1996 Polanyi Award Lecture
Proton reactions in clusters[1]

Raymond Kapral, Styliani Consta, and Daniel Laria

Abstract: Reactions in mesoscopic, molecular clusters may proceed by mechanisms and with rates that differ from those in bulk solvents. Two examples of reactions in large, liquid-state, molecular clusters are described to illustrate the distinctive features of these reactions: acid dissociation and proton transfer in aprotic, polar solvents. Both of these reactions involve proton dynamics so methods for dealing with mixed quantum–classical systems must be utilized to investigate the reaction dynamics. Surface versus bulk solvation effects play an important role in determining the reaction mechanisms as do the strong cluster fluctuations. Mechanisms for proton transfer within clusters that have no bulk analogs will be described.

Key words: proton reactions, mesoscopic clusters.

Résumé : Les mécanismes de réactions qui se produisent dans des agrégats moléculaires mésoscopiques peuvent être différents de ceux observés dans les masses de solvants. Pour illustrer les caractéristiques particulières de ces réactions, on décrit deux exemples de réactions effectuées dans de grands agrégats moléculaires, à l'état liquide : la dissociation acide et le transfert de proton dans des solvants polaires aprotiques. Ces deux réactions impliquent la dynamique des protons; pour étudier la dynamique de ces réactions, on doit donc utiliser les méthodes qui s'appliquent aux systèmes de quantum–classique mixtes. Par rapport aux effets de solvatation, les effets de surface jouent un rôle plus important dans la détermination des mécanismes de réaction; il en est de même pour les fortes variations dans les agrégats. On décrira les mécanismes de transfert de proton dans les agrégats qui n'ont aucune ressemblance avec ceux impliqués dans les masses de solvant.

Mots clés : réactions de proton, agrégats mésoscopiques.

[Traduit par la rédaction]

1. Introduction

Clusters composed of tens to hundreds of molecules are sufficiently large that their chemistry differs from that of few-molecule clusters, yet they are so small that they cannot be classified as macroscopic objects. Important features that enter the description of chemical properties and dynamics are the cluster density and shape fluctuations and the strong effects that surface forces have on the position and orientation of molecules in the cluster. A number of different aspects of cluster reactions have been studied (see, for example, ref. 1) but here we examine reaction dynamics in mesoscopic, liquid-state clusters.

Since these clusters provide environments that differ significantly from either small molecular aggregates or bulk liquids, it is of interest to inquire if reaction rates or mechanisms have distinctive features in such media. By means of two examples, acid ionization and proton transfer, we shall show that this is indeed the case. The mechanisms of both reactions are known to be influenced by the solvent in which they take place; in fact, the solvent is responsible for the very existence of reactant and product states. In addition, the two examples involve protons so one must consider the quantum character of the proton in any description of the reaction dynamics.

In Sect. 2 we examine acid ionization processes in aprotic, polar, molecular solvents. In particular, we consider the ionization of HCl in acetonitrile and dimethyl sulfoxide, two solvents with similar dipole moments but very different solvation properties (2). We determine whether solvent-separated ion pairs can exist in clusters and examine the influence of surface forces on the solvation structure. Section 3 considers proton transfer in a proton–ion complex consisting of two ions and a proton. This complex is a constituent of a polar molecular cluster and again the focus is on how the cluster environment can alter the mechanism and rate of the transfer reaction (3, 4). The conclusions are presented in Sect. 4.

2. Ionization of acids in clusters

The equilibria of ions dissolved in polar solvents present some interesting features that have consequences for the mechanisms of reactions. Consider an acid HA dissolved in

Received July 30, 1996.

R. Kapral[2] and S. Consta. Chemical Physics Theory Group, Department of Chemistry, University of Toronto, Toronto, ON M5S 3H6, Canada.
D. Laria. Departamento Química de Reactores, Comisión Nacional de Energía Atómica, 1429 Capital Federal, Argentina.

[1] This is an invited review article based on the 1996 J.C. Polanyi Award Lecture presented by Professor Kapral at the annual conference of the Canadian Society for Chemistry in St. John's, Nfld., in June 1996.

[2] Author to whom correspondence may be addressed. Telephone: (416) 978-6106. Fax: (416) 978-5325. E-mail: rkapral/@gatto.chem.utoronto.ca

© 1997 NRC Canada

Can. J. Chem. Downloaded from www.nrcresearchpress.com by 92.62.229.171 on 09/08/12
For personal use only.

Can. J. Chem. Downloaded from www.nrcresearchpress.com by 92.62.229.171 on 09/08/12
For personal use only.

a polar solvent S. We may schematically represent the ionization process as

[1] $HA \longrightarrow H^+||A^- \longrightarrow H^+(S) + A^-(S)$

The configuration $H^+ \,||\, A^-$ denotes a solvent-separated ion pair (SSIP), a metastable configuration corresponding to a local minimum in the free energy as a function of the separation between the H^+ and A^- ions (5). In this section we shall investigate this process for HCl in acetonitrile (ACN) and dimethyl sulfoxide (DMSO) clusters and bulk. In particular we shall describe the computation of the free energy for this quantum ionization process and determine if a local minimum does indeed exist so that a SSIP species may be identified (2).

A. Potential of mean force

The equilibrium structure is determined by the potential of mean force, $W(r)$, as a function of the separation between the H^+ and Cl^- ions. This quantity may be determined from a knowledge of the probability density, $P(r')$, for finding a particular numerical value r' of the separation r according to the formula

[2] $$W(r') \sim -kT \ln P(r') = -kT \ln \langle \delta(r - r') \rangle$$

where $\langle \cdots \rangle$ signifies an equilibrium ensemble average and $\delta(r)$ is the Dirac delta function. The mean force is related to the mean potential by

[3] $$F(r') = -\frac{dW(r')}{dr'}$$

From eq. [2] we see that in order to compute $W(r)$ one must consider a fixed value of the separation $r = r'$ and average over an equilibrium distribution of all other degrees of freedom. This calculation was carried out using the constrained-reaction-coordinate-dynamics (CRCD) ensemble (6, 7) by applying a holonomic constraint to the equations of motion that fixes the separation at a prescribed value (8).

B. Quantum description of the proton

Since the proton is a quantum mechanical particle and the chloride ion and solvent are classical particles to a good approximation, a scheme must be devised for the computation of the potential of mean force that takes this feature into account. If only static properties are of interest this is easily accomplished by using a Feynman path integral representation of the proton (9). In this scheme the similarity between the Boltzmann factor $\exp(-\beta\hat{H})$ and the quantum mechanical propagator $\exp(-i\hat{H}t/\hbar)$ is utilized with the identification of $\beta \rightarrow it/\hbar$ as the imaginary time where β^{-1} is Boltzmann's constant times the temperature. If the imaginary time is discretized into P segments, where P is determined by the de Broglie wavelength of the particle, the quantum proton is represented as a classical ring polymer composed of P monomers (9, 10). In this representation the effective potential of the system, solvent plus chloride ion and proton, is given by

[4] $$V_{\text{eff}} = V_{\text{cl}}(\boldsymbol{R}^N) + \frac{Pm_{\text{p}}}{2(\beta\hbar)^2} \sum_{i=1}^{P} (\boldsymbol{r}_i - \boldsymbol{r}_{i+1})^2 + \frac{1}{P} V_{\text{p}}(\boldsymbol{r}^P, \boldsymbol{R}^N)$$

where m_{p} is the proton mass. Here $V_{\text{cl}}(\boldsymbol{R}^N)$ is the potential energy for all the classical particles and $V_{\text{p}}(\boldsymbol{r}^P, \boldsymbol{R}^N)$ is the interaction energy between the proton monomers and the classical particles. A value $P = 20$ suffices for an accurate description of the proton.

If one assigns a fictitious mass m^* to the proton monomers and adds a kinetic energy term to the effective potential energy a Hamiltonian may be constructed for this system:

[5] $$H = \sum_{i=1}^{P} \frac{1}{2} m^* \dot{\boldsymbol{r}}_i^2 + \sum_{j=1}^{N} \frac{1}{2} M_j \dot{\boldsymbol{R}}_j^2 + V_{\text{eff}}$$

where the second term on the right hand side is the usual kinetic energy term for the classical particles. This Hamiltonian may be used to generate the dynamics of the classical particles and proton monomers. While this dynamics is fictitious due to the introduction of the proton monomer kinetic energy, the equilibrium properties are independent of the kinetic energy and thus the trajectories may be used to compute equilibrium averages making use of the usual replacement of ensemble averages by time averages over the system trajectory.

The proton position was taken to be the centroid of the proton polymer (11)

[6] $$\boldsymbol{r}_{\text{c}} = \frac{1}{P} \sum_{i=1}^{P} \boldsymbol{r}_i$$

The mean force on the ion pair separated by a distance $r = |\boldsymbol{R}_{\text{Cl}} - \boldsymbol{r}_{\text{c}}|$ was calculated from the formula (12)

[7] $$F(r) = \left\langle \sum_{i=1}^{P} \boldsymbol{F}_i \cdot \hat{\boldsymbol{r}} \right\rangle_r + \frac{2}{\beta r}$$

where $\boldsymbol{F}_i$ is the force exerted by the Cl^- and the solvent particles upon the ith proton monomer, $\hat{\boldsymbol{r}} = \boldsymbol{r}/|\boldsymbol{r}|$ and $\langle \ldots . \rangle_r$ signifies a time average computed using the constrained reaction coordinate dynamics ensemble (6). The situation is shown schematically in Fig. 1. The mean potential $W(r)$ was computed from an integration of the mean force:

[8] $$W(r) = W(r_0) + \int_{r_0}^{r} dr' \, F(r')$$

C. Ionization in ACN and DMSO clusters

The potential of mean force is shown in Fig. 2 for bulk phase ACN and DMSO as well as for a cluster containing 30 DMSO solvent molecules. These results for bulk solvent show that SSIPs are found in DMSO but not in ACN. The free energy barrier for passage from the SSIP configuration at $r_{\text{s}} = 7.5$ Å to the bound ion pair is $\Delta W_{\text{DMSO}} = W_{\text{DMSO}}(r_{\text{max}}) - W_{\text{DMSO}}(r_{\text{s}}) = 5.4$ kcal/mol, where r_{max} is the position of the maximum between the bound ion pair configuration and the SSIP. In contrast, ACN has only a very shallow minimum whose magnitude is within the statistical uncertainty of our results.

The cluster free energy shows that SSIPs are also found in

© 1997 NRC Canada

Fig. 1. Schematic diagram showing the constrained separation r between the Cl^- ion and the proton centroid. In the molecular dynamics simulation r is constrained but all other coordinates (apart from those fixed by bond constraints) are allowed to evolve according to the equations of motion.

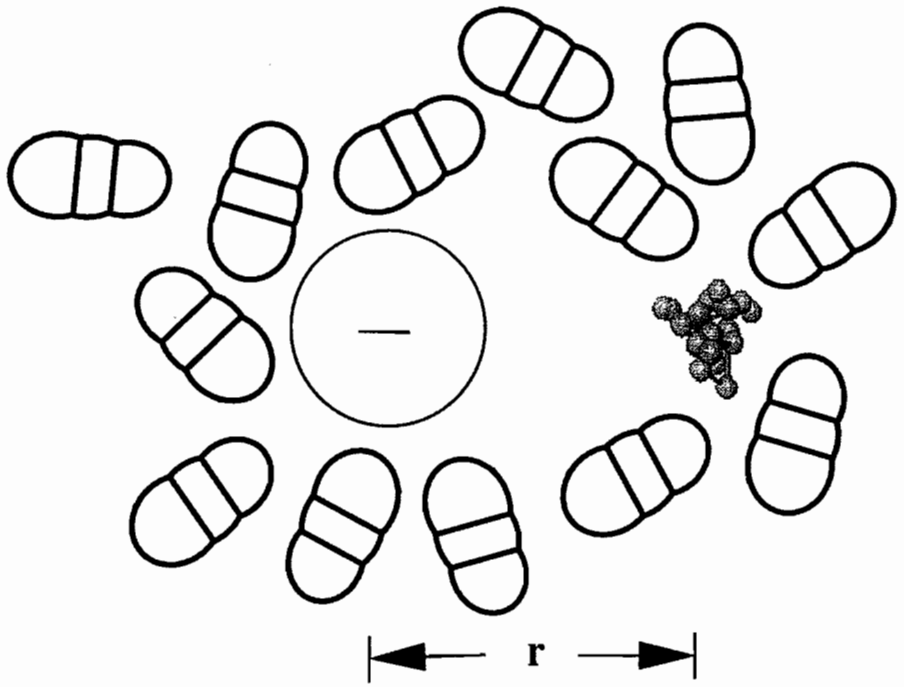
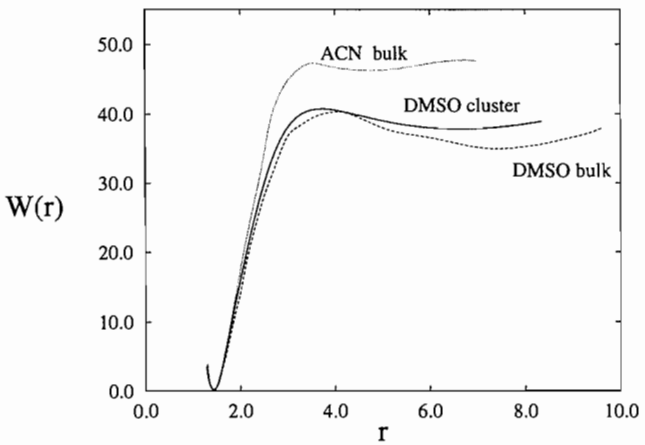


Fig. 2. Potential of mean force $W(r)$ in kcal/mol for bulk ACN, bulk DMSO, and a $N = 30$ DMSO cluster.



four nearest solvent molecules around the proton. Examina- the $N = 30$ DMSO cluster with a free energy barrier between the SSIP and bound ion pair states of $\Delta W_{DMSO}(n = 30) = 1.8$ kcal/mol. The solvation structure in the bulk and cluster phases is subtly different for both solvents. In either solvent case there is similar coordination and orientation of roughly tion of the solvation structure reveals qualitatively similar configurations at r values in the vicinity of the metastable minimum. In the ACN cluster, which is not shown in Fig. 2, the free energy presents no SSIP minimum.

In spite of the qualitative similarities in the solvation structure there are differences that are responsible for both the widely different ionization constants in these two solvents and the existence of SSIPs in DMSO. For example, the solvent structure in the transition region between bound ion pair and SSIP configurations is different in the two solvents. The dipolar density shows that the ACN molecules have a considerable degree of orientational variability so that when the molecular dipole moment is projected onto the z-axis of the ion pair the projection can take either sign. However, the dipolar density of DMSO shows no such effect, implying that the DMSO molecules are much more rigidly ordered in the first solvation shell. Consequently, it appears that, in ACN, fluctuations are sufficiently large to promote dipolar orientations that favor passage from SSIP to bound ion pair states. In DMSO a much more structured three-dimensional solvent network exists that hinders molecular rotations and leads to a larger free energy barrier.

The cluster environment has an important influence on the ionization process. For ion pair separations as large as that for the SSIP state, the cluster potential of mean force closely corresponds to that of the bulk, even for clusters with as few as $n = 14$ solvent molecules. If the separation between the H^+ and Cl^- ions is large, the finite size of the cluster gives rise to changes in the mean potential as reflected in the "rubber band"-like solvent configurations (cf. Fig. 3) that lead to attractive forces between the ions that cannot exist in the bulk.

3. Proton transfer in clusters

The transfer of a proton between two ions in a proton–ion

© 1997 NRC Canada

Can. J. Chem. Downloaded from www.nrcresearchpress.com by 92.62.229.171 on 09/08/12
For personal use only.

Fig. 3. Sample configurations showing solvent fluctuations when the ion pair is constrained to lie at a large internuclear separation, $r = 27$ Å.

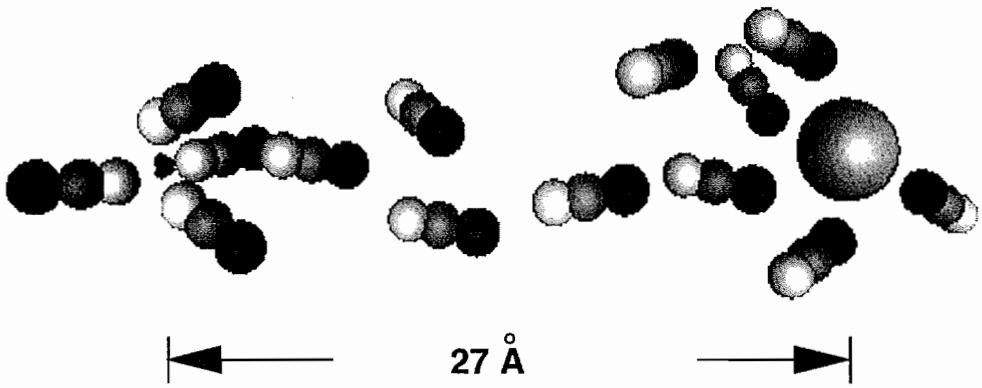
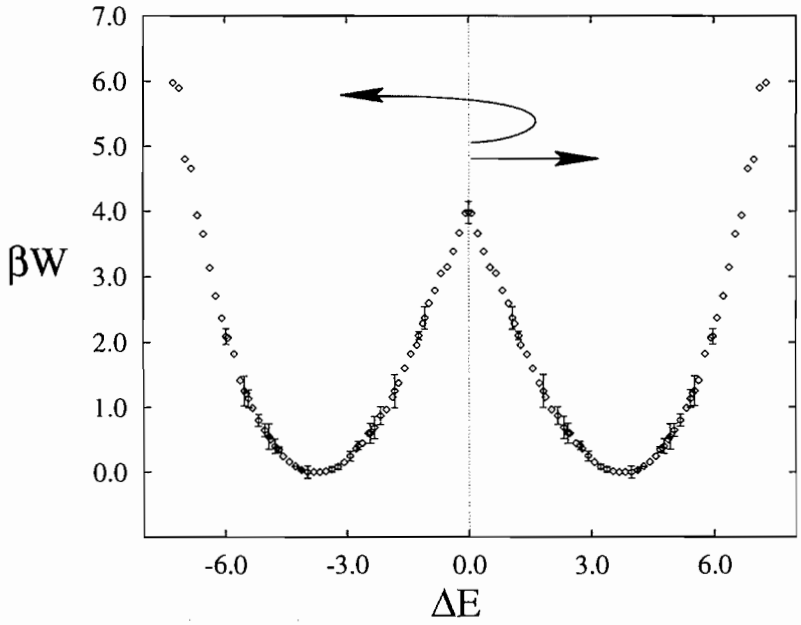


Fig. 4. Potential of mean force and a schematic representation of direct and recrossing trajectories.



complex within a molecular cluster will now be considered (3). The two ions may be taken to represent ion sites in an intramolecular proton transfer or free ions in an intermolecular proton transfer. Since the internuclear separation is fixed, we neglect contributions of the internal modes of the proton–ion complex to the proton transfer reaction. The proton transfer reaction may be written as

[9] $\mathrm{A} - \mathrm{H} \cdots \mathrm{A}^- \rightleftharpoons \mathrm{A}^- \cdots \mathrm{H} - \mathrm{A}$

The solvent molecules comprising the cluster are rigid diatomic molecules with molecular dipole moment $\mu = 5.0$ D (3). We consider liquid-state clusters with $N = 20$ and 67 molecules.

A. Adiabatic dynamics

If the ground state protonic energy level is well separated from the excited states for all solvent configurations the dynamics of the quantum proton in the classical solvent may be treated in the Born–Oppenheimer approximation (for bulk-phase studies, see ref. 13). The Schrödinger equation for the proton in the fixed field of the classical particles is

[10] $$\hat{H}_\mathrm{p}(\nabla_u, u; \boldsymbol{R}^N)\Psi_n(u; \{\boldsymbol{R}\}) = \left[-\frac{\hbar^2}{2m_\mathrm{p}}\nabla_u{}^2 + V_\mathrm{p}(u, \boldsymbol{R}^N)\right]\Psi_n(u; \boldsymbol{R}^N) = \epsilon_n(\boldsymbol{R}^N)\Psi_n(u; \boldsymbol{R}^N)$$

Here $\hat{H}_\mathrm{p}$ is the total proton Hamiltonian, $2\pi\hbar$ is Planck's constant, and n labels the protonic state. The potential energy V_p is the sum of the intrinsic, V_int, and Coulomb, V_c, potentials.

The intrinsic potential has essentially no barrier so that we model proton transfer in a strongly hydrogen-bonded system (see, for instance, ref. 14). Solvent effects are especially large in such a circumstance and in the present model are responsible for the existence of reactant and product species. The free energy along the reaction coordinate is shown in Fig. 4 and indicates the formation of reactant and product states

© 1997 NRC Canada

Can. J. Chem. Downloaded from www.nrcresearchpress.com by 92.62.229.171 on 09/08/12
For personal use only.

Can. J. Chem. Downloaded from www.nrcresearchpress.com by 92.62.229.171 on 09/08/12
For personal use only.

as a result of solvent interactions. The time evolution of the classical particles is given by Newton's equations of motion

$$[11] \quad m_i\ddot{\boldsymbol{R}}_i = -\nabla_{\boldsymbol{R}_i} V_s(\boldsymbol{R}^N) - \nabla_{\boldsymbol{R}_i}\langle\Psi_0(\boldsymbol{R}^N)|\hat{H}_p(\boldsymbol{R}^N)|\Psi_0(\boldsymbol{R}^N)\rangle$$

where the first term on the right hand side is the force due to all classical particles and the second term is the Hellmann–Feynman force. The Schrödinger equation was solved at each molecular dynamics time step by expanding the wave function in a Gaussian basis and solving the resulting non-orthogonal eigenvalue problem (3).

B. Reaction coordinate

Two reaction coordinates were used to monitor the progress of the reaction. The first is the expectation value of the proton position in the adiabatic ground state,

$$[12] \quad \xi(\boldsymbol{R}^N) = \bar{z}_p(\boldsymbol{R}^N) = \langle\Psi_0(\boldsymbol{R}^N) \mid u \mid \Psi_0(\boldsymbol{R}^N)\rangle$$

While this reaction coordinate monitors the position of the proton one should note that it is a function of the solvent configuration through the dependence of the adiabatic wave function on $\boldsymbol{R}^N$. The second reaction coordinate monitors the progress of the reaction through the solvent polarization (15),

$$[13] \quad \xi(\boldsymbol{R}^N) = \Delta E(\boldsymbol{R}^N) = \sum_{i,a} z_a e\left(\frac{1}{|\boldsymbol{R}_i^a - \boldsymbol{s}|} - \frac{1}{|\boldsymbol{R}_i^a - \boldsymbol{s}'|}\right)$$

where $\boldsymbol{s}$ and $\boldsymbol{s}'$ are two points in the vicinities of the reactant and product configurations. Using this reaction coordinate one views the reaction as being driven by the solvent polarization fluctuations. The transition state corresponds to a symmetrically solvated proton–ion complex in which $\Delta E = 0$ (cf. Fig. 4). In fact, there is a third possibility for the choice of reaction coordinate, the centroid of the polymer chain representing the proton in the Feynman path integral representation, as in the acid dissociation problem considered in the previous section. We have considered this reaction coordinate for cluster proton transfer reactions (4) but here we focus on the first two choices. Both choices of reaction coordinate, $\bar{z}_p(\boldsymbol{R}^N)$ and $\Delta E(\boldsymbol{R}^N)$, provide equivalent descriptions of the transfer process.

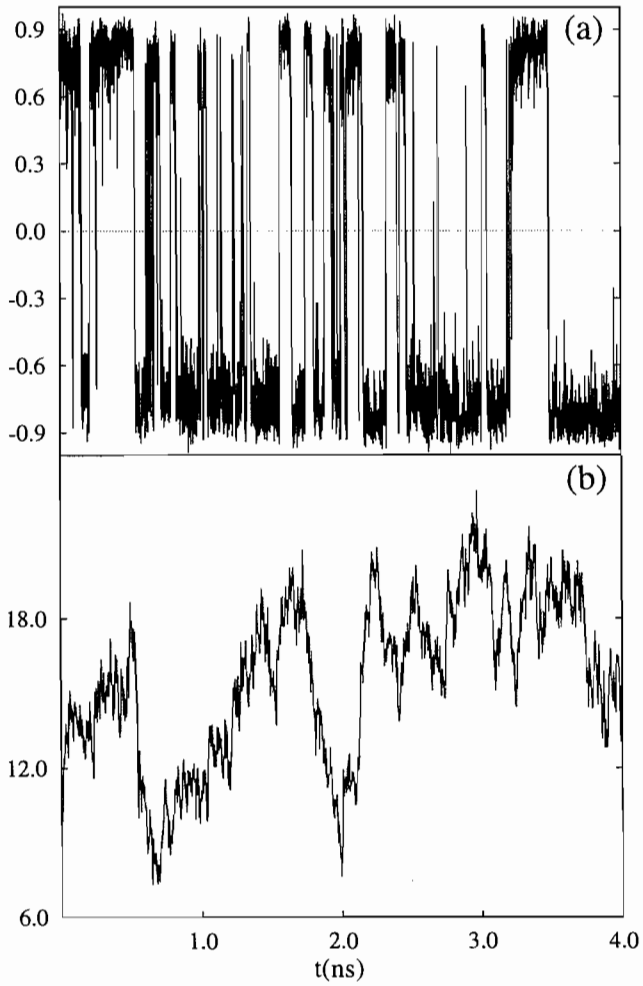
C. Reaction mechanism and rate In the bulk phase the proton transfer reaction is driven by solvent polarization fluctuations due primarily to solvent reorientation. We now consider how the transfer occurs in mesoscopic molecular clusters where surface forces and strong solvent orientational and translational fluctuations play an important role. The mechanism of such transfer events depends on the cluster size, even within the mesoscopic domain. As an example we consider one case, a cluster with $N = 67$ solvent molecules, to illustrate some features of the cluster mechanism. This cluster size is large enough to support two solvent shells around the proton–ion complex.

Reactions occur both in the interior of the cluster and on its surface. This can be seen from a comparison of the time series of the reaction coordinate (here $\bar{z}_p(\boldsymbol{R}^N)$) and the distance, $d = |\boldsymbol{d}|$, between the center of mass (CM) of the proton–ion complex and the center of mass of the solvent molecules in the cluster

$$[14] \quad \boldsymbol{d} = N^{-1}\sum_{i=1}^{N} \boldsymbol{R}_i^{CM} - \boldsymbol{R}_{CM} = N^{-1}\sum_{i=1}^{N} \boldsymbol{d}_i$$

where $\boldsymbol{d}_i$ is the vector from the center of mass of the complex to that of the ith solvent molecule, $\boldsymbol{d}_i = \frac{1}{2}(\boldsymbol{R}_{i,1} + \boldsymbol{R}_{i,2}) - \boldsymbol{R}_{CM} = \boldsymbol{R}_i^{CM} - \boldsymbol{R}_{CM}$. This quantity provides a rough measure of the position of the complex within the cluster. One sees in panel (*a*) of Fig. 5 a large number of flips between the reactant and product states of the complex. In the course of this reaction the complex resides for long portions of time on the surface of the cluster but also makes excursions to the interior of the cluster. There is some evidence from this figure that proton transfers are more rapid when the complex is within the cluster. This is not surprising in view of the fact that in this circumstance it is more likely to find symmetric solvent configurations that correspond to the transition state configurations through which the transfer process occurs. In fact, in smaller clusters ($N = 20$) proton transfer occurs only within the interior of the cluster on the several nanosecond time scale on which the simulations were carried out (3).

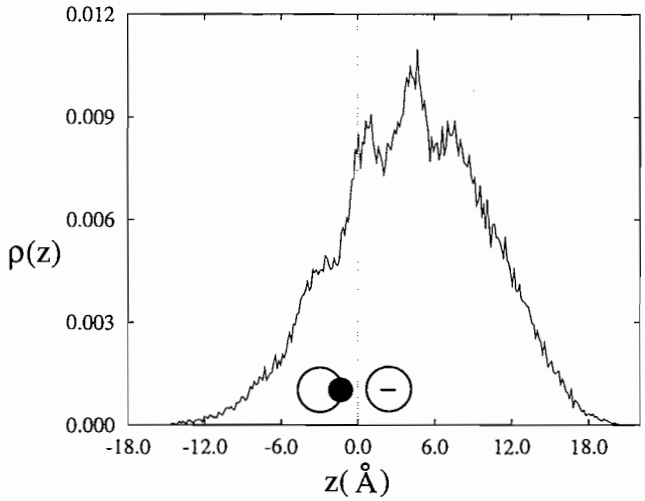
Fig. 5. (*a*) The reaction coordinate $\bar{z}_p(\boldsymbol{R}^N)$ versus time for a cluster with 67 solvent molecules. (*b*) The distance d versus time for the same trajectory.



© 1997 NRC Canada

Can. J. Chem. Downloaded from www.nrcresearchpress.com by 92.62.229.171 on 09/08/12
For personal use only.

Fig. 6. Probability density of the solvent molecule center of mass projected on the proton–ion complex internuclear axis.

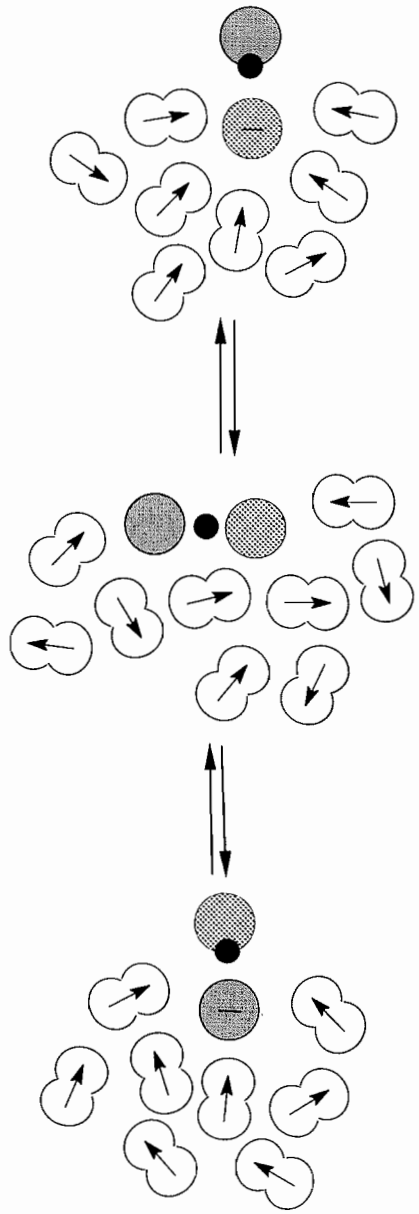


In the somewhat larger clusters, where there are on average approximately two solvent shells, the distinction between bulk and surface manifests itself more clearly. The surface reaction is controlled by the specific solvation structure associated with the proton–ion complex (3, 4). For the complex A—H ··· A^-, the solvent–solvent interactions are stronger than the solvent–(A—H) interactions, while the solvent–A^- interactions are very strong. These considerations suggest that the A^- end of the complex will tend to be strongly solvated within the cluster while the (A—H) end will tend to reside on the surface. In addition to energetic factors, entropic factors favor configurations where the complex resides close to the surface of the cluster. This is indeed the case as can be seen from Fig. 6, which shows the probability density for finding the center of mass of a solvent molecule projected on the z-axis along the interionic bond in the proton–ion complex. This probability density was computed directly from the molecular dynamics trajectory by sampling configurations only when the proton was in the reactant (or product) configuration. The high and asymmetric probability density confirms that the exposed ion is strongly solvated and that the cluster accommodates to the state of the proton–ion complex. Thus, the tendency is for the complex to float on the surface of the cluster like a fishing bob on the surface of a lake: the A^- end is in the cluster and the (A—H) end is out. The reaction occurs as a result of the orientational and positional fluctuations of the complex and solvent. These fluctuations can lead to an orientational change of the complex relative to the surface so that the complex lies parallel to the surface. Also, solvent fluctuations can lead to configurations where the solvation is more nearly symmetrical without deep excursions of the complex to the interior of the cluster. These situations will favor a proton transfer. Once the transfer takes place the original solvation structure is no longer favorable and the proton–ion complex "bob" flips and adopts a configuration with the opposite ion strongly solvated within the cluster. This situation is depicted schematically in Fig. 7.

The rate constant of the reaction was computed using the reactive flux correlation expression (7, 16)

$$[15] \quad k(t) = \frac{\langle \Delta\dot{E}(0)\delta(\Delta E(0))\theta[\Delta E(t)]\rangle}{\langle\theta[\Delta E(t)]\rangle} = k^{\mathrm{TST}}\kappa(t)$$

Fig. 7. Schematic picture showing the dominant solvation structures of the proton–ion complex in the reactant and product configurations and the process responsible for the proton transfer.



where the angular brackets represent a canonical ensemble average, and $\theta(\Delta E(t))$ is the Heaviside function. Here we have used the solvent polarization coordinate $\Delta E(\boldsymbol{R}^N)$ to monitor the progress of the reaction. The ensemble averages were computed in the CRCD ensemble. The breakup of $k(t)$ into a transition state theory rate constant, k^{TST}, and a time-dependent transmission coefficient, $\kappa(t)$, is a convenient way to view the reaction dynamics. Figure 4 shows the free energy along the reaction coordinate and a schematic representation of trajectories starting at the free energy barrier that go directly to products and contribute to the TST rate constant, and recrossing trajectories that lower the TST rate and lead to a κ value that is less than unity. Provided there is a large time scale separation between the reactive and other processes, the full rate constant k can be determined as $k(t^*)$

© 1997 NRC Canada

where t^* is a time of order $t_{mic} \ll t^* \ll t_{chem}$ with t_{mic} a microscopic time and t_{chem} the chemical relaxation time (7, 16, 17).

Computations show that for the 67-molecule cluster the free energy barrier is $\Delta W = 4.47\ kT(T = 260K)$ leading to a TST rate constant of $k^{TST} = 0.04\ ps^{-1}$, and the transmission coefficient is found to be $\kappa = 0.4$ giving $k = 0.016\ ps^{-1}$ (3).

D. Non-adiabatic dynamics

Adiabatic dynamics is most likely to break down in the vicinity of the transition state configuration where the configuration of solvent molecules in the cluster provides a nearly symmetrical solvation structure around the proton–ion complex. In this configuration the two lowest adiabatic states may be separated by energies that are a fraction of a kT unit. Since this is the region that influences the reaction dynamics, it is of interest to examine the extent to which the reaction rate is modified if account is taken of the excited protonic states.

In Tully's surface-hopping, stochastic model (18) an ensemble of trajectories is evolved on the adiabatic surfaces with hops between the adiabatic states determined from a master equation. The time-dependent quantum wave function of the proton $\Phi(u, \boldsymbol{R}^N, t)$ is expanded in terms of the adiabatic states as

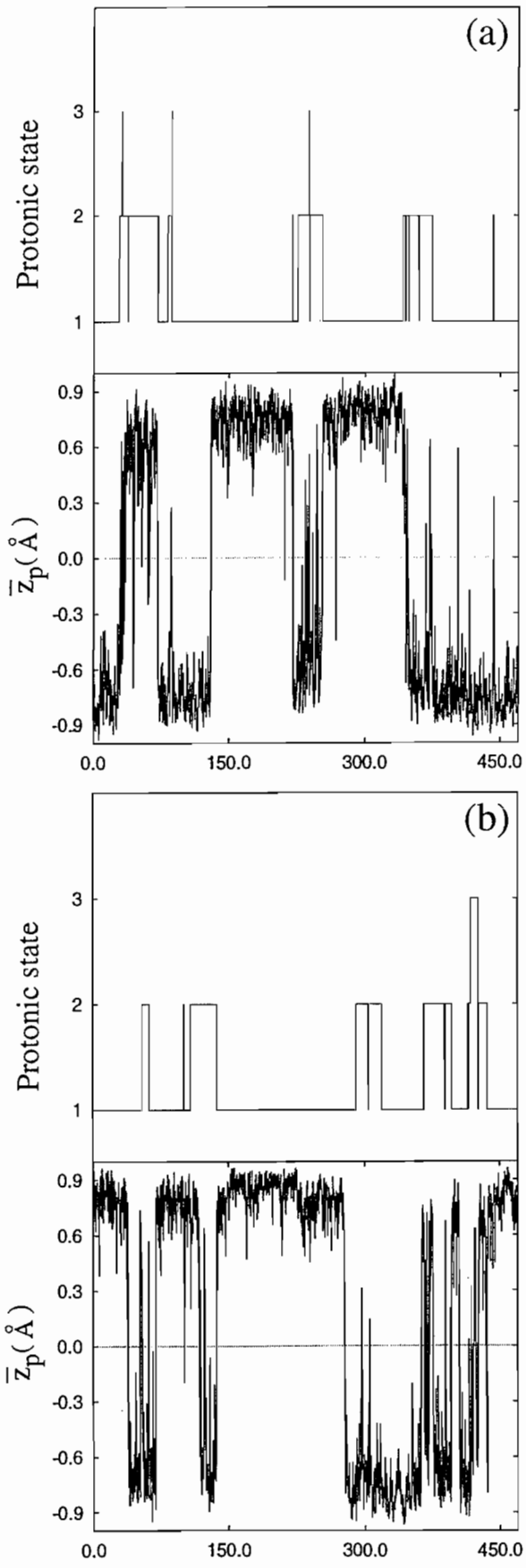
$$[16] \quad \Phi(u, \boldsymbol{R}^N, t) = \sum_n c_n(t)\Psi_n(u; \boldsymbol{R}^N)$$

The Schrödinger equation for the expansion coefficients is solved along with Newton's equations of motion to determine the time evolution of the system. The probability of a hop from state k at time t to state j in the time interval between t and $t+\Delta$ is given by $g_{kj} = (b_{jk}(t+\Delta)\Delta)/a_{kk}(t+\Delta)$ if $g_{kj} \geq 0$ and zero otherwise. Here $a_{kj} = c_k c_j^*$ and $b_{jk} = -2$ Re $(a_{jk}^* \dot{\boldsymbol{R}} \cdot \boldsymbol{d}_{kj})$ where $\boldsymbol{d}_{kj}$ is the non-adiabatic coupling vector

$$[17] \quad \boldsymbol{d}_{kj}(\boldsymbol{R}^N) = \langle \Psi_k(\boldsymbol{R}^N) | \nabla_{\boldsymbol{R}^N} | \Psi_j(\boldsymbol{R}^N) \rangle$$

In non-adiabatic dynamics we use $\bar{z}_p^n = \langle \Psi_n | u | \Psi_n \rangle$ as the reaction coordinate. In Fig. 8 (*a* and *b*) for a 67-molecule cluster we see that transitions of the proton from the ground state to the excited states frequently occur in the transition state region. From a series of non-adiabatic trajectories it was estimated that (*a*) the number of proton transfers while the proton is in an excited state is comparable to that when the proton is in the ground state (note that the proton spends 88% of the time in the ground state) and (*b*) the number of recrossings of the transition state is much higher when the proton is in an excited state compared to that when the proton is in the ground state. These observations are consistent with the fact that the excited state proton charge density is more expanded along the interionic axis than the ground state charge density. Therefore, the Hellman–Feynman forces determined by the excited state densities lead to solvent configurations that favour the transition state. The rate of the reaction computed from the direct observation of reactive transitions was found to be $k = 0.017\ ps^{-1}$ (1/59.0 ps). Recall that the value using adiabatic dynamics was $k = 1/62.5$ ps. The similarity of the adiabatic and non-adiabatic rate constants may arise from a cancellation of effects. The proton excited state charge density may favor transition state configurations where proton transfer is likely but it also appears to favor increased tran-

Fig. 8. Protonic state (upper panel) and reaction coordinate (lower panel) as a function of time for nonadiabatic dynamics.



© 1997 NRC Canada

Can. J. Chem. Downloaded from www.nrcresearchpress.com by 92.62.229.171 on 09/08/12
For personal use only.

sition surface recrossings that lower the rate. These effects deserve further detailed study.

4. Conclusions

The two examples described above have served to illustrate only a few aspects of the unique chemistry that is possible on the mesoscale domain in liquid-state molecular clusters. The principal factors that come into play determining the reaction rates and mechanisms are the specific solvation effects and strong fluctuations for such clusters. The rather large surface-to-volume ratio makes surface forces very important and these surface forces can influence the solvation of species within the cluster. They may determine whether a species resides within the cluster or on its surface, as was the case for the proton–ion complex we studied. This in turn will have implications for the mechanism of a reaction. The precise nature of these surface-specific solvation effects will of course depend on the nature of the solvent and reactants: for example, whether they are charged or polar and the relative magnitudes of solvent–solvent versus solvent–solute forces. Effects of this kind have been seen in studies of S_N2 reactions in water clusters (19).

The liquid-state clusters we examined are dynamic objects with strong particle and shape fluctuations. The extent to which these cluster environments can be modeled by simple stochastic theories is an open problem but, clearly, models of the reactive dynamics that neglect these fluctuations are likey to miss important aspects of the reaction mechanism.

We have focused on liquid-state clusters. The general aspects of such cluster reactions could have implications for the reactive processes occurring in the atmosphere. Normally one is concerned with reactive dynamics in much larger liquid clusters where macroscopic concepts have greater validity. However, large clusters grow from small ones and one must consider the dynamics on these smaller scales, which is still "terra incognito" and deserves further exploration. Of course, clusters in the same size domain but in other physical states, such as solid clusters and mixed clusters, are also interesting environments in which to examine fundamental questions of condensed-phase reaction dynamics.

Acknowledgements

We would like to thank G. Ciccotti and M. Ferrario for many discussions on topics in this area that have formed the background for the work described here. This work was supported in part by a grant from the Natural Sciences and Engineering Research Council of Canada.

References

1. A.W. Castleman, Jr. and R.G. Keesee. Science, **241**, 36 (1988); R.G. Keesee and A.W. Castleman, Jr. J. Phys. Chem. Ref. Data, **15**, 1011 (1986); R. Naamen. Adv. Chem. Phys. **70**, 181 (1988); H.-P. Kaukonen, U. Landman, and C.L. Cleveland. J. Chem. Phys. **97**, 4997 (1991), and refs. therein; D. Laria and R. Fernández-Prini. Chem. Phys. Lett. **205**, 260 (1993); J. Chem. Phys. **102**, 7664 (1995); J. Jortner, R.D. Levine, and B. Pullman (*Editors*). Reaction dynamics in clusters and condensed phases. Kluwer Academic Publishers, Dordrecht. 1994.
2. D. Laria, R. Kapral, D. Estrín and G. Ciccotti. J. Chem. Phys. **104**, 6560 (1996).
3. S. Consta and R. Kapral. J. Chem. Phys. **104**, 4581 (1996).
4. S. Consta and R. Kapral. J. Chem. Phys. **101**, 10908 (1994).
5. S. Winstein, E. Clippenger, A.H. Fainber, and G.C. Robinson. J. Am. Chem. Soc. **76**, 259 (1954).
6. E.A. Carter, G. Ciccotti, J.T. Hynes, and R. Kapral. Chem. Phys. Lett. **156**, 472 (1989).
7. G. Ciccotti, M. Ferrario, D. Laria, and R. Kapral. *In* Progress in computational physics of matter. *Edited by* L. Reatto and F. Manghi. World Scientific, New Jersey. 1995. p. 150.
8. J.P. Ryckaert, G. Ciccotti, and H.J.C. Berendsen. J. Comput. Phys. **23**, 327 (1977).
9. R.P. Feynman. Phys. Rev. **56**, 340 (1939).
10. D. Chandler and P.G. Wolynes. J. Chem. Phys. **74**, 4078 (1981).
11. M. Gillan. J. Phys. C: Solid State Phys. **20**, 3621 (1987); G.A. Voth, D. Chandler, and W.H. Miller. J. Chem. Phys. **91**, 7749 (1989).
12. D. Laria, G. Ciccotti, M. Ferrario, and R. Kapral. Chem. Phys. **180**, 181 (1994).
13. D. Laria, G. Ciccotti, M. Ferrario, and R. Kapral. J. Chem. Phys. **97**, 378 (1992); H. Azzouz and D. Borgis. J. Chem. Phys. **98**, 7361 (1993); D. Borgis, G. Tarjus, and H. Azzouz. J. Phys. Chem. **96**, 3188 (1992); J. Chem. Phys. **97**, 1390 (1992).
14. M.D. Joesten and L.J. Schaad. Hydrogen bonding. Marcel Deckker, Inc., New York. 1974.
15. R.A. Marcus and N. Sutin. Biochim. Biophys. Acta, **811**, 265 (1985); A. Warshel. J. Am. Chem. Soc. **86**, 2218 (1982).
16. T. Yamamoto. J. Chem. Phys. **33**, 281 (1960); D. Chandler. J. Chem. Phys. **68**, 2959 (1978).
17. R. Kapral. Adv. Chem. Phys. **48**, 71 (1981).
18. J.C. Tully. J. Chem. Phys. **93**, 1061 (1990); Int. J. Quantum Chem. Quantum Chem. Symp. **25**, 299 (1991); S. Hammes-Schiffer and J.C. Tully. J. Chem. Phys. **101**, 4657 (1994).
19. M. Re and D. Laria. J. Chem. Phys. **105**, 4584 (1996).

Can. J. Chem. Downloaded from www.nrcresearchpress.com by 92.62.229.171 on 09/08/12
For personal use only.

© 1997 NRC Canada

The mechanism of oxidation of 3-mercaptopropionic acid

Paula Forlano, José A. Olabe, Jorge F. Magallanes, and Miguel A. Blesa

Abstract: The mechanism of the oxidation of 3-mercaptopropionic acid (3-MPA) by hydrogen peroxide was studied in the acidic pH range. The nucleophilic attack by sulphur on the peroxide bond controls the rate. Extrapolation of the pH dependency suggests that the rate of attack by the deprotonated dianion is highest. Traces of Fe(III), at levels below 10^{-7} mol dm^{-3}, do not catalyze efficiently the process through one-electron mechanisms; at higher concentrations, or on the surface of iron(III) oxides, this type of catalysis becomes important. The electrochemical oxidation of 3-MPA was also studied, using differential pulse polarography and cyclic voltammetry techniques. The mechanism is of the EC_2E type, the second electron transfer step corresponding to the oxidation of the disulphide RS-SR. The rate constant for the dimerization of the RS$^{\bullet}$ radicals was 1.8×10^3 mol^{-1} dm^3 s^{-1}; the slowness of this step agrees with the mechanisms observed in the course of one-electron oxidations by metal ions.

Key words: electrochemistry, kinetics, 3-mercaptopropionic acid, autooxidation.

Résumé : Opérant dans la plage acide des pH, on a étudié le mécanisme d'oxydation de l'acide 3-mercaptopropanoïque («3-MPA») par le peroxyde d'hydrogène. La vitesse de la réaction est fixée par l'attaque nucléophile du soufre sur la liaison peroxyde. Une extrapolation de la dépendance sur le pH suggère que l'attaque par le dianion déprotoné est celle qui se fait avec la vitesse la plus grande. Le fer(III), à l'état de traces, à des niveaux inférieurs à 10^{-7} mol dm^{-3}, ne catalyse pas le processus d'une façon efficace par le biais de mécanismes à un électron; à des concentrations plus élevées, ou sur la surface d'oxydes de fer(III), ce type de catalyse devient important. On a aussi examiné l'oxydation électrochimique du «3-MPA» en faisant appel à des techniques de polarographie différentielle pulsée et de voltampérométrie cyclique. Le mécanisme de cette réaction est du type EC_2E, l'étape du deuxième transfert d'électron correspondant à l'oxydation du disulfure RS-SR. La constante de vitesse de dimérisation des radicaux RS$^{\bullet}$ est égale à $1,8 \times 10^3$ mol^{-1} dm^3 s^{-1}; la lenteur de cette étape est en accord avec les mécanismes observés lors des oxydations à un électron en présence d'ions métalliques.

Mots clés : électrochimie, cinétique, acide 3-mercaptopropanoïque, autooxydation.

[Traduit par la rédaction]

Introduction

The oxidation of mercaptocarboxylic acids is a reaction of importance in biological systems, and has therefore been studied by several authors (1–7). The oxidation of other organic compounds, such as thiourea or thiols, has also been the subject of extensive research (8–11). It seems clear that no single mechanism is involved in all cases, although the disulphide is generally the main "initial" product. The formation of disulphide may be mediated by sulphenic acids R-SOH originating in the attack of hydrogen peroxide on the deprotonated R-S$^-$ moiety, or by R-S$^{\bullet}$ free radicals formed by attack of OH$^{\bullet}$ on R-S-(H$^+$), the OH$^{\bullet}$ radical having been formed by radiolysis, or by chemical means from H_2O_2 (metal ion catalysis).

The present note reports a study of the oxidation of 3-mercaptopropionic acid both by hydrogen peroxide and in an electrochemical cell. In the former case, the influence of added Fe(III) was cursorily explored to define the limits of relevance of direct attack and radical, Fenton-like mechanisms. The intervention of these latter mechanisms was also explored in heterogeneous media, i.e., under conditions of iron oxide catalyzed H_2O_2 decomposition.

Experimental

All reagents were analytical grade; tridistilled water was used to prepare the solutions, the last two distillations being made in a quartz apparatus. Hydrogen peroxide free of stabilizers was used as solutions freshly prepared and titrated against a $KMnO_4$ standard solution. Fe(III) stock solution was prepared by oxidation with H_2O_2 of a Fe(II) solution obtained by dissolving the metal in $HClO_4$ and titrated potentiometrically against standard $K_2Cr_2O_7$.

Received March 29, 1996.[1]

P. Forlano and J.A. Olabe. Instituto de Química Física de Materiales, Medio Ambiente y Energía (INQUIMAE), Departamento de Química Inorgánica, Analítica y Química Física, Facultad de Ciencias Exactas y Naturales, Universidad de Buenos Aires, Ciudad Universitaria, Pabellón II, 1428 Buenos Aires, Argentina.

J.F. Magallanes and M.A. Blesa.[2] Instituto de Química Física de Materiales, Medio Ambiente y Energía (INQUIMAE), Departamento de Química Inorgánica, Analítica y Química Física, Facultad de Ciencias Exactas y Naturales, Universidad de Buenos Aires, Ciudad Universitaria, Pabellón II, 1428 Buenos Aires, Argentina, and Unidad de Actividad Química, Comisión Nacional de Energía Atómica, Avenida del Libertador 8250, 1429 Buenos Aires, Argentina.

[1] Revision received November 4, 1996.

[2] Author to whom correspondence may be addressed. Telephone: (54-1) 704-1367. Fax: (54-1)-704-1164. E-mail: miblesa@cnea.edu.ar

© 1997 NRC Canada

Can. J. Chem. Downloaded from www.nrcresearchpress.com by 92.62.229.171 on 09/08/12
For personal use only.

Can. J. Chem. Downloaded from www.nrcresearchpress.com by 92.62.229.171 on 09/08/12
For personal use only.

The ionic strength was kept constant at 4×10^{-3} M using $HClO_4$ and $NaClO_4$ solutions. This ionic strength was high enough to ensure appropriate behavior of the differential pulse polarography (dpp) waves in the experiments described below. The reversibility of 3-MPA oxidation was checked, and the width at half-peak height ($W_{1/2}$) of dpp was found to agree with the theoretical values of the Heijne and Van der Linden (12) treatment, over the whole 3-MPA concentration range explored ($4 \times 10^{-5} - 4 \times 10^{-4}$ M).

Oxidation by hydrogen peroxide

The kinetics of the oxidation of 3-MPA by H_2O_2 was studied in the pH range 2.4–6. The decrease of the 3-MPA peak height during oxidation was followed by measuring the height of the dpp wave. The concentration was obtained from the linear calibration plot (peak height vs. concentration) previously determined for each pH value. Solutions of 10^{-4} M 3-MPA were prepared and the pH adjusted with $HClO_4$. The solution was placed in the thermostatted (25°C) cell of a PAR 174A polarographic analyzer, with a dropping or hanging drop Hg electrode, a Pt wire auxiliary electrode, and the reference electrode. All potentials were measured against a Ag/AgCl, KCl saturated reference electrode. Differential pulse polarograms (dpp) were obtained at $t = 0$ and sequentially after the addition of the adequate amount of hydrogen peroxide; all experiments were conducted under conditions of excess H_2O_2. The 3-MPA oxidation wave is found in the range between −0.35 and 0.40 V, with $E_{1/2} = -0.15$ V. At concentrations higher than 7×10^{-4} mol dm^{-3}, a new wave appears at more positive potentials, due to multilayer formation on the adsorbed monolayer (13). The reaction is slow enough to permit the sequential determination of 3-MPA. Occasionally, hydrogen peroxide was determined using its reduction wave in the range −0.35 to −1.85 V ($E_{1/2} = -0.96$ V) (14).

To assess the possible operation of metal ion catalysis, measurements were also carried out in the presence of EDTA, or in the presence of added iron(III) perchlorate, in the concentration range 10^{-8}–10^{-6} mol dm^{-3}.

Electrochemical oxidation

The mechanism of the electrochemical oxidation was explored by using polarographic and cyclic voltammetric (CV) techniques at pH = 2.4. The dependence of $E_{1/2}$ on the 3-MPA concentration and the $W_{1/2}$ of differential pulse polarography was measured. Experiments were also carried out at different drop times.

A complementary set of CV experiments were done at sweep rates between 10 and 200 mV s^{-1} and various 3-MPA concentrations. In the range $3 \times 10^{-4} - 5 \times 10^{-3}$ mol dm^{-3} of 3-MPA, no multilayer effect is observed.

Results and discussion

Oxidation by hydrogen peroxide

At constant pH and $[H_2O_2]$, plots of $\ln([MPA]/[MPA]_o)$ vs. time yield straight lines from which pseudo-first-order rate constants can be obtained. Figure 1 shows the plot of the pseudo-first-order constants at pH = 2.4 as a function of $[H_2O_2]$, which demonstrates that the kinetic law is

$$[1] \quad R = k[MPA][H_2O_2]$$

Fig. 1. Dependence of the pseudo-first-order rate constants upon $[H_2O_2]$ at pH = 2.4 and 298 K, ionic strength 4×10^{-3} M.

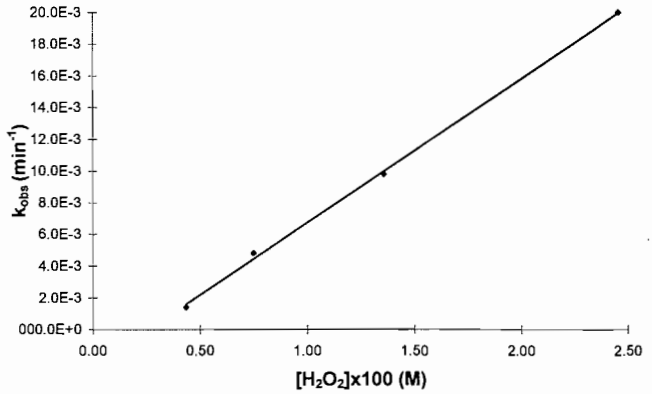
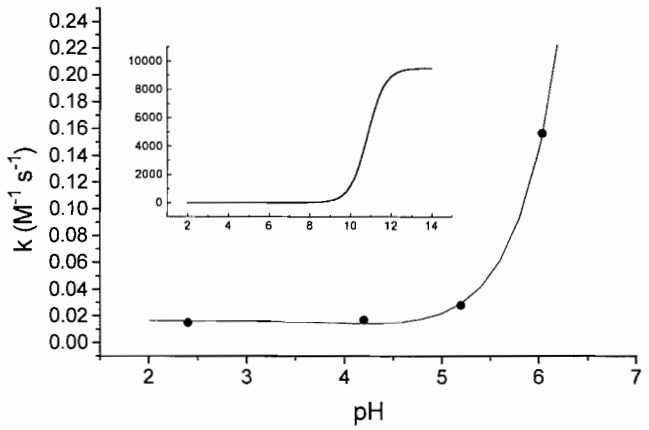


Fig. 2. pH dependence of the second-order rate constant for the reaction of 3-MPA upon H_2O_2 at 298 K, ionic strength 4×10^{-3} M: (•) experimental points; (—) eq. [2]. Inset: pH dependence of the empirical rate constant k (eq. [1]) according to eq. [2].



where [MPA] represents the total (analytical) concentration of 3-mercaptopropionic acid.

The straight line in Fig. 1 extrapolates to an apparent negative rate for $[H_2O_2] = 0$; this behavior is most probably an experimental artifact associated with some decomposition of hydrogen peroxide.

Figure 2 shows the pH dependency of k, together with the curve drawn assuming that the general eq. [2] can be used to describe the pH effects in terms of the contribution of three parallel pathways to eq. [1], each path corresponding to the reaction with hydrogen peroxide of each of the three protolysis species of 3-MPA. The values $pK_{a1} = 4.34$ and $pK_{a2} = 10.84$ (taken from ref. 15) were used to calculate the concentration of each species at each pH.

$$[2] \quad k = (k_1[H_2X] + k_2[HX^-] + k_3[X^{2-}])/[MPA]$$

where X^{2-} represents the dianion of 3-MPA.

The data were collected in a pH range well below pK_{a2} and the steep rise in rate at the highest pH explored can be accounted for only if it is assumed that the reactivity is essentially governed by the dianion. From our data, it is not possible to derive a value for k_2; only an upper limit can be given. The

© 1997 NRC Canada

Can. J. Chem. Downloaded from www.nrcresearchpress.com by 92.62.229.171 on 09/08/12
For personal use only.

second-order rate constants that yield the best fit shown in Fig. 2 are (in mol^{-1} dm^3 s^{-1}) $k_1 = 1.6 \times 10^{-2}$; $k_2 = 10^{-2}$; $k_3 = 9.5 \times 10^3$.

This kinetic law is compatible with a rate-determining direct attack by sulphur on hydrogen peroxide, the rate being highest for the deprotonated sulphur of the dianion:

[3] $$^{-}R\text{-}S^{-} + HO\text{-}OH \rightarrow [^{-}R - S - \underset{OH}{OH^{-}}]^{\#} \rightarrow {}^{-}R\text{-}SOH + OH^{-}$$

This mechanism involves a nucleophilic attack on hydrogen peroxide. The ensuing population of the LUMO of H_2O_2 (mainly antibonding about the peroxide bond) results in O—O bond breaking. The simplest stoichiometry of the reaction results from the further fast reaction of the sulphenic derivative RSOH with RSH:

[4] $$RSOH + RSH \rightarrow RS\text{-}SR + H_2O$$

but other products may also form in the presence of excess oxidant (7, 16).

Barton et al. (3) have studied the analogous reactions of cysteine and cysteamine, and report second-order rate constants of 12.4 and 10 mol^{-1} dm^3 s^{-1} for the corresponding zwitterionic species, $^{+}H_3N\text{-}R\text{-}S^{-}$. These two values are strikingly similar, taking into account that cysteine bears a net negative charge due to the ionized carboxylate group. It is also reported that the corresponding anions $H_2N\text{-}R\text{-}S^{-}$ react more slowly. Of particular interest is the comparison of cysteine (2-amino-3-mercaptopropionic acid) and 3-MPA. The dianion $^{-}O_2CCH_2CH_2S^{-}$ is more basic than $^{-}O_2CCH(NH_2)CH_2S^{-}$ (the corresponding pK_a values of the conjugate acids are 10.84 and 8.53, respectively). The former dianion is also more reactive towards H_2O_2, and 3-MPA reacts faster at any given pH value (correspondingly, the pH range spanned in our study is lower than that explored by Barton et al. (3)). The presence of the amino group in the 2-position is seen to affect profoundly the basicity of the $R\text{-}S^{-}$ group. The decrease in basicity is related to the very large decrease in the rate of attack on the peroxide bond. In agreement, in a separate study, we have found that the rates of coordination through sulphur to $[Ru^{III}(edta)H_2O]^{-}$ by various R-SH ligands correlate with the pK_a values of the -SH group.[3] Also in agreement, we have shown previously that the rate of reductive attack on iron(III) oxides by 3-MPA is much larger than that of cysteine (17). An important consequence is that the amino group gives some protection to cysteine against hydrogen peroxide attack at physiological pH.

Protonation of the leaving OH group of hydrogen peroxide at low pH catalyzes the attack of thiourea on H_2O_2 (8); a related phenomenon has been involved in the reaction of the cysteine zwitterion, even though the bulk pH in this case precludes equilibrium protonation of H_2O_2. Acid catalysis is totally ruled out under our experimental conditions. The very small effect of the carboxylate group, as documented by the comparison of cysteine and cysteamine, still remains unexplained.

[3] V. Povse and J.A. Olabe. Work in progress.

The influence of Fe(III)

It is well known that Fe(III) oxidizes mercaptocarboxylic acids to disulphides, through an inner-sphere reaction (4). This reaction takes place both with dissolved Fe(III) salts and with suspended iron(III) oxides (17) (in this case, the anaerobic oxidation of 3-MPA by Fe(III) takes place along with oxide dissolution). In the heterogeneous case, addition of excess hydrogen peroxide shifts the stoichiometry of the reaction to the catalyzed oxidation of 3-MPA, with negligible dissolution.

The coupling of the internal redox decomposition of Fe(III)-mercaptocarboxylate complexes and the reoxidation of Fe(II) by hydrogen peroxide may lead to the catalytic oxidation of mercaptocarboxylic acids:

[5] $$Fe(III)\text{-}{}^{-}S\text{-}R \rightarrow Fe(II) + {}^{\cdot}SR$$

[6] $$Fe(II) + H_2O_2 \rightarrow Fe(III) + OH^{-} + OH^{\cdot}$$

[7] $$Fe(III) + {}^{-}S\text{-}R \rightarrow Fe(III)\text{-}{}^{-}S\text{-}R$$

The reaction scheme is completed with the fast scavenging of $OH^{\cdot}$ by HSR.

The possible contribution of free radicals due to Fenton-type reactions of hydrogen peroxide with metal ion impurities was explored in a series of experiments with added EDTA and added Fe(III). In the presence of EDTA, the measured rates were identical to those discussed above. Added Fe(III), on the other hand, led to erratic rate changes; for example, a fivefold rate enhancement was observed when [Fe(III)] = 10^{-7} mol dm^{-3}. Although the rate generally increased upon addition of Fe(III), no clear relationship could be observed between the rates and [Fe(III)]. Although this reaction pathway may become important under adequate experimental conditions, at pH 2.4 the stability of the complex and rates of internal redox decomposition are low enough to make the rate of the catalyzed reaction (at [Fe(III)] below 10^{-7} mol dm^{-3}) slow in comparison with the direct bimolecular reaction. The rate values reported above are therefore not affected by contributions of this type.

Electrochemical oxidation

As early as 1940 Kolthoff, Barnum, and Lingane (18, 19, and refs. therein) studied the polarographic anodic oxidation of cysteine. They found that the reaction is not reversible, even in 0.1 M $HClO_4$. At higher pH (> 2) abnormal waves are obtained because of the strong adsorption on the mercury electrode. At low concentration (0.002 M) the reaction is diffusion controlled, but at higher concentration the film formation controls the current. After considering several possible mechanisms, including the EC_2 (EDIM), these authors conclude that the reaction mechanism is simply

$$RSH + Hg \rightleftarrows HgSR + H^{+} + e^{-}$$

The dimerization stage of $RS^{\cdot}$ radicals to yield the disulphide is therefore inhibited by the stability of adsorbed Hg(I) salt. Birke and Mazorra report that $Hg(SR)_2$ layers may be formed in the oxidation of several thiols. Our results in the oxidation of 3-mercaptopropionic acid at pH 2.4 bear some similarities, but there is clear evidence for an EC_2E (EDIME) mechanism, in which the disulphide RS-SR is involved, as discussed below.

© 1997 NRC Canada

Can. J. Chem. Downloaded from www.nrcresearchpress.com by 92.62.229.171 on 09/08/12
For personal use only.

Fig. 3. The dpp traces of the oxidation of 3-MPA at pH = 2.4 for various drop times. (*a*): 0.5 s, (*b*): 1 s, (*c*): 2 s, (*d*): 5 s.

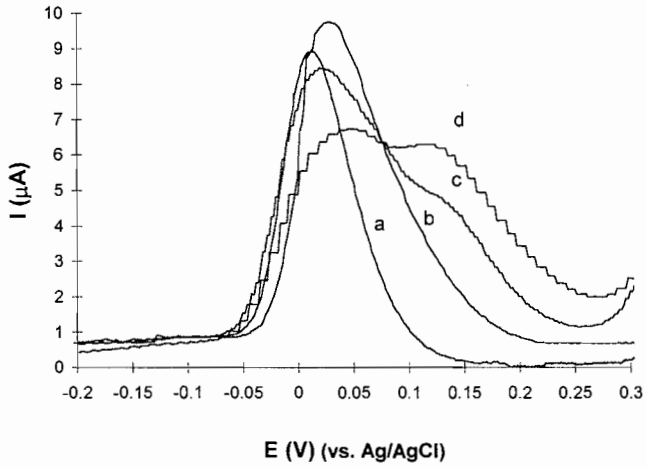
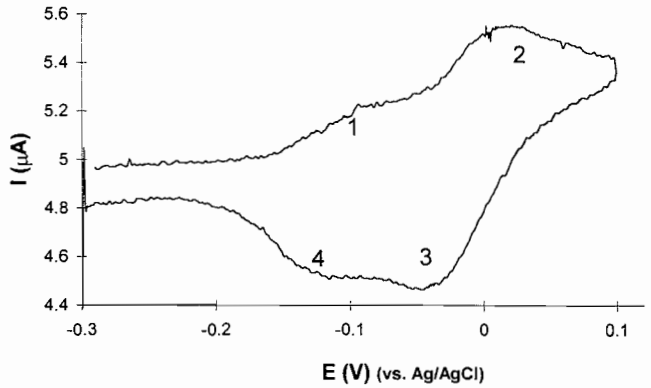


Fig. 4. Voltammogram of 3-MPA at pH 2.4, scan rate 100 mV s^{-1}. Peaks 1 and 2 correspond to reaction steps [9] and [11], respectively (see text).



The dpp of 3-MPA in 4×10^{-3} mol dm^{-3} $HClO_4$ shows a value of $W_{1/2}$ = 80.5 mV, appreciably lower than the theoretical value for reversible one-electron transfer, 92.8 mV (12). This observation suggests that more than one electron is transferred in the overall reaction.

When the 3-MPA concentration is increased, the maximum of the dpp oxidation wave E_p shifts to more negative potentials. As $E_p = E_{1/2} + \Delta E/2$ (where ΔE is the modulation potential) the shift in E_p with concentration is identical with the shift in $E_{1/2}$, and the observed behavior is indicative of an EC-type mechanism (20), at variance with the mechanism postulated by Kolthoff and Barnum for cysteine. The plot of $E_{1/2}$ vs. ln [MPA] is linear, the slope being 13.3 mV/decade. This value is identical within the error limits with the theoretical slope for an EC_2 (EDIM) mechanism involving one-electron transfer and surface reaction of adsorbed species, $RT/2nF$ = 12.85 mV at 25°C (20). For an EDIM mechanism involving a "volume" reaction (no adsorption), Mairanovskii (20) and Koutecky and Hanus (22) found that this slope is $RT/3nF$ = 8.5 mV.

Figure 3 shows a set of dpp traces at different drop times. At short drop times, a single wave is observed; when the drop time increases, a second wave at more positive potentials emerges progressively. For a modulation potential of 25 mV and drop time 1 s, the difference between the potentials of both waves is 28 mV; separate experiments with pure disulphide demonstrated that the dpp oxidation wave of this compound reaches the maximum at a potential positively shifted from the value for 3-MPA by 22.2 mV. In view of the different experimental conditions (no adsorbed reactant, no overlapped waves), the agreement is reasonably good, and it may be concluded that the second wave observed in Fig. 3 is due to the oxidation of RS-SR. This process may be observed only when the drop time is long enough to permit dimer formation, and an EC_2E mechanism is thus suggested, involving a second electron transfer stage that produces reversibly an otherwise undefined oxidation product. No experimental evidence on the nature of this product is available. Several experimental characteristics of the disulphide oxidation indicate a one-electron reaction. In CV experiments (Fig. 4, peaks 2 and 3), the ΔE_{peak} (anodic − cathodic) is 63 mV; also, the peak position does not shift with the sweep rate. Finally, in dpp, $W_{1/2}$ = 94 mV indicates a reversible one-electron transfer. This mechanism also accounts for the small difference between the theoretical and the calculated slope in the $E_{1/2}$ vs. ln [MPA] plots:

[9] $RSH \rightleftarrows RSH^{\bullet+} + e^-$

[10] $2\,RSH^{\bullet+} \rightarrow RS\text{-}SR + 2\,H^+$

[11] $RS\text{-}SR \rightleftarrows$ oxidation products + e^-

The voltammograms of 3-MPA show four peaks, corresponding to the two electron transfers, the intensity and position of which are dependent on sweep rate. Figure 4 shows an example; although the definition of some peaks was poor (for instance peaks 1 and 4 in Fig. 4), it was possible to draw clear conclusions from the analysis of the whole set of voltammograms. In particular, the ratio of the heights of peaks 2 and 4 is strongly dependent on the sweep rate: I_{p2}/I_{p4} decreases when the sweep rate increases, as expected for the above mechanism. From the values of I_{p2}/I_{p4} for various 3-MPA concentrations, measured at two sweep rate values, v = 50 and 100 mV s^{-1}, the value of the radical dimerization (eq. [10]) rate constant k_{dim} may be calculated. The calculations must be done by simulation of the I_{p2}/I_{p4} ratio as a function of the dimensionless rate constant k_{sim}, defined by eqs. [12] and [13]:

[12] $k_{sim} = k_{dim}([MPA]/a)$

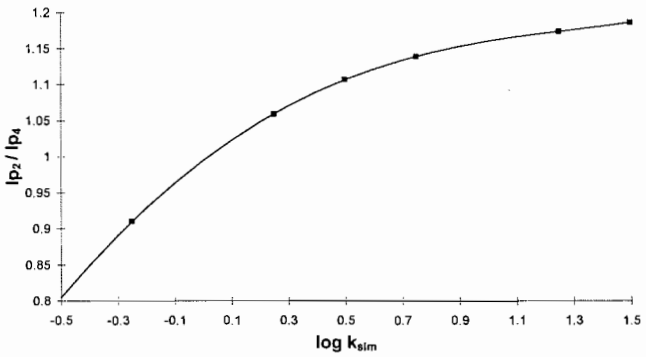
where:

[13] $a = nFv/RT$

An explicit digital simulation, based on the exponential expanded space grid method developed by S.W. Feldberg (23) was used. Details of this program applied to a similar mechanism are explained in ref. 24. Due to the overlapping of $I_{p1}|I_{p2}$ and $I_{p3}|I_{p4}$, the ratio would be difficult to measure using the basic analytical theories of voltammetry. However, because the separation between $E_{1/2}$ for reactions [9] and [11] is measured experimentally, the digital simulation of the system leads to a set of partially overlapped waves, similar to those

© 1997 NRC Canada

Fig. 5. Simulated I_{p2}/I_{p4} ratio as a function of log k_{sim} (see text for further details).



obtained in practice. The simulated and experimental I_{p2}/I_{p4} ratios behave similarly.

Figure 5 shows the simulated function $I_{p2}/I_{p4} = f(\log k_{sim})$; interpolation of the experimental I_{p2}/I_{p4} values yields values of k_{sim} from which k_{dim} may be obtained, using eq. [12]. The dependence of k_{sim} on the concentration at constant sweep rates is indeed linear, and from the slopes at v = 50 and 100 mV s^{-1}, the derived values of k_{dim} are $1.7(\pm 0.2) \times 10^3$ and $1.97(\pm 0.04) \times 10^3$ mol dm^{-3} s^{-1}.

As a further check, simulated voltammograms were computed using these k_{dim} values; a reasonable coincidence between simulated and experimental traces was obtained. Also, the relative heights of the dpp waves at different drop times can be calculated using k_{dim} to estimate the concentration of 3-MPA on the electrode surface. For drop times of 2 and 5 s, the height ratio is calculated to be 0.74, as compared with an experimental ratio of 0.83. The lack of data at other drop times precludes further elaboration of this point.

The slowness of radical dimerization poses a certain limitation to the operation of one-electron chemical oxidation of 3-MPA, because the reverse regeneration of the dianion may become important. In fact, in the course of oxidation by one-electron metallic oxidants such as Fe(III), the activated complex composition normally reflects the need to bring together two oxidants, thus allowing the formation of the disulphide in a more efficient way (17). In view of the large atom transfer rate constant between the dianion of 3-MPA and hydrogen peroxide, it is not surprising that the radical pathway does not contribute significantly to the reaction mechanism.

Acknowledgments

This work was partially supported by grants from the University of Buenos Aires and Fundación Antorchas. J.A.O. and M.A.B. are members of the National Research Council (CONICET).

References

1. R.G. Neville. J. Am. Chem. Soc. **79**, 2456 (1957).
2. I. Pascal and D.S. Tarbell. J. Amer. Chem. Soc. **79**, 6015 (1957).
3. J.P. Barton, J.E. Packer, and R.J. Sims. J. Chem. Soc. Perkin Trans. 2, 1547 (1973).
4. C. Baiocchi, E. Mentasti, and P. Arselli. Transition Met. Chem. (London), **8**, 40 (1983), and refs. therein.
5. R.F. Jameson, W. Linert, A. Tschinkowitz, and V. Gutmann. J. Chem. Soc. Dalton Trans. 943 (1988) (correction on p. 2243 (1988)).
6. R.F. Jameson, W. Linert, and A. Tschinkowitz. J. Chem. Soc. Dalton Trans. 2109 (1988).
7. E. Deutsch, M.J. Root, and D.L. Nosco. Adv. Inorg. Bioinorg. Mech. 269 (1983).
8. M.R. Hoffmann and J.O. Edwards. Inorg. Chem. **16**, 3333 (1977).
9. K. Leung and M.R. Hoffmann. J. Phys. Chem. **89**, 5267 (1985).
10. K. Leung and M.R. Hoffmann. J. Phys. Chem. **93**, 431 (1989).
11. M.R. Hoffmann. *In* Aquatic chemical kinetics. *Edited by* W. Stumm. Wiley, New York. 1990. pp. 71–111.
12. G.J.M. Heijne and W.E. Van der Linden. Anal. Chim. Acta, **82**, 231 (1976).
13. R.L. Birke and M. Mazorra. Anal. Chim. Acta, **118**, 257 (1980).
14. I.M. Kolthoff and J.J. Lingane. *In* Polarography. Vol. 2. Interscience Publishers, New York. 1952. pp. 552–553.
15. E.A. Martell and R.M. Smith. *In* Critical stability constants. Vol. 1. Plenum Press, New York. 1974.
16. F.A. Davis and R.L. Billmers. J. Am. Chem. Soc. **103**, 7016 (1981).
17. E.B. Borghi, P.J. Morando, and M.A. Blesa. Langmuir, **7**, 1652 (1991).
18. I.M. Kolthoff and C. Barnum. J. Am. Chem. Soc. **62**, 3061 (1940).
19. I.M. Kolthoff and J.J. Lingane. *In* Polarography. Vol. 2. Interscience Publishers, New York. 1952. pp. 781–791.
20. S.G. Mairanovskii. *In* Catalytic and kinetic waves in polarography. Plenum Press, New York. 1968. pp. 228–231.
21. E. Laviron and R. Meunier-Prest. J. Electroanal. Chem. **375**, 79 (1994).
22. J. Koutecky and V. Hanus. Collect. Czech. Chem. Commun. **28**, 446 (1970).
23. S.W. Feldberg. J. Electroanal. Chem. **127**, 1 (1981).
24. J.M. Marioli, J.F. Magallanes, and L. Sereno. Bol. Soc. Chil. Quim. **36**, 157 (1991).

Can. J. Chem. Downloaded from www.nrcresearchpress.com by 92.62.229.171 on 09/08/12
For personal use only.

© 1997 NRC Canada

Characterization of humic substances extracted from Canadian lake sediments

Nelson Belzile, Helen A. Joly, and Hongbo Li

Can. J. Chem. Downloaded from www.nrcresearchpress.com by 92.62.229.171 on 09/08/12
For personal use only.

Abstract: Humic substances (HS) were extracted from the sediments of four Sudbury area lakes, namely, Tilton, Clearwater, Silver, and Ramsey Lakes, with the aid of 0.1 M $Na_4P_2O_7$ and 0.5 M NaOH solutions . The HS (humic and fulvic acids) were purified and characterized using the methods of elemental analysis, visible spectroscopy (E_4/E_6 ratio), FTIR, and solid-state ^{13}C CPMAS NMR. A substantial amount of information with regard to the composition and chemical nature of lake sediment HS was obtained. The results obtained for the Sudbury area lake sediments were compared with one another and with HS from other sources, such as soils. The elemental composition, atomic ratios, E_4/E_6 ratios, and FTIR and NMR features of the samples from the above lakes were found to be nearly identical, suggesting that HS formed in the Sudbury area have similar chemical properties. Compared with soil HS, the Sudbury lake sediments HS have undergone a low degree of aromatic condensation and are considerably more aliphatic in nature.

Key words: humic substances, characterization, lake sediments, extraction, ^{13}C NMR.

Résumé : Des substances humiques (SH) ont été extraites des sédiments de quatre lacs de la région de Sudbury : les lacs Tilton, Clearwater, Silver et Ramsey, au moyen de solutions de $Na_4P_2O_7$ 0.1 M et de NaOH 0.5 M. Les SH (acides humiques et fulviques) ont été purifiées et caractérisées à l'aide des méthodes d'analyse élémentaire, de la spectroscopie visible (rapport E_4/E_6), FTIR et état solide RMN ^{13}C CPMAS. Une quantité substantielle d'information a été obtenue sur la composition et la nature chimique de SH des sédiments lacustres. Les résultats obtenus pour les sédiments lacustres de la région de Sudbury ont pu être comparés entre eux et avec des SH provenant d'autres sources tels les sols. La composition élémentaire, les rapports atomiques, les rapports E_4/E_6, les caractéristiques FTIR et RMN des échantillons des lacs étudiés se sont montrés presqu'identiques ce qui suggère que les SH formées dans la région de Sudbury ont des propriétés chimiques semblables. En comparaison avec les SH des sols, les SH des sédiments lacustres de Sudbury ont subi un moindre degré de condensation aromatique et sont considérablement plus aliphatiques en nature.

Mots clés : substances humiques, caractérisation, sédiments lacustres, extraction, RMN ^{13}C.

Introduction

Organic matter (OM) constitutes a minor but important fraction of lake sediment. It is made up of a complex mixture of lipids, carbohydrates, proteins, and other biochemicals originating from the tissues of living benthic micro-organisms and the detritus of organisms formerly living in the lake and its watershed. Humic substances (HS) are formed from these biochemical starting materials and represent the major constituent of the organic materials found in lake sediments (1). HS play a vital role in terrestrial and aquatic ecosystems; consequently they have long been a subject of scientific interest.

Operational definition of HS

HS can be classified as humic acid, fulvic acid or humin depending on their solubility in alkali and acid. More specifically, *humic acid* (HA) is defined as the fraction of the HS that is soluble in dilute alkali but is coagulated by acidification of the alkaline extract (below pH 2); *fulvic acid* (FA) is the fraction of the HS that remains in solution when the alkaline extract is acidified, that is, the fraction that is soluble in both dilute alkali and dilute acid; *humin* is the fraction of the HS that cannot be extracted from the soil by dilute base or acid. These definitions have survived the test of time because of their practical utility. Solubility is an effective criterion for the classification of substances because of its dependence on important chemical characteristics, such as the number of acidic functional groups present, molecular weight, aromaticity, etc. (2). The definitions described above have been accepted by most scientists and specialists investigating humic materials (3). It is important to note that other classification schemes for natural organic matter exist. These schemes are based on the biochemical classification and the physical form of the natural organic matter (4).

Roles

HS, being an important source of organic matter in all terrestrial and aquatic environments, participate in a variety of biochemical and geochemical processes and serve as a major reservoir of organic carbon in soils and oceans for the global carbon cycle. HS can be nutrients on which plants, benthic animals, and microbes live and grow. As well, HS play an

Received May 6, 1996.

N. Belzile,[1] H.A. Joly, and H. Li. Department of Chemistry and Biochemistry, Laurentian University, Ramsey Lake Road, Sudbury, ON P3E 2C6, Canada.

[1] Author to whom correspondence may be addressed. Telephone: (705) 675-1151, ext. 2114. Fax.: (705) 675-4844. E-mail: BELZILE@NICKEL.LAURENTIAN.CA

© 1997 NRC Canada

Can. J. Chem. Downloaded from www.nrcresearchpress.com by 92.62.229.171 on 09/08/12
For personal use only.

important role in the cycles of nutrient elements such as nitrogen and phosphorus (3). One of the most striking characteristics of HS is their ability to interact with metal ions (5–8), oxides, hydroxides, and minerals (9), to form water-soluble and water-insoluble complexes of widely differing chemical and biological stabilities. Through the formation of water-soluble complexes, humic materials can dissolve, mobilize, and transport metals and organics in soil and water, while the formation of water-insoluble complexes brings about their accumulation in certain soil horizons and in sediments (3). In addition, organic compounds with appropriate functional groups can bind to HS through the formation of hydrogen bonds. Such interactions affect the environmental behaviour of these materials, including the rate of chemical degradation, photolysis, volatilization, migration, and biological uptake of the organic compound (3). For instance, the presence of high concentrations of humic materials in water increases the solubility of toxic pollutants such as DDT (10, 11) and aromatic hydrocarbons in water (12). Finally, HS can produce degradation products that are harmful to the environment. For example, the degradation of HS found in chlorinated municipal drinking water can lead to the formation of haloforms which are a health hazard even at low concentration (2, 13, 14).

Organic matter in lakes and lake sediments originates both from aquatic organisms living in the lake (autochthonous) and from organic matter that is washed into the lake from surrounding soils and streams (allochthonous). Therefore, the amount and composition of the organic matter in lake sediments are dependent on various factors such as the trophic level, climate, drainage into the lake, and chemical, biological, and geological characteristics of the surrounding environments. HS are clearly the major constituent of organic matter in lake sediments and thus should play a central role in the geochemical cycling of carbon compounds in lakes, lake sediments, and sedimentary rocks (15). It should be pointed out that because HS are a complex mixture of organic matter it has not been possible to elucidate their exact composition and structure. Hence, as more detailed information on the structure and composition of HS becomes available it will be possible to comment on their nature, origin, and geochemical roles.

Characterization

The most common techniques used to obtain structural and compositional information on HS include elemental analysis, visible, infrared, and ^{13}C NMR spectroscopies, and degradation methods. The elemental composition (C,H,N,O,S,P) of HS, determined with the aid of an elemental analyzer, can establish the nature and origin of these compounds. The elemental composition of a substance is often expressed in terms of atomic ratios because errors due to ash content are then factored out. The ratios of H/C, O/C, and N/C have been used (16): (*i*) to identify different types of HS, (*ii*) to monitor the structural changes of humates in soils and sediments, and, (*iii*) to elucidate structural formulae for humates. For instance, the O/C ratio is believed to be an indicator of the carbohydrate content of a humic substance and can be used to compare HS from different origins.

Visible spectroscopy is a simple but important method used to characterize HS. The ratio of optical densities or absorbances of dilute aqueous HA and FA solutions at 465 and 665 nm is widely used for the characterization of these materials. This ratio, usually referred to as E_4/E_6, is independent of the concentrations of humic materials, but varies for humic materials of different soil types (17, 18). Schnitzer (18) suggests that the absorption of light by aqueous HA and FA solutions in the visible region of the electromagnetic spectrum is dependent upon (*i*) the total carbon content of the material, (*ii*) the number of aromatic residues versus the number of aliphatic residues, and (*iii*) the molecular weight of the HS. Attempts have been made to extract structural information by relating the E_4/E_6 ratio for HS to such characteristics as viscosity, carbon content, oxygen content, and total acidity (19).

Infrared (IR) spectroscopy has been widely used for the characterization of HS (18, 20–23). Since HS comprise complex mixtures, each type of functional group present in the HS exists in a variety of different chemical environments. As a result, the spectra usually consist of relatively few bands, which are very broad. However, the development of high-performance FTIR has resulted in improved transmission spectra of HS obtained from various sources (22–24).

Recently, ^{13}C nuclear magnetic resonance (NMR) spectroscopy has become a powerful tool in elucidating the structure of HS. The nondestructive technique makes use of the signals recorded from the small proportion of ^{13}C in naturally occurring substances. It has several inherent advantages over conventional ^{1}H NMR spectroscopy in that it provides direct information on the carbon skeleton of organic substances. In addition, the large chemical shifts associated with ^{13}C nuclei allow signals of carbon atoms with only slightly different magnetic environments to be resolved. Furthermore, a comparison of the peak areas of the signals found in the aromatic and aliphatic regions of the ^{13}C NMR spectra of HS is indicative of the degree of aromaticity vs. aliphaticity of the HS (25–28). Macromolecular substances can also be studied by determining the structure of the molecular fragments that make up the long molecular chain. The degradation methods used to fragment macromolecular substances include chemical oxidation with alkaline permanganate (29) or alkaline cupric oxide (30, 31) and thermal degradation. Recently, the thermal degradation products of HS have been analyzed by coupling of a pyrolysis unit to a gas chromatograph, which is in turn coupled to a mass spectrometer (32–37).

It should be pointed out that the methods most frequently used to characterize HS, namely elemental analysis, IR, NMR, etc., provide general information with respect to the origin of the organic matter, the degree of humification, the nature of the functional groups present in the organic matter, and the degree of aromaticity associated with the organic matter. Thermal and chemical degradation techniques, on the other hand, provide information concerning the building blocks that make up the HS. Unfortunately, information on how the fragments were assembled in the original material is not given by the degradation techniques.

In this study, we present the results of the chemical and structural characterization of HA and FA isolated from the sediment of four Sudbury Lakes using elemental analysis, FTIR, and solid-state ^{13}C NMR. The chemical characteristics of the HS originating from the different lake sediments are compared in order to study the influence of water pH, contaminants, surrounding vegetation, etc. on the HS. We also compare the chemical characteristics of the lake sediment HS with those from other environments such as

© 1997 NRC Canada

soil, lake water, etc., in order to establish the differences and similarities.

Methodology

Sampling sites and sample collection

Sediment samples were collected from four different lakes located in the Sudbury region, namely, Tilton, Clearwater, Silver, and Ramsey. The four lakes chosen in this area differ in pH, levels of metal contamination, surrounding vegetation, and in the amount of dissolved organic matter in the water. Three sampling points were selected for each lake and surficial sediments were collected by using a sediment grab. The sediments obtained from the three points were mixed to give one sample. The sediments were stored in plastic containers and taken to the laboratory. After being air-dried at room temperature for 7 days, the sediment samples were ground and sieved through a 2 mm sieve. The sediment samples were stored in sealed plastic bottles for further analysis.

Sequential extraction of organic matter

(i) Hexane extraction

Sediment (25.0 g) in a single thickness Whatman extraction thimble (43 × 123 mm) was extracted in a Soxhlet apparatus for 48 h with 300 mL of spectroscopic grade *n*-hexane (Caledon). The hexane extract was filtered and reduced in volume with the aid of a rotary evaporator. The residue was transferred to a preweighed 4 mL vial and reduced to dryness under a gentle stream of N_2.

(ii) Chloroform extraction

The residual sediment in the extraction thimble was subsequently extracted with 300 mL of spectrograde chloroform (Caledon) for 48 h using the method described above. The filtered extract was concentrated with the aid of a rotary evaporator and transferred to a preweighed 4 mL vial. A gentle stream of N_2 was used to evaporate the remaining chloroform. As before, the weight of the residue was determined.

(iii) $Na_4P_2O_7$ extraction

The residual dried sediment in the extraction thimble was transferred to a 250 mL polyethylene centrifuge bottle containing 250 mL of a 0.1 M $Na_4P_2O_7$ solution (pH ≃ 10.5). The bottle was flushed with N_2 to displace air, sealed tightly, and shaken on a reciprocal shaker at room temperature for 24 h. The $Na_4P_2O_7$ extract was separated from the insoluble sediment by centrifugation at 10 400 *g* for 10 min followed by vacuum filtration using a Millipore filter system (0.45 μm pore).

(iv) NaOH extraction

Next, 250 mL of a 0.5 M NaOH solution was added to the centrifuge bottle containing the residual sediment. The contents of the bottle were shaken under N_2 for 24 h. The NaOH extract was centrifuged at 10 400 *g* and filtered. Both the $Na_4P_2O_7$ extract (from step *iii*) and the NaOH extract (from step *iv*) were used in the following separation of FA and HA, respectively.

Separation and purification of HA and FA

Both the $Na_4P_2O_7$ and the NaOH extracts were adjusted to pH 1.0 with 6 N HCl. The solutions were allowed to stand at room temperature for 24 h. The supernatant (FA fraction) was separated from the coagulate (HA fraction) by centrifugation at 10 400 *g* for 10 min followed by vacuum filtration. The FA fraction was adjusted to pH 8.0 with a 5 N NaOH solution and was allowed to stand for 4 h. It was next centrifuged at 10 400 *g* for 10 min and filtered. The clear solution was reduced to 20 mL on a rotary evaporator and dialyzed in a dialysis bag tubing (100 mm, Spectra/Por, Spectrum Medical Industries, Houston, Texas) with a molecular weight cutoff point of 3500 amu to allow removal of Na^+ and Cl^-. The dialysis procedure was repeated until a negative chloride test was obtained (ca. 72 h). The dialysed FA solution was subjected to freeze-drying and the dried FA was stored in a vacuum desiccator ready for further characterization.

The HA fraction was dissolved in 20 mL of a 0.1 M KOH solution under a N_2 atmosphere. Potassium chloride (0.3 g) was added to make the system 0.3 M in K^+. The inorganic colloid in the solution precipitated more easily at this ionic strength. After standing for 4 h, the solution was centrifuged at 10 400 *g* for 10 min. The supernatant was decanted to another centrifuge bottle and the remaining solid residue was discarded. The clear HA supernatant was acidified to pH 1.0 with 6 M HCl and the HA allowed to coagulate. The solid was separated from the liquid phase by centrifugation at 10 400 *g* for 10 min. The liquid was discarded and the solid was subsequently shaken on a reciprocal shaker for 24 h at room temperature with 250 mL of a HCl–HF solution (0.5% v/v of each acid). The HA was separated from the liquid phase by centrifugation at 10 400 *g* for 10 min. The solid (HA) remaining after decantation was treated with an additional 250 mL of the HCl–HF mixture. The solution was shaken for 24 h at which point the HA was separated from the liquid phase by centrifugation as described above. The solid (HA) was next washed with distilled H_2O. The residual water was removed from the HA with the aid of a freeze dryer. The dried HA was stored in a vacuum desiccator pending further characterization.

Characterization of sediment, HA, and FA samples

Determination of C, H, and N

Carbon, hydrogen, and nitrogen present in samples of lake sediments and in the HA and FA extracted from the sediment were determined on a Perkin–Elmer 2400 CHN elemental analyzer. The coefficients of variability for three replicate reference analyses were 0.20% for C, 2.2% for H, and 0.19% for N. The %O was calculated by difference, i.e., %O = 100 − %C − %H − %N, and can therefore include trace fractions of S or P.

Moisture and ash content

Weighed sediment, FA, or HA samples were placed in dry, preweighed porcelain crucibles. The crucibles and their contents were dried in an oven at 105°C for 4 h. After being allowed to cool in a desiccator the crucibles were reweighed. The process was repeated until a constant weight was obtained. The % moisture was calculated using eq. [1]:

$$[1] \quad \%\ \text{moisture} = \frac{w_0 - w_{105}}{w_0} \times 100$$

© 1997 NRC Canada

Can. J. Chem. Downloaded from www.nrcresearchpress.com by 92.62.229.171 on 09/08/12
For personal use only.

Can. J. Chem. Downloaded from www.nrcresearchpress.com by 92.62.229.171 on 09/08/12
For personal use only.

where w_0 is the initial weight of the sample and w_{105} is the weight of the sample after being heated at 105°C. Similarly, to determine the ash content, weighed samples of the sediment, FA, or HA in dry preweighed crucibles were placed in a muffle furnace at 750°C for 4 h. The weight of the remaining residue (w_{750}) and eq. [2] were used to determine the % ash content of the sample:

$$[2] \quad \% \text{ ash} = \frac{w_{105} - w_{750}}{w_{105}} \times 100$$

E_4/E_6 ratios:
The E_4/E_6 ratios, defined as the ratio of absorbance found at 465 and 665 nm, respectively, were determined for a series of FA and HA samples. More specifically, the absorbance of a 0.04% (w/v) solution of FA or HA in 0.05 M $NaHCO_3$ was measured at 465 nm and 665 nm on a Beckman DU-65 spectrophotometer. A 0.05 M $NaHCO_3$ solution was used as the reference solution.

IR analysis
The Fourier-transform infrared (FTIR) spectra of the *n*-hexane and chloroform extracts were recorded on smears between NaCl plates. The FTIR spectra of FA and HA were run in the form of potassium bromide pellets. Potassium bromide pellets were made from a mixture of 0.5 mg of a FA or HA sample and 200 mg of KBr which had been dried at 200°C for 12 h. The FTIR spectra of the KBr pellets were recorded on a Bomen Michelson-100 FTIR spectrophotometer between 4000 and 650 cm^{-1}. A pellet consisting of only KBr was used as the reference material.

NMR analysis
The solid state CPMAS ^{13}C NMR spectra were recorded at the laboratory of the U.S. Geological Survey, Denver, Colorado. The following parameters were used to record the ^{13}C NMR spectra of the various HA and FA samples: spectrometer frequency: 50.30 MHz; 90 degree pulse width: 4.5 μs; contact time : 1.00 ms. Determination of optimum contact and relaxation time was done prior to ^{13}C NMR analysis being performed. Spectra were interpreted in the manner described by Malcolm (28). Each NMR spectrum was divided into five regions based on the type of the carbon nucleus. The relative quantities of C in each region were calculated according to the method described by Novak and Smeck (38). Briefly, the areas under the peaks found in a particular region of the spectrum were estimated by dropping verticals to the baseline. The error associated with estimating the area of well-defined peaks in ^{13}C NMR spectra is approximately ±5% (26). The aliphaticity and aromaticity of humic and fulvic acids were determined using the following formulae (3), eqs. [3] and [4]:

$$[3] \quad \% \text{ aliphaticity} = \frac{\text{peak area for C signals from 0–110 ppm}}{\text{peak area for C signals from 0–160 ppm}} \times 100$$

$$[4] \quad \% \text{ aromaticity} = \frac{\text{peak area for C signals from 110–160 ppm}}{\text{peak area for C signals from 0–160 ppm}} \times 100$$

Table 1. Some characteristics of the four lakes located in the Sudbury area.[a]

Lake	pH	Colour[b]	Cond[c]	Cl[d]	DOC[e]	Vegetation
Silver	4.0	0.5	384.0	81.4	0.4	+
Clearwater	4.8	1.0	84.0	10.0	0.5	++
Tilton	5.6	3.5	60.0	3.8	1.9	++
Ramsey	7.5	7.5	321.0	60.4	3.0	+

[a]Unpublished data provided by the Ontario Ministry of Natural Resources with exception of pH and vegetation.
[b]Colour was measured on a relative scale (total colour unit: 0–500).
[c]Conductivity, μS/cm.
[d]Chloride ion content, mg/L.
[e]Dissolved organic carbon content, mg/L.

Table 2. The moisture, ash, and TOM content of the sediments collected from four Sudbury lakes.

Lakes	% Moisture[a]	% Ash[a]	% TOM[a]
Silver	2.78 ± 0.47	74.08 ± 0.09	23.05 ± 0.09
Ramsey	1.01 ± 0.22	90.59 ± 0.10	8.43 ± 0.10
Clearwater	0.72 ± 0.21	93.65 ± 0.03	5.63 ± 0.03
Tilton	0.22 ± 0.02	96.78 ± 0.05	3.03 ± 0.07

[a]Average of three replications ± standard deviation (SD).

Results and Discussion

Sediments

Some characteristics of the lakes studied are listed in Table 1. It is interesting to note that both the colour index and the dissolved organic matter (DOC) reflect the same trend as found with the pH, i.e., the values for colour index and DOC increase in the order Silver, Clearwater, Tilton, and Ramsey. The conductivity measurements and the chloride ion concentration are high for Silver and Ramsey and relatively low for Tilton and Clearwater. The high chloride content of the lakes could be due to road salting (39) as Silver and Ramsey Lake are very close to the city and are therefore more susceptible to the effects of human activity. Finally, the area surrounding Tilton and Clearwater Lake is highly vegetated compared to that of Ramsey and Silver Lake.

Total organic matter (TOM) refers to the total amount of organic substances present in the sediments. TOM was calculated for the four lakes using eq. [5].

$$[5] \quad \text{TOM (\%)} = 100 - \text{moisture (\%)} - \text{ash (\%)}$$

The moisture, ash, and TOM contents of the four lake sediments are shown in Table 2. The moisture content of the sediments was found to range from 0.22 to 2.78%. The ash content, which corresponds to noncombustible material, was found to range from 74.08 to 96.78%. The TOM in these sediments ranged from 3.03 to 23.05%. The sediments collected from Silver Lake were found to contain the highest percentage of TOM. The primary source of organic matter for lake sediments is the debris of plants that have lived in the waters and on the land surrounding the lake (1). The TOM content of lake sediment therefore depends on the degree of vegetation sur-

© 1997 NRC Canada

Table 3. Elemental contents of the sediments and elemental composition of TOM.

Lakes	C	H	N	C	H	N	O	N/C
	Sediments (g/100 g) (moisture free)[a]			Percentage of TOM in sediments[b]				
Silver	11.08 ± 0.66	2.14 ± 0.08	0.92 ± 0.06	48.1	9.3	4.0	38.6	0.071
Ramsey	3.83 ± 0.18	0.71 ± 0.03	0.31 ± 0.01	45.7	9.3	3.7	41.3	0.069
Clearwater	2.36 ± 0.15	0.51 ± 0.04	0.18 ± 0.01	42.1	9.1	3.2	45.6	0.065
Tilton	1.24 ± 0.11	0.25 ± 0.03	0.10 ± 0.02	41.3	8.3	3.3	47.1	0.069

[a]Average of three replications ± SD.

[b]$\text{C, H, N\%} = \frac{\text{C, H, N g/100 g of the sediment (moisture free)}}{\text{TOM g/100 g of the sediment}} \times 100$

O% = 100 − C(%) − H(%) − N(%).

rounding the lake and the abundance of plants in the lake and watershed. The fact that the sediments taken from Silver Lake have a relatively high TOM content suggests a high contribution from plants in the water and (or) on the land surrounding the lake. This is somewhat surprising because the current level of vegetation surrounding the lake is sparse. The low pH of Silver Lake water could, however, contribute to the precipitation of HS, which as stated earlier is the primary source of organic matter (OM) found in sediments. This would have the effect of increasing the content of TOM in the sediment, and cause the lake water to be relatively low in DOC, as was in fact observed. However, it should be noted that the pH alone cannot be used to explain the high TOM content of Silver Lake sediments. Further investigation will be needed to explain the high content of TOM in the lake sediment as little information is known about the history of the activities that could have affected Silver Lake sediment when vegetation was probably more abundant. The TOM appears to be correlated with the moisture content. For instance, the sediment collected from Silver Lake has the highest TOM content as well as the highest moisture content. This phenomenon could be related to the structural composition of the OM. It is a well-known fact that HS contain many polar groups such as -OH, -COOH, etc. (4). These groups have a strong affinity for water owing to the formation of hydrogen bonds. As a result it is more difficult to air-dry the sediments, which are richer in organic matter. Finally, it follows that the % ash is inversely proportional to the % moisture and % TOM.

The elemental composition of the sediments was obtained through analysis of C, H, and N in the sediment samples. The percentage of O in the TOM was calculated by difference. The amount of C, H, and N (expressed in g/100 g of sediment) found in the four lake sediments as well as the elemental composition of the TOM of sediments is presented in Table 3. The C content of the sediments was found to range from 1.24 to 11.08 g/100 g. The H content was found to range from 0.25 to 2.14 g/100 g while the range of the N content was 0.10–0.92 g/100 g. Ishiwatari (15) reported the average values of organic C and N in lake sediments as 4.42 g/100 g and 0.44 g/100 g, respectively. The values of the C and N content of the sediment collected from Tilton, Clearwater, and Ramsey lakes are lower than the average values, while the Silver Lake sediment has much higher values of C and N content. The high values are consistent with the high TOM content of the Silver Lake sediment. Although the elemental content of the Silver Lake sediment is significantly different from that of the other lake sediments, the elemental compositions of the TOM in all the lake sediments are similar. With regard to the elemental composition of TOM in the different lake sediments, C was found to range from 41.3 to 48.1%, H was found to range from 8.3 to 9.3%, N ranged from 3.2 to 4.0%, and O ranged from 38.6 to 47.1%. The fact that the elemental composition of the TOM varies very slightly suggests that the organic matter in the sediments collected from the four lakes may have a similar composition and structure.

The N/C ratios of the lake sediments were calculated and can be found in the last column of Table 3. They range from 0.065 to 0.071. The N/C ratios of organic matter are considered to be an indicator of the source of TOM in lake sediments. It has been reported that N/C ratios are dependant on whether cellulose is present in the plants contributing organic matter to lake sediments (1). Nonvascular aquatic plants have high N/C ratios, typically between 0.1 and 0.25, whereas vascular land plants, which contain cellulose, have N/C ratios of 0.05 and lower. Lakes for which the contribution of organic matter from vascular land plants is small show higher N/C ratios in their sediments (values between 0.11 and 0.16) than do lakes receiving important amounts of vascular plant debris (values between 0.072 and 0.077) (1). The fact that low N/C ratios were found in the organic matter of the four lake sediments suggests that land plants are the major contributor to the organic matter. In addition, the similarity in N/C ratios indicates that the sources of the organic matter are similar for the different lakes (40).

Extracted HA and FA

In the sequential extraction method used in this study, the extractants included organic solvents (*n*-hexane and chloroform), as well as $Na_4P_2O_7$ and NaOH. The organic solvents were used to extract alkanes, fatty acids, long-chain alcohols, and wax esters. With the exception of Silver Lake, OM extracted by hexane and chloroform represented less than 2% of TOM. Values of the OM extracted from the soil samples by the same two organic solvents were reported as ranging from 0.04 to 0.06% (41). FTIR spectra of each chloroform and hexane extract were recorded to obtain information on the compounds extracted. A summary of the FTIR bands observed is presented in Table 4. There is not much difference between

© 1997 NRC Canada

Can. J. Chem. Downloaded from www.nrcresearchpress.com by 92.62.229.171 on 09/08/12
For personal use only.

Table 4. FTIR bands of *n*-hexane and chloroform extracted OM of the lake sediments.

		FTIR bands (cm^{-1})						
Lakes	Extractants	~2920	~2850	~1730	~1460	1370~1240	1165~1100	~730
Tilton	*n*-Hexane	+++	+++	+	++	+	±	+
	Chloroform	+++	+++	++	+	±	±	+
Clearwater	*n*-Hexane	+++	+++	+	++	+	±	+
	Chloroform	+++	+++	++	+	±	±	++
Silver	*n*-Hexane	+++	+++	+	++	+	±	+
	Chloroform	+++	+++	++	+	±	±	+
Ramsey	*n*-Hexane	+++	+++	+	++	+	±	+
	Chloroform	+++	+++	++	+	+	+	++

Note: +++ = very strong signal; ++ = strong signal; + = weak signal; ± = very weak signal.

the FTIR spectra of the material extracted from the lake sediments by *n*-hexane and chloroform. More important, the OM extracted from the four different lake sediments does not seem to differ significantly. The most prominent IR absorption bands are at ~2920 cm^{-1} (asymmetric C–H stretch of CH_2) and ~2850 cm^{-1} (symmetric C–H stretch of CH_2). Some strong absorptions are also found at ~1730 cm^{-1} (C=O stretch of CO_2H), ~1460 cm^{-1} (CH_3 bending), and 730 cm^{-1} ($(CH_2)_n$ bending of paraffins). In addition, there are minor bands at ~1370 cm^{-1} (CH_3 bending), ~1270 cm^{-1} (C–OH stretch), and ~1130 cm^{-1} (C–C or C–OH stretch), all indicative of the presence of paraffins and fatty acids. The intensity of the bands at ~1730 cm^{-1} and 1460 cm^{-1} differs slightly when comparing the OM obtained from the *n*-hexane extraction and that obtained from the chloroform extractions. The band at 1730 cm^{-1} is more intense than at 1460 cm^{-1} in the chloroform-extracted material suggesting that the concentration of fatty acids is greater. These results are similar to those reported in the literature (41), suggesting that the *n*-hexane extracts more specifically alkanes and fatty acids while the chloroform removes mainly fatty acids, long-chain alcohols, and wax esters from the soil samples. These are believed to be compounds that are trapped in the complex matrix that makes up HS. The fact that more material was extracted by chloroform from the Silver Lake sediment suggests that the sediment contained more fatty acids, long-chain alcohols, and wax esters than the other lake sediments studied.

The two extraction reagents most often used in the studies of HS are $Na_4P_2O_7$ and NaOH. HS extracted by the two reagents have been known to be slightly different. More specifically, the molecular weight of the HS extracted from soils by $Na_4P_2O_7$ is smaller. The HS are also more aromatic in nature than those extracted by NaOH (42). The use of both reagents ensures that a maximum amount of HS is extracted from the lake sediments. The extraction procedure generated the following four samples for each sediment sample: 1. FA–$Na_4P_2O_7$ (the FA extracted using $Na_4P_2O_7$); 2. HA–$Na_4P_2O_7$ (the HA extracted using $Na_4P_2O_7$); 3. FA–NaOH (the FA extracted using NaOH); 4. HA–NaOH (the HA extracted using NaOH).

The amount of FA–$Na_4P_2O_7$ from a 25 g sediment sample ranges from 40.5 to 309.9 mg while the amount of FA–NaOH ranges from 59.8 to 237.6 mg. The total amount of FA extracted constitutes 0.4–2.19% of the sample weight and 9.27–13.02% of the TOM. The amount of HA–$Na_4P_2O_7$ from a 25 g sediment sample ranges from 23.5 to 639.7 mg and HA–NaOH ranges from 40.6 to 875.7 mg. HA makes up 0.26–6.04% of the sample weight and 8.27–25.90% of the TOM. Small amounts of FA and HA are found in the sediment samples collected from Tilton, Clearwater, and Ramsey lakes while relatively large amounts of FA and HA are observed in the Silver Lake sediments. These findings correlate well with the sediments. A comparison of these results with that reported (42) for the HA content of soils (2.08–18.8% by weight) indicates that lake sediments are relatively deficient in HA. Although there is a large difference in the amounts of FA and HA recovered from the four lake sediments (ranging from 0.40 to 2.19% for FA and from 0.26 to 6.04% for HA), the percentage of FA and HA in the TOM of the lake sediments is similar (ranging from 9.27 to 13.02% for FA and 8.27 to 25.9% for HA). The results in this study also agree with the observations (15) that FA make up 6–23% and HA 8–24% of the OM found in lake sediments. Our results show that the sediments are richer in HA than FA. This is because FA have higher solubility in lake water than HA. The highest HA content was found in the Silver Lake sediments, possibly due to the relatively low pH of the lake water (pH = 4.0).

Elemental composition of HA and FA

Once the FA and HA were separated from the lake sediments, they were analyzed for carbon, hydrogen, nitrogen, and oxygen content. The carbon, hydrogen, nitrogen, and oxygen composition of the FA and HA extracted from the four lake sediments is presented in Table 5. The percentage of carbon in the FA–$Na_4P_2O_7$ ranges from 37.47 to 46.15. The hydrogen ranges from 6.40 to 6.93%, the nitrogen ranges from 2.48 to 3.89%, and the oxygen ranges from 43.44 to 53.60%. The FA extracted from the Silver Lake sediments with $Na_4P_2O_7$ is lower in carbon, lower in nitrogen, and higher in oxygen when compared to that of the other sediments. The percentage of carbon in FA–NaOH ranges from 45.1 to 48.01. The hydrogen ranges from 6.59 to 6.94%, the nitrogen ranges from 4.95 to 5.76%, and the oxygen ranges from 40.36 to 42.75%. The elemental composition of FA extracted from all four sediments by NaOH is similar. It should be noted that in comparing the FA extracted from the lake sediment by NaOH with that obtained by using $Na_4P_2O_7$ the NaOH extracts contain higher carbon (except for Tilton), hydrogen, and nitrogen but lower

Can. J. Chem. Downloaded from www.nrcresearchpress.com by 92.62.229.171 on 09/08/12
For personal use only.

© 1997 NRC Canada

Can. J. Chem. Downloaded from www.nrcresearchpress.com by 92.62.229.171 on 09/08/12
For personal use only.

Table 5. Elemental composition of FA and HA extracted from the lake sediments.

Lakes	Extractants	Elemental composition (%) C	H	N	O
Fulvic acids					
Tilton	0.1 M $Na_4P_2O_7$	46.15 ± 0.02	6.40 ± 0.01	3.89 ± 0.01	43.55 ± 0.09
	0.5 M NaOH	45.15 ± 0.12	6.94 ± 0.12	5.15 ± 0.03	42.75 ± 0.12
Clearwater	0.1 M $Na_4P_2O_7$	45.88 ± 0.06	6.55 ± 0.09	3.67 ± 0.02	43.90 ± 0.13
	0.5 M NaOH	46.63 ± 0.23	6.71 ± 0.05	4.94 ± 0.03	41.71 ± 0.22
Silver	0.1 M $Na_4P_2O_7$	37.47 ± 0.21	6.45 ± 0.23	2.48 ± 0.02	53.60 ± 0.45
	0.5 M NaOH	48.01 ± 0.19	6.66 ± 0.06	4.96 ± 0.01	40.36 ± 0.25
Ramsey	0.1 M $Na_4P_2O_7$	42.83 ± 0.71	6.93 ± 0.19	3.70 ± 0.09	46.55 ± 0.92
	0.5 M NaOH	47.24 ± 0.16	6.59 ± 0.10	5.76 ± 0.03	40.42 ± 0.28
Humic acids					
Tilton	0.1 M $Na_4P_2O_7$	51.16 ± 0.54	5.76 ± 0.02	4.70 ± 0.08	38.87 ± 0.63
	0.5 M NaOH	52.69 ± 0.03	6.27 ± 0.07	5.23 ± 0.02	35.81 ± 0.12
Clearwater	0.1 M $Na_4P_2O_7$	48.78 ± 0.34	5.16 ± 0.09	4.26 ± 0.03	41.80 ± 0.45
	0.5 M NaOH	52.79 ± 0.35	5.98 ± 0.13	4.94 ± 0.03	36.29 ± 0.48
Silver	0.1 M $Na_4P_2O_7$	53.41 ± 0.19	5.23 ± 0.04	4.34 ± 0.02	37.03 ± 0.24
	0.5 M NaOH	54.67 ± 0.33	6.21 ± 0.16	4.85 ± 0.02	34.27 ± 0.50
Ramsey	0.1 M $Na_4P_2O_7$	51.38 ± 0.08	4.52 ± 0.03	4.64 ± 0.01	39.46 ± 0.06
	0.5 M NaOH	53.97 ± 0.06	5.83 ± 0.05	5.19 ± 0.01	35.01 ± 0.04

Table 6. A comparison of elemental composition of FA and HA from different lake sediments.

Element	Reported values[a] (%)	Values determined in this study (%)
Fulvic acids		
Carbon	44.98 ± 3.90	44.94 ± 3.39
Hydrogen	5.12 ± 1.24	6.65 ± 0.20
Nitrogen	7.63 ± 0.56	4.31 ± 1.07
Oxygen	42.27 ± 4.69	44.11 ± 4.34
Humic acids		
Carbon	52.05 ± 3.61	52.36 ± 1.87
Hydrogen	5.67 ± 0.65	5.26 ± 0.60
Nitrogen	5.63 ± 1.08	4.77 ± 0.36
Oxygen	36.55 ± 4.27	37.32 ± 2.54

[a]The values reported by Ishiwatari (15).

oxygen. In the HA–$Na_4P_2O_7$, the carbon ranges from 48.78 to 53.41%, the hydrogen ranges from 4.52 to 5.16%, the nitrogen ranges from 4.26 to 4.70%, and oxygen ranges from 37.03 to 41.80%. The carbon in the HA–NaOH ranges from 52.69 to 54.67%, the hydrogen ranges from 5.83 to 6.27%, the nitrogen ranges from 4.85 to 5.23%, and the oxygen ranges from 34.27 to 36.29%. In each extract, there are small variations of the elemental composition of HA among the lake sediments. But, as was the case for FA, the HA resulting from extraction by NaOH contains higher carbon, hydrogen, and nitrogen but lower oxygen than the $Na_4P_2O_7$ extracts. These results suggest that the NaOH and $Na_4P_2O_7$ extracted OM from the lake sediments differs in composition.

Average values of the elemental composition of FA and HA reported (15) for different lake sediments of Japan are summarized in Table 6 where they are compared to the values calculated from our data for the NaOH and $Na_4P_2O_7$ extracted materials (Table 5). The values of the elemental composition of the HA determined in this study are close to the average values reported (15). The FA found in the Sudbury area lake sediments appear to be slightly higher in hydrogen content and lower in nitrogen content.

When comparing the FA and HA one notices that the carbon content of fulvic acid is lower than that of humic acid while oxygen displays the opposite trend (Table 5). The nitrogen content of HA–$Na_4P_2O_7$ is slightly higher than that of FA–$Na_4P_2O_7$ but there is no such trend found in the NaOH extracts. The results also show that the hydrogen content for FA appears to be higher than that for HA (Table 5).

Elemental ratios of HA and FA

The elemental ratios most often used in the study of HS are H/C, N/C, and O/C. By using the H, C, N, and O elemental analysis data, H/C, N/C, and O/C ratios of fulvic and humic acids extracted from the four lake sediments were calculated (Table 7). The H/C ratio varies from 1.66 to 2.06 in the FA–$Na_4P_2O_7$ and from 1.66 to 1.84 in the FA–NaOH. The H/C ratio varies from 1.05 to 1.35 in the HA–$Na_4P_2O_7$ and from 1.30 to 1.43 in the HA–NaOH. Higher H/C ratios were found in the FA than in the HA. In addition, for the HA, the H/C ratios of the NaOH extracts appear to be slightly higher than that of the $Na_4P_2O_7$ extracts. The N/C ratio varies from 0.057 to 0.074 in the FA–$Na_4P_2O_7$ and from 0.089 to 0.105 in the FA–NaOH. The ranges of the N/C ratio are 0.070 to 0.078 in the HA–$Na_4P_2O_7$ and 0.076 to 0.085 in the HA–NaOH. The HA extracted by both NaOH and $Na_4P_2O_7$ produces N/C ratios that are within experimental error of one other. The FA extracted by $Na_4P_2O_7$ have lower N/C ratios than those observed for the NaOH extracted FA. The O/C ratio varies from 0.708 to 1.07 in the FA–$Na_4P_2O_7$ and from 0.630 to 0.710 in the FA–NaOH. The ratio varies from 0.520 to 0.643

© 1997 NRC Canada

Table 7. Elemental ratios of FA and HA extracted from the lake sediments.

Lakes	Extractants	Elemental ratios H/C	N/C	O/C
Fulvic acids				
Tilton	0.1 M $Na_4P_2O_7$	1.66 ± 0.03	0.072 ± 0.001	0.708 ± 0.001
	0.5 M NaOH	1.84 ± 0.04	0.098 ± 0.001	0.710 ± 0.003
Clearwater	0.1 M $Na_4P_2O_7$	1.71 ± 0.03	0.069 ± 0.001	0.718 ± 0.003
	0.5 M NaOH	1.73 ± 0.02	0.091 ± 0.001	0.671 ± 0.007
Silver	0.1 M $Na_4P_2O_7$	2.06 ± 0.06	0.057 ± 0.001	1.07 ± 0.02
	0.5 M NaOH	1.66 ± 0.01	0.089 ± 0.001	0.630 ± 0.007
Ramsey	0.1 M $Na_4P_2O_7$	1.94 ± 0.04	0.074 ± 0.001	0.815 ± 0.030
	0.5 M NaOH	1.67 ± 0.02	0.105 ± 0.001	0.642 ± 0.007
Humic acids				
Tilton	0.1 M $Na_4P_2O_7$	1.35 ± 0.01	0.078 ± 0.001	0.563 ± 0.150
	0.5 M NaOH	1.43 ± 0.02	0.085 ± 0.001	0.509 ± 0.001
Clearwater	0.1 M $Na_4P_2O_7$	1.27 ± 0.01	0.075 ± 0.001	0.643 ± 0.011
	0.5 M NaOH	1.36 ± 0.03	0.080 ± 0.001	0.516 ± 0.010
Silver	0.1 M $Na_4P_2O_7$	1.18 ± 0.01	0.070 ± 0.001	0.520 ± 0.005
	0.5 M NaOH	1.36 ± 0.02	0.076 ± 0.001	0.470 ± 0.010
Ramsey	0.1 M $Na_4P_2O_7$	1.05 ± 0.01	0.077 ± 0.001	0.576 ± 0.002
	0.5 M NaOH	1.30 ± 0.02	0.083 ± 0.001	0.486 ± 0.001

in the HA–$Na_4P_2O_7$ and from 0.470 to 0.516 in the HA–NaOH. Higher O/C ratios were found in the FA than in the HA and the ratios of the $Na_4P_2O_7$ extracts appear to be higher than those of the NaOH extracts for both the FA and HA.

From Table 7, the elemental ratios for the FA and HA can be summarized as follows: for **FA:** H/C: 1.66–2.06; N/C: 0.057–0.11; O/C: 0.63–1.07; for **HA:** H/C: 1.05–1.43; N/C: 0.070–0.085; O/C: 0.47–0.64. Using the average elemental ratios, the empirical formulae for the FA and HA extracted from lake sediments are: **FA:** C:H:O:N = 12:22:9:1 and **HA:** C:H:O:N = 12:16:6:1. The elements present in FA and HA decrease in the order: H > C > O > N.

Larger amounts of H and O found in the FA with respect to HA suggest that FA molecules contain a greater number of carbohydrate and carboxylic acid groups. This has been further confirmed by the ^{13}C NMR spectra of the FA and HA (see further in the text). In addition, for the HA, the NaOH extracted material has a higher H/C ratio and a lower O/C ratio than the $Na_4P_2O_7$ extracted material. This appears to suggest that the material extracted by the 0.5 M NaOH solution could be more aliphatic in nature than that extracted by the 0.1 M $Na_4P_2O_7$ solution. Using ^{13}C NMR, it has been reported (42) that HA extracted by 0.1 M $Na_4P_2O_7$ solution are more aromatic than those removed from the same soils by 0.5 M NaOH solution. The ^{13}C spectra in our study also indicate the same results.

A comparison of elemental ratios of FA and HA from different sources was made and the results are shown in Table 8. Ishiwatari (15) summarized the average values of elemental ratios for FA from sediments of Japanese lakes. The FA in the present study have a slightly higher H/C (1.66–2.06) and O/C ratio (0.63–1.07) while the N/C ratio (0.057–0.11) is lower than the average values published by Ishiwatari. Organic material with a relatively high O-alkyl and carboxylic acid composition would result in high H/C and O/C ratios. Therefore, the FA isolated from the Sudbury area lake sediments would seem to contain a higher proportion of O-alkyl and carboxylic acid functionalities than those studied thus far based on the H/C and O/C ratios. The values for the HA in the present study (H/C = 1.05–1.43, N/C = 0.070–0.085, and O/C = 0.47–0.64) are essentially in the same range as those previously reported for lake sediments (15).

The data in Table 8 show that there are significant differences among the values of the elemental ratios for FA and HA derived from lake sediments and other sources such as soil, river water, and groundwater. It can been seen that FA and HA extracted from lake sediments produce relatively high H/C, O/C, and N/C ratios compared to those for FA and HA extracted from soil, river, and groundwater. High N/C ratios suggest that lake sediment FA and HA are closely related to their precursory materials (e.g., the N/C ratios for phytoplankton range from 0.11 to 0.16 (1)) and have a relatively low degree of humification (15). High H/C and O/C ratios reflect high carbohydrate content and the high aliphatic character of lake sediment FA and HA. These trends have also been observed in the analysis of the ^{13}C NMR spectra in this study.

E_4/E_6 ratios of HA and FA

The E_4/E_6 ratio refers to the ratio of the absorbances of dilute aqueous FA or HA solution at 465 and 665 nm. The ratio is inversely related to the molecular weight or particle size of FA or HA (42) as larger molecules have higher absorbances at long wavelengths than at the shorter ones. As shown in Table 9, the E_4/E_6 ratio of the FA–$Na_4P_2O_7$ ranges from 11.11 to 12.40 and the E_4/E_6 ratio of the FA–NaOH ranges from 8.81 to 11.03, while the E_4/E_6 ratio of the HA–$Na_4P_2O_7$ ranges from 5.59 to 5.88 and the E_4/E_6 ratio of the HA–NaOH ranges from 4.23 to 4.66. There are two trends observed from the E_4/E_6

© 1997 NRC Canada

Can. J. Chem. Downloaded from www.nrcresearchpress.com by 92.62.229.171 on 09/08/12
For personal use only.

Can. J. Chem. Downloaded from www.nrcresearchpress.com by 92.62.229.171 on 09/08/12
For personal use only.

Table 8. Elemental ratios of fulvic and humic acids from different sources.

Sources	Elemental ratios H/C	N/C	O/C	References
Fulvic acids				
Soil	0.83–1.4	0.03–0.06	0.64–0.74	16
River	0.81–1.05	0.01–0.03	0.54–0.63	16
Groundwater	0.90–1.3	0.001–0.03	0.34–0.47	16
Lake sediment	1.10–1.58	0.13–0.16	0.57–0.86	15
Lake sediment	1.66–2.06	0.057–0.11	0.63–1.07	This study
Humic acids				
Soil	0.80–1.10	0.01–0.06	0.46–0.57	16
River	0.82–1.11	0.02–0.03	0.50–0.59	16
Groundwater	0.69–0.98	0.04–0.09	0.28–0.39	16
Lake sediment	1.17–1.43	0.075–0.11	0.44–0.63	15
Lake sediment	1.05–1.43	0.070–0.085	0.47–0.64	This study

Table 9. E_4/E_6 ratios of FA and HA extracted from the lake sediments.

Lakes	Extractants	E_4/E_6 ratios[a] Fulvic acids	Humic acids
Tilton	0.1 M $Na_4P_2O_7$	11.83 ± 0.04	5.60 ± 0.03
	0.5 M NaOH	9.85 ± 0.12	4.23 ± 0.01
Clearwater	0.1 M $Na_4P_2O_7$	11.50 ± 0.40	5.88 ± 0.11
	0.5 M NaOH	8.81 ± 0.15	4.47 ± 0.04
Silver	0.1 M $Na_4P_2O_7$	11.11 ± 0.06	5.59 ± 0.06
	0.5 M NaOH	10.21 ± 0.06	4.66 ± 0.06
Ramsey	0.1 $Na_4P_2O_7$	12.40 ± 0.07	5.68 ± 0.04
	0.5 M NaOH	11.03 ± 0.04	4.54 ± 0.06

[a] E_4/E_6 ratio = $\frac{\text{Absorbance at 465 nm}}{\text{Absorbance at 665 nm}}$

Table 10. Correlation coefficients (r) for E_4/E_6 ratios and %C, %H, %O, H/C, and O/C.

Pairs of values	r
E_4/E_6 ratios and %C	−0.85[a]
E_4/E_6 ratios and H/C	0.84[a]
E_4/E_6 ratios and %O	0.78[a]
E_4/E_6 ratios and O/C	0.77[a]
E_4/E_6 ratios and %H	0.66[a]
E_4/E_6 ratios and %N	0.43[b]
E_4/E_6 ratios and N/C	0.004[c]

[a] Significant at $P = 0.01$.
[b] Significant at $P = 0.05$.
[c] Significant at $P > 0.1$.

values. Firstly, the E_4/E_6 ratios of FA are higher than those of HA, suggesting that the molecular weight of FA is lower than those of HA. These are similar to the E_4/E_6 ratios of HA (3.95 ± 0.16) and FA (10.66 ± 0.49) reported for fulvic acid extracted from Lake Huron sediment (43). Secondly, the E_4/E_6 ratios of the $Na_4P_2O_7$ extracted FA and HA are higher than those of the NaOH extracted material. This suggests that the NaOH extracted material has a higher molecular weight than the $Na_4P_2O_7$ extracted material. Piccolo and Mirabella (44) also found that 0.1 M NaOH extracted OM from soil with higher molecular weight than did a 0.1 M $Na_4P_2O_7$ solution.

In addition, E_4/E_6 ratios, being a function of molecular weight or particle size, are expected to be related to the elemental composition of the molecules. Plots were drawn of the E_4/E_6 ratio versus %C, %H, %N, %O, H/C, N/C, and O/C, respectively, and the resulting correlation coefficients are presented in Table 10. The negative correlation coefficient indicates that the E_4/E_6 ratio decreases as %C increases. HA have higher %C and lower E_4/E_6 ratios while FA have a lower %C and higher E_4/E_6 ratios. As the %H increases, the E_4/E_6 ratios also increase. HA have lower E_4/E_6 ratios and lower %H while FA have higher E_4/E_6 ratios and higher %H. There is no obvious trend between the E_4/E_6 ratio and %N. The r value seems to indicate that the lower molecular weight material (high E_4/E_6 ratios) has a variable amount of N (~2.5–6%) while the N in higher molecular weight material has a narrower range (4.2–5.2%). The data in Table 10 suggest that the larger molecular weight materials (low E_4/E_6 ratios) have a relatively low %O (~34–42%) while the smaller molecular weight materials have a relatively high %O (~40–54%). E_4/E_6 ratios appear to increase as H/C and O/C ratios increase. HA have lower E_4/E_6 H/C and O/C ratios than FA. No relationship was observed between the E_4/E_6 ratios and N/C ratios. However, as in the case of the E_4/E_6 versus %N plot, the N/C ratio of the FA (high E_4/E_6) is highly variable (0.057–0.105) while HA have a much narrower range of N/C ratios (0.07–0.085). In summary, for lake sediment FA and HA, a low E_4/E_6 ratio is associated with a molecule that has a high carbon content, but is relatively low in hydrogen and oxygen. A high E_4/E_6 ratio, in contrast, indicates that the molecule has a low carbon content, but is relatively high in hydrogen and oxygen. These are consistent with the observations made for soil FA and HA (42), the

© 1997 NRC Canada

Table 11. FTIR bands of fulvic and humic acids from the lake sediments.

Lakes	Extractants	FTIR bands[a] ~3350	~2935	~2860	~1720	~1625	~1525	~1400	~1220	~1080	~800
Fulvic acids											
Tilton	$Na_4P_2O_7$	+++	+	–	–	+++	–	++	+	+++	±
	NaOH	+++	+	–	–	++	–	+	+	++	+
Clearwater	$Na_4P_2O_7$	+++	±	–	–	++	–	+	+	++	+
	NaOH	+++	±	–	–	++	–	+	±	++	+
Silver	$Na_4P_2O_7$	+++	±	–	–	++	–	+	+	+++	++
	NaOH	++	±	–	–	++	±	+	±	++	+
Ramsey	$Na_4P_2O_7$	+++	±	–	–	++	±	+	–	++	++
	NaOH	+++	+	±	–	+++	–	++	–	+++	+
Humic acids											
Tilton	$Na_4P_2O_7$	+++	++	+	+	+++	+	±	±	+	–
	NaOH	+++	++	+	+	++	+	±	+	++	±
Clearwater	$Na_4P_2O_7$	+++	++	+	+	+++	±	±	++	++	–
	NaOH	+++	+++	++	+	+++	+	±	++	++	–
Silver	$Na_4P_2O_7$	+++	++	+	+	+++	±	±	++	++	–
	NaOH	+++	+++	++	+	+++	+	±	++	++	–
Ramsey	$Na_4P_2O_7$	+++	++	+	+	+++	±	±	++	++	–
	NaOH	+++	++	++	+	+++	++	+	++	++	–

[a]+++ = v. strong signal; ++ = strong signal; + = weak signal; ± = v. weak signal; – = no signal.

Can. J. Chem. Downloaded from www.nrcresearchpress.com by 92.62.229.171 on 09/08/12
For personal use only.

correlation coefficients for E_4/E_6 ratios with %C and %O were −0.73 and 0.82, respectively.

FTIR spectroscopy of HA and FA

Fourier-transform infra red spectroscopy (FTIR) is a very useful method for determining the functional groups present in HS. In this study, FTIR spectra of FA and HA samples extracted from Sudbury area lakes were recorded in the form of KBr pellets. A summary of the major bands found in the FTIR spectra is presented in Table 11. The FTIR spectra of the FA and HA are relatively simple. There are no apparent structural differences between the FA and HA extracted from the four lake sediments according to the infrared analysis. McCarthy and Rice (24) comment that the most striking feature of the infrared spectra of HS is the overall simplicity of the spectra and the similarity suggests that the chemical structures of these compounds are closely related. When compared to the infrared spectra of a commercial humic acid and a peat fulvic acid (not shown), it is immediately obvious that their spectra resemble closely those recorded in the present study. Although there are relatively few bands, which are generally very broad and nondescript, some structural information regarding the lake sediment FA and HA can be extracted from the spectra. It should be noted, however, that infrared spectroscopy is not sensitive enough to uncover minor structural differences that may exist between HS. The FTIR spectra of FA exhibit the following features: a broad band around 3300–3400 cm^{-1} (OH stretching vibration, or H_2O, contribution from aliphatic OH stretching vibration, and possibly NH stretching vibration), a small shoulder around 2935 cm^{-1} (asymmetric CH stretching vibration of $-CH_2-$), a well-pronounced peak at 1625 cm^{-1} (aromatic C=C stretching vibration and (or) asymmetric $-COO^-$ stretching vibration), a peak at around 1400 cm^{-1} (-CH bending vibration of $-CH_2$ and $-CH_3$), a small peak at 1220 cm^{-1} (-C–O stretching vibration and OH bending vibration of -COOH), a major peak at around 1080 cm^{-1} (-C–OH stretching vibration of polysaccharides) and an absorption band at around 800 cm^{-1} (=C–H out-of-plane bending vibration, characteristic of aromatics or alkene).

The FTIR spectra of HA exhibit basically the same features as those of FA except for a shoulder at ca. 2860 cm^{-1} (aliphatic CH stretching vibration), a band at 1720 cm^{-1} (-C=O stretch of -COOH), and a peak at ca. 1530 cm^{-1} (aromatic C=C stretching vibration). These FTIR spectra indicate that FA and HA extracted from the lake sediments are composed of aromatic groups (bands at around 1620 cm^{-1} and 900 cm^{-1}), aliphatic groups (bands in the 2860–2930 cm^{-1} region and at around 1422 cm^{-1}), carboxylic groups (bands at around 1720 cm^{-1} and 1220 cm^{-1}), and polysaccharide-like components (bands at 1040 cm^{-1}). The band at 1040 cm^{-1} is more intense for the FA samples, than that found for the HA samples, indicating that the FA contains more polysaccharide components. This has been confirmed by the solid-state ^{13}C NMR analysis carried out in the present study. The bands observed at ca. 1720 cm^{-1} (due to C=O stretching vibration of COOH) in the spectra of HA appear to reflect the relatively high acidity of the HA. This finding is consistent with the results of the PY–GC–MS analysis (37), as many components of fatty acids were found in the pyrolysis products of HA. It is worth noting that the band at 1625 cm^{-1} is of similar intensity in both FA and HA spectra, indicating that the aromatic character of FA and HA is similar. This observation was confirmed by the

© 1997 NRC Canada

Table 12. Distribution of C (as percentage of total organic C) in humic and fulvic acids from the lake sediments.

Lakes	Extractants	Aliphatic C 0–50 (ppm)	O-Alkyl C 50–110 (ppm)	Aromatic C 110–160 (ppm)	Carboxylic C 160–190 (ppm)	Carbonyl C 190–230 (ppm)	Ali.[a]	Aro.[b]
Humic acids								
Tilton	0.1 M $Na_4P_2O_7$	38.9	24.0	22.7	11.0	3.4	73.5	26.5
	0.5 M NaOH	43.7	30.5	11.1	14.7	6.6	87.0	13.0
Clearwater	0.1 M $Na_4P_2O_7$	44.0	25.1	8.9	15.6	6.4	88.9	11.4
	0.5 M NaOH	45.4	31.4	9.2	10.8	3.2	83.3	10.7
Silver	0.1 M $Na_4P_2O_7$	31.8	30.8	22.1	12.4	2.9	73.9	26.1
	0.5 M NaOH	44.0	27.8	9.2	12.8	6.2	88.7	11.3
Ramsey	0.1 M $Na_4P_2O_7$	28.1	30.6	24.2	13.5	3.6	70.8	29.2
	0.5 M NaOH	44.4	24.4	11.2	12.9	7.2	86.0	14.0
Fulvic acids								
Silver	0.1 M $Na_4P_2O_7$	22.6	34.7	21.5	17.0	4.2	72.7	27.3
	0.5 M NaOH	23.5	37.1	19.1	17.9	2.4	76.0	24.0
Ramsey	0.1 M $Na_4P_2O_7$	21.9	35.0	22.3	18.3	2.6	71.8	28.2
	0.5 M NaOH	34.1	31.0	8.6	21.2	5.1	88.3	11.7

[a] $\text{Aliphaticity (\%)} = \frac{\%C\ (0\text{–}110\ ppm)}{\%C\ (0\text{–}160\ ppm)} \times 100.$

[b] $\text{Aromaticity (\%)} = \frac{\%C\ (110\text{–}160\ ppm)}{\%C\ (110\text{–}160\ ppm)} \times 100.$

analysis of the ^{13}C spectra of the FA and HA samples. This is interesting as IR and ^{13}C NMR data of soil HS (38) indicated that the aromatic character of FA was less than that of HA.

Solid-state CPMAS ^{13}C NMR spectroscopy of HA and FA

Solid samples of FA and HA were subjected to cross polarization magic-angle spinning (CPMAS) ^{13}C NMR analysis. As described earlier, each ^{13}C NMR spectrum was divided into five chemical shift regions, corresponding to aliphatic C (0–50 ppm), O-substituted alkyl C (50–110 ppm), aromatic C (110–160 ppm), carboxylic acid C (160–190 ppm), and carbonyl C (190–240 ppm), respectively. Relative quantities of each type of C found in the five regions were determined by planimetry and are expressed as a percentage of the total organic carbon content. Spectral identification was facilitated by using the chemical shift data for FA and HA reported by Malcolm (28). The distribution of C in the five regions of the spectra is presented in Table 12. The spectra have five well-resolved and three poorly resolved peaks. The well-resolved peaks are in the regions of 15–40 ppm (methyl, methylene, and methine groups), 50–60 ppm (methoxy groups), 60–90 ppm (C–O groups), 115–145 ppm (aromatic carbons), and 160–190 ppm (carboxyl and ester groups). The poorly resolved peaks occur between 95 and 108 ppm (anomeric carbons), 145 and 160 ppm (phenolic carbons), and 190 and 215 ppm, (carbonyl groups). The most intense peak in the HA spectra is found at around 35 ppm, which corresponds to the aliphatic C region (0–50 ppm) (28). The percentage of C in this region varies from 28.1 to 44.0 for the $Na_4P_2O_7$ extracted material and from 43.7 to 45.4 for the NaOH extracted material (Table 12). This suggests that the structure of HA from the lake sediments is primarily aliphatic in nature. Furthermore, the higher percentage of C in the aliphatic region for the NaOH extracts than that for the $Na_4P_2O_7$ extracts indicates that the organic material extracted by the 0.5 M NaOH solution possesses more aliphatic groups than that extracted by the 0.1 M $Na_4P_2O_7$ solution. In the O-alkyl region (50–110 ppm), two well-resolved peaks at 54 and 76 ppm as well as a small peak at 104 ppm were evident in the spectra of all the HA samples. The peak at 54 ppm has been attributed to methoxy groups associated with lignin and lignin-like products (28, 45, 46). The peak at 76 ppm is thought to correspond to ring carbons of polysaccharides (28, 47), whereas the signal at 104 ppm has been assigned to anomeric carbons in polysaccharides (28). The intensity of the signals found in the 50–110 ppm region of the spectra suggests that HA from the lake sediments contain a substantial amount of carbohydrate-like matter. More specifically, the percentage of the O-alkyl carbons with respect to the total organic carbon varies from 24.0 to 30.8% for both extracts (Table 12). This is the second highest percentage of carbon in the five regions considered. Hence, the groups with O-alkyl carbons (which might include carbohydrate O-methylene and methine, and aromatic O-methyl and methylene) constitute the second major structural component of HA. In the aromatic C region (110–160 ppm), a well-resolved peak at 130 ppm has been attributed to aromatic structures substituted with alkyl groups. A minor peak, indicative of phenolic groups, also occurs at 153–154 ppm in all the spectra recorded for the samples of HA. The fact that peaks in the aromatic C region are less intense than those in the aliphatic and O-alkyl regions indicates that aromatic structure is not the major component of lake sediment HA. The percentage of aromatic carbon relative to the total organic carbon varies from 8.9 to 24.2% (Table 12), which is a relatively low percentage. It should be noted that significantly more aromatic carbon containing material (21.1–24.2%) is extracted from the sediments of Tilton, Silver, and Ramsey lakes by the 0.1 M $Na_4P_2O_7$ solution than by the 0.5 M NaOH solution (9.2–11.2%). In the region between 160 and 190 ppm, all lake sediment HA spectra exhibit a prominent peak between 173 and 174 ppm, which

© 1997 NRC Canada

Can. J. Chem. Downloaded from www.nrcresearchpress.com by 92.62.229.171 on 09/08/12
For personal use only.

Table 13. A comparison of the C distribution in humic and fulvic acids from different sources.

Sources	Total organic C				
	Aliphatic C	O-Alkyl C	Aromatic C	Carboxylic C	Carbonyl C
Humic acids					
Soils[a]	16–26	19–29	30–42	14–18	1.4–4.7
Lake waters[b]	30–31	29–30	21–22	14–16	4.1–5.6
Lake sediments[c]	36–44	27–29	9.1–17	12–13	4.6–5.4
Fulvic acids					
Soils[a]	23–27	23–30	18–19	23–28	3.5–5.2
Lake waters[b]	43–44	21–22	14–15	16–17	4.7–5.1
Lake sediments[c]	23–28	33–35	15–20	17–19	3.3–3.8

[a]Reported by Novak and Smeck (38).
[b]Reported by Boerchke et al. (48).
[c]This study.

is characteristic of the carboxyl, amido, and ester functionalities. The percentage of carbon in this region varies from 10.8 to 15.6 for both extracts (Table 12). Minor peaks in the carbonyl region (190–230 ppm) are evident in the spectra of the four HA samples. The similarities between the ^{13}C NMR spectra of the HA extracted from the four lake sediment samples show that their structures are virtually identical. In comparing the % carbon in the five regions of the HA spectra one finds that: %aliphatic C > %O-alkyl C > %aromatic C > %carboxylic C > %carbonyl C.

In addition, HA from Clearwater Lake has a relatively low aromatic C content. The aromaticity and aliphaticity of HA, calculated using the formulae provided by Schnitzer (3), vary from 10.7 to 29.2% and from 83.3 to 70.8%, respectively (Table 12). It should be noted that the aromaticity for material extracted with 0.1 M $Na_4P_2O_7$ is higher than that for material extracted with 0.5 M NaOH. Schnitzer and Schuppli (42) also found in their study of the soil HA that the $Na_4P_2O_7$ extracted OM was more aromatic in nature.

Solid-state CPMAS ^{13}C NMR spectra of FA extracted from Silver Lake and Ramsey Lake were recorded. The percentages of carbon in the five regions of the spectra are shown in Table 12. The spectra of FA extracted from those two lake sediments by both $Na_4P_2O_7$ and NaOH are similar. The FA spectra differ significantly from those obtained for HA extracted from the same lake sediments. The most intense signal occurs at 176 ppm (in the carboxylic C region) rather than at 31 ppm (in the aliphatic region) as was observed in the HA spectra. In contrast to HA, the signal at 76 ppm (in the O-alkyl region) of the FA spectra is also higher than the 31 ppm peak. Table 12 shows that the percentage of the O-alkyl C and the carboxylic C in the FA extracted from the sediments of Silver and Ramsey lakes varies from 31.0 to 37.1% and from 17.0 to 21.2%, respectively, which are higher than those determined for HA. On the other hand, the percentage of the aliphatic C in the FA varies from 21.6 to 34.1%, which is lower than that calculated for HA. This suggests that there are more O-alkyl groups, which are attributed to carbohydrate-like compounds, and more carboxylic groups in the structure of the FA than in the structure of the HA. It is also worth noting from Table 12 that the aromatic C content of the FA (8.6–22.3%) is close to that of HA (9.2–24.2%). The aromaticity of the FA obtained from the sediments of Silver Lake (27.3% for 0.1 M $Na_4P_2O_7$ and 24.0% for 0.5 M NaOH) is even slightly higher than that calculated for the HA extracted from the sediments of the same lake (26.1% for 0.1 M $Na_4P_2O_7$ and 11.3% for 0.5 M NaOH).

A comparison of the distribution of C in HA and FA from soils (38), lake waters (48), and lake sediments (this study) can be found in Table 13. The relative amount of aromatic carbon in the structure of HA is dependent upon the origin. The percentage of aromatic C in the lake sediment HA (9.1–17%) and lake waters (20.6–21.9%) is much lower than in the soil HA (30–42%). Thus, the highest contribution of C in the structure of the lake HA is in the aliphatic (0–50 ppm) rather than in the aromatic region (110–160 ppm). This suggests that the aromaticity of soil HA is higher than that of lake HA. Boerschke et al. (48) reported the aromaticity of HA from Ramsey Lake water to be 25%, which is slightly higher than those aromaticity of the sediment HA (21%). Lake sediment FA have a slightly higher amount of O-alkyl carbons and a lower amount of carboxylic carbons than those found for soil FA. Fulvic acid from lake water appears to contain a relatively high number of aliphatic carbon groups in its structure. The structural implications of the information obtained from the different techniques are summarized in Table 14.

Conclusions

In this study, organic matter was extracted from the sediment of four Sudbury area lakes, with the aid of *n*-hexane, chloroform, 0.1 M $Na_4P_2O_7$, and 0.5 M NaOH solutions. The different FA and HA fractions were characterized using a number of different analytical methods. In general, the HS from the different lake sediments were shown to have similar chemical composition and structure. Such similarities suggest that the factors that play major roles in the formation and preservation of HS, such as the nature of the sediments, climatic and botanical environments, etc., are quite similar in the lakes tested and

© 1997 NRC Canada

Can. J. Chem. Downloaded from www.nrcresearchpress.com by 92.62.229.171 on 09/08/12
For personal use only.

Table 14. Structural implications of the information obtained from the various techniques.

	Aliphatic		O-Alkyl		Aromatic		Carboxylic		Carbonyl	
Techniques	HA	FA	HA	FA	HA	FA	HA	FA	HA	FA
Larger H and O content			L[a]	G			L	G		
H/C and O/C ratios	L	G	L	G			L	G		
Higher E_4/E_6 ratios	L	G	L	G			L	G		
FTIR			L	G	S	S				
NMR			L	G	S	S	L	G		

[a]Symbols indicate that structures may be present to a greater (G), lower (L), or similar degree.

Can. J. Chem. Downloaded from www.nrcresearchpress.com by 92.62.229.171 on 09/08/12
For personal use only.

that the pH of lakewater does not significantly affect the HS composition. A careful analysis of the data showed that the HS from the lake sediments have low aromaticity and relatively high carbohydrate content compared to the soil HS. The data on the composition and structure of the organic matter obtained from this study should provide useful information for the investigation of the interaction of organic matter in the lakes with trace metals, pollutants, etc.

The results of this study are summarized as follows:

1. The TOM in the four Sudbury area lakes range from 3 to 23% with Silver Lake being the highest. This could be related to the intense acidification of the lake watershed.
2. A very small portion of organic matter in the sediments was extracted by *n*-hexane and chloroform. Similar FTIR spectra were found for both the *n*-hexane and chloroform extracts. The spectra indicate that the material extracted from the lake sediments by the two organic solvents are a mixture of alkanes, fatty acids, long-chain alcohols, and wax esters.
3. The HS of lake sediments were found to contain a greater proportion of HA than FA. This could be due to the higher solubility of the smaller molecular weight FA in lakewater.
4. Elemental analysis showed that higher H/C and O/C ratios were found for FA than for HA, suggesting that the FA molecules contain more carbohydrate and carboxylic-like groups. The NaOH extracted material had a higher H/C ratio than the $Na_4P_2O_7$ extracted material, indicating that the material extracted by the 0.5 M NaOH solution is more aliphatic in nature than that extracted by the 0.1 M $Na_4P_2O_7$ solution.
5. E_4/E_6 ratios indicate that the molecular weight of HA is higher than that of FA and the 0.1 M $Na_4P_2O_7$ solution extracted smaller molecular weight material from the lake sediments than did the 0.5 M NaOH solution.
6. No apparent structural differences between the FA and HA extracted from the four lake sediments were detected by FTIR spectroscopy. The spectra indicate that both FA and HA possess aromatic, aliphatic, O-alkyl, and carboxylic functional groups.
7. The ^{13}C NMR spectra of FA and HA extracted from the lake sediments confirm that there are aliphatic, O-alkyl, aromatic, carboxylic, and carbonyl carbon nuclei in the FA and HA. The higher alkyl C and carboxylic C content found in the FA with respect to HA suggests that FA contain more carbohydrate and carboxylic groups than HA. Analysis of the spectra also showed that FA and HA extracted from the lake sediments are highly aliphatic. The aromaticity of lake HA is lower than that of soil HS. The ^{13}C NMR spectra of the $Na_4P_2O_7$ and NaOH extracts show that the aromatic C content found in the $Na_4P_2O_7$ extracts is higher than that found in the NaOH extracts, confirming that the $Na_4P_2O_7$ extracted material is more aromatic in nature than the NaOH extracted material.

Acknowledgements

Financial support from the Natural Sciences and Engineering Research Council of Canada and the Laurentian University Research Fund is acknowledged. Technical assistance provided by R. Boerschke and the U.S. Geological Survey, Denver, Colorado, is gratefully acknowledged.

References

1. P.A. Meyer and R. Ishiwatari. Org. Geochem. **20**, 867 (1993).
2. G.R. Aiken, D.M. McKnight, R.L. Wershaw, and P.MacCarthy. *In* Humic substances in soil, sediment and water. *Edited by* G.R. Aiken et al. John Wiley, New York. 1985. pp. 1–9.
3. M. Schnitzer. Soil Sci. **151**, 41 (1991).
4. J. Buffle. *In* Complexation reactions in aquatic systems: an analytical approach. Ellis Horwood Ltd., Chichester. 1988. pp. 90–145.
5. R. Saar and J. Webber. Geochim. Cosmochim. Acta, **44**, 1381 (1980).
6. G. Peschel and T. Wildt. Water Res. **22**, 105 (1988).
7. R.J. Carter, A. Hoxey, and T.V. Verheyem. Sci. Total Environ. **125**, 25 (1992).
8. A. Tessier, D. Fortin, N. Belzile, R.R. De Vitre, and G.G. Leppard. Geochim. Cosmochim. Acta, **60**, 387 (1996).
9. F.R. Livens. Environ. Pollut. **70**, 183 (1991).
10. R.L. Wershaw, P.J. Burcar, and M.C. Goldberg. Environ. Sci. Technol. **3**, 271 (1969).
11. W. Carter and I. Suffet. Environ. Sci. Technol. **16**, 735 (1982)
12. S. Johnsen and I.S. Gribbestad. Sci. Total Environ. **107**, 99 (1991).
13. J. Rook. Environ. Sci. Technol. **11**, 478 (1977).
14. R.F. Christman, J.D. Johnson, F.K. Pfaender, D.L. Norwood, M.R. Webb, J.R. Haas, and M.J. Babenrieth. *In* Water chlorina-

© 1997 NRC Canada

tion: environmental impact and health. Vol. 3. *Edited by* R.L. Jolly et al. Ann Arbor Science, Ann Arbor, Mich. 1980. pp. 75–84.
15. R. Ishiwatari. *In* Humic substances in soil, sediment and water. *Edited by* G.R. Aiken et al. John Wiley, New York. 1985. pp. 147–180.
16. C. Steelink. *In* Humic substances in soil, sediment and water. *Edited by* G.R. Aiken et al. John Wiley, New York. 1985. pp. 457–476.
17. T. Koyama. Coal Sci. Adv. Chem. Ser. **55**, 43 (1966).
18. M. Schnitzer. *In* Soil biochemistry. Vol. 2. *Edited by* D.W. Robertson and J.G.D. Lamb. Marcel Dekker, New York. 1971. pp. 60–95.
19. Y. Chen, N. Senesi, and M. Schnitzer. Soil Sci. Soc. Am. J. **42**, 352 (1977).
20. F.J. Stevenson and K.M. Goh. Geochim. Cosmochim. Acta, **35**, 471 (1971).
21. A.U. Baes and P.R. Bloom. Soil Sci. Soc. Am. J. **53**, 695 (1989).
22. Y. Inbar, Y. Chen, and Y. Hadar. Soil Sci. Soc. Am. J. **53**, 1695 (1989).
23. J. Niemeyer, Y. Chen, and J.-M. Bollag. Soil Sci. Soc. Am. J. **56**, 135 (1992).
24. P. MacCarthy and J.A. Rice. *In* Humic substances in soil, sediment and water. *Edited* by G.R. Aiken et al. John Wiley, New York. 1985. pp. 527–543.
25. M.A. Wilson. Soil Sci. **32**, 167 (1981).
26. P.G. Hatcher, I. A. Breger, L. W. Dennis, and G. E. Maciel. *In* Aquatic and terrestrial humic materials. *Edited by* R.F. Christian and E.T. Gjessing. Ann Arbor Science, Ann Arbor, Mich. 1983. pp. 37–81.
27. R.L. Wershaw. *In* Humic substances in soil, sediment and water. *Edited by* G.R. Aiken et al. John Wiley, New York. 1985. pp. 561–84.
28. R.L. Malcolm. *In* Humic substances II. *Edited by* M.H.B. Hayes et al. John Wiley, New York. 1989. pp. 339–372.
29. S.M. Griffith and M. Schnitzer. *In* Humic substances II. *Edited* by M.H.B. Hayes et al. John Wiley, New York. 1989. pp. 69–98.
30. J.P. Martin, K. Haider, and C. Saiz-Jimenez. Soil Sci. Soc. Am. Proc. **38**, 760 (1974).
31. M. Schnitzer and J.A. Neyroud. Soil Biol. Biochem. **7**, 365 (1975).
32. C. Saiz-Jimenez. Environ. Sci. Technol. **28**, 1773 (1994a).
33. C. Saiz-Jimenez. Environ. Sci. Technol. **24**, 197 (1994b).
34. G. Chiavari, G. Torsi, D. Fabbri, and G.C. Galletti. Analyst, **119**, 1141 (1994).
35. F. Martin, F.J. Gonzalez-Vila, J.C. del Rio, and T. Verdejo. J. Anal. Appl. Pyrolysis. **28**, 71 (1994).
36. F. Martin, J.C. del Rio, F.J. Gonzalez-Vila, and T. Verdejo. J. Anal. Appl. Pyrolysis, **31**, 75 (1995).
37. H.A. Joly, H. Li, and N. Belzile. J. Anal. Appl. Pyrolysis. Submitted.
38. J.M. Novak and N. E. Smeck. Soil Sci. Soc. Am. J. **55**, 96 (1991).
39. D.J. Landry. M.Sc. Thesis, Laurentian University, Sudbury. 1995.
40. H. Li. M.Sc. Thesis, Laurentian University, Sudbury. 1995.
41. M. Schnitzer and P. Schuppli. Soil Sci. Soc. Am. J. **53**, 1418 (1989a).
42. M. Schnitzer and P. Schuppli. Can. J. Soil Sci. **69**, 253 (1989b).
43. A. Bourbonnière and P.A. Meyers. Can. J. Spectrosc. **23**, 35 (1978).
44. A. Piccolo and A. Mirabella. Sci. Total Environ. **62**, 39 (1987).
45. P.G. Hatcher, D.L. Vanderhart, and W.L. Earl. Org. Geochem. **2**, 87 (1980).
46. E.G. Piotrowski, K.M. Valentine, and P.E. Pfeffer. Soil Sci. **137**, 194 (1984).
47. C.M. Preston and J.A. Ripmeester. Can. J. Spectrosc. **27**, 99 (1982).
48. R.C. Boerschke, E.A. Gallie, N. Belzile, R.N. Gedye, and J.R. Morris. Can. J. Chem. **74**, 2460 (1996).

Can. J. Chem. Downloaded from www.nrcresearchpress.com by 92.62.229.171 on 09/08/12
For personal use only.

© 1997 NRC Canada

Annulated derivatives of 2,2′-biimidazole, 2-(2′-imidazolyl)benzimidazole, and 2,2′-bibenzimidazole

James R. Ames, Melissa A. Houghtaling, Deborah L. Terrian, and Timothy P. Mitchell

Abstract: Preparation of bisannulated salts of 2,2′-biimidazole, 2-(2′-imidazolyl)benzimidazole, 2,2′-bibenzimidazole, and annulated salts of 1,1′-dimethyl-2,2′-biimidazole, 1,1′-dimethyl-2-(2′-imidazolyl)benzimidazole, and 1,1′-dimethyl-2,2′-bibenzimidazole is accomplished by direct alkylation of the parent azaheterocycle with excess 1,*n*-dihaloalkane. Discussions of the product conformations use electronic absorption spectra and NMR. The redox potentials of these salts are measured in DMF and CH_3CN, and become increasingly more negative and less reversible as the systems become less planar.

Key words: electrochemistry, bridged azabiaryl salts.

Résumé : On a fait appel à une alkylation directe des azahétérocycles parents à l'aide d'un excès de 1,*n*-dihalogénoalcane pour effectuer la préparation des sels à deux anneaux des 2,2′-biimidazole, 2-(2′-imidazolyl)benzimidazole, 2,2′-bibenzimidazole et des sels à un anneau des 1,1′-diméthyl-2,2′-biimidazole, 1,1′-diméthyl-2-(2′-imidazolyl)benzimidazole et 1,1′-diméthyl-2,2′-bibenzimidazole. On discute des conformations des produits en fonction des spectres d'absorption électronique et de la RMN. On a mesuré les potentiels rédox de ces sels dans le DMF et dans le CH_3CN; lorsque les systèmes adoptent des conformations de moins en moins planaires, ils deviennent de plus en plus négatifs et moins réversibles.

Mots clés : électrochimie, sels azabiaryles pontés.

[Traduit par la rédaction]

Introduction

The organic chemist has long been intrigued by biaryl molecules, the prototype being 1,1′-biphenyl, and the π-interaction between the two covalently bound rings. Researchers have used ultraviolet spectroscopy and ^1H NMR to examine the twisted nature of bridged biphenyls (1, 2).

The biphenyl work was soon extended to the diaza analogue, 2,2′-bipyridine. Homer and Tomlinson studied the electronic spectrum and reduction potential as a function of the length of the *N,N′* bridges quaternizing the nitrogens in 2,2′-bipyridine (3). They found that conjugation between the rings was affected by the length of the quaternizing chain.

Bridged diquaternary salts of 2,2′-biimidazole, **1**, and 2,2′-bibenzimidazole, **2**, have also been studied with respect to their redox and electronic properties (4–6). These 1,4-diaza systems differ significantly from that of 2,2′-bipyridine. For example, the chelation angle has been estimanted to be about 20° less for 2,2′-biimidazole than for 2,2′-bipyridine, causing a larger *N,N′* distance. Therefore, bridging between these sites should be affected, and the dihedral angle between the rings resulting from bridging should be reduced. In fact, molecular mechanics calculations on bridged 2,2′-biimidazoles have given dihedral angles of up to 20° less than the corresponding 3,3′-bridged-2,2′-bipyridines (4). The increased *N,N′* distance in the 2,2′-biimidazole molecule has prevented the synthesis of the *N,N′*-bis(dimethylene)-bridged salt (4). Furthermore, the doubly bridged 2,2′-biimidazolium and 2,2′-bibenzimidazolium salts are of interest because of their redox behavior — a neutral, tetraazaethylene derivative can be formed after two-electron reduction. These species are of great interest because they are aza analogues of tetrathiafulvene, an important donor in conducting charge transfer salts.

Thummel has demonstrated the importance of the effect of annulation on aromaticity in other heteroaromatics. His group has prepared mono- and bisannulated derivatives of 2,2′-bipyridine (7, 8), 2,2′-biquinoline (9), 2,2′-bi-1,8-naphthyridine (10), 2,2′-biimidazole (4), 2,2′-bithiazole (11), and 2,2′-bibenzimidazole (6).

As an extension of the 2,2′-biimidazolium (4) and 2,2′-bibenzimidazolium (5, 6) studies, the preparation, and spectral and redox properties of more than 20 mono- and bisannulated diquaternary salts of **1**, **2**, 2-(2′-imidazolyl)benzimidazole, **3**, 1,1′-dimethyl-2,2′-biimidazole, **4**, 1,1′-dimethyl-2,2′-bibenzimidazole, **5**, and 1,1′-dimethyl-2-(2′-imidazolyl)benzimidazole, **6**, is now reported. It is hoped that these studies will allow the prediction of the reduction potential for the unknown salt **7** (bis-dimethylene bridged). Table 1 indicates the structures of the diquaternary salts.

Received February 28, 1996.[1]

J.R. Ames,[2] M.A. Houghtaling, D.L. Terrian, and T.P. Mitchell. Department of Chemistry, University of Michigan–Flint, Flint, MI 48502-2186. U.S.A.

[1] Revision received September 30, 1996.

[2] Author to whom correspondence may be addressed. Telephone: 810-762-3275. Fax: 810-766-6693. E-mail: jimames@umich.edu

© 1997 NRC Canada

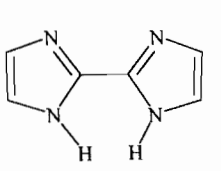
Can. J. Chem. Downloaded from www.nrcresearchpress.com by 92.62.229.171 on 09/08/12
For personal use only.

Results and discussion

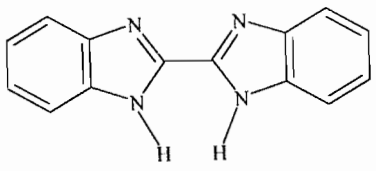
A. Synthesis

Diquaternary salts in this study are prepared by one of two methods (see experimental section). Treatment of the parent azaheterocycle with an excess of 1,*n*-dibromoalkane in refluxing solvent generates the symmetrically bridged bisannulated salts and the monoannulated salts. For example, preparation of compound **7***b* involves the direct treatment of 2,2′-biimidazole with an excess of 1,3-dibromopropane. The yields of these reactions are typically 40–80%. However, the yield of compound **9***a* was only 10%. The corresponding 2,2′-biimidazolium salt is unknown (4) and Hunig et al. (5) have reported a 40% yield of **8***a*. The more facile bridging in the 2-(2′-imidazolyl)benzimidazole and the 2,2′-bibenzimidazole systems is likely due to the increased N1-C2-N3 bond angle resulting from the benzo-ring fusion.

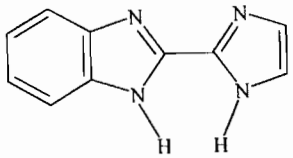
Preparation of the unsymmetrically bridged salts **7***a*, **9***b*, **9***c*, and **9***e* is accomplished by first treating either **1** or **3** with a slight excess of 1-bromo-*n*-chloroalkane to give the bridged species. This is followed by reaction with 1,*n*-dihaloalkane to give the salt.



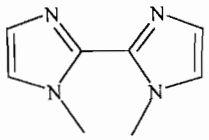
1



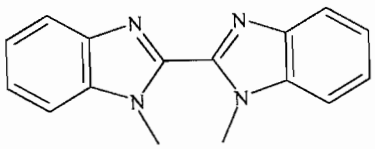
2



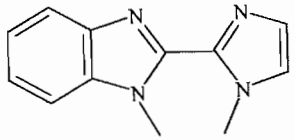
3



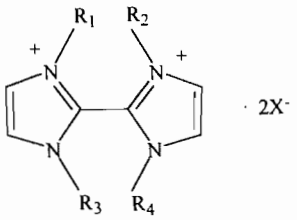
4



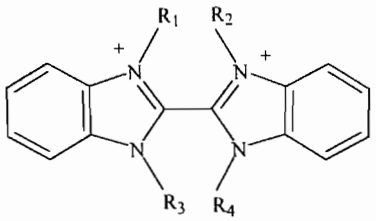
5



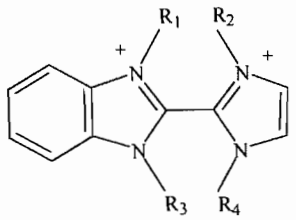
6



7



8



9

B. Spectroscopic properties

Spectroscopic properties and molecular modeling may be used to gain information about the dihedral angle between the rings of bridged azabiaryl compounds. Early work correlated the dihedral angle with the ultraviolet absorption maxima (3). Proton NMR spectra have also been related to the dihedral angle. Vogtle and Brombach (12) studied differences in the chemical shift of H_3 and H_5 of 2,2′-bipyridines, while Font and co-workers (13) and Thummel et al. (4, 7–9, 11, 14) analyzed the conformational mobility of biaryl systems by the coupling constants and the multiplicity of the bridge protons.

Several trends become apparent from the absorbance data given in Tables 2 and 3. First, as the *N,N′* bridges increase, there is a clear hypsochromic shift. In the case of the 1,1′-dimethyl salts the shift is consistently about 20 nm per CH_2 unit. The intensity of these absorptions is less consistent but shows a general trend wherein absorptions for the more planar systems are generally more intense. Both the shifts to higher energy and to lower intensity correspond with decreasing planarity (3).

The absorption maximum value is greatly influenced by the presence of an ethylene bridge. For example, the absorption maximum is 359 nm for **8***a* and **8***d*, near 335 nm for **8***e*, **9***a*, **9***d*, and **9***e*, and 300 nm for **7***a* and **7***d*. The differences in absorption maxima as a result of the parent nucleus, cf., **7***b*, **8***b*, and **9***d*, is expected.

Finally, incorporation of a second bridge imposes added rigidity to the salt. That is, increasing the bridge size from two to three carbon units appears not to greatly alter the dihedral angle as evidenced by the small change in absorption maxima, cf., **8***a* and **8***b*, or **9***a* and **9***d*. The greatest amount of molecular distortion is indicated for the bis(tetramethylene) bridged systems **7***c*, **8***c*, and **9***f*. The change is less for **9***e*; apparently, the trimethylene bridge affects the conformation to some degree. The results from the UV observations reflect a diminished π-delocalization resulting from the concurrent decrease in conjugative interaction between the two aromatic rings as the tethers increase, as expected for twisting about an essentially single bond in a conjugated system.

Supporting information can be obtained by examination of

Can. J. Chem. Downloaded from www.nrcresearchpress.com by 92.62.229.171 on 09/08/12
For personal use only.

© 1997 NRC Canada

Can. J. Chem. Downloaded from www.nrcresearchpress.com by 92.62.229.171 on 09/08/12
For personal use only.

Table 1. Structures of diquaternary salts.

Salt	R_1	R_2	R_3	R_4	X^-
7*a*	CH_2CH_2		$CH_2CH_2CH_2$		Br
7*b*	$CH_2CH_2CH_2$		$CH_2CH_2CH_2$		Br
7*c*	$CH_2CH_2CH_2CH_2$		$CH_2CH_2CH_2CH_2$		Br
7*d*	CH_3	CH_3	CH_2CH_2		Br
7*e*	CH_3	CH_3	$CH_2CH_2CH_2$		Br
7*f*	CH_3	CH_3	$CH_2CH_2CH_2CH_2$		I
8*a*	CH_2CH_2		CH_2CH_2		Br
8*b*	$CH_2CH_2CH_2$		$CH_2CH_2CH_2$		Br
8*c*	$CH_2CH_2CH_2CH_2$		$CH_2CH_2CH_2CH_2$		Br
8*d*	CH_3	CH_3	CH_2CH_2		Br
8*e*	CH_3	CH_3	$CH_2CH_2CH_2$		Br
8*f*	CH_3	CH_3	$CH_2CH_2CH_2CH_2$		Br
9*a*	CH_2CH_2		CH_2CH_2		Br
9*b*	CH_2CH_2		$CH_2CH_2CH_2$		Br
9*c*	CH_2CH_2		$CH_2CH_2CH_2CH_2$		Br
9*d*	$CH_2CH_2CH_2$		$CH_2CH_2CH_2$		Br
9*e*	$CH_2CH_2CH_2$		$CH_2CH_2CH_2CH_2$		Br
9*f*	$CH_2CH_2CH_2CH_2$		$CH_2CH_2CH_2CH_2$		Br
9*g*	CH_3	CH_3	CH_2CH_2		Br
9*h*	CH_3	CH_3	$CH_2CH_2CH_2$		Br
9*i*	CH_3	CH_3	$CH_2CH_2CH_2CH_2$		I

Table 2. Reduction potentials and ultraviolet absorption data for bisannulated diquaternary salts.[a]

	$E_{1/2}$(V)			
Salt	DMF	CH_3CN	$\lambda_{max(nm)}$	log ε
7*a*	−1.15(75), −1.46(ir)	−1.16(80), −1.52(ir)	300	—
7*b*	−1.20(140)	−1.18(90), −1.37(ir)	300	4.23
7*c*	−1.44(ir)	−1.47(ir)[b]	272	4.07
8*a*	−0.56(ir),[c] −1.47(ir)	−0.59(ir)	359	4.23
8*b*	−0.62(70), −0.84(75)	−0.64(70), −0.93(70)	356	4.41
8*c*	−0.81(75), −0.95(80)	−0.77(ir)	326	4.21
9*a*	−0.80(ir)	−0.82(ir)	334	4.13
9*b*	−0.87(70), −1.05(60)	−0.85(75), −1.14(ir)	330	4.27
9*c*	−1.08(105), −1.22(ir)	−1.07(80), −1.30(ir)	306	4.23
9*d*	−0.85(80), −1.15(100)	−0.86(75), −1.26(ir)	337	4.39
9*e*	−0.86(70), −1.20(ir)	−0.86(70), −1.26(ir)	337	4.31
9*f*	−1.03(ir)	−1.02(ir)	320	—

[a]Potentials are given for 0.5 mM solutions with 0.1 M tetraethylammonium perchlorate, recorded at a scan rate of 100 mV/s. The difference between cathodic and anodic peak potentials (mV) is given in parentheses; ir indicates irreversible, and for these systems the potential given is the peak of the cathodic wave.

[b]The value is −1.39 V (ir) in CH_3CN with tetrabutylammonium perchlorate as electrolyte.

[c]Reference 5 questioned the reversibility of the reduction.

the ^1H NMR. In the ethano-bridged salts, the methylene protons in trifluoroacetic acid-*d* appear as singlets in the δ 5.1–5.4 range, indicating that for these quasi-planar systems bridge protons are equivalent. Differences in shielding of the different π-systems is evident. For example, bridge protons in salt **8***b* give a triplet at 5.23 (8H) and a quintet at 3.25 ppm (4H), while salt **9***d* gives triplets at 4.88 and 4.77 (4H each), with a quintet at 2.77 ppm (4H). The two triplets are due to the unsymmetrical shielding effects of the two rings. These results suggest that the structures are conformationally mobile at room temperature on the NMR time scale; the added methylene unit allows for added flexibility. Thummel has reported on

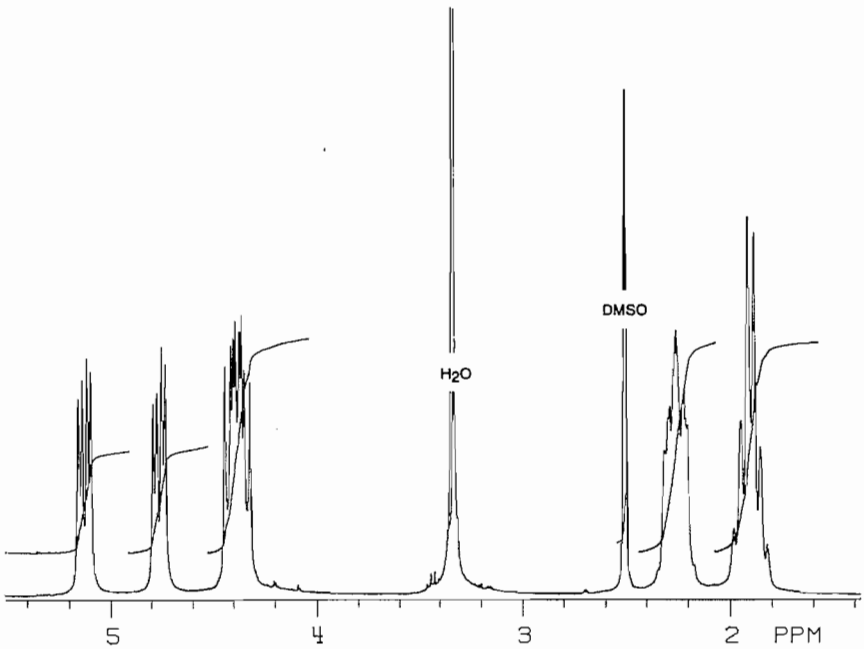
© 1997 NRC Canada

Table 3. Reduction potentials and ultraviolet absorption data for monoannulated diquaternary salts.[a]

Salt	$E_{1/2}$(V) DMF	$E_{1/2}$(V) CH_3CN	$^{\lambda}$max(nm)	log ε
7*d*	−1.18 (ir)	−1.21(ir)	304	4.18
7*e*	−1.32 (140)	−1.31(ir)	283	4.14
7*f*	−1.41 (ir)	−1.44(ir)	265	3.93
8*d*	−0.60 (ir)	−0.62(70), −0.97(ir)	359	—
8*e*	−0.76 (90), −0.82 (80)	−0.76(60), −0.94(ir)	338	4.28
8*f*	−0.87 (110)	−0.86(60), −1.03(70)	320	4.30
9*g*	−0.86 (90), −1.07 (ir)	−0.89(70), −1.10(ir)	333	4.30
9*h*	−1.04 (ir)	−1.00(90)	314	4.28
9*i*	−1.12 (ir)	−1.12(ir)	300	4.27

[a]Potentials are given for 0.5 mM solutions with 0.1 M tetraethylammonium perchlorate, recorded at a scan rate of 100 mV/s. The difference between cathodic and anodic peak potentials (mV) is given in parentheses; ir indicates irreversible, and for these systems the potential is the peak of the cathodic wave.

Fig. 1. 360 MHz ^{1}H NMR spectrum of the upfield region of 1:1′,3:3′-bis(tetramethylene)-2-(2′-imidazolyl)-benzimidazolium dibromide (DMSO-d_6), **9***f*.



the fluxional nature of trimethylene bridged salts of 2,2′-biimidazole (4), 2,2′-bibenzimidazole (6), and bithiazole (11) at room temperature. Conversely, a tetramethylene bridge introduces rigidity on the NMR time scale. Salt **8***c* provides an AA′BB′ pattern centered at 8.21 (8H), two doublet of doublets at 5.16 (4H) and 4.58 (4H), a multiplet at 2.33 (4H), and a quintet at 1.97 (4H). At 360 MHz, salt **9***f* gives well-separated resonances for the bridge protons (Fig. 1). Examination of models shows that some of the geminal α-protons lie more in the plane of the adjacent aromatic ring, accounting for the downfield shift in these salts.

In direct contrast to the bis-bridged salts **8***b* and **9***d*, magnetic nonequivalence for the α-methyl protons is indicated by broad, relatively unresolved peaks in the aliphatic region for the trimethylene bridged salts **7***e*, **8***e*, and **9***h*. Spotswood and Tanzer found evidence for conformational rigidity in di-, tri-, and tetramethylene bridged 3,3′-dimethyl-2,2′-bipyridines, which they attributed to the steric repulsions between the methyl groups (15). Salts **7***f*, **8***f*, and **9***i* all give four poorly resolved peaks for the bridge protons. In addition, there is a shift of about 0.1 ppm upfield per methylene addition for the methyl resonances in the mono-bridged salts. Models indicate that, as the bridges lengthen, the methyl groups point more toward the shielding region of the adjacent ring. Apparently, there is a significant amount of steric repulsion between the methyl groups even with the larger chelation angles present in these salts.

In the ^{13}C NMR, an interesting trend is observed for the C-2 resonance, which shifts steadily to higher field as the length of the N,N′ bridge is increased. The mono-annulated salts will be

© 1997 NRC Canada

Can. J. Chem. Downloaded from www.nrcresearchpress.com by 92.62.229.171 on 09/08/12
For personal use only.

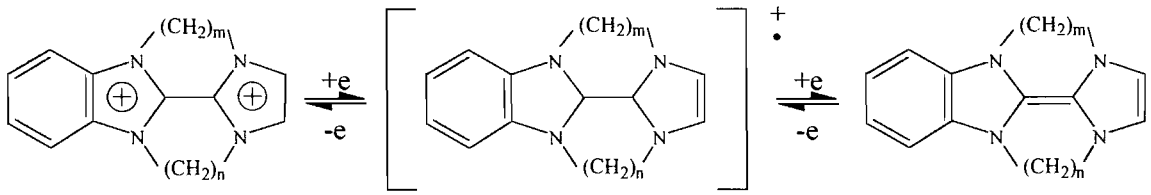
discussed first. The resonances change from 128.5 ppm (**7***d*) to 125.6 (**7***f*); 132.4, 128.3 (**9***g*) to 130.1, 125.7 (**9***i*); and 134.5 (**8***d*) to 130.3 (**8***f*). A similar trend is observed for the bisannulated salts where $n \geq 3$. For example, 129.0 ppm (**7***b*) to 125.8 (**7***c*); 133.6 (**8***b*) to 130.7 (**8***c*); and 133.8, 128.9 (**9***d*) to 130.6, 126.2 (**9***f*). Interestingly, the values for **8***a* (131.2 ppm) and **9***a* (131.8, 128.3) are between those for the corresponding $n = 3$ and $n = 4$ salts. This is possibly due to the strain on the molecule imposed by such short *N,N′* bridges. The general implication of the C-2 results is that positive charge density at this carbon is decreasing as the delocalization becomes inhibited by nonplanarity.

C. Redox properties

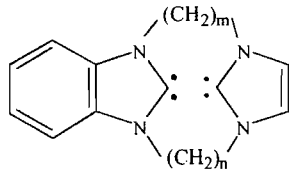
The ability of diquaternary salts of azabiaryl systems to undergo two one-electron reductions has been extensively studied (3–5, 7, 11, 16). Electron uptake depends on the electrophilicity of the material being reduced and the stability of the generated species (3, 17).

The salts in this study are capable of undergoing the same type of redox chemistry, as illustrated in **9** →**11** →**12**. For the intermediate radical cations (**11**) to be the most stable, delocalization over the entire aromatic framework should be possible.

The reduction potentials for all salts, determined in dimethylformamide and acetonitrile, are reported in Tables 2



9 **11** **12**



13

and 3. Representative voltammograms are presented in Figs. 2 and 3. The slight differences between the reduction values for **7***a–c* in this study and a previous one (see Table 2 and ref. 4) are due to differences in the conditions under which they were collected. The reduction properties for salt **7***c* become identical if our electrolyte system is changed to the previously reported system in CH_3CN.

The first obvious trend is the shift to more negative potentials as the bridges lengthen. Furthermore, with the exception of **7***d–f* and the most highly strained salts, the reductions (in CH_3CN) also become more irreversible. The least planar systems, e.g., **7***c*, **9***f*, and **9***i*, all show a single irreversible wave.

Secondly, as with the NMR data, a larger dihedral angle for the 1,1′-dimethyl salts is implied by comparing the reduction potentials of these salts to the corresponding bisannulated salts. The reduction potentials of salts **7***d*, **8***d*, and **9***g* are nearly identical to the bisannulated salts with one more methylene unit in the *N,N′* bridge, i.e., **7***b*, **8***b*, and **9***d*, respectively.

The irreversible nature of many of the reductions in this study implies that the species formed upon reduction undergoes some other process faster than it can be oxidized back to the original salt. The typical processes that might interfere with reoxidation include a conformational change, a subsequent chemical reaction, or adsorption of the reduced species onto the electrode surface. The formation of species such as **11** and **12** may involve a conformational change as a discrete step that occurs after electron transfer. Normally the energy barrier for this process is low enough that it does not interfere with the reversibility of the electron transfer. However, for systems such as **7***c*, **8***c*, and **9***e*, we know from the NMR studies that the barrier has become large enough that its importance cannot be ignored. Furthermore, an appreciable barrier is evident in the methyl-containing salts that accounts for the decreased reversibility of the reductions in the mono-bridged salts. The nature of the reductions of salts **8***a* and **9***a* may be explained by the strain put on the systems by the short bridges. Perhaps reduction is accompanied by a chemical change. Thummel has recently discussed possible *bis*-carbene formation (similar to **13**) for bisbenzimidazole, **8***b* and *c* (18), and bisimidazole, **7***c* and $R_{1\text{-}4} = CH_3$, (19). The bridges may impose steric and conformational effects restraining dimerization. Furthermore, it has been noted that radical cations formed from reduction of bridged 2-(2′-pyridyl)quinolinium salts (20) and bridged 2,2′-bithiazolium salts (11) could not always be completely oxidized (chemically or electrochemically) back to the parent.

Finally, it is noteworthy that the reduction potentials for salts **9***d*, and **9***f–i* are nearly intermediate between those of the corresponding structures, which predict potentials of −0.91 V

Can. J. Chem. Downloaded from www.nrcresearchpress.com by 92.62.229.171 on 09/08/12
For personal use only.

© 1997 NRC Canada

Can. J. Chem. Downloaded from www.nrcresearchpress.com by 92.62.229.171 on 09/08/12
For personal use only.

Fig. 2. Cyclic voltammograms of 0.5 mM solutions of salts **9***b* (top), **9***d* (middle), and **9***f* (bottom) in dimethylformamide at a scan rate of 100 mV/s.

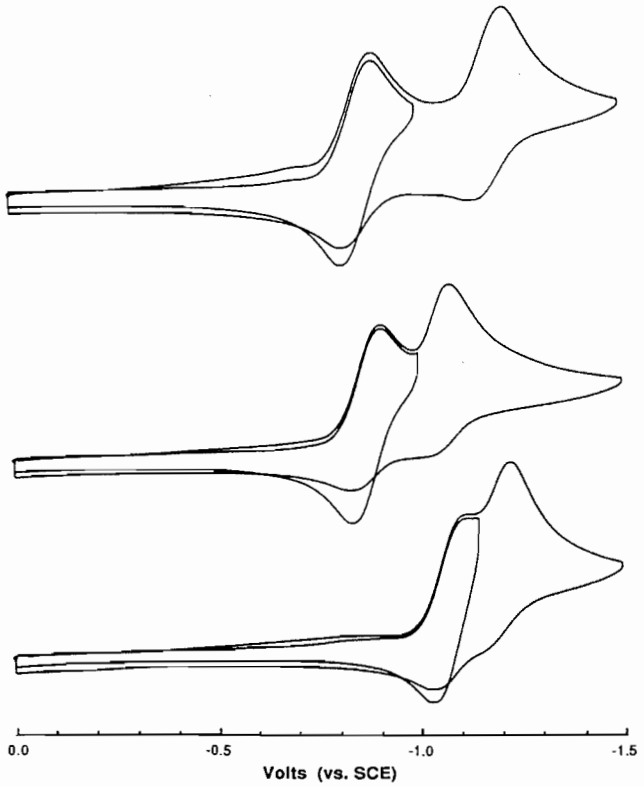
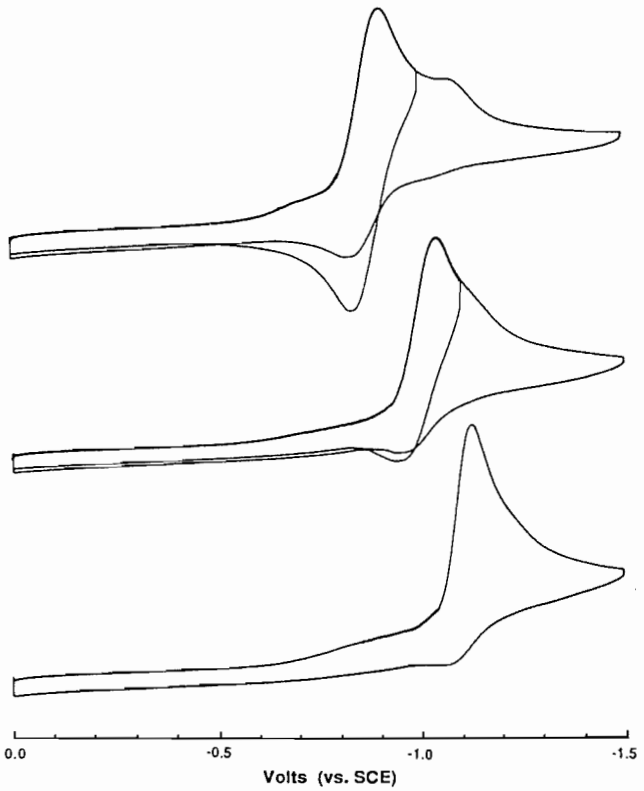


Fig. 3. Cyclic voltammograms of 0.5 mM solutions of salts **9***g* (top), **9***h* (middle) and **9***i* (bottom) in CH_3CN of a scan rate of 100 mV/s.



for **9***d*, −1.12 V for **9***f*, −0.90 V for **9***g*, −1.04 V for **9***h*, and −1.14 V for **9***i*. Therefore, the incorporation of the fused electron-attracting benzo substituent in these compounds has an additive effect of about 0.3 V, which is similar to the value found when comparing methylene-bridged 2,2′-bipyridinium and 2-(2′-pyridyl)quinolinium salts (20). Subtracting 0.3 V from the reduction value for **9***a* leads to a predicted reduction potential of about −1.1 V for the hypothetical salt **7** (bis-dimethylene bridged). Further support for this value comes from the examination of the differences in reduction potentials for salts **8** and **9**, when the bridge size decreases from three to two. There is, on average, about a 70 mV change in the positive direction as the methylene bridges contract. Decreasing the value for **7***b* by the same amount would lead to the predicted reduction potential.

Experimental

2,2′-Biimidazole, **1**, 2,2′-bibenzimidazole, **2** (5, 21), 2-(2′-imidazolyl)benzimidazole, **3** (22), 1,1′-dimethyl-2,2′-biimidazole, **4** (23), 1,1′-dimethyl-2,2′-bibenzimidazole, **6** (24), and **8***a*, **8***b* (5), **8***d* (24), and **7***a* (4) were prepared according to literature procedures. Salts **7***b*, **7***c*, and **8***c* were synthesized by modifications to the literature (4, 6) methods. Ultraviolet spectra were obtained, in EtOH, on a Milton Roy Spectronic 3000 spectrophotometer. All solvents were reagent grade, and all melting points are uncorrected. Details of the electrochemical experiments are given elsewhere (25, 26). Half-wave potentials were calculated as the average of the cathodic and anodic peak potentials (27). Microanalyses were performed by Desert Analytics, Tucson, Ariz. Nuclear magnetic resonance spectra were generally recorded on a JEOL FX-90Q spectrometer: ^1H (90 MHz) (CF_3CO_2D or DMSO-d_6); ^{13}C (20 MHz) (D_2O with dioxane as reference). The 360 MHz NMR spectra were collected by Spectral Data Services, Inc., Champaign, Ill.

1,1′-Dimethyl-2-(2′-imidazolyl)benzimidazole (6)

To a refluxing solution of 3 g (0.016 mol) of 2-(2′-imidazolyl)benzimidazole, 45 mL of absolute ethanol, and 20 mL of 20% NaOH, 7.7 g (0.081 mol) of dimethyl sulfate was added dropwise. The solution was refluxed for 14 h. After cooling, filtering, and neutralizing with HCl, it was evaporated to dryness. The resulting solid was then dissolved in 35 mL of water and extracted with 150 mL of chloroform. The chloroform extracts were washed with 8% NaOH to remove any monomethylated product. The $CHCl_3$ layer was dried over anhydrous sodium sulfate and evaporated to dryness. The resulting thick yellow liquid, which solidified on standing, was chromatographed (alumina) with $CHCl_3$. Evaporation of the solvent gave 1.6 g (47%) of a yellow solid. ^1H NMR (CF_3CO_2D) δ: 7.99 (s, 6H), 4.29 (s, 3H), 4.24 (s, 3H). ^{13}C NMR (22.5 MHz, $CHCl_3$-*d*) δ: 32.1, 35.7, 109.7, 119.7, 122.4, 123.2, 123.8, 128.5, 135.9, 138.1, 142.4.

1,1′-Dimethyl-3,3′-(dimethylene)-2,2′-biimidazolium dibromide (7*d*)

1,1′-Dimethylbiimidazole (0.15 g, 0.92 mmol) was refluxed in 8.8 g (0.047 mol) of 1,2-dibromoethane for 24 h to yield 0.30 g

© 1997 NRC Canada

Can. J. Chem. Downloaded from www.nrcresearchpress.com by 92.62.229.171 on 09/08/12
For personal use only.

(94%) of crude product. The product was recrystallized from EtOH (95%); mp 288°C. ^{1}H NMR (CF_3CO_2D) δ: 7.83 (AA′BB′, 4H), 5.07 (s, 4H), 4.47 (s, 6H). ^{13}C NMR (D_2O, dioxane) δ: 39.2, 45.4, 124.8, 127.5, 128.5. Anal. calcd. for $C_{10}H_{14}N_4Br_2$: C 34.31, H 4.03, N 16.00; found: C 34.17, H 3.98, N 15.91.

1,1′-Dimethyl-3,3′-(trimethylene)-2,2′-biimidazolium dibromide (*7e*)

1,1′-Dimethyl-2,2′-biimidazole (0.21 g, 1.3 mmol) and 12.1 g (60 mmol) of 1,3-dibromopropane were refluxed in 5 mL of 2-methoxyethanol for 18 h. The solution was cooled and 10 mL of ether was added to afford 0.20 g (43%) of the product. Recrystallization from ethanol (95%) – ether gave a material with mp 241°C (dec.). ^{1}H NMR (CF_3CO_2D) δ: 7.99 (AA′BB′, 4H), 4.78 (bm, 4H), 4.36 (s, 6H), 2.95 (m, 2H). ^{13}C NMR (D_2O, dioxane) δ: 29.8, 37.5, 46.3, 126.8, 127.5. Anal. calcd. for $C_{22}H_{16}N_4Br_2 \cdot H_2O$: C 35.41, H 4.86, N 15.02; found: C 35.20, H 4.59, N 14.92.

1,1′-Dimethyl-3,3′-(tetramethylene)-2,2′-biimidazolium diiodide (*7f*)

1,1′-Dimethyl-2,2′-biimidazole (0.24 g, 1.45 mmol) and 4.13 g (1.33 mmol) of 1,4-diiodobutane were heated at 125°C in 1 mL of 2-methoxyethanol for 4 h. The solution was cooled and 10 mL of ether was added to afford 0.41 g (59%) of the product. Recrystallization from ethanol gave a material with mp 252°C (dec.). ^{1}H NMR (CF_3CO_2D) δ: 8.00 (s, 4H), 4.79 (m, 2H), 4.45 (m, 2H), 4.28 (s, 6H), 2.29 (bm, 4H). ^{13}C NMR (D_2O, dioxane) δ: 27.1, 36.9, 50.4, 125.6, 127.0, 128.4. Anal. calcd. for $C_{12}H_{18}N_4I_2$: C 30.53, H 3.84, N 11.87; found: C 30.71, H 3.80, N 11.96.

1,1′-Dimethyl-3,3′-(dimethylene)-2,2′-bibenzimidazolium Dibromide (*8d*)

The method of Rochling was used to prepare this material, mp 280°C (lit. (14) mp 275–277°C). ^{1}H NMR (CF_3CO_2D) δ: 8.02 (s, 8H), 5.44 (s, 4H), 4.74 (s, 6H). ^{13}C NMR (D_2O, dioxane) δ: 36.4, 42.6, 113.6, 114.1, 130.0, 130.1, 131.3, 133.9, 134.5.

1,1′-Dimethyl-3,3′-(trimethylene)-2,2′-bibenzimidazolium Dibromide (*8e*)

1,1′-Dimethyl-2,2′-bibenzimidazole (0.68 g, 2.6 mmol) and 6.25 g (30.9 mmol) of 1,3-dibromopropane was refluxed in 1.5 mL of 2-methoxyethanol for 20 h. After cooling, 10 mL of ethyl ether was added and the solution was filtered and washed with ice-cold ethanol. Recrystallization from ethanol (95%) yielded 0.41 g (34%) of an off-white material; mp 266–270°C (dec.). ^{1}H NMR (CF_3CO_2D) δ: 8.04 (s, 8H), 5.16 (m, 2H), 4.88 (m, 2H), 4.61 (s, 6H), 3.14 (m, 2H); (DMSO-d_6) δ: 8.46 (m, 4H), 8.03 (m, 4H), 5.43 (m, 2H), 4.69 (m, 2H), 3.34 (s, H_2O), 2.84 (m, 2H). ^{13}C NMR (D_2O, dioxane) δ: 29.5, 35.0, 43.1, 113.4, 114.1, 129.8, 129.9, 132.0, 132.4, 133.6. Anal. calcd. for $C_{19}H_{20}N_4Br_2 \cdot \frac{1}{2}H_2O$: C 48.22, H 4.47, N 11.84; found: C 47.96; H 4.51, N 11.78.

1,1′-Dimethyl-3,3′-(tetramethylene)-2,2′-bibenzimidazolium dibromide (*8f*)

A procedure similar to that for **8***e* was used. Recrystallization from ethanol (95%) yielded 0.26 g (40%) of an off-white material; mp 217–221°C (dec.). ^{1}H NMR (CF_3CO_2D) δ: 8.08 (s, 8H), 5.51–5.00 (bm, 2H), 4.94–4.60 (bm, 2H), 4.53 (s, 6H), 2.48 (bm, 4H); (DMSO-d_6) δ: 8.43 (m, 4H), 8.03 (m, 4H), 5.22 (m, 2H), 4.55 (m, 2H), 3.48 (s, H_2O), 2.25 (m, 2H), 2.01 (m, 2H). ^{13}C NMR (D_2O, dioxane) δ: 25.7, 34.2, 47.1, 113.7, 114.2, 129.9, 130.3, 132.5, 133.8. Anal. calcd. for $C_{20}H_{22}N_4Br_2 \cdot \frac{1}{2}H_2O$: C 49.29, H 4.76, N 11.49; found: C 49.32; H 4.91, N 11.32.

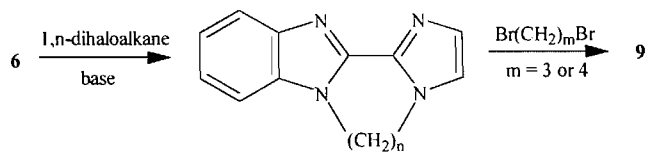
1,1′:3,3′-Bis(dimethylene)-2-(2′-imidazolyl)-benzimidazolium dibromide (*9a*)

Method A

2-(2′-Imidazolyl)benzimidazole (0.5 g, 2.7 mmol), 1.0 g (7.8 mmol) of *N,N′*-diisopropylethylamine, and 21.98 g (0.117 mol) of 1,2-dibromoethane were heated at reflux in 12 mL of 2-methoxyethanol for 48 h. After cooling, the cream solid 0.11 g (10%) was filtered and recrystallized from EtOH (95%) – MeOH (1:1); mp 330°C (dec.). ^{1}H NMR (CF_3CO_2D) δ: 7.92 (s, 6H), 5.39 (s, 4H); (200 MHz, DMSO-d_6) δ: 8.29 (s, 2H), 7.83–8.26 (AA′BB′ centered at 8.04, 4H), 5.06–5.19 (m, 8H), 3.33 (s, H_2O). ^{13}C NMR (D_2O, dioxane) δ: 44.4, 46.6, 114.3, 126.0, 128.3, 129.1, 131.8, 132.3. Anal. calcd. for $C_{14}H_{14}N_4Br_2$: C 42.24, H 3.54, N 14.07; found: C 41.91; H 3.57, N 13.75.

Method B

10*a* (0.05 g, 0.24 mmol) was refluxed with stirring in 3 mL (34 mmol) of 1,2-dibromoethane for 4 h. After cooling, filtration, and recrystallization from EtOH (95%) – MeOH, the material (52%) had identical properties as that prepared by Method A.



10
a = 2
b = 3

1,1′-(Dimethylene)-3,3′-(trimethylene)-2-(2′-imidazolyl)-benzimidazolium dibromide (*9b*)

Method A

A mixture of 0.05 g (0.24 mmol) of **10***a* and 2 mL (20 mmol) of 1,3-dibromopropane was heated at 167°C for 4 h. After cooling, filtering, and recrystallization from EtOH (95%) – MeOH (1:1), the product yield was 0.05 g (51.0%). The melting point of the purified product was 361°C (dec.). ^{1}H NMR (360 MHz, DMSO-d_6) δ: 8.32 (m, 2H), 8.29–7.82 (AA′BB′ centered at 8.05, 4H), 5.08 (m, 2H), 4.96 (m, 4H), 4.82 (m, 2H), 3.33 (s, H_2O), 2.61 (quintet, 2H). ^{13}C NMR (D_2O, dioxane) δ: 36.2, 39.6, 42.5, 45.7, 113.4, 113.9, 126.0, 128.3, 128.8, 129.4, 129.6, 130.9, 132.4, 133.3. Anal. calcd. for $C_{15}H_{16}N_4Br_2 \cdot H_2O$: C 41.88, H 4.21, N 13.03; found: C 42.13, H 3.94, N 12.75.

Method B

Similarly 0.035 g (0.16 mmol) of **10***b* and 3 mL (34 mmol) of 1,2-dibromoethane were stirred at reflux for 4 h. The product, 0.057 g (88%), had a melting point of 360°C after recrystallization from EtOH (95%) – MeOH (1:1).

© 1997 NRC Canada

Can. J. Chem. Downloaded from www.nrcresearchpress.com by 92.62.229.171 on 09/08/12
For personal use only.

1,1′-(Dimethylene)-3,3′-(tetramethylene)-2-(2′-imidazolyl)benzimidazolium dibromide (9*c*)

Via the procedure described above for **9***b*, 0.05 g (0.24 mmol) of **10***a* and 3 mL (25 mmol) of 1,4-dibromobutane were used to obtain 0.06 g (59.4%) of product. After recrystallization from ethanol (95%), the melting point was 285–287°C. ^{1}H NMR (200 MHz, DMSO-d_6) δ: 8.35 (s, 2H), 8.29–7.86 (AA′BB′, centered at 8.08, 4H), 4.82–5.08 (m, 8H), 3.32 (s, H_2O), 2.29 (m, 4H). ^{13}C NMR (D_2O, dioxane) δ: 29.6, 34.7, 37.9, 42.7, 46.7, 113.2, 113.9, 127.6, 128.3, 129.3, 129.5, 132.0, 132.2, 133.2. Anal. calcd. for $C_{16}H_{18}N_4Br_2 \cdot H_2O$: C 43.26, H 4.53, N 12.61; found: C 42.90, H 4.58, N 12.31.

1,1′:3,3′-Bis(trimethylene)-2-(2′-imidazolyl)-benzimidazolium dibromide (9*d*)

Method A

Via the procedure described for **9***a*, 0.5 g (2.7 mmol) of 2-(2′-imidazolyl)benzimidazole, 1.0 g of *N,N*′-diisopropylethylamine, and 23.7 g (0.18 mol) of 1,3-dibromopropane gave a cream product in 90% yield. The material was recrystallized from EtOH (95%) – MeOH; mp 334–335°C. ^{1}H NMR (360 MHz, DMSO-d_6) δ: 8.33 (s, 2H), 8.31–7.87 (AA′BB′ centered at 8.10, 4H), 4.88 (t, 4H), 4.77 (t, 4H), 3.32 (s, H_2O), 2.77 (quintet, 4H). ^{13}C NMR (D_2O, dioxane) δ: 26.0, 47.1, 50.1, 113.5, 127.6, 128.9, 129.4, 132.5, 133.8. Anal. calcd. for $C_{16}H_{18}N_4Br_2 \cdot H_2O$: C 43.26, H 4.53, N 12.61; found: C 43.06, H 4.26, N 12.43.

Method B

A mixture 0.05 g (0.22 mmol) of **10***b* and 2 mL (20 mmol) of 1,3-dibromopropane was heated at 167°C for 4 h. After cooling and filtering, 0.08 g (84.2%) of product was obtained and recrystallized from EtOH (95%) to give an identical melting point with that prepared by Method A.

1,1′-(Trimethylene)-3,3′-(tetramethylene)-2-(2′-imidazolyl)benzimidazolium dibromide (9*e*)

Via the procedure described for **9***d*, 0.05 g (0.22 mmol) of **10***b* and 3 mL (25 mmol) of 1,4-dibromobutane were used to obtain 0.05 g (51.0%) of product. After recrystallization from 2-propanol, the melting point was 265°C. ^{1}H NMR (60 MHz, DMSO-d_6) δ: 8.6–8.3 (m, 4H), 8.2–7.7 (m, 2H), 4.85 (m, 8H), 3.63 (s, H_2O), 2.95 (m, 2H), 2.25 (m, 4H). ^{13}C NMR (D_2O, dioxane) δ: 25.7, 27.0, 34.1, 37.3, 47.0, 50.7, 113.6, 114.1, 125.8, 127.7, 128.9, 129.7, 130.1, 132.2, 133.6. Anal. calcd. for $C_{17}H_{20}N_4Br_2 \cdot 2H_2O$: C 42.87, H 5.07, N 11.76; found: C 42.94, H 4.92, N 11.64.

1,1′:3,3′-Bis(tetramethylene)-2-(2′-imidazolyl)-benzimidazolium dibromide (9*f*)

Compound **3** (0.5 g, 2.7 mmol), 1.0 g of *N,N*′-diisopropylethylamine, and 25.3 g (0.12 mol) of 1,4-dibromobutane were heated under reflux in 15 mL of 2-methoxyethanol for 48 h. Filtration yielded 85% of an off-white product that was recrystallized from EtOH (95%) – MeOH (mp 283°C (dec.)). ^{1}H NMR (360 MHz, DMSO-d_6) δ: 8.47 (s, 2H), 8.41–7.91 (AA′BB′ centered at 8.15, 4H), 5.12 (dd, 2H), 4.76 (dd, 2H), 4.38 (m, 4H), 3.33 (s, H_2O), 1.90 (m, 4H). ^{13}C NMR (D_2O, dioxane) δ: 29.6, 30.6, 42.9, 46.9, 47.6, 50.9, 113.2, 113.6, 127.5, 127.7, 129.3, 129.4, 132.2, 132.3, 132.6. Anal. calcd. for $C_{18}H_{22}N_4Br_2 \cdot H_2O$: C 44.09, H 5.35, N 11.42; found: C 43.74, H 5.39, N 11.31.

1,1′-Dimethyl-3,3′-(dimethylene)-2-(2′-imidazolyl)-benzimidazolium dibromide (9*g*)

A similar procedure to that for **8***e* was used. Recrystallization from ethanol (95%) yielded 0.37 g (56%) of a light yellow material; mp 322–325°C (dec.). ^{1}H NMR (CF_3CO_2D) δ: 7.96 (m, 6H), 5.25 (s, 4H), 4.63 (s, 3H), 4.58 (s, 3H). ^{13}C NMR (D_2O, dioxane) δ: 36.1, 39.6, 42.4, 45.6, 113.3, 113.8, 125.9, 128.3, 128.8, 129.4, 129.5, 130.9, 132.4, 133.3. Anal. calcd. for $C_{14}H_{16}N_4Br_2$: C 42.02, H 4.03, N 14.00; found: C 42.12, H 4.03, N 14.04.

1,1′-Dimethyl-3,3′-(trimethylene)-2-(2′-imidazolyl)-benzimidazolium dibromide (9*h*)

A similar procedure to that for **8***e* was used. Recrystallization from ethanol (95%) yielded 0.48 g (48%) of an off-white material; mp 220°C (dec.). ^{1}H NMR (CF_3CO_2D) δ: 8.00 (m, 6H), 5.18–4.71 (bm, 4H), 4.53 (s, 3H), 4.46 (s, 3H), 3.07 (m, 2H). ^{13}C NMR (D_2O, dioxane) δ: 29.6, 34.7, 37.9, 42.7, 46.7, 113.2, 113.9, 127.6, 128.3, 129.3, 129.5, 132.0, 132.2, 133.2. Anal. calcd. for $C_{15}H_{18}N_4Br_2 \cdot H_2O$: C 41.69, H 4.66, N 12.96; found: C 41.37, H 4.31, N 12.83.

1,1′-Dimethyl-3,3′-(tetramethylene)-2-(2′-imidazolyl)-benzimidazolium diiodide (9*i*)

A procedure similar to that for **7***f* yielded 0.42 g (55%) of product from 0.31 g (1.45 mmol) of 1,1′-dimethyl-2,2′-biimidazole and 4.53 (1.46 mmol) of 1,4-diiodobutane. Recrystallization from ethanol (95%) gave a material with mp 257°C (dec.). ^{1}H NMR (CF_3CO_2D) δ: 8.00 (m, 6H), 5.05 (m, 2H), 4.65 (m, 2H), 4.46 (s, 3H), 4.36 (s, 3H), 2.35 (bm, 4H). ^{13}C NMR (D_2O, dioxane) δ: 25.7, 26.9, 34.1, 37.3, 46.9, 50.6, 113.5, 114.1, 125.7, 127.6, 128.9, 129.6, 130.1, 132.2, 133.6. Anal. calcd. for $C_{16}H_{20}N_4I_2 \cdot H_2O$: C 36.80, H 3.86, N 10.73; found: C 37.08, H 3.90, N 10.74.

1,1′-Dimethylene-2-(2′-imidazolyl)benzimidazole (10*a*)

To a well stirred solution of 1.0 g (5.4 mmol) of **3** and 13 mL of DMF, 1.0 mL of 35% NaOH was added. After stirring for 2 h, 1.5 g (10.5 mmol) of 1-bromo-2-chloroethane was slowly added to the reaction mixture, which was then stirred overnight. The reaction mixture was vacuum filtered and the solid was washed with ethanol. The filtrate was evaporated to dryness under vacuum and the residue was washed with hot acetonitrile. The acetonitrile was evaporated and the residue recrystallized from EtOH to yield 0.11 g (9.7%) of creamy yellow crystals, mp 255–257°C. ^{1}H NMR (200 MHz, DMSO-d_6) δ: 7.1–7.7 (m, 6H), 4.59 (s, 4H). Anal. calcd. for $C_{12}H_{10}N_4$: C 68.55, H 4.79, N 26.65; found: C 68.42, H 4.74, N 26.81.

1,1′-Trimethylene-2-(2′-imidazolyl)benzimidazole (10*b*)

Compound **3** (1.0 g, 5.4 mmol) and 0.59 g (11 mmol) of $NaOCH_3$ were refluxed in 50 mL of absolute EtOH, with a drying tube, for 1 h with stirring followed by the dropwise addition of 1-bromo-3-chloropropane (10.5 mmol). After an additional 20 h of refluxing, the mixture was cooled, filtered, and the filtercake was extracted with EtOH. The ethanol filtrate was evaporated to dryness and extracted with boiling

© 1997 NRC Canada

CH_3CN. The acetonitrile was evaporated to dryness to yield a residue of 0.20 g (17%), which was recrystallized from EtOH–H_2O; mp 187–200°C. ^1H NMR (200 MHz, DMSO-d_6) δ: 7.1–7.7 (m, 6H), 4.35–4.46 (m, 6H), 2.47 (quintet, 2H). Anal. calcd. for $C_{13}H_{12}N_4$: C 69.62, H 5.39, N 24.98; found: C 69.22, H 5.25, N 25.20.

Acknowledgments

This project was supported in part by grants from the Faculty Research Grant/Fellowship Program and the Faculty Development Fund of the University of Michigan–Flint. We thank Robert M. Smith, Bobbi Beckers, Vicki H. Larsen, Christopher Houston, and Timothy Lauer for experimental assistance.

References

1. G.H. Beaven and E.A. Johnson. J. Chem. Soc. 651 (1957).
2. K. Mislow, M.A.W. Glass, H.B. Hopps, E. Simon, and G.H. Wall. J. Am. Chem. Soc. **86**, 1710 (1964).
3. R.F. Homer and T.E. Tomlinson. J. Chem. Soc. 2498 (1960).
4. R.P. Thummel, V. Goulle, and B. Chen. J. Org. Chem. **54**, 3057 (1989).
5. S. Hunig, D. Scheutzow, and H. Schlaf. Liebigs Ann. Chem. **765**, 126 (1972).
6. Z. Shi and R.P. Thummel. J. Org. Chem. **60**, 5935 (1995).
7. R.P. Thummel, F. Lefoulon, and R. Mahadevan. J. Org. Chem. **50**, 3824 (1985).
8. R.P. Thummel, F. Lefoulon, S. Chirayil, and V. Goulle. J. Org. Chem. **53**, 4745 (1988).
9. R.P. Thummel and F. Lefoulon. J. Org. Chem. **50**, 666 (1985).
10. R.P. Thummel, F. Lefoulon, D. Cantu, and R. Mahadevan. J. Org. Chem. **49**, 2208 (1984).
11. V. Goulle, S. Chirayil, and R.P. Thummel. Tetrahedron Lett. **31**, 1539 (1990).
12. F. Votgtle and D. Brombach. Chem. Ber. **108**, 1682 (1975).
13. C. Campa, J. Camps, J. Font, and P. de March. J. Org. Chem. **52**, 521 (1987).
14. R.P. Thummel, Y. Decloitre, and F. Lefoulon. J. Heterocycl. Chem. **23**, 689 (1986).
15. T. McL. Spotswood and C.I. Tanzer. Aust. J. Chem. **20**, 1213 (1967).
16. S. Hünig and H. Bernneth. Top. Curr. Chem. **92**, 1 (1980).
17. V.P. Kadysh, Y.P. Stradyn, E.S. Lavrinovich, and P.P. Zarin. Chem. Heterocycl. Cmpd. **11**, 588 (1975).
18. Z. Shi and R.P. Thummel. Tetrahedron Lett. **36**, 2741 (1995).
19. Z. Shi and R.P. Thummel. Tetrahedron Lett. **37**, 2357 (1996).
20. A.L. Black and L.A. Summers. J. Chem. Soc. (C), 2271 (1971).
21. G. Holan, E.L. Samuel, B.C. Ennis, and R.W. Hinde. J. Chem. Soc. (C), 20 (1967).
22. B.C. Ennis, G. Holan, and E.L. Samuel. J. Chem. Soc. (C), 33 (1967).
23. P. Melloni, E. Dradi, and W. Logemann. J. Med. Chem. **15**, 926 (1972).
24. H. Rochling. Z. Naturforsch. B: Anorg. chem. Org. Chem. Biochem. Biophys. Biol. **25B**, 931 (1970).
25. J.R. Ames. J. Pharmaceut. Sci. **80**, 293 (1991).
26. J.R. Ames, M.A. Houghtaling, and D.L. Terrian. Electrochim. Acta, **37**, 1433 (1992).
27. A.J. Bard and L.R. Faulkner. *In* Electrochemical methods. Wiley, New York. 1980. p. 227.

Can. J. Chem. Downloaded from www.nrcresearchpress.com by 92.62.229.171 on 09/08/12
For personal use only.

© 1997 NRC Canada

Rhenium(V) complexes with benzimidazole (BzimH) and crystal structure of the hemiprotonated compound $[ReO_2(BzimH)_4][ReO(OH)(BzimH)_4](ReO_4)_3$

Suzanne Bélanger, Sébastien Fortin, and André L. Beauchamp

Can. J. Chem. Downloaded from www.nrcresearchpress.com by 92.62.229.171 on 09/08/12
For personal use only.

Abstract: *trans*-$[ReO_2(BzimH)_4]I$ is generated by reacting $ReO_2I(PPh_3)_2$ with excess BzimH in methanol, but free ligand is difficult to eliminate from the product. Pure samples of the *trans*-$[ReO_2(BzimH)_4]BPh_4$ salt and of the protonated oxo-hydroxo form $[ReO(OH)(BzimH)_4](BF_4)_2$ are isolated. Recrystallization of the dioxo complex in acetone–ether yields a pink solid. Red crystals suitable for X-ray diffraction are obtained by recrystallization of this solid in ethanol. The crystallographic study reveals a hemiprotonated $[ReO_2(BzimH)_4][ReO(OH)(BzimH)_4](ReO_4)_3$ phase (*Acam*, $a = 10.794$, $b = 21.520$, $c = 27.196$ Å, $R = 0.049$). The O═Re═O fragments are parallel to one another along the unit cell *c* axis, forming layers of dimeric units consisting of one dioxo and one oxo-hydroxo species connected by a very short O—H···O hydrogen bond of 2.44 Å. The ReO_4^- anions form hydrogen bonds with ligand N-H groups. The complexes are characterized by solution (^1H and ^{13}C) and solid-state (^{13}C CP-MAS) NMR, UV–VIS, and IR spectroscopies. ^1H NMR reveals that the benzimidazole protons in close proximity to the rhenium–oxo multiple bond or adjacent benzimidazole ligands are very sensitive to nonbonded magnetic effects.

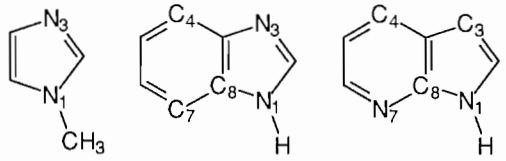
Key words: rhenium, oxo complexes, benzimidazole, X-ray diffraction.

Résumé : Le complexe *trans*-$[ReO_2(BzimH)_4]I$ est obtenu par réaction de $ReO_2I(PPh_3)_2$ avec un excès de BzimH dans le méthanol, mais le ligand libre est difficile à éliminer du produit. Des échantillons purs du sel *trans*-$[ReO_2(BzimH)_4]BPh_4$ et de la forme protonée oxo-hydroxo $[ReO(OH)(BzimH)_4](BF_4)_2$ ont été isolés. La recrystallization du complexe dioxo dans un mélange acetone–éther conduit à un solide rose. Des cristaux rouges sont isolés par recristallisation de cet échantillon dans l'éthanol et leur étude par diffraction des rayons X révèle une phase mixte stoechiométrique $[ReO_2(BzimH)_4][ReO(OH)(BzimH)_4](ReO_4)_3$ (*Acam*, $a = 10{,}794$, $b = 21{,}520$, $c = 27{,}196$ Å, $R = 0{,}049$). Les fragments O═Re═O sont orientés parallèlement les uns aux autres selon l'axe *c* de la maille, où ils forment des couches de motifs dimères comprenant un cation dioxo et un cation oxo-hydroxo reliés par une liaison hydrogène O—H···O très courte de 2,44 Å. Les anions ReO_4^- forment des liaisons hydrogène avec les groupes N-H des ligands. Les composés préparés sont caractérisés par spectroscopies RMN en solution (^1H et ^{13}C) et à l'état solide (^{13}C CP-MAS), UV–visible et infrarouge. La RMN ^1H indique que les protons du benzimidazole se trouvant à proximité du lien multiple rhenium–oxo ou des ligands benzimidazole voisins sont très sensibles aux effets magnétiques à travers l'espace.

Mots clés : rhénium, complexes oxo, benzimidazole, diffraction des rayons X.

Introduction

Rhenium(V) oxo complexes with imidazoles and related nitrogen heterocyclic ligands are currently being investigated in this laboratory. These compounds are of interest not only for their particular optical properties (1), but also because various compounds containing Re═O and Re≡N groups are being considered for potential applications of radioactive Re isotopes in radiopharmacy (2). In general, $[ReO_2L_4]^+$ is readily generated by reacting excess ligand with $ReO_2I(PPh_3)_2$ or $ReOCl_3(PPh_3)_2$, but stability problems are often encountered with the compounds once isolated. Complexes of pyridines and imidazoles as chloride salts tend to decompose slowly (3, 4). Although stable complexes of imidazoles were obtained as iodides and tetraphenylborates (5), we recently found that controlled decomposition of the 1-methylimidazole (**1**, 1-MeIm) complex *trans*-$[ReO_2(1\text{-MeIm})_4]^+$ in low pH aqueous solution generates an unusual oxo-bridged trinuclear complex (6). In less acidic media, when air is not excluded, oxidation occurs at some point, generating ReO_4^- ions. The latter process undoubtedly produces H^+, since some protonated $[ReO(OH)L_4]^{2+}$ complex is formed, as observed in the non-stoichiometric 1,2-dimethylimidazole $[ReO_2(1,2\text{-}Me_2Im)_4]^+$/$[ReO(OH)(1,2\text{-}Me_2Im)_4]^{2+}$ phase (3).



1 **2** **3**

With the goal of identifying factors affecting these processes, our work on imidazoles was extended to rigid and ster-

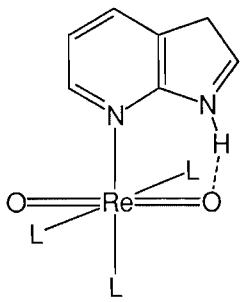
Received July 30, 1996.

S. Bélanger, S. Fortin, and A.L. Beauchamp.[1] Département de Chimie, Université de Montréal, Montréal, QC H3C 3J7, Canada.

[1] Author to whom correspondence may be addressed. Telephone: (514) 343-6446. Fax: (514) 343-7586. E-mail: beauchmp@ere.umontreal.ca

© 1997 NRC Canada

ically more demanding ligands. In a previous study (7), the reactivity 7-azaindole (**3**, Haza) was investigated. Coordination was found to take place via the pyridine ring (N7) and the crystal structure of $[ReO_2(Haza)_4]Cl$ showed an all-upright conformation stabilized by N1—H···oxo intramolecular hydrogen bonding (**4**).



4

The present work deals with benzimidazole (**2**, BzimH), a ligand with a similar steric demand, which was expected to lead to conformational differences, since the hydrogen-bonding five-membred ring of azaindole is replaced by a hydrophobic benzene ring in benzimidazole. As anticipated, a compound similar to $[ReO_2(Haza)_4]^+$ could be obtained, but it showed an unusually high preference to form a *stoichiometric* $[ReO_2L_4]^+/[ReO(OH)L_4]^{2+}$ phase. The preparation and protonation of *trans*-$[ReO_2(BzimH)_4]^+$ are described in the present paper.

Experimental

Reactants and methods

Reactants and solvents (reagent grade) from Aldrich, except for HI (Anachemia), HBF_4, and $NaBF_4$ (Johnson-Matthey), were used as received. $ReO_2I(PPh_3)_2$ was prepared from $KReO_4$ according to literature (8, 9). IR spectra were recorded as CsI pellets on a 1750 Perkin–Elmer Fourier-transform spectrophotometer. Routine solution ^1H and ^{13}C NMR spectra were run on either a Varian VXR-300 or a Bruker AMX-300 spectrometer. Solid-state ^{13}C CP-MAS spectra were obtained at 75.43 MHz on the Varian instrument. The (^1H–^1H) COSY spectra were recorded on a Bruker ARX-400 spectrometer. Chemical shifts are expressed in ppm relative to TMS. The residual CD_3OD signal was used as internal reference for solution spectra (^1H, δ 3.30; ^{13}C, δ 49.0 ppm). The aromatic signal of hexamethylbenzene (δ = 132.1 ppm) was used as an external reference for the solid-state ^{13}C NMR experiments. Electronic spectra were recorded on a UV–VIS/NIR Varian/Cary-5E spectrophotometer.

Preparative work

$[ReO_2(BzimH)_4]I$

Samples free of uncoordinated BzimH could not be obtained, since attempts to remove excess BzimH inevitably yielded a partially protonated material. A typical run is described here.

Under argon, methanol is added to $ReO_2I(PPh_3)_2$ (2.15 g; 2.27 mmol) and benzimidazole (1.65 g; 15.3 mmol), and the mixture is stirred at room temperature. All the solid dissolves and a brown solution is obtained within minutes. The mixture is allowed to react for 60–70 min, after which time toluene (80 mL) is added and the solution is evaporated under reduced pressure until all the complex has come out of solution as a sticky brick-red material. Toluene is decanted and acetone (20 mL) is added. A brownish-red suspension is obtained in which about half of the original material has dissolved. The mixture is filtered and a first crop (0.58 g) of solid is isolated and washed with ether. Its composition roughly corresponds to $[ReO_2(BzimH)_4]I{\cdot}2BzimH$ as determined from ^1H NMR. Whether it is a mixture of $[ReO_2(BzimH)_4]I$ and BzimH, or a stoichiometric phase containing uncoordinated lattice BzimH molecules was not checked. To the filtrate, excess ether is added until no more precipitate forms. The peach solid is filtered and washed with ether (yield: 1.43 g). On the basis of elemental analysis, the sample contains ~30% of protonated complex whose charge is balanced by ReO_4^- counterions. IR (cm^{-1}): 792 (s), ν_{as}(O═Re═O); ~920 (w), $\nu_{as}(ReO_4^-)$/ν(Re═O) of O═Re-OH. ^{13}C CP-MAS (ppm): ~142 (sh, C2), 140.6 (C9), 133.1 (C8), 123.8 (C5/C6), 117.6 (C4), 113.5 (C7). Anal. calcd. for $C_{28}H_{27.3}N_8O_2I(ReO_4)_{0.3}{\cdot}0.5\ (CH_3)_2CO$: C 38.43, H 2.98, N 12.15; found: C 38.26, H 2.88, N 12.13.

UV–VIS and solution NMR data were obtained after adding 0.5 equivalent of CH_3ONa to the half-protonated compound described below, to make sure that any $[ReO(OH)(BzimH)_4]^{2+}$ species is converted back to $[ReO_2(BzimH)_4]^+$. UV–VIS (CH_3OH): 472 nm (ε = 681 M^{-1} cm^{-1}), ~570 nm (sh) (ε = ~139 M^{-1} cm^{-1}). ^1H NMR (CD_3OD) (ppm): 8.27 (s, H2), 7.63 (d, H4), 7.57 (d, H7), 7.29 (t, H6), 7.02 (t, H5), ($^3J_{45}$ = $^3J_{67}$ = 8.3 Hz, $^3J_{56}$ = ~8 Hz). ^{13}C NMR (CD_3OD) (ppm): 146.2 (C2), 141.9 (C9), 134.2 (C8), 125.7 (C6), 124.8 (C5), 119.0 (C4), 113.9 (C7).

$[ReO_2(BzimH)_4]/[ReO(OH)(BzimH)_4](I)_3{\cdot}2H_2O$

The dioxo species is generated as above with 60 min reaction time, up to obtention of the oily residue, which is precipitated in this case by addition of ether. To recrystallize the sample from acetone, large quantities of solvent are required and subsequent addition of excess ether affords a fine pink solid. The suspension is allowed to crystallize overnight and the resulting pink sample is filtered and washed with ether. Elemental analysis reveals a hemiprotonated complex containing two crystallization water molecules. Yield based on $ReO_2I(PPh_3)_2$: 0.55 g, 59%. IR (cm^{-1}): 795 (m), ν_{as} (O═Re═O); 920 (m, br), ν(Re═O). UV–VIS (CH_3OH): 472 nm (ε = 592 M^{-1} cm^{-1}). ^1H NMR (CD_3OD) (ppm): 8.27 (s, H2), 7.58 (d, br, superimposed H4/H7), 7.30 (t, H6), 7.03 (t, H5), ($^3J_{45}$ = $^3J_{67}$ = 8.7 Hz, $^3J_{56}$ = ~8 Hz). ^{13}C NMR (CD_3OD) not significantly different from above, because the ^{13}C spectra of all forms reported here are quite similar and because the protonated form may be partly dissociated. ^{13}C CP-MAS (ppm): ~142 (C2), 140.8 (C9), 132.7 (C8), 123.5 (C5/C6), 117.9 (C4), 114.1 (C7). Anal. calcd. for $C_{56}H_{53}N_{16}O_6I_3Re_2$: C 37.38, H 2.97, N 12.46; found: C 37.32, H 2.91, N 12.16.

Slow recrystallization of the pink sample in ethanol gave red crystals of the stoichiometric mixed phase $[ReO_2(BzimH)_4][ReO(OH)(BzimH)_4](ReO_4)_3$, which were used for X-ray work (see below). IR (cm^{-1}): 792 (m), ν_{as} (O═Re═O); 918 (s)/925 (sh), $\nu_{as}(ReO_4^-)$/ν(Re═O) of O═Re-OH.

Can. J. Chem. Downloaded from www.nrcresearchpress.com by 92.62.229.171 on 09/08/12
For personal use only.

© 1997 NRC Canada

Can. J. Chem. Downloaded from www.nrcresearchpress.com by 92.62.229.171 on 09/08/12
For personal use only.

$[ReO_2(BzimH)_4]BPh_4$

The reaction is effected with a 1:6 $ReO_2I(PPh_3)_2$:benzimidazole ratio in methanol at room temperature for 1 h. To the orange-brown solution, $NaBPh_4$ (2 equiv.) in methanol is added dropwise. The resulting solution is stirred for a few minutes and evaporated to dryness. Dissolution in methanol and partial evaporation of the solvent affords an orange solution and a beige residue (PPh_3 and excess $NaBPh_4$), which is removed by filtration. The orange solution is evaporated and the dioxo complex is isolated as a sticky brown residue. Addition of ether gives a brick-brown solid, which is filtered and washed with ether. Yield: 0.35 g; 60%. IR (cm^{-1}): 792 (s), ν_{as} (O═Re═O). ^1H NMR (CD_3OD) (ppm): 8.25 (s, H2), 7.65 (d, H4), 7.54 (d, H7), ~7.3 (H6, interference with BPh_4^-), 7.02 (t, H5), ($^3J_{45} = {}^3J_{67} = 8.4$ Hz, $^3J_{56} = \sim 7.5$ Hz), ~7.3 (m, BPh_4^-), 6.94 (t, 7.4 Hz, BPh_4^-), 6.79 (t, 7.3 Hz, BPh_4^-). ^{13}C CP-MAS (ppm): ~142 (C2), 140.3 (C9/BPh_4^-), 133.1 (C8/BPh_4^-), ~128 (sh) (BPh_4^-), 124.1 (C5/C6), 118.2 (C4), 116.9 (C7).

$[ReO(OH)(BzimH)_4](BF_4)_2 \cdot 0.5\ (CH_3)_2CO$

One drop of concentrated HBF_4 is added to $[ReO_2(BzimH)_4]I$ (0.362 g, 0.443 mmol) dissolved in a minimum volume (2–3 mL) of methanol. To the purple solution, $NaBF_4$ (0.194 g, 1.76 mmol) in methanol is added with stirring. Addition of ether to the solution initiates the precipitation of a lavender powder, which is filtered. The sample contains excess $NaBF_4$ and is purified by stirring in aqueous HBF_4 (pH ~1) for a few minutes. The lavender compound is filtered and washed with ether after recrystallization in acetone–ether to remove water. Yield: 0.22 g, 56%. IR (cm^{-1}): 931, ν (Re═O). UV–VIS (CH_3OH): 535 nm ($\varepsilon = 526\ M^{-1}\ cm^{-1}$). ^1H NMR (CD_3OD) (ppm): 8.20 (s, H2), 7.65 (t, H7), 7.38 (d, H4), 7.37 (t, H6), 7.10 (t, H5), ($^3J_{45} = {}^3J_{67} = 8.3$ Hz, $^3J_{56} = \sim 7.5$ Hz). ^{13}C CP-MAS (ppm): ~140 (C9), ~133 (C8), 123.8 (C6), 122.6 (C5), 115.8 (C4), 113.5 (C7), C2 not observed. Anal. calcd. for $C_{29.5}H_{28}B_2F_8N_8O_{2.5}Re$: C 39.24, H 3.12, N 12.42; found: C 39.33, H 2.69, N 12.50.

Table 1. Crystallographic data for $[ReO_2(BzimH)_4][ReO(OH)(BzimH)_4](ReO_4)_3$.

Formula	$C_{56}H_{49}N_{16}O_{16}Re_5$
Formula weight	1066.58
Cell system	Orthorhombic
Space group	*Acam*
a, Å	10.794(3)
b, Å	21.520(6)
c, Å	27.196(14)
V, Å^3	6317(4)
Z	4
T, K	220
Radiation	Cu Kα
λ, Å	1.54056
μ, mm^{-1}	18.22
D_{calcd}, g cm^{-1}	2.243
Crystal size, mm (faces)	0.038 {001}
	0.137 {010}
	0.593 {100}
Transmission range	0.05-0.53
Scan	ω/2θ
$2\theta_{max}$, deg	140
Standards (number, fluctuation)	4, ±4.8%
No. of unique reflections	3073
No. of observed reflections	1915
R_{av}	0.078
Rejection criterion, $I/\sigma(I)$	< 2.0
Refinement method	Full-matrix on F^2
No. of parameters varied	221
No. of restraints	10
R^a	0.049
$wR2^a$	0.113
Goodness-of-fit on F^2, S^a	0.865

$^aR = \Sigma(\|F_o| - |F_c\|)/\Sigma(|F_o|)$; $wR2 = [\Sigma[w(F_o^2-F_c^2)^2]/\Sigma[w(F_o^2)^2]]^{1/2}$; $S = [\Sigma[w(F_o^2-F_c^2)^2]/(\text{no. of reflns} - \text{no. of params})]^{1/2}$.

Crystallographic measurement and structure resolution

Experimental data collection details are collected in Table 1. X-ray work was carried out on an Enraf–Nonius CAD-4 diffractometer (graphite-monochromatized CuKα radiation). The reduced cell was determined from a rotation picture and checked with axial photographs. An *A*-centred orthorhombic cell was indicated from the Niggli matrix and *mmm* Laue symmetry was verified on a limited set of data. The orthorhombic cell was refined with 25 reflections ($22.5° < \theta < 25°$). Systematic absences (*hkl k+l* odd; *0kl k,l* odd; *h0l h,l* odd) indicated *Aba*2 (no. 41) or *Acam* (no. 64) as possible space groups. Intensities were collected in the entire sphere and averaged to one octant (*hkl*) at this stage. These data were corrected for the effects of Lorentz, polarization, and absorption (Gaussian integration).

The crystal structure was solved in the *Acam* space group, which is an alternate definition of *Cmca* (16-fold general equipoint of *Acam*: x,y,z; $x+1/2,-y+1/2,-z$; $-x+1/2,y+1/2,-z$; $-x,-y,z$; $-x,-y,-z$; $-x+1/2,y+1/2,z$; $x+1/2,-y+1/2,z$; $x,y,-z$, and corresponding sites translated by 0,1/2,1/2). The stoichiometry is unambiguously determined from the crystal structure. The rhenium atoms were located from the Patterson map and all non-hydrogen atoms from difference Fourier maps. The $ReO_2(BzimH)_4$ unit is found to lie on a crystallographic twofold axis (Re1, O1, and O2 on equipoint *8d*) and contains two independent benzimidazole ligands in general positions. ReO_4^- ions are present on two different sites. One of them occupies a mirror plane: Re3, O301, and O302 on equipoint *8f*, O303 in general position. For the second ReO_4^- anion, the Re2 atom is also found on equipoint *8f*, equally disordered over two sites near, but not exactly on, equipoint *4b* (*2/m* symmetry). In addition, this anion shows orientational disorder about the twofold axis, so that each oxygen atom (general position) has an occupancy of 0.25. Therefore, the unit cell contains 1.5 ReO_4^- ion per $ReO_2(BzimH)_4$ unit, indicating that only half of these units are $[ReO_2(BzimH)_4]^+$, the other half having been protonated to $[ReO(OH)(BzimH)_4]^{2+}$. A packing pattern reveals that two such units are facing each other across the origin with an O···O separation of 2.44 Å indicative of O═Re-O-H···O═Re═O hydrogen bonding. All $ReO_2(BzimH)_4$ units being symmetry equivalent, "O═Re-O-H···O═Re═O" and "O═Re═O···H-O-Re═O" pairings are equally probable, so that each pair of hydrogen-bonded ions is involved in twofold disorder. However, this does not introduce appreciable disorder in most of the atomic positions.

© 1997 NRC Canada

Can. J. Chem. Downloaded from www.nrcresearchpress.com by 92.62.229.171 on 09/08/12
For personal use only.

Table 2. Atomic coordinates and equivalent isotropic displacement parameters ($Å^2$, $\times 10^2$) for $[ReO_2(BzimH)_4][ReO(OH)(BzimH)_4](ReO_4)_3$.

Atom	x	y	z	U_{eq}[a]
Re1	0.0000	0.0000	0.11107(2)	3.58(2)
O1	0.0000	0.0000	0.1730(4)	4.3(2)
O2	0.0000	0.0000	0.0448(4)	4.9(3)
N11	0.2661(10)	0.1390(4)	0.0787(5)	5.0(3)
C21	0.1632(12)	0.1062(5)	0.0743(4)	4.7(3)
N31	0.1485(9)	0.0644(4)	0.1086(3)	3.8(2)
C41	0.2850(13)	0.0389(6)	0.1810(5)	6.0(4)
C51	0.396(2)	0.0581(7)	0.2027(5)	7.5(5)
C61	0.4698(14)	0.1050(8)	0.1834(6)	7.5(5)
C71	0.4366(14)	0.1356(6)	0.1424(5)	5.5(3)
C81	0.3265(12)	0.1172(5)	0.1203(4)	4.4(3)
C91	0.2530(10)	0.0696(5)	0.1389(4)	3.8(3)
N12	–0.2770(10)	0.1347(5)	0.0818(5)	5.3(3)
C22	–0.2151(11)	0.0819(6)	0.0755(4)	4.8(3)
N32	–0.1255(8)	0.0749(4)	0.1086(3)	3.8(2)
C42	–0.0686(14)	0.1430(6)	0.1798(5)	5.7(4)
C52	–0.101(2)	0.1983(6)	0.2025(5)	7.4(5)
C62	–0.194(2)	0.2356(6)	0.1835(6)	7.6(5)
C72	–0.2643(14)	0.2209(6)	0.1450(5)	5.8(4)
C82	–0.2313(12)	0.1648(6)	0.1222(5)	4.7(3)
C92	–0.1355(12)	0.1272(5)	0.1390(4)	4.0(3)
Re2[b]	0.4937(3)	0.02299(9)	0.0000	8.46(7)
O201[b]	0.344(2)	0.0157(11)	0.005(2)	6.6(9)
O202[b]	0.538(2)	0.1000(10)	0.002(3)	6.7(8)
O203[b]	0.591(3)	–0.0193(14)	0.0277(11)	7.3[c]
O204[b]	0.517(5)	0.007(3)	–0.0661(9)	8.7(13)
Re3	0.46404(7)	0.25579(4)	0.0000	4.36(2)
O301	0.4605(14)	0.3351(6)	0.0000	7.4(4)
O302	0.3187(12)	0.2302(6)	0.0000	6.7(4)
O303	0.5395(9)	0.2297(4)	0.0516(3)	7.6(3)

[a] $U_{eq} = (1/3)\Sigma_i\Sigma_j U_{ij} a^*_i a^*_j \boldsymbol{a}_i \cdot \boldsymbol{a}_j$.
[b] Occupancy factor: Re2, 0.5; O201–O204, 0.25.
[c] Refined isotropically with constrained $U_{iso} = [U_{eq}(O201)+U_{eq}(O202)+U_{eq}(O204)]/3$.

Both perrhenate ions were described with an idealized tetrahedral geometry. The Re—O distances were constrained to be equal, but allowed to refine with a common bond length. To maintain tetrahedral geometry, a similar constraint was applied to the O—O distances. Hydrogen atoms of benzimidazole were calculated at idealized positions (N—H = 0.87 Å, C—H = 0.94 Å) using a riding model. The isotropic displacement factors were adjusted to a value 20% higher than that of the bonded atom. All non-hydrogen atoms were refined anisotropically, except for the oxo ligands, for which only isotropic refinement was suitable, since their positions in O═Re═O and H-O-Re═O groups apparently differ appreciably. The disordered perrhenate oxygens were refined isotropically. O203 was assigned a fixed isotropic thermal parameter, because of its proximity to the symmetry-generated Re2 atom. The position of the "half-proton" involved in the Re-O-H···O hydrogen bond was not determined with certainty: the ΔF map showed a residual at the origin and this proton was arbitrarily fixed at this position (U_{iso} fixed at 0.05 $Å^2$). The final ΔF map contains a residual of 3.8 e $Å^{-3}$ near the disordered Re2 atom, a few more of |1.4–0.9| e $Å^{-3}$ near Re or disordered O atoms, whereas the general background is below ±0.8 e $Å^{-3}$. Refined coordinates are listed in Table 2.[2] All calculations were done using NRCVAX (10), SHELXS-86 (11), and SHELXL-93 (12).

The structure was also interpreted in terms of the corresponding non-centric *Aba2* space group (no. 41) after averag-

[2] The supplementary material includes distances and angles in the ligand and perrhenate anions, hydrogen atom coordinates, anisotropic displacement factors, and distances to the weighted least-squares planes. The complete set of data (6 pages) can be purchased from: The Depository of Unpublished Data, Document Delivery, CISTI, National Research Council Canada, Ottawa, Canada ON K1A 0S2. The lists of coordinates and of distances and angles have also been deposited with the Cambridge Crystallographic Data Centre. The can be obtained from The Director, Cambridge Crystallographic Data Centre, University Chemical Laboratory, 12 Union Road, Cambridge, CB2 1EZ, U.K. A table of observed and calculated structure factors (13 pages) can be obtained from the corresponding author.

© 1997 NRC Canada

Can. J. Chem. Downloaded from www.nrcresearchpress.com by 92.62.229.171 on 09/08/12
For personal use only.

ing the data set to octants *hkl* and *hkl̄*: refinement was very unstable, disorder on the ReO_4^- ions was not removed, and the *R* factor was not improved. Other space groups in which one set of glide planes is removed were also considered. Replacing either glide plane by a mirror would generate superimposed non-coincident images of the benzimidazole ligands: since no disorder or abnormal thermal motion was noted in this part of the structure for the *Acam* model, these possibilities were discarded. The two remaining groups, namely $A2_1am$ (no. 36) and *Ac2m* (no. 39), in which the glide planes are replaced by two-fold axes, were tested. Again, refinement was extremely unstable and the ReO_4^- ions remained disordered. Thus, the *Acam* solution was retained.

Results

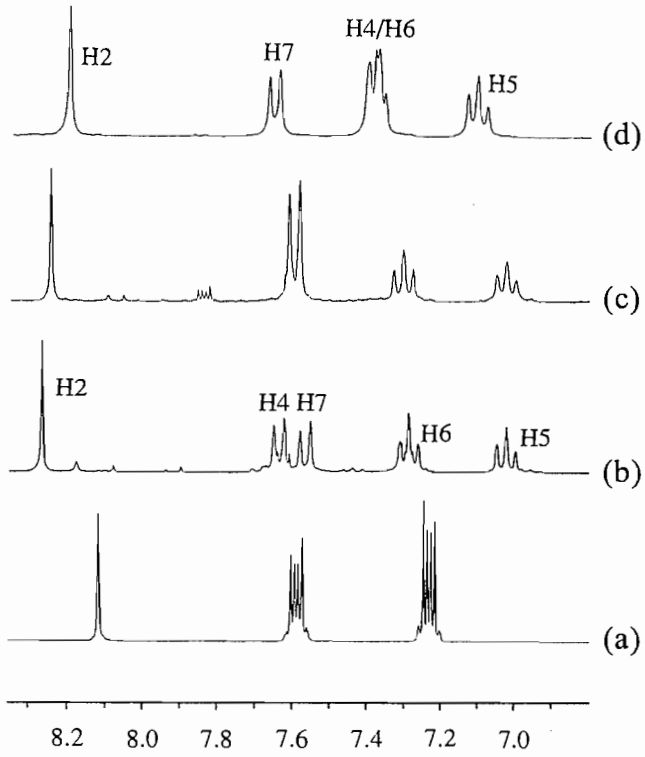
trans-$[ReO_2(BzimH)_4]I$ is formed by reacting BzimH with $ReO_2I(PPh_3)_2$ as described for imidazoles (5), but pure samples of this iodide salt cannot be isolated: reacting a stoichiometric amount or slight excess of ligand gives incomplete conversion, whereas large excess leaves large amounts of unreacted BzimH difficult to separate. The typical case described in the experimental section yields a sample containing two BzimH molecules per complex. When attempting to purify the sample by recrystallization in acetone–ether, the solution quickly turns pink and yields a protonated material, whose elemental analysis reveals an exactly hemiprotonated form of the complex. Recrystallization of this pink compound in ethanol gives red crystals, whose structure determined by X-ray diffraction shows a stoichiometric mixed phase $[ReO_2(BzimH)_4]^+/[ReO(OH)(BzimH)_4]^{2+}$ with perrhenate counterions. $[ReO_2(BzimH)_4]^+$ can be isolated as the BPh_4^- salt and the fully protonated complex as $[ReO(OH)(BzimH)_4](BF_4)_2$.

Infrared spectroscopy

The dominant spectral feature is the rhenium–oxygen stretching band. The asymmetric O═Re═O stretch in $[ReO_2(BzimH)_4]I$ is observed at 795 cm^{-1}, which compares well with related imidazole and other nitrogen–ligand systems (765–825 cm^{-1}) (5). In the hemiprotonated sample obtained after recrystallization from acetone, partial protonation of the oxo ligand is apparent, since the ν_{as}(O═Re═O) band loses intensity, while a new band arising from the protonated oxo group is found near 920 cm^{-1}. In the completely protonated compound, the ν(Re═O) frequency is located at 931 cm^{-1}. This mode has been observed in the 955–973 cm^{-1} range for related oxo-hydroxo and oxo-methoxo systems (5, 13–15).

The IR spectrum of benzimidazole undergoes several modifications upon coordination. The tentative assignments used here are based on the literature spectrum of the free ligand (16). Besides the disappearance of combination bands at 1700–2000 cm^{-1}, coordination introduces noticeable effects in various spectral regions. Near 1600 cm^{-1}, the benzimidazole C═C stretching band at 1588 cm^{-1} moves to 1602 cm^{-1} and loses intensity. The most obvious changes occur in the 1400–1500 cm^{-1} region, where benzimidazole shows ν(C═C) bands at 1410, 1459, and 1478 cm^{-1}. In the coordinated ligand, the lowest frequency mode is split in two components at 1425/1440 cm^{-1}, the vibration at 1459 cm^{-1} loses much intensity, whereas the most intense vibration in this region is found at 1510 cm^{-1}. Complexation also results in reduced intensity for other vibration modes, such as ν(C-N) at 1350 and 1370 cm^{-1}, δ(C-H) at 1135 and 1205 cm^{-1}, ν(C═C) at 1276 cm^{-1}, and γ(C-H) at 885 cm^{-1}.

Fig. 1. ^1H NMR spectra (CD_3OD) of (*a*) free benzimidazole, (*b*) $[ReO_2(BzimH)_4]^+$, (*c*) $[ReO_2(BzimH)_4]^+/[ReO(OH)(BzimH)_4]^{2+}$, and (*d*) $[ReO(OH)(BzimH)_4]^{2+}$.



NMR spectroscopy

The ^1H NMR spectrum of free benzimidazole in D_2O has been previously reported (17), but assignments differ from those adopted here for CD_3OD solution, which are made by comparison with 1-methylbenzimidazole (18, 19). Only three C-H signals are found because of fast tautomeric exchange of the N-H proton between the two N sites (Fig. 1*a*). H2 appears as a singlet at 8.12 ppm. We attribute the multiplet centred at 7.59 ppm to H4/H7 and the multiplet at 7.23 ppm to H5/H6 ($^3J_{45} = {}^3J_{67} = 8.1$, $^3J_{56} = 6.9$, $^4J_{46} = {}^4J_{57} = 1.1$ Hz) (see **2** for ring numbering). The coupling constants for this AA′XX′ spectrum were calculated as described by Sohár (20), assuming $^5J_{47} = 0$. The following data have been reported for 1-methylbenzimidazole in acetone–water: 8.19 (H2), 7.75 (H4), 7.58 (H7), 7.32 (H5), and 7.36 (H6) with the same coupling constants (19). Our interpretation is consistent with these results, since the chemical shifts for H5/H6 and H4/H7 are close to the mean values for the corresponding protons in 1-methylbenzimidazole (19).

Monodentate coordination of benzimidazole to the metal centre removes tautomerism. Hence, five distinct signals appear in the ^1H NMR spectrum of $[ReO_2(BzimH)_4]^+$ (Fig. 1*b*): two pseudo-triplets (H5 and H6) at high field, one singlet (H2) at low field, and two intermediate doublets (H4 and H7). From signal multiplicity, H4 and H7 can be unambiguously

© 1997 NRC Canada

Fig. 2. ORTEP drawing of the $ReO_2(BzimH)_4$ unit showing the numbering scheme. The Re–O bonds lie along a crystallographic twofold axis. Ellipsoids are drawn at a 50% probability level. Hydrogens are omitted.

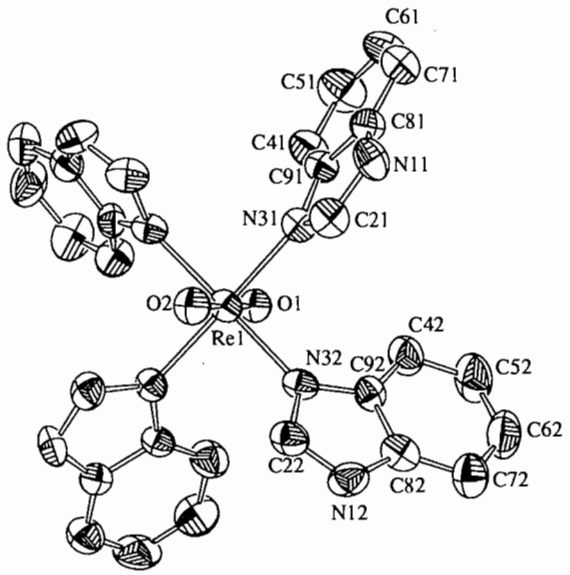
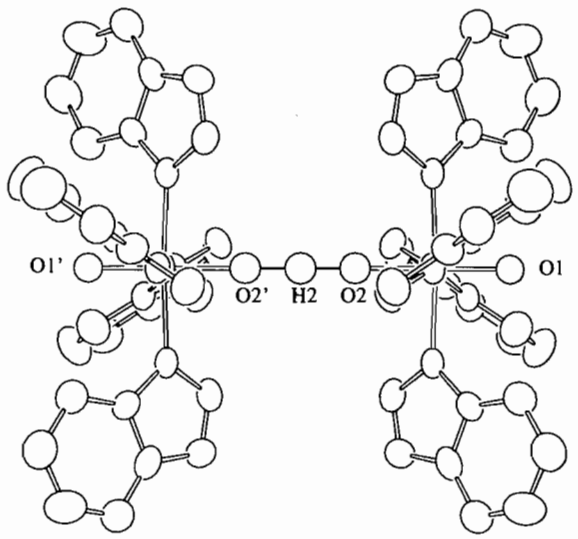


Fig. 3. Representation of the dimeric hemiprotonated $[ReO_2(BzimH)_4]^+/[ReO(OH)(BzimH)_4]^{2+}$ ion pair showing the short O2–O2′ contact along *c* and the orientation of the benzimidazole ligand relative to the Re–O bonds. The O-Re-O unit lies on a crystallographic twofold axis and the O—H···O proton was fixed at the origin (2/*m* site symmetry).



differentiated from H5 and H6. Identification of the next neighbour(s) of each proton is made from a ^1H–^1H COSY experiment. Final assignment is based on the safe assumption that H7 occurs upfield from H4: this trend is followed by free 1-methylated benzimidazoles (18, 19, 21), as well as Ni (22), Co (21), and Ru complexes (23). This is consistent with the relative insensitivity of H7 to its environment, as expected from its being remote from the coordination centre. Alessio et al. (23) have recently described a detailed NMR study on conformationally rigid Ru complexes with 1,5,6-trimethylbenzimidazole and found that, regardless of the conformation, the chemical shift of H7 remains in a narrow range. This gives further support to our assignments, since the doublet assigned to H7 (7.54–7.65 ppm) is much less affected by the protonation state than the other (7.38–7.63 ppm) assigned to H4 (Fig. 1*b*–*d*). The signals in the complexes being broader than in the free ligand, the ^4J couplings (~1 Hz) were rarely resolved. The observed ^3J coupling constants (7–9 Hz) are similar to those of free benzimidazole.

The spectra obtained with $[ReO_2(BzimH)_4][ReO(OH)(BzimH)_4](I)_3$ and $[ReO(OH)(BzimH)_4](BF_4)_2$ are given in Fig. 1(*c*, *d*). In the former case, a single set of averaged signals is observed as expected for a fast exchange between the two forms. Since protonation of the oxo group increases the positive charge at the Re centre, all signals should be shifted downfield. This is indeed what happens when 1-methylbenzimidazole is N3-methylated to generate the N1,N3-dimethylbenzimidazolium cation (24). For the Re complex, downfield shifts of ~0.08 are actually observed on H5, H6, and H7, but H2 and H4 move *upfield* by 0.07 and 0.25 ppm, respectively. The opposite displacement observed for the inner protons H2 and H4 indicates particular sensitivity to the environment in the complex, probably originating from anisotropic effects. With the ligand orientation observed in the crystal structure (Figs. 2 and 3), anisotropy from the Re═O multiple bond is likely felt by H2 and H4. At the same time, these protons can be influenced by the anisotropy of the adjacent benzimidazole ligands and, considering the recent detailed analysis of Alessio et al. (23) on Ru complexes with 1,5,6-trimethylbenzimidazole, this effect is very sensitive to conformation. Protonation is known to introduce significant structural modifications in the coordination sphere: bond orders change in the $[O{=}Re{=}O]^+$ unit and the four Re—N bonds are displaced 4°–5° away from the $[O{=}Re\text{-}OH]^{2+}$ multiple bond (see Crystal structure below). Unpredictable changes in the orientation of the benzimidazole ligands can also take place. In related imidazole systems (5), protonation has been found to shift H2 downfield by ~0.2 ppm, which is opposite to what is observed here for this proton. The much higher upfield shift on H4 could be explained by its greater distance from the Re—N bond: a small rotation about the Re—N bond produces large displacements for this remote proton, thereby changing considerably its position relative to the groups responsible for anisotropy.

Our ^{13}C NMR data for free benzimidazole in CD_3OD (141.5 (C2), 137.9 (C8/C9), 122.9 (C5/C6), 115.4 ppm (C4/C7)) compare well with those previously reported in D_2O (25). A solid-state spectrum was recorded in order to remove averaging due to fast tautomeric N–H exchange and obtain distinct chemical shifts for C4/C7 and C5/C6: 142.6 (C2), 141.0 (C9), 135.8 (C8), 132.4 (C6), 121.7 (C5), 118.8 (C4), 113.4 (C7) ppm. ^{13}C NMR data, both in solution and in the solid state, for the various complexes were assigned by comparison with related nickel complexes (22). Shifts between the coordinated ligand and its free solid-state spectrum are small. Only C2, which is adjacent to the coordination site, appears to be appreciably shifted (+3.4 ppm) upon coordination to the rhenium centre.

© 1997 NRC Canada

Can. J. Chem. Downloaded from www.nrcresearchpress.com by 92.62.229.171 on 09/08/12
For personal use only.

Table 3. Selected bond lengths (Å) and angles (°) for $[ReO_2(BzimH)_4][ReO(OH)(BzimH)_4](ReO_4)_3$.

Complex cation			
Re1—O1	1.682(10)	O1-Re1-O2	180.0
Re1—O2	1.805(11)	Re1-O2-H2[a]	180.0
Re1—N31	2.119(9)	O1-Re1-N31	91.9(2)
Re1—N32	2.106(9)	O1-Re1-N32	91.9(2)
		O2-Re1-N31	88.1(2)
		O2-Re1-N32	88.1(2)
		N31-Re1-N32	89.1(3)
		N31-Re1-N32[e]	90.7(3)
		N31-Re1-N31[e]	176.3(5)
		N32-Re1-N32[e]	176.2(5)
Hydrogen bonds			
(A—H···B)	A—B	A—H[a]	A-H-B
O2—H2[a]···O2[b]	2.436(21)	1.218	180.0
N11—H11···O302	2.960(15)	0.87	165.5(5)
N12—H12···O303[c]	2.962(14)	0.87	141.9(4)
N12—H12···O202[c]	3.05(5)	0.87	133.4(6)
N12—H12···O202[d]	3.11(6)	0.87	133.6(6)

[a]Not refined.
[b]$-x, -y, -z$.
[c]$-1+x, y, z$.
[d]$-1+x, y, -z$
[e]$-x, -y, z$.

Crystal structure of $[ReO_2(BzimH)_4]$-$[ReO(OH)(BzimH)_4][ReO_4]_3$

Crystallographic work unambiguously establishes the presence of a hemiprotonated phase. The unit cell contains 1.5 ReO_4^- ions per Re complex, which requires an extra positive charge for each pair of $[ReO_2(BzimH)_4]^+$ species. Furthermore, the short O···O distance between two centrosymmetrically related units necessitates an O—H···O bond in this region. However, the $[ReO_2(BzimH)_4]^+$ and $[ReO(OH)(BzimH)_4]^{2+}$ ions occupy symmetry-equivalent crystallographic sites, with the consequence that the geometry represented in Fig. 2 and the bond lengths and angles in Table 3 are averages over these two species.

Overall geometry and individual parameters involving the BzimH ligands are not expected to differ appreciably in the two forms. The Re—N bonds (2.11 Å) are similar to those found in imidazole compounds (5, 13). Coordination takes place approximately along the expected lone-pair direction, as indicated by the small difference between the C2-N3-Re and C9-N3-Re angles (~125° and 130°, respectively). The O1-Re-O2 angle is 180°, as required by symmetry. Two distinct rhenium–oxo distances are present in the structure. The longer Re1—O2 distance (1.805(11) Å) on the side of the O—H···O interaction is intermediate between the Re=O distance in $[ReO_2L_4]^+$ (1.765 Å) (5) and the Re—OH distances (~1.90 Å) in $[ReO(OH)(1,2\text{-}Me_2Im)_4]^{2+}$ (5) and $[ReO(OH)(CN)_4]^{2-}$ (26), as expected for disorder. The "outside" Re=O distance of 1.682(10) Å is close to the value found for $[ReO(OH)(O_1cyclam)]^{2+}$ (O_1cyclam = 1,4,8,11-tetraazacyclodecan-2-one) (1.685(8) Å) (27). The four heterocycles are similarly oriented with the phenyl groups away from the O—H···O region. Rotations about the Re—N bonds bring the plane of the rings at 32.4(9)° (ring 1) and 36.3(9)° (ring 2) from the O-Re-O direction. The Re—N bonds are slightly displaced towards the O—H···O region, producing an "umbrella" deformation with O1-Re1-N angles of 91.9(2)°. Again, this is intermediate between the ~90° angles observed in dioxo compounds and the ~94° angles introduced by the steric constrains of the higher multiplicity Re1=O1 bond in oxo-hydroxo species (5, 26, 27). The geometry of the BzimH ligands is normal (supplementary material).

Extensive hydrogen bonding takes place in the crystal. The most interesting is the strong O—H···O bond between centrosymmetrically related complex cations, leading to dimeric units (Fig. 3). The protonated oxo ligand O2 is close (2.44(2) Å) to its symmetry generated position O2′ (Table 3), but this O···O separation is not unprecedented, the lower limit for an intermolecular O···O interaction in the solid state being considered to be ~2.40 Å (28). Hydrogen bonds in the 2.40–2.50 Å range are nevertheless considered to be very short.

The position of the proton could not be reliably determined in the crystallographic study. It was fixed on the origin, since no electron density was found elsewhere in the ΔF map on or near the c axis. Nevertheless, this position is quite consistent with various correlations made for O—H···O hydrogen bonds between O—H, H···O′, and O···O′ distances and O-H···O′ angles (28). According to Olovsson and Jönsson (28), the shorter the O···O′ distance, the more linear the interaction and the more equal the O—H and H···O′ distances are expected to get. The model proposed here with the proton at the origin follows these trends, with an O-H-O′ angle of 180°, a short O···O′ separation (2.44(2) Å) and equal O—H and H—O′ distances of 1.22 Å.

The view of the unit cell represented in Fig. 4 clearly shows the arrangement of anions and cations in the crystal: layers of ReO_4^- ions are intercalated between two layers of $[ReO_2(BzimH)_4]^+/[ReO(OH)(BzimH)_4]^{2+}$ ions, in the region containing the connecting O—H···O bonds, where they form hydrogen bonds with ligand N-H groups. The linear O-Re-O groups are all oriented parallel to the c axis. The phenyl rings of all BzimH ligands are pointing away from this hydrophilic region, towards the surfaces of these three-decker sheets, thereby providing hydrophobic van der Waals contacts between the sheets.

Distances and angles related to the N—H···O(perrhenate) hydrogen bonds are reported in Table 3. Interactions are present between N11 and O302 (2.960(15) Å) and between N12 and O303 (2.962(14) Å), two oxygens belonging to the undisordered ReO_4^- ion. The N···O separations are in the normal range (2.6–3.2 Å) (29) and the N-H···O angles (165.5(5)° and 141.9(4)°, respectively) are favourable. Extra N—H···O bonds exist between N12 and O202 (3.05(5) Å), and between N12 and O202′ (3.11(6) Å). The fact that these interactions are much weaker accounts for the disorder observed for perrhenate ion Re2.

Discussion

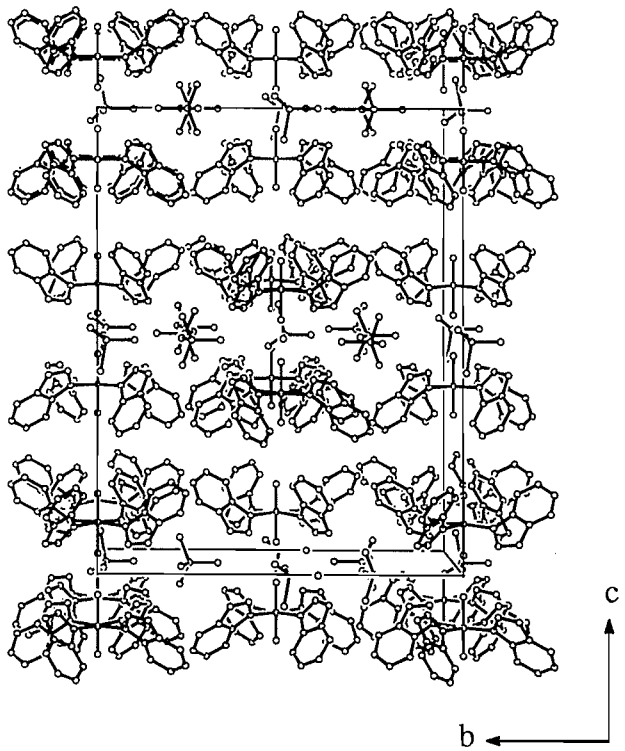
Under mild conditions, excess benzimidazole reacts well with $ReO_2I(PPh_3)_2$, forming *trans*-$[ReO_2(BzimH)_4]I$, but under stoichiometric conditions (4:1 ligand:Re ratio), the reaction does not proceed to completion even after 24 h. With excess ligand, conversion into $[ReO_2(BzimH)_4]^+$ is nearly quantita-

Can. J. Chem. Downloaded from www.nrcresearchpress.com by 92.62.229.171 on 09/08/12
For personal use only.

© 1997 NRC Canada

Can. J. Chem. Downloaded from www.nrcresearchpress.com by 92.62.229.171 on 09/08/12
For personal use only.

Fig. 4. View of the unit cell down the *a* axis, showing alternating layers of hydrogen-bonded cation pairs and perrhenate ions. Hydrogens are omitted and atoms are represented with spheres of arbitrary size for clarity.



tive, but removal of excess free ligand proved to be problematic, since some protonation usually occurs during recrystallization. Protonation is easily detected by the reddish-brown dioxo complexes taking a pink coloration even when protonation is only partial. In the IR spectrum, the ν(Re=O) mode of $[ReO(OH)(BzimH)_4]^{2+}$ appears at 931 cm^{-1}, whereas the ν_{as}(O=Re=O) mode of $[ReO_2(BzimH)_4]^+$ at 795 cm^{-1}, which is the most intense vibration in the spectrum of a non-protonated sample, loses intensity. From concentrated acetone solutions, nearly ligand-free *trans*-$[ReO_2(BzimH)_4]I$ can be isolated, but partial protonation is nevertheless present. From very dilute solutions in acetone, an unusual exactly hemiprotonated iodide salt $[ReO_2(BzimH)_4][ReO(OH)(BzimH)_4](I)_3$ is isolated. Slow recrystallization from alcohols results in ligand loss and partial decomposition, and the hemiprotonated material precipitates as the perrhenate salt. Nonprotonated ligand-free $[ReO_2(BzimH)_4]^+$ could be obtained as the tetraphenylborate salt.

More robust reaction conditions do not help. Refluxing mixtures of $ReO_2I(PPh_3)_2$ and benzimidazole (stoichiometric amounts or excess) yields a dark reddish-brown material. From IR spectroscopy, this sample is believed to be a mixture of products, including the dioxo complex (ν_{as}(O=Re=O) at 795 cm^{-1}) and an oxo-bridged dimer (medium bands at 965 and 700 cm^{-1} for ν(Re=O) and ν_{as}(Re-O-Re), respectively) (30).

Both the dioxo and the oxo-hydroxo complexes are unstable in methanol, free protonated ligand being present in aged (several minutes) NMR solutions. The instability towards oxidation observed here in alcohol solutions is not uncommon for *trans*-dioxo compounds of Re(V) (27, 31). Mixed $[O=Re=O]^+/[O=Re\text{-}OH]^{2+}$ phases have been reported and structurally characterized for 1,2-dimethylimidazole (3). Partial protonation could also be responsible for unexplained colour changes in *trans*-$[TcO_2L_4]^+$ complexes (32, 33). Pink solids were isolated from initially orange solutions when acetone was used to recrystallize $[TcO_2L_4]Cl$ imidazole complexes (32). These reports possibly involve partly protonated mixed phases of the type described in this paper, since a very small amount of protonation could lead to colour variations. The crystal structure of these Tc complexes shows no obvious signs of protonation, with normal Tc=O bonds (1.71(2) Å), although the relatively large uncertainties and the symmetry equivalence of the two oxo ligands could mask a small bond length variation due to a partly protonated Tc=O bond. The oxygen atoms in *trans*-dioxo systems are nucleophilic and are good hydrogen bond acceptors from water or other protic crystallization solvents. Traces of protonation would imply a slight excess of Cl^- counterions, but the extra electron density could go unnoticed if the anion lies approximately on the same site as a solvent molecule.

In contrast with the $[ReO_2(1,2\text{-}Me_2Im)_4]^+/[ReO(OH)(1,2\text{-}Me_2Im)_4]^{2+}$ phases, which are only partially protonated and non-stoichiometric (3), the mixed phase isolated here with benzimidazole is exactly hemiprotonated. In both cases, hydrogen bonding has a determining effect. In the 1,2-Me_2Im materials, a lattice water molecule lying on a crystallographic 3-fold axis is surrounded by three complex cations and it plays the double role of hydrogen-bond donor and acceptor: most water molecules act as hydrogen-bond donor to two Re=O groups and as acceptor for one Re-OH group. The high symmetry of the cubic unit cell provides each Re=O or Re-OH group with a suitable hydrogen-bonding partner. However, water is disordered over two close positions, so that it can move away from the third group when it is Re=O instead of Re-OH. As a consequence, the crystal lattice can accommodate a certain range of $[ReO_2(1,2\text{-}Me_2Im)_4]^+/[ReO(OH)(1,2\text{-}Me_2Im)_4]^{2+}$ composition and non-stoichiometric phases are obtained.

In the present case, although hydrogen bonding also plays a crucial role, the bulky benzimidazole ligands also control the structure to a large extent. In the first place, all benzimidazole side-rings adopt head-to-head orientations, hence providing enough space on the other side for the Re-OH group of one cation and the Re=O group of another one to approach each other and form the O—H···O bond. Secondly, the Re-O-H···O=Re segments should not deviate much from linearity since repulsions would develop between the benzimidazoles in the two cations. Thirdly, these restrictions at the dimer level generate sheets with a hydrophilic interior, where extra N—H···perrhenate hydrogen bonds are formed, and hydrophobic surfaces where inter-sheet contacts are taking place. It is difficult to decide which of these three factors plays the most important role in determining the structure, but this type of structure could not exist if it did not contain exactly the same amount of $[ReO_2(BzimH)_4]^+$ and $[ReO(OH)(BzimH)_4]^{2+}$, since two Re=O groups or two Re-OH groups could not face each other at the very short O···O distance observed. However, the same structural pattern could be retained in the iodide

© 1997 NRC Canada

salt $[ReO_2(BzimH)_4][ReO(OH)(BzimH)_4](I)_3$ prepared here, where the ReO_4^- ions would be replaced by I^- ions with the same charge and a similar size.

Another interesting structural aspect is revealed from a comparison with the related $[ReO_2(Haza)_4]Cl$ compound (7). In both complexes, the cations all have mutually parallel and linearly stacked O-Re-O segments. The azaindole complexes adopt a "windmill" conformation with all ligands parallel to the O═Re═O axis to favour intramolecular N—H···oxo hydrogen bonding. In the benzimidazole compound, the rings are tilted about 35° away from the axis, leading to a "propeller" conformation. This results in the 7-azaindole complex crystallizing as *chains* of cations, while the crystal structure of the benzimidazole complex shows *layers* of dimeric units.

Although the "all head-to-head" conformer discussed in this communication is no doubt the major conformer, the presence of weak secondary signals was sometimes detected in the NMR spectra of non-recrystallized samples. Whether these signals should be attributed to "head-to-tail" $[ReO_2L_4]^+$ conformers or chemically different species is not known. From the X-ray diffraction study, it is reasonable to think that the structure should promote preferential crystallization of the "all head-to-head" conformer, leading to a "conformationally pure" sample.

^{1}H NMR shows that oxo protonation produces unexpected effects on the H2 and H4 protons close to the coordination sphere, the effect being particularly large for H4. Such effects may become efficient ways of studying conformation in these systems, but a detailed discussion must await a better understanding of Re═O multiple bond anisotropy.

Acknowledgments

We wish to thank M. Simard and F. Bélanger-Gariépy for help in collecting the X-ray data, R. Mayer for running the CP-MAS spectra, and S. Bilodeau who did the COSY experiments. The financial support of the Natural Sciences and Engineering Research Council of Canada and the Fonds FCAR du Ministère de l'Éducation du Québec is gratefully acknowledged.

References

1. C. Savoie, C. Reber, S. Bélanger, and A.L. Beauchamp, Inorg. Chem. **34**, 3851 (1995).
2. M. Nicolini, G. Bandoli, and U. Mazzi (*Editors*). Technetium and rhenium in chemistry and nuclear medicine. S.G. Editoriali, Padova. 1995.
3. A.M. Lebuis, J.M.C. Young, and A.L. Beauchamp. Can. J. Chem. **71**, 2070 (1993).
4. J.C. Brewer. Ph.D. Thesis, California Institute of Technology, 1991.
5. S. Bélanger and A.L. Beauchamp. Inorg. Chem. **35**, 7836 (1996).
6. S. Bélanger. Thèse de Ph.D., Université de Montréal. 1997.
7. A.M. Lebuis and A.L. Beauchamp. Can. J. Chem. **71**, 2060 (1993).
8. G.F. Ciani, G. D'Alfonso, P.F. Romiti, A. Sironi, and M. Freni. Inorg. Chim. Acta, **72**, 29 (1983).
9. J.C. Brewer and H.B. Gray. Inorg. Chem. **28**, 3334 (1989).
10. E.J. Gabe, Y. Le Page, J.-P. Charland, F.L. Lee, and P.S. White. J. Appl. Crystallogr. **22**, 384 (1989).
11. G.M. Sheldrick. SHELXS-86: Program for the solution of crystal structures. University of Gottigen, Germany. 1985.
12. G.M. Sheldrick. SHELXL-93. Program for crystal structure refinement. University of Göttingen, Germany. 1995.
13. S. Bélanger and A.L. Beauchamp. Inorg. Chem. Submitted.
14. M.S. Ram, L.M. Skeens-Jones, C.S. Johnson, X.L. Zhang, C. Stern, D.I. Yoon, D. Selmarten, and J.T. Hupp. J. Am. Chem. Soc. **117**, 1411 (1995).
15. A. Paulo, A. Domingos, and I. Santos. Inorg. Chem. **35**, 1798 (1996).
16. S. Mohan, N. Sundaraganesan, and J. Mink. Spectrochim. Acta, **47A**, 1111 (1991).
17. F. Kratz, B. Nuber, J. Weib, and B.K. Keppler. Polyhedron, **11**, 487 (1992).
18. J. de Mendoza, M.L. Castellanos, J.-P. Fayet, M.-C. Vertut, and J. Elguero. J. Chem. Res. **50**, 514 (1980).
19. R. Benassi, R. Grandi, U.M. Pagnoni, and F. Taddel. Magn. Reson. Chem. **24**, 415 (1986).
20. P. Sohár. *In* Nuclear magnetic resonance spectroscopy. Vol. 1. Chemical Rubber Company Press, Boca Raton, Fla. 1983, p. 126.
21. W.O. Parker, Jr., E. Zangrando, N. Bresciani-Pahor, P.A. Marzilli. L. Randaccio, and L.G. Marzilli, Inorg. Chem. **27**, 2170 (1988).
22. J.-P. Costes, G. Commenges, and J.-P. Laurent. Inorg. Chim. Acta, **134**, 237 (1987).
23. E. Alessio, M. Calligaris, M. Iwamoto, and L.G. Marzilli. Inorg. Chem. **25**, 2538 (1996).
24. A.F. Pozharskii, V.V. Kruz, C. Foces-Foces, A.L. Llamsa-Saiz, R.M. Claramunt, D. Sanz, and J. Elguero. J. Chem. Soc. Perkin Trans. 2, 841 (1994).
25. R.J. Pugmire and D.M. Grant. J. Am. Chem. Soc. **93**, 1880 (1971).
26. W. Purcell, A. Roodt, S.S. Basson, and J.G. Leipoldt. Transition Met. Chem. **5–6**, 5 (1989).
27. B.W. Tsang, J. Reibenspies, and A.E. Martell. Inorg. Chem. **32**, 988 (1993).
28. I. Olovsson and P.-G. Jönsson. The hydrogen bond: recent developments in theory and experiments. Vol. 2. *Edited by* P. Schuster, G. Zundel, and C. Sandorfy. North-Holland Publishing Company, Amsterdam. 1976. p. 395.
29. G.H. Stout and L.H. Jensen. *In* X-ray structure determination, a practical guide. MacMillan, London. 1968. p. 303.
30. B. Jezowska-Trzebiatowska, J. Hanuza, and M. Baluka. Spectrochim. Acta, **27A**, 1752 (1971).
31. Y.-P. Wang, C.-M. Che, K.-Y. Wong, and S.-M. Peng. Inorg. Chem. **32**, 5827 (1993).
32. P.H. Fackler, M.J. Lindsay, M.J. Clarke, and M.E. Kastner. Inorg. Chim. Acta, **109**, 39 (1985).
33. M.E. Kastner, P.H. Fackler, M.J. Clarke, and E. Deutsch. Inorg. Chem. **23**, 4683 (1984).

Can. J. Chem. Downloaded from www.nrcresearchpress.com by 92.62.229.171 on 09/08/12
For personal use only.

© 1997 NRC Canada

The X-ray structure of a sodium peroxide hydrate, $Na_2O_2 \cdot 8H_2O$, and its reactions with carbon dioxide: relevance to the brightening of mechanical pulps

Geoffrey S. Hill, David G. Holah, Stephen D. Kinrade, Vincent R. Magnuson, Valery Polyakov, and Todd A. Sloan

Can. J. Chem. Downloaded from www.nrcresearchpress.com by 84.22.46.98 on 09/08/12
For personal use only.

Abstract: The main component of the solid originally believed to be a peroxosilicate with pulp-brightening properties has been shown to be $Na_2O_2 \cdot 8H_2O$. The solid crystallizes in the monoclinic space group *C2/c*, with an empirical formula H_8O_5Na, and with a = 14.335(3), b = 6.461(1), c = 11.432(2) Å, β = 118.28(3)°, and Z = 8. The centrosymmetric structure consists of a peroxide anion with an O—O distance of 1.499(2) Å. Each of these oxygen atoms is at the apex of an approximate square-based pyramid, the base of which consists of four oxygen atoms of water molecules. The bases of the two pyramids are staggered when viewed down the peroxide bond. Each sodium is at the centre of an approximate octahedron of water molecules, four of which bridge other sodium atoms and two bridge to the peroxide anions. One hydrogen atom of each of these two water molecules is terminal and the other two are hydrogen bonded to peroxide oxygen atoms. The compound reacts very rapidly with CO_2 in moist air to form Na_2CO_3, but in drier conditions, formation of the carbonate can take many days and proceeds via a percarbonate, believed to be Na_2CO_4. This has been identified by infrared spectroscopy and X-ray powder diffraction and can persist for long periods in dry air.

Key words: sodium peroxide hydrate, sodium percarbonate, pulp brightening, X-ray diffraction, infrared.

Résumé : On démontre que le produit principal d'un solide, auquel on avait originalement attribué la structure d'un peroxosilicate ayant des propriétés de blanchiment de la pulpe, est formé de $Na_2O_2 \cdot 8H_2O$. Le solide, de formule empirique de H_8O_5Na, cristallise dans le groupe d'espace monoclinique *C2/c*, avec a = 14,335(3), b = 6,461(1), et c = 11,432(2) Å, β = 118,28(3)°, et Z = 8. La structure centrosymétrique comporte un anion peroxyde dans lequel la longueur de la liaison O—O est égale à 1,499(2) Å. Chacun de ces atomes d'oxygène se trouve au sommet d'une pyramide à base approximativement carrée dont la base est formée de quatre atomes d'oxygène des molécules d'eau. Lorsqu'on les regarde le long de la liaison du peroxyde, les bases des deux pyramides sont décalées. Chaque atome de sodium se trouve approximativement au centre d'un octaèdre de molécules d'eau, dont quatre forment des ponts avec d'autres atomes de sodium et deux forment des ponts avec des anions peroxydes. L'un des atomes d'hydrogène de chacune de ces molécules d'eau est terminal et les deux autres forment des liaisons hydrogènes avec les atomes d'oxygène du peroxyde. Le composé réagit rapidement avec le CO_2, dans l'air humide, pour conduire à la formation de Na_2CO_3; toutefois, dans des conditions plus sèches, la formation du carbonate nécessite plusieurs jours et elle implique un intermédiaire percarbonate que l'on croit être le Na_2CO_4. Celui-ci a été identifié par spectroscopie infrarouge et par diffraction de poudre des rayons X et il peut exister pour de longues périodes dans de l'air sec.

Mots clés : hydrate de peroxyde de sodium; percarbonate de sodium; blanchiment de la pulpe; diffraction des rayons X; infrarouge.

[Traduit par la rédaction]

Introduction

The work described here arose during research aimed at improving the procedures for the lignin-preserving brightening of mechanical wood pulps. (Bleaching more often refers to the production of pure cellulose by delignification with reagents such as Cl_2, ClO_2, O_2, etc. in Kraft pulps; for a general reference, see Smook (1)). The most widely used brightening reagent is an alkaline solution of hydrogen peroxide and its successful use in mills requires the presence of a variety of additional reagents (2) whose primary goals are to stabilize the peroxide and minimize its autodecomposition and its decomposition catalyzed by transition metal ions in the wood (2, 3). The most common additives include sodium silicate, magnesium ions, and the sodium salt of diethylenetriaminepentaacetic acid. Because of the enormous amounts of mechanical pulps being produced, and since hydrogen peroxide is the most expensive chemical used in such mills, it is of consider-

Received July 30, 1996.

G.S. Hill, D.G. Holah[1], S.D. Kinrade, and T.A. Sloan. Department of Chemistry, Lakehead University, Thunder Bay, ON P7B 5E1, Canada.
V.R. Magnuson and V. Polyakov. Chemistry Department, University of Minnesota–Duluth, Duluth, MI 55812, U.S.A.

[1] Author to whom correspondence may be addressed. Telephone: (807) 343-8297. Fax: (807) 346-7775. E-mail: David.Holah@lakeheadu.ca

© 1997 NRC Canada

Fig. 1. The structure of $Na_2O_2 \cdot 8H_2O$ showing the environment of the Na atoms.

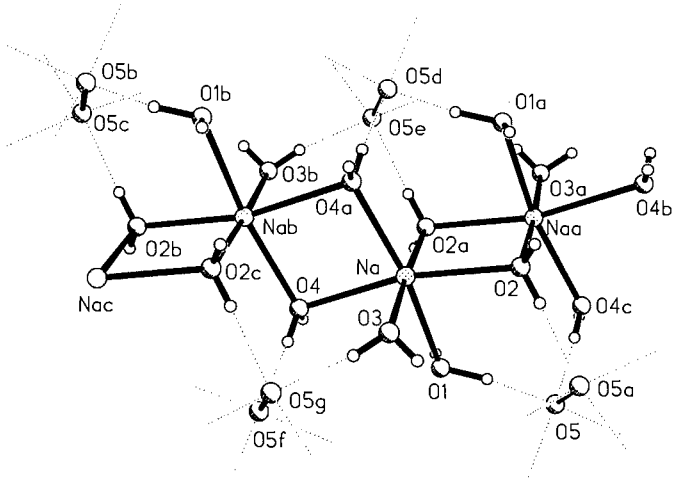
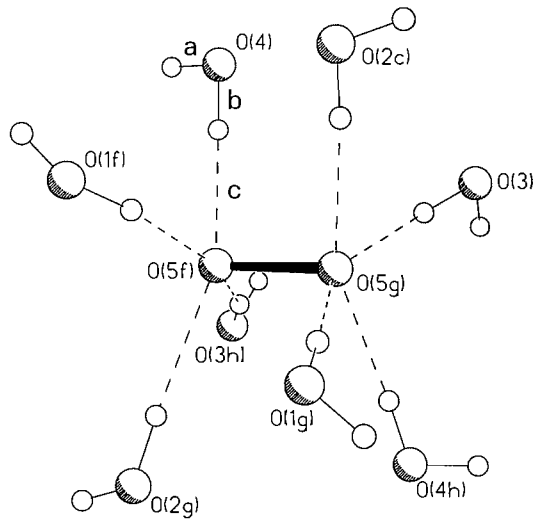


Fig. 2. The structure of $Na_2O_2 \cdot 8H_2O$ showing the environment of the peroxide anion.



able economic importance to understand the chemistry involved in these processes so that peroxide losses can be minimized. For example, there has been much discussion and speculation on the specific role(s) of the silicate (4). It has been shown (3) that a major (but not total (5)) function is the deactivation of metal cations involved in catalyzing peroxide decomposition. In addition, it has long been suspected that peroxosilicates are involved (3), and there are several reports describing the solid obtained when solutions of hydrogen peroxide and sodium silicate solutions are mixed at high pH values as $Na_2SiO_3 \cdot xH_2O_2$ (6), sodium persilicate (7), and sodium peroxysilicate (3, 8, 9). The solid has brightening properties (7, 8), but no evidence has been presented to support any of the above formulations. This paper describes the structure of the only crystalline compound, $Na_2O_2 \cdot 8H_2O$, present in the solid and its reactions with CO_2.

Results and discussion

The presence of silicon in the very unstable solid obtained in bulk from solutions containing silicate, hydrogen peroxide, and sodium hydroxide, and generally referred to as a peroxosilicate, has been confirmed by strong signals in the ^{29}Si nmr spectra, by ir spectroscopy, and by energy-dispersive X-ray microanalysis. Since this solid shows brightening properties (7, 8), and is of unknown composition, it was of importance to establish its composition. We have shown previously (4) that, compared to pure silicate, there are minor changes in the ^{29}Si nmr spectra of solutions from which the solid crystallizes and that these are probably due to the formation of labile complexes of dissolved silicates and radical H_2O_2 decomposition products. No evidence for the existence of peroxide coordinated to silicate was found in such solutions.

Well-formed crystals were obtained from a variety of solutions (especially at very high pH) containing NaOH, SiO_2, and H_2O_2, prepared in connection with the ^{29}Si nmr studies (4). These crystals are colourless, transparent plates that become opaque very rapidly when removed from the mother liquor in air. Decomposition is slightly less rapid under nitrogen at room temperature, but to preserve a crystal for data collection, it was necessary to transfer crystals rapidly, under nitrogen, to sealed Lindemann capillaries for storage at liquid nitrogen temperatures.

Results from the structural determination (see below) show that the compound is $Na_2O_2 \cdot 8H_2O$, which was made previously (10) either by reacting sodium peroxide with water or, more conveniently (11), from mixtures of hydrogen peroxide and sodium hydroxide. It is reported as a white powder that reacts readily with carbon dioxide and water vapour. The stabilization of this compound for industrial use has formed the subject of patents (12).

Views of the structure, showing the arrangement of the water molecules about each Na atom and about each peroxide ion, are shown in Figs. 1 and 2, with selected bond lengths and angles recorded in Table 1. From Fig. 1, it can be seen that each Na (Nab for example) is surrounded by O atoms from six water molecules. Four of these (O2b, O2c, O4a, and O4) are from water molecules that essentially act as bridges to other Na atoms. Two (O1b and O3b) serve to bridge Nab to O5b and O5e, the oxygen atoms of peroxide anions. Na—O distances are in the range 2.376(12)–2.508(12) Å, and the O-Na-O angles approximate to 90° so that each Na ion is in the centre of an approximate octahedron.

Effects of hydrogen bonding can be seen by considering the distances labelled ***a***, ***b***, and ***c*** in Fig. 2 and tabulated below.

	a	*b*	*c*	*d*
O1	0.787(25)	1.032(31)	1.555(1)	2.582(1)
O2	0.768(25)	0.847(25)	1.897(1)	2.742(1)
O3	0.791(22)	0.855(27)	1.788(1)	2.622(1)
O4	0.795(25)	0.865(25)	1.802(1)	2.665(2)

Distance ***b*** is greater than distance ***a*** for all lattice waters. This fact is consistent with the H atom oriented towards the peroxide being hydrogen bonded to the peroxide O atom, whereas the second H atom is terminal, with little or no hydrogen bonding as distances range from 1.958 to 2.581 Å. It is apparent from Fig. 2 and from a comparison of ***d***, the peroxide O to

© 1997 NRC Canada

Can. J. Chem. Downloaded from www.nrcresearchpress.com by 84.22.46.98 on 09/08/12
For personal use only.

Can. J. Chem. Downloaded from www.nrcresearchpress.com by 84.22.46.98 on 09/08/12
For personal use only.

Table 1. Selected bond lengths (Å) and angles (°). See supplementary material for complete data.

Na—O(4a)	2.3710(12)
Na—O(3)	2.3913(13)
Na—O(2a)	2.4160(13)
Na—O(2)	2.4223(12)
Na—O(1)	2.4428(12)
Na—O(4)	2.5009(12)
Na—Na(a)	3.5229(12)
Na—Na(b)	3.6366(12)
O5—O5(a)	1.499(2)
O(4a)-Na-O(3)	93.15(3)
O(4a)-Na-O(2a)	88.49(5)
O(3)-Na-O(2a)	177.13(4)
O(4a)-Na-O(2)	109.64(4)
O(3)-Na-O(2)	90.69(4)
O(2a)-Na-O(2)	86.54(4)
O(4a)-Na-O(1)	166.15(4)
O(3)-Na-O(1)	94.88(5)
O(2a)-Na-O(1)	83.98(5)
O(2)-Na-O(1)	81.56(4)
O(4a)-Na-O(4)	83.47(4)
O(3)-Na-O(4)	88.96(4)
O(2a)-Na-O(4)	93.57(4)
O(2)-Na-O(4)	166.90(4)
O(1)-Na-O(4)	85.41(4)
O(4a)-Na-Na(a)	102.29(4)
O(3)-Na-Na(a)	133.89(4)
O(2a)-Na-Na(a)	43.34(3)
O(2)-Na-Na(a)	43.20(3)
O(1)-Na-Na(a)	80.05(3)
O(4)-Na-Na(a)	135.43(4)
O(4a)-Na-Na(b)	43.10(3)
O(3)-Na-Na(b)	91.34(4)
O(2a)-Na-Na(b)	91.47(4)
O(2)-Na-Na(b)	152.72(4)
O(1)-Na-Na(b)	125.31(4)
O(4)-Na-Na(b)	40.37(3)
Na(a)-Na-Na(b)	128.95(4)
Na(a)-O(2)-Na	93.46(4)
Na(b)-O(4)-Na	96.53(4)

water O distance, with the sum of ***b*** and ***c*** that the hydrogen bond is approximately linear (angles range from 164.4° to 176.2°).

The environment of the anions can also be seen in Fig. 1 and, more clearly, in Fig. 2. Each O atom of the O_2^{2-} is approximately 0.5 Å above a plane formed by four O atoms from neighbouring water molecules. When viewed down the O—O bond, the eight O atoms are in a staggered configuration. Distances from a peroxide O to its closest four water O atoms are 2.582(2)–2.742(1) Å, with angles of the type O(5f)-O(5g)-O(2c) ranging between 100° and 110°. The O—O distance of 1.499(2) Å is comparable to that found in the related $SrO_2 \cdot 8H_2O$ and in fact the two structures are quite similar (10, 13). In previous work, the space group of $Na_2O_2 \cdot 8H_2O$ was reported as either *Cc* or *C2/c*, with a unit cell of $a = 13.5$, $b = 6.5$, $c = 11.5$ Å, $\beta = 100.5$ and $Z = 4$ (14).

The solid obtained by literature methods (7, 8) in high yields from mixtures of NaOH, Na_2SiO_3, and H_2O_2 is very sticky because of the high NaOH content. After washing with small amounts of ethanol and H_2O_2, small well-formed crystals are clearly visible in the bulk solid, suggesting that the original precipitate is a mixture. The powder diffraction patterns of several samples at various stages of washing are the same as that of the pure octahydrate (see experimental section). The observed pattern agrees very closely with that calculated from the single crystal data and is only slightly different from that on file (15) in the ICDD data bank. Data from ir, nmr, and energy-dispersive X-ray spectrometry suggest that the amorphous, silicon-containing contaminant is sodium silicate, which is more soluble in water (16) or H_2O_2 than is $Na_2O_2 \cdot 8H_2O$ and explains why the pure octahydrate is the only solid remaining after washing.

There is a clear phase change when the pure octahydrate is pumped under vacuum for 5 h, and the powder pattern of the new phase corresponds to that reported for the dihydrate (15), obtained when the octahydrate is allowed to stand over desiccants (11).

Because decomposition of the peroxide begins as soon as the solid is exposed to atmosphere, samples for ir measurements were handled under dry nitrogen. The ir spectrum (Fig. 3) consists of a series of broad absorptions due to the lattice water and peaks in the 500–1000 cm^{-1} region. The peak at 985 cm^{-1} is possibly due to νO—O, which is typically (17) found in this region. There are additional peaks in the 500–850 cm^{-1} region but, significantly, no peaks between 1000 and 1600 cm^{-1}, and therefore the sample is carbonate free at this point (18).

The rate of decomposition and the product formed greatly depend on the amount of moisture present in the atmosphere. Exposure to moist air (relative humidity ~80%) results in the rapid (within minutes) appearance of the very intense signal at ~1450 cm^{-1} due to CO_3^{2-} (18). Transformation is complete in a few hours. This accounts for the previously published spectra (19) of both $Na_2O_2 \cdot 8H_2O$ and $Na_2O_2 \cdot 8D_2O$, which are dominated by absorptions due to water (~3000 cm^{-1}) and to sodium carbonate at ~1450 cm^{-1} (very strong), ~880, and ~700 (very weak) cm^{-1} (18). In fact there is little evidence of any peroxide remaining in the samples used to record these spectra, which were also used to argue that the structure of $Na_2O_2 \cdot 8H_2O$ does not consist of units of $2NaOH \cdot H_2O_2 \cdot 6H_2O$.

However, in drier air (relative humidity ~20%), dehydration is accompanied by the appearance, within minutes, of new signals that continue to grow in intensity over several hours. The changes after 20 h are shown in Fig. 3. There is little peroxide remaining, almost all the water has been lost, and a small amount of CO_3^{2-} is present. The three peaks due to the latter continue to increase with time, but many days are required for complete conversion to CO_3^{2-}. The remaining peaks in the spectrum in Fig. 3 are most likely due to a surprisingly stable, colourless sodium percarbonate.

A detailed analysis of ir and Raman spectra of various percarbonates suggests that the spectra of most species are best interpreted on the basis of the centrosymmetric $(C_2O_6)^{2-}$ anion (20). The ir spectra of $Na_2C_2O_6 \cdot nH_2O$ ($n = 0$–1) and three coloured (orange and blue) forms of $K_2C_2O_6$, prepared by reactions between CO_2, KOH, and H_2O_2, have been analyzed (20). In addition, ("yellowish") $Na_2C_2O_6$ has been reported from $Na_2O_2 \cdot 8H_2O$ and CO_2 (21). Percarbonates formulated as

© 1997 NRC Canada

Can. J. Chem. Downloaded from www.nrcresearchpress.com by 84.22.46.98 on 09/08/12
For personal use only.

CO_4^{2-} are less well known. Attempts to prove the existence of Li_2CO_4 by X-ray powder diffraction methods were unsuccessful and it was concluded that the compound does not exist at room temperature (22). It was later obtained from LiOH–H_2O_2–CO_2 mixtures and characterized by elemental analysis and ir spectroscopy (20); its (unpublished) powder pattern does not contain lines due to Li_2CO_3, LiOH, LiO_2H, or Li_2O_2 (20). There is a report of CO_4^{2-} coordinated to Pt (23).

The ir spectrum of the colourless percarbonate shown in Fig. 3 closely resembles that of $Li_2CO_4 \cdot H_2O$. The one difference is that the very strong 1350 cm^{-1} peak in the Li compound, assigned to the C--O stretching vibration (20), appears as a doublet at 1371 and 1339 cm^{-1} in Fig. 3. These may be the symmetric and antisymmetric modes. The spectrum is quite different from that of $Na_2C_2O_6$ (20). The X-ray powder pattern of this sample (see experimental section) shows it to be mostly the percarbonate, contaminated by approximately 5% Na_2CO_3, with no detectable amount of $Na_2O_2 \cdot 8H_2O$. The pattern is also quite different from that reported for $Na_2C_2O_6$ (21) and is therefore probably due to Na_2CO_4.

There is a variety of adducts of H_2O_2 and Na_2CO_3 (20, 24) and it appears to be common practice in the literature (see, for example, ref. 25) to refer to these, particularly the important bleaching agent $Na_2CO_3 \cdot 1.5H_2O_2$, as percarbonates. The crystal structure of the latter (24, 26) shows that it contains H_2O_2 molecules hydrogen bonded to CO_3^{2-}, and is therefore not a percarbonate. Its powder pattern and ir spectrum (20) are quite different from the compound prepared in this work.

Relationship to pulp brightening

All the evidence now points to the fact that the bulk solid obtained from NaOH, H_2O_2, and Na_2SiO_3 mixtures, previously described as sodium peroxysilicate (3, 8, 9) with pulp-brightening properties (7, 8), is in fact a mixture of $Na_2O_2 \cdot 8H_2O$ and amorphous Na_2SiO_3. The pulp-brightening properties of such solids are due to the title compound. The presence of other known crystalline species, such as $Na_2O_2 \cdot xH_2O_2 \cdot yH_2O$ ($x = 2$, $y = 4$ and $x = 4$, $y = 0$) (27), $Na_2(HO_2)_2 \cdot H_2O_2$ (10), and $Na_2SiO_3 \cdot xH_2O_2 \cdot yH_2O$ (particularly with $x = 3$, $y = 0$ (7) and $x = 2$, $y = 1$ (28)) can be also ruled out from powder pattern data. The compound containing the hydroperoxide anion would be particularly important since this anion is believed to be the major active pulp-brightening agent (1). Isolation of peroxide adducts of silicate require that silicate–peroxide solutions be taken to dryness under vacuum (6, 28). In addition, they are very water soluble when first formed and therefore would likely not precipitate under the conditions studied in this work.

Experimental

Physical measurements and syntheses

Infrared spectra as both Nujol mulls and KBr discs were recorded on a Bruker IFS 66 FTIR spectrophotometer. Scanning electron microscopy (SEM) spectra were collected from a Hitachi 570 energy-dispersive X-ray microanalysis instrument equipped with a Tracor Northern 5502 energy-dispersive X-ray spectrometer. X-ray powder data were recorded on a 114.83 mm diameter Debye–Scherrer camera using Ni-filtered Cu-K_α radiation from a Phillips PW 1010 generator. Samples were contained in sealed Lindemann capillaries.

The title compound was made by the literature method (11), and also obtained from mixtures of NaOH, Na_2SiO_3, and H_2O_2 (7, 8) by careful washing with H_2O_2. Optimum conditions for the growth of single crystals suitable for structural determination occur when solutions contain 3.0 mol dm^{-3} SiO_2, 2.0 mol dm^{-3} H_2O_2, and 6.5–7.0 mol dm^{-3} NaOH, crystallization being complete after 48 h; ir (KBr): 3625, 3533, 3446, 3305 (w on broad background, νOH), 2920 (w,vb), 1918 (w,b), 1672 (m, δHOH), 985 (s, νO–O), 833 (sh), 717 (m), 627 (m), 537 (m) cm^{-1}. When exposed to air new peaks due to CO_4^{2-} occur at 1664 (vs, νC═O), 1645 (sh, δHOH?), 1369, 1342 (d,s), 1016 (m), 877 (m), 818 (m), 724 (m) cm^{-1}. In addition, peaks due to CO_3^{2-} occur at 1450 (vs,b), 878 (m) and 724 (w) cm^{-1}.

The first 25 lines in the powder pattern of Na_2CO_4, *d*-spacing in Å (relative intensities): 5.10(2), 4.88(2), 4.30(1), 3.7395), 3.65(2), 3.42(2), 3.29(5), 3.08(20), 2.99(10), 2.915(20), 2.800(2), 2.750(5), 2.700(100), 2.610(2), 2.530(80) br, 2.37(5), 2.300(100), 2.275(5), 2.205(5).

X-ray crystallography

A small crystal was mounted in a sealed Lindemann capillary under nitrogen, and immediately placed in liquid nitrogen.

Data were collected on an Enraf–Nonius CAD4 diffractometer using graphite-monchromatized Mo-K_α radiation at 173 K; 1343 independent reflections were measured in the range $-20 \le h \le 17, 0 \le k \le 9, 0 \le l \le 6$ with a 2θ (max) = 59.96°. Of these, 1064 had $F_o > 4\sigma(F_o)$ and were used for further computation of *wR*2. The Enraf–Nonius peak search, centering, and indexing program was used to determine the initial choice for crystal class and space group. Unit cell parameters were obtained by least-squares analysis of 25 low-angle reflections. The stability of the crystal was measured by periodically monitoring three standard reflections; no systematic intensity variations were observed. Intensity data were corrected for Lorentz and polarization factors. NRCVAX programs (29; PC version of the system) were used for scaling and data reduction. Atomic scattering factors were taken from tabulated values (30).

Crystal data were as follows: H_8O_5Na, $F_w = 111.05$, monoclinic, *C*2/*c*; $a = 14.335(3)$, $b = 6.461(1)$, $c = 11.432(2)$ Å, $\beta = 118.28(3)°$, $V = 932.44$ Å^3, $Z = 8$, $D_c = 1.582$ g cm^{-3}, $F(000) = 472.0$, $\lambda = 0.71073$ Å, μ(Mo-K_α) = 0.24 mm^{-1}, $T = 173$ K.

The structure was solved by a combination of direct methods and difference Fourier cycles. The Na and the O atoms were refined anisotropically and H atoms were refined isotropically. Coordinates of all atoms were refined. Full-matrix least-squares refinement on F^2, for 1064 data ($F_o > 4\sigma(F_o)$), 0 restraints, and 87 parameters resulted in a gof on $F^2 = 1.129$, $R1 = 0.0313$, and $wR2 = 0.0760$.[2] The largest peaks in the final difference Fourier were 0.243 and −0.223 e/Å^3. Positional thermal parameters are shown in Table 2.[3]

[2] $R1 = \sigma||F_o|-|F_c||/\sigma|F_o|$ and $wR2 = [\sigma[w(F_o^2-F_c^2)^2]/\sigma[w(F_o^2)^2]]^{0.5}$.

[3] Tables of atomic coordinates and displacement parameters, complete bond lengths and angles, and other refinement data may be purchased from: The Depository of Unpublished Data, Document Delivery, CISTI, National Research Council Canada, Ottawa, Canada K1A 0S2. This supplementary material has also been deposited with the Cambridge Crystallographic Data Centre, and can be obtained on request from The Director, Cambridge Crystallographic Data Centre, University Chemical Laboratory, 12 Union Road, Cambridge, CB2 1EZ, U.K.

© 1997 NRC Canada

Fig. 3. IR spectra of $Na_2O_2 \cdot 8H_2O$ (dotted line) and, probably, Na_2CO_4 (solid line). Contamination by Na_2CO_3 is revealed by the very strong band marked by * due to ν_3 of CO_3^{2-}. Arrows indicate the positions of the peaks in the spectrum of the analogous $Li_2CO_4 \cdot H_2O$; relative peak intensities are also very similar (20).

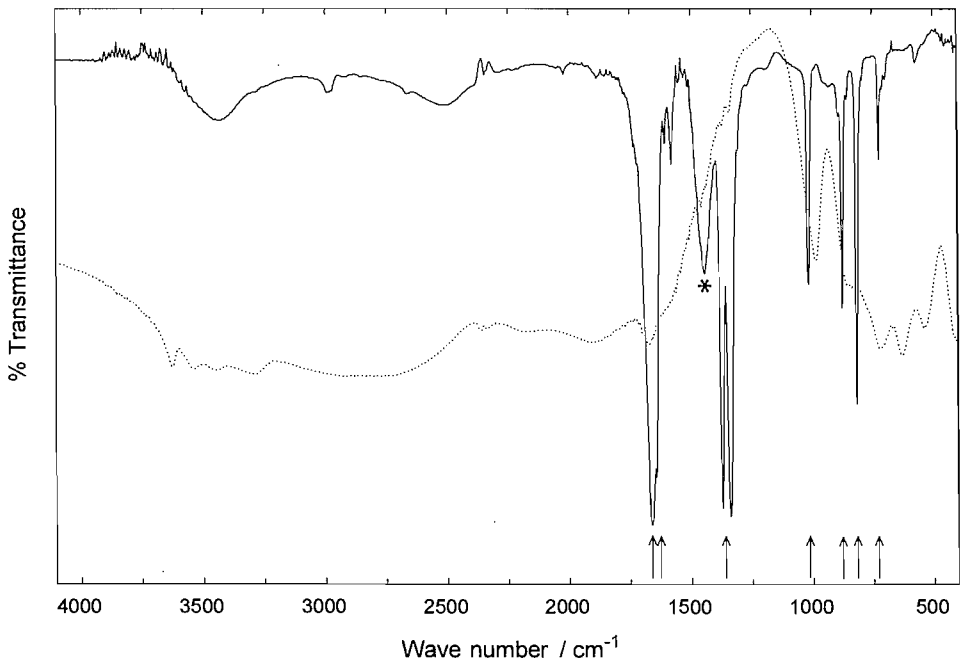


Table 2. Atomic coordinates ($\times 10^4$) and equivalent isotropic displacement parameters ($A^2 \times 10^3$). $U_{(eq)}$ is defined as one third of the trace of the orthogonalized U_{ij} tensor.

	x	*y*	*z*	$U_{(eq)}$
Na	3002(1)	49(1)	682(1)	20(1)
O(1)	4603(1)	1634(2)	834(1)	22(1)
O(2)	2844(1)	3414(2)	1505(1)	22(1)
O(3)	3855(1)	−1302(2)	2894(1)	21(1)
O(4)	3566(1)	−3115(2)	−79(1)	23(1)
O(5)	5203(1)	5174(2)	2004(1)	21(1)
H(11)	4398(16)	1803(32)	53(22)	46(6)
H(12)	4794(19)	3022(41)	1231(23)	69(8)
H(21)	2469(16)	3553(29)	1801(19)	35(5)
H(22)	3439(17)	4003(33)	2002(20)	45(6)
H(31)	4288(15)	−443(30)	3225(19)	31(5)
H(32)	4225(17)	−2364(39)	2857(21)	62(7)
H(41)	3769(16)	−2769(35)	−582(20)	45(6)
H(42)	4109(17)	−3635(33)	600(21)	47(6)

Refinement calculations were carried out on a PC Express computer with the SHELX program system (31) .

Acknowledgments

Support of this work by a National Centres of Excellence (Mechanical Pulping Project) grant provided by the Government of Canada (to D.G.H.) is gratefully acknowledged. We thank also the Natural Sciences and Engineering Research Council of Canada and the Lakehead University Senate Research Committee for additional financial support. We gratefully acknowledge the technical assistance provided by the staff of the Lakehead University Instrumentation Laboratory.

References

1. G.A. Smook. Handbook for pulp and paper technologists. Canadian Pulp and Paper Association, Montreal and Tappi, Atlanta, Ga. 1982.
2. J.T. Burton, L.L. Campbell, and G.P. Donnini. Pulp Pap. Can. **88**, T224 (1987).
3. J.L. Colodette, S. Rothenberg, and C.W. Dence. J. Pulp Pap. Sci. **15**, J3 (1989); **15**, J45 (1989).
4. S.D. Kinrade, D.G. Holah, G.S. Hill, K.E. Menuz, and C.R. Smith. J. Wood Chem. Technol. **15**, 202 (1995).
5. T. Ali, D. McArthur, D. Scott, M. Fairbank, and P. Whiting. J. Pulp Pap. Sci. **12**, J166 (1986).
6. Von G. Rietz and H. Kopp. Z. Anorg. Allg. Chem. **382**, 31 (1971); **384**, 19 (1971); Von G. Rietz and J. Losher. Z. Anorg. Allg. Chem. **382**, 37 (1971).
7. H. Horiuchi, T. Ariyoshi, and J. Maekawa. Jpn. Kokai (patent) 77 19, 199 (1977); Chem. Abstr. **87**, 7874t (1977).
8. J.T. Burton. J. Pulp Pap. Sci. **12**, J95 (1986).
9. Von A. Blaschette and J.M. Saad. Holzforchung, **23**, 163 (1969); Von A. Blaschette. Z. Anorg. Allg. Chem. **384**, 177 (1971).
10. N.-G. Vannerberg. Prog. Inorg. Chem. **4**, 125 (1962).
11. R.A. Penneman. Inorg. Synth. **3**, 1 (1950); R.J. Seyse and G. Gordon. J. Inorg. Nucl. Chem. **34**, 477 (1972).
12. D.L. Schecter and J.J. Leddy. U.S. Patents 3,305,310; 3,304,618 (Chem. Abstr. **66**, 77836x; **66**, 96947a (1967)).
13. N.-G. Vannerberg. Ark. Kemi, **14**, 17 (1959).
14. V. Kotov. J. Phys. Chem. USSR, **13**, 829 (1939).
15. International Centre for Diffraction Data, Newton Square, Pa.
16. R.K. Iler. The chemistry of silica. Wiley, New York. 1979.
17. W.P. Griffith and T.D. Wickins. J. Chem. Soc. (A), 397 (1968); J.C. Evans. J. Chem. Soc. Chem. Commun. 682 (1969).

Can. J. Chem. Downloaded from www.nrcresearchpress.com by 84.22.46.98 on 09/08/12
For personal use only.

© 1997 NRC Canada

18. M.H. Brooker and J.B. Bates. J. Chem. Phys. **54**, 4788 (1971).
19. E.G. Brame, S. Cohen, J.L. Margrave, and V.W. Meloche. J. Inorg. Nucl. Chem. **4**, 90, (1957).
20. D.P. Jones and W.P. Griffith. J. Chem. Soc. Dalton Trans. 2526 (1980).
21. V.I. Sokol, V.M. Bakulina, E.Y. Filatov, and T.P. Firsova. Russ. J. Inorg. Chem. **13**, 1211 (1968).
22. A.J. Cohen. J. Am. Chem. Soc. **74**, 3762 (1952).
23. P.J. Hayward, D.M. Blake, G. Wilkinson, and C.J. Nyman. J. Am. Chem. Soc. **92**, 5873 (1970).
24. M.A.A.F. de C.T. Carrondo, W.P. Griffith, D.P. Jones and A.C. Skapski. J. Chem. Soc., Dalton Trans. 2323 (1977).
25. (*a*) R. Oura. Senshoku Kogyo, **41**, 557 (1993); Chem. Abstr. **120**, 194518 (1994); (*b*) R. Marton, A. Czerkies, and S.G. Granzow. Tappi J. **69**, 98 (1986).
26. J.M. Adams and R.G. Pritchard. Acta Crystallogr. Sect. B: Struct. Crystallogr. Cryst. Chem. **B33**, 3650 (1977).
27. A.M. Chernyshova and T.A. Dobrynina. Chem. Abstr. **82**, 148848w (1975); **82**, 90708 (1975); T.A. Dobrynina. Chem. Abstr. **83**, 21027 (1975).
28. F. Krauss and C. Oettner. Z. Anorg. Allg. Chem. **204**, 318 (1932).
29. E.J. Gabe, Y. Le Page, J.P. Charland, F.L. Lee, and P.S. White. J. Appl. Crystallogr. **22**, 384 (1989).
30. D.T. Cromer and J.T. Waber. International tables for X-ray crystallography. Vol. 4. Kynoch Press, Birmingham. 1974.
31. G.M. Sheldrick. SHELXL-93, Program system for X-ray structure determination. University of Cambridge, 1993.

Can. J. Chem. Downloaded from www.nrcresearchpress.com by 84.22.46.98 on 09/08/12
For personal use only.

© 1997 NRC Canada

The complexation of glucose and other monosaccharides with cyclodextrins[1]

Frank Hacket, Jose-Miguel Coteron, Hans-Jörg Schneider, and Vladimir P. Kazachenko

Abstract: Equilibrium constants of complexes between β-cyclodextrin and glucose, galactose, or mannose have been determined by fluorometric competition titrations in water to be as low as $K = 1–0.5\ M^{-1}$, in sharp contrast to recently published values for glucose around $K = 400\ M^{-1}$. The pentoses ribose, xylose, and arabinose show association constants between 6.3 and $1.5\ M^{-1}$, in agreement with published values. Preliminary computer-aided molecular modelling studies suggest that the small values observed for the hexoses are not due to steric hindrance of an intracavity inclusion but to a smaller number of intermolecular hydrogen bonds and to some strain as a result of cyclodextrin deformation. Calorimetric measurements of the glucose–β-cyclodextrin complex show, again in contradiction with the literature, an **endo**thermic reaction, or a free enthalpy value close to zero.

Key words: cyclodextrin complexes, sugar complexation, glucose complexation, calorimetry, computer-aided molecular modelling.

Résumé : Faisant appel à des titrages fluorométriques compétitifs et opérant dans l'eau, on a déterminé que les constantes d'équilibre des complexes formés entre la β-cyclodextrine et le glucose, le galactose ou le mannose peuvent avoir des valeurs aussi faibles que $K = 1$ ou $0{,}5\ M^{-1}$; ces valeurs sont en opposition avec les valeurs de $K = 400\ M^{-1}$ rapportées récemment pour le glucose. Les constantes d'association des pentoses, comme le ribose, le xylose et l'arabinose, se situent entre 6,3 et $1{,}5\ M^{-1}$. Des études préliminaires de modelage moléculaire assisté par ordinateur suggèrent que les faibles valeurs observées avec les hexoses ne sont pas le résultat d'un empêchement stérique à une inclusion intracavité, mais à la présence de moins de liaisons hydrogènes intermoléculaires et à une tension résultant d'une déformation de la cyclodextrine. Des mesures calorimétriques du complexe glucose–β-cyclodextrine indiquent, encore une fois en contradiction avec ce qui a été rapporté dans la littérature, que la réaction est **endo**thermique ou que son enthalpie libre est très proche de zéro.

Mots clés : complexes de la cyclodextrine, complexation des sucres, complexation du glucose, calorimétrie, modelage moléculaire assisté par ordinateur.

[Traduit par la rédaction]

Introduction

Several authors have recently investigated interactions of cyclodextrins with sugars, with, however, quite conflicting results (2–4). Although the interactions between the hydrophilic guest molecules with cycloamyloses in water must be expected to be small, the most recent publication by Hirsch et al. (2) claims for the complex between D-glucose and β-cyclodextrin an association constant of $450\ M^{-1}$, based on measurements with a glucose-sensitive electrode, or of $380\ M^{-1}$, on competition with methyl orange as optical indicator. This is in sharp contrast to earlier data from Aoyama et al. (3) and de Namor et al. (4), who reported that binding of cyclodextrins with aldohexoses, and in particular with glucose, is barely measurable. We have shown (5) that efficient binding of saccharides in cyclodextrins requires the presence of additional groups on the cycloamylose ring. As not only the most recent paper (2) reports binding that by far exceeds any predictions and earlier measurements, but also the others (3, 4) contain some discrepancies, or K values of "0" (3), we have remeasured some association constants with a competition assay using the fluorescence dye 8-anilinonaphthalen-1-sulfonate ANS, and carried out some calorimetric measurements. To provide firmer grounds for the inclusion modes discussed in the earlier papers (2–4) we also performed some preliminary computer-aided molecular modelling studies on cyclodextrin complexes with glucose and ribose.

Received July 28, 1996.

F. Hacket, J.-M. Coteron, and H.-J. Schneider.[2]
FR Organische Chemie der Universität des Saarlandes, D 66041 Saarbrücken, Germany.
V.P. Kazachenko. IPAC, Russian Academy of Science, Chernogolovka/Moscow Region, 142432 Russia.

[1] This is part 69 of the Saarbrücken series Supramolecular chemistry. For part 68, see ref. 1.

[2] Author to whom correspondence may be addressed. Telephone: 681-302-3209/2269. Fax: 681-302-4105/3209. E-mail: CH12hsvr@sbusol.rz.uni-sb.de

Results

Experimental and computational details

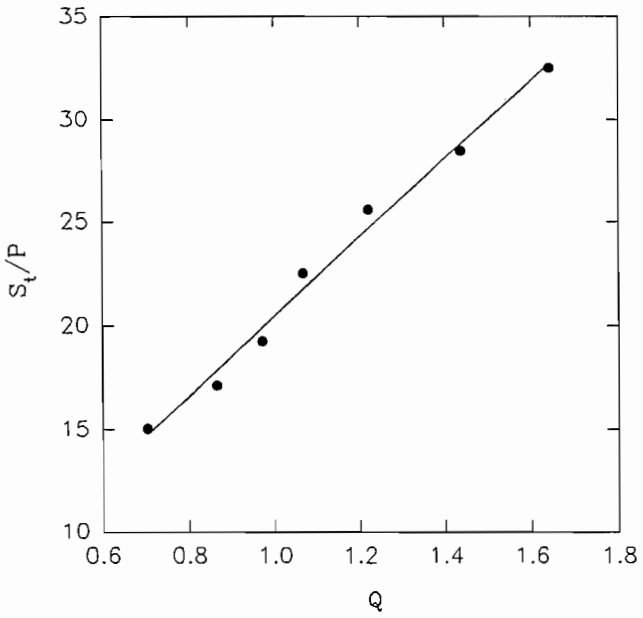
β-Cyclodextrin, ANS, TNS (6-toluidinonaphthalene-2-sulfonate), and the monosaccharides were commercially available and were dried prior to use without further purification.

© 1997 NRC Canada

Can. J. Chem. Downloaded from www.nrcresearchpress.com by 92.62.229.171 on 09/08/12
For personal use only.

Can. J. Chem. Downloaded from www.nrcresearchpress.com by 92.62.229.171 on 09/08/12
For personal use only.

Fig. 1. Example of a linear least-squares fit to eq. [1] for a titration of β-CD, ANS, and D-ribose.



Competition titrations (Table 1) with ANS were carried out at 298°C by adding a stock solution of the monosacchcaride (1.0 M) to a solution of β-CD (1.5×10^{-2} M) and ANS (1×10^{-4} M) in buffer solution at pH = 7.0 (Na_2HPO_4 + NaOH), measuring a fluorescence decrease from, for example, 1500 to 800 relative units. The instrument used was a Hitachi fluorescence spectrophotometer F-2000. The association constant K for ANS + β-CD (measured in a fluorescence titration by adding a stock solution of β-CD (1.5×10^{-2} M) to a solution of 1×10^{-4} M ANS) was 110 M^{-1} (±7%), in accord with published values (6). With TNS instead of ANS, we obtained an association constant with ß-CD of $K = 2.5 \times 10^3$ M^{-1} (corresponding to a free energy of association of ΔG = 19.4 kJ/mol). (With TNS, longer exposure times in the fluorimeter lead to changes of the emission intensity.)

The data were evaluated by a linear least-squares fit to eq. [1] (ref. 7); Fig. 1 shows an example of the fitting.

[1] $S_t/P = (K_I/K_{11})\ Q + 1$

where $P = L_t - 1/QK_I - I_t/Q + 1$
$Q = (e - e_{IL}) / (e_I - e)$
S = [Monosaccharide], S_t = [Monosaccharide]total
L = βCD, L_t = [βCD]total
I = ANS, I_t = [ANS]total
K_I = [IL]/[I] [L], K_{11} = [SL]/[S] [L]
e = measured fluorescence intensity
e_I = fluorescence intensity of ANS without βCD
e_{IL} = fluorescence intensity of the complex ANS–βCD

K is in M^{-1}; S, P and L in M; other parameters are dimensionless.

Heats of complexation of cyclodextrins with α-D-glucose in fresh doubly distilled water at 298 K were measured with a LKB-2107 microcalorimetry system. Aqueous solutions of cyclodextrins (2 mL) in the calorimetric vessel were titrated with the α-D-glucose–water solutions contained in a 1 mL gastight motor-driven Hamilton syringe (for concentrations see below). Dilution heats of glucose were automatically taken into account by differential calorimetry, adding parallel glucose solutions to pure water. Dilution heats of cyclodextrins were negligible, as checked by a separate experiment.

The following total concentrations of the reagents were used in calorimetric titrations (we could not reach the concentration 0.08–0.10 mol/L reported in the literature (4) for α-CD in water).

Cyclodextrin	[Cyclodextrin] (mmol/L)	[Glucose] mmol/L
α-CD	25.2–28.3	14.9–92.5
	67.8–73.2	107.0–231.4
β-CD	25.8–29.4	7.5–92.5
	17.2–19.4	7.5–46.7

The reliability of the calorimetric equipment was checked by measuring in duplicate and by measuring stability constants and enthalpies of a well-known reaction. Thus. for the 1:1 complexation of 18-crown-6 with KNO_2 in H_2O at 298 K, values of log K 1.98(0.01) and ΔH −25.8(0.2) kJ/mol were obtained, in close agreement with published calorimetric data (log K 2.03, ΔH −26.0 kJ/mol) (8).

The calorimetric data were analyzed using the multipurpose computer program CHEM-EQUI as described elsewhere (9). For the complexation of cyclodextrins (CD) with α-D-glucose (G) fitting was satisfactory for a simple 1:1 (CD+G ⇌ CD–G) complexation model.

Molecular modelling was carried out with QUANTA/CHARMm (version 4.0) from MSI on a SGI workstation, with a constant dielectric value of ε = 3 D; minimizations were done by the steepest descent method followed by the Adapted Newton Raphson technique. Several start geometries were generated by manual docking of the sugar within the cyclodextrins.

Discussion

The discrepancies documented in Tables 1 and 2 provide an illustration of the serious problems involved in measurements of very weak complexes. The association constants K obtained from the fluorescence titrations are believed to be fraught with less error in view of the relatively large signal intensity changes. It should be noticed that the cyclodextrins and the sugars are ideal candidates for fluorescence titrations in view of their inactivity in luminescence. However, the necessity to use concentrations around 1 M of the excess compound (sugar) for complexes with K around 1 M^{-1} may well lead to problems arising from the varying self-association and from changes in bulk properies of the medium. Nevertheless, we have been able to replace for the hexose complexes the "zero" K values published until now (3) by discrete numbers, showing that indeed the glucose, galactose, and mannose are complexed close to or a little below 50% at standard conditions (1 M solution of either host or guest, or both). The larger association constants obtained for the pentoses agree with the earlier reported values (3) (Table 1), within the experimental error.

© 1997 NRC Canada

Table 1. Association free energies ΔG^0 (kJ/mol) and association constants K (M^{-1}) of monosaccharides with β-cyclodextrin.[a]

	$\Delta G^{0\,b}$	K^b	K^c	$\Delta G^{0\,d}$	$\Delta G^{0\,e}$
Hexoses:					
D-Glucose	+1.3 (±0.9)	0.6	"0"	—	−15(±0.9)
D-Galactose	+1.7 (±0.5)	0.5	"0"	—	—
D-Mannose	0.0 (±0.3)	1.0	"0"	—	—
Pentoses:					
D-Ribose	−4.8 (±0.1)	6.3	−5.3 (±20%)	—	—
D-Xylose	−1.2 (±0.6)	1.6	−1.0 (±20%)	−6.96 (±0.54)	—
D-Arabinose	−1.0 (±0.5)	1.5	−0.7 (±20%)	−6.91 (±1.82)	—

[a]in phosphate buffer pH = 7.0 at 298 K.
[b]From competition titration with ANS, this work.
[c]Reference 3, from competition titration with ANS.
[d]Reference 4, from microcalorimetric titration.
[e]Reference 2, from titration with glucose-sensitive electrode.

Table 2. Calorimetric data for the complex of D-glucose[a] with cyclodextrins in water.

	ΔH^b	ΔH^c	ΔH^d
α-CD	+3.4 (±2.5)	−11 (±4)	−0.14 (±0.03)
β-CD	+1.6 (±1.5)	−15 (±5)	—

[a]Free enthalpies ΔH in kJ/mol, at 298 K.
[b]This work.
[c]Reference 2.
[d]Reference 4.

The problems arising from weak complexes become much more serious with calorimetric determinations as here the measurement signal is a function of the then usually low reaction heat, and therefore susceptible to even greater error. The measurements by Danil de Namor et al. (4) were carried out with very sensitive microcalorimetric equipment and showed for the measured systems remarkably high reproducibilities and low errors. It is noteworthy, however, that their measurements were restricted to complexes with association constants above 15 M^{-1}. In view of the weak complex with glucose, we tried to measure with as high concentrations as possible, using the observation that the β-CD solubility was enhanced in the presence of glucose. Our calorimetric analysis with glucose and ß-CD was hampered by considerable error, yet demonstrates unequivocally that the formation of the glucose complex is either **endo**thermic, or has values of ΔH close to zero, in agreement with the spectroscopic measurements, and in sharp contrast to other published values (2).

With respect to the binding of different monosaccharides little more can be said other than that a better defined and useful cyclodextrin–glucose complex requires chemical modification of the cycloamylose before one can come even near the claimed (2) association constants around 400 M^{-1}. Several arguments have been put forward (3, 4) for the slightly better binding of pentoses, based on the assumption of intracavity inclusion of the sugars. While we have been able to prove intracavity inclusion for aminocyclodextrins and ribosephosphate by intermolecular NOEs (*5b*), this method is totally unsuited for the extremely weak complexes studied here, which are characterized by a multitude of rapidly exchanging conformers. One cannot even exclude the possibility that the sugars are associated *outside* the cavity, as this has been demonstrated recently by intermolecular NOEs between protons outside the CD host cavity and those of cyclohexanecarboxylate.[3]

Our molecular mechanics calculations at least demonstrate that a larger pyranose with a CH_2OH side chain can also be accommodated within the β-CD cavity (Fig. 2). Although we have not scanned systematically all possible conformations in view of the almost countless orientations,[4] the unknown role of water, and the absence of experimental constraints, it is noteworthy that a complex with the glucose outside the cavity (**OC**) yields a **smaller** calculated association energy than the intracavity complex **IC**. The gas-phase calculations yield for the intracavity complex **IC** an enthalpy 13 kJ/mol below the **OC** complex; **OC** shows four intermolecular hydrogen bonds, **IC** only one, which replaces the intramolecular glucose–hydrogen bond. The simulations suggest deformation of the CD ring. In the **OC** complex, however, the deformations seem to be larger than in the case of **IC**. Thus, at distances between the different glycosidic oxygens of 1–4 glucose, parts of the CD ring change by 0.45–0.89 Å for the **OC** case, and by 0.05–0.19 Å in the **IC** case. The concomitant strain built up during intracavity inclusion is calculated to be as large as 15 kJ/mol, and must be compensated for by large dispersion interactions, which can only materialize within the cavity.

Acknowledgement

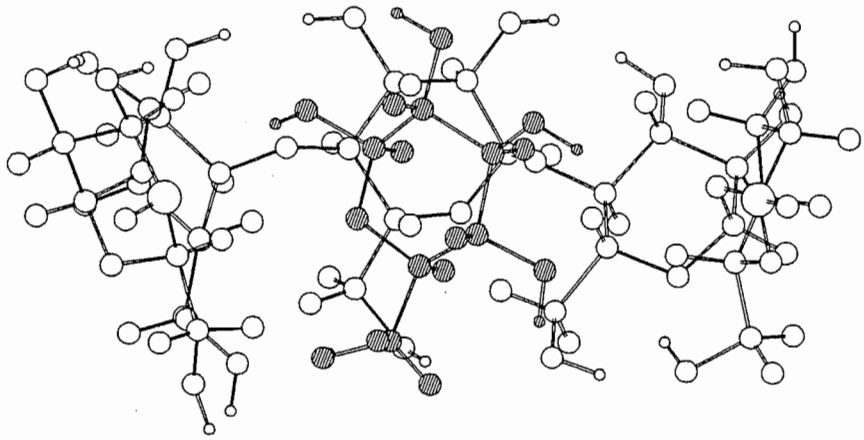
Our work in Saarbrücken is supported by the Deutsche Forschungsgemeinschaft, Bonn, and the Fonds der Chemischen Industrie, Frankfurt. Support from the VW-Stiftung, Hannover, is also gratefully acknowledged.

[3] A Gadre, V. Rüdiger, H.-J. Schneider, and K.A. Connors. Unpublished work.
[4] For molecular mechanics/dynamics calculations on cyclodextrin complexes, see recent references (10).

© 1997 NRC Canada

Can. J. Chem. Downloaded from www.nrcresearchpress.com by 92.62.229.171 on 09/08/12
For personal use only.

Fig. 2. Complex **IC** with D-glucose inside the β-cyclodextrin cavity. The front part of the cyclodextrin is omitted for clarity.



References

1. O.A. Raevsky, V.P. Solov'ev, A.F. Solofnov, H.-J. Schneider, and V. Rüdiger. J. Org. Chem. In press.
2. W. Hirsch, T. Muller, R. J. Pizer, and P.J. Ricatto. Can. J. Chem. **73**, 12 (1995).
3. Y. Aoyama, Y. Nagai, J.-i. Otsuki, K. Kobayashi, and H. Toi. Angew. Chem. Int. Ed. Engl. **31**, 745 (1992).
4. A.F. Danil de Namor, P.M. Blackett, M.C. Cabaleiro, and J.M.L Al Rawi. J. Chem. Soc. Faraday Trans. **90**, 845 (1994).
5. A.V. Eliseev and H.-J. Schneider. (*a*) Angew. Chem. Int. Ed. Engl. **32**, 1331 (1993); (*b*) J. Am. Chem. Soc. **116**, 6081 (1994).
6. H.-J. Schneider, Th. Blatter, and S. Simova. J. Am. Chem. Soc. **113**, 1996 (1991), and refs. cited therein.
7. K. Connors. Binding constants. John Wiley & Sons, New York. 1987.
8. R.M. Izatt, R.E. Terry, B.L. Haymore, L.D. Hansen, N.K. Dalley, A.G. Avondet, and J.J. Christensen. J. Am. Chem. Soc. **98**, 7620 (1976).
8. (*a*) R.M. Izatt, D.V. Dearden, P.R. Brown, J.S. Bradshaw, J.D. Lamb, and J.J. Christensen. J. Am. Chem. Soc. **105**, 1785 (1983).
9. V.P. Solov'ev, E.A. Vnuk, N.N. Strakhova, and O.A. Raevsky. Thermodynamics of complexation of the macrocyclic polyethers with salts of alkali and alkaline-earth metals (in Russian) VINITI, Moscow. 1991.
10. (*a*) M.E. Amato, K.B. Lipkowitz, G.M. Lombardo, and G.C. Pappalarado. J. Chem. Soc. Perkin Trans. 2, **3**, 321 (1996); (*b*) G. Fronza, A. Mele, E. Redenti, and P. Ventura. J. Org. Chem. **61**, 909 (1996); (*c*) F. Perez, C. Jaime, and X. Sanchezruiz. J. Org. Chem. **60**, 3840 (1995); (*d*) C.T. Klein, G. Kohler, B. Mayer, K. Mraz, and S. Reiter. J. Inclusion Phenom. Mol. Recognit. Chem. **22**, 15 (1995); (*e*) J.E.H. Köhler, M. Hohla, M. Richters, and W.A. König. Chem. Ber. **127**, 119 (1994); (*f*) M. Fathallah, F. Fotiadu, and C. Jaime. J. Org. Chem. **59**, 1288 (1994); (*g*) M.E. Amato, G.M. Lombardo, G.C. Pappalardo, and G. Scarlata. J. Mol. Struct. **350**, 71 (1995); (*h*) C. Wolf, W.A. König, and C. Roussel. Liebigs Ann. Chem. **5**, 781 (1995).

Can. J. Chem. Downloaded from www.nrcresearchpress.com by 92.62.229.171 on 09/08/12
For personal use only.

© 1997 NRC Canada

Acid-catalyzed hydrolysis of 4-diazo-isothiochroman-3-one. Comparison with the acyclic analog and the corresponding oxygen system

E.A. Jefferson, A.J. Kresge, and S.W. Paine

Can. J. Chem. Downloaded from www.nrcresearchpress.com by 92.62.229.171 on 09/08/12
For personal use only.

Abstract: The acid-catalyzed hydrolysis of the cyclic diazothiolactone, 4-diazoisochroman-3-one (**3**) was found to occur with the hydronium-ion isotope effect, $k_{H^+}/k_{D^+} = 2.04$ and to give the ring-contracted product, 1,3-dihydrobenzo[*c*]thiophene-1-carboxylic acid (**4**). This shows that protonation of the diazo carbon atom occurs in the rate-determining step and that the reaction also involves migration of the thio group. The hydronium-ion catalytic coefficient for this reaction, $k_{H^+} = 4.04 \times 10^{-3}$ M^{-1} s^{-1}, is 45 times less than that for hydrolysis of its acyclic thio ester analog, *S*-methyl phenyldiazothioacetate (**5**). Semiempirical AM1 molecular orbital calculations support the idea that this difference in reactivity is the result of increased delocalization of negative charge into the aromatic ring in the case of the cyclic substrate, which reduces the negative charge on the diazo carbon atom and makes it less susceptible to protonation.

Key words: hydrolysis, diazoalkanes, charge delocalization, AM1 calculations, thio group migration.

Résumé : On a observé que l'hydrolyse acidocatalysée de la diazothiolactone, 4-diazoisochroman-3-one (**3**), se produit avec un effet isotopique de l'ion hydronium, $k_{H^+}/k_{D^+} = 2{,}04$, et conduit à un produit résultant d'une contraction de cycle, l'acide 1,3-dihydrobenzo[*c*]thiophène-1-carboxylique (**4**). Ces résultats démontrent que, dans l'étape qui détermine la vitesse de la réaction, il se produit une protonation de l'atome de carbone du diazo et que la réaction implique aussi la migration du groupe thio. Le coefficient catalytique de l'ion hydronium pour cette réaction, $k_{H^+} = 4{,}04 \times 10^{-3}$ M^{-1} s^{-1}, est 45 fois moins important que celui observé lors de l'hydrolyse du thioester acyclique analogue, le phényldiazoacétate de *S*-méthyle (**5**). Des calculs d'orbitales moléculaires semiempiriques AM1 supportent l'hypothèse d'après laquelle cette différence de réactivité résulte du fait que, dans le cas du substrat cyclique, il se produit une augmentation de la délocalisation de la charge négative par le noyau aromatique qui réduit la charge négative sur l'atome de carbone du groupe diazo et qui le rend moins susceptible à la protonation.

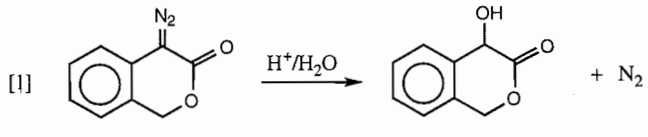
Mots clés : hydrolyse, diazoalcanes, délocalisation le la charge, calculs AM1, migration du groupe thio.

[Traduit par la rédaction]

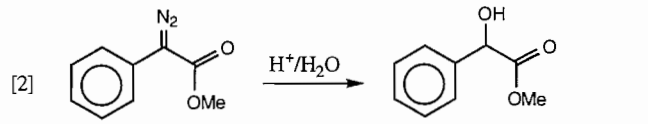
Introduction

We recently reported (1) that the acid-catalyzed hydrolysis of 4-diazoisochroman-3-one, **1**, eq. [1], occurs almost two orders of magnitude more slowly than that of its acyclic analog, methylphenyldiazoacetate, **2**, eq. [2], and we were able, with the aid of semiempirical molecular orbital AM1 calculations, to attribute this difference in reactivity to enforced near-coplanarity of the diazo and phenyl groups in the cyclic substrate as opposed to a staggered arrangement of these groups in the acyclic system.

We have now extended that work to the corresponding thiolactone, 4-diazoisothiochroman-3-one, **3**, whose hydrolytic reactivity we find to be similarly decreased below that of its acyclic analog, *S*-methyl phenyldiazothioacetate, **5** (2). These sulfur systems, however, are unlike their oxygen counterparts, where, as shown in eqs. [1] and [2], hydrolysis involves simple replacement of the diazo group by hydroxyl. In the sulfur analogs, hydrolysis is accompanied by thio group migration to give the ring-contracted product, 1,3-dihydrobenzo-



1



2

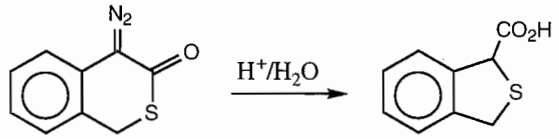
Received August 26, 1996.

E.A. Jefferson, A.J. Kresge,[1] and S.W. Paine. Department of Chemistry, University of Toronto, Toronto, ON M5S 3H6, Canada.

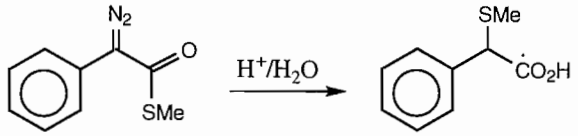
[1] Author to whom correspondence may be addressed. Telephone: (416) 978-7259. Fax: (416) 978-7259. E-mail: akresge@alchemy.chem.utoronto.ca

© 1997 NRC Canada

[c]thiophene-1-carboxylic acid, **4**, eq. [3], in the cyclic case and the correspondingly rearranged product, α-(methylthio)phenylacetic acid, **6**, eq. [4] in the acyclic case (2).

[3] 

3 **4**

[4] 

5 **6**

Once again, we have found AM1 calculations to be helpful in understanding these phenomena.

Experimental section

Materials

4-Diazoisothiochroman-3-one was prepared from isothiochroman-3-one (3)[2] by a diazo transfer reaction using *p*-acetamidobenzenesulfonyl azide as the diazo transfer reagent and triethylamine as the base (4). The product, mp 49–50°C, was obtained in 51% yield. Its spectral properties are as follows: ^{1}H NMR (200 MHz, $CDCl_3$); δ/ppm: 7.40–7.01 (m, 4H, Ar), 4.19 (s, 2H, CH_2); ^{13}C NMR (50 MHz, $CDCl_3$), δ/ppm: 186.96 (C=O), 128.29 (Ar), 127.77 (Ar), 125.80 (Ar), 125.32 (Ar), 121.05 (Ar), 72.83 (C=N_2), 32.70 (CH_2); HRMS, M^+ for $C_9H_6N_2OS$, *m/e*: 190.0201 (calcd.); 190.0197 (found).

All other materials were best available commercial grades.

Kinetics

Rates of hydrolysis of 4-diazoisothiochroman-3-one were determined spectrophotometrically by monitoring the decrease in absorbance of this diazo compound at λ = 325 nm. Measurements were made at substrate concentrations of ca. 10^{-5} M using a Cary model 2200 spectrometer whose cell compartment was thermostatted at 25.0 ± 0.05°C. The rate data fit the first-order rate law well, and observed first-order rate constants were calculated by least-squares fitting of an exponential function.

Molecular Orbital Calculations

Semiempirical AM1 (5) molecular orbital calculations were performed using the program MOPAC 93 (6) in conjunction with a Hewlett Packard 755 computer. The geometries of the singlet ground state for all molecules studied were fully optimized, and energy minima were identified as having all positive eigenvalues and all positive vibrational frequencies.

[2] ^{1}H NMR (200 MHz, $CDCl_3$), δ/ppm: 7.34–7.19 (m, 5H, Ar), 4.22 (s, 2H, CH_2S), 3.80 (s, 2H, CH_2CO).

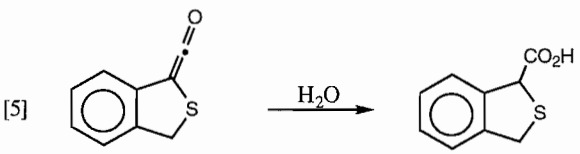
Table 1. Rates of hydrolysis of 4-diazoisothiochroman-3-one in aqueous perchloric acid solutions at 25°C.[a]

[Acid]/10^{-2} M	$k_{obs}/10^{-5}$ s^{-1}
H_2O	
10.0	38.4, 37.8, 37.1
8.00	30.7, 30.6
6.00	21.6, 21.0, 21.1
4.00	14.2, 14.0
2.00	5.70, 5.77, 5.38
$k_{obs}/s^{-1} = -(2.42 \pm 0.36) \times 10^{-5} + (4.04 \pm 0.05) \times 10^{-3}[HClO_4]$	
D_2O	
10.0	19.7, 20.2, 19.2
8.00	16.2, 16.3, 16.1
6.00	12.2, 12.1, 12.2
4.00	8.44, 8.04, 8.28
2.00	4.20, 4.10, 3.99
$k_{obs}/s^{-1} = -(2.49 \pm 1.03) \times 10^{-6} + (1.98 \pm 0.02) \times 10^{-3}[DClO_4]$	
$k_{H^+}/k_{D^+} = 2.04 \pm 0.03$	

[a]Ionic strength = 0.10 M ($NaClO_4$).

Results

The acid-catalyzed hydrolysis of 4-diazoisothiochroman-3-one was found to give 1,3-dihydrobenzo[*c*]thiophene-1-carboxylic acid (**4**) as the sole reaction product. This was established by allowing a 10^{-4} M solution of the substrate in 0.1 M aqueous perchloric acid to stand in the dark for 48 h and then extracting the reaction mixture with ethyl acetate. Removal of the extraction solvent gave a residue whose ^{1}H NMR spectrum was identical with that of an authentic sample of the acid, prepared by hydration of the corresponding ketene, **7**, eq. [5],

[5] 

7

itself obtained by photo-Wolff rearrangement of 4-diazoisothiochroman-3-one.[3] This spectrum also showed the absence of any other substance.

Rates of hydrolysis of 4-diazoisothiochroman-3-one were measured in H_2O and D_2O solutions of perchloric acid over a range of acid concentrations. The data are summarized in Table 1. Observed first-order rate constants proved to be accurately proportional to acid concentration, and linear least-squares analysis gave the hydronium ion catalytic coefficients, $k_{H^+} = 4.04 \times 10^{-3}$ M^{-1} s^{-1} and $k_{D^+} = 1.98 \times 10^{-3}$ M^{-1} s^{-1}, whose ratio provides the kinetic isotope effect $k_{H^+}/k_{D^+} = 2.04$.

Semiempirical AM1 molecular orbital calculations were performed to obtain minimum energy structures for 4-diazoisothiochroman-3-one and *S*-methyl phenyldiazothioacetate. Two minimum energy structures were found for the latter, cor-

[3] E.A. Jefferson, unpublished work.

© 1997 NRC Canada

Can. J. Chem. Downloaded from www.nrcresearchpress.com by 92.62.229.171 on 09/08/12
For personal use only.

Table 2. Results of AM1 calculations.

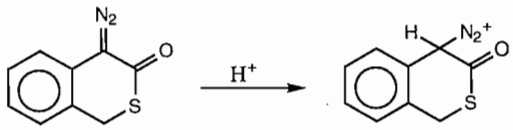
Substance	Dihedral angle between diazo and phenyl groups/degrees	Charge/electrons[a]	
		Diazo carbon	Phenyl group
4-Diazoisothiochroman-3-one	30	–0.27	+0.11
S-Methyl s-*cis*-phenyldiazothioacetate	90	–0.37	+0.19

[a]Charge distributions obtained by the molecular field potential method (7).

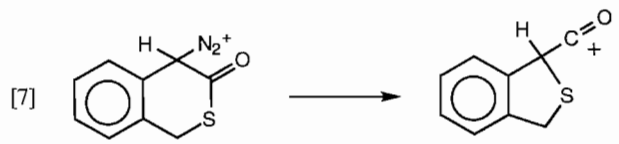
responding to s-*cis* and s-*trans* conformations about the bond connecting the diazoalkane and carbonyl groups, with the s-*cis* isomer being the more stable by 2.5 kcal mol^{-1}. Some selected results of the calculations for this isomer and the cyclic substrate are given in Table 2.

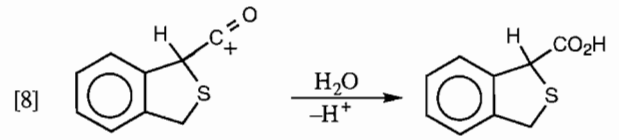
Discussion

The present work shows that the hydrolysis of 4-diazoisothiochroman-3-one is an acid-catalyzed reaction with a substantial hydronium-ion kinetic isotope effect in the normal direction: $k_{H^+}/k_{D^+} = 2.04$. This is classic evidence for rate-determining proton transfer to carbon (8), and it implies that the site of protonation by the acid catalyst in this reaction is the diazo carbon atom, eq. [6]. Another potential site for protonation is the carbonyl oxygen atom, and such a mechanism has been found to operate in the hydrolysis of some diazocarbonyl compounds (9). Proton transfer to oxygen, however, is generally fast and reversible, and that should give an inverse isotope effect, $k_{H^+}/k_{D^+} < 1$, contrary to present observation. Protonation on carbon could also be fast and reversible rather than rate determining, and there is evidence that such a mechanism operates in some cases as well (10, 11), but that too would give an inverse isotope effect. It seems clear, therefore, that the present reaction occurs by rate-determining proton transfer to the diazo carbon atom.

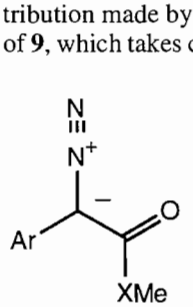
[6] 

In the hydrolysis of diazocompounds, proton transfer to carbon is usually followed by displacement of nitrogen by a water molecule. In the present case, however, because the sole reaction product is the ring-contracted 1,3-dibenzo[*c*]thiophene-1-carboxylic acid (eq. [3]), displacement by water must be being replaced by thio group migration. Such thio group migration had been observed before, in the hydrolysis of the acyclic analog of the present reaction (eq. [4]) (2). It was argued then that migration could be concerted with proton transfer, but it was also pointed out that such a concerted mechanism would require a rather contorted transition state in which proton transfer, migration, and leaving group departure all were occurring at the same time; a stepwise mechanism with migration taking place after proton transfer might therefore be more plausible. Such a stepwise mechanism would convert the diazonium ion formed by proton transfer, as shown in eq. [6], into an acylium ion, eq. [7], which could then be hydrated to give the final reaction product, eq. [8].

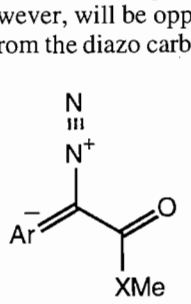
[7] 

[8] 

Comparison of the hydronium-ion catalytic coefficient for hydrolysis of 4-diazoisothiochroman-3-one determined here with that found before for the acyclic analog, *S*-methyl phenyldiazothioacetate, eq. [4] (2), shows the cyclic compound to be 45 times less reactive. This is similar to the 57-fold reduction observed before in a comparison of the rates of hydrolyses of cyclic and acyclic substrates in the corresponding oxygen series, eqs. [1] and [2] (1). It was suggested then that this rate reduction is produced by a change in the balance of contributions provided by the various resonance forms that make up the structure of these diazo compounds. The rate of reaction might be expected to increase in proportion to the importance of resonance form **8**, which puts negative charge on the carbon atom that is protonated in the rate-determining step. The contribution made by this form, however, will be opposed by that of **9**, which takes charge away from the diazo carbon atom and puts it into the aromatic group. Such charge delocalization into the aromatic group will be most efficient when the *p*-orbital of the sp^2 hybridized diazo carbon atom is parallel to the *p*-orbitals of the aromatic ring and the dihedral angle between the diazo and aromatic groups is zero. This is more likely to be the case in the cyclic substrate, whose small heterocyclic ring



8



9

Can. J. Chem. Downloaded from www.nrcresearchpress.com by 92.62.229.171 on 09/08/12
For personal use only.

© 1997 NRC Canada

enforces near coplanarity of the diazo and aromatic groups, than in the acyclic substrate, where steric interference between the side chain and aromatic hydrogens at the *ortho* positions encourages twisting about the diazo carbon – aromatic bond.

This argument is supported here, as it was in the oxygen series, by AM1 calculations. As the results summarized in Table 2 show, the dihedral angle between diazo and aromatic groups is considerably less for the cyclic than for the acyclic substrate, and the increased charge delocalization that this produces is reflected in a less negative charge on the diazo carbon and a more negative (less positive) charge in the aromatic group for the cyclic substrate.

Acknowledgement

We are grateful to the Natural Sciences and Engineering Research Council of Canada and the United States National Institutes of Health for financial support of this research.

References

1. E.A. Jefferson, A.J. Kresge, and S.W. Paine. Can. J. Chem. **74**, 1369 (1996).
2. J. Jones, Jr. and A.J. Kresge. J. Org. Chem. **58**, 2658 (1993).
3. C. Lemaire, A. Luxen, L. Christiaens, and M. Guillaume. J. Heterocycl. Chem. **20**, 811 (1983).
4. J.S. Baum, D.A. Shook, H.M.L. Davies, and H.D. Smith. Synth. Commun. **17**, 1709 (1987).
5. M.J.S. Dewar, E.G. Zoebisch, E.F. Healy, and J.J.P. Stewart. J. Am. Chem. Soc. **107**, 3902 (1985).
6. MOPAC 93.00 Manual, J.J.P. Stewart, Fujitsu Limited, Tokyo, Japan. 1993.
7. B.H. Besler, K.M. Merz, Jr., and P.A. Kollman. J. Comput. Chem. **11**, 431 (1990).
8. J.R. Keeffe and A.J. Kresge. *In* Techniques of Chemistry. Vol. VI. Investigations of rates and mechanisms of reactions. 4th ed. *Edited by* C.F. Bernasconi. Wiley–Interscience, New York. 1986. Chap. XI.
9. M. Regitz and G. Maas. Diazo compounds, properties and synthesis. Academic Press, New York. 1986. pp. 122–123.
10. R.P. Bell. The proton in chemistry. 2nd ed. Cornell University Press, Ithaca, N.Y. 1973. pp. 164–171.
11. A.J. Kresge and V.V. Popik. Electronic conference on heterocyclic chemistry. 1996. http://hackberry.chem.niu.edu.ECHET96/papers/037/index.htm.

Can. J. Chem. Downloaded from www.nrcresearchpress.com by 92.62.229.171 on 09/08/12
For personal use only.

© 1997 NRC Canada

Substituent effects on basicity in Group 15 compounds: an analysis based on proton affinities, charge distributions, and dipole polarizabilities

S.T. Howard, J.P. Foreman, and P.G. Edwards

Can. J. Chem. Downloaded from www.nrcresearchpress.com by 92.62.229.171 on 09/08/12
For personal use only.

Abstract: Ab initio calculations on a series of trisubstituted amines, phosphines, and arsines are presented at the MP2/6-311G(d,p) level. Specifically, the species studied are XH_3, XF_3, and $X(Me)_3$, where X = N, P, or As. The influence of the substituents on the proton affinity is analyzed in terms of the charge distribution, its topology, some one-electron properties (dipole moments, electric field gradients), and dipole polarizabilities. An atoms-in-molecules decomposition of the charge distribution, energetics, and polarizabilities also proves informative. There seems to be no straightforward way of rationalizing the basicities of these compounds on the basis of electrostatic properties (i.e., properties of the charge distribution in the unprotonated bases). However, substituent effects on basicities can be correlated with response properties, such as the molecular (and atoms-in-molecules) polarizability tensors, and the amount of charge that a substituent group or atom donates on protonation.

Key words: quantum chemistry, proton affinity, electron density, lone pairs, polarizability, basicity, dipole moment, electric field gradient.

Résumé : On a effectué des calculs ab initio, au niveau MP2/6-311G(d,p), sur une série d'amines, des phosphines et d'arsines trisubstituées. D'une façon spécifique, les espèces étudiées sont : XH_3, XF_3 et $X(Me)_3$ dans lesquelles X = N, P ou As. On a analysé l'influence des substituants sur l'affinité protonique en fonction de la distribution de la charge, de sa topologie, de quelques-unes de ses propriétés impliquant un électron (moments dipolaires, gradients des champs électriques) et des polarisabilités dipolaires. Une décomposition de la distribution de charge, des énergies et des polarisabilités, effectuée en fonction de la théorie des atomes dans les molécules, s'est aussi avérée utile pour fournir de l'information. Il ne semble pas y avoir de façons simples de rationaliser les basicités de ces composés sur la base des propriétés électrostatiques (c'est-à-dire des propriétés de la distribution de charge dans les bases qui ne sont pas protonées). Toutefois, on peut établir une corrélation entre les effets des substituants sur les basicités et les propriétés de réponse, telles que les tenseurs de polarisabilité moléculaire (et des atomes dans les molécules) et la quantité de charge donnée par un atome ou un groupe substituant lors de sa protonation.

Mots clés : chimie quantique, affinité protonique, densité électronique, paires libres, polarisabilité, basicité, moments dipolaires, gradient du champ électrique.

[Traduit par la rédaction]

Introduction

The concept of basicity is a cornerstone of chemistry. It has traditionally been defined in a dichotomous way: as the ability of an atom to furnish an electron pair (the Lewis definition), or as a scale based on acid–base equilibrium constants (Brønsted–Lowry definition). If these two definitions are really describing the same phenomena, then it ought to be possible to link the lone pair electron distributions in a series of related monofunctional bases, and their corresponding (thermodynamic) basicities. Some recent theoretical attempts to do just this in simple amine (1) and phosphine (2) bases have met with only limited success. Other theoretical approaches for rationalizing substituent effects on basicity utilize response functions, such as softness and hardness (3). The remaining parameter often used in predicting basicity trends, electronegativity (χ), is also effectively a response function, since Nagle has shown that atomic dipole polarizabilities (α's) and χ's are closely correlated (4).

In this work we present high-level calculations on a series of simple amines, phosphines, and arsines, looking at both electrostatic and response properties, in order to see which (if any) act as indicators for the proton affinity (PA). We also apply Bader's Atoms-In-Molecules (AIM) decomposition of the charge distribution (5) to the ground state charge distribution of the free bases, and to the α tensors (6–8). In this way it is possible to focus on the properties of the central

Received August 2, 1996.

S.T. Howard,[1] J.P. Foreman, and P.G. Edwards.
Department of Chemistry, University of Wales, Cardiff, Cardiff CF1 3TB, U.K.

[1] Author to whom correspondence may be addressed. Telephone: +44 (01222) 874950. Fax: +44 (01222) 874029. E-mail: howardst@cardiff.ac.uk

© 1997 NRC Canada

Table 1. MP2/6-311G(d,p) geometries (Å, deg) and proton affinities[a] (kJ mol^{-1}).

XR_3	X—R	$[X—R]H^+$	R—X—R	$[R—X—R]^+$	PA	Exptl. PA (ref.)
NH_3	1.014	1.025	106.1	109.5	871.0 (847.5)	853.1 (29)
NF_3	1.366	1.313	102.2	108.9	569.8 (551.5)	554.0 (30)
NMe_3	1.454	1.498	110.0	111.5	956.5 (936.3)	933.5 (31)
PH_3	1.410	1.390	94.3	109.5	799.6 (788.0)	782.4 (31)
PF_3	1.588	1.508	97.7	108.5	664.8 (644.0)	669.0 (32)
PMe_3	1.866	1.813	100.6	111.5	955.8 (944.7)	935.1 (31)
AsH_3	1.512	1.481	93.0	109.5	761.0 (754.0)	756.9 (31)
AsF_3	1.736	1.660	96.2	107.2	523.7 (510.4)	—
$AsMe_3$	1.985	1.926	98.4	111.3	908.3 (899.0)	881.2 (33)

[a]Including ZPE corrections computed at the HF/6-31G(d,p) level, scaled by 0.9 (14). Values in parentheses include a counterpoise correction.

Can. J. Chem. Downloaded from www.nrcresearchpress.com by 92.62.229.171 on 09/08/12
For personal use only.

basic atom. This work additionally addresses the following questions:

(*i*) are the conclusions of our earlier Hartree–Fock (HF) level study on substituent effects in phosphines (2) (hereafter Paper I) still valid when correlated charge distributions are considered?

(*ii*) do similar effects operate in amines and arsines?

(*iii*) is the "chemistry" of Group 15 compounds (e.g., enthalpy changes in subsequent chemical interactions) actually reflected in the basic atom charge distribution, especially in the lone pair region?

The last point is of particular relevance to experimental, diffraction-based studies of charge distributions (9, 10), where it is widely supposed that measuring the charge distribution of a compound must give us detailed information about its chemistry.

We note that most of the amine and phosphine PAs reported here were previously known from both experiment and quantum chemical calculations, but the results for substituted arsines appear to be new. Moreover, these results are presented at a consistent (correlated) level, and include a number of properties such as polarizabilities and electric field gradients (EFGs) that are hitherto unreported.

Computational details

The geometries of NH_3, PH_3, AsH_3, NF_3, PF_3, AsF_3, NMe_3, PMe_3, $AsMe_3$, and their protonated cations were optimized at the HF level with the standard 6-31G(d,p) basis set, and subsequently using 2nd order Møller–Plesset (frozen core) perturbation theory (MP2) with the standard 6-311G(d,p) basis sets on C, H, F, N, and P. Arsenic 6-31G(d,p) and 6-311G(d,p) basis sets were taken from refs. 11 and 12, respectively. The calculations were performed using GAUSSIAN 94/DFT (13) running on a Convex C3860 supercomputer at the University of London Computing Centre. C_{3v} symmetry was assumed throughout, except for the (tetrahedral) XH^{4+} cations. Harmonic frequency calculations performed on all species at the RHF/6-31G(d,p) level verified that all optimized structures were true minima (MP2 optimized structures, starting from the HF results, were assumed to be minima). Changes in zero point energy (ZPE) on protonation are included in the computed PAs, using HF/6-31G(d,p) level frequencies scaled by a factor of 0.9 (14). Basis set superposition error was estimated using the counterpoise method (15). Molecular dipole polarizabilities were computed using the MP2/coupled perturbed Hartree–Fock technique as implemented in GAUSSIAN 94. Finite-field single-point calculations with an electric field of 0.001 au were also carried out at this level, in order to determine AIM α's based on the method of Bader et al. and Howard (6–8). EFGs at the nitrogen, phosphorus, and arsenic nuclei in the various compounds were computed at the MP2 level, and will be reported in a traceless tensor form.

The critical point (CP) analyses of $\nabla^2\rho$ were carried out using Laidig's program BUFFALO, part of the AIMPAC suite of programs (16). The program PROAIMV, also part of AIMPAC, was used to compute integrated atomic properties (energies, charges, dipoles, and α's).

Results and discussion

Structures and proton affinities (Table 1)

In both phosphines and arsines, protonation decreases the X—R bond length with the largest shortening observed in the fluoro compounds. In amines the length of the X—R bond varies on protonation according to the type of substituent present. In all compounds the R-X-R angle increases on protonation (due to loss of bond pair – lone pair repulsions), with much larger changes being observed in phosphines and arsines.

The last column of Table 1 contains a number of experimentally determined gas phase PAs. It should be noted that these experimental values are measured at 300 K (except for the NH_3 value, which is a 0 K extrapolated PA), and some are subject to substantial uncertainties. Despite this, there is generally good agreement between the theoretical and experimental values, where the latter are available.

PAs relative to XH_3 are enhanced by methyl substitution and diminished by fluorine substitution in all compounds. The reductions of PA caused by fluorination are almost twice as large as the enhancements caused by methylation. Methylation of phosphine and arsine causes significantly larger enhancements in PA than for ammonia. Fluorination causes the opposite behaviour — the largest reduction in PA is ob-

© 1997 NRC Canada

Can. J. Chem. Downloaded from www.nrcresearchpress.com by 92.62.229.171 on 09/08/12
For personal use only.

Table 2. MP2/6-311G(d,p) molecular dipole moments[a] (D), dipole polarizabilities (au), and electric field gradients at the basic atom nucleus (au).

		Polarizability		Electric field gradient[b]	
	Dipole moment	$\alpha_{xx} = \alpha_{yy}$	α_{zz}	$E_{xx} = E_{yy}$	E_{zz}
NH_3	−1.75	+10.01	+7.90	−0.505	1.012
NF_3	+0.15	+13.93	+7.65	−0.795	1.589
NMe_3	−0.62	+45.54	+39.69	−0.602	1.203
PH_3	−0.74	+23.86	+21.20	−0.632	1.264
PF_3	+1.53	+20.68	+15.34	−0.934	1.869
PMe_3	−1.38	+62.22	+52.44	−0.751	1.501
AsH_3	−0.45	+29.44	+27.28	−1.212	2.424
AsF_3	+2.72	+24.96	+19.96	−1.569	3.138
$AsMe_3$	−1.08	+68.22	+56.53	−1.401	2.803

[a]Here a negative dipole points *from* the basic atom down the symmetry axis through the plane containing the substituents.

[b]Traceless tensor values are reported, e.g.,

$$E_{xx} = 2\left(\frac{\partial^2 V}{\partial x^2}\right) - \left(\frac{\partial^2 V}{\partial y^2}\right) - \left(\frac{\partial^2 V}{\partial z^2}\right)$$

where V is the electrostatic potential at the nucleus.

Table 3. MP2/6-311G(d,p) basic atom properties (au).

			Polarizability		
	Charge	Dipole moment [a]	$\alpha_{xx} = \alpha_{yy}$	α_{zz}	Energy (au)
NH_3	−1.006	−0.204	−0.4	+3.8	−54.9261
NF_3	+0.831	−0.994	−1.1	+2.0	−53.9503
NMe_3	−1.002	−0.279	−2.9	+2.6	−55.1192
PH_3	+1.715	−2.258	+9.1	+7.7	−340.1388
PF_3	+2.309	−2.186	+7.4	+5.9	−339.6767
PMe_3	+1.543	−2.203	+6.5	+11.3	−340.2847
AsH_3	+0.973	−1.684	+8.5	+9.5	−2234.0169
AsF_3	+1.957	−1.866	+7.9	+7.8	−2233.5133
$AsMe_3$	+0.957	−1.777	+6.6	+11.7	−2234.1031

[a]Dipole directions defined as in Table 2.

served for ammonia. These observations make sense in terms of simple ideas about hardness and softness, i.e., combination of the "hardest" acid and base (fluorine and nitrogen) causes the largest decrease in basicity; combination of the "softest" acid and base (methyl and phosphorus/arsenic) gives rise to the largest increase in basicity. The expected trend in PA down the group

$$NH_3 > PH_3 > AsH_3$$

is observed. Trends that are less predictable include

$$PF_3 > NF_3 > AsF_3$$

and

$$NMe_3 \approx PMe_3 > AsMe_3$$

(the equivalence of PMe_3 and NMe_3 PAs has been noted before by Ikuta and Kebarle (17)). The observed enhancements in basicity of methylated amines and phosphines have been discussed at length in the literature, and are neatly summarized by Ikuta and Kebarle. Qualitative concepts of polarizability and especially "group polarizability" are often invoked (quite plausibly), although we are unaware of a quantitative analysis of these effects in terms of actual α tensors. It will be shown that dipole polarizabilities may provide a basis for explaining the substituent effects on the PAs.

Charges and dipole moments (Tables 2 and 3)

In phosphine and arsine, the molecular dipole moment is enhanced by methylation. On fluorination, the dipole moment reverses polarity, which is reflected in the large changes in

© 1997 NRC Canada

Can. J. Chem. Downloaded from www.nrcresearchpress.com by 92.62.229.171 on 09/08/12
For personal use only.

magnitude (and in sign) of phosphorus and arsenic atomic charges. So, the dipole moment does show an approximate relationship with PA in these compounds.

The dipole moment of ammonia, however, is diminished on methylation, and all but disappears on fluorination. Staley and Beauchamp (18) have argued that this is due to rehybridization of the nitrogen atom on substitution, such that the lone pair "shrinks" (acquiring more *s*-type character). As can be seen in Table 3 the dipole moment of the nitrogen atom, which effectively measures how much electronic charge is located in the lone pair, is in fact larger in NMe_3 than in NH_3. The molecular dipole moment P_z can be expressed as a sum over the individual atomic charges q_i and dipoles $p_{z,i}$

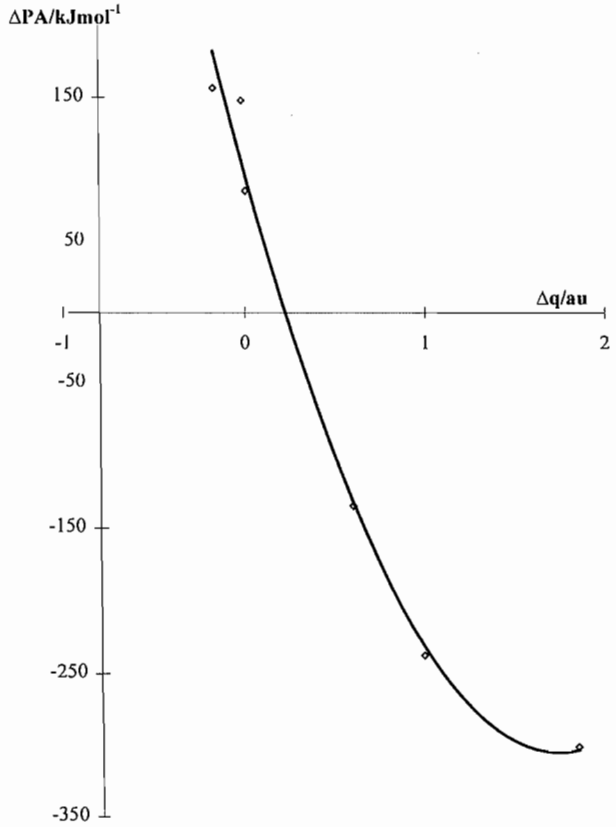
$$[1] \quad P_z = \sum_i p_{z,i} + q_i \cdot z_i$$

In NH_3 the contribution of the atomic dipoles to the total moment is very small (+0.15 D) compared to the charge terms (−1.89 D). In NMe_3 the atomic dipole contributions (+1.19 D) more effectively cancel the charge contribution (−1.80 D), due to the large and positive dipole polarizations of the methyl carbons and their associated hydrogens. So the arguments of Staley and Beauchamp are incorrect — it is the (intrinsic) opposing dipole polarization of the methyl groups that reduces the total dipole moment of NMe_3 relative to NH_3, rehybridization of the nitrogen having a minor effect (the nitrogens have almost identical charges and similar dipoles in NH_3 and NMe_3).

A small "methyl-inductive" effect is apparent only in the phosphine atomic charges, the charge on the basic atom remaining virtually unchanged in NMe_3 and $AsMe_3$ compared to NH_3 and AsH_3. This is in contrast to the fluoro substituted compounds where a marked withdrawing effect (relative to nitrogen in NH_3) is always observed in the basic atom charge. There appears to be a relationship between the *change* in the basic atom charge on fluorination or methylation, and the corresponding reduction/enhancement of the PA (Fig. 1). It is also true that the basic atom is always energetically destabilized by fluorination and stabilized by methylation, although the magnitudes of the energy changes do not correlate with the reduction/enhancement of the PA.

In Paper I it was observed that so-called alkyl-inductive effects were not manifest in the charge distribution of substituted phosphine bases. Instead, the enhanced PAs of alkylated species could be explained by noting that methyl groups donated more charge than hydrogen or fluorine on protonation, which has the effect of stabilizing phosphorus (it loses less charge to the added proton). Figure 2 illustrates the same analysis applied to amines, phosphines, and arsines in this work, based on the MP2 atomic charges in Table 3. Indeed, the same effects do operate in amines and arsines: on protonation, methyl groups donate more charge (and fluorine groups donate less charge) to the basic atom, than does hydrogen. This therefore provides a general basis for understanding substituent effects in Group 15 compounds. The ability of a group or atom to donate charge on chemical change is certainly linked to the density functional concepts of chemical potential, softness and hardness (19). These indices have as their basis the relationship between total energy and changes in *electronic* population (i.e., $\delta E/\delta N$). In practice, the softness or hardness tensor for a molecule is computed in a finite difference approximation using the changes in atomic populations between the associated (open shell) anion and cation ($\delta N = 2$). Since protonation changes only the total nuclear charge of the system ($\delta N = 0$), the information contained in Fig. 2 would complement an analysis based on chemical potential equalization, i.e., this represents a distinct approach.

Fig. 1. Relationship between the change in PA on methylation/fluorination, and the change in basic atom net charge (MP2 level).



The basic atom dipole moment is slightly enhanced by methylation in amines and arsines, and more significantly enhanced by fluorination. This reflects the increase in lone pair electron density (verified by the analysis of $\nabla^2\rho$ reported in the next section) accompanying both methylation and fluorination, first noted for phosphines in Paper I. Curiously, in the phosphine compounds the phosphorus atomic dipole varies very little with substituent, even for fluorination.

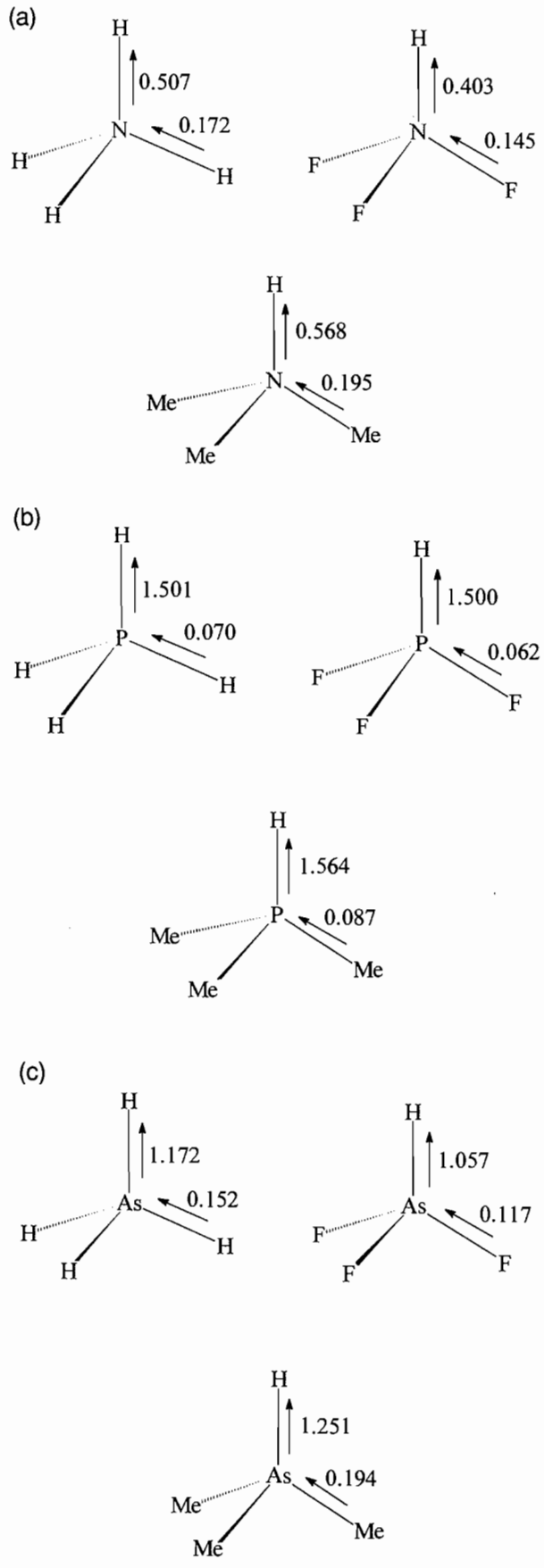
Dipole polarizabilities (Tables 2 and 3)

In every case, methylation enhances the (lone-pair directed) α_{zz} component of the (total) α, and fluorination diminishes it. So this is a physical property that reflects substituent effects on basicity across all the compounds. It must be noted, however, that the difference in α_{zz} between NH_3 and NF_3 is sufficiently small that it could disappear at a higher level of theory. The α_{xx} component behaves similarly in the phosphines and arsines, but fails to reflect substituent effects in the same way as α_{zz} for the amines.

© 1997 NRC Canada

Can. J. Chem. Downloaded from www.nrcresearchpress.com by 92.62.229.171 on 09/08/12
For personal use only.

Fig. 2. Charge flow upon protonation (MP2 level).



At the atomic level, α_{zz} for the basic atom also reflects electron-withdrawing and -donating substituent effects quite well in the phosphines and arsines, but this breaks down for the amines, where both methylation and fluorination decrease α_{zz}. The α_{xx} component bears no relationship to substituent effects on basicity.

It should be pointed out that AIM α's are necessarily origin dependent, because of the finite charge transfer term (8). The AIM α's reported here are based only on the response of the basic atom's dipole moment to an applied field, i.e., the charge transfer term has been ignored (equivalently, the basic atom has been translated to the origin). The charge transfer terms obtained in the finite field calculations appeared to be unrelated to the substituent effects on the PA, so they are not reported.

Electric field gradients (Table 2)

There appear to be no previously reported studies on the relationship between EFGs of Group 15 atoms and basicity. This parameter, obtainable from nuclear quadrupole resonance spectroscopy, is known to be closely linked with the LP distribution of electrons in amines (20–22). Hence it is feasible that EFGs evaluated at the basic atom nuclei might reflect substituent effects on PA's.

In all cases, E_{xx} of the basic atom (X) in the XMe_3 compounds are more negative than in the corresponding XH_3 compounds. Fluorination causes even larger negative shifts in the E_{xx} of X, relative to its value in XH_3. Consequently, these EFGs don't correlate with substituent effects on the PAs. The E_{zz} (lone pair directed) components similarly fail to reflect substituent effects on the PAs, since both methylation and fluorination cause positive shifts relative to the E_{zz} values in XH_3.

Lone pair analyses (Table 4)

The electronic shell structure of atoms is revealed by $-\nabla^2\rho$: local maxima in $-\nabla^2\rho$ effectively locate lone pairs (LPs) and bonded pairs (BPs) of electrons (23–25). In Paper I it was shown that both electron-donating and -withdrawing substituents on phosphorus appear to increase the electron density in the LP region, so such LP properties do not correctly indicate substituent effects on PAs of phosphines. The values of ρ_c and $|\nabla^2\rho_c|$ reported in Table 4 verify that the same is true for amines and arsines — either methylation or fluorination produces an increase in the density and concentration of density at the LP centroid in amines and arsines, as well as phosphines. The HF results in Paper I for phosphines are borne out at the MP2 correlated level.

The analysis of the basic atom dipole moment in the previous section indicated that it may be misleading to characterize the LP by only monitoring its properties at the local maximum in $-\nabla^2\rho$. The Hessian eigenvalues $\{\mu_i\}$ of $-\nabla^2\rho$ at this point contain information on the shape of the LP (see Table 4). All three eigenvalues are necessarily negative: the most negative eigenvalue μ_3 corresponds to the curvature of $\nabla^2\rho$ along the C_3 axis. Taking the *product* of these eigenvalues provides a possible measure of the LP effective volume. However, since all three eigenvalues are increased in magnitude by substitution of an electron-withdrawing *or* -donating group/atom, it is evident that this product also fails to correlate with substituent effects on basicity.

© 1997 NRC Canada

Table 4. MP2/6-311G(d,p) properties[a] at the lone pair critical point in $-\nabla^2\rho$ (au).

				Hessian eigenvalues of $\nabla^2\rho$	
	r_c	ρ_c	$\nabla^2\rho_c$	$\mu_1 = \mu_2$	μ_3
NH_3	0.7404	0.5720	−2.6361	−8.45	−172.86
NF_3	0.7021	0.6941	−4.5169	−18.50	−277.66
NMe_3	0.7369	0.5882	−2.8360	−9.74	−179.48
PH_3	1.4470	0.1283	−0.3073	−0.32	−9.13
PF_3	1.4098	0.1513	−0.4445	−0.57	−12.73
PMe_3	1.4431	0.1336	−0.3322	−0.38	−9.49
AsH_3	1.7870	0.0937	−0.0167	−0.07	−2.34
AsF_3	1.7513	0.1031	−0.0418	−0.11	−3.40
$AsMe_3$	1.7788	0.0980	−0.0285	−0.09	−2.58

[a] r_c is the distance from the basic atom nucleus to the lone pair CP.

$-\nabla^2\rho$ Distributions (Figs. 3*a*–3*i*)

Figures 3*a*–3*i* show the $-\nabla^2\rho$ distribution in a mirror plane, so each map represents a section through the LP critical point. The LP is seen as a charge concentration adjacent to the basic atom nucleus. The width of the valence shell of charge concentration (VSCC) along the direction from the basic atom nucleus through the LP centroid provides another way of estimating the LP effective volume, and it contradicts the previous LP volume measure considered earlier. Methylation or fluorination clearly increases the LP radial extent in the substituted amines and arsines (the expansion is less obvious for phosphines). This is in agreement with the atomic dipole moment analysis for the basic atom that we discussed earlier, where only phosphorus fails to register an increase on fluorination or methylation. So the $\{\mu_i\}$ are only indicative of the LP distribution of charge very near to the LP centroid, and do not accurately reflect the size of the LP region.

These maps computed at the MP2 level show the same polarization of the charge distribution in the bonds of NH_3 versus NF_3 and PH_3 versus PF_3 shown previously at the HF level (23). The $-\nabla^2\rho$ distribution in AsF_3 (Fig. 3*h*) similarly indicates substantial ionic character of these bonds. It is also noteworthy that the arsenic LP regions are much thinner in radial extent than those of nitrogen or phosphorus.

Conclusions

It seems that there is no electrostatic property (i.e., a property derived from the charge distribution of the unprotonated bases) that can act as a consistent indicator for substituent effects on basicity in amines, phosphines, and arsines. Changes in molecular dipole moments on substitution of hydrogen by Me or F correlate with substituent effects on proton affinities in phosphines and arsines, but not in amines. Looking at the atomic level does not help, since the basic atom dipole moment magnitude is enhanced by either methylation *or* fluorination in amines and arsines, and is reduced (slightly) by both substituents in phosphines. Other properties, such as the electric field gradient at the basic atom nucleus, show similar behaviour.

The α_{zz} component of the molecular dipole polarizability tensor seems to be the only physical property that follows substituent effects on the proton affinities of Group 15 compounds. Even in this case, it is a very "nonlinear" indicator, e.g., methylation of NH_3 increases its proton affinity and α_{zz} by 10% and ≈400%, respectively; fluorination causes corresponding decreases of 35% and 3%. Again, looking at the atomic level seems to be even less helpful in this case, since in amines the atomic dipole polarizability of nitrogen in both NF_3 *and* NMe_3 is lower than in NH_3.

The atoms-in-molecules analysis does reveal that *changes* in atomic charges and energies on protonation are clearly linked to substituent effects on basicity. Similar conclusions were reached in previous Hartree–Fock level studies on amines and alcohols (26), carbocations (27), and phosphines (2). Both the change in charge of the basic atom X, and the flow of charge $\Delta Q(Y)$ from Y→X on protonation of XY_3, correlate with the changes in basicity for a given Group 15 atom, i.e.,

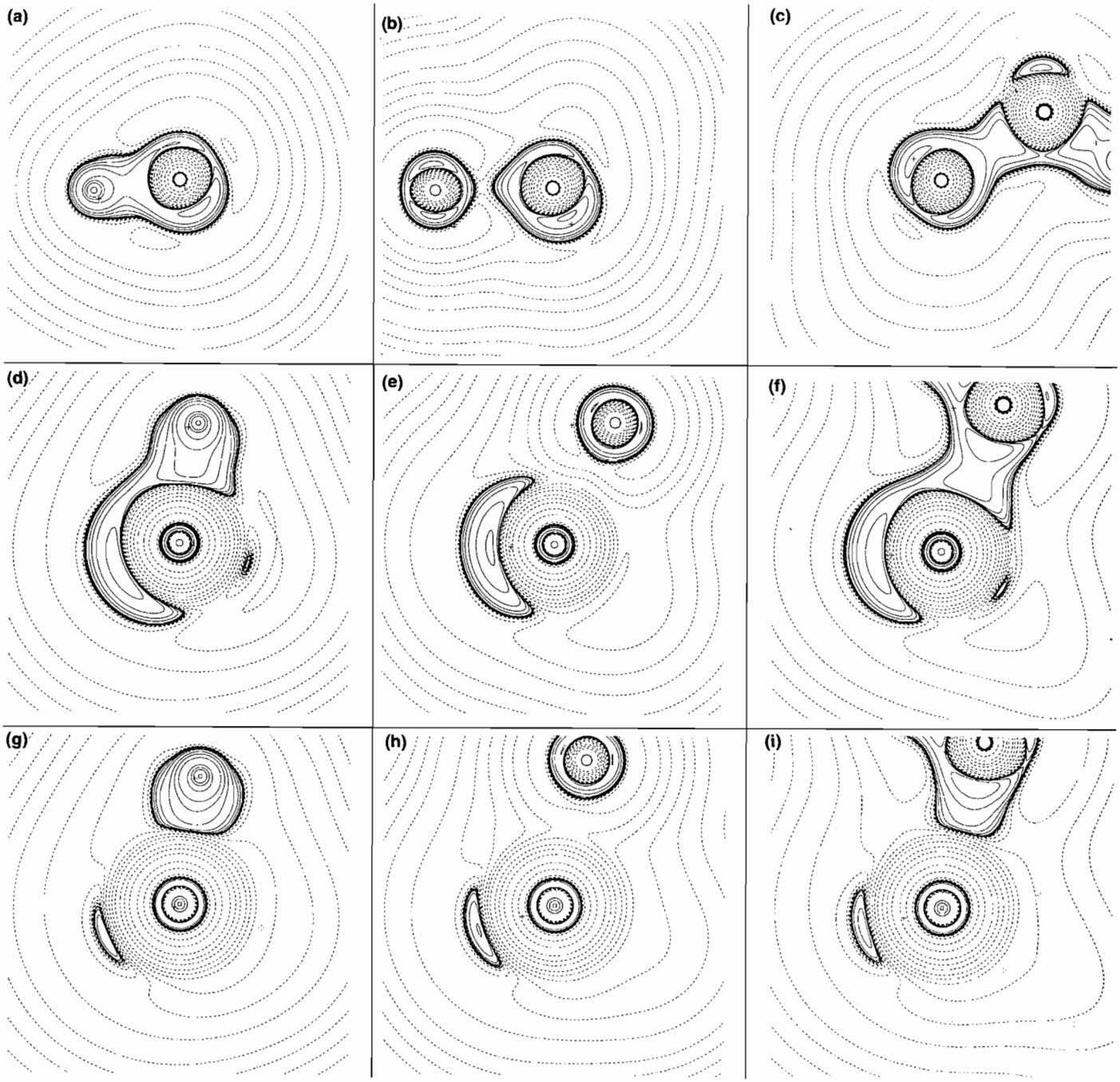
$$\Delta Q(\text{Me}) > \Delta Q(\text{H}) > \Delta Q(\text{F})$$

On the face of it, this just reflects what we might have predicted on the basis of atomic/group electronegativity differences. Although the concept of charge flow on chemical bond formation is behind most χ scales, the χ values for an atom or group (Y) have always been based on indirect information, such as the mean of the atomic ionization energy and electron affinity, or the distance from Y to the bond critical point in YH (28). Looking at the charge flow on protonation, ΔQ is clearly a more direct way of analyzing substituent effects, and it differs in an important conceptual sense. Definitions of χ are invariably based on either properties of the associated free atom, or on the value of some theoretical/physical property of the atom in various compounds. ΔQ values as defined here measure how the charge distribution of an anisotropic atom Y bonded in a molecule is modified when the compound undergoes a subsequent chemical interaction (protonation). A systematic study of ΔQ values at a suitably high level of theory could therefore provide a valuable set of data

© 1997 NRC Canada

Can. J. Chem. Downloaded from www.nrcresearchpress.com by 92.62.229.171 on 09/08/12
For personal use only.

Fig. 3. Maps of $-\nabla^2\rho$ in the LP-X-Y plane (MP2 level): (*a*) NH_3; (*b*) NF_3; (*c*) NMe_3; (*d*) PH_3; (*e*) PF_3; (*f*) PMe_3; (*g*) AsH_3; (*h*) AsF_3; (*i*) $AsMe_3$. Negative contours correspond to the solid lines. Contours plotted at ±0.002, ±0.004, ±0.008, ±0.02, ±0.04, ±0.08, ±0.2, ±0.4, ±0.8, ±2, ±4, ±8, ±20, ±40, and ±80 e $Bohr^{-5}$.



for interpretation and prediction of substituent effects on basicity.

Three ways of characterizing the size and amount of charge in the lone pair region were considered: (*i*) atomic dipole moment; (*ii*) ρ and $\nabla^2\rho$ at the lone pair centroid; (*iii*) the physical extent of the valence shell of charge concentration. All three methods agree that both withdrawing and donating substituents act to increase the charge density, the concentration of charge density, and the overall size of the lone pair in amines and arsines. (In phosphines, (*i*) and (*iii*) register only very small changes on substitution, which nevertheless do not fit in with this trend, while (*ii*) does behave as in amines and arsines.) So the phenomenon first reported for phosphines in ref. 2 occurs in general in Group 15 compounds. This enables us to generalize the main conclusion of the phosphine study — it is the ability (inability) of the methyl (fluoro)

© 1997 NRC Canada

Can. J. Chem. Downloaded from www.nrcresearchpress.com by 92.62.229.171 on 09/08/12
For personal use only.

group to donate charge *on protonation* which accounts for donating (withdrawing) substituent effects on proton affinities of trivalent Group 15 compounds. This contrasts with the essentially anecdotal belief that substituent effects on basicity in such compounds are due to a corresponding enhancement/depletion of density in the basic atom's lone pair.

This is an important point for experimental studies of charge densities. It tells us that the distribution of density in the lone pair region of an atom, even if it can be measured accurately, tells us little or nothing about the compound's basicity. It might be thought that these results reveal the Lewis concept of basicity as fundamentally incorrect, but that isn't necessarily the case. Lewis's definition refers to an atom's "ability to furnish a lone pair." If we read this as a dynamical statement about *how the lone pair atom modifies its charge distribution* when it bonds to a proton, or coordinates to a metallic centre, then there is nothing in these findings that contradicts Lewis's definition of basicity. If Lewis's definition has a failing, it is perhaps that it appears to identify basicity as an intrinsic lone pair property. It is evident from these results that basicity is only rationalized by looking at the response to the perturbation on a molecular scale.

Acknowledgements

The authors thank the U.K. Engineering and Physical Sciences Research Council for an Advanced Fellowship (S.T.H.) and a CASE Ph.D. Studentship (J.P.F.), the latter being partly supported by I.C.I. Wilton.

References

1. T.-H. Tang, W.-J. Hu, D.-Y. Yan, and Y.-P. Cui. J. Mol. Struct. (THEOCHEM), **207**, 327 (1990).
2. S.T. Howard and J.A. Platts. J. Phys. Chem. **99**, 9027 (1995).
3. A. Baeten, F. De Proft, and P. Geerlings. Chem. Phys. Lett. **235**, 17 (1995).
4. J.K. Nagle. J. Am. Chem. Soc. **112**, 4741 (1990).
5. R.F.W. Bader. Atoms in molecules; a quantum theory. Oxford University Press, Oxford. 1990.
6. R.F.W. Bader, T.A. Keith, K.N. Gough, and K.E. Laidig. Mol. Phys. **75**, 1167 (1989).
7. K.E. Laidig and R.F.W. Bader. J. Chem. Phys. **93**, 7213 (1990).
8. S.T. Howard. Molec. Phys. **85**, 395 (1995).
9. P. Coppens. J. Phys. Chem. **93**, 7979 (1989).
10. P. Coppens. Annu. Rev. Phys. Chem. **43**, 663 (1992).
11. R.C. Binning, Jr. and L.A. Curtiss. J. Comput. Chem. **11**, 1206 (1990).
12. A.D. Mclean and G.S. Chandler. J. Chem. Phys. **72**, 5639 (1980); R. Krishnan, J.S. Binkley, R. Seeger, and J.A. Pople. J. Chem. Phys. **72**, 650 (1980).
13. M.J. Frisch, G.W. Trucks, H.B. Schlegel, P.M.W. Gill, B.G. Johnson, M.A. Robb, J.R. Cheeseman, T. Keith, G.A. Petersson, J.A. Montgomery, K. Raghavachari, M.A. Al-Laham, V.G. Zakrzewski, J.V. Ortiz, J.B. Foresman, J. Cioslowski, B.B. Stefanov, A. Nanayakkara, M. Challacombe, C.Y. Peng, P.Y. Ayala, W. Chen, M.W. Wong, J.L. Andres, E.S. Replogle, R. Gomperts, R.L. Martin, D.J. Fox, J.S. Binkley, D.J. Defrees, J. Baker, P.J. Stewart, M. Head-Gordon, C. Gonzalez, and J.A. Pople, Gaussian 94, Revision C.3. Gaussian, Inc., Pittsburgh, Pa. 1995.
14. R.F. Hout, B.A. Levi, and W.J. Hehre. J. Comput. Chem. **3**, 234 (1982).
15. S.F. Boys and F. Bernardi. Mol. Phys. **19**, 553 (1970).
16. F.W. Biegler-König, R.F.W. Bader, and T. Tang. J. Comput. Chem. **3**, 317 (1982).
17. S. Ikuta and P. Kebarle. Can. J. Chem. **61**, 97 (1983).
18. R.H. Staley and J.L. Beauchamp. J. Am. Chem. Soc. **96**, 6252 (1974).
19. R.F. Nalewajski and J. Korchowiec. J. Mol. Catal. **54**, 324 (1989).
20. Y. Aray, C. Gatti, and J. Murgich. J. Chem. Phys. **101**, 9800 (1994).
21. Y. Aray, J.C. Casilimas, and J. Murgich. J. Phys. Chem. **100**, 5291 (1996).
22. K. Woźniak, H. Heyong, J. Klinowski, B. Nogaj, D. Lemański, D.E. Hibbs, M.B. Hursthouse, and S.T. Howard. J. Chem. Soc. Faraday Trans. **91**, 3925 (1995).
23. R.F.W. Bader, P.J. MacDougall, and C.D.H. Lau. J. Am. Chem. Soc. **106**, 1594 (1984).
24. R.F.W. Bader and P.J. MacDougall. J. Am. Chem. Soc. **107**, 6788 (1985).
25. R.J. Gillespie and I. Hargittai. The VSEPR model of molecular geometry, Allyn and Bacon, Boston. 1991.
26. N.J.C. Stutchbury and D.L. Cooper. J. Phys. Chem. **79**, 4967 (1983).
27. R.F.W. Bader. Can. J. Chem. **64**, 1036 (1986).
28. R.J. Boyd and K.E. Edgecombe. J. Am. Chem. Soc. **110**, 4182 (1988).
29. J.M.L. Martin and T.J. Lee. Chem. Phys. Lett. **258**, 136 (1996).
30. K. Hiraoka, M. Nasu, S. Fujimaki, and S. Yamabe. J. Phys. Chem. **99**, 15822 (1995).
31. J.F. Wolf, R.H. Staley, I. Koppel, M. Taagepera, R.T. McIver, J.L. Beauchamp, and R.W. Taft. J. Am. Chem. Soc. **99**, 5417 (1977).
32. R.R. Cordermann and J.L. Beauchamp. Inorg. Chem. **17**, 1585 (1978).
33. R.V. Hodges and J.L. Beauchamp. Inorg. Chem. **14**, 1887 (1975).

Can. J. Chem. Downloaded from www.nrcresearchpress.com by 92.62.229.171 on 09/08/12
For personal use only.

© 1997 NRC Canada

Use of aldolases in the synthesis of non-carbohydrate natural products. Stereoselective synthesis of aspicilin C-3—C-9 fragment

Robert Chênevert, Michèle Lavoie, and Mohammed Dasser

Can. J. Chem. Downloaded from www.nrcresearchpress.com by 92.62.229.171 on 09/08/12
For personal use only.

Abstract: The C-3—C-9 main fragment of aspicilin was prepared via a fructose 1,6-diphosphate aldolase reaction. The same fragment was also synthesized by chemical transformation starting from D-arabinose.

Key words: aldolase, aspicilin, arabinose, synthesis.

Résumé : Le fragment principal (C-3 à C-9) de l'aspiciline a été préparé via une réaction de l'aldolase du fructose 1,6-diphosphate. Le même fragment a été obtenu par une série de réactions non-enzymatiques à partir du D-arabinose.

Mots clés : aldolase, aspiciline, arabinose, synthèse.

Introduction

The development of methods for stereoselective C—C bond formation using the aldol reaction is a major focus of interest in organic synthesis. Both chemical (1) and enzymatic (2) aldol reactions with high level of asymmetric induction have recently been developed. The use of aldolases in the synthesis of carbohydrates and close analogs (azasugars, cyclitols) has been amply demonstrated (2, 3). However, the application of aldolases for the synthesis of natural products other than sugars has received very little attention. The synthesis of brevicomin, an insect pheromone, represents a rare example of this strategy (4). More recently, Shimagaki et al. (5) reported the synthesis of the C-11—C-16 fragment of pentamycin using an aldolase catalyzed reaction as the key step. The most prominent and easily available representative of these enzymes is fructose-1,6-diphosphate aldolase (FDP aldolase). This aldolase catalyzes the reversible aldol reaction of dihydroxyacetone phosphate (DHAP) and a broad range of aldehydes with the formation of a C—C bond having the D-*threo* (3*S*, 4*R*) configuration.

In this paper, we describe a FDP aldolase catalyzed stereoselective C—C bond formation leading to the main (C-3—C-9) fragment of (+)-aspicilin. (+)-Aspicilin (**1**) is a 18-membered lactone isolated from the lichen *Aspicilia gibbosa* (6). Several different nonenzymatic approaches for the synthesis of (−) or (+)-aspicilin have been reported (7).

Received June 15, 1996.

R. Chênevert,[1] M. Lavoie, and M. Dasser. Département de chimie, Faculté des sciences et de génie, Université Laval, Québec, QC G1K 7P4, Canada.

[1] Author to whom correspondence may be addressed. Telephone: (418) 656–3283. Fax: (418) 656–7916. E-mail: robert.chenevert@chm.ulaval.ca

Results and discussion

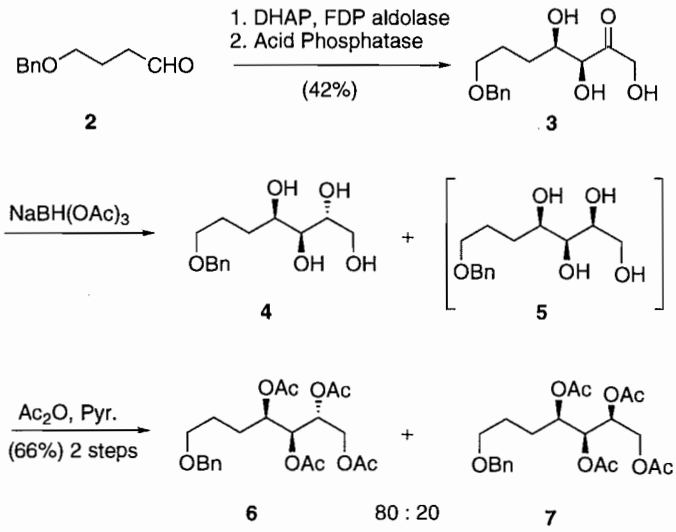
The reaction of aldehyde **2** (7*c*) with DHAP in the presence of FDP aldolase in water/DMF (10/1), followed by hydrolysis in situ of the intermediate phosphate ester with acid phosphatase, afforded ketotriol **3** in 42% overall yield (Scheme 1). Ketotriol **3** was reduced by using a variety of reagents and conditions. Sodium or lithium borohydride gave low diastereoselectivity. Evans et al. (8) reported that reduction of acyclic β-hydroxyketones with tetramethylammonium triacetoxyborohydride consistently affords 1,3-*anti* diols with high diastereoselectivity. The proposed mechanism involves a ligand exchange of acetate for substrate alcohol by the triacetoxyborohydride; the resultant intermediate, presumably an alkoxydiacetoxyborohydride, reduces the ketone by intramolecular hydride delivery (8). Reduction of **3** with triacetoxyborohydrides gave the desired 1,3-*anti* diastereoisomer **4** as the dominant product along with some 1,3–*syn* diastereoisomer **5** (1,3-*anti* **4**/1,3-*syn* **5** ~ 4/1). The separation of these diastereoisomers by flash chromatography provided the desired *anti*-**4** in a pure form but the minor *syn*-**5** isomer was still contaminated. A sample of the mixture **4**–**5** was acylated by acetic anhydride in pyridine in the presence of 4-dimethylaminopyridine (DMAP) and the resulting diastereomeric esters **6**–**7** were separated by flash chromatography. The nature of the triacetoxy borohydrides (sodium or tetramethylammonium triacetoxyborohydride, tetramethylammonium borohydride in acetic acid) did not significantly affect the stereoselectivity of this reduction. The lower diastereoselectivity of our reduction reaction can be explained by the presence of three additional oxygen atoms interfering with the formation of the intermediate alkoxydiacetoxyborohydride. Presumably, several directed reduction reactions compete with opposite stereochemical preferences.

Compounds **4** and **6** are presumed to have the 2*R*,3*S*,4*R* absolute configuration. To prove this configuration beyond any doubt, we synthesized authentic (2*R*,3*S*,4*R*)-**4** and -**6** by chemical transformation starting from D-arabinose (Scheme 2).

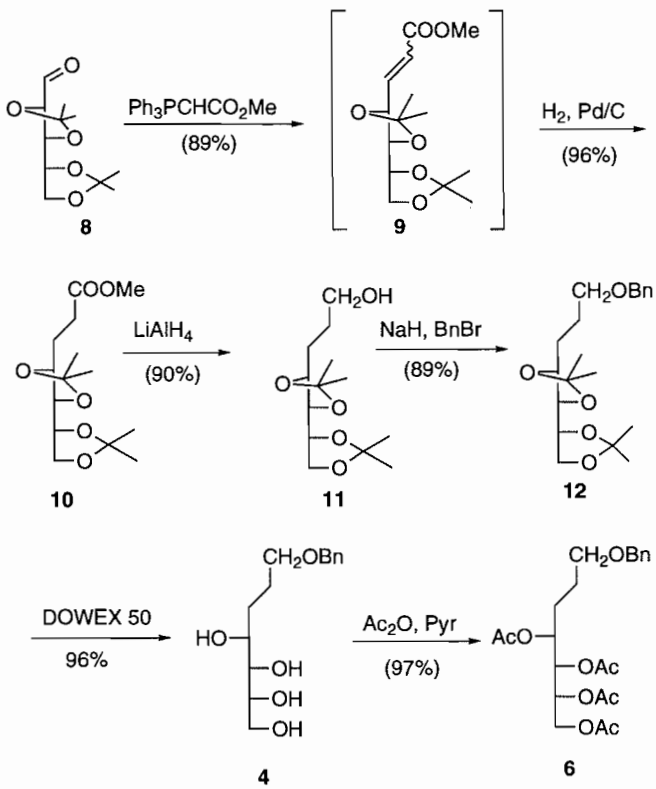
© 1997 NRC Canada

Can. J. Chem. Downloaded from www.nrcresearchpress.com by 92.62.229.171 on 09/08/12
For personal use only.

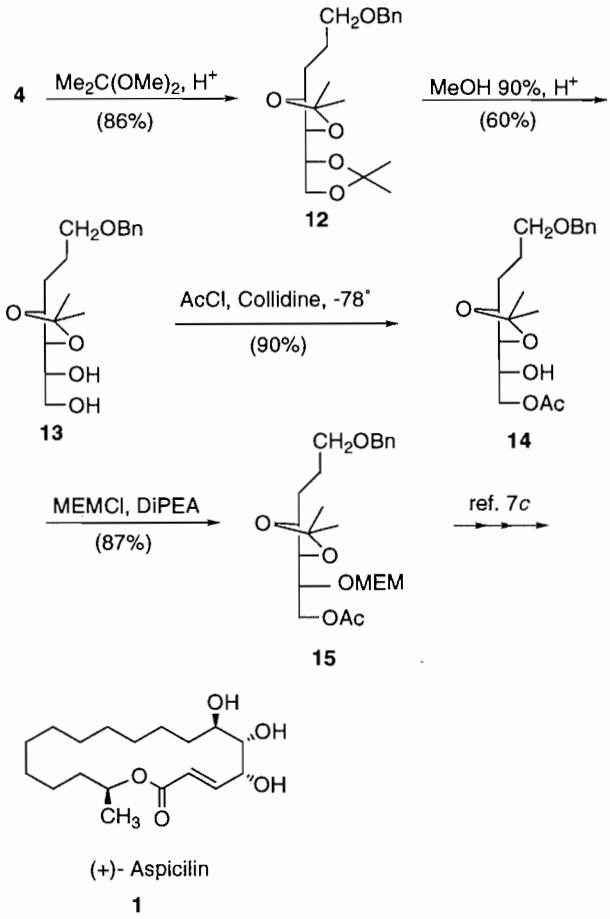
Scheme 1.



Scheme 2.



Scheme 3.



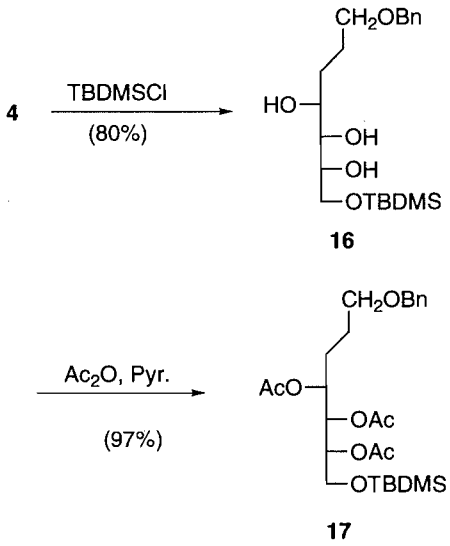
D-Arabinose was transformed into di-*O*-isopropylidene-D-arabinose **8** in a three-step sequence according to known procedures (9). The Wittig reaction of **8** with (carbomethoxymethylene)triphenylphosphorane in benzene afforded **9** as a mixture in which the *trans* isomer was predominant (*E*/*Z* ratio = 6). Catalytic hydrogenation of ester mixture **9** furnished the dihydro derivative **10**. Ester **10** was reduced with $LiAlH_4$ in ether to afford alcohol **11**. Alcohol **11** was benzylated with benzyl bromide in the presence of NaH to give **12**. Deprotection of isopropylidenes in **12** was achieved satisfactorily using acidic resin in water at 60°C to give tetraol **4**. A sample of tetraol **4** was acetylated with acetic anhydride in pyridine in the presence of DMAP. Compounds **4** and **6** prepared from D-arabinose were identical in all respects with the samples obtained via the enzymatic addition–reduction sequence. This correlation proved that the aldolase catalyzed reaction provided an addition product with a 3*S*,4*R* configuration and that the subsequent reduction gave the 2*R*,3*S*,4*R* tetraol **4** as the major product.

Compound **15** corresponding to the C-3—C-9 fragment of aspicilin was easily prepared in a few steps from tetraol **4** (from the enzymatic condensation) or from **12** (from arabinose). Compound **4** was treated with dimethoxypropane in acidic medium to give **12** (Scheme 3). Selective deprotection of **12** was achieved by treatment with methanol in the presence of an acidic resin (Dowex 50W-X8) (10). The primary alcohol of **13** was selectively acylated with acetyl chloride in the presence of collidine at −78°C in CH_2Cl_2 (11). Mono-alcohol **14** was converted into the corresponding 2-methoxyethoxymethyl (MEM) ether **15** in high yield by reaction with MEMCl in the presence of *N*,*N*-diisopropylethylamine (DiPEA). This sequence constitutes a formal synthesis of aspicilin since the transformation of **15** into aspicilin has been reported by Solladié et al. (7*c*).

Compound **4** has also been transformed in two steps into **17**, another compound corresponding to the C-3—C-9 fragment of aspicilin with orthogonal protection (Scheme 4). The primary alcohol of **4** was selectively protected by reaction with

© 1997 NRC Canada

Scheme 4.



tert-butyldimethylsilyl chloride (TBDMSCl) followed by acylation of the remaining alcohol functionalities in compound **16** with acetic anhydride.

In conclusion, we have completed a formal synthesis of (+)-aspicilin via an aldolase-catalyzed condensation. The main C-3—C-9 fragment was obtained in six steps and 10% overall yield. The same fragment was also prepared from D-arabinose in 10 steps and 22% overall yield. The synthesis of this fragment from D-arabinose not only provides unambiguous establishment of the relative and absolute stereochemistry of the intermediate but also provides an alternative pathway for the formal synthesis of (+)-aspicilin. The present work demonstrates that the aldolase-catalyzed condensation is an efficient process in the asymmetric synthesis of natural products other than carbohydrates. Applications of this strategy for the stereospecific synthesis of other non-carbohydrate natural products are underway.

Experimental section

Aldolase (D-fructose-1,6–biphosphate-D-glyceraldehyde-3-phosphate-lyase; EC 4.1.2.13, from rabbit muscle) and acid phosphatase (from wheat germ, EC 3.1.3.2) were purchased from Sigma Chem. Co. Melting points are uncorrected. NMR spectra were recorded at 300 MHz (^{1}H), 75.44 MHz (^{13}C).

(3*S*,4*R*)-7-Benzyloxy-1,3,4-trihydroxyheptan-2-one (3)
Aldehyde **2** (166.2 mg, 0.94 mmol) was added to a solution of DHAP (12) (180.0 mg, 1.06 mmol) in 10 mL of water containing 10% DMF under nitrogen atmosphere and the pH was adjusted to 6.8 with 1 N NaOH. Aldolase was added (8.6 mg, 102 U) and the mixture was shaken at room temperature. After 24 h, the pH was readjusted to 6.8, additional aldolase (7.8 mg, 92 U) and DHAP (98 mg, 0.58 mmol) were added, and the mixture was stirred for another 45 h. The pH was then set at 4.8 with 1 N HCl, the acid phosphatase (40 mg, 16 U) was added, and the mixture was stirred at room temperature for 12 h. Additional phosphatase (40 mg, 16 U) was added and the mixture was stirred for 12 h. The pH was then raised to 7 with 1 N NaOH. The solution was freeze-dried, the residue was taken up in ethyl acetate, and the solution was filtered and evaporated. The crude product was purified by flash chromatography on silica gel (CH_2Cl_2/MeOH, 19:1 as eluant) to afford **3** as an oil (106 mg, 42%). $[\alpha]_D^{23}$ +14.0 (*c* 3.1, $CHCl_3$); IR (neat): 3650–3000, 2980–2800, 1720, 1490, 1140–1000 cm^{-1}; ^{1}H NMR ($CDCl_3$): 7.31 (m, 5H), 4.51 (d, J = 19 Hz, 1H), 4.48 (s, 2H), 4.34 (d, J = 19 Hz, 1H), 4.14 (s, 1H), 3.91 (m, 1H), 3.89 (br s, 3H), 3.71 (m, 2H), 1.59–1.71 (m, 4H); ^{13}C NMR ($CDCl_3$): 211.87, 137.70, 128.37, 127.73, 77.82, 72.98, 72.03, 70.12, 66.56, 30.47, 26.05. MS (CI, isobutane) *m/e* (rel. intensity): 269 (MH^+, 25), 91 (100).

(2*R*,3*S*,4*R*)-7-Benzyloxy-1,2,3,4-tetrahydroxyheptane (4)
To a solution of sodium triacetoxyborohydride (127 mg, 0.60 mmol) in anhydrous acetic acid (4 mL) at 10°C was added dropwise a solution of **3** (40 mg, 0.15 mmol) in acetic acid (10 mL). The solution was stirred for 3 h at 10°C. Ice water (5 mL) was added and the solvent were eliminated by freeze-drying. Flash chromatography on silica gel (CH_2Cl_2/MeOH, 9:1) gave diastereoisomer **4** (24.4 mg, 60%) as a white solid along with a fraction of impure **5**. Compound **4**: mp 114.5–115.5°C (recrystallized from AcOEt:EtOH, 9/1); $[\alpha]_D^{23}$ +5.9 (*c* 0.7, MeOH); IR (neat): 3300–3600, 3000–3100, 2850–2990, 1100–1300 cm^{-1}; ^{1}H NMR (CD_3OD): 7.31 (m, 5H), 4.55 (s, 2H), 3.58–3.83 (m, 6H), 3.4 (dd, J_1 = 8.0 Hz, J_2 = 2.2 Hz, 1H), 1.5–1.8 (m, 4H); ^{13}C NMR (CD_3OD): 129.44, 128.96, 128.72, 74.71, 73.96, 73.28, 71.56, 71.41, 65.16, 31.46, 27.93. MS (CI, isobutane) *m/e* (rel. intensity): 271 (MH^+, 17.5), 145 (100). Anal. calcd. for $C_{14}H_{22}O_5$: C 62.20, H 8.20; found: C 62.22, H 8.39.

(2*R*,3*S*,4*R*) and (2*S*,3*S*,4*R*)-7-Benzyloxy-1,2,3,4-tetraacetoxyheptane (6 and 7)
The crude reduction product (40 mg, 0.15 mmol, mixture of **4** and **5**), DMAP (10 mg), and acetic anhydride (2 mL) were dissolved in pyridine (4 mL) and the solution was stirred for 36 h at room temperature. CH_2Cl_2 (75 mL) was added and the resulting organic layer was washed with 1 N HCl (3 × 30 mL), saturated aqueous $NaHCO_3$ (2 × 30 mL), brine (2 × 30 mL), and then dried over $MgSO_4$ and evaporated. Flash chromatography on silica gel (ether/petroleum ether, 3:2) gave diastereoisomer **6** (34 mg) and diastereoisomer **7** (9 mg). Total yield: 66%; compound **6**: mp 50–51°C; $[\alpha]_D$ + 13.8 (*c* 0.8, $CHCl_3$); IR (neat): 2990–3100, 2850–2980, 1740, 1490, 1100–1300 cm^{-1}; ^{1}H NMR ($CDCl_3$): 7.31 (m, 5H), 5.31 (dd, J_1 = 8 Hz, J_2 = 3 Hz, 1H), 5.17–5.25 (m, 2H), 4.47 (s, 2H), 4.24 (dd, J_1 = 12 Hz, J_2 = 3 Hz, 1H), 4.13 (dd, J_1 = 12 Hz, J_2 = 6 Hz, 1H), 3.46 (m, 2H), 2.11 (s, 3H), 2.04 (s, 9H), 1.61 (m, 4H); ^{13}C NMR ($CDCl_3$): 170.59, 170.39, 169.91, 169.82, 138.48, 128.35, 127.58, 72.83, 70.41, 69.51, 68.48, 61.97, 27.69, 25.50, 20.82, 20.68, 20.62. MS (CI, isobutane) *m/e* (rel. intensity): 439 (MH^+, 41), 289 (72), 229 (100). Anal. calcd. for $C_{22}H_{30}O_9$: C 60.26, H 6.89; found: C 60.44, H 6.90.

Diastereoisomer **7**: $[\alpha]_D^{23}$ +6.4 (*c* 0.4, $CHCl_3$); IR (neat): 3100–2990, 2850–2980, 1740, 1490, 1100–1300 cm^{-1}; ^{1}H NMR ($CDCl_3$): 7.32 (m, 5H), 5.30 (m, 3H), 4.48 (s, 2H), 4.35 (dd, J_1 = 12 Hz, J_2 = 6 Hz, 1H), 3.50 (m, 2H), 2.05 (m, 12H), 1.70 (m, 4H); ^{13}C NMR ($CDCl_3$): 170.15, 169.82, 138.27, 128.23, 127.55, 127.48, 72.78, 71.33, 69.44, 69.34, 61.85, 27.43, 25.16, 20.73, 20.57, 20.48, 20.23. MS (CI, isobutane)

Can. J. Chem. Downloaded from www.nrcresearchpress.com by 92.62.229.171 on 09/08/12
For personal use only.

© 1997 NRC Canada

Can. J. Chem. Downloaded from www.nrcresearchpress.com by 92.62.229.171 on 09/08/12
For personal use only.

m/e (rel. intensity): 439 (MH^+, 64), 229 (100); Anal. calcd. for $C_{22}H_{30}O_9$: C 60.26, H 6.89; found: C 60.30, H 7.11.

Methyl 2,3-dideoxy-4,5:6,7-di-O-isopropylidene-D-*arabino*-hept-2-enoate (9)

A solution of aldehyde **8** (1.730 g, 7.513 mmol) and carbomethoxymethylene triphenyl phosphorane (2.782 g, 8.32 mmol) in benzene (30 mL) was refluxed for 3 h. The solvent was evaporated and the crude product was purified by flash chromatography on silica gel (ethyl acetate/hexane 1:4) to give **9** as an oil (1.92 g, 89%). This compound was a *trans*/*cis* (6:1) mixture. *trans*-**9**: $[\alpha]_D^{25}$ −1.27 (*c* 2.62, $CHCl_3$) (lit. (13, 14) $[\alpha]_D^{19}$ −1.1 (*c* 3.0, ethanol); IR (neat): 2850–3000, 1735, 1660, 1375, 1385, 1000–1300 cm^{-1}; ^1H NMR ($CDCl_3$): 6.94 (dd, J_1 = 15.5 Hz, J_2 = 4.5 Hz, 1H), 6.1 (dd, J_1 = 15.5 Hz, J_2 = 1.6 Hz, 1H), 4.46 (m, 1H), 4.05 (m, 2H), 3.90 (m, 1H), 3.68 (s, 3H), 3.60 (t, *J* = 7.7 Hz, 1H), 1.35 (s, 3H), 1.33 (s, 6H), 1.27 (s, 3H); ^{13}C NMR ($CDCl_3$): 166.48, 145.17, 120.86, 110.12, 109.71, 81.06, 78.79, 77.30, 67.37, 51.45, 26.79, 26.57, 26.52, 25,02.

Methyl 2,3-dideoxy-4,5:6,7-di-*O*-isopropylidene-D-*arabino*-heptonate (10)

The *cis*/*trans* mixture of olefin **9** (600 mg, 2.1 mmol) was subjected to hydrogenation (18 h) at a 40 psi pressure (1 psi = 6.8-kPa) and room temperature in the presence of Pd/C (60 mg) in EtOH (30 mL). The suspension was then filtered and the solvent evaporated. The crude product was purified by flash chromatography (ethyl acetate/hexane 1:4) to give **10** (580 mg, 96%) as an oil; $[\alpha]_D^{23}$ +16.5 (*c* 2, $CHCl_3$); IR (neat): 3000–2850, 1730, 1300–1000, 1380, 1370 cm^{-1}; ^1H NMR ($CDCl_3$): 4.10 (dd, J_1 = 8.1 Hz, J_2 = 5.9 Hz, 1H), 3.95 (m, 1H), 3.89 (m, 2H), 3.64 (s, 3H), 3.52 (t, *J* = 7.7 Hz, 1H), 2.48 (m, 2H), 2.08 (m, 1H), 1.84 (m, 1H), 1.37 (s, 3H), 1.33 (s, 3H), 1.31 (s, 3H), 1.30 (s, 3H); ^{13}C NMR ($CDCl_3$): 173.71, 109.61, 109.03, 81.09, 79.45, 67.74, 51.50, 30.49, 28.81, 27.24, 26.98, 26.70, 25.27. MS (CI, isobutane) *m/e* (rel. intensity): 289 (MH^+, 16), 231 (100), 129 (70).

5,6-Dideoxy-1,2:3,4-di-*O*-isopropylidene-D-*lyxo*-heptitol (11)

To a suspension of $LiAlH_4$ (80 mg, 2.1 mmol) in 10 mL of ether was added dropwise a solution of ester **10** (1.32 mmol) in 5 mL of ether at 0°C. The mixture was stirred for 0.5 h at 0°C, then for 14 h at room temperature under dry atmosphere. The resulting mixture was cooled at 0°C and quenched with 1 N HCl (2 mL). Ether (50 mL) was added and the layers were separated. The organic layer was washed with water (1 × 25 mL), saturated aqueous $NaHCO_3$ (1 × 25 mL), and brine (2 × 25 mL), dried over $MgSO_4$ and concentrated. The residue was then purified by flash chromatography (ethyl acetate/hexane, 3:7) to afford alcool **11** (310 mg, 90%) as an oil; $[\alpha]_D^{25}$ +13.7 (*c* 2.1, $CHCl_3$); IR (neat): 3500–3000, 3000–2800, 1373, 1380 cm^{-1}; ^1H NMR ($CDCl_3$): 4.10 (dd, J_1 = 8 Hz, J_2 = 6 Hz, 1H), 4.00 (m, 1H), 3.93 (m, 2H), 3.64 (m, 2H), 3.52 (t, *J* = 7.7 Hz, 1H), 2.48 (br s, 1H), 1.9 (m, 1H), 1.72 (m, 2H), 1.58 (m, 1H), 1.37 (s, 3H), 1.36 (s, 3H), 1.32 (s, 3H), 1.31 (s, 3H); ^{13}C NMR ($CDCl_3$): 109.49, 108.75, 81.03, 80.28, 77.33, 67.57, 62.46, 30.13, 29.27, 27.14, 26.82, 26.53, 25.12. MS (CI, isobutane) *m/e* (rel. intensity): 261 (MH^+, 10), 203 (90), 145 (100).

7-*O*-Benzyl-5,6-dideoxy-1,2:3,4-di-*O*-isopropylidene-D-*lyxo*-heptitol (12)

To a suspension of NaH (36 mg, 1.5 mmol) in dry THF (2 mL) at 0°C and under dry nitrogen atmosphere was added dropwise a solution of **11** (260 mg, 1.00 mmol) in THF (20 mL). The mixture was stirred for 20 min at 0°C and then benzylbromide (256.5 mg, 1.5 mmol) and a catalytic amount (2 mg) of Bu_4NI were added. The mixture was stirred for 30 min at 0°C and then for 24 h at room temperature. The mixture was then filtered through Celite and the filtrate was evaporated. The residue was taken up by EtOAc (40 mL) and this organic phase was washed with water (2 × 15 mL), dried over $MgSO_4$, and evaporated. Flash chromatography on silica gel (EtOAc/hexane, 1:9) gave **12** (311 mg, 89%) as a colorless oil; $[\alpha]_D^{23}$ +13.9 (*c* 2.03, $CHCl_3$); IR (neat): 3000–3100, 2900–3000, 1380, 1370 cm^{-1}; ^1H NMR ($CDCl_3$): 7.33 (m, 5H), 4.52 (s, 2H), 4.11 (dd, J_1 = 7.65 Hz, J_2 = 5.85 Hz, 1H), 4.06 (m, 1H), 3.92 (m, 2H), 3.56 (m, 3H), 1.83 (m, 2H), 1.75 (m, 1H), 1.62 (m, 1H), 1.39 (s, 3H), 1.38 (s, 3H), 1.34 (s, 6H); ^{13}C NMR ($CDCl_3$): 138.73, 128.32, 127.55, 127.46, 109.55, 108.82, 81.33, 80.25, 76.61, 72.95, 70.13, 67.68, 30.29, 27.41, 27.06, 26.73, 26.18, 25.35; MS (CI, isobutane) *m/e* (rel. intensity): 351 (MH^+, 20), 293 (100), 185 (82.5).

Preparation of 4 from 12

A suspension of **12** (200 mg, 0.57 mmol) in water (10 mL) was stirred for 18 h at 60°C in the presence of an acidic Dowex 50 resin (3 g). The mixture was filtered and the filtrate was evaporated. Flash chromatography on silica gel (CH_2Cl_2/methanol, 9:1) provided **4** (148 mg, 96%). Physical and spectral data were identical with those reported above.

Preparation of 6 from 4 (sequence 12 → 4 → 6)

To a solution of **4** (140 mg, 0.52 mmol) and DMAP (3 mg, catalytic amount) in pyridine 3 mL at 0°C was added dropwise 4 mL of acetic anhydride. The solution was stirred for 18 h at room temperature. Ether (20 mL) was added and the resulting organic layer was washed with 3 N HCl (5 mL), water (2 × 10 mL), and brine (3 × 10 mL), and then dried over $MgSO_4$ and evaporated. Flash chromatography on silica gel (petroleum ether/ether, 3:2) afforded **6** (221 mg, 97%) as a colorless oil. Spectral and physical data were identical with those reported above.

Preparation of 12 from 4 (from the enzymatic reaction)

Dimethoxypropane (5.8 mmol, 0.71 mL) was added dropwise to a suspension of tetraol **4** (165 mg, 0.58 mmol) in CH_2Cl_2 (3 mL) in the presence of pyridinium *p*-toluenesulfonate (30 mg, 0.12 mmol). The solution was stirred for 3 h at room temperature under dry nitrogen atmosphere. Dichloromethane was added (25 mL) and the resulting organic layer was washed with water (1 × 10 mL), saturated aqueous $NaHCO_3$ (1 × 10 mL), and brine (2 × 10 mL), dried over $MgSO_4$, and evaporated. Flash chromatography (EtOAc/hexane, 1:9) provided **12** (170 mg, 86%). Physical and spectral data were identical to those described above.

7-*O*-Benzyl-5,6-dideoxy-3,4-*O*-isopropylidene-D-*lyxo*-heptitol (13)

To a solution of diacetonide **12** (140 mg, 0.40 mmol) in 90% methanol (10 mL) was added the Dowex 50W-X8 resin

© 1997 NRC Canada

Can. J. Chem. Downloaded from www.nrcresearchpress.com by 92.62.229.171 on 09/08/12
For personal use only.

(154 mg). The reaction mixture was stirred for 24 h at room temperature. The resin was removed by filtration and the solution was treated with aqueous saturated $NaHCO_3$ (1 mL), and evaporated. Ethyl acetate was added and the organic phase was washed with brine, dried over $MgSO_4$, and evaporated. Flash chromatography (gradient from EtOAc/hexane 1:9 to 3:7 and then pure EtOAc) provided **13** (75 mg, 60%) along with starting material (24 mg) and fully deprotected compound **4** (10 mg). Compound **13** (colorless oil): $[\alpha]_D^{23}$ +5.52 (*c* 4.5, $CHCl_3$); IR (neat): 3600–3200, 3100–2900, 2900–2800, 1390–1380, 1300–1100 cm^{-1}; ^1H NMR ($CDCl_3$): 7.32 (m, 5H), 4.49 (s, 2H), 4.0 (m, 1H), 3.6–3.8 (m, 4H), 3.52 (m, 2H), 2.65 (br s, 1H), 3.10 (br s, 1H), 1.6–1.9 (m, 4H), 1.37 (s, 3H), 1.34 (s, 3H); ^{13}C NMR ($CDCl_3$): 138.12, 128.27, 127.63, 127.52, 108.64, 80.90, 78.95, 72.80, 72.50, 70.07, 63.70, 30.73, 27.21, 26.92, 25.89. MS (CI, isobutane) *m/e* (rel. intensity): 311 (MH^+, 100), 253 (93).

1-*O*-Acetyl-7-*O*-benzyl-5,6-dideoxy-3,4-*O*-isopropylidene-D-*lyxo*-heptitol (14)

To a solution of **13** (44 mg, 0.14 mmol) in dry CH_2Cl_2 (3 mL) cooled at −78°C was added 2,4,6-collidine (12 μL, 2 equiv.). After stirring for 5 min, acetyl chloride (12 μL, 1.2 equiv.) was added dropwise and the solution was stirred for 2 h at −78°C. CH_2Cl_2 (25 mL) was added and the resulting organic phase was washed with water (1 × 10 mL), saturated aqueous $NaHCO_3$ (1 × 10 mL), and brine (2 × 10 mL), and then dried over $MgSO_4$ and evaporated. Flash chromatography on silica gel (hexane/EtOAc, 3:7) gave **14** (45 mg, 90%); $[\alpha]_D^{23}$ +18.76 (*c* 2.1, $CHCl_3$); IR (neat): 3600–3200, 2850–3000, 3050–3150, 1740, 1360 cm^{-1}; ^1H NMR ($CDCl_3$): 7.22 (m, 5H), 4.43 (s, 2H), 4.26 (dd, J_1 = 2.9 Hz, J_2 = 11.7 Hz, 1H), 4.04 (dd, J_1 = 6.7 Hz, J_2 = 11.7 Hz, 1H), 3.97 (m, 1H), 3.74 (m, 1H), 3.55 (t, J = 7 Hz, 1H), 3.45 (m, 2H), 2.54 (d, J = 4.8 Hz, 1H), 2.03 (s, 3H), 1.54–1.79 (m, 4H), 1.43 (s, 3H), 1.31 (s, 3H); ^{13}C NMR ($CDCl_3$): 171.3, 138.31, 128.23, 127.56, 127.43, 108.87, 80.08, 79.06, 72.75, 71.38, 70.03, 66.18, 30.89, 27.28, 26.92, 25.98, 20.74. MS (CI, isobutane) *m/e* (rel. intensity): 253 (MH^+, 100), 277 (38), 187 (54).

1-*O*-Acetyl-7-*O*-benzyl-5,6-dideoxy-3,4-*O*-isopropylidene-2-*O*-[2′-(methoxyethoxy)methyl]D-*lyxo*-heptitol (15)

To a solution of **14** (42 mg, 0.12 mmol) in CH_2Cl_2 (1 mL) at 0°C were added DIPEA (62 μL, 0.357 mmol, 3 equiv.) and MEMCl (34 μL, 0.298 mmol, 2.5 equiv.). The solution was stirred for 0.5 h at 0°C, then for 48 h at room temperature under dry atmosphere. CH_2Cl_2 (25 mL) was added and the organic layer was washed with water (1 × 10 mL), with saturated aqueous $NaHCO_3$ (2 × 10 mL), and with brine (2 × 10 mL), dried over $MgSO_4$, and evaporated. Flash chromatography on silica gel (EtOAc/petroleum ether, 3:7) provided **15** (45 mg, 87%) as a colorless oil; $[\alpha]_D^{25}$ +18.4 (*c* 1.1, acetone) (lit. (*7c*) $[\alpha]_D^{25}$ −18.7 (c. 1.87, acetone) for the opposite enantiomer). IR (neat): 2900–3100, 2800–2900, 1740, 1370, 1000–1200 cm^{-1}; ^1H NMR ($CDCl_3$): 7.31 (m, 5H), 4.84 (d, J = 7.1 Hz, 1H), 4.73 (d, J = 7.1 Hz, 1H), 4.48 (s, 2H), 4.1 (dd, J_1 = 6 Hz, J_2 = 12 Hz, 1H), 4.42 (dd, J_1 = 12 Hz, J_2 = 3 Hz, 1H), 4.02 (m, 1H), 3.85 (m, 1H), 3.77 (m, 1H), 3.68 (m, 2H), 3.47–3.59 (m, 4H), 3.51 (s, 3H), 2.05 (s, 3H), 1.59–1.85 (m, 4H), 1.37 (s, 3H), 1.34 (s, 3H); ^{13}C NMR ($CDCl_3$): 170.62, 138.48, 128.19, 127.45, 127.36, 108.89, 94.89, 79.54, 78.85, 75.64, 72.70, 71.53, 69.96, 67.33, 63.54, 58.89, 30.73, 27.30, 26.90, 26.20, 20.75. MS (CI, isobutane) *m/e* (rel. intensity): 441 (MH^+, 4), 365 (100), 307 (46), 157 (67).

(2*R*,3*S*,4*R*)-1-*tert*-Butyldimethylsilyloxy-7-benzyloxy-2,3,4-heptanetriol (16)

To a solution of **4** (135 mg, 0.50 mmol) in acetonitrile–pyridine (1:1, 2 mL) in the presence of TMG (12.5 μL, 0.1 mmol) was added TBDMSCl (90 mg, 1.2 equiv.) and the solution was stirred for 3.5 h at room temperature under dry nitrogen atmosphere. CH_2Cl_2 (20 mL) was added and the organic layer was washed with 1 N HCl (10 mL), saturated aqueous $NaHCO_3$ (10 mL), and brine (2 × 10 mL), and dried over $MgSO_4$ and evaporated. Flash chromatography on silica gel (EtOAc/hexane, 3:7) provided **16** (155 mg, 80%); $[\alpha]_D^{23}$ +4.0 (*c* 2.54, $CHCl_3$); IR (neat): 3100–3600, 3030–3090, 2850–3000, 1100–1200 cm^{-1}; ^1H NMR ($CDCl_3$): 7.23 (m, 5H), 4.42 (s, 2H), 3.34–3.76 (m, 7H), 1.60–1.74 (m, 4H), 0.88 (s, 9H), 0.06 (s, 6H); ^{13}C NMR ($CDCl_3$): 73.91, 72.83, 72.03, 70.33, 70.22, 64.29, 30.78, 26.14, 25.62, 17.99, −5.67. MS (CI, isobutane) *m/e* (rel. intensity): 385 (MH^+, 14), 270 (100).

(2*R*,3*S*,4*R*)-1-*tert*-Butyldimethylsilyloxy-7-benzyloxy-2,3,4-triacetoxyheptane (17)

To a solution of **16** (140 mg, 0.36 mmol) and DMAP (10 mg) in pyridine (1 mL) was added acetic anhydride (0.5 mL) and the solution was stirred for 24 h at room temperature. EtOAc (50 mL) was added and this organic layer was washed with 1 N HCl (3 × 10 mL), with saturated aqueous $NaHCO_3$ (2 × 10 mL), with brine (3 × 10 mL), then dried over $MgSO_4$ and evaporated. Flash chromatography on silica gel (EtOAc/hexane, 1:9) provided **17** (180 mg, 97%) as an oil; $[\alpha]_D^{23}$ +15.7 (*c* 2.8, $CHCl_3$); IR (neat): 3020–3090, 2850–3000, 1740, 1360, 1100–1300 cm^{-1}; ^1H NMR ($CDCl_3$): 7.29 (m, 5H), 5.29 (dd, J_1 = 8.3 Hz, J_2 = 3.3 Hz, 1H), 4.98 (ddd, J_1 = 8.3 Hz, J_2 = 5.1 Hz, J_3 = 3.6 Hz, 1H), 4.45 (s, 2H), 3.71 (dd, J_1 = 11.2 Hz, J_2 = 3.6 Hz, 1H), 3.61 (dd, J_1 = 11.2 Hz, J_2 = 5.1 Hz, 1H), 3.42 (m, 2H), 2.07 (s, 3H), 2.01 (s, 3H), 2.00 (s, 3H), 1.61 (m, 4H), 0.85 (s, 9H), 0.0 (s, 6H); ^{13}C NMR ($CDCl_3$): 170.39, 169.97, 169.63, 138.49, 128.30, 127.55, 127.46, 72.76, 71.13, 70.96, 70.72, 69.60, 61.50, 25.68, 27.76, 25.44, 20.68, 20.85, 20.91, 5.58. MS (CI, isobutane) *m/e* (rel. intensity): 511 (MH^+, 28), 451 (100), 303 (62), 228 (61).

Acknowledgements

The authors would like to thank the Natural Sciences and Engineering Research Council of Canada (NSERC) for financial support as well as "le Fonds pour les chercheurs et l'aide à la recherche, Québec", for a postgraduate scholarship to M.D.

References

1. B.M. Trost and I. Fleming (*Editors*). Comprehensive organic synthesis. Vol. 2. Pergamon, New York. 1991.
2. C.H. Wong and G.M. Whitesides. *In* Enzymes in synthetic organic chemistry. Pergamon, New York. 1994. Chap. 4.
3. (*a*) E.J. Toone, E.S. Simon, and M.D. Bednarski. Tetrahedron, **45**, 5365 (1989); (*b*) C.H. Wong, R.L. Halcomb, Y. Ichikawa, and T. Kajimoto. Angew. Chem. Int. Ed. Engl. **34**, 412 (1995);

© 1997 NRC Canada

(*c*) W.D. Fessner and G. Sinerius. Angew. Chem. Int. Ed. Engl. **33**, 209 (1994).
4. M. Schultz, H. Waldmann, W. Vogt, and H. Kunz. Tetrahedron Lett. **31**, 867 (1990).
5. M. Shimagaki, H. Muneshima, M. Kubota, and T. Oishi. Chem. Pharm. Bull. **41**, 282 (1993).
6. (*a*) S. Huneck, K. Schreiber, and W. Steglich. Tetrahedron, **29**, 3687 (1973); (*b*) G. Quinkert, N. Heim, J.W. Bats, H. Oschkinat, and H. Kessler. Angew. Chem. Int. Ed. Engl. **24**, 987 (1985).
7. (*a*) D. Enders and O.F. Prokopenko. Justus Liebigs Ann. Chem. 1185 (1995); (*b*) S.C. Sinha and E.J. Keinan. J. Org. Chem. **59**, 949 (1994); (*c*) G. Solladié, I. Fernandez, and C. Maestro. Tetrahedron: Asymmetry, **2**, 801 (1991); (*d*) P.P. Waanders, L. Thijs, and B. Zwanenburg. Tetrahedron Lett. **28**, 2409 (1987); (*e*) G. Quinkert, H. Becker, and G. Dürner. Tetrahedron Lett. **32**, 7397 (1991); (*f*) G. Quinkert, N. Heim, J. Glenneberg, U.M. Billhardt, V. Autze, J.W. Bats, and G. Dürner. Angew. Chem. Int. Ed. Engl. **26**, 362 (1987); (*g*) G. Quinkert, E. Fernholz, P. Eckes, D. Newmann, and G. Dürner. Helv. Chim. Acta, **72**, 1753 (1989).
8. D.A. Evans, K.T. Champman, and E.M. Carriera. J. Am. Chem. Soc. **110**, 3560 (1988).
9. H. Zinner, E. Wittenburg, and G. Rembarz. Chem. Ber. **92**, 1614 (1959).
10. K.H. Park, Y.J. Yoon, and S.G. Lee. Tetrahedron Lett. **35**, 9737 (1994).
11. K. Ishihara, H. Kurihara, and H. Yamamoto. J. Org. Chem. **58**, 3791 (1993).
12. R.L. Pederson, J. Esker, and C.H. Wong. Tetrahedron, **47**, 2643 (1991).
13. I.W. Lawston and T.D. Inch. J. Chem. Soc. Perkin Trans. 1, 2629 (1983).
14. I. Dyong and W. Hohenbrink. Chem. Ber. **110**, 3655 (1977).

Can. J. Chem. Downloaded from www.nrcresearchpress.com by 92.62.229.171 on 09/08/12
For personal use only.

© 1997 NRC Canada

Kinetic isotope effects from reactions of muonium atoms in water with various ketones, and acetaldehyde: contrasts with hydrogen atoms

John M. Stadlbauer, Krishnan Venkateswaran, and David C. Walker

Can. J. Chem. Downloaded from www.nrcresearchpress.com by 92.62.229.171 on 09/08/12
For personal use only.

Abstract: This paper presents data showing that in dilute aqueous solutions of butanone, 3-pentanone, cyclohexanone, di-*tert*-butyl ketone, and acetaldehyde the addition reaction of muonium atoms occurs with a rate constant close to 1×10^8 M^{-1} s^{-1}. The same value was obtained previously for acetone. Thus the reaction rate is virtually independent of the group attached to the C=O, be it a methyl, methylene, *tert*-butyl, or even a hydrogen atom. This is in sharp contrast to the reactivity of ordinary ^1H atoms, whose rate constants are much slower and dependent on adjacent groups. In fact muonium and ^1H react by different mechanisms, to form different products, so their rate ratio represents a complex kinetic isotope effect.

Key words: kinetic isotope effects, muonium atoms, muon spin rotation, ketones, hydrogen atom reactions.

Résumé : Dans ce travail, on présente des données montrant que, en solutions diluées, la butanone, la pentan-3-one, la cyclohexanone, l'acétaldéhyde et la di-*tert*-butylcétone conduisent à des réactions d'addition des atomes de muonium pour lesquelles la constante de vitesse est de l'ordre de 1×10^8 M^{-1} s^{-1}. La même valeur avait antérieurement été obtenue avec l'acétone. La constante de vitesse est donc virtuellement indépendante de la nature du groupe attaché au C=O, que ce soit méthyle, méthylène, *tert*-butyle ou même un atome d'hydrogène. Cette observation diffère considérablement de la réactivité des atomes de ^1H ordinaires pour lesquels les constantes de vitesse, beaucoup plus lentes, varient avec la nature des groupes adjacents. En fait, le muonium et le ^1H réagissent par des mécanismes différents et ils forment des produits différents; les rapports de leurs constantes de vitesse représentent donc un effet isotopique cinétique complexe.

Mots clés : effets isotopiques cinétiques, atomes de muonium, rotation de spin du muon, cétones, réactions des atomes d'hydrogène.

[Traduit par la rédaction]

Introduction

Hydrogen atoms are of special interest in the study of kinetic isotope effects (hereafter abbreviated to KIE) because H undergoes a variety of different types of reaction, and possesses four available isotopes, two of which can be studied via their radioactivity. Here we present data on the comparison of ^1H with muonium (Mu), the light radioactive isotope of hydrogen with a short-lived (2 μs) positive muon as nucleus with one-ninth the mass of a proton. These studies involve Mu reactions with solutes in dilute aqueous solution, where a 10^4-fold range of classical and quantum-mechanical KIEs has been reported in the past (1).

Received October 3, 1996.

J.M. Stadlbauer,[1] K. Venkateswaran,[2] and D.C. Walker.[3]
Chemistry Department and TRIUMF, University of British Columbia, Vancouver, BC V6T 1Y6, Canada.

[1] Permanent address: Chemistry Dept., Hood College, Frederick, MD 21701, U.S.A.
[2] Permanent address: Hindustan Lever Research Centre, Bombay 400 099, India.
[3] Author to whom correspondence may be addressed. Telephone: (604) 822-3187. Fax: (604) 822-2847. E-mail: Walker@Triumf.ca

Acetone is a solute which was found to react with Mu atoms ~60 times faster than with ^1H atoms in water (1–4). Chemical analysis of the products of the ^1H-atom reaction revealed two competing processes occurring with comparable rates (33/67%) corresponding to "addition" and "abstraction" reactions (2). This competition is represented by reaction [1] for addition and reaction [2] for abstraction, given here for Mu:

[1] $\mathrm{Mu} + (\mathrm{CH_3})_2\mathrm{CO} \rightarrow (\mathrm{CH_3})_2\dot{C}(\mathrm{OMu})$

[2] $\mathrm{Mu} + (\mathrm{CH_3})_2\mathrm{CO} \rightarrow \mathrm{HMu} + \mathrm{CH_3CO\dot{C}H_2}$

The observed overall rate of reaction of Mu with acetone is virtually independent of pH (3, 5), and it is well documented that the $(\mathrm{CH_3})_2\dot{C}(\mathrm{OMu})$ radical is produced. This muonated free radical has been unequivocally characterized by both high-field muon spin rotation studies of pure liquid acetone and concentrated aqueous solutions (6), and by muon level-crossing resonance spectroscopy in dilute solutions in water, and hexane (5). There is some quantitative evidence that reaction [1] dominates for Mu in pure water, but that reaction [2] takes over in micelles (7). A lingering question was whether these effects are peculiar to acetone or common to other carbonyls where Mu-adduct radicals have been observed (8).

In recent studies of H atoms in dilute aqueous acidic solutions, Mezyk and Bartels (4) found butanone (methyl ethyl

© 1997 NRC Canada

Can. J. Chem. Downloaded from www.nrcresearchpress.com by 92.62.229.171 on 09/08/12
For personal use only.

ketone) to react 20 times faster than acetone with ^{1}H, and aldehydes to be faster still. Consequently, we have undertaken a study of the dependence of Mu-atom reactions towards carbonyls with different alkyl groups adjacent to the C=O, to compare with this H-atom finding. To that end, we have determined the absolute reaction rate constants of Mu with butanone (one CH_3 + one CH_2 adjacent group), 3-pentanone (two CH_2 groups), cyclohexanone (all CH_2 groups, no CH_3 groups present), di-*tert*-butyl ketone (2,2,4,4-tetramethylpentanone) hereafter referred to as DTBK (no H atoms β to the carbonyl, only γ-CH_3 groups), and acetaldehyde (one H and one CH_3 group), for direct comparison with each other and with acetone, and to evaluate their KIEs where possible.

Experimental

Muonium atom rate constants were measured by the muon spin rotation method (μSR), fully described previously (1, 7, 8). This involved bombarding a solution with high-energy positive muons and observing the decay positrons in a low transverse magnetic field, one muon at a time. In dilute aqueous solutions only a small fraction of the incident muons formed thermalized Mu atoms at the end of the muon track; but most of those that did, reacted with additives in the water during the muon's microsecond lifetime. The rates of those reactions were then extracted from the overall muon decay signals by computer-fitting to a semiempirical analytical equation, which includes a decay constant (λ) for the component precessing at the characteristic frequency of Mu atoms. λ is thus equivalent to a pseudo-first-order chemical reaction constant for Mu in a given solution.

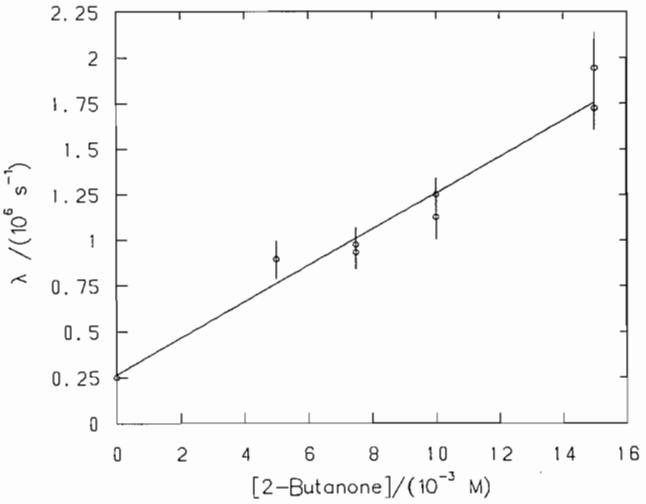
These experiments were conducted on the M9B "backward" muon channel of the TRIUMF cyclotron in Vancouver employing the SFUMu apparatus. Histograms from two counters were composed separately using at least 10 million events each and fitted independently to give a pair of values of λ for each solution. All solutions were prepared from reagent-grade chemicals or equivalent (acetone, butanone, 3-pentanone, cyclohexanone, di-*tert*-butyl ketone, acetaldehyde, *n*-heptane) and triply distilled water. They were all thoroughly deoxygenated by bubbling with pure nitrogen immediately prior to study. The experiments were conducted at 22 ± 1°C at neutral pH.

Results

Figure 1 shows λ increasing with the concentration of the solute in solution for the case of butanone. The intercept corresponds to a small "background" relaxation λ_0 (ostensibly due to fluctuations and inhomogeneities in the magnetic field, but possibly because of reaction with impurities in the water (9)). The slope equals the second-order rate constant, k_M, for reaction of Mu with the solute. Our values of k_M as determined this way are reported in Table 1.

All the data except for DTBK were obtained from direct measurements in water. DTBK was insufficiently soluble in water to allow a direct measurement, so a value for k_M was determined in *n*-heptane solution, and acetone was also measured in *n*-heptane. Mu reactions are faster in hydrocarbons than in water (acetone by a factor of ~10, evidently), so the DTBK result in *n*-heptane was "normalized" to water by assuming the water-to-heptane ratio for acetone would be similar to that for DTBK (see footnote (*d*) to Table 1).

Fig. 1. Plot of λ (/10^6 s^{-1}) against concentration of butanone (/10^{-3} M) in water at 295 K. (The two points at 5 mM coincide.)



Discussion

The major finding of this study is that Mu reacts at virtually the same rate with all these ketones, with $k_M = (10 \pm 2) \times 10^7$ M^{-1} s^{-1}. This means that the reaction rate is not affected significantly by which alkyl groups are attached to the carbonyl group, be they -CH_3, -CH_2, or -$C(CH_3)_3$. Even when -H is adjacent, as in acetaldehyde, the rate increases only by 75% or so. These data strongly imply that the abstraction reaction of a neighbouring hydrogen atom by Mu atoms, as in reaction [2], plays a very minor role. This then adds credence to the notion that the Mu reaction is predominantly that of addition to the carbonyl to give a muonated free radical, analogous to that indicated for acetone in reaction [1]. We take these results to mean that the addition reaction dominates when Mu reacts with any of these ketones (with acetaldehyde, perhaps, showing abstraction as well).

This is in sharp contrast to the situation for H-atom reactions, where the rate constant, k_H, depends significantly on the structure (and probably bond strength) of the groups adjacent to the carbonyl. Thus, k_H increases from 2×10^6 M^{-1} s^{-1} for acetone to 38×10^6 M^{-1} s^{-1} for butanone just as a result of replacing one of the CH_3 groups by a CH_2 group (4). It increases further to $\sim 1 \times 10^8$ M^{-1} s^{-1} for an adjacent H atom, as in propanal and butanal (4), though only to 3×10^8 M^{-1} s^{-1} for acetaldehyde (2). Although 3-pentanone, cyclohexanone, and DTBK do not seem to have been reported yet with regard to their H-atom reactivity, the k_H data that do exist are consistent with the notion that H reacts predominantly by "abstracting" a hydrogen atom from an adjacent site. In fact, abstraction was shown by chemical analysis of products to be 67% predominant in the case of acetone (2) and at least 95% so for butanone (4).

With different reactions occurring for Mu and H it is clear that the ratio of the observed rate constants, k_M/k_H, cannot be described as a single KIE. At best it is an admixture of two opposite isotopic effects. It equals the sum of Mu's addition

© 1997 NRC Canada

Table 1. Rate constants determined for the reaction of Mu with various carbonyl compounds in water at pH = 6–7 and T = 295(±1)K.

Solute	k_M	k_H	k_M/k_H
Acetone	10 (±1)[a]	0.17[b]	60
Butanone	9.9 (±1.0)	3.8[c]	2.6
3-Pentanone	8.4 (±1.5)	–	–
Cyclohexanone	11.7 (±2.0)	–	–
DTBK	6.5 (±~3)[d]	–	–
Acetaldehyde	17.5 (±2.0)	3.1[e]	5.6

All k's are given in units of 10^7 M^{-1} s^{-1}. Column 3 records the published data on the reaction with ^1H, where available, and the final column shows the observed "overall" KIE as k_M/k_H.

[a]This is already published data: $k_M = 1.1 \times 10^8$ M^{-1} s^{-1} for acetone at pH = 7 (5), and 0.87×10^8 M^{-1} s^{-1} at pH = 2 (3).

[b]Taking the more recent value for the "overall" k_H, ref. 4.

[c]From ref. 4.

[d]DTKB (2,2,4,4-tetramethylpentanone) was measured in n-heptane solution. The measured values of k_M in n-heptane for DTBK and acetone were, respectively, $(6.6 \pm 1.5) \times 10^8$ M^{-1} s^{-1} and $(10.5 \pm 2.0) \times 10^8$ M^{-1} s^{-1}. By assuming the same ratio in water-to-heptane for both acetone and DTBK, k_M for DTBK was deduced to be 6.5 based on the value of acetone in water. Because of this assumption and larger experimental errors in n-heptane due to its bigger background λ_0 due to impurities, an error bar of up to 50% seems appropriate. For the direct measurements in water an overall reproducibility error of < ±20% is estimated.

[e]From ref. 2.

plus abstraction rates divided by the sum of H's analogous rates; but due to the dominance of addition for Mu and abstraction for H, this reduces to k_M^{add}/k_H^{abst}. And as the addition rate constant for Mu (k_M^{add}) is almost constant, the changes seen in the observed k_M/k_H reflect directly the changes of k_H^{abst} for individual ketones

We suggest it is the differences in the quantum mechanical properties of zero-point vibrational frequency and tunneling efficiency that change the two reaction rates in opposite senses for Mu and H. This implies that tunneling is more important for the addition reaction, so that Mu as the lighter atom is favoured there; and that the abstraction reaction depends more on barrier height, so that the heavier H wins there (Mu has the higher barrier due to the higher zero point vibrational energy of its transition states).

Subtle differences in reaction paths for Mu and H have been noted before. Mu was found to be a weak nucleophile in its reactions towards substituted benzenes (10) and N-heterocyclic compounds (11), whereas H has always been known as a weak electrophile (12). Again, there are two competing reaction paths, one at an electron-rich centre, the other at an electron-deficient centre. These involve different "mechanisms," each path with its own KIE — and they must be of quite different magnitude to account for Mu and H adding to different sites on the aromatic rings. And its origin might be similar, namely, additions at electron-deficient sites carrying much larger tunneling probabilities than addition at electron-excess centres.

Such switches in reaction path do not seem to have been observed on interchanging ^1H with deuterium or tritium. They may require the particularly small atomic mass of Mu in order to occur, and to be detectable, especially at room temperature and in solution.

Acknowledgement

We gratefully acknowledge assistance with the experiments by Professor Jerry Porter and Dr. Mary Barnabas, and for technical help by Dr. D. Arseneau, Curtis Ballard, and Mel Good. Financial support from the Natural Sciences and Engineering Research Council of Canada (NSERC) is recorded with appreciation. J.M.S. also thanks the Hood College Board of Associates for financial assistance.

References

1. (*a*) J.H. Brewer, K.M. Crowe, F.N. Gygax, R.F. Johnson, D.G. Fleming, and A. Schenk. Phys. Rev. A: Gen. Phys. **9**, 495 (1974); (*b*) P.W.Percival, E. Roduner and H. Fischer. Chem. Phys. **32**, 353 (1978); (*c*) D.G. Fleming, D.M. Garner, L.C. Vaz, D.C. Walker, J.H. Brewer, and K.M. Crowe. Adv. Chem. Ser. **175**, 279 (1979); (*d*) D.C.Walker. J. Phys. Chem. **85**, 3960 (1981); (*e*) S.F.J. Cox. J. Phys. C: Solid State Phys. **20**, 3187 (1987).
2. R.A. Witter and P. Neta. J. Org. Chem. **38**, 484 (1973).
3. P.W. Percival, E. Roduner, H. Fischer, M. Camani, F.N. Gygax, and A. Schenck. Chem. Phys. Lett. **47**, 11 (1977).
4. S.P. Mezyk and D.M. Bartels. Can. J. Chem. **72**, 2516 (1994).
5. K. Venkateswaran, R.F. Kiefl, M.V. Barnabas, J.M. Stadlbauer, B.W. Ng, and D.C. Walker. Chem. Phys. Lett. **145**, 289 (1988).
6. (*a*) E. Roduner, P.W. Percival, D.G. Fleming, J. Hochmann, and H. Fischer. Chem. Phys. Lett. **57**, 37 (1978); (*b*) A. Hill, M.C.R. Symons, S.F.J. Cox, R. de Renzi, C.A. Scott, C. Bucci, and A. Vecli. J. Chem. Soc. Faraday Trans. 1, **81**, 433 (1985); (*c*) S.F.J. Cox and M.C.R. Symons. Radiat. Phys. Chem. **27**, 53 (1985); (*d*) E. Roduner. Radiat. Phys. Chem. **28**, 75 (1986).
7. (*a*) D.C. Walker. Can. J. Chem. **68**, 1719 (1990); (*b*) J.M. Stadlbauer, K. Venkateswaran, H.A. Gillis, G.B. Porter, and D.C. Walker. Can. J. Chem. **74**, 1945 (1996).
8. S.F.J. Cox, D.A. Geeson, C.J. Rhodes, E. Roduner, C.A. Scott, and M.C.R. Symons. Hyperfine Interact. **32**, 763 (1986).
9. D.C. Walker. Muon and muonium chemistry. Cambridge University Press, Cambridge. 1983, pp. 46–47.
10. (*a*) J.M. Stadlbauer, B.W. Ng, R. Ganti, and D.C. Walker. J. Am. Chem. Soc. **106**, 3151 (1984); (*b*) J.M. Stadlbauer, B.W. Ng, and D.C. Walker. Hyperfine Interact. **32**, 721 (1986); (*c*) J.M. Stadlbauer, Y. Miyake, B.W. Ng, E.C. Phillips, and D.C. Walker. Radiat. Phys. Chem. **28**, 95 (1986).
11. (*a*) Z. Wu, M.V. Barnabas, J.M. Stadlbauer, K. Venkateswaran, G.B. Porter, and D.C. Walker. J. Am. Chem. Soc. **113**, 9096 (1991); (*b*) Z. Wu, J.M. Stadlbauer, and D.C. Walker. J. Am. Chem. Soc. **114**, 3988 (1992).
12. (*a*) P. Neta and R.H. Schuler. J. Am. Chem. Soc. **94**, 1056 (1972); (*b*) P. Neta. Chem. Rev. **72**, 533 (1972); (*c*) W.A. Pryor, T.H. Lin, J.P. Stanley, and R.W. Henderson. J. Am. Chem. Soc. **95**, 6993 (1973).

Can. J. Chem. Downloaded from www.nrcresearchpress.com by 92.62.229.171 on 09/08/12
For personal use only.

© 1997 NRC Canada

On sodium clusters in C_{60} fullerides

M. Apostol, F. Rachdi, C. Goze, and L. Hajji

Abstract: Sodium (Na) clusters in octahedral cages of Na-intercalated fullerides Na_6C_{60} and $Na_{11}C_{60}$ are studied within a Thomas–Fermi model. It is shown that the tetrahedral Na_4 cluster in Na_6C_{60} has an electric charge $\sim+2.7$ (in electron charge units), while the body-centered cubic Na_9 cluster in $Na_{11}C_{60}$ is almost electrically neutral.

Key words: sodium clusters, alkali fullerides, Thomas–Fermi theory, ionization charge.

Résumé : En faisant appel au modèle de Thomas–Fermi, on a étudié les agrégats de sodium (Na) dans des cages octaédriques de fullerures dans lesquels du sodium a été intercalé, Na_6C_{60} et $Na_{11}C_{60}$. On a établique l'agrégat tétraédrique de Na_4 dans le Na_6C_{60} a une charge électrique d'environ +2,7 eV alors que l'agrégat cubique à corps centré de Na_9 présent dans le $Na_{11}C_{60}$ est pratiquement neutre.

Mots clés : agrégats de sodium, fullerures alcalins, théorie de Thomas–Fermi, potentiel d'ionisation.

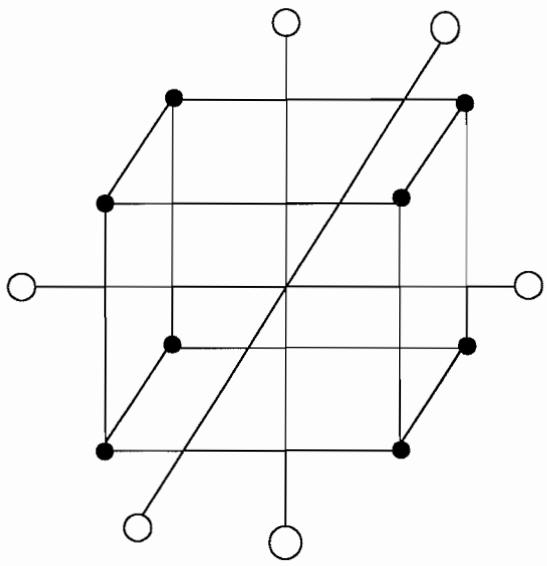
[Traduit par la rédaction]

Introduction

There has recently been a great deal of interest in studying the fullerene molecule and the alkali-doped fullerides by means of the Thomas–Fermi model. This approach has successfully been used to investigate the stability of the fullerene molecule (1) and the endohedral rare gas fullerenes (2). The Thomas-Fermi model for molecules, clusters, and solids has a long history, originating, probably, in ref. 3. In this paper we employ this model to study the sodium (Na) clusters embedded in fulleride solids, with the aim of computing their valence charges (4).

The nature of metallic clusters is currently receiving a great deal of interest (see, for example, the recent reviews in ref. 5). Metallic clusters trapped in zeolite cages can be studied by various magnetic resonance techniques (6–8) and, in this respect, the nature of chemical bonding, the distinction between metallic and covalent bonding, and the degree of ionicity of the clusters are of utmost importance. The existence of Na clusters in the octahedral cages of Na-doped C_{60}-fullerite has recently been suggested by X-ray analysis (9, 10). Similar clusters of calcium (Ca) in Ca-doped C_{60} were previously pointed out (11). Tetrahedral-shaped Na_4 clusters seem to build up in the octahedral cages of the face-centered cubic (fcc) Na_6C_{60} (9), with the Na atoms disposed alternately on the corners of a cube of side 2 Å. Similarly, body-centered cubes of nine sodium atoms (Na_9 cluster) seem to occur in the octahedral cages of the fcc-$Na_{11}C_{60}$ (10), with a cube side of 3.2 Å. A schematic configuration of these clusters

Fig. 1. A schematic cluster configuration in an octahedral cage of alkali-doped fullerites. The open circles represent the centres of the fullerene molecules, while the corners of the cube indicate the positions of the Na nuclei; an additional Na atom may be placed at the centre of the cube as in the case of the Na_9 cluster.



is shown in Fig. 1. This is in contrast with the C_{60}-fullerite doped with heavier species, such as A_6C_{60}, A = K, Rb, Cs, where the alkali cations push through the fcc structure of the host, pristine C_{60}, and distort it into a bcc structure, while acquiring a conventional ionic character (12). The stability and the chemical bonding of isolated, small-size alkali clusters, such as Na and Li clusters, have been extensively studied (13–16). Recently, the formation of Na clusters in Na_6C_{60} has been challenged on computational grounds (17). Here we present a Thomas–Fermi model of Na clusters in Na_6C_{60} and $Na_{11}C_{60}$, discuss its equilibrium, and compute the distri-

Received July 30, 1996.

M. Apostol.[1] Department of Theoretical Physics, Institute of Atomic Physics, Magurele-Bucharest MG-6, PO Box MG-35, Romania.

F. Rachdi, C. Goze, and L. Hajji. Université Montpellier II, GDPC-026, 34095 Montpellier, France.

[1] Author to whom correspondence may be addressed. Fax: 40-1-420-91-01. E-mail: apoma@theor1.ifa.ro

© 1997 NRC Canada

Can. J. Chem. Downloaded from www.nrcresearchpress.com by 92.62.229.171 on 09/08/12
For personal use only.

Can. J. Chem. Downloaded from www.nrcresearchpress.com by 92.62.229.171 on 09/08/12
For personal use only.

bution of electric charges and the degree of ionization of the clusters.

Results and discussion

We start with the main observation that the Na–Na distance in these Na clusters is much shorter than the Na–Na distance of 3.7 Å in bulk metallic sodium, though slightly larger than twice the Na^+ radius of 1.15 Å. Indeed, the Na–Na distance in the tetrahedral Na_4 cluster in $Na_6C_{60}(10)$ is $2\sqrt{2}$ Å = 2.82 Å, while in the cubic Na_9 cluster in $Na_{11}C_{60}$ (10) this distance (the shortest) is $3.2\sqrt{3}/2$ Å = 2.75 Å. This indicates that, in comparison with bulk metallic sodium, the Na clusters in doped C_{60} are squeezed (or compressed) in the octahedral cages provided by the neighbouring fullerene molecules. In the octahedral coordination of the fcc-C_{60} the fullerene molecules are placed at ~7.1 Å from the coordination centre (18, 19) and, allowing for the fullerene molecule radius of ~3.5 Å, one obtains a distance of ~3.6 Å from the coordination centre to the intersections of the fullerene molecules with the octahedral axes. The distance from the coordination centre to the plane passing through these intersection points may be taken as an average radius of the octahedral cage; we obtain thereby an average radius $R_0 = 3.6/\sqrt{3}$ Å = 2 Å for the octahedral cage (9, 10). For the tetrahedral Na_4 cluster, whose atoms are placed at $R = 2\sqrt{3}/2$ Å = 1.73 Å from the coordination centre, this cage provides an average atomic radius of $2^{1/3}$ (≅1.26) Å, and an average interelectron separation much smaller than the Bohr radius. This suggests that a Thomas–Fermi model is suitable for describing the Na_4 cluster. The confinement of the cluster in the octahedral cage is ensured by the electronic clouds of carbon atoms on the surface of the fullerene molecules, which, in order to be penetrated, require electrons of higher energy. They act as very high potential barriers. The confinement of electrons in the much narrower tetrahedral sites of the fcc-C_{60} (whose radius is estimated at ~1.12 Å (11) may certainly provide them with enough energy to make them capable of penetrating the confinement, which may explain the absence of clusters in these cages. Similar considerations apply for heavier-alkali atoms in the octahedral cages, and even for the Na_9 cluster in $Na_{11}C_{60}$, whose atoms, placed at $R = 3.2\sqrt{3}/2$ Å = 2.75 Å, are clearly exceeding the 2 Å limit found above. However, the penetration of the electronic clouds of the C atoms proceeds gradually and, in the octahedral cages, the C atoms provide another limit of about 4 Å in the (111) directions: this is the distance from the coordination centre to the octahedral faces passing through the centres of the fullerene molecules. We may take, tentatively, a mean value of these two limits (2 Å and 4 Å), and set up an average cage radius $R_0 \sim 3$ Å for the Na_9 cluster. This gives an average atomic radius $3^{1/3}$ (≅1.44) Å, which again justifies a Thomas–Fermi model for this Na_9 cluster. It is worth remarking at this point that the resistance of the cage walls to the penetrating electrons (which may also apply in the case of the zeolite cages) is an expression of the Pauli exclusion principle, which requires fast varying (in space) wave functions for the latter (and therefore higher energy) if they are going to penetrate into the space regions already occupied by atomic-core electrons. This confining effect of the cage boundaries on an atomic cluster may be formalized as an external field "pseudo-potential," much in the same manner as has already been done for bulk metals (20). It can easily be seen that these "pseudo-potentials" would vary strongly over short distances (as in the short-range parts of the interatomic Lennard–Jones or Born–Mayer potentials), and their functional dependence on distance (which would depend, among others, on the number of confined electrons) will provide an effective cage radius R_0 for a given cluster, as we shall discuss below in more detail.

As is well known, the Thomas–Fermi model is a quasi-classical theory of interacting electrons and atomic nuclei, which assumes that the Fermi wave vector k_F of the electrons, and the electron density n, vary slowly in space.

$$[1] \qquad n = \frac{1}{3\pi^2} k_F^3$$

This is true (except for distances very close to the nuclei) due to the effective screening of the nuclear charges accomplished by the high-density electrons. We shall see that this assumption is consistent also in the present Thomas–Fermi model of clusters. Under this assumption the particular shape of the atomic cluster is no longer very relevant, so that we may introduce an additional simplification by assuming that the total charge z of the nuclei is uniformly distributed over a spherical shell of radius R, plus a central Na nucleus of charge +11 (in electron charge units) in the case of the Na_9 cluster. We denote by V the electrostatic potential created by the distribution of positive charges, and note that its particular expression is not very important in subsequent calculations; the only requirement on the positive charge distribution is that of symmetry, from obvious reasons of stability, and the approximation made is that of radial symmetry. Later on in this paper we will estimate the error introduced by this approximation. In the high-density limit the electron exchange interaction is a higher order contribution (as well as other contributions to the electron interaction energy), and we may assume that an electrostatic potential φ is generated by the electron distribution, which does not depend on k_F. We may therefore set up the basic Thomas–Fermi relationship (in atomic units Bohr radius $a_H = \hbar^2/me^2 = 0.53$ Å, $e^2/a_H = 27.2$ eV, and $\hbar = 1$)

$$[2] \qquad \frac{1}{2} k_F^2 - \varphi - V - U = -\varphi_0$$

where U is the potential well of the cage and φ_0 is the chemical potential; the latter should be constant, in order to ensure the local equilibrium, and equal to the "pseudo-potential" of the external field at the cage frontier R_0, to prevent any flux of electrons pouring in and out of the cage. The variation of this external "pseudo-potential" over the distance R_0 may be taken as the depth U of the potential well. Using eqs. [1] and [2] we may rewrite the Poisson equation $\Delta\varphi = 4\pi n$ as

$$[3] \qquad \Delta(\varphi + V + U - \varphi_0) = \frac{8\sqrt{2}}{3\pi} (\varphi + V + U - \varphi_0)^{3/2}$$

everywhere except for $r = R$; introducing the reduced vari-

© 1997 NRC Canada

Can. J. Chem. Downloaded from www.nrcresearchpress.com by 92.62.229.171 on 09/08/12
For personal use only.

ables $x = r/R_0$ and

$$[4] \quad \varphi + V + U - \varphi_0 = \left(\frac{3\pi}{8\sqrt{2}R_0^2}\right)^2 \frac{\chi}{x}$$

we arrive at the Thomas–Fermi equation

$$[5] \quad x^{1/2}\chi'' = \chi^{3/2}$$

for any x between 0 and 1 except for $x = a = R/R_0$. Since n is a continuous function, φ and its first and second derivatives must be continuous functions; it follows that the function χ has a slope discontinuity (but is itself continuous) exactly as has the derivative of V, i.e., at $x = a$; the magnitude of this slope jump will be obtained below by Gauss' law. It is therefore convenient to define $\chi_1(x) = \chi(x)$ for $0 < x < a$ and $\chi_2(x) = \chi(x)$ for $a < x < 1$, with the continuity condition

$$[6] \quad \chi_1(a) = \chi_2(a)$$

The number of electrons inside a sphere of radius x is easily obtained from eqs. [1]–[5] as

$$[7] \quad N(x) = 4\pi R_0^3 \int_0^x dx \cdot x^2 n = \frac{9\pi^2}{128R_0^3} \int_0^x dx[x\chi' - \chi]$$

$$= \left\{ \begin{array}{ll} \dfrac{9\pi^2}{128R_0^3}[x\chi_1' - \chi_1 + \chi_1(0)], & 0 < x < a \\ \dfrac{9\pi^2}{128R_0^3}\{x\chi_2' - \chi_2 + a[\chi_1'(a) - \chi_2'(a)] + \chi_1(0)\}, & a < x < 1 \end{array} \right\}$$

and one notes that it is continuous at $x = a$. The total number of electrons in the cage is obtained from eq. [7] as

$$[8] \quad N = \frac{9\pi^2}{128R_0^3}\{\chi_2'(1) - \chi_2(1) + a[\chi_1'(a) - \chi_2'(a)] + \chi_1(0)\}$$

By Gauss' law we easily obtain the net charge inside the sphere of radius x as

$$[9] \quad q(x) = \frac{9\pi^2}{128R_0^3}(\chi - x\chi')$$

whence, by using eq. [7], we obtain the positive charge

$$[10] \quad q_{1+}(x) = \frac{9\pi^2}{128R_0^3}\chi_1(0)$$

inside the sphere of radius $x < a$. We note that, if it exists, it is concentrated at $x = 0$. Obviously, for the Na_4 cluster we should require

$$[11] \quad \chi_1(0) = 0$$

while for the body-centered cubic Na_9 cluster the corresponding boundary condition is

$$[12] \quad \frac{9\pi^2}{128R_0^3}\chi_1(0) = 11$$

The total charge inside the sphere of radius x, $a < x < 1$, given by eq. [9] consists of z positive charges distributed over the spherical shell of the cluster, a charge of +11 at the centre, if this is the case, and $-N(x)$ electron charges; whence, by using eq. [7], we obtain the magnitude

$$[13] \quad z = \frac{9\pi^2}{128R_0^3} a[\chi_1'(a) - \chi_2'(a)]$$

in the slope discontinuity of the function χ, as expected; eq. [13] provides the third boundary condition for our problem, with $z = 44$ for the Na_4 cluster and $z = 88$ for the Na_9 cluster. The fourth boundary condition needed for the unique solution of eq. [5] is provided by the equilibrium condition of the positive shell of the cluster. It is easy to get the electric self-field acting on the shell; in the absence of the central atom it is given by

$$[14] \quad E_s = z/2R^2$$

while in the case of the centered cluster we obtain

$$[15] \quad E_s = z/2R^2 + 11/R^2$$

The electric field on the shell due to the electrons is readily obtained as

$$[16] \quad E_e = -\frac{\partial\varphi}{\partial r}\bigg|_{r=R} = \frac{9\pi^2}{128R_0^5}\frac{1}{a^2}[\chi_1(a) - a\chi_1'(a) - \chi_1(0)]$$

(or equivalently in terms of χ_2), and we note that, in contrast to eqs. [14] and [5], it is negative, i.e., the electrons try to stabilize the exploding cluster shell. Using eq. [13] we arrive easily at the equilibrium condition

$$[17] \quad 2\chi_1(a) = a[\chi_1'(a) + \chi_2'(a)]$$

both for the noncentered and for the centered cluster. Equation [5] is solved numerically with the boundary conditions given by eqs. [6], [11]–[13], and [17], both for the Na_4 and the Na_9 clusters, and the results are described below. In each case we were especially interested in the total charge

$$[18] \quad q = \frac{9\pi^2}{128R_0^3}[\chi_2(1) - \chi_2'(1)]$$

in the cage, as given by eq. [9].

We note that eq. [5] is a second-order differential equation for two distinct functions, $\chi_1(x)$ over the range 0–a, and $\chi_2(x)$ over a–1; consequently, we need four boundary conditions in order to uniquely determine the solution, and they are indeed provided by eq. [6], one of eqs. [11] and [12], [13], and [17]. As a matter of fact, we start with $\chi_1(0)$ as given by eqs. [11] or [12] and with an arbitrary slope at $x = 0$; the values $\chi_1(a)$ and $\chi_1'(a)$ are then uniquely determined, and, from eqs. [6] and [13] we get $\chi_2(a)$ and $\chi_2'(a)$, so that the solution $\chi_2(x)$ is completely determined; finally, we look for that arbitrary initial slope at the origin, to satisfy eq. [17]. The physical solution is therefore completely determined and we compute the corresponding total charge in the cage, as given by eq. [18].

In the case of the Na_4 cluster we used $R = 1.73$ Å and $R_0 = 2$ Å ($a = R/R_0 = 0.86$), as suggested by the X-ray diffraction data (9, 11). The function χ is plotted versus x

© 1997 NRC Canada

Can. J. Chem. Downloaded from www.nrcresearchpress.com by 92.62.229.171 on 09/08/12
For personal use only.

Fig. 2. The function χ vs. x for the Thomas–Fermi model of the Na_4 cluster with $z = 44, R = 1.73$ Å, and $R_0 = 2$ Å, corresponding to a total charge $q = +2.72$.

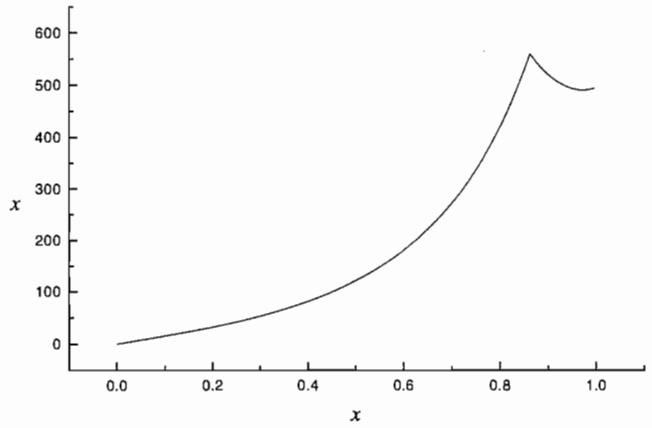
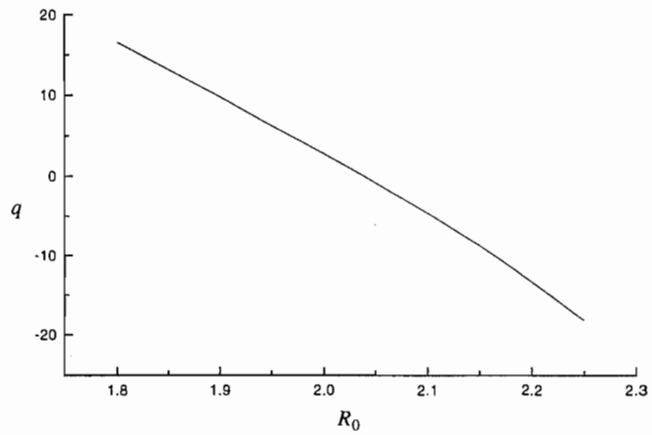


Fig. 3. The total charge q vs. the cage radius R_0 for the Na_4 cluster with $R = 1.73$ Å.



in Fig. 2; it corresponds to a total charge $q = +2.72$, i.e., an average charge of +0.68 for each Na ion. The variation of the total charge in this case is also plotted versus R_0 in Fig. 3. As discussed above, the numerical results obtained for the function χ are valid everywhere except for a range of about twice the Bohr radius around the position of the positive shell of charges, where the variation of χ/x is too large; even so, one can estimate that almost half of the electrons are located there, thus ensuring the screening of the positive charges. Another limitation of the present calculations occurs from the assumption of radial symmetry for the function χ. We can estimate the error introduced by this approximation as follows. Assuming the same variation of electron density per unit length in all directions, the relative contribution of the angular part of the variation of the potential derivative with respect to the radial part is $\delta\varphi_a'/\delta\varphi_r' \sim \sqrt{4\pi/s}$, for a cluster consisting of s atoms; on the other hand, as these small variations are proportional to the variations of the distance, we have $(\delta\varphi_r')^2 + 2\left(\delta\varphi_a'\right)^2 = (\delta\varphi_r')_0^2$, where the latter corresponds to neglecting the angular part. As the variations of the potential derivatives are also proportional to the charge (from the Poisson equation), we then easily find that the relative error made in estimating the charge is at most $\sim 1 - \sqrt{1 + 8\pi/s}/(1 + 2\sqrt{4\pi/s})$. In the case of the Na_4 cluster this amounts to $\sim 40\%$; one can see that the radial-symmetry approximation improves its accuracy for large s.

Increasing the amount of negative charge on the cluster, the position of the maximum value of χ moves toward smaller values of x (smaller values of R), and it exhibits the opposite behaviour on increasing the degree of ionization. The variation of χ with respect to the cage radius R_0 brings into discussion the energy of the cluster. One can easily check that the density of the electronic kinetic energy is given by

$$[19] \quad \varepsilon_{kin} = \frac{1}{2\pi^2} \int_0^{k_F} dk \cdot k^4 = \frac{9\,(3\pi/32)^3}{10R_0^{10}} \cdot \frac{\chi^{5/2}}{x^{5/2}}$$

where eqs. [2] and [4] have been used; from this the total kinetic energy of the electrons can be calculated:

$$[20] \quad \mathscr{E}_{kin} = \frac{3(3\pi/8)^4}{20R_0^7} \int_0^1 dx \cdot \frac{\chi^{5/2}}{x^{1/2}}$$

We similarly obtain the potential energy of the electrons

$$[21] \quad \mathscr{E}_{pot} = -\frac{(3\pi/8)^4}{4R_0^7} \int_0^1 dx \cdot \frac{\chi^{5/2}}{x^{1/2}} - N\varphi_0$$

so that the electronic energy may be expressed as $\mathscr{E}_{el} = \mathscr{E}_1 - N\varphi_0$, where

$$[22] \quad \mathscr{E}_1 = -\frac{(3\pi/8)^4}{10R_0^7} \int_0^1 dx \cdot \frac{\chi^{5/2}}{x^{1/2}}$$

The self-energy of the positive charges is given by $\mathscr{E}_s = \mathscr{E}_0 - zU$ for the noncentered cluster and $\mathscr{E}_s = \mathscr{E}_0 - (z+11)U$ for the centered one, where $\mathscr{E}_0 = z^2/2R$ in the former case and $\mathscr{E}_0 = z^2/2R + 11z/R$ in the latter. On the other hand, expressing the interaction energy of the shell with the electrons in two distinct ways, namely, $z\varphi(R) = -\int d\boldsymbol{r}nV$, we get

$$[23] \quad U - \varphi_0 = \frac{9\pi^2}{128R_0^4}\,\chi_2'(1)$$

Summing up all these contributions we obtain the total energy of the cluster as

$$[24] \quad \mathscr{E} = \mathscr{E}_0 + \mathscr{E}_1 + \mathscr{E}_2 - (2z - q)\varphi_0$$

where $\mathscr{E}_2 = -z(U - \varphi_0)$ as given above; in the case of the centered cluster we should replace z by $z + 11$ in eq. [24]. The numerical integration gives $\mathscr{E}_1 = -28$ and $\mathscr{E}_2 = -42$ for the Na_4 cluster, while $\mathscr{E}_0 = 296$; the total energy, consisting of eq. [24] and the energy of the electrons transferred to the cage walls, must be negative, in order that the cluster be formed. For small values of the total charge of the cluster the latter contribution to the total energy is small, so that we may estimate that the energy E given by eq. [24] must acquire negative values. Hence it follows that φ_0 must be of the order of $(296 - 28 - 42)/N \sim 2.6$ (for $N = 44$). On the other hand, φ_0 equals the external "pseudo-potential" at the cage frontier R_0, as we discussed before, whence one can estimate the magnitude of this "pseudo-potential." One can see, therefore, that it acquires high values, to ensure the con-

© 1997 NRC Canada

Fig. 4. Same as in Fig. 1 for the centered-cubic Na_9 cluster with $z = 88$, $R = 2.75$ Å, and $R_0 = 3.15$ Å, and a vanishing total charge ($q \sim 0$).

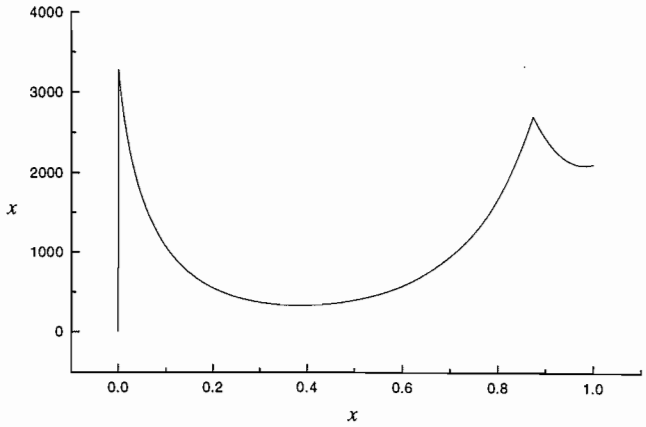
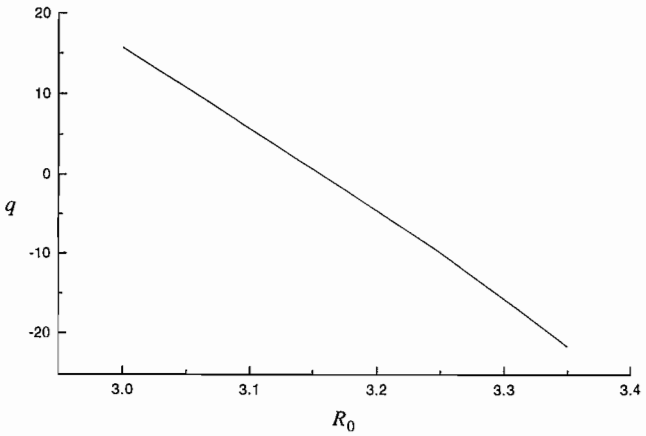


Fig. 5. The total charge q vs. the cage radius R_0 for the Na_9 cluster with $R = 2.75$ Å.



finement of the squeezed cluster within the R_0 range. In addition, as the present estimations are valid over a scale length larger than the Bohr radius, one can also see that the external "pseudo-potential" has a high variation over short distances. This illustrates again the gradual resistance developed by the inner-core electrons of the environment to the penetrating "pressure" of the confined cluster. The electron density also varies rapidly over short distances at the frontier of the cage, in order to ensure the delimitation of the compressed cluster from its confining environment. The "pressure" exerted by the cluster electrons on their environment results in the deformation of the electronic clouds of the surrounding atoms. Having determined φ_0 by the external "pseudo-potential" at the cage frontier R_0, the two remaining parameters R_0 and R will be obtained, within a complete theory, by minimizing the total energy of the cluster (given by eq. [24]) and the electrons transferred to the cage walls. Of course, this first requires the computation of the "pseudo-potential."

From the discussion above one can see that the results of the computation are very sensitive to the values of R and R_0; this sensitivity may result in a higher inaccuracy for clusters consisting of a greater number of atoms. This is evident in the case of the Na_9 cluster, where, according to the experimental data suggested by the X-ray analysis (10), we used $R = 2.75$ Å and $R_0 = 3.15$ Å ($a = R/R_0 = 0.87$). The function χ vs. x is plotted in Fig. 4; it corresponds, within errors of ± 0.03 Å in R and R_0, to a total charge of the cluster $q \sim \pm 1$. At this level of approximation we may conclude that the centered-cubic Na_9 cluster is practically neutral. The dependence of the total charge q on the cage radius R_0 is also included in Fig. 5 for this case. The same discussion regarding the screening and the value of the chemical potential φ_0 (~ 2.4) applies here as for the Na_4 cluster. It is worth noting that a similar calculation for a noncentered cubic cluster consisting of eight atoms of Na gives a total charge $q \sim +1$, for the same values of R and R_0. Finally, noticing that the theory contains the charge z only in the product zR_0^3 (see, for example, eqs. [12], [13], and [18]) we can say that similar clusters formed by lithium may also form in the octahedral cages of the fullerite with a smaller size or, equivalently, with a diminished cluster size and ionization charge.

Conclusions

In conclusion, one may say that the calculations presented here indicate a metallic bonding of the Na_4 and Na_{11} clusters squeezed into the octahedral cages of the Na-fullerites. We emphasize that this squeezing is a central feature of the picture presented here, whose direct consequence is that of affecting all the electron states in the cluster; enough electronic energy may be gained in this way to stabilize the cluster at lower values of R, as compared with R_0. This is in contrast, at least for the Na_4 cluster, with recent claims (17) that the Na atoms in Na_6C_{60} are fully ionized and that the octahedral Na ions are placed much further away from the coordination centre. These claims, based on numerical simulations within the local-density approximation, make use of a certain distinction between the valence and the core electrons, which may be inappropriate for the squeezed clusters. As we have seen from the present calculations, almost half of the electrons seem to be affected by the presence of the neighbouring atoms in the cluster, which indicates a drastic change in the inner electronic states of the isolated atoms. The metallic character of the alkali clusters in fullerites can be tested by various techniques, most notably by Raman and ^{23}Na NMR spectroscopies (see, for example, ref. 19). In addition, it is worth mentioning that metallic clusters squeezed in atomic cages may exhibit two types of collective modes, one associated with the vibrations of the positively charged ions, and another with the oscillations of the electron density. Preliminary calculations indicate that these two modes are in the range of ultraviolet optical spectroscopy and electron spectroscopy.

References

1. D.P. Clougherty and X. Zhu. e-print 9607001 chem-ph@xxx.lanl.gov
2. D.P. Clougherty. Can. J. Chem. **74**, 965 (1996).
3. N.H. March. Proc. Cambridge. Philos. Soc. **48**, 665 (1952).
4. M. Apostol. J. Theor. Phys. **9**, 1 (1995); see also e-print 9603009 mtrl-th@xxx.lanl.gov
5. W.A. de Heer. Rev. Mod. Phys. **65**, 611 (1993); M. Brack. Rev. Mod. Phys. **65**, 677 (1993).
6. M.R. Harrison, P.P. Edwards, J. Klinowski, and J.M. Thomas. J. Solid State Chem. **54**, 330 (1984).

© 1997 NRC Canada

Can. J. Chem. Downloaded from www.nrcresearchpress.com by 92.62.229.171 on 09/08/12
For personal use only.

7. E. Trescos, F. Rachdi, L.C. de Menorval, F. Fajula, T. Nunes, and G. Feio. J. Phys. Chem. **97**, 11885 (1993).
8. A. Bifone, T. Pietrass, J. Kritzenberger, A. Pines, and B.F. Chmelka. Phys. Rev. Lett. **74**, 3277 (1995).
9. M.J. Rosseinsky, D.W. Murphy, R.M. Fleming, R. Tycko, A.P. Ramirez, T. Siegrist, G. Dabbagh, and S.E. Barrett. Nature, **356**, 416 (1992).
10. T. Yildirim, O. Zhou, J.E. Fischer, N. Bykovetz, R.A Strongin, M.A. Cichy, A.B. Smith III, C.L. Lin, and R. Jelinek. Nature, **360**, 568 (1992).
11. A.R. Kortan, N. Kopylov, S. Glmarum, E.M. Gyorgy, A.P. Ramirez, R.M. Fleming, F.A. Thiel, and R.C. Haddon. Nature, **355**, 529 (1992).
12. O. Zhou, J.E. Fischer, N. Coustel, S. Kycia, Q. Zhu, A.R. McGhie, W.J. Romanow, J.P. McCauley, Jr., A.B. Smith III, and D.E. Cox. Nature, **351**, 462 (1991).
13. I. Boustani, W. Pawestorf, P. Fantucci, V. Bonacic-Koutecky, and J. Koutecky. Phys. Rev. B: Condens. Matter, **B35**, 9437 (1987).
14. V. Bonacic-Koutecky, P. Fantucci, and J. Koutecky. Phys. Rev. B: Condens. Matter, **B37**, 4369 (1988).
15. U. Rothlisberger and W. Andreoni. J. Chem. Phys. **94**, 8129 (1991).
16. M.R. Prince, and R.W. Hall. J. Phys. Chem. **99**, 8562 (1995).
17. W. Andreoni, P. Giannozzi, and M. Parinello. Phys. Rev. Lett. **72**, 848 (1994).
18. P.W. Stephens, L. Mihaly, P.L. Lee, R.L. Whetten, S.M. Huang, R. Kaner, F. Diederich, and K. Holczer. Nature, **351**, 632 (1991).
19. D.W. Murphy, M.J. Rosseinsky, R.M. Fleming, R. Tycko, A.P. Ramirez, R.C. Haddon, T. Siegrist, G. Dabbagh, J.C. Tully, and R.E. Walstedt. J. Phys. Chem. Solids, **53**, 1321 (1992).
20. J.R. Chelikowsky. Phys. Rev. B: Condens. Matter, **B21**, 3074 (1980).

Can. J. Chem. Downloaded from www.nrcresearchpress.com by 92.62.229.171 on 09/08/12
For personal use only.

© 1997 NRC Canada

Effect of β-cyclodextrin on the reaction of α-amino acid anions with *p*-nitrophenyl acetate and *p*-nitrophenyl hexanoate

Oswald S. Tee, Timothy A. Gadosy, and Javier B. Giorgi

Can. J. Chem. Downloaded from www.nrcresearchpress.com by 92.62.229.171 on 09/08/12
For personal use only.

Abstract: The effects of β-cyclodextrin (β-CD) on the kinetics of the reaction of α-amino acid anions with *p*-nitrophenyl acetate (pNPA) and *p*-nitrophenyl hexanoate (pNPH) have been investigated. Pseudo-first-order rate constants obtained with various concentrations of nucleophile and β-CD, in aqueous solution at pH 9.88, were analyzed to yield rate constants for reaction of the nucleophiles with free ester (k_N) and with ester bound to β-CD (k_{cN}). For pNPA reacting with amino acids that bind weakly to β-CD, if at all, the ratio k_{cN}/k_N is very close to one, but for amino acids that bind appreciably to β-CD this ratio is greater than one (up to 3.5). Generally similar behaviour is observed for reactions with pNPH, but the rate ratios are smaller and all less than one. These findings are comparable to those obtained in this laboratory for the CD-mediated reactions of *p*-nitrophenyl alkanoate esters with other nucleophiles, including simple alkylamines that bind quite strongly to CDs, but they differ from those reported in an earlier study of the reaction of pNPA with amino acid anions (Can. J. Chem. **69**, 1124 (1991)) where the data analysis suggested more substantial catalysis by cyclodextrins.

Key words: amino acids, cyclodextrin, ester cleavage, kinetics, catalysis.

Résumé : On a étudié les effets de la β-cyclodextrine (β-CD) sur la cinétique de la réaction des anions des acides α-aminés avec l'acétate de *p*-nitrophényle («pNPA») et hexanoate de *p*-nitrophényle («pNPH»). On a analysé les constantes de vitesse de pseudo-premier ordre obtenues avec divers concentrations du nucléophile et de la β-CD, en solution aqueuse, à un pH de 9,88 et on en a tiré les constantes de vitesse pour la réaction des nucléophiles avec l'ester libre (k_N) et avec l'ester lié à la β-CD (k_{cN}). Pour la réaction du «pNPA» avec les acides aminés qui se lient, au mieux, faiblement à la β-CD, le rapport k_{cN}/k_N se rapproche de l'unité, mais pour les acides aminés qui se lient facilement à la β-CD, ce rapport est supérieur à un (jusqu'à 3,5). En général, on observe un comportement semblable pour les réactions avec le «pNPH»; toutefois, les rapports des vittesses sont plus faibles et, dans tous les cas, ils sont inférieurs à un. Ces résultats se comparent à ceux obtenus dans ce laboratoire pour les réactions, effectuées sous l'influence de la CD, des alcanoates de *p*-nitrophényle avec d'autres nucléophiles, y compris les alkylamines simples qui se lient fortement à la CD; ils diffèrent toutefois de ceux rapportés dans un travail antérieur sur la réaction du «pNPA» avec les anions des acides aminés (Can. J. Chem. **69**, 1124 (1991), dans lequel une analyse des données avait suggéré la présence d'une catalyse beaucoup plus substantielle par les cyclodextrines.

Mots clés : acides aminés, cyclodextrine, clivage des esters, cinétique, catalyse.

[Traduit par la rédaction]

Introduction

Three recent studies in this laboratory have been concerned with the effects of cyclodextrin hosts (1) on acyl transfer reactions of included esters (2, 3).[2] The first involved the reaction of *p*-nitrophenyl acetate (pNPA) and *p*-nitrophenyl hexanoate (pNPH) with four nucleophiles (NH_2OH, imidazole, $CF_3CH_2O^-$, and $HOCH_2CH_2S^-$) that do not bind appreciably to cyclodextrins (CDs). For these nucleophiles, it was found that pNPA bound to β-CD has 70–140% of the reactivity of free pNPA, but pNPH bound to β-CD has only 20–55% of the reactivity of the free ester, the actual percentage depending on the nucleophile (2). Similar results were obtained for esters with acyl chain lengths up to C_{10}, and the variation in reactivity of the CD-bound esters towards $CF_3CH_2O^-$ was rationalized in terms of a switch in the mode of ester binding in the transition state, from aryl group to acyl group inclusion (3). Overall, the binding of *p*-nitrophenyl esters to CDs affects their susceptibility to attack by simple nucleophiles, but not greatly so (2, 3).

By contrast, Barra and de Rossi reported earlier that the reaction of α-amino acid anions with pNPA bound to β-CD is accelerated, up to 20- or 30-fold (4). The catalytic effect was attributed to reaction within a weak ternary complex, {pNPA·CD·AA^-}, formed by hydrogen bonding of the carboxylate group of the amino acid anion (AA^-) to secondary hydroxy groups on the CD. Since the reaction of imidazole with pNPA (and pNPH) is not greatly affected by the presence of β-CD (2), we were interested to see whether the amino acid histidine, which has an imidazole side chain, and which was not studied previously (4), would also show appreciable catal-

Received August 14, 1996.

O.S. Tee,[1] T.A. Gadosy, and J.B. Giorgi. Department of Chemistry and Biochemistry, Concordia University, Montréal, QC H3G 1M8, Canada.

[1] Author to whom correspondence may be addressed. Telephone: (514) 848-3348. Fax: (514) 848-2868. E-mail: ostee@vax2.concordia.ca

© 1997 NRC Canada

Can. J. Chem. Downloaded from www.nrcresearchpress.com by 92.62.229.171 on 09/08/12
For personal use only.

ysis. If it did so, the enhanced reactivity could provide further support for the mechanism just mentioned. However, when we measured the reactivity of histidine with pNPA in the presence of β-CD we found that it reacted more slowly (vide infra); it did not show any catalysis.

In probing more deeply to understand the different behaviour of histidine, we discovered that the previous results on amino acids are not described particularly well by the parameters reported, raising doubts about the extent of catalysis. Consequently, in order to try to clarify matters, we carried out further studies of the effect of β-CD on the reaction of amino acid anions with pNPA, as well as with pNPH, which are reported below.

Results

Using stopped-flow spectrophotometry, we measured the kinetics of the reaction of several α-amino acids anions with *p*-nitrophenyl acetate (pNPA) and with *p*-nitrophenyl hexanoate (pNPH) in the presence and absence of β-CD, in basic aqueous solution. To keep our work comparable to that of Barra and de Rossi (4), the reaction medium was buffered at pH 9.88 where most of the amino acids are 50% or more as their anions, $NH_2CH(R)COO^-$. However, we generally used higher concentrations of the amino acids and β-CD than previously (4), to maximize the contribution of the aminolysis pathways, relative to the background reactions.

Pseudo-first-order rate constants obtained at various concentrations of amino acid, with and without β-CD, were analyzed to yield rate constants for reaction of the nucleophiles with free and CD-bound ester, using the same approach as in previous studies (2, 3).[2] This approach is based on consideration of four processes: hydrolysis of the ester (S) in the medium (eq. [1]); ester cleavage through an {ester·CD} complex (eq. [2]), or its kinetic equivalent (5); reaction of the free ester with the nucleophile (Nuc)(eq. [3]); reaction of the {ester·CD} complex with the nucleophile (eq. [4]).[3] These four reactions together require that k_{obs} varies with [Nuc] and [CD] in the manner expressed in eq. [5].

[1] $S \xrightarrow{k_u} \text{products}$

[2] $S + CD \underset{K_S}{\rightleftharpoons} S{\cdot}CD \xrightarrow{k_c} \text{products}$

[3] $S + Nuc \xrightarrow{k_N} \text{products}$

[4] $S{\cdot}CD + Nuc \xrightarrow{k_{cN}} \text{products}$

[5] $$k_{obs} = \frac{(k_u K_S + k_c[CD]) + (k_N K_S + k_{cN}[CD])[Nuc]}{(K_S + [CD])}$$

Fig. 1. Rate constants for the cleavage of pNPA in the presence of β-CD and L-alanine, at pH 9.88. The symbols correspond to the following concentrations of L-alanine (in mM): ◆, none; ■, 25; □, 50; ▼, 75; ∇, 100. The curves were calculated with eq. [5] and fitted parameters. Note that the addition of L-alanine causes comparable increases in k_{obs} at each [β-CD], meaning that free and CD-bound pNPA have very similar reactivities.

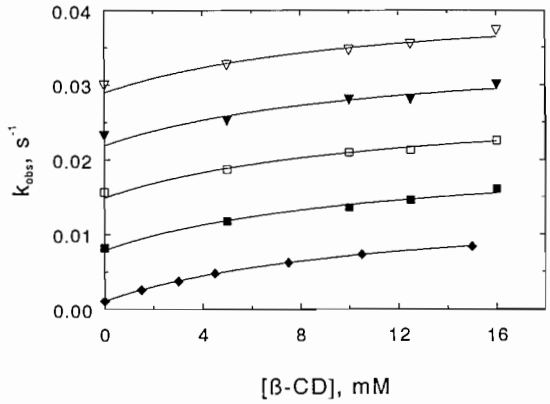


Fig. 2. The data for the cleavage of pNPA in the presence of β-CD and L-alanine, plotted according to eq. [6], with the same symbols as in Fig. 1. Multiple regression analysis of the 20 points for which [Nuc] ≠ 0 affords the values of k_N and k_{cN} given in Table 1.

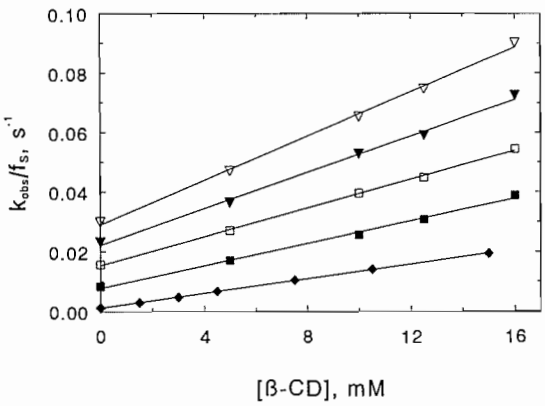


Figure 1 shows kinetic data for the cleavage of pNPA at various levels of β-CD and L-alanine, with curves drawn using eq. [5] and fitted constants. It is seen that the effect of the added nucleophile at each β-CD concentration is virtually the same, meaning that pNPA bound to β-CD has essentially the same reactivity as free pNPA towards L-alanine. This assertion is supported by the following analysis, which is based on eq. [5].

First, to simplify matters, eq. [5] is linearized by dividing it by $f_S = K_S/(K_S + [CD])$, the fraction of unbound ester, to give eq. [6].[4] According to this equation, plots of k_{obs}/f_S against

[2] O.S. Tee, T.A. Gadosy, and M.J. Boyd. Manuscript in preparation.

[3] The reaction of free ester and {CD·Nuc}, which is kinetically equivalent to the process in eq. [4], is considered explicitly in the Discussion.

[4] The form of f_S assumes that [CD] >> [S·CD] ≤ $[S]_0$, which was valid for the concentrations used. The value of K_S was determined in the normal way from experiments with varying β-CD concentration (6), and no added amino acid (i.e., the lowest curve in Fig. 1).

© 1997 NRC Canada

Can. J. Chem. Downloaded from www.nrcresearchpress.com by 92.62.229.171 on 09/08/12
For personal use only.

Table 1. Constants for the reaction of α-amino acids with *p*-nitrophenyl acetate and *p*-nitrophenyl hexanoate in the presence of β-cyclodextrin.[a,b]

Amino acid	K_N (mM)	k_N (M^{-1} s^{-1})	k_{cN} (M^{-1} s^{-1})	k_{cN}/k_N	K_{TS} (mM)
(*a*) *p*-Nitrophenyl acetate (K_S = 11.3 mM)					
Glycine	—[c]	1.36 ± 0.01	1.32 ± 0.03	0.97	11.7
Glycylglycine	—[c]	0.141 ± 0.004	0.133 ± 0.011	0.94	12.0
L-Histidine[d]	—[c]	0.0741 ± 0.0005	0.0561 ± 0.0030	0.76	14.9
L-Cysteine[e]	Large	5.90 ± 0.08	5.42 ± 0.19	0.92	12.3
L-Alanine	Large	0.281 ± 0.017	0.278 ± 0.019	0.99	11.4
DL-Norvaline	2500	0.283 ± 0.005	0.235 ± 0.008	0.83	13.6
L-Valine	255	0.239 ± 0.006	0.294 ± 0.013	1.2	9.2
DL-Norleucine	158	0.287 ± 0.011	0.374 ± 0.020	1.3	8.7
L-Leucine	107	0.206 ± 0.019	0.444 ± 0.032	2.2	5.2
L-Tryptophan	45.1	0.232 ± 0.005	0.495 ± 0.011	2.1	5.3
L-Phenylalanine	19.8	0.0885 ± 0.0022	0.306 ± 0.010	3.5	3.3
(*b*) *p*-Nitrophenyl hexanoate (K_S = 1.60 mM)					
Glycine	—[c]	0.728 ± 0.011	0.121 ± 0.006	0.17	9.6
L-Cysteine[e]	Large	3.89 ± 0.02	1.57 ± 0.04	0.40	4.0
L-Alanine	Large	0.125 ± 0.002	0.0302 ± 0.0020	0.24	6.6
DL-Norvaline	2500	0.119 ± 0.009	0.0318 ± 0.0020	0.27	6.0
L-Valine	255	0.0936 ± 0.0024	0.0281 ± 0.0008	0.30	5.3
DL-Norleucine	158	0.130 ± 0.014	0.0696 ± 0.0040	0.54	3.0
L-Leucine	107	0.105 ± 0.008	0.0600 ± 0.0030	0.57	2.8

[a]At 25°C, in an aqueous borate (0.1 M) buffer of pH 9.88 (μ = 0.2 M, with KCl; 0.025 or 0.050% (v/v) CH_3CN). The values of K_N are taken from earlier work (6); K_S for pNPA was determined under the reaction conditions in this work; K_S for pNPH (16) is the same as used in previous studies (2, 3).

[b]The entry "large" under K_N indicates that no significant binding to β-CD was detected earlier (6). The rate constant k_{cN} is for reaction of CD-bound ester and free nucleophile (eq. [4]). The apparent dissociation constant $K_{TS} = k_N K_S/k_{cN}$, as previously (2, 3).

[c]Assumed to be nonbinding with β-CD.

[d]In a 0.1 M borate buffer at pH 8.00 (μ = 0.2 M, with KCl). The reaction takes place on the imidazole group.

[e]Reaction on the thiolate group.

[CD] should be linear for each fixed [Nuc], and such is the case for the alanine data of Fig. 1, as shown in Fig. 2. Multiple linear regression of the data in terms of eq. [6], with [Nuc], [CD], and [Nuc][CD] as three "X" variables, for [Nuc] ≠ 0, gives slope parameters that lead to the estimates of k_N and k_{cN} reported in Table 1 and used to calculate the curves in Fig. 1. From these rate constants, the ratio $k_{cN}/k_N = 0.99 \pm 0.01$, so bound and free pNPA have the same reactivity towards L-alanine, as surmised above.

$$[6] \quad k_{obs}/f_S = k_u + k_N[\text{Nuc}] + k_c[\text{CD}]/K_S + k_{cN}[\text{Nuc}][\text{CD}]/K_S$$

In their work, Barra and de Rossi made the reasonable assumption that the amino acids they studied did not bind significantly to CDs at the low concentrations used (4). Since we intended to use higher [β-CD] and much higher concentrations of the amino acids, wherever feasible, it was necessary to determine if such complexation (eq. [7]) is important under the reaction conditions. As reported recently, along with binding studies of other amino compounds (6), we found that α-amino acids with hydrophobic side chains do bind to β-CD and the strength varies with the size of the side chain (see K_N in Table 1), but amino acids with small side chains do not bind measurably. Since L-alanine and L-cysteine do not bind significantly to β-CD, and norvaline binds only very weakly (Table 1), we have assumed that glycine, glycylglycine, and histidine do not bind.

$$[7] \quad \text{CD} + \text{Nuc} \underset{K_N}{\rightleftharpoons} \text{CD}\cdot\text{Nuc}$$

The analysis based on eq. [6] is also valid for cases where the nucleophile binds to the cyclodextrin, as long both [CD] and [Nuc] are corrected for formation of the {CD·Nuc} complex.[2] Figure 3 shows data for the effect of different levels of β-CD on the reaction of L-leucine with pNPA, transformed according to eq. [6], and using corrected [CD] and [Nuc]. Multiple regression analysis of the data yields values of k_N and k_{cN} (Table 1) from which the ratio $k_{cN}/k_N = 2.15 \pm 0.04$, implying that pNPA bound to β-CD is about twice as reactive towards L-leucine as free pNPA.

The ability of eq. [5] to reproduce the experimental data can be judged from Fig. 4, which shows values of k_{calc}, calculated with fitted parameters, plotted against the corresponding values of k_{obs}, for the alanine and leucine data sets. All 40 points sit very close to the diagonal line of slope one, showing that

© 1997 NRC Canada

Fig. 3. Data for the cleavage of pNPA by β-CD and L-leucine, plotted according to eq. [6], with [CD] and [Nuc] corrected for binding between β-CD and the amino acid. The symbols are for the following [β-CD] (in mM): ▲, none; ▽, 4.0; ▼, 8.0; □, 12.0; ■, 15.0. Multiple regression analysis of all 20 data points affords the values of k_N and k_{cN} given in Table 1. The curves are calculated from eq. [6] and parameters from the regression.

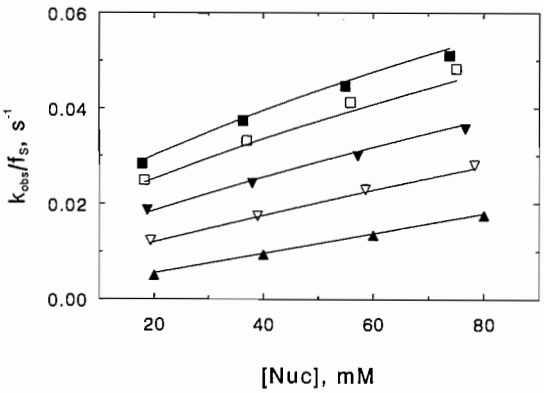
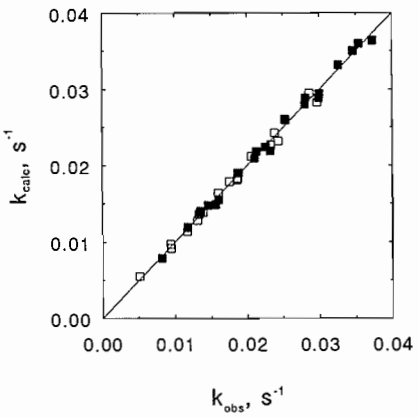


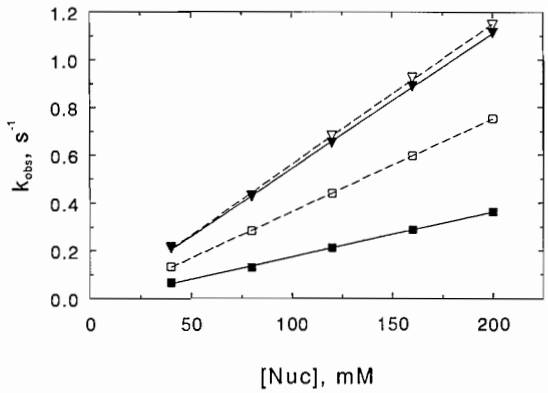
Fig. 4. Correlation between calculated rate constants (k_{calc}), obtained from eq. [5] and fitted parameters, and observed rate constants (k_{obs}) for reaction of pNPA with L-alanine (■) and L-leucine (□) in the presence of β-CD, corresponding to the data plotted in Figs. 2 and 3. The diagonal line has a slope of one and goes through the origin.



the analysis based on eq. [6] works well for the reaction of pNPA with alanine and leucine in the presence of β-CD, as it does for various other esters, nucleophiles, and cyclodextrins (2, 3).[2]

Having established the validity of eq. [5] for alanine and leucine, we used a simpler procedure for other amino acids and for the reactions with pNPH. This procedure, which entails fewer measurements and has been used before (2, 3), consists of two sets of experiments with varying [Nuc]: one at zero CD and the other with a high [CD], so that much of the ester is bound to the CD. In the absence of CD, $k_{obs} = k_u + k_N[Nuc]$, and k_N is simply the slope of k_{obs} vs. [Nuc]. With CD present, the full form of eq. [5] must be used and the slope of the linear plot of k_{obs} vs. [Nuc] is $(k_N K_S + k_{cN}[CD])/(K_S + [CD])$, from which k_{cN} can be estimated, knowing [CD], k_N, and K_S. This

Fig. 5. Rate constants for the cleavage of pNPA (▽,▼) and of pNPH (□, ■) by cysteine. The slopes of the lines through the open symbols (no added CD) are k_N. The slopes of the lines through the solid symbols (10 mM added β-CD) are $(k_N K_S + k_{cN}[CD])/(K_S + [CD])$, from eq. [5]. Note that for both esters the background reaction is negligible. Also, for pNPA it is clear that $k_{cN} \approx k_N$ whereas for pNPH $k_{cN} < k_N$ (Table 1).



approach furnished most of the values of k_N and k_{cN} for the amino acids that do not bind appreciably to β-CD.

Figure 5 shows data for the cleavage of pNPA and pNPH by L-cysteine[5] in the presence and absence of β-CD. For pNPA, the two series of rate constants are very close, meaning that the free and CD-bound forms of the ester have very similar reactivities ($k_{cN}/k_N = 0.92$) whereas pNPH reacts more slowly in the presence of β-CD because its bound form is less reactive ($k_{cN}/k_N = 0.40$, Table 1). Note that cysteine is sufficiently reactive that the background cleavage of the esters is negligible (Fig. 5) and so the rate constants k_N and k_{cN} can be determined with good precision. Similar considerations apply to the reactions of the esters with glycine, which has a comparable reactivity under the reaction conditions (Table 1).

Rate constants for the reaction of pNPA with glycylglycine and L-valine are plotted in Fig. 6. In the case of valine, the plotting and analysis allow for its binding to β-CD, even though this is weak ($K_N = 255$ mM). The data analysis was carried out by multiple linear regression of both data sets (with and without β-CD) because [CD] varies upon the addition of the nucleophile. For both amino acids, the strong parallelism of the two plots for reaction with and without added β-CD (Fig. 6), indicates that $k_{cN} \approx k_N$ (Table 1).

Finally, Fig. 7 presents data for DL-norleucine reacting with pNPA and pNPH. Again, the binding of the amino acid, though not particularly strong ($K_N = 158$ mM), is taken into account in the plotting and the data analysis. Clearly, the relative slopes of the plots[6] mean that $k_{cN} \approx k_N$ for pNPA and k_{cN}

[5] At pH 9.88, the amino group of cysteine is largely protonated and its thiol group is deprotonated, so that the reaction with pNPA and pNPH is a thiolysis, not an aminolysis (7).

[6] Because of complexation of the amino acid by β-CD, the plots should be curved when β-CD is present. However, the binding of valine and norleucine is sufficiently weak that the curvature is not apparent, and so in Figs. 6 and 7 we have simply drawn straight lines through the data. With tryptophan and phenylalanine, which bind more strongly, the curvature is quite noticeable.

© 1997 NRC Canada

Can. J. Chem. Downloaded from www.nrcresearchpress.com by 92.62.229.171 on 09/08/12
For personal use only.

Can. J. Chem. Downloaded from www.nrcresearchpress.com by 92.62.229.171 on 09/08/12
For personal use only.

Fig. 6. Rate constants for the cleavage of pNPA by glycylglycine (□, ■) and by L-valine (▽,▼) in the absence of β-CD (open symbols) and in the presence of 10 mM β-CD (solid symbols). Clearly, for both amino acids, $k_{cN} \approx k_N$ (Table 1).

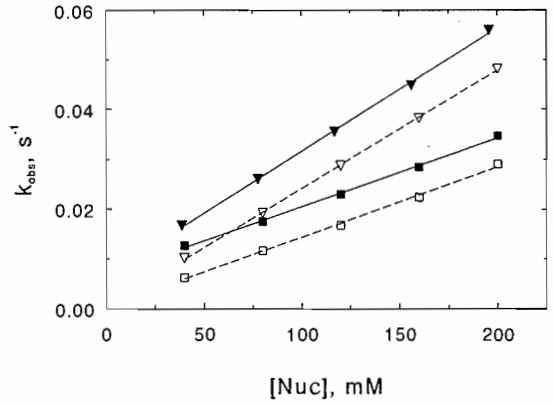
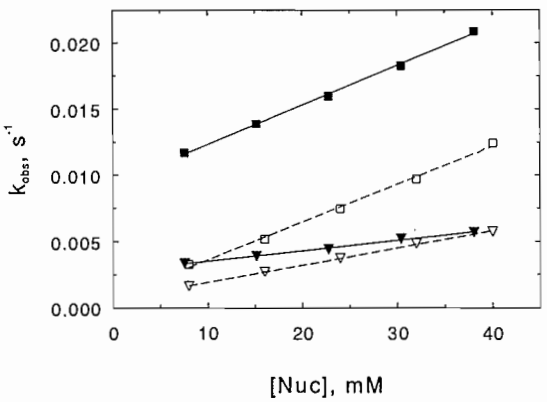


Fig. 7. Rate constants for the cleavage of pNPA (□, ■) and pNPH (▽, ▼) by DL-norleucine in the presence of no β-CD (open symbols) and 10 mM β-CD (solid symbols). Again, for pNPA it is apparent that $k_{cN} \approx k_N$ whereas for pNPH $k_{cN} < k_N$ (Table 1).

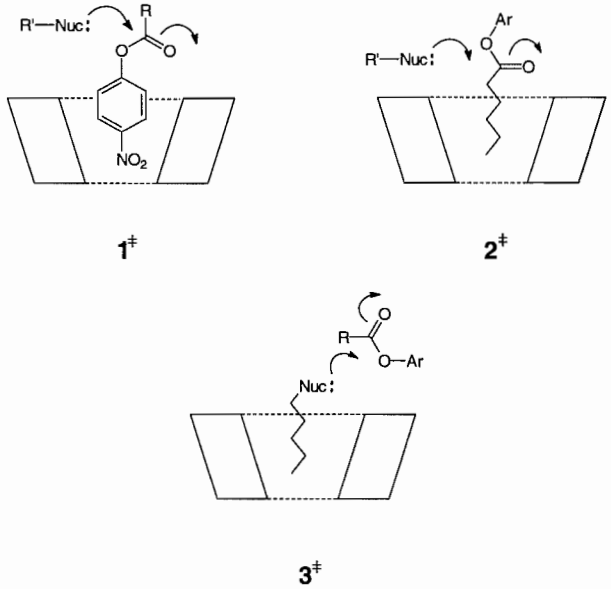


$< k_N$ for pNPH, as is the case with most of the amino acids studied (Table 1).

Before proceeding with the Discussion, we wish to point out that the rate constants k_N (Table 1) found for reaction of the free esters with amino acid anions (AA^-) are not exceptional. When allowance is made for the pH of the experiments and the pK_as of the nucleophiles, our results agree well with those in the literature for the reaction of pNPA with the anions of cysteine (7), glycine (8), glycylglycine (9), alanine, leucine, and tryptophan (4). Note also that values of k_N for amino acid anions with a simple alkyl substituent show little variation with structure and for steric reasons they are about five times smaller than k_N for glycine.[7] Likewise for normal steric reasons (10), the k_N values for pNPH are roughly half those for pNPA, as found for other nucleophiles (2, 3),[2] including hydroxide ion (10, 11).

Discussion

Attack by a simple nucleophile on a *p*-nitrophenyl alkanoate ester bound in a cyclodextrin cavity can basically occur in either of two ways: it can take place with the aryl group of the ester in the cavity ($\mathbf{1}^{\ddagger}$) or with its acyl group in the cavity ($\mathbf{2}^{\ddagger}$). Short-chain esters like pNPA react through the aryl-bound form ($\mathbf{1}^{\ddagger}$) but for longer esters ($\geq C_6$) the more stable, acyl-bound form (11) is more reactive ($\mathbf{2}^{\ddagger}$) (3). With nucleophiles such as alkylamines, which bind appreciably to CDs, reaction may also occur between the CD-bound nucleophile and free ester ($\mathbf{3}^{\ddagger}$). In particular cases, there may even be reaction through a transition state



$\mathbf{1}^{\ddagger}$ $\mathbf{2}^{\ddagger}$ $\mathbf{3}^{\ddagger}$

in which parts of both the nucleophile and the ester are bound to the CD, if its cavity is large enough to accommodate them. Evidence of all four of these situations has been presented in previous work (2, 3),[2] using the dependence of kinetic parameters on structure as the criterion of mechanism.

Our usual approach to discussing modes of reactions of CD-mediated processes involves explicit consideration of transition state binding (2, 3, 5, 11*b*). For this purpose we employ an apparent equilibrium constant (K_{TS}) for dissociation of the {transition state · CD} complex because variations of K_{TS} (and of $pK_{TS} = -\log K_{TS}$) with structure can serve as a probe of transition state binding (5, 12). In the case of CD-mediated nucleophilic attack, the constant is given by $K_{TS} = k_N K_S / k_{cN}$ (2, 3), and relevant values are listed in Table 1. Besides K_{TS}, we will also make use of reactivity ratios, such as k_{cN}/k_N, which focus attention on the apparent catalysis by specific pathways.

Reactivity ratios (k_{cN}/k_N and k_{Nc}/k_N)

The ratios k_{cN}/k_N measure the relative reactivities of the CD-bound and free ester towards nucleophiles. For the reaction of

[7] It is also noteworthy that for *n*-alkylamines (RCH_2NH_2) $k_2 \sim 15$ M^{-1} s^{-1} (8)[2] whereas for analogous amino acid anions ($RCH(CO_2^-)NH_2$) $k_2 \sim 0.5$ M^{-1} s^{-1} (after correction for pH). Thus, the presence of the negatively charged carboxylate group in AA^- appreciably reduces the nucleophilicity of the adjacent amino group, presumably for steric reasons and because negative charge is developed in the transition state for aminolysis.

© 1997 NRC Canada

Can. J. Chem. Downloaded from www.nrcresearchpress.com by 92.62.229.171 on 09/08/12
For personal use only.

Table 2. Constants for the reaction of *p*-nitrophenyl acetate and *p*-nitrophenyl hexanoate with α-amino acids bound to β-cyclodextrin.[a]

		pNPA (K_S = 11.3 mM)		pNPH (K_S = 1.60 mM)	
Amino acid	K_N (mM)	k_{Nc} (M^{-1} s^{-1})	k_{Nc}/k_N	k_{Nc} (M^{-1} s^{-1})	k_{Nc}/k_N
DL-Norvaline	2500	52.0	184	49.7	418
L-Valine	255	6.63	28	4.48	48
DL-Norleucine	158	5.23	18	6.87	53
L-Leucine	107	4.20	20	4.01	39
L-Tryptophan	45.1	1.98	8.5		
L-Phenylalanine	19.8	0.54	6.1		

[a]As in Table 1. The rate constant $k_{Nc} = k_{cN}K_N/K_S$ (see Discussion and footnote 9).

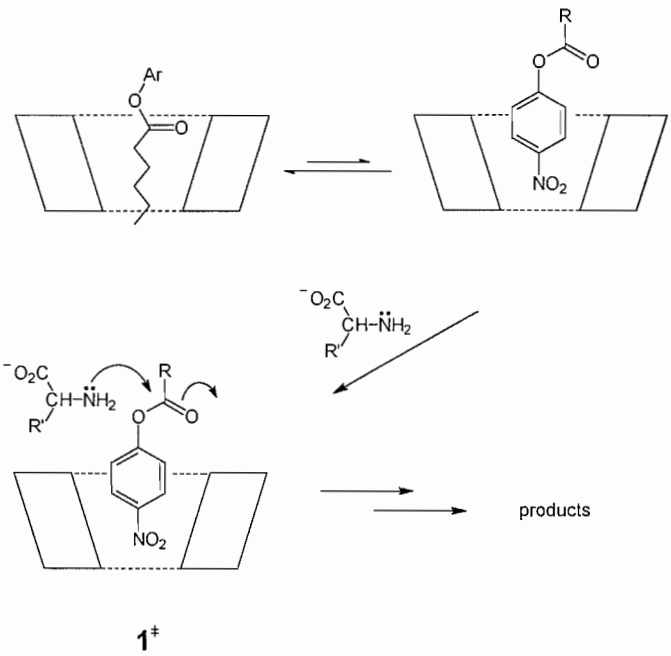
pNPA with amino acid anions[8] that bind weakly, if at all, to β-CD, the ratios are in the range 0.76–0.99 (Table 1), which are similar to those found for other nonbinding nucleophiles (2, 3) and consistent with the CD-mediated reaction taking place by nucleophilic attack upon pNPA bound to β-CD through its aryl group (**1**‡). That the rate ratio is close to one is taken to mean that pNPA, which is bound to β-CD by its *p*-nitrophenyl group (11*a*, 13), has its carbonyl group exposed to the bulk medium and fairly accessible to external nucleophiles (2).

Larger AA^- that bind more strongly to β-CD have reactivity ratios k_{cN}/k_N that increase modestly with the strength of binding, from 1.2 for L-valine (K_N = 255 mM) to 3.5 for L-phenylalanine (K_N = 19.8 mM). Since the efficiency of the CD-mediated reaction seems to be related to the strength of binding of the nucleophile to β-CD, it is appropriate to consider whether the reaction takes place by way of attack of CD-bound nucleophile on the free ester (eq. [8]), as in **3**‡. This process is kinetically equivalent to that in eq. [4], and so rate constants for it may be calculated easily from $k_{Nc} = k_{cN}K_N/K_S$.[9]

$$[8] \quad S + CD{\cdot}Nuc \xrightarrow{k_{Nc}} \text{products}$$

Values of k_{Nc} for amino acid anions that bind to β-CD are given in Table 2, along with the reactivity ratios k_{Nc}/k_N. For reaction with pNPA, these ratios range from 6.1 to 184, implying a modest to appreciable catalytic effect for reaction as in eq. [8] (transition state **3**‡). The highest ratio is for DL-norvaline, which binds very weakly to β-CD, and it seems more likely that this nucleophile reacts as in eq. [4] (transition state **1**‡) for which the ratio k_{cN}/k_N is modest (0.83), as it is for nonbinding AA^- (Table 1). Whether or not any of the amino acid anions react through the pathway in eq. [8] is considered again, later, in the discussion of transition state binding.

Scheme 1.



1‡

For the reaction of the hexanoate ester (pNPH) with AA^-, all of the reactivity ratios k_{cN}/k_N are less than one (0.22–0.58) (Table 1). Similar behaviour has been found for pNPH reacting with other nucleophiles that bind weakly or not at all to β-CD (2, 3) and only with *n*-alkylamines that bind strongly do such ratios approach or exceed one.[2] Since the dominant mode of binding of pNPH to β-CD is by its acyl chain (11), the rate constants k_{cN} and the ratios k_{cN}/k_N refer to reaction taking place as in **2**‡, rather than **1**‡. However, when pNPH is bound by its acyl chain it seems that its carbonyl group is more or less inside the CD cavity, so that it is not readily accessible to nucleophiles in the surrounding medium (3). As a result, nucleophilic attack may occur on the less stable, aryl-bound complex of the ester, in equilibrium with the major acyl-bound form (Scheme 1). Assuming that the aryl-bound complex has a dissociation constant K_S' = 10 mM (cf. K_S = 11.3 mM for pNPA), whereas the acyl-bound form has K_S = 1.6 mM, the rate constants for reaction of the aryl-bound complex with amino acid anions (k_{cN}') are 10/1.6 = 6.25 times larger than

[8] To be comparable to earlier experiments with imidazole (2), those with histidine were carried out at pH 8.00. Consequently, the reaction with histidine is on its imidazole moiety and not on the amino group, which is protonated at pH 8.

[9] The third-order rate constant for S + CD + Nuc → products is given by $k_3 = k_{cN}/K_S$ or k_{Nc}/K_N, depending on whether the reaction is viewed as taking place as in eq. [4] or as in eq. [8].

© 1997 NRC Canada

Can. J. Chem. Downloaded from www.nrcresearchpress.com by 92.62.229.171 on 09/08/12
For personal use only.

Fig. 8. Correlation of transition state binding (pK_{TS}) for the reaction of amino acid anions with pNPA (■) and with pNPH (□), mediated by β-CD, with pK_N for binding of the amino acid anions to β-CD. The slopes of the lines are 0.29 for pNPA and 0.23 for pNPH.

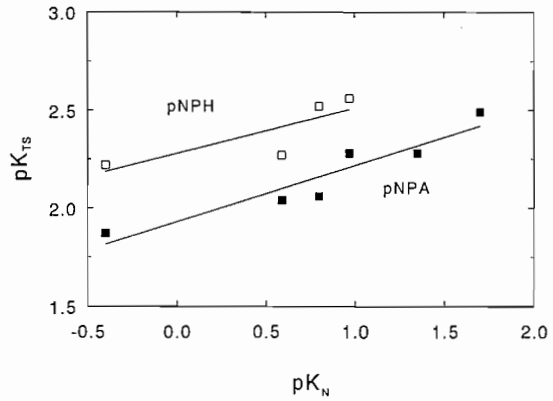
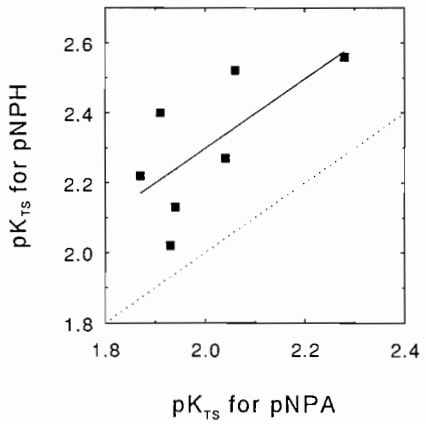


Fig. 9. Relation between the transition state binding (pK_{TS}) for the reaction of amino acid anions with pNPH and with pNPA, mediated by β-CD. Note that the slope of the correlation line is essentially one and that the values for pNPH are greater than those for pNPA – all the points are above the dotted line.



k_{cN}. More important, the appropriate reactivity ratios, k_{cN}'/k_N, are in the range 1.1–3.6, not very different from those for pNPA reacting with AA^- (Table 1) and other nucleophiles (2) by the same reaction mode ($\mathbf{1}^{\ddagger}$). Thus, it appears quite feasible that the reaction of pNPH with amino acid anions takes place as depicted in Scheme 1.

With amino acid anions that bind significantly to β-CD it is possible that pNPH reacts as free ester with CD-bound nucleophile (eq. [8] and $\mathbf{3}^{\ddagger}$). Values of k_{Nc} for this process are collected in Table 2, together with the ratios k_{Nc}/k_N. These ratios range from 39 to 418, suggesting a substantial catalytic effect *if* the reaction takes place as in $\mathbf{3}^{\ddagger}$. However, as with pNPA, the largest value is for the weakly binding DL-norvaline and we think it more likely that the free nucleophile reacts with CD-bound pNPH (eq. [4]), as in $\mathbf{2}^{\ddagger}$ ($k_{cN}/k_N = 0.27$, Table 1) or as in $\mathbf{1}^{\ddagger}$ (Scheme 1) ($k_{cN}'/k_N = 1.7$, assuming $K_S' = 10$ mM).

To try to get a clearer idea of how both pNPA and pNPH react with the amino acid anions, as in $\mathbf{1}^{\ddagger}$, $\mathbf{2}^{\ddagger}$, or in $\mathbf{3}^{\ddagger}$, or through some other pathway, we will look at transition state binding, and how it relates to binding of the nucleophiles.

Transition state binding (K_{TS} and pK_{TS})

For the CD-mediated reaction of pNPA with amino acid anions that do not bind measurably to β-CD, K_{TS} = 11–15 mM (Table 1), which is very close to K_S = 11.3 mM for substrate binding. These values are perfectly compatible with the reaction taking place through transition state $\mathbf{1}^{\ddagger}$, which has the aryl group of the ester in the CD cavity and the nucleophile external to it. Transition state binding is slightly stronger (K_{TS} = 3.3–9.2 mM) for amino acid anions that bind to β-CD (K_N = 20–255 mM) and there is a fair correlation between pK_{TS} and pK_N, as seen in Fig. 8, but the slope is only 0.29. For the reaction of pNPH, the trends are similar and the plot of pK_{TS} against pK_N has a slope of 0.23 (Fig.8). In neither case is the slope large enough to justify postulating reaction between free ester and CD-bound nucleophile (eq. [8] and transition state $\mathbf{3}^{\ddagger}$). In the case of pNPA, it probably means that reaction takes place as in $\mathbf{1}^{\ddagger}$, but for amino acid anions having hydrophobic side chains there is a weak interaction that provides a small, additional amount of stabilization to the CD-bound transition state. Assuming that pNPH reacts in the same way ($\mathbf{1}^{\ddagger}$), there must be an isomerization from the principal, acyl-bound form of the {ester·CD} complex to the aryl-bound form (Scheme 1), as well as some weak interaction of the amino acid side chain. Alternatively, pNPH could react through its acyl-bound form, as in $\mathbf{2}^{\ddagger}$, but there must still be some interaction of the amino acid side chains to account for the greater transition stabilization (larger pK_{TS}) for those AA^- that bind to β-CD.

Comparing the pK_{TS} values for pNPH and pNPA reacting with all the amino acid anions common to both esters, the correlation between the two sets is not particularly good, but the slope is about one (Fig. 9). What is more noteworthy is that for each nucleophile, pK_{TS} is larger for pNPH than for pNPA, implying some additional stabilization for the hexanoate ester. Conceivably, this could be evidence that pNPH reacts by way of acyl group binding ($\mathbf{2}^{\ddagger}$) whereas pNPA reacts by aryl group binding ($\mathbf{1}^{\ddagger}$). In previous work on a series of *p*-nitrophenyl alkanoates (C_2 to C_{10}) reacting with two nonbinding nucleophiles ($CF_3CH_2O^-$ and $HOCH_2CH_2S^-$) in the presence of β-CD, the chain length dependence of pK_{TS} and other parameters provided strong evidence of a switch in the mode of reaction from $\mathbf{1}^{\ddagger}$ to mode $\mathbf{2}^{\ddagger}$, with the break point coming precisely at the hexanoate ester (3).

Conclusions

The results presented above show that the reaction of pNPA with amino acid anions is not greatly affected by added β-cyclodextrin, and in most cases the CD-bound ester appears to have a reactivity very close to that of the free ester ($k_{cN} \sim k_N$); only with nucleophiles that bind appreciably to β-CD is the ratio $k_{cN}/k_N > 1$. Almost certainly, the CD-mediated reaction of pNPA takes place between CD-bound ester and free nucleophile, as in $\mathbf{1}^{\ddagger}$, rather than between free ester and CD-bound nucleophile ($\mathbf{3}^{\ddagger}$).

The behaviour of pNPH is generally similar but the ratios k_{cN}/k_N are all less than one, presumably because the carbonyl group of the acyl-bound ester is not so accessible to nucleophiles in the bulk medium. As a result, the reaction may take place by nucleophilic attack on a more reactive, aryl-bound form of the ester (Scheme 1, $\mathbf{1}^{\ddagger}$), rather than on the acyl-bound

© 1997 NRC Canada

Can. J. Chem. Downloaded from www.nrcresearchpress.com by 92.62.229.171 on 09/08/12
For personal use only.

form ($\mathbf{2}^{\ddagger}$). On the other hand, transition state binding (pK_{TS}) is somewhat greater for pNPH than for pNPA, which could be due to pNPH reacting by its acyl-bound form ($\mathbf{2}^{\ddagger}$), as is the case for longer esters and other nucleophiles (3).

For the cleavage of both pNPA and pNPH, amino acid anions having hydrophobic side chains show slightly elevated reactivity in the CD-mediated reaction, implying that there is some additional transition state stabilization due to these substituents. However, the shallow dependence of the transition state binding (pK_{TS}) on structure, compared to binding of the nucleophile (pK_N), does not indicate a large component of nucleophile binding in the transition state and it does not support a complete switch from reaction of free nucleophile and CD-bound ester ($\mathbf{1}^{\ddagger}$ or $\mathbf{2}^{\ddagger}$) to reaction between CD-bound nucleophile and free ester ($\mathbf{3}^{\ddagger}$).

There remains the question of why our findings are different from those of Barra and de Rossi (4), specifically for the β-CD-mediated reaction of pNPA with alanine and leucine. The difference could have arisen from the fact that the kinetic effects they observed were not particularly large and the analysis of them was based upon subtraction of the contributions of the three processes [1]–[3]. Thus, any errors in estimating these contributions, *from whatever source*, could have a large effect on the estimated k_{cN} values. Compared to our results, the major deviations appear to be with the previous k_{obs} obtained with constant $[Nuc]_0$ and varying $[\beta\text{-CD}]_0$. It was precisely these results that were analyzed to find k_{cN}. In our experiments we tried to avoid problems by having both $[\beta\text{-CD}]_0$ and $[Nuc]_0$ high, to maximize the contribution of the CD-mediated aminolysis, and by estimating both k_N and k_{cN} from parallel or combined experiments carried out with solutions made up from common stock solutions. As seen in Figs. 1–7, the results obtained under these conditions show that k_{cN} is not very different from k_N for pNPA reacting with various amino acid anions.

Experimental

The reactants were purchased as follows: pNPA and pNPH from Sigma; amino acids from Sigma or ICN Biochemicals; β-cyclodextrin from Aldrich. These materials were used as supplied.

The pK_a of the ammonium group of L-alanine is 9.87 and values for other simple amino acids are very close (14). Barra and de Rossi carried out their studies at pH 9.878 ± 0.001 (μ = 0.2 M), and for ease of comparison we tried to do likewise. Obviously, at this pH the amino acids exist in their anionic forms, $NH_2CH(R)CO_2^-$, to the extent of about 50%.

A stock solution (A) of borate buffer (0.2 M) containing 0.2 M KCl was made up and its pH was adjusted to 9.878 ± 0.003. An amino acid was dissolved in some of solution A to give a stock nucleophile solution (B) and its pH was also adjusted. Other concentrations of amino acid were obtained by dilution of B with A. Ester solutions (C) (100 μM for pNPA and 50 μM for pNPH) were made by dilution of a stock ester solution (0.1 M) in acetonitrile into water. For low concentrations of β-CD, this was incorporated into stock solution A, and hence into B. However, for higher [β-CD] (>7 mM), the CD was added to A and thus B, and to the ester solution C, because β-CD is not particularly soluble (~16 mM) in water (1). Reactions were initiated by stopped-flow mixing of equal volumes of solutions B and C, so the final concentrations of the constituents were halved, except for β-CD if it was in both B and C. The range of $[Nuc]_0$ used in many of the experiments can be judged from Figs. 1, 3, 5–7. For other nucleophiles, the concentration ranges were: norvaline, 20–200 mM; phenylalanine, 16–80 mM; tryptophan, 5–25 mM; histidine, 25–100 mM. In the case of histidine, the pH of solutions A and B was adjusted to 8.000 ± 0.004.

Kinetic procedures were similar to those in previous, related studies (2, 3). Ester cleavage was followed by monitoring the first-order appearance of the *p*-nitrophenoxide ion at 405 nm, using an Applied Photophysics SX17MV stopped-flow spectrophotometer, with the cell maintained at 25.0 ± 0.1°C. Pseudo-first-order rate constants were obtained by fitting a single exponential function to the absorbance increases, and values of k_{obs} were taken as averages of 5–10 determinations, differing by <5%.

As outlined in the text, and detailed earlier (2, 3), analysis of the data from experiments with varying $[CD]_0$ and $[Nuc]_0$ was based on eq. [5] and its linear form eq. [6]. In many cases the analysis to find k_N and k_{cN} used multiple linear regression (15) in terms of eq. [6], with [CD], [Nuc], and [CD][Nuc] as three "X" variables. In several cases where binding of the amino acid to β-CD was unimportant, k_N and k_{cN} were obtained more simply from the slopes of the linear variation of k_{obs} with $[Nuc]_o$, for $[CD]_o$ = 0 and 10 mM, respectively (see text).

Where complexation of the amino acid by β-CD was important (6), the analysis was carried out with [CD] and [Nuc], corrected for formation of the CD·Nuc complex (eq. [7]), rather than $[CD]_0$ and $[Nuc]_0$. To find [CD] one solves the quadratic in [CD] obtained by expansion of:

$$K_N = [CD][Nuc]/[CD\cdot Nuc]$$

$$= [CD]([Nuc]_0 - [CD]_0 + [CD])/([CD]_0 - [CD])$$

which comes from the definition of K_N and the two equations for mass balance: $[Nuc]_0 = [Nuc] + [CD\cdot Nuc]$; $[CD]_0 = [CD] + [CD\cdot Nuc]$. The solution of the quadratic equation is $[CD] = \{-b + (b^2 + 4K_N[CD]_0)^{1/2}\}/2$, where $b = (K_N - [CD]_0 + [Nuc]_0)$. Then, by difference, $[Nuc] = [Nuc]_0 - [CD\cdot Nuc] = [Nuc]_0 - ([CD]_0 - [CD])$. All of the calculations involved in the data analysis were executed in spreadsheets, using Lotus 1-2-3 software (15).

The analysis based on eq. [6] requires a known value of K_S for binding of the ester to the CD. For pNPH the value of 1.60 mM was taken from earlier work (16), but for pNPA it was redetermined in the 0.10 M borate buffer at pH 9.88. Under these conditions, we found $k_u = 0.00111\ s^{-1}$ and nonlinear fitting of the normal saturation equation (5, 11*b*, 16) to the variation of k_{obs} with [β-CD] (lower curve in Fig. 1) gave $k_c = 0.0139 \pm 0.0003\ s^{-1}$ and $K_S = 11.3 \pm 0.4$ mM ($r = 0.9998$). By way of comparison, Barra and de Rossi (4) reported $k_u = 0.000815\ s^{-1}$ and nonlinear fitting to their kinetic data gives $k_c = 0.0112 \pm 0.0022\ s^{-1}$ and $K_S = 15.4 \pm 5.4$ mM ($r = 0.9938$), for reaction at pH 9.878, in 2% (v/v) aqueous DMSO, and apparently no buffer.

The values of K_N needed to account for binding of the amino acids to β-CD were determined by a fluorescent probe method, as reported earlier (6). Note that when K_N is large in relation to $[\beta\text{-CD}]_0$, as it was in most cases, the value of k_{cN}

© 1997 NRC Canada

(and hence k_{cN}/k_N) derived from the analysis in terms of eq. [6] is not particularly sensitive to the precise value of K_N. For example, for the reaction of pNPA with L-leucine, treatment of the data (Fig. 3) with the measured value of K_N = 107 mM (6) gave $k_{cN} = 0.44 \pm 0.03\ M^{-1}\ s^{-1}$ whereas for K_N = 250 mM it gives $k_{cN} = 0.37 \pm 0.03\ M^{-1}\ s^{-1}$. At the extreme, if binding of leucine was insignificant, then $k_{cN} = 0.31 \pm 0.03\ M^{-1}\ s^{-1}$.

Acknowledgements

We thank the Natural Sciences and Engineering Research Council of Canada for an operating grant, a post-graduate scholarship, a summer studentship, and an equipment grant towards the purchase of the stopped-flow spectrophotometer. We are also grateful to Dr. Monica Barra and Professor Rita de Rossi for correspondence and discussions about the differences between their results and ours.

References

1. (*a*) M. Bender and M. Komiyama. Cyclodextrin chemistry. Springer Verlag, New York. 1978; (*b*) J. Szejtli. Cyclodextrins and their inclusion complexes. Akademiai Kiado, Budapest. 1982.
2. O.S. Tee and T.A. Gadosy. J. Chem. Soc. Perkin Trans. 2, 2307 (1994).
3. T.A. Gadosy and O.S. Tee. J. Chem. Soc. Perkin Trans. 2, 71 (1995).
4. M. Barra and R.H. de Rossi. Can. J. Chem. **69**, 1124 (1991).
5. (a) O.S. Tee. Carbohydr. Res. **192**, 181 (1989); (*b*) Adv. Phys. Org. Chem. **29**, 1 (1994).
6. O.S. Tee, T.A. Gadosy, and J.B. Giorgi. Can. J. Chem. **74**, 736 (1996).
7. J.W. Ogilvie, J.T. Tildon, and B.S Strauch. Biochemistry, **3**, 754 (1964).
8. W.P. Jencks and J. Carriuolo. J. Am. Chem. Soc. **82**, 675 (1960).
9. W.L. Koltun and F.R.N. Gurd. J. Am. Chem. Soc. **81**, 301 (1959).
10. (*a*) J.P. Guthrie. Can. J. Chem. **51**, 3494 (1973); (*b*) O.S. Tee and J.A. Enos. Can. J. Chem. **66**, 3027 (1988).
11. (*a*) G.M. Bonora, R. Fornasier, P. Scrimin, and U. Tonellato. J. Chem. Soc. Perkin Trans. 2, 367 (1985); (*b*) O.S. Tee, C. Mazza, and X.-X. Du. J. Org. Chem. **55**, 3603 (1990).
12. A.J. Kirby. Angew. Chem. Int. Ed. Engl. **35**, 707 (1996).
13. M. Komiyama and H. Hirai. Chem. Lett. 1471 (1980).
14. (*a*) G.D. Fasman (*Editor*). Handbook of biochemistry and molecular biology. Vol. I. 3rd ed. CRC Press, Cleveland, Ohio. 1976; (*b*) J.A. Dean (*Editor*). Handbook of organic chemistry. McGraw–Hill, New York. 1987.
15. L.M. Mezei. Practical spreadsheet statistics and curve-fitting for scientists and engineers. Prentice-Hall, Englewood Cliffs, N.J. 1990.
16. O.S. Tee, M. Bozzi, N. Clement, and T.A. Gadosy. J. Am. Chem. Soc. **115**, 3509 (1995).

Can. J. Chem. Downloaded from www.nrcresearchpress.com by 92.62.229.171 on 09/08/12
For personal use only.

© 1997 NRC Canada

Exploratory study of the quenching of photosensitizers by initiators of free radical "living" polymerization

J.C. Scaiano, Terrence J. Connolly, Nadereh Mohtat, and Claudette N. Pliva

Abstract: Several compounds of the type $PhCR^1R^2$-TEMPO (where TEMPO = 2,2,6,6-tetramethylpiperidine-*N*-oxide) have been prepared and examined as potential photosensitized initiators for "living" free radical polymerizations. For example, these compounds are excellent quenchers of triplet xanthone (rate constants in the range $(8.0–13) \times 10^8\ M^{-1}\ s^{-1}$) and result in the formation of benzylic and TEMPO radicals. The importance of excited state energy and nature of the excited triplet state have also been explored. We also tested pyrene as a possible singlet sensitizer. While pyrene fluorescence is efficiently quenched, the process does not lead to cleavage of the C—O bond. A model is proposed to account for this anomaly in the photosensitized decomposition of these TEMPO adducts.

Key words: TEMPO, laser flash photolysis, time resolved emission spectroscopy, sensitizers, quenching, photoinitiator.

Résumé : On a préparé plusieurs composés du type $PhCR^1R^2$-TEMPO (dans lesquels TEMPO = 2,2,6,6-tétraméthylpipéridine, *N*-oxyde de) et on a évalué leurs propriétés comme photosensibilisateurs potentiels de polymérisations par radicaux libres «vivants». Par exemple, ces composés sont excellents pour désactiver l'état triplet de la xanthone (constantes de vitesse de 8,0 à $13 \times 10^8\ M^{-1}\ s^{-1}$) et ils conduisent à la formation de radicaux benzylique et TEMPO. On a aussi étudié l'importante de l'énergie de l'état excité et de la nature de l'état triplet excité. On a aussi évalué les propriétés du pyrène comme sensibilisateur potentiel d'états singulets. Même si la fluorescence du pyrène est désactivée d'une façon efficace, le processus ne conduit pas à la rupture de la liaison C—O. On propose un modèle pour expliquer cette anomalie lors de la décomposition photosensibilisée de ces adduits avec TEMPO.

Mots clés : TEMPO, photolyse éclair au laser, spectroscopie d'émission résolue en fonction du temps, désactivation, photoinitiateur.

[Traduit par la rédaction]

Introduction

The 1993 report by Georges et al. (1) showing that low polydispersity polystyrene could be prepared by free radical polymerization of styrene in the presence of TEMPO (2,2,6,6-tetramethyl-1-piperidinyloxy, free radical) has triggered a widespread research effort in this area (2–14). The mechanism of polymerization is believed to involve reversible capping of the polystyrene chain by TEMPO, a stable radical that is known to scavenge a wide range of free radicals with rate constants somewhat below the diffusion limit (15–17). Thus, these TEMPO-capped polystyrene chains effectively become dormant polymers, ready to continue free radical polymer growth if the cap dissociates (14). The mechanism of reaction is shown in Scheme 1, where P_nT is the TEMPO capped dormant polymer, $P_n^{\cdot}$ is the active, growing polymer, and $T^{\cdot}$ is TEMPO.

Received August 19, 1996.

J.C. Scaiano,[1] T.J. Connolly, N. Mohtat, and C.N. Pliva.
Department of Chemistry, University of Ottawa, Ottawa, ON K1N 6N5, Canada.

[1] Author to whom correspondence may be addressed. Telephone: (613) 562-5728. Fax: (613) 562-5170. E-mail: tito@photo.chem.uottawa.ca

Scheme 1.

$$[1]\quad P_nT \underset{k_{-L}}{\overset{k_L}{\rightleftharpoons}} P_n^{\cdot} + T^{\cdot}$$

$$[2]\quad P_n^{\cdot} + \text{styrene} \xrightarrow{k_P} P_{n+1}^{\cdot}$$

Note that the self-reaction of two polymer chains ($P_m^{\cdot}$ + $P_n^{\cdot}$) to give polymer P_{m+n} has not been included in Scheme 1. It is now well established that under normal polymerization conditions, there is a steady state or residual TEMPO concentration, always present, which effectively makes reaction [1] much faster than reaction [3]. This has been observed experimentally, modeled successfully (9, 14), and can be readily predicted from work carried out by Fischer a decade ago (18, 19). Additionally, the concentration of active chain ends at any time is quite low, which makes bimolecular reactions less likely. Fukuda et al. recently estimated the equilibrium constant for eq. [1] to be 2.1×10^{-11} mol L^{-1} at 125°C (20).

$$[3]\quad P_m^{\cdot} + P_m \xrightarrow{k_T} P_{m+n}$$

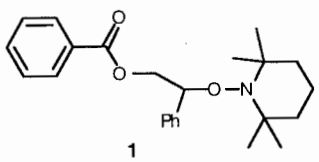
The capping reaction (see eq. [1]) is not reversible at room temperature, where P_nT is stable, and polymerizations follow-

© 1997 NRC Canada

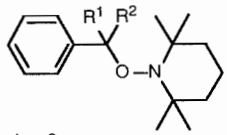
Can. J. Chem. Downloaded from www.nrcresearchpress.com by 92.62.229.171 on 09/08/12
For personal use only.

ing the mechanism of Scheme 1 are typically carried out at temperatures around 125°C, where k_{-L}, the rate constant for release of the growing polymer chain, is sufficiently large to activate the dormant polymer, P_nT.

A number of recent reports have dealt with the thermal and photochemical synthesis of initiators for living free radical polymerizations, such as molecules **1–6** (7, 10, 21–23).



1



2: $R^1=R^2=H$
3: $R^1=CH_3$; $R^2=H$
4: $R^1=Et$; $R^2=H$
5: $R^1=R^2=CH_3$
6: $R^1=H$;$R^2=Ph$

In addition to being good initiators for TEMPO-mediated thermal polymerizations, molecules **1–6** are also good models for the polymers themselves and have occasionally been described as "unimers." We are interested in establishing possible photochemical routes for dissociation of the TEMPO cap. Direct photolysis at wavelengths below 280 nm is known to cleave **2–6** readily, although it is likely that in polymers much of the energy will be absorbed away from the active site.

In this communication, we explore the possibility of photosensitized decomposition of **2–5** as a potential method for the initiation of "living" free radical polymerization. Such decomposition can potentially facilitate polymerizations at lower temperatures, not only allowing additional flexibility, but also avoiding some of the problems (e.g., autopolymerizations) of high-temperature styrene polymerization. To examine these reactions we have employed laser flash photolysis and time-resolved emission spectroscopy.

Experimental

Materials

All solvents used for synthesis and laser flash photolysis studies were of the highest grade commercially available (BDH, Omnisolv grade) and were used without further purification. Compounds **2–5** were prepared and purified as previously described (10). TEMPO and 4-benzoylbiphenyl (4-phenylbenzophenone) were purchased from Aldrich and used as received. Xanthone, pyrene, and thioxanthen-9-one were purchased from Aldrich and were recrystallized from ethanol. 1-Azaxanthone was purchased from Maybridge and was recrystallized from ethanol prior to use.

Laser flash photolysis

The samples, contained in 7×7 mm^2 Suprasil quartz cuvettes saturated with oxygen-free nitrogen at room temperature, were excited by pulses using the third harmonic, 355 nm, of a Surelite Nd/YAG laser ($\leq$ 25 mJ per 7 ns pulse). A Tektronix 2440 digitizer was used to capture the transient absorption signals from the monochromator–photomultiplier system. The data were transferred via GPIB interface to a PowerMacintosh computer that controls the experiment and provides processing facilities through a home-developed program using LabVIEW 3.1.1 software from National Instruments. Further details on similar laser systems have been provided elsewhere (24, 25).

Emission spectroscopy and lifetimes

A Hamamatsu C-4334 streak camera was used to measure the time-resolved luminescence from pyrene. Pyrene samples in acetonitrile were prepared in concentration low enough (0.035 mM) to ensure that interference from the excimer did not occur. Samples prepared as above were photoexcited at 355 nm with the third harmonic from the same Surelite Nd/YAG nanosecond laser, the beam of which was attenuated to $\leq$ 2 mJ/pulse.

Steady state irradiations

The samples of sensitizer, dissolved in 50 mM solutions of **2** in acetonitrile contained in 7×7 mm^2 Suprasil quartz cuvettes saturated with oxygen-free nitrogen at room temperature, were irradiated in a Rayonet photoreactor with six RPR 3500 lamps at 30°C. The concentration of sensitizer was adjusted so that the absorbance at 355 nm matched that for the sensitizer used in the laser flash photolysis experiments.

Laser drop photolysis

The beam from a Surelite Nd/YAG laser (355 nm, 30 mJ, 7 ns pulse) was focused using a quartz lens on a drop of a solution of xanthone (absorbance at 355 nm was 0.7) in 50 mM **2** in acetonitrile suspended from a needle (20 gauge) in a specially constructed cell. The flow rate of the solution was adjusted using a Sage Instruments model 355 syringe pump, so that each shot of the laser irradiated a fresh drop. Further details of our laser drop system have been published elsewhere (26, 27).

Results

This section is divided according to the multiplicity of the sensitizers used, since this property largely determines the experimental technique employed.

Excited triplet sensitizers

Laser flash photolysis with nanosecond resolution was the technique of choice in this case. We describe in some detail the case of xanthone, which is representative of the method employed in all cases.

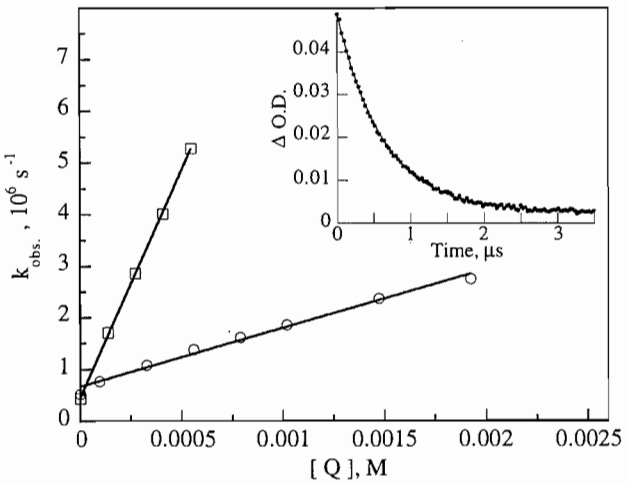
Xanthone has an excited triplet energy of ~74 kcal/mol and its triplet state has predominant n,π^* character in nonpolar solvents and π,π^* character in polar or hydrogen-bonding media (24, 28). In acetonitrile, where our experiments were performed, the low-lying triplet has π,π^* character. Under these conditions, the triplet–triplet absorption of xanthone shows λ_{max} at 635 nm. Triplet decay was usually monitored at 640 nm. The triplet state was produced by 355 nm laser excitation, a wavelength at which xanthone has a suitable absorption, but where the quenchers **2–5** are transparent. The triplet is formed following rapid and efficient intersystem crossing of excited singlet xanthone. Typical triplet lifetimes in the absence of quenchers are in the 5–10 μs range, and are largely determined by self-quenching, nonradiative decay and possibly residual traces of oxygen. Addition of initiators **2–5** leads to a shortening of the triplet lifetime. The rate constant for quenching, k_q, can be derived from a plot of the observed pseudo-first-order rate constant for decay ($k_{obs} = \tau^{-1}$) as a function of the quencher concentration, eq. [4] and Fig. 1,

$$[4] \quad k_{obs} = k_o + k_q[Q]$$

Can. J. Chem. Downloaded from www.nrcresearchpress.com by 92.62.229.171 on 09/08/12
For personal use only.

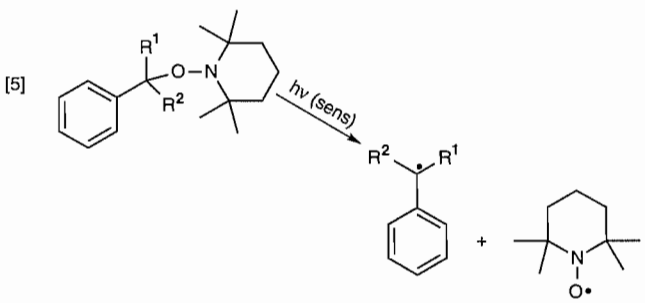
© 1997 NRC Canada

Fig. 1. Quenching of xanthone triplets by TEMPO (□) and **3** (○) in acetonitrile. *Inset:* Decay of triplet xanthone monitored at 640 nm in the presence of 0.8 mM **3**.



where k_0 is the rate constant for triplet decay in the absence of added quenchers. All plots were linear, and lead to the rate constants of Table 1.

With all sensitizers, it is important to examine the quenching of the excited state by TEMPO itself, since sensitized decomposition of the initiators can lead to the formation of TEMPO according to reaction [5].



Recombination of the benzylic radical with TEMPO to reform starting material is usually slower than the combination of two benzylic radicals (15–17, 29), thus leading to some accumulation of TEMPO in the samples. While we have used fresh samples throughout this work, special care was taken whenever the quenching rate constant was 1% or less of the TEMPO value.

Among the other sensitizers, 1-azaxanthone (73 kcal/mol) has essentially the same triplet energy as xanthone, but its lowest triplet has n,π^* character in both polar and nonpolar media. Lower energy sensitizers, such as 4-phenylbenzophenone (61 kcal/mol) and thioxanthone (~65.5 kcal/mol) were also tested, although it soon became evident that not only were the quenching rate constants much slower than for xanthone and 1-azaxanthone but, in addition, the fraction of quenching events leading to fragmentation was very small. This is indicated in Table 1 by the signs "+" and "−" for detectable and undetectable benzylic radicals, respectively. Clearly, as the triplet energy decreases, the rate constant for quenching drops dramatically even for energies that are well in excess of the O—C bond energies. No radicals were detected in the case of 4-phenylbenzophenone. While interference from triplet–triplet absorption makes this experiment difficult, we are confident that the radical yield is very small or zero. Similarly, no radicals were detected in the case of thioxanthone. The case of azaxanthone is particularly difficult because samples that have a suitable absorption (usually ~0.3) at the laser wavelength (355 nm) are strongly absorbing in the 310–330 nm region where benzylic radicals absorb. In spite of these problems, it was possible to establish the presence of benzylic radicals in at least two systems (see Table 1).

In an attempt to determine the yield of benzylic radicals, the decomposition of adduct **2** was sensitized by xanthone. This sensitizer was chosen since results from the laser flash photolysis had shown that the benzylic radical was formed when the xanthone triplet was quenched. Steady state irradiation at 350 nm with a sensitizer concentration similar to that used in the laser flash photolysis study and a 50 mM concentration of adduct did not result in the detection of bibenzyl as would be expected from benzylic radical recombination. Most likely, accumulation of small amounts of TEMPO rapidly makes radical cross-combination (i.e., trapping by TEMPO) more favorable than self-reaction (18). In an attempt to increase the concentration of radicals without TEMPO accumulation, recourse was made to the laser drop technique. Although developed in our laboratory to study multiphotonic processes, it is also possible to use the technique to study monophotonic reactions, and increase the yield of transient species generated, thus favoring second-order processes. Laser drop photolysis of a 50 mM solution of **2** in acetonitrile containing enough xanthone to have an absorbance of 0.7 at 355 nm resulted in the formation of bibenzyl, detected by GC and confirmed by GC–MS with authentic samples. The yield of bibenzyl was 5%. Repeating the laser drop cycle did not increase the yield of bibenzyl, although this is not surprising given the fact that there will be an accumulation of TEMPO as the reaction proceeds, and the known efficiency of TEMPO quenching of the excited state.

Excited pyrene as a singlet sensitizer

Pyrene, with its long singlet lifetime and moderately high singlet excited state energy (~83 kcal/mol) was an obvious choice as a singlet sensitizer (30, 31). Quenching can be readily examined by monitoring the effect of quenchers **2**–**5** on the fluorescence from pyrene. The analysis is much the same as in the case of triplet sensitizers described earlier. Figure 2 shows quenching plots obtained using a static system. The rate constant for TEMPO was also examined and has been included in Table 2.

Discussion

Nitroxides are excellent quenchers of excited states, normally promoting intersystem crossing to the ground state in the case of triplets, and a mixture of crossing to the triplet state (32) and probably to the ground state in the case of excited singlets. Where data for TEMPO quenching are available from earlier work, our values agree well with those in the literature (32–38). As indicated earlier, it is important to know the quenching rate constants for TEMPO in order to evaluate accurately the possibility of quenching interference due to TEMPO released

© 1997 NRC Canada

Can. J. Chem. Downloaded from www.nrcresearchpress.com by 92.62.229.171 on 09/08/12
For personal use only.

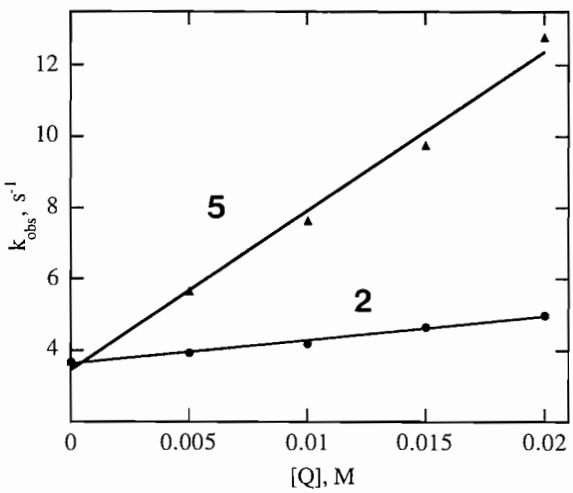
Can. J. Chem. Downloaded from www.nrcresearchpress.com by 92.62.229.171 on 09/08/12
For personal use only.

Table 1. Quenching of triplet photosensitizers by initiators **2–5** and by TEMPO in acetonitrile at room temperature.

Sensitizer	Quencher	$k_q/M^{-1}\ s^{-1}$	Radical[a] detection
Xanthone	TEMPO	$(8.9 \pm 0.1) \times 10^9$	n/a
(73.4 kcal/mol)	**2**	$(8.0 \pm 0.2) \times 10^8$	+
	3	$(1.1 \pm 0.1) \times 10^9$	+
	4	$(1.2 \pm 0.1) \times 10^9$	+
	5	$(1.3 \pm 0.1) \times 10^9$	+
1-Azaxanthone	TEMPO	$(1.3 \pm 0.1) \times 10^{10}$	n/a
(73 kcal/mol)	**2**	$(3.6 \pm 0.2) \times 10^9$	+
	3	$(4.5 \pm 0.2) \times 10^9$	Not checked
	4	$(4.8 \pm 0.2) \times 10^9$	Not checked
	5	$(6.9 \pm 0.3) \times 10^9$	+
Thioxanthone	TEMPO	$(5.1 \pm 0.1) \times 10^9$	n/a
(65.5 kcal/mol)	**2**	$(3.1 \pm 0.1) \times 10^7$	–
	3	$(3.7 \pm 0.1) \times 10^7$	Not checked
	4	$(2.8 \pm 0.1) \times 10^7$	Not checked
	5	$(3.2 \pm 0.1) \times 10^8$	–
4-Phenylbenzophenone	TEMPO	$(2.4 \pm 0.1) \times 10^9$	n/a
(61 kcal/mol)	**2**	$<5.1 \times 10^6$	–
	3	$<1.0 \times 10^7$	–
	4	$<5.4 \times 10^7$	–
	5	$(1.1 \pm 0.1) \times 10^8$	–

[a]Refers to benzylic radicals and is not applicable to the examples of TEMPO quenching.

Fig. 2. Quenching of pyrene fluorescence by **2** and **5** in acetonitrile at room temperature.



in the photoreactions under study. Given the fast rates measured (see Tables 1 and 2), and the fact that cleavage only occurs in the case of the faster triplet systems, it seems unlikely that minor traces of TEMPO will be enough to shorten significantly the lifetimes of excited sensitizers. To further verify this conclusion, in the case of xanthone we determined the rate constants using fresh samples (our standard procedure) and then repeated the determination with these pre-used (i.e., already exposed) samples. The rate constants obtained in the two experiments were identical, thus confirming that nitroxide accumulation is not a problem.

Table 2. Quenching rate constants for pyrene fluorescence in acetonitrile at room temperature.

Quencher	$k_q/M^{-1}\ s^{-1}$
TEMPO	$(1.6 \pm 0.1) \times 10^{10}$
2	$(6.6 \pm 0.4) \times 10^7$
3	$(6.1 \pm 0.1) \times 10^7$
4	$(6.8 \pm 0.4) \times 10^7$
5	$(4.5 \pm 0.2) \times 10^8$

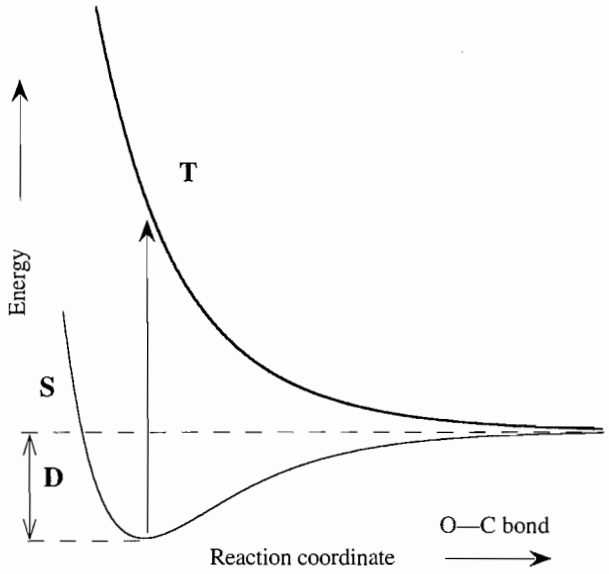
The results of Tables 1 and 2 should be examined in the context of the bonds being broken. While there is still some question concerning the strength of the O—C (see eq. [5]) bond being broken, all estimates seem to fall in the 25–40 kcal/mol range (12–14, 22, 39). Bond energies in this range are also consistent with the failure to produce **5** by thermal methods (21). Thus, all the sensitizers employed carry enough excitation energy that the sensitized cleavage of reaction [5] should be at least 20 kcal/mol exothermic. However, some fail to sensitize this process, as reflected by slow rate constants for thioxanthone and 4-phenylbenzophenone, and the failure to detect benzylic radicals with these sensitizers even when quenching takes place. It is clear that generating a benzylic radical is key to sensitized decomposition. Turro and co-workers have reported that *O*-alkyl-TEMPO adducts do not quench benzophenone triplets (40).

The following trends are observed in the case of triplet sensitizers.

© 1997 NRC Canada

Can. J. Chem. Downloaded from www.nrcresearchpress.com by 92.62.229.171 on 09/08/12
For personal use only.

Fig. 3. Qualitative potential energy profile showing the energetics in the singlet and triplet surfaces as a function of the C—O bond length. The shape shown is based on Morse-type curves.



1. Only sensitizers with triplet energies ≥ 63 kcal/mol are efficiently quenched by all the substrates examined.
2. For comparable triplet energies, quenching is faster for n,π^* (1-azaxanthone) than for π,π^* (xanthone) triplet states.
3. Triplet energies of at least ~66 kcal/mol are required for cleavage to occur.
4. It seems reasonable to assume that O—C bond energies will follow the order **2** > **3** ≈ **4** > **5**. Quenching rate constants generally follow this order.

We believe that the simplest way to rationalize these results is to invoke a quenching mechanism similar to that proposed for peroxides. We have proposed that sensitized decomposition of peroxides involves energy transfer to the repulsive triplet surface associated with the O—O bond (41). We suggest that similar concepts apply in this case, as illustrated in Fig. 3. Clearly, reaching the triplet surface requires energies well in excess of the bond energy, "*D*." It seems that the critical energy for rapid quenching and efficient cleavage must be in the 65–70 kcal/mol. In the case of *O*-alkyl TEMPO adducts studied by Turro (40), the stronger C—O bond leads to an even slower rate of quenching.

Steric hindrance must increase in the order **2** < **3** ≈ **4** < **5**. Thus, we would have expected quenching by **5** to be the slowest if steric effects were rate determining. This order is not observed with any of the sensitizers. In the case of 4-phenylbenzophenone, where the energetics are probably borderline, only **5**, which is expected to have the weakest bond, shows significant quenching.

The excited singlet energy of pyrene is around 83 kcal/mol and is, by analogy with triplet states, sufficient to overcome energy requirements for bond cleavage. As expected, rates of quenching are very fast (see Table 2), although not diffusion limited. Yet, in all these systems we systematically failed to detect benzylic radicals, in spite of the efficient quenching and the intense absorption of the radicals in the UV region. It is tempting to suggest that this is due to rapid recombination within the solvent cage from which the radicals of reaction [5] never escape. However, this argument is probably flawed. For example, in the case of **2** the rate constant for benzyl radical scavenging by TEMPO in acetonitrile is $(9.5 \pm 0.7) \times 10^7$ M^{-1} s^{-1} (17). The value should be multiplied by four, since for a singlet radical pair in the solvent cage no correction for spin statistics is needed, in contrast with the case of random encounters where only one quarter can be effective. Even the corrected (×4) value is only $\sim 4 \times 10^8$ M^{-1} s^{-1}, significantly below the diffusion limit in acetonitrile, which is around 2×10^{10} M^{-1} s^{-1}. This implies that a pair of radicals (such as TEMPO and 1-phenylethyl) in a solvent cage are expected to undergo a considerable degree of separation. Thus, the two possible explanations for the low radical yield under pyrene sensitization are either that quenching does not involve cleavage of the C—O bond, or that the geminate radical pair is different from that formed in a random encounter in solution. We favor the latter explanation. We suggest that the reason why escape is not efficient is that many collisions take place in random encounters before one occurs with the correct orientation for reaction. In contrast, the nascent radical pair generated by singlet pyrene sensitization is born with the correct spin and orientation for recombination, with no solvent molecules separating the radical partners. Thus, under these unique "contact" conditions, back reaction may occur with remarkable efficiency.

From the perspective of initiation of living free radical polymerization, it is clear that triplet sensitizers should be preferred over singlet ones. Further, it would appear that energies near 70 kcal/mol are required for efficient quenching *and* formation of free radicals, albeit in low yields. However, efficient polymerization should still occur, since it is well established that the concentration of active "living" polymer is quite low in other thermal "living" systems . Among the sensitizers used here, xanthone should probably be preferred. It may appear upon cursory examination of the rate constants that 1-azaxanthone may be a better sensitizer. However, we note that 1-azaxanthone has an n,π^* triplet character in all solvents, which makes it very prone to radical-like reactions, such as hydrogen abstraction. In contrast, xanthone has a low-lying π,π^* state in polar or hydrogen-bonding solvents where it is a poor hydrogen abstractor. Thus, we expect fewer complications in the case of xanthone.

Acknowledgments

This work has been supported by Natural Sciences and Engineering Research Council of Canada through a research grant (J.C.S.) and a graduate scholarship (N.M.). J.C.S. is the recipient of a Killam Fellowship awarded by the Canada Council. We are also grateful to Drs. Roger Sinta and George Barclay of Shipley Company for valuable exchanges of ideas.

References

1. M.K. Georges, R.P.N. Veregin, P.M. Kazmaier, and G.K. Hamer. Macromolecules, **26**, 2987 (1993).
2. M.K. Georges, R.P.N. Veregin, P.M. Kazmaier, G.K. Hamer, and M. Saban. Macromolecules, **27**, 7228 (1994).

© 1997 NRC Canada

Can. J. Chem. Downloaded from www.nrcresearchpress.com by 92.62.229.171 on 09/08/12
For personal use only.

3. M.K. Georges, R.P.N. Veregin, P.M. Kazmaier, and G.K. Hamer. Polym. Prepr. (Am. Chem. Soc. Div. Polym. Chem.) **35**, 582 (1994).
4. M.K. Georges, M. Saban, R.P.N. Veregin, P.M. Kazmaier, and G.K. Hamer. Polym. Prepr. (Am. Chem. Soc. Div. Polym. Chem.) **35**, 737 (1994).
5. M.K. Georges, R.P.N. Veregin, P.M. Kazmaier, and G.K. Hamer. Polym. Prepr. (Am. Chem. Soc. Div. Polym. Chem.) **35**, 870 (1994).
6. C.J. Hawker, E. Elce, J.L. Dao, W. Volksen, T.P. Russell, and G.G. Barclay. Macromolecules, **29**, 3346 (1996).
7. C.J. Hawker. J. Am. Chem. Soc. **116**, 11185 (1994).
8. R.D. Puts and D.Y. Sogah. Macromolecules, **29**, 3323 (1996).
9. M.V. Baldoví, N. Mohtat, and J.C. Scaiano. Macromolecules, **29**, 5497 (1996).
10. T.J. Connolly, M.V. Baldovi, N. Mohtat, and J.C. Scaiano. Tetrahedron Lett. **37**, 4919 (1996).
11. K. Matyjaszewski, T. Shigemoto, J.M.J. Frechet, and M. Leduc. Macromolecules, **29**, 4167 (1996).
12. R.P.N. Veregin, M.K. Georges, P.M. Kazmaier, and G.K. Hamer. Macromolecules, **26**, 5316 (1993).
13. R.P.N. Veregin, M.K. Georges, G.K. Hamer, and P.M. Kazmaier. Macromolecules, **28**, 4391 (1995).
14. R.P.N. Veregin, P.G. Odell, L.M. Michalak, and M.K. Georges. Macromolecules, **29**, 2746 (1996).
15. J. Chateauneuf, J. Lusztyk, and K.U. Ingold. J. Org. Chem. **53**, 1629 (1988).
16. V.W. Bowry and K.U. Ingold. J. Am. Chem. Soc. **114**, 4992 (1992).
17. A.L.J. Beckwith, V.W. Bowry, and K.U. Ingold. J. Am. Chem. Soc. **114**, 4983 (1992).
18. H. Fischer. J. Am. Chem. Soc. **108**, 3925 (1986).
19. D. Rüegge and H. Fischer. Int. J. Chem. Kinet. **21**, 703 (1989).
20. T. Fukuda, T. Terauchi, A. Goto, K. Ohno, Y. Tsujii, T. Miyamoto, S. Kobatake, and B. Yamada. Macromolecules, **29**, 6393 (1996).
21. C.J. Hawker, G.G. Barclay, A. Orellano, and J. Dao. Macromolecules, **29**, 5245 (1996).
22. I. Li, B.A. Howell, A. Ellaboudy, P.E. Kastl, and D.B. Priddy. Polym. Prepr. (Am. Chem. Soc. Div. Polym. Chem.) **36**, 469 (1995).
23. E.C. Korolenko, F.L. Cozens, and J.C. Scaiano. J. Phys. Chem. **99**, 14123 (1995).
24. J.C. Scaiano. J. Am. Chem. Soc. **102**, 7747 (1980).
25. J.C. Scaiano, M. Tanner, and D. Weir. J. Am. Chem. Soc. **107**, 4396 (1985).
26. J.T. Banks and J.C. Scaiano. J. Am. Chem. Soc. **115**, 6409 (1993).
27. J.C. Scaiano and J.T. Banks. J. Braz. Chem. Soc. **6**, 211 (1995).
28. A. Garner and F. Wilkinson. J. Chem. Soc. Faraday Trans. 2, **72**, 1010 (1976).
29. J. Lusztyk and J.M. Kanabus Kaminska. *In* Handbook of organic photochemistry. *Edited by* J.C. Scaiano. CRC Press, Boca Raton, Fl. 1989. p. 177.
30. T. Förster. *In* The exciplex. *Edited by* M. Gordon and W.R. Ware. Academic Press, New York. 1975. p. 1.
31. F.M. Winnik. Chem. Rev. **93**, 587 (1993).
32. V.A. Kuzmin and A.S. Tatikolov. Chem. Phys. Lett. **51**, 45 (1977).
33. J.C. Scaiano. Chem. Phys. Lett. **79**, 441 (1981).
34. M.V. Encinas, E.A. Lissi, and J. Alvarez. Photochem. Photobiol. **59**, 30 (1994).
35. S.S. Atik and L.A. Singer. Chem. Phys. Lett. **59**, 519 (1978).
36. A.R. Watkins. Chem. Phys. Lett. **70**, 262 (1980).
37. A.R. Watkins. Chem. Phys. Lett. **29**, 526 (1974).
38. J.A. Green II and L.A. Singer. J. Am. Chem. Soc. **96**, 2730 (1974).
39. P.M. Kazmaier, K.A. Moffat, M.K. Georges, R.P.N. Veregin, and G.K. Hamer. Macromolecules, **28**, 1841 (1995).
40. E.N. Step, N.J. Turro, M.E. Gande, and P.P. Klemchuk. J. Photochem. Photobiol. A: **74**, 203 (1993).
41. J.C. Scaiano and G.G. Wubbels. J. Am. Chem. Soc. **103**, 640 (1981).

© 1997 NRC Canada

1996 Hoffman–LaRoche Award Lecture Photochemistry and photobiology of perylenequinones[1]

James William Lown

Can. J. Chem. Downloaded from www.nrcresearchpress.com by 92.62.229.171 on 09/08/12
For personal use only.

Abstract: Photodynamic therapy relies on the selective accumulation of photosensitizers within neoplastic tissue, followed by light activation to generate cytotoxic singlet oxygen. At present, Photofrin™, a preparation of hematoporphyrin derivatives (HPD) with the bulk of the porphyrin monomers removed, is the only clinically approved photosensitizer. Intravesical administration of Photofrin or HPD has failed to photosensitize bladder tumors. Bladder cancer is the second most common genitourinary malignancy. In 1994 there were an estimated 51 200 cases of bladder cancer with 10 600 deaths in the United States. The predominant histopathology is transitional cell carcinoma, occurring in 90–95% of these cases. Most patients (85%) have superficial disease at the time of initial diagnosis. Superficial bladder cancer is defined as disease involving the mucosa with carcinoma in situ or papillary lesions and invasion limited to submucosa. To address these limitations we have been conducting preclinical studies with perylenequinones (PQs). The majority of our effort has focused on developing and characterizing derivatives of PQs. Following site-directed modifications, we have identified certain congeners that warrant further preclinical development. These compounds are monomeric and do not effect cutaneous photosensitization beyond 24 h. With clinically relevant drug and light doses we have cured >90% of experimental subcutaneous murine tumors.

Key words: photodynamic therapy, perylenequinones, photobiology, photochemistry.

Résumé : La thérapie photodynamique repose sur l'accumulation sélective de photosensibilisateurs dans le tissu néoplastique, suivie d'une activation par la lumière pour générer l'oxygène singulet cytotoxique. Actuellement le seul photosensibilisateur approuvé cliniquement est la Photofrine™, une préparation à base de dérivés de l'hématoporphyrine (HPD) dans laquelle on a supprimé l'encombrement de la porphyrine monomère. L'administration intravésiculaire de la Photofrine n'a pas permis de photosensibiliser les tumeurs de la vessie. Le cancer de la vessie est en importance la deuxième des plus communes tumeurs malignes affectant les fonctions urinaires ou génitales. En 1994, aux États Unis, on dénombré environ 51 200 cas de cancer de la vessie dont 10 600 ont entraîné la mort. L'histopathologie prédominante est un carcinome de transition, se produisant dans environ 90–95% des cas. La plupart des patients (85%) ont des maladies superficielles au moment du premier diagnostique. Le cancer superficiel de la vessie est défini comme une maladie impliquant la muqueuse avec un carcinome in situ ou des lésions papillaires et une invasion limitée de la sous-muqueuse. Dans le but de comprendre ces limitations nous avons effectué des études précliniques avec des pérylènequinones (PQs). Nous avons concentré nos efforts dans le développement et la caractérisation des dérivés des PQs. Après des modifications de site, nous avons identifié certains congénères qui justifient un développement préclinique plus poussé. Ces composés sont des monomères et n'affectent pas la photosensibilisation cutanée après 24 h. Utilisant un médicament clinique appropriée et à des doses légères nous avons soigné plus de 90% des tumeurs sous-cutanées développées expérimentalement sur des cobayes.

Mots clés : thérapie photodynamique, pérylènequinones, photobiologie, photochimie.

[Traduit par la rédaction]

Introduction

The ultimate goal of pharmacology is the development of therapeutic agents that selectively destroy the target tissue while sparing the non-target tissue. Unfortunately, in many disorders including cancer, such a discrimination is hard to achieve. Recently, considerable attention has been paid to photodynamic therapy (PDT) to maximize the therapeutic ratio (1–8). This approach is based on the use of drugs (photosensitizers) that acquire the desired activity when excited by light, but that are relatively innocuous in the absence of light. It permits dual selectivity since the simultaneous presence of both photosensitizer and light is required, so ideally the healthy regions of the system are not affected. The selectivity depends on both the degree of preferential accumulation of the photosensitizer in the target tissue and the extent of spatial localization of light energy to the target tissue. In this modality, a photosensitizer is intravenously injected and then allowed to distribute within the animal (Fig. 1). When the concentration ratio of the photosensitizer between target and non-target tissues reaches a max-

Received June 20, 1996.

J.W. Lown.[2] Department of Chemistry, University of Alberta, Edmonton, AB T6G 2G2, Canada.

[1] This Hoffman-La Roche 1996 Award Lecture was presented by Professor Lown at the 79th Conference of the Canadian Society for Chemistry, St. John's, Newfoundland, June 23–26, 1996.

[2] Telephone: (403) 492-3646. Fax: (403) 492-8231.

© 1997 NRC Canada

Can. J. Chem. Downloaded from www.nrcresearchpress.com by 92.62.229.171 on 09/08/12
For personal use only.

imum, light is directed at the tumor, and then the PDT effect will affect primarily the target tissue. A typical protocol is available for Photofrin (9).

A photosensitizer can be activated by both Type I and (or) Type II pathways (10). Briefly, the photosensitizer is first excited into the short-lived singlet state following the absorption of light. The singlet state of the photosensitizer is converted into the triplet state via an intersystem crossing process, which results in more stable and longer lived species compared with the singlet state. Usually, photosensitization occurs via the triplet state; therefore, a high quantum yield of triplet state formation is required for efficient photosensitizers. The excited triplet state of the photosensitizer can undergo two kinds of reactions. It can directly react with substrate via electron and (or) hydrogen atom transfer to produce radical forms of the substrate and (or) the photosensitizer that, after interaction with oxygen, generate peroxides, hydroxy radical, superoxide anion radical ($O_2^{\cdot-}$), and other oxygenated products (Type I reaction) (9–11). The Type I mechanism is extremely concentration dependent, and is favored when the photosensitizers are bound or associated with readily oxidized biomolecules (12).

Alternatively, the triplet state of the photosensitizer can transfer its energy to the ground state of oxygen to generate singlet oxygen ($^1O_2$), a highly reactive species (Type II reaction). The electrophilic nature of $^1O_2$ makes it very efficient in producing oxidized forms of biomolecules and to initiate most types of PDT[3] damage (10, 11, 13, 17). The properties and biological roles of $^1O_2$ have been well documented (14–16, 18–20).

Type I and Type II reactions (Fig. 2) may occur simultaneously, and the relative contribution of the two processes depends on the nature and concentrations of the substrate and photosensitizer, oxygen concentration, and the binding of the photosensitizer to the substrate. From the above it is evident that the PDT effect should be oxygen dependent. For most photosensitizers, the PDT effect is mediated by $^1O_2$. There are several lines of evidence to suggest that $^1O_2$ is a major damaging species in PDT. However, other activated species, such as $O_2^{\cdot-}$ and hydroxy radical (·OH) may also be involved in some aspects of PDT damage (21, 22).

Although the concept of PDT was proposed 90 years ago (23), with eosin and acridine as prototype photosensitizers, substantial progress was not made until HPD (Fig. 3) was shown in clinical trials to have improved tumor localization properties (24, 25). Since then, extensive basic and clinical investigations have been made with HPD, and the results obtained, which are promising, are summarized in several excellent reviews (2, 3, 6, 8, 11, 26–31). Nowadays, the utilization of sophisticated electrooptical techniques (especially the application of optical fibers in PDT), and advances of knowledge on photophysical and photochemical processes occurring in microheterogeneous systems, have enhanced the efficacy of PDT (11, 32). A variety of phototherapeutic procedures have been developed, some of which have currently reached the stage of clinical application (1, 2, 6, 23, 33, 34).

As laser and optical techniques develop rapidly (such as the application of endoscopy illumination), PDT depends more and more critically on the development of photosensitizers with superior properties. These include, especially, strong absorption in the "phototherapeutic window" region from 600 to 950 nm, in which tissue light scattering is low and there is little competing absorption from endogeneous biomolecules, such as hemoglobin, melanin, and water. This would permit deep light penetration into tissue and render PDT potentially feasible for many clinically important tumors. In addition, high preferential tumor localization and minimal dark toxicity to enhance the therapeutic ratio, as well as rapid clearance from normal tissue to suppress prolonged photosensitivity side effects, would also have beneficial effects (17, 35).

Although promising results have been obtained with HPD, there are disadvantages with this agent. Specifically, HPD has little absorption in the "phototherapeutic window" region, limiting its PDT efficiency, and it is retained in several types of normal tissue, such as skin, for extended time (about 4–6 weeks), resulting in severe prolonged skin photosensitivity (3, 9). To overcome these problems with HPD, renewed interest in the synthesis and evaluation of new photosensitizers for the treatment of malignant and infectious disorders has arisen.

Perylenequinones

4,9-Dihydroxy-3,10-perylenequinones comprise a relatively small but growing group of natural pigments that possess unique chemical and biological properties (36–38). The natural PQs of this class identified to date include hypocrellins, cercosporin, phleichrome, elsinochromes, erythroaphins, and calphostins (see Fig. 4). Most of them are produced by a wide variety of molds and act as photodynamic phototoxins of their hosts, except that erythroaphins are isolated from aphids. Substantial progress has been made recently in the application of PQs in the PDT of human malignancies (38–40), anticancer (41), and possibly anti-HIV (42–44). The latter property was related to the potent specific inhibition of protein kinase C by PQs (45, 46).

Occurrence, isolation, and synthesis

Although fungi were considered as the richest sources of PQs, there exist other sources to produce PQs, such as certain kinds of soil and insects (36, 37). Erythroaphins were the first isolated and characterized members of the PQ class, after which elsinochromes, cercosporin, cladochrome, and phleichrome were isolated and identified. Recently, two new kinds of PQs, hypocrellins and calphostins, have been reported (38, 46–49).

Hypocrellin, which includes hypocrellin A (HA) and hypocrellin B (HB), derives its name from *Hypocrella bombuase (B. et Br) sacc.*, a parasitic fungus of *Sinarundinaria sp.* which grows abundantly in the northwestern region of Yunnan Province and the southeastern region of Xizang Autonomous Region of the People's Republic of China (P.R.C.) and also in

[3] **Abbreviations:** AHBD, amino-substituted hypocrellin B derivatives; ATPase, adenosine triphosphatase; AcEase, acetic ester, acetyl hydrolase; ^{14}C-HB, hypocrellin B labeled with ^{14}C in methoxy groups; CHO, Chinese hamster ovary; DABCO, 1,4-diazabicyclo[2,2,2]octane; DMAP, dimethylaminopyridine; EPR, electron paramagnetic resonance; G-6-Pase, guanosine-6-phosphatase; GAPDH, glycol-3-phosphate dehydrogenase; HA, hypocrellin A; HB, hypocrellin B;HIV, human immunodeficiency virus; HPD, hematoporphyrin derivative; PDT, photodynamic therapy; PQ, perylenequinone; SOD, superoxide dismutase; TFA, trifluoracetic acid.

© 1997 NRC Canada

Fig. 1. Scheme summarizing the procedure for administration of photodynamic therapy (PDT).

PDT is the treatment of malignant lesions with 600-1000 nm light (called a "phototherapeutic window") following the systemic administration of drug (photosensitizer).

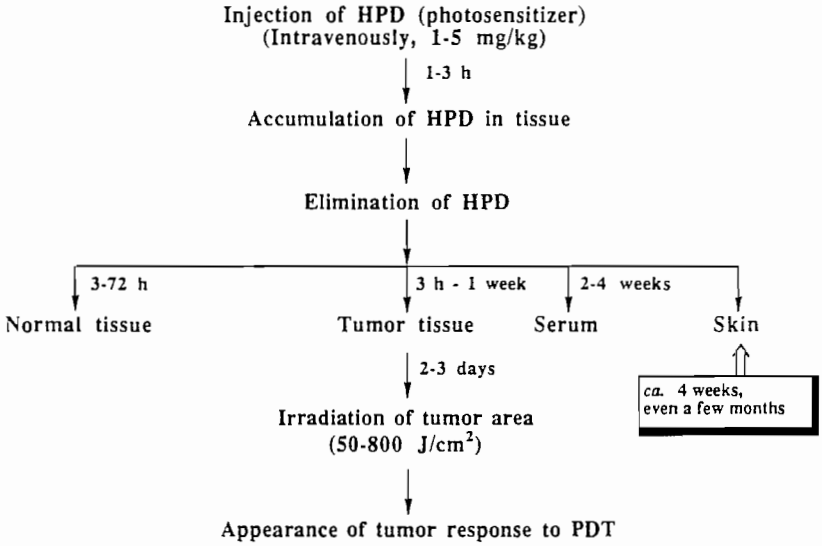


Fig. 2. Main characteristics of PDT.

The Molecular Mechanism for PDT

$$PS \xrightarrow{h\nu} {}^1PS \longrightarrow {}^3PS \qquad \text{(EXCITATION)}$$

$$PS^* + SUB \longrightarrow PS^{\cdot-} + SUB^{\cdot+} \qquad \text{(TYPE I)}$$

$${}^3PS + {}^3O_2 \longrightarrow PS + {}^1O_2 \qquad \text{(TYPE II)}$$

Requirements for Optimal PDT Photosensitizer

(1) Strong absorption above 600 nm.
(2) High quantum yield of triplet formation.
(3) High tumor-retained selectivity.
(4) Minimal dark toxicity
(5) Rapid clearence from normal tissue.

certain parts of Sri Lanka. Hypocrellin constitutes up to 4% of the fungus (37). *Shiraia bombusicola P. Heen* also contains the same pigments that are structurally related to the general class of pigments. In addition to hypocrellin, other perylenequinonoid pigments are isolated from other microbial sources found in other countries, such as cercosporin, phleichrome, elsinochrome A, B, C, and D, cladochrome, and erythroaphin. The structural similarities of these pigments led to some common properties among them and occasioned comparative studies between hypocrellin and the other related pigments. However, the fungus that generates individual perylenequinonoid pigments generally exists only in certain regions of the P.R.C. This has stimulated the study of methods by which the perylenequinonoid pigments can be totally synthesized (37).

Mei and Luo (50) reported the first case in which oral administration of hypocrellin caused hypericism, a state of skin sensitivity to visible light in animals. Twenty years later, it was proved that the photosensitizing effects caused by hypocrellin depend on the presence of oxygen, and thus it was recognized as a photodynamic action. Interestingly, hypocrellin has also been utilized as a potent phototherapeutic agent for white lesions of vulva, keloid, vitiligo, psorasis, tinea capitis, and lichen amyloidosis (38). Recently it has also been shown that HA has a strong PDT effect (39). In addition, hypocrellin has bactericidal and other physiological activities (38). In the past, the hypocrellin-containing *Hypocrella bambuase* was used to treat rheumatoid arthritis and gastric disease.

Although, as early as in 1954, Calderbank et al. prepared 4,9-dihydroxy-3,10-perylenequinone, the parent compound of the natural perylenequinonoid pigments (51), it was not until 1972 that Weisgraber and Weiss synthesized the first derivative of this class bearing methoxy groups, a characteristic substituent in natural perylenequinones, starting from commercial homoveratric acid (52*a*). However they later modified the assigned perylenequinonoid structure to be dinaphthofuranedione (52*bc*). Until recently, relatively few efforts have been devoted to the synthesis of perylenequinone structures. Dallacker and Leidig prepared a methoxylated perylenequinone but this compound still lacked some indispensable functionalized groups at appropriate positions (53). Subsequently Chao and Zhang synthesized another perylenequinone bearing methoxy groups and acetic ester side chains in their correct positions by two different methods, which were then modified to provide natural perylenequinone (54).

In the first route of Chao and Zhang, and in that of Dallacker and Leidig, a biphenyl, formed from an Ulmann coupling reaction, was elaborated into the desired pentacycle. The second route developed by Chao and Zhang utilized a double oxidative coupling reaction of a 5-bromo-1,2-naphthalenediol to generate the perylenequinonoid nucleus. However, the required 5-bromo-1,2-naphthalenediol in the second route of

Can. J. Chem. Downloaded from www.nrcresearchpress.com by 92.62.229.171 on 09/08/12
For personal use only.

© 1997 NRC Canada

Fig. 3. Representative porphyrin photosensitizers.

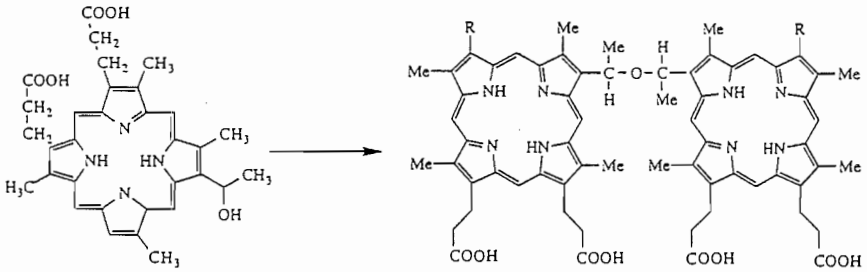
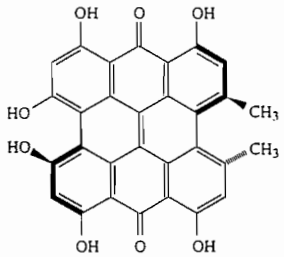
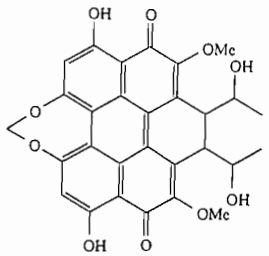
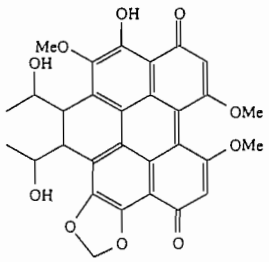
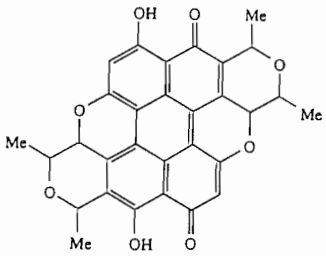


Fig. 4. Representative perylenequinone structures.









Chao and Zhang is difficult to prepare and readily decomposes (vide infra). An alternative route for the preparation of a 5-bromo-1,2-dioxygenated naphthalene, based on a Diels–Alder cycloaddition, was later developed by Coleman and Grant, but this naphthalene lacked the three carbon side chains found in natural perylenequinones (55). Subsequently, a selective and stereospecific approach was developed for the total synthesis of phleichrome, the first successful synthesis of a natural perylenequinone. However, this approach requires at least 26 steps starting from commercially available reagents, and several of these steps require stringent experimental conditions (56). Thus the procedure is inconvenient and ill-adapted for the preparation of various functionalized perylenequinones with different substituents at different positions. Therefore, we reexamined and attempted to improve upon the double coupling method of Chao and Zhang to synthesize certain perylenequinones. During this research, we developed a convenient and higher-yielding route to perylenequinones (Fig. 5).

Total synthesis of hypocrellin B

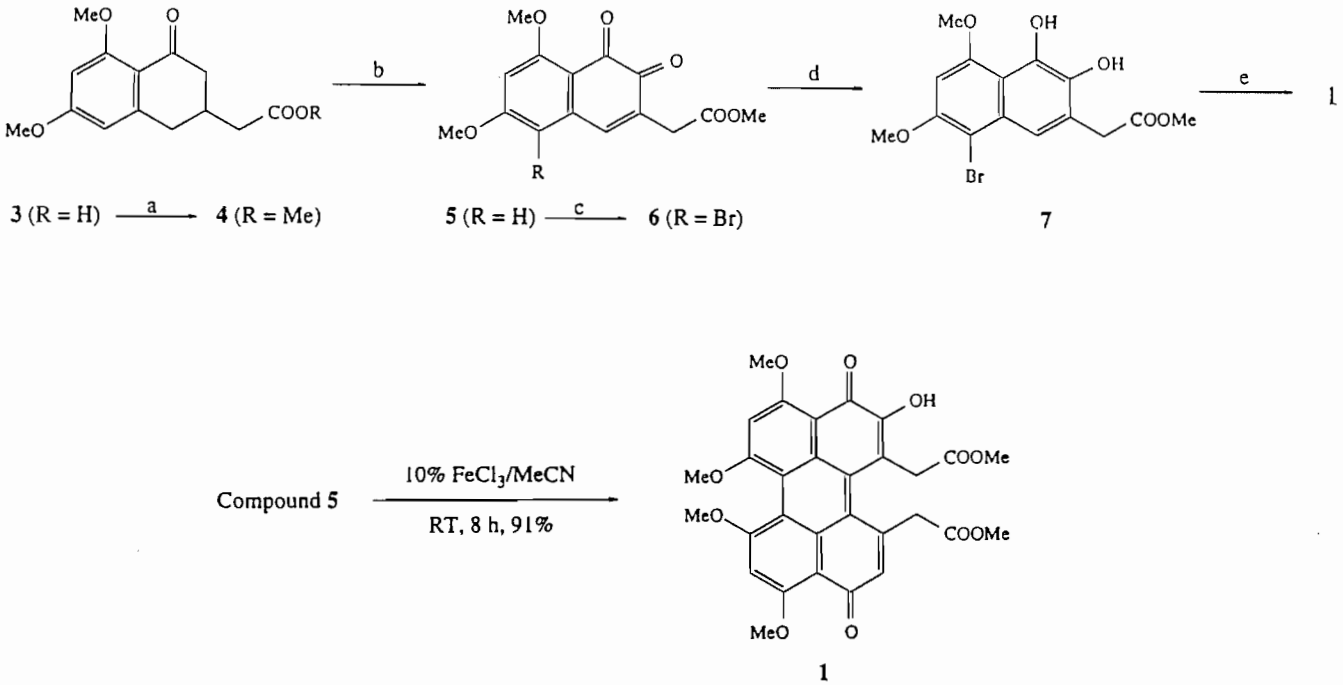
The synthetic approach toward HB that we have initiated is outlined in Fig. 6. Simplification of HB by a retro-aldol condensation of methyl ketone provides **1**; cleavage of the two biaryl bonds of **1** in a retrosynthetic sense affords 3-acetonyl-6,8-dimethoxy-1,2-naphthoquinone **2**. Takuwa et al. (57*a*) reported a one-pot photochemical reaction to prepare 3-(2-oxoalkyl)-1,2-naphthoquinone; however, it afforded only very low yield of the precursor **2**. Recently, Hauser and co-workers reported the total synthesis of calphostin D and gave a method to prepare precursor **3** in high overall yield (57*b*). Hydrolysis of **3** followed by oxidation affords **2** in high yield. The precursor **2** is unstable and was used immediately for the next coupling reaction by $FeCl_3$ or TFA, but no anticipated product was obtained.

An efficient total synthesis of HB was accomplished using another precursor **6** as shown in Fig. 6. The commercially available 3,5-dimethoxybenzaldehyde was converted to compound **5** via seven reaction steps according to the procedure of

© 1997 NRC Canada

Can. J. Chem. Downloaded from www.nrcresearchpress.com by 92.62.229.171 on 09/08/12
For personal use only.

Fig. 5. Synthesis of perylenequinones from one-step double coupling reaction of 1,2-naphthoquinone. Reagents and conditions: a. MeOH/H_2SO_4, reflux, 95%; b. SeO_2/HAc, 80–90°C, 71%; c. NBS/H_2SO_4/THF, RT, 41%; d. SO_2/MeOH·H_2O, reflux, 96%; e. $FeCl_3$/MeCN, RT, 28%.



Hauser and co-workers (57*b*). Oxidation of **5** with benzeneseleninic anhydride in anhydrous THF gave the 1,2-naphthoquinone **6** in 87% yield (59). Attempted coupling of **6** to the corresponding perylenequinone by TFA and $FeCl_3$ was not successful but coupling of its ester, which was prepared in the presence of Ac_2O, pyridine, and a catalytic amount of DMAP in 95% yield, gave perylenequinone **7** in 88% yield. Methylation of **7** with methyl iodide and CsF in anhydrous THF led to compound **8** quantitatively. Hydrolysis of **8** in K_2CO_3 and MeOH·H_2O solution, followed by oxication with CrO_3 and pyridine in CH_2Cl_2, gave the methyl ketone **1** in 63% overall yield (60). Compound **9**, which was obtained from **1** in 85% yield by an intramolecular aldol condensation reaction, was demethylated selectively with 48% hydrobromic acid to afford a 1:1 mixture of enantiomers HB (90%), which was identical in all respects (TLC, IR, and NMR) with the natural product HB. This synthesis now provides an entry to the synthesis of other important perylenequinones (Fig. 6). We have reported additional synthetic routes to certain related perylenequinone structures (108).

Photophysical and photochemical properties of perylenequinones

In terms of photophysical and photochemical studies of natural PQs, hypocrellins and cercosporin have received the most attention. As a general rule, PQs have three visible absorption bands, which are respectively assigned to a $\pi\pi^*$ transition of their conjugated systems and charge transfer. Their fluorescence emission spectra consist of a major peak of the neutral species with a shoulder peak attributed to the zwitterions, which are formed via intramolecular proton transfer (37, 61). The excimers of hypocrellin A (HA) and hypocrellin B (HB) were detected both in concentrated solution and in the crystalline states of the hypocrellins (61). In addition, HA and HB may act as molecular probes for the diagnosis of cancer, since the environmental effects of their fluorescence spectra have been well characterized (37, 62).

The singlet states of PQs were investigated by means of static and time-resolved fluorescence spectroscopy (38, 63). Relatively few investigations have been made concerning the triplet states of PQs, since no phosphorescence or triplet–triplet absorption spectra were recorded. However, some significant triplet parameters (such as lifetime, energy level, and quantum yield) were indirectly estimated for HA, HB, and cercosporin on the basis of the relationship between delayed fluorescence and phosphorescence (38, 63).

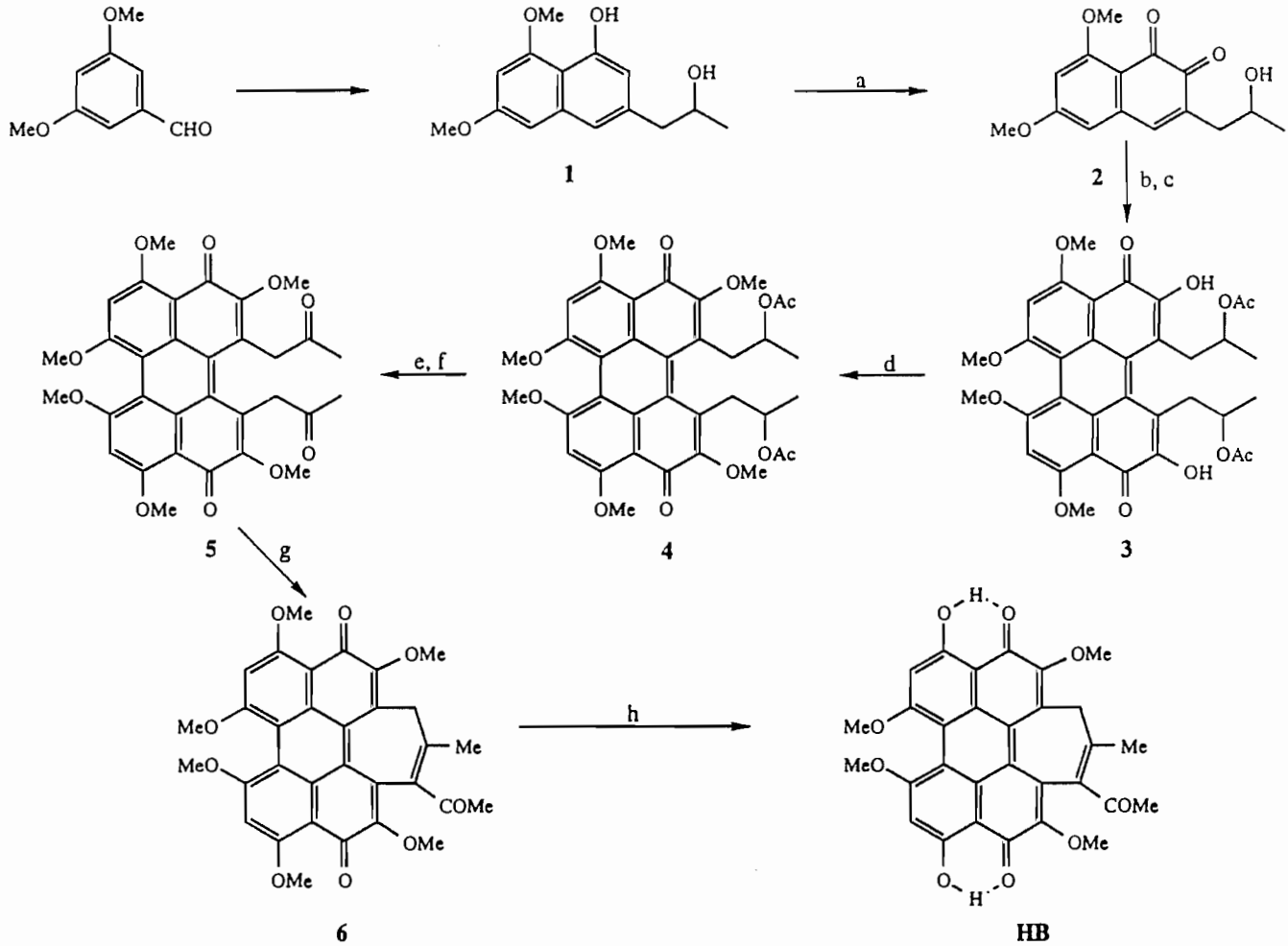
PQs are an efficient class of $^1O_2$ generators with quantum yields comparable with those of porphyrins. In aerobic solution, the production of $^1O_2$ by PQs was detected by means of chemical trapping reactions, spin trapping, and $^1O_2$ luminescence (64, 65). On the basis of a series of comparative studies, the 4,9-dihydroxy-3,10-perylenequinonoid chromophore was determined to be the essential structural requirement for the generation of $^1O_2$ by the quinones, and the side chains of the quinones had little effect on the production of $^1O_2$. This conclusion is a key finding for the design of PDT agents, which are now required to contain the 4,9-dihydroxy-3,10-perylenequinonoid chromophore, efficiently producing $^1O_2$, appropriate side chains, promoting cellular uptake, and, ideally, the selective localization of the sensitizers in tumor tissue (22).

In addition to $^1O_2$, $O_2^{\cdot-}$ is also generated by PQs on illumination via the reduction of oxygen by the semiquinone radicals of the PQs in aerobic solution, but to a lesser extent than $^1O_2$. This process is significantly enhanced by the presence of electron donors (22). There were several lines of evidence for

Can. J. Chem. Downloaded from www.nrcresearchpress.com by 92.62.229.171 on 09/08/12
For personal use only.

© 1997 NRC Canada

Fig. 6. Total synthesis of the perylenequinone pigment hypocrellin B. Reagents and conditions: a. $(PhSeO)_2O$, THF, 50°C, 20 min, 87%. b. Ac_2O, Py, DMAP (cat.), $CHCl_3$, RT, 3 h, 95%. c. TFA then $FeCl_3$, RT, 2 h, 88%. d. MeI, CsF, THF, RT, 16 h, 94%. e. K_2CO_3, $MeOH{\cdot}H_2O$, RT, 12 h, 96%. f. CrO_3–Py, CH_2Cl_2, RT, 3 min, 66%. g. LiOH, $MeOH{\cdot}H_2O$, RT, 1 h, 85%. h. 48% HBr, $CHCl_3$, RT, 1 h, 90%.



the photoproduction of OH by PQs, but for which the exact mechanism is still obscure (22, 65).

Besides the reactive oxygen species, semiquinone radicals of PQs were also detected in the photosensitizations of PQs. In anaerobic solution, the semiquinone radicals are predominantly photoproduced via self-electron transfer between excited and ground state species (38, 67). The semiquinone radicals of HA, HB, elsinochrome A, and cercosporin display well-defined EPR spectra, which were assigned by reference to simulated spectra. The presence of electron donors significantly promotes the production of the semiquinone radicals (66, 67).

Evidently the photodynamic action of PQs involves a number of processes (3, 22, 63, 67–70). Although $^1O_2$ was determined to be a major active intermediate for PQ photosensitization, the supplemental roles of other reactive species, such as $O_2^{\cdot-}$, $\cdot OH$, H_2O_2, and the semiquinone radicals of the sensitizers, should also be considered. Oxygen consumption and EPR studies confirmed that oxygen concentration plays a key role in the mutual transformation between $^1O_2$ (Type II) and the semiquinone radicals (Type I) (22).

The degradation of some biological molecules (such as amino acids, peptides, protein, bases, DNA, lipids) sensitized by HA has also been investigated extensively. These reactions may be mediated by Type I and (or) Type II pathways, depending upon the reaction conditions, such as the nature of substrate, oxygen concentration, pH, etc. (38). The photooxidations of tryptophan and its derivatives were demonstrated to have some biological relevance to the phototherapeutic mechanism of hypocrellins (71–73). Like many photosensitizers, hypocrellins, cercosporin, and calphostins were demonstrated to sensitize the inactivation of some enzymes, such as ATPase, GAPDHase, AcEase, and protein kinase C (38, 74).

Perylenequinonoid pigments, novel singlet oxygen sensitizers

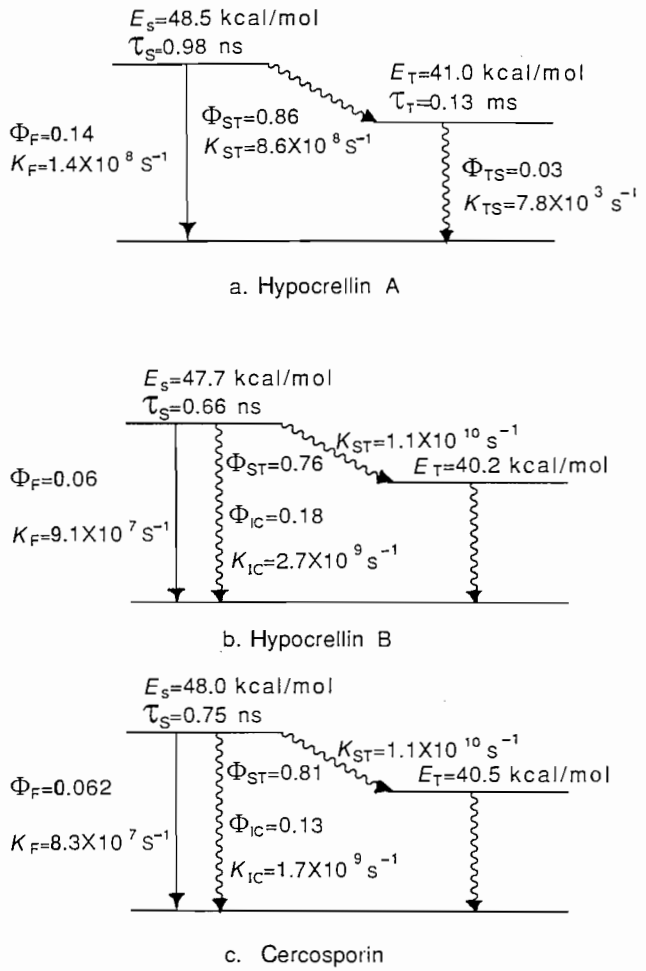
The marked photosensitizing properties of perylenequinonoid pigments, now a promising class of the agents for photodynamic therapy of human tumors, have been recognized but quantitative information on their excited states are lacking. For the first time, some fundamental photophysical parameters of hypocrellins A, B and cercosporin in solution have been determined (63). For hypocrellin A, $K_F = 1.4 \times 10^8\ s^{-1}$,

© 1997 NRC Canada

Can. J. Chem. Downloaded from www.nrcresearchpress.com by 92.62.229.171 on 09/08/12
For personal use only.

Can. J. Chem. Downloaded from www.nrcresearchpress.com by 92.62.229.171 on 09/08/12
For personal use only.

Fig. 7. Energetics of photoexcitation processes for the representative perylenequinones hypocrellin A and B and cercosporin.



$\Phi_F = 0.14$, $\tau_s = 0.98$ ns, $E_s = 48.5$ kcal/mol, $\Phi_{ST} = 0.86$, $K_{ST} = 8.6 \times 10^8$ s^{-1}, $\Phi_{TS} = 0.03$, $K_{TS} = 7.8 \times 10^3$ s^{-1}, $\tau_T = 4.5$ μs (in the presence of oxygen), $\tau_T \geq 0.13$ ms (in the absence of oxygen), and $E_T = 41.0$ kcal/mol (63). For hypocrellin B, $K_F = 9.1 \times 10^7$ s^{-1}, $K_{IC} = 2.7 \times 10^9$ s^{-1}, $K_{ST} = 1.1 \times 10^{10}$ s^{-1}, $\Phi_F = 0.06$, $\Phi_{IC} = 0.18$, $\tau_s = 0.66$ ns, $E_s = 47.7$ kcal/mol, $\Phi_{ST} = 0.176$, and $E_T = 40.2$ kcal/mol. For cercosporin, $K_F = 8.3 \times 10^7$ s^{-1}, $K_{IC} = 1.7 \times 10^9$ s^{-1}, $K_{ST} = 1.1 \times 10^{10}$ s^{-1}, $\Phi_F = 0.062$, $\Phi_{IC} = 0.13$, $\tau_s = 0.75$ ns, $E_s = 48.0$ kcal/mol, $\Phi_{ST} = 0.81$, and $E_T = 40.5$ kcal/mol.

In addition, the energy diagrams of hypocrellins A, B and cercosporin were established (Fig. 7). Differences are apparent between the decay process of singlet hypocrellin A and those of singlet hypocrellin B and cercosporin. The quantum yields of singlet oxygen formation by these agents were also determined, $\Phi_{^1O_2}$ (HA) = 0.83, $\Phi_{^1O_2}$ (HB) = 0.76, and $\Phi_{^1O_2}$ (CP) = 0.81 (63). As well, these perylenequinonoid agents have been shown to act as excellent singlet oxygen sensitizers (Fig. 8). The characteristics of the sensitizer play a key role in any sensitized photooxygenations. The marked photophysical and photochemical characteristics of the PQ pigments qualify them as a new class of efficient $^1O_2$ sensitizers with the following advantages warranting their application in photosensitized reactions: (*i*) large molar absorptivity at the appropriate wavelength; (*ii*) high quantum yield of $^1O_2$ formation; (*iii*) large adaptability for solubility; (*iv*) small solvent effect to simplify photochemical reactions; (*v*) wide irradiation wavelength region; (*vi*) large concentration tolerance, and (*vii*) low tendency toward hydrogen abstraction and self-photooxidation, causing their bleaching and high thermal stability.

The photooxidation of hypocrellin A. A mechanism study using ^{18}O labelling

For the PDT of human tumors, the photooxidation of the sensitizer employed appeared to be a critical factor, which therefore needed to be comprehensively examined. On the one hand photooxidation of the sensitizer should be minimized because it destroys sensitizer, thereby decreasing photodynamic therapeutic efficiency, but on the other hand it can also be utilized as a basis for the selective destruction of the sensitizer following PDT treatment to obviate long-term photosensitivity (75).

Among the natural PQs, cercosporin, elsinochromes, and erythroaphins are not readily photooxidized, and only the photooxidations of hypocrellins and phleichrome have been observed (76). In 1981, Chen et al. (77) suggested that HA photooxidation results in an endoperoxide via the [2+4] addition of singlet oxygen ($^1O_2$) formed during irradiation to ground state HA.

However, they deduced this mechanism only on the basis of the assigned structure of the photooxidized product of HA, and did not supply any evidence for the involvement of $^1O_2$ in the photooxidation of HA (77). In fact, the assigned structure of the photooxidized products of HA has been also revised by Liang's X-ray diffraction data. In 1985, Zhang et al. (78) proposed that HA photooxidation proceeds via the reaction of excited (singlet and (or) triplet) HA with ground state oxygen (instead of $^1O_2$).

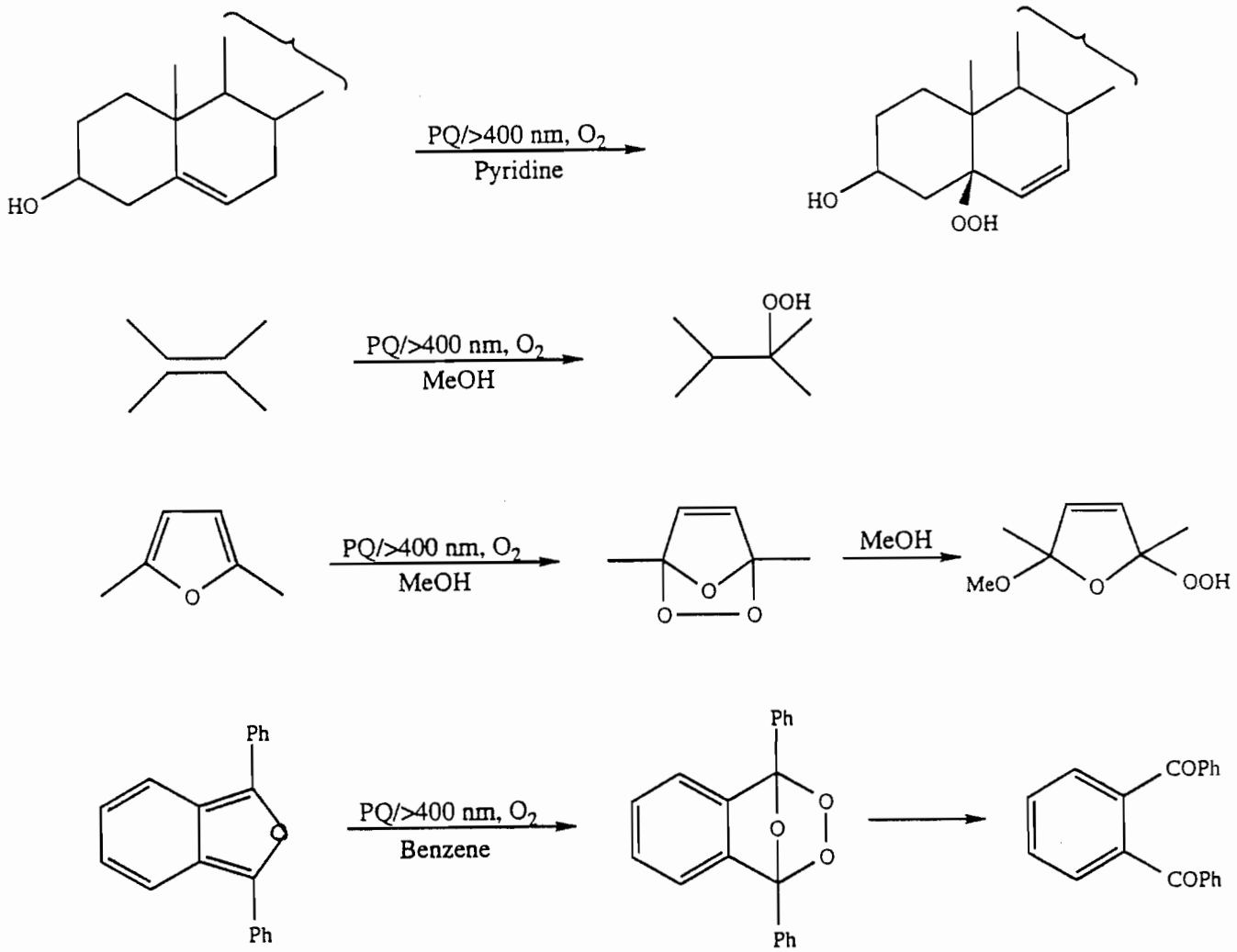
Subsequently Zhao et al. reassigned the main photooxidized product of HA as the dioxetane generated from the [2+2] addition of ground state oxygen to excited HA instead of the endoperoxide proposed by Chen et al. (77, 79). The correct structure of the photooxidized product of HA was established, by X-ray diffraction in 1988, to be a di-α-naphthoquinone compound (38).

Nevertheless, Arone et al. observed that the photooxidation of phleichrome, an HA analog, does form endoperoxides, typical $^1O_2$ photooxidized products, and that prolonged irradiation also leads to the formation of a di-α-naphthoquinone as in HA photooxidation (80, 81). Again, unfortunately, a mechanistic study of the photooxidation of phleichrome is not available. Consequently it appears that the photooxidation mechanism of HA is confusing, and that of phleichrome is ambiguous. It is evident that our knowledge of the photooxidation mechanisms of PQs is incomplete. For example, it was necessary to establish whether $^1O_2$ is involved in the photooxidation of PQ.

Hypocrellin A was selected as a representative structure for investigating the mechanism of the photooxidations of perylenequinonoid pigments. The following processes were determined to be involved in the photooxidation of perylenequinonoid pigments using ^{18}O atom labelling. After perylenequinonoid pigment is photoexcited, it tautomerizes and

© 1997 NRC Canada

Fig. 8. Selection of characteristic photochemical processes sensitized by perylenequinones.



dissociates to produce the anion, which reacts with singlet oxygen generated during irradiation, resulting in formation of an *endo* peroxide. The *endo* peroxide then rearranges to form a dioxetane, which undergoes cycloreversion to produce the final product, a di-α-naphthoquinone (Fig. 9).

As demonstrated above, $^1O_2$ plays a crucial role in HA photooxidation. However, the photoexcitation of HA itself should also be considered. The pH of the solution, the nature of the solvent, and irradiation wavelength exert certain effects on HA photooxidation. Among these factors, the pronounced effect of pH on HA photooxidation has important biological implications in the PDT of human tumors. This specific effect can be taken advantage of as a basis for the selective localization of HA in tumor tissue since tumor tissue has a somewhat lower average pH than normal tissue (82, 83). On the basis of the proposed photooxidation mechanism of PQs, one can envisage the design and synthesis of improved PQ photosensitizers with selectivity for tumor tissue localization for the PDT of human malignancies by means of manipulating the pK_a of the photosensitizer. Consequently one can expect that a PQ photosensitizer with pK_a = ~7.0 should meet this condition where the photosensitizer in normal tissue (existing in the form of the anion) will be photooxidized much faster than that in tumor tissue (existing in the form of the neutral molecule). Therefore, the relative amount of HA in tumor tissue will increase substantially during photobleaching. Thus the administration of low HA concentrations and high light exposure may be advantageous in order to reduce the damaging effects of the treatment to normal tissue and to eliminate residual photosensitivity and phototoxicity that result from the use of hematoporphyrin derivatives.

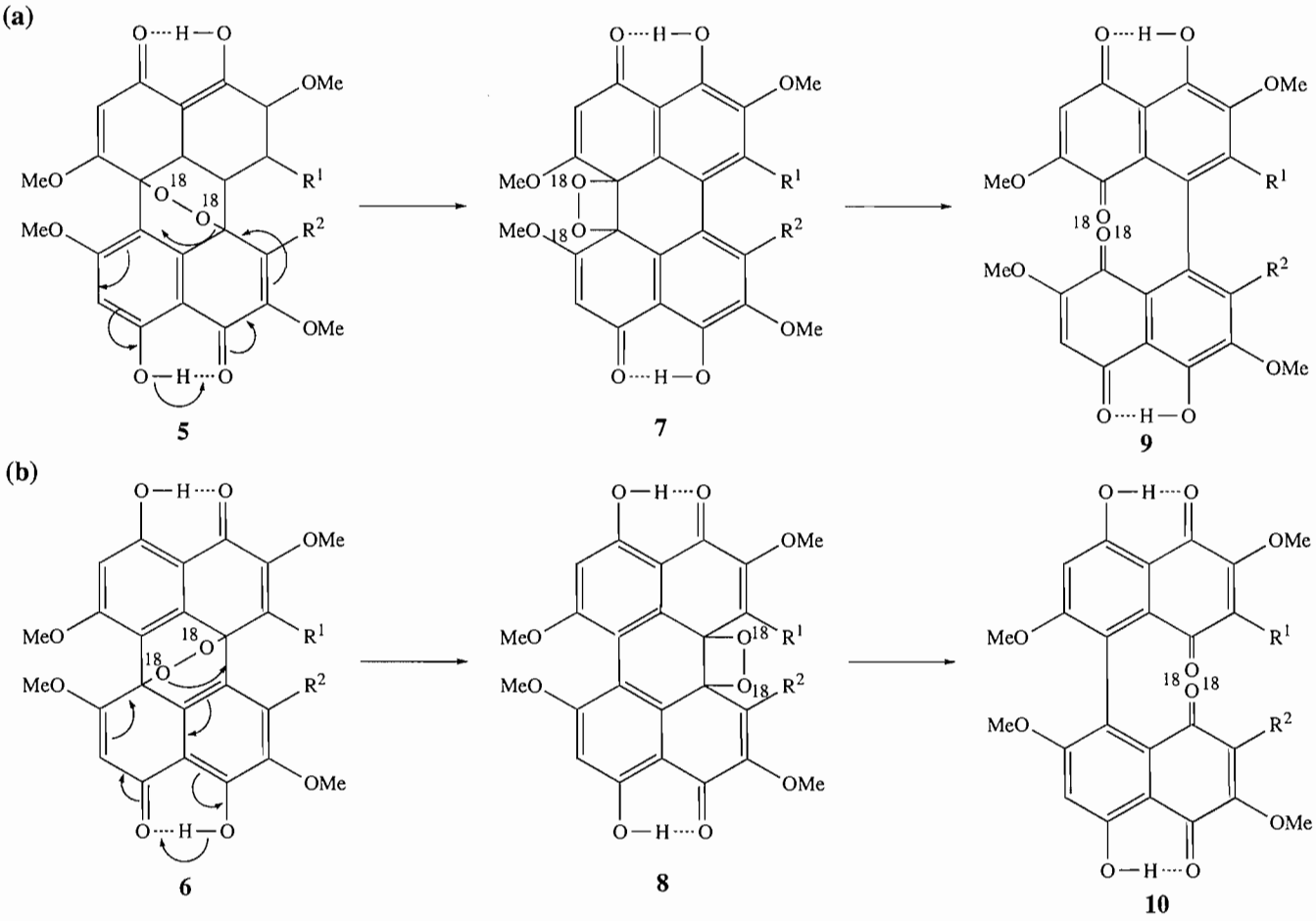
Preparation and photodynamic properties of amino-substituted hypocrellin derivatives

We have shown that PQs are a new class of efficient singlet oxygen ($^1O_2$) generators and demonstrate some advantages over the established $^1O_2$ sensitizers (such as porphyrins, rose bengal, and methylene blue, etc.). These advantages include wide UV–VIS absorption, high quantum yield of $^1O_2$ generation, high stability, good solubility, and small solvent and concentration effects (63, 84). More significantly PQs have been proven to be potential sensitizers for the PDT of tumors, quite

© 1997 NRC Canada

Can. J. Chem. Downloaded from www.nrcresearchpress.com by 92.62.229.171 on 09/08/12
For personal use only.

Fig. 9. Mechanistic elucidation using ^{18}O labelling of the photooxidation of hypocrellin A to an inactive bis-naphthoquinone.



different in properties from the existing PDT porphyrins and phthalocyanines (3, 11, 39, 40, 85, 86).

Preliminary data have demonstrated that some PQs exert a much stronger photodynamic action on EMT6/Ed tumor cells than photofrin-II (39, 40, 70, 85). Hypocrellins, representative of PDT applications of PQs, exhibit several advantages over the presently used HPD, i.e., ready preparation and easy purification relative to HPD (58), low aggregation tendency (which decreases PDT efficiency in the case of HPD) (37), high triplet quantum yield (84), strong red light absorptivity, and significantly reduced normal tissue photosensitivity because of their rapid metabolism in vivo (39, 40, 85, 86).

Nevertheless, as in the case of HPD, natural PQs themselves do not exhibit absorptivity longer than 600 nm sufficiently strong for PDT, and this limits their PDT applications at present. Accordingly we prepared certain amino-substituted hypocrellin B derivatives (AHBDs), which demonstrate significantly enhanced red absorptivities and strong $^1O_2$-generating properties. These attributes are necessary for improved PDT performance (3, 11, 69). The photophysical and photochemical properties of the amino-substituted hypocrellin B derivatives were investigated, and their significantly enhanced red absorptivities and strong $^1O_2$-generating functions qualify them as promising photodynamic therapeutic agents. In addition, the superoxide anion radical was also determined to be implicated in the photosensitization of the amino-substituted hypocrellin B derivatives.

As discussed above, the new AHBDs have demonstrated several photodynamic therapeutic advantages over the commonly used HPD, especially their significantly enhanced red absorptivities and strong $^1O_2$-generating functions (Tables 1, 2), which qualify them as potential photodynamic therapeutic agents (Fig. 10). These in vitro studies have been corroborated by recent in vivo experiments in which complete eradication of implanted EMT6/Ed tumor in mice has been achieved employing HBEA-Ra (Fig. 11). The photosensitizations of AHBDs are primarily mediated by $^1O_2$, but the supplemental roles of other reactive oxygen species such as $O_2^{\cdot-}$, hydroxy radical, and hydrogen peroxide also need to be considered and further investigated.

Photodynamic action of perylenequinone derivatives

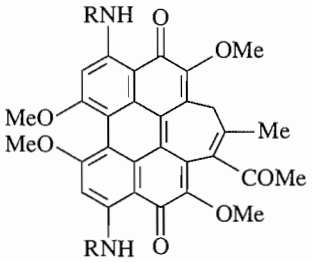
Perylenequinones as photosensitizers — molecular level studies

Comparative studies have shown that the 3,10-dihydroxy-4,9-perylenequinone moiety is essential for the photodynamic action of the perylenequinonoid pigments (86). This explains why amphicercosporin, neocercosporin, and protocercosporin

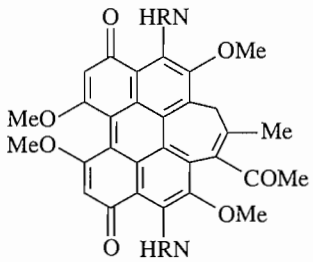
© 1997 NRC Canada

Can. J. Chem. Downloaded from www.nrcresearchpress.com by 92.62.229.171 on 09/08/12
For personal use only.

Table 1. Photodynamic properties of amino-substituted hypocrellin derivatives.



Compounds 2A–9A



Compounds 2B–9B

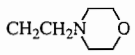
Compound	R	Quantum yield
2	Me	0.80
3	CH_2CH_2OH	0.70
4	$CH_2CH_2CH_2Me$	0.60
5	$CH_2CH_2N(Et)_2$	0.36
6	$CH_2CH_2CH_2N(Me)_2$	0.42
7	$CH_2CH_2NHCH_2CH_2OH$	0.72
8	$CH_2CH_2OCH_2CH_2OH$	0.67
9		0.70

Table 2.

(*a*) Photophysical properties.

Compound	ε_{630} ($\times 10^{-3}$)	$\Phi_{^1O_2}$
HB	1.00	0.74
HBEA-R1	6.23	0.6
HBBA-R2	6.19	0.32
HBDP-R1	4.80	0.42

(*b*) Photosensitizers tested in vitro.

Compound	Photopotentiation (light/dark kill ratio)
Porphyrin	3
HBBA-R2	205–615
HBEA-R1	135
HBDP-R1	15–50

do not exhibit any photodynamic action although cercosporin shows photodynamic action on plant tissues (87).

It has been observed that activated oxygen species are produced by HA-photosensitization, including singlet oxygen ($^1O_2$), superoxide ($O_2^{\cdot-}$), hydroxy radical (·OH), and hydrogen peroxide (H_2O_2) (65, 84, 88, 89). $^1O_2$ is presumed to be generated by energy transfer from the excited triplet HA to ground state oxygen. Similarly $O_2^{\cdot-}$ is thought to be produced when ground state oxygen is reduced by the monovalent anion radical of HA, and H_2O_2 to be formed when ground state oxygen is reduced by its divalent anion. $^1O_2$, $O_2^{\cdot-}$, and H_2O_2 are formed in the primary reaction of the photosensitization by HA, but ·OH is produced only in the presence of some substrates (such as indole, tryptophan, and kynurenine) (84). The addition of reduced compounds (such as indole, lysine, histidine, methionine, tryptophan, 5-hydroxytryptophan, cysteine, hydroquinone, reduced glutathione, and ascorbic acid) markedly enhances the yield of $O_2^{\cdot-}$ by HA-photosensitization, as does cercosporin (68, 84). Zhang et al. (89) have demonstrated that HB can also produce $^1O_2$ and $O_2^{\cdot-}$ upon illumination with visible light like HA.

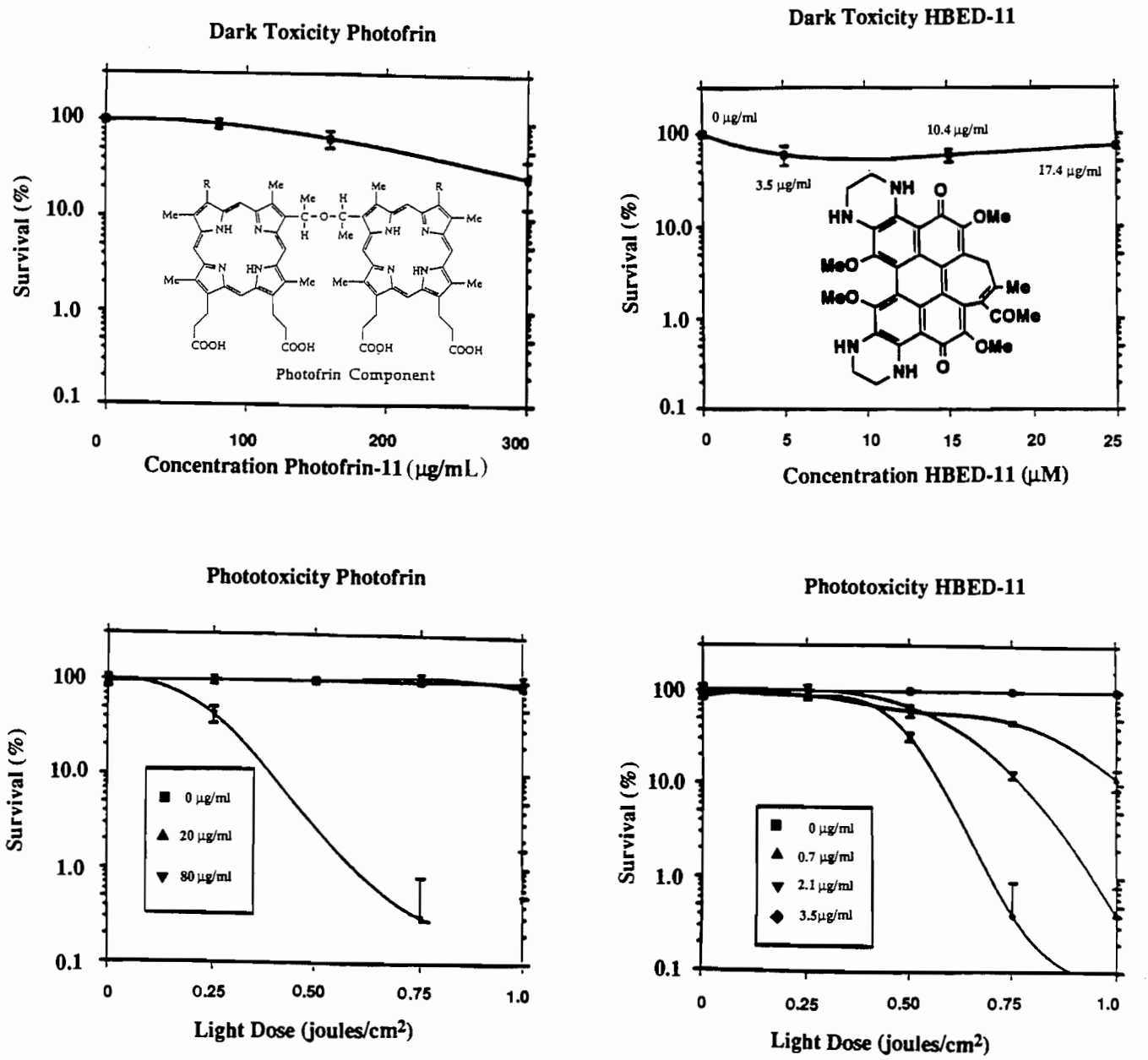
The HA-sensitized photooxidations of tetramethylethylene, 2,5-dimethylfuran, anthracene, 9,10-diphenylanthracene, reduced glutathione, furfuryl alcohol, fatty acids, cholesterol, prostaglandins, and histidine follow a reaction path similar to the photooxidations by other sensitizers, such as rose bengal, eosin, HPD, and methylene blue, i.e., wherein Type II is the main process (84, 88, 90–92). However, the photooxidation of *trans*-stilbene sensitized by HA is different from that sensitized by other sensitizers, and several novel products were isolated and identified (88). HA sensitizes the photooxidations of guanine and thymine in processes that are regarded as involving the participation of $^1O_2$, but does not sensitize those of cytosine and adenine.

Wang et al. (92) observed that HB sensitizes the photooxidation of purine bases. The photooxidations of caffeine and theophylline are mediated by $^1O_2$, and that of tetramethyl uric acid by $O_2^{\cdot-}$. However HB does not photosensitize pyrimidine bases. In micellar solution, visible light can also induce HA to produce $^1O_2$ to oxidize 1,3-diphenylisobenzofuran and bilirubin (93, 94). The HA-sensitized photooxidations of tyrosine, dopa, and aliphatic amines were ascribed to Type I processes (37, 94). In the HA-sensitized photooxidations of indoles, tryptophans, and indole alkaloids, $^1O_2$ appears to play an important role, although Type II processes cannot be excluded as a contributing factor, and some new reactive intermediates and products have been found (37, 86).

© 1997 NRC Canada

Can. J. Chem. Downloaded from www.nrcresearchpress.com by 92.62.229.171 on 09/08/12
For personal use only.

Fig. 10. EMT6 cancer cell survival illustrating the respective dark and light mediated toxicities of Photofrin and a representative aminoperylenequinone derivative HBED-II.



The mechanism of HA-sensitized photooxidation of diphenylamine markedly depends on the solvent; for example, in acetonitrile, the amine was oxidized to *N*-phenyl-*p*-benzoquinone via a Type II reaction, and in methanol via a Type I process (95). The HA-sensitized photooxidation of bilirubin is also affected by solvent. Thus in aprotic solvent, HA photooxidizes biliverdin and the degraded molecules via Type II, and in alkaline protic media by Type I. Thus Type II, and other free radical reactions, may be involved simultaneously (94). The HA-sensitized photooxidation of phenols was considered to proceed via a competition between Type I and Type II reactions.

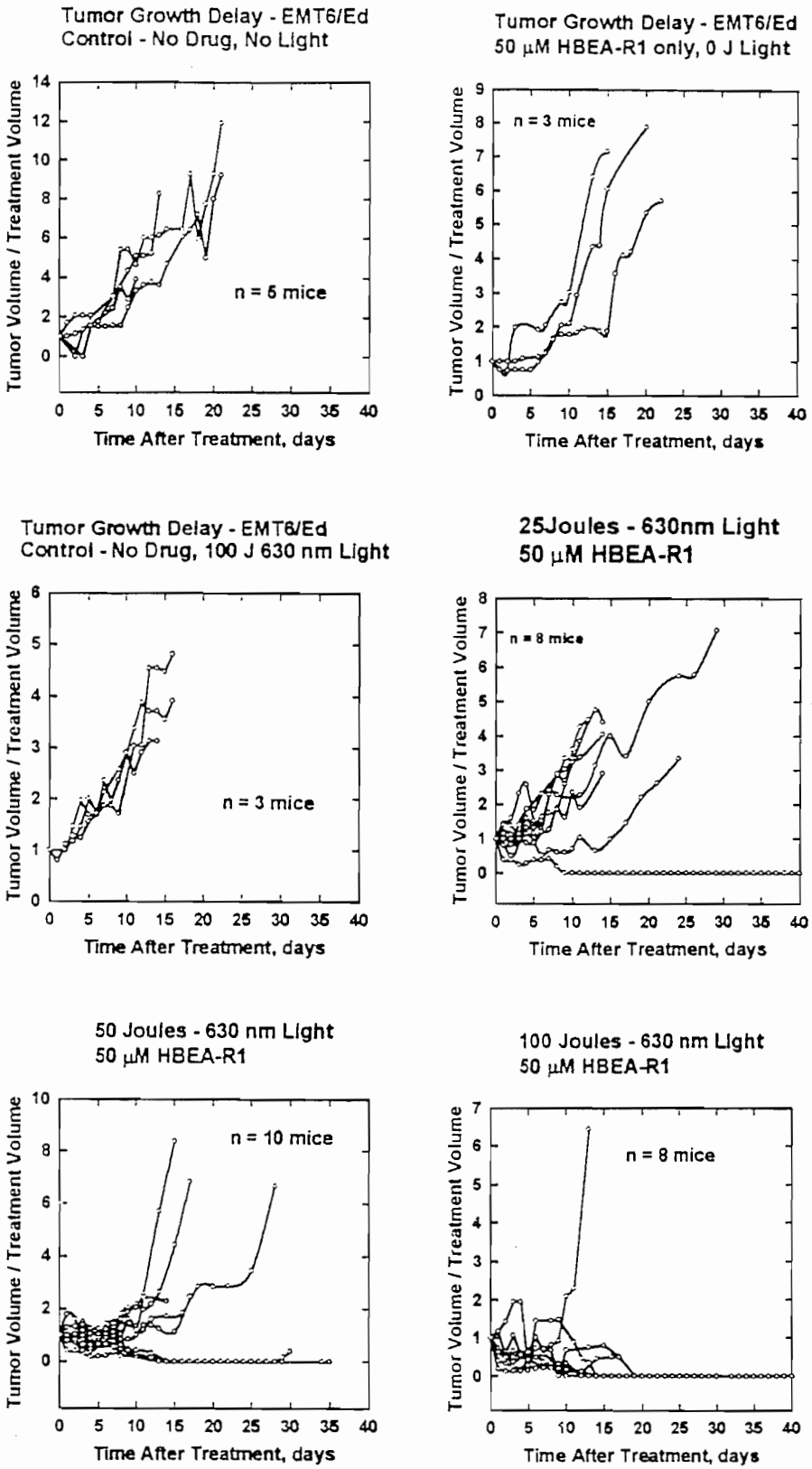
Perylenequinones as photosensitizers for photodynamic therapy: a screening evaluation

Evidence from EMT6/Ed cells in vitro and in rodents suggests that hypocrellins, products of a fungal bamboo parasite, have demonstrable photosensitizing properties, with favorable properties of cytotoxicity and pharmacokinetics. In addition, the hypocrellins are characterized by high quantum yields of singlet oxygen ($^1O_2$), and are amenable to site-directed chemical modification to enhance any of the above properties. The parent hypocrellins A and B share an absorption peak at 648 nm. These molecules may therefore be considered as useful progenitors of derivatives that absorb more strongly in the red,

Can. J. Chem. Downloaded from www.nrcresearchpress.com by 92.62.229.171 on 09/08/12
For personal use only.

© 1997 NRC Canada

Fig. 11. Tumor growth delay under various conditions of HBEA-R1 PDT, of the EMT6/Ed tumor growing in the flanks of Balb/c mice. Transcutaneous illumination (non-hyperthermic).



Can. J. Chem. Downloaded from www.nrcresearchpress.com by 92.62.229.171 on 09/08/12
For personal use only.

© 1997 NRC Canada

Can. J. Chem. Downloaded from www.nrcresearchpress.com by 92.62.229.171 on 09/08/12
For personal use only.

considering that the ideal sensitizer should absorb in the 650–800 nm range, beyond the absorption range of hemoglobin, and where light penetration in tissues is maximized through reduced scattering. A series of pure, monomeric PQ derivatives was tested for properties of cellular uptake, dark cytotoxicity, and photosensitizing potential by clonogenic assay in monolayer cultures of EMT6/Ed cells. Their respective toxicities are compared on a molar basis relative to one another. The in vitro screening assay has, to date, resulted in the selection of four agents for further development as photosensitizers for photodynamic therapy (85). Dose escalation studies are underway in rodents to establish nominal concentrations commensurate with adequate photosensitization of EMT6/Ed tumors grown in the flanks of Balb/c mice, with acceptable systemic toxicity.

Of the 21 hypocrellin derivatives screened to date, all have shown acceptable levels of cytotoxicity in vitro (Table 3). At least seven of the compounds photopotentiate toxicity by a factor of 10, with four of exceptional photopotentiating efficiency (Fig. 12). Direct molar comparison of the hypocrellin concentrations required to effect a given degree of cytotoxicity or photopotentiation with those for Photofrin-II is not possible, since the molecular weight of the photosensitizing component(s) of Photofrin-II can only be estimated. Under the conditions of preincubation employed in this screening study, Photofrin-II appeared to be a poor photosensitizer, possibly due to limited time of penetration and sensitization of the cells. Considering the low molecular weights characteristic of the hypocrellin derivatives, and their predominance as monomeric forms, we did not deem it necessary to adhere to the tradition of longer drug preincubation times characteristic of porphyrins. Preincubation kinetics studies confirm that varying the preincubation time for intervals up to 24 h has no significant effect on the drug concentration required to exert 50% cytotoxicity or photopotentiation of cell death. Preliminary cellular uptake studies using ^{14}C-HB confirm this concept, in that uptake occurs in a linear fashion for the first 10-12 min of incubation, and then plateaus for incubation times at least up to 120 min (85). Detailed uptake kinetic studies for selected photosensitizers were then undertaken (see below).

Perylenequinones as photosensitizers — cell studies

Gram positive bacteria were found to be sensitive to HA-photokilling, but Gram negative bacteria were not (96). This behavior is similar to that of porphyrins but different from that of cercosporin, which inhibits equally the growth of both Gram positive and Gram negative bacteria (97). In the case of elsinochromes, Gram positive bacteria are more sensitive to photosensitization than Gram negative bacteria (97, 98). Yamazaki et al. (97) and Guo et al. (98) have compared the inactivation of Chinese hamster ovary (CHO) cells induced by HA-photosensitization and that by UV exposure, and found that the photodamage caused by HA is greater than that by UV light. The analysis of survival curve parameters showed that the repair of sublethal damage and potential lethal damage of CHO cells induced by HA-photosensitization is less efficient than that induced by UV light. The results suggested that the main target of HA-photosensitization is the cell membrane, in which HA concentrates as a result of its lipophilicity.

Wang and Cheng (99) demonstrated that the binding of HA to erythrocyte membrane and liposomes is greater than to albumin, histone, and DNA. Accordingly, contractile protein bound to membrane is more sensitive to HA-photosensitization than is free contractile protein (100). Several types of membrane damage were found in the erythrocyte membrane treated with HA and light. For example, there was a considerable decrease in the content of some amino acids, especially tryptophan and cysteine, as well as amino and thiol groups in the membrane. Other reactions were observed, including lipid peroxidation, and the cross-linking of proteins, especially contractile protein (such as actin) (100); changes in membrane permeability, membrane mobility, and the configuration of membrane protein, which were thought to be partially related to the chelation of HA with metal ions in membrane (37); K^+ release, as well as photohemolysis and the inactivation of some enzymes (vide infra). The photooxidation of thiol groups and lipid peroxidation induced by HA and light are not inhibited by NaN_3, 1,4-diazabicyclo[2,2,2]octane (DABCO), or superoxide dismutase (SOD), suggesting that neither $^1O_2$ nor $O_2^{\cdot-}$ is involved in the two processes. The cross-linking of membrane proteins caused by HA-photosensitization is partially inhibited by NaN_3, which was considered to be an indication of the participation of $^1O_2$ to this process (101). Furthermore, it was shown, by the specific modification of different groups of membrane proteins, that the HA-sensitized cross-linking of membrane proteins is caused by the condensing reaction of the amino groups in the membrane with the carbonyl group-containing compounds derived from the photooxidations of amino acid residues, in which the photooxidized products of tryptophan and histidine were considered to play a key role (101). Finally, in the HA-photosensitization of erythrocyte membranes, the cross-linking of membrane proteins, photooxidation of the thiol groups and lipid peroxidation were deduced to be independent of one another (102).

As in the case of other perylenequinonoid pigments, HA sensitizes the inactivation of some enzymes. Cheng et al. found that HA sensitizes the inactivation of some enzymes in the following descending order of efficiency: Ca^{2+}–Mg^{2+} ATPase > Na^+–K^+ ATPase > GAPDHase > AcEase. Generally, the enzymes bound to membranes are more sensitive to photosensitization than free enzymes. The inactivation of AcEase was demonstrated to be mediated by $^1O_2$, and the inactivating mechanism of other enzymes is under investigation.

Cao and Cheng (103) made comparative studies between cellular DNA damage in Hela cells by HA-photosensitization and that by γ-ray irradiation, and found that there exists a considerable difference in the content and rate of repair of DNA single strand breaks between the two processes. At equivalent levels of strand breakage, the rate of repair for HA-sensitized strand breaks is smaller than that induced by γ-ray. The HA-sensitized photoconversion of closed circular DNA to open circular DNA was proved by NaN_3 inhibition to be mediated by $^1O_2$ (104).

Uptake kinetics and intracellular localization of hypocrellin by confocal microscopy

The availability of reliable markers for cellular organelles has facilitated detailed analysis of the intracellular distribution of several promising new hypocrellin photosensitizers varying

© 1997 NRC Canada

Can. J. Chem. Downloaded from www.nrcresearchpress.com by 92.62.229.171 on 09/08/12
For personal use only.

Table 3. Physical and chemical properties for hypocrellins of potential use in PDT.

	Name of compound	Chemical formula	F.W.	Abs. peak in red spectral region (nm)	A_{max}/solvent	A_{630}[c]	$\varepsilon_{630} \times 10^3$[c]	$^1O_2$ yield (μM)	LD_{50} dark (μM)	LD_{50} light	Photo-potentiation factor
HA	Hypocrellin A	$C_{30}H_{26}O_{10}$	546	658[a]	0.093/DMF	0.086	0.86	0.84	15	3–5	3–5
HB	Hypocrellin B	$C_{30}H_{24}O_9$	528	658[a]	0.118/DMF	0.100	1.00	0.74	20	1.5–2	10–13
HA-Mg^{2+}	HA-$Mg^{2+}(Ac)_2$	$C_{34}H_{28}O_{12}Mg$	652	616	0.958/EtOH	0.447	4.47	0.71	>25	>5	5
HB-Mg^{2+}	HB-Mg^{2+}	$C_{34}H_{26}O_{11}Mg$	634	622	0.604/EtOH	0.527	5.27	0.53	10	1	10
DAHA-Mg^{2+}	Deacetylated HA-Mg^{2+}	$C_{32}H_{24}O_{10}Mg$	592	622	0.651/EtOH	0.570	5.70	0.51	>25	>5	—
HBAC-1	Cystamine-HB	$C_{32}H_{27}O_8NS$	585	646	0.417/$CHCl_3$	0.388	3.88	0.40	12.5	1	12.5
HBAC-2	Cystamine-HB	$C_{32}H_{27}O_8NS$	585	600	0.337/DMSO	0.244	2.44	0.31	12.5	5	2.5
HBBA-R2	Butylamine HB	$C_{36}H_{60}N_4O_7$	780	616[a]	0.628/$CHCl_3$	0.619	6.19	0.32	>100	0.2–0.6	167–500
HBAM-R1	4-2-(2-Amioethyl)morpholine-HB	$C_{42}H_{48}N_4O_9$	752	658				0.70	>25	4	>6.25
HBDD-R2	2-(*N,N*-Diethylamino)ethylamine-HB	$C_{42}H_{52}N_4O_7$	696	646[a]	0.508/$CHCl_3$	0.055	0.55	0.36	>25	7.5	>3.3
HBDP-R1	2-(*N,N*-Dimethylamino)propylamine-HB	$C_{40}H_{48}N_4O_7$	724	640[a]	0.463/$CHCl_3$	0.480	4.80	0.42	>25	0.5–1.5	>16.6–50
HBEA-R1	Ethanolamine-HB	$C_{34}H_{34}N_2O_9$	614	696[a]	0.625/DMSO	0.623	6.23	0.60	15–25	0.15	100–167
HBEA-R2	Ethanolamine-HB	$C_{34}H_{34}N_2O_9$	614	634[a]	0.162/DMSO	0.127	1.27	0.70	25	7.5	3.3
HBED-R2	Ethylenediamine-HB	$C_{38}H_{32}N_8O_6$	696	614[a]	1.449/DMSO	1.239	12.39	0.50	>25	3–5	5–8.3
HBMA-IV	Methylamine-HB	$C_{30}H_{33}N_3O_6$	696	640	0.246/$CHCl_3$	0.246	2.46	0.80	8.5	1	8.5
DBHB	5,8-Dibromo-HB	$C_{30}H_{23}O_9Br_2$	631	ND	ND	ND	ND	0.62	10	3	3.3
DMHB	Demethylated HB	$C_{28}H_{16}O_9$	686	648[a]	0.469/EtOH	0.477	4.77	0.42	>25	3–5	>5–8.3
JL-1-1		$C_{30}H_{26}O_{12}$	578	594	0.478/$CHCl_3$	0.062	0.62	0.72	>70	2–4	>18.5–35
P-II	Photofrin II®	N/A	N/A	630[b]	ND	ND	ND	ND	160	40–60	2.5–4

[a]Significant light absorption at 700 nm.

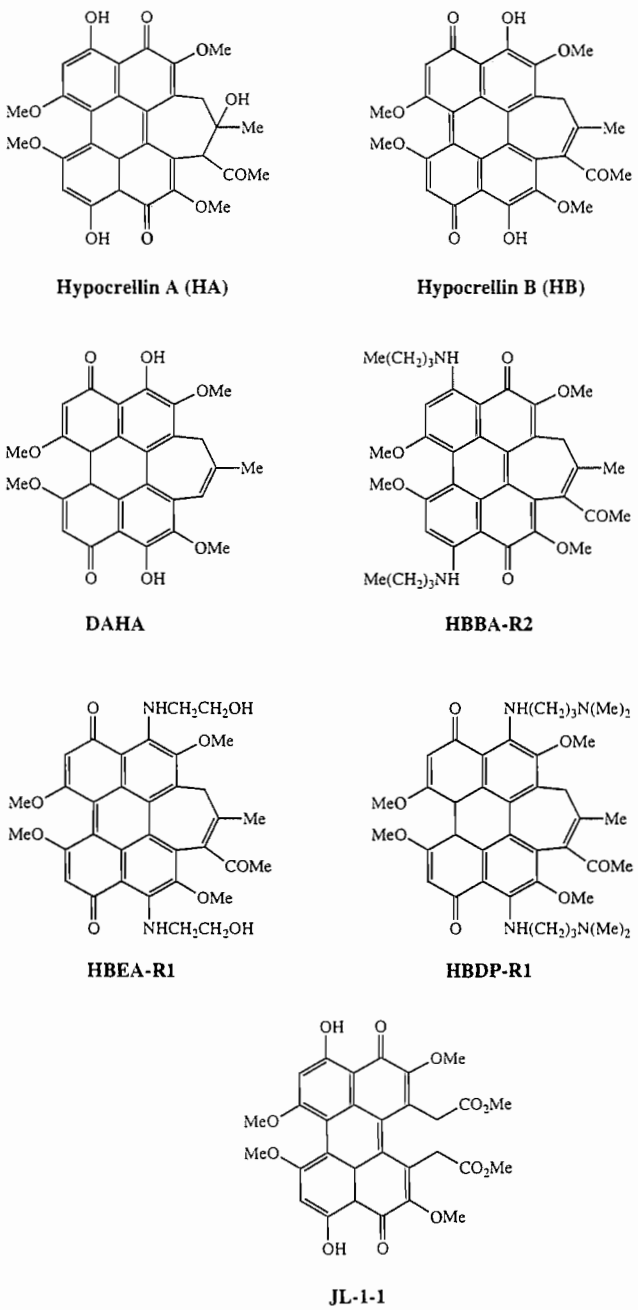
[b]Solvent unknown. HBBA-R2, HBDP-R1, HBEA-R1, and JL-1-1 demonstrate average, or lower than average toxicity, with excellent photopotentiation. N/A = not applicable/ ND, not done. For the purposes of the screening study, the LD_{50} light dose was not fixed. It may be seen in Fig. 4 that, for the compounds tested, this dose is 0.75–1.00 J/cm^2 of 630 nm light.

[c]Absorbance properties are quoted at 630 nm for comparison purposes since this is the wavelength customarily used in clinical PDT protocols.

© 1997 NRC Canada

Can. J. Chem. Downloaded from www.nrcresearchpress.com by 92.62.229.171 on 09/08/12
For personal use only.

Fig. 12. Structures of the parent hypocrellin A and certain photoactive aminoperylenequinones.



with respect to charge and partition coefficient. The close agreement of uptake kinetics using ^{14}C-labelled HB vs. uptake determined by confocal microscopy indicates that the latter technique is a reliable means of determining the fate of fluorescent hypocrellins following administration in vitro and in vivo. The evident advantages of this approach are that it will be possible to estimate the optimal time of photoactivation, based on accumulation of a given sensitizer to its most sensitive intracellular target. Additionally, intratumoral compartmentalization characteristics of each compound are readily visualized, rendering valuable information on the mechanism(s) of tumor destruction. It will be possible to distinguish between likely mechanisms of photodynamic effects, including damage to tumor endothelium leading to stasis of vascular flow; or more direct tumoricidal mechanisms including stromal destruction; or ablation of tumor cell populations — based on patterns of fluorescence observed in histological material. Fluorescent markers for vascular functional patency, such as Hoechst 33342 (105), as well as for cellular hypoxia used in combination with the hypocrellins, will provide further detail on phototoxic mechanisms. It should be pointed out that measurement of sub-cellular drug localization by confocal microscopy is qualitative and may be subject to variations in yield of fluorescence according to the local environment.

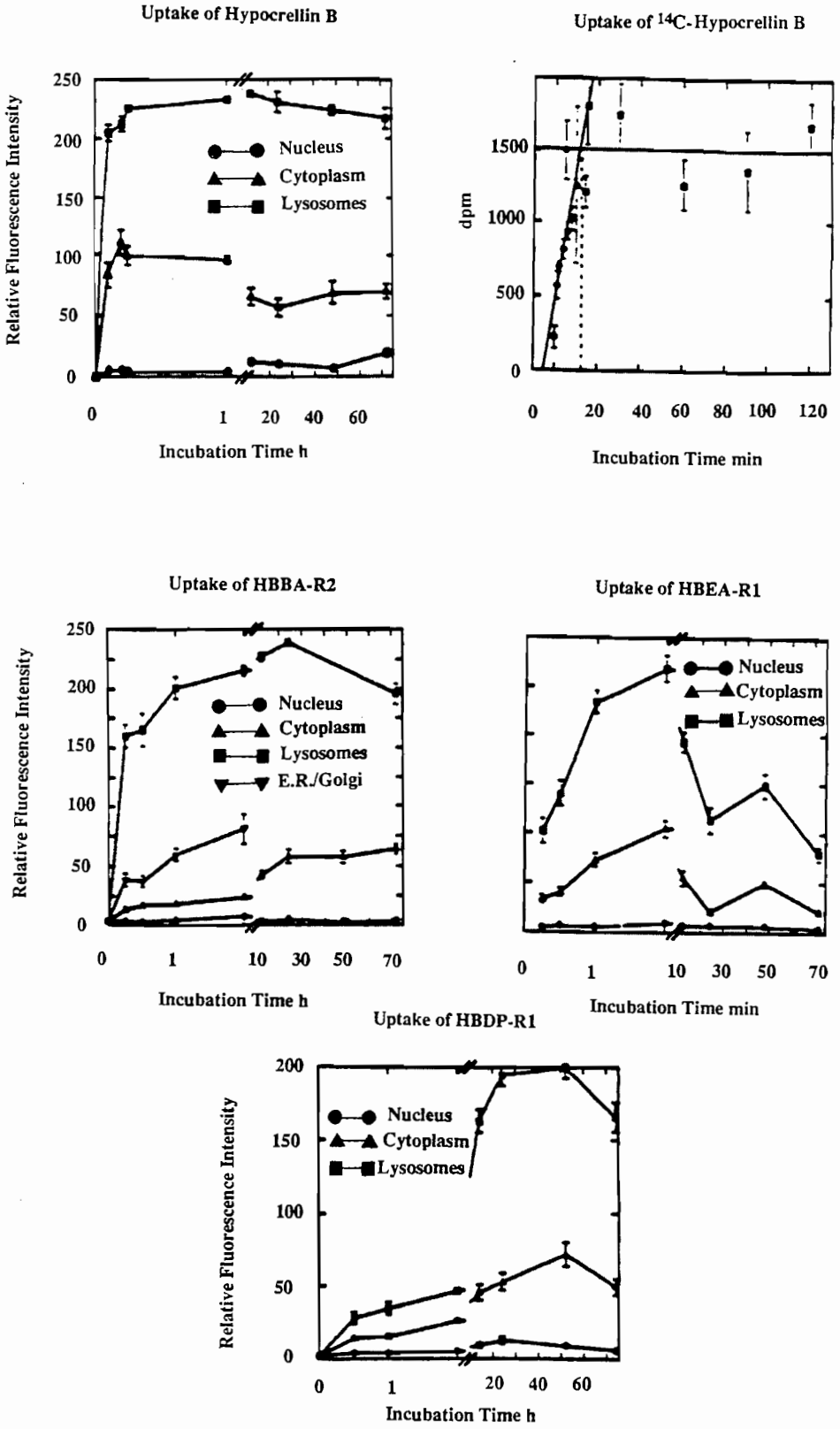
The unique uptake kinetics demonstrated by each hypocrellin may provide a useful avenue of approach to optimize therapeutic ratios among different tumor/adjacent normal tissue combinations encountered clinically. For example, HB is incorporated to the full extent into lysosomes within 15 min. In contrast, lysosomal uptake of HBDP-R1 peaks some 20 h following administration. HBEA-R1 and HBBA-R2 peak in lysosomes at 2 h (Fig. 13). Comprehensive pharmacokinetic studies will be necessary to identify which tumor/normal tissue combinations are most amenable to treatment with a given hypocrellin congener, based on maximal tumor cell uptake vs. minimal uptake in critical targets of surrounding tissues. There are additional possibilities for combined administration of hypocrellins of differing uptake kinetics and fractionated illumination, provided that the first sensitizer does not act via stasis of vascular flow. It will be necessary to determine the relative contributions to phototoxicity of mitochondria, Golgi apparatus, plasma membrane, and endoplasmic reticulum, since it is premature to assume that phototoxicity is predicated uniquely upon the level of uptake. Since only a small number of hypocrellins (selected on the basis of excellent photopotentiation) was analyzed, it is not yet possible to establish general predictive estimates of intracellular distribution based on physicochemical properties. HBBA-R2 and HBEA-R1 (Fig. 11) are cationic congeners, while HB and HBDP-R1 are neutral. Mitochondrial uptake of HBEA-R1 is consistent with its cationic attributes. Each of the four compounds is insoluble in water under neutral conditions (63), which would be consistent with integration into cellular membranes, as well as uptake via the endosomal system, as has been demonstrated (106). Interestingly, a water-soluble, sulfonated derivative of HB did not demonstrate marked photopotentiation of EMT6/Ed cell killing in vitro (data unpublished). It will be useful to examine the intracellular distribution of this, and other, hydrophilic sensitizers to determine why they are generally less effective.

Preferential accumulation of each of the hypocrellins in the lysosomal compartment (106), coupled with their inherently low cytotoxicity and individual uptake kinetics, may render these fluorescent compounds extremely useful agents with which to observe the process of endocytosis in a wide variety of tumor and normal cell types (for review, see ref. 107).

Recent studies have shown that 688 nm light produces phototoxicity equivalent to that of 630 nm light when EMT6/Ed cells are illuminated in the presence of HBEA-R1 or HBBA-R2. Both compounds have been employed in dose-escalation studies in Balb/c mice, with no evidence of toxicity over a 30-

© 1997 NRC Canada

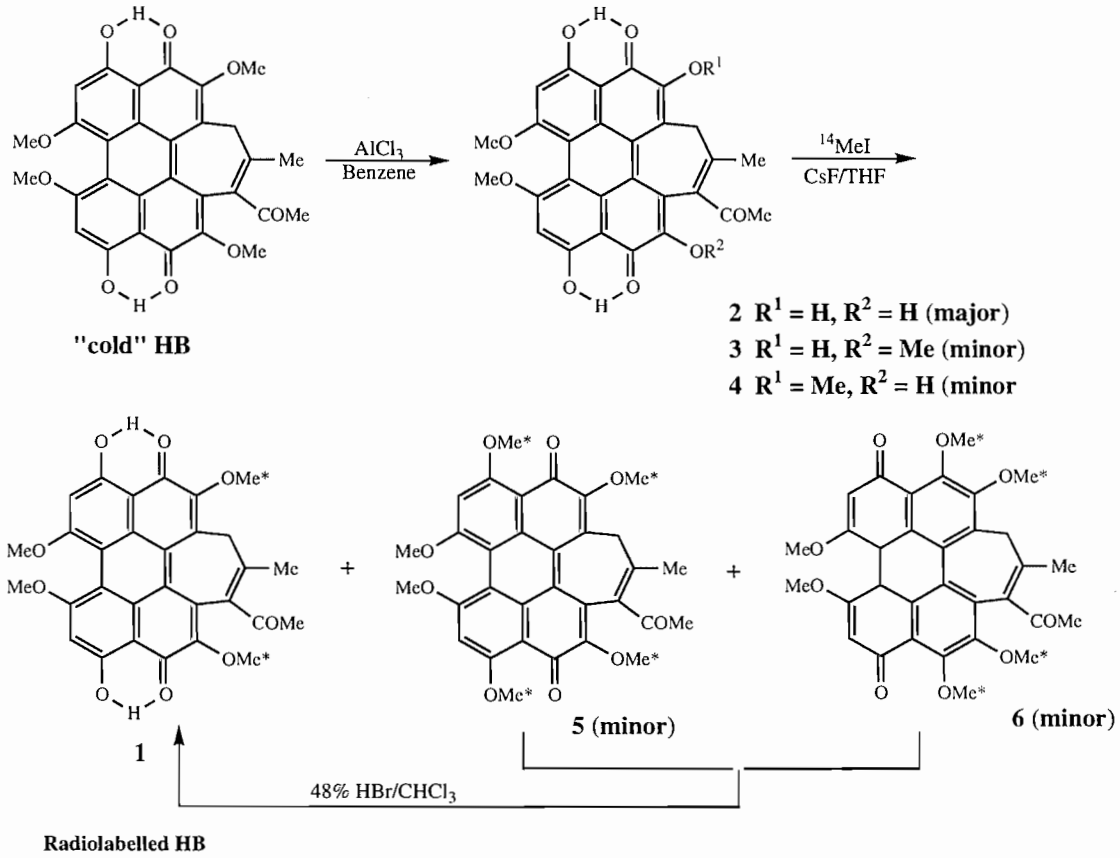
Fig. 13. Cellular uptake and subcellular fractionation of representative perylenequinones.



Can. J. Chem. Downloaded from www.nrcresearchpress.com by 92.62.229.171 on 09/08/12
For personal use only.

© 1997 NRC Canada

Fig. 14. Schematic summary of the synthesis of ^{14}C-radiolabelled hypocrellin B.



Can. J. Chem. Downloaded from www.nrcresearchpress.com by 92.62.229.171 on 09/08/12
For personal use only.

day test period, to maximum "total body" doses of 50 μM. Based on favorable findings related to photopotentiation and pharmacokinetics reported elsewhere, we are proceeding with tumor growth delay assays to establish whether the hypocrellin congeners reported here will have potential for use in the treatment of human tumors.

Synthesis and pharmacokinetics of ^{14}C-radiolabelled hypocrellin B

Radiolabelled hypocrellin B (HB) with the ^{14}C atom incorporated in either or both the 4- and 13-methoxy groups was synthesized with a specific activity of 2.11 mCi per mmol. The purified, ^{14}C-HB, prototype photodynamic therapy photosensitizer was used to determine the kinetics of uptake in EMT6/Ed cells in monolayer culture, and the kinetics of tumor and tissue distribution in Balb/c mice bearing the EMT6/Ed tumor (108).

In vitro cellular uptake studies were performed using EMT6/Ed experimental mammary tumor model. EMT6/Ed mouse mammary carcinoma cells were propagated as monolayer cultures in our laboratory as previously reported (109). Briefly, the cultures were serially passaged in Waymouth's medium containing 13% fetal calf serum (GIBCO) at 37°C, in a water-saturated atmosphere containing 5% CO_2. At 3-month intervals the tumor cells were routinely passaged in the flanks of Balb/c mice to maintain vigor of the tumor cell line.

Cellular uptake of ^{14}C-radiolabelled hypocrellin B

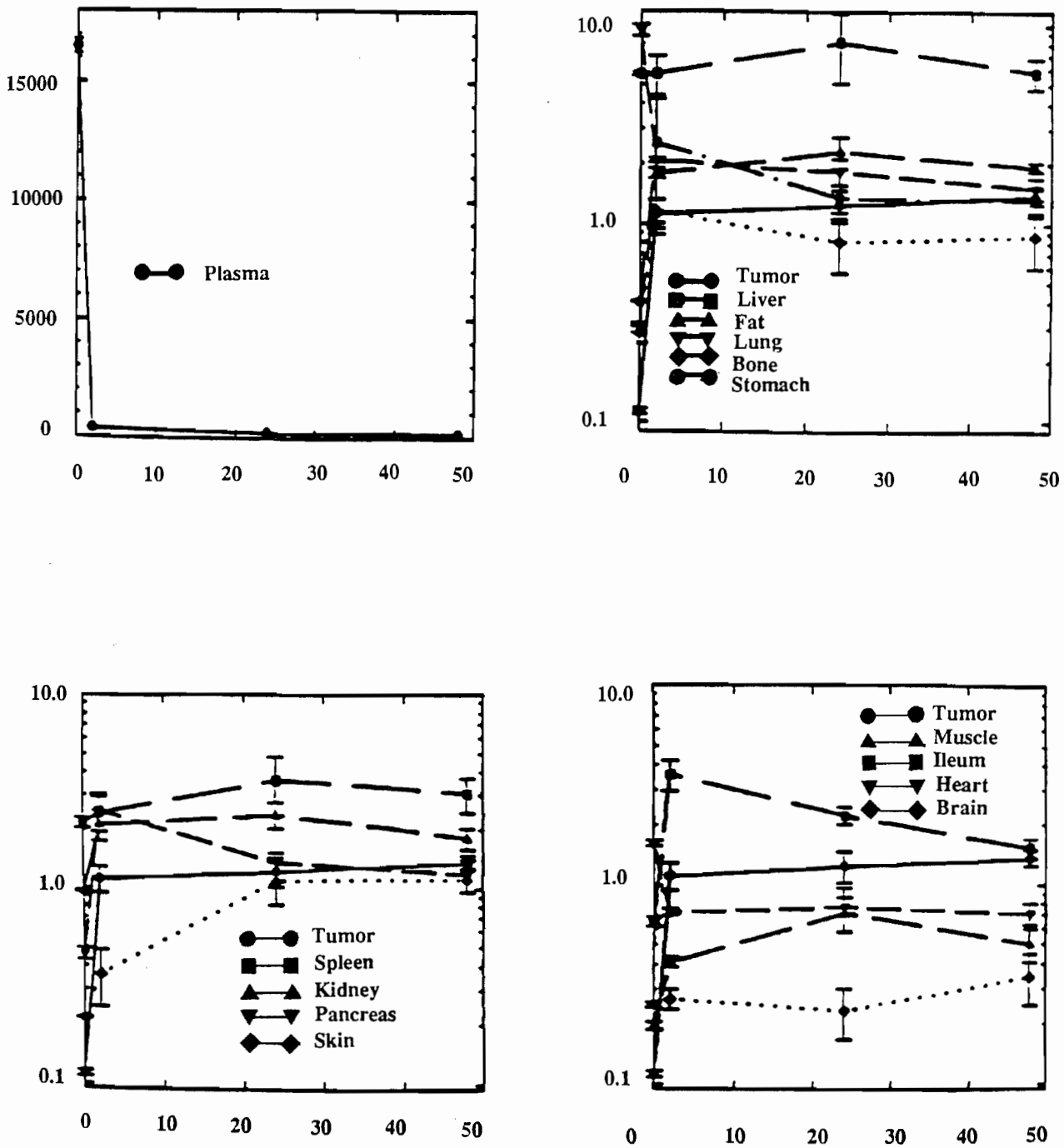
Cellular uptake of ^{14}C-HB (Fig. 14) was determined by plating 5.0×10^5 cells in 2 mL of Waymouth's medium containing 13% fetal calf serum in 35 mm Petri plates and incubating for graded time intervals with ^{14}C-HB at a final concentration of 11.79 μM {$(1.0 \times 10^5$ disintegrations per minute (dpm)}. Free ^{14}C-HB was removed from the plates by three gentle washes with 1.0 mL phosphate-buffered saline (pH 7.4). The cells were quantitatively lysed with 0.2 mL of 1.0 N NaOH and neutralized with an equal volume of 1.0 N HCl. The lysate was transferred to a scintillation vial and 15 mL of CytoScint (ICN) were added for counting. Cellular uptake was standardized to dpm/10^6 cells.

Pharmacokinetics of ^{14}C-radiolabelled hypocrellin B

Tissue and tumor distribution were assessed for 48 h following administration of ^{14}C-HB, in Balb/c mice bearing EMT6/Ed tumors bilaterally on the flanks (Fig. 15). Approximately 7 days before drug administration, 10^5 tumor cells were suspended in 100 μL of Hank's balanced salts solution and injected into each flank of each of 10 mice. When the tumors reached an approximate volume of 250 μL, 14C-HB was administered either intraperitoneally (i.p.), or intravenously in the caudal vein (i.v.) to a final "total body" concentration of HB of 11.79 μM (10^6 dpm). At intervals of 0, 2, 24, and 48 h, the mice were euthanized by i.p. injection of Euthanyl (MTC

© 1997 NRC Canada

Fig. 15. Uptake of ^{14}C-HB in various tissues of Balb/c mice bearing the EMT6/Ed tumor. Ordinate: a. dpm/g plasma; b–d. dpm/g tissue relative to plasma level. Abscissa: Time after administration of the radiolabelled compound, h.



Pharmaceuticals). Samples (10–80 mg) of various tissues and tumor were dissected from the mice, weighed, and placed in glass scintillation vials. Blood samples were centrifuged, and the resulting plasma aliquots were treated the same as tissue samples. For each time point, three animals were used, with two replicate tissue/plasma samples per animal. Tissue uptake was normalized to dpm/g, and the results were expressed as the ratio of tissue to plasma radioactivity.

Perylenequinones as photosensitizers for PDT

Although only preliminary information is available, it is clear that hypocrellin selectively accumulates in some types of tumor tissues, and efficiently sensitizers photodamage in such tissues. Animal experiments have shown that the maximum concentration of HA in tumor tissue is reached at the sixth hour after injection at which time its strongest PDT effect is evident. It was reported that Hela cells and implanted S-180

© 1997 NRC Canada

Can. J. Chem. Downloaded from www.nrcresearchpress.com by 92.62.229.171 on 09/08/12
For personal use only.

tumors in Kuming mice treated with 50 mg/kg HA undergo necrosis after irradiation with 200 J/cm^2 of 632 nm He–Ne laser (39). The mitochondria and microsomes of hepatoma cells were considered to be the targets of HA-photosensitization. With a 105 mW/cm^2 high-pressure sodium lamp illuminating hepatoma cells for 10 min in the presence of 25 μg/mL HA, the mitochondrial ATPase and microsomal G-6-Pase are extensively inhibited, but their mitochondrial monoamine oxidases are not affected. The sulfhydryl contents of the cells are significantly reduced, and lipid peroxidation is greatly enhanced (39). Dong et al. (109) observed that HA-photosensitization retards the synthesis of protein, RNA, and DNA in cancer cells. Cercosporin and phleichrome were also shown to cause photodamage of mitochondria and microsomes of mouse liver cells (110).

Although hypocrellin is phototoxic, it is eliminated from the living organism very quickly, i.e., within about 24 h. This greatly decreases its photosensitizing side effect in PDT. In the absence of light, hypocrellin is nontoxic. In fact, hypocrellin has been used for several hundred years as an oral Chinese traditional medicine. The metabolism of hypocrellin is similar to that of cercosporin. These agents distribute throughout the whole body except the central nervous system. In the dark, they are excreted via intraperitoneum → blood → liver → bile → duct → small intestine → feces, but in the presence of light, they are transported by blood, cell, and tissues before elimination, and thus are toxic to bacteria, mice, and plant cells only when illuminated (110, 111). Clearly more studies of the properties of hypocrellins as photosensitizers in vivo need to be carried out.

Conclusions and prospects

Whether for use in treatment, diagnosis, or prevention, an important aspect of drug pharmacology is selectivity, which is the key to chemotherapy. Advantages of photochemotherapy over other chemotherapeutic techniques are (*i*) the ability to control the duration of the reaction by light, e.g., one can "turn the reaction on or off" since no reaction occurs in the absence of light, and (*ii*) the dual selectivity that both the photosensitizer and the actinic light can be preferentially directed to the locations to be treated, so ideally the healthy regions of the system are not affected. So far some promising clinical results have been obtained with HPD. Therefore, the discovery, synthesis, and evaluation of new photosensitizers for the treatment of malignant and infectious disorders continues to be an active area of investigation. Structural modification of the dyes can then be made in order to improve their light absorption, tumor deliverability, and retention. Chemical alterations can also enhance their yields of light-induced reactive oxygen species. These efforts have led to a new generation of photosensitizers, as summarized above.

Since cancer is a large family of diseases with widely different clinical patterns, it is unlikely that a single sensitizer can serve all purposes. For example, in some cases, a highly selective uptake of the sensitizer in the tumor is required, whereas in other cases, the photosensitizing efficiency of the sensitizer may be the crucial factor. Therefore, it is necessary to develop various kinds of photosensitizers to treat various kinds of cancers. In addition, it may be feasible to devise a combination photochemotherapy, utilizing multiple photosensitizers, gaining the benefits of different localization phototoxicity of different photosensitizers.

The available information on the photochemical properties of the perylenequinones, as reviewed above, is encouraging and clearly suggests that PQs and their derivatives have an array of properties that could make them very valuable sensitizers for PDT. They are readily obtained, easily purified, very stable, low in toxicity, and do not form the aggregates that would decrease their photodynamic activity as is the case for HPD. In addition, some of these agents can utilize superior tissue-penetrating red light much more efficiently than the HPD presently being used for PDT. Therefore, full-scale studies are indicated for a wide variety of PQs as possible PDT anticancer agents. We may therefore see a rapid expansion of both basic and clinical aspects of research on these unique compounds in the near future.

Acknowledgments

The work described was carried out with a group of outstanding and dedicated students, postdoctoral fellows, and colleagues in the Department of Chemistry, University of Alberta, and in the Department of Surgery, W.W. Cross Cancer Institute, and their names appear on the quoted publications. We thank the National Cancer Institute of Canada for a Terry Fox Program Project, as well as the Alberta Heritage Foundation for Medical Research and the Alberta Cancer Foundation for support.

References

1. G. Jori and C. Perria (*Editors*). Photodynamic therapy of tumor and other diseases. Edizioni Libreria Progetto, Padova. 1985.
2. C.J. Gomer (*Editor*). Photodynamic therapy. Pergamon Press, New York. 1987.
3. C.J. Gomer. Photochem. Photobiol. **54**, 1093 (1991).
4. C.J. Gomer, N. Rucker, A. Ferrario, and S. Wong. Radiat. Res. **120**, 1 (1989).
5. T.J. Dougherty. Semin. Surg. Oncol. **5**, 6 (1989).
6. D. Kessel (*Editor*). Photodynamic therapy of neoplastic disease. Vols. I and II. CRC Press, Boston. 1990.
7. G. Morstyn and A.H. Kaye (*Editors*). Phototherapy of cancer. Harwood Academic Publishers, New York. 1990.
8. C.W. Lin. Cancer Cells, **3**, 437 (1991).
9. G. Jori. Photochem. Photobiol. **52**, 439 (1990).
10. J. Spikes. *In* The science of photobiology. *Edited by* K.C. Smith. Plenum Press, New York. 1989. p. 79.
11. B.W. Henderson and T.J. Dougherty. Photochem. Photobiol. **55**, 145 (1992).
12. J. Amagasa. Photochem. Photobiol. **33**, 947 (1981).
13. K. Weishaupt, C.J. Gomer, and T.J. Dougherty. Cancer Res. **36**, 2326 (1976).
14. T.J. Dougherty. CRC Crit. Rev. Oncol. Hematol. **2**, 83 (1984).
15. C.S. Foote. *In* Light-activated pesticides. *Edited by* J.R. Heitz and K.R. Downum. American Chemical Society, Washington, D.C. 1987. p. 22.
16. C.S. Foote. *In* Reactive oxygen species in chemistry, biology and medicine. *Edited by* A. Quintanilha. Plenum Press, New York. 1988. p. 107.
17. J. Moan. J. Photochem. Photobiol. B: **5**, 521 (1990).
18. B.G. Ranby and J.F. Rabek (*Editors*). Singlet oxygen reactions with compounds and polymers. Wiley–Interscience Publication, Sydney. 1978.

Can. J. Chem. Downloaded from www.nrcresearchpress.com by 92.62.229.171 on 09/08/12
For personal use only.

© 1997 NRC Canada

Can. J. Chem. Downloaded from www.nrcresearchpress.com by 92.62.229.171 on 09/08/12
For personal use only.

19. H.H. Wasserman and R.W. Murray (*Editors*). Organic chemistry, a series of monographs. Vol. 40. Singlet oxygen. Academic Press, New York. 1979.
20. A.A. Frimer (*Editor*). Singlet O_2. Vol. I. Vol. II, part 1. Vol. III, part 2. Vol. IV. CRC Press, Inc. Boca Raton, Fla. 1985.
21. M. Athar, C.A. Elmets, D.R. Bickers, and H. Mukhtar. J. Clin. Invest. **83**, 1137 (1989).
22. Z.J. Diwu and J.W. Lown. J. Photochem. Photobiol. B: **18**, 131 (1993).
23. O. Raab. Z. Biol. **39**, 524 (1900).
24. R. Lipson, E. Baldes, and A. Olson. J. Natl. Cancer Inst. **267**, 1 (1961).
25. H. Gregorie, E. Horder, J. Ward, J.F. Green, T. Richards, H.C. Robertson, and T.B. Stevenson. Ann. Surg. **67**, 820 (1968).
26. D. Kessel and T.J. Dougherty (*Editors*). Porphyrin photosensitization. Plenum Press, New York. 1983.
27. D.R. Doiron and C.J. Gomer (*Editors*). Porphyrin localization and treatment of tumors. Alan R. Liss, New York. 1984.
28. A. Andreoni and R. Cubeddu (*Editors*). Porphyrins in tumor phototherapy. Plenum Press, New York. 1984.
29. D. Kessel. Photochem. Photobiol. **39**, 851 (1984).
30. D. Kessel (*Editor*). Methods in porphyrin photosensitization. Plenum Press, New York. 1985.
31. J. Moan. Photochem. Photobiol. **43**, 681 (1986).
32. B.C. Wilson and M.S. Patterson. Phys. Med. Biol. **31**, 327 (1986).
33. C.J. Gomer (*Editor*). New directions in photodynamic therapy. SPIE Press, Bellingham. 1990.
34. C.J. Gomer (*Editor*). Future directions and applications in photodynamic therapy. SPIE Press, Bellingham. 1990.
35. T.J. Dougherty. Photochem. Photobiol. **45**, 879 (1987).
36. U. Weiss, L. Merlini, and G. Nasini. Prog. Chem. Org. Nat. Prod. **52**, 1 (1987).
37. Z.J. Diwu. Ph.D. Thesis. Institute of Chemistry, Academia Sinica, Beijing.
38. Z.J. Diwu and J.W. Lown. Photochem. Photobiol. **52**, 609 (1990).
39. N.W. Fu, Y.X. Chu, L.X. Yuan, J.Y. An, and Z.J. Diwu. Chin. J. Oncol. **10**, 80 (1988).
40. G.G. Miller, K.M. Brown, E.P. Estey, Z.J. Diwu, J.W. Lown, J. Tulip, and M.S. McPhee. *In* Proc. 40th Annu. Meet. Radiat. Res. Soc. Salt Lake City, Utah. 1992. p. 109.
41. H. Nakano, E. Kobayashi, I. Takahashi, K. Ando, M. Yoshida, S. Akinaga, and T. Iida. European Patent Application. EP284358. 1988.
42. D. Meruelo, G. Lavie, and D. Lavie. Proc. Natl. Acad. Sci. U.S.A. **85**, 5230 (1988).
43. D. Meruelo and G. Lavie. PCT International Application. WO 8909055 and WO 8909056. 1989.
44. I. Takahashi, S. Nakanishi, E. Kobayashi, H. Nakano, K. Suzuki, and T. Tamaoki. Biochem. Biophys. Res. Commun. **165**, 1207 (1989).
45. A.P. Fields, D.P. Bednarik, A. Hess, and W.S. May. Nature, **333**, 278 (1988).
46. E. Kobayashi, K. Ando, H. Nakano, T. Tida, H. Ohno, M. Morimoto, and T. Tamaoki. J. Antibiot. **42**, 1470 (1989).
47. H. Wu, X. Lao, Q. Wang, and R. Lu. J. Nat. Prod. **52**, 948 (1989).
48. T. Iida, E. Kobayashi, M. Yoshida, and H. Sano. J. Antibiot. **42**, 1475 (1989).
49. T. Kishi, S. Tahara, N. Taniguchi, M. Tsuda, C. Tanaka, and S. Takahashi. Planta Med. **57**, 376 (1991).
50. G.D. Mei and H.C. Luo. Chin. J. Dermatol. **6**, 434 (1958).
51. A. Calderbank, A.W. Johnson, and A.R. Todd. J. Chem. Soc. 1285 (1954).
52. (*a*) K.H. Weisgraber and U. Weiss. J. Chem. Soc. Perkin Trans. 1, 83 (1972); (*b*) U. Weiss, H.M. Fales, and K.H. Weisgraber. Liebigs Ann. Chem. 914 (1979); H.M. Fales, U. Weiss, and T. Jaouni. Liebigs Ann. Chem. 367 (1983).
53. F. Dallacker and H. Leidig. Chem. Ber. **112**, 2672 (1979).
54. C. Chao and P. Zhang. Tetrahedron Lett. **29**, 225 (1988).
55. R.S. Coleman and E.B. Grant. J. Org. Chem. **56**, 1357 (1991).
56. C.A. Broka. Tetrahedron Lett. **32**, 859 (1991).
57. (*a*) A. Takuwa, I. Hidetoshi, Y. Nishigaichi, and K. Yamanak. Synthesis, 315 (1993); (*b*) F.M. Hauser, D. Sengupta, and S.A. Colert. J. Org. Chem. **59**, 1967 (1994).
58. Z.J. Diwu and J.W. Lown. Tetrahedron, **48**, 45 (1992).
59. D.H.R. Barton. J. Chem. Soc. Perkin Trans. 1, 1473 (1981).
60. R. Ratcliffe and R. Rodehorst. J. Org. Chem. **35**, 4000 (1970).
61. Z.J. Diwu, L.J. Jiang, and M.H. Zhang. Sci. Sin. (B), **32**, 113 (1989).
62. Z.J. Diwu, L.J. Jiang, and M.H. Zhang. Acta Phys. Chem. Sin. **5**, 250 (1989).
63. Z.J. Diwu and J.W. Lown. J. Photochem. Photobiol. A: **64**, 273 (1992).
64. D.C. Dobrowolski and C.S. Foote. Angew. Chem. Int. Ed. Engl. **22**, 720 (1983).
65. Z.Y. Zhang, L.Y. Zang, G.R. Xu, L.B. Tao, and D.H. Wang. Sci. Sin. (B), **32**, 361 (1989).
66. R.J.J.Ch. Lousberg and U. Weiss. J. Chem. Soc. (C), 2152 (1970).
67. Z.J. Diwu and J.W. Lown. J. Photochem. Photobiol. A: **69**, 191 (1992).
68. P.E. Hartman, W.J. Dixon, T.A. Dahl, and M.E. Daub. Photochem. Photobiol. **47**, 699 (1988).
69. Z.J. Diwu and J.W. Lown. Tetrahedron, **48**, 45 (1992).
70. Z.J. Diwu and J.W. Lown. *In* Proc. 1st Bilateral Canada–China Symp. Org. Chem. *Edited by* T. Chen. Banff, Alta. 1992. p. 5.
71. Z.J. Diwu, M.H. Zhang, and L.J. Jiang. Acta Chim. Sin. **47**, 246 (1989).
73. Z.J. Diwu, M.H. Zhang, and L.J. Jiang. Chin. Sci. Bull. (Engl. Ed.), **34**, 401 (1989).
74. J.D. Spikes and R. Livingston. *In* Advances in radiation biology. *Edited by* L.G. Augenstein, R. Mason, and M. Zeele. Academic Press, New York. 1969. p. 29.
75. J.F. Rabek (*Editor*). Experimental methods in photochemistry and photophysics, part 2. John Wiley & Sons, New York. 1982. p. 944.
76. U. Weiss and G. Nasini. Prog. Chem. Org. Nat. Prod. **52**, 1 (1987).
77. W.X. Chen, Y.T. Chen, X.Y. Wan, E. Friedrichs, H. Puff, and E. Breitmainer. Justus Liebigs Ann. Chem. 1880 (1981).
78. M.H. Zhang, J.Y. An, Z.J. Ni, and L.J. Jiang. Kexue Tongbao (Engl. Ed.), **30**, 75 (1985).
79. K.H. Zhao, J.L. Jiang, and X.Y. Sun. Kexue Tongbao, **32**, 1559 (1987).
80. A. Arone, L. Camarda, and G. Nasini. J. Chem. Soc. Perkin Trans. 1, 1387 (1985).
81. A. Arone, G. Assante, T. Caronna, V.D. Modugno, and G. Nasini. Phytochemistry, **27**, 1669 (1988).
82. C.D. Stevens, P.M. Quinlin, M.A. Meinken, and A.M. Kock. Science, **112**, 5461 (1950).
83. D.E.V. Wilman and T.A. Connors. *In* Molecular aspects of anticancer drug action. *Edited by* S. Neidle and M.J. Waring. The Macmillan Press Limited, London. 1983. p. 233.
84. Z.J. Diwu, M.H. Zhang, and L.J. Jiang. *In* Advances in photochemistry. *Edited by* B.W. Zhang, Z.H. Tung, and S.K. Wu. International Academic Publishers, Beijing. 1989. p. 176.
85. E.P. Estey, G.G. Miller, Z.J. Diwu, J. Tulip, J.W. Lown, and M.S. McPhee. Presented at the Alberta cancer board research initiative program annual scientific meeting. Kananaskis, Alta. 1991.
86. Z.J. Diwu and J.W. Lown. Pharmacol. Ther. **63**, 1 (1994).

© 1997 NRC Canada

87. F. Macri and M. Vianello. Plant Cell Environ. **2**, 267 (1979).
88. J.Y. An, M.H. Zhang, G.Y. Wu, J.Y. Liu, G.Z. Ma, and L.J. Jiang. Sci. Sin. (B), 975 (1985).
89. M.H. Zhang, Z.J. Wang, S. Chen, and L.J. Jiang. *In* Advances in photochemistry. *Edited by* B.W. Zhang, C.H. Tung, and S.K. Wu. International Academic Publishers, Beijing. 1989. p. 298.
90. S. Chen. M.H. Zhang, and L.J. Jiang. *In* Advances in photochemistry. *Edited by* B.W. Zhang, C.H. Tung, and S.K. Wu. International Academic Publishers, Beijing. 1989. p. 274.
91. N.H. Wang, J.Y. An, and L.J. Jiang. *In* Advances in photochemistry. *Edited by* B.W. Zhang, C.H. Tung, and S.K. Wu. International Academic Publishers, Beijing. 1989. p. 294.
92. Z.J. Wang, L.J. Jiang, and M.H. Zhang. *In* Advances in photochemistry. *Edited by* B.W. Zhang, C.H. Tung, and S.K. Wu. International Academic Publishers, Beijing. 1989. p. 369.
93. X.F. Jiang and D.Y. Wang. *In* Advances in photochemistry. *Edited by* B.W. Zhang, C.H. Tung, and S.K. Wu. International Academic Publishers, Beijing. 1989. p. 282.
94. J.S. Ma and G.R. Leu. *In* Advances in photochemistry. *Edited by* B.W. Zhang, C.H. Tung, and S.K. Wu. International Academic Publishers, Beijing. 1989. p. 290.
95. J.N. Ma, J.Y. Zhang, and L.J. Jiang. Sci. Sin. (B), **31**, 411 (1988).
96. X.Y. Wan and Y.T. Chen. Kexue Tongbao (Engl. Ed.), **26**, 1040 (1981).
97. S. Yamazaki, A. Okubo, Y. Akiyama, and K. Fuwa. Agric. Biol. Chem. **39**, 287 (1975).
98. S.W. Guo, D.J. Tang, Z.Q. Ye, and Z.M. Liu. Acta Biophys. Sin. **3**, 69 (1987).
99. J.Z. Wang and L.S. Cheng. Acta Biophys. Sin. **3**, 33 (1987).
100. L.S. Cheng and J.Z. Wang. Acta Biol. Exp. Sin. **18**, 89 (1985).
101. J.H. Zheng and L.S. Cheng. Acta Biophys. Sin. **2**, 312 (1986).
102. L.S. Cheng and X. Liu. Acta Biol. Exp. Sin. **20**, 373 (1987).
103. E.H. Cao and L.S. Cheng. Acta Biol. Exp. Sin. **21**, 79 (1988).
104. H.T. Jia, Y.P. Fu, and C.Y. Dong. Chin. J. Biochem. **5**, 335 (1989).
105. D.J. Chaplin, R.E. Durand, and P.L. Olive. Br. J. Cancer, **51**, 569 (1985).
106. G.G. Miller, K. Brown, R.B. Moore, Z. Diwu, J. Liu, L. Huang, J.W. Lown, D.A. Begg, V. Chlumecky, J. Tulip, and M.S. McPhee. Photochem. Photobiol. **61**, 632 (1995).
107. J. Swanson. *In* Methods in cell biology. Vol. 29. Academic Press, Inc., New York. 1991. p. 137.
108. J. Liu, G.G. Miller, L. Huang, Z. Diwu, J.W. Lown, K. Brown, R.B. Moore, J. Tulip, and M.S. McPhee. J. Labelled Compounds Radiopharmaceuticals **36**, 815 (1995).
109. J.D. Chapman, K. Baer, and J. Lee. Cancer Res. **43**, 1523 (1983).
110. C.Y. Dong, H.T. Jia, and C.M. Ma. Chin. J. Biochem. **3**, 468 (1987).
111. F. Macri and M. Vianello. Plant Cell Environ. **2**, 267 (1979).

Can. J. Chem. Downloaded from www.nrcresearchpress.com by 92.62.229.171 on 09/08/12
For personal use only.

© 1997 NRC Canada

Reactions of dialkoxycarbenes with tethered triple bonds to form heterocyclic compounds

Karim Kassam and John Warkentin

Abstract: Dialkoxycarbenes with a tethered triple bond, generated from the corresponding oxadiazolines, undergo an intramolecular cyclization with the tethered alkyne moiety to give 3,3-dialkoxyvinylcarbene/1,3-dipole intermediates. The regioselectivity of the carbene cyclization is highly dependent upon the nature of the alkyne substituent. In the cases where an exocyclic vinylcarbene is generated, the vinylcarbene intermediate can undergo a synthetically useful [3+2] cycloaddition with either an appropriate olefin or an alkyne. This approach allows the rapid construction of some interesting heterocyclic ring systems.

Key words: carbene, dialkoxycarbene, vinylogous dialkoxycarbene, heterocycle.

Résumé : Les dialcoxycarbènes attachés à une triple liaison, générés à partir des oxadiazolines correspondantes, subissent une cyclisation intramoléculaire avec la portion alcyne auxquels ils sont attachés et ils conduisent à des intermédiaires 1,3-dipolaires, 3,3-dialcoxyvinylcarbènes. La régiosélectivité de la cyclisation du carbène dépend fortement de la nature du substituant alcyne. Dans les cas où il y a génération d'un vinylcarbène exocyclique, l'intermédiaire vinylcarbène peut alors subir une cycloaddition [3+2], utile d'un point de vue synthétique, soit avec une oléfine appropriée ou avec un alcyne. Cette approche permet de construire rapidement quelques systèmes hétérocycliques intéressants.

Mots clés : carbène, dialcoxycarbène, dialcoxycarbène vinylogue, hétérocycle.

[Traduit par la rédaction]

Introduction

It was recently demonstrated that oxadiazolines (**1**) are convenient and efficient thermal sources of a variety of interesting dialkoxycarbenes (**2**) (1). Oxadiazolines are easily prepared (1, 2), and are stable at room temperature. However, upon thermolysis at 110°C, in an inert solvent such as benzene or toluene, oxadiazolines yield the corresponding dialkoxycarbenes (Scheme 1). The major by-product, acetone, is easily removed following reaction of the carbene with an appropriate trap. That is one of a number of advantages of oxadiazolines over other well-established thermal dialkoxycarbene sources, such as norbornadienone ketals (3), diazirines (4), and other sources (5).

The potential of oxadiazolines for the efficient formation of ring systems was illustrated with the thermolysis (toluene/reflux) of oxadiazoline **3a**, which gave the tricyclic cyclobutanone ketal **4a** as the major product, in 74% yield (Scheme 2) by a remarkable cascade of reactions (1*d*, 6) (vide infra). This product has five contiguous stereocentres and was obtained as a single (±) diastereomer. The mechanism (1*d*, 7) that accounts for the formation of this tricyclic product comprises up to 10 sequential steps and involves an unprecedented intramolecular cyclization of a dialkoxycarbene (**5a**) onto a tethered triple bond to give a 3,3-dialkoxyvinylcarbene **6a**. The intermediacy of this novel endocyclic 3,3-dialkoxyvinylcarbene (**6a**), formed regioselectively, was of particular interest. There was no evidence for the generation of the alternative exocyclic vinylcarbene **7a**.

In an extensive study, Boger and Brotherton (8) have shown that simple acyclic 3,3-dialkoxyvinylcarbenes, which are isoelectronic with 1,3 dipoles, can be generated from the thermal ring opening of the corresponding cyclopropenone ketals, and have been found to undergo a variety of mechanistically interesting and synthetically useful reactions with a number of different substrates. One reaction of the 3,3-dioxyvinylcarbenes/1,3-dipoles that has considerable synthetic potential is a [3+2] cycloaddition with highly electron-deficient olefins, such as benzylidenemalononitrile, to give substituted cyclopentenes (Scheme 3). In this reaction, unique to this particular class of vinylcarbenes, the 3,3-dialkoxyvinylcarbene behaves formally as a 1,3-dipole. The mechanism for the "Boger cycloaddition" is believed likely to involve a single electron transfer from the electron-rich vinylcarbene to the electron-deficient alkene, followed by a subsequent radical-cation/radical-anion collapse (8*a*). In contrast to most [3+2] cycloadditions, which afford heterocycles (9), this transformation is one of a few known all-carbon [3+2] cycloadditions (10) and may provide a valuable complement to the Diels–Alder reaction. The endocyclic vinylcarbene **6a**, however, is different from the 3,3-dioxyvinylcarbenes studied by Boger in that it cannot undergo a similar [3+2] cycloaddition without forming a highly strained product with a bridgehead double bond.

Herein we report a study of the thermolysis of analogs of oxadiazoline **3a**, having either a methyl or a methoxycarbonyl substituent at the alkyne carbon atom. It was found that the alkyne substituent controlled the regioselectivity of dialkoxy-

Received October 17, 1996.

K. Kassam and J. Warkentin.[1] Department of Chemistry, McMaster University, Hamilton, ON L8S 4M1, Canada.

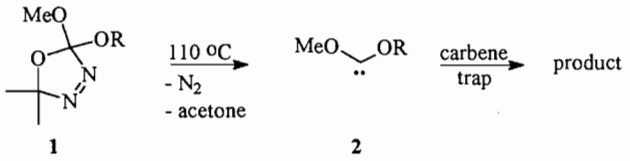
[1] Author to whom correspondence may be addressed. Telephone: (905) 525-9140. Fax: (905) 522-2509. E-mail: warkent@mcmaster.ca

© 1997 NRC Canada

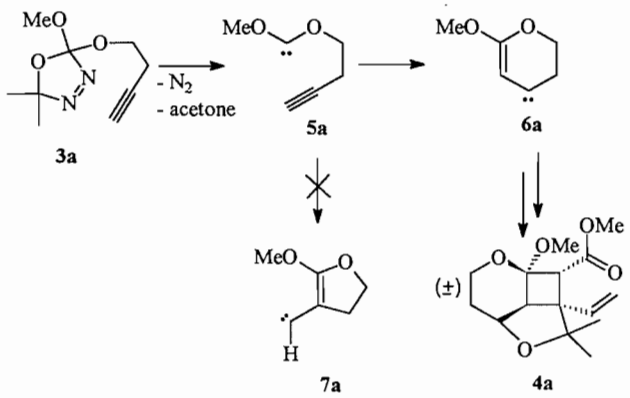
Can. J. Chem. Downloaded from www.nrcresearchpress.com by 92.62.229.171 on 09/08/12
For personal use only.

Can. J. Chem. Downloaded from www.nrcresearchpress.com by 92.62.229.171 on 09/08/12
For personal use only.

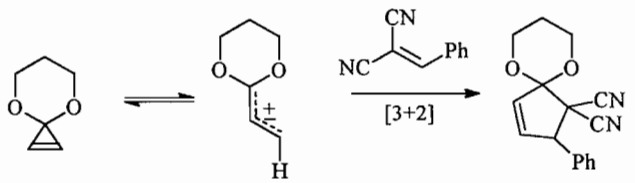
Scheme 1.



Scheme 2.



Scheme 3.

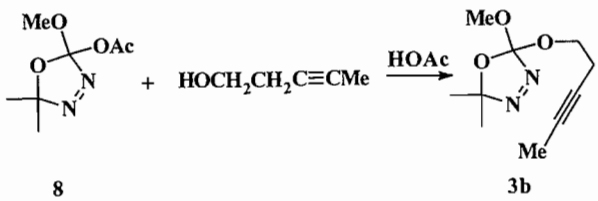


carbene cyclization completely, to allow the generation of either an endocyclic or an exocyclic 3,3-dialkoxyvinylcarbene. Moreover, in the cases where an exocyclic vinylcarbene was formed, it could be intercepted by a [3+2] cycloaddition reaction with an appropriate electron-deficient olefin or alkyne, for the rapid and efficient construction of some new heterocyclic compounds.

Results and discussion

Oxadiazoline **3b** was obtained in 67% yield by acid-catalyzed exchange (2) between the acetoxy methoxy oxadiazoline **8** and commercially available 3-pentyn-1-ol (eq. [1]). It was pre-

[1]

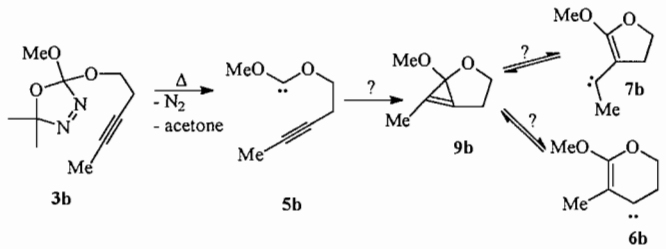


+ HOAc

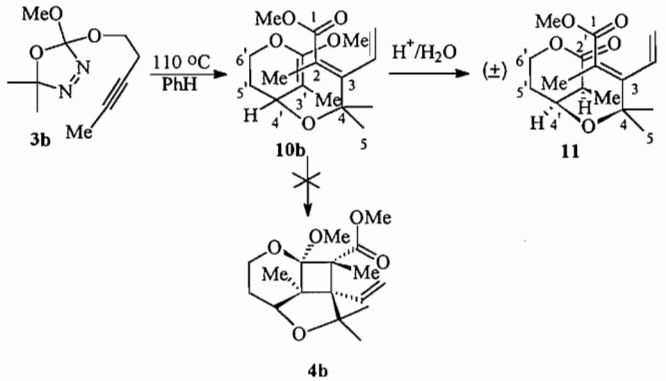
3b was hydrolyzed during attempted purification by the same method.

The product obtained from the thermolysis of **3b** was shown to be **10b**, on the basis of spectroscopic data. As further evidence of the structure, **10b** (a ketene acetal) was hydrolyzed with dilute aqueous acid to give lactone **11**, as a single diastereomer that was isolated as the major product by chromatography. The magnitude of the coupling constant (^3J = 4.3 Hz) between the methine protons on the ring indicates that the hydrolysis had proceeded with π-facial selectivity, by proto-

Scheme 4.



Scheme 5.

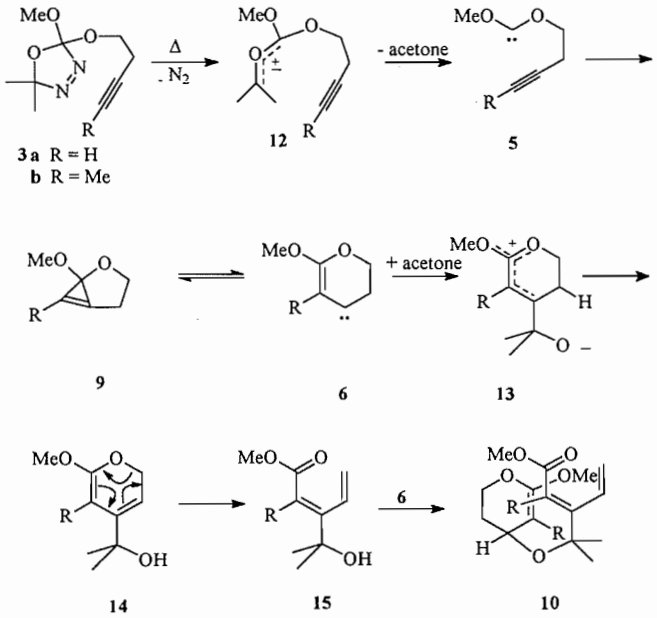


pared in order to check the possibility that **5a**, generated from **3a**, had cyclized regioselectively to the endocyclic vinylcarbene **6a** because of the choice of generating a secondary over a primary carbene site (Scheme 2). It is clear that the cyclization of **5b**, generated from **3b**, gives a secondary 3,3-dialkoxyvinylcarbene (**6b** or **7b**) in either case (Scheme 4). The cyclization could either be a concerted closure, followed by regioselective ring opening of a cyclopropenone ketal intermediate **9b**, as illustrated in Scheme 4, or a direct nucleophilic attack (not shown) of the dialkoxycarbene onto one of the two alkyne carbon atoms to afford **7b** and (or) **6b** directly.

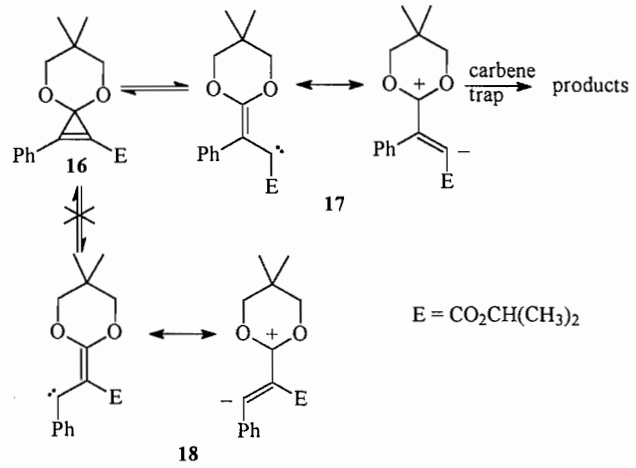
Thermolysis of **3b** in benzene (110°C/sealed tube) afforded a single identifiable product (>80% by NMR) that had the mass of two carbene units and one unit of acetone. Although this product was of the correct composition to be a dimethyl analogue of **4a** (i.e., **4b**) (Scheme 5), its ^{13}C NMR spectrum differed significantly from that of **4a**. Furthermore, **4a** was easily purified by chromatography whereas the product from

© 1997 NRC Canada

Scheme 6.



Scheme 7.



nation of the ketene acetal only on the face *anti* to the unsaturated ester moiety. A molecular mechanics calculation with PC Model gave $^3J(cis)$ = 4.4 Hz, consistent with the assignment of stereochemistry, and $^3J(trans)$ = 10.7 Hz.

Formation of **10b** can be attributed to a mechanism analogous to that proposed for the formation of **4a** (1*d*) with the exception that the final step, an intramolecular thermal [2+2] cycloaddition, does not proceed in this case. As shown in Scheme 6, the mechanism that gives **10b** begins with the thermal generation of dialkoxycarbene **5b** from oxadiazoline **3b** (1), either via fragmentation of an initially formed carbonyl ylide (**12b**) (11, 12) or by the concerted loss of both acetone and nitrogen, as proposed by Smith (7). Once formed, the dialkoxycarbene (**5b**) undergoes an intramolecular cyclization onto the tethered alkyne, either by direct nucleophilic attack of the carbene onto the methyl-substituted alkyne carbon atom, or via regioselective ring opening of a cyclopropenone ketal intermediate (**9b**) to give the endocyclic 3,3-dialkoxyvinylcarbene **6b** (8, 13). The high degree of *endo*-regioselectivity in this step is the same as that observed in the cyclization of **5a** and, therefore, the regioselective formation of **6a** does not seem to be attributable to the choice of a secondary over a primary carbene site. Vinylcarbene **6b** goes on to react with acetone, generated earlier in the decomposition of **3b**, to give **13b**. Dipole **13b**, whether formed directly from the nucleophilic attack of **6b** onto acetone or by other pathways (1*d*), affords **14b** by an intramolecular proton abstraction or by an analogous diradical mechanism. An electrocyclic ring opening (14) of **14b** then gives **15b**. The intermediacy of **15b**, from thermolysis of **3b**, is supported by the fact that **15a** was isolated previously in low yield (approx. 5%) from the thermolysis of **3a** (1*d*).

Since alcohols are highly efficient carbene traps (15), **15b** does not accumulate under the reaction conditions but reacts with **6b** by an overall O-H insertion to give the observed major product, **10b**. Compound **10b** does not undergo an intramolecular thermal [2+2] cycloaddition (16) between the electron-rich ketene acetal and the electron-deficient α,β-unsaturated ester, as observed for **10a**. This result is in agreement with findings of Scheeren's group that disubstituted ketene acetals do not undergo thermal [2+2] cycloadditions with electron-deficient olefins that have only one electron-withdrawing substituent (16*a*). Formation of **10b** (Scheme 6) verifies that **10a** is indeed an intermediate in the thermolysis of **3a** as postulated in our previous paper (1*d*). Moreover, the fact that **10b** was formed in high yield indicates that the cyclization of **5b** proceeds with the same high *endo*-regioselectivity as observed for **5a**.

Nakamura and co-workers (13) have reported that anion stabilizing groups, such as ester or phenylthio, exert control over the regioselectivity of the ring opening of cyclopropenone ketals. For example, the thermal ring opening of cyclopropenone ketal **16** (Scheme 7) proceeds at room temperature to give only the ester-substituted vinylcarbene/1,3-dipole **17** as inferred from various trapping experiments. Products derived from vinylcarbene/1,3-dipole **18** were not found.

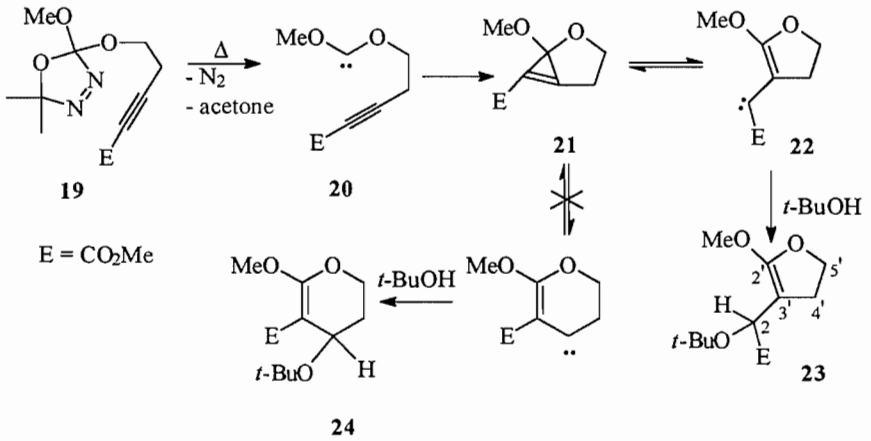
Oxadiazoline **19** was prepared in order to investigate whether the ester functional group could be used to direct the cyclization of dialkoxycarbene **20**, which might involve an intermediate cyclopropenone ketal (**21**), toward the exocyclic vinylcarbene **22** (Scheme 8). Upon thermolysis of oxadiazoline **19** in the presence of *tert*-butyl alcohol at a low concentration (to prevent capture of the initially formed **20**), ketene acetal **23**, derived from the capture of carbene **22**, was obtained in high yield (>85% by ^{1}H NMR spectroscopy). The absence of other carbene + alcohol trapping products (e.g., **24**) detectable by GC–MS clearly implies that carbene **20** had undergone regioselective cyclization to give only the exocyclic vinylcarbene (**22**).

As mentioned previously, Boger et al. (8) demonstrated that 3,3-dialkoxyvinylcarbenes behave as highly efficient 1,3-dipoles in their reactions with benzylidenemalononitrile, and analogous highly electron-deficient olefins, to yield substituted cyclopentenone ketals (Scheme 3). The regioselective formation of the exocyclic vinyl carbene **22** led us to attempt to trap it with an olefin in a [3+2] cycloaddition reaction.

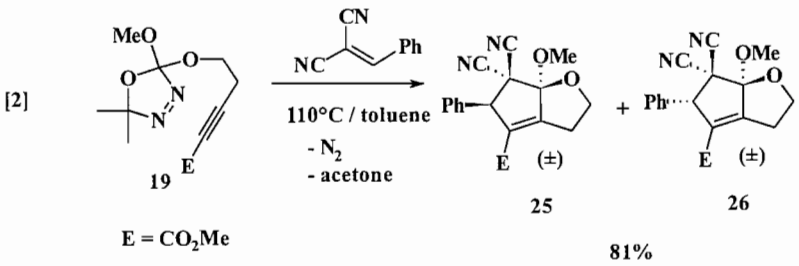
© 1997 NRC Canada

Can. J. Chem. Downloaded from www.nrcresearchpress.com by 92.62.229.171 on 09/08/12
For personal use only.

Scheme 8.



Thermolysis of **19** in the presence of benzylidenemalononitrile at a low concentration (to prevent reaction with the initially formed **20**) led to the clean formation of a diastereomeric mixture of cycloadducts, **25** and **26** (ratio 45:55), which were isolated by chromatography in a combined yield of 81% (eq. [2]). Although separation of the diastereomers by chromatography was not achieved, this tandem sequence, involving an intramolecular carbene cyclization followed by an intermolecular [3+2] cycloaddition, leads rapidly and efficiently to an interesting bicyclic ring system.



Thermolysis of oxadiazoline **19** in the presence of dimethyl acetylenedicarboxylate (DMAD) (low concentration) led to the formation of a bicyclic product (**27**) that was isolated in 30% yield (eq. [3]). Formation of this product is attributed to an initial [3+2] cycloaddition between the intermediate vinylcarbene **22** (Scheme 8) and DMAD, followed by an apparent[2] 1,5-sigmatropic methoxy shift. To the best of our knowledge, this is the first reported example of a 1,5-sigmatropic methoxy shift in a cyclopentadiene ring system, although an analogous chlorine shift is known (17). The ^{1}H NMR spectrum of the crude thermolysis product indicated that **27** was the major product (>80%) of this reaction although it was isolated in only up to 30% yield because of partial decomposition during chromatography. The initial [3+2] cycloadduct could not be detected (<3%) in the crude thermolysis product, indicating that the rearrangement is facile under the reaction conditions (refluxing toluene) and favours the formation of **27** thermodynamically. In contrast to the above result, Boger and Brotherton reported that the thermal generation of a 3,3-dialkoxyvinylcarbene, from the corresponding 3,3-dialkoxycyclopropenone ketal, in the presence of DMAD failed to give a [3+2] adduct (8*c*). The ester substituent may play a role in the successful cycloaddition of **22** with DMAD.

Extension of the alkyne tether by one methylene unit was found not to alter the observed chemistry of the oxadiazoline. Thermolysis of oxadiazoline **28** in the presence of benzylidenemalononitrile (low concentration) led to the clean formation of a diastereomeric mixture of **29** and **30** (46:54 ratio), which were isolated by chromatography in a combined yield of 76% (eq. [4]). In this case the diastereomers were separable by chromatography.

In contrast to the above thermal reaction of **19** with DMAD (eq. [3]), the thermolysis of oxadiazoline **28** in the presence of DMAD (low concentration) gave a mixture of two isomeric heterocycles, **31** and **32**, which were formed in 55:45 ratio as estimated from the ^{1}H NMR spectrum of the crude thermolysis product (eq. [5]). These compounds were separated by chromatography in 36% and 31% yield, respectively.

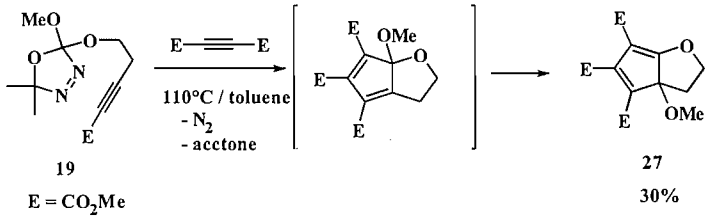
The formation of **31** can be attributed to a [3+2] cycloaddition between the intermediate vinylcarbene and DMAD. Product **32** may be derived from **31** by a thermal 1,5-methoxy shift as seen previously (eq. [3]). Heating a pure sample of either **31**

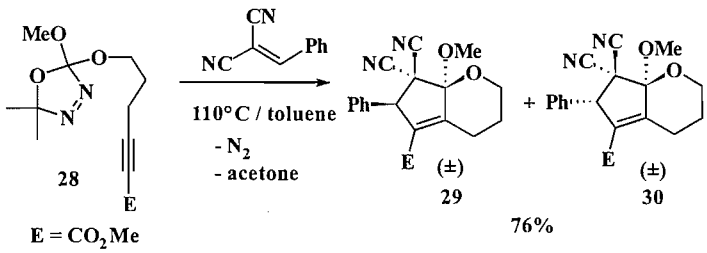
[2] A reviewer pointed out that the same result might be expected from conjugate addition followed by elimination. Although the methanol required for that mechanism was not present initially, the possibility that some was generated from adventitious water has not been excluded.

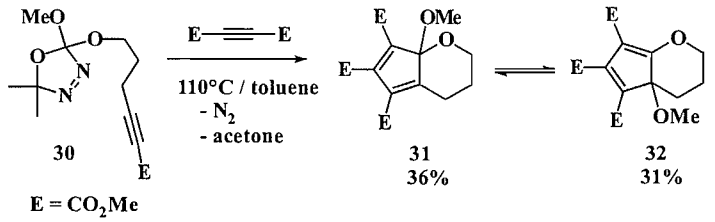
Can. J. Chem. Downloaded from www.nrcresearchpress.com by 92.62.229.171 on 09/08/12
For personal use only.

© 1997 NRC Canada

Can. J. Chem. Downloaded from www.nrcresearchpress.com by 92.62.229.171 on 09/08/12
For personal use only.

[3] 

[4] 

[5] 

or **32** at 110°C for 12 h gave a mixture of **31** and **32** in the same ratio as that observed for the crude thermolysis product, indicating that in this case the 1,5-methoxy shift is an equilibrium process with $K \cong 0.8$ (eq. [5]), and that equilibrium was established during the thermolysis.

Conclusion

As demonstrated first by Boger et al., and then by Nakamura and co-workers, 3,3-dialkoxyvinylcarbenes/1,3-dipoles are interesting and synthetically useful reactive intermediates. Both endocyclic and exocyclic 3,3-dialkoxyvinylcarbenes were generated selectively, in situ, by the intramolecular reaction of a dialkoxycarbene with a tethered triple bond. The regioselectivity of formation of the vinylcarbene is controlled by the alkyne substituent. A consequence of forming an exocyclic 3,3-dialkoxyvinylcarbene/1,3-dipole is efficient [3+2] cycloaddition with an appropriate olefin or alkyne, for the rapid construction of new bicyclic products. We are currently investigating the application of this methodology for the construction of other ring systems.

Experimental

General methods

NMR spectra were recorded on a Bruker AM-500, AC-300, or AC-200 spectrometer. Chemical shifts for ^{1}H NMR spectra were measured with TMS, C_6H_6 (δ = 7.15), or $CHCl_3$ (δ = 7.24) as internal reference, while ^{13}C NMR spectra were referenced to the chloroform-*d* triplet (δ = 77.0) or the benzene-d_6 triplet (δ = 128.0). Mass spectra were recorded on a ZAB-E double-focusing mass spectrometer or on a Hewlett Packard MSD GCMS. FTIR spectra were obtained with a Bio-Rad, FTS-40 instrument. Benzene, toluene, and THF were distilled from sodium benzophenone ketyl and dichloromethane was distilled from calcium hydride. Chromatography solvents (EtOAc, hexanes) were distilled before use. All reactions were carried out under a nitrogen atmosphere.

Preparation of 2-acetoxy-2-methoxy-5,5-dimethyl-Δ^3-1,3,4-oxadiazoline (8) (ref. 2)

To an ice-cooled heterogeneous mixture of lead tetraacetate (162 g, 366 mmol) and acetic acid (2 mL) in CH_2Cl_2 (160 mL) was added a solution of the carbomethoxy hydrazone of acetone (42.0 g, 325 mmol) in CH_2Cl_2 (100 mL). Addition was slow, by means of an addition funnel, and the mixture was stirred with a mechanical stirrer and continuously purged with N_2. Following addition of the hydrazone, the ice-bath was removed and the mixture was allowed to warm slowly to room temperature with continued stirring (ca. 1 h). The mixture was then filtered (Buchner funnel/aspirator), and the filtrate was washed with aqueous (4%) bicarbonate. The organic layer was then collected and the aqueous layer was extracted (2 × 20 mL) with methylene chloride. The combined organic extracts were then dried over anhydrous sodium sulfate. Evaporation of the solvent in vacuo gave a mixture of **8** and a single impurity in a ratio of 75:25; combined yield of 90%. The impurity is an acyclic isomer of the oxadiazoline (2). Purification of the oxadiazoline is possible by slow bulb-to-bulb distillation but separation is not required and the mixture was used in the subsequent reactions.

© 1997 NRC Canada

Can. J. Chem. Downloaded from www.nrcresearchpress.com by 92.62.229.171 on 09/08/12
For personal use only.

2-Acetoxy-2-methoxy-5,5-dimethyl-Δ^3-1,3,4-oxadiazoline (ref. 2): FTIR (NaCl cell, CCl_4) cm^{-1}: 2993, 2951, 2849, 1832, 1771, 1715, 1462, 1443, 1380, 1369, 1260, 1214, 1208, 1180, 1158, 1085, 1061, 1013, 981, 924, 910, 851, 625, 561; ^1H NMR (200 MHz, $CDCl_3$) δ: 1.51 (s, 3H), 1.62 (s, 3H), 2.10 (s, 3H), 3.58 (s, 3H); ^{13}C NMR (50.3 MHz, $CDCl_3$) δ: 19.7, 21.7, 24.2, 52.6, 122.3, 134.0, 166.4; MS (e.i.) *m/z*: 129, 117, 73, 59, 43 (100 %) (mol. ion not observed); MS (c.i., NH_3) *m/z*: 206 $(M+NH_4)^+$, 189 $(M+H)^+$.

Typical procedure for the acetoxy exchange method. Preparation of Δ^3-1,3,4-oxadiazoline (3b)

To the above-mentioned crude 2-acetoxy-2-methoxy-5,5-dimethyl-Δ^3-1,3,4-oxadiazoline (**8**) (0.88 g, 3.5 mmol of oxadiazoline) in CH_2Cl_2 (20 mL) was added 3-pentyn-1-ol (0.30 g, 3.6 mmol) and acetic acid (ca. 1.0 mL). The resulting solution was allowed to stand at room temperature for 48 h. This mixture was concentrated in vacuo and then subjected to chromatography (Chromatotron, 2 mm plate, 10–20% EtOAc–hexanes) to give **3b** as a clear oil in 67% yield (0.50 g, 2.4 mmol). ^1H NMR (200 MHz, $CDCl_3$) δ: 1.47 (s, 3H, CH_3), 1.48 (s, 3H, CH_3), 1.73 (d, ^5J = 2.6 Hz, 3H, alkynyl CH_3), 2.44 (tq, ^3J = 7.3 Hz, ^5J = 2.6 Hz, 2H, CH_2), 3.43 (s, 3H, CH_3O), 3.72 (dt, ^3J = 7.3 Hz, ^2J = 9.5 Hz, 1H, CH_2O), 3.84 (dt, ^3J = 7.3 Hz, ^2J = 9.5 Hz, 1H, CH_2O); ^{13}C NMR (50 MHz, $CDCl_3$) δ: 3.3 (CH_3), 20.0 (CH_3), 23.8 (CH_3), 24.0 (CH_2), 51.7 (CH_3O), 63.2 (CH_2O), 74.9 (*C*≡C), 76.9 (C≡*C*), 119.1 (C5), 136.7 (C2); MS (e.i.) *m/z* (rel. intensity): 129 (20), 125 (8), 111 (48), 67 (100) (mol. ion not observed); MS (c.i., NH_3) *m/z*: 230 $(M+NH_4)^+$.

Thermolysis of 2-methoxy-5,5-dimethyl-2-(3-pentynoxy)-Δ^3-1,3,4-oxadiazoline (3b)

At atmospheric pressure, 40 mL of benzene was distilled from a solution of 2-methoxy-5,5-dimethyl-2-(3-pentynoxy)-Δ^3-1,3,4-oxadiazoline (**3b**, 361 mg, 1.70 mmol) in 80 mL of dry benzene to remove adventitious water by azeotropic distillation. The solution was then sealed into a 100 mL glass tube after degassing at 0.1 Torr (1 Torr = 133.3 Pa) by three freeze–pump–thaw sequences. The tube was kept in an oil bath operating at 110 ± 0.1°C for 20 h before it was cooled and opened. The crude reaction mixture was concentrated in vacuo to yield a yellow oil (258 mg, ca. 49%). Spectroscopy of the residue showed that it consisted primarily (>90%) of methyl (*E*)-3-ethenyl-4-(5,6-dihydro-2-methoxy-3-methyl-2*H*-pyran-4-oxy)-2,4-dimethylpent-2-enoate (**10b**). The spectral data below are those of the crude thermolysis product, which was primarily (>90%) **10b**. ^1H NMR (500 MHz, C_6D_6) δ: 1.14 (s, 3H, CH_3), 1.24 (s, 3H, CH_3), 1.4–1.7 (m, complex, 2H, H5′a and H5′b), 1.83 (s, 3H, CH_3 on C3′), 2.22 (d, ^5J = 1.7 Hz, 3H, CH_3 on C2), 3.35 (s, 3H, OCH_3), 3.42 (s, 3H, OCH_3), 3.82 (m, $^2J_{6'a,6'b}$ = 10.2 Hz, $^3J_{5'a,6'a}$ = 3.7 Hz, $^3J_{5'b,6'a}$ = 3.7 Hz, $^4J_{4',6'a}$ = 1.2 Hz, 1H, H6′a), 3.98 (m, $^3J_{4',5'a}$ = 6.9 Hz, $^3J_{4',5'b}$ = 6.9 Hz, $^3J_{4',6'a}$ = 1.2 Hz, 1H, H4′), 4.04 (m, $^2J_{6'a,6'b}$ = 10.2 Hz, $^3J_{5'a,6'b}$ = 12.5 Hz, $^3J_{5'b,6'b}$ = 2.3 Hz, 1H, H6′b), 4.88 (dd, $^3J_{bx}$ = 10.9 Hz, $^2J_{ab}$ = 2.3 Hz, 1H, Hb), 5.10 (dd, $^3J_{ax}$ = 17.2 Hz, $^2J_{ab}$ = 2.3 Hz, 1H, Ha), 6.25 (m, $^3J_{ax}$ = 17.2 Hz, $^3J_{bx}$ = 10.9 Hz, $^5J_{x,Me}$ = 1.7 Hz, 1H, Hx); ^{13}C NMR (75 MHz, C_6D_6) δ: 13.2 (CH_3), 17.8 (CH_3), 26.6 (CH_3), 27.8 (CH_3), 31.5 (CH_2), 51.1 (OCH_3), 54.9 (OCH_3), 63.6 (C6′), 67.3 (C4′), 76.8 (C4), 83.5 (C3′), 116.9 (CH_2=*C*H), 130.7 (C2), 139.0 (*C*H_2=CH), 146.2 (C2′), 155.5 (C3), 172.0 (C=O); MS (e.i.) *m/z* (rel. intensity): 310 (M^+, 58), 295 ($M^+ - CH_3$, 18), 279 ($M^+ - CH_3O$, 9), 279 ($M^+ - CO_2CH_3$, 37), 168 (82),143 (100); MS (c.i., NH_3) *m/z*: 311 $(M + H)^+$.

Attempts to purify this ketene acetal by chromatography led to its hydrolysis to methyl (*E*)-3-ethenyl-4-(tetrahydro-4*H*-pyran-2-on-4-oxy)-2,4-dimethylpent-2-enoate (**11**) as the major isolated hydrolysis product, in 60–70% yield. ^1H NMR of **11** (500 MHz, C_6D_6) δ: 0.97 (s, 3H, CH_3), 1.05 (s, 3H, CH_3), 1.17 (d, ^3J = 7.0 Hz, 3H, CH_3 on C3′), 1.19–1.26 (m, complex, 1H, H5′), 1.55 (m, ^2J = 14.2, ^3J = 8.5, ^3J = 5.6 Hz, ^3J = 5.6 Hz, 1H, H5′), 2.05 (dq, ^3J = 7.0 Hz, ^3J = 4.3 Hz, 1H, H3′), 2.10 (d, ^5J = 1.7 Hz, 3H, CH_3 on C2), 3.34 (s, 3H, OCH_3), 3.36 (m, complex, 1H, H4′), 3.51 (m, $^2J_{6'a,6'b}$ = 11.5 Hz, $^3J_{5'a,6'a}$ = 5.1 Hz, $^3J_{5'b,6'a}$ = 8.5 Hz, 1H, H6′a), 3.90 (m, $^2J_{6'a,6'b}$ = 11.5 Hz, $^3J_{5'a,6'b}$ = 11.5 Hz, $^3J_{5'b,6'b}$ = 5.8 Hz, 1H, H6′b), 4.88 (dd, $^3J_{bx}$ = 10.9 Hz, $^2J_{ab}$ = 2.2 Hz, 1H, Hb), 5.03 (dd, $^3J_{ax}$ = 17.2 Hz, $^2J_{ab}$ = 2.2 Hz, 1H, Ha), 6.16 (m, $^3J_{ax}$ = 17.2 Hz, $^3J_{bx}$ = 10.9 Hz, $^5J_{x,Me}$ = 1.7 Hz, 1H, Hx). ^{13}C NMR (50 MHz, C_6D_6) δ: 12.9 (CH_3), 17.9 (CH_3), 26.1 (CH_3), 27.3 (CH_3), 29.7 (CH_2), 41.1 (C3′), 51.2 (OCH_3), 64.5 (C6′), 68.8 (C4′), 77.7 (C4), 117.3 (CH_2=*C*H), 131.1 (C2), 138.6 (*C*H_2=CH), 145.0 (C3), 172.0 (C=O), 172.4 (C=O); MS (e.i.) *m/z* (rel. intensity): 296 (M^+, 25), 281 ($M^+ - CH_3$, 5), 265 ($M^+ - CH_3O$, 13), 238 (9), 168 (100); MS (c.i., NH_3) *m/z*: 314 $(M + NH_4)^+$, 297 $(M + H)^+$.

2-(3-Butyn-1-oxy)-2-methoxy-5,5-dimethyl-Δ^3-1,3,4-oxadiazoline (3a) (ref. 2)

Prepared in 86% yield by the acetoxy exchange method (2) (see above) using 3-butyn-1-ol. ^1H NMR (200 MHz, $CDCl_3$) δ: 1.52 (s, 3H), 1.53 (s, 3H), 1.94 (t, ^4J = 2.7 Hz, 1H), 2.49 (dt, ^3J = 7.2 Hz, ^4J = 2.7 Hz, 2H), 3.42 (s, 3H), 3.76 (dt, ^3J = 7.2 Hz, ^2J = 9.3 Hz, 1H), 3.84 (dt, ^3J = 7.2 Hz, ^2J = 9.3 Hz, 1H); ^{13}C NMR (50.3 MHz, $CDCl_3$) δ: 19.9, 24.0, 24.2, 51.9, 62.8, 69.7, 80.4, 119.4, 136.7; MS (e.i.) *m/z* (rel. intensity): 167, 129 (100), 111, 97, 73, 59 (mol. ion not observed); MS (c.i., NH_3) *m/z*: 216 $(M+NH_4)^+$. Combustion analysis, calcd. for $C_9H_{14}N_2O_3$: C 54.52, H 7.12, N 14.14; found: C 54.32, H 7.22, N 13.75.

2-Methoxy-2-(4-methoxycarbonyl-3-butyn-1-oxy)-5,5-dimethyl-Δ^3-1,3,4-oxadiazoline (19)

A stirred solution of 2-(3-butyn-1-oxy)-2-methoxy-5,5-dimethyl-Δ^3-1,3,4-oxadiazoline (0.76 g, 3.9 mmol) in dry THF was cooled at −78°C under nitrogen for 30 min. *n*-Butyllithium in hexanes (1.6 M, 2.4 mL, 3.8 mmol) was then added dropwise. This solution was stirred at −78°C for 1 h before addition of methylchloroformate (0.75 mL, 9.8 mmol). The reaction mixture was allowed to reach room temperature overnight with the cooling bath left in place. Water (25 mL) was then cautiously added and most of the THF was removed from the aqueous solution by rotary evaporation. The aqueous residue was extracted with CH_2Cl_2 (3 × 20 mL) and the combined extracts were dried over anhydrous Na_2SO_4, and then concentrated in vacuo. Chromatography (Chromatotron, 4 mm plate, 10% EtOAc–hexanes) gave **19** as a yellow oil in 76% yield. ^1H NMR (200 MHz, $CDCl_3$) δ: 1.54 (s, 3H, CH_3), 1.56 (s, 3H, CH_3), 2.67 (t, ^3J = 6.9 Hz, 2H, CH_2), 3.43 (s, 3H, CH_3O), 3.75 (s, 3H, CH_3O), 3.88 (dt, ^3J = 6.9 Hz, ^2J = 9.7 Hz, 1H, ^1H of CH_2O), 3.96 (dt, ^3J = 6.9 Hz, ^2J = 9.7 Hz, 1H, ^1H of CH_2O); ^{13}C NMR (50 MHz, $CDCl_3$) δ: 19.9 (CH_3), 23.6 (CH_3), 23.9

© 1997 NRC Canada

Can. J. Chem. Downloaded from www.nrcresearchpress.com by 92.62.229.171 on 09/08/12
For personal use only.

(CH_2), 51.6 (CH_3O), 52.3 (CH_3O), 61.4 (CH_2O), 73.6 (EC≡C), 85.2 (EC≡*C*), 119.3 (C5), 136.4 (C2), 153.5 (C=O); MS (c.i., NH_3) *m/z*: 274 $(M + NH_4)^+$.

Thermolysis of 2-methoxy-2-(4-methoxycarbonyl-3-butyn-1-oxy)-5,5-dimethyl-Δ^3-1,3,4-oxadiazoline (19) in the presence of *tert*-butyl alcohol

At atmospheric pressure, 20 mL of toluene was distilled from a solution of 2-methoxy-2-(4-methoxycarbonyl-3-butyn-1-oxy)-5,5-dimethyl-Δ^3-1,3,4-oxadiazoline (**19**) (119 mg, 0.465 mmol) in 130 mL of dry toluene, to remove adventitious water by azeotropic distillation. *tert*-Butyl alcohol (90 mg, 1.2 mmol) was added and the solution was refluxed under a nitrogen atmosphere for 20 h. Concentration of this solution in vacuo gave an oil. The spectral data of the residue indicated that it was primarily (>80%) methyl 2-*tert*-butoxy-2-(2-methoxy-4,5-dihydro-3-furanyl)-ethanoate (**23**). ^{1}H NMR (500 MHz, C_6D_6) δ: 1.32 (s, 9H, $(CH_3)_3$), 2.85 (m, $^2J_{4'\alpha,4'\beta}$ = 19.4 Hz, $^3J_{4'\alpha,5'\beta}$ = 7.9 Hz, $^3J_{4'\alpha,5'\alpha}$ = 7.9 Hz, $^4J_{2,4'\alpha}$ = 2.9 Hz, 1H, H4′α), 2.99 (m, $^2J_{4'\alpha,4'\beta}$ = 19.4 Hz, $^3J_{4'\beta,5'\beta}$ = 6.1 Hz, $^3J_{4'\beta,5'\alpha}$ = 8.1 Hz, $^4J_{2,4'\beta}$ = 2.8 Hz, 1H, H4′β), 3.09 (s, 3H, OCH_3), 3.36 (s, 3H, OCH_3), 3.61 (m, $^2J_{5'\alpha,5'\beta}$ = 8.0 Hz, $^3J_{4'\alpha,5'\beta}$ = 8.1 Hz, $^3J_{4'\beta,5'\beta}$ = 6.1 Hz, 1H, H5′β), 3.64 (m, $^2J_{5'\alpha,5'\beta}$ = 8.0 Hz, $^3J_{4'\alpha,5'\alpha}$ = 5.8 Hz, $^3J_{4'\beta,5'\alpha}$ = 7.9 Hz, 1H, H5′α), 6.26 (dd, $^4J_{2,4'\beta}$ = 2.8 Hz, $^4J_{2,4'\alpha}$ = 2.9 Hz, 1H, H2); ^{13}C NMR (75 MHz, C_6D_6) δ: 30.2 (+)(C4′), 30.3 (−)($(CH_3)_3$), 49.6 (−)(CH_3O), 50.8 (−)(CH_3O), 64.1 (+)(C5′), 64.2 (+)(*C*$(CH_3)_3$), 76.7 (+)(C3′), 114.0 (−)(C2), 158.9 (+)(C2′), 167.0 (+)(CO).

Typical [3+2] cycloaddition with dimethyl acetylenedicarboxylate (DMAD). Thermolysis of 2-methoxy-2-(4-methoxycarbonyl-3-butyn-1-oxy)-5,5-dimethyl-Δ^3-1,3,4-oxadiazoline (19) in the presence of DMAD

Toluene (20 mL) was distilled from a solution of **19** (180 mg, 0.703 mmol) in dry toluene (180 mL) to remove adventitious water by azeotropic distillation. DMAD (140 mg, 0.986 mmol) was added before the solution was refluxed for 20 h. Following concentration in vacuo the crude thermolysis product was purified by chromatography (Chromatotron, 2 mm plate, 10–20 % EtOAc–hexanes) to give the [3+2] cycloadduct **27** as a yellow oil in 30% yield. ^{1}H NMR (300 MHz, $CDCl_3$) δ: 2.18 (m, ^2J = 13.2 Hz, ^3J = 10.7 Hz, ^3J = 7.7 Hz, 1H, CH_2), 2.50 (m, ^2J = 13.2 Hz, ^3J = 4.1 Hz, ^3J = 0.0 Hz, 1H, CH_2), 3.23 (s, 3H, ether CH_3O), 3.73 (s, 3H, CH_3O), 3.75 (s, 3H, CH_3O), 3.91 (s, 3H, CH_3O), 4.99 (m, ^2J = 8.4 Hz, ^3J = 7.7 Hz, ^3J = 0.0 Hz, 1H, OCH_2), 5.38 (m, ^2J = 8.4 Hz, ^3J = 10.7 Hz, ^3J = 7.7 Hz, ^3J = 4.1 Hz, 1H, OCH_2); ^{13}C NMR (125 MHz, C_6D_6) δ: 34.5 (+)(C3), 51.1 (−)(CH_3O), 51.2 (−)(CH_3O), 51.9 (−)(CH_3O), 52.3 (−)(CH_3O), 86.0 (+)(OCH_2), 91.0 (+) (C4), 101.3 (+), 118.5 (+), 153.3 (+)(3 × vinyl), 161.3 (+)(2 × C=O), 164.5 (+)(C=O), 183.6 (+)(C8). Assignment of C4 was based on a two- and three-bond ^{1}H–^{13}C correlation (HETCOR) NMR experiment that showed correlation of the resonance at 91.0 ppm to the ether OCH_3 hydrogens. In addition, assignment of C8 was based on the fact that the resonance at 183.6 ppm showed a correlation to both C2 and C3 protons. MS (e.i.) *m/z* (rel. intensity): 312 (M^+, 100), 297 ($M^+ - CH_3$, 7), 281 ($M^+ - OCH_3$, 47), 269 (27), 253 ($M^+ - CO_2CH_3$, 59), 221 (55), 84 (100); MS (HR) *m/z*, calcd. for $C_{14}H_{16}O_8$(M^+): 312.0845; found: 312.0844.

Typical [3+2] cycloaddition with benzylidenemalononitrile. Thermolysis of 2-methoxy-2-(4-methoxycarbonyl-3-butyn-1–oxy)-5,5-dimethyl-Δ^3-1,3,4-oxadiazoline (19) in the presence of benzylidenemalononitrile

Toluene (20 mL) was distilled from a solution of **19** (136 mg, 0.531 mmol) and benzylidenemalononitrile (90 mg, 0.58 mmol) in 150 mL of dry toluene to remove adventitious water by azeotropic distillation before the solution was refluxed for 20 h. Following concentration in vacuo the crude thermolysis product was purified by chromatography (Chromatotron, 1 mm plate, 5–15% EtOAc–hexanes) to give the [3+2] cycloadducts **25** and **26** as a 54:46 mixture of diastereomers in 81% combined yield. Chromatographic separation was not achieved. Melting point 140–158°C. ^{1}H NMR of **25** and **26** with approximate integrations based on ca. 1:1 ratio (300 MHz, $CDCl_3$) δ: 2.78–3.09 (m, 2H, allylic CH_2) , 3.22–3.45 (m, 2H, allylic CH_2), 3.50 (s, 3H, CH_3O), 3.54 (s, 3H, CH_3O), 3.67 (s, 3H, CH_3O), 3.76 (s, 3H, CH_3O), 4.45–4.57 (m, 2H, OCH_2), 6.62–4.75 (m, 2H, OCH_2), 5.05 (d, ^5J = 1.8 Hz, 1H, benzylic CH), 5.21 (dd, ^5J = 1.6 Hz, ^5J = 4.7 Hz, 1H, CH), 7.29–7.46 (m, 10H); ^{13}C NMR (50 MHz, $CDCl_3$) δ: 26.4 (2 × CH_2), 48.8 ($C(CN)_2$), 51.1 ($C(CN)_2$), 51.8 (CH_3O), 52.0 (CH_3O), 52.4 (CH_3O), 53.2 (CH_3O), 62.2 (CPh), 64.2 (CPh), 74.2 (CH_2O), 74.5 (CH_2O), 111.0 (OCO), 111.3 (OCO), 111.8 (CN), 114.0 (CN), 114.8 (CN), 116.0 (CN), 126.9, 127.6, 128.2, 128.6, 128.7, 129.1, 129.2 (8 × aryl + 2 C=*C*E), 155.1 (*C*=CE), 155.5 (*C*=CE), 162.9 (C=O), 163.3 (C=O); MS (e.i.) *m/z* (rel. intensity): 324 (M^+, 100), 309 ($M^+ - CH_3$, 3), 293 ($M^+ - OCH_3$, 8), 265 ($M^+ - CO_2CH_3$, 35), 237 (24), 205 (44), 111 (71); MS (HR) *m/z*, calcd. for $C_{18}H_{16}N_2O_4$ (M^+): 324.1110; found: 324.1100.

2-Methoxy-5,5-dimethyl-2-(4-pentyn-1-oxy)-Δ^3-1,3,4-oxadiazoline

Prepared in 78% by the acetoxy exchange method (2) with 4-pentyn-1-ol. ^{1}H NMR (300 MHz, $CDCl_3$) δ: 1.50 (s, 3H, CH_3), 1.51 (s, 3H, CH_3), 1.81 (tt, ^3J = 6.2 Hz, ^3J = 6.9 Hz, 2H, CH_2), 1.91 (t, ^4J = 2.7 Hz, 1H, C≡CH), 2.26 (dt, ^3J = 6.9 Hz, ^4J = 2.7 Hz, 2H, CH_2), 3.42 (s, 3H, CH_3O), 3.74 (dt, ^3J = 6.2 Hz, ^2J = 9.7 Hz, 1H, OCH_2), 3.83 (dt, ^3J = 6.2 Hz, ^2J = 9.7 Hz, 1H, OCH_2); ^{13}C NMR (75 MHz, $CDCl_3$) δ: 15.0, 24.0, 24.1, 28.4, 51.8, 63.0, 68.7, 83.3, 119.1, 136.9; MS (e.i.) *m/z* (rel. intensity): 181 ($M^+ - OCH_3$, 2), 129 ($M^+ - O(CH_2)_3CCH$, 10), (mol. ion not observed); MS (c.i., NH_3) *m/z*: 230 $(M+NH_4)^+$.

2-Methoxy-2-[5-methoxycarbonyl-4-pentyn-1-oxy]-5,5-dimethyl-Δ^3-1,3,4-oxadiazoline (28)

A stirred solution of 2-methoxy-5,5-dimethyl-2-(4-pentyn-1-oxy)-Δ^3-1,3,4-oxadiazoline (1.00 g, 4.72 mmol) in dry THF (50 mL) was cooled at −78°C for 30 min under nitrogen. *n*-Butyllithium in hexanes (1.6 M, 3.3 mL, 5.2 mmol) was then added dropwise. This solution was stirred at −78°C for 1 h before addition of methyl chloroformate (1.0 mL, 12 mmol). The reaction mixture was allowed to reach room temperature overnight with the cooling bath left in place. Water (25 mL) was then added cautiously and most of the THF was evaporated from the aqueous mixture by rotary evaporation. The aqueous residue was extracted with CH_2Cl_2 (3 × 20 mL) and the combined extracts were dried over anhydrous Na_2SO_4 and

© 1997 NRC Canada

Can. J. Chem. Downloaded from www.nrcresearchpress.com by 92.62.229.171 on 09/08/12
For personal use only.

then concentrated in vacuo. Chromatography (Chromatotron, 4 mm plate, 10% EtOAc–hexanes) gave **30** as an oil in 60% yield. ^{1}H NMR (200 MHz, $CDCl_3$) δ: 1.49 (s, 3H, CH_3), 1.50 (s, 3H, CH_3), 1.84 (m, ^3J = 7.2 Hz, ^3J = 6.5 Hz, ^3J = 6.0 Hz, 2H, CH_2), 2.41 (t, ^3J = 7.2 Hz, 2H, CH_2), 3.38 (s, 3H, CH_3O), 3.70 (s, 3H, CH_3O), 3.71 (dt, ^2J = 9.9 Hz, ^3J = 6.5 Hz, 1H, 1H of OCH_2), 3.80 (dt, ^2J = 9.9 Hz, ^3J = 6.0 Hz, 1H, 1H of OCH_2); ^{13}C NMR (50 MHz, $CDCl_3$) δ: 15.4 (CH_2), 23.9 (CH_3), 24.1 (CH_3), 27.6 (CH_2), 51.8 (CH_3O), 52.5 (CH_3O), 62.8 (CH_2O), 73.2 (EC≡C), 88.4 (EC≡*C*), 119.2 (C5), 136.9 (C2), 154.0 (C=O); MS (e.i.) (rel. intensity) *m/z*: 239 ($M^+ - OCH_3$, 3), 169 (5), 239 ($M^+ - O(CH_2)_3C{\equiv}C$-E, 15), 125 (65), 93 (68), 59 (100); MS (c.i., NH_3) *m/z*: 288 $(M + NH_4)^+$.

Thermolysis of 2-methoxy-2-[5-methoxycarbonyl-4-pentyn-1-oxy]-5,5-dimethyl-Δ^3-1,3,4-oxadiazoline (28) in the presence of benzylidenemalononitrile

The typical procedure for [3+2] cycloaddition with benzylidenemalononitrile (above) was followed. Thermolysis of 2-methoxy-2-[5-methoxycarbonyl-4-pentyn-1-oxy]-5,5-dimethyl-Δ^3-1,3,4-oxadiazoline (**28**) (134 mg, 0.496 mmol) in the presence of benzylidenemalononitrile gave **29** and **30** in 55:45 ratio. These products were separated by chromatography (Chromatotron, 2 mm plate, 5–10% EtOAc–hexanes) in a combined yield of 76%. They were distinguished from each other from the magnitudes of the homoallylic coupling constants (^5J) in the ^{1}H NMR spectra (18).

*Data for **29***: FTIR (NaCl) cm^{-1}: 2980–2849, 2250 (CN), 1724, 1456, 1438, 1281, 1252, 1051; ^{1}H NMR (300 MHz, $CDCl_3$) δ: 1.83–1.93 (m, 2H, CH_2), 2.60 (m, ^2J = 15.1 Hz, ^3J = 10.2 Hz, ^3J = 8.0 Hz, ^5J = 2.2 Hz, 1H, allylic CH_2), 3.49 (m, ^2J = 15.1 Hz, ^3J = 3.9 Hz, ^3J = 3.9 Hz, ^4J = 1.7 Hz, 1H, allylic CH_2), 3.53 (s, 3H, CH_3O), 3.62 (s, 3H, CH_3O), 3.86 (m, ^2J = 10.7 Hz, ^3J = 8.5 Hz, ^3J = 6.2 Hz, 1H, OCH_2), 4.09 (m, ^2J = 10.7 Hz, ^3J = 3.2 Hz, ^3J = 3.2 Hz, ^4J = 1.7 Hz, 1H, OCH_2), 4.71 (d, ^5J = 1.7 Hz, 1H, allylic CH), 7.26–7.36 (m, 5H); ^{13}C NMR (50 MHz, $CDCl_3$) δ: 23.2 (CH_2), 25.0 (CH_2), 48.0 ($C(CN)_2$), 50.4 (CH_3O), 52.0 (CH_3O), 58.6 (CPh), 64.7 (CH_2O), 108.8 (OCO), 111.9 (CN), 114.5 (CN), 127.1, 128.7, 129.0, 134.8 (phenyl + C=*C*E), 149.9 (*C*=CE), 163.5 (C=O); MS (e.i.) *m/z* (rel. intensity): 338 (M^+, 70), 323 ($M^+ - CH_3$, 3), 307 ($M^+ - OCH_3$, 22), 279 ($M^+ - CO_2CH_3$, 23), 273 (100), 247 (32), 219 (35), 125 (87); MS (HR) *m/z*, calcd. for $C_{19}H_{18}N_2O_4$ (M^+): 338.1267; found: 338.1265.

*Data for **30***: IR (NaCl) cm^{-1}: 2965–2848, 2250 (CN), 1724, 1456, 1437, 1280, 1255, 1048; ^{1}H NMR (300 MHz, $CDCl_3$) δ: 1.90–2.12 (m, 2H, CH_2), 2.53 (m, ^2J = 13.9 Hz, ^3J = 12.5 Hz, ^3J = 6.0 Hz, ^5J = 3.5 Hz, 1H, allylic CH_2), 3.48 (m, ^2J = 13.9 Hz, ^3J = 6.0 Hz, ^3J = 4.0 Hz, ^4J = 2.0 Hz, 1H, allylic CH_2), 3.56 (s, 3H, CH_3O), 3.65 (s, 3H, CH_3O), 3.94 (m, ^2J = 11.5 Hz, ^3J = 11.7 Hz, ^3J = 3.2 Hz, 1H, OCH_2), 4.11 (m, ^2J = 11.5 Hz, ^3J = 4.8 Hz, ^3J = 1.8 Hz, ^4J = 2.0 Hz, 1H, OCH_2), 4.80 (d, ^5J = 3.5 Hz, 1H, allylic CH), 7.13–7.38 (m, 5H); ^{13}C NMR (50 MHz, $CDCl_3$) δ: 26.8 (2 × CH_2), 50.9 ($C(CN)_2$), 49.3 (CH_3O), 51.8 (CH_3O), 58.2 (CPh), 64.9 (CH_2O), 108.7 (OCO), 111.3 (CN), 113.7 (CN), 126.7, 128.3, 128.9, 129.1 (phenyl + C=*C*E), 150.3 (C=CE), 163.7 (C=O); MS (e.i.) *m/z* (rel. intensity): 338 (M^+, 80), 323 ($M^+ - CH_3$, 5), 307 ($M^+ - OCH_3$, 22), 279 ($M^+ - CO_2CH_3$, 26), 273 (100), 247 (39), 219 (31), 125 (100); MS (HR) *m/z*, calcd. for $C_{19}H_{18}N_2O_4$ (M^+): 338.1267; found: 338.1247.

Thermolysis of 2-methoxy-2-[5-methoxycarbonyl-4-pentyn-1-oxy]-5,5-dimethyl-Δ^3-1,3,4-oxadiazoline (28) in the presence of DMAD

The typical procedure for [3+2] cycloaddition with DMAD (above) was followed. Thermolysis of 2-methoxy-2-[5-methoxycarbonyl-4-pentyn-1-oxy]-5, 5-dimethyl-Δ^3-1,3,4-oxadiazoline (**28**) (133 mg, 0.493 mmol) in the presence of DMAD gave two products **31** and **32** in 53:47 ratio, by ^{1}H NMR. These products, both oils, were isolated by chromatography (Chromatotron, 1 mm plate, 10–20% EtOAc–hexanes) in 36 and 31% yields, respectively. Heating either one of the two isolated isomeric cycloadducts (**31** or **32**) led to a 53:47 mixture of the two.

*Spectral data of **31***: ^{1}H NMR (300 MHz, C_6D_6) δ: 1.16–1.34 (m, 2H, CH_2), 2.06 (m, 1H, allylic CH_2), 3.03 (s, 3H, CH_3O), 3.28 (s, 3H, CH_3O), 3.33 (m, 1H, allylic CH_2), 3.36 (s, 3H, CH_3O), 3.39 (m, 1H, OCH_2), 3.71 (s, 3H, CH_3O), 3.81 (m, 1H, OCH_2); ^{13}C NMR (50 MHz, C_6D_6) δ: 24.9 (CH_2), 28.8 (allylic CH_2), 50.9 (CH_3O), 51.4 (2 × CH_3O), 52.1 (CH_3O), 61.5 (OCH_2), 105.8 (CH_3OCOCH_2), 123.2 (vinyl), 132.3 (vinyl), 147.7 (vinyl), 161.4 (C=O), 162.6 (C=O), 163.1 (C=O), 165.2 (E-C=*C*CH_2); MS (e.i.) *m/z* (rel. intensity): 326 (M^+, 100), 311 ($M^+ - CH_3$, 11), 295 ($M^+ - OCH_3$, 80), 283 (17), 267 ($M^+ - CO_2CH_3$, 82), 235 (50); MS (HR) *m/z*, calcd. for $C_{15}H_{18}O_8$ (M^+): 326.1002; found: 326.1001.

*Spectral data of **32***: ^{1}H NMR (500 MHz, C_6D_6) δ: 1.01 (m, ^2J = 17.4 Hz, ^3J = 6.1, ^3J = 4.7, ^3J = 4.2, 1H, CH_2), 1.26–1.35 (m, 2H, 1H of CH_2 and 1H of homoallylic CH_2), 2.72 (m, ^2J = 15.3 Hz, ^3J = 9.6 Hz, ^3J = 4.7 Hz, 1H of homoallylic CH_2), 2.96 (s, 3H, CH_3O), 3.49 (s, 3H, CH_3O), 3.54 (s, 3H, CH_3O), 3.76 (m, ^2J = 10.5 Hz, ^3J = 6.1 Hz, ^3J = 2.4 Hz, 1H, OCH_2), 4.32 (m, ^2J = 10.5 Hz, ^3J = 11.5 Hz, ^3J = 4.2 Hz, 1H, OCH_2); ^{13}C NMR (50 MHz, C_6D_6) δ: 17.2 (CH_2), 27.1 (CH_2), 51.1 (2 × CH_3O), 52.0 (CH_3O), 52.2 (CH_3O), 68.0 (OCH_2), 83.7 (CH_3OCCH_2), 105.3, 121.7, 150.1 (3 × vinyl), 161.4 (C=O), 161.9 (C=O), 165.5 (C=O), 175.0 (O*C*=C); MS (e.i.) *m/z* (rel. intensity): 326 (M^+, 79), 311 ($M^+ - CH_3$, 11), 295 ($M^+ - OCH_3$, 52), 283 (14), 267 ($M^+ - CO_2CH_3$, 100), 235 (60); MS (HR) *m/z*, calcd. for $C_{15}H_{18}O_8$ (M^+): 326.1002; found: 326.1002.

Acknowledgments

The authors gratefully acknowledge financial support from the Natural Sciences and Engineering Research Council of Canada (NSERC) and the assistance of Drs. Richard Smith and Don Hughes with the mass spectrometry and NMR spectroscopy, respectively.

References

1. (*a*) M. El-Saidi, K. Kassam, D.L. Pole, T. Tadey, and J. Warkentin. J. Am. Chem. Soc. **114**, 8751 (1992); (*b*) L. Isaacs and F. Diederich. Helv. Chim. Acta, **76**, 2454 (1993); (*c*) W.W. Win, M. Kao, M. Eiermann, J.J. McNamara, F. Wudl, D. L. Pole, K. Kassam, and J. Warkentin. J. Org. Chem **59**, 5871 (1994); (*d*) K. Kassam and J. Warkentin. J. Org. Chem. **59**, 5071 (1994); (*e*) D.L. Pole and J. Warkentin. Liebigs Ann. 1907 (1995); (*f*) A. de

© 1997 NRC Canada

Can. J. Chem. Downloaded from www.nrcresearchpress.com by 92.62.229.171 on 09/08/12
For personal use only.

Meijere, S.I. Kozhushkov, D.S. Yufit, R. Boese, T. Haumann, D.L. Pole, P.K. Sharma, and J. Warkentin. Liebigs Ann. 601 (1996); (*g*) D. Suh, D.L. Pole, J. Warkentin, and J.K. Terlouw. Can. J. Chem. **74**, 544 (1996); (*h*) D.L. Pole, P.K. Sharma, and J. Warkentin. Can. J. Chem. **74**, 1335 (1996).

2. K. Kassam, D.L. Pole, M. El-Saidi, and J. Warkentin. J. Am. Chem. Soc. **116**, 1161 (1994).
3. (*a*) R.W. Hoffmann. Angew. Chem. **83**, 595 (1971); (*b*) Angew. Chem. Int. Ed. Engl. **10**, 529 (1971); (*c*) R.W. Hoffmann and H. Häuser. Tetrahedron, **21**, 891 (1965); (*d*). Tetrahedron Lett 197 (1964); (*e*) D.M. Lemal, E.P. Gosselink, and S.D. McGregor. J. Am. Chem. Soc. **88**, 582 (1966).
4. (*a*) R.A. Moss. Acc. Chem. Res. **22**, 15 (1989); (*b*) *In* Chemistry of diazirines. Vol. 1. *Edited by* M.T.H. Liu. CRC Press, Boca Raton, Fla. 1986. p. 99; (*c*) R.A. Moss, M. Włostowski, J. Terpinski, G. Kmiecik-Lawrynowicz, and K. Krogh-Jespersen. J. Am. Chem. Soc. **109**, 3811 (1987); (*d*) R.A. Moss, M. Włostowski, S. Shen, K. Krogh-Jespersen, and A. Matro. J. Am. Chem. Soc. **110**, 444 (1988); (*e*) R.A. Moss, H. Fan, L.M. Hadel, S. Shen, J. Włostowska, M. Włostowski, and K. Krogh-Jespersen. Tetrahedron Lett. **28**, 4779 (1987); (*f*) R.A. Moss, S. Shen, and M. Włostowski. Tetrahedron Lett. **29**, 6417 (1988).
5. (*a*) R.W. Hoffmann, K.K. Steinbach, and W. Lilienblum. Chem. Ber. **109**, 1759 (1976); (*b*) R.A. Moss and D.P. Cox. Tetrahedron Lett. **26**, 1931 (1985); (*c*) R.A. Olofson, S.W. Walinsky, J.P. Marino, and J.L. Jernow. J. Am. Chem. Soc. **90**, 6554 (1968); (*d*) J.W. Scheeren, R.J.F.M. Staps, and R.J.F. Nivard. Recl. Trav. Chim. Pays-Bas, **92**, 11 (1973); (*e*) E.J. Corey and R.A.E. Winter. J. Am. Chem. Soc. **85**, 2677 (1963).
6. J.F. Britten, K. Kassam, and J. Warkentin. Acta Crystallogr. Sect. C: Cryst. Struct. Commun. **C53**, 243 (1997).
7. W.B. Smith. J. Org. Chem. **60**, 7456 (1995).
8. (*a*) D.L. Boger and C.E. Brotherton-Pleiss. Advances in cycloaddition. Vol. 2. *Edited by* D.P Curran. JAI Press, Greenwich, Conn. 1990; p. 147; (*b*) D.L. Boger and R.J. Wysocki, Jr. J. Org. Chem. **53**, 3408 (1988); (*c*) D.L. Boger and C.E. Brotherton. J. Am. Chem. Soc. **108**, 6695 (1986); (*d*) J. Am. Chem. Soc. **108**, 6713 (1986); (*e*) Tetrahedron, **42**, 2777 (1986); (*f*) J. Org. Chem. **50**, 3524 (1985); (*g*) J. Am. Chem. Soc. **106**, 805 (1984); (*h*) Tetrahedron Lett. **25**, 5611 (1984); (*i*) D.L. Boger, C.E. Brotherton, and G.I. Georg. Tetrahedron Lett. **25**, 5615 (1984).
9. (*a*) R. Huisgen. 1,3-Dipolar cycloaddition chemistry. *Edited by* A. Padwa. Wiley–Interscience, New York. 1984; (*b*) S. Yamago and E. Nakamura. J. Am. Chem. Soc. **111**, 7285 (1989); (*c*) J. Org. Chem. **55**, 5553 (1990).
10. J.A. Berson, D.M. McDaniel, and L.R. Corwin. J. Am. Chem. Soc. **94**, 5509 (1972).
11. R.W. Hoffmann and H.J. Luthardt. Tetrahedron Lett. 411 (1966).
12. (*a*) M. Békhazi and J. Warkentin. J. Am. Chem. Soc. **103**, 2473 (1981); (*b*) Can. J. Chem. **61**, 619 (1983); (*c*) M. Békhazi, P.J. Smith, and J. Warkentin. J. Am. Chem. Soc. **62**, 1646 (1982); (*d*) M. Békhazi and J. Warkentin. Can. J. Chem. **60**, 2914 (1982); (*e*) M.W. Majchrzak and J. Warkentin. Can. J. Chem. **67**, 175 (1989); (*f*) Can. J. Chem. **68**, 759 (1990).
13. (*a*) E. Nakamura. J. Synth. Org. Chem. Jpn. **52**, 935 (1995); (*b*) H. Tokuyama, M. Nakamura, and E. Nakamura. Tetrahedron Lett. **34**, 7429 (1993); (*c*) H. Tokuyama, M. Isaka, and E. Nakamura. J. Am. Chem. Soc. **114**, 5523 (1992).
14. E.N. Marvell. Thermal electrocyclic reactions. Academic Press, New York. 1980. p. 305.
15. (*a*) D. Griller, M.T.H. Liu, and J.C. Scaiano. J. Am. Chem. Soc. **104**, 5549 (1982); (*b*) R.A. Moss, S. Shen, and M. Włostowski. Tetrahedron Lett. **29**, 6417 (1988); (*c*) G. Hömberger, W. Kirmse, and R. Lelgemann. Chem. Ber. **124**, 1867 (1991); (*d*) G.B. Bulter, K.H. Herring, P.L. Lewis, V.V. Sharpe III, and R.L. Veazey. J. Org. Chem. **42**, 679 (1977).
16. (*a*) J.W. Scheeren. Recl. Trav. Chim. Pays-Bas, **105**, 71 (1986); (*b*) H.W. Scheeren, A.J.R. van Rossum, and R.J.F. Nivard. Tetrahedron, **39**, 1345 (1983).
17. I.E. Mikhailov, G.A. Dushenko, A.V. Kisin, C. Mugge, A. Zschunke, and V.I. Minkin. Mendeleev Commun. 85 (1994).
18. H. Booth. Prog. Nucl. Magn. Reson. Spectrosc. **5**, 149 (1969).

© 1997 NRC Canada

The oxidation of secondary alcohols by potassium tetraoxoferrate(VI)

Bruce E. Norcross, William C. Lewis, Huifa Gai, Nazih A. Noureldin, and Donald G. Lee

Abstract: The kinetics of the oxidation of 2-propanol, 1,1,1-trifluoro-2-propanol, 1,1,1,3,3,3-hexafluoro-2-propanol, 1-phenyl-2,2,2-trifluoroethanol, 1-(4-methylphenyl)-2,2,2-trifluoroethanol, 1-(3-bromophenyl)-2,2,2-trifluoroethanol, and 1-(3-nitrophenyl)-2,2,2-trifluoroethanol by potassium tetraoxoferrate(VI) have been studied under basic conditions. The products are ketones, formed in almost quantitative yields, iron(III) hydroxide, and dioxygen. The reactions are characterized by substantial enthalpies of activation (40–60 kJ/mol), very unfavorable entropies of activation, large primary deuterium isotope effects, and a positive Hammett ρ value. Both acid and base catalysis are observed. Acid catalysis is attributed to formation of a more reactive oxidant, $HFeO_4^-$, at low pH. Base catalysis is attributed partly to the conversion of the reductants to alkoxide ions at high pH, and partly to the reaction of hydroxide ion with tetraoxoferrate(VI) to give a five-coordinated species, $HOFeO_4^{3-}$, that reacts rapidly with nucleophiles. A reaction mechanism involving formation of an intermediate ferrate ester is proposed.

Key words: oxidation, alcohols, potassium tetraoxoferrate(VI), ferrate esters, base catalysis, acid catalysis.

Résumé : On a étudié, en milieu basique, la cinétique de l'oxydation des 2-propanol, 1,1,1-trifluoro-2-propanol, 1,1,1,3,3,3-hexafluoro-2-propanol, 1-phényl-2,2,2-trifluoroéthanol, 1-(4-méthylphényl)-2,2,2-trifluoroéthanol, 1-(3-bromophényl)-2,2,2-trifluoroéthanol et 1-(3-nitrophényl)-2,2,2-trifluoroéthanol par le tétraoxoferrate(VI) de potassium. Les produits sont des cétones, formées avec des rendements quasi-quantitatifs, le fer(III), l'hydroxyde et l'oxygène O_2. Les réactions sont caractérisées par des enthalpies d'activation substantielles (40–60 kJ/mol), par des entropies d'activation très défavorables, par des effets isotopiques primaires du deutérium assez importants, et par une valeur positive ρ de Hammett. On a observé à la fois la catalyse acide et basique. On attribue à une catalyse acide la formation d'un oxydant plus réactif $HFeO_4^-$ à pH faible. La catalyse basique est attribuée partiellement à la transformation du réducteur en ions alcoolates à fort pH, et partiellement à la réaction de l'ion hydroxyde avec le tétraoxoferrate(VI) pour donner une espèce pentacoordonnée, $HOFeO_4^{3-}$, qui réagit rapidement avec les nucléophiles. On propose un mécanisme réactionnel qui implique la formation d'un ester ferrate intermédiaire.

Mots clés : oxydation, alcools, tétraoxoferrate(VI) de potassium, esters ferrates, catalyse basique, catalyse acide.

[Traduit par la rédaction]

Introduction

Increasing environmental concerns over the possible spread of toxic heavy metals may eventually result in a required decrease in the use of some high-valent transition metal oxides as oxidants in organic synthesis. The response to such a requirement will involve the development of catalytic processes (coupled to dioxygen) that utilize only small amounts of transition metals and (or) the use of nontoxic oxidants. Both of these objectives can potentially be met by the utilization of iron oxides as catalysts or stoichiometric reagents.

Received May 2, 1996.

B.E. Norcross[1] and W.C. Lewis. Department of Chemistry, State University of New York at Binghamton, Binghamton, NY 13902-6000, U.S.A.
H. Gai, N.A. Noureldin, and D.G. Lee.[1] Department of Chemistry, University of Regina, Regina, SK S4S 0A2, Canada.

[1] Authors to whom correspondence may be addressed. (B.E.N.) Telephone: (607) 777-2797. Fax: (607) 777-4478. (D.G.L.) Telephone: (306) 585-4247. Fax: (306) 585-4894. E-mail: dglee@meena.cc.uregina.ca

Iron, because of its widespread occurrence in the environment, and the consequent large tolerance that living systems have to its presence, is considered to be environmentally benign. Whether or not the use of iron as an oxygen carrier in compounds such as hemoglobin and myoglobin (1) is a consequence of evolutionary development in an iron-rich environment remains a question for speculation and possible investigation. However, it is a fact that iron and iron oxides do not present a toxic threat to human life, nor to the lives of most other animals and plants.

Although the use of ferrate has not as yet found wide application in organic synthesis, it has been shown to be a good stoichiometric oxidant, particularly for alcohols. Primary alcohols are converted into aldehydes and secondary alcohols into ketones. The yields are highest for products in which the carbonyl is conjugated to an aromatic ring. For example, benzyl alcohol and its ring-substituted derivatives yield the corresponding benzaldehydes in 80–95% yield (2, 3) and 1-phenylethanol is converted into acetophenone in 90% yield (3). The reported yields for the oxidation of aliphatic alcohols are lower; about 30% for the formation of heptanal from 1-heptanol or cyclohexanone from cyclohexanol (3, 4). A useful selectivity has been observed when carbohydrates are oxi-

© 1997 NRC Canada

Can. J. Chem. Downloaded from www.nrcresearchpress.com by 92.62.229.171 on 09/08/12
For personal use only.

Can. J. Chem. Downloaded from www.nrcresearchpress.com by 92.62.229.171 on 09/08/12
For personal use only.

dized by ferrate; hydroxymethyls are oxidized much more readily than secondary hydroxyls (5, 6).

Amines are also oxidized by ferrate. For example, benzylamine and 1-amino-1-phenylethane are converted into benzaldehyde and acetophenone, respectively, both in 70% yield (3). In addition, it has been reported that sulfides are oxidized to sulfoxides by this reagent, but no yields were reported (7).

Ferrate has also been used as a selective oxidant for allylic and benzylic alcohols in a two-phase water–benzene system containing a phase transfer agent. For example, cinnanyl and benzyl alcohols were converted into the corresponding aldehydes in quantitative yields (8). Ferrate adsorbed on silica gel can also be used as a heterogeneous oxidant (9). The method is particularly effective for the oxidation of secondary aliphatic alcohols that often give low yields under homogeneous conditions.

The catalytic capabilities of iron porphyrins as oxidation catalysts are well known (10) and preliminary work has shown that noncomplexed iron-oxo compounds also have potential use as catalysts for the oxidation of organic compounds (11). Hence, it is important to achieve a better understanding of the chemical properties and potential applications of these reagents in both catalytic and stoichiometric reactions. Therefore, in this paper we wish to describe a kinetic study of the stoichiometric oxidation of alcohols by tetraoxoferrate(VI) (FeO_4^{2-}) under alkaline conditions. Since ferrate(VI) reacts rapidly with water in neutral or acidic solutions to give iron(III) and dioxygen, the study was limited to solutions with a pH of 8 or greater (12–16).

Experimental

Materials

Potassium tetraoxoferrate(VI) was prepared using procedures previously described in the literature (17–19). The purity of various batches of the oxidant, determined by titration with ferrous chloride using diphenylamine as an indicator (20), was found to be 90–99%.

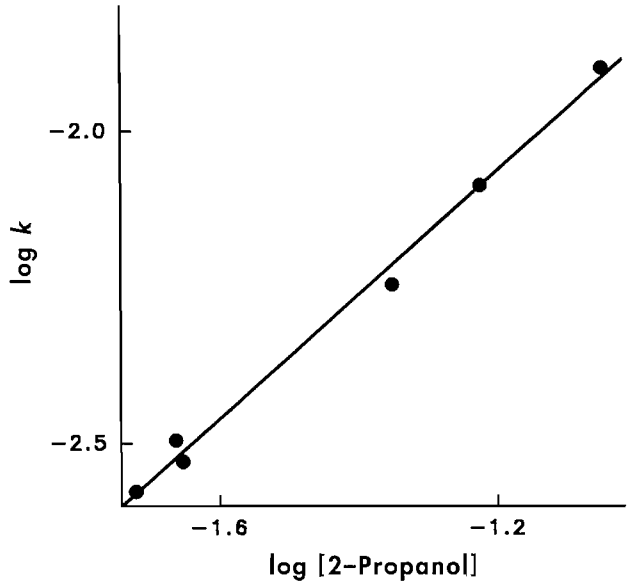
2-Propanol was obtained commercially from Aldrich. 1,1,1-Trifluoro-2-propanol, 1,1,1,3,3,3-hexfluoro-2-propanol, 1-phenyl-2,2,2-trifluoroethanol, and 1-(4-methylphenyl)-2,2,2-trifluoroethanol were prepared by reduction of the corresponding ketones with lithium aluminum hydride and purified by use of gas–liquid chromatography (glc). The physical and spectroscopic properties of the products agreed with those reported in the literature (21–24).

1-(3-Bromophenyl)-2,2,2-trifluoroethanol was also prepared by the reduction of *m*-bromotrifluoroacetophenone with lithium aluminum hydride and purified by glc (10% polypropylene glycol on Chromasorb W, 45–60 mesh, 200°C) to give a liquid product (n_D^{29} = 1.5028; lit. (21) n_D^{27} = 1.5005) that crystallized on standing to give a white solid, mp 27–29°C. The yield obtained in this reaction was 89%.

1-(3-Nitrophenyl)-2,2,2-trifluoroethanol was prepared by the reduction of *m*-nitrotrifluoroacetophenone by potassium borohydride in methanol. A solution of the ketone (10 g, 0.045 mol) was added dropwise to a well-stirred solution of potassium borohydride (2.7 g, 0.05 mol) in 100 mL of methanol. The solution was stirred for 2 h at room temperature, acidified with HCl, and extracted with ether (3 × 50 mL). The ether extract was dried, flash evaporated, and the resulting brown oil distilled (104–106°C/2 Torr; 1 Torr = 133.3 Pa). The distillate slowly crystallized, giving pale yellow crystals, mp 45–52°C. Recrystallization from benzene and petroleum ether gave pale yellow crystals with mp 48–51°C (lit. (21) mp 47–48°C). 1-(3-Nitrophenyl)-2,2,2-trifluoroethanol-1-*d* was prepared by the reduction of *m*-nitrotrifluoroacetophenone with sodium borodeuteride using the procedure just described for preparation of the unlabelled compound, mp 48–51°C (lit. (22) mp 51.5–52.5°C).

2-Propanol-2-*d* and 1-phenyl-2,2,2-trifluoroethanol-1-*d* were prepared by reduction of the corresponding ketones with lithium aluminum deuteride and purified by fractional distillation and gas–liquid chromatography, respectively (22, 23).

Fig. 1. Plot of log k_{cor} vs. log[2-propanol] for defining the order of the reaction with respect to 2-propanol. [KOH] = 8.0 M. Temp. = 25.1°C. Slope = 1.00 ± 0.04; r = 0.997.



Kinetic methods

The rate of reduction of ferrate was determined by monitoring the decrease in absorbance at 508 nm using either a Cary model 14 or a Hewlett–Packard 8450A spectrophotometer equipped with a thermostated cell compartment. Thermostated solutions of ferrate and alcohol (of known concentrations) were mixed in either 5.0 or 10.0 cm quartz cells and placed in the spectrophotometer. When the concentration of alcohol was much higher than the concentration of ferrate, plots of ln(absorbance − final absorbance) vs. time were linear over 2–4 half-lives, indicating that the reaction is first order in oxidant. Because ferrate is also slowly reduced in the absence of organic reductants, it was necessary to correct the pseudo-first-order rate constants obtained for alcohol oxidation by subtracting the first-order-rate constants for the reaction that occurs in the absence of alcohol.

The corrected pseudo-first-order rate constants were found to be directly dependent on the concentration of alcohol (Fig. 1), indicating that the reaction is also first order with respect to the reductant. Second-order rate constants obtained from division of the pseudo-first-order rate constants by alcohol con-

© 1997 NRC Canada

Can. J. Chem. Downloaded from www.nrcresearchpress.com by 92.62.229.171 on 09/08/12
For personal use only.

Table 1. Isolation of acetone from the oxidation of excess 2-propanol by potassium tetraoxoferrate(VI).[a]

K_2FeO_4 (mmol)	Acetone (mmol)[b]	Yield(%)[c]
41.3	38.9	94
44.0	41.6	95
44.2	46.5	105

[a]0.5 M KOH, 3.5 M KF, 25°C.
[b]Isolated as 1,5-di(2-hydroxyphenyl)-1,4-pentadien-3-one, the product obtained from the condensation of acetone with salicylaldehyde (26).
[c]Yield, based on a 1:1 stoichiometry.

centration were then determined for several alcohols under a variety of conditions and temperatures.

For kinetic experiments in 0.5 M KOH, potassium fluoride (3.5 M) was added to prevent precipitation of iron(III) hydroxide, which interferes with spectrophotometric measurements.

Product isolation and identification

Acetone was identified as the product obtained from the oxidation of 2-propanol as its 2,4-dinitrophenylhydrazone derivative, mp 124–125°C (lit. (25) mp 126°C). Also, as indicated by the data in Table 1, when acetone was isolated after condensation with salicylaldehyde (26), one mole of acetone was produced for each mole of ferrate reduced. It has previously been observed that this reaction is accompanied by the formation of one equivalent of dioxygen (0.25 mol) as in eq. [1] (27).

[1] $$FeO_4^{2-} + CH_3CHOHCH_3 + 1.5H_2O \longrightarrow Fe(OH)_3 + CH_3COCH_3 + 0.25O_2 + 2OH^-$$

m-Nitrotrifluoroacetophenone was quantitatively isolated and identified from the reaction of 1-(3-nitrophenyl)-2,2,2-trifluoroethanol (82.1 mg, 0.372 mmol) with K_2FeO_4 (53.6 mg, 0.232 mmol) in 25 mL of 0.5 M KOH for 1 h at room temperature. The basic solution was acidified, extracted with ether (3 × 50 mL), dried over anhydrous magnesium sulfate, and chromatographed on a 3 in. × 3/8 in. column of Woeln activity V alumina using ether as the eluent. Evaporation of the ether left *m*-nitrotrifluoroacetophenone (54.7 mg, 0.25 mmol). The yield is therefore quantitative, assuming a 1:1 stoichiometry. The yields of the corresponding ketones obtained from the oxidation of 1-phenyl-2,2,2-trifluoroethanol, 1-(3-bromophenyl)-2,2,2-trifluoroethanol, and 1-(4-methylphenyl)-2,2,2-trifluoroethanol were determined by gas chromatography of the product mixtures to be 87%, 96%, and 95%, respectively.

Although the ratio of ferrate reduced to ketone produced when 1-phenyl-2,2,2-trifluoroethanols are oxidized is clearly 1:1, as described above, the amount of dioxygen produced was not quantified. However, it was noted that dioxygen evolution usually continued for a short time after all of the ferrate had been reduced (as evidenced by the fading of the characteristic purple color of FeO_4^{2-}). This suggests that dioxygen formation is due to the reaction of iron(IV) with water as in the following sequence:

[2] $$Fe(VI) + RCHOHR' \longrightarrow Fe(IV) + RCOR'$$

[3] $$Fe(IV) + H_2O \longrightarrow Fe(III) + 0.25O_2$$

The latter reaction (eq. [3]) has been observed to occur when iron(IV) pyrophosphate is dissolved in water at pH 10 (28, 29) and when Ba_2FeO_4 or Sr_2FeO_4 is treated with aqueous mineral acid (30).

The presence of ferric hydroxide in the product was indicated by the formation of a blood-red complex with thiocyanate ion (31). Carr et al. (12) have shown that the presence of small amounts of iron(II) in these products can be detected by complexing it with 1,10-phenanthroline and measuring the absorbance at 510 nm (ε = 10 880 M^{-1} cm^{-1}). Using this approach it was found that the product obtained contained 15–18% iron(II). However, in a separate experiment, iron(III) was found to be slowly reduced to iron(II) by alcohols under these conditions, suggesting that a slow reduction of iron(III) is responsible for the presence of iron(II) in the product.

The products obtained from the oxidation of cyclobutanol can be used to distinguish between one- and two-electron transfer oxidants (32); the use of two-electron transfer oxidants results in the formation of cyclobutanone while one-electron oxidants produce only acylic products (33–37). Therefore, to determine if ferrate was a two-electron oxidant, the products obtained from the oxidation of cyclobutanol were analyzed for the presence of cyclobutanone. When this was done, only two nonvolatile products (cyclobutanone and γ-butyrolactone) were detected, both in low yields. Attempts to improve the yields by varying the ratio of oxidant to reductant or changing the order of mixing the reactants were unsuccessful. Moreover, it was observed, in a separate experiment, that cyclobutanone and ferrate reacted very readily with the evolution of volatile products under these conditions. Cyclobutanone is therefore an intermediate rather than a final product, thus precluding the possibility of obtaining it in high yields. In a typical procedure, potassium ferrate (1.5 g, 7.6 mmol) was slowly added to cyclobutanol (0.50 g, 6.9 mmol) in 25 mL of buffer, pH = 9.3. The reaction, mildly exothermic, proceeded with the evolution of volatile products. After the addition was completed (1 h with stirring) the solution was acidified with concentrated HCl and extracted with ether. After drying over anhydrous magnesium sulfate, the ether extract was analyzed by gc–ms. The compounds present were cyclobutanol (94%), *m/z* (%): 72 (M^+, 0.3), 39(9), 27(17), 44(100); cyclobutanone (1.2%), *m/z* (%): 70 (M^+, 17), 27(19), 43(100); γ-butyrolactone (4.5%), *m/z* (%): 86 (M^+, 24), 56(22), 28(88), 42(100). The gc retention times for cyclobutanol and cyclobutanone were identical to those for authentic samples.

Results and discussion

When tetraoxoferrate(VI) is reduced by excess alcohol, good pseudo-first-order kinetics, as defined by eq. [4], are obtained (where k_{cor} is the observed first-order rate constant, k_{obs}, corrected for the slow reduction of ferrate in the absence of alcohol).

[4] $$-d[FeO_4^{2-}]/dt = k_{cor}[FeO_4^{2-}]$$

The observation that the values of k_{cor} are directly proportional to the concentration of alcohol indicates that the reaction is also first order in alcohol, as in eq. [5] where $k_2 = k_{cor}/[Alcohol]$.

[5] $$-d[FeO_4^{2-}]/dt = k_2[FeO_4^{2-}][Alcohol]$$

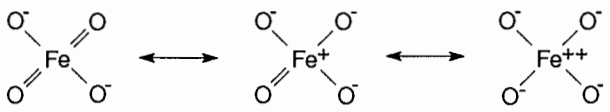
© 1997 NRC Canada

Can. J. Chem. Downloaded from www.nrcresearchpress.com by 92.62.229.171 on 09/08/12
For personal use only.

The second-order rate constants obtained in this way are dependent upon the pH of the solution, the temperature of the solution, the structure of the reductant, and isotopic substitutions. From a consideration of the way in which the magnitude of the rate constants change with each of these variables, it is possible to limit mechanistic options and to arrive at a "most probable" mechanism for these reactions. To begin with, however, it is necessary to consider the evidence available concerning the structure of ferrate ion in alkaline solutions.

Structure of the oxidant

X-ray powder pattern studies have indicated that the ferrate ion is tetrahedral when present in solid K_2FeO_4 crystals (38). In aqueous solutions, the infrared spectrum of ferrate is also consistent with a tetrahedral geometry (39) and isotopic oxygen exchange studies have indicated that all oxygens are kinetically equivalent (40). From the knowledge that metal oxos are strongly polarized ($L_nM = O \leftrightarrow L_nM^+—O^-$) (41, 42), it can be concluded that the ferrate ion is best visualized as a positively charged iron cation surrounded by four equivalent oxygens, each bearing a partial negative charge; i.e., a resonance hybrid of three canonical structures, **1**–**3**.



1 **2** **3**

In a theoretical study, Ziegler, Rauk, and Baerends (43) concluded, using the Hartree–Fock–Slater Discrete Variational Method to investigate electronic structures, that tetrahedral oxyanions of transition metals would have *d*-orbital populations close to those of the corresponding M^{2+} ions; i.e., that **3** would be the most important canonical structure. An independent study using symmetry adapted cluster (SAC) and SAC – configuration interaction (SAC–CI) theories, reported by Jitsuhiro, Nakai, Hada, and Nakatsuji (44), predicted that the charge on the central metal of comparable compounds ranges from 1.04 to 1.44, suggesting that both **2** and **3** strongly contribute to the structure of ferrate.

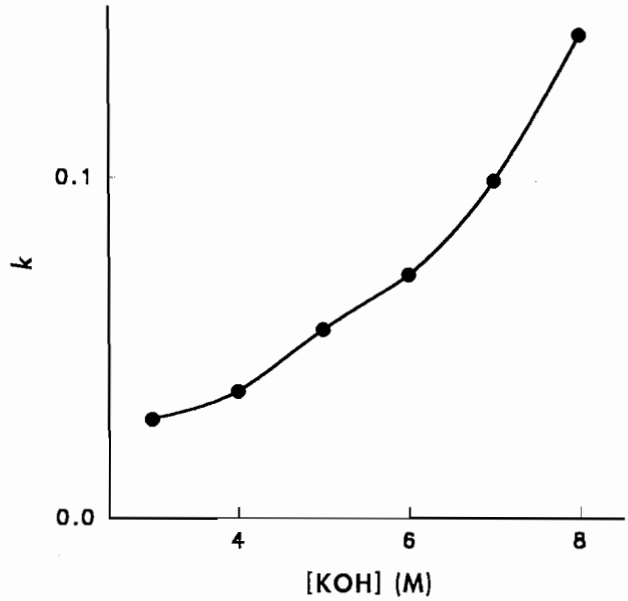
Base catalysis

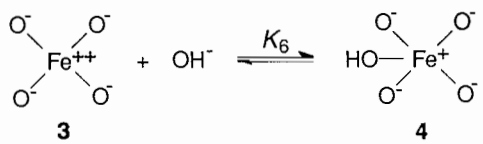
It is apparent that the rate of reduction of ferrate by 2-propanol (Table 2) is subject to base catalysis; the observed second-order rate constants increase from 0.03 M^{-1} s^{-1} in 3.0 M KOH to 0.14 M^{-1} s^{-1} in 8.0 M KOH. By comparison with studies on the reduction of ferrate by water in alkaline solutions (14), it seems likely that this rate acceleration is associated with the formation of a reactive pentacoordinated iron(VI) oxyanion, **4**, as in eq. [6]. Reaction of **4** with a reductant such as 2-propanol would then give an octahedral intermediate, **5**, that could convert to products as described below. A five-coordinated species such as **4** would be expected to react readily with nucleophilic reductants to give an octahedral product, **5**, as in eq. [7].

A compound similar to **4**, formed by the reaction of hydroxide ions with $HFeO_4^-$, has been suggested as a possible intermediate in the exchange of isotopic oxygen between ferrate and water (40).

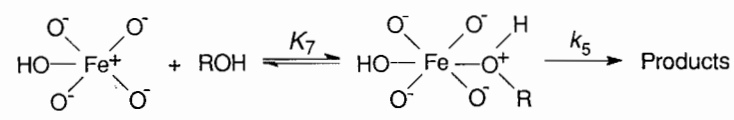
The rate law for a sequence consisting of reaction [6] followed by reaction [7] would be first order in hydroxide ion concentration (eq. [8]) and the second-order rate constants should be directly dependent on $[OH^-]$ (eqs. [9] and [10]). However, a plot of k_2 vs. $[OH^-]$ is not linear (Fig. 2) and a plot of log k_2 vs. log $[OH^-]$ has a slope much greater than unity in strongly basic solutions. This steep increase in rate at high basicities is likely due to ionization of 2-propanol ($pK_a = 17.1$ (45)) in these solutions; alkoxide ions, formed as in eq. [11], are known to be more rapidly oxidized by other comparable oxidants such as permanganate (46*a*, 47).

Fig. 2. Dependence of k_2 for the oxidation of 2-propanol on base concentration.



[6] 

3 **4**

[7] 

4 **5**

© 1997 NRC Canada

Can. J. Chem. Downloaded from www.nrcresearchpress.com by 92.62.229.171 on 09/08/12
For personal use only.

Table 2. Rate constants for the oxidation of 2-propanol under various conditions.[a]

[2-Propanol] ($M \times 10^2$)	[K_2FeO_4] ($M \times 10^3$)	KOH (M)	Temp. (°C)	k_{obs}[b] ($s^{-1} \times 10^3$)	k_{cor}[c] ($s^{-1} \times 10^3$)	k_2[d] ($M^{-1}s^{-1} \times 10$)
1.91	0.20	8.0	25.1	2.84	2.65	1.39
1.91	0.16	8.0	31.8	4.07	3.91	2.05
1.91	0.24	8.0	38.5	5.62	5.39	2.82
1.91	0.30	8.0	45.2	8.19	7.89	4.13
1.91	0.52	8.0	45.2	7.68	7.16	3.74
2.18	0.19	8.0	25.1	3.38	3.20	1.47
2.23	0.15	8.0	25.1	3.11	2.96	1.55
4.46	0.14	8.0	25.1	5.83	5.69	1.28
5.95	0.13	8.0	25.1	8.36	8.23	1.38
8.92	0.13	8.0	25.1	12.8	12.7	1.42[e]
2.11	0.25	7.0	25.1	2.20	2.09	0.991
2.13	0.20	6.0	25.1	1.73	1.52	0.715
1.91	0.34	5.0	25.1	1.40	1.06	0.555
1.97	0.31	4.0	25.1	0.976	0.666	0.338
3.17	0.49	4.0	25.1	1.79	1.30	0.410
3.98	0.35	3.0	25.1	1.51	1.16	0.292[e]
7.15	0.38	5.0[f]	25.1	5.53	5.16	0.722
7.26	0.16	3.0[g]	25.1	3.70	3.55	0.489
7.37	0.54	1.0[h]	25.1	2.07	1.53	0.207

[a]Each rate constant is the average of two or more experiments that agree within ±9%.
[b]k_{obs} is the observed pseudo-first-order rate constant obtained from the slope of a plot of $\ln(A - A_f)$ vs. time.
[c]k_{cor} is the observed pseudo-first-order rate constant minus the first-order rate constant for the reduction of ferrate in the absence of alcohol.
[d]$k_2 = k_{cor}$/[2-propanol].
[e]Obtained from a single experiment.
[f]Containing KF (1.0 M).
[g]Containing KF (3.0 M).
[h]Containing KF (5.0 M).

[8] $\text{Rate} = k_5K_6K_7[FeO_4^{2-}][\text{2-Propanol}][OH^-]$

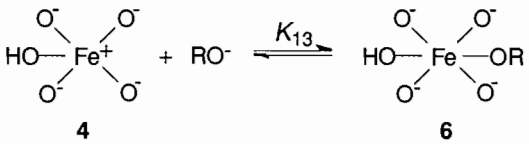
[9] $k_2 = k_5K_6K_7[OH^-]$

[10] $\log k_2 = \log[OH^-] + \log k_5K_6K_7$

[11] $ROH + OH^- \rightleftharpoons RO^- + H_2O$

Assuming that ferrate could be reduced by both the alcohol and the alkoxide ion requires an expansion of the rate law expressed in eq. [8] to that in eq. [12], where K_{13} is the equilibrium constant for the reaction between **4** and the alkoxide ion as in eq. [13], while k_5 and k_6 are the rate constants for conversion of **5** and **6**, respectively, into products. The concentration of alkoxide ion can be calculated from eq. [14], using the acidity function ($H_- = -\log h_-$) defined for concentrated KOH solutions (48).

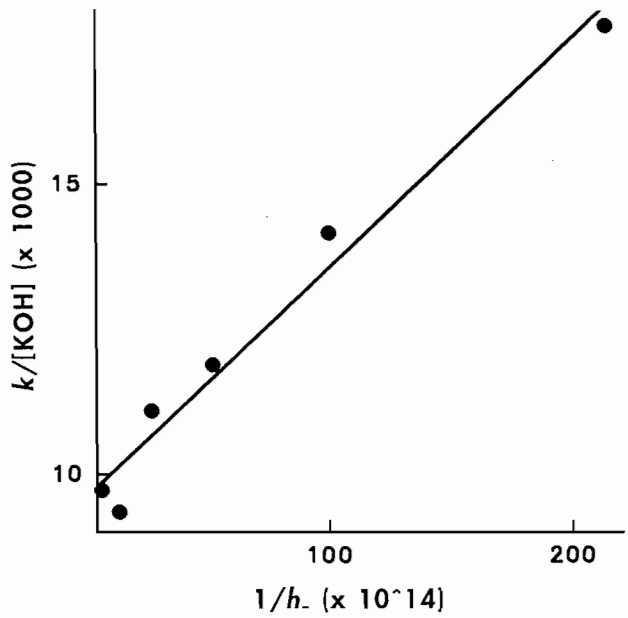
[12] $\text{Rate} = K_6(k_5K_7[ROH] + k_6K_{13}[RO^-])[FeO_4^{=}][OH^-]$

[13] 

4 6

[14] $[RO^-] = K_a[ROH]/h_-$

Fig. 3. Plot of eq. [17], $k_2/[KOH] = k_5K_6K_7 + k_6K_6K_{13}K_a/h_-$. Slope = $(3.98 \pm 0.33) \times 10^{-19}$. Intercept = $(9.58 \pm 0.33) \times 10^{-3}$ M^{-2} s^{-1}; r = 0.99.



© 1997 NRC Canada

Can. J. Chem. Downloaded from www.nrcresearchpress.com by 92.62.229.171 on 09/08/12
For personal use only.

Table 3. Rate constants for the oxidation of 1,1,1,3,3,3-hexafluoro-2-propanol by tetraoxoferrate(VI).

pH	k_{obs} [a] ($s^{-1} \times 10^3$)	k_{cor} [b] ($s^{-1} \times 10^3$)	k_2 [c] ($M^{-1}s^{-1} \times 10^2$)
8.00	24.6 ± 0.6	23.8 ± 0.7	79.3 ± 2.3
8.15	19.4 ± 0.3	18.8 ± 0.3	62.7 ± 1.0
8.42	12.5 ± 0.3	12.1 ± 0.3	40.3 ± 1.0
8.60	8.81 ± 0.24	8.55 ± 0.24	28.5 ± 0.8
8.70	7.51 ± 0.24	7.24 ± 0.24	24.1 ± 0.8
9.02	5.21 ± 0.11	5.09 ± 0.11	17.0 ± 0.4
9.30	4.49 ± 0.14	4.41 ± 0.15	14.7 ± 0.5
9.70	3.49 ± 0.04	3.43 ± 0.04	11.4 ± 0.1
9.95	2.82 ± 0.09	2.76 ± 0.09	9.20 ± 0.30
10.14	2.94 ± 0.05	2.87 ± 0.06	9.57 ± 0.20
10.69	3.01 ± 0.05	2.58 ± 0.07	8.60 ± 0.23

[a] k_{obs} is the observed pseudo-first-order rate constant obtained from the slope of a plot of $\ln(A - A_t)$ vs. time.

[b] k_{cor} is the observed pseudo-first-order rate constant minus the first-order rate constant for the reduction of ferrate in the absence of alcohol.

[c] $k_2 = k_{cor}/[1,1,1,3,3,3\text{-hexafluoro-2-propanol}] = k_{cor}/0.0030$ M.

Substitution of eq. [14] into eq. [12] gives eq. [15], from which an expression for the observed second-order rate constants can be derived (eq. [16]). The fact that plots of $k_2/[OH^-]$ vs. $1/h_-$ are linear (Fig. 3), as predicted from eq. [17], indicates that this reaction sequence is in quantitative agreement with the available data.

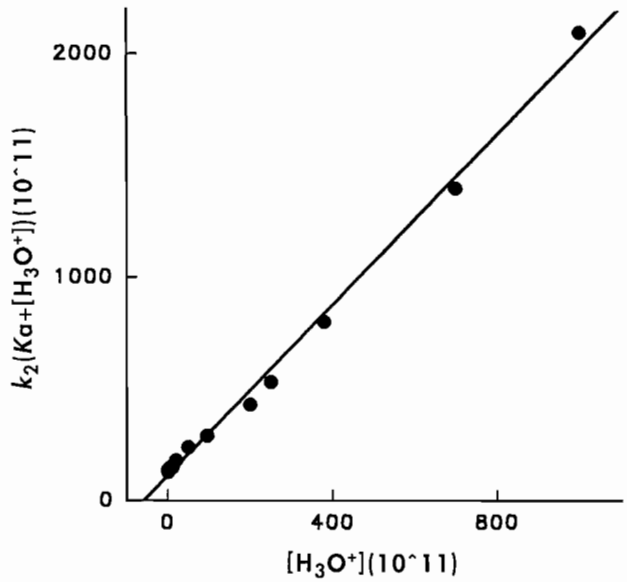
[15] $\text{Rate} = K_6(k_5K_7 + k_6K_{13}K_a/h_-)[FeO_4^{2-}][ROH][OH^-]$

[16] $k_2 = (k_5K_6K_7 + k_6K_6K_{13}K_a/h_-)[OH^-]$

[17] $k_2/[OH^-] = k_5K_6K_7 + k_6K_6K_{13}K_a/h_-$

Although it is not possible to obtain absolute values for the rate constants for the reduction of ferrate by 2-propanol and isopropoxide ion, relative values can be obtained from the ratio of the slope of the plot in Fig. 3 to its intercept; slope/intercept = $k_6K_{13}K_a/k_5K_7$. Since the value for K_a is known (7.84×10^{-18} (45)), the magnitude of k_6K_{13}/k_5K_7, which is the relative rate for the oxidation of isopropoxide ion compared to 2-propanol, can be calculated to be 5.3. Hence, it appears that the alkoxide is, as expected, oxidized more rapidly than the corresponding alcohol. It is not clear, however, if this acceleration is associated with the equilibrium constant for reaction [13] as compared to reaction [7] or if it is due to the rates at which **6** and **5**, respectively, are converted into products.

Fig. 4. Dependence of k_2 for the oxidation of 1,1,1,3,3,3-hexafluoro-2-propanol on $[H_3O^+]$. Slope = $(7.22 \pm 0.17) \times 10^{-4}$ M^{-2} s^{-1}. Intercept = $(9.94 \pm 0.68) \times 10^{-2}$ M^{-1} s^{-1}.



Acid catalysis

When the pH is less than 9, the reaction is subject to acid catalysis as indicated by the data in Table 3 for the oxidation of 1,1,1,3,3,3-hexafluoro-2-propanol. Since this alcohol is a very weak base, it can be assumed that the observed acceleration is not due to protonation of the reductant. Instead, it must be associated with formation of the hydrogen ferrate ion (pK_a = 7.8 (49)) as in eq. [18].

[18] $HFeO_4^- + H_2O \rightleftharpoons FeO_4^{2-} + H_3O^+$

The kinetics under these conditions could, therefore, be expressed as in eqs. [19]–[21], where $[Fe(IV)]_T$ indicates the total iron(VI) concentration.

[19] $\text{Rate} = (k_{11}[FeO_4^{2-}] + k_{12}[HFeO_4^-])[ROH]$

$= k_2[Fe(VI)]_T[ROH]$

[20] $k_2 = (k_{11}K_a + k_{12}[H_3O^+])/(K_a + [H_3O^+])$

[21] $k_2(K_a + [H_3O^+]) = k_{11}K_a + k_{12}[H_3O^+]$

© 1997 NRC Canada

Can. J. Chem. Downloaded from www.nrcresearchpress.com by 92.62.229.171 on 09/08/12
For personal use only.

Table 4. Kinetic deuterium isotope effects.

Reductant	Conditions	k_H (M^{-1} s^{-1} × 10)	k_D (M^{-1} s^{-1} × 10)	k_H/k_D
2-Propanol	8.0 M KOH, 25.1°C	1.39 ± 0.13	0.139 ± 0.011	10 ± 2
2-Propanol	8.0 M KOH, 31.8°C	2.05 ± 0.18	0.172 ± 0.008	12 ± 2
2-Propanol	8.0 M KOH, 38.5°C	2.82 ± 0.25	0.270 ± 0.015	10 ± 2
1-Phenyl-2,2,2-trifluoroethanol	0.5 M KOH,[a] 25.1°C	7.65 ± 0.45	1.45 ± 0.11	5.3 ± 0.7
1-(3-Nitrophenyl)-2,2,2-trifluoroethanol	0.5 M KOH,[a] 25.1°C	23.6 ± 0.4	3.74 ± 0.70	6.3 ± 1.5

[a]3.5 M KF.

Fig. 5. Effect of ionic strength on the rate constants for the oxidation of 1,1,1,3,3,3-hexafluoro-2-propanol by tetraoxoferrate(VI) at pH 9.33. Temp. = 25.0°C. Slope = 0.18 ± 0.03; r = 0.95.

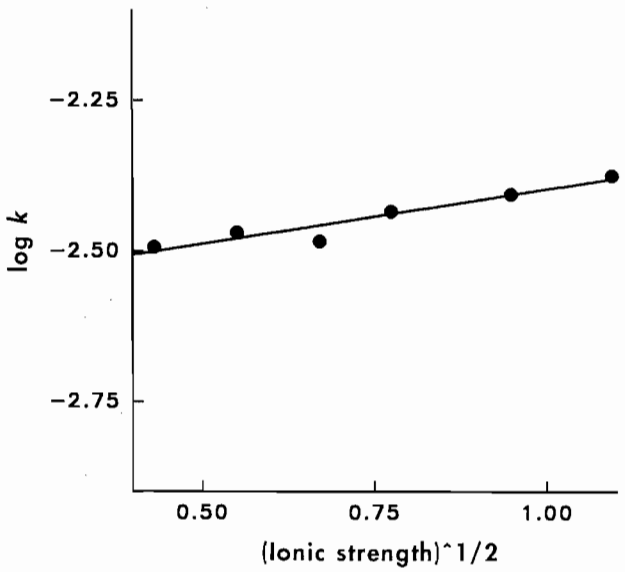
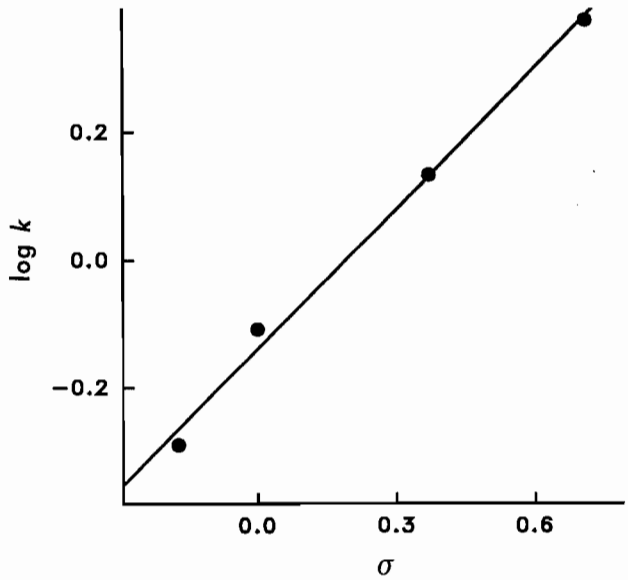


Fig. 6. Hammett plot for the oxidation of 1-aryl-2,2,2-trifluoroethanols by tetraoxoferrate(VI) in 0.50 M KOH containing 3.5 M KF. Temp. = 25.1°C. Slope = 0.73 ± 0.04; r = 0.997.



Values for k_{11} and k_{12} obtained from nonlinear curve fitting of eq. [20] are k_{11} = 0.0764 ± 0.0076 M^{-1} s^{-1} and k_{12} = 1.87 ± 0.04 M^{-1} s^{-1} (r^2 = 0.993).[2] Equation [20] can also be rearranged into a linear form as indicated in eq. [21]. From the corresponding plot, presented in Fig. 4, the values obtained for k_{11} and k_{12} are k_{11} = 0.0708 ± 0.0071 M^{-1} s^{-1} and 1.91 ± 0.04 M^{-1} s^{-1} (r^2 = 0.995). The ratio, k_{12}/k_{11}, indicates that hydrogen ferrate ($HFeO_4^-$) reacts with 1,1,1-trifluoro-2-propanol about 25 times faster than ferrate (FeO_4^{2-}) under comparable conditions. This observation is consistent with Stewart's conclusion that acid catalysis in similar reactions is also due to protonation of the oxidant (46). For example, the rates of permanganate (50), chromate (51), manganate (52), and ruthenate (53) oxidations all increase as the acidity of the medium is increased.

[2] Nonlinear plots were studied using the computer program, *Table Curve*, Jandel Corporation, 1986–1995.

Ionic strength

When the ionic strength of the medium was increased by increasing buffer concentrations, little or no effect on the reaction rate could be detected as indicated by the plot in Fig. 5. The polarities of the ground and transition states for this reaction must, therefore, be similar.

In highly basic solutions, where buffering is not possible, the addition of KF to prevent the precipitation of iron(III) hydroxide did cause an increase in rate as indicated by the last three entries in Table 2; however, such increases are most likely associated with an increase in basicity of the medium. Addition of KF would salt out the hydroxide ion, causing the basicity of the solution to increase.

Substituent effects

The oxidations of 1-phenyl-2,2,2-trifluoroethanol and its ring-substituted derivatives were carried out in 0.50 M KOH containing a high concentration of KF (3.5 M) to prevent precipitation of iron(III) hydroxide. As noted above, the effect of

© 1997 NRC Canada

Can. J. Chem. Downloaded from www.nrcresearchpress.com by 92.62.229.171 on 09/08/12
For personal use only.

this added salt will be to increase the basicity of these solutions beyond that of 0.5 M KOH (h_- = 13.7 (48)). Considering that 1-phenyl-2,2,2-trifluoroethanol has a pK_a of 11.90 (21), it would be at least 98.4% ionized under the conditions in which the data in Table 4 were collected. Similarly, the 4-methyl, 3-bromo, and 3-nitro derivatives, which have pK_a's of 12.04, 11.50, and 11.23 (21), would be ionized to at least 98.0%, 99.4%, and 99.7%, respectively, under these conditions. Consequently, it is possible to be confident that the Hammett ρ value does not contain a significant contribution from ionization equilibria occurring prior to oxidation; it is a consequence only of the change in electron density that occurs at the α-carbon as the oxidation reaction proceeds from the ground state to the transition state. Since the ρ value is positive (ρ = 0.73, Fig. 6) it is apparent that the electron density on the carbon adjacent to the aromatic ring must be greater in the transition state.

Isotope effect

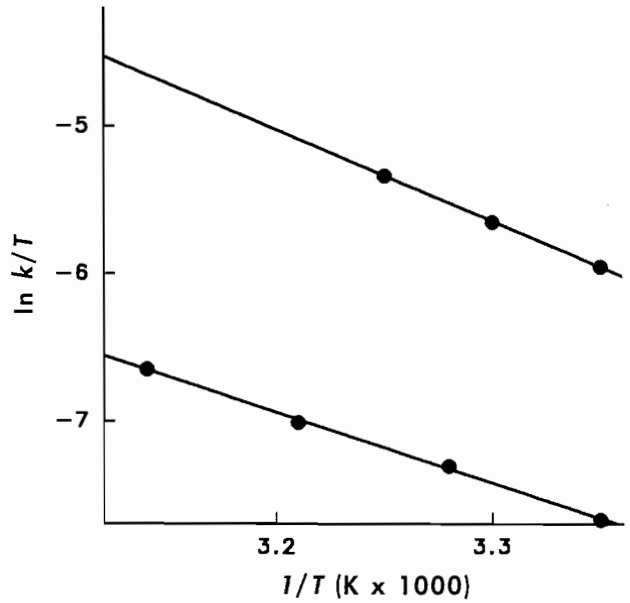
Primary kinetic isotope effects were observed when the hydrogen adjacent to the hydroxyl group was replaced by deuterium. As the data in Table 4 indicate, the magnitude of the effect is much greater for 2-propanol than for 1-phenyl-2,2,2-trifluoroethanol or 1-(3-nitrophenyl)-2,2,2-trifluoroethanol, suggesting that C—H cleavage is more symmetrical for 2-propanol. According to the theory initially elaborated by Westheimer (54), the magnitude of an isotope effect is dependent on the symmetry of the transition state, with the largest effects being observed when bond cleavage and bond formation are approximately balanced. Since the Hammett ρ value is positive, the hydrogen must be transferred as a proton to an available base. The 1-aryl-2,2,2-trifluoroethanols would be more capable of accommodating proton loss from the α-carbon, suggesting that the smaller isotope effect occurs because proton transfer is more advanced in the transition state. The larger isotope effect observed for the oxidation of 2-propanol indicates a more symmetrical transition state with respect to proton transfer and the possible involvement of tunneling (55).

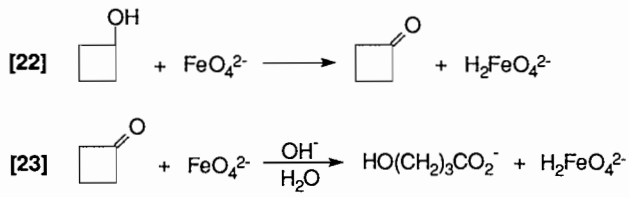
The oxidation of cyclobutanol

The products obtained from the oxidation of cyclobutanol were examined in an attempt to determine if ferrate(VI) is a one- or two-electron oxidant. Empirical evidence indicates that two-electron oxidants convert cyclobutanol into cyclobutanone; however, if free radicals are formed (by a one-electron transfer oxidant), the resulting cyclobutyl free radical undergoes rapid ring opening resulting in the formation of acyclic products (32–37). A previous report indicated that only traces of cyclobutanone along with a number of acyclic products are obtained from the oxidation of cyclobutanol by ferrate(VI) (19). A reexamination of this reaction has, however, led to the observation that cyclobutanone is also rapidly oxidized by ferrate(VI) under these conditions to yield only volatile products. Attempts to obtain a better yield of cyclobutanone from the oxidation of cyclobutanol by varying the relative amounts of oxidant and reductant, the temperature, and the order of mixing all resulted in the formation of primarily volatile products, along with small amounts of cyclobutanone (~1%) and γ-butyrolactone (~5%).

Although these results are not conclusive, a most likely scenario is that cyclobutanone and 4-hydroxybutanoate are formed in successive two-electron oxidations as in eqs. [22] and [23]. Acidification of the solution forms 4-hydroxybutanoic acid, which is isolated as its lactone as in eq. [24]. The volatile products would come from the oxidation of water to dioxygen by iron(IV), as previously described (28–30), and from the oxidative degradation of 4-hydroxybutanoate.

Fig. 7. Eyring plots for the oxidation of 1-phenyl-2,2,2-trifluoroethanol (top) and 2-propanol (bottom). For the top plot, slope = −6180 ± 80 K, intercept = 14.8 ± 0.3, r = 0.999. For the bottom plot, slope = −4810 ± 134 K, intercept = 8.45 ± 0.44; r = 0.999.





[24] $HO(CH_2)_3CO_2^- \longrightarrow HO(CH_2)_3CO_2H \longrightarrow O(CH_2)_3CO$

These results, therefore, appear to be most consistent with the suggestion that ferrate(VI) is a two-electron oxidant. However, because of the highly equivocal nature of this data, one-electron mechanisms must also remain under active consideration.

Temperature effects

Rate constants obtained for a range of temperatures were used to prepare Eyring plots (Fig. 7) from which activation parameters can be calculated (56). The results obtained from these studies, Table 5, indicate that the reaction of alcohols with ferrate(VI) is marked by relatively high activation enthalpies and large unfavorable activation entropies. The very unfavorable entropies of activation indicate that the transition state is more highly organized than the ground state.

Reaction mechanism

The oxidation of alkoxide ions most likely occurs in two steps,

© 1997 NRC Canada

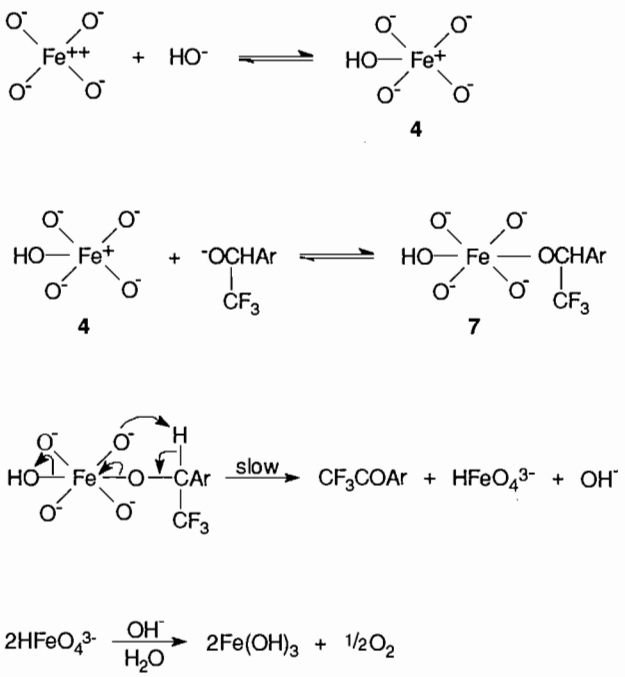
Can. J. Chem. Downloaded from www.nrcresearchpress.com by 92.62.229.171 on 09/08/12
For personal use only.

Table 5. Activation parameters for the reduction of tetraoxoferrate(VI) by alcohols.

Alcohol	Conditions	Temp. range (°C)	$\Delta H^{\ddagger}$ (kJ mol^{-1})	$\Delta S^{\ddagger}$ (J mol^{-1} K^{-1})	$\Delta G^{\ddagger}$ (kJ mol^{-1})	r^b
2-Propanol	8 M KOH	25–45	40.0	−127	77.9	0.999
1,1,1-Trifluoro-2-propanol	8 M KOH	15–40	44.0	−110	76.8	0.993
1,1,1,3,3,3-Hexafluoro-2-propanol	8 M KOH	20–40	42.8	−114	76.8	0.998
1-Phenyl-2,2,2-trifluoroethanol	0.5 M KOH[a]	25–35	51.4	−74.9	73.7	0.9999
1-(4-Methylphenyl)-2,2,2-trifluoroethanol	0.5 M KOH[a]	20–35	45.0	−99.4	74.6	0.996
1-(3-Bromophenyl)-2,2,2-trifluoroethanol	0.5 M KOH[a]	15–30	61.2	−37.2	72.3	0.999
1-(3-Nitrophenyl)-2,2,2-trifluoroethanol	0.5 M KOH[a]	15–32	53.7	−57.9	71.0	0.999

[a]3.5 M KF.
[b]Correlation coefficient for the Eyring plot.

Scheme 1. A possible mechanism for the oxidation of 1-aryl-2,22-trifluoroethanols by tetraoxoferrate(VI) under basic conditions.



an addition in which $HFeO_5^{3-}$, **4**, combines with an alkoxide ion to form an ester, **6**, followed by a reductive elimination resulting in the reduction of ferrate and the oxidation of the alkoxide ion. From the isotope and substituent effects it appears as if the reductive elimination must be accompanied by heterolytic cleavage of the α-C—H bond. This could be achieved by either a transfer of a proton to an external base (such as hydroxide ion) or an internal cyclic transfer to an oxygen attached to iron. The latter appears to be more likely because involvement of additional base in the rate-limiting step would not be consistent with the observed dependence of the rate on the basicity of the solution that was discussed above. A cyclic mechanism is also more consistent with the highly unfavorable entropies of activation observed in the temperature studies. Heterolytic cleavage of the Fe—O bond must occur in rapid succession of, or concurrently with, proton transfer as outlined in Scheme 1.

The third step in Scheme 1, which involves cleavage of the α-C—H bond, would be rate limiting as required by the observed isotope effect. The positive Hammett ρ value indicates an electron-rich transition state, suggesting that the rate-limiting step is initiated by proton transfer as indicated. The relatively low value of ρ (0.73) means, however, that there is only a small increase in the electron density at α-carbon in the transition state and is more consistent with a concerted mechanism in which electron transfer occurs concurrently with proton transfer. The insensitivity of the reaction rate to changes in the ionic strength is also consistent with a concerted mechanism.

The reaction depicted in Scheme 1 involves the transfer of a proton and two electrons to the oxidant; i.e., the overall result is hydride transfer. Therefore, another mechanism that could be considered would be direct hydride transfer as in eq. [25]. In such a reaction, however, the electron density at the α-carbon is decreasing and a negative ρ value would be expected. A direct hydride transfer is, therefore, not as consistent with the experimental evidence as the synchronized proton/2-electron mechanism depicted in Scheme 1.

[25] $RR'CHO^- + HOFeO_4^{3-} \longrightarrow RR'CO + HOFeO_3^{3-} + HO^-$

In addition, because the results obtained from the oxidation of cyclobutanol do not unambiguously establish that the reaction is a two-electron oxidation, a hydrogen atom transfer mechanism must also be considered as a possibility. As indicated by eq. [26], hydrogen atom transfer would lead to formation of a radical anion that could undergo a subsequent single electron transfer (eq. [27]).

[26] $RR'CHO^- + HOFeO_4^{3-} \longrightarrow RR'\dot{C}O^- + (HO)_2FeO_3^{3-}$

[27] $RR'\dot{C}O^- + (HO)_2FeO_3^{3-} \longrightarrow RR'CO + HOFeO_3^{3-} + HO^-$

© 1997 NRC Canada

Such a hydrogen atom transfer mechanism has been established for the oxidation of these same aryl-2,2,2-trifluoroethanols by permanganate under basic conditions (46*b*, 47). In that reaction, however, the Hammett ρ value is approximately zero, as might be expected for a process that does not cause much change in the electron density of the α-carbon (24). Hence, a direct hydrogen atom transfer, in common with a direct hydride ion transfer, is not as consistent with the experimental evidence as the mechanism depicted in Scheme 1.

Conclusions

It has been found that the oxidation of alcohols by ferrate(VI) is subject to both acid and base catalysis. The increased rate in acidic solutions has been proposed to be due to the formation of the acid ferrate ion, $HFeO_4^-$, a more reactive oxidant than FeO_4^{2-}. Rate acceleration under basic conditions has been attributed partly to formation of alkoxide ions, which are more reactive reductants than neutral alcohols, and partly to formation of $HOFeO_4^{3-}$, which, it has been proposed, is more susceptible to nucleophilic attack by alcohols and alkoxide ions.

The possible reactions can therefore be summarized as in eqs. [28]–[30].

$$[28]\quad HOFeO_4^{3-} + RO^- \xrightarrow{k_b} \text{products}$$

$$[29]\quad FeO_4^{2-} + ROH \xrightarrow{k_n} \text{products}$$

$$[30]\quad HFeO_4^- + ROH \xrightarrow{k_a} \text{products}$$

Kinetic studies on the oxidation of 2-propanol suggest that the ratio, k_b/k_n, is about 5, while similar studies on the oxidation of 1,1,1-trifluoro-2-propanol indicate that the ratio, k_a/k_n, is about 25. The results obtained from isotope and substituent effects, along with temperature and ionic strength studies, are most consistent with a mechanism that involves formation of an intermediate ferrate ester, **7**, as in Scheme 1.

Acknowledgments

The authors are pleased to acknowledge the financial assistance of the Natural Sciences and Engineering Research Council of Canada and the Petroleum Research Foundation of the American Chemical Society.

References

1. R.E. Dickerson and I. Geis. Hemoglobin: structure, function, evolution and pathology. Benjamin/Cummings, Menlo Park, Calif. 1983.
2. Y. Tsuda and S. Nakajima. Chem. Lett. 1397 (1978).
3. R.J. Audette, J.W. Quail, and P.J. Smith. Tetrahedron Lett. 279 (1971).
4. M. Fieser and L.F. Fieser. Reagents for organic synthesis. Vol. 4. Wiley–Interscience, New York. (1974). p. 405.
5. J.N. BeMiller and S.D. Darling. US Patent 3,632,802 (1972).
6. J.N. BeMiller, V.G. Kumari, and S.D. Darling. Tetrahedron Lett. 4143 (1972).
7. R.L. Bartzatt and J. Carr. Transition Met. Chem. **11**, 116 (1986).
8. K.S. Kim, Y.K. Chang, S.K. Bae, and C.S. Hahn. Synthesis, 866 (1984).
9. L. Delaude and P. Laszlo. J. Org. Chem. **61**, 6360 (1996); H. Gai. Ph.D. Thesis, The University of Regina, 1996.
10. F. Montanari and L. Casella. Metalloporphyrins catalyzed oxidations. Kluwer, Boston. 1994.
11. D.H.R. Barton and D. Doller. Acc. Chem. Res. **25**, 504 (1992), and refs. therein.
12. J.D. Carr, P.B. Kelter, A. Tabatabai, D. Splichal, J. Erickson, and C.W. McLaughlin. Water chlorination: chemistry, environmental impact and health effects. Proceedings of the Fifth Conference on Water Chlorination. Vol. 5. Williamsburg, Va. 1984. p. 1285.
13. T. Ernst, M. Wawrzenczyk, M. Cyfert, and M. Wronska. Bull. Acad. Pol. Sci. **27**, 773 (1979).
14. B. Jezowska-Trzebiatowska. Catal. Chem. Kinet. 217 (1964).
15. B. Jezowska-Trzebiatowska and M. Wronska. Bull. Acad. Pol. Sci. **5**, 659 (1957).
16. J.M. Schreyer and L.T. Ockerman. Anal. Chem. **23**, 1312 (1951).
17. J.M. Schreyer, G.W. Thompson, and L.T. Ockerman. Inorg. Synth. **4**, 164 (1953).
18. R.L. Bartzatt. Ph.D. Thesis, University of Nebraska–Lincoln, 1982.
19. D.G. Lee and H. Gai. Can. J. Chem. **71**, 1394 (1993).
20. J.M. Schreyer, G.W. Thompson, and L.T. Ockerman. Anal. Chem. **22**, 1426 (1950).
21. R. Stewart and R. Van der Linden. Can. J. Chem. **38**, 399 (1960).
22. R. Stewart and D.G. Lee. Can. J. Chem. **42**, 439 (1964); D.G. Lee. Ph.D. Thesis, The University of British Columbia, 1963.
23. D.G. Lee and R. Stewart. J. Org. Chem. **32**, 2868 (1967).
24. R. Stewart and R. Van der Linden. Tetrahedron Lett. 28 (1960).
25. R.L. Shriner, R.C. Fuson, and D.Y. Curtin. The systematic identification of organic compounds. Wiley, New York. 1956. p. 316.
26. G.E. Ginther and R.C. Finch. Anal. Chem. **32**, 1894 (1960).
27. B.E. Norcross and W.C. Lewis. Abstract of papers. 146th Meeting of the ACS, 1964. p. 35c.
28. B.H.J. Bielski. Free Rad. Res. Commun. **12–13**, 469 (1991).
29. J.D. Melton and B.H.J. Bielski. Radiat. Phys. Chem. **36**, 725 (1990).
30. W. Levason and C.A. McAuliffe. Coord. Chem. Rev. **12**, 151 (1974).
31. C.H. Sorum. Introduction to semimicro qualitative analysis. 3rd ed. Prentice Hall, Englewood Cliffs, N.J. 1960. p. 134.
32. W.C. Cheng, W.Y. Yu, C.K. Li, and C.M. Che. J. Org. Chem. **60**, 6840 (1995).
33. D.G. Lee and L.N. Congson. Can. J. Chem. **68**, 1774 (1990).
34. D.G. Lee, U.A. Spitzer, J. Cleland, and M.E. Olson. Can. J. Chem. **54**, 2124 (1976).
35. J. Rocek and D.E. Aylward. J. Am. Chem. Soc. **97**, 5452 (1995).
36. J. Rocek and A.E. Radkowski. J. Am. Chem. Soc. **95**, 7123 (1973).
37. K. Meyer and J. Rocek. J. Am. Chem. Soc. **94**, 1209 (1972).
38. V.H. Krelis. Z. Anorg. Allg. Chem. **263**, 175 (1950); R. Scholder, H. Bunsen, F. Kinderwater, and W. Zeiss. Z. Anorg. Allg. Chem. **282**, 268 (1955).
39. W.P. Griffith. J. Chem. Soc. A, 1467 (1966).
40. H. Goff and R.K. Murmann. J. Am. Chem. Soc. **93**, 6058 (1971).
41. K.B. Sharpless, A.Y. Teranishi, and J.E. Blackvall. J. Am. Chem. Soc. **99**, 3120 (1977).
42. W.A. Howard and G. Parkin. J. Am. Chem. Soc. **116**, 606 (1994).

Can. J. Chem. Downloaded from www.nrcresearchpress.com by 92.62.229.171 on 09/08/12
For personal use only.

© 1997 NRC Canada

43. T. Ziegler, A. Rauk, and E.J. Baerends. Chem. Phys. **16**, 209 (1976).
44. S. Jitsuhiro, H. Nakai, M. Hada, and H. Nakatsuji. J. Chem. Phys. **101**, 1029 (1994).
45. R. Stewart. The proton: applications to organic chemistry. Academic Press, New York. 1985. p. 43.
46. R. Stewart. *In* Oxidation in organic chemistry. Part A. *Edited by* K.B. Wiberg. Academic Press, New York. 1960. (*a*) p. 35; (*b*) p. 50.
47. A. Thibblin. J. Phys. Org. Chem. **8**, 186 (1995).
48. C.H. Rochester. Acidity functions. Academic Press, New York. 1970. p. 237.
49. V.H.J. Bielski and M.J. Thomas. J. Am. Chem. Soc. **109**, 7761 (1987).
50. A.G. Sikkander and K.A.B. Ahamed. Ind. J. Chem. **31A**, 845 (1992).
51. F.H. Westheimer and A. Novick. J. Chem. Phys. **11**, 506 (1943).
52. D.G. Lee and T. Chen.J. Am. Chem. Soc. **111**, 7534 (1989).
53. D.G. Lee and L.N. Congson. Can. J. Chem. **68**, 1774 (1990).
54. F.H. Westheimer. Chem. Rev. **61**, 265 (1961).
55. L. Melander. Isotope effects on reactions rates. Ronald Press, New York. 1960. p. 11; E.F. Caldin. Chem. Rev. **69**, 135 (1969).
56. H. Maskill. The physical basis of organic chemistry. Oxford University Press, London. 1985. p. 247.

Can. J. Chem. Downloaded from www.nrcresearchpress.com by 92.62.229.171 on 09/08/12
For personal use only.

© 1997 NRC Canada

Synthesis, high-field NMR, X-ray structure, and conformational analysis of a 10-membered diamide disulfide ring

Rabindranath B. Maharajh, James P. Snyder, James F. Britten, and Russell A. Bell

Can. J. Chem. Downloaded from www.nrcresearchpress.com by 92.62.229.171 on 09/08/12
For personal use only.

Abstract: *N,N'*-[Dimethyl-(2,2'-dithiobisacetyl)]ethylenediamine (**1**) has been synthesized in 30% overall yield from *N,N'*-dimethylethylenediamine and thioacetic acid by an improved procedure involving simultaneous deprotection and oxidative cyclization with iodine. This cyclic diamide disulfide exists in solution as a mixture of two *Z,Z* and one *Z,E* disulfide, and amide ring conformers and has been characterized by nuclear Overhauser effect (NOE), ^1H–^1H, ^1H–^{13}C shift-correlated 2D-NMR and molecular modelling studies. Among the *Z,Z* ring conformers Z,Z_1 and Z,Z_2, the former predominates and interconverts with the latter isomer by rotation about the S—S bond with an activation energy of 14.5 ± 1.3 kcal/mol. Coalescence of N-CH_3 signals occurred at ca. 127°C (500 MHz), which corresponded to an approximate barrier to amide rotation of 19.3 kcal/mol. Aromatic solvent-induced shifts in C_6D_6 corroborated molecular mechanics and NOE predictions of amide stereochemistry. The structure of the *Z,E* stereoisomer of **1** has been determined by single-crystal X-ray diffraction at 296 K. A large geminal N-CH_2 inequivalence (>2 ppm in $CDCl_3$) was observed for the *Z,Z* conformers. Proton chemical shifts have been calculated for the conformers of **1** and related molecular fragments with DFT/GIAO theory. Absolute chemical shifts are modelled within 0.2 ppm of experiment. The unusual nonequivalence of geminal N-CH_2 and S-CH_2 protons can be understood as a combination of shielding mechanisms derived from short N-methyl contacts, amide group orientation, and sulfur lone-pair disposition. An implication of these results is the possibility of using α-C*H* (and eventually α-*C*H) shifts to probe the local conformational space in cyclic peptides and other conformationally constrained rings.

Key words: amide/disulfide rotamers, conformational analysis, density functional theory, DFT/GIAO NMR shift calculations, methylene nonequivalence, molecular modelling.

Résumé : On a synthétisé la *N,N'*-[diméthyl-(2,2'-dithiobisacetyl)]éthylènediamine (**1**), avec un rendement global de 30% à partir de la *N,N'*-diméthyléthylènediamine et de l'acide thioacétique, à l'aide d'une méthode améliorée impliquant une déprotection et une cyclisation oxydante simultanées sous l'influence de l'iode. En solution, ce disulfure diamide cyclique existe sous la forme d'un mélange de deux disulfures *Z,Z* et d'un *Z,E*, en plus des conformères du cycle amide; on l'a caractérisé par effet Overhauser nucléaire (eOn), par des études de RMN 2D avec corrélation de déplacements ^1H–^1H et ^1H–^{13}C et des études de modélisation moléculaire. Parmi les conformères *Z,Z* du cycle, Z,Z_1 et Z,Z_2, le premier est prédominant et les deux subissent une interconversion par le biais d'une rotation autour de la liaison S—S avec une énergie d'activation de 14,5 ± 1,3 kcal/mol. La coalescence des signaux se produit aux environs de 127°C (500 MHz); ceci correspond à une barrière de la rotation de l'amide d'environ 19,3 kcal/mol. Les déplacements induits par un solvant aromatique, C_6D_6, ont permis de confirmer les conclusions de la mécanique moléculaire et les prédictions basées sur l'eOn pour la stéréochimie de l'amide. On a déterminé la structure du stéréoisomère *Z,E* de **1** par diffraction des rayons X par un cristal unique, à 296 K. Avec les conformères *Z,Z*, on a observé une importante inéquivalence géminale pour le N-CH_2 (>2 ppm, dans $CDCl_3$). En se basant sur la théorie de la densité fonctionnelle («DGT/GIAO»), on a calculé les déplacements chimiques des protons des conformères du composé **1** et de fragments moléculaires apparentés. On peut faire la modélisation des déplacements chimiques absolus à 0,2 ppm près des valeurs observées expérimentalement. On peut expliquer la non équivalence exceptionnelle des protons géminés des N-CH_2 et S-CH_2 en se faisant appel à une combinaison de mécanismes de blindage dérivés des contacts à courte distance des N-méthyles, de l'orientation du groupe amide et de l'arrangement de la paire d'électrons non partagée du soufre. Ces résultats impliquent qu'il est possible

Received March 19, 1996.

The authors dedicate this manuscript to the memory of Professor Colin J.L. Lock of McMaster University.

R.B. Maharajh.[1] R&D Laboratory, Nu·Pharm Inc., Richmond Hill, ON L4C 5H2, Canada.
J.P. Snyder. Department of Chemistry, Emory University, Atlanta, GA, 30322, U.S.A.
J.F. Britten and R.A. Bell.[1] Department of Chemistry, McMaster University, Hamilton, ON L8S 4M1, Canada.

[1] Authors to whom correspondence may be addressed. Telephone: R.B.M., (905) 884-0470; R.A.B., (905) 525-9140, ext. 23479. Fax: R.B.M., (905) 884-9876. E-mail: R.B.M., ae149@freenet.hamilton.on.ca

© 1997 NRC Canada

d'utiliser les déplacements des α-C*H* (et éventuellement un α-*C*H) comme sonde pour étudier l'espace conformationnel localisé dans les peptides cycliques ainsi que d'autres cycles conformationnellement restreints.

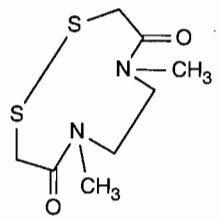
Mots clés : rotamères amide/disulfure, analyse conformationnelle, théorie de la densité fonctionnelle («DFT/GIAO»), calculs de déplacements chimiques de RMN, non équivalence de méthylènes, modélisation moléculaire.

[Traduit par la rédaction]

Introduction

Structures similar to *N,N'*-ethylenebis(2-thioacetamide) are frequent precursors to complexing reagents for technetium and have been used extensively in Tc-based radioimaging work both at research and clinical levels (1–5). In addition to forming very stable Tc complexes (5), these diamide disulfur (DADS) ligands are highly amendable to modification using standard synthetic techniques and commercial reagents and, as such, represent an attractive ligand system to systematically evaluate structure–activity requirements for the development of tissue-specific technetium chelates. To illustrate, N-C_α carboxylated analogues of DADS ligands are currently being investigated in the targeted delivery of radioactivity in bifunctional chelate strategies (5, 6). However, as examples of ^{99m}Tc radiopharmaceuticals employed for imaging the nonexcretory organs are few, further research in this area is highly desirable. This limited success of existing ^{99m}Tc complexes has been ascribed in part to a lack of sufficient lipid solubility required for adequate membrane transport through capillaries and other lipid barriers (7–9).

In a program to develop cyclic diamide disulfides into lipophilic, bifunctional DADS chelators for ^{99m}Tc radioimaging, we noted the complexity of NMR spectra in a number of nonsymmetric derivatives and the dearth of literature on the conformational properties and a reliable synthetic approach to such compounds. Hence, the preparation of the symmetric diamide disulfide **1** was undertaken as both a conformational and synthetic model and we present herein its synthesis, NMR properties, and solid state and solution state structures. An investigation into the conformational properties of such simple ring systems also allows for a better understanding of peptide conformation and an improved approach towards the rational design of conformationally constrained peptides that possess important biological activities (10).



1

Results and discussion

Synthesis

The 10-membered heterocycle **1** was synthesized from 2-mercaptoacetic acid and *N,N'*-dimethylethylenediamine in four steps in 30% overall yield as shown in Scheme 1. Tritylation of thioacetic acid under Lewis acid catalysis readily afforded the *S*-protected acid **2**, which was subsequently reacted with 1,3-dicyclohexylcarbodiimide (DCC) and *N*-hydroxysuccinimide (NHS) to give the activated ester **3**. Treatment of two equivalents of **3** with *N,N'*-dimethylethylenediamine in dry dimethoxyethane allowed for the acylation of both nitrogens and the formation of the diamide **4** in 76% yield. Deprotection of **4** was effected with 1.1 equivalents of iodine in ethanol–acetonitrile and, by maintaining high dilution conditions to preclude intermolecular disulfide formation, in situ intramolecular oxidative cyclization readily generated the monomeric disulfide **1** in 66% yield.

The choice of the *S*-protecting group for thioacetic acid and the method for its cleavage were crucial for the efficiency of the synthesis. The S atom in these compounds is normally protected as aryl thioethers, hemithioacetals, or thioesters (11); however, deprotection frequently requires harsh conditions that can lead to decomposition when sensitive functional groups are present. Moreover, the sulfur products of these acidic or basic deprotection schemes can also engage in side reactions, including acid-catalyzed *N*- to *S*-acyl transfer initiated by SH attack to neighbouring amide groups[2] and disulfide polymerization via thiolate coupling (14, 15). The instability of unprotected sulfur atoms compounded with harsh deprotection methods makes this synthetic strategy less desirable for the development of radioimaging precursors.

For the development of chemically sensitive radiopharmaceuticals incorporating the DADS ligand, an exceedingly mild *S*-deprotection method was required. Iodine has been used in the removal of trityl groups from sulfur with facile, in situ oxidation to acyclic disulfides (16). Moreover, disulfides are stable, readily prepared, and easy to cleave with mild reductants (for example, $SnCl_2$) and as such represent attractive precursors to Tc chelants, particularly in the clinical setting. The synthesis was therefore undertaken with trityl as the sulfur protecting agent and iodine as the deprotectant.

Conformational analysis

(a) ^{1}H and ^{13}C NMR data

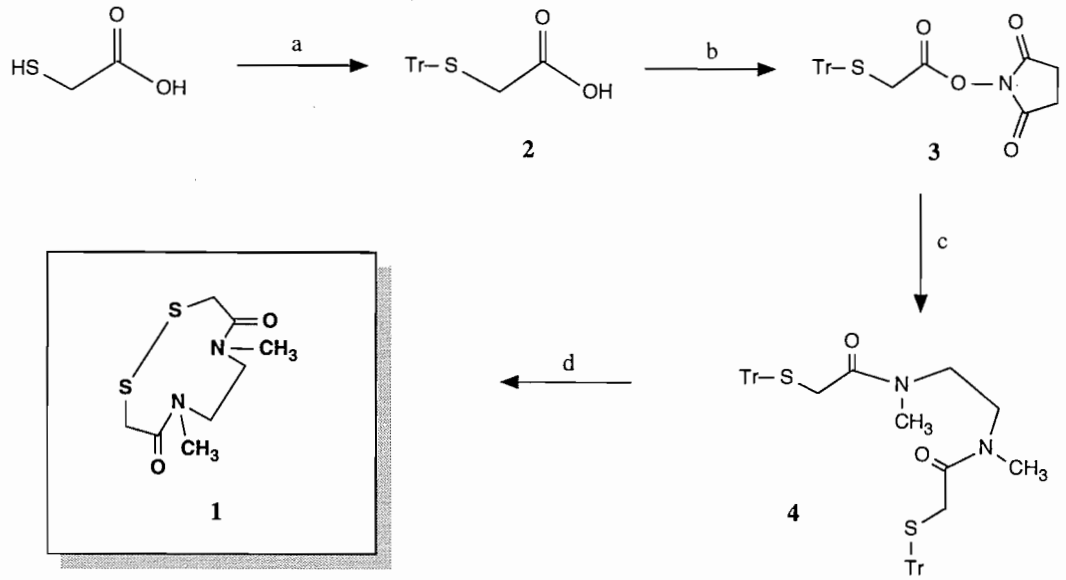
The product (**1**) ran as one spot when examined by thin-layer chromatography and melted over a 1.0°C range, indicating good sample homogeneity. Infrared, Raman, and mass spectra of the product were consistent with its proposed monomeric structure (see Experimental methods). The ^{1}H and ^{13}C NMR

[2] Decomposition of C_{11} substituted DADS fatty acid amide conjugates has been noted in our lab during *S*-detritylation using the CF_3COOH–Et_3SiH method (12). This is suspected to proceed via nucleophilic attack of the unmasked SH group to the C=O function at the C_{11} amide, resulting in a six-membered thiolactone and the corresponding 11-amino fatty acid. This mechanism is based on analogy to ref. 13.

Can. J. Chem. Downloaded from www.nrcresearchpress.com by 92.62.229.171 on 09/08/12
For personal use only.

© 1997 NRC Canada

Scheme 1.



(a) Ph_3C-OH, BF_3·etherate, AcOH, 70°C; (b) NHS, DCC, dry DME, 0–5°C; (c) 0.5 equiv. $CH_3NHCH_2CH_2NHCH_3$, NEt_3, AN; (d) I_2, AN/EtOH, [**4**] = 5mM. NHS = *N*-hydroxysuccinimide; DCC = *N,N'*-dicyclohexylcarbodiimide; DME = dimethoxyethane; AN = acetonitrile.

analyses (Fig. 1 and Tables 1 and 2), however, showed dramatically complex signal profiles despite the established chemical purity of the sample and its symmetry-related, isolated sets of ^1H and ^{13}C nuclei. That this multiplicity of lines arose from the presence of different ring conformers was suggested from the ^{13}C spectrum, which showed 12 lines (Table 2) in the aliphatic region (δ 30–50) rather than the anticipated three.[3] This increased number of lines was rationalized by noting that each amide group can exist in either *Z* or *E* stereochemistry because of restricted amide rotation: this enables the cyclic disulfide to adopt, in principle, three conformations with the amide groups *Z,Z*, *Z,E*, and *E,E*.

(b) ^1H dynamic NMR studies

Variable-temperature ^1H NMR was employed to determine the presence of conformational isomers. Spectra recorded in the temperature range −61.5 to 30.0°C in $CDCl_3$ indicated that the proposed conformers were in slow exchange at room temperature and below. At higher temperatures in DMSO-d_6, interconversion rates increased, as evidenced from the gradual coalescence of all resonances (Fig. 2). However, it was not possible to observe the three signals expected in the regime of fast exchange at 500 MHz, as this would require heating the sample to an impractically high level.

To further confirm the exchange process as restricted amide rotation, the free energy of activation, $\Delta G^{\ddagger}$, was estimated using a modified form of the Eyring formulation (17):

$$[1] \quad \Delta G^{\ddagger} = RT_c[22.96 + \ln(T_c/\Delta\nu)]$$

The coalescence temperature T_c was estimated from Fig. 2 to be about 127°C at 500 MHz, based on the coalescence of the singlets at 2.42 and 2.71 ppm.[4] This afforded $\Delta G^{\ddagger}_{127} \approx 19.3$ kcal/mol. The measured barrier is consistent with those typically reported for substituted *N,N'*-dimethylamides (e.g., dimethylacetamide, $\Delta G^{\ddagger}_{25.2} = 17.4$ kcal/mol; dimethylpropanamide, $\Delta G^{\ddagger}_{25.2} = 16.7$ kcal/mol) (18). Restricted rotation associated with the S—S linkage (19, 20)[5] and ring inversion presumably contributes to this composite $\Delta G^{\ddagger}$, thus magnifying it in relation to typical acyclic amide rotational barriers.

A heteronuclear ^1H–^{13}C 2D NMR shift-correlated experiment at room temperature identified the geminal pairs of diastereotopic protons for *three* geometric isomers and, with the aid of standard chemical shifts, permitted the location of their NCH_2CH_2N groupings (Fig. 3). Two of these appeared as sets of A_2B_2 (or AA'BB') spin systems in the F_1 (^1H) domain, consistent with two symmetrical isomers, and the third as a more complex ABCD spin system for an unsymmetrical isomer. The experiment also enabled the assignment of carbon signals associated with the three isomers. The ^1H–^1H connectivity patterns in each isomer were confirmed through a homonuclear 2D COSY-45 NMR experiment (data not shown).

The data from the 2D and dynamic NMR (DNMR) experiments, as well as patterns in signal multiplicity, were fully consistent with the presence of three, interconvertible, conformational isomers of **1** at room temperature. The amide configurations of these ring conformers have been assigned as Z,Z_1, *Z,E*, and Z,Z_2. The designation Z,Z_1 refers to the major *Z,Z* ring conformer while Z,Z_2 indicates the minor one. These proposed

[3] Signal averaging for lengthy periods revealed the presence of additional signals, which presumably arises from trace amounts of other ring conformers.

[4] Later ascribed to the N-CH_3 resonances of the unsymmetrical *Z,E* ring isomer.

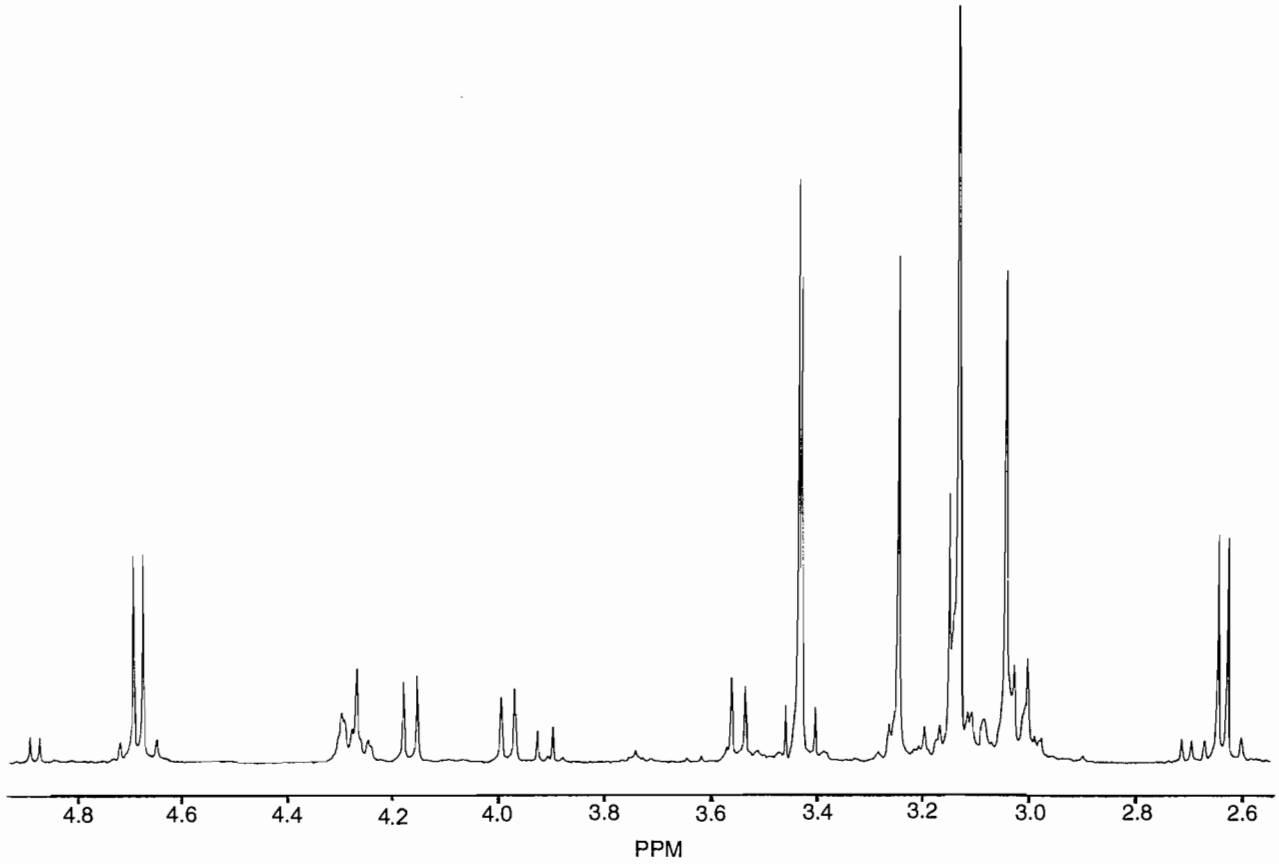
[5] The barrier to S—S rotation in the ring conformers Z,Z_1 and Z,Z_2 is addressed later on.

Can. J. Chem. Downloaded from www.nrcresearchpress.com by 92.62.229.171 on 09/08/12
For personal use only.

© 1997 NRC Canada

Can. J. Chem. Downloaded from www.nrcresearchpress.com by 92.62.229.171 on 09/08/12
For personal use only.

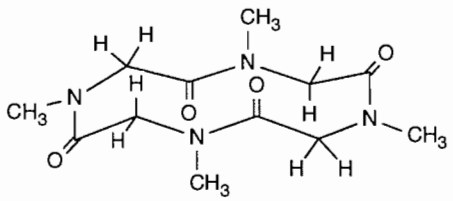
Fig. 1. The 500 MHz ^{1}H NMR spectrum of **1** in $CDCl_3$ at 303 K between 2.5 and 5.0 ppm.



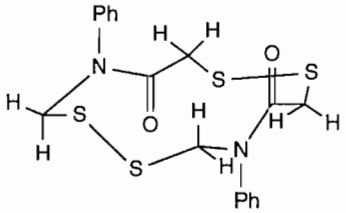
geometries have been shown to be consistent with the results of other experiments, including benzene dilution ^{1}H NMR shifts, nuclear Overhauser effect (NOE) experiments, single-crystal X-ray diffraction studies, molecular modelling, and proton shielding calculations (vide infra).

Proton integrals and ^{13}C resonance intensities (Tables 1 and 2) suggested the following stability trend among the conformers: $Z,Z_1 > Z,E > Z,Z_2$. This finding can be rationalized from an analysis of the sterically driven, conformational preferences governing *N,N'*-dialkylamides: for large-membered lactams, the *Z* stereochemistry is energetically favored over *E* (21). Therefore, the *Z* configuration in **1** can be expected to be the predominant amide stereochemistry in solution. Based on the ratio of intensities of the N-CH_3 ^{13}C signals (Table 2) and, assuming a Boltzmann population distribution at 303 K, the Z,Z_1 ring conformer was favored over the *Z,E* by 0.61 kcal/mol and *Z,E* over the Z,Z_2 by 0.87 kcal/mol. Table 3 presents the corresponding percentage compositions in $CDCl_3$, as well as in DMSO-d_6 and C_6D_6 solvents. The results suggest that the isomeric composition of **1** appeared to be relatively independent of solvent.

The most noteworthy feature in the NMR spectrum of **1** is the large geminal shift differences ($\Delta\delta_{OBS}$) between the N-CH_2 protons of the *Z,Z* and, to a lesser extent, *Z,E* conformers. In $CDCl_3$, the largest $\Delta\delta_{OBS}$ was measured at 2.17 ppm for the minor Z,Z_2 isomer, while the Z,Z_1 and *Z,E* configurations recorded 2.04, 1.18, and 1.26 ppm, respectively (Table 1). The chemical shift differences were invariant with the concentration of **1** in $CDCl_3$, precluding any effects due to intermolecular association. These results suggested that the N-CH_2 (and S-CH_2) groups in the symmetrical *Z,Z* isomers are pairwise



5



6

© 1997 NRC Canada

Table 1. 500 MHz ^{1}H NMR assignments (ppm (multiplicity, integral,[a] amide stereochemistry[b])) for **1** in $CDCl_3$ at 303 K.

	Conformer		
Signal	Z,Z_1	Z,E	Z,Z_2
N-CH_3	3.13(s,~6H)	3.04(s,~3H,*E*) 3.24(s,~3H,*Z*)	3.15(s,~6H)
N-$(CH_2)_2$	2.64(dd,2H)[c] 4.68(dd,2H)[c] ^2J = −13.7 Hz[e] $^3J_{ax\text{-}ax}$ = 11.2 Hz[f] $^3J_{ax\text{-}eq}$ = 4.8 Hz $^3J_{eq\text{-}eq}$ = 1.4 Hz	3.01(m,~1H,*Z*)[c] 4.27(obs[d] m,~1H,*Z*)[c] ^2J = −14.41 Hz 3.09(obs m,~1H,*E*)[c] 4.27(obs m,~1H,*E*)[c] $^3J_{ax\text{-}ax}$ = 11.6 Hz $^3J_{eq\text{-}ax}$ = 3.6, 3.9 Hz $^3J_{eq\text{-}eq}$ = 2.4 Hz	2.71(dd,2H)[c] 4.88(dd,2H)[c] ^2J = −13.5 Hz $^3J_{ax\text{-}ax}$ = 11.1 Hz $^3J_{ax\text{-}eq}$ = 5.1 Hz $^3J_{eq\text{-}eq}$ = 1.3 Hz
S-CH_2	3.42(AB d,2H)[c] 3.45(AB d,2H)[c] ^2J = −12.7 Hz	3.55(AB d,1H,*E*)[c] 3.99(AB d,1H,*E*)[c] ^2J = −13.2 Hz 3.03(obs AB d,~1H,*Z*)[c] 4.16(AB d,1H,*Z*)[c] ^2J = −12.8 Hz	3.19(obs AB d,~2H)[c] 3.91(AB d,2H)[c] ^2J = −14.7 Hz

[a]Integrals are relative within a conformer series.
[b]Assignments of amide stereochemistry was based on NOE, MM2, and X-ray crystallographic data.
[c]Geminally coupled (determined from ^{1}H–^{13}C chemical shift correlated experiment).
[d]Obscured.
[e]All ^2J couplings were assumed to be negative.
[f]All ^3J couplings were measured from MMX-calculated structures.

Table 2. 126 MHz *J*-modulated ^{13}C NMR assignments (ppm (relative intensity, amide stereochemistry[a])) for **1** in $CDCl_3$ at 303 K.

	Conformer		
Signal	Z,Z_1	Z,E	Z,Z_2
N-CH_3	36.58(–98)	33.59(–17,*E*) 41.17(–18,*Z*)	37.10
S-CH_2	36.98(144)	37.49(31,*Z*) 42.17(20,*E*)	40.69(18)
N-$(CH_2)_2$	44.23(127)	48.20(26) 48.99(22)	46.17(16)
CO-NH	166.55(14)	168.84(6) 169.46(5)	—

[a]Stereochemical assignments are based on the analysis of NOE and ^{1}H–^{13}C shift correlated data.

equivalent or enantiotopic and that the N-CH_2 protons have markedly different magnetic environments. Large geminal proton chemical shift differences have been observed in a few semi-rigid, polyamide systems (22–24). In cyclotetrasarcosyl, **5**, the isochronous pairs of the *N*-methylene protons are separated by about 2 ppm (in $CDCl_3$) (23), while one set of those for the tetrathiacyclododecane **6** have a chemical shift difference of 1.78 ppm (in $CDBr_3$) (24).

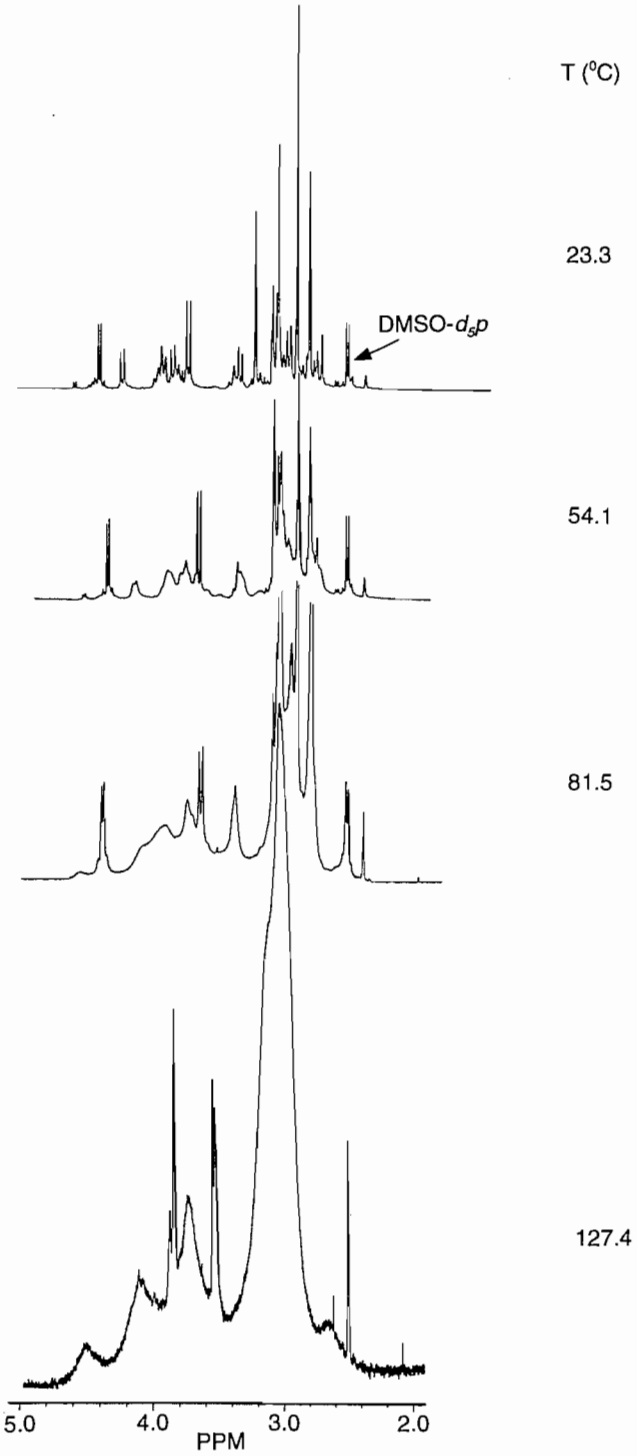
Invariably, such large (i.e., >1.5 ppm) N-carbinyl splittings appear to be associated with the sterically favored *Z* amide stereochemistry, which places these protons in or close to the respective amide planes pointing toward the C=O groups

© 1997 NRC Canada

Can. J. Chem. Downloaded from www.nrcresearchpress.com by 92.62.229.171 on 09/08/12
For personal use only.

Can. J. Chem. Downloaded from www.nrcresearchpress.com by 92.62.229.171 on 09/08/12
For personal use only.

Fig. 2. 500 MHz ^{1}H NMR variable temperature spectra of **1** in DMSO-d_6.

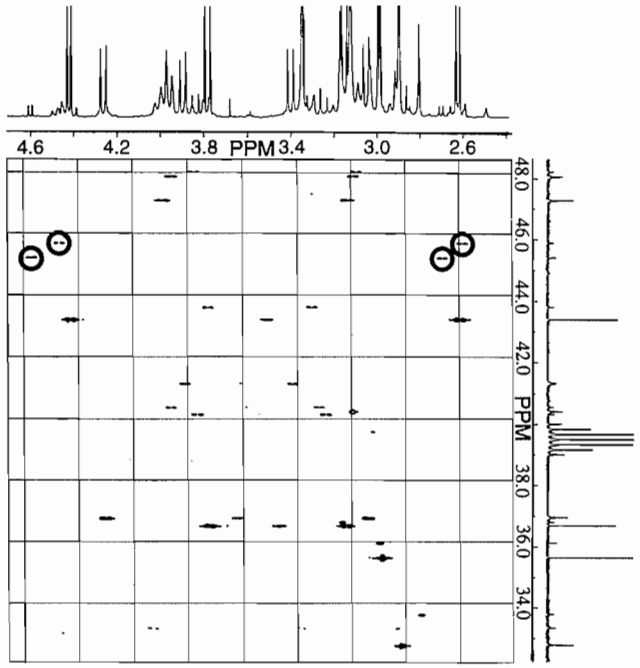


(25).

(c) NOE data

To further define the solution state conformations of **1**, NOE experiments were carried out in $CDCl_3$ at 303 K on signals of the two major isomers. Representive difference NOE spectra for these isomers are shown in Figs. 4 and 5. The inserts illustrate NOE interactions for a given geometric isomer, together with their interatomic distances as determined from MM2-calculated structures.

Fig. 3. ^{1}H-^{13}C chemical shift correlated spectra of **1** in DMSO-d_6 at 303 K. The diastereotopic N-CH_2 protons of the *Z,Z* isomers are circled.



In the major isomer, irradiation of the AB S-CH_2 quartet at 3.43 ppm resulted in a large NOE of the *N*-methyl protons at 3.13 ppm (Fig. 4(*a*)), indicative of a pseudoaxial S-C*H* and N-CH_3 proximity about a *Z* amide configuration. This enhancement was not expected for an *E* stereochemistry, as a larger distance would separate the appropriate protons. The observation of a NOE between the shielded N-CH_2 (2.64 ppm) and N-CH_3 protons (Fig. 4(*b*)) was consistent with a *Z* geometry, where the former protons occupy a pseudoequatorial position *syn* to the adjacent CH_3 group. Irradiation of the N-CH_3 resonance caused NOEs at not only the expected positions of the shielded N-CH_2 and S-CH_2 protons, but also at the deshielded N-C*H* at 4.68 ppm (Fig. 4(*c*)). The weaker enhancement of the deshielded N-C*H* (relative to the shielded protons) suggested a transannular proximity with its *opposite* N-CH_3 group — an interaction made possible through pseudoaxial configurations[6] for both groups. Thus, a C_2 symmetric *Z,Z* conformation best matched the NOE observations noted for the major solution conformation of **1** (see **1a**, Fig. 8).

In the nonsymmetric isomer, irradiation of the S-C*H* signal at 3.55 ppm induced a strong enhancement of its geminal partner at 3.99 ppm as well as a weaker enhancement of the N-CH_2 protons at 4.27 ppm (Fig. 5(*a*)). According to molecular models, the latter NOE was only possible between the pseudoaxial S-C*H* (H(3b)) and the pro-*R* N-C*H* (H(6b))

[6] N-CH_2 protons that occupy either pseudoaxial or pseudoequatorial positions in the symmetrical *Z,Z* isomers are denoted as H_{ax} or H_{eq}, respectively.

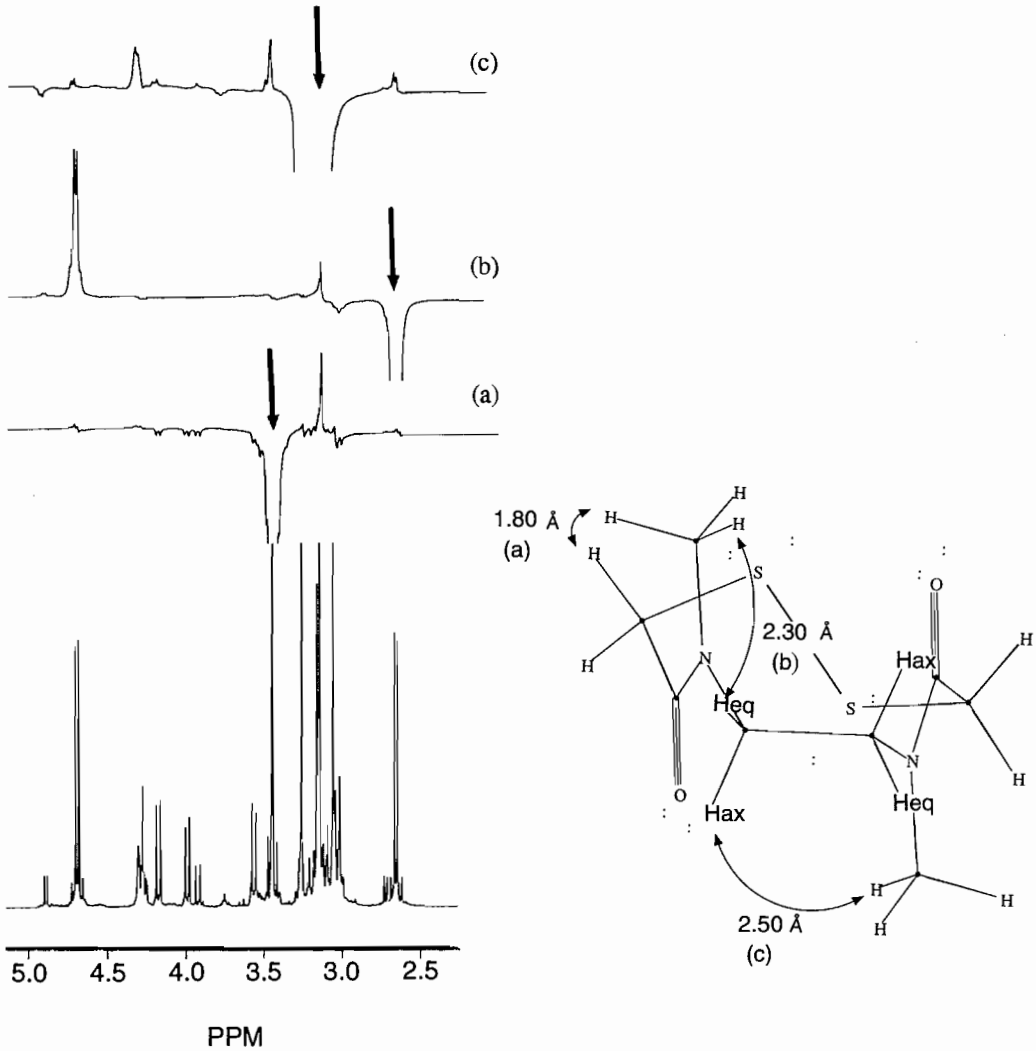
© 1997 NRC Canada

Table 3. Calculated and observed population distributions for conformers Z,Z_1, Z,E, and Z,Z_2 at 303 K.

Conformer	Calcd. E_{Steric} (kcal/mol)	Calcd. population distribution (%)[a]	Observed population distributions[a,b] (%)		
			$CDCl_3$	DMSO-d_6[c]	C_6D_6
Z,Z_1 (**1a**)	0	82	53	54	54
Z,E (**1c**)	2.03	3	39	29	38
Z,Z_2 (**1b**)	1.15	15	8	6	8

[a]According to the Boltzmann relationship: $n_2/n_1 = \exp(-\Delta G/RT)$, T = 303 K.
[b]Based on ^{1}H NMR integrals.
[c]Small amounts (<12%) of additional conformers were detected and measured using ^{13}C NMR intensities.

Fig. 4. 500 MHz NOE difference spectra (*a*)–(*c*) of the Z,Z_1 stereoisomer of **1** in $CDCl_3$ at 303 K. The irradiated peak is indicated at the arrowed frequency.

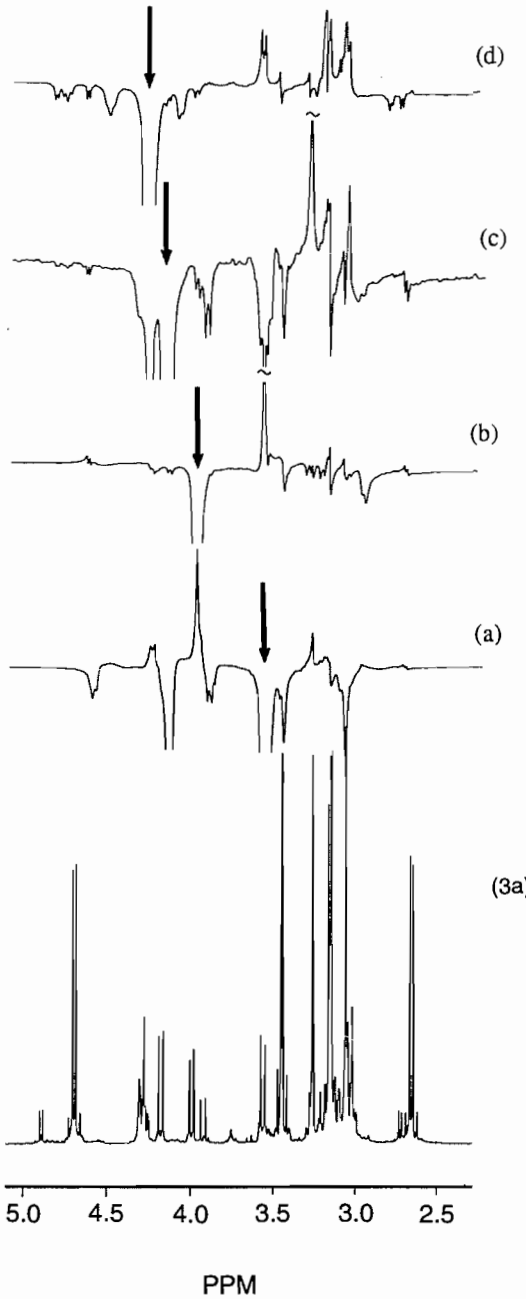


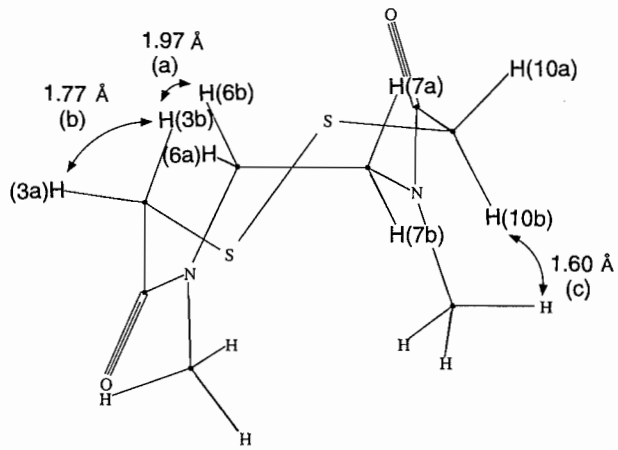
about the *E* amide group. The X-ray structure and molecular mechanics calculations (Figs. 6 and 8, **1c**) supported this result: with an interatomic separation of 1.97 Å, the electron clouds of these protons were overlapping by about 0.4 Å. The positive N-CH_3 enhancement at 3.24 ppm was most likely a result of saturation transfer (26) to S-C*H* (H(10a)) at 4.16 ppm by which it is strongly relaxed (Fig. 5(*c*)). Barring geminal enhancements, NOEs were not observed for the second *E* S-C*H* (H(3a)) signal at 3.99 ppm: this was consistent with a pseudoequatorial position (Fig. 5(*b*)).

© 1997 NRC Canada

Can. J. Chem. Downloaded from www.nrcresearchpress.com by 92.62.229.171 on 09/08/12
For personal use only.

Fig. 5. 500 MHz NOE difference spectra (*a*)–(*d*) of the *Z,E* stereoisomer of **1** in $CDCl_3$ at 303 K. The irradiated peak is indicated at the arrowed frequency.





Irradiation of the S-C*H* (H(10a)) resonance at 4.16 ppm (Fig. 5(*c*)) induced strong enhancement of the downfield N-CH_3 protons at 3.24 ppm, which was indicative of a di-pseudoaxial disposition of protons about a *Z* amide bridge. Examination of the *Z,E* molecular model revealed that the point of closest approach of these protons was ca. 1.6 Å. The NOE was therefore consistent with a *Z* amide stereochemistry and supported the prediction (27) that the *downfield* N-CH_3 (and N-CH_3 by ^1H–^{13}C shift correlation, Fig. 3) belonged to the *Z* amide group in the *Z,E* conformer.

Irradiating the co-resonating, downfield N-CH_2 protons (H(6b) and H(7a)) at 4.27 ppm created moderate NOEs at 3.55, 3.10, and 3.01 ppm (Fig. 5(*d*)). The 3.55 ppm enhancement arises from interaction of H(6b) with H(3b) (as in Fig. 5(*a*)). The latter two enhancements most likely arose from geminal interactions with the shielded *Z* and *E* N-CH_2 protons (H(7b) and H(6a), respectively) and was further evidence that the nonsymmetric component of **1** (see **1c**, Fig. 8) possessed a *Z,E* geometry.

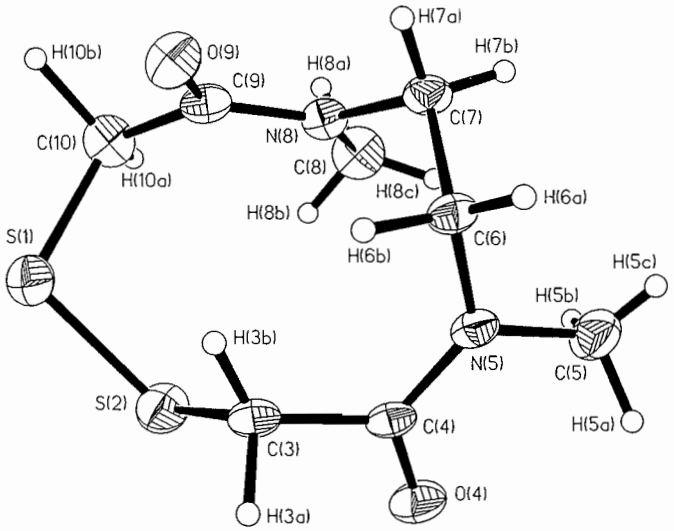
Unfortunately, it was not possible to obtain definitive NOE data for the Z,Z_2 isomer, largely because of its low abundance and intensity complications arising from saturation transfer from more abundant isomers. Although saturation transfer effects were also observed for the *Z,E* and, to a lesser extent,

© 1997 NRC Canada

Can. J. Chem. Downloaded from www.nrcresearchpress.com by 92.62.229.171 on 09/08/12
For personal use only.

Can. J. Chem. Downloaded from www.nrcresearchpress.com by 92.62.229.171 on 09/08/12
For personal use only.

Fig. 6. The crystal structure of the *Z,E* isomer of **1**. 30% probability thermal ellipsoids are shown for non-hydrogen atoms.



the Z,Z_1 conformers, their relatively intense signals allowed for the extraction of useful conformational information from their NOE spectra.

(d) Aromatic solvent-induced shift (ASIS) studies

The lack of NOE data for the Z,Z_2 stereoisomer prompted an ASIS investigation to determine its solution state geometry. Studies on a variety of amides (28–31) have consistently showed that aromatic solvents shift the signals of the N-C_α protons *trans* to the carbonyl group *upfield* to a greater extent than those at the *cis* position. By comparison of their relative proton shifts in aromatic and nonaromatic solvents, these resonances can be assigned to a particular amide stereochemistry.

The ^{1}H NMR spectrum of **1** in benzene-d_6 revealed that the N-CH_3 (and N-CH_2) resonances of both major (Z,Z_1) and minor (Z,Z_2) isomers exhibited very similar upfield aromatic solvent-induced shifts (0.56 and 0.61 ppm relative to the $CDCl_3$ shifts, data not shown). Since the NOE experiments confirmed the major isomer to have the *Z,Z* geometry, the benzene dilution experiments suggested that the minor isomer also possesses the *Z,Z* configuration. The relatively large ASIS values were also consistent with a *Z* geometry (32). An *E,E* stereochemistry in the minor isomer would have resulted in a smaller ASIS value and an increased separation between the N-CH_3 resonances of the major and minor isomers upon benzene-d_6 dilution. It is worth noting that in benzene-d_6, the N-CH_2 splittings for the Z,Z_1 and Z,Z_2 ring conformers increased to 2.58 and 2.69 ppm, respectively.

(e) Solid state structure analysis

An X-ray diffraction study of **1** was undertaken to establish unambiguously the geometry that could give rise to the enormous NMR shift differences observed for the geminal methylene protons.

The geometry and numbering of the X-ray structure of **1** is shown in Fig. 6; atomic coordinates, bond length, and bond angles are listed in Tables 4–8. As the structure analysis revealed, **1** crystallized with the *Z,E* geometry. This was a surprising result since NMR data had shown the Z,Z_1 isomer to be the dominant geometry in solution (Table 3). A survey of the bond angles and bond lengths of **1** indicated no unusual deviations from normal values. The disulfide and amide torsional angles (Table 7) are very close to ground state values (i.e., 90° and planarity, respectively) indicating low torsional strain in the *Z,E* ring.

Table 4. Atomic coordinates ($\times 10^4$) and equivalent isotropic displacement coefficients ($Å^2 \times 10^3$).

Atom	*x*	*y*	*z*	U_{eq}[a]
S(1)	2354(2)	581(2)	1211(1)	57(1)
S(2)	1815(2)	2637(2)	2470(1)	56(1)
C(3)	2612(7)	4613(7)	1793(5)	40(2)
C(4)	3905(7)	6481(7)	2911(4)	37(2)
O(4)	3040(6)	6847(6)	3814(3)	55(2)
N(5)	5926(6)	7663(5)	2905(4)	38(2)
C(5)	7114(9)	9380(8)	4057(5)	60(3)
C(6)	7089(7)	7342(7)	1883(4)	37(2)
C(7)	8656(7)	6622(7)	2219(5)	39(2)
N(8)	7584(6)	4821(5)	2511(3)	35(2)
C(8)	7751(9)	4980(8)	3888(5)	55(3)
C(9)	6531(7)	3148(7)	1506(5)	39(2)
O(9)	6581(6)	3115(5)	382(3)	50(2)
C(10)	51177(9)	1295(8)	1766(5)	49(3)

[a]Equivalent isotropic *U* defined as one third of the trace of the orthogonalized U_{ij} tensor.

Table 5. Bond lengths (Å) with estimated standard deviations in parentheses.

Bond	Length	Bond	Length
S(1)—S(2)	2.035(2)	S(1)—C(10)	1.835(6)
S(2)—C(3)	1.836(6)	C(3)—C(4)	1.517(6)
C(4)—O(4)	1.229(7)	C(4)—N(5)	1.342(6)
N(5)—C(5)	1.468(6)	N(5)—C(6)	1.461(7)
C(6)—C(7)	1.520(9)	C(7)—N(8)	1.466(7)
N(8)—C(8)	1.479(7)	N(8)—C(9)	1.353(5)
C(9)—O(9)	1.234(7)	C(9)—C(10)	1.515(8)

The unit cell contains two *Z,E* molecules of **1**, which are related by a center of inversion. Molecules stack in columns with a high degree of packing efficiency given the unsymmetrical nature of the *Z,E* isomer. The most significant intermolecular contact is O(4)···C(8), which is 3.23 Å. Intramolecular nonbonding contacts were observed between O(9) and H(7a), and between H(3b) and H(6b). These nuclei, separated by 2.35 Å and 2.01 Å, respectively, are within the sum of the accepted van der Waals radii for oxygen and hydrogen (1.4–1.6 and 1.2 Å, respectively) (33, 34). These contacts may contribute to the rather large NMR shift differences observed for geminal hydrogen nuclei of the *Z,E* conformation (vide infra).

The excellent agreement between the crystal structure of the *Z,E* isomer and the NOE-derived conformational model established a link to proton shift assignments. The direction and magnitude of proton shifts may be qualitatively explained by the positions of the geminal protons relative to

© 1997 NRC Canada

Table 6. Bond angles (deg) with estimated standard deviations in parentheses.

Bond	Angle	Bond	Angle
S(2)-S(1)-C(10)	104.0(2)	S(1)-S(2)-C(3)	104.4(2)
S(2)-C(3)-C(4)	106.6(4)	C(3)-C(4)-O(4)	117.6(4)
C(3)-C(4)-N(5)	120.5(4)	O(4)-C(4)-N(5)	122.0(4)
C(4)-N(5)-C(5)	117.2(4)	C(4)-N(5)-C(6)	125.8(3)
C(5)-N(5)-C(6)	116.9(4)	N(5)-C(6)-C(7)	112.9(4)
C(6)-C(7)-N(8)	111.4(4)	C(7)-N(8)-C(8)	117.1(3)
C(7)-N(8)-C(9)	117.7(4)	C(8)-N(8)-C(9)	125.1(5)
N(8)-C(9)-O(9)	121.3(5)	N(8)-C(9)-C(10)	119.2(5)
O(9)-C(9)-C(10)	119.4(4)	S(1)-C(10)-C(9)	108.8(5)

Table 7. Torsional angles (deg) with estimated error in parentheses.

Bond	Angle	Bond	Angle
C(10)-S(1)-S(2)-C(3)	85.9(0.3)	S(2)-S(1)-C(10)-C(9)	−69.2(0.4)
S(2)-S(1)-C(10)-H(10A)	61.7(0.4)	S(2)-S(1)-C(10)-H(10B)	−170.5(0.3)
S(1)-S(2)-C(3)-C(4)	−135.8(0.3)	S(1)-S(2)-C(3)-H(3A)	115.4(0.3)
S(1)-S(2)-C(3)-H(3B)	−5.9(0.3)	C(8)-N(8)-C(9)-O(9)	−175.1(0.6)
C(8)-N(8)-C(8)-H(8B)	−43.3(0.9)	C(7)-N(8)-C(9)-O(9)	4.5(0.8)
C(7)-N(8)-C(9)-C(10)	−172.4(0.5)	C(9)-N(8)-C(8)-H(8B)	−43.2(0.9)
C(9)-N(8)-C(8)-H(8C)	−162.3(0.5)	C(9)-N(8)-C(8)-H(8A)	59.1(0.6)
C(7)-N(8)-C(8)-H(8B)	137.2(0.6)	C(7)-N(8)-C(8)-H(8C)	18.1(0.8)
C(7)-N(8)-C(8)-H(8A)	−120.5(0.5)	C(9)-N(8)-C(7)-C(6)	79.8(0.6)
C(9)-N(8)-C(7)-H(7A)	−32.4(0.7)	C(9)-N(8)-C(7)-H(7B)	−154.5(0.5)
C(8)-N(8)-C(7)-C(6)	−100.5(0.5)	C(8)-N(8)-C(7)-H(7A)	147.2(0.5)
C(8)-N(8)-C(7)-H(7B)	25.1(0.7)	C(4)-N(5)-C(6)-C(7)	−102.5(0.6)
C(4)-N(5)-C(6)-H(6A)	131.9(0.6)	C(4)-N(5)-C(6)-H(6B)	20.4(0.8)
C(5)-N(5)-C(6)-C(7)	74.1(0.6)	C(5)-N(5)-C(6)-H(6A)	−51.5(0.7)
C(5)-N(5)-C(6)-H(6B)	−163.0(0.5)	C(6)-N(5)-C(4)-O(4)	179.5(0.6)
C(6)-N(5)-C(4)-C(3)	0.3(0.9)	C(5)-N(5)-C(4)-O(4)	2.9(0.9)
C(5)-N(5)-C(4)-C(3)	−176.3(0.6)	C(6)-N(5)-C(5)-H(5A)	143.4(0.6)
C(6)-N(5)-C(5)-H(5B)	−111.0(0.6)	C(6)-N(5)-C(5)-H(5C)	11.4(1.1)
C(4)-N(5)-C(5)-H(5A)	−39.7(0.9)	C(4)-N(5)-C(5)-H(5B)	65.9(0.7)
C(4)-N(5)-C(5)-H(5C)	−171.8(0.8)	N(5)-C(6)-C(7)-N(8)	57.5(0.4)
N(5)-C(6)-C(7)-H(7A)	174.3(0.3)	N(5)-C(6)-C(7)-H(7B)	−67.1(0.5)
H(6A)-C(6)-C(7)-N(8)	−176.0(0.4)	H(6A)-C(6)-C(7)-H(7A)	−59.2(0.5)
H(6A)-C(6)-C(7)-H(7B)	59.4(0.6)	H(6B)-C(6)-C(7)-N(8)	−66.0(0.5)
H(6B)-C(6)-C(7)-H(7A)	50.8(0.5)	H(6B)-C(6)-C(7)-H(7B)	169.4(0.4)
N(8)-C(9)-C(10)-S(1)	109.0(0.5)	N(8)-C(9)-C(10)-H(10A)	−12.6(1.0)
N(8)-C(9)-C(10)-H(10B)	−144.2(0.5)	O(9)-C(9)-C(10)-S(1)	−68.1(0.7)
O(9)-C(9)-C(10)-H(10A)	170.4(0.6)	O(9)-C(9)-C(10)-H(10B)	38.8(0.7)
O(4)-C(4)-C(3)-S(2)	−58.2(0.7)	O(4)-C(4)-C(3)-H(3A)	59.5(0.7)
O(4)-C(4)-C(3)-H(3B)	−174.1(0.6)	N(5)-C(4)-C(3)-S(2)	121.0(0.5)
N(5)-C(4)-C(3)-H(3A)	−121.3(0.6)	N(5)-C(4)-C(3)-H(3B)	5.2(1.0)

their adjacent carbonyl group: in general, a proton will be increasingly deshielding as it approaches the plane and (or) midpoint of a carbonyl group (25). In the *Z* amide system, H(7a) and H(7b) (see Fig. 6) are 10.4° and 13.9° out of the amide plane defined by atoms O(9)-C(9)-N(8) and are located 2.36 and 3.36 Å, respectively, from the midpoint of the C═O bond. Thus, H(7a) should resonate *downfield* (4.27 ppm) from H(7b) (3.01 ppm). Similarily, H(6b) and H(6a) of the *E* amide are 170.6° and 151.6° removed from the O(4)-C(4)-N(5) plane and are situated at distances of 3.27 and 3.65 Å, respectively, from the midpoint of the carbonyl bond. Since H(6b) is "closer" to its adjacent amide group, it should appear downfield (4.27 ppm) of its geminal partner (3.09 ppm). It is interesting to note that the very similar deshielding influences on H(7a) and H(6b) appear to result from two different orientations of the protons, namely, H(7a) is close to the O atom of one C═O group, while H(6b) is near the C atom of the other. The ab initio shift calculations (see Table 12) provided addi-

Can. J. Chem. Downloaded from www.nrcresearchpress.com by 92.62.229.171 on 09/08/12
For personal use only.

© 1997 NRC Canada

Fig. 7. The 25 MHz CP-MAS ^{13}C spectrum of **1** at 303 K.

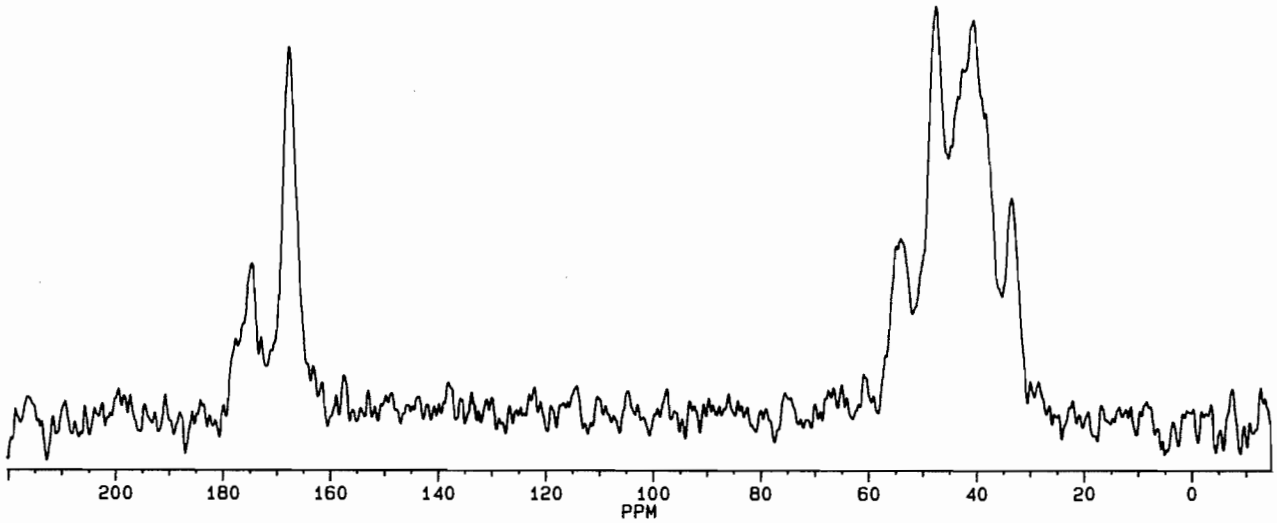


Table 8. Hydrogen atom coordinates ($\times 10^4$) and equivalent isotropic displacement coefficients ($Å^2 \times 10^3$).

Atom	*x*	*y*	*z*	*U*
H(3A)	1310	4855	1499	80
H(3B)	3234	4124	1042	80
H(5A)	6271	10070	4465	80
H(5B)	7334	8860	4893	80
H(5C)	8323	10241	4063	80
H(6A)	7774	8433	1645	80
H(6B)	5952	6293	960	80
H(7A)	9204	6338	1359	80
H(7B)	9867	7622	2946	80
H(8A)	8451	4127	3840	80
H(8B)	6348	4137	3992	80
H(8C)	8162	6271	4375	80
H(10A)	5285	1229	2691	80
H(10B)	5578	231	904	80

tional confirmation of the above qualitative assessment of proton assignments.

To further assess the relationship between the solution and solid state geometries of **1**, the cross-polarization, magic angle spinning (CP-MAS) ^{13}C NMR spectrum of a larger sample of crystalline **1** (0.10 g) was determined in the solid state at 25.2 MHz (Fig. 7). Unfortunately, excessive broadening of the ^{13}C resonances caused by dipolar coupling to ^{14}N nuclei, as well as signal overlap and sensitivity complications, prevented an unequivocal correlation of characteristic shifts between the solid state and solution state spectra in the 30–50 ppm range. Spectra recorded at a higher field and (or) higher sample concentration would probably resolve this inadequacy.

An interesting outcome of the solid state experiment, however, was noted in the carbonyl region: two broad signals of unequal intensity (167.30 and 174.39 ppm) suggested the presence of at least two conformers in the sample. If the recrystallized sample of **1** consisted *only* of the *Z,E* geometric isomer, then only two, *equally intense* resonances should be observed for the carbonyls. Based on chemical shift and intensity comparisons with the solution state ^{13}C data (Table 2), the more intense signal at 167.30 ppm was ascribed to the Z,Z_1 structure, while the unresolved resonance at 174.39 ppm was assigned to the *Z,E* conformer. The observation of two species in the solid state NMR could be rationalized by the presence of both *Z,Z* and *Z,E* crystals in the sample. The rather high barriers to amide isomerization could promote the crystallization of the *Z,Z* and *Z,E* amide ring conformers into *separate* lattice structures. Examples of acyclic monoamides have been reported to crystallize in either the *Z* or *E* geometry, with only one geometric rotamer in each unit cell (35).

Computational analysis

While the X-ray structure provided a link between the ^1H NMR chemical shift and geometry for the *Z,E* isomer, no such benefits were available for the *Z,Z* isomers. Consequently, a number of computational methods were investigated to aid in chemical shift assignment and to provide insight into the origins of the unusually large N-CH_2 anisochronism and its apparent absence for the S-CH_2 protons.

(a) MMX calculations

Molecular mechanics calculations were performed using PCMODEL (version 4.0) to evaluate the conformational geometries and energies of the Z,Z_1 and Z,Z_2 structures. From over 90 unique starting geometries, five conformers were found for **1** within 5 kcal/mol of the global minimum structure (Table 9, Fig. 8). Conformers **1a** (*Z,Z*), **1b** (*Z,Z*), and **1c** (*Z,E*) agreed well with the structural models inferred from NOE, thermodynamic, X-ray, and NMR symmetry data. Based on this correlation, the observed conformers in the NMR spectra of **1** — Z,Z_1, Z,Z_2, and *Z,E* — were proposed to have similar structures as **1a**, **1b**, and **1c**, respectively.

The *Z,E* isomer (Fig. 6) was taken as the source of the unsymmetrical set of NMR resonances and, among the set of *Z,E* isomers, **1c** provided the best correlation between calcu-

© 1997 NRC Canada

Can. J. Chem. Downloaded from www.nrcresearchpress.com by 92.62.229.171 on 09/08/12
For personal use only.

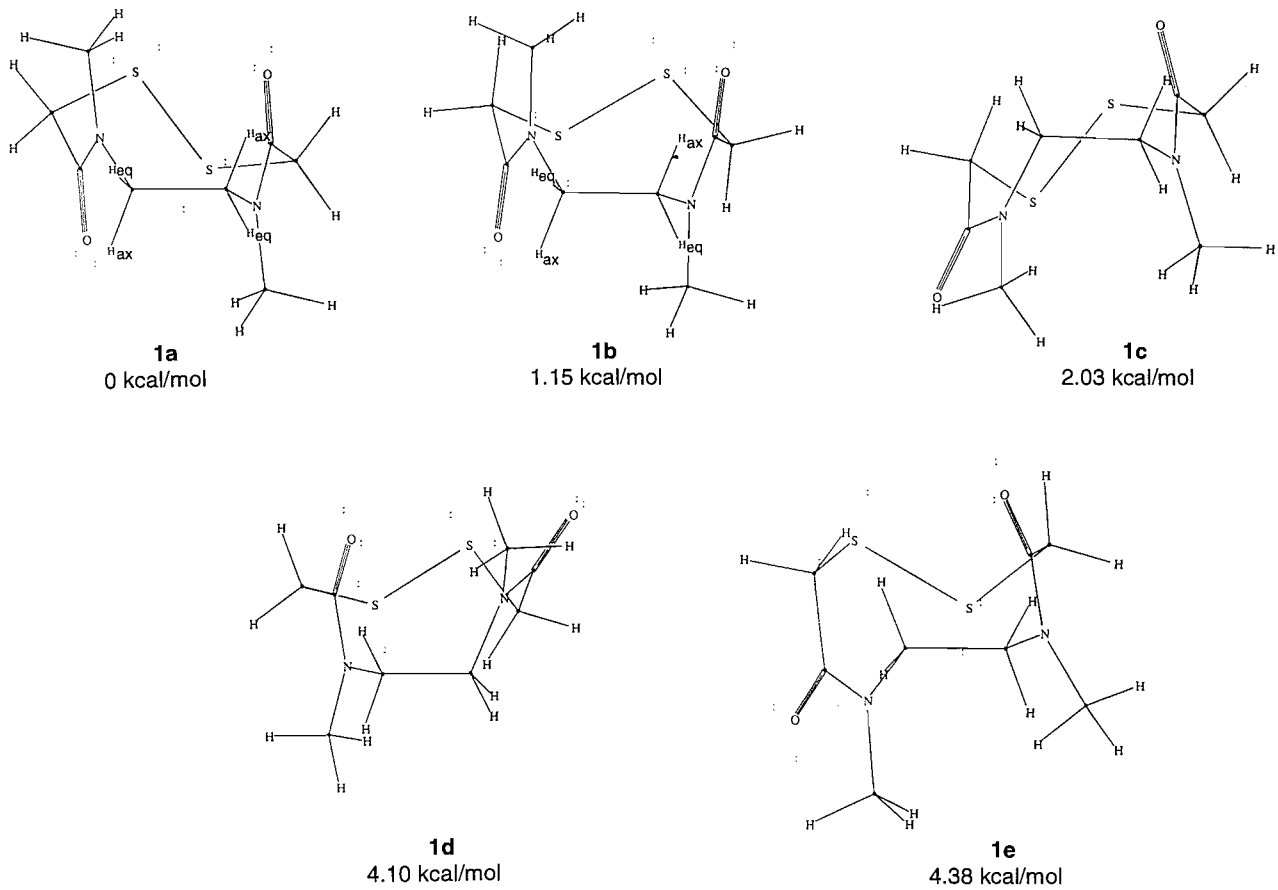
Can. J. Chem. Downloaded from www.nrcresearchpress.com by 92.62.229.171 on 09/08/12
For personal use only.

Table 9. Characterization data for the five lowest energy MMX conformers (**1a–1e**) of **1**.

Conformer	E_{Steric}[a] (kcal/mol)	Symmetry group	Disulfide chirality[b]	C-S-S-C torsional angle (deg)	CH_3-N-C=O torsional angle (deg)		$C\text{-}C_{sp2}\text{-}N$ bond angle (deg)		S-S bond length (Å)
					E	*Z*	*E*	*Z*	
1a (*Z,Z*)	0	C_2	R	−104.2	—	177.2	—	119.3	2.073
					—	177.2	—	119.3	
1b (*Z,Z*)	1.15	C_2	L	94.6	—	171.8	—	119.7	2.073
					—	172.4	—	119.6	
1c (*Z,E*)	2.03	—	L	86.9	1.8	173.1	121.5	120.0	2.070
1d (*Z,E*)	4.10	—	L	87.3	11.1	178.0	120.4	119.4	2.072
1e (*Z,E*)	4.38	—	R	−82.2	0.9	173.0	121.0	119.4	2.070
X-ray (*Z,E*)	—	—	L	85.9	2.9	175.1	120.5	119.2	2.035

[a]Relative steric energy.
[b]R = right-handed chirality; L = left-handed chirality.

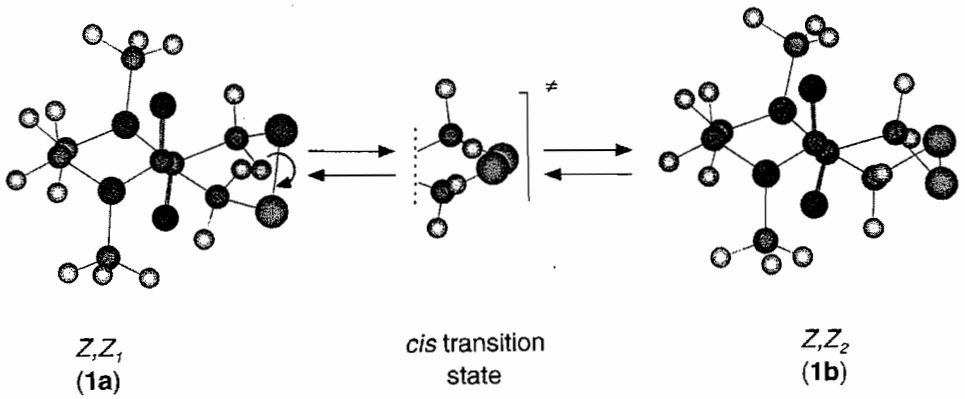
Fig. 8. Stick plots of the five lowest MMX energy conformers of **1** (**1a–1e**). The ethylene moiety is located at the front of each conformation and is aligned along the *x*-axis for all plots.



lated and experimental Boltzmann distributions (see Table 3). Moreover, when **1c** was overlapped with the X-ray structure in PCMODEL, it was evident that they were similar (RMS deviation of atoms = 0.037 Å). To achieve a more realistic comparison, conformational changes that might be imposed on **1** by crystal lattice forces were removed from the X-ray structure by subjecting the molecule to the PCMODEL force field energy minimization program. The observed change amounted to approximately 0.6 kcal/mol energy loss upon minimization. The resultant "minimized X-ray" structure was then superimposed on **1c** and **1d** to afford a virtually complete overlay with **1c** (RMS deviation of atoms = 0.021 Å) but gave a poorer alignment with **1d** (RMS deviation of atoms = 0.198 Å). Molecular mechanics had thus accurately predicted the solid

© 1997 NRC Canada

Fig. 9. Ball and stick plots of the MMX-calculated diastereomers **1a** and **1b**, illustrating rotational isomerization about the S—S bond.



Can. J. Chem. Downloaded from www.nrcresearchpress.com by 92.62.229.171 on 09/08/12
For personal use only.

state geometry of the *Z,E* conformer. This fact, coupled with the strong similarities between NOE and computed structural models, suggested that the MM2 force field was a reasonable probe for generating the solution state conformations of **1**. Conformer **1e** is simply the enantiomer of **1c**.

Conformers **1a** and **1b** possess C_2 symmetry and an antiparallel,[7] *Z,Z* configuration with both amide functions essentially coplanar. This antiparallel *Z,Z* arrangement has been reported for other *N*-substituted polyamide heterocycles, including cyclic amides **5** and **6** (23, 24). Steric and electronic factors may account for the configurational preference found in these systems. For example, in the parallel conformation, transannular methyl–methyl contacts and a large internal dipole moment (resulting from the sum of the moments from the parallel C═O groups) will undoubtedly be quite destabilizing.

Analysis of the molecular modelling data and mechanical models led to the conclusion that isomers Z,Z_1 and Z,Z_2 are disulfide ring conformers. At room temperature, interconversion of these rotational isomers was sufficiently slow on the NMR time scale to allow detection by ^{13}C NMR spectroscopy (Table 2). Interconversion occurs presumably through the *cis* transition state by ca. 180° rotation about the asymmetric S—S bond (Fig. 9) and a ^{13}C DNMR study was carried out with the objective of validating the molecular modelling results.

(b) Measurement of the S—S rotational barrier for the $Z,Z_1 \rightleftarrows Z,Z_2$ *equilibrium via* ^{13}C *DNMR*

The simple Arrhenius equation (eq. [2]) was used because previous studies on conformational processes in reasonably inert solvents have shown that $\Delta G^{\ddagger}$ values vary only slightly with temperature (36) and lie within the range of experimental error.

$$[2] \quad k = A \exp(-\Delta G^{\ddagger}/RT)$$

Warming a sample of **1** in DMSO-d_6 from 25.0 to 56.7°C resulted in a temperature-dependent broadening and a subtle high-field migration of the Z,Z_2 N-C_α signal at 45.4 ppm. Rate constants, *k*, for this chemical exchange process were evaluated using the complete bandshape (CBS) method (37). Based on a two-site exchange of the Z,Z_1 and Z,Z_2 N-CH_2 resonances (43.4 and 45.4 ppm, respectively) between 27.0 and 40.2°C, the barrier to $Z,Z_1 \rightleftarrows Z,Z_2$ interconversion ($\Delta G^{\ddagger}$) was measured to be 14.5 ± 1.3 kcal/mol (Table 10). The height of this barrier lies close to the range reported for disulfide rotations in cyclic systems. For example, the barriers to inversion for 1,2-dithiane and 3,3,6,6-tetramethyl-1,2-dithiane have been reported to be 11.6 and 13.6 kcal/mol, respectively (38, 39).

Table 10. Calculated rate constants (from CBS analysis) and Arrhenius parameters for the $Z,Z_1 \rightleftarrows Z,Z_2$ conformational equilibrium.

T (K)	*k* (s^{-1})	1/*T* (K^{-1})	ln *k*
298.5	0.6	0.00335	–0.5108
300.0	0.9	0.00333	–0.1054
302.0	1.0	0.00331	0
304.2	1.2	0.00329	0.1823
306.3	1.2	0.00326	0.1823
309.8	1.8	0.00323	0.5878
311.1	2.2	0.00321	0.7885
313.2	2.4	0.00319	0.8755
317.6	2.7	0.00315	0.9932
329.7	4.6	0.00303	1.5261

The barrier of 14.5 kcal/mol was too low to be attributed to an amide rotation, particularly one occurring in a cyclic system and, although it was at the high end for reported disulfide rotations, it was reasonable to attribute the $Z,Z_1 \rightleftarrows Z,Z_2$ chemical exchange process to a disulfide rotational mechanism as illustrated in Fig. 9. A large component of the observed barrier is reflected in the energy profile of the acyclic disulfide bond, which has a maximum of ca. 8–10 kcal/mol at a CSSC dihedral angle of 0° (i.e., for the *S-cis* transition state) and a minimum at 90° (40) with the barrier considered to arise from the mutual repulsion between the unshared pairs of 3*pz* nonbonded electrons on adjacent sulfur atoms (41). In cyclic disulfides such as **1**, however, the presence of transannular electrostatic and steric interactions will increase the height of the disulfide rotational barrier. Moreover, the amide groups presumably confer additional rigidity to the ring and likely contribute to the relatively high barrier.

[7] The term antiparallel refers to the opposite relative orientation of the amide groups.

© 1997 NRC Canada

Can. J. Chem. Downloaded from www.nrcresearchpress.com by 92.62.229.171 on 09/08/12
For personal use only.

It is interesting to note that S—S rotation generated diastereomeric conformations, and not the enantiomers that are commonly observed in acyclic, unsymmetric disulfides (42). The asymmetric nature of the ring introduces a second source of chirality, which, in combination with asymmteric disulfide rotation, confers a diastereomeric relation between the Z,Z_1 and Z,Z_2 stereoisomers.

Unlike the Z,Z_2 isomer, the S-CH_2 protons in the Z,Z_1 structure did not possess pseudoaxial geometry (**1a**, Fig. 8). Analysis of space-filling, mechanical models of the Z,Z_2 structure indicated that a pseudoaxial, S-CH_2 configuration brought one set of lone electron pairs on oppositely related O and S atoms into close proximity. It appeared that the compromised, dipseudoequatorial geometry of the Z,Z_1 conformation defused this transannular interaction by directing the electrons away from each other. Moreover, a pseudoequatorial configuration of S-CH_2 protons was expected to be sterically preferable to a pseudoaxial one as 1,3-diaxial interactions with the methyl groups will destabilize the latter conformation. Some combination of these electronic and steric effects may serve to explain the calculated and observed population distributions between the Z,Z_1 and Z,Z_2 ring conformers (Table 3).

The calculated, MMX conformational energies agreed moderately well with those of the observed populations (Table 3). Since the molecular mechanics calculations mimic isolated molecules in their gaseous state, exact agreement between calculated and experimental populations is unattainable given the present level of computational sophistication. This situation arises from the inability to accurately incorporate solvent effects into the calculations. In addition, certain conformations may be differentially stabilized by solvation (43), particularly in higher energy geometries. In this case, the more energetic, gas-phase *Z,E* (**1c**) conformer will be stabilized to a greater extent than the lower energy Z,Z_2 structure, resulting in a thermodynamic reversal of solution state population levels. The effect may serve to rationalize the differences between calculated and experimental population distributions (Table 3), particularly for the *Z,E* structure.

In analogy to the chemical shift assignments made for protons of the *Z,E* crystal structure (vide supra), the orientation of a MMX-calculated N-CH proton, in relation to its adjacent C=O group, will primarily determine its chemical shift. Consequently, for isomers **1a** and **1b** (Fig. 8), one isochronous N-CH_{ax} pair occupied a pseudoaxial configuration that was essentially *cis* coplanar to the C=O group (i.e., 9.2° and 1.4° removed from the amide plane defined by the atoms O, C, and N) and, therefore, should be the low-field protons at 4.68 and 4.88 ppm, respectively. An interesting confirmation of this pseudoaxial geometry was noted in a ^1H–^1H COSY experiment, where the 4.68 ppm signal was weakly correlated to the N-CH_3 resonance at 3.13 ppm. This was indicative of a stereospecific, four-bond coupling originating from the "W" configuration (44) that is often observed between axial protons α to C-18 or C-19 methyl groups in steroids. Four-bond coupling to the methyl protons was not possible for the pseudoequatorial (H_{eq}) protons in this molecular configuration.

The second, isochronous set of geminal N-CH_{eq} protons in the Z,Z_1 and Z,Z_2 ring isomers occupied pseudoequatorial positions that were approximately 20.9° and 15.6° out of the amide plane. Their respective shifts at 2.64 and 2.71 ppm implied that they were shielded in comparison to the rotationally averaged, *Z,Z* N-CH_2 shift of 3.28 ppm for the open-chain precursor **4** (cf. Table 13). A comparison at a more quantitative level suggests that the H_{eq} protons were shielded by about 0.6 ppm, while the H_{ax} protons were deshielded by 1.5 ppm, respectively. Clearly, the shielding mechanisms (particularly the deshielding forces) at work in the conformational isomers of **1** were quite significant and worthy of further investigation.

Shielding calculations

The objective of this section is to investigate the extent to which it is possible to identify the origins of and to quantify the large N-CH_2 nonequivalences observed in the Z,Z_1 and Z,Z_2 conformers. In addition, we examine the pattern of S-CH_2 nonequivalencies for the *Z,Z* and *Z,E* conformations.

For the purpose of calculating chemical shifts, we have employed a combination of nonlocal density functional theory (DFT) and the guage-independent atomic orbital (GIAO) method using two common ab initio basis sets: Becke3LYP/3-21G* and Becke3LYP/6-31G*. Previous workers have successfully employed a similar level of theory for shift predictions of organic molecules using both DFT (45) and correlated as well as uncorrelated HF (46) methodologies.

*(a) Shift predictions for conformers **1a**, **1b**, and **1c***

The results are presented in Table 11 for the three proton environments as absolute shifts in ppm downfield from TMS. Three primary points derive from the tabulation. First, the calculated shift differences (Δδ) for the eight N-CH_2 and S-CH_2 geminal proton pairs accurately reproduce the measurement with a maximum deviation of 0.2 ppm (cf. Table 1). Second, the absolute shifts from TMS (δ^1H) for the same protons are only slightly less well reproduced, with the majority of deviations from experiment at 0.1–0.2 ppm. The N-CH_3 proton shifts are uniformly overestimated by 0.3–0.5 ppm. However, the calculated values are simple averages over a single N-methyl conformation and are thus subject to the greatest error. The numbers are still quantitatively representative of the spectroscopic outcome. Finally, the economical 3-21G* basis set performs as well as the extended 6-31G* version, both delivering impressive matches with the measured shifts.

(b) Origins of chemical shift differences

The observed chemical shift difference, $\Delta\delta_{OBS}$, between a geminal pair of protons can be broken down heuristically into a number of overlapping effects as depicted by eq. [3] (47).

$$[3] \quad \Delta\delta_{OBS} = \Delta\delta_{MAG} + \Delta\delta_{EL} + \Delta\delta_{SOL} + \Delta\delta_{VDW}$$

The terms $\Delta\delta_{MAG}$, $\Delta\delta_{EL}$, $\Delta\delta_{SOL}$, and $\Delta\delta_{VDW}$ refer to the *net* chemical shift between N-CH_2 or S-CH_2 protons ascribed to shielding contributions from magnetic anisotropy, electric field, solvent, and van der Waals effects of all neighbouring groups in the molecule.

The $\Delta\delta_{MAG}$ and $\Delta\delta_{EL}$ contributions arise from the perturbation of a proton by the magnetic field and electric dipoles of polar groups such as amide functionalities by an obtained through-space mechanism. Rough estimates can be estimated by applying modified forms of McConnell's (48) and Buckingham's (49) equations, respectively. The polar character of the amide group can also contribute to $\Delta\delta_{OBS}$ through the polarization of the solvent via a reaction field. However, this

© 1997 NRC Canada

Table 11. Becke3LYP/GIAO ^{1}H NMR chemical shift (ppm) predictions for MMX optimized disulfide conformers **1a**, **1b**, and **1c** with the 3-21G* and 6-31G* basis sets.[a,b]

	Conformer					
	Z,Z$_1$		Z,E		Z,Z$_2$	
Signal	δ^1H	$\Delta\delta$	δ^1H	$\Delta\delta$	δ^1H	$\Delta\delta$
N-CH$_2$						
3-21G*	2.6(0.0)	2.0(0.0)	3.1(0.1)	1.2(0.1)	2.7(0.0)	2.3(0.1)
	4.6(0.1)		4.3(0.0)		5.0(0.1)	
			3.3(0.2)	1.0(0.2)		
			4.3(0.0)			
6-31G*	2.7(0.1)	1.9(0.1)	3.1(0.1)	1.3(0.0)	2.8(0.1)	2.2(0.0)
	4.6(0.1)		4.4(0.1)		5.0(0.2)	
			3.2(0.1)	1.2(0.0)		
			4.4(0.1)			
S-CH$_2$						
3-21G*	3.1(0.3)	0.0(0.0)	3.4(0.2)	0.6(0.2)	3.3(0.1)	0.5(0.2)
	3.1(0.4)		4.0(0.0)		3.8(0.1)	
			3.1(0.1)	0.9(0.2)		
			4.0(0.2)			
6-31G*	3.2(0.2)	0.2(0.2)	3.5(0.1)	0.5(0.1)	3.2(0.0)	0.6(0.1)
	3.4(0.1)		4.0(0.0)		3.8(0.1)	
			3.0(0.0)	1.0(0.1)		
			4.0(0.2)			
N-CH$_3$[c]						
3-21G*	3.5(0.4)		3.4(0.4)		3.5(0.3)	
			3.7(0.5)			
6-31G*	3.5(0.4)		3.4(0.4)		3.6(0.4)	
			3.7(0.5)			

[a]Relative to TMS at the same basis set with MP2/6-31G* optimized geometry; isotropic ^{1}H shifts: 3-21G* 32.9 ppm; 6-31G* 32.3 ppm.

[b]Parenthetical values are the absolute chemical shift differences in ppm between the measured (Table 1) and calculated values.

[c]Tabulated chemical shifts are simple averages for the three methyl protons.

shift contribution from the solvent ($\Delta\delta_{SOL}$) was demonstrated by Clayden and Williams to be unimportant in determining the methylene nonequivalence in cyclotetrasarcosyl, **5** (50). The absence of exchangeable protons and a concentration dependence for the magnitude of the N-C*H*$_2$ shift difference in **1** indicates that specific solvent–solute and (or) solute–solute interactions are not likely shift factors either.

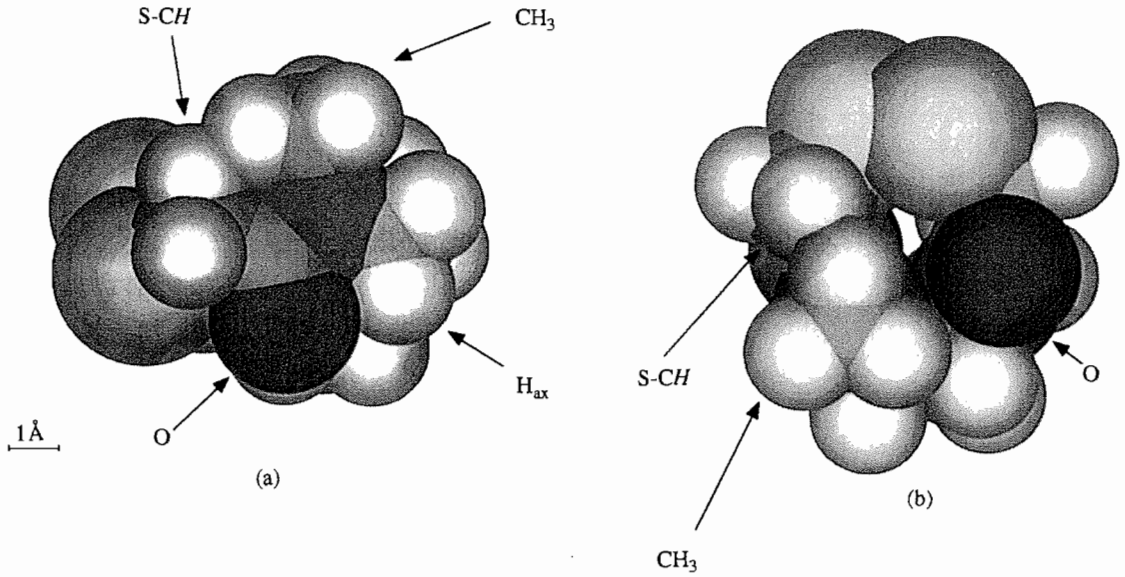
The expression $\Delta\delta_{VDW}$ reflects the operation of shielding effects when hydrogen atoms are subject to intramolecular steric or van der Waals interactions with proximate nuclei (51). Qualitatively, the direction of shielding can be associated with the net nuclear charge on the resonant proton, which, in turn, depends on the predominance of either an attractive or repulsive interaction. For example, if the resonant proton feels an *attractive* van der Waals interaction with a proximate group, its effective nuclear charge will be increased, resulting in an *upfield* shift (shielding) of the hydrogen nucleus. Conversely, in the *repulsive* van der Waals regime, electrostatic repulsion of interacting electron clouds will induce charge polarization in the H→C bond direction and will produce a *downfield* shift (deshielding) of the resonant proton (52). In general, intramolecular separations at, or smaller than, the sum of the van der Waals radii of the interacting groups usually result in repulsive van der Waals interactions, while attractive interactions will dominate at slightly larger interatomic distances. The attractive interaction is relatively weak compared to its stronger repulsive counterpart, so deshielding effects are generally much larger and more common than the shielding ones (53). Instances of such deshieldings have been observed mostly in rigid systems, where one or more hydrogen atoms is forced too close to other groups because of rigid geometrical constraints (51). For example, the magnitude of the δ_{VDW} shift and N-C*H*$_2$ nonequivalence in a series of hindered amides has been linearly correlated to the size and number of the interacting groups (54).

In contrast to **5** (50), a $\Delta\delta_{VDW}$ contribution to $\Delta\delta_{OBS}$ cannot be ruled out for **1** since van der Waals contacts involving the downfield H_{ax} protons were detected in the calculated MMX

© 1997 NRC Canada

Can. J. Chem. Downloaded from www.nrcresearchpress.com by 92.62.229.171 on 09/08/12
For personal use only.

Fig. 10. Space-filling models of **1b** from (*a*) side and (*b*) top perspectives. Note the van der Waals compression of the S-CH pseudoaxial proton with the N-CH_3 protons, and the carbonyl oxygen with H_{ax}. The N-CH_3 group has been rotated by ca. 60° to illustrate steric compression.



Can. J. Chem. Downloaded from www.nrcresearchpress.com by 92.62.229.171 on 09/08/12
For personal use only.

and crystal structures. An example of these through-space contacts is illustrated for the Z,Z_2 conformer (Fig. 10). CPK space-filling representations are used to illustrate an "effective size" for each atomic electron cloud based on their characteristic van der Waals radii (r_{VDW}). Intra-atomic measurements showed that the oxygen (r_{VDW} = 1.5 Å) (34) and methyl (r_{VDW} = 2.0 Å) groups protrude into the electron cloud of the H_{ax} (r_{VDW} = 1.2 Å) protons by at least 0.2 and 0.1 Å, respectively. Thus, a downfield shift is predicted for the H_{ax} protons. In contrast, the H_{eq} protons are not expected to be influenced by a paramagnetic van der Waals shift given its sterically unencumbered, pseudoequatorial geometry. A quantitative assessment of the $\Delta\delta_{VDW}$ contributions to methylene shift nonequivalences was provided by ab initio shift calculations (vide infra).

(c) The N-CH_2 protons

Our strategy for deconvoluting the various intramolecular influences on the differential chemical shifts of geminal protons is to carve the molecule into smaller fragments of identical structural geometries and to compute the corresponding chemical shifts using the ab initio methodology employed for the whole molecule (Table 11). Consequently, seven substructures were prepared (see Experimental) and subjected to a DFT/GIAO evaluation for comparison with **1a-1c** (Table 12). The following analysis shows that the observed shieldings are a complex blend arising from the amide dipole, N–CH steric effects, and, in the case of S-CH_2 protons, the sulfur lone pairs.

Consider the 2.0 ppm difference between the geminal pseudoaxial and equatorial N-CH_2 protons in **1a** (Z,Z_1). A comparison of 1,2-diaminoethane, ((OHCN-CH_2)$_2$ and N-demethyl **1a** with the corresponding N-methyl structures (Table 12) demonstrates that methylation causes the geminal proton *syn* to the methyl group (H_{syn}) to shift upfield by 0.3–0.5 ppm. By contrast, H_{anti} is deshielded by 0.1–0.3 ppm upon methyl addition. The resulting difference is around 0.6 ppm. Further addition of the CHO unit induces a small deshielding of −0.1 to −0.2 for H_{syn}, but a much larger deshielding of −1.5 to −1.8 ppm results for H_{anti}. Overall, H_{syn} experiences an approximate 0.2–0.3 ppm upfield shift (relative to the protons in diaminoethane) largely as a result of an attractive van der Waals interaction with the N-methyl group. H_{anti}, on the other hand, is pulled 1.8 ppm downfield mainly by dipolar effects of the amide group, but supplemented by a small δ_{VDW} contribution from N-methyl contact. The net geminal proton separation is 2.0–2.1 ppm, as observed and predicted for **1a** (Table 11).

Precisely the same situation applies to the minor conformation **1b** (Z,Z_2). Here, the observed geminal splitting of 2.2 ppm is due to the effect of amide group deshielding (ca. 1.8–2.0 ppm) with a diminutive contribution of 0.3 ppm from steric interaction with the N-CH_3 group. The axial H_{anti} is somewhat nearer the C═O oxygen in **1b** than **1a** (2.41 vs. 2.44 Å, respectively), while the C═O and C—H bonds are closer to a common plane (ϕ(H—C---C═O) = 12.3° and 24.5°, respectively).

A similar analysis for the third conformer, **1c** (Z,E), shows that the presence or absence of the N-methyl function has little effect on the N-CH_2 shift difference (≤0.1 ppm, Table 12). The *trans* and *cis* amide groups contribute the most, providing 1.0 and 1.2 ppm, respectively, to the observed geminal splitting. On the *trans* half of the molecule, the axial N-CH_2 ($H_{anti,1}$) is situated 2.54 Å from the amide oxygen and twisted out of the H—C---C═O plane by 39°. Both factors cause a reduction in the geminal split relative to **1a** and **1b**, which is 1.1 ppm based on the fragment analysis (Table 12). On the *cis* side, the axial N-CH_2 proton ($H_{anti,2}$) is too far from the adjacent C═O to significantly experience any electronic effects, but lies only 2.7 Å cross-ring from the oxygen of the *trans* amide. A more revealing description of its location sites the proton 1.74 Å *above* the plane of the *trans* amide but shifted 2.01 Å away from the carbonyl oxygen (Fig. 11). This is to be compared with $H_{anti,1}$,

© 1997 NRC Canada

Table 12. Becke3LYP/GIAO ^{1}H NMR geminal X-CH_2 chemical shift (ppm) predictions for MMX optimized disulfide conformers **1a**, **1b**, and **1c** and capped fragments with the 3-21G* and 6-31G* basis sets.[a,b,c]

	Conformer								
	Z,Z_1 3-21G* (6-31G*)			Z,E[d] 3-21G* (6-31G*)			Z,Z_2 3-21G* (6-31G*)		
Signal	H_{syn}	H_{anti}	Δδ	H_{syn}	H_{anti}	Δδ	H_{syn}	H_{anti}	Δδ
1 (N-CH_2)	2.6(2.7)	4.6(4.6)	2.0(1.9)	3.3(3.2)	4.3(4.4)	1.0(1.2)	2.7(2.8)	5.0(5.0)	2.3(2.2)
				3.1(3.1)	4.3(4.4)	1.2(1.3)			
(H_2N-CH_2)$_2$	2.9(3.0)	2.9(2.9)	0.1(0.0)	2.8(2.8)	3.0(3.2)	0.2(0.4)	2.9(3.1)	2.7(2.8)	0.2(0.3)
				3.0(3.1)	2.7(2.9)	0.3(0.2)			
(MeHN-CH_2)$_2$	2.4(2.6)	3.2(3.2)	0.8(0.6)	2.9(3.0)	3.1(3.3)	0.2(0.3)	2.4(2.6)	3.2(3.2)	0.8(0.6)
				2.7(2.8)	2.7(2.9)	0.0(0.1)			
(OHCNH-CH_2)$_2$	3.0(2.9)	4.7(4.7)	1.7(1.8)	3.1(2.8)	4.3(4.3)	1.2(1.5)	3.0(2.9)	4.9(4.8)	1.9(1.9)
				3.2(3.1)	4.3(4.3)	1.1(1.2)			
MeHN-CH_2-	2.8(2.2)	3.2(2.6)	0.4(0.4)	3.1(3.1)	3.5(3.6)	1.1(1.1)	2.7(2.9)	3.2(3.1)	0.5(0.2)
CH_2-NMeCHO	2.4(2.4)	4.7(4.7)	2.3(2.3)	3.1(3.0)	3.3(3.4)	1.1(1.1)	2.4(2.4)	4.8(4.8)	2.4(2.4)
				3.0(2.8)	4.1(3.9)	0.4(0.5)			
				2.7(3.0)	3.8(4.1)	0.2(0.4)			
(OHCNMe-CH_2)$_2$	2.6(2.6)	4.7(4.7)	2.1(2.1)	3.1(3.0)	4.3(4.4)	1.2(1.8)	2.6(2.6)	4.9(4.8)	2.3(2.2)
				3.0(3.0)	4.2(4.3)	1.2(1.3)			
1 (NH/N-CH_2)[e]	3.0(3.0)	4.4(4.5)	1.4(1.5)	3.1(3.0)	4.1(4.2)	1.0(1.2)	3.0(3.0)	4.7(4.8)	1.7(1.8)
				3.2(3.2)	4.2(4.3)	1.0(1.1)			
1 (S-CH_2)	3.1(3.2)	3.1(3.4)	0.0(0.2)	4.0(4.0)	3.1(3.0)	0.9(1.0)	3.8(3.8)	3.3(3.2)	0.5(0.6)
				4.0(4.0)	3.4(3.5)	0.6(0.5)			
HCH_2-S-S-CH_2H	2.1(2.2)	2.9(3.0)	0.8(0.8)	2.7(2.9)	2.2(2.2)	0.5(0.7)	2.4(2.6)	2.3(2.4)	0.1(0.2)
				3.1(3.2)	2.0(2.2)	1.1(1.0)			
1 (NH/S-CH_2)[e]	2.7(2.8)	3.2(3.5)	0.5(0.7)	3.0(3.0)	3.4(3.3)	0.4(0.3)	2.8(2.9)	3.5(3.4)	0.7(0.5)
				4.0(4.0)	3.3(3.3)	0.7(0.7)			

[a]H_{syn} is the CH_2 proton *syn* to CH_3 or H of the N-R group; H_{anti} is defined similarly. The shift values are given in ppm relative to TMS; cf. footnote *a*, Table 1.

[b]Parenthetical values are those calculated from the 6-31G* basis set.

[c]Δδ is the chemical shift difference between NCH_2 and SCH_2 geminal protons in ppm.

[d]*trans*-Amide values are listed first; *cis*-amide, second.

[e]Bis-*N*-demethyl **1**.

which is 0.70 Å *below* the *trans* amide plane and likewise shifted from the carbonyl oxygen by 2.47 Å.

Qualitatively, we can predict that both $H_{anti,1}$ and $H_{anti,2}$ are deshielded relative to their geminal partners because of their positions inside the deshielding space of the *trans* C=O shielding cone. Their observed shifts and splittings are accurately reproduced by the shift calculations (Table 11) and confirmed to be primarily a deshielding effect of the (*trans*) amide (Table 12) by the fragment shielding treatment. The latter analysis suggests a geminal separation of 1.3 ppm (H_{anti}: (H_2N-CH_2)$_2$ vs. (OHCNH-CH_2)$_2$, Table 12), in agreement with experiment.

(d) The S-CH_2 protons

The observed splittings for the geminal protons α to sulfur are considerably less than those α to nitrogen (Table 1). Superficially, one might conclude that the local "magnetic" environments are therefore similar. On the other hand, there is no obvious intuitive reason for drawing this inference based on molecular geometry. Both the N-CH_2 and S-CH_2 sites are equally asymmetric: a pseudoaxial and a pseudoequatorial proton residing at each center. Magnetic similarity must then arise from the near cancellation of effects. To accomplish the analysis, we examine chemical shifts in the S-CH_2 moieties of **1**, N-demethyl **1**, and the dimethyldisulfide fragment given in Table 12.

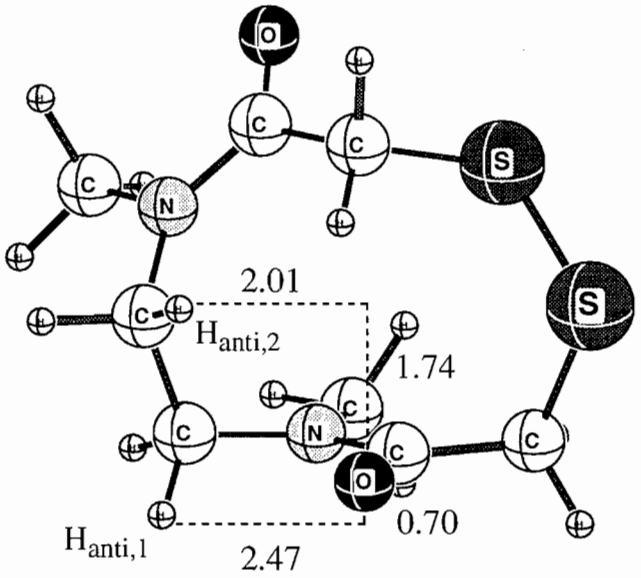
The abundant conformer **1a** (Z,Z_1) exhibits its S-CH_2 protons as magnetically equivalent (Tables 1 and 11). Yet, the dimethyldisulfide fragment reveals a 0.8 ppm difference between geminal protons (Table 12). This surprisingly large isochrony can be appreciated by recognizing that H_{anti} resides almost directly above the S—S bond and is consequently deshielded by both lone pairs on the adjacent sulfur (Fig. 8, **1a**). From MeSSMe to **1a**, H_{syn} experiences a 1.0 ppm downfield shift as a result of its position close to the amide plane and its steric interaction with the N-methyl group, the latter repulsive van der Waal contact contributing 0.4 ppm. H_{anti} is simultaneously deshielded by only 0.2 ppm, derived entirely from dipolar interaction with the amide. The net result is that both protons experience almost identical shifts, although each is influenced significantly and dissimilarly by the S—S, (N)Me, and amide moieties. A parallel analysis can also serve

© 1997 NRC Canada

Can. J. Chem. Downloaded from www.nrcresearchpress.com by 92.62.229.171 on 09/08/12
For personal use only.

Can. J. Chem. Downloaded from www.nrcresearchpress.com by 92.62.229.171 on 09/08/12
For personal use only.

Fig. 11. A ball and stick plot of the MMX diamide **1c**, showing the H_{syn} and H_{anti} positions relative to the *trans* carbonyl oxygen. Numerical values correspond to distances in Å.



to rationalize the S-CH_2 $\Delta\delta_{OBS}$ for **1b** (Z,Z_2). However, the shielding forces affecting H_{syn} and H_{anti} are greater (owing to their stricter pseudoaxial and pseudoequatorial geometries) and are manifest as a larger, geminal shift difference of 0.7 ppm (Table 1).

Conformer **1c** (*Z,E*) exhibits $\Delta\delta$'s of similar magnitude for protons α to N and S around the *trans*-amide functionality. While they arise from alternative factors, a decomposition analysis from values in Table 12 provides a quantitative assessment. Noteworthy is the situation for the geminal hydrogen pair adjacent to the *cis*-amide center, which sustains a rather small observed isochrony of 0.4 ppm (Table 1). The C—H bond containing H_{anti} is nearly eclipsed with the S—S bond (ϕ = 12.0°), while the same bond involves an unusually short, H---H van der Waals contact (1.97 Å) with a *cis*-disposed H_{anti} of the adjacent N-CH_2 group (respectively, H(3b) and H(6b), Fig. 5 inset). The combination promotes a 1.4 ppm deshielding that is matched by a nearly identical H_{syn} deshielding of 0.9 ppm from the *cis*-amide moiety (cf. MeSSMe and **1**, Table 12). Once again, large and compensatory effects lead to a diminutive geminal $\Delta\delta$.

Experimental

Materials

Acetonitrile was distilled from P_2O_5 and the distillate was redistilled from CaH_2, discarding the first 5 and the last 10%. Ethanol (EtOH) was dried and purified via distillation from magnesium turnings and stored over freshly activated 4 Å molecular sieves. All chemicals were purchased from Aldrich Chemical Company (Milwaukee, Wis.).

Melting points (mp) were recorded on a Gallenkamp capillary tube melting point apparatus and are uncorrected.

Analytical thin-layer chromatography (TLC) and column chromatography (according to the "flash" method of Still et al. (55)) were carried out on E. Merck silica gel 60 F_{254} coated Al plates of 0.2 mm thickness and 0.040–0.063 mm (230–400 mesh), respectively. TLC visualization was achieved using a combination of either a UV lamp at 254 nm or I_2 vapour and treatment with a phosphomolybdic acid spray (20 g of phosphomolybdic acid hydrate and 15 g $Ce(SO_4)_2$ dissolved in 1 L of 10% H_2SO_4) followed by heating to ca. 130°C.

Electrospray (ES) mass spectrometry (MS) was performed on a Fisons VG Platform LC–MS electrospray mass spectrometer. Other mass spectra were obtained on a VG ZAB-E mass spectrometer with sample introduction via a direct inlet system. Infrared spectra (IR) were recorded on a Perkin–Elmer 283 spectrometer using either liquid cells with methylene chloride or chloroform as solvents or potassium bromide pellets. The abbreviations (s) = strong, (m) = medium, and (w) = weak are used to describe the intensity of particular bands in the IR spectra.

X-ray diffraction

$C_8H_{14}N_2O_2S_2$ fw = 234.3

Triclinic, a = 7.0570(10), b = 8.071(2), c = 11.012(2) Å, α = 106.05(2)°, β = 93.41(1)°, γ = 114.93(1)°, V = 535.3(3) $Å^3$, Z = 2, ρ_c = 1.454 g cm^{-3}, μ = 4.342 mm^{-1} (23°C; CuKα_1, λ = 1.54178 Å)

Crystals of **1** were grown by very slow recrystallization from freshly distilled tetrahydrofuran at −15°C. A colorless plate having approximate dimensions of 0.20 × 0.05 × 0.15 mm was mounted on a glass fiber. All measurements were made on a Rigaku AFC6R diffractometer with graphite-monochromated CuKα radiation and a rotating anode generator.

Cell constants and an orientation matrix for data collection were obtained from a least-squares refinement using the setting angles of 24 carefully centered reflections in the range 7.0 < 2θ < 45.0°. Based on packing considerations, a statistical analysis of intensity distribution and the successful solution and refinement of the structure, the space group was determined to be $P\bar{1}$ (no. 2).

The data were collected at a temperature of 23 ± 1°C using the ω–2θ scan technique to a maximum 2θ value of 110.1°. Scans of (1.21 + 0.30 tan θ)° were made at a speed of 32.0°/min (in ω). The weak reflections ($I < 10.0\sigma_I$) were rescanned (maximum of nine rescans) and the counts were accumulated to assure good counting statistics. Stationary background counts were recorded on each side of the reflection. The ratio of peak counting time to background counting time was 2:1. The diameter of the incident beam collimator was 0.5 mm and the crystal-to-detector distance was 400.0 mm.

Of the 1479 reflections that were collected, 1362 were unique (R_{int} = 0.032). The intensities of three representative reflections, which were measured after every 150 reflections, remained constant throughout data collection, indicating crystal and electronic stability (no decay correction was applied). The data were corrected for Lorentz and polarization effects.

The structure was solved by direct methods. All non-hydrogen atoms were refined with anisotropic thermal parameters. Hydrogen atoms were placed geometrically and not refined. A correction was made for extinction (χ = 0.005(3) where $F^* = F[1 + 0.002\chi F^2/\sin 2\theta]^{-1/4}$) and an absorption correction was applied using the program DIFABS (56), employing transmission factors ranging from 0.69 to 1.20. Atomic scattering fac-

© 1997 NRC Canada

Can. J. Chem. Downloaded from www.nrcresearchpress.com by 92.62.229.171 on 09/08/12
For personal use only.

tors for all atoms and corrections for anomalous dispersion for C, O, N, and S were taken from the International Tables for Crystallography, Vol. C (57). Refinement minimized the function $\Sigma\omega(|F_o| - |F_c|)^2$, with $\omega = (\sigma^2F + 0.0008F^2)^{-1}$. The final solution, with $R = 4.67\%$ ($R = \Sigma(||F_o| - |F_c||)\Sigma F_o$) and $\omega R = 6.80\%$ for 1006 reflections ($I > 2\sigma_I$), showed no significant peaks in the final difference map. The goodness-of-fit was $S = 1.51$. The program SHELXTL PC was used for all calculations (58).[8]

NMR spectroscopy

Proton nuclear magnetic resonance (^{1}H NMR) spectra were recorded on Varian EM 390, Bruker MSL-100, AC-200, WM-250, or AM-500 spectrometers, with the majority of experiments acquired at 500.135 MHz on the latter instrument using a 5 mm dual-frequency ^{1}H–^{13}C probe. Spectra were obtained in eight scans in 16K data points over a 5.000 kHz spectral width (1.638 s acquisition time). Sample temperature was maintained at 303 K by a Bruker BVT-1000 variable temperature unit. The free induction decay (FID) was processed using exponential multiplication (line broading: 0.2 Hz) and was zero-filled to 32K before Fourier transformation. The abbreviations s = singlet, d = doublet, t = triplet, q = quartet and m = multiplet refer to the multiplicities of the signals observed.

Broad band decoupled, natural abundance carbon-13 nuclear magnetic resonance (^{13}C NMR) spectra were recorded on a Bruker AM-500 spectrometer at 125.759 MHz using the 5 mm dual frequency ^{1}H–^{13}C probe, except in one experiment, which was acquired on a Bruker WP-80 instrument at 20.115 MHz. The spectra were acquired over a 30.0 kHz spectral width in 16K data points (0.279 s acquisition time). The ^{13}C pulse width was 2.5 μs (35° flip angle). A 0.5 s relaxation delay was used. For spectral editing, the standard *J*-modulated spin-sort pulse sequence was used, incorporating a 7.3 μs ^{13}C 90° pulse width and a relaxation delay of 2.5 s. The FIDs were processed using exponential multiplication (line broading: 3.5 Hz) and zero-filled to 32K before Fourier transformation.

NOE difference spectra were obtained by subtraction of the off-resonance control FID from the on-resonance FID under non-spinning conditions and employing a sweep rate of 19 Hz. The signal of interest was selectively saturated for 5 s and the decoupler was gated off during acquisition. This saturation period also served as the relaxation delay. Normally, eight scans were acquired for each irradiation with the cycle of irradiation repeated 10 times. Free induction decays were processed using exponential multiplication with a line broadening of 4.0 Hz before Fourier transformation. The sample was not degassed, so the enhancements are not quantitative.

The ^{13}C–^{1}H 2-D chemical shift correlation spectrum was acquired using the standard pulse sequence incorporating the BIRD pulse during the evolution period for the ^{1}H–^{1}H decoupling in F_1 (59–61). The spectra in F_2 were recorded over a spectral width of 3.76 kHz in 4K data points. The 256 FIDs in F_1 were obtained over a ^{1}H spectral width of 1.52 kHz. Each FID was acquired in 200 scans. The fixed delays in the pulse sequence were a 1.0 s relaxation delay, BIRD pulse and polarization transfer delays ($1/2\ ^1J_{CH}$) of 0.003 571 s, and a refocussing delay ($1/4\ ^1J_{CH}$) of 0.001 786 s. The ^{13}C 90° pulse width was 6.4 μs while the ^{1}H 90° pulse width through the decoupler channel was 18.6 μs. The data were processed using exponential multiplication (line broadening: 5.0 Hz) in F_2 and unshifted sine bell in F_1. Zero-filling in F_1 resulted in a 2048 × 1024 data matrix.

^{13}C DNMR spectra were recorded over a 2.066 kHz spectral width in 8K data points (1.98 s acquisition time) incorporating a 5.5 μs pulse width and a 9.0 s relaxation delay to optimize sensitivity and digital resolution. The sample and probe were allowed a 10 min equilibration period per 5°C increment. An external digital thermocouple was used to measure the probe temperature to an accuracy of ±0.5°C. Rate constants were estimated by visual fitting of experimental to computer-simulated spectra measured for a given temperature. The calculated spectra were generated on an IBM PS/2 model 30 (286) microcomputer equipped with a HP 7550A graphics plotter using the simulation program EXCHANGE (available from R.E.D. McClung, Department of Chemistry, University of Alberta, Edmonton, AB T6G 2G2, Canada). The intrinsic linewidth of 0.35 Hz was obtained from a measurement of the peak width at one-half peak height of the S-*C*H$_2$ resonance at 35.61 ppm at 25.5°C. The $\Delta G^{\ddagger}$ for disulfide rotation was calculated from the slope of the regression line derived from an Arrhenius plot of ln k versus $1/T$ in Quattro Pro (3.01). The data points corresponding to T = 298.5, 317.6, and 329.7 K were omitted from the regression analysis. The error in $\Delta G^{\ddagger}$ was measured by the standard deviation of the regression coefficient. The theoretical line was drawn by fitting the $1/T$ data series to the regression equation.

The solid state, CP-MAS ^{13}C spectrum was obtained at 25.18 MHz on a Bruker MSL-100 spectrometer operating at 2.35 T using a **1** ms contact time and a recycle time of 10 s. Crystals of **1** (0.10 g), obtained by slow evaporation of a THF solution of the compound, were pulverized and diluted with KBr prior to analysis.

The compounds analyzed via NMR were dissolved in either deuterated acetone, deuterated benzene, deuterochloroform, or deuterated dimethyl sulfoxide (CD_3COCD_3, C_6D_6, $CDCl_3$, or DMSO-d_6, respectively) obtained from MSD Isotopes. ^{1}H and ^{13}C chemical shifts are reported in parts per million (ppm) using either TMS (0.0 ppm) as an internal reference or the residual signal of the following solvents: CD_3COCD_3 (2.04; 29.8 ppm), C_6D_6 (7.15; 128.0 ppm), $CDCl_3$ (7.26; 77.0 ppm), and DMSO-d_6 (2.49; 39.5 ppm).

Molecular mechanics calculations

Steric energies and conformations were calculated and minimized in PCMODEL V4.0 (available from K. Gilbert, Serena Software, Box 3076, Bloomington, IN 47402-3076, U.S.A.) using the MMX force field derived from the MM2 force field of N.L. Allinger (available from Quantum Chemistry Pro-gram Exchange, Chemistry Department, Indiana University, Bloomington, IN 47405, U.S.A.). The calculations were performed on an IBM PS/2 model 70 (486) microcomputer. The MMX force field includes the parameters necessary for the minimization calculations. Calculated steric energies were reported relative to the global minimum structure. Vicinal coupling constants

[8] Tables of observed and calculated structure factor amplitudes and atomic coordinates (ref.: R.B.M. Ph.D. Dissertation, McMaster University; data deposited in 1992 on 5 $\frac{1}{4}$ in. floppy diskette) may be purchased from: The Depository of Unpublished Data, Document Delivery, CISTI, National Research Council Canada, Ottawa, Canada K1A 0S2.

© 1997 NRC Canada

Table 13. ^{1}H NMR (500 MHz) characterization of **4** in $CDCl_3$ at 303 K.

	Conformer		
Signal	*Z,Z*	*Z,E*	*E,E*
	ppm (multiplicity, integral[a])		
N-CH_3	2.60(s,6H)	2.42(s,3H) 2.71(s,3H)	2.52(s,6H)
S-CH_2	2.79(s,4H)	2.77(s,2H) 2.84(s,2H)	2.72(s,4H)
(N-CH_2)$_2$	3.28(s,4H)	3.08(t,2H) 3.16(t,2H)	2.93(s,4H)
Aromatic		7.14–7.38(m,32H[b])	

[a]Integrals are relative within a geometrical isomer.
[b]Overlapping residual $CHCl_3$.

Table 14. ^{13}C NMR (126 MHz), *J*-modulated characterization of **4** in $CDCl_3$ at 303 K.

	Conformer					
Signal	*Z,Z*	*Z,E*	*E,E*	*Z,Z/Z,E*	*Z,Z/E,E*	*Z,E/E,E*
	ppm (relative intensity)					
N-CH_3	35.98(–52)	34.02(–10) 36.67(–10)	—	2.6	—	—
S-CH_2	35.10(55)	34.64(11) 34.83(11)	33.88(5)	2.5	11.0	4.4
(N-CH_2)$_2$	44.76(52)	46.94(11) 47.53(11)	—	2.4	—	—
Aromatic	126.64–129.73, 143.80(4), 143.92(17), 144.00(18), 144.05(18)					
C-Tr	66.71(11)	66.81(3.03) 66.94(2.74)				
CO-NH	168.77(26)	168.24(6) 168.52(7)				

measured from energy-minimized structures were calculated using the Altona modification of the Karplus equation, which takes into account substituent electronegativity (62).

To ensure a comprehensive search of conformational space, initial geometries were generated by either systematic or random methods (63). Systematic geometry searches were typically conducted by merging all combinations of accepted ground state geometries of the disulfide, amide, and ethyl functional groups of **1**; i.e., 90° torsional angle for the disulfide linkage, 180° (*trans*) and (or) 0° (*cis*) torsional angles for the amide groups, and a staggered configuration for the ethyl fragment. Random geometries were typically generated by either random or pseudorandom atomic variations on either minimized structures or two-dimensionally drawn images. After a crude starting geometry was produced, it was allowed to relax into an optimized geometry by the MMX force field. The search was terminated when new minima within 5 kcal/mol of the global minimum ceased be to found. Starting geometries were preminimized without hydrogen atoms and then reminimized with added hydrogens. This procedure avoids forcing hydrogens and lone electron pairs into high-energy configurations (64). Minimized structures were finally reminimized to ensure full convergence.

Shielding calculations

As a preliminary, the MMX optimized structures of **1a**, **1b**, and **1c** were modified by structural fragmentation. For example, the full structures were converted from N-CH_3 to N-H by eliminating the methyl protons and replacing the carbon by hydrogen with an N—H bond. Similarly, the other cut-down structures were generated from the three key conformations by retaining the MMX geometry, but eliminating various fragments. Heavy-atom replacements were made by hydrogen. The resulting N—H and C—H bond length were assigned values of 1.00 and 1.10 Å, respectively, but no additional changes to molecular geometry were made. The series of structures generated are listed in Tables 11 and 12. To obtain absolute chemical shifts, the structure of tetramethylsilane (TMS) was optimized with the MP2(Full)/6-31G* protocol to give r(Si—C) = 1.884 Å, r(C—H) = 1.094 Å, θ(Si-C-H) = 111.3° and θ(C-Si-C) = 109.47°.

All chemical shift evaluations were performed as single-point calculations on the original and modified structures using the Gaussian-94 series of programs (65). Becke's nonlocal density functional theory (DFT) (66, 67) was combined with two standard basis sets to generate the wave functions, Becke3LYP/3-31G* and Becke3LYP/6-31G*. Each calcula-

Can. J. Chem. Downloaded from www.nrcresearchpress.com by 92.62.229.171 on 09/08/12
For personal use only.

© 1997 NRC Canada

Can. J. Chem. Downloaded from www.nrcresearchpress.com by 92.62.229.171 on 09/08/12
For personal use only.

tion was followed with a Gauge-Independent Atomic Orbital (GIAO) (68) evaluation. The resulting isotropic magnetic shieldings are presented in Tables 11 and 12.

2-(Triphenylmethyl)thioacetic acid (2)

This synthesis was performed according to the method of Brenner et al. (12). A solution of triphenylmethanol (48.0 g, 184.0 mmol), mercaptoacetic acid (12.2 mL, 184.0 mmol), and glacial acetic acid (160 mL) was heated to 70°C. Boron trifluoride etherate (32.0 mL) was added and the resulting brown solution was stirred at room temperature for 50 min. The reaction mixture was poured into ice-cold distilled water, depositing a clear oil that solidified over 18 h at 5°C. The solid was broken and washed with distilled water, then with a small amount of diethyl ether, and was dried in vacuo to give a white solid (40.0 g, 65%). A further crop (4.3 g, 7%) was recovered from the ether washings and purified by recrystallization from toluene; mp 155.0–157.0°C (lit. (6, 12) mp 158.5–160.0°C).

***N*-Succinimido 2-(triphenylmethylthio) acetate (3)**

This synthesis was performed according to the method of Brenner et al. (12). To an ice-cooled solution of acid **2** (5.01 g, 15.00 mmol) and *N*-hydroxysuccinimide (1.72 g, 15.00 mmol) in DME (38 mL) was added DCC (3.20 g, 1.1 equiv., 15.5 mmol) such that the temperature remained at approximately 0°C. The resulting mixture was then stored at 5°C for 18 h and then filtered and washed with ice-cold CH_2Cl_2. The filtered, white crystalline solid (DCU) was collected and discarded. The combined CH_2Cl_2 filtrate and washings were pooled and concentrated in vacuo to afford a white solid. Residual amounts of DCU were removed via recrystallization from ethyl acetate to give large, opaque prisms (5.43 g, 84%); mp 178.5–180.0°C (lit. (6, 12) 178.5–179.5°C).

***N,N′*-{Dimethyl-bis[2-(triphenylmethyl)thioacetyl]}-ethylenediamine (4)**

To a stirred solution of the succinimidoyl ester **3** (1.00 g, 2.32 mmol) in acetonitrile (10 mL) was added a solution of *N,N′*-dimethylethylenediamine (120 μL, 1.1 mmol) in AN (1 mL) and NEt_3 (2 drops) under a N_2 atmosphere. After 12 h, the milky-white suspension was concentrated to 2 mL, diluted with 0.5 N HCl (100 mL), and extracted with CH_2Cl_2 (200 mL). The organic layer was backwashed with 0.5 N HCl (200 mL), with 0.5 N $NaHCO_3$ (200 mL), and dried over $MgSO_4$ for 1 h. Filtration and concentration of the filtrate in vacuo afforded a white solid (621 mg, 76%). Chromatographic purification of the resultant crude (stepwise elution: 100% CH_2Cl_2 followed by 2% MeOH in CH_2Cl_2) gave a white solid; mp 71.0–72.5°C; R_f 0.79 (10% MeOH in CH_2Cl_2); IR(KBr pellet): 3055(w) (aromatic C═C-H), 2930, 2850 (w)(aliphatic C-H); 1645(s) (C═O, amide I); 1485, 1440(s) (aromatic C═C); 1400(m), 735, 695(s) (monosubstituted aromatic C-H); ^{1}H NMR: see Table 13; ^{13}C NMR: see Table 14. MS(+ES), *m/z* (RI%): 766(4)[M + $2Na^+$], 759(3)[M + K^+], 743(7)[M + Na^+], 721(4)[M + 1], 243(100)[Tr^+].

***N,N′*-[Dimethyl-(2,2′-dithiobisacetyl)]ethylenediamine (1)**

This synthesis was a modification of the method of Kamber (16). Resublimed I_2 (848 mg, 1.1 equiv., 3.30 mmol) was added to a solution of tritylthio ether **4** (1.16 mg, 3.00 mmol) in a degassed 2:1 v/v mixture (1.5 L) of acetonitrile and absolute EtOH under a N_2 atmosphere. The amber solution was further degassed for 30 min under aspirator vacuum (15 Torr; 1 Torr = 133.3 Pa), vented to dry N_2 gas, and allowed to stir at room temperature. After 12 h, the solution was concentrated to 20 mL, diluted with doubly distilled H_2O, decolorized with 1.0 N $Na_2S_2O_3$, and extracted with diethyl ether. A white solid was seen at the solvent interface. The organic phase was decanted and, after salting the aqueous layer, the precipitate was extracted into $CHCl_3$ and dried over $MgSO_4$ for 2 h. Filtration and rotary evaporation of the filtrate afforded an off-white, semi-solid (466 mg, 66%). The residue was suspended in isopropyl alcohol, chilled at −15°C, and filtered to separate most of the insoluble trityl carbinol. Recrystallization from peroxide-free THF gave opaque, non-geometric plates; mp 139.0–140.0°C; R_f 0.49 (10% MeOH in CH_2Cl_2); IR(KBr pellet): 2930, 2853 (m)(C-H); 1629 (s) (C═O, amide I); 1458 (m); 1396 (m); Raman: 645 (m)(CH_2-S), 510 (s)(S-S); ^{1}H NMR: see Table 1; ^{13}C NMR: see Table 2; MS(+NH_3 DCI), *m/z*(RI%): 252(100)[M + 18], 235(48)[M + 1], 205(10).

Acknowledgements

The authors gratefully acknowledge the financial support of the Natural Sciences and Engineering Research Council of Canada. We also thank Drs. A.D. Bain, D.W. Hughes, J.D. Laposa, L. Li, and M.J. McGlinchey for helpful discussions.

References

1. M.K. Dewanjee. Semin. Nucl. Med. **20**, 5, (1990).
2. D. Eshima, A.R. Fritzburg, and A. Taylor, Jr. Semin. Nucl. Med. **20**, 28 (1990).
3. H.F. Kung. Semin. Nucl. Med. **20**, 150 (1990).
4. W.C. Klingensmith III, A.R. Fritzburg, V.M. Spitzer, D.L. Johnson, C.C. Kuni, M.R. Williamson, G. Washer, and R. Weil. J. Nucl. Med. **25**, 42 (1984).
5. A.R. Fritzburg, P.G. Abrams, P.L. Beaumier, S. Kasina, A.C. Morgan, T.N. Reno, J.A. Sanderson, A. Srinivasan, D.S. Wilbur, and J.-L. Vanderheyden. Proc. Natl. Acad. Sci. U.S.A. **85**, 4025 (1988).
6. A. Capretta, R.B. Maharajh, and R.A. Bell. Carbohydr. Res. **267**, 49 (1995).
7. J.G. McAfee. *In* Radiopharmaceuticals. *Edited by* G. Subramanian, B.A. Rhodes, J.F. Cooper, and V.J. Sodd. The Society of Nuclear Medicine Inc., New York. 1975.
8. E. Livini, M.A. Davis, and V.D. Warner. J. Med. Chem. **22**, 580 (1979).
9. M.D. Loberg, E.H. Corder, A.T. Fields, and P.S. Callery. J. Nucl. Med. **20**, 1181 (1979).
10. B. Ivanov, W. Grzesik, and F.A. Robey. Bioconjugate Chem. **6**, 269 (1995).
11. T. W. Greene. Protecting groups in organic chemistry. J. Wiley, New York. 1981. p. 320.
12. D. Brenner, A. Davison, J. Lister-James, and A.G. Jones. Inorg. Chem. **23**, 3793 (1984).
13. S.Z. Lever, K.E. Baidoo, A.V. Kramer, and H.D. Burns. Tetrahedron Lett. **29**, 3219, 1988.
14. J. Xan, E.A. Wilson, L.D. Roberts, and N.H. Horton. J. Am. Chem. Soc. **63**, 1139 (1941).
15. R.H. Mach, H.F. Kung, P. Jungwiwattanaporn, and Y.-Z. Guo. Tetrahedron Lett. **30**, 4069 (1989).
16. B. Kamber. Helv. Chim. Acta, **54**, 417 (1971).
17. R.J. Abraham and P. Loftus. Proton and carbon-13 NMR spectroscopy — an integrated approach. Heyden, London. 1979. p. 169.

© 1997 NRC Canada

18. T.H. Siddhall and W.E. Stewart. J. Chem. Phys. **48**, 2928 (1968).
19. G. Claeson, G. Androes, and M. Calvin. J. Am. Chem. Soc. **83**, 9357 (1961).
20. C.H. Bushweller and M.H. Gianni. *In* The chemistry of ethers, crown ethers, hydroxyl groups and their sulphur analogues. Part 1. *Edited by* S. Patai. Interscience, Chichester. 1980. pp. 221–222.
21. M.B. Robin, F.A. Bovey, and H. Basch. *In* The chemistry of amides. *Edited by* S. Patai and J. Zabicky. Interscience, New York. 1970. p. 21.
22. F. Bohlmann and D. Schumann. Tetrahedron. Lett. **28**, 2435 (1965).
23. J. Dale and K. Titlestad. J. Chem. Soc. Chem. Commun. 656 (1969).
24. Z. Lidert. Tetrahedron, **27**, 967 (1981).
25. L.M. Jackman and S. Sternhell. Applications of nuclear magnetic resonance spectroscopy in organic chemistry. 2nd ed. Pergamon Press, Oxford. 1969. p. 91.
26. D. Neuhaus and M. Williamson. The nuclear Overhauser effect in structural and conformational analysis. VCH Publishers, New York. 1989. pp. 143–148.
27. S. Gronowitz and Z. Lidert. Chem. Scr. **16**, 97 (1980), and refs. therein.
28. W.E. Stewart and T.H. Siddall III. Chem. Rev. **70**, 517 (1970).
29. M. Frucht, A.H. Lewin, and F.A. Bovey. Tetrahedron Lett. **42**, 3707 (1970).
30. J.V. Hatton and R.E. Richards. Mol. Phys. **5**, 139 (1963). 31. L.A. LaPlanche and M.T. Rogers. J. Am. Chem. Soc. **85**, 3728 (1963).
32. L.L. Graham and M.R. Miller. Org. Magn. Reson. **4**, 327 (1972).
33. R.C Weast (*Editor*). CRC handbook of chemistry and physics. 68th ed. CRC Press, Boca Raton, Fla. 1987. p. D-188.
34. J.P. Idoux, J.M. Scandrett, and J.A. Sikorski. J. Am. Chem. Soc. **99**, 4577 (1977).
35. T.H. Siddall III, W.E. Stewart, and A.L. Marston. J. Phys. Chem. **72**, 2135 (1968).
36. M.A. Cremonini, L. Lunazzi, G. Placucci, R. Okazaki, and G. Yamamoto. J. Am. Chem. Soc. **112**, 2915 (1990).
37. J. Sandrström. Dynamic NMR spectroscopy. Academic Press, London. 1982. pp. 77, 86–91.
38. G. Claeson, G. Androes, and M. Calvin. J. Am. Chem Soc. **83**, 4357 (1961).
39. C.H. Bushweller, J. Golini, G. Rao, and J.W. O'Neil. J. Am. Chem. Soc. **92**, 3055 (1970).
40. A. Komornicki and J.W. McIver. J. Am. Chem. Soc. **95**, 4512 (1973).
41. O. Foss. *In* Organic sulfur compounds. Vol I. *Edited by* N. Kharash. Pergamon Press, New York. 1961. p. 77.
42. R. Rahman, S. Safe, and A. Taylor. Qt. Rev. **24**, 208 (1970).
43. A. Lidén, C. Roussel, T. Liljefors, M. Chanon, R.E. Metzger, and J. Sandström. J. Am. Chem. Soc. **98**, 2853 (1976).
44. M. Barfield, A.M. Dean, C.J. Fallick, R.J. Spear, S. Sternhell, and P.W. Westerman. J. Am. Chem. Soc. **97**, 1482 (1975).
45. V.G. Malkin, O.L. Malkina, L.A. Eriksson, and D.R. Salahub. *In* Theoretical and computational chemistry. Vol 2. *Edited by* J.M. Seminario and P. Politzer. Elsevier Science, B.V., New York. 1995. p. 273.
46. D.B. Chesnut. Annu. Rep. NMR. Spectrosc. **29**, 71 (1994); J. Gauss, M. Hofmann, and P.v.R. Schleyer. J. Am. Chem. Soc. **115**, 12385 (1993), and refs. therein.
47. R.F. Zürcher. *In* Progress in NMR spectroscopy. Vol II. *Edited by* J.W. Emsley, J. Feeney, and L.H. Sutcliffe. Pergamon Press, Oxford. 1967. p. 205.
48. H.M. McConnell. J. Chem. Phys. **27**, 226 (1957).
49. A.D. Buckingham. Can. J. Chem. **38**, 300 (1960).
50. N.J. Clayden and R.J.P. Williams. J. Magn. Reson. **49**, 383 (1982).
51. S. Winstein, P. Carter, F.A.L. Anet, and A.J.R. Bourn. J. Am. Chem. Soc. **87**, 5247 (1965).
52. S. Li and N.L. Allinger. Tetrahedron, **44**, 1339 (1988).
53. D.B. Chestnut and W.P. Johnson. J. Magn. Reson. **65**, 110 (1985).
54. B. Staskun. J. Org. Chem. **46**, 1643 (1981).
55. W.C. Still, M. Kahn, and A.J. Mitra. J. Org. Chem. **43**, 2923 (1978).
56. N. Walker and D. Stuart. Acta Crystallogr. Sect. A: Found. Crystallogr. **A39**, 158 (1983).
57. A.J.C. Wilson (*Editor*). International tables for cystallography. Vol. C. Kluwer Academic Publishers, Dordrecht. 1992. pp. 477–87.
58. SHELXTL PC. Version 4.1. Siemens Analytical X-Ray Instruments, Inc., Madison, Wis. May, 1990.
59. A. Bax. J. Magn. Reson. **53**, 517 (1983).
60. V. Rutar. J. Magn. Reson. **58**, 306 (1984).
61. J.A. Wilde and P.H. Bolton. J. Magn. Reson. **59**, 343 (1984).
62. C.A.G. Haasnoot, F.A.A.M. de Leeuw, and C. Altona. Tetrahedron, **36**, 2783 (1980).
63. M. Saunders, K.N. Houk, Y.-D. Wu, W.C. Still, M. Lipton, G. Chang, and W.C. Guida. J. Am. Chem. Soc. **112**, 1419 (1990).
64. PCMODEL user's guide. Version 4.0. Serena Software, Bloomington, Ind. p. 32.
65. M.J. Frisch, G.W. Trucks, H.B. Schlegel, P.M.W. Gill, B.G. Johnson, M.A. Robb, J.R. Cheeseman, T. Keith, G.A. Petersson, J.A. Montgomery, K. Raghavachari, M.A. Al-Laham, V.G. Zakrewski, J.V. Oortiz, J.B. Foresman, C.Y. Peng, P.Y. Ayala, W. Chen, M.W. Wong, J.L. Andres, E.S. Replogle, R. Gomperts, R.L. Martin, D.J. Fox, J.S. Binkley, D.J. Defrees, J. Baker, J.P. Stewart, M. Head-Gordon, C. Gonzalez, and J.A. Pople. Gaussian 94. Gaussian, Inc., Pittsburgh, Pa. 1994.
66. A.D. Becke. J. Chem. Phys. **98**, 5648 (1993).
67. P.J. Stevens, F.F. Devlin, C.F. Chabalowski, and M.J. Frisch. J. Phys. Chem. **98**, 11623 (1994).
68. K. Wolinski, J.F. Hilton, and P. Pulay. J. Am. Chem. Soc. **112**, 8251 (1990).

Can. J. Chem. Downloaded from www.nrcresearchpress.com by 92.62.229.171 on 09/08/12
For personal use only.

© 1997 NRC Canada

Electrochemical studies on sulphonephthaleins. Part 3.[1] Kinetics of electrochemical reduction of xylenol orange and square-wave adsorptive cathodic stripping voltammetry of its lanthanum complex

Refat Abdel-Hamid, Hussein M. El-Sagher, and Mostafa K. Rabia

Can. J. Chem. Downloaded from www.nrcresearchpress.com by 92.62.229.171 on 09/08/12
For personal use only.

Abstract: The electrochemical reduction behaviour of xylenol orange, XO, in aqueous medium was studied over a pH range of 2.3–9.6 at a hanging mercury drop electrode, HMDE, on the basis of cyclic voltammetric, and double-potential step chronoamperometric and chronocoulometric data. The experimental results indicate that in acid medium (pH 2.28) the reduction of XO proceeds via an ECEC, first-order mechanism giving a single two-electron diffusion-controlled cyclic voltammetric wave. It was concluded that the rate-determining step is the protonation of the protonated anion intermediate to the final product, with rate constant k_2 of 0.26 s^{-1}. At pH 7.25 the reduction follows an ECE kinetics along two cyclic voltammetric waves in which the first wave was attributed to an EC, first-order process and the second wave to an irreversible electron transfer step, E. On addition of lanthanum(III) to xylenol orange, it forms 1:1 and 1.2 La(III)–XO chelates, which are adsorbed and reduced on the HMDE at more negative potentials than the peak potential of free XO. The adsorptive cathodic stripping voltammetry, ACSV, of these chelates was studied using the square-wave, SW, method. It was found that the SW-ACSV of La(III)–XO can be applied to the determination of lanthanum at the nanomole level. Optimum conditions and the analytical method of determination were presented and discussed.

Key words: electrochemical, reduction mechanism, xylenol orange, lanthanum complex, double potential step chronoamperometry and chronocoulometry, stripping voltammetric determination.

Résumé : En se basant sur des données de voltampérométrie cyclique, de chronoampérométrie à double potentiel et de chronocoulométrie, on a étudié le comportement du xylénol orange, XO, lors de sa réduction électrochimique en solution aqueuse, à des pH allant de 2,3 à 9,6, par une électrode de mercure à goutte tombante, EMGT. Les données expérimentales indiquent que, en milieu acide (pH de 2,28), la réduction du XO se produit par le biais d'un mécanisme ECEC du premier ordre conduisant à une seule vague de voltampérométrie cyclique à deux électrons, contrôlée par la diffusion. On en conclut que l'étape qui détermine la vitesse de la réaction correspond à la protonation de l'anion intermédiaire protoné conduisant au produit final avec une constante de vitesse k_2 de 0.26 s^{-1}. À un pH de 7,25, la réduction suit une cinétique ECE le long de deux vagues de voltampérométrie cyclique dans lesquelles la première peut être attribuée à un processus EC du premier ordre et la deuxième à l'étape de transfert irréversible de l'électron, E. Par addition de lanthane(III) au xylénol orange, il se forme des chélates 1 : 1 et 1 : 2 de La(III)–XO qui sont adsorbés et réduits sur l'EMGT à des potentiels plus négatifs que celui du potentiel maximal de XO libre. On a étudié ces chélates par la voltampérométrie absorbante avec redissolution cathodique (VARC), en faisant appel à la méthode de l'onde carrée (OC). On a trouvé que l'on peut appliquer la technique de la VARC-OC à la détermination du lanthane au niveau de la nanomole. On présente et on discute des conditions optimales et de la détermination de la méthode analytique.

Mots clés : électrochimie, mécanisme de réduction, xylénol orange, complexe du lanthane, chronoampérométrie et chronocoulométrie avec étape à double potentiel, analyse par voltampérométrie avec redissolution.

[Traduit par la rédaction]

Received February 12, 1996.[2]

R. Abdel-Hamid,[3] H.M. El-Sagher, and M.K. Rabia. Department of Chemistry, Faculty of Science, University of South Valley, Sohag, Egypt.

[1] For Part 2, see ref. 1.

[2] Revision received November 7, 1996.

[3] Author to whom correspondence may be addressed. Fax: 093 601950. E-mail: janobwadi@frcu.eun.eg

© 1997 NRC Canada

Can. J. Chem. Downloaded from www.nrcresearchpress.com by 92.62.229.171 on 09/08/12
For personal use only.

Introduction

The rare earth elements are important components of some special technological and metallurgical materials. In general, analyses of small amounts of metals by means of voltammetric methods are easy to perform. Unfortunately, most of rare earth ions except Eu, Sm, and Yb are not reducible at the mercury electrode in aqueous solutions. On the other hand, several dyes and organic reagents that are reducible at the mercury electrode can be used as complexing ligands in which they form adsorptive complexes with the rare earths (2–7). For example, it was found previously that the phenolphthalein dyes, *o*-cresolphthalexon (5, 7) and thymolphthalexon (6), form adsorptive complexes with the rare earths. The adsorptive waves can then be used for the determination of trace rare earth contents in ores.

The electrochemical behaviour of xylenol orange is important due to its use as a metallochromic indicator (8) in the electrochemical microdetermination of europium in plants (9), in electrocatalysis of nitrite and nitric oxide reduction (10), and in adsorptive cathodic stripping voltammetry of lead in sea water (11). The kinetics of the electrochemical reduction of xylenol orange and the redox behaviour of its lanthanum(III) complex will be studied here. The applicability of square-wave cathodic adsorptive stripping voltammetry at the hanging mercury drop electrode, HMDE, for direct micro determination of La(III) will be tested.

In previous paper the electrochemical reduction mechanism of one of sulphonephthaleins, catechol violet, was studied (1). It shows a single diffusion-controlled two-electron cyclic voltammetric wave at lower pH (<7) and the reduction pathway follows an ECEC, first-order kinetics. At higher pH, two diffusion-controlled monoelectronic cv waves were seen and the reduction proceeds via an EEC, first-order process.

One objective of the present electrochemical investigation was to ascertain the kinetics of the reduction of another sulphonephthalein, xylenol orange, in aqueous solutions at the hanging mercury drop electrode. The study was performed utilizing a variety of electrochemical techniques including cyclic voltammetry, and double-potential step chronoamperometry and chronocoulometry. The second objective was to study the redox behaviour of a xylenol orange – lanthanum(III) complex. Finally, the study was extended to include the adsorptive cathodic stripping voltammetry, ACSV, of the La(III) complex using the square-wave, SW, voltammetric method. It was intended to lower the lanthanum detection limit to nanomole levels. The SW-ACSV method appears to combine the best features of the two methods. It was demonstrated that SW-ACSV gives a response 6 times greater than other stripping methods (12). It offers a method having a short analysis time and, in addition, surpasses the other pulse techniques in sensitivity and discrimination against the charging current background. Its utility has been demonstrated experimentally in conjunction with the stationary mercury drop electrode (13).

Experimental

Reagents and solutions

Rare earth nitrates of Y, La, interfering metal nitrates, anion salts, and xylenol orange sodium salt of analytical grade purity were used. Stock solutions of 5.0 mM in triply distilled water were prepared for the metal ions, anions, and XO and were diluted as required for standard solutions. The rare earth solutions were standardized chelatometrically. Britton–Robinson and acetic acid – sodium acetate buffer solutions were prepared from analytical grade chemicals.

Instrumentation

The cell and the instruments used for cyclic and square-wave voltammetry (SWV), chronoamperometry, and chronocoulometry have been described elsewhere (1). For all experiments, an Ag/Ag^+ electrode was used as the reference electrode. The HMDE in medium hanging drop mode was used throughout. The electrode area was 1.18×10^{-4} cm^2. For square-wave experiments, La(III)–XO complex characterization, calibration, and determination of La(III) measurements, the electrochemical analyzer was operated at a square-wave frequency, f, of 200 Hz since, as previously shown (14), the maximum sensitivity in SWV should be obtained for a maximum value of τ corresponding to a frequency of 200 Hz, and square-wave amplitude of 25 mV.

Procedure

All measurements were obtained at 298 ± 0.1 K. The general procedure used to produce square-wave adsorptive stripping voltammograms was as follows: A 10 cm^3 analyte solution in 20 mM acetic acid – sodium acetate/0.1 mol dm^{-3} sodium perchlorate solution was used. Solutions were deaerated by purging with pure nitrogen. After formation of a new HMDE drop at a deposition potential of –0.30 V, the solution was stirred for 60 s (accumulation time) and equilibrated for 10 s. A negative potential scan was recorded using the square-wave mode.

Results and discussion

1. Xylenol orange, XO

Xylenol orange, 3,3′-bis(*N*,*N*-bis(carboxymethyl)amino)-methyl-*o*-cresol sulphonephthalein, has the structural formula shown in Scheme 1 and is abbreviated as XO or H_6 XO.

1a. Cyclic voltammetry

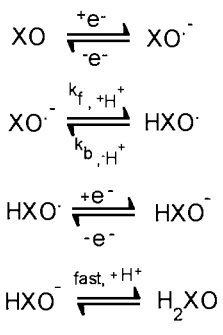
Cyclic voltammetric behaviour of XO was studied in aqueous Britton–Robinson buffer solutions at different pH's. The cyclic voltammogram of 1.0×10^{-3} mol dm^{-3} XO shows a single cathodic cv wave with a peak potential at –0.443 V versus Ag/Ag^+ at pH 2.28 and scan rate of 50 mV/s. No evidence of reversibility is noticed as indicated by the lack of an anodic partner corresponding to the oxidation of the product of reduction on reversing the potential. Since xylenol orange has the same reducible center as catechol violet, it is expected that the number of electrons and protons participating in the reduction process at lower pHs is two (1, 15, 16). The cv wave splits into two waves, each corresponding to one electron, in which the first one shifts to more negative potentials while the second does not change on increasing the pH of the solution (>2.3). This reveals that hydrogen ions participate in the reduction process along the first wave, whereas in the second one they do not. On plotting the peak potential, E_p, against the pH, two linear segments are obtained in the pH range 2.3 – 9.6. They are represented by the following linear least-square equations for the first cv wave:

© 1997 NRC Canada

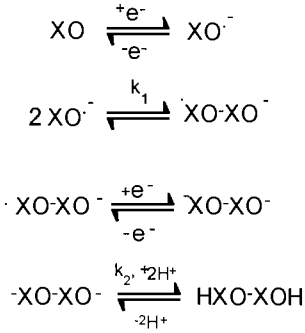
Scheme 1.

At pH = 2.28

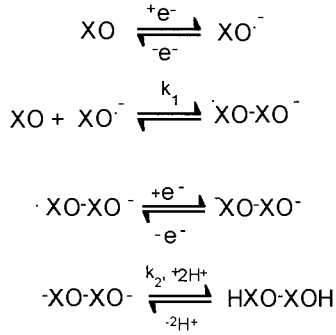
(a) ECE, first order



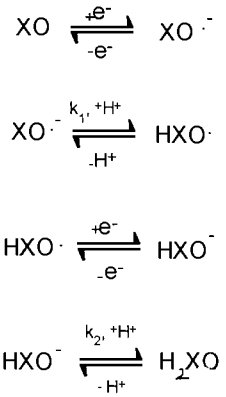
(b) ECEC, radical - radical dimerization



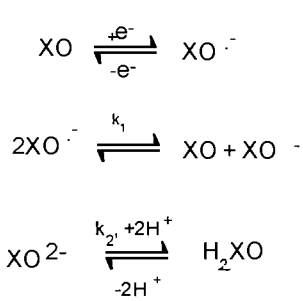
(c) ECEC, parent - radical dimerization

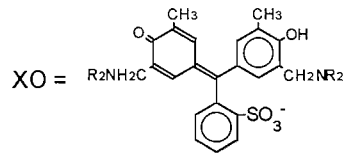


(d) ECEC, first order



(e) ECC, disproportionation





R=CH_2COOH

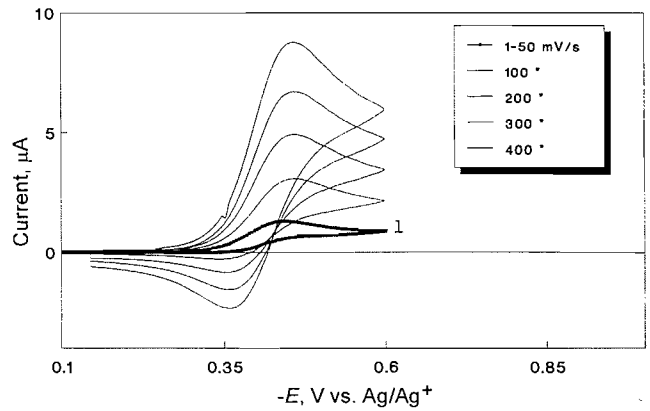
[1] $E_p = -0.330 - 0.959$ pH, $r = 0.994$

[2] $E_p = -0.151 - 0.086$ pH, $r = 0.995$

The two segments intercept at pH 6.7, which may correspond to dissociation of the -OH group. The number of protons involved during the first reduction step is calculated to be one from the relationship $S = (m/n) \times 59$ mV (at 298 K) (17) where S is the slope of E_p vs. pH, m is the number of protons, and n is the number of electrons.

At pH 2.28, xylenol orange exhibits a single irreversible cv wave at lower scan rates ($\nu = 50$ mV/s). On increasing the scan rate, the cv wave tends to be reversible (cf. Fig. 1). The anodic counterpart develops the peak current ratio, i_{pa}/i_{pc}, estimated according to Nicholson and Shain (18), increases with increasing scan rate and reaches unity at $\nu = 5.0$ V/s. Furthermore, the peak current, i_p, depends on the square root of the scan rate, $\nu^{1/2}$, with a correlation coefficient of 0.998. On increasing the scan rate, the peak potential does shift to more negative values, the current function, $i_p/\nu^{1/2}$, decreases, and the peak width, $E_p - E_{p/2}$, increases. These data suggest that the reduction of xylenol orange at pH 2.28 proceeds via a two-electron diffusion-controlled cv wave following an ECE mechanism in which the

Fig. 1. Cyclic voltammograms for the reduction of 1.0 mM xylenol orange on HMDE at pH 2.28 aqueous Britton–Robinson buffer solution at different scan rates.



difference between the standard electrode potentials for the two electron transfer steps, ΔE, equals 0 (18).

On the other hand, at higher pH's, the voltammograms of XO show two mono-electronic irreversible cv waves. At pH 7.25, the peak potentials of the two waves shift cathodically by

Can. J. Chem. Downloaded from www.nrcresearchpress.com by 92.62.229.171 on 09/08/12
For personal use only.

© 1997 NRC Canada

Can. J. Chem. Downloaded from www.nrcresearchpress.com by 92.62.229.171 on 09/08/12
For personal use only.

40.0 and 29.4 mV per decade for the first and second waves, respectively, on increasing the scan rate. Furthermore, the peak currents correlated with the square root of the scan rate (r = 0.996 and 0.999 for the first and second waves, respectively). The current function for the first wave decreases while for the second one it more or less has a constant value of 0.5 on increasing the scan rate. Thus, these findings lead to an initial suggestion that the electrochemical reduction of xylenol orange at higher pH's follows an EC mechanism for the first wave and an irreversible electron transfer process for the second (18). The overall kinetics of the reduction process is ECE.

1b. Chronoamperometry and chronocoulometry

Two basic electrochemical approaches were used for the investigation of the electrode mechanism, one-step and two-step methods. The one-step method, for example, includes the analysis of peak shape, potential, and current variations of the cyclic voltammetric waves. Unfortunately, the one-step methods are used in qualitative measurements and are subject to several limitations. The two-step methods, on the other hand, are more generally applicable for quantitative electrode mechanism studies. The two-step methods used herein are double-potential step chronoamperometry and chronocoulometry. In the first step of electrolysis, the potential is stepped to a value where the cathodic current is determined solely by diffusion of the subject ions to the electrode. Then at some switching time, τ, the potential is suddenly returned to the initial value. The resulting anodic current, which is determined by the diffusion-controlled reoxidation of the reduced form generated, gives a measure of the unreacted subject molecules.

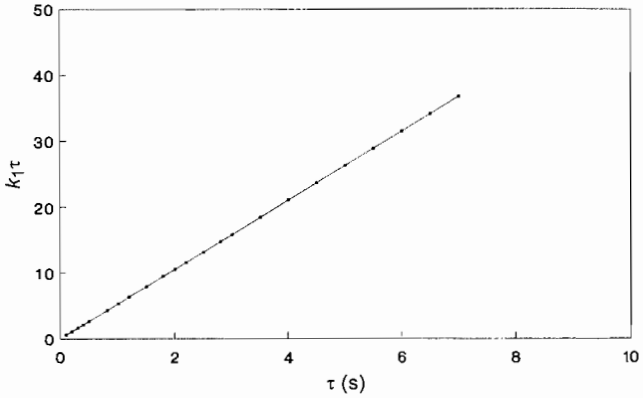
At lower pH's (pH 2.28) the electrode potential is stepped from –0.1 V, at which no faradaic current flows, to –0.45 V, sufficiently cathodic, to the cyclic voltammetric peak potential. Then at variable switching duration times, τ, the potential is suddenly returned to the initial potential value of –0.1 V. The cathodic chronoamperograms and chronocoulograms are analysed using eqs. [3] and [4], respectively, where (i)(t) and

$$[3] \quad i(t < \tau) = \frac{nFAD^{1/2}C^*}{(\pi t)^{1/2}}$$

$$[4] \quad Q(t < \tau) = 2nFAD^{1/2}C^* \left[\frac{t}{\pi}\right]^{1/2}$$

$Q(t)$ are the current and charge, respectively, that have passed at time t since the application of the potential step, C^* and D^* are the concentration and diffusion coefficient of the substrate, respectively, A is the surface area of the electrode, and n and F have their usual significance. According to the Cottrell equation, eq. [3], the diffusion coefficient of xylenol orange is determined (a) from the slope of the ic vs. $t^{-1/2}$ plot or (b) from the linear least-squares intercept of $it^{1/2}$ vs. $t^{-1/2}$ plots. It has been reported that chronoamperometric data obtained at short times are often unreliable and that such data cannot be used for accurate determinations (19); thus, long-duration time experiments were used. Linear dependence was obtained for the ic and $it^{1/2}$ vs. $t^{-1/2}$ plots, with correlation coefficients of 0.999 for the entire range of duration times (1.0 – 7.5 s). This is indicative of the diffusion-controlled nature of the electrochemical reduction of the subject substrate. The diffusion coefficient of

Fig. 2. $k_1\tau$ vs. τ relationship for the ECEC, first-order mechanism for the reduction of xylenol orange at pH = 2.28.



XO was calculated and found to be (1.02 ± 0.02) × 10^{-6} cm^2/s. On analysing the chronocoulograms using eq. [4], it is seen that the charge, $Q(t < \tau)$, has a direct proportionality to the square root of time, $t^{1/2}$. Linear least-squares fits were obtained with a correlation coefficient of 0.999 for different duration times. This is in agreement with chronoamperometric results showing that the cathodic current for the subject compound at such conditions is controlled by diffusion. Moreover, the diffusion coefficient of XO was calculated to be (1.10 ± 0.04) × 10^{-6} cm^2/s. This value agrees well with those calculated above.

Analysis of the chronocoulometric data, the cathodic–anodic chronocoulograms, involves the measure of the charge ratio, Q_r, for a series of different duration times. The double-potential step chronocoulometric results were fitted using the theoretical working curves developed by Hanafey et al. (20) for various mechanisms, in an attempt to find a satisfactory match. The first few points of data arising from the double layer charging current were ignored. Different electrode reaction mechanisms, in addition to the ECE process, were considered as possible pathways for the electrochemical reduction of XO in such circumstances (cf. Scheme 1). These include ECEC, radical–radical dimerization; ECEC, parent–radical dimerization; ECEC, first–order; and ECC disproportionation. It is reasonable to exclude the dimerization and disproportionation pathways, since the resultant radical anion intermediate and the parent substrate are very bulky and sterically hindered species. Furthermore, it is found that he experimental results satisfactorily fit the theoretical working curves for the ECEC first-order mechanism with k_2/k_1 = 0.05. So the ECEC first-order pathway is likely the mechanism for the electrochemical reduction of xylenol orange. The rate-determining step is concluded to be the protonation of the protonated anion intermediate to the final product, with a rate constant of k_2. These results are similar to the electrochemical reduction mechanism of catechol violet studied elsewhere (1), since they have the same reducible center.

On plotting the values of $k_1\tau$, the kinetic parameter obtained from the matched experimental data plots of Q_r vs. log $k_1\tau$, as function of τ, the value of k_1 is estimated directly from the slope. Linear least-squares plots passing through the origin are obtained with correlation coefficients of 1.0. A typical plot is presented in Fig. 2. The rate constant k_1 obtained is found to be

© 1997 NRC Canada

Can. J. Chem. Downloaded from www.nrcresearchpress.com by 92.62.229.171 on 09/08/12
For personal use only.

Scheme 2.

At pH 7.25:
First cv wave:

(a) EC, first order

$$XO \underset{-e^-}{\overset{+e^-}{\rightleftharpoons}} XO^{\cdot -}$$

$$XO^{\cdot -} \underset{k_b,\ -H^+}{\overset{k_f,\ +H^+}{\rightleftharpoons}} HXO^{\cdot}$$

(b) EC, radical - radical dimerization

$$XO \underset{-e^-}{\overset{+e^-}{\rightleftharpoons}} XO^{\cdot -}$$

$$2XO^{\cdot -} \underset{k_b}{\overset{k_f}{\rightleftharpoons}} {}^{\cdot}XO\text{-}XO^{\cdot -}$$

(c) EC, parent - radical dimerization

$$XO \underset{-e^-}{\overset{+e^-}{\rightleftharpoons}} XO^{\cdot -}$$

$$XO + XO^{\cdot -} \underset{k_b}{\overset{k_f}{\rightleftharpoons}} {}^{\cdot}XO\text{-}XO^{\cdot -}$$

Second cv wave:

E, slow electron transfer

$$HXO^{\cdot} \xrightarrow{+e^-} HXO^-$$

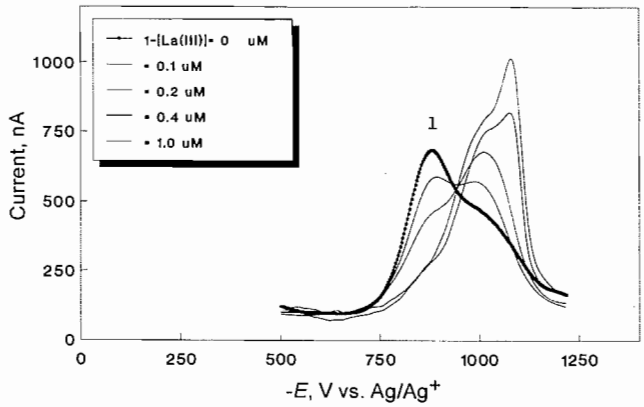
$$HXO^{\cdot} \underset{+H^+}{\overset{\text{fast},\ +H^+}{\rightleftharpoons}} H_2XO$$

$5.25 \pm 0.01\ s^{-1}$. The rate constant k_2 for the second protonation step is calculated to be $0.26 \pm 0.003\ s^{-1}$.

At higher pH's (7.25), the electrode potential was stepped from E_1 to E_2 to E_1 in which $E_1 = -0.60$ and $E_2 = -0.80$ V for the first wave. The cathodic chronoamperograms were analysed according to Cottrell equation. On plotting ic or $ict^{1/2}$ against $t^{-1/2}$, linear dependences with correlation coefficients of 0.999 were obtained. This reveals that the electrochemical reduction of XO at pH 7.25 is a diffusion-controlled process. Similar correlations were obtained on analysis of the chronocoulograms. The values of the diffusion coefficient of XO were determined and the average value is $(1.11 \pm 0.02) \times 10^{-6}\ cm^2/s$. This value is consistent with the value obtained at pH 2.28.

On matching the experimental charge ratio plots, Q_r vs. log τ with the theoretical working curves of Hanafey et al. (20), considering different possible electrode reaction pathways, it was found that the reduction of xylenol orange follows EC kinetics. These pathways are EC, first-order; EC, radical–radical dimerization; and EC, parent–radical dimerization (cf. Scheme 2). As stated before, the dimerization pathways are excluded. It was concluded that a good fit is obtained with the experimental data for the EC first-order mechanism in which $k_f/k_b = 0.01$. The first-order rate constant, k_f, was estimated following the method mentioned above. It was found to be 30.45 $\pm$ 0.04 s^{-1}. The rate constant, k_b, was calculated to be $0.30 \pm 0.02\ s^{-1}$. Thus the electrochemical reduction of XO at pH 7.25 in the entire range of potential for the first wave follows the EC first-order kinetics. The mechanism at higher pH's is ECE.

Fig. 3. Square-wave voltammograms of 1.0 μM xylenol orange containing different concentrations of lanthanum(III), in 20 mM acetic acid – acetate/0.1 M $NaClO_4$ buffer solution, pH 6.05, preconcentration time 60 s, frequency 200 Hz.



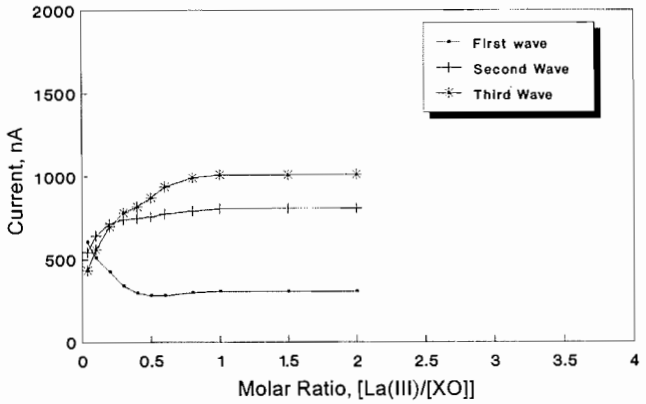
2. Lanthanum(III) – xylenol orange

Cyclic and square-wave voltammograms of 1.0×10^{-6} mol dm^{-3} xylenol orange mixed with concentrations of lanthanum(III) varying from 0 to 3.0 molar ratio, La(III)–XO, in 0.1 mol dm^{-3} acetate/0.1 mol dm^{-3} sodium perchlorate aqueous solution at pH 6.05, show three irreversible reduction waves in the entire voltage sweep, –0.1 to –1.4 V. These waves are located at peak potentials of –0.886, –1.015, and –1.077 v. The first wave attributed to the reduction of the uncomplexed XO, since it is located at the peak potential of free XO. The two more negative waves are due to the reduction of the La(III)–XO complexes, since the reduction wave of XO is shifted to more negative potentials on complexation with La(III). An enhancement of the voltammetric response is achieved after adsorption of the electroactive species on the HMDE on stirring the solution mixture. The SW-ADSV behaviour of La(III)–XO is presented in Fig. 3. It is worth emphasizing that the adsorbed complexes of La(III)–XO have the same peak potentials as those obtained in solution. On addition of La(III) to XO, a spontaneous colour, a decrease in the peak current of the XO reduction wave, and the development of a second wave at more negative potentials were observed. Thus the reaction between XO and La(III) is rapid. Increasing the concentration of La(III) shows a further decrease in the first wave and growth of the second. At molar ratios higher than 0.3, the third wave tends to develop. The third wave grows with further increase in the molar ratio of La(III). The composition of the metal complexes was determined by plotting the peak current versus molar ratio, [M]:[L] (21–23). The results are presented in Fig. 4. It is seen that the peak current for free XO, the first wave, decreases on increasing the mole ratio of La(III), reaching a more or less constant value at the 0.5 mole ratio. This is indicative of formation of a complex with a composition of 1:2, La(III):XO, under such conditions. Some authors (24–26) have reported the formation of 1:2 complexes with methyl thymol blue, which has a similar sulphonephthalein

© 1997 NRC Canada

Can. J. Chem. Downloaded from www.nrcresearchpress.com by 92.62.229.171 on 09/08/12
For personal use only.

Fig. 4. Variation of peak current with mole ratio of La(III) for La–XO system at the conditions cited in Fig. 3 for the three waves.



structure. On the other hand, for the second wave, the peak current increases on increasing the mole ratio [La(III)]/[XO] and levels off at a molar ratio of 1.0. The graph has two breaks at molar ratios of 0.5 and 1.0, which are due to the change of the composition of the reducible species. This reveals the formation of two types of complexes of 1:2 and 1:1 composition (La(III):XO). Moreover, from the i_p vs. [La(III)]/[XO] relationship, at the third wave, it is evident that La(III) forms complexes with XO with a stoichiometric ratio of 1:2 and 1:1 (La–XO). This supports the composition suggested from the data at the first and the second waves.

Xylenol orange has two 3-bis[*N*,*N*-bis(carboxymethyl)amino] methyl chelating groups on each side of the large sulphonephthalein molecule. It was reported that each chelating group reacts with metal ions independently (27). Thus, the donor atoms in the XO molecule are two carboxylic oxygens, a quinoyl oxygen, and a tertiary nitrogen. At the given pH, 6.05, the carboxylic groups dissociate and coordinate to the La(III) ion. The colour, and the cyclic and square-wave voltammetry corresponding to the complexes are quite different from those of the free XO. This suggests that the quinoyl oxygen is the other ligating site, since it is the electroactive center (28). At this pH, the tertiary nitrogen is protonated and is not involved in the coordination. Thus, XO behaves as a terdentate ligand and the lanthanum ion is hexa-coordinated to xylenol orange in the 1:2 (La–XO) chelates, thus using fully the three ligating sites. In 1:1 chelates, the metal ion tri-coordinates the subject ligand through its ligating sites and completes its hexa-coordination with three water molecules (29).

The peak potential for the reduction of adsorbed La–XO chelate does shift to more negative values on increasing the pH. It is evident from the dependence of E_p on pH that the maximum separation between the E_p of XO and La(III)–XO exists at pH 6.05. The peak current of La(III)–XO depends on the concentration of acetate, preconcentration time, and accumulation potential. The effect of these parameters was tested in order to optimize the conditions for the determination of lanthanum. The peak current of La(III)–XO decreases with increasing concentration of acetate. This is presumably due to the competitive complexation of La(III). The recommended buffer concentration of acetate is 20 mM. The adsorption peak for La(III)–XO is found to be dependent on the adsorption time. It grows with time to a limiting value and then levels off. From the data obtained, it is evident that the optimum preconcentration time is 60 s. The effect of accumulation potential on the height of the La(III)–XO adsorptive peak was investigated and it is revealed that the optimum accumulation potential is –0.30 V.

3. Characterization of adsorbed La(III)–XO

It was demonstrated that double-potential step chronocoulometry provides a useful method for the quantitative characterization of an adsorption process independent of both the relative reduction potentials of the diffusing and adsorbed species and the kinetics of their electrode reactions (30). On considering that only La–XO is adsorbed on the electrode surface, additional terms must be added to eq. [4] for the cathodic response.

$$[5]\quad Q_f(t<\tau) = 2nFAD^{1/2}C^*\left[\frac{t}{\pi}\right]^{1/2} + nFA\Gamma_0 + Q_{dl}$$

where Γ_0 is the amount of the adsorbed reactant in mol/cm^2 and Q_{dl} is the charge consumed by the electrode – electrolyte double layer when the potential is changed from its initial to its final value. The terms on the right-hand side represent the contribution of dissolved, adsorbed, and double-layer charging, respectively. For the anodic response, according to the approximation of Christie et al. (31), the charge is given by the following equation:

$$[6]\quad Q_r(t>\tau) = 2nFAD^{1/2}C^*\left[\frac{1}{\pi}\right]^{1/2}\left[1+\frac{a_1nAFT_0}{Q_c}\right]\theta + a_0nFA\Gamma_0 + Q_{dl}$$

where $\theta = \tau^{1/2} + (t-\tau)^{1/2} - t^{1/2}$, Q_c is the total charge arising from the diffusing species during the forward step, and a_0 and a_1 are usually assumed to be –0.069 and –0.97, respectively.

On considering the quantity of change removed in the reversal step, $Q_r(t>\tau)$, which experimentally is the difference $Q(\tau) - Q(t>\tau)$, the anodic response is

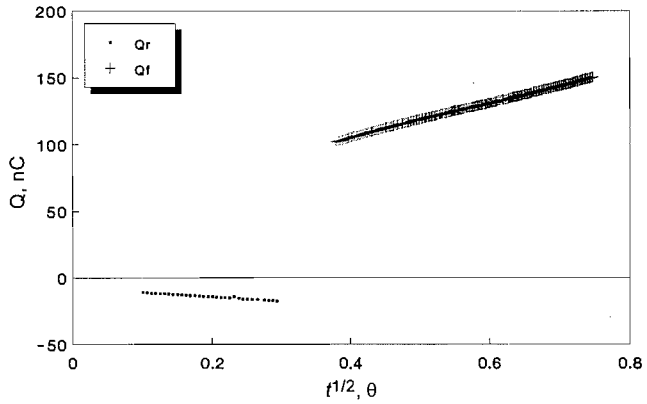
$$[7]\quad Q_r(t>\tau) = 2nFAD^{1/2}C^*\left[\frac{1}{\pi}\right]^{1/2}\theta + Q_{dl}$$

The plot of $Q_r(t>\tau)$ versus θ should be linear with an intercept of Q_{dl}.

Chrononcoulometric data for a 1.0×10^{-6} mol dm^{-3} 1:1 La(III)–XO complex at pH 6.05 were obtained on stepping the electrode potential from –0.7 to –0.95 V and then returning it to its initial value (–0.70 V). The data were analysed according to eqs. [5] and [7], cf. Fig. 5. On plotting $Q_f(t<\tau)$ vs. $t^{1/2}$ and $Q_r(t>\tau)$ vs. θ, good straight lines were obtained with regression coefficients of 0.997 and 0.998, respectively. They have different slopes and intersect each other above, rather than on, the t-axis. This demonstrates the adsorption of the La(III)–XO chelate on the electrode surface. From the slope of the $Q_f(t<\tau)$ vs. $t^{1/2}$ plot, the diffusion coefficient of the chelate was calculated to be $(2.33 \pm 0.06) \times 10^{-7}$ cm^2/s which is lower than that of XO. The amount of adsorbed complex, the surface excess Γ_0, is determined from the difference between the intercepts of the two lines in Fig. 5, which is simply $nFA\Gamma_0$. This difference cancels Q_{dl} and leaves only a net faradaic

© 1997 NRC Canada

Fig. 5. Double-potential step chronocoulometric dependence of Q_f on $t^{1/2}$ and Q_r on θ for La–XO chelate.



charge due to adsorbate. The double layer charge is determined from the intercept according to eq. [7] to be 5.77 ± 0.5 *nC*.

4. Analytical determination of La(III)

According to the above-mentioned results, the optimum conditions for the analytical determination of La(III) by SW-ASCV at HMDE are as follows: pH 6.05, accumulation time 60 s, accumulation potential –0.30 V, SW height 25 mV, frequency 200 Hz, and the presence of 1.0×10^{-6} mol dm^{-3} xylenol orange. Under these conditions, the response of the peak current as a function of La(III) concentration is linear over the range 100.0 – 500 nM dm^{-3} La(III) at the three peak potentials, E_p, of –0.886, –1.0125, and –1.077 V. For concentrations beyond the above range, the calibration curve is no longer linear. However, higher La concentrations can be adjusted by dilution to bring them within the recommended concentration range or, alternatively, shorter deposition times may be used. Using standard La(III) solution, the method gave linear calibration curves. The slopes of the calibration lines obtained (sensitivity) with correlation coefficients of 0.994, 0.999, and 0.997, respectively, were 1.13, 1.18, and 1.39 nA/nM/60 s, for the three waves. The detection limit (DL) was estimated by sue of signal-to-noise ratio, r_d = 3, pooled standard deviation, *S*, and the slopes of calibration, *b*, from the formula DL = $r_d S/b$. It was found to be 1.06, 1.02, and 0.86 nM, respectively, for the first, second, and third waves.

The interference of a number of cations and anions was tested in the determination of La(III) using 1.0 nM xylenol orange with 0.1 nM La(III), with addition of various metal ions. It was found that electrochemically inactive ions such as Na^+, K^+, Ca^{2+}, as well as most commonly occuring anions, do not interfere with the determination of lanthanum. Fe(III), Co(II), Ni(II), Cu(II), Zn(II), Pb(II), and Cd(II) do not interfere at the 0.5 mM dm^{-3} level. They form adsorbed complexes with XO under such conditions and are reduced at a lower potential than that for the reduction of the La(III)–XO complex. On the other hand, addition of Y(III) and Ce(III) shows peaks overlapping with those for La(III)–XO. Thus Y(III) and Ce(III) interfere and the peak current for La(III) decreases due to adsorption competition.

References

1. R. Abdel-Hamid. J. Chem. Soc. Perkin Trans 2, 691 (1996).
2. X. Gao, N. Li, L. Zhang, K. Jlao, and M. Zhang. Kexue Tongbao (Chin. Ed.) **28**, 914 (1983).
3. X. Gao, M. Zhang, and T. Ho. Fenxi Huaxue, **11**, 762 (1983).
4. Z. Wa, X. Teng, X. Gao, K. Jlao, and M. Zhang. Zhongguo Xitu Xuebao, **1**, 70 (1983).
5. X. Gao and M. Zhang. Anal. Chem. **56**, 1912 (1984).
6. M. Zhang and X. Gao. Anal. Chem. **56**, 1917 (1984).
7. J. Wang, P.A.M. Farias, and J.S. Mahmoud. Anal. Chim. Acta, **171**, 215 (1985).
8. K.M.M. K. Prasad, P. Vijayalekshmi, and C.K. Sastri. Analyst, **119**, 2817 (1994).
9. X. Gao and M. Zhang. Sci. Sin. Ser. B: **25**, 690 (1982).
10. J.J. Zhang, A.B.P. Lever, and W.J. Pietro. Inorg. Chem. **33**, 1392 (1994).
11. Q. Wu and G.E. Batley. Anal. Chim. Acta, **309**, 95 (1995).
12. S.P. Kounaves, J.J. O'Dea, P. Chanadresekhar, and J. Osteryoung. Anal. Chem. **59**, 386 (1987).
13. M. Wojiechowski, W. Go, and J. Osteryoung. Anal. Chem. **57**, 155 (1985).
14. L. Ramaley and M.S. Krause, Jr. Anal. Chem. **41**, 1362 (1969).
15. D.V. Vukomanovic, J.A. Page, and G.W. VanLoon. Can. J. Chem. **69**, 1418 (1991).
16. D.V. Vukomanovic and G.W. VanLoon. Talanta, **41**, 387 (1994).
17. T.M. Florence and W.L. Belew. J. Electroanal. Chem. **21**, 157 (1969).
18. R.S. Nicholson and I. Shain. Anal. Chem. **36**, 706 (1964); **37**, 178 190 (1965).
19. W.T. Yap and L.M. Doane. Anal. Chem. **54**, 2399 (1982).
20. M.K. Hanafey, R.L. Scott, T.H. Ridgway, and C.N. Reilley. Anal. Chem. **50**, 116 (1978).
21. K. Ogura and K. Arinobu. J. Electroanal. Chem. **89**, 175 (1978).
22. K. Ogura, K. Seneo, S. Murakami, and T. Yoshino. J. Inorg. Nucl. Chem. **42**, 1165 (1980).
23. K. Ogura. Y. Fushima, and I. Aomizu. J. Electroanal. Chem. **107**, 271 (1980).
24. T.V. Mal'kova, N.D. Medvedeva, and K.S. Yatsimirskii. Zh. Neorg. Khim. **9**, 2347 (1964).
25. V.A. Nazarenko and E.M. Nevskaya. Zh. Anal. Khim. **24**, 839 (1969).
26. T.V. Mal'kova, V.D. Ovchinnikova, and T.B. Boloshina. Izv. Vyssh. Uchebn. Zaved. Khim. Khim. Tekhnol. **14**, 1635 (1971).
27. M. Otomo. Bunseki Kagaku, **21**, 436 (1972).
28. K. Ogura, S. Murakami, and K. Seneo. J. Inorg. Nucl. Chem. **43**, 1243 (1981).
29. S. Murakami. J. Inorg. Nucl. Chem. **41**, 209 (1979).
30. A.J. Bard and L.R. Faulkner. Electrochemical methods: fundamentals and applications. John Wiley & Sons, New York. 1980. p. 535.
31. J.H. Christie, R.A. Osteryoung, and F.C. Anson. J. Electroanal. Chem. **13**, 236 (1967).

Can. J. Chem. Downloaded from www.nrcresearchpress.com by 92.62.229.171 on 09/08/12
For personal use only.

© 1997 NRC Canada

Synthesis, structure, and properties of oligo-tridentate ligands; covalently assembled precursors of coordination arrays

Garry S. Hanan, Ulrich S. Schubert, Dirk Volkmer, Emmanuel Rivière, Jean-Marie Lehn, Nathalie Kyritsakas, and Jean Fischer

Can. J. Chem. Downloaded from www.nrcresearchpress.com by 92.62.229.171 on 09/08/12
For personal use only.

Abstract: Oligo-tridentate ligands based on alternating pyridines and pyrimidines were synthesised by Stille-type carbon–carbon bond-forming reactions. The terpyridine-like sites are designed to coalign upon metal complexation, giving rise to organized and rigidly spaced metal ions. Peripheral functionalization of the basic bis-tridentate framework was explored. The heterocycles in the ligands are in an all-*trans* conformation about the interannular bonds as indicated by comparison of their ^{1}H NMR spectra. An X-ray crystal structure analysis of the nonchiral tris-tridentate ligand **2***a* reveals a helical structure in the solid state. The seven heterocycles form a helical structure with resulting overlap of the terminal pyridines. Their centroid-to-centroid distance is 4.523 Å with 38.8° between the planes. NMR investigations support a helical conformation in solution as well. Electrochemical and UV absorption measurements indicate that the LUMO resides on the pyrimidine moiety of the ligands.

Key words: nitrogen-containing ligands, Stille coupling, helical structure, supramolecular chemistry.

Résumé : Nous avons développé une route synthétique pour la synthèse de ligands oligo-tridentates basée sur le couplage carbone–carbone de Stille. La disposition des sites tridentates a été conçue en vue de la complexation d'ions métalliques de façon colinéaire. La structure de base a été fonctionalisée de manière à construire des systèmes plus étendus. La structure rayons-X du ligand tris-tridentate **2***a* révèle sa forme hélicoidale. Les groupes pyridine terminaux s'empilent l'un sur l'autre à une distance centre–centre de 4.523 Å avec un angle de 38.8° entre les planes. Le spectre de RMN du proton est en accord avec l'existence de la forme hélicoidale aussi en solution. Les études d'électrochimie et d'absorption d'UV indiquent que la plus basse orbitale inoccupée est localisée principalement sur le groupe pyrimidine.

Mots clés : ligands azoté hétérocycliques, couplage Stille, structure hélicoidale, chimie supramoléculaire.

Introduction

Recent work that exploits hydrogen-bonding (1–3), metal–ligand (4, 5), and cation–π (6) interactions has demonstrated that information stored into molecular components may be read out by various non-covalent interactions to bring about a desired structure (7). Functional supramolecular structures are of current interest for the development of molecular-level devices (8, 9). Interesting structures exploiting metal–ligand interactions based on commercially available compounds have been constructed; however, most contain infinite lattices and some only exist in the solid state (10, 11). Increasingly, chemists must look to more and more complex components to assemble structures presenting desired properties. Molecular components with repeating sub-units simplify the overall synthesis of relatively complex target molecules (12) and this approach has been exploited here to synthesize oligo-tridentate ligands capable of binding metal ions in a predetermined arrangement (13).

We sought to develop models for information storage based on coordination *arrays*, multimetallic complexes of precise nuclearity and geometry, in particular inorganic architectures of two-dimensional geometries and $[m \times n]$ nuclearity. The basic geometries may be termed *racks* [*n*]R, *ladders* [2*n*]L, and *grids* $[m \times n]$G (Fig. 1), where the nuclearity of the R, L, and G species is given by [*n*], [2*n*], and $[m \times n]$, in sequence of increasing complexity. In addition to serving as centres for ligand binding and positioning, metal ions also introduce a range of electrochemical, photochemical, and reactional properties.

The metal-directed self-assembly of molecules of rack, ladder, and grid type requires judicious choice of metal and binding site. Transition metal ions with octahedral coordination geometry are expected to cover a wider range of elements and properties than ladder- (14) and grid-type (15) complexes with tetrahedral metal ions. The two ligand moieties, therefore, must be tridentate to maintain an orthogonal disposition about an octahedral metal ion (16). Terpyridine (tpy) forms stable complexes with a wide variety of octahedral metals (17) and is a well-suited tridentate motif. It also sustains a variety of oxidative and reductive conditions (18, 19), and has accessible π* orbitals (20).

Linking tpy's together in the 4, 3′ positions as depicted in Fig. 2*a* would produce a ligand strand where the individual tpy

Received July 20, 1996.

G.S. Hanan, U.S. Schubert, D. Volkmer, E. Rivière, and J.-M. Lehn.[1] Laboratoire de chimie supramoléculaire (CNRS, URA 422), Université Louis Pasteur, 4, rue Blaise Pascal, F-67000 Strasbourg, France.
N. Kyritsakas and J. Fischer. Laboratoire de cristallochimie et de chimie structurale (CNRS, URA 424), Université Louis Pasteur, 4, rue Blaise Pascal, F-67000 Strasbourg, France.

[1] Author to whom correspondence may be addressed. Fax: 33-388-41 10 20.

© 1997 NRC Canada

Fig. 1. Inorganic architectures of rack (left), ladder (center), and grid (right) type.

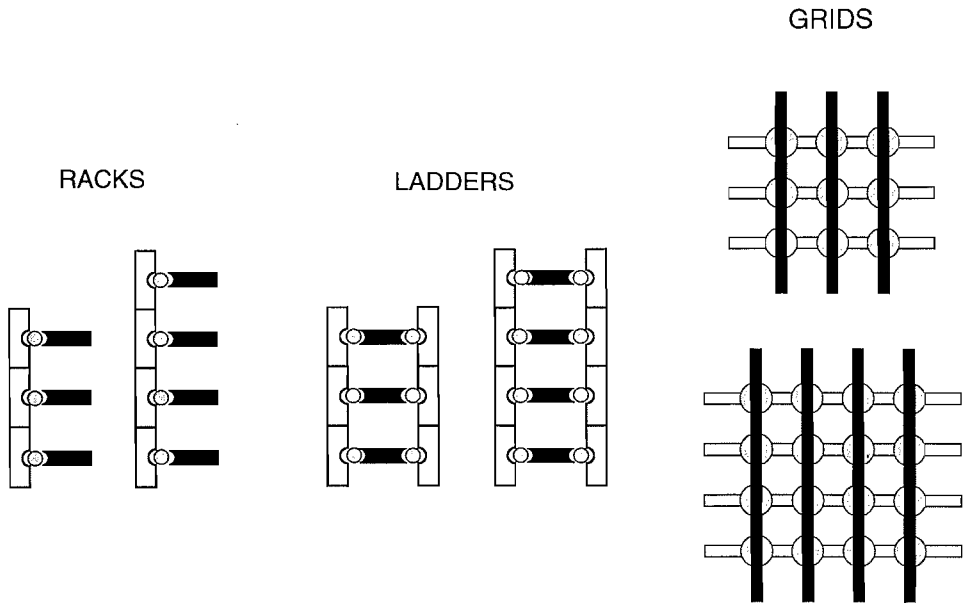
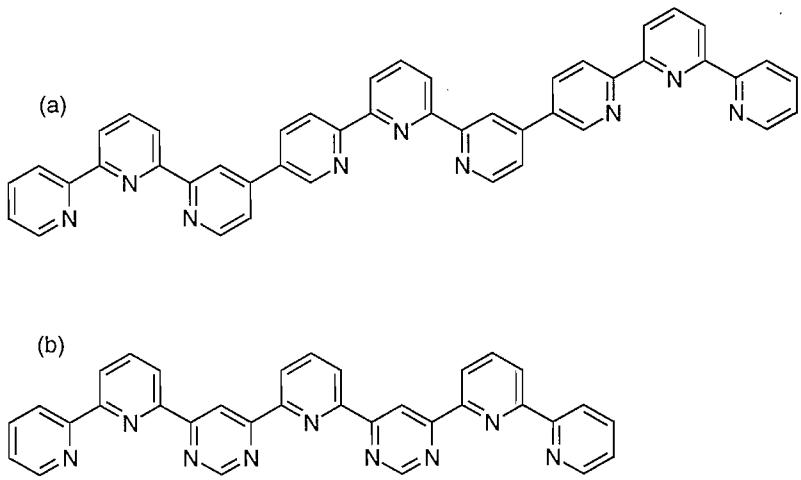


Fig. 2. Types of oligo-tridentate ligands for the assembly of metal ion arrays.



sub-units may not coalign properly in the complex due to rotation about the interannular bonds. To enforce alignment and to promote metal–metal interaction (21), a condensed-ring structure was chosen by using bridging pyrimidines (Fig. 2*b*). The synthesis and characterization of the bis-tridentate (**1***a–f*) and tris-tridentate ligands (**2***a–c*) based on pyridine and pyrimidine is presented in the present work.

Experimental

2,2′-Bipyridine-*N*-oxide (22), 6-chloro-2,2′-bipyridine (23), 2-tributylstannylpyridine (24), 2-bromo-5-methylpyridine (25), and 4,6-dichloro-2-phenylpyrimidine (26) were prepared as described. Materials were obtained from commercial suppliers and used without further purification. Dimethylformamide (DMF) was purchased anhydrous from Aldrich Chemical Company. Diethyl ether (ether) and tetrahydrofuran (THF) were distilled under argon from sodium–benzophenone immediately prior to use in lithiation reactions. Dichloromethane (DCM) was dried over CaH_2. Organic extracts were dried over $MgSO_4$. Chromatography was carried out on Merck 60 silica gel (0.040–0.063 mm), Merck, activity II-III, alumina (0.063–0.200 mm). ^1H and $^{13}C\{^1H\}$ NMR spectra were recorded at 200 and 50 MHz, respectively, on a Bruker AC 200 spectrometer in $CDCl_3$. ^1H NMR spectra were also recorded at 400 MHz on a Bruker AM 400 spectrometer in $CDCl_3$ where indicated. The chemical shifts were calibrated to the residual solvent peak. Melting points were measured on a digital Thomas–Hoover (Electrotherma) apparatus. Infrared absorption spectra were measured on a Perkin Elmer 1600 series FTIR spectrometer as KBr disks. Electronic absorption spectra were measured on a Cary 219 spectrometer in DCM, with λ_{max} in nm and 10^{-4} ε/dm^3 mol^{-1} cm^{-1}. Cyclic voltammograms were measured using a EDT potentiostat/galvanostat

Can. J. Chem. Downloaded from www.nrcresearchpress.com by 92.62.229.171 on 09/08/12
For personal use only.

© 1997 NRC Canada

Can. J. Chem. Downloaded from www.nrcresearchpress.com by 92.62.229.171 on 09/08/12
For personal use only.

with a Tacussel IG5-LN integrator and IFELEC-IF 3802 recorder: the working electrode was a platinum disc, the auxiliary electrode was a coiled platinum wire, and the reference electrode was a SCE.

Preparation of 6-bromo-2,2′-bipyridine (*6a*)

(i) Via 6-chloro-2,2′-bipyridine (5)

To 6-chloro-2,2′-bipyridine **5** (2.00 g, 10.5 mmol) was added phosphorous tribromide (50 mL) and the reaction mixture was stirred at 165°C for 5 h. The reaction mixture was cooled to room temperature, poured on crushed ice, carefully basicified with ammonia to basic pH (**Caution:** *exothermic reaction, continuous addition of crushed ice required*), and extracted with ether (4 × 50 mL). The combined organic phases were dried and evaporated. The black residue was extracted with pentane (2 × 100 mL) and the pentane was evaporated. The resulting pale, yellow solid was sublimed (0.75 Torr (1 Torr = 133.3 Pa), 75°C) giving **6***a* (2.30 g, 93%) as a white solid.

(ii) Via 2,6-dibromopyridine (9)

To 2-(tributylstannyl)pyridine **8***a* (43.0 g, 0.117 mol), 2,6-dibromopyridine **9** (48.0 g, 0.205 mol), and tetrakis(triphenylphosphine)palladium ($Pd(PPh_3)_4$) (1.86 g, 1.4 mol%) was added THF (100 mL) and the reaction mixture was stirred at reflux for 72 h. The solvent was evaporated and HCl (6 M, 100 mL) was added to the remaining tar. The aqueous phase was extracted with DCM (5 × 100 mL) and basified with ammonia. To the aqueous solution was added $NiCl_2 \cdot 6H_2O$ until a deep-green colour persisted. The aqueous solution was reextracted with DCM (7 × 200 mL) and the latter organic phases were combined, dried, and evaporated. Sublimation (0.75 Torr, 75°C) of the residue gave **6***a* (10.0 g, 36%) as a white solid, mp 70–71°C (lit. (23) mp 70–71°C). ^{1}H NMR, δ (ppm): 8.67 (d, $H_{6'}$, J = 4.7 Hz, 1H), 8.41 (dt, $H_{3'}$, J = 7.9, 0.9 Hz, 1H), 8.37 (dd, $H_{3\text{ or }5}$, J = 7.6, 0.9 Hz, 1H), 7.82 (td, $H_{4'}$, J = 7.6, 1.7 Hz, 1H), 7.67 (t, H_4, J = 7.8 Hz, 1H), 7.49 (dd, $H_{3\text{ or }5}$, J = 7.8, 0.9 Hz, 1H), 7.33 (ddd, $H_{5'}$, J = 7.5, 4.8, 1.2 Hz, 1H). ^{13}C{^{1}H} NMR (DEPT), δ (ppm): 149.0, 139.3, 137.4, 128.1, 124.4, 121.7, 119.9. MS *m/z*+ (EI): 235 (M+1, 6%), 234 (M, 52%), 155 (M−79 (−Br), 100%), 128 (M−107 (−CNH, Br), 14%). R_f: 0.68 on alumina (DCM).

Preparation of 2-tributylstannyl-5-methylpyridine (*8b*)

To a solution of 2-bromo-5-methylpyridine **7***a* (10.00 g, 0.058 mol) in THF (150 mL) was added *n*-butyllithium (37.6 mL, 1.6 M, 0.060 mol) while the solution temperature was kept at −78°C. After stirring 75 min at −78°C, tributyltin chloride (18.5 mL, 0.068 mol) was added during 15 min to the reaction mixture, which was further stirred for 4 h at −78°C. The temperature was left to rise to room temperature, at which time water (50 mL) was added and the phases separated. The aqueous phase was extracted with ether (3 × 100 mL) and the combined organic phases were dried and evaporated. The residue was distilled (Kugelrohr, 0.5 Torr, 130–135°C) and chromatographed on alumina, eluting with DCM, to afford **8***b* (5.09 g, 84%) as a colourless oil. ^{1}H NMR, δ (ppm): 8.58 (d, H_6, J = 0.5 Hz, 1H), 7.30 (dd, $H_{3\text{ or }4}$, J = 8.0, 0.5 Hz, 1H), 7.30 (d, $H_{3\text{ or }4}$, J = 1.2 Hz, 1H), 2.28 (s, H_{methyl}, 3H), 1.57 (m, H_{CH_2}, 6H), 1.37 (m, H_{CH_2}, 6H), 1.15 (m, H_{CH_2}, 6H), 0.87 (t, H_{CH_3}, 9H). ^{13}C{^{1}H} NMR, δ (ppm): 169.5, 151.3, 134.0, 131.8, 131.1, 29.1, 27.3, 18.5, 13.7, 9.7. MS *m/z*+ (FAB): 384 (M + 1, 11%), 326 (M − 58 (Bu + H), 17%), 268 (M − 112 (−2 Bu), 14%), 212 (M − 170 (−3 Bu), 100%). Anal. calcd. for $C_{18}H_{33}NSn$: C 56.57, H 8.70, N 3.67; found: C 56.29, H 8.53, N 3.64. R_f: 0.79 on alumina (CH_2Cl_2).

Preparation of 6-bromo-5′-methyl-2,2′-bipyridine (*6b*)

To 2-tributylstannyl-5-methylpyridine **8***b* (18.69 g, 0.049 mol), 2,6-dibromopyridine **9** (27.25 g, 0.116 mol), and $Pd(PPh_3)_4$ (1.84 g, 2.7 mol%) was added toluene (150 mL) and the reaction mixture was stirred at reflux for 72 h. The solvent was evaporated and HCl (6 M, 50 mL) was added to the remaining tar. The aqueous phase was extracted with DCM (5 × 100 mL) and basified with ammonia. To the aqueous solution was added $NiCl_2 \cdot 6H_2O$ until a deep-green colour persisted. The aqueous solution was reextracted with DCM (5 × 200 mL) and the latter organic phases were combined, dried, and evaporated. Chromatography of the residue on silica (CH_2Cl_2:CH_3OH 99:1) gave **6***b* (8.82 g, 72%) as a white solid, mp 126–128°C. ^{1}H NMR, δ (ppm): 8.48 (d, $H_{6'}$, J = 1.6 Hz, 1H), 8.33 (d, H_5, J = 7.8 Hz, 1H), 8.29 (d, $H_{3'}$, J = 7.8 Hz, 1H), 7.64 (t, H_4, J = 7.8 Hz, 1H), 7.61 (dd, $H_{4'}$, J = 7.8, 1.6 Hz, 1H), 7.45 (d, H_3, J = 7.8 Hz, 1H), 2.39 (s, H_{methyl}, 3H). ^{13}C{^{1}H} NMR (DEPT), δ (ppm): 157.5, 152.0, 149.7, 141.5, 139.1, 137.9, 134.1, 127.6, 121.0, 119.4, 18.4. MS *m/z*+ (FAB): 249 (M, 100%), 169 (M−79 (−Br), 28%). Anal. calcd. for $C_{11}H_9BrN_2$: C 53.04, H 3.64, N 11.25; found: C 53.09, H 3.59, N 11.39. R_f: 0.86 on alumina (DCM).

Preparation of 6-tributylstannyl-2,2′-bipyridine (*10a*)

To a solution of 6-bromo-2,2′-bipyridine **6***a* (3.02 g, 0.0128 mol) in ether (80 mL) was added *n*-butyllithium (8.0 mL, 1.6 M, 0.0128 mol) while the solution temperature was maintained at −90°C. After stirring 30 min, tributyltin chloride (3.63 mL, 0.0128 mol) was added to the reaction mixture over 10 min. The temperature of the solution was left to rise to room temperature, at which time water (30 mL) was added and the phases separated. The aqueous phase was extracted with ether (3 × 50 mL). The combined organic phases were dried and evaporated. The residue was distilled (0.5 Torr, 135–140°C) to afford **10***a* (5.09 g, 89%) as a pale brown oil. IR (neat): 2925, 1574, 1549, 1421, 1074, 770, 691. ^{1}H NMR, δ (ppm): 8.66 (d, $H_{6'}$, J = 4.8 Hz, 1H), 8.53 (d, $H_{3'}$, J = 8.0, 1.0 Hz, 1H), 8.25 (d, $H_{3\text{ or }5}$, J = 8.0, 1.3 Hz, 1H), 7.80 (td, $H_{4'}$, J = 7.6, 1.8 Hz, 1H), 7.63 (dd, H_4, J = 8.0, 7.3 Hz, 1H), 7.40 (dd, $H_{3\text{ or }5}$, J = 7.3, 1.3 Hz, 1H), 7.27 (ddd, $H_{5'}$, J = 7.6, 4.8, 1.2 Hz, 1H), 1.62 (m, H_{CH_2}, 6H), 1.37 (m, H_{CH_2}, 6H), 1.16 (m, H_{CH_2}, 6H), 0.90 (t, H_{CH_3}, 9H). ^{13}C{^{1}H} NMR, δ (ppm): 173.2, 157.0, 155.9, 136.6, 134.0, 132.3, 123.4, 121.1, 119.2, 119.1, 29.1, 27.3, 13.7, 10.1. MS *m/z*+ (FAB): 447 (M + 2, 90%), 389 (M − 58 (Bu + H), 65%), 333 (M − 112 (−2 Bu), 18%), 275 (M − 175 (bpy), 100%). Anal. calcd. for $C_{22}H_{34}N_2Sn$: C 59.34, H 7.71, N 6.29; found: C 59.04, H 7.66, N 6.44. R_f: 0.78 on alumina (5% CH_3CN – $CHCl_3$).

Preparation of 6-tributylstannyl-5′-methyl-2,2′-bipyridine (*10b*)

To a solution of 6-bromo-5′-methyl-2,2′-bipyridine **6***b* (6.94 g, 0.028 mol) in THF (200 mL) was added *n*-butyllithium (18.2 mL, 1.6 M, 0.029 mol) while the solution temperature was maintained at −90°C. After stirring 45 min, tributyltin

© 1997 NRC Canada

Can. J. Chem. Downloaded from www.nrcresearchpress.com by 92.62.229.171 on 09/08/12
For personal use only.

chloride (8.34 mL, 0.029 mol) was added to the reaction mixture over 15 min, while the solution warmed up to −78°C. The temperature of the solution was left to rise to room temperature, at which time water (100 mL) was added. Ether (50 mL) was added and the phases separated. The aqueous phase was extracted with ether (5 × 100 mL). The combined organic phases were dried and evaporated. The residue was distilled (Kugelrohr, 0.5 Torr, 150–155°C) and chromatographed on alumina, eluting with DCM to afford **10***b* (10.55 g, 82%) as a colourless oil. ^{1}H NMR, δ (ppm): 8.48 (dd, $H_{6'}$, J = 2.0, 0.8 Hz, 1H), 8.42 (d, $H_{3'}$, J = 8.1 Hz, 1H), 8.20 (ddd, H_5, J = 8.1, 8.0, 1.2 Hz, 1H), 7.61 (td, H_4, J = 8.0, 7.3 Hz, 1H), 7.61 (ddd, $H_{4'}$, J = 8.0, 2.0, 0.8 Hz, 1H), 7.37 (ddd, H_3, J = 8.0, 7.3, 1.2 Hz, 1H), 2.39 (s, H_{methyl}, 3H), 1.62 (m, H_{CH_2}, 6H), 1.37 (m, H_{CH_2}, 6H), 1.15 (m, H_{CH_2}, 6H), 0.89 (t, H_{CH_3}, 9H). ^{13}C{^{1}H} NMR, δ (ppm): 173.1, 156.0, 154.5, 149.3, 137.3, 134.0, 133.0, 132.0, 120.7, 118.9, 29.1, 27.4, 18.4, 13.7, 10.0. MS *m/z*+ (FAB): 461 (M+1, 48%), 403 (M − 58, 46%), 289 (M − 170, 100%). Anal. calcd. for $C_{23}H_{36}N_2Sn$: C 60.15, H 7.90, N 6.10; found: C 59.92, H 7.78, N 5.99. R_f: 0.73 on alumina (CH_2Cl_2).

Preparation of 4,6-dichloro-2-methylpyrimidine (11*b*)

A solution of 2-methyl-4,6-dihydroxypyrimidine (4.11 g, 32.6 mmol) in $POCl_3$ (170 mL) was heated to reflux for 5 h. The $POCl_3$ was evaporated, water (100 mL) was added to the residue, and the mixture was extracted with ether (4 × 50 mL). The combined organic phases were dried and evaporated. The crude solid was sublimed (0.1 Torr, 40°C) to afford **11***b* (3.40 g, 64%) as a white solid, mp 46–47°C (lit. (32) mp 46–48°C). ^{1}H NMR, δ (ppm): 7.20 (s, H_5, 1H), 2.65 (s, H_a, 3H). ^{13}C{^{1}H} NMR, δ (ppm): 169.7, 161.5, 118.3, 25.6.

Preparation of 2-(9-anthryl)-4,6-dichloropyrimidine (11*d*)

To 9-bromoanthracene (5.42 g, 0.0211 mol) in a two-necked, 250 mL, round-bottom flask fitted with a low-temperature thermometer and Ar inlet was added diethyl ether (150 mL). The mixture was cooled to −10°C and *n*-butyllithium (13.8 mL, 0.0221 mol) was added while maintaining the temperature below 0°C. The solution was stirred at 0°C for 20 min and then was cooled to −35°C. To this mixture was added 4,6-dichloropyrimidine (2.99 g) in diethyl ether (30 mL) over 15 min. After stirring at −30°C for 20 min, the temperature was left to rise to 0°C. To this mixture was added acetic acid (1.2 mL), water (0.2 mL), and THF (4 mL) followed by DDQ (4.50 g) in THF (20 mL). The solution was stirred at room temperature for 10 min, brought to 0°C, and NaOH (3 M, 8 mL) was added while vigorously stirring the solution. Water (20 mL) was added to the solution, the phases were separated, and the aqueous phase was extracted with ether (3 × 50 mL). The combined organic phases were dried, concentrated, and chromatographed on alumina, eluting with DCM to afford **11***d* (2.58 g, 40%) as a pale-yellow solid, mp 188.8–190.8°C. IR: 1529, 1306, 1276, 1106, 894, 862, 847, 820, 730, 637. UV–VIS: 249 (11.1), 256 (15.0), 366 (1.01), 385 (1.04). ^{1}H NMR, δ (ppm): 8.60 (s, H_{A10}, 1H), 8.06 (m, H_{A1}, 2H), 7.60 (m, H_{A4}, 2H), 7.59 (s, H_5, 1H), 7.52–7.43 (m, $H_{A2,A3}$, 4H). ^{13}C{^{1}H} NMR (DEPT), δ (ppm): 168.5, 162.4, 131.2, 129.6, 129.5, 128.7, 127.0, 125.3, 124.8, 119.7. MS *m/z*+ (CI): 325.2 (M+H, 100%), 289.2 (M−35 (Cl), 10%). Anal. calcd. for $C_{18}H_{10}N_2Cl_2$: C 66.48, H 3.11, N 8.62; found: C 66.42, H 8.53, N 3.25. R_f: 0.46 on silica (DCM/hexane, 1:1).

General procedure for the in situ preparation of 6-tributylstannyl-2,2′-bipyridines (10*a*,*b*)

To a stirred solution of **6***a* or **6***b* (1 equiv.) in THF at −90°C was added *n*-butyllithium (1.05 equiv.) over 15 min. The temperature of the mixture was maintained at −90°C for another 30 min and was brought to −70°C during the addition of tributyltin chloride (1.05 equiv. over 10 min). The mixture was stirred at −50°C for another 30 min. The THF was evaporated and the residue was used without purification in subsequent reactions. The estimated yield of **10***a*,*b* was 90%.

General procedure for the preparation of the bis-tridentate ligands (1*a*,*e*)

To the residue of **10***a* or **10***b* (2.1 equiv., prepared in situ, vide supra) was added 4,6-dichloro-2-*R*-pyrimidine (1 equiv.), bis(triphenylphosphine)dichloropalladium $Pd(PPh_3)_2Cl_2$ (0.1 equiv.), and dry DMF. The reaction mixtures were stirred at the temperatures and for the times indicated below. The reaction mixtures were cooled and the DMF was evaporated under reduced pressure. The resulting black residues were purified by the procedures described below.

*Preparation of 4,6-bis(2″,2′-bipyrid-6′-yl)pyrimidine (1*a*)*

To 6-tributylstannyl-2,2′-bipyridine **10***a* (prepared in situ from **6***a* (2.00 g, 8.51 mmol), *n*-butyllithium (5.6 mL, 1.6 M, 8.96 mmol), and tributyltin chloride (2.92g, 8.96 mmol)), 4,6-dichloropyrimidine (0.54 g, 3.65 mmol), and $Pd(PPh_3)_2Cl_2$ (0.54 g, 9 mol%) was added DMF (8 mL) and the reaction mixture was stirred at 100°C for 15 h. The DMF was evaporated and the residue was extracted with acetone–methanol (1:1, 3 × 25 mL). The remaining solid was recrystallized from acetonitrile–chloroform to afford **1***a* (0.34 g, 24%) as a off-white solid. The combined filtrates were concentrated and chromatographed on alumina, eluting with DCM to give more **1***a* (0.36 g, 25%). Total yield: 0.70 g (49%); mp: 233–236°C. IR: 1560, 1532, 1474, 1429, 1380, 827, 763, 653. ^{1}H NMR (400 MHz), δ (ppm): 9.78 (d, H_5, J = 1.3 Hz, 1H), 9.40 (d, H_2, J = 1.3 Hz, 1H), 8.79 (dt, $H_{3''}$, J = 8.0, 0.9 Hz, 2H), 8.75 (d, $H_{6''}$, J = 4.7 Hz, 2H), 8.61 (dd, $H_{3' \text{ or } 5'}$, J = 7.9, 1.0 Hz, 2H), 8.57 (dd, $H_{3' \text{ or } 5'}$, J = 7.8, 1.0 Hz, 2H), 8.05 (t, $H_{4'}$, J = 7.8 Hz, 2H), 7.89 (dt, $H_{4''}$, J = 7.7, 1.8 Hz, 2H), 7.39 (ddd, $H_{5''}$, J = 7.6, 4.8, 1.2 Hz, 2H). ^{13}C{^{1}H} NMR, δ (ppm): 164.0, 158.6, 155.9, 155.8, 153.4, 149.3, 138.2, 136.7, 124.0, 122.6, 121.7, 121.2, 114.0. MS *m/z*+ (EI): 389 (M+1, 12%), 388 (M, 57%), 387 (M−1, 100%), 360 (M−28 (CNH), 4%), 310 (M–78 (py), 3%). Anal. calcd. for $C_{24}H_{16}N_6$: C 74.20, H 4.16, N 21.64; found: C 73.95, H 4.02, N 21.43. R_f: 0.06 on alumina (DCM).

*Preparation of 4,6-bis(2″,2′-bipyrid-6′-yl)-2-methylpyrimidine (1*b*)*

To 6-tributylstannyl-2,2′-bipyridine **10***a* (prepared in situ from **6***a* (2.10 g, 8.93 mmol), *n*-butyllithium (6.1 mL, 1.6 M, 9.883 mmol), and tributyltin chloride (3.20 g, 9.83 mmol)), 4,6-dichloro-2-methylpyrimidine **11***b* (0.62 g, 3.83 mmol), and $Pd(PPh_3)_2Cl_2$ (0.56 g, 10 mol%) was added DMF (4 mL) and the reaction mixture was stirred at 110°C for 20 h. During this time, a precipitate formed and, upon cooling to 4°C, more solid precipitated out of solution. The solid was collected by filtration, washed with methanol (3 × 25 mL), dissolved in boiling chloroform, and filtered. The filtrate was evaporated and the unreacted starting material and by-products were sub-

© 1997 NRC Canada

Can. J. Chem. Downloaded from www.nrcresearchpress.com by 92.62.229.171 on 09/08/12
For personal use only.

limed (10^{-5} Torr, 180°C) and the residue was resublimed (10^{-5} Torr, 200°C) to give **1***b* (0.73 g, 48%) as a white solid, mp 274–276°C. IR: 2922, 1599, 1560, 1542, 1475, 1432, 1385, 993, 789, 764, 653. ^{1}H NMR, δ (ppm): 9.55 (s, H_5, 1H), 8.80 (d, $H_{3''}$, J = 8.0 Hz, 2H), 8.74 (d, $H_{6''}$, J = 4.8 Hz, 2H), 8.58 (d, $H_{3',5'}$, J = 7.8 Hz, 4H), 8.03 (t, $H_{4'}$, J = 7.8 Hz, 2H), 7.89 (td, $H_{4''}$, J = 1.8, 7.8 Hz, 2H), 7.38 (ddd, $H_{5''}$, J = 7.5, 4.8, 1.1 Hz, 2H), 2.94 (s, CH_3, 3H). ^{13}C{^{1}H} NMR (DEPT, CH), δ (ppm): 149.3, 138.2, 136.8, 124.1, 122.5, 121.8, 121.3, 111.1. MS *m/z*$^+$ (FAB): 403.2 (M+1, 100%). Anal. calcd. for $C_{25}H_{18}N_6$: C 74.60, H 4.52, N 20.88; found: C 74.57, H 4.49, N 20.79. R_f: 0.73 on alumina (5% CH_3CN–$CHCl_3$); 0.41 on alumina ($CHCl_3$).

*Preparation of 4,6-bis(2″,2′-bipyrid-6′-yl)-2-phenylpyrimidine (**1**c)*

To 6-tributylstannyl-2,2′-bipyridine **10***a* (prepared in situ from **6***a* (0.99 g, 4.21 mmol), *n*-butyllithium (2.8 mL, 1.6 M, 4.43 mmol), and tributyltin chloride (1.39 g, 4.43 mmol)), 4,6-dichloro-2-phenylpyrimidine **11***c* (0.406 g, 1.804 mmol), and $Pd(PPh_3)_2Cl_2$ (0.266 g, 9 mol%) was added DMF (5 mL) and the reaction mixture was stirred at 100°C for 15 h. The DMF was evaporated and the residue was washed with methanol (3 × 25 mL). The remaining solid was recrystallized from DCM giving **1***c* (0.43 g, 51%) as an off-white solid. The combined filtrates were concentrated and chromatographed on alumina, eluting with DCM to give more **1***c* (0.043 g, 5.1%). Total yield: 0.473 g (56%); mp 242–243°C. IR: 1551, 1531, 1475, 1430, 1376, 781, 753, 693, 651. ^{1}H NMR, δ (ppm): 9.69 (s, H_5, 1H), 8.84 (dt, $H_{3''}$, J = 0.9, 8.0 Hz, 2H), 8.78 (m, H_o, 2H), 8.78–8.74 (m, $H_{6'',3' \text{ or } 5'}$, 4H), 8.62 (dd, $H_{3' \text{ or } 5'}$, J = 7.9, 1.0 Hz, 2H), 8.08 (t, $H_{4'}$, J = 7.9 Hz, 2H), 7.91 (td, $H_{4''}$, J = 7.8, 1.8 Hz, 2H), 7.62–7.55 (m, $H_{m,p}$, 3H), 7.40 (ddd, $H_{5''}$, J = 7.5, 4.8, 1.2 Hz, 2H). ^{13}C{^{1}H} NMR (DEPT, CH), δ (ppm): 149.4, 138.2, 136.8, 130.8, 128.7, 128.5, 124.1, 122.6, 121.9, 121.4, 111.8. MS *m/z*+ (CI): 465.4 (M+H, 63%). Anal. calcd. for $C_{30}H_{20}N_6$: C 77.56, H 4.35, N 18.09; found: C 77.48, H 4.34, N 18.20. R_f: 0.65 on alumina ($CHCl_3$).

*Preparation of 2-(9-anthryl)-4,6-bis(2″,2′-bipyrid-6′-yl)-pyrimidine (**1**d)*

To 6-tributylstannyl-2,2′-bipyridine **10***a* (4.60 g, 0.0103 mol), 2-(9-anthryl)-4,6-dichloropyrimidine **11***d* (1.60 g, 0.00492 mol), and $Pd(PPh_3)_2Cl_2$ (0.72 g, 9 mol%) was added DMF (30 mL) and the reaction mixture was stirred at 105°C. After 36 h, TLC indicated the presence of starting material as well as product. Another aliquot of $Pd(PPh_3)_2Cl_2$ (0.20 g, 2 mol%) was added to the reaction mixture. After an additional 24 h, the DMF was evaporated and the resulting residue was extracted with boiling chloroform (8 × 25 mL) and filtered. The combined filtrates were evaporated and the resulting solid was washed with boiling ethanol (3 × 25 mL) and filtered. The solid was recrystallized from chloroform–hexane to afford **1***d* (1.66 g, 60%) as a pale-yellow solid. The filtrates were combined, concentrated, and filtered, giving more pure **1***d* (0.15 g, 5.4%) as a pale-yellow solid. Total yield: (1.81 g, 65%); mp 270–274°C. IR: 1560, 1531, 1474, 1430, 1379, 1262, 1080, 773, 742, 698, 653. ^{1}H NMR, δ (ppm): 9.92 (s, H_5, 1H), 8.90 (dt, $H_{3''}$, J =8.0 Hz, 2H), 8.78 (d, $H_{6''}$, J = 4.7 Hz, 2H), 8.64 (s, H_{A10}, 1H), 8.61 (dd, $H_{3' \text{ or } 5'}$, J = 8.0, 0.9 Hz, 2H), 8.57 (d, $H_{3' \text{ or } 5'}$, J = 7.7, 1.0 Hz, 2H), 8.11 (d, H_{A1}, J = 7.7 Hz, 2H), 7.96 (t, $H_{4'}$, J = 7.9 Hz, 2H), 7.95 (td, $H_{4''}$, J = 7.9, 1.3 Hz, 2H), 7.86 (d, H_{A4}, J = 8.8 Hz, 2H), 7.45 (m, $H_{5'', A2, A3}$, 6H). ^{13}C{^{1}H} NMR, δ (ppm): 167.0, 164.8, 156.1, 155.9, 153.7, 149.4 (CH), 138.3 (CH), 136.9 (CH), 134.2, 131.6, 130.0, 128.7 (CH), 128.3 (CH), 126.2 (CH), 126.1 (CH), 125.3 (CH), 124.1 (CH), 122.8 (CH), 122.4 (CH), 121.3 (CH), 112.0 (CH). MS *m/z*+ (FAB): 565.1 (M+1, 100%), Anal. calcd. for $C_{38}H_{24}N_6$: C 80.82, H 4.29, N 14.89; found: C 80.81, H 4.35, N 14.78. R_f: 0.48 on alumina (DCM).

*Preparation of 4,6-bis(5″-methyl-2″,2′-bipyrid-6′-yl)pyrimidine (**1**e)*

To 6-tributylstannyl-5′-methyl-2,2′-bipyridine **10***b* (prepared in situ from **6***b* (6.94 g, 0.028 mol), *n*-butyllithium (18.2 mL, 1.6 M, 0.029 mol), and tributyltin chloride (9.95 g, 0.029 mol)), 4,6-dichloropyrimidine (1.82 g, 0.012 mol), and $Pd(PPh_3)_2Cl_2$ (1.75 g, 9 mol%) was added DMF (20 mL) and the reaction mixture was stirred at 100°C for 24 h. The DMF was evaporated and the residue was chromatographed on silica (DCM with 1–5% MeOH) and alumina (DCM), giving **1***e* (2.45 g, 49%); mp 239–241°C. ^{1}H NMR, δ (ppm): 9.62 (d, H_5, J = 1.3 Hz, 1H), 9.31 (d, H_2, J = 1.3 Hz, 1H), 8.79 (dt, $H_{3''}$, J = 8.0, 0.9 Hz, 2H), 8.75 (d, $H_{6''}$, J = 4.7 Hz, 2H), 8.61 (dd, $H_{3' \text{ or } 5'}$, J = 7.9, 1.0 Hz, 2H), 8.57 (dd, $H_{3' \text{ or } 5'}$, J = 7.8, 1.0 Hz, 2H), 8.05 (t, $H_{4'}$, J = 7.8 Hz, 2H), 7.94 (t, $H_{4'}$, J = 7.8, 2H), 7.39 (ddd, $H_{5''}$, J = 7.6, 4.8, 1.2 Hz, 2H), 2.40 (s, H_{CH_3}, 3H). ^{13}C{^{1}H} NMR, δ (ppm): 165.9, 158.4, 155.7, 153.3, 153.2, 149.6, 137.9, 137.1, 133.6, 122.2, 121.2, 120.6, 113.8, 18.4. MS *m/z*+ (FAB): 417 (M+1, 100%). Anal. calcd. for $C_{26}H_{20}N_6$: C 74.98, H 4.84, N 20.18; found: C 74.70, H 4.83, N 20.35. R_f: 0.41 on alumina (DCM with 1% MeOH).

*Preparation of 4,6-bis(5″-(bromomethyl)-2″,2′-bipyrid-6′-yl)-pyrimidine (**1**f)*

A mixture of 4,6-bis(5″-methyl-2″,2′-bipyrid-6′-yl)pyrimidine **1***e* (0.106 g, 0.25 mmol), *N*-bromosuccinimide (0.460 g, 0.0026 mol), and 2,2′-azobis(2-methylpropionitrile) (0.0021 g, 0.13 mmol) in 20 mL carbon tetrachloride was heated under reflux for 70 min (monitored by TLC). The mixture was filtered hot and the filtrate was cooled to 0°C. The white precipitate was collected and chromatographed on silica (DCM with 1–5% MeOH), giving **1***f* (39 mg, 27%); mp 231–233°C. ^{1}H NMR, δ (ppm): 9.72 (d, H_5, J = 1.2 Hz, 1H), 9.40 (d, H_2, J = 1.2 Hz, 1H), 8.75 (d, $H_{6''}$, J = 2.3 Hz, 2H), 8.75 (d, $H_{3''}$, J = 7.7 Hz, 2H), 8.60 (dd, $H_{3' \text{ or } 5'}$, J = 7.7, 0.9 Hz, 2H), 8.57 (dd, $H_{3' \text{ or } 5'}$, J = 7.7, 0.3 Hz, 2H), 8.05 (t, $H_{4'}$, J = 7.7 Hz, 2H), 7.94 (dd, $H_{4'}$, J = 7.7, 2.1, 2H), 4.61 (s, H_{CH_2}, 4H). ^{13}C{^{1}H} NMR, δ (ppm): 163.0, 158.6, 155.8, 155.2, 153.5, 149.3, 138.3, 137.5, 134.0, 122.8, 121.9, 121.2, 114.1, 29.7. MS *m/z*+ (FAB): 575 (M+1, 100%), 496 (M − Br, 29%), 415 (M − 2 Br, 24%), 242 (45%). HRMS (M$^+$) calcd. for $C_{26}H_{18}N_6Br_2$: 573.0039; found: 573.0036. R_f: 0.42 on alumina (DCM with 1% MeOH).

Preparation of 4-(2″,2′-bipyrid-6′-yl)-6-chloropyrimidine (12*a*)

To 6-tributylstannyl-2,2′-bipyridine **10***a* (prepared in situ from **6***a* (1.01 g, 4.30 mmol), *n*-butyllithium (2.65 mL, 1.6 M, 4.73 mmol), and tributyltin chloride (1.54 g, 4.73 mmol)), 4,6-dichloropyrimidine **11***a* (1.15 g, 7.74 mmol), and $Pd(PPh_3)_2Cl_2$ (0.27 g, 10 mol%) was added DMF (10 mL); the reaction mixture was stirred at 90°C for 10 h and subsequently

© 1997 NRC Canada

Can. J. Chem. Downloaded from www.nrcresearchpress.com by 92.62.229.171 on 09/08/12
For personal use only.

cooled to room temperature. To the mixture was added a saturated aqueous solution of KF (20 mL) and ether (30 mL). The mixture was stirred vigorously for 1 h. Water (100 mL) was added and the mixture was extracted with diethyl ether (3 × 50 mL). The combined organics were washed with water (3 × 50 mL), dried, and evaporated. The residue was chromatographed on alumina, eluting with DCM to afford pure **12***a* (0.476 g, 41%) as a white solid, mp 151.8–152.2°C. IR: 1561, 1530, 1447, 1428, 1350, 769, 760. ^{1}H NMR, δ (ppm): 9.08 (d, H_2, J = 1.0 Hz, 1H), 8.72 (d, $H_{6''}$, J = 4.0 Hz, 1H), 8.62–8.50 (m, $H_{5,3',5'',3''}$, 4H), 8.03 (t, $H_{4'}$, J = 7.9 Hz, 1H), 7.91 (td, $H_{4''}$, J = 7.8, 1.7 Hz, 1H), 7.38 (ddd, $H_{5''}$, J = 7.5, 4.7, 1.1, 1H). ^{13}C{^{1}H} NMR, δ (ppm): 158.7, 149.3, 138.3, 137.0, 124.2, 123.4, 122.1, 121.2, 118.0. MS *m/z*+ (EI): 268 (M, 100%), 240 (M–28 (CHN), 5%), 233 (M−35 (Cl), 36%), 206 (M−62 (Cl + CHN), 34%), 155 (M−113 (py + Cl), 13%), 78 (M−190 (bpy+ Cl), 21%). Anal. calcd. for $C_{14}H_9ClN_4$: C 62.57, H 3.38, N 20.85; found: C 62.58, H 3.35, N 20.91. R_f: 0.36 on alumina (DCM).

Preparation of 4-(2″,2′-bipyrid-6′-yl)-6-chloro-2-methylpyrimidine (12*b*)

To 6-tributylstannyl-2,2′-bipyridine **10***a* (prepared in situ from **6***a* (3.76 g, 16.0 mmol), *n*-butyllithium (10.5 ml, 1.6 M, 16.8 mmol), and tributyltin chloride (5.21 g, 16.0 mmol)), 4,6-dichloro-2-methylpyrimidine **11***b* (2.77 g, 17.0 mmol), and $Pd(PPh_3)_2Cl_2$ (1.0 g, 9 mol%) was added DMF (25 mL); the reaction mixture was stirred at 90°C for 14 h and subsequently cooled to room temperature. To the mixture was added a saturated aqueous solution of KF (50 mL) and ether (100 mL). The mixture was stirred vigorously for 2 h. Water (300 mL) was added and the mixture was extracted with diethyl ether (3 × 150 mL). The combined organics were washed with water (3 × 50 mL), dried, and evaporated. The residue was filtered over a short alumina column, eluting with DCM to afford a crude yellow powder. Recrystallization from acetonitrile afforded white needles of **12***b* (2.83 g, 67%), mp 142°C. IR: 1561, 1537, 1472, 1424, 1393, 1344, 1324, 1260, 1154, 1068, 876, 848, 834, 787, 761, 740, 666. ^{1}H NMR, δ (ppm): 8.69 (d, $H_{6''}$, J = 4.7 Hz, 1H), 8.55 (d, $H_{3'}$, $H_{5'}$, J = 7.8 Hz, 2H), 8.48 (dd, $H_{3''}$, J = 7.8, 1.0 Hz, 1H), 8.35 (s, H_5, 1H), 7.97 (t, $H_{4'}$, J = 7.8 Hz, 1H), 7.87 (dt, $H_{4''}$, J = 7.8, 1.7 Hz, 1H), 7.34 (ddd, $H_{5''}$, J = 7.3, 4.7, 1.2 Hz, 1H), 2.79 (s, CH_3, 3H). ^{13}C{^{1}H} NMR, δ (ppm): 168.9, 164.6, 162.0, 155.9, 155.5, 152.2, 149.2, 138.1, 136.9, 124.1, 123.1, 122.0, 121.2, 114.6, 25.9. MS *m/z*+ (FAB): 283.1 (M+H, 100%), 206.1 (M−76 (py), 6%). Anal. calcd. for $C_{15}H_{11}ClN_4$: C 63.72, H 3.92, N 19.82; found: C 63.61, H 3.68, N 19.90. R_f: 0.66 on alumina (DCM).

Preparation of 4-(2″,2′-bipyrid-6′-yl)-6-chloro-2-phenylpyrimidine (12*c*)

To 6-tributylstannyl-2,2′-bipyridine **10***a* (prepared in situ from **6***a* (1.42 g, 6.04 mmol), *n*-butyllithium (4.15 mL, 1.6 M, 6.64 mmol), and tributyltin chloride (2.16 g, 6.64 mmol)), 4,6-dichloro-2-phenylpyrimidine **11***b* (0.42 g, 6.04 mmol), and $Pd(PPh_3)_2Cl_2$ (0.42 g, 10 mol%) was added DMF (25 mL); the reaction mixture was stirred at 90°C for 13.5 h and subsequently cooled to room temperature. To the mixture was added a saturated aqueous solution of KF (20 mL) and ether (30 mL). The mixture was stirred vigorously for 1 h. Water (100 mL) was added and the mixture was extracted with diethyl ether (3 × 50 mL). The combined organics were washed with water (3 × 50 mL), dried, and evaporated. The residue was chromatographed on alumina, eluting with DCM–hexane 1:1 to afford **12***c* (1.00 g, 48%) as a white solid, mp 187–189°C. IR: 1559, 1546, 1530, 1430, 1374, 1332, 1077, 826, 785, 754, 696, 650. ^{1}H NMR, δ (ppm): 8.73 (d, $H_{6''}$, J = 4.7 Hz, 1H), 8.69 (dd, $H_{3'}$ or $H_{5'}$, J = 7.8, 0.9 Hz, ^{1}H), 8.64–8.58 (m, $H_{3'}$ or $H_{5'}$, $H_{3'',o}$, 4H), 8.45 (s, H_5, 1H), 8.05 (t, $H_{4'}$, J = 7.8 Hz, 1H), 7.91 (td, $H_{4''}$, J = 7.8, 1.7 Hz, 1H), 7.58–7.51 (m, $H_{m,p}$, 3H), 7.38 (ddd, $H_{5''}$, J = 7.5, 4.8, 1.1 Hz, 1H). ^{13}C{^{1}H} NMR, δ (ppm): 165.1, 164.7, 162.7, 156.0, 155.6, 152.4, 149.3, 138.2, 137.0, 136.4, 131.5, 128.7, 124.2, 123.2, 122.2, 121.3, 115.3 (missing one C). MS *m/z*+ (EI): 344 (M, 100%), 309 (M−35 (Cl), 83%), 242 (M+H−103 (C_6H_5+CN), 6%), 206 (M−138 (C_6H_5+CN+Cl), 60%), 155 (M+H−190 (bpy+ Cl), 32%). Anal. calcd. for $C_{20}H_{13}ClN_4$: C 69.66, H 3.81, N 16.25; found: C 69.88, H 3.94, N 16.22. R_f: 0.48 on alumina (DCM/hexane, 1:1).

Preparation of 2,6-bis(tributylstannyl)pyridine (13)

To 2,6-dibromopyridine **9** (17.3 g, 0.0730 mol) in THF (240 mL) was added *n*-butyllithium (28 mL, 10.0 M, 0.28 mol) dropwise over 2 h while the solution temperature was maintained below −90°C. The solution was stirred for 2 h at −90°C and tributyltin chloride (75 mL, 0.28 mol) was added over 1 h while the solution temperature was kept below −75°C. The solution temperature was allowed to rise to room temperature and the THF was evaporated. Water (30 mL) was added to the residue and the aqueous phase was extracted with DCM (3 × 20 mL). The combined organic phases were dried and evaporated. The residue was purified by two Kugelrohr distillations (5 × 10^{-6} Torr, 140–150°C) to afford **13** (8.15 g, 17%) as a pale-brown oil. ^{1}H NMR, δ (ppm): 7.30–7.20 (m, $H_{3,4}$, 3H), 1.70–1.55 (m, CH_2, 6H), 1.46–1.21 (m, CH_2, 6H), 1.16–1.04 (m, CH_2, 6H), 0.92 (t, CH_3, 9H). ^{13}C{^{1}H} NMR, δ (ppm): 174.51 (C_2, J_{Sn-C} = 255, 28 Hz), 130.63 (C), 130.33 (C), 29.25 (CH2, J_{Sn-C} = 10.8 Hz), 27.48 (CH_2, J_{Sn-C} = 27.4 Hz), 13.81 (CH_3), 10.05 (CH_2, J_{Sn-C} = 37.2, 7.2 Hz). MS *m/z*+ (EI): 597 (M−58 (H + butyl), 100%), 540 (M−115 (H, 2 × butyl), 18%). Anal. calcd. for $C_{29}H_{57}NSn_2$: C 52.99, H 8.76, N 2.13; found: C 53.20, H 8.91, N 2.34. R_f: 0.80 on alumina ($CHCl_3$).

Preparation of 2,6-bis(6′-(2‴,2″-bipyrid-6″-yl)-pyrimidin-4′-yl)-pyridine (2*a*)

To 2,6-bis(tributylstannyl)pyridine **13** (0.4586 g, 0.6978 mmol), 4-(2′,2″-bipyrid-6′-yl)-6-chloropyrimidine **12***a* (0.4125 g, 1.535 mmol), and $Pd(PPh_3)_2Cl_2$ (0.108 g, 10 mol%) was added DMF (5 mL); the reaction mixture was stirred at 120°C for 48 h. The DMF was evaporated, DCM (50 mL) was added to the residue, and the organic phase was extracted with aqueous HCl (5 × 50 mL). The combined aqueous phases were extracted with DCM (4 × 50 mL), basified, and reextracted with DCM (5 × 75 mL). The latter organic phases were combined, dried, and evaporated. The residue was chromatographed on alumina, eluting with DCM to afford **2***a* (0.118 g, 31%) as a white solid, mp 292–293°C. IR: 1601, 1576, 1564, 1531, 1468, 1457, 1431, 1372, 1247, 1273, 990, 827, 771, 661. ^{1}H NMR (400 MHz), δ (ppm): 9.99 (d, H_5, J = 1.3 Hz, 2H), 9.44 (d, H_2, J = 1.3 Hz, 2H), 8.70 (d, $H_{3'''}$, J = 7.8 Hz, 2H), 8.62 (dd, $H_{3'\text{ or }5'}$, J = 7.7, 1.0 Hz, 2H), 8.38 (dd, $H_{3'\text{ or }5'}$, J

© 1997 NRC Canada

Can. J. Chem. Downloaded from www.nrcresearchpress.com by 92.62.229.171 on 09/08/12
For personal use only.

= 7.9, 1.0 Hz, 2H), 8.33 (d, $H_{6''}$, J = 4.8 Hz, 2H), 8.31 (dt, $H_{3''}$, J = 7.7, 1.0 Hz, 2H), 8.14 (t, $H_{4'''}$, J = 7.8 Hz, 1H), 8.02 (t, $H_{4'}$, J = 7.8 Hz, 2H), 6.85 (ddd, $H_{5''}$, J = 7.4, 4.7, 1.2 Hz, 2H), 6.72 (td, $H_{4''}$, J = 7.6, 1.9 Hz, 2H). $^{13}C\{^1H\}$ NMR, δ (ppm): 164.2, 163.8, 158.8, 156.0, 154.8, 153.9, 153.1, 148.5, 138.6, 138.0, 135.8, 123.7, 123.2, 122.7, 121.3, 121.2, 114.0. MS *m/z*+ (EI): 544 (M+1, 22%), 543 (M, 38%), 542 (M−1, 86%), 543 (M−2, 46%), 515 (M−27 (CNH), 4%), 465 (M−77 (py), 86%), 388 (M−154 (bpy), 6%); HRMS *m/z* calcd. for $C_{33}H_{22}N_9$ (MH^+): 544.1998; found: 544.1985. Anal. calcd. for $C_{33}H_{21}N_9$: C 72.90, H 3.90, N 23.19; found: C 71.96, H 3.72, N 23.14. R_f: 0.16 on alumina ($CHCl_3$).

Preparation of 2,6-bis(6′-(2‴,2″-bipyrid-6″-yl)-2′-methylpyrimidin-4′-yl)-pyridine (2*b*)

To 2,6-bis(tributylstannyl)pyridine **13** (1.45 g, 2.2 mmol), 4-(2″,2′-bipyrid-6′-yl)-6-chloro-2-methylpyrimidine **12***b* (1.30 g, 4.6 mmol), and $Pd(PPh_3)_2Cl_2$ (0.25 g, 16 mol%) was added DMF (15 mL); the reaction mixture was stirred at 120°C for 44 h and subsequently cooled to room temperature. The solid precipitate was filtered off and it was washed thoroughly, first with DMF and then with acetonitrile. The combined filtrates were evaporated to dryness. The remaining residue was treated with a mixture of ether and hexane (1/1) to yield a second crop of the desired product. The crude product was suspended in chloroform and refluxed for 12 h. Filtration of the hot mixture yields **2***b* as an off-white powder (0.56 g, 45%), mp 334°C. IR: 1599, 1538, 1474, 1429, 1371, 1259, 1131, 1095, 1070, 993, 826, 788, 766, 742, 634. ^1H NMR, δ (ppm): 9.80 (s, H_5, 2H), 8.65 (d, $H_{3'''}$, J = 7.7 Hz, 2H), 8.63 (dd, $H_{3'}$ or $H_{5'}$, J = 7.9, 1.0 Hz, 2H), 8.40 (dd, $H_{3'}$ or $H_{5'}$, J = 7.9, 1.0 Hz, 2H), 8.37–8.34 (m, $H_{6''}$, $H_{3''}$, 4H), 8.10 (t, $H_{4'''}$, J = 7.7 Hz, 1H), 8.00 (t, $H_{4'}$, J = 7.7 Hz, 2H), 6.86 (ddd, $H_{5''}$, J = 7.4, 4.6, 1.2 Hz, 2H), 6.77 (td, $H_{4''}$, J = 7.9, 1.8 Hz, 2H), 2.97 (s, CH_3, 6H). $^{13}C\{^1H\}$ NMR, δ (ppm): insufficiently soluble. MS *m/z*+ (FAB): 572.1 (M+H, 100%), 493.1 (M−78 (py), 5%). HRMS *m/z*+ calcd. for $C_{35}H_{26}N_9$ (MH+): 572.2309; found: 572.2322. Anal. calcd. for $C_{35}H_{25}N_9$: C 73.54, H 4.41, N 22.05; found: C 73.73, H 4.11, N 22.27. R_f: 0.12 on alumina ($CHCl_3$).

Preparation of 2,6-bis(6′-(2‴,2″-bipyrid-6″-yl)-2′-phenylpyrimidin-4′-yl)-pyridine (2*c*)

To 2,6-bis(tributylstannyl)pyridine **13** (0.194 g, 0.29 mmol), 4-(2′,2″-bipyrid-6′-yl)-6-chloro-2-phenylpyrimidine **12***c* (0.200 g, 0.580 mmol), and $Pd(PPh_3)_2Cl_2$ (0.06 g, 10 mol%) was added DMF (10 mL); the reaction mixture was stirred at 110°C for 60 h. The DMF was evaporated and the residue was washed with methanol (3 × 25 mL). The remaining solid was recrystallized from chloroform to afford **2***c* (0.0606 g, 30%) as a white solid. The combined filtrates were evaporated and the residue was washed with boiling diethyl ether and recrystallized from chloroform to give more pure **2***c* (0.0553 g, 27%). Total yield: 0.116 g (57%); mp 262–264°C. IR: 1560, 1538, 1476, 1429, 1368, 1261, 992, 823, 788, 757, 697, 652, 634. ^1H NMR (400 MHz), δ (ppm): 9.97 (s, H_5, 2H), 8.93 (d, $H_{3'''}$, J = 7.9 Hz, 2H), 8.85 (dd, $H_{3'\text{ or }5'}$, J = 7.7, 1.0 Hz, 2H), 8.83 (dd, H_o, J = 8.0, 1.8 Hz, 4H), 8.43 (d, $H_{3'\text{ or }5'}$, J = 8.2 Hz, 2H), 8.41 (d, $H_{3''}$, J = 7.6 Hz, 2H), 8.35 (d, $H_{6''}$, J = 5.0 Hz, 2H), 8.21 (t, $H_{4'''}$, J = 7.8 Hz, 1H), 8.07 (t, $H_{4'}$, J = 7.9 Hz, 2H), 7.65–7.58 (m, $H_{m,p}$, 6H), 6.87 (ddd, $H_{5''}$, J = 7.3, 5.0, 1.2 Hz, 2H), 6.78 (td, $H_{4''}$, J = 7.3, 1.8 Hz, 2H). $^{13}C\{^1H\}$ NMR (DEPT): δ (ppm): 148.5, 138.4, 139.0, 135.9, 130.9, 128.7, 128.6, 123.7, 123.2, 122.6, 121.5, 121.4, 111.8. MS *m/z*+ (FAB): 696.2 (M+H, 100%), 617 (M−78 (py), 4%); HRMS *m/z* calcd. for $C_{45}H_{30}N_9$ (MH^+): 696.2624; found: 696.2618. Anal. calcd. for $C_{45}H_{29}N_9 \cdot H_2O$: C 75.71, H 4.39, N 17.66; found: C 76.06, H 4.57, N 17.39. R_f: 0.33 on alumina (DCM).

Crystal structure determination

X-Ray data for **2**: ($C_{33}H_{21}N_9$), M = 543.6; colourless crystals; monoclinic; a = 12.396(3), b = 12.307(3), c = 17.358(5) Å, ß = 95.49(2)°, V = 2636.0 Å^3, Z = 4, ρ_{calc} = 1.370, μ = 6.502 cm^{-1}, space group $C2/c$. A suitable crystal of **2**, (0.28 × 0.20 × 0.14 mm^3) was mounted on the end of a glass fibre: 2891 + $h \pm k \pm l$ reflections were collected on a Philips PW1100/16 instrument at 20°C with Cu graphite monochromated radiation (λ = 1.5418 Å), θ/2θ flying step scans, step width = 0.03°, scan speed = 0.020° s^{-1}, scan width = 0.80 + 0.14 tg(θ)°, 3° < θ < 52°. Three standard reflections measured every hour during the data collection period showed no significant trend. The raw data were converted to intensities and corrected for Lorentz and polarization factors. The structure was solved using direct methods: 1036 independent reflections with $I > 3\sigma(I)$ were used to determine and refine the structure. Hydrogen atoms were introduced as fixed contributors by their computed coordinates (C—H = 0.95 Å) and isotropic temperature factors such as $B_H = 1.3\ B_{eqv}(C)$ Å^2. Empirical absorption corrections were applied (DIFABS): Molen on a Vax computer was used for all calculations. Final $R(F)$ = 0.035. Atomic coordinates, bond lengths and angles, and thermal parameters have been deposited at the Cambridge Crystallographic Data Centre.

Results and discussion

The basic ligand design is shown in Fig. 2*b*. Modification of the substituent in the pyrimidine 2-position will influence the metal-binding properties as well as the shape of the ligand upon metal complexation. Various R groups (hydrogen, methyl, phenyl, and 9-anthryl) were incorporated into the framework by attaching bipyridyl subunits onto substituted pyrimidines by carbon–carbon bond-forming reactions. To use such ligands as building blocks for larger systems requires the functionalization of the terminal pyridines; this was done by introducing a functionalized methyl group in the 5-position of the terminal pyridine ring, so as not to interfere with metal complexation.

The key material, 6-bromo-2,2′-bipyridine **6***a*, was synthesized in two different ways. In the first approach (Fig. 3), bipyridine (bpy) **3** and *m*-CPBA gave 2,2′-bipyridine-*N*-oxide **4** in 46% yield (22). Excess $POCl_3$ and **4** gave two chlorobipyridine isomers, 4-chloro-2,2′-bipyridine and 6-chloro-2,2′-bipyridine **5** in 99% yield (27). The 6-isomer is isolated by selectively complexing the 4-isomer with $Ni(II)Cl_2 \cdot 6H_2O$ in water (28). The bpy **5** is extracted into DCM and isolated in 45% yield and is converted to 6-bromo-2,2′-bipyridine **6***a* in 93% yield with excess PBr_3 heated to reflux. The overall yield of **6***a* from bpy over the four steps is 19% (Fig. 3).

We investigated whether **6***a* could be prepared by organotin chemistry in good yields in the steps outlined in Fig. 3. Other direct methods to synthesize **6***a* resulted in moderate yields or multistep procedures (29–31). 2-Tributylstannylpyridine (24)

© 1997 NRC Canada

Can. J. Chem. Downloaded from www.nrcresearchpress.com by 92.62.229.171 on 09/08/12
For personal use only.

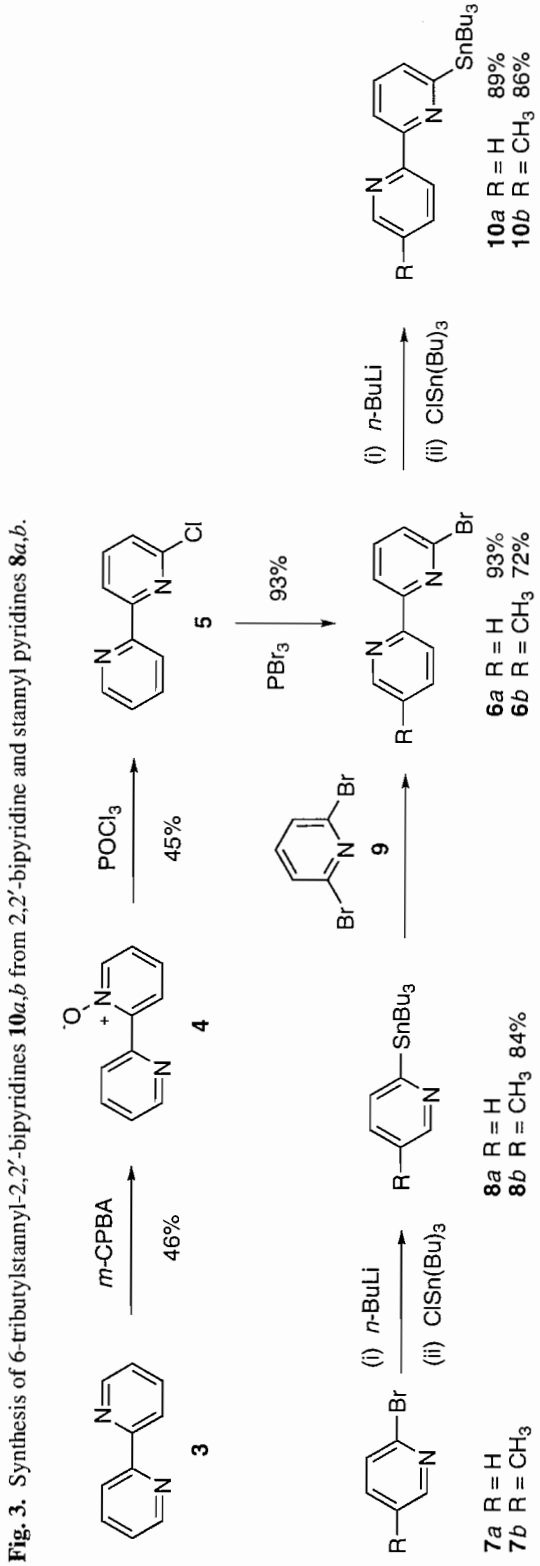


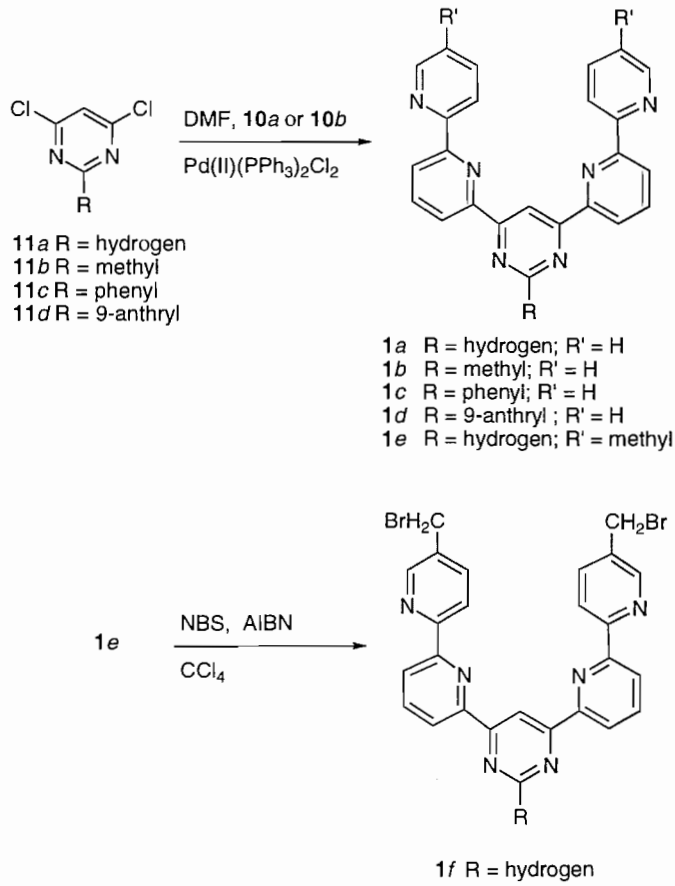
Fig. 3. Synthesis of 6-tributylstannyl-2,2′-bipyridines **10***a*,*b* from 2,2′-bipyridine and stannyl pyridines **8***a*,*b*.

Table 1. Reaction conditions for the synthesis of the bipyridine derivative **6***a* via Stille-type coupling.

	Reagent ratio[a]	
Conditions	1:1	1:2
Toluene 70°C, 73 h	35%	—
Toluene 90°C, 24 h	54%	67%
THF 67°C, 24 h	29%	36%
Dioxane 90°C, 21 h	43%	—
Dimethoxy ethylene glycol 70°C, 71 h	56%	—

[a]Ratio of **8***a* to **9**, 5 mol% $Pd(PPh_3)_4$ for all reactions except in THF, where 5 mol% $Pd(PPh_3)_2Cl_2$ was used.

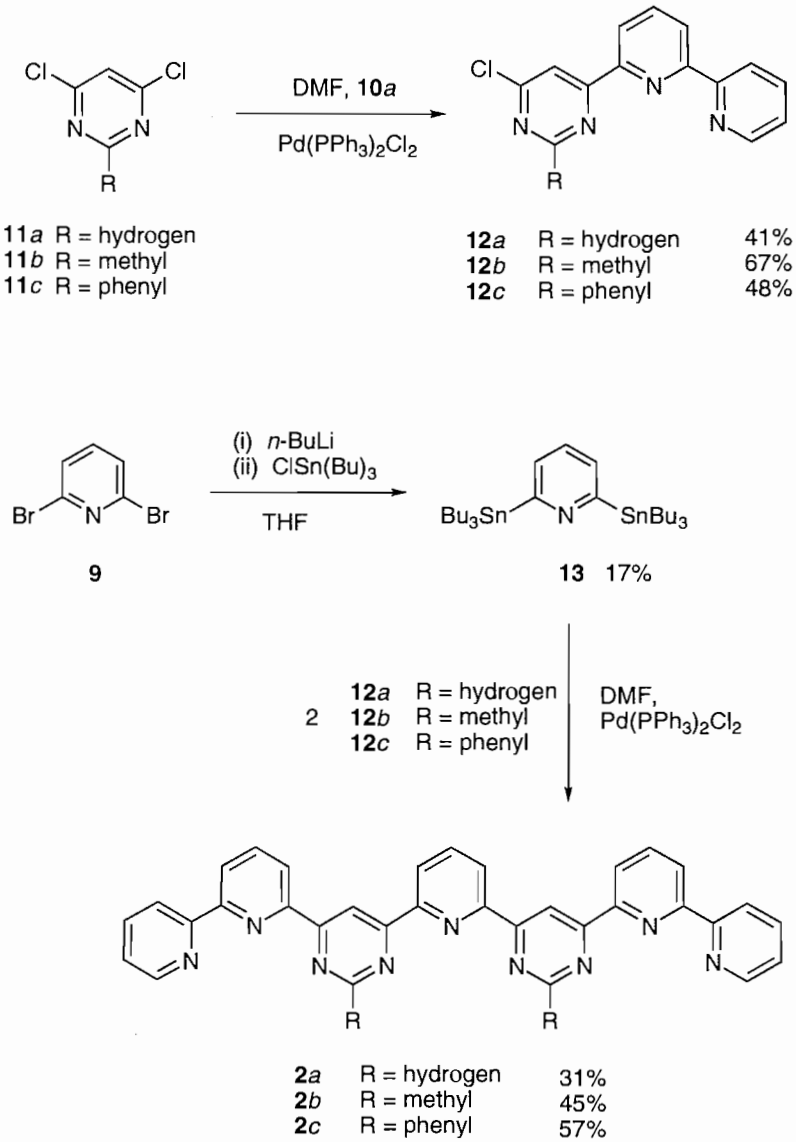
Fig. 4. Synthesis of the bis-tridentate ligands **1***a–e* and of the bromo-substituted ligand **1***f*.



8*a* and 2,6-dibromopyridine **9** are heterocoupled using the conditions listed in Table 1. The bpy **6***a* is easily separated from the starting materials and organotin by-products by acidification of the reaction mixture and subsequent extraction with organic solvents. Stannylpyridine **8***a*, 2,6-dibromopyridine **9**, and tributyltin chloride are extracted into the organic phase of a 1 M HCl – DCM mixture, whereas **6***a* and the side-product tpy are not. Nickel dichloride hexahydrate, added to the neutralized aqueous phase, separates tpy from **6***a* quantitatively following extraction with DCM. Excess **9** favours the formation of **6***a* over tpy. Unreacted **9** is recovered by column

© 1997 NRC Canada

Fig. 5. Synthesis of tris-tridentate ligands **2***a–c*.



chromatography along with the tributyltin bromide formed as a by-product. The synthesis can also be performed in a single procedure. The lithiation of 2-bromopyridine in THF at −78°C with *n*-butyllithium followed by the addition of tributyltin chloride gives pyridine **8***a*. After adding an excess of **9** and palladium catalyst, the reaction mixture is heated to reflux for 2 days. The bpy **6***a* and tpy are isolated as described above. Reaction times are shorter if one removes the THF under reduced pressure and replaces it with higher boiling solvents (Table 1).

To obtain 2-bromo-5-methyl-2,2′-bipyridine **6***b* we used a similar strategy starting from 2-bromo-5-methylpyridine, which is easily obtained from commercially available 2-amino-5-methylpyridine (25). Low-temperature lithiation and reaction with tributyltin chloride gave 2-tributylstannylpyridine **8***b*, which was heterocoupled with 2,6-dibromopyridine **9** to afford **6***b* in 72% yield. The reaction conditions and work-up procedures are similar to those described for **6***a*.

Following low-temperature lithiation of **6***a*,*b* with *n*-butyllithium, the lithiobipyridine is quenched with tributyltin chloride. Purification by distillation affords the 6-tributylstannyl functionalized bipyridines **10***a*,*b* in yields of 89 and 86%, respectively. Upon prolonged standing, small quantities of the dimerization product of **10***a*, 2,2′:6′,2″:6″,2‴-quaterpyridine, solidify out of the oil.

The pyrimidines are all synthesized in one step from commercially available materials. Reacting 4,6-dihydroxy-2-methylpyrimidine with $POCl_3$ gives 4,6-dichloro-2-methylpyrimidine **11***b*. Purification in an analogous fashion to that of **5**, followed by sublimation (instead of fractional distillation as reported (32)) affords **11***b* in 64% yield. 4,6-Dichloro-2-phenylpyrimidine **11***c* is produced by the addition of phenyllithium to **11***a*, followed by oxidation of the addition product with DDQ (26). In an analogous fashion, 9-lithioanthracene, generated by treatment of 9-bromoanthracene with *n*-butyllithium, reacts with **11***a* to afford 2-(9-anthryl)-4,6-dichloropyrimidine **11***d* in 40% yield. The reaction of two equivalents of bpy **10***a* with the 2-substituted-4,6-dichloropyrimidines

Can. J. Chem. Downloaded from www.nrcresearchpress.com by 92.62.229.171 on 09/08/12
For personal use only.

© 1997 NRC Canada

Table 2*a*. ^{1}H NMR chemical shifts for the various ligands (in ppm).[a,d]

	6″	5″	4″	3″	5′	4′	3′	5	2	3‴	4‴
11*a*								7.44	8.81		
12*a*	8.72	7.38	7.91	8.56[b]	8.56[b]	8.03	8.56[b]	8.56[b]	9.08		
1*a*	8.75	7.39	7.89	8.79	8.61[c]	8.05	8.57[c]	9.78	9.40		
12*a*	8.33	6.85	6.72	8.31	8.62[c]	8.02	8.38[c]	9.99	9.44	8.70	8.14
11*b*								7.20			
12*b*	8.69	7.34	7.87	8.48	8.55	7.97	8.55	8.35			
1*b*	8.74	7.38	7.89	8.80	8.58	8.03	8.58	9.55			
2*b*	8.36[b]	6.86	6.77	8.36[b]	8.63[c]	8.00	8.40[c]	9.80		8.65	8.10
11*c*								7.27			
12*c*	8.73	7.38	7.91	8.61[b]	8.69[c]	8.05	8.61[b,c]	8.45			
1*c*	8.76[b]	7.40	7.91	8.84	8.76[b,c]	8.08	8.62[c]	9.69			
2*c*	8.35	6.87	6.78	8.41	8.85[c]	8.07	8.43[c]	9.97		8.93	8.21
11*d*								7.59			
1*d*	8.78	7.45[b]	7.95	8.90	8.61[c]	7.96	8.57[c]	9.92			
1*e*	8.49		8.58	8.57	8.50[c]	7.94	8.46[c]	9.62	9.31		
1*f*	8.75		7.94	8.75	8.60[c]	8.05	8.57[c]	9.72	9.40		
tpy	8.69	7.35	7.88	8.64	8.47	7.96					

[a]In $CDCl_3$.
[b]Denotes central position of multiplet.
[c]Uncertainty in peak assignment.
[d]^{1}H labelling in Fig. 6.

Table 2*b*. ^{1}H NMR chemical shifts for the R groups of the various ligands and their precursors (in ppm).[a,b]

	H_{Me}	H_o	H_m	H_p	A_{10}	A_1	A_2	A_3	A_4
11*b*	2.65								
12*b*	2.79								
1*b*	2.94								
2*b*	2.97								
11*c*		8.44	7.51[c]	7.51[c]					
12*c*		8.61[c]	7.54[c]	7.54[c]					
1*c*		8.78	7.59[c]	7.59[c]					
2*c*		8.83	7.52[c]	7.52[c]					
11*d*					8.60	8.07	7.48[c]	7.48[c]	7.60[c]
1*d*					8.64	8.11	7.45[c]	7.45[c]	7.86

[a]In $CDCl_3$.
[b]R group labelling in Fig. 6.
[c]Denotes central position of multiplet.

11*a–d* in DMF with $Pd(II)(PPh_3)_2Cl_2$ as catalyst yields the bis-tridentate ligands **1***a–d* in 49, 48, 56, and 65% yield, respectively (Fig. 4). Similarly, the terminal pyridine methyl-substituted bis-tridentate ligand **1***e* can be obtained in 49% yield. Further functionalization with NBS resulted in a mixture of different brominated products. The bisbromomethyl ligand **1***f* was isolated via column chromatography in 27% yield (Fig. 4).

2,6-Bis(tributylstannyl)pyridine **13** is obtained via transmetallation of 2,6-dilithiopyridine (33) with tributyltin chloride in 17% yield (Fig. 5). 4-(2′,2″-Bipyrid-6′-yl)-6-chloropyrimidines **12***a–c* are synthesized in an analogous manner to the bis-tridentate ligands (Fig. 5). The bpy **10***a* and an excess of pyrimidines **11***a–c* are reacted in DMF with $Pd(II)(PPh_3)_2Cl_2$ as the catalyst, giving **12***a–c* in yields of 41, 67, and 48%, respectively. The reaction of **13** with **12***a–c* proceeded under similar conditions to yield 31, 45, and 57% of the respective tris-tridentate ligands **2***a–c*.

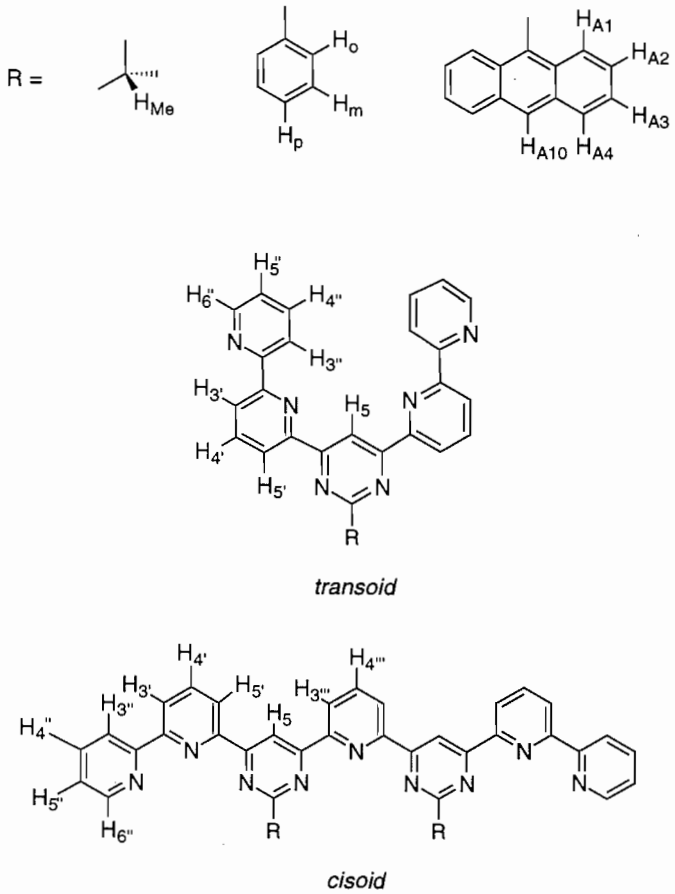
Solution structure of **1***a–f* and **2***a–c*

Information concerning the orientation of the bis- and tris-tridentate ligands in solution was deduced from ^{1}H NMR chemical shifts (Fig. 6, Table 2). In the *cisoid* conformation, $H_{3''}$ would have no nitrogen lone pairs in proximity, whereas in the *transoid* conformation, $H_{3''}$ is close to two nitrogen lone pairs, accounting for its deshielding relative to H_3 in tpy. The chemical shifts of $H_{3'}$ and $H_{5'}$ are similar (a single doublet in **1***b* at 200 MHz), demonstrating that the pyrimidine N lone pair has

© 1997 NRC Canada

Can. J. Chem. Downloaded from www.nrcresearchpress.com by 92.62.229.171 on 09/08/12
For personal use only.

Fig. 6. Labelling of the *transoid* bis-tridentate and *cisoid* tris-tridentate ligands.



a similar deshielding effect to that of the pyridine N lone pair. The minor differences in the chemical shifts of H_2 in **11***a*, **12***a*, **1***a*, and **2***a* suggests that there is no intramolecular interaction between H_2 and the rest of the molecule. Intramolecular interactions involving H_5 are demonstrated by significant changes in its chemical shift in the aforementioned compounds. The greatest deshielding of H_2 and H_5 occurs after the addition of the first and second bipyridyl moieties to **11***a* (for **12***a*: +0.27 and +1.12, respectively; for **1***a*: +0.32 and +1.22 ppm, respectively). In **2***a*, the deshielding of H_2 (+0.04 ppm) and H_5 (+0.21 ppm) is modest relative to **1***a*. Evidently, the proximity of more nitrogen lone pairs deshields H_5. Although three nitrogen lone pairs point into a central cavity in **2***a*, one is far from H_5, resulting in only minor deshielding effects when compared to **1***a*.

The large upfield shift of the terminal pyridine protons in **2***a–c* may be attributed to shielding effects resulting from π–π interactions between the two terminal pyridines. Significant upfield shifts are observed when comparing **1***a* to **2***a*: −0.44, −0.54, −1.17, and −0.48 ppm for $H_{6''}$–$H_{3''}$, respectively. Similar upfield shifts occur between **1***b* and **2***b* (−0.38, −0.52, −1.12, and −0.44 ppm for $H_{6''}$–$H_{3''}$, respectively) and **1***c* and **2***c* (−0.41, −0.53, −1.13, and −0.43 ppm for $H_{6''}$–$H_{3''}$, respectively), suggestings similar environments for the terminal pyridines. The ^{1}H NMR spectra of **2***a–c* indicate similar solution structures.

The ^{1}H ROESY NMR spectrum of **2***a* reveals no interannular NOE interactions between adjacent heterocycles, supporting an all-*trans* conformation. The only prevalent NOE interaction occurs between $H_{3''}$ and H_5, indicating partial curling up of the ligand. The symmetry of the molecule on the NMR time scale does not allow differentiation of the three-ring (partial curling-up of the ligand) and five-ring (full curling-up of the ligand) interactions between $H_{3''}$ and H_5. No NOE interactions between $H_{3'''}$ and H_5 are observed, further supporting a *transoid* conformation at the central tridentate site.

The overlap between the terminal pyridines requires that the nonchiral linear molecule be curled up into a helical shape. Three basic features dictate this behaviour: (*a*) an alternating sequence of pyridine and pyrimidine units; (*b*) linkage of these units at appropriate positions; (*c*) *transoid* conformation around the linkage bonds based on the preference for a *trans* orientation of nitrogen sites and concomitant *cis* orientation of CH and N sites as found in 2,2′-bipyridine (12).

Solid state structure of 2*a*

X-ray crystallographic studies indicate a helical structure in the solid state (Figs. 7 and 8). The unit cell is centrosymmetric and contains the two enantiomeric helices. The molecule has a twofold rotation axis passing through the central pyridine N and C-4. Molecule **2***a* adopts an overall helical conformation in which the nitrogen sites have the expected *transoid* orientation about the interannular bonds. The interior of the helical strand is lined with alternating CH and N sites. The central cavity is 5.42 Å across and of a size comparable to that in cyclosexipyridine and 18-crown-6.

$H_{3''}$ is directed into the cavity formed by the helix, with a distance of 3.0 and 3.4 Å between $H_{3''}$ and H_5 for the three-ring and five-ring interaction, respectively. The angle between the least-squares planes (16.5 (2)°) is greatest between the pyrimidine (ring C) and central pyridine (ring D) (Fig. 8). The most coplanar rings are B and C (3.8 (8)°). The angle (8.6 (3)°) between the pyridine rings in the bipyridyl moieties is slightly greater than that found in terpyridine (5.1° and 7.1°) (34).

The interannular bond lengths in molecule **2***a* are typical of C—C single bonds between sp^2 hybridized carbon atoms, and lie between 1.484 (3) and 1.489 (4) Å. The pyridine and pyrimidine C—N bond lengths range from 1.334 (3) to 1.346 (4) Å and from 1.329 (4) to 1.344 (3) Å, respectively. The angles about the interannular bonds fall into two separate sets for the pyridines and pyrimidines: those which include a nitrogen atom and those which include a carbon atom. The C-C-C angles are between 3.5° and 9.2° greater than the N-C-C angles.

The interlamellar distance in graphite (3.354 Å) (35) is a reference for an optimal π-stacking distance. The terminal pyridines in **2***a* lie between an edge-to-face and a face-to-face orientation with a least-squares-planes angle of 38.8° and a centroid-to-centroid distance of 4.523 Å. The closest interactions between the terminal pyridines are those of C-3–C-3 (3.600 Å) and C-2-C-3 (3.755 Å), although C-3 and C-4 of the terminal pyridine are closer to the nitrogen of pyridine ring B, at 3.559 and 3.598 Å, respectively. The terminal pyridines are, therefore, slightly offset from one another, and are partially

Can. J. Chem. Downloaded from www.nrcresearchpress.com by 92.62.229.171 on 09/08/12
For personal use only.

© 1997 NRC Canada

Fig. 7. Solid state structure of **2***a*.

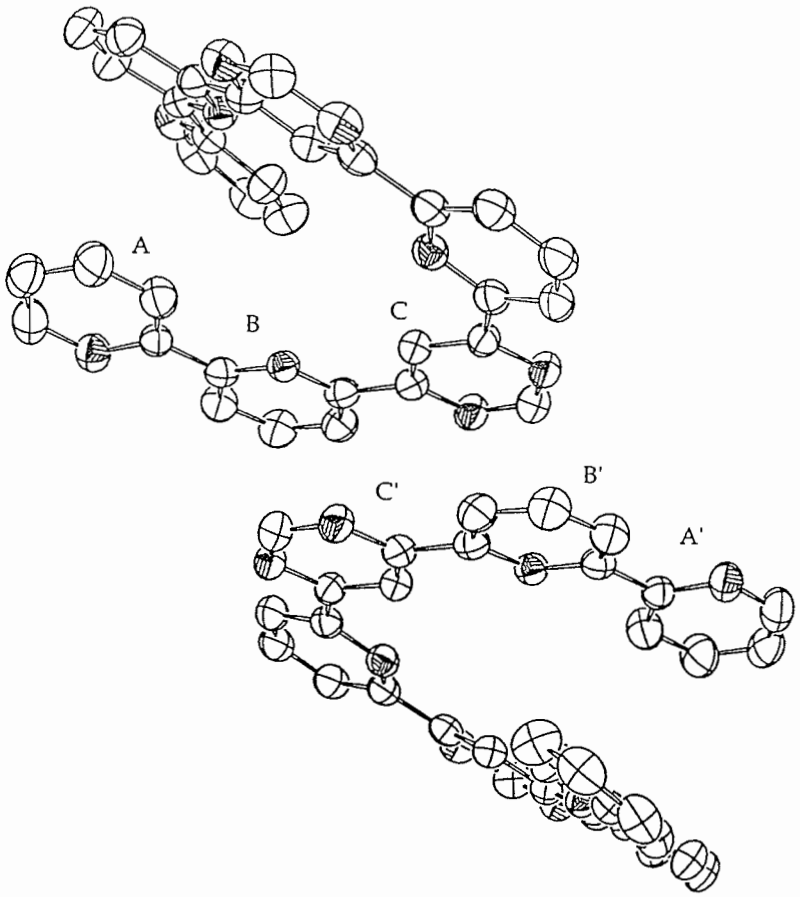


Table 3. Electrochemical reduction potentials $E^{\circ\prime}$ of the bis- and tris-tridentate ligands.[a,b]

	1*a*	**1***b*	**1***c*	**1***d*	**1***e*	**1***f*	**2***a*	**2***c*
$E^{\circ\prime}$ (1)	−1.44 (70)	−1.49 (60)	−1.43 (60)	−1.46 (70)	−1.54 (90)	−1.32[c]	−1.38 (70)	−1.41 (60)
$E^{\circ\prime}$ (2)	−2.07[c]	−2.17[c]	−2.06[c]	−1.96[c]	−2.22[c]	−1.46 (80)	−1.62 (70)	−1.64 (80)
$E^{\circ\prime}$ (3)				−2.06[c]				

[a]In DMF vs. SCE, except **1***e* and **1***f* vs. ferrocene (+0.45 V). The difference between cathodic and anodic peak potentials (mV) is given in parentheses.
[b]**2***b* not soluble enough for accurate measurements.
[c]Irreversible wave.

above the B rings (least-squares-planes angle = 33.2(1)°). $H_{4''}$ is directed above the B ring, whereas $H_{3''}$, $H_{5''}$, and $H_{6''}$ are above the other terminal pyridine. These interactions lead to the significant upfield shift of the ^{1}H NMR signals of these protons (36).

Ring B and ring C′ from each of the two enantiomeric helices have a centroid-to-centroid distance of 3.79 Å (Fig. 7). The least-squares-planes angle between the rings is 3.8 (7)°. The rings are slightly offset from one another, which may lead to favourable π–π interaction (36). Based on the above observations, we conclude that the solid state and solution structures of this molecule are helical and similar.

Heterocyclic ligands exhibit electrochemical reduction potentials that approximate their relative π* levels (37). The bis-tridentate ligands **1** present a reversible pyrimidine-based reduction (between −1.43 and −1.49 V; $E^{\circ\prime}_{\text{pyrimidine}} = -1.87$ V (38)) followed by an irreversible pyridine-based reduction (between −2.06 and −2.17 V; $E^{\circ\prime}_{\text{pyridine}} = -2.09$ V (38)) in DMF (Table 3). The 9-anthryl substituted ligand **1***d* also shows another irreversible reduction at −1.96 V in DMF, presumably due to the 9-anthryl moiety ($E^{\circ\prime}_{\text{anthracene}} = -1.92$ V, 2.5 V (39)).

The tris-tridentate ligands **2***a* and **2***c* exhibit two reversible reductions, the first near −1.40 V and the second near −1.63 V (Table 3), which may be considered as pyrimidine based, with the first lower and the second higher in energy than the first reduction of the bis-tridentate ligands **1**. Clearly, the pyrimidine moieties provide electronic communication that may involve extended delocalization through the central pyridine and electrostatic interaction. No subsequent reductions of the

© 1997 NRC Canada

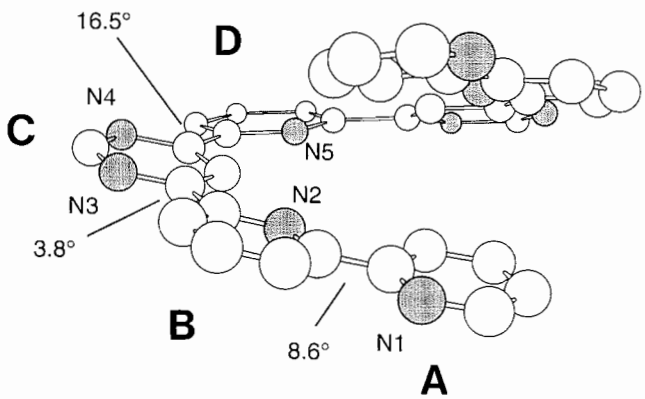
Can. J. Chem. Downloaded from www.nrcresearchpress.com by 92.62.229.171 on 09/08/12
For personal use only.

Table 4. Electronic spectra of the bis- and tris-tridentate ligands **1** and **2**.[a]

Compound	Absorption bands (λ_{max}, nm (ε, 10^4 dm^{-3} mol cm^{-1}))
1*a*	236 (3.8), 286 (3.3), 308 (2.6), 320 (3.2)
1*b*	237 (4.9), 284 (3.0), 304 (2.5), 322 (1.9)
1*c*	236 (4.8), 256 (3.2), 275 (3.8), 284 (sh, 3.5), 322 (1.4), 333 (1.0)
1*d*	236 (sh, 14), 250 (20), 257 (28), 285 (5.6), 320 (sh, 3.6), 348 (1.4), 366 (2.0), 386 (1.8)
1*e*	241 (5.7), 289 (4.0), 298 (sh, 3.5), 312 (sh, 2.4), 322 (sh, 2.0)
1*f*	244 (5.55), 295 (5.1), 321 (sh, 2.4)
2*a*	232 (7.7), 281 (sh, 3.5), 294 (3.9), 318 (sh, 2.4)
2*b*	233 (8.8), 291 (sh, 5.2), 302 (5.3), 320 (sh, 3.3)
2*c*	230 (8.3), 255 (5.1), 273 (5.5), 311 (2.4), 332 (1.5)

[a]In CH_2Cl_2.

Fig. 8. Angles between the least-squares planes between heterocyclic rings A–D in **2***a*.



pyridyl groups are observed. The poor solubility of **2***b* precluded determination of its reduction potentials.

The absorption spectra of the bis-tridentate ligands **1***a–f* (Table 4) display high-energy absorption bands like those found in pyridine (251, 270 nm) and pyrimidine (243, 298 nm) (40). They contain common absorption bands near 236, 286, 308, and 320 nm. The lowest energy band is ascribed to a pyrimidine-based transition, while the high-energy ones may be due to either pyridine- or pyrimidine-based absorptions. The low-energy absorption is expected to occur at lower energies than those of pyridine and pyrimidine, as bpy and tpy low-energy bands are at lower energies than those of pyridine (41). The same was found in other polyaromatic compounds, where conjugative interaction gives an extended π-system with a lowered HOMO–LUMO energy gap (42).

The phenyl- (**1***c*) and 9-anthryl-substituted (**1***d*) ligands exhibit additional UV bands (256 and 333 nm; and 250, 257, 348, 366, and 386 nm, respectively) that correspond reasonably well to the absorption bands of benzene (204, 256 nm) and anthracene (221, 256, 375 nm) (40). The molar absorptivity of **1***d* is higher than that of the other bis-tridentate ligands at all the common wavelengths as the 9-anthryl moiety has higher ε values than the other R groups at these wavelengths. As for the absorption maxima, the molar absorptivities for the chromophoric components in the ligands are approximately additive.

The tris-tridentate ligands **2***a–c* exhibit absorption spectra similar to those of their bis-tridentate counterparts **1***a–c*. The molar absorptivities of the transitions are more intense due to the greater number of heterocycles present and the λ_{max} positions are closer together.

Conclusion

We have developed a synthetic pathway for the synthesis of bis- and tris-tridentate ligands for metal complexation based on pyridine and pyrimidine units. The stepwise synthesis of the ligands proceeded via Stille carbon–carbon bond-forming reactions. The solution structures of the ligands were deduced by ^{1}H NMR, exemplified by pronounced deshielding of the protons adjacent to the interannular bond. When seven alternating pyridine–pyrimidine heterocycles are connected together, a helical structure is formed, as indicated by solution and solid state data. Longer multisite versions of these ligands are being investigated. The ligands **1***e–f*, functionalized at the terminal pyridine, represent potential building blocks for more extended systems.

Acknowledgement

G.S.H. thanks the Natural Sciences and Engineering Research Council of Canada for a post-graduate fellowship. U.S.S. thanks the Stiftung Stipendien-Fonds der Chemischen Industrie e.V. (Germany) for a postdoctoral fellowship. D.V. thanks the Alexander von Humboldt-Stiftung (Germany) for a postdoctoral fellowship.

References

1. D.S. Lawrence, T. Jiang, and M. Levett. Chem. Rev. 2229 (1995).
2. M. Kotera, J.-M. Lehn, and J.-P. Vigneron. J. Chem. Soc. Chem. Commun. 197 (1994).
3. R.M. Grotzfeld, N. Branda, and J.J. Rebek. Science, **271**, 487 (1996).
4. J.-M. Lehn, A. Rigault, J. Siegel, J. Harrowfield, B. Chevrier, and D. Moras. Proc. Natl. Acad. Sci. U.S.A. **84**, 2565 (1987).
5. E.C. Constable. Prog. Inorg. Chem. **42**, 67 (1994).
6. D.A. Dougherty. Science, **271**, 163 (1996).
7. J.-M. Lehn. *In* Supramolecular chemistry — concepts and perspectives. VCH, Weinheim. 1995. Chap. 9.

© 1997 NRC Canada

Can. J. Chem. Downloaded from www.nrcresearchpress.com by 92.62.229.171 on 09/08/12
For personal use only.

8. V. Balzani and F. Scandola. *In* Supramolecular chemistry. Horwood, Chichester, U.K. 1991.
9. J.-M. Lehn. *In* Supramolecular chemistry — concepts and perspectives. VCH, Weinheim. 1995. Chap. 8.
10. B.F. Abrahams, M.J. Hardie, B.F. Hoskins, R. Robson, and G.A. Williams. J. Am. Chem. Soc. **114**, 10641 (1992).
11. E.C. Constable, A.J. Edwards, D. Phillips, and P.R. Raithby. Supramol. Chem. **5**, 93 (1995).
12. G.S. Hanan, J.-M. Lehn, N. Kyritsakas, and J. Fischer. J. Chem. Soc. Chem. Commun. 765 (1995).
13. G.S. Hanan, C.R. Arana, J.-M. Lehn, and D. Fenske. Angew. Chem. Int. Ed. Engl. **34**, 1122 (1995).
14. P. Baxter, G.S. Hanan, and J.-M. Lehn. J. Chem. Soc. Chem. Commun. 2019 (1996).
15. P. Baxter, J.-M. Lehn, J. Fischer, and M.-T. Youinou. Angew. Chem. Int. Ed. Engl. **33**, 2284 (1994).
16. G.S. Hanan, C.R. Arana, J.-M. Lehn, G. Baum, and D. Fenske. Chem. Eur. J. **2**, 2019 (1996).
17. G. Morgan and F.H. Burstall. J. Chem. Soc. 1649 (1937).
18. W.R. McWhinnie and J.D. Miller. Adv. Inorg. Chem. Radiochem. **12**, 135 (1969).
19. E.C. Constable. Adv. Inorg. Chem. Radiochem. **30**, 69 (1986).
20. J.R. Kirchhoff, D.R. McMillin, P.A. Marnot, and J.-P. Sauvage. J. Am. Chem. Soc. **107**, 1138 (1985).
21. P.J. Steel. Coord. Chem. Rev. **106**, 227 (1990).
22. D. Wenkert and R.B. Woodward. J. Org. Chem. **48**, 283 (1983).
23. F.H. Case. J. Org. Chem. **31**, 2398 (1966).
24. C. Bolm, M. Erwald, M. Felder, and G. Schingloff. Chem. Ber. **125**, 1169 (1992).
25. P.-M. Windscheif and F. Vögtle. Synthesis, 87 (1994).
26. D.B. Harden, M.J. Mokrosz, and L. Strekowski. J. Org. Chem. **53**, 4137 (1988).
27. D.B. Moran, G.O. Morton, and J.D. Albright. J. Heterocycl. Chem. **23**, 1071 (1986).
28. A.J. Downard, G.E. Honey, L.F. Phillips, and P.J. Steel. Inorg. Chem. **30**, 2259 (1991).
29. J. Uenishi, T. Tanaka, K. Nishiwaki, S. Wakabayashi, S. Oae, and H. Tsukube. J. Org. Chem. **58**, 4382 (1993).
30. J.E. Parks, B.E. Wagner, and R.H. Holm. J. Organomet. Chem. **56**, 73 (1973).
31. T. Garber and D.P. Rillema. Synth. Commun. **20**, 1233 (1990).
32. H.R. Henze, W.J. Clegg, and C.W. Smart. J. Org. Chem. **17**, 1320 (1952).
33. G.R. Newkome and J.M. Roper. J. Organomet. Chem. **186**, 147 (1980).
34. C.A. Bessel, R.F. See, D.L. Jameson, M.R. Churchill, and K.L. Takeuchi. J. Chem. Soc. Dalton Trans. 3223 (1992).
35. F.A. Cotton and G. Wilkinson. *In* Advanced inorganic chemistry. John Wiley & Sons, Toronto. 1988.
36. C.A. Hunter and J.K.M. Sanders. J. Am. Chem. Soc. **112**, 5525 (1990).
37. S.D. Ernst and W. Kaim. Inorg. Chem. **28**, 1520 (1989).
38. P. Ford, D.F.P. Rudd, R. Gaunder, and H. Taube. J. Am. Chem. Soc. **90**, 1187 (1968).
39. A. Bard and L.R. Faulkner. *In* Electrochemical methods, fundamentals and applications. John Wiley & Sons, New York. 1980.
40. A.J. Boulton and A. McKillop. *In* Comprehensive heterocyclic chemistry. Vol. 2. *Edited by* A.R. Katritzky and C.W. Rees. Pergamon Press Ltd., London. 1984.
41. K. Nakamoto. J. Phys. Chem. **64**, 1420 (1960).
42. U. Müller, M. Adam, and K. Müllen. Chem. Ber. **127**, 437 (1994).
43. R.M. Silverstein, G.C. Bassler, and T.C. Merrill. *In* Spectrometric identification of organic compounds. John Wiley & Sons, New York. 1981.

Can. J. Chem. Downloaded from www.nrcresearchpress.com by 92.62.229.171 on 09/08/12
For personal use only.

© 1997 NRC Canada

Reactions of hydroxamidovanadate with peptides: Aqueous equilibria and crystal structure of oxobis(hydroxamido)-glycylglycinatovanadium(V)[1]

Pradip C. Paul, Sarah J. Angus-Dunne, Raymond J. Batchelor, Frederick W.B. Einstein, and Alan S. Tracey

Abstract: Bis(hydroxamido)hydroxooxovanadate has been found to undergo favourable condensation reactions with simple peptides such as glycylglycine, glycylglycylglycine, or glycyltyrosine to afford, in each case, three products in the approximate ratio 1:3.5:0.2. The three products had the same ligand stoichiometry and, in the case of glycylglycine, an overall formation constant of 3.3×10^3 M^{-1} for the addition of GlyGly to bis(hydroxamido)vanadate. The ^{51}V chemical shift range of the products (close to −850 ppm) overlaps that of the starting complexes and the products may well have a coordination geometry similar to the parent complexes. The chemical shifts observed for these materials are in the range of chemical shifts observed for peroxovanadium complexes. A crystalline monomeric complex with a single glycylglycinato ligand was obtained and its crystal structure determined. The complex is zwitterionic and has a pentagonal bipyramidal coordination at vanadium with the glycine-NH_2 functionality coordinated in the plane of the two hydroxyalamine ligands and the amido carbonyl oxygen in the apical position. Some comparisons with peroxovanadium complexes are drawn. Crystal structure of $V(O)(ONH_2)_2(GlyGly)\cdot H_2O$: monoclinic, space group *Cc*; $Z = 4$; $a = 9.1340(9)$ Å; $b = 16.3355(15)$ Å; $c = 7.1149(6)$ Å; β (°) = 103.020(7); $V = 1034.31$ Å^3; $T = 295$ K; $R_F = 0.21$ for 2513 data ($I_0 \geq 2.5\sigma(I_0)$) and 197 variables.

Key words: vanadate, hydroxylamine, *N*-methylhydroxylamine, oxobis(hydroxamido)glycylglycinatovanadium(V), peptide complex, glycylglycine, ^{51}V NMR, crystal structure.

Résumé : Le bis(hydroxamido)hydroxooxovanadate selon une réaction de condensation favorable avec les peptides simples tels la glyglycine, la glycylglycylglycine, ou la glycyltyrosine conduit, dans chaque cas, à trois produits dans le rapport approximatif de 1 : 3, 5 : 0,2. La stoechiométrie du ligand est la même dans ces trois produits et, dans le cas de la glycylglycine, la constante globale de formation est de $3{,}3 \times 10^3$ M^{-1} pour l'addition de GlyGly sur le bis(hydroxamido)vanadate. L'intervalle des déplacements chimiques du ^{51}V de ces produits (voisin de −850 ppm) recouvre celui des complexes de départ et les produits peuvent bien avoir une géométrie de coordination similaire à celles des complexes dont ils sont issus. Les déplacements chimiques observés pour ces produits se situent dans l'intervalle des déplacements chimiques observés pour les complexes de peroxovanadium. On a obtenu un complexe monomère cristallin avec un seul ligand glycylglycinato et on a déterminé sa structure cristalline. Le complexe est un zwitterion et sa coordination est pentagonale bipyramidale au niveau du vanadium avec la fonction NH_2 de la glycine coordonnée dans le plan des deux ligands hydroxylamines et avec l'oxygène du carbonyle du groupe amide en position apicale. On a établi quelques comparaisons avec les complexes de peroxovanadium. Structure cristalline du $V(O)(ONH_2)_2(GlyGly)\cdot H_2O$: groupe d'espace monoclinique, *Cc*; $Z = 4$; $a = 9{,}1340(9)$ Å; $b = 16{,}3355(15)$ Å; $c = 7{,}1149(6)$ Å; $\beta(°) = 103{,}020(7)$; $V = 1034{,}31$ Å^3; $T = 295$ K; $R_F = 0{,}21$ pour 2513 données ($I_0 \geq 2{,}56\sigma(I_0)$) et 197 variables.

Mots clés : vanadate, hydroxylamine, *N*-méthylhydroxylamine, oxobis(hydroxamido)glycylglycinatovanadium(V), complexe de peptide, glycylglycine, ^{51}V RNM, structure cristalline.

[Traduit par la rédaction]

Received October 3, 1996.

P.C. Paul, S.J. Angus-Dunne, R.J. Batchelor,[2] F.W.B. Einstein,[2] and A.S. Tracey.[3] Department of Chemistry, Simon Fraser University, Burnaby, BC V5A 1S6, Canada.

[1] This work was presented in part at the 31st International Conference on Coordination Chemistry, Vancouver, August 18–23, 1996.
[2] X-ray crystal laboratory, Department of Chemistry.
[3] Author to whom correspondence may be addressed. Telephone: (604) 291-4464. Fax: (604) 291-3765. E-mail: tracey@sfu.ca

© 1997 NRC Canada

Can. J. Chem. Downloaded from www.nrcresearchpress.com by 92.62.229.171 on 09/08/12
For personal use only.

Can. J. Chem. Downloaded from www.nrcresearchpress.com by 92.62.229.171 on 09/08/12
For personal use only.

Introduction

Vanadium is now known to be an important metal for the function of a number of enzymatic systems. It is found in marine algae (1) and a number of terrestial lichens (2) and fungi, (3, 4), where vanadate (V(V)) is required for the function of vanadium-dependent haloperoxidases (5, 6). Nitrogenases that require vanadium for their nitrogen-fixing function have also been found in bacteria (7–9). These discoveries have stimulated a great deal of interest in the aqueous chemistry of vanadate and of peroxovanadates. For the latter there has been interest in their formation (10–15), their reactivity with heteroligands (16–19), and in their oxidative capabilities (16–23). This interest has been further piqued by the insulin-mimetic properties of peroxovanadates (24–27) and by the fact that vanadate can activate some types (28) and inhibit other types (29) of phosphate-metabolizing enzymes.

Hydroxamidovanadates offer a convenient point of departure from the study of peroxovanadates. The ligands are isoelectronic with each other and hydroxylamine offers the advantage of being asymmetrical so that further details of the reactions are accessible. A detailed study of reactions of dimethylhydroxylamine[4] and of methylhydroxylamine and hydroxylamine[5] have revealed that, unlike the case with hydrogen peroxide, two distinct types of bisligand complexes are formed. If the bonds to the hydroxylamine ligand are formally treated as unidentate, then the crystal structure studies show a tetrahedral coordination about vanadium for one type of complex, the other type is thought to correspond to a trigonal bipyramidal coordination.[4] In the presence of certain heteroligands, it seems probable that further reaction of the bishydroxamidovanadate to generate additional products can occur, as is well known for bisperoxovanadate complexes (16–18). However, because of the occurrence of two types of coordination for the bis(hydroxamido)vanadate complex compared to only one type for for the corresponding bisperxovanadate complex, it is quite feasible that hydroxamido(heteroligand) vanadate complexes that are structurally different from those derived from peroxovanadate will be formed. Initial studies show that this, to an extent, is the case and, for the ligands of this study, the reaction scheme does not correspond to that for the peroxovanadates.

Experimental

Materials

Reagents used were of commercially available reagent grade quality. Hydroxylamine hydrochloride, N-methylhydroxylamine hydrochloride, glycylglycine, glycylglycineOEt, triglycine, glycyltyrosine, and tetraethylammonium hydroxide (20% aqueous solution) were obtained from Sigma Chemical Co. Vanadium(V) oxide (99.99%) and HEPES buffer were obtained from Aldrich Chemical Co. All chemicals were used as supplied.

Stock solutions of KCl (2 M), hydroxylamine(100 mM), HEPES buffer (200 mM), and of the heteroligands (100 mM) were prepared at pH 6.5. The vanadate stock solution (100 mM) was prepared at pH 9. The stock solutions were combined appropriately with added distilled water to give the final concentrations of reactants. All final solutions were prepared at 1.0 M ionic strength with added KCl, 20 mM HEPES buffer, the indicated amounts of hydroxylamine, and heteroligand at pH 7.1. Care was taken to ensure that pH adjustments on vanadate-containing solutions did not require addition of acid (stock solutions were adjusted appropriately, if necessary).

Under locally acidic conditions, vanadate rapidly oligomerizes to decavanadate, which hydrolyzes only very slowly.

Synthesis of $[VO(ONH_2)_2(GlyGly)]\cdot H_2O$

Vanadium pentoxide (0.10 g; 0.55 mmol), tetraethylammonium hydroxide (1 mL), and a small amount of water (~2 mL) was taken in a beaker. The resultant mixture was warmed to 60°C, with continuous stirring to get a clear solution of tetraethylammonium vanadate. The pH of the vanadate solution was about 11. To this vanadate solution a solution of hydroxylamine hydrochloride (0.15 g; 2.16 mmol) dissolved in water (2 mL) at pH 7 (adjusted by tetraethylammonium hydroxide) was added with continuous stirring. The pH was maintained between 8.5 and 9.5. This solution was cooled in an ice bath and glycylglycine (0.15 g; 1.1 mmol) dissolved in water (2 mL) was added with continuous stirring. The pH of the final solution was adjusted to 9.0. The reaction mixture was maintained at about 2°C. After about 30 min, pale yellow crystals were obtained. After crystallization was complete, the solution was filtered and the crystalline product washed with cold water and dried in vacuo. The compound was found to be stable at room temperature. Yield 0.17 g (60%).

The crystals were light yellow coloured and very hard in nature. They were not found to be soluble in water and common organic solvents. This precluded dissolution studies of this compound. The structure of this compound was determined from single crystal X-ray diffraction studies.

^{51}V NMR spectroscopy

Spectra were acquired at 105 MHz using a Bruker AMX400 NMR spectrometer. 4K data set sizes were obtained with 0.05 s aquisition times and 60° pulse widths. The spectra were zero filled to 16 K and a line-broadening factor of 40 Hz applied before Fourier transformation. Fourier transformation, baseline corrections and spectral integration were done using the instrument manufacturer's software.

Equilibrium analysis

Equilibrium expressions were obtained and the data analysis carried out as outlined in the text. Errors in parameters are reported at the 3σ level.

Crystal structure

A crystal was mounted on a glass fiber. Data were recorded at ambient temperature with an Enraf Nonius CAD4F diffractometer using graphite monochromatized Mo K_α radiation. Empirical absorption corrections were applied (30). Data reduction included corrections for Lorentz and polarization effects.

Coordinates for all atoms were refined. Two restraints were

[4] P.C. Paul, S.J. Angus-Dunne, R.J. Batchelor, F.W.B. Einstein, and A.S. Tracey. Can J. Chem. Submitted.

[5] S.J. Angus-Dunne, P.C. Paul, and A.S. Tracey. Can J. Chem. Submitted.

© 1997 NRC Canada

Can. J. Chem. Downloaded from www.nrcresearchpress.com by 92.62.229.171 on 09/08/12
For personal use only.

Table 1. Crystallographic data for the structure determination of $V(O)(ONH_2)_2(GlyGly) \cdot H_2O$.

Parameter		Parameter	
Formula	$VO_7N_4C_4H_{13}$	Crystal system	Monoclinic
FW	280.11	Space Group	*Cc*
a (Å)[a]	9.1340(9)	ρ_c (g cm^{-3})	1.799
b (Å)	16.3355(15)	λ(Mo Kα_1) (Å)	0.70930
c (Å)	7.1149(6)	μ(Mo Kα) (cm^{-1})	9.6
β (°)	103.020(7)	min–max 2θ (°)	4–70
V (Å^3)	1034.31	Transmission[b]	0.818–0.867
Z	4	Crystal dimensions (mm)	0.25 × 0.28 × 0.35
T(K)	295	R_F[d]	0.022
GoF[c]	1.34	R_{wF}[e]	0.025

[a]Cell dimensions were determined from 48 reflections ($40° \leq 2\theta \leq 56°$).

[b]The data were corrected empirically for the effects of absorption using the product of the experimental ψ dependance and a (spherical) 2θ correction.

[c]GoF = $[\Sigma(w(F_o - F_c)^2)/\text{degrees of freedom}]^{1/2}$.

[d]$R_F = \Sigma||F_o| - |F_c||/\Sigma|F_o|$, for 2513 data ($I_0 \geq 2.5\sigma(I_0)$).

[e]$R_{wF} = [\Sigma(w(|F_o| - |F_c|)^2)/\Sigma(wF_o^2)]^{1/2}$ for 2513 data ($I_0 \geq 2.5\sigma(I_0)$); $w = [\sigma(F_o)^2 + 0.0001F_o^2]^{-1}$.

used to fix the origin. Anisotropic thermal parameters were refined for all non-hydrogen atoms. Independent isotropic temperature factors for all hydrogen atoms were also refined. The Flack (31) enantiopole parameter, which refined to 0.00 (2), unambiguously established the correct polarity for the crystal. Of the incidentally measured sets of Friedel related reflections, for which $|F_c^+| - |F_c^-|/\sigma(F_o) \geq 5$, all 29 showed the correct sign of $|F_o^+| - |F_o^-|$, supporting the model. A weighting scheme based on counting statistics was applied such that $\langle w(|F_o| - |F_c|)^2 \rangle$ was near constant as a function of both $|F_o|$ and sin θ/λ. Final full-matrix least-squares refinement of 197 parameters for 2513 data ($I_0 \geq 2.5\sigma(I_0)$) converged at $R = 0.022$. Crystallographic details are summarized in Table 1. Final fractional atomic coordinates are listed in Table 2.

Analysis of the anisotropic thermal parameters, using a rigid-body (32) model for the non-hydrogen atoms of the complex, $V(O)(ONH_2)_2(GlyGly)$, yielded $R = 0.174$ for the agreement between observed and calculated U_{ij} and an r.m.s. discrepancy of 0.0035 Å^2. The resultant bond length corrections ranged from +0.001 to +0.005 Å.

The computer programs used were: DIFRAC (33) for data collection; NRCVAX (34) for absorption correction, data reduction, structure solution, and graphical output; and CRYSTALS (35) for structure refinement and rigid body thermal motion analysis. Complex scattering factors for neutral atoms (36) were used in the calculation of structure factors. Computations were carried out on a Pentium computer.

Results and discussion

Hydroxylamine, in the presence of vanadate under neutral aqueous conditions, gives rise to one major monoligand and four major bisligand products, their formation and relative proportions being highly pH dependent.[5] The four major products are readily separated into two groups of two complexes each. In the ^{51}V NMR spectrum at pH 7, one set of two broad signals and a second set of two relatively sharp signals are observed. With increase in pH the broad signals decrease in intensity relative to the sharp ones. In the presence of glycylglycine, the four signals are replaced by a set of three sharp signals occurring near −850 ppm. This suggests that the product complexes are coordinated similarly to the products corresponding to the sharp pair of the four signals in the precursor complexes. Figure 1 shows the spectra obtained in the absence (A) and presence (B) of glycylglycine. In Fig. 1A, the signal of the monohydroxamido complex is observed at −672 ppm while the signals of the bisligand complexes are centred near −840 ppm. As can be seen from Fig 1B, the product complexes also give signals near −840 ppm. The chemical shifts of these complexes are within the range of chemical shifts observed for peroxo (17, 37, 38) and hydroxamido-derived (37, 39) complexes of vanadate and this is consistent with a side-on coordination of the hydroxamido ligand. The only other product signal is found at −570 ppm and is thought to derive from an ester-like product formed from reaction at the hydroxyl group of hydroxylamine.

In the case of bis(dimethylhydroxamido)vanadate, it has been proposed,[4] on the basis of an X-ray study and dissolution studies, that the similarly broad signals observed in that system correspond to a six-coordinate complex (tetrahedral-like, if the bonds to the dimethylhydroxylamine are formally assumed to be monodentate) and this seems to correspond to the situation here. With this ligand, the broad signals also are retained in solution with decrease in pH while the single sharp signal vanishes from the spectrum. The opposite situation is obtained with increasing pH. The sharper signal has been assigned to a complex with a pentagonal bipyramidal coordination and this assignment is in agreement with observations here where the GlyGly products give rise to sharp signals.

It was possible to show that the three heteroligand products had the same ligand stoichiometry by varying the glycylglycine and hydroxylamine concentrations. It was found that the product ratio was independent of the glycylglycine concentration. Furthermore, if the glyclyglycine concentration was maintained at 20 mM in the presence of 1 mM total vanadate

© 1997 NRC Canada

Can. J. Chem. Downloaded from www.nrcresearchpress.com by 92.62.229.171 on 09/08/12
For personal use only.

Table 2. Fractional atomic coordinates and isotropic or equivalent isotropic temperature factors (Å^2) for $V(O)(ONH_2)_2(GlyGly)\cdot H_2O$.

Atom	x	y	z	$U_{eq/iso}$[a]
V	0.04103(10)	0.34826(1)	0.99031(13)	0.0186
O(1)	0.05143(17)	0.45582(8)	1.09265(21)	0.0283
O(2)	−0.12755(18)	0.32822(9)	1.09608(21)	0.0312
O(3)	0.17322(18)	0.30032(8)	1.13407(21)	0.0286
O(4)	−0.12564(16)	0.39700(7)	0.74561(18)	0.0223
O(5)	−0.46615(19)	0.36331(8)	0.16287(24)	0.0331
O(6)	−0.58335(19)	0.47532(9)	0.22567(26)	0.0350
O(7)	−0.58549(22)	0.63781(10)	0.27506(26)	0.0344
N(1)	0.14806(18)	0.45351(9)	0.96588(22)	0.0247
N(2)	−0.11749(21)	0.26129(10)	0.97772(23)	0.0287
N(3)	−0.21466(19)	0.39811(10)	0.42300(21)	0.0233
N(6)	0.10715(17)	0.30191(8)	0.74351(22)	0.0199
C(1)	−0.47586(21)	0.42616(10)	0.25846(26)	0.0241
C(2)	−0.34592(21)	0.44719(12)	0.42593(26)	0.0272
C(4)	−0.11377(19)	0.37821(9)	0.57941(22)	0.0190
C(5)	0.02372(22)	0.33207(11)	0.55553(24)	0.0248
H(1)	0.2350(39)	0.4530(19)	1.0263(46)	0.054(9)
H(2)	0.1041(32)	0.4825(17)	0.8613(39)	0.044(7)
H(3)	−0.1147(34)	0.2153(20)	1.0409(49)	0.056(9)
H(4)	−0.1866(32)	0.2581(17)	0.8852(40)	0.041(7)
H(21)	−0.3235(27)	0.5037(14)	0.4360(32)	0.024(5)
H(22)	−0.3825(36)	0.4421(18)	0.5314(47)	0.051(8)
H(30)	−0.1983(35)	0.3777(19)	0.3326(46)	0.052(8)
H(51)	0.0849(40)	0.3670(20)	0.5018(54)	0.063(9)
H(52)	0.0009(30)	0.2892(17)	0.4756(42)	0.047(8)
H(61)	0.1858(28)	0.3145(14)	0.7465(34)	0.025(6)
H(62)	0.1044(22)	0.2576(13)	0.7420(30)	0.015(4)
H(71)	−0.5494(49)	0.6397(20)	0.3968(60)	0.070(11)
H(72)	−0.5891(37)	0.5998(18)	0.2513(44)	0.045(9)

[a] U_{eq} is the cube root of the product of the principal axes of the thermal ellipsoid.

and the hydroxylamine concentration varied between 2 and 20 mM, there also was no change in the product ratio of the three products. In this latter case, overall, the −850 ppm product signals increased relative to the −672 ppm signals. This is in keeping with a monohydroxamido (−672 ppm) and bishydroxamido (−850 ppm) stoichiometry. No evidence was obtained for the formation of a monohydroxamidoGlyGly–vanadate complex.

These preliminary studies suggested that product formation can be written as in eq. [1], where L refers to hydroxylamine and GG to glycylglycine. Equation [1] can be reexpressed as in eq. [2].

$$[1]\quad V + 2L + GG \overset{K_1}{\rightleftharpoons} VL_2GG$$

$$[2]\quad [L]^2K_1 = [VL_2GG]/[V][GG]$$

Figure 2 shows the experimental result when the concentration of NH_2OH was varied while the overall vanadate (3.0 mM) and glycylglycine (20.0 mM) were maintained constant. For this plot, the total integrated intensity for the three signals near −850 ppm was used. The individual products were found in the ratio of 1:3.5:0.23 for the −839, −848, and −861 ppm products, respectively. The overall formation constant of $(4.3 \pm 0.4) \times 10^8$ M^{-3} can then be partitioned according to the ratio of the individual products.

The formation constant for the GlyGly complex from VL_2 corresponding to the reaction of eq. [3] can be obtained from the value of K_1 for eq. [1] and the known formation constant, K', for VL_2

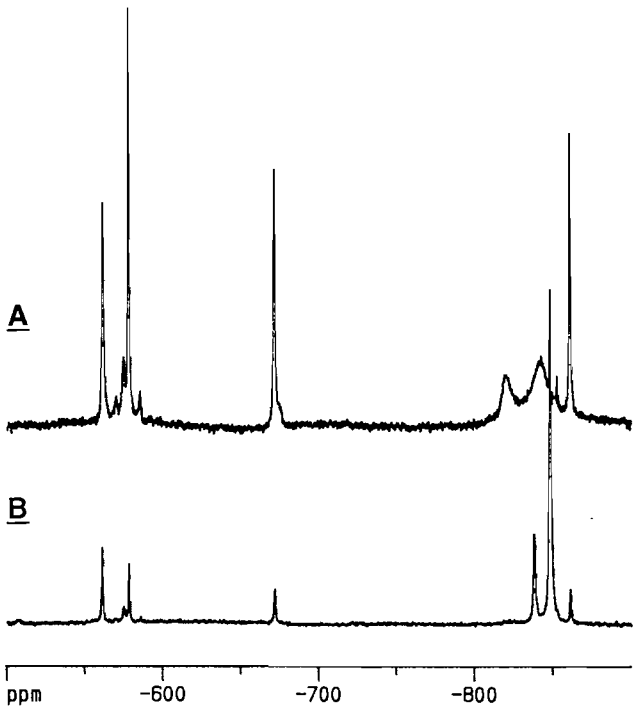
$$[3]\quad VL_2 + GG \overset{K_2}{\rightleftharpoons} VL_2GG$$

from vanadate and hydroxylamine for the pH of this study; $K' = (1.3 \pm 0.2) \times 10^5$ M^{-2} (footnote 5). K_1 is then equal to $K'K_2$ and $K_2 = (3.3 \pm 0.5) \times 10^3$ M^{-1}. There is no evidence from the study of bisperoxovanadates in the presence of glycylglycine or other dipeptides that products, similar to those found here, are formed. Indeed, only monoperoxopeptidovanadate complexes are formed to any appreciable extent and such products are highly favoured (40). Product formation is different in another way. With monoperoxovanadate, the N-terminal amino, the amido NH, and the C-terminal carboxylate are necessary for product formation. With the hydroxyamine–vanadate complex, three products with ^{51}V NMR chemical shifts and formation constants similar to those

© 1997 NRC Canada

Can. J. Chem. Downloaded from www.nrcresearchpress.com by 92.62.229.171 on 09/08/12
For personal use only.

Fig. 1. ^{51}V NMR spectra showing the spectrum of the starting equilibrium mixture of compounds (A) and the result after addition of glycylglycine (B). The signals near −670 ppm arise from monohydroxamidovanadate complexes, those near −850 ppm from bis(hydroxamido)vanadate complexes. The signals near −570 ppm occur in the order, low to high field, V_1, V-ONH_2, V_2, V_4 and V_5. Conditions of the experiments: 1-A: 3.0 mM vanadate; 6.0 mM NH_2OH, pH 7.2; ambient temperature. 1-B: as for 1-A but with 20 mM glycylglycine.



from glycylglycine are obtained with GlyGlyOEt, GlyGlyGly, and glycyltyrosine. It is evident that the carboxylate group is not required for the product to form and it also appears that a bulky side chain has little influence on product formation. An isolated carboxylate group, as in acetate for instance, can react with bishydroxamidovanadate, but even 400 mM acetate at pH 7 converts only about one half of the reactant complex to products. For comparison, 20 mM GlyGly converts about 90% of the starting complex to products. Ethylamine does have some influence on the hydroxylamine complex, but much less so than does acetate.

Attempts to obtain a crystalline glycylglycinatohydroxamidovanadate complex proved successful. The crystalline complex was found to be zwitterionic ($V(O)(ONH_2)_2$(GlyGly)) and its structure is shown in Fig. 3. Bond distances and angles are given in Table 3. A single water of crystallization, (O(7)), was also found in the unit cell. The vanadium atom has a seven-coordinate, approximately pentagonal bipyramidal environment with O(3) and O(4) occupying the axial positions. Alternatively, the complex might be described as trigonal bipyramidal — considering the center of the N—O bond in each hydroxylamine as one vertex in the equatorial plane. The complex deviates from mirror symmetry and this, presumably, is a consequence of the intermolecular interactions. The coordination mode of the glycylglycine ligand (via the amide carbonyl oxygen and the amine nitrogen atoms) seems unusual. In

Fig. 2. Graphical display of the overall formation of the product complexes as function of added hydroxylamine at constant total glyclylglycine concentration. Conditions of the experiments: 20 mM glyclycine; 3 mM vanadate; pH 7.0; variable NH_2OH (0.5–6.0 mM).

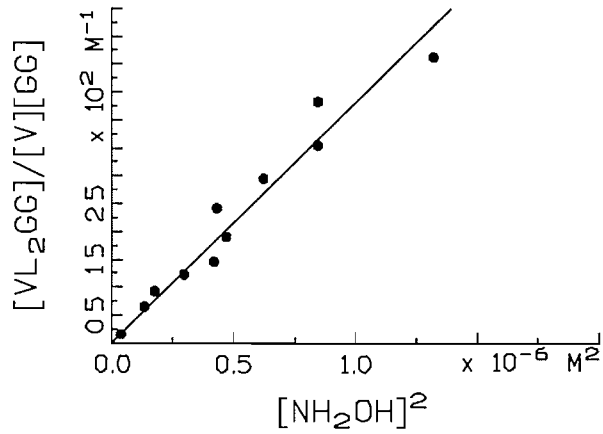
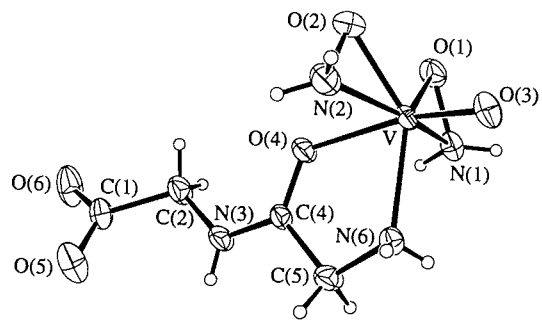


Fig. 3. The molecular structure of $V(O)(ONH_2)_2$(GlyGly) at 295 K. 50% probability thermal ellipsoids are shown for all non-hydrogen atoms. Hydrogen atoms are depicted by spheres of arbitrary radius.



the bisperoxovanadate case, similar complexes are not formed if this type of coordination is forced by esterifying the terminal carboxylate group. In this case no product was found (18, 38). The complex is zwitterionic, carrying a negative charge on the uncomplexed carboxylate group and the positive charge in the region of the vanadium. The form of the complex presumably is stabilized by the extensive intermolecular hydrogen bonding found in the crystal.

The relative orientations and dimensional parameters of the hydroxylamine ligands are similar to those for the dimethylhydroxylamine ligands of $[V(O)(ONMe_2)_2]_2O$ (footnote 4) and $[V(O)(ONEt_2)_2]_2O$ (41), in which, however, vanadium is only six-coordinate. Differences in the related bond angles at vanadium in these structures are commensurate with the introduction of a seventh coordinate bond. The most notable difference in analogous bond lengths is that the V—N bonds (2.0046(14) and 2.0160(19) Å, Table 3) average about 0.06 Å shorter than those in $[V(O)(ONMe_2)_2]_2O$ (2.066(2) and 2.069(2) C)[4] and about 0.07 Å shorter than those in $[V(O)(ONEt_2)_2]_2O$ (2.079(4), 2.061(4), 2.094(4), and 2.079(4), Å) (41). This difference is a reasonable consequence of the fact that in $V(O)(ONH_2)_2$(GlyGly) both of the hydroxylamine protons are involved in hydrogen bonds. The V—O(hydroxamido) bonds are perhaps very slightly longer in $V(O)(ONH_2)_2$(GlyGly) (see

© 1997 NRC Canada

Can. J. Chem. Downloaded from www.nrcresearchpress.com by 92.62.229.171 on 09/08/12
For personal use only.

Table 3. Selected intramolecular distances (Å)[a] and angles (°) for $V(O)(ONH_2)_2(GlyGly)\cdot H_2O$.

V—O(1)	1.8961(14)	O(4)—C(4)	1.2498(21)
V—O(2)	1.8886(20)	O(5)—C(1)	1.2457(23)
V—O(3)	1.6003(16)	O(6)—C(1)	1.2490(24)
V—O(4)	2.1882(14)	N(3)—C(2)	1.446(3)
V—N(1)	2.0046(16)	N(3)—C(4)	1.3158(20)
V—N(2)	2.0160(19)	N(6)—C(5)	1.4673(21)
V—N(6)	2.1211(19)	C(1)—C(2)	1.5196(24)
O(1)—N(1)	1.3974(25)	C(4)—C(5)	1.507(3)
O(2)—N(2)	1.3957(23)		
O(1)-V-O(2)	88.99(8)	O(3)-V-O(4)	167.44(8)
O(1)-V-O(3)	104.05(7)	O(3)-V-N(1)	99.36(8)
O(1)-V-O(4)	86.22(5)	O(3)-V-N(2)	96.57(7)
O(1)-V-N(1)	41.87(7)	O(3)-V-N(6)	92.29(8)
O(1)-V-N(2)	130.05(9)	O(4)-V-N(1)	83.36(6)
O(1)-V-N(6)	130.52(7)	O(4)-V-N(2)	81.78(6)
O(2)-V-O(3)	103.06(9)	O(4)-V-N(6)	75.41(6)
O(2)-V-O(4)	84.06(7)	N(1)-V-N(2)	163.73(8)
O(2)-V-N(1)	129.83(7)	N(1)-V-N(6)	89.94(7)
O(2)-V-N(2)	41.73(7)	N(2)-V-N(6)	92.71(7)
O(2)-V-N(6)	132.67(7)	O(5)-C(1)-O(6)	125.28(17)
V-O(1)-N(1)	73.23(9)	O(5)-C(1)-C(2)	118.38(16)
V-O(2)-N(2)	74.03(11)	O(6)-C(1)-C(2)	116.32(16)
V-O(4)-C(4)	118.05(11)	N(3)-C(2)-C(1)	111.53(15)
V-N(1)-O(1)	64.91(9)	O(4)-C(4)-N(3)	123.10(17)
V-N(2)-O(2)	64.24(10)	O(4)-C(4)-C(5)	118.80(14)
C(2)-N(3)-C(4)	123.34(16)	N(3)-C(4)-C(5)	118.10(15)
V-N(6)-C(5)	116.64(12)	N(6)-C(5)-C(4)	109.88(15)

[a] An analysis of the thermal parameters suggests bond length corrections in the range +0.001 – +0.005 Å (see text).

Table 3) than in $[V(O)(ONMe_2)_2]_2O$ (1.880(2) and 1.881(2) Å), while the N—O bond lengths are not significantly different.

A number of bisperoxovanadate complexes (42–46), which have a bidentate chelating ancillary ligand bonded to vanadium via one axial and one equatorial position are structurally very similar to the complex described here. Perhaps the best comparison is with the structures of the doubly anionic bisperoxovanadate complexes with pyridine-2-carboxylate and 3-hydroxypyridine-2-carboxylate (42). Both these ancillary ligands form five-membered chelate metallocycles having nitrogen in the equatorial position and oxygen in the axial position. In these complexes, the V—N bond lengths are 2.123(5) and 2.137(2) Å, respectively, and the V—O bond lengths are 2.290(4) and 2.314(2) Å, respectively (cf. V—N(6) 2.1211(19) Å and V—O(4) 2.1882(14) Å in the present structure). Very similar arrangements for the vanadium environment are also observed in related bisperoxovanadyl complexes having, instead, two monodentate ancillary ligands in these positions (47–49), although the axial ligand *trans* to the vanadyl oxygen is often only weakly coordinated.

Extensive hydrogen bonding in the crystals of $V(O)(ONH_2)_2(GlyGly)\cdot H_2O$ produces a three-dimensionally extended structure (see Figure 4). Every N-H or O-H hydrogen atom is involved in an intermolecular hydrogen bond. Each $V(O)(ONH_2)_2(GlyGly)$ unit is hydrogen bonded directly to eight different neighbouring complexes and to four different water molecules. In addition, each water molecule (O(7)) links four complexes by forming hydrogen bonds individually to O(6) and O(5) of two different carboxylate groups and also acts as an H-bond receptor for hydrogen atoms from a hydroxylamine and the (glycine)amine group of two additional neighbouring complexes. The oxygen atoms of the pendant carboxylate group (O(5) and O(6)) are each the receptors for two hydrogen bonds. The only "heteroatom" (O or N) not involved in hydrogen bonding is the carbonyl oxygen, O(4). A stereo diagram depicting all molecules that protrude into one unit cell and the hydrogen bonds between them is given in Fig. 4. The hydrogen-bonded interactions are summarized in Table 4. Additional crystallographic details, anisotropic thermal parameters, additional bond lengths and angles, torsion angles, and least-squares planes are provided as supplementary material.[6]

[6] Copies of material on deposit may be purchased from: The Depository of Unpublished Data, Document Delivery, CISTI, National Research Council, Ottawa, Canada K1A 0S2. Crystallographic details and tables of bond lengths and angles have also been deposited with the Cambridge Crystallographic Data Centre, and can be obtained on request from The Director, Cambridge Crystallographic Data Centre, University Chemical Laboratory, 12 Union Road, Cambridge, CB2 1EZ, U.K.

© 1997 NRC Canada

Fig. 4. Stereo packing diagram of $V(O)(ONH_2)_2(GlyGly)\cdot H_2O$. The entire contents of one unit cell plus atoms to complete all molecules are shown. H-bonds are depicted as dotted lines.

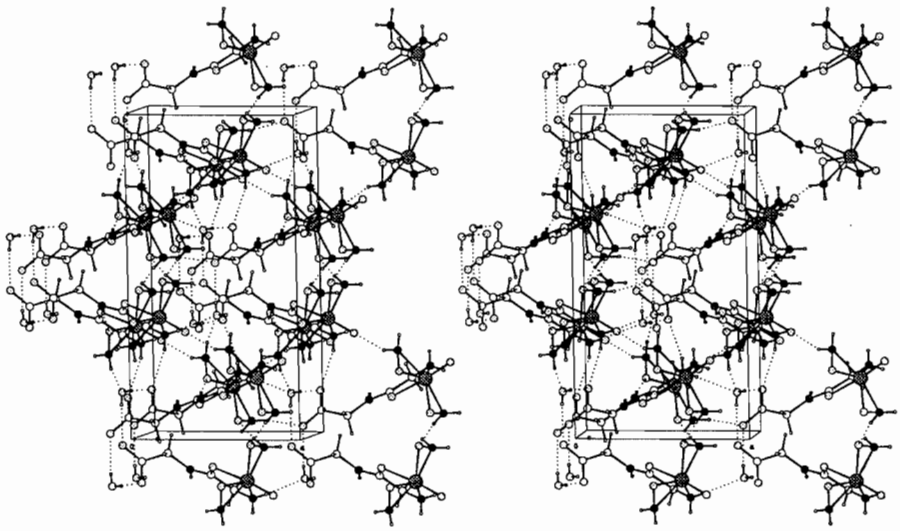


Table 4. Hydrogen-bonded distances (Å) for $V(O)(ONH_2)_2(GlyGly)\cdot H_2O$.

O(1)—(H)N(1)[a]	2.995(2)	O(2)—(H)N(3)[b]	2.860(2)
O(3)—(H)N(2)[c]	2.922(2)	O(5)—(H)O(7)[d]	2.729(2)
O(5)—(H)N(6)[e]	2.809(2)	O(6)—(H)O(7)	2.678(2)
O(6)—(H)N(1)[f]	2.742(2)	O(7)—(H)N(2)[g]	2.890(2)
O(7)—(H)N(6)[h]	2.936(2)		

[a](x, 1 − y, 1/2 + z)
[b](x, y, 1 + z)
[c](1/2 + x, 1/2−y, 1/2 + z)
[d](x, 1 − y, −1/2 + z)
[e](−1/2 + x, 1/2−y, −1/2 + z)
[f](−1 + x, y, −1 + z)
[g](−1/2 + x, 1/2 + y, −1 + z)
[h](−1 + x, 1 − y, −1/2 + z)

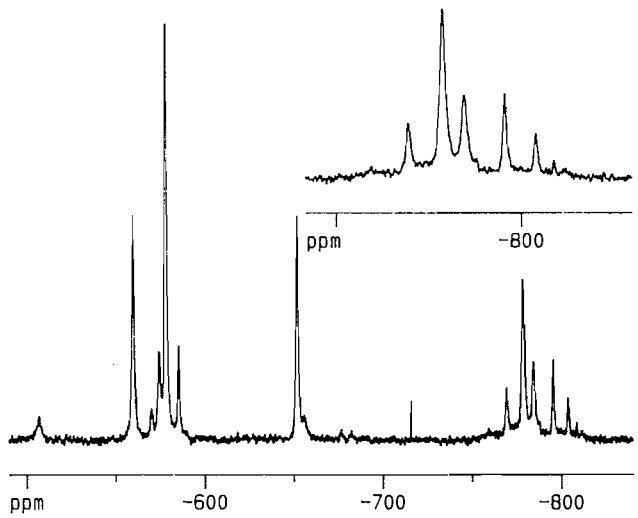
The crystalline material is very hard and, despite the zwitterionic character of the complex, is virtually insoluble in water and dipolar aprotic solvents such as dimethyl sulfoxide and dimethylformamide. This insolubility, presumably, is a consequence of the extensive hydrogen-bonded network within the crystalline structure that makes dissolution thermodynamically unfavourable. Despite this inability to do dissolution studies, it seems very likely that the solution products have a coordination similar to that of the crystalline material. GlyGlyOEt and GlyGlyGly both give three products with a product distribution and ^{51}V chemical shifts virtually indistinguishable from those of the glycylglycine products. This clearly shows that the terminal carboxylate group is not required for the complex to form, as would be predicted from the crystal structure. There is no indication of any complex formation that cannot be assigned to the above possibility. The formation of the three solution complexes can then be accounted for quite simply from the structure of the solid. One product, probably the major one, can be assigned a structure similar to that found in the crystalline material where a *cis* arrangement, with the two oxygens of the two hydroxamide ligands in close proximity, is found. The other two crystal structures of hydroxylamine-derived complexes (footnote 4 and ref. 41) show the same arrangement, relative to each other, as the two hydroxylamine ligands in the complex here. This may suggest that there is an underlying principle giving rise to this preference for this orientation of the two ligands, perhaps steric but more likely electronic in origin. In some cases where heteroligands are also complexed (50), the two nitrogens, rather than the oxygens, are in close proximity to each other. The second product could correspond to the situation where both hydroxamido groups have undergone an end-to-end rotation so that the hydroxamido ligands are in the alternate *cis* orientation to one another. End-to-end isomerization has been shown to occur quite quickly in bis(dimethylhydroxamido)hydroxooxovanadate.[4] The third product would then correspond to the *trans* orientation where only one ligand has rotated. Although this offers a plausible explanation for the occurrence of three products, there are other possibilities that could include, for instance, a 180° rotation of the GlyGly ligand or a change in coordination.

The reaction of *N*-methylhydroxamidovanadate with gly-

© 1997 NRC Canada

Can. J. Chem. Downloaded from www.nrcresearchpress.com by 92.62.229.171 on 09/08/12
For personal use only.

Fig. 5. ^{51}V NMR spectrum showing the products formed in the equilibration of glycylglycine in the methylhydroxylamine–vanadate system. The signals near −652 ppm are from mono(*N*-methylhydroxamido)vanadate complexes, those in the range −760 to −820 ppm from bis(*N*-methylhydroxamido)GlyGly complexes. The signal at −505 ppm is from a glycylglycinatovanadate complex (52) while those near −570 ppm are from V_1, V-ONH_2, V_2, V_4, and V_5, respectively, from low to high field strength. Conditions of the experiments: 3 mM vanadate; 4 mM methylhydroxylamine; 20 mM glycylglycine; pH 7.5.



cylglycine follows closely the pattern of the non-methylated complex. Of some interest is the observation that a minimum of six product signals are observable in the vanadium NMR spectrum (Fig. 5). The observation of more than three signals shows that methyl group isomerization is quite slow, less than about 100 s^{-1}, as estimated from the chemical shift separations between signals. In principle, nine product signals might have been expected, three for each of the possible *cis* or *trans* N-O orientations. However, some signals may well be hidden under others or, as judged from Fig. 1, may simply be of an intensity too low to observe under the conditions of the experiments. It is unlikely that methyl group reorientation is stopped and it would be of interest to ascertain from kinetics experiments whether there is coupling between the end-for-end isomerization of the hydroxamido group and methyl reorientation.

The mode of complexation observed here, for the glycylglycinato ligand, involving the amine nitrogen and the carbonyl oxygen, is very different from that in the peroxovanadate system where the preferred product contains only one peroxo group and glycylglycine is complexed in a tridentate fashion through the terminal H_2N-, the terminal -CO_2^-, and the amide nitrogen, which is deprotonated in the complex (18, 38–40). This latter mode of coordination of a peptide is also found in oxovanadium(V) complexes (51, 52). Of course, bidentate complexation in the bisperoxovanadate system is well known (47, 48, 53), for instance with picolinic acid (47, 54) or oxalic acid (48, 55, 56). The differences in the chemistry toward additional ligands observed for the bishydroxamido complexes compared to the bisperoxo complexes will find its origin in the influence that the primary ligands have on the ability of the vanadium centre to accept electrons from the hetero-ligand and it may be that, with suitable ligands, similar products will be formed with bisperoxovanadate.

The coordination of dipeptides by vanadate found here by aqueous solution studies and established by the crystal structure analysis, coupled with the possibility of participation by side chains, opens up a potentially new means of complexation of vanadate by proteins. The functional groups on side chains such as those in serine, histidine, or lysine in conjunction with a peptide carbonyl oxygen provide the groups through which complexation could occur. Folding of a protein to bring the groups into an appropriate juxtaposition, as in the active site of an enzyme, certainly provides for the possibility of this mode of complex formation and it cannot be ignored.

Acknowledgements

Thanks are gratefully extended to the Natural Sciences and Engineering Research Council of Canada for its financial support of this work in the form of an operating grant to A.S.T.

References

1. E. de Boer, Y. van Kooyk, M.G.M. Tromp, H. Plat, and R. Wever. Biochim. Biophys. Acta, **869**, 48 (1986).
2. H. Plat, B.E. Krenn, and R. Wever. Biochem. J. **248**, 277 (1987).
3. E.G.M. Vollenbroek, L.H. Simons, J.W.P.M. Schijndel, P. Barnett, M. Balzar, H. Dekker, C. van der Linden, and R. Wever. Biochem. Soc. Trans. **23**, 267 (1995).
4. A. Messershmidt and R. Wever. Proc. Natl. Acad. Sci. U.S.A. **93**, 392 (1996).
5. R. Wever and B.E. Krenn. *In* Vanadium in biological systems. *Edited by* N.D. Chasteen. Kluwer Academic Publishers, Dordrecht, Boston, London. 1990. pp. 81–97.
6. H. Vilter. Met. Ions Biol. Syst. **31**, 325 (1995).
7. R.E. Eady. Tetrahedron, **8**, 1695 (1989).
8. R.L. Robson, R.E. Eady, T.H. Richardson, R.W. Miller, M. Hawkins, and J.R. Postgate. Nature, **322**, 388 (1986).
9. B.J. Hales, E.E. Case, J.E. Morningstar, M.F. Dzeda, and L.A. Mauterer. Biochemistry, **25**, 7251 (1986).
10. A.T. Harrison and O.W. Howarth. J. Chem. Soc. Dalton Trans. 1173 (1985).
11. O.W. Howarth and J.R. Hunt. J. Chem. Soc. Dalton Trans. 1388 (1979).
12. J.S. Jaswal and A.S. Tracey. Inorg. Chem. **30**, 3718 (1991).
13. S. Ramanadham, C. Heyliger, M.J. Gresser, A.S. Tracey, and J.H. McNeill. Biol. Trace Elem. Res. **30**, 119 (1991).
14. P. Schwendt. Proc. 13th Conf. Coord. Chem. 243 (1991).
15. N.J. Campbell, A.C. Dengel, and W.P. Griffith. Polyhedron, **8**, 1379 (1989).
16. A. Butler, M.J. Clague, and G.E. Meister. Chem. Rev. **94**, 625 (1994).
17. A.S. Tracey and J.S. Jaswal. Inorg. Chem. **32**, 4235 (1993).
18. A.S. Tracey and J.S. Jaswal. J. Am. Chem. Soc. **114**, 3835 (1992).
19. M. Bhattacharjee, M.K. Chaudhuri, N.S. Islam, and P.C. Paul. Inorg. Chim. Acta, **169**, 97 (1990).
20. M.J. Clague and A. Butler. J. Am. Chem. Soc. **117**, 3475 (1995).
21. M. Bonchio, V. Conte, F. Di Furia, G. Modena, S. Moro, and J.O. Edwards. Inorg. Chem. **33**, 1631 (1994).
22. A. Butler. *In* Vanadium in biological systems. *Edited by* N.D. Chasteen. Kluwer Academic Publishers, Dordrecht, Boston, London. 1990. pp. 25–49.
23. A.F. Ghiron and R.C. Thompson. Inorg. Chem. **29**, 4457 (1990).

© 1997 NRC Canada

Can. J. Chem. Downloaded from www.nrcresearchpress.com by 92.62.229.171 on 09/08/12
For personal use only.

24. B. Leighton, G.J.S. Cooper, C. DaCosta, and E.A. Foot. Biochem. J. **276**, 289 (1991).
25. D. Heffetz, I. Bushkin, R. Dror, and Y. Zick. J. Biol. Chem. **265**, 2896 (1990).
26. B.I. Posner, R. Faure, J.W. Burgess, A.P. Bevan, D. Lachance, G. Zhang-Sun, I.G. Fantus, J.B. Ng, D.A. Hall, B. Soo Lum, and A. Shaver. J. Biol. Chem. **269**, 4596 (1994).
27. S. Kadota, I.G. Fantus, G. Deragon, H.J. Guyda, B. Hersh, and B.I. Posner. Biochem. Biophys. Res. Commun. **147**, 259 (1987).
28. P.J. Stankiewicz and A.S. Tracey. Met. Ions Biol. Syst. **31**, 259 (1995).
29. P. J. Stankiewicz, A.S. Tracey, and D.C. Crans. Met. Ions Biol. Syst. **31**, 287 (1995).
30. A.C.T. North, D.C. Phillips, and F.S. Mathews. Angew. Chem. Int. Ed. Engl. **24**, 351 (1968).
31. H. Flack. Acta Crystallogr. Sect. A: Found Crystallogr. **A39**, 876 (1983).
32. V. Shomaker and K.N. Trueblood. Acta Crystallogr. Sect. B: Struct. Crystallogr. Cryst. Chem. **B24**, 63 (1968).
33. E.J. Gabe, P.S. White, and G.D. Enright. *In* DIFRAC: a Fortran 77 control routine for 4-circle diffractometers. National Research Council, Ottawa. 1995.
34. E.J. Gabe, Y. LePage, J.-P. Charland, F.L. Lee, and P.S. White. J. Appl. Crystallogr. **22**, 384 (1989).
35. D.J. Watkin, J.R. Carruthers, and P.W. Betteridge. *In* CRYSTALS. Chemical Crystallography Laboratory, University of Oxford, Oxford, England. 1984.
36. International tables for X-ray crystallography. IV. Kynoch Press, Birmingham. 1975. p. 99.
37. O.W. Howarth. Prog. Nucl. Magn. Reson. Spectrosc. **22**, 453 (1990).
38. J.S. Jaswal and A.S. Tracey. J. Am. Chem. Soc. **115**, 5600 (1993).
39. D. Rehder and K. Wieghardt. Z. Naturforsch. B: Anorg. Chem. Org. Chem. **36B**, 1251 (1981).
40. F.W.B. Einstein, R.J. Batchelor, S.J. Angus-Dunne, and A.S. Tracey. Inorg. Chem. **35**, 1680 (1996).
41. L. Saussine, H. Mimoun, A. Mitschler, and J. Fisher. Nouv. J. Chim. **4**, 235 (1980).
42. A. Shaver, J.B. Ng, D.A. Hall, B. Soo Lum, and B.I. Posner. Inorg. Chem. **32**, 3109 (1993).
43. D. Begin, F.W.B. Einstein, and J. Field. Inorg. Chem. **14**, 1785 (1975).
44. H. Szentivanyi and R. Stomberg. Acta Chem. Scand. Ser. A: **A37**, 709 (1983).
45. R. Stomberg. Acta Chem. Scand. Ser. A: **A39**, 725 (1985).
46. R. Stomberg, S. Olson, and I.-B. Svensson. Acta Chem. Scand. Ser. A: **A38**, 653 (1984).
47. R.E. Drew and F.W.B. Einstein. Inorg. Chem. **11**, 1079 (1972).
48. R. Stomberg and S. Olson. Acta Chem. Scand. Ser. A: **A38**, 801 (1984).
49. R. Stomberg. Acta Chem. Scand. Ser. A: **A38**, 541 (1984).
50. M. Shao, J. Leng, and Z. Pan. Wuji Huaxue Xuebao, **6**, 443 (1990).
51. D. Rehder. Inorg. Chem. **27**, 4312 (1988).
52. J.S. Jaswal and A.S. Tracey. Can. J. Chem. **69**, 1600 (1991).
53. C.E. Holloway and M. Melnik. Rev. Inorg. Chem. **7**, 75 (1985).
54. B. Galeffi and A.S. Tracey. Inorg. Chem. **28**, 1726 (1989).
55. P.M. Ehde, L. Pettersson, and J. Glaser. Acta Chem. Scand. **45**, 998 (1991).
56. A.S. Tracey, M.J. Gresser, and K.M. Parkinson. Inorg. Chem. **26**, 629 (1987).

Can. J. Chem. Downloaded from www.nrcresearchpress.com by 92.62.229.171 on 09/08/12
For personal use only.

© 1997 NRC Canada

Three-dimensional electron delocalization: a theoretical study based on the pentacyclo[3.3.1.1^{3,7}.0^{1,3}.0^{5,7}]decane system

Mary S.W. Chan and Donald R. Arnold

Abstract: The concept of electron delocalization, and the possibility of aromaticity in three dimensions has been introduced, but remains relatively unexplored. This work examines the structure and energy of a series of ions generated from pentacyclo[3.3.1.1^{3,7}.0^{1,3}.0^{5,7}]decane (**1**). The ions considered are the dication (**1**$^{2+}$), the radical cation (**1**$^{+\bullet}$), the radical anion (**1**$^{-\bullet}$), and the dianion (**1**$^{2-}$). The dication belongs to a small group of organic compounds that shows three-dimensional electron delocalization and it has been classified as "three-dimensionally homoaromatic." The relative stability of these ions is estimated by the enthalpy change of isodesmic and disproportionation reactions using energies obtained from HF, MP2, and DFT methods. The structural changes and the reorganization of the frontier orbitals when electrons are successively added to or removed from the neutral molecule (**1**) are also explored. The results confirm the three-dimensional electron delocalization in **1**$^{2+}$ and indicate that it is stable relative to a localized structure with similar features; however, it is highly unstable compared to the radical cation (**1**$^{+\bullet}$). The dianion (**1**$^{2-}$), on the other hand, did not show any evidence for electron delocalization and it is unstable relative to the radical anion (**1**$^{-\bullet}$).

Key words: three-dimensional aromaticity, electron delocalization, resonance, radical cations, radical anions.

Résumé : Le concept de la délocalisation des électrons et la possibilité d'aromaticité en trois dimensions a été proposé, mais ils n'ont pratiquement pas été explorés. Dans ce travail, on examine la structure et l'énergie d'une série d'ions générés à partir du pentacyclo[3.3.1.1^{3,7}.0^{1,3}.0^{5,7}]décane (**1**). Les cations considérés sont le dication (**1**$^{2+}$), le cation radical (**1**$^{+\bullet}$), l'anion radical (**1**$^{-\bullet}$), et le dianion (**1**$^{2-}$). Le dication appartient à un petit groupe de composés organiques qui présentent de la délocalisation électronique en trois dimensions et il a été classifé comme « tridimensionnellement homoaromatique ». On a évalué les stabilités relatives de ces ions par le biais des changements d'enthalpie des réactions isodesmiques et de dismutation en faisant appel aux énergies obtenues à l'aide des méthodes « HF », « MP2 » et « DFT ». On a aussi examiné les changements structuraux et la réorganisation des orbitales frontières résultant quand les électrons sont ajoutés ou enlevés successivement de la molécule neutre (**1**). Les résultats obtenus confirment la délocalisation tridimensionnelle des électrons dans l'espèce **1**$^{2+}$ et ils indiquent qu'elle est stable par rapport à une structure localisée comportant des caractéristiques semblables; toutefois, elle est hautement instable comparée au cation radical (**1**$^{+\bullet}$). Par ailleurs, aucune donnée suggère que le dianion (**1**$^{2-}$) présente de la délocalisation électronique et il est instable par rapport à l'anion radical (**1**$^{-\bullet}$).

Mots clés : aromaticité tridimensionnelle, délocalisation d'électrons, résonance, cations radicaux, anions radicaux.

[Traduit par la rédaction]

Introduction

Kekulé marked the beginning of a new era in organic chemistry in 1865 by referring to benzene and its derivatives as aromatic (1). The parent compound, benzene, has been considered the archetypical example of this class of compounds ever since. In the intervening years, aromaticity has become a vital concept in our understanding of organic chemistry because of the role it plays in explaining molecular structure, stability, and reactivity. Although the term "aromatic" now refers to a wider variety of structures, generally associated with enhanced stability and low reactivity, most of these examples are still two-dimensional, i.e., planar molecules. In fact, planarity was originally stated to be one of the requirements for aromaticity (for a general discussion of aromaticity see ref. 2)! The concept of electron delocalization, and therefore the possibility of aromaticity, in three dimensions remains relatively unexplored. However, this concept is becoming increasingly important because of the need for more sophisticated models to describe the bonding topology in unusual molecules like corannulene, buckminsterfullerene, and [5.5.5]trefoilene (3–5).

Three-dimensional electron delocalization in a polyhedral structure occurs in a variety of ways, and a number of theories have been developed for electron-counting rules to describe their bonding arrangements (6). This work is focused on electron delocalization in a volume contained by a polyhedron

Received September 4, 1996.

This manuscript is dedicated to Marshall D. Gates, my (D.R.A.) former mentor, on the occasion of his 81st birthday (September 25, 1915).

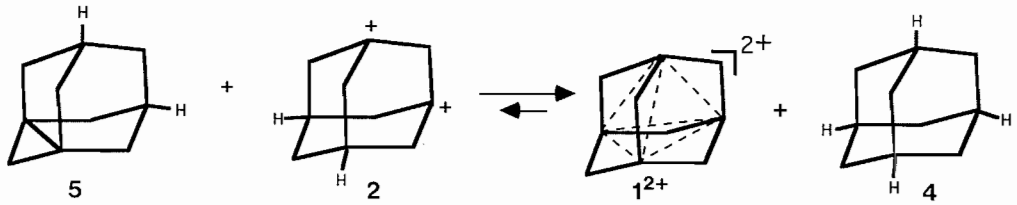
M.S.W. Chan and D.R. Arnold.[1] Department of Chemistry, Dalhousie University, Halifax, NS B3H 4J3, Canada.

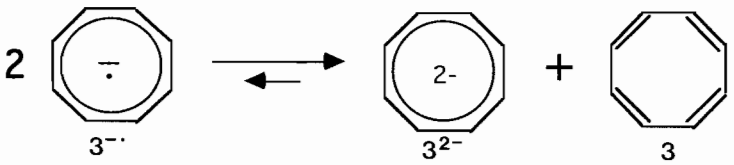
[1] Author to whom correspondence may be addressed. Telephone: (902) 494-3714. Fax: (902) 494-1310. E-mail: arnold@ac.dal.ca

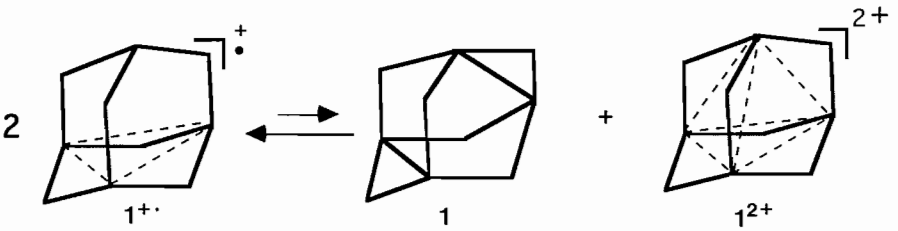
© 1997 NRC Canada

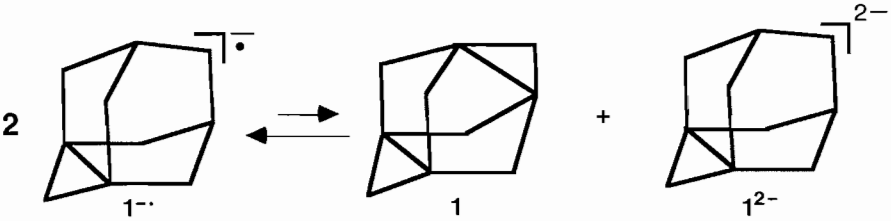
Can. J. Chem. Downloaded from www.nrcresearchpress.com by 92.62.229.171 on 09/08/12
For personal use only.

Can. J. Chem. Downloaded from www.nrcresearchpress.com by 92.62.229.171 on 09/08/12
For personal use only.

[1] 

[2] 

[3] 

[4] 

resulting from the mutual overlap of orbitals pointing towards the center of the structure. Electron delocalization of this type was first recognized in boron cage compounds with the general formulae $B_nH_n^{2-}$ ($6 \leq n \leq 12$) and $C_2B_{n-2}H_n$ ($5 \leq n \leq 12$). A number of theoretical models have been developed to explain the bonding in these electron-deficient clusters (7). A similar type of electron delocalization can be found in pyramidal cations (8). Three-dimensional electron delocalization in a hydrocarbon $(CH)_5^+$ was first suggested by Williams from analogy to the square pyramidal (D_{4d}) skeleton of pentaborane (9). This idea was further developed by Stohrer and Hoffman using molecular orbital calculations (10). Theoretical and experimental evidence for this square pyramidal cation intermediate has been presented for numerous substituted systems (11), even though the parent cation has now been shown to prefer a vinyl cyclopropene structure (12). A $4n + 2$ interstitial electron rule has been introduced to predict electron delocalization in these pyramidal (organic and inorganic) molecules (13).

A beautiful example of three-dimensional electron delocalization in a purely organic compound is Schleyer's dication: 1,3,5,7-tetradehydrotricyclo[3.3.1.1^{3,7}]decandiylium ($\mathbf{1}^{2+}$) (14). This dication adopts T_d symmetry with the four bridgehead carbon atoms forming the vertices of a tetrahedron. These atoms are strategically positioned such that one valence orbital from each atom points directly toward the center of the adamantyl cage. The in-phase combination of this set of atomic orbitals provides a bonding molecular orbital and, with the population of two electrons, this molecular orbital is a rare example of a four-center–two-electron bond. The structure of this dication has been confirmed by NMR spectroscopy and theoretical calculations (14, 15). The stability associated with this structure has also been demonstrated (14, 16). In particular, Schleyer chose to compare $\mathbf{1}^{2+}$ ($C_{10}H_{12}$) with tricyclo[3.3.1.1^{3,7}]decan-1,3-diylium (**2**) ($C_{10}H_{14}$), taking the enthalpy change of the isodesmic reaction [1] ($\Delta H = -197$ kJ/mol, MINDO/3) to be a measure of the stability for $\mathbf{1}^{2+}$. Schleyer classified $\mathbf{1}^{2+}$ as "three-dimensionally homoaromatic" based on these structural features and the enhanced stability estimated by reaction [1].

The structural features of a planar, cyclic, conjugated system are dictated in part by the number of π-electrons. Hückel molecular orbital theory demonstrated that for n-membered (n is an integer) monocyclic conjugated systems with D_{nh} symmetry, all π molecular orbitals are doubly degenerate except for the lowest bonding orbital and the highest anti-bonding orbital if n is even. If n is odd, all but the lowest bonding orbital are doubly degenerate. The degeneracy of these molecular orbitals leads to the well-known Hückel $4n + 2$ π-electron rule for predicting aromaticity in two dimensions (17).

The consequence of this rule is illustrated by the 1,3,5,7-cyclooctatetraene system. The neutral molecule **3** contains eight π-electrons and is an unstable open-shell system in the D_{8h} point group because of the degeneracy of the molecular

© 1997 NRC Canada

Can. J. Chem. Downloaded from www.nrcresearchpress.com by 92.62.229.171 on 09/08/12
For personal use only.

orbitals. This molecule, therefore, distorts from planarity to a D_{2d} tub-shaped structure (18). The double bonds are localized and behave chemically as isolated unconjugated double bonds (19). However, if two electrons are removed, the dication ($\mathbf{3}^{2+}$) becomes a six π-electron system. According to the Hückel $4n + 2$ rule, this is the correct number of electrons to achieve a stable closed-shell configuration and the molecule becomes planar to achieve maximum π-orbital overlap for electron delocalization. Ab initio molecular orbital calculations have demonstrated the planar (D_{8h}) structure and enhanced stability of this dication (20). Although the dication of the parent compound is not known, experimental evidence for methyl-substituted systems has been reported. The chemical shifts from both ^{1}H and ^{13}C NMR spectroscopy confirm the coplanarity of the eight ring carbon atoms in the dications of 1,4-dimethyl and 1,3,5,7-tetramethyl-cyclooctatetraene (21). The dianion ($\mathbf{3}^{2-}$), obtained from adding two electrons to **3**, also has the right number of electrons to attain a closed-shell configuration in the D_{8h} point group. Semiempirical calculations found the structure $\mathbf{3}^{2-}$ to have equal carbon–carbon bond lengths and bond orders (22). Experimentally, $\mathbf{3}^{2-}$ can be readily produced by alkali metal reduction; both X-ray diffraction and NMR studies have confirmed it to be a planar (D_{8h}) aromatic species (23).

The enhanced stability associated with aromaticity has historically been related to resonance energies. A variety of methods based on this concept have been introduced. For all methods used, both $\mathbf{3}^{2+}$ and $\mathbf{3}^{2-}$ have more than two-thirds of the aromatic stability of benzene (24). Another method is to measure the thermodynamic stability from equilibrium constants. The classical illustration of the stability of the aromatic doubly charged anion in the cyclooctatetraene system is the disproportionation of the radical anion (reaction [2]). Experimental evidence showed that this equilibrium constant is dependent on the solvent and the counterion. The values range from 2×10^0 ($\Delta G = -1.7$ kJ/mol) in ammonia, with lithium as the counterion, to 3×10^8 ($\Delta G = -47.8$ kJ/mol) in tetrahydrofuran, with potassium as the counterion (25). Both $\mathbf{3}^{2+}$ and $\mathbf{3}^{2-}$ are considered to be aromatic because of these structural features and enhanced stability.

The behavior of the cyclooctatetraene system provides an interesting two-dimensional model for the study of aromaticity in three dimensions. For example, can such systems be expected to behave the same as two-dimensional aromatic systems and is there an analogy between Schleyer's dication and the cyclooctatetraene dication? The addition of two electrons to $\mathbf{1}^{2+}$ leads to a neutral species whose Lewis structure can be represented by pentacyclo[3.3.1.1^{3,7}.0^{1,3}.0^{5,7}]decane (**1**). Ab initio and density function theory (DFT) molecular orbital calculations were employed to determine the geometry and energy of the species necessary for a study analogous to the cyclooctatetraene system in the pentacyclo[3.3.1.1^{3,7}.0^{1,3}.0^{5,7}] decane system: $\mathbf{1}^{2+}$, $\mathbf{1}^{+\cdot}$, **1**, $\mathbf{1}^{-\cdot}$, $\mathbf{1}^{2-}$. To determine the stability of the doubly charged ions, the energies obtained from these calculations were used to estimate the enthalpy change for the disproportionation reaction of the radical cation ($\mathbf{1}^{+\cdot}$) (reaction [3]) and the radical anion ($\mathbf{1}^{-\cdot}$) (reaction [4]).

Computational details

The Gaussian 92 package of programs was employed for all ab initio molecular orbital calculations and the Gaussian 94 package was employed for DFT calculations (26, 27). The geometry of the closed-shell systems was fully optimized at the restricted Hartree–Fock level with the 6-31G* basis set (6-31+G* for anions).[2] The neutral molecule (**1**) was optimized using both basis sets. The Hartree–Fock geometry then served as a starting point for optimization using Becke's three-parameter exchange function with Predew and Wang's 1991 gradient-corrected correlation (B3PW91) (29, 30). The structures of the open-shell systems were obtained in the same manner using the unrestricted formalism. All of the structures were optimized using the Berny optimization procedure (31) without symmetry constraints and were confirmed, by harmonic frequency analysis, to be local minima on their respective potential energy surfaces. Single-point energies were calculated to second order in Møller–Plesset perturbation theory (MP2) using the 6-31G* basis set (6-31+G* for anions) at the HF/6-31G* (HF/6-31+G* for anions) optimized geometries, and were corrected for spin contamination where necessary (32). The charge and spin density distributions were obtained from Mulliken and natural population analyses (33, 34).

Results

It has been emphasized that higher levels of theory are required to accurately predict the structure and energy of nonclassical cations (35). Therefore we recalculated the enthalpy change of reaction [1] using ab initio molecular orbital theory up to the HF/6-31G* level. Geometry optimization of tricyclo[3.3.1.1^{3,7}]decane (**4**), commonly known as adamantane, gave the expected highly symmetric T_d structure. Both **2** and tetracyclo[3.3.1.1^{3,7}.0^{5,7}]decane (**5**) gave C_{2v} structures.

A pictorial representation of the B3PW91/6-31G* (B3PW91/6-31+G* for anions) fully optimized structures of the five species in the pentacyclo[3.3.1.1^{3,7}.0^{1,3}.0^{5,7}]decane system are shown in Figs. 1–5. Selected geometrical parameters can be found in Tables 1–5. The DFT optimizations were performed to include electron correlation in the optimization procedure. Conventional MP2 optimization was not possible for the anions due to the large memory requirements of this method. The MP2 optimized geometry of $\mathbf{1}^{+\cdot}$ is reported along with the DFT geometry in Table 2. The B3PW91 optimized geometry is very similar to the MP2 geometry with an average difference of 0.007 Å for bond lengths, 0.3° for bond angles, and 0.4° for dihedral angles. This is consistent with results obtained from other research groups (36).

Where appropriate, the charge and spin density distributions obtained from Mulliken and natural population analysis for these species are listed in Table 6. The two methods are generally within good agreement for the spin density of the two radical species $\mathbf{1}^{+\cdot}$ and $\mathbf{1}^{-\cdot}$. However, there are large discrepancies in their charge assignment. One of the limitations of Mulliken population analysis is evident in its charge assignment of the anions. It shows a tendency to place large positive charge density on the bridgehead carbon atoms with large negative charge density on the methylene groups to compensate.

[2] For a general discussion of theoretical methods and basis sets see ref. 28.

© 1997 NRC Canada

Can. J. Chem. Downloaded from www.nrcresearchpress.com by 92.62.229.171 on 09/08/12
For personal use only.

Fig. 1. B3PW91/6-31G* optimized structure of $\mathbf{1}^{2+}$.

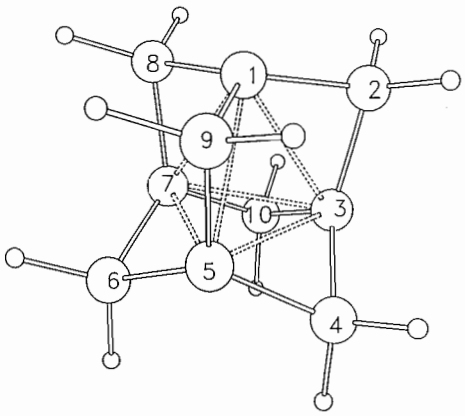


Fig. 2. B3PW91/6-31G* optimized structure of $\mathbf{1}^{+\cdot}$.

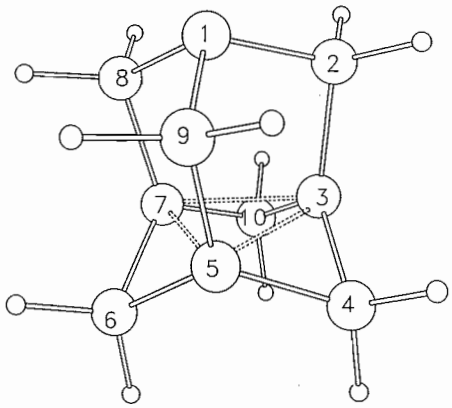
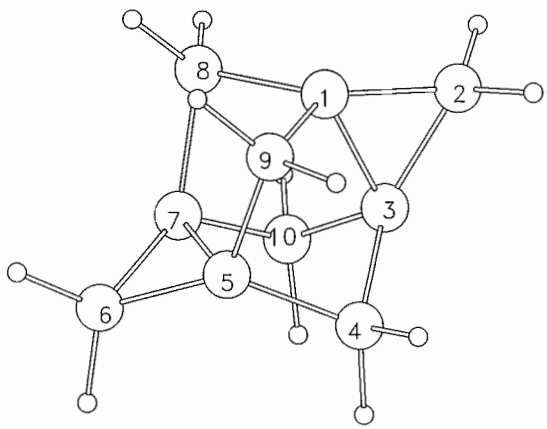


Fig. 3. B3PW91/6-31G* optimized structure of **1**.



This charge separation is not observed in natural population analysis where the bridgehead carbon atoms carry more negative charge than the methylene groups. In general, the results obtained from natural population analysis are more consistent with the structures suggested by the optimized geometries, in agreement with previously reported results (37). A graphical representation of the frontier molecular orbitals of the closed-shell species for the pentacyclo[3.3.1.1^{3,7}.0^{1,3}.0^{5,7}]decane system is shown in Fig. 6.

Fig. 4. B3PW91/6-31+G* optimized structure of $\mathbf{1}^{-\cdot}$.

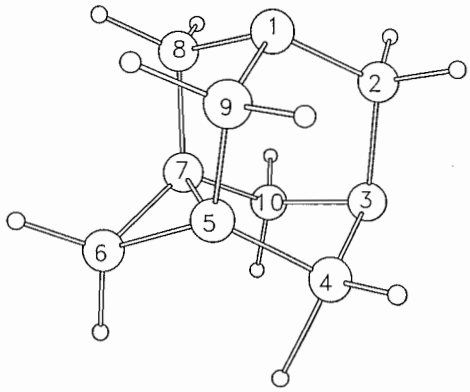
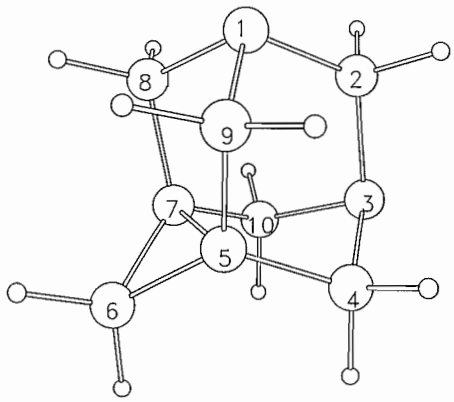


Fig. 5. B3PW91/6-31+G* optimized structure of $\mathbf{1}^{2-}$.



Geometry optimization of **1** produced a D_{2d} structure with completely localized σ-bonds. This fully optimized structure was used as the starting point for geometry optimizations of all ions in this series. Geometry optimization of $\mathbf{1}^{2+}$ using this procedure reproduced the T_d structure reported by Schleyer and co-workers (14). The structure of the radical cation $\mathbf{1}^{+\cdot}$, obtained in this manner, can be described as a C_{3v} distonic radical cation (38). The charge and spin distribution from both population analyses showed that the spin is located on C_1, whereas most of the charge is delocalized over the cyclohexyl moiety. The total overlap population between the remaining three bridgehead atoms in $\mathbf{1}^{+\cdot}$ is stronger than that in $\mathbf{1}^{2+}$, justifying the dotted-line representation shown in Fig. 2. The structure of the radical anion $\mathbf{1}^{-\cdot}$, shown in Fig. 4, does not show spin and charge separation. The spin density is concentrated on two bridgehead carbon atoms (C_1 and C_3). The same two atoms carry one-half of the negative charge, with the rest delocalized over the remaining bridgehead carbon atoms. Unlike the radical cation, the charge is not symmetrically distributed; C_1 and C_3 carry significantly more of the negative charge than the other two bridgehead carbon atoms (C_5 and C_7). As a result, the C_5—C_7 bond remains intact, distorting the structure to C_{2v} symmetry. The optimized structure of $\mathbf{1}^{2-}$ also belongs to the C_{2v} point group. It is similar to the structure of $\mathbf{1}^{-\cdot}$ in that the bond between C_1 and C_3 is broken while the bond between C_5 and C_7 remains. In fact, this bond (C_5—C_7)

© 1997 NRC Canada

Fig. 6. Frontier molecular orbital of the dication ($\mathbf{1}^{2+}$), the neutral molecule (**1**), and the dianion ($\mathbf{1}^{2-}$).

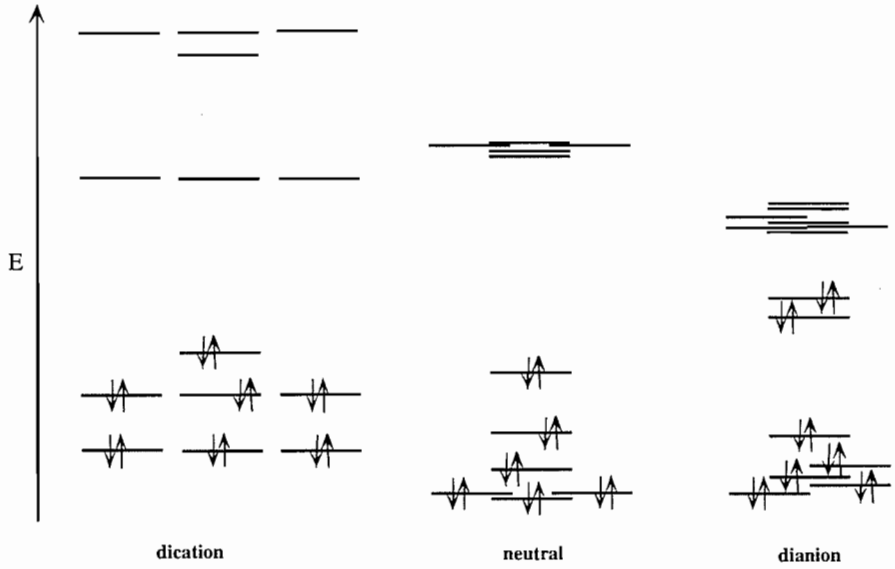


Table 1. Geometrical parameters for the B3PW91/6-31G* optimized structure of $\mathbf{1}^{2+}$.

Interatomic distance (Å)		Angles (deg)		Dihedral angles (deg)	
C_1C_2	1.505	$C_1C_2C_3$	87.1	$C_2C_1C_3C_4$	119.7
C_1C_3	2.074	$C_1C_3C_5$	60.0	$C_3C_4C_5C_6$	75.9
		$C_2C_3C_4$	117.9	$C_3C_4C_5C_7$	30.5
		$C_2C_3C_5$	99.6	$C_8C_1C_3C_4$	−120.7
				$C_9C_1C_3C_4$	0.0

Table 2. Geometrical parameters for the B3PW91/6-31G* and MP2/6-31G* optimized structure of $\mathbf{1}^{+\cdot}$.

Interatomic distance (Å)			Angles (deg)			Dihedral angles (deg)		
	MP2	B3PW91		MP2	B3PW91		MP2	B3PW91
C_1C_2	1.529	1.529	$C_1C_2C_3$	100.2	99.7	$C_1C_2C_3C_4$	−79.2	−80.1
C_1C_3	2.336	2.332	$C_1C_3C_5$	65.4	65.6	$C_2C_3C_5C_6$	122.7	123.1
C_2C_3	1.516	1.521	$C_2C_3C_4$	119.0	119.1	$C_3C_4C_5C_6$	81.2	82.0
C_3C_4	1.495	1.495	$C_2C_1C_8$	107.3	107.3	$C_3C_4C_5C_7$	31.1	31.1
C_3C_5	1.947	1.925	$C_3C_4C_5$	81.3	80.1	$C_4C_3C_5C_6$	−11.3	−117.3
			$C_3C_5C_7$	60.0	60.0	$C_{10}C_3C_5C_6$	0.0	0.0

Table 3. Geometrical parameters for the B3PW91/6-31+G* optimized structure of **1**.

Interatomic distance (Å)		Angles (deg)		Dihedral angles (deg)	
C_1C_2	1.504	$C_1C_2C_3$	64.5	$C_2C_1C_3C_4$	129.6
C_1C_3	1.604	$C_1C_3C_2$	57.8	$C_3C_4C_5C_6$	97.5
C_3C_4	1.545	$C_1C_3C_4$	103.3	$C_8C_1C_3C_4$	−100.7
		$C_2C_3C_4$	130.4	$C_9C_1C_3C_4$	0.0
		$C_3C_4C_5$	92.3		
		$C_4C_3C_{10}$	97.1		

Can. J. Chem. Downloaded from www.nrcresearchpress.com by 92.62.229.171 on 09/08/12
For personal use only.

© 1997 NRC Canada

Can. J. Chem. Downloaded from www.nrcresearchpress.com by 92.62.229.171 on 09/08/12
For personal use only.

Table 4. Geometrical parameters for the B3PW91/6-31+G* optimized structure of $\mathbf{1}^{-\cdot}$.

Interatomic distance (Å)		Angles (deg)		Dihedral angles (deg)	
C_1C_2	1.561	$C_1C_2C_3$	112.2	$C_1C_2C_3C_4$	−53.5
C_1C_3	2.592	$C_2C_3C_4$	110.1	$C_1C_9C_5C_4$	78.1
C_3C_5	2.361	$C_4C_3C_{10}$	98.0	$C_3C_4C_5C_6$	95.5
C_3C_4	1.533	$C_4C_5C_6$	125.4	$C_6C_7C_5C_4$	122.9
C_4C_5	1.547	$C_4C_5C_9$	108.8	$C_8C_7C_5C_4$	−114.3
C_5C_6	1.509	$C_5C_6C_7$	61.3	$C_9C_5C_7C_8$	0.0
C_5C_7	1.539				

Table 5. Geometrical parameters for the B3PW91/6-31+G* optimized structure of $\mathbf{1}^{2-}$.

Interatomic distance (Å)		Angles (deg)		Dihedral angles (deg)	
C_1C_2	1.582	$C_1C_2C_3$	119.3	$C_1C_2C_3C_4$	−51.3
C_1C_3	2.731	$C_2C_3C_4$	106.4	$C_1C_9C_5C_4$	79.1
C_3C_5	2.390	$C_4C_3C_{10}$	96.9	$C_3C_4C_5C_6$	95.2
C_3C_4	1.540	$C_4C_5C_6$	124.4	$C_4C_5C_7C_8$	−116.6
C_4C_5	1.548	$C_4C_5C_9$	111.0	$C_6C_5C_7C_8$	121.7
C_5C_6	1.502	$C_5C_6C_7$	61.5	$C_9C_5C_7C_8$	0.0
C_5C_7	1.536				

Table 6. Charge and spin density distributions from Mulliken and natural poplulation analysis.

	$\mathbf{1}^{2+}$		$\mathbf{1}^{+\cdot}$				$\mathbf{1}^{-\cdot}$				$\mathbf{1}^{2-}$	
	Charge[a]		Charge[a]		Spin[a]		Charge[a]		Spin[a]		Charge[a]	
Atom number	Mulliken	Natural	Mulliken	Natural	Mulliken	Natural	Mulliken	Natural	Mulliken	Natural	Mulliken	Natural
1	0.06	0.28	0.08	0.16	0.95	0.91	0.31	−0.24	0.64	0.48	1.78	−0.49
2	0.30	0.15	0.11	0.02	−0.04	−0.02	−0.28	−0.09	−0.03	−0.02	−1.87	−0.15
3			0.03	0.16	0.05	0.05						
4			0.17	0.10	0.01	0.01	−0.40	−0.05	−0.09	−0.01	−0.84	−0.11
5							0.31	−0.11	0.04	0.04	−0.09	−0.13
6							0.31	0.01	0.04	−0.01	−0.17	−0.16

[a]All charge and spin density of the directly bonded hydrogen atoms are summed into the carbon atom.

is shorter than the corresponding bond in the neutral molecule (**1**).

The enthalpy changes (ΔH) of reactions [1], [3], and [4], calculated at various theoretical levels, are shown in Table 7. The ΔH values reported are estimated by taking the difference between the self-consistent field (SCF) energy of the products and reactants. The rotational, translational, and vibrational (including zero point) energies are not large enough to make a significant difference. The total of these components contributes less than 0.4% to ΔH at the HF/6-31G* level. Ab initio molecular orbital calculations predict reaction [1] to be exothermic, consistent with the MINDO results, although smaller in magnitude. The enthalpy change is positive for the disproportionation of both radical ions ($\mathbf{1}^{+\cdot}$ and $\mathbf{1}^{-\cdot}$), illustrated by reactions [3] and [4], for all theoretical models investigated.

Discussion

It is evident from Table 7 that the calculated enthalpy change (ΔH) for each reaction is dependent on the theoretical model employed. For reaction [1], the ΔH value does not change significantly when the split-valence (3-21G) basis set is used instead of the minimal (STO-3G) basis set. The total energies of the reactants and the products must decrease by about the same amount for there to be no significant change in ΔH. The magnitude of ΔH nearly doubles when the polarized (6-31G*)

© 1997 NRC Canada

Table 7. Estimated enthalpy changes for reactions [1], [3], and [4] calculated at various theoretical levels.

Theoretical model	Enthalpy change (kJ/mol)		
	Reaction [1]	Reaction [3]	Reaction [4]
HF/STO-3G//HF/STO-3G	−81	830	694
HF/3-21G//HF/3-21G	−83	716	600
HF/6-31G*//HF/6-31G*	−154	688	566
MP2/6-31G*//HF/6-31G*		544	
B3PW91/6-31G*//B3PW91/6-31G*		563	
HF/6-31+G*//HF/6-31+G*			509
B3PW91/6-31+G*//B3PW91/6-31+G*			427

basis set is employed. Closer inspection of the total energy of each species revealed that this change in ΔH is caused by a significant decrease in the total energy of $\mathbf{1}^{2+}$. This suggests that the polarization functions on the carbon atoms play a more important role in determining the bonding structure in $\mathbf{1}^{2+}$ than in the classical structure of compounds **2**, **4** and **5**. The enthalpy change at the HF/6-31G* level for reaction [1] shows that the delocalized dication $\mathbf{1}^{2+}$ is 154 kJ/mol more stable than **2**, in agreement with the principle that delocalization leads to stability. Geometry optimization of $\mathbf{1}^{2+}$, starting from the structure of the neutral molecule **1**, without symmetry constraints, gave the same structure as that reported by Schleyer and co-workers (14). The fact that identical structures were obtained starting from different geometries provides additional evidence that this non-classical structure is the most stable minimum on the potential energy surface of this system. Further evidence for the stability associated with the four-center–two-electron bonding arrangement similar to that observed in $\mathbf{1}^{2+}$ have been reported. Glukhovtsev et al. showed that the tetrahedral structure is the only minimum on the potential energy surfaces of Li_4^{2+} and Na_4^{2+} (39). The electron density distributions of these T_d structures showed that there is no direct bonding between the atoms. The four positively charged atoms are essentially held together by a large negative charge density located at the center of the tetrahedral. The Coulombic repulsion in these small, doubly charged species is significant; therefore the stability associated with this bonding arrangement must be very large in order to overcome the repulsion energy and produce a minimum.

The structural changes that occur upon sequential oxidation and reduction of **1** are quite interesting. The symmetry of **1** can be easily predicted from its Lewis structure. However, the optimized structure of **1** serves as a good reference to analyze the changes that occur when electrons are successively removed or added. Transformation to the structure of $\mathbf{1}^{+\cdot}$ involves cleavage of the C_1—C_3 bond to generate a radical center at C_1 and a cationic center at C_3 (Fig. 2). Delocalization of the positive charge due to electron donation to C_3 from the cyclopropane bond (C_5—C_7) produces the C_{3v} distonic radical cation. This delocalization requires dramatic structural changes and the driving force for this reorganization is the overlap of the valence orbitals on the remaining three bridgehead carbon atoms (excluding the one bearing the spin) to produce the molecular orbital that will lead to delocalization, forming a tris-homoaromatic ($4n + 2$, $n = 0$) species similar to the tris-homocyclopropenyl cation (40). The magnitude of the net stabilization gained by this type of homoaromatic interaction has been estimated to be 85 kJ/mol (41). The spin distribution, combined with the observation that the singly occupied molecular orbital of $\mathbf{1}^{+\cdot}$ is composed mainly of the one p orbital of C_1, indicates that the radical portion is essentially localized on this single atom. For this particular system, the stability achieved by the delocalization of two electrons to form the homoaromatic structure is obviously greater than that of spin delocalization.

The overall stability of $\mathbf{1}^{+\cdot}$ is illustrated by the energetics of reaction [3]. The ΔH value for reaction [3] decreases significantly when the 3-21G basis set is used instead of the STO-3G basis set. Inspection of the changes in the total energy of each species shows that this is primarily due to a large decrease in the total energy of **1**. The small change observed when the basis set is further increased to 6-31G* is a consequence of the large decrease in the total energy of $\mathbf{1}^{2+}$ and $\mathbf{1}^{+\cdot}$, but the total energy of **1** remained fairly constant; therefore, ΔH remains about the same. This observation implies that the split-valence basis set is more important in predicting the structure of **1**, presumably because of the high p character of the cyclopropane bonds. Electron correlation also has a significant effect on the ΔH value for this reaction. This is expected because the number of electron pairs is not equal on both sides of the equation. Becke's hybrid method gave similar results as the MP2 single point calculations: $\mathbf{1}^{+\cdot}$ is ~550 kJ/mol more stable than $\mathbf{1}^{2+}$. This indicates that more energy is required to remove an electron from $\mathbf{1}^{+\cdot}$ to produce $\mathbf{1}^{2+}$ than is necessary to convert **1** to $\mathbf{1}^{+\cdot}$. This result is not too surprising when factors other than aromaticity are taken into account. For example, in order to bring all four bridgehead atoms within bonding distance, the adamantane cage has to be compressed, which causes a decrease in the C-CH_2-C angles (87.1° in $\mathbf{1}^{2+}$). This large deviation from the normal tetrahedral angle (109°) of an sp^3 hybridized carbon atom creates a large strain energy. The structure of $\mathbf{1}^{2+}$ is a compromise between optimal overlap and strain energy. The result is that three of the C-CH_2-C bond angles are smaller in $\mathbf{1}^{2+}$ than in $\mathbf{1}^{+\cdot}$, with concomitant increases in strain energy. The effectiveness of delocalization in $\mathbf{1}^{2+}$ is reduced because of the longer distances between the bridgehead atoms so that optimal overlap cannot be achieved. The total overlap between the bridgehead atoms in $\mathbf{1}^{2+}$ is only

Can. J. Chem. Downloaded from www.nrcresearchpress.com by 92.62.229.171 on 09/08/12
For personal use only.

© 1997 NRC Canada

Can. J. Chem. Downloaded from www.nrcresearchpress.com by 92.62.229.171 on 09/08/12
For personal use only.

half the magnitude of the overlap between the bridgehead atoms in the cyclohexyl moiety of $\mathbf{1}^{+\cdot}$. Furthermore, since $\mathbf{1}^{2+}$ carries twice the charge in essentially the same volume, the total repulsion energy will be significantly higher than in $\mathbf{1}^{+\cdot}$. All of these factors increase the total energy of $\mathbf{1}^{2+}$ relative to $\mathbf{1}^{+\cdot}$. The enthalpy change of reaction [3] represents the difference between the first and second ionization potentials of **1**. The first ionization involves transformation from a localized molecule to an aromatic radical cation, while the second ionization only serves to expand the electron delocalization in $\mathbf{1}^{+\cdot}$ to the fourth bridgehead carbon atom. Evidently, the first process is more favorable.

The response of the neutral molecule **1** to the addition of electrons is also the cleavage of the C_1—C_3 bond. The B3PW91/6-31+G* optimized structures of the radical anion $\mathbf{1}^{-\cdot}$ and the dianion $\mathbf{1}^{2-}$ are similar. In the case of the radical anion, both Mulliken and natural population analysis agree that the spin and charge are essentially located on two bridgehead carbon atoms (C1 and C_3). These two carbon atoms also carry the highest charge density in the dianion, but in contrast to $\mathbf{1}^{-\cdot}$, the methylene groups also carry a significant amount of negative charge along with the remaining bridgehead carbon atoms. As a result of the large repulsion between the two anionic centers in $\mathbf{1}^{2-}$, the C_1—C_3 interatomic distance is significantly longer than in $\mathbf{1}^{-\cdot}$ (Tables 4 and 5). This also causes corresponding increases in the C_1-C_2-C_3 and C_3-C_4-C_5 angles that would alleviate some of the strain in $\mathbf{1}^{2-}$. Although natural population analysis assigns small negative charges to the methylene groups and the bridgehead atoms C_5 and C_7, the optimized geometry of $\mathbf{1}^{2-}$ suggests that the electrons in $\mathbf{1}^{2-}$ are largely localized on C_1 and C_3 rather than delocalized over the entire molecule as in $\mathbf{1}^{2+}$.

The enthalpy change for the disproportionation of the radical anion (reaction [4]) is positive for all theoretical models studied. The enthalpy change decreases as the basis set increases. The largest decrease occurred upon going from the minimal (STO-3G) to the split valence (3-21G) basis set. This is caused by a large decrease in the total energy of $\mathbf{1}^{2-}$, which again can be related back to the importance of the *p*-orbitals in describing the bonding of cyclopropane structures. The next largest decrease in the enthalpy change is upon the inclusion of electron correlation. Again, the most dramatic change in total energy was observed in $\mathbf{1}^{2-}$. The positive ΔH of reaction [4] indicates that more energy is required to add an electron to the radical anion than to the neutral molecule; $\mathbf{1}^{-\cdot}$ is more stable than $\mathbf{1}^{2-}$. The structures of these two species are very similar and hence the strain energy in $\mathbf{1}^{2-}$ should not be significantly higher than in $\mathbf{1}^{-\cdot}$. The instability of $\mathbf{1}^{2-}$ relative to $\mathbf{1}^{-\cdot}$ can be attributed to the Coulombic repulsion of the two negative charges in the dianion. The enthalpy change estimated at the B3PW91/6-31+G* level for this reaction is 427 kJ/mol. Since $\mathbf{1}^{-\cdot}$ does not show any special structural feature that would lead to significant stabilization (in contrast to $\mathbf{1}^{+\cdot}$), this large positive ΔH indicates that there is no special stabilization in $\mathbf{1}^{2-}$ either. The energies of these calculations confirm the conclusion reached from the structural analysis: $\mathbf{1}^{2-}$ does not exhibit extra stabilization due to electron delocalization.

All known organic molecules exhibiting three-dimensional electron delocalization contain two or six delocalized electrons (8, 11*c*, 42). These numbers follow the Hückel $4n + 2$ π-electron rule for two-dimensionally aromatic compounds. However, Fig. 6 shows that the frontier orbitals of the three closed-shell species in the pentacyclo[3.3.1.$1^{3,7}$.$0^{1,3}$.$0^{5,7}$]decane system do not resemble the pattern predicted by Hückel theory. The lowest unoccupied molecular orbital (LUMO) of $\mathbf{1}^{2+}$ is triply degenerate, suggesting that six more electrons have to be added in order to reach the next closed-shell configuration in the T_d point group. If Schleyer's dication $\mathbf{1}^{2+}$ is considered as the first member of an aromatic series with T_d symmetry in three dimensions, the next member of this series would contain eight delocalized electrons. Fig. 6 also shows how the frontier orbitals of the three-dimensional pentacyclo[3.3.1.$1^{3,7}$.$0^{1,3}$.$0^{5,7}$]decane system rearrange to accommodate additional electrons. When two electrons are added to $\mathbf{1}^{2+}$, an unstable open shell arrangement occurs in the T_d point group due to the degeneracy of the LUMO. Consequently, the neutral molecule **1** in this system distorts to a lower (D_{2d}) symmetry. This is similar to the behavior in the two-dimensional cyclooctatetraene system. However, the open shell configuration still remains when four electrons are added to produce the dianion $\mathbf{1}^{2-}$ because the LUMO of $\mathbf{1}^{2+}$ is triply degenerate. Therefore, instead of reverting to T_d symmetry, $\mathbf{1}^{2-}$ distorts further to a lower C_{2v} symmetry. The degeneracy of the frontier molecular orbitals observed for these three closed-shell species indicates that a different rule for predicting the number of delocalized electrons will be required for aromaticity in three dimensions.

The results from this study illustrate the importance of symmetry in determining the degeneracy of molecular orbitals, which in turn dictates the possible number of delocalized electrons a molecule may accommodate. The degeneracy of the molecular orbitals in any given molecular species is governed by the point group of the molecule. The Hückel $4n + 2$ π-electron rule for aromaticity in two dimensions depends on the presence of doubly degenerate levels ensured by the D_{nh} symmetry of the molecules for which this rule is normally invoked (43). A number of different symmetry groups, such as T_d and O_h, may facilitate delocalization of electrons in three dimensions. This implies that a number of different rules are required to predict the number of delocalized electrons for aromaticity in three dimensions: one for each conceivable point group.

Conclusion

The structure and charge density of $\mathbf{1}^{2+}$ obtained from these calculations confirm that two electrons are delocalized in a three-dimensional space in this dication. However, the results obtained in the same manner for the dianion $\mathbf{1}^{2-}$ are more consistent with a structure where the electrons are localized in σ-bonds and specific atoms rather than a delocalized structure. The fully optimized structure of $\mathbf{1}^{2-}$ did not reveal any unusual features that indicate special stabilization. The large positive enthalpy change of the disproportionation reaction for the radical anion, estimated by using the total energies of the appropriate species, also confirms that $\mathbf{1}^{2-}$ does not possess any special stability compared to the radical anion. The relative stability of $\mathbf{1}^{2+}$ was estimated by two different reactions (reactions [1] and [3]). Reaction [1] shows that the extra stabilization due to electron delocalization is on the order of 150 kJ/mol. However, reaction [3] indicates that the disproportionation reaction for the radical cation is endothermic by 563

© 1997 NRC Canada

Can. J. Chem. Downloaded from www.nrcresearchpress.com by 92.62.229.171 on 09/08/12
For personal use only.

kJ/mol, implying that the radical species is much more stable than the dication.

The enthalpy change of reaction [1] confirmed that there is stability associated with electron delocalization in $\mathbf{1}^{2+}$. In spite of this, $\mathbf{1}^{+\cdot}$ is more stable than the dication as indicated by the large positive ΔH of reaction [3]. Reaction [4] shows that the dianion $\mathbf{1}^{2-}$ is also less stable than the radical anion $\mathbf{1}^{-\cdot}$. It is recognized that these are gas phase calculations, and that solvent and counterion effects may shift the equilibrium of these reactions. In the case of the cyclooctatetraene system, the enthalpy change of the disproportionation reaction for the radical anion (reaction [2]) is also positive in the gas phase, with magnitudes similar to those obtained with reactions [3] and [4] (44). In fact, the dianion has not been observed experimentally in the gas phase (45]). Once in solution, this equilibrium shifts to the right with the help of ion pairing and solvation effects. This leads to the conclusion that, in the gas phase, the Coulombic repulsion in the doubly charged ions is larger than the stabilization from aromatic electron delocalization. Therefore, it is plausible that solvent and counterion effects would also shift the equilibrium of reactions [3] and [4].

In contrast to the cyclooctatetraene system, the dianion $\mathbf{1}^{2-}$ does not revert to the same symmetry as the dication $\mathbf{1}^{2+}$ due to the fact that the pattern of the frontier orbitals for the closed-shell species of the three-dimensional pentacyclo[3.3.1.1^{3,7}.0^{1,3}.0^{5,7}]decane system does not resemble the Hückel pattern. This is to be expected since Hückel theory only applies to planar molecules with D_{nh} symmetry, and cannot be extended to aromaticity in three dimensions. The degeneracy of the frontier orbitals obtained from these calculations suggests that six more electrons must be added to $\mathbf{1}^{2+}$ to achieve the next closed-shell configuration in the T_d point group. This implies that for three-dimensional aromaticity different rules are needed to predict the number of delocalized electrons. Furthermore, symmetry dictates that more than one rule is necessary: one for each point group, which may facilitate electron delocalization in three dimensions.

Acknowledgments

We thank Dr. R. J. Boyd and his research team for their valuable assistance with computational details, Ms. V. Hannon at University Computing and Information Services (UCIS) at Dalhousie University for hardware support, Dr. N. Burford for helpful discussion on symmetry, and the Natural Sciences and Engineering Research Council of Canada for funding. Computer time was arranged through Dr. Boyd's group and UCIS at Dalhousie University.

References

1. (*a*) A. Kekulé. Bull. Soc. Chim. Paris, **3**, 98 (1865); (*b*) Bull. Acad. R. Belg. **19**, 551 (1865); (*c*) Liebigs Ann. **137**, 129 (1866).
2. (*a*) P.J. Garratt. Aromaticity. John Wiley & Sons, Toronto. 1986; (*b*) G.M. Badger. Aromatic character and aromaticity. Cambridge University Press, New York. 1969; (*c*) J.P. Snyder. Nonbenzenoid aromatics. Academic Press, New York. 1969.
3. (*a*) W.E. Barth and R.G. Lawton. J. Am. Chem. Soc. **88**, 380 (1966); (*b*) J. Am. Chem. Soc. **93**, 1730 (1971).
4 H.W. Kroto, J.R. Heath, S.C. O'Brien, R.F. Curl, and R.E. Smalley. Nature, **318**, 162 (1985).
5. T. Fukunaga, H.E. Simmons, J.J. Wendoloski, and M.D. Gordon. J. Am. Chem. Soc. **105**, 2729 (1983).
6. (*a*) M.J. Goldstein and R. Hoffmann. J. Am. Chem. Soc. **93**, 6193 (1971); (*b*) R.W. Rudolph. Acc. Chem. Res. **9**, 446 (1976); (*c*) K. Wade. Adv. Inorg. Chem. Radiochem. **18**, 1 (1976); (*d*) J.-I. Aihara. J. Am. Chem. Soc. **100**, 3339 (1978); (*e*) D.M.P. Mingos. Acc. Chem. Res. **17**, 311 (1984); (*f*) V.I. Minkin, M.N. Glukhovtsev, and B.Ya. Simkin. Aromaticity and antiaromaticity, electronic structure and structual aspects. John Wiley & Sons, Inc., Toronto. 1994. Chaps. 8, 9, 10.
7. (*a*) R.B. King and D.H. Rouvray. J. Am. Chem. Soc. **99**, 7834 (1977); (*b*) R.B. King, B. Dai, and B.M. Gimarc. Inorg. Chim. Acta, **167**, 213 (1990); (*c*) R.B. King. J. Math. Chem. **4**, 69 (1990); (*d*) M. Zhao and B.M. Gimarc. Inorg. Chem. **32**, 4700 (1993).
8. H. Hogeveen and P.W. Kwant. Acc. Chem. Res. **8**, 413 (1975).
9. R.E. Williams. Inorg. Chem. **10**, 210 (1971).
10. W.-D. Stohrer and R. Hoffman. J. Am. Chem. Soc. **94**, 1661 (1972).
11. (*a*) S. Masamune, M. Sakai, A.V. Kemp-Jones, H. Ona, A.Venot, and T. Nakashima. Angew. Chem. Int. Ed. Engl. **12**, 769 (1973); (*b*) S. Masamune, M. Sakai, H. Ona, and A.J. Jones. J. Am. Chem. Soc. **94**, 8956 (1972); (*c*) H. Hart and M. Kuzuya. J. Am. Chem. Soc. **94**, 8958 (1972); (*d*) G. Maier, H. Rang, and H.-O. Kalinowski. Angew. Chem. Int. Ed. Engl. **28**, 1232 (1989).
12. (*a*) J. Feng, J. Leszczynski, B. Weiner, and M.C. Zerner. J. Am. Chem. Soc. **111**, 4648 (1989); (*b*) M.N. Glukhovtsev, R.D. Bach, and S. Laiter. J. Phys. Chem. **100**, 10952 (1996).
13. E.D. Jemmis and P.v.R. Schleyer. J. Am. Chem. Soc. **104**, 4781 (1982).
14. M. Bremer, P.v.R. Schleyer, K. Schötz, M. Kausch, and M. Schindler. Angew. Chem. Int. Ed. Engl. **26**, 761 (1987).
15. P. Buzek, P.v.R. Schleyer, and S. Sieber. Chem. Unserer Zeit, **26**, 116 (1992).
16. (*a*) P.v.R. Schleyer, C. Maerker, A. Dransfeld, H. Jiao, and N.J.R.v.E. Hommes. J. Am. Chem. Soc. **118**, 6317 (1996); (*b*) P.v.R. Schleyer and H. Jiao. Pure Appl. Chem. **68**, 209 (1996).
17. (*a*) E. Hückel. Z. Phys. **70**, 204 (1931); (*b*) Z. Phys. **76**, 628 (1932); (*c*) Z. Phys. **83**, 632 (1933); (*d*) Z. Elektrochem. **43**, 827 (1937).
18. (*a*) I.L. Karle. J. Chem. Phys. **20**, 65 (1952); (*b*) M. Traetteberg. Acta Chem. Scand. **20**, 1724 (1966); (*c*) J. Bordner, R.G. Parker, and R.H. Stanford. Acta Crystallogr. Sect. B: Struct. Crystallogr. Cryst. Chem. **B28**, 1069 (1972).
19. (*a*) G. Schröder. Cyclooctatetraene. Verlag Chemie, Heidelberg. 1965; (*b*) L. A. Paquette. Tetrahedron, **31**, 2855 (1975).
20. L. Radom and H.F. Schaefer III. J. Am. Chem. Soc. **99**, 7522 (1977).
21. G.A. Olah, J.S. Staral, G. Liang, L.A. Paquette, W.P. Melega, and M.J. Carmody. J. Am. Chem. Soc. **99**, 3349 (1977).
22. K. Jug. J. Org. Chem. **49**, 4475 (1984).
23. (*a*) T.J. Katz. J. Am. Chem. Soc. **82**, 3784 (1960); (*b*) S.Z. Goldberg, K.N. Raymond, C.A. Harmon, and D.H. Templeton. J. Am. Chem. Soc. **96**, 1348 (1974).
24. (*a*) B.A. Hess, Jr. and L.J. Schaad. J. Am. Chem. Soc. **93**, 2413 (1971); (*b*) M.J. Cook, A.R. Katritzky, and P. Linda. Adv. Hetercycl. Chem. **17**, 255 (1974); (*c*) J.-I. Aihara. J. Am. Chem. Soc. **98**, 2750 (1976); (*d*) I. Gutman, M. Milun, and N. Trinajstic. J. Am. Chem. Soc. **99**, 1692 (1977); (*e*) J.-I. Aihara. Bull. Chem. Soc. Jpn. **50**, 3057 (1977); (*f*) R.C. Haddon. J. Am. Chem. Soc. **101**, 1722 (1979); (*g*) P. Ilic and N. Trinajstic. J. Org. Chem. **45**, 1738 (1980); (*h*) K. Jug. J. Org. Chem. **48**, 1344 (1983).
25. (*a*) H.L. Strauss, T.J. Katz, and G.K. Fraenkel. J. Am. Chem. Soc. **85**, 2360 (1963); (*b*) F.J. Smentowski and G.R. Stevenson.

© 1997 NRC Canada

J. Phys. Chem. **73**, 340 (1969); (*c*) G.R. Stevenson and J.G. Concepción. J. Phys. Chem. **76**, 2176 (1972).
26. M.J. Frisch, G.W. Trucks, H.B. Schlegel, P.M.W. Gill, B.G. Johnson, M.W. Wong, J.B. Foresman, M.A. Robb, M. Head-Gordon, E.S. Replogle, R. Gomperts, J.L. Andres, K. Raghavachari, J.S. Binkley, C. Gonzalez, R.L. Martin, D.J. Fox, D.J. Defrees, J. Baker, J.P. Stewart, and J.A. Pople. Gaussian 92/DFT, Revision F.2. Gaussian, Inc.; Pittsburgh, Pa. 1993.
27. M.J. Frisch, G.W. Trucks, H.B. Schlegel, P.M.W. Gill, B.G. Johnson, M.A. Robb, J.R. Cheeseman, T. Keith, G.A. Petersson, J.A. Montgomery, K. Raghavachari, M.A. Al-Laham, V.G. Zakrzewski, J.V. Ortiz, J.B. Foresman, J. Cioslowski, B.B. Stefanov, A. Nanayakkara, M. Challacombe, C.Y. Peng, P.Y. Ayala, W. Chen, M.W. Wong, J.L. Andres, E.S. Replogle, R. Gomperts, R.L. Martin, D.J. Fox, J.S. Binkley, D.J. Defrees, J. Baker, J.P. Stewart, M. Head-Gordon, C. Gonzalez, and J.A. Pople. Gaussian 94, Revision B.2. Gaussian, Inc., Pittsburgh, Pa. 1995.
28. W.J. Hehre, L. Radom, P.v.R. Schleyer, and J.A. Pople. Ab initio molecular orbital theory. Wiley–Intersciences, New York. 1986.
29. A.D. Becke. J. Chem. Phys. **98**, 5648 (1993).
30. J.P. Perdew and Y. Wang. Phys. Rev. B: Condens. Matter, **45**, 13244 (1992).
31. (*a*) H.B. Schlegel. J. Chem. Phys. **77**, 3676 (1982); (*b*) J. Comput. Chem. **3**, 214 (1982).
32. C. Møller and M.S. Plesset. Phys. Rev. **46**, 618 (1934).
33. (*a*) R.S. Mulliken. J. Chem. Phys. **23**, 1833 (1955); (*b*) J. Chem. Phys. **23**, 1841 (1955)
34. A.E. Reed, R.B. Weinstock, and F. Weinhold. J. Chem. Phys. **83**, 735 (1985).
35. R.C. Haddon and K. Raghavachari. J. Am. Chem. Soc. **105**, 118 (1983).
36. (*a*) J. Wang, L.A. Eriksson, B.G. Johnson, and R.J. Boyd. J. Phys. Chem. **100**, 5274 (1996); (*b*) J. Hrusák, H. Friedrichs, H. Schwarz, H. Razafinjanahary, and H. Chermette. J. Phys. Chem. **100**, 100 (1996); (*c*) R.H. Mitchell, Y. Chen, V.S. Iyer, D.Y.K. Lau, K.K. Baldridge, and J.S. Siegel. J. Am. Chem. Soc. **118**, 2907 (1996).
37. K.B. Wiberg and P.R. Rablen. J. Comput. Chem. **14**, 1504 (1993).
38. B.F. Yates, W.J. Bouma, and L. Radom. J. Am. Chem. Soc. **106**, 5805 (1984).
39. M.N. Glukhovtsev, P.v.R. Schleyer, and A. Stein. J. Phys. Chem. **97**, 5541 (1993).
40. (*a*) S. Masamune, M. Sakai, A.V. Kemp-Jones, and T. Nakashima. Can. J. Chem. **52**, 855 (1974); (*b*) G.N. Olah, G.K. Surya Prakash, T.N. Rawdah, D. Whittaker, and J.C. Rees. J. Am. Chem. Soc. **101**, 3935 (1979); (*c*) G.K. Surya Prakash, M. Arvanaghi, and G.A. Olah. J. Am. Chem. Soc. **107**, 6017 (1985).
41. M. Bremer, K. Schötz, P.v.R. Schleyer, U. Fleischer, M. Schindler, W. Kutzelnigg, W. Koch, and P. Pulay. Angew. Chem. Int. Ed. Engl. **28**, 1042 (1989).
42. (*a*) H. Schwarz. Angew. Chem. Int. Ed. Engl. **20**, 991 (1981); (*b*) A.V. Kemp-Jones, N. Nakamura, and S. Masamune. J. Chem. Soc. Chem. Commun. 109 (1974).
43. (*a*) C.A. Coulson, B. O'Leary, and R.B. Mallion. Hückel theory for organic chemists. Academic Press, New York. 1978, pp. 74–87; (*b*) M.H. Palmer, J.R. Wheeler, R.H. Findlay, N.P.C. Westwood, and W.M. Lau. J. Mol. Struct. **86**, 193 (1981).
44. (*a*) H. Zuilhof and G. Lodder. J. Phys. Chem. **99**, 8033 (1995); (*b*) M.J.S. Dewar, A. Harget, and E. Haselbach. J. Am. Chem. Soc. **91**, 7521 (1969).
45. G.R. Stevenson. *In* Molecular structure and energetics. *Edited by* J.F. Liebman and A. Greenberg. VCH Publishers Inc., Deerfield Beach, Fla. 1986. Chap. 2.

Can. J. Chem. Downloaded from www.nrcresearchpress.com by 92.62.229.171 on 09/08/12
For personal use only.

© 1997 NRC Canada

Micellar catalysis of organic reactions. Part 37.[1] A comparison of the catalysis of ester and amide hydrolysis by copper-containing micelles

Trevor J. Broxton and Abdulla Nasser

Can. J. Chem. Downloaded from www.nrcresearchpress.com by 92.62.229.171 on 09/08/12
For personal use only.

Abstract: The hydrolysis of a number of nitroactivated esters and amides has been studied in the presence of copper-containing metallomicelles at neutral pH. The relative rates of hydrolysis in the pure metallomicelle and in co-micelles with either cetyltrimethylammonium bromide (ctab) or Triton X-100 depends on the hydrophobicity of the substrate and whether it is completely solubilized by the copper micelle. Thus it depends on the concentration of the copper micelle. At low concentrations of copper micelle (0.2 mM) where the substrate is incompletely solubilized, the reaction is faster when 2 mM ctab is added. At higher concentrations (>0.6 mM) where the substrate may be almost completely solubilized by the copper micelle, the reaction is slower when 2 mM ctab is added. For ester hydrolysis the presence of either a carboxylic acid group or a heterocyclic nitrogen atom close to the reaction centre resulted in much larger catalysis by the metallomicelle than for model compounds without these additional groups. It is postulated that these groups coordinate with the metal ion and thus present the reaction centre close to a metal-bound hydroxyl resulting in a significant increase in the rate of bond formation, which is the rate-determining step for ester hydrolysis. For amide hydrolysis the presence of a carboxyl group *ortho* to the reaction centre did not lead to larger catalysis by the copper micelle than for the compound without this group. This difference is attributed to the different rate-determining steps for amide and for ester hydrolysis.

Key words: metallomicelles, ester and amide hydrolysis.

Résumé : Opérant à un pH neutre, en présence de métallomicelles contenant du cuivre, on a étudié l'hydrolyse d'un certain nombre d'esters et d'amides activés par des groupes nitro. Les vitesses relatives d'hydrolyse dans la métallomicelle pure et dans des comicelles comportant soit du bromure de cétyltriméthylammonium («ctab») soit du Triton X-100 dépend du caractère hydrophobe du substrat et de sa solubilité dans la micelle de cuivre. Elles dépendent donc de la concentration de micelle de cuivre. À de faibles concentrations de micelle de cuivre (0,2 mM), alors que le substrat ne se solubilise pas complètement, la vitesse de la réaction est accélérée par l'addition de 2 mM de «ctab». À des concentrations plus élevées (>0,6 mM), alors que le substrat est pratiquement solubilisé par la micelle de cuivre, la réaction est ralentie par l'addition de 2 mM de «ctab». Lors de l'hydrolyse de l'ester en présence soit d'un groupe acide carboxylique soit d'un atom d'azote hétérocyclique à proximité du centre réactionnel, la catalyse par la métallomicelle est beaucoup plus importante que dans les cas de composés modèles ne portant pas ces groupes. On fait l'hypothèse que ces groupes se coordonnent à l'ion métallique et rapprochent donc le centre réactionnel du groupe hydroxyle lié au métal; il en résulte une augmentation de la vitesse de formation de la liaison qui est l'étape déterminante dans l'hydrolyse de l'ester. Par rapport à l'hydrolyse de composés modèles ne comportant pas ces groupes, l'hydrolyse d'amides comportant un groupe carboxyle en position *ortho* du centre réactionnel ne conduit pas à des niveaux de catalyse par la micelle de cuivre plus élevés.

Mots clés : métallomicelles; hydrolyse, ester et amide.

[Traduit par la rédaction]

Introduction

The study of the catalysis of organic reactions by metallomicelles is currently of interest (1–4). We have previously reported (5) strong catalysis of amide hydrolysis in neutral solution by micelles formed after complexation of a hydrophobic ligand, *N,N,N′*-trimethyl-*N′*-hexadecylethylenediamine, with cupric chloride. The amide studied was 5-nitro-2-(trifluoroacetylamino)benzoic acid **1**. It is now of interest to determine whether the carboxylic acid group *ortho* to the amide reaction centre is essential for maximal catalysis by the copper-containing micelle and furthermore to compare ester and amide hydrolysis in pure metallomicelles and in the presence of co-micelles with either cetyltrimethylammonium bromide (ctab), a cationic surfactant, or with Triton X-100, a neutral surfactant. Engbersen and co-workers (6) reported stronger catalysis of the hydrolysis of phenyl picolinate in co-micelles of a copper-containing metallo-

Received March 28, 1996.[2]

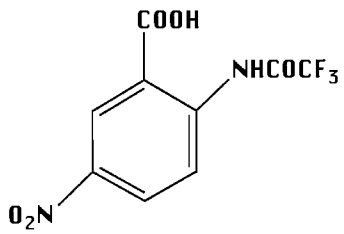
T.J. Broxton[3] and A. Nasser. School of Chemistry, La Trobe University, Bundoora, Victoria, Australia 3083.

[1] Part 36: see ref. 17.
[2] Revision received October 8, 1996.
[3] Author to whom correspondence may be addressed. Telephone: 613-9479 2552. Telex: AA 33143. Fax: 613 9479 1399. E-mail: chetjb @ lure latrobe.edu.au

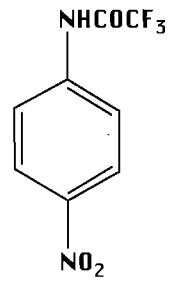
© 1997 NRC Canada

micelle with both ctab and with Brij 35 than in the pure metallo micelles.

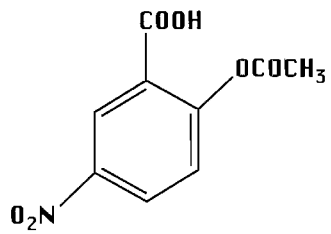
We now report the catalyzed hydrolysis of amides 5-nitro-2-(trifluoroacetylamino)benzoic acid **1** and *N*-4-nitrophenyltrifluoroacetamide **2** and esters 2-acetoxy-5-nitrobenzoic acid **3**, 4-acetoxy-3-nitrobenzoic acid **4**, 8-acetoxy-5-nitroquinoline **5**, *p*-nitrophenylacetate **6**, and *o*-nitrophenyl acetate **7** in the presence of copper-containing metallomicelles. We have chosen to use the tetradecyl ligand *N,N,N′*-trimethyl-*N′*-tetradecylethylenediamine to prepare the metallomicelle, to avoid some solubility problems encountered with the hexadecyl compound.



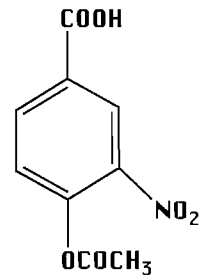
1



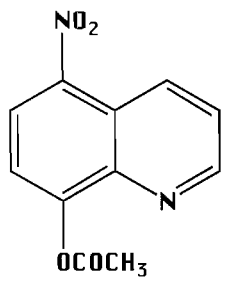
2



3



4



5

Table 1. Pseudo-first-order rate constants ($10^4 \times k_1/s^{-1}$) for the hydrolysis of amides (*a*)**1** and (*b*)(**2**) in the presence of copper-containing metallomicelles.

(*a*) 5-Nitro-2-trifluoroacetylamino benzoic acid (**1**)

[Cu(L)] (mM)	Chloride	Acetate	Nitrate
0	0.217	0.217	0.217
0.20	1.88		
0.20 + 2 mM Triton	0.305		
0.25	2.84	2.77	2.80
0.25 + 1 mM Triton	—	2.01	
0.40	3.12		
0.40 + 2 mM Triton	0.809		
0.50	6.54	6.83	6.57
0.50 + 1 mM Triton	—	6.37	
0.50 + 1 mM ctab	—	5.14	
0.60	5.43		
0.60 + 2 mM Triton	1.59		
0.75	8.96	9.11	8.95
0.75 + 1 mM Triton	—	8.59	
1.00	9.35	9.62	9.96
1.00 + 1 mM Triton	8.13	9.11	9.20
1.00 + 1 mM ctab	3.97	4.56	4.99
2.00	9.99	10.3	10.2
2.00 + 1 mM Triton	9.80		10.2
2.00 + 1 mM ctab	6.29	6.81	6.74

(*b*) Model compound *N*-4-nitrophenyltrifluoroacetamide (**2**)

[Cu(L)] (mM)	Chloride	Acetate	Nitrate
0	0.162	0.162	0.162
0.20	0.439	—	
0.20 + 2 mM Triton	0.307		
0.20 + 2 mM ctab	0.761		
0.25 + 1 mM Triton	0.52		
0.40	1.12	—	
0.40 + 2 mM Triton	0.673		
0.40 + 2 mM ctab	1.41		
0.50	1.43	1.49	1.39
0.50 + 1 mM Triton	—	1.29	
0.60	1.83	—	
0.60 + 2 mM Triton	1.11		
0.60 + 2 mM ctab	2.32		
0.75	3.00	2.85	3.02
0.75 + 1 mM Triton	—	2.46	
1.00	3.97	—	4.35
1.00 + 1 mM ctab	3.57	4.71	
1.00 + 1 mM Triton	3.57	7.54	3.62
2.00	7.78		6.67
2.00 + 1 mM ctab	6.49	7.41	
2.00 + 1 mM Triton	7.03	—	6.67

Results and discussion

1. Amide hydrolysis

Pseudo-first-order rate constants for the hydrolysis of amides **1** and **2** are given in Table 1. With both the chloride and acetate salts, identical rate constants were obtained for reactions using solutions obtained by dissolving solid samples of the copper–ligand complex (method *a*), and for solutions obtained by preparing the complex in situ (method *b*), see experimental section. For the nitrate salt, the rate constants were only obtained by method *b*, i.e., in solutions obtained by mixing the copper nitrate and ligand in situ, see experimental section.

Can. J. Chem. Downloaded from www.nrcresearchpress.com by 92.62.229.171 on 09/08/12
For personal use only.

© 1997 NRC Canada

Can. J. Chem. Downloaded from www.nrcresearchpress.com by 92.62.229.171 on 09/08/12
For personal use only.

For both compounds, similar rates were obtained with the chloride, acetate, and nitrate metallomicelles and the maximum observed catalysis for each compound was also similar for each micelle. This indicates that the reaction of the amide substrate is with a copper-bound hydroxyl rather than with hydroxide ion from the bulk solution. In the latter case we would have expected significant differences between the rates obtained in chloride, acetate, and nitrate micelles based on the pseudophase ion exchange kinetic model of micellar catalysis (7, 8), because the hydroxide ion would be competing with different counterions for available sites on the micelle surface. This is consistent with conclusions drawn by Menger et al. (1) for the copper-catalyzed hydrolysis of phosphate esters.

In most cases it can be seen that the rate of hydrolysis of compound **1** is slightly faster (1.3- to 4.9-fold) than that for compound **2**. The maximum observed catalysis of the hydrolysis of both compounds is similar, ranging from 46 to 47.5 for compound **1** and from 41 to 48 for compound **2**.

The rate–detergent profile in the miceles with chloride counterions showed an increase in rate as the detergent concentration was increased from 0.2 to 2 mM. Even at 0.2 mM the rate of hydrolysis was more than 10 times faster than in pure water alone. This is consistent with a critical micelle concentration (cmc) of 0.18 mM as reported by Menger et al. (1) for this micelle.

Effect of co-micelles

For compound **1**, which should be well solubilized by the metallomicelle due to the electrostatic attraction between the ionized carboxylic acid group and the cationic micelle, the rate of hydrolysis in the presence of a co-micelle was slower than in the pure metallomicelle. This inhibiting effect was larger for ctab co-micelles than for Triton X-100 co-micelles.

For compound **2**, which is less well solubilized by the metallomicelle since it is a neutral compound, the addition of co-micelles of ctab at low concentrations of copper micelle (0.2–0.4 mM) resulted in a rate increase. At higher copper micelle concentrations the addition of co-micelles of ctab caused a reduction in the rate of hydrolysis. At all copper concentrations the addition of co-micelles of Triton X-100 resulted in a reduction in the rate of hydrolysis. The effect of these co-micelles on the rate of hydrolysis depends on how well the substrate is solubilized by the copper micelle alone and hence on the copper micelle concentration. If the substrate is completely solubilized by the copper micelle, then the addition of a co-micelle reduces the rate of hydrolysis, presumably as a result of the dilution of the substrate in the micellar pseudophase. On the other hand, if the substrate is not completely solubilized by the copper micelle, then the addition of a co-micelle improves solubilization of the substrate by the micelles and hence increases the rate of hydrolysis. Engbersen and co-workers (6) observed that the rate of hydrolysis of *p*-nitrophenylpicolinate in the presence of zinc- or copper-containing metallomicelles was increased by the addition of co-micelles of either ctab or Brij-35. This work was carried out at a low metallomicelle concentration (0.4 mM), so presumably the ester substrate was not fully solubilized and hence the addition of co-micelles increased solubilization of the substrate in the micellar pseudophase, thus increasing the observed rate of hydrolysis.

2. Ester hydrolysis

Pseudo-first-order rate constants for the hydrolysis of esters **3**, **4**, and **5** are given in Table 2. For 2-acetoxy-5-nitrobenzoic acid, **3**, the rate of hydrolysis increased to a maximum at 2 mM copper micelle. At this concentration the catalysis was 7100-fold compared to reaction in water. For *p*-nitrophenylacetate, a model compound without the acid group, the observed catalysis, was only 5-fold. For the isomer 4-acetoxy-3-nitro benzoic acid, **4**, the optimum rate of hydrolysis was also obtained at 2 mM copper micelle but in this case the catalysis was only 58-fold. The model compound without the acid group, *o*-nitrophenylacetate, had only a 4.5-fold catalysis. For 8-acetoxy-5-nitroquinoline, **5**, the rate increased to a maximum at 0.6 mM copper micelle, reflecting the hydrophobicity of this compound. The catalysis at this concentration was 66-fold. The model compound without the heterocyclic nitrogen atom, *p*-nitrophenyl acetate, had only 5-fold catalysis as above.

Thus the presence of an ionized carboxylate group *ortho* to the reaction centre (as in compound **3**) or a quinoline nitrogen atom close to the reaction centre (as in compound **5**) is very beneficial to the magnitude of catalysis of ester hydrolysis by copper-containing metallomicelles, in contrast to the situation observed above for amide hydrolysis. The beneficial effect of a pyridine nitrogen atom on the magnitude of catalysis of the hydrolysis of aryl esters of picolinic acid in metallomicelles has previously been reported (9). This was attributed to coordination of the nitrogen with the metal ion.

The presence of the carboxylic acid group *para* to the reaction centre, while beneficial to the magnitude of catalysis by copper metallomicelles, is less effective than one *ortho* to the reaction centre. This suggests that the effect of the ionized carboxylate group is not merely to assist in the solubilization of the substrate by the copper-containing cationic micelle, but rather to orient the substrate within the micelle so that the reaction centre is close to the metal ion and hence the metal-bound hydroxide. The quinoline nitrogen atom close to the reaction centre in compound **5** presumably has a similar effect.

The different behaviour of ester and amide hydrolysis to the copper-containing metallomicelles is of interest. It may possibly result from different rate-determining steps for the two reactions. For ester hydrolysis the rate-determining step is bond formation (10). However, for trifluoroacetanilides the rate-determining step has been shown to be solvent-assisted C—N bond breaking (11). Thus it follows that for ester hydrolysis with bond formation between the ester and the metal-bound hydroxide being rate determining, the proximity of these species within the micelle is catalytically important (see Scheme 1). For amide hydrolysis, however, with C—N bond breakage being rate determining, the substrate is already bound to the copper micelle and hence the orientational differences between compounds **1** and **2** in the micelle are not kinetically important.

As for amide hydrolysis, the rate of hydrolysis of the esters is faster in a pure metallomicelle solution than in the presence of co-micelles except at very low metallomicelle concentrations. At 0.2 mM $CuCl_2$ the hydrolysis of compound **5** is more than 8 times faster than the uncatalyzed hydrolysis in water, once again indicating a cmc less than 0.2 mM. Addition of ctab (2 mM) to this reaction mixture resulted in a fivefold rate increase. At higher $CuCl_2$ concentrations (0.6–2.0 mM), how-

© 1997 NRC Canada

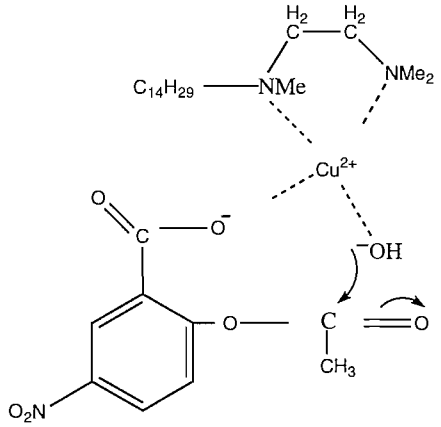
Can. J. Chem. Downloaded from www.nrcresearchpress.com by 92.62.229.171 on 09/08/12
For personal use only.

Table 2. Pseudo-first-order rate constants for the hydrolysis[a] of ester **3–5** in the presence of copper-containing metallomicelles.

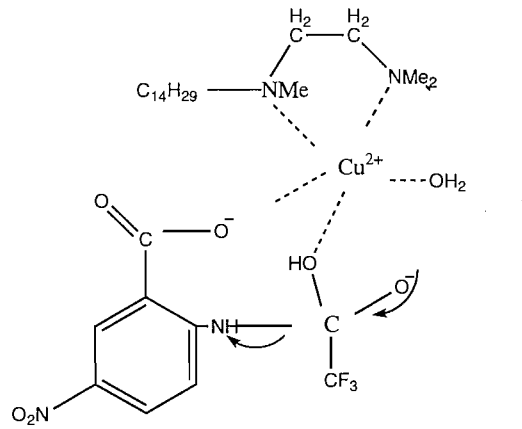
Conditions	$10^4\ k_1/s^{-1}$
2-Acetoxy-5-nitrobenzoic acid 3	
Water	0.02
0.50 mM $CuCl_2$	32.2
1.00 mM $CuCl_2$	101
2.00 mM $CuCl_2$	142
3.00 mM $CuCl_2$	140
1.00 mM $CuCl_2$ + 1 mM ctab	64.2
8-Acetoxy-5-nitroquinoline 5	
Water	0.66
2.00 mM ctab	0.465
4.00 mM ctab	0.350
6.00 mM ctab	0.377
0.20 mM $CuCl_2$	5.44
0.20 mM $CuCl_2$ + 2 mM ctab	27.9
0.40 mM $CuCl_2$	16.9
0.40 mM $CuCl_2$ + 2 mM ctab	17.1
0.50 mM $CuCl_2$	26.1
0.50 mM $CuCl_2$ + 1.5 mM ctab	20.1
0.50 mM $CuCl_2$ + 3 mM ctab	17.4
0.50 mM $CuCl_2$ + 1. mM Triton	40.4
0.50 mM $CuCl_2$ + 1.5 mM Triton	24.8
0.60 mM $CuCl_2$	43.7
0.60 mM $CuCl_2$ + 2 mM ctab	19.5
1.00 mM $CuCl_2$	29.2
1.00 mM $CuCl_2$ + 1 mM ctab	24.5
1.00 mM $CuCl_2$ + 2 mM ctab	23.5
1.00 mM $CuCl_2$ + 1 mM Triton	26.5
1.00 mM $CuCl_2$ + 2 mM Triton	23.7
2.00 mM $CuCl_2$	30.0
2.00 mM $CuCl_2$ + 1 mM Triton	26.8
3.00 mM $CuCl_2$	30.6
Model compound 4-nitrophenyl acetate	
Water	0.10
0.50 mM $CuCl_2$	0.27
1.00 mM $CuCl_2$	0.26
3.00 mM $CuCl_2$	0.542
4-Acetoxy-3-nitrobenzoic acid 4	
Water	0.17
0.20 mM $CuCl_2$	0.54
0.20 mM $CuCl_2$ + 2 mM Triton	0.25
0.40 mM $CuCl_2$	0.82
0.40 mM $CuCl_2$ + 2 mM Triton	0.54
0.60 mM $CuCl_2$	2.02
0.60 mM $CuCl_2$ + 2 mM Triton	1.21
1.00 mM $CuCl_2$	4.37
2.00 mM $CuCl_2$	9.93
3.00 mM $CuCl_2$	6.22
1.00 mM $CuCl_2$ + 1 mM ctab	2.74
Model compound 2-nitrophenyl acetate	
Water	0.134
0.50 mM $CuCl_2$	0.179
2.00 mM $CuCl_2$	0.547
3.00 mM $CuCl_2$	0.601

[a]Conditions: T = 31°C, pH 7.00 (Tris buffer 2.4 mM free base and 32.6 mM Tris HCl).

Scheme 1. Proposed mechanisms of copper-catalyzed amide and ester hydrolysis.



Rate-determining transition state for ester hydrolysis



Rate-determining transition state for amide hydrolysis

ever, the addition of ctab resulted in a reduction of the rate of hydrolysis.

This difference is most likely due to the differences in the extent of solubilization of the substrate by the copper micelles as described above for amide hydrolysis. This effect is similar to that observed in micellar reactions at concentrations higher than the optimum micelle concentration. Typically the rate vs. detergent concentration profile shows a decrease in the rate of reaction once the optimum concentration of surfactant is exceeded. The optimum rate of hydrolysis of compound **5** is observed at 0.6 mM copper micelle, the rate decreasing at higher concentrations. This indicates that the substrate is indeed completely solubilized at 0.6 mM.

Experimental section

Materials

The required ligand was prepared by the method of Menger (1) using 1-bromotetradecane and *N,N,N'*-trimethylethylenediamine in basic solution. The complex with cupric chloride

© 1997 NRC Canada

was prepared in absolute ethanol and the resulting blue-green precipitate was recrystallized from acetonitrile to give blue crystals; mp 104–105°C (lit. (1) mp 104–105°C). The identity of this product was confirmed by electrospray mass spectrometry.

The complex with copper acetate, mp 88–90°C, was prepared in an analogous way. The positive ion electrospray mass spectra (ESMS) of all of the complexes were identical, with peaks corresponding to the protonated ligand m/z = 299.1 and $Cu(L)CH_3COO^+$ m/z = 420 and 422. The presence of acetate in the ion in all of the complexes was attributed to the ESMS mobile phase, which contained methanol, water, and acetic acid. The co-micellar ctab and Triton X-100 were available commercially (BDH).

Purified water was prepared from distilled water by treatment with a Millipore system to achieve a resistivity of at least 17 MΩ cm^{-1}.

Tris buffer pH 7.0 was prepared from Tris free base (50 mL, 0.1 M) and hydrochloric acid (46.6 mL, 0.1 M). This mixture was then diluted to 100 mL with purified water.

Substrates

Compound **1** was available from previous work (5). *N*-4-Nitrophenyltrifluoroacetamide **2**, mp 150°C (lit. (12) mp 147°C), was prepared by trifluoroacetylation of *p*-nitroaniline with trifluoroacetic anhydride in dry ether at 0–5°C. Iced water then added to the reaction mixture and the precipitate was filtered and recrystallized from a mixture of methanol and ethanol. Esters **3**, **4**, and **5** were prepared by acetylation of the corresponding phenols with acetic anhydride using the method of Ciampa (13): 2-acetoxy-5-nitrobenzoic acid **3**, mp 152–154°C (lit. (14) mp 153–154°C); 4-acetoxy-3-nitrobenzoic acid **4**, mp 150°C (lit. (15) mp 152°C); 8-acetoxy-5-nitroquinoline **5**, mp 110°C (lit. (16) mp 112–113°C).

Kinetics

(a) Using previously prepared complex ($Cu(L)Cl_2$ or acetate

A stock solution of the complex (10 mM) was prepared in purified water. The required volume of this solution was added to a volumetric flask; then the required volume of Tris buffer (pH 7.0) was added and the solution was diluted to the mark with purified water. A sample of this solution (3 mL) was then thermally equilibrated in a cuvette in the cell compartment of the Varian DMS 70 UV–VIS spectrophotometer. The reaction was initiated by the addition (microsyringe) of a stock solution (20 μL) of the required substrate (0.01 M) in acetonitrile. Product formation was followed at 375 nm for compounds **1** and **2**, at 380 nm for compounds **3** and **6**, at 415 nm for compounds **4** and **7**, and at 430 nm for compound **5** using a linear recorder. The infinity value and rate constant were calculated by a computer program designed to give the best straight line fit to data (time–absorbance pairs) collected over at least two half-lives. Good agreement between experimental and calculated rate constants and infinity values was obtained for all reaction systems.

(b) Using mixed solutions of ligand and $CuCl_2$, acetate, or nitrate

The required volumes of solutions of the copper salt in water and ligand in water were mixed to provide equimolar amounts of each species and then the required volume of Tris buffer was added. The reactions were initiated and followed as above (*a*).

(c) Using co-micelles

Required volumes of ligand and copper salt were mixed to obtain equimolar amounts of both species followed by aliquots of either ctab or Triton X-100 and Tris buffer (pH 7.0). The mixture was diluted to the mark with purified water. The reactions were initiated and followed as described above (*a*).

Mass spectra

Electrospray mass spectra were obtained on a VG Bio-Q triple quadrupole mass spectrometer (VG Bio Tech, Altringham, Cheshire, U.K.) using a mobile phase of 50:50 aqueous methanol also containing 1% acetic acid. Electrospray mass spectra of each preformed complex and the corresponding ligand – copper salt mixture were identical.

References

1. F.M. Menger, L.H. Gan, E. Johnson, and D.H. Durst. J. Am. Chem. Soc. **109**, 2800 (1987).
2. G. De Santi, P. Scrimin, and U. Tonellato. Tetrahedron Lett. 4791 (1990).
3. R. Fornasier, P. Scrimin, P. Tecilla, and U. Tonellato. J. Am. Chem. Soc. **111**, 224 (1989).
4. J.H. van Esch, A.L.H. Stols, and R.J.M. Nolte. J. Chem. Soc. Chem. Commun. 1658 (1990).
5. T.J. Broxton and R.A. Cox. Can. J. Chem. **71**, 670 (1993).
6. J.G.J. Weinjen, A. Koudijs, and J.F.J. Engbersen. J. Chem. Soc. Perkin Trans. **2**, 1121 (1991).
7. F.M. Menger and C.E. Portnoy. J. Am. Chem. Soc. **89**, 4698 (1967).
8. C.A. Bunton. Catal. Rev. Sci. Eng. **20**, 1 (1979).
9. K. Ogino, H. Yamamoto, T. Yoshida, and W. Tagaki. Chem. Commun. 691 (1995).
10. P. Sykes. A guidebook to mechanism in organic chemistry. 6th ed. Longman Group Ltd., London. pp. 238–239. 1986.
11. R.L. Schowen, C.R. Hopper, and C.M. Bazikian. J. Am. Chem. Soc. **94**, 3095 (1972).
12. M.J. Saxby. Org. Mass. Spectrom. **2**, 835 (1969).
13. G. Ciampa. Ann. Chim. (Rome), **44**, 975 (1964); Chem. Abstr. **62**, 14559a (1965).
14. A.R. Fersht and A.J. Kirby. J. Am. Chem. Soc. **89**, 4853 (1967).
15. C.G. Overberger, T. St. Pierre, N. Vorcheimer, J. Lee, and S. Yoroslavsky. J. Am. Chem. Soc. **87**, 296 (1965).
16. J. Komives, A.F. Marton, and F. Dutka. Acta Acad. Sci. Hung. **88**, 183 (1976); Chem. Abs. **85**, 4818a (1976).
17. T.J. Broxton and M.J. Lucas. J. Phys. Org. Chem. **7**, 442 (1994).

Can. J. Chem. Downloaded from www.nrcresearchpress.com by 92.62.229.171 on 09/08/12
For personal use only.

© 1997 NRC Canada

Excess molar volumes and isothermal vapor–liquid equilibria in the tetrahydrofuran with propan-1-ol and propan-2-ol systems at 298.15 K

Julio A. Salas, Eleuterio L. Arancibia, and Miguel Katz

Can. J. Chem. Downloaded from www.nrcresearchpress.com by 92.62.229.171 on 09/08/12
For personal use only.

Abstract: Densities and vapor-liquid equilibria were determined for tetrahydrofuran with propan-1-ol and propan-2-ol systems at 298.15 K. From the experimental results, excess molar volumes and excess Gibbs free energies were calculated. Information could be obtained from the possible interaction between both chemical species in the two systems. The Prigogine–Flory–Patterson method was applied to calculate excess molar volumes. Liquid activity coefficients were calculated and correlated with different expressions existing in the literature.

Key words: excess molar volumes, vapor–liquid equilibria, activity coefficients, excess Gibbs free energies, tetrahydrofuran, propan-1-ol, propan-2-ol.

Résumé : Opérant à 298 K, on a déterminé les densités et les équilibres vapeur–liquide des systèmes formés de tétrahydrofurane et de propan-1-ol ou de propan-2-ol. Utilisant les données expérimentales, on a calculé les volumes molaires en excès ainsi que les énergies libres de Gibbs en excès. On a pu obtenir de l'information sur les interactions possibles entre les deux espèces chimiques dans chacun de ces deux systèmes. On a appliqué la méthode de Prigogine–Flory–Patterson au calcul des volumes molaires en excès. On a calculé les coefficients d'activité liquide et on a établi une corrélation avec les diverses expressions qui existent dans la littérature.

Mots clés : volumes molaires en excès, équilibres vapeur–liquide, coefficients d'activité, énergies libres de Gibbs en excès, tétrahydrofurane, propan-1-ol, propan-2-ol.

[Traduit par la rédaction]

Introduction

Excess thermodynamic properties such as excess molar volumes (V^E) and excess molar Gibbs free energies (G^E) were determined to obtain some information about interactions between molecules of tetrahydrofuran (THF) and the propanol (1-PR) and (2-PR) systems at 298.15 K. This is a continuation of our research on the thermodynamic properties of binary mixtures of non-electrolytes (1, 2).

With density data, V^E values have been calculated and the interactions between THF and propanols can be discussed in terms of Prigogine–Flory–Patterson (PFP) theory, which take into consideration only the physical aspects (Heintz and co-workers (3)). The chemical aspects can be calculated following ERAS's method (3), which takes into consideration the autoassociation of the alcohols, and gives great errors, probably because of the small values for V^E.

This paper presents also vapor–liquid equilibria (VLE) data on the two binary systems mentioned above. Different equations exist in the literature that calculate the activity coefficients in the liquid phase. In this work, some equations have been applied and the results compared with experimental data.

Received May 10, 1996.

J.A. Salas, E.L. Arancibia, and M. Katz.[1] Cátedra de Fisicoquimica, Instituto de Ingeniería Química, Facultad de Ciencias Exactas y Tecnologia, U.N.T. Avenida Independencia 1800, S.M. de Tucumán (4000), R. Argentina.

[1] Author to whom all correspondence may be addressed. Telephone: (081)-364093 (203). Fax: 54-81-248025. E-mail: termfis@herrera.unt. edu.ar

Experimental

The methods used in our laboratory have been described previously (1, 2). Densities were determined with an AP digital densimeter, model DMA 45. A thermostatically controlled bath constant to 0.01 K was used. Calibration was carried out with air and doubly distilled water, with an uncertainty of ±0.2 kg m^{-3}. Temperatures were read in a Digitec digital thermometer. Vapor–liquid equilibria data were determined using a modified version of the Boublik–Benson (4) still. Pressures were determined using a barocel transducer type 590, and a digital pressure display and controller model 1501 B. The estimated error was ±0.005 kPa in pressures.

The compositions of liquid and vapor condensed phases were determined from measurements of their densities at 298.15 K, using eq. [1]:

$$[1] \qquad \rho = x_1\rho_1 + x_2\rho_2 + x_1x_2\sum_{j=1}^{n} a_j(1-2x_1)^{j-1}$$

where x_1 and x_2 are the mole fractions of components 1 and 2, and ρ, ρ_1 and ρ are the densities of the solution and of the pure components, respectively. The parameters a_j were

© 1997 NRC Canada

Can. J. Chem. Downloaded from www.nrcresearchpress.com by 92.62.229.171 on 09/08/12
For personal use only.

Table 1. Densities and excess molar volumes at 298.15 K.

THF(1) + 1-PR(2)			THF(1) + 2-PR(2)		
x_1	$\rho \times 10^{-3}$ (kg m^{-3})	$V^E \times 10^6$ (m^3 mol^{-1})	x_1	$\rho \times 10^{-3}$ (kg m^{-3})	$V^E \times 10^6$ (m^3 mol^{-1})
0.0000	0.7996	—	0.0000	0.7813	—
0.0993	0.8044	0.038	0.0967	0.7905	0.106
0.1884	0.8153	0.084	0.2009	0.8007	0.177
0.3030	0.8253	0.068	0.2942	0.8099	0.221
0.3958	0.8341	−0.024	0.4083	0.8212	0.256
0.4864	0.8423	−0.0087	0.5034	0.8307	0.265
0.5961	0.8516	−0.119	0.5983	0.8402	0.262
0.6948	0.8595	−0.118	0.6969	0.8492	0.236
0.8050	0.8680	−0.101	0.8091	0.8620	0.152
0.8882	0.8742	−0.077	0.8949	0.8709	0.093
0.9106	0.8757	−0.057	1.0000	0.8819	—
1.0000	0.8819	—			

Table 2. Coefficients a_j and standard deviations σ determined by the method of least squares for THF(1) + 1-PR(2) and THF(1) + 2-PR(2) at 298.15 K.

	THF(1) + 1-PR(2)	THF(1) + 2-PR(2)
a_1	0.009777	−0.005106
a_2	−0.016246	0.001580
a_3	0.013345	0.000510
a_4	0.067158	−0.005047
a_5	−0.067752	—
a_6	−0.141271	—
ρ	4×10^{-4}	3×10^{-5}

determined by a linear least-squares equations-fitting procedure.

In each case, the optimum number of coefficients was ascertained from an examination of the variation of the standard error of estimate with n:

$$[2] \qquad \sigma = \{\sum(\rho_{obs} - \rho_{cal})^2/(n_{obs} - n)\}^{1/2}$$

(THF) (Merck puriss.) was used without further purification. (1-PR) and (2-PR) (Merck puriss.) were distilled and the middle fractions collected. Mixtures were prepared by mixing weighed amounts of the pure components. Caution was taken to prevent evaporation.

Results and discussion

Table 1 shows the densities and excess molar volumes of the two binary systems. Table 2 shows the adopted coefficients a_j and standard deviations of densities associated with the use of eqs. [1] and [2].

The excess molar volumes were calculated using the following expression:

$$[3] \qquad V^E = x_1 M_1(\rho^{-1} - \rho_1^{-1}) + x_2 M_2(\rho^{-1} - \rho_2^{-1})$$

where M_1 and M_2 are the molar masses of components 1 and 2, x_1 and x_2 are the mole fractions of the components, and ρ, ρ_1, and ρ_2 are the densities of the solutions and of the pure components. Each set of results was fitted using Redlich–Kister equations of the type:

$$[4] \qquad V^E = x_1 x_2 \sum_{k=1}^{n} a_k (1 - 2x_1)^{k-1}$$

and Table 3 shows the values of the coefficients a_k and their standard deviations defined by eq. [2].

Figure 1 shows the experimental values of V^E for the two systems at 298.15 K. The continuous curves were calculated from eq. [3], using the adopted values for the coefficients.

One of the systems (with 1-PR) shows a sigmoid curve for V^E, while the other system shows positive values of V^E. We deduce that, in a qualitative form, dispersion forces are dominant in the mixture with secondary alcohol, while in the mixture with 1-PR specific interactions exist. The alcohols are liquids associated by hydrogen bonds, and this association diminishes in the secondary alcohol. The addition of THF, which is a polar molecule but not associated in its pure state, produces a breaking in this association causing positive values of V^E in the mixture with 2-PR. In the other mixture, the addition of molecules of 1-PR to THF produces a breaking of association in the alcohol, leading to an association of alcohol monomers with THF of the type H—O- - -H (5) with a volume contraction greater than the dispersion forces. This effect is small; at $x_1 = 0.5$ it is about -0.25×10^{-6} m^3 mol^{-1}.

The application of ERAS's method in this case, assuming the constancy of autoassociation of the alcohol and equilibrium between the two components, gives great errors. Thus, we applied the PFP (6) theory, where V^E can be calculated with the following expression:

$$[5] \qquad \frac{V^E}{x_1 V_1^* + x_2 V_2^*} = \frac{(\tilde{V}^{1/3} - 1)\tilde{V}^{2/3}}{\frac{4}{3}\tilde{V}^{-1/3} - 1}\psi_1\theta_2\frac{X_{12}}{P_1^*} - \frac{(\tilde{V}_1 - \tilde{V}_2)^2(\frac{14}{9}\tilde{V}^{-1/2} - 1)}{(\frac{4}{3}\tilde{V}^{-1/3} - 1)\tilde{V}}\psi_1\psi_2 + \frac{(\tilde{V}_1 - \tilde{V}_2)(P_1^* - P_2^*)}{P_2^*\psi_1 + P_1^*\psi_2}\psi_1\psi_2 = \Delta V_{int} - \Delta V_F + \Delta V_{p*}$$

where the first term is the interactional contribution, the second term the free volume contribution, and the third one is the characteristic pressure contribution.

The various parameters involved in eq. [5] for the pure components (with subscripts) and the mixture (without subscripts) are obtained through the theory of Flory et al. (7). Table 4 shows the parameters used for the three substances, and Table 5 the values of X_{12} and the other contributions from eq. [5] and compared with experimental results.

Figure 1 shows the curves obtained with PFP theory, which agree well with experimental data in the THF (1) + 1-PR (2) system, showing a sigmoid curve, and indicating that the chemical interaction between the components is very small. In the other mixture, the agreement is not good when compared with experimental data.

© 1997 NRC Canada

Can. J. Chem. Downloaded from www.nrcresearchpress.com by 92.62.229.171 on 09/08/12
For personal use only.

Table 3. Coefficients from eq. [3] and σ for V^E at 298.15 K.

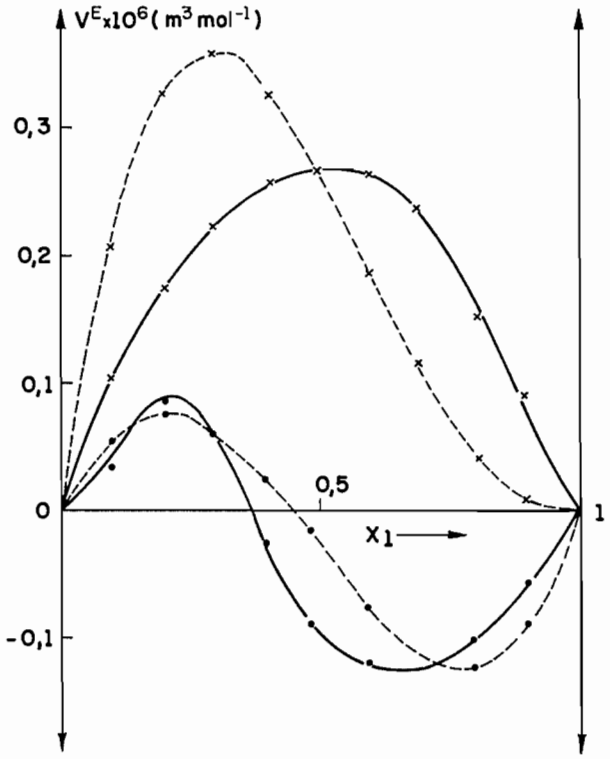
System	a_1	a_2	a_3	a_4	a_5	a_6	ρ
THF(1) + 1-PR (2)	−0.369	1.01	1.82	0.60	−2.37	−1.70	0.008
THF(1) + 2-PR (2)	1.07	−0.08	0.0	0.40	—	—	0.004

Table 4. Parameters for the pure liquids at 298.15 K.

Substance	$a \times 10^4$ (K^{-1})	$\kappa \times 10^7$ (kPa^{-1})	$V^* \times 10^6$ ($m^3\ mol^{-1}$)	$P^* \times 10^{-6}$ ($J\ m^{-3}$)	$\tilde{V}$	$\tilde{T}$
THF	18.40[a]	1.045[b]	58.4970	1026	1.3977	0.075573
1-PR	10.04[a]	1.026[a]	60.1971	455	1.2485	0.057117
2-PR	10.64[a]	1.332[a]	81.0130	379	1.2607	0.058948

[a]Reference 15.
[b]Reference 16.

Fig. 1. Excess molar volumes: (·····) THF(1) + 1-PR(2); (× × × ×) THF(1) + 2-PR(2) at 298.15 K. Continuous curves are calculated from eq. [3]. (— — —): curves calculated from eq. [5].



Analysis of the three contributions to V^E shows that the interactional contribution is the most important, negative in all cases, and larger than the free volume. The P^* also are important, due to the large difference that exists between the characteristic pressures.

The activity coefficients of the components in the liquid phase were calculated from the experimental data by employing the following equation:

$$[6] \qquad \ln \gamma_i = \ln \frac{y_i P}{x_i P_i} + \frac{(B_{ii} - V_i)(P - P_i)}{RT} + (1 - y_i)^2 \frac{P\delta}{RT}$$

Table 5. Experimental and theoretical V^E at 298.15 K.

	THF(1) + 1-PR(2) $x_1 = 0.4864$	THF(1) + 2-PR(2) $x_1 = 0.5034$
$X_{12} \times 10^6$ ($m^3\ mol^{-1}$)	−121.6	−107.0
ΔV_{int} ($m^3\ mol^{-1}$)	-2.2×10^{-2}	-2.2×10^{-2}
ΔV_F ($m^3\ mol^{-1}$)	7.1×10^{-3}	5.5×10^{-3}
ΔV_{P^*} ($m^3\ mol^{-1}$)	2.9×10^{-2}	3.2×10^{-2}
V^E ($m^3\ mol^{-1}$)	-1.8×10^{-2}	0.261
V^e ($m^3\ mol^{-1}$)	-8.7×10^{-2}	0.265

Table 6. Experimental VLE results and activity coefficients for the THF(1) + 1-PR(2) system at 298.15 K.

x_1	y_1	P (kPa)	γ_1	γ_2
0.049	0.359	4.15	1.434	0.990
0.302	0.805	10.33	1.283	1.022
0.379	0.848	11.90	1.240	1.033
0.441	0.874	13.15	1.213	1.047
0.511	0.897	14.35	1.171	1.071
0.559	0.909	15.20	1.150	1.100
0.665	0.933	16.80	1.095	1.178
0.750	0.950	18.03	1.059	1.278
0.800	0.959	18.50	1.045	1.367
0.877	0.972	19.70	1.015	1.532

where x_1 and y_i are the mole fractions in the liquid phase and vapor phase, respectively. P and P_i are the vapor pressures of the mixture and of the pure components; V_i is the molar volume of the pure components. The values of $\delta = 2B_{12} - B_{11} - B_{22}$ where B_{11} and B_{22} are the virial coefficients and B_{12} the cross virial coefficient. For THF, $B_{11} = -1280 \times 10^{-6}$ m^3 mol^{-1}; for 1-PR, $B_{22} = -2609 \times 10^{-6}$ m^3 mol^{-1}; for 2-PR, $B_{22} = -2407 \times 10^{-6}$ m^3 mol^{-1}. For the mixtures THF(1) + 2-PR (2), $B_{12} = -1879 \times 10^{-6}$ m^3 mol^{-1} and for THF(1) + 2-PR (2), $B_{12} = -1852 \times 10^{-6}$ m^3 mol^{-1}.

These values were estimated from the method of Hayden and O'Connell (8). Tables 6 and 7 show the molar fractions of liquid, vapor pressures, and activity coefficients calculated with eq. [6].

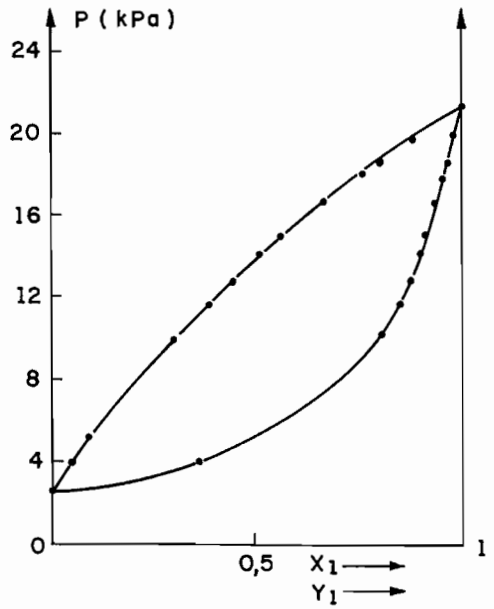
© 1997 NRC Canada

Can. J. Chem. Downloaded from www.nrcresearchpress.com by 92.62.229.171 on 09/08/12
For personal use only.

Table 7. Experimental VLE results and activity coefficients for the THF(1) + 2-PR(2) system at 298.15 K.

x_1	y_1	P (kPa)	γ_1	γ_2
0.118	0.400	8.50	1.344	0.998
0.195	0.530	10.07	1.275	1.013
0.250	0.595	11.00	1.219	1.022
0.300	0.647	11.89	1.193	1.033
0.354	0.695	12.90	1.180	1.045
0.404	0.730	13.85	1.145	1.067
0.470	0.769	14.69	1.117	1.098
0.546	0.809	15.86	1.091	1.143
0.613	0.838	16.80	1.086	1.204
0.721	0.878	18.15	1.045	1.380
0.880	0.943	20.10	0.998	1.627

Fig. 2. Vapor pressures vs. mole fractions of THF(1) + 1-PR(2) system at 298.15 K.



Figures 2 and 3 show the vapor pressure for both systems versus x_i and y_i.

The thermodynamic consistency of the VLE was determined using the method of Barker described by Fredenslund et al. (9).

Knowing activity coefficients, we can calculate the excess molar Gibbs free energies with the following expression:

$$[7] \qquad G^E = RT(x_1 \ln \gamma_1 + x_2 \ln \gamma_2)$$

which gives positive values for both systems. To calculate the entropy of these systems, we need enthalpies, which could be calculated by the UNIFAC method (10). For both systems the values of entropies are positive and small, indicating that dispersion forces are dominant in this case.

The experimental data of VLE were correlated with the three-suffix Margules (11) equation, Wilson (12) equations, NRTL (13) equations, and UNIFAC (14) methods.

The parameters in these equations were obtained by minimizing the root-mean-square deviations in P and y. The procedure is known as Barker's method. Values of P and y are calculated with the following expressions:

Fig. 3. Vapor pressures vs. mole fractions of THF(1) + 2-PR(2) system at 298.15 K.

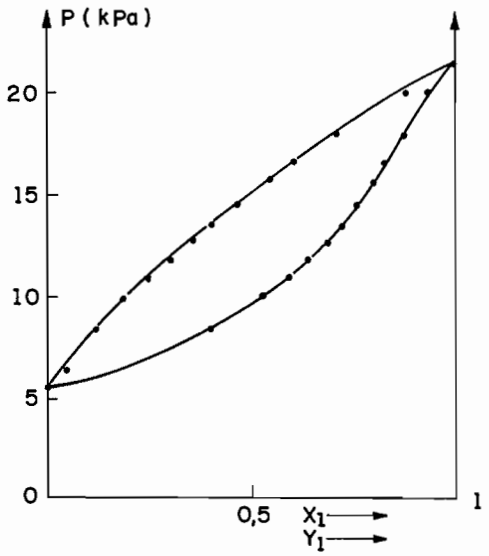


Table 8. Standard deviations in P and y for both systems at 298.15 K.

	THF(1) + 1-PR(2)		THF(1) + 2-PR(2)	
	SD_p (kPa)	SD_y	SD_p (kPa)	SD_y
Margules	0.07	0.005	0.05	0.007
Wilson	0.06	0.001	0.33	0.01
NRTL	0.05	0.002	0.34	0.01
UNIFAC	0.68	0.016	1.35	0.03

$$[8] \qquad P_{cal} = x_1\gamma_1 P_1^0 + x_2\gamma_2 P_2^0$$

$$[9] \qquad y_{cal} = x_1\gamma_1 P_1^0 / P_{cal}$$

over the complete concentration range, where P_i^0 is

$$[10] \qquad P_i^0 = P_i \exp\left[\frac{(V_i - B_{ii})(P - P_i)(1 - y_i)^2}{RT}\right]$$

The standard deviations (SD) in pressures and in vapor phase mole fractions are calculated by:

$$[11] \qquad SD = \left[\frac{\sum(M_{exp}^E - M^E)}{n}\right]^{1/2}$$

where M is P or y. These values are shown in Table 8.

Conclusions

From the Margules equations $A = 0.2896$ and $B = 0.6852$ for THF(1) + 1-PR(2) and $A = 0.3084$, $B = 0.4353$ for the THF(1) + 2-PR(2) system. For the Wilson equations

© 1997 NRC Canada

$\Lambda_{12} = 1.3479$ and $\Lambda_{21} = 0.3491$ for THF(1) + 1-PR(2) and $\Lambda_{12} = 1.4761$, $\Lambda_{21} = 0.3491$ for THF(1) + 2-PR(2). For the NRTL equations with $\alpha = 0.30$ as a constant, $A = 1.3359$, $B = 0.5553$ for THF(1) + 1-PR(2) and $A = 1.4558$, $B = 0.6511$ for the THF(1) + 2-PR(2) system. The contribution groups of UNIFAC theory (14) is the last method applied to the two systems. Table 8 shows that for mole fractions the Wilson equations agree very well with minor deviation, and the Margules equations for the THF(1) + 2-PR(2).

For pressures, NRTL for THF(1) + 1-PR(2) and the Margules equations for THF(1) + 2-PR(2) show minor deviation. The UNIFAC method gives great errors in both mole fractions and pressures.

Acknowledgment

This work was financed by a research grant from the Consejo de Investigaciones, Universidad Nacional de Tucumán (CIUNT).

References

1. S.M. Bardavid, G.C. Pedrosa, and M. Katz. Lat. Am. Appl. Res. **22**, 225 (1992).
2. I.L. Acevedo, E.L. Arancibia, and M. Katz. J. Solution Chem. **22**, 191 (1993).
3. H. Kaur, N.S. Samra, B.S. Mahl, J.R. Khurma, M. Bender, and A. Heintz. Fluid Phase Equilib. **67**, 241 (1991).
4. T. Boublik and C. Benson. Can. J. Chem. **47**, 539 (1969).
5. A. Nath and F. Bender. Fluid Phase Equilib. **7**, 276 (1981).
6. T.M. Letcher and R.C. Baxter. J. Solution Chem. **18**, 65 (1989).
7. P.J. Flory, R.A. Orwoll, and A. Vrij. J. Am. Chem. Soc. **86**, 3507 (1964).
8. J.G. Hayden and J.P. O'Connell. Ind. Eng. Chem. Process. Des. Dev. **14**, 209 (1975).
9. A. Fredenslund, J. Gmehling, and P. Rasmussen. Vapor–liquid equilibrium using UNIFAC. Elsevier Scientific Publishing Company, Amsterdam. (1977).
10. P. Dang and D.P. Tassios Ind. Eng. Chem. Process Des. Dev. **25**, 22 (1986).
11. J.M. Prausnitz. *In* Molecular thermodynamics of fluid phase equilibria. *Edited by* N.R. Admunson. Prentice Hall, Inc. Englewood Cliffs, N.J. 1969.
12. A.G. Wilson. J. Am. Chem. Soc. **86**, 127 (2964).
13. H. Renon and J.M. Prausnitz. AIChEJ. **14**, 135 (1968).
14. J. Gmehling, P. Rasmussen, and A. Fredenslund. Ind. Eng. Chem. Process, Des. Dev. **21**, 116 (1982).
15. J.A. Riddick, W.B. Bunger, and T.K. Sakano. Organic solvents. 4th ed. Wiley & Sons, New York. 1988.
16. A.J. Richard and K.S. Rogers. Can. J. Chem. **49**, 3956 (1971).

Can. J. Chem. Downloaded from www.nrcresearchpress.com by 92.62.229.171 on 09/08/12
For personal use only.

© 1997 NRC Canada

Metal complexes of propane-1,2,3-triamine. Potentiometric and calorimetric investigations

Renzo Cini, Antonio Sabatini, Alberto Vacca, and Fabrizio Zanobini

Abstract: The complexes formed by the ions Co^{2+}, Ni^{2+}, Cu^{2+}, and Zn^{2+} with the ligand propane-1,2,3-triamine (L^1) in 0.15 mol dm^{-3} aqueous NaCl at 25°C have been studied by potentiometry and calorimetry (ligand to metal molar ratio, 1–3; pH range from 3.0 to 6.5–11.0). Stability constants have been obtained from potentiometric data by means of the least-squares program HYPERQUAD for the following species: $[M(L^1)]^{2+}$ and $[MH(L^1)]^{3+}$ for all four metal cations; $[M(L^1)_2]^{2+}$ and $[MH(L^1)_2]^{3+}$ for Ni^{2+}, Cu^{2+}, and Zn^{2+}; $[MH_2(L^1)_2]^{4+}$ for Ni^{2+} and Cu^{2+}; and $[M(OH)(L^1)]^{+}$ for Cu^{2+} only. Stabilities increase in the order Zn < Co < Ni < Cu. The complexes of L^1 have approximately the same stability as the corresponding ones formed by the related triamines 2-methyl (2-methylamine) propane-1,3-diamine (L^3) and 2-ethyl (2-methylamine)propane-1,3-diamine (L^4). The stability constants have been used to obtain, from the calorimetric titration experiments, the formation enthalpies of all the metal complexes except those for cobalt(II) as well as the corresponding entropy changes. The thermodynamic quantities are compared with the corresponding values previously found for L^3, in order to derive information about the coordination ability of the ligand. The analysis suggests that the unprotonated ligand forms a *fac*-tridentate complex in most cases, but for some species, such as $[Cu(L^1)_2]^{2+}$, $[CuH(L^1)_2]^{3+}$, and $[Zn(L^1)]^{2+}$, the thermodynamic quantities indicate that at least one of the nitrogen atoms of the triamine is either loosely bonded or not coordinated to the metal ion. A gas-phase molecular mechanics analysis shows that the strain energies of the *fac*-$[Co(L^1)_2]^{2+}$ and -$[Ni(L^1)_2]^{2+}$ symmetrical (s) and unsymmetrical (u) isomers are very similar. If the same solvation energy is assumed for the two isomers, each isomer will be present in roughly equal amounts in solution.

Key words: propane-1,2,3-triamine, potentiometry, calorimetry, complexation, cobalt, nickel, copper, zinc.

Résumé : On a étudié les complexes formés par les ions Co^{2+}, Ni^{2+}, Cu^{2+} et Zn^{2+} avec le ligand propane-1,2,3-triamine (L^1) dans du NaCl aqueux 0.15 mol dm^{-3} à 25°C en utilisant la potentiométrie et calorimétrie (ligand : métal = 1–3; dans des intervalles de pH compris entre 3 et 6,5–11,0). Les constantes de stabilité ont été obtenues à partir des données potentiométriques par la méthode des moindres carrés du programme HYPERQUAD pour les espèces suivantes : $[M(L^1)]^{2+}$ et $[MH(L^1)]^{3+}$ pour les quatre cations métalliques; $[M(L^1)_2]^{2+}$ et $[MH(L^1)_2]^{3+}$ pour les cations Ni^{2+}, Cu^{2+} et Zn^{2+}; $[MH_2(L^1)_2]^{4+}$ pour les cations Ni^{2+} et Cu^{2+} et $[M(OH)(L^1)]^{+}$ pour l'ion Cu^{2+} seulement. Les constantes de stabilité augmentent dans l'ordre Zn < Co < Ni < Cu. La stabilité des complexes de L^1 est approximativement la même que celle des complexes correspondants formés avec les triamines apparentées 2-methyl(2-méthylamine)propane-1,3-diamine (L^3) et 2-éthyl(2-méthylamine)propane-1,3-diamine (L^4). On a utilisé les constantes de stabilité pour obtenir, par titration calorimétrique, les enthalpies de formation de tous les complexes exceptés ceux du cobalt(II) ainsi que les variations d'entropie correspondantes. On a comparé les quantités thermodynamiques aux valeurs correspondantes, trouvées antérieurement pour L^3 dans le but d'obtenir des informations sur la capacité de coordination du ligand. L'analyse suggère que le ligand non protoné forme, dans la plupart des cas, un complexe *fac*-tridenté, mais pour quelques espèces comme $[Cu(L^1)_2]^{2+}$, $[CuH(L^1)_2]^{3+}$ et $[Zn(L^1)]^{2+}$, les valeurs des entités thermodynamiques suggèrent qu'au moins un des atomes de la triamine est faiblement lié ou pas du tout coordonné à l'ion métallique. Une analyse de mécanique moléculaire en phase gazeuse montre que les énergies de tension des isomères *fac*-$[Co(L^1)_2]^{2+}$ et -$[Ni(L^1)_2]^{2+}$ symétriques (s) et non symétriques (u) sont très similaires. Si on suppose que les deux isomères ont la même énergie de solvatation, chacun d'eux devrait alors être approximativement en quantités égales, dans la solution.

Mots clés : propane-1,2,3-triamine, potentiométrie, calorimétrie, complexation, cobalt, nickel, cuivre, zinc.

Received August 7, 1996.

R. Cini.[1] Dipartimento di Scienze e Tecnologie Chimiche e dei Biosistemi, Universitá di Siena, Pian dei Mantellini 44, I-53100 Siena, Italy.
A. Sabatini and A. Vacca. Dipartimento di Chimica, Universitá di Firenze, Via Maragliano 77, I-50144 Firenze, Italy.
F. Zanobini. Istituto per lo Studio della Stereochimica ed Energetica dei Composti di Coordinazione, Consiglio Nazionale delle Ricerche, Via I. Nardi 39, I-50132 Firenze, Italy.

[1] Author to whom correspondence may be addressed. Telephone: ++39 577 298041. Fax: ++39 577 280004. E-mail: cini@unisi.it

© 1997 NRC Canada

Can. J. Chem. Downloaded from www.nrcresearchpress.com by 92.62.229.171 on 09/08/12
For personal use only.

Can. J. Chem. Downloaded from www.nrcresearchpress.com by 92.62.229.171 on 09/08/12
For personal use only.

Introduction

Polyamines and metal cations have a very important place in the biochemistry of nucleic acids, in many processes of living cells, in the treatment of human diseases, and being useful as well as probes for the investigation of the structure of biopolymers (1–12). Natural polyamines like spermine, putrescine, and spermidine are required for optimal growth and development of cells (13). The presence of metal cations is often an important factor (either stimulating or inhibiting) in determining the activity of polyamines (13). As biological polyamines are linear aliphatic chain molecules, the interactions of branched polyamines with biopolymers have not been so extensively investigated. A knowledge of the coordination chemistry of polyamines is important for the understanding of structure–thermodynamic and structure–spectroscopic relationships; it is also crucial in the understanding of reaction mechanism pathways (14–16). We now report the results of a detailed investigation into the relationship between structure and coordinating ability in some small branched triamines. The complexes formed in aqueous solution between Co(II), Ni(II), Cu(II), and Zn(II) and the ligand propane-1,2,3-triamine (Scheme 1, L^1) have been examined by potentiometry and calorimetry. The careful analysis of the data has led to a deep speciation of the systems investigated. A ^{13}C NMR spectroscopy and molecular mechanics investigation on $[CoL^1]^{3+}$ was reported previously (17).

The four ligands shown in Scheme 1 are potentially tridentate and may form a *fac* octahedral complex. When all the nitrogen atoms are coordinated to the metal ion three chelate rings result. With L^2, L^3, and L^4 all three rings are six-membered, whereas with L^1 one ring is six-membered and the other two are five-membered. We have therefore been able to obtain some information regarding the strain energy associated with the formation of this type of condensed chelate ring system by molecular mechanics calculations.

Experimental

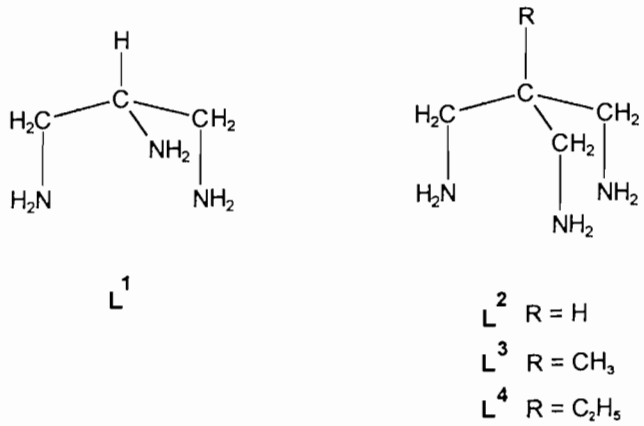
Materials

Propane-1,2,3-triamine (L^1) hydrochloride was obtained according to the procedure outlined in ref. 18. Preparation, recrystallization, and analysis of the hydrochloride, $L^1 \cdot 3HCl$, has been reported previously (19). A stock solution of 0.1 mol dm^{-3} $L^1 \cdot 3HCl$ was prepared by dissolving the crystalline solid in 0.15 mol dm^{-3} NaCl. The content of L^1 in the solution was measured by alkalimetric titration, by using the procedure previously described (19).

Analytical grade cobalt(II), nickel(II), copper(II), and zinc(II) chlorides were obtained from Merck and C. Erba. Suprapur NaCl was obtained from Merck. All the salts were used without any further purification. Approximately 0.1 mol dm^{-3} metal chloride stock solutions were prepared by dissolving the salts in 0.15 mol dm^{-3} NaCl. The metal content was accurately determined by standard analytical methods (20).

Solutions of HCl and NaOH were prepared by dilution of concentrated solutions taken from Merck ampoules. The NaOH solution was standardized as before (19). The potentiometric cell was calibrated by the Gran procedure (21). K_w in 0.15 mol dm^{-3} NaCl solution at 25°C was taken as 1.72×10^{-14} mol^2 dm^{-6} ($pK_w = 13.76$).

Scheme 1.



Potentiometric titrations

The titrations were carried out at 25.0 ± 0.1°C by using the same instrumentation and procedure described before (19). All the solutions were maintained under ultrapure nitrogen during the titrations. With the cobalt(II)–L^1 system either nitrogen, first passed through a 1/4 in. OXY-TRAP column (Alltech), or ultrapure argon were used.

The basicity constants of the ligand have been reported previously (19). The cobalt(II)–, nickel(II)–, copper(II)–, and zinc(II)–L^1 systems were studied by acid–base titrations performed with an experimental procedure similar to that used for the determination of the protonation constants. The solutions contained known amounts of $L^1 \cdot 3HCl$ (ca. 2 mmol dm^{-3}, 25 cm^3) and metal salts. The ligand–metal molar ratio ranged from 1.5 to 3.0. During the titrations of the cobalt(II)–, copper(II)–, and zinc(II)–L^1 systems, the emf values became stable within ca. 10 s from the titrant addition. The collection parameters were as follows. The time interval between two consecutive blocks of 10 readings, 3 s; the maximum allowed standard deviation and the tolerance between the first and the tenth mean value were both 0.05 mV. About 20 emf readings were usually enough to get steady values with Co, Cu, and Zn, but more readings were necessary in the Ni titrations because of the relative inertness of the Ni(II) complexes (22). The starting pH values for all the M–L^1 systems were about 3. There was no backwards drift in electrode readings up to pH 6.5, 11.0, 8.2, and 9.5 for the cobalt(II)–, nickel(II)–, copper(II)–, and zinc(II)–L^1 systems, respectively.

The formation constants of the metal complexes were calculated with the least-squares computer program HYPERQUAD (23). In this program the sum of the weighted squared residuals on the observed emf values is minimized. The weights were derived from the estimated errors in emf (0.2 mV) and titrant volume (0.002 cm^3). The most probable chemical model was selected by following a strategy (24) based on statistical inferences applied to σ^2. The sample standard deviation should be 1, in the absence of systematic errors and when a correct weighting scheme is used. However, the agreement is considered good for standard deviation values smaller than 3 ($\sigma^2 < 9$). Values of σ^2 lower than 7 were obtained for all the refined equilibrium models in the present work.

© 1997 NRC Canada

Table 1. Logarithms of the cumulative formation constants of the M^{II}–L^1 complexes determined in aqueous 0.15 M NaCl solution at 298 K.[a]

M	$[ML^1]^{2+}$	$[MHL^1]^{3+}$	$[ML^1_2]^{2+}$	$[MHL^1_2]^{3+}$	$[MH_2L^1_2]^{4+}$	$[M(OH)L^1]^+$
Co	7.18(2)	14.024(7)				
Ni	9.35(2)	15.613(6)	17.398(8)	24.318(8)	30.24(1)	
Cu	10.41(4)	18.26(1)	19.60(2)	27.77(2)	35.21(2)	2.46(2)
Zn	6.66(1)	13.97(1)	11.55(2)	19.49(4)		

[a]Values in parentheses are estimated standard deviations in the last significant figure.

Can. J. Chem. Downloaded from www.nrcresearchpress.com by 92.62.229.171 on 09/08/12
For personal use only.

Calorimetric titrations

Stepwise titrations were performed using an LKB thermal activity monitor (model 2277) equipped with a perfusion/titration system and a Hamilton pump (model Microlab M). Both the calorimetric system and the Hamilton pump were controlled by means of a personal computer (IBM PS/2 model 30) running the program AUTOTAM (25). Chemical calibration of the apparatus was accomplished by measuring the heat of neutralization of hydrochloric acid by sodium hydroxide in aqueous 0.15 mol dm^{-3} NaCl. The value obtained, $\Delta H° = -56.0 \pm 0.2$ kJ mol^{-1}, is in excellent agreement with the values previously reported (26). A typical calorimetric titration consisted of 10–15 injections (10–15 mm^3 each) of 0.2 mol dm^{-3} aqueous NaOH into the reaction cell; the cell contained 1.5 cm^3 of a 2×10^{-3} mol dm^{-3} solution of $L^1 \cdot 3HCl$ in the presence of variable quantities of the appropriate metal(II) chloride (ligand to metal molar ratio ranging from 1 to above 2) in aqueous NaCl (0.15 mol dm^{-3}). The enthalpies of complex formation were calculated using the least-squares program KK95, an updated version of the program previously used by this group (27). The values of the enthalpies of stepwise protonation of the ligand used in the calculations ($\Delta H°_1 = 45.9 \pm 0.2$, $\Delta H°_2 = 46.3 \pm 0.3$, $\Delta H°_3 = 35.6 \pm 0.3$ kJ mol^{-1}) were taken from ref. 19. Calorimetric measurements involving the oxidizable cobalt(II) complexes have not been attempted since an inert atmosphere cannot be maintained inside the calorimeter.

Calculations

The strain energies of the complexes $[M(L^1)_2]^{2+}$ (M = Co, Ni) were computed as the sum of bond length deformation, valence angle deformation, torsional angle deformation, nonbonding interaction, and electrostatic contribution: $E_{tot} = E_b + E_\theta + E_\phi + E_{nb} + E_\varepsilon$. The MM2 force field (28) was used in the MacroModel package version 3.0 implementation (29). The force field was extended to take into account interactions between the metal center and the donor atoms. The atomic charges (see deposited material[2]) were computed through the molecular orbital extended-Hückel method of the ICONC&INPUTC package (30) without any optimization of the geometry and with distance-dependent weighted Wolfsberg–Helmholz formulas. The self-consistent charge interaction calculation on the Co and Ni atom was performed on the complex molecules. The VSIE (valence state ionization energy) parameters for the metal ions are those implemented in the ICONC&INPUTC package. The force field parameters were tested against the structure of s-*fac*-$[Co^{III}(L^1)_2]Cl_3$ (31) (s = symmetrical) and are in good agreement with values previously published (32). The starting structures of the s/u-*fac*-$[M^{II}(L^1)_2]^{2+}$ (u = unsymmetrical) complexes were generated from the s-*fac*-$[Co^{III}(L^1)_2]^{3+}$ structure via MacroModel at an Evans & Sutherland PS390 graphics terminal. Details of the molecular mechanics calculations are as before (33).

[2] Copies of material on deposit may be purchased from: The Depository of Unpublished Data, Document Delivery, CISTI, National Research Council Canada, Ottawa, Canada K1A 0S2.

Results and discussion

Characterization of the equilibrium models

Table 1 shows the values of the logarithms of the cumulative formation constants of the metal complexes that have been identified as being present in appreciable concentrations under the experimental conditions of the titrations. The relevant equilibria are described by eq. [1] and the corresponding equilibrium constants β_{pqr} are defined as in eq. [2].

$$[1] \quad pM^{2+} + qH^+ + rL = M_pH_qL_r^{(2p+q)+}$$

$$[2] \quad [M_pH_qL_r^{(2p+q)+}] = \beta_{pqr}[M^{2+}]^p[H^+]^q[L]^r$$

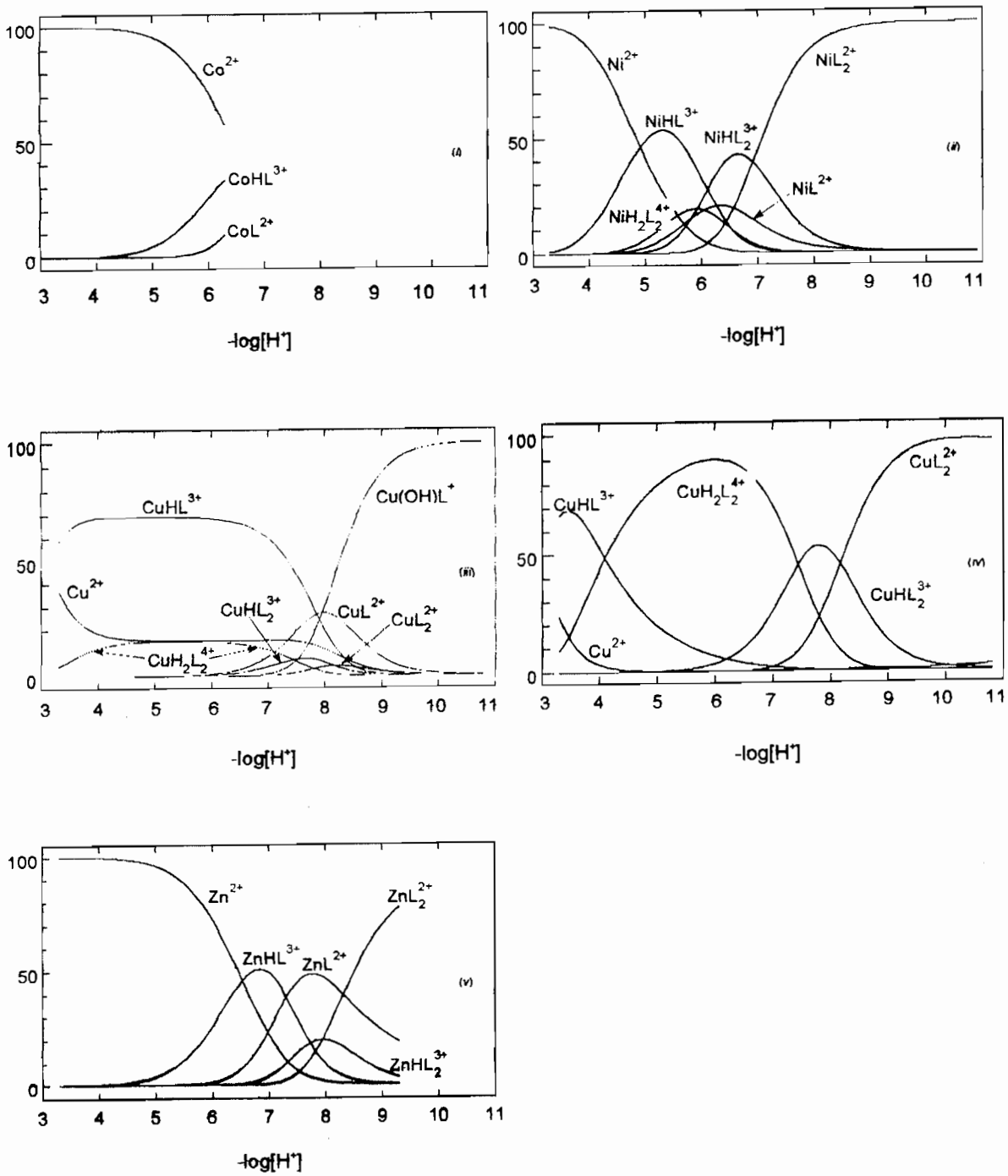
The results can be compared both with those obtained previously for the same ligand (34) and with those of the other ligands shown in Scheme 1, 1,1,1-tris(aminomethyl)alkanes L^2 (35, 36), L^3 (37), and L^4 (38). Distribution curves for the M^{II}–L^1 systems are shown in Figure 1.

In the cobalt(II)–L^1 system, emf measurements could not be carried out above pH 6.5 owing to precipitation and (or) oxidation reactions in spite of stringent precautions. The limited pH interval does not allow extensive coordination of the metal ion to occur: only the $[CoHL^1]^{3+}$ and $[CoL^1]^{2+}$ complexes are formed, with a total degree of formation of less than 50%. The species that we have found are the same as those found by Prue and Schwarzenbach (34). The values of the equilibrium constants given by those authors for reactions at 20°C in the medium 0.1 mol dm^{-3} KCl, $\log \beta_{101} = 6.8$, $\log \beta_{111} = 13.7$, are in satisfactory agreement with the values obtained by us at 25°C in 0.15 mol dm^{-3} NaCl. In the cobalt(II)–L^2 system (36), the diprotonated complex $[CoH_2L^2]^{4+}$ was also characterized.

In the titration of a mixture of nickel(II) and L^1 (molar ratio 1:2) appreciable concentrations of $[Ni(L^1)]^{2+}$, $[NiH(L^1)]^{3+}$, $[Ni(L^1)_2]^{2+}$, $[NiH(L^1)_2]^{3+}$, and $[NiH_2(L^1)_2]^{4+}$ were found within the pH range studied. The complex $[Ni(L^1)_2]^{2+}$ is practically the only species present at pH above 9. The first two complexes were identified in an earlier investigation (34); the

© 1997 NRC Canada

Fig. 1. Distribution diagrams for the M–L^1 systems. The percentages of the complexes are calculated for titration curves where the analytical concentrations of metal ion and ligand are as follows: (*i*) T_{Co} = 2 mM, T_L = 2 mM; (*ii*) T_{Ni} = 1 mM, T_L = 2 mM; (*iii*) T_{Cu} = 2 mM, T_L = 2 mM; (*iv*) T_{Cu} = 1 mM, T_L = 2 mM; (*v*) T_{Zn} = 1 mM, T_L = 2 mM.



reported values of the formation constants, log β_{101} = 9.3 and log β_{111} = 15.6, are in excellent agreement with the corresponding values determined in the present study. With L^2, only $[NiL^2]^{2+}$ and $[NiHL^2]^{3+}$ were previously found (35, 36), whereas the same species identified in this study with L^1, except for $[NiH_2(L^1)_2]^{4+}$, had been found before in the case of L^3 and L^4 (37, 38).

Reaction of copper(II) with L^1 produces six different complexes, $[CuL^1]^{2+}$, $[CuHL^1]^{3+}$, $[Cu(L^1)_2]^{2+}$, $[CuH(L^1)_2]^{3+}$, $[CuH_2(L^1)_2]^{4+}$, and $[Cu(OH)L^1]^+$, corresponding to the set of species already identified with similar triamines: L^3 and L^4 (37, 38). Prue and Schwarzenbach (34) characterized only $[CuL^1]^{2+}$. The agreement between the values of the formation constants determined in that study (log β = 11.1, 18.4, 20.1, and 28.0) and those obtained in the present work is satisfactory. The formation of $[CuH_2L^2]^{4+}$ has also been reported (36).

© 1997 NRC Canada

Can. J. Chem. Downloaded from www.nrcresearchpress.com by 92.62.229.171 on 09/08/12
For personal use only.

Table 2. Thermodynamic functions $\Delta G°$, $\Delta H°$ (kJ mol^{-1}), and $\Delta S°$ (J K^{-1} mol^{-1}) for stepwise reactions involving cobalt(II), nickel(II), copper(II), and zinc(II) complexes of L^1 and L^3 at 298 K.[a]

	L = L[1b]			L = L[3c]		
	$-\Delta G°$	$-\Delta H°$	$\Delta S°$	$-\Delta G°$	$-\Delta H°$	$\Delta S°$
$Co^{2+} + L = [CoL]^{2+}$	41.0(2)					
$Co^{2+} + HL^{+} = [CoHL]^{3+}$	25.00(6)					
$[CoL]^{2+} + H^{+} = [CoHL]^{3+}$	39.1(1)					
$Ni^{2+} + L = [NiL]^{2+}$	53.4(1)	41(1)	42(4)	57.95(4)	44.6(3)	45(1)
$[NiL]^{2+} + L = [NiL_2]^{2+}$	45.9(1)	42(3)	13(10)	40.63(8)	46.0(3)	−18(1)
$[NiHL]^{3+} + L = [NiHL_2]^{3+}$	49.69(3)	44(3)	19(10)	48.6(3)	40(1)	29(4)
$Ni^{2+} + HL^{+} = [NiHL]^{3+}$	34.03(3)	30(1)	14(3)	30.7(1)	31.4(8)	−2(3)
$[NiL]^{2+} + HL^{+} = [NiHL_2]^{3+}$	30.4(1)	33(3)	−9(10)	21.3(4)	27(2)	−19(8)
$[NiHL]^{3+} + HL^{+} = [NiH_2L_2]^{4+}$	28.4(1)	33(4)	−15(14)			
$[NiL]^{2+} + H^{+} = [NiHL]^{3+}$	35.73(6)	35(1)	2(4)	30.7(1)	36.0(8)	−18(3)
$[NiL_2]^{2+} + H^{+} = [NiHL_2]^{3+}$	39.50(3)	36(2)	12(7)	38.7(3)	30(2)	29(8)
$[NiHL_2]^{3+} + H^{+} = [NiH_2L_2]^{4+}$	33.79(6)	34.3(4)	−2(2)			
$Cu^{2+} + L = [CuL]^{2+}$	59.4(2)	59(3)	1(11)	62.63(8)	63.6(8)	−3(3)
$[CuL]^{2+} + L = [CuL_2]^{2+}$	52.5(3)	46(4)	22(14)	44.1(1)	31.8(8)	41(3)
$[CuHL]^{3+} + L = [CuHL_2]^{3+}$	54.28(6)	50(2)	14(7)	49.41(8)	42.7(4)	23(2)
$Cu^{2+} + HL^{+} = [CuHL]^{3+}$	49.20(6)	51.9(8)	−9(3)	46.99(4)	52.1(1)	−17.1(5)
$[CuL]^{2+} + HL^{+} = [CuHL_2]^{3+}$	44.1(3)	43(4)	4(14)	33.8(1)	31.0(8)	9(3)
$[CuHL]^{3+} + HL^{+} = [CuH_2L_2]^{4+}$	41.77(5)	47.7(8)	−20(3)	33.18(8)	46.4(4)	−44(2)
$[CuL]^{2+} + H^{+} = [CuHL]^{3+}$	44.8(2)	39(3)	19(11)	42.34(8)	37.7(8)	16(3)
$[CuL_2]^{2+} + H^{+} = [CuHL_2]^{3+}$	46.63(6)	43(1)	12(4)	47.66(8)	48.5(4)	−3(2)
$[CuHL_2]^{3+} + H^{+} = [CuH_2L_2]^{4+}$	42.47(6)	43.5(8)	−3(3)	41.76(8)	53.1(8)	−38(3)
$[CuL]^{2+} + OH^{-} = [Cu(OH)L]^{+}$	33.2(3)	17.6(4)	52(1)	31.5(1)	2(3)	99(10)
$Zn^{2+} + L = [ZnL]^{2+}$	38.0(2)	22.2(4)	53(2)	37.74(4)	25.4(3)	41(1)
$[ZnL]^{2+} + L = [ZnL_2]^{2+}$	27.9(1)	26(1)	6(4)	24.3(3)	21(1)	11(4)
$[ZnHL]^{3+} + L = [ZnHL_2]^{3+}$	31.5(2)	22.6(8)	30(3)			
$Zn^{2+} + HL^{+} = [ZnHL]^{3+}$	24.71(6)	19.8(2)	16(1)	19.2(2)	19.7(8)	−2(3)
$[ZnL]^{2+} + HL^{+} = [ZnHL_2]^{3+}$	18.2(3)	21(1)	−9(4)			
$[ZnL]^{2+} + H^{+} = [ZnHL]^{3+}$	41.7(1)	43.5(4)	−2(2)	39.5(2)	43.1(8)	−12(3)
$[ZnL_2]^{2+} + H^{+} = [ZnHL_2]^{3+}$	45.3(2)	39.7(4)	19(2)			

[a]Values in parentheses are estimated standard deviations on the last significant figure.
[b]This work, I = 0.15 mol dm^{-3} NaCl.
[c]Reference 6, I = 0.5 mol dm^{-3} KNO_3.

The species $[Cu(L^1)_2]^{2+}$, $[CuH(L^1)_2]^{3+}$, and $[CuH_2(L^1)_2]^{4+}$ are formed even when the Cu:ligand ratio is 1:1, though their concentrations are relatively low. The protonated complex $[CuHL^1]^{3+}$ prevails in the acid region, whereas above pH 9 the hydroxo complex $[Cu(OH)L^1]^{+}$ appears to be the dominant species. When the Cu:ligand ratio is 1:2, $[CuHL^1]^{3+}$ is present at low concentration in the acidic region (it becomes the prevailing species below pH 4), with $[Cu(L^1)_2]^{2+}$, $[CuH(L^1)_2]^{3+}$, and $[CuH_2(L^1)_2]^{4+}$ being the dominant species over the whole pH range, $[Cu(L^1)_2]^{2+}$ dominating at high pH.

The four species that have been characterized in the zinc(II)–L^1 system are $[ZnL^1]^{2+}$, $[ZnHL^1]^{3+}$, $[Zn(L^1)_2]^{2+}$, and $[ZnH(L^1)_2]^{3+}$. Log β values for the first two species of 6.75 and 13.84 were reported previously (34), in very good agreement with the values obtained in this study. The ligand L^2 gave the two protonated complexes $[ZnHL^2]^{3+}$ and $[ZnH_2L^2]^{4+}$ (36), but with L^3 and L^4 the species $[ZnHL_2]^{3+}$ were not found before (37, 38). It should be noted that, although zinc–hydroxo complexes are usually found in systems like this, we were unable to confirm the presence of the species $[Zn(OH)L]^{+}$ and $[Zn(OH)_2L]$ that had been suggested before (37, 38).

Thermodynamics of complex formation

Values of the thermodynamic functions $-\Delta G°$, $-\Delta H°$ and $\Delta S°$ for the stepwise reactions involving metal complexes of L^1 are shown in Table 2. The values for the relevant L^3–metal complexes (39) are also given for comparison purposes.

The addition of one ligand molecule to a nickel(II) ion results in a less favourable free energy change for L^1 than for L^3 in the first step, whereas the opposite happens in the second step. These results may be ascribed to the less favourable enthalpy contribution in the first stage, whereas the entropy contribution outweighs the still unfavourable enthalpy change in the second step. The two enthalpy changes for the stepwise

© 1997 NRC Canada

Can. J. Chem. Downloaded from www.nrcresearchpress.com by 92.62.229.171 on 09/08/12
For personal use only.

Can. J. Chem. Downloaded from www.nrcresearchpress.com by 92.62.229.171 on 09/08/12
For personal use only.

Table 3. Selected force field parameters[a] for the molecular mechanics calculations on $[ML^1_2]$ complexes carried out with MM2 (25) implemented in MacroModel (26).

	Co^{III}		Co^{II}		Ni^{II}	
Parameter	R_o/θ_o (Å/°)	k (mdyn Å^{-1}/ mdyn rad^{-1})	R_o/θ_o (Å/°)	k (mdyn Å^{-1}/ mdyn rad^{-1})	R_o/θ_o (Å/°)	k (mdyn Å^{-1}/ mdyn rad^{-1})
M—N	1.94	1.75	2.17	1.10	2.12	1.20
N-M-N	90/180	0.34		0.21		0.25
M-N-C	110	0.20		0.12		0.15
M-N-H	110	0.15		0.10		0.12

[a]MM2 substructure (atom type from MacroModel) for the coordination sphere is: N3(.Z0(.N3)(.N3)(.N3))-C3-C3(-N3.2)-C3-N3(.2)

addition of L^1 are approximately equal and the entropy changes exhibit the usual decreasing trend. The $-\Delta H°$ values for the protonation of the coordinated ligand in $[NiL^1]^{2+}$, $[Ni(L^1)_2]^{2+}$, and even in $[NiH(L^1)_2]^{3+}$ are roughly equal and definitely lower than the corresponding value for the protonation of the free ligand (45.9 kJ mol^{-1}) (19). This is an indication that the triamine behaves as a tridentate ligand in both $[ML^1]^{2+}$ and $[M(L^1)_2]^{2+}$. Further support for this hypothesis is afforded by the result that the addition of the monoprotonated ligand HL^+ is clearly less exothermic than the addition of the neutral ligand.

The free energies of ligation in the copper complexes follow the same trends as in the nickel complexes, but for different reasons: the enthalpy contribution is less favourable with L^1 than with L^3 in the first step, but is more favourable in the second step. Protonation of the coordinated ligand is more exothermic for copper(II) than for nickel(II). The $-\Delta H°$ values for protonation of $[Cu(L^1)_2]^{2+}$ and $[CuH(L^1)_2]^{3+}$ are close to the value obtained for the protonation of the free ligand. This means that at least one of the unprotonated nitrogen atoms is either weakly bonded or even nonbonded to the metal in these complexes. On the other hand, protonation of $[CuL^1]^{2+}$ is less exothermic than the corresponding reaction of $[Cu(L^1)_2]^{2+}$ or $[CuH(L^1)_2]^{3+}$, indicating that, at least for this complex, all the nitrogen atoms are bonded to the copper ion. The values of the thermodynamic functions for the addition of the protonated ligand HL^{1+} to Cu^{2+} are consistent with a bidentate coordination in this case. The reaction of hydroxide ion with $[CuL^1]^{2+}$ is slightly exothermic and the corresponding entropy change is markedly positive owing to the decrease of the total ionic charge. Similar observations were made with L^3 and L^4.

The stepwise $-\Delta G°$ values for the formation of $[ZnL]^{2+}$ and $[ZnL_2]^{2+}$ (where L = L^1 and L^3) follow the same trends as just described for the corresponding nickel and copper complexes. The enthalpy change is less favourable for L^1 in the first step but more favourable in the second step. The $\Delta S°$ values for the two steps are close to those observed for the corresponding reactions of nickel, which suggests that the corresponding complexes have similar structures. The $-\Delta H°$ values for the addition of one ligand molecule fall in the range 22–26 kJ mol^{-1}, whereas the corresponding reactions of the monoprotonated HL^+ ion are slightly less exothermic (20 and 21 kJ mol^{-1}). The $-\Delta H°$ value for the protonation of the coordinated ligand in $[ZnL^1]^{2+}$ is high, being close to the first protonation enthalpy of the free triamine. These facts can be explained by postulating that in $[ZnL^1]^{2+}$ at least one of the amino groups of the ligand is only weakly bonded to the metal ion because of conformational strain.

Table 4. Total strain energy (kJ mol^{-1}) for the *fac*-$[ML^1_2]^{n+}$ complexes.

Isomer	Co^{III}	Co^{II}	Ni^{II}
s	386.70	65.58	69.59
u	386.82	65.99	69.10

The thermodynamic properties of the 1:1 complexes do not exhibit a regular pattern. Thus, while $[NiL]^{2+}$ and $[CuL]^{2+}$ are more stable for L^3 than for L^1 due to a more favourable enthalpy, the entropy term is nearly equal for the two ligands. In contrast, the two $[ZnL]^{2+}$ complexes (L = L^1, L^3) have about the same stability as the result of conflicting contributions from enthalpy (in favour of L^3) and entropy (in favour of L^1). The addition of a ligand molecule to both $[ML]^{2+}$ and $[MHL]^{3+}$ is always favoured for L^1 with respect to L^3, mainly because of the different enthalpy contribution. The $-\Delta H°$ values for the reaction of HL^+ with M^{2+} are strongly dependent on the metal ion (Zn < Ni < Cu) but nearly equal for the two ligands. The slightly higher values of the corresponding equilibrium constants for L^1 are the result of more favourable entropy terms. The addition of HL^+ to both $[ML]^{2+}$ and $[MHL]^{3+}$ is more spontaneous for L^1 than for L^3; this is probably the reason because the formation of $[MH_2(L^3)_2]^{4+}$ has not been observed.

Strain energies

The force field parameters and the total strain energy values for the energy-minimized structures of s-*fac*- and u-*fac*-$[Co^{III}(L^1)_2]^{3+}$, -$[Co^{II}(L^1)_2]^{2+}$, and -$[Ni^{II}(L^1)_2]^{2+}$ (see Scheme 2) are given in Tables 3 and 4. Selected geometrical parameters are listed in Table 5.

The total strain energy of s- and u-*fac* isomers for tridentate ligands related to L^1 has been the subject of debate (ref. 32*b* and refs. cited therein, ref. 17).

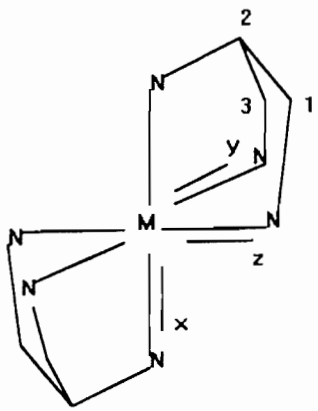
© 1997 NRC Canada

Can. J. Chem. Downloaded from www.nrcresearchpress.com by 92.62.229.171 on 09/08/12
For personal use only.

Table 5. Selected bond lengths (Å) and angles (°) for the isomers of s-*fac*-$[Co^{III}L^1_2]^{3+}$, $[Co^{II}L^1_2]^{2+}$, and $[Ni^{II}L^1_2]^{2+}$, as obtained from the molecular mechanics geometry optimization.

	Co^{III}	Co^{II}	Ni^{II}
Lengths			
M—N(1)	1.976	2.135	2.100
M—N(2)	1.968	2.125	2.074
N(1)—C(1)	1.502	1.501	1.500
C(2)—N(2)	1.499	1.501	1.501
Angles			
N(1)-M-N(2)	87.6	85.7	86.7
N(1)-M-N(3)	86.1	83.1	84.2
M-N(1)-C(1)	105.7	103.1	103.3
M-N(2)-C(2)	96.7	94.0	94.2
N(1)-C(1)-C(2)	109.1	112.0	111.3
C(1)-C(2)-N(2)	106.1	108.5	108.1
C(1)-C(2)-C(3)	113.4	113.9	113.9

Scheme 2.



It is evident that the u and s isomers have almost the same strain energy, the differences being -0.41 kJ mol^{-1} for the cobalt(II) complex and 0.49 kJ mol^{-1} for the nickel(II) complex. It should be noted that the difference is very small for both species. An important contribution to the strain energy comes from the valence angle deformation of M-N(2)-C(2). This effect contributes an average of 2.80 kJ mol^{-1} for the four structures of the Co^{2+} and Ni^{2+} complexes and it is almost 10 times larger than the contributions of the deformations of M-N(1)-C(1) and M-N(3)-C(3). Previous molecular mechanics studies on *fac*-$[Co(dien)_2]^{3+}$ (dien = diethylenetriamine) found almost identical strain energies for the s and u isomers (40) even though studies of the equilibrium isomer distributions in solution indicated that the u isomer is more stable than the s isomer by about 2.93 kJ mol^{-1}. Bond et al. (32*b*) computed a difference of ca. 5.86 kJ mol^{-1} between the more stable conformer of the u and s-*fac* isomers.

A difference of -0.10 kJ·mol^{-1} has been found for *fac*-$[Co(L^1)_2]^{3+}$ in this work and it compares well with the respective value reported in ref. 17 (-0.72 kJ mol^{-1}). If it is assumed that the s and u isomers of *fac*-$[Co(L^1)_2]^{2+}$ and -$[Ni(L^1)_2]^{2+}$ have the same solvation energy, which is a reasonable assumption, then the two isomers should be present in nearly equal amounts in solution.

Conclusions

The complex species that have been identified in this work are not the same as those that were reported previously (34–38). This can be largely attributed to the fact that earlier workers used graphical methods for the treatment of experimental data whereas we have used the more rigorous least-squares method. It must be noted that the chemical models selected for complexes of the ligand L^1 are, with minor exceptions, the same as the models found by least-squares methods for complexes of the ligands L^3 and L^4.

The stability constants of the complexes of L^1 are comparable to those of the analogous complexes of L^3 and L^4 even though L^1 is notably less basic than the other two ligands. It seems likely that when L^1 forms a tridentate complex containing two five-membered and one six-membered rings the strain energy is less than in tridentate complexes of L^3 and L^4 where there are three six-membered rings, and that the reduced strain energy compensates for the lower basicity of the ligand L^1.

Addition of L to $[ML]^{2+}$ is more favourable for L^1 than for L^3. Although this behaviour was observed for all the metals studied it happens for different reasons: a more favourable enthalpy term for copper(II) and zinc(II) but a more favourable entropy term for nickel(II). Lastly, it may be noted that the unsymmetrical ligand L^1 may form either u or s isomers of the bis-complex $[ML_2]^{2+}$. The results of molecular mechanics calculations indicate that the two isomers have nearly the same strain energies in the (hypothetical) gaseous state, so that both are likely to be present in equal amounts in solution.

Acknowledgements

We thank Dr. G. Giorgi (Centro Interdipartimentale de Analisi e Determinazioni Strutturali, University of Siena) for performing some of the titrations and for doing some preliminary molecular mechanics analyses during his work for the Tesi di Dottorato. We gratefully acknowledge the financial support of the European Community for the Human Capital and Mobility programme "Metals and Environmental Problems" (1995–1997) and the Italian Ministero dell'Università e della Ricerca Scientifica e Tecnologica.

References

1. T. Thomas and T.J. Thomas. Biochemistry, **32**, 14068 (1993).
2. C. Romano, K. Williams, S. DePriest, R. Seshadri, G.R. Marshall, M. Israel, and P.B. Molinoff. Mol. Pharmacol. **41**, 785 (1992).
3. M. Egli, L.D. Williams, Q. Gao, and A. Rich. Biochemistry, **30**, 11388 (1991).
4. A.I. Sacaan and K.M. Johnson. Mol. Pharmacol. **38**, 705 (1991).
5. G.L. Eichhorn, E. Tarien, G.A. Elgavish, J.J. Butzow, and Y.A. Shin. *In* Biomolecular stereodynamics. Vol. II. *Edited by* R.H. Sarma. Adenine Press, New York. 1981. p. 185.

© 1997 NRC Canada

6. A. Rich, G.J. Quigley, and A.H.-J. Wang. *In* Biomolecular stereodynamics. Vol. I. *Edited by* R.H. Sarma. Adenine Press, New York. 1981. p. 35.
7. R. Lavery, A. Pullman, and S. Corbin. *In* Biomolecular stereodynamics. Vol. I. *Edited by* R.H. Sarma. Adenine Press, New York. 1981. p. 185.
8. C.F. Mills. Zinc in human biology. Springer-Verlag, Heidelberg. 1989.
9. W. Guschlbauer and W. Saeger (*Editors*). DNA–ligand interaction: from drugs to protein. NATO ASI Ser. A: **137** (1987).
10. H. Sigel (*Editor*). Metal ions in biological systems. Vol. 14. Marcel Dekker, Inc., New York. 1983.
11. C.H. Evans. *In* Biochemistry of the lanthanides. *Edited by* E. Frieden. Plenum Press, New York. 1990.
12. C. Navarro-Raminger, J.M. Pérez, F. Zamora, V.M. Gonzalez, J.R. Masaguer, and C. Alonso. J. Inorg. Biochem. **52**, 37 (1993).
13. C.W. Tabor and H. Tabor. Annu. Rev. Biochem. **53**, 749 (1984).
14. B.R. Cameron, D.A. House, and A. McAuley. J. Chem. Soc. Dalton Trans. 1019 (1993).
15. A.D. Kirk and C. Namasivayam. Inorg. Chem. **32**, 2815 (1993).
16. A.M. Calafat and L.G. Marzilli. Inorg. Chem. **32**, 2906 (1993).
17. P.Comba, T.W. Hambley, and L. Zipper. Helv. Chim. Acta, **71**, 1875 (1988).
18. K. Henrick, M.McPartlin, S. Munjoma, P.G. Owston, R. Peters, S.A. Songokoya, and P.A. Tasker. J. Chem. Soc. Dalton Trans. 225 (1982).
19. R. Cini, G. Giorgi, D. Masi, A. Sabatini, and A. Vacca. J. Chem. Soc. Perkin Trans. 2, 765 (1991).
20. I.M. Kolthoff and E.B. Sandell. Textbook of quantitative inorganic analysis. The MacMillan Company, New York. 1953.
21. F.J.C. Rossotti and H. Rossotti. J. Chem. Educ. **42**, 375 (1965); G. Gran. Analyst (London), **77**, 661 (1952).
22. F. Basolo and R.G. Pearson. Mechanisms of inorganic reactions, a study of metal complexes in solution. J. Wiley and Sons, New York. 1967.
23. A. Sabatini, A. Vacca, and P. Gans. Coord. Chem. Rev. **120**, 389 (1992); P. Gans, A. Sabatini, and A. Vacca. Talanta, **43**, 1739 (1996).
24. L. Bologni, A. Sabatini, and A. Vacca. Inorg. Chim. Acta, **69**, 71 (1983).
25. M. Fontanelli and M. Micheloni. Proc. 1st Spanish–Italian Congress on Thermodynamics of Metal Complexes. Peñiscola, Spain. 1990. p. 41.
26. R.M. Smith and A.E. Martell. NIST critically selected stability constants of metal complexes database. Version 2.0. U.S. Department of Commerce, National Institute of Standards and Technology, Gaithersburg, Md. 1995.
27. R. Barbucci, L. Fabbrizzi, P. Paoletti, and A. Vacca. J. Chem. Soc. Dalton Trans. 1763 (1973).
28. N.L. Allinger. J. Am. Chem. Soc. **99**, 8127 (1977).
29. W.C. Still, F. Mohammadi, N.G.J. Richards, W.C. Guida, M. Lipton, G. Chang, T. Hendrickson, F. DeGunst, and W. Hasel. MacroModel V3.0. Department of Chemistry, Columbia University, New York. 1990.
30. (*a*) G. Calzaferri and M. Brandle. ICONC&INPUTC. QCPE program No QCMP116. University of Berne, Switzerland. 1992; (*b*) G. Calzaferri, L. Forss, and I. Kamber. J. Phys. Chem. **93**, 5366 (1989); (*c*) G.Calzaferri and R. Hoffmann. J. Chem. Soc. Dalton Trans. 917 (1991); ICONC&INPUTC documentation.
31. K. Henrick, M. McPartlin, S. Munjoma, P.G. Owston, R. Petrs, S.A. Sangokoya, and P.A. Tasker. J. Chem. Soc. Dalton Trans. 226 (1982).
32. (*a*) T.W. Hambley. Inorg. Chem. **27**, 2496 (1988); (*b*) A.M. Bond, T.W. Hambley, and M.R. Snow. Inorg. Chem. **24**, 1920 (1985).
33. (*a*) R. Cini, R. Pogni, R. Basosi, A. Donati, C. Rossi, L. Sabadini, L. Rollo, S. Lorenzini, R. Gelli, and R. Marcolongo. Metal Based Drugs, **2**, 43 (1995); (*b*) L. Hansen, R. Cini, A. Taylor, Jr., and L.G. Marzilli. Inorg. Chem. **31**, 2801 (1992).
34. J.E. Prue and G. Schwarzenbach. Helv. Chim. Acta, **33**, 995 (1950).
35. T.G. Spiro and C.J. Ballhausen. Acta Chem. Scand. **15**, 1707 (1961).
36. G. Anderegg. Helv. Chim. Acta, **45**, 1303 (1962).
37. A. Sabatini and A. Vacca. Coord. Chem. Rev. **16**, 161 (1975).
38. M. Micheloni, A. Sabatini, and A. Vacca. Inorg. Chim. Acta, **25**, 41 (1977).
39. A. Sabatini and A. Vacca. J. Chem. Soc. Dalton Trans. 519 (1980).
40. (*a*) M. Dwyer and G.H. Searle. J. Chem. Soc. Chem. Commun. 726 (1972); (*b*) Y. Yoshikawa. Bull. Chem. Soc. Jpn. **49**, 159 (1976).

Can. J. Chem. Downloaded from www.nrcresearchpress.com by 92.62.229.171 on 09/08/12
For personal use only.

© 1997 NRC Canada

^{1}H NMR study of paramagnetic rhenium(III) monomers with nitrogen heterocycles. Crystal structures of $ReCl_3L_2(PPh_3)$ complexes (L = pyridine, 3-picoline, and 1-methylimidazole)

Céline Pearson and André L. Beauchamp

Abstract: Rhenium(III) monomers of the type $ReCl_3L_n(PPh_3)_{3-n}$, where n = 1, 2, and 3, were prepared for simple nitrogen heterocyclic ligands L and characterized mainly by ^{1}H NMR and IR spectroscopies. Most of the ^{1}H NMR signals of these paramagnetic compounds were assigned by using methylated pyridines. A *mer-cis* octahedral geometry slightly distorted by triphenylphosphine was determined by X-ray diffraction for three $ReCl_3L_2(PPh_3)$ complexes: L = pyridine, triclinic, $P\bar{1}$, a = 11.379, b = 13.532, c = 18.160 Å, α = 80.16°, β = 89.57, γ = 86.27°, Z = 4, R = 0.076; L = 3-picoline, triclinic, $P\bar{1}$, a = 10.557, b = 12.580, c = 13.153 Å, α = 66.80°, β = 67.46°, γ = 75.89°, Z = 2, R = 0.021; L = 1-methylimidazole, monoclinic, $P2_1/c$, a = 15.437, b = 9.436, c = 18.607 Å, β = 92.23°, Z = 4, R = 0.046. The same structure was deduced from ^{1}H NMR data for these compounds in solution, whereas the other types of complexes were found to exist as the *mer,trans*-$ReCl_3L(PPh_3)_2$ and *mer*-$ReCl_3L_3$ isomers. In contrast with these complexes, which contain the *mer*-$ReCl_3$ core, the starting material $ReCl_3$(benzil)(PPh_3) is found to be the *fac* isomer in solution. The typical low-field shifted pattern of ^{1}H NMR signals for PPh_3 is not greatly perturbed by changes in the number or arrangement of the remaining ligands in the coordination sphere, but the signals for protons on conjugated systems directly bonded to the metal atoms are much more affected by the unpaired electrons.

Key words: paramagnetic NMR, crystal structures, rhenium(III) complexes, imidazole, pyridine, triphenylphoshine.

Résumé : Des monomères de formule $ReCl_3L_n(PPh_3)_{3-n}$, où n = 1, 2 et 3, ont été préparés pour certains hétérocycles azotés simples L et caractérisés principalement par spectroscopies RMN ^{1}H et IR. La plupart des signaux RMN ^{1}H de ces composés paramagnétiques ont pu être attribués en utilisant des pyridines méthylées. La géométrie octaédrique *mer-cis* légèrement déformée par la triphénylphosphine a été déterminée par diffraction des rayons X pour trois complexes $ReCl_3L_2(PPh_3)$: L = pyridine, triclinique, $P\bar{1}$, a = 11,379, b = 13,532, c = 18,160 Å, α = 80,16°, β = 89,57°, γ = 86,27°, Z = 4, R = 0,076; L = 3-picoline, triclinique, $P\bar{1}$, a = 10,557, b = 12,580, c = 13,153 Å, α = 66,80°, β = 67,46°, γ = 75,89°, Z = 2, R = 0,021; L = 1-méthylimidazole, monoclinique, $P2_1/c$, a = 15,437, b = 9,436, c = 18,607 Å, β = 92,23°, Z = 4, R = 0,046. D'après les données RMN ^{1}H, ces complexes conservent la même structure en solution, alors que les autres catégories de composés existent sous forme des isomères *mer,trans*-$ReCl_3L(PPh_3)_2$ et *mer*-$ReCl_3L_3$. Contrairement à ces systèmes renfermant le motif *mer*-$ReCl_3$, le composé de départ $ReCl_3$(benzil)(PPh_3) se trouve sous forme de l'isomère *fac*. Le déplacement des signaux RMN ^{1}H à champ faible, caractéristique de PPh_3, dépend relativement peu des changements apportés au nombre ou à l'arrangement des autres ligands dans la sphère de coordination, mais les signaux des protons de systèmes conjugués directement liés au métal sont beaucoup plus perturbés par les électrons non appariés.

Mots clés : RMN paramagnétique, structure cristalline, complexes de rhénium(III), imidazole, pyridine, triphénylphosphine.

Can. J. Chem. Downloaded from www.nrcresearchpress.com by 92.62.229.171 on 09/08/12
For personal use only.

Introduction

As part of our ongoing research on monomeric Re(III) complexes as routes to purine-bridged metal–metal bonded dimers (1) and to materials of interest for radioactive Re labelling in radiopharmacy (2), we noticed that preparative work was considerably hampered by the absence of standard guidelines for assigning signals and extracting structural information from the ^{1}H NMR spectra of these paramagnetic compounds. We therefore decided to search for useful trends in NMR data by systematically looking at a few series of simple complexes.

In our earlier paper (3), we reported that $ReCl_3(RCN)(PAr_3)_2$ complexes with various combinations of nitriles and arylphosphines gave relatively sharp ^{1}H NMR spectra in which couplings were often observed, and all protons could be identified from their constant patterns of chemical shifts. We have now moved one step further and examined compounds containing simple nitrogen heterocycles. The $ReCl_3py_2(PPh_3)$ and $ReCl_3py_3$ compounds, described and

Received July 13, 1996.

C. Pearson and A.L. Beauchamp.[1] Département de chimie, Université de Montréal, C.P. 6128, Succ. Centre-ville, Montréal, QC H3C 3J7, Canada

[1] Author to whom correspondence may be addressed. Telephone: (514) 343-6446. Fax: (514) 343-7586. E-mail: beauchmp@ere.umontreal.ca

© 1997 NRC Canada

Can. J. Chem. Downloaded from www.nrcresearchpress.com by 92.62.229.171 on 09/08/12
For personal use only.

briefly characterized by Rouschias and Wilkinson (4), were prepared. The sample was enlarged by including the related ligands 3-picoline (3-pic), 4-picoline (4-pic), and 1-methylimidazole (1-meim). $ReCl_3L(PPh_3)_2$ compounds with 1-methylimidazole and pyridine were also isolated for the first time.

Experimental section

Reactants and methods

$KReO_4$ and PPh_3 were used as received from Aldrich. $ReCl_3(MeCN)(PPh_3)_2$ (**1**) was prepared as described in the literature (4) and checked by ^1H NMR (3). All experiments were run under argon using Schlenk techniques. Toluene was distilled over sodium and CH_2Cl_2 over calcium chloride. Ligands (py, 3-pic, 4-pic, 1-meim) were dried over molecular sieves.

^1H NMR spectra were recorded on a Bruker AMX-300 spectrometer, spectral width: 160 to −160 ppm. The residual signals ($CDCl_3$, 7.27; CD_2Cl_2, 5.32; $(CD_3)_2CO$, 2.04 ppm) were used as internal standard and chemical shifts were converted to the usual TMS scale. Infrared spectra were recorded on a Perkin–Elmer 1600 FT-IR spectrometer as CsI pellets. The mass spectrometry data (FAB^+) were recorded on a VG-Autospec Q instrument in nitrobenzylic alcohol. Magnetic moments were determined at room temperature with an Evans magnetic susceptibility balance (Johnson–Matthey), calibrated with $HgCo(SCN)_4$ ($\chi = 16.44 \times 10^{-6}$ cgsemu). Corrections for diamagnetism were calculated from Pascal's constants (5). UV–visible spectra (230–800 nm) were recorded on a Varian Cary 5E spectrophotometer in CH_2Cl_2. Elemental analyses were performed by Guelph Chemical Laboratories, Guelph, Canada.

Preparative work

*$ReCl_3L_2(PPh_3)$ (L = py (**2**), 3-pic (**3**), 4-pic (**4**))*

These compounds were obtained by refluxing $ReCl_3(MeCN)(PPh_3)_2$ in a 50-fold excess of the dry neat pyridine ligand for 1 min, as described by Rouschias and Wilkinson (4) for pyridine. The orange-brown product was precipitated by addition of ether. Yields: 73% (py), 61% (3-pic), 49% (4-pic). μ (B.M.): 1.72 (py), 1.78 (3-pic), 1.70 (4-pic). UV–VIS. (λ nm ($\varepsilon \times 10^{-3}$ M^{-1} cm^{-1})): L = py, 407 (4.58), 374 (4.72), 310 (4.58), 278 (sh, 6.65), 259(sh, 10.9); L = 3-pic, 407 (5.32), 372 (5.37), 309 (5.50), 259 (13.84); L = 4-pic, 407 (4.38), 369 (4.45), 306 (5.34), 240 (21.51). The same products were also obtained by refluxing a 1:2 mixture of $ReCl_3(MeCN)(PPh_3)_2$ and the pyridine ligand (as a 1% CH_2Cl_2 solution) for 6 h. The yields were lower, but this method could eventually be applied to other systems involving solid ligands where a large excess cannot be conveniently used.

*$ReCl_3(1\text{-}meim)_2(PPh_3)$ (**5**)*

A mixture of $ReCl_3(MeCN)(PPh_3)_2$ (3.0 g) and 1-methylimidazole (0.5 mL) in toluene (200 mL) was refluxed for 4 h. The brownish orange product was filtered under argon. Yield: 84%. μ (B.M.): 1.62. UV–VIS (λ nm ($\varepsilon \times 10^{-3}$ M^{-1} cm^{-1})): 345 (2.74), 263 (9.35). Anal. calcd. for $C_{26}H_{27}N_4Cl_3PRe$: C 43.4, H 3.8, N 7.8, Cl 14.8; found: C 43.1, H 3.4, N 8.0, Cl 14.8.

*$ReCl_3(1\text{-}meim)(PPh_3)_2$ (**6**)*

$ReCl_3(MeCN)(PPh_3)_2$ (3.0 g) and 1-methylimidazole (0.25 mL) in toluene (125 mL) were refluxed for 3.5 h. The impure green precipitate was filtered under argon and purified by column chromatography on a precoated TLC plate (10 mm silica gel) using a 70:30 CH_2Cl_2:hexane mixture as eluent. The pure compound is yellow. Yield: 55%. UV–VIS. (λ nm ($\varepsilon \times 10^{-3}$ M^{-1} cm^{-1})): 417 (2.00), 253 (24.8), 233 (31.8). Anal. calcd. for $C_{40}H_{36}N_2Cl_3P_2Re$: C 53.4, H 4.0, N 3.1, Cl 11.8; found: C 53.8, H 4.2, N 3.1, Cl 12.0.

*$ReCl_3py(PPh_3)_2$ (**7**)*

$ReCl_3(MeCN)(PPh_3)_2$ (0.2 g) and a 1% solution of pyridine in CH_2Cl_2 (1.9 mL) were refluxed for 20 min. Ether was added to precipitate the yellow solid. The reaction mixture contained a large amount of unreacted starting complex. To obtain the NMR spectrum, a small amount was purified by chromatography on silica gel using a 70:30 CH_2Cl_2:hexane mixture as eluent.

*$ReCl_3(benzil)(PPh_3)$ (**8**)*

The purple product was prepared as described in the literature (4). μ (B.M.): 1.66. UV–VIS. (λ nm ($\varepsilon \times 10^{-3}$ M^{-1} cm^{-1})): 722 (0.13), 550 (15.98), 336 (9.90), 240 (30.98).

*$ReCl_3py_3$ (**9**)*

The red-brown product was obtained as described in the literature (4). Yield: 57%. μ (B.M.): 1.42. UV–VIS spectrum (λ nm ($\varepsilon \times 10^{-3}$ M^{-1} cm^{-1})): 474 (6.32), 444 (6.95) 420 (6.74), 354 (5.47), 253 (16.84). FAB^+: m/z = 529 ($(ReCl_3py_3)^+$), 450 ($(ReCl_3py_2)^+$).

*$ReCl_3(4\text{-}pic)_3$ (**10**)*

A mixture of $ReCl_3(benzil)(PPh_3)$ (0.3 g) and 4-picoline (4.0 mL) was refluxed for 30 min, diluted with benzene (5 mL), and poured into ether (50 mL). Yield: 64%. μ (B.M.): 1.89. UV–VIS (λ nm ($\varepsilon \times 10^{-3}$ M^{-1} cm^{-1})): 431 (6.86), 352 (5.14), 289 (5.52), 253 (14.90).

*$ReCl_3(1\text{-}meim)_3$ (**11**)*

The compound was obtained by refluxing 0.3 g of $ReCl_3(benzil)(PPh_3)$ with 3.8 mL of 1-meim for 5 min. Benzene (4.0 mL) was added and the solution was poured into ether. Crystallization in CH_2Cl_2–benzene gave a brown-green solid. UV–VIS (λ nm (relative intensities)): 420 (0.01), 357 (0.02), 325 (0.15), 316 (0.20), 298 (0.30), 281 (0.30), 252 (0.47), 247 (0.54). Poor solubility precluded ε calculations.

Crystallographic work on the $ReCl_3L_2PPh_3$ compounds

In all cases, orange-brown crystals were grown in a CH_2Cl_2–ether mixture. X-ray work was carried out on an Enraf–Nonius CAD-4 diffractometer with graphite-monochromatized CuKα (L = py, 1-meim) or MoKα radiation (L = 3-pic). The reduced cells were determined from 25 centred reflections and the Niggli parameters clearly indicated that no higher symmetry was present. During data collection, orientation was monitored every 200 measurements and intensity was checked every hour with standard reflections. Crystallographic data and conditions of data collection are summarized in Table 1. Corrections for the effects of Lorentz, polarization, and absorption (Gaussian integration) were applied.

© 1997 NRC Canada

Can. J. Chem. Downloaded from www.nrcresearchpress.com by 92.62.229.171 on 09/08/12
For personal use only.

Table 1. Crystallographic data for the $ReCl_3L_2(PPh_3)$ compounds.

Compound	$ReCl_3py_2(PPh_3)$	$ReCl_3(3\text{-pic})_2(PPh_3)$	$ReCl_3(1\text{-meim})_2(PPh_3)$
Formula	$C_{28}H_{25}Cl_3N_2PRe$	$C_{30}H_{29}Cl_3N_2PRe$	$C_{26}H_{27}Cl_3N_4PRe$
Formula weight	713.06	741.11	719.06
Space group	$P\bar{1}$	$P\bar{1}$	$P2_1/c$
a, Å	11.379(5)	10.557(2)	15.437(3)
b, Å	13.532(6)	12.580(3)	9.436(2)
c, Å	18.160(7)	13.153(3)	18.607(3)
α, deg	80.16(3)	66.80(2)	90
β, deg	89.57(3)	67.46(2)	92.23(2)
γ, deg	86.27(3)	75.89(2)	90
Volume, Å^3	2749(2)	1474.1(6)	2708.3(9)
D_{meas}, g cm^{-3}	1.714	1.654	1.742
D_{calcd}, g cm^{-3}	1.723	1.670	1.764
Z	4	2	4
Radiation wavelength	1.54178	0.71069	1.54178
Temperature, K	216	298	220
μ, cm^{-1}	118.0	45.3	120.0
Number of unique reflections	10410	5171	5133
Number of observed reflections	7393	4531	4259
Range of *hkl*	$0 \le h \le 14$	$-11 \le h \le 12$	$-18 \le h \le 18$
	$-16 \le k \le 16$	$0 \le k \le 14$	$0 \le k \le 11$
	$-22 \le l \le 22$	$-13 \le l \le 15$	$0 \le l \le 22$
R^a	0.076	0.021	0.046
$R_w{}^a$	0.075	0.023	0.058
GOF	2.24	1.41	1.69

$^aR = \Sigma||F_o| - |F_c||/\Sigma|F_o|$; $R_w = [\Sigma w(|F_o| - |F_c|)^2/\Sigma w|F_o|^2]^{1/2}$.

The structures were solved by the heavy-atom method. The non-hydrogen atoms were refined anisotropically by the least-squares procedures of SHELX-76 (6) (L = py) or NRCVAX (7) (L = 3-pic, 1-meim). Hydrogen positions and temperature factors were fixed: C—H = 0.95 Å, $U_H = U_C + 0.01$ Å^2. Poor crystal quality for the pyridine compound led to a higher R factor, but the overall structure is nevertheless reliably defined. The refined coordinates are listed in Table 2. The thermal parameters and hydrogen coordinates are given as supplementary material.[2]

Results and discussion

$ReCl_3L_2(PPh_3)$ complexes with L = py (**2**), 3-pic (**3**), 4-pic (**4**), and 1-meim (**5**) were obtained by reacting excess ligand with $ReCl_3(MeCN)(PPh_3)_2$, as described by Rouschias and Wilkinson (4). The reaction was slower with 1-meim than with pyridines. Simple displacement of MeCN to obtain $ReCl_3L(PPh_3)_2$ was found to be difficult and gave poor yields: under mild conditions, conversion was only partial even after several hours, whereas more vigorous conditions led directly to $ReCl_3L_2(PPh_3)$. A satisfactory yield of the $ReCl_3L(PPh_3)_2$ compound could be obtained with the less reactive 1-meim ligand. $ReCl_3L_3$ compounds were prepared from $ReCl_3$(benzil)(PPh_3) as described (4). All compounds are paramagnetic with magnetic moments in the range 1.4–1.9 B.M. typical of low-spin d^4 Re(III) complexes.

^{1}H NMR spectroscopy

Two unpaired electrons in the Re(III) centre cause signal broadening and unusually large chemical shifts in the ^{1}H NMR spectra, as exemplified by the spectrum of $ReCl_3py_2(PPh_3)$ shown in Fig. 1. The NMR data are collected in Table 3.

The phosphine gives well defined peaks at 18.06 ppm (*ortho*), 10.09 ppm (*meta*), and 10.88 ppm (*para*). A similar pattern, in which the *ortho* protons close to the paramagnetic centre are the most displaced, has been observed for the $ReCl_3(RCN)(PR'_3)_2$ compounds (3) and other complexes with aryl-phosphines (8). Spin–spin couplings are not visible in Fig. 1, but have been detected for other cases discussed below. The signals of pyridine were more difficult to detect, because they correspond to a relatively small number of protons and their presence on a conjugated system directly connected to the paramagnetic centre results in greater signal displacement and line broadening than the remote phosphine protons. Nevertheless, two sets of signals were found, in agreement with the *mer-cis* geometry indicated by the X-ray diffraction work below. They follow the trends discussed by Davison and co-

[2] The supplementary material includes tables of refined temperature factors, hydrogen coordinates, interatomic distances and bond angles, and least-squares plane calculations (35 pages). Copies of material on deposit may be purchased from: The Depository of Unpublished Data, Document Delivery, CISTI, National Research Council Canada, Ottawa, Canada K1A 0S2.

Tables of hydrogen coordinates, and distances and angles have also been deposited with the Cambridge Crystallographic Data Centre and can be obtained on request from the Director, Cambridge Crystallographic Data Centre, University Chemical Laboratory, 12 Union Road, Cambridge, CB2 1EZ, U.K.

© 1997 NRC Canada

Table 2. Atomic coordinates and equivalent isotropic temperature factors ($Å^2 \times 10^2$) for the $ReCl_3L_2(PPh_3)$ compounds.

Atom	*x*	*y*	*z*	U_{eq}
L = pyridine				
Re(1)	0.34874(5)	0.28003(4)	0.13644(3)	2.59(2)
Re(2)	0.28686(6)	0.77313(5)	0.41344(3)	2.82(2)
Cl(11)	0.3855(3)	0.1038(3)	0.1696(2)	3.9(1)
Cl(12)	0.5264(3)	0.2845(3)	0.0648(2)	3.8(1)
Cl(13)	0.3181(3)	0.4574(3)	0.1097(2)	3.7(1)
Cl(21)	0.2611(3)	0.9501(3)	0.3801(2)	3.8(1)
Cl(22)	0.1835(3)	0.7771(3)	0.5283(2)	3.7(1)
Cl(23)	0.3364(3)	0.5980(3)	0.4519(2)	4.0(1)
P(11)	0.2290(3)	0.2631(3)	0.0300(2)	2.5(1)
P(21)	0.1052(3)	0.7671(3)	0.3431(2)	3.1(1)
N(11)	0.1966(10)	0.2727(10)	0.2124(6)	3.1(4)
N(12)	0.4531(10)	0.3058(9)	0.2323(6)	3.0(4)
N(21)	0.3932(11)	0.7654(10)	0.3157(6)	3.5(4)
N(22)	0.4494(11)	0.7934(10)	0.4727(7)	3.6(4)
C(112)	0.1851(14)	0.1931(12)	0.2656(8)	3.8(5)
C(113)	0.0888(15)	0.1847(15)	0.3134(9)	5.1(6)
C(114)	0.0033(15)	0.2636(16)	0.3067(10)	5.5(7)
C(115)	0.0162(15)	0.3475(15)	0.2531(9)	5.0(6)
C(116)	0.1119(12)	0.3509(12)	0.2059(8)	3.7(5)
C(122)	0.4119(14)	0.3698(12)	0.2774(8)	3.9(5)
C(123)	0.4776(16)	0.3925(13)	0.3351(9)	4.8(6)
C(124)	0.5866(16)	0.3430(13)	0.3511(9)	4.7(6)
C(125)	0.6324(16)	0.2763(13)	0.3050(10)	5.1(6)
C(126)	0.5591(13)	0.2570(12)	0.2476(8)	3.7(5)
C(131)	0.0717(12)	0.2734(10)	0.0547(7)	2.8(4)
C(132)	0.0279(11)	0.1988(10)	0.1043(8)	3.2(5)
C(133)	−0.0878(14)	0.2078(13)	0.1308(8)	4.1(5)
C(134)	−0.1573(12)	0.2934(13)	0.1044(9)	4.1(6)
C(135)	−0.1156(13)	0.3690(13)	0.0536(9)	4.4(6)
C(136)	0.0008(12)	0.3625(12)	0.0268(8)	3.3(5)
C(141)	0.2435(12)	0.1451(10)	−0.0065(8)	3.0(4)
C(142)	0.3568(13)	0.1049(11)	−0.0206(7)	3.5(5)
C(143)	0.3696(15)	0.0198(11)	−0.0537(8)	4.3(5)
C(144)	0.2746(15)	−0.0266(11)	−0.0749(9)	4.3(5)
C(145)	0.1618(15)	0.0135(12)	−0.0631(9)	4.4(6)
C(146)	0.1452(13)	0.0993(11)	−0.0284(9)	3.9(5)
C(151)	0.2439(11)	0.3519(10)	−0.0583(7)	2.7(4)
C(152)	0.3322(13)	0.4201(11)	−0.0693(8)	3.4(5)
C(153)	0.3439(14)	0.4816(12)	−0.1382(9)	4.1(5)
C(154)	0.2699(14)	0.4757(13)	−0.1959(9)	4.5(6)
C(155)	0.1807(14)	0.4094(13)	−0.1862(9)	4.5(6)
C(156)	0.1692(13)	0.3458(12)	−0.1187(8)	3.7(5)
C(212)	0.3925(14)	0.6853(12)	0.2797(8)	3.8(5)
C(213)	0.4609(17)	0.6814(15)	0.2151(10)	5.9(7)
C(214)	0.5322(17)	0.7558(17)	0.1899(10)	6.7(8)
C(215)	0.5374(18)	0.8374(17)	0.2264(10)	6.8(8)
C(216)	0.4646(15)	0.8413(15)	0.2886(9)	5.3(6)
C(222)	0.5512(14)	0.7388(14)	0.4661(10)	4.9(6)
C(223)	0.6535(15)	0.7519(16)	0.5020(11)	6.1(8)
C(224)	0.6522(19)	0.8218(18)	0.5490(11)	7.0(9)
C(225)	0.5503(17)	0.8779(15)	0.5557(10)	5.6(7)
C(226)	0.4479(15)	0.8624(12)	0.5180(9)	4.5(6)

Can. J. Chem. Downloaded from www.nrcresearchpress.com by 92.62.229.171 on 09/08/12
For personal use only.

© 1997 NRC Canada

Table 2 (*continued*)

Atom	*x*	*y*	*z*	U_{eq}
C(231)	0.1337(14)	0.7736(12)	0.2428(8)	3.9(5)
C(232)	0.1203(14)	0.6908(12)	0.2063(9)	4.1(5)
C(233)	0.1556(16)	0.6988(14)	0.1315(9)	5.1(6)
C(234)	0.2028(18)	0.7848(15)	0.0937(9)	5.6(7)
C(235)	0.2150(16)	0.8659(14)	0.1312(9)	4.8(6)
C(236)	0.1810(15)	0.8601(12)	0.2043(8)	4.2(5)
C(241)	–0.0087(15)	0.8701(12)	0.3434(8)	4.1(5)
C(242)	–0.0343(13)	0.9055(12)	0.4106(9)	4.3(5)
C(243)	–0.1318(15)	0.9756(13)	0.4156(11)	5.2(6)
C(244)	–0.2014(17)	1.0085(15)	0.3521(11)	6.2(7)
C(245)	–0.1758(18)	0.9743(16)	0.2855(11)	6.5(8)
C(246)	–0.0810(14)	0.9030(14)	0.2829(9)	4.8(6)
C(251)	0.0138(14)	0.6587(12)	0.3674(8)	3.7(5)
C(252)	0.0735(19)	0.5593(14)	0.3827(11)	6.5(8)
C(253)	0.0127(21)	0.4743(15)	0.4029(12)	7.0(8)
C(254)	–0.1065(23)	0.4842(17)	0.4104(11)	7.2(9)
C(255)	–0.1668(23)	0.5772(16)	0.3946(13)	8.3(10)
C(256)	–0.1023(17)	0.6639(15)	0.3744(12)	6.5(8)
L = 3-picoline				
Re	0.17047(1)	0.21890(1)	0.18855(1)	2.414(6)
Cl(1)	0.19284(10)	0.39214(8)	0.02628(8)	3.71(5)
Cl(2)	0.40930(9)	0.19507(9)	0.16618(9)	3.95(5)
Cl(3)	0.14732(10)	0.03558(8)	0.33799(8)	3.65(5)
P	0.11501(9)	0.34174(8)	0.30732(8)	2.55(4)
N(1)	–0.0420(3)	0.2256(3)	0.2046(3)	3.0(2)
N(2)	0.2240(3)	0.1240(3)	0.0675(3)	3.0(2)
C(12)	–0.1378(4)	0.1814(3)	0.3096(3)	3.4(2)
C(13)	–0.2743(4)	0.1836(4)	0.3243(4)	4.5(3)
C(14)	–0.3154(4)	0.2362(4)	0.2273(5)	6.0(3)
C(15)	–0.2208(5)	0.2814(4)	0.1196(5)	5.6(3)
C(16)	–0.0840(4)	0.2747(4)	0.1098(4)	4.1(2)
C(17)	–0.3738(5)	0.1314(5)	0.4422(5)	7.1(4)
C(22)	0.3345(4)	0.1479(3)	–0.0309(3)	3.4(2)
C(23)	0.3772(4)	0.0904(3)	–0.1098(3)	3.6(2
C(24)	0.3016(4)	0.0035(3)	–0.0874(4)	4.0(2)
C(25)	0.1873(4)	–0.0209(3)	0.0110(4)	4.0(2)
C(26)	0.1516(4)	0.0410(3)	0.0860(3)	3.6(2)
C(27)	0.5018(5)	0.1224(4)	–0.2160(4)	5.4(3)
C(31)	–0.0707(3)	0.3902(3)	0.3509(3)	2.8(2)
C(32)	–0.1574(4)	0.3556(4)	0.4652(3)	3.6(2)
C(33)	–0.2984(4)	0.3817(4)	0.4898(4)	4.7(2)
C(34)	–0.3547(4)	0.4419(4)	0.4018(4)	4.5(2)
C(35)	–0.2688(4)	0.4803(4)	0.2879(4)	3.8(2)
C(36)	–0.1274(4)	0.4548(3)	0.2622(3)	3.2(2)
C(41)	0.1555(3)	0.2829(3)	0.4446(3)	2.8(2)
C(42)	0.2157(4)	0.3474(4)	0.4748(3)	4.1(2)
C(43)	0.2397(5)	0.3036(4)	0.5807(4)	5.0(3)
C(44)	0.2031(5)	0.1964(4)	0.6570(4)	4.8(3)
C(45)	0.1442(5)	0.1318(4)	0.6282(4)	4.7(2)
C(46)	0.1201(4)	0.1745(4)	0.5221(3)	4.1(2)
C(51)	0.1934(3)	0.4788(3)	0.2367(3)	2.8(2)
C(52)	0.3319(4)	0.4797(3)	0.1689(3)	3.5(2)

Can. J. Chem. Downloaded from www.nrcresearchpress.com by 92.62.229.171 on 09/08/12
For personal use only.

© 1997 NRC Canada

Table 2 (*concluded*).

Atom	*x*	*y*	*z*	U_{eq}
C(53)	0.3952(4)	0.5808(4)	0.1232(4)	4.2(2)
C(54)	0.3225(5)	0.6801(4)	0.1442(4)	4.4(2)
C(55)	0.1862(4)	0.6791(4)	0.2124(4)	4.4(2)
C(56)	0.1214(4)	0.5794(3)	0.2581(3)	3.7(2)
L = 1-methylimidazole				
Re	0.32217(2)	0.86338(3)	0.86754(2)	1.57(1)
Cl(1)	0.27564(13)	0.64836(20)	0.81230(10)	2.56(7)
Cl(2)	0.27913(12)	0.99331(20)	0.76181(9)	2.37(7)
Cl(3)	0.38144(12)	1.06729(20)	0.92572(10)	2.44(7)
P	0.18371(11)	0.91353(20)	0.92052(9)	1.59(6)
N(11)	0.3914(5)	0.5625(8)	1.0324(4)	3.0(3)
C(11)	0.3773(8)	0.4293(12)	1.0706(6)	4.6(5)
C(12)	0.3469(6)	0.6074(9)	0.9738(4)	2.6(3)
N(13)	0.3715(4)	0.7365(7)	0.9547(3)	2.1(2)
C(14)	0.4370(5)	0.7749(9)	1.0043(4)	2.6(3)
C(15)	0.4486(6)	0.6679(11)	1.0534(5)	3.2(4)
N(21)	0.5871(4)	0.8328(7)	0.8027(4)	2.7(3)
C(21)	0.6809(6)	0.8621(11)	0.8144(6)	3.7(4)
C(22)	0.5241(5)	0.8786(9)	0.8441(5)	2.8(3)
N(23)	0.4474(4)	0.8307(7)	0.8196(3)	2.2(2)
C(24)	0.4632(6)	0.7543(12)	0.7598(5)	3.6(4)
C(25)	0.5507(6)	0.7553(12)	0.7484(5)	3.6(4)
C(31)	0.1637(5)	0.8245(8)	1.0055(4)	1.7(2)
C(32)	0.0873(5)	0.7578(8)	1.0204(4)	2.1(3)
C(33)	0.0763(6)	0.6927(10)	1.0866(5)	3.0(3)
C(34)	0.1419(6)	0.6916(11)	1.1384(5)	3.3(4)
C(35)	0.2195(6)	0.7601(10)	1.1249(4)	2.8(3)
C(36)	0.2307(5)	0.8244(9)	1.0598(4)	2.3(3)
C(41)	0.0842(5)	0.8723(8)	0.8672(4)	2.1(3)
C(42)	0.0201(5)	0.9757(10)	0.8523(4)	2.7(3)
C(43)	−0.0560(6)	0.9381(12)	0.8143(5)	3.6(4)
C(44)	−0.0700(6)	0.8023(13)	0.7921(5)	3.8(4)
C(45)	−0.0082(6)	0.6975(12)	0.8064(5)	3.7(4)
C(46)	0.0693(5)	0.7346(10)	0.8441(5)	3.1(3)
C(51)	0.1707(4)	1.1016(8)	0.9435(4)	1.7(3)
C(52)	0.1830(5)	1.2038(9)	0.8902(4)	2.4(3)
C(53)	0.1735(6)	1.3448(9)	0.9047(5)	3.0(4)
C(54)	0.1525(6)	1.3894(8)	0.9731(6)	3.0(4)
C(55)	0.1416(6)	1.2903(10)	1.0262(5)	3.1(3)
C(56)	0.1501(5)	1.1469(8)	1.0116(4)	2.3(3)

Can. J. Chem. Downloaded from www.nrcresearchpress.com by 92.62.229.171 on 09/08/12
For personal use only.

workers (9) for $TcCl_3py_3$. The *meta* protons give sharp peaks at ~35 ppm, whereas the *ortho* and *para* protons are found at very high field. The *ortho* signals are assigned to the peaks at −58.59 and −76.53 ppm, broadened by their proximity to the paramagnetic centre. The weaker and sharper peaks at −46.88 and −77.66 ppm are due to the *para* protons.

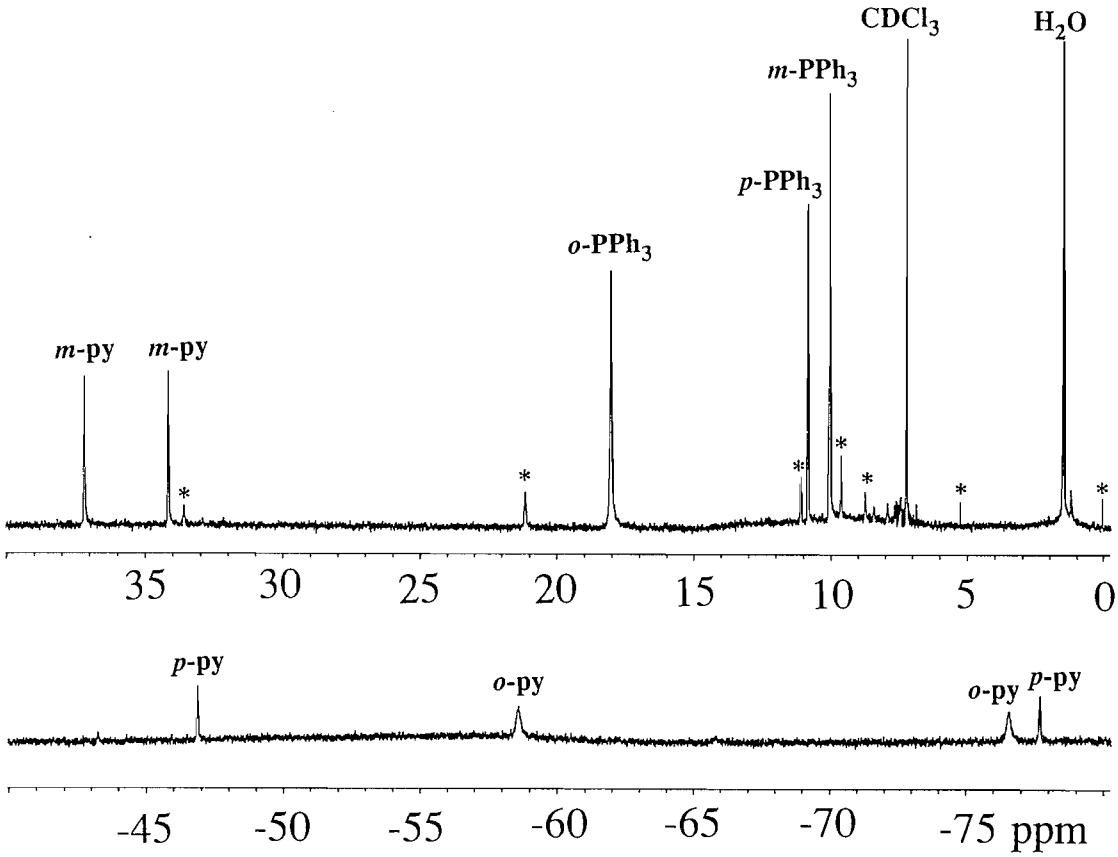
These assignments are confirmed by the spectra of the picoline complexes (Table 3), where the signals occur at the same places. In the 4-picoline complex, the high-field *para* resonances are replaced by very low-field signals for the methyl protons at 70.64 and 100.11 ppm, respectively. With 3-picoline, only one *meta* resonance is found near 33 ppm for each ring, the methyl groups giving upfield signals at −14.23 and −22.29 ppm, respectively.

The alternation between upfield and downfield shifts around the ring and the lack of attenuation of isotropic shift for remote protons has been ascribed to spin delocalization occurring via the pyridine π-system (9, 10). The fact that the ring C-H protons and those of a methyl group bound to the same carbon show displacements in opposite directions is also consistent with this mechanism.

For each type of pyridine proton, the higher-field signal was assigned to the same ligand, as noted for $ReCl_3py_3$ (below) and $TcCl_3py_3$ (9). It is probably the one sitting *trans* to Cl,

© 1997 NRC Canada

Fig. 1. ^{1}H NMR spectrum of $ReCl_3py_2(PPh_3)$ in $CDCl_3$. * = Weak signals due to traces of unidentified impurities.



where metal-to-pyridine π bonding is more favoured than for the other position, where the pyridine and PPh_3 compete for π back-bonding.

$ReCl_3py(PPh_3)_2$ (**7**) must be the *trans*-PPh_3 isomer, since the spectrum contains a single set of phosphine signals, at slightly higher field than for the above compounds. The pyridine protons show spin–spin splitting, allowing unambiguous assignments from intensity and multiplicity: doublet at −4.00 ppm to the *ortho* protons, triplet at 11.57 ppm for the *meta* protons, and half-intensity triplet at 4.23 ppm to the *para* protons. The alternating *ortho/meta/para* pattern in the pyridine ring is similar to the one noted above, although the amplitudes are smaller. Interestingly, in *trans*-$[ReCl(py)(en)_2](PF_6)_2$, where py is also *trans* to Cl, the *ortho* and *meta* protons appear at roughly the same places, although their *para* proton occurs at much higher field (11). In contrast, the chemical shifts are drastically different for *cis*-$[ReCl(py)(en)_2](PF_6)_2$, showing that the remaining ligands in the coordination sphere play a crucial role.

The spectra obtained with the $ReCl_3L_3$ complexes of pyridine and 4-picoline raised particular questions. In contrast with the $TcCl_3L_3$ complexes, which give relatively narrow coupled peaks (9), very broad signals were obtained for the *ortho* and *para* protons in the $ReCl_3L_3$ analogues (Fig. 2): for instance, the linewidth of the *ortho* signal is ~35 Hz for $TcCl_3py_3$ and ~600 Hz for $ReCl_3py_3$. This does not reflect instrinsic trends for these two metal centres, since Duatti et al. (12) have noted that, for Schiff base complexes, Tc(III) gives broader peaks than Re(III). On the other hand, our chemical shifts are strikingly different from those recently reported by Tisato et al. (10)[3] for $ReCl_3py_3$: 3.16, 16.93, and −0.32 ppm for the *trans* ligands; 6.1, 13.9, and −2.4 ppm (values estimated from their Fig. 3) for the unique ligand. After testing different variables, the magnetic field was identified as being responsible for these differences: our spectra were recorded on 300 and 400 Hz instruments, those of Tisato et al. on a 200 MHz instrument. Thus, it appears that this particular set of compounds shows extreme sensitivity to field strength, probably because the electronic ground state of the metal centre changes between these two fields. Having identified the reason for these discrepancies, we believe comparisons can safely be made between our data and those of the $TcCl_3L_3$ compounds, which were also studied at 300 MHz (9). The presence of two sets of signals with different integrations is consistent with a *mer* geometry. The narrow *meta* protons (21.32 and 18.87 ppm) are shifted downfield from the free ligand, whereas the *ortho* and *para* protons between −11.0 and −16.3 ppm are shifted upfield. The proximity of the very broad *ortho* and *para* signals precluded reliable integration and unambiguous identification. From the Tc compound (9, 13), it was assumed that the signals in the mutually *trans* pair of ligands are downfield from those of the *unique* pyridine, since the former must compete for π-back-bonding. Again, the methyl signals for $ReCl_3(4\text{-pic})_3$ occur at very high field, that is, in the opposite direction to that for the *para* protons of

[3] Also, F. Tisato, private communication.

Can. J. Chem. Downloaded from www.nrcresearchpress.com by 92.62.229.171 on 09/08/12
For personal use only.

© 1997 NRC Canada

Table 3. ^{1}H NMR data.[a]

		PPh_3			Other ligand			
		ortho	*meta*	*para*	*ortho*	*meta*	*para*	CH_3
$ReCl_3py(PPh_3)_2$ (**7**)		13.55	8.49	8.49	−4.00(d)	11.57(t)	4.23(t)	
trans-$[ReClpy(en)_2]^{2+}$ [b]					−6.66	11.71	−12.86	
cis-$[ReClpy(en)_2]^{2+}$ [b]					16.66	14.66	13.41	
$ReCl_3py_2(PPh_3)$ (**2**)		18.06	10.09	10.88	−58.59	34.17	−46.88	
					−76.53	37.18	−77.66	
$ReCl_3(3\text{-pic})_2(PPh_3)$ (**3**)		17.89	10.03	10.92	−51.18	31.65	−48.65	−14.23
					−66.17	35.17	−80.08	−22.29
					−67.88			
					−86.98			
$ReCl_3(4\text{-pic})_2(PPh_3)$ (**4**)		17.94	9.98	10.97	−58.21	33.87		70.64
					−74.09	36.18		100.11
$ReCl_3py_3$ (**9**)[c]	*trans*				−11.07[d]	21.32	−15.56[d]	
	unique				−13.08[d]	18.87	−16.29[d]	
$ReCl_3(4\text{-pic})_3$ (**10**)[c]	*trans*				~−30 [e]	24.38		~44 [e]
	unique				~−30	22.40		~44
$TcCl_3py_3$[f]					−6.77	23.44	−0.81	
					−17.88	16.68	−2.20	
$TcCl_3(4\text{-pic})_3$[f]					−6.07	23.95		30.01
					−20.88	16.87		21.52
$ReCl_3$(benzil)(PPh_3) (**8**)[g]		14.37(d)	8.86(t)	8.72(t)	~8.65[h]	0.44(t)[h]	15.23(t)[h]	
					H2	H4	H5	CH_3
$ReCl_3(1\text{-meim})(PPh_3)_2$ (**6**)[i]		13.35	8.49	8.49	−10.90[j]	−10.17[j]	4.96[j]	5.08
$ReCl_3(1\text{-meim})_2(PPh_3)$ (**5**)[i]		13.54	8.85	8.35	9.01	14.61	12.86	10.61
					−13.11	−8.92[j]	5.88[j]	5.75
$ReCl_3(1\text{-meim})_3$ (**11**)[i]	*trans*				−4.89[j]	0.87[j]	9.16[j]	8.93
	unique				7.06[j]	7.24[j]	8.07[j]	3.81

[a]In $CDCl_3$, unless otherwise stated.
[b]Reference 11.
[c]Spectra sensitive to magnetic field strength (see text).
[d]Broad, ~600 Hz, some assignments could be interchanged.
[e]Very broad, ~2600 Hz.
[f]Reference 9.
[g]In $(CD_3)_2CO$.
[h]Protons on phenyl rings of benzil.
[i]In CD_2Cl_2.
[j]Individual assignment of imidazole protons uncertain.

$ReCl_3py_3$. Thus, our data follow the trends observed for the $TcCl_3L_3$ compounds (9) and for the two above types of Re(III) complexes.

Spectra were recorded for the three types of 1-meim complexes. The ring protons of 1-meim were sometimes hard to detect, because they are nonequivalent and produce very weak peaks compared with those of the phosphine. Nevertheless, all signals were detected and they indicated the same stereochemistries as the pyridine analogs: a single set of PPh_3 signals was observed for *mer,trans*-$ReCl_3(1\text{-meim})(PPh_3)_2$ (**6**), two sets of 1-meim resonances of the same intensity for *mer,cis*-$ReCl_3(1\text{-meim})_2(PPh_3)$ (**5**), and two sets in a 2:1 ratio for *mer*-$ReCl_3(1\text{-meim})_3$ (**11**).

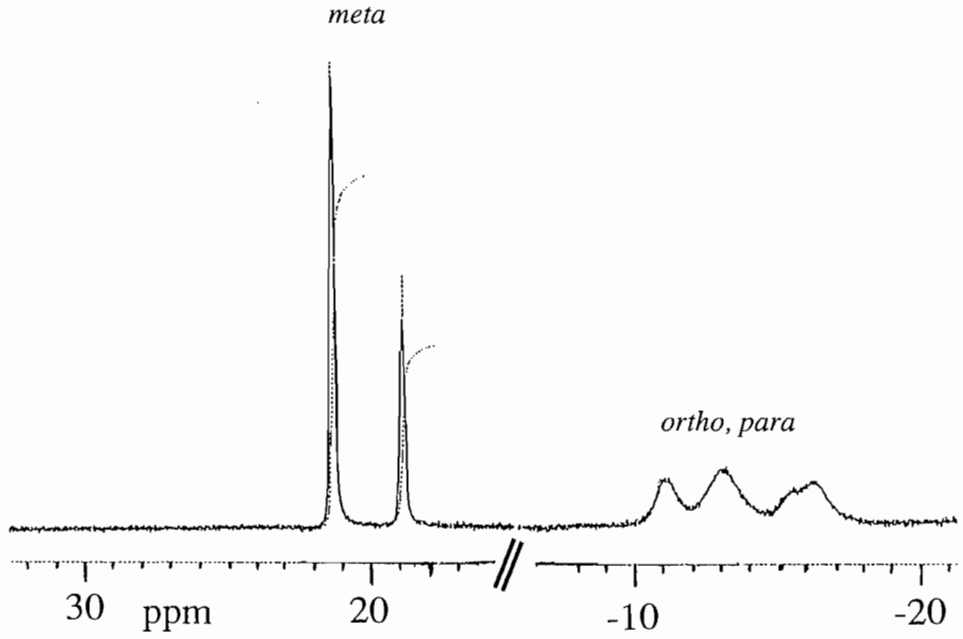
Although the PPh_3 protons could be readily assigned, the situation was less straightforward for those of 1-meim. Data on complexes with other metal centres indicate that the alternating pattern of chemical shifts of pyridines is not found for the five-membered imidazole ring. In a series of Ru(III) species (14, 15), the three ring protons of imidazole were shifted upfield in the order H2 > H4 > H5. In various Fe(III) compounds (16, 17), these protons were not found to occur in a uniform order, but H2 was always found to be the most displaced, although on the downfield side.

A NOE difference experiment was run for $ReCl_3(1\text{-meim})_2(PPh_3)$, from which the set of signals originating from the same type of ligand were identified. It allowed us to identify most of the ring protons, an ambiguity remaining concerning H4 and H5 in one of the rings. The ligand showing peaks at −13.11, −8.92, 5.88, and 5.75 ppm is believed to be *trans* to Cl, since $ReCl_3(1\text{-meim})(PPh_3)_2$ gives a similar pattern, which is assigned similarly. For $ReCl_3(1\text{-meim})_3$ (**11**), the set of resonances belonging to each type of 1-meim ligand can be identified from relative intensities, but assignments to individual ring protons are only tentative at this time.

Can. J. Chem. Downloaded from www.nrcresearchpress.com by 92.62.229.171 on 09/08/12
For personal use only.

© 1997 NRC Canada

Fig. 2. ^{1}H NMR spectrum of $ReCl_3py_3$ in $CDCl_3$ (300 MHz).



The spectrum of $ReCl_3$(benzil)(PPh_3) used as starting material to prepare the *mer*-$ReCl_3L_3$ complexes **9–11** was recorded. Besides the usual phosphine pattern, the ^{1}H spectrum in acetone shows a single set of signals for the benzil protons, whose couplings are clearly detected. This observation requires a *fac* arrangement of the chloride ligands in order to produce equivalency in the two benzil phenyl rings. Well-separated resonances at 15.23 and 0.44 ppm are found for the *para* and *meta* protons, respectively, whereas the *ortho* protons appear at ~8.65 ppm and are partly masked by the PPh_3 signal at 8.72 ppm. The shifts around the phenyl ring of benzil follow the alternating pattern found for pyridine, but the amplitude is much smaller and the peaks are very sharp. This is consistent with spin delocalization occurring via the π system, but at a greater distance from the metal centre.

Comparison of the data for PPh_3 protons in Table 3 shows that the *ortho* protons systematically occur downfield from the *meta* and *para* protons, which are sometimes not resolved. It is interesting to point out that the three resonances are displaced downfield for the three $ReCl_3L_2(PPh_3)$ compounds with pyridines, whereas the 13.5/8.5/8.5 ppm pattern of *mer,trans*-$ReCl_3(RCN)(PPh_3)_2$ is retained for the remaining compounds including *fac*-$ReCl_3$(benzil)PPh_3 and *mer*-$ReCl_3$(1-meim)$_2(PPh_3)$. Therefore, chemical shifts do not depend on a single feature such as ligand composition or stereochemistry, since they are sensitive to subtle changes such as replacing pyridine by imidazole. Systematic studies on other series of complexes are needed before general trends can be proposed.

Infrared spectroscopy

The 4000–600 cm^{-1} region includes a number of ligand bands that are not greatly affected by coordination. The more interesting 600–200 cm^{-1} region is presented in Table 4.

Bands at 544 and 496 cm^{-1} for $ReCl_3(4\text{-pic})_3$ (**10**) and 466/454 cm^{-1} for $ReCl_3py_3$ (**9**) are assigned to the pyridine ligands (18, 19). A pattern of two bands at 280 and 306 cm^{-1} (the latter containing a high-frequency shoulder) is consistently found in the present series of compounds and can be assigned to Re–Cl stretching, for which three IR active modes are expected in a *mer*-$ReCl_3$ unit. The absence of significant absorption at ~280 cm^{-1} for $ReCl_3(1\text{-meim})_3$ remains unclear. For related Rh and Ir complexes, bands near 280 cm^{-1} were assigned as M–N stretching (19, but the presence of this band in $ReCl_3(MeCN)(PPh_3)_2$ (**1**) and other pyridine-free $ReCl_3(RCN)(PAr_3)_2$ compounds (3) supports our assignments as ν(Re–Cl).

The remaining complexes all contain PPh_3, which shows two characteristic sets of bands. The typical triplet (3, 20, 21) with an intensity pattern opposite to that of free PPh_3 is observed at 523/513/498 cm^{-1} (first two components not resolved for **2**). Two weaker characteristic bands are also observed at 450 and 430 cm^{-1}, masking those of pyridine or picolines (18, 19). Nevertheless, a weak band is detected for $ReCl_3(4\text{-pic})_2(PPh_3)$ (**4**) at 545 cm^{-1}. A weak feature at ~380 cm^{-1} for $ReCl_3(1\text{-meim})_2(PPh_3)$ (**5**) and a stronger band at 391 cm^{-1} for $ReCl_3(1\text{-meim})_3$ (**11**) are likely due to an imidazole mode (22, 23). This absorption is probably too weak to be detected in the spectrum for $ReCl_3(1\text{-meim})(PPh_3)_2$ (**7**) dominated by the strong features of the two PPh_3 ligands. The ν(Re–Cl) pattern described above is not affected by the presence of PPh_3.

The ν(Re–P) bands should appear near 200 cm^{-1} (24, 25) and are not expected to show in our spectra. Weak bands at 247 and ~230 cm^{-1} in the $ReCl_3L_3$ compounds **9–11** could be due to ν(Re–N) motion. Weak features in the same region are detected for most other complexes with py, 3-pic, 4-pic, and 1-meim. However, since this spectral region is poorly defined and weak signals are also found for compounds **1** and **8** devoid of Re—N bonds, no assignments are attempted below 250 cm^{-1}.

Can. J. Chem. Downloaded from www.nrcresearchpress.com by 92.62.229.171 on 09/08/12
For personal use only.

© 1997 NRC Canada

Table 4. IR data (600–200 cm^{-1}) for the complexes.

	$ReCl_3L_3$			$ReCl_3L_2(PPh_3)$					$ReCl_3L(PPh_3)_2$	
Assignment	L = py **9**	4-pic **10**	1-meim **11**	py **2**	3-pic **3**	4-pic **4**	1-meim **5**	1/2 benzil **8**	1-meim **7**	MeCN **1**
4-pic		544 w				545 w				
PPh_3				526 vs	525 vs	524 vs	526 vs	526 vs	518 vs	520 vs
PPh_3				512 s	513 s	513 vs		507 m		513 s
PPh_3				496 s	496 s	494 vs	502 s	498 m	494 s	498 s
4-pic		496 s								
benzil								488 m		
py	466 m									
py	454 m									
PPh_3, py				446 w	450 w	451 m	448 m	460 w	455 m	456 m
3-pic				436 w	424 m	430 m	420 m	440 w	434 w	436 w
4-pic				427 w					414 m	417 w
benzil								416 vw		
1-meim			391 m				380 vw			
benzil								330 m		
	315 sh	312 sh		317 sh	318 sh	314 sh	312 sh	344 s	312 w	325 m
ν(Re–Cl)	306 vs	307 vs	313vs	308 s	309 s	309 vs	301 vs	293 vs	300 s	307 s
	280 m	279 m		281 m	281 m	278 m	276 m		270 m	285 m
							267 vw			
	247 m	247 w	238 m							
ν(Re–N)	232 m	229 w	222 m							
				248 vw		258 vw	256 vw	247 vw		
				237 vw		236 vw	237 vw		234 vw	

The spectrum of the $ReCl_3$(benzil)(PPh_3) complex used as starting material was also recorded. The ^1H NMR spectra discussed above indicate the presence of a *fac*-$ReCl_3$ unit in this molecule. The IR spectrum shows the typical features for PPh_3, as well as strong bands at 488 and 330 cm^{-1}, probably corresponding the 470 and 328 cm^{-1} bands, respectively, of uncoordinated benzil. The two remaining strong bands at 344 and 293 cm^{-1} probably originate from ν(Re–Cl) modes. Therefore, shifts to higher frequencies seem to take place between *mer* and *fac* configurations.

Crystallographic work

The $ReCl_3L_2(PPh_3)$ molecules with 3-picoline, pyridine (two crystallographically independent molecules), and 1-methylimidazole adopt the same *cis-mer* geometry (Figs. 3*a–d*). The 4-picoline analogue adopts the same arrangement, since its ^1H NMR spectrum shows two sets of proton signals for the picoline ring.

Interatomic distances and bond angles are listed in Table 5. The Re–Cl distances *trans* to a Re—N bond (mean 2.390 Å) are appreciably longer than the mutually *trans* Re—Cl bonds (2.369 Å). A similar *trans* influence of a pyridine ligand has already been noted in related Tc complexes (13), as well as for the complexes with Ti(III) (26) and Os(III) (27). However, this is not a general trend, since it is not followed by complexes with Fe(III) (28), Rh(III) (29), Mo(III) (30), Cr(III) (31), and V(III) (32). The Re—P distances (mean 2.436 Å) are slightly shorter than those found in $ReCl_3$(MeCN)(PPh_3)$_2$ (33) and related phosphines, where the presence of two PPh_3 ligands introduces greater steric hindrance. The Re—N bonds also show some significant differences: the Re—N(1) bond, *trans* to Cl, tend to be ~0.03 Å shorter than the other, *trans* to the phosphine.

A number of significant deviations from the ideal 90° value are noted around the metal, but they generally remain within 5°, which is relatively small considering that the van der Waals envelopes as seen from the metal are quite different for the phosphine and the heterocyclic ligands. However, a region of steric strain is found for the complexes with 3-picoline and pyridine (molecule 2), where the rotation about the Re—P bond and the orientation of the phosphine rings bring an *ortho* proton (C(46)-H and C(252)-H, respectively) close to Cl(3), increasing the P-Re–Cl(3) angle to ~100°. This steric effect does not seem to introduce repulsive contacts with the heterocyclic ligands (type 1) roughly coplanar with the $ReCl_3$ plane, since the dihedral angles (~18°) are smaller than for the other two cases (~33°), where the P-Re-Cl(3) angles are normal. The other heterocyclic ligands (type 2) make dihedral angles of ~45° with the underlying Re—Cl or Re—N bonds for the three molecules containing pyridine ligands, whereas 1-methylimidazole is rotated towards the Re–Cl(1)-Cl(3)-P plane, with which it makes a dihedral angles of 22°.

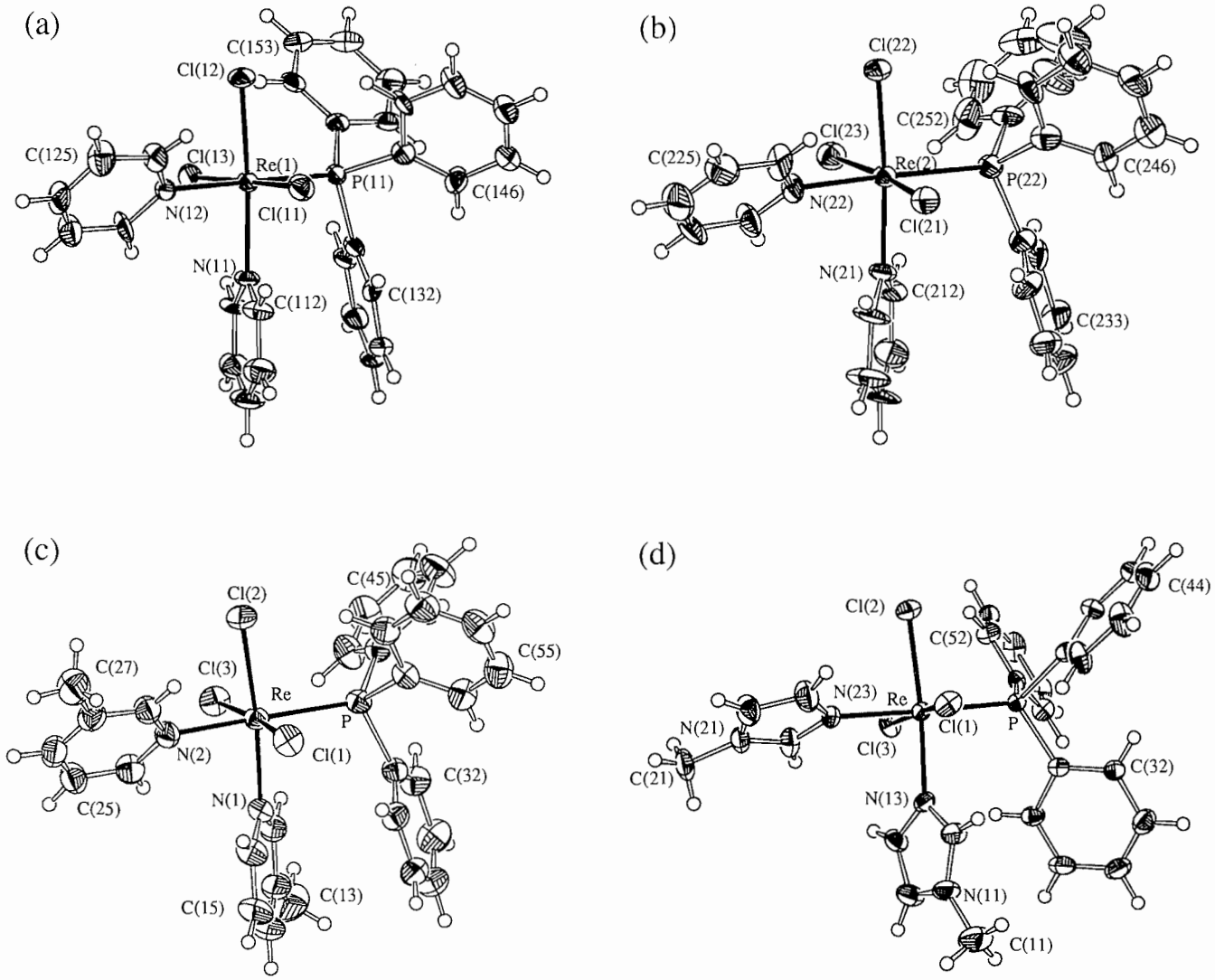
Concluding remarks

All the $ReCl_3L(PPh_3)_2$ and $ReCl_3L_2(PPh_3)$ compounds studied here show the typical pattern of three slightly downfield-shifted phosphine signals observed for $ReCl_3(RCN)(PAr_3)_2$

Can. J. Chem. Downloaded from www.nrcresearchpress.com by 92.62.229.171 on 09/08/12
For personal use only.

© 1997 NRC Canada

Fig. 3. ORTEP drawings of $ReCl_3L_2(PPh_3)$ molecules. (*a*) L = pyridine, molecule 1; (*b*) L = pyridine, molecule 2; (*c*) L = 3-picoline; (*d*) L = 1-methylimidazole. Thermal ellipsoids correspond to 50% probability. Hydrogens are shown as spheres of arbitrary size.



(3), but its position cannot be correlated at this time with a single variable in the complex, since it occurs approximately at the same place for *mer,trans*-$ReCl_3py(PPh_3)_2$, *mer,trans*-$ReCl_3(1\text{-meim})(PPh_3)_2$, *fac*-$ReCl_3(benzil)(PPh_3)$, and *mer,cis*-$ReCl_3(1\text{-meim})_2(PPh_3)$, but it is displaced several ppm downfield for the *mer,cis*-$ReCl_3L_2(PPh_3)$ complexes with pyridine, 3-picoline, and 4-picoline. In all cases, the pyridine protons were found to follow a systematic pattern: *ortho* and *para* upfield, *meta* downfield, opposite displacements for a given proton and those of methyl groups at the same position. The number of signals was useful to confirm the presence of a single stereoisomer in solution and identify its stereochemistry, but no obvious correlation with chemical shift values can be proposed at this time. As to the imidazole ligands, no definite pattern could be deduced. Our work suggests that useful structural information can be extracted from ^1H NMR spectra of these paramagnetic Re(III) compounds, but further work is needed to define guidelines allowing prediction of ligand composition and stereochemistry.

Acknowledgment

We wish to thank M. Simard and F. Bélanger-Gariépy for their assistance in collecting and interpreting the crystallographic data, Phan Viet Minh Tan for valuable assistance with the NOE experiment, and F. Sauriol for assistance in recording the 200 MHz NMR spectra. We are particularly grateful to Dr. F. Tisato, who provided data and samples of $ReCl_3py_3$ from which the extreme sensitivity of the ^1H NMR signals to field strength was uncovered. The financial support of the Natural

© 1997 NRC Canada

Can. J. Chem. Downloaded from www.nrcresearchpress.com by 92.62.229.171 on 09/08/12
For personal use only.

Table 5. Selected distances (Å) and angles (°) for the $ReCl_3L_2(PPh_3)$ compounds.

	L = py[a]		L = 3-pic	L = 1-meim
Re—Cl(1)	2.368(4)	2.367(4)	2.3582(11)	2.373(2)
Re—Cl(2)	2.394(3)	2.394(3)	2.3803(10)	2.390(2)
Re—Cl(3)	2.369(4)	2.385(4)	2.3615(11)	2.374(2)
Re—P	2.424(3)	2.451(4)	2.4354(11)	2.435(2)
Re—N(1)	2.202(11)	2.154(12)	2.154(3)	2.133(6)
Re—N(2)	2.203(11)	2.202(12)	2.181(3)	2.182(6)
Cl(1)-Re-Cl(2)	88.5(1)	91.3(1)	92.02(4)	90.71(7)
Cl(1)-Re-Cl(3)	176.6(1)	173.0(1)	173.90(4)	174.50(7)
Cl(1)-Re-P	92.3(1)	86.4(1)	86.65(4)	94.93(7)
Cl(1)-Re-N(1)	89.6(3)	90.6(3)	90.22(9)	86.7(2)
Cl(1)-Re-N(2)	91.4(3)	88.4(3)	87.87(8)	87.7(2)
Cl(2)-Re-Cl(3)	91.6(1)	89.9(1)	89.39(4)	92.84(7)
Cl(2)-Re-P	92.7(1)	92.9(1)	91.92(4)	90.76(6)
Cl(2)-Re-N(1)	174.3(3)	175.1(3)	174.51(8)	173.5(2)
Cl(2)-Re-N(2)	88.2(3)	87.9(3)	87.78(8)	87.6(2)
Cl(3)-Re-P	91.1(1)	100.4(1)	99.24(4)	89.23(6)
Cl(3)-Re-N(1)	90.0(3)	87.7(3)	87.87(9)	89.3(2)
Cl(3)-Re-N(2)	85.3(3)	84.8(3)	86.26(8)	88.2(2)
P-Re-N(1)	92.8(3)	91.7(3)	93.21(8)	95.4(2)
P-Re-N(2)	176.2(3)	174.8(3)	174.49(8)	176.9(2)
N(1)-Re-N(2)	86.4(4)	87.7(5)	87.29(11)	86.3(2)

[a]Two independent molecules in the asymmetric unit.

Can. J. Chem. Downloaded from www.nrcresearchpress.com by 92.62.229.171 on 09/08/12
For personal use only.

Sciences and Engineering Research Council of Canada and of the Fonds FCAR du Ministère de l'Éducation du Québec is gratefully acknowledged.

References

1. A.M. Lebuis and A.L. Beauchamp. Inorg. Chim. Acta, **216**, 131 (1994).
2. M. Nicolini, G. Bandoli, and U. Mazzi. Technetium and rhenium in chemistry and nuclear medicine. Sgeditoriali, Padova. 1995.
3. C. Pearson and A.L. Beauchamp. Inorg. Chim. Acta, **237**, 13 (1995).
4. G. Rouschias and G. Wilkinson. J. Chem. Soc. A, 993 (1967).
5. R.S. Drago. *In* Physical methods in chemistry. Saunders, Toronto. 1977.
6. G. Sheldrix. SHELX-76. Crystallographic program system. Cambridge University, U.K. 1976.
7. E.J. Gabe, Y. LePage, J.P. Charland, F.L. Lee, and P.S. White. J. Appl. Crystallogr. **22**, 384 (1989).
8. X.L.R. Fontaine, E.H. Fowles, T.P. Layzell, B.L. Shaw, and M. Thornton-Pett. J. Chem. Soc. Dalton Trans. 1519 (1991).
9. A.I. Breikss, A. Davison, and A.G. Jones. Inorg. Chim. Acta, **170**, 75 (1990).
10. F. Tisato, F. Refosco, M. Nicolini, and E. Deutsch. *In* Technetium and rhenium in chemistry and nuclear medicine. Vol. 4. *Edited by* M. Nicolini, G. Bandoli, and U. Mazzi. Sgeditoriali, Padova. 1995. pp. 155–163.
11. S.D. Orth, J. Barrera, M. Sabat, and W.D. Harman. Inorg. Chem. **32**, 594 (1993).
12. A. Duatti, A. Marchi, S.A. Luna, G. Bandoli, U. Mazzi, and F. Tisato. J. Chem. Soc. Dalton Trans. 867 (1987).
13. J. Lu, A. Yamano, and M.J. Clarke. Inorg. Chem. **29**, 3483 (1990).
14. C. Anderson and A.L. Beauchamp. Can. J. Chem. **73**, 471 (1995).
15. C. Anderson and A. L. Beauchamp. Inorg. Chem. **34**, 6065 (1995).
16. J.D. Satterlee and G.N. La Mar. J. Am. Chem. Soc. **98**, 2804 (1976).
17. I. Vernik and D.V. Stynes. Inorg. Chem. **35**, 2011 (1996).
18. N.S. Gill and H.J. Kingdon. Aust. J. Chem. **19**, 2197 (1966).
19. R.J.H. Clark and C.S. Williams. Inorg. Chem. **4**, 350 (1965).
20. K. Shobatake, C. Postmus, J.R. Ferraro, and K. Nakamoto. Appl. Spectrosc. **23**, 12, 1969.
21. G.B. Deacon and J.H.S. Green. Spectrochim. Acta, Part A: **24A**, 845 (1968).
22. D.M.L. Goodgame, M. Goodgame, and G.W. Rayner-Canham. Inorg. Chim. Acta, **3**, 406 (1969).
23. C. Perchard and A. Novak. J. Chim. Phys. **65**, 1964 (1968).
24. J.T. Wang, C. Udovich, K. Nakamoto, A. Quattrochi, and J.R. Ferraro. Inorg. Chem. **9**, 2675 (1970).
25. V. Alexander. Inorg. Chim. Acta, **204**, 109 (1993).
26. S.I. Troyanov, M.Yu. Furkalyuk, and M.A. Simonov. Vestn. Mosk. Univ. Ser. 2: Khim. **30**, 281 (1989). R.K. Collins and M.G.B. Drew. Inorg. Nucl. Chem. Lett. **8**, 975 (1972).
27. A.J. Blake, G.A. Heath, G. Smith, L.J. Yellowlees, and D.W.A. Sharp. Acta Crystallogr. Sect C: Cryst. Struct. Commun. **C44**, 1836 (1988).
28. A. Hoser, Z. Kaluski, M. Januszczyk, J. Pietrzak, and T. Gowiak. Acta Crystallogr. Sect. C: Cryst. Struct. Commun. **C39**, 1039 (1983).
29. K.R. Acharya, S.S. Tavale, and T.N.G. Row. Acta Crystallogr. Sect. C: Cryst. Struct. Commun. **C40**, 1327 (1984).
30. J.V. Brencic. Z. Anorg. Allgem. Chem. **403**, 218 (1974).
31. S.A. Howard and K.I. Hardcastle. J. Crystallogr. Spectrosc. Res. **15**, 643 (1985).
32. K.L. Sorensen, J.W. Ziller, and N.M. Doherty. Acta Crystallogr. Sect. C: Cryst. Struct. Commun. **C50**, 407 (1994).
33. D. Zargarian, F. Bélanger-Gariépy, and A.L. Beauchamp. Acta Crystallogr. Sect. C: In press.

© 1997 NRC Canada

The design of radical clocks to probe the reactivity of the intermediates in arylmethyl ester photochemistry

S.M. Nevill and J.A. Pincock

Can. J. Chem. Downloaded from www.nrcresearchpress.com by 92.62.229.171 on 09/08/12
For personal use only.

Abstract: The photochemistry in methanol of the esters **1–6** was examined. These reactions normally proceed through radical pairs that result from homolytic cleavage of the carbon–oxygen bond in the excited singlet state. Each of the esters was designed to probe the intervention and reactivity of the substituted arylmethyl radical by incorporating a potential radical clock at the carbon of the reactive bond. For esters **1–5**, the products isolated indicated that the radical clock was not reactive enough to compete with the very rapid alternate processes of the radical pair, namely, electron transfer to form the corresponding ion pair and decarboxylation of the phenylacyloxy radical ($k = 4.6 \times 10^9$ s^{-1}). Ester **6**, which incorporates the extremely rapid fluorenylcyclopropylcarbinyl clock, showed very unusual reactivity. On thermal solvolysis in methanol, **6** rearranged quantitatively to the ester **20**. No methyl ethers were detected. In contrast, photolysis of **6** in benzene resulted in an alternate rearrangement to the cyclobutyl ester, **22**, resulting from the aryl version of the cyclopropyl–π-methane photochemical rearrangement. No ester cleavage occurred on excitation. A rationale for the latter conversion was based on stereoelectronic arguments provided by a crystal structure of **6**.

Key words: photochemistry of arylmethyl esters, radical clocks.

Résumé : On a étudié la photochimie des esters **1–6** en solution dans le méthanol. Ces réactions se produisent généralement par le biais de paires de radicaux résultant du clivage homolytique de la liaison carbone–oxygène dans l'état singulet excité. Chacun de ces esters a été synthétisé pour évaluer l'intervention et la réactivité du radical arylméthyle substitué en leur incorporant une horloge radicalaire potentielle au niveau du carbone de la liaison réactive. Dans les cas des esters **1–5**, les produits isolés indiquent que l'horloge radicalaire n'est pas assez réactive pour être en compétition avec les processus alternatifs très rapides de la paire de radicaux, soit le transfert d'électron conduisant à la formation de la paire d'ions correspondante et la décarboxylation du radical phénylacyloxy ($k = 4{,}6 \times 10^9$ s^{-1}). L'ester **6**, qui incorpore l'horloge extrêmement rapide fluorénylcyclopropylcarbinyle, présentait une réactivité très inhabituelle. Lors de sa solvolyse thermique dans le méthanol, le composé **6** se réarrange quantitativement en ester **20**. On ne peut détecter d'éthers méthyliques. Par ailleurs, la photolyse du produit **6** dans le benzène conduit à un réarrangement alternatif en ester cyclobutylique, **22**, qui découle de la version arylée du réarrangement photochimique cyclopropyl–π-méthane. Il ne se produit aucun clivage par excitation. On a expliqué cette dernière conversion en se basant sur des arguments stéréoélectroniques fournis par une structure cristalline du produit **6**.

Mots clés : photochimie d'esters arylméthyles, horloges radicalaires.

[Traduit par la rédaction]

Introduction

The photochemistry of arylmethyl compounds with leaving groups ($ArCH_2$-LG) leads to products derived from both radical ($ArCH_2{}^{\cdot}$ $^{\cdot}$LG) and ion ($ArCH_2{}^+$ $^-$LG) pairs (1–4) and the partitioning between these pathways is controlled by many variables that are not yet clearly understood. Our detailed observations (5) on arylmethyl esters are best explained by a mechanism dominated by homolytic cleavage of the arylmethyl–oxygen bond from the excited singlet state to give the radical pair ($ArCH_2{}^{\cdot}$ $^{\cdot}$O(CO)R). Product yields are then controlled by two rate constants: the rate constant for decarboxylation of the acyloxy radical and that for electron transfer converting the radical pair to the ion pair ($ArCH_2{}^+$ $^-$O(CO)R). Direct heterolytic cleavage of the excited state to form the ion pair seems to be of only minor importance.

One of the now standard ways of probing both the intervention and the reactivity of radicals is by the use of "radical clocks" (6). In fact, in ester photochemistry, the rate of decarboxylation of the acyloxy radical serves as the clock necessary to obtain rate constants for electron transfer for converting the radical pair to the ion pair. However, we have an interest in studying other leaving groups that do not have an internal radical clock.

The obvious solution for timing the radical reactivity is to put the clock on the arylmethyl carbon. Such an approach was taken by Givens and Singh (7) using the well-established 5-hexenyl clock in a benzylic phosphate, eq. [1]. The idea was to probe the reactivity (k_{rad}) of the initially formed radical pair by the competing cyclization (k_{cycl}). In the absence of the phenyl group, the rate constant for the cyclization is $\sim 10^5$ s^{-1} (8). Our

Received October 4, 1996.

S.M. Nevill and J.A. Pincock.[1] Department of Chemistry, Dalhousie University, Halifax, NS B3H 4J3, Canada.

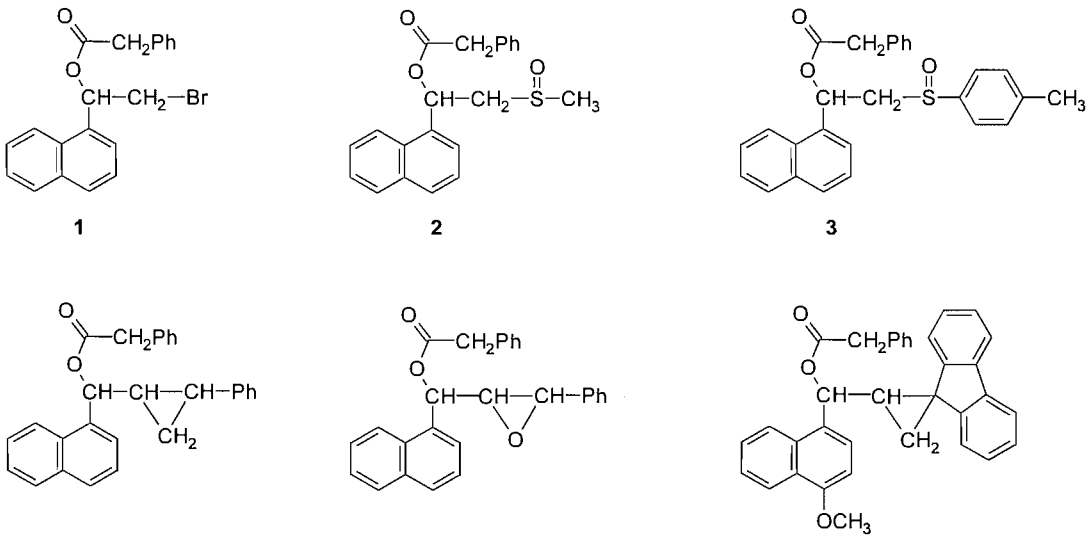
[1] Author to whom correspondence may be addressed. Telephone: (902) 494-3324. Fax: (902) 494-1310. E-mail: PINCOCK@CHEM1.CHEM.DAL.CA

© 1997 NRC Canada

Can. J. Chem. Downloaded from www.nrcresearchpress.com by 92.62.229.171 on 09/08/12
For personal use only.

estimates of the rate constants for the reactivity of the radical pair in ester photochemistry are in the 10^9–10^{11} s^{-1} range. Therefore, a much faster radical clock is necessary in order to obtain significant yields of products from the clock process. This difficulty is apparent in the results from the phosphate in eq. [1] where only very low yields of cyclized products were obtained.

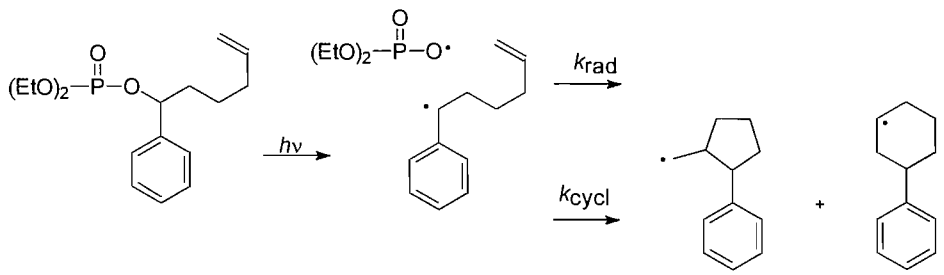
With this in mind we have synthesized and studied the photochemistry of six esters, **1**–**6**.[2] All were chosen so that the excitation would be localized in the chromophore of lowest energy, the naphthalene ring (Naph). Cleavage of the ester bond would then give the radical pair, eq. [2], and the clock built into **1r**–**6r** would then compete with the other processes of the radical pair, namely, electron transfer to give the ion



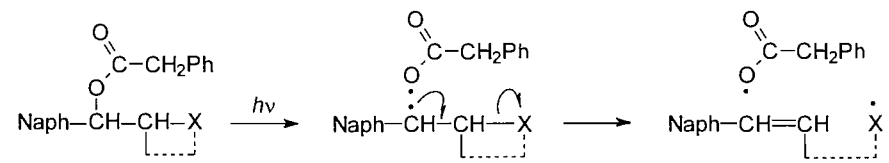
1 **2** **3**

4 **5** **6**

[1]



[2]



1 - 6 **1r - 6r**

pair and decarboxylation of the acyloxy radical. Product yields could then be used to determine the radical clock rate constant.

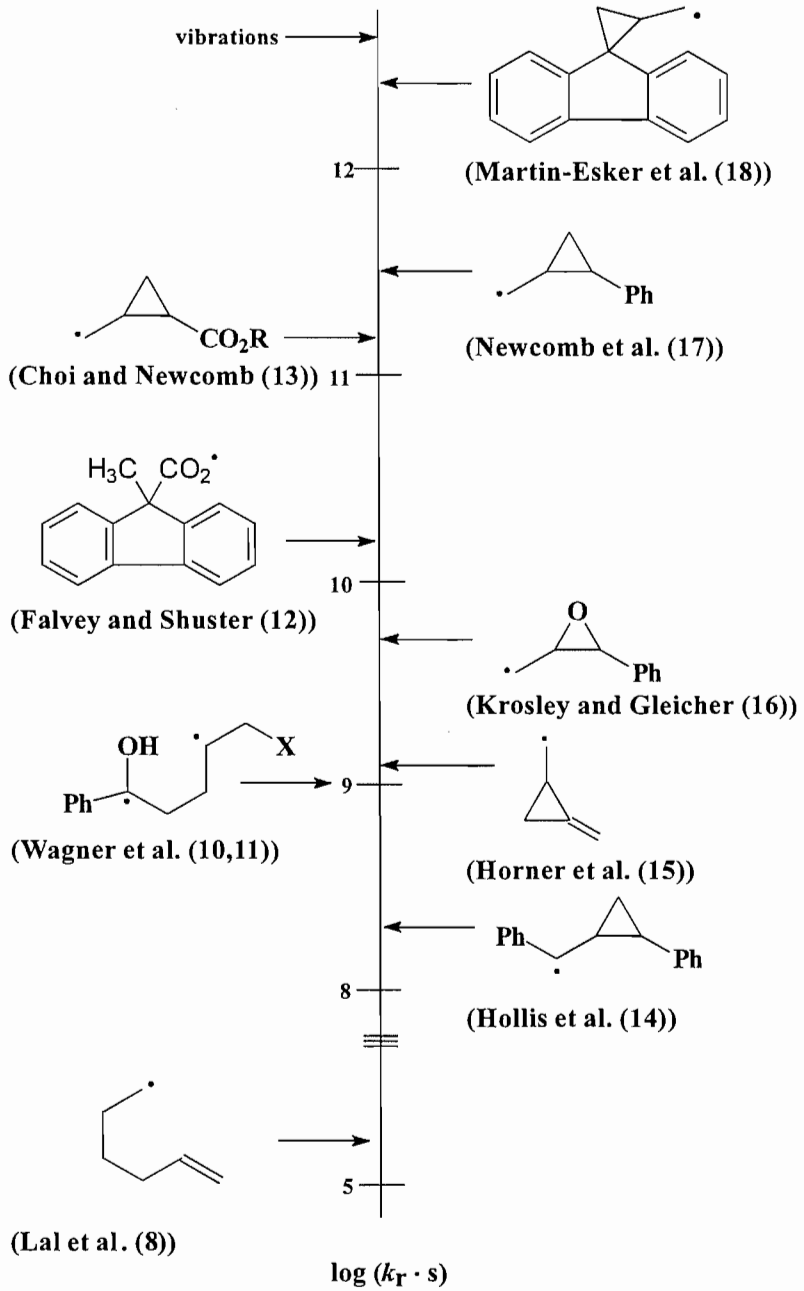
The choice of this set of compounds was based on literature expectations for the reactivity of the radicals. For compounds **1**–**3**, the β-cleavage reaction of biradicals (without the 1-naphthyl group) generated in the Norrish type II reaction of δ-substituted arylketones has been reported (10, 11). For compounds **4**–**6**, the β-cleavage reaction opens the three-membered rings. A summary of rate constants and references (12–18) for their determination is given in Fig. 1 (adopted from a similar figure by Newcomb (19)).

The difficulties inherent in designing a fast arylmethyl radical clock are exemplified by the rate constants for ring opening obtained for three cyclopropylcarbinyl radicals. For the unsubstituted case (20), $k = 1 \times 10^8$ s^{-1}. For the phenyl-

[2] A preliminary account of the photochemistry of **6** has appeared (9).

© 1997 NRC Canada

Fig. 1. Summary of rate constants for radical clocks.



substituted case, the value (17) increases by more than three orders of magnitude to $\sim 5 \times 10^{11}$ s^{-1}, reflecting the increased stability of the ring-opened radical. A second phenyl substitution on the carbinyl carbon decreases the rate constant (14), $k \sim 2 \times 10^{8}$ s^{-1}, nearly back to the original value for the unsubstituted case. The stabilization of the cyclopropylcarbinyl radical by aryl substitution slows down the ring-opening process.

As a historical note, compounds **1**–**6** are ordered in the same sequence in which they were studied. Thus, faster radical clocks were sought after the initial ones were shown to be unsuitably slow.

Results and discussion

Synthesis of esters 1–6

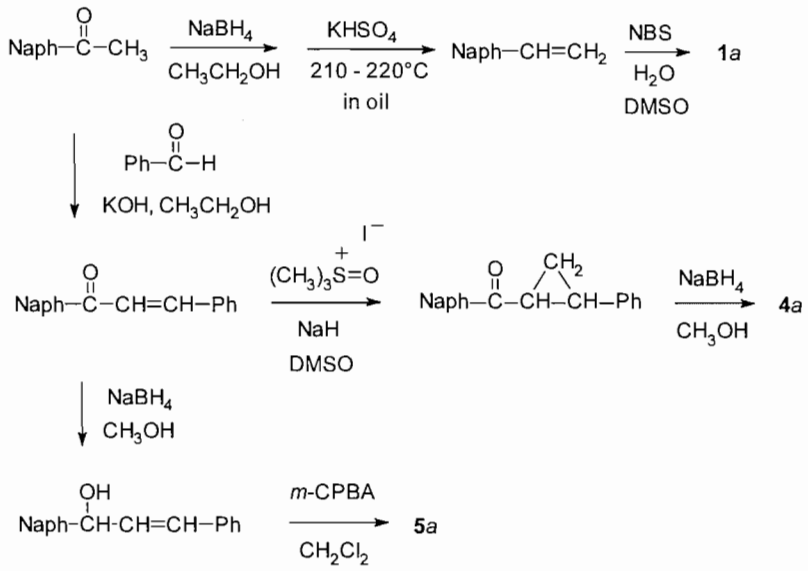
The esters were synthesized from the corresponding alcohols, **1***a*–**6***a*, with phenylacetyl chloride and pyridine in benzene for **1**, **5**, and **6** and with phenylacetic acid and *N,N*-carbonyldiimidazole for **2**, **3**, and **4**.

The successful synthetic routes to the alcohols are summarized in Scheme 1 for **1***a*, **4***a*, and **5***a*, in Scheme 2 for **2***a* and **3***a*, and in Scheme 3 for **6***a*. For all alcohols except **1***a*, the possibility of diastereomeric products created problems for both

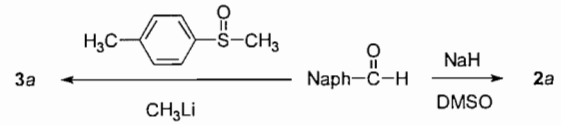
© 1997 NRC Canada

Can. J. Chem. Downloaded from www.nrcresearchpress.com by 92.62.229.171 on 09/08/12
For personal use only.

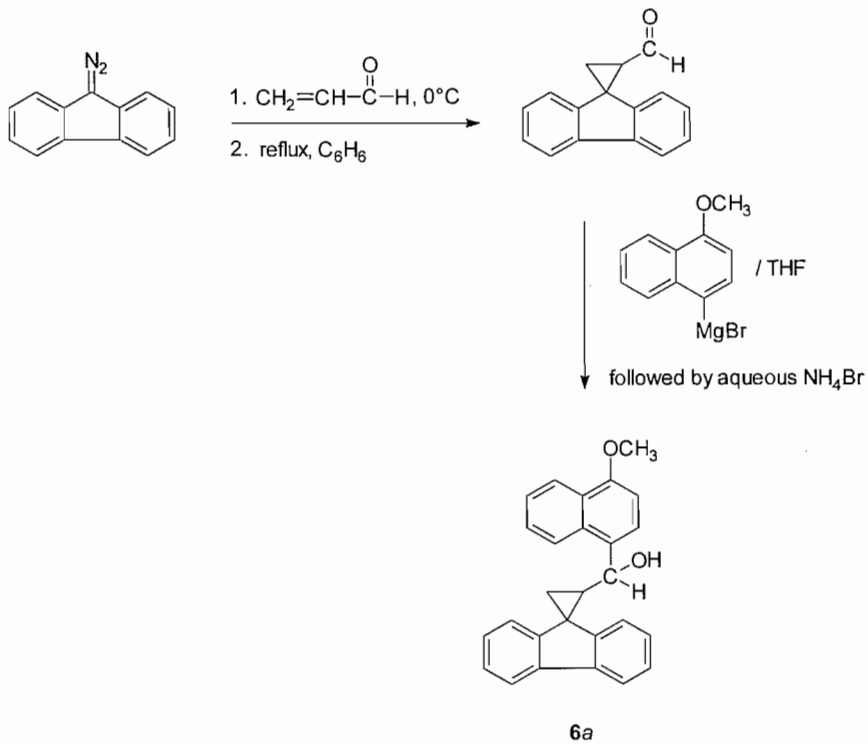
Scheme 1. Synthesis of alcohols **1***a*, **4***a*, and **5***a*.



Scheme 2. Synthesis of alcohols **2***a* and **3***a*.



Scheme 3. Synthesis of alcohol **6***a*.



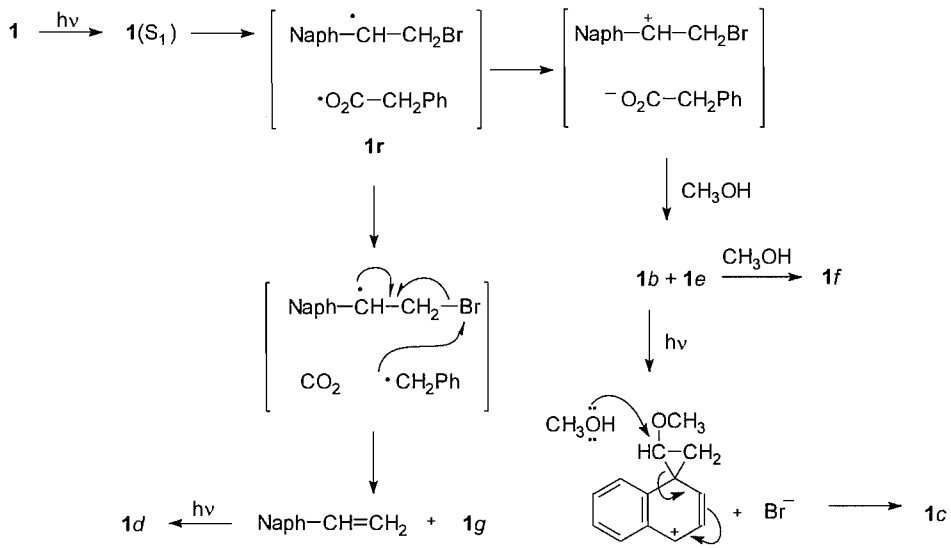
yield and purification. For both **2***a* and **3***a*, with two stereogenic centers, only two diastereomers are possible. By ^{1}H NMR, two similar but distinct ABX patterns at nearly equal intensities were obvious. These diastereomers were not separated and the spectra were not assigned to specific isomers. For the esterification reactions, these mixtures were used in order to maximize yields.

For **4***a* and **5***a*, there are three stereogenic centers, but the

© 1997 NRC Canada

Can. J. Chem. Downloaded from www.nrcresearchpress.com by 92.62.229.171 on 09/08/12
For personal use only.

Scheme 4. Mechanism for the photolysis of **1** in methanol.



possibility of four isomers was reduced to two because of the more stable *trans* geometry through the cyclopropane and oxirane rings. This results because the precursor enone, synthesized by aldol condensation, is the *E* isomer. This assignment was confirmed for the oxirane, **5***a*, by the small coupling constant of 1.5 Hz for the *trans* protons in the three-membered ring (21). For **4***a*, the two diastereomers were formed in a 2:1 ratio, and for **5***a* in a 3:1 ratio. Neither of these mixtures was separated.

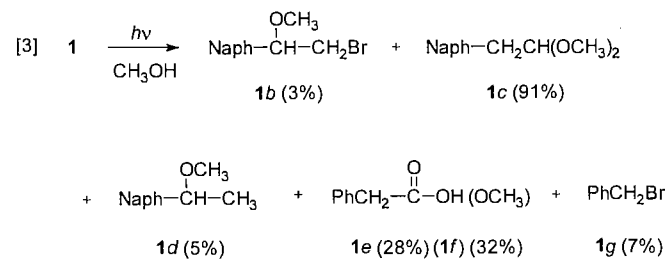
For **6***a*, with two stereogenic centers, the diastereomeric alcohols were formed in a ratio of greater than 9:1 and, in this case, separation and purification of the major isomer was achieved. An X-ray crystal structure determination,[3] Fig. 2, of the ester **6**, made from this isomer, showed that it is of the *R,R/S,S* configuration. The dihedral angle between the two hydrogens on these stereogenic centers is 166°; the large vicinal coupling constant of 10.1 Hz between these same two hydrogens strongly suggests that the stable conformation in solution has a similarly large dihedral angle (ref. 21, p. 197).

Photochemistry of esters 1–6

The esters were photolyzed in nitrogen-purged methanol using a Pyrex-filtered 200 W medium-pressure Hanovia mercury lamp. For preparative runs, high conversions were used. The products were then separated by silica gel chromatography and their structures determined by spectroscopic methods. Once again, the problems of diastereomeric products, as discussed above for the ester substrates, often complicated the separations. In some cases, where yields were low, authentic samples were prepared by independent synthesis. For quantitative runs, lower conversions were used and the yields of products were determined by calibrated HPLC. These yields are given in the equation for each photolysis.

Photochemistry of 1 in methanol

The products for the bromo ester, **1**, are shown in eq. [3]. The major product, **1***c*, was synthesized from 1-naphthylacetic acid by borane–THF reduction to the alcohol, chromium trioxide – pyridine oxidation to the aldehyde, followed by dimethylacetal formation using methanol and an ion exchange resin as the acid catalyst. The bromo ether, **1***b*, was prepared by addition of bromine to vinylnaphthalene in methanol. The other ether was prepared from 1-(1-naphthyl)ethanol using sodium hydride in DMF followed by methyl iodide. Control experiments with **1***b* demonstrated that it was converted to **1***c* by irradiation in methanol. This reaction did not occur in the dark. Therefore, the major product, **1***c*, is not a primary photoproduct. The ratio of **1***e*:**1***f* slowly decreased as a function of



irradiation time, indicating slow ground state esterification of the primary product, the carboxylic acid.

These products can be rationalized by the mechanism outlined in Scheme 4. Initial homolytic cleavage from the excited singlet state gives the radical pair, **1r**. The preferred reaction of the radical pair is electron transfer to give the ion pair, which is then trapped by methanol to give the ether, **1***b*, and phenylacetic acid. Based on the yields of **1***b* and **1***c*, this pathway accounts for 94% of the products. For the related compound, **7**, without the bromine clock, this channel accounts for 84% of the products.

The formation of the ether, **1***d*, is of interest because the

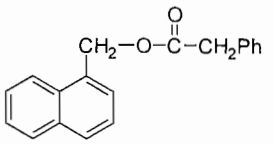
[3] W. Kwiatkowski, Department of Chemistry, Dalhousie University, unpublished results (1996). Lists of atomic coordinates, bond lengths and angles, torsion angles, and anisotropic thermal parameters have been deposited at the Cambridge Crystallographic Data Centre, 12 Union Road, Cambridge, CB2 1EZ, U.K.

Can. J. Chem. Downloaded from www.nrcresearchpress.com by 92.62.229.171 on 09/08/12
For personal use only.

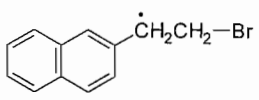
© 1997 NRC Canada

Can. J. Chem. Downloaded from www.nrcresearchpress.com by 92.62.229.171 on 09/08/12
For personal use only.

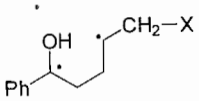
loss of bromine implies that the potential clock reaction of **1r** is competing, though not very efficiently, with the electron transfer process. Based on analogy with the photoprotonation reactions studied by McEwen and Yates (22), the initially formed 1-vinylnaphthalene would be expected to add methanol in the Markovnikov sense to give **1***d*, particularly since it will absorb at longer wavelengths and with a higher molar absorptivity than **1**. However, recent laser flash photolysis results on the closely related 2-bromo-1-(2-naphthyl)ethyl radical, **8**, show that it is very long lived (>5 μs) and that it



7



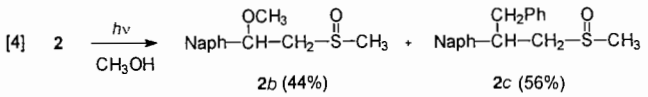
8



9*a*, X = Br
9*b*, X = $SOCH_2CH_2CH_2CH_3$
9*c*, X = SOPh

decays, not by unimolecular fragmentation to 2-vinylnaphthalene and a bromine atom, but in a bimolecular process (23). It is an unreasonable expectation that the positional change from 2-naphthyl to 1-naphthyl for the radical, **1r**, obtained in the photolysis of **1**, would increase the rate constant for this unimolecular process by more than three orders of magnitude. We had originally chosen **1** as a potential probe for arylmethyl reactivity based on the estimated rate constant of 3×10^8 s^{-1} for β-cleavage of the bi-radical **9***a*, obtained in the Norrish type II reaction (10, 11). Again we see that the change from an unsubstituted radical center, as in **9***a*, to an aryl-substituted one, as in **1r**, slows the rate of fragmentation by several orders of magnitude.

Therefore, the pathway for formation of 1-vinylnaphthalene and hence the ether, **1***d*, in the photolysis of **1** is probably not

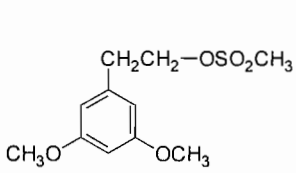


[4] 2 $\xrightarrow[CH_3OH]{h\nu}$ Naph–CH(OCH$_3$)–CH$_2$–S(=O)–CH$_3$ + Naph–CH(CH$_2$Ph)–CH$_2$–S(=O)–CH$_3$

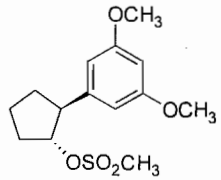
2*b* (44%) **2***c* (56%)

by unimolecular fragmentation of **1r**. A more likely possibility is suggested by the observation of the formation of benzyl bromide, **1***g*, in yields comparable to that for **1***d*. In-cage disproportionation by bromine atom transfer between the benzyl radical and **1r** gives benzyl bromide and 1-vinylnaphthalene. The transfer of the bromine atom from a 1° carbon to a benzylic one is endothermic by about 12 kcal/mol (24) but the compensating formation of the double bond makes this process highly exothermic. The rate constant for decarboxylation of the phenylacetyloxy radical (25), 4.6×10^9 s^{-1}, is great enough that benzyl radicals will be generated before cage escape.

The photochemical conversion of **1***b* to **1***c* probably proceeds by the mechanism shown in Scheme 4. Photochemical activation of leaving groups by β-aryl participation has not been extensively studied (1) but there is precedent for phenonium ion intermediates. Photolysis of the methane sulfonates, **10** (26) and **11** (27), in methanol–water leads to products that result from symmetrical bridged (or equilibrating) species.



10



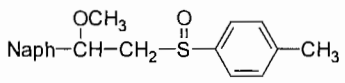
11

Photochemistry of 2 and 3 in methanol

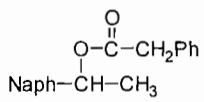
The relative reactivity for loss of X from the radicals **9***a–c* has been estimated at 1:1.2:9.7 for X = Br, SO-$CH_2CH_2CH_2CH_3$, and SO-Ph (11). In the photolysis of **1**, eq. [3], unimolecular loss of a bromine atom from **1r** did not compete with other processes of the radical pair. Therefore, fragmentation of **2r** should also not compete with other processes.

This was confirmed by the products observed, **2***b* resulting from trapping of the ion pair by methanol and **2***c* by in-cage coupling of the substituted 1-naphthylmethyl radical and the benzyl radical, eq. [4]. No products were detected that resulted from loss of the methane sulfinyl group.

The photochemistry of **3** was not studied in detail because preliminary experiments indicated it would not be a suitable precursor for an arylmethyl radical clock. All photolyses resulted in recovery, after chromatography, of less than 10% of the consumed starting material even when conversions were kept as low as 50%. One of the products isolated was the expected methyl ether, **3***b*, but another was **3***c*, resulting from carbon–sulfur bond cleavage at the sulfoxide functional



3*b*



3*c*

group. This bond cleavage was apparently competitive with the usual ester photochemistry. Both the poor mass balance and this unexpected alternate photochemical pathway precluded further study of compound **3**.

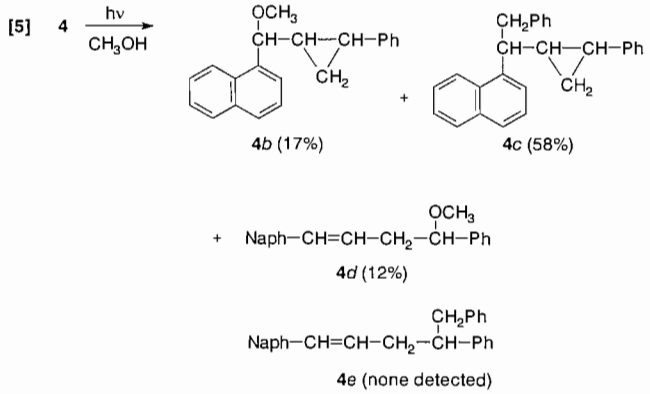
Photochemistry of 4 in methanol

Based on the results for esters **1–3**, a simple homolytic cleavage, even with weak C—X bonds, does not compete with other processes of the radical pair. The substrates, **4–6**, were chosen so that the rate for bond cleavage would be assisted by the thermodynamic driving force provided by cleavage of the three-membered ring. The products and yields for the photolysis of **4** are shown in eq. [5]. The cyclopropyl ether, **4***b*, was independently synthesized from the alcohol, **4***a*, using sodium hydride in DMSO followed by methyl iodide. Products **4***b* and **4***c*, which account for 75% of the mass balance, both retain the cyclopropane ring. The ratio of ether to hydrocarbon (0.29) is now considerably lower than observed (5.2) for the model compound **7**, suggesting that the electron transfer process to form the ion pair is considerably slower for the radical pair, **4r**.

© 1997 NRC Canada

Can. J. Chem. Downloaded from www.nrcresearchpress.com by 92.62.229.171 on 09/08/12
For personal use only.

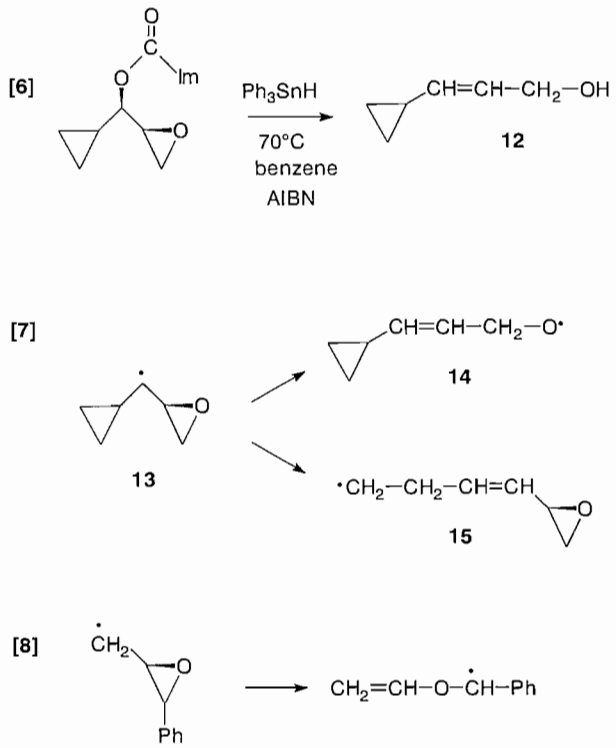
The ring-opened ether **4***d* is clearly suggestive of radical clock reactivity. However, there are two quite distinct mechanistic possibilities for its formation. The first is ring opening at the radical stage followed by electron transfer oxidation to the cation; the second is initial formation by electron transfer of the ring-closed cation followed by ring opening. To probe the reactivity of the cation, the ground state solvolysis of **4** in methanol was examined. Complete conversion required refluxing in methanol (65°C) for 24 h. The ethers **4***b* and **4***d* were again formed but the ratio of 0.42 was considerably lower than the value of 1.42 observed in the room temperature photolysis. A likely explanation for this observation is that the higher temperature required for the solvolysis causes the rate of ring opening of the cation to be faster than trapping by the solvent, methanol. This experiment establishes the fact that the ring-opened cation can be formed, as expected, from the ring-closed one but does not rule out partial intervention of the radical clock possibility for the formation of the ether, **4***d*.



However, an important potential product, **4***e*, that would have established the radical clock pathway, was not detected. Careful examination of the hydrocarbon fraction from silica gel chromatography (which contained **4***c*) by ^{1}H and ^{13}C NMR did not reveal any signals that could be attributed to the alkene functional group. Since the yield of the ring-closed hydrocarbon, **4***c*, is 58%, an upper limit for the yield of **4***e* is probably around 2%. Assuming that the rate constant of electron transfer for the radical pair, **4r**, is $\sim 10^{10}$ s^{-1}, an upper limit for the rate of ring opening for **4r** is $\sim 2 \times 10^{8}$ s^{-1}, a value essentially identical to that previously observed for the 2-phenylcyclopropylcarbinyl radical with a second phenyl substituent at the carbinyl carbon (14).

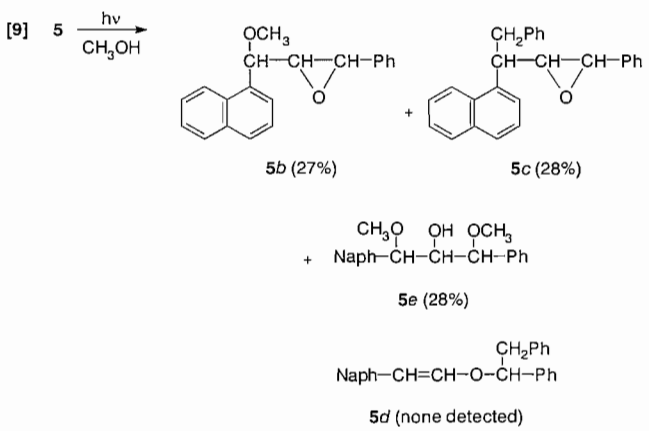
Photochemistry of 5 in methanol

In 1993, Krosley and Gleicher (16) reported that oxiranylmethyl radicals are more reactive to ring opening than cyclopropylmethyl radicals by approximately two orders of magnitude. This was based on the exclusive formation (by NMR analysis) of **12**, eq. [6], the product expected from the radical **13** after rearrangement to **14**, eq. [7]. No evidence was obtained for the intervention of the alternate possibility, **15**. The authors comment that "...no report of chemical trapping or spectroscopic observation of these species prior to rearrangement has appeared." Moreover, oxiranylmethyl radicals that are aryl substituted on the three-membered ring are known to give products derived from ring opening of the carbon–carbon bond rather than the carbon–oxygen bond, eq. [8] (16). With these ideas in mind, we synthesized **5** as a potential clock probe for arylmethyl radical reactivity.



Photolysis of **5** in methanol gave the products shown in eq. [9]. Surprisingly, no products were isolated that were derived from the ring opening of the oxiranyl radical, **5r**, perhaps **5***d* being the most obvious choice. Again, careful examination of ^{1}H NMR spectra of fractions containing **5***c* gave no evidence for alkene hydrogens. The ring-opened product, **5***e*, is a secondary one, derived from addition of methanol to **5***b*, as has been observed in the photochemistry of other oxiranes (28).

One reason for the absence of **5***d* may be its expected high reactivity in methanol both because it is a vinyl ether and because it has a chromophore that will absorb at longer wavelengths than the starting ester. The mass balance in this photolysis is not extremely high (~70%) so the possibility certainly exists that degradation products of **5***d* account for some of this missing mass.

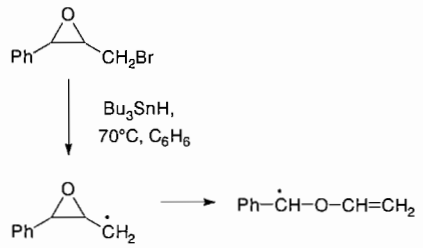


© 1997 NRC Canada

Can. J. Chem. Downloaded from www.nrcresearchpress.com by 92.62.229.171 on 09/08/12
For personal use only.

Of interest is the isolation of the coupling product, **5***c*, which must be derived from in-cage coupling of the benzyl radical with the ring-closed oxiranyl radical, **5r**, proving that under suitable conditions oxiranylalkyl radicals can be trapped, although not yet reported, in a bimolecular process.

Recent results on trapping experiments for the radicals **16** and **17** derived from **15**, eq. [10], indicate that, although **16** is kinetically preferred, **17** is thermodynamically favoured and the conversion of **16** to **15** is reversible (29). As well, allyloxy radicals that are tertiary are capable of cyclizing to oxiranylcarbinyl radicals, so in those cases the equilibrium constant

[10] 

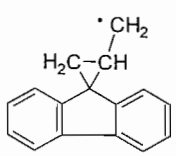
16 15 17

favours the closed form (30). These results all suggest that oxiranylcarbinyl radicals are more stable to ring opening than previously expected. Therefore, **5r**, the 1-naphthyl-substituted analogue of **15**, is stabilized enough by aryl substitution, as in the cyclopropylcarbinyl cases, so that it does not open as rapidly as required to be a useful clock in arylmethyl photochemistry.

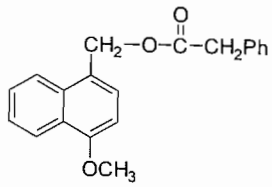
Photochemistry of 6 in methanol and benzene (ref. 9)

In 1994, Martin-Esker et al. (18) reported on the ring-opening reactivity of the (spiro[cyclopropane-1,9′-fluorene]-2-yl)-methyl radical, **18**, and, using bimolecular trapping experiments with benzeneselenol, estimated a rate constant of 6×10^{12} s^{-1}. Even with the assumption of a decrease of two orders of magnitude in this value for 1-naphthyl substitution at the methylene carbon, a value competitive with electron transfer in radical pairs seemed probable. We therefore synthesized the ester **6**.

The change from naphthyl to 4-methoxy-1-naphthyl was necessary to insure that the excitation energy would still be localized in the naphthalene chromophore. This seemed essential in order to observe ester rather than fluorenylcyclopropane photochemistry. Irradiation through Pyrex glass would be quite selective for naphthalene excitation. This expectation was confirmed by fluorescence results in methanol for **6**, which gave a 0,0 value for the singlet excited state at 87.7 kcal/mol, very similar to the reported value of 89 kcal/mol (31) for 4-methoxynaphthalene. Fluorene has a significantly higher



18



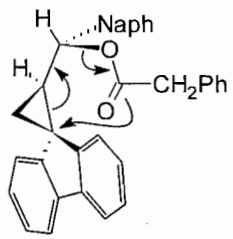
19

singlet excited state energy of 95 kcal/mol (ref. 31, p. 27). Somewhat surprisingly, the quantum yield of fluorescence for **6** (0.12) was considerably lower than that observed (0.27) for the analogue, **19**, without the cyclopropylfluorene clock. This, of course, implies a higher excited state reactivity.

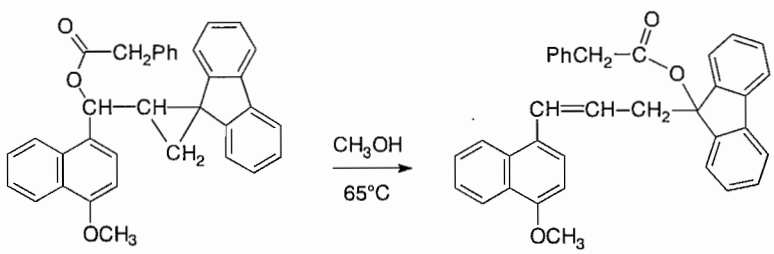
Preliminary irradiations in methanol were not encouraging since HPLC analysis indicated many minor products but no major one. However, the observation was made that **6** slowly underwent ground state conversion at room temperature to a new compound. With the idea that the identity of this compound would be useful in understanding the reactivity of the ion pair, the solvolysis of **6** was examined.

Refluxing **6** in methanol resulted in quantitative conversion to **20**, eq. [11]; the rate constant as determined by HPLC analysis of peak heights is 1.3×10^{-4} s^{-1} ($t_{1/2}$ = 1.4 h). The structure of **20** was established by spectral analysis. The lack of a stereogenic center in **20** removes the diastereotopic character of the benzylic CH_2, which now appears as a singlet in the ^1H NMR. Moreover, the fluorenyl moiety is now symmetric and has only six sp^2 carbon signals (2 singlets, 4 doublets) in the ^{13}C NMR in contrast to the 12 signals for **6**. The ^1H NMR spectrum of the allyl group could be simulated as an A_2XY pattern with J_{XY} = 15.9 Hz, the latter value indicating a *trans* geometry through the double bond.

This conversion was unexpected since all previous solvolysis studies of these esters in methanol resulted in the formation of methyl ethers. The contrast suggested that perhaps the mechanism was concerted via a Cope-like transition state, **21**. This possibility was dismissed after no rearrangement of **6**



21

[11] 

6 20

© 1997 NRC Canada

Can. J. Chem. Downloaded from www.nrcresearchpress.com by 92.62.229.171 on 09/08/12
For personal use only.

was observed after 24 h in either refluxing hexane or acetonitrile. The conclusion is that **6** rearranges to **20** by a very tight ion pair that does not allow trapping by methanol.

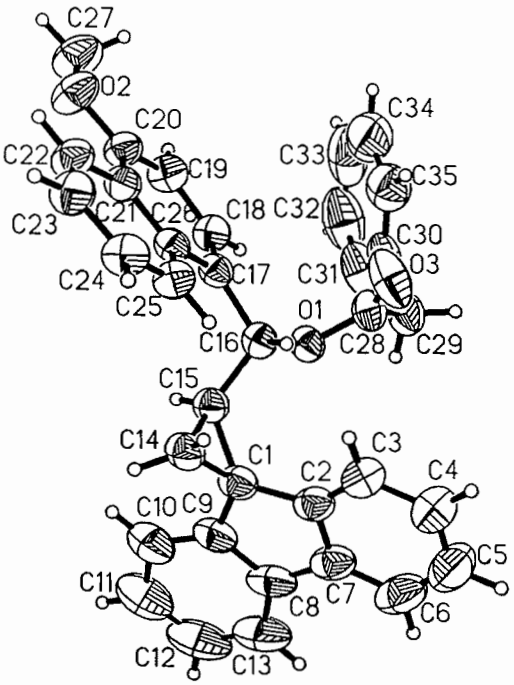
To understand the reactivity of the expected radical pair, **6** was subsequently photolyzed in benzene. In contrast to the results for methanol photolysis, only one major product, **22**, was observed (75% yield after 68% conversion of **6**), Scheme 5.[4] More extended photolysis resulted in disappearance of **22**. The same conversion occurred in acetonitrile but the maximum yield of **22** was lower. Careful silica gel chromatography allowed separation of **6** from **22**. Although **22** could be recrystallized from methanol, the solid samples obtained were inadequate for crystal structure determination. Therefore, proof of the structure of **22** relied entirely on spectroscopic analysis.

The fact that **22** was an ester, isomeric with **6**, was confirmed by IR (carbonyl band at 1720 cm^{-1}) and MS ($M^{\cdot+}$ at *m/z* 496). The assymetry in **22** was revealed by the benzylic methylene as a doublet of doublets (J = 15.5 Hz) in the ^1H NMR and the observation of 12 fluorenyl sp^2 carbons (4 singlets and 8 doublets) in the ^{13}C NMR. Decoupling experiments in the ^1H NMR showed that the lowest field (δ 5.91) cyclobutane hydrogen at the ester carbon (C3) was coupled only to the other methine hydrogen at C2. That methine hydrogen and the cyclobutyl methylene hydrogens could be simulated as an ABX system (calculated coupling constants are given in the experimental section). A hydrogen/carbon NMR HETCOR clearly established that the AB hydrogens were on the same carbon at δ 33.8. Enhancements between one of these hydrogens and a hydrogen (δ 7.56) at C1 of the fluorenyl moiety were shown by NOE experiments; a similar enhancement was seen between the same fluorenyl hydrogen and the cyclobutane hydrogen at C3. There was no enhancement between the two cyclobutane methine hydrogens at C2 and C3. This evidence is all consistent with structure **22** as shown in Scheme 5, including the *trans* substitution on the cyclobutane ring.

The suggested mechanism for conversion of **6** to **22** is also shown in Scheme 5. It represents the "aryl version of the cyclopropyl–π-methane photochemical rearrangement," a variant of the di-π-methane rearrangement. This variant was first suggested by Zimmerman and Carpenter (32) in their report on the photochemistry of **23**, Scheme 6.[5] The hoped-for rearrangement product, **26**, was formed only in trace quantities. The alkenes, **24** and **25**, were shown to be photoproducts of **26** (prepared by independent synthesis) but, in the irradiation of **23**, these alkenes were primary, not secondary, photoproducts. The conclusion was that the 1,4-biradical, **27**, preferentially fragmented to the alkenes rather than cyclizing to form **26**.

The reason for the differences in the photochemistry between the ester **6** and the cyclopropane **23** can be ascribed mainly to stereoelectronic effects. Examination of the X-ray structural data for **6**, Fig. 2, gives a calculated dihedral angle for the vicinal hydrogens of 166°, i.e., nearly *anti*. The large vicinal coupling constant of 10.1 Hz for the same two hydrogens strongly suggests that the solution conformation has a similarly large dihedral angle. One consequence of this geometry is that C4 of the naphthalene ring[4] is ideally placed to induce cyclopropyl C1 to C2 bond cleavage. The distance in the solid between C4 and C2 is only 2.46 Å and the C2-C3-C4-C5 dihedral angle is 98°. Apparently, this leads to enhanced excited state reactivity as indicated by the decreased quantum yield of fluorescence for **6** relative to **19**. The other consequence is that ester reactivity is not favourable from this geometry. The potentially reactive C—O bond of the ester is nearly orthogonal to the naphthalene chromophore; the O-C3-C4-C5 dihedral angle is only 19°. In fact, this compound is the first arylmethyl ester we have studied that does not undergo excited state C—O bond cleavage.

Fig. 2. X-ray structure of **6**.



The difference in reactivity between the diradicals, **27** in Scheme 6 and **28** in Scheme 5, can also be ascribed to stereoelectronic effects. As predicted by Zimmerman and Carpenter (32) and observed for **28**, the biradical is formed in a *cisoid* geometry and collapses with inversion of configuration at C3 to the *trans* cyclobutane, **22**. In contrast, **27** is less likely to be formed in the required geometry so that conversion to **26** is disfavoured. Fragmentation to the alkenes **24** and **25** occurs. The possibility that **28** is still on the S_1 hypersurface, where collapse to cyclobutane is preferred (32), may also be a factor.

Conclusions

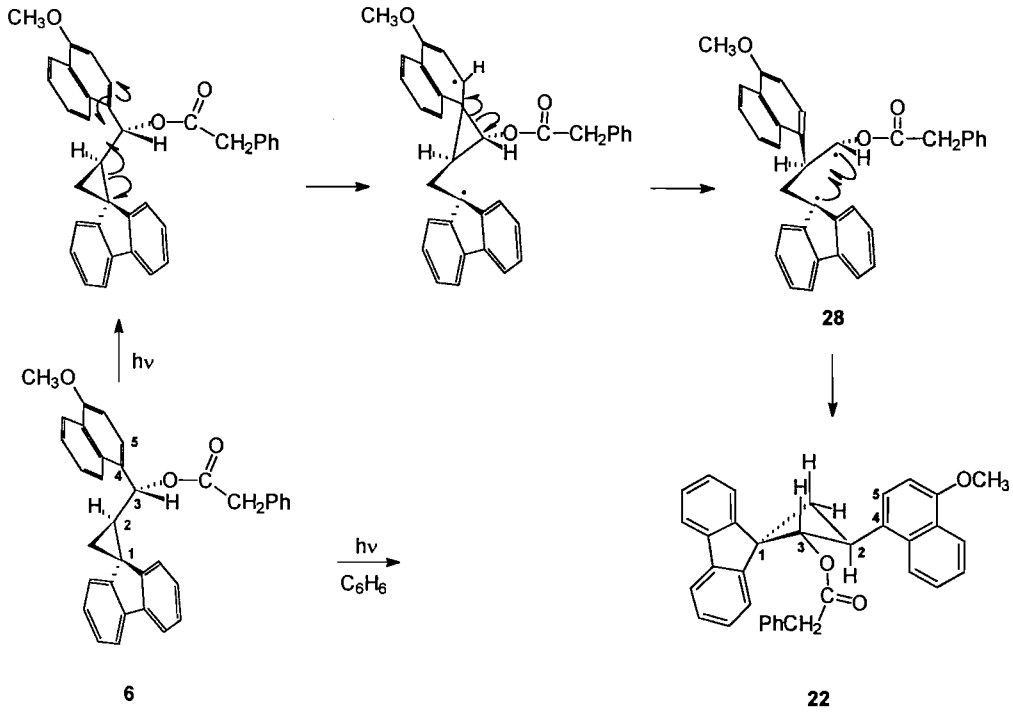
The principal conclusion from the results reported here is that we were unable to design a clock reaction capable of timing the reactivity of photochemically generated arylmethyl radicals. On a positive note, the difficulties in designing such a clock are now understood and will serve as a guide in future attempts. Particularly surprising was the reactivity of **6** where the potential clock never had a chance to operate because of an alternate, more efficient, photoreaction. If the reactivity of **6** is

[4] The numbering on the carbons of **6** and **22** in Scheme 5 does not follow nomenclature rules but rather shows the five carbons critical to the rearrangement mechanism.

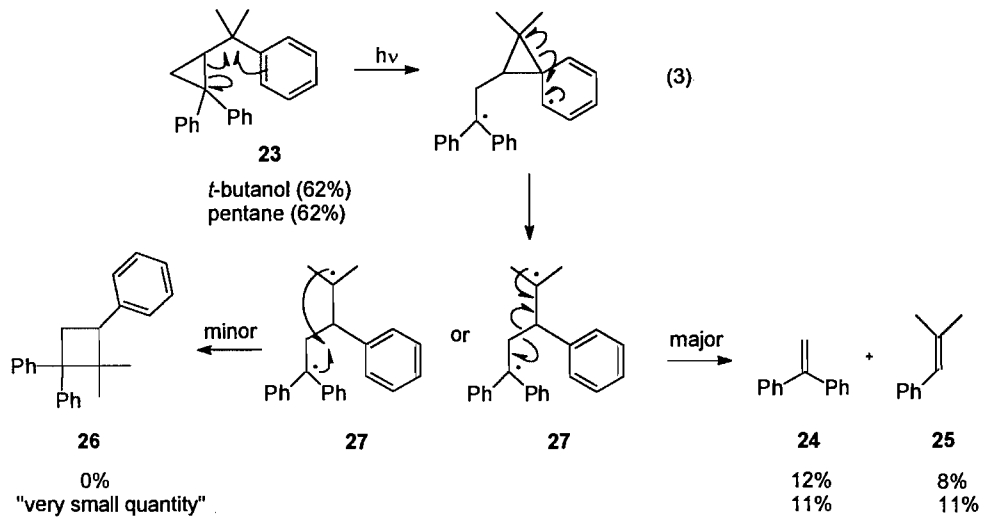
[5] The percent values under **23** in Scheme 6 are for the yield of reisolated starting material.

© 1997 NRC Canada

Scheme 5. Mechanism for the photolytic conversion of **6** to **22** in benzene.



Scheme 6. Products and mechanism for the photolysis of **23**.



controlled by the stereoelectronic effects suggested, then an interesting possibility is presented. These arguments are only likely to hold for the particular diastereomer studied, the *R,R*/*S,S* one. The other isomer, with reversed stereochemistry at the ester carbon, may have a geometry that favors ester photolysis and thus may allow the clock reaction to occur. Other possibilities are also suggested by the recent report of picosecond decarboxylations of acyloxy radicals (33).

Experimental

General experimental

Melting points were determined on a Fisher–Johns melting point apparatus and are uncorrected. Proton (^{1}H) and carbon (^{13}C) nuclear magnetic resonance (NMR) spectra were obtained in $CDCl_3$ on an AC 250 F NMR spectrometer in automation mode or on an AMX 400 NMR spectrometer. Some ^{1}H and ^{13}C NMR spectra were obtained on a Varian Gemini 200 as indicated. High-resolution mass measurements were done on a CEC 21-110B instrument. THF, previously dried with phosphorus pentoxide, was refluxed over sodium with benzophenone until the blue colour of the ketyl radical anion developed, and then distilled. Other general experimental details have been reported previously (34).

The following compounds were purchased from the Aldrich Chemical Company: 1-acetonaphthone, acrolein, benzalde-

Can. J. Chem. Downloaded from www.nrcresearchpress.com by 92.62.229.171 on 09/08/12
For personal use only.

© 1997 NRC Canada

Can. J. Chem. Downloaded from www.nrcresearchpress.com by 92.62.229.171 on 09/08/12
For personal use only.

hyde, *N*-bromosuccinimide, *N,N*-carbonyldimidazole, *m*-chloroperbenzoic acid, dibromoethane, fluorenone hydrazone, magnesium metal, mercuric oxide (yellow), 1-methoxynaphthalene, methyl iodide, methyllithium, 1-naphthaldehyde, 1-naphthylacetic acid, phenylacetic acid, phenylacetyl chloride, sodium borohydride, sodium hydride.

Synthesis of alcohols 1*a*–6*a*

2-Bromo-1-(1-naphthyl)ethanol, ***1****a*

Excess sodium borohydride (3.13 g, 8.24×10^{-2} mol) was slowly added to a solution of 1-acetonaphthone (40.2 g, 2.36×10^{-1} mol) in ethanol (200 mL) with stirring. During the addition of sodium borohydride, the reaction mixture was occasionally cooled to maintain a room-temperature solution. The reaction solution was stirred for 3 h and then water (100 mL) was added. The aqueous layer was extracted twice with dichloromethane (2×40 mL). The organic layers were combined and dried with anhydrous magnesium sulfate and the solvent was removed under reduced pressure to give the impure alcohol. Recrystallization from light petroleum ether gave fluffy, colourless crystals of 1-(1-naphthyl)ethanol: yield 15.4 g, 38%; mp 63.0–63.5°C (lit. (35) mp 66°C). The procedure for the dehydration of the alcohol of Klemm et al. (36) was used for the synthesis of 1-vinylnaphthalene: yield 8.9 g, 71%. The ^{1}H NMR spectrum was the same as previously reported (37).

The generalized procedure for formation of bromohydrins developed by Dalton et al. was used to synthesize 2-bromo-1-(1-naphthyl)ethanol (38). To a stirred solution of 1-vinylnaphthalene (8.9 g, 5.8×10^{-2} mol), DMSO (1 mL), and water (2.1 mL, 0.12 mol) at ~10°C was added *N*-bromosuccinimide (20.3 g, 0.114 mol) in one portion. The reaction mixture was stirred for 15 min, and then water (25 mL) was added. The product was then extracted into ether (25 mL). The ether was then washed with saturated sodium chloride solution and water to remove any excess DMSO, dried over anhydrous magnesium sulfate, and the solvent was removed to obtain the crude product. The resulting bromohydrin was purified using column chromatography, with dichloromethane as eluant to give a yellow oil: yield 3.48 g, 39%; ^{1}H NMR ($CDCl_3$) δ: 7.90 (d, 1H, J = 8.1 Hz), 7.89 (d, 1H, J = 8.5 Hz), 7.83 (d, 1H, J = 8.2 Hz), 7.70 (d, 1H, J = 7.3 Hz), 7.51 (m, 3H), 5.70 (dd, 1H, J = 9.6 and 2.5 Hz, C-H), 3.74 (dd, 1H, J = 10.6 and 2.5 Hz, CH_2-Br), 3.73 (dd, 1H, J = 10.6 and 9.7 Hz, CH_2-Br), 2.8 (bs, 1H, OH); ^{13}C ($CDCl_3$) δ: 133.9, 133.4, 130.7, 129.9, 126.7, 126.1, 125.3, 124.6, 122.6, 46.1, 33.6; GC–MS: 252 (18), 250 (17, M^+), 170 (11), 158 (12), 157 (100), 154 (15), 153 (38), 152 (24), 142 (10), 141 (47), 139 (10), 129 (88), 128 (51), 127 (33), 126 (12), 115 (24), 77 (11), 76 (12), 75 (11), 63 (12).

2-Methylsulfinyl-1-(1-naphthyl)ethanol, ***2****a*

The procedure used was that of Corey and Chaykovsky (39). Sodium hydride (56–58% in mineral oil) (1.24 g, 2.90×10^{-2} mol) was washed twice with hexane. Under nitrogen, DMSO (15 mL) was added, and the reaction mixture was heated to 65–70°C until no more hydrogen was evolved (45 min). To the sodium salt was added 1-naphthaldehyde (1.70 mL, 1.25×10^{-2} mol) over 1 min, while cooling the reaction in a water bath at 15°C. The solution was stirred for 1 h at room temperature. Water (50 mL) was added to destroy any excess NaH. The aqueous layer was extracted with chloroform (2×50 mL). The organic layers were combined and washed with water and brine, dried over anhydrous magnesium sulfate, and the solvent was removed under reduced pressure to give a mixture of diastereomers in a ratio of 1.3:1 based on ^{1}H NMR integration of the CH_3SO signals at δ: 2.60 (minor) and 2.55 (major). These could be separated by column chromatography on silica gel using chloroform as eluant. Diastereomer 1 (yield 0.22 g, 8%): ^{1}H NMR ($CDCl_3$) δ: 8.1–8.0 (m, 1H), 7.9–7.7 (m, 3H), 7.5–7.2 (m, 3H), 6.15 (dd, 1H, J = 8.6 and 3.7 Hz, C-H), 4.8 (bs, 1H, OH), 3.15–3.00 (m, 2H, CH_2-S(O)), 2.55 (s, 3H, CH_3-S(O)); MS: 234 (2, M^+), 200 (22), 185 (14), 184 (12), 170 (71), 169 (21), 158 (51), 157 (19), 153 (57), 152 (22), 141 (58), 129 (100), 128 (55), 127 (40), 115 (21). Diastereomer 2 (yield 0.26 g, 10%): mp 154–156°C; ^{1}H NMR ($CDCl_3$) δ: 8.1–8.0 (m, 1H), 7.9–7.7 (m, 3H), 7.5–7.2 (m, 3H), 6.18 (dd, 1H, J = 7.9 and 4.3 Hz, C-H), 4.6 (bs, 1H, OH), 3.15–3.00 (m, 2H, CH_2-S(O)), 2.60 (s, 3H, CH_3-S(O)); ^{13}C NMR ($CDCl_3$) δ: 137.7 (C), 133.7 (C), 129.5 (C), 129.0 (CH), 128.5 (CH), 126.6 (CH), 125.8 (CH), 125.6 (CH), 123.3 (CH), 122.5 (CH), 64.9 (CH), 61.8 (CH_2), 38.4 (CH_3).

2-(4-Methylphenylsulfinyl)-1-(1-naphthyl)ethanol, ***3****a*

The oxidation of methyl 4-methylphenyl sulfide to the sulfoxide used the procedure of Drabowicz and Mikolajczyk (40): yield 11.1 g, 99%; the ^{1}H NMR was the same as that described previously (41). To a stirred solution of the sulfoxide (1.64 g, 1.06×10^{-2} mol) in anhydrous THF (50 mL) under nitrogen at 0°C was slowly added methyllithium (1.4 M) (10 mL, 1.4×10^{-2} mol). The reaction mixture was stirred for 30 min, and then naphthaldehyde (2.22 g, 1.42×10^{-2} mol) was slowly added. The solution was stirred for a further 60 min, and then saturated ammonium chloride solution was added. The two layers were separated, and the aqueous layer was extracted with dichloromethane (3×50 mL), dried over anhydrous magnesium sulfate, and rotoevaporated to give the β-hydroxy sulfoxide as a mixture of diastereomers in a ratio of 1:1 (yield 0.9 g, 29%). These could be separated by column chromatography on silica gel using 40:60 ethyl acetate:hexane as eluant: Diastereomer 1: ^{1}H NMR ($CDCl_3$) δ: 7.9–7.2 (m, 11H, aromatic), 6.10 (d, 1H, J = 9.6 Hz), 4.4 (bs, 1H, OH), 3.25 (dd, 1H, J = 13.4 and 9.6 Hz, CH_2-S(O)), 3.15 (dd, 1H, J = 13.4 and 2.3 Hz, CH_2-S(O)), 2.42 (s, 3H, Ph-CH_3); ^{13}C NMR ($CDCl_3$) δ: 142.2 (C), 140.3 (C), 137.4 (C), 133.8 (C), 130.2 (CH), 129.5 (C), 129.2 (CH), 128.5 (CH), 126.5 (CH), 125.6 (CH), 124.2 (CH), 123.5 (CH), 122.3 (CH), 67.8, 63.4, 21.5 (CH_3). Diastereomer 2: ^{1}H NMR ($CDCl_3$) δ: 7.9–7.2 (m, 11H, aromatic), 6.10 (d, 1H, J = 9.0 Hz), 5.0 (bs, 1H, OH), 3.30 (dd, 1H, J = 14 and 9 Hz, CH_2-S(O)), 3.0 (d, 1H, J = 14 Hz, CH_2-S(O)), 2.44 (s, 3H, Ph-CH_3); ^{13}C NMR ($CDCl_3$) δ: 141.8 (C), 139.2 (C), 137.6 (C), 133.6 (C), 130.1 (CH), 129.4 (C), 129.0 (CH), 128.2 (CH), 126.3 (CH), 125.7 (CH), 125.5 (CH), 124.2 (CH), 123.4 (CH), 122.2 (CH), 65.1, 63.3, 21.4 (CH_3).

1-Naphthyl-2-(phenylcyclopropyl)methanol, ***4****a*

To a solution of potassium hydroxide (16.6 g, 0.297 mol) in water (110 mL) was added ethanol (100 mL). The resulting solution was cooled and 1-acetonaphthone (53.6 mL, 0.357 mol) was added with stirring. While keeping the solution at room temperature, benzaldehyde (38 mL, 0.374 mol) was added. The reaction mixture was stirred at room temperature for 1 h, and then left for 3 h at 0°C. The oil that resulted was

© 1997 NRC Canada

Can. J. Chem. Downloaded from www.nrcresearchpress.com by 92.62.229.171 on 09/08/12
For personal use only.

extracted from the aqueous solution with dichloromethane. The organic layer was washed with 10% HCl and water, then dried over anhydrous magnesium sulfate. The solvent was removed under reduced pressure, and the α,β-unsaturated ketone was fractionally distilled: yield 80.1 g, 87%. The ^{1}H NMR was the same as that previously reported (42).

The α,β-unsaturated ketone was converted to the cyclopropane according to the procedure of Prestwich et al. (43). To a stirred solution of sodium hydride (56% in mineral oil) (3.25 g, 76 mmol) and trimethylsulfoxonium iodide (17.6 g, 80 mmol) in DMSO (75 mL) under nitrogen gas at 0°C was added 1-naphthyl-3-phenylpropenone (15.4 g, 60 mmol) in DMSO (75 mL). The reaction was stirred under nitrogen for a further 16 h at room temperature. The resulting reaction mixture was poured into water (100 mL), and extracted with ether (3 × 100 mL). The organic layers were combined, and washed with brine and water. The impure cyclopropyl ketone was isolated by drying the organic layer over anhydrous magnesium sulfate and removing the solvent under reduced pressure. The ketone was purified by recrystallization from 100% ethanol: yield 7.0 g, 43%. The ^{1}H NMR was identical with that described previously.

The cyclopropyl ketone was reduced according to the procedure of Dickinson et al. (44). To a solution of cyclopropyl ketone (9.57 g, 35 mmol) in methanol was added sodium borohydride (2.89 g, 70 mmol) in small portions. After stirring the solution for 1 h, the solvent was removed under reduced pressure. Ethyl acetate (25 mL) was added, and the organic layer was washed with water (2 × 25 mL). The solvent was dried over anhydrous magnesium sulfate, and rotoevaporated to give the crude alcohol as a pale yellow oil: yield 10.8 g, quantitative; ^{1}H NMR ($CDCl_3$) δ: 8.1–7.0 (m, 12H), 5.06 (d, 1H, J = 7.0 Hz) (the other minor diastereomer had a doublet at δ 4.96), 2.36 (bs, 1H, OH), 2.0–1.9 (m, 1H), 1.8–1.65 (m, 1H), 1.15–0.86 (m, 2H); ^{13}C NMR ($CDCl_3$) for the major diastereomer δ: 142.4 (C), 138.4 (C), 133.9 (C), 131.2 (C), 128.8 (CH), 128.4 (CH), 126.1 (CH), 125.9 (CH), 125.6 (CH), 125.4 (CH), 123.7 (CH), 73.6 (CH-OH), 29.4 (CH), 22.0 (CH_2), 14.0 (CH).

1-Naphthyl-3-(2-phenyloxiranyl)methanol, ***5***a

The procedure for the synthesis of the alcohol and the epoxy alcohol was that by Dickinson et al. (44). A solution of *m*-chloroperbenzoic acid (57–86%) (7.44 g, 25 mmol) in dichloromethane (40 mL) was slowly added to a stirred solution of the enol (4.53 g, 17 mmol) in dichloromethane (30 mL). After stirring for 3 h, the solution was washed with aqueous sodium sulphite (3 × 20 mL), saturated sodium bicarbonate (3 × 20 mL), and saturated sodium chloride solution (20 mL). The organic layer was dried over anhydrous magnesium sulfate and the solvent was removed under reduced pressure. The impure epoxy alcohol was chromatographed using 10:90 ethyl acetate:hexane. The epoxy alcohol, as a mixture of diastereomers, was isolated as a pale yellow oil: yield 2.84 g, 59%; ^{1}H NMR ($CDCl_3$) δ: 8.1–7.1 (m, 12H), 5.7 and 5.4 (two d's, 1H from each diastereomer), 4.1-4.0 (m, 1H), 3.5–3.4 (m, 1H), 3.1 (bs, 1H).

2-(Spiro[cyclopropane-1,9′-fluorene])(4-methoxy-1-naphthyl)methanol, ***6***a

The procedure of Schöberg et al. (45) was used for the synthesis of 9-diazofluorene: yield 18.5 g, 74%; mp 94–97°C (lit. (45) mp 94–97°C).

The spirocyclopropylfluorenyl aldehyde was synthesized, with minor alterations, according to the procedure of Martin-Esker et al. (18). To a stirred solution of acrolein (350 mL) at 0°C was added 9-diazofluorene (35.0 g, 0.208 mol) in one portion. After 15 min at 0°C, the solution was allowed to warm to room temperature. The excess acrolein was removed under reduced pressure. Some of the acrolein polymerized, and the resulting polymer was rinsed with dichloromethane to remove the aldehyde. The intermediate pyrazoline was then refluxed overnight in benzene. After removal of the benzene at reduced pressure, the aldehyde was chromatographed using 5:95 ethyl acetate:hexane. The aldehyde was a pale yellow oil: yield 19.9 g, 49%; ^{1}H NMR ($CDCl_3$)[6] (Varian) δ: 9.69 (d, 1H, J = 4.2 Hz), 7.86–7.80 (m, 2H), 7.45–7.10 (m, 5H), 7.09–7.06 (m, 1H), 2.95–2.84 (dt, 1H, J = 8.2 and 4.2 Hz), 2.68–2.60 (dd, 1H, J = 7.4 and 5.4 Hz), 2.31–2.24 (dd, 1H, J = 8.2 and 5.4 Hz); ^{13}C NMR ($CDCl_3$) (Varian) δ: 197.8 (CH═O), 146.2 (C), 142.4 (C), 141.5 (C), 140.4 (C), 127.9 (CH), 127.9 (CH), 127.5 (CH), 123.2 (CH), 120.8 (CH), 120.5 (CH), 119.3 (CH), 40.7 (CH), 40.0 (C), 20.9 (CH_2). The resulting aldehyde was sufficiently pure to use in the Grignard reaction.

The alcohol was synthesized using the procedure of Dickinson et al. (44). To a suspension of magnesium metal (0.63 g, 26 mmol) in THF was added dibromoethane (0.15 g, 0.8 mmol) and a small amount of 1-bromo-4-methoxynaphthalene (46). Once the reaction started, the remainder of the 1-bromo-4-methoxynaphthalene was added dropwise (total 4.08 g, 16 mmol). The solution was refluxed for 1 h and then stirred at room temperature for 1 h. To the stirred solution was then added the aldehyde (0.868 g, 3.9 mmol) at 0°C. This solution was stirred at 0°C for 1 h, and then overnight at room temperature. Saturated ammonium chloride solution was added to quench the reaction mixture. The aqueous solution was extracted with diethyl ether, and the organic layer was washed with water. After drying the ether layer with anhydrous magnesium sulfate and filtering, the solvent was removed under reduced pressure. This crude alcohol was chromatographed with 5:95 ethyl acetate:hexane to give the alcohol as an oil and as a mixture of diastereomers (9:1 ratio): yield 0.923 g, 63%. Major diastereomer: ^{1}H NMR ($CDCl_3$)[6] δ: 8.39–8.33 (m, 2H), 7.96–7.86 (m, 2H), 7.71–7.25 (m, 8H), 7.03 (d, 1H, J = 7.6 Hz), 6.86 (d, 1H, J = 7.9 Hz), 5.65 (d, 1H, J = 10.1 Hz), 4.04 (s, 3H), 2.73–2.62 (m, 1H, J = 10.1, 8.5 and 8.3 Hz), 2.04–1.93 (m, 2H), 1.70 (bs, 1H); ^{13}C NMR ($CDCl_3$) δ: 155.5 (C), 148.1 (C), 144.0 (C), 141.4 (C), 139.1 (C), 131.9 (C), 130.3 (C), 127.2 (CH), 127.0 (CH), 126.8 (CH), 126.7 (CH), 126.3 (CH), 126.1 (C), 125.1 (CH), 124.5 (CH), 123.8 (CH), 122.8 (CH), 121.1 (CH), 120.7 (CH), 120.0 (CH), 118.6 (CH), 103.2 (CH), 71.5 (CH-OH), 55.6 (OCH_3), 39.4 (CH), 34.8 (C), 23.0 (CH_2). Minor diastereomer: ^{1}H NMR ($CDCl_3$)[6] δ: 8.23–8.16 (m, 1H), 8.09–8.05 (m, 1H), 7.81–7.77 (m, 2H), 7.46–7.18 (m, 7H), 7.09–7.02 (m, 2H), 6.47 (d, 1H, J = 8.0 Hz), 5.49 (d, 1H, J = 7 Hz), 3.85 (s, 3H), 2.62–2.52 (m, 1H, J = 9.5, 7.2 and 7.0 Hz), 2.30–2.23 (m, 1H, J = 7.2 and 5.5), 2.20–2.13 (m, 2H, J = 9.5

[6] The coupling constants reported here are by simulation using NMRSIM: T.P. Forrest, Department of Chemistry, Dalhousie University, Halifax, NS B3H 4J3, Canada.

© 1997 NRC Canada

Can. J. Chem. Downloaded from www.nrcresearchpress.com by 92.62.229.171 on 09/08/12
For personal use only.

and 5.5 Hz), 2.12 (bs, 1H, OH); ^{13}C NMR ($CDCl_3$) δ: 155.3 (C), 148.0 (C), 144.3 (C), 141.0 (C), 139.4 (C), 131.6 (C), 131.1 (C), 127.0 (CH), 126.6 (CH), 126.5 (CH), 126.2 (CH), 126.1 (CH), 126.0 (C), 125.0 (CH), 124.0 (CH), 123.8 (CH), 122.5 (CH), 121.8 (CH), 120.1 (CH), 119.7 (CH), 118.6 (CH), 102.8 (CH), 70.8 (CH-OH), 55.4 (OCH_3), 36.7 (CH), 35.4 (C), 21.8(CH_2).

Synthesis of esters 1–6

Method A for **1**, **5**, and **6**: by reaction of the alcohol with phenylacetyl chloride in benzene with pyridine (5).

Method B for **2**, **3**, and **4**: by reaction of phenylacetic acid with *N,N*-carbonyldiimidazole followed by the alcohol according to the procedure developed by Staab and Rohr (47) and Carpenter and Moore (48). Example of procedure for **2**: To a stirred solution of *N,N*-carbonyldiimidazole (0.69 g, 4.3×10^{-3} mol) in anhydrous THF (25 mL) was added phenylacetic acid (0.69 g, 5.07×10^{-3} mol) in anhydrous THF (25 mL). After stirring the solution for 1 h at room temperature, 2-methylsulfinyl-1-(1-naphthyl)ethanol, ***2a*** (0.51 g, 2.18×10^{-3} mol), in anhydrous THF (15 mL) was added in one portion, and a small piece of sodium metal was added. The reaction was refluxed until completion, while the extent of the reaction was monitored by HPLC. Upon completion of the reaction, the solvent was removed under reduced pressure. Water was added (50 mL) and the product was extracted into ether (3×25 mL). The organic layers were combined, washed with 1 M Na_2CO_3, water, and then dried over anhydrous magnesium sulfate. The solvent was rotoevaporated to give the crude ester, which was purified by column chromatography.

2-Bromo-1-(1-naphthyl)ethyl phenylacetate, ***1***: yield 93%; IR (neat): 1750 cm^{-1}, ^{1}H NMR ($CHCl_3$) δ: 8.02 (d, 1H, J = 8.6 Hz), 7.87 (d, 1H, J = 8.4 Hz), 7.78–7.82 (m, 1H), 7.45–7.67 (m, 2H), 7.25–7.40 (m, 7H), 6.70 (dd, 1H, J = 7.2 and 5.2 Hz, CH-O), 3.76 (dd, 2H, $PhCH_2$), 3.7–3.5 (m, 2H, CH_2-Br); ^{13}C NMR ($CHCl_3$) δ: 170.2 (C═O), 133.6 (C), 133.5 (C), 133.2 (C), 129.9 (C), 129.3 (CH), 129.2 (CH), 128.9 (CH), 128.4 (CH), 127.1 (CH), 126.7 (CH), 125.8 (CH), 125.1 (CH), 124.1 (CH), 122.4 (CH), 72.6 (CH-O), 41.2 (CH_2), 33.9 (CH_2); GC–MS: 370 (15), 368 (15, M^+), 235 (16), 233 (16), 171 (15), 170 (61), 157 (36), 155 (19), 154 (85), 153 (100), 152 (23), 127 (12), 91 (98), 65 (12); HRMS mass calcd. for $C_{20}H_{17}O_2Br$: 368.0412; found: 368.0420.

2-Methylsulfinyl-1-(1-naphthyl)ethyl phenylacetate, ***2***: yield 32%, as a mixture of diastereomers; ^{1}H NMR ($CDCl_3$) δ: 8.15–8.05 (m, 1H), 7.9–7.7 (m, 2H), 7.6–7.4 (m, 2H), 7.4–7.2 (m, 5H), 7.00–6.95 (m, 1H, CH-O), 3.76 (dd, 2H, Ph-CH_2), 3.4–3.2 (m, 2H, CH_2-S(O)), 2.54 (s, 3H, CH_3-S(O)); ^{13}C NMR ($CDCl_3$) (major diastereomer) δ: 169.8 (CO), 134.1 (C), 133.8 (C), 133.5 (C), 129.5 (CH), 129.4 (CH), 129.2 (CH), 129.0 (C), 128.7 (CH), 127.4 (CH), 127.3 (CH), 127.0 (CH), 126.1 (CH), 125.3 (CH), 123.2 (CH), 122.7 (CH), 67.7 (CH), 61.1 (CH_2), 41.5 (CH_2), 39.4 (CH_3); MS 352 (3, M^+), 170 (20), 154 (17), 153 (39), 92 (100). Anal. calcd. for $C_{21}H_{20}SO_3$: C 71.56, H 5.72; found: C 71.76, H 5.68.

2-(4-Methylphenylsulfinyl)-1-(1-naphthyl)ethyl phenyaceate, ***3***: yield 52% as a mixture of diastereomers; ^{1}H NMR ($CDCl_3$) (major diastereomer) δ: 8.25–8.15 (t, 1H), 8.0–7.2 (m, 15H), 6.73 (dd, 1H, J = 8 and 3 Hz, CH-O), 3.55 (dd, 1H, J = 12 and 8 Hz), 3.48 (dd, 2H, J = 15 Hz, $PhCH_2$), 3.25 (dd, 1H, J = 12 and 3 Hz), 2.40 (s, 3H, Ph-CH_3); ^{13}C NMR ($CDCl_3$) (major diastereomer) δ: 170.0 (C═O), 142.1 (C), 139.9 (C), 134.1 (C), 133.8 (C), 133.4 (C), 130.2 (CH), 129.5 (C), 129.3 (CH), 129.2 (CH), 128.6 (CH), 127.2 (CH), 127.0 (CH), 126.0 (CH), 125.2 (CH), 124.5 (CH), 123.5 (CH), 122.3 (CH), 67.1 (CH), 62.1 (CH_2), 41.1 (CH_2), 21.5 (CH_3); MS: 400 (12, $M^+ - CO$), 308 (13), 153 (38), 152 (100), 91 (42); HRMS calcd. for $C_{27}H_{24}O_3S$: 428.5508.

1-Naphthyl-2-(phenylcyclopropyl)methyl phenylacetate, ***4***: ^{1}H NMR ($CDCl_3$) (major diastereomer) δ: 8.11–6.80 (m, 17H), 6.20 (d, 1H, J = 8.2 Hz), 3.50 (s, 2H), 2.08–2.04 (m, 1H), 1.80–1.75 (m, 1H), 0.93–0.83 (m, 2H); ^{13}C NMR ($CDCl_3$) (major diastereomer) δ: 171.3 (C═O), 142.1 (C), 135.3 (C), 134.3 (C), 134.2 (C), 131.1 (C), 129.5 (CH), 129.1 (CH), 128.8 (CH), 128.6 (CH), 127.3 (CH), 126.6 (CH), 126.4 (CH), 126.1 (CH), 126.0 (CH), 125.5 (CH), 124.1 (CH), 77.0 (CH-OH), 41.9 (CH_2), 27.8 (CH), 23.1 (CH_2), 13.4 (CH); MS: 392 (2, M^+), 288 (28), 257 (13), 256 (51), 171 (14), 170 (100), 167 (13), 165 (18), 152 (11), 141 (16), 91 (95); HRMS calcd. for $C_{28}H_{24}O_2$: 392.1776; found 392.1804.

1-Naphthyl-3-(2-phenyloxiranyl)]methyl phenylacetate, ***5***: yield 48% as a mixture of diastereomers: IR (neat): 1746 (C═O), 1142 (C-O) cm^{-1}; ^{1}H NMR ($CDCl_3$) (major diastereomer) δ:8.2–7.1 (m, 17H, aromatic), 6.60 (d, 1H, J = 5 Hz, CH-O), 3.84–3.77 (m, 3H), 3.55 (dd, 1H, J = 5 and 1.5 Hz, CH); ^{13}C NMR ($CDCl_3$) (major diastereomer) δ: 170.5 (C═O), 136.0 (C), 133.8 (C), 132.3 (C), 129.4 (CH), 128.9 (CH), 128.6 (CH), 128.4 (CH), 127.2 (CH), 126.6 (CH), 125.9 (CH), 125.6 (CH), 125.2 (CH), 123.3 (CH), 73.0 (CH-O), 63.2 (Ph-CH), 56.9 (CH-CH-Naph), 41.4 (CH_2); MS: 394 (6), 275 (28), 258 (12), 171 (22), 170 (50), 169 (11), 157 (14), 155 239(14), 153 (13), 152 (14), 120 (12), 92 (10), 91 (100). Anal. calcd. for $C_{27}H_{22}O_3$: C 82.21, H 5.62; found: C 81.92, H 5.52.

2-(Spiro[cyclopropane-1,9′-fluorene])(4-methoxy-1-naphthyl)methyl phenylacetate, ***6***: yield 80%; mp 128–130°C; IR (film): 1720 cm^{-1}; ^{1}H NMR ($CDCl_3$) δ: 8.40–8.30 (m, 1H), 8.30–8.20 (m, 1H), 7.92 (t, 2H), 7.58–7.29 (m, 8H), 7.11–7.06 (m, 3H), 6.98 (d, 1H, J = 7.6 Hz), 6.81 (d, 1H, J = 8.2 Hz), 6.73–6.69 (m, 2H), 6.52 (d, 1H, J = 10.1 Hz, CH-O), 4.03 (s, 3H, CH_3O), 3.14 (dd, 2H, J = 15.9 Hz, Ph-CH_2), 2.70 (q, 1H), 1.97 (d, 2H). This apparently simple pattern for the cyclopropane hydrogens could be simulated[6] as an ABX system with $J_{AB} = -5.5$ Hz, $J_{AX} = 9.5$ Hz (*trans*), and $J_{BX} = 10.2$ Hz (*cis*). ^{13}C NMR ($CDCl_3$) δ: 170.2 (C═O), 155.8 (C), 147.9 (C), 143.9 (C), 140.9 (C), 139.5 (C), 133.5 (C), 131.4 (C), 129.1 (CH), 128.3 (C), 128.2 (CH), 127.0 (CH), 126.8 (CH), 126.6 (CH), 126.5 (CH), 126.1 (C), 125.9 (CH), 125.2 (CH), 123.8 (CH), 122.9 (CH), 121.2 (CH), 120.3 (CH), 119.9 (CH), 118.6 (CH), 103.3 (CH), 75.7 (CH-O), 55.6 (CH_3O), 40.7 (CH_2Ph), 35.1 (fluorenyl C9), 22.7 (CH_2); MS: 360 (4.2, $M^{\cdot+}$ – $PhCH_2CO_2H$), 136 (19), 92 (14), 91 (100), 65 (13); HRMS calcd. for $C_{27}H_{20}O$: 360.1514; found: 360.1509.

Preparative scale and quantitative photolyses of esters 1*a*–6*a*

The general procedures used have been described (25).

© 1997 NRC Canada

Can. J. Chem. Downloaded from www.nrcresearchpress.com by 92.62.229.171 on 09/08/12
For personal use only.

Characterization of photoproducts

Ethers **1**b–**5**b

2-Bromo-1-methoxy-1-(1-naphthyl)ethane, **1**b
A solution of bromine (0.95 mL, 1.85×10^{-2} mol) in methanol (10 mL) was slowly added to a solution of 1-vinylnaphthalene (prepared as described above) (2.85 g, 1.85×10^{-2} mol) in methanol (10 mL). The reaction mixture was poured into 5% sodium bisulfite (25 mL), and then was extracted into dichloromethane (2 × 25 mL). The organic layers were combined, washed with water (2 × 25 mL) and with saturated $NaHCO_3$ solution (2 × 25 mL), dried over anhydrous magnesium sulfate, and the solvent was removed under reduced pressure. The product was purified using column chromatography with 90:10 hexane:dichloromethane as eluant. The resulting bromoether was isolated as a pale yellow oil: yield 1.15 g (23%); ^{1}H NMR ($CDCl_3$) δ: 8.03–7.14 (m, 7H), 4.97 (t, 1H, J = 7 Hz), 3.44 (d, 2H, J = 7 Hz), 3.18 (s, 3H); GC–MS: 266 (7), 264 (6), 172 (13), 171 (100), 153 (14), 152 (11), 141 (11), 128 (14); HRMS calcd. for $C_{13}H_{13}OBr$: 264.0150; found: 264.0147.

General synthesis of ethers **2**b–**5**b
To a stirred solution of the alcohol (15 mmol) in dimethyl sulfoxide (15 mL) was added sodium hydride (57% by weight in mineral oil) (25 mmol) under nitrogen gas. After stirring for 1 h, methyl iodide (50 mmol) in DMSO (10 mL) was added. After stirring for an additional hour, the reaction mixture was poured into water (10 mL), and the product was extracted with dichloromethane (15 mL). The organic layer was then washed with water (10 mL) and brine solution (10 mL) several times to remove any DMSO. The solvent was dried over anhydrous magnesium sulfate and then removed under reduced pressure. The resulting ether was purified using column chromatography with ethyl acetate:hexane as eluant. The spectra of these compounds are below.

Methyl 2-methoxy-2-(1-naphthyl)ethyl sulfoxide, **2**b: (major diastereomer) IR (neat): 1100 (C-O), 1040 (C-O), 782 (SO) cm^{-1}; ^{1}H NMR ($CDCl_3$) δ: 8.20 (d, 1H, J = 8 Hz), 7.92–7.82 (m, 2H), 7.65–7.47 (m, 4H), 5.52 (dd, 1H, J = 5.2 and 3.4 Hz), 3.40 (s, 3H, OCH_3), 3.2–3.1 (m, 2H), 2.62 (s, 3H, $CH_3(SO)$); ^{13}C NMR ($CDCl_3$) δ: 134.7 (C), 134.0 (C), 130.5 (C), 129.1 (CH), 128.8 (CH), 126.7 (CH), 125.9 (CH), 125.5 (CH), 123.8 (CH), 122.7 (CH), 74.6 (CH), 62.9 (CH_3), 57.4 (CH_2), 39.4 (CH_3); MS: 248 (6, M^+), 185 (14), 184 (66), 183 (13), 171 (29), 155 (10), 154 (20), 153 (100), 152 (16), 141 (27), 128 (11), 127 (11).

(2-Phenyl-1-cyclopropyl)(1-naphthyl)methyl methyl ether, **4**b: (as a mixture of diastereomers in a ratio of 3:1) ^{1}H NMR ($CDCl_3$) δ: 8.35–7.00 (12H); (major diastereomer) δ: 4.58 (d, 1H, J = 4.3 Hz), 3.30 (s, 1H), 1.97–1.92 (m, 1H), 1.80–1.74 (m, 1H),, 0.95–0.84 (m, 2H); (minor diastereomer) δ: 4.70 (d, 1H, J = 4.0 Hz), 1.10–1.00 (m, 1H); ^{13}C NMR ($CDCl_3$) δ: 142.5 (C), 136.3 (C), 134.0 (C), 131.5 (C), 128.9 (CH), 128.3 (CH), 126.0 (CH), 126.0 (CH), 125.6 (CH), 125.4 (CH), 125.0 (CH), 124.8 (CH), 124.1 (CH), 124.0 (CH); (major) δ: 84.2 (CH), 56.9 (OCH_3), 28.3 (CH), 22.8 (CH), 12.8 (CH_2); (minor) δ: 83.3 (CH), 56.7 (OCH_3), 28.1 (CH), 20.9 (CH), 14.4 (CH_2); MS: 288 (1, $M^{\cdot+}$), 185 (14), 184 (100), 171 (12), 141 (16), 134 (25), 128 (11); HRMS calcd. for $C_{21}H_{20}O$: 288.1514; found: 288.1513.

1-(1-Naphthylmethoxymethyl)-2-phenyloxirane, **5**b: (as a mixture of diasteremers) ^{1}H NMR ($CDCl_3$) (1st diastereomer) δ: 8.3–7.1 (m, 12H), 5.10 (d, 1H, J = 3.3 Hz), 4.12 (d, 1H, J = 1.9 Hz), 3.39 (s, 3H), 3.36 (dd, 1H, J = 3.3 and 2.1 Hz); (2nd diastereomer) δ: 8.3–7.1 (m, 12H), 4.89 (d, 1H, J = 5.5 Hz), 3.83 (d, 1H, J = 1.9 Hz), 3.42 (s, 3H), 3.5 (dd, 1H, J = 5.5 and 2.1 Hz); ^{13}C ($CDCl_3$) δ: 137.0 (C), 136.7 (C), 134.1 (C), 134.0 (C), 133.6 (2 C's), 131.4 (2 C's), 129.1 (CH), 129.0 (CH), 128.5 (CH), 128.2 (CH), 126.4 (CH), 125.8 (CH), 125.7 (CH), 125.6 (CH), 125.5 (CH), 125.5 (CH), 123.7 (CH), 123.5 (CH), 82.0 (CH), 80.1 (CH), 64.8 (OCH3), 64.3 (OCH3), 57.6 (CH), 57.2 (CH), 56.5 (CH), 56.4 (CH); MS: 290 (5, M^+), 199 (18), 186 (12), 184 (11), 172 (13), 171 (100), 141 (12), 128 (16).

1,1-Dimethoxy-2-(1-naphthyl)ethane, **1**c: The preparation of 2-(1-naphthyl)ethanol was by the general procedure of Brown and co-workers (49). To a stirred solution of 1-naphthylacetic acid (10.9 g, 6.36×10^{-2} mol) in anhydrous THF (25 mL) at 0°C was slowly added 1 M borane:THF solution (76 mL) under nitrogen. The solution was stirred for an hour at room temperature. A 1:1 water:THF solution (80 mL) was slowly added, and the resulting mixture was saturated with potassium carbonate. The product was extracted into ether (2 × 100 mL) and the organic layers were combined, dried over anhydrous magnesium sulfate, and concentrated to give the product as a colourless oil: yield 9.84 g, 90%; the ^{1}H NMR was the same as that previously reported (50).

The method of Ratcliffe and Rodehorst was used to synthesize 2-(1-naphthyl)ethanal (51).

Preparation of reagents: Chromium trioxide was stored overnight in a vacuum desiccator using phosphorus pentoxide as desiccant. Barium oxide was added to pyridine, and the pyridine was distilled and stored over 4 Å molecular sieves until needed. Dichloromethane was washed with concentrated sulfuric acid (100 mL), water (100 mL), and brine (100 mL) and then distilled and stored over 4 Å molecular sieves until needed.

To a stirred solution of pyridine (19.0 g, 0.24 mol) in dichloromethane (150 mL) was added chromium trioxide (12.5 g, 0.12 mol). The reaction vessel was kept at 0°C during the addition. The mixture was stirred for 15 min, and then 2-(1-naphthyl)ethanol (0.71 g, 4.13×10^{-3} mol) in dichloromethane (5 mL) was added to the reaction mixture in one portion. The reaction was stirred for a further 15 min. The dichloromethane was decanted off, and the residue was washed with ether (200 mL). The organic layers were combined, and then washed with 5% NaOH (3 × 100 mL), 5% HCl (100 mL), 5% $NaHCO_3$ (100 mL), and saturated NaCl solution (100 mL), dried over anhydrous magnesium sulfate, and the solvent was removed under reduced pressure. The product was then diluted with dichloromethane (20 mL) and was washed with cold 5% HCl (4 × 75 mL) to remove the excess pyridine. The aldehyde was isolated as a pale yellow oil: yield 0.21 g, 30%; ^{1}H NMR ($CDCl_3$) δ: 9.74 (t, 1H, J = 2 Hz, C(O)H), 7.32–7.95 (m, 7H), 4.01 (d, 2H, J = 2 Hz).

Preparation of the ion exchange resin: Amberlite (IR-120

© 1997 NRC Canada

Can. J. Chem. Downloaded from www.nrcresearchpress.com by 92.62.229.171 on 09/08/12
For personal use only.

PLUS, Alfa) (50 g) was washed with 5% HCl until the solution was acidic, then washed with distilled water until the solution was neutral, and finally washed with Na distilled methanol to remove the water.

To a solution of 2-(1-naphthyl)ethanal (0.21 g, 1.23×10^{-3} mol) in methanol (200 mL) was added the Amberlite resin (1 g) and 3 Å molecular sieves. The reaction mixture was refluxed and the extent of the reaction was monitored by HPLC. After 1.5 h the ion exchange resin and the molecular sieves were filtered off and the solvent was removed under reduced pressure. The resulting acetal was purified using bulb-to-bulb distillation to give a yellow oil; ^{1}H NMR ($CDCl_3$) δ: 8.06 (d, 1H, J = 7 Hz), 7.82 (d, 1H, J = 7 Hz), 7.72 (t, 1H, J = 4.7 Hz), 7.55–7.35 (m, 4H), 4.71 (t, 1H, J = 5.5 Hz), 3.37 (d, 2H, J = 5.5 Hz), 3.32 (s, 6H); ^{13}C NMR ($CDCl_3$) δ: 133.8 (C), 133.2 (C), 132.2 (C), 128.8 (CH), 127.7 (CH), 127.2 (CH), 125.9 (CH), 125.5 (CH), 125.5 (CH), 125.43 (CH), 123.8 (CH), 104.8 (CH), 53.5 (CH_3), 36.9 (CH_2).

4-Methoxy-1-(1-naphthyl)-4-phenyl-1-butene, **4**d: ^{1}H NMR ($CDCl_3$) δ: 7.72–6.94 (m, 12H), 6.96 (d, 1H, J = 16 Hz), 6.07 (dt, 1H, J = 16 and 7.3 Hz), 4.20 (t, 1H, J = 6.5 Hz), 3.17 (s, 3H), 2.81–2.69 (m, 1H), 2.65–2.51 (m, 1H); ^{13}C NMR ($CDCl_3$) δ: 141.7 (C), 135.5 (C), 133.6 (C), 131.1 (C), 129.7 (CH), 129.6 (CH), 128.5 (CH), 128.4 (CH), 127.7 (CH), 127.5 (CH), 126.9 (CH), 125.8 (CH), 125.7 (CH), 124.1 (CH), 123.7 (CH), 84.0 (CH), 56.8 (OCH_3), 42.1 (CH_2); MS: 288 (3, $M^{\cdot+}$), 181 (12), 171 (13), 165 (23), 152 (12), 128 (13), 127 (12), 121 (100), 105 (11), 91 (35), 77 (15).

Methyl 2-(1-naphthyl)-3-phenylpropyl sulfoxide, **2**c: ^{1}H NMR ($CDCl_3$) δ: 8.14 (d, 1H, J = 8.3 Hz), 7.84 (m, 1H), 7.74 (m, 1H), 7.53–7.04 (m, 9H), 4.44 (m, 1H), 3.38–3.20 (m, 3H), 3.02 (m, 1H), 2.42 (s, 3H, CH_3(SO)); ^{13}C NMR ($CDCl_3$) δ: 138.4 (C), 137.6 (C), 134.0 (C), 131.1 (C), 129.3 (CH), 129.0 (CH), 128.2 (CH), 127.7 (CH), 126.4 (CH), 126.4 (CH), 125.7 (CH), 125.1 (CH), 122.6 (CH), 60.1 (CH_2), 40.4 (CH_2Ph), 38.9 (CH_3), 35.2 (CH); MS: 308 (13, $M^{\cdot+}$), 245 (23), 244 (81), 167 (14), 154 (56), 153 (100), 152 (33), 141 (12), 117 (15), 115 (11), 91 (88), 43 (16).

1-(1-Naphthyl)-1-(2-phenylcyclopropyl)-2-phenylethane, **4**c: (mixture of diastereomers) ^{1}H NMR ($CDCl_3$) δ: 8.13–6.83 (m, 17H), 3.41–2.90 (m, 3H), 1.54 (m, 1H), 1.07–1.00 (m, 1H), 0.94–0.86 (m, 1H), 0.75–0.65 (m, 1H); ^{13}C NMR ($CDCl_3$) δ: 143.2, 140.7, 140.4, 140.3, 140.2, 134.0, 131.9, 129.6, 129.4, 129.1, 128.2, 128.1, 128.0, 126.9, 126.8, 126.0, 125.7, 125.6, 125.4, 124.7, 124.5, 123.2, 46.6, 43.4, 43.2, 29.8, 28.8, 27.4, 25.0, 21.9, 17.1, 14.4; MS: 348 (0.2, $M^{\cdot+}$), 334 (25), 244 (17), 243 (75), 230 (11), 203 (11), 168 (32), 166 (27), 153 (10), 152 (16), 151 (33), 140 (12), 139 (43), 138 (12), 127 (32), 115 (20), 77 (100).

1-(1-(1-Naphthyl)-2-phenylethyl)-2-phenyloxirane, **5**c: IR (neat): 1598, 1495, 1455 (aromatic), 794 (C-O) cm^{-1}; ^{1}H NMR ($CDCl_3$) δ: 8.1–6.9 (m, 12H), 3.9–3.8 (m, 1H), 3.4–3.1 (m, 4H); ^{13}C NMR ($CDCl_3$) δ (major): 139.8 (C), 137.4 (C), 137.2 (C), 134.0 (C), 132.0 (C), 129.2 (CH), 129.0 (CH), 128.6 (CH), 128.2 (CH), 127.9 (CH), 127.5 (CH), 125.5 (CH), 125.5 (CH), 123.1 (CH), 65.6 (CH-Ph), 59.1 (*c*H-CH-Naph), 44.4 (Naph-CH), 39.6(CH_2); (minor): 139.0 (C), 137.1 (C), 137.0 (C), 133.9 (C), 131.7 (C), 129.3 (CH), 128.1 (CH), 128.0 (CH), 127.4 (CH), 126.4 (CH), 126.2 (CH), 126.4 (CH), 126.1 (CH), 125.6 (CH), 125.0 (CH), 124.8 (CH), 124.2 (CH), 123.0 (CH), 65.8 (CH-Ph), 58.3 (*c*H-CH-Naph), 44.4 (Naph-CH), 39.7 (CH_2). Accounting for all the aromatic methine carbons in the two diastereomers was not possible because some peaks were coincident. MS: 350 (9, $M^{\cdot+}$), 259 (34), 241 (12), 231 (11), 229 (10), 217 (13), 171 (24), 156 (13), 155 (23), 154 (14), 153 (100), 152 (40), 151 (10), 141 (13), 128 (22), 127 (26), 121 (60), 115 (13), 105 (11), 91 (51), 77 (23).

1-(Spiro[4-(4-methoxy-1-naphthyl)cyclobutane-2,9′-fluorene]) phenylacetate, **22**: mp 73–75°C; IR (film): 1720 cm^{-1}; ^{1}H NMR ($CDCl_3$) δ: 8.35–8.33 (m, 1H), 8.01 (d, 1H, J = 7.9 Hz), 7.89 (d, 1H, J = 7.4 Hz), 7.74 (d, 1H, J = 7.6 Hz), 7.68–7.66 (m, 1H), 7.6–7.1 (m, 10H), 7.18–7.16 (m, 2H), 6.88–6.84 (m, 2H), 5.91 (d, 1H, J = 8.2 Hz), 4.82 (m, 1H, J = 9.5, 8.5, and 8.2 Hz), 4.02 (s, 3H), 3.26 (dd, 2H, J = 15.5 Hz), 3.02 (m, 1H, J = 13 and 8.5 Hz), 2.74 (m, 1H, J = 13 and 9.5 Hz). The pattern for the cyclobutane hydrogens could be simulated as an ABX system giving the above coupling constants.[6] Decoupling experiments showed that the hydrogen at δ: 5.91 was only coupled to that at δ: 4.82. ^{13}C NMR ($CDCl_3$) δ: 169.8 (C═O), 154.8 (C), 149.0 (C), 145.6 (C), 141.4 (C), 139.6 (C), 133.6 (C), 132.5 (C), 129.3 (C), 129.2 (CH), 128.5 (CH), 127.8 (CH), 127.7 (CH), 127.1 (CH), 126.9 (CH), 126.7 (CH), 126.1 (C), 125.3 (CH), 124.7 (CH), 123.8 (CH), 122.9 (CH), 122.8 (CH), 120.1 (CH), 119.7 (CH), 103.3 (CH), 78.0 (CH-O), 55.6 (CH_3O), 55.0 (fluorenyl C9), 41.0 (CH_2Ph), 40.0 (CH), 33.9 (CH_2); MS ($M^{\cdot+}$): 496 (1.5) 360 (12), 318 (19), 284 (19), 257 (14), 256 (37), 202 (12), 186 (44), 185 (28), 180 (70), 178 (15), 171 (25), 152 (22), 131 (19), 129 (18), 128 (14), 119 (12), 91 (55), 83 (21), 76 (16), 73 (24), 69 (100), 57 (32); HRMS calcd. for $C_{27}H_{20}O$ ($M^{\cdot+}$ − $PhCH_2CO_2H$): 360.1514; found: 360.1528.

Ground state solvolysis of 2-(spiro[cyclopropane-1,9′-fluorene])(4-methoxy-1-naphthyl)methyl phenylacetate, 6: 9-fluorenyl-3-(1-[4-methoxy-naphthyl])-2-propene phenylacetate, 20

The ester, **6**, (180 mg) was refluxed in 100 mL of methanol. The progress of the reaction was monitored by HPLC. After 10 h, the methanol was removed by rotoevaporation and the residue taken up in CH_2Cl_2, which was then extracted with brine, dried ($MgSO_4$), and then rotoevaporated to give a quantitative yield of **20**; ^{1}H NMR ($CDCl_3$) δ: 8.20 (m, 1H), 7.60–7.18 (m, 18H), 6.69 (d, 1H, J = 16 Hz), 6.59 (d, 1H, J = 7.9 Hz), 5.75 (dt, 1H, J = 16 and 7.3 Hz), 3.89 (s, 3H), 3.04 (d, 2H, J = 7.3 Hz), 2.86 (s, 2H); ^{13}C NMR ($CDCl_3$) δ: 154.8 (CO), 145.1 (C), 140.8 (C), 131.9 (C), 131.1 (CH), 129.6 (CH), 129.0 (CH), 128.8 (CH), 128.3 (C), 127.7 (CH), 127.1 (C), 126.2 (CH), 126.2 (CH), 125.3 (C), 125.0 (CH), 124.5 (CH), 124.1 (CH), 123.9 (CH), 122.2 (CH), 120.0 (CH), 103.7 (CH), 88.2 (C), 55.5 (OCH_3), 51.7 (CH_2), 44.0 (CH_2); MS: 392 (35), 198 (18), 197 (84), 197 (100), 180 (39), 166 (11), 91 (24); HRMS calcd. for $C_{27}H_{20}O$ ($M^{\cdot+}$ − $PhCO_2H$): 360.1514; found: 360.1504.

Acknowledgment

This research was supported by the Natural Sciences and

© 1997 NRC Canada

Engineering Research Council of Canada (NSERC). S.M.N. thanks the Faculty of Graduate Studies at Dalhousie University and The Walter C. Sumner Foundation for financial support, Drs. G.P Arsenault and J.P. LaPlante from the Royal Military College (RMC) in Kingston for providing laboratory facilities and support for the completion of her doctorate, Robert Whitehead at RMC for NMR assistance, and Dr. R. Lemieux and Susan Swansburg at Queen's University. We also thank Gloria Jocys, Alexandra Pincock, and Susan Swansburg for experimental assistance.

References

1. S. Cristol and T.H. Bindel. Org. Photochem. **6**, 327 (1983).
2. P.J. Kropp. Acc. Chem. Res. **17**, 131 (1984).
3. P.K. Das. Chem. Rev. **93**, 119 (1993).
4. W.M. McGowan and E.F. Hilinski. J. Am. Chem. Soc. **117**, 9019 (1995).
5. J.A. Pincock. Acc. Chem. Res. **30**, 43 (1997).
6. D. Griller and K.U. Ingold. Acc. Chem. Res. **13**, 317 (1980).
7. R.S. Givens and R. Singh. Tetrahedron Lett. **32**, 7013 (1991).
8. D. Lal, D. Griller, S. Husband, and K.U. Ingold. J. Am. Chem. Soc. **96**, 6355 (1974).
9. S.M. Nevill, A.L. Pincock, and J.A. Pincock. J. Org. Chem. In press.
10. P.J. Wagner, J.H. Sedon, and M.J. Lindstrom. J. Am. Chem. Soc. **100**, 2579 (1978).
11. P.J. Wagner, M.J. Lindstrom, J.H. Sedon, and D.R. Ward. J. Am. Chem. Soc. **103**, 3842 (1981).
12. D.E. Falvey and G.B. Shuster. J. Am. Chem. Soc. **108**, 7419 (1986).
13. S.-Y. Choi and M. Newcomb. Tetrahedron Lett. **51**, 657 (1995).
14. R. Hollis, L. Hughes, V.W. Bowry, and K.U. Ingold. J. Org. Chem. **57**, 4284 (1992).
15. J.H. Horner, F.N. Martinez, O.M. Musa, M. Newcomb, and H.E. Shahin. J. Am. Chem. Soc. **117**, 11124 (1995).
16. K.W. Krosley and G.J. Gleicher. J. Phys. Org. Chem. **6**, 228 (1993).
17. M. Newcomb, C.C. Johnson, M.B. Manek, and R. Varick. J. Am. Chem. Soc. **114**, 10915 (1992).
18.. Martin-Esker, C.C. Johnson, J.H. Horner, and M. Newcomb. J. Am. Chem. Soc. **116**, 9174 (1994).
19. M. Newcomb. Tetrahedron, **49**, 1151 (1993).
20. (*a*) M. Newcomb and A.G. Glenn. J. Am. Chem. Soc. **111**, 275 (1989); (*b*) A.L.J. Beckwith and V.W. Bowry. J. Org. Chem. **54**, 2681 (1989), and refs. therein.
21. R.M. Silverstein, G.C. Bassler, and T.C. Morrill. Spectrometric identification of organic compounds. 5th ed. J. Wiley and Sons, New York. 1991. p. 221.
22. J. McEwen and K. Yates. J. Phys. Org. Chem. **4**, 193 (1991), and refs. therein.
23. B. Zhang, C.R. Pandit, and W.G. McGimpsey. J. Phys. Chem. **98**, 7022 (1994).
24. D.F. McMillen and D.M. Golden. Annu. Rev. Phys. Chem. **33**, 493 (1982).
25. D.P. DeCosta and J.A. Pincock. J. Am. Chem. Soc. **115**, 2180 (1993).
26. D.A. Jaeger. J. Am. Chem. Soc. **98**, 6401 (1976).
27. D.A. Jaeger and E.A. Bernhardt. Tetrahedron Lett. **24**, 5421 (1983).
28. N.R. Bertoniere and G.W. Griffin. Organic photochemistry. Vol. 3. *Edited by* O. Chapman. Marcel Dekker, New York. 1973. p. 115.
29. F.E. Ziegler and A.K. Peterson. J. Org. Chem. **60**, 2666 (1995).
30. P. Galatsis and S.D. Millan. Tetrahedron Lett. **51**, 7493 (1991).
31. S.L. Murov, I. Carmichael, and G.L. Hug. Handbook of photochemistry. 2nd ed. Marcel Dekker, New York. 1993. p. 33.
32. H.E. Zimmerman and C.W. Carpenter. J. Org. Chem. **53**, 3298 (1988).
33. T.M. Bockman, S.M. Hubig, and J.K. Kochi. J. Am. Chem. Soc. **118**, 4502 (1996).
34. J.M. Kim and J.A. Pincock. Can J. Chem. **73**, 885 (1995).
35. R.H. Pickard and J. Kenyon. J. Chem. Soc. 1115 (1914).
36. L.H. Klemm, J.W. Spraque, and H. Ziffer. J. Org. Chem. **53**, 2374 (1988).
37. P.J. Card, F.F. Freidli, and H. Shechter. J. Am. Chem. Soc. **105**, 6104 (1983).
38. D.R. Dalton, V.P. Dutta, and D.C. Jones J. Am. Chem. Soc. **90**, 5498 (1968).
39. E.J. Corey and M. Chaykovsky. J. Am. Chem. Soc. **87**, 1345 (1965).
40. J. Drabowicz and M. Mikolajczyk. Synth. Commun. **11**, 1025 (1981).
41. M.N. Yoon, C.S. Pak, H.C. Brown, S. Krishnamurthy, and T.P. Stocky. J. Org. Chem. **38**, 2786 (1973).
42. L. Bonsign, S. Cabiddu, A. Maccioni, and E. Marongiu. Gazz. Chim. Ital. **106**, 617 (1976).
43. G.D. Prestwich, J.W. Kuo, S.K. Park, D.N. Loury, and B.D. Hammock. Arch. Biochem. Biophys. **242**, 11 (1985).
44. J.M. Dickinson, J.A. Murphy, C.W. Patterson, and N.F. Wooster. J. Chem. Soc., Perkin Trans. 1, 1179, (1990).
45. A. Schōberg, W.I. Awad, and N. Latif. J. Chem. Soc. 1368 (1951).
46. H. Konishi, K. Aritomi, T. Okano, and J. Kiji. Bull. Chem. Soc. Jpn. **62**, 591 (1989).
47. H.A. Staab and W. Rohr. Syntheses using heterocyclic amides (azolides). *In* Newer methods of preparative organic chemistry. Academic Press, Germany. 1968.
48. J.G.D. Carpenter and J.W. Moore. J. Chem. Soc. C, 1610 (1969).
49. M.N. Yoon, C.S. Pak, H.C. Brown, S. Krishnamurthy, and T.P. Stocky. J. Org. Chem. 2786 (1973).
50. C. Pouchert. The Aldrich library of NMR spectra. ed. II. Aldrich Chemical Co., Inc., Milwaukee, Wis. 1983.
51. R. Ratcliffe, and R. Rodehorst. J. Org. Chem. **35**, 4000 (1970).

Can. J. Chem. Downloaded from www.nrcresearchpress.com by 92.62.229.171 on 09/08/12
For personal use only.

© 1997 NRC Canada

1996 Clara Benson Award Lecture
The kinetics of the reaction of carbon with oxygen[1]

M.H. Back

Can. J. Chem. Downloaded from www.nrcresearchpress.com by 88.146.161.215 on 09/08/12
For personal use only.

Abstract: The results of studies of the kinetics of the reaction of oxygen with thin films of carbon are described with special emphasis on the role, in the mechanism of the reaction, of the stable complex formed between oxygen and the carbon surface. A key part of the proposed mechanism is the reaction between gaseous oxygen and the stable complex to form the product carbon dioxide. Measurements of the total pressure and the products formed as a function of time of the reaction have allowed estimates of the rate constants for the elementary reactions that make up the mechanism. This in turn has led to the application of computer modelling to the mechanism of the reaction and to the development of a more detailed mechanism involving two types of reactive sites on the carbon surface.

Key words: carbon, oxygen, kinetics, mechanism, computer modelling.

Résumé : On décrit les résultats d'études sur la cinétique de la réaction de l'oxygène avec des films minces de carbone, en insistant sur le rôle du complexe stable qui se forme entre l'oxygène et la surface du carbone dans le mécanisme de la réaction. La réaction entre l'oxygène gazeux et le complexe stable, conduisant à la formation du bioxyde de carbone, est une étape clé du mécanisme proposé. Des mesures de la pression totale et des produits formés en fonction du temps de la réaction ont permis d'évaluer les constantes de vitesse des réactions élémentaires impliquées dans le mécanisme. Celles-ci ont par la suite permis de faire un modelage par ordinateur du mécanisme de la réaction et de développer un mécanisme plus détaillé impliquant deux types de sites réactifs sur la surface du carbone.

Mots clés : carbone, oxygène, cinétique, mécanisme, modelage par ordinateur.

[Traduit par la rédaction]

Introduction

Carbon, as an element, plays an important role in the chemical world (for a summary of studies of the reactivity of carbon, see ref. 1). We are familiar with the two forms of carbon, graphite and diamond, and many teachers of chemistry are fond of pointing out the remarkable differences in the properties of these two forms as a result of what might be described as a minor difference in structure. The addition of a third form, fullerenes, has been an exciting development, which has generated intense interest over the past several years.

Graphite is, of course, the most common form of carbon. Carbon fibres and carbon composites provide a dense, strong material, valuable in the aerospace industry (2). As an adsorbent, carbon is indispensable in purification procedures and its high surface area makes a good catalyst support (3). As a reactant, carbon is decidedly inert. Reaction with hydrogen or water vapour, for example, requires temperatures in excess of about 900°C. Carbon will, however, be consumed by oxygen at lower temperatures and it is the kinetics of this reaction that I want to describe in this paper.

In a recent review of the kinetics of the reaction of carbon with oxygen, Walker, Taylor, and Ranish (4) state in the opening sentence: "The carbon–oxygen reaction is arguably the most important reaction known." Stoichiometrically the reaction is simple. Oxygen reacts with carbon to form carbon dioxide or carbon monoxide.

$$C + O_2 \rightarrow CO_2$$

$$C + \tfrac{1}{2} O_2 \rightarrow CO$$

The general features of the kinetics have been well documented (5). With moderate pressures of oxygen the rate becomes measurable at about 550°C and with low pressures rates may be measured up to about 900°C. The major product at low temperatures and high pressures of oxygen is carbon dioxide and the activation energy for its formation is in the range 160–200 kJ mol^{-1}. Carbon monoxide becomes important at higher temperatures and lower pressures of oxygen and the activation energy of its rate is larger, 250–300 kJ mol^{-1}. The order of the rate with respect to the pressure of oxygen varies between 1 and 0.5. But how does this reaction occur? By what series of elementary processes is solid carbon converted into carbon dioxide and carbon monoxide by reaction with gaseous oxygen?

In spite of decades of studies of the kinetics of this reaction,

Received June 14, 1996.

M.H. Back.[2] Department of Chemistry, Ottawa–Carleton Chemistry Institute, Ottawa, ON K1N 6N5, Canada.

[1] This is an invited review article based on the 1996 Clara Benson Award lecture presented by Professor Back at the 79th Annual Conference of the Canadian Society for Chemistry, St. John's, Newfoundland, June 23–26, 1996.

[2] Telephone: (613) 236-7166.
E-mail: mback@AIX1.uottawa.ca

© 1997 NRC Canada

Can. J. Chem. Downloaded from www.nrcresearchpress.com by 88.146.161.215 on 09/08/12
For personal use only.

the elementary processes of adsorption, migration, rearrangement, dissociation, and desorption that make up the overall reaction have not been correlated into a general mechanism that can describe the rate over a range of temperature, of pressures of oxygen, and other conditions. One of the difficulties in formulating a general mechanism is the variation in the properties of carbon in its graphitic form, which depend heavily on the source and the method of preparation. Graphite from natural sources, for example, may contain heavy metals that act as catalysts. Also, a variety of techniques have been used for kinetic studies, for example, static or flow systems (6), shock tubes (7), molecular beams (8), and surface microscopy (9), each of which gives results under widely different conditions.

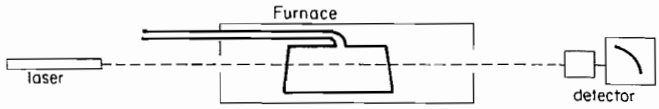
Of central importance in the oxidation reaction is the strongly bound complex formed on adsorption of oxygen on the surface of carbon (10). When oxygen is admitted to a carbon surface at about 300°C, oxygen is adsorbed, but reaction, to give carbon dioxide or carbon monoxide, does not occur. When unadsorbed oxygen is removed and the carbon is heated, no further oxygen is released, but beginning at about 700°C carbon monoxide and small amounts of carbon dioxide are evolved. This result has been interpreted to indicate that oxygen adsorbs dissociatively on a carbon surface, forming a strongly bound complex that is released only at high temperatures as carbon monoxide.

The properties of the complex have been studied by various techniques, including adsorption and desorption kinetics (11), spectroscopic measurements (12), and chemical analysis (13). Studies using electron microscopy have shown that the complex forms on edge carbon atoms of graphite crystals (14). The importance of the complex in the oxidation process was first recognized by Walker and co-workers through their extensive studies of the kinetics of the reaction (10). They proposed that the amount of carbon monoxide released could be correlated with a number of "active" carbon atoms on the surface and they converted this quantity into an Active Surface Area, ASA. The ASA for many samples of graphitic carbon was typically a few percent of the total surface area measured by the BET technique, that is, by using an adsorbent that does not chemically interact with the surface.

The role of the complex in the oxidation process has been difficult to define. It must first be realized that the reaction of oxygen with carbon cannot be described by a simple sequence of adsorption, formation of complex, and desorption to give products. First, reaction with oxygen begins at about 550°C, at least 100 degrees below temperatures at which the complex is released. Second, the complex is released as carbon monoxide and does not account for the formation of carbon dioxide. Third, the activation energy for formation of carbon dioxide is in the range of 160–200 kJ mol^{-1} and not the value of 280 kJ mol^{-1} required for desorption of the complex.

It should also be noted that the effect of the complex on the processes taking place on the surface is difficult to test experimentally. During a gasification reaction the carbon surface changes dramatically and such changes would have a profound influence on the properties and reactions of the complex. Some results have been interpreted to show that the complex blocks active sites and may actually inhibit the reaction (10). Other experiments have shown that the complex enters into the oxidation process and may be an intermediate in a series of surface processes (15). The importance of the complex in the kinetics was recognized but the identification of the elementary processes, the measurement of their rates, and the formulation of a general mechanism was not achieved.

Fig. 1. Schematic diagram of the reaction vessel showing the passage of the light beam from a He-Ne laser through the reaction vessel. The attenuation of the beam was measured by the photo diode detector and Keithley electrometer.



The purpose of our experiments was to explore in detail the kinetics of the reaction of carbon with oxygen with particular emphasis on the role of the complex in the mechanism. An important part of the study was a careful measurement of the time course of the reaction under a variety of conditions as a means of defining the mechanism in terms of concurrent and consecutive processes. A static system was used in which carbon was formed by pyrolysis of methane as a thin film on the surface of the reaction vessel. A technique had been developed in our laboratory for the quantitative measurement of the amount of carbon in the film and for the continuous monitoring of the removal of carbon during its reaction with oxygen (16). The results of these studies allowed further interpretation of the role of the complex in the reaction and this paper will describe these results and the general mechanism that was developed as an interpretation of the results.

Experimental

The reaction was studied in a static system. A detailed description has been given previously (16). Carbon was formed as a thin film on the surface of the quartz reaction vessel by pyrolysis of 40 Torr (1 Torr = 133.3 Pa) of methane at 1223 K. This produced a film of uniform thickness, usually between 10 and 20 nm, of high purity, and with surface area comparable to the geometric area of the reactor (17). The amount of carbon in the film was measured by the attenuation of a He-Ne laser beam passed axially through the vessel, as illustrated in Fig. 1. Calibration was made by oxidation of the carbon to carbon dioxide and carbon monoxide followed by analysis by gas chromatography. The absorbance was a linear function of the total amount of carbon in the film and an extinction coefficient of 2.2×10^6 cm^2mol^{-1} was obtained. The consumption of carbon by reaction with oxygen could thus be monitored continuously throughout the course of the reaction by the measurement of the light attenuation. The total pressure was also measured continuously and reactants and products were removed for analysis at the end of a reaction or at any stage during reaction. Following removal of reactants and products, the amount of complex adsorbed on the carbon surface at that point was measured by temperature-programmed desorption of the complex, followed by analysis of the products: carbon monoxide with minor amounts of carbon dioxide and traces of water. By such an analysis of the time course of the reaction in a static system the primary, secondary, and tertiary products may be distinguished and a better understanding of the mechanism achieved.

© 1997 NRC Canada

Can. J. Chem. Downloaded from www.nrcresearchpress.com by 88.146.161.215 on 09/08/12
For personal use only.

Results

The kinetics of the reaction were studied over a wide range of temperature, 750–1175 K, and of pressures of oxygen, 0.5–120 Torr. At temperatures below 898 K the formation of carbon monoxide was negligible and all the carbon was converted to carbon dioxide. Therefore we may write

$$-\frac{dC}{dt} = \frac{dCO_2}{dt}$$

$$P_T = P_{O_2} + P_{CO_2}$$

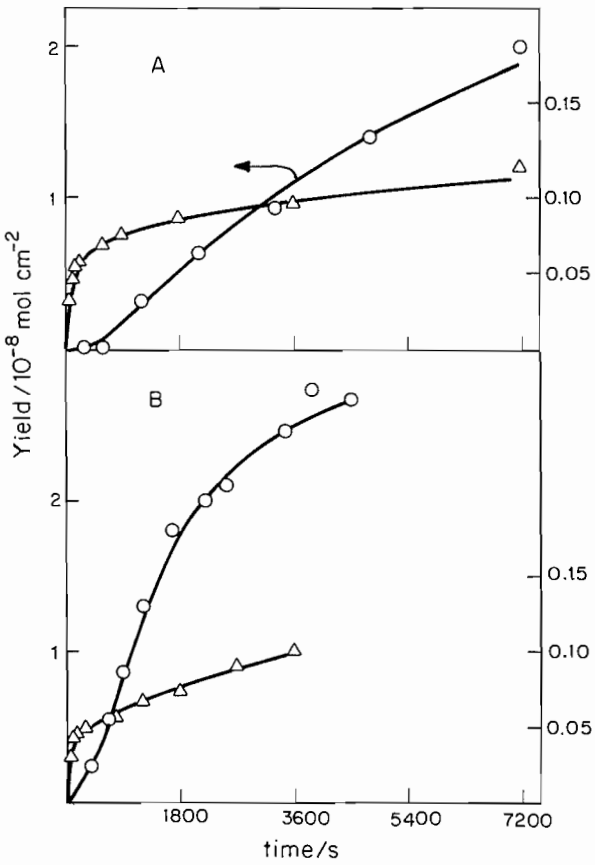
$$P_T - P^0_{O_2} = -\Delta P = O_2 \text{ adsorbed}$$

where P_T, P_{O_2}, and P_{CO_2} refer to the total pressure, the pressure of O_2, and the pressure of CO_2, respectively, at any time during the reaction. $P^0_{O_2}$ is the initial pressure of O_2. If no carbon monoxide is formed there will be no pressure increase. A pressure decrease will indicate adsorption of oxygen on the surface. We equated this decrease to the formation of the stable complex. In addition, the presence of the complex on the surface was confirmed by termination of the reaction at various stages in the conversion, removal of the reactants and products, followed by temperature-programmed desorption to recover the complex. These measurements of the complex correlated well with the values deduced from the pressure change. It should be pointed out that these measurements also show that adsorbed oxygen must be rapidly converted to the stable complex, since only the stable complex could remain on the surface following removal of reactants and products.

The results of the measurements of the loss of carbon and the total pressure are shown converted to formation of complex and of carbon dioxide in Fig. 2, where the left-hand scale refers to the yield of carbon dioxide and the right-hand scale, which is 10 times smaller, to the yield of complex. These yield–time curves obtained in the low-temperature region clearly show that formation of carbon dioxide involved an induction period whereas no induction period was observed for adsorption of oxygen on the carbon surface, as measured by the decrease in pressure, with subsequent formation of the stable complex. Furthermore, the maximum rate of formation of carbon dioxide correlates roughly with the maximum yield of complex. It is also evident that the induction period is shortened at higher temperatures. These results strongly suggest that the complex is an intermediate in the formation of carbon dioxide.

Several types of experiments were performed for the purpose of testing the role of the complex in the reaction. The experiments were designed to compare, in various ways, the rate of oxidation in the presence and absence of the complex. In one series a carbon film was allowed to react with oxygen in two stages, removing about 25% of the initial amount of carbon in each stage. In the first stage oxygen was admitted to the system and the rate was measured as usual. The reaction was stopped by evacuating the products and remaining reactant. A temperature-programmed desorption to 1223 K was then performed to remove the stable complex remaining on the surface. The temperature of the film was then reduced to the reaction temperature and the oxygen was readmitted for reaction in stage 2.

Fig. 2. Yield of carbon dioxide (left-hand scale) and formation of complex (right-hand scale) as a function of time in the low-temperature region. ○: CO_2; Δ: complex. *A*: 848 K; initial pressure of O_2: 1.0 Torr. *B*: 908 K; initial pressure of O_2: 0.8 Torr.

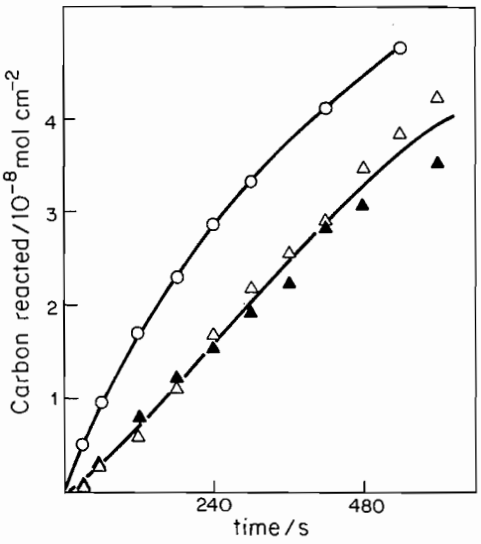


A second series of experiments with a new film, identical to the first, was performed, except that the complex was not removed after stage 1. Thus the difference between the two series of experiments is that, prior to reaction at stage 2, the complex was not present on the surface in the first series but was present in the second series. A typical result of these oxidations is shown in Fig. 3. This figure shows two important features of this set of experiments. First, the magnitude and the kinetic characteristics of the rate are practically the same for the oxidation in stage 1 with a new film and for the oxidation in stage 2 after removal of the complex. Thus the partial oxidation in stage 1 did not noticeably change the number of active sites on the surface. Second, the rate was signficantly increased when the complex was present on the surface before admission of oxygen. Furthermore, other types of experiments showed that the presence of the complex on the surface before the reaction shortened the induction period, an effect consistent with the interpretation of the complex as an intermediate in the reaction. The complex therefore played a significant role in the mechanism of the oxidation.

At temperatures higher than about 925 K the induction period was much shorter and carbon monoxide was an important product. In this region the decrease in pressure caused by the formation of complex was negligible compared to the

© 1997 NRC Canada

Fig. 3. Effect of the presence of the complex on the rate of removal of carbon. Initial pressure of O_2: 1.0 Torr. T = 998 K. Δ: Stage 1, new film; ▲: stage 2, complex removed after stage 1; ○: stage 2, complex not removed after stage 1.



increase caused by the production of carbon monoxide. Under these conditions we may write

$$-\frac{dC}{dt} = \frac{dCO_2}{dt} + \frac{dCO}{dt}$$

$$P_T = P_{O_2} + P_{CO_2} + P_{CO}$$

$$P_T - P^0_{O_2} = \Delta P = P_{CO}$$

Yield–time curves for the formation of products and loss of carbon obtained from these measurements at 1048 K are shown in Fig. 4.

The measured activation energy for the rate of formation of carbon monoxide was approximately 290 kJ mol^{-1}, a value similar to the energy required for desorption of the complex as measured by temperature-programmed desorption. It seems reasonable therefore that desorption of the complex is the source of carbon monoxide. An Arrhenius plot for the rate of formation of carbon monoxide is shown in Fig. 5.

In order that the activation energy for the rate of formation of carbon monoxide may be identified with the energy required for release of the complex, the rate of occupation of the active sites, or rate of formation of the complex, must be fast compared to the rate of desorption. In other words, complete coverage of the active sites must be maintained. As the temperature is increased and the rate of desorption increases, a point will be reached, observed first at low pressure, where complete coverage cannot be maintained. The rate of desorption will then no longer conform to the Arrhenius dependence observed at lower temperatures and will fall below a rate extrapolated from the low-temperature region. This effect is evident from the results shown in Fig. 5. This apparent decrease in activation energy at high temperatures is often observed in catalytic processes when the number of active sites on a surface can no longer be maintained. The effect is quite different from the decrease in rate observed in other experiments on the reaction of carbon with oxygen at temperatures above about 1200 K, which has been accounted for by diffusion effects (18).

As carbon monoxide accumulated in the products a secondary reaction with oxygen occurred and the ratio CO/CO_2 fell with increasing conversion. This secondary reaction was sometimes so rapid that we realized we were observing the explosive reaction of carbon monoxide and oxygen (19, 20). This reaction is catalyzed by traces of water vapour and in our system minute amounts of water vapour are formed as a gaseous product from oxidation of traces of hydrogen in the films of pyrolytic carbon.

Figure 6 shows a portion of the chart record of the pressure and the transmitted light intensity for an experiment where an explosion occurred. As the reaction proceeds, both the pressure and the transmitted light increase smoothly initially, indicating formation of carbon monoxide as well as carbon dioxide and consumption of carbon. After removal of a certain amount of carbon, the amount depending on the conditions of the experiment, a sudden drop in pressure occurs, reducing almost to the initial value, preceded by a momentary jump in pressure. This behaviour, which has been observed in comparable systems and discussed in detail by Bond, Gray, and Griffiths (21), indicates that an ignition has occurred. The momentary pressure pulse, also observed in previous studies, is a consequence of a temperature pulse caused by the exothermic reactions associated with the explosion. This figure also shows that the explosion was accompanied by a dramatic increase in the rate of gasification. The explosive reaction was studied in some detail and we were able to show that explosions occurred when the concentration of water vapour in the gas phase achieved the levels required to initiate the chain-branching reactions.

It was also shown that the presence of inert gas could prevent the explosion by stabilization of the intermediate, HO_2. The dissociative reaction of hydrogen atoms with oxygen is a critical step in the chain-branching reactions leading to explosion.

$$H + O_2 \rightarrow HO_2$$

$$HO_2 \rightarrow OH + O$$

$$HO_2 + M \rightarrow HO_2 + M$$

If HO_2 is stabilized branching does not occur. Effects of inert gases on the rate of oxidation of carbon (22), and some other catalytic processes (23), had previously been reported and explanations had, not very satisfactorily, invoked various types of surface processes, including effects on the reactivity of the active sites on carbon. On the other hand, the results of our experiments showed that at temperatures above about 900 K both water vapour and inert gases could induce radical reactions in the gas phase that had a profound effect on the rate of the overall reaction (24). Clearly, interpretation of the effects of water vapour and of inert gas on the kinetics of the carbon–oxygen reaction should not be confined to effects on the surface.

The mechanism

The picture of the oxidation process that emerges involves, as a first step, rapid adsorption of oxygen on the carbon surface

© 1997 NRC Canada

Can. J. Chem. Downloaded from www.nrcresearchpress.com by 88.146.161.215 on 09/08/12
For personal use only.

Fig. 4. Carbon consumed and CO and CO_2 formed as a function of time in the high-temperature region. ○: carbon removed; Δ: CO; ◇; CO_2. *A*: 1048 K, initial pressure of oxygen: 1 Torr. *B*: 1148 K, initial pressure of oxygen: 3 Torr.

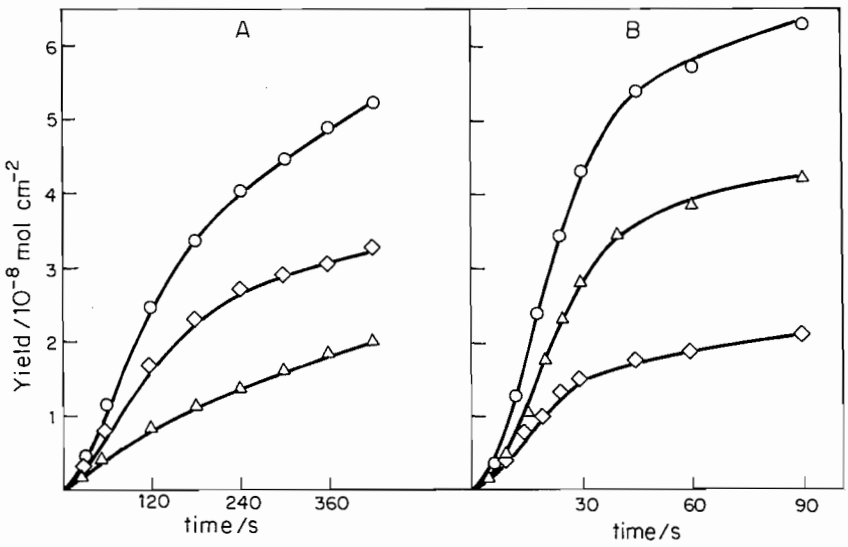


Fig. 5. Arrhenius plot for the rate of formation of carbon monoxide. Initial pressure of oxygen: ○: 3 Torr; Δ: 1 Torr, ◇: 0.5 Torr.

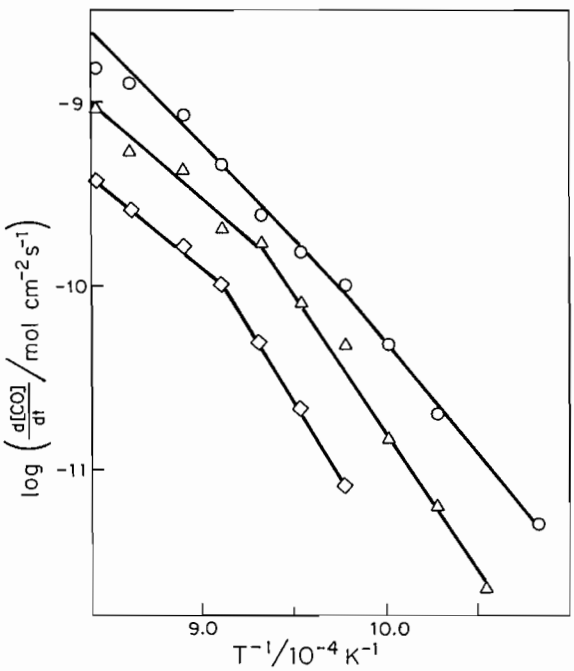
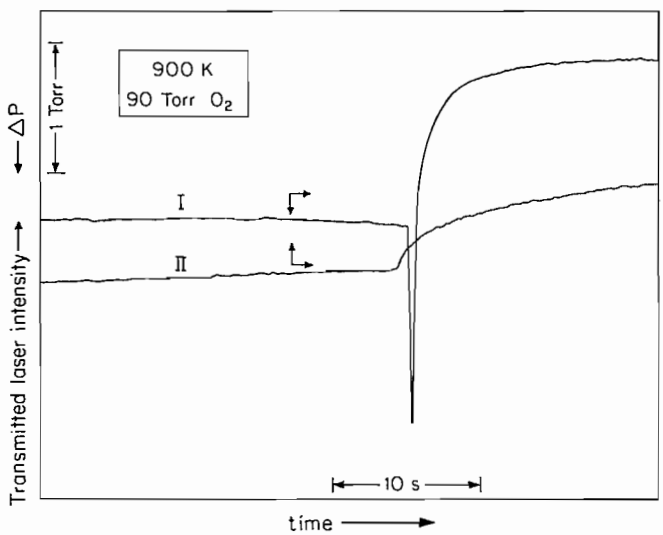


Fig. 6. Part of the chart record of the time course of an oxidation of carbon leading to an explosion. I: Pressure; II: intensity of transmitted light.



followed by formation of the stable complex. In the low-temperature region carbon dioxide is produced after accumulation of the complex on the surface. We suggested that this process occurs by reaction of the complex with gaseous oxygen in an Eley–Rideal type of mechanism (16). The following five reactions describe the main features of this picture, where C_F refers to an edge carbon atom (a free site), $C(O_2)$ refers to an adsorbed molecule of oxygen before formation of the complex, and $(CO)_C$ is the stable complex on the surface.

[1] $C_F + O_2 \rightarrow C(O_2)$

[2] $C_F + C(O_2) \rightarrow 2(CO)_C$

[3] $(CO)_C \rightarrow CO(g) + C_F$

[4] $C_F + (CO)_C + O_2 \rightarrow CO_2 + (CO)_C + C_F$

[5] $(CO)_C + C(O_2) \rightarrow CO_2 + (CO)_C + C_F$

Reactions [1] and [2] describe the formation of the complex, reaction [3] is the desorption of the complex to give carbon monoxide, and reactions [4] and [5] represent the reaction of

© 1997 NRC Canada

Can. J. Chem. Downloaded from www.nrcresearchpress.com by 88.146.161.215 on 09/08/12
For personal use only.

the complex with either gaseous or adsorbed oxygen to give carbon dioxide.

These latter two reactions are the most important feature of the mechanism and describe reactions, other than simple desorption, by which the complex could participate in the formation of products. The activation energy for the rate of formation of carbon dioxide was, from our measurements, 160 kJ mol^{-1}. Values in the range 160–200 kJ mol^{-1} have been reported. These values are much less than the energy required (about 280 kJ mol^{-1}) for desorption of the complex. The energy requirement for reactions [4] or [5] should be considerably less than required for simple desorption, since the process of conversion of the complex into gaseous carbon dioxide involves formation of new bonds as well as rupture of the carbon lattice. Interaction with the complex thus provides a low-energy path for formation of carbon dioxide. These reactions also account for the observed first-order dependence of the rate on the pressure of oxygen.

The formation of each product molecule, carbon monoxide and carbon dioxide, is accompanied by regeneration of a free site and the possibility of formation of another complex. The complex may thus be regarded as a catalyst. On this basis, the rate of reaction or, at low temperature, the rate of formation of carbon dioxide should be directly related to the concentration of the complex. Rates measured with a variety of different types of carbon and under a variety of reaction conditions should be comparable if the rates are normalized to the number of active sites, as measured by the complex. Ahmed and Back (16) examined rates of oxidation measured over a wide range of temperature and pressures of oxygen and for a variety of types and sources of carbon in systems where the active surface area, as defined by the concentration of complex, was reported. Remarkable agreement was observed among these normalized rates, taking into account the uncertainties expected from the extrapolations and interpolations required for the comparisons. Undoubtedly the surface complex provides some indication of the reactivity of the carbon surface. In reality, the complex itself is not a single structure and each carbon surface has different types of active centers so that the activity of a particular sample may not be fully described by the measurement of the complex present under particular conditions. It is not surprising that the role of the complex in the oxidation process is still not clearly understood.

Application of computer modelling

The ideas presented in the simple mechanism suggested here appeared to offer a plausible explanation for some features of the kinetics of the reaction and to at least provide a starting point for further development of a detailed mechanism. As a first step, quantitative evaluation of the importance of the individual elementary steps was required. Analytical solutions of rate equations based on steady-state assumptions are of limited value in achieving this understanding, partly because details of the mechanism may be obscured by the representation of the rate by a single rate constant. Computer modelling techniques, on the other hand, do not require an analytical solution and provide great sensitivity and scope for the evaluation of mechanisms. The main requirement is reliable measurements of the rate constants for each elementary process in the mechanism (25).

The measurements described in the previous section provided us with a basis for estimating the rate of each individual step in the mechanism, including adsorption, formation of complex, reactions of the complex, and desorption of the complex. Before making the kinetic measurements, the characterization of the carbon surface in terms of the number of active sites was estimated according to the procedures defined by Laine, Vastola, and Walker (10). The film was saturated with oxygen at about 573 K, followed by temperature-programmed desorption up to 1223 K, with analysis of the carbon monoxide and carbon dioxide desorbed. The number of active sites on the carbon surface at the beginning of a reaction, C_F^0, was given as

$$[6] \quad C_F^0 = CO + 2CO_2$$

With the films used in our experiments this quantity was always reproducible.

At temperatures below about 900 K, where the formation of carbon monoxide is negligible, the reaction does not involve a change in pressure. A small but measurable drop in pressure occurred in the early stages of the reaction, showing that oxygen was adsorbed on the surface. Because the initial rate of pressure drop was fast and the activation energy for the process was only about 40 kJ mol^{-1}, this rate was assumed to correspond to reaction [1] and the rate constant was calculated from the expression

$$[7] \quad -\frac{d[O_2]}{dt} k_1 C^0{}_F [O_2]^0$$

This equation assumes that in the initial stages reaction [2] is not important or, in other words, that conversion of $C(O_2)$ into the strongly bound complex is slow compared to its formation. As an estimate, k_2 was taken as 0.1 k_1 at 748 K and its value was allowed to vary with temperature with an activation energy of some 80–120 kJ mol^{-1}. The ratio k_2/k_1 was subsequently adjusted in developing the kinetic model, but the changes did not invalidate the use of eq. [7].

The rate of reaction [3] was estimated from the results of temperature-programmed desorption measurements, which gave an average activation energy for desorption of 270 kJ mol^{-1}. Assuming a frequency factor of 10^{13} s^{-1}, direct desorption is negligible compared to the overall rate of the reaction below about 900 K, in agreement with the dominance of carbon dioxide in the product.

Estimation of the rate constants for reactions [4] and [5] required values for the concentration of each complex on the surface, $C(O_2)$ and $(CO)_C$, as well as the concentration of free sites, C_F, at any time. The concentration of the strongly bound complex, $(CO)_C$, was obtained, at any stage of the reaction, by removing reactants, products, and $C(O_2)$ by evacuation, leaving only $(CO)_C$ on the surface. Temperature-programmed desorption to 1223 K, with measurement of the carbon monoxide and carbon dioxide evolved, gave directly the number of moles of $(CO)_C$.

Since two complexes must interact to give CO_2

$$2(CO)_C = CO_2 + C_F$$

Can. J. Chem. Downloaded from www.nrcresearchpress.com by 88.146.161.215 on 09/08/12
For personal use only.

© 1997 NRC Canada

Can. J. Chem. Downloaded from www.nrcresearchpress.com by 88.146.161.215 on 09/08/12
For personal use only.

therefore the total moles of complex will be given as follows:

[8] $(CO)_C = CO + 2CO_2$

At any time during the reaction the difference between the measured pressure and the initial pressure indicated formation of both $C(O_2)$ and $(CO)_C$ as follows,

[9] $-\Delta P = -\Delta O_2 = 2(CO)_C + C(O_2)$

Thus from eqs. [8] and [9] the quantity of $C(O_2)$ was obtained.

Finally, C_F, the concentration of free sites at any time, was given as the difference between the initial value, C_F^0, and the sum of sites occupied by $C(O_2)$ and $(CO)_C$:

[10] $C_F = C_F^0 - [(CO)]_C + C(O_2)]$

The rate constants for reactions [4] and [5] were estimated by two approaches. The rate of disappearance of oxygen after the initial stage of the reaction and the rate of formation of carbon dioxide are given by the equations:

[11] $$-\frac{d[O_2]}{dt} = k_1 C_F[O_2] + k_4 C_F[(CO)_C][O_2]$$

[12] $$\frac{d[CO_2]}{dt} = k_4 C_F[CO)_C][O_2] + k_5[(CO)_C][O_2]$$

Using the value of k_1 calculated from the initial rate of disappearance of oxygen, eq. [7], and the estimates of C_F and $(CO)_C$ described, k_4 may be obtained from eq. [11]. Using this value of k_4 in eq. [12] gives a value for k_5. Alternatively, k_4 and k_5 may be obtained from simultaneous solutions of eq. [12] using rates of formation of carbon dioxide measured at different times during the course of the reaction. These procedures gave values of k_4 and k_5 in agreement within a factor of two.

The rates of formation of products calculated on the basis of the simple mechanism provided an accurate picture of the early stages of the reaction but were not adequate to describe the observed variations of reactant and products during the complete course of the reaction. Significant improvement was achieved by the introduction of two types of reactive sites on the carbon surface, a feature long recognized from a variety of experimental studies (for a summary, see ref. 1*b*). One site, designated CA, adsorbs oxygen rapidly and is identified as the site responsible for the initial sharp decrease in the oxygen pressure. Such sites are quickly saturated and play only a small part in the subsequent chemistry. A second kind of site, designated CB, adsorbs oxygen much more slowly. Its concentration therefore decreases slowly and it is able to participate in other reactions without requiring unacceptably large rate constants.

This extension of the mechanism gave partial improvement, but much better agreement between calculated and observed yields was obtained by allowing some interchange between the chemical reactions of A and B sites. A detailed discussion of the types of reactions of the complexes on both sites and of the sensitivitity analysis that identifies the important reactions has been given previously (26). The final minimum set of reactions required to give quantitative agreement with experimental measurements is given below.

[1A] $CA + O_2 \rightarrow C(O_2)_A$

[2A] $CA + C(O_2)_A \rightarrow 2(CO)_{CA}$

[3B] $(CO)_{CB} \rightarrow CO + CB$

[1B] $CB + O_2 \rightarrow C(O_2)_B$

[13B(*a*)] $CB + (CO)_{CB} + O_2 \rightarrow CO_2 + (CO)_{CB} + 2\,CB$

[13B(*b*)] $CB + (CO)_{CB} + O_2 \rightarrow CO_2 + (CO)_{CB} + CB$

[13B(*c*)] $CB + (CO)_{CA} + O_2 \rightarrow CO_2 + (CO)_{CB} + CA$

[14A] $CB + C(O_2)_A \rightarrow (CO)_{CA} + (CO)_{CB}$

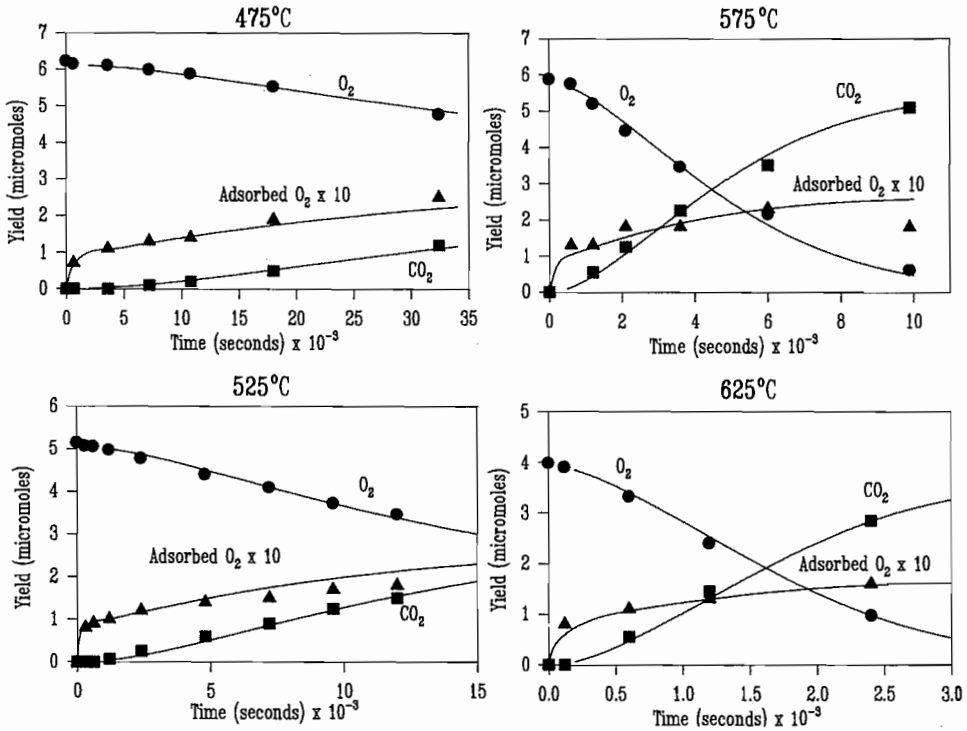
Because reaction with oxygen has been generally observed to increase reactivity of the surface, reaction [13B(*a*)] is written to allow for an increase in the number of sites. The relative rates of reactions [13B(*a*)] and [13B(*b*)] were adjusted to give the increase in rate observed. The mechanism does not include a loss process for $C(O_2)_B$ because direct conversion of oxygen adsorbed on B sites to form $(CO)_{CB}$ is too slow in the low-temperature region to make a significant contribution. Formation of the complex on B sites occurs more readily by reactions [13B(*c*)] and [14A]. Only a small loss of oxygen occurs by reaction [1B]. The yields of products calculated on the basis of this mechanism are shown as the solid lines in Fig. 7 with the experimental measurements as the points. The mechanism thus provides a satisfactory description of the reaction in the low-temperature region.

The values of the rate constants used in the computation together with the Arrhenius parameters were listed in an earlier paper (26). Although the reactions as written may not be truly elementary processes, nevertheless the rate constants conform to an Arrhenius temperature dependence, at least in the low-temperature region. In fitting a model to experimental results adjustment of rate constants is constrained by the experimental measurements and is guided by sensitivity analysis. This procedure identifies the rate constants that require the smallest change for the largest effect on the rate and allows the elimination of reactions that make negligible contributions to the rate.

The model provided a reasonably quantitative description of the processes occurring during the reaction of oxygen with carbon in the temperature range 750–900 K at oxygen pressures in the neighbourhood of 100 Pa (1 Torr). A more demanding test of a model is its application to results obtained outside the range of conditions for which it was developed. For this we chose the detailed yield–time data obtained by Laine, Vastola, and Walker (10) where measurements were made with a different type of carbon, Graphon (highly purified graphitized carbon black), at much lower pressures (10^{-3} Torr) than used in the experiments of Ahmed and Back. By introducing two alterations to the mechanism good agreement was obtained between the calculated and observed results (27). First, the reactivity of the A sites was increased by increasing the rate constants for reactions [1A] and [3A]

© 1997 NRC Canada

Fig. 7. Comparison of experimental measurements and calculated values for consumption of oxygen and formation of products at four temperatures. Experimental data are represented by points. Calculated values are represented by lines. ●: O_2; ▲: complex; ■: CO_2.



[3A] $(CO)_{CA} \rightarrow CO + CA$

by factors of 14 and 120, respectively. Such changes in reactivity would be expected between different types of carbon and are in accord with the high reactivity of Graphon. A second adjustment was the addition of a new type of adsorption site, designated C_{AA}, which rapidly but loosely binds oxygen and provides a new route to the formation of $(CO)_A$. Again this type of adjustment reflects differences in the structure and hence in types of active sites of carbon formed from different sources. The new reactions were

[15] $C_{AA} + O_2 \rightarrow C(O_2)_{AA}$

[16] $C_A + C(O_2)_{AA} \rightarrow (CO)_{AA} + (CO)_A$

The rate of reaction [15] is the key factor in reproducing the decay curves of oxygen observed by Laine, Vastola, and Walker (10). The new type of site binds a single oxygen atom particularly strongly and may be the very stable complex suggested by these authors.

Calculated and experimental results are shown in Fig. 8 for the results of both Ahmed and Back (16), using the original mechanism, and Laine, Vastola, and Walker (10), with the revised mechanism, at the same temperature. The major difference between the two sets of results is in the product distribution. At pressures of 1 Torr, carbon dioxide is the major product because the rate of reaction [13] greatly exceeds that of reaction [3], the desorption of carbon monoxide. At pressures of 10^{-3} Torr, on the other hand, carbon monoxide is the major product. At such low pressures the rate of reaction [13] is reduced and reaction [3] is now the faster.

Discussion

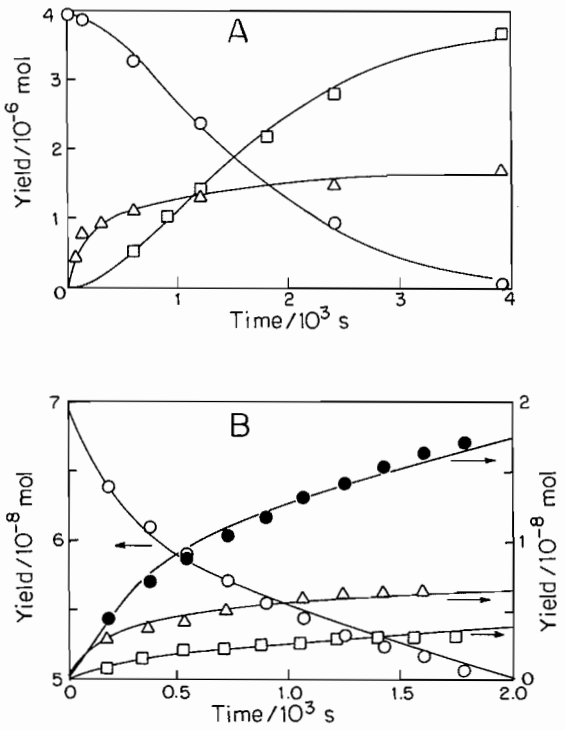
The most significant features of the model are the existence of at least two distinct types of active sites on the carbon surface, with different reactivities, and the introduction of the general type of reaction given by eq. [4], where a gas-phase molecule of oxygen reacts with the chemisorbed complex. The idea that the carbon surface may contain more than one type of active site has been suggested many times, based on results from a variety of studies. The sites labelled CA are the most active in terms of adsorption of oxygen and are rapidly saturated. Oxygen therefore is initially rapidly adsorbed, followed by a more gradual loss as sites CB contribute. CA sites do not contribute appreciably to subsequent reactions to produce carbon dioxide, which all involve CB sites. The very different nature of adsorption on CB sites is reflected in the larger activation energy of reaction [1B], 190 kJ mol^{-1}, compared to that for reaction [1A], 50 kJ mol^{-1}. The two adsorbed oxygen species, $C(O_2)_A$ and $C(O_2)_B$, also had different reactivities. Reaction of $C(O_2)_A$ with CB sites was the dominant mechanism for formation of the complex and the corresponding reaction with $C(O_2)_B$ did not contribute. Conversion of the complexes $(CO)_A$ and $(CO)_B$ into carbon dioxide probably occurs following adsorption of oxygen on a neighbouring CB site. Interaction of the adsorbed oxygen with the complex leads to formation of carbon dioxide. Following desorption of carbon dioxide a new complex and new active sites remain on the surface. These reactions regenerate the appropriate proportions of CA and CB sites at all stages in the reaction.

An additional feature of the mechanism is the prediction, often suggested by various experimental measurements, that

© 1997 NRC Canada

Can. J. Chem. Downloaded from www.nrcresearchpress.com by 88.146.161.215 on 09/08/12
For personal use only.

Fig. 8. Comparison of experimental measurements and calculated 2222 values for the reaction of oxygen with carbon at 898 K. Experimental measurements are represented by points. Calculated values are represented by lines. ○: O_2; ●: CO; □ : CO_2; Δ: complex. *A*: Results of Ahmed and Back. Initial pressure 1 Torr. *B*: Results of Laine, Vastola, and Walker. Initial pressure 10^{-3} Torr.



the concentration of oxide complex on the surface rapidly rises to a small value that remains nearly constant as the reaction proceeds, as a result of the balance between the rates of formation and disappearance. The complex is an intermediate in the reaction, continuously occupying and releasing new active carbon atoms. Thus the role of the complex resembles that of active sites in a catalytic process.

The results of this first attempt at computer modelling of the carbon–oxygen reaction represent only a beginning in the development of a mechanism that may, with suitable values for the rate constants for each individual step, describe the kinetics of the reaction under all conditions. The rate constants used in the present calculations were based on measurements made with a particular type of carbon and the relative values for these rate constants as well as the relative concentrations of the sites would be expected to change with different types of carbon. Nevertheless the basic features of the mechanism should be generally applicable. The value of the method lies in its ability to test, under a range of conditions, a complex mechanism involving a wide variety of elementary steps. The results of the tests clearly show the importance of certain types of reactions as opposed to the ineffectiveness of others. The mechanism presented undoubtedly needs additions and modifications and improved estimates for rate constants. As new measurements provide these, the mechanism may be developed in ways that will provide new insights into the complexities of the reaction and the role of the various surface oxides in the gasification process.

Acknowledgments

The author acknowledges the contributions of C.-J. Chen, in the development of the method of formation and analysis of carbon, of S. Ahmed, in the measurements of the kinetics of the reaction of carbon with oxygen, and of Professor J.R. Roscoe in the computer modelling of the mechanism of the reaction. The author also expresses her appreciation of the many valuable discussions with her late husband, Robert A. Back, while these ideas were brought to fruition. Generous support by the Natural Sciences and Engineering Research Council of Canada was greatly appreciated.

References

1. (*a*) 20th Biennial Conference on Carbon, University of California, Santa Barbara, California, American Carbon Society. 1991; (*b*) J. Lahaye and P. Ehrburger (*Editors*). Fundamental issues in control of carbon gasification reactivity. NATO ASI Ser. E, **192** (1991).
2. D.J. Johnson. Chem. Phys. Carbon, **20**, 1 (1988).
3. F. Rodriguez-Reinoso and A. Linares-Solano. Chem. Phys. Carbon, **21**, 2 (1989).
4. P.L. Walker, R.L. Taylor, and J.M. Ranish. Carbon, **29**, 411 (1991).
5. H. Marsh. Spec. Publ. – Chem. Soc. 32, p. 13 (1978).
6. R.J. Tyler, H.J. Wouterlood, and M.F.R. Mulcahy. Carbon, **14**, 271 (1976).
7. C. Park and J. Appleton. Combust. Flame, **20**, 369 (1973).
8. D.R. Olander, W. Siekhaus, R. Jones, and J.A. Schwartz. J. Chem. Phys. **57**, 408 (1972).
9. R.T. Yang. Chem. Phys. Carbon, **19**, 163 (1984).
10. N.R. Laine, F.J. Vastola, and P.L. Walker. J. Phys. Chem. **67**, 2030 (1963).
11. G. Tremblay, F.J. Vastola, and P.L. Walker. Carbon, **16**, 35 (1978).
12. F.G. Fischer and A.R. Feichtinger. 15th Bienn. Conf. Carbon, Philadelphia, Pennsylvania. 1981. p. 472.
13. R. Phillips, F.J. Vastola, and P.L. Walker. Carbon, **8**, 205 (1970).
14. G.R. Hennig. Chem. Phys. Carbon, **1**, 122 (1965).
15. H. Marsh and A.D. Foord. Carbon, **11**, 421 (1973).
16. S. Ahmed and M.H. Back. Carbon, **23**, 513 (1985).
17. S.B. Tong, P. Pareja, and M.H. Back. Carbon, **20**, 191 (1982).
18. I.W. Smith, D.J. Harris, M.G. Valix, and D.L. Trimm. *In* Fundamental issues in control of carbon gasification reactivity. *Edited by* J. Lahaye and P. Ehrburger. NATO ASI Ser. E, **192** (1991).
19. S. Ahmed and M.H. Back. Int. J. Chem. Kinet. **18**, 181 (1986).
20. S. Ahmed and M.H. Back. Int. J. Chem. Kinet. **18**, 801 (1986).
21. J.R. Bond, P. Gray, and J.F. Griffiths. Proc. R. Soc. London, Ser. A: **375**, 43 (1981).
22. P.L. Walker, L. Pentz, D.L. Biederman, and F.J. Vastola. Carbon, **15**, 165 (1977).
23. W.G. Rhodey, P.M. Reilly, P.L. Silveston, and R.R. Hudgins. J. Catal. **42**, 312 (1976).
24. S. Ahmed and M.H. Back. Carbon, **25**, 783 (1987).
25. M.H. Back. Carbon, **29**, 1287 (1991).
26. S. Ahmed, M.H. Back, and J.M. Roscoe. Combust. Flame, **70**, 1 (1987).
27. S. Ahmed, M.H. Back, and J.M. Roscoe. Symp. Fundamentals of Gasification, ACS Division of Fuel Chemistry, **34** (1989).

Can. J. Chem. Downloaded from www.nrcresearchpress.com by 88.146.161.215 on 09/08/12
For personal use only.

© 1997 NRC Canada

Solubility of *trans*-stilbene in organic nonelectrolyte solvents. Comparison of observed versus predicted values based upon mobile order theory

Kristin A. Fletcher, Mary E.R. McHale, Karen S. Coym, and William E. Acree, Jr.

Can. J. Chem. Downloaded from www.nrcresearchpress.com by 92.62.229.171 on 09/08/12
For personal use only.

Abstract: Experimental solubilities are reported at 25.0°C for *trans*-stilbene dissolved in 28 different organic nonelectrolyte solvents containing methyl, ether, hydroxy, and *tert*-butyl functional groups. Results of these measurements are used to test the applications and limitations of expressions derived from Mobile Order theory. For the 20 solvents for which predictions could be made, computations show that Mobile Order theory does provide fairly reasonable (although by no means perfect) estimates of the saturation mole fraction solubilities. Average absolute deviation between predicted and observed values is ca. 24%. In comparison, the average absolute deviation increases significantly to 935% when ideal solution behavior is assumed.

Key Words: *trans*-stilbene solubilities, organic nonelectrolyte solvents, solubility predictions.

Résumé : On a déterminé les solubilités expérimentales, à 25°C, du *trans*-stilbène dissous dans 28 solvants organiques non-électrolytiques différents comportant des groupes fonctionnels méthyle, éther, hydroxy et *tert*-butyle. On a utilisé les valeurs ainsi obtenues pour évaluer les applications et les limitations d'expressions dérivées de la théorie de l'ordre mobile. Les 20 solvants pour lesquels il est possible de faire des prédictions à l'aide de calculs montrent que la théorie de l'ordre mobile permet d'obtenir des évaluations assez correctes (même si elles sont loin d'être parfaites) de solubilité à saturation des fractions molaires. Les déviations moyennes absolues entre les valeurs prédites et observées sont d'environ 24%. En comparaison, la déviation moyenne absolue augmente d'une façon phénoménale à 935% lorsqu'on fait l'hypothèse que le comportement de la solution est idéal.

Mots clés : solubilités du *trans*-stilbène, solvants organiques non-électrolytiques, prédictions des solubilités.

[Traduit par la rédaction]

Introduction

Solid–liquid equilibrium data of organic nonelectrolyte systems are becoming increasingly important in the petroleum industry, particularly in light of present trends towards heavier feedstocks and known carcinogenicity/mutagenicity of many of the larger polycyclic aromatic compounds. Solubility data for a number of polycyclic aromatic hydrocarbons (e.g., anthracene and pyrene) and heteroatom polynuclear aromatics (e.g., carbazole, dibenzothiophene, and xanthene) have been published in the recent chemical literature (for listing of references see Acree (1–3)). Despite efforts by experimentalists and scientific organizations, both in terms of new experimental measurements and critically evaluated data compilations, there still exist numerous systems for which solubility data are not readily available.

To address this problem, researchers have turned to group contribution methods and semiempirical expressions to predict desired quantities. Group contribution methods have proved fairly successful in estimating solid solubility in pure and binary solvent mixtures from structural information (4–11). Practical application, however, is limited to systems for which all group interaction parameters are known. Interaction parameters can be evaluated from liquid–vapor, liquid–liquid, and solid–liquid equilibria data. It is important that the data base contain as many different functional groups as possible, preferably with adequate representation from both mono- and multi-functional solute/solvent molecules to permit evaluation of potential synergistic effects. The data base should contain sufficient experimental values near infinite dilution in the event that one wishes to determine separate interaction parameters for finite concentration and infinite dilution activity coefficient predictions. For this reason, we have measured *trans*-stilbene solubilities in 28 different organic solvents. Functional groups represented include ethers, and hydroxy and saturated hydrocarbons. These measurements will be used to further test the applications and limitations of predictive expressions derived from Mobile Order theory.

Received November 8, 1996.

K.A. Fletcher, M.E.R. McHale, K.S. Coym, and W.E. Acree, Jr.[1] Department of Chemistry, University of North Texas, Denton, TX 76203-0068, U.S.A.

[1] Author to whom correspondence may be addressed. Fax: (817) 565-4318. E-mail: Acree@cas1.unt.edu

Materials and methods

trans-Stilbene (Aldrich, 96%) was recrystallized several times from methanol. 1-Pentanol (Aldrich, 99+%), ethanol (Aaper Alcohol and Chemical Company, absolute), methanol

© 1997 NRC Canada

Can. J. Chem. Downloaded from www.nrcresearchpress.com by 92.62.229.171 on 09/08/12
For personal use only.

(Aldrich, 99.9+%), 1-propanol (Aldrich, 99+%, anhydrous), 2-propanol (Aldrich, 99+%, anhydrous), 1-butanol (Aldrich HPLC, 99.8+%), 2-butanol (Aldrich, 99+%, anhydrous), 1-hexanol (Alfa Aesar, 99+%), 1-heptanol (Alfa Aesar, 99+%), 2-methyl-2-butanol (Acros, 99+%), 2-methyl-1-propanol (Aldrich, 99+%, anhydrous), 3-methyl-1-butanol (Aldrich, 99+%, anhydrous), 1-octanol (Aldrich, 99+%, anhydrous), 2-pentanol (Acros, 99+%), 4-methyl-2-pentanol (Acros, 99+%), 2-ethyl-1-hexanol (Aldrich, 99+%), 2-methyl-1-pentanol (Aldrich, 99%), dibutyl ether (Aldrich, 99%), methyl *tert*-butyl ether (Arco, 99.9+%), *tert*-butylcyclohexane (Aldrich, 99+%), *n*-hexane (Aldrich, 99%), *n*-heptane (Aldrich, HPLC), *n*-octane (Aldrich, 99+%, anhydrous), cyclohexane (Aldrich, HPLC), methylcyclohexane (Aldrich, 99+%, anhydrous), cyclooctane (Aldrich, 99+%), 2,2,4-trimethylpentane (Aldrich, HPLC), and cyclopentanol (Aldrich, 99%) were stored over molecular sieves before use. Gas chromatographic analysis showed solvent purities to be 99.7 mol% or better.

Excess solute and solvent were placed in amber glass bottles and allowed to equilibrate in a constant temperature water bath at 25.0 ± 0.1°C for at least 3 days (often longer). Attainment of equilibrium was verified both by repetitive measurements after several additional days and by approaching equilibrium from supersaturation by pre-equilibrating the solutions at a higher temperature. Aliquots of saturated *trans*-stilbene solutions were transferred through a coarse filter into a tared volumetric flask to determine the amount of sample, and were diluted quantitatively with methanol for spectrophotometric analysis at 294 nm on a Bausch and Lomb Spectronic 2000. Concentrations of the dilute solutions were determined from a Beer–Lambert law absorbance versus concentration working curve for nine standard solutions ranging in concentration from 1.38×10^{-5} to 4.62×10^{-5} M. The calculated molar absorptivity of $\varepsilon \approx 28\,750$ L mol^{-1} cm^{-1} was constant over the concentration range. Experimental molar concentrations were converted to (mass/mass) solubility fractions by multiplying by the molar mass of *trans*-stilbene, volume(s) of volumetric flask(s) used, and any dilutions required to place the measured absorbances on the Beer–Lambert law absorbance versus concentration working curve, and then dividing by the mass of the saturated solution analyzed. Mole fraction solubilities were computed from (mass/mass) solubility fractions using the molar masses of the solute and solvent. Experimental *trans*-stilbene solubilities, X_A^{sat}, in 28 organic solvents studied are listed in Table 1. Numerical values represent the average of between four and eight independent determinations, with the measurements being reproducible to ±2%.

Table 1. Experimental *trans*-stilbene mole fraction solubilities in select organic solvents at 25.0°C.

Organic solvent	X_A^{sat}
n-Hexane	0.009 60
n-Heptane	0.010 85
n-Octane	0.012 41
Cyclohexane	0.013 74
Methylcyclohexane	0.014 13
Cyclooctane	0.020 80
2,2,4-Trimethylpentane	0.008 03
tert-Butylcyclohexane	0.015 70
Methanol	0.001 96
Ethanol	0.003 21
1-Propanol	0.004 03
2-Propanol	0.002 79
1-Butanol	0.005 33
2-Butanol	0.003 82
2-Methyl-1-propanol	0.003 30
1-Pentanol	0.006 91
2-Pentanol	0.005 31
3-Methyl-1-butanol	0.005 02
2-Methyl-2-butanol	0.005 78
1-Hexanol	0.008 41
2-Methyl-1-pentanol	0.006 00
4-Methyl-2-pentanol	0.005 06
1-Heptanol	0.010 92
1-Octanol	0.012 51
2-Ethyl-1-hexanol	0.008 63
Cyclopentanol	0.008 23
Dibutyl ether	0.027 83
Methyl *tert*-butyl ether	0.028 87

Results and discussion

Solvents studied include both noncomplexing alkanes and self-associating alcohols. Of the many solution models proposed in recent years, Mobile Order theory is perhaps the only one that is capable of describing solute behavior in such a wide range of solvent mixtures. The basic model (12–19) assumes that all molecular groups perpetually move, and that neighbors of a given kind of external atom in a molecule constantly change identity. All molecules of a given kind dispose of the same volume, equal to the total volume V of the liquid divided by the number N_A of molecules of the same kind, i.e., Dom A = V/N_A. The center of this domain perpetually moves. The highest mobile disorder is achieved whenever groups visit all parts of their domain without preference. Preferential contacts lead to deviations with respect to this "random" visiting. This is especially true in the case of hydrogen bonding, as specific interactions result in a specific orientation of the "donor" molecule with respect to an adjacent "acceptor" molecule.

In the case of an inert crystalline solute dissolved in a self-associating solvent, Mobile Order theory expresses the volume fraction saturation solubility, ϕ_A^{sat}, as

$$[1]\quad \ln \phi_A^{sat} = \ln a_A^{solid} - 0.5(1 - V_A/V_{solvent})\phi_{solvent} + 0.5 \ln [\phi_A^{sat} + \phi_{solvent}(V_A/V_{solvent})] - \phi_{solvent}^2 V_A(\delta_A' - \delta_{solvent}')^2(RT)^{-1} - r_{solvent}(V_A/V_{solvent})\phi_{solvent}$$

where the $r_{solvent}(V_A/V_{solvent})\phi_{solvent}$ term represents the contributions resulting from hydrogen-bond formation between the solvent molecules. For most of the published applications, $r_{solvent}$ was assumed to be unity for strongly associated solvents with single hydrogen-bonded chains such as monofunctional alcohols, to be two for water or diols, and to equal zero for nonassociated solvents such as saturated hydrocarbons. A more exact value for alcoholic solvents can be calculated based upon

© 1997 NRC Canada

Can. J. Chem. Downloaded from www.nrcresearchpress.com by 92.62.229.171 on 09/08/12
For personal use only.

Table 2. Comparison between experimental *trans*-stilbene mole fraction solubilities and predicted values based upon Mobile Order theory.

Organic solvent	$(X_A^{sat})^{exp}$	$(X_A^{sat})^{calc}$	% Dev[a]
n-Hexane	0.009 60	0.010 25	6.8
n-Heptane	0.010 85	0.010 80	−0.4
n-Octane	0.012 41	0.012 24	−1.4
Cyclohexane	0.013 74	0.013 16	−4.3
Methylcyclohexane	0.014 13	0.014 14	0.1
Cyclooctane	0.020 80	0.018 14	−12.8
2,2,4-Trimethylpentane	0.008 03	0.008 12	1.1
tert-Butylcyclohexane	0.015 70	0.018 64	18.7
Dibutyl ether	0.027 83	0.044 98	61.6
Methanol	0.001 96	0.002 09	6.5
Ethanol	0.003 21	0.003 87	20.5
1-Propanol	0.004 03	0.005 19	28.8
2-Propanol	0.002 79	0.005 97	114.0
1-Butanol	0.005 33	0.006 82	27.9
2-Butanol	0.003 82	0.005 47	43.1
2-Methyl-1-propanol	0.003 30	0.004 41	33.7
1-Pentanol	0.006 91	0.007 61	10.1
1-Hexanol	0.008 41	0.007 46	−11.4
1-Heptanol	0.010 92	0.008 58	−21.4
1-Octanol	0.012 51	0.006 18	−50.6

[a]Deviations (%) = 100 $[(X_A^{sat})^{calc} - (X_A^{sat})^{exp}]/(X_A^{sat})^{exp}$.

$$[2] \quad r_{solvent} = (K_{solvent}\phi_{solvent}/V_{solvent})/(1 + K_{solvent} \times \phi_{solvent}/V_{solvent})$$

with a numerical value of $K_{solvent}$ = 5000 cm^3 mol^{-1} assumed for all monofunctional alcohols.

If complexation does occur between the crystalline solute and solvent, then an additional term involving the solute–solvent equilibrium constant, $K_{ASolvent}$, must be introduced to describe the solubility enhancement that arises as a result of specific interactions. A slightly more complex expression applies in the case of solute complexation with a self-associating solvent. The symbols δ_A' and $\delta_{solvent}'$ denote the modified solubility parameters of the solute and solvent, respectively, V_i is the molar volume, and a_A^{solid} is the activity of the solid solute. This latter quantity is defined as the ratio of the fugacity of the solid to the fugacity of the pure hypothetical supercooled liquid. The numerical value of a_A^{solid} can be computed from the solute's molar enthalpy of fusion, ΔH_A^{fus}, at the normal melting point temperature, T_{mp}. Contributions from nonspecific interaction are incorporated into Mobile Order theory through the $\phi_{solvent}^2 V_A(\delta_A' - \delta_{solvent}')^2(RT)^{-1}$ term. Ruelle and co-workers (15–19) have presented a very impressive set of comparisons between experimental and predicted values for anthracene, naphthalene, pyrene (see also Powell et al. (20)), biphenyl, carbazole, benzil (see also Fletcher et al. (21)), *p*-benzoquinone, tricosane, octacosane, 10-nonadecanone, 11-heneicosanone, and 12-tricosanone in a wide range of both noncomplexing and complexing solvents to document the predictive ability of Mobile Order theory.

Table 3. Solvent and solute properties used in Mobile Order predictions.

Component (i)	V_i(cm^3 mol^{-1})	δ_i'/(MPa$^{1/2}$)[a]
n-Hexane	131.51	14.56
n-Heptane	147.48	14.66
n-Octane	163.46	14.85
Cyclohexane	108.76	14.82
Methylcyclohexane	128.32	15.00
2,2,4-Trimethylpentane	166.09	14.30
Cyclooctane	134.9	15.40
tert-Butylcyclohexane	173.9	15.50
Dibutyl ether	170.3	17.45
Methanol	40.7	19.25
Ethanol	58.7	17.81
1-Propanol	75.10	17.29
2-Propanol	76.90	17.60
1-Butanol	92.00	17.16
2-Butanol	92.4	16.60
2-Methyl-1-propanol	92.8	16.14
1-Pentanol	108.6	16.85
1-Hexanol	125.2	16.40
1-Heptanol	141.9	16.39
1-Octanol	108.6	16.38
trans-Stilbene[b]	177.0	19.69[c]

[a]Tabulated values are taken from a compilation given in Ruelle et al. (15, 16, 19).

[b]The numerical value of a_A^{solid} = 0.062 27 was calculated from the molar enthalpy of fusion, ΔH_A^{fus} = 27 400 J mol^{-1} (22) at the normal melting point temperature of the solute, T_{mp} = 398.15 K.

[c]Numerical value was calculated using the measured *trans*-stilbene mole fraction solubilities in *n*-hexane, *n*-heptane, and *n*-octane, in accordance with eqs. [1] and [3]; with $r_{solvent}$ = 0 and (or) $K_{ASolvent}$ = 0.

$$[3] \quad \ln \phi_A^{sat} = \ln a_A^{solid} - 0.5(1 - V_A/V_{solvent})\phi_{solvent} + 0.5 \ln [\phi_A^{sat} + \phi_{solvent}(V_A/V_{solvent})] - \phi_{solvent}^2 V_A(\delta_A' - \delta_{solvent}')^2(RT)^{-1} + \ln [1 + \phi_{solvent}(K_{Asolvent}/V_{solvent})]$$

$$[4] \quad \ln a_A^{solid} = -\Delta H_A^{fus}(T_{mp} - T)/(RTT_{mp})$$

Predictive application of eqs. [1] and [3] is relatively straightforward. First, an average numerical value of $\delta_{stilbene}'$ = 19.69 MPa$^{1/2}$ is computed by requiring that each equation (with $r_{solvent}$ = 0 and (or) $K_{ASolvent}$ = 0) perfectly describes our *trans*-stilbene mole fraction solubility data in *n*-hexane ($\delta_{stilbene}'$ = 19.78 MPa$^{1/2}$), *n*-heptane ($\delta_{stilbene}'$ = 19.68 MPa$^{1/2}$), and *n*-octane ($\delta_{stilbene}'$ = 19.60 MPa$^{1/2}$). The numerical value of a_A^{solid} = 0.062 27 is calculated using eq. [4] with ΔH_A^{fus} = 27 400 J mol^{-1} (22), and T_{mp} = 398.15 K. A numerical value of $V_{stilbene}$ = 177 cm^3 mol^{-1} was used for the molar volume of the hypothetical subcooled liquid solute.

Table 2 summarizes the predictive ability of Mobile Order theory for the 20 different organic solvents for which both *trans*-stilbene solubility data and modified solubility parameters could be found. Solvent molar volumes and modified solubility parameters are listed in Table 3. The modified

© 1997 NRC Canada

solubility parameters account for only nonspecific interactions, and in the case of the alcoholic solvents the hydrogen-bonding contributions have been removed. Numerical values of $\delta'_{solvent}$ were obtained from published compilations (15, 16, 19), and were either deduced by regressing actual solubility data of solid *n*-alkanes in organic solvents in accordance with the configurational entropic model of Huyskens and Haulait-Pirson (23) or estimated using known values for similar organic solvents. Examination of the entries in Table 2 reveals that Mobile Order theory does provide fairly reasonable (though by no means perfect) estimates of the solubility behavior of *trans*-stilbene in a wide range of organic solvents. Average absolute deviation between predicted and observed values is circa 24%. Readers are reminded that in evaluating the applicability of Mobile Order theory one must realize that many of these particular systems are highly nonideal, and that the experimental solubility data cover up to a 14-fold range in mole fraction. Had an ideal solution been assumed, then the predicted mole fraction solubility would be $X_A^{sat} = a_A^{solid} = 0.062\ 27$ for each solvent. The ideal solution approximation corresponds to a considerably larger average absolute deviation of 935% between predicted and observed values.

References

1. W.E. Acree, Jr. Polycyclic aromatic hydrocarbons in pure and binary solvents. Solubility Data Ser. Vol. 54. Oxford University Press, Oxford, U.K. 1994.
2. W.E. Acree, Jr. Polycyclic aromatic hydrocarbons: binary non-aqueous systems: Part 1 (Solutes A–E). Solubility Data Ser. Vol. 58. Oxford University Press, Oxford, U.K. 1995.
3. W.E. Acree, Jr. Polycyclic aromatic hydrocarbons: binary non-aqueous systems: Part 2 (Solutes F–Z). Solubility Data Ser. Vol. 59. Oxford University Press, Oxford, U.K. 1995.
4. W.E. Acree, Jr. Int. J. Pharm. **18**, 47 (1984).
5. U. Domanska and T. Hofman. J. Solution Chem. **14**, 531 (1985).
6. U. Domanska. Fluid Phase Equilib. **35**, 217 (1985).
7. R.S. Basu, H. Pham, and D.P. Wilson. Int. J. Pharm. **7**, 319 (1986).
8. A.B. Ochsner and T.D. Sokoloski. J. Pharm. Sci. **74**, 634 (1985).
9. R. Carta and S. Dernini. J. Chem. Eng. Data, **28**, 328 (1983).
10. W.E. Acree, Jr. and J.H. Rytting. Int. J. Pharm. **13**, 197 (1983).
11. A. Martin, P.L. Wu, A. Adjei, A. Beerbower, and J.M. Prausnitz. J. Pharm. Sci. **70**, 1260 (1981).
12. P.L. Huyskens and G.G. Siegel. Bull. Soc. Chim. Belg. **97**, 821 (1988).
13. G.G. Siegel, P.L. Huyskens and G. Vanderheyden. Ber. Bunsenges. Phys. **94**, 549 (1990).
14. P.L. Huyskens. J. Mol. Struct. **274**, 223 (1992).
15. P. Ruelle, C. Rey-Mermet, M. Buchmann, H. Nam-Tran, U.W. Kesselring, and P.L. Huyskens. Pharm. Res. **8**, 840 (1991).
16. P. Ruelle, M. Buchmann, H. Nam-Tran, and U.W. Kesselring. Int. J. Pharm. **87**, 47 (1992).
17. P. Ruelle, M. Buchmann, and U.W. Kesselring. J. Pharm. Sci. **83**, 396 (1994).
18. P. Ruelle, E. Sarraf, and U.W. Kesselring. Int. J. Pharm. **104**, 125 (1994).
19. P. Ruelle, E. Sarraf, L. Van den Berge, K. Seghers, M. Buchmann, and U.W. Kesselring. Pharm. Acta Helv. **68**, 49 (1993).
20. J.R. Powell, D. Voisinet, A. Salazar, and W.E. Acree, Jr. Phys. Chem. Liq. **28**, 269 (1994).
21. K.A. Fletcher, S. Pandey, M.E.R. McHale, and W.E. Acree, Jr. Phys. Chem. Liq. **33**, 181 (1996).
22. W.E. Acree, Jr. Thermochim. Acta, **189**, 37 (1991).
23. P.L. Huyskens and M.C. Haulait-Pirson. J. Mol. Liq. **31**, 135 (1985).

Can. J. Chem. Downloaded from www.nrcresearchpress.com by 92.62.229.171 on 09/08/12
For personal use only.

© 1997 NRC Canada

Chemical modification of chlorophyll *a*: synthesis of new regiochemically pure benzoporphyrin and dibenzoporphyrin derivatives

Lifu Ma and David Dolphin

Abstract: Starting from pheophorbide *a* methyl ester (**5**), a degradation product of chlorophyll *a*, routes for the preparation of 3-vinylporphyrins **6** and **9** and of an [A,C]-divinylporphyrin **16** are described. These porphyrins were obtained as a result of chemical modification of **5** on ring D and the exocyclic ring E. Diels–Alder reactions of these (di)vinylporphyrins with dimethyl acetylenedicarboxylate, to afford new regiochemically pure benzoporphyrin derivatives **29** and **30** and dibenzoporphyrin derivative **33** for potential use as sensitizers in photodynamic therapy of tumors, were also investigated.

Key words: Diels–Alder, (di)vinylporphyrins, (di)benzoporphyrins, photodynamic therapy, chlorophyll.

Résumé : On décrit des voies de synthèse pour la préparation des 3-vinylporphyrines **6** et **9** et d'une [A,C]-divinylporphyrine (**16**) à partir de l'ester méthylique de l'acide phéophorbide *a* (**5**). On a obtenu ces porphyrines par modification chimique du cycle D et du cycle exocyclique E du produit **5**. On a aussi examiné les réactions de Diels–Alder de ces (di)vinylporphyrines avec l'acétylènedicarboxylate de diméthyle pour préparer les dérivés benzoporphyrines **29** et **30** et le dérivé dibenzoporphyrine **33** régiochimiquement purs, qui pourraient s'avérer utiles comme sensibilisateurs dans la thérapie photodynamique des tumeurs.

Mots clés : Diels–Alder, (di)vinylporphyrines, (di)benzoporphyrines, thérapie photodynamique, chlorophylle.

[Traduit par la rédaction]

Introduction

Among long-wavelength absorbing photosensitizers, chlorins and bacteriochlorins have received increasing attention as potential candidates for use in photodynamic therapy (PDT) since they absorb strongly in the red region (>670 nm) and thereby enable deeper penetration of light through tissues (1). Some naturally occurring chlorins and bacteriochlorins have previously been reported as effective photosensitizers both in vitro and in vivo (2). However, these compounds, by virtue of their di- and tetrahydro reduction states, can be readily oxidized back to the parent porphyrin accompanied by the loss of their long-wavelength absorption bands (3). This potential lack of stability has led us to examine other ways of producing chlorin-like and bacteriochlorin-like chromophores.

A number of years ago Johnson and co-workers (4) reported a facile synthesis of compounds possessing the chlorin-like chromophore by using the Diels–Alder reaction on vinylporphyrins. We extended this methodology to vinyl- and [A,C]-divinylporphyrins and prepared a series of benzoporphyrin derivatives (BPD) (5) and dibenzoporphyrin derivatives (DBPD) (6) (bacteriochlorins). In the BPD series, benzoporphyrin derivative monoacid A (BPD-MA) (**1**), a second-generation photosensitizer that has shown promising photophysical properties, is currently in Phase II clinical trials and has been proposed as a possible alternative to Photofrin™, a commercial variant of hematoporphyrin derivative, used in the clinic for the treatment of solid tumors (7). Preliminary biological evaluation also indicated that the dibenzoporphyrin (**2**) is highly photocytotoxic and has potential as a useful therapeutic compound (8).

Further biological investigation of DBPD (**2**) as a potential phototoxin in PDT was complicated by problems associated with the availability of the [A,C]-divinylporphyrin **3** since the total synthesis of **3**, via a stepwise route from pyrrolic precursors using the MacDonald dipyrromethane approach, requires a large number of steps and therefore considerable effort in order to obtain the quantities required for biological investigations (6, 9). For the synthesis of BPD-MA (5), protoporphyrin IX dimethyl ester (**4**) is reacted with dimethyl acetylenedicarboxylate (DMAD) in refluxing toluene (Scheme 1). The ring A Diels–Alder adduct (i.e., 1,4-cyclohexadiene derivative) is then separated by crystallization from the ring B adduct and is subsequently rearranged with base (DBU). The rearranged

Received March 26, 1996.[1]

L. Ma[2] and D. Dolphin.[3] Department of Chemistry, The University of British Columbia, 2036 Main Mall, Vancouver, BC, V6T 1Z1, Canada.

[1] Revision received November 20, 1996.

[2] Present address: Howard Hughes Medical Institute, Department of Chemistry, University of California, Berkeley, CA 94720, U.S.A.

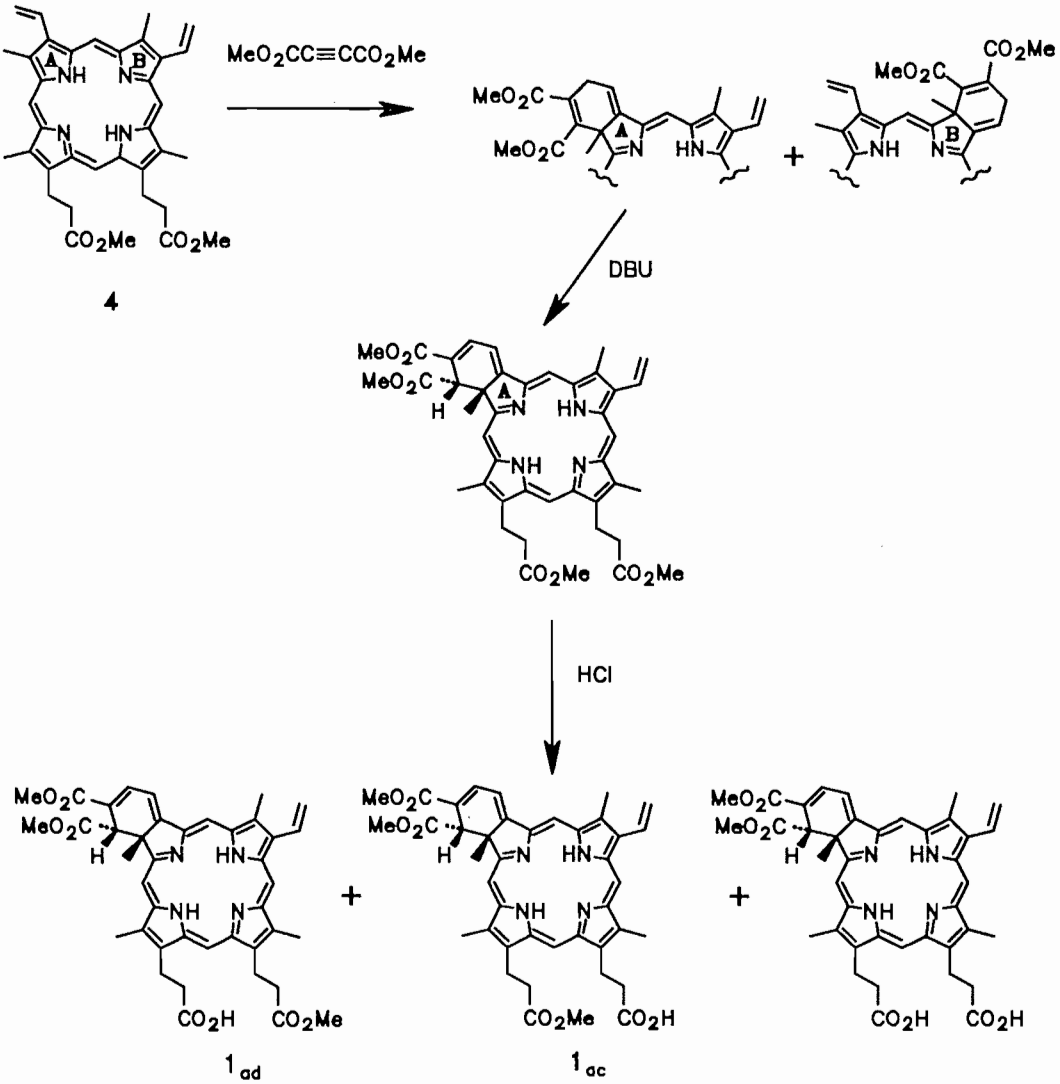
[3] Author to whom correspondence may be addressed. Telephone: (604) 822-4571. Fax: (604) 822-9678. E-mail: david@dolphin.chem.ubc.ca

© 1997 NRC Canada

Can. J. Chem. Downloaded from www.nrcresearchpress.com by 88.146.161.215 on 09/08/12
For personal use only.

Can. J. Chem. Downloaded from www.nrcresearchpress.com by 88.146.161.215 on 09/08/12
For personal use only.

Scheme 1



ring "A" 1,3-cyclohexadiene derivative is then partially hydrolyzed to afford, after purification, the two regioisomers, $\mathbf{1}_{ac}$ and $\mathbf{1}_{ad}$, which are used for biological studies (5). From the biological data reported so far, photodynamic activity is maximized for BPD when: (*a*) "ring A" of the porphyrin nucleus is modified by the Diels–Alder cycloaddition – base rearrangement procedure; (*b*) only one of the two methyl propionate groups is hydrolyzed to the free acid (7).

To eliminate the problem of regioisomer formation in the preparation of BPD-MA, we sought to acquire vinylporphyrins that contain one vinyl group (in ring A) and one propionic side chain. Similar studies were recently reported by Pandey et al. after the submission of this paper (10). These vinylporphyrins should thus afford regiochemically pure BPD-MA derivatives and would subsequently lead to less ambiguity at the biological screening stage. Further, it was envisioned that performing a partial synthesis of [A,C]-divinylporphyrins, from readily available natural tetrapyrroles, might facilitate and greatly simplify the synthetic sequence to [A,C]-divinylporphyrins.

Results and discussion

With our recent progress on chemical modifications of chlorophyll derivatives on ring D and the exocyclic ring E (11–15), the way was opened for synthesis of vinylporphyrins and [A,C]-divinylporphyrins from a chlorophyll degradation product. More specifically, these studies demonstrated the feasibility of transforming pheophorbide *a* methyl ester (**5**), readily available from the blue alga, *Spirulina maxima*, into 3-vinylporphyrin **6** (13). This substance, with a vinyl group at position 3, will produce only a ring "A" chlorin (after the Diels–Alder reaction) and only one propionic ester side chain, which can be hydrolyzed to the corresponding monocarboxylic acid at the final step of the synthesis, and serves as an ideal precursor to a regiochemically pure BPD-MA derivative. As a

© 1997 NRC Canada

Can. J. Chem. Downloaded from www.nrcresearchpress.com by 88.146.161.215 on 09/08/12
For personal use only.

continuation of our research on chemical modifications of chlorophyll *a*, pheophorbide *a* methyl ester (**5**) was chosen as the key intermediate in this work.

A. Preparation of 3-vinylporphyrins 6 and 9

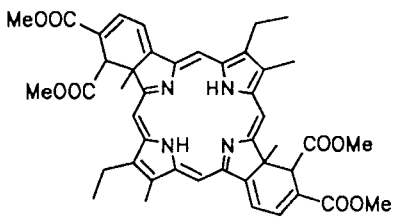
3-Vinylporphyrin **6** was obtained by the direct transformation of 13^1-hydroxychlorin **7** using a procedure described in a recent report (13). Demethoxycarbonylation of pheophorbide *a* methyl ester (**5**) in collidine afforded pyropheophorbide *a* methyl ester (**8**), which was reduced by NaBH4 to give a diastereomeric mixture of 13^1-deoxo-13^1-hydroxypyropheophorbide *a* methyl ester (**7**). Reaction of **7** with 1.2 equivalents benzoyl chloride in DMF gave vinylporphyrin **6** in 73% yield after recrystallization from dichloromethane–hexane.

3-Vinylrhodoporphyrin XV dimethyl ester (**9**), another substrate suitable for the synthesis of regiochemically pure BPD derivatives, was prepared from the oxidation of purpurin-7 trimethyl ester (**10**) (16), which was obtained from two routes. Thus, pheophorbide *a* methyl ester (**5**) was transformed into **10** by dissolution in pyridine, dilution with ether, and addition of KOH in *n*-propanol. After aeration for 30 min Fischer's "unstable chlorin" was obtained (16). Esterification of "unstable chlorin" (**11**) with diazomethane gave purpurin-7 trimethyl ester (**10**). The overall yield from **5** was 58%. Deglyoxylation and concomitant oxidation of purpurin-7 trimethyl ester in collidine furnished a 76% yield (44% overall yield from **5**) of 3-vinylrhodoporphyrin XV dimethyl ester (**9**).

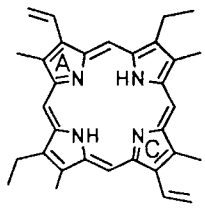
One important characteristic of the above method is that **11** was somewhat unstable and had a tendency to oxidize further in the aerial oxidation step. The esterification with diazomethane therefore produced both purpurin-18 methyl ester (**12**) in addition to the desired purpurin-7 trimethyl ester (**10**). Separation of purpurin-18 methyl ester from purpurin-7 trimethyl ester by chromatography is difficult due to their very close structures and polarities. Based on our synthetic methods (11, 12, 14) developed in the research of natural antioxidative chlorins, an alternate route to synthesize purpurin-7 trimethyl ester (**10**) was via 15^1-hydroxypurpurin-7-lactone methyl ester (**13**). Hydroxylation (14) of pheophorbide *a* methyl ester (**5**) using commercially available (−)-(1*R*)-(10-camphorsulfonyl)oxaziridine and 1,8-diazabicyclo[5.4.0]-undec-7-ene (DBU) (17) gave 13^2*R*-hydroxypheophorbide *a* methyl ester (**14**(*R*)) (90% d.e.) in 94% yield. Periodate oxidation of 13^2*R*-hydroxypheophorbide *a* methyl ester to 15^1-hydroxypurpurin-7-lactone methyl ester, followed by esterification with diazomethane, gave purpurin-7 trimethyl ester (**10**) in 79% yield (73% overall yield from **5**). This route has the advantages of higher yield and facile separations although it necessitates two extra steps compared to the original aerial oxidation of pheophorbide *a* methyl ester.

B. Synthesis of [A,C]-divinylporphyrin 16 via 3-vinylpurpurin 15

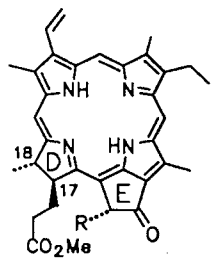
Attention was then focused on the development of a new and efficient route to obtain an [A,C]-divinylporphyrin from a chlorophyll derivative. To keep the number of chemical modifications involved in this sequence to a minimum, 3-vinylpurpurin **15** was chosen as the required precursor to an [A,C]-divinylporphyrin. With a 3-vinyl group at ring A and a 13-formyl group at ring C, purpurin **15** was subjected to a Wittig olefination reaction on the 13-formyl group to form a second vinyl group at ring C and, after further decarboxylation and oxidation, to give the desired target [A,C]-divinylporphyrin **16**. It was reasoned that the glyoxylic ester group at position 15 of the purpurin **15** could be lost with concomitant oxidation of the chlorin macrocycle into the porphyrin **17** in a one-pot procedure as was used in the transformation of purpurin-7 trimethyl ester (**10**) into



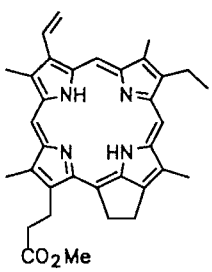
2



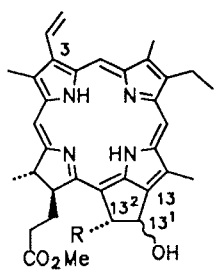
3



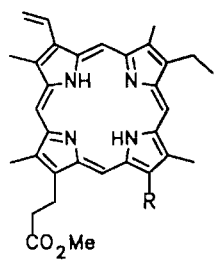
5. R=COOMe
8. R=H



6

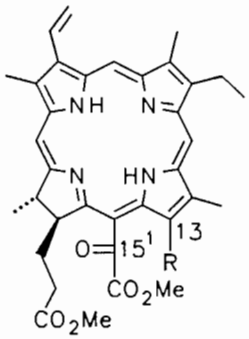


7. R=H
20. R=COOMe

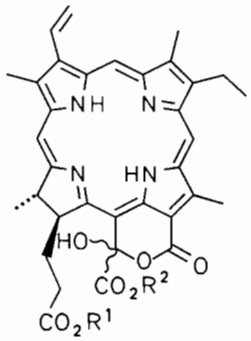


9. R=COOMe
17. R=CHO

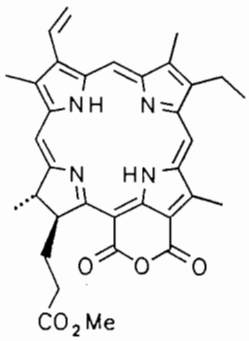
© 1997 NRC Canada



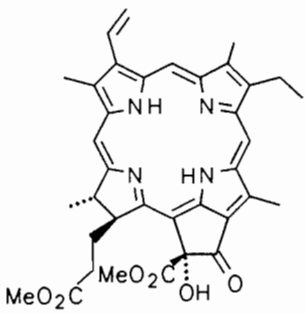
10. R=COOMe
15. R=CHO



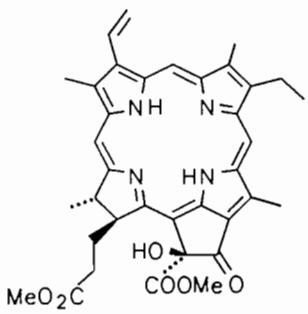
11. $R^1=R^2=H$
13. $R^1=R^2=Me$



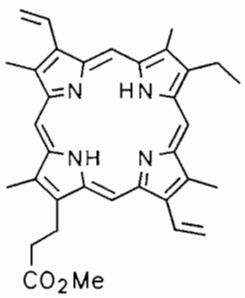
12



14 *(R)*



14 *(S)*



16

3-vinylrhodoporphyrin XV dimethyl ester (**9**) (18) in collidine at 170°C. Further, Wittig olefination of the resulting **17** with methylene triphenylphosphorane would furnish the desired [A,C]-divinylporphyrin **16**. Alternatively the [A,C]-divinylporphyrin **16** may be formed first by a Wittig olefination of the purpurin **15**, to furnish the [A,C]-divinylpurpurin **18**, followed by deglyoxylation of the ester and oxidation in situ in refluxing collidine. Both pathways appeared plausible because of the known transformation procedures and the ready availability of the starting material **15** from the synthetic method described above.

For the preparation of 3-vinylpurpurin **15**, two synthetic pathways were investigated and the one giving the higher overall yield was subsequently used to make **15** on a 400 mg scale. Initially, 3-vinylpurpurin **15** was derived from the photooxidation of 13^1-deoxo-13^1,13^2-dehydropheophorbide *a* methyl ester (**19**) (13). In this synthetic approach, the first step was $NaBH_4$ reduction of pheophorbide *a* methyl ester (**5**) to give a diastereomeric mixture of 13^1-deoxo-13^1-hydroxypheophorbide *a* methyl ester (**20**) (13, 19), followed by elimination of a molecule of trifluoroacetic acid (via proton sponge), to provide the desired compound **19** in 80% yield. Although **19** (mp >300°C) has high thermal stability, it is extremely photosensitive, and reaction (in dichloromethane solution) in air with sunlight (20 min) oxidatively cleaved the 13^1-13^2 double bond to quantitatively give vinylpurpurin **15**. In a second method, 3-vinylpurpurin **15** was derived from the periodate oxidation of the diastereomeric mixture, 13^2-deoxo-13^1-hydroxy-13^2R-hydroxypheophorbide *a* methyl ester (**21**), which was in turn obtained from the $NaBH_4$ reduction of 13^2R-hydroxypheophorbide *a* methyl ester (**14**(*R*)) (13). Using this second method, purpurin **15** has been obtained in 67% overall yield from pheophorbide *a* methyl ester (**5**), in contrast to an 80% overall yield from **5** in the first method by means of photooxidation.

When purpurin **15** was heated in collidine at 170°C for 45 min, 13-decarboxy-13-formyl-3-vinylrhodoporphyrin XV methyl ester (**17**) was obtained in only 15% yield; the remainder of the starting material decomposed or was overoxidized under these conditions. Attempts to avoid these side reactions by reducing reflux time and temperature (using pyridine instead of collidine) were all unsuccessful. The problem seemed to be due to the susceptibility of the 13-formyl group, which led to overoxidation during the purpurin-into-porphyrin conversion. Protection of the 13-formyl function to circumvent this unwanted side reaction was therefore considered

© 1997 NRC Canada

Can. J. Chem. Downloaded from www.nrcresearchpress.com by 88.146.161.215 on 09/08/12
For personal use only.

Can. J. Chem. Downloaded from www.nrcresearchpress.com by 88.146.161.215 on 09/08/12
For personal use only.

next. The ethylene acetal **22** was readily formed in 90% yield by heating purpurin **15** with ethylene glycol in THF and *p*-toluenesulfonic acid as catalyst. The salient features of the electronic spectrum of acetal **22** (λ_{max} = 660 nm), which looks similar to such hydroxychlorins as **7** and **20**, are the hypsochromic shift of its Q band (λ_{max} = 660 nm) in comparison with that of the purpurin **15** (λ_{max} = 686 nm) and the appearance of a strong absorption band at 496 nm, which suggested that the electron-withdrawing group at C-13 was removed.

Unfortunately, when the ethylene acetal **22** was refluxed in collidine even for 4 h, no reactions occurred and the starting material was recovered. Various attempts to achieve the purpurin-into-porphyrin conversion for the ethylene acetal **22** were all unsuccessful. It appears that an electron-withdrawing group at position 13 is required for the loss of the 15-glyoxylic ester group and concomitant oxidation of a purpurin macrocycle to a porphyrin, as observed with purpurin-7 trimethyl ester (**10**) and purpurin **15**. The key reason appears to be the dramatic change in the oxidation potential of the ethylene acetal **22** with the protection of the 13-formyl group. The presence of an electron-withdrawing group at position 13 in these purpurins seems to render the molecule easier to oxidize than the corresponding protected derivative.

The conversion of purpurin-7 trimethyl ester (**10**) into 3-vinylrhodoporphyrin XV dimethyl ester (**9**) was originally investigated by Fischer and Orth (20), who found the loss of the glyoxylic ester residue from purpurin-7 trimethyl ester (**10**) occurred upon refluxing in pyridine. Later, Kenner et al. (18) reported that the use of refluxing collidine in place of pyridine results in higher yield for the purpurin-into-porphyrin conversion, because prolonged reflux in pyridine often gives rise to decomposition products. Interestingly, we found that the presence of oxygen in the reaction medium has a beneficial effect on the conversion, but is not required, since the conversion was also observed under oxygen-free conditions.

Given the anticipated difficulty in the purpurin-into-porphyrin conversion for the [A,C]-divinylpurpurin **18**, a purpurin with a non-electron-withdrawing group (i.e., vinyl) at position 13, the planned synthetic route to [A,C]-divinylporphyrin **16** via the [A,C]-divinylpurpurin **18** was abandoned. Finally, we came back to the direct conversion of purpurin **15** and prepared sufficient 13-decarboxy-13-formyl-3-vinylrhodoporphyrin XV methyl ester (**17**) by refluxing purpurin **15** in collidine. Treatment of **17** with zinc(II) acetate in methanol–dichloromethane gave a zinc complex, which was subjected to a Wittig reaction to give, after removal of the zinc by treatment with trifluoroacetic acid, a 71% yield of the desired [A,C]-divinylporphyrin **16**. With this synthetic approach the [A,C]-divinylporphyrin **16** was obtained in six steps from pheophorbide *a* methyl ester (**5**) in 9% overall yield. Compound **16** has a very similar electronic absorption spectrum to that of the divinylporphyrin **3** reported by Dolphin and coworkers (6).

C. Synthesis of [A,C]-divinylporphyrin 16 via porphyrin 9

At this point, it was felt that the 15% yield of the formylrhodoporphyrin XV (**17**) obtained by the oxidation and deglyoxylation of purpurin **15** in collidine was unsatisfactory and should be improved upon by pursuing an alternative approach. Previous studies led us to conclude that the 13-methoxycarbonyl group and other (non-formyl) groups are advantageous in this regard. 3-Vinylrhodoporphyrin XV dimethyl ester (**9**) was chosen as the starting material since it is readily available from the oxidation of purpurin-7 trimethyl ester (**10**) as described above.

In this approach, 3-vinylrhodoporphyrin XV dimethyl ester (**9**) was hydrolyzed to its diacid form and was partially remethylated on the propionic side chain using 5% H_2SO_4 in methanol to give the 3-vinylrhodoporphyrin XV monomethyl ester (**23**) in 70% overall yield (21). The resulting monomethyl ester (**23**) was added to a solution of *N,N'*-carbonyldiimidazole in THF and heated to reflux for 30 min (22). The desired imidazolide **24** was obtained in 91% yield after flash chromatography on silica gel. The nucleophilic displacement (21) of the imidazolide **24** with the magnesium salt of methyl hydrogen malonate (23) gave the expected β-keto-ester **25** in 70% yield. This step was based on a method that was introduced by Bram and Vilkas (23) and later improved by Kenner and coworkers (21). The magnesium salt of methyl hydrogen malonate was prepared by treatment of methyl hydrogen malonate with 2 equivalents of isopropylmagnesium bromide in THF. The advantage of this procedure was its selectivity, which allowed the reaction to proceed without deprotonation of the porphyrin macrocycle to the green dianion.

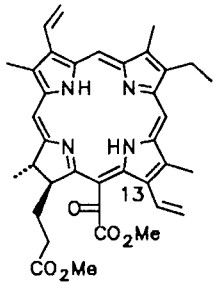
With the enolizable β-keto-ester **25** in hand, we were able to attempt the decarboxylation step. A high yield of the desired acetylporphyrin **26** was obtained by modifying the decarboxylation method described by Taber et al. (24). In this reaction, the β-keto-ester **25** was stirred in a solution of 4-(dimethylamino)pyridine (4-DMAP) in phosphate buffer (pH = 7) at 90°C for 12 h under nitrogen to effect the demethoxycarbonylation (75% yield). The progress of the reaction was monitored by TLC and its completion was indicated by the disappearance of the less mobile enolizable β-keto-ester **25**. The electronic spectrum of this compound was almost the same as that of the imidazoylporphyrin **24** (oxorhodo-type spectrum). The ^{1}H NMR spectrum of porphyrin **26** showed the H-13^2 (i.e., 13-$COCH_3$) appearing as a singlet at δ 3.32 ppm. This observation indicated the presence of the desired 13-$COCH_3$ moiety.

The acetylporphyrin **26** was reduced with $NaBH_4$ in THF to give the expected hydroxyporphyrin **27**. With the absence of an electron-withdrawing group at position 13, hydroxyporphyrin **27** exhibited a rhodo-type electronic spectrum in contrast to an oxorhodo-type spectrum in the starting material **26**, suggesting that only one rhodofying group (i.e., the 3-vinyl moiety) was present in the molecule. The last step in the synthetic sequence involved the generation of the 13-vinyl group. This transformation was achieved by subjecting the hydroxyporphyrin **27** to benzoyl chloride in DMF at 105°C for 2 h (25). Under these conditions, the hydroxyporphyrin **27** was dehydrated to give the desired [A,C]-divinylporphyrin **16** in 60% yield after chromatography. This material was found to be identical to the divinylporphyrin prepared from the Wittig reaction of 13-formylporphyrin **17**. With this synthetic approach, the [A,C]-divinylporphyrin **16** was prepared in nine steps from pheophorbide *a* methyl ester (**5**) in 12% overall yield.

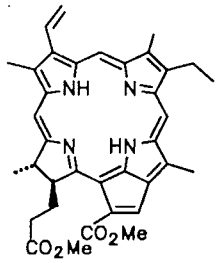
Diels–Alder reactions on vinylporphyrins

Porphyrin **9** was heated in degassed toluene at 110°C with a 50-fold molar excess of DMAD for 28 h and afforded the

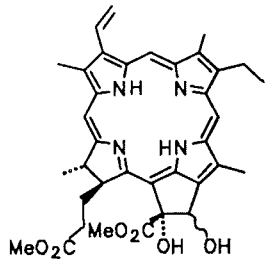
© 1997 NRC Canada



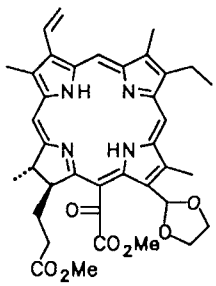
18



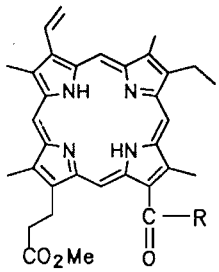
19



21



22

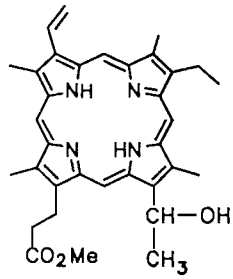


23. R=OH

24. R= 

25. R=CH_2COMe

26. R=Me



27

cycloadduct **28** in 50% yield. The ring A 1,4-cyclohexadiene derivative **28** was treated with DBU in dichloromethane to provide the chlorin-like BPD 1,3-cyclohexadiene dimethyl ester **29** in 90% yield after chromatography (45% overall yield from **9**). This rearrangement gave the thermodynamically more stable product, i.e., the carbomethoxy substituent attached at 2^1 and the angular methyl group located at C-2 are in a *trans* orientation. This *transoid* orientation was confirmed by a positive nOe effect observed for the C-2^1 proton (δ 5.04 ppm) and the methyl group at C-2 (δ 1.79 ppm).

The absorption spectrum (Fig. 1) of BPD **29** is characteristic of a chlorin-like chromophore but it has an unusually broad Soret band and the lowest energy absorption (Q band) at 672 nm (ε 14 600) is blue-shifted some 18 nm in comparison with that (690 nm) (5) of BPD-MA. This difference is due to the presence of an 8-vinyl group in BPD-MA, which extends the conjugation of the molecule. Pandey et al. (26) have recently exploited chemistry similar to that described above, and obtained a similar Diels–Alder adduct **29** from 3-vinylrhodoporphyrin XV dimethyl ester and DMAD. However, these authors reported a 23% overall yield (**29** from **9**) in contrast to a 45% total yield for the same reaction sequence in our hands.

For the preparation of BPD **30**, reaction of porphyrin **6** with DMAD in refluxing toluene under nitrogen gave the desired chlorin **31** in 42% yield. Compound **31** was then treated with DBU in dichloromethane to provide the fully conjugated chlorin **30** in 91% yield (36% overall yield) after chromatography. The reaction progress was monitored by UV–VIS spectroscopy, which showed a new absorbance at 686 nm (ε 37 000) (Fig. 1) and the disappearance of the peak at 648 nm of compound **31**.

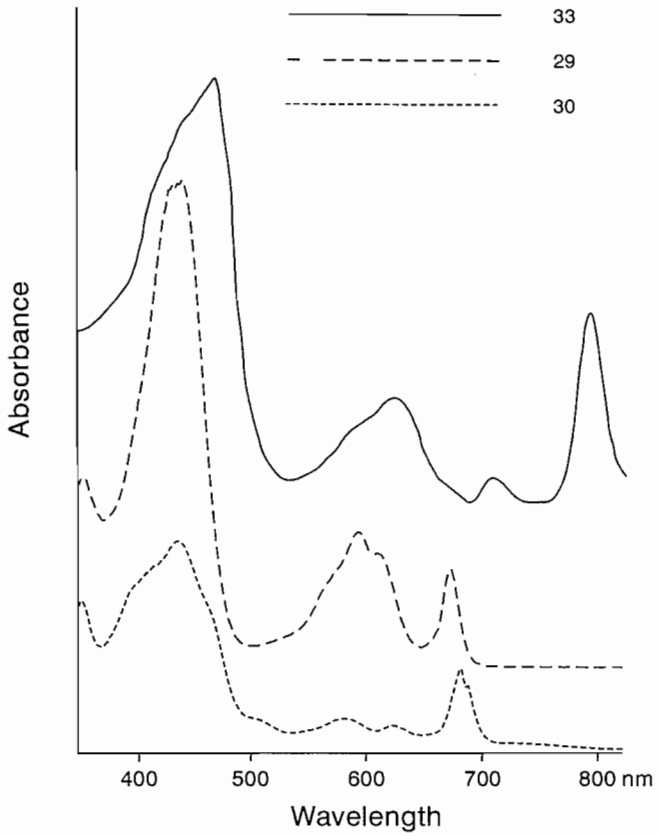
As has already been mentioned, the synthetic strategy for the [A,C]-dibenzoporphyrin derivative relied on two cycloaddition reactions on an [A,C]-divinylporphyrin system. Refluxing the [A,C]-divinylporphyrin **16** with 100-fold molar excess of DMAD in toluene for 3 days gave a mixture with a strong absorption at 720 nm, a bacteriochlorin-like chromophore. The desired bis-adduct **32** was obtained as the major product along with a small amount of chlorin in which only one of the vinyl groups (either ring A and ring C) was transformed (identified by spectrophotometry). The best reaction time was found to be 80 h with a yield of ~30%, while prolonged reflux resulted in decomposition and thus gave the product **32** in a lower yield. Flash chromatography on a silica gel column followed by further purification by preparative TLC plate gave the bis-adduct **32** in 25% yield.

Can. J. Chem. Downloaded from www.nrcresearchpress.com by 88.146.161.215 on 09/08/12
For personal use only.

© 1997 NRC Canada

Can. J. Chem. Downloaded from www.nrcresearchpress.com by 88.146.161.215 on 09/08/12
For personal use only.

Fig. 1. UV–VIS spectra (CH_2Cl_2) of regiochemically pure benzoporphyrin derivatives **29** and **30**, and [A,C]-dibenzoporphyrin derivative **33**.



When the above bis-adduct **32** was stirred overnight with DBU at room temperature, a dramatic bathochromic shift was observed (λ_{max} = 784 nm, ε = 38 000) (Fig. 1). This [A,C]-dibenzoporphyrin derivative **33** showed almost the same electronic spectrum as the DBPD **2** reported by Dolphin and coworkers (6). The most significant features in the ^{1}H NMR spectrum of the new adduct **33** were the appearance of a signal at δ 4.89 ppm for the new sp^3 center generated at C-2^1 and C-12^1 and two doublets at δ 7.30 and δ 7.81 ppm for the new sp^2 centers. This observation indicated an isomerization of the double bonds in both 1,4-cyclohexadienes, thus extending the conjugation in the molecule.

As described earlier, the monocarboxylic acid analogue of benzoporphyrin derivative BPD-MA shows better photosensitizing efficacy than its corresponding diester. Therefore, to parallel the structural requirements for this biologically active benzoporphyrin derivative and to satisfy our originally planned goals, the new regiochemically pure benzoporphyrin derivatives **29** and **30**, and the [A,C]-dibenzoporphyrin derivative **33** were partially hydrolyzed with 25% HCl at the propionic ester side chain to afford the corresponding monocarboxylic acids **34**, **35**, **36** (i.e., propionic acid analogues). These monocarboxylic acids, together with their corresponding esters described herein, are being evaluated for their photodynamic ability.

Conclusion

Two series of new regiochemically pure benzoporphyrin derivatives **29** and **30** have been synthesized from Diels–Alder reactions on 3-vinylrhodoporphyrin XV dimethyl ester (**9**) and 3-vinylporphyrin (**6**) with dimethyl acetylenedicarboxylate. The corresponding monocarboxylic analogues of these new regiochemically pure BPDs have been prepared by partial hydrolysis. These new photosensitizers have characteristics that meet or exceed the promising chemical features of BPD-MA, a second-generation photosensitizer in Phase-II clinical trials. The [A,C]-divinylporphyrin **16** was synthesized via two routes and its Diels–Alder reaction with dimethyl acetylenedicarboxylate was studied. The resulting bis-adduct **33**, being a stable bacteriochlorin-like chromophore, absorbs strongly at 784 nm, a fact that, according to current thinking, renders it eminently desirable as a photosensitizer for treatment of large tumors or tumors that are deeply seated within the body.

In conclusion, the present work has led to the synthesis of a class of compounds, via chemical modifications of chlorophyll *a*, with potential as future drugs in the field of photodynamic therapy.

Experimental

General procedures

Melting points were measured on a Thomas–Bristoline microscopic hot stage apparatus and are uncorrected. ^{1}H NMR spectra were recorded using a Bruker WH-400 or Bruker AC-200 spectrometer and ^{13}C NMR spectra were run on a Varian XL-300 or a Bruker AMX-500 spectrometer (residual $CHCl_3$ as internal standard, δ_H 7.24 ppm, δ_C 77.0 ppm). Silica gel 60 (70–230 mesh, Merck; usually silica III, i.e., deactivated with 6% water, or silica V, i.e., deactivated with 15% water) or neutral alumina (usually Brockman Grade III, deactivated with 6% water, or Brockman Grade V, deactivated with 15% water) was used for column chromatography. Preparative thin-layer chromatography was carried out on 20 × 20 cm glass plates coated with Merck G_{254} silica gel (0.5 mm, 1 mm thick). The deactivated silica gel plates, when necessary, were prepared by a blank development with 10% methanol in dichloromethane followed by air drying before use. Electronic absorption spectra were measured using a HP 8452A diode array spectrophotometer. Mass spectra were recorded by fast atom bombardment (FAB) and electron impact (EI). Elemental analyses were carried out in the departmental microanalytical laboratory at UBC using a Carlo Erba elemental analyzer 1106. Reactions were monitored by TLC and spectrophotometry and were carried out under nitrogen and in the dark. Pheophorbide *a* methyl ester (**5**) was obtained from *Spirulina maxima* alga using a literature method (15). Pyropheophorbide *a* methyl ester (**8**) was obtained (98% yield) from decarboxylation of pheophorbide *a* methyl ester (**5**) in collidine (15, 27). Tetrahydrofuran (THF) and dioxane were dried overnight with calcium hydride and distilled from sodium wire and benzophenone; other solvents were of reagent grade.

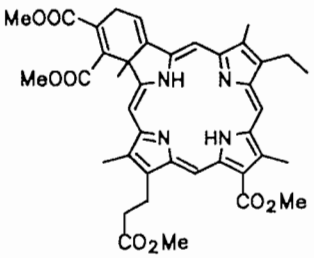
Synthesis of 3-vinylporphyrins 6 and 9

13^1-Deoxo-13^1-hydroxypyropheophorbide a *methyl ester (7)*

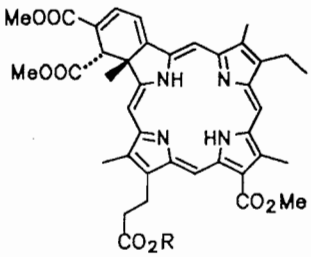
Pyropheophorbide *a* methyl ester (**8**) (150 mg, 0.274 mmol)

© 1997 NRC Canada

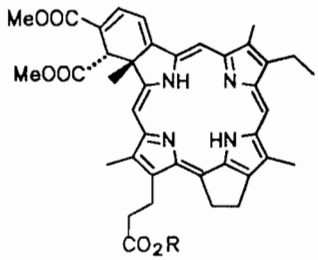
Can. J. Chem. Downloaded from www.nrcresearchpress.com by 88.146.161.215 on 09/08/12
For personal use only.



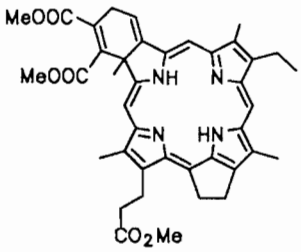
28



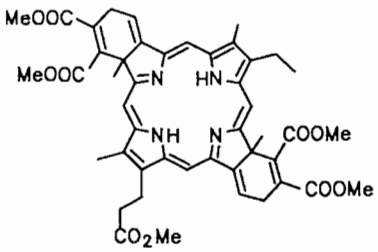
29. R=Me
34. R=OH



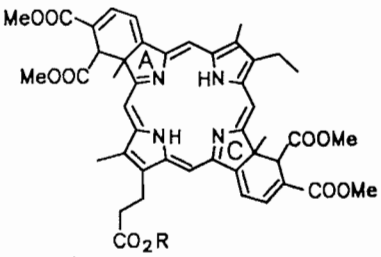
30. R=Me
35. R=OH



31



32



33. R=Me
36. R=OH

was dissolved in 100 mL of pyridine–methanol solution (pyridine:methanol = 1:1) and the solution was stirred at room temperature. $NaBH_4$ (200 mg) was added and the reaction mixture was stirred for 2 h, at which time the UV–VIS spectrum indicated no more starting material. The green reaction mixture was poured into cooled 2 N HCl and the chlorin was extracted with CH_2Cl_2. The organic layer was carefully washed once with water, twice with saturated $NaHCO_3$, three times with water, and then dried over anhydrous Na_2SO_4, filtered, and evaporated. The residue was purified by flash chromatography on silica III, eluting with 1% MeOH in CH_2Cl_2. The main band was collected, evaporated, and recrystallized from CH_2Cl_2–hexane to give the title compound (129 mg, 86% yield) as a dark-green powder; mp 178–180°C; UV–VIS λ_{max} (CH_2Cl_2): 402 nm (ε 117 600), 502 (9100), 654 (32 900); ^{1}H NMR (200 MHz, $CDCl_3$) δ: 9.98 (s, 1H, H-10), 9.82 (s, 1H, H-5), 9.05 (s, 1H, H-20), 8.30 (dd, 1H, H-3^1), 6.45 (dd, 1H, H-3^2(*E*)), 6.32 (s, 1H, H-3^2(*Z*)), 6.27 (dd, 1H, H-13^1), 5.30 (m, 1H, H-13^1), 4.48 (m, 2H, 13^2), 4.20 (m, 1H, H-18), 4.10 (m, 1H, H-17), 3.90 (q, 2H, H-8^1), 3.83, 3.72, 3.65, 3.40, 3.15 (5s, 12H, H-2^1, H-7^1, H-12^1, and H-17^4), 2.70 (m, 2H, H-17^1), 2.30 (m, 2H, H-17^2), 1.95 (d, 3H, H-18^1), 1.82 (t, 3H, H-8^2), −1.40 (br s, 1H, NH), −3.10 (br s, 1H, NH); LREIMS (*m/z*): 550 (M^+, 5%), 532 ($M^+ - H_2O$, 100%); LRFABMS (*m/z*): 551 ([M + H]$^+$, 100%); HREIMS, $C_{34}H_{36}N_4O_2$ ([M − H_2O]$^+$), calcd.: 532.2838; obsd.: 532.2828; HRFABMS, $C_{34}H_{39}N_4O_3$ ([M + H]$^+$), calcd.: 551.3021; obsd.: 551.3019.

*3-Vinyl-13^1-deoxo-phytoporphyrin methyl ester (**6**)*

13^1-Deoxo-13^1-hydroxypyropheophorbide *a* methyl ester (**7**) (105 mg, 0.191 mmol) was dissolved in dry DMF (50 mL) and the solution was stirred at 100°C under N_2. Benzoyl chloride (0.250 mmol) was added via a syringe and the reaction mixture (which turned red after 40 min) was stirred at this temperature for a further 120 min, at which time the UV–VIS spectrum indicated no more starting material. The reaction mixture was poured into ice-cooled 10% NaOH and the porphyrin was extracted with CH_2Cl_2. The organic layer was washed three times with water, and then dried over anhydrous Na_2SO_4, filtered, and evaporated. The residue was purified by flash chromatography on silica, eluting with CH_2Cl_2. The main band was collected, evaporated, and the residue was recrystallized from CH_2Cl_2–hexane to give the title compound (74.0 mg, 73% yield) as a purple solid; mp >300°C; UV–VIS λ_{max} (CH_2Cl_2): 404 nm (ε 161 300), 504 (15 900), 540 (7800), 566 (8300), 620 (5800); ^{1}H NMR (400 MHz, $CDCl_3$) δ: 10.10 (s, 1H, H-10), 9.99 (s, 1H, H-5), 9.93 (s, 1H, H-20), 8.26 (dd, 1H, H-31, *J* = 17.9 and 11.6 Hz), 6.27 (dd, 1H, H-3^2(*E*), *J* = 17.9 and 1.7 Hz), 6.11 (dd, 1H, H-3^2(*Z*), *J* = 11.6 and 1.7 Hz), 5.20 (br s, 2H, H-13^2), 4.25 (t, 2H, H-17^1, *J* = 8.3 Hz), 4.10

© 1997 NRC Canada

Can. J. Chem. Downloaded from www.nrcresearchpress.com by 88.146.161.215 on 09/08/12
For personal use only.

(q, 2H, H-8^1, J = 7.1 Hz), 3.96 (br s, 2H, H-13^1), 3.78 (s, 3H, H-12^1), 3.65 (s, 6H, H-17^4 and H-7^1), 3.59 (s, 3H, H-18^1), 3.52 (s, 3H, H-2^1), 3.03 (t, 2H, H-17^2, J = 8.3 Hz), 1.86 (t, 3H, H-8^2, J = 7.1 Hz), −3.02 (br s, 1H, NH), −3.89 (br s, 1H, NH); LREIMS (*m/z*): 532 (M^+, 100%), 459 ($M^+ - CH_2COOMe$, 47%); HREIMS, $C_{34}H_{36}N_4O_2$ (M^+); calcd.: 532.2838, obsd.: 532.2835; Anal. calcd. for $C_{34}H_{36}N_4O_2$: C 76.66, H 6.81, N 10.52%; found: C 76.50, H 6.85, N 10.58%.

*Purpurin-7 trimethyl ester (**10**) (14, 18, 28)*

Pheophorbide *a* methyl ester (**5**) (1.09 g, 1.75 mmol) was dissolved in warm pyridine (25 mL) and the solution was diluted with ether (700 mL). The solution was stirred with a stream of air passing through it, and a solution of potassium hydroxide (11.5 g) in *n*-propanol (40 mL) was added. The bright-green mixture (containing precipitated KOH) was stirred and aerated for 30 min and then extracted with water (2 × 300 mL). The ethereal solution was discarded; the aqueous extracts were combined, acidified with concentrated H_2SO_4 (11.5 mL) in water (60 mL), and then extracted with methylene chloride (2 × 350 mL). The extracts were washed with water (350 mL) and immediately treated with an excess of ethereal diazomethane. The brownish-purple solution was left at room temperature for 10 min, and then evaporated in vacuo. Chromatography (alumina V) of the residue (elution with methylene chloride) gave a major band that was collected, evaporated, and subjected to preparative TLC separation on deactivated silica plates (elution with 0.5% MeOH in CH_2Cl_2) to give the desired product (660 mg, 58% yield) after crystallization from CH_2Cl_2–hexane, along with 35 mg of a unseparated mixture of purpurin-18 methyl ester (**12**) and purpurin-7 trimethyl ester (**10**) as the other products.

*3-Vinylrhodoporphyrin XV dimethyl ester (**9**) (18)*

Purpurin-7 trimethyl ester (**10**) (450 mg, 0.69 mmol) was heated in an oil bath at 180–185°C in 2,4,6-collidine (60 mL) for 2 h. After cooling, the solvent was evaporated at 0.5 Torr (1 Torr = 133.3 Pa) and the residue was recrystallized from $CHCl_3$–CH_3OH, giving the title porphyrin (295 mg, 76%) as purple needles; mp 266–267°C (lit. (18) mp 271–272.5°C); UV–VIS λ_{max} (CH_2Cl_2): 408 nm (ε 187 000), 514 (10 000), 552 (20 000), 576 (11 000), 636 (1600); ^{1}H NMR (400 MHz, $CDCl_3$) δ: 10.81, 9.89, 9.82, 9.68 (4s, 4H, H-5, H-10, H-15, and H-20), 8.12 (dd, 1H, H-3^1, J = 18.4 and 11.8 Hz), 6.23 (dd, 1H, H-3^2(*E*), J = 18.4 and 1.6 Hz), 6.10 (dd, 1H, H-3^2(*Z*), J = 11.8 and 1.6 Hz), 4.42 (s, 3H, H-13^2), 4.30 (t, 2H, H-171, J = 8.0 Hz), 3.93 (q, 2H, H-8, J = 8.0 Hz), 3.84, 3.67, 3.52, 3.50, 3.48 (5s, 15H, H-2^1, H-7^1, H-12^1, H-18^1, and H-17^4), 3.23 (t, 2H, H-17^2, J = 8.0 Hz), 1.79 (t, 3H, H-8^2, J = 8.0 Hz), −4.50 (br s, 2H, NH); LREIMS (*m/z*): 564 (M^+, 100%); Anal. calcd. for $C_{34}H_{36}N_4O_4$: C 72.32, H 6.43, N 9.92%; found: C 71.98, H 6.45, N 9.65%.

Synthesis of [A,C]-divinylporphyrin 16 via purpurin 15

13^1-Deoxo-13^1-hydroxypheophorbide a *methyl ester (**20**)*

Pheophorbide *a* methyl ester (**5**) (100 mg, 0.16 mmol) was dissolved in 50 mL of pyridine–methanol solution (pyridine:methanol = 1:1) and the solution was stirred at room temperature. $NaBH_4$ (90 mg) was added and the reaction mixture was stirred for 2 h, at which time the UV–VIS spectrum indicated that the starting material had been consumed. The reaction mixture (bright green) was poured into cooled 2 N HCl and the chlorin was extracted with CH_2Cl_2. The green organic layer was carefully washed once with water, twice with saturated $NaHCO_3$, three times with water, and then dried over anhydrous Na_2SO_4, filtered, and evaporated. The residue was chromatographed on an alumina III column, eluting with 1% MeOH in CH_2Cl_2. The main band was collected, evaporated, and recrystallized from $CHCl_3$–hexane to give the required compound (83.7 mg, 86% yield) as a dark-green powder; mp 135-136°C; UV–VIS λ_{max} (CH_2Cl_2): 400 nm (ε 124 400), 498 (12 000), 656 (35 800); ^{1}H NMR (200 MHz, $CDCl_3$) δ (the major epimer): 9.84 (s, 1H, H-10), 9.60 (s, 1H, H-5), 8.88 (s, 1H, H-20), 8.20 (dd, 1H, H-3^1), 6.63 (dd, 1H, H-13^1), 6.34 (dd, 1H, H-3^2(*E*)], 6.18 (s, 1H, H-3^2(*Z*)), 5.90 (s, 1H, H-13^2), 4.60 (m, 1H, H-18), 4.45 (m, 1H, H-17), 3.81, 3.55, 3.55, 3.39, 3.22 (5s, 15H, H-2^1, H-7^1, H-12^1, H-13^4, and H-17^4), 3.80 (q, 2H, H-8^1), 2–2.70 (m, 4H, H-17^1 and H-17^2), 1.90 (d, 3H, H-18^1), 1.75 (t, 3H, H-8^2), −1.39 (br s, 1H, NH), −3.05 (br s, 1H, NH); LREIMS (*m/z*): 608 (M^+, 100%); HREIMS, $C_{36}H_{40}N_4O_5$ (M^+), calcd.: 608.2999; obsd.: 608.2993; Anal. calcd. for $C_{36}H_{40}N_4O_5$: C 71.03, H 6.62, N 9.20%; found: C 70.81, H 6.79, N 8.97%.

13^1-Deoxo-13^1,13^2-dehydropheophorbide a *methyl ester (**19**)*

13^1-Deoxo-13^1-hydroxypheophorbide *a* methyl ester (**20**) (50 mg, 0.0822 mmol) was dissolved in pyridine (20 mL) and the solution stirred at 0°C under N_2. Excess trifluoroacetylimidazole (150 mg) was added via a syringe and the reaction mixture was stirred for 5 mins. After addition of proton sponge (1.81 mmol), the reaction mixture was kept at 0°C for 30 min and then at 25°C for 3 h, at which time the UV–VIS spectrum indicated no more starting material. The reaction mixture (bright green) was poured into water and the chlorin was extracted with CH_2Cl_2. The green organic layer was washed three times with water, and then dried over anhydrous Na_2SO_4, filtered, and evaporated. The residue was chromatographed on a silica column eluting with CH_2Cl_2. The main band was collected, evaporated, and the residue was recrystallized from $CHCl_3$–MeOH to give the title compound (45.6 mg, 94% yield) as a dark-green powder; mp >300°C; UV–VIS λ_{max} ($CHCl_3$): 354 nm (ε 55 600), 434 (67 900), 586 (4100), 630 (11 600), 760 (4100), 820 (4100); ^{1}H NMR (400 MHz, 1.5 mg/0.6 mL $CDCl_3$) δ: 8.41(s, 1H, H-10), 8.33 (s, 1H, H-5), 7.42 (s, 1H, H-20), 7.42 (dd, 1H, H-3^1, J = 18.5 and 11.8 Hz), 7.19 (s, 1H, H-13^1), 6.01 [d, 1H, H-3^2(*E*), J = 18.5 Hz), 5.94 (d, 1H, H-3^2(*Z*), J = 11.8 Hz), 4.77 (d, 1H, H-17, J = 8.6 Hz), 3.93 (s, 3H, H-13^4), 3.77 (q, 1H, H-18, J = 8.5 Hz), 3.57 (s, 3H, H-17^4), 3.25 (q, 2H, H-8^1, J = 7.1 Hz), 2.96 (s, 3H, H-12^1), 2.91 (s, 3H, H-2^1), 2.80 (s, 3H, H-7^1), 2.44 (dd, 1H, H-17^1, J = 8.6 Hz), 2.20 (dd, 2H, H-17^2), 1.85 (dd, 1H, H-17^1), 1.69 (d, 3H, H-18^1, J = 8.5 Hz), 1.45 (t, 3H, H-8^2, J = 7.1 Hz); LREIMS (*m/z*): 590 (M^+, 100%); HREIMS, $C_{36}H_{38}N_4O_4$ (M^+); calcd.: 590.2893; obsd.: 590.2895; Anal. calcd. for $C_{36}H_{38}N_4O_4$: C 73.21, H 6.48, N 9.48%; found: C 72.73, H 6.53, N 9.21%.

*13^1-Deoxo-13^1-hydroxy-13^2*R*-hydroxypheophorbide* a *methyl ester (**21**)*

13^2*R*-Hydroxypheophorbide *a* methyl ester (**14**) (90% d.e.) (11, 14) (50 mg, 0.0803 mmol) was dissolved in 25 mL of

© 1997 NRC Canada

Can. J. Chem. Downloaded from www.nrcresearchpress.com by 88.146.161.215 on 09/08/12
For personal use only.

pyridine–methanol solution (pyridine:methanol = 1:1) and the solution was stirred at room temperature. $NaBH_4$ (70 mg) was added and the reaction mixture was stirred for 3 h, at which time the UV–VIS spectrum indicated the absence of starting material. The reaction mixture was poured into ice-cooled 2 N HCl and the chlorin was extracted with CH_2Cl_2. The organic layer was carefully washed once with water, twice with saturated $NaHCO_3$, three times with water, and then dried over anhydrous Na_2SO_4, filtered, and evaporated. The residue was purified by flash chromatography on silica III, eluting with 1% MeOH in CH_2Cl_2. The main band was collected (44.5 mg, 89% yield) and was analyzed by ^{1}H NMR to be a diastereomeric mixture of 56% 13^1-deoxo-13^1*R*-hydroxy-13^2*R*-hydroxypheophorbide *a* methyl ester (**21***RR*) and 44% 13^1-deoxo-13^1*S*-hydroxy-13^2*R*-hydroxypheophorbide *a* methyl ester (**21***SR*). Further purification of this diastereomeric mixture (20 mg) by preparative TLC on silica (developed by 2% MeOH, 5% acetone in dichloromethane) gave the optically pure 13^1-deoxo-13^1*R*-hydroxy-13^2*R*-hydroxypheophorbide *a* methyl ester (**21***RR*) (100% d.e. from ^{1}H NMR) (8.5 mg) as a green solid after recrystallization from CH_2Cl_2–hexane; mp 180°C; UV–VIS λ_{max} (CH_2Cl_2): 400 nm (ε 114 100), 498 (10 700), 656 (33 700), 682 (6200); ^{1}H NMR (400 MHz, 1.4 mg/0.6 mL $CDCl_3$) δ: 9.80 (s, 1H, H-10), 9.65 (s, 1H, H-5), 8.80 (s, 1H, H-20), 8.20 (dd, 1H, H-3^1, *J* = 18.3 and 12.0 Hz), 6.42 (br s, 1H, OH-13^2), 6.33 (dd, 1H, H-3^2(*E*), *J* =18.3 and 1.4 Hz), 6.16 (dd, 1H, H-3^2(*Z*), *J* = 12.0 and 1.4 Hz), 5.60 (s, 1H, H-13^1), 4.93 (d, 1H, H-17, *J* = 8.2 Hz), 4.59 (q, 1H, H-18, *J* = 7.5 Hz), 4.48 (m, 2H, 13^2), 3.81 (q, 2H, H-8^1, *J* = 7.6 Hz), 3.57 (s, 3H, H-17^4), 3.55 (s, 3H, H-13^4), 3.54 (s, 3H, H-12^1), 3.53 (s, 3H, H-7^1), 3.38 (s, 3H, H-2^1), 2.45 (ddd, 1H, H-17^1), 2.32 (ddd, 1H, H-17^2), 2.10 (ddd, 1H, H-17^1), 1.96 (ddd, 1H, H-17^2), 1.74 (d, 3H, H-18^1, *J* = 7.5 Hz), 1.71 (t, 3H, H-8^2, *J* = 7.6 Hz), −1.40 (br s, 1H, NH), −3.10 (br s, 1H, NH); ^{13}C NMR (75 MHz, 12 mg/1.0 mL $CDCl_3$) δ: 176.03 (C-13^3), 173.81 (C-17^3), 167.27 (C-19), 163.05 (C-16), 150.59 (C-6), 150.48 (C-9), 143.18 (C-14), 142.49 (C-8), 139.81 (C-1), 138.18 (C-11), 136.49 (C-3), 135.63 (C-4), 134.48 (C-7), 132.21 (C-2), 129.88 (C-3^1), 128.83 (C-12), 128.41 (C-13), 121.56 (C-3^2), 108.87 (C-15), 99.75 (C-10), 99.29 (C-5), 95.00 (C-13^2), 93.46 (C-20), 82.41 (C-13^1), 53.32 (C-13^4), 51.57 (C-17^4), 50.98 (C-17), 49.95 (C-18), 30.66 (C-17^1), 29.33 (C-17^2), 23.54 (C-18^1), 19.64 (C-8^1), 17.71 (C-8^2), 12.31 (C-12^1), 11.43 (C-2^1), 11.43 (C-7^1); LREIMS (*m/z*): 624 (M^+, 38%); HREIMS, $C_{36}H_{40}N_4O_6$ (M^+), calcd.: 624.2948; obsd.: 624.2938; Anal. calcd. for $C_{36}H_{40}N_4O_6$: C 69.20, H 6.46, N 8.97%; found: C 68.97, H 6.44, N 8.70%.

*13-Decarboxy-13-formyl-purpurin-7 dimethyl ester (**15**)*

Method A: A solution of 13^1-deoxo-13^1,13^2-dehydropheophorbide *a* methyl ester (**19**) (20 mg, 0.0339 mmol) in CH_2Cl_2 (100 mL) was stirred in Vancouver sunlight for 20 min. Removal of solvent in vacuo and crystallization from CH_2Cl_2–hexane gave a brown powder of the aldehyde **15** (21 mg, 100% yield).

Method B: A solution of 13^2-deoxo-13^1-hydroxy-13^2*R*-hydroxypheophorbide *a* methyl ester (**21**) (31 mg, 0.05 mmol) in dioxane (20 mL) was stirred with an aqueous solution (20 mL) of periodic acid dihydrate (900 mg, 3.95 mmol) at room temperature for 20 h before the mixture was extracted with dichloromethane (2 × 40 mL). The organic layer was dried over sodium sulfate, filtered, and evaporated in vacuo. The residue was purified by flash chromatography on silica III, eluting with dichloromethane. Recrystallization from dichloromethane–hexane gave the title compound as a brown powder (24.8 mg, 80%); mp 216-217°C; UV–VIS λ_{max} (CH_2Cl_2): 414 nm (ε 113 200), 508 (7400), 544 (10 600), 630 (7000), 680 (35 400), 686 (31 700); ^{1}H NMR (400 MHz, 1.5 mg/0.6 mL $CDCl_3$) δ: 10.93 (s, 1H, H-13^1), 9.50 (s, 1H, H-10), 9.20 (s, 1H, H-5), 8.45 (s, 1H, H-20), 7.90 (dd, 1H, H-3^1, *J* = 18.2 and 11.9 Hz), 6.30 (d, 1H, H-3^2(*E*), *J* = 18.2 Hz), 6.11 (d, 1H, H-3^2(*Z*), *J* = 11.9 Hz), 4.48 (dd, 1H, H-17, *J* = 9.4 Hz), 4.28 (q, 1H, H-18, *J* = 9.0 Hz), 3.93 (s, 3H, H-12^1), 3.66 (s, 3H, H-17^4), 3.61 (q, 2H, H-8^1, *J* = 7.5 Hz), 3.52 (s, 3H, H-15^3), 3.30 (s, 3H, H-2^1), 3.13 (s, 3H, H-7^1), 2.35 (m, 1H, H-17^1), 2.10 (m, 2H, H-17^2), 1.80 (m, 1H, H-17^1), 1.73 (d, 3H, H-18^1, *J* = 9.0 Hz), 1.65 (t, 3H, H-8^2, *J* = 7.5 Hz), 0.2 (br s, 2H, NH); ^{13}C NMR (75 MHz, 15 mg/1.0 mL $CDCl_3$) δ: 186.83 (C-13^1), 184.92 (C-15^1), 174.85 (C-15^2), 173.30 (C-17^3), 168.22 (C-19), 163.28 (C-16), 157.05 (C-6), 149.12 (C-9), 145.98 (C-14), 143.24 (C-8), 140.40 (C-1), 137.34 (C-11), 136.62 (C-3), 135.97 (C-4), 134.20 (C-7), 131.90 (C-2), 129.56 (C-12), 124.36 (C-13), 128.57 (C-3^1), 122.89 (C-3^2), 106.90 (C-5), 105.80 (C-15), 100.45 (C-10), 93.74 (C-20), 53.27 (C-17), 52.63 (C-15^3), 51.53 (C-17^4), 49.71 (C-18), 31.44 (C-17^2), 30.93 (C-17^1), 22.78 (C-18^1), 19.40 (C-8^1), 17.47 (C-8^2), 11.90 (C-12^1), 11.39 (C-2^1), 11.06 (C-7^1); LREIMS (*m/z*): 622 (M^+, 15%), 563 (M^+ − COOMe, 27%), 535 (M^+ − COOMe − CO, 27%); HREIMS, $C_{36}H_{38}N_4O_6$ (M^+), calcd.: 622.2791; obsd.: 622.2786; Anal. calcd. for $C_{36}H_{38}N_4O_6$: C 69.44, H 6.15, N 9.00%; found: C 69.11, H 5.93, N 8.92%.

*13-Decarboxy-13-formyl-3-vinylrhodoporphyrin XV methyl ester (**17**)*

Purpurin **15** (150 mg, 0.24 mmol) was heated in an oil bath at 180–185°C in 2,4,6-collidine (30 mL) for 45 min. After cooling, the solvent was evaporated at 0.5 Torr and the residue was recrystallized from $CHCl_3$–CH_3OH, giving the title porphyrin (19.3 mg, 15% yield) as purple needles; mp 245–246°C; UV–VIS λ_{max} (CH_2Cl_2): 414 nm (ε 189 000), 518 (9000), 560 (21 400), 582 (15 300), 636 (2500); ^{1}H NMR (400 MHz, $CDCl_3$) δ: 11.40 (s, 1H, 13-CHO), 10.70, 9.92, 9.88, 9.76 (4s, 4H, H-5, H-10, H-15, and H-20), 8.15 (dd, 1H, H-3^1, *J* = 17.5 and 11.0 Hz), 6.29 (dd, 1H, H-3^2(*E*), *J* = 17.5 and 1.0 Hz), 6.15 (dd, 1H, H-3^2(*Z*), *J* = 11.0 and 1.0 Hz), 4.37 (t, 2H, H-17^1, *J* = 7.5 Hz), 4.00 (q, 2H, H-8^1, *J* = 8.3 Hz), 3.80, 3.69, 3.58, 3.58, 3.58 (5s, 15H, H-2^1, H-7^1, H-12^1, H-18^1, and H-17^4), 3.23 (t, 2H, H-17^2, *J* = 7.5 Hz), 1.80 (t, 3H, H-8^2, *J* = 8.3 Hz), −4.50 (br s, 2H, NH); LREIMS (*m/z*): 534 (M^+, 100%); HREIMS, $C_{33}H_{34}N_4O_3$ (M^+); calcd.: 534.2631; obsd.: 534.2634.

*13-Decarboxy-13-(ethyleneacetal)-purpurin-7 dimethyl ester (**22**)*

The foregoing purpurin **15** (20 mg, 0.032 mmol) in dry THF (50 mL) under nitrogen was stirred in a three-necked round-bottom flask equipped with a Soxhlet apparatus containing 4Å molecular sieves. Ethylene glycol (0.9 mL) and *p*-toluenesulfonic acid (2 mg) were added to the solution and the reaction mixture was brought to reflux. Progress of the reac-

© 1997 NRC Canada

Can. J. Chem. Downloaded from www.nrcresearchpress.com by 88.146.161.215 on 09/08/12
For personal use only.

tion was followed by spectrophotometry, using the change in absorption spectrum from λ_{max} = 686 nm to λ_{max} = 660 nm; the reaction was complete after 1 h. The mixture was diluted with methylene chloride (50 mL), washed with water (3 × 50 mL), dried over Na_2SO_4, and evaporated to dryness. The residue was chromatographed on alumina V (elution with methylene chloride) to give the principal green band. Removal of solvent in vacuo and recrystallization from CH_2Cl_2–hexane gave a dark-green powder of the title acetal **22** (19.2 mg, 90% yield); mp 265°C; UV–VIS λ_{max} (CH_2Cl_2): 400 nm (ε 149 000), 496 (13 000), 606 (5000), 660 (39 000); ^{1}H NMR (400 MHz, 1.5 mg/0.6 mL $CDCl_3$) δ: 10.93 (s, 1H, H-13^1), 9.75 (s, 1H, H-10), 9.68 (s, 1H, H-5), 8.80 (s, 1H, H-20), 8.12 (dd, 1H, H-3^1, *J* = 18.3 and 11.7 Hz), 6.33 (d, 1H, H-3^2(*E*), *J* = 18.3 Hz), 6.15 (d, 1H, H-3^2(*Z*), *J* = 11.7 Hz), 4.70 (m, 1H, 13^1-OCH_2OCH_2), 4.40 (q, 1H, H-18, *J* = 7.3 Hz), 4.18 (dd, 1H, H-17, *J* = 13.3 and 3.6 Hz), 4.06 (s, 3H, 15^1-$COOCH_3$), 4.01 (m, 3H, 13^1-OCH_2OCH_2), 3.79 (q, 2H, H-8^1, *J* = 7.56 Hz), 3.59 (s, 3H, H-17^4), 3.50 (s, 3H, H-12^1), 3.44 (s, 3H, H-2^1), 3.33 (s, 3H, H-7^1), 2.38 (m, 1H, H-17^1), 2.20 (m, 1H, H-17^2), 1.89 (m, 1H, H-17^1), 1.82 (d, 3H, H-18^1, *J* = 7.3 Hz), 1.80 (m, 1H, H-17^2), 1.73 (t, 3H, H-8^2, *J* = 7.6 Hz), −1.85 (br s, 1H, NH), −2.03 (br s, 1H, NH); LREIMS (*m/z*): 666 (M^+, 100%); HREIMS, $C_{38}H_{42}N_4O_7$ (M^+), calcd.: 666.3053; obsd.: 666.3061.

13-Decarboxy-3,13-divinylrhodoporphyrin XV methyl ester (16)

Method A: 13-Decarboxy-13-formyl-3-vinylrhodoporphyrin XV methyl ester (**17**) (18 mg, 0.0337 mmol) was dissolved in methylene chloride (10 mL), and a saturated solution of $Zn(OAc)_2$ in methanol (0.5 mL) was added. The resulting solution was stirred at room temperature for 3 h, at which time TLC and UV–VIS spectroscopy showed full conversion to the desired compound. The solvent was removed by evaporation in vacuo and the product was redissolved in methylene chloride, filtered through a short bed of alumina V, and evaporated to dryness. The Zn(II) porphyrin was further dried, under vacuum, at 0.5 Torr, for 4 h.

Dry methyltriphenylphosphonium bromide (30 mg, 0.084 mmol) in dry THF (25 mL) and diisopropylamine (0.5 mL) were treated with *n*-butyllithium in *n*-hexane (50 mL, 1.6 M). The resulting ylide was stirred at 0°C under nitrogen gas and a THF solution (10 mL) of the above Zn(II) porphyrin was added via a cannula. After 30 min the solution was evaporated to dryness to give a residue that was taken into methylene chloride (30 mL), filtered through anhydrous sodium sulfate, and then evaporated again to dryness. The residue was dissolved in trifluoroacetic acid (3 mL) and washed twice with water (30 mL). The organic phase was evaporated to dryness and the residue was chromatographed on alumina III (elution with methylene chloride). The red eluates were evaporated to dryness to furnish a residue that was recrystallized from $CHCl_3$–hexane to give the title porphyrin (12.6 mg, 71%) as a purple-red powder.

Method B: The foregoing hydroxyporphyrin **27** (55 mg, 0.1 mmol) was dissolved in dry DMF (20 mL) and stirred at 105°C under nitrogen. Benzoyl chloride (1 mL) was added to this solution via a syringe and the mixture was kept at this temperature for 2 h. The solution was then diluted with methylene chloride (100 mL), and successively washed with 2 M sodium hydroxide (75 mL) and water (2 × 100 mL). The organic layer was dried over $MgSO_4$, filtered, and evaporated in vacuo. The residue was chromatographed on silica III (elution with methylene chloride) to give a major red band. The appropriate fractions were collected, evaporated, and recrystallized from CH_2Cl_2–hexane to give the title divinylporphyrin **16** (31.9 mg, 60%) as a purple-red solid. This material was found identical to the compound prepared from the Wittig reaction of 13-formylporphyrin **17**; mp 227°C; UV–VIS λ_{max} (CH_2Cl_2): 404 nm (ε 108 000), 506 (7500), 544 (9800), 572 (5600), 630 (1500); ^{1}H NMR (400 MHz, $CDCl_3$) δ: 10.16, 10.15, 10.08, 10.07 (4s, 4H, H-5, H-10, H-15, and H-20), 8.27 (dd, 2H, H-3^1 and H-13^1), 6.33 (dd, 2H, H-3^2(*E*) and H-13^2(*E*)), 6.15 (dd, 2H, H-3^2(*Z*) and H-13^2(*Z*)), 4.42 (t, 2H, H-17^1, *J* = 7.6 Hz), 4.10 (q, 2H, H-8^1, *J* = 7.5 Hz), 3.69, 3.67, 3.66, 3.65, 3.63 (5s, 15H, H-2^1, H-7^1, H-12^1, H-18^1, and H-17^4), 3.26 (t, 2H, H-17^2, *J* = 7.6 Hz), 1.86 (t, 3H, H-8^2, *J* = 7.5 Hz), −3.75 (br s, 2H, NH); LRFABMS (*m/z*): 533 (M^+, 100%); HRFABMS, $C_{34}H_{37}N_4O_2$ (M^+); calcd.: 533.2916; obsd.: 533.2916.

Synthesis of [A,C]-divinylporphyrin 16 via porphyrin 9

3-Vinylrhodoporphyrin XV methyl ester (23) (21)

Vinylrhodoporphyrin XV dimethyl ester (**9**) (850 mg) in warm pyridine (175 mL) was refluxed for 4 h with a solution of potassium hydroxide (20 g) in water (25 mL) and methanol (150 mL). The solution was cooled, diluted with ice-water (1 L), acidified with concentrated sulfuric acid (15 mL) in water (100 mL), and then stirred for 10 min. The precipitated porphyrin diacid was filtered onto Celite, and washed with warm water followed by dry methanol. A mixture of dry methanol (650 mL) and concentrated sulfuric acid (20 mL) was passed slowly through the bed of Celite, thereby dissolving the porphyrin, and the resultant solution was kept at room temperature in the dark for 16 h before addition to water (1.5 L). The porphyrin was extracted with methylene chloride (3 × 500 mL) and the extracts were washed with water (1 L), dried over anhydrous $MgSO_4$, and evaporated. The residue was recrystallized from THF–benzene to give the title porphyrin monocarboxylic acid (605 mg, 70%) as a dark-red powder; mp >300°C (lit. (21) mp >300°C); UV–VIS λ_{max} (CH_2Cl_2): 408 nm (ε 154 000), 514 (7900), 554 (16 300), 578 (9500) (lit. (21) λ_{max} (pyridine): 409 nm (ε 189 000), 511(10 000), 552 (17 200), 579 (9200); λ_{max} ($CHCl_3$–HCl): 427 nm (ε 206 000), 569 (12 000), 620 (12 900); λ_{max} (0.1 M NaOMe – MeOH): 399 nm (ε 146 000), 503 (10 500), 550 (12 000), 572 (6700), 624 (1900)); ^{1}H NMR (400 MHz, CF_3COOD) δ: 11.90, 11.20, 11.00, 10.95 (4s, 4H, H-5, H-10, H-15, and H-20), 8.28 (dd, 1H, H-3^1, *J* = 18.3 and 11.0 Hz), 6.65 (d, 1H, H-3^2(*Z*), *J* = 11.0 Hz), 6.40 (d, 1H, H-3^2(*E*), *J* = 18.3 Hz), 4.62 (t, 2H, H-17^1), 4.25 (q, 2H, H-8^1), 4.19, 3.80, 3.78, 3.76, 3.72 (5s, 15H, H-2^1, H-7^1, H-12^1, H-18^1, and H-17^4), 3.40 (t, 2H, H-17^2), 1.82 (t, 3H, H-8^2); LREIMS (*m/z*): 550 (M^+, 100%), 506 ($M^+ - CO_2$, 30%); HREIMS, $C_{33}H_{34}N_4O_4$ (M^+), calcd.: 550.2580; obsd.: 550.2580; Anal. calcd. for $C_{33}H_{34}N_4O_4$: C 71.98, H 6.22, N 10.17%; found: C 71.93, H 6.16, N 9.86%.

© 1997 NRC Canada

Can. J. Chem. Downloaded from www.nrcresearchpress.com by 88.146.161.215 on 09/08/12
For personal use only.

*13-Imidazoyl-3-vinylrhodoporphyrin XV methyl ester (**24**)*

A mixture of 3-vinylrhodoporphyrin XV methyl ester (**23**) (600 mg, 1.09 mmol) and *N,N'*-carbonyldiimidazole (600 mg) was refluxed for 30 min in THF (125 mL). The solution was evaporated to about 60 mL and then applied to a short alumina column (Brockman Grade V; elution with methylene chloride). The appropriate eluates were evaporated and the residue was recrystallized from CH_2Cl_2–benzene to give the title porphyrin (595 mg, 91%) as a dark-red powder; mp 239°C; UV–VIS λ_{max} (CH_2Cl_2): 408 nm (ε 160 000), 514 (6900), 554 (15 300), 574 (9900); ^{1}H NMR (400 MHz, $CDCl_3$) δ: 10.01, 9.97, 9.88, 9.70 (4s, 4H, H-5, H-10, H-15, and H-20), 8.38 (s, 1H, H-imidazole), 8.12 (dd, 1H, H-3^1, J = 17.5 and 12.0 Hz), 7.95 (s, 1H, H-imidazole), 7.35 (s, 1H, H-imidazole), 6.29 (dd, 1H, H-3^2(*E*), J = 17.5 and 1.5 Hz), 6.15 (dd, 1H, H-3^2(*Z*), J = 17.5 and 1.5 Hz), 4.25 (t, 2H, H-17^1, J = 8.1 Hz), 4.00 (q, 2H, H-8^1, J = 8.0 Hz), 3.67, 3.65, 3.55, 3.53, 3.51 (5s, 15H, H-2^1, H-7^1, H-12^1, H-18^1, and H-17^4), 3.18 (t, 2H, H-17^2, J = 8.1 Hz), 1.80 (t, 3H, H-8^2, J = 8.0 Hz), −4.30 (br s, 2H, NH); LRFABMS (*m/z*): 601 ([M + H]$^+$, 73%), 533 (M$^+$ − C_3H_3N2, 100%); LREIMS (*m/z*): 533 (M$^+$ − $C_3H_3N_2$, 100%); HRFABMS, $C_{36}H_{37}N_6O_3$ ([M + H]$^+$); calcd.: 601.2927; obsd.: 601.2929; HREIMS, $C_{33}H_{33}N_4O_3$ (M$^+$ − $C_3H_3N_2$): calcd.: 533.2552; obsd.: 533.2551.

*13-Decarboxy-13-methoxycarbonylacetyl-3-vinylrhodoporphyrin XV methyl ester (**25**) (21)*

A solution of 2-PrMgBr was prepared by refluxing, under dry nitrogen, a mixture of Mg turnings (1.2 g) and 2-PrBr (4 g) in freshly distilled THF (150 mL). When the metal had dissolved, the solution was cooled to 0°C and redistilled methyl hydrogen malonate (23) (3 g) in dry THF (30 mL) was added via a cannula. The mixture was warmed to 65°C and stirred for 10 min before introduction of a solution of 13-imidazoyl-3-vinylrhodoporphyrin XV methyl ester (**24**) (400 mg) in dry THF (200 mL). Stirring was maintained for 2.5 h while heating under reflux, and glacial acetic acid (15 mL) was then added. Heating and stirring were continued for a further 15 min, after which the mixture was diluted with chloroform (1400 mL), washed with 0.1 M HCl (1100 mL) and water (2 × 800 mL), and then dried over anhydrous Na_2SO_4 and evaporated to dryness. The residue was chromatographed on alumina V (elution with 5% acetone in methylene chloride) and after evaporation of the appropriate eluates the product was recrystallized from CH_2Cl_2–hexane to give the required porphyrin-β-ketoester **25** (280 mg, 70%) as a dark-red solid; mp 270–274°C (lit. (21) mp 250–254°C); UV–VIS λ_{max} (CH_2Cl_2): 410 nm (ε 140 000), 512 (7400), 552 (14 000), 576 (9200) (lit. (21) λ_{max} (CH_2Cl_2): 409 nm (ε 176 000), 512 (7200), 553 (15 400), 574 (9900), 635 (1300); λ_{max} (CH_2Cl_2–CF_3COOH): 412 nm (ε 267 000), 559 (12 200), 608 (8600); λ_{max} (0.1 M NaOMe – MeOH): 401 nm (ε 154 000), 504 (10 500), 542 (12 400), 572 (6900), 625 (2200)); ^{1}H NMR (400 MHz, $CDCl_3$) δ (the enol tautomer): 13.30 (s, 1H, OH), 10.62, 10.62, 10.42, 9.75 (4s, 4H, H-5, H-10, H-15, and H-20), 6.10 (s, 1H, H-13^2); δ (the ketone tautomer): 9.98, 9.97, 9.86, 9.85 (4s, 4H, H-5, H-10, H-15, and H-20), 4.70 (s, 2H, H-13^2); δ (their mixture): 8.10 (m, 1H, H-3^1), 6.25 (m, 1H, H-3^2(*E*)), 6.12 (m, 1H, H-3^2(*Z*)), 4.41 (t, 2H, H-17^1), 3.98 (q, 2H, H-8^1), 4.02–3.45 (6s, 18H, H-2^1, H-7^1, H-12^1, H-18^1, H-17^4, and 13^2-$COOCH_3$), 3.25 (t, 2H, H-17^2), 1.83 (t, 3H, H-8^2), −4.26 (br s, 1H, NH), −4.30 (br s, 1H, NH); LRFABMS (*m/z*): 607 ([M + H]$^+$, 16%); HRFABMS, $C_{36}H_{39}N_4O_5$ ([M + H]$^+$); calcd.: 607.2920; obsd.: 607.2919.

*13-Acetyl-13-decarboxy-3-vinylrhodoporphyrin XV methyl ester (**26**)*

A mixture of porphyrin-β-ketoester **25** (180 mg, 0.297 mmol), 4-(dimethylamino)pyridine (36 mg, 2.92 mmol), 1.0 M phosphate buffer (pH = 7) (40 mL), and toluene (150 mL) was stirred at 90°C for 12 h, at which time TLC analysis showed the full disappearance of the porphyrin-β-ketoester band and appearance of a more mobile red band. The reaction mixture was extracted with ethyl acetate (250 mL) and the organic layer was washed once with saturated NH_4Cl, twice with water (200 mL), dried over $MgSO_4$, filtered, and evaporated. The residue was chromatographed on silica III (elution with methylene chloride) to give a major red band. The appropriate eluates were evaporated and the residue was recrystallized from CH_2Cl_2–hexane to give the title acetylporphyrin (122 mg, 75%) as purple-red small leaves; mp 284°C; UV–VIS λ_{max} (CH_2Cl_2): 410 nm (ε 147 000), 514 (7400), 554 (13 800), 576 (8600), 608 (1300); ^{1}H NMR (400 MHz, $CDCl_3$) δ: 10.75, 10.10, 10.07, 9.98 (4s, 4H, H-5, H-10, H-15, and H-20), 8.20 (dd, 1H, H-3^1, J = 17.4 and 12.5 Hz), 6.30 (d, 1H, H-3^2(*E*), J = 17.4 Hz), 6.12 (d, 1H, H-3^2(*Z*), J = 12.5), 4.43 (t, 2H, H-17^1, J = 7.5 Hz), 4.09 (q, 2H, H-8^1, J = 8.8 Hz), 3.88, 3.67, 3.65, 3.61, 3.61 (5s, 15H, H-2^1, H-7^1, H-12^1, H-18^1, and H-17^4), 3.33 (t, 2H, H-17^2, J = 7.5 Hz), 3.32 (s, 3H, H-13^2), 1.85 (t, 3H, H-8^2, J = 8.8 Hz), −3.80 (br s, 2H, NH); LRFABMS (*m/z*): 549 ([M + H]$^+$, 100%); HRFABMS, $C_{34}H_{36}N_4O_3$ ([M + H]$^+$); calcd.: 549.2865; obsd.: 549.2861.

*13-Decarboxy-13-(α-hydroxy)ethyl-3-vinylrhodoporphyrin XV methyl ester (**27**)*

To a mixture of the foregoing porphyrin **26** (100 mg, 0.182 mmol) in methylene chloride (80 mL) and methanol (15 mL) was added sodium borohydride (80 mg). The mixture was stirred for 90 min at room temperature, after which time TLC monitoring indicated reduction of the acetyl group to be complete. The reaction was quenched by slow addition of ice-cooled 1 M HCl. The organic layer was separated, washed twice with water, dried over $MgSO_4$, filtered, and evaporated. The residue was chromatographed on silica V (elution with 0.5% methanol in methylene chloride) to give a major red band. The appropriate eluates were evaporated and the residue was recrystallized from CH_2Cl_2–hexane to give the title hydroxyporphyrin (82 mg, 82%) as a purple solid; mp 219°C; UV–VIS λ_{max} (CH_2Cl_2): 404 nm (ε 178 000), 502 (10 600), 540 (12 000), 572 (9300), 624 (2700); ^{1}H NMR (400 MHz, $CDCl_3$) δ: 10.18, 10.00, 9.88, 9.88 (4s, 4H, H-5, H-10, H-15, and H-20), 8.20 (dd, 1H, H-3^1, J = 17.1 and 11.4 Hz), 6.31 (dd, 1H, H-3^2(*E*), J = 17.1 and 1.9 Hz), 6.15 (dd, 1H, H-3^2(*Z*), J = 12.5 and 1.9 Hz), 4.27 (t, 2H, H-17^1, J = 8.5 Hz), 4.00 (q, 2H, H-8^1, J = 8.2 Hz), 3.58, 3.58, 3.54, 3.51, 3.49 (5s, 15H, H-2^1, H-7^1, H-12^1, H-18^1, and H-17^4), 3.45 (q, 1H, H-13^1, J = 7.0 Hz), 3.16 (t, 2H, H-17^2, J = 8.5 Hz), 2.72 (br s, 1H, OH-13^1), 2.14 (d, 3H, H-13^2, J = 7.0 Hz), 1.81 (t, 3H, H-8^2, J = 8.2 Hz), −4.30 (br s, 2H, NH); LRFABMS (*m/z*): 551 ([M + H]$^+$, 100%); HRFABMS, $C_{34}H_{39}N_4O_3$ ([M + H]$^+$): calcd.: 551.3022; obsd.: 551.3011.

© 1997 NRC Canada

Can. J. Chem. Downloaded from www.nrcresearchpress.com by 88.146.161.215 on 09/08/12
For personal use only.

Diels–Alder reactions with vinylporphyrins

*$2^1,2^2$-Bis(methoxycarbonyl)-8-ethyl-13-methoxycarbonyl-17-methoxycarbonylethyl-2,7,12,18-tetramethyl-2^3-hydrobenzo[*b*]porphyrin (**28**)*

3-Vinylrhodoporphyrin XV dimethyl ester (**9**) (57 mg, 0.1 mmol) and DMAD (710 mg, 5 mmol) were suspended in degassed toluene (N_2) (20 mL) and the mixture heated at 110°C for 28 h. After removal of the toluene in vacuo, the residue was chromatographed on silica (methylene chloride eluant). After elution of the excess dienophile, the solvent polarity was increased to 2% methanol in methylene chloride to elute the major reaction product. After evaporation to dryness, the residue was recrystallized from CH_2Cl_2–hexane to afford the 1,4-cyclohexadiene adduct **28** as a green solid (35 mg, 50% yield); mp 244-245°C; UV–VIS λ_{max} (CH_3COCH_3): 410 nm (peak ratio, 1.40), 516 (0.119), 646 (0.138); ^{1}H NMR (400 MHz, $CDCl_3$) δ: 10.75, 9.80, 9.25, 9.01 (4s, 4H, H-5, H-10, H-15, and H-20), 7.40 (dd, 1H, H-3^1, J = 7.4 and 2.1 Hz), 4.31 (t, 2H, H-17^1, J = 8.3 Hz), 3.95 (dd, 1H, H-2^3, J = 3.0 and 0.5), 3.94 (q, 2H, H-8^1, J = 7.5 Hz), 3.62 (s, 1H, H-2^3, J = 3.3 and 0.5 Hz), 3.25 (t, 2H, H-17^2, J = 8.3 Hz), 4.33, 4.02, 3.89, 3.75, 3.69, 3.45, 3.41 (7s, 21H, H-7^1, H-12^1, H-18^1, H-17^4, 2^1-$COOCH_3$, and 2^2-$COOCH_3$), 2.07 (s, 3H, 2-CH_3), 1.78 (t, 3H, H-8^2, J = 7.5 Hz), −2.26 (br s, 1H, NH), −2.30 (br s, 1H, NH); LREIMS (*m/z*): 706 (M^+, 100%), 690 ($M^+ - CH^4$, 60%).

*$2^1,2^2$-Bis(methoxycarbonyl)-8-ethyl-13-methoxycarbonyl-17-methoxycarbonylethyl-2,7,12,18-tetramethyl-2^1-hydrobenzo[*b*]porphyrin (**29**)*

The adduct **28** (32 mg, 0.045 mmol) was dissolved in methylene chloride and a few drops of DBU were added. The reaction mixture was stirred in the dark and monitored by visible spectroscopy (complete in 4 h). The mixture was poured into 1 M HCl and extracted with methylene chloride. The organic layer was washed twice with brine, once with water, and dried over anhydrous magnesium sulfate. The solvent was evaporated in vacuo and the compound was chromatographed on silica gel (1% MeOH in CH_2Cl_2 eluent). The pure 1,3-cyclohexadiene fraction was evaporated in vacuo yielding 29 mg (90% yield) of tiny dark-green needles after recrystallization from CH_2Cl_2–hexane; mp 248–249°C; UV–VIS λ_{max} (CH_2Cl_2): 356 nm (ε 27 000), 440 (70 400), 592 (19 900), 672 (14 600); ^{1}H NMR (400 MHz, $CDCl_3$) δ: 10.70, 9.80, 9.30, 8.90 (4s, 4H, H-5, H-10, H-15, and H-20), 7.80 (d, 1H, H-2^4, J = 6.0 Hz), 7.42 (d, 1H, H-2^3, J = 6.0 Hz), 5.40 (s, 1H, H-2^1), 4.29 (t, 2H, H-17^1, J = 7.7 Hz), 3.92 (q, 2H, H-8^1, J = 7.9 Hz), 3.25 (t, 2H, H-17^2, J = 7.7 Hz), 4.34, 3.98, 3.75, 3.70, 3.43, 3.40, 2.98 (7s, 21H, H-7^1, H-12^1, H-18^1, H-17^4, 2^1-$COOCH_3$, and 2^2-$COOCH_3$), 1.79 (s, 3H, 2-CH_3), 1.76 (t, 3H, H-8^2, J = 7.9 Hz), −1.95 (br s, 1H, NH), −2.00 (br s, 1H, NH); LREIMS (*m/z*): 706 (M^+, 100%); HREIMS, $C_{40}H_{42}N_4O_8$ (M^+); calcd.: 706.3002, obsd.: 706.3010; Anal. calcd. for $C_{40}H_{42}N_4O_8$: C 67.97, H 5.99, N 7.93%; found: C 68.03, H 5.96, N 7.92%.

*$2^1,2^2$-Bis(methoxycarbonyl)-13,15-ethano-8-ethyl-17-methoxycarbonylethyl-2,7,12,18-tetra-methyl-2^1-hydrobenzo[*b*]porphyrin (**30**)*

3-Vinylporphyrin **6** (27 mg, 0.05 mmol) and DMAD (360 mg, 25 mmol) were suspended in degassed toluene (N_2) (20 mL) and the mixture was heated at 110°C for 30 h. After removal of the toluene in vacuo, the residue was chromatographed on silica (methylene chloride eluant). After elution of the excess dienophile, the solvent polarity was increased to 2% methanol in methylene chloride to elute the major reaction product. After evaporation to dryness, 14 mg (42% yield) of the 1,4-cyclohexadiene adduct **31** (λ_{max} = 404, 550, 650 nm) was obtained.

The adduct **31** (14 mg, 0.02 mmol) was dissolved in methylene chloride and a few drops of DBU were added. The reaction mixture was stirred in the dark and monitored by visible spectroscopy (completed in 6 h). The mixture was poured into 1 M HCl and extracted with methylene chloride. The organic layer was washed twice with brine, once with water, and dried over anhydrous magnesium sulfate. The solvent was evaporated in vacuo and the compound was chromatographed on silica gel (1% MeOH in CH_2Cl_2 eluent). The pure 1,3-cyclohexadiene fraction was evaporated in vacuo, yielding 12.7 mg (91% yield) of tiny dark-green needles after recrystallization from CH_2Cl_2–hexane; mp 258°C; UV–VIS λ_{max} (CH_2Cl_2): 354 nm (ε, 86 000), 438 (120 000), 580 (18 000), 620 (14 000), 680 (47 000), 686 (37 000); ^{1}H NMR (400 MHz, $CDCl_3$) δ: 9.59 (s, 1H, H-10), 9.30 (s, 1H, H-5), 8.95 (s, 1H, H-20), 7.83 (d, 1H, H-2^4, J = 5.8 Hz), 7.45 (d, 1H, H-2^3, J = 5.8 Hz), 5.20 (t, 2H, H-13^2), 5.05 (s, 1H, H-2^1), 4.30 (m, 2H, H-17^1), 3.93 (m, 2H, H-13^1), 3.93 (q, 2H, H-8^1, J = 7.9 Hz), 3.10 (t, 2H, H-17^2), 3.97, 3.78, 3.46, 3.42, 3.39, 2.92 (6s, 18H, H-7^1, H-12^1, H-18^1, H-17^4, 2^1-$COOCH_3$, and 2^2-$COOCH_3$), 1.78 (t, 3H, H-8^2, J = 7.9 Hz), 1.77 (s, 3H, 2-CH_3), −1.42 (br s, 1H, NH), −2.22 (br s, 1H, NH); LRFABMS (*m/z*): 675 ($[M + H]^+$, 100%); HRFABMS, $C_{40}H_{43}N_4O_6$ ($[M + H]^+$); calcd. 675.3182; obsd.: 675.3176.

*$2^1,2^2,12^1,12^2$-Tetrakis(methoxycarbonyl)-8-ethyl-17-methoxycarbonylethyl-2,7,12,18-tetramethyl-$2^3,12^3$-dihydrobenzo[*b*,*l*]porphyrin (**32**)*

The foregoing 3,13-divinylporphyrin **16** (30 mg, 0.0564 mmol) and DMAD (800 mg, 5.6 mmol) were suspended in degassed toluene (N2) (20 mL) and the mixture heated at 110°C for 80 h. After removal of the toluene in vacuo, the residue was chromatographed on silica (methylene chloride eluant). After elution of the excess dienophile, the solvent polarity was increased to 2% methanol in methylene chloride to elute the major reaction product. After evaporation to dryness, the resulting residue was subjected to preparative TLC on silica (1 mm thick plate; elution with 2% methanol in methylene chloride). The more mobile band was found to be the mono-adduct (exhibiting a band at 656 nm), present in a trace amount; the major band was found to be the bis-adduct, which was recrystallized from CH_2Cl_2–hexane to afford the bis-adduct **32** as a green solid (10.8 mg, 25% yield); mp 198°C; UV–VIS λ_{max} (CH_3COCH_3): 406 nm (peak ratio, 1.10), 484 (0.21), 538 (0.15), 666 (0.13), 720 (0.338); LREIMS (*m/z*): 816 (M^+, 100%).

*$2^1,2^2,12^1,12^2$-Tetrakis(methoxycarbonyl)-8-ethyl-17-methoxycarbonylethyl-2,7,12,18-tetra-methyl-$2^1,12^1$-dihydrobenzo[*b*,*l*]porphyrin (**33**)*

The bis-adduct **32** (9 mg, 0.011 mmol) was dissolved in methylene chloride and a few drops of DBU were added. The reaction mixture was stirred in the dark and monitored by visible spectroscopy (completed in 16 h). The mixture was poured

© 1997 NRC Canada

into 1 M HCl and extracted with methylene chloride. The organic layer was washed twice with brine, once with water, and dried over anhydrous magnesium sulfate. The solvent was evaporated in vacuo and the compound was chromatographed on silica gel (1% MeOH in CH_2Cl_2 eluent). The pure 1,3-cyclohexadiene fraction was evaporated in vacuo, yielding 8.0 mg (90% yield) of a dark-green solid after recrystallization from CH_2Cl_2–hexane; mp 289-291°C; UV–VIS λ_{max} (CH_2Cl_2): 468 nm (ε 81 000), 620 (20 900), 700 (4700), 784 (38 000); ^{1}H NMR (400 MHz, $CDCl_3$) δ: 9.15, 9.15, 8.74, 8.74 (4s, 4H, H-5, H-10, H-15, and H-20), 7.82 (d, 2H, H-2^4 and H-12^4, J = 7.8 Hz), 7.35 (d, 2H, H-2^3 and H-12^3, J = 7.8 Hz), 4.95 (s, 2H, H-2^1 and H-12^1), 4.10 (t, 2H, H-17^1, J = 8.1 Hz), 3.98 (q, 2H, H-8^1, J = 7.7 Hz), 3.25 (t, 2H, H-17^2, J = 7.7 Hz), 3.90, 3.86, 3.63, 3.60, 3.32, 3.01 (6s, 18H, H-7^1, H-18^1, H-17^4, 2^1-$COOCH_3$, 2^2-$COOCH_3$, 12^1-$COOCH_3$, and 12^2-$COOCH_3$), 1.81 (s, 6H, 2-CH_3), 1.74 (t, 3H, H-8^2, J = 7.7 Hz), −1.90 (br s, 2H, NH); LRFABMS (*m/z*): 817 ([M + H]$^+$, 100%); HRFABMS, $C_{46}H_{49}N_4O_{10}$ ([M + H])$^+$; calcd.: 817.3455, obsd.: 817.3449.

Acknowledgement

This work was supported by the Natural Sciences and Engineering Research Council of Canada.

References

1. H.I. Pass. J. Natl. Cancer Inst. **85**, 443 (1993).
2. E.M. Beems, T.M.A.R. Dubbelman, L. Lugtenburg, J.A.V. Best, M.F.M.A. Smeets, and P.S. Boegheim. Photochem. Photobiol. **46**, 639 (1987).
3. D. Dolphin. Can. J. Chem. **72**, 1005 (1994).
4. H.J. Callot, A.W. Johnson, and A. Sweeney. J. Chem. Soc. Perkin Trans. 1, 1424 (1973).
5. A.M. Richter, B. Kelly, J. Chow, J.D. Liu, G.H.N. Towers, J. Levy, and D. Dolphin. J. Natl. Cancer Inst. **52**, 501 (1990), and refs. therein.
6. P. Yon-Hin, T.P. Wijesekera, and D. Dolphin. Tetrahedron Lett. **32**, 2875 (1991).
7. E. Sternberg and D. Dolphin. Curr. Med. Chem. **3**, 293 (1996).
8. P. Yon-Hin. Ph.D. Dissertation, University of British Columbia (1989).
9. R.K. Pandey, F. Shiau, K. Ramachandran, T.J. Dougherty, and K.M. Smith. J. Chem. Soc. Perkin Trans. 1, 1377 (1992).
10. R.K. Pandey, N. Jagerovic, J.M. Ryan, T.J. Dougherty, and K.M. Smith. Tetrahedron, **52**, 5349 (1996).
11. L. Ma and D. Dolphin. Tetrahedron: Asymmetry, **6**, 313 (1995).
12. L. Ma and D. Dolphin. Pure Appl. Chem. **68**, 765 (1996).
13. L. Ma and D. Dolphin. Tetrahedron Lett. **36**, 7791 (1995), and refs. therein.
14. L. Ma and D. Dolphin. J. Org. Chem. **61**, 2501 (1996).
15. L. Ma and D. Dolphin. Tetrahedron, **52**, 849 (1996).
16. H. Fischer and H. Orth. *In* Die Chemie des Pyrroles. Vol. II. Part 2. Johnson Reprint Corporation, New York. 1968. pp. 108–112.
17. L. Ma and D. Dolphin. J. Chem. Soc. Chem. Commun. 2251 (1995), and refs. therein.
18. G.W. Kenner, S.W. McCombie, and K.M. Smith. J. Chem. Soc. Perkin Trans. 1, 2517 (1973).
19. H. Scheer and H. Wolf. Tetrahedron, **28**, 5839 (1972).
20. H. Fischer and H. Orth. *In* Die Chemie des Pyrroles. Vol. II. Part 2. Johnson Reprint Corporation, New York. 1968. pp. 229–233.
21. M.T. Cox, A.H. Jackson, G.W. Kenner, S.W. McCombie, and K.M. Smith. J. Chem. Soc. Perkin Trans. 1, 516 (1974).
22. S. Ohta, A. Shimabayashi, M. Aono, and M. Okamoto. Synthesis, 833 (1982).
23. G. Bram and M. Vilkas. Bull. Soc. Chim. Fr., 945 (1964).
24. D.F. Taber, J.C. Amedio, and F. Gulino. J. Org. Chem. **54**, 3474 (1989).
25. K.M. Smith, E.M. Fujinari, K.C. Langry, D.W. Parish, and H. D. Tabba. J. Am. Chem. Soc. **105**, 6638 (1983).
26. R.K. Pandey, N. Jagerovic, J.M. Ryan, T.J. Dougherty, and K.M. Smith. Bioorg. Med. Chem. Lett. **3**, 2615 (1993).
27. K.M. Smith, D.A. Goff, and D.J. Simpson. J. Am. Chem. Soc. **107**, 4946 (1985).
28. H.H. Inhoffen, P. Jager, R. Mahlhop, and C.D. Mergler. Liebigs Ann. Chem. **704**, 188 (1967).

Can. J. Chem. Downloaded from www.nrcresearchpress.com by 88.146.161.215 on 09/08/12
For personal use only.

© 1997 NRC Canada

FTIR spectroscopic investigation of matrix-isolated isomerization and decomposition products of ionized acetone: generation and characterization of 1-propen-2-ol

Xiaokui K. Zhang, J. Mark Parnis, Errol G. Lewars, and Raymond E. March

Can. J. Chem. Downloaded from www.nrcresearchpress.com by 92.62.229.171 on 09/08/12
For personal use only.

Abstract: An electron bombardment – matrix isolation apparatus was used to generate and isolate products from acetone isomerization and decomposition for infrared spectroscopic examination. Bombardment of a dilute acetone/argon gas mixture (1:400) above a 12 K matrix isolation substrate leads to the direct observation of neutral fragmentation and isomerization products. A major product is 1-propen-2-ol, the enolic tautomer of acetone, whose IR absorption spectrum, and that of its perdeutero analog, are interpreted with the aid of ab initio computations. The observation of matrix-isolated decomposition products of acetone such as acetyl radicals, ketene, methane, and CH_3· is interpreted in terms of ion and neutral decomposition processes occurring in the gas phase above the matrix surface and during matrix condensation. The detection of matrix-isolated 1-propen-2-ol is consistent with a process involving acetone ionization, isomerization, neutralization, and stabilization, an approach that may have general utility in the generation of other thermodynamically unfavourable neutral isomers of organic molecules.

Key words: enol, isomerization, acetone, infrared, ionization, 1-propen-2-ol.

Résumé : On a utilisé un appareil de bombardement électronique avec isolement dans une matrice pour générer et isoler les produits d'isomérisation et de décomposition de l'acétone à des fins d'études par spectroscopie infrarouge. Le bombardement d'un mélange gazeux dilué d'acétone dans l'argon (1 : 400) au-dessus d'un substrat matriciel d'isolement maintenu à 12 K permet d'observer directement la fragmentation neutre et les produits d'isomérisation. Un des produits majeurs est le prop-1-én-2-ol, le tautomère énolique de l'acétone, dont le spectre d'absorption IR et celui de son analogue perdeutéré ont pu être interprétés à l'aide de calculs ab initio. L'observation de produits de décomposition l'acétone, comme les radicaux acétyles, le cétène, le méthane et le radical CH_3·, isolés dans une matrice peut être interprétée en fonction de processus de décompositions neutres et ioniques se produisant en phase gazeuse au-dessus de la surface matricielle et au cours de la condensation de la matrice. La détection de prop-1-én-2-ol isolé dans la matrice est en accord avec un processus impliquant l'ionisation, l'isomérisation, la neutralisation et la stabilisation de l'acétone, une approche qui peut être d'une utilité générale pour la production d'autres isomères neutres, thermodynamiquement défavorisés, de molécules organiques.

Mots clés : énol, isomérisation, acétone, infrarouge, ionisation, prop-1-én-2-ol.

[Traduit par la rédaction]

Introduction

The investigation of decomposition and isomerization processes that follow the ionization of gaseous molecules is one of the central and fundamental foci of mass spectrometry. Due to the ease with which they may be detected and manipulated, ionic products generated in the ionization process have been, in general, the predominant source of information used in the investigation of the structure and decomposition mechanisms of precursor molecules. In contrast, investigation of neutral products of ion fragmentation processes cannot be carried out directly by mass spectrometry unless the neutral species are reionized, such as in neutralization–reionization mass spectrometric (NRMS) techniques (1). Most neutral products of ion decomposition remain implicated but undetected players in the overall picture of the events that follow gas-phase ionization.

Matrix isolation has been used successfully for the isolation of highly unstable or very short-lived neutral and ionic species for spectroscopic investigation (2). A number of efforts (3–5) have been made to link matrix isolation techniques with gas-phase ionization methods, mainly to collect and to investigate spectroscopically ionic species generated in an ionization process. Recently, some success has been met in the matrix isola-

Received December 27, 1995.[1]

X.K. Zhang,[2] J.M. Parnis,[3,4] E.G. Lewars, and R.E. March.[4]
Department of Chemistry, Trent University, Peterborough, ON K9J 7B8, Canada.

[1] Revision received January 2, 1997.

[2] Formerly a Ph.D. student in the Trent–Queen's Cooperative Graduate Program. Present address: Laboratory of Biophysical Chemistry, National Heart, Lung, and Blood Institute, Bethesda, MD 20892, U.S.A.
[3] Author to whom correspondence may be addressed: Telephone: (705) 748-1505. Fax: (705) 748-1625. E-mail: mparnis@trentu.ca
[4] Holds an adjunct appointment in the Chemistry Department, Queen's University, Kingston, ON K7L 3N6, Canada.

© 1997 NRC Canada

Can. J. Chem. Downloaded from www.nrcresearchpress.com by 92.62.229.171 on 09/08/12
For personal use only.

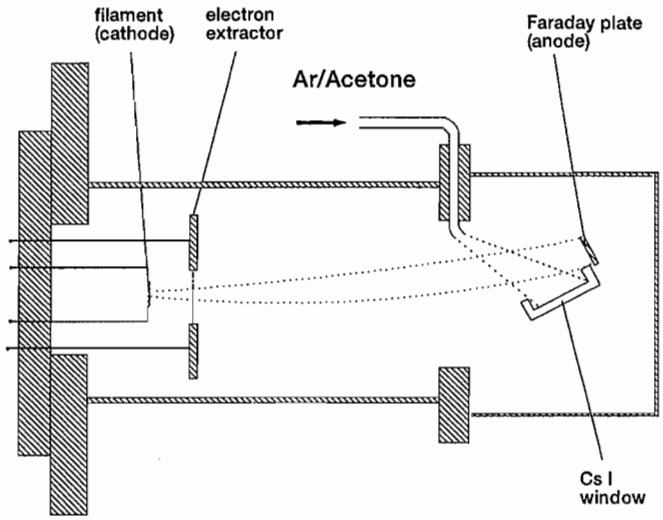
tion of mass-selected ions, such as CF_3^+ and CO_2^+ (5). Much less effort has been dedicated to the stabilization and observation of neutral products of ionization processes, which could include both neutral decomposition fragments and neutralized ionic species. In principle, the spectroscopic investigation of such isolated neutral species would provide information that would otherwise not be accessible by conventional mass spectrometry. With this idea in mind, a series of experiments has been carried out in our laboratory, combining a conventional matrix isolation apparatus with either an electron bombardment source or a quadrupole ion trap, for the isolation and spectroscopic characterization of neutral or ionic species generated in the ionization processes of organic molecules. In this paper, we report the results of our investigation into the isomerization and decomposition processes occurring following the ionization of acetone.

In this work, the enol form of acetone, 1-propen-2-ol, was isolated in a cryogenic matrix, providing evidence for its participation, or that of its ionic precursor, in acetone ionization processes. Several fragments, including the acetyl radical, are also identified and their roles in the overall decomposition processes are discussed. Acetone is an appealing choice of organic molecule in the context of this work, since it is one of the simplest members of a group of carbonyl compounds of the [CH_3COR] type. In this group, which includes aliphatic aldehydes, ketones, acids, and esters, the relative thermodynamic stability of the enol to the keto forms of a given ion is reversed with respect to that of the corresponding neutral forms (6, 7). The gas-phase heats of formation of the enolic ions of these compounds have been measured by Holmes and Lossing (6), showing that the enolic ions studied are 59–130 kJ/mol more stable thermochemically than their ketonic counterpart ions; the neutral keto forms are generally more stable than the corresponding neutral enol forms. The endothermic isomerization of enol acetone cation to its keto form prior to dissociation has been studied by a few groups (8, 9) in the context of the nonergodic decomposition of the enol ion. The reverse exothermic isomerization of the keto molecular ion to its enol form has never been observed directly even though it has been implicated (7, 10) in studies on the dissociation behaviour of the acetyl cation with acetone as a precursor molecule (see below).

Experimental approach

The apparatus used in this work was a modification of the design of Szczepanski et al. (11) and is illustrated schematically in Fig. 1. It consists of an electron source, an ionization zone through which accelerated electrons pass and intersect a stream of matrix support gas containing acetone, and a matrix condensation region where products are trapped. The filament was biased at −70 to −100 V, and a current at 3.0–3.5 A was passed through it to generate thermionically emitted electrons. A centre-meshed steel plate, which served as an electron extractor for acceleration of the electron beam, had an applied positive voltage of +20–30 V. A piece of very thin metal placed perpendicularly to the cold crystal surface on one side of the copper block functioned as a Faraday plate for measurement of electron current, to which a voltage between +50–130 V was applied. Typical kinetic energies of the electron beam ranged from 120 to 250 eV. To minimize undesired interference from photons emitted from the filament, the copper block was rotated about 45 degrees with respect to the central axis during matrix deposition. In the absence of a gas sample, the current reading on the Faraday plate represents the actual number of electrons entering the ionization zone, and was typically 4–10 μA. During sample preparation, the current was observed to increase by two- to three fold. The accelerated electron beam intersected the gas sample flow almost perpendicularly, and immediately above the surface of the cold window. Ionization products, together with the neutral precursor and excess Ar gas, were then co-condensed to form the matrix.

Fig. 1. Details of the ionization housing for the electron impact/matrix isolation (EI/MI) apparatus, showing the electron trajectory profile.



The CsI substrate was cooled to 12 K by means of an APD Cryogenics Displex closed-cycle helium refrigeration system. Acetone (Caledon) or d_6-acetone (MSD Isotopes) was degassed in a series of freeze–pump–thaw cycles in an all-metal, high-vacuum line. Research grade argon gas (>99.9995%) was supplied by Matheson Canada. Mole ratios of Ar/acetone vapour were of the order of 250/1 to 800/1. The premixed gas was introduced through the gas inlet line, which pointed directly at the cold surface (see Fig. 1). The flow of the gas mixture was controlled by a MKS mass-flow controller, typically set to 0.8 cm^3/min. The voltages on the cathode and anode were further adjusted within a small range to maintain a current reading at 80–120 μA. The deposition time was normally 8–12 h.

Fourier-transform infrared absorption spectra were recorded using a Bomem-102 FTIR spectrometer. Minor modifications were made to the sample compartment to accommodate the vacuum manifold. Typical spectra were taken at 1 cm^{-1} resolution with 300–600 scans averaged per spectrum. After the infrared spectrum of the initial deposition was collected, the prepared matrix was exposed to the full (200–1000 nm) or filtered irradiation (cut-off filter: >590 nm and >300 nm) from a xenon arc lamp (150 W). Irradiation time varied from 30 to 60 min for each individual experiment (see below).

© 1997 NRC Canada

Can. J. Chem. Downloaded from www.nrcresearchpress.com by 92.62.229.171 on 09/08/12
For personal use only.

Fig. 2. Infrared spectra of an ionized mixture (upper spectrum) and a non-ionized mixture (lower spectrum) of acetone in argon (1:400) in the range 1500–1000 cm^{-1}. New absorptions only observed following ionization are annotated as E (1-propen-2-ol), K (ketene), M (methane).

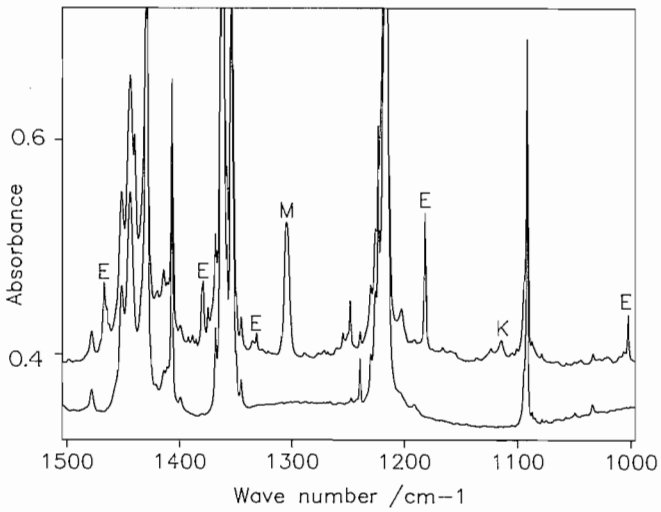
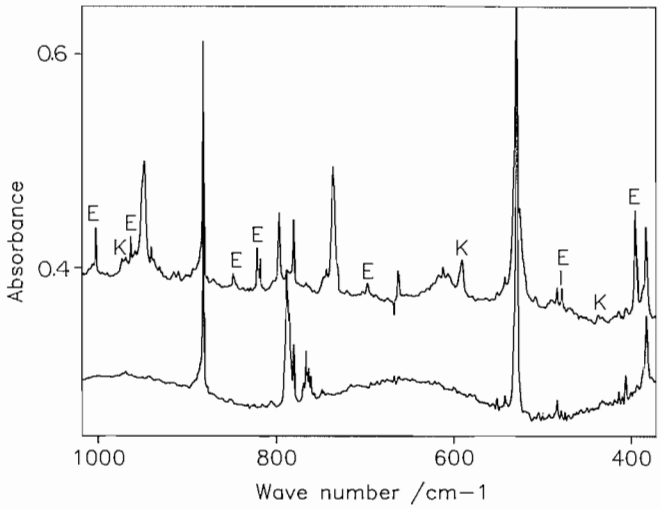


Fig. 3. Infrared spectra of an ionized mixture (upper spectrum) and a non-ionized mixture (lower spectrum) of acetone in argon (1:400) in the range 1000–375 cm^{-1}. New absorptions only observed following ionization are annotated as E (1-propen-2-ol) and K (ketene).



Computational methods

All calculations were done with Spartan[5] except for the potential energy surface scans, and normal mode frequency calculations used for comparison with experiment, for which GAUSSIAN 92 (12) was used; the ab initio (13) HF/6-31G*-optimized geometry and analytical second derivatives were used for the HF/6-31G* frequencies reported here. The semiempirical AM1 method (14) and the ab initio HF/3-21G level were used for PES scans to locate stationary points, and these yielded qualitatively similar surfaces. Examination of the stationary points by geometry optimization and normal-mode vibrational frequencies at the AM1 and the ab initio HF/3-21G and HF/6-31G* levels showed that, at these levels, conformers **1** and **2** are the only minima (see below).

Experimental results

A series of experiments was carried out in which a mixture of Ar/acetone or Ar/d_6-acetone (400:1) was ionized under the conditions outlined above. Spectra obtained under these conditions are hereafter referred to as ionization spectra. For purposes of comparison, similar matrices were also made in which all conditions were held constant except that the electron beam was turned off. With the electron beam on or off, matrices were formed that exhibited absorptions associated with isolated neutral acetone (15), and the hydrogen-bonded acetone–water complex (16). Absorptions due to the common impurities of the vacuum system, CO_2, H_2O, and CO, increased dramatically in the ionization mode, presumably due to the more vigorous outgassing of the filament or metal surfaces. Many new absorption features were also observed only under ionization conditions (see Figs. 2 and 3). The relative intensity of these new absorptions following various irradiations are summarized in Table 1.

The dominant new spectral features observed only under ionization conditions were intense absorptions assigned below to 1-propen-2-ol; the fundamental vibrational mode wave numbers and their associated spectroscopic assignments are listed in Table 2. Selected regions of the absorption spectra are illustrated in Figs. 2 and 3, together with the absorption spectrum of neutral acetone, for comparison. The intensities of the 1-propen-2-ol absorption bands did not change systematically when the electron energy was varied over the range 120–250 eV, and no change followed irradiation of matrices with light in the range of 200–1000 nm for periods in excess of 1 h. The isotopic counterparts of these absorption features were observed following ionization of Ar containing d_6-acetone, and are listed in Table 2.

Other neutral species generated in the ionization process were identified by the behaviour of spectral absorption features following various periods of filtered irradiation (see Table 1), and by comparison with published data. New spectral features observed at 1875, 1321, and 3678 cm^{-1} disappeared following irradiation with >590 nm light for 30 min. The positions of these bands agree very well with three relatively intense bands of the six absorption bands assigned by Jacox (17) to acetyl radicals, generated by abstraction of CHO hydrogen atoms from CH_3CHO molecules by F atoms. No isotopic counterparts for these absorptions were detected in the d_6-acetone experiment. The absorptions at 607 cm^{-1} and the pair at 2138 and 2142 cm^{-1} are attributed to CH_3˙ (18*a*) and CO (18*b*), respectively. These absorptions showed a slight increase in intensity following >590 nm irradiation. The photodecomposition threshold of CH_3CO˙ to form CH_3˙ and CO has been measured at approximately 600 nm (17), which is consistent with the observation in the present study. Clearly identifiable as other neutral products are ketene CH_2CO (19) and CH_4 (20), which are responsible for the absorption features listed in Table 1.

[5] Spartan SGI Version 3.1.3 GL: Wavefunction Inc., 18401 Von Karman, Suite 370, Irvine, Calif. 1994.

© 1997 NRC Canada

Can. J. Chem. Downloaded from www.nrcresearchpress.com by 92.62.229.171 on 09/08/12
For personal use only.

Table 1. Relative intensity of absorbances (excluding those of 1-propen-2-ol) associated with new features present on deposition of ionized mixture of Ar/acetone (400/1), and following various irradiations.

	Relative intensity				
Wave number (cm^{-1})	Initial intensity	>500 nm 60 min	>300 nm 30 min	>200 nm 30 min	Annealing (20 K, 20 s)
$CH_3CO^{\cdot}$					
1875	0.0012	0.0	0.0	0.0	0.0
1321	0.0026	0.0	0.0	0.0	0.0
3678	0.0011	0.0	0.0	0.0	0.0
$CH_3^{\cdot}$					
607	0.0032	0.0053	0.0053	0.0053	0.0053
CO					
2138	0.6517	0.6725	0.7183	0.7411	0.8056
2142	0.6861	0.7027	0.7422	0.7609	0.7958
CH_2CO					
436.4	0.0052	0.0059	0.0062	0.0066	0.0066
591.0	0.0282	0.0296	0.0314	0.0332	0.0338
973.0	0.0065	0.0065	0.0070	0.0081	0.0088
1114.3	0.0118	0.0122	0.0131	0.0135	0.0142
1379.3	0.0402	0.0424	0.0424	0.0424	0.0475
2142	0.6861	0.7027	0.7422	0.7609	0.7958
3153.0	0.0129	0.0141	0.0152	0.0153	0.0174
3062.6	0.0540	0.0554	0.0569	0.0569	0.0603
CH_4					
1305	0.1243	0.1292	0.1375	0.1408	0.1533
3019	0.1864	0.1882	0.1890	0.1914	0.2014
Unassigned					
611.8	0.0089	0.0089	0.0181	0.0281	0.0231
736.4	0.1174	0.1213	0.1313	0.1376	0.1376
796.5	0.0639	0.0656	0.0764	0.0782	0.0745
1123.2	0.0066	0.0066	0.0056	0.0036	0.0050
1247.9	0.0429	0.0429	0.0341	0.0328	0.0328
1559.2	0.0183	0.0171	0.0040	0.0040	0.0
1565.0	0.4961	0.4961	0.4946	0.4882	0.4882
2098.3	0.2273	0.1952	0.1356	0.1225	0.1636

Discussion

Spectral assignment of 1-propen-2-ol

The major new absorption features observed following ionization of acetone are consistent with the fundamental vibrational mode frequencies of matrix-isolated 1-propen-2-ol (CH_3-C(OH)=CH_2), the enol isomer of acetone. In Table 2 are summarized the wave numbers of absorptions attributed to 1-propen-2-ol, together with the corresponding isotopically shifted absorption wave numbers observed in experiments with d_6-acetone. Also included in Table 2 are the scaled (21) wave number predictions for h_6- and d_6-1-propen-2-ol, based upon ab initio SCF calculations of the equilibrium geometry and energy of 1-propen-2-ol. Several of the absorption features attributed to 1-propen-2-ol are similar to those of matrix-isolated vinyl alcohol CH_2=CHOH, the enolic tautomer of acetaldehyde (22). For example, the OH and C=C stretching modes of vinyl alcohol (OH stretching: 3625.0 cm^{-1}; C=C stretching: 1631.0 cm^{-1}) are similar to those of 1-propen-2-ol (OH stretching: 3622.4 cm^{-1}; C=C stretching: 1673.1 cm^{-1}). The main difference between the two spectra is the observation of stretching, deformational, and rocking modes that are characteristic of a methyl group in 1-propen-2-ol; in the vinyl alcohol spectrum these absorption features are absent.

The spectral assignment is supported by the remarkable agreement between the observed and calculated wave numbers of the h_6 and d_6 forms of 1-propen-2-ol. This agreement is illustrated for 1-propen-2-ol in Fig. 4. Two closely related local minimum energy conformations (**1** and **2**, Fig. 5), both of C_s symmetry, were found for 1-propen-2-ol in computations performed using both 3-21G and 6-31G* basis sets. The total energies for conformations **1** and **2** are −191.932 342 and −191.937 924 hartrees (6-31G*), respectively. Therefore, conformation **1**, with energy 14.7 kJ/mol lower than that of conformation **2**, is predicted to be the minimum energy conformation. With either the 6-31G* or 3-21G basis sets, the predicted wave numbers for conformation **1** generally match the experimental data better than do those for conformation **2**,

© 1997 NRC Canada

Can. J. Chem. Downloaded from www.nrcresearchpress.com by 92.62.229.171 on 09/08/12
For personal use only.

Table 2. Observed and calculated (6-31G*) vibrational mode wave number values for h_6-1-propen-2-ol and d_6-1-propen-2-ol. Calculated values have been scaled by a factor of 0.89.

$CH_3C(OH)CH_2$			$CD_3C(OD)CD_2$			
Obsd.	Calcd.	Int.[a]	Obsd.	Calcd.		Assignment[b]
3622.4	3652.6	w	2639.4	2659.4	$\nu_1(A')$	ν(OH str.)
2992.2	3050.2	w	—	2271.8	$\nu_2(A')$	ν(CH_2 asym. str.)
2978.7	2966.7	w	2195.9	2184.4	$\nu_3(A')$	ν(CH_2 sym. str.)
2950.2	2945.0	w	2183.5	2178.9	$\nu_4(A')$	ν(CH_3 asym. str.)
2921.4	2911.2	w	2125.0	2156.7	$\nu_{17}(A'')$	ν(CH_3 asym. str.)
2835.5	2861.4	w	2083.7	2058.8	$\nu_5(A')$	ν(CH_3 sym. str.)
1673.1	1683.2	w	1625.0	1624.1	$\nu_6(A')$	ν(C═C str.)
1466.7	1456.6	m	1293.0	1287.7	$\nu_7(A')$	δ(CH_3 def./CH_2 scis.)
1439.3	1440.0	w	1104.7	1108.4	$\nu_{18}(A'')$	δ(CH_3 def.)
—	1425.9		1055.6	1056.8	$\nu_8(A')$	ν(CC str./CH_2 scis.)
1379.0	1392.0	m	—	1045.7	$\nu_9(A')$	δ(CH_3 def./CO str.)
1331.2	1326.0	w	—	1038.0	$\nu_{10}(A')$	ν(CO str./CCC bend)
1181.7	1183.3	s	922.3	928.0	$\nu_{11}(A')$	ν(O-C-C asym. str.)
1050.4	1051.7	w	848.6	876.7	$\nu_{19}(A'')$	ρ_r(CH_3 rock)
1002.4	1002.3	m	843.0	824.5	$\nu_{12}(A')$	ρ_r(CH_3 rock/CO str.)
963.3	955.4	w	—	756.4	$\nu_{13}(A')$	δ(CH_2 def./OCC str.)
848.6	840.6	w	—	715.4	$\nu_{20}(A'')$	δ(CH_2 def.)
821.6	821.3	w	642.7	673.0	$\nu_{14}(A')$	ν(O-C-C sym. str.)
697.2	712.8	w	—	461.2	$\nu_{21}(A'')$	ρ_t(C═CH_2 torsion)
494.1	494.8	w	—	403.4	$\nu_{22}(A'')$	δ(CCOC framework def.)
478.3	462.4	w	396.1	397.4	$\nu_{15}(A')$	ρ_w(OH wag)
395.4	393.9	s	—	329.2	$\nu_{23}(A'')$	ρ_t(C-OH torsion)
—	388.5		276.0	287.1	$\nu_{16}(A')$	ρ_w(CH_3 wag)
—	178.9		—	129.7	$\nu_{24}(A'')$	ρ_t(C-CH_3 torsion)

[a]Observed spectroscopic absorption intensity.

[b]Assignment refers to configuration **1** of h_6-1-propen-2-ol described in the text. The labels sym. and asym. refer to symmetric and antisymmetric motions under its local symmetry. Modes for which more than one qualitative descriptor are given indicate those involving strong coupling.

suggesting that matrix-isolated 1-propen-2-ol is likely to be in conformation **1**. Most observed vibrational frequencies agree with the 6-31G* predicted values within ± 10 cm^{-1} when a scaling factor of 0.89 is employed (21), except for some vibrational mode frequencies, such as OH stretching and the asymmetric CH stretching modes, for which agreement is less satisfactory.

Assignment of the vibrational modes of 1-propen-2-ol was made in conjunction with the calculated normal mode wave numbers and their predicted atomic displacement descriptions. The normal modes of 1-propen-2-ol are predicted to involve strong coupling between C–O stretching and C–C stretching or CH_3 deformational motions, the former giving rise to essentially symmetric and antisymmetric coupled stretching motions. The C–O stretching motion is predicted to be coupled also to the framework C═C-C bending motion. Thus, calculations suggest that there is no clearly assignable C–O stretching mode in this molecule, since significant C–O stretching is involved in each of ν_9, ν_{10}, ν_{11}, and ν_{14}. In addition, the scissoring motion of the CH_2 group is coupled strongly to the CH_3 umbrella-type deformation and the C–C stretch.

Mechanistic considerations

Since the only significant decomposition process for acetone cations in gas-phase electron impact and collision-induced dissociation experiments is formation of acetyl cations and methyl radicals following C—C bond cleavage (23), it is necessary to consider additional neutralization processes in order to explain the origin of the products observed in the present study. The relatively large internal energy associated with cation–electron recombination processes, implicated in the present work by the observation of predominantly neutral products, appears to allow a significantly richer chemistry to occur.

The presence of free electrons in the ionization region above the matrix surface, along with the requirement of charge balance in the matrix, suggests that many cationic species formed above the matrix surface would be neutralized as they are carried by the matrix gas flow toward the cold substrate, or following matrix condensation. That such processes are important in the present work would appear to be evidenced by the absence of spectral features attributable to cationic species. When neutralization occurs far from the matrix surface,

© 1997 NRC Canada

Fig. 4. Spectral line diagrams illustrating the (*A*) calculated 6-31G* and (*B*) observed wave number positions and intensities for vibrational modes of 1-propen-2-ol. The calculated wave number positions have been scaled by a factor of 0.89.

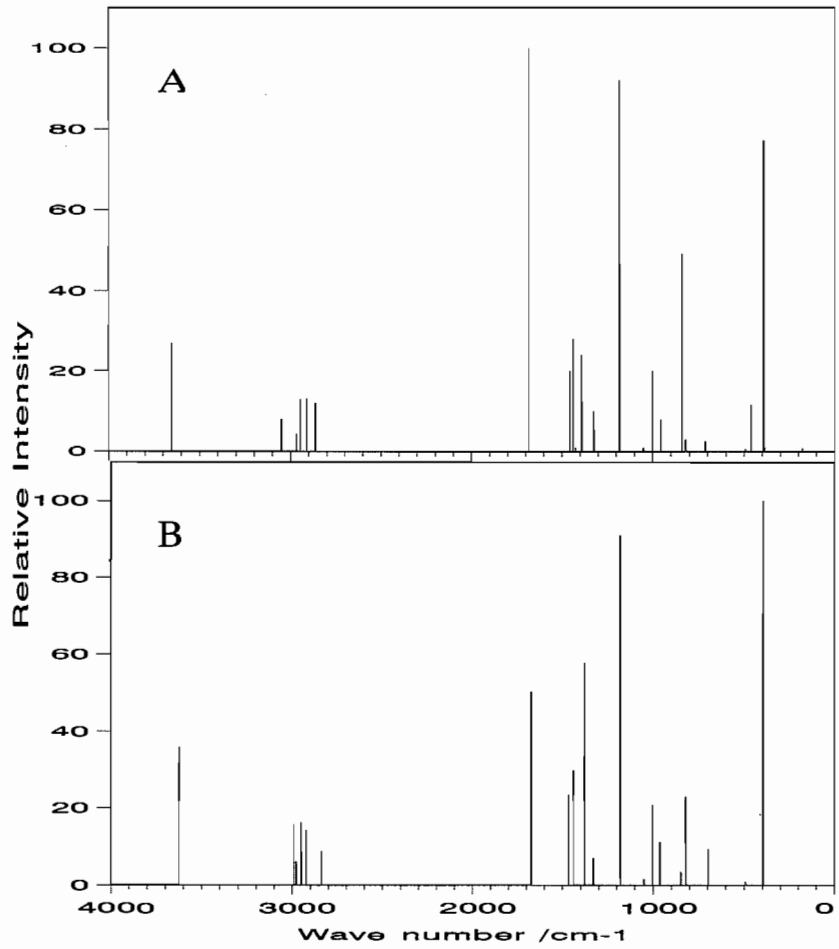
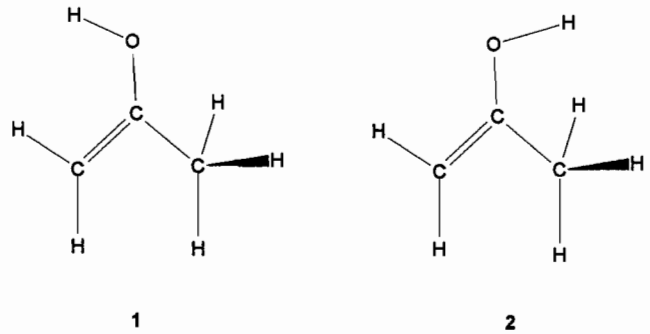


Fig. 5. Illustration of the 6-31G* optimized geometries of conformations **1** and **2** of 1-propen-2-ol.



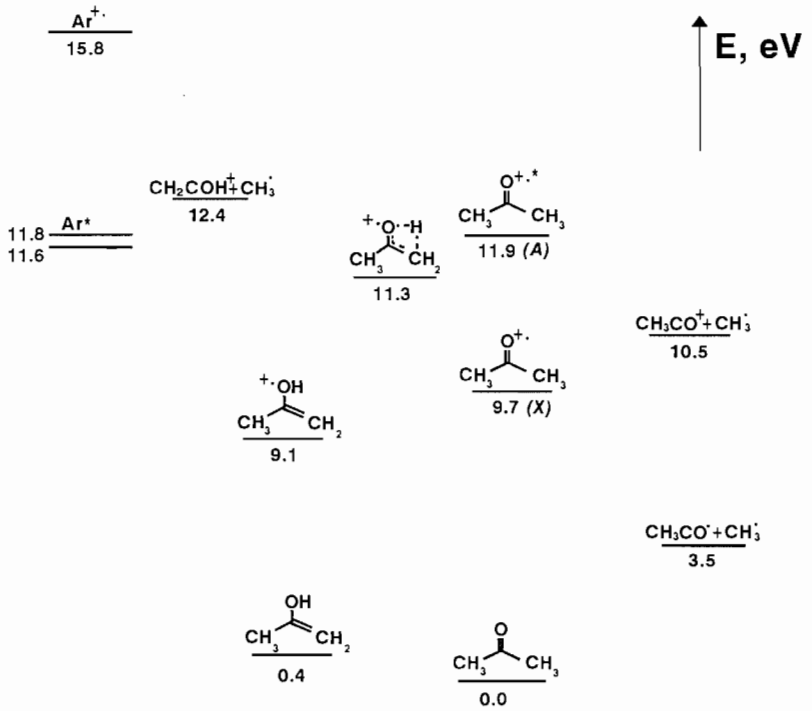
gas-phase unimolecular decomposition of the newly formed neutral species would be expected to dominate due to the extremely large amounts of energy involved in cation–electron recombination processes. In the case of acetone, energy of the order of its ionization potential (9.71 eV) would be released, which is much greater than the endothermicity associated with the activation energy for decomposition of acetone to $CH_3CO^{\cdot}$ + $CH_3^{\cdot}$, given that the homolytic bond dissociation energy of neutral acetone to form $CH_3CO^{\cdot}$ + $CH_3^{\cdot}$ is 3.56 eV (24). Indeed, sufficient energy is available to allow decomposition to 2 CH_3 + CO to occur as well. Should neutralization occur at or beneath the matrix surface, the neutralized species would be expected to lose excess energy rapidly through energy transfer interactions with Ar atoms. When energy transfer to the matrix quenches unimolecular decomposition, or when cage effects significantly inhibit dissociation processes through matrix-induced fragment recombination, the neutralized species would be stabilized and isolated in the rigid Ar matrix. Thus, the fate of ions neutralized by electron recombination processes is expected to depend heavily upon whether recombination occurs in the gas phase above the matrix, or within the matrix solid.

Electron bombardment of dilute mixtures of acetone vapour in Ar can lead to the ionization of acetone molecules by direct electron impact, or via charge exchange and Penning ionization. The large excess of Ar atoms in the gas mixture suggests that the primary electron impact processes would be ionization of Ar atoms (IE(Ar)) = 15.76 eV (24) and electronic excitation of neutral Ar atoms, for which the minimum excitation energy is 11.6 eV (25) (see Fig. 6). Ionization of acetone can then

Can. J. Chem. Downloaded from www.nrcresearchpress.com by 92.62.229.171 on 09/08/12
For personal use only.

© 1997 NRC Canada

Fig. 6. Energy level diagram for neutral and ionized acetone, 1-propen-2-ol, and Ar, and associated fragments in the acetone system. Relative energies are cited from refs. 9, 24, 26, and 30.



occur by both charge exchange (CE) reactions (transfer of an electron from acetone to Ar^+) and Penning ionization (PI) reactions (ionization of acetone following collision with Ar^*). Both processes are highly exothermic, and would lead directly to formation of acetone cations with up to about 6 eV (CE) or 2 eV (PI) excess internal energy. This excess is much greater than the 0.8 eV endothermicity associated with the activation energy of the lowest energy decomposition pathway for the ground electronic state *X* of acetone cations, leading to the formation of acetyl cations and methyl radicals (24). Given that acetone cations are known to decompose from the *X* state on a picosecond time scale following collisional excitation (27), it is likely that any acetone cations formed in the X state would decompose essentially instantaneously in the gas phase above the matrix surface. It is, therefore, unlikely that isomerization of the acetone radical cation in its ground *X* state would be a viable source of enol cations. The presence of methyl radicals in the matrix spectra of ionized acetone is likely due in part to this primary decomposition process. Subsequent hydrogen atom abstraction from acetone or scavenging of H-atoms by methyl radicals is a likely source of methane.

The absence of spectral features attributable to the acetyl cation suggests that any such cations formed in decomposition of ground state acetone cations are subject to subsequent ion decomposition, or neutralization through electron capture. However, it is known that acetyl cations do not survive electron transfer in NRMS experiments (23), suggesting that acetyl radical decomposition fragments, and not acetyl radicals themselves, should be observed here as the final products of acetone cation recombination processes, should recombination occur in the gas phase. Such a process may contribute to the formation of ketene, a major product in this work, since ketene ions are the major product of acetone cation neutralization–reionization experiments when K vapour is employed as a neutralization gas (23).[6] Alternately, electron recombination following isolation of the acetyl cation in the matrix solid would favour stabilization of the intact acetyl radical and is likely the major source of the acetyl observed in this work.

Formation of the 1-propen-2-ol cation directly from the ground-state acetone cation would appear to be highly unlikely. However, several studies have implied that the first excited electronic *A* state of the acetone cation is also formed in small amounts following electron impact ionization of acetone (27, 28). Molecular ions formed in the *A* state are stable for at least 30 μs (29, 30), and Bombach et al. (27) have attributed this unusually long lifetime to a reversible, symmetry-allowed isomerization to form the 1,2-epoxypropane radical cation in its electronic ground state. Metastable 1,2-epoxypropane cations may also isomerize to form the 1-propen-2-ol radical cation. Therefore, formation of the *A* state of the acetone radical cation may be a route to formation of the enol cation, via the following scheme:

$$\text{Acetone (A)}^+ \rightleftharpoons \text{1,2-epoxypropane}^+ \rightleftharpoons \text{1-propen-2-ol}^+$$

Other experimental evidence to support the feasibility of such keto→enol cation isomerization is provided by unimolecular

[6] Note that ketene ion formation is not observed when Xe is used as the neutralization gas, suggesting that the formation of ketene is a high-energy process. In the present work, neutral acetone formed by electron capture would have nearly twice the 5.37 eV internal energy released in K vapour NRMS, such that the high-energy route to ketene formation would likely be highly favoured.

© 1997 NRC Canada

Can. J. Chem. Downloaded from www.nrcresearchpress.com by 92.62.229.171 on 09/08/12
For personal use only.

Can. J. Chem. Downloaded from www.nrcresearchpress.com by 92.62.229.171 on 09/08/12
For personal use only.

(7) and collision-induced dissociation (10) studies of $C_2H_3O^+$ ions generated by electron impact ionization of acetone, both of which suggest that a minor fraction of ionized acetone converts to the enol form prior to decomposition.

If the 1-propen-2-ol cation were formed as a result of isomerization from the long-lived *A* state of the acetone cation, its fate following neutralization would depend also upon where the subsequent neutralization reaction occurred. If the neutralization happens far from the matrix surface, the 1-propen-2-ol molecule would most likely isomerize back to acetone due to its high relative thermodynamic instability and the relatively modest barrier[7] to enol–keto isomerization compared with the energy of electron–cation recombination. If the neutralization reaction occurs during the condensation process, the newly formed and highly energized neutral 1-propen-2-ol molecule might be stabilized through energy transfer to the matrix solid and isolated by the surrounding Ar atoms, thereby allowing it to retain its enol configuration. Once stabilized, the barrier to enol–keto isomerization would be formidable, given the limited internal energy present at 12 K. We consider this route to be the most likely source of the 1-propen-2-ol in the matrix following ionization of acetone.

Further spectroscopic studies of the products of electron bombardment of dihalomethanes, in combination with mass spectroscopic studies and theoretical calculations, have demonstrated that this experimental approach also leads to the generation of iso-dihalomethanes, which will be described elsewhere (32).

Conclusion

This work has shown that a small fraction of acetone molecular ions may tautomerize to 1-propen-2-ol ions, possibly via the *A* state. In addition, infrared spectra of the highly unstable neutral 1-propen-2-ol and its deuterated analog are presented for the first time. These observations signal a new approach for synthesis and stabilization of highly unstable organic species in the matrix environment, which we refer to as the ionization–isomerization–neutralization–stabilization method. It is possible that this synthesis technique can be developed further to generate and to isolate other unstable organic isomers, so long as their ionic counterparts can be formed, either through isomerization or decomposition, in the ionization process.

Acknowledgements

The financial support of the Natural Sciences and Engineering Research Council of Canada (Operating Grants program) is gratefully acknowledged. X.K.Z. wishes to thank Queen's University for graduate research fellowship support.

References

1. J.L. Holmes. Mass Spectrom. Rev. **8**, 513 (1989); N. Goldberg and H. Schwartz. Acc. Chem. Res. **27**, 347 (1994); F.W. McLafferty. Int. J. Mass Spectrom. Ion Processes, **118–119**, 221 (1992); J.K. Terlouw. Adv. Mass Spectrom. **11B**, 984 (1989); C. Wesdemiotis and F.W. McLafferty. Chem. Rev. **87**, 485 (1987).
2. (*a*) L. Andrews. *In* Chemistry and physics of matrix-isolated species. *Edited by* L. Andrews and M. Moskovits. Elsevier, New York. 1989. pp. 17–46; (*b*) M.E. Jacox. *In* Chemistry and physics of matrix-isolated species. *Edited by* L. Andrews and M. Moskovits. Elsevier, New York. 1989. pp. 77–105.
3. L. Andrews. *In* Molecular ions: spectroscopy, structure and chemistry. *Edited by* T.A. Miller and V.E. Bondebey. Elsevier, New York. 1983.
4. D. Forney, M. Jakobi, and J.P. Maier. J. Chem. Phys. **90**, 600 (1989).
5. (*a*) T.H. Halasinski, J.T. Godbout, J. Allison, and G.E. Leroi. J. Phys. Chem. **98**, 3930 (1994); (*b*) J.T. Godbout, T.H. Halasinski, G.E. Leroi, and J. Allison. J. Phys. Chem. **100**, 2892 (1996).
6. J.L. Holmes and F.P. Lossing. J. Am. Chem. Soc. **102**, 1591 (1980).
7. P.C. Burgers, J.L. Holmes, J.E. Szulejko, A.A. Mommers, and J.K. Terlouw. Org. Mass Spectrom. **18**, 254 (1983).
8. F. Tureček and F.W. McLafferty. J. Am. Chem. Soc. **106**, 2525 (1984).
9. T.H. Osterheld and J.I. Brauman. J. Am Chem. Soc. **115**, 10311 (1993).
10. F. Tureček and F.W. McLafferty. Org. Mass Spectrom. **18**, 608 (1983).
11. J. Szczepanski, D. Roser, W. Personette, M. Eyring, R. Pellow, and M. Vala. J. Phys. Chem. **96**, 7876 (1992).
12. M.J. Frisch, G.W. Trucks, M. Head-Gordon, P.M.W. Gill, M.W. Wong, J.B. Foresman, B.G. Johnson, H.B. Schlegel, M.A. Robb, E.S. Replogle, R. Gomperts, J.L. Andres, K. Raghavachari, J.S. Binkley, G. Gonzales, R.L. Martin, D.J. Fox, D.J. DeFrees, J. Baker, J.J.P. Stewart, and J.A. Pople. GAUSSIAN 92. Gaussian, Inc., Pittsburgh, Pa. 1992.
13. W.J. Hehre, L. Radom, P. v. R. Schleyer, and J.A. Pople. Ab initio molecular orbital theory. Wiley–Interscience, New York. 1986.
14. M.J.S. Dewar, E.G. Zoebisch, E.F. Healy, and J.J.P. Stewart. J. Am. Chem. Soc. **107**, 3902 (1985).
15. G. Dellepiane and J. Overend. Spectrochim. Acta, **22**, 593 (1966).
16. X.K. Zhang, E.G. Lewars, R.E. March, and J.M. Parnis. J. Phys. Chem. **97**, 4320 (1993).
17. M.E. Jacox. Chem. Phys. 69, 407 (1982).
18. (*a*) M.E. Jacox. J. Mol. Spectrosc. **66**, 272 (1977); (*b*) H. Dubost and A. Abouaf-Marguin. Chem. Phys. Lett. **17**, 269 (1972).
19. C.B. Moore and G.C. Pimentel. J. Chem. Phys. **38**, 2816 (1963).
20. K. Nakamoto. Infrared and Raman spectra of inorganic and coordination compounds. Wiley, New York. 1986.
21. J.B. Foresman and A. Frisch. Exploring chemistry with electronic structure methods. Gaussian, Inc, Pittsburg, Pa. 1993. p. 78.
22. M. Hawkins and L. Andrews. J. Am. Chem. Soc. **105**, 2525 (1983).
23. P.C. Burgers, W. Kulik, C. Versluis, and J.K. Terlouw. Int. J. Mass Spectrom. Ion Processes, **98**, 247 (1990).
24. S.G. Lias, J.E. Bartmess, J.F. Liebman, J.L. Holmes, R.D. Levin, and W.G. Mallard. J. Phys. Chem. Ref. Data, **17**, Supp. 1 (1988).
25. M.T. Bowers (*Editor*). Gas phase ion chemistry. Vol. 3. Ions and light. Academic Press, New York. 1984.
26. J.H. Futrell, A.K. Shukla, R. Zhao, and R. Chawla. Proc. 42th Annu. Conf. Am. Soc. Mass Spectrom., Chicago, Ill. 1994. p. 210.

[7] The analogous barrier for the conversion of hydroxyethylidene to vinyl alcohol has been calculated to be 235 kJ mol^{-1} (31).

© 1997 NRC Canada

27. R. Bombach, J.P. Stadelmann, and J. Vogt. Chem. Phys. **72**, 259 (1982).
28. K. Qian, A. Shukla, and J. Futrell. J. Chem. Phys. **10**, 5988 (1990).
29. D.M. Mintz and T. Baer. Int. J. Mass Spectrom. Ion Phys. **25**, 39 (1977).
30. K. Qian, A. Shukla, S. Howard, S. Anderson, and J. Futrell. J. Phys. Chem. **93**, 3889 (1989).
31. B.J. Smith, M.T. Nguyen, W.J. Bouma, and L. Radom. J. Am. chem. Soc. **113**, 6452 (1991).
32. X.K. Zhang, J.M. Parnis, E.G. Lewars, and R.E. March. Manuscript in preparation.

Can. J. Chem. Downloaded from www.nrcresearchpress.com by 92.62.229.171 on 09/08/12
For personal use only.

© 1997 NRC Canada

Equilibrium acidities of some carbon acids in acetonitrile

W. Galezowski, M. Stanczyk, and A. Jarczewski

Abstract: The pK_a values for C-acids (4-nitrophenylnitroalkanes, 4-nitrophenyl-(4-X-phenyl)cyanomethanes, 2,4,6-trinitrotoluene, and 9-cyanofluorene) in acetonitrile have been measured. These values were determined spectrophotometrically in buffer solutions consisting of a strong amine base and its picrate or perchlorate using known potentiometric pK_a's of amines, and they range from 19 for bis(4-nitrophenyl)cyanomethane to 25.1 for ethyl bis(4-nitrophenyl)acetate.

Key words: C-acids, pK_a values, equilibrium, reactivity, proton transfer reaction.

Résumé : On a mesuré les pK_a de C-acides (4-nitrophénylnitroalcanes, 4-nitrophényl-(4-X-phényl)cyanométhanes, 2,4,6-trinitrotoluène et 9-cyanofluorène) en solution dans l'acétonitrile. On a déterminé ces pK_a d'une façon spectrophotométrique, en solutions dans des tampons formés d'une amine fortement basique et de son picrate ou de son perchlorate, en utilisant des pK_a potentiométriques connus d'amines; ces valeurs varient de 19 pour le bis(4-nitrophényl)cyanométhane à 25,1 pour le bis(4-nitrophényl)acétate d'éthyle.

Mots clés : C-acides, valeurs de pK_a, équilibre, réactivité, réaction de transfert de proton.

[Traduit par la rédaction]

Can. J. Chem. Downloaded from www.nrcresearchpress.com by 92.62.229.171 on 09/08/12
For personal use only.

Introduction

Over several years the mechanism of proton transfer reactions in solutions has attracted the attention of a number of laboratories (1–5). One of the most useful solvents for carrying out the kinetic and equilibrium experiments appears to be acetonitrile (6–9). This highly polar, aprotic solvent was successfully used to study the effect of the polarity on deuterium kinetic isotope effects (KIE) (10, 11). The KIE is sensitive to the symmetry of the transition state, which is a function of the strength of the C-acid and of the base (1, 2, 12, 13). Therefore the pK_a values of reacting bases and C-acids are of interest. The reaction products in acetonitrile were thought to be ion pairs, and pseudo Benesi–Hildebrand equilibrium constants were measured (8, 10). In addition to the fact that they had no physical meaning, the equilibrium constants derived from equilibrium and kinetic measurements were often different from each other. This stemmed, in part, from the non-reproducible concentration of the amine cation. Therefore, taking advantage of the fact that the potentiometric pK_a's of numerous amine bases in acetonitrile are known, pK_a's of some C-acids have been conveniently determined in appropriate buffer solutions. For years most of the C-acids have been used extensively in proton transfer studies focused on kinetic isotope effects and proton tunneling.

Received September 12, 1996.

W. Galezowski, M. Stanczyk, and A. Jarczewski.[1] Faculty of Chemistry, A. Mickiewicz University, Grunwaldzka 6, Poznań, Poland.

[1] Author to whom correspondence may be addressed. Telephone: 659-562. Fax: 011-4861-658008. E-mail: arnold@chem.amu.edu.pl

Results and discussion

At spectrophotometric concentrations, the product of the reaction of a relatively strong carbon acid with amine bases in acetonitrile is extensively dissociated into free ions (8, 10). The equilibrium can be described by eq. [1]:

$$[1] \quad K = f^2[BH^+][A^-]/([B][AH])$$

The measurements should be carried out in buffers consisting of a base and its salt, so that the concentration of BH^+ can be controlled.

At a constant concentration of BH^+ a Benesi–Hildebrand equation is followed,

$$[2] \quad C_{AH}/A = 1/\varepsilon + 1/(\varepsilon K_{Ben} C_B)$$

where A is the absorbance of the product, ε the molar extinction coefficient, and K_{Ben} the pseudo equilibrium constant by the Benesi–Hildebrand method. K_{Ben}'s and ε's are found from a C_{AH}/A vs. $1/C_B$ plot at a constant C_{AH} and $[BH^+]$.

The values of K, quoted in Table 1, were calculated using eq. [3].

$$[3] \quad K = K_{Ben} f^2[BH^+]$$

In this paper, for some C-acids, K_{Ben} values were determined for several concentrations of $[BH^+]$ and the resulting equilibrium constants K did not depend significantly on $[BH^+]$.

The pK_a values were calculated using eq. [4]. The results are summarized in Table 2. The average pK_a values were taken.

$$[4] \quad pK_a = -\log K + pK_{BH^+}$$

© 1997 NRC Canada

Can. J. Chem. Downloaded from www.nrcresearchpress.com by 92.62.229.171 on 09/08/12
For personal use only.

Table 1. Results of spectrophotometric studies of C-acids in buffer solutions in acetonitrile at 25°C.

C-acid	Base (pK_{BH^+})	$10^3[BH^+]$	$10^3[B]$	K_{Ben}	ε	K	pK_a
1	PhTMG (20.6 (30))	0.5(picrate)	1–100	1770 ± 150	27200 ± 600	0.763	20.7
2	TMG (23.3 (31))	0.5(perchl.)	1–100	610 ± 80	25000 ± 2000	0.26	23.9
4	TMG	2.5(perchl.)	2–25	620 ± 20	13700 ± 200	1.13	23.2
4	TMG	2.5(picrate)	2–25	820 ± 10	13380 ± 40	1.51	23.1
6	TMG	1.25(perchl.)	1–250	3780 ± 100	40900 ± 300	3.74	22.7
6	TMG	2.5(perchl.)	1–250	1790 ± 20	41800 ± 200	3.30	22.8
6	TMG	5(perchl.)	1–250	1050 ± 20	41400 ± 400	3.48	22.7
6	TMG	12.5(perchl.)	1–250	552 ± 4	41200 ± 300	3.80	22.7
6	TMG	1.25(picrate)	1–250	3200 ± 100	42500 ± 300	3.20	22.8
6	TMG	2.5(picrate)	1–250	1870 ± 40	42600 ± 300	3.44	22.7
6	TMG	4(picrate)	1–250	1320 ± 20	42100 ± 300	3.62	22.7
7	TMG	2.5(perchl.)	1–250	700 ± 10	54800 ± 600	1.29	23.2
7	TMG	1(picrate)	1–250	1950 ± 10	54690 ± 80	1.59	23.1
7	TMG	2.5(picrate)	1–250	800 ± 20	53200 ± 500	1.48	23.1
8	PhTMG	0.5(picrate)	1–10	470 ± 50	38600 ± 3000	0.20	21.3
9	TBA (18.1 (16))	0.4(perchl.)	1–10	336 ± 5	68900 ± 900	0.117	19.0
10	TMG	0.5(picrate)	1.25–40	41 ± 1	30600 ± 500	0.017	25.1
10	TMG	1(picrate)	1.25–40	22 ± 2	31800 ± 300	0.017	25.1
11	TBA	0.2(perchl.)	10–80	9.5 ± 0.7	26000 ± 2000	0.0019	20.8

Table 2. Equilibrium acidities of C-acids ($CHR^1R^2R^3$) in acetonitrile at 25°C.

C-acid	R^1	R^2	R^3	pK_a	Relevant kinetic studies
1	NO_2	4-Nitrophenyl	H	20.7, 20.6 (13)	22, 23
2	NO_2	4-Nitrophenyl	Ethyl	23.9	8
3	NO_2	4-Nitrophenyl	i-Pr	25.9 (10)	8
4	2,4,6-Trinitrophenyl	H	H	23.2	24, 25
5	CN	4-Nitrophenyl	H	25.4 (10)	7
6	CN	4-Nitrophenyl	Phenyl	22.7	7, 12, 26, 27
7	CN	4-Nitrophenyl	4-Methoxyphenyl	23.1	27
8	CN	4-Nitrophenyl	4-Bromophenyl	21.3	27
9	CN	4-Nitrophenyl	4-Nitrophenyl	19.0	27, 28
10	COOEt	4-Nitrophenyl	4-Nitrophenyl	25.1	29
9-Cyanofluorene (**11**)				20.8	

Activity coefficients were calculated using a partially extended Debye–Hückel equation (14).

$$[5] \quad -\log f = 1.53\ \mu^{1/2}/(1 + (4.8 \times 10^7)a\mu^{1/2})$$

An a value of 6 Å was taken for all ions.

For some C-acids, measurements were run with amine perchlorates and picrates as the salt component of the buffer and satisfactory agreement was achieved. For example, see results for **6** in Table 1. The pK_a's seem reliable within 0.1 pK unit.

Some ion association can be expected for alkanenitronates (15), which would lead to an overestimation of equilibrium acidity as defined by eqs. [1] and [4]. For instance, the dissociation constant for tetramethylguanidinium 4-nitrophenyl methanenitronate is 6.9×10^{-3} (conductometric value) (15) or $(8.4–9) \times 10^{-3}$ (spectrophotometric values) (15). Therefore for the 4-nitrophenylnitromethane reaction, measurements were run at low cation concentration and the resulting pK_a is identical within 0.1 pK unit with that reported by Gandler and Bernasconi (13), who used benzoate buffer. With TNT and nitrophenylcyanoalkanes, ion association is negligible (15). A change in ε, as determined from eq. [2], with $[BH^+]$ would be symptomatic of ion association. Such changes were observed with 9-cyanofluorene and this could distort its pK_a. Again, as in the case of nitroalkanes, a small concentration of the salt was used to minimize ion-association effects.

Using amine bases to determine pK_a has some disadvantages as compared to anionic bases. One possible threat is the homoconjugation of the BH^+ cation. This should not influence our results in the ranges of concentrations used. Tributylam-

© 1997 NRC Canada

Can. J. Chem. Downloaded from www.nrcresearchpress.com by 92.62.229.171 on 09/08/12
For personal use only.

monium cations do not form homoconjugates $(Bu_3N)_2H^+$ (16). With guanidines, homoconjugation constants determined potentiometrically are not large: 5.3 and 1.9 M^{-1} for TMG and PhTMG (17). Some absorbances were measured in the base concentration range in which homoconjugation becomes important, to make estimation of ε exact, but they had little impact on the slopes of the Benesi–Hildebrand plots and thus on the K_{Ben}'s. Molar absorptivities of the anions should not be affected by homoconjugation of the base. There are also reports of extensive dimerization of TMG base (18). This would complicate the system. However, our differential vapor pressure measurements showed that there is no substantial dimerization up to 1 M TMG (17).

A number of pK_a's for various C-acids have been determined in DMSO (19), but most of the C-acids were weaker than those studied in this work. The values that can be compared are 12.3 (20), 8.3 (19), and 8.6 (21) for **5**, **11**, and **1**, respectively. The resulting $\Delta pK_{a\ (MeCN-DMSO)}$ values of 13.1, 12.5, and 12.1 (for **5**, **11**, and **1**, respectively) are similar to that of 12.9 for phenolphthalein (31).

Using data from ref. 27 and Table 2 a Brönsted plot for the reaction of C-acids **6–9** with TMG was constructed. It gave $\alpha = 0.46 \pm 0.02$ for proton transfer and $\alpha = 0.50 \pm 0.03$ for deuteron transfer, with good correlation coefficients.

Experimental

The syntheses of C-acids have been described elsewhere: 4-nitrophenylnitromethane (**1**) (6), 4-nitrophenyl-1-nitropropane (**2**) (8), 4-nitrophenylphenylcyanomethane (**6**) (32), 4-methoxyphenyl-4-nitrophenylcyanomethane (**7**) (33), 4-bromophenyl-4-nitrophenylcyanomethane (**8**) (33), bis(4-nitrophenyl)cyanomethane (**9**) (10), ethyl bis(4-nitrophenyl)acetate (**10**) (34), and 9-cyanofluorene (**11**) (35). All C-acids were recrystallized from alcohol except **9** (10).

1,1,3,3-Tetramethylguanidine (**TMG**), the commercial product by Aldrich, was stored over KOH pellets and fractionally distilled at 4 Torr (1 Torr = 133.3 Pa). 2-Phenyl-1,1,3,3-tetramethylguanidine (**PhTMG**) was synthesized according to the method of Bredereck (36) and purified as described above for **TMG**. Tributylamine from Aldrich was stored over KOH pellets and fractionally distilled.

The bases were protected from atmospheric moisture and carbon dioxide. Picrates of amine bases were readily obtained and recrystallized from alcohol. Melting points were the same as previously reported.

Perchlorates of TMG and PhTMG were prepared by mixing aliquots of the base and 70% perchloric acid in alcohol. With PhTMG, upon removal of the solvents under vacuum, at temperatures up to 50°C, white crystals formed. These were dissolved in absolute ethanol and the solvent was removed again. These operations were repeated until the weight of residue corresponded to the stoichiometric amount of the salt.

With $TMGHClO_4$, crystallization did not occur unless initiated with Dry Ice. The perchlorates were dissolved in dry acetonitrile to obtain stock solutions of the salts. Acetonitrile, a good spectrometric grade from Romil, was shaken with CaH_2, distilled from P_2O_5, then fractionally distilled from CaH_2. The distillate was protected from CO_2 and moisture.

Most of the absorbances were measured on an HP 8452 diode-array spectrophotometer fitted with thermostated cell holder. The solutions of base and C-acid were prethermostated before mixing to minimize the time needed for equilibration and thus the effect of oxidation. Product decay was particularly important for nitriles and **10**. Except for **10**, within some 15 min the decrease in absorbance did not affect K_{Ben} values, but did affect the ε's. This weak dependence of K_{Ben} on time of measurement may stem from comparable rates of product decay in cells with different C_B. If the analytical concentration of C-acid was at any moment the same in all solutions, i.e., decreasing with time but independent of C_B, using the initial value of C'_{AH} in eq. [2] instead of the true value C_{AH} would make both the slope and intercept of the Benesi–Hildebrand plot C'_{AH}/C_{AH} times larger than the correct values, and this would result in reduced $\varepsilon' = \varepsilon C_{AH}/C'_{AH}$ and unchanged $K'_{Ben} = K_{Ben}$.

Taking advantage of the fact that ionization of nitriles is faster than product decay, for some reactions an Applied Photophysics stopped-flow spectrophotometer was used to avoid ambiguities. The ε's were somewhat higher than those obtained with the HP diode array but there was no essential change in pK_a.

The product of the relatively slow ionization reaction of **10** is very susceptible to oxidation. Reproducible results were obtained on the diode array spectrophotometer when a small amount of antioxidant, ascorbic acid, was used. The concentration of the antioxidant in the cell was 8×10^{-5} M, which was about three times higher than the concentration of the C-acid.

Product decay can lead to unreasonably large differences in ε's for the same ion of C-acid in acetonitrile, for instance, for reactions of the same C-acid with different bases (37). Therefore the stopped-flow technique should be used for equilibrium measurements of fast reactions with unstable products.

Except for **11**, the intense absorption bands of the products do not interfere with absorption of the buffer solutions, even when picrates are used, and absorbances measured at λ_{max} of the product were taken for calculations of K_{Ben} and ε, as follows: **1** (490 nm), **2** (504 nm), **4** (520 nm), **6** (580 nm), **7** (582 nm), **8** (582 nm), **9** (648 nm), **10** (630 nm). With **11**, perchlorate needed to be used, and the analytical wavelength was 300 nm. Small corrections for absorbance of buffer solution were applied where needed.

Acknowledgements

The authors are grateful for financial support from KBN Grant 2 P 303 121 07.

References

1. R.P. Bell. The proton in chemistry. 2nd ed. Chapman and Hall, London. 1973.
2. E.F. Caldin and V. Gold (*Editors*). Proton transfer reactions. Chapman and Hall, London. 1975.
3. A. Müller, H. Ratajczak, W. Junge, and E. Diemann. Electron and proton transfer in chemistry and biology. Elsevier, Amsterdam. 1992.
4. Special issue. Chem. Phys. **136** (1989).
5. E. Buncel and C.C. Lee. Isot. Org. Chem. **2** (1975).
6. E.F. Caldin, A. Jarczewski, and K.T. Leffek. Trans. Faraday Soc. **67**, 1100 (1971).
7. P. Pruszyński, A. Jarczewski. J. Chem. Soc. Perkin Trans. 2, 1117 (1986).

© 1997 NRC Canada

8. W. Galezowski and A. Jarczewski. J. Chem. Soc. Perkin Trans. 2, 1647 (1989).
9. G. Schroeder, B. Leska, A. Jarczewski, B. Nowak-Wydra, and B. Brzezinski. J. Mol. Struct. **344**, 77 (1995).
10. W. Galezowski and A. Jarczewski. Can. J. Chem. **70**, 935 (1992).
11. K.T. Leffek and P. Pruszyński. Can. J. Chem. **66**, 1454 (1988).
12. A. Jarczewski and P. Pruszyński. Pol. J. Chem. **58**, 1175 (1984).
13. J.R. Gandler and C.F. Bernasconi. J. Am. Chem. Soc. **114**, 631 (1992).
14. I.M. Kolthoff and M.K. Chantooni, Jr. J. Am. Chem. Soc. **91**, 2875 (1969).
15. W. Galezowski, I. Grzeskowiak, M. Stanczyk, and A. Jarczewski. J. Chem. Soc. Perkin Trans. 2. 2647 (1996).
16. J.F. Coetzee and G.R. Padmanabhan. J. Am. Chem. Soc. **87**, 5005 (1965).
17. W. Galezowski, A. Jarczewski, M. Stanczyk, B. Brzezinski, F. Bartl, and G. Zundel. J. Chem. Soc. Faraday Trans. Submitted.
18. I.M. Kolthoff and M.K. Chantooni, Jr. J. Am. Chem. Soc. **97**, 1376 (1975).
19. W.S. Matthews, J.E. Bares, J.E. Bartmess, F.G. Bordwell, F.J. Cornforth, G.E. Drucker, Z. Margolin, R.J. McCallum, G.J. McCollum, and N.R. Vanier. J. Am. Chem. Soc. **97**, 7006 (1975).
20. E.A. Walters. J. Phys. Chem. **81**, 1995 (1977).
21. J.R. Keeffe, J. Morey, C.A. Palmer, and J.C. Lee. J. Am. Chem. Soc. **101**, 1297 (1979).
22. E.F. Caldin and S. Mateo. J. Chem. Soc. Faraday Trans. 1, **71**, 1876 (1975).
23. J.H. Blanch, O. Rogne, and L.I. Rossemyr. J. Chem. Soc. Faraday Trans. 1, **76**, 1905 (1980).
24. P. Pruszyński and A. Jarczewski. Rocz. Chem. **51**, 2171 (1977).
25. N. Sugimoto and M. Sasaki. J. Chem. Soc. Faraday Trans. 1, **81**, 1441 (1985), and refs. therein.
26. G. Schroeder, B. Brzezinski, and A. Jarczewski. J. Mol. Struct. **274**, 83 (1992).
27. M. Hojatti and K.T. Leffek. Can. J. Chem. **62**, 2653 (1983).
28. P. Pruszyński and K.T. Leffek. Can. J. Chem. **69**, 205 (1991).
29. G. Schroeder and A. Jarczewski. Z. Phys. Chem. **271**, 175 (1990).
30. K.T. Leffek, P. Pruszyński, and K. Thanapaalasingham. Can. J. Chem. **67**, 590 (1989).
31. I.M. Kolthoff, M.K. Chantooni, Jr., and S. Bhowmik. J. Am. Chem. Soc. **90**, 23 (1968).
32. H. Neresheimer and W. Rupple. US Patent 2080057 (1937); Chem. Abstr. **31**, 4830 (1937).
33. L.C. Prizzini and R.B. Davis. J. Org. Chem. **25**, 1884 (1966).
34. R.S. Yost and C.R. Hauser. J. Am. Chem. Soc. **69**, 2325 (1947).
35. W. Wislicenus and K. Russ. Ber. Dtsch. Chem. Ges. **43**, 2719 (1910).
36. H. Bredereck and K. Bredereck. Chem. Ber. **94**, 2278 (1961).
37. M. Dworniczak and K.T. Leffek. Can. J. Chem. **68**, 1657 (1990).

Can. J. Chem. Downloaded from www.nrcresearchpress.com by 92.62.229.171 on 09/08/12
For personal use only.

© 1997 NRC Canada

Photolysis of 5,5-dibenzyl-Δ^3-1,3,4-oxadiazolines[1]

John Warkentin and John McK.R. Woollard

Abstract: Photolysis of dibenzyl-Δ^3-1,3,4-oxadiazolines (**3**) in the presence of dimethyl acetylenedicarboxylate (DMAD) gives only modest yields of the expected symmetrical 3,3-dibenzylcyclopropenes (**4**), but these are accompanied by more than six by-products, including unsymmetrical cyclopropenes, methylenecyclopropanes, and various pyrazoles. The origin of this array of products can be explained by a series of steps starting with photolysis of **3** to form a diazoalkane that undergoes 1,3-dipolar cycloaddition to DMAD, generating a 3*H*-pyrazole as initial product. The latter is further photolyzed to a symmetrical cyclopropene in competition with benzyl group migration by thermal 1,5-sigmatropic or ion-pair rearrangement to afford a 4*H*-pyrazole. The 4*H*-pyrazole in turn undergoes photolysis to an unsymmetrical cyclopropene, which rearranges to a methylenecyclopropane. The 4*H*-pyrazole also undergoes autoxidation, in the presence of air, to afford a benzoyl-4*H*-pyrazole. Additionally, in competition with rearrangement, the various pyrazoles lose a benzyl group or a methoxycarbonyl group to afford pyrazoles with one less substituent.

Key words: 5,5-dibenzyl-Δ^3-1,3,4-oxadiazolines, photolysis of; 3,3-dibenzyl-3*H*-pyrazoles, rearrangement of; 3,4-dibenzyl-4*H*-pyrazoles, autoxidation of; 3,4-dibenzyl-4*H*-pyrazoles, photolysis of; cyclopropenes, rearrangement to methylenecyclopropanes.

Résumé : La photolyse des dibenzyl-Δ^3-1,3,4-oxadiazolines (**3**) en présence d'acétylènedicarboxylate de diméthyle (ADCD) ne fournit que de faibles rendements des 3,3-dibenzylcyclopropènes (**4**) symétriques attendus; toutefois, ceux-ci sont accompagnés par plus de six sous-produits incluant des cyclopropènes non symétriques, des méthylènes cyclopropanes et divers pyrazoles. On peut expliquer l'origine de cette série de produits par une série d'étapes commençant par la photolyse du produit **3** conduisant à un diazoalcane qui subit une cycloaddition 1,3-dipolaire sur l'ADCD pour conduire au 3*H*-pyrazole comme produit initial. Ce dernier peut subir une photolyse subséquente en cyclopropène symétrique, en compétition avec une migration sigmatropique-1,5 thermique du groupe benzyle ou une transposition de la paire d'ions qui conduit à un 4*H*-pyrazole. Le 4*H*-pyrazole subit à son tour une photolyse en cyclopropène non symétrique qui se réarrange en un méthylènecyclopropane. Le 4*H*-pyrazole subit aussi une autooxydation, en présence d'air, qui conduit au benzoyl-4*H*-pyrazole. De plus, en compétition avec les réarrangements, les divers pyrazoles perdent un groupe benzyle ou un groupe méthoxycarbonyle pour fournir des pyrazoles important un substituant de moins.

Mots clés : photolyse de 5,5-dibenzyl-Δ^3-1,3,4-oxadiazolines, réarrangement de 3,3-dibenzyl-3*H*-pyrazoles, autooxydation et photolyse de 3,4-dibenzyl-4*H*-pyrazoles, réarrangement de cyclopropènes, à méthylènecyclopropanes.

[Traduit par la rédaction]

Introduction

As part of our ongoing studies of reactive intermediates, we wished to prepare a series of dibenzylcyclopropenes with the general structure **4***a–e*. Earlier experience with three-membered rings indicated that **4** ought to be formed by extended photolysis of a mixture of dimethyl acetylenedicarboxylate (DMAD) and appropriate Δ^3-1,3,4-oxadiazolines (**3**), available in good yield from simple dibenzylketones (**1***a–e*) by oxidation of their acetylhydrazones (**2**) using lead tetraacetate (LTA) (1–3) (Scheme 1).

The crucial photolysis stage giving **4** would consist of a sequence of five steps, for each of which there is ample precedence. First, photolytic cleavage of **3** would form diazoalkane **5**, which would be trapped by DMAD to give 3*H*-pyrazole **6** (2). Further irradiation in situ would convert **6** into vinyl diazo compound **7**. This in turn would readily lose nitrogen on continued photolysis to give a vinyl carbene (**8**), which characteristically can collapse to the desired cyclopropene (**4**) (4–8) (Scheme 2).

Judging from previous reports, the conversion of a 3*H*-pyrazole to a cyclopropene is highly efficient, normally occurring with yields approaching 100% (4, 6, 9), and the method can even be used to generate more highly strained ring systems such as cyclopropabenzenes (10); similarly the

Received May 23, 1996.[2]

J. Warkentin[3] and J.McK.R. Woollard.[3,4] Chemistry Department, McMaster University, 1280 Main Street West, Hamilton, ON L8S 4M1, Canada.

[1] Presented in part at the 75th Annual Conference of the Canadian Society for Chemistry, Edmonton, Alberta, Canada, 1–4 June, 1992.

[2] Revision received December 13, 1996.

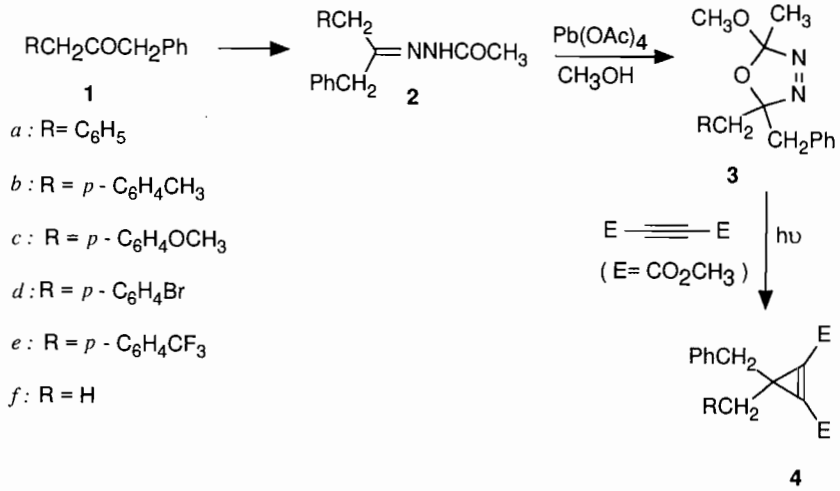
[3] Correspondence may be addressed to either author.
J.W. — Telephone: (905) 525-9140. Fax: (905) 522-2509.
E-mail: warkent@mcmaster.ca
J.McK.R.W. — Telephone: (403) 479-9292.
Fax: (403) 474-1933.
E-mail: woollard@math.concordia.edmonton.ab.ca

[4] Present address: Chemistry Department, Concordia University College of Alberta, 7128 Ada Boulevard, Edmonton, AB T5B 4E4, Canada.

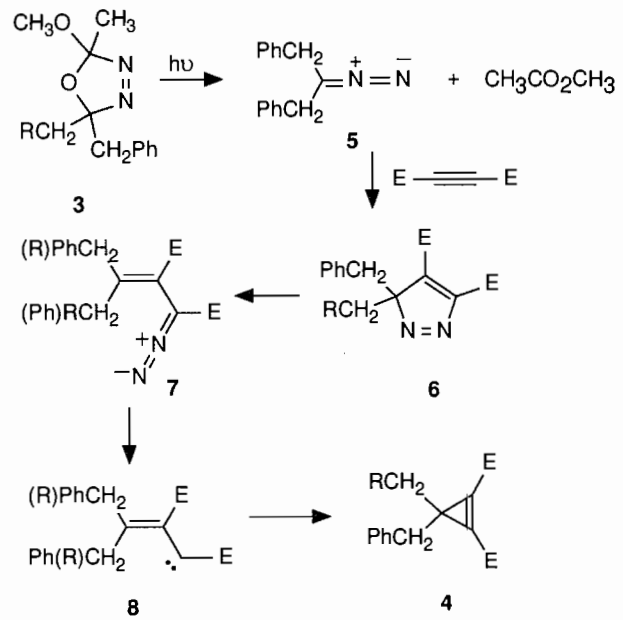
© 1997 NRC Canada

Can. J. Chem. Downloaded from www.nrcresearchpress.com by 92.62.229.171 on 09/08/12
For personal use only.

Scheme 1.



Scheme 2.



(R as in Scheme 1, *a* - *e*)

3*H*-pyrazole is obtained from the oxadiazoline typically in yields of about 70% (2). Although the photolytic steps each require somewhat different wavelengths for optimum efficiency, in practice either a Hanovia medium-pressure mercury lamp (4) or a Rayonet apparatus with 300 nm lamps (2) can provide enough spectral width to make a "one-pot" process feasible. We had anticipated, then, that this composite photolysis stage would give something like 60% of the desired three-membered ring and that, overall, we would have an attractive and simple route to our target molecules. It was thus surprising and disappointing to discover that the cyclopropenes (**4**) were produced in only low yields during the photolysis, and that they were accompanied by a wide range of other products in comparable amounts. One of these additional products has already been reported (3), and it is the purpose of this paper to clarify the nature of the other products, to suggest their origins, and to present details of a set of versatile and potentially useful reactions.

Results and structural assignments

As outlined above, the major products from the photolysis of Δ^3-1,3,4-oxadiazolines in the presence of DMAD were expected to be cyclopropenes (**4**). As for possible by-products, inspection of the literature suggested that these would include azines (**9**) formed by self-reaction of two molecules of the diazoalkanes (2), dienes (**10**) formed from vinyl carbenes (**8**) by a hydrogen shift (4, 7), 1:2 adducts (**11**) formed by cycloaddition of a molecule of a diazoalkane to a 3*H*-pyrazole such as **6** (11), oxiranes (**12**) formed by loss of nitrogen from the oxadiazolines (2), and 4*H*-pyrazoles (**13**) produced by migration of a group from the 3-position of 3*H*-pyrazoles (**6**) (6).

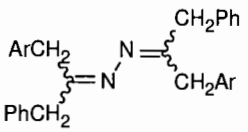
In practice, it was found that not only were the desired cyclopropenes formed in yields of merely 10–30%, but also that the six or more by-products fitted none of the precedents described above. Thus the mixture of by-products nearly always included 1,3-diarylpropenes (**14** and **15**), unsymmetrical cyclopropenes (**16**), methylenecyclopropenes (**17** and **18**), dibenzylpyrazoles (**19**), monobenzylpyrazoles (**20**), and pyrazole N-oxides (**25**), plus frequently one or more of the benzoyl pyrazoles **21**, **22**, and **23**.

Separation and isolation of the various products was achieved using centrifugal chromatography, a particularly sensitive process in this study owing to the presence of strongly absorbing chromophores in all the products. Structures followed from analysis of their spectroscopic properties, and some of the more significant features of those spectra are given below. Assignment of structure to compounds in the series **16** has already been outlined (3) and ^{13}C NMR data are summarized in Table 1.

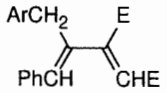
The compounds **17** and **18** initially presented a challenge, since they co-eluted under every elution condition tried. Moreover when a *para* substituent was present in the starting material, there were generally two isomers of each, giving a total of four isomers in the mixture. Fortunately, the last system examined proved to be an exception; with a *para*-trifluo-

Can. J. Chem. Downloaded from www.nrcresearchpress.com by 92.62.229.171 on 09/08/12
For personal use only.

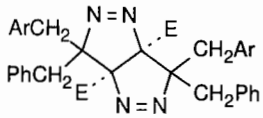
© 1997 NRC Canada



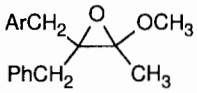
9



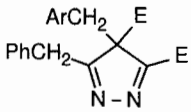
10



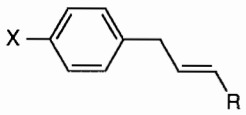
11



12



13



14

a : X = H, R = C_6H_5

b : X= CH_3, R= C_6H_5

c : X = H, R = *p* - $C_6H_4CH_3$

d : X = CH_3O, R= C_6H_5

e : X = H, R = *p* - $C_6H_4OCH_3$

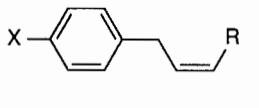
f : X = Br, R = C_6H_5

g : X = H, R = *p* - C_6H_4Br

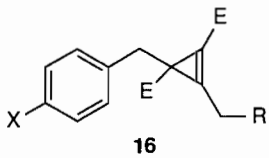
h : X = CF_3 , R = C_6H_5

i : X = H, R = *p* - $C_6H_4CF_3$

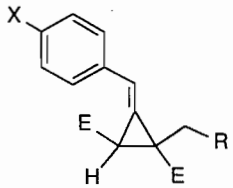
j : X= R= H



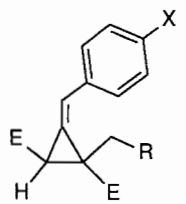
15



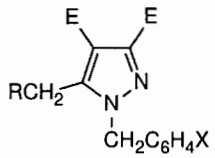
16



17



18



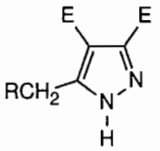
19

romethyl group present, *only two* isomers were produced, **17***h* and **18***h*, which, with some care, could be cleanly separated, and their formulae established. Furthermore, their spectra permitted disentanglement of the spectra of the mixed isomers from other experiments. In their ^{1}H NMR spectra each compound showed one proton (δ ca. 3.4 ppm) coupled (J = 2 Hz) to a single vinyl proton (δ ca. 6.7 ppm), and both sets of compounds had signals from one methylene group. In the series **17** this was a singlet, by coincidental equivalence of diastereotopic protons, whereas in series **18** the CH_2 signal was an AB quartet, presumably in consequence of the closer proximity of the other aryl group. Long-range C-H correlation spectra for **17***h* confirmed that the *para*-trifluoromethylphenyl group was bonded to the vinyl group, and a similar investigation on a mixture enriched in **18***a* identified a carbonyl carbon (δ = 170.3 ppm in the ^{13}C NMR spectrum; see Table 2) as being close to the methylene group. The geometry indicated for these compounds followed from NOE experiments. Thus in **17***h*, irradiation at the frequency of the methylene hydrogens gave signal enhancement for both the vinyl-H and the *ortho*-H of the phenyl ring, whereas irradiation of the methine-H caused signal enhancement for the *ortho*-H of the trifluoromethylphenyl group but not of the vinyl or the methylene hydrogens, showing that the methine-H was close to the aryl group on the exocyclic double bond, and *trans* to the methylene group. In contrast, irradiation of the methine-H in **18***a* gave no enhancement of the signal from the methylene hydrogens but a small enhancement of the vinyl-H signal.

Although compounds **21**, **22**, and **23** were isolated directly from the photolysis mixtures on different occasions, they were also formed regularly, although in varying amounts, from an unstable compound, described below, and it thus appeared they were closely related. In support of this hypothesis, the three products **21***a*, **22***a*, and **23***a*, apparently derived from **6**, all showed strong peaks in their mass spectra at m/z = 105, suggestive of the benzoyl fragment, whose presence was also indicated by a series of characteristic signals in their ^{1}H NMR spectra. Both **22***a* and **23***a* had prominent IR peaks at ca. 3300 cm^{-1} indicating the presence of an N-H group, and the ^{13}C NMR spectrum of **23***a* made an excellent fit with that for the corresponding acetyl compound **23***d* (12). The ^{1}H NMR spectra of compounds **22** showed that they had one ester group and one benzyl group. The signal from the methylene group of the latter, at ca. 4.5 ppm, indicated a fairly deshielded environ-

Can. J. Chem. Downloaded from www.nrcresearchpress.com by 92.62.229.171 on 09/08/12
For personal use only.

© 1997 NRC Canada



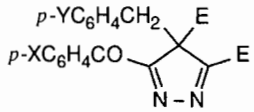
20

a : R = Ph

b : R = *p* - $C_6H_4CH_3$

c : R = *p* - C_6H_4Br

d : R = H



21

a : X = Y = H

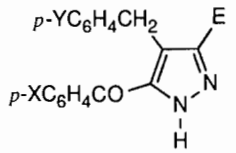
b: X = H, Y = CH_3

c : X = H, Y = OCH_3

d : X = Br, Y = H

e : X = H, Y = Br

f : X = CF_3, Y = H



22

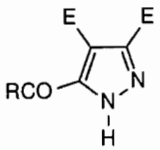
a : X = Y = H

b : X = H, Y = CH_3

c : X = H, Y = OCH_3

d : X = H, Y = Br

e : X = CF_3, Y = H



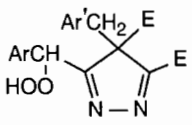
23

a : R = Ph

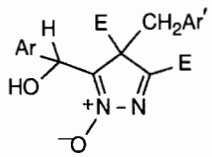
b : R = *p* - C_6H_4Br

c : R = *p* - $C_6H_4CF_3$

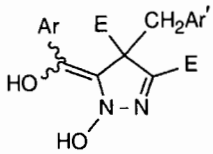
d : R = CH_3



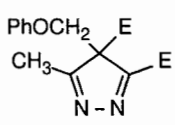
24



25



26



27

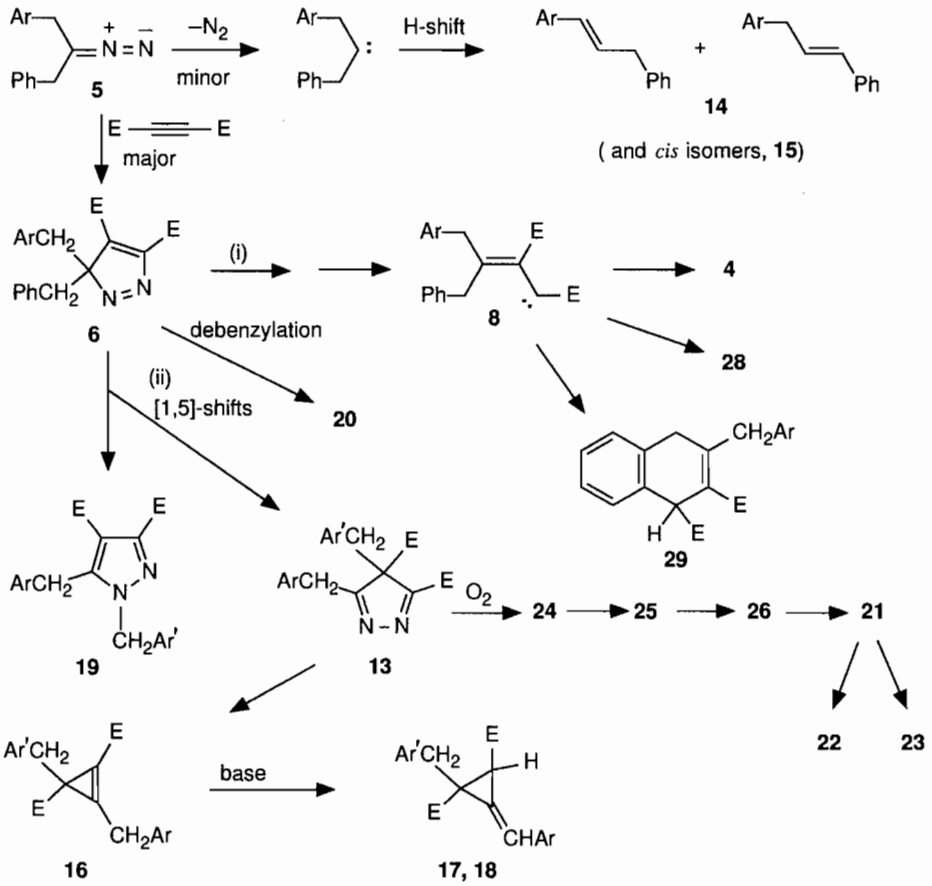
ment, consistent with the placement shown. Compounds **21** gave infrared spectra without N-H peaks. In the ^{1}H NMR spectrum of **21***a* the methylene group appeared as an AB quartet at ca. 3.8 ppm suggesting the presence of a benzyl group bonded to a quaternary carbon, and in the ^{13}C NMR spectrum there was one signal at ca. 78 ppm, typical of a quaternary carbon bearing electron-withdrawing groups. Further information was obtained from a long-range C-H correlation investigation. Thus the hydrogens of the methoxyl at 3.7 ppm coupled with the ester carbonyl carbon at 163 ppm, and those at 4.1 ppm coupled with the carbonyl carbon at 160 ppm, thus indicating clearly which low-field carbons were from carbonyl groups, the former presumably being from the sp^3-bound ester group. Consequently, the signals at 173 and 168 ppm have to be assigned to the ring sp^2 carbons, and appropriately both showed coupling with the methylene hydrogens, which in turn also couple with the quaternary carbon at ca. 78 ppm. These relationships, plus mass constraints and the fact that the quaternary carbon of a 4*H*-pyrazole typically absorbs at ca. 63–80 ppm (13, 14), dictate that compounds **21** must have a 4*H*-pyrazole nucleus.

The common source of **21**, **22**, and **23** appeared to be a yellow compound that was formed consistently in all experiments. Although the yellow material could be preserved for months when stored under N_2, exposure to air quickly gave rise to mixtures of **21**, **22**, and smaller amounts of **23**. The assignment of a structure for this yellow precursor proved to be difficult. In the UV spectra there were longer wavelength absorption maxima at 282 and 372 nm and in the IR spectra there were strong peaks at 3300 cm^{-1} pointing to an OH or NH group, a feature confirmed by the effect of added D_2O (exchange) on the ^{1}H NMR spectrum. In the ^{1}H NMR spectra, signals included a one-proton exchangeable singlet at ca. 8.0 ppm, a one-proton singlet at ca. 5.7 ppm, and an AB quartet with signals located at ca. 3.3 and 3.8 ppm, along with two methyl ester groups and an appropriate number of aromatic hydrogens (without any indication of pronounced deshielding). Apparently one benzyl group had been modified in some way at the methylene group, while the other evidently remained intact. In the ^{13}C NMR spectra, salient features included two sp^2 carbon signals very close together at ca. 143 ppm, a methine carbon signal at ca. 100 ppm, a quaternary carbon signal at ca. 64 ppm, and one methylene carbon signal at ca. 43 ppm. A single-bond C-H correlation spectrum of the yellow compound from **3***d* confirmed that there were no other methine groups, and that the proton giving the signal at 8.1 ppm was not attached to a carbon. Long-range C-H correlation experiments on the yellow compounds from both **3***a* and **3***c* showed coupling of the methylene protons to both the carbon at 64 ppm and one (or both?) of the carbons at 143 ppm, but unfortunately did not pick out any coupling between the methine-H and nearby carbons, nor other helpful structural

Can. J. Chem. Downloaded from www.nrcresearchpress.com by 92.62.229.171 on 09/08/12
For personal use only.

© 1997 NRC Canada

Scheme 3.



relationships. In NOE experiments on the yellow compound from **3***d*, irradiation of either of the methylene hydrogens caused enhancement of the signal at 8.0 ppm and that at 5.7 ppm, as well as of that of an *ortho*-H of the unsubstituted phenyl group. Irradiation of the proton absorbing at 5.7 ppm caused enhancement of the signal at 8.0 ppm as well as of those *ortho*-H of the bromophenyl group and one of the methylene protons. Lastly, irradiation of the proton at 8.0 ppm caused enhancement of the signal from the *ortho*-H of the bromophenyl group.

Bearing in mind that the yellow materials in question decomposed to benzoyl pyrazoles (**21**–**23**) and absorbed at 3300 cm^{-1} in the infrared, hydroperoxide **24** was first considered as a possible structure. In this, the groups are disposed suitably to fit the observed interactions in the long-range correlation experiments, and the quaternary carbon signal at 64 ppm well suits C4 of a 4*H*-pyrazole (13, 14). Moreover, this structure is mechanistically reasonable, for it is known that 4*H*-pyrazoles are readily formed from 3*H*-pyrazoles (6, 15), and autoxidation of benzylic compounds, such as cumene, to hydroperoxides is well precedented. It had to be noted, however, that in similar 4*H*-pyrazoles the sp^2 carbons of that ring usually give signals at 160–180 ppm rather than at ca. 143 ppm as observed (cf. compounds **21**, **27**, and **34**, and examples in refs. 13 and 14), and it was not clear how a hydroperoxy group could significantly affect the chemical shifts of the sp^2 carbons of the pyrazole ring. Further, the yellow colour was not an obvious consequence of the structure **24**. Nevertheless **24** is a plausible product from **13**, and a solution to the puzzle was sought based on the premise that **24** is indeed formed by radical chain autoxidation of **13**, but it is then converted swiftly to the yellow compound **25**.

Given that hydrogen peroxide or peracids are effective reagents for converting *N*-heterocycles to corresponding *N*-oxides, we propose that **24** are rapidly converted to corresponding pyrazole *N*-oxides (**25**) by intramolecular reaction. Models for **25** do have absorptions in the UV/visible spectrum (16, 17) and the exchangeable OH, the IR, and the NOE results fit well. Moreover, with an *N*-oxide structure, the chemical shifts of the ring carbons should be significantly affected. Finally, the formation of benzoyl pyrazoles **21**, **22**, and **23** from **25** can be accounted for nicely, as described in the Discussion.

Discussion

The origin of the various products can be ascribed to transformation of the diazoalkane **5** by one minor and two major pathways, each followed by further reaction as in Scheme 3. The minor pathway is loss of nitrogen from **5** to give a carbene, but both major pathways derive from trapping of **5** by the DMAD to produce the 3*H*-pyrazole **6**. This then either rearranges (path ii) or loses nitrogen (path i) to give the vinyl carbene **8** that collapses to some of the products of Scheme 3.

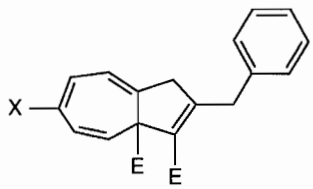
© 1997 NRC Canada

Can. J. Chem. Downloaded from www.nrcresearchpress.com by 92.62.229.171 on 09/08/12
For personal use only.

Can. J. Chem. Downloaded from www.nrcresearchpress.com by 92.62.229.171 on 09/08/12
For personal use only.

This basic scheme is supported by the results from photolysis of oxadiazoline **3***a* (without DMAD) at −70°C in toluene-d_8. After 4 h it had been converted almost totally to methyl acetate and the diazoalkane **5***a*, in whose carbon spectrum the diazocarbon appeared at 48 ppm. During storage at −20°C for 15 h, approximately 70% of the compound had decomposed to azine **9***a* plus smaller amounts of propenes **14***a* and **15***a*, and after 5 days the decomposition was complete. In no other experiment was any trace of such an azine found, indicating that the rate of reaction of the diazoalkane with DMAD is substantially faster than its self-reaction. On the other hand, since propenes were consistently found in modest amounts in both this and all other photolysis experiments, photolytic loss of nitrogen from **5** was competitive with dipolar cycloaddition to DMAD. Once a carbene was generated by nitrogen loss, a rapid H-shift gave propenes. Moreover, since only hydrogen shifts seem to have occurred, without any evidence for a phenyl shift, the precursor carbene presumably reacted from the singlet state (18). As might be expected, when propenes **14** and **15** were produced, the yields of *trans* isomer tended to exceed those of the *cis* isomer, and when a *para* substituent was present in **3**, both positional isomers of the two propenes were produced in essentially equal amounts.

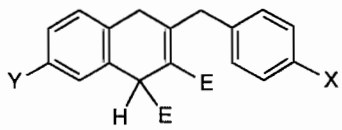
The nitrogen-loss pathway (i) from the 3*H*-pyrazole (Scheme 3) was the route we had expected the bulk of the material to follow. Although the expected cyclopropenes (**4**) were indeed produced, the yields were low and the product mixtures also included, on occasion, small amounts of dihydroazulenes (**28**) and substances believed to be dihydronaphthalenes (**29**). Those compounds are also produced in small amounts by thermolysing the pure cyclopropenes (**4**) in an inert solvent, and presumably arise by attack of the intermediate vinyl carbene **8***a* on one of the aromatic rings (3, 19, 20). Additional evidence for the intermediacy of the carbene **8***a* was provided by photolysis of **3***a* in methanol (in the presence of DMAD), when ether **30** was produced, in an amount comparable to that of symmetric cyclopropene **4***a*, by carbene insertion into the O—H bond of the alcohol (18–20). In principle, carbene insertion can follow several pathways (21–25), including direct insertion into the O—H bond, attack on the carbene by the nucleophilic oxygen to give a zwitterion that then undergoes an H-shift, and protonation of the carbene to give a cation that combines with the counterion. Which pathway occurs is dependent on the structure of the carbene, but the last pathway is known for at least some vinyl carbenes (26). If this last pattern were followed, protonation of vinyl carbene **8***a* would form an allylic cation that ought to give two ethers, **30** and **31**, of which, if anything, **31** should be favoured. However, since **31** could not be detected, it seems unlikely that a cationic pathway is followed in this system.



28

a : X = H

b : X= Br

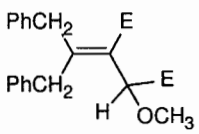


29

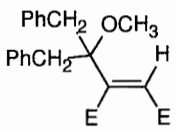
a : X = Y = H

b : X= H, Y= OCH_3

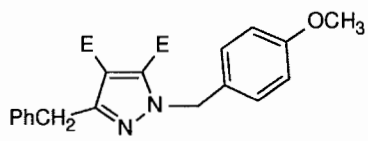
c : X= OCH_3, Y= H



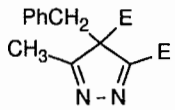
30



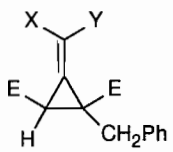
31



32

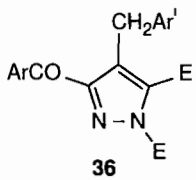


33



34 : X= Ph, Y= H

35 : X= H, Y= Ph



36

That the other major pathway for reaction of the 3*H*-pyrazole was rearrangement is supported by the finding, in every case, of compounds **16**, **19**, and **17** and **18** (Scheme 3). The thermal rearrangement of 3*H*-pyrazoles has been called the VanAlphen–Hüttel rearrangement after its discoverers (27), and in most cases can be considered as taking place by a thermally allowed [1,5]-sigmatropic shift of a group from the 3-position either to the 1-position, or to the 4-position (6, 15,

© 1997 NRC Canada

Can. J. Chem. Downloaded from www.nrcresearchpress.com by 92.62.229.171 on 09/08/12
For personal use only.

28–31). Although 1*H*-pyrazoles are more stable than 4*H*-pyrazoles, the latter frequently constitute the predominant rearrangement product, pointing to kinetic control and late development of aromatic character in the transition state (5). Not surprisingly, ease of migration is a function of substituent, and it has been found that ester and acyl groups are much more mobile than alkyl, aryl, or benzyl groups, so that 3*H*-pyrazoles with ester or acyl groups in the 3-position rearrange rapidly at room temperature (29, 30), frequently not even being isolable (31). One explanation for this, based on careful work with the comparable indene system, is that the energy barrier for the process is reduced by secondary interaction between a vacant π^* orbital of the migrating group and an occupied orbital of the five-membered ring (32). Although steric factors also play a part, clearly when there is no π^* orbital, i.e., with alkyl and benzyl groups, no such lowering of the barrier is possible, and the rearrangement should be slow. Thus for our systems we would not have expected a rapid rearrangement.

On the other hand, the conjugate acid of the pyrazole can also undergo concerted rearrangement (33) and in acetic acid solution benzyl groups do migrate much faster than other alkyl groups. This suggests there is substantial charge transfer in the transition state for such reactions, and that migrating tendency then also becomes a function of ability to stabilize a positive charge (33). However, the rearrangement of 3*H*-pyrazoles is not always concerted, and we recently reported strong evidence for a two-step process in which an ion pair is formed when the migrating group can form a particularly stable cation (34). There thus appears to be a mechanistic spread ranging from a one-step (concerted) process to a two-step, ion-pair process.

To check whether the benzyl migration was being catalyzed by adventitious acid, some photolyses were performed in tubes that had been washed with ammonia and others in solvents containing a small amount of triethylamine. However, those precautions made no significant difference to the proportion of products arising from rearrangement. Temperature also seemed to have little effect. Although most experiments were run at ambient temperature, essentially identical results were found in one experiment performed using dichloromethane as solvent with the temperature maintained at or below −15°C until work-up. It was also striking that, in contrast to earlier work, in our reactions there was no evidence for any ester migration from the putative 4*H*-pyrazole intermediate **13**, which might have been expected to behave this way (27, 30, 34).

In light of these findings, we believe that 3, 3-dibenzyl-3*H*-pyrazoles (e.g., **6**) rearrange by the two-step, ion-pair mechanism (cf. ref 34). Calculations have shown that such a process is reasonable for cyclopentadiene systems (35) and, in the present case, five observations support this interpretation. First, although 1-benzyl-1*H*-pyrazoles were produced, there was always formed a small amount of debenzylated compound (**20***a–e*), indicating that the migrating benzyl group could become detached. The result is formally similar to the debenzylation reported by others (36) from reactions at a much higher temperature (205°C). Secondly, when photolysis of **3***a* was performed in the more polar solvent methanol, the yield of debenzylated product **20***a* from unrearranged 3*H*-pyrazole was increased at the expense of the yield of cyclopropene **4***a*. Thirdly, the *para*-substituted systems (**6***b–e*) gave evidence of preferential migration in the sense *p*-$MeOC_6H_4CH_2$ > $C_6H_5CH_2$ > *p*-$CF_3C_6H_4CH_2$, paralleling ability to support a benzylic cation. Fourthly, with *p*-methoxybenzyl, the isomeric 1*H*-pyrazole **32** was also formed, a compound most simply accounted for by assuming that the ion-pair intermediate is loose enough for collapse to occur at either nitrogen. Lastly, in the photolysis of the related oxadiazoline **3***f* in methanol-d_4, the products included not only both cyclopropenes **4***f* and **16***j* and the 1-benzyl-1*H*-pyrazole **19***j*, but also the 4-benzyl-4*H*-pyrazole **33** and the debenzylated 1*H*-pyrazole **20***d*.

Additional evidence for Scheme 3 came from the finding that, if the diazoalkane was first generated (at low temperature) and then DMAD was added, the "missing" 3*H*-pyrazoles (**6***a*, **6***b*, and **6***d*) could be isolated. They are not stable at room temperature, decomposing to give a product mixture similar to that from direct photolysis. Moreover, it was not possible to isolate **6***c* under these conditions, suggesting that the *p*-methoxybenzyl group can migrate rapidly even at room temperature.

Thus the crucial steps proposed in Scheme 3 for the production from **6** of products **16**, **17** and **18**, and **19** are the following. First, there is a shift of a benzyl group, by a pathway involving a tight ion-pair intermediate (loose in the case of *p*-$MeOC_6H_4CH_2$) to give some **19** but mainly the 4*H*-pyrazole **13** (compare findings in ref. 37), as well as small amounts of **20**, by complete loss of the migrating group. Then **13** generates the unsymmetrical cyclopropene **16** by photochemical loss of nitrogen (3). The two isomeric methylenecyclopropenes (**17** and **18**) are then produced from **16** either by a base-catalyzed proton shift or by [1,5]-sigmatropic rearrangement to the more acidic ester enol (not shown), which then undergoes a base-catalyzed allylic rearrangement. There are many precedents in cyclopropene chemistry for base-catalyzed rearrangements (38), and since a benzylic hydrogen vinylogous to an ester is weakly acidic, strong bases do not have to be sought. Either the traces of base introduced deliberately or, in cases where that was omitted, the diazoalkane (39), can be assigned to that role. In the latter case, some of the diarylpropenes (**14** and **15**) would have originated from 1,3-diaryl-2-propyl cations, rather than from carbenes. It is possible that **17** and **18** are also subject to photochemical interconversion, but this was not investigated.

Base-catalyzed isomerization of **16** was confirmed by two observations. First, when the photolysis of **3***a* was conducted in the presence of added base, no **16***a* was present in the product mixture, although both **17***a* and **18***a* were found. Secondly, treatment of pure cyclopropene **16***a* with triethylamine in chloroform caused total isomerization within a few minutes. In the latter case, along with **17***a* and **18***a* in approximately equal amounts, there were found much smaller amounts of **34** and **35**, whose structures followed from their NMR spectra and NOE experiments. Since the isomerization is presumably equilibrium controlled, structures **17** and **18** must be more stable than both cyclopropene **16**, and its isomers **34** and **35**. The fact that **34** and **35** were not observed as co-products of the photolyses could simply mean that the yields of these compounds were too small.

The sequence of reactions leading to benzoyl pyrazoles **21**, **22**, and **23** is probably the following. First **6** rearranges, by preferential migration of that benzyl group with the better cationic stabilization, to afford 4*H*-pyrazole **13**. The doubly acti-

© 1997 NRC Canada

vated methylene group of **13** then undergoes autoxidation, by a radical chain mechanism, to afford hydroperoxide **24**, which is short lived, undergoing intramolecular *N*-oxidation to afford the yellow pyrazole-*N*-oxide **25**. A 1,4-sigmatropic H-shift in **25** affords the enolic hydroxylamine **26**, which leads to acyl pyrazole **21** in one of two ways. One of these is 1,4-elimination of water and the alternative involves ketonization followed by 1,2-elimination of water. The 4*H*-pyrazoles **21** can also generate 5-acylpyrazoles **22** and **23** by loss of one of the groups at C4, the driving force presumably being the fact that the products are aromatic. The route may involve ion pairs or nucleophilic attack on the ester group that is lost.

Conclusion

Dimethyl 3,3-dibenzyl-3*H*-pyrazole-4,5-dicarboxylates, produced by photolysis of oxadiazolines in the presence of DMAD, undergo benzyl shifts at ambient temperatures by an ion-pair mechanism, to give mainly 3,4-dibenzyl-4*H*-pyrazole-4,5-dicarboxylates as initial products. The latter undergo further photolysis to afford cyclopropenes by loss of nitrogen. These 4*H*-pyrazoles are unusually sensitive to air, and are also converted, through unstable hydroperoxide and *N*-oxide intermediates, to benzoyl pyrazoles **21**, **22**, and **23**.

Experimental

Melting points were determined on a Thomas Hoover capillary melting point apparatus. NMR spectra were recorded on Varian EM-390, Bruker AM-500, or, when unspecified, Bruker AM-200 spectrometers using $CDCl_3$ as solvent and for internal reference either TMS (proton spectra) or solvent $CDCl_3$ (δ = 77.20 for ^{13}C spectra). Centrifugal chromatography was carried out on silica gel (Merck Kieselgel 60 PF_{254}) plates in a model 7924T Chromatotron apparatus, under nitrogen, using a gradient elution protocol starting with low-boiling petroleum spirit containing 5% diethyl ether plus 0.1% methanol, and finishing with neat acetonitrile. Infrared spectra were recorded as thin films for liquids or Nujol mulls for solids.

General procedure for preparation of dibenzylketones (1)
For those which were not commercially available, an adequate synthesis was available (40) by reaction of dibenzyl cadmium with the appropriate 4-substituted phenylacetyl chloride, obtained from the corresponding acid using thionyl chloride (41). Brief characteristics of compounds, some of them new, follow.

(4-Trifluoromethylphenyl)acetyl chloride, a clear oil, bp 75–80°C/0.5 Torr (1 Torr = 133.3 Pa). ^1H NMR, δ: 7.58 (d, J = 8.0 Hz, H-3, H-5), 7.34 (d, J = 8.0 Hz, H-2, H-6), 4.15 (s, CH_2).

*1-(4-Methylphenyl)-3-phenylpropan-2-one (1*b*)*, clear oil (44%), bp 148–155°C/0.4 Torr (lit (40*a*) bp 143°C/0.3 Torr). IR (cm^{-1}): 3035 w, 2925 w, 1719 s, 1603 w, 1514 m, 1496 m, 1453 m. ^1H NMR (90 MHz) δ: 7.35–7.00 (m, 9H), 3.68 (s, 2H), 3.65 (s, 2H), 2.31 (s, 3H); this fits well the published ^1H NMR data (40*b*).

*1-(4-Methoxyphenyl)-3-phenylpropan-2-one (1*c*)*, a clear oil (29%), bp 175–185°C/0.7 Torr (lit (40*a*) bp 152–154°C/0.4 Torr. ^1H NMR (90 MHz) δ: 7.35-6.80 (m, 9H), 3.77 (s, 3H), 3.68 (s, 2H), 3.62 (s, 2H).

*1-(4-Bromophenyl)-3-phenylpropan-2-one (1*d*)*, yellowish oil (44%), bp 180–200°C/0.02 Torr (lit. (42) mp 54°C). IR (cm^{-1}): 3085 w, 3065 w, 3030 w, 2920 w, 1718 s, 1600 m, 1590 m, 1487 s, 1451 m, 1404 m. ^1H NMR (90 MHz) δ: 7.50–7.05 (m, 9H), 3.68 (s, 2H), 3.62 (s, 2H).

In one preparation of **1***d*, dibenzyl(4-bromobenzyl)carbinol was also produced, as a pasty solid. IR (mull) cm^{-1}: 3570(sharp) m, 3025 m, 1598 w, 1483 s. ^1H NMR, δ: 7.40 (d, J = 8.3 Hz, 2H, H-3, H-5 of Ar), 7.31–7.17 (m, 10H), 7.09(d, J = 8.3 Hz, 2H, H-2, H-6 of Ar), 2.73 (s, 4H), 2.70 (s, 2H).

*1-Phenyl-3-(4-trifluoromethylphenyl)propan-2-one (1*e*)* (38%), bp 130–140°C/0.3 Torr. IR (cm^{-1}): 3065 w, 3035 w, 2915 w, 1722 s, 1618 m, 1605(sh), 1585 m, 1494 m, 1452 w, 1418 m. ^1H NMR, δ: 7.55 (d, J = 8.0 Hz, 2H, H-3, H-5 of Ar), 7.4–7.3 (m, 3H), 7.25–7.15 (m, 4H), 3.78 (s, 2H), 3.74 (s, 2H). ^{13}C NMR, δ: 204.8 (CO), 138.1(br, Ar-C1), 133.7 (Ph-C1), 130.0 (Ar-C2), 129.6 (Ph-C2), 129.0 (Ph-C3), 127.5 (Ph-C4), 125.6 (q, J_{CF} = 3.8 Hz, Ar-C3), 49.9 (C3), 48.5 (C1), signals from Ar-C4 and CF_3 too dispersed for detection.

Also produced with **1***e* was dibenzyl(4-trifluoromethylbenzyl)carbinol (11%), bp 185–190°C/0.5 Torr. IR (cm^{-1}): 3580 m, 3070 w, 3060 w, 3035 m, 1615 m, 1600 m, 1581 w, 1491 m, 1445 s, 1413 s. ^1H NMR, δ: 7.50 (d, 2H, H-3, H-5 of Ar), 7.40–7.15 (m, 12H), 2.81 (s, 2H), 2.77 (s, 2H), 1.49 (s, OH). MS (ci, NH_3) *m/z*: 388 (M + NH_4^+, 100%), 108 (15%), 91 (22%); MS (ei) *m/z*: 279 (M − Bn^+, 30%), 261 (5%), 211 (M − $ArCH_2^+$, 10%), 159 ($ArCH_2^+$, 25%), 119(10%), 91 (100%).

General procedure for preparation of oxadiazolines (3)
A two-step process was used, involving oxidation of the acetylhydrazone (**2**) formed from the corresponding dibenzyl ketone. Virtually quantitative yields of the hydrazone were obtained by overnight refluxing of equimolar amounts of the ketone and acetylhydrazine in methanol, in the presence of a trace of acetic acid.

Acetylhydrazones (2)

*Hydrazone (2*a*)*, mp 118–119°C. IR, cm^{-1}: 3240 m, 3205 m, 3060 m, 3030 m, 2855 m, 1687 m, 1667 m, 1631 m, 1602 w, 1532 m, 1493 m, 1439 m, 1427 m, 1405. ^1H NMR (90 MHz), δ: 9.4 (s, NH), 7.3–7.0 (m, 10H), 3.56 (s, 4H), 2.24 (s, 3H, MeCO). ^{13}C NMR, δ: 173.7 (CO), 151.7 (C—N), 136.8 and 134.3 (2 × Ph-C1), 129.4 and 129.3 and 128.8 and 128.5 (2 × Ph-C2 and 2 × Ph-C3), 127.3 and 127.0 (2 × Ph-C4), 44.1 and 34.3 (2 × CH_2), 20.6 (Me).

*Hydrazone (2*b*)*, mixture of two isomers. IR (cm^{-1}): 3210 m, 3090(sh), 3055(sh), 3035 m, 2925 m, 1710(sh), 1673 s, 1615 m, 1513 m, 1495 m, 1450 m, 1423 m. ^1H NMR (90 MHz), δ: 8.6(br, NH), 7.3–6.9 (m, 9H, aryl-H), 3.57 and 3.53 and 3.48 and 3.45 (all s, 4H, 2 pairs of CH_2), 2.32 (s, 3H, MeCO), 2.30 and 2.29 (both s, 3H, ArMe).

*Hydrazone (2*c*)*, mixture of two isomers, mp 115–117°C. IR (cm^{-1}): 3190 m, 3110 w, 3080 w, 3025 w, 1671 s, 1630 w, 1610 w, 1583 w, 1509 m, 1492 m. ^1H NMR (90 MHz) δ: 8.63 (br, 1H, NH), 7.4–6.8 (m, 9H aryl-H), 3.80 (s, 3H, OMe), 3.57 and 3.50 and 3.47 and 3.42 (all s, 4H, 2 pairs of CH_2), 2.28 (s, 3*H*, MeCO).

© 1997 NRC Canada

Can. J. Chem. Downloaded from www.nrcresearchpress.com by 92.62.229.171 on 09/08/12
For personal use only.

Can. J. Chem. Downloaded from www.nrcresearchpress.com by 92.62.229.171 on 09/08/12
For personal use only.

*Hydrazone (**2**d)*; initial solid was essentially a single isomer, mp 121-124°C. IR (cm^{-1}): 3180 m, 3085 w, 3065 w, 3030 w, 1717 w, 1687 s, 1635 w, 1483 m. ^1H NMR (90 MHz) δ: 9.25 (s, br, 1H), 7.45–7.00 (m, 7H), 6.89 (d, 2H, H-3, H-5 of Ar), 3.54 (s, 2H), 3.49 (s, 2H), 2.24 (s, 3H, MeCO). Later crops of crystals were mixtures of both isomers.

*Hydrazone (2*e*)*; mixture of two isomers, first batch mp 113–126°C, second batch mp 131–137°C. ^1H NMR, δ: 9.45 and 9.28 (both s, br, 1H, NH), 7.54 (d, J = 7.5 Hz, 2H, 3-H, 5-H of Ar), 7.4–7.0 (m, 7H), 3.60 and 3.56 (both s, 4H, 2 × CH_2), 2.25 and 2.22 (two s, 3H, MeCO).

*Oxadiazolines (**3**)*

The oxidation of the hydrazones was accomplished using lead tetraacetate (1–3), and gave mixtures of by-products similar to those reported (3). Characterizations of new compounds are given below; first the target molecules, then the by-products.

*5-Benzyl-2-methoxy-2-methyl-5-(4-methylbenzyl)-Δ^3-1,3,4-oxadiazoline (**3**b)*; (80%), colourless oil, approximately equal amounts of the two isomers. IR (cm^{-1}): 3030 s, 3005 s, 2940(sh), 2930 s, 1738 m, 1605 w, 1575 w, 1515 s, 1498 s, 1454 s, 1433 s, 1405 m. ^1H NMR, δ: 7.30–6.85 (m, 9H), 3.31 and 3.26 (two d, J = 14.1 Hz, 2H, two halves of two AB quartet from CH_2 groups), 3.24 (d, J = 14 Hz, 2H, two coincident halves of two AB quartets from CH_2 groups), 3.17 and 3.13 (two s, 3H, 2 × OMe), 3.04 and 2.99 and 2.93 and 2.89 (four d, J = 14 Hz, 4H, two AB quartets from CH_2 groups), 2.32 and 2.24 (two s, 3H, 2 × ArMe), 1.00 and 0.93 (two s, 3H, 2 × 2-Me).

*5-Benzyl-2-methoxy-5-(4-methoxybenzyl)-2-methyl-Δ^3-1,3, 4-oxadiazoline (**3**c)* (73%), colourless oil consisting of the two isomers. ^1H NMR, δ: 7.4–6.9 (m, 9H), 3.81 and 3.74 major (two s, 3H, ArOMe); 3.33 and 2.93 (two d, J = 14.2 Hz), and 3.28 and 3.01 (two d, J = 14.4 Hz) (2 × CH_2, minor); 3.29 and 3.06 (two d, J = 14.2 Hz) and 3.24 and 2.90 (two d, J = 14.4 Hz) (2 × CH_2 major); 3.21 and 3.19 major (two s, 3H, 2-OMe); 1.04 major and 0.96 (two s, 2-Me). ^{13}C NMR, δ (major): 158.7 (Ar-C4), 134.3 (Ph-C1), 133.7 (C2), 131.6 (Ar-C2), 131.0 (Ph-C2), 127.9 (Ph-C3), 126.9 (Ph-C4), 126.8 (Ar-C1), 124.0 (C5), 113.7 (Ar-C3), 55.1 (ArOMe), 51.0 (2-OMe), 43.3 and 42.6 (2 × CH_2), 20.6 (Me); (minor): 158.8 (Ar-C4), 134.9 (Ph-C1), 133.7 (C2), 132.0 (Ar-C2), 130.6 (Ph-C2), 128.3 (Ph-C3), 127.0 (Ph-C4), 126.1 (Ar-C1), 124.2 (C5), 113.3 (Ar-C3), 55.0 (ArOMe), 50.9 (2-OMe), 41.47 and 40.7 (2 × CH_2), 20.4 (Me).

*5-Benzyl-5-(4-bromobenzyl)-2-methoxy-2-methyl-Δ^3-1,3,4-oxadiazoline (**3**d)* (62%), colourless oil consisting of the two isomers. IR (cm^{-1}): 3065 m, 3035 m, 3000 m, 2940 m, 2915(sh), 2840 w, 1740 m, 1605 w, 1595 w, 1575 w, 1490 s, 1455 m. ^1H NMR, δ (major): 7.45 (d, J = 8.3 Hz, H-3, H-5 of Ar), 7.30–7.15 (m, 3H of Ph), 7.04 (m, 2H of Ph), 6.89 (d, J = 8.2 Hz, H-2, H-6 of Ar); 3.25 and 2.89 (two d, J = 14.2 Hz, CH_2), 3.22 and 3.03 (two d, J = 14.0 Hz, CH_2); 3.21 (s, OMe), 1.07 (s, 2-Me); (minor): 7.30–7.15 (m, aryl-H); 3.31 and 2.92 (two d, J = 14.2 Hz, CH_2); 3.25 and 3.01 (two d, J = 14.2 Hz, CH_2); 3.19 (s, OMe), 0.98 (s, 2-Me). ^{13}C NMR, δ (major): 134.8 (Ph-C1), 134.1 (C-2), 133.4 (Ar-C1), 132.8 (Ar-C2), 131.6 (Ar-C3), 131.2 (Ph-C2), 128.6 (Ph-C3), 127.3 (Ph-C4), 123.7 (C5), 121.3 (Ar-C4), 51.3 (OMe), 43.7 and 41.1 (2 × CH_2), 20.6 (Me); (minor): 134.1 (Ph-C1), 134.0 (C2), 133.9 (Ar-C1), 132.5 (Ar-C2), 131.1 (Ar-C3), 130.7 (Ph-C2), 128.1 (Ph-C3), 127.2 (Ph-C4), 123.7 (C5), 121.2 (Ar-C4), 51.3 (OMe), 43.1 and 41.8 (2 × CH_2), 20.3 (2-Me).

*5-Benzyl-2-methoxy-2-methyl-5-(4-trifluoromethylbenzyl)-Δ^3-1,3,4-oxadiazoline (**3**e)* (31%), a mixture of the two isomers one of which formed crystals preferentially. IR (cm^{-1}): 3070 w, 3035 w, 3000 w, 2945 w, 2840 w, 1740 w, 1620 m, 1575 w, 1492 w, 1435 m, 1429 m, 1418 m. ^1H NMR, δ: 7.59 (d, J = 8.2 Hz, 2H, H-3, H-5 of Ar), 7.43 (d, J = 8.0 Hz, 2H, H-2, H-6 of Ar), 7.25–7.19 and 7.0 (m, 5H of Ph); 3.35 and 2.95 and 3.34 and 3.15 (two AB quartets, J = 14.2 Hz, 2 × CH_2); 3.20 (s, OMe), 0.98 (s, 2-Me). ^{13}C NMR, δ: 139.1 (Ar-C1), 134.2 (Ph-C1), 133.9 (C2), 131.14 (Ar-C2), 131.11 (Ph-C2), 128.1 (Ph-C3), 127.3 (Ph-C4), 125.3 (q, J_{CF} = 3.7 Hz, Ar-C3), 123.7 (C5), 51.4 (OMe), 43.5 and 41.9 (2 × CH_2), 20.1 (2-Me). Other isomer (from spectra of mixture): ^1H NMR, δ: 7.6–7.4 (m, H-3, H-5 of Ar), 7.4–7.0 (m, H-2, H-6 of Ar and 5H of Ph); 3.38 and 3.05 and 3.29 and 3.04 (two AB quartets, J = 14.2 Hz, 2 × CH_2); 3.23 (s, OMe), 1.03 (s, 2-Me). ^{13}C NMR, δ: 138.6 (Ar-C1), 134.7 (Ph-C1), 133.9 (C2), 131.5 (Ar-C2), 130.7 (Ph-C2), 128.6 (Ph-C3), 127.4 (Ph-C4), 124.9 (q, J_{CF} = 3.9 Hz, Ar-C3), 123.7 (C5), 51.3 (OMe), 43.7 and 41.3 (2 × CH_2), 20.3 (Me).

By-products from LTA oxidation

2-Methoxy-1-(4-methoxyphenyl)-3-phenylpropane: ^{13}C NMR, δ: 158.1 (Ar-C4), 139.2 (Ph-C1), 131.1 (Ar-C1), 130.5 (Ar-C2), 129.6 (Ph-C2), 128.4 (Ph-C3), 126.2 (Ph-C4), 113.8 (Ar-C3), 83.9 (C2), 57.6 (2-OMe), 55.3 (Ar-OMe), 40.3 and 39.4 (2 × CH_2).

2-Methoxy-1-phenyl-3-(4-trifluoromethylphenyl)propane: IR (cm^{-1}): 3065 w, 3030 w, 2930 m, 2825 w, 1615 w, 1490 w, 1450 w, 1432 w, 1412 w. ^1H NMR, δ: 7.52 (d, J = 8.0 Hz, 2H, H-3, H-5 of Ar), 7.35–7.20 (m, 7H, H-2, H-6 of Ar and Ph-H_5), 3.60 (quintet, J = 6.2 Hz, 1H, H-2), 3.24 (s, 3H, OMe), 2.7–2.9 (m, 4H, 2 × CH_2); ^{13}C NMR, δ: 143.4 (br, Ar-C1), 138.7 (Ph-C1), 129.9 (Ar-C2), 129.6 (Ph-C2), 128.5 (Ph-C3), 126.4 (Ph-C4), 125.2 (q, J_{CF} = 4 Hz, Ar-C3), 83.3 (C2), 57.7 (OMe), 40.3 and 40.1 (C1 and C3).

Co-eluting with **3***d* was a small amount of 2-acetoxy-1-(4-bromophenyl)-3-phenylpropane (7%), its presence being deduced from characteristic NMR signals in the mixture. ^1H NMR (partial), δ: 5.26 (quintet, J = 6.6 Hz, H-2), 2.79 (d, J = 6.6 Hz, 2 × CH_2), 1.91 (s, MeCO). ^{13}C NMR (partial), δ: 170.5 (CO), 137.5 (Ph-C1), 136.5 (Ar-C1), 131.3 (Ar-C2), 129.5 (Ph-C2), 128.5 (Ph-C3), 126.8 (Ph-C4), 75.0 (C2), 39.8 (CH_2).

Co-eluting with **3***e* was a small amount of 2-acetoxy-1-phenyl-3-(4-trifluoromethylphenyl)propane (8%). IR (cm^{-1}): 3065 w, 3030 w, 2950 w, 2925 w, 2850 w, 1740 s, 1616 w, 1605(sh), 1581 w, 1490 w, 1450 w, 1432 w, 1413 w. ^1H NMR, δ: 7.53 (d, J = 8.0 Hz, H-3, H-5 of Ar), 7.34–7.16 (m, H-2, H-6 of Ar and Ph-H_5), 5.31(quintet, H-2), 2.9–2.8 (m, 2 × CH_2), 1.93 (s, MeCO). ^{13}C NMR, δ: 170.4 (CO), 141.8 (Ar-C1), 137.2 (Ph-C1), 129.9 (Ar-C2), 129.6 (Ph-C2), 128.7

© 1997 NRC Canada

Can. J. Chem. Downloaded from www.nrcresearchpress.com by 92.62.229.171 on 09/08/12
For personal use only.

(Ph-C3), 126.9 (Ph-C4), 125.4 (q, J_{CF} = 3.7 Hz, Ar-C3), 74.9 (C2), 40.3 and 39.9 (C1 and C3), 21.2 (COMe).

2-Acetoxy-5-benzyl-2-methyl-5-(4-methylbenzyl)-Δ^3-1,3,4-oxadiazoline (9%), a mixture of the two isomers. IR (cm^{-1}): 3060 w, 3030 w, 2940(sh), 2925 w, 1760 s, 1724 m, 1606 w, 1515 w, 1498 w, 1453 m, 1436 m. ^{1}H NMR (90 MHz), δ: 7.3–7.0 (m, 9H), 3.7–2.9 (m, 4H, two pairs of CH_2); 2.32 and 2.26 (two s, 3H, ArMe), 1.79 (s, 3H, MeCO), 1.20 and 1.16 (two s, 3H, two 2-Me).

2-Acetoxy-5-benzyl-5-(4-methoxybenzyl)-2-methyl-Δ^3-1,3,4-oxadiazoline (12%), a mixture of the two isomers. IR (cm^{-1}): 3065 w, 3035 w, 3003 w, 2950(sh), 2930 w, 2838 w, 1755(br) s, 1611 s, 1583 m, 1510 s, 1498 s, 1455 m, 1440 m. ^{1}H NMR (90 MHz) δ: 7.3–6.7 (m, 9H); 3.78 and 3.76 (two s, 3H, 2 × ArOMe); 3.6–2.9 (m, 4H, 2 × CH_2); 1.82 and 1.79 (two s, 3H, 2 × MeCO); 1.27 and 1.25 (two s, 3H, 2 × 2-Me). ^{13}C NMR, δ (major): 168.0 (CO), 159.0 (Ar-C4), 134.4 (Ph-C1), 132.3 (Ar-C2), 131.2 (C2), 130.9 (Ph-C2), 128.5 (Ph-C3), 128.38 (C5), 127.3 (Ph-C4), 125.7 (Ar-C1), 113.6 (Ar-C3), 55.4 (Ar-OMe), 43.7 and 41.8 (2 × CH_2), 21.9 (MeCO), 21.0 (Me); (minor): 168.0 (CO), 159.0 (Ar-C4), 133.8 (Ph-C1), 131.9 (Ar-C2), 131.3 (Ph-C2), 128.4 (C5), 128.2 (Ph-C3), 127.3 (Ph-C4), 126.3 (Ar-C1), 114.0 (Ar-C3), 55.4 (Ar-OMe), 43.0 and 42.4 (2 × CH_2), 21.2 (MeCO), 20.9 (Me), C2 not observed.

2-Acetoxy-5-(4-bromobenzyl)-5-benzyl-2-methyl-Δ^3-1,3,4-oxadiazoline (12%), as a 7:3 mixture of the two isomers, mp 78–95°C. ^{1}H NMR, δ (major): 7.4–6.9 (m, aryl-H); 3.53 and 3.33 and 3.17 and 3.08 (two AB quartets, J = 14.2 Hz, 2 × CH_2); 1.79 (s, MeCO), 1.15 (s, Me); (minor): 7.4–6.9 (m, aryl-H); 3.47 and 3.00 (AB quartet, J = 14.2 Hz, one CH_2; signals from other CH_2 obscured); 1.82 (s, MeCO), 1.29 (s, Me). ^{13}C NMR, δ (major): 167.8 (CO), 133.4 (Ph-C1), 133.2 (Ar-C1), 132.6 (Ar-C2), 131.6 (Ar-C3), 131.5 (C2), 131.2 (Ph-C2), 128.2 (Ph-C3), 127.8 (C5), 127.5 (Ph-C4), 121.5 (Ar-C4), 43.0 and 42.8 (2 × CH_2), 21.8 (MeCO), 20.9 (Me); (minor): 167.8 (CO), 134.1 (Ph-C1), 132.9 (Ar-C2), 131.4 (Ar-C3), 131.2 (C2), 130.8 (Ph-C2), 128.6 (Ph-C3), 127.7 (C5), 127.5 (Ph-C4), 121.5 (Ar-C4), 43.8 and 41.7 (2 × CH_2), 21.8 (COMe), 21.1 (Me), Ar-C1 not observed.

General procedure for photolysis of oxadiazolines (3)

In the general method adopted (3) the oxadiazoline (typically 1.5 mmol) and dimethyl acetylenedicarboxylate (in 10% excess) were mixed in benzene (typically 6.0 mL, giving a concentration of ca. 0.25 M) in a quartz tube, and photolyzed with 300 nm light in a Rayonnet apparatus. The reaction mixture became yellow almost at once, and a gentle stream of gas (presumably nitrogen) was evolved. For the initial runs, progress of the reaction was monitored by running ^{1}H NMR spectra at hourly intervals, and typically after 5 h the amount of starting oxadiazoline had dropped to about 5%. In later experiments, therefore, photolysis was halted at this time. The solvent was removed on a rotary evaporator, and the residue was separated by centrifugal chromatography on 4 mm silica gel plates. Between 10 and 17 distinct bands were usually present, although not all fractions could be satisfactorily identified. As a general picture, the first fraction from the plate would be mixed 1, 3-diarylpropenes (**14** and **15**), followed by unchanged starting materials, followed by methylenecyclopropene isomers (**17** and **18**), closely followed by symmetrical cyclopropene **4** and unsymmetrical cyclopropene **16**, followed by the unstable yellow compound **25**, just in front of 1, 5-dibenzyl-1*H*-pyrazole (**19**) and, lastly, 5-benzyl-1*H*-pyrazole (**20**). A variety of other compounds were formed on one or two occasions only. Usually several fractions needed further purification on thinner plates; sometimes equivalent fractions from different runs were combined for this. Yields are of isolated material and are corrected for recovered starting material.

*Photolysis of dibenzyl oxadiazoline (**3**a) (12 runs)*

Typical results from one run are as follows. Similar results were found in other runs, but percentages varied with run and conditions, as did the presence of occasional minor products, which are detailed later.

The known (3) *1,3-diphenylpropenes **14**a and **15**a* (2%).

*Dimethyl 3,3-dibenzylcyclopropene-1,2-dicarboxylate (**4**a)* (35%), was obtained as a pale yellow oil, together with dimethyl (*E*)-1-benzyl-3-(phenylmethylene)cyclopropane-*trans*-1,2-dicarboxylate (**17***a*) and dimethyl (*Z*)-1-benzyl-3-(phenylmethylene)cyclopropane-*trans*-1,2-dicarboxylate (**18***a*) (3%) in approximately 1:1 ratio. It proved impossible to separate these cleanly using the Chromatotron, but partial enrichment of each allowed assignment of signals in NMR spectra. For **17***a*, ^{1}H NMR, δ: 7.5–7.2 (m, Ph-H), 6.79 (d, J = 2.4 Hz, vinyl-H); 3.69 and 3.66 (two s, 2 × OMe); 3.47 (d, J = 2.3 Hz, methine-H), 3.38 (s, CH_2). In an NOE experiment, irradiation of the doublet at 6.79 δ gave enhancement of a phenyl-H signal at 7.4 δ, irradiation of doublet at δ = 3.47 gave enhancement of a phenyl-H signal at 7.3 δ, and irradiation of singlet at δ = 3.38 gave enhancement of vinyl-H at 6.79 δ and of phenyl-H at 7.3 δ. For ^{13}C NMR data see Table 2. MS (ei) on mixture, *m/z*: 336 (M^+, 5%), 304 (15%), 276 ($M - EH^+$, 15%), 245 ($M - Bn^+$, 25%), 217 ($276 - E^+$, 65%), 214 (5%), 202 (35%), 189 (10%), 115 (65%), 91 (100%), 77 (35%). MS (ci, NH_3) *m/z*: 354 ($M + NH_4^+$, 100%), 337 ($M + H^+$, 12%), 305 ($M - OMe^+$, 10%), 252 (12%), 228 (10%), 202 (5%), 121 (7%).

For **18***a*, ^{1}H NMR, δ: 7.5–7.2 (m, Ph-H), 6.88 (d, J = 2 Hz, vinyl-H); 3.91 and 3.11 (AB quartet, J = 16 Hz, CH_2); 3.70 and 3.55 (two s, 2 × OMe); 3.44 (d, J = 2 Hz, methine-H). In an NOE experiment, irradiation of the doublet at δ = 6.88 gave enhancement at phenyl-H signal at 7.38 δ, and slight enhancement of doublet at 3.44 δ. Irradiation of doublet at δ = 3.44 gave possible enhancement at 6.88 δ, but not of methylene signals.

*Dimethyl 2,3-dibenzylcyclopropene-1,3-dicarboxylate (**16**a)* (14%), pale yellow oil. ^{1}H NMR (500 MHz) δ: 7.27 (t, br, J = 7 Hz, 3*H* of Ph), 7.24–7.16 (m, 3*H* of Ph), 7.10 (d, J = 7 Hz, 2H, H-2, H-6 of Ph), 7.04 (d, J = 7 Hz, 2H, H-2, H-6 of Ph); 3.77 and 3.67 (AB quartet, J = 17.8 Hz, 2H, 2-CH_2); 3.71 and 3.55 (two s, 6H, 2 × OMe); 3.32 and 3.24 (AB quartet, J = 14.2 Hz, 2H, 3-CH_2); for ^{13}C NMR see Table 1.

The known (3) *dihydroazulene **28**a*, (2%).

*Pyrazole-N-oxide (**25**a)*, bright yellow oil. UV (1.66 mg/mL MeOH) λ_{max}, nm: 282 (ε = 550), 372 (ε = 420). ^{1}H NMR, δ:

© 1997 NRC Canada

Can. J. Chem. Downloaded from www.nrcresearchpress.com by 92.62.229.171 on 09/08/12
For personal use only.

Table 1. Comparative ^{13}C NMR data for unsymmetrical dibenzylcyclopropenes (**16**).

	16*a*	**16***b*	**16***c*	**16***d*	**16***e*	**16***f*	**16***g*	**16***h*	**16***i*
1-COO*C*H$_3$	52.4	52.3	52.4	52.4	52.5	52.3	52.3	52.4	52.5
1-*C*OOMe	159.6	159.6	159.6	159.6	159.6	159.5	159.4	159.4	159.4
3-COO*C*H$_3$	52.2	52.1	52.0	52.2	52.0	52.5	52.5	52.6	52.3
3-*C*OOMe	174.2	174.2	174.2	174.2	174.2	173.8	174.0	172.2	174.0
C1	104.0	104.0	104.0	104.0	103.9	103.8	104.4	104.3	105.0
C2	129.2	129.3	129.2	129.3	obsc	129.1	129.0	obsc	129.28
C3	35.4	35.4	35.4	35.6	35.6	35.2	35.5	35	35.6
2-*C*H$_2$	32.2	32.2	31.2	32.2	31.4	32.1	31.7	32.1	32.0
3-*C*H$_2$	37.6	37.1	37.6	36.7	37.7	37.3	37.6	37.9	37.6
2-CH$_2$-Ar									
C1	134.7	134.8	131.6	134.8	126.4	134.5	133.8	134.4	139.0
C2	129.0	129.0	128.9	129.0	129.9	129.0	130.7	129.0	129.34
C3	128.7	128.6	129.3	128.7	114.5	128.8	131.8	128.9	125.6 (q, J_{CF} =3.8 Hz)
C4	127.2	127.2	136.7	127.2	159.1	127.4	121.1	127.4	obsc
3-CH$_2$-Ar									
C1	138.6	135.4	138.6	130.6	138.7	137.7	138.5	142.9	138.5
C2	129.8	129.7	129.8	130.8	129.6	131.49	129.9	130.0	129.9
C3	128.4	129.1	128.4	113.9	128.4	131.54	128.5	125.3 (q, J_{CF} = 3.5 Hz)	128.6
C4	126.4	135.8	126.4	158.2	126.4	120.4	126.5	obsc	126.6
Aryl-subst.		21.2 (CH$_3$)	21.2 (CH$_3$)	55.4 (OCH$_3$)	55.5 (CH$_3$O)	—	—	obsc(CF$_3$)	obsc(CF$_3$)

8.05 (s, 1H, OH), 7.05–7.4 (m, 10H), 5.76 (s, 1H, >CH-), 3.90 and 3.78 (two s, 6H, 2 × OMe), 3.41 and 3.23 (AB quartet, J = 12 Hz, 2H, CH$_2$); for ^{13}C NMR see Table 3.

*Methyl 5-benzoyl-4-benzyl-1*H*-pyrazole-3-carboxylate (**22**a)* (1%). IR (cm^{-1}): 3270(br) m, 3090 w, 3065 w, 3035 w, 2955 w, 2930(sh), 1724 s, 1654 s, 1598 m, 1575 w, 1563 w, 1489 m, 1449 s, 1442(sh). ^1H NMR, δ: 8.02 (d, br, J = 7.8 Hz, 2H, H-2, H-6 of Bz), 7.58 (t, br, J = 7.6 Hz, 1H, H-4 of Bz), 7.46 (t, br, J = 7.8 Hz, 2H, H-3, H-5 of Bz), 7.3–7.1 (m, 5H), 4.51 (s, 2H, CH$_2$), 3.95 (s, 3*H*, OMe). ^{13}C NMR, δ: 189.1 (PhCO), 160.2 (*C*OOMe), 148.4 (C3 and C5), 140.4 (Bn-C1), 137.8 (Bz-C1), 133.2 (C4), 133.0 (Bz-C4), 130.4 (Bz-C2), 128.7 (Bn-C2), 128.4 (Bn-C3 and Bz-C3), 126.2 (Bn-C4), 52.5 (OMe), 29.1 (CH$_2$). MS (ei) *m/z*: 321 (10%), 320 (M$^+$, 55%), 288 (M − 32$^+$, 35%), 183 (288-PhCO$^+$, 15%), 155 (30%), 127 (15%), 105 (PhCO$^+$, 100%).

The known (3) *dimethyl 1,5-dibenzyl-1*H*-pyrazole-3,4-dicarboxylate (**19**a)* (3.3%), yellow oil. HRMS, Exact Mass calcd. for $C_{21}H_{20}N_2O_4$: 364.1423; found: 364.1420.

*Dimethyl 5-benzyl-1*H*-pyrazole-3,4-dicarboxylate (**20**a)*, trace of a yellow oil. IR (cm^{-1}): 3480 m, 3280(br) s, 3060, 3030, 2955 s, 1730(br) s, 1603 m, 1569 m, 1496 s, 1453 s, 1436 s. ^1H NMR, δ: 7.33–7.15 (m, 5H), 4.25 (s, 2H, CH$_2$), 3.87 and 3.81 (two s, 6H, 2 × OMe). ^{13}C NMR, δ: 163.3 and 162.4 (2 × CO), 148.4 (C3), 143.2 (C4), 136.7 (Ph-C1), 129.0 and 128.9 (Ph-C2 and Ph-C3), 127.2 (Ph-C4), 111.7 (C5), 52.7 and 52.0 (2 × OMe), 31.8 (5-CH$_2$). MS (ei) *m/z*: 274 (M$^+$, 20%), 242 (M − 30$^+$, 100%), 210 (85%), 182 (M − 92$^+$, 25%), 155 (45%), 154 (40%), 91 (35%). MS (ci, NH$_3$) *m/z*: 275 (M + H$^+$, 80%), 192 (55%), 175 (100%), 160 (10%). HRMS, Exact Mass calcd. for $C_{14}H_{14}N_2O_4$: 274.0954; found: 274.0960.

On keeping in solution for some weeks, **25***a* decomposed to a mixture of **21***a*, **22***a*, and **23***a*.

*Dimethyl 5-benzoyl-4-benzyl-4*H*-pyrazole-3,4-dicarboxylate (**21**a)*: IR (cm^{-1}): 3065 w, 3035 w, 2960 m, 1765 s, 1731 s, 1656 s, 1596 m, 1578 w, 1546 w, 1528 w, 1492 w, 1441 s. ^1H NMR, δ: 8.06 (d, J = 8 Hz, 2H, H-2, H-6 of Bz), 7.66 (t, J = 7.3 Hz, 1H, H-4 of Bz), 7.47 (t, J = 7.6 Hz, 2H, H-3, H-5 of Bz), 7.17–7.03 (m, 3*H*, H-3, H-4, H-5 of Bn), 6.79 (d, J = 7.4 Hz, 2H, H-2, H-6 of Bn); 4.07 and 3.73 (two s, 6H, 2 × OMe); 3.92 and 3.82 (AB quartet, J = 14 Hz, 2H, CH$_2$). ^{13}C NMR, δ: 186.4 (Ph-CO), 163.4 and 160.3 (2 × *C*OOMe), 173.1 and 168.1 (C3 and C5), 134.9 (Bz-C4), 134.6 (Bz-C1), 133.0 (Bn-C1), 131.3 (Bz-C2), 128.8 (Bn-C2 and Bn-C3 and Bz-C3), 128.2 (Bn-C4), 77.7 (C4), 54.1 and 53.8 (2 × OMe), 37.5 (CH$_2$). MS (ei) *m/z*: 378 (M$^+$, 5%), 346 (5%), 287 (M − Bn$^+$, 10%), 213 (15%), 105 (Bz$^+$, 100%), 91 (85%), 77 (55%). MS (ci, NH$_3$) *m/z*: 379 (M + H$^+$, 30%), 289 (100%). HRMS, Exact Mass calcd. for $C_{21}H_{18}N_2O_5$: 378.1216; found: 378.1210.

*Dimethyl 5-benzoyl-1*H*-pyrazole-3,4-dicarboxylate (**23**a)*: IR (cm^{-1}): 3450 m, 3240(br) m, 3060 w, 2955 m, 2927 w, 2850 w, 1738 s, 1658 m, 1598 w, 1576 w, 1492 w, 1450 m. ^1H NMR, δ: 8.10 (d, br, J = 8 Hz, 2H, H-2, H-6 of Bz), 7.63 (t, br, J = 7.2 Hz, 1H, H-4 of Bz), 7.49 (t, br, J = 7.5 Hz, 2H, H-3,

© 1997 NRC Canada

Table 2. Comparative ^{13}C NMR data for (*E*)- and (*Z*)-methylenecyclopropanes (**17** and **18**).

	17*a*	**17***f*[a]	**17***g*[a]	**17***h*	**18***a*	**18***f*[a]	**18***g*[a]	**18***h*
$COOCH_3$	52.6	52.6	52.6	52.7	52.4	52.4	52.5	52.7
	52.9	52.9	52.9	53.0	53.1	53.1	53.1	53.0
2-*C*OOMe	168.9	168.6	168.6	168.5	169.7	169.5	169.7	169.3
1-*C*OOMe	171.0	170.9	171.0	170.7	170.3	170.2	170.3	170.0
CH_2	32.8	32.8	32.2	32.8	32.4	32.4	31.8	32.8
	33.8	34.0	33.6	34.0	37.3	37.4	37.0	34.0
	30.7	30.6	30.7	30.7	27.3	(27.6)[c]	27.6	30.7
	125.2	126.1	124.8	128.0	125.8	126.6	125.3	129.7
=CH-	121.2	120.3	121.5	120.1	121.9	121.1	122.3	120.9
Benzyl Ar								
C1	138.8	138.6	137.9	138.5	138.0	(137.7)	137.2	137.7
C2	129.1[b]	129.03[b]	131.0	129.1	129.0	(129.0)	130.6	128.8
C3	128.41	128.45	131.5	128.5	128.42[b]	128.49	131.4	128.5
C4	126.5	126.6	(120.3)[c]	126.7	126.5	(126.5)	120.5	126.7
Vinyl Ar								
C1	135.5	134.5	135.4	139.0	135.2	134.2	135.1	138.6
C2	127.6	129.05[b]	127.6	127.7	127.8	129.2	127.7	127.8
C3	128.9[b]	132.0	128.93	125.8 (q, J_{CF} = 3.9 Hz)	128.6[b]	132.1	128.94	125.9 (q, J_{CF} = 3.5 Hz)
C4	128.40	122.5	128.6	obsc	128.38	122.4	128.40	obsc
Aryl subst.	—	—	—	obsc(CF_3)	—	—	—	obsc(CF_3)

[a]Spectrum obtained at 125 MHz from a mixture with its three isomers.
[b]These assignments may be interchanged.
[c]Parentheses indicate presumed position of signal, obscured by others in sample.

H-5 of Bz); 3.97 and 3.83 (two s, 6H, 2 × OMe). ^{13}C NMR, δ: 186.2 (PhCO), 163.4 (COOMe), 159.1 (COOMe), 147.9 (C3, C5), 136.2 (Ph-C1), 135.2 (C4), 133.8 (Ph-C4), 130.3 (Ph-C2), 128.7 (Ph-C3), 119.4 (C4), 53.2, 53.1. MS (ei) *m/z*: 288 (M^+, 5%), 257 (M − OMe^+, 10%), 225 (10%), 105 (Bz^+, 63%), 91 (60%), 77 (100%). MS (ci, NH_3) *m/z*: 289 (M + H^+, 100%), 275 (15%), 257 (8%). HRMS, Exact Mass calcd. for $C_{14}H_{12}N_2O_5$: 288.0746; found: 288.0755.

Other products from photolysis of ***3****a in the presence of DMAD*

On several occasions dimethyl 1,3,5,7-cyclooctatetraene-1,8-dicarboxylate was isolated (ca. 8%). IR (cm^{-1}): 3060 w, 3020 m, 2955 m, 2910 w, 2850 w, 1722 s, 1656 m, 1640 m, 1605 w, 1495 w, 1435 m. ^1H NMR, δ: 7.19 (d, *J* = 3.3 Hz, 2H, H-2, H-7), 6.07 (dd, *J* = 11.5, 3.3 Hz, 2H, H-3, H-6), 5.95 (d, *J* = 11.1 Hz, 2H, H-4, H-5), 3.88 (s, 6H, OMe). ^{13}C NMR, δ: 166.1 (CO), 143.2 (C-2), 132.8 and 130.2 (C-3 and C-4), 132.2 (C-1), 52.3 (OMe). MS (ei) *m/z*: 220 (M^+, 35%), 188 (35%), 161 (M − E^+, 75%), 160 (100%), 133 (90%), 102 (85%), 91 (75%), 76 (35%). MS (ci, NH_3) *m/z*: 238 (M + NH_4^+, 30%), 221 ($M+H^+$, 100%), 189 (M − OMe^+, 10%), 160 (5%). The NMR data fit well with those in the literature (43), and the IR data fit moderately well with published mull data (44).

On one occasion, a small amount of an unidentified compound was obtained with ^1H NMR, δ: 9.3 (s, br, 1H), 7.20 (dd, *J* = 6.6 Hz, 2.1 Hz, ca. 2H), 6.85 (dd, *J* = 6.6 Hz, 2.1 Hz, ca. 2H), 3.79 (s, 3H, OMe), 3.59 (s, 2H, CH_2), 2.01(s, 3H, Me). ^{13}C NMR (spin sort mode) δ: 176.8 (CO), 167.9 (CO), 158.9 (), 130.5 (intense, =CH-), 125.8 (), 114.2 (intense, =CH-), 102.6 (quat-C), 55.4 (OMe), 40.3 (CH_2), 20.7 (Me).

On a few occasions, and contaminated with other components, small amounts of what is probably the dihydronaphthalene ***29****a* (ca. 1.5%), were isolated. Partial spectrum: ^1H NMR, δ: 4.91(s, br, 1H), 4.16 and 4.10 (AB quartet, *J* = 14.2 Hz, 2H, CH_2), 3.80 and 3.66 (two s, 2 × OMe), 3.34 (d, *J* = 20 Hz, 1H, upfield half of an AB quartet).

*Photolysis of oxadiazoline (****3****a) in methanol (1 run)*

Oxadiazoline (***3****a*) was photolyzed as described above, but using methanol as solvent. The majority of the products were the same as with benzene as solvent, but one new component was methyl 4-benzyl-3-methoxycarbonyl-2-methoxy-5-phenylpent-3-enoate (**30**) (4%). IR (cm^{-1}): 3080 w, 3065 w, 3030 w, 3000 w, 2955 m, 2830 w, 1760 s, 1729 s, 1652 w, 1600 w, 1490 m, 1450 m, 1433 m. ^1H NMR (500 MHz) δ: 7.30–7.25(m, 4H of Ph), 7.22(t, *J* = 7 Hz, 2H of Ph), 7.17 (d, *J* = 7 Hz, 2H, H-2, H-6 of Ph), 7.14 (d, *J* = 7 Hz, 2H, H-2, H-6 of Ph), 4.86 (s, 1H, methine-H), 3.81 (s, 3H, 1-OMe), 3.77 (s, 3H, 3-COOMe); 3.63 and 3.59 (AB quartet, *J* = 14.5 Hz, 2H, CH_2 *cis* to 3-E); 3.53 (s, 2H, CH_2 *cis* to CHEOMe), 3.41 (s, 3H, 2-OMe). ^{13}C NMR, δ: 170.6 (C1, i.e., *C*OOMe), 167.9 (3-*C*OOMe), 150.0 (C4), 138.4 and 137.9 (2 × Ph-C1), 131.3 (C3), 129.3 and 129.1 and 128.8 and 128.7 (C2

Can. J. Chem. Downloaded from www.nrcresearchpress.com by 92.62.229.171 on 09/08/12
For personal use only.

© 1997 NRC Canada

Can. J. Chem. Downloaded from www.nrcresearchpress.com by 92.62.229.171 on 09/08/12
For personal use only.

Table 3. Comparative ^{13}C NMR data for 4*H*-pyrazole *N*-oxides (**25**).

	25*a*	**25***b*	**25***c*	**25***d*	**25***e*
3-COO*C*H$_3$	52.5	52.5	52.5	52.6	52.7
3-*C*OOMe	161.7	161.7	161.7	161.6	161.5
4-COO*C*H$_3$	53.4	53.4	53.3	53.5	53.6
4-*C*OOMe	169.7	169.8	169.7	169.5	169.3
4-CH$_2$	42.7	42.5	42.0	42.7	42.7
5-CH(OH)	100.2	100.1	100.1	99.0	98.5
C3	143.5	143.6	143.5	144.13	144.6
C4	63.7	63.8	63.9	64.0	64.3
C5	143.6	145.4	143.8	144.09	145.3
4-CH$_2$-Ar					
C1	135.1	131.9	127.0	134.9	134.7
C2	130.2	130.1	131.1	130.1	130.1
C3	128.4	129.1[a]	113.8	128.4	128.5
C4	127.31	138.2	158.9	127.4	127.4
5-CH(OH)Ar					
C1	135.7	135.7	135.7	134.6	139.3
C2	127.34	127.3	127.3	128.9	127.5
C3	129.3	129.3[a]	129.3	132.4	126.2 (q, J_{CF} = 3.5 Hz)
C4	126.8	126.7	126.8	120.3	obsc
Aryl subst	—	22.8(CH$_3$)	53.4(OCH$_3$)	—	obsc(CF$_3$)

[a]Assignments may be interchanged.

and C3 of Ph's), 126.9 and 126.7 (2 × C4 of Ph), 77.9 (C2), 57.9 (2-OMe), 52.5 (1-OMe), 52.2 (3-COO*Me*), 39.5 (CH$_2$ *cis* to 3-E), 37.4 (CH$_2$ *cis* to CHEOMe). MS (ci, NH$_3$) *m/z*: 386 (M + NH$_4^+$, 35%), 369 (M + H$^+$, 35%), 354 (65%), 337 (M − OMe$^+$, 100%), 309 (M − E$^+$, 20%), 245 (30%), 91 (27%).

Low-temperature photolysis of **3**a *(2 runs)*

Compound **3***a* was photolyzed in the presence of DMAD in toluene at −40°C, using a thin-walled NMR tube. After 5 h the mixture contained the unstable 3*H*-pyrazole **6***a*, but only about half the oxadiazoline had reacted. Also present was a small amount of symmetric cyclopropene (**4***a*), but apparently no unsymmetrical cyclopropene (**16***a*). After 4 days in solution, compound **6***a* had disappeared, and some of the new signals could be assigned to the 1, 5-dibenzyl 1*H*-pyrazole **19***a*.

In a repeat run, most of the oxadiazoline had been consumed after 10 h. Separation gave propenes **14***a* and **15***a* (2%), unchanged starting material, cyclopropene **4***a* (22%), as well as an unidentified compound with ^1H NMR, δ: 7.35–7.15 (m, ca. 8H), 7.02 (d, *J* = 7 Hz, 2H), 3.89 (s, 2H, CH$_2$), 3.80 and 3.76 (two s, 2 × OMe), 3.49 (s, 2H, CH$_2$). ^{13}C NMR, δ: 166.8 and 158.1 (2 × CO), 138.1 and 137.3 (2 × C1 of Ph), 129.2 and 128.9 and 128.8 (CH of Ph), 126.9 and 126.7 (2 × C4 of Ph), 52.5 (2 × OMe), 40.4 and 38.8 (2 × CH$_2$). Final components were unsymmetric cyclopropene **16***a* (11%), benzoyl 4*H*-pyrazole **21***a* (5%), and monobenzyl 1*H*-pyrazole **20***a* (2%).

*Photolysis of oxadiazoline (***3**b*) (1 run)*

Separation gave a mixture of 1, 3-diarylpropenes (**14***b*, **14***c*, **15***b*, and **15***c*) in ratio approximately 3:3:1:1 (3%), and the following additional compounds in this order. Methylenecyclopropanes **17***c* and **18***c* in approximately equal amounts, but each occurring with about 25% of the positional isomers **17***b* and **18***b* (combined total yield: 10%). This mixture of four components could not be separated on the Chromatotron. IR (mixture) (cm^{-1}): 3030 w, 3005 w, 2950 w, 2925 w, 1728 s, 1510 w, 1494 w, 1448(sh), 1431 m. ^1H NMR (**18***c*), δ: 7.45–7.00 (m, aryl-H), 6.87 (d, *J* = 2.0 Hz, vinyl-H); 3.85 and 3.08 (AB quartet, *J* = 15.7 Hz, 2H, CH$_2$), 3.70 and 3.58 (two s, 2 × OMe), 3.40 (d, *J* = 2.2 Hz, 1H, methine-H), 2.28 (s, 3H, ArMe); **18***b* includes 6.85 (d, *J* = 2.0 Hz, vinyl-H); 3.92 and 3.09 (AB quartet, *J* = 15.9 Hz, CH$_2$); 3.54 (s, OMe), 2.36 (s, ArMe); **17***c* includes 6.75 (d, *J* = 2.3 Hz, vinyl-H); 3.69 and 3.65 (two s, 2 × OMe); 3.45 (d, *J* = 2.3 Hz, methine-H), 3.33 (s, CH$_2$), 2.32 (s, ArMe); (**17***b*) includes 6.79 (d, *J* = 2.3 Hz, vinyl-H), 3.37 (s, CH$_2$), 2.34 (s, ArMe).

*Dimethyl 3-benzyl-3-(4-methylbenzyl)cyclopropene-1,2-dicarboxylate (***4**b*) (16%). IR (cm^{-1}): 3030 w, 2955 w, 2915 w, 2850 w, 1833 m, 1713 s, 1605 w, 1510 w, 1491 w, 1445(sh), 1430 m. ^1H NMR, δ: 7.4–6.9 (m, 9H), 3.74 (s, 6H, 2 × OMe); 3.11 and 3.08 (two s, 2 × CH$_2$), 2.28 (s, 3*H*, ArMe). ^{13}C NMR, δ:160.0 (CO), 138.3 (Ph-C1), 135.9 (Ar-C4), 135.1 (Ar-C1), 129.8 (Ph-C2), 129.7 (Ar-C2), 129.2 (Ar-C3), 128.5 (Ph-C3), 126.8 (C1 and C2), 126.5 (Ph-C4), 52.7 (OMe), 43.0 and 42.6 (2 × CH$_2$), 41.3 (C3), 21.2 (Ar-Me).

*Dimethyl 2-benzyl-3-(4-methylbenzyl)cyclopropene-1,3-dicarboxylate (***16**b*) and dimethyl 3-benzyl-2-(4-methylbenzyl)-cyclopropene-1,3-dicarboxylate (***16**c*)* as a 2:1 mixture (25%). The isomers could not be separated. IR (of mixture) cm^{-1}: 3030 w, 3005 w, 2950 w, 2920 w, 1867 m, 1720 s, 1605 w, 1510 m, 1492 w, 1445 (sh), 1430 m. ^1H NMR of **16***b* (from the

© 1997 NRC Canada

Can. J. Chem. Downloaded from www.nrcresearchpress.com by 92.62.229.171 on 09/08/12
For personal use only.

mixture), δ: 7.3–6.9 (m, aryl-H), 3.72 and 3.54 (two s, 2 × OMe); 3.8–3.5 (m, 2-CH_2; partly obscured), 3.29 and 3.18 (AB quartet, J = 14.4 Hz, 3-CH_2); 2.28 (s, ArMe). Partial ^{1}H NMR of **16***c* (remaining signals obscured by those of **16***b*), δ: 3.71 and 3.56 (two s, 2 × OMe); 3.31 and 3.22 (AB quartet, J = 14 Hz, 3-CH_2) 2.31 (s, ArMe).

Pyrazole-N-*oxide* (**25**b), bright yellow oil (3%). ^{1}H NMR, δ: 8.06 (s, br, 1H, OH), 7.4–6.9 (m, 9H), 5.75 (s, 1H, >CH-), 3.90 and 3.77 (two s, 2 × OMe), 3.72 and 3.28 (AB quartet, J = 13.5 Hz, CH_2) 2.25 (s, ArMe). This compound was unstable, and after 2 weeks' exposure to air at room temperature had changed to a complex mixture. Based on the major signals in the ^{1}H NMR spectrum of the mixture the principal component was methyl 5-benzoyl-4-(4-methylbenzyl)-1*H*-pyrazole-3-carboxylate (**22***b*). ^{1}H NMR, δ: 8.02 (d, J = 7 Hz, 2H, H-2, H-6 of Bz), 7.56 (t, J = 7 Hz, 1H, H-4 of Bz), 7.44 (t, J = 7 Hz, 2H, H-3, H-5 of Bz), 7.16 (d, J = 8.0 Hz, 2H, H-2, H-6 of Ar), 7.02 (d, J = 8.0 Hz, 2H, H-3, H-5 of Ar), 4.46 (s, 2H, 4-CH_2), 3.94 (s, 3*H*, OMe), 2.26 (s, 3H, Ar-Me).

*Dimethyl 5-benzyl-1-(4-methylbenzyl)-1*H*-pyrazole-3,4-dicarboxylate (19*b) (6%). IR (cm^{-1}): 3035 w, 3005 m, 2955 m, 2930 (sh), 2860 w, 1730 s, 1602 w, 1531 w, 1511 w, 1491 m, 1477 m, 1445(sh), 1432 s. ^{1}H NMR, δ: 7.3–6.9 (m, 9H), 5.13 (s, 2H, N-CH_2), 4.16 (s, 2H, 5-CH_2), 3.96 and 3.81 (two s, 2 × OMe); 2.31 (s, 3H, ArMe). ^{13}C NMR, δ: 163.6 and 162.8 (2 × CO), 145.3 (C3), 138.1 (Ar-C4), 136.1 (Ph-C1), 132.0 (Ar-C1), 129.7 (Ar-C3), 129.0 (Ph-C3), 128.3 (Ph-C2), 127.1 (Ph-C4), 127.0 (Ar-C2), 114.2 (C4), 54.3 (*N*-CH_2), 52.7 and 52.1 (2 × OMe), 30.3 (5-CH_2), 21.3 (Ar-Me), signal from C5 not clearly visible. MS(ei) *m/z*: 378 (M^+, 10%), 346 (M − $MeOH^+$, 10%), 314 (5%), 273 (M − $ArCH_2^+$, 25%), 241 (20%), 105 ($ArCH_2^+$, 100%), 91 (25%), 77 (20%). HRMS, Exact Mass calcd. for $C_{22}H_{22}N_2O_4$: 378.1580; found: 378.1583.

Compound **20**a *and dimethyl 5-(4-methylbenzyl)-1*H*-pyrazole-3,4-dicarboxylate (**20**b)* as a 3:2 mixture (ca. 4%). Because of overlap by signals from **20***a*, only partial spectra are available for **20***b*. ^{1}H NMR, δ: 4.23 (s, CH_2); 3.92 and 3.84 (two s, 2 × OMe); 2.33 (s, ArMe). ^{13}C NMR, δ: 163.3 and 162.3 (2 × CO), 137.2 (Ar-C4), 133.3 (Ar-C1), 129.9 (Ar-C3), 129.0 (Ar-C2), 52.8 and 52.0 (2 × OMe), 21.2 (Ar-Me).

Photolysis of para-*methoxybenzyl oxadiazoline (***3**c*) (1 run)* Separation gave first a mixture of the 1,3-diarylpropenes **14***d*, **14***e*, **15***d*, and **15***e* in approximate ratio 2:2:1:1 (2%), then the following additional products.

*Dimethyl 3-benzyl-3-(4-methoxybenzyl)cyclopropene-1,2-dicarboxylate (**4**c)* (6%). IR(cm^{-1}): 3065 w, 3030 w, 3005 w, 2955 m, 2915 m, 1834 m, 1715 s, 1610 m, 1581 w, 1509 m, 1495 m, 1450 m, 1430 s. ^{1}H NMR (90 MHz) δ: 7.17–7.10 (m, 3H of Ph), 7.05–7.01 (m, 2H of Ph), 6.92 (d, J = 8.6 Hz, 2H, H-2, H-6 of Ar), 6.69 (d, J = 8.6 Hz, 2H, H-3, H-5 of Ar), 3.68 (s, 9H, ArOMe and 2 × COOMe), 3.03 and 2.99 (two s, 2 × CH_2). ^{13}C NMR, δ: 160.1 (CO), 158.3 (Ar-C4), 138.4 (Ph-C1), 130.8 (Ar-C2), 130.3 (Ar-C1) 129.8 (Ph-C2), 128.5 (Ph-C3), 126.9 (C1 and C2), 126.5 (Ph-C4), 114.0 (Ar-C3), 55.3 (Ar-OMe), 52.7 (COO*Me*), 43.0 and 42.2 (2 × CH_2), 41.5 (C3).

*Dimethyl (*E*)-1-(4-methoxybenzyl)-3-phenylmethylenecyclopropane*-trans-*1,2-dicarboxylate (**17**e) and dimethyl (*Z*)-1-(4-methoxybenzyl)-3-phenylmethylenecyclopropane*-trans-*1, 2-dicarboxylate (**18**e)* in 1:1 ratio, as a mixture (2.5%). Characteristic ^{1}H NMR signals were discernable as follows; for **17***e*, δ: 6.77 (d, J = 2.2 Hz, vinyl-H), 3.70 and 3.66 (two s, 2 × OMe), 3.44 (d, J = 2.3 Hz, methine-H), 3.30 (s, CH_2); for **18***e*, δ: 6.87 (d, J = 2.0 Hz, vinyl-H), 3.71 and 3.60 (two s, 2 × OMe), 3.38 (d, J = 1.9 Hz, methine-H), 3.06 (d, J = 15.6 Hz, half of CH_2 AB quartet; other half obscured by ester signals).

*The methoxy analogue of **29**a*, as a mixture of two isomers; presumably **29***b* and **29***c*. Distinguishable signals in the ^{1}H NMR spectrum: major isomer, δ: 4.86 (s, br, 1H), 4.19 and 4.06 (AB quartet, J = 14.4 Hz, CH_2), 3.72 and 3.71 and 3.60 (three s, 2 × COOMe and ArOMe); minor isomer, δ: 4.90 (s, br, 1H), 4.10 and 3.99 (AB quartet, J = 13.8 Hz, CH_2), 3.73 and 3.70 and 3.59 (three s, 2 × COOMe and ArOMe).

*Dimethyl 2-benzyl-3-(4-methoxybenzyl)cyclopropene-1,3-dicarboxylate (**16**d)*. ^{1}H NMR, δ: 7.3–7.1 (m, 5H of Ph), 6.92 (d, J = 8.7 Hz, 2H, H-2, H-6 of Ar), 6.74 (d, J = 8.7 Hz, 2H, H-3, H-5 of Ar), 3.79 (m, 2H, 2-CH_2), 3.76 and 3.72 (two s, 9H, 2 × COOMe and ArOMe), 3.22 (m, 2H, 3-CH_2).

*Dimethyl 3-benzyl-1-(4-methoxybenzyl)-1*H*-pyrazole-4,5-dicarboxylate (**32**)* (5%), as a yellow oil. IR (cm^{-1}): 3060 w, 3030 w, 3000 w, 2950 m, 2835 w, 1725 s, 1610 m, 1582 w, 1535 m, 1510 s, 1491 m, 1461 m, 1451 m, 1431 m. ^{1}H NMR, δ: 7.26–7.18 (m, 5H of Ph), 7.16 (d, J = 8.6 Hz, 2H, H-2, H-6 of Ar), 6.88 (d, J = 8.6 Hz, 2H, H-3, H-5 of Ar), 5.40 (s, 2H, N-CH_2), 4.18 (s, 2H, 3-CH_2), 3.82 and 3.78 and 3.74 (three s, 2 × COOMe and ArOMe). In an NOE experiment, irradiation at δ = 5.40 caused enhancement of the doublet at 7.16 δ but had no effect on the singlet at 4.18 δ; equally, irradiation at δ = 4.18 enhanced the multiplet at δ = 7.2, but had no effect on the singlet at δ = 5.4. ^{13}C NMR, δ: 163.3 and 161.1 (2 × CO), 159.4 (Ar-C4), 152.0 (C3), 139.1 (C5), 135.7 (Ph-C1), 129.3 and 128.9 (Ar-C2 and Ph-C3), 128.1 (Ph-C2), 126.3 (Ph-C4 and Ar-C1(?)), 114.3 (C4), 113.6 (Ar-C3), 55.4 (ArOMe), 54.7 (N-CH_2), 53.0 and 51.8 (2 × COO*Me*), 33.4 (3-CH_2). MS(ei) *m/z*: 394 (M^+, 10%), 362 (M − 32$^+$, 10%), 307 (15%), 275 (5%), 121 ($MeOBn^+$, 100%), 91 (Bn^+, 20%).

Pyrazole-N-*oxide* (**25**c) as a bright yellow oil. IR (cm^{-1}): 3350(br) w, 3030 w, 3000 w, 2955 w, 2835 w, 1740 s, 1710 s, 1655 m, 1611 w, 1600 w, 1555 m, 1511 m, 1450 s, 1411 m. ^{1}H NMR, δ: 8.04 (s, br, OH), 7.40–7.35 (m, 2H of Ph), 7.25–7.18 (m, 3H of Ph), 6.98 (d, J = 8.7 Hz, 2H, H-2, H-6 of Ar), 6.70 (d, J = 8.7 Hz, 2H, H-3, H-5 of Ar), 5.74 (s, 1H, >CH-), 3.96 and 3.77 (two s, 2 × COOMe), 3.74 (s, ArOMe), 3.71 and 3.27 (AB quartet, J = 13.7 Hz, CH_2). MS (ei) *m/z*: 394 (M^+, 5%), 121 ($MeOBn^+$, 100%), 105 (10%), 77 (12%). On exposing the solution to the atmosphere for several days, **25***c* was converted primarily to methyl 5-benzoyl-4-(4-methoxybenzyl)-1*H*-pyrazole-3-carboxylate (**22***c*). IR (cm^{-1}): 3270(br) m, 3070 w, 3040 w, 3005 w, 2960 m, 2842 w, 1730 s, 1655 s, 1613 m, 1601 m, 1582 w, 1511 s, 1452 s, 1442 s. ^{1}H NMR, δ: 8.02 (d, J = 7.0 Hz, 2H, H-2, H-6 of Bz), 7.59 (t, J = 7.3 Hz, 1H, H-4 of

© 1997 NRC Canada

Can. J. Chem. Downloaded from www.nrcresearchpress.com by 92.62.229.171 on 09/08/12
For personal use only.

Bz), 7.46 (t, J = 7.7 Hz, 2H, H-3, H-5 of Bz), 7.20 (d, J = 8.7 Hz, 2H, H-2, H-6 of Ar), 6.76 (d, J = 8.7 Hz, 2H, H-3, H-5 of Ar), 4.44 (s, 2H, CH_2), 3.97 (s, 3H, COOMe), 3.74 (s, 3H, ArOMe). ^{13}C NMR, δ (partial spectrum): 189.1 (PhCO), 160.1 (*C*OOMe), 158.1 (Ar-C4), 137.9 (Ph-C1), 133.0 (Ph-C4), 132.8 (Ar-C1), 129.8 (Ar-C2), 128.4 (Ph-C3), 113.9 (Ar-C3), 55.4 (Ar-OMe), 52.5 (COO*Me*), 28.2 (CH_2).

*Dimethyl 5-benzyl-1-(4-methoxybenzyl)-1*H*-pyrazole-3,4-dicarboxylate (**19**d)* (25%). IR (cm^{-1}): 3050 w, 3025 w, 2995 w, 2945 m, 2830 w, 1735 s, 1718 s, 1611 m, 1584 w, 1531 m, 1512 s, 1493 s, 1477 s, 1453 s, 1438 s. ^{1}H NMR, δ: 7.2 (m, 3H of Ph), 7.06 (m, 2H of Ph), 6.96 (d, J = 8.8 Hz, 2H, H-2, H-6 of Ar), 6.79 (d, J = 8.6 Hz, 2H, H-3, H-5 of Ar), 5.11 (s, 2H, N-CH_2), 4.19 (s, 2H, 5-CH_2), 3.96 and 3.81 (two s, 2 × COOMe), 3.77 (s, 3H, ArOMe). ^{13}C NMR, δ: 163.4 and 162.7 (2 × CO), 159.6 (Ar-C4), 145.1 (C3), 143.0 (C5), 136.0 (Ph-C1), 129.0 (Ph-C3), 128.6 (Ar-C2), 128.2 (Ph-C2), 127.1 (Ar-C1), 127.0 (Ph-C4), 114.3 (Ar-C3), 114.0 (C4), 55.4 (Ar-OMe), 53.9 (N-CH_2), 52.6 and 52.0 (2 × COO*Me*), 30.2 (5-CH_2).

Finally, dimethyl 5-benzyl-1*H*-pyrazole-3, 4-dicarboxylate (**20***a*) (7%) was isolated.

Photolysis of para*-bromobenzyl oxadiazoline (**3**d) (2 runs)*
Separation after first run gave a mixture of 1,3-diarylpropenes **14***f*, **14***g*, **15***f*, and **15***g* (5%), then the following compounds in this sequence. First a ca. 4:4:3:2 mixture of methylenecyclopropenes **18***g*, **17***f*, **17***g*, and **18***f* (combined yield, 3%). The isomers could not be cleanly separated, and the spectra are those of mixtures, with not all signals being resolved. ^{1}H NMR data, partial spectra: dimethyl 3-(*E*)-(4-bromophenylmethylene)-1-benzylcyclopropane-*trans*-1,2-dicarboxylate (**17***f*), δ: 6.75 (d, J = 2.4 Hz, 1H, vinyl-H), 3.72 and 3.66 (two s, 2 × OMe), 3.46 (d, J = 2.4 Hz, 1H, methine-H), 3.22 (s, 2H, CH_2); dimethyl 1-(4-bromobenzyl)-3-(*E*)-(phenylmethylene)cyclopropane-*trans*-1,2-dicarboxylate (**17***g*), δ: 6.72 (d, J = 2.3 Hz, 1H, vinyl-H), 3.69 and 3.67 (two s, 2 × OMe), 3.45 (d, J = 2.4 Hz, 1H, methine-H), 3.36 (s, 2H, CH_2); dimethyl 1-benzyl-3-(Z)-(4-bromophenylmethylene)cyclopropane-*trans*-1,2-dicarboxylate (**18***f*), δ: 6.83 (d, J = 2.0 Hz, 1H, vinyl-H), 3.82 and 3.13 (AB quartet, J = 15.8 Hz, CH_2), 3.57 (s, OMe); dimethyl 1-(4-bromobenzyl)-3-(*Z*)-(phenylmethylene)cyclopropane-*trans*-1,2-dicarboxylate (**18***g*), δ: 6.89 (d, J = 2.0 Hz, 1H, vinyl-H), 3.77 and 3.11 (AB quartet, J = 15.8 Hz, CH_2), 3.71 and 3.60 (two s, 2 × OMe), 3.39 (d, J = 1.8 Hz, 1H, methine-H).

A minor component, eluting with the methylenecyclopropenes, was not fully purified. Based on comparison with literature data (3), it was probably *2-benzyl-6-bromo-3,3a-bis(methoxycarbonyl)-1,3a-dihydroazulene (**28**b)*. ^{1}H NMR (500 MHz) includes δ: 6.47 and 6.36 (two d, J = 2.6 Hz, 2 × =CH-), 6.09 and 5.75 (two d, J = 5.8 Hz, 2 × =CH-), 4.17 and 3.86 (AB quartet, J = 14.5 Hz, 2-CH_2), 3.77 and 3.64 (two s, 2 × OMe), 2.96 and 2.52 (AB quartet, J = 18.5 Hz, 2 × H-1). ^{13}C NMR (125 MHz), tentative assignments, δ: 173.0 (3a-*C*OOMe), 165.6 (3-*C*OOMe), 157.1 (C2), 143.2 and 139.6 (2 × CH), 138.1 (Ph-C1), 136.0 and 133.4 (2 × CH), 132.1 (C8a), 131.1 (C3 or C6), 129.0 and 128.7 (Ph-C2, Ph-C3), 127.6 (C6 or C3), 126.6 (Ph-C4), 60.8 (C3a), 52.3 and 51.3 (2 × OMe), 47.4 (C1), 36.5 (2-CH_2).

*Dimethyl 3-benzyl-3-(4-bromobenzyl)cyclopropene-1,2-dicarboxylate (**4**d)* (16%). IR (cm^{-1}): 3075 w, 3055 w, 3020 w, 2995 w, 2945 m, 2910 w, 2835 w, 2075 w, 1835 m, 1720 s, 1600 w, 1485 m, 1431 m. ^{1}H NMR, δ: 7.35 (d, J = 8.3 Hz, 2H, H-3, H-5 of Ar), 7.3–7.1 (m, 3H, Ph-H), 7.07 (d, J = 7 Hz, 2H, H-2, H-6 of Ph), 6.97 (d, J = 8.3 Hz, 2H, H-2, H-6 of Ar), 3.76 (s, 6H, 2 × OMe), 3.09 and 3.07 (two s, 2 × CH_2). ^{13}C NMR δ: 159.9 (CO), 138.0 (Ph-C1), 137.2 (Ar-C1), 131.6 (Ar-C2 and Ar-C3), 129.8 (Ph-C2), 128.6 (Ph-C3), 126.7 (C1 and C2), 126.6 (Ph-C4), 120.5 (Ar-C4), 52.8 (OMe), 43.1 and 42.4 (2 × CH_2), 40.8 (C3).

An approximately 10:7 mixture of the asymmetric cyclopropenes, *dimethyl 2-benzyl-3-(4-bromobenzyl)cyclopropene-1,3-dicarboxylate (**16**f) and dimethyl 3-benzyl-2-(4-bromobenzyl)cyclopropene-1,3-dicarboxylate (**16**g)*. ^{1}H NMR assignments from spectrum of mixture: **16***g*, δ: 7.4–6.8 (m, 9H), 3.8-3.6 (m, 2-CH_2), 3.73 and 3.55 (two s, 2 × OMe), 3.23 and 3.13 (AB quartet, J = 14.6 Hz, 3-CH_2); **16***f*, partial spectrum, δ: 3.71 and 3.59 (two s, 2 × OMe), 3.38 and 3.25 (AB quartet, J = 14.6 Hz, 3-CH_2). MS (ei) of mixture *m/z*: 416/414 (M^+, 8%), 384/382 (9%), 357/355 (10%), 325/323 (M − Bn^+, 5%), 297/295 (8%), 245 (20%), 215 (100%), 171/169 (*p*-$BrBn^+$, 60%), 115 (5%), 91 (50%).

Pyrazole-*N*-oxide (**25***d*) eluted in ca. 1:1 ratio with 1*H*-pyrazole (**19***g*) (ca. 3%).
*Compound (**25**d)*. ^{1}H NMR, δ: 7.99 (s, 1H, OH; disappears on shaking with D_2O), 7.47 (d, J = 8.4 Hz, 2H, H-3, H-5 of Ar), 7.4–7.1 (m, 3H, of Ph), 7.07–7.02 (m, 4H, H-2, H-6 of Ar and Ph), 5.66 (s, 1H, >CH-), 3.91 and 3.78 (two s, 2 × OMe), 3.31 (d, J = 13.6 Hz, upfield half of CH_2 AB quartet: other half presumably hidden by ester signals). A one-bond C-H correlation experiment confirmed the assignments as given. In an NOE experiment irradiation of the doublet at δ = 3.31 gave enhancement at 7.99, 5.66, and 3.78 δ whereas irradiation at δ = 3.76 gave enhancement at 7.99, 7.02(d, *ortho*-H of Ph), and 3.31 δ and negative enhancement at 5.67 δ. Irradiation of singlet at δ = 5.67 gave enhancement of signals at 7.99, 7.07(d, *ortho*-H of Ar), and slightly at 3.31 δ. Irradiation of singlet at δ = 7.99 gave enhancement of the signal at δ = 7.07(d, of Ar). There was no change on keeping the mixture with D_2O under nitrogen at −15°C for 4 months.

*Dimethyl 1-benzyl-5-(4-bromobenzyl)-1*H*-pyrazole-3,4-dicarboxylate (**19**g)*. ^{1}H NMR, δ: 7.36 (d, J = 8.4 Hz, 2H, H-3, H-5 of Ar), 7.3–7.0 (m, 5H, of Ph), 6.89 (d, J = 8.5 Hz, 2H, H-2, H-6 of Ar), 5.19 (s, 2H, *N*-CH_2), 4.12 (s, 2H, 5-CH_2), 3.97 and 3.82 (two s, 2 × OMe). ^{13}C NMR, δ: 163.4 and 162.7 (2 × CO), 144.9 (C3), 143.3 (C5), 135.0 (Ph-C1), 134.9 (Ar-C1), 132.1 (Ar-C3), 129.9 (Ar-C2), 129.1 (Ph-C3), 128.4 (Ph-C4), 127.0 (Ph-C2), 121.1 (Ar-C4), 114.2 (C4), 54.5 (*N*-CH_2), 52.8 and 52.1 (2 × OMe), 29.8 (5-CH_2); MS (ei) *m/z*: 444/442 (M^+, 8%), 412 (12%), 380/378 (10%), 353/351 (M − Bn^+, 13%), 331 (5%), 240 (15%), 171/169 (*p*-$BrBn^+$, 10%), 115 (10%), 91 (100%). HRMS, Exact Mass calcd. for $C_{21}H_{19}{}^{79}BrN_2O_4$: 442.0528; found: 442.0522.

The final compound eluted was **20***a* mixed with about 20%

© 1997 NRC Canada

*dimethyl 5-(4-bromobenzyl)-1*H*-pyrazole-3,4-dicarboxylate (**20***c*). Overlap meant that only partial ^{1}H NMR data could be determined for **20***c*, signals for which included (δ): 7.44 (d, *J* = 8.4 Hz, H-3, H-5 of Ar), 7.10 (d, *J* = 8.4 Hz, H-2, H-6 of Ar), 4.22 (s, CH_2), 3.93 and 3.83 (two s, 2 × OMe). ^{13}C NMR, δ: 132.2 (Ar-C3), 130.7 (Ar-C2), 32.0 (5-CH_2). HRMS (on high molecular mass component of mixture), Exact Mass calcd. for $C_{14}H_{13}{}^{79}BrN_2O_4$: 352.0059; found: 352.0056.

On exposure to the atmosphere for several days, the solution of **25***d* was converted to *dimethyl 4-benzyl-5-(4-bromobenzoyl)-4*H*-pyrazole-3,4-dicarboxylate **21**d* (2% overall). IR (cm^{-1}): 3340(br) w, 3090 w, 3070 w, 3040 w, 2960 m, 2930 m, 2855 w, 1765 s, 1733 s, 1657 m, 1585 m, 1568 w, 1487 m, 1438 m. ^{1}H NMR, δ: 7.93 (d, *J* = 8.6 Hz, 2H, H-2, H-6 of Ar), 7.61 (d, *J* = 8.6 Hz, 2H, H-3, H-5 of Ar), 7.2–7.0 (m, 3*H*, of Ph), 6.76 (d, *J* = 6.6 Hz, 2H, H-2, H-6 of Ph), 4.08 and 3.73 (two s, 2 × OMe), 3.9–3.8 (m, 2H, CH_2). ^{13}C NMR, δ (partial spectrum): 185 (Ar-CO), 173 (C3 or C5), 133.4 (Ph-C1), 132.7 (Ar-C2), 132.2 (Ar-C3), 128.8 (Ph-C2), 128.7 (Ph-C3), 128.3 (Ph-C4), 54.1 and 53.8 (2 × OMe), 37.5 (CH_2).

Performing the photolysis of **3***d* in the presence of triethylamine (1 drop) gave a similar mix of products, but also included dimethyl 1-(diethylamino)maleate. IR (cm^{-1}): 2995 m, 2960 m, 1750 s, 1701 s, 1661 m, 1575 s, 1519 w, 1450 s, 1440 s, 1428 m, *cf.* values in ref 45. ^{1}H NMR, δ: 4.61 (s, 1H), 3.94 and 3.63 (two s, 2 × OMe), 3.18 (q, *J* = 7.1 Hz, 4H, 2 × CH_2), 1.18 (t, *J* = 7.1 Hz, 6H, 2 × CH_3). This spectrum is in good agreement with that published (45, 46). ^{13}C NMR, δ: 168.5 and 166.3 (2 × CO), 129.1 (=C<), 83.1 (=CH-), 54.3 and 50.8 (2 × OMe), 45.1 br (CH_2), 12.8 br (CH_3). This is reasonably concordant with values tabulated for the corresponding dimethyl compound (47).

Photolysis of para*-trifluoromethylbenzyl oxadiazoline (**3**e) (2 runs)*

Separation gave a mixture of 1,3-diarylpropenes **14***h*, **14***i*, **15***h*, and **15***i* as well as the following additional products.

Dimethyl (E)*-1-benzyl-3-(4-trifluoromethylphenylmethylene)-cyclopropane*-trans*-1,2-dicarboxylate (**17**h)* (5%). IR (cm^{-1}): 3080(sh), 3060 w, 3030 w, 3005 w, 2955 m, 2930 w, 2850 w, 1733 s, 1615 m, 1491 w, 1445(sh), 1434 m, 1421(sh), 941 m, 872 m, 822 m, 795 w. ^{1}H NMR, δ: 7.60 (d, *J* = 8.4 Hz, 2H, H-3, H-5 of Ar), 7.51 (d, *J* = 8.3 Hz, 2H, H-2, H-6 of Ar), 7.3–7.2 (m, 5H, of Ph), 6.81 (d, *J* = 2.2 Hz, 1H, vinyl-H), 3.70 and 3.68 (two s, 2 × OMe), 3.50 (d, *J* = 2.2 Hz, 1H, methine-H), 3.37 (s, 2H, CH_2). MS (ei) *m/z*: 404 (M^+, 7%), 385 (M − F^+, 3%), 372 (17%), 344 (M − EH^+, 12%), 313 (M − Bn^+, 15%), 285 (50%), 215 (25%), 183 (10%), 159 (*p*-$CF_3C_6H_4CH^+2$, 22%), 115 (30%), 91 (100%). HRMS, Exact Mass calcd. for $C_{22}H_{19}F_3O_4$: 404.1235; found: 404.1241.

Dimethyl (Z)*-1-benzyl-3-(4-trifluoromethylphenylmethylene)-cyclopropane*-trans*-1,2-dicarboxylate (**18**h)* (3%). IR (cm^{-1}): 3080(sh), 3060 w, 3030 w, 2955 m, 2925 m, 2845 w, 1731 s, 1613 w, 1490 w, 1445(sh), 1432 m, 1420(sh), 964 w, 914 w, 869 m, 839 w, 821 w. ^{1}H NMR, δ: 7.57 (d, *J* = 8.3 Hz, 2H, H-3, H-5 of Ar), 7.43 (d, *J* = 8.3 Hz, 2H, H-2, H-6 of Ar), 7.15 (s, br, 5H, of Ph), 6.93 (d, *J* = 2.0 Hz, 2H, vinyl-H), 3.80 and 3.16 (two d, *J* = 15.7 Hz, CH_2), 3.73 and 3.59 (two s, 2 × OMe), 3.42 (d, *J* = 1.8 Hz, 1H, methine-H). MS(ei) *m/z*: 404 (M^+, 12%), 385 (M − F^+, 7%), 372 (M − 32^+, 55%), 344 (M − EH^+, 35%), 329 (5%), 313 (45%), 285 (100%), 215 (55%), 183 (22%), 159 (25%), 115 (22%), 91 (93%). HRMS, Exact Mass calcd. for $C_{22}H_{19}F_3O_4$: 404.1235; found: 404.1243.

*Dimethyl 2-benzyl-3-(4-trifluoromethylbenzyl)cyclopropene-1,3-dicarboxylate (**16**h)* (ca. 5%). ^{1}H NMR, δ: 7.45 (d, *J* = 8.1 Hz, 2H, H-3, H-5 of Ar), 7.3–7.05 (m, 7H), 3.72 and 3.57 (two s, 2 × OMe), ca. 3.7 (m, 2H, 2-CH_2), 3.35 and 3.19 (two d, *J* = 14.5 Hz, 3-CH_2).

*Dimethyl 3-benzyl-2-(4-trifluoromethylbenzyl)cyclopropene-1,3-dicarboxylate (**16**i)* (5%). IR (cm^{-1}): 3080 w, 3055 w, 3025 w, 2945 m, 2840 w, 1863 w, 1719(br) s, 1611 w, 1578 w, 1488 w, 1442(sh), 1428 m, 1413 m. ^{1}H NMR, δ: 7.52 (d, *J* = 8.0 Hz, 2H, H-3, H-5 of Ar), 7.26–7.15 (m, 5H), 7.05–7.00 (m, 2H), 3.71 and 3.59 (two s, 2 × OMe), 3.7 (m, 2H, 2-CH_2), 3.44 and 3.21 (two d, *J* = 14.3 Hz, 3-CH_2).

*Dimethyl 3-benzyl-3-(4-trifluoromethylbenzyl)cyclopropene-1,2-dicarboxylate (**4**e)* (12%). IR (cm^{-1}): 3065 w, 3035 w, 2955 w, 2925 w, 2845 w, 1837 m, 1722 s, 1617 w, 1602 w, 1491 w, 1448(sh), 1443 s, 1418 m. ^{1}H NMR, δ: 7.5–7.4 (m, 4H, of Ar), 7.30–7.17 (m, 3H, of Ph), 7.10–7.06 (m, 2H, of Ph), 3.76 (s, 6H, 2 × OMe), 3.17 and 3.11 (two s, 2 × CH_2). ^{13}C NMR, δ: 159.9 (CO), 142.4 br (Ar-C1), 137.9 (Ph-C1), 130.2 (Ar-C2), 129.8 (Ph-C2), 128.7 (Ph-C3), 126.8 (C1 and C2), 126.6 (Ph-C4), 125.4 (q, J_{CF} = 3.6 Hz, Ar-C3), 52.9 (OMe), 43.1 and 42.9 (2 × CH_2), 40.7 (C3), signals for Ar-C4 and CF_3 too dispersed for detection. *Pyrazole*-N*-oxide (**25**e)* as a yellow oil. IR (cm^{-1}): 3350 w, 3065 w, 3035 w, 2955 w, 1740 s, 1713 s, 1652 m, 1611 m, 1565 s, 1490 w, 1445 s, 1439(sh). ^{1}H NMR, δ: 8.08 (s, 1H, HO), 7.61 and 7.29 (two d, *J* = 8.2 Hz, 4H of Ar), 7.20–7.15 (m, 3H, Ph-H), 7.07–7.01 (m, 2H, Ph-H), 5.76 (s, 1H, >CH-), 3.92 and 3.79 (two s, 2 × OMe), 3.78 and 3.34 (AB quartet, *J* = 13.5 Hz, CH_2).

*Dimethyl 1-benzyl-5-(4-trifluoromethylbenzyl)-1*H*-pyrazole-3,4-dicarboxylate (**19**i)* (34%). IR (cm^{-1}): 3065 w, 3055 w, 3000 w, 2955 w, 1736 s, 1724 s, 1617 w, 1541 w, 1476 m, 1451 m, 1435 m, 1418 m. ^{1}H NMR, δ: 7.47 (d, *J* = 8.2 Hz, 2H, H-3, H-5 of Ar), 7.26–7.22 (m, 3H, of Ph), 7.11 (d, *J* = 7.9 Hz, 2H, H-2, H-6 of Ar), 6.98–6.94 (m, 2H, of Ph), 5.21 (s, 2H, N-CH_2), 4.25 (s, 2H, 5-CH_2), 3.98 and 3.82 (two s, 2 × OMe). ^{13}C NMR, δ: 163.4 and 162.7 (2 × OMe), 144.5 (C3), 143.4 (C5), 140.1 (Ar-C1), 134.7 (Ph-C1), 129.1 (Ph-C3), 128.6 (Ar-C2), 128.5 (Ph-C4), 126.9 (Ph-C2), 125.9 (q, J_{CF} = 4.0 Hz, Ar-C3), 114.3 (C4), 54.6 (N-CH_2), 52.8 and 52.2 (2 × OMe), 30.2 (5-CH_2), Ar-C4 and CF_3 signals too dispersed for detection.

Compound **25***e* was stable in $CDCl_3$ under nitrogen at −20°C for over 4 weeks, but on exposure to air, gave *methyl 4-benzyl-5-(4-trifluoromethylbenzoyl)-1*H*-pyrazole-3-carboxylate (**22**e)*. ^{1}H NMR, δ: 8.15 (d, *J* = 8.0 Hz, 2H, H-2, H-6 of Ar), 7.71 (d, *J* = 8.2 Hz, 2H, H-3, H-5 of Ar), 7.2–7.1 (m, 5H, of Ph), 4.54 (s, 2H, CH_2), 3.98 (s, 3H, OMe). ^{13}C NMR, δ: 193.2 (ArCO), 159.9 (COOMe), 148.5 (C3 and C5), 140.7 (Ar-C1), 140.2 (Ph-C1), 133.7 (C4), 130.8 (Ar-C2), 128.7 (Ph-C2), 128.5 (Ph-C3), 126.3 (Ph-C4), 125.3 (q, J_{CF} = 3.6 Hz, Ar-C3), 52.6 (OMe), 29.1 (CH_2), signals from Ar-C4

Can. J. Chem. Downloaded from www.nrcresearchpress.com by 92.62.229.171 on 09/08/12
For personal use only.

© 1997 NRC Canada

Can. J. Chem. Downloaded from www.nrcresearchpress.com by 92.62.229.171 on 09/08/12
For personal use only.

and CF_3 too dispersed for detection. HRMS, Exact Mass calcd. for $C_{20}H_{15}F_3N_2O_3$: 388.1035; found 388.1031.

Photolysis of benzyl methyl oxadiazoline ***4f*** *in methanol (1 run)*

Oxadiazoline ***3f*** (0.5 mmol) in methanol-d_4 (1 g) in a thin-walled NMR tube was photolyzed for 5 h. Standard work-up and separation gave the known (ref. 3) symmetrical cyclopropene ***4f*** (9%), and unsymmetrical cyclopropene ***16j*** (4%), along with the pyrazoles described below.

*Dimethyl 1-benzyl-5-methyl-1*H*-pyrazole-3,4-dicarboxylate (**19**j)* (13%). IR (cm^{-1}): 3060 w, 3035 w, 3000 w, 2950 m, 2850 w, 1737 s, 1720 s, 1605 w, 1548 m, 1480 m, 1452 m, 1439 s. ^{1}H NMR, δ: 7.30–7.26 (m, 3H of Ph), 7.14–7.09 (m, 2H, H-2, H-6 of Ph), 5.36 (s, 2H, CH_2), 3.95 and 3.84 (two s, 2 × OMe), 2.39 (s, 3H, 5-Me). In an NOE experiment, irradiation of the singlet at δ = 2.39 caused enhancement of signals at both 5.36 and 7.1 δ. ^{13}C NMR, δ: 163.6 and 162.8 (2 × CO), 144.0 and 143.1 (C3 and C5), 135.7 (Ph-C1), 129.1 (Ph-C3), 128.4 (Ph-C4), 127.0 (Ph-C2), 113.2 (C4), 54.2 (*N*-CH_2), 52.7 and 51.9 (2 × OMe), 11.0 (5-Me). HRMS, Exact Mass calcd. for $C_{15}H_{16}N_2O_4$: 288.1110; found 288.1109.

*Dimethyl 4-benzyl-5-methyl-4*H*-pyrazole-3,4-dicarboxylate (**33**)* (18%). ^{1}H NMR, δ: 7.2 (m, 3*H* of Ph), 6.95 (m, 2H of Ph), 3.96 and 3.72 (two s, 2 × OMe), 3.84 and 3.50 (two d, *J* = 14 Hz, 4-CH_2), 2.39 (s, 3H, 5-Me). In an NOE experiment, irradiation of singlet at δ = 2.39 gave enhancement of the methylene-H at 3.50 δ and an *ortho*-H at 6.9 δ. ^{13}C NMR, δ: 176.4 (C3), 166.8 (C5), 165.4 (4-CO), 160.9 (3-CO), 132.8 (Ph-C1), 128.9 and 128.6 (C2 and C3 of Ph), 128.2 (Ph-C4), 76.4 (C4), 53.9 and 53.3 (2 × OMe), 37.6 (CH_2), 14.0 (5-Me).

*Dimethyl 5-methyl-1*H*-pyrazole-3,4-dicarboxylate (**20**d)* (5%). IR (cm^{-1}): 3500(sh) br, 3250(br) s, 2950 s, 2925 s, 2855 s, 1710 s, 1565 m, 1490 m, 1445 s. ^{1}H NMR, δ: 3.94 and 3.86 (two s, 2 × OMe), 2.53 (s, 5-Me). ^{13}C NMR, δ: 163 and 162.4 (2 × CO), 146.2 (C3), 114 (C4), 52.8 and 52.0 (2 × OMe), 11.7 (5-CH_3), C5 not clearly visible. MS (ei) *m/z*: 198 (M^+, 20%), 167 (M − OMe^+, 95%), 166 (100%), 135 (40%), 79 (20%). MS(ci, NH_3) *m/z*: 199 (M + H^+, 40%), 167 (M − OMe^+, 100%), 152 (5%).

Isolation of diazoalkane **5**a

Oxadiazoline (***3a***) (0.21 mmol) in toluene-d_8 (0.5 mL) in a thin-walled NMR tube was photolyzed at −70°C for 4 h, giving the typical pinkish-yellow solution observed in all of the above procedures. The solution was transferred at the temperature of liquid nitrogen to the precooled probe of the 500 MHz NMR spectrometer, and spectra were recorded as the temperature was gradually raised to ambient. The proton spectrum showed that negligible amounts of starting material remained, while the new signals were consistent with the presence of methyl acetate and 2-diazo-1,3-diphenylpropane (***5a***). ^{1}H NMR (in C_7D_8) δ: 7.10–7.05 (m, 6H), 6.85 (d, *J* = 6.9 Hz, 4H), 2.81 (s, 4H). ^{13}C NMR, δ: 138.2 (Ph-C1), 128.76 and 128.67 (Ph-C2 and Ph-C3), 126.8 (Ph-C4), 48.1 (), 32.3 (CH_2). There was little change during the 2 h needed to warm up to −20°C, and even after being kept overnight in the freezer (at ca. −15°C), about 30% of diazo-alkane was left intact. After a further 3 days at −15°C, the diazo-alkane had gone completely and the solution was virtually colourless. About 7% of the diazo-alkane had been converted to the 1,3-diphenylpropenes ***14a*** and ***15a*** in about 2:1 ratio, but the major product was the azine ***9a***. IR (cm^{-1}): 3080 w, 3060 m, 3030 s, 2920 m, 1737 s, 1630 m, 1600 m, 1493 s, 1451 w, 1426 m. ^{1}H NMR, δ: 7.34–7.14 (m, 6H), 7.06–7.01 (m, 4H), 3.70 and 3.58 (two s, 2 × CH_2). ^{13}C NMR, δ: 165.2 (), 138.0 and 137.2 (2 × Ph-C1), 129.6 and 129.5 and 128.7 and 128.6 (2 × Ph-C2 and 2 × Ph-C3), 126.7 and 126.5 (2 × Ph-C4), 42.9 and 36.2 (2 × CH_2). MS (ei) *m/z*: 416 (M^+, 1%), 325 (M − Bn^+, 1%), 194 (22%), 91 (100%). MS (ci, NH_3) *m/z*: 417 (M + H^+, 1%), 314 (3%), 272 (41%), 228 (100%).

Sequential trapping experiments

Oxadiazoline **3** in toluene containing one drop of triethylamine was photolyzed at −65°C for several h, before addition of a solution of dimethyl acetylenedicarboxylate in toluene. Then the solvent and excess volatiles were removed by a stream of nitrogen as the solution warmed up to ambient. Typically this gave a viscous yellow residue.

The product from ***3a*** was essentially pure *dimethyl 3,3-dibenzyl-3*H*-pyrazole-4,5-dicarboxylate (**6**a)*. ^{1}H NMR, δ: 7.35–7.10 (m, 6H), 7.05–6.90 (m, 4H), 3.87 and 3.79 (two s, 2 × OMe), 3.86 and 3.46 (two 2H d, *J* = 13.4 Hz, 2 × CH_2). ^{13}C NMR, δ: 162.6 and 160.3 (2 × CO), 148.7 (C5), 148.1 (C4), 133.6 (Ph-C1), 129.6 (Ph-C3), 128.1 (Ph-C2), 127.4 (Ph-C4), 105.1 (C3), 52.8 and 52.7 (2 × OMe), 41.3 (CH_2).

This solution was divided into two: one portion (still in $CDCl_3$) was photolyzed at −65°C for a further 6 h. The ^{1}H NMR spectrum of the product mixture indicated that 1,5-dibenzyl-1*H*-pyrazole ***19a***, yellow pyrazole-*N*-oxide ***25a***, and unsymmetrical cyclopropene ***16a*** were major components, in ratio ca. 1:1:2, along with the symmetrical cyclopropene ***4a*** as a minor component.

The other portion was stored at room temperature for some days, before separation of decomposition products. The following were isolated: yellow pyrazole-*N*-oxide ***25a*** (22%) and 1,5-dibenzyl-1*H*-pyrazole ***19a*** (20%). The solution of ***25a*** was fairly stable when stored in $CDCl_3$ under nitrogen at −20°C, but after 10 weeks the ***25a*** had been converted exclusively to benzoyl 4*H*-pyrazole (***21a***).

Similarly, oxadiazoline ***3b*** gave *dimethyl 3-benzyl-3-(4-methylbenzyl)-3*H*-pyrazole-4,5-dicarboxylate (**6**b)*: IR (cm^{-1}): 3055 w, 3030 w, 2955 w, 2925 w, 1730 s, br, 1655 w, 1635 w, 1600 w, 1545 w, 1513 w, 1495 m, 1450 m, 1438 m. ^{1}H NMR, δ: 7.23–7.10 (m, 3*H* of Ph), 7.00–6.86 (m, 6H), 3.89 and 3.76 (two s, 2 × OMe), 3.86 + 3.83 and 3.45 + 3.41 (four d, *J* = 13.4 Hz, 2 × CH_2 as AB quartets), 2.23 (s, ArMe). The solvent was removed, the residue was taken up in benzene-d_6, and the resulting solution was heated at 65°C in a sealed tube. After 20 min, signals from the dibenzyl 1*H*-pyrazole ***19b*** began to be evident, and within 3.5 h those of starting material had virtually disappeared. Based on the ^{1}H NMR spectra, the final mixture contained ***19b*** and ***25b*** in the ratio 4:3. As judged from satellite peaks in the ^{1}H NMR spectrum, compound ***19b*** was also contaminated by approximately 10% of the positional isomer ***19c***.

In the same way, oxadiazoline ***3d*** gave ***6d***, as evidenced by

© 1997 NRC Canada

Can. J. Chem. Downloaded from www.nrcresearchpress.com by 92.62.229.171 on 09/08/12
For personal use only.

appearance of two overlapping doublets at ca. 3.44 and 3.43 ppm in the crude photolysate. After further photolysis, these signals disappeared, and in the spectrum of the crude product the only signals assignable belonged to isomeric 1,5-dibenzyl-1*H*-pyrazoles **19***f* and **19***g*. Chromatography gave the following compounds: the isomeric 1, 3-diarylpropenes **14***f*, **14***g*, **15***f*, and **15***g* (together ca. 5%); cyclopropene **4***d* (5%); benzoyl 4*H*-pyrazole **21***d* (4%); and its isomer, *dimethyl 5-benzoyl-4-(4-bromobenzyl)-4*H*-pyrazole-3,4-dicarboxylate (**21***e*)* (8%): IR (cm^{-1}): 3300(br) w, 3070 w, 3035 w, 2965 s, 2925(sh), 2855 w, 1765 s, 1732 s, 1656 s, 1585 m, 1488 m, 1443 s, 1405 m. ^{1}H NMR, δ: 8.12 (d, J = 7.4 Hz, 2H, H-2, H-6 of Bz), 7.63 (m, 1H, H-4 of Bz), 7.50 (t, J = 7.2 Hz, 2H, H-3, H-5 of Bz), 7.21 (d, J = 8.3 Hz, 2H, H-3, H-5 of Ar), 6.69 (d, J = 8.3 Hz, 2H, H-2, H-6 of Ar), 4.06 and 3.73 (two s, 2 × OMe), ca. 3.86 and ca. 3.80 (AB quartet, only centre two lines visible, CH_2). An approximately 2:1 mixture of dibenzyl 1*H*-pyrazole **19***g* and its isomer, dimethyl 5-benzyl-1-(4-bromobenzyl)-1*H*-pyrazole-3,4-dicarboxylate **19***f*, with partial ^{1}H NMR, δ: 6.89 (d, J = 8.4 Hz, H-2, H-6 of Ar), 5.12 (s, N-CH_2), 4.18 (s, 5-CH_2), 3.97 and 3.83 (two s, 2 × OMe), and, finally, monobenzyl 1*H*-pyrazoles **20***a* and **20***c* (ca. 6% together), were obtained.

In contrast, the same procedure applied to methoxy oxadiazoline **3***c* did not appear to give any **6***c*. Chromatography gave 1,3-diarylpropenes **14***d*, **14***e* and **15***d*, **15***e* (together 13%), dibenzyl 1*H*-pyrazole (**19***d*) (42%), and pyrazole-*N*-oxide **25***c*. Compound **25***c* was fairly stable when stored in $CDCl_3$ under nitrogen at −20°C for over four weeks, but gradually decomposed to benzoyl monoester **22***c*, plus an unidentified compound with the following partial ^{1}H NMR spectrum, δ: 7.4–7.3 (m, 5H), 7.20 (d, J = 8.6 Hz, 2H, H-2, H-6 of Ar), 6.84 (d, J = 8.6 Hz, 2H, H-3, H-5 of Ar), 6.47 (s, 1H), 5.50 (s, 2H), 3.85 (s, 3H) and 3.78 (s, 3H) (2 × OMe), 3.71 (s, 3H, ArOMe). Irradiation of the singlet at δ = 5.50 gave enhancement at 7.20 δ, while irradiation at δ = 6.47 gave enhancement at 7.34 δ. The implication is that the compound contains the unit *p*-MeO-C_6H_4-CH_2-, in a rather deshielded environment, but that there is no benzoyl group.

*Base-catalyzed isomerization of unsymmetric cyclopropene **16**a*

To unsymmetrical dibenzylcyclopropene **16***a* (0.2 mmol) in $CDCl_3$ (0.4 mL) was added triethylamine (1 drop). The solution changed from yellow to rich gold, and an ^{1}H NMR spectrum run at once showed no sign of starting material. Separation gave a mixture of methylenecyclopropanes **17***a* and **18***a* in approximately equal amounts (42%), followed by a 3:2 mixture (10%) of *dimethyl 1-benzyl-3-(*E*)-(phenylmethylene)cyclopropane-*cis*-1,2-dicarboxylate (**34**) and its (*Z*) isomer (**35**)*. For **34**: ^{1}H NMR (500 MHz) δ: 7.46 (d, J = 8 Hz, 2H, H-2, H-6 of Ph), 7.34–7.15 (m, 8H), 6.95 (d, J = 2.4 Hz, 1H, vinyl-H), 3.69 and 3.63 (two s, 2 × OMe), 3.59 and 2.79 (two d, J = 14.0 Hz, CH_2), 2.75 (d, J = 2.4 Hz, 1H, methine-H). In an NOE experiment, irradiation of doublet at δ = 6.95 enhanced the signal at 7.46 δ (*ortho*-H of vinyl-Ph), but apparently none of the signals at 2.75, 3.59, or 2.79 δ; the remaining signals from the mixture were too close together for unambiguous results. ^{13}C NMR, δ: 169.7 and 168.8 (2 × CO), 137.3 and 135.6 (2 × Ph-C1), 129.2 and 128.83 and 128.6 and 127.7 (2 × Ph-C2 and 2 × Ph-C3), 128.4 and 127.2 (2 × Ph-C4), 123.7 (C3), 122.5 (=CH-), 52.57 and 52.54 (2 × OMe), 41.0 (C1), 31.5 (CH_2), 27.9 (C2). IR (of mixture)(cm^{-1}) 3070 w, 3035 m, 3010 w, 2960 m, 2850 w, 1730(br) s, 1603 w, 1495 m, 1450(sh), 1435 s. MS (ei) on mixture *m/z*: 336 (M^+, 10%), 304 (15%), 276 (10%), 245 (M − Bn^+, 20%), 217 (50%), 202 (20%), 115 (45%), 91 (100%). MS (ci, NH_3) *m/z*: 354 (M + NH_4^+, 100%), 337 (M + H^+, 45%), 322 (10%), 305 (10%), 217 (5%). For **35**; ^{1}H NMR (500 MHz) δ: 7.44 (d, J = 8 Hz, 2H, H-2, H-6 of Ph), 7.34–7.15 (m, 6H), 7.08–7.06 (m, 2H, H-2, H-6 of Bn), 6.87 (d, J = 2.0 Hz, 1H, vinyl-H), 3.69 and 3.68 (two s, 2 × OMe), 3.38 (s, 2H, CH_2), 2.37 (d, J = 2.0 Hz, 1H, methine-H). In an NOE experiment, irradiation of doublet at δ = 6.87 gave enhancement at 7.44 δ (*ortho*-H of vinyl-Ph) and 2.37 δ; whereas irradiation of singlet at δ = 3.38 enhanced the signal at 7.07 δ (*ortho*-H of Bn) and methine doublet at 2.37 δ. ^{13}C NMR (assignments tentative), δ: 170.1 and 169.2 (2 × CO), 136.1 and 135.5 (2 × Ph-C1), 130.0 and 128.78 and 128.5 and 128.0 (2 × Ph-C2 and 2 × Ph-C3), 128.3 (1 × Ph-C4; other C4 obscured), 123.8 (C3), 124.0 (=CH-), 52.7 and 52.45 (2 × OMe), 37.6 (C1), 38.6 (CH_2), 34.3 (C2).

Acknowledgements

We thank the Natural Sciences and Engineering Research Council of Canada for financial support. The assistance of Dr Richard Smith and Mr Fajar Ramelan with mass spectrometry, and of Dr Donald Hughes and Mr Brian Sayer with some of the NMR spectroscopy is gratefully acknowledged.

References

1. (*a*) J. Warkentin. Synthesis, 279 (1970), and refs. therein; (*b*) M. Békhazi and J. Warkentin. J. Am. Chem. Soc. **103**, 2473 (1981); (*c*) J. Am. Chem. Soc. **105**, 1289 (1983); (*d*) M. Békhazi, P.A. Risbood, and J. Warkentin. J. Am. Chem. Soc. **105**, 5675 (1983); (*e*) M. Békhazi and J. Warkentin. Can. J. Chem. **61**, 619 (1983).
2. M.W. Majchrzak, M. BJkhazi, I. Tse-Sheepy, and J. Warkentin. J. Org. Chem. **54**, 1842 (1989).
3. M.W. Majchrzak, J. Warkentin, and J.McK.R. Woollard. Struct. Chem. **2**, 137 (1991).
4. G.L. Closs, W.A. Böll, H. Heyn, and V. Dev. J. Am. Chem. Soc. **90**, 173 (1968).
5. D.R. Arnold, R.W. Humpreys, W.J. Leigh, and G.E. Palmer. J. Am. Chem. Soc. **98**, 6225 (1976).
6. W.J. Leigh and D.R. Arnold. Can. J. Chem. **57**, 1186 (1979).
7. C. Dietrich-Buchecker and M. Franck-Neumann. Tetrahedron, **33**, 751 (1977).
8. (*a*) M. Franck-Neumann. Angew. Chem. Int. Ed. Engl. **6**, 79 (1967); (*b*) M. Franck-Neumann, M. Miesch, and H. Kempf. Tetrahedron, **43**, 853 (1987).
9. M. Franck-Neumann and C. Dietrich-Buchecker. Tetrahedron Lett. **9**, 15 (1969).
10. (*a*) H. Dürr, W. Schmidt, and R. Sergio. Justus Liebigs Ann. Chem. 1132 (1974); (*b*) H. Dürr and H. Schmitz. Angew. Chem. Int. Ed. **14**, 647 (1975).
11. (*a*) M. Franck-Neumann. Angew. Chem. Int. Ed. Engl. **6**, 79 (1967); (*b*) C. Dietrich-Buchecker and M. Franck-Neumann. Tetrahedron, **33**, 745 (1977).
12. O. Tsuge, S. Kanemasa, T. Suzuki, and K. Matsuda. Bull. Chem. Soc. Jpn. **59**, 2851 (1986).
13. (*a*) H. Dürr, H. Kober, R. Sergio, and V. Formacek. Chem. Ber. **107**, 2037 (1974); (*b*) H. Dürr, and W. Schmidt. Justus Liebigs Ann. Chem. 1140 (1974).

© 1997 NRC Canada

14. K.L.M. Stanley, J. Dingwall, J.T. Sharp, and T.W. Naisby. J. Chem. Soc. Perkin Trans. I, 1433 (1979).
15. M.P. Sammes and A.R. Katritzky. Adv. Heterocycl. Chem. **34**, 1 (1983).
16. W.M. Williams and W.R. Dolbier, Jr. J. Am. Chem. Soc. **94**, 3955 (1972).
17. J.F. Hanson, Y.I. Kim, L.J. Griswold, G.H. Hoelle, D.T. Taylor, and O.E. Vietti. J. Org. Chem. **45**, 76 (1980).
18. M. Pomerantz and T.H. Witherup. J. Am. Chem. Soc. **95**, 5977 (1973).
19. (*a*)H.E. Zimmerman and C.J. Samuel. J. Am. Chem. Soc. **97**, 4025 (1975); (*b*) A. Padwa, C.S. Chou, R.J. Rosenthal, and B. Rubin. J. Am. Chem. Soc. **103**, 3057 (1981).
20. D. Bethell, A.R. Newall, and D. Whittaker. J. Chem. Soc. B, 23 (1971).
21. W. Kirmse, K. Loosen, and H.-D. Sluma. J. Am. Chem. Soc. **103**, 5935 (1981).
22. N.C. Mathur, M.S. Snow, K.M. Young, and J.A. Pincock. Tetrahedron, **41**, 1509 (1985).
23. W. Kirmse, J. Kilian, and S. Steenken. J. Am. Chem. Soc. **112**, 6399 (1990).
24. W. Kirmse, T. Meinert, D.A. Modarelli, and M.S. Platz. J. Am. Chem. Soc. **115**, 8918 (1993).
25. W. Kirmse. *In* Advances in carbene chemistry. Vol. 1. *Edited by* U.H. Brinker. JAI Press, Greenwich, Conn. 1994. pp. 1–57.
26. J.A. Pincock, R. Morchat, and D.R. Arnold. J. Am. Chem. Soc. **95**, 7536 (1973).
27. (*a*) J. Van Alphen. Recl. Trav. Chim. Pays-Bas, **62**, 485 (1943); (*b*) R. Hhttel, K. Franke, H. Matin, and J. Riedl. Chem. Ber. **93**, 1433 (1960).
28. M.I. Komendantov, A.P. Zavgorodnyaya, I.N. Domnin, and R.R. Bakmukhametov. J. Org. Chem. USSR (Engl. transl.), **22**, 1389 (1986).
29. (*a*) M. Franck-Neumann and C. Dietrich-Buchecker. Tetrahedron Lett. **17**, 2069 (1976); (*b*) R. Huisgen, H.-U. Reissig, and H. Huber. J. Am. Chem. Soc. **101**, 3647 (1979).
30. (*a*) M. Franck-Neumann and C. Dietrich-Buchecker. Tetrahedron Lett. **13**, 937 (1972); (*b*) Angew. Chem. Int. Ed. Engl. **12**, 240 (1973); (*c*) R. Huisgen, M.P.B. Verderol, A. Gieren, and V. Lamm. Angew. Chem. Int. Ed. Engl. **20**, 694 (1981).
31. T. Yamazaki and H. Shechter. Tetrahedron Lett. **13**, 4533 (1972).
32. (*a*) D.J. Field, D.W. Jones, and G. Kneen. J. Chem. Soc. Perkin Trans. I, 1050 (1978); (*b*) R.J. Bushby and D.W. Jones. J. Chem. Soc. Chem. Commun. 688 (1979).
33. (*a*) G. Wittig and J.J. Hutchinson. Justus Liebigs Ann. Chem. **741**, 89 (1970); (*b*) R. Baumes, J. Elguero, R. Jacquier, and G. Tarrago. Tetrahedron Lett. **14**, 3781 (1973); (*c*) P. Schiess, and H. Stalder. Tetrahedron Lett. **21**, 1413 (1980); (*d*) Tetrahedron Lett. **21**, 1417 (1980).
34. M.W. Majchrzak, E. Jefferson, and J. Warkentin. J. Am. Chem. Soc. **112**, 2449 (1990).
35. S.D. Kahn, W.J. Hehre, N.G. Rondan, and K.N. Houk. J. Am. Chem. Soc. **107**, 8291 (1985).
36. (*a*) R.K. Bramley, R. Grigg, G. Guilford, and P. Milner. Tetrahedron, **29**, 4159 (1973); (*b*) I.I. Grandberg, A.P. Krasnoshchek, A.N. Kost, and G.K. Faizova. J. Gen. Chem. USSR (Engl. transl.), **33**, 2521 (1963).
37. E. Jefferson and J. Warkentin. J. Am. Chem. Soc. **114**, 6318 (1992).
38. M.S. Baird. Top. Curr. Chem. **144**, 147 (1988).
39. R. Huisgen, A. Mitra, and J.R. Moran. Heterocycles, **24**, 2429 (1986).
40. (*a*) R.C. Elderfield and K.L. Burgess. J. Am. Chem. Soc. **82**, 1975 (1960); (*b*) N.J. Turro and G.C. Weed. J. Am. Chem. Soc. **105**, 1861 (1983).
41. L.F. Fieser and M. Fieser. Reagents for organic synthesis. Vol. 1. Wiley, New York. 1967. pp. 1158–1159.
42. S.B. Coan and E.I. Becker. J. Am. Chem. Soc. **76**, 501 (1954).
43. R.C. Kerber, D. Glasser, and B. Luck. Organometallics, **3**, 840 (1984).
44. D. Bryce-Smith and J.E. Lodge. J. Chem. Soc. 695 (1963).
45. F.E. Herkes and H.E. Simmons. J. Org. Chem. **38**, 2845 (1973).
46. A.V. Prosyanik, A.S. Moskalenko, S.V. Bondarenko, and V.I. Markov. J. Org. Chem. USSR (Engl. transl.), **21**, 594 (1985).
47. S. Braun. Org. Magn. Reson. **11**, 197 (1978).

Can. J. Chem. Downloaded from www.nrcresearchpress.com by 92.62.229.171 on 09/08/12
For personal use only.

© 1997 NRC Canada

Excess enthalpies of ternary mixtures of an *n*-alkane with methyl *tert*-butyl ether and di-*n*-butyl ether

Zhangfa Tong, Dankui Liao, George C. Benson, and Benjamin C.-Y. Lu

Abstract: Excess molar enthalpies, measured at 298.15 K, are reported for the two ternary systems consisting of either *n*-heptane or *n*-decane, together with methyl *tert*-butyl ether and di-*n*-butyl ether. Smooth representations of the results were used to construct constant enthalpy contours on Roozeboom diagrams. It was found that the Flory theory can provide good estimates of the ternary enthalpies.

Key words: excess enthalpies, ternary mixtures, *n*-alkanes, ethers, Flory theory.

Résumé : Opérant à 298,15 K, on a mesuré les enthalpies molaires en excès de deux systèmes ternaires formés soit d'heptane ou de décane en mélange avec de l'oxyde de *tert*-butyle et de méthyle et de l'oxyde de dibutyle. On a utilisé des représentations aplanies pour construire des contours d'enthalpie constante sur des diagrammes de Roozeboom. On a trouvé que la théorie de Flory peut conduire à de bonnes évaluations des enthalpies ternaires.

Mots clés : enthalpies en excès, mélanges ternaires, *n*-alcanes, éthers, théorie de Flory.

[Traduit par la rédaction]

Can. J. Chem. Downloaded from www.nrcresearchpress.com by 92.62.229.171 on 09/08/12
For personal use only.

Introduction

The use of ethers as oxygenating agents in gasoline technology has resulted in an increased interest in the thermodynamic properties of hydrocarbon + ether systems. A recent paper (1) from our laboratory described measurements of the excess molar enthalpies of ternary mixtures containing either *n*-heptane (nC7) or *n*-decane (nC10), together with methyl *tert*-butyl ether (MTBE) and *tert*-amyl methyl ether (TAME). As a continuation of that investigation, we have made similar measurements for the analogous systems where di-*n*-butyl ether (DNBE) replaced the TAME used previously.

Experimental

Pure Grade nC7 from the Phillips Chemical Co. was used in the present work. The nC10, MTBE (HPLC Grade), and DNBE (Gold Label) were obtained from the Aldrich Chemical Co. In all cases, the purities stated by the manufacturers exceeded 99 mol%, and all of the component liquids were used without further purification. Their densities, measured at 298.15 K, were 679.79, 726.37, 735.58, and 764.02 kg m^{-3}, for nC7, nC10, MTBE, and DNBE, respectively. These values are in reasonable agreement with the literature (2, 3).

Received October 8, 1996.

Z. Tong, D. Liao, G.C. Benson,[1] and B.C.-Y. Lu. Department of Chemical Engineering, University of Ottawa, Ottawa, ON K1N 6N5, Canada.

[1] Author to whom correspondence may be addressed. Telephone: (613) 562-5800 (6118). Fax: (613) 562-5172. E-mail: gbenson@eng.uottawa.ca

An LKB flow microcalorimeter (model 10700-1) was used to measure excess molar enthalpies H^E_m at (298.150 ± 0.003) K. Details of this equipment and its operation have been described previously (4). The excess molar enthalpies of the ternary mixtures were investigated by measuring the excess molar enthalpies $H^E_{m,1+23}$ for several pseudo-binary mixtures, in which component 1 (either nC7 or nC10) was added to binary mixtures of components 2 (MTBE) and 3 (DNBE), having a fixed mole ratio x_2/x_3. These binaries were prepared by weighing. The excess molar enthalpy $H^E_{m,123}$ of the ternary mixture was then obtained from the relation:

$$[1] \quad H^E_{m,123} = H^E_{m,1+23} + (1 - x_1)H^E_{m,23}$$

where $H^E_{m,23}$ is the excess molar enthalpy of the particular MTBE + DNBE binary. Over most of the mole fraction range, the errors in the excess molar enthalpies are estimated to be less than ±0.5%. Errors in the mole fractions of the ternary mixtures are estimated to be less than 5×10^{-4}.

Results and discussion

Excess molar enthalpies $H^E_{m,ij}$ $(i < j)$, at 298.15 K, for four of the five constituent binaries of present interest, have been reported in the literature: nC7 + MTBE (1), nC7 + DNBE and nC10 + DNBE (5), nC10 + MTBE (6). Table 1 summarizes the present experimental measurements for the binary ether system MTBE + DNBE. The smoothing function:

$$[2] \quad H^E_{m,ij} = x_i(1 - x_i) \sum_{k=1}^{n} h_k(1 - 2x_i)^{k-1}$$

was fitted to these results by the method of least squares with

© 1997 NRC Canada

Fig. 1. Excess molar enthalpies, $H^E_{m,1+23}$ at 298.15 K, for the addition of nC7 to binary mixtures of MTBE + DNBE to form $x_1CH_3(CH_2)_5CH_3 + x_2(CH_3)_3COCH_3 + x_3[CH_3(CH_2)_3]_2O$. Experimental results: △, $x_2/x_3 = 3.0128$; ○, $x_2/x_3 = 1.0006$; ▽, $x_2/x_3 = 0.3352$. Curves: •—•—, $x_3 = 0$, Tong et al. (1); ····, $x_2 = 0$, Benson et al. (5); —, calculated from the representation of the results by eqs. [3] and [4], using the ternary term $H^E_{m,T}$ given in the footnote of Table 3; ----, estimated from the Flory theory.

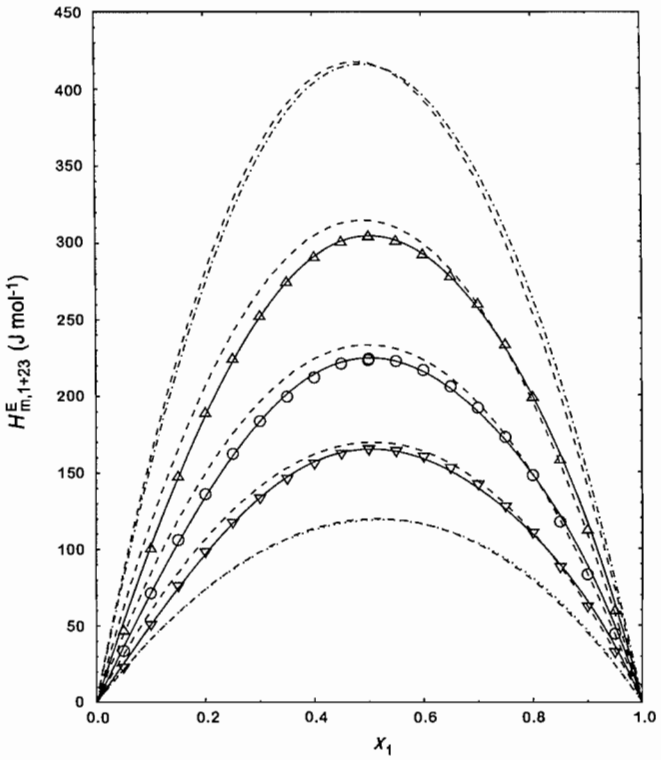
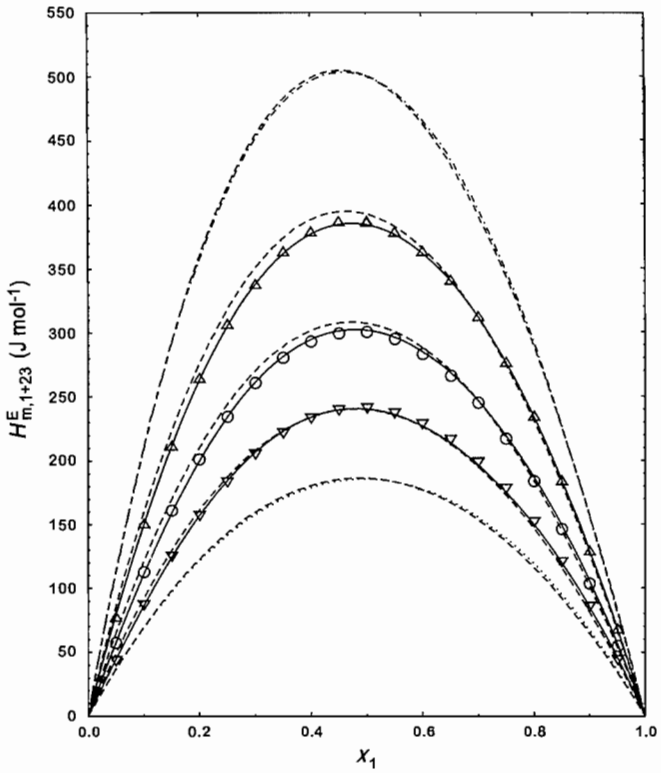


Fig. 2. Excess molar enthalpies, $H^E_{m,1+23}$ at 298.15 K, for the addition of nC10 to binary mixtures of MTBE + DNBE to form $x_1CH_3(CH_2)_8CH_3 + x_2(CH_3)_3COCH_3 + x_3[CH_3(CH_2)_3]_2O$. Experimental results: △, $x_2/x_3 = 3.0006$; ○, $x_2/x_3 = 0.9973$; ▽, $x_2/x_3 = 0.3352$. Curves: •—•—, $x_3 = 0$, Wang et al. (6); ····, $x_2 = 0$, Benson et al. (5); —, calculated from the representation of the results by eqs. [3] and [4], using the ternary term $H^E_{m,T}$ given in the footnote of Table 4; ----, estimated from the Flory theory.



all points weighted equally. The number, n, of coefficients employed in the fit was selected on the basis of the changes in the values of the standard deviation s, for increasing values of n (F-test). Values of the coefficients h_k are listed in Table 2, along with those for the representations of the four other binary systems. Also included in Table 2 are the values of the standard deviation s for each of the representations.

The experimental results for $H^E_{m,1+23}$ and the corresponding values of $H^E_{m,123}$ are listed in Tables 3 and 4 for the nC7 and nC10 ternary systems, respectively. Plots of $H^E_{m,1+23}$ against x_1 are given in Figs. 1 and 2. Also included in these figures are the smooth representations of the excess molar enthalpies of the constituent binaries, corresponding to the cases $x_2 = 0$ and $x_3 = 0$. These were calculated from eq. [2] using the coefficients in Table 2. In all cases, the maximum values of $H^E_{m,1+23}$ and $H^E_{m,123}$ occur near $x_1 = 0.5$ and, for comparable values of x_2/x_3, the maximum is larger for the mixture with nC10. The enthalpies increase as x_2/x_3 increases, for both systems at constant x_1.

As in our previous work (1), the values of $H^E_{m,1+23}$ were represented as a sum of binary terms with an added ternary correction:

$$[3] \quad H^E_{m,1+23} = [x_2/(1 - x_1)]H^E_{m,12} + [x_3/(1 - x_1)]H^E_{m,13} + H^E_{m,T}$$

where the values of the $H^E_{m,ij}$ were calculated from the appropriate smoothing functions. The ternary term was assumed to have the form:

$$[4] \quad H^E_{m,T}(\text{J mol}^{-1}) = x_1x_2x_3(c_0 + c_1x_1 + c_2x_2 + c_3x_1^2 + c_4x_1x_2 + c_5x_2^2 + \cdots)$$

and the values of the parameters c_k were obtained from least-squares analyses, in which eqs. [3] and [4] were fitted to the experimental $H^E_{m,1+23}$ in Tables 3 and 4. The results of these analyses are given in the footnotes of the tables, where the standard deviations s of the representations are also indicated. The solid curves in Figs. 1 and 2 were calculated from these representations.

Can. J. Chem. Downloaded from www.nrcresearchpress.com by 92.62.229.171 on 09/08/12
For personal use only.

© 1997 NRC Canada

Table 1. Experimental excess molar enthalpies $H^E_{m,23}$ (J mol^{-1}) at 298.15 K for $x_2(CH_3)_3COCH_3 + (1 - x_2)[CH_3(CH_2)_3]_2O$.

x_2	$H^E_{m,23}$	x_2	$H^E_{m,23}$	x_2	$H^E_{m,23}$	x_2	$H^E_{m,23}$	x_2	$H^E_{m,23}$
0.0501	16.60	0.2501	69.13	0.4504	96.10	0.5999	95.54	0.7996	67.46
0.1000	31.96	0.3000	78.76	0.5000	96.81	0.6494	92.15	0.8500	54.03
0.1501	45.66	0.3500	86.08	0.5002	97.06	0.6996	86.09	0.8999	38.18
0.2001	58.07	0.4001	92.02	0.5497	97.12	0.7510	77.94	0.9500	18.48

Table 2. Parameters h_k and standard deviations s for the representation of $H^E_{m,ij}$ at 298.15 K by eq. [2].

Component								
i	j	h_1	h_2	h_3	h_4	h_5	h_6	s
MTBE	DNBE	389.02	−33.19	31.02	−89.09	−57.24	121.80	0.32
nC7	MTBE[a]	1662.94	70.87	42.38	−58.64			1.06
nC7	DNBE[b]	475.32	−35.68	20.31				0.52
nC10	MTBE[c]	2000.50	313.32	110.94	100.36	−87.36		1.18
nC10	DNBE[b]	742.66	15.25	20.29				0.21

[a]Tong et al. (1).
[b]Benson et al. (5).
[c]Wang et al. (6).

Table 3. Experimental excess molar enthalpies $H^E_{m,1+23}$ (J mol^{-1}) at 298.15 K for the addition of nC7 to MTBE + DNBE to form $x_1CH_3(CH_2)_5CH_3 + x_2(CH_3)_3COCH_3 + x_3[CH_3(CH_2)_3]_2O$, and values of $H^E_{m,123}$ (J mol^{-1}) calculated from eq. [1] using the smooth representation of $H^E_{m,23}$ (J mol^{-1}) by eq. [2].

x_1	$H^E_{m,1+23}$[a]	$H^E_{m,123}$	x_1	$H^E_{m,1+23}$[a]	$H^E_{m,123}$	x_1	$H^E_{m,1+23}$[a]	$H^E_{m,123}$
x_2/x_3 = 0.3352, $H^E_{m,23}$ (J mol^{-1}) = 69.5								
0.0500	22.8	88.8	0.4003	155.7	197.4	0.7002	142.0	162.8
0.1000	50.7	113.2	0.4500	162.1	200.4	0.7499	127.5	144.8
0.1500	75.8	134.9	0.4994	165.2	200.0	0.7999	110.2	124.1
0.2000	98.1	153.6	0.4999	164.7	199.5	0.8500	87.8	98.2
0.2501	117.3	169.4	0.5501	163.7	195.0	0.9000	62.3	69.3
0.3001	133.2	181.8	0.6006	160.0	187.7	0.9500	32.7	36.1
0.3502	146.0	191.1	0.6500	152.7	177.0			
x_2/x_3 = 1.0006, $H^E_{m,23}$ (J mol^{-1}) = 97.3								
0.0501	33.6	126.0	0.3999	211.9	270.3	0.7001	191.9	221.0
0.0999	71.3	158.9	0.4496	220.8	274.4	0.7499	172.8	197.1
0.1499	105.9	188.6	0.4991	223.0	271.7	0.8000	147.9	167.3
0.1999	135.9	213.7	0.5001	223.9	272.6	0.8498	117.4	132.0
0.2504	162.3	235.2	0.5501	222.4	266.2	0.8999	83.1	92.8
0.3004	183.6	251.6	0.6000	216.5	255.4	0.9500	44.6	49.4
0.3501	199.5	262.7	0.6500	205.8	239.9			
x_2/x_3 = 3.0128, $H^E_{m,23}$ (J mol^{-1}) = 78.1								
0.0500	46.8	121.0	0.4004	290.3	337.1	0.6999	259.4	282.9
0.1001	100.4	170.7	0.4499	300.1	343.1	0.7498	232.9	252.4
0.1500	147.4	213.8	0.5000	303.9	342.9	0.8000	198.8	214.4
0.2000	188.9	251.4	0.5002	303.5	342.5	0.8500	157.9	169.6
0.2504	224.2	282.7	0.5502	300.6	335.7	0.9000	112.0	119.8
0.3000	252.0	306.7	0.5995	291.7	322.9	0.9500	59.7	63.6
0.3496	274.2	325.0	0.6499	277.5	304.8			

[a]Ternary term for representation of $H^E_{m,1+23}$ by eqs. [3] and [4]: $H^E_{m,T}$ (J mol^{-1}) = $x_1x_2x_3(-1701.78 + 2630.20x_1 + 1773.32x_2 + 644.97x_1^2 - 4458.57x_1x_2 - 2345.65x_2^2 - 7058.68x_1^3)$, s = 2.3.

Can. J. Chem. Downloaded from www.nrcresearchpress.com by 92.62.229.171 on 09/08/12
For personal use only.

© 1997 NRC Canada

Can. J. Chem. Downloaded from www.nrcresearchpress.com by 92.62.229.171 on 09/08/12
For personal use only.

Table 4. Experimental excess molar enthalpies $H^E_{m,1+23}$ (J mol^{-1}) at 298.15 K for the addition of nC10 to MTBE + DNBE to form $x_1CH_3(CH_2)_8CH_3 + x_2(CH_3)_3COCH_3 + x_3[CH_3(CH_2)_3]_2O$, and values of $H^E_{m,123}$ (J mol^{-1}) calculated from eq. [1] using the smooth representation of $H^E_{m,23}$ (J mol^{-1}) by eq. [2].

x_1	$H^E_{m,1+23}$ [a]	$H^E_{m,123}$	x_1	$H^E_{m,1+23}$ [a]	$H^E_{m,123}$	x_1	$H^E_{m,1+23}$ [a]	$H^E_{m,123}$
x_2/x_3 = 0.3352, $H^E_{m,23}$ (J mol^{-1}) = 69.5								
0.0501	44.1	110.1	0.3999	233.8	275.4	0.7000	199.3	220.2
0.1000	87.7	150.2	0.4497	239.8	278.1	0.7501	178.6	196.0
0.1501	125.7	184.7	0.5002	241.4	276.1	0.7999	152.2	166.1
0.2000	157.6	213.1	0.5005	241.6	276.3	0.8501	120.8	131.2
0.2497	184.1	236.2	0.5495	237.6	268.8	0.9000	86.1	93.0
0.3000	205.9	254.5	0.5997	229.2	257.0	0.9500	44.8	48.2
0.3502	222.2	267.4	0.6499	216.8	241.1			
x_2/x_3 = 0.9973, $H^E_{m,23}$ (J mol^{-1}) = 97.2								
0.0500	57.4	149.8	0.3997	292.8	351.2	0.7001	244.9	274.0
0.1001	112.8	200.4	0.4500	299.1	352.6	0.7500	216.9	241.2
0.1501	161.0	243.7	0.4997	300.2	348.8	0.8000	183.7	203.2
0.1996	201.2	279.0	0.5001	300.3	348.9	0.8500	146.0	160.6
0.2501	234.5	307.4	0.5502	294.7	338.4	0.8999	103.3	113.0
0.2999	260.8	328.8	0.6007	282.9	321.8	0.9500	54.8	59.7
0.3499	280.4	343.6	0.6506	265.9	299.9			
x_2/x_3 = 3.0006, $H^E_{m,23}$ (J mol^{-1}) = 78.2								
0.0500	76.9	151.2	0.3996	378.3	425.3	0.6998	311.3	334.7
0.1001	150.2	220.6	0.4496	386.2	429.2	0.7501	275.6	295.2
0.1500	211.4	277.8	0.4997	385.5	424.6	0.7999	233.8	249.5
0.1999	263.9	326.5	0.4999	386.3	425.4	0.8500	183.6	195.4
0.2499	305.9	364.6	0.5498	377.8	413.0	0.9000	128.4	136.2
0.3000	337.3	392.1	0.6000	362.6	393.9	0.9500	67.4	71.3
0.3502	362.8	413.6	0.6502	340.0	367.4			

[a]Ternary term for representation of $H^E_{m,1+23}$ by eqs. [3] and [4]: $H^E_{m,T}$ (J mol^{-1}) = $x_1x_2x_3(-1314.44 + 4197.67x_1 - 634.45x_2 - 6200.96x_1^2 - 3142.80x_1x_2)$, s = 1.6.

Equations [1]–[4] were also used to calculate the constant $H^E_{m,123}$ contours plotted on the Roozeboom diagrams in Figs. 3*a* and 4*a*. The general characteristics of these are very similar and are similar to those found for the corresponding systems with TAME (1). All of the contours extend to the edges of the triangle and there is no indication of an extremum lying within the triangle.

For the analogous systems containing TAME (1) in place of DNBE, it was found that the Flory theory (7), as applied to multicomponent systems (8), provided reasonable estimates of the ternary enthalpies, when only properties of the pure components and their binary mixtures were used. The same approach was investigated for the present systems. The equations for the treatment have been outlined by Wang et al. (6), and will not be repeated here.

The parameters used in the calculations are summarized in Table 5. The characteristic pressures p^*, molar volumes V^*_m, and temperatures T^* were taken from our previous publications (5, 6), where sources of the values of the primary thermodynamic properties are indicated. In evaluating the ratio of molecular surface areas of contact per segment between components i and j, it was assumed that the molecules were spherical. The values of the interchange-energy parameters X_{ij}, given in the footnotes of the table, were obtained by fitting the Flory formula for $H^E_{m,ij}$ to the smooth representations of the experimental results for each binary mixture by eq. [2].

Using the values of the parameters given in Table 5, $H^E_{m,1+23}$ and $H^E_{m,123}$ were estimated for the present ternary mixtures. The results for $H^E_{m,1+23}$ are shown as broken curves in Figs. 1 and 2. In general, these estimates tend to be higher than the experimental results at low alkane mole fractions and to fall below the results at higher mole fractions. The mean absolute relative deviations of the 60 points for the nC7 system in Table 3 and the 60 points for the nC10 system in Table 4 amount to 3.6% and 2.2%, respectively.

Constant $H^E_{m,123}$ contours were also estimated on the basis of the Flory theory. For both systems, the overall characteristics of these are quite similar to those derived from the representations of the experimental data by eqs. [1]–[4]. The results of the estimations are shown on the Roozeboom diagrams in Figs. 3*b* and 4*b*. It is clear from a comparison of parts (*a*) and (*b*) in these figures that, for the present type of systems, the Flory theory provides useful estimates of $H^E_{m,123}$ without requiring the direct investigation of the excess enthalpies of any ternary mixtures.

© 1997 NRC Canada

Can. J. Chem. Downloaded from www.nrcresearchpress.com by 92.62.229.171 on 09/08/12
For personal use only.

Fig. 3. Contours for constant values of $H^E_{m,123}$/(J mol^{-1}) for the system nC7 + MTBE + DNBE at 298.15 K. (*a*) Calculated from the representation of the experimental results by eqs. [1]–[4] with $H^E_{m,T}$ from the footnote of Table 3. (*b*) Estimated from the Flory theory.

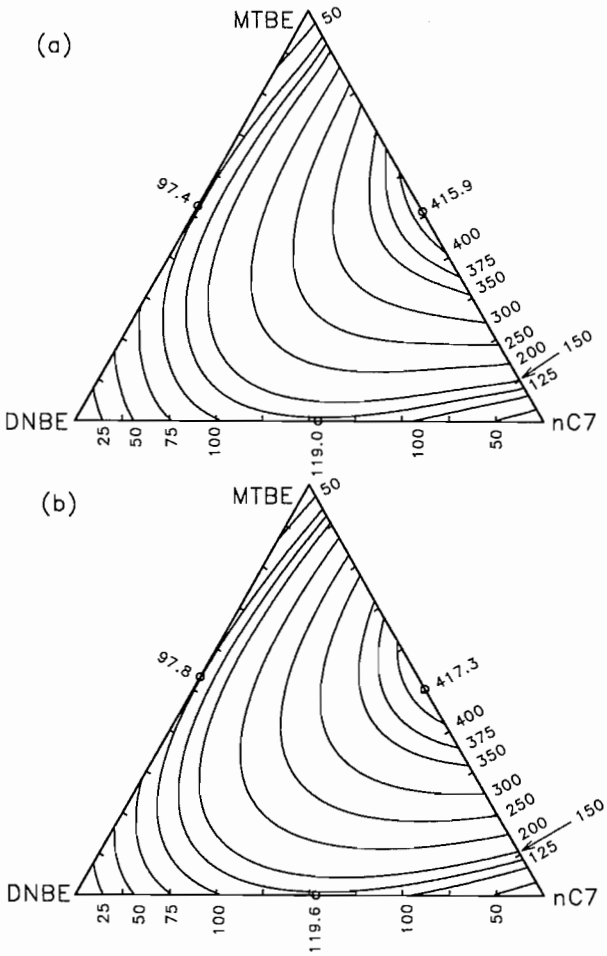


Fig. 4. Contours for constant values of $H^E_{m,123}$/(J mol^{-1}) for the system nC10 + MTBE + DNBE at 298.15 K. (*a*) Calculated from the representation of the experimental results by eqs. [1]–[4] with $H^E_{m,T}$ from the footnote of Table 4. (*b*) Estimated from the Flory theory.

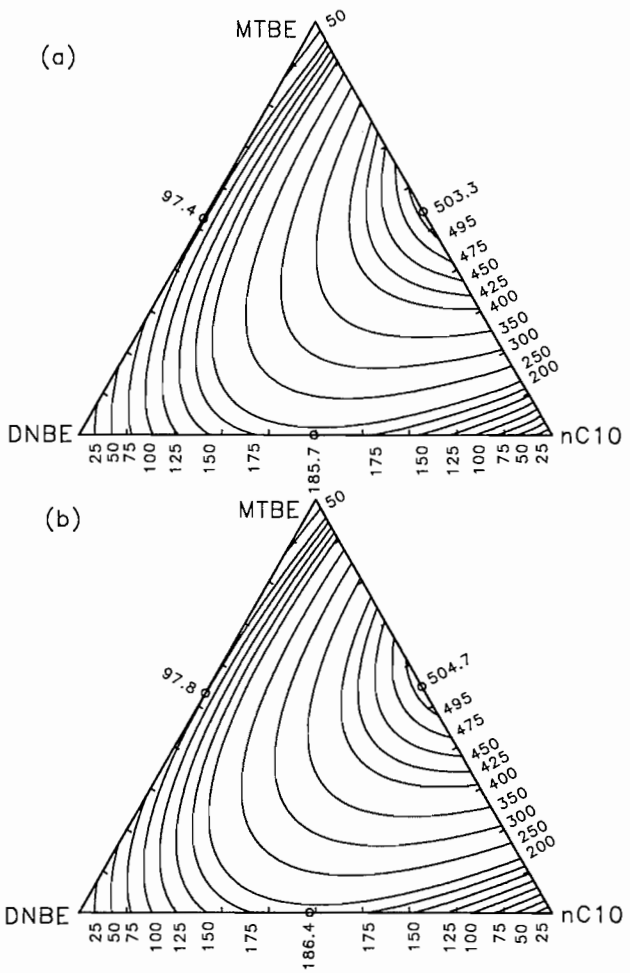


Table 5. Parameters used in Flory theory calculations at 298.15 K for nC7 + MTBE + DNBE[a] and nC10 + MTBE + DNBE.[b]

Component	p^* (J cm^{-3})	V^*_m (cm^3 mol^{-1})	T^* (K)	Reference
nC7	431.9	113.60	4648.1	Benson et al. (5)
nC10	447.0	155.75	5091.4	Benson et al. (5)
MTBE	442.9	90.20	4385.0	Wang et al. (6)
DNBE	450.7	133.93	4909.8	Benson et al. (5)

Note: Interchange-energy parameters X_{ij} (J cm^{-3}) are as follows:
[a]X_{12} = 15.0620; X_{13} = 3.8999; X_{23} = 4.1801.
[b]X_{12} = 15.6509; X_{13} = 4.8536; X_{23} = 4.1801.

© 1997 NRC Canada

Acknowledgements

The authors are indebted to the Natural Sciences and Engineering Research Council of Canada (NSERC) for financial support of this work.

References

1. Z. Tong, G.C. Benson, L.L. Wang, and B.C.-Y. Lu. J. Chem. Eng. Data, **41**, 865 (1996).
2. TRC thermodynamic tables — hydrocarbons. Thermodynamics Research Center, The Texas A&M University System, College Station, Tex. 1988. p. a-1010.
3. TRC thermodynamic tables — non-hydrocarbons. Thermodynamics Research Center, The Texas A&M University System, College Station, Tex. 1988. pp. a-6030, a-6040.
4. R. Tanaka, P.J. D'Arcy, and G.C. Benson. Thermochim. Acta, **11**, 163 (1975); F. Kimura, G.C. Benson, and C.J. Halpin. Fluid Phase Equilib. **11**, 245 (1983).
5. G.C. Benson, B. Luo, and B.C.-Y. Lu. Can. J. Chem. **66**, 531 (1988).
6. L. Wang, G.C. Benson, and B.C.-Y. Lu. Thermochim. Acta, **213**, 83 (1993).
7. P.J. Flory. J. Am. Chem. Soc. **87**, 1833 (1965); A. Abe and P.J. Flory. J. Am. Chem. Soc. **87**, 1838 (1965).
8. W. Brostow and J.S. Sochanski. J. Mater. Sci. **10**, 2134 (1975).

Can. J. Chem. Downloaded from www.nrcresearchpress.com by 92.62.229.171 on 09/08/12
For personal use only.

© 1997 NRC Canada

Determination of the absolute configuration of the fragments composing the phytotoxin phomalide

M. Soledade C. Pedras

Abstract: The absolute configurations of the residues constituting phomalide (**1**) were determined on the products resulting from acidic hydrolysis. The configurations of the amino acids Val and Leu were determined as (*S*) and (*R*), respectively, by chiral GC analysis (Chirasil-Val capillary column), employing *N*-trifluoroacetyl (TFA) amino acid methyl ester derivatives. The configurations of the hydroxy acids O-Phe and O-Leu were determined as (*S*) by ^{1}H NMR of the Mosher's esters of the isopropyl ester derivatives. The method described allowed for the unambiguous assignment of the absolute configuration of the α-amino and α-hydroxy acid residues composing phomalide (**1**).

Key words: absolute configuration, depsipeptide, Mosher's ester.

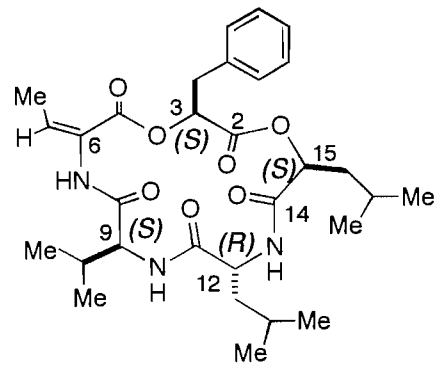
Résumé : En se basant sur les produits de son hydrolyse acide, on a déterminé les configurations absolues des divers résidus formant le phomalide (**1**). Grâce à une analyse par CG chirale (colonne capillaire Chirasil-Val) sur les dérivés *N*-trifluoroacétyles (TFA) des esters méthyliques des acides aminés, on a déterminé que les configurations absolues des acides aminés Val et Leu sont respectivement (*S*) et (*R*). Faisant appel à la RMN du ^{1}H des esters isopropyliques des esters de Mosher, on a déterminé que les configurations des acides hydroxylés O-Phe et O-Leu sont (*S*). La méthode décrite permet d'attribuer sans ambiguïté la configuration des acides α-aminés et α-hydroxylés formant le phomalide (**1**).

Mots clés: configuration absolue, depsipeptide, ester de Mosher.

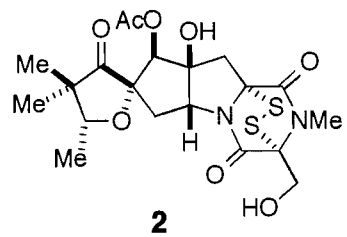
[Traduit par la rédaction]

The depsipeptide phomalide (**1**) is a host-selective toxin produced by the blackleg fungus (*Leptosphaeria maculans* (Desm.) Ces. et de Not., asexual stage *Phoma lingam* (Tode ex Fr.) Desm.) of brassicas (1). Diverse phytotoxic depsipeptides are produced by phytopathogenic fungi, as for example the destruxins from *Alternaria brassicae* (2) and AM-toxins from *A. mali* (3). Phomalide is, however, an unusual depsipeptide in that it has a 15-membered ring composed of five residues; more common depsipeptides, and cyclic peptides as well, incorporate typically either four or more than five residues (4). Remarkably, phomalide is produced by the blackleg fungus in liquid cultures only for a short period (24–60 h); older fungal cultures produce nonselective phytotoxins (epipolythiodioxopiperazines) such as sirodesmin PL (**2**).[2] This unusually short production period was attributed to an inhibitory effect of sirodesmin PL (**2**) on the biosynthesis of phomalide.

The structure of phomalide (**1**) was assigned from analysis of spectroscopic data, including HMBC and HMQC (1). The



1



2

configuration of the double bond of the rare amino acid dehydrothreonine (DhThr) residue was assigned as (*E*) based on NOE experiments on phomalide (1); chemical degradation was required to establish the absolute configuration of the four stereogenic centers. However, due to the small quantities of compound obtained from fungal cultures and the need for its

Received September 26, 1996.

M.S.C. Pedras.[1] Department of Chemistry, University of Saskatchewan, Science Place 110, Saskatoon, SK S7N 5C9, Canada.

[1] Telephone: (306) 966-4772. Fax: (306) 966-4730. E-mail: pedras@sask.usask.ca

[2] For a recent review of phytotoxins produced by the blackleg fungus see ref. 5.

© 1997 NRC Canada

Can. J. Chem. Downloaded from www.nrcresearchpress.com by 92.62.229.171 on 09/08/12
For personal use only.

Can. J. Chem. Downloaded from www.nrcresearchpress.com by 92.62.229.171 on 09/08/12
For personal use only.

biological evaluation, the use of chemical degradation presented a significant dilemma. Additionally, while the absolute configuration of the amino acid residues valine (Val) and leucine (Leu) present in phomalide (**1**) could be determined by microscale chiral GC analysis of the derivatized hydrolysis products (6), the determination of the absolute configuration of the hydroxy acid residues 3-phenyllactic acid (O-Phe) and leucic acid (O-Leu) required the development of specific methodology. The determination of the absolute configurations of the four stereogenic centers present in phomalide (**1**) is now reported here.

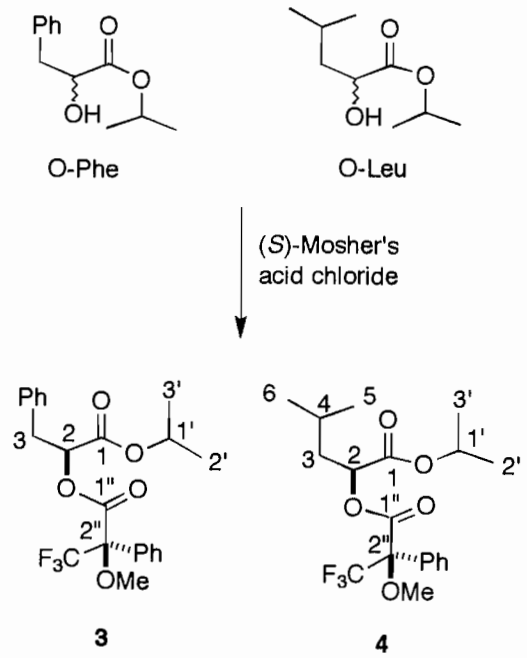
Results and discussion

The absolute configurations of the residues composing phomalide (**1**) were determined by analysis of the products resulting from acidic hydrolysis. The configurations of the amino acids Val and Leu were determined as (*S*) and (*R*), respectively, by chiral GC analysis (Chirasil-Val capillary column), employing the *N*-trifluoroacetyl (TFA) amino acid methyl ester derivatives. The configurations of the hydroxy acids O-Phe and O-Leu were determined as (*S*) by ^{1}H NMR analysis of the Mosher's esters of the isopropyl ester derivatives, as described below.

Initially, efforts were made to determine the absolute configuration of the two hydroxy residues by chiral GC analysis of the corresponding methyl, 2-propyl, and 3-pentyl ester derivatives (7). Although chiral GC analysis of the 2-propyl ester of racemic O-Leu acid indicated the presence of the enantiomeric pair (confirmed by chiral GC–MS), similar analysis could not resolve the 2-propyl, the 3-pentyl, or the methyl esters of racemic O-Phe acid (8).[3] Next, different diastereomeric derivatives of 2-propyl esters of racemic O-Phe and O-Leu were prepared to identify a suitable derivative for assignment of the absolute configuration. Thus, esterification of the O-Phe and O-Leu 2-propyl esters with (*S*)-2-methoxy-2-phenylacetyl chloride and with (*S*)-2-methoxy-2-trifluoromethyl-2-phenylacetyl chloride (Mosher's acid chloride, MPTACl) gave diastereomeric mixtures, which were analyzed by TLC and ^{1}H NMR. The two pairs of diastereomeric products resulting from reaction with the (*S*)-MPTACl were clearly distinguishable by ^{1}H NMR spectroscopy, and separable by TLC. Although the diastereomeric products resulting from reaction of 2-propyl (*R,S*)-O-Leu ester with (*S*)-2-methoxy-2-phenylacetyl chloride could be separated by TLC, those from 2-propyl (*R,S*)-O-Phe ester were inseparable. Therefore, determination of the configurations of the O-Leu and O-Phe residues present in phomalide proceeded employing derivatization of the 2-propyl esters with (*S*)-MPTACl.[4]

Phomalide was hydrolyzed by heating in aqueous HCl in a sealed tube, and the reaction mixture was extracted with Et_2O. Both the Et_2O extract (containing hydroxy acids) and the remaining aqueous phase (containing amino acids) were concentrated to dryness. The amino acid fraction was methylated with CH_2N_2, followed by acetylation with TFAA. The resulting mixture was analyzed by chiral GC and the retention times compared with authentic standards of the (*S*), (*R*), and racemic *N*-TFA amino acid methyl ester derivatives. The hydroxy acid fraction was first esterified with 2-propanol, followed by reaction with the (*S*)-MPTACl (9). The ^{1}H NMR spectrum of the reaction mixture showed characteristic proton signals due to the MeO groups at δ 3.33 and 3.53 (q, J = 1.0 Hz). These two signals allowed the unambiguous assignment of the configurations; since the signal at δ 3.33 could only be due to the derivative of (*S*)-O-Phe (**3**, cf. experimental section), the signal at δ 3.53 had to result from the (*S*)-O-Leu derivative (**4**). Analysis of the remaining proton signals of the mixture confirmed these assignments; for example, the two doublets at δ 0.92 and 0.91 (J = 6.2 Hz) due to H-5/H-6 confirmed the presence of the (*S*)-O-Leu derivative (cf. δ 0.82 and 0.80 for the (*R*)-O-Leu derivative). Furthermore, the coupling constants for the proton signal at δ 5.34 (dd, J = 10.0, 3.7 Hz, H-2) corroborated the presence of the (*S*)-O-Phe derivative (**3**) (cf. J = 8.2, 4.2 Hz, H-2, for the (*R*) isomer). These assignments have now been confirmed by the total synthesis of phomalide (10).

Scheme 1. Absolute configuration of phomalide fragments.



In summary, a method for determining the absolute configuration of small amounts of depsipeptides was developed. The method described allowed for the unambiguous assignment of the absolute configuration of the α-hydroxy acid residues composing phomalide (**1**). This method may also be applicable to other hydroxy acids of various depsipeptides.

Experimental

General

All chemicals were purchased from Aldrich Chemical Company, Inc., Madison, Wis., or Sigma Chemical Company,

[3] It appears that chiral GC methods are less likely to resolve α-hydroxy acids than α-aminoacids; see for example ref. 8.

[4] Note that the *R,S* descriptor for the absolute configuration of MPTACl is opposite to that of the precursor acid or the derived ester because the presence of the chlorine atom changes the relative Cahn–Ingold–Prelog priorities.

© 1997 NRC Canada

Can. J. Chem. Downloaded from www.nrcresearchpress.com by 92.62.229.171 on 09/08/12
For personal use only.

St. Louis, Mo. All solvents were HPLC grade and used as such, unless indicated otherwise. Preparative TLC: (Merck, Kieselgel 60 F_{254}), 20 × 20 cm × 0.25 mm; analytical TLC (Merck, Kieselgel 60 F_{254}, aluminum sheets) 5 × 2 cm × 0.2 mm; compounds were visualized by exposure to UV light and by dipping the plates in a 5% aqueous (w/v) phosphomolybdic acid solution containing a trace of ceric sulfate and 4% (v/v) H_2SO_4, followed by heating at 200°C.

GC analysis was carried out with a Hewlett–Packard 5880 gas chromatograph, equipped with a chiral capillary column (Chirasil-Val® column, Alltech, 25 m × 0.32 mm id, film thickness 0.2 μm), with He as carrier gas (flow 30 cm/s, measured at 50°C); detector at 250°C; injector at 220°C; oven temperature 70–200°C, at 4°C min^{-1}; samples were injected in split mode (ca. 1:30) with CH_2Cl_2 as solvent. NMR spectra were recorded on a Bruker AMX 500 or AM 360 spectrometer; for ^1H (360 MHz), δ values were referenced to $CHCl_3$ (7.24 ppm) and for ^{13}C (125.8 MHz) referenced to $CDCl_3$ (77.0 ppm). Mass spectra (MS) were obtained on a VG 70-250 SEQ hybrid mass spectrometer or a Finnigan Mat model 4500 mass spectrometer (electron impact (EI), or chemical ionization (CI) with ammonia as carrier gas), employing a solids probe in both cases.

Hydrolysis of phomalide

Degassed 6 M HCl (1 mL) was added to phomalide (**1**) (4 mg, 0.007 mmol) and the mixture was heated in a sealed tube at 110°C for 20 h. The reaction mixture was diluted with distilled H_2O (5 mL) and extracted with Et_2O (4 × 5 mL). The Et_2O extract, containing the hydroxy acids, was dried, filtered through a cotton plug, concentrated, and derivatized as described below. The aqueous extract, containing the amino acids, was concentrated to dryness and derivatized as described below.

Derivatization of hydrolysis products: preparation of *N*-trifluoroacetyl methyl esters of α-amino acids

One third of the residue from the aqueous extract (containing amino acid mixture) obtained from hydrolysis of phomalide was dissolved in MeOH (200 μL) and excess ethereal CH_2N_2 (1 mL) was added. After 15 min, the reaction mixture was concentrated (rotary evaporator), dissolved in CH_2Cl_2 (200 μL), and a solution of TFAA in CH_2Cl_2 (10 μL of a 25% solution, v/v) was added (6). After 1 h at room temperature, the reaction mixture was concentrated with a slow stream of N_2. The *N*-trifluoroacetyl amino acid methyl ester derivatives were analyzed by chiral GC employing a chiral capillary column.

Derivatization of hydrolysis products: preparation of 2-propyl Mosher's esters of α-hydroxy acids

The residue from the Et_2O extract (containing hydroxy acid mixture) obtained from hydrolysis of phomalide (above) was dissolved in 2-propanol (200 μL) containing 10% AcCl (v/v) in a ReactiVial and heated at 110°C for 15 min. The reaction mixture was concentrated (rotary evaporator), the residue was dissolved in $CHCl_3$ (300 μL), and Et_3N (4 μL, 0.03 mmol) and DMAP (4 mg, 0.033 mmol) were added. This solution was added to the neat (*S*)-MPTACl (6.5 mg, 0.026 mmol) (9). After 10 min the reaction mixture was concentrated (rotary evaporator) and analyzed by TLC and ^1H NMR.

Preparation of *N*-trifluoroacetyl methyl esters of Val and Leu

The *N*-trifluoroacetyl methyl esters (*N*-TFA) of both (*R*)-valine, (*R*)-leucine, and of both (*R,S*)-valine and (*R,S*)-leucine were prepared by a modification of an established method (6). Typically, to the amino acid (7.7 μmol) solution in MeOH (200 μL), a solution of CH_2N_2 in Et_2O (1.5 mL) was added at room temperature. After 30 min, the reaction mixture was concentrated (rotary evaporator) and the residue was dissolved in 25% TFAA in CH_2Cl_2 (v/v). Subsequent evaporation of the TFAA solvent with a gentle N_2 stream yielded the *N*-TFA methyl esters of the amino acids. GC analysis of the amino acid derivatives dissolved in CH_2Cl_2 and of the standards purchased from Sigma were carried out as described above; under those conditions the retention times were the following: *N*-TFA-(*R*)-Val Me ester, 5.6 min; *N*-TFA-(*S*)-Val Me ester, 6.0 min; *N*-TFA-(*R*)-Leu Me ester, 10.1 min; *N*-TFA-(*S*)-Leu Me ester, 9.2 min.

Preparation of Mosher's esters of 2-propyl O-Leu and 2-propyl O-Phe

The 2-propyl esters of hydroxy acids (*R*)-O-Leu, (*R*)-O-Phe, (*R,S*)-O-Leu, and (*R,S*)-O-Phe were prepared by a modification of an established method (7). Typically, a solution of the hydroxy acid (0.028 mmol) in AcCl–2-propanol (10:90, v/v, 200 μL) was heated to 110°C for 60 min. After concentration (rotary evaporator), Et_3N (15 μL) and DMAP (1 mg) were added to the reaction mixture dissolved in $CHCl_3$ (500 μL); this solution was added to the neat acid chloride of the (*R*) Mosher's acid ((*R*)-2-methoxy-2-phenyl-2-trifluoromethylacetic acid), prepared according to published procedure (9). The diastereomeric products (ca. 90% yield) obtained from derivatization of (*R,S*) O-Phe were separated by prep TLC (hexane–EtOAc, 10:1, v/v; multiple development); the diastereomeric products obtained from derivatization of (*R,S*) O-Leu were separated by prep TLC (hexane–EtOAc, 20:1, v/v; multiple development).

*1′-Methylethyl (*R*)-2-[(*R*)-2″-methoxy-2″-phenyl-2″-trifluoromethyl] acetoxy-3-phenylpropanoate*: ^1H NMR (360 MHz, $CDCl_3$) δ: 7.50–7.05 (m, 10 H's), 5.32 (dd, J = 8.2, 4.2 Hz, H-2), 5.05 (sept, J = 6.3 Hz, H-1′), 3.53 (q, J = 1.0 Hz, OMe), 3.18 (dd, J = 14.4, 4.2 Hz, H-3), 3.09 (dd, J = 14.4, 8.2 Hz, H-3), 1.20 (d, J = 6.3 Hz, H-2′/H-3′), 1.17 (d, J = 6.3 Hz, H-3′/H-2′); ^{13}C NMR (90.5 MHz, $CDCl_3$) δ: 168.0, 166.1, 135.1, 132.0, 129.4 (2 C's) 129.3 (2 C's), 128.33 (2 C's), 128.27 (2 C's), 127.4, 127.0, 123.0 (q, J_{C-F} = 289 Hz), 84.4 (q, $^2J_{C-F}$ = 28 Hz) 74.9, 69.8, 55.6, 37.1, 21.6, 21.6; CIMS (NH_3) *m/z*: (relative abundance): 442 (M + 18, 100); EIMS *m/z*: 189 (100), 148 (23).

*1′-Methylethyl (*S*)-2-[(*R*)-2″-methoxy-2″-phenyl-2″-trifluoromethyl] acetoxy-3-phenylpropanoate (**3**)*: ^1H NMR (360 MHz, $CDCl_3$) δ: 7.33–7.19 (m, 10 H's), 5.34 (dd, J = 10.0, 3.7 Hz, H-2), 5.06 (sept, J = 6.2 Hz, H-1′), 3.33 (q, J = 1.0 Hz, OMe), 3.28 (dd, J = 14.6, 3.7 Hz, H-3), 3.08 (dd, J = 14.6, 10.0 Hz, H-3), 1.22 (d, J = 6.2 Hz, H-2′), 1.21 (d, J = 6.2 Hz, H-3′); ^{13}C NMR (90.5 MHz, $CDCl_3$) δ: 167.9, 166.1, 135.5, 131.9, 129.5 (2 C's), 129.4 (2 C's), 128.6 (2 C's), 128.2 (2 C's), 127.5, 127.2, 123.1 (q, J_{C-F} = 289 Hz), 84.5 (q, $^2J_{C-F}$ = 28 Hz), 75.2, 69.8, 55.3, 37.1, 21.6 (2 C's); CIMS (NH_3) *m/z* (relative abun-

© 1997 NRC Canada

dance): 442 (M + 18, 100); EIMS *m/z* (relative abundance): 189 (100), 148 (20).

1′-Methylethyl (R)-2-[(R)-2″-methoxy-2″-phenyl-2″-trifluoromethyl] acetoxy-4-methylpentanoate: ^{1}H NMR (360 MHz, $CDCl_3$) δ: 7.68–7.63 (m, 2H); 7.39–7.36 (m, 3H); 5.08 (dd, J = 10.0, 3.5 Hz, H-2), 5.09 (sept, J = 6.3 Hz, H-1′), 3.64 (q, J = 1.0 Hz, OCH_3), 1.80 (m, 1H), 1.58 (m, 2H), 1.27 (d, J = 6.3 Hz, H-2′/H-3′), 1.23 (d, J = 6.3 Hz, H-3′/H-2′), 0.82 (d, J = 6.5 Hz, H-5/H-6), 0.80 (d, J = 6.5 Hz, H-6/H-5); ^{13}C NMR (90.5 MHz, $CDCl_3$) δ: 169.4, 166.4, 132.2, 129.6, 128.3 (2 C′s), 127.5 (2 C′s), 123.3, (q, J_{C-F} = 289 Hz), 84.5 (q, $^2J_{C-F}$ = 28), 73.0, 69.5, 55.7, 39.5, 24.2, 21.7, 21.7, 20.9; CIMS (NH_3) *m/z* (relative abundance): 408 (M + 18, 100); EIMS *m/z* (relative abundance): 189 (100), 115 (62).

*1′-Methylethyl (S)-2-[(R)-2″-methoxy-2″-phenyl-2″-trifluoromethyl] acetoxy-4-methyl pentanoate (**4**)*: ^{1}H NMR (360 MHz, $CDCl_3$) δ: 7.56–7.52 (m, 2 H′s), 7.40–7.37 (m, 3 H′s), 5.11 (dd, J = 10.0, 3.8 Hz, H-2), 5.06 (sept, J = 6.3 Hz, H-1′), 3.53 (q, J = 1.0 Hz, OCH_3), 1.84 (m, H-3), 1.73 (m, H-4), 1.65 (m, H-3), 1.24 (d, J = 6.3 Hz, H-2′/H-3′), 1.23 (d, J = 6.3 Hz, H-3′/H-2′), 0.92 (d, J = 6.2 Hz, H-5/H-6), 0.91 (d, J = 6.2 Hz, H-6/H-5); ^{13}C NMR (90.5 MHz, $CDCl_3$) δ: 169.1, 166.4, 131.7, 129.6, 128.3 (2 C′s), 127.8 (2 C′s), 123.2 (q, J_{C-F} = 289 Hz), 84.6 (q, $^2J_{C-F}$ = 28), 73.2, 69.4, 55.4, 39.5, 24.4, 23.0, 21.6 (2 C′s), 21.2; CIMS (NH_3) *m/z* (relative abundance): 408 (M + 18, 100); EIMS *m/z* (relative abundance): 189 (100), 115 (60).

Acknowledgment

I thank Professor D. E. Ward, University of Saskatchewan, for advice in preparing the Mosher's esters.

References

1. M.S.C. Pedras, J.L. Taylor, and T.T. Nakashima. J. Org. Chem. **58**, 4778 (1993).
2. W.A. Ayer and L.M.P. Rodriguez. J. Nat. Prod. **50**, 400 (1987).
3. S. Nishimura and K. Kohmoto. Annu. Rev. Phytopathol. **21**, 87 (1983).
4. W.B Turner and D.C. Aldridge. Fungal metabolites II. Academic, New York. 1983. pp. 436–442; H. Kleinkauf and H. von Doheren. Eur. J. Biochem. **192**, 1 (1990).
5. M.S.C. Pedras. Rev. Latinoam. Quim. **24**, 177 (1996).
6. H. Bruckner and M. Hausch. Chromatographia, **28**, 487 (1989).
7. B. Koppenhoefer, H. Ailmendinger, G.J. Nicholson, and E. Bayer. J. Chromatogr. **260**, 63 (1983).
8. H. Frank, J. Gerhardt, G.J. Nicholson, and E. Bayer. J. Chromatogr. **270**, 159 (1983).
9. D.E. Ward and C.K. Rhee. Tetrahedron Lett. **32**, 7165 (1991).
10. D.E. Ward, A. Vazquez, and M.S.C. Pedras. J. Org. Chem. **61**, 8008 (1996).

Can. J. Chem. Downloaded from www.nrcresearchpress.com by 92.62.229.171 on 09/08/12
For personal use only.

© 1997 NRC Canada

Synthesis and characterization of 4-alkenyl and 4,4′-dialkenyl-2,2′-bipyridyl ligands bearing π-donor substituents

Manuel Bourgault, Thierry Renouard, Barbara Lognoné, Chakour Mountassir, and Hubert Le Bozec

Abstract: The synthesis of a new series of π-donor mono- and disubstituted vinyl bipyridines (donor = 4-R_2N-C_6H_4-; 4-RO-C_6H_4-; (C_5H_5)Fe(C_5H_4-); (C_5H_5)Ru(C_5H_4-)) has been achieved by reaction of the mono- and dilithio species of 4,4′-dimethyl-2,2′-bipyridine and the monolithio species of 4-nonyl-4′-methyl-2,2′-bipyridine with the appropriate aldehydes. Their ^{1}H NMR and UV–visible characterizations are reported.

Key words: 2,2′-bipyridines, π-donor substituents, UV–visible, ^{1}H NMR, nonlinear optics.

Résumé : La synthèse d'une nouvelle série de ligands mono- et di-alcényles 2,2′-bipyridines substitués par des groupements conjugués π-donneurs (donneur = 4-R_2N-C_6H_4-; 4-RO-C_6H_4-; (C_5H_5)Fe(C_5H_4-); (C_5H_5)Ru(C_5H_4-)) a été réalisée par réaction des espèces mono- et di-lithiées de la 4,4′-diméthyl-2,2′-bipyridine et mono-lithiée de la 4-nonyl-4′-méthyl-2,2′-bipyridine avec les aldéhydes appropriés. Leurs caractérisations RMN ^{1}H et UV–visible sont également décrites.

Mots clés : 2,2′-bipyridines, substituants π-donneurs, UV–visible, RMN ^{1}H, optique non lineaire.

Introduction

Recent work in our laboratory has focused on the design, synthesis, and second-order nonlinear optical (NLO) properties of new bipyridyl metal complexes. We have previously reported the synthesis of a series of 4-alkenyl-4′-methyl-2,2′-bipyridine complexes of rhenium, zinc, and mercury, in which the alkenyl fragment bears a π-donor group such as di-*n*-butylaminophenyl (1). The molecular hyperpolarizabilities of these new dipolar organometallic compounds were examined using the EFISH technique and large β values were found, especially for the bipyridyl zinc complex (**I**). In addition, we have recently discovered a giant octupolar nonlinearity, among the highest β values ever reported, for the octahedral trisubstituted ruthenium complexes (**II**) containing the bis-4,4′-di-*n*-butylaminostyryl-2,2′-bipyridine ligand (2). To gain insight into the potential scope of dipolar and octupolar bipyridyl metal complexes as NLO materials, we have carried out the preparation of a series of donor-substituted bipyridines. In this paper we report the synthesis and spectroscopic and electronic characterizations of 4-alkenyl- and 4,4′-dialkenyl-2,2′-bipyridyl ligands containing π-donor dialkylaminophenyl, alkoxyphenyl, or metallocenyl groups.

Received September 12, 1996.

M. Bourgault, T. Renouard, B. Lognoné, C. Mountassir, and H. Le Bozec.[1] Laboratoire de chimie de coordination organique, Unité de recherche associée n° 415 du Centre national de la recherche scientifique, Campus de Beaulieu, Université de Rennes 1, F-35042 Rennes, France.

[1] Author to whom correspondence may be addressed. Telephone: (33) 2 99.28.62.81. Fax: (33) 2 99.28.69.39. E-mail: lebozec@univ-rennes1.fr

Results and discussion

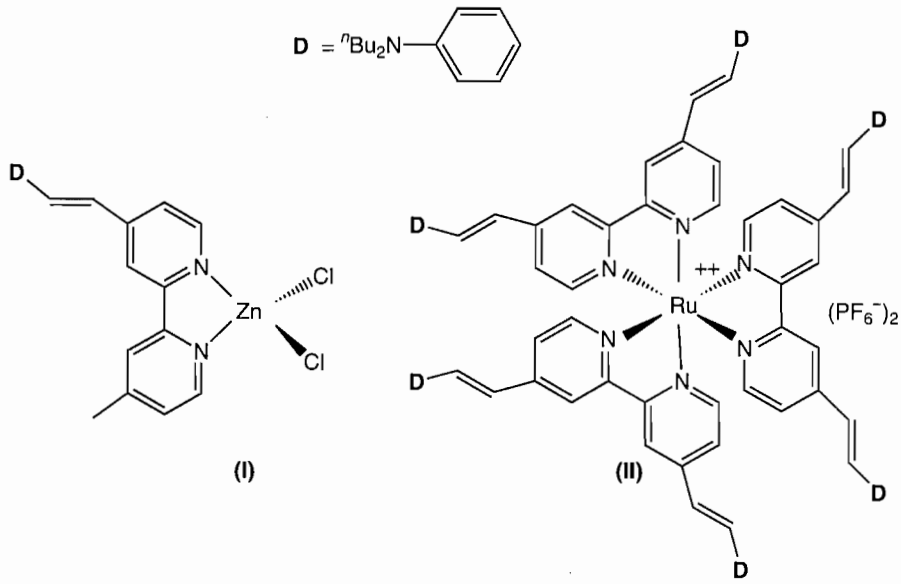
The 4-alkenyl-2,2′-bipyridyl ligands were prepared from 4,4′-dimethyl-2,2′-bipyridine **1** by an approach analogous to that used by Beer et al. in the preparation of 4-methyl-4′-ferrocenylvinyl-2,2′-bipyridine **6** (3). Reaction of **1** with one equivalent of lithium diisopropylamide (LDA) is known to generate the mono-lithio species (4). The reaction of this anion with the appropriate aldehydes gave the corresponding alcohols, and subsequent treatment with *p*-toluenesulfonic acid yielded the respective 4-methyl-4′-alkenyl-2,2′-bipyridines **3***a–d*, **4**, **6**, and **7** in 49–96% yield (Scheme 2). The dialkylaminobenzaldehyde precursors were obtained by formylation (Vilsmeier reaction) of the aniline derivatives (5) whereas the 4-alkoxybenzaldehydes were synthesized from 4-hydroxybenzaldehyde and the appropriate alkyl bromide or mesylate reagents (see experimental section) (6). To enhance the solubility of the resultant complexes in common organic solvents, which is the prerequisite condition to measure the dipole moments μ and the molecular hyperpolarizabilities β, the synthesis of 4-nonyl-4′-alkenyl-2,2′-bipyridines **5** and **8** was attempted. Compound **5** was synthesized in 37% yield from 4-nonyl-4′-methyl-2,2′-bipyridine **2** (7, 8) by using the same previous procedure, whereas **8** was conveniently prepared (68% yield) in a one-pot reaction from **1** using a step by step lithiation and the successive addition of ferrocene carbaldehyde and octyl bromide (Scheme 2).

The symmetrical 4,4′-disubstituted 2,2′-bipyridines compounds were obtained from **1** upon treatment with two equivalents of LDA followed by addition of the appropriate aldehydes (Scheme 3) (6, 9, 10). Dehydration of the dialdehydes was accomplished either with *p*-toluenesulfonic acid or with pyridium *p*-toluenesulfonate and afforded the new bis-4,4′-alkenyl-2,2′-bipyridines **9**, **10**, and **12** in moderate to

© 1997 NRC Canada

Can. J. Chem. Downloaded from www.nrcresearchpress.com by 88.146.161.215 on 09/08/12
For personal use only.

Scheme 1.



good yield (Table 1). Ligands **11** and **13** were also synthesized from the chiral (S)-(+)-4-[*N*-methyl-*N*-(2-methylbutyl)amino]benzaldehyde and (*S*)-(+)-4-(2-methylbutoxy)benzaldehyde, respectively, in order to promote the noncentrosymmetric crystallization of the corresponding organometallic materials (Scheme 3).

These compounds were easily characterized by means of their analytical data (see experimental section) and ^{1}H NMR and UV–visible data (Table 1). The configuration of the double bond formed after dehydration was in every case established as *E* on the basis of the proton-proton coupling constant, $J_{H^7H^8} \approx 16$ Hz. The aromatic region of **3–8** shows six different signals ($H^{3,3'}$, $H^{5,5'}$, $H^{6,6'}$) characteristic of disymmetric substituted bipyridines. In all cases the lowest field resonances are H^6 and $H^{6'}$ as expected from the deshielding by the adjacent nitrogen. The protons H^3 and $H^{3'}$ are also found at lower field than H^5 and $H^{5'}$, which is known to be due to the *transoid* conformation of the bipyridines (11). In the case of symmetric ligands **9–13** the aromatic region gives rise, as expected, to only three signals. The optical absorption spectra for the mono- and bis-dialkylaminostyryl bipyridines are all characterized by intense broad transitions in the region 350–400 nm (**3***a–c*: $\varepsilon \approx 22\,000$; **9–11**: $\varepsilon \approx 50\,000$), which are assigned to intramolecular charge transfer transitions (ICT). In addition, this absorption band exhibits a solvatochromic shift characteristic of a large dipole moment change between the ground and the excited states and suggestive of appreciable microscopic nonlinearities. A less intense ICT band is observed at higher energy for compounds **3***c*, **4**, **5**, **12**, and **13** ($\lambda \approx 330$–350 nm), which is consistent with the following relative ordering of donor strength: $N(^nBu)_2 > N(Me)_2 > N(Et)(Ar) > O(Alk)$. The visible absorption spectra of the ferrocenylvinyl bipyridines **6** and **8** exhibit two broad bands at ca. 475 and 375 nm that can be assigned to metal-to-ligand charge transfer and π–π^* transitions, respectively (12). These two bands are hypsochromically shifted ($\lambda = 310$ and 345 nm) for the ruthenium analog **7**, as expected for the replacement of ferrocene by the less electron-rich ruthenocene (12). An extensive investigation regarding the coordination studies of these ligands to form mono- and tris-bipyridine metal complexes, along with studies of their optical nonlinearities, will be described in the future.

Experimental

All reactions were conducted under argon or nitrogen atmosphere. The solvents were dried by standard methods. Infrared spectra were recorded on a Nicolet 205 FT-IR spectrometer. Electronic absorption spectra were recorded on a Uvikon 941+ spectrophotometer. Proton (300.13 MHz) NMR spectra were recorded on a Bruker AM 300 spectrometer at 297 K using $CDCl_3$ as solvent and referenced to TMS. High-resolution mass spectra were obtained on a Varian MAT 311 at CRMPO, University of Rennes. Elemental analyses were performed by the Service Central de Microanalyses du CNRS at Lyon, France. Melting points, uncorrected, were taken on a Kofler apparatus.

Materials

4,4′-Dimethyl-2,2′-bipyridine (13) and ruthenocenecarbaldehyde (14) were prepared by described procedures. 4-(*N,N*-Dimethylamino)benzaldehyde, 9-ethyl-3-carbazole carboxaldehyde, 4-methoxybenzaldehyde, and ferrocenecarbaldehyde were commercial products (Aldrich or Acros).

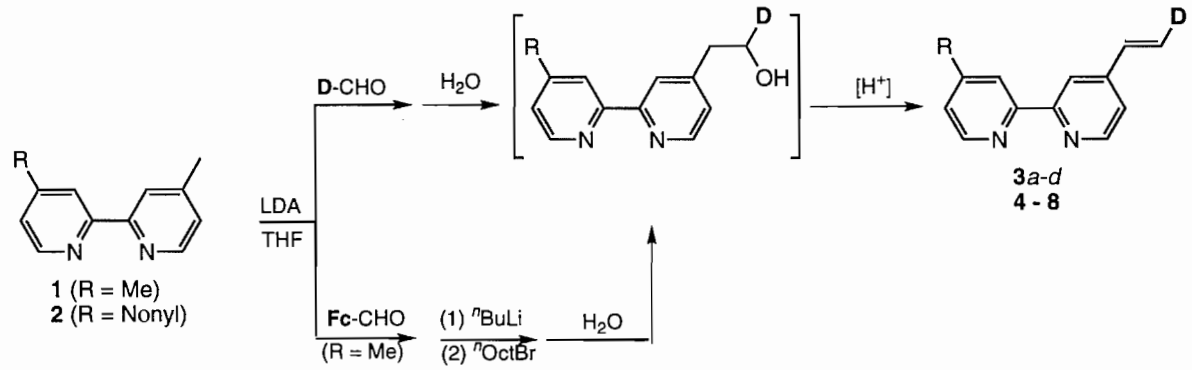
4-(*N,N*-Di-*n*-butylamino)benzaldehyde (ref. 5)

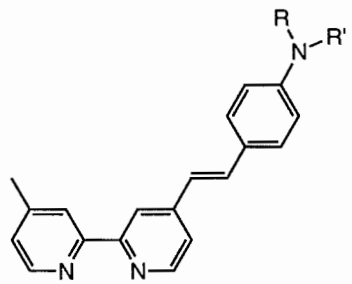
Dimethylformamide (10 mL) was cooled to 0°C and treated dropwise with phosphorus oxychloride (2.1 mL, 22.5 mmol). The solution was stirred at 0°C for 1 h and then at room temperature for 1 h. To the red solution was added dropwise *N,N*-di-*n*-butylaniline (4.53 mL, 20 mmol). The mixture was heated at 60°C for 10 h and then cooled to 0°C. A solution of 2 g of sodium acetate in 20 mL of cold water was added slowly with stirring. The reaction mixture was then stirred for an additional 1 h, and the resulting solution was extracted with

Can. J. Chem. Downloaded from www.nrcresearchpress.com by 88.146.161.215 on 09/08/12
For personal use only.

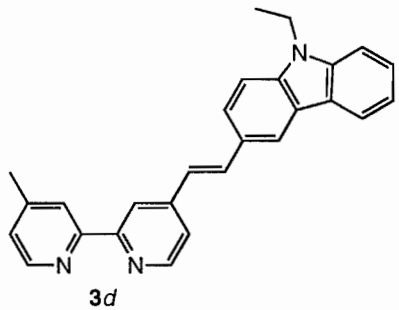
© 1997 NRC Canada

Scheme 2.

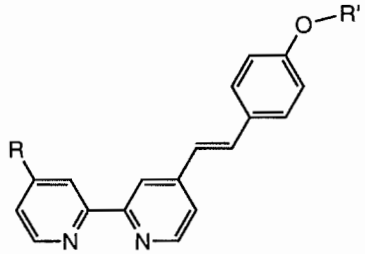




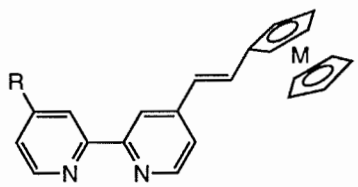
3*a* : R , R' = ^{n}Bu , ^{n}Bu
3*b* : R , R' = Me , Me
3*c* : R , R' = Me , ^{n}Oct



3*d*



4 : R = Me , R' = ^{n}Oct
5 : R = Nonyl , R' = Me



6 : R = Me , M = Fe
7 : R = Me , M = Ru
8 : R = Nonyl , M = Fe

ether. The combined extract was washed with saturated aqueous sodium bicarbonate and then with water, and the organic layer was dried over $MgSO_4$. The solvent was removed under reduced pressure, and the residue was distilled in vacuum at 147–150°C/1 Torr (= 133.3 Pa) to yield 4-(*N*,*N*-di-*n*-butylamino)benzaldehyde as a yellow liquid (4.37 g, 90%); IR, ν_{max}(cm^{-1}): 1686 (C=O); ^{1}H NMR, δ: 9.67 (s, 1H, CHO), 7.66 (dd, 2H, *J* = 9.0 and 2.7 Hz, C_6H_4-), 6.62 (dd, 2H, *J* = 9.0 and 2.7 Hz, C_6H_4-), 3.32 (t, 4H, *J* = 7.7 Hz, N-CH_2-), 1.58 (m, 4H, CH_2-), 1.35 (m, 4H, CH_2-), 0.35 (t, 6H, *J* = 7.3 Hz, CH_3).

(*N*-Methyl-*N*-octyl)aniline

To an ice-cooled solution of *N*-methylaniline (6.5 g, 60 mmol) in 20 mL of freshly distilled THF was added 1.6 M *n*-butyllithium (40 mL, 66 mmol) dropwise. The resulting mixture was stirred for 0.5 h and octylbromide (11.5 mL, 66 mmol) was added slowly. The solution was allowed to warm to room temperature. The orange solution was cooled in an ice-water bath and hydrolysed with 10 mL of water. The organic layer was separated, dried over $MgSO_4$, and filtered, and the solvent was evaporated to dryness. The title compound was obtained as an orange oil (11.8 g; 90%); ^{1}H NMR, δ: 7.33 (dd, 2H, *J* = 7 and 8.8 Hz, C_6H_5-), 6.80 (m, 3H, C_6H_5-), 3.40 (t, 2H, *J* = 7.5 Hz, N-CH_2-), 3.02 (s, 3H, N-CH_3), 1.68 (m, 2H, N-CH_2-CH_2-), 1.41 (m, 10H, $(CH_2)_5$-), 1.01 (t, 3H, *J* = 7.5 Hz, CH_2-CH_3).

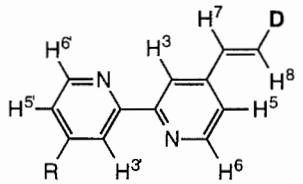
4-(*N*-Methyl-*N*-octylamino)benzaldehyde

The title compound was obtained as an orange oil (12.5 g, 74%) from (*N*-methyl-*N*-octyl)aniline (15 g, 73 mmol), phosphorus oxychloride (7 mL, 75 mmol) and dimethylformamide (30 mL); bp 110°C at 0.03 Torr; IR, ν_{max}(cm^{-1}): 1682 (C=O);

© 1997 NRC Canada

Can. J. Chem. Downloaded from www.nrcresearchpress.com by 88.146.161.215 on 09/08/12
For personal use only.

Table 1. Yield, selected ^{1}H NMR, and UV–visible data for bipyridines **1**–**13**.



Compound	% Yield	^{1}H NMR (δ_{ppm} ; J_{Hz})[a]						UV–visible[b]
		$H^{6,6'}$	$H^{3,3'}$	$H^{5,5'}$	H^8	H^7	J_{7-8}	λ_{max} (nm)
1	—	8.47	8.16	7.05				—
2	75	8.47	8.23	7.11				—
3*a*	96	8.53, 8.50	8.48, 8.27	7.30, 7.11	7.35	6.88	16.2	388
3*b*	74	8.59, 8.58	8.48, 8.30	7.36, 7.16	7.42	6.92	16.3	374
3*c*	61	8.51, 8.50	8.46, 8.25	7.31, 7.13	7.36	6.89	16.3	389
3*d*	51	8.62, 8.59	8.55, 8.27	7.49, 7.16	7.66	7.15	16.3	351
4	70	8.61, 8.57	8.48, 8.25	7.33, 7.15	7.40	6.97	16.3	329
5	37	8.56, 8.52	8.51, 8.26	7.34, 7.14	7.40	7.00	16.4	325
6	69	8.53, 8.52	8.45, 8.27	7.29, 7.15	7.28	6.73	16.1	375, 472
7	49	8.50, 8.49	8.39, 8.25	7.20, 7.12	7.14	6.65	16.2	310, 345
8	68	8.58, 8.58	8.43, 8.25	7.27, 7.15	7.27	6.70	16.1	378, 469
9	83	8.60	8.46	7.33	7.38	6.88	16.2	401
10	80	8.60	8.46	7.33	7.39	6.90	16.2	394
11	51	8.60	8.47	7.33	7.39	6.90	16.2	394
12	20	8.64	8.51	7.36	7.41	6.98	16.3	337
13	23	8.64	8.51	7.36	7.41	6.98	16.3	336

[a]Data in $CDCl_3$.
[b]Data in CH_2Cl_2.

^{1}H NMR, δ: 9.62 (s, 1H, CHO), 7.62 (dd, 2H, J = 9.0 Hz, C_6H_4-), 6.59 (dd, 2H, J = 9.0 Hz, C_6H_4-), 3.31 (t, 2H, J = 7.6 Hz, N-CH_2-), 2.95 (s, 3H, N-CH_3), 1.52 (t, 2H, J = 6.9 Hz, N-CH_2-CH_2-), 1.22 (m, 10H, $(CH_2)_5$-), 0.80 (t, 3H, J = 6.7 Hz, CH_2-CH_3).

(*N*-Methyl-*N*-2-methylbutyl)aniline

The title compound was obtained as a yellow oil (3.54 g, 66%) from *N*-methylaniline (3.2 g, 30 mmol), (*S*)-(+)-2-methylbutylmesylate (5.5 g, 33 mmol), and 1.6 M *n*-butyllithium (20 mL, 32 mmol) in 20 mL of freshly distilled THF; ^{1}H NMR, δ: 7.30 (m, 2H, C_6H_5-), 6.76 (m, 3H, C_6H_5-), 3.21(2 × q, 2H, J = 6.8 and 14.5 Hz, N-CH_2-), 3.03 (s, 3H, N-CH_3), 1.92 (m, 1H, CH-CH_3), 1.56 (m, 1H, CH_2-CH_3), 1.20 (m, 1H, CH_2-CH_3), 1.02 (t, 3H, J = 7.3 Hz, CH_2-CH_3), 0.99 (d, 3H, J = 6.7 Hz, CH-CH_3).

(*S*)-(+)-4-(*N*-Methyl-*N*-(2-methylbutyl)amino)-benzaldehyde

The title compound was obtained as an orange oil (3.5 g, 85%) from (*N*-methyl-*N*-2-methylbutyl)aniline (3.54 g, 20 mmol), $POCl_3$ (2 mL, 20 mmol), and DMF (10 mL); $[\alpha]_D$ +26 (c = 1.0, CH_2Cl_2); IR, ν_{max}(cm^{-1}): 1684 (C═O); ^{1}H NMR, δ: 9.64 (s, 1H, CHO), 7.63 (d, 2H, J = 9.0 Hz, C_6H_4-), 6.60 (d, 2H, J = 9 Hz, C_6H_4-), 3.17 (2 × q, 2H, J = 6.8 and 14.6 Hz, N-CH_2-), 2.97 (s, 3H, N-CH_3), 1.77 (m, 1H, CH-CH_3), 1.37 (m, 1H, CH_2-CH_3), 1.07 (m, 1H, CH_2-CH_3), 0.86 (t, 3H, J = 7.4 Hz, CH_2-CH_3), 0.82 (d, 3H, J = 6.6 Hz, CH-CH_3).

4-Octyloxybenzaldehyde (ref. 6)

To a solution of 4-hydroxybenzaldehyde (6.11 g, 50 mmol) in 300 mL of ethanol was added potassium carbonate (17 g, 123 mmol). The resulting mixture was stirred for 0.5 h at room temperature and octylbromide (8.6 mL, 50 mmol) was added slowly. The yellow solution was refluxed for 70 h and then cooled to room temperature. The mixture was filtered and the solvent evaporated. The yellow residue was dissolved in ether and washed with water (until the washings were neutral). The solution was dried over $MgSO_4$, and the solvent evaporated to dryness. The title compound was obtained as a yellow oil (9.6 g, 82%); IR, ν_{max}(cm^{-1}): 1696 (C═O); ^{1}H NMR, δ: 9.84 (s, 1H, CHO), 7.79 (dd, 2H, J = 8.8 and 2.6 Hz, C_6H_4-), 6.95 (dd, 2H, J = 8.8 and 2.6 Hz, C_6H_4-), 4.0 (t, 2H, J = 6.5 Hz, O-CH_2), 1.78 (m, 2H, CH_2-), 1.5–1.1 (m, 10H, $(CH_2)_5$-), 0.86 (t, 3H, J = 6.6 Hz, CH_3).

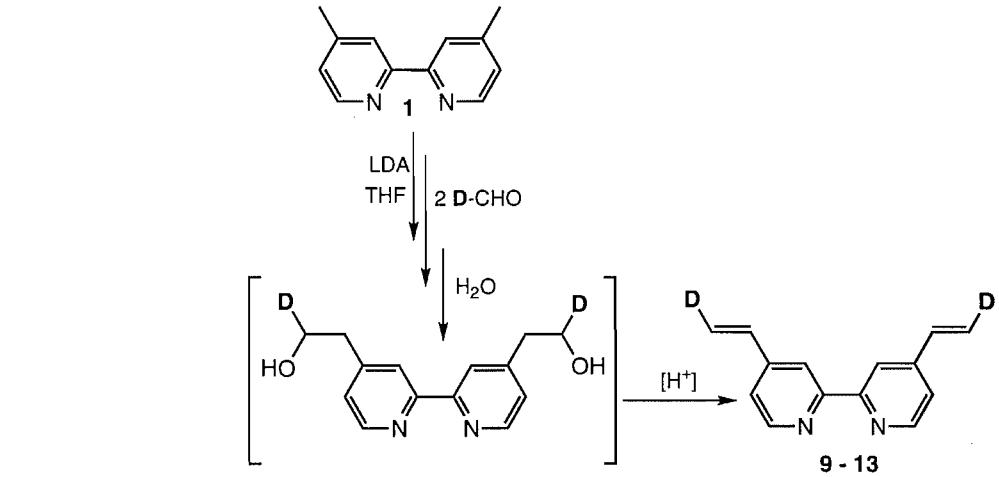
(*S*)-(+)-4-(2-Methylbutoxy)benzaldehyde

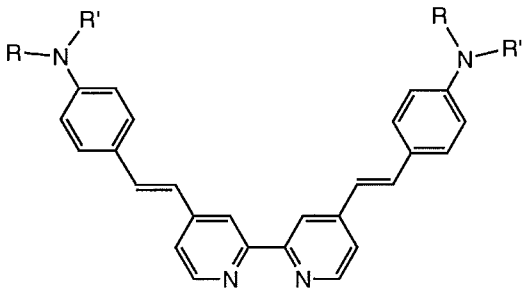
The title compound was obtained as a yellow oil (3.3 g, 57%) from 4-hydroxybenzaldehyde (3.66 g, 30 mmol), potassium carbonate (17 g, 123 mmol), and 4.98 g of (*S*)-(+)-2-methylbutylmesylate; $[\alpha]_D$ +7 (c = 1.6, CH_2Cl_2); IR, ν_{max}(cm^{-1}): 1694 (C═O); ^{1}H NMR, δ: 9.72 (s, 1H, CHO), 7.67 (dd, 2H, J = 8.8 and 2.6 Hz, C_6H_4-), 6.84 (dd, 2H, J = 8.8 and 2.6 Hz, C_6H_4-), 3.74 (dd, 1H, J = 9.1 and 6.0 Hz, O-CH_2-), 3.66 (dd, 1H, J = 9.1 and 6.0 Hz, O-CH_2-), 1.74 (m, 1H, CH-CH_3), 1.42 (m, 1H, CH_2-), 1.12 (m, 1H, CH_2-), 0.88 (d, 3H, J = 6.7 Hz, CH_3), 0.80 (t, 3H, J = 7.4 Hz, CH_3).

Can. J. Chem. Downloaded from www.nrcresearchpress.com by 88.146.161.215 on 09/08/12
For personal use only.

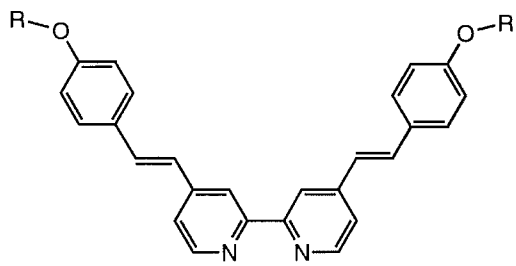
© 1997 NRC Canada

Scheme 2.





9 : R , R' = ^{n}Bu , ^{n}Bu
10 : R , R' =Me , ^{n}Oct
11 : R , R' = Me ,$CH_2CH(Me)(Et)$



12 : R = ^{n}Oct
13 : R = $CH_2CH(Me)(Et)$

4-Nonyl-4′-methyl-2,2′-bipyridine 2

A solution of 4,4′-dimethyl-2,2′-bipyridine **1** (1.84 g, 10 mmol) in 30 mL THF was added dropwise to a stirred solution of freshly prepared LDA (12.9 mmol) in 40 mL THF at 0°C. The resulting red mixture was stirred 1 h at 0°C. Octylbromide (2 mL, 10 mmol) was added and the mixture was stirred for an additional 1 h at 0°C, treated with water, and evaporated in vacuo. The yellow oil was dissolved in 100 mL CH_2Cl_2, washed with water (2 × 75 mL), dried over $MgSO_4$, and evaporated. Recrystallization from hexane (15 mL) yielded **2** as white crystals (2.21 g); mp 42–45°C; ^{1}H NMR, δ: 8.47 (d, 2H, $H^{6,6'}$), 8.23 (m, 2H, $H^{3,3'}$), 7.11 (m, 2H, $H^{5,5'}$), 2,66 (t, 2H, J = 8.0 Hz, CH_2-), 2.40 (s, 3H, CH_3), 1.65 (m, 2H, CH_2-), 1.40–1.15 (m, 12H, $(CH_2)_6$-), 0.85 (t, 3H, J = 8.0 Hz, CH_3). Anal. calcd. for $C_{20}H_{28}N_2$: C 81.03; H 9.52; found: C 80.96, H 10.39.

4-[*p*-(*N*,*N*-Dibutylamino)styryl]-4′-methyl-2,2′-bipyridine *3a*

To a stirred solution of freshly prepared LDA (51.6 mmol) in 60 mL of THF at −78°C was added dropwise a solution of **1** (7.9 g, 43 mmol) in 120 mL of THF. The red solution was stirred for 15 min at −78°C and 1 h at 0°C. A solution of 4-(*N*,*N*-dibutylamino)benzaldehyde (10 g, 43 mmol) in 40 mL of THF was then added dropwise and the yellow-green solution was stirred for 2 h at 0°C and overnight at room temperature. The mixture was quenched with 50 mL of water and extracted with CH_2Cl_2 (3 × 100 mL). The combined extract was dried over $MgSO_4$ and evaporated in vacuo. The crude product was chromatographed on silica gel with dichloromethane–methanol – ammonium hydroxide (100/5/1) as the eluant. The resulting alcohol was then dissolved in 250 mL of toluene and treated with *p*-toluenesulfonic acid monohydrate (500 mg, 2.6 mmol). The mixture was refluxed for 4 h, then cooled to room temperature, washed with saturated aqueous sodium bicarbonate, dried over $MgSO_4$, and evaporated in vacuo to give **3***a* as an orange oil (16.4 g); UV, λ_{max} (nm): 382 (toluene), 388 (CH_2Cl_2), 397 (DMF); ^{1}H NMR, δ: 8.53 (d, 1H, J = 5.1 Hz, H^6), 8.50 (d, 1H, J = 5.0 Hz, $H^{6'}$), 8.48 (d, 1H, J = 1.6 Hz, H^3), 8.27 (s, 1H, $H^{3'}$), 7.40 (d, 2H, J = 9.0 Hz, C_6H_4-), 7.35 (d, 1H, J = 16.2 Hz, CH=), 7.30 (dd, 1H, J = 5.1 and 1.6 Hz, H^5), 7.11 (dd, 1H, J = 5.0 and 0.9 Hz, $H^{5'}$), 6.88 (d, 1H, J = 16.2 Hz, CH=), 6.63 (d, 2H, J = 9.0 Hz, C_6H_4-), 3.29 (t, 4H, J = 7.8 Hz, N-CH_2-), 2.42 (s, 3H, CH_3), 1.57 (m, 4H, CH_2-), 1.35 (m, 4H, CH_2-), 0.95 (t, 6H, J = 7.3 Hz, CH_3). Anal. calcd. for $C_{27}H_{33}N_3$: C 81.16, H 8.32, N 10.52; found: C 81.32, H 8.59, N 10.21.

4-[*p*-(*N*,*N*-Dimethylamino)styryl]-4′-methyl-2,2′-bipyridine *3b*

The title compound was prepared analogously as described for

Can. J. Chem. Downloaded from www.nrcresearchpress.com by 88.146.161.215 on 09/08/12
For personal use only.

© 1997 NRC Canada

Can. J. Chem. Downloaded from www.nrcresearchpress.com by 88.146.161.215 on 09/08/12
For personal use only.

3*a*, using **1** (2.76 g, 15 mmol) and 4-(*N*,*N*-dimethylamino)benzaldehyde (2.4 g, 15 mmol) as starting materials, and was isolated as yellow-orange microcrystals after recrystallization from dichloromethane–ether (3.54 g); mp 140°C; ^{1}H NMR, δ: 8.59 (d, 1H, J = 5.2 Hz, H^6), 8.58 (d, 1H, J = 4.9 Hz, $H^{6'}$), 8.48 (d, 1H, J = 1.2 Hz, H^3), 8.30 (s, 1H, $H^{3'}$), 7.47 (d, 2H, J = 8.9 Hz, C_6H_4-), 7.42 (d, 1H, J = 16.3 Hz, CH═), 7.36 (dd, 1H, J = 5.2 and 1.7 Hz, H^5), 7.16 (dd, 1H, J = 4.9 and 1.7 Hz, $H^{5'}$), 6.92 (d, 1H, J = 16.3 Hz, CH═), 6.73 (d, 2H, J = 8.9 Hz, C_6H_4-), 3.02 (s, 6H, N-CH_3), 2.46 (s, 3H, CH_3). Anal. calcd. for $C_{21}H_{21}N_3$: C 79.97, H 6.71, N 13.32; found: C 79.23, H 6.76, N 13.00. HRMS *m/z*, calcd.: 315.1735; found: 315.1733.

4-[*p*-(*N*-Methyl-*N*-octyl)aminostyryl]-4′-methyl-2,2′-bipyridine 3*c*

The title compound was prepared analogously as described for **3***a*, using **1** (0.92 g, 5 mmol) and 4-(*N*-methyl-*N*-octyl)aminobenzaldehyde (1.25 g, 5.1 mmol) as starting materials, and was isolated as an orange oil after flash chromatography on silica gel with dichloromethane–methanol (90:10) as the eluant (1.26 g); ^{1}H NMR, δ: 8.51 (d, 1H, J = 5.2 Hz, H^6), 8.50 (d, 1H, J = 4.0 Hz, $H^{6'}$), 8.46 (d, 1H, J = 1.2 Hz, H^3), 8.25 (s, 1H, $H^{3'}$), 7.42 (d, 2H, J = 8.9 Hz, C_6H_4), 7.36 (d, 1H, J = 16.3 Hz, CH═), 7.31 (dd, 1H, J = 5.2 and 1.7 Hz, H^5), 7.13 (dd, 1H, J = 4.8 and 0.9 Hz, $H^{5'}$), 6.89 (d, 1H, J = 16.3 Hz, CH═), 6.66 (d, 2H, J = 8.9 Hz, C_6H_4-), 3.32 (t, 2H, J = 7.7 Hz, N-CH_2-), 2.94 (s, 3H, N-CH_3), 2.41 (s, 3H, CH_3), 1.56 (m, 2H, CH_2-), 1.28 (m, 10H, $(CH_2)_5$-), 0.86 (t, 3H, J = 6.9 Hz, CH_3); HRMS *m/z* calcd. for $C_{28}H_{35}N_3$: 413.2831; found: 413.2847.

4-[(9-Ethyl-3-carbazolyl)vinyl]-4′-methyl-2,2′-bipyridine 3*d*

The title compound was prepared analogously as described for **3***a*, using **1** (2.76 g, 15 mmol) and 9-ethyl-3-carbazole carboxaldehyde (3.33 g, 15 mmol) as starting materials, and was isolated as a yellow solid after flash chromatography on alumina with dichloromethane–acetonitrile (90:10) as the eluant (3.0 g); mp 174°C; ^{1}H NMR, δ: 8.62 (d, 1H, J = 5.1 Hz, H^6), 8.59 (d, 1H, J = 5.0 Hz, $H^{6'}$), 8.55 (d, 1H, J = 1.5 Hz, H^3), 8.27 (s, 2H, $H^{3'}$ and H arom), 8.13 (d, 1H, J = 7.7 Hz, H arom), 7.71 (dd, 1H, J = 8.5 and 1.5 Hz, H arom), 7.66 (d, 1H, J = 16.3 Hz, CH═), 7.49 (m, 1H, H arom), 7.49 (m, 3H, H^5 and H arom), 7.26 (m, 1H, H arom), 7.16 (dd, 1H, J = 5.0 and 0.9 Hz, $H^{5'}$), 7.15 (d, 1H, J = 16.3 Hz, CH═), 4.36 (q, 2H, J = 7.2 Hz, CH_2-), 2.45 (s, 3H, CH_3), 1.44 (t, 3H, J = 7.2 Hz, CH_3). Anal. calcd. for $C_{27}H_{23}N_3$: C 83.26, H 5.95, N 10.79; found: C 82.35, H 5.99, N 10.55. HRMS *m/z*, calcd.: 389.1892; found: 389.1892.

4-[*p*-(Octyloxy)styryl]-4′-methyl-2,2′-bipyridine 4

The title compound was prepared analogously as described for **3***a*, using **1** (1 g, 5.4 mmol) and 4-octyloxybenzaldehyde (1.27 g, 5.4 mmol) as starting materials, and was isolated as a white solid after recrystallization from ethyl acetate (1.51 g); mp 60–62°C; ^{1}H NMR, δ: 8.61 (d, 1H, J = 5.1 Hz, H^6), 8.57 (d, 1H, J = 5.0 Hz, $H^{6'}$), 8.48 (s, 1H, H^3), 8.25 (s, 1H, $H^{3'}$), 7.48 (d, 2H, J = 8.7 Hz, C_6H_4-), 7.40 (d, 1H, J = 16.3 Hz, CH═), 7.33 (dd, 1H, J = 5.1 and 1.6 Hz, H^5), 7.15 (dd, 1H, J = 5.0 and 0.9 Hz, $H^{5'}$), 6.97 (d, 1H, J = 16.3 Hz, CH═), 6.91 (d, 2H, J = 8.7 Hz, C_6H_4-), 3.98 (t, 2H, J = 6.5 Hz, O-CH_2-), 2.44 (s, 3H, CH_3), 1.78 (m, 2H, CH_2-), 1.50–1.20 (m, 10H, $(CH_2)_5$-), 0.89 (t, 3H, J = 6.9 Hz, CH_3). Anal. calcd. for $C_{27}H_{32}N_2O{\cdot}0.5\ H_2O$: C 79.22, H 8.31, N 6.85; found: C 79.08, H 7.87, N 7.07.

4-[*p*-(Methoxy)styryl]-4′-nonyl-2,2′-bipyridine 5

The title compound was prepared analogously as described for **3***a*, using **2** (1.73 g, 5.8 mmol) and 4-methoxybenzaldehyde (1.12 g, 7 mmol), and was isolated as a white solid after flash chromatography on silica gel with dichloromethane–ethanol as the eluant (0.88 g); mp 62–64°C; ^{1}H NMR, δ: 8.56 (d, 1H, J = 5.1 Hz, H^6), 8.52 (d, 1H, J = 5.0 Hz, $H^{6'}$), 8.51 (s, 1H, H^3), 8.26 (s, 1H, $H^{3'}$), 7.51 (d, 2H, J = 8.7 Hz, C_6H_4-), 7.40 (d, 1H, J = 16.4 Hz, CH═), 7.34 (dd, 1H, J = 5.1 and 1.7 Hz, H^5), 7.14 (dd, 1H, J = 5.0 and 1.6 Hz, $H^{5'}$), 7.0 (d, 1H, J = 16.4 Hz, CH═), 6.91 (d, 2H, J = 8.7 Hz, C_6H_4-), 3.81 (s, 3H, CH_3), 2.68 (t, 2H, J = 7.4 Hz), 1.67 (m, 2H, CH_2-), 1.35–1.20 (m, 12H, $(CH_2)_6$-), 0.85 (t, 3H, J = 6.9 Hz, CH_3); HRMS *m/z* calcd. for $C_{28}H_{34}N_2O$: 414.2671; found: 414.2670.

4-Ferrocenylvinyl-4′-methyl-2,2′-bipyridine 6 (ref. 4)

The title compound was prepared analogously as described for **3***a*, using **1** (2.76 g, 15 mmol) and ferrocenecarbaldehyde (3.21 g, 15 mmol) as starting materials, and was isolated as a red solid after flash chromatography on alumina with dichloromethane–methanol as the eluant (3.97 g); mp 156°C (dec.); ^{1}H NMR, δ: 8.53 (d, 1H, J = 5.2 Hz, H^6), 8.52 (d, 1H, J = 5.4 Hz, $H^{6'}$), 8.45 (d, 1H, J = 1.6 Hz, H^3), 8.27 (d, 1H, $H^{3'}$), 7.29 (dd, 1H, J = 5.2 and 1.7 Hz, H^5), 7.28 (d, 1H, J = 16.1 Hz, CH═), 7.15 (d, 1H, J = 4.9 Hz, $H^{5'}$), 6.73 (d, 1H, J = 16.1 Hz, CH═), 4.51 (t, 2H, J = 1.8 Hz, C_5H_4-), 4.33 (t, 2H, J = 1.8 Hz, C_5H_4-), 4.13 (s, 5H, C_5H_5), 2.42 (s, 3H, CH_3). Anal. calcd. for $C_{23}H_{20}N_2Fe$: C 72.65, H 5.30, N 7.37; found: C 72.22, H 5.17, N 7.45. HRMS *m/z*, calcd.: 380.0976; found: 380.0980.

4-Ruthenocenylvinyl-4′-methyl-2,2′-bipyridine 7

The title compound was prepared analogously as described for **3***a*, using **1** (1.5 g, 8.15 mmol) and ruthenocenecarbaldehyde (2.1 g, 8.15 mmol), and was isolated as a pale yellow solid after recrystallization from ethyl acetate–pentane (1.7 g); mp 120°C (dec.); ^{1}H NMR, δ: 8.50 (d, 1H, J = 4.8 Hz, H^6), 8.49 (d, 1H, J = 4.6 Hz, $H^{6'}$), 8.39 (d, 1H, J = 1.5 Hz, H^3), 8.25 (s, 1H, $H^{3'}$), 7.20 (dd, 1H, J = 5.1 and 1.7 Hz, H^5), 7.14 (d, 1H, J = 16.2 Hz, CH═), 7.12 (dd, 1H, J = 4.6 and 0.9 Hz, $H^{5'}$), 6.65 (d, 1H, J = 16.2 Hz, CH═), 4.90 (t, 2H, J = 1.7 Hz, C_5H_4-), 4.64 (t, 2H, J = 1.7 Hz, C_5H_4-), 4.52 (s, 5H, C_5H_5), 2.40 (s, 3H, CH_3). Anal. calcd. for $C_{23}H_{20}N_2Ru$: C 64.94, H 4.71, N 6.59; found: C 64.85, H 4.89, N 6.90.

4-Ferrocenylvinyl-4′-nonyl-2,2-bipyridine 8

To a stirred solution of freshly prepared LDA (6.0 mmol) in 10 mL THF at −78°C was added dropwise a solution of **1** (1.0 g, 5.4 mmol) in 50 mL THF. The red solution was stirred for 15 min at −78°C and 1 h at 0°C. A solution of ferrocenecarbaldehyde (1.16 g, 5.4 mmol) in 40 mL THF was added dropwise and the yellow-green solution was stirred for 2 h at 0°C. The reaction mixture was then cooled to −78°C and treated with 1.6 M butyllithium solution in hexane (3.8 mL, 6.1 mmol). After being stirred for 1 h at 0°C, octylbromide (1.05 g, 5.4 mmol) was slowly added and the solution was stirred for 2 h at 0°C and then overnight at 25°C. The mixture was quenched with 50 mL water, extracted with ethyl acetate (3 × 75 mL), dried over $MgSO_4$, and evaporated. The crude product was

© 1997 NRC Canada

Can. J. Chem. Downloaded from www.nrcresearchpress.com by 88.146.161.215 on 09/08/12
For personal use only.

purified by chromatography on alumina using ether–ethanol as the eluant. The resulting red oil was dissolved in 125 mL dry toluene, *p*-toluenesulfonic acid monohydrate (500 mg, 2.6 mmol) was added, and the mixture was refluxed for 4 h and then cooled to room temperature. The solution was washed with 100 mL saturated water solution of $NaHCO_3$, dried, and evaporated in vacuo. Recrystallization from ethyl acetate yielded **8** as red crystals (1.8 g); ^{1}H NMR, δ: 8.58 (d, 2H, J = 5.0 Hz, H^6 and $H^{6'}$), 8.43 (d, 1H, J = 1.5 Hz, H^3), 8.25 (d, 1H, J = 1.0 Hz, $H^{3'}$), 7.27 (d, 1H, J = 16.1 Hz, CH═), 7.27 (dd, 1H, J = 5.0 and 1.5 Hz, H^5), 7.15 (dd, 1H, J = 5.0 and 1.5 Hz, $H^{5'}$), 6.70 (d, 1H, J = 16.1 Hz, CH═), 4.50 (t, 2H, J = 1.8 Hz, C_5H_4-), 4.36 (t, 2H, J = 1.8 Hz, C_5H_4-), 4.14 (s, 5H, C_5H_5), 2.69 (t, 2H, J = 7.7 Hz, CH_2-), 1.69 (m, 2H, CH_2-), 1.40–1.10 (m, 12H, $(CH_2)_6$-), 0.86 (t, 3H, J = 7.0 Hz, CH_3). Anal. calcd. for $C_{31}H_{36}N_2Fe$: C 75.63, H 7.32, N 5.69; found: C 75.82, H 7.32, N 5.73.

4,4′-Bis[*p*-(*N*,*N*-dibutylamino)styryl]-2,2′-bipyridine 9

To a stirred solution of freshly prepared LDA (21 mmol) in 30 mL THF at −78°C was added slowly a solution of **1** (1.84 g, 10 mmol) in 75 mL THF. The red-brown solution was stirred for 1.5 h at −78°C. A solution of 4-(*N*,*N*-dibutylamino)benzaldehyde (4.66 g, 20 mmol) in 20 mL THF was then added dropwise and the yellow-green solution was stirred for 2 h at −78°C and then overnight at 25°C. The mixture was quenched with 100 mL water and extracted with CH_2Cl_2 (2 × 100 mL). The combined extract was dried over $MgSO_4$ and evaporated in vacuo. The crude product was purified by chromatography on silica gel with dichloromethane–methanol – ammonium hydroxide (100/5/1) as the eluant. The resulting diol was then dissolved in 250 mL toluene and treated with pyridinium *p*-toluene sulfonate (0.1 g, 0.4 mmol). The mixture was refluxed for 4 h, then cooled to room temperature, washed with saturated aqueous sodium bicarbonate, dried over $MgSO_4$, and evaporated in vacuo. Recrystallization from ethyl acetate yielded **9** as orange microcrystals (5.2 g); mp 140°C; ^{1}H NMR, δ: 8.60 (d, 2H, J = 5.1 Hz, $H^{6,6'}$), 8.46 (d, 2H, J = 1.1 Hz , $H^{3,3'}$), 7.42 (d, 4H, J = 8.8 Hz, C_6H_4-), 7.38 (d, 2H, J = 16.2 Hz, CH═), 7.33 (dd, 2H, J = 5.1 and 1.1 Hz, $H^{5,5'}$), 6.88 (d, 2H, J = 16.2 Hz, CH═), 6.63 (d, 4H, J = 8.8 Hz, C_6H_4-), 3.30 (t, 8H, J = 7.6 Hz, N-CH_2-), 1.59 (m, 8H, CH_2-), 1.36 (m, 8H, CH_2-), 0.96 (t, 12H, J = 7.3 Hz, CH_3). Anal. calcd. for $C_{42}H_{54}N_4$: C 82.04, H 8.85, N 9.11; found: C 81.96, H 8.73, N 8.94.

4,4′-Bis[p-[(*N*-methyl-*N*-octyl)amino]styryl]-2,2′-bipyridine 10

The title compound was prepared analogously as described for **9**, using **1** (1.84 g, 10 mmol) and 4-(*N*-methyl-*N*-octylamino)benzaldehyde (5.0 g, 20 mmol) as starting materials, and was isolated as orange microcrystals after recrystallization from ethyl acetate (5.0 g); mp 136°C; ^{1}H NMR, δ: 8.60 (d, 2H, J = 5.2 Hz, $H^{6,6'}$), 8.46 (s, 2H, $H^{3,3'}$), 7.44 (d, 4H, J = 8.8 Hz, C_6H_4-), 7.39 (d, 2H, J = 16.2 Hz, CH═), 7.33 (dd, 2H, J = 5.2 and 1.5 Hz, $H^{5,5'}$), 6.90 (d, 2H, J = 16.2 Hz, CH═), 6.67 (d, 4H, J = 8.8 Hz, C_6H_4-), 3.33 (t, 4H, J = 7.5 Hz, N-CH_2-), 2.97 (s, 6H, N-CH_3), 1.59 (m, 4H, CH_2-), 1.29 (m, 20H, $(CH_2)_5$-), 0.88 (t, 6H, J = 6.6 Hz, CH_3); HRMS *m/z*, calcd. for $C_{44}H_{58}N_4$: 642.4661; found: 642.470.

(*S*)-(+)-4,4′-Bis[*p*-[*N*-methyl-*N*-(2-methylbutyl)amino]-styryl]-2,2′-bipyridine 11

The title compound was prepared analogously as described for **9**, using **1** (1.48 g, 8 mmol) and 4-[*N*-methyl-*N*-(2-methylbutyl)amino]benzaldehyde (3.4 g, 16 mmol) as starting materials, and was isolated as yellow-orange microcrystals after recrystallization from ethanol (2.3 g); mp 184°C; $[\alpha]_D$ = +12 (c = 1.0, CH_2Cl_2); ^{1}H NMR, δ: 8.60 (d, 2H, J = 5.2 Hz, $H^{6,6'}$), 8.47 (s, 2H, $H^{3,3'}$), 7.44 (d, 4H, J = 8.9 Hz, C_6H_4-), 7.39 (d, 2H, J = 16.2 Hz, CH═), 7.33 (dd, 2H, J = 5.2 and 1.5 Hz, $H^{5,5'}$), 6.90 (d, 2H, J = 16.2 Hz, CH═), 6.67 (d, 4H, J = 8.9 Hz, C_6H_4-), 3.28 (dd, 2H, J = 14.6 and 6.8 Hz, N-CH_2-), 3.10 (dd, 2H, J = 14.6 and 7.9 Hz, N-CH_2-), 3.00 (s, 6H, N-CH_3), 1.86 (m, 2H, CH-), 1.46 (dq, 2H, CH_2-), 1.13 (dq, 2H, CH_2-), 0.91 (m, 2 × 6H, CH-CH_3 and CH_2-CH_3). Anal. calcd. for $C_{38}H_{46}N_4$: C 81.68, H 8.30, N 10.03; found: C 80.53, H 8.26, N 9.76. HRMS *m/z*, calcd: 558.3722; found: 558.368.

4,4′-Bis[*p*-(octyloxy)styryl]-2,2′-bipyridine 12

The title compound was prepared analogously as described for **9**, using **1** (1.50 g, 8.14 mmol) and 4-octyloxybenzaldehyde (3.81 g, 16.28 mmol) as starting materials, and was isolated as white microcrystals after recrystallization from ethyl acetate (1.0 g); mp 146°C; ^{1}H NMR, δ: 8.64 (d, 2H, J = 5.2 Hz, $H^{6,6'}$), 8.51 (d, 2H, J = 1.6 Hz, $H^{3,3'}$), 7.49 (d, 4H, J = 8.7 Hz, C_6H_4-), 7.41 (d, 2H, J = 16.3 Hz, CH═), 7.36 (dd, 2H, J = 5.2 and 1.6 Hz, $H^{5,5'}$), 6.98 (d, 2H, J = 16.3 Hz, CH═), 6.91 (d, 4H, J = 8.7 Hz, C_6H_4-), 3.98 (t, 4H, J = 6.6 Hz, O-CH_2-), 1.79 (m, 4H, CH_2-), 1.60–1.20 (m, 20H, $(CH_2)_5$-), 0.88 (t, 6H, J = 6.6 Hz, CH_3). Anal. calcd. for $C_{42}H_{52}N_2O_2$: C 81.78, H 8.50, N 4.54; found: C 81.20, H 8.54, N 4.27.

(*S*)-(+)-4,4′-Bis[*p*-[(2-methyl)butoxy]styryl]-2,2′-bipyridine 13

The title compound was prepared analogously as described for **9**, using **1** (1.19 g, 6.45 mmol) and 4-(2-methylbutoxy)benzaldehyde (2.48 g, 12.90 mmol) as starting materials, and was isolated as pale yellow microcrystals after recrystallization from ethyl acetate (0.8 g); mp > 200°C; ^{1}H NMR, δ: 8.64 (d, 2H, J = 5.2 Hz, $H^{6,6'}$), 8.51 (d, 2H, J = 1.7 Hz, $H^{3,3'}$), 7.49 (d, 4H, J = 8.7 Hz, C_6H_4-), 7.41 (d, 2H, J = 16.3 Hz, CH═), 7.36 (dd, 2H, J = 5.2 and 1.7 Hz, $H^{5,5'}$), 6.98 (d, 2H, J = 16.3 Hz, CH═), 6.91 (d, 4H, J = 8.7 Hz, C_6H_4-), 3.85 (dd, 4H, J = 9.0 and 6.0 Hz, O-CH_2-), 1.86 (m, 2H, CH-), 1.56 (m, 2H, CH_2-), 1.25 (m, 2H, CH_2-), 0.95 (t, 6H, J = 6.7 Hz, CH_3), 0.95 (t, 6H, J = 7.4 Hz, CH_3). Anal. calcd. for $C_{36}H_{40}N_2O_2$: C 81.16, H 7.47, N 5.26; found: C 80.33, H 7.58, N 5.23.

Acknowledgements

We thank the Conseil Régional de Bretagne for a grant to M.B., and the Ministère de l'Enseignement Supérieur et de la Recherche for a grant to T.R.

References

1. M. Bourgault, C. Mountassir, H. Le Bozec, I. Ledoux, G. Pucetti, and J. Zyss. J. Chem. Soc. Chem. Commun. 1623 (1993).

© 1997 NRC Canada

2. C. Dhénaut, I. Ledoux, I.D.W. Samuel, J. Zyss, M. Bourgault, and H. Le Bozec. Nature, **374**, 339 (1995).
3. P.D. Beer, O. Kocian, and R.J. Mortimer. J. Chem. Soc. Dalton. Trans. 3283 (1990).
4. P.K. Ghosh and T.G. Spiro. J. Am. Chem. Soc. **102**, 5543 (1980).
5 A. Ulman, C.S. Willand, W. Köhler, D.R. Robello, D.J. Williams, and L. Handley. J. Am. Chem. Soc. **112**, 7083 (1990).
6. R. Brette, D.A. Dunmur, N.J. Hindley, and C.M. Marson. J. Chem. Soc. Perkin Trans. 1, 775 (1993).
7. C.G. Griggs and D.J.H. Smith. J. Chem. Soc. Perkin Trans. 1, 3041 (1982).
8. D.K. Ellison and R.T. Iwamoto. Tetrahedron Lett. **24**, 31 (1983).
9. A. Juris, S. Campagna, I. Bidd, J.-M. Lehn, and R. Ziessel. Inorg. Chem. **27**, 4007 (1988).
10. O. Kocian, R.J. Mortimer, and P.D Beer. J. Chem. Soc. Perkin Trans. 1, 3203 (1990).
11. S. Castellano, H. Gunther, and S. Ebersole. J. Phys. Chem. **69**, 4166 (1965).
12. J.C. Calabrese, L.-T. Cheng, J.C. Green, S.R. Marder, and W. Tam. J. Am. Chem. Soc. **113**, 7227 (1991).
13. S.J. Valenty and G.L. Gaines, Jr. J. Am. Chem. Soc. **99**, 1285 (1977).
14. O. Hofer and K. Schlögl. J. Organomet. Chem. **13**, 443 (1968).

Can. J. Chem. Downloaded from www.nrcresearchpress.com by 88.146.161.215 on 09/08/12
For personal use only.

© 1997 NRC Canada

Ketene acetals from thermolysis of aryloxy methoxy oxadiazolines. Evidence for carbonyl ylide intermediates

Philippe Couture, Manal El-Saidi, and John Warkentin

Abstract: Thermolysis of oxadiazolines (**5**) in benzene at 110°C leads to ketene acetals (**11**) as minor products. Carbonyl ylide intermediates (**6**), and oxiranes (**7**), presumably in equilibrium with those ylides, are implicated as unstable precursors of the ketene acetals although none of the oxiranes (carbonyl protected α-lactones) were isolable and only one of the ketene acetals was isolable in pure form. The evidence points to the two-step sequence of thermolysis of oxadiazolines, namely, initial cycloreversion to N_2 and carbonyl ylide (**6**), rather than concerted fragmentation to N_2, acetone, and carbene (**12**). The first-formed ylide does fragment to carbene and acetone in a second step that competes with oxirane formation. A tentative mechanism for reaction of **7** with **12**, to afford **11**, is advanced.

Key words: carbonyl ylide, dioxy oxirane, ketene acetal, oxadiazoline.

Résumé : La thermolyse des oxadiazolines (**5**), dans le benzène à 110°C, conduit à des acétals de cétènes (**11**) comme produits mineurs. Des intermédiaires ylures de carbonyle (**6**), et les oxiranes (**7**) qui sont probablement en équilibre avec ces ylures, sont impliqués comme précurseurs instables des acétals de cétènes, même s'il n'est pas possible d'isoler d'oxiranes (α-lactones dont le carbonyle est protégé) et qu'un seul des acétals de cétènes a pu être isolé à l'état pur. Des données suggèrent que la thermolyse des oxadiazolines se fait en deux étapes, avec cycloréversion initiale en N_2 et en ylure de carbonyle (**6**), plutôt qu'une fragmentation concertée en N_2, acétone et carbène (**12**). L'ylure qui se forme en premier se fragmente en carbène et en acétone dans une deuxième étape qui est en compétition avec la formation de l'oxirane. On propose un mécanisme pour la réaction des produits **7** et **12** conduisant au produit **11**.

Mots clés : ylure de carbonyle, dioxy-oxirane, acétal de cétène, oxadiazoline.

[Traduit par la rédaction]

Can. J. Chem. Downloaded from www.nrcresearchpress.com by 92.62.229.171 on 09/08/12
For personal use only.

Introduction

2,2-Dialkoxy oxadiazolines (1–12) and 3,3-dialkoxy diazirines (13–16) are now established precursors of dialkoxycarbenes (**2a**). Methoxyphenoxycarbene (**2b**) also has been generated by the latter route (17). Oxadiazolines have the advantage of shelf stability, over corresponding diazirines (14–18) but, unlike the latter, the oxadiazolines are only converted thermally to those carbenes, Scheme 1. Photolysis of 2-alkoxy or 2,2-dialkoxy oxadiazolines with 300 nm light leads to diazoalkanes (**3**) (19–21).

The mechanism of thermolysis of oxadiazolines **1** has long been thought to involve successive fragmentation rather than a single step (8, 12, 21–25). The stepwise mechanism, Scheme 2, seemed likely, the first step being an orbital-symmetry-allowed [4π + 2π] cycloreversion analogous, except for its reverse sense, to the numerous and well-known 1,3-dipolar cycloadditions (26–31). Many, but not all, such cycloadditions appear to be concerted reactions (28). In the case of ylide **4**, the mechanism of the reverse reaction (with N_2 to form **1**) is not known, of course, because such cycloadditions do not occur.

Recently, Smith presented computational results to indicate that a dioxy oxadiazoline (**1**, $R^1 = R^3 = R^4 = Me$, R^2 = 3-butynyl) may thermolyze by a concerted mechanism, avoiding a carbonyl ylide intermediate altogether (32). While those results pertain to only one 2,2-dialkoxy oxadiazoline, the implication that concerted decomposition could be a more general feature of the chemistry of related oxadiazolines comes naturally to mind.[2] We now present evidence for carbonyl ylide intermediates **6**, and therefore for stepwise fragmentation of oxadiazolines **5**, Scheme 3. Evidence for the first carbonyl-protected α-lactones (**7**) as unstable intermediates is also presented.[3]

Methods, results, and discussion

Oxadiazolines **5** were prepared from the appropriate phenols and 2-acetoxy-2-methoxy-Δ^3-1,3,4-oxadiazoline (**8**), by the

Received October 31, 1996.

P. Couture, M. El-Saidi, and J. Warkentin.[1] Department of Chemistry, McMaster University, Hamilton, ON L8S 4M1, Canada.

[1] Author to whom correspondence may be addressed. Telephone: (905) 525-9140. Fax: (905) 522-2509. E-mail: warkent@mcmaster.ca

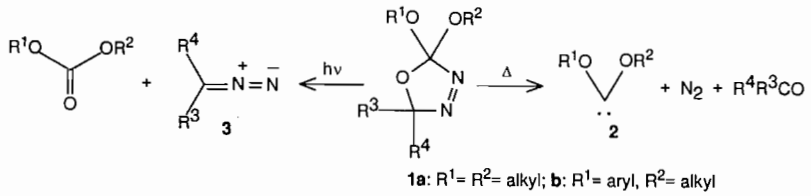
[2] Smith was careful to restrict his conclusions to the system that he had investigated (32).

[3] None of these compounds could be isolated. Given that they were present in very low concentration, together with other products at much higher concentration, it was impossible to gather any NMR data. Only GC–MS data could be obtained and therefore the structures were not established with the customary rigour.

© 1997 NRC Canada

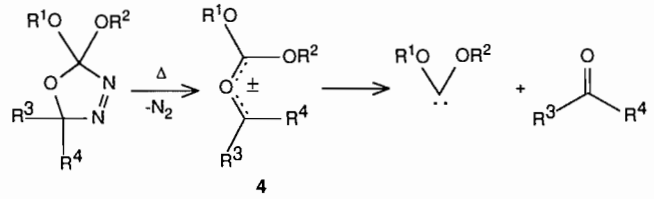
Can. J. Chem. Downloaded from www.nrcresearchpress.com by 92.62.229.171 on 09/08/12
For personal use only.

Scheme 1.

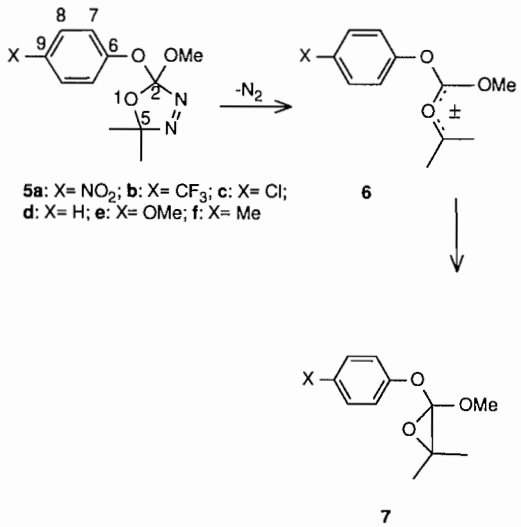


1a: $R^1 = R^2$ = alkyl; **b**: R^1 = aryl, R^2 = alkyl

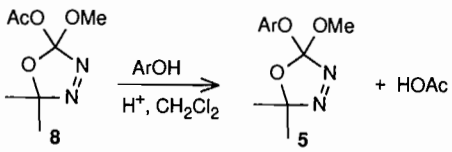
Scheme 2.



Scheme 3.



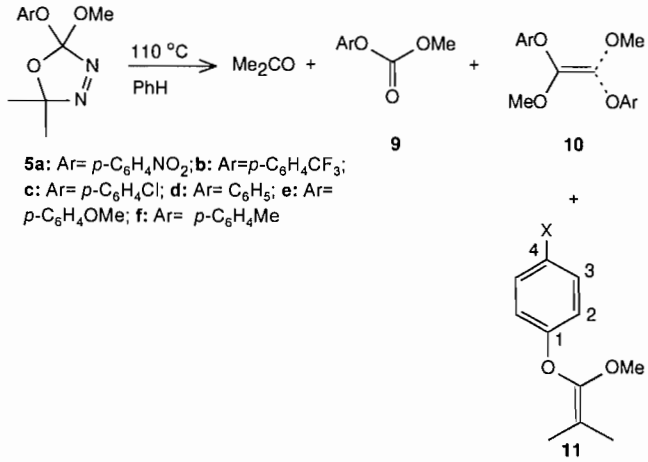
Scheme 4.



exchange method (7), Scheme 4. They were stable enough to be purified by chromatography on basic silica and their identities followed from their ^{13}C NMR spectra, which showed the C2 and C5 signals, at 134–136 and 120–121 ppm, respectively, characteristic of 2,2-dioxyoxadiazolines (8, 12, 33), indicating that the azo functional group was present. Thermolyses were carried out with benzene solutions of **5** (ca. 5×10^{-4} mol of **5** in 10 mL of benzene) sealed into glass tubes.

Thermolysis of **5a** resulted in a complex mixture of products, including carbonate **9a**, *E*- and *Z*-dimers (**10a**) of an apparent aryloxymethoxycarbene intermediate, and, in ca. 7% yield, ketene acetal **11a**, Scheme 5. While **11a**, like other ketene acetals, was sensitive to moisture, its hydrolysis to *p*-nitrophenol and methyl isobutyrate during chromatography (Chromatotron plate coated with SiO_2, pre-treated with Et_3N)

Scheme 5.



5a: Ar= *p*-$C_6H_4NO_2$; **b**: Ar=*p*-$C_6H_4CF_3$; **c**: Ar= *p*-C_6H_4Cl; **d**: Ar= C_6H_5; **e**: Ar= *p*-C_6H_4OMe; **f**: Ar= *p*-C_6H_4Me

Table 1. Partial ^1H NMR data ($CDCl_3$) of ketene acetals **11**.

	δ (OMe)	δ (Me)
11a	3.52	1.56, 1.75
11b	3.51	1.57, 1.74
11c	3.45	1.58, 1.72
11d	3.48	1.56, 1.75
11e	3.47	1.56, 1.74

was incomplete. This circumstance, undoubtedly attributable to the nitro group, permitted isolation of pure **11a** and acquisition of its ^1H and ^{13}C NMR spectra as well as a high-resolution mass spectrum. The ^1H NMR characteristics could then be used to infer the presence of less stable ketene acetals (**11b–11e**) in crude product mixtures from the corresponding oxadiazolines **5b–5e**. Those ketene acetals hydrolyzed too rapidly upon exposure to the atmosphere to permit their isolation by chromatography. Given their sensitivity, and the fact that they constituted less than 10% of the products, only partial ^1H NMR data, assigned by analogy to the ^1H NMR spectrum of **11a**, could be acquired. The available methoxy and methyl chemical shifts are listed in Table 1.

Gas chromatography did separate the ketene acetals (**11**) from other products, and mass spectra could be acquired by GC–MS. In each case a species with the mass of the molecular ion was observed as a relatively intense signal, comprising 18–36% of the intensity of the base peak. The latter corresponded, in each case, to M − 59. This pattern also is in keeping with a common connectivity, but the identity of the

© 1997 NRC Canada

Scheme 6.

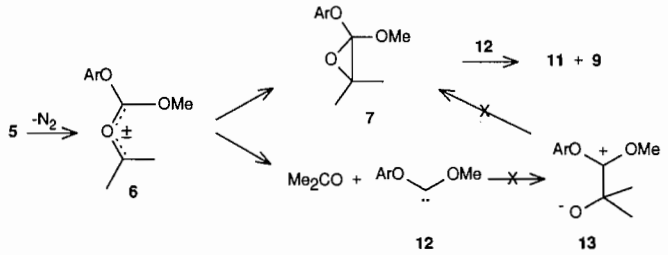


Table 2. Yields of products from **5c**.

	Yields (%)[a]			
$[\mathbf{5c}]_{initial}$ (mM)	Carbonate (**9c**)	Oxirane (**7c**)	Ketene acetal (**11c**)	Ratio (**11c**:**7c**)
36.5	16.7 ± 0.7	0.95 ± 0.07	2.89 ± 0.33	3.1
61.8	16.2 ± 0.5	0.63 ± 0.10	3.35 ± 0.24	5.4
83.9	15.9 ± 0.8	0.44 ± 0.19	3.42 ± 0.23	8.7
120	16.3 ± 0.6	0.39 ± 0.03	4.12 ± 0.20	10.5
154	16.8 ± 1.0	0.41 ± 0.03	4.54 ± 0.29	11.1
194	15.9 ± 0.4	0.40 ± 0.03	4.54 ± 0.15	11.3

[a]Yield numbers are averages ± standard deviation for five GC measurements on the same solution of crude thermolysate.

fragment giving rise to the M − 59 signal is not known. One possibility is that M − 59 is the cation $ArCMe_2$, formed by loss of MeO and CO from the molecular ion.

Given that a ketene acetal **11** is formed during thermolysis of each **5**, it was of interest to probe for their origin. The fact that the *gem* dimethyl portion of **5** is retained in **11** is strongly indicative of one or other of the mechanisms of Scheme 6. In the first of these, a carbonyl ylide (**6**) from [3+2] fragmentation of the oxadiazoline precursor cyclizes to the corresponding oxirane (**7**), thereby forming the new CC bond required for **11**. In the second mechanism, the carbonyl ylide fragments to carbene **12** and acetone. Subsequent attack of the carbene at the carbonyl carbon of acetone to afford dipole **13**, which cyclizes, or else direct [1+2] cycloaddition of **12** to acetone, leads to the same oxirane (**7**).

The basic mechanisms are distinguishable because one of them should result in incorporation of added acetone from solution. Precedents for attack of dialkoxycarbenes on acetone are unknown, although methoxymethylcarbene attacks acetone (25) and a vinylogous dialkoxycarbene does so as well (8). Two probes were applied with **5a**, one involving addition of acetone-d_6, and the other of cyclopentanone, to the solvent prior to thermolysis. In each case, the cross product expected if ketone from solution had been incorporated was not detectable. Thus the mechanism involving reaction of a free carbene intermediate (**12**) with acetone to form **13**, or a concerted attack of **12** on acetone to afford **7** directly, is unlikely to be correct, leaving the contentious (32) carbonyl ylide mechanism as the most obvious alternative.

The carbonyl ylide mechanism requires the intermediacy of oxiranes **7** ("acetals" of α-lactones), which are unknown as a class. Kopecky et al. (34) have considered tetramethoxyoxirane as a potential reactive intermediate from ozonolysis of tetramethoxyethylene. They were unable to detect it and concluded that it must be very short lived, even at −90°C, if it had actually been formed at all. In the present study it was possible (in five cases out of six) by means of GC, but not ^{1}H NMR, to see an intermediate to which we have tentatively assigned structure **7**. Each **5** except **5a** afforded a species that eluted ahead of the corresponding ketene acetal **11**. The mass spectra (GC–MS) of the species **7b–f** gave highest *m/z* signals, corresponding to dioxycarbene + H (aryloxymethoxymethyl cation) or for an isomeric structure, of course.

Experiments to support the assignment of the oxirane structure to **7** were based on the expectation that the yield ratio (**11**:**7**) might be sensitive to the initial concentration of oxadiazoline precursor. Compound **5c** was chosen, and thermolyses were carried out with the initial concentrations shown in Table 2, and with the same thermolysis time. The ratios of yields (**11c**:**7c**) were determined by GC, with ethyl benzoate as added standard. It is clear that the ratio increased, from about 3 to about 11, as a result of changing the initial oxadiazoline concentration from 36.5 to 194 mM. That is the expected trend[4] for a scenario in which **7**, by reaction with an intermediate from **5**, serves as the precursor of **11**. Yields of carbonate

[4] The kinetic scheme is complicated, but ketene acetal formation is of higher order in oxadiazoline than oxirane formation. Presumably the ratio is also time dependent, if **7** is only moderately stable at 110°C, and it was for this reason that the time was kept the same for the series of experiments.

© 1997 NRC Canada

Can. J. Chem. Downloaded from www.nrcresearchpress.com by 92.62.229.171 on 09/08/12
For personal use only.

Can. J. Chem. Downloaded from www.nrcresearchpress.com by 92.62.229.171 on 09/08/12
For personal use only.

9c were independent of initial oxadiazoline concentration, within experimental error, and much higher than expected if the only source of carbonate were deoxygenation of oxirane. The source of additional carbonate is under investigation at this time; competitive fragmentation of the oxadiazoline to diazopropane and carbonate is one possibility.

A simple mechanism, then, that accounts for the ketene acetal has the initial ylide formation of Scheme 6, and subsequent attack of carbene (**12**) on oxirane (**7**). Although there are precedents for deoxygenation of oxiranes by carbenes, the carbenes known to do so are electrophilic or ambiphilic species that attack at oxygen to afford an ylide intermediate (35). Nucleophilic carbenes might be expected to attack oxiranes at carbon. The carbenes in this study should range from nucleophilic to ambiphilic (14, 36–40). Unfortunately the yields were too low, with a large uncertainty as a consequence, to permit any inference about effects of substituents on the efficiency of ketene acetal formation.[5] We assume for simplicity that the carbene intermediates did attack corresponding oxiranes at oxygen, although a more complex mechanism can also accommodate the results.[6]

Carbene dimers (**10**) were formed with small *Z* vs. *E* discrimination as indicated in the Experimental. That is not a surprising result, for the coupling results in two new bonds and must therefore be very exothermic. Consequently the transition state should resemble starting material (41), with those new bonds only poorly developed and with only a moderate difference in steric hindrance between transition states leading to *Z* and *E* isomers. The fact that the *Z*:*E* ratio exceeds unity for the unsubstituted case and for some of the donor-substituted systems (GC data) was surprising, and suggests that there is a favourable nonbonded interaction between the aromatic rings at the transition state that can overcome the moderate steric hindrance for carbene coupling.

In summary, thermolysis of alkoxyaryloxyoxadiazolines **5** is a sequential process involving corresponding carbonyl ylide intermediates. A fraction of those ylides undergo fragmentation to acetone and the appropriate alkoxyaryloxycarbenes (**12**). The carbenes dimerize and presumably deoxygenate oxirane **7**, formed by electrocyclic ring closure of the ylides, to afford ketene acetals **11**, Scheme 6. Although it does not follow that dialkoxy oxadiazolines fragment by an analogous mechanism, it is possible to rationalize their chemistry in the same way, simply by recognizing that corresponding ylides probably fragment more rapidly, to afford more stabilized carbenes, and therefore afford oxiranes in undetectable (or zero) yields.

Experimental

General

^{1}H NMR spectra were obtained with Bruker instruments operating at 200, 300, or 500 MHz. ^{13}C NMR spectra were run on Bruker instruments operating at the frequencies indicated. Mass spectra (ei) were obtained with a Hewlett Packard MSD GC–MS and chemical ionization, as well as high-resolution mass spectra, with a ZAB-E double focusing instrument. MS peaks less intense than 5% of the base peak are not included unless they were of highest or next highest *m/z*, and fragments with *m/z* less than 55 are also excluded. Weak IR bands are not labelled; medium and strong bands have symbols m and s, respectively, attached.

Chromatography refers to elution from a layer of silica gel coated onto a glass plate in a Chromatotron apparatus.

Synthesis of 2-aryloxy-2-methoxy-Δ^3-1,3,4-oxadiazolines (**5**)

To a mixture of 2-acetoxy-2-methoxy-Δ^3-1,3,4-oxadiazoline (**8**, 0.9 g, 3.6 mmol) and acyclic isomer (7) (ca. 70% oxadiazoline) in CH_2Cl_2 (35 mL) was added the appropriate phenol (7.2 mmol) and acetic acid (1.0 mL). The resulting solution was refluxed for 72 h before it was cooled and most of the solvent was stripped off. KOH pellets (ca. 2.0 g) were added and, after stirring for 1 h, water (50 mL) was added to the heterogeneous mixture. After further stirring (10 min), the organic layer was separated and dried over $MgSO_4$. Evaporation of the solvent left **5**, in some cases in nearly pure form. Chromatography on SiO_2 was used in all cases to remove remaining impurities.

*2-Methoxy-5,5-dimethyl-2-(4-nitrophenoxy)-Δ^3-1,3,4-oxadiazoline (**5a**)*

Off-white solid, mp 55–57°C, yield 60%. ^{1}H NMR (200 MHz, $CDCl_3$) δ: 1.49 (s, 3H), 1.66 (s, 3H), 3.54 (s, 3H), 7.39 (d, 2H, ^3J = 9.3 Hz), 8.22 (d, 2H, ^3J = 9.3 Hz). ^{13}C NMR (50 MHz, $CDCl_3$) δ: 22.3 (Me), 22.5 (Me), 51.1 (OMe), 118.4 (C7), 120.3 (C5), 123.7 (C8), 134.3 (C2), 142.2 (C9), 155.8 (C6). MS (ei) *m/z* (rel. intensity): 236 (M^+ − OMe, 4), 180 (19), 150 (22), 129 (100), 122 (14), 108 (9), 92 (10), 73 (12), 59 (11). MS (ci, NH_3) *m/z*: 285 ($(M + NH_4)^+$,14) 182 (30), 152 (32), 129 (100), 110 (31), 60 (19).

*2-Methoxy-5,5-dimethyl-2-(4-trifluoromethylphenoxy)-Δ^3-1,3,4-oxadiazoline (**5b**)*

Oil, yield 58%. ^{1}H NMR (200 MHz, $CDCl_3$) δ: 1.42 (s, 3H), 1.62 (s, 3H), 3.55 (s, 3H), 7.34 (d, ^3J = 8.6 Hz, 2H), 7.57 (d, ^3J = 8.6 Hz, 2H).^{13}C NMR (50 MHz) δ: 23.9 (Me), 23.9 (Me), 52.5 (OMe), 120.1 (C5), 120.5 (C7), 124.1 (q, $^1J_{CF}$ = 271 Hz, CF_3), 126.2 (q, $^2J_{CF}$ = 33 Hz, C9), 126.6 (C8), 136.1 (C2), 154.7 (C6). ^{19}F NMR (282.4 MHz, ref. ext CF_3Cl) δ: −62.2. MS (ei, ZAB-E instrument) *m/z*: 290 (M^+, ca. 0.3%, clear signal at 300-fold amplification; CA on the fragment with *m/z* = 290 showed it to be linked to the base peak at *m/z* = 129), 275 (M^+ − Me, ca. 0.2%), 259 (9), 203 (23), 173 (95), 145 (21), 129 (100). MS (ci, NH_3) *m/z*: 308 ($(M + NH_4)^+$, 27), 261 (27), 220 (30), 205 (80), 203 (52), 188 (100), 171 (11), 129 (100), 58 (51).

*2-(4-Chlorophenoxy)-2-methoxy-5,5-dimethyl-Δ^3-1,3,4-oxadiazoline (**5c**)*

Oil, yield 68%. ^{1}H NMR (200 MHz, $CDCl_3$) δ: 1.35 (s, 3H) 1.59 (s, 3H), 3.58 (s, 3H), 7.14 (d, ^3J = 6.6 Hz, 2H), 7.27 (d, ^3J = 6.6 Hz, 2H). ^{13}C NMR (50 MHz, $CDCl_3$) δ: 23.8 (Me), 24.1 (Me), 52.5 (OMe), 120.8 (C5), 122.7 (C7), 129.2 (C8), 129.7

[5] It is also recognised that the yields of ketene acetals may be determined in part by other factors, such as competitions from other primary processes that consume **5**.

[6] For example, a carbene **12** could react with **7** in a nucleophilic ring-opening reaction that could lead to an oxetane. Fragmentation of the latter could then afford **11** and carbonate **9**.

© 1997 NRC Canada

Can. J. Chem. Downloaded from www.nrcresearchpress.com by 92.62.229.171 on 09/08/12
For personal use only.

(C9), 136.4 (C2), 150.6 (C6). MS (ei) for ^{35}Cl *m/z* (rel. intensity): 225 (M^+ − OMe, 7), 213 (11), 169 (32), 153 (22), 139 (55), 129 (100), 127 (42), 111 (30), 99 (40), 84 (39), 73 (49), 59 (24). MS (ci, NH_3) *m/z*: 276 ($(M + NH_4)^+$, 33) 274 (100), 227 (20), 225 (55), 204 (60), 186 (17), 171 (95), 169 (46).

*2-Methoxy-5,5-dimethyl-2-phenoxy-Δ^3-1,3,4-oxadiazoline (**5d**)*

Oil, yield 61%. ^1H NMR (200 MHz, $CDCl_3$) δ: 1.28 (s, 3H), 1.57 (s, 3H), 3.62 (s, 3H), 7.12–7.31 (m, 5H). ^{13}C NMR (50 MHz, $CDCl_3$) δ: 23.2 (Me), 23.8 (Me), 52.1 (OMe), 120.2 (C5), 121.3 (C7), 124.2 (C9), 128.9 (C8), 136.4 (C2), 151.7 (C6). MS (ei) *m/z* (rel. intensity): 191 (M^+ − OMe, 12), 179 ($M^+ - N_2$ − Me, 17), 162 (12), 153 (12), 135 (49), 129 (M^+ − OPh, 100), 119 (23), 105 (74), 94 (12), 77 (60). MS (ci, NH_3) *m/z*: 240 ($(M + NH_4)^+$, 5), 191 (3), 170 (24), 129 (100), 58 (19).

*2-Methoxy-2-(4-methoxyphenoxy)-5,5-dimethyl-Δ^3-1,3,4-oxadiazoline (**5e**)*

Oil, yield 68%. ^1H NMR (200 MHz, $CDCl_3$) δ: 1.22 (s, 3H), 1.54 (s, 3H), 3.63 (s, 3H), 3.78 (s, 3H), 6.80 (d, ^3J = 9.1 Hz, 2H), 7.08 (d, ^3J = 9.1 Hz, 2H). ^{13}C NMR (50 MHz, $CDCl_3$) δ: 23.3 (Me), 24.1 (Me), 52.3 (MeO at C2), 55.3 (ArOMe), 113.9 (C8), 120.1 (C5), 123.2 (C7), 136.8 (C2), 145.1 (C6), 156.6 (C9). MS (ei) *m/z* (rel. intensity): 221 (M^+ − Me, 27), 205, (M^+ − OMe, 42), 149 (100), 135 (33), 129, (58), 123 (45), 95 (15), 73 (44). MS (ci, NH_3) *m/z*: 221 (8), 200 (17), 167 (38), 149 (39), 129 (100), 124 (11), 58 (10).

*2-Methoxy-5,5-dimethyl-2-(4-methylphenoxy)-Δ^3-1,3,4-oxadiazoline (**5f**)*

Oil, yield 65%. ^1H NMR (200 MHz, $CDCl_3$) δ: 1.27 (s, 3H), 1.56 (s, 3H), 2.31 (s, 3H), 3.61 (s, 3H), 7.08 (s, 4H). ^{13}C NMR (50 MHz, $CDCl_3$) δ: 20.7 (Me), 23.6 (Me), 24.2 (Me), 52.5 (OMe), 120.4 (C5), 121.6 (C7), 129.6 (C8 and C9, signals also coincident in corresponding phenol), 134.2 (C2), 149.6 (C6), C9. MS (ei) *m/z* (rel. intensity): 205 (M^+ − OMe, 95), 199 ($M^+ - N_2$ − Me, 29), 176 (18), 149 (72), 129 (88), 119 (100), 107 (39), 91 (58), 73 (55). MS (ci, NH_3) *m/z*: 254 ($(M + NH_4)^+$, 10), 205 (5), 184 (42), 129 (100), 58 (28).

Thermolyses of oxadiazolines 5 and thermolysis products

A solution of an oxadiazoline (**5**, 0.5 mmol) in dry benzene (10 mL) was sealed into a glass tube after three cycles of freeze–pump–thaw degassing at 10^{-2} Torr (1 Torr = 133.3 Pa). The tube was kept in an oil bath at 110 ± 0.1°C for 24 h before it was opened at room temperature for stripping off solvent and volatile products with a rotary evaporator. Spectra of the residue, including GC–MS, were recorded before it was placed on a 1 mm silica plate for centrifugal chromatography, with 5–20% ethyl acetate in hexanes as eluting solvent. This procedure usually separated most of the aryl methyl carbonates (**9**) from the diaryloxydimethoxy ethylenes (**10**) but the latter were not always cleanly separated from one another. Only in the case of **5a** was the ketene acetal (**11a**) isolable by chromatography. The NMR spectra of the carbene dimers (below) are those of *E/Z* mixtures, except in cases where a separation was accomplished, and it is assumed that the isomer eluting first from silica or from GC columns was the *E* isomer, with zero dipole moment. The carbonates eluted first from silica gel followed closely by the *E* isomers, usually slightly contaminated with carbonate, and then by the *Z* isomers. Proton spectra of the carbonates could be subtracted from composite spectra. Some ^{13}C NMR signals were also assigned tentatively on the basis of relative intensities of signals from corresponding atoms of *E* and *Z* isomers, but others could not be assigned with confidence, in part because there was generally a shortfall from the number of signals expected, suggesting coincidence of some signals from *E* and *Z* isomers. Mass spectra of separated *E/Z* isomers were not significantly different and they are therefore not reported separately. Those spectra, by GC–MS, are not contaminated with signals from corresponding carbonates.

Thermolysis of 5a in the presence of acetone-d_6

The procedure described above was used with **5a** (50 mg, 0.19 mmol) and 0.44 g (6.9 mmol) of acetone-d_6 in enough benzene to make 6 mL of solution. In the ^1H NMR spectrum of **11a** in the crude product, the integral for each C-CH_3 signal was the same as the integral of the O-CH_3 signal, indicating non-incorporation of acetone from solution. The GC–MS of the product mixture was not distinguishable from that of the analogous mixture arising from reaction without added acetone-d_6.

Thermolysis of 5a in the presence of cyclopentanone

The procedure described above was used with **5a** (135 mg, 0.51 mmol) and cyclopentanone (92 mg, 1.1 mmol) in enough benzene to make 9 mL of solution. Analysis of the product mixture by means of ^1H NMR spectroscopy and GC–MS revealed **11a** but not the analogous compound from incorporation of cyclopentanone.

*1-Methoxy-2,2-dimethyl-1-(4-nitrophenoxy)ethylene (**11a**)*: IR (CCl_4) cm^{-1}: 1715m, 1612, 1594m, 1530s, 1492m, 1456, 1438, 1372, 1344s, 1263m, 1225s, 1207m, 1160m, 1124s, 1017m, 927, 863, 851m. ^1H NMR (200 MHz, $CDCl_3$) δ: 1.56 (s, 3H), 1.75 (s, 3H), 3.52 (s, 3H), 7.02–7.16 (m, 2H), 8.14–8.29 (m, 2H). ^{13}C NMR (50 MHz, $CDCl_3$) δ: 16.17 (2 × Me), 57.08 (OMe), 100.67(=*C*Me_2), 115.88 (Ar C2,6), 125.87 (Ar C3,5), 142.67 (Ar C4), 147.94 (=*C*(OR)(OMe)), 161.23 (Ar C1). MS (ei) *m/z*: 223 (M^+, 30), 208 (1), 180 (5), 164 (100), 148 (7), 136 (16), 118 (16), 106 (15), 91 (12), 85 (12), 76 (23), 70 (67), 63 (27). MS (ci, NH_3) *m/z*: 241 $(M + NH_4)^+$, 224 $(M + H)^+$. HRMS calcd. for $C_{11}H_{13}NO_4(M^+)$: 223.0845; found: 223.0845.

*1-Methoxy-2,2-dimethyl-1-(4-trifluoromethylphenoxy)ethylene (**11b**)*: GC–MS (ei) *m/z*: 246 (M^+, 36), 227 (14), 187 (100), 159 (83), 145 (42), 125 (18), 113 (17), 95 (19), 70 (50), 55 (25).

*1-(4-Chlorophenoxy)-1-methoxy-2,2-dimethylethylene (**11c**)*: GC–MS (ei) *m/z*: 214 (M^+ for ^{37}Cl, 7), 212 (M^+ for ^{35}Cl, 21), 197 (2), 169 (9), 155 (36), 153 (100), 142 (6), 127 (23), 125 (37), 111 (18), 99 (33), 85 (21), 75 (43), 70 (73), 63 (20), 63 (20), 55 (39).

*1-Methoxy-2,2-dimethyl-1-phenoxyethylene (**11d**)*: GC–MS (ei) *m/z*: 178 (M^+, 29), 135 (10), 119 (100), 107 (12), 91 (74), 77 (56), 65 (41), 55 (32).

© 1997 NRC Canada

Can. J. Chem. Downloaded from www.nrcresearchpress.com by 92.62.229.171 on 09/08/12
For personal use only.

*1-Methoxy-1-(4-methoxyphenoxy)-2,2-dimethylethylene (**11e**)*: GC–MS (ei) *m/z*: 208 (M^+, 18), 149 (100), 138 (6), 123 (41), 109 (16), 95 (21), 77 (19), 70 25), 63 (14), 55 (15).

*1-Methoxy-2,2-dimethyl-1-(4-methylphenoxy)ethylene (**11f**)*: GC–MS (ei) *m/z*: 192 (M^+, 26), 149 (9), 133 (100), 121 (8), 105 (55), 91 (23), 77 (31), 70 (28), 65 (19), 55 (16).

*2-Methoxy-3,3-dimethyl-2-(4-trifluoromethylphenoxy)oxirane (**7b**)*: GC–MS (ei) *m/z*: 205 (44), 162 (8), 145 (28), 113 (14), 75 (100).

*2-(4-Chlorophenoxy)-2-methoxy-3,3-dimethyloxirane (**7c**)*: GC–MS (ei) *m/z*: 173 (11), 171 (30), 154 (2), 130 (6), 128 (18), 113 (5), 111 (13), 101 (5), 99 (16), 75 (100), 65(8), 63 (14).

*2-Methoxy-3,3-dimethyl-2-phenoxyoxirane (**7d**)*: GC–MS (ei) *m/z*: 137 (79), 109 (12), 94 (36), 77 (58), 75 (100), 65 (46).

*2-Methoxy-2-(4-methoxyphenoxy)-3,3-dimethyloxirane (**7e**)*: GC–MS (ei) *m/z*: 167 (42), 152 (2), 139 (14), 124 (36), 109 (30), 95 (17), 81 (18), 75 (100), 63 (18).

*2-Methoxy-3,3-dimethyl-2-(4-methylphenoxy)oxirane (**7f**)*: GC–MS (ei) *m/z*: 151 (54), 123 (15), 107 (27), 91 (27), 75 (100), 65 (13).

*1,2-Dimethoxy-1,2-di(4-nitrophenoxy)ethylene (**10a**)*
Viscous oil, yield 52%. *Z:E* ratio 1:3.1 by ^{1}H NMR. Isomers separated by chromatography. ^{1}H NMR (200 MHz, $CDCl_3$) (*Z* isomer) δ: 3.61 (s, 3H), 7.22 (d, ^3J = 9.2 Hz, 2H), 8.29 (d, ^3J = 9.2 Hz, 2H); (*E* isomer) δ: 3.77 (s, 3H), 7.11 (d, ^3J = 9.2 Hz, 2H), 8.21 (d, ^3J = 9.2 Hz, 2H). ^{13}C NMR of isomer mixture (50 MHz, $CDCl_3$) δ: 58.4 (OMe, *Z*), 58.8 (OMe, *E*), 116.0, 125.7, 138.1, 143.2, 160.3, 160.7. MS (ei) *m/z* (rel. intensity): 362 (M^+, 53), 347 (M^+ − Me, 100), 331 (11), 319 (29), 240 (31) 182 (100), 122 (8), 75 (7). MS (ci, NH_3) *m/z*: 380 (($M + NH_4$)$^+$, 100), 294 (15), 182 (25), 133 (25). HRMS calcd. for $C_{16}H_{14}N_2O_8$: 362.0750; found: 362.0751.

*1,2-Dimethoxy-1,2-di(4-trifluoromethylphenoxy)ethylene (**10b**)*
Oil, yield 57%. *Z:E* ratio 1:1.4 by ^{1}H NMR; 1:1.7 by GC. ^{1}H NMR of separate isomers (200 MHz, $CDCl_3$) (*Z* isomer) δ: 3.59 (s, 3H), 7.21 (d, ^3J = 8.4 Hz, 2H), 7.64 (d, ^3J = 8.4 Hz, 2H); (*E* isomer) δ: 3.74 (s, 3H), 7.10 (d, ^3J = 8.5 Hz, 2H), 7.56 (d, ^3J = 8.5 Hz, 2H). ^{13}C NMR of mixture (50 MHz, $CDCl_3$) δ: 58.2 (OMe, *Z*), 58.5 (OMe, *E*), 117.2 , 120.1, 138.2, 154.5, signals from carbons coupled to ^{19}F not identified. ^{19}F NMR (282.4 MHz, $CDCl_3$, rel. ext CF_3Cl) δ: −62.2. MS (ei) *m/z* (rel. intensity): 408 (M^+, 50), 393 (M^+ − Me, 29), 365 (22), 335 (10), 263 (90), 205 (100), 145 (28). MS (ci, NH_3) *m/z*: 409 ((M^+ + H), 15), 263 (25), 205 (100), 118 (25), 60 (83). HRMS calcd. for $C_{18}H_{14}F_6O_4$: 408.0796; found: 408.0796.

*1,2-Di(4-chlorophenoxy)-1,2-dimethoxyethylene (**10c**)*
Oil, yield 56%. *Z:E* ratio 1:1.1 by ^{1}H NMR; 1:1.7 by GC. ^{1}H NMR (200 MHz, $CDCl_3$) δ: 3.57 (s, OMe, *Z*), 3.71 (s, OMe, *E*), 6.97 (d, ^3J = 9.1 Hz, *E*), 7.06 (d, ^3J = 9.1 Hz, *Z*), 7.24 (d, ^3J = 9.1 Hz, *E*), 7.31 (d, ^3J = 9.1 Hz, *Z*). ^{13}C NMR (50 MHz, $CDCl_3$) δ: 57.9 (OMe, *Z*), 58.1 (OMe, *E*), 117.1, 127.6, 127.7, 129.2, 129.3, 138.1, 154.6, 154.9. MS (ei) *m/z* (rel. intensity): 344 (M^+, 2 × ^{37}Cl, 4), 342 (M^+, ^{37}Cl and ^{35}Cl, 18), 340 (M^+, 2 × ^{35}Cl, 25), 329 (5), 327 (22), 325 (34), 301 (10), 299 (45), 297 (67), 238 (13), 236 (9), 229 (11), 218 (8), 203 (6), 197 (7), 175 (9), 168 (6), 155 (6), 144 (7), 142 (22), 129 (14), 127 (42), 113 (34), 111 (100), 101 (15), 99 (46), 75 (56), 63 (15), 59 (34).

*1,2-Dimethoxy-1,2-diphenoxyethylene (**10d**) (17)*
Oil, yield 46%. Isomers (both oils) separated by chromatography. *Z:E* ratio 1:0.78 by ^{1}H NMR; 1:0.83 by GC. ^{1}H NMR (200 MHz, $CDCl_3$) (*Z* isomer) δ: 3.59 (s, 3H), 7.02–7.43 (m, 5H); (*E* isomer) δ: 3.73 (s, 3H), 6.98–7.35 (m, 5H). ^{13}C NMR of mixture (50 MHz, $CDCl_3$) δ: 57.9 (s, OMe, *E*), 58.1 (s, OMe, *E*), 115.7, 115.9, 122.6, 122.9, 129.3, 129.4, 138.2, 155.8, 156.1. MS (ei) *m/z* (rel. intensity): 272 (M^+, 17), 257 (M^+ − Me, 30), 229 (37), 195 (6), 170 (16), 152 (17), 141 (7), 108 (11), 93 (10), 77 (100), 65 (26), 59 (19). MS (ci, NH_3) *m/z*: 273 ((M^+ + 1), 100), 257 (10), 229 (9), 195 (20), 137 (23). HRMS calcd. for $C_{16}H_{16}O_4$: 272.1049; found: 272.1044.

*1,2-Dimethoxy-1,2-di(4-methoxyphenoxy)ethylene (**10e**)*
Oil, yield 57%. *Z:E* ratio 1:0.49 by ^{1}H NMR; 1:0.94 by GC. ^{1}H NMR (200 MHz, $CDCl_3$) δ: 3.60 (s, OMe, *Z*), 3.71 (s, OMe, *E*), 3.78 (s, OMe of Ar, *E*), 3.80 (s, OMe of Ar, *Z*), 6.65 (d, ^3J = 9.1 Hz, *E*), 6.74 (d, ^3J = 9.1 Hz, *Z*), 6.87 (d, ^3J = 9.1 Hz, *E*), 6.95 (d, ^3J = 9.1 Hz, *Z*). ^{13}C NMR (50 MHz, $CDCl_3$) δ: 55.4, 57.8, 58.0, 114.3, 114.5, 116.7, 116.9, 138.4, 149.7, 149.9, 155.1. MS (ei) *m/z* (rel. intensity): 332 (M^+, 34), 317 (M^+ − Me, 27), 289 (72), 257 (6), 230 (19), 225 (8), 215 (8), 198 (7), 193 (21),187 (5), 165 (11), 151 (9), 138 (18), 135 (22), 123 (100), 107 (16), 95 (26), 92 (47), 77 (48), 64 (21), 59 (9). MS (ci, NH_3) *m/z*: 331 ((M^+ + H), 100), 289 (10), 167 (40). HRMS calcd. for $C_{18}H_{20}O_6$: 332.1260; found: 332.1264.

*1,2-Dimethoxy-1,2-di(4-methylphenoxy)ethylene (**10f**)*
Oil, yield 60%. *Z:E* ratio 1:0.76 by ^{1}H NMR; 1:0.90 by GC. ^{1}H NMR (200 MHz, $CDCl_3$) δ: 2.30 (s, Me, *E*), 2.33 (s, Me, *Z*), 3.58 (s, OMe, *Z*), 3.70 (s, OMe, *E*), 6.92 (d, ^3J = 8.8 Hz), 7.01 (d, ^3J = 8.8 Hz), 7.04 (d, ^3J = 8.8 Hz), 7.08 (d, ^3J = 8.8 Hz). ^{13}C NMR (50 MHz, $CDCl_3$) δ: 20.2, 57.6, 57.8, 115.5, 115.6, 129.6, 129.7, 131.7, 131.8, 138.1, 154.0, 154.1. MS (ei) *m/z* (rel. intensity): 300 (M^+, 32), 285 (33), 257 (100), 225 (9), 209 (13), 198 (31), 177 (18), 166 (16), 149 (8), 135 (6), 122 (22), 107 (40), 91 (99), 77 (36), 65 (50), 59 (15). MS (ci, NH_3) *m/z*: 301 ((M^+ + H), 100), 285 (20), 257 (15), 209 (40), 193 (12), 151 (100), 108 (10). HRMS calcd. for $C_{18}H_{20}O_4$: 300.1362; found: 300.1375.

*Carbonates (**9**) and methyl isobutyrate*
Identification of the carbonates in question by GC–MS and by ^{1}H NMR spectroscopy was routine. **9a**: ^{1}H NMR (200 MHz, $CDCl_3$) δ: 3.96 (s, 3H), 7.39 (d, ^3J = 9.2 Hz, 2H), 8.30 (d, ^3J = 9.2 Hz). MS (ei) *m/z* (rel. intensity): 197 (M^+, 4), 153 (4), 123 (100), 107 (5), 95 (19), 92 (24), 77 (20), 63 (42), 59 (21). **9b**: ^{1}H NMR (200 MHz, $CDCl_3$) δ: 3.94 (s, 3H), 7.33 (d, ^3J = 8.5 Hz, 2H), 7.68 (d, ^3J = 8.5 Hz, 2H). MS (ei) *m/z* (rel. intensity): 220 (M^+, 32), 201 (14), 176 (100), 161 (9), 157 (49), 145 (80), 133 (95), 127 (30), 113, (80), 107 (12), 96 (25), 90 (18), 83 (51), 79 (24), 75 (22), 71 (13), 63 (41), 59 (37). **9c**: ^{1}H NMR (200 MHz, $CDCl_3$) δ: 3.92 (s, 3H), 7.12 (d, ^3J = 9.0 Hz, 2H),

© 1997 NRC Canada

7.36 (d, ^3J = 9.0 Hz, 2H). MS (ei) *m/z* (rel. intensity): 188 (M^+ for ^{37}Cl, 9), 186 (24), 144 (13), 142 (40), 129 (20), 127 (66), 113 (6), 111 (15), 101 (33), 99 (100), 75 (25), 73 (33), 63 (31), 59 (13). **9d**: ^1H NMR (200 MHz, $CDCl_3$) δ: 3.92 (s, 3H), 7.1–7.5 (m, 5H). MS (ei) *m/z* (rel. intensity): 152 (M^+, 30), 108 (25), 93 (16), 78 (66), 65 (100), 59 (13). **9e**: ^1H NMR (200 MHz, $CDCl_3$) δ: 3.82 (s, 3H), 3.91 (s, 3H), 6.8–7.2 (m, 4H). MS (ei) *m/z* (rel. intensity): 182 (M^+, 20), 138 (6), 123 (100), 107 (3), 95 (55), 80 (7), 77 (6), 63 (12), 59 (8). **9f**: ^1H NMR (200 MHz, $CDCl_3$) δ: 2.36 (s, 3H), 3.91 (s, 3H), 6.75–7.20 (m, 4H). MS (ei) *m/z* (rel. intensity): 166 (M^+, 36), 121 (51), 107 (55), 91 (30), 77 (100), 63 (16), 59 (15). Methyl isobutyrate: ^1H NMR (200 MHz, $CDCl_3$) δ: 1.18 (d, ^3J = 7.0 Hz, 6H), 2.58 (sept, ^3J = 7.0 Hz, 1H), 3.69 (s, 3H).

Acknowledgments

Financial support from the Natural Sciences and Engineering Research Council of Canada (NSERC) is gratefully acknowledged. Dr. Richard Smith and Mr. Fajar Ramelan acquired the high-resolution mass spectra and some other mass spectra. We are indebted to Prof. J.K. Terlouw and Dave Lavorato who took special care to obtain the mass spectrum of **5b**. Dr. Don Hughes and Mr. Brian Sayer assisted with the ^{19}F NMR spectra. M. E.-S. was the recipient of a Canadian International Development Agency scholarship and P.C. held an Ontario Graduate Scholarship award.

References

1. A. de Meijere, S.I. Kozhushkov, D.S. Yufit, R. Boese, T. Haumann, D.L. Pole, P.K. Sharma, and J. Warkentin. Liebigs Ann. 601 (1996).
2. R. González, F. Wudl, D.L. Pole, P.K. Sharma, and J. Warkentin. J. Org. Chem. **61**, 5837 (1996).
3. D.L. Pole, P.K. Sharma, and J. Warkentin. Can. J. Chem. **74**, 1335 (1996).
4. D. Suh, D.L. Pole, J. Warkentin, and J.K. Terlouw. Can. J. Chem. **74**, 544 (1996).
5. D.L. Pole and J. Warkentin. Liebigs Ann. 1907 (1995).
6. F. Diederich, L. Isaacs, and D. Philp. Chem. Soc. Rev. 243 (1994).
7. K. Kassam, D.L. Pole, M. El-Saidi, and J. Warkentin. J. Am. Chem. Soc. **116**, 1161 (1994).
8. K. Kassam and J. Warkentin. J. Org. Chem. **59**, 5071 (1994).
9. W.W. Win, M. Kao, M. Eiermann, J.J. McNamara, F. Wudl, D.L. Pole, K. Kassam, and J. Warkentin. J. Org. Chem. **59**, 5871 (1994).
10. T. Wong, J. Warkentin, and J.K. Terlouw. Int. J. Mass Spectrom. Ion Processes, **115**, 33 (1992).
11. L. Isaacs and F. Diederich. Helv. Chim. Acta, **76**, 2454 (1993).
12. M. El-Saidi, K. Kassam, D.L. Pole, T. Tadey, and J. Warkentin. J. Am. Chem. Soc. **114**, 8751 (1992).
13. C.-S. Ge, E.A. Jefferson, and R.A. Moss. Tetrahedron Lett. **34**, 7549 (1993).
14. R.A. Moss, M. Włostowski, S. Shen, K. Krogh-Jespersen, and A. Matro. J. Am. Chem. Soc. **110**, 4443 (1988).
15. R.A. Moss, S. Shen, and M. Włostowski. Tetrahedron Lett. **29**, 6417 (1988).
16. X.-M. Du, H. Fan, J.L. Goodman, M.A. Kesselmayer, K. Krogh-Jespersen, J.A. LaVilla, R.A. Moss, S. Shen, and R.S. Sheridan. J. Am. Chem. Soc. **112**, 1920 (1990).
17. R.A. Moss, M. Włostowski, J. Terpinski, G. Kmiecik-Lawrynowicz, and K. Krogh-Jespersen. J. Am. Chem. Soc. **109**, 3811 (1987).
18. J. Włostowska, R.A. Moss, W. Guo, and M.J. Chang. J. Chem. Soc. Chem. Commun. 432 (1982).
19. J.P. Pezacki, B.D. Wagner, C. Lew, J. Warkentin, and J. Lusztyk. J. Am. Chem. Soc. **119**, 1789 (1997).
20. W. Adam and R. Finzel. Tetrahedron Lett. 863 (1990).
21. M.W. Majchrzak, M. Békhazi, I. Tse-Sheepy, and J. Warkentin. J. Org. Chem. **54**, 1842 (1989).
22. P. Sharma and J. Warkentin. Tetrahedron Lett. **36**, 7591 (1995).
23. M. Békhazi, W. Lawrynowicz, and J. Warkentin. Can. J. Chem. **69**, 1398 (1991).
24. M.W. Majchrzak and J. Warkentin. Can. J. Chem. **67**, 1753 (1989).
25. M. Békhazi and J. Warkentin. J. Am. Chem. Soc. **105**, 1289 (1989).
26. T. Golz, S. Hammes, and F.-G. Klärner. Chem. Ber. **126**, 485 (1993).
27. R. Huisgen. 1,3-Dipolar Cycloadditions. *In* 1,3-Dipolar cycloaddition chemistry. *Edited by* A. Padwa. Wiley–Interscience, New York. 1984. pp. 1–176 .
28. R. Huisgen. Pure Appl. Chem. **53**, 171 (1981).
29. R. Huisgen. Pure Appl. Chem. **52**, 2283 (1980).
30. K.N. Houk, N.G. Rondan, C. Santiago, C.J. Gallo, R.W. Gandour, and G.W. Griffin. J. Am. Chem. Soc. **102**, 1504 (1980).
31. R. Huisgen and S. Sustmann. Heterocycles, **5**, 141 (1976).
32. W.B. Smith. J. Org. Chem. **60**, 7456 (1995).
33. H. Tomioka, K. Hirai, and T. Nakayama. J. Am. Chem. Soc. **115**, 1285 (1993).
34. K.R. Kopecky, J. Molina, and R. Rico. Can. J. Chem. **66**, 2234 (1988).
35. C.J. Shields and G.B. Schuster. Tetrahedron Lett. **28**, 853 (1987).
36. R.A. Moss, C.-S. Ge, J. Włostowska, E.G. Jang, E.A. Jefferson, and H. Fan. Tetrahedron Lett. **36**, 3083 (1995).
37. R.A. Moss, S. Xue, W. Liu. J. Am. Chem. Soc. **116**, 1583 (1994).
38. R.A. Moss. Acc. Chem. Res. **22**, 15 (1989).
39. R.S. Sheridan, R.A. Moss, B.K. Wilk, S. Shen, M. Włostowski, M.A. Kesselmayer, R. Subramanian, G. Kmiecik-Lawrynowicz, and K. Krogh-Jespersen. J. Am. Chem. Soc. **110**, 7563 (1988).
40. R.A. Moss, S. Shen, L.M. Hadel, G. Kmiecik-Lawrynowicz, J. Włostowska, and K. Krogh-Jespersen. J. Am. Chem. Soc. **109**, 4341 (1987).
41. G.S. Hammond. J. Am. Chem. Soc. **77**, 334 (1955).

Can. J. Chem. Downloaded from www.nrcresearchpress.com by 92.62.229.171 on 09/08/12
For personal use only.

© 1997 NRC Canada

Spectroscopic and crystallographic studies of phosphino adducts of gallium(III) iodide

Martyn A. Brown, Jesus A. Castro, and Dennis G. Tuck

Abstract: The solid state structures of the compounds $GaI_3 \cdot PPh_3$ and $Ga_2I_6 \cdot$dppe (dppe = 1,2-bis(diphenylphosphino)ethane) have been determined. For the former, in which the GaI_3P core has C_{3v} symmetry, the structure is trigonal, with a = 14.961(2) Å, c = 16.509(3) Å, V = 3199.5(4) Å^3, Z = 6, space group $R\bar{3}$. In $Ga_2I_6 \cdot$dppe, the ligand bridges two GaI_3P centres; the structure is monoclinic, a = 10.196(7) Å, b = 15.363(1) Å, c = 23.027(9) Å, β = 98.735(4)°, V = 3565.1(3.2) Å^3, Z = 4, space group $P2_{1/n}$. The use of ^{31}P NMR spectroscopy shows that $GaI_3 \cdot PPh_3$ is slightly dissociated in nonaqueous solution, and the effect of adding Ph_3P or I^- has been investigated. Similar studies with $Ga_2I_6 \cdot$dppe are also reported. In each system, four-coordination at gallium is dominant; an equally important factor is the dimerization of uncomplexed GaI_3 to Ga_2I_6 in these solutions.

Key words: gallium(III) iodide, complexes, phosphorus, NMR, crystallography.

Résumé : On a déterminé les structures des composés $GaI_3 \cdot PPh_3$ et $Ga_2I_6 \cdot$dppe (dppe = 1,2-bis(diphénylphosphino)éthane) à l'état solide. Dans le cas du premier composé, dans lequel la symétrie du groupe GaI_3P fondamental est C_{3v}, la structure est trigonale, groupe d'espace $R\bar{3}$, avec a = 14,961(2) et c = 16,509(3) Å, V = 3199,5(4) Å^3 et Z = 6. Dans le composé $Ga_2I_6 \cdot$dppe, le coordinat fait le pont entre deux centres GaI_3; la structure est monoclinique, groupe d'espace $P2_{1/n}$, avec a = 10,196(7), b = 15.363(1) et c = 23.027(9) Å , β = 98,735(4)°, V = 3565,1(3.2) Å^3 et Z = 4. La spectroscopie RMN du ^{31}P permet de démontrer que le $GaI_3 \cdot PPh_3$ est légèrement dissocié en solution non aqueuse et d'étudier l'effet de l'addition de PPh_3 ou de I^- sur cette dissociation. On a aussi effectué des études semblables avec le $Ga_2I_6 \cdot$dppe. Dans chacun de ces systèmes, le gallium tétracoordinant est dominant; un facteur qui est aussi important est la dimérisation du GaI_3 non-complexé en Ga_2I_6 dans ces solutions.

Mots clés : iodure de gallium(III), complexes, phosphore, RMN, cristallographie.

[Traduit par la rédaction]

Introduction

The adducts formed by the trihalides of the Group III elements (B, Al, Ga, In, Tl) with neutral or anionic donors have played a fundamental role in the overall development of coordination chemistry, and a variety of investigations have established the basic features of both the solid state and solution chemistry. In a recent paper (1), we used multinuclear NMR spectroscopy and X-ray crystallography to extend the understanding of the behaviour of the InI_3/Ph_3P system, and showed that the 1:1 and 1:2 complexes are closely related in their solution and crystal chemistry, and that both four- and five-coordinate adducts can be formed. With InI_3/dppe (dppe = bis(diphenylphosphino)ethane) the 1:1 adduct is a five-coordinate linear polymer, but four-coordinate species are important in solution.

In addition to the intrinsic interest of such complexes, their solution chemistry is germane to that of *ortho*- and *para*-quinone complexes, currently under investigation in this laboratory. An important factor in all of these studies is the effect of the size, and hence maximum coordination number, of the metallic elements in question, and it therefore seemed reasonable to investigate the chemistry of gallium compounds analogous to the indium species discussed in ref. 1. We have identified significant differences in the behaviour of these two groups of compounds in both the solid and solution state.

Two earlier investigation of GaI_3/Ph_3P and GaI_3/dppe systems have been reported. Balls, Greenwood, and Straughan (2) prepared a number of phosphino derivatives of the gallium(III) halides, and analysed the infrared spectra, while Carty (3, 4) used both infrared and conductivity measurements in attempts to identify the structures of these compounds in the solid state and in solution.

Received November 1, 1996.

M.A. Brown, J.A. Castro,[1] and D.G. Tuck.[2] Department of Chemistry and Biochemistry, University of Windsor, Windsor, ON N9B 3P4, Canada.

[1] Permanent address: Departamento de Quimica Pura y Aplicada, Universidade de Vigo, 36200 Vigo, Galicia, Spain.

[2] Author to whom correspondence may be addressed. Telephone: (519) 253-4232, ext. 3541. Fax: (519) 973-7098. E-mail: DGTuck@uwindsor.ca

Experimental section

General techniques

Gallium(III) iodide was prepared by reacting gram quantities of the elements in refluxing xylene. Triphenylphosphine and bis(diphenylphosphino)ethane (Aldrich) were recrystallized before use. Solvents were distilled from suitable drying agents, and stored over molecular sieves.

Phosphorus-31 NMR spectra were recorded on a Bruker 300 instrument, operating at 81.0 MHz, with 85% H_3PO_4 = 0. Infrared spectra were run on a Nicolet 4DX instrument, and the Raman spectra of finely ground solids were recorded with a Jobin Yvon S3000 spectrometer. Microanalysis was by Canadian Microanalytical Services Ltd.

© 1997 NRC Canada

Can. J. Chem. Downloaded from www.nrcresearchpress.com by 92.62.229.171 on 09/08/12
For personal use only.

Table 1. Summary of crystal data, intensity collection, and structural refinement.

	1	2
Chemical formula	$C_{18}H_{15}GaPI_3$	$C_{26}H_{24}Ga_2P_2I_6$
M	712.72	1299.29
Crystal system	Trigonal	Monoclinic
Space group	$R\bar{3}$ (No.148)	$P2_{1/n}$ (No. 14)
a/Å	14.961(2)	10.196(7)
b/Å	14.961(6)	15.363(11)
c/Å	16.509(3)	23.027(9)
β (deg)	90.00	98.735(54)
V/Å^3	3199.5(4)	3565.1(3.2)
Z	6	4
F(000)	1968	2160
D_c/g cm^{-3}	2.22	2.42
Crystal dimensions/mm	0.1 × 0.1 × 0.1	0.1 × 0.2 × 0.3
Absorption coeff/cm^{-1}	57.05	68.14
2θ° (max)	50	50
Total reflections measured	1379	6938
Unique data used	1253	6545
T/°C	23	23
No. of parameters	71	196
R	0.040	0.063
R_w	0.034	0.058
Max. shift/error in final cycle	0.16	0.07
Max., min. peaks in final difference map/e Å^{-3}	+0.67, −0.67	+1.47, −1.54

Can. J. Chem. Downloaded from www.nrcresearchpress.com by 92.62.229.171 on 09/08/12
For personal use only.

Preparative

Triphenylphosphine adduct: the procedure involved mixing solutions of GaI_3 and PPh_3 in toluene, following the method of Carty (3). The precipitate was recrystallized from toluene. Anal. calcd. for $C_{18}H_{15}GaPI_3$: C 30.3, H 2.12; found: C 30.7, H 2.17.

Immediate precipitation occurred when ethyl acetate solutions of GaI_3 (0.45 g, 1 mmol) and dppe (0.20 g, 0.5 mmol) were mixed, and the product, Ga_2I_6·dppe, was collected, washed, and recrystallized from the same solvent. Anal. calcd. for $C_{26}H_{24}Ga_2P_2I_6$: C 24.0, H 1.86; found: C 24.2, H 2.01.

Crystallographic analysis

(*i*) In the study of GaI_3·PPh_3, **1**, a colourless crystal mounted on a glass fibre was sited in a Rigaku AFC6S diffractometer, equipped with graphite-monochromated Mo-Kα radiation (λ = 0.71069 Å) and a rotating anode generator. Cell constants, and orientation matrices for data collection, were obtained from least-squares refinements, using 20 carefully centred reflections in the range 8.59° < 2θ < 16.07°. Based on the systematic absences *hkl*: $-h + k + l \neq 3n$, the space group was uniquely identified as $R\bar{3}$ (No. 148), and this was confirmed by subsequent solution and refinement of the structure. Details of the intensity collection are given in Table 1.

The intensities of three representative reflections were measured after every 150 reflections. Over the course of data collection, the standard increased 1%, and a linear correction factor was applied to the results. The linear absorption coefficient (57.05 cm^{-1}) required an absorption correction, using PSI Scan, with transmission factors between 0.80 and 1.00. The results were also corrected for Lorentz and polarization effects. The structure was solved by direct methods, and expanded using Fourier techniques. The non-hydrogen atoms were refined isotropically; hydrogen atoms on carbon were included in ideal positions but were not refined. The final cycle of full-matrix least-squares refinement was based on 761 observed reflections ($I > 3\sigma(I)$) and 71 variable parameters, and the solution converged at $R = 0.040$ and $R_w = 0.034$. A final Fourier difference map calculation showed no peaks of chemical significance; the maximum and minimum peaks corresponded to + and − 0.67 e Å^{-3}, respectively.

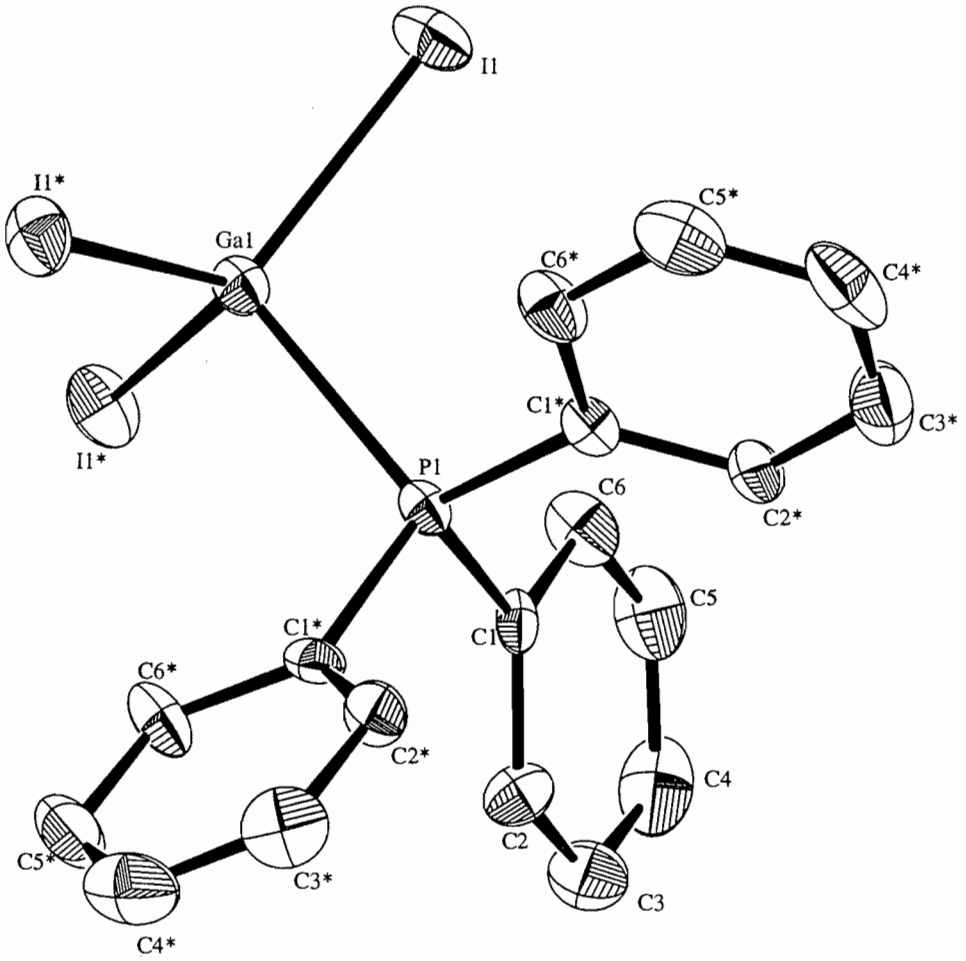
(*ii*) The structural study of crystals of Ga_2I_6·dppe, **2**, followed essentially the same procedure. The space group was identified as $P2_{1/n}$ (No. 14). The data were corrected for decay absorption, Lorentz and polarization effects, and the structure was again solved by direct methods. The final Fourier calculation showed no peaks of chemical significance; the maximum and minimum peaks corresponded to 1.47 and −1.54 e Å^{-3}, respectively. The solution converged at $R = 0.063$ and $R_w = 0.058$.

In both sets of calculations, neutral-atom scattering factors were taken from Cromer and Waber (5). Anomalous dispersion effects were included in the calculations (6); the values for $\Delta f'$ and $\Delta f''$ were those published by Cromer (7). All calculations were performed using the TEXSAN (8) crystallographic software package. The structure of the molecules are shown in Figs. 1 and 2; the positional parameters are in Tables 2 and 4, and important bond distances and angles in Tables 3 and 5.

Tables of hydrogen-atom coordinates and thermal parameters, anisotropic thermal parameters for other atoms, and bond

© 1997 NRC Canada

Fig. 1. The molecular structure of $GaI_3 \cdot PPh_3$, **1**, showing the numbering system. ORTEP diagram, with 30% probability ellipsoids.



lengths and angles other than those in Tables 3 and 5, are available as supplementary data.[3]

Results and discussion

Crystallographic studies

The triphenylphosphine adducts of GaI_3 (**1**) and InI_3 are, not surprisingly, isostructural, with the stereochemistry at metal and phosphorus being essentially C_{3v} in each case. The complex **2** shows the same structural features at the metal centre, and differs from **1** only in the sense that the ligand is effectively $P(C_6H_5)_2CH_2^-$. This structure represents a departure from $InI_3 \cdot$dppe, in which an infinite chain of planar InI_3 units is linked by bridging dppe to give five-coordinate indium. The Ga—I bond distance in **1** is 2.5212(9) Å, to be compared with the range of 2.533(5)–2.481(5) Å in **2**, for which the average r(Ga—I) is 2.513 Å. The average Ga—P bond distances in **1** (2.416(5) Å) and **2** (2.407(9) Å) are also identical within the experimental error, all of which emphasizes the close relationship in the structural chemistry of the gallium centres in these two molecules in the solid state, and the predominance of four-coordination, in contrast to the analogous indium complexes.

Preparative

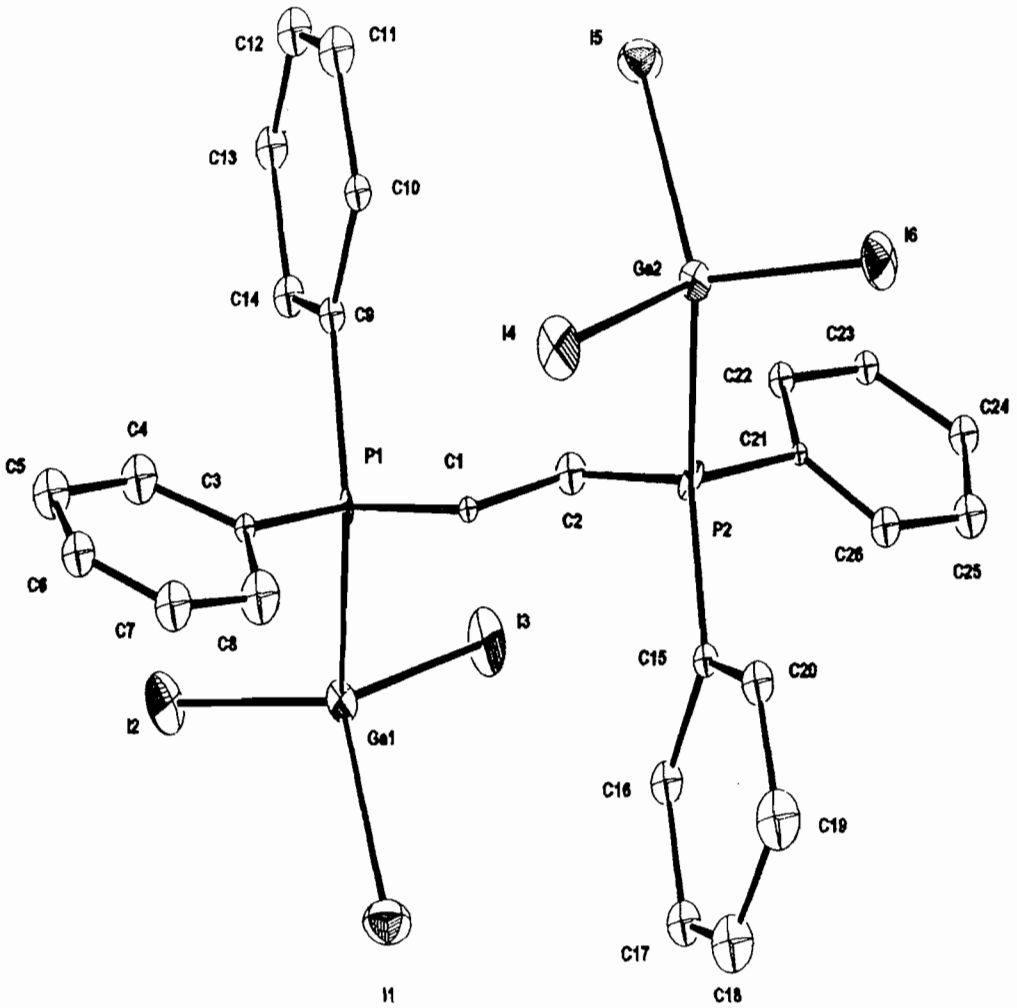
The first point to note is that the preparative chemistry of the GaI_3/PPh_3 system appears much simpler than for the indium analogue, in which both 1:1 and 1:2 adducts were characterized and shown to readily interconvert in nonaqueous solution (1). None of the previous workers reported such behaviour in the gallium system, and our results are in keeping with their findings (2–4). Similarly, the reaction with dppe gives a single species, whereas with indium triiodide and dppe, both $[InI_3(dppe)]_\infty$ and $(InI_3)_3(dppe)_2$ have been identified crystallographically (1, 9). These comparisons and contrasts emphasize that here, as in other parts of this paper, the maximum coordination number for gallium in these systems is four, and the apparent inability to exceed this underlies the differences between gallium and indium.

[3] Copies of material on deposit can be purchased from: The Depository of Unpublished Data, Document Delivery, CISTI, National Research Council Canada, Ottawa, Canada K1A 0S2. The tables of H-atom coordinates have also been deposited with the Cambridge Crystallographic Data Centre, and can be obtained on request from The Director, Cambridge Crystallographic Data Centre, University Chemical Laboratory, 12 Union Road, Cambridge, CB2 1EZ, U.K.

Can. J. Chem. Downloaded from www.nrcresearchpress.com by 92.62.229.171 on 09/08/12
For personal use only.

© 1997 NRC Canada

Fig. 2. The molecular structure of Ga_2I_6·dppe, **2**, showing the numbering system. ORTEP diagram, with 30% probability ellipsoids.



^{31}P NMR studies of GaI_3·PPh_3

A solution of GaI_3·PPh_3 in acetone (0.1 M) at 23°C has two ^{31}P resonances, at 28.35 ppm, half-width 10.1 Hz, and −3.91 ppm, half-width 46.5 Hz. Since triphenylphosphine in the same solvent gives a signal at −4.77 ppm, $w_{1/2}$ = 9 Hz, this spectrum establishes immediately that the 1:1 complex, for which $\delta(^{31}P)$ = 28.35 ppm, undergoes partial dissociation, with the simplest equilibrium being

[1] $GaI_3 \cdot PPh_3 \rightleftharpoons GaI_3 + PPh_3$

The ratio of the peak heights for complex:PPh_3 is 12.0, so that the equilibrium constant for eq. [1] is ca. 0.08 mol L^{-1}. The rather large half-width for Ph_3P in this solution suggests a relatively slow exchange process in eq. [1], which is at first sight surprising, since adduct formation is presumed to be fast (but see below). There is a smooth change in the ratio of the peak heights for the complex and free PPh_3 as PPh_3 is added (Fig. 3*a*) and the half-width for free PPh_3 also decreases over the range studied (Fig. 3*b*).

Figure 4 shows the effect of adding iodide ion (as *n*-Bu_4NI) to the solution. At low I^-:complex ratios, PPh_3 is released as the result of the reaction

[2] $GaI_3 \cdot PPh_3 + I^- \rightarrow GaI_4^- + PPh_3$

but beyond an I^-:complex mole ratio of 0.6, a sharp rise in the amount of free PPh_3 is detected. The interpretation of these results is complicated by the presence of a small quantity of PPh_3 in the solution due to the dissociation described in eq. [1], and clearly the quantity of GaI_3·PPh_3 is also lowered by the effect of eq. [2]. At I^- = 0, the quantity of PPh_3 from dissociation of GaI_3·PPh_3 is ca. 8% (see above), which accounts for the point at −4.7 ppm, peak height = 0.1, in Fig. 4. At added I^- = 0.05 M, the quantity of free PPh_3 is more than 10 times greater, and the correction for eq. [1] is of the order of 1% and therefore negligible. The dotted line in Fig. 4 is an approximate correction to allow for PPh_3 arising via eq. [1] rather than eq. [2].

With or without this correction, Fig. 4 shows a linear dependence up to a mole ratio of approx. 0.5, followed by a steep rise in the quantity of Ph_3P released, reaching a maximum at the equimolar point. Further addition of iodide beyond this

© 1997 NRC Canada

Can. J. Chem. Downloaded from www.nrcresearchpress.com by 92.62.229.171 on 09/08/12
For personal use only.

Can. J. Chem. Downloaded from www.nrcresearchpress.com by 92.62.229.171 on 09/08/12
For personal use only.

Table 2. Positional parameters for non-hydrogen atoms in $GaI_3 \cdot PPh_3$ (**1**).

Atom	*x*	*y*	*z*	*B*(eq)
I(1)	0.18102(6)	0.04565(6)	0.62089(5)	4.49(2)
Ga(1)	0	0	0.6595(1)	2.86(3)
P(1)	0	0	0.8058(3)	2.4(6)
C(1)	−0.0216(7)	−0.1211(7)	0.8462(6)	2.7(2)
C(2)	−0.0927(8)	−0.1722(8)	0.9061(6)	3.6(3)
C(3)	−0.108(1)	−0.265(1)	0.9340(7)	5.3(3)
C(4)	−0.054(1)	−0.310(1)	0.9022(9)	6.0(4)
C(5)	0.015(1)	−0.258(1)	0.8409(8)	5.1(4)
C(6)	0.0330(9)	−0.1645(8)	0.8128(7)	4.1(3)
I(1*)	−0.13537(6)	−0.18102(6)	0.62089(5)	4.49(2)
I(1*)	−0.04565(6)	0.13537(6)	0.62089(5)	4.49(2)
C(1*)	0.1211(7)	0.0994(7)	0.8462(6)	2.7(2)
C(1*)	−0.0944(7)	0.0216(7)	0.8462(6)	2.7(2)
C(2*)	0.1722(8)	0.0795(8)	0.9061(6)	3.6(3)
C(2*)	−0.0795(8)	0.0927(8)	0.9061(6)	3.6(3)
C(3*)	0.2852(10)	0.157(1)	0.934(7)	5.3(3)
C(3*)	0.01574(10)	0.108(1)	0.934(7)	5.3(3)
C(4*)	0.31(1)	0.2556(10)	0.9022(9)	6.0(4)
C(4*)	−0.256(1)	0.054(10)	0.9022(9)	6.0(4)
C(5*)	0.258(1)	0.2737(10)	0.8409(8)	5.1(4)
C(5*)	−0.274(1)	−0.0153(10)	0.8409(8)	5.1(4)
C(6*)	0.1645(9)	0.1976(8)	0.8128(7)	4.1(3)
C(6*)	−0.01978(9)	−0.033(8)	0.8128(7)	4.1(3)

Table 3. (*a*) Bond distances (Å) and (*b*) angles (deg) in $GaI_3 \cdot PPh_3$ (**1**).

(*a*)

Atom	Atom	Distance	Atom	Atom	Distance
I(1)	Ga(1)	2.5212(9)	C(1)	C(2)	1.37(1)
Ga(1)	P(1)	2.416(5)	C(1)	C(6)	1.39(1)
P(1)	C(1)	1.801(9)	C(2)	C(3)	1.37(1)
			C(3)	C(4)	1.38(2)
			C(4)	C(5)	1.37(2)
			C(5)	C(6)	1.37(1)

(*b*)

Atom	Atom	Atom	Angle	Atom	Atom	Atom	Angle
I(1)	Ga(1)	I(1)	113.85(4)	C(1)	P(1)	C(1)	107.1(3)
I(1)	Ga(1)	P(1)	104.62(5)	C(2)	C(1)	C(6)	120(1)
Ga(1)	P(1)	C(1)	111.7(3)	C(1)	C(2)	C(3)	120(1)
P(1)	C(1)	C(2)	121.8(8)	C(2)	C(3)	C(4)	121(1)
P(1)	C(1)	C(6)	118.2(8)	C(3)	C(4)	C(5)	118(1)
				C(4)	C(5)	C(6)	122(1)
				C(1)	C(6)	C(5)	119(1)

point produces no change. The half-width of the ^{31}P resonance of the complex is constant at 12.3 ± 0.1 Hz throughout this series, whereas the value for the free ligand changes monotonically from a value of 46.5 Hz for $I^- = 0$ to 15.5 Hz at the equimolar point; this latter is characteristic of free Ph_3P in acetone (see above).

These results, and those for the addition of Ph_3P, suggest a set of equilibria more complicated than eqs. [1] and [2]. The

© 1997 NRC Canada

Can. J. Chem. Downloaded from www.nrcresearchpress.com by 92.62.229.171 on 09/08/12
For personal use only.

Table 4. Positional parameters for non-hydrogen atoms in $Ga_2I_6 \cdot$dppe (**2**).

Atom	*x*	*y*	*z*	*B*(eq)
I(1)	0.4443(3)	−0.1022(2)	0.3537(1)	4.8(2)
I(2)	0.3215(2)	0.0745(2)	0.4771(1)	3.8(1)
I(3)	0.1371(2)	0.0747(2)	0.3036(1)	3.9(1)
I(4)	0.8561(2)	0.1597(2)	0.1904(1)	4.0(1)
I(5)	0.5479(3)	0.3426(2)	0.1503(1)	4.2(1)
I(6)	0.6520(2)	0.1766(2)	0.0185(1)	3.7(2)
Ga(1)	0.3478(3)	0.0431(2)	0.3739(2)	2.0(2)
Ga(2)	0.6406(3)	0.1977(3)	0.1256(2)	1.9(2)
P(1)	0.5155(7)	0.1379(6)	0.3462(4)	1.1(4)
P(2)	0.4751(7)	0.0999(6)	0.1526(4)	1.2(4)
C(1)	0.556(3)	0.112(2)	0.275(1)	1.0(6)
C(2)	0.441(3)	0.128(2)	0.223(1)	2.3(7)
C(3)	0.668(3)	0.127(2)	0.394(1)	1.0(6)
C(4)	0.771(4)	0.076(2)	0.384(2)	4(1)
C(5)	0.896(3)	0.070(2)	0.422(2)	3.3(8)
C(6)	0.906(3)	0.116(2)	0.472(2)	2.9(8)
C(7)	0.805(3)	0.166(3)	0.493(2)	3.5(9)
C(8)	0.684(3)	0.171(2)	0.451(1)	2.5(8)
C(9)	0.477(3)	0.254(2)	0.347(1)	1.6(7)
C(10)	0.550(3)	0.314(2)	0.318(1)	2.1(7)
C(11)	0.522(3)	0.402(2)	0.325(2)	3.3(8)
C(12)	0.428(3)	0.429(3)	0.355(2)	3.2(8)
C(13)	0.354(3)	0.374(2)	0.380(1)	2.6(7)
C(14)	0.374(3)	0.283(2)	0.377(1)	2.1(7)
C(15)	0.518(3)	−0.012(2)	0.153(1)	1.6(7)
C(16)	0.463(3)	−0.071(2)	0.185(1)	2.4(7)
C(17)	0.487(3)	−0.156(2)	0.183(1)	2.5(7)
C(18)	0.568(4)	−0.185(3)	0.152(2)	5(1)
C(19)	0.627(4)	−0.127(3)	0.112(2)	4(1)
C(20)	0.603(3)	−0.042(2)	0.114(2)	2.9(8)
C(21)	0.320(3)	0.112(2)	0.100(1)	1.1(6)
C(22)	0.224(3)	0.168(2)	0.114(1)	1.8(7)
C(23)	0.111(3)	0.171(2)	0.073(1)	1.5(6)
C(24)	0.089(3)	0.120(2)	0.023(1)	1.8(7)
C(25)	0.187(3)	0.062(2)	0.018(2)	2.9(8)
C(26)	0.302(3)	0.056(2)	0.056(1)	2.4(7)

most important factor is that the dimerization of gallium(III) halides is an important process in nonaqueous solution, and that ligand addition, and hence dissociation, must go via this dimer (10–12). We therefore rewrite eq. [1], and add the successive processes

[3] $2\ GaI_3 \cdot PPh_3 \rightleftharpoons 2\ GaI_3 + 2PPh_3$

[4] $2\ GaI_3 \rightleftharpoons Ga_2I_6$

[5] $Ga_2I_6 + PPh_3 \rightleftharpoons Ga_2I_6 \cdot PPh_3$

[6] $Ga_2I_6 \cdot PPh_3 \rightleftharpoons GaI_3 + GaI_3 \cdot PPh_3$

The sum of eqs. [3]–[6] is of course eq. [1]. We postulate that the equilibria [3] and [4] are rapidly established, and that [4] lies strongly to the right. In the presence of added PPh_3, eq. [5] becomes important, since this step accounts for the uptake of the ligand to yield the complex $GaI_3 \cdot PPh_3$ via eqs. [5] + [6]. We further suggest that eq. [5] is the rate-controlling step in the sequence, and that the decreasing ^{31}P line width shown in Fig. 3*b* is caused by increasingly rapid exchange between PPh_3 as the quantity of free ligand is increased.

Similar equilibria can also be used to understand the processes implicit in the addition of I^- (Fig. 4). Equations [3] and [4] are here followed by

[7] $Ga_2I_6 + I^- \rightleftharpoons Ga_2I_7^-$

[8] $Ga_2I_7^- \rightleftharpoons GaI_4^- + GaI_3$

[9] $GaI_3 + I^- \rightleftharpoons GaI_4^-$

The addition of I^- to a solution of $GaI_3 \cdot PPh_3$, already in equilibrium via eqs. [1] and [2] with Ga_2I_6 and PPh_3, leads via eq. [7] to $Ga_2I_7^-$, which is the anionic analogue of $Ga_2I_6 \cdot PPh_3$ (eq. [5]). If eq. [7] lies to the right, then the formation of a steady concentration of $Ga_2I_7^-$ will occur at the mole ratio

© 1997 NRC Canada

Can. J. Chem. Downloaded from www.nrcresearchpress.com by 92.62.229.171 on 09/08/12
For personal use only.

Table 5. (*a*) Bond distances (Å) and (*b*) angles (deg.) in Ga_2I_6·dppe (**2**).

(*a*)

Atom	Atom	Distance	Atom	Atom	Distance
I(1)	Ga(1)	2.512(5)	P(1)	C(1)	1.80(3)
I(2)	Ga(1)	2.481(5)	P(1)	C(3)	1.78(3)
I(3)	Ga(1)	2.533(5)	P(1)	C(9)	1.82(3)
I(4)	Ga(2)	2.530(4)	P(2)	C(2)	1.76(3)
I(5)	Ga(2)	2.518(5)	P(2)	C(15)	1.78(3)
I(6)	Ga(2)	2.506(5)	P(2)	C(21)	1.85(3)
Ga(1)	P(1)	2.404(9)	C(1)	C(2)	1.56(3)
Ga(2)	P(2)	2.410(9)			

(*b*)

Atom	Atom	Atom	Angle	Atom	Atom	Atom	Angle
I(1)	Ga(1)	I(2)	116.9(2)	I(5)	Ga(2)	P(2)	101.0(2)
I(1)	Ga(1)	I(3)	111.7(2)	I(6)	Ga(2)	P(2)	108.2(2)
I(1)	Ga(1)	P(1)	100.1(2)	Ga(1)	P(1)	C(1)	112(1)
I(2)	Ga(1)	I(3)	111.8(2)	Ga(1)	P(1)	C(3)	112(1)
I(2)	Ga(1)	P(1)	108.8(2)	Ga(1)	P(1)	C(9)	115(1)
I(3)	Ga(1)	P(1)	106.4(2)	C(1)	P(1)	C(3)	104(1)
I(4)	Ga(2)	I(5)	113.1(2)	C(1)	P(1)	C(9)	108(1)
I(4)	Ga(2)	I(6)	112.7(2)	C(3)	P(1)	C(9)	105(1)
I(4)	Ga(2)	P(2)	106.4(3)	Ga(2)	P(2)	C(2)	109(1)
I(5)	Ga(2)	I(6)	114.3(2)	Ga(2)	P(2)	C(15)	115(1)
Ga(2)	P(2)	C(21)	109(1)	P(1)	C(3)	C(4)	125(3)
C(2)	P(2)	C(15)	109(2)	P(1)	C(3)	C(8)	119(2)
C(2)	P(2)	C(21)	108(1)	P(1)	C(9)	C(10)	121(2)
C(15)	P(2)	C(21)	106(1)	P(1)	C(9)	C(14)	119(2)
P(1)	C(1)	C(2)	115(2)	P(2)	C(15)	C(16)	122(3)
P(2)	C(2)	C(1)	116(2)	P(2)	C(15)	C(20)	119(3)
				P(2)	C(21)	C(22)	119(2)
				P(2)	C(21)	C(26)	116(2)

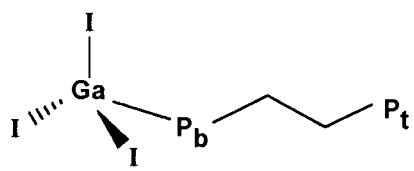
Phenyl rings, average values

C3–C8	1.41(4)	120(3)
C9–C14	1.38(4)	120(3)
C15–C20	1.37(5)	120(4)
C21–C26	1.37(4)	120(4)

I^-:GaI_3·PPh_3 = 0.5, and only beyond that point can further uptake of I^- (and hence further dissociation of GaI_3·PPh_3) occur by eqs. [8] and [9]. This mechanism accepts that direct nucleophilic attack of I^- on GaI_3·PPh_3 via a five-coordinate intermediate cannot be important, and in this context the molecular structure of Ga_2I_6·dppe, in which gallium prefers four-coordination to the alternative GaI_3P_2 mode, is significant. An important conclusion of these studies is that four-coordination at gallium(III) is predominant in the solution chemistry of GaI_3/PPh_3/I^- systems.

We also investigated the effect of temperature change on the ^{31}P spectra of GaI_3·PPh_3, in the hope of identifying some of the kinetic parameters. For a 0.1 M solution in acetone at 283 K, the only resonance observed is at 27.4 ppm, with $w_{1/2}$ = 15 Hz. Over the temperature range 283–323 K, the resonance of free PPh_3 appears at −5.7 ppm, but we did not observe any signs of coalescence, and therefore chose not to extend these studies.

Scheme 1.



^{31}P NMR studies of GaI_3·dppe

The ^{31}P spectrum of a solution of Ga_2I_6·dppe in acetone (0.1 M) at 23°C consists of two sharp doublets at 33.61, 33.46 and −(11.87, 11.52) ppm. The half-width for each is ca. 75 Hz. These resonances are assigned to the bound and terminal

© 1997 NRC Canada

Can. J. Chem. Downloaded from www.nrcresearchpress.com by 92.62.229.171 on 09/08/12
For personal use only.

Table 6. Vibrational spectra (in cm^{-1}) of $GaI_3 \cdot PPh_3$ and $Ga_2I_6 \cdot dppe$ in the metal–ligand region.

Molecule	Core symmetry	Spectra	Assignment
GaI_4^{-a}	T_d	ν_1 145, ν_2 52, ν_3 222, ν_4 73	
$GaI_3 \cdot PPh_3$	C_{3v}	ν_1 395 (w) (IR)	ν(Ga–P)
		ν_3 264 (m), 245(s)(R)	
		266 (w), 245(s) (IR)	ν(Ga–I)
$Ga_2I_6 \cdot dppe$	C_{2v}	ν_1 350 (m)(R)	ν(Ga–P)
		ν_3 260 (w), 250 (w), 238 (m) (R)	
		257(s), 246(s), 233(s) (IR)	ν(Ga–I)

[a]Values from ref. 13.

Fig. 3. Effect of adding PPh_3 to a solution of $GaI_3 \cdot PPh_3$, 0.1 M in acetone; (*a*) change in ^{31}P peak height ratio, (*b*) change in line width at half-height for PPh_3 resonance.

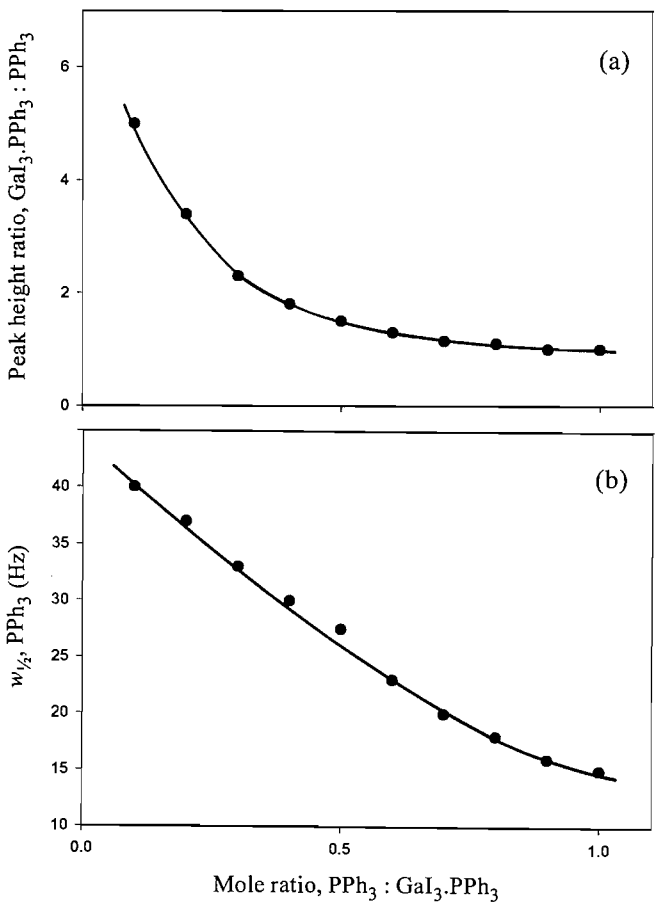
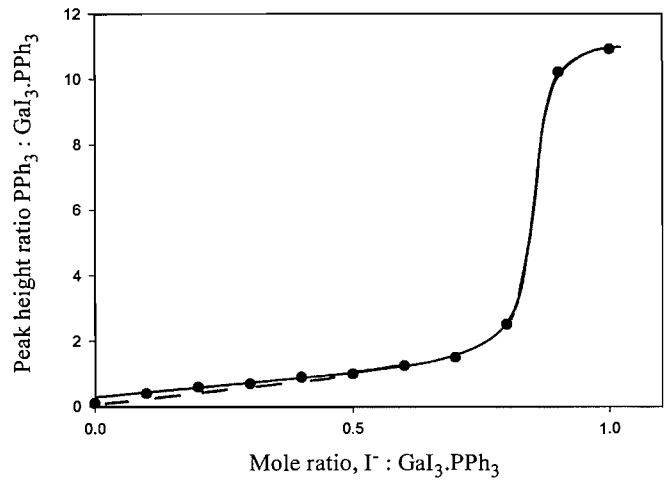


Fig. 4. Effect of adding I^- to a solution of $GaI_3 \cdot PPh_3$, 0.1 M in acetone; change in ^{31}P peak height ratio.



phosphorus atoms of the species based on the ^{31}P resonance of dppe in acetone, at −12.45 ppm, $w_{1/2}$ = 14 Hz, and the positive shift observed for this ligand, and for PPh_3, on coordination (ref. 1, and above). This pair of doublets is observed in all experiments in which $Ga_2I_6 \cdot dppe$ is present in solution, and the average value of J = 42 Hz is ascribed to long-range P–P coupling. The four-coordinate complex of Scheme 1 arises from the processes

[10] $Ga_2I_6 \cdot dppe \rightleftharpoons GaI_3 \cdot dppe + GaI_3$

[11] $GaI_3 \rightleftharpoons \frac{1}{2} Ga_2I_6$

in which all the species are undergoing exchange. The addition of dppe causes no initial change in the ^{31}P NMR spectrum, since the process

[12] $\frac{1}{2} Ga_2I_6 + dppe \rightleftharpoons GaI_3 \cdot dppe$

removes free ligand. As more dppe is added, the ^{31}P spectrum remains essentially constant, but at the mole ratio dppe:$Ga_2I_6 \cdot dppe$ = 1.0, a new signal appears at −12.1 ppm, indicating the presence of free dppe, and the absence of uncomplexed GaI_3 (or Ga_2I_6). Beyond this point, the addition

© 1997 NRC Canada

Can. J. Chem. Downloaded from www.nrcresearchpress.com by 92.62.229.171 on 09/08/12
For personal use only.

of dppe (up to a mole ratio of 1.8) causes an increased intensity of the resonance at −12.15 ppm, which masks that assigned to P_t (Scheme 1); the doublet at ca. 34 ppm remains throughout this sequence. Similarly the addition of Ga_2I_6 causes the gradual disappearance of the P_t resonance, which is completely absent beyond the equimolar point. In this region, the ^{31}P spectrum consists of a doublet at 33.71, 33.38, establishing the presence of $I_3Ga{\cdot}dppe{\cdot}GaI_3$ (i.e., the solid state structure **2**) in the solution. We conclude that although $GaI_3{\cdot}$dppe does not give rise to a crystalline 1:1 adduct under the preparative conditions used in this, and earlier (2–4), work, this molecule can exist in nonaqueous solution, as described by eq. [10]. Equally, the solid state species in which dppe bridges two four-coordinate gallium(III) entities can also be formed in solution in the presence of excess gallium(III) iodide. These results provide yet another example of the effect of differing solution and solid state stabilizing factors on the properties, and especially the stoichiometry, of such adducts.

Following eqs. [10] and [11], the addition of I^- to a solution of $Ga_2I_6{\cdot}$dppe in fact involves the interaction of I^- with $GaI_3{\cdot}$dppe and (or) Ga_2I_6. At low I^-:complex mole ratios, there is no change in the ^{31}P spectrum, since the dominant process is

[13] $\frac{1}{2}\,Ga_2I_6 + I^- \rightleftharpoons GaI_4^-$

When sufficient I^- has been added to complex all the Ga_2I_6 as the stable GaI_4^- anion, displacement of dppe from $GaI_3{\cdot}$dppe occurs

[14] $GaI_3{\cdot}dppe + I^- \rightleftharpoons GaI_4^- + dppe$

and this release of dppe results in the growth of the resonance at −12.2 ppm. The continued addition of I^- causes an increase in the height of this signal relative to that for bound dppe; at the mole ratio I^-:Ga_2I_6 = 1.4, approximately 48% of the dppe has been displaced, and at a mole ratio of 2.0, this rises to 96%. Beyond this ratio, only free dppe is detected in the ^{31}P spectrum since all the gallium is present as GaI_4^-. The half-width of the ^{31}P resonance is almost constant at 80 Hz throughout.

Vibrational spectroscopy

The earlier investigations of the phosphino complexes of gallium(III) iodide depended in large measure on infrared spectroscopy for the elucidation of the solid state structures (2–4). We have recorded the Raman and far infrared spectra of both $GaI_3{\cdot}PPh_3$ and $Ga_2I_6{\cdot}$dppe, with the results shown in Table 6. Given the similarities in the coordination kernels of the two complexes, it is not surprising that the vibrational spectra are very similar in the metal–ligand stretching region. This conclusion is easily reached in the light of the crystallographic results not available to the earlier workers.

General conclusions

It is useful to compare and contrast the behaviour of gallium and indium in terms of the complexation of MI_3 with PPh_3 and dppe. Four-coordination is an exclusive feature of gallium chemistry in such systems, and this factor also accounts for the significance of Ga_2I_6 in nonaqueous solution. For indium, four-coordination is important, but five-coordinate species are also found in crystalline $InI_3(PPh_3)_2$ and $[InI_3(dppe)]_\infty$. The bisphosphino adduct of InI_3 dissociates completely in nonaqueous solution to the 1:1 adduct, but this process can be reversed somewhat by the addition of excess ligand. The preparative chemistry of InI_3–PPh_3 and InI_3–dppe systems is therefore complicated to an extent which is not apparent in the analogous gallium chemistry. The spectroscopic investigations of these various species in nonaqueous solution provide an explanation in terms of the different equilibria involved. No doubt comparable dissimilarities will be found in further investigations of related systems.

Acknowledgments

This work was supported in part by Research Grants (to D.G.T.) from the Natural Sciences and Engineering Research Council of Canada. One of us (J.A.C.) thanks the Universidade de Vigo, and the Xunta de Galicia, for the award of a Travel Grant.

References

1. M.A. Brown, D.G. Tuck, and E.J. Wells. Can. J. Chem. **74**, 1535 (1996).
2. A. Balls, N.N. Greenwood, and B.P. Straughan. J. Chem. Soc. (A), 753 (1968).
3. A.J. Carty. Can. J. Chem. **43**, 3187 (1967).
4. A.J. Carty. Can. J. Chem. **45**, 344 (1967).
5. D.T. Cromer and J.T. Waber. International tables for X-ray crystallography. Vol. IV. Kynoch Press, Birmingham, U.K. 1974. Table 2.2A.
6. J.A. Ibers and W.C. Hamilton. Acta Crystallogr. **17**, 781 (1974).
7. D.T. Cromer. International tables for X-ray crystallography. Vol. IV. Kynoch Press, Birmingham, U.K. 1974. Table 2.3.1.
8. TEXSAN–TEXRAY Structure analysis package, Molecular Structure Corporation, The Woodlands, Tex. 1958.
9. I.A. Degnan, N.W. Alcock, S.M. Roe, and M.G.H. Wallbridge. Acta Crystallogr. Sect. C: Cryst. Struct. Commun. **C48**, 995 (1992).
10. H.C. Brown, L.O. Eddy, and R. Wong. J. Am. Chem. Soc. **75**, 6275 (1953).
11. C. Hambly and J.B. Raynor. J. Chem. Soc. Dalton Trans. 604 (1974).
12. Z. Černý, J. Macháček, J. Fusek, B. Čásenský, O. Kříž, and D.G. Tuck. Inorg. Chem. Acta, **247**, 119 (1996).
13. L.A. Woodward and G.H. Singer. J. Chem. Soc. 716 (1958).

© 1997 NRC Canada

Comparison of crystal and solution structures and ^{1}H and ^{13}C chemical shifts for grandiflorenic acid, kaurenoic acid, and monoginoic acid

Raul G. Enriquez, Julie Barajas, Benjamin Ortiz, Alan J. Lough, William F. Reynolds, Margaret Yu, Ismael Leon, and Dino Gnecco

Abstract: The crystal structure of monoginoic acid, **3**, is determined and compared with previously reported structures of kauradienoic acid, **1**, and kaurenoic acid, **2**. ^{1}H and ^{13}C chemical shifts are assigned for all three diterpenes and solution and crystal structure conformations are confirmed with the aid of solution NOE measurements. The overall shapes of **2** and **3** are very similar while **1** is significantly dissimilar. These differences may be partially responsible for the reported greater in vitro uterotropic activity of **1**, relative to **2** and **3**.

Key words: monoginoic acid, kaurodienoic acid, kaurenoic acid.

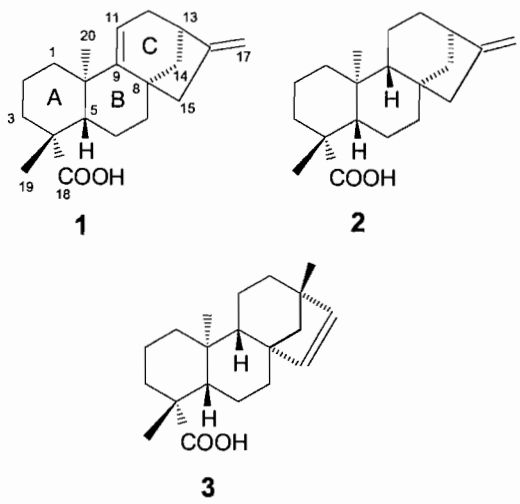
Résumé : On a déterminé la structure cristalline de l'acide monoginoïque, **3**, et on l'a comparée aux structures rapportées antérieurement pour les acides kauradiénoïque, **1**, et kaurénoïque, **2**. On a attribué les déplacements chimiques du ^{1}H et du ^{13}C pour les trois diterpènes et les conformations des structures cristallines et de celles en solution ont pu être confirmées à l'aide de mesures d'EON en solution. Les formes globales des composés **2** et **3** sont très semblables alors que celle du composé **1** est très dissimilaire. Il est possible que ces différences soient partiellement responsables de l'activité utérotropique in vitro plus élevée rapportée pour le composé **1** par rapport aux composés **2** et **3**.

Mots clés : l'acide monoginoïque, l'acide kaurodiénoïque, l'acide kaurénoïque.

[Traduit par la rédaction]

Introduction

The plant known as "zoapatle" (*Montanoa tomentosa* Cerv. ssp. *tomentosa*) is widely used in Mexican traditional medicine, both as an abortifacient in early stages of pregnancy and to induce labour in late stages of pregnancy (1). Among the secondary metabolites isolated from zoapatle are three kaurane derivatives: grandiflorenic acid ((4α)-kaura-9(11),16-dien-18-oic acid), **1**, kaurenoic acid ((4α)-kaur-16-en-18-oic acid), **2**, and monoginoic acid (13-methyl-(4α)-norkaur-15-en-18-oic acid), **3** (2). There are conflicting reports concerning the possible role of any or all of these three derivatives in the pharmacological activity of zoapatle. For example, Gallegos, in a patent, reported in vivo (uterine evacuating) activity for all three compounds, with **1** being most effective (3). In vitro uterine stimulating activity has been reported for **1** and **2** (4) and it has also been reported that a mixture of **1** and **2** shows even higher levels of activity (5). However, other workers, while confirming the in vitro activity of **1**, failed to find evidence of in vivo activity for any of the three compounds (6, 7). Interestingly, **1** and **2** were also recently isolated from the leaves of *Aspilia mossambicensis* (8). The leaves of this plant and others of the genus *Aspilia* are consumed preferentially by female chimpanzees in Africa, possibly as fertility regulators (8).



Received June 7, 1996.

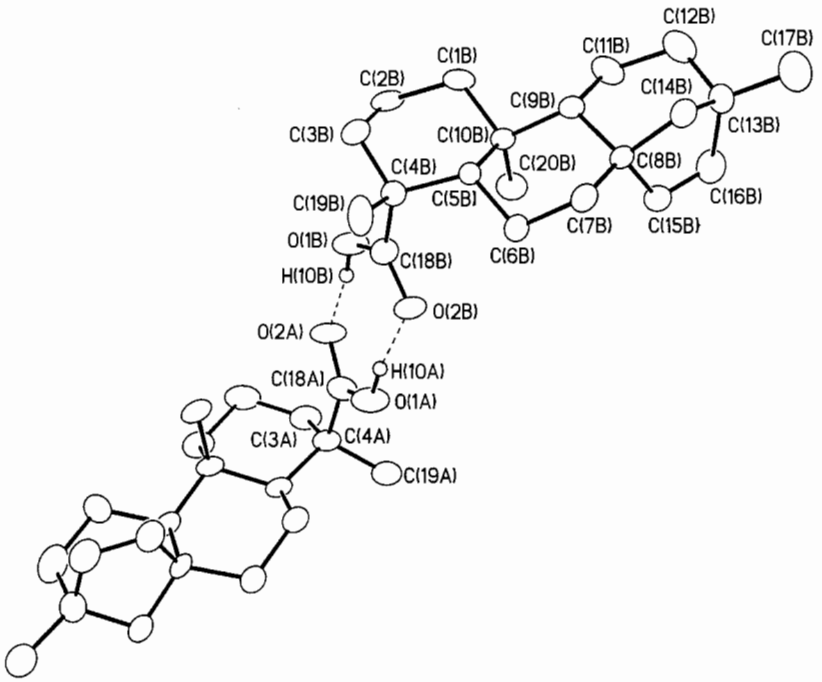
R.G. Enriquez,[1] J. Barajas, and B. Ortiz. Instituto de Quimica, Universidad Nacional Autonoma de Mexico, Circuito Exterior, Ciudad Universitaria, Mexico 04510, D.F.
A.J. Lough, W.F. Reynolds,[1] and M. Yu. Department of Chemistry, University of Toronto, Toronto, ON M5S 3H6, Canada.
I. Leon. Facultad de Ciencies, Universidad Autonoma del Estado de Morelos, Cuernavaca 62210, Morelos, Mexico.
D. Gnecco. Centro de Quimica, Instituto de Ciencias, Universidad Autonoma de Puebla, Puebla, Mexico.

[1] Authors to whom correspondence may be addressed. (W.F.R.) Telephone: (416) 978-3563. Fax: (416) 978-8775. E-mail: bgranozi@alchemy.chem.utoronto.ca

© 1997 NRC Canada

Can. J. Chem. Downloaded from www.nrcresearchpress.com by 92.62.229.171 on 09/08/12
For personal use only.

Fig. 1. ORTEP drawing of **3**, illustrating the hydrogen-bonded dimer and giving numbering of molecules A and B in unit cell.



There have also been conflicting reports on whether **1**–**3** are present in aqueous herbal extracts of zoapatle (9, 10). This is critical since the absence of these compounds from the aqueous "tea" would rule out any role for them in the pharmacological activity of this traditional medicine. However, we recently conclusively demonstrated the presence of significant amounts of **1**–**3** in the aqueous herbal extracts by using GC–MS measurements in conjunction with 2D NMR measurements (11). This positive result has encouraged us to further investigate possible structure–activity relations.

We previously reported complete ^{1}H and ^{13}C spectral assignments for **1** (12) and, more recently, a crystal structure determination for the same compound (13). A crystal structure has also been reported for **2** (14). We believed that it would be useful to have complete spectral assignments and crystal structure determinations for all three compounds as a starting point for better understanding of the disputed structure–activity relationships for these derivatives. The crystal structure of **3** and complete ^{13}C and ^{1}H spectral assignments for **2** and **3** are provided here, along with comparisons of the solid state and solution structures for the three compounds.

Results and discussion

X-ray crystal structures of 3

The atomic coordinates for **3** are summarized in Table 1 while an ORTEP drawing is given in Fig. 1. Inspection of the structure shows that all three six-membered rings are in chair or near-chair conformations while most bond lengths and bond angles are unexceptional. Tables of bond lengths, bond angles, H-atom coordinates, and anisotropic thermal parameters are available as supplementary material.[2]

When comparing the crystal structures of **1**, **2**, and **3**, one finds significant differences, particularly between **1** and the other two compounds. The geometry of ring A is very similar in all three cases. However, in **1**, ring B adopts a boat conformation, probably due to the 9,11 double bond (13). As a result, the 16,17 double bond is well above the β face of the molecule while ring C is near the plane formed by ring A. On the other hand, ring B of **2** is in a chair form. However, due to the *cis* B–C ring junction in **2**, ring C is well below (i.e., on the α face of) the mean plane of the ring carbons of ring A (but still in a chair conformation) while the exocyclic 16,17 double bond is near this mean plane. In **3**, due to the *trans* B–C ring junction, rings A, B, and C form essentially a single plane with all three rings in chair conformations. The double bond is well below this plane while the C-20 methyl carbon is almost in the same location as the C-17 methylene carbon in **2**. The overall "shapes" of **2** and **3** are surprisingly similar.

These features are illustrated in Figs. 2 and 3. Figure 2 shows a side view of structures **1** and **3** with ring A superimposed while Fig. 3 provides a similar view of **2** and **3**. The dif-

[2] The supplementary material can be purchased from: The Depository of Unpublished Data, Document Delivery, CISTI, National Research Council Canada, Ottawa, Canada K1A 0S2. Tables of atomic positional parameters, bond distances and bond angles for monoginoic acid have also been deposited with the Cambridge Crystallographic Data Center and can be obtained on request from the Director, Cambridge Crystallographic Data Center, Univeristy Chemical Laboratory, 12 Union Road, Cambridge, CB2 1EZ, U.K.

Can. J. Chem. Downloaded from www.nrcresearchpress.com by 92.62.229.171 on 09/08/12
For personal use only.

© 1997 NRC Canada

Can. J. Chem. Downloaded from www.nrcresearchpress.com by 92.62.229.171 on 09/08/12
For personal use only.

Table 1. Atomic coordinates and equivalent isotropic displacement coefficients (Å^2).

Atom	x	y	z	U(eq)[a]
O(1A)	0.6005(4)	0.8362(4)	0.2524(3)	0.087(3)
O(2A)	0.6954(4)	0.9783(4)	0.2663(3)	0.081(2)
C(1A)	0.4739(7)	1.1049(5)	0.3837(4)	0.071(4)
C(2A)	0.5475(7)	1.1398(6)	0.3309(5)	0.079(4)
C(3A)	0.5070(7)	1.0961(6)	0.2725(4)	0.071(4)
C(4A)	0.4914(6)	0.9831(6)	0.2708(4)	0.055(3)
C(5A)	0.4236(6)	0.9484(5)	0.3273(4)	0.050(3)
C(6A)	0.3984(6)	0.8349(5)	0.3305(4)	0.058(3)
C(7A)	0.3076(7)	0.8134(6)	0.3772(3)	0.061(3)
C(8A)	0.3345(6)	0.8525(6)	0.4396(3)	0.049(3)
C(9A)	0.3755(6)	0.9638(5)	0.4361(3)	0.051(3)
C(10A)	0.4656(6)	0.9880(5)	0.3887(4)	0.048(3)
C(11A)	0.4069(7)	1.0004(6)	0.4995(4)	0.073(4)
C(12A)	0.3270(10)	0.9650(8)	0.5484(5)	0.107(5)
C(13A)	0.2863(8)	0.8520(7)	0.5422(4)	0.069(4)
C(14A)	0.2329(7)	0.8466(6)	0.4815(3)	0.064(3)
C(15A)	0.4179(8)	0.7867(5)	0.4744(5)	0.064(3)
C(16A)	0.3944(8)	0.7958(6)	0.5338(5)	0.079(4)
C(17A)	0.2137(8)	0.8251(8)	0.5945(4)	0.104(5)
C(18A)	0.6021(7)	0.9276(7)	0.2633(4)	0.063(3)
C(19A)	0.4222(7)	0.9596(7)	0.2141(4)	0.076(4)
C(20A)	0.5823(6)	0.9464(6)	0.4051(4)	0.066(3)
O(1B)	0.8781(4)	0.8591(4)	0.2629(3)	0.085(3)
O(2B)	0.7840(4)	0.7260(4)	0.2329(3)	0.074(2)
C(1B)	1.1585(5)	0.7921(6)	0.1664(4)	0.067(4)
C(2B)	1.1244(6)	0.8434(7)	0.2254(4)	0.075(4)
C(3B)	1.0815(6)	0.7715(6)	0.2710(4)	0.069(4)
C(4B)	0.9839(6)	0.7072(6)	0.2497(4)	0.053(3)
C(5B)	1.0153(5)	0.6564(6)	0.1886(3)	0.040(3)
C(6B)	0.9317(6)	0.5830(5)	0.1632(3)	0.052(3)
C(7B)	0.9836(7)	0.5166(6)	0.1167(3)	0.056(3)
C(8B)	1.0367(6)	0.5738(5)	0.0648(3)	0.044(3)
C(9B)	1.1138(5)	0.6601(6)	0.0894(3)	0.047(3)
C(10B)	1.0609(5)	0.7278(5)	0.1397(3)	0.044(3)
C(11B)	1.1670(7)	0.7180(6)	0.0376(4)	0.073(4)
C(12B)	1.2058(7)	0.6550(7)	−0.0161(4)	0.084(4)
C(13B)	1.1233(7)	0.5703(7)	−0.0311(4)	0.066(4)
C(14B)	1.1099(6)	0.5067(6)	0.0255(3)	0.057(3)
C(15B)	0.9580(7)	0.6137(6)	0.0182(4)	0.057(3)
C(16B)	1.0057(8)	0.6130(7)	−0.0350(4)	0.075(4)
C(17B)	1.1663(9)	0.5138(9)	−0.0850(4)	0.108(5)
C(18B)	0.8764(7)	0.7693(6)	0.2475(4)	0.061(3)
C(19B)	0.9632(8)	0.6270(7)	0.2965(4)	0.086(4)
C(20B)	0.9686(6)	0.7972(6)	0.1148(4)	0.064(3)

[a]Equivalent isotropic U defined as one third of the trace of the orthogonalized U_{ij} tensor.

ferent locations of the exocyclic double bond in **1** and **2** are clearly seen while **2** and **3** are more nearly superimposed. Top views (not shown) confirm the similarity in overall shape of **2** and **3**, with **1** being significantly different. However, before one can reach any conclusions about whether these differences might be pharmacologically significant, it is first necessary to determine whether the molecules adopt similar conformations in solution.

^{13}C and ^{1}H spectral assignments and preferred conformations of 1–3 in solution

Complete ^{1}H and ^{13}C spectral assignments for **1–3** are given in Table 2. The data for **1** are essentially the same as those reported previously (12), except for minor chemical shift changes since the spectra were obtained for a more dilute solution than originally used. ^{1}H and ^{13}C spectral assignments were carried out with the aid of COSY (15), HETCOR (16),

© 1997 NRC Canada

Fig. 2. Side view of crystal structures of **1** (broken lines) and **3** (solid lines) with ring A atoms superimposed as closely as possible.

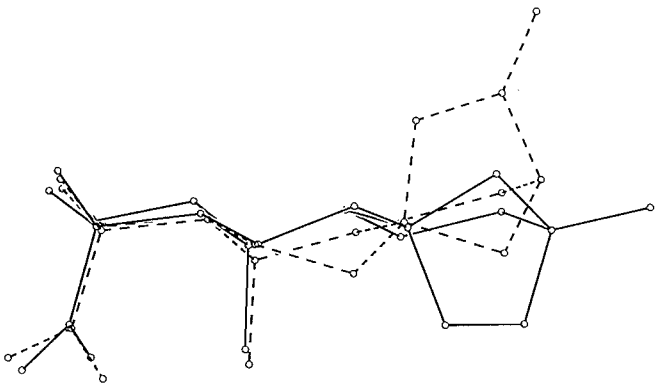
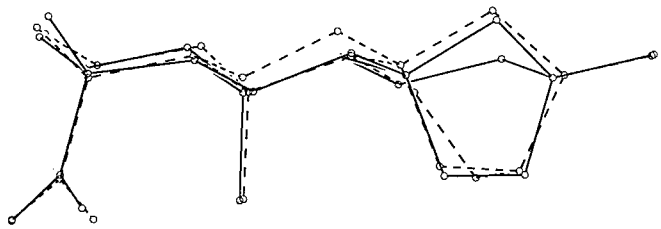


Fig. 3. Side view of crystal structures of **2** (broken lines) and **3** (solid lines) with ring A atoms superimposed as closely as possible.



HMQC (17), FLOCK (18), and HMBC (19) spectra, using methodologies similar to those reported earlier (12).

Solution conformations were investigated with the aid of NOESY and NOE difference spectra. In addition, cross sections for the HETCOR or HMQC spectra at specific ^{13}C frequencies allowed determination of the numbers of large splittings (*anti*-vicinal and geminal) for each proton, aiding in assignment of protons as axial or equatorial and, consequently α or β. However, the most important evidence for confirming the close similarity of solution and crystal structures was provided by NOE difference and NOESY experiments. For example, irradiation of the H-20 methyl protons of **1** resulted in an 7% enhancement of the proton assigned as H-7_α, confirming the boat conformation for ring B in **1**, since this kind of 1–4 ("flagpole") interaction is only possible for a boat conformation. In the case of **3**, the key observation is a strong NOE enhancement of 10% for the olefinic proton H-15 on irradiation of H-20. There are also significant enhancements of both H-16 and H-6_α on irradiation of H-15, as expected from the crystal conformation. Similarly in **2**, a 9% NOE enhancement is observed for H-14_α on irradiating H-20, suggesting that ring C is locked in a single chair conformation, identical to that in the solid state, even though it has a *cis* ring junction. A complete listing of significant NOESY cross peaks for the three compounds is provided in Table 3.

Comparisons of ^1H and ^{13}C chemical shifts for **1**–**3** show that, for ring A, carbons 2, 3, 4, 18, and 19 as well as the C-2 and C-3 methylene proton chemical shifts are quite similar for all three compounds. However, there are significant differ-

Table 2. Assigned ^{13}C and ^1H chemical shifts for **1**, **2**, and **3**.[a]

	1			**2**			**3**		
Carbon	δ_C	$\delta_{H\alpha}$	$\delta_{H\beta}$	δ_C	$\delta_{H\alpha}$	$\delta_{H\beta}$	δ_C	$\delta_{H\alpha}$	$\delta_{H\beta}$
1	40.75	1.93	1.24	40.70	1.88	0.82	39.49	1.69	0.91
2	20.16	1.88	1.50	19.09	1.86	1.42	19.17	1.80	1.41
3	38.31	2.16	1.02	37.83	2.16	1.02	37.88	2.16	1.02
4	44.69	—	—	43.71	—	—	43.76	—	—
5	46.56	—	1.67	57.04	—	1.06	57.04	—	1.11
6	18.48	2.47	1.68	21.83	⟨1.82⟩[b]		21.52	⟨1.82⟩[b]	
7	29.66	1.97	1.46	33.10	1.47	1.62	33.07	⟨1.25⟩[b]	
8	42.27	—	—	44.23	—	—	49.08	—	—
9	158.56	—	—	55.11	—	1.04	52.22	—	0.97
10	38.79	—	—	39.66	—	—	37.91		
11	114.90	5.24[c]		18.43	1.56	1.60	20.41	1.25	1.53
12	37.93	2.43	1.99	41.27	1.52	1.45	37.56	1.67	1.28
13	41.24	2.77	—	43.85	2.63	—	43.62	—	—
14	44.94	1.60	1.50	39.70	1.99	1.13	60.99	1.46	1.01
15	50.32	2.20	2.62	48.96	⟨2.05⟩[b]		134.78	5.75[c]	
16	155.92	—	—	155.90	—	—	136.47	5.45[c]	
17	105.48	4.91[c,d]	4.80	102.98	4.80[c,d]	4.73	24.87	—	1.00
18	182.74	—	—	183.74	—	—	184.12	—	—
19	28.23	—	1.24	28.96	—	1.24	29.11	—	1.24
20	23.62	1.02	—	15.60	0.95	—	13.76	0.67	—

[a]In ppm relative to internal $(CH_3)_4$ Si in $CDCl_3$.
[b]Average chemical shift for unresolved methylene protons.
[c]α, β designation is not applicable to olefinic hydrogens.
[d]Proton *cis* to C-13.

Can. J. Chem. Downloaded from www.nrcresearchpress.com by 92.62.229.171 on 09/08/12
For personal use only.

© 1997 NRC Canada

Can. J. Chem. Downloaded from www.nrcresearchpress.com by 92.62.229.171 on 09/08/12
For personal use only.

Table 3. Significant long-range[a] NOE peaks observed for NOESY spectra of **1–3**.[a]

Compound		
1	**2**	**3**
H-1_β/H-3_β[b]	H-1_β/H-3_β	H-1_β/H-5_β[d]
H-1_α/H-20	H1_α/H-20	H-1_α/H-20
H-1_β/H-5_β	H-1_β/H-5_β	H-3_α/H-19
H-2_α/H-20	H-1_β/H-9_β	H-3_β/H-19
H3_β/H-5_β	H-11/H-11_α	H-5_β/H-19
H-3_α/H-19	H-3_α/H-19	H-6_α/H-15
H-3_β/H-19	H-3_β/H-19	H-6_β/H-19
H-5_β/H-19	H-5_β/H-7_β	H-6_α/H-20
H-5_β/H-15_β	H-5_β/H-19	H-11_α/H-20
H-7_α/H-14_α	H-6_β/H-19	H-11_α/H-16
H-7_α/H-20	H-6_α/H-20	H12_β/H-17
H-11/H-20	H-9_β/H-11_β	H-15/H-20
H-13_α/H-17c[c]	H-11_α/H-20	
H-15_α/H-17t[c]	H-13_α/H-17c[c]	
H-15_β/H-17t	H-14_α/H-20	
	H-15_α/H-17t[c]	
	H-15_β/H-17t[c]	

[a]Excluding NOE cross peaks between geminal or vicinal pairs of protons. Tabulated cross peaks have intensities at least 1/3 of that between geminal pairs.

[b]Cross-peak assignments from spectra in C_6D_6 as well as $CDCl_3$ due to numerous spectral overlaps in $CDCl_3$.

[c]H-17c is *cis* to H-13_α; H-17t is *trans* to H-13.

[d]Not all expected cross peaks were observed for H-1_β and H-3_β due to similar chemical shifts for H-1_β, H-3_β, and H-5_β.

Table 4. Summary of crystal data and details of intensity collection and least-squares refinement parameters.

Empirical formula	$C_{20}H_{30}O_2$
M_r	302.4
Crystal size, mm	0.20 × 0.10 × 0.10
Crystal class	Orthorhombic
Space group	$P2_12_12_1$
a, Å	11.855(2)
b, Å	13.303(3)
c, Å	22.387(4)
V, Å^3	1483.7(7)
Z	8
D_{calc}, Mg m^{-3}	1.138
μ(MoKα), mm^{-1}	0.071
F(000)	1328
ω scan width, °	0.6 + 0.35 tan θ
Range 2θ collected, °	3–45
Index ranges; *h*, *k*, *l*	0 to 12, −14 to 0, −24 to 0
Total no. refls.	2643
No. obsd. data ($F > 6.0\sigma(F)$)	1420
Weighting *G*	0.0007
R	0.045
R_w	0.054
Goodness of fit	1.43
Largest/mean Δ/σ	0.02/0.0
Parameters refined	399
Max/min density in Δ*F* map, e/Å^3	0.29/−0.16

ences for C-1, H-1_α, H-1_β, C-5, H-5_β, C-10, and particularly for C-20 and H-20, reflecting structural differences in rings B and C. The unusual ^{1}H chemical shift for H-20 in **3** may also be due to the anisotropic shielding effect of the proximal C=C bond. In the case of ring B, all of the ^{13}C and ^{1}H chemical shifts for **1** are significantly different from those in **2** and **3**, reflecting the difference between boat and chair conformations. Between **2** and **3**, C-5, H-5, C-6, H-6_α, H-6_β, and C-7 chemical shifts are generally similar while H-7_α and H-7_β show significant differences, possibly reflecting different anisotropic shielding effects of the different double bond locations. C-8 and C-9 also show significant chemical shift differences, probably due to the different B–C ring junctions in **2** and **3**. Comparisons for ring C are generally meaningless due to the different structures of the three compounds. However, the much larger δ value for C-14 in **3** than in to **1** and **2** is noteworthy.

Conclusion

Each of the kaurane derivatives, **1–3**, has similar solid state and solution conformations. There are at least four differences among these compounds that could account for differences in pharmacological activity. The first two are the obvious structural differences, i.e., the additional double bond in **1** and the endocyclic double bond in **3** compared to the exocyclic double bonds in **1** and **2**. However, the two additional differences revealed in this investigation are the significantly different spatial locations of the endocyclic or exocyclic double bond in the three compounds and the fact that **2** and **3** have very similar shapes while **1** has a significantly different shape. These differences may allow an understanding of the structure–activity relationships between these compounds, once their in vivo pharmacological activities have been unambigously established.

Experimental

Isolation of 1–3

Dried roots of *Montanoa tomentosa* (300 g) were ground to a coarse power and macerated three times with CH_2Cl_2 for periods of 24 h. The combined extracts were evaporated in vacuo, yielding 18 g of a viscous oily residue. The latter was submitted to column chromatography with SiO_2, eluting with a gradient of hexane: ethyl acetate from a 9:1 to a 7:3 ratio. **2** (mp 179–181°C (lit. (20) mp 179–180°C)) was clearly separated while **1** and **3** occurred in nearby fractions with **1** as the major component. Fractional crystallization was used to separate pure **1** (mp 154–156°C, (lit. (21) mp 155–157°C)) while **3** was further purified using 2 mm SiO_2 preparative thin-layer chromatography, eluting three times with a 93:7 ratio of hexane: ethyl acetate (mp 179–180°C, (lit. (2) mp 180°C)). **3** was subsequently recrystallized from slowly cooled hot hexane to obtain crystals suitable for X-ray diffraction.

Crystal structure determination

X-ray intensity data were collected on an Enraf–Nonius CAD-4 diffractometer at room temperature, using graphite monochromated Mo K^α radiation (λ = 0.71073 Å). The ω–2θ scan technique was applied with variable scan speeds (1.83–5.49°/min in ω). Accurate cell dimensions were determined from the

© 1997 NRC Canada

setting angles of 24 reflections in the range $20° < 2\theta < 25.2°$. Two standard reflections measured every two hours showed no decrease in intensity. The data were corrected for Lorentz and polarization effects but not for absorption.

The structure was solved by direct methods. C and O atoms were refined anisotropically by full-matrix least squares to minimize $\Sigma w(F_o - F_c)^2$, where $w^{-1} = \sigma^2(F) + gF^2$. Hydrogen atoms were positioned on geometric grounds (C—H 0.96 Å) and included in the calculations as riding atoms. An overall hydrogen atom thermal parameter refined to a value of 0.082(4) $Å^2$. The electron density contours of the hydroxyl hydrogen atoms were visible from a difference Fourier map calculated in the plane of the four oxygen atoms of the dimer molecule. In the final cycles of least-squares the hydroxyl hydrogen atoms were included in the refinement in calculated positions and fixed thermal parameters (O—H 0.87 Å, 0.08 $Å^3$).

Crystal data, data collection, and least-squares parameters are listed in Table 4. All calculations were performed using SHELXTL PC (22) on a 486-66 personal computer.

NMR spectroscopy

Spectra were obtained on Varian Unity-400 and Unity-500 spectrometers, the former fitted with a computer-switchable ^{1}H-heteronuclear probe optimized for ^{13}C detection while the latter was equipped with a 5 mm inverse detection probe. Initial 2D NMR measurements were carried out on the Unity-400, using ca. 30 mg of sample dissolved in 1 mL $CDCl_3$ while ^{13}C and ^{1}H spectra were obtained using 3 mg of sample. Further inverse detection experiments were carried out on the UNITY-500 using the more dilute samples since there seemed to be significant dilution shifts, particularly for protons and carbons close to the carboxylic acid function.

References

1. A.J. Gallegos. Contraception, **27**, 211 (1983).
2. Y. Caballero and F. Walls. Bol. Inst. Quim. Univ. Nac. Auton. Mex. **22**, 103 (1970).
3. A.J. Gallegos. U.S. Pat., 4,491,593; Chem. Abstr. **102**, 137790 (1985).
4. X. Lozoya, R.G. Enriquez, E. Bejor, A.V. Estrada, H. Giron, H. Ponce-Monter, and A.J. Gallegos. Contraception, **27**, 267 (1983).
5. A.J. Gallegos. Contraception, **31**, 487 (1985).
6. H.H.S. Fong, Y. Oshima, A. Martin, S. Sasnick, Y. Zhu, C. Konno, Z. Tu, Z. Lin, D.O. Soejarto, G.A. Cordell, and D.P. Walker. Proc. Int. Symp. on Traditional Medicines and Modern Pharmacology, Beijing, PRC, p. 100. 1987.
7. Z.-Z. Lu, H.-Z. Xue, Z.-B. Tu, C. Konno, D.P. Waller, D.O. Soejarto, G.A. Cordell, and H.H.S. Fong. J. Nat. Prod. **50**, 996 (1987).
8. J.I. Page, F. Balza, T. Nishida, and G.H.N. Towers. Phytochemistry, **31**, 3437 (1992).
9. R.G. Enriquez, L.I. Escobar, M.L. Romero, M.A. Chavez, and X. Lozoya. J. Chromatogr. **258**, 297 (1983).
10. X. Dong, M.O. Hamburger, G.A. Cordell, and H.H.S. Fong. Planta Med. **55**, 185 (1989).
11. R.G. Enriquez, B. Ortiz, I. Leon, G. Magos, S. Capella, A. Pena, W.F. Reynolds, and D. Gnecco. Planta Med. **62**, 569 (1996).
12. W.F. Reynolds, R.G. Enriquez, L.I. Escobar, and X. Lozoya. Can. J. Chem. **62**, 2421 (1984).
13. W.F. Reynolds, A.J. Lough, J.F. Sawyer, R.G. Enriquez, B. Ortiz, and F. Walls. Acta. Crystallogr. Sect. C: Cryst. Struct. Commun. C **47**, 973 (1991).
14. C. Brassy, B. Bachet, and E. Wollenweber. Acta. Crystallogr. Sect. C: Cryst Struct. Commun. C. **44**, 528 (1988).
15. A. Bax and R. Freeman. J. Magn. Reson., **44**, 542 (1981)
16. (*a*) A. Bax and G.A. Morris. J. Magn. Reson. **42**, 501 (1981); (*b*) A. Bax. J. Magn. Reson. **53**, 517 (1983).
17. A. Bax and S. Subramamian. J. Magn. Reson. **67**, 565 (1986).
18. W.F. Reynolds, S. McLean, M. Perpick-Dumont, and R.G. Enriquez. Magn. Reson. Chem. **27**, 162 (1989).
19. A. Bax and M.F. Summers. J. Am. Chem. Soc. **108**, 2093 (1986).
20. J.R. Cannon, P.W. Chow, P.F. Jefferies, and G. Meechan. Aust. J. Chem. **19**, 861 (1966).
21. C.H. Brieskorn and E. Poblaman. Chem. Ber. **102**, 2621 (1969).
22. G. Sheldrick. SHELXTL PC. Siemens Analytical X-ray Instruments, Madison, Wis. 1990.

Can. J. Chem. Downloaded from www.nrcresearchpress.com by 92.62.229.171 on 09/08/12
For personal use only.

© 1997 NRC Canada

The steric course of some electrophilic additions to the tetrahydropyridazine ring moiety of benzo[*g*]pyridazino[1,2-*b*]-phthalazine-6,13-dione derivatives. II.[1]

María del Carmen Cano, Fernando Gómez-Contreras, Ana María Sanz, and María Josefa Rodríguez Yunta

Abstract: The stereochemical features involved in electrophilic additions to the ring A moiety in diazatetracyclic analogues of anthracyclinones have been investigated. The 1-methyl and 1,3-dimethyl derivatives **2a** and **2b** were selected as the substrates and made to react with bromine azide, iodine azide, and NBS–EtOH in order to evaluate the influence of the C-1 substituent on the product distributions. Electrophilic attack at the C-2/C-3 double bond occurs mainly in the less hindered *anti* fashion. The nucleophilic step governs the stereochemistry of the reaction products. Conformational factors are predominant over the steric and electronic effects originated by the ring A substituents, since axial antiparallel attack of the nucleophile on the intermediate epihalonium ion is clearly preferred to the equatorial approach.

Key words: diazatetracycles, Diels–Alder reaction, electrophilic addition, anthracyclinone analogues, pyridazine ring.

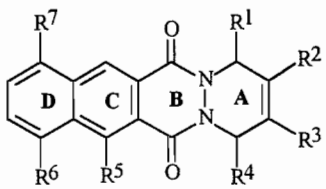
Résumé : On a étudié les caractéristiques stéréochimiques impliquées dans les additions électrophiliques sur le cycle A d'analogues diazatétracycliques d'anthracyclinones. Dans le but d'évaluer l'influence du substituant en C-1 sur la distribution des produits, on a choisi les dérivés 1-méthylé et 1,3-diméthylé, **2a** et **2b**, comme substrats pour des réactions avec les azotures de brome et d'iode ainsi qu'avec le NBS–EtOH. L'attaque électrophilique sur la double liaison en C-2/C-3 se fait principalement de la façon *anti* la moins empêchée. L'étape nucléophilique détermine la stéréochimie des produits réactionnels. Les facteurs conformationnels prédominent sur les effets stériques et électroniques provenant des substituants présents sur le cycle A; cette conclusion découle du fait que l'attaque axiale antiparallèle du nucléophile sur l'ion épihalogénium est nettement favorisée par rapport à celle impliquant un rapprochement équatorial.

Mots clés : diazatétracycles, réaction de Diels–Alder, addition électrophilique, analogues d'anthracyclinone, noyau pyridazine.

[Traduit par la rédaction]

Quite a number of papers have appeared concerning the total synthesis of anthracyclinones, the aglycons of the highly active anticancer anthracyclines (1). Diverse strategies have been also developed for the preparation of non-natural analogues (2), in an effort to minimize the dose-dependent cardiotoxicity shown by most of the known anthracyclines (3). The modification of redox properties by introducing heteroatoms in the carbocyclic backbone appears as a promising means of reducing toxicity and improving neoplastic activity (4).

In earlier publications (for a review, see ref. 5) we described an efficient method for the synthesis of the benzo[*g*]-pyridazino[1,2-*b*]phthalazine-6,13-dione system, **1**, via the Diels–Alder cycloaddition of benzo[*g*]phthalazine-1,4-dione, an unstable compound available by the in situ lead tetraacetate oxidation of benzo[*g*]phthalic hydrazide (6), with substituted 1,3-butadienes. These diazatetracyclic compounds exhibit the main features required for the intercalating action of anthracyclinones: an aromatic moiety providing an adequate planar area, a quinone-like system, and a conformationally flexible ring A that can be functionalized in order to allow the proper intermolecular binding to the third pair of DNA bases (7).



1

R^1 = COOR, Me, Ph, NR_2, H
R^2 = COR, Et, Me, COOR, H
R^3 = Me, H
R^4 = Me, Ph, H
R^5, R^6, R^7 = OH, OR, H

Received June 6, 1996.[2]

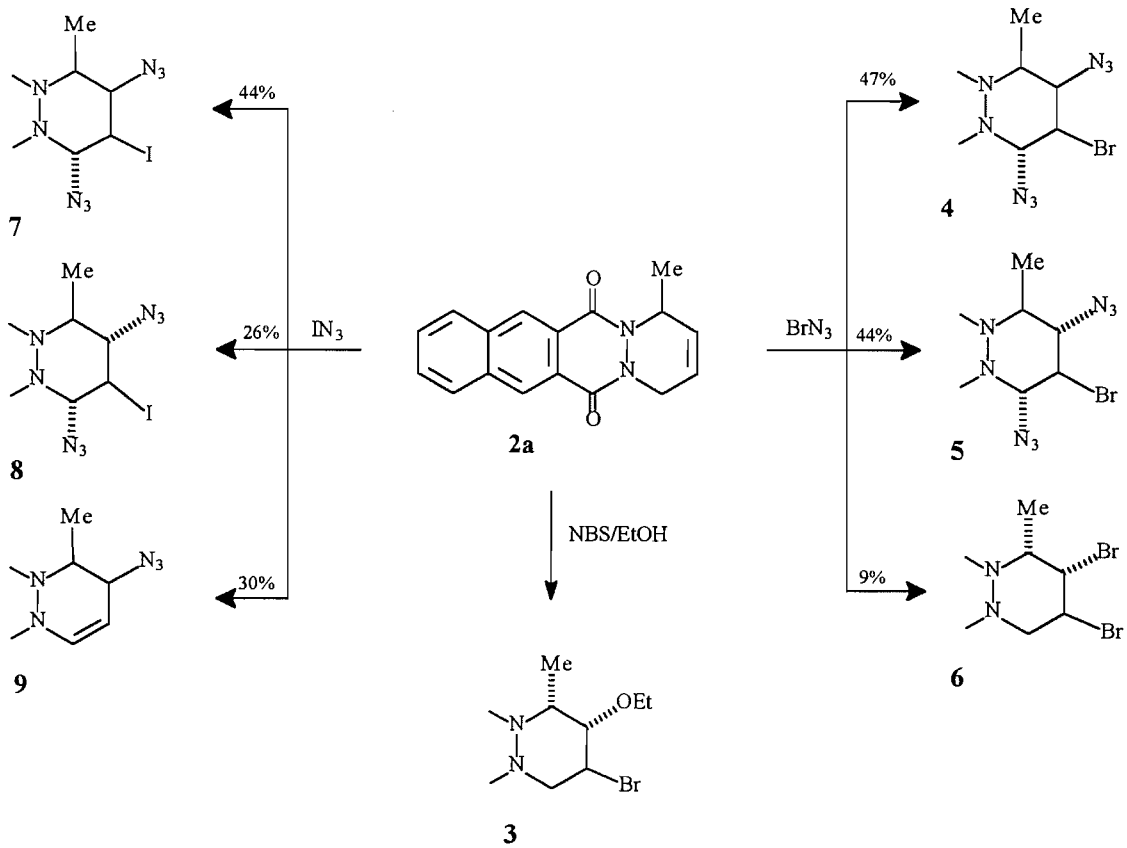
M.C. Cano, F. Gómez-Contreras,[3] A.M. Sanz, and M.J.R. Yunta. Departamento de Química Orgánica I, Facultad de Ciencias Quimicas, Universidad Complutense, Avenida Complutense s/n, 28040 Madrid, Spain.

[1] Part I: ref. 8.
[2] Revision received January 23, 1997.
[3] Author to whom correspondence may be addressed. Telephone: (341) 394-4229. Fax: (341) 394-4103. E-mail: Fercon@eucmax.sim.ucm.es

© 1997 NRC Canada

Can. J. Chem. Downloaded from www.nrcresearchpress.com by 92.62.229.171 on 09/08/12
For personal use only.

Scheme 1.



The introduction of electronegative substituents into the terminal tetrahydropyridazine ring moiety of **1** is essential for achieving the required interaction with DNA chains. Furthermore, both the stereochemistry of these substituents and the conformation adopted by ring A have a decisive influence on the intercalating properties of anthracyclinones (7). In the preceding paper of this series (8) we reported on the steric course of some electrophilic additions to the C-2/C-3 double bond of 2-methyl and 2,3-dimethyl-substituted diazatetracyclic compounds of type **1**, in an effort to evaluate the electronic and stereoelectronic factors involved. However, the stereochemical influence of substituents at the C-1 or C-4 positions has not yet been evaluated. In this respect, it should be noted that substitution at C-1 greatly affects the geometry of ring A (9), because destabilizing interactions with the C=O groups at the ring B moiety arise when the substituent is equatorially oriented.

Therefore, we report in this paper on some electrophilic additions to the 1-methyl and 1,3-dimethyl-substituted substrates **2a** and **2b**. As in the preceding paper (8), bromine azide, iodine azide, and *N*-bromosuccinimide–EtOH were the reactants of choice. As usual, high amounts of unchanged **2** were recovered in every reaction performed, due to the lack of reactivity caused by the electron-withdrawing effect of the amido groups. The use of more stringent reaction conditions led to ring opening and gave large amounts of benzo[*g*]phthalic anhydride. Conditions described in the experimental part are those combining the highest yield of addition products with the least extent of ring opening. In fact, the formation of ring-opening products was not detected under the conditions reported here. A range of experiments were run for every reaction in order to confirm the reproducibility of the regio- and stereochemical results.

Scheme 1 displays the compounds obtained by treatment of 1-methyl-1,4-dihydrobenzo[*g*]pyridazino[1,2-*b*]phthalazine-6,13-dione **2a** with every reactant. The reaction with NBS–EtOH–H_2SO_4 at 50°C afforded exclusively the *t*-3-bromo-*c*-2-ethoxy-*r*-1-methyl (**3**) derivative. Bromine azide in dichloromethane–nitromethane at room temperature gave the *t*-4,*c*-2-diazido-*c*-3-bromo-*r*-1-methyl (**4**) and *t*-2,*t*-4-diazido-*c*-3-bromo-*r*-1-methyl (**5**) derivatives,[4] together with a small amount of the dibromo compound (**6**), in relative percentages of 47:44:9. Iodine azide in chloroform–acetonitrile yielded the *c*-2,*t*-4-diazido-*c*-3-iodo-*r*-1-methyl (**7**) and *t*-2,*t*-4-diazido-*c*-3-iodo-*r*-1-methyl (**8**) derivatives,[4] together with allylazide (**9**), in a 44:26:30 relation. The products were isolated after laborious preparative TLC work, and 300 MHz ^{1}H NMR spectroscopic analyses were made previously in order to confirm that no structural changes had occurred during the purification procedure. Distribution of the addition derivatives

[4] Addition products have been numbered in all cases by assigning the lower number to the carbon atom attached to the methyl group, in order to make easier the discussions on stereochemical features.

© 1997 NRC Canada

Can. J. Chem. Downloaded from www.nrcresearchpress.com by 92.62.229.171 on 09/08/12
For personal use only.

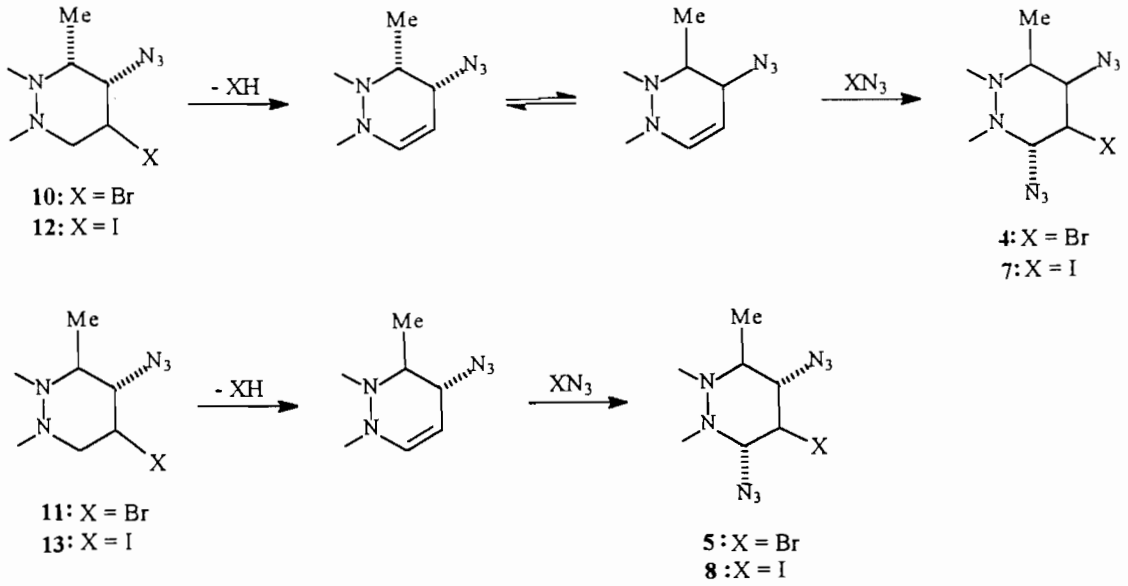
Can. J. Chem. Downloaded from www.nrcresearchpress.com by 92.62.229.171 on 09/08/12
For personal use only.

Table 1. Some analytical and spectroscopic data for the addition products from **2a,b**.

Compound	Yield[a] (%)	R_f[b]	MS *m/e* (%)			IR KBr, cm^{-1}		
3	28	0.46	402(53,M^+)	387(13)	308(6)	1645(C=O)	1155(C-O)	670(C-Br)
4	52	0.65	437(15,M^+)	357(4)	277(18)	2100(N_3)	1660(C=O)	670(C-Br)
5	48	0.65	437(15,M^+)	398(20)	277(18)	2100(N_3)	1665(C=O)	670(C-Br)
6	5	0.51	438(10,M^+)	357(3)	277(18)	1655(C=O)	1150(C-O)	670(C-Br)
7	11	0.39	488(4,M^+)	446(10)	319(30)	2095(N_3)	1650(C=O)	1620(C=C)
8	14	0.31	488(9,M^+)	369(10)	277(77)	2100(N_3)	1660(C=O)	1625(C=C)
9	33	0.19	319(2,M^+)	277(100)	254(10)	2100(N_3)	1655(C=O)	1625(C=C)
14	8	0.38	416(5,M^+)	372(3)	291(14)	1650(C=O)	1620(C=C)	670 (C-Br)
15	17	0.48	462(5,M^+)	417(47)	293(17)	1655(C=O)	1620(C=C)	675(C-Br)
16	7	0.31	336(84,M^+)	291(49)	276(10)	1645(C=O)	1625(C=C)	1170(C-O)
18	9	0.48	456(8,M^+)	414(4)	291(33)	2100(N_3)	1665(C=O)	620(C-Br)
19	7	0.44	456(8,M^+)	414(4)	291(33)	2100(N_3)	1665(C=O)	620(C-Br)
20	6	0.06	333(14,M^+)	291(42)	254(100)	2110(N_3)	1645(C=O)	1620(C=C)
21	6	0.39	452(77,M^+)	373(27)	291(74)	1660(C=O)	1625(C=C)	665(C-Br)
23	5	0.38	461(24,M^+)	334(1)	292(7)	2095(N_3)	1645(C=O)	1095(C-O)
24	5	0.38	461(24,M^+)	334(1)	292(7)	2105(N_3)	1665(C=O)	1615(C=C)

[a]Whole yields taking into account the percentage of unreacted adduct recovered.
[b]Measured under conditions described in the experimental part.

Scheme 2.



in the reaction mixtures was calculated from integration of the methyl group signals in the ^1H NMR spectra. Table 1 displays some analytical properties concerning the products of addition to **2a**.

As established in previous work for the 2-methyl and 2,3-dimethyl-substituted substrates (8), bromodiazides **4** and **5** should be formed from the addition products **10** and **11**, respectively, through dehydrohalogenation of the initial electrophilic addition product and further regiospecific addition to the C-1/C-2 double bond, according to the sequences shown in (Scheme 2). In the case of **4**, it implies nitrogen inversion of the intermediate allylazide favored by the decrease of steric hindrance between the carbonyl group at ring B and the C-1 methyl, as the latter moves from a pseudoequatorial to a pseudoaxial orientation (9). In a similar way, iododiazides **7** and **8** should derive from iodoazides **12** and **13**, the former via the isolated allylazide **9.**

Stereo- and regiochemical features in the ring A moiety have been elucidated mainly on the basis of high-resolution ^1H NMR spectra (Table 2). In contrast to the behaviour of less substituted analogues (10), the tri- and tetrasubstituted compounds isolated have been shown to be conformationally homogeneous. Proton chemical shifts at ring A are strongly affected by the nature of the substituent attached to the same carbon ($\delta_{H\text{-}C\text{-}Br}$, $\delta_{H\text{-}C\text{-}I} > \delta_{H\text{-}C\text{-}OEt}$, $\delta_{H\text{-}C\text{-}N3}$). This fact has been used for assignment purposes (11) (see, for instance, H-2 and

© 1997 NRC Canada

Table 2. ^{1}H NMR chemical shifts (ppm, δ scale) and coupling constants (Hz) at the terminal tetrahydropyridazine ring of the addition products of **2a**, measured in $CDCl_3$.[a]

Compound	δ_{H1}	δ_{H2}	δ_{H3}	δ_{H4a}	δ_{H4e}	$\delta_{HMe\text{-}C1}$	J_{H1-H2}	J_{H2-H3}	J_{H3-H4a}	J_{H3-H4e}	J_{H2-H4e}
3	5.46(m)	3.68(m)	4.38(m)	4.06(dd)	4.93(o)	1.57(d)	3.4	2.3	3.1	3.1	1.0
4	4.89(m)	3.84(dd)	4.22(dd)	—	6.59(d)	1.50(d)	5.2	7.5	—	2.4	—
5	5.49(m)	4.49(dd)	4.62(dd)	—	6.77(d)	1.59(d)	3.4	4.5	—	3.3	—
6	5.55(m)	4.70(m)	4.65(m)	4.47(dd)	4.98(o)	1.58(d)	3.2	2.5	3.2	3.5	1.5
7	4.87(m)	3.79(dd)	4.27(dd)	—	6.63(d)	1.57(d)	5.8	8.1	—	3.4	—
8	5.17(m)	3.73(t)	4.59(dd)	—	6.66(d)	1.52(d)	4.7	4.5	—	3.5	—
9	5.52(m)	3.87(dd)	5.60(dd)	7.88(d)	—	1.25(d)	5.6	<1	<1	—	—

[a]TMS as internal standard.

Table 3. Torsion angles (°) calculated for the tetrahydropyridazine terminal ring of some addition products to **2a**.

Compound	ϕ_{H1-H2}	ϕ_{H2-H3}	ϕ_{H3-H4e}	ϕ_{H3-H4a}
3	315.6	289.9	59.5	305.5
4	315.9	30.4	63.5	—
6	307.8	294.3	55.4	307.1
7	320.2	26.7	55.3	—

H-3 chemical shifts in **6**). On the other hand, vicinal and long-range coupling constants can be easily applied to determine the relative orientations of the substituents, as there are protons attached to every carbon of the ring. The C-1 methyl group is axially oriented in compounds **4**, **5** and **7–9**, but it has an equatorial position in **3** and **6** (hashed bonds).

From the experimental J_{H2-H3} and J_{H1-H2} values obtained for the tetrasubstituted derivatives **4** and **7**, substantial deviations from the pure chair conformations can be assumed (12). This is due to the coexistence of a diversity of unfavored steric interactions: *syn*-1,3-diaxial between the C-1 and C-3 substituents, $A^{1,3}$ between the C-1 and C-4 substituents and the neighbouring carbonyls (9), and also *gauche* between the C-2 azido group and the halogen at C-3. In fact, J_{H2-H3} and J_{H3-H4} are higher in **7** (8.1 and 3.4 Hz) than in **4** (7.5 and 2.4 Hz) owing to the presence of the bulky iodine atom in **7**. Conversely, the axial orientation of the C-2 azido group in **5** and **8** reduces steric hindrance and, therefore, coupling constants are closer to those expected for a chair form (13). *W* long-range couplings are not observed due to the lack of coplanarity between 1,3-diequatorial protons. However, trisubstituted derivatives **3** and **6** present long-range J_{H2-H4e} couplings (1.0 and 1.5 Hz), confirming both the axial orientation of the substituents at C-2 and C-3 and the prevalence of a classical chair conformation.

Calculation of the torsion angles from the experimental coupling constants by means of the Altona equation (14) (Table 3) confirms a significant flattening of the C-1/C-2/C-3/C-4 moiety in **4** and **7**, which is increased when the C-2 substituent is an iodine atom. On the contrary, the less hindered dibromo (**6**) and bromoethoxy (**3**) derivatives exhibit much less distorted geometries.

Analogous treatment of 1,3-dimethyl-1,4,6,13-tetrahydrobenzo[*g*]pyridazino[1,2-*b*]phthalazine-6,13-dione, **2b**, led to results displayed in Scheme 3. The reaction of **2b** with NBS–EtOH–H_2SO_4 afforded the *c*-2-bromo-*t*-3-ethoxy-*r*-1-methyl (**14**), *t*-3-bromo-*c*-2,*c*-4-diethoxy-*r*-1-methyl (**15**), and *c*-2-ethoxy-*r*-1-methyl (**16**) derivatives in 25:56:19 ratio. As usual (8), compound **15** arises from the dehydrohalogenation of **17** and further regiospecific addition of bromine and ethoxyl (Scheme 4). Treatment with bromine azide led to isolation of the isomeric *c*-2,*t*-4-diazido-*c*-3-bromo-*r*-1-methyl (**18**) and *c*-2,*c*-4-diazido-*t*-3-bromo-*r*-1-methyl (**19**) derivatives, accompanied by the *c*-allylazide **20** and the dibromide **21**, in relative percentages of 34:25:16:25. Compounds **18–20** should derive from the bromoazide **22** as shown in Scheme 4 (nitrogen inversion of the elimination product to give allylazide **20** is sterically favored due to the pseudoaxial orientation of the C-1 methyl group (9)) In the presence of iodine azide, the stereoisomeric azidoiodo derivatives **23** and **24** were characterized together with allylazide **20** in 22:22:56 percentages. In this last reaction analytical TLC showed the presence of much smaller amounts of two other compounds that could not be isolated or identified.

The higher percentages of halodiazides obtained from both **2a** and **2b** with bromine azide (and also from other substrates (8)) can be explained on the basis of the more electrophilic character of the bromonium ion.

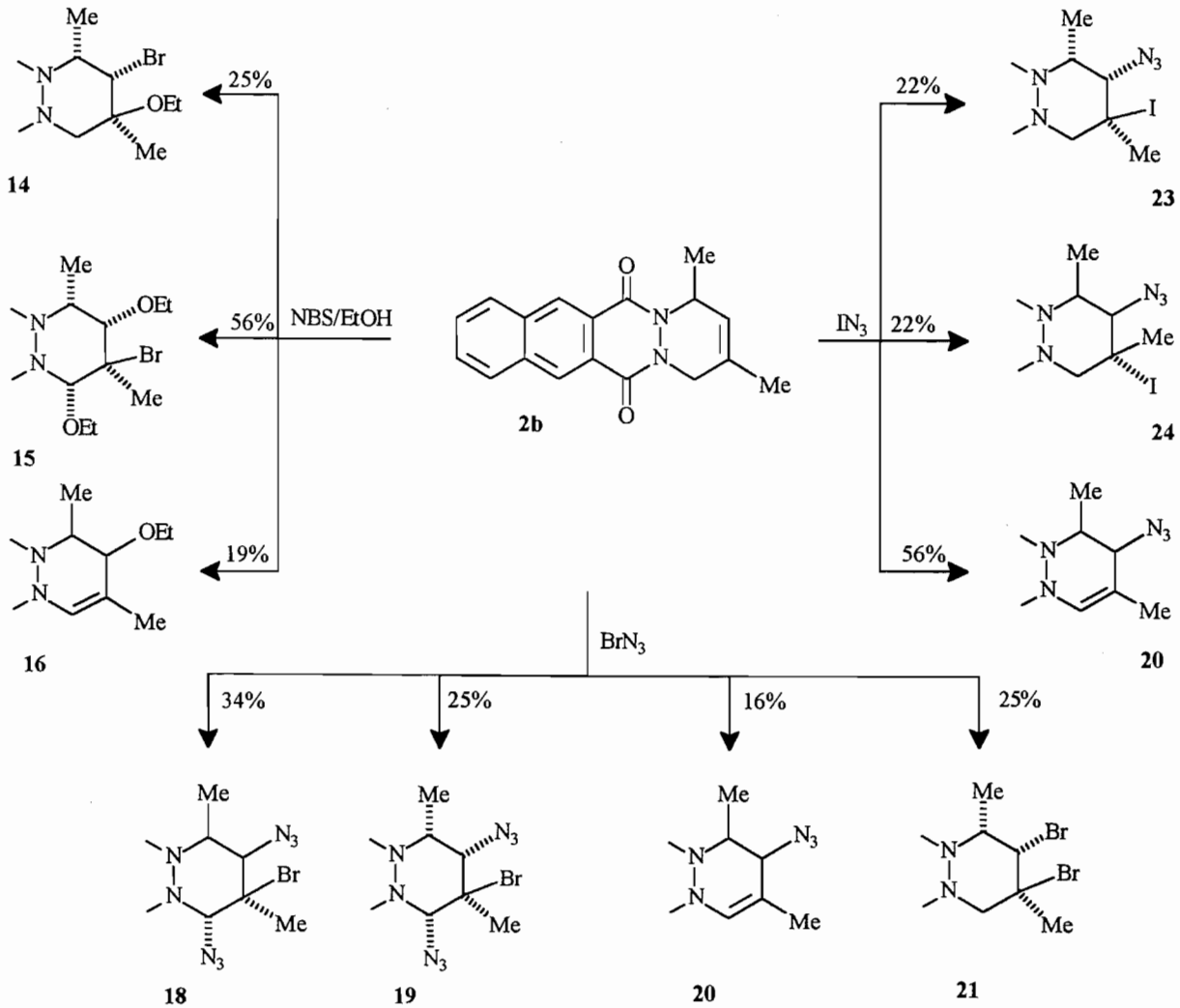
Table 4 displays the chemical shifts and coupling constants of ring A protons obtained from the 300 MHz ^{1}H NMR spectra, which were used to assign the position and orientation of the ring substituents. As in previous series, the nature of the C-3 substituents can be accurately deduced from the δ values measured for the C-3 methyl groups (8), and the same applies for the C-4 substituents and the H-4 chemical shifts, as $\delta_{CH\text{-}OEt} > \delta_{CH\text{-}N3}$. J_{H1-H2} coupling constants show the stereochemical relationship between the C-1 methyl and the C-2 substituent (J_{He-Ha} values are high owing to chair deformations due to steric hindrance). The C-1 methyl stereochemistry is confirmed from $J_{Me\text{-}C1}$ values, which increase when the methyl group is axially oriented.[5] On the other hand, *W* long-range

[5] This fact is due to the antiperiplanar arrangement that may adopt the hydrogen atoms of an axial methyl group with respect to the neighbouring bridgehead nitrogen, which reduced the *J* value. That arrangement is not possible when the alkyl substituent is equatorially oriented because of steric hindrance with the neighbouring carbonyl group at ring B. Such effects will be considered in full in the following part of this series.

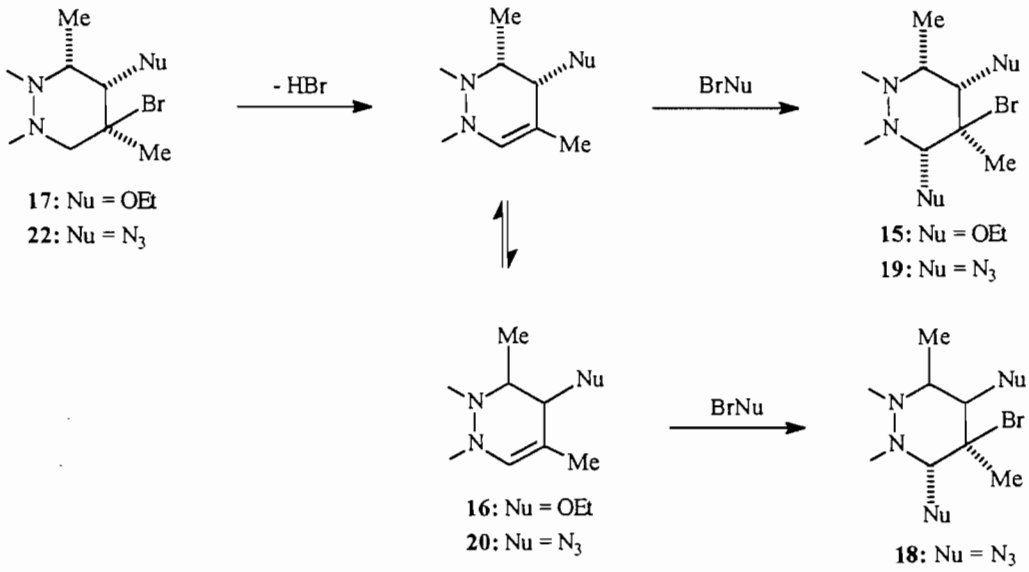
© 1997 NRC Canada

Can. J. Chem. Downloaded from www.nrcresearchpress.com by 92.62.229.171 on 09/08/12
For personal use only.

Scheme 3.



Scheme 4.



Can. J. Chem. Downloaded from www.nrcresearchpress.com by 92.62.229.171 on 09/08/12
For personal use only.

© 1997 NRC Canada

Table 4. ^{1}H NMR chemical shifts (δ scale) and coupling constants (Hz) at the terminal tetrahydropyridazine ring of the addition products from **2b,** measured in $CDCl_3$.[a]

Compound	δ_{H1}	δ_{H2}	δ_{H4a}	δ_{H4e}	$\delta_{Me\text{-}C1}$	$\delta_{Me\text{-}C3}$	$J_{H1\text{-}H2}$	$J_{H1\text{-}Me}$	$J_{H2\text{-}H4e}$	$J_{H4a\text{-}H4e}$
14	5.44(o)	4.20(dd)	3.54(d)	4.96(dd)	1.50(d)	1.40(s)	3.6	7.2	0.9	13.9
15	5.36(o)	3.48(dd)	—	6.13(d)	1.42(d)	1.95(s)	3.6	7.2	2.2	—
16	5.66(o)	3.66(d)	—	7.58(s)	1.30(d)	2.10(s)	1.6	6.0	—	—
18	4.95(o)	3.85(d)	—	6.66(s)	1.51(d)	2.03(s)	4.2	6.7	—	—
19	5.25(o)	3.53(d)	—	6.41(s)	1.56(d)	2.01(s)	4.6	7.2	—	—
20	5.53(o)	3.97(m)	—	7.50(d)	1.16(d)	2.08(s)	1.2	6.7	—	—
21	5.65(o)	4.73(m)	3.91(d)	5.00(dd)	1.66(d)	2.10(s)	3.8	7.5	1.5	15.1
23	5.40(o)	4.28(dd)	4.42(d)	4.66(dd)	1.70(d)	1.94(s)	2.8	7.2	1.4	14.1
24	5.54(o)	3.89(d)	4.02(d)	4.14(d)	1.84(d)	2.15(s)	4.2	6.9	—	15.0

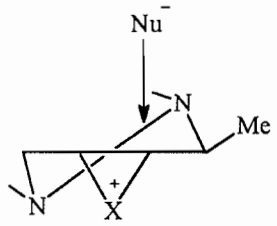
[a]TMS as internal standard.

couplings between H-2 and H-4e are found in compounds **14**, **15**, **21**, and **23**, confirming the axial orientation of the substituents attached to C-2 and C-4. The only exception is bromodiazide **19**, in which substitution at C-4 leads to 1,3-*syn*diaxial interaction between the two azido groups that must preclude coplanarity between H-2 and H-4. Last, the C-3 methyl group of **24** is deshielded by 0.21 ppm with respect to that of **23**, in spite of having the same substituents at C-2 and C-3. This may be due to the 1,3-*syn*diaxial interaction between the two methyls of iodoazide **24** (15), and agrees with the stereochemical assignments described above.

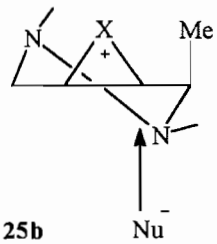
If we consider now the regio- and stereochemical implications of the product distributions obtained from these substrates, it should be pointed out that the presence of the C-1 methyl group in both **2a** and **2b** introduces a new steric factor with respect to the 2-methyl and 2,3-dimethyl-substituted substrates studied in the previous work (8). The stereoselectivity of the electrophilic attack is shown in Table 5 for the different reactants employed. Attack occurs preferentially over the less hindered side of ring A to give the sterically favored *anti* epihalonium ion. This implies a remarkable steric effect of the C-1 methyl, probably due to its high tendency to move away from the neighbouring carbonyl group at ring B (9). With respect to the nucleophilic step, different explanations should be considered regarding the behaviour of **2a** and **2b**. In **2a**, opening of the *trans* epihalonium ion takes place always through axial antiparallel attack over C-2, conformationally more favored than equatorial attack at C-3 (16), in spite of the steric hindrance involved with the pseudoequatorial C-1 methyl (**25a**). The *cis* epihalonium ion is opened by antiparallel attack on C-2, with the C-1 methyl in a pseudoaxial orientation (**25b**). Therefore, it is shown that conformational requirements prevail in all cases both over steric and electronic considerations.

The 1,3-dimethyl-substituted substrate matches the steric effect of the C-1 methyl with the electronic one of the second methyl group. However, the influence of the latter seems to be negligible, since Table 5 shows that the nucleophile attaches very selectively to the C-2 position. As seen for **2a**, axial antiparallel attack on C-2 with the C-1 methyl pseudoequatorially oriented is clearly predominant in the nucleophilic step (**25c**).

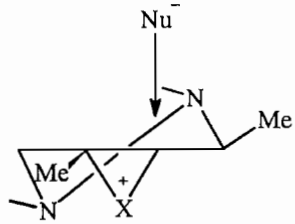
In consequence, it may be concluded that the C-1 methyl orientation is the essential factor controlling the regioselectivity, since the substituent directs nucleophilic attack towards C-2 or C-3 according to its axial or equatorial disposition. The high predominance of *anti* addition products with the C-1 methyl equatorially oriented indicates that *syn*-1,3-diaxial interactions between the methyl group and the nucleophile are more destabilizing than $A^{1,3}$ hindrance between the equatorial methyl and the nearby carbonyl group. These facts should be taken into account when making electrophilic additions to the ring A moiety in order to achieve stereochemical results approximating the geometry of the anthracyclinone models.



25a



25b



25c

Experimental

Melting points are uncorrected, and were determined in open capillary tubes with a Gallenkamp apparatus. IR spectra were recorded in KBr pellets on a Perkin–Elmer 257 spectrophotometer. NMR spectra were obtained with a Varian XL-300 spectrophotometer for solutions in $CDCl_3$ or d_6-DMSO with

© 1997 NRC Canada

Can. J. Chem. Downloaded from www.nrcresearchpress.com by 92.62.229.171 on 09/08/12
For personal use only.

Can. J. Chem. Downloaded from www.nrcresearchpress.com by 92.62.229.171 on 09/08/12
For personal use only.

Me_4Si as internal reference. Assignments were made by appropriate decoupling experiments and comparison of the spectra of related structures. Direct inlet mass spectra were measured on a Hitachi Perkin–Elmer RMV-GM6 spectrometer. Chromatographic separations were carried out by using 20 × 20 cm preparative TLC plates coated with a 2 mm layer of silica gel $60PF_{254}$ Merck. Dichloromethane was refluxed over P_2O_5 and distilled. Chloroform was purified by washing with 2 N NaOH, concentrated H_2SO_4, and water, drying with K_2CO_3, and distillation, and was used immediately. Dry ethanol was obtained via the formation of the magnesium ethanolate and distillation. Nitromethane was purified by standing for a day with H_2SO_4, washing with water, drying over $MgSO_4$, and distillation. Acetonitrile was shaken with molecular sieves and, subsequently, with CaH_2 until no further hydrogen was evolved, and was fractionally distilled over CaH_2. $MgSO_4$ was always used as the drying agent in the work-up for addition reactions.

Benzo[*g*]phthalic hydrazide was obtained from α,α,α′,α′-tetrabromo-*o*-xylene and maleic anhydride according to Cava et al. (17). Substrates **2a** and **2b** were prepared by oxidation of the hydrazide in the presence of the appropriate diene, following a procedure previously described (9).

The haloazide solutions were prepared as follows:

Bromine azide: To a suspension of 0.05 mol of sodium azide in 30 mL of dichloromethane, 7 mL of 37% HCl were added. The heterogeneous mixture was stirred for 10 min at 0°C and 0.05 mol of molecular bromine was addded. After 30 min stirring, the organic layer was collected and used without further purification.

Iodine azide: Commercial chlorine iodide (0.006 mol) was added to a solution of 0.01 mol of sodium azide in 30 mL of dry acetonitrile cooled to 0°C. The mixture was stirred for 10 min and used without further purification.

The reaction mixtures of the electrophilic additions consisted of an appreciable amount of unreacted alkene and the addition products described above, and the percentages were calculated from integration of the signals displayed by the methyl groups in the 300 MHz ^1H NMR spectra. Several runs were carried out for every condition and results reported are average values. The reaction mixtures were chromatographed, and IR, NMR, and mass spectra were obtained for each one of the recovered fractions in order to confirm the identity and solve the stereochemistry of the compounds involved. The stereoisomeric mixtures **4/5**, **7/8**, **18/19**, and **23/24** could not be separated, as they gave only one spot in analytical TLC, but were assigned on the basis of the NMR spectra.

Addition reaction conditions

(a) With NBS–EtOH

Equimolecular amounts of **2a,b** and *N*-bromosuccinimide were suspended in dry ethanol and stirred for 5 h at 50°C. After addition of water, the solvent was removed to half of the initial volume and the remaining solution was filtered. The precipitate was repeatedly washed with water, dried, and submitted to preparative TLC over silica gel by using toluene/ethanol (98:2) as the eluent.

(b) With BrN_3

2a,b (0.03 mol) in 30 mL of nitromethane was added to 35 mL of a solution of bromine azide in dichloromethane prepared as described above. After 30 min stirring at room temperature the solvent was evaporated at reduced pressure to give a yellow residue, which was submitted to preparative TLC over silica gel by using toluene/ethanol (98/2) as the eluent.

(c) With IN_3

2a,b (0.03 mol) in 30 mL of chloroform was added to 35 mL of a solution of iodine azide in acetonitrile prepared as described above. After 24 h stirring at room temperature the reaction mixture was poured into 100 mL of cold water, extracted three times with 50 mL of chloroform, and the organic layer was successively washed with 0.1 N NaOH, 0.1 N HCl, and aqueous sodium bicarbonate. After drying and evaporation of the solvent under reduced pressure, the residue was submitted to preparative TLC over silica gel by using toluene/ethanol (98/2) as the eluent.

Acknowledgements

Support of this work by a grant from the Comisión Asesora de Investigación Científica y Técnica de la Presidencia del Gobierno of Spain (Project PB89-0101) is gratefully acknowledged. The authors also thank Professor M. Pardo for helpful discussions concerning the stereochemical assignments.

References

1. (*a*) T.R. Kelly. Tetrahedron, **40**, 4539 (1984); (*b*) M. Braun. Tetrahedron, **40**, 4585 (1984); (*c*) M.J. Broadhurst, C.H. Hassall, and G. Thomas. Chem. Ind. (London), 106 (1985); (*d*) K. Krohn. Angew. Chem. Int. Ed. Engl. **25**, 790 (1986); (*e*) Tetrahedron, **46**, 291 (1990).
2. (*a*) K. Krohn, K. Tolkiehn, V. Lehne, H.W. Schmalle, and H.F. Grützmacher. Liebigs Ann. Chem. 1311 (1985); (*b*) T. Antonsson and P. Vogel. Tetrahedron Lett. **31**, 89 (1990); (*c*) B. Deguin, J.C. Florent, and C. Monneret. J. Org. Chem. **56**, 405 (1991).
3. (*a*) T. Oki and T. Takeuchi. J. Synth. Org. Chem. Jpn. **40**, 2 (1982); (*b*) F. Arcamone. Med. Res. Rev. **4**, 153 (1984); (*c*) J.W. Lown. Anthracycline and anthracenedione-based anticancer agents. Elsevier Science Publishers, Amsterdam. 1988. pp. 1–236; (*d*) J.W. Lown, S.M. Shondi, S.B. Mandel, and S.J. Murphy. J. Org. Chem. **47**, 4304 (1982); (*e*) N.R. Bachur, S.L. Gordon, and M.V. Gee. Mol. Pharmacol. **13**, 901 (1977).
4 (*a*) P. Nebois, R. Barret, and H. Fillion. Tetrahedron Lett. **31**, 2569 (1990); (*b*) K.T. Potts, E.B. Walsh, and D. Bhattacharjee. J. Org. Chem. **52**, 2285 (1987); (*c*) L. Campayo, F. Gómez-Contreras, and P. Navarro. Bull. Soc. Chem. Jpn. **40**, 2905 (1992).
5. F. Gómez-Contreras and M. Lora-Tamayo. Heterocycles, **13**, 389 (1979).
6. M. Quinteiro, C. Seoane, and J.L. Soto. Heterocycles, **9**, 1771 (1978).
7. (*a*) F. Arcamone. Doxorubicin anticancer antibiotics. *In* Medicinal chemistry. Vol. 17. Academic Press, New York. 1981; (*b*) R. Mondelli, E. Ragg, G. Fronza, and A. Arnone. J. Chem. Soc. Perkin Trans. 2, 15 (1987); (*c*) E. Ragg, R. Mondelli, and S. Penco. J. Chem. Soc. Perkin Trans. 2, 1673 (1988); (*d*) J.W. Lown and H.H. Chen. Can. J. Chem. **59**, 3212 (1981); (*e*) V. Malatesta, S. Penco, N. Sacchi, L. Valentini, A. Vigevani, and F. Arcamone. Can. J. Chem. **62**, 2845 (1984); (*f*) F. Matsuda, M.

© 1997 NRC Canada

Kawasaki, M. Ohsaki, K. Yamada, and S. Terashima. Chem. Lett. 653 (1988).
8. M.C. Cano, F. Gómez-Contreras, A.M. Sanz, and M.J.R. Yunta. Tetrahedron, **49**, 243 (1993).
9. M.C. Cano, F. Gómez-Contreras, and M. Lora-Tamayo. J. Chem. Soc. Perkin Trans 1, 273 (1991).
10. F. Gómez-Contreras and P. Navarro. J. Heterocycl. Chem. **16**, 1035 (1979).
11. (*a*) R.C. Cambie, R.C. Hayward, P.S. Rutledge, T. Smith-Palmer, and P.D. Woodgate. Chem. Soc. Perkin Trans. 1, 840 (1976); (*b*) M. Adinolfi, G. Barone, R. Lanzetta, G. Laonigro, L. Manzoni, and M. Parrilli. Tetrahedron, **40**, 2183 (1984).
12. A.F. Casy and K.M.J. McErlane. J. Chem. Soc. Perkin Trans. 1, 334 (1972).
13. P.L.Barilli, G. Bellucci, G. Ingrosso, F. Marioni, and I. Morelli. Tetrahedron, **28**, 4583 (1972).
14. C.A.G. Haasnoot, F.A.A.M. de Leeuw, and C. Altona. Tetrahedron, **36**, 2783 (1980).
15. P. Sohar. NMR spectroscopy. Vol. 2. CRC Press, Boca Raton, Fla. 1983.
16. (*a*) E. Toromanoff. Tetrahedron, **36**, 1971 (1980); (*b*) P. Kokovsky, I. Stary, J. Zajicek, F. Turecek, and S. Vasickova. J. Chem. Soc. Perkin Trans. 1, 2297 (1988).
17. M.P. Cava, A.A. Deana, and K.J. Muth. J. Am. Chem. Soc. **81**, 6458 (1959).

Can. J. Chem. Downloaded from www.nrcresearchpress.com by 92.62.229.171 on 09/08/12
For personal use only.

© 1997 NRC Canada

Energétique des liaisons inter- et intramoléculaires dans les trois isomères du benzènediamine

Raphaël Sabbah et Laurence Perez

Résumé : Le présent travail porte sur l'étude thermodynamique des trois isomères du benzènediamine (BDA) de formule générale : $C_6H_8N_2$. Il a été réalisé en utilisant quatre techniques : la calorimétrie de combustion de faibles quantités de substance (quelques milligrammes par essai), la calorimétrie de sublimation, l'analyse thermique différentielle et la mesure de capacités calorifiques. Cette étude nous a permis : de déterminer les enthalpies de combustion, de sublimation et de fusion de ces composés ainsi que la température de leur point triple; de préciser la stabilité relative des trois isomères; de déterminer les énergies de conjugaison expérimentales et de les comparer aux valeurs théoriques; de déterminer les enthalpies d'atomisation des trois composés et de vérifier qu'elles sont compatibles avec les valeurs calculées à partir des contributions énergétiques précédemment obtenues au laboratoire; de déterminer qualitativement et quantitativement les interactions intermoléculaires; de discuter de l'existence d'une liaison hydrogène intramoléculaire dans l'isomère *ortho*.

Mots clés : isomères du benzènediamine; enthalpie de combustion, de sublimation, de fusion, des liaisons inter- et intramoléculaires.

Abstract: The present work is concerned with a thermodynamic study of the three benzenediamine (BDA) isomers (general formula: $C_6H_8N_2$). It was achieved using four techniques: combustion calorimetry of small amounts of substance (a few milligrams), sublimation calorimetry, differential thermal analysis, and heat capacity measurements. From this study it was possible: to determine the enthalpies of combustion, sublimation, and fusion of these compounds as well as their triple point temperatures; to discuss the relative stability of the three molecules; to determine the experimental resonance energies and to compare them with the theoretical values; to determine the atomization enthalpies and to compare them with the values calculated from the energetical contributions previously obtained in our laboratory; to determine the intermolecular enthalpy bonds; to consider the existence of an intramolecular hydrogen bond in the *ortho* isomer.

Key words: benzenediamine isomers; enthalpy of combustion, of sublimation, of fusion, of inter- and intramolecular bonds.

1. Introduction

Les trois isomères *ortho*, *méta* et *para* du benzènediamine (BDA) possèdent de multiples applications industrielles : tous trois entrent dans la composition de nombreux pigments colorés mais aussi de certains fongicides (isomère *ortho*) (1, 2). Par ailleurs, et depuis peu, l'isomère *para* trouve également sa place dans le domaine de la chimie des matériaux, ses propriétés durcissantes faisant de lui un produit intermédiaire dans la synthèse de polymères (3). Ces substances, toxiques de surcroît, peuvent donc, selon leur comportement, avoir un sérieux impact sur l'environnement et la santé de l'homme. Il est à noter que l'isomère *para* semble être le plus nocif (4).

Les données thermodynamiques relatives aux benzènediamines, rapportées dans la littérature, sont rares (5–7). Il en est de même des informations relatant la structure cristalline de ces composés et concernant essentiellement l'isomère *para* (8, 9).

Ce travail a pour but de mettre en évidence le lien existant entre les grandeurs énergétiques des substances étudiées et leur structure moléculaire. Il trouve sa place aussi bien dans le domaine de la recherche fondamentale qu'appliquée et, notamment, dans celui de la protection de l'environnement (aptitude à la dégradation et au stockage de ces substances, problèmes liés à l'élimination des déchets par incinération, dépollution de l'eau, dépollution de l'atmosphère...).

2. Partie expérimentale

2.1. Produits utilisés

Les trois substances analysées sont des produits Aldrich de pureté supérieure à 99%. L'analyse thermique différentielle ayant confirmé ce résultat, les trois isomères ont été étudiés sans repurification préalable. Signalons, au passage, que ces trois substances sont nocives par inhalation, ingestion et contact avec la peau. Leur manipulation, réalisée sous hotte aspirante, a donc nécessité quelques précautions telles que le port de masque et gants appropriés.

Enfin, ces composés sont photosensibles et brunissent lorsqu'ils sont exposés à la lumière. Aussi, les avons-nous stockés à l'abri de celle-ci.

Reçu le 8 octobre 1996.

R. Sabbah[1] **et L. Perez.** Centre de thermodynamique et de microcalorimétrie du Centre national de la recherche scientifique, 26, rue du 141ème R.I.A., 13331 Marseille, Cedex 03, France.

1. Auteur à qui adresser toute correspondance. Téléphone : 33 4 91 28 20 62. Fax : 33 4 91 50 38 29.
E-mail : raphael.sabbah@ctm.cnrs-mrs.fr

© 1997 NRC Canada

Can. J. Chem. Downloaded from www.nrcresearchpress.com by 88.146.161.215 on 09/08/12
For personal use only.

Can. J. Chem. Downloaded from www.nrcresearchpress.com by 88.146.161.215 on 09/08/12
For personal use only.

2.2. Appareillages, techniques et modes opératoires

2.2.1. Analyse thermique différentielle

Nous avons utilisé la version moyenne température de l'analyseur thermique différentiel et les cellules expérimentales en verre décrites dans la référence 10.

Dans toutes nos expériences : (*i*) la vitesse de montée en température du four a été de 0,2 K min^{-1}; (*ii*) la masse de substance utilisée a été d'environ 100 mg, déterminée par double pesée à l'aide d'une balance Mettler, type M5, sensible au μg et dont l'exactitude des pesées est de ±2 μg; (*iii*) la préparation des échantillons et leur mise en container ont été conduites de la façon décrite dans la référence 10.

La mesure des températures a été faite à l'aide de deux thermocouples (thermocoax, type 2ABI 15); l'un est solidaire de l'échantillon, l'autre de la référence (alumine-α). La différence entre les f.e.m. délivrées par ces deux thermocouples est amplifiée par un microvoltmètre AOIP, type EVA, sensibilité 100 μV pleine échelle. Le signal ainsi amplifié est envoyé simultanément à un enregistreur Sefram, type Gépérac, pour le visualiser, et à un multimètre Keithley, modèle 175, pour le digitaliser. Un autre multimètre Keithley modèle 196, sensibilité 300 mV (résolution 100 nV), est utilisé pour mesurer la f.e.m correspondant à la température de l'échantillon. Les données issues de ces deux multimètres sont envoyées vers un ordinateur en vue de leur traitement à l'aide d'un programme écrit et mis au point au laboratoire. En appliquant l'équation de Clausius–Clapeyron à l'équilibre solide ⇔ liquide et la loi de Raoult, ce programme permet de déterminer la pureté de l'échantillon, son enthalpie de fusion ainsi que la température de son point triple.

Comme indiqué dans la référence 10, l'étalonnage (*i*) en température, de notre analyseur thermique a été réalisé à partir d'échantillons rigoureusement purs de naphtalène, de fluorène, d'acides benzoïque, diphénylacétique et anisique, de carbazole et d'anthraquinone, dont la température de leur point triple est bien connue dans la littérature; celle-ci est comprise entre 353 et 558 K; (*ii*) en énergie, a été réalisé à partir d'échantillons rigoureusement purs de naphtalène, de fluorène, d'acides benzoïque et diphénylacétique, dont l'enthalpie de fusion est bien connue dans la littérature.

2.2.2. Calorimétrie de combustion

Les enthalpies de combustion de nos composés ont été déterminées en utilisant un calorimètre isotherme, à flux thermique, monopile, basculant, CRMT (sensibilité : 0,0623 V W^{-1}) équipé d'une microbombe en acier inoxydable (Superimphy 625) de volume interne égal à 43,3 cm^3 à la température ambiante.

Le signal issu du calorimètre est amplifié par un microvoltmètre électronique AOIP, modèle EVA, sensibilité 30 mV pleine échelle, avant son envoi simultané sur un intégrateur éléctronique, conçu, réalisé et mis au point au laboratoire, qui détermine l'aire des thermogrammes $dQ/dt = f(t)$, et sur un enregistreur potentiométrique (Sefram, modèle Servotrace) qui le visualise.

La rotation du calorimètre suivant plusieurs plans permet à toutes les génératrices de la bombe d'être lavées par l'eau déminéralisée placée en son fond (1 cm^3).

Comme indiqué dans la référence 11, les substances à étudier sont mises sous forme de pastilles. À cet effet, nous avons utilisé un ensemble piston-moule façonné dans un acier trempé, ce qui a pour effet d'éviter l'entraînement dans les pastilles de traces de métal et d'augmenter ainsi la qualité des résultats.

Les pesées ont été effectuées sur une microbalance Mettler, modèle UM3, équipée d'un jeu de poids étalonnés par le N.I.S.T. Sa portée est de 3 g et sa sensibilité de 0,1 μg. L'erreur commise avec cette balance sur une pesée de quelques milligrammes est de l'ordre de ±0,2 μg. Dans toutes nos pesées, nous avons tenu compte des corrections de poussée de l'air pour calculer les masses réelles.

Une fois garnie, la bombe est remplie d'oxygène sous une pression de 3,04 MPa. L'oxygène N45, utilisé à cet effet, provient de l'Air Liquide et son degré de pureté est supérieur à 99,995% (fraction molaire d'azote < 10^{-5}). La durée d'une expérience a toujours été de 120 min à partir du moment de la mise de feu.

Après chaque expérience, nous avons déterminé, dans la phase aqueuse, les concentrations d'acide nitrique par titrage acido-basique en présence de phénolphtaléine avec une solution de soude préalablement titrée à l'aide d'une solution d'acide chlorhydrique de concentration connue; et vérifié, à l'aide des tubes de Dräger, l'absence d'oxyde de carbone et d'oxydes d'azote (NO, NO_2) dans la phase gazeuse (sensibilité des tubes < 1 ppm pour CO et < 0,1 ppm pour NO et NO_2).

2.2.3. Calorimétrie de sublimation

Nous avons utilisé un calorimètre Tian–Calvet (sensibilité 0,0621 V W^{-1}) associé à un montage différentiel doté de cellules d'effusion de Knudsen pour déterminer les enthalpies de sublimation de nos composés. L'étalonnage de notre système calorimétrique a été réalisé par effet Joule avant et après chaque série d'expériences. Le mode opératoire a été décrit dans la référence 12. Précisons que :

(*i*) le signal issu du calorimètre est amplifié par un nanovoltmètre Keithley modèle 147, sensibilité 100 μV pleine échelle, puis digitalisé par un multimètre numérique Keithley modèle 175 et enregistré sur un enregistreur potentiométrique, Sefram, modèle Servotrace;

(*ii*) l'isomère *ortho* a été étudié à 298,15 K alors que les deux autres isomères l'ont été à 319 K en raison de leur faible pression de vapeur saturante (égale à 0,09 Pa à 298,15 K, 0,6 et 0,2 Pa à 319 K respectivement dans le cas du 1,2-, 1,3- et 1,4-BDA). Compte tenu de ces faibles valeurs, nous avons admis l'identité $\Delta_{sub}H_m(T) \equiv \Delta_{sub}H^\circ_m(T)$

(*iii*) le diamètre des trous d'effusion pratiqués dans des joints en téflon de 0,2 mm d'épaisseur est de 1,5, 0,7 et 1 mm respectivement dans le cas du 1,2-, 1,3- et 1,4-BDA;

(*iv*) l'ouverture et la fermeture de l'orifice d'effusion des cellules sont pilotées par l'ordinateur;

(*v*) toutes les pesées ont été effectuées à l'aide d'une balance Mettler, type UM3.

L'acquisition et le traitement des données sont réalisés à l'aide d'un ordinateur et d'un programme conçu et mis au point au laboratoire. Il permet, entre autres, de déterminer l'aire des thermogrammes et, à partir du coefficient d'étalonnage, l'enthalpie de sublimation de nos composés à la température de l'expérience $\Delta_{sub}H^\circ_m(T)$.

2.2.4. Mesure des capacités calorifiques

Pour calculer $\Delta_{sub}H^\circ_m$ (298,15 K) à partir de $\Delta_{sub}H^\circ_m(T)$, il est

© 1997 NRC Canada

Can. J. Chem. Downloaded from www.nrcresearchpress.com by 88.146.161.215 on 09/08/12
For personal use only.

Tableau 1. Grandeurs physiques des substances utilisées à 298,15 K.

Substance	Formule	M^a (g mol^{-1})	ρ (g cm^{-3})	$-(\partial U/\partial P)_T$ (J g^{-1} MPa^{-1})
Acide benzoïque	$C_7H_6O_2$	122,1234	1,32[b]	0,12[b]
Coton	$CH_{1,791}O_{0,850}$	27,4157	1,50[b]	0,29[b]
1,2-BDA	$C_6H_8N_2$	108,1430	1,21[c]	0,13[d]
1,3-BDA	$C_6H_8N_2$	108,1430	1,21[d]	0,13[d]
1,4-BDA	$C_6H_8N_2$	108,1430	1,21[d]	0,13[d]

[a]Calculée à partir de la référence 14.
[b]Référence 15.
[c]Référence 9.
[d]Valeurs estimées.

Tableau 2. Analyse thermique différentielle des trois isomères du BDA.

Isomère	Pureté (mol %)	T_{pt}[a] notre résultat (K)	T_{pt} littérature[b] (K)	$\Delta_{fus}H_m$ notre résultat (kJ mol^{-1})	$\Delta_{fus}H_m$ littérature[b] (kJ mol^{-1})
1,2-BDA	99,98 ± 0,00$_5$	374,70 ± 0,02	373,9 ± 0,5	18,61 ± 0,17	23,1 ± 0,3
1,3-BDA	99,97 ± 0,00$_5$	336,25 ± 0,04	335,5 ± 0,4	12,03 ± 0,07	15,4 ± 0,2
1,4-BDA	99,96 ± 0,00$_5$	414,31 ± 0,03	412,3 ± 0,5	20,12 ± 0,18	21,7 ± 0,2

[a]Températures du point triple définies par rapport à l'EIT-90.
[b]Référence 5.

nécessaire de connaître : (*i*) le comportement thermique de nos substances entre 298,15 K et *T*. Nous nous sommes donc assurés que nos substances ne présentaient aucun changement de phase dans cet intervalle; (*ii*) la capacité calorifique à pression constante des phases condensée et gazeuse des substances étudiées à 298,15 K et *T* de façon à pouvoir appliquer la relation suivante :

$$\Delta_{sub}H^\circ_m(298{,}15\ \text{K}) = \Delta_{sub}H^\circ_m(T) + \int_T^{298{,}15\ \text{K}} [C^\circ_{p,m}(\text{g}) - C^\circ_{p,m}(\text{s})]\, dT$$

La différence enthalpique $H^\circ_m(T) - H^\circ_m(298{,}15\ \text{K})$ à l'état solide a été calculée par la méthode de chute à l'aide d'un calorimètre Tian–Calvet et d'un four maintenus respectivement à 298,15 K et *T*. Le calorimètre a été préalablement étalonné en utilisant des échantillons d'alumine-α.

Quant aux valeurs des capacités calorifiques à l'état gazeux $C^\circ_{p,m}(\text{g})$ et aux températures 298,15 K et *T*, elles ont été déterminées à partir d'une méthode incrémentale en utilisant, à chacune de ces deux températures, les capacités calorifiques à l'état gazeux des molécules de benzène et d'aniline (13). Ceci nous a permis, dans un premier temps et à chacune de ces deux températures, de déterminer la part du chaînon NH_2, puis, de calculer une valeur moyenne de $C^\circ_{p,m}$ pour les trois isomères du benzènediamine en ajoutant cette quantité au $C^\circ_{p,m}$ de l'aniline.

Les différents calorimètres et analyseur thermique, leurs périphériques ainsi que les balances sont placés dans des salles thermorégulées à (19,0 ± 0,2) °C.

3. Résultats

Les constantes physiques de nos composés sont résumées dans le tableau 1.

3.1. Analyse thermique différentielle

Les résultats obtenus ainsi que ceux qui sont empruntés à la littérature sont rassemblés dans le tableau 2. Notons que :

(*i*) Le 1,3-BDA reste en surfusion à température ambiante; d'où la nécessité de le recristalliser avant chaque expérience en l'abandonnant au réfrigérateur pendant une vingtaine de minutes.

(*ii*) Le 1,4-BDA prend une teinte bleutée après la première fusion et la conserve par la suite. L'analyse par diffraction de rayons X nous a permis de conclure à une très légère dénaturation.

(*iii*) Aucune des trois substances ne semble se décomposer de façon appréciable entre la température ambiante et son point de fusion.

Comme on peut le constater, à partir du tableau 2, si les valeurs relatives à la température du point triple sont peu différentes de celles de la référence 5, il n'en est pas de même pour les valeurs des enthalpies de fusion. À ce sujet, nous nous permettons d'émettre certaines critiques quant au mode opératoire adopté par les auteurs de cette référence. Tout d'abord, le type de cellule de travail utilisée (conçue en acier inoxydable et sertie d'un joint en aluminium) n'exclut pas toute possibilité de réaction avec l'échantillon à analyser. De plus, l'étalonnage du système calorimétrique a été réalisé par effet Joule dans des conditions qui diffèrent des conditions expérimentales. Enfin, la vitesse de montée en température utilisée est, à notre avis, trop élevée (2 K min^{-1}) lorsque l'on souhaite déterminer une enthalpie de fusion avec fiabilité.

© 1997 NRC Canada

Tableau 3. Combustion des trois isomères du BDA à 298,15 K.

$m_{subst.}$ (mg)	m_{coton} (mg)	n (HNO_3) (10^{-6} mol)	A (V s)	$-\Delta U$ (J)	$-W_1$ (J)	W_2 (J)	$-\Delta_c U°m$ (kJ mol^{-1})
			1,2-BDA				
5,2858	0,1649	9,63	10,803 339	175,106	2,705	0,709	3512,67
4,9217	0,2335	8,56	10,128 786	164,172	3,830	0,638	3509,14
5,3372	0,1908	9,63	10,920 234	177,000	3,129	0,711	3508,59
5,5017	0,2211	10,2	11,280 051	182,833	3,626	0,748	3507,83
4,9931	0,2045	9,10	10,243 173	166,023	3,354	0,671	3508,71
5,2813	0,1571	11,0	10,762 911	174,450	2,577	0,790	3503,21
			1,3-BDA				
5,6938	0,1663	11,2	11,563 425	187,426	2,728	0,814	3492,52
5,1642	0,1603	10,2	10,519 374	170,503	2,629	0,737	3500,00
5,2163	0,1768	10,2	10,619 511	172,126	2,900	0,739	3493,04
5,4880	0,1767	10,4	11,180 721	181,223	2,898	0,762	3498,93
5,4909	0,1685	10,7	11,160 186	180,890	2,764	0,777	3492,87
5,3053	0,1645	10,7	10,795 275	174,975	2,698	0,772	3495,95
			1,4-BDA				
5,2793	0,1431	10,7	10,731 939	173,948	2,347	0,771	3499,35
5,2054	0,1756	9,10	10,617 450	172,093	2,880	0,676	3501,38
5,4686	0,1530	11,1	11,121 381	180,261	2,509	0,797	3499,31
5,4841	0,1677	9,81	11,174 283	181,118	2,750	0,725	3503,00
5,3866	0,1659	9,45	10,959 132	177,631	2,721	0,702	3497,46
5,1122	0,1435	9,63	10,382 571	168,286	2,354	0,704	3495,22
5,6824	0,1872	10,7	11,561 163	187,389	3,070	0,783	3492,90

A = aire des thermogrammes, ΔU = variation de l'énergie interne de la bombe et de son contenu, W_1 = énergie de combustion du coton, W_2 = corrections pour passer à l'état de référence.

	1,2-BDA	1,3-BDA	1,4-BDA
$-\Delta_c U°_m$(cr, 298,15 K)/kJ mol^{-1}	3508,4 ± 1,2	3495,5 ± 1,3	3498,4 ± 1,3
$-\Delta_c H°_m$(cr, 298,15 K)/kJ mol^{-1}	3510,8 ± 1,2	3498,0 ± 1,3	3500,9 ± 1,3
$\Delta_f H°_m$(cr, 298,15 K)/kJ mol^{-1}	6,5 ± 1,3	−6,4 ± 1,4	−3,5 ± 1,4

3.2. Calorimétrie de combustion

L'équivalent énergétique du système calorimétrique (U_{calor}) a été déterminé à partir de neuf combustions d'acide benzoïque, échantillon 39i du N.I.S.T. pour lequel $\Delta_c u°$(cr, 298,15 K) = (−26 414 ± 3) J g^{-1} (16). Dans chaque expérience, nous avons utilisé environ 5 mg d'acide et 0,2 mg de coton (dont l'énergie de combustion, préalablement déterminée au laboratoire, a pour valeur $\Delta_c u°$(cr, 298,15 K) = (−16 399 ± 23) J g^{-1} (17)). Nous avons trouvé U_{calor} = (16,209 ± 0,006) J V^{-1} s^{-1}.

Les enthalpies standard de combustion de nos composés concernent la réaction suivante :

$$C_6H_8N_2(cr) + 8\ O_2(g) \rightarrow 6\ CO_2(g) + 4\ H_2O(l) + N_2(g)$$

et sont calculées, à l'aide d'un ordinateur et d'un programme écrit et mis au point au laboratoire, à partir de nos valeurs expérimentales en tenant compte des corrections dites de Washburn.

La combustion des trois isomères s'est révélée complète, aucune trace de cendre ne subsistant dans le corps de la bombe et dans le creuset une fois l'expérience terminée et les dosages par tubes colorimétriques de Dräger n'ayant révélé aucune présence de CO dans la phase gazeuse.

Les résultats relatifs à ces manipulations sont résumés dans le tableau 3.

Nous avons remarqué qu'environ 11% de l'azote contenu dans nos composés se trouvaient, à l'issue de la combustion, sous forme d'acide nitrique. L'expérience a montré que la quantité d'acide nitreux formé est excessivement faible et peut être négligée.

La comparaison de nos résultats avec les très rares données de la littérature montre un accord satisfaisant. En effet et comme nous pouvons le constater, nos valeurs expérimentales de l'enthalpie de combustion s'écartent d'environ ±0,2% des valeurs reportées dans la littérature pour les isomères *ortho* ((−3504,1 ± 4,2) kJ mol^{-1} (7)) et *para* ((−3509,3 ± 0,6) kJ mol^{-1} (6)). En revanche, le résultat obtenu pour le 1,3-BDA est parfaitement compatible avec celui de la référence 7 ((−3496,6 ± 4,2) kJ mol^{-1}). Signalons, au passage, que les résultats de la littérature ont été obtenus par calorimétrie de combustion classique.

© 1997 NRC Canada

Can. J. Chem. Downloaded from www.nrcresearchpress.com by 88.146.161.215 on 09/08/12
For personal use only.

Can. J. Chem. Downloaded from www.nrcresearchpress.com by 88.146.161.215 on 09/08/12
For personal use only.

Tableau 4. Sublimation des trois isomères du BDA.

Isomère	m (mg)	$\Delta_{sub}H_m(T)^a$ (kJ mol^{-1})	$\Delta_{sub}H_m(T)a$ (kJ mol^{-1})	$\int_{298,15\ K}^{T} C°_{p,m}(g)dT$ (kJ mol^{-1})	$\int_{298,15\ K}^{T} C°_{p,m}(s)dT$ (kJ mol^{-1})	$\Delta_{sub}H°_m(298,15\ K)$ (kJ mol^{-1})
1,2-BDA	8,2950	86,10				
	7,8057	84,80				
	8,1980	84,84	85,51 ± 0,29			85,51 ± 0,29
	8,1542	86,37				
	8,1858	84,98				
1,3-BDA	11,8830	88,87				
	11,1846	87,50				
	11,4487	90,01				
	11,6149	88,15	88,79 ± 0,36	2,93 ± 0,01	4,50 ± 0,02	90,36 ± 0,36
	12,0115	88,82				
	11,5402	88,15				
	11,7016	90,03				
1,4-BDA	7,8200	90,17				
	8,7135	91,20				
	8,6102	90,21	90,75 ± 0,24	2,93 ± 0,01	4,40 ± 0,03	92,22 ± 0,24
	8,4629	90,29				
	7,9550	91,20				
	7,7744	91,41				

[a]1,2-BDA: T = 298,15 K; 1,3- et 1,4-BDA: T = 319 K.

3.3. Calorimétrie de sublimation et mesures des capacités calorifiques

Les enthalpies de sublimation de nos substances ainsi que les variations enthalpiques à l'état solide et gazeux entre 319 et 298,15 K sont consignées dans le tableau 4.

Il est à noter que nous n'avons trouvé dans la littérature aucune donnée relative aux enthalpies de sublimation et aux pressions de vapeur saturante de nos substances.

3.4. Enthalpie de formation à l'état gazeux

En utilisant les résultats expérimentaux obtenus par calorimétrie de combustion et de sublimation, nous avons calculé l'enthalpie molaire standard de formation à l'état gazeux de chacun des trois isomères. Celle-ci est égale à (92,0 ± 1,3) kJ mol^{-1}, (84,0 ± 1,4) kJ mol^{-1} et (88,7 ± 1,4) kJ mol^{-1} respectivement pour les isomères *ortho*, *méta* et *para*.

3.5. Enthalpie d'atomisation

À une température donnée, la réaction d'atomisation des BDA s'écrit :

$$C_6H_8N_2\ (g) \rightarrow 6\ C(g) + 8\ H(g) + 2\ N(g)$$

En conséquence, à 298,15 K, l'enthalpie liée à cette réaction est égale à :

$$\Delta_{a,exp}H°_m = 6\ \Delta_fH°_m\ [C(g)] + 8\ \Delta_fH°_m\ [H(g)] + 2\ \Delta_fH°_m[N(g)] - \Delta_fH°_m\ [C_6H_8N_2\ (g)]$$

Les valeurs de $\Delta_{a,exp}H°_m$(298,15 K) de nos substances (tableau 5) ont été calculées en utilisant les valeurs de $\Delta_fH°_m$(g, 298,15 K) de C, H et N consignées dans la référence 18 et qui valent respectivement (716,67 ± 0,44), (217,997 ± 0,006) et (472,68 ± 0,40) kJ mol^{-1}.

Tableau 5. Enthalpies d'atomisation expérimentales et calculées des trois isomères du BDA.

Isomère	$\Delta_{a,exp}H°_m$(298,15 K) (kJ mol^{-1})	$\Delta_{a,calc}H°_m$(298,15 K) (kJ mol^{-1})
1,2-BDA	6897,4 ± 1,9	6893,6
1,3-BDA	6905,4 ± 2,0	6893,1
1,4-BDA	6900,7 ± 2,0	6893,1

Dans le présent travail, l'incertitude qui accompagne les résultats expérimentaux représente l'écart moyen, $\sigma_m = \pm \{(x - x_0)^2 / n(n-1)\}^{1/2}$, x étant chacune des n valeurs entrant dans le calcul de la moyenne x_0. Lorsque la valeur expérimentale est fonction de plusieurs variables, l'incertitude calculée tient compte de l'erreur sur chacune de ces variables.

4. Discussion

4.1. Energie de conjugaison

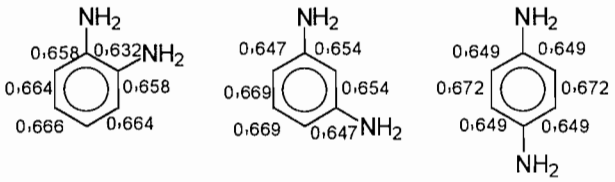
L'énergie de conjugaison est la différence entre l'énergie réelle de la molécule et l'énergie qu'elle aurait si les divers systèmes insaturés qu'elle comporte étaient indépendants. Sur le plan pratique, pour la déterminer, il suffit d'utiliser les enthalpies standard de combustion à l'état gazeux de la molécule réelle et de la molécule fictive non conjuguée. La première de ces grandeurs s'obtient expérimentalement et la seconde nécessite le recours aux systématiques. En ce qui nous concerne, nous avons utilisé celle de Klages qui est consignée dans la référence 19.

© 1997 NRC Canada

Tableau 6. Energies de conjugaison expérimentales et théoriques des trois isomères du BDA.

Isomère	$E_{conj,exp}$ (kJ mol^{-1})	$E_{conj,théor}$ (kJ mol^{-1})
1,2-BDA	165,1	179,5
1,3-BDA	170,1	179,1
1,4-BDA	165,4	179,4

Fig. 1. Indices de liaison des trois isomères du BDA.



1,2-BDA 1,3-BDA 1,4-BDA

Nous avons également calculé l'énergie de conjugaison théorique à l'aide de la méthode de calcul indiquée dans la référence 20 et ce, en utilisant les paramètres suivants : $\alpha_N = \alpha + 2{,}250\ \beta_0$; $\beta_{(C\text{-}N)} = 0{,}750\ \beta_0$ (β_0 est l'intégrale de recouvrement de la molécule de benzène; elle est égale à 131,7 kJ mol^{-1}).

Les valeurs de l'énergie de conjugaison expérimentale et théorique (tableau 6) ainsi obtenues sont compatibles. Toutefois, nous pensons que le fait que les valeurs de l'énergie de conjugaison théorique soient supérieures aux valeurs expérimentales peut s'expliquer par un manque de planéité des molécules réelles.

4.2. Liaisons intramoléculaires dans les BDA

Par définition, l'enthalpie d'atomisation d'une molécule est égale à la somme des liaisons intramoléculaires compte tenu des facteurs de stabilisation et de déstabilisation. Pour retrouver, par le calcul, l'enthalpie d'atomisation de nos composés, nous avons tenu compte du principe de la transférabilité et avons utilisé, entre autres, les valeurs énergétiques des liaisons intramoléculaires préalablement déterminées au laboratoire.

Pour ce qui est des liaisons C_b—C_b du cycle benzénique, nous avons adopté le procédé de calcul consigné dans la référence 11. Celui-ci fait intervenir un paramètre lié à la géométrie de la molécule, l'indice de liaison l_{rs} entre deux atomes directement liés r et s, obtenu à partir du calcul théorique de l'énergie de conjugaison (fig.1). La relation reliant H_{rs} à l_{rs} s'écrit (H_{rs} / kJ mol^{-1}) = 246,0 l_{rs} + 342,6. Quant à H(C_b—H) et H(C_b—NH_2), nous avons respectivement utilisé les valeurs 415,88 (21) et 1102,37 kJ mol^{-1} (21)

Les valeurs ainsi calculées sont consignées dans le tableau 5 et sont en très bon accord avec les valeurs expérimentales (différence $\leq$ 0,18%).

4.3. Liaisons intermoléculaires dans les BDA

L'enthalpie de sublimation d'une substance organique est liée aux interactions intermoléculaires. Dans le cas des BDA, ces interactions sont du type van der Waals et concernent les forces de dispersion et d'interactions dipolaires. À côté de ces interactions, il existe aussi des liaisons hydrogène intermoléculaires. Il nous a donc paru intéressant de déterminer la part énergétique de chacune d'elles. Pour ce faire, nous avons appliqué un procédé de calcul déjà utilisé au laboratoire (22–27). Il consiste, dans notre cas, à déterminer la contribution énergétique des forces de dispersion (London) en considérant qu'elle est égale à l'enthalpie de sublimation des diméthylbenzènes, composés isoélectroniques des BDA.

À une température donnée (ici 298,15 K), la différence Δ_1 des enthalpies de sublimation des BDA et des diméthylbenzènes correspondants représente la somme des énergies d'interaction dipolaire et des liaisons hydrogène intermoléculaires (tableau 7).

Afin de déterminer la contribution énergétique des interactions dipolaires Δ_2, nous avons comparé les enthalpies de sublimation des dichlorobenzènes (composés isoélectroniques des BDA et des diméthylbenzènes, qui présentent un moment dipolaire mais ne forment pas de liaisons hydrogène intermoléculaires) à celles des diméthylbenzènes correspondants. Comme on peut le constater, celle-ci est faible.

La différence $\Delta_1 - \Delta_2$, soit 27,07 kJ mol^{-1}(en prenant la molécule de 1,4-BDA comme référence), représente la part énergétique pouvant être attribuée à la somme des liaisons hydrogène intermoléculaires mises en évidence par des études cristallographiques (8, 9). Étant donné qu'il ne se forme que deux ponts hydrogène par molécule de 1,4-BDA, l'enthalpie d'une liaison hydrogène peut être estimée à (27,07/2) = 13,54 kJ mol^{-1}. Cette valeur est compatible avec toutes celles qui ont été précédemment déterminées au laboratoire (22, 24–27).

4.4. Existence d'une liaison hydrogène intramoléculaire dans l'isomère *ortho*

Si nous comparons entre elles les valeurs des enthalpies de sublimation des isomères *ortho* et *para*, nous observons que la première est plus faible de 6,71 kJ mol^{-1}. Cette différence pourrait être attribuée au fait que le 1,2-BDA présente moins de liaisons hydrogène intermoléculaires que l'isomère *para* en raison d'une possible formation de liaison hydrogène intramoléculaire.

Bien que la seule référence 9 traitant de la structure de l'isomère *ortho* n'y fasse pas allusion, quelques observations faites sur les propriétés physico-chimiques des BDA laisseraient supposer l'existence de cette liaison hydrogène intramoléculaire dans ce composé :

1. L'isomère 1,2-BDA a pu être sublimé à 298,15 K alors que les deux autres isomères n'ont pu être étudiés, par calorimétrie de sublimation, qu'à 319 K. En conséquence, la pression de vapeur saturante du 1,2-BDA est plus forte que celle du 1,4-BDA.

2. La température du point triple et l'enthalpie de fusion, qui renseignent sur la force des liaisons intermoléculaires, sont plus élevées dans le cas de l'isomère *para* que dans celui de l'isomère *ortho*.

3. L'isomère *para* est soluble dans un solvant polaire tel que l'eau alors que l'isomère *ortho* peut être dissous dans un solvant apolaire comme le benzène (28). Ceci est dû au fait que la première molécule présente avec le solvant des associations intermoléculaires par liaisons hydrogène plus nombreuses que la seconde.

Comme il a été fait mention dans le cas de la molécule de 1,2-aminophénol (22*a*), on pourrait expliquer les quelques observations précédentes en supposant que les liaisons

© 1997 NRC Canada

Can. J. Chem. Downloaded from www.nrcresearchpress.com by 88.146.161.215 on 09/08/12
For personal use only.

Tableau 7. Comparaison des enthalpies de sublimation des BDA, diméthyl- et dichlorobenzènes.

	$\Delta_{sub}H°_m$(298,15 K) (kJ mol^{-1})		
	ortho	*méta*	*para*
di-NH_2 A	85,51	90,36	92,22
di-Cl B	64,35 (13, 31)	62,78 (13, 31)	65,15 (13, 31)
di-CH_3 C	59,82 (13, 31)	58,26 (13, 31)	60,18 (13, 31)
Δ_1 = A–C	25,69	32,10	32,04
Δ_2 = B–C	4,53	4,52	4,97
$\Delta = \Delta_1 - \Delta_2$	21,16	27,58	27,07

hydrogène intermoléculaires, qui associent les molécules par deux dans l'isomère *ortho*, soient suffisamment fortes pour qu'un certain nombre de ces molécules passe de l'état solide à l'état gazeux sous forme de dimères. Dans ce cas, l'enthalpie de sublimation de cet isomère ne tiendrait pas compte de toutes les liaisons hydrogène intermoléculaires et serait inférieure à l'enthalpie de sublimation de l'isomère *para* pour lequel seules des molécules monomères existent en phase gazeuse.

Enfin, il y a lieu de préciser que si elle existe, cette liaison hydrogène intramoléculaire est faible et du même ordre de grandeur que celles que l'on rencontre dans le cas du 1,2-dihydroxybenzène (6,63 kJ mol^{-1}) (24) et du 1,2-aminophénol (6,73 kJ mol^{-1}) (22a).

4.5. Calcul de l'enthalpie de sublimation du 1,4-BDA par voie incrémentale

Nous avons tenté de retrouver l'enthalpie de sublimation de l'isomère *para* à partir de valeurs incrémentales. Pour cela, nous avons déterminé la contribution du chaînon NH_2 en retranchant à la valeur de $\Delta_{sub}H°_m$(298,15 K) de la molécule d'aniline celle de la molécule de benzène. Ces dernières sont, en première approximation, calculées à partir de la relation :

$$\Delta_{sub}H°_m(298{,}15\ \text{K}) = \Delta_{fus}H_m(298{,}15\ \text{K}) + \Delta_{vap}H°_m(298{,}15\ \text{K})$$

où $\Delta_{fus}H$(298,15 K) est obtenue à l'aide de la règle de Sidgwick (29) :

$$\Delta_{fus}H_m(298{,}15\ \text{K}) = \Delta_{fus}H_m(T_{fus}) - 0{,}055\ (T_{fus} - 298{,}15\ \text{K})$$

Les valeurs relatives à la molécule de benzène sont empruntées aux références 30 et 31, celles correspondant à l'aniline aux références 32 et 33. Après calcul, nous trouvons que $\Delta_{sub}H°_m$(298,15 K) est égale à 44,86 kJ mol^{-1} et à 68,08 kJ mol^{-1} respectivement pour le benzène et l'aniline. La part du chaînon NH_2 est donc estimée à 23,22 kJ mol^{-1}.

Il s'ensuit que l'enthalpie de sublimation du 1,4-BDA, à 298,15 K, calculée en ajoutant à l'enthalpie de sublimation du benzène deux fois la contribution énergétique du chaînon NH_2 à cette température, est égale à 91,30 kJ mol^{-1}. Elle diffère seulement d'environ 1% de la valeur expérimentale.

Bibliographie

1. H.G. Franck et J.W. Stadelhofer. Industrial aromatic chemistry, raw materials, processes, products. Springer, Berlin. 1988.
2. J. Fournier. Chimie des pesticides. Agence de Coopération Culturelle et Technique, Paris. 1988.
3. F. Cataldo. Eur. Polym. J. **32**, 43 (1996).
4. N. Irving Sax. Dangerous properties of industrial materials. 4th ed. Van Nostrand Reinhold, New York. 1975.
5. P. Bret-Dibat et A. Lichanot. Thermochim. Acta, **147**, 261 (1989).
6. G.M. Kibler et H. Hunt. J. Phys. Chem. **53**, 955 (1949).
7. J.B. Pedley, R.D. Naylor et P. Kirby. Thermodynamic data of organic compounds. 2nd ed. Chapman et Hall, New York. 1986.
8. Z.P. Povet'eva et Z.V. Zvonkova. Sov. Phys. Crystallogr. **20**, 37 (1975).
9. C. Stålhandske. Cryst. Struct. Commun. **10**, 1081 (1981).
10. (*a*) R. Sabbah et L. El Watik. J. Therm. Anal. **36**, 2291 (1990); (*b*) R. Sabbah et I. Antipine. J. Therm. Anal. **32**, 1929 (1987).
11. R. Sabbah et I. Antipine. Bull. Soc. Chim. Fr. **3**, 392 (1987).
12. R. Sabbah, I. Antipine, M. Coten et L. Davy. Thermochim. Acta, **115** , 153 (1987).
13. D.R. Stull, E.F. Westrum, Jr. et G.C. Sinke. The chemical thermodynamics of organic compounds. Wiley, New York. 1969.
14. Atomic weights of the elements 1993. Pure Appl. Chem. **66**, 2423 (1994).
15. W.D. Good et N.K. Smith. J. Chem. Eng. Data, **14**, 102 (1969).
16. J.D. Cox et G. Pilcher. Thermochemistry of organic and organometallic compounds. Academic Press, London. 1970.
17. R. Sabbah et M. Coten. Thermochim. Acta, **49**, 307 (1981).
18. Report of the codata task group on key values of thermodynamics. J. Chem. Thermodyn. **10**, 903 (1978).
19. G.W. Wheland. Resonance in organic chemistry. Wiley, New York. 1955. Chap. 3.
20. R. Sabbah, M. Gilbert et A. Julg. Thermochim. Acta, **10**, 345 (1974).
21. R. Sabbah et M. Laffitte. Thermochim. Acta, **25**, 376 (1978).
22. (*a*) R. Sabbah et M. Gouali. Can. J. Chem. **74**, 500 (1996); (*b*) Aust. J. Chem. **47**, 1651 (1994).
23. R. Sabbah et O. Pemenzi. C.R. Acad. Sci. Paris, **317**, 575 (1993).
24. R. Sabbah et E.N.L.E. Buluku. Can. J. Chem. **69**, 481 (1991).
25. P. Knauth et R. Sabbah. Can. J. Chem. **68**, 731 (1990).
26. P. Knauth et R. Sabbah. Bull. Soc. Chim. Fr. **5**, 834 (1988).
27. S. Skoulika et R. Sabbah. Thermochim. Acta, **61**, 203 (1983).
28. D.R. Lide. Handbook of chemistry and physics. 71 ed. CRC, Boca Raton, Fla. 1990–1991.

Can. J. Chem. Downloaded from www.nrcresearchpress.com by 88.146.161.215 on 09/08/12
For personal use only.

© 1997 NRC Canada

29. T.L. Cottrell. The strengths of chemical bonds. 2nd ed. Butterworths, London. 1958.
30. G.D. Oliver, M. Eaton et H.M. Huffman. J. Am.Chem. Soc. **70**, 1502 (1948).
31. V. Majer, V. Svoboda et H.V. Kehiaian. Enthalpies of vaporization of organic compounds: a critical review and data compilation: I.U.P.A.C. Chemical Data Series N° 32. Blackwell, Oxford. 1985.
32. W.E. Hatton, D.L. Hildebrandt, G.C. Sinke et D.R. Stull. J. Chem. Eng. Data, **7**, 229 (1962).
33. K. Kusano et I. Wadsö. Bull. Chem. Soc. Jpn. **44**, 1705 (1971).

Can. J. Chem. Downloaded from www.nrcresearchpress.com by 88.146.161.215 on 09/08/12
For personal use only.

© 1997 NRC Canada

Electronic absorption spectra and structure of hydroxycoumarin derivatives and their ionized forms

Valery F. Traven, Larisa I. Vorobjeva, Tatjana A. Chibisova, Edward Andrew Carberry, and Noelle Jean Beyer

Can. J. Chem. Downloaded from www.nrcresearchpress.com by 88.146.161.215 on 09/08/12
For personal use only.

Abstract: Electronic absorption spectra of 18 hydroxycoumarin derivatives and their ionized forms have been studied. Close agreement between experimental and the PPP CI calculated electron absorption band energies has been found in most cases. Strong polarization of the carbonyl function of the pyrone ring in the 7-hydroxycoumarin derivatives, H-bonding between the hydroxyl group and neighboring substituent in the *ortho*-substituted hydroxycoumarins, as well as their tautomeric transformations, have been suggested in the discussion of the electronic absorption spectra of the hydroxycoumarin derivatives. In accord also with calculational results, ionization of the hydroxyl function leads to a bathochromic shift of the longest-wavelength absorption bands in the spectra of 7-hydroxycoumarin derivatives. The ionization has no effect on the electronic absorption of the 4-hydroxycoumarin derivatives. Relative stabilities of the tautomeric forms of hydroxycoumarin derivatives and their ionized forms have also been compared by MNDO calculations.

Key words: hydroxycoumarins, intramolecular H-bonding, ionization, electronic absorption spectra, keto–enol tautomerism.

Résumé : On a étudié les spectres d'absorption électronique de 18 dérivés de l'hydroxycoumarine et de leurs formes ionisées. Dans la plupart des cas, il existe un bon accord entre les énergies expérimentales des bandes d'absorption électronique et celles calculés par la méthode «PPP CI». Dans la discussion des spectres d'absorption électronique des dérivés de l'hydroxycoumarine, on a suggéré l'existence d'une forte polarisation de la fonction carbonyle du cycle pyrone des dérivés 7-hydroxycoumarines, l'existence d'une liaison hydrogène entre le groupe hydroxyle et le substituant voisin des hydroxycoumarines substituées en *ortho*, ainsi que la possibilité de leurs transformations tautomériques. En accord encore une fois avec les résultats des calculs, la valeur de l'ionisation de la fonction hydroxyle conduit, dans les spectres des dérivés de la 7-hydroxycoumarine, à un déplacement bathochromique des bandes d'absorption aux longueurs d'onde les plus élevées. En se basant sur des calculs «MNDO», on a comparé les stabilités relatives des formes tautomériques des dérivés de l'hydroxycoumarine et de leurs formes ionisées.

Mots clés : hydroxycoumarines, liaison hydrogène intramoléculaire, ionisation, spectres d'absorption électronique, tautomérie céto–énolique.

[Traduit par la rédaction]

Introduction

Natural hydroxycoumarins and their derivatives possess many remarkable properties. Some of these coumarins, viz, 7-hydroxycoumarins, are known for their high photosensitivity, lasing effect, and application as luminescent colorants for biosubstrates and fluorescent whiteners for polyester and polyamide fabrics (1, 2). Many oxygenated coumarins, e.g., 4-hydroxycoumarin derivatives, show marked biological activity, such as enzyme inhibition, hypotoxicity, and carcinogenicity, and anticoagulant and antibiotic action. Therefore, the electronic structure of hydroxycoumarins, including their UV light absorption ability, has become the subject of much interest (3–12).

A reasonable interpretation of the electronic absorption spectra of coumarin and 4-hydroxycoumarin has already been elaborated (6–9). Three long-wavelength absorption bands of coumarin have been assigned to the $\pi \rightarrow \pi^*$ transitions. The high intensity as well as solvent independence of these bands agree with this assignment. For example, the maximum positions of electronic absorption for the coumarin derivatives in ethanol are very close to those in cyclohexane (9). In accord with the $\pi \rightarrow \pi^*$ assignment, the long-wavelength bands have been accurately predicted by PPP CI calculations.

The first absorption band of coumarin belongs to the one-configurational transition, possessing 85% HOMO→LUMO participation (9). This transition is mostly localized on the carbon atoms of the benzene ring and the lactone ethylene

Received October 3, 1996.

V.F. Traven,[1] L.I. Vorobjeva, and T.A. Chibisova. D. Mendeleev University of Chemical Technology of Russia, Miusskaja 9, Moscow, 125047, Russia.
E.A. Carberry[1] and N.J. Beyer. Southwest State University, Marshall, MN 56258, U.S.A.

[1] Authors to whom correspondence may be addressed. VFT: Fax: +7 095 200 4204. E-mail: traven@orgchem.mhti.msk.su EAC: Telephone: (507) 537-71-31. Fax: 507-537-71-54. E-mail: carberry@ssu.southwest.msus.edu

© 1997 NRC Canada

Can. J. Chem. Downloaded from www.nrcresearchpress.com by 88.146.161.215 on 09/08/12
For personal use only.

bond. The first band is polarized near the long axis of the coumarin molecule. The second spectral band is due to the (HOMO-1)→LUMO transition; the direction of its polarization is close to that of the first transition (the angle between directions is equal to 14°). The third band belongs to the transition between the HOMO and the (LUMO+1). The direction of polarization of this transition is very different from those of the first and the second transitions, as it is close to being perpendicular to the first transition moment (7).

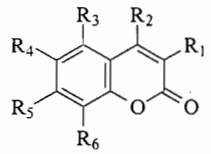
Although these results have mainly been provided by quantum chemical calculations in the *p*-approximation, EHMO and CNDO calculations (where all valence atomic orbitals are included in the basis set) agree with the main conclusions (6, 7) .

The effect of the hydroxyl function on the electronic absorption spectra of coumarins has also been discussed (9, 10), even though some results seem to be rather controversial. Generally, the electronic absorption of a hydroxycoumarin depends on the hydroxyl group location. The hydroxyl function, which is located in position 4, changes the spectral properties of coumarin only slightly (6, 7). The angle between the first and second band transition moments decreases to 14°, while the third transition is also polarized in a direction perpendicular to the first and the second transitions.

The results of a study of the 7-hydroxycoumarin electronic absorption spectrum are not so definite (7–11). Since the longest-wavelength band is shifted in this spectrum to lower energy, its $\pi\rightarrow\pi^*$ assignment has been assumed. Abu-Eitah Rafie et al. suggested that the band at 370 nm is due to the first $\pi\rightarrow\pi^*$ transition in the electronic absorption spectrum of 7-hydroxycoumarin (10). However, this band can be assigned to the absorbance of its ionized form (4, 13). The appearance of this form cannot be excluded when electronic absorption spectra of hydroxycoumarins are recorded in basic and ionizing solvents. It is known that hydroxycoumarins are rather acidic and partly ionized even in the presence of water (13). The absorption of 7-hydroxycoumarin at 324 nm seems to be more reasonably assigned to the longest-wavelength $\pi\rightarrow\pi^*$ transition (10). Its bathochromic shift when compared to the coumarin absorption has been explained by charge transfer between the 7-hydroxyl function and the carbonyl group.

Electronic absorption spectra of substituted hydroxycoumarins have not yet been systematically studied. We have analyzed the electron absorption spectra of 18 substituted 4- and 7-hydroxycoumarins, studying the effect on the spectral properties of methyl, phenyl, acetyl, and hydroxyl functional groups as substituents. Analysis is based on quantum chemical calculations by the PPP CI method. The effect of intramolecular H-bonding on the electronic absorption of *ortho*-substituted hydroxycoumarins has been evaluated from the calculations. Electronic absorption spectra of ionized forms of substituted hydroxycoumarins have also been studied. The heats of formation, $\Delta H_f°$, of neutral and ionized forms of hydroxycoumarin derivatives have been calculated by the MNDO method.

The structures of the hydroxycoumarin derivatives studied are shown as follows (substituents R different from H are only listed for the compounds **2**–**18**):



1: R_1–R_6 = H;
2: R_2 = OH;
3: R_5 = OH;
4: R_2 = Me, R_5 = OH;
5: R_1 = Ph, R_5 = OH;
6: R_2 = Ph, R_5 = OH;
7: R_2 = Me, R_4 = OH;
8: R_2 = OH, R_4 = Me;
9: R_1 = C(O)Me, R_2 = OH;
10: R_1 = C(O)Me, R_2 = OH, R_4 = Me;
11: R_5 = OH, R_6 = C(O)Me;
12: R_2 = Me, R_5 = OH, R_6 = C(O)Me;
13: R_2 = R_3 = OH;
14: R_2 = R_5 = OH;
15: R_4 = R_5 = OH;
16: R_2 = Me, R_4 = R_5 = OH;
17: R_2=Me, R_5 = R_6 = OH;
18: R_4 = OMe, R_5 = OH.

Experimental section

Materials and UV spectra

Compounds **1**–**14** and **16** were synthesized by known procedures and purified by recrystallization. Their melting points (uncorrected) are in agreement with literature data and are listed in Table 1.

Electronic absorption spectra of neutral forms of hydroxycoumarin were recorded in 95% ethanol, at a concentration of 5.0×10^{-5} mol/L, using a Perkin–Elmer model 323 UV–VIS–IR spectrophotometer. Electronic absorption spectra of *ortho*-substituted hydroxycoumarins, where intramolecular H-bonding is possible, were also recorded in *n*-hexane and carbon tetrachloride. Electronic absorption spectra of the ionized forms of hydroxycoumarin were recorded in 95% ethanol mixed in 5-mL cuvettes with one drop of 10% NaOH aqueous solution. The experimental procedure of hydroxycoumarin derivative ionization was developed in accordance with previously published methods (13–16).

Methods of MO calculations

The Pariser–Parr–Pople CI method was used for quantum chemical calculations of the electronic absorption spectra in the *p*-approximation (17). The standard values of parameters only were used for the calculations of electronic absorption spectra of hydroxycoumarin derivatives in their neutral forms (17). Electronic absorption spectra of hydroxycoumarins in their ionized forms were calculated using both the standard parameter values of phenoxide oxygen and new parameters of the ionized OH group, which turned out to be in the best agreement with experimental data. All parameters of neutral, H-bonded, and ionized hydroxyl functions used are listed below:

	J, eV	*A*, eV
OH group, neutral	32.90	11.40
OH group, H-bonded	28.00	10.00
O^-, phenoxide oxygen standard parameters	17.70	2.47
O^- group (ionized OH group new parameters)	20.00	5.00

Standard parameters only were used in the MNDO calculations of heats of formation, $DH_f°$. Input atomic coordinates were evaluated via MMX calculations.

© 1997 NRC Canada

Can. J. Chem. Downloaded from www.nrcresearchpress.com by 88.146.161.215 on 09/08/12
For personal use only.

Table 1. Melting points of the hydroxycoumarin derivatives.

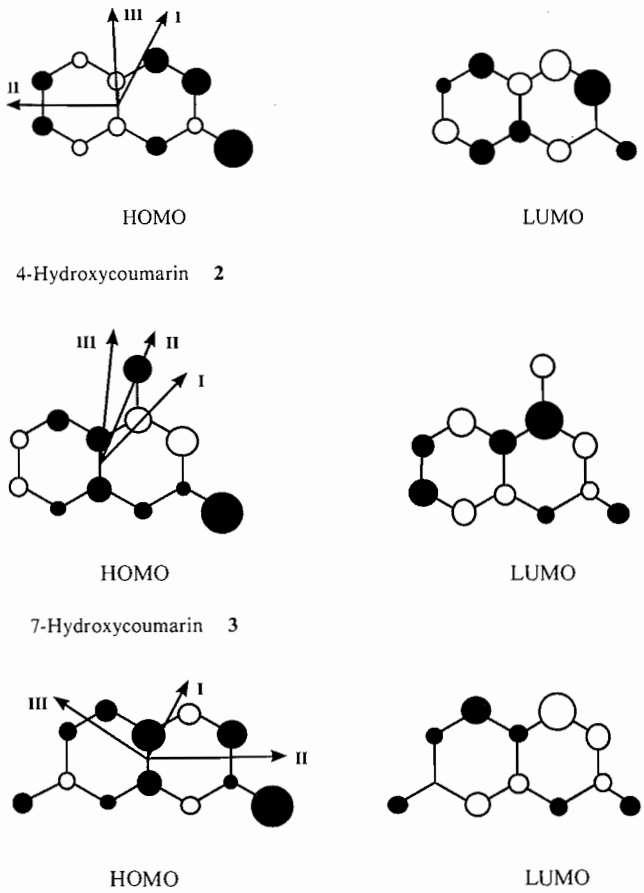
Compound	R_1	R_2	R_3	R_4	R_5	R_6	Melting point, °C
1	H	H	H	H	H	H	68–69
2	H	OH	H	H	H	H	209–210
3	H	H	H	H	OH	H	227–228
4	H	CH_3	H	H	OH	H	191–192
5	Ph	H	H	H	OH	H	207–208
6	H	Ph	H	H	OH	H	249–250
7	H	CH_3	H	OH	H	H	242–243
8	H	H	OH	CH_3	H	H	253–254
9	$COCH_3$	OH	H	H	H	H	138–139
10	$COCH_3$	OH	H	CH_3	H	H	143–144
11	H	H	H	H	OH	$COCH_3$	169–170
12	H	CH_3	H	H	OH	$COCH_3$	166–167
13	H	OH	OH	H	H	H	217–218
14	H	OH	H	H	OH	H	273–274
16	H	CH_3	H	OH	OH	H	271–272

Results and discussion

Partial results of the PPP CI calculations of absorption spectra of the hydroxycoumarin derivatives are given in Tables 2 and 3. The calculated longest-wavelength band positions (and intensities), λ_{max} (lg ε), the frontier orbital energies, E_{HOMO} and E_{LUMO}, the frontier orbital transition participation, HOMO→LUMO, %, and the parameter $\beta_{C=O}$ values used are listed. We found good agreement between the experimental and calculated results in most cases. First of all, it was certainly true for the 4-hydroxycoumarin derivatives: the electronic absorption of 4-hydroxycoumarin itself is only slightly changed when compared with that of coumarin. The longest-wavelength band has 87% participation of the HOMO→LUMO transition in the spectrum of 4-hydroxycoumarin and 84% of that in the spectrum of coumarin. The electron density at the oxygen atom of the carbonyl group in 4-hydroxycoumarin is also, as is that of coumarin, greatly changed under UV excitation: the O(C=O) charge is equal to −0.36 in the ground state and to −0.06 in the first excited state. The decrease of electron density at the carbonyl group is in accord with its increase at the carbon–carbon double bond of the pyrone ring and carbon atoms of the benzene moiety. The corresponding data are listed in Table 2. The shapes of the frontier molecular orbitals and polarization directions of the first, second, and third transitions of compounds **1**–**3** are compared in Fig. 1.

On the whole, energies (and oscillator strengths) of the long-wavelength bands are rather close to previously published results (6, 7). However, the calculated directions of the electronic transition polarizations turned out to be somewhat different from those reported earlier. According to Moore et al. (7), both the first and second transition directions in the electronic absorption spectra of coumarin and 4-hydroxycoumarin are nearly parallel to the long axis of the molecules. The angles between their polarization directions are not higher than 16°. Our results show the first electronic transition polarization directions to be perpendicular to the long axis both for coumarin and 4-hydroxycoumarin (as can be seen in Fig. 1).

Fig. 1. Frontier orbital shapes and polarization directions of three π→π* transitions in coumarin **1**, 4-hydroxycoumarin **2**, and 7-hydroxycoumarin **3** predicted by the PPP CI calculations.



Moreover, the second transition has been found to be HOMO→(LUMO+1) and the third transition is due to (HOMO-1)→LUMO. This sequence is the reverse of that previously published (7).

© 1997 NRC Canada

Table 2. Experimental data and calculated parameters of the first transition of the electron absorption spectra of hydroxycoumarin derivatives (solvent: 95% ethanol).

Compound	Experimental data λ_{max}, nm (lg ε)	PPP CI calculated data λ_{max}, nm (*f*)	E_{HOMO}, eV	E_{LUMO}, eV	HOMO→LUMO, %	$-\beta_{C=O}$, eV
1	310(3.78)	310(0.36)	9.18	2.17	85	2.46
2	308(3.78)	310(0.34)	8.82	1.91	87	2.46
3	324(4.15)	313(0.51)	9.21	2.37	90	2.46
		322(0.56)	8.76	2.05	88	2.46
4	323(3.78)	321(0.56)	8.71	2.00	88	2.00
5	342(4.3)	348(0.86)	8.56	2.28	94	2.00
6	333(3.02)	336(0.59)	8.65	2.38	92	2.00
7	344(3.7)	330(0.31)	8.81	2.02	87	2.46
		341(0.27)[a]	8.61	1.95	88	2.46
8	309(3.81)	311(0.33)	8,79	1.88	85	2.46
13	312(3.9)	299(0.24)	8.76	1.66	70	2.46
		301(0.29)[a]	8.61	1.59	80.6	2.46
14	310(4.06)	310(0.46)	8.57	1.65	83	2.46
15	347(4.06)[b]	339(0.50)	8.47	1.93	86	2.00
		348(0.46)[a]	8.33	1.88	89	2.00
16	348(4.18)	348(0.51)[a]	8.33	1.74	93	2.00
17	328(4.10)[c]	316(0.34)	8.64	1.88	74	2.00
		324(0.48)[a]	8.49	1.82	75	2.00
18	345(4.1)	336(0.55)	8.95	2.37	94	2.00
		341(0.45)[a]	8.72	2.14	94	2.00

[a]Calculated with the parameters: J_{OH} = 28.00 eV; A_{OH} = 10.00 eV (structures **7-1**, **15-1**, **17-1**, and **18-1**, respectively; see text for comments).
[b]Experimental data are given by ref. 18.
[c]Experimental data are given by ref. 19.

Table 3. Experimental data and calculated parameters of the first transition of the electron absorption spectra of *ortho*-acetyl-hydroxycoumarins.

Compound	Experimental data λ_{max}, nm (lg ε)	PPP CI calculated data λ_{max}, nm (*f*)	E_{HOMO}, eV	E_{LUMO}, eV	HOMO→LUMO, %	$-\beta_{C=O}$, eV
9	342(3.91)[a]	341(0.45)[c,d]	8.95	2.38	94	2.46
		350(0.36)[c,d]	9.06	2.50	95	2.46
	321(4.03)[b]	318(0.27)[d,e]	9.28	2.30	93	2.46
10	347(3.78)[a]	350(0.37)[c,d]	9.04	2.47	97	2.46
	330(3.75)[b]	328(0.27)[d,e]	9.24	2.26	94	2.46
11	344(4.05)[a]	330(0.32)[f]	9.01	2.33	76	2.00
	337(4.05)[b]	340(0.29)[d,f]	8.95	2.52	82	2.00
		430(0.20)[d,g]	8.58	2.95	94	2.00
12	342(3.92)[a]	338(0.33)[d,f]	8.90	2.49	81	2.00
	334(3.92)[b]					

[a]*n*-Hexane as solvent.
[b]95% Ethanol as solvent.
[c]Calculated for the 3-acetyl-4-hydroxy-2-chromenone form.
[d]Standard parameters of H-bond are used (see text for comments).
[e]Calculated for the 3-acetyl-2,4-chromandione enol form **9-2** (see text for comments).
[f]Calculated for the 8-acetyl-7-hydroxy-2-chromenone form **11-1**.
[g]Calculated for the form **11-2** (see text for comments).

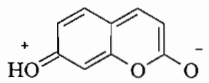
© 1997 NRC Canada

Can. J. Chem. Downloaded from www.nrcresearchpress.com by 88.146.161.215 on 09/08/12
For personal use only.

Can. J. Chem. Downloaded from www.nrcresearchpress.com by 88.146.161.215 on 09/08/12
For personal use only.

The introduction of a methyl group into position 6 of 4-hydroxycoumarin does not change the electronic absorption spectrum parameters of the molecule. The longest-wavelength band positions, changes of electron densities on atoms under UV excitation, and polarization directions of the first bands are very close for both hydroxycoumarins **2** and **8**.

In contrast with the coumarin and 4-hydroxycoumarin derivatives, the standard value of the resonance integral $\beta_{C=O}$ = −2.46 eV does not provide satisfactory results in calculations of the electronic absorption spectra of 7-hydroxycoumarin derivatives. A strong intramolecular interaction between the 7-hydroxyl group and the carbonyl group (cf. resonance structure **3–1**) can be suggested as an explanation of this result. Significant participation of structure **3–1** in the *p*-electron delocalization of 7-hydroxycoumarin has already



3 − 1

λ_{max} (PPP)=322 nm

been suggested (10, 20). However, the specificity of intramolecular charge transfer beween the 7-hydroxyl group and the carbonyl function of the lactone ring has never been analyzed in terms of parameterization of the PPP quantum chemical calculations.

We have approximated the decrease of covalence of the carbonyl group in 7-hydroxycoumarins by changing the resonance integral $\beta_{C=O}$ from the standard value of −2.46 eV to a value of −2.0 eV. In Table 2 one can see better agreement between the 7-hydroxycoumarin experimental data and the results calculated with this value of the resonance integral $\beta_{C=O}$. Since the longest-wavelength band is mostly due to the excitation of electrons between the frontier orbitals of hydroxycoumarins, the increase in energy of the highest occupied molecular orbital, equal to 0.42 eV, seems to be responsible for the observed bathochromic shift of the first absorption band of 7-hydroxycoumarin. The increase in energy of the LUMO is much smaller and equal to 0.12 eV. It should also be mentioned that the HOMO has a rather large value of the eigencoefficient at position 7.

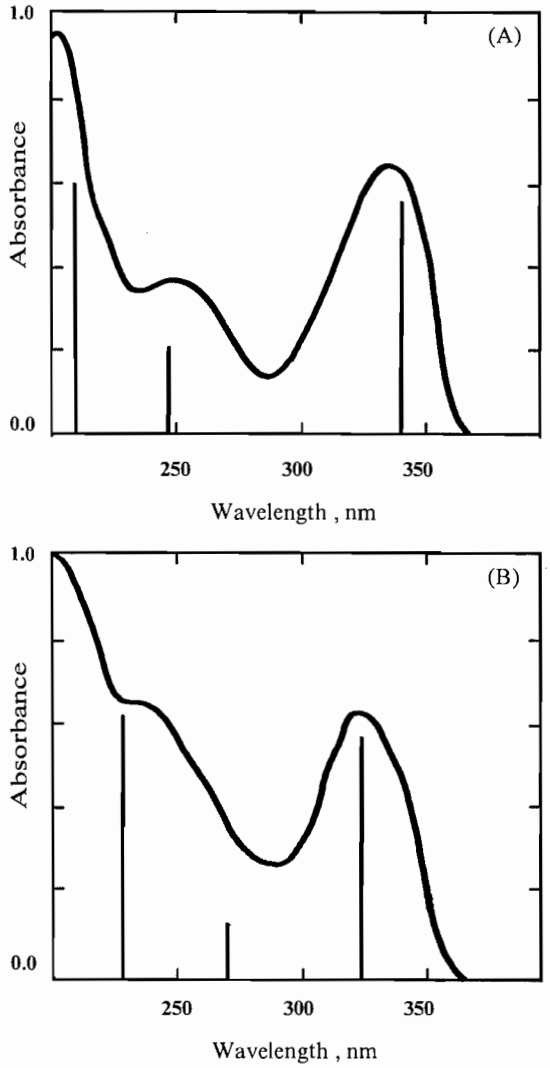
One should note that the bathochromic shift of the 7-hydroxycoumarin electronic absorption is much larger than that of coumarin; the intensive long-wavelength bands in the benzene and phenol EA spectra are located at 203 and 210 nm, respectively.

As shown in Fig. 1, the HOMO→LUMO transition character (88% participation) of the first electronic transition of 7-hydroxycoumarin and the direction of its polarization are rather close to those of coumarin and 4-hydroxycoumarin. The second electronic transition direction is nearly parallel to the long axis of the molecule.

As in the series of 4-hydroxycoumarins, introduction of a methyl group into position 4 of 7-hydroxycoumarin has no effect on the parameters of the electronic absorption spectra. According to the PPP calculations, a methyl group slightly increases the energies of both the HOMO and the LUMO.

On the other hand, the effect of a phenyl group on electronic transitions in the 7-hydroxycoumarins is much larger. Electronic absorption spectra of the 3- and 4-phenyl-7-hydroxy-

Fig. 2. Electron absorption spectra of 7-hydroxy-3-phenylcoumarin **5** (curve *A*) and 7-hydroxy-4-phenylcoumarin **6** (curve *B*) in ethanol. The PPP CI calculated band positions λ_{max} and oscillator strengths *f* are indicated by the vertical lines.



coumarins are compared in Fig. 2 (curves *A* and *B*, respectively). Comparison of the experimental and calculated electronic absorption data is also shown. On the whole, the introduction of a phenyl group leads to extension of the *p*-conjugated system and provides definite bathochromic shifts of the first absorption bands, of 18 and 8 nm, respectively. Since these bands are still based on one-configurational transitions, their bathochromic shifts in both spectra are due to the corresponding changes of the frontier orbital energies: the increase of the HOMO energies, 0.2 and 0.11 eV, and the decrease of the LUMO energies, 0.23 and 0.33 eV, for 3- and 4-phenyl-7-hydroxycoumarins, respectively. The phenyl group in position 3 has no noticeable effect on the polarization of the first band of 7-hydroxycoumarin. As can be seen from the diagrams given in Fig. 3, electron densities on the carbon atoms of the phenyl ring are not much changed under the first electronic excitation in compound **5**.

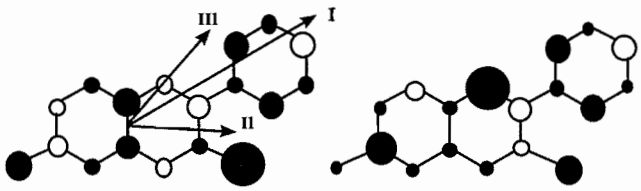
The introduction of a phenyl group in position 4 of umbel-

© 1997 NRC Canada

Can. J. Chem. Downloaded from www.nrcresearchpress.com by 88.146.161.215 on 09/08/12
For personal use only.

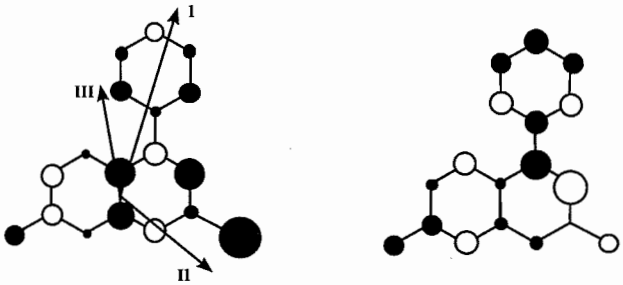
Fig. 3. Frontier orbital shapes and polarization directions of three $\pi\rightarrow\pi^*$ transitions in 7-hydroxy-3-phenylcoumarin **5** and 7-hydroxy-4-phenylcoumarin **6** predicted by the PPP CI calculations.

7-Hydroxy-3-phenylcoumarin **5**



HOMO LUMO

7-Hydroxy-4-phenylcoumarin **6**



HOMO LUMO

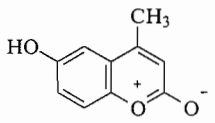
lyferone affects the electronic transition parameters to a larger extent. It changes the direction of polarization of the first electronic transition due to definite changes of electron densities on the phenyl-substituted carbon atoms under UV excitation. Shapes of the frontier molecular orbitals of compound **6** are also shown in Fig. 3.

A hydroxyl group in position 6 of coumarin provides an even larger bathochromic shift in the electronic absorption spectrum of 6-hydroxycoumarin when compared with that of 7-hydroxycoumarin. One can note the higher transfer of electron density from the hydroxyl group located at position 6 under UV excitation and the maximal value of the HOMO eigencoefficient at that position in the 6-hydroxycoumarin molecule. Better agreement between experimental data and calculated results can be seen when higher electron donation of the position-6 hydroxyl group has been taken into consideration via parameterization of the PPP calculations (see Table 2):

	J, eV	*A*, eV
OH-group, increased electron-donation parameters	28.00	10.00

This suggestion is in accord with a partial positive charge located at the lactone oxygen atom, in *para*-position to the hydroxyl group in compound **7** as seen in the resonance form **7–1**.

Electronic absorption spectra of *ortho*-acetylhydroxycoumarins have never been discussed. Absorption spectra of neutral forms of 8-acetyl-7-hydroxycoumarin and 3-acetyl-4-hydroxycoumarin are shown in Fig. 4. The bathochromic shifts of the first absorption bands in spectra of both 4-hydroxycoumarin and 7-hydroxycoumarin acetyl derivatives, recorded in ethanol, are about 12–13 nm when compared with unsubstituted 4- and 7-hydroxycoumarins, respectively. In accordance with the calculated results, a carbonyl function adjacent to a hydroxyl group in hydroxycoumarin derivatives does not change the nature of the longest-wavelength band. This band continues to be due to the frontier orbital electronic transition.

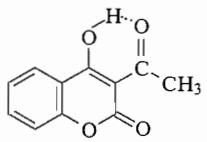


7 – 1

λ_{max} (PPP)=341 nm

H-Bonding between neighboring carbonyl and hydroxyl functions may be at least partly responsible for the bathochromic shifts mentioned. H-Bonding effects were approximated as an electrostatic interaction between the corresponding functional groups in previous quantum chemical calculations (21). Some attempts were also made to account for H-bonding effects in the PPP calculations (17). We carried out PPP CI calculations of the electronic absorption spectra of compounds **9–12** with the standard "H-bonded" parameters given above (see Experimental section). These parameters provide better agreement between the experimental data and the calculational results for all *ortho*-acetyl substituted hydroxycoumarins **9–12** (the corresponding data are compared in Table 3).

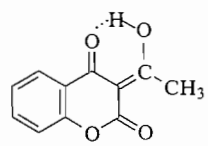
3-Acetyl-4-hydroxycoumarins **9**, **10** and 8-acetyl-7-hydroxycoumarins **11**, **12** turned out to be very different in respect to the solvent effect on their electronic absorption spectra. As can be seen in Fig. 4, absorption curves of 3-acetyl-4-hydroxycoumarin recorded in ethanol – carbon tetrachloride mixtures show an isobestic point. Tautomeric transformations of compound **9** are suggested in explanation, since none of these solvents can provide ionization of the hydroxyl function at position 4 of the coumarin ring.



9 – 1

ΔH_f°(MNDO)= – 124.5 kcal/mol

λ_{max} (PPP)=341 nm



9 – 2

ΔH_f°(MNDO)= – 122.9 kcal/mol

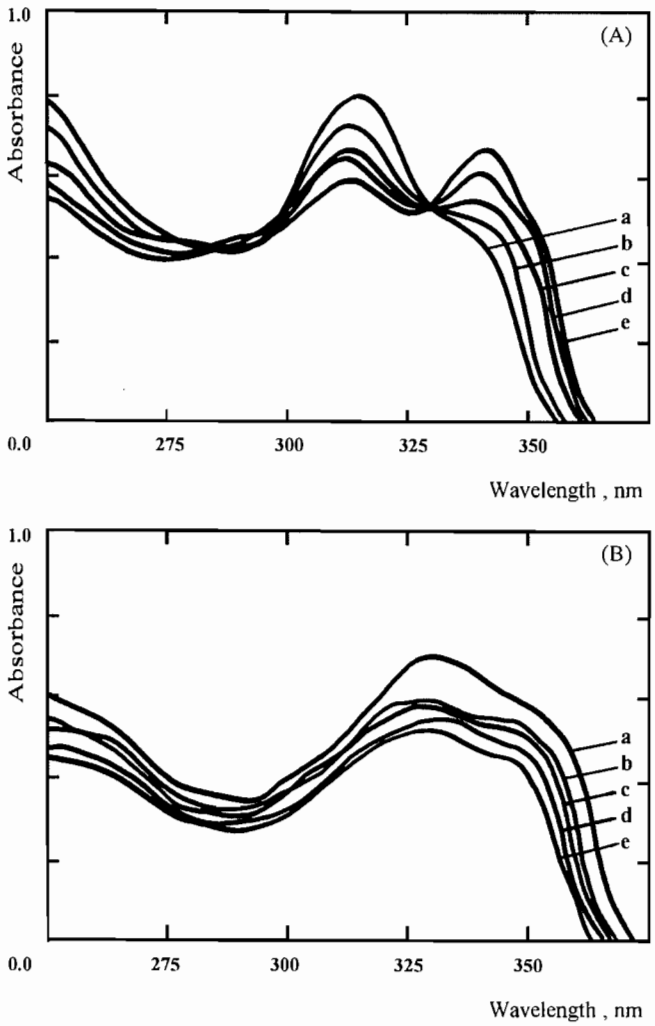
λ_{max} (PPP)=318 nm

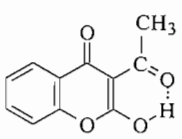
Compound **9** can be considered to exist in the following tautomeric forms: **9-1**, **9-2**, **9-3**, **9-4**, and **9-5**. According to MNDO calculational results, forms **9-4** and **9-5** are distinguished by rather large heats of formation ΔH_f°. As a result, these structures do not seem to participate strongly in the electronic absorption of the neutral form of compound **9**. According to both the PPP CI calculated longest-wavelength band positions and the MNDO calculated heats of formation, the 3-acetyl-4-hydroxycoumarin H-bonded form **9-1** can be suggested to be predominant in nonpolar solvents (carbon tetrachloride, *n*-hexane). On the other hand, for the enol form of

© 1997 NRC Canada

Can. J. Chem. Downloaded from www.nrcresearchpress.com by 88.146.161.215 on 09/08/12
For personal use only.

Fig. 4. Electronic absorption spectra of 3-acetyl-4-hydroxycoumarin **9** (curve *A*) and 8-acetyl-7-hydroxycoumarin **11** (curve *B*) in ethanol – carbon tetrachloride mixtures: (*a*) 100% ethanol; (*b*) 80% ethanol + 20% CCl_4; (*c*) 50% ethanol + 50% CCl_4; (*d*) 20% ethanol + 80% CCl_4; (*e*) 100% CCl_4.

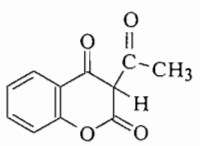




9 – 3

ΔH_f°(MNDO)= – 123.5 kcal/mol

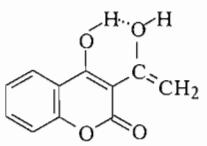
λ_{max} (PPP)=330 nm



9 – 4

ΔH_f°(MNDO)= – 118.5 kcal/mol

λ_{max} (PPP)= no data

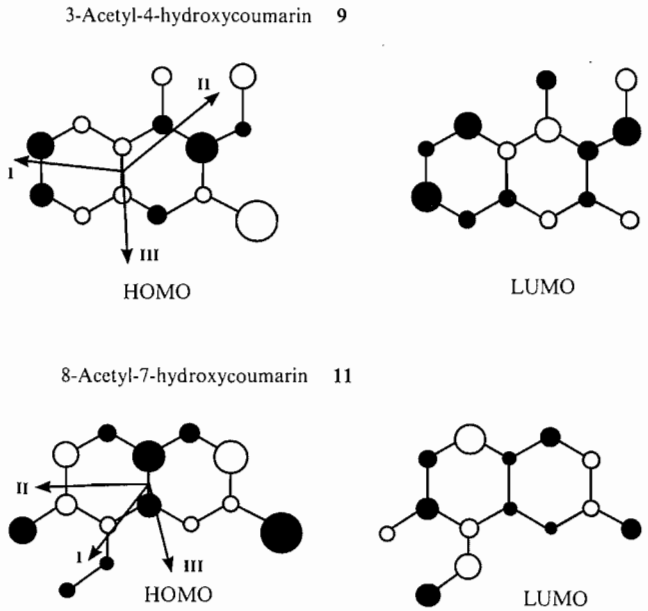


9 – 5

ΔH_f°(MNDO)= – 119.1 kcal/mol

λ_{max} (PPP)=344 nm

Fig. 5. Frontier orbital shapes and polarization directions of three $\pi \rightarrow \pi^*$ transitions in 3-acetyl-4-hydroxycoumarin **9** and 8-acetyl-7-hydroxycoumarin **11** predicted by the PPP CI calculations.



3-acetyl-2,4-chromandione, **9-2**, the calculated results are in better agreement with the electronic absorption spectrum of compound **9** recorded in a polar solvent, such as ethanol, even though the form **9-2** and 3-acetyl-2-hydroxy-4-chromenone form **9-3** are rather close in their MNDO-calculated ΔH_f° values.

The 2,4-chromandione tautomeric forms (similar to **9-2** and **9-4**) have often been discussed in the study of keto–enol tautomerism of 4-hydroxycoumarin derivatives. Some of the 2,4-chromandione derivatives have been found as reactive intermediates (22–24). Other derivatives have even been isolated as stable final structures (25, 26).

Predominance of the form **9-1** in nonpolar solvents is worthy of additional comment, since according to both the MNDO and PPP calculations this form is more polar than the form **9-2**: e.g., the PPP-calculated dipole moment values of these two forms are 5.58 and 3.3 D, respectively. The relative stability of form **9-1** seems to be due to its stronger intramolecular H-bonding than that of form **9-2**. Nonpolar solvents, e.g., *n*-hexane and carbon tetrachloride, do not affect intramolecular H-bonds, accounting for the predominance of form **9-1**.

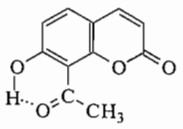
No notable changes in the electronic absorption spectra of compound **11** can be seen when these spectra are recorded in nonpolar and polar solvents (Fig. 4). PPP CI calculational results for the 8-acetyl-7-hydroxy-2-chromenone form **11-1** are in good agreement with the experimental spectra. The enol structure **11-2** of 8-acetyl-7-hydroxycoumarin **11** turned out to be invalid according to both the MNDO-calculated heat of formation data and the PPP CI-calculated longest-wavelength absorption band positions.

The differences between *ortho*-acetyl-substituted 4- and 7-hydroxycoumarins can also be seen from the calculational results. The shapes of the frontier molecular orbitals of compounds **9** and **11** are shown in Fig. 5. The minimal value of the

© 1997 NRC Canada

Can. J. Chem. Downloaded from www.nrcresearchpress.com by 88.146.161.215 on 09/08/12
For personal use only.

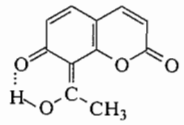
negative charge on the acetyl oxygen atom in compound **11** (structure **11-1**) agrees well with a weakness of the H-bond



11–1

ΔH_f^o(MNDO)= – 125.9 kcal/mol

λ_{max} (PPP)=340 nm



11–2

ΔH_f^o(MNDO)= – 107.6 kcal/mol

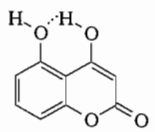
λ_{max} (PPP)=430 nm

between the hydroxyl and carbonyl functions in the 7-hydroxycoumarin derivatives. On the other hand, high negative charge on the acetyl oxygen atom in compound **9** (structure **9-1**) supports the suggestion concerning the strong intramolecular H-bonding in the 4-hydroxycoumarin derivatives, **9** and **10**.

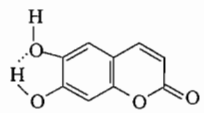
Intramolecular H bonding increases significantly changes of electron density on the hydroxyl oxygen atoms under UV excitation. According to the calculational results, an H-bonded hydroxyl function provides a stronger electron donation along the first electron transition than does a free hydroxyl group (the corresponding data are given in Table 4). Increase of electron donation of the oxygen atom of the hydroxyl function via H-bonding (or ionization, see further discussion) seems to be one of the reasons for the recorded bathochromic shifts of the longest-wavelength bands in electronic absorption spectra of *ortho*-hydroxyl- and *ortho*-acetyl-substituted hydroxycoumarins. Increased electron donation of the H-bonded hydroxyl function is evident from comparison of parameter values of free, H-bonded, and ionized hydroxyl groups. As seen in the Experimental section, parameters J and A of the H-bonded hydroxyl function are intermediate in value between those of the neutral and ionized forms.

The differences between the 3-substituted 4-hydroxycoumarins and the 8-substituted 7-hydroxycoumarins can also be illustrated by their reactivity. While studying ionization phenomena of some hydroxycoumarin derivatives, we found that introduction of an acetyl group into position 8 of 7-hydroxycoumarin increases the ionization constant K_{ion} due to stabilization of the resulting conjugate base by the electron-withdrawing effect of the acetyl function (compare compounds **3** and **11**). On the other hand, introduction of an acetyl group into position 3 definitely decreases the ionization potential of the 4-hydroxycoumarins.[2] These data can be explained by the acetyl group in position 3 transforming the corresponding 4-hydroxycoumarin derivative to another tautomeric form, which seems to be characterized by a different ionization potential. In such cases, comparison of the ionization constants of compounds **2** and **9** becomes meaningless.

PPP CI calculations with standard parameters also provide a good representation of energies and intensities of the longest-wavelength bands in the electronic absorption spectra of some dihydroxycoumarins. We refer, first of all, to the electronic absorption experimental data and calculated results for 4,7-dihydroxycoumarin **14** (these data are also listed in Table 2). The differences between experimental and calculated data become larger for the dihydroxycoumarins **13**, **15**, and **16**, which have neighboring hydroxyl functions: e.g., the differences between the experimental data and the calculated longest-wavelength band positions in the 6,7-dihydroxycoumarin electronic absorption spectra are 13–15 nm. H-Bonding between neighboring hydroxyl groups can be suggested as a structural effect that is responsible for the observed discrepancy. The corresponding structures **13-1**, **15-1**, and **17-1** are listed below.



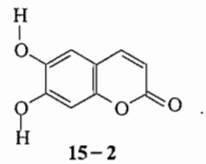
13–1



15–1

ΔH_f^o(MNDO)= – 135.5 kcal/mol

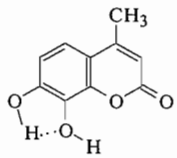
λ_{max} (PPP)=348 nm



15–2

ΔH_f^o(MNDO)= – 134.4 kcal/mol

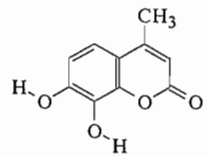
λ_{max} (PPP)=339 nm



17–1

ΔH_f^o(MNDO)= – 136.6 kcal/mol

λ_{max} (PPP)=324 nm



17–2

ΔH_f^o(MNDO)= – 134.4 kcal/mol

λ_{max} (PPP)=316 nm

We have found that the H-bonded 6-hydroxyl group model (structure **15-1**) provides the best agreement between experimental and calculated electronic transition energies of 6,7-dihydroxycoumarin when those of the non-H-bonded hydroxyl group model (structure **15-2**) and those of the H-bonded 7-hydroxyl group model are compared. Significantly different acidities of the hydroxyl functions located at different positions of the coumarin ring are in accord with these results. The 7-hydroxyl group is known to be much more acidic than the 6-hydroxyl group (pK_a values of the 7- and 6-hydroxycoumarins are 7.45 and 9.05, respectively (9)).

The same is true for 6,7-dihydroxy-4-methylcoumarin **16** and 7,8-dihydroxy-4-methylcoumarin **17**. For example, electronic transition energies calculated for the structure **17-1** (hydroxyl group at position 8 is H-bonded) are in better agreement with the experimental data than the results calculated for the structure in which the hydroxyl group at position 7 is H-bonded, and the structure **17-2** (where no H-bonds are possible at all).

The preference for structures **15-1** and **17-1** compared with structures **15-2** and **17-2** has also been confirmed by MNDO

[2] We have measured the K_{ion} values of compounds **3** and **11** using piperidine as a base, and of compounds **2** and **9** using imidazole as a base. These values are given below (compound number and the K_{ion} value are listed): **3**, 0.030; **11**, 0.064; **2**, 0.94; **9**, 0.22. These data will be published in detail elsewhere (for a preliminary report, see ref. 27).

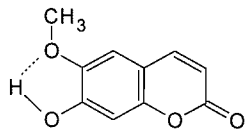
© 1997 NRC Canada

Table 4. Changes of electron density on the oxygen atom of the hydroxyl function in the first electronic transition of hydroxycoumarin derivatives.

	Change of electron density on oxygen atom of hydroxyl function		
Structure	Free OH	H-bonded OH	Ionized OH
9-1	−0.0007	−0.0015	−0.0280
11-1	−0.0270	−0.0610	−0.2220
13-1	−0.0207	−0.0557	−0.1350
16-1	−0.0310	−0.0700	−0.0900

calculations (the heats of formation $\Delta H_f°$ are given under the formulas): H-bonded structures **15-1** and **17-1** turned out to be 1–2 kcal/mol more stable.

The hypothesis of H-bonding in *ortho*-dihydroxycoumarins is supported by good agreement between the calculated and experimental electronic absorption spectra of 7-hydroxy-6-methoxycoumarin **18**: the H-bonded methoxyl group (structure **18-1**) is used in the calculations, since H-bonding of the 7-hydroxyl group in this compound is impossible (see data in Table 2 for illustration).

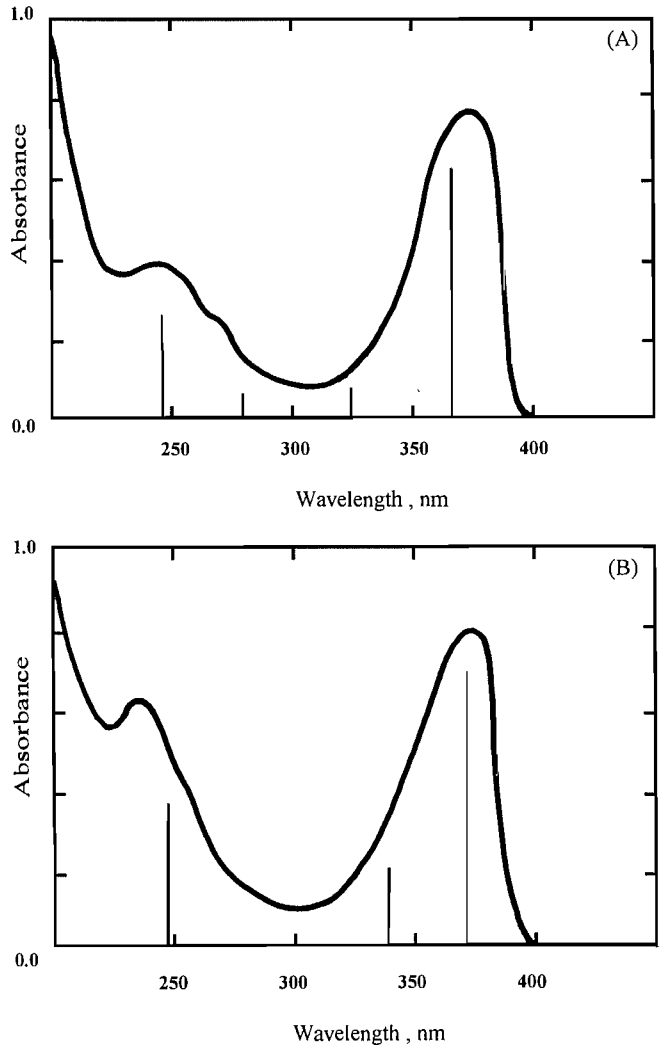


18 – 1

In previous studies electronic absorption spectra of ionized forms of hydroxycoumarin were mostly used for analytical purposes (14–16). Only a few reports discuss the absorption spectra of the ionized forms in a quantitative way (4, 28). Perel'son has calculated these spectra by the Hückel MO method and suggested that the decrease of parameter *d* under ionization of the hydroxyl function is due to the corresponding increase of its electron donation (4). Chatterjee and Douglas analyzed a dependence of the PPP calculational results on the resonance integral *b*, ionization potential *J*, and electron affinity *A* parameters (28). The parameters *J* were found to be the most effective in providing good agreement between the experimental data and the calculated results. On the other hand, resonance integral *b* changes show no significant effect.

We have also recorded electronic absorption spectra of hydroxycoumarin derivatives in their ionized forms. These spectra are partly shown in Figs. 6 and 7. On the whole, better agreement between the experimental data and the calculated results was found when the standard parameters of phenoxide oxygen atom were changed for the new parameters (see Experimental section and Table 5 data). First, this is true for the 7-hydroxycoumarin derivatives, which show excellent agreement of the experimental and calculated longest-wavelength band positions. One can see that ionization of the 7-hydroxycoumarin derivatives leads to a significant bathochromic shift of the longest-wavelength absorption bands (compare spectra given in Fig. 6 as an example). This shift is due to an increase in electron donation of the hydroxyl function upon ionization. The phenoxide-like ionized form is a result of ionization of the 7-hydroxycoumarin derivative. The ionization leads to a significant increase of HOMO energy in 7-hydroxycoumarins (compare also Table 4 data) and thus to bathochromic band shifts in their electronic absorption spectra.

Fig. 6. Electronic absorption spectra of 7-hydroxycoumarin **3** (curve *A*) and 8-acetyl-7-hydroxycoumarin **11** (cruve *B*) ionized forms in ethanol. The PPP CI calculated band positions λ_{max} and oscillator strengths *f* are indicated by the vertical lines (parameters used: J_{O^-} = 20.0 eV, A_{O^-} = 5.0 eV, $\beta_{C=O}$ = −2.00 eV).



On the other hand, ionization of the hydroxyl function

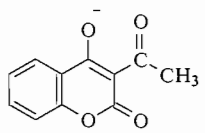
Can. J. Chem. Downloaded from www.nrcresearchpress.com by 88.146.161.215 on 09/08/12
For personal use only.

© 1997 NRC Canada

located at position 4 has no significant effect on the electronic absorption spectra of the monohydroxycoumarin derivatives (compare data in Tables 2 and 5). 4-Hydroxycoumarin and 4-hydroxy-6-methylcoumarin have no shifts of their longest-wavelength bands in the EA spectra under ionization, although the eventual direction of polarization of the corresponding transitions turned out to be definitely different. Moreover, parameters of the negatively charged oxygen atom (which are well suited for calculations of the phenoxide-like ionized form of 7-hydroxycoumarin) seem to be unsuccessful for the ionized form of 4-hydroxycoumarin as can be seen from the data in Table 5. 4-Hydroxy-2-chromenone seems to undergo a tautomeric transformation under ionization (see more detailed discussion below).

The ionized form of 8-acetyl-7-hydroxycoumarin has an electronic absorption spectrum that is very similar to the spectrum of the ionized form of 7-hydroxycoumarin (these spectra are compared in Fig. 6). This similarity supports the assumption that H-bonding is responsible for the bathochromic shifts in the electronic absorption spectra of neutral forms of 7-hydroxycoumarins **11** and **12**. As a whole, the PPP CI calculated results provide a good approximation of the electronic absorption spectra of 7-hydroxycoumarin derivatives in both their ionized and neutral forms. The 8-acetyl-7-hydroxycoumarins **11** and **12** do not show any tautomeric transformations under ionization, and the ionized form of structure **11-1** seems to be a good model for the ionization phenomena of these 7-hydroxycoumarins.

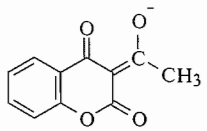
It is not surprising that calculational results of the ionized form of 3-acetyl-4-hydroxycoumarin (obtained with both standard and new atomic parameters for phenoxide oxygen) are not close to the experimental electronic absorption spectrum data (see Fig. 7). Effective delocalization of negative charge in the ionized form of 3-acetyl-4-hydroxycoumarin can be suggested as an explanation. As seen from the MNDO calculated heats of formation, ΔH_f° (values given below the structure numbers), the enolate ion forms **9i-1** and **9i-2**, as well as the carbanion form **9i-4**, seem to be almost equivalent in their stabilities. The 3-acetyl-2-hydroxy-4-chromenone ionized form **9i-3** and the enolate ion form **9i-5** are the least stable ones. On the whole, the structure of the enolate ion form **9i-2** appears to be the form most fitted to the experimental data and the calculational results, even though participation of the carbanion form **9i-4** in electronic absorption cannot reliably be evaluated by the PPP CI calculations due to lack of parameters for the negatively charged carbon atom.



9i-1

ΔH_f°(MNDO)= − 172.0 kcal/mol

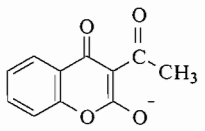
λ_{max} (PPP)=351 nm



9i-2

ΔH_f°(MNDO)= − 173.0 kcal/mol

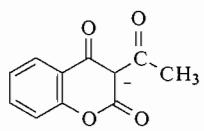
λ_{max} (PPP)=326 nm



9i-3

ΔH_f°(MNDO)= − 168.0 kcal/mol

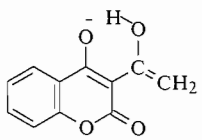
λ_{max} (PPP)=336 nm



9i-4

ΔH_f°(MNDO)= − 172.9 kcal/mol

λ_{max} (PPP)= no data

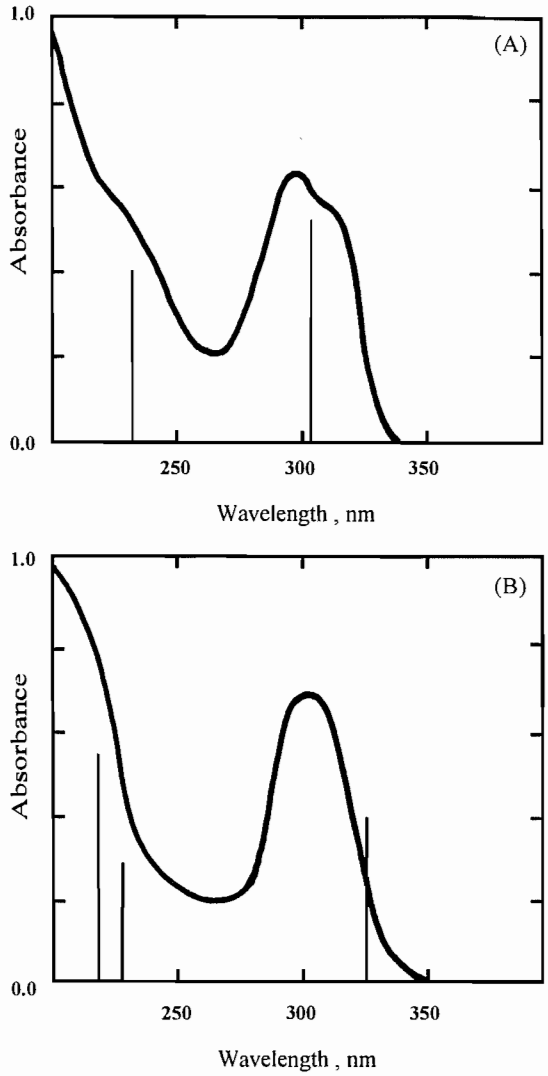


9i-5

ΔH_f°(MNDO)= − 164.1 kcal/mol

λ_{max} (PPP)=353 nm

Fig. 7. Electronic absorption spectra of ionized forms of 4-hydroxycoumarin **2** (curve *A*) and 3-acetyl-4-hydroxycoumarin **9** (curve *B*) in ethanol. The PPP CI calculated band positions λ_{max} and oscillator strengths *f* are indicated by the vertical lines (parameters used: J_{O^-} = 20.0 eV, A_{O^-} = 5.0 eV, $\beta_{C=O}$ = −2.00 eV).



Can. J. Chem. Downloaded from www.nrcresearchpress.com by 88.146.161.215 on 09/08/12
For personal use only.

© 1997 NRC Canada

Table 5. Experimental and calculated EAS maxima of the ionized forms of hydroxycoumarin derivatives.

Compound	Experimental data λ_{max}, nm (lg ε)	PPP CI calculated data λ_{max}, nm (*f*)	J_{O^-}, eV	A_{O^-}, eV	$-\beta_{C=O}$, eV
2	301(3.91)	348(0.10)	20.0	5.0	2.46
		399(0.15)	17.1	2.47	2.46
		305(0.45)	20.0	10.0	2.46
3	369(4.11)	369(0.70)	20.0	5.00	2.00
		393(0.66)	17.7	2.47	2.00
5	392(4.40)	390(0.95)	20.0	5.00	2.00
		436(1.12)	17.7	2.47	2.00
6	383(3.03)	390(0.48)	20.0	5.00	2.00
		436(0.40)	20.0	2.00	
		489(0.40)	17.7	2.47	2.00
7	392(3.60)	398(0.20)	20.0	5.00	2.46
		489(0.13)	17.7	2.47	2.46
9	303(4.15)	385(0.35)	20.0	5.00	2.46
		375(0.15)	17.7	2.47	2.46
		326(0.54)	20.0	10.0	2.46
11	373(4.33)	364(0.65)	20.0	5.00	2.00
		389(0.23)	17.7	2.47	2.00

Can. J. Chem. Downloaded from www.nrcresearchpress.com by 88.146.161.215 on 09/08/12
For personal use only.

It is quite reasonable that ionization of both 3- and 4-phenyl-substituted 7-hydroxycoumarins **5** and **6** does not remove the bathochromic shift that is seen in the absorption spectra of their neutral forms (when compared with 7-hydroxycoumarin itself), since intramolecular H-bonding has no effect on their neutral molecules.

It is worth noting that electronic absorption spectra of ionized forms of the dihydroxycoumarin derivatives are also in good accord with the calculational results. Ionization of both hydroxyl groups was assumed in the PPP CI calculations. The largest bathochromic shift (about 65 nm) was recorded in the electronic absorption spectrum of the ionized form of 4,5-dihydroxycoumarin. The ionization of two hydroxyl groups in this compound increases the HOMO energy and does not appreciably change the LUMO energy of this molecule.

On the other hand, ionization of two hydroxyl functions in the 4,7-dihydroxycoumarin increases both the HOMO and the LUMO energies and thus provides a rather small bathochromic shift, about 13 nm.

Conclusions

Electronic absorption spectra of hydroxycoumarins depend on the location of the hydroxyl function, its intramolecular H-bonding with a neighboring substituent, and ionization via interaction of hydroxycoumarin with a base.

7-Hydroxycoumarin and its methyl-, phenyl-, hydroxyl-, and acetyl-substituted derivatives exist in the 2-chromenone tautomeric form both in polar (ethanol) and in nonpolar (carbon tetrachloride and *n*-hexane) solvents. Ionization of these derivatives yields phenoxide-like ionized forms. The following parameters of the negatively charged oxygen atom (J = 20.0 eV, A = 5.00 eV) and resonance integral $\beta_{C=O}$ equal to −2.00 eV provide close agreement between the calculated and experimental electronic absorption spectral data.

3-Acetyl-4-hydroxycoumarins exist in the 4-hydroxy-2-chromenone tautomeric form in nonpolar solvents. The 2,4-chromandione enol form of this compound seems to be predominant in polar solvents. Ionization of 4-hydroxycoumarin derivatives seems to lead to their transformation to the 2,4-chromandione ionized forms.

H-Bonding of the hydroxyl function and its ionization produce a bathochromic shift of the longest-wavelength bands in the electronic absorption spectra of substituted hydroxycoumarins due to an increase of its electron donation under UV excitation.

Acknowledgements

This work was generously funded by the Highest Education State Committee of the Russian Federation (program "Fine Organic Synthesis") and by the Otto Bremer Foundation (Minnesota, U.S.A.).

References

1. R.D.H. Murray. The natural coumarins, occurrence, chemistry and biochemistry. Wiley–Interscience, New York. 1982.
2. R.D.H. Murray. Nat. Prod. Rep. **6**, 551 (1989).
3. M.E. Perel'son and Yu. N. Sheinker. Teor. Eksp. Khim. (USSR), **4**, 697 (1968).
4. M.E. Perel'son and Yu. N. Sheinker. Teor. Eks. Khim. (USSR), **4**, 185 (1968).
5. P.S. Song. Can. J. Spectrosc. **26**, 59 (1981).
6. P.S. Song and W.H. Gordon. J. Phys. Chem. **74**, 4234 (1970).
7. T.A. Moore, M.L. Harter, and P.S. Song. J. Mol. Spectrosc. **40**, 144 (1971).
8. I.V. Sokolova and L.I. Loboda. Zh. Strukt. Khim. (USSR), **23**, 37 (1982).

© 1997 NRC Canada

9. H. Nakazumi, T. Ucyama, T. Kitaguchi, and T. Kitao. Phosphorus Sulfur, **16**, 59 (1983).
10. H. Abu-Eitah Rafie and A.H. El-Tawl Bahgat. Can. J. Chem. **63**, 1173 (1985).
11. O.A. Ponomarev, E.R. Vasina, V.G. Mitina, and S.N. Yarmolenko. Zh. Obsch. Khim. (USSR), **55**, 179 (1990).
12. O.A. Ponomarev, E.R. Vasina, V.G. Mitina, and A.A. Suchorukov. Zh. Fiz. Khim. (USSR), **64**, 974 (1990).
13. D.N. Robertson and K.P. Link. J. Am. Chem. Soc. **75**, 1883 (1953).
14. R.M. Horowitz and B. Gentili. J. Org. Chem. **25**, 2183 (1960).
15. N.R. Krishnaswami, T.R. Seshadri, and B.R. Sharm. Indian J. Chem. **4**, 120 (1960).
16. F.M. Dean and B. Parton. J. Chem. Soc. C, 526 (1969).
17. J. Griffiths. Dyes Pigm. **3**, 211 (1982).
18. G.M. Haitink and H. Diehl. Talanta, **21**, 1193 (1974).
19. S. Marciant. Z. Naturforsch. **26B**, 1129 (1971).
20. P.K. McCarthy and G.J. Blanchard. J. Phys. Chem. **94**, 12205 (1993).
21. V.P. Bulichev and N.D. Sokolov. *In* Hydrogen bond. *Edited by* N.D. Sokolov. Nauka, Moscow. 1981. pp. 10–29.
22. G. Appendino, G. Cravotto, S. Tagliapietra, and G.M. Nano. Helv. Chim. Acta, **73**, 1865 (1990).
23. G. Appendino, G. Cravotto, S. Tagliapietra, S. Ferraro, G.M. Nano, and G. Palmisano. Helv. Chim. Acta, **74**, 1451 (1991).
24. G. Appendino, G. Cravotto, L. Toma, R. Annunziata, and G. Palmisano. J. Org. Chem. **59**, 5556 (1994).
25. D. Anker and J. Massicot. Bull. Soc. Chim. Fr. **6**, 2181 (1969).
26. A.S. Shawali, N.M.S. Harb, and K.O. Badahdah. J. Heterocycl. Chem. **22**, 1397 (1985).
27. V.F. Traven, L.I. Vorobjeva, T.A. Chibisova, E.A. Carberry, and N.J. Beyer. Ionization of hydroxycoumarin derivatives by amines. Abstr. 211th ACS Natl. Meeting, New Orleans, March 24–28, 1996. Abstract no. 286.
28. R.K. Chatterjee and B.E. Douglas. Spectrochim. Acta, **21**, 1625 (1965).

Can. J. Chem. Downloaded from www.nrcresearchpress.com by 88.146.161.215 on 09/08/12
For personal use only.

© 1997 NRC Canada

Keto–enol tautomerism, NMR spectra, and H–D exchange of 4-hydroxycoumarins

Valery F. Traven, Vadim V. Negrebetsky, Larisa I. Vorobjeva, and Edward Andrew Carberry

Abstract: 4-Hydroxycoumarin **1**, 4,5-dihydroxycoumarin **2**, and 4,7-dihydroxycoumarin **3** undergo H–D exchange at the C(3) atom of the lactone ring. Although only the 4-hydroxy-2-chromenone tautomeric forms are seen in the ^{1}H and ^{13}C NMR spectra of compounds **1–3**, the equilibrium between the 4-hydroxy-2-chromenone and 2,4-chromandione forms is suggested to be the key step in the H–D exchange reaction. 4,5-Dihydroxycoumarin shows the highest rate of the reaction, since H-bonding between 5-hydroxyl and 4-keto functional groups can provide relative stability to the 5-hydroxy-2,4-chromandione tautomeric form, a probable intermediate of the exchange. NMR spectra and tautomeric transformations of 3-(4-methoxyphenylazo)-4-hydroxycoumarin **4** and 3-acetyl-4-hydroxycoumarin **5** are also discussed. The stabilities of different tautomeric forms of compounds **1–5** have been evaluated by MNDO calculations.

Key words: 4-hydroxycoumarin derivatives, keto-enol tautomerism, H–D-exchange.

Résumé : Les 4-hydroxycoumarine (**1**), 4,5-dihydroxycoumarine (**2**) et 4,7-dihydroxycoumarine (**3**) subissent un échange H–D au niveau de l'atome C(3) du noyau lactonique. Même si on n'observe que les formes tautomériques 4-hydroxychrom-2-énones dans les spectres RMN ^{1}H et ^{13}C des composés **1–3**, on est porté à croire que l'existence d'un équilibre entre les formes 4-hydroxychrom-2-énone et chromane-2,4-dione est l'étape clé dans la réaction d'échange H–D. La 4,5-dihydroxycoumarine présente la vitesse de réaction la plus élevée; ce résultat découle probablement de l'existence d'une liaison hydrogène entre les groupes fontionnels 5-hydroxyle et 4-céto qui fournit une stabilité relative accrue à la forme tautomérique 5-hydroxychromane-2,4-dione, l'intermédiaire probable de l'échange. On discute aussi des spectres RMN et des transformations tautomériques des 3-(4-méthoxyphénylazo)-4-hydroxycoumarine (**4**) et 3-acétyl-4-hydroxycoumarine (**5**). On a évalué les stabilités des diverses formes tautomériques des composés **1–5** par le biais de calculs «MNDO».

Mots clés : dérivés de la 4-hydroxycoumarine, tautomérie céto-énolique, échange H–D.

[Traduit par la rédaction]

Introduction

Natural hydroxycoumarins are of great interest, since many of them show prominent biological activity (1, 2). Some 3-substituted 4-hydroxycoumarins are the most effective anticoagulant drugs known for prevention and treatment of thromboembolic disorders (3–5). It has been suggested that enol–keto tautomeric transformations of the 4-hydroxycoumarin moiety are responsible for that activity. The 2,4-chromandione form has been proposed to react with nucleophilic centers of the enzyme Vitamin K Epoxide Reductase, thus inhibiting the Vitamin K – Vitamin K Epoxide cycle that provides the prothrombin synthesis (5).

Received October 3, 1996.

V.F. Traven,[1] **V.V. Negrebetsky, and L.I. Vorobjeva.** D. Mendeleev University of Chemical Technology of Russia, Miusskaja 9, Moscow, 125047, Russia.
E.A. Carberry.[1] Southwest State University, Marshall, MN 56258, U.S.A.

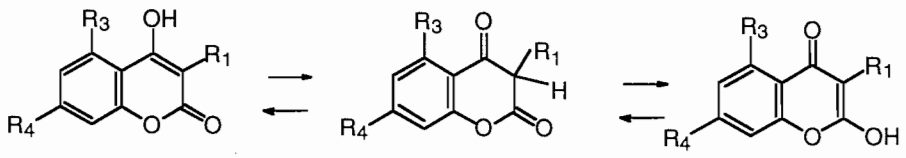
[1] Authors to whom correspondence may be addressed. VFT: Fax: +7 095 200 4204. E-mail: traven@orgchem.mhti.msk.su EAC: Telephone: (507) 537-7131. Fax: (507) 537-7154. E-mail: carberry@ssu.southwest.msus.edu

The following tautomeric forms of 4-hydroxycoumarin **1** and its derivatives have been discussed in most earlier studies: 4-hydroxy-2-chromenone **1***a*, 2.4-chromandione **1***b*, and 2-hydroxy-4-chromenone **1***c*. The possible transformations of these forms have been intensively examined by different methods. Some of the conclusions were based on chemical reactivity data (6–14). Arndt et al. have suggested the existence of the forms **1***a* and **1***c* under treatment of 4-hydroxycoumarin by CH_2N_2 (6). The 2,4-chromandione form **1***b* (an ionized state) has been suggested as an intermediate in the 4-acetoxycoumarin rearrangement to 3-acetyl-4-hydroxycoumarin (7). 3-Substituted 2,4-chromandione forms have also been suggested as intermediates in the 1,2-addition of α,β-unsaturated aldehydes to 4-hydroxycoumarin (10). Treatment of 3,3′-alkylidene-4,4′-dihydroxybis(coumarins) with $NaBH_3CN$ in refluxing methanol has been suggested to lead to the formation of 3-alkylidene-2,4-chromandiones as intermediates. These intermediates have been trapped using hydride ion in several reactions with dienes and dienophiles (11, 12).

Although 2,4-chromandione **1***b* has never been isolated as a stable product or as an intermediate, 3,3′-disubstituted 2,4-chromandiones have been shown to be stable final products in some reactions. For example, 3,3′-dialkyl-2,4-chromandiones have been prepared under treatment of the silver salt of 4-hydroxycoumarin by alkyl halides (8). Also, 3-arylhydrazono-2,4-chromandiones were found to be stable products of the

© 1997 NRC Canada

Can. J. Chem. Downloaded from www.nrcresearchpress.com by 88.146.161.215 on 09/08/12
For personal use only.



1*a* - **5***a* **1***b* - **5***b* **1***c* -**5***c*

azo-coupling reaction between 4-hydroxycoumarin and arene diazonium compounds (14).

Tautomeric transformations of 4-hydroxycoumarins have also been studied by spectroscopic and calculational methods (15–24). Knobloch et al. studied the electronic absorption spectra of 4-hydroxycoumarin and reported the existence of both tautomeric forms 4-hydroxy-2-chromenone **1***a* and 2-hydroxy-4-chromenone **1***c* (15). Wolfbeis and Uray concluded that the fluorescence spectra of 4-hydroxycoumarin derivatives show the predominance of the tautomeric form **1***c* (16).

Experimental section

Compounds **1**–**6** were synthesized by known procedures and purified by recrystallization from ethanol or acetic acid. Their melting points (uncorrected, in °C) are given below (reference data are shown in parentheses): **1**, 216–218 (217–218 (25)); **2**, 216–218 (218–219 (26)); **3**, 273–274 (274–275 (27)); **4**, 236–237 (236 (14)); **5**, 136–137 (137–139 (28)); **6**, 125 (125 (6)).

^{1}H and ^{13}C NMR spectra were recorded on a Bruker NMR spectrometer (200 MHz); DMSO-d_6 and methanol-d_4 were used as solvents. The ^{13}C NMR spectra of compounds **4** and **5** were not recorded in methanol-d_4 due to their low solubility.

The H–D exchange reactions were studied by measurement of the intensity of the H(3) signal in the corresponding 4-hydroxycoumarin ^{1}H NMR spectra at room temperature. Methanol-d_4 was used as solvent in reactions of compounds **1**–**3** and **6**. An acetonitrile-d_3 – methanol-d_4 mixture (3:1 ratio) was used in measurements of the reaction rate of compound **4** because of the compound's low solubility in pure methanol-d_4. Measured concentrations were treated by the first-order reaction law; the accuracy of measurement of the H–D exchange rate constant was equal to 10%.

Quantum chemical calculations were done by the MNDO method using standard programs and parameters (29). Starting atomic coordinates were evaluated via PC Model calculations.

Results and discussion

The MNDO method was successfully used for the calculation of ground state parameters of organic compounds, including π-conjugated heteroarenes (29, 30). We evaluated the stabilities of compounds **1**–**6** in different tautomeric forms by calculation of their heats of formation $\Delta H_f°$. These data, dipole moments μ, ionization potentials IP_1, and electron affinities EA_1 are given in Table 1.

Although an equilibrium between the 2- and 4-chromenone forms **1***a* and **1***c* has been suggested in the discussion of 4-hydroxycoumarin electronic absorption spectra, Song reported excellent agreement between the experimental data and PPP CI calculational results for the form **1***a* (18). Porter and coworkers studied infrared spectra of the 2-^{13}C and 3-D labelled

Table 1. Heats of formation ($H_f°$ (kcal/mol), dipole moments μ(D), ionization potentials IP_1 (eV), electron affinities EA_1 (eV) of tautomeric forms of 4-hydroxycoumarin derivatives.

Tautomeric form	$-\Delta H_f°$	μ	IP_1	EA_1
1*a*	88.27	4.31	9.29	0.99
1*b*	87.41	2.94	9.63	0.98
1*c*	85.05	4.30	9.26	0.61
2*a*	133.64	3.96	9.13	1.02
2*b*	133.70	2.15	9.32	1.06
2*c*	132.03	3.84	9.07	0.67
3*a*	137.24	5.59	9.11	0.93
3*b*	136.20	2.39	9.53	0.96
3*c*	131.94	1.32	9.31	0.57
4*a*	27.93	4.40	8.92	1.44
4*b*	20.59	3.55	9.56	0.94
4*c*	23.70	2.32	8.84	1.04
4*d*	16.89	2.90	8.98	1.13
5*a*	124.50	5.48	9.53	1.27
5*b*	118.50	3.54	9.70	1.07
5*c*	121.00	3.70	9.49	0.75
6	80.26	4.64	9.24	0.88

4-hydroxycoumarins in solution, and found no sign of the tautomeric form **1***c* (19, 20).

^{13}C NMR spectra of 4-hydroxycoumarin and its derivatives have also been recorded (21–23) and did not show the presence of any other tautomeric forms than 4-hydroxy-2-chromenone form *a*.

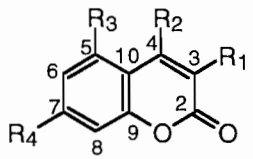
Some calculational results should also be mentioned. The resonance energies (calculated in the *p*-approximation) did not differentiate between the 4-hydroxy-2-chromenone and the 2-hydroxy-4-chromenone tautomeric forms **1***a* and **1***c* but showed a definite predominance of the 2,4-chromandione tautomeric form **1***b* (24).

As one can see, tautomeric transformations of 4-hydroxycoumarin and its derivatives are important for understanding their reactivity and spectral properties, even though some of the conclusions reported seem to be rather controversial.

We have studied the keto–enol tautomerism of 4-hydroxycoumarin and its derivatives, recording their ^{1}H and ^{13}C NMR spectra and looking for the H–D exchange reaction at the 3 position of the coumarin ring. The compounds studied (4-hydroxycoumarin **1**, 4,5-dihydroxycoumarin **2**, 4,7-dihydroxycoumarin **3**, 4-hydroxy-3-(4′-methoxyphenylazo)-coumarin **4**, 3-acetyl-4-hydroxycoumarin **5** and 4-methoxycoumarin **6**) are listed as follows (only R substituents different from H are given):

Can. J. Chem. Downloaded from www.nrcresearchpress.com by 88.146.161.215 on 09/08/12
For personal use only.

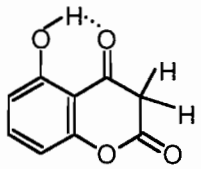
© 1997 NRC Canada



1: R^2 = OH; **4**: R^1 = *p*-CH_3O-C_6H_4-N = N-, R^2 = OH;
2: $R^2 = R^3$ = OH; **5**: R^1 = $C(O)CH_3$, R^2 = OH;
3: $R^2 = R^4$ = OH; **6**: R^2 = OCH_3.

4-Hydroxy-2-chromenone forms **1***a*–**5***a* turned out to be the most stable forms for each of the compounds **1**–**5**, since these forms have minimal values of heats of formation $\Delta H_f°$. On the whole, 2,4-chromandione forms **1***b*–**5***b* are less stable than the forms **1***a*–**5***a*. However, the forms **1***b*–**5***b* differ in their unstability. The differences of the values $\Delta H_f°$ between forms **1***a*–**5***a* and forms **1***b*–**5***b* turned out to be −0.86, 0.06, −1.04, −7.34 and −6.0 kcal/mol, respectively.

The highest relative stability of the 2,4-chromandione tautomeric form **2***b* of 4,5-dihydroxycoumarin can be understood in terms of the possible intramolecular H-bonding between the 4-keto and the 5-hydroxyl functional groups. H-Bonding of the same energy is out of the question in the tautomeric form **2***a*.



2*b*

Tautomerism of compound **4** is worth additional comments. Even though the 4-hydroxy-3-(4-methoxyphenylazo)-coumarin form **4***a* turns out to be more stable according to the MNDO calculations, form **4***d* should also was taken into consideration in accordance with reference data (14) (see discussion below).

Forms **1***a*–**5***a* seem to be preferable to forms **1***b*–**5***b* and **1***c*–**5***c* in polar solvents (methanol and dimethyl sulfoxide) due to the higher values of the dipole moments calculated by the MNDO method and given in Table 1.

The first ionization potentials and electron affinity values of the tautomeric forms of compounds **1**–**6** calculated by the MNDO method are also listed in Table 1. As one can see, 2,4-chromandione forms **1***b*–**3***b* exhibit increased electron affinity values. These results are in good accord with the proposed higher reactivity to nucleophilic reagents of the 2,4-chromandione forms of 4-hydroxycoumarin derivatives, when these forms are available, due to the corresponding structural effects (5).

The 2-hydroxy-4-chromenone enol forms **1***c*–**3***c* turned out to be the least stable forms. These conclusions agree well with most of experimental data (6–18).

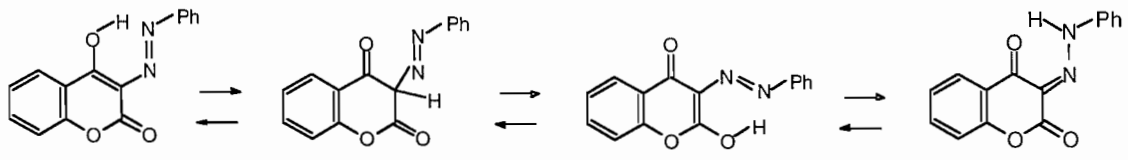
We have recorded the ^1H and ^{13}C NMR spectra of compounds **1**–**6**. The ^1H NMR spectral data are listed in Table 2. Assignment of the spectral patterns was made by using homonuclear ($^1H - ^1H$) (COSY) and heteronuclear ($^1H - ^{13}C$) correlation of chemical shifts. Quaternary and carbonyl carbon atom signals were assigned with use of the APT method and heteronuclear correlation of long-range coupling constants (HETCOR $^3J_{CH}$). The coupling constants $^1J_{CH}$ and $^3J_{CH}$ were determined by the GATE technique (31).

NMR spectral patterns were compared with the MNDO calculational results. In agreement with the quantum chemical calculations, only the 4-hydroxy-2-chromenone forms **1***a* and **3***a* were registered in the ^1H NMR spectra of compounds **1** and **3**. As one can see from the data given in Table 2, there is no sign of the presence of 2,4-chromandione form *b* in these ^1H NMR spectra. Surprisingly, the same is true for 4,5-dihydroxycoumarin **2** although forms **2***a* and **2***b* have almost the same MNDO-calculated heat of formation values. The ^1H NMR spectrum does not show an equilibrium between these forms, since proton signals are noted only for form **2***a*.

Analysis of the ^{13}C NMR spectra supports these conclusions. The corresponding data are listed in Tables 3 and 4. For example, signals at 161.79 and 165.52 ppm in the low-field ^{13}C NMR spectrum of compound **1** belong to the C(2) and to C(4) atoms, respectively. Splitting pattern analysis of ^{13}C NMR spectra shows the signal of the C(2) atom to be a doublet ($^2J_{CH}$, 2.3 Hz) due to its interaction with the only proton at position 3. If the form **1***c* were predominant, an additional splitting on the 2-hydroxyl group proton should also be registered. The signals of the C(4) atoms in the ^{13}C NMR spectra of coumarins **1** and **3** are multiplets (doublets of doublets) due to splitting on the H(3) and H(5) atoms. These signals are also broadened due to their scalar interaction with the solvated proton of the hydroxyl group.

Although signals of the 2,4-chromandione forms **1***b*–**3***b* have not been noted in the ^1H and ^{13}C NMR spectra even at different temperatures (from +30 to −60°C), the use of methanol-d_4 instead of DMSO-d_6 broadens the signals in the ^1H NMR spectra. 2-Carbon and 4-carbon atoms seem to become more equivalent in methanol, since the difference between C(2) and C(4) chemical shifts in the ^{13}C NMR spectra is diminished in this solvent: 2.35 ppm (CD_3OD) instead of 3.73 ppm (DMSO-d_6).

4-Hydroxycoumarins are more strongly solvated in methanol. We suggest that this solvation may provide the 2,4-chromandione tautomeric form *b*, even at a relatively low concentration. We have already shown that alcohols provide keto–enol tautomeric transformations in a series of 4-hydroxycoumarin derivatives (32). In particular, this was noted in the electronic absorption spectra of 3-acetyl-4-hydroxycoumarins when nonpolar solvents (such as *n*-hexane or carbon tetrachloride) are exchanged for polar solvents such as ethanol or methanol, transforming the 3-acetyl-4-hydroxy-



4*a* **4***b* **4***c* **4***d*

Can. J. Chem. Downloaded from www.nrcresearchpress.com by 88.146.161.215 on 09/08/12
For personal use only.

© 1997 NRC Canada

Can. J. Chem. Downloaded from www.nrcresearchpress.com by 88.146.161.215 on 09/08/12
For personal use only.

Table 2. ^{1}H NMR spectra of hydroxycoumarins **1–6** (solvent, DMSO-d_6; chemical shifts and splitting constants are given in Hz).

	Compound					
Atom	**1**	**2**	**3**	**4**[a]	**5**[b]	**6**
H-3	5.61,1H, s	5.46,1H, s	5.39,1H, s	5.55,1H, s (form ***4a***)	—	5.65,1H, s
H-5	7.84,1H, d,	—	7.65,1H, d,	7.90–8.00,[c] 7.76[d]	8.00,1H, d,	7.59,1H, d,
H-6	7.66,1H, t, H6–H5,7.8	6.75,1H,dd, H6–H7,8.2, H6-H8,0.8	6.79,1H,dd, H6–H5,8.6, H6–H8,2.3	7.32,1H, t, H6–H5,7.9	7.44,1H, t, H6–H5,7.9	6.76,1H,dd H6–H5,8.8,
H-7	7.36,1H, t, H7–H8,7.8	7.45,1H, d, H7–H8,8.2	—	7.59,1H, t, H7–H8,8.1	7.83,1H, t, H7–H8,8.0	
H-8	7.39,1H, d,	6.83,1H,dd,	6.68,1H, d,	7.29,1H, d,	7.41,1H, d,	6.67,1H, d,
H-11	—	—	— H11–H12,9.4	7.69,2H, d,	—	—
H-12	—	—	—	7.05,2H, d,		

[a]Other protons: OCH_3, 3.77, 3H, s; OH, 16.00, s (form **4*a***); OH, 12.44, s (form **4*c***); NH, 14.00, s (form **4*d***).
[b]Other protons: $COCH_3$, 2.66, 3H, s; OH, 13.30, 1H, s.
[c]0.5 H, d, H5–H6, 8.0, forms **4*a***, **4*c***, **4*d***.
[d]0.5 H, d, H5–H6, 7.9, form **4*b***.

Table 3. ^{13}C NMR spectra of hydroxycoumarins **1–3**, **5**, and **6** (solvent, DMSO-d_6, chemical shifts and splitting constants are given in Hz).

	Compound				
Atom	**1**	**2**	**3**	**5**[a]	**6**[b]
C-2	161.79,d C2–H3,2.3	161.70,s	162.34,s	159.4,s	162.13,s
C-3	90.87,d, C3–H3,167.6	89.69,d, C3–H3,167.5	87.73,d, C3–H3,166.9	101.7,s	86.87,d, C3–H3,169.3
C-4	165.52,dd, C4–H3,3.5 C4–H5,4.6	167.77,s	166.11,d, C4–H5,3.2	178.2,d, C4–H5,4.8	166.42,d, C4–H5,3.7
C-5	123.85,dd, C5–H5,163.4, C5–H7,7.8	155.62,d, C5–H7,10.7	124.45,d, C5–H5,163.6	125.2,dd, C5–H5,165.5 C5–H7,8.0	124.09,d, C5–H5,163.7
C-6	123.10,dd, C6–H6,164.7, C6–H8,8.0	110.77,dd, C6–H6,162.9, C6–H8,7.7	112.46,dd, C6–H6,162.9, C6–H8,4.9	125.5,dd, C6–H6,166.3 C6–H8,8.0	112.80,dd, C6–H6,162.9, C6–H8,4.4
C-7	132.63,dd, C7–H7,161.5, C7–H5,8.7	132.78,d, C7–H7,162.4	161.61,d, C7–H5,11.1	137.0,dd, C7–H7,163.3	161.64,d, C7–H5,10.8 C7–H5,8.0
C-8	116.28,dd, C8–H8,164.5, C8–H6,7.7	107.41,dd, C8–H8,166.5, C8–H6,7.8	101.89,dd, C8–H8,162.3, C8–H6,4.4	117.1,dd, C8–H8,166.3 C8–H6,7.5	101.99,dd, C8–H8,162.9, C8–H6,4.3
C-9	153.41,dd, C9–H7,9.6, C9–H5,8.0	154.63,d, C9–H7,10.1	155.36,dd, C9–H7,9.6, C9–H6,4.1	154.4,dd, C9–H7,9.0, C9–H5,8.0	154.59,dd, C9–H7,9.7, C9–H6,4.3
C-10	115.67,dd, C10–H8,8.9, C10–H6,5.0	103.71,d, C10–H8,8.7	107.59,d, C10–H8,8.2	115.0,dd, C10–H8,8.0, C10–H6,4.5	107.05,d, C10–H8,9.1

[a]Other carbons: C(CO), acetyl, 205.8, q, $J_{C(CO)-H(CH_3)}$, 6.4, CH_3, 29.9, s.
[b]Other carbons: OCH_3, 56.7, q, $J_{C(CH_3)-H(CH_3)}$, 147.0.

© 1997 NRC Canada

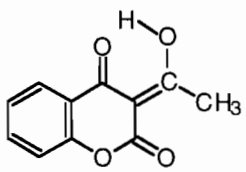
Can. J. Chem. Downloaded from www.nrcresearchpress.com by 88.146.161.215 on 09/08/12
For personal use only.

Table 4. ^{13}C NMR spectra of hydroxycoumarins **1–3** and **6** (solvent, methanol-d_4, chemical shifts and splitting constants are given in Hz).

	Compound			
Atom	**1**	**2**	**3**	**6**[a]
C-2	166.06,d, C2–H3,2.1	165.70,s	167.01,s	166.06,s
C-3	91.71,d, C3–H3,167.7	91.27,d, C3–H3,167.6	88.56,d, C3–H3,167.2	87.39,d, C3–H3, 168.6
C-4	168.41,d, C4–H5,4.3	169.62,s	169.13,d, C4–H5,3.9	169.24,d, C4–H5,4.0
C-5	125.32,dd, C5–H5,165.5, C5–H7,8.3	156.72,d, C5–H7,10.9	125.91,d, C5–H5,164.4	125.52,d, C5–H5, 164.3
C-6	124.63,dd, C6–H6,163.4, C6–H8,7.8	111.98,dd, C6–H6,163.0, C6–H8,7.8	114.09,dd, C6–H6,162.7, C6–H8,5.0	114.26,dd, C6–H6, 163.1, C6–H8,5.6
C-7	133.99,dd, C7–H7,162.0, C7–H5,9.4	134.41,d, C7–H7,162.1	163.67,d, C7–H5,10.9	163.47,d, C7–H5,10.6
C-8	117.60,dd, C8–H8,164.0, C8–H6,7.7	109.31,dd, C8–H8,166.6, C8–H6,7.5	103.12,dd, C8–H8,162.2, C8–H6,4.3	—
C-9	155.23,d, C9–H7,12.1	156.14,d, C9–H7,12.0	157.14,dd, C9–H7,9.3, C9–H5,4.1	157.23,dd, C9–H7, 9.6, C9–H5, 4.1
C-10	117.30,d, C10–H8,8.5	104.92,d, C10–H8,5.4	109.38,d, C10–H8,7.5	109.03,d, C10–H8,8.9

[a]Other carbons: OCH_3, 57.2, q, $J_{C(CH_3)-H(CH_3)}$, 145.8.

2-chromenone tautomeric form **5***a* to the 3-acetyl-2,4-chromandione derivative form **5***d*.



5*d*

We also have found that methanol allows the H–D exchange reaction at the C(3) atom in compounds **1–3** and **4**. The H–D exchange proceeds by a pseudo-first-order reaction in methanol-d_4. The measured rate constants k_1 are given below.

Compound	**1**	**2**	**3**	**4**
k_1,s^{-1}	1.1×10^{-3}	1.8×10^{-2}	1.0×10^{-3}	1.0×10^{-4}

Two possible mechanisms for the H–D exchange in 4-hydroxycoumarins can be suggested. One of them is an electrophilic aromatic substitution mechanism $S_E(Ar)$, leading to H–D exchange in aromatic hydrocarbons and heteroarenes (33). This scheme might work with the 4-hydroxycoumarins as well, since heteroaromaticity of the coumarin moiety (including the 2-pyrone ring) has been illustrated many times. Some electrophilic reactions of 4-hydroxycoumarin at position 3 (including bromination (34) and formylation (35)) can be used as examples.

As a rule, $S_E(Ar)$ reactions in arenes and heteroarenes proceed according to orbital control in their orientation patterns: the HOMO electron densities of a substrate determine whether it will be attacked by electrophilic reagents (36, 37).

Graphical representations of the HOMOs of compounds **1–3**, and **6** in their most probable tautomeric forms **1***a*–**3***a*, and **6***a* are shown in Fig. 1. The values of the eigencoefficients are proportional to the sizes of the circles on the given atoms. As one can see, these compounds are certainly different in their frontier molecular orbitals. The HOMOs of the tautomers **1***a*, **3***a*, and **6***a* have maximal eigencoefficient values at position 3. However, these HOMO electron densities do not seem to correlate with the relative rates of position 3 H–D exchange for the 4-hydroxycoumarins. For example, 4,5-dihydroxycoumarin **2** does not have the highest electron density at position 3 in the HOMO of the tautomeric form **2***a*, but this compound shows the maximal rate of the H–D exchange. On the other hand, 4-methoxycoumarin **6** has maximal eigencoefficient value at position 3 in the HOMO of the tautomeric form **6***a*, but this compound does not show any sign of the H–D exchange at all.

Conjugated addition of D^+ (in CD_3OD) to the ionized form of 4-hydroxycoumarin **1***a* followed by the formation of 2,4-chromandione tautomeric form **1***b* seems to be a more reason-

© 1997 NRC Canada

Scheme 1.

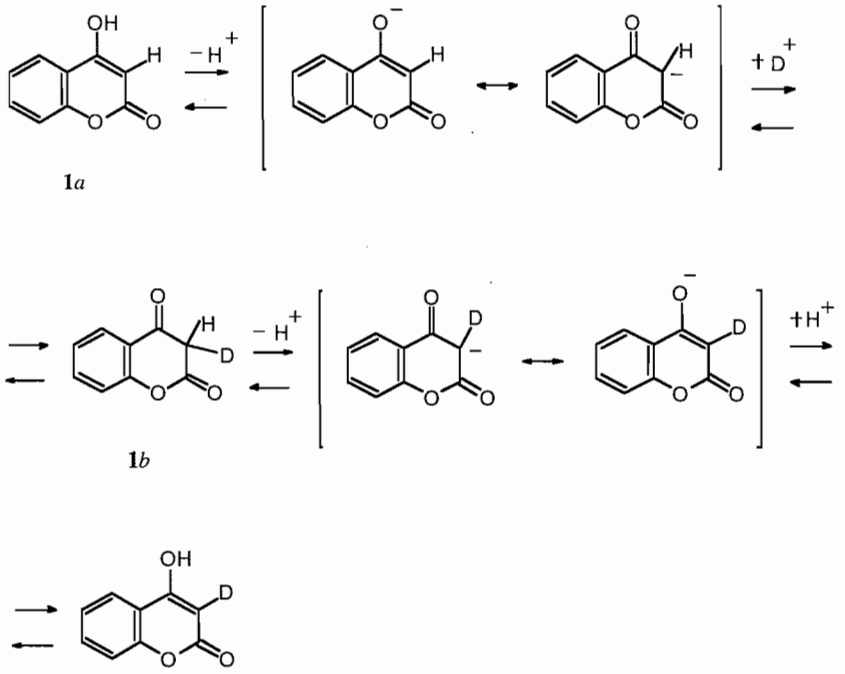
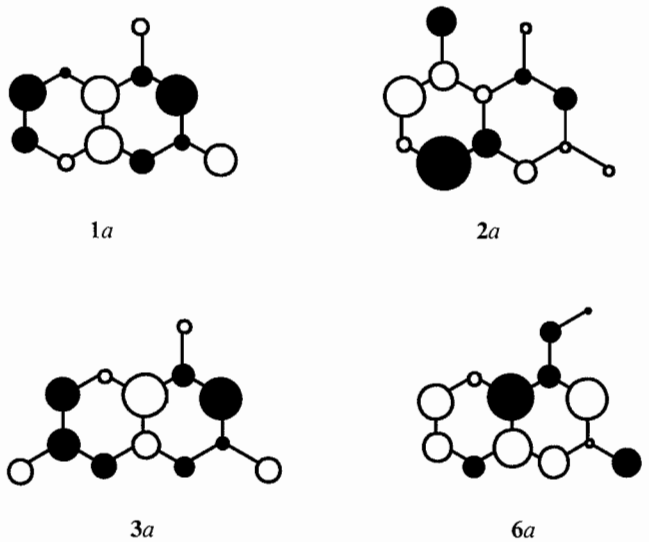


Fig. 1. Highest occupied molecular orbital (HOMO) shapes of compounds **1–3** and **6** in their 4-hydroxy-2-chromonone tautomeric forms *a* (according to the MNDO calculations).



able path (as shown in Scheme 1 for D-incorporation into position 3 of the 4-hydroxycoumarin substrate). Partial ionization of 4-hydroxycoumarin in methanol seems to be reasonable because of the high acidity of the 4-hydroxyl function in hydroxycoumarins (38).

In terms of this mechanism, any effect in 4-hydroxycoumarins that provides relative stability of 2,4-chromandione form *b* would increase the rate of H–D exchange at position 3. Following this proposal, the highest rate of H–D exchange in 4,5-dihydroxycoumarin **2** would be due to the relative stability of its 2,4-chromandione form **2***b* because of H-bonding between 5-hydroxyl and 4-keto functions in its structure (see discussion above).

In agreement with the conjugated D^+ addition scheme, the 2,4-chromandione forms *b* themselves do not seem to be reactive in the H–D exchange. Although the ^{1}H NMR spectrum of 4-hydroxy-3-(4-methoxyphenylazo)coumarin **4** indicates the existence of forms **4***b* and **4***d* (compare the Table 2 data and results given in ref. 14), it shows a rather low rate of H–D exchange. The intensity of the H(3) signal was decreased by only a factor of 3 after 3 h in the presence of methanol-d_4 (acetonitrile-d_3 had been used as solvent). The low reactivity of compound **4** in the H–D exchange agrees well with the low content of the 4-hydroxyl enol form **4***a* in its tautomeric equilibrium. According to the ^{1}H NMR spectra, compound **4** exists predominantly in the form **4***b* (50% in dimethyl sulfoxide-d_6 and 83% in acetonitrile-d_3 as a solvent).[2]

The suggestion that the H–D exchange at position 3 is based on the equilibrium between tautomeric forms 4-hydroxy-2-chromenone *a* and 2,4-chromandione *b* also seems to be true for compound **5**. Its ^{1}H NMR spectrum does not contain signals for 3-acetyl-2,4-chromandione form **5***b*. This form also was not found in a study of electronic absorption spectra of ketone **5** (32).

The importance of 2,4-chromandione forms *b* in the H–D exchange reaction is also illustrated by the complete lack of D-incorporation into position 3 of compound **6**, since no keto–enol tautomeric transformations of this 4-hydroxycoumarin analog are possible.

[2] NMR spectra and tautomerism of azo dyestuffs based on hydroxycoumarins will be discussed in more detail elsewhere.

© 1997 NRC Canada

Can. J. Chem. Downloaded from www.nrcresearchpress.com by 88.146.161.215 on 09/08/12
For personal use only.

Conclusions

Keto–enol tautomerism of 4-hydroxycoumarins depends on their structure. Substituents located at positions 3 and 5 affect the tautomeric transformations. The 5-hydroxyl functional group is supposed to stabilize the 2,4-chromandione tautomeric form via intramolecular H-bonding to thus provide H–D exchange at position 3. Introduction of the phenylazo functional group at position 3 transforms the 4-hydroxy-2-chromenone tautomeric form to the 2,4-chromandione derivative tautomeric forms, one of which undergoes H–D exchange. H–D exchange is not observed in 3-acetyl-4-hydroxycoumarin, since its most probable tautomeric forms do not contain an H atom at position 3.

Acknowledgements

This work was generously funded by the Highest Education State Committee of the Russian Federation (program "Fine Organic Synthesis") and by the Otto Bremer Foundation (Minnesota, U.S.A.).

References

1. R.D.H. Murray. The natural coumarins, occurrence, chemistry and biochemistry. Wiley–Interscience, New York. 1982.
2. R.D.H. Murray. Nat. Prod. Rep. **6**, 551 (1989).
3. W.G. Levine. *In* The pharmacological basis of therapeutics. 5th ed. *Edited by* L.S. Goodman and A. Gilman. MacMillan, New York. 1975.
4. R.A. O'Reilly. Annu. Rev. Med. **27**, 245 (1976).
5. R.B. Silverman. J. Am. Chem. Soc. **103**, 3910 (1981).
6. F. Arndt, L. Loewe, R. Un, and E. Ayca. Chem. Ber. **84**, 319 (1951).
7. H.R. Eisenhauer and K.P. Link. J. Am. Chem. Soc. **75**, 2044 (1953).
8. D. Anker and J. Massicot. Bull. Soc. Chim. Fr. **6**, 2181 (1969).
9. N. Matzat, H. Wamhoff, and F. Korte. Chem. Ber. **102**, 3122 (1969).
10. G. Appendino, G. Cravotto, S. Tagliapietra, and G.M. Nano. Helv. Chim. Acta, **73**, 1865 (1990).
11. G. Appendino, G. Cravotto, S. Tagliapietra, S. Ferraro, G.M. Nano, and G. Palmisano. Helv. Chim. Acta, **74**, 1451 (1991).
12. G. Appendino, G. Cravotto, L. Toma, R. Annunziata, and G. Palmisano. J. Org. Chem. **59**, 5556 (1994).
13. M. Rahman, Kh. Z. Khan, Z. S. Siddigi, and A. Zaman. Indian J. Chem. **29B**, 941 (1990).
14. A.S. Shawali, N.M.S. Harb, and K.O. Badahdah. J. Heterocycl. Chem. **22**, 1397 (1985).
15. E. Knobloch, B. Kakai, and F. Macha. Chem. Listy, **46**, 416 (1952).
16. O.S. Wolfbeis and G. Uray. Monatsh. Chem. **109**, 123 (1978).
17. Th. A. Moore, M. L. Harter, and P.-S. Song. J. Mol. Spectrosc. **40**, 144 (1971).
18. P.-S. Song. Can. J. Spectrosc. **26**, 59 (1981).
19. A.O. Obaseka, W.R. Porter, and W.F. Trager. J. Heterocycl. Chem. **19**, 385 (1982).
20. W.R. Porter and W.F. Trager. J. Heterocycl. Chem. **19**, 475 (1982).
21. S.A. Cussans and T.N. Huckerbyb. Tetrahedron, **21**, 2719 (1975).
22. A. Patra, A.K. Mukhopadhyay, and A.K. Mitra. Ind. J. Chem. **25B**, 1167 (1986).
23. S.A. Soika. J. Org. Chem. **40**, 1175 (1975).
24. P. Ilic, B. Mohar, J.V. Knop, A. Juric, and N. Trinajstic. J. Heterocycl. Chem. **19**, 625 (1982).
25. V.R. Shah, J.L. Bose, and R.C. Shah. J. Org. Chem. **25**, 677 (1960).
26. G. Jacobson. J. Am. Chem. Soc. **107**, 1055 (1985).
27. A. Buckle. J. Med. Chem. **18**, 391 (1975).
28. J. Klosa. Arch. Pharm. **288**, 356 (1955).
29. M.J.S. Dewar and W. Thiel. J. Am. Chem. Soc. **99**, 4907 (1977).
30. M.J.S. Dewar, A.J. Harget, N. Trinajstic, and S.D. Worley. Tetrahedron, **26**, 4505 (1970).
31. Atta-ur-Rahman. One and two dimensional NMR spectroscopy. Elsevier, New York. 1989.
32. V.F. Traven, L.I. Vorobjeva, T.A. Chibisova, E.A. Carberry, and N.J. Beyer. Can. J. Chem. **75**, 365 (1997).
33. O.A. Reutov, I.P. Belezkaya, and K.P. Butin. The CH-acids. Nauka, Moscow. 1980.
34. H.R. Eisenhauer and K.P. Link. J. Am. Chem. Soc. **76**, 1647 (1954).
35. E. Ziegler and H. Maier. Monatsh. Chem. **89**, 787 (1958).
36. K. Fukui et al. J. Chem. Phys. **22**, 1433 (1954).
37. V.F. Traven. Frontier orbitals and properties of organic molecules. Ellis Horwood, Chichester. 1992.
38. V.P. Georgievskyi. Khim. Prir. Soedin. **6**, 770 (1985).

Can. J. Chem. Downloaded from www.nrcresearchpress.com by 88.146.161.215 on 09/08/12
For personal use only.

© 1997 NRC Canada

The importance of conformational effects on the carbon–carbon bond cleavage of β-phenethyl ether radical cations[1]

A.L. Perrott, H.J.P. de Lijser, and D.R. Arnold

Can. J. Chem. Downloaded from www.nrcresearchpress.com by 88.146.161.215 on 09/08/12
For personal use only.

Abstract: The photosensitized (electron transfer) bond cleavage of some β-phenylethyl ether radical cations has been investigated. In previous studies the feasibility of the bond cleavage was thought to depend on the bond dissociation energy (BDE). However, this simple hypothesis led to several incorrect predictions and therefore additional criteria, conformational effects, were added to the hypothesis. This study has now been extended and additional examples of the importance of the conformation on the carbon–carbon bond cleavage of radical cations are provided. The four β-phenylethyl ethers studied are 2-methoxy-3-phenylbutane (**9**, both diastereomers), and *cis*- and *trans*-2-methyl-3-phenyltetrahydropyran (**10***c*, **10***t*). Generally, bond cleavage will occur if the (calculated) BDE in the radical cation is less than 55 kJ/mol, and if there is significant overlap between the singly occupied molecular orbital (SOMO) and the vulnerable (C—C or C—H) bond. In the case of a β-phenylethyl ether radical cation, the alkoxy group must also be oriented so that an oxygen lone pair of electrons can overlap with the C—C *sigma* antibonding (σ*) orbital. The calculated BDE values of the vulnerable C—C bond in the radical cations of the four ethers studied here are well below the threshold value, 55 kJ/mol, and C—C cleavage will therefore be governed by conformational effects. Molecular mechanics (MM3) calculations were used to identify the most stable conformers of the neutral molecules. Based on the calculated angles and overlap between orbitals it was predicted that the global-minimum conformers of the ethers **9** and **10***c* would not give C—C bond cleavage products or deprotonation to any significant extent. The global minimum of ether **10***t* is well oriented for C—C cleavage but not for deprotonation. Irradiation of an electron-accepting photosensitizer, 1,4-dicyanobenzene (**2**), in the presence of the ethers showed that the ethers **9** did not cleave efficiently; no deprotonation or isomerization was observed. This is in good agreement with the predictions based on the MM3 calculations. Both ethers **10***c* and **10***t* gave reasonable yields of the C—C cleavage products; in fact, ether **10***c* cleaved more efficiently than **10***t*. This can be explained by the fact that a conformer of **10***c*, only 4.35 kJ/mol higher in energy than the global minimum, is perfectly aligned for cleavage. Ether **10***t* did not show any evidence for deprotonation whereas **10***c* did. This is also in good agreement with the calculations.

Key words: photoinduced electron transfer, radical cations, bond cleavage, conformation, molecular mechanics calculations.

Résumé : On a étudié le clivage photosensibilisé (transfert d'électron) de quelques cations radicaux d'éthers comportant un groupe β-phényléthyle. Dans des études antérieures, on croyait que la possibilité de cliver la liaison dépendait de l'énergie de dissociation de la liaison (EDL). Toutefois, cette hypothèse simple a conduit à plusieurs prédictions incorrectes et on a donc ajouté des critères additionnels, comme les effets conformationnels, à cette hypothèse. On a maintenant étendu cette étude et on présente de nouveaux exemples démontrant l'importance de la conformation sur le clivage de la liaison carbone–carbone de cations radicaux. On a étudié les quatre éthers β-phényléthylés suivants : 2-méthoxy-3-phénylbutane (**9**, deux diastéréomères) et les *cis*- et *trans*-2-méthyl-3-phényltétrahydropyranes (**10***c*, **10***t*). En général, le clivage de la liaison a lieu lorsque l'EDL (calculée) est inférieure à 55 kJ mol^{-1} et s'il existe un recouvrement significatif entre l'orbitale moléculaire à un seul occupant («SOMO») et la liaison vulnérable (C—C ou C—H). Dans le cas d'un cation radical d'éther β-phényléthylé, le groupe alcoxyle doit être orienté d'une façon telle que la paire d'électrons non appariée de l'oxygène puisse effectuer un recouvrement avec l'orbitale antiliante (σ*) *sigma* de C—C. Les valeurs calculées d'EDL de la liaison C—C vulnérable des cations radicaux des quatre éthers étudiés sont bien inférieures à la valeur limite de 55 kJ mol^{-1}; il en découle que le clivage de la liaison C—C sera gouvernée par les effets conformationnels. On a utilisé des calculs de mécanique moléculaire (MM3) pour identifier les conformères les plus stables des molécules neutres. Sur la base des angles et des recouvrement calculés des orbitales, il a été possible de prédire que les conformères d'énergie globale minimale des éthers **9** et **10***c* ne pourraient pas conduire à des degrés importants de produits de clivage de la liaison C—C ou de déprotonation. Dans sa conformation d'énergie globale minimale, le composé **10***t* est bien orienté pour donner un clivage C—C, mais ce n'est pas le cas pour la déprotonation. L'irradiation d'un photosensibilisateur pouvant accepter des électrons, le 1,4-dicyanobenzène (**2**), en présence des éthers a permis de monter que

Received November 26, 1996.

A.L. Perrott, H.J.P. de Lijser, and D.R. Arnold.[2] Department of Chemistry, Dalhousie University, Halifax, NS B3H 4J3, Canada.

[1] This is Part 40 of the series Radical Ions in Photochemistry; see refs. 1 and 2 for the preceding parts of this series.

[2] Author to whom correspondence may be addressed. Telephone: (902) 494-3714. Fax: (902) 494-1310. E-mail: arnold@chem1.chem.dal.ca

© 1997 NRC Canada

les éthers **9** ne se clivent pas d'une façon efficace; on n'a observé ni déprotonation ni isomérisation. Ces observations sont en bon accord avec les prédictions faites sur la base des calculs MM3. Les éthers tant **10***c* que **10***t* donnent des rendements raisonnables de produits provenant d'un clivage C—C; en fait, l'éther **10***c* se clive d'une façon plus efficace que le produit **10***t*. On peut expliquer cette différence par le fait qu'un conformère du produit **10***c*, dont l'énergie ne se trouve qu'à 4,35 kJ mol^{-1} au-dessus de celle du conformère d'énergie minimale, est parfaitement aligné pour donner le clivage. Avec l'éther **10***t*, on n'observe aucune indication de déprotonation alors que le composé **10***c* en donne. Ceci aussi est en accord avec les calculs.

Mots clés : transfert photoinduit d'électron, cations radicaux, clivage de liaison, conformation, calculs de mécanique moléculaire.

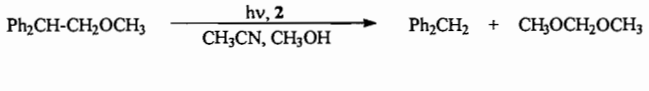
[Traduit par la rédaction]

Can. J. Chem. Downloaded from www.nrcresearchpress.com by 88.146.161.215 on 09/08/12
For personal use only.

Introduction

Several examples of photosensitized (electron transfer) carbon–carbon bond cleavage have been reported (3). One of the first examples of this type of reaction was the C—C bond cleavage of methyl 2,2-diphenylethyl ether (**1**) when irradiated in the presence of 1,4-dicyanobenzene (**2**) in an acetonitrile–methanol (3:1) solution (reaction [1]) (3*a*).

Reaction [1] (3a)



1

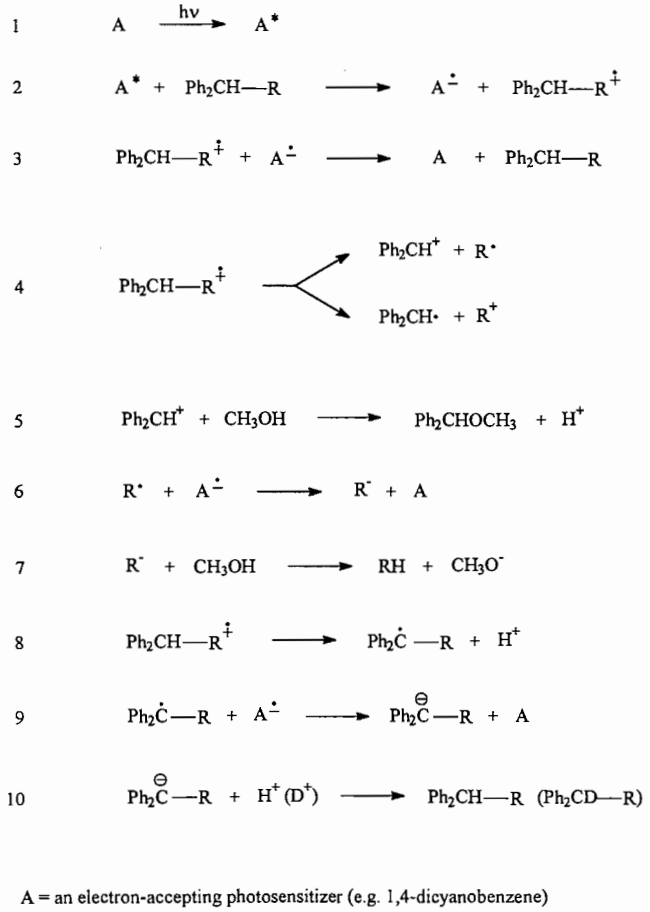
2 = 1,4-dicyanobenzene

The mechanism proposed for the photosensitized (electron transfer) bond cleavage is shown in Scheme 1 where A is an electron-accepting photosensitizer (e.g., 1,4-dicyanobenzene (**2**)). Step 4 shows the actual cleavage of the radical cation to yield radical and cationic fragments. Cleavage can obviously occur in two ways and the preferred mode can be predicted based on the oxidation potentials of the alternative radical fragments (3*a*,*h*).

The feasibility of photosensitized (electron transfer) carbon–carbon bond cleavage is known to depend on the dissociation energy of the vulnerable bond in the radical cation and on the conformation of the radical cation.[3] From previous studies, an upper threshold of 55 kJ/mol has been estimated for the bond dissociation energy (BDE) in the radical cation (3*h*). When the BDE of the radical cation is well below this threshold, cleavage of the radical cation usually occurs readily. If the BDE is above the threshold, no cleavage is observed. Generalizations are more difficult when the BDE approaches the threshold value and using the BDE as the only criterion for cleavage has led to some erroneous predictions. For example, although the calculated BDE for cleavage of the radical cation of *cis*-1-methoxy-2-phenylcyclopentane (**3**) is only 18 kJ/mol

[3] It must be noted that under these conditions (photosensitized electron transfer) there is a third factor involved, namely back electron transfer (BET). Carbon–carbon bond cleavage is in competition with BET and the overall efficiency of the cleavage reaction might be decreased when BET becomes more important.

Scheme 1. Proposed mechanism for the photosensitized carbon–carbon and carbon–hydrogen bond cleavage of radical cations.



A = an electron-accepting photosensitizer (e.g. 1,4-dicyanobenzene)

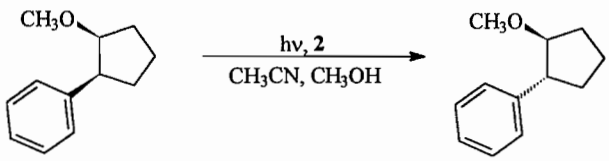
(4), no bond cleavage was observed experimentally (reaction [2]). Deprotonation of the radical cation, reduction of the radical, and reprotonation leads ultimately to the *trans* isomer. To improve the predictive power of the hypothesis, conformational criteria were included.

It has been well established that the acidity of a radical cation is much greater than that of the neutral molecule (5). However, in order for deprotonation to take place, the singly occupied orbital of a radical cation must overlap with the C—H bond that is breaking. This was clearly shown by studying *cis*- and *trans*-1-methyl-2-phenylcyclopentane (**4***c*, **4***t*). The *cis* isomer, when irradiated in acetonitrile in the presence of an electron-accepting photosensitizer (1,4-dicyanobenzene (**2**)) and a non-nucleophilic base (2,4,6-collidine), was

© 1997 NRC Canada

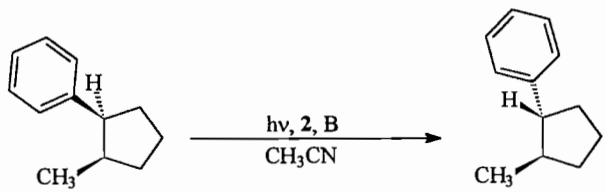
Can. J. Chem. Downloaded from www.nrcresearchpress.com by 88.146.161.215 on 09/08/12
For personal use only.

Reaction [2] (3i)



3c 3t

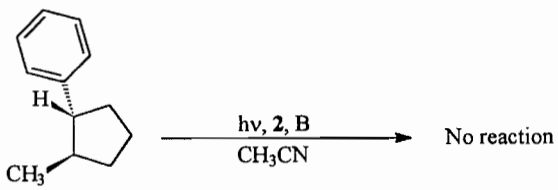
Reaction [3] (4)



4c 4t

B = 2,4,6-collidine

Reaction [4] (4)

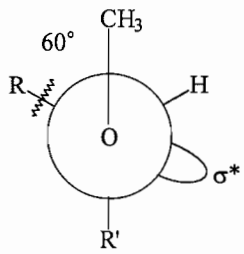


4t

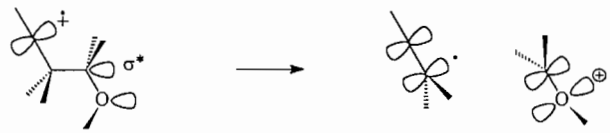
B = 2,4,6-collidine

Fig. 1. Preferred conformation for carbon–carbon bond cleavage of the radical cation; (*a*) illustrated with a Newman projection along the O—C bond; (*b*) illustrated with dashed–wedged line notation.

(a)



(b)



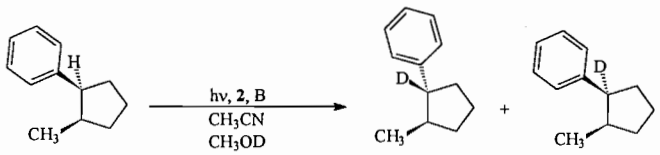
converted into the *trans* isomer. Under the same conditions, the *trans* isomer did not react (reactions [3], [4]). When the reaction was carried out in a 3:1 acetonitrile–methanol-*O-d* solution, starting with the *cis* isomer, deuterium was incorporated in both the *cis* and *trans* isomers. No deuterium was incorporated under these conditions, starting with the *trans* isomer (reactions [5], [6]). Molecular mechanics calculations revealed that the angle between the plane of the phenyl ring and the benzylic C—H bond (ϕ) in the global minimum of the *trans* isomer is 1°. The orbital overlap between the singly occupied molecular orbital (SOMO) and the benzylic C—H bond will be maximum when the angle between the C—H bond and the plane of the phenyl ring (ϕ) is 90°. The magnitude of this interaction follows a $1 - \cos^2(\phi)$ relationship, i.e., the orbital overlap in the *trans* isomer is ca. 0%. The calculated angle (ϕ) in the global minimum of the *cis* isomer was 34° (31% effective orbital overlap, MM3; 51°, 60%, MMP2). Despite the fact that the overlap between the SOMO and the benzylic C—H bond is not optimal, deprotonation does occur and isomerization to the *trans* isomer is observed.

Based on these results for C—H bond cleavage it seemed reasonable to suggest that, in order for C—C bond cleavage to occur, the SOMO must also overlap with the vulnerable C—C bond; methyl *cis*- and *trans*-2-phenylcyclohexylether (**7**) and 6-phenyl-1,4-dioxaspiro[4.5]decane (**8**) were therefore expected to cleave. However, whereas the diphenyl systems (**5** and **6**) did show C—C bond cleavage, the monophenyl systems (**7** and **8**) did not (Reactions [7]–[10]). The new hypothesis that was formulated recognized that in order for the radical cation of a β-phenylethyl ether to cleave, the alkoxy group must also be oriented so that a lone pair of electrons on the oxygen can overlap with the C—C *sigma* antibonding (σ^*) orbital. The preferred conformation for cleavage is shown in Fig. 1.

The goal of this research was to provide additional examples of C—C bond cleavage in β-phenylethyl ether radical

© 1997 NRC Canada

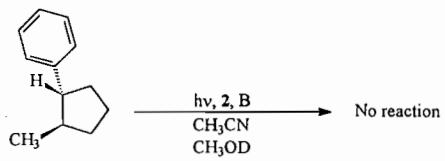
Reaction [5] (4)



4c 4t 4c

B = 2,4,6-collidine

Reaction [6] (4)



4t

B = 2,4,6-collidine

cations and to formulate rules useful for predicting this reactivity. The diastereomers of 2-methoxy-3-phenylbutane (**9**) and the *cis* and *trans* isomers of 2-methyl-3-phenyltetrahydropyran (**10**) were chosen as analogues of the methyl 2-phenylcycloalkyl ethers investigated previously (reactions [3]–[6]) (3*j*). The BDE of these radical cations are similar to those of the cycloalkyl compounds; differences in reactivity can therefore be attributed to differences in conformation. The preferred conformations of the neutral species have been identified using molecular mechanics calculations (6). The conformers of these neutral species have been used to rationalize the reactivities of their corresponding radical cations. This is a valid approach: the SOMO in the radical cations of these β-phenylethyl ethers will be largely associated with the phenyl group and the relative energies of the conformers should therefore not be greatly affected upon formation of the radical cation. It must be noted that in some cases removal of an electron could lead to a significant change in geometry, especially if the C—C or C—H bond that is about to be cleaved may provide hyperconjugative stabilization to the π radical cation and does not do so in the neutral compound. However, in all the cases studied in the past, the results of the MM calculations (on the neutral molecules) have been in good agreement with the results of the experiments (involving the radical cations), indicating that this assumption is valid.

Cleavage of the C—C bond in these ethers will lead to 1,6-radical cations. These species could have significant synthetic utility, and a general rule for predicting whether radical cations will undergo C—C bond cleavage or deprotonation is important.

Results

Molecular modeling (MM3)

The structures of both diastereomers of 2-methoxy-3-phenylbutane (**9**) and the *cis* and *trans* isomers of 2-methyl-3-phenyltetrahydropyran (**10**) were optimized (steric energies were minimized) with the 1988 force field of the MM3 program. The initial geometries of these molecules were obtained by using PCModel.[4] For each molecule, a number of starting conformations were considered and the stochastic search option was used to find stationary points. Not all initial conformations led to distinct conformers. Selected dihedral angles for all of the conformers identified are tabulated in Tables 1–4.

Preparation of starting materials

The syntheses of the ethers, 2-methoxy-3-phenylbutane (**9**) (both diastereomers) and *cis*- and *trans*-2-methyl-3-phenyltetrahydropyran (**10**), are outlined in Schemes 2–4. The details of these syntheses are given in the experimental section.

Irradiations

Solutions of the ether and 1,4-dicyanobenzene (**2**), the electron-accepting photosensitizer, in acetonitrile–methanol (3:1) solution were degassed by nitrogen ebullition and irradiated with a medium-pressure mercury vapour lamp, through Pyrex, in a constant temperature bath held at 10°C. Reaction progress was followed by gas chromatography with a flame ionization detector (gc/fid) and gas-chromatography with a mass-selective detector (gc/ms). The results of the irradiations are summarized in reactions [11] and [12].

All four of the ethers cleaved, some inefficiently. The two diastereomers of 2-methoxy-3-phenylbutane (**9**) give the same products in almost the same yield (reaction [11]). Identification of the products was made by comparison of gc/ms retention times and mass spectra with those of authentic samples, and from ^{1}H and ^{13}C nmr spectra. Identification (tentatively) of trace amounts of the diastereomers of 2,3-diphenylbutane (**13**) rests on the observed mass spectra. The crude photolysates from the irradiations of the diastereomers of **9** were chromatographed on silica gel: the yield of 1-(4-cyanophenyl)-1-phenylethane (**12**) was determined by analysis of ^{1}H nmr spectra of fractions containing a mixture of **12** and recovered ether **9**. The yield of ethylbenzene (**11**) was determined by calibrated gc/ms and gc/fid using cyclododecane as an internal standard.

The cleavage products obtained upon irradiation of *cis*- and *trans*-2-methyl-3-phenyltetrahydropyran (**10***c*, **10***t*) were 4-phenylbutyl (1-methoxyethyl) ether (**14**), and 4-(4-cyanophenyl)-4-phenylbutyl (1-methoxyethyl) ether (**15**)

[4] K. Gilbert. PCModel. Serena Software, Box 3076, Bloomington, IN 47402-706, U.S.A. (1987).

Can. J. Chem. Downloaded from www.nrcresearchpress.com by 88.146.161.215 on 09/08/12
For personal use only.

© 1997 NRC Canada

Can. J. Chem. Downloaded from www.nrcresearchpress.com by 88.146.161.215 on 09/08/12
For personal use only.

Table 1. Conformers of (2*R*,3*R*)-2-methoxy-3-phenylbutane (**9**).

Energy above global minimum (kJ/mol)	$\lvert\phi_{Ph\text{-}CH}\rvert$, (overlap)	$\lvert\phi_{Ph\text{-}CC}\rvert$, (overlap)	$\lvert\phi_{OCH_3}\rvert$, (overlap)
27.5 (Me *anti* H)	6°, (1%)	71°, (89%)	97°, (64%)
22.7 (Me *anti* OMe)	14°, (6%)	79°, (96%)	90°, (75%)
10.8 (Me *anti* OMe)	24°, (17%)	89°, (100%)	84°, (83%)
9.83 (Me *anti* Me)	2°, (0%)	63°, (79%)	69°, (98%)
9.54 (Me *anti* OMe)	23°, (15%)	89°, (100%)	164°
6.53 (Me *anti* H)	8°, (2%)	72°, (90%)	160°
0.0 (Me *anti* Me)	1°, (0%)	62°, (78%)	160°

Table 2. Conformers of (2*S*,3*R*)-2-methoxy-3-phenylbutane (**9**).

Energy above global minimum (kJ/mol)	$\lvert\phi_{Ph\text{-}CH}\rvert$, (overlap)	$\lvert\phi_{Ph\text{-}CC}\rvert$, (overlap)	$\lvert\phi_{OCH3}\rvert$, (overlap)
23.6 (Me *anti* OMe)	24°, (17%)	90°, (100%)	100°, (59%)
19.0 (Me *anti* Me)	23°, (15%)	88°, (100%)	98°, (62%)
10.6 (Me *anti* OMe)	1°, (0%)	59°, (73%)	67°, (99%)
4.77 (Ph *anti* OMe)	27°, (21%)	89°, (100%)	80°, (88%)
4.48 (Ph *anti* OMe)	27°, (21%)	89°, (100%)	160°
1.4 (Me *anti* OMe)	5°, (1%)	67°, (85%)	153°
0.0 (Me *anti* Me)	9°, (2%)	72°, (90%)	164°

Table 3. Conformers of *cis*-2-methyl-3-phenyltetrahydropyran (**10***c*)

Energy above global minimum (kJ/mol)	$\lvert\phi_{Ph\text{-}CH}\rvert$, (overlap)	$\lvert\phi_{Ph\text{-}CC}\rvert$, (overlap)	$\lvert\phi_{OR}\rvert$, (overlap)
4.35 (Ph eq)	23°, (15%)	89°, (100%)	59°, (100%)
0.0 (Ph ax)	19°, (11%)	40°, (41%)	64°, (100%)

Table 4. Conformers of *trans*-2-methyl-3-phenyltetrahydropyran (**10***t*).

Energy above global minimum (kJ/mol)	$\lvert\phi_{Ph\text{-}CH}\rvert$, (overlap)	$\lvert\phi_{Ph\text{-}CC}\rvert$, (overlap)	$\lvert\phi_{OR}\rvert$, (overlap)
21.3 (Ph ax)	28°, (22%)	31°, (26%)	56°, (100%)
0.0 (Ph eq)	2°, (0%)	59°, (74%)	65°, (99%)

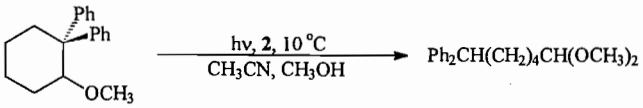
(reaction [12]). These compounds were identified after acid hydrolysis of the reaction mixture to yield 4-phenyl-1-butanol (**16**) and 4-(4-cyanophenyl)-4-phenyl-1-butanol (**17**). The retention time and mass spectrum of alcohol **16** were compatible with an authentic sample. Alcohol **17** was isolated and fully characterized. The percent conversion of the starting materials and the yields of the alcohols **16** and **17** were determined by using calibrated gc/ms, with cyclododecane as an internal standard.

Deuterium incorporation studies were carried out as described above, using acetonitrile–methanol-*O*-*d* (3:1) solutions. The reactions were followed by gc/ms, using selected ion monitoring. There was no evidence of deuterium incorporation in either diastereomer of **9**, or in ether **10***t*. Ether **10***c* did show some deuterium incorporation. Isomerization was also observed: ether **10***t* was formed from **10***c* and vice versa.

Oxidation potentials of the ethers were determined by cyclic voltammetry. The free energies of the electron transfer reactions were calculated by using the Weller equation (eq. [1]) (7). The values are summarized in Table 5.

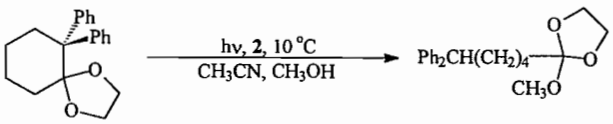
© 1997 NRC Canada

Reaction [7] (3j)



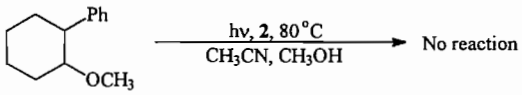
5

Reaction [8] (3j)



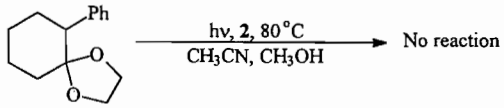
6

Reaction [9] (3j)



7
(*cis* and *trans*)

Reaction [10] (3j)



8

[1] $\Delta G_{et} = F[E^{ox}_{½}(D) - E^{red}_{½}(A) - e/\epsilon\alpha] - E_{0,0}(A)$

Discussion

The first three steps of the proposed mechanism for the cleavage reaction (Scheme 1) should occur readily. Calculated values of the free energy for electron transfer between the singlet excited state of 1,4-dicyanobenzene (**2***) and the ethers are all exergonic by more than −20 kJ/mol (Table 1); electron transfer should take place at the diffusion-controlled rate (7). Back electron transfer (step 3) is extremely exergonic: this deactivation pathway is the most likely for the radical cation.

Step 4 is the actual carbon–carbon bond cleavage of the radical cation. For all of the ethers considered in this investigation, the BDEs of the radical cations are expected to be below the threshold value. Therefore, if the conformations are suitable, the radical cations of the diastereomers of 2-methoxy-3-phenylbutane (**9**) and the two isomers of 2-methyl-3-phenyltetrahydropyran (**10**) should undergo photosensitized (electron transfer) carbon–carbon bond cleavage.

In previous cases (3*i*,*j*), lack of reactivity has been attributed to insufficient overlap of the singly occupied molecular orbital (SOMO) with the carbon–carbon bond expected to cleave and (or) due to a lack of overlap between the lone pair of electrons on the oxygen with the adjacent C—C *sigma* antibonding (σ*) orbital. In the radical cations of all the compounds under investigation, the SOMO is largely associated with the phenyl group. Therefore, the optimum orientation for cleavage to occur has the plane of the phenyl ring perpendicular to the benzylic C—C bond. Also, the O-R moiety of the ether should be *gauche* to the vulnerable C—C bond.

Step 8 is the deprotonation step of the radical cation. This is a fragmentation pathway in competition with the C—C bond cleavage; the conformation of the radical cation is also important here. The SOMO must overlap with the benzylic C—H bond in order for deprotonation to take place.

A Karplus-type relationship can be used to evaluate the degree of overlap between orbitals as a function of angle (8). The fraction of maximum overlap is $(1 - \cos^2\phi_{Ph\text{-}CH})$, where $\phi_{Ph\text{-}CH}$ is the dihedral angle between the C—H bond and the plane of the phenyl ring. The overlap between the SOMO and the benzylic C—H bond is maximum when the angle between the phenyl group and the C—H bond is 90°. Similarly, in order for carbon–carbon bond cleavage to take place, the dihedral angle between the plane of the phenyl group and the C—C bond should approach 90°: the magnitude of orbital overlap is $(1-\cos^2\phi_{Ph\text{-}CC})$. If ϕ_{OCH_3} is the dihedral angle between the C—C bond and the O-CH_3 bond, then the degree of overlap between an sp^3-type lone pair of electrons on oxygen and the C—C *sigma* antibonding (σ*) orbital is $\cos^2(\phi_{OCH_3} - 60°)$; 60° is the angle at which this overlap will be maximum.

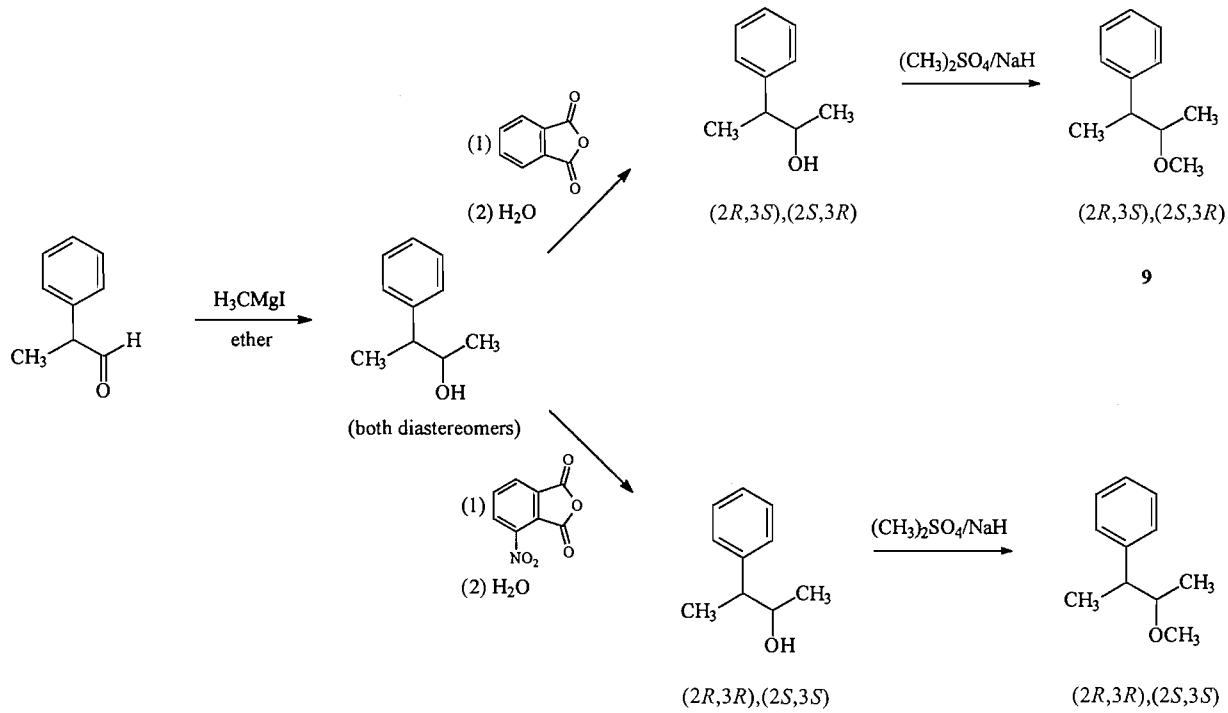
The results of the calculations on the (2*R*,3*R*) isomer of 2-methoxy-3-phenylbutane (**9**) are tabulated in Table 2. The global minimum conformer is predicted not to cleave, due to an unfavourable orientation of the OCH_3 group. Because the plane of the phenyl group is parallel to the geminal hydrogen, deprotonation is also unlikely. However, two potentially reactive conformers were found 9.83 and 10.8 kJ/mol above the global minimum. Both of these conformers could undergo carbon–carbon bond cleavage; the (2*R*,3*R*) isomer will cleave if the populations of these conformers are sufficient. No conformers that might undergo deprotonation (isomerization) were found.

Similarly, the global-minimum conformer of the (2*S*,3*R*) isomer was predicted to be inert under the irradiation conditions (Table 3). The orientation of the methoxy group would prevent the cleavage of the three most stable conformers. However, a conformer was found 4.77 kJ/mol above the global minimum in which the methoxy group is more favourably

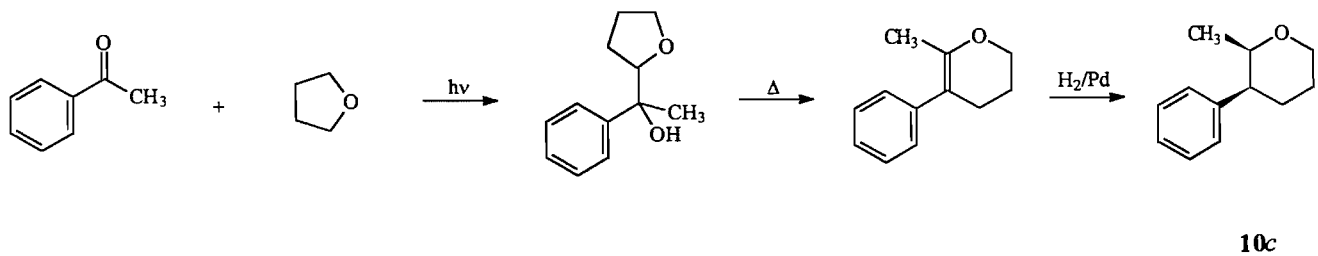
Can. J. Chem. Downloaded from www.nrcresearchpress.com by 88.146.161.215 on 09/08/12
For personal use only.

© 1997 NRC Canada

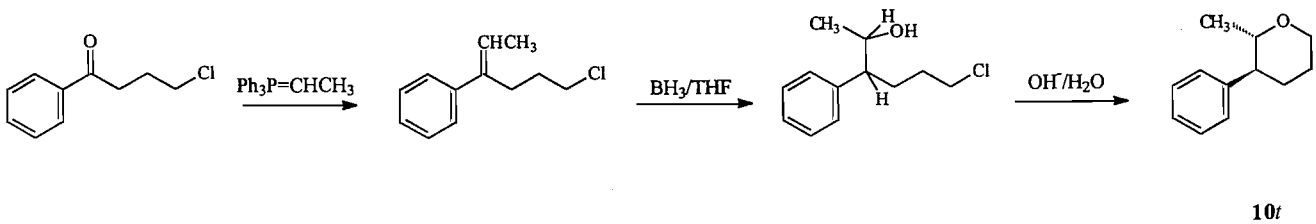
Scheme 2. Synthesis of the diastereomers of 2-methoxy-3-phenylbutane (**9**); see experimental for details.



Scheme 3. Synthesis of *cis*-2-methyl-3-phenyltetrahydropyran (**10***c*); see experimental for details.



Scheme 4. Synthesis of *trans*-2-methyl-3-phenyltetrahydropyran (**10***t*); see experimental for details.



aligned. Therefore, cleavage of the (2*S*,3*R*) isomer also seemed feasible.

Although there was no evidence for deprotonation of either diastereomer, it was found that both diastereomers of **9** cleaved inefficiently when subjected to the standard irradiation conditions. Cleavage of **9** produces a secondary 1-phenylethyl radical and a secondary α-oxy carbocation. Reduction of the radical by the radical anion of the sensitizer ($\mathbf{2}^{-\bullet}$) and subsequent protonation gives ethylbenzene (observed in ca. 7% yield, calibrated gc/ms). Coupling of the radical fragments gives 2,3-diphenylbutane (**13**, two diastereomers, which were detected in trace amounts). Coupling of the radical fragment at the *ipso* position of $\mathbf{2}^{-\bullet}$ followed by loss of cyanide anion yields 1-(4-cyanophenyl)-1-phenylethane (**12**), which was the major product from both diastereomers.

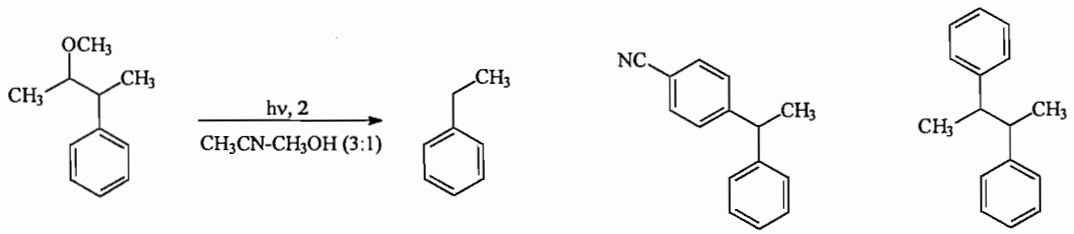
All of the observed products involve the initial formation of the benzylic radical fragment. The relative amounts of these products are related to the reduction potential of the radical.

© 1997 NRC Canada

Can. J. Chem. Downloaded from www.nrcresearchpress.com by 88.146.161.215 on 09/08/12
For personal use only.

Can. J. Chem. Downloaded from www.nrcresearchpress.com by 88.146.161.215 on 09/08/12
For personal use only.

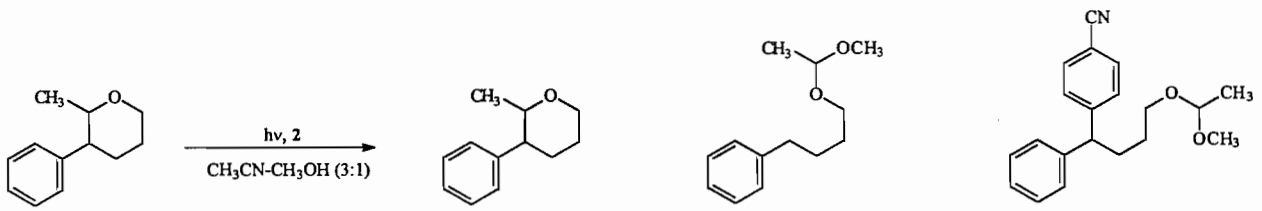
Reaction [11]



9 **11** **12** **13**

[a]	(2*R*,3*S*),(2*S*,3*R*)	8%	20%	trace
[b]	(2*R*,3*R*),(2*S*,3*S*)	6%	24%	trace

Reaction [12]



10 **10** **14** **15**

[a]	*cis*	*trans*: 6%	20%	31%
[b]	*trans*	*cis*: 1%	23%	37%

The reduction potential of **2** is −1.66 V (vs. SCE), while the reduction potential of the 1-phenylethyl radical is −1.60 V (9). Therefore, reduction of the radical to the carbanion by $\mathbf{2}^{-\bullet}$ should be exergonic. However, the difference between these two reduction potentials is not great, and it is not surprising that products resulting from reaction of both the radical and the carbanion are formed.

2-Methyl-3-phenyltetrahydropyran (**10**) was of special interest. The rotational barriers in the acyclic systems are low and it is difficult to predict a priori which conformation(s) will be most favourable. However, since tetrahydropyrans can be expected to adopt chair conformations, the equatorial lone pair of electrons on the oxygen atom will be antiperiplanar to the C—C bond to be cleaved.

An MM2 study by Allinger and Tribble (10) has shown that the most stable conformer of phenylcyclohexane has the phenyl group in the equatorial position, with the ring parallel to the geminal C—H bond. This orientation minimizes repulsive interactions between the *ortho* hydrogens and the equatorial hydrogens on C2 and C6. However, if additional substituents on the cyclohexane ring force the phenyl ring to be in the axial position, the most favourable conformer will have the phenyl ring perpendicular to the geminal C—H bond. In this conformation, the repulsive interactions between the *ortho* hydrogens of the phenyl group and the axial hydrogens on the cyclohexane ring are minimized. The free energy difference between these two conformers of phenylcyclohexane (i.e., the *A*-value) is 8.4 – 13 kJ/mol in favour of the equatorial conformer (11). Allinger has calculated the free energy difference to be 15.3 kJ/mol. Since there is no substituent geminal to the phenyl group in **10**, it was initially expected that the phenyl group would be in the equatorial position, oriented parallel to the geminal C—H bond. Although this would make deprotonation unlikely, it would give reasonably good overlap

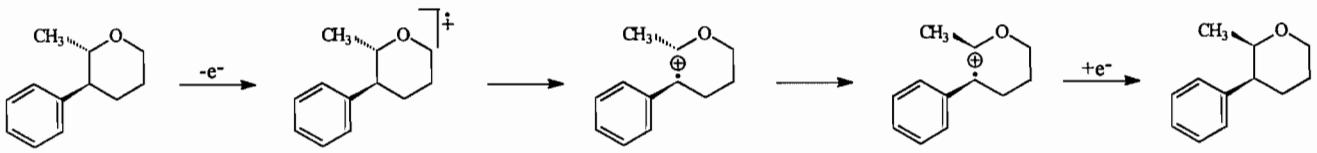
© 1997 NRC Canada

Table 5. Oxidation potentials and calculated free energies for electron transfer from ethers **9** and **10**.

Compound	$E^{ox}_{½}$ (V)[a]	ΔG_{et} (kJ/mol)[b]
(2*R*,3*S*)- and (2*S*,3*R*)-2-Methoxy-3-phenylbutane (**9**)	2.36	–25.9
(2*R*,3*R*)- and (2*S*,3*S*)-2-Methoxy-3-phenylbutane (**9**)	2.27	–34.6
cis-2-Methyl-3-phenyltetrahydropyran (**10***c*)	2.19	–42.3
trans-2-Methyl-3-phenyltetrahydropyran (**10***t*)	2.16	–45.2

[a]Reported vs. saturated calomel electrode (sce), see experimental for details.
[b]Free energy for electron transfer from the ether to the electronically excited singlet state of **2** based upon the Weller equation (eq. 1, ref. 7): $E_{0,0}$ (**2**) 408.4 kJ/mol; $E^{red}_{½}$(**2**) –1.66 V; the Coulombic attraction term was taken to be 5.40 kJ/mol (2*c*).

Scheme 5. Possible mechanism for the isomerization of *trans*-2-methyl-3-phenyltetrahydropyran (**10***t*) to *cis*-2-methyl-3-phenyltetrahydropyran (**10***c*).



10*t* **10***c*

between the SOMO and the C—C bond. As mentioned above, the orientation of a lone pair of electrons on oxygen is favourable.

Two of the starting conformers used in the optimization of **10***c* were based on a chair structure: one with the phenyl group in the axial position and the other with the phenyl group equatorial. Structures with the six-membered ring in a boat conformation were all at least 21.4 kJ/mol higher in energy than the chair-based global minimum.

The global-minimum structure of **10***c* does not have the phenyl group in the equatorial position; the conformer with the axial phenyl group is 4.35 kJ/mol more stable than the equatorial conformer. This calculated result is supported by the ^{1}H nmr spectrum of the compound. The proton geminal to the phenyl group has no coupling constant larger than 4 Hz, indicating that this proton must be in the equatorial position. In retrospect, this result is not surprising. In this conformation of the tetrahydropyran ring, the axial phenyl group has a 1,3-diaxial interaction with only one hydrogen. Although the conformation of the ring does indeed guarantee that one lone pair of electrons can assist the C—C bond cleavage, the axial phenyl group is twisted so that overlap of the C—C bond and the SOMO is only 41% of the maximum (Table 4). At best, cleavage of this conformer would be inefficient. The higher-energy conformer, with the phenyl group in the equatorial position, is perfectly aligned for cleavage. The energy gap between this conformer and the global-minimum is only 4.35 kJ/mol (Table 4). Calculation of the Boltzmann distribution at 10°C leads to a value of 0.16, i.e., one out of six molecules will be populating the higher-energy conformer.

Irradiating the *cis* isomer under standard conditions resulted in ca. 60% conversion of the starting material. This was more than expected based upon reaction of just the global minimum. This indicates clearly that the other low-energy conformer is also present. The two observed C—C bond cleavage products are the acetals **14** and **15**. Acid hydrolysis yielded the alcohols **16** and **17**, which were isolated and fully characterized. The relative yields of **16** (20%) and **17** (31%) show again that there is a competition between reduction of the intermediate benzylic radical and addition of the radical to the radical anion of the electron acceptor. The competition is in favour of addition, which is consistent with the results from the irradiation of the diastereomers of **9**.

There is some overlap between the benzylic C—H bond and the SOMO of the phenyl ring in both of these conformers and therefore some deprotonation can be expected. Irradiation of the *cis* isomer in acetonitrile–methanol-*O*-*d* (3:1) in the presence of a sensitizer (**2**) showed that deprotonation does indeed take place. Isomerization to the *trans* isomer (6%) was also observed.

Only chair conformations of the *trans* isomer (**10***t*) were considered. This isomer was calculated to be 12.0 kJ/mol more stable than the *cis* isomer. In this isomer (**10***t*), the structure with the equatorial phenyl group was indeed found to be lower in energy than the conformer with the phenyl group in the axial position. This was confirmed by the ^{1}H nmr spectrum of this compound; the proton (δ 4.07) adjacent to the benzylic hydrogen has a coupling constant (^3J) of 11.25 Hz, which is also present in the signal of the benzylic proton (δ 2.41) indicating that both these protons are in the axial position. In agreement with the original expectations, the most stable conformer had the equatorial phenyl group aligned parallel to the geminal hydrogen. This orientation would inhibit deprotonation and subsequent isomerization to the *cis* isomer. However, this conformer is well aligned for C—C bond cleavage.

As predicted, no deuterium incorporation was observed when the irradiation was performed in acetonitrile–methanol-*O*-*d*. However, there was some (≈1%) isomerization to the *cis*

Can. J. Chem. Downloaded from www.nrcresearchpress.com by 88.146.161.215 on 09/08/12
For personal use only.

© 1997 NRC Canada

Can. J. Chem. Downloaded from www.nrcresearchpress.com by 88.146.161.215 on 09/08/12
For personal use only.

isomer. This indicates that isomerization may occur without the deprotonation-reprotonation steps. Obviously, another possible pathway involves C—C bond cleavage followed by isomerization, back electron transfer, and C—C bond formation (Scheme 5). This mechanism for isomerization has been observed before (*1f*).

The *trans* isomer also undergoes efficient C—C bond cleavage under the standard irradiation conditions but this process is somewhat less efficient than that of the *cis* isomer; 44% conversion was observed. This is surprising when only the global minima of the *cis* and *trans* isomers are considered. However, as pointed out earlier, other low- energy conformers are involved in the reaction as well. In the case of the *cis* isomer this results in a more efficient cleavage (the higher-energy conformer is favourably aligned for cleavage) whereas there is no such conformer available for the *trans* isomer.

Conclusions

The carbon–carbon and carbon–hydrogen bond cleavage in radical cations is governed by energetic (bond dissociation energy) and conformational criteria. Radical cations can undergo carbon–carbon bond cleavage when the activation barrier is lower than 55 kJ/mol. When the conformation is suitable, the bond dissociation energy is a good estimate of the activation barrier for cleavage. However, when the plane of the phenyl group is parallel to the vulnerable benzylic bond or when the alkyl portion of the alkoxy group is antiperiplanar to the C—C bond, the barrier is substantially higher than the bond dissociation energy, and cleavage becomes much less likely.

The radical cations that were considered in this study, (2*R*,3*R*)- and (2*S*,3*R*)-2-methoxy-3-phenylbutane (**9**) and *cis*- and *trans*-2-methyl-3-phenyltetrahydropyran (**10***c*, **10***t*), all have C—C bond dissociation energies below the threshold value. Molecular mechanics (MM3) calculations have been used to determine whether the radical cations of these ethers are suitably aligned for cleavage. The global minimum conformers of the diastereomers of **9** and of the *cis* isomer of **10** were all predicted to be unreactive toward C—C bond cleavage and deprotonation. However, for all three of these ethers, other higher-energy conformers that might undergo C—C cleavage were identified. The *trans* isomer of 2-methyl-3-phenyltetrahydropyran (**10***t*) was expected to cleave efficiently since the global minimum conformer is aligned for C—C bond cleavage but not for deprotonation.

The two diastereomers of **9** both cleaved inefficiently and no deprotonation or isomerization was observed. This is in good agreement with the predictions. The *cis* isomer of ether **10** cleaved efficiently and also showed evidence of deprotonation. This can only be explained on the basis of the reactivity of both the global minimum and a higher-energy conformer. The cleavage of the *trans* isomer was less efficient than that of the *cis* isomer. No deprotonation was detected; however, some isomerization to the *cis* isomer did occur, indicating that isomerization could occur through C—C bond cleavage. All the observations can be explained on the basis of the molecular mechanics calculations. These calculations are a valuable tool when predicting C—C and (or) C—H bond cleavage reactions.

Experimental

General information

The ^{1}H and ^{13}C nmr spectra were recorded on a Nicolet Instruments Corp. narrow-bore 360-MHz spectrometer or on a Bruker AC250 spectrometer as noted. Chemical shifts are reported in parts per million relative to tetramethylsilane. Infrared spectra were recorded on a Perkin–Elmer 283B spectrometer or a Nicolet 205 FT-IR spectrometer and frequencies are reported in cm^{-1}. Exact Mass determinations were obtained using a CEC 21-110B spectrometer. Gas chromatography with mass selective detection (gc/ms) was carried out on a Hewlett Packard (HP) 5890 gc coupled to an HP 5970 mass selective detector. Samples were analyzed on a 25 m × 0.2 mm, 5% phenyl methyl silicone on fused silica column (film thickness: 0.25 μm). Gas chromatography with flame ionization detection (gc/fid) was carried out on an HP 5890 gc equipped with a 25 m × 0.25 mm OV-1701 fused silica column. Preparative gas chromatography (prep-gc) was carried out using a Varian Aerograph 920 equipped with an SE-30 (20%) on Chromosorb W 60/80 column (6 ft. × 1/4 in.) and a thermal conductivity detector. Combustion analyses were performed by Canadian Microanalytical Service Ltd., Delta, B.C.

Electrochemical measurements

Oxidation potentials were obtained by cyclic voltammetry in acetonitrile solution using a three-electrode cell that has been described previously (12). The working electrode was a platinum sphere (1 mm diameter) and the counter electrode was a platinum wire. The electrolyte was 0.1 M tetraethylammonium perchlorate (TEAP) in acetonitrile. Substrate concentrations were approximately 1 mM. The peak potentials were measured with a 100 mV/s sweep rate. Since the anodic wave was irreversible, the half-wave potential was taken as 0.028 V before the anodic peak potential (13).

Materials

Solvents were distilled prior to use. Acetonitrile and 1,4-dicyanobenzene (**2**) (Aldrich) were purified as reported previously (*3f*). Tetrahydrofuran (BDH) was distilled from sodium. DL-2-Phenylpropionaldehyde, phthalic anhydride, 3-nitrophthalic anhydride, dimethyl sulfate, 4-phenyl-1-butanol (**15**), 4-chlorobutyrophenone, (ethyl)triphenylphosphonium bromide, sodium amide, and borane–tetrahydrofuran complex (1.0 M) were all obtained from Aldrich Chemical Company and were used as received. Iodomethane and sodium hydroxide were obtained from BDH, acetophenone and hydrogen peroxide (30%) were obtained from Fisher, lithium bromide was obtained from Sigma, and cyclododecane was obtained from K&K laboratories.

Calculations

Molecular mechanics calculations were carried out on a VAX 8800 mainframe computer. The 1988 force field of MM3 was used. PCModel[4] was used for the initial molecular mechanics calculations.

Preparations

Preparation of 3-phenyl-2-butanol

Phenyl-2-butanol was prepared from DL-2-phenylpropionalde-

© 1997 NRC Canada

Can. J. Chem. Downloaded from www.nrcresearchpress.com by 88.146.161.215 on 09/08/12
For personal use only.

hyde via a Grignard reaction. Iodomethane (100 mL, 228 g, 1.61 mol) was added dropwise with stirring to magnesium metal (50 g, 2.1 mol) in anhydrous diethyl ether. The flask was chilled in an ice bath throughout the addition. After the addition was complete, DL-2-phenylpropionaldehyde (106 mL, 107 g, 0.799 mol) was added dropwise. The resulting mixture was stirred for 16 h and then poured into a slurry of saturated NH_4Cl and ice. Concentrated HCl was added until the aqueous layer was acidic. The aqueous layer was extracted several times with ether; the combined organic extracts were washed with 5% $NaHCO_3$, dilute $NaHSO_3$, and distilled water. The solution was dried over anhydrous $MgSO_4$ and the ether was evaporated. A mixture of the diastereomers of 3-phenyl-2-butanol was obtained by vacuum distillation (107.8 g, 89.8% yield).

Separation of the diastereomers of 3-phenyl-2-butanol

The diastereomers were separated with a few slight modifications of Cram's procedure (14*a*). A mixture of the isomers of 3-phenyl-2-butanol (80.5 g, 0.536 mol) was refluxed with phthalic anhydride (60.0 g, 0.405 mol) and pyridine (100 mL) for 2 h. The mixture was cooled and diluted with an equal volume of benzene. The solution was washed with excess 1 M H_2SO_4 and with water, and was then dried over $MgSO_4$. The solvent was evaporated, and the residue was diluted with two volumes of ethyl acetate. Low-boiling petroleum ether was added until the solution became slightly turbid. The crystals that formed upon standing were recrystallized from ethyl acetate and petroleum ether to yield 21.4 g of the acid phthalates of the (2*R*,3*S*) and (2*S*,3*R*) enantiomers of the alcohol (14*b*). Some of these crystals (10.0 g) were hydrolyzed back to the alcohol by refluxing for 16 h with a solution of NaOH (8.0 g) in water (40 mL). The crude hydrolysis mixture was extracted with diethyl ether, and the organic layer was washed with water. The solution was dried over $MgSO_4$, and the ether was evaporated. The conversion from the acid phthalate to the alcohol was quantitative.

The (2*R*,3*R*),(2*S*,3*S*) pair of isomers (14*b*) was obtained by refluxing a mixture of the alcohol diastereomers (24.3 g, 0.162 mol) with 3-nitrophthalic anhydride (23.4 g, 0.121 mol) in pyridine (35 mL) for 1 h. The solution was diluted with an equal volume of benzene, washed with excess 1 M H_2SO_4 and distilled water, and dried over $MgSO_4$. The solvent was evaporated, and the crude reaction mixture was chromatographed on silica gel, using ethyl acetate as the eluant. Some of the fractions were induced to crystallize by adding two volumes of ethyl acetate, followed by sufficient petroleum ether to produce turbidity. The resulting solid was recrystallized from ethyl acetate and petroleum ether to yield 1.2 g of the acid 3-nitrophthalate. This ester was hydrolyzed to the alcohol by refluxing for 14 h with a solution of NaOH (2.0 g) in water (20 mL); work-up of the reaction mixture as before yielded the diastereomeric alcohol in 77% yield.

*Preparation of 2-methoxy-3-phenylbutane (**9**)*

The separated diastereomers of 3-phenyl-2-butanol were methylated with dimethyl sulfate. The (2*R*,3*S*),(3*R*,2*S*) alcohol mixture (5.20 g, 0.0346 mol) was dissolved in anhydrous diethyl ether (150 mL). NaH (6.0 g of a 60% suspension in mineral oil, 0.15 mol) was added, followed by dropwise addition of dimethyl sulfate (14 mL, 19 g, 0.15 mol). After the suspension was refluxed for 29 h, more dimethyl sulfate (10 mL, 13 g, 0.11 mol) was added and the mixture was refluxed for an additional 23 h. The reaction was quenched by the addition of distilled water. The aqueous layer was extracted with diethyl ether and the combined organic extracts were washed with concentrated NH_4OH and saturated NaCl. This solution was dried over anhydrous $MgSO_4$ and the solvent was removed from the potentially volatile ether by distillation through a fractionating column. The residue was chromatographed on silica gel using CH_2Cl_2–hexanes (1:4) to give 2-methoxy-3-phenylbutane (**9**) in quantitative yield; integration of the gc/ms spectrum gave the ratio of diastereomers as 95:5. The ^1H nmr spectrum corresponded to the one reported in the literature (14*b*): ^1H nmr (AC250, $CDCl_3$), δ: 7.23 (m, 5 Hz), 3.43 (dq, 1H, 6.3 Hz, 5.8 Hz), 3.27 (s, 3H), 2.93 (dq, 1H, 7.2 Hz, 5.8 Hz), 1.25 (d, 3H, 7.2 Hz), 1.05 (d, 3H, 6.3 Hz).

The same procedure was used to methylate the (2*R*,3*R*),(2*S*,3*S*) isomers of 3-phenyl-2-butanol (78% yield, 96:4 ratio of diastereomers). The recorded ^1H nmr spectrum corresponded to that reported in the literature (14*b*): ^1H nmr (AC250, $CDCl_3$), δ: 7.31–7.16 (m, 5H), 3.35 (s, 3H), 3.34 (dq, 1H, 6.1 Hz, 6.6 Hz), 2.73 (dq, 1H, 7.2 Hz, 6.6 Hz), 1.25 (d, 3H, 7.2 Hz), 0.96 (d, 3H, 6.1 Hz).

Preparation of cis*-2-methyl-3-phenyltetrahydropyran (**10**c)*

2-Methyl-3-phenyl-5,6-dihydropyran was prepared via a two-step synthesis, following the method of Descotes et al. (15). The first step involved the synthesis of α-methylphenyltetrahydrofuryl carbinol. A stirred solution of acetophenone (12 mL, 12 g, 0.10 mol) in tetrahydrofuran (200 mL, 177 g, 2.46 mol) was irradiated through Pyrex with a 450-W medium-pressure mercury vapour lamp. Nitrogen was bubbled through the solution during the irradiation; the total irradiation time was 24 h. Evaporation of the excess THF left 28 g of a mixture containing the carbinol. This crude mixture was used in the next step without purification.

α-Methylphenyltetrahydrofuryl carbinol was converted to 2-methyl-3-phenyl-5,6-dihydropyran by pyrolysis on neutral alumina (activity 1). The pyrolysis was carried out in a cylindrical electric multiple-unit furnace (Cenco) at 320°C. The alumina (14 g) was packed into a Pyrex tube (2 cm diameter), which was clamped vertically in the furnace. The crude carbinol mixture was pyrolyzed in batches of ca. 5 g each. With the entire apparatus under vacuum (0.25 Torr; 1 Torr = 133.3 Pa), the carbinol was allowed to drop onto the alumina, and the product was collected in a flask immersed in liquid nitrogen. On average, about 40% of the mass of the carbinol mixture was recovered. The pyrolysis mixture was chromatographed on silica gel, using a 1:1 mixture of CH_2Cl_2 and hexanes. The fractions containing the pyran were combined and hydrogenated, at atmospheric pressure, over 10% Pd on activated carbon. Filtration of the suspension and careful distillation of the solvent from the volatile product gave 1.0 g of product.

cis*-2-Methyl-3-phenyltetrahydropyran* (**10**c, 6% yield): ir (PE, neat), ν: 3080 (w), 3050 (w), 3020 (w), 2940 (s), 2840 (s), 1600 (m), 1495 (s), 1450 (s), 1380 (s), 1340 (m), 1270 (s), 1225 (s), 1190 (s), 1140 (m), 1110 (s), 1090 (s), 1075 (s), 1040 (s), 1030 (m), 960 (w), 930 (w), 880 (w), 850 (s), 835 (w), 810 (w), 745 (s), 730 (m), 690 (s), 655 (w); ^1H nmr (360 MHz,

© 1997 NRC Canada

Can. J. Chem. Downloaded from www.nrcresearchpress.com by 88.146.161.215 on 09/08/12
For personal use only.

$CDCl_3$), δ: 7.42–7.14 (m, 5H), 4.03 (m, 1H), 3.92 (dq, 1H, 3.26 Hz, 6.7 Hz), 3.61 (m, 1H), 2.83 (m, 1H), 1.91 (m, 4H), 1.04 (d, 3H, 6.7 Hz); ^{13}C nmr (90 MHz, $CDCl_3$), δ: 142.6 (s), 129.2 (d), 128.0 (d), 125.9 (d), 75.4 (d), 66.5 (t), 44.7 (d), 28.8 (t), 22.1 (t), 17.6 (q); ms, *m/z*: 176 ($M^{+\bullet}$, 12%), 132 (10), 117 (14), 115 (10), 104 (100), 91 (20). Anal. calcd. for $C_{12}H_{16}O$: C 81.77, H 9.15; found: C 81.42, H 9.08.

Preparation of trans-*2-methyl-3-phenyltetrahydropyran* (***10t***)
A mixture of 1.0 g (2.56×10^{-2} mol) sodium amide and 10.0 g (2.69×10^{-2} mol) (ethyl)triphenylphosphonium bromide in 50 mL tetrahydrofuran (THF) was refluxed for 1 h. The orange-red coloured solution was cooled to room temperature and a mixture of 1.75 g (9.58×10^{-3} mol) 4-chlorobutyrophenone and 1.1 g (1.27×10^{-2} mol) LiBr in 10 mL THF was added dropwise. The solution was stirred for 2 h after which the solid residue was filtered off. The solvent was evaporated and the residue was chromatographed on silica gel to yield 0.35 g of the alkene (both *cis* and *trans* isomers), which was used without further purification in the next step.

A solution of 0.35 g (1.81×10^{-3} mol) of the alkene from step 1 in 30 mL THF was flushed with nitrogen for 15 min. After this period 15 mL of a 1.0 M BH_3–THF complex was added dropwise and this solution was then refluxed for 10 h. The mixture was poured into water and cooled in an ice bath. A solution consisting of 8 mL 6 M NaOH and 6 mL H_2O_2 (30% aqueous solution) was added dropwise and the resulting mixture was stirred for 2 h. The solution was extracted with ether and the combined ether layers were washed with distilled water, saturated NH_4Cl, and saturated NaCl, and dried over anhydrous $MgSO_4$. The mixture of alcohols (0.27 g) that was obtained after evaporation of the solvent was used in the third step without further purification.

The alcohol (0.27 g, 1.27×10^{-3} mol) was added to 25 mL of a 6 M NaOH aqueous solution and refluxed for 10 h. The aqueous solution was extracted with ether and the combined ether layers were dried over anhydrous $MgSO_4$. Evaporation of the solvent followed by column chromatography of this residue on silica gel yielded pure *cis*- (40 mg) and *trans*-2-methyl-3-phenyltetrahydropyran (0.12 g). These compounds were further purified by prep-gc.

trans-*2-Methyl-3-phenyltetrahydropyran* (**10***t*, 0.12 g): ir (Nicolet, $CDCl_3$), ν: 3082 (w), 3061 (w), 3029 (w), 2961 (s), 2932 (s), 2850 (s), 1603 (w), 1494 (m), 1452 (m), 1378 (m), 1343 (w), 1264 (s), 1221 (m), 1186 (w), 1103 (s), 1083 (s), 1022 (s), 939 (w), 901 (w), 870 (m), 854 (m), 848 (m), 800 (s), 757 (m), 701 (s); ^1H nmr (360 MHz, $CDCl_3$), δ: 7.35–7.15 (m, 5H), 4.07 (dd, 1H, 2.45 Hz, 11.25 Hz), 3.57 (m, 1H+1H), 2.41 (m, 1H), 1.97 (m, 2H), 1.73 (m, 2H), 0.98 (d, 3H, 5.86 Hz); ^{13}C nmr (90 MHz, $CDCl_3$), δ: 143.79 (s), 128.48 (d), 127.69 (d), 126.44 (d), 78.25 (d), 68.43 (t), 50.61 (d), 32.24 (t), 26.55 (t), 20.07 (q); ms, *m/z*: 176 ($M^{+\bullet}$, 14%), 132 (9), 117 (19), 115 (13), 104 (100), 91 (21), 78 (15), 77 (13), 65 (7), 59 (7), 51 (9); actual mass of ion $C_{12}H_{16}O$: 176.1201; measured: 176.1199.

Irradiations

All irradiations were carried out in Pyrex tubes, at 10°C, using a General Electric 1-kW medium-pressure mercury vapour lamp. The samples were degassed by nitrogen ebullition for five minutes prior to irradiation.

*Irradiation of a mixture of (2R,3S)- and (2S,3R)-2-methoxy-3-phenylbutane (**9**) and 1,4-dicyanobenzene (**2**) in acetonitrile–methanol (3:1) (reaction [11a])*
A solution of 2-methoxy-3-phenylbutane (**9**, (2*R*,3*S*) and (2*S*,3*R*) enantiomers) (0.2085 g, 1.27×10^{-3} mol), 1,4-dicyanobenzene (**2**) (0.1147 g, 8.95×10^{-4} mol), and cyclododecane (38.0 mg, 2.26×10^{-4} mol) in acetonitrile–methanol (3:1) (30 mL) was irradiated through Pyrex (nmr tubes) for 1 week. The conversion of **9** after this period was 22%. The yield of ethylbenzene (**11**) was 8% (calibrated gc/ms). Trace amounts of the diastereomers of 2,3-diphenylbutane (**13**) were also detected. The identification of these diastereomers is based on the observed mass spectra (see below). The solvent was evaporated and the residue was chromatographed on silica gel with hexanes and CH_2Cl_2. The attempt at chromatographic separation was only partially successful: the yield of 1-(4-cyanophenyl)-1-phenylethane (**12**, 20%) was determined by analysis of fractions containing **12** and recovered starting material (**9**).

1-(4-Cyanophenyl)-1-phenylethane (***12***): ^1H nmr (AC 250, $CDCl_3$), δ: 7.56 (d, 2H, 6.6 Hz), 7.32–7.16 (m, 7H) 4.19 (q, 1H, 7.1 Hz), 1.64 (d, 3H, 7.1 Hz); ^{13}C nmr (AC 250, $CDCl_3$), δ: 151.9, 144.7, 132.3, 129.1, 128.7, 128.4, 127.5, 119.0, 110.0, 44.9, 21.4; ms, *m/z*: 207 ($M^{+\bullet}$, 38%), 192 (100), 165 (35), 105 (5), 77 (18).

2,3-Diphenylbutane (**13**, trace): *m/z*: 210 ($M^{+\bullet}$, 1%), 105 (100), 77 (14).

*Irradiation of a mixture of (2R,3S)- and (2S,3R)-2-methoxy-3-phenylbutane (**9**) and 1,4-dicyanobenzene (**2**) in acetonitrile–methanol-*O*-d (3:1)*
A solution of 2-methoxy-3-phenylbutane (**9**, (2*R*,3*S*) and (2*S*,3*R*) enantiomers) (45.4 mg, 2.76×10^{-4} mol) and 1,4-dicyanobenzene (**2**) (27.0 mg, 2.11×10^{-4} mol) in 3:1 acetonitrile–methanol-*O-d* (2 mL) was irradiated for 7 d through Pyrex. The reaction was monitored by gc/ms with selected ion monitoring. There was no evidence for deuterium incorporation in the starting material.

*Irradiation of a mixture of (2R,3R)- and (2S,3S)-2-methoxy-3-phenylbutane (**9**) and 1,4-dicyanobenzene (**2**) in acetonitrile–methanol (3:1) (reaction [11b])*
A solution of 2-methoxy-3-phenylbutane (**9**, (2*R*,3*R*),(2*S*,3*S*) enantiomers) (0.1491 g, 9.08×10^{-4} mol), 1,4-dicyanobenzene (**2**) (0.0791 g, 6.17×10^{-4} mol), and cyclododecane (35.1 mg, 2.09×10^{-4} mol) in acetonitrile–methanol (3:1) (20 mL) was placed in nmr tubes and irradiated for 7 d through Pyrex, resulting in a 22% conversion of **9**. The yield of ethylbenzene (**11**) was 6% (calibrated gc/ms). Trace amounts of the diastereomers of 2,3-diphenylbutane (**13**) were also detected. The solvent was evaporated and the residue was chromatographed on silica gel using a hexanes–CH_2Cl_2 gradient. The yield of 1-(4-cyanophenyl)-1-phenylethane (**12**) was determined as before (24% yield).

*Irradiation of a mixture of (2R,3S)- and (2S,3R)-2-methoxy-3-phenylbutane (**9**) and 1,4-dicyanobenzene (**2**) in acetonitrile–methanol-*O*-d (3:1)*
A solution of 2-methoxy-3-phenylbutane (**9**, (2*R*,3*R*),(2*S*,3*S*) enantiomers) (21.3 mg, 1.30×10^{-4} mol) and 1,4-dicyanoben-

© 1997 NRC Canada

Can. J. Chem. Downloaded from www.nrcresearchpress.com by 88.146.161.215 on 09/08/12
For personal use only.

zene (**2**) (16.3 mg, 1.27×10^{-4} mol) acetonitrile–methanol-*O-d* (3:1) (1 mL) was irradiated for 7 d through Pyrex. Monitoring of the reaction by gc/ms with selected ion monitoring showed that there was no evidence for isomerization or deuterium incorporation in the starting material.

Irradiation of cis-*2-methyl-3-phenyltetrahydropyran (**10**c) and 1,4-dicyanobenzene (**2**) in acetonitrile–methanol (3:1): identification of products*

A solution of *cis*-2-methyl-3-phenyltetrahydropyran (**10***c*) (0.197 g, 1.12×10^{-3} mol), 1,4-dicyanobenzene (**2**) (0.1025 g, 8.01×10^{-4} mol), and cyclododecane (25 mg, 1.49×10^{-4} mol) in acetonitrile–methanol (3:1) (8 mL) was irradiated for 84 h through Pyrex. Analysis by gc/ms indicated the presence of two cleavage products: the acetals **14** and **15**. The solvent was removed by rotary evaporation and the residue was subjected to acid hydrolysis by adding 5 N HCl (10 mL) and refluxing the solution for 1 h. The mixture was extracted with ether and the combined organic layers were washed with saturated $NaHCO_3$ and with water before drying with $MgSO_4$. Analysis of the mixture by gc/ms before and after the acid hydrolysis showed the disappearance of the acetal peaks and the appearance of two new (alcohol) peaks, attributed to 4-phenyl-1-butanol (**16**) and to 3-(4-cyanophenyl)-4-phenyl-1-butanol (**17**). Dry column flash chromatography (16) was used to separate the two alcohols. Alcohol **16** (10.5 mg, 12%) was positively identified after comparison of the retention time (gc/fid and gc/ms) and the mass spectrum with an authentic sample (Aldrich).

3-(4-Cyanophenyl)-4-phenyl-1-butanol (**17**, 29 mg, 21%): ir (Nicolet, $CDCl_3$), ν: 3636 (w), 3407 (s), 3061 (m), 3030 (m), 2939 (s), 2871 (m), 2229 (s), 1604 (m), 1497 (m), 1452 (m), 1413 (m), 1384 (w), 1346 (w), 1304 (w), 1174 (w), 1116 (w), 1059 (s), 1030 (m), 992 (w), 914 (m), 833 (m), 805 (m), 764 (m), 732 (s), 702 (s), 648 (m), 618 (m); ^{1}H nmr (360 MHz, $CDCl_3$), δ: 7.58–7.52 (d, 2H, 8.31 Hz), 7.38–7.32 (d, 2H, 8.32 Hz), 7.32–7.16 (m, 5H), 5.29 (s, 1H), 3.97 (t, 2H, 7.83 Hz), 3.65 (t, 2H, 6.36 Hz), 2.14 (m, 2H), 1.52 (m, 2H); ^{13}C nmr (90 MHz, $CDCl_3$), δ: 150.63 (s), 143.24 (s), 132.30 (d), 128.75 (d), 128.63 (d), 127.80 (d), 126.75 (d), 118.90 (s), 110.04 (s), 62.50 (t), 51.20 (d), 31.50 (t), 30.97 (t); ms, *m/z*: 251 ($M^{+\bullet}$, 5%), 233 (33), 218 (7), 205 (58), 192 (100), 190 (49), 177 (9), 165 (42), 152 (6), 140 (5), 115 (6), 91 (6), 51 (5); actual mass of ion $C_{17}H_{17}NO$: 251.1310; measured: 251.1316.

Irradiation of cis-*2-methyl-3-phenyltetrahydropyran (**10**c) and 1,4-dicyanobenzene (**2**) in acetonitrile–methanol (3:1) (reaction [12a])*

A solution of *cis*-2-methyl-3-phenyltetrahydropyran (**10***c*) (32 mg, 1.82×10^{-4} mol), 1,4-dicyanobenzene (**2**) (28 mg, 2.19×10^{-4} mol), and cyclododecane (4.5 mg, 2.68×10^{-5} mol) in 3:1 CH_3CN–CH_3OH (2 mL) was irradiated for 36 h through Pyrex. The irradiation resulted in a 61% conversion of the starting material. Isomerization to the *trans* isomer accounted for 6% of the conversion. Yields of the cleavage products were determined after acid hydrolysis by calibrated gc/ms using cyclododecane as an internal standard: 4-phenyl-1-butanol (**16**): 20%; 3-(4-cyanophenyl)-4-phenyl-1-butanol (**17**): 31%.

Irradiation of cis-*2-methyl-3-phenyltetrahydropyran (**10**c) and 1,4-dicyanobenzene (**2**) in acetonitrile–methanol*-O-d *(3:1)*

A solution of *cis*-2-methyl-3-phenyltetrahydropyran (**10***c*) (30 mg, 1.70×10^{-4} mol) and 1,4-dicyanobenzene (**2**) (25 mg, 1.95×10^{-4} mol) in acetonitrile–methanol-*O-d* (3:1) (2 mL) was irradiated for 36 h through Pyrex. Selected ion monitoring with the gc/ms showed that deuterium was incorporated in the molecular ion.

Irradiation of trans-*2-methyl-3-phenyltetrahydropyran (**10**t) and 1,4-dicyanobenzene (**2**) in acetonitrile–methanol (3:1) (reaction [12b])*

A solution of *trans*-2-methyl-3-phenyltetrahydropyran (**10***t*) (30 mg, 1.70×10^{-4} mol), 1,4-dicyanobenzene (**2**) (24 mg, 1.90×10^{-4} mol), and cyclododecane (3.5 mg, 2.08×10^{-5} mol) in acetonitrile–methanol (3:1) (2 mL) was irradiated for 36 h through Pyrex. The irradiation resulted in a 44% conversion of the starting material. Isomerization to the *cis* isomer accounted for 1% of the conversion. Yields of the cleavage products were determined as before: 4-phenyl-1-butanol (**16**): 23%; 3-(4-cyanophenyl)-4-phenyl-1-butanol (**17**): 37%.

Irradiation of trans-*2-methyl-3-phenyltetrahydropyran (**10**t) and 1,4-dicyanobenzene (**2**) in acetonitrile–methanol*-O-d *(3:1)*

A solution of *trans*-2-methyl-3-phenyltetrahydropyran (**10***t*) (30 mg, 1.70×10^{-4} mol) and 1,4-dicyanobenzene (**2**) (25 mg, 1.95×10^{-4} mol) in acetonitrile–methanol-*O-d* (3:1) (2 mL) was irradiated for 36 h through Pyrex. Selected ion monitoring with the gc/ms showed that there was no (within experimental error) deuterium incorporation in the molecular ion.

Acknowledgements

This work was supported by a grant from the Natural Sciences and Engineering Research Council (NSERC) of Canada. We thank Drs. D.L. Hooper and M.D. Lumsden at the Atlantic Regional Magnetic Resonance Centre for the high-field NMR spectra and for help in the preparation of the manuscript. We also thank Dr. G. Deslongchamps, University of New Brunswick, for a useful suggestion regarding the synthesis of one of the ethers. A.L.P. and H.J.P.dL. are grateful for scholarships from the Izaak Walton Killam Memorial Foundation.

References

1. (*a*) D.R. Arnold, M.S.W. Chan, and K.A. McManus. Can. J. Chem. **74**, 2143 (1996); (*b*) H.J.P. de Lijser and D.R. Arnold. J. Phys. Chem. **100**, 3996 (1996); (*c*) D.R. Arnold, D.A. Connor, K.A. McManus, P.K. Bakshi, and T.S. Cameron. Can. J. Chem. **74**, 602 (1996); (*d*) K.A. McManus and D.R. Arnold. Can. J. Chem. **73**, 2158 (1995); (*e*) D.A. Connor, D.R. Arnold, P.K. Bakshi, and T.S. Cameron. Can. J. Chem. **73**, 762 (1995); (*f*) D.R. Arnold, X. Du, and H.J.P. de Lijser. Can. J. Chem. **73**, 522 (1995); (*g*) D.R. Arnold, X. Du, and J. Chen. Can. J. Chem. **73**, 307 (1995); (*h*) K.A. McManus and D.R. Arnold. Can. J. Chem. **72**, 2291 (1994); (*i*) H.J.P. de Lijser and D.R. Arnold. J. Chem. Soc. Perkin Trans. 2. In press.
2. (*a*) A.J. Maroulis, Y. Shigemitsu, and D.R. Arnold. J. Am. Chem. Soc. **100**, 535 (1978); (*b*) R.M. Borg, D.R. Arnold, and T.S. Cameron. Can. J. Chem. **62**, 1785 (1984); (*c*) D.R. Arnold and M.S. Snow. Can. J. Chem. **66**, 3012 (1988).

© 1997 NRC Canada

3. (*a*) D.R. Arnold and A.J. Maroulis. J. Am. Chem. Soc. **98**, 5931 (1976); (*b*) D.F. Eaton. Pure Appl. Chem. **56**, 1191 (1984); (*c*) L.W. Reichel, G.W. Griffin, A.J. Muller, P.K. Das, and S.N. Ege. Can. J. Chem. **62**, 424 (1984); (*d*) H.F. Davis, P.K. Das, L.W. Reichel, and G.W. Griffin. J. Am. Chem. Soc. **106**, 6968 (1984); (*e*) A. Okamoto and D.R. Arnold. Can. J. Chem. **63**, 2340 (1985); (*f*) A. Okamoto, M.S. Snow, and D.R. Arnold. Tetrahedron, **42**, 6175 (1986); (*g*) D.R. Arnold, B.J. Fahie, L.J. Lamont, J. Wierzchowski, and K.M. Young. Can. J. Chem. **65**, 2734 (1987); (*h*) R. Popielarz and D.R. Arnold. J. Am. Chem. Soc. **112**, 3068 (1990); (*i*) D.R. Arnold and L.J. Lamont. Can. J. Chem. **67**, 2119 (1989); (*j*) D.R. Arnold, L.J. Lamont, and A.L. Perrott. Can. J. Chem. **69**, 225 (1991); (*k*) F.D. Saeva. Top. Curr. Chem. **156**, 59 (1990); (*l*) P. Maslak, Top. Curr. Chem. **168**, 1 (1993); (*m*) E.R. Gaillard and D.G. Whitten. Acc. Chem. Res. **29**, 292 (1996).
4. A.L. Perrott and D.R. Arnold. Can. J. Chem. **70**, 272 (1992).
5. (*a*) A.M. de P. Nicholas and D.R. Arnold. Can. J. Chem. **60**, 2165 (1982); (*b*) F.D. Lewis. Acc. Chem. Res. **19**, 401 (1986); (*c*) F.G. Bordwell, J.-P. Cheng, and M.J. Bausch. J. Am. Chem. Soc. **110**, 2867 (1988); (*d*) L.M. Tolbert and R.K. Khanna. J. Am. Chem. Soc. **109**, 3477 (1987); (*e*) L.M. Tolbert, R.K. Khanna, A.E. Popp, L. Gelbaum, and L.A. Bottomley. J. Am. Chem. Soc. **112**, 2373 (1990).
6. (*a*) U. Buckert and N.L. Allinger. Molecular mechanics. ACS Monograph No. 117, Washington, D.C. 1982; (*b*) N.L. Allinger. *In* Accurate molecular structures: their determination and importance. *Edited by* A. Domenicano and I. Hargittai. Oxford University Press, New York. 1992. p. 336; (*c*) J. Am. Chem. Soc. **99**, 8127 (1977); (*d*) N.L. Allinger, Y.H. Yuh, and J.-H. Lii. J. Am. Chem. Soc. **111**, 8551 (1989); (*e*) N.L. Allinger, M. Rahman, and J.-H. Lii. J. Am. Chem. Soc. **112**, 8293 (1990).
7. (*a*) A. Weller. Pure Appl. Chem. **16**, 115 (1965); (*b*) D. Rehm and A. Weller. Isr. J. Chem. **8**, 259 (1970).
8. (*a*) M. Karplus. J. Chem. Phys. **30**, 11 (1959); (*b*) J. Am. Chem. Soc. **85**, 2870 (1963).
9. (*a*) D.D.M. Wayner, J.J. Dannenberg, and D. Griller. Chem. Phys. Lett. **131**, 189 (1986); (*b*) D.D.M. Wayner, D.J. McPhee, and D. Griller. J. Am. Chem. Soc. **110**, 132 (1988).
10. N.L. Allinger and M.T. Tribble. Tetrahedron Lett. **35**, 3259 (1971).
11. J.A. Hirsch. *In* Topics in stereochemistry. *Edited by* N.L. Allinger and E.L. Eliel. Vol. 1. Wiley–Interscience, New York. 1967, p. 207.
12. D.R. Arnold and D.D.M. Wayner. Can. J. Chem. **64**, 100 (1986).
13. (*a*) R.S. Nicholson and I. Shain. Anal. Chem. **36**, 706 (1964); (*b*) Anal. Chem. **37**, 178 (1965).
14. (*a*) D.J. Cram. J. Am. Chem. Soc. **71**, 3863 (1949); (*b*) B. Scholl and H.-J. Hansen. Helv. Chim. Acta, **63**, 1823 (1980).
15. (*a*) G. Descotes, J.-C. Martin, and G. Labrit. Bull. Soc. Chim. Fr. **11**, 4151 (1969); (*b*) J.-P. Decor and G. Descotes. Bull. Soc. Chim. Fr. **8–9**, 3112 (1970).
16. L.M. Harwood. Aldrichimica Acta, **18**, 25 (1985).

Can. J. Chem. Downloaded from www.nrcresearchpress.com by 88.146.161.215 on 09/08/12
For personal use only.

© 1997 NRC Canada

A study of formation and fragmentation of ionic metal complexes of substituted benzoic and cinnamic acids with Al(III)–glycerol by fast atom bombardment mass spectrometry

Mandapati Saraswathi and Jack M. Miller

Can. J. Chem. Downloaded from www.nrcresearchpress.com by 88.146.161.215 on 09/08/12
For personal use only.

Abstract: Substituted benzoic and cinnamic acids were studied by FAB mass spectrometry using matrix-based Al(III) ions. Complex ions derived from these acids, such as $(M + 117)^+$ (117 = (Al + glycerol − 2H)$^+$), $(M + 159)^+$ (159 = [2Al + 2glycerol − 5H − 74(epoxypropanol)]$^+$), and $(M + 233)^+$ (233 = (2Al + 2glycerol − 5H)$^+$), when subjected to collisionally activated dissociation (CAD), gave an ion corresponding to $(M - OH)^+$. Formation of this ion was explained by the transfer of the carboxylic -OH group to the (Al + glycerol − 2H)$^+$, (2Al + 2glycerol − 5H − 74)$^+$, and (2Al + 2glycerol − 5H)$^+$ portion of the complexes. This transfer is more pronounced in the case of *meta*- and *para*-substituted acids. The CAD of the $(M + 117)^+$ ions yielded $(M + Al(III))^+$ ions resulting from the insertion of Al(III) into the carboxylic acid, which was followed by the elimination of CO to produce $(M + Al(III) - CO)^+$ ions. Interpretation of spectral data was clarified by study of the formation and fragmentation of ions produced from deuterated benzoic and cinnamic acids.

Key words: substituted benzoic and *trans*-cinnamic acids, Al(III)–glycerol, FAB mass spectrometry, ionic metal complexes, collisionally induced dissociation, Al(III) insertion, carbonyl cations.

Résumé : On a étudié une série d'acides benzoïques et cinnamiques substitués par spectrométrie de masse «FAB», en utilisant des ions d'Al(III) insérés dans des matrices. Les ions complexes obtenus à partir de ces acides, tels que ceux à $(M + 117)^+$ (117 = (Al + glycérol − 2H)$^+$), $(M + 159)^+$ (159 = [2Al + 2glycérol − 5H − 74(époxypropanol)]$^+$) et $(M + 233)^+$ (233 = (2Al + 2glycérol − 5H)$^+$), soumis ensuite à une dissociation activée par collision (DAC), conduisent à un ion correspondant à $(M - OH)^+$. On a expliqué la formation de cet ion par le transfert du groupe -OH du carboxyle aux portions (Al + glycérol − 2H)$^+$, (2Al + 2glycérol − 5H − 74)$^+$ et (2Al + 2glycérol − 5H)$^+$ des complexes. Ce transfert est plus important dans les cas des acides substitués en *méta* et en *para*. La DAC des ions $(M + 117)^+$ conduit aux ions $(M + Al(III))^+$ qui résultent de l'insertion du Al(III) dans l'acide carboxylique, suivie d'une élimination de CO conduisant aux ions (M + Al(III) − CO). L'interprétation des données spectrales a été clarifiée par l'étude de la formation et de la fragmentation des ions produits à partir d'acides benzoïques et cinnamiques deutérés.

Mots clés : acides benzoïques et *trans*-cinnamiques substitués, Al(III)–glycérol, spectrométrie de masse «FAB», complexes métalliques ioniques, dissociation induite par collision, insertion de Al(III), cations carbonyles.

[Traduit par la rédaction]

Introduction

Reactions of metal ions with amino acids (1), peptides (2), nucleotides (3), and crown ethers (4) have been studied by fast atom bombardment and electrospray mass spectrometry. However, the gas phase chemistry of the aluminum ion has not been as well explored as that of alkali, alkaline earth, and transition metal ions. There are a few reports on gas phase ion–molecule reactions of Al^+, generated from aluminum foil or $AlCl_3$, with alkyl halides, alcohols, ketones, and esters (5). We reported that aluminum chloride in a glycerol matrix, under FAB ionization conditions, generated a complex ion (Al + Gly − 2H)$^+$ (Gly = glycerol) in addition to some other matrix-based Al(III) ions (6).

Reactions of (Al + Gly − 2H)$^+$ ions (*m/z* 117) have been studied with α-amino acids (7), peptides (7), and polydentate ligands such as crown ethers (6), polyethylene glycols (6), and nucleobase-substituted glymes (8). All these ligands formed abundant ionic complexes with the (Al + Gly − 2H)$^+$. Nucleobase-substituted glymes also formed $(M + 141)^+$ (M = analyte) ions by displacement of amide protons of the nucleobase, i.e., formation of a covalent bond between Al(III) and N_3 of two nucleobases (8). Complex ions generated from α-amino acids and Al(III) species on collisionally activated decomposition (CAD) gave fragment ions where the Al(III) is covalently bound to amino and carboxylic groups by substitution of acidic protons (7). The acidic protons of these amino and carboxylic groups were involved in the elimination of glycerol attached to the Al(III). Similar elimination of glycerol was also observed in the fragmentation of adduct ions derived from peptides by substituting the amide protons with Al(III) (7). The CAD spectra of cluster ions obtained from crown

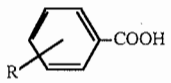
Received September 26, 1996.

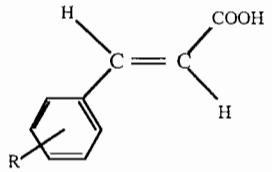
M. Saraswathi and J.M. Miller.[1] Department of Chemistry, Brock University, St. Catharines, ON L2S 3A1, Canada.

[1] Author to whom correspondence may be addressed. Telephone: (905) 688-5550, ext. 3402. Fax: (905) 682-9020. E-mail: jmiller@sandcastle.cosc.brocku.ca

© 1997 NRC Canada

Fig. 1. A list of substituted benzoic and cinnamic acids investigated.





R =
1. H; **2**. 2-CH_3; **3**. 3-CH_3; **4**. 2-OH; **5**. 4-OH; **6**. 2-OCH_3; **7**. 3-OCH_3; **8**. 4-OCH_3; **9**. 2,4-OCH_3; **10**. 2,6-OCH_3; **11**. 3,5-OCH_3; **12**. 3-NO_2; **13**. 2-NO_2-3-CH_3; **14**. 2-NH_2; **15**. 3-NH_2.

R =
16. 4-CH_3; **17**. 2-OH; **18**. 3-OH; **19**. 4-OH; **20**. 2-OCH_3; **21**. 3-OCH_3; **22**. 4-OCH_3;

Can. J. Chem. Downloaded from www.nrcresearchpress.com by 88.146.161.215 on 09/08/12
For personal use only.

ethers and polyethylene glycols also appeared in the formation of covalently bound $(M + AlO)^+$ ionic complexes, which was followed by the loss of neutral C_2H_4O units (6). In this study we discuss the reactions of Al(III)–glycerol ions with benzoic and *trans*-cinnamic acids.

Results and discussion

Cluster ions generated by fast atom bombardment of a matrix mixture consisting of glycerol (25–30 mg), $AlCl_3$ (3–4 mg), TFA (2,2,2-trifluoroacetic acid, 2 μL), and H_2O (2 μL) are observed at *m/z* 117 $(Al + Gly - 2H)^+$, 231 $(Al + Gly + TFA - 2H)^+$, and 233 $(2Al + 2Gly - 5H)^+$ (Gly = glycerol), along with the species produced by substitution of one hydroxy proton of these with 116u (Al + Gly − 3H) and 114u (TFA), as observed in our earlier studies (6–8). All substituted aromatic carboxylic acids form significant adduct ions such as $(M + 117)^+$, $(M + 159)^+$, $(M + 233)^+$, $(M + 347)^+$, and $(M + 349)^+$ (M = analyte). The relative intensities of the ions containing Al(III) produced by the reactions between aromatic carboxylic acids **1**–**15** (Fig. 1) and Al(III)–glycerol ions are listed in Table 1. From methyl (**2** and **3**) and methoxy (**6**–**11**) substituted acids, ions corresponding to $(M + 103)^+$ are observed in addition to other cluster ions. The formation of a number of cluster ions depends on the amount of $AlCl_3$ added to the glycerol matrix. The solubility of the carboxylic acids in the matrix mixture could be increased by the addition of a mixture of ethyl acetate and ethyl alcohol to the matrix. These solvents do not interfere with the formation of ions from these acids. Addition of TFA to the matrix results in the formation of the protonated analyte, which is followed by dehydration of the $(M + H)^+$ ions. Metal-chelated ions are also observed in significant abundances. Accurate mass measurements on the $(M + 117)^+$ ion of **3** give $C_{11}H_{14}O_5Al$ as the elemental composition with a 2.5 ppm deviation (theor. 253.06565; obsd. 253.06630). Similar experiments on the $(M + 159)^+$ ion of **6** fit the molecular formula $C_{11}H_{13}O_7Al_2$ (theor. 311.02919; obsd. 311.02883, Δ = 1.1 ppm). The elemental composition, $C_{14}H_{19}O_9Al_2$, is in agreement within an error of 3.5 ppm for the $(M + 233)^+$ ion of **6** (theor. 385.06597; obsd. 385.06735).

The FAB mass spectra of *trans*-cinnamic acids **16**–**22** (Fig. 1) show abundant metal-complexed ions at $(M + 117)^+$, $(M + 159)^+$, $(M + 233)^+$, $(M + 347)^+$, and $(M + 349)^+$. The relative abundances of metal-coordinated ions are given in Table 2. Aliphatic carboxylic acids also react with Al(III)–glycerol species and form adduct ions. With the increase of alkyl chain length the solubility of aliphatic acids is reduced. Therefore, further studies on these systems were not carried out. The site of coordination of the metal ion is likely at the carboxylate group.

The FAB spectra obtained with *d*-labelled acids such as **3**, **6**, **7**, **10**, **14**, **15**, **18**, and **21** with $AlCl_3$ and glycerol-d_3, TFA, and D_2O show an increase of 2, 1, and 2 mass units in the formation of $(M + 117)^+$, $(M + 159)^+$, and $(M + 233)^+$ ions, respectively. In the case of hydroxy (M = **18**) and amino (M = **14**, **15**) substituted acids, there is observed an additional increase of mass by 1 and 2u. The $(M + 103)^+$ ion from **3** and **6** shows an increase of 3u in the mass.

1. The collisionally activated dissociation of adduct ions from benzoic acids

(a) $(M + 117)^+$ ($P^+ = (M + Al + Gly - 2H)^+$)

The CAD of $P^+ = (M + 117)^+$ ions of **3**–**7**, **9**, **10**, **14**, and **15** were studied using "daughter ion" linked scans by keeping the *B/E* ratio constant. The fragmentation of $P^+ = (M + 117)^+$ ions of **3**–**7** gives ions due to $(P - OH)^+$, $(P - H_2O)^+$, $(P - CH_2O)^+$, $(P - 44)^+$, $(P - RH)^+$, and $(P - R)^+$ (R = substituent). The formation of the $(P - H_2O)^+$ ion is always followed by the loss of CH_2O to give the $(P - 48)^+$ ion. Other abundant ions observed are $(P - 28)^+$, $(P - 74)^+$, $(P - 90)^+$, $(P - 118)^+$, and $(P - 134)^+$ or substituted benzoyl cations. Loss of 74u (epoxypropanol) from the P^+ ion yielding the $(M + AlO)^+$ ion is consistent with our previous observations (6, 7). The $(P - 90)^+$ ion can be formed by the insertion of Al(III) into the carboxylate group after the elimination of the neutral dideprotonated glycerol moiety attached to the metal ion. Hydroxy acids **4** and **5** also show a $(P - 90)^+$, i.e., $(M + Al(III))^+$ ion at *m/z* 165, which is common in other acids. From this ion, elimination of a carbonyl group gives a significant ion at *m/z* 137, i.e., the $(P - 118)^+$ or $(M + Al(III) - CO)^+$ ion. The $(P - 92)^+$ ion is observed only from **4**, which involves the elimination of

© 1997 NRC Canada

Table 1. Relative abundances of the ions above the molecular region obtained from substituted benzoic acids and Al(III)–glycerol.

Compound no.	$(M + H)^+$	$(M + 117)^+$	$(M + 159)^+$	$(M + 233)^+$	$(M + 347)^+$	$(M + 349)^+$
1	11	10	25	45	23	14
2	7	5	15	17	—	—
3	10	24	26	27	6	10
4	28	100	8	59	15	5
5	100	57	3	13	6	—
6	22	28	7	10	4	2
7	17	44	59	60	21	22
8	30	12	40	52	—	—
9	16	13	14	14	4	6
10	26	15	3	9	4	3
11	14	14	26	28	10	10
12	53	100	—	30	—	—
13	—	53	45	100	42	32
14	99	38	3	7	3	6
15	100	34	14	20	10	10

Other ions, *m/z* (%)

1: 221(5), 225(15), 269(17), 271(18), 329(19), 331(16), 447(15), 499(19)
2: 239(14), 265(8), 283(8), 357(26), 431(9), 475(10), 505(12), 549(8), 567(5), 592(3), 665(5)
3: 179(8), 205(6), 235(10), 239(17), 241(11), 265(11), 283(11), 285(10), 357(30), 431(9), 505(16), 527(13)
4: 237(15), 509(16)
6: 251(5)
7: 195(21), 221(11), 251(16), 255(45), 257(38), 275(22), 281(27), 299(26), 389(34), 427(15), 477(13), 521(13), 537(14), 559(17)
8: 255(39), 273(11), 281(18), 297(13), 299(25), 301(25), 329(12), 389(32), 407(22), 477(22), 481(13), 501(18), 537(14)
9: 285(4), 507(6)
10: 413(9)
11: 285(16), 287(12), 311(13), 327(7), 329(10), 331(11), 449(12)
12: 266(48), 492(12), 568(15)
14: 180(5), 182(5), 346(6), 368(9), 506(5), 598(3)
15: 177(12), 236(17)

Unless otherwise noted the base peak is $(MH - H_2O)^+$.

a glycerol molecule to form a six-membered ring. The fragmentation of the adduct ions of **6** and **7** also produces $(P - CH_2)^+$, $(P - CH_3)^+$, $(P - CH_4)^+$, $(P - CO)^+$, $(P - CH_2O)^+$, $(P - CH_2, CO)^+$/$(P - CO_2)^+$ equal to $(P - 44)^+$, $(P - 74)^+$, $(P - 90)^+$, or $(M + Al(III))^+$ and $(P - 118)^+$ or $(M + Al - CO)^+$ ions, in addition to other less abundant ions at *m/z* 121, 92, and 77. The formation of product ions from **3** and **6** is confirmed by the dissociation of labelled P^+ ions.

The fragmentation of $P^+ = (M + 117)^+$ ions for positional isomers **9** and **10** yields enormous differences in the abundance of the $(P - H_2O)^+$ and $(P - 90)^+$ ions. The ion due to the insertion of Al(III) into the carboxylic acid group at *m/z* 209 ($(P - 90)^+$ or $[M + Al(III)]^+$) is the base peak in the spectrum of **10**, whereas, M = **9** produces a $(P - H_2O)^+$ ion as the most abundant ion. Formation of other ions from these two compounds, such as $(P - CH_2O)^+$, $(P - 134)^+$, and the loss of CH_4 from the parent ion as well as from the $(P - CH_2O)^+$ ion is quite similar to the fragmentation of $(M + 117)^+$ ions from other compounds. The CAD of the deuterated P^+ ion (*m/z* 301) of **10** gives ions at *m/z* 210, 211, and 212 that correspond to the ion at *m/z* 209 in the unlabelled P^+ ion. Therefore, the ion at *m/z* 209 (301 deuterated) may undergo H/D exchange in the exited state after collisional activation.

The dissociation of the P^+ complex of **14** and **15** also yields $(P - OH)^+$, $(P - H_2O)^+$, $(P - 74)^+$, $(P - 90)^+$, $(P - 118)^+$, and $(P - 134)^+$ ions. The *d*-labelled $(M + 117)^+$ ion of **14** and **15** appears at *m/z* 258. On fragmentation, this ion gives three ions at *m/z* 238, 239, and 240. The ion at *m/z* 240 may be due to the loss of OD. Since there is no acidic H that is unlabelled in this ion, the loss of an HDO molecule from the parent ion would not explain the ion at *m/z* 239. Therefore, this ion may be related to the loss of neutral ND_2H, which would have the same mass as an OH group in the unlabelled adduct ion. Since the elimination of ND_3 or D_2O accounts for the same mass, we cannot be clear whether or not the hydroxy proton of the reagent is involved in the elimination of ammonia. However, the loss of ND_2H does indicate the involvement of aromatic hydrogen. Ions due to $(P - D_2O/ND_3)^+$ and $(P - ND_2H)^+$ are equally abundant. The fragmentation of labelled P^+ ion also yields the loss of one deuterium atom in the formation of $(P - 74)^+$, $(M + Al(III))^+$ ions and amino benzoyl cations ($(P - 134)^+$). The formation of the $(M + H)^+$ ion is not a common process in the decomposition of an $(M + 117)^+$ ion. However, dissociation of the $(M + 117)^+$ ion of **14** yields a low-abundance $(M + H)^+$ ion. This can be attributed to the higher proton affinity of aminobenzoic acids compared to the other substituted acids studied.

We explain the production of substituted benzoyl cations

© 1997 NRC Canada

Can. J. Chem. Downloaded from www.nrcresearchpress.com by 88.146.161.215 on 09/08/12
For personal use only.

Table 2. Relative abundances of metal-containing ions obtained from substituted cinnamic acids **16–23** using Al(III)/glycerol/TFA/H_2O.

Compound no.	$(M + 117)^+$	$(M + 159)^+$	$(M + 233)^+$	$(M + 347)^+$	$(M + 349)^+$
16	29	26	28	12	7
17	82	27	27	12	8
18	34	47	31	24	9
19	29	20	19	9	9
20	16	46	54	17	18
21	16	29	35	18	12
22	7	31	49	25	12

Other metal-containing ions, *m/z* (%)

16: 265 (19), 267(15), 323(14), 435(14), 479(8), 487(6)
17: 373(19), 489(12)
18: 373(9), 437(12), 489(9), 529(12), 533(7)
19: 373(6), 437(6), 489(6)
20: 281(21), 301(19), 307(19), 323(17), 327(13)
21: 281(16), 283(14), 307(14)
22: 283(13), 479(24), 503(19), 547(15), 575(11)

Unless otherwise noted the base peak is $(MH - H_2O)^+$.

$((P - 134)^+)$ as the transfer of the OH group of the acids to Al(III). The amount of the benzoyl cation formed depends on the ease of cleavage of the C—OH bond and the approach of the metal ion to transfer the OH to the $(Al + Gly - 2H)^+$ portion of the P^+ ion. Among the positional isomers, the abundance of the benzoyl cation $((P - 134)^+)$ is greater in *meta*- and *para*-substituted acids, which are sterically less hindered to the approach of the $(Al + Gly - 2H)^+$ ion than are the *ortho*-substituted acids.

(b) $(M + 233)^+$ ($C^+ = (M + 2Al + 2Gly - 5H)^+$)

The CAD of the $C^+ = (M + 233)^+$ ion from **2–4**, **6–8**, **14**, and **15** yields $(C - 74)^+$, $(C - 104)^+$, $(C - 86)^+$, and $(C - 130)^+$ ions. However, the formation of the $(M + 117)^+$ ion is a very minor process. The formation of a benzoyl cation is observed from all these acids. Production of an ion corresponding to the $(M + 103)^+$ or $(C - 130u)^+$ ion from **2–4**, **6–8**, **14**, and **15** is explained with reference to the fragmentation of *d*-labelled $(M + 233)^+$ ions from **6** and **14** (Scheme 1). The CAD spectra of labelled C^+ of these acids show a loss of one deuterium each in the formation of the $(C - 74)^+$ (i.e., loss of $CH_2(O)CHCH_2OD$) and $(C - 130)^+$ ions and retention of all deuteriums in the $(C - 86)^+$ ion. The $(C - 130)^+$ and $(C - 86)^+$ ions are abundant for all acids studied and no substituent effect is involved in their formation. Thus, we conclude that the ion from which these two originate is from the $(2Al + 2Gly - 5H)^+$ ion. It follows that the $(C - 130)^+$ ion is an adduct of an Al(III)–glycerol species corresponding to 103u plus the analyte $((M + 103)^+)$. From the $(C - 130)^+$ ion, the loss of a water molecule can give rise to an ion at *m/z* 222 and 223 from **14** or **15** and **4**, respectively, because loss of substituent **2** shows the loss of 16u from the $(M + 103)^+$ ion. If the structure of the ion at *m/z* 233 generated from the matrix is "**a**", as proposed in our earlier studies, then there will be facile routes to formation of the $(M + 117)^+$ ion, as already observed for amino acids and peptides (7). The formation of the $(M + 117)^+$ ion is insignificant in the CAD spectra of the $(M + 233)^+$ ion. Therefore, we suggest that the ion at *m/z* 233 from the matrix may have another isomeric structure "**b**", dependent on the pH of the matrix solution.

The fragmentation of the $(M + 103)^+$ ion of **2**, **3**, **6**, and **7** gives an abundant ion corresponding to a substituted benzoyl cation. The $(M + 103)^+$ ion at *m/z* 239 from **2** and **3** and at *m/z* 255 from **6** and **7**, formed from the $(M + 117)^+$ ion on dissociation, is due to the loss of a methylene group. It follows that the fragmentation of the $(M + 103)^+$ ion should give a fragment ion corresponding to the $(M + 103 - CH_2OCHCH_2OH)^+$ ion due to the loss of epoxypropanol. This is a commonly observed fragment ion from the dissociation of the $(M + 117)^+$ ion. It also follows that there should not be the formation of a substituted benzoyl cation at *m/z* 119 for M = **2** and **3** and at 135 for M = **6** and **7** and loss of CH_4 from the $(M + 103)^+$ ion. Therefore, the $(M + 103)^+$ ion is something different from the $(M + 117 - CH_2)^+$ ion. The high-resolution measurements on the $(M + 103)^+$ ion from **6** show that it is composed of two ions, resolved at 10 000 resolving power. The less abundant ion of mass 255.04570u shows a 3.0 ppm deviation from the molecular formula $C_{10}H_{12}O_6Al$ (theor. 255.04492). The higher-abundance ion observed at *m/z* 255.0023 shows 2.6 ppm deviation from the elemental composition $C_8H_9O_6Al_2$ (theor. 255.00297; obsd. 255.0023). The dissociation of the $C^+ = (M + 233)^+$ ion shows an increase of one mass unit when compared with the dissociation of the labelled $(M + 233)^+$ ion of **6** and **14**. The $(M + 103)^+$ ion from **3** and **6** overlaps with other ions in D_2O exchange experiments. Therefore, the structure of this ion has not been established.

2. Dissociation of adduct ions from *trans*-cinnamic acids

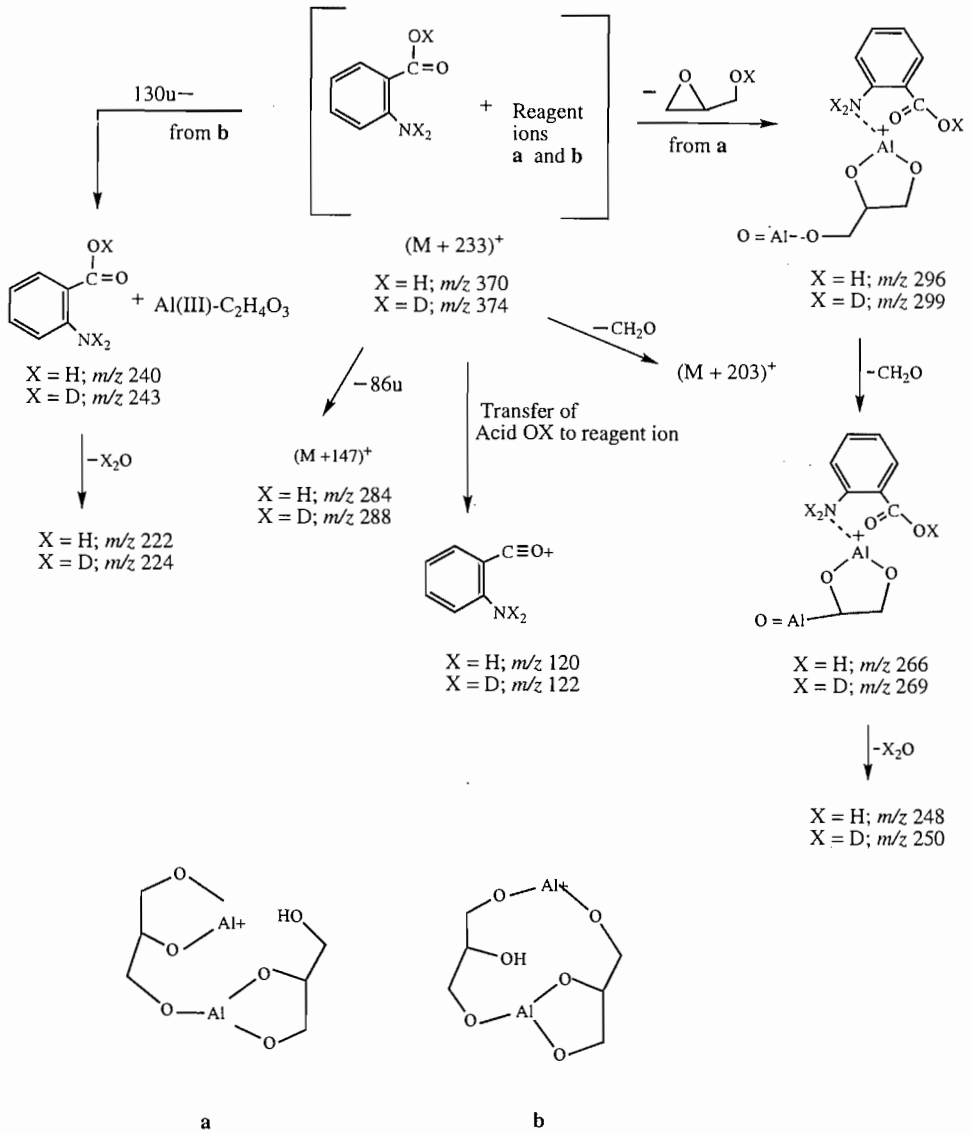
(a) $(M + 117)^+$ ($P^+ = (M + Al + Gly - 2H)^+$)

The decomposition of $P^+ = (M + 117)^+$ ions from **17–19** gives $(P - OH)^+$, $(P - H_2O)^+$, $(P - CH_2O)^+$, $(P - 44)^+$, $(P - 72)^+$,

Can. J. Chem. Downloaded from www.nrcresearchpress.com by 88.146.161.215 on 09/08/12
For personal use only.

© 1997 NRC Canada

Scheme 1. The collisionally activated dissociation of the $(M + 233)^+$ ion from **14**.



$(P - 74)^+$, $(P - 90)^+$, $(P - 92)^+$, $(P - 118)^+$, and $(P - 134)^+$ and is followed by loss of CH_2O neutral (formaldehyde) from the $(P - H_2O)^+$ ion. The loss of water from the $(P - CH_2O)^+$ ion may also give rise to the ion at $(P - 48)^+$. The $(P - 74)^+$ ion is an adduct of AlO^+ with analyte, i.e., $(M + AlO)^+$ formed by the loss of epoxypropanol. The ion at *m/z* 209 ($(P - 72)^+$) can be formed from these acids by the removal of an acrylic acid unit (72u). Insertion of Al(III) into the carboxylic acids can form the $(P - 90)^+$ or $((M + Al(III))^+$ ion by removal of the neutral dideprotonated glycerol moiety. The loss of CO from the $(M + Al(III))^+$ ion gives the $(M + Al(III) - CO)^+$ ion at *m/z* 163. The $(P - 92)^+$ ions are due to the substitution of acidic protons with Al(III), i.e., the formation of $(M + Al - 2H)^+$ ions by elimination of the glycerol molecule from the $P^+ = (M + 117)^+$ ion of **17**. Its intensity is reduced significantly where M = **18** and **19**. The transfer of the OH group from the carboxylic acid to $(Al + Gly - 2H)^+$ ions leads to the formation of carbonyl cation at *m/z* 147 ($(P - 134)^+$) as observed for benzoic acids. Ions $(P - CH_2)^+$, $(P - CH_3)^+$, $(P - CH_4)^+$, $(P - OH)^+$, $(P - H_2O)^+$, $(P - CH_2O)^+$, $(P - CO)^+$, $(P - 44)^+$, $(P - 72)^+$, and $(P - 74)^+$ are observed from the dissociation of the P^+ ion of methoxy-substituted acids **20–22**. The loss of C_2H_2/26u from the $(P - CH_2O)^+$ and $(P - CO)^+$ ions, and an ion at *m/z* 161 corresponding to the carbonyl cation ($(P - 134)^+$) from the analyte was also observed. These $(P - CH_2O)^+$ and $(P - CO)^+$ ions are more significant in **21** and **22**. The fragmentation of the P^+ ion of **20** gives the $(P - CH_2)^+$ ion as the base peak whereas the other two acids **21** and **22** produce the $(P - H_2O)^+$ ion as the base peak. The fragmentation of $(M + 117)^+$ ions from methoxy and hydroxy acids is established based on the dissociation of labelled P^+ ions as illustrated in Scheme 2.

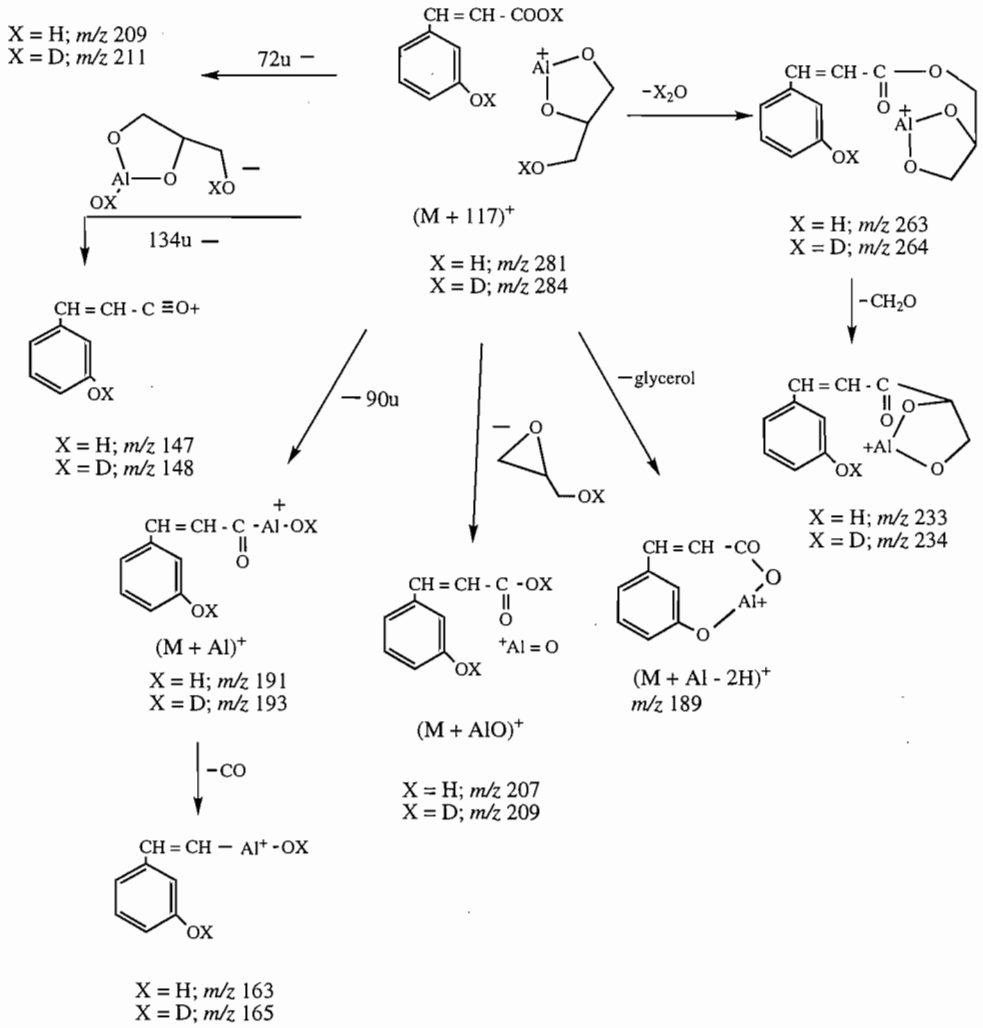
(b) $(M + 233)^+$ ($C^+ = (M + 2Al + 2Gly - 5H)^+$)

The CAD dissociation of the $C^+ = (M + 233)^+$ ion from **17–19** gives $(M + 159)^+$, i.e., $(C - 74)^+$, as the most abundant ion in the spectrum as well as less-abundant $(C - 86)^+$ and $(C - 130)^+$ ions. The loss of CH_2O and 72u (CH_2=CH-COOH)

Can. J. Chem. Downloaded from www.nrcresearchpress.com by 88.146.161.215 on 09/08/12
For personal use only.

© 1997 NRC Canada

Scheme 2. The collisionally activated dissociation of the $(M + 117)^+$ ion from **18**.



from the $(M + 159)^+$ ion gives rise to ions at *m/z* 293 and 251, respectively. The ion at *m/z* 293 gives an ion at *m/z* 249 by the loss of CO_2 (44u). However, there is less probability of formation of the $(M + 117)^+$ ion from the C^+ of **17–19**. The CAD of the $C^+ = (M + 233)^+$ ion from **20–22** also yields an $A^+ = (M + 159)^+$ ion with a high abundance. The significant ions at *m/z* 307 and 161 correspond to $(C - 104)^+$ and the carbonyl cation $(C - 250)^+$, respectively. From the C^+ ion, the transfer of an OH group to the $(2Al + 2Gly - 5H)^+$ ion produces $(C - 250)^+$ ions as observed for benzoic acids. These fragmentation pathways are confirmed by comparing the fragmentation of *d*-labelled adduct ions.

The dissociation of $A^+ = (M + 159)^+$ ions from **20–22** yields $(A - CH_2)^+$, $(A - CH_4)^+$, $(A - CO)^+$, $(A - CH_2O)^+$, $(A - 40)^+$, $(A - 42)^+$, $(A - 44)^+$, and ions at *m/z* 161 and 265. The $(M + 159)^+$ ion from the hydroxy acids **17–19** appears at *m/z* 323. The ion generated from the matrix corresponding to $(Al + 2Gly + TFA - 2H)^+$ also appears at *m/z* 323. Therefore, the *B/E* analysis of *m/z* 323 was used to determine that the fragments from this species are primarily due to the matrix.

Conclusions

Though the solubility of substituted benzoic acids and cinnamic acids is low in the highly polar matrix glycerol, we were able to study them with the addition of a mixture of ethyl acetate and ethanol to the matrix, without affecting the spectra significantly. The dissociation of $P^+ = (M + 117)^+$ ions produced an interesting fragment ion due to insertion of Al(III) into carboxylic acids, which is followed by the elimination of CO to yield $(M + Al(III) - CO)^+$ ions. The formation of $(P - 134)^+$ or carbonyl cations from the dissociation of $(M + 117)^+$, $(M + 159)^+$, and $(M + 233)^+$ ions depends on the ease of transfer of the hydroxyl anion to the metal ion. In contrast with the fragmentation of the same ions derived from amino acids and peptides, the production of fragment ions from the dissociation of $(M + 233)^+$ ions is attributed to the difference in the pH of the matrix solution.

Experimental

All experimental work was carried out using a Kratos (Manchester, U.K.) Concept 1S double focusing (EB geome-

Can. J. Chem. Downloaded from www.nrcresearchpress.com by 88.146.161.215 on 09/08/12
For personal use only.

© 1997 NRC Canada

try) mass spectrometer, equipped with an Ion Tech (Teddington, U.K.) fast atom gun. The standard FAB source was used for the FAB spectra of carboxylic acids (2–3 mg) in a mixture of glycerol (25–30 mg) with $AlCl_3$ (3–5 mg), TFA (2 μL), and H_2O (2 μL) as a matrix. Where noted, a mixture of 2 μL of ethyl acetate and ethyl alcohol (~1:2 v/v) was added to the matrix solution to increase the solubility of some analytes. For each sample, 1 μL of prepared solution was loaded on to the 1 mm wide FAB probe tip and bombarded with xenon fast atoms produced at 6–8 kV using an emission current of 0.5–1 mA. The source housing pressure was maintained at (1–2) × 10^{-5} Torr (1 Torr = 133.3 Pa). The ions produced were accelerated to 8 kV. All the spectra were acquired at a resolution of ~1100 at a scan rate of 8 s/decade with an inter scan delay of 2 s over a mass range of 11–950 amu. All experiments were repeated three to four times to check the reproducibility. Each spectrum was the result of an average of 6–9 scans. The background was subtracted using the Kratos DART/MACH3 data system running on a SUN SPARC Station 10. Collisionally activated dissociation spectra were recorded by colliding the ion beam with helium in the first field-free region, which caused reduction of main beam intensity by 40–50%. Accurate mass measurements were made at a resolving power of 10 000 and 8 kV accelerating potential.

All the materials used are commercially available (Aldrich, Milwaukee, Wis.; Chem Service, West Chester, Pa.). Deuterium labelled acids and glycerol-d_3 were prepared by repeating the addition and evaporation of deuterium oxide.

Acknowledgment

The authors are indebted to the Natural Sciences and Engineering Research Council of Canada for operating and equipment grants to J.M.M. and to T.R.B. Jones for technical assistance.

References

1. (*a*) G. Bojesen, T. Breindahl, and U.N. Andersen. Org. Mass Spectrom. **28**, 1448 (1993); (*b*) D. Wen, T. Yalcin, and A.G. Harrison. Rapid Commun. Mass Spectrom. **9**, 1155 (1995); (*c*) C.L. Gatlin, F. Turecek, and T. Vaisar. J. Am. Chem. Soc. **117**, 3637 (1995); (*d*) J. Mass Spectrom. **30**, 1605 (1995); (*e*) J. Mass Spectrom. **30**, 1617 (1995); (*f*) C.L. Gatlin and F. Turecek. J. Mass Spectrom. **30**, 1636 (1995).
2. (*a*) M.L. Gross. Acc. Chem. Res. **27**, 361 (1994); (*b*) C.L. Gatlin, R.D. Rao, F. Tureck, and T. Vaisar. Anal. Chem. **68**, 263 (1996), and refs. cited therein.
3. (*a*) L.M. Mallis and D.H. Russell. Int. J. Mass Spectrom. Ion Processes, **78**, 147 (1987).
4. (*a*) R.A.W. Johnstone and M.E. Rose. J. Chem. Soc. Chem. Commun. 1268 (1983); (*b*) R.A.W. Johnstone and I.A.S. Lewis. Int. J. Mass Spectrom. **46**, 451 (1983); (*c*) R.A.W. Johnstone, I.A.S. Lewis, and M.E. Rose. Tetrahedron, **39**, 1597 (1983); (*d*) R. Colton, S. Mitchell, and J.C. Traeger. Inorg. Chim. Acta, **231**, 87 (1995); (*e*) M. Vincenti. J. Mass Spectrom. **30**, 925 (1995); (*f*) G.J. Langley, D.G. Hamilton, and M.C. Grossel. J. Chem. Soc. Perkin Trans. 2, 929 (1995); (*g*) B. Kralj, O.S. Timofeev, D. Zigon, T.I. Kirichenko, and J. Marsel. Rapid Commun. Mass Spectrom. **10**, 850 (1996).
5. R.V. Hodges, P.B. Armentrout, and J.L. Beauchamp. Int. J. Mass Spectrom. Ion Phys. **29**, 375 (1979); (*b*) A.K. Chowdhury and C.L. Wilkins. Int. J. Mass Spectrom. Ion Processes, **82**, 163 (1988).
6. M. Saraswathi and J.M. Miller. Can. J. Chem. **74**, 2221 (1996).
7. M. Saraswathi and J.M. Miller. Rapid Commun. Mass Spectrom. **10**, 1706 (1996).
8. M. Saraswathi and J.M. Miller. J. Chem. Soc. Dalton Trans. 341 (1997).

Can. J. Chem. Downloaded from www.nrcresearchpress.com by 88.146.161.215 on 09/08/12
For personal use only.

© 1997 NRC Canada

Complex formation between D-lactobionate and bivalent metal ions. Studies in solution and in the solid state

Alejandro A. Frutos, Graciela M. Escandar, Juan Manuel Salas Peregrin, Manuel Gonzalez Sierra, and Luis F. Sala

Can. J. Chem. Downloaded from www.nrcresearchpress.com by 88.146.161.215 on 09/08/12
For personal use only.

Abstract: The equilibrium reactions between deprotonated D-lactobionic acid (4-*O*-β-D-galactopyranosyl-D-gluconic acid) and cobalt(II), nickel(II), copper(II), zinc(II), cadmium(II), and mercury(II) have been studied by potentiometric and spectrophotometric methods in aqueous solution. All measurements have been carried out at a temperature of 20.0 ± 0.1°C and at an ionic strength of 0.100 M ($NaNO_3$) with the corresponding stability constants calculated by applying computational methods. The interactions between the proposed cations with deprotonated D-lactobionic acid were compared with those corresponding to D-gluconic acid. Compounds of type: $Co(C_{12}H_{21}O_{12})_2 \cdot 2H_2O \cdot C_2H_5OH$, $Ni(C_{12}H_{21}O_{12})_2 \cdot 2H_2O \cdot C_2H_5OH$, $Cu(C_{12}H_{21}O_{12})_2 \cdot 2H_2O \cdot C_2H_5OH$, $Zn(C_{12}H_{21}O_{12})_2 \cdot 2H_2O \cdot C_2H_5OH$, and $Cd(C_{12}H_{21}O_{12})_2 \cdot 2H_2O \cdot 0.5C_2H_5OH$ have been isolated. These metal–sugar salts were characterized by elemental, thermogravimetric, and susceptibility analyses and FT-IR, UV–visible absorption, diffuse reflectance, and ^{13}C NMR spectroscopies.

Key words: D-lactobionate, metal complexes, equilibrium constants, potentiometry, solid state studies.

Résumé : Opérant en solutions aqueuses et faisant appel à des méthodes potentiométriques et spectrophotométriques, on a étudié les réactions d'équilibre entre l'acide D-lactobionique déprotoné (acide 4-*O*-β-D-galactopyranosyl-D-gluconique) et des ions cobalt(II), cuivre(II), zinc(II), cadmium(II) et mercure(II). Toutes les mesures ont été effectuées à une température de 20,0 ± 0,1°C, à une force ionique de 0,100 M ($NaNO_3$); les constantes de stabilités correspondantes ont été calculées en appliquant diverses méthodes de calcul. On a comparé les interactions entre les cations proposés et l'acide D-lactobionique déprotoné avec les interactions correspondantes avec l'acide D-gluconique. On a pu isoler des composés des types : $Co(C_{12}H_{21}O_{12})_2 \cdot 2H_2O \cdot C_2H_5OH$, $Ni(C_{12}H_{21}O_{12})_2 \cdot 2H_2O \cdot C_2H_5OH$, $Cu(C_{12}H_{21}O_{12})_2 \cdot 2H_2O \cdot C_2H_5OH$, $Zn(C_{12}H_{21}O_{12})_2 \cdot 2H_2O \cdot C_2H_5OH$ et $Cd(C_{12}H_{21}O_{12})_2 \cdot 2H_2O \cdot 0{,}5C_2H_5OH$. On a caractérisé ces sels métalliques de sucre par des analyses élémentaires, thermogravimétriques et de susceptibilité ainsi que par spectroscopies «FT-IR», d'absorption UV–visible, de réflexion diffuse et de RMN du ^{13}C.

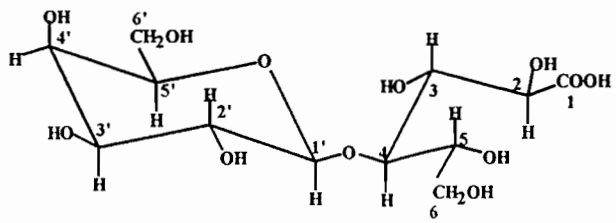
Mots clés : D-lactobionate, complexes métalliques, constantes d'équilibre, potentiométrie, études à l'état solide.

[Traduit par la rédaction]

Introduction

As part of our program on the coordination chemistry of sugar acids (1–7) we have set out to elucidate the complexometric behavior of deprotonated D-lactobionic acid (4-*O*-β-D-galacto-pyranosyl-D-gluconic acid) with Co(II), Ni(II), Cu(II), Zn(II), Cd(II), and Hg(II) ions. We have already reported that the importance of studying the interaction between D-gluconic acid and transition metal ions is related to the use of this natural ligand as a sequestering agent for both essential and toxic metal ions present in biological media (1, 5). D-Lactobionic acid (LBA) (Scheme 1) is a natural disaccharide constituted by D-galactose and D-gluconic acid joined through a glycosidic linkage, which is usually employed by nature in biological media as a chelating agent of transition and heavy metal

Scheme 1.



D-lactobionic acid

Received November 15, 1996.

A. Frutos and L.F. Sala.[2] Departamento de Química Fisica, Facultad de Ciencias Bioquímicas y Farmacéuticas, Universidad Nacional de Rosario, Suipacha 531 (2000) Rosario, Argentina.
G.M. Escandar. Departamento de Química Analítica, Facultad de Ciencias Bioquímicas y Farmacéuticas, Universidad Nacional de Rosario, Suipacha 531 (2000) Rosario, Argentina.
J.M. Salas Peregrin. Departamento de Química Inorgánica, Facultad de Ciencias, Universidad de Granada, Granada, Spain 18071.
M. Gonzalez Sierra. Departamento de Química Orgánica, Facultad de Ciencias Bioquímicas y Farmacéuticas, Universidad Nacional de Rosario, Suipacha 531 (2000) Rosario, Argentina.

[1] Presented at the 31st Int. Conf. Coord. Chem. August 1996, Vancouver, Canada.

[2] Author to whom correspondence may be addressed. Fax: 54-41-350214. E-mail: inquibir@satlink.com

© 1997 NRC Canada

Can. J. Chem. Downloaded from www.nrcresearchpress.com by 88.146.161.215 on 09/08/12
For personal use only.

ions. Presently, LBA is employed to chelate Cu(II) for its incorporation in milk as a nutritional supplement (8).

The interaction of sugar acids containing both carboxylate and hydroxyl groups with metal ions is of great interest in the biochemistry of these metals related to environmental and toxicological problems. We have studied the composition of some isolated lactobionate complexes with the metal ions indicated above. Structural information was obtained by means of elemental, thermogravimetric, and susceptibility analyses, complemented by ^{13}C NMR, UV–visible, and diffuse reflectance spectroscopies, and the investigation was extended to the coordination in aqueous solution. The computer program selected to process the data allowed us to provide an accurate description of the aqueous coordination chemistry of the systems under investigation.

Experimental

Reagents

D-Lactobionic free acid was obtained from Sigma. Its purity was checked by elemental analysis and pH titration. The stability of lactobionic acid in acidic and basic media was confirmed by paper chromatography. Stock solutions of Co(II), Ni(II), Cu(II), Zn(II), Cd(II), and Hg(II) (0.010–0.020 M) were prepared from their nitrates of analytical grade (Merck). With the purpose of avoiding the Hg(II) hydrolysis, its solution was prepared in 0.05 M nitric acid and the exact amount of this acid was evaluated by a Gran's plot (9). The exact concentrations of the cation solutions were determined by titration with ethylenediaminetetraacetic acid (EDTA) solution (10). Stock solutions of NaOH and HNO_3 were standardized against potassium hydrogenphthalate and sodium carbonate, respectively. Gran's method was applied for the determination of carbonate on NaOH solutions (9).

Potentiometry

The equilibrium constants for D-lactobionate metal complexes were determined by using a Corning 350 research pH meter equipped with glass and calomel reference electrodes calibrated with HNO_3 and acetic acid at an ionic strength (μ) of 0.100 M to read pH as p[H]. Titrations were carried out under a nitrogen atmosphere. The temperature was maintained at 20.0 ± 0.1°C and μ was adjusted to 0.100 M by addition of $NaNO_3$. The solutions of metal and D-lactobionic acid were diluted, in different ratios, to a volume of 100 mL, with final concentrations in the range $(1–3) \times 10^{-3}$ M. In this way, those low concentrations did not contribute significantly to the ionic strength of the medium.

Equilibrium pH values were determined at every incremental addition of NaOH or HNO_3 to the experimental solutions. These increments were sufficiently small as to provide a ratio of experimental points per a value of higher than 10:1 (a = moles of base per mol of D-lactobionic acid or metal). Reversibility of the reactions was suggested by the fact that the direct and inverse titration data were coincident, within the investigated pH range (2.5–11).

Potentiometric equilibrium constants calculation

Since all the complexes studied were not fully formed at low pH, their stability constants could be determined by direct potentiometric titration, with the aid of the BEST program (11*a*).

Spectrophotometric measurements

The spectra were recorded on a Metrolab 1700 spectrophotometer. The spectrophotometric titrations were performed in the visible region of the spectra in order to evaluate the equilibrium constants for the complexes produced by Cu(II) and Ni(II) ions, respectively. For the Cu(II) system the metal to D-lactobionic acid ratios were 1:1 and 1:2, while for Ni(II) it was 1:1. The system produced between D-lactobionate and Co(II) could not be evaluated employing the present method because in alkaline media (the region where complex formation takes place) the required high concentrations of reactants led to oxidation of the metal ion. The metal concentrations employed in the spectrophotometric experiments were in the range 2×10^{-3} to 1×10^{-2} M and those for the D-lactobionic acid in the range 4×10^{-3} to 2×10^{-2} M. Beer's law was checked previous to performing each experiment. The titrations were carried out under nitrogen at 20.0 ± 0.1°C at μ = 0.100 M ($NaNO_3$). An excess of 0.5 M NaOH was added to the experimental solution and a back titration was performed with 0.1 M HNO_3. After each addition of acid, an exact aliquot of the solution was extracted and the absorbance measured at the wavelength at which the absorbance is a maximum for each system under study: 652, 666, and 391 nm for 1:2 Cu(II) – D-lactobionic acid, 1:1 Cu(II) – D-lactobionic acid, and 1:1 Ni(II) – D-lactobionic acid systems, respectively.

The plots of absorbance vs. pH were computationally processed employing the EPSILON program (12), which allows estimation of the value of equilibrium constants and molar absorptivities of the species proposed on each system.

^{13}C NMR

All spectra were acquired on a Bruker AC-200 E pulsed Fourier-transform instrument with a 4.3 T supercon magnet, at a carbon-13 resonance frequency of 50.1 MHz. All measurements were conducted at 22°C. The samples were prepared by dissolving D-lactobionic acid in distilled water until a concentration of 0.3 M with 10% D_2O to provide the deuterium lock. For the diamagnetic metal ions the metal concentration was equal to that of the D-lactobionic acid, whereas for the paramagnetic ion a metal concentration ranging from 2×10^{-3} to 2×10^{-2} M was employed.

Preparation of metal ion – D-lactobionate complexes in the solid state

The metal ion – D-lactobionate complexes were synthesized following the procedure described by Melson and Pickering (13). Specifically, the metal ion (0.0075 mol) as either carbonate (Co(II), Ni(II), and Cu(II)) or oxide (Zn(II) and Cd(II)) was added to a previously boiled (5 min) aqueous solution containing 0.015 mol of free D-lactobionic acid. The final mixture was boiled for 2 h. To avoid a redox reaction (production of copper(I) oxide), the copper(II) – D-lactobionic acid solution was boiled for only 45 min. Ethanol was added to the solution until a precipitate was obtained. The solid was removed by filtration, and recrystallized three times from (1:1) ethanol–water. The final product was washed with ethanol, dried under vacuum over phosphorus pentoxide at room temperature, ground to a fine powder, and again dried at 80°C under vacuum over P_2O_5.

The purity of the isolated salts was checked by elemental analysis.

© 1997 NRC Canada

Can. J. Chem. Downloaded from www.nrcresearchpress.com by 88.146.161.215 on 09/08/12
For personal use only.

Analysis of the solid complexes

Microanalyses of C and H were determined by the Center of Scientific Research of the University of Granada, using a Fisons 1108 CHNS microanalyser. The metal percentages in the complexes were determined by complexometric titration with EDTA employing appropriate indicators (10). DSC data were obtained on a Shimadzu DSC-50 differential scanning calorimeter, using a heating speed of 10°C min^{-1}. Thermogravimetric curves were obtained in an atmosphere of pure air using a Shimadzu TGA-50H, with a heating speed of 20°C min^{-1}, equipped with a Nicolet model 550 IR gas analyzer and Fisons model Thermolab mass detector. IR spectra were recorded on a FTIR Nicolet 20 SX8 spectrophotometer. Magnetic measurements were carried out on a Manics DSM-8 instrument in the 80–290 K temperature range. The diffuse reflectance spectra of the solid complexes were obtained with a Cary-5E refractometer provided with a praying mantis module.

Results and discussion

Studies in solution

Potentiometric measurements

Figure 1 shows selected potentiometric profiles of the systems under study (the figure is divided into two plots for clarity). Table 1 displays the equilibrium constant values for the complexes formed in such systems. The D-lactobionic acid protonation constant used in the calculation is log K_H = 3.53 (4). The log K_w employed throughout the whole work is −13.87 (20°C, μ = 0.1 M) (14). The overall hydrolysis constants for Co(II) and Hg(II) metal ions are log K_{CoH-1} = −9.85 and log K_{HgH-1} = −3.60 respectively (15*a*, 15*b*). There was no need of invoking hydrolytic species for the other metal ions involved in the present study.

Co(II) – D-lactobionate system

A blue precipitate was observed around pH 9 that was attributed to a basic cobalt(II) salt. In the soluble region the $[CoLH_{-2}]^-$ complex was detected. The negative stoichiometric coefficient under the H represents the number of protons displaced upon complex formation, which could arise either from D-lactobionic acid hydroxyl groups or from coordinated water molecules. It was not necessary to introduce either intermediates $[CoL^+]$ and $[CoLH_{-1}]$ or other complexes with different metal to D-lactobionic acid ratios.

Ni(II) – D-lactobionate system

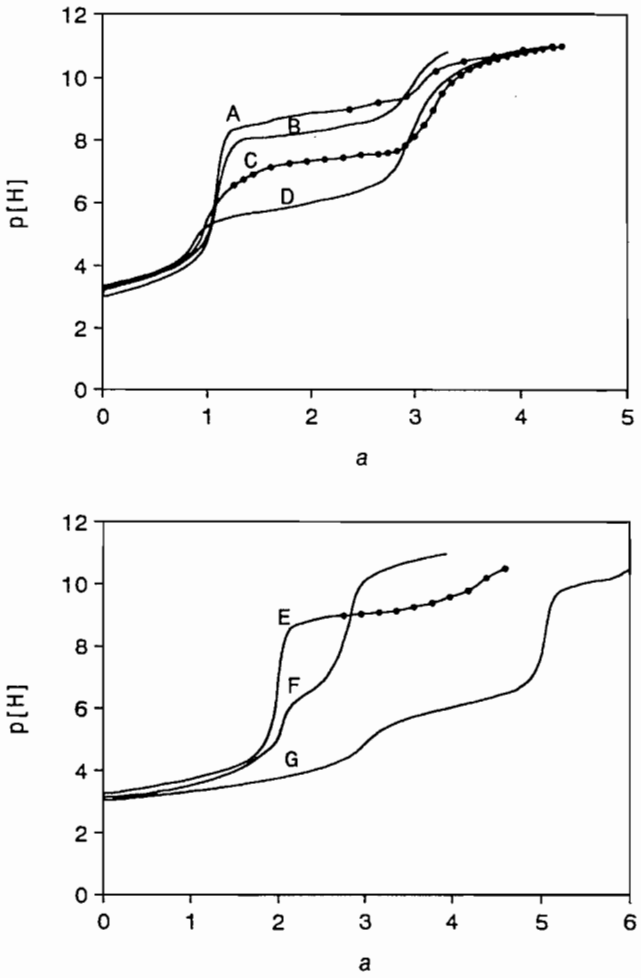
The potentiometric curves of Ni(II) – D-lactobionic acid did not show precipitation, independently of the metal to D-lactobionic acid ratio. Only two species were detected: $[NiL]^+$ and $[NiLH_{-2}]^-$. This case differs from the systems produced between Ni(II) and D-gluconic acid, where only species of 1:2 stoichiometry were detected (1).

Cu(II) – D-lactobionate system

1:1, 1:2, and higher metal to D-lactobionic acid ratios were tried, and no precipitation took place during the potentiometric determination. For the 1:1 ratio, the potentiometric profile showed a first break at a = 1 and a second one at a = 3. This was indicative of a total displacement of three moles of hydrogen ion due to the chelation process between the metal ion and the aldobionic acid. The titration curves were fitted by considering $[CuL]^+$ and $[CuLH_{-2}]^-$ as the major complex species. The first mole of the released proton was attributed to dissociation of the carboxylic group of the D-lactobionic acid and the other two might be attributed either to the deprotonation of coordinated water molecules or to the hydroxyl group of the saccharidic chain being dissociated. The $[CuL]^+$ species only reaches a maximum of 11% with respect to the total analytical metal ion concentration. Thus, the equilibrium constant was determined from five replicates and the error was informed with a 95% confidence level by applying the Student test (Table 1). The second complex species was detected above pH 5.6 and is predominant above pH 9.6.

When 1:2 and higher Cu(II) – lactobionic acid ratios were employed, $[CuL_2]$, $[CuL_2H_{-1}]^-$, $[CuL_2H_{-2}]^{-2}$, and $[CuL_2H_{-4}]^{4-}$

Fig. 1. Potentiometric equilibrium curves of A: Co(II)–LBA (C_M = 1.875×10^{-3} M, C_L = 1.890×10^{-3} M); B: Ni(II)–LBA (C_M = 3.265×10^{-3} M, C_L = 3.266×10^{-3} M); C: Zn(II)–LBA (C_M = 1.020×10^{-3} M, C_L = 1.020×10^{-3} M); D: Cu(II)–LBA (C_M = 9.050×10^{-4} M, C_L = 9.050×10^{-4} M); E: Cd(II)–LBA (C_M = 8.540×10^{-4} M, C_L = 1.710×10^{-3} M); F: Hg(II)–LBA (C_M = 1.101×10^{-3} M, C_L = 2.203×10^{-3} M); G: Cu(II)–LBA (C_M = 1.002×10^{-3} M, C_L = 3.005×10^{-3} M); μ = 0.100 M ($NaNO_3$); t = 20.0°C. Precipitate is indicated by solid circles.



© 1997 NRC Canada

Table 1. Protonation and equilibrium constant values for D-lactobionate and its metal complexes, and extinction coefficients corresponding to the Cu(II) and Ni(II) complexes.

Metal ion	Quotient	log K Potentiometry	log K Spectrophotometry	ε (M^{-1} cm^{-1})
	[HL]/[H] [L]	3.53 (0.01)[a]		
Co(II)	$[H]^2$ $[MLH_{-2}]$/[M] [L]	−15.64 ± 0.03		
Ni(II)	[ML]/[M] [L]	2.13 ± 0.03	2.29 ± 0.15	14 ± 2 (391)
	$[H]^2[MLH_{-2}]$/[M] [L]	−13.77 ± 0.02	−13.2 ± 0.2	15 ± 1 (391)
Cu(II)	[ML]/[M] [L]	2.28 ± 0.05[b]	1.9 ± 0.2	27 ± 3 (666)
	$[H]^2[MLH_{-2}]$/[M] [L]	−8.64 ± 0.01	−8.2 ± 0.2	41.0 ± 0.4 (666)
	$[ML_2]$/[M] $[L]^2$	5.40 ± 0.02	4.4 ± 0.9	16 ± 5 (652)
	[H] $[ML_2H_{-1}]$/[M] $[L]^2$	−0.44 ± 0.02		
	$[H]^2[ML_2H_{-2}]$/[M] $[L]^2$	−6.29 ± 0.01	−6.3 ± 0.06	34.0 ± 0.3 (652)
	$[H]^4[ML_2H_{-4}]$/[M] $[L]^2$	−27.14 ± 0.02		
Cd(II)	$[H]^2$ $[MLH_{-2}]$/[M] [L]	−15.54 ± 0.15[b]		
Hg(II)	[H] $[MLH_{-1}]$/[M] [L]	−0.29 ± 0.02		
	$[H]^2[MLH_{-2}]$/[M] [L]	−6.64 ± 0.02		

μ = 0.100 M ($NaNO_3$), 20.0 ± 0.1°C. The wavelengths (in nm) are shown within parentheses.
[a]Reference 4.
[b]See text. Standard deviations refer only to random errors.

complexes were identified (Fig. 2) that were coincident with the ones reported by Bouhsina et al. (16).

Zn(II) – D-lactobionate system

The titration curve shown in Fig. 1 is very similar to the one found for the Zn(II) – D-gluconic acid system (1). Two breaks can be observed, one at $a = 1$ (dissociation of carboxylate group) and the second one at $a = 3$. This latter inflection may be explained by the $[ZnH_{-2}L]^-$ complex formation.

Unfortunately, the solid phase produced at pH 7 prevented the stability constant computation. In the present experimental conditions, the formation of chelate containing a 1:2 metal to D-lactobionic acid ratio was not detected.

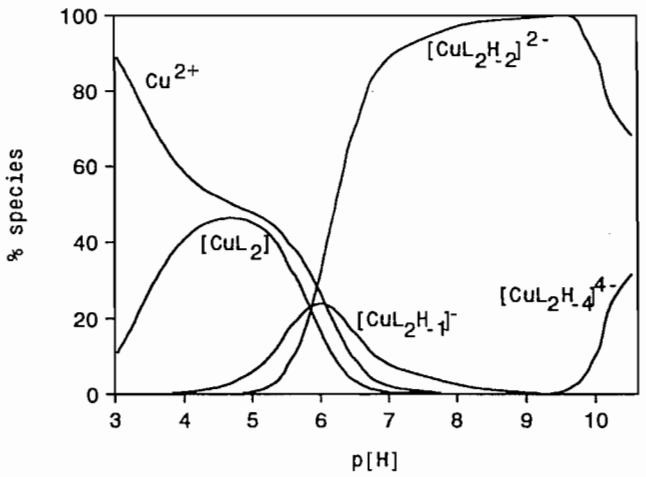
Cd(II) – D-lactobionate system

In this system, and for different metal to D-lactobionic acid ratios, $Cd(OH)_2$ precipitates above pH 8. In the soluble region, only $[CdLH_{-2}]^-$ was found as the principal species. This differs from the Cd(II) – D-gluconic acid system, where an additional complex was detected: $[CdL]^+$. Through the equilibrium constant value, it can be seen that the $[CdLH_{-2}]^-$ species (where L is the D-lactobionate) shows the same stability as the analogous one in the D-gluconic acid system (log $K_{CdGH-2} = -15.7$) (1). Owing to its low concentration in solution (not higher than 20% with respect to the analytical concentration of the metal ion), its equilibrium constant has a considerable uncertainty. Therefore, it is reported with a 95% confidence limit, employing the Student test parameter for six potentiometric determinations. Each potentiometric measurement afforded a σ_{fit} of less than 0.01 (11*b*).

Hg(II) – D-lactobionate system

No precipitation was observed within the pH range studied. To explain the potentiometric results for the Hg(II) system, the presence of $[HgLH_{-1}]$ and $[HgLH_{-2}]^-$ complexes was proposed, similar to those found for the Hg(II) – D-gluconic acid system. The complex species arising from the interaction of Hg(II) with D-gluconic acid are more stable (log $K_{HgGH-1} = -0.09$ and log $K_{HgGH-2} = -4.03$) (1) than those produced in the Hg(II) – D-lactobionate system.

Fig. 2. Distribution of species as a function of p[H] in the 1:3 Cu(II) – D-lactobionic acid system. $C_M = 1.002 \times 10^{-3}$ M, $C_L = 3.005 \times 10^{-3}$ M; μ = 0.100 M ($NaNO_3$); t = 20.0°C.



Spectrophotometric determinations

The electronic spectral patterns at different pH values of the colored Cu(II) – D-lactobionate system present weak bands in the visible region that are due to *d–d* transitions. The signals in the UV region can be assigned to charge transfer bands (17).

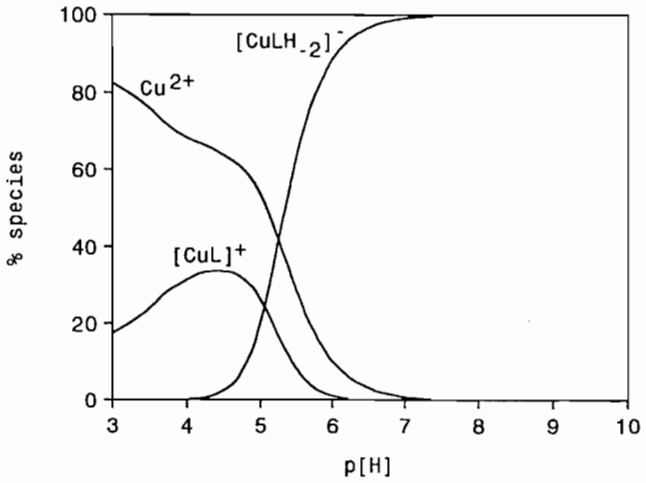
The spectrophotometric titrations of 1:1 metal – D-lactobionic acid solutions afforded the same species found during the potentiometric determination: $[CuL]^+$ and $[CuLH_{-2}]^-$. The equilibrium constant values obtained through these two inde-

© 1997 NRC Canada

Can. J. Chem. Downloaded from www.nrcresearchpress.com by 88.146.161.215 on 09/08/12
For personal use only.

Can. J. Chem. Downloaded from www.nrcresearchpress.com by 88.146.161.215 on 09/08/12
For personal use only.

Fig. 3. Distribution of species as a function of p[H] in the 1:1 Cu(II) – D-lactobionic acid system obtained from spectrophotometric titration data; $C_M = 1.260 \times 10^{-3}$ M, $C_L = 1.262 \times 10^{-3}$ M; $\mu = 0.100$ M ($NaNO_3$); $t = 20.0$°C.



pendent methods were very similar (Table 1). Hydrolytic species of Cu(II) ion were not found. According to the species distribution plot (Fig. 3) the cationic $[CuL]^+$ species is predominant at pH 4.5 and the anionic $[CuLH_{-2}]^-$ species at alkaline pH. At pH lower than 3.7, where no complex formation was detected, the only band present was at 808 nm, which has been attributed to the Cu(II) aqueous complex (17, 18*a*).

The computational processing of the spectrophotometric data for a 1:2 metal to D-lactobionic acid ratio only yielded the presence of both $[CuL_2]$ and $[CuL_2H_{-2}]^{2-}$ chelates. In this case the spectrophotometric method was ambiguous for determining the other complex species, which were detected potentiometrically. At the same time, overlapping of the absorbance bands for the different complex species in equilibrium at different pH impeded the assignment of the correct absorption band of the electronic spectra for the 1:2 system. Nevertheless, when the pH was lowered, the wide band at 666 nm (pH 11.7) shifted to higher wavelengths, and thus a distorted octahedral geometry was proposed for the Cu(II)–D-lactobionic species detected through the present method (19*a*).

The visible spectra of nickel(II) complexes show three distinct absorption maxima at pH 12: 391, 671, and 1073 nm, which are in agreement with *d–d* transitions in an octahedral structure (18*b*, 19*b*).

The spectrophotometric titration of the 1:1 Ni(II) – D-lactobionic acid system showed the presence of two main bright-green complexes: $[NiL]^+$ and $[NiLH_{-2}]^-$. The stoichiometry and equilibrium constant values for both complexes were similar to that found through the potentiometric method (Table 1).

^{13}C NMR spectra

The observation of selective line broadening and (or) chemical shift displacement of signals in the ^{13}C NMR spectra of metal complexes is a useful means of obtaining qualitative information about possible coordination sites (20). We previously analyzed and assigned the solution (D_2O) ^{13}C NMR spectra of D-lactobionic acid alone (6). This work compares the present results with those obtained with D-gluconic acid (1).

The ^{13}C NMR spectra of the Co(II)–D-lactobionate system were obtained at pH 9, where the main complex species was $[CoLH_{-2}]^-$. The signals ascribed to C-1, C-2, and C-3 of the D-lactobionic acid suffer significant broadening. Taking into account these results, we suggest that in the chelation process the carboxylate group and the deprotonated hydroxyl of C-2 and C-3 are involved in the chelate ring. This is coincident with the conclusions obtained at pH 10 for the Co(II) – D-gluconic acid system (1).

The NMR experiments in the Ni(II)–D-lactobionate system were performed at pH 10, where the main complex is $[NiLH_{-2}]^-$. The ^{13}C NMR spectra recorded for the Ni(II) complex showed both broadening and changes in the chemical shifts for C-1, C-2, and C-4. This fact suggests that in the coordination of the Ni(II) complex the metal ion is octahedrally bonded to the carboxylate group, to the deprotonated hydroxyl group at C-2, and to the lone electron pair of the C-4 oxygen. In agreement with the complex stoichiometry and the ^{13}C NMR data, the additional mole of displaced proton may belong to a coordinated water molecule.

The species distribution plot for the Cu(II)–D-lactobionate system showed the predominance at pH 8 and 11 of the following chelates: $[CuL_2H_{-2}]^{2-}$ and $[CuL_2H_{-4}]^{4-}$, respectively. The ^{13}C NMR experiments performed at both pH's showed that the most affected (broadened) signals were for C-1, C-2, and C-3 for $[CuL_2H_{-2}]^{2-}$ and C-2, C-3, and C-5 for $[CuL_2H_{-4}]^{4-}$. For the first complex, the metal ion should coordinate with the carboxylate group and the deprotonated hydroxyl groups at C-2 and C-3, while with the second complex only deprotonated hydroxyl groups would be involved, belonging to C-2, C-3, and C-5, without participation of the carboxylate group. It should be noticed that, both for $[CuL_2H_{-2}]^{2-}$ and $[CuL_2H_{-4}]^{4-}$, there are more non-carboxylic affected carbons than protons released per ligand. Therefore, in each complex, the lactobionate units should coordinate through different carbons. Specific assignments may not be obtained from this kind of experiments. Bouhsina et al. (16) indicated this possible coordination mode, although we were able to identify the hydroxyl groups involved.

The ^{13}C NMR spectra in the Zn(II)–D-lactobionate system were registered at pH 8, avoiding high pH values due to the hydroxide precipitation. Table 2 shows small changes in the signals of C-1, C-3, and C-4. The $[ZnLH_{-2}]^-$ species might be predominant at this pH, which means that the Zn(II) interacts with the carboxylate group, the deprotonated hydroxyl group bonded to C-3, and the lone pair electrons of the glycosidic linkage. The second mole of displaced protons should belong to a coordinated water molecule. For the Zn(II) – D-gluconic acid system the most affected signals were C-1, C-2, and C-3 (1).

The ^{13}C NMR spectra registered for the Cd(II) system at pH 8 (where the main complex species is $[CdLH_{-2}]^-$) showed that the affected carbons were C-1, C-3, and C-5 (see Table 2). This kind of chelation implies two chelate rings, which help to increase the thermodynamic stability of the system. The ^{13}C NMR spectra registered for the Cd(II) – D-gluconic acid system at pH = 4.5 and 10 showed that the affected carbons were C-1, C-2, and C-4, involving a coordination to the carboxylate groups and the deprotonated hydroxyl group of C2 and C4 (1). D-Lactobionic acid bears no free hydroxyl group at C-4, and that at C-5 is involved in the coordination process, instead of a

© 1997 NRC Canada

Can. J. Chem. Downloaded from www.nrcresearchpress.com by 88.146.161.215 on 09/08/12
For personal use only.

Table 2. ^{13}C NMR chemical shifts corresponding to D-lactobionic acid and Zn(II), Cd(II), and Hg(II) lactobionate complexes.

	δ (ppm)			
Carbon	LBA	Zn(II) system	Cd(II) system	Hg(II) system
C1	181.0	181.2	181.2	179.5
C1′	106.0	106.1	106.0	105.9
C4	83.9	84.1	84.0	83.3
C5′	77.9	77.9	77.9	77.8
C3′	75.2	75.2	75.2	75.2
C2	75.0	75.0	75.0	76.7
C5	74.4	74.3	74.2	74.0
C3	74.2	74.0	76.0	73.8
C2′	73.8	73.7	73.7	73.7
C4′	71.3	71.3	71.3	71.3
C6	64.6	64.7	64.6	64.7
C6′	63.7	63.7	63.7	63.7

$C_{Zn} = C_L = 0.27$ M (pH 8); $C_{Cd} = C_L = 0.27$ M (pH 8); $C_{Hg} = C_L = 0.72$ M (pH 3).

Table 3. Elemental analyses and colors of the synthesized complexes.

		% C		% H		% M	
Complex	Color	Calcd.	Found	Calcd.	Found	Calcd.	Found
$Co(C_{12}H_{21}O_{12})_2 \cdot 2H_2O \cdot C_2H_5OH$	Pink	36.50	36.33	6.13	6.37	6.89	6.79
$Ni(C_{12}H_{21}O_{12})_2 \cdot 2H_2O \cdot C_2H_5OH$	Green	36.51	36.58	6.13	6.33	6.86	6.88
$Cu(C_{12}H_{21}O_{12})_2 \cdot 2H_2O \cdot C_2H_5OH$	Blue	36.30	36.55	6.09	6.08	7.39	7.28
$Zn(C_{12}H_{21}O_{12})_2 \cdot 2H_2O \cdot C_2H_5OH$	White	36.20	36.46	6.08	6.13	7.55	7.58
$Cd(C_{12}H_{21}O_{12})_2 \cdot 2H_2O \cdot 0.5C_2H_5OH$	White	33.90	33.70	5.60	5.80	12.7	12.4

coordinated water molecule. This makes a difference when compared with the same kind of complex suggested for Zn(II)–D-lactobionate.

Under the NMR experimental conditions for the mercury system, precipitation of the corresponding oxide is detected above pH 3. Therefore, the spectrum was measured at this pH value. In this system carbons C-1 and C-2 suffer chemical shift modifications (Table 2). Since the predominant complex species is $[HgLH_{-1}]$, the 1,2 chelation mode is proposed.

Solid state analysis

The analytical results of the solid complexes formed between D-lactobionate and the metal ions under investigation are reported in Table 3. All the complexes were obtained in solvated form. Coordinated molecules of water and ethanol were observed, although all samples were dried under vacuum at 80°C over 2 h. For the complex species with the diamagnetic metal ions Zn(II) and Cd(II), the content of ethanol was determined by ^1H NMR spectroscopy. Since a redox reaction took place, it was not possible to isolate the Hg(II) – D-lactobionate solid complex.

Thermogravimetric curves

The main process occurring in the TGA curves is a pyrolytic decomposition that takes place above 200°C. Usually, this is accompanied by a previous loss of solvent in the range 100–190°C (see Table 3 for composition of complexes). The release of ethanol is detected together with the dehydration process, except for the solid complexes of Cd(II) and Ni(II) with D-lactobionate, where the loss of organic solvent takes place at a temperature above 200°C. These results were confirmed by IR spectra of the lost products. The temperature for loss of water and ethanol molecules might indicate that these molecules are coordinated to the metal.

Figure 4 shows a typical thermal decomposition of the solid complexes under study, in this particular case for the Cd(II)–D-lactobionate complex.

The Cd(II) and Ni(II) lactobionates suffered dehydration in one step (DGTA maxima: 155 and 165°C, respectively); Cu(II)–D-lactobionate dehydrates and partially loses ethanol in one step (DGTA maximum: 171°C), and Co(II) and Zn(II) complexes release water and ethanol in two steps (DGTA maxima at 151, 182°C and 155, 179°C respectively).

The pyrolytic process of the ligand took place at 200°C in three steps except for the Cu(II) complex, which presented a four-step pyrolytic process. The pyrolytic products were water, carbon monoxide, carbon dioxide, and ethanol. The final pyrolytic residues at 400–600°C were determined as

© 1997 NRC Canada

Fig. 4. Thermogravimetric curve of the $Cd(C_{12}H_{21}O_{12})_2 \cdot 2H_2O \cdot 0.5C_2H_5OH$ complex (4.733 mg sample).

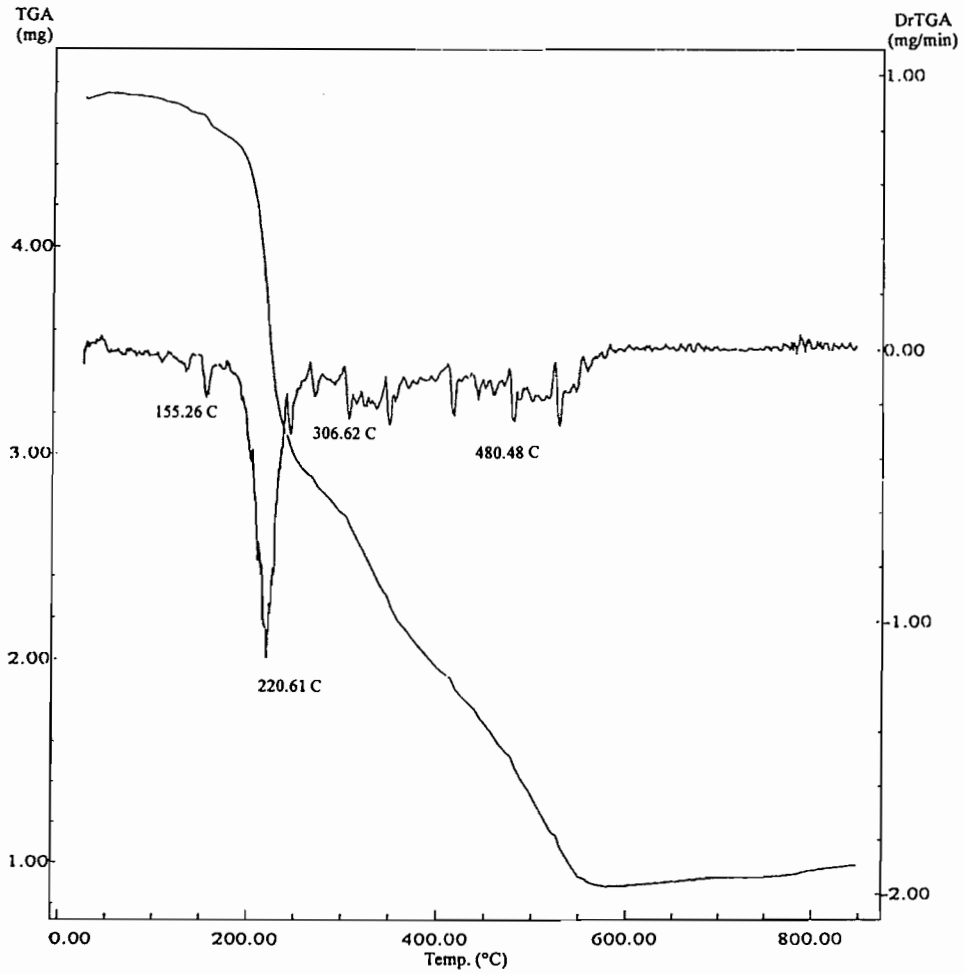


Table 4. Magnetic moments for the solid D-lactobionate complexes.

Complex	Temperature (K)	θ (K)	μ_{eff}(BM)
$Co(C_{12}H_{21}O_{12})_2 \cdot 2H_2O \cdot C_2H_5OH$	81–290	–22.4	5.21
$Ni(C_{12}H_{21}O_{12})_2 \cdot 2H_2O \cdot C_2H_5OH$	81–290	–10.4	3.34
$Cu(C_{12}H_{21}O_{12})_2 \cdot 2H_2O \cdot C_2H_5OH$	80–290	–44.6	2.27

mixtures of carbonates and oxides of the corresponding metal ion.

Magnetic susceptibility

In Table 4 the magnetic data obtained for the isolated compounds have been collected. The Curie–Weiss law ($\chi_m = C/(T-\theta)$, where χ_m is the molar susceptibility, C is the Curie constant, T is absolute temperature, and θ is the Weiss constant) was applied. The equation used to calculate magnetic moments was $\mu_{eff} = 2.84\sqrt{C}$. Corrections for diamagnetism were done using the values of -157×10^{-6} and -12.8×10^{-6} for the diamagnetic susceptibilities of D-lactobionate and the metal ions, respectively.

The magnetic moment for Co(II) reveals a high-spin octahedral geometry. The value of $\mu_{eff} = 5.21$ MB was higher than the theoretical value of 3.87 MB, consistent with a distorted octahedral geometry (see below). The same situation was found for the Ni(II) complex.

The magnetic susceptibility values for the Cu(II) complex suggested magnetic interactions at low temperatures. Presently, we are performing experiments at liquid helium temperatures.

Reflectance spectra

The diffuse reflectance spectra of Co(II), Ni(II), and Cu(II) complexes were measured and the corresponding bands are shown in Table 5.

The bands of the spectra of both Co(II) and Ni(II) com-

© 1997 NRC Canada

Can. J. Chem. Downloaded from www.nrcresearchpress.com by 88.146.161.215 on 09/08/12
For personal use only.

Table 5. Electronic absorption spectral data in the solid phase.

Complex	v1	v2	v3	$\Delta_0{}^a$ (cm^{-1})	B^a (cm^{-1})
$Co(C_{12}H_{21}O_{12})_2 \cdot 2H_2O \cdot C_2H_5OH$	$^4T_{2g} \leftarrow {}^4T_{1g}$ (8.07×10^3 cm^{-1})	$^4T_{1g(P)} \leftarrow {}^4T_{1g}$ (1.50×10^4 cm^{-1})	$^4A_{2g} \leftarrow {}^4T_{1g}$ (1.88×10^4 cm^{-1})	1.07×10^4	639
$Ni(C_{12}H_{21}O_{12})_2 \cdot 2H_2O \cdot C_2H_5OH$	$^3T_{2g} \leftarrow {}^3A_{2g}$ (8.53×10^3 cm^{-1})	$^3T_{1g(F)} \leftarrow {}^3A_{2g}$ (1.42×10^4 cm^{-1})	$^3T_{1g(P)} \leftarrow {}^3A_{2g}$ (2.56×10^4 cm^{-1})	8.53×10^3	947
$Cu(C_{12}H_{21}O_{12})_2 \cdot 2H_2O \cdot C_2H_5OH$	$^2T_{2g} \leftarrow {}^2E_g$ (1.24×10^4 cm^{-1})			1.24×10^4	

[a]Calculated according to ref. 22.

plexes were those expected for the electronic transitions of d^7 and d^8 metal ions in octahedral arrangements, respectively. The assignments given for the Co(II) complex are in agreement with those observed for octahedral cobalt(II) oxo complexes (19*c*).

The second band of the Ni(II) spectrum (704 nm) was found to be split into two signals, probably due either to spin-orbit coupling or to interactions with the nearest electronic level ^1E_g. The relationship between the first two bands in this case gave a value of 1.76, which was an indication that the metal ion should be involved in an octahedral arrangement. The energy value corresponding to the first transition (8.53×10^3 cm^{-1}) gives the magnitude of the splitting field Δ_0.

The reflectance spectra for the Cu(II)–D-lactobionate showed a single wide band at 807 nm, which was coincident with the value of the crystal field splitting and belongs to the electronic transition $^2T_{2g} \leftarrow {}^2E_g$. This result was in agreement with a tetragonal distortion of the octahedral geometry.

FT-IR spectra

IR spectra for the solid complexes were recorded in the region 4000–400 cm^{-1} and the interpretation was based on a comparison with the free D-lactobionic acid and structurally related compounds.

The intense broad band observed at ca. 3500–3100 cm^{-1} in the spectra of the free D-lactobionic acid was assigned to the strongly hydrogen-bonded OH groups. The interaction between the sugar hydroxyl groups and the metal produces broadening but no shift of the sugar OH stretching vibrations. The CH and CH_2 stretching vibrations, which appear at 2800–3000 cm^{-1} in the infrared spectra of the complexes, are similar to those found in the spectrum of the free D-lactobionic acid. The main change was observed in the carbonyl stretching vibration region, which appears at 1744 cm^{-1} in the free D-lactobionic acid. This band disappears in the solid complexes and a new band appears at 1610 cm^{-1}, assigned to an antisymmetric stretching carboxyl frequency (21). The concomitant carboxylate symmetric frequency (usually appearing at 1400–1100 cm^{-1}) could not be assigned due to overlapping with strong sugar C–O stretching vibrations. Because of this it was not possible to evaluate the difference in values between both types of bands and to obtain additional coordination data.

Conclusions

The interaction between D-lactobionate and bivalent metal ions afforded mainly 1:1 species, except for the Cu(II) system where the 1:1 and 1:2 complex species were found. The equilibrium constant values for the D-gluconate complexes were higher than those for D-lactobionate complexes. This could be attributed to the preferred rigid conformation of the acid disaccharide in solution, which restricts the coordination modes. The stoichiometric ratios and equilibrium constant values determined by the potentiometric and spectrophotometric methods were coincident. ^{13}C NMR spectroscopy allowed us to determine which hydroxyl groups of the D-lactobionic acid chain were involved in the chelation process, with concomitant participation of coordinated water molecules.

In the solid phase, the complexes produced between the metal ions employed in the present study and D-lactobionate presented a 1:2 stoichiometry and the spectroscopic studies allowed us to determine that the preferred coordination mode is the octahedral one.

Acknowledgments

We are grateful for financial support from the Universidad Nacional de Rosario (UNR) and from the Agreement between Consejo Nacional de Investigaciones Científicas y Técnicas (CONICET) and the Universidad de Granada, Spain.

References

1. G.M. Escandar, J.M. Salas Peregrin, M. Gonzalez Sierra, D. Martino, M.I. Santoro, A.A. Frutos, S.I. García, G. Labadié, and L.F. Sala. Polyhedron, **15**, 2251 (1996).
2. G.M. Escandar, F.H. Gandolfo, and L.F. Sala. An. Asoc. Quím. Argent. **78**, 37 (1990).
3. G.M. Escandar and L.F. Sala. Can. J. Chem. **70**, 2053 (1992).
4. G.M. Escandar, A.C. Olivieri, M. Gonzalez Sierra, and L.F. Sala. J. Chem. Soc. Dalton Trans. 1189 (1994).
5. G.M. Escandar, M. Gonzalez Sierra, J.M. Salas Peregrin, G. Labadié, M.I. Santoro, A.A. Frutos, and L.F. Sala. Polyhedron, **13**, 909 (1994).
6. G.M. Escandar, A.C. Olivieri, M. Gonzalez Sierra, A.A. Frutos, and L.F. Sala. J. Chem. Soc. Dalton Trans. 799 (1995).
7. G.M. Escandar, M. Gonzalez Sierra, and L.F. Sala. Polyhedron, **13**, 143 (1994).
8. J. Hegenauer, P. Saltman, D. Ludwig, L. Ripley, and Ph. Bajo. J. Agric. Food Chem. **27**, 860 (1979).
9. J.F. Rossotti and H. Rossotti. J. Chem. Educ. **7**, 375 (1965).
10. G. Schwarzenbach. Complexometric titrations. Interscience, New York. 1960. pp. 79, 81–83, 87.
11. A.E. Martell and R.J. Motekaitis. The determination and use of stability constants. 2nd ed. VCH, New York. 1992. (*a*) p. 143; (*b*) p. 25.
12. C.A. Araujo, G.A. Ibañez, G.N. Ledesma, G.M. Escandar, and A.C. Olivieri. Talanta. Submitted.

© 1997 NRC Canada

Can. J. Chem. Downloaded from www.nrcresearchpress.com by 88.146.161.215 on 09/08/12
For personal use only.

13. G.A. Melson and W.F. Pickering. Aust. J. Chem. **21**, 2889 (1968).
14. H.S. Harned and B.B. Owen. The physical chemistry of electrolytic solutions. 3rd. ed. Chapman and Hall, New York. 1964. pp. 641–645.
15. C.F. Baes, Jr. and R.E. Mesmer. The hydrolysis of cations. R. E. Krieger, Malabar (U.S.A), 1986. (*a*) p. 85; (*b*) p. 241; (*c*) p. 312.
16. S. Bouhsina, P. Decock, H. Kozlwski, G. Micera, and J. Swiatek. J. Inorg. Biochem. **42**, 57 (1991).
17. R.B. Martin. Metal ions in biological systems. Vol. 1. *Edited by* H. Sigel. Marcel Dekker, New York. 1974. Chap. 4.
18. D. Sutton. Espectros electrónicos de los complejos de los metales de transición. Reverté, Barcelona. 1975. (*a*) p. 141; (*b*) pp. 119–122.
19. A.B.P. Lever Inorganic electronic spectroscopy. 2nd ed. Elsevier, New York. 1984. (*a*) pp. 560–567; (*b*) pp. 507–511, p. 742.
20. B. Gyurcsik, T. Gajda, L. Nagy, and K. Burger. J. Chem. Soc. Dalton Trans. 2787 (1992).
21. K. Nakamoto. Infrared spectra of inorganic and coordination compounds. Wiley, New York. 1963.
22. Y.-s. Dou. J. Chem. Educ. **67**, 134 (1994).

Can. J. Chem. Downloaded from www.nrcresearchpress.com by 88.146.161.215 on 09/08/12
For personal use only.

© 1997 NRC Canada

Electrolytic conductivity of crystal violet based quaternary ammonium polyelectrolytes in *N,N′*-dimethylformamide and dimethyl sulfoxide

Meenakshi Singh, Anil Kumar, Shirley Easo, and B.B. Prasad

Abstract: Electrolytic conductivities of crystal violet based quaternary ammonium polyelectrolytes in very dilute solutions of dimethylformamide and dimethyl sulfoxide at 25°C have been investigated. The electrolytic conductivity (κ) as a function of concentration for systems having a reduced charge density (ξ) greater than unity revealed a very narrow range of linearity in the dilute region. A modest correlation has been made with the counterion condensation and the polycation conformations in order to explain the relative magnitude of limiting equivalent conductivities.

Key words: conductance, polyelectrolyte, aprotic solvent, solvation, counterion condensation.

Résumé : Opérant à 25°C, on a mesuré les conductivités électrolytiques de solutions très diluées de polyélectrolytes de sels d'ammonium quaternaire reliés au cristal violet dans le diméthylformamide et de diméthylsulfoxyde. Un examen de la relation entre la conductivité électrolytique (κ) et la concentration des systèmes ayant des densités de charge réduite (ξ) plus grande que l'unité permet de mettre en évidence une plage très étroite de linéarité dans la région diluée. Il a été possible d'établir une modeste corrélation entre le degré de condensation du contreion et les conformations du polycation qui devrait permettre d'expliquer l'amplitude relative des conductivités équivalentes limites.

Mots clés : conductance, polyélectrolyte, solvant aprotique, solvation, condensation du contreion.

[Traduit par la rédaction]

Introduction

Macroion mobility has proved to be an important property for providing an insight into the sizes, frictional coefficients, as well as conformations of polyelectrolytes (1–4). In dilute polyelectrolyte solutions, which still involve long-range intermolecular interactions, their conformational alterations are unexpectedly pronounced. The rapid increase of equivalent conductivity in dilute solution characterizes the behaviour of most polyelectrolyte solutions. However, counterion condensation may play a key role in determining the limiting equivalent conductivity of the polyions. In this sense, the present paper explores the typical behaviour of a few nitrogen-based polyelectrolytes in dipolar aprotic solvents, viz., *N,N′*-dimethylformamide (DMF) and dimethyl sulfoxide (DMSO). The polyions studied have distinctive structural constituents carrying ethylene, xylylene, and 2,5-thiophenylene links in their repeating units of the polymeric chain. This covers a wide range of quaternary nitrogen centres: (*i*) where quaternary nitrogens are located on the main chain (not as side-chain constituents); (*ii*) where backbone quaternary centres constitute a parallel cationic track with quaternized nitrogens on the side groups of the molecules; and (*iii*) where the heterocyclic ring nitrogens are quaternized with acyl derivatives in the repeating unit of the chain. The surge of interest for investigation in DMF and DMSO is primarily due to their dipolar aprotic characteristics, which avoid any proton interference with the conductivity of the polyions. The solubility restriction in the present instance in media of high dielectric constant does not allow for characterization of transport properties over a range of varying dielectric constants. Nevertheless, the moderately intermediate dielectric constant values at 25°C (DMF 36.1 and DMSO 46.6) and reasonably large Gutmann's donor number (DMF 26.6 and DMSO 29.8 kcal mol^{-1}) result in their good solvent behaviour, particularly that for which ion–dipole-type solute–solvent interactions are preferred. The anion solvation ability of DMF and DMSO (5) is negligibly small. Therefore, the interactions of a polycationic system with intermediate environments of varying dielectric constants are considered worthy of investigation in aprotic solvents.

Experimental

Solvents DMF and DMSO (99% pure, Sarabhai-Merck, stated purity 99 mol% (CO_2 < 0.02 mol%; H_2O < 0.03 mol%; conductivities, 1.6×10^{-8} S cm^{-1} (25°C) (DMF) and 1.1×10^{-8} S cm^{-1} (25°C) (DMSO)) were purified and stored as described elsewhere (6). All other chemicals were either high-purity materials or were purified before use. An automatic burette fitted into a sealed container was used as the solvent dispenser under pure nitrogen gas to avoid contamination with CO_2 and water from the air. Materials that fulfill the desired structural

Received October 1, 1996.

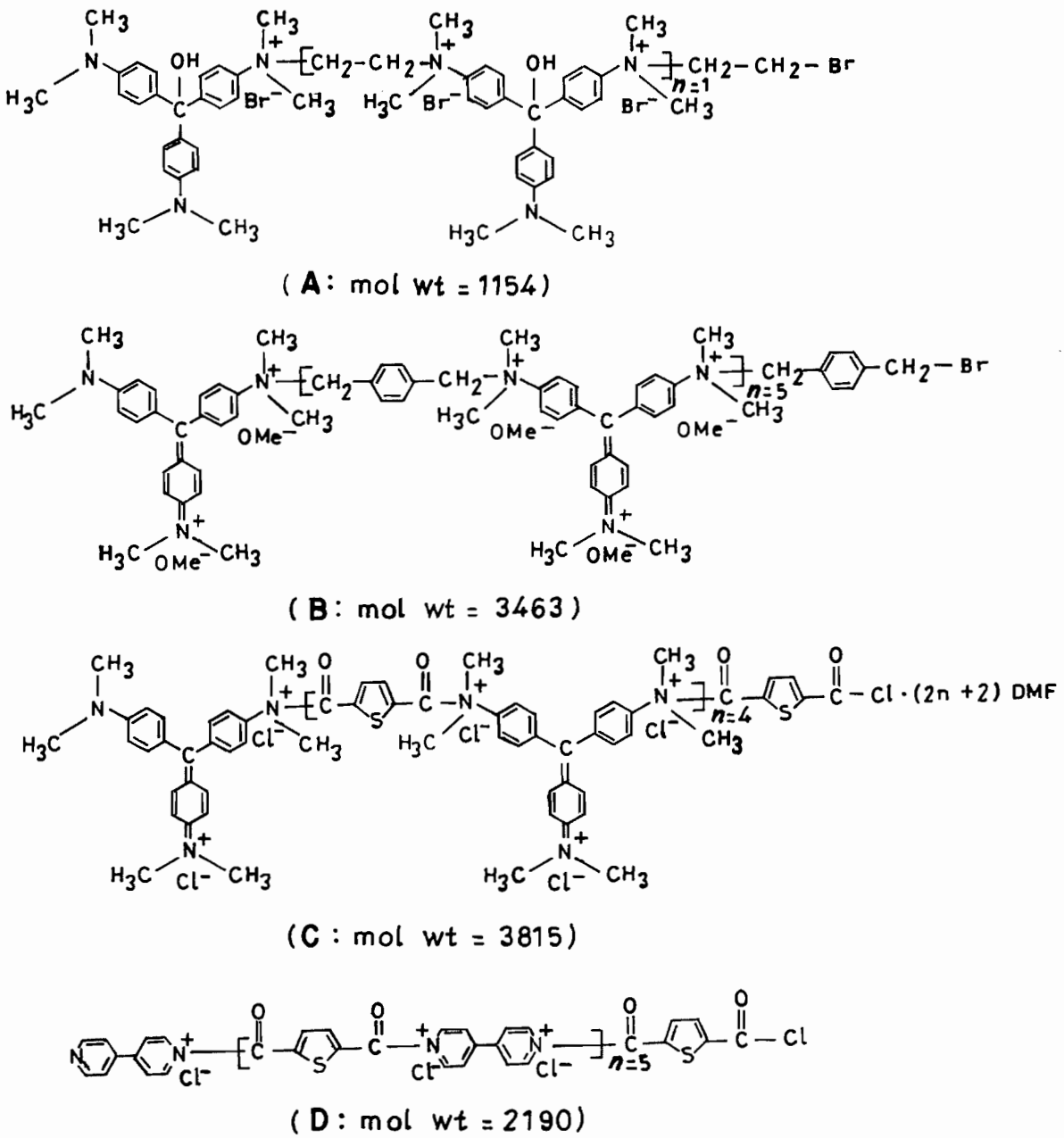
M. Singh, A. Kumar, S. Easo, and B.B. Prasad.[1] Department of Chemistry, Banaras Hindu University, Varanasi-221005, India.

[1] Author to whom correspondence may be addressed. Fax: 91-542-317074.

© 1997 NRC Canada

Can. J. Chem. Downloaded from www.nrcresearchpress.com by 88.146.161.215 on 09/08/12
For personal use only.

Fig. 1. Structures of the polyelectrolytes.



distinctions as stated above are as follows: **A**, poly(*N*-ethylene monohydroxy crystal violet dibromide]; **B**, poly[*N*-*p*-*x*ylylene crystal violet trimethoxide]; **C**, poly[*N*-2,5-diacylthiophenylene crystal violet trichloride], and **D**, poly[*N*-2, 5-diacylthiophenylene-4,4′-bipyridinium dichloride]. Details of the syntheses, characterizations, and purity of these polycations (structures in Fig. 1) have been reported elsewhere (7).

The reported equivalent conductances are calculated on the basis of equivalents of counterions available per mole of the different compounds studied, and are corrected for the solvent conductance.

The effect of possible adsorption in very dilute solution of the polycations was apparently negligible, as the conductivity for a certain concentration was always found to be very reproducible with a variation within $\pm 1 \times 10^{-7}$ S cm^{-2} after the attainment of thermal equilibrium. All conductances were measured at (25 ± 0.05)°C in the conventional way (8) using an immersion-type special conductivity cell with bright platinum electrodes having cell constant 0.6055 cm^{-1}. A Beckman RC 18 A conductance bridge and a WTW (model LBR/B) instrument were used; no significant variations in resistances were noted at frequencies 0.05, 1, and 3 kHz.

Furthermore, the possible absorption of traces of water molecules with nonaqueous solution over long periods of exposure in air (20 ± 5 h) did not affect the measurement, as repeated measurements with a given solution, between which the cell was conditioned with solutions of different concentrations, always led to identical results. The relative standard

© 1997 NRC Canada

Can. J. Chem. Downloaded from www.nrcresearchpress.com by 88.146.161.215 on 09/08/12
For personal use only.

Can. J. Chem. Downloaded from www.nrcresearchpress.com by 88.146.161.215 on 09/08/12
For personal use only.

deviation or coefficient of variation was found to be less than 0.03% in DMF and 0.02% in DMSO for five successive measurements with the level of certainty better than 95% (χ-test). However, as a preventive measure, all experiments were carried out using freshly prepared solutions, which were found by Karl Fischer titrations to be devoid of any detectable traces of water.

Theoretical background

The limiting equivalent conductivity of an electrolyte is generally obtained by extrapolation of the plot of Λ_c vs. $C^{1/2}$. However, this is not feasible in the case of a polyelectrolyte since equivalent conductivities (Λ_C) may vary upward or downward due to the changes in conformation and (or) counterion condensation. Thus, an alternative procedure for extrapolation is considered by using the equation

$$[1] \quad \kappa = \kappa_0 + \Lambda_0 \cdot C + C \cdot \phi(C)$$

where κ and κ_0 are electrolytic conductivities of the solution and solvent, respectively, C is the equivalent concentration, and the function $\phi(C)$ denotes the effect of interionic interactions. The slope ($d\kappa/dc$) of a plot of κ against C approximates the limiting conductivity (Λ_0), provided other derivatives $d\kappa_0/dC$ and $d[C\,\phi(C)]/dC$ in the differential form of the eq. [1] are neglected as compared to Λ_0. However, Λ_0 may be determined from conductivity data obtained at extreme dilution, provided the κ vs. C curve is linear over a sufficiently wide range of concentration (4).

$$[2] \quad \frac{d\kappa}{dC} = \frac{d\kappa_0}{dC} + \Lambda_0 + \frac{d}{dC}[C \cdot \phi(C)]$$

Another empirical approach for evaluation of polyion limiting conductivities from the conductance data is based on the Lattey equation (9):

$$[3] \quad \Lambda_0 - \Lambda_c = \frac{\sqrt{C}}{D + G\sqrt{C}}$$

which was originally suggested for simple electrolytes and has the same form as that of the relationship proposed by Robinson and Stokes (10) from an extension of the Onsager theory for ions of finite sizes. However, unlike the Onsager theory, the values of D and G in the case of polyelectrolytes are unfortunately not physically interpretable.

Expressing Λ_0 in terms of the limiting equivalent conductivities of the individual ions, one obtains the equation

$$[4] \quad \Lambda_0 = \Lambda_{0_{ip}} = f[\lambda_{0_i} + \lambda_{0_p}]$$

where $f \leq 1$ is an interaction parameter denoting the apparent degree of ionization and the fraction of free counterions (11). (The subscripts i and p denote the counterion and polyion, respectively.) The parameter f is expressed by

$$[5a] \quad f = 1 - [0.55\,\xi^2/(\pi + \xi)]; \qquad \xi \leq 1$$

$$[5b] \quad f = 0.866\,\xi^{-1}; \qquad \xi \geq 1$$

The model chosen for the polyion, which is used to obtain the equilibrium structure of the solution, is an infinitely long line charge. This is characterized by a dimensionless charge density parameter (reduced charge density) ξ (4, 12) as given by the expression

$$[6] \quad \xi = \frac{l_B}{b} = \frac{e^2}{\epsilon\, k_B\, Tb}$$

where l_B is the Bjerrum length at which two electronic charges (e) in a solvent of permittivity (ϵ) interact with an energy k_BT and b is the average charge spacing along the axis of real polyion chain (i.e., contour length divided by number of charged groups) (b = 9.40 (**A**), 8.20 (**B**), 10.20 (**C**), and 7.00 cm (**D**)). For dilute solutions of polyions, Manning's theory (12) states that the effective spacing of the charged groups on the polyion can not be less than a critical value corresponding to $\xi = 1$ in the case of monovalent charge groups and monovalent counterions. Therefore, for $\xi > 1$, the fraction $(1 - \xi^{-1})$ of counterions will condense on the polyion to lower the effective value of ξ and the dissociated counterions behave in accordance with the Debye–Hückel approximation.

The limiting equivalent conductivity of the polyion (λ_{0_p}) also depends directly on α, the degree of ionization, according to the relation

$$[7] \quad \lambda_{0_p} = \frac{F^2\,\alpha\,|Z_p|}{f_{pw}}$$

where F is the Faraday constant, $|Z_p|$ is the stoichiometric charge number of the polyion, and f_{pw} is its hydrodynamic friction coefficient, that is, the interactions resulting on account of the viscous drag exerted by the polyion on the electroneutral solvent. For $\xi < 1$, α becomes unity, whereas for $\xi > 1$, α approximates to the reciprocal of the charge density. The parameter f_{pw} could be related to the respective diffusion coefficients (D) on the basis of the Einstein relation (4), i.e.,

$$[8] \quad D = RT/f_{pw}$$

Results and discussion

The results of conductivity measurements on polyelectrolyte systems **A**, **B**, **C**, and **D** in DMF and DMSO at 25°C are presented in Tables 1 and 2 (the system **A** could not be studied in DMF because of the solubility restriction). In the case of DMF-soluble systems, the nature of Λ_c vs. $\sqrt{C}$ curves (Figs. 2 and 3) is very interesting. For systems **B** and **C**, the curves do not, as generally observed, increase uninterruptedly but surprisingly bend downward at very low concentrations, giving rise to a maximum at $3.70_5 \times 10^{-3}$ g-equiv L^{-1} for **B** and 0.70×10^{-3} g-equiv L^{-1} for **C**. However, the "normal" behaviour (increasing equivalent conductivity with dilution) is observed for the compound **D** in DMF (Fig. 3). It should be noted that reduced viscosities also assume a maximum in their respective concentration plots (13). One may find the rationale for this typical behaviour in terms of specific solvation characteristics of the system concerned. The decreasing trend of Λ_c with dilution in the case of compounds **B** and **C** resembles in every respect their corresponding partial molar volume (14) and viscosity behaviours (13). These behaviours are in conformity with the transition, as suggested for branched polyelectrolytes

© 1997 NRC Canada

Table 1. Conductance of various polyelectrolytes in dimethylformamide at 25°C.

B			C			D		
10^3C (g-equiv L^{-1})	$10^5\kappa$ (S cm^{-1})	$\Lambda_c{}^a$ (S cm^2 $equiv^{-1}$)	10^3C (g-equiv L^{-1})	$10^5\kappa$ (S cm^{-1})	$\Lambda_c{}^a$ (S cm^2 $equiv^{-1}$)	10^3C (g-equiv L^{-1})	$10^5\kappa$ (S cm^{-1})	$\Lambda_c{}^a$ (S cm^2 $equiv^{-1}$)
0.98	0.44	4.49_5	0.30	1.56	52.52_5	0.46	2.29	49.67
1.79	0.82	4.57	0.76	4.47	58.97	0.94	3.90	41.40
3.70_5	1.77	4.78	1.52	7.48	49.33	1.48	5.91	39.85
5.87	2.72	4.63	1.82_5	6.72	36.81_5	2.56_5	8.32_5	33.28
7.76	3.18	4.10	2.21	9.23	41.78	3.00_5	5.97	19.87
10.11	3.90	3.85	2.94	10.92	37.17	3.49	3.40	9.75
12.15	4.43	3.65	3.72	11.56	31.10	4.13	4.50	10.90
			4.53	15.44	34.05	5.78	11.79	20.41
			5.16	15.44	29.90_5			
			5.87	15.85	27.02			
			8.73	20.07	22.99			
			9.92	20.79	20.96			

[a]Relative standard deviation or coefficient of variation: ≤0.3%.

(4), into a more compact bent-rod (semicircular arc model) conformation owing to the possible contraction of the polyion chain, in extremely dilute solutions. The contraction in molecule **B** is chiefly due to crystal violet shrinkage, whereas the major constriction in compound **C** involves intramolecular Coulombic interactions in crystal violet and in 2,5-diacylthiophene moieties as well (14). The subsequent decrease of Λ_0 beyond maximum with increasing concentration is due to an increased screening of polyion charges through counterion associations. On the other hand, the concomitant increase of Λ_c upon dilution in the case of **D** conforms to normal polyelectrolyte behaviour (4). This is associated with the curled shape assuming an "impermeable coil" model under the force of common counterions associated with the bare quaternary nitrogens and including, to some extent, the intramolecular Coulombic attraction in diacylthiophenylene residues of the polycations (13, 14). However, the observed decrease in Λ_c, until a minimum (a characteristic kink, Fig. 3) is attained at the relatively higher concentration (3.49×10^{-3} g-equiv L^{-1}), reflects an increased counterion binding toward the concentrated region. The reason for the observed minimum in the Λ_c–$\sqrt{C}$ plot (Fig. 3) is perhaps due to the complete overlapping of the domains of individual molecules, yielding an optimum compact entanglement under the pool of common associated counterions, with increasing population of polyions. This facilitates an easier mode of incorporation of the solvent into the free volume of intermolecular spacings (14) and, consequently, a minimum in conductance is observed. However, at higher concentrations beyond this minimum, further addition of polyions may eventually destabilize the entanglement, leading to the separation of individual molecules. This results in lower hydrodynamic friction coefficients (f_{pw}, cf. Table 3) and thereby increased conductivity after the minimum.

A close perusal of the conductivity curves (Λ_c vs. $\sqrt{C}$) for **B**, **C**, and **D** in DMF (Figs. 2 and 3) reveals the following interesting facts: the conductivity is higher for **C** over the wide range of concentrations studied despite its larger molecular weight. The appreciable magnitude of Λ_c for **C** and the drastic reduction in conductivity for **B** (**B** and **C** have somewhat similar molecular weight) over the entire range of concentrations are expected, due to the lesser degree of counterion condensation arising from the lower charge density parameter (ξ) of **C** in comparison with **B** (Table 3). This ensures that equivalent conductance is based largely on the nature of the polyelectrolyte under study rather than on its molecular weight. Despite the observed constrictions and bent-rod conformations of both compounds **B** and **C**, the extremely small equivalent conductivity of **B** is the consequence of higher degree of counterion condensation and thereby screening of the positive charge by methoxide counterions. Irrespective of the high charge density (Table 3) of the polymeric chain of **D**, it is the geometrical conformation (impermeable coil) (14) of **D** in DMF that augments the transport phenomenon to an appreciable magnitude to render higher conductivity.

The concentration dependence of electrolytic conductivity (κ) for DMF-soluble systems is depicted in Fig. 4. This reveals an interesting feature of a very narrow range of linearity, indicating that the term $d\kappa_0/dc$ has a dominating influence on eq. [2] due to the presence of polyion (4). Furthermore, all the systems have considerable interionic interactions (including counterion condensation and intramolecular bending as revealed from ϕ_v (14) and η_{sp}/C (13) results) throughout the wide range of concentrations studied. Therefore, the derivative $d[C\cdot\phi(C)]/dC$ cannot be ignored in comparison with Λ_0, and measurements in this region have to be discarded in the determination of Λ_0. Despite these restrictions, limiting equivalent conductivities were evaluated from the limiting slope of smaller linear portions of the κ vs. C curve, assuming that the interionic interactions in this range of concentration are limited to interaction between the polyion and its counterion atmosphere. The accuracy of the evaluated Λ_0 values appeared highly questionable and erroneous through this treatment. Thus, no critical appraisal of the Λ_0 values seems possible in the present instance. However, the order **C** (46.46) > **D** (39.05) > **B** (4.21), in which the Λ_0 values appear, is based primarily on the chemical nature irrespective of such other parameters as size and molecular weight of the individual system concerned. The accurate determination of Λ_0 through the treat-

© 1997 NRC Canada

Can. J. Chem. Downloaded from www.nrcresearchpress.com by 88.146.161.215 on 09/08/12
For personal use only.

Can. J. Chem. Downloaded from www.nrcresearchpress.com by 88.146.161.215 on 09/08/12
For personal use only.

Table 2. Conductance of various polyelectrolytes in dimethyl sulfoxide at 25°C.

A			B			C			D		
10^3C (g-equiv L^{-1})	$10^5\kappa$ (S cm^{-1})	Λ_c^a (S cm^2 equiv^{-1})	10^3C (g-equiv L^{-1})	$10^5\kappa$ (S cm^{-1})	Λ_c^a (S cm^2 equiv^{-1})	10^3C (g-equiv L^{-1})	$10^5\kappa$ (S cm^{-1})	Λ_c^a (S cm^2 equiv L^{-1})	10^3C (g-equiv L^{-1})	$10^5\kappa$ (S cm^{-1})	Λ_c^a (S cm^2 equiv^{-1})
0.53	2.41	45.49_5	0.20	0.20	9.99_5	0.76	2.81	36.80	0.20	0.53	26.35
1.06	4.63	43.72	1.01	0.44	4.34	1.52	5.24	34.37	0.81_5	1.90	23.28
1.58	6.70	42.33	2.03	0.66	3.24	2.23	7.27	32.66	2.04	4.33	21.25
2.41	9.74	40.46	2.92	0.76	2.61	3.71	10.60	28.56	3.03	5.66	18.69
4.74	18.32	38.68	4.06	1.14	2.81	6.61	15.50	23.46	4.25	7.59	17.87
			4.87	0.97	1.99	8.54	18.32_5	21.46	5.05	8.74	17.33
			5.85	1.57	2.68				6.07	10.07	16.60
			8.13	1.99_5	2.45				6.89	10.32	14.97_5
			8.78	1.93	2.20				7.85	11.85	15.09
			9.75	2.14	2.19				8.92	12.21	13.68
									9.70	13.14	13.55

[a]Relative standard deviation or coefficient of variation: ≤0.2%.

Fig. 2. Concentration dependence of equivalent conductivity for **B** in dimethylformamide.

Fig. 3. Concentration dependence of equivalent conductivity for **C** (X) and **D** (○) in dimethylformamide.

ment based on the Lattey equation is no longer feasible in the present instance because of the unusual constrictions of polyelectrolytes in the dilute range of concentrations in DMF. Moreover, polyion–polyion interactions become significant at higher concentrations, bringing further complications. Therefore, the existing models for linear polyelectrolytes seem inapplicable to the present systems.

In DMSO, all the systems demonstrated normal linear polyelectrolyte behaviour, as the limiting equivalent conductivities increased uninterruptedly with decreasing concentration (Figs. 5–7). However, there was levelling in the $\Lambda_c - \sqrt{C}$ plots beyond ~0.0036 g-equiv L^{-1} for systems **A** and **B**, due to the possible optimization of agglomeration at the higher concentrations. This offers somewhat constant frictional coefficients (f_{pw}, Table 3) to the transport processes. The conductivity curves representing κ vs. C for DMSO-soluble systems **A**, **B**,

© 1997 NRC Canada

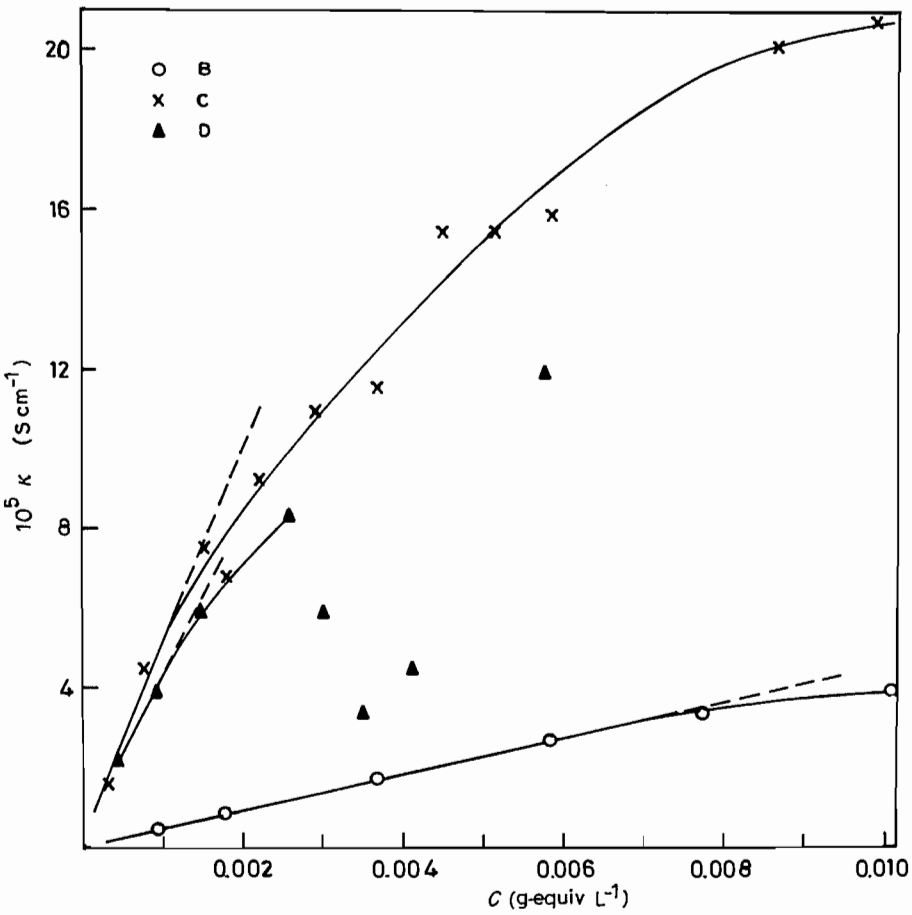
Can. J. Chem. Downloaded from www.nrcresearchpress.com by 88.146.161.215 on 09/08/12
For personal use only.

Table 3. Parameters derived on the basis of counterion condensation on polycations at 25°C.

System	ξ	f	α	$f_{pw} \times 10^{-8}$ (kg s^{-1} mol^{-1})	$D \times 10^{6}$ (cm^2 s^{-1})	λ_{op} (S cm^2 mol^{-1})
B/DMF	2.11	0.41	0.47	[a]	[a]	[a]
C/DMF	1.69	0.51	0.59	21.40	1.16	35.90
D/DMF	2.47	0.35	0.40_5	7.35	3.36	56.47
A/DMSO	1.47	0.59	0.68	4.80	5.17	39.62
B/DMSO	1.69	0.51	0.59	[a]	[a]	[a]
C/DMSO	1.36	0.64	0.74	6.92	3.60	138.65
D/DMSO	1.98	0.44	0.50	4.08	6.10	126.72

[a]These values could not be calculated in absence of data for the conductivity of counterion (MeO^-) in DMF and DMSO.

Fig. 4. Concentration dependence of electrolytic conductivity in dimethylformamide: **B** (○), **C** (×), and **D** (▲).



C, and **D** are depicted in Fig. 8. The linear parts of the κ vs. *C* curves are apparently shrinking for polyelectrolytes **B**, **C**, and **D**, which unfortunately does not favour the measurement of Λ_0 on the basis of the treatment suggested by eq. [1]. The dimeric system **A**, however, which has a lower charge density all along the polyion chain, shows largely linear variations of κ with concentration. Moreover, the effect of interionic interactions ϕ(C) and counterion binding may apparently be marginal in a medium like DMSO (ϵ = 46.6) at finite dilution. This allows the estimation of Λ_0 (36.36 ohm^{-1} cm^2 equiv^{-1}) in this instance from the slope of the linear region of the κ vs. *C* plot.

A modest attempt was made to evaluate Λ_0 values by the application of the Lattey equation, since all systems follow the usual polyelectrolyte behaviour in DMSO and no complica-

© 1997 NRC Canada

Can. J. Chem. Downloaded from www.nrcresearchpress.com by 88.146.161.215 on 09/08/12
For personal use only.

Fig. 5. Concentration dependence of equivalent conductivity for **A** in dimethyl sulfoxide.

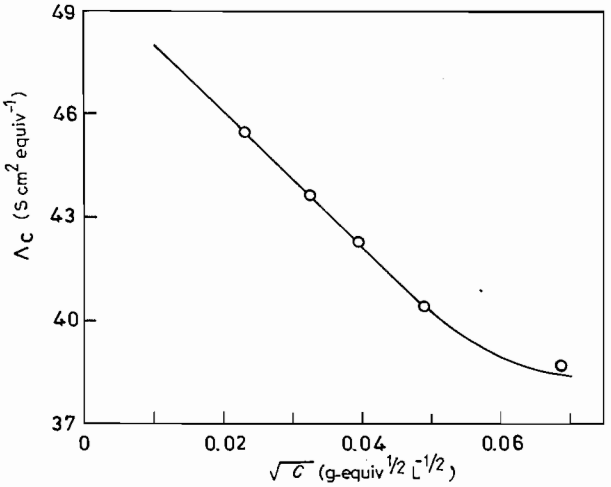


Fig. 6. Concentration dependence of equivalent conductivity for **B** in dimethyl sulfoxide.

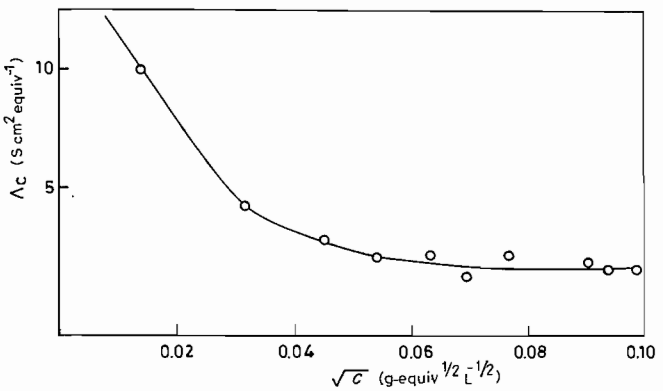
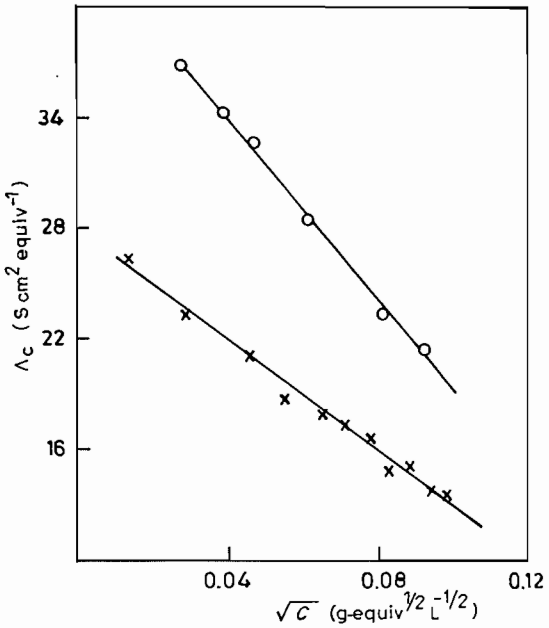


Fig. 7. Concentration dependence of equivalent conductivity for **C** (○) and **D** (×) in dimethyl sulfoxide.



tions as were observed for DMF arose in the present case. A representative Lattey equation plot in the form $\sqrt{C}/(\Lambda_0-\Lambda_c)$ vs. $\sqrt{C}$ is shown in Fig. 9 for system **A** in DMSO, for which the different trial values of Λ_0 that yielded a linear plot were chosen as the limiting equivalent conductance of the system concerned. The values of the limiting conductances thus obtained are: 55 (**A**), 30 (**B**), 124 (**C**), and 80 (**D**) ohm^{-1} cm^2 equiv^{-1}. The least-squares values of **D** and **G** obtained for the minimum Λ_0 line are given in Table 4. System **C** has larger value of Λ_0 in DMSO in spite of its larger molecular weight and the larger partial molar volume (14). With the least counterion association in comparison to other systems in DMSO (Table 3) this system enjoys the highest degree of coiling to attain a "globular" model, which resulted in smaller hydrodynamic resistances during the dynamic flow of the solution in viscosity measurements (13) and thereby larger mobility. Excluding the exceptional case of **A**, for which Λ_0 is somewhat unexpectedly small despite its lower molecular weight and smaller size with rigid-rod conformation (13), the Λ_0 values derived for other three systems **B**, **C**, and **D** follow the sequence **C** > **D** > **B**. This seems to agree with the observed trend of intrinsic viscosities (0.410, 0.568, and 0.754_5 dL/g at 25°C (14)) and in all possibility may reflect the effect of an increase in hydrodynamic sizes of the respective systems in that order. The systems **B** and **D** are reported, from a viscosity study, to possess a free-draining coil. Furthermore, despite the larger f_{pw}, molecular weight, and the least ξ (Table 3), the coiling tendency of **C** is considered to be a main factor in determining its position in the conductivity sequence. The higher f_{pw} approximates its conformation to a loose extended coil that is being changed to an impermeable "globular" shape during the solution transport. The Λ_0 values determined from both treatments (36.36 ohm^{-1} cm^2 equiv^{-1} from the κ–C plot, 55 ohm^{-1} cm^2 equiv^{-1} from the Lattey equation plot) for **A** are somewhat dissimilar; however, its decreased value might be attributed to the screening of positive charge density by the lone-pair electrons of the unquaternized nitrogens of the pendant moieties. The dramatic decrease in the limiting conductivity of **B** in DMSO is due to the reduction of the effective charge of the polyion with a subsequent decrease in the number of "free" counterions as a result of the higher tendency of counterion binding of methoxide ions, even at infinite dilution. It is to be noted that the effect of ion pairing for this system is more pronounced in the relatively low dielectric constant medium DMF, which gives rise to an extremely small Λ_0. It should be further mentioned that limiting conductivities are found mainly dependent on the extent of counterion condensations in DMF, whereas the DMSO-soluble systems display Λ_0 values primarily in accordance with their sizes and conformations in the solution. This reveals an active role of DMF, as compared with DMSO, that demonstrates specific polymer–solvent contacts.

On further inspection of the results listed in Table 3, it is observed that the hydrodynamic friction coefficient (f_{pw}) decreases steadily with increasing charge density of the polyelectrolytes studied in both solvents. This is because the extent of counterion condensation is reasonably enhanced with the increase of charge density that alters the polymer conforma-

© 1997 NRC Canada

Fig. 8. Concentration dependence of electrolytic conductivity in dimethyl sulfoxide: **A** (×), **B** (●), **C** (□), and **D** (△).

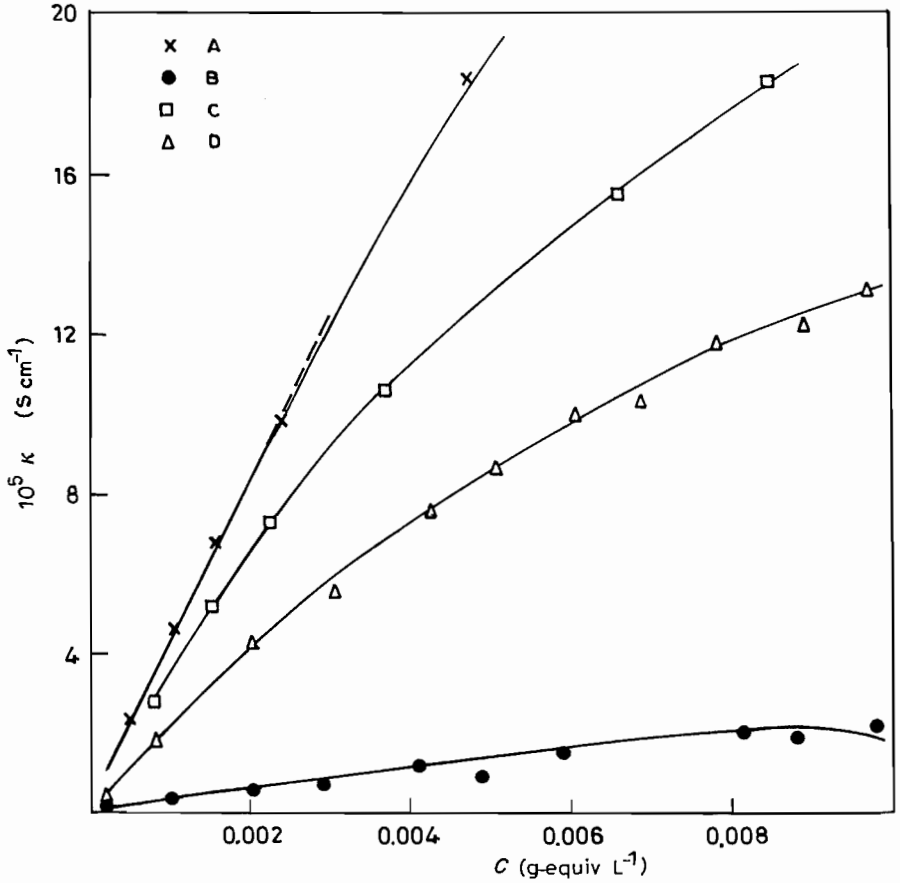
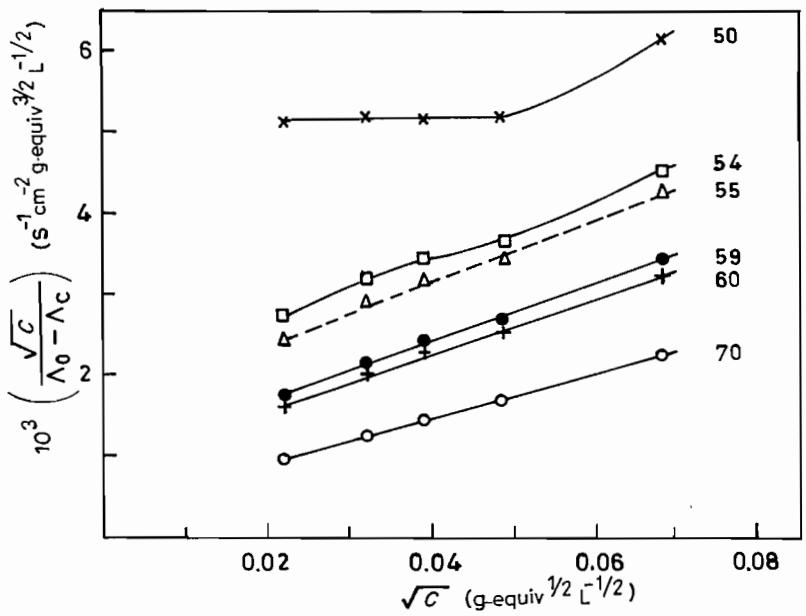


Fig. 9. Lattey equation plots for **A** in dimethyl sulfoxide using different values of Λ_0: 50 (×); 54 (□); 55 (△); 59 (●); 60 (+); 70 (○). The plot shown for $\Lambda_0 = 55$ represents the least-squares line.



Can. J. Chem. Downloaded from www.nrcresearchpress.com by 88.146.161.215 on 09/08/12
For personal use only.

© 1997 NRC Canada

Table 4. Parameters D and G derived from the Lattey equation[a] in dimethyl sulfoxide.

	A	B	C	D
10^4 D (S^{-1} cm^{-2} $equiv^{3/2}$ $dm^{-3/2}$)	15.90	1.70	0.80	0.10
10^2 G (S^{-1} cm^{-2} $equiv$)	3.79	3.41	0.88	0.14

[a] $C^{1/2} / (\Lambda_0 - \Lambda_c) = D + GC^{1/2}$

tion with appreciable coiling in the solution. The exceptionally high value of Λ_0 for **C** in DMSO is because of unusual coiling of **C**, as already explained.

It should be noted that deviation from Manning's condensation theory is quite likely because an isolated molecule of a high molecular weight flexible polyelectrolyte cannot maintain a rodlike conformation, even in very dilute solutions. The current polyelectrolyte theories based on simple electrostatic models are unable to rationalize the conductivity behaviour of such flexible polyelectrolytes and, therefore, a judicious scrutiny of the solvation effect in support of the conformational alterations of polycations has to be adopted.

Acknowledgements

One of us (M.S.) is grateful to the Council of Scientific and Industrial Research (CSIR), New Delhi, for a Senior Research Fellowship to carry out this project.

References

1. B.B. Prasad, A. Kumar, M. Singh, and S. Singh. J. Chem. Eng. Data, **40**, 79 (1995).
2. M. Singh and B.B. Prasad. J. Chem. Eng. Data, **41**, 409 (1996).
3. A.R. Bizzari, C. Cametti, and F. Bordi. J. Phys. Chem. **94**, 2166 (1990), and refs. therein.
4. H. Vink. J. Chem. Soc. Faraday Trans. 1, **77**, 2439 (1981); **79**, 1403 (1983); **83**, 801 (1987).
5. K. Burger. *In* Studies in analytical chemistry. Vol. 6. *Edited by* E. Pungor, W. Simon, and J. Inczédy. Elsevier, Amsterdam. 1983. pp. 25, 32.
6. B.B. Prasad, M. Singh, and S. Singh. Polym. J. **27**, 49 (1995).
7. B.B. Prasad, S. Easo, and A. Kumar. Polym. J. **26**, 251 (1994).
8. S.K. Srivastava, B.B. Prasad, and D. Singh. J. Electroanal. Chem. **25**, 71 (1988).
9. R.T. Lattey. Philos. Mag. **4**, 831 (1927).
10. R.A. Robinson and R.H. Stokes. J. Am. Chem. Soc. **76**, 1991 (1954).
11. A. Schmitt and R. Varoqui. J. Chem. Soc. Faraday Trans. 2, **69**, 1087 (1973).
12. G.S. Manning. J. Chem. Phys. **51**, 924 (1969); **51**, 934 (1969).
13. M. Singh, A. Kumar, S. Easo, and B.B. Prasad. J. Chem. Eng. Data. Submitted.
14. B.B. Prasad, S. Easo, and A. Kumar. Polymer, **35**, 2874 (1994).

Can. J. Chem. Downloaded from www.nrcresearchpress.com by 88.146.161.215 on 09/08/12
For personal use only.

© 1997 NRC Canada

Quinones and hydroxyquinones as generators and quenchers of singlet molecular oxygen

Isela Gutiérrez, Sonia G. Bertolotti, M.A. Biasutti, Arnaldo T. Soltermann, and Norman A. García

Abstract: The role of quinones and hydroxyquinones as sensitizers and as quenchers in Type II photooxygenations has been examined. The second aspect is discussed here, through a systematic study, for the first time in the open literature. Quinonic compounds are excellent generators of $O_2(^1\Delta_g)$ in aprotic solvents (excluding those quinones possessing substituents in positions adjacent to the carbonyl groups, in the case of anthraquinone derivatives). Benzoquinones, anthraquinones, and hydroxy derivatives are good $O_2(^1\Delta_g)$ quenchers upon dye-sensitized photoirradiation. The excited oxygen species is deactivated with rate constants in the range 10^6–10^7 M^{-1} s^{-1} depending on the solvent employed. The quenching process deactivates $O_2(^1\Delta_g)$ without further destruction of the quinone. The main interaction with $O_2(^1\Delta_g)$ is driven by the quinone moiety, in spite of the presence of potentially active nuclear substituents. The quenching mechanism could involve a reversible charge transfer intermediate, with the quinonic compound acting as an electron donor.

Key words: photooxidation, quenching, quinones, rose bengal, singlet oxygen.

Résumé : On a évalué le rôle des quinones et des hydroxyquinones dans la sensibilisation et la désactivation des réactions de photooxygénations de type II. Grâce à une revue systématique de la littérature effectuée pour la première fois, on peut discuter ici du deuxième aspect. Les composés quinoniques sont d'excellents générateurs d'$O_2(^1\Delta_g)$ dans les solvants aprotiques (à l'exception des dérivés de l'anthraquinone possédant des substituants dans les positions adjacentes aux groupes carbonyles). Lors d'irradiations sensibilisées par des colorants, les benzoquinones, les anthraquinones et leurs dérivés hydroxylés sont de bons désactivateurs d'$O_2(^1\Delta_g)$. La vitesse de désactivation de l'oxygène excité est de l'ordre de 10^6–10^7 M^{-1} s^{-1}, dépendant de la nature du solvant utilisé. Le processus de désactivation d'$O_2(^1\Delta_g)$ se fait par la portion quinone, malgré la présence de substituants nucléaires potentiellement actifs. Le mécanisme de désactivation pourrait impliquer un intermédiaire de transfert de charge réversible qui transformerait le composé quinonique en un électrodonneur.

Mots clés : photooxydation, désactivation, quinones, rose de Bengale, oxygène singulet.

[Traduit par la rédaction]

Introduction

Quinones and hydroxyquinones belong to an important class of biologically active and commercially valuable compounds. They are involved in a huge number of electron transfer processes representing individual steps in a variety of enzymatic systems. The participation of quinone derivatives in light-induced processes therefore constitutes a topic of special interest. Quinones have been extensively studied in connection to their near-uv–visible absorbing characteristics and potential photosensitizing properties for Type I and Type II photoreactions (1–8). In this area, Gollnick and Held (6) in 1992 published a study on hydroxyanthraquinones as sensitizers for singlet molecular oxygen ($O_2(^1\Delta_g)$) photooxidations. Subsequently Gollnick et al., in 1993, reported (7) on the properties of the same compounds as sensitizers for electron transfer reactions. As well, photosensitizing mechanisms of the antitumor agents represented by aminoanthraquinones (4) and anthracyclines (2, 5) have been widely investigated. As a final example of photosensitization we can cite anthraquinone itself, which is a photosensitizer often detected in sea water, frequently employed to mimic natural photooxidation processes in the marine environment (3, 8). These few cases illustrate the significance of the interaction of quinonic derivatives with light in nature and in technology and, in this context, the importance of the photosensitizing action of quinones for Type II reactions (photopromoted $O_2(^1\Delta_g)$ generation) becomes evident.

The quality of a given sensitizer, such as the quinone family in the present case, must be evaluated in conjunction with the properties as eventual selfquenchers of the transient species generated in the sensitizing process. In this manner, the information obtained can contribute to the interpretation of experiments or events in which direct irradiation of quinones is carried out. However, almost no information about the behaviour of these derivatives as potential $O_2(^1\Delta_g)$ quenchers is available.

Following this line, in this work we carried out a kinetic study on the properties of different quinones and hydroxy-

Received August 26, 1996.

I. Gutiérrez. Departamento de Química, Facultad de Ciencias Naturales, Universidad Nacional de La Patagonia, SJB, 9000 Comodoro Rivadavia, Argentina.
S.G. Bertolotti, M.A. Biasutti, A.T. Soltermann, and N.A. García.[1] Departamento de Química y Física, Universidad Nacional de Río Cuarto, 5800 Río Cuarto, Argentina.

[1] Author to whom correspondence may be addressed.

© 1997 NRC Canada

Can. J. Chem. Downloaded from www.nrcresearchpress.com by 88.146.161.215 on 09/08/12
For personal use only.

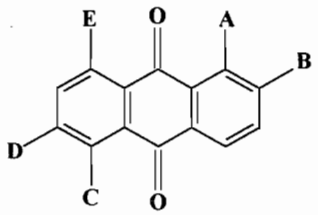
Can. J. Chem. Downloaded from www.nrcresearchpress.com by 88.146.161.215 on 09/08/12
For personal use only.

quinones as $O_2(^1\Delta_g)$ deactivators. In parallel, the quantum yields for $O_2(^1\Delta_g)$ generation (Φ_Δ) of several quinonic derivatives of interest, not previously reported in the literature, were determined.

Experimental

Materials

Rose bengal (RB) and rubrene (R) were from Sigma Chem. Co. Perinaphthenone (1*H*-phenalen-1-one, PN), 9,10-dimethylanthracene (DMA), furfuryl alcohol (FFA), and the quinones benzoquinone (BQ), tetramethyl benzoquinone (DQ), anthraquinone (AQ), 2,6-dihydroxyanthraquinone (2,6-DOHAQ), 1,8-dihydroxyanthraquinone (1,8-DOHAQ), 1,2-dihydroxyanthraquinone (1,2-DOHAQ), anthraquinone-2-sulfonic acid (2-SAQ), and anthraquinone-1,5-disulfonic acid (1,5-DSAQ) were purchased from Aldrich. The compounds 2,6-dihydroxyanthraquinone (2,6-DOHAQ) and 1,5-dihydroxyanthraquinone (1,5-DOHAQ) were from Pfaltz and Bauer. Perinaphthenone-2-sulfonic acid (1*H*-phenalen-1-one-2-sulfonic acid PNS) was synthesized as described in the literature (9). For the kinetic determinations the following solvents were employed: benzene (Bz), acetonitrile (MeCN), and ethanol (EtOH) all from Sintorgan, 2-propanol (iPrOH) from Mallinkrodt, and D_2O (99.9% D) from Sigma Chem. Co. Water was triply distilled.



Molecule	A	B	C	D	E
AQ	H	H	H	H	H
2,6DOHAQ	H	OH	H	OH	H
1,5 DOHAQ	OH	H	OH	H	H
1,8 DOHAQ	OH	H	H	H	OH
1,2 DOHAQ	OH	OH	H	H	H
2 SAAQ	H	SO_3H	H	H	H
1,5 DSAAQ	SO_3H	H	SO_3H	H	H

The quinones were purified as follows: 1,5-DSAAQ was recrystallized from acetic acid. DQ and 1,5-DOHAQ were sublimated. The dihydroxy derivatives 1,8-DOHAQ and 1,2-DOHAQ were passed through a chromatographic column of silica gel, employing as eluents Bz and Bz – ethyl acetate 85:15 (v:v), respectively. The quinones BQ, AQ, and 2-SAAQ were used as received.

Methods

Kinetic measurements

(a) Time-resolved phosphorescence detection (TRPD): The laser kinetic spectrophotometer has been previously described (10). Briefly, it consists of a Laser Optics nitrogen laser with pulses of 5 mJ and 7 ns (337 nm) halfwidth as the excitation source. The emitted radiation (mainly 1270 nm) is detected at right angles (using an amplified Judson J16/8Sp germanium detector) after having passed through appropriate filters. The output of the detector is coupled to a digital oscilloscope and to a personal computer to carry out the signal processing. Usually 16 shots were needed for averaging, in order to get a good signal/noise ratio, from which the decay times were calculated. The sensitizer (RB or PN in organic solvents and PNS in D_2O) had an Abs_{336} = 0.5–0.6. The $O_2(^1\Delta_g)$ lifetimes in Bz, MeCN, and D_2O were 28, 40, and 64 μs, respectively.

The $O_2(^1\Delta_g)$ lifetimes were evaluated in the absence (τ^0) and in the presence (τ) of the quencher, and their ratio plotted as a function of quinone concentration, according to a simple Stern–Volmer treatment (eq. [1]):

$$[1] \quad \tau^0/\tau = 1 + k_t\tau^0\,[\text{quinone}]$$

k_t (the *total* or *overall* rate constant for $O_2(^1\Delta_g)$ quenching) is given by the addition of the respective rate constants for *physical* deactivation to ground-state molecular oxygen $O_2(^3\Sigma_g)$ (k_q, eq. [2]) and *chemical* or *reactive* quenching (k_r, eq. [3]).

$$[2] \quad O_2(^1\Delta_g) + \text{quinone} \xrightarrow{k_q} O_2(^3\Sigma_g^-) + \text{quinone}$$

$$[3] \quad O_2(^1\Delta_g) + \text{quinone} \xrightarrow{k_r} P$$

For solvents such as EtOH and iPrOH, k_t was evaluated employing the method of Carlsson et al. (11), given that the $O_2(^1\Delta_g)$ lifetime in the presence of quenchers was too low to be determined by our TRPD instrument (time response approximately 4 μs). This method is based on the self-sensitized photooxidation of rubrene. The ratio of initial rates of rubrene photooxidation in the absence (V_0) and in the presence (V) of different concentrations of the quinone was plotted against the quinone concentration, and k_t was calculated from eq. [4]:

$$[4] \quad V_0/V = 1 + k_t[\text{quinone}]/(k_d + k_{rR}[R])$$

In the present case $k_{rR}[R] \sim 370\ s^{-1}$ (assuming $k_{rR} = 4.4 \times 10^7\ M^{-1}\ s^{-1}$, see ref. 11). Under these conditions the denominator of eq. [4] can be practically taken as equal to k_d. The values for $1/k_d$ employed in the calculations were 11 and 15 μs, respectively, for EtOH and iPrOH, obtained from TRPD experiments.

(b) Static photolysis: The irradiation device, including the specific oxygen electrode, has been described elsewhere (12). A set of cutoff filters was employed to ensure that all electromagnetic radiation was absorbed only by the sensitizers.

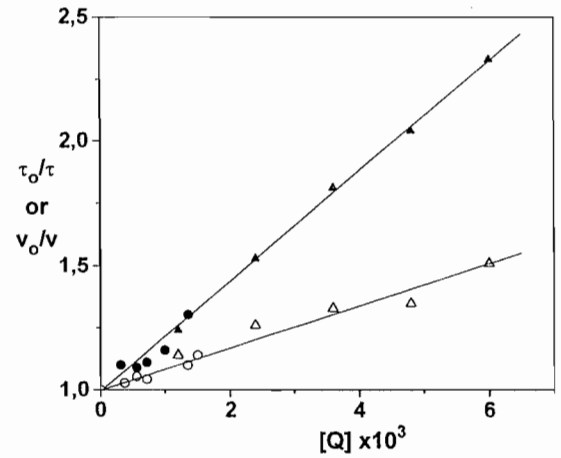
Determination of the photooxidizability of quinones

The reactivity of quinones (i.e., their effectiveness for chemical reaction with $O_2(^1\Delta_g)$) was determined by different comparative methods (already described (13)), depending on the solvent. In all cases, knowledge of the reactive rate constant for the sensitized photooxidation of a reference compound (Ref) is required. In water the rates of oxygen uptake for the quinones and the reference compound, upon sensitized irradiation, were compared. Ref was FFA with $k_r = 1.2 \times 10^8\ M^{-1}\ s^{-1}$

© 1997 NRC Canada

Can. J. Chem. Downloaded from www.nrcresearchpress.com by 88.146.161.215 on 09/08/12
For personal use only.

Fig. 1. Stern–Volmer plots for the quenching of AQ (empty symbols) and BQ (full symbols) in Bz. Triangles correspond to the data of TRPD and circles correspond to the determination by the method of Carlsson et al. (11) (see the experimental section).



(14) and the sensitizer RB (Abs_{560} = 0.5). The oxygen electrode (Orion 97-08) has a membrane that can be used only in media containing a high percent of water (typically, more than 95%). Ref was 9,10-dimethylanthracene (DMA), whose k_r value, determined by TRPD, is 5.5×10^7 M^{-1} s^{-1} in MeCN. In organic media the method for k_r determination was essentially the same as in water, except that in this case the loss of substrate and of reference compound must be compared. The loss of DMA upon sensitized irradiation was monitored spectrofluorimetrically employing 395 nm and 450 nm, respectively, as excitation and emission wavelengths. The eventual loss of quinones was monitored through their absorption spectrum.

Ground state absorption measurements were carried out with a Hewlett Packard 8452A diode array spectrophotometer.

Determination of singlet oxygen quantum yields

The determination of Φ_Δ was made by the comparative method already described (15). Briefly, the dependence of $O_2(^1\Delta_g)$ phosphorescence intensity I_0 on the laser fluence E_L extrapolated to zero time was measured for solutions of the quinones. Several absorbances of the quinones were employed, at the laser emission wavelength, 337 nm. The laser fluence was varied, employing filters of neutral density. The Φ_Δ values were calculated by comparison of the slopes of the linear plots I_0 vs. E_L × fraction of absorbed light, for the reference and sample. The references were PN in MeCN (Φ_Δ = 0.95)(9) and PNS in D_2O (Φ_Δ = 1)(9).

Results

Overall interaction quinones–$O_2(^1\Delta_g)$

As described in the experimental section, k_t values were calculated from the lifetimes measured by TRPD, through a simple Stern–Volmer plot (typical cases, for BQ and AQ in Bz are shown in Fig. 1). For some quinones, in organic media, k_t was also determined according to the method of Carlsson et al. (11). As can be seen in Fig. 1, the set of experimental points employing this method lie exactly on the same curve as those corresponding to the time-resolved results.

Table 1. Rate constants for overall quenching of $O_2(^1\Delta_g)$ by quinones and derivatives (k_t, M^{-1} s^{-1}), and quantum yields for $O_2(^1\Delta_g)$ generation in MeCN by the same compounds, upon direct 337-nm photoirradiation.

Quinone	Solvent	$k_t \times 10^{-6}$	Φ_Δ
BQ	Bz	9.2	
	MeCN	2.8	0.38
	EtOH	23.0(34)[a]	
	iPrOH	11.0	
AQ	Bz	3.0	
	MeCN	2.2	0.62; 0.70[b]
	EtOt	21.0	
	iPrOH	42.0	
DQ	Bz	5.0	
	MeCN	4.0	0.89; 0.80[d]
	EtOH	10.0	
	iPrOH	11.0	
2,6-DOHAQ	MeCN	8.0	0.34[b]
	EtOH	11.0	
	iPrOH	14.0	
1,5-DOHAQ	Bz	4.0	
	MeCN		n.g.[c]
1,8-DOHAQ	Bz	4.0	
	MeCN	4.4	0.69[b]
	EtOH	15.0	
	iPrOH	15.0	
1,2-DOHAQ	Bz	6.0	
	MeCN	7.0	0.034; 0.03[b]
	EtOH	25.0	
2-SAAQ	D_2O	45.0	n.g.[c]
	MeCN		0.69
1,5-DSAAQ	D_2O	16.0	n.g.[c]
	MeCN		n.g.[c]

[a]From ref. 17.
[b]From ref. 6.
[c]No $O_2(^1\Delta_g)$ generation.
[d]Error quoted ±20% from ref. 25.

Results (Table 1) reveal that quinones are good $O_2(^1\Delta_g)$ quenchers. Solvents of different characteristics were explored. It is worth mentioning at this stage that k_t increases in alcoholic solvents, as compared to non-protic solvents, whereas the higher k_t values were obtained for the sulfonic derivatives in heavy water.

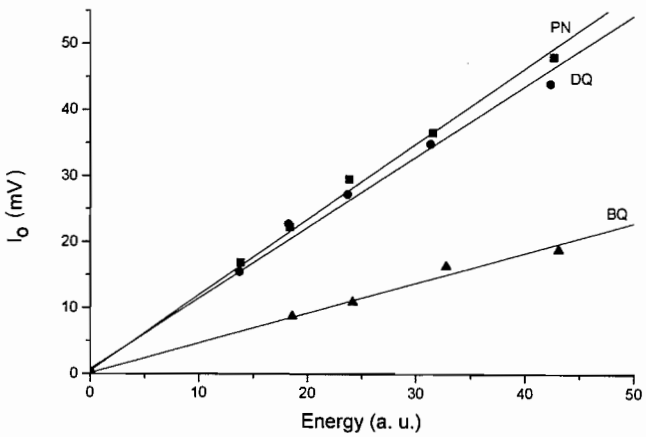
The absence of chemical reaction of singlet molecular oxygen $O_2(^1\Delta_g)$ with quinones

We attempted the evaluation of the hypothetical k_r values for quinones, employing the comparative methods described in the experimental section. After prolonged sensitized irradiation no changes in the absorption spectrum of the quinones could be observed. We employed the well-known $O_2(^1\Delta_g)$ chemical scavenger 9,10-DMA for comparative purposes. Under identical experimental conditions this reference compound was practically completely consumed after a period 50 times shorter than that employed as a photolysis time for the quinones.

© 1997 NRC Canada

Can. J. Chem. Downloaded from www.nrcresearchpress.com by 88.146.161.215 on 09/08/12
For personal use only.

Fig. 2. Laser fluence dependence of the amplitude at zero-time I_0 of the $O_2(^1\Delta_g)$ phosphorescence signal in MeCN for PN, DQ, and BQ.



For water-soluble sulfonic derivatives, we assayed the measurement of oxygen consumption upon sensitized irradiation. Again, a relatively fast oxygen consumption was observed for the reference compound (FFA). After a few minutes it was totally oxidized via an $O_2(^1\Delta_g)$-mediated process, as estimated by auxiliary spectroscopic determinations. In contrast, no oxygen consumption could be detected for quinones, even when the irradiation time was several times greater than that employed for FFA.

On the basis of the above-mentioned results and considering the detection limits of the apparatus and methodologies employed, we can roughly estimate a value of $10^4\ M^{-1}\ s^{-1}$ as an upper limit for k_r for the quinones listed in Table 1.

The Φ_Δ values for quinonic compounds

The capacity of several quinones for $O_2(^1\Delta_g)$ generation upon direct irradiation, Φ_Δ, was investigated in MeCN and D_2O solutions. The quantum yield for singlet oxygen formation is given by the sum of contributions from oxygen quenching of the lowest singlet (S) and triplet (T) excited states of the quinones.

$$[5] \quad \Phi_\Delta = \Phi_\Delta(S) + \Phi_\Delta(T)$$

For air-saturated solutions (oxygen concentration in MeCN 1.9 mM (16)) the contribution from the quinones excited singlet state (lifetime in the order of nanoseconds or subnanoseconds (6)) can be neglected. Hence, the expression for the quantum yield of $O_2(^1\Delta_g)$ formation is reduced to:

$$[6] \quad \Phi_\Delta = S_\Delta\, \Phi_T$$

Where S_Δ represents the proportion of triplet quinone–$O_2(^3\Sigma^-_g)$ that leads to the formation of $O_2(^1\Delta_g)$ and Φ_T is the quantum yield for excited triplet state generation.

The Φ_Δ values for AQ, DQ, 1,5-DOHAQ, and the sulfonic derivatives from Table 1 have not been previously reported, according to our knowledge. In Fig. 2 are shown typical experimental results, in this case allowing the determination of Φ_Δ values for DQ and BQ in MeCN.

As shown in Table 1, we obtained a value of 0.034 for 1,2-DOHAQ, in good agreement with the value of 0.03 reported by Gollnick and Held (6). For 1,5-DOHAQ in MeCN and the for the sulfonated derivatives in D_2O no signal at all for $O_2(^1\Delta_g)$ generation could be detected.

Discussion

The total absence of evidence for quinone photooxidation, as monitored by substrate and oxygen consumption, clearly indicates that the interaction with $O_2(^1\Delta_g)$ must be largely ascribed to a physical process.

Only two inconclusive references regarding kinetic data on the interaction quinones–$O_2(^1\Delta_g)$ have been published (17, 18). The first one (Koka and Song) concerns the protective effect by several substrates, including benzoquinone, against $O_2(^1\Delta_g)$-mediated photooxidation of chlorophyll *a*. In it, k_t values of 3.40 and $1.60 \times 10^7\ M^{-1}\ s^{-1}$ for benzoquinone in EtOH and EtOH–Bz, respectively, were reported. The second reference (18) (Croux et al.) reports k_t values of 1.8 and $0.59 \times 10^7\ M^{-1}\ s^{-1}$ for 5- and 6-hydroxy-1,4-naphthoquinone in MeOH, respectively. No comment on photooxidation of the naphthoquinones was made.

Turning to our data in Table 1, we can distinguish two sets of compounds: the *pure* quinonic derivatives and the dihydroxyquinones. The presence of -OH groups as aromatic ring substituents in the second set suggests the possibility that some of these compounds could behave as phenolic derivatives, from the point of view of their reactivity towards $O_2(^1\Delta_g)$. It is known that phenols are efficient $O_2(^1\Delta_g)$ quenchers (19). Typical k_t values for phenolic derivatives such as phenol itself and some dihydroxybenzenes range from 10^6 to $10^8\ M^{-1}\ s^{-1}$ in organic solvents (19). Besides, k_t values for phenols dramatically increase with the increase of solvent polarity. This argument is not supported by our data in Table 1. The k_t values are practically the same when the solvents Bz and MeCN are compared, the respective rate constants in EtOH and iPrOH being definitely higher. Nevertheless, the differences between k_t for both alcohols are not significant. The alcohols and MeCN possess similar values for their respective dielectric constants and both are much higher than the dielectric constant for Bz (16). Hence we can neglect the possibility of a solvent polarity effect on k_t, for the case of quinones. Furthermore, if the k_t values for anthraquinone and the four dihydroxy derivatives from Table 1 are compared, only a slight difference in favour of the hydroxyquinones can be observed. This is clear evidence that the main interaction for these compounds with $O_2(^1\Delta_g)$ is driven by the quinonic moiety.

The increase in the rate constant observed in alcoholic solvents when compared to Bz as a solvent was already detected by Koka and Song (17) for BQ, going from EtOH to an EtOH-Bz mixture, but this observation was not discussed further. It could in principle be related to the fact that the quinonic structure in protic solvents is in equilibrium with the corresponding hydroquinone derivative, which is an efficient $O_2(^1\Delta_g)$ scavenger as stated earlier. Nevertheless, the absence of reaction products, typical in the photooxidation of dihydroxybenzenes (19), even upon prolonged sensitized irradiation, imposes some doubts about this possibility. At the same time, the similarity between k_t values obtained in EtOH and iPrOH also makes improbable the involvement of reversible hydrogen atom abstraction in the reaction mechanism for $O_2(^1\Delta_g)$ quenching.

© 1997 NRC Canada

Can. J. Chem. Downloaded from www.nrcresearchpress.com by 88.146.161.215 on 09/08/12
For personal use only.

Several authors have examined the reactivity of $O_2(^1\Delta_g)$ toward different families of aromatic compounds. In most of the cases, the initial formation of an intermediate complex with some degree of charge transfer character, leading to physical and (or) chemical quenching, was postulated (20, 21). The occurrence of an exclusive reversible charge transfer process within the complex should lead to predominant physical quenching, such as that observed in the present case for quinone derivatives. In this field there can be cited a number of examples of $O_2(^1\Delta_g)$ physical quenching by amines, indoles, phenols, and sulfides (for a review see ref. 19) acting in all cases as the electron donors. This kind of interaction, involving a reverse electron transfer process, was also invoked by Darmayan in 1993 (23) to explain the interaction of $O_2(^1\Delta_g)$ with solvent molecules. The author, through experimental evidence, demonstrated that a charge transfer process to $O_2(^1\Delta_g)$ occurs from organic molecules possessing ionization potentials (Ip) as high as 11 eV. The parent compounds in Table 1 (BQ and AQ) exhibit Ip values of 10 and 9.24 eV, respectively (16). Furthermore, the difference in their respective k_t values may reflect the aforementioned tendency for electron-donor activity.

In the present case, no solvent polarity effect on k_t could be observed when aprotic solvents were employed. The higher values of k_t in protic solvents might be explained on the basis of the higher polarization of the quinone molecule due to solvent–hydrogen bonding, favouring the charge transfer interaction and increasing the stabilization of the transition state.

The photophysical properties of quinones and derivatives, in particular those of triplet states, have been sufficiently investigated. Triplet lifetimes and triplet quantum yields depend on the π–π^* or n–π^* nature of the excited state involved (2, 6). Gollnick and Held (6) established that, in general, S_Δ seems to be large when Φ_T is large (see eq. [6]). Moore et al. (2) proposed that quinones with substituents in position 1, possibly due to interaction with the adjacent carbonyl group, possess T_1 states that are π–π^* in nature. This implies a consequent decrease in triplet quantum yields. Quinones substituted in position 2, on the contrary, mainly populate n–π^* triplet states, which are accompanied by longer lifetimes and higher triplet quantum yields. These observations are in agreement with our experimental results. No signal for $O_2(^1\Delta_g)$ generation could be observed for 1,5-dihydroxyanthraquinone (possessing two substituents in positions of potential interaction with the carbonyl groups). The same was true for 1,5-DSAAQ in both D_2O and MeCN, whereas for 2SAAQ a Φ_Δ value of 0.69 was obtained in MeCN. For this compound no signal for $O_2(^1\Delta_g)$ generation could be detected in heavy water, possibly due to two concurrent factors: an intrinsic low value for Φ_Δ accompanied by the extremely low quantum yield for the radiative transition $O_2(^1\Delta_g) \rightarrow O_2(^3\Sigma_g^-)$ in D_2O, which certainly precludes the neat observation of the emissive signal (22). The first assumption could be in agreement with previous results from Oliveros et al. (24) for carbonyl-containing sensitizers. For cases in which solvent-induced state inversion occurs, as commented upon above for the anthraquinones, the Φ_Δ values drop to near zero in protic solvents (19).

Concluding remarks

Quinones and hydroxy derivatives (excluding those derivatives with substituents in positions adjacent to the carbonyl groups) are excellent sensitizers for $O_2(^1\Delta_g)$ generation in aprotic solvents. In parallel, they are moderate quenchers of $O_2(^1\Delta_g)$. This fact should be carefully considered when the possible extent of the Type II sensitizing effect of quinones, in a given environment, is evaluated. The quenching process, exclusively physical in nature, deactivates the oxygen-excited species generated, without further destruction of the quinone. In substituted quinones, the main $O_2(^1\Delta_g)$–quinone interaction is driven by the quinone moiety, in spite of the potentially active nuclear substituents. Even when the ability of quinones to act as electron acceptors is a recognized fact, experimental evidence indicates that the quenching mechanism could involve a reversible charge transfer intermediate, the quinonic compound acting as an electron donor. In this context, the mechanistic way mentioned agrees with the poor k_t values exhibited by the quinones as compared to those observed (one to two orders of magnitude higher) for electron donor $O_2(^1\Delta_g)$ quenchers (19, 25).

Acknowledgements

Thanks are given to CONICET (República Argentina), CONICOR (Pcia. de Córdoba), and SECyT UNRC for financial support. The technical work of Miss Marcela de Alba is gratefully acknowledged. We also thank Dr. Mario Reta for his advice on the purification of hydroxyanthraquinones.

References

1. S. Oishi, Y. Watanabe, and Y. Kuriyama. Chem. Lett. 2187 (1994).
2. J.N. Moore, D. Phillips, N. Nakashima, and K. Yoshihara. J. Chem. Soc. Faraday Trans. 2, **83**, 1487 (1987).
3. F.R. Rontani and G. Giusti. J. Photochem. Photobiol. A: **40**, 107 (1987).
4. K.J. Reszka, P. Bilski, C.F. Chignell, J.A. Hartley, N. Kahn, R. Souhami, A.J. Mendonca, and W. Lown. J. Photochem. Photobiol. B: **15**, 317 (1982).
5. A. Andreoni, A. Colasanti, and G. Roberti. J. Photochem. Photobiol. B: **14**, 319 (1992).
6. K. Gollnick and S. Held. J. Photochem. Photobiol. A: **70**, 135 (1993).
7. K. Gollnick, S. Held, D.O. Mártire, and S.E. Braslavsky. J. Photochem. Photobiol. A: **69**, 155 (1992).
8. M. Ehrhardt and G. Petrick. Mar. Chem., **16**, 227 (1985).
9. S. Nonell, M. González, and F.R. Trull. Afinidad, **448**, 445 (1993).
10. S. Miskoski, S. Bertolotti, N.A. García, and G. Arguello. Amino Acids, **4**, 101 (1993).
11. D.J. Carlsson, T. Suprunchuk, and D.M. Wiles. Can. J. Chem. **52**, 3728 (1974).
12. S.G. Bertolotti, G.A. Arguello, and N.A. García. J. Photochem. Photobiol. B: **10**, 57 (1991).
13. S. Nonell, L. Moncayo, F. Trull, F. Amat-Guerri, E.A. Lissi, A.T. Soltermann, S. Criado, and N.A. García. J. Photochem. Photobiol. B: **29**, 157 (1995).
14. W.R. Hagg and J. Hoigné. Environ. Sci. Technol. **20**, 341 (1986).
15. A.T. Soltermann, D. de la Pena, S. Nonell, F. Amat-Guerri, and N.A. García. Polym. Degrad. Stab. **49**, 371 (1995).
16. S.L. Murov. Handbook of photochemistry. M. Dekker, New York. 1973.
17. P. Koka and P.-S. Song. Photochem. Photobiol. **28**, 509 (1978).
18. S. Croux, M.-T. Maurette, M. Hocquaux, A. Ananides, A.M. Braun, and E. Olveros. New J. Chem. **14**, 161 (1990).

© 1997 NRC Canada

19. N.A. García. J. Photochem. Photobiol. B: **22**, 185 (1994).
20. A.A. Gorman, G. Lovering, and M.A.J. Rodgers. J. Am. Chem. Soc. **101**, 3050 (1979).
21. A.A. Gorman, I.R. Gould, I. Hamblett, and M.C. Standen. J. Am. Chem. Soc. **106**, 6956 (1984).
22. A.P. Losev, I.M. Byteva, and G.P. Gurinivich. Chem. Phys. Lett. **143**, 127 (1988).
23. A.P. Darmayan. Chem. Phys. Lett. **215**, 477 (1993).
24. E. Oliveros, P. Suardi-Murasecco, T. Aminian-Saghafi, A.M. Braun, and H.-J. Hansen. Helv. Chim. Acta, **74**, 79 (1991).
25. F. Wilkinson, W.P. Helman, and A.B. Ross. J. Phys. Chem. Ref. Data, **24**, 663 (1995).

Can. J. Chem. Downloaded from www.nrcresearchpress.com by 88.146.161.215 on 09/08/12
For personal use only.

© 1997 NRC Canada

Reactions of vanadate with *N,N*-dimethylhydroxylamine: aqueous equilibria and the crystal structure of the uncharged oxygen-bridged dimer of bis(*N,N*-dimethylhydroxamido)hydroxooxovanadate

Pradip C. Paul, Sarah J. Angus-Dunne, Raymond J. Batchelor, Frederick W.B. Einstein, and Alan S. Tracey

Can. J. Chem. Downloaded from www.nrcresearchpress.com by 88.146.161.215 on 09/08/12
For personal use only.

Abstract: ^{51}V nuclear magnetic resonance spectroscopy has been utilized in the investigation of the reactions of vanadate with *N,N*-dimethylhydroxylamine in aqueous medium. The major components of the reaction products were mono- and bisliganded mononuclear vanadate compounds with ^{51}V chemical shifts near −630 and −740 ppm, respectively. Variation of the concentration of the reactants enabled the determination of stoichiometry and formation constants of the products. The two major signals near −740 ppm were assigned to two stereoisomers of a bisligand product. The proton stoichiometries and pK_a values of the major products were determined from pH variation studies. A crystalline product of the type $[V(O)(ONMe_2)_2]_2O$ was isolated from the reaction of vanadate with dimethylhydroxylamine and its structure determined from X-ray diffraction studies. The compound possesses a dimeric oxo-bridge structure with a six-coordinate vanadium core. The arrangement about each vanadium may be described as approximately tetrahedral considering the center of the N—O bond in each dimethylhydroxamide ligand as one vertex. Hydrolysis of the crystalline solid in D_2O provided two isomers that corresponded to the two bisligand products. A variable temperature ^1H NMR study in D_2O and 50% $D_2O/(CD_3)_2CO$ mixture revealed the existence of reasonably fast chemical exchange between the two predominant isomers. The nature of coordination of these and related compounds is discussed. Crystal structure of $[V(O)(ONMe_2)_2]_2O$: orthorhombic, space group $P22_12_1$; $Z = 2$; $a = 7.0955(9)$ Å; $b = 10.2313(12)$ Å; $c = 11.5942(11)$ Å; $V = 841.69$ Å^3; $T = 213$ K; $R_F = 0.021$ for 1141 data ($I_0 \geq 2.5\sigma(I_0)$) and 137 variables.

Key words: bis(*N,N*-dimethylhydroxamido)hydroxooxovanadate, vanadate, dimethylhydroxylamine, vanadium NMR, aqueous equilibria, peroxovanadate.

Résumé : On a fait appel à la RMN du ^{51}V pour étudier les réactions du vanadate avec la *N,N*-diméthylhydroxylamine, en solution aqueuse. Les produits principaux de la réaction sont des vanadates mononucléaires mono- et bicoordinés dont les déplacements chimiques du ^{51}V sont respectivement de −630 et −740 ppm. La variation de la concentration des réactifs a permis de déterminer la stoechiométrie et les constantes de formation des produits. Les deux signaux importants près de −740 ppm ont été attribués à deux stéréoisomères d'un produit bicoordiné. On a déterminé les stoechiométries et les valeurs de pK_a des produits principaux en se basant sur des études de variation de pH. À partir des produits de la réaction du vanadate avec la diméthylhydroxylamine, on a isolé un produit cristallin du type $[V(O)(ONMe_2)_2]_2O$ dont on a déterminé la structure par diffraction des rayons X. Le composé possède une structure dimère à pont oxo comportant un vanadium hexacoordiné central. L'arrangement autour de chaque vanadium peut être décrit comme pratiquement tétraédrique si l'on considère le centre de la liaison N—O de chaque coordinat diméthylhydroxamide comme un sommet. L'hydrolyse du solide cristallin dans du D_2O fournit deux isomères qui correspondent aux deux produits bicoordinés. Une étude par RMN du ^1H à température variable, dans du D_2O et dans un mélange 50/50 de $D_2O/(CD_3)_2CO$ a permis d'établir l'existence d'un échange chimique relativement rapide entre les deux isomères prédominants. On discute de la nature de la coordination de ces composés et de composés apparentés. Structure cristalline du $[V(O)(ONMe_2)_2]_2O$: orthorhombique, groupe d'espace $P22_12_1$; $Z = 2$; $a = 7,0955(9)$, $b = 10,2313(12)$ et $c = 11,5942(11)$ Å; $V = 841,69$ Å^3; $T = 213$ K; $R_F = 0,021$ for 1141 données ($I_0 \geq 2,5\sigma(I_0)$) et 137 variables.

Mots clés : bis(*N,N*-diméthylhydroxamido)hydroxooxovanadate, vanadate, diméthylhydroxylamine, RMN du vanadium, équilibre aqueux, peroxovanadate.

[Traduit par la rédaction]

Received November 1, 1996.

P.C. Paul, S.J. Angus-Dunne, R.J. Batchelor,[1] F.W.B. Einstein,[1] and A.S. Tracey.[2] Department of Chemistry and Institute of Molecular Biology and Biochemistry, Simon Fraser University, Burnaby, BC V5A 1S6, Canada.

[1] X-ray Crystal Laboratory, Department of Chemistry.
[2] Author to whom correspondence may be addressed. Telephone: (604) 291 4464. Fax: (604) 291 3765. E-mail: tracey@sfu.ca

© 1997 NRC Canada

Can. J. Chem. Downloaded from www.nrcresearchpress.com by 88.146.161.215 on 09/08/12
For personal use only.

Introduction

Vanadium-dependent enzymes are found in haloperoxidases of some marine algae (1), in lichens and fungi (2, 3), and also in certain nitrogenases of a variety of nitrogen-fixing bacteria (4–6). The occurrence of these enzymes has generated interest in vanadium chemistry and this interest has been greatly stimulated by the findings that oxovanadium(IV), oxovanadium(V), and peroxovanadium(V) complexes give rise to a number of biological responses, the insulin-mimetic effects of vanadates and peroxovanadates being of predominant interest. For comprehensive reviews of these and other topics concerning vanadium biochemistry, the readers are referred to two recent compendiums (7, 8).

Because of the biochemical influences of peroxovanadates, a considerable amount of effort has gone into expanding our understanding of the aqueous chemistry of these materials. Complex formation with heteroligands (9–14), oxidative mechanisms (14–16), and oxygen transfer reactions (14, 17, 18) have been the topics of numerous studies. Our interest in the biochemistry of peroxovanadates, and also because they are interesting systems in their own right, has led us to extend our studies to include hydroxylamines. The reactions of aqueous vanadate with hydroxylamines provided a convenient point of departure from the studies with hydrogen peroxide. Also, the hydroxylamine ligand is found in the naturally occurring V(IV) product, amavadin (19, 20), models of which have been prepared and characterized by X-ray structure studies. It has also been shown that, electrochemically, the vanadium in amavadin is readily oxidized to the V(V) state with no apparent changes in coordination (21). Hydroxylamine and hydrogen peroxide are isoelectronic with each other and they undergo similar reactions with vanadate. However, the replacement of OH by NH_2 or $N(CH_3)_2$ provides sufficient differences from the peroxide chemistry to allow development of our insight into the reactions characteristic of these systems. Investigations into the H_2NOH–V reactions proved to be complicated somewhat by the slow decomposition of hydroxylamine. Because of this, it proved rewarding to turn to the dimethyllated hydroxylamine for initial studies into the aqueous chemistry of these systems. The results gathered from these studies allowed for a detailed interpretation of the hydroxylamine and methylhydroxylamine reactions (22). In addition, we have obtained a crystalline dimethylhydroxylamine–vanadate derivative that provided detailed structural information. Dissolution studies of the crystalline material using water and acetone–water solutions, in conjunction with known properties of the solution products from equilibrium studies, allowed structural assignments of many of the solution products to be made.

Experimental section

Materials

All chemicals used in this work are of reagent grade. Vanadium(V) oxide, 99.99% (Aldrich Chemical Co.), *N,N*-dimethylhydroxylamine (DMHA) hydrochloride (Aldrich Chemical Co.), *N*-(2-hydroxyethyl)-piperazine-*N'*-ethanesulfonic acid (HEPES) buffer (Boehringer Mannheim Gmbh), and tetraethylammonium hydroxide 20% aqueous solution (Sigma Chemical Co.) were used without further purification.

Solutions

A stock solution of sodium vanadate was prepared by adding 0.500 molar equivalents of V_2O_5 to a 1.00 M solution of NaOH in distilled water. The mixture was then stirred until all vanadium pentoxide went into solution and the solution became colourless (generally overnight). This solution was diluted with distilled water to a concentration of 0.100 M.

An *N,N*-dimethylhydroxylamine (DMHA) solution of concentration 0.100 M was prepared by dissolving the required amount of amine in distilled water. The 1.0 M HEPES buffer and 2.0 M KCl stock solutions were both prepared in distilled water. The ionic strength of all the final solutions, before recording the spectra, was brought to 1.0 M with KCl. The initial pH of the KCl stock solution was adjusted downward by the addition of HCl, then upward with NaOH, if required, so that when the HEPES buffer, DMHA, and vanadate solutions were added in a sequential fashion, the resultant pH was in the range 6.3–6.5. The various vanadate–ligand solutions of different concentrations were prepared by adding appropriate amounts of vanadate stock (0.100 M), ligand stock (0.100 M), and HEPES buffer stock (1.0 M) solutions to the pH-adjusted KCl solution (2.0 M). This solution was then diluted to near the desired final volume using distilled water. This process avoids the formation of decavanadate. The final upward adjustment of the pH of the final solution was done by using small aliquots of NaOH and the final volume was obtained with added distilled water. For the pH studies (6.5–8.0), the composition of the solution was maintained as: 3.00 mM total vanadate; 3.00 mM DMHA hydrochloride ; 20 mM HEPES buffer, and 1.0 M KCl, unless stated otherwise. Studies in the acidic pH range, i.e, at pH below 6, were carried out by keeping the ligand concentration in excess; a concentration of 3.00 mM vanadate, 20.0 mM DMHA hydrochloride, 20 mM HEPES, and 1.0 M KCl was used. Ligand and vanadate concentration studies at pH >9 were done with the composition, 2–4.5 mM total vanadate; 8–15 mM ligand; 20 mM HEPES, and 1.0 M KCl. A three- to fivefold excess ligand concentration was required in order to identify products of low formation constants in highly alkaline medium.

Synthesis of $V_2O_3(C_2H_6NO)_4$

Solid V_2O_5 (0.10 g; 0.55 mmol) was added to a solution of 20% tetraethylammonium hydroxide (0.75 mL) and water (~2 mL). The resultant slurry was warmed to 60°C with continuous stirring, to obtain a clear solution of tetraethylammonium vanadate. The pH of the vanadate solution was about 10. A solution of *N,N*-dimethylhydroxylamine hydrochloride (0.213 g; 2.19 mmol) dissolved in water (~2 mL) at pH 6 (adjusted by tetraethylammonium hydroxide) was added to the above vanadate solution with continuous stirring to give a yellow solution with the pH maintained between 7 and 8. The pH of the yellow solution was finally adjusted to 8.0. The reaction solution was then stirred for ~10 min, whereupon a yellow crystalline solid began to crystallize from solution. After crystallization was complete, the yellow solid was filtered, washed with cold water, and dried in vacuo. This material was stored at room temperature for several months without observable deterioration. Yield 0.15 g (70%).

^1H NMR spectra of $V_2O_3(C_2H_6NO)_4$ in D_2O, $(CD_3)_2CO$, and $CDCl_3$ solvents were recorded in order to check the stability of the compound in the respective solvents. Variable tem-

© 1997 NRC Canada

Can. J. Chem. Downloaded from www.nrcresearchpress.com by 88.146.161.215 on 09/08/12
For personal use only.

perature studies were carried out in D_2O and 50% $(CD_3)_2CO$–D_2O solutions.

Spectroscopy

^{51}V NMR spectra were obtained using a Bruker AMX-400 NMR spectrometer operating at 105.2 MHz at ambient temperature. Vanadium chemical shifts are quoted relative to the external reference $VOCl_3$ assigned to 0 ppm. Baseline corrections were applied to all spectra prior to their integration. NMR spectral parameters were the following: pulse widths, 60°; spectral widths, 60 kHz; acquisition times, 0.05 s; line broadening , 40 Hz; frequency domain size, 16K data points.

The acquisition parameters for the ^1H spectra were as follows: spectral window, 5000 Hz; pulse width, 60° (4 μs); time domain data points, 32 K; transform data points, 32 K; line broadening, 0.5 Hz. For the variable temperature studies a recycle delay of 2 s was also utilized during the acquisition of the spectra.

^{51}V spectra of freshly prepared solutions of V_2O_3-$(C_2H_6NO)_4$ in D_2O and $CDCl_3$ were recorded. The spectrum in $CDCl_3$ exhibited one signal at −728 ppm, while in D_2O two signals, found at −726 and −740 ppm, were observed. A separate experiment was also done in order to examine the change in the ^{51}V spectral pattern of $V_2O_3(Me_2NO)_4$ as the solvent was changed from pure acetone to a 50% acetone–water mixture. Approximately 5 mg of the powdered crystalline compound was dissolved in 3 mL of pure acetone in a 10 mm NMR tube and the spectrum was recorded. To this solution 3 mL of water was added in steps of 0.5 mL each to a total of 3 mL and spectra recorded for each addition.

For the variable temperature studies, approximately 1.5 mg of the powdered crystalline compound, $V_2O_3(Me_2NO)_4$, was dissolved in 0.5 mL D_2O in a 5 mm NMR tube and the proton NMR spectrum recorded as a function of temperature in the range 275–298 K. A similar study was carried out for the temperature range 248–73 K using a 1:1 $(CD_3)_2CO$—D_2O solvent.

X-ray diffraction

A yellow-colored needle-shaped crystal was mounted on a glass fiber. Data were recorded with an Enraf Nonius CAD4F diffractometer equipped with an in-house modified low-temperature attachment and using graphite monochromatized Mo K_α radiation. Absorption corrections were made using the Gaussian integration method. Data reduction included corrections for Lorentz and polarization effects.

Appropriate coordinates and anisotropic thermal parameters for all non-hydrogen atoms were refined. Hydrogen atoms were readily located in an electron density difference map and their coordinates were refined. A single parameter was refined for the isotropic thermal motion of the hydrogen atoms of each methyl group. Refinement of a chirality parameter unambiguously confirmed the correct hand for the crystal selected. An extinction parameter was also refined. A weighting scheme based on counting statistics was applied such that $\langle w(|F_o|-|F_c|)^2\rangle$ was near constant as a function of both $|F_o|$ and $\sin\theta/\lambda$. Final full-matrix least-squares refinement of 137 parameters for 1141 data ($I_0 \geq 2.5\sigma(I_0)$) converged at $R = 0.021$. Crystallographic details are summarized in Table 1. Final fractional atomic coordinates are listed in Table 2.

The computer programs used were: DIFRAC (23) for data collection; NRCVAX (24) for absorption correction, data reduction, structure solution, and graphical output; and CRYSTALS (25) for structure refinement and rigid body thermal motion analysis. Complex scattering factors for neutral atoms (26) were used in the calculation of structure factors. Computations were carried out on a Pentium-based computer.

Analysis of the anisotropic thermal parameters, using a rigid-body (27) model for one $OVO(ONMe_2)_2$ unit, yielded $R = 0.089$ for the agreement between observed and calculated U_{ij} and an r.m.s. discrepancy of 0.0020 Å^2. The resultant, corrected bond lengths are included in Table 3.

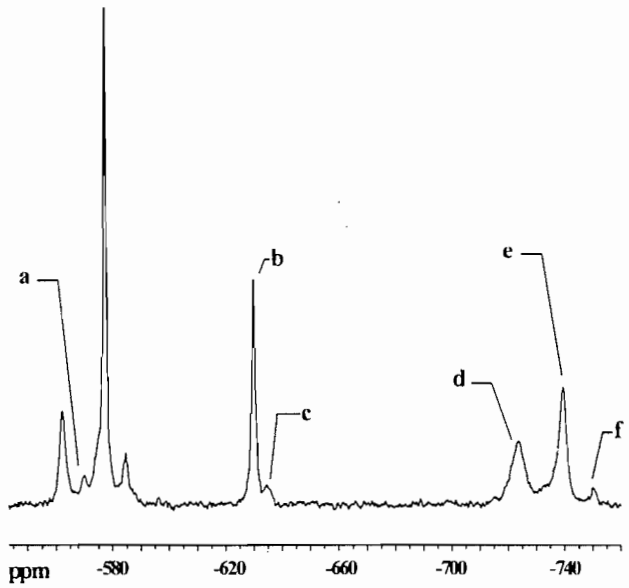


Fig. 1. ^{51}V NMR spectra showing the formation of the various vanadium complexes of *N,N*-dimethylhydroxylamine. Signal **a** may correspond to a product arising from complexation at the hydroxyl group of *N,N*-dimethylhydroxylamine ligand, signals **b**, **c**, and **d**, **e** and **f** correspond to the mono- and bisliganded bidentate products, respectively. The unassigned signals near −570 ppm, in order from low to high field, correspond to V_1, V_2 (partially superimposed on V_4), V_4, and V_5. Conditions of the experiments: 1.0 M KCl; 20 mM HEPES buffer; pH 7.2; 3.0 mM total vanadate; 3.0 mM *N,N*-dimethylhydroxylamine.

Results and discussion

N,N-Dimethylhydroxylamine (DMHA) reacts with vanadate to give a yellow solution consisting of a number of product complexes as evidenced by ^{51}V NMR spectroscopy. Figure 1 shows the results of mixing dimethylhydroxylamine with vanadate. The ^{51}V NMR spectrum shows two sets of product signals, one located near −630 ppm and the second near −740 ppm. These signals lie in the chemical shift region typical for peroxovanadium complexes (11, 12, 28–30). Within the −740 ppm set of signals, two types were observed (Fig. 1). Two broad (Fig. 1; **d**, **e**) and one comparatively sharp signal (Fig. 1; **f**) were found. A minor component was also observed in the −630 ppm region of the spectrum. This component (Fig. 1; **c**) gave rise to a rather broad signal compared to the major product (Fig. 1; **b**) in this region of the spectrum.

© 1997 NRC Canada

Can. J. Chem. Downloaded from www.nrcresearchpress.com by 88.146.161.215 on 09/08/12
For personal use only.

Table 1. Crystallographic data for the structure determination of $[V(O)(ONMe_2)_2]_2O$ at 213 K.

Parameter		Parameter	
Formula	$V_2O_7N_4C_8H_{24}$	Crystal system	Orthorhombic
fw	390.18	Space group	$P22_12_1$
a (Å) [a]	7.0955(9)	ρ_c (g cm^{-3})	1.540
b (Å)	10.2313(12)	λ(Mo Kα_1) (Å)	0.70930
c (Å)	11.5942(11)	μ(Mo Kα) (cm^{-1})	11.1
V (Å^3)	841.69	Min–max 2θ (°)	4–56
Z	2	Transmission [b]	0.779–0.842
Temperature (K)	213	Crystal dim. (mm)	0.13 × 0.22 × 0.40
GoF[c]	1.46	R_F [d]	0.021
		R_{wF} [e]	0.024

[a]Cell dimensions were determined from 64 reflections ($40° \le 2\theta \le 50°$).
[b]The data were corrected for the effects of absorption by the Gaussian integration method.
[c]GoF = $[\Sigma(w(F_o - F_c)^2)$ /degrees of freedom$]^{1/2}$.
[d]$R_F = \Sigma||F_o| - |F_c||/\Sigma|F_o|$, for 1141 data ($I_0 \ge 2.5\sigma(I_0)$).
[e]$R_{wF} = [\Sigma(w(|F_o| - |F_c|)^2)/\Sigma(wF_o^2)]^{1/2}$ for 1141 data ($I_0 \ge 2.5\sigma(I_0)$); $w = [\sigma(F_o)^2 + 0.0001F_o^2]^{-1}$.

Table 2. Fractional atomic coordinates and equivalent isotropic or isotropic temperature factors (Å^2) for $[V(O)(ONMe_2)_2]_2O$ at 213 K.

Atom	x	y	z	$U_{eq/iso}$ [a]
V	0.22494(5)	0.11343(3)	0.11404(3)	0.0194
O(1)	0.16739(32)	0.00000	0.00000	0.0225
O(2)	0.39623(23)	0.08001(17)	0.19877(14)	0.0311
O(3)	0.01704(24)	0.16789(16)	0.20231(14)	0.0268
O(4)	0.2448(3)	0.29005(14)	0.07080(15)	0.0305
N(1)	0.0225(3)	0.03235(17)	0.22060(16)	0.0219
N(2)	0.3842(3)	0.22873(19)	0.00493(19)	0.0263
C(1)	–0.1465(4)	–0.0323(3)	0.17804(22)	0.0277
C(2)	0.0611(4)	0.0023(3)	0.34198(22)	0.0325
C(3)	0.3463(4)	0.2397(3)	–0.1190(3)	0.0355
C(4)	0.5715(5)	0.2752(3)	0.0369(3)	0.0407
H(11)	–0.131(4)	–0.126(3)	0.1809(22)	0.036(4)
H(12)	–0.248(4)	–0.007(3)	0.2196(23)	0.036(4)
H(13)	–0.164(4)	–0.014(3)	0.1078(23)	0.036(4)
H(21)	0.083(4)	–0.090(3)	0.3468(22)	0.043(5)
H(22)	0.175(5)	0.037(3)	0.369(3)	0.043(5)
H(23)	–0.035(4)	0.029(3)	0.384(3)	0.043(5)
H(31)	0.417(4)	0.179(3)	–0.1596(22)	0.031(4)
H(32)	0.216(4)	0.2242(25)	–0.1305(24)	0.031(4)
H(33)	0.365(4)	0.322(3)	–0.1446(21)	0.031(4)
H(41)	0.663(4)	0.229(3)	–0.002(3)	0.048(5)
H(42)	0.576(4)	0.365(3)	0.0175(25)	0.048(5)
H(43)	0.589(4)	0.269(3)	0.118(3)	0.048(5)

[a]U_{eq} is the cube root of the product of the principal axes of the thermal ellipsoid.

An additional product signal was observed at −571 ppm (Fig. 1; **a**). This latter signal is thought to originate from an ester type of product formed between vanadate and the hydroxyl group of the ligand as is typically observed for alcohols (31–33). The stoichiometry of the products formed can easily be ascertained by vanadate and ligand concentration studies. The initial concentration study indicates that the ratios of vanadium to DMHA are 1:1 and 1:2 for the −630 and −740 ppm products, respectively. The equilibrium equation for the formation of two kinds of products can be written as eqs. [1] through [3], where V_1 refers to vanadate, ℓ to ligand (DMHA) and $V\ell_1$ and $V\ell_2$ represent, overall, the mono- and bisligand products, respectively. The formation constants for the individual components of each set are then readily obtained from the relative concentrations within each set.

$$[1] \quad [V_1] + [\ell] \overset{K_{01}}{\rightleftharpoons} [V\ell_1], \qquad [V_1]\,[\ell]\,K_{01} = [V\ell_1]$$

© 1997 NRC Canada

Table 3. Selected intramolecular distances (Å) and angles (°) for $[V(O)(ONMe_2)_2]_2O$ at 213 K.

		Corr.[a]			Corr.[a]
V—O(1)	1.806(1)	1.815	O(3)—N(1)	1.403(3)	1.409
V—O(2)	1.600(2)	1.608	O(4)—N(2)	1.398(3)	1.404
V—O(3)	1.880(2)	1.887	N(1)—C(1)	1.455(3)	1.461
V—O(4)	1.881(2)	1.887	N(1)—C(2)	1.466(3)	1.472
V—N(1)	2.069(2)	2.073	N(2)—C(3)	1.467(4)	1.473
V—N(2)	2.066(2)	2.070	N(2)—C(4)	1.459(4)	1.465
V-O(1)-V′[b]		153.87(14)	O(2)-V-O(4)		108.19(8)
O(1)-V-O(2)		118.95(8)	O(2)-V-N(1)		94.31(8)
O(1)-V-O(3)		114.31(9)	O(2)-V-N(2)		94.73(8)
O(1)-V-O(4)		116.05(6)	O(3)-V-O(4)		85.36(7)
O(1)-V-N(1)		91.29(7)	O(3)-V-N(2)		126.39(8)
O(1)-V-N(2)		92.43(7)	O(4)-V-N(1)		126.63(7)
O(2)-V-O(3)		108.98(8)	N(1)-V-N(2)		167.05(8)
V-N(1)-C(1)		123.49(15)	V-N(2)-C(3)		122.90(16)
V-N(1)-C(2)		121.84(16)	V-N(2)-C(4)		121.92(18)
O(3)-N(1)-C(1)		112.03(18)	O(4)-N(2)-C(3)		111.79(19)
O(3)-N(1)-C(2)		110.95(18)	O(4)-N(2)-C(4)		111.05(20)
C(1)-N(1)-C(2)		112.58(20)	C(3)-N(2)-C(4)		113.02(22)

[a]Distances corrected for thermal motion using a rigid-body model.
[b]Prime(′) indicates the symmetry-related position $(x, -y, -z)$.

Can. J. Chem. Downloaded from www.nrcresearchpress.com by 88.146.161.215 on 09/08/12
For personal use only.

[2] $[V_1] + 2[\ell] \overset{K_{02}}{\rightleftharpoons} [V\ell_2], \qquad [V_1]\,[\ell]^2\,K_{02} = [V\ell_2]$

[3] $[V\ell_1] + [\ell] \overset{K_{12}}{\rightleftharpoons} [V\ell_2], \qquad [V\ell_1]\,[\ell]\,K_{12} = [V\ell_2]$

Initial studies revealed that the overall formation constants are large for both the Vℓ and Vℓ_2 products. As a consequence it was necessary to use the conservation equation, eq. [4], in order to properly specify the free ligand concentration as a

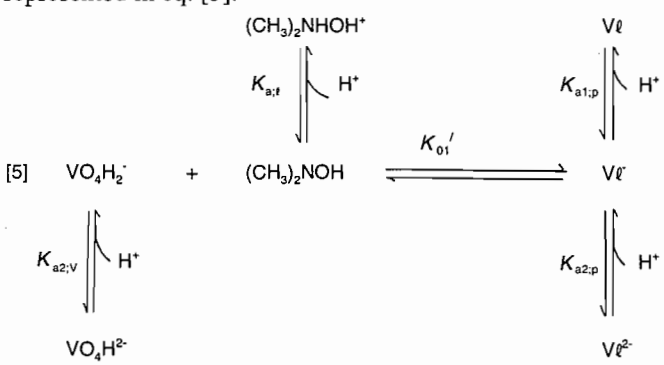
[4] $c\ell_t = [\ell] + [V\ell] + 2[V\ell_2]$

function of total ligand concentration ($c\ell_t$) and concentration of mono- and bisligand products.

The results of the ligand concentration study for both mono- and bisligand products at constant pH are summarized in Fig. 2. The total concentration of the products centered around −630 ppm (**b** + **c**, Fig. 2*A*) and those around −740 ppm (**e** + **f**, Fig. 2*B*) were utilized to obtain the pH-dependent formation constants K_{01}, K_{02}, and K_{12} ($K_{02} = K_{01}\,K_{12}$). These formation constants have the values $(7.5 \pm 0.2) \times 10^3\ M^{-1}$, $(8.1 \pm 0.7) \times 10^6\ M^{-2}$, and $(1.1 \pm 0.1) \times 10^3\ M^{-1}$, respectively, at pH 6.7. See Table 4 for a more detailed breakdown of these values.

The study of the vanadium and DMHA systems with varying pH showed that the signals originating from bisligand products are sensitive towards hydrogen ion concentration, while the signals at −630 ppm are pH insensitive. A gradual increase in pH led to a change in relative signal intensities of the broad and sharp components of the bisligand products. With a stepwise increase in pH from pH 6.5 to pH 8.0, there was a corresponding decrease and increase in intensities of the broad and sharp components, respectively. Figure 3 shows the change in spectral pattern as a function of hydrogen ion concentration within the pH range 6.5–8.0. Above pH 8.0 the intensity of the sharper signal starts decreasing and ultimately, at about pH 9.1, it no longer appears in the spectrum. At higher ligand concentrations, the pH range over which this signal is observed would doubtless be extended. Interestingly, an additional product signal is observed in the pH range above pH 9.2, but it is only easily observed when the ligand concentration is significantly in excess. The intensity of this signal attains its maximum at about pH 9.5 and the chemical shift at this pH value is −698 ppm. Ligand and vanadate concentration studies of the product at pH 9.5 show that it also is a monovanadium bisligand compound with a comparatively low formation constant, $K_{12} = 46 \pm 2\ M^{-1}$ (Fig. 4). The chemical shift of this signal was found to vary with pH, suggesting the product has a pK_a. However, because of its rather limited range of occurrence under the conditions of our studies, no quantitative analysis of the pH variation studies of this compound was made.

Detailed analysis of a pH-variation study requires consideration of the pK_a's of both the reactants and products. The pH-dependent equilibrium equation for the monoligand product is represented in eq. [5].



© 1997 NRC Canada

Can. J. Chem. Downloaded from www.nrcresearchpress.com by 88.146.161.215 on 09/08/12
For personal use only.

Fig. 2. A graphical representation of the results from ligand concentration studies carried out at constant pH. The linear relationships of these graphs are consistent with *A*, $V\ell$ (eq. [1]), and *B*, $V\ell_2$ (eq. [2]), stoichiometry, respectively, for the −630 ppm and −740 ppm products of Fig. 1. Conditions of the experiments: 1.0 M KCl; 20 mM HEPES buffer; pH 6.7; 3.0 mM total vanadate; variable *N,N*-dimethylhydroxylamine total concentration, 1–3.8 mM.

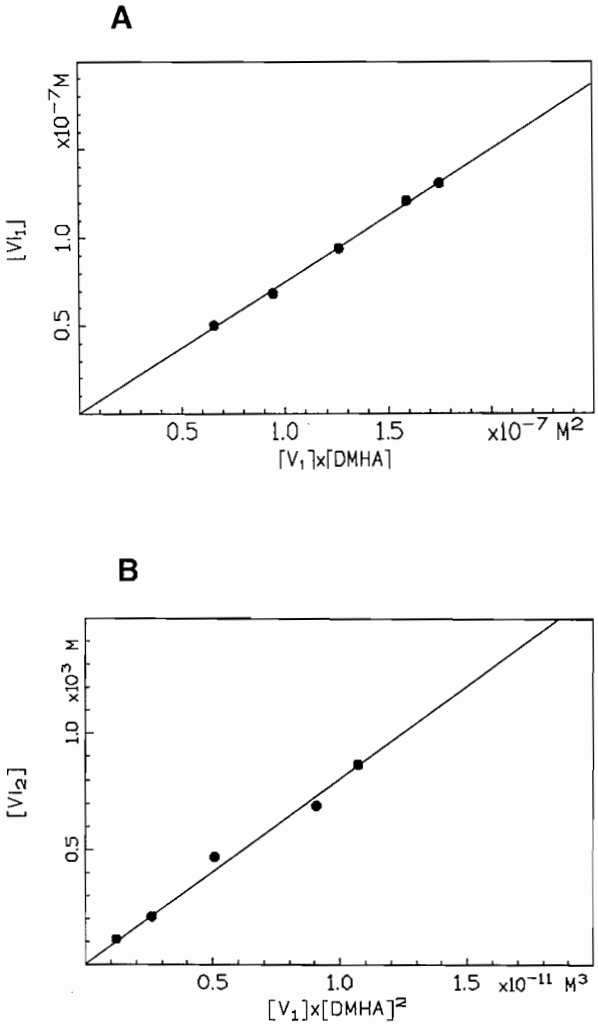


Fig. 3. ^{51}V spectra showing the influence of pH on the products of the reaction of vanadate with *N,N*-dimethylhydroxylamine. Conditions of the experiments: 1.0 M KCl; 20 mM HEPES buffer; 3 mM total vanadate; 5 mM total *N,N*-dimethylhydroxylamine; variable pH, pH 6.5–8.0, top to bottom spectra.

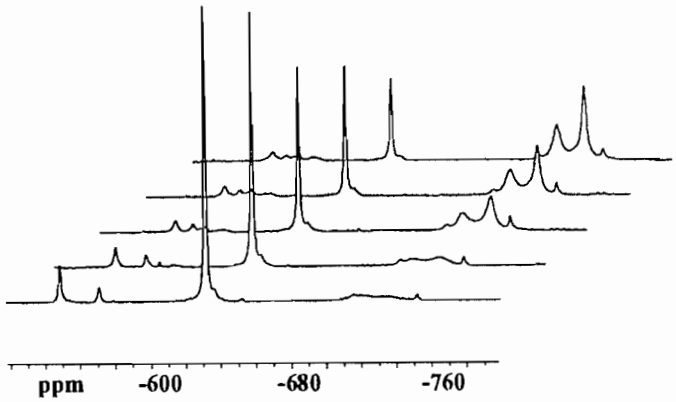
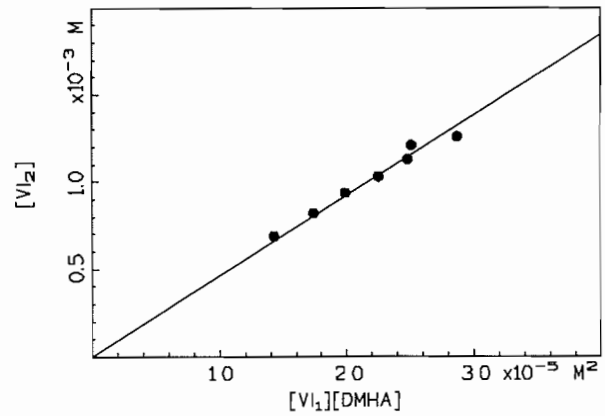


Fig. 4. A graphical representation of the formation of the −698 ppm product as a function of added vanadate at pH 9.5. The linear relationship is consistent with the occurrence of a single vanadium in this product. Conditions of the experiments: 1.0 M KCl; 20 mM HEPES buffer; 15 mM *N,N*-dimethylhydroxylamine; variable total vanadate concentration, 2.0–5.0 mM.



Since the values for $pK_{a2;V}$ (8.2), $pK_{a;\ell}$ (5.28)(34), and pH are known, all other quantites required for analysis of the pH-independent results can be obtained from eq. [5]. Initial studies revealed that the chemical shift of the monoligand product is pH independent. This suggested that the monoligand product does not have a pK_a within the pH range of this study, and was supported by plotting the total concentration of the monoligand products, $[V\ell]$, against the left-hand-side quantitities, $[VO_4H_2^-][(CH_3)_2NOH]$, of eq. [5] as a function of the hydrogen ion concentration. A linear relationship was obtained. This means that, for this pH range, there is no significant change in charge state of the product. If there were, curvature would be observed in this graph. The value $K'_{01} = (6.5 \pm 0.2) \times 10^3$ M^{-1} was obtained from the slope of the plot. To confirm that the product had no pK_a within the range of pH variation of this study, ligand concentration studies were carried out at various pH values and the results analysed according to eq. [1]. These pH-dependent, K_{01}, formation constants can then be written in terms of the pH-independent constant, K'_{01}, of eq. [5], and the hydrogen ion concentration. The relationship between K_{01} and K'_{01} is given by eq. [6], where it is assumed that the product can lose a proton as the pH is raised. A similar equation can be written if a proton were gained in the reaction.

$$[6] \quad (1 + K_{a2;V}/[H^+])\,(1 + [H^+]/K_{a;\ell})\,K_{01} = K'_{01}\,(1 + K_{a1;p}/[H^+])$$

A plot of the term on the left of eq. [6] versus $1/[H^+]$ gave a straight line with no observable slope. Since the line had no slope, it is evident that a proton is neither being gained nor released within the pH range (6.5–8.0) of this study. From the intercept of this line a value for K'_{01} of $(6.4 \pm 0.5) \times 10^3$ was obtained. With this value for K'_{01} and, because it cannot be observed, by neglecting the term in $K_{a1;p}$, eq. [6] can be used to calculate the pH-dependent formation constant, K_{01}, for any

© 1997 NRC Canada

Can. J. Chem. Downloaded from www.nrcresearchpress.com by 88.146.161.215 on 09/08/12
For personal use only.

Table 4. ^{51}V chemical shifts and formation constants for various products of the reaction of aqueous vanadate with dimethylhydroxylamine.

Equilibrium equation	Chemical shift[a] (ppm)	Equilibrium constant[b]	pH
$V_1 + \ell \rightleftharpoons V\ell$	−571 (**a**)	$(7.2 \pm 1.4) \times 10^2$ M^{-1}	6.7
$V_1 + \ell \rightleftharpoons V\ell$	−630 (**b**)	$(6.6 \pm 0.2) \times 10^3$ M^{-1}	6.7
$V_1 + \ell \rightleftharpoons V\ell$	−635 (**c**)	$(0.9 \pm 0.3) \times 10^3$ M^{-1}	6.7
$V_1 + 2\ell \rightleftharpoons V\ell_2$[c]	−724 (**d**), −740 (**e**)	$(7.5 \pm 0.2) \times 10^6$ M^{-2}	6.7
$V_1 + 2\ell \rightleftharpoons V\ell_2$	−750 (**f**)	$(0.6 \pm 0.1) \times 10^6$ M^{-2}	6.7
$V\ell + \ell \rightleftharpoons V\ell_2$[c]	−724 (**d**), −740 (**e**)	$(1.1 \pm 0.1) \times 10^3$ M^{-1}	6.7
$V\ell + \ell \rightleftharpoons V\ell_2$	−698	46 ± 2 M^{-1}	9.5
$V_1^- + \ell \rightleftharpoons V\ell^-$	−630 (**b**)	$(6.5 \pm 0.2) \times 10^3$ M^{-1}	6.5–8.0
$V_1^- + 2\ell^+ \rightleftharpoons V\ell_2 + H^+$[c]	−724 (**d**), −740 (**e**)	$(1.3 \pm 0.1) \times 10^3$ M^{-1}	6.5–8.0
$V\ell_2H^+ \rightleftharpoons V\ell_2 + H^+$	−724 (**d**, var)	$(2.2 \pm 0.8) \times 10^3$	1.5–7.0
$V\ell_2H^+ \rightleftharpoons V\ell_2 + H^+$	−740 (**e**, var)	$(6.3 \pm 0.8) \times 10^3$	1.5–7.0

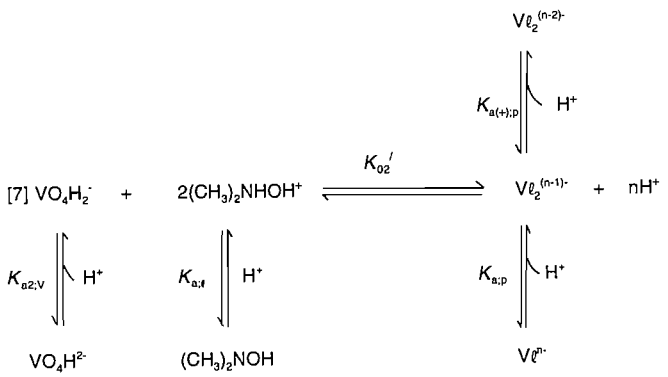
[a]All chemical shifts are for pH 7.2 except that for the pH 9.4 value of the −698 ppm product. The assignments **a**, **b**, **c**, **d**, **e**, **f** correspond to the products so labelled in Fig. 1, var means the chemical shift varies from the pH 7.2 value with change in pH.

[b]The pH-independent formation constants and any corresponding pK_a values can be used to calculate formation constants for any pH that falls within the range of the pH study (see text).

[c]The formation constants are for the total of the two products that, above pH 5, are formed in an approximate 1:1 ratio for the −724 and −740 ppm products, respectively. Below pH 5, the pK_a values influence the ratio of products.

pH. The possibility of the existence of a pK_a for the monoligand product outside the pH range of this study can not be ruled out.

A pH variation study, for the range 6.5–8.0, was also carried out at higher ligand concentration in order to gather information concerning the bisligand product. The equilibrium reaction for these products can be written in a manner analogous to eq. [5]. The chemical shift of the signals originating from the



bisligand products remained the same over the pH range 6.5–8. This observation suggested, but certainly did not prove, that none of the bisligand products had a pK_a within the pH range of our study. Other studies had suggested that the products giving rise to the broader NMR signals had pK_a's below 6.5. To test this, ^{51}V NMR spectra were recorded for the acidic pH range of 1.5–7.0. For this study, an excess of ligand (V:ligand molar ratio of ~3 mM:20 mM) was used. Under these conditions, the vast majority of vanadate is converted into complexes so that no observable amounts of decavanadate were formed.

The decrease in pH led to a sharpening of the broad signals and an accompanying change in chemical shift. The behavior of the sharp component, Fig. 1: **f**, of the bisligand product signals was quite different from the other components. The intensity of the sharper component decreased with the increase in hydrogen ion concentration and the signal was not observed below pH 5.5. These observations are in keeping with the higher pH study and support the suggestion that the vanadium is coordinated in two different geometries. The pH dependence of the chemical shift values was utilized to determine the pK_a of the products giving rise to the broad NMR signals. In Fig. 5, chemical shift values for signals **d** and **e** of Fig. 1 are plotted against pH and the plots show an inflection point in both the cases. This pH-dependent chemical shift derives from protonation/deprotonation of the products and can be related to their pK_a's by eq. [8],

$$[8] \quad pH = pK_a + \log [(\delta_L - \delta_O) / (\delta_O - \delta_H)]$$

where δ_O is the observed chemical shift, δ_L is the limiting chemical shift at low pH, and δ_H is the corresponding value at high pH. A plot of pH versus the logarithm term provided a line of intercept pK_a and unit slope. The pK_a's were 3.35 ± 0.15 and 3.80 ± 0.15, for the bisligand products **d** and **e** (Fig. 1), respectively.

The pK_a values obtained for the major bisligand products fall within the acidic pH range and suggest that the quantitative analysis of the results of the pH variation study from pH 6.5 to 8.0 does not require consideration of a protonation/deprotonation state of the products. The total vanadate and ligand concentration was maintained constant throughout the pH-variation study. On plotting the data appropriately for eq. [7], (Fig. 6) a linear relationship was obtained only for a value of $n = 1$ for the major product and no evidence of curvature was obtained. This result showed that the product does not carry a charge and the absence of curvature in the graph was consistent with the above proposal that these products do not

© 1997 NRC Canada

Can. J. Chem. Downloaded from www.nrcresearchpress.com by 88.146.161.215 on 09/08/12
For personal use only.

Fig. 5. The influence of variation in pH on the chemical shifts of the major bisligand products. Conditions of the experiments: variable pH, 1.2–7.0; 3.0 mM total vanadate; 20 mM total *N,N*-dimethylhydroxylamine; 1.0 M KCl; 20 mM HEPES buffer.

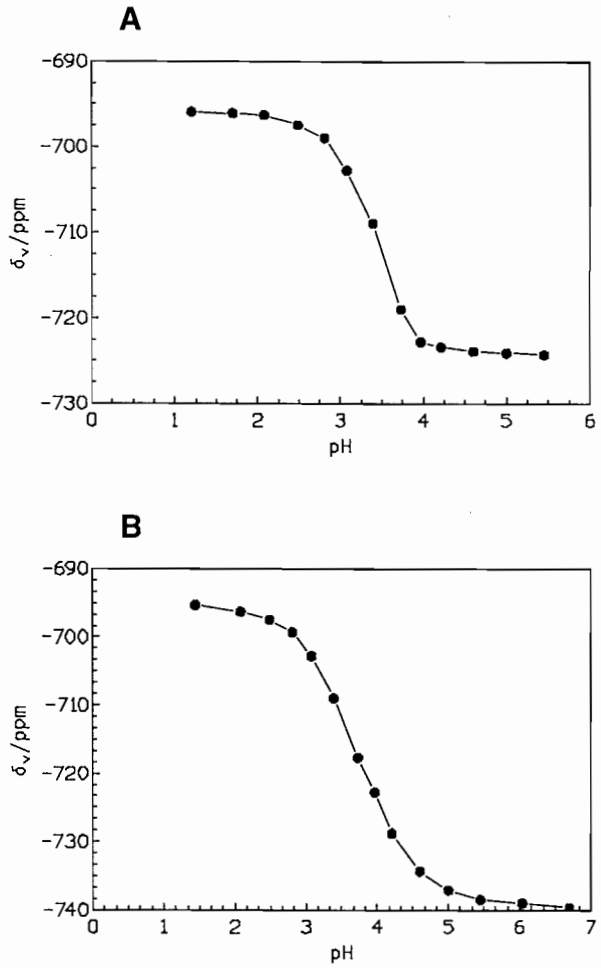


Fig. 6. Graphical representation of the formation of the bisligand products as a function of pH. The graph is plotted in accordance with eq. [7]. Conditions of the experiments: variable pH, pH 6.8–8.0; 3.0 mM total vanadate; 3.0 mM total *N,N*-dimethylhydroxylamine; 1.0 M KCl; 20 mM HEPES buffer.

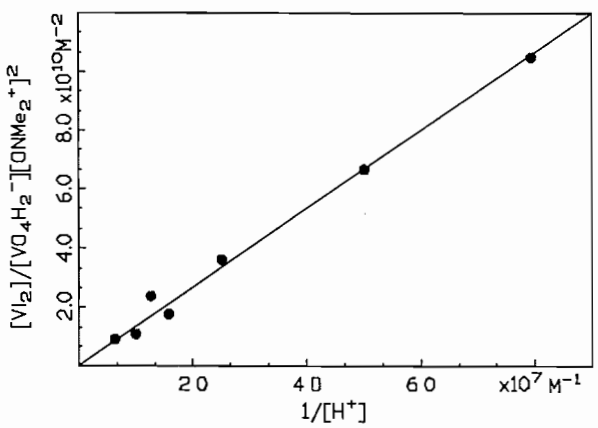
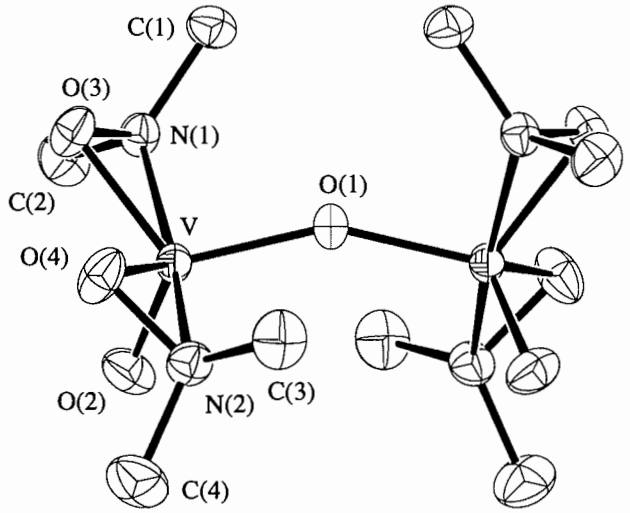


Fig. 7. The molecular structure of $[V(O)(ONMe_2)_2]_2O$ at 213 K. 50% Probability thermal ellipsoids are shown for all non-hydrogen atoms.



have a pK_a near this pH range. This is in keeping with the rapid loss of this product with increase in pH. The overall pH-independent formation constant K'_{02} for the major bisligand products (**d** + **e**, Fig. 1) was determined to be $(1.3 \pm 0.1) \times 10^3$ M^{-1}. The minor bisligand product persists with increase in pH and this suggests this product does have a pK_a and possibly a different charge state from the major products. Studies of methylhydroxylamine–vanadate have, however, shown that, for that system, the corresponding compound does not carry a charge. Although the major products do not carry a charge at neutral pH, they are protonated at lower pH. Taken together, this evidence clearly shows that there are two types of bisligand compound that probably vary in their coordination geometry. The two broad signals, corresponding to the major bisligand products, are assigned to one type of complex and are ascribed to stereoisomers. From the studies here, it is not possible to know whether there is a change in coordination when the neutral products are protonated. Table 4 summarizes the formation constants measured for the various products.

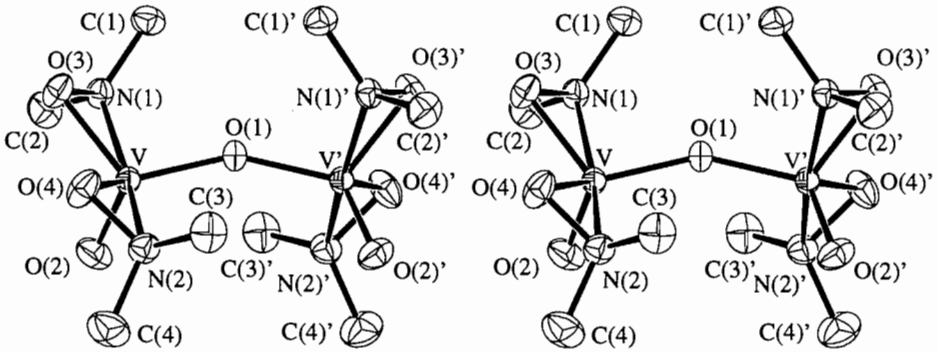
To obtain more information about these materials, an attempt was made to obtain a product in solid form. This proved successful and reaction of tetraethylammonium vanadate with DMHA at pH 8 (see Experimental) afforded a yellow crystalline solid in good yield (70%). The yellow, needle-shaped crystals were stable at room temperature for extended periods of time and suitable for X-ray structural studies.

The molecular structure is shown in Fig. 7. Bond distances and angles are given in Table 3.[3] In the structure of this com-

[3] Additional crystallographic details, and tables of anisotropic thermal parameters, additional bond lengths and angles, torsion angles, and least-squares plane have been put on deposit. Copies of materials on deposit may be purchased from: The Depository of Unpublished Data, Document Delivery, CISTI, National Research Council Canada, Ottawa, Canada K1A 0S2. The crystallographic details and tables of bond lengths and angles have also been deposited with the Cambridge Crystallographic Data Centre, and can be obtained on request from The Director, Cambridge Crystallographic Data Centre, University Chemical Laboratory, 12 Union Road, Cambridge, CB2 1EZ, U.K.

© 1997 NRC Canada

Fig. 8. A molecular stereodiagram of $[V(O)(ONMe_2)_2]_2O$ at 213 K. 50% Probability thermal ellipsoids are shown for all non-hydrogen atoms.



pound, no intermolecular separations significantly less than the sums of the appropriate van der Waals radii (35) were found. A structurally similar diethylhydroxamidovanadium(V) complex was previously prepared in a nonaqueous solvent system (36). This correspondence in structure, perhaps, is not surprising since neither complex is ionic.

The molecule has crystallographic twofold symmetry, the *2* axis passing through O(1). The vanadium atom is six-coordinate. As can be judged from the stereodiagram, Fig. 8, the arrangement about vanadium might be described as approximately tetrahedral, considering the center of the N—O bond in each dimethylhydroxamide as one vertex. The N and O atoms of the two dimethylhydroxamido ligands on each vanadium are very nearly coplanar. Similar coplanarity is ubiquitous in bisperoxovanadium complexes and this suggests the operation of a fundamental physical process leading to this characteristic behaviour. The deviations from the best least-squares plane through the four atoms are: O(3) −0.011(3) Å, O(4) 0.012(3) Å, N(1) 0.009(3), and N(2) −0.011(3) Å. The fact that both the bridging and terminal oxo groups lie well out of this plane on either side (O(1) −1.317(4) Å, O(2) 1.569(3) Å), while the vanadium atom is only slightly displaced towards the terminal oxo (0.087(2) Å), precludes describing this geometry as a pentagonal pyramid as is often found for oxoperoxovanadate(V) complexes. For example, in $[V(O)(O_2)_2(NH_3)][NH_4]$ (37), where the complex anion lies on a mirror plane and thus the atoms of the two mirror-related peroxo groups are precisely coplanar, the deviations of the other atoms from this plane are N(ammine) 0.29 Å, O(vanadyl) 2.12 Å, and V 0.52 Å. The pentagonal pyramidal or bipyramidal arrangements in such complexes (37–43) appear to be a consequence of coordination by a seventh ligand, such as the long (2.926(3) Å) intermolecular secondary bond to an adjacent vanadyl oxygen atom in $[V(O)(O_2)_2(NH_3)][NH_4]$.

The structure can also be compared to that exhibited by the $[(V(O)(O_2)_2)_2O]^{4-}$ anion as displayed in its tetraammonium salt (44). A major difference is the absence, in the dimethylhydroxylamine complex, of the seventh coordination site *trans* to the terminal oxo group. In $[(V(O)(O_2)_2)_2O][NH_4]_4$, this seventh site is occupied by a peroxo-oxygen atom that is primarily bound to the other vanadium atom within the molecule. The methyl groups in the present structure apparently preclude the formation of an analogous N—V secondary coordinate bond as well as obstructing further vanadium contacts to adjacent molecules and dictating the stereochemistry of the complex. The absence of intramolecular bridging by the dimethylhydroxylamine group allows the V-O(1)-V′ angle to open out to 153.87(14)° as compared to 98.9(1)° in $[(V(O)(O_2)_2)_2O][NH_4]_4$ (44). A further consequence is that the V—O(1) bond is much shorter (1.806(1) Å) than the analogous V—O bonds in $[(V(O)(O_2)_2)_2O][NH_4]_4$ (2.013(2), 1.994(2) Å). The implication of bond order greater than 1 for the V—O(1) bond and possible π-orbital conjugation through O(1) is supported by the approximately orthogonal torsional juxtaposition of the two $V(O)(ONMe_2)_2$ groups when projected along the V--V′ vector (e.g., N(1)-V--V′-N(1)′ 90.1(1)°; N(2)-V--V′-N(2)′ 113.4(1)°; O(2)-V--V′-O(2)′ −73.3(1)°; where (′) indicates the symmetry equivalent position (x, $-y$, $-z$)). Furthermore, the 153.87(14)° V-O(1)-V′ bond angle does not appear to be sterically imposed as there are no contacts between the ligands on the opposing vanadium atoms less than the sums of the appropriate atomic van der Waals radii.

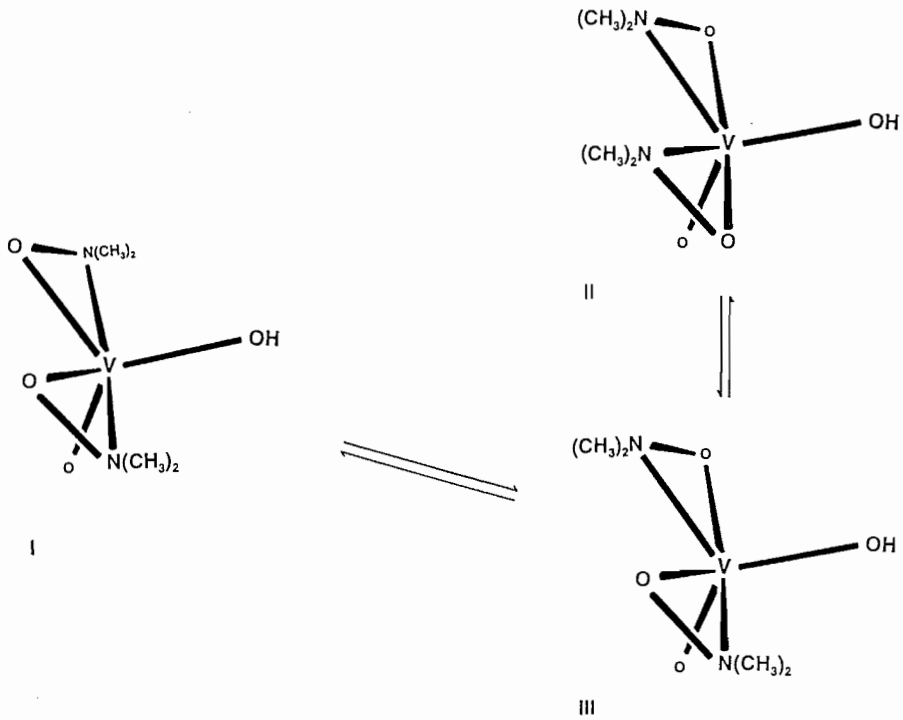
The other V—O bond lengths are in good agreement with their counterparts in the array of known structures of oxobisperoxovanadate(V) complexes (37–43), while the V—N distances (V—N(1) 2.069(2) Å, V—N(2) 2.066(2) Å) are, quite reasonably, longer than the analogous V—O distances (typically about 1.9 Å). Consistent with this are the somewhat shorter O—N bonds (O(3)—N(1) 1.403(3) Å, O(4)—N(2) 1.398(3)) compared to the range of corresponding O—O bond lengths (1.451(6) – 1.474(4) Å).

The crystals dissolved readily in many organic solvents but were less soluble in water. When $CDCl_3$ was used as the solvent, a single signal at −728 ppm was observed in the ^{51}V NMR spectrum. This chemical shift is close to that reported for vanadate complexes with *N,N*-diethylhydroxylamine (−711 ppm) and *N,N*-dibenzylhydroxylamine (−696 ppm). When dissolved in D_2O, two signals, −726 ppm and −740 ppm, were found. Since these signals were of different intensities, the presence of two different complexes was evident. ^1H NMR spectra of the complex also were recorded for $CDCl_3$ and D_2O solvents and the results obtained were in keeping with the vanadium NMR spectra. The important feature of the proton spectrum in $CDCl_3$ was the presence of two sharp signals at 3.3 and 3.0 ppm that are assignable to the two types of ligand methyl groups in the dimeric complex. In D_2O, the spectrum exhibited two very broad signals in the range 2.5–3.5 ppm. This spectrum was indicative of a reasonably fast equilibration between the two different forms of the complex.

Can. J. Chem. Downloaded from www.nrcresearchpress.com by 88.146.161.215 on 09/08/12
For personal use only.

© 1997 NRC Canada

Scheme 1.



The ^{51}V NMR spectrum of the $[V(O)(ONMe_2)_2]_2O$ complex in acetone (3 mL) exhibited a sharp signal at −726 ppm. Gradual addition of water (total of 3 mL in 0.5 mL portions) to the above solution led to decrease in intensity of this peak. Simultaneously with the decrease in intensity of this peak, two other peaks, −722 to −738 ppm, appeared in the spectrum. The intensity of these two peaks increased with each addition of water. These three species, in each acetone–water solution, rapidly attained equilibrium, after which no appreciable change in intensities was observed. The signal at −726 ppm is attributed to a dimeric $[V(O)(ONMe_2)_2]_2O$ with a structure corresponding to the crystalline solid.

An ^1H NMR variable temperature study of the crystalline compound dissolved in D_2O (298–275 K) and in $(CD_3)_2CO/D_2O$ (273–248 K) revealed that the broad signal observed at room temperature sharpened with decrease in temperature, to give a well-resolved spectrum of several signals at the lowest temperature. This suggested that the broadening derived from a chemical exchange process that interconverted the two isomers. The low-temperature spectrum was somewhat complicated by the presence of more than two sets of signals, probably because of the presence of binuclear isomers. Since the vanadium signals, in frequency units, were much farther apart than the proton signals (~1600 Hz compared to ~300 Hz) the exchange broadening was not clearly observed in the vanadium spectrum. It is evident from these studies that, in an aqueous environment, hydrolysis of the dimer occurs to provide at least two product complexes that correspond to the broad signals of the equilibrium studies. In principle, a third product is possible. Its vanadium NMR signal may lie under either of those from the other products or its formation may be disfavoured because of steric interations or possibly electronic effects. Steric interactions could arise from the presence of the ligand methyl groups while electronic influences would result from the relative orientations of the oxygens and nitrogens of the two hydroxamido ligands.

[9] $V\ell_2(1) \rightleftharpoons V_2\ell_4 \rightleftharpoons V\ell_2(2)$

As found from the variable temperature proton spectra, these two products are undergoing quite rapid equilibration. This is in keeping with our previous suggesion that they are stereoisomers. This proposal is supported by a longer term study that showed that hydrolysis to free vanadate or the monoligand compound is, comparatively, very slow, requiring in the order of hours for hydrolysis to occur. This strongly suggests that the isomerization does not involve bond breaking but rather corresponds to a simple, in-plane, end-for-end rotation of the hydroxamido group. Any bond breakage in the kinetic pathway would be expected to promote dissociation.

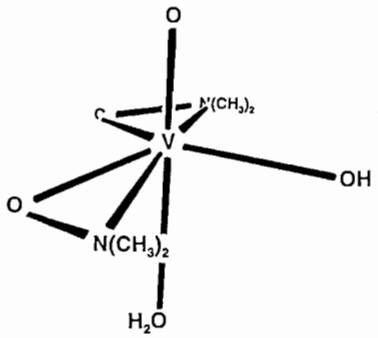
In agreement with the results of the equilibium pH variation study that shows these two products do not carry a charge, it is proposed that the coordination about vanadium in the two major bisligand products is similar to that found in the crystalline material, that is, the tetrahedral-like coordination depicted in Scheme 1. In Scheme 1, compound III is thought to correspond to the stereoisomer for which no vanadium NMR signal has been observed in this study. This isomer, of the three possible, has been selected on the basis that no X-ray study has yet reported a bishydroxamidovanadium complex for which the hydroxamido groups are in a *trans* arrangement to each other. Such an arrangement, however, could possibly occur and the corresponding complex be present in solution. Several X-ray

Can. J. Chem. Downloaded from www.nrcresearchpress.com by 88.146.161.215 on 09/08/12
For personal use only.

© 1997 NRC Canada

Can. J. Chem. Downloaded from www.nrcresearchpress.com by 88.146.161.215 on 09/08/12
For personal use only.

Scheme 2.



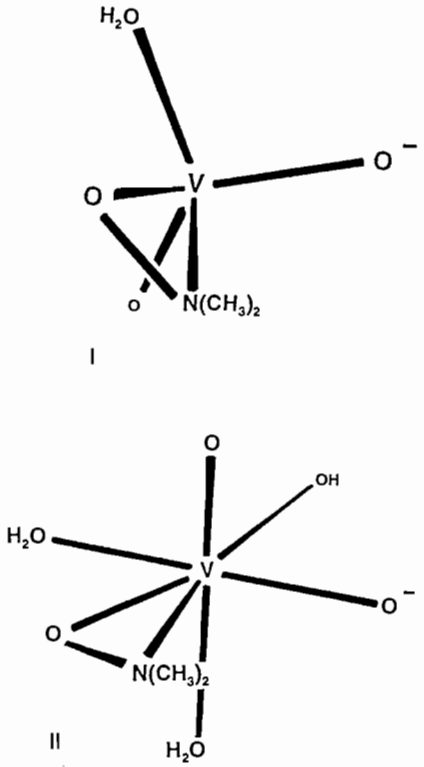
studies have reported structures where the oxygens of the two ligands are in close proximity as in Scheme 1, I (this work and refs. 36 and 45), and one report has shown the two nitrogens to be in close proximity, similar to Scheme 1, II (46). A very different arrangement in which the two hydroxamido moieties are oriented perpendicular to each other is found in a certain structural analogue of amavadin but, in this case, the multidentate ligand is constraining the system (47). The perpendicular orientation will, presumably, correspond to the intermediate in the isomerization observed here in the variable temperature ^{1}H NMR studies.

The minor bisligand complex (corresponding to signal **f**, Fig. 1) has different proton requirements than the major bisproducts. On this basis, it must have a different coordination geometry. It seems likely that it is heptacoordinate (Scheme 2), after the fashion proposed for bisperoxovanadates (12, 48). It should, however, be recognized that both pentagonal pyramidal (13, 49) and eight-coordinate structures (30) have been proposed for bisperoxovanadates. Formation of this product seems to be disfavoured by the presence of the two methyl groups on the nitrogen since a similar product is relatively much more readily formed from hydroxylamine and methylhydroxylamine (22). The influence may principally be a consequence of electronic influences since the pK_a values for *N,N*-dimethylhydroxylamine (pK_a = 5.28) is significantly lower than for *N*-methylhydroxylamine (pK_a = 6.00) and hydroxylamine (pK_a = 6.01) (34). On the other hand, the relative change in populations is not large enough to rule out small steric influences.

An additional bisligand compound is observed above pH 9. It is not highly favoured under the conditions of this study, having a formation constant a factor of 20 smaller than the major products (see Table 4). Its coordination geometry is unknown.

The coordination about vanadium in the monoligand products also is not known. The observation of two products suggests two different coordination schemes. Unless forced otherwise by the ligand, the tendency of vanadate coordination is to favour tetrahedral geometry so it seems likely that, if the predominant bisligand product has a tetrahedral-like coordination, the major monoligand product also does. In this case, a hydroxyl group would replace one of the DMHA ligands to give $(CH_3)_2NOVO(OH)_2$, which deprotonates to form the monoanionic product observed (Scheme 3, I). The second monoligand product, which is formed to an extent of about 12% of the total monoligand product, would then correspond to a higher coordination number complex (Scheme 3, II), most

Scheme 3.



probably a coordination similar to that proposed above for the minor bisligand product and for monoperoxovanadate (11,12).

A few other complexes are formed, all in very low proportions. Of these, only the product giving rise to the NMR signal at −571 ppm can be assigned a structure. It is highly likely that this signal corresponds to a vanadate ester formed between the hydroxylamine hydroxyl group and monovanadate. Its formation (Table 4) is relatively unfavoured when compared to the major products of this study but is highly favoured when compared to aromatic (32, 50) and aliphatic (33, 51, 52) alcohols.

The formation of these complexes with *N,N*-dimethylhydroxylamine compares very favourably with those from hydrogen peroxide (10, 28). In fact, the monoanionic monoligand product ($K_{01}' = (6.5 \pm 0.2) \times 10^3$ M^{-1}), Vℓ, is actually favoured by about a factor of 10 over that of the corresponding hydrogen peroxide complex ($K_{01}' = (6 \pm 2) \times 10^2$ M^{-1} (28)). The incorportion of the second ligand cannot be so easily compared because of the different proton requirements. However, at pH 6.7 the value for the reaction $V\ell + \ell \rightleftharpoons V\ell_2$ is K_{12} = $(1.7 \pm 0.6) \times 10^5$ M^{-1} for the formation of the bisperoxo derivative compared to $K_{12} = (1.1 \pm 0.1) \times 10^3$ M^{-1} for the corresponding reaction with *N,N*-dimethylhydroxylamine. The formation of the bisperoxo derivative from the monoligand precursor is therefore favoured by a factor of 100 compared to the corresponding reaction with dimethylhydroxylamine.

The observation of a reasonably fast rotational isomerization of the dimethylhydroxamide ligand suggests that a similar isomerization occurs with peroxo ligands. In this case, such an isomerization might be observed by partially ^{17}O enriching the hydrogen peroxide and observing the ^{17}O NMR spectrum.

© 1997 NRC Canada

The observation of a product that can be assigned to an end-on coordination to give a vanadate ester has potential implications for the function of haloperoxidases since it is very likely that similar complexes are formed with hydrogen peroxide and could have a role in the function of these enzymes.

Perhaps one of the most interesting findings of this study is that the dimethylhydroxamide ligand favours the formation of tetrahedral-like complexes rather than the trigonal bipyramidal-like structures of the hydrogen peroxide ligand. The more efficient electron donation by O-N compared to O-O could account for this. With increased electron density at the vanadium nucleus, there will be less propensity towards accepting ligands and thus expanding the coordination sphere. As discussed elsewhere for other ligands (29, 33, 53), similar subtle electronic influences have a significant impact on vanadate coordination and chemistry.

Acknowledgments

Thanks are gratefully extended to the Natural Sciences and Engineering Research Council of Canada for its financial support of this work.

References

1. E. de Boer, Y. van Kooyk, M.G.M. Tromp, H. Plat, and R. Wever. Biochim. Biophys. Acta, **869**, 48 (1986).
2. J.W.P.M. van Schijndel, L.H. Simons, E.G.M. Vollenbroek, and R. Wever. FEBS Lett. **336**, 239 (1993).
3. H. Plat, B.E. Krenn, and R. Wever. Biochem. J. **248**, 277 (1987).
4. R.E. Eady. Met. Ions Biolog. Syst. **31**, 363 (1995).
5. B.J. Hales, E.E. Case, J.E. Morningstar, M.F. Dzeda, and L.A. Mauterer. Biochemistry, **25**, 7251 (1986).
6. R.L. Robson, R.E. Eady, T.H. Richardson, R.W. Miller, M. Hawkins, and J.R. Postgate. Nature, **322**, 388 (1986).
7. H. Sigel and A. Sigel (*Editors*). *In* Metal ions in biological systems. Vol. 31. Marcel Dekker, Inc., New York, Basel, Hong Kong. 1995.
8. N.D. Chasteen (*Editor*). Vanadium in biological systems. Kluwer Academic Publishers, Dordrecht, Boston, London. 1990.
9. P. Schwendt, J. Tyrselova, and F. Pavelcik. Inorg. Chem. **34**, 1964 (1995).
10. A. Butler, M.J. Clague, and G.E. Meister. Chem. Rev. **94**, 625 (1994).
11. A.S. Tracey and J.S. Jaswal. Inorg. Chem. **32**, 4235 (1993).
12. A.S. Tracey and J.S. Jaswal. J. Am. Chem. Soc. **114**, 3835 (1992).
13. P. Schwendt. 13th Conf. Coord. Chem. Proc. 243 (1991).
14. A. Butler. *In* Vanadium in biological systems. *Edited by* N.D. Chasteen. Kluwer Academic Publishers, Dordrecht, Boston, London. 1990. pp. 25–49.
15. M.J. Clague and A. Butler. J. Am. Chem. Soc. **117**, 3475 (1995).
16. M. Bonchio, V. Conte, F. Di Furia, G. Modena, S. Moro, and J.O. Edwards. Inorg. Chem. **33**, 1631 (1994).
17. A.F. Ghiron and R.C. Thompson. Inorg. Chem. **29**, 4457 (1990).
18. H. Mimoun, L. Saussine, E. Daire, M. Postel, J. Fischer, and R. Weiss. J. Am. Chem. Soc. **105**, 3101 (1983).
19. E. Bayer, E. Koch, and G. Anderegg. Angew. Chem. Int. Ed. Engl. **26**, 545 (1987).
20. E. Bayer. Met. Ions Biolog. Syst. **31**, 407 (1995).
21. M.A. Nawi and T.L. Riechel. Inorg. Chim. Acta, **136**, 33 (1987).
22. P.C. Paul, S.J. Angus-Dunne, and A.S. Tracey. Can. J. Chem. **75**, 183 (1997).
23. E.J. Gabe, P.S. White and G.D. Enright. DIFRAC. A Fortran 77 control routine for 4-circle diffractometers. National Research Council, Ottawa. 1995.
24. E.J. Gabe, Y. LePage, J.-P. Charland, F.L. Lee, and P.S. White. J. Appl. Crystallogr. **22**, 384 (1989).
25. D.J. Watkin, J.R. Carruthers, and P.W. Betteridge. CRYSTALS. Chemical Crystallography Laboratory, University of Oxford, Oxford, England. 1984.
26. International tables for X-ray crystallography. IV. Kynoch Press, Birmingham. 1975. p. 99.
27. V. Shomaker and K.N. Trueblood. Acta Crystallogr. Sect. B: Struct. Crystallogr. Cryst. Chem. **B24**, 63 (1968).
28. J.S. Jaswal and A.S. Tracey. Inorg. Chem. **30**, 3718 (1991).
29. O.W. Howarth. Prog. Nucl. Magn. Reson. Spectrosc. **22**, 453 (1990).
30. A.T. Harrison and O.W. Howarth. J. Chem. Soc. Dalton Trans. 1173 (1985).
31. D.C. Crans, S.M. Schelble, and L.A. Theisen. J. Org. Chem. **56**, 1266 (1991).
32. B. Galeffi and A.S. Tracey. Can. J. Chem. **66**, 2565 (1988).
33. A.S. Tracey, B. Galeffi, and S. Mahjour. Can. J. Chem. **66**, 2294 (1988).
34. T.C. Bissot, R.W. Parry, and D.H. Campbell. J. Am. Chem. Soc. **79**, 796 (1957).
35. A. Bondi. J. Phys. Chem. **68**, 441 (1964).
36. L. Saussine, H. Mimoun, A. Mitschler, and J. Fisher. Nouv. J. Chim. **4**, 235 (1980).
37. R.E. Drew and F.W.B. Einstein. Inorg. Chem. **11**, 1079 (1972).
38. D. Begin, F.W.B. Einstein, and J. Field. Inorg. Chem. **14**, 1785 (1975).
39. R.E. Drew and F.W.B. Einstein. Inorg. Chem. **12**, 829 (1973).
40. A. Shaver, J.B. Ng, D.A. Hall, B. Soo Lum, and B.I. Posner. Inorg. Chem. **32**, 3109 (1993).
41. H. Szentivanyi and R. Stomberg. Acta Chem. Scand. **A37**, 709 (1983).
42. R. Stomberg. Acta Chem. Scand. Ser. A. **A38**, 541 (1984).
43. R. Stomberg and S. Olson. Acta Chem. Scand. Ser. A: **A38**, 801 (1984).
44. R. Stomberg, S. Olson, and I.-B. Svensson. Acta Chem. Scand. Ser. A: **A38**, 653 (1984).
45. F.W.B. Einstein, R.J. Batchelor, S.J. Angus-Dunne, and A.S. Tracey. Inorg. Chem. **35**, 1680 (1996).
46. M. Shao, J. Leng, and Z. Pan. J. Inorg. Chem. (Chinese) **6**, 443 (1990).
47. M.A.A.F. de C.T. Carrondo, M.T.L.S. Duarte, J.C. Pessoa, J.A.L. Silva, J.J.R.F. da Silva, M.C.T.A. Vaz, and L.F. Vilas-Boas. J. Chem. Soc. Chem. Commun. 1158 (1988).
48. N.J. Campbell, A.C. Dengel, and W.P. Griffith. Polyhedron, **8**, 1379 (1989).
49. P. Schwendt and M. Pisarcik. Spectrochim. Acta, Part A: **46A**, 397 (1990).
50. A.S. Tracey and M.J. Gresser. Proc. Natl. Acad. Sci. (U.S.A.), **83**, 609 (1986).
51. M.J. Gresser and A.S. Tracey. J. Am. Chem. Soc. **107**, 4215 (1985).
52. A.S. Tracey and M.J. Gresser. Can. J. Chem. **66**, 2570 (1988).
53. A.S. Tracey, M.J. Gresser, and K.M. Parkinson. Inorg. Chem. **26**, 629 (1987).

Can. J. Chem. Downloaded from www.nrcresearchpress.com by 88.146.161.215 on 09/08/12
For personal use only.

© 1997 NRC Canada

Reexamination of the Kirkwood–Westheimer theory of electrostatic effects. V. Effect of charged substituents on the rates of alkaline hydrolysis of substituted strychnines

Khamis A. Abbas, Phillip Hurst, and John T. Edward

Abstract: The rates of hydrolysis in aqueous sodium hydroxide of the alkaloid strychnine and seven of its derivatives have been determined at 50 and 75°C. The kinetic data indicate that all the compounds, except strychninesulfoni acid-I, hydrolyze by competing second- and third-order mechanisms, involving one and two hydroxide ions, respectively; strychninesulfonic acid-I hydrolyzes by the second-order mechanism only. The quantitative effect of positively charged groups in enhancing, and negatively charged groups in depressing, the rates of hydrolysis is in rough agreement with calculations using Kirkwood–Westheimer theory.

Key words: Kirkwood–Westheimer theory; strychnine derivatives, hydrolysis of; lactams, hydrolysis of; electrostatic effects on rates of alkaline hydrolysis; alkaloids, reactions of.

Résumé : On a déterminé, à des températures de 50 et de 75°C et dans l'hydroxyde de sodium aqueux, les vitesses d'hydrolyse de strychnine et de sept dérivés. Les données cinétiques indiquent que tous les composés, à l'exception de l'acide strychninesulfonique-I, subissent l'hydrolyse selon un mécanisme compétitif d'ordre 2 et 3, impliquant un et deux ions hydroxydes respectivement; l'acide strychninesulfonique-I s'hydrolyse uniquement selon un mécanisme d'ordre 2. L'effet quantitatif des groupes chargés positivement et des groupes chargés négativement sur l'augmentation et la diminution respectives des vitesses d'hydrolyses est grossièrement en accord avec les calculs utilisant la théorie de Kirkwood–Westheimer.

Mots clés : théorie de Kirkwood–Westheimer, hydrolyse des dérivés de la strychnine, hydrolyse des lactames, effets électrostatiques sur la vitesse de l'hydrolyse alcaline, réactions des alcaloïdes.

[Traduit par la rédaction]

Following earlier ideas of Bjerrum (1), Ingold (2), Eucken (3) and others, Kirkwood and Westheimer (KW) (4) elaborated a theory of electrostatic effects on reaction rates and equilibria that is still being investigated (5–11). Tests of the theory are best carried out with cage molecules of rigidly defined geometry, but the synthesis of such molecules is usually very time-consuming. However, many readily available alkaloids have cage structures, and in this paper we describe studies of the rates of alkaline hydrolysis of the alkaloid strychnine and of seven of its derivatives shown in Scheme 1. The derivatives (except brucine) carry charged or dipolar groups, which can be expected to affect their rates of hydrolysis, and each can be prepared in a few days, as compared with the months required by Roberts and Moreland (16) to synthesize the 1,4-disubstituted bicyclo[2.2.2]octanes used in their classic study of KW theory. We have already used the three isomeric strychninesulfonic acids shown in Scheme 1 to study the effect of the negatively charged sulfonate group on rates of detritiation from the methylene adjacent to the amide carbonyl in alkaline solution (17).

The opening of the lactam ring of strychnine **1** by alkaline hydrolysis to give the anion of the amino acid **2** has been known for almost a century (18–20), but its rate has never been measured. Since the lactam is a cyclic anilide, its alkaline hydrolysis would be expected to take place by competing second- and third-order paths, involving the singly and doubly charged intermediates Int^{1-} and Int^{2-} shown in Scheme 2 (21–26). However, the lactam rings of the compounds of Scheme 1 are all considerably more stable than most anilides, which hydrolyze at convenient rates at 25°C, and we have had to work at 50 and 75°C. Rates have been measured over a range of concentrations of sodium hydroxide, and results have been extrapolated back to zero concentration in order to apply KW theory (7, 27). The need to do this has sometimes been overlooked (28).

Experimental

Materials

Strychnine and brucine were commercial products, and were recrystallized to have melting points reported in the literature.

Received July 8, 1996.[1]

K.A. Abbas,[2] P. Hurst, and J.T. Edward.[3] Department of Chemistry, McGill University, 801 Sherbrooke Street W., Montreal, QC H3A 2K6, Canada.

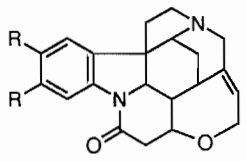
[1] Revision received January 9, 1997.

[2] Department of Chemistry, Yarmouk University, Irbid, Jordan.
[3] Author to whom correspondence may be addressed. Telephone: (514) 398-6233 (W), 489-1663 (H). Fax: (514) 398-3797.

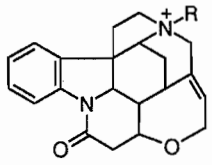
© 1997 NRC Canada

Can. J. Chem. Downloaded from www.nrcresearchpress.com by 88.146.161.215 on 09/08/12
For personal use only.

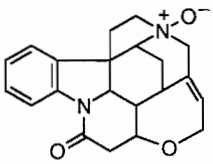
Scheme 1. Names and structures of strychnine derivatives, with literature references to methods for preparing them.



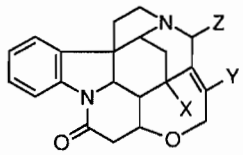
Strychnine (R=H)
Brucine (R=OCH_3)



N-Methylstrychninium chloride (R=CH_3) (12)
N-Benzylstrychninium bromide (R=CH_2Ph) (13)

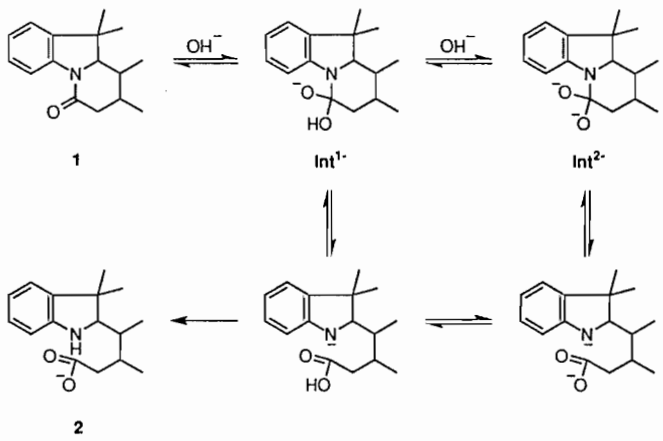


Strychnine *N*-oxide (14)



Strychninesulfonic acid anions
I (X=SO_3^-, Y=Z=H) (15)
II (Y=SO_3^-, X=Z=H) (15)
III (Z=SO_3^-, X=Y=H) (15)

Scheme 2.



Other compounds were prepared and purified by the methods given in the references of Scheme 1. Sodium hydroxide solutions (0.100 N, 0.500 N, 1.00 N, 5.00 N) were Fisher carbonate-free products. Other concentrations were prepared by dilution of these solutions with carbon dioxide-free water.

Kinetic measurements

Sodium hydroxide (10 mL in a volumetric flask) of known concentration was brought to a temperature of 50 or 75°C by immersion in a thermostatted bath for 30 min. A 5.0 μL aliquot of a stock solution in trifluoroacetic acid of the compound being investigated was injected into the sodium hydroxide solution, and after rapid mixing the solution was poured into a cuvette, which was stoppered and put into the compartment of a Unicam SP 800 spectrophotometer. The latter was thermostatted by water circulating from a Haake model F5/FE circulator. Hydrolysis was followed by the decrease in peak absorbance A (at 265 nm for brucine, 250–256 nm for strychnine and its derivatives). Good isosbestic points (at 316 nm for brucine, 287.5–292 nm for strychnine and its derivatives) were obtained. Pseudo-first-order rate constants k_ψ were determined by least-squares plots of log $(A_t - A_\infty)$ against t, where A_t and A_∞ are the absorbances at time t and at infinite time. For slow (s) reactions A_0^s was calculated by $A_\infty^s = A_\infty^f A_0^s/A_0^f$, where A_∞^f is the experimentally determined absorbance for a fast reaction after a sufficient time for change in absorbance to be complete, and A_0^f and A_0^s are the absorbances of the fast and slow reaction at zero time. A_∞^s was tested by taking a slightly lower and slightly higher value, and comparing the regression coefficients (R) for the slopes of log $(A_t - A_\infty)$ against t, using the new values of A_∞^s, with R for the slope using the original A_∞^s.

Results and discussion

In the large excess of sodium hydroxide used, the rates of hydrolysis of the compounds of Scheme 1 all followed pseudo-first-order kinetics.[4] We now consider the kinetics of hydrolysis of the different types of molecules, starting with those lacking a charged group.

Hydrolysis of uncharged molecules (strychnine, brucine, and strychnine *N*-oxide)

The change in the pseudo-first-order rate constant k_ψ with change in hydroxide ion concentration [OH^-] shows that hydrolysis of the uncharged molecules S involves competing second- and third-order routes via Int^{1-} and Int^{2-} of Scheme 2. Assuming transition states ‡(1) and ‡(2) close to Int^{1-} and Int^{2-} in structure, application of the Bronsted–Bjerrum treatment gives

$$[1] \quad k_\psi = k_\psi^{(1)} + k_\psi^{(2)} = k_0^{(1)}[OH^-] f_S f_{OH^-}/f_{\ddagger(1)} + k_0^{(2)}[OH^-]^2 f_S f_{OH^-}^2/f_{\ddagger(2)}$$

k_0 representing a rate constant at ionic strength $\mu = 0$, and f representing molar activity coefficients, referred to infinitely dilute solution in water as the standard state.

Biechler and Taft (29) found that the rates of alkaline hydrolysis of *N*-methylanilides in aqueous sodium hydroxide were unaffected by changes in ionic strength over the range 0–0.577 M, the activity coefficient terms cancelling out, so that for these compounds eq. [1] becomes

[4] Tables 1S and 2S of experimental pseudo-first-order rate constants at 50 and 75°C are available as supplementary material and can be purchased from: The Depository of Unpublished Data, CISTI, National Research Council Canada, Ottawa, Canada K1A 0R6. Also available from this source are figures and details of computations mentioned later in the paper.

Can. J. Chem. Downloaded from www.nrcresearchpress.com by 88.146.161.215 on 09/08/12
For personal use only.

© 1997 NRC Canada

Table 1. Second-order rate constants $k_0^{(1)}$ (in mol^{-1} s^{-1}), third-order rate constants $k_0^{(2)}$ (in mol^{-2} s^{-1}), and β coefficients at 50 and 75°C.

Compound	50°C				75°C			
	$10^5k_0^{(1)}$	β	$10^5k_0^{(2)}$	β	$10^5k_0^{(1)}$	β	$10^5k_0^{(2)}$	β
Strychnine	0.85	—	2.95	—	5.84	—	10.2	—
Brucine	2.10	—	2.51	—	—	—	—	—
Strychnine *N*-oxide	2.18	—	36.6	—	30.2	—	66.6	—
N-Methylstrychninium chloride	10.5	−0.077	15.1	0.13	58.9	0.40	661	−0.004
N-Benzylstrychninium bromide	11.2	−0.86	17.4	0.079	74.1	−1.94	832	−0.13
Strychninesulfonic acid-I	0.10	0.37	—	—	0.46	0.39	—	—
Strychninesulfonic acid-II	0.29	0.82	0.19	0.19	2.69	0.099	0.81	0.068
Strychninesulfonic acid-III	0.89	0.23	0.16	0.16	3.16	0.27	0.93	0.027

[2] $$k_\psi + k_0^{(1)}[OH^-] + k_0^{(2)}[OH^-]^2$$

which can be rearranged to

[3] $$k_\psi/[OH^-] = k_0^{(1)} + k_0^{(2)}[OH^-]$$

Hence plots of $k_\psi/[OH^-]$ against $[OH^-]$ gave straight lines of slope $k_0^{(2)}$ and intercept $k_0^{(1)}$. We find the same behaviour for the uncharged compounds strychnine, brucine, and strychnine *N*-oxide. This is shown in Fig. 1 for strychnine and strychnine *N*-oxide at 50°C. Over the range 0–2 M sodium hydroxide for strychnine and 0–0.5 M for strychnine *N*-oxide, rates of hydrolysis followed eq. [3], with linear plots of log $k_\psi/[OH^-]$ against $[OH^-]$ (correlation coefficients *r* better than 0.980). The values of $k_0^{(1)}$ and $k_0^{(2)}$ obtained from these plots are given in Table 1. Similar plots[4] gave values of $k_0^{(1)}$ and $k_0^{(2)}$ at 75°C (Table 1).

At higher concentrations of sodium hydroxide the second-order pathway becomes progressively less important, accounting for less than 26% of the product from the hydrolysis of strychnine and for less than 8% of the product from the hydrolysis of strychnine *N*-oxide in concentrations above 1 M. The difference between the two compounds would be expected from simple electrostatic theory: the *N*-oxide dipole will stabilize Int^{2-} more than Int^{1-}, and hence favour the third- over the second-order route.

Hydrolysis of positively charged ions: the rate becomes almost exclusively third order in concentrations of sodium hydroxide above about 0.5 M

Even more than the *N*-oxide dipole, the positively-charged nitrogen atom of the methyl- and benzylstrychninum ions S^+ should stabilize Int^{2-} more than Int^{1-}, and favour the third-order route. We show below that, in fact, in concentrations of sodium hydroxide above about 0.5 M the contribution of the second-order route becomes negligible.

Consequently, in these concentrations,

[4] $$k_\psi = k_0^{(2)}[OH^-]^2 f_{S^+} f_{OH^-}^2 / f_{\ddagger(2)}$$

[4*a*] $$\log k_\psi = \log k_0^{(2)} + 2\log[OH^-] + \log(f_{S^+} f_{OH^-}^2 / f_{\ddagger(2)})$$

In reactions between ions, unlike reactions between an ion and a neutral molecule (30), the last term does not cancel out even in dilute solution, but must be calculated by Debye–Huckel theory (30–33). This theory (34) indicates that for a second-order reaction between ions 1 and 2 having unit charges z_1 and z_2, the rate constant *k* will vary with $\mu^{1/2}$ according to the equation:

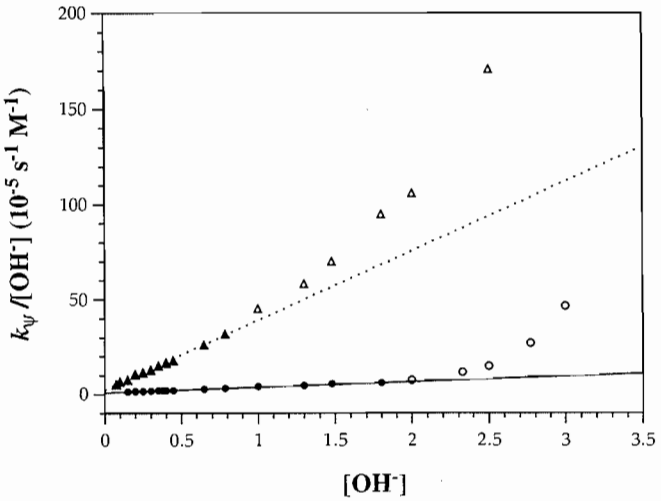


Fig. 1. Plots of $k_\psi/[OH^-]$ for strychnine (○) and strychnine *N*-oxide (△) against concentrations of sodium hydroxide at 50°C. Straight-line plots are based on solid points (●, ▲). (▲ ·····) $y = 2.1817 + 36.615x$; $R = 0.99767$. (● ——) $y = 0.85388 + 2.9473x$; $R = 0.99666$.

[5] $$\log k = \log k_0 + \frac{2z_1zA\mu^{1/2}}{1 + B\mathring{a}\mu^{1/2}}$$

where $\mathring{a}$ is the mean diameter of the ions and *A* and *B* are quantities varying with temperature, and calculable by Debye–Hückel theory (30–32). In higher concentrations of electrolyte it is necessary to add a term βμ (30–32):

[6] $$\log k = \log k_0 + \frac{2z_1zA\mu^{1/2}}{1 + B\mathring{a}\mu^{1/2}} + \beta\mu$$

where β is an empirically determined constant. For a third-order reaction involving ions 1, 2, and 3 having charges z_1, z_2, and z_3 the equation becomes (30)

[7] $$\log k = \log k_0 + 2(z_1z_2 + z_1z_3 + z_2z_3)\frac{A\mu^{1/2}}{1 + B\mathring{a}\mu^{1/2}} + \beta\mu$$

Can. J. Chem. Downloaded from www.nrcresearchpress.com by 88.146.161.215 on 09/08/12
For personal use only.

© 1997 NRC Canada

Can. J. Chem. Downloaded from www.nrcresearchpress.com by 88.146.161.215 on 09/08/12
For personal use only.

For the third-order reaction of methyl- or benzylstrychninium ions with two hydroxide ions, $(z_1z_2 + z_1z_3 + z_2z_3) = -1$. Accepting Weller's values (33) for A and $B\mathring{a}$, for hydrolyses at 50°C (31, 32, 35) eq. [4*a*] becomes

$$[8] \quad \log k_\psi^{(2)} = \log k_0^{(2)} + 2 \log [OH^-] - \frac{1.08\mu^{1/2}}{1 + 2.03\mu^{1/2}} + \beta\mu$$

This equation requires that (as long as the second-order reaction can be neglected) a plot of $y = \log k_\psi - 2 \log [OH^-] + 1.08\mu^{1/2}/(1 + 2.03\mu^{1/2})$ against μ should give a straight line of slope β and intercept $\log k_0^{(2)}$.

In fact, it can be seen that in concentrations of sodium hydroxide above about 0.8 M (Fig. 2) plots for the methyl- and benzylstrychninium ion are reasonably linear, so that in these concentrations the second-order pathway can be ignored. The slopes and intercepts of these plots give the values of β and $k_0^{(2)}$ recorded in Table 1. The values of β and $k_0^{(2)}$ at 75°C were obtained in similar fashion.[4]

Hydrolysis of methyl- and benzylstrychninium ions by competing second- and third-order mechanisms in dilute sodium hydroxide

In concentrations of sodium hydroxide below 0.5 M the experimental points in Fig. 2 diverge increasingly from the straight-line plots, showing that $k_\psi^{(1)}$ is making an increasingly important contribution to k_ψ and can no longer be ignored.

We can calculate $k_\psi^{(1)} = k_\psi - k_\psi^{(2)}$ by calculating $k_\psi^{(2)}$ at 50°C in 0–0.5 M sodium hydroxide from eq. [8] using the values of $k_0^{(2)}$ and β recorded in Table 1. The values of $k_\psi^{(1)}$ thus calculated should agree with those given by the equation

$$[9] \quad \log k_\psi^{(1)} = \log k_0^{(1)} + \log [OH^-] - \frac{1.08\mu^{1/2}}{1 + 2.03\mu^{1/2}} + \beta\mu$$

for data at 50°C. (The sign and magnitude of the term in $\mu^{1/2}$ comes from $z_1z_2 = -1$: see eq. [5].) This equation requires that plots of $y = \log k_\psi^{(1)} - \log [OH^-] + 1.08\mu^{1/2}/(1 + 2.03\mu^{1/2})$ against μ should give straight lines. We can see in Fig. 3 that scatter of points about the straight lines is appreciable. However, errors in $k_\psi^{(1)} = k_\psi - k_\psi^{(2)}$ would be expected to be large, not only because of experimental errors in k_ψ but also because of substantial errors in $k_\psi^{(2)}$, whose calculation depends upon a value of $k_0^{(2)}$ obtained by a lengthy extrapolation. We can accordingly expect much larger errors in $k_0^{(1)}$ and β, given by the slopes and intercepts of the straight-line plots in Fig. 3, than in $k_0^{(2)}$ and β for the termolecular reactions. These values are all given in Table 1. Similar computations and plots[4] give the corresponding values for 75°C recorded in the table.

Qualitatively, these values are those expected by simple electrostatic theory. The positive nitrogen atom of the strychninium ions causes $k_0^{(1)}$ to be 10–12 times greater than $k_0^{(1)}$ of strychnine, in which the nitrogen has no formal charge, and causes $k_0^{(2)}$ of the ions to be 51–82 times greater than $k_0^{(2)}$ of strychnine.

Hydrolysis of anions of the strychninesulfonic acids-I, -II, and -III

The sulfonic acids-I, -II, and -III exist as zwitterions in neutral solution (15), but as the anions depicted in Scheme 1 in alkaline solution.

Fig. 2. Plots of $y = \log k_\psi - 2 \log [OH^-] + 1.08\ \mu^{1/2}/(1 + 2.03\ \mu^{1/2})$ for hydrolysis at 50°C of methylstrychninium chloride (○) and benzylstrychninium bromide (Δ) in aqueous sodium hydroxide against ionic strength μ of the hydroxide solution. Straight-line plots are based on solid points (●, ▲). (● ——) $y = -2.8187 + 0.13024x$; $R = 0.99353$. (▲ ·····) $y = -2.7592 + 0.07908x$; $R = 0.95659$.

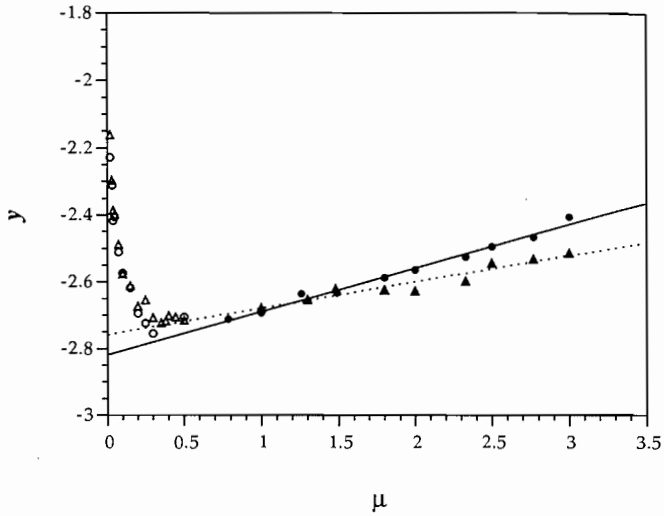
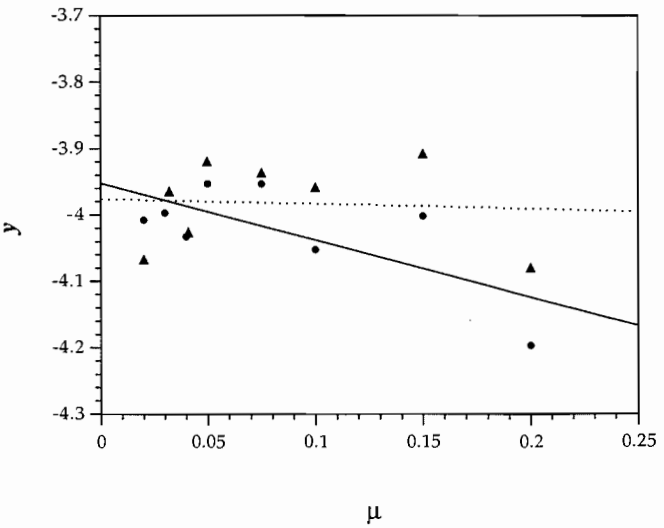


Fig. 3. Plots of $y = \log k_\psi^{(1)} - \log [OH^-] + 1.08\mu^{1/2}/(1 + 2.03\mu^{1/2})$ for hydrolysis of methyl (●) and benzylstrychninium ions (▲) at 50°C against ionic strength μ of the aqueous sodium hydroxide. Calculated straight line plots: methyl —; benzyl ---. (● ——) $y = -3.9528 + -0.85917x$; $R = 0.70145$. (▲ ·····) $y = -3.9767 + -0.076721x$; $R = 0.072815$.



On the basis of simple electrostatic theory, it would be expected that these anions would be hydrolyzed more slowly than strychnine, and furthermore that the rate for the third-order pathway via Int^{2-} would be more depressed than the rate for the second-order pathway via Int^{1-}. Both expectations were realized (Table 1). The kinetic data were analysed in the same fashion as the data for methyl- and benzylstrychninium ions, the equation for the third-order pathway being identical

© 1997 NRC Canada

Can. J. Chem. Downloaded from www.nrcresearchpress.com by 88.146.161.215 on 09/08/12
For personal use only.

Table 2. Distances R between charges or between charge and dipole, and calculated and experimental values of logarithms of ratios of second-order rate constants $\Delta \log k_0^{(1)}$ at 50 and 75°C.

Compound	R(Å)	$\Delta \log k_0^{(1)}$ (50°C) Calcd.	Exptl.	$\Delta \log k_0^{(1)}$ (75°C) Calcd.	Exptl.
Strychnine *N*-oxide	7.17	0.48	0.41	0.50	0.71
N-Methylstrychninium chloride	6.46	1.24	1.09	1.22	1.00
N-Benzylstrychninium bromide	6.46	1.24	1.12	1.22	1.10
Strychninesulfonic acid-I	6.17	−0.95	−0.93	−0.92	−1.10
Strychninesulfonic acid-II	8.41	−0.43	−0.47	−0.42	−0.34
Strychninesulfonic acid-III	8.89	−0.38	0.02	−0.37	−0.25

Table 3. Calculated and experimental values of logarithms of ratios of third-order rate constants $\Delta \log k_0^{(2)}$ at 50 and 75°C.

Compound	50°C Calcd.	Exptl.	75°C Calcd.	Exptl.
Strychnine *N*-oxide	0.96	1.09	1.00	0.84
N-Methylstrychninium chloride	2.48	1.71	2.44	1.81
N-Benzylstrychninium bromide	2.48	1.77	2.44	1.91
Strychninesulfonic acid-II	−0.86	−1.19	−0.84	−1.10
Strychninesulfonic acid-III	−0.76	−1.26	−0.74	−1.04

with eq. [8], except for change in sign and magnitude of the coefficient for the term in $\mu^{1/2}$ determined by the fact that now $(z_1z_2 + z_1z_3 + z_2z_3) = +3$. The equation for the second-order pathway was identical with eq. [9], except for the sign of the term in $\mu^{1/2}$ ($z_1z_2 = +1$). The details of the computations and the plots are given elsewhere;[4] the results are given in Table 1.

Calculation of the increases in rates of hydrolysis caused by positive charges: *N*-methyl- and *N*-benzylstrychninium ions

The positively charged nitrogen atom in *N*-methyl- and *N*-benzylstrychninium ions causes their rate constants for hydrolysis by the second-order ($k_0^{(1)}$) and third-order ($k_0^{(2)}$) routes to be greater than the corresponding rates $k_0^{(1)}$(S), $k_0^{(2)}$(S) of the parent strychnine molecule, and for the effect to be greater on $k_0^{(2)}$ than on $k_0^{(1)}$ (see Table 1). Consequently the logarithms of the ratios $\log k_0^{(1)}/k_0^{(1)}$ (S) = $\Delta \log k_0^{(1)}$ and $\log k_0^{(2)}/k_0^{(2)}$ (S) = $\Delta \log k_0^{(2)}$ are positive and (based on the experimental data in Table 1) are gathered in Tables 2 and 3.

Also in these tables are the ratios calculated by KW theory. For this calculation we assume that the transition state for the second-order route (Scheme 1) is close to Int^{1-}, and hence has a charge close to unit electronic charge, distributed equally between the two geminal oxygen atoms and effectively localized midway between them. Similarly, for the third-order route it is assumed that a charge close to $2e$ is effectively localized at the same point. The distance R between this point and the centre of N^+ of the methyl and benzyl ion can be calculated from atomic coordinates given by an X-ray study of a strychnine derivative (36), and is given in Table 2. KW theory (4, 27) states that $\Delta \log k_0^{(1)}$ depends on R:

$$[10] \quad \Delta \log k_0^{(1)} = e^2/2.3\ \kappa T R D_{\text{eff}}$$

where κ is Boltzmann's constant, T the absolute temperature, and D_{eff} the effective dielectric constant, having a value intermediate between the dielectric constant D_e of the solvent (water at 50 and 75°C) and the dielectric constant D_i of the hydrocarbon framework of the solute molecule (assumed to be $D_i = 2$ (4, 37)). The third-order $\Delta \log k_0^{(2)}$ will be twice as great, if the charge on Int^{2-} is twice as great as on Int^{1-}.

For the particular case of molecules having the shape of a prolate ellipsoid with charges located at the foci, Kirkwood and Westheimer (4) calculated D_{eff} as a function of D_e and λ_0, the ratio of the major axis to the interfocal distance in the ellipsoid. The shapes of the strychnine molecule and its various derivatives approximate prolate ellipsoids, as shown in Fig. 4 for Int^{2-} for the *N*-methylstrychninium ion.

The most convenient method for obtaining λ_0 is that of Tanford (38, 39), in which each charged focus is located at a distance d beneath the end surface of the ellipsoid. Then

$$[11] \quad \lambda_0 = (R + 2d)/R$$

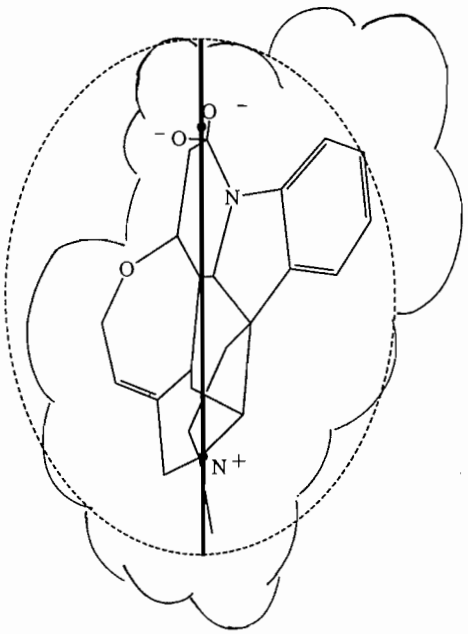
For the particular case of charged groups such as NH_3^+ and CO_2^- Tanford showed that the experimental data were accommodated with d = 1.0 Å, 0.9 Å less than the van der Waals radius of about 1.9 Å for NH_3^+ (cf. 2.0 Å for CH_3 (40)). In the *N*-methylstrychninium ion the distance from N^+ to the surface of the methyl group can be calculated (40) to be about 3.5 Å. Following Tanford, we reduce this by 0.9 Å to d = 2.6 Å for N^+ in methyl and benzyl ions. Retaining Tanford's d = 1.0 Å for the depth of the negative charges on oxygen[5] in Int^{1-} and Int^{2-}, we obtain an average d of 1.8 Å, which is used in drawing the ellipsoid in Fig. 4. The volume V_{Tan} calculated from d and R (315 Å^3: refs. 4 and 39) turns out to be only slightly less

[5] We (39) and Reynolds (41) differ from Eucken (3), Kirkwood and Westheimer (4), and workers following them in the precise nature and location of interacting charges, for reasons set out elsewhere (39, 41).

© 1997 NRC Canada

Can. J. Chem. Downloaded from www.nrcresearchpress.com by 88.146.161.215 on 09/08/12
For personal use only.

Fig. 4. Molecular model of Int^{2-} (Scheme 2) for *N*-methylstrychninium ion, drawn by Personal CAChe Software (version for Macintosh), from CAChe Scientific. Tanford ellipse, drawn to scale, is superimposed with N^+ at one focus and midpoint between two O^- at the other; interfocal instance *R*, 6.56 Å; major axis *R* + 2d, 10.16 Å.



than the van der Waals volume V_w of 325 Å^3 for Int^{2-} calculated by addition of van der Waals increments (42). (Only very rarely does V_{Tan} approach V_w (39).)

From eq. [11] we calculate λ_o = 1.55, which requires D_{eff} = 28.0 at 50°C and 26.5 at 75°C (4). With these values in eq. [12] we calculate $\Delta \log k_0^{(1)}$ (Table 2) and $\Delta \log k_0^{(2)}$ (Table 3). If we assume that the additional benzene ring of the *N*-benzylstrychninium ion has a negligible effect on D_{eff}, we obtain the same $\Delta \log k_0^{(1)}$ and $\Delta \log k_0^{(2)}$ for this ion. In fact, the agreement with experimental $\Delta \log k_0^{(1)}$ (Table 2) and $\Delta \log k_0^{(2)}$ (Table 3) is good. The experimental $\Delta \log k_0^{(1)}$ values are about 10% lower than the calculated values, which would be expected if the transition states have charges of about 0.9*e*, distributed between the two oxygen atoms, rather than the charge of 1.0*e* of Int^{1-}. The experimental $\Delta \log k_0^{(2)}$ values are about 30% lower than calculated values, expected if the two oxygen atoms of the transition state share a charge of 1.4*e*, rather than the charge of 2.0*e* of Int^{2-}.

Calculation of the decreases in rates of hydrolysis caused by negative charges: strychninesulfonic acids-I, -II, and -III

X-ray studies (36) show the sulfur atom of the SO_3^- group in strychninesulfonic acid – I to be roughly tetrahedral. We have located the negative charges of the SO_3^- groups in these zwitterionic acid anions at the midpoint between the three oxygen atoms, and obtained intercharge distances *R* (Table 2) by calculation from atomic coordinates given by X-ray measurements (36).

Models of the intermediates Int^{1-} and Int^{2-} involved in the hydrolysis of the strychninesulfonic acids-II and -III[6] show them to approximate Tanford ellipsoids with charges at the foci as required by KW theory. No value has been reported for the depth *d* of the negative charge of the SO_3^- group, although it might be expected to be greater than *d* = 1.0 Å for the CO_2^- group. We have adopted *d* = 1.4 Å, which gives, along with the *R* values reported in Table 2, volumes V_{Tan} of the Tanford ellipsoids (323 Å^3 for acid-II, 354 Å^3 for acid-III) in reasonable agreement with the van der Waals volume V_w (341 Å^3) calculated for Int^{2-} for all three sulfonic acids (42).

Using λ_0 and thence D_{eff} values obtained with these values of *R* and *d* (eq. [11]), we calculate (eq. [10]) $\Delta \log k_0^{(1)}$ (Table 2) and $\Delta \log k_0^{(2)}$ (Table 3). These turn out to be in reasonable agreement with experiment. In the case of $\Delta \log k_0^{(2)}$, experimental values were about 70% of calculated values, possibly again because the geminal oxygen atoms in the transition state share a total charge of about 1.4*e* and not 2.0*e* as used in the calculation. The experimental $\Delta \log k_0^{(1)}$ values probably have greater errors, which would account for the anomalous positive value of $\Delta \log k_0^{(1)}$ for strychninesulfonic acid-III at 50°C.

KW calculations for strychninesulfonic acid-I were expected to be very much in error. Examination of a model (see Fig. 1 in ref. 36) shows that while the midpoint between the geminal oxygens of Int^{1-} and Int^{2-} will again be close to the focus of any ellipsoid enclosing the molecule, the SO_3^- will not; i.e., that the Tanford ellipsoid will not enclose the bulk of the molecule. This is confirmed by the wide discrepancy between the volume of the Tanford ellipsoid for Int^{2-} (V_{Tan} = 200 Å^3) and the van der Waals volume (341 Å^3). In spite of this failure to fit the molecule into the ideal KW ellipsoid, the agreement between calculated and experimental values of $\Delta \log k_0^{(1)}$ is surprisingly good (Table 2).

Calculation of the increase in rate of hydrolysis of strychnine *N*-oxide

For a transition state having the shape of a prolate ellipsoid with a charge *ze* (*z* = number of electronic charges) at one focus and a point dipole of moment *M* at the other focus, Kirkwood and Westheimer (4, 27) showed that the effect of the dipole of moment *M* should be given by

$$[12] \quad \Delta \log k_0^{(z)} = \log k_0^{(z)}/k_0^{(z)}(S) = zeM \cos\theta/2.3\,\kappa TR^2 D_{eff}$$

where *R* is the distance from the charge to the centre of the dipole and θ is the angle between the line *R* joining the foci and the dipole vector. The effective dielectric constant D_{eff} is related to D_e of the solvent and λ_0 of the ellipsoid (but the relationship is not the same as that for two charges interacting from opposite foci of the ellipsoid).

Tanford (38) found eq. [12] valid for a large number of prolate ellipsoidal compounds having interacting charges and dipoles if he assumed *d* = 1.5 Å for both the charged group (e.g., NH_3^+, CO_2^-) and the dipole. (The contradiction that CO_2^- has *d* = 1.0 Å when interacting with another charged group and *d* = 1.5 Å when interacting with a dipole is not explained.) We have adopted *d* = 1.5 Å for strychnine

[6] The model took account of the stereochemistry (43).

© 1997 NRC Canada

Can. J. Chem. Downloaded from www.nrcresearchpress.com by 88.146.161.215 on 09/08/12
For personal use only.

N-oxide; *R* (Table 2) and θ (24.4°) were calculated from atomic coordinates given by X-ray diffraction results (36) and from the known bond length of N^+—O^- (44). With this *R* value and d = 1.5 Å, eq. [11] yielded λ_0 and thence D_{eff}. Then, with the dipole moment M (5.24 *D*) given in the literature (45), eq. [14] gave values of $\Delta \log k_0^{(1)}$ (z = 1.0: Table 2) and $\Delta \log k_0^{(2)}$ (z = 2.0: Table 3) in rough agreement with experiment.

Conclusions

Using the Tanford approximation, the KW equations have proved adequate in calculating the increase in rate of alkaline hydrolysis of the lactam ring of strychnine brought about by the presence of a positive charge (*N*-methyl- and *N*-benzylstrychninium ions), the decrease brought about by negative charges (strychninesulfonic acids- I, -II, and -III), and the increase brought about by a suitably oriented dipole (strychnine *N*-oxide). Furthermore, the results serve to confirm the mechanism of Scheme 2: the effects of charged substituents are greater on the rates of the third-order reactions than on the rates of the second-order reactions, as expected from the greater electrostatic interactions.

The behaviour of the strychninesulfonic acids is interesting. Rumpf (46) showed that in the ω-aminosulfonic acid zwitterions H_3N^+-$(CH_2)_n$-SO_3^- the negative sulfonate group, which should stabilize the ammonium group (i.e., should increase pK_{BH^+}), in fact does this only when $n > 5$; for n = 1–3 the ammonium ions are stronger rather than weaker acids, as expected. Hoefnagel et al. (7) have given further examples, and the same anomaly is observed in the pK_{BH^+} values of the strychninesulfonic acid-I, -II, and -III zwitterions (15). This behaviour has been explained by Bell (47), who assumes that the sulfur atom of the negative sulfonate group has a charge of +2 and the three oxygen atoms each a charge of −1. When n = 1–3 in the ω-aminosulfonic acid zwitterions, the effect of the positive sulfur atoms is more important than that of the more distant oxygen atoms. When $n \geq 5$, the difference in distance of sulfur and oxygen atoms becomes less important, and the sulfonate group can be regarded as a point negative charge. The latter is true for the reactions involving Int^{1-} and Int^{2-} in this paper and for the detritiation reactions described in a previous paper (17), reactions in which the distances of the sulfonate group from the reaction centres are sufficiently great.

More generally, the results in this paper point to the usefulness of the rigid cage structure of the strychnine and other alkaloid molecules for physical organic studies. Strychnine is cheap, has a rich chemistry (48), and has a variety of groups whose reaction rates would be expected to be affected by variously disposed charged centres, such as those of the compounds of Scheme 1. Thus the benzene ring undergoes various substitution reactions; the basic nitrogen atom undergoes the Menschutkin reaction; the double bond can be oxidized; the methylene adjacent to the amide carbonyl forms benzylidene derivatives; and so forth. Results from such reactions would serve to test the newer methods of Ehrenson (49–53) and Orttung (54) for deriving the effective dielectric constant of bodies more irregular than the ideal prolate ellipsoids of Kirkwood and Westheimer, and to discover the useful limits of eqs. [10] and [12].

Acknowledgement

The financial support of the Natural Sciences and Engineering Research Council of Canada is gratefully acknowledged. We are grateful to James Connolly for help with computations and for Fig. 4, to Professor Jik Chin for use of computers and programs, to Professor O.S. Tee and to a referee for helpful advice, and to members of the Mansfield Philosophical Society for encouragement and support.

References

1. N. Bjerrum Z. Phys. Chem. **106**, 219 (1923).
2. C.K. Ingold. J. Chem. Soc. 2179 (1931).
3. A. Eucken. Z. Angew. Chem. **45**, 203 (1932).
4. J.G. Kirkwood and F.H. Westheimer. J. Chem. Phys. **6**, 506 (1938). F.H. Westheimer and J.G. Kirkwood. J. Chem. Phys. **6**, 513 (1938).
5. K. Bowden. J. Chim. Phys. Phys.-Chim. Biol. **89**, 1647 (1992).
6. Z. Friedl. J. Hapala, and O. Exner. Collect. Czech. Chem. Commun. **44**, 2928 (1979).
7. A.J. Hoefnagel, M.A. Hoefnagel, and B.M. Wepster. J. Org. Chem. **43**, 4720 (1978); A.J. Hoefnagel and B.M. Wepster. J. Org. Chem. **47**, 2318 (1982).
8. O. Exner and Z. Friedel. Prog. Phys. Org. Chem. **19**, 259 (1993).
9. C.K. Ingold. Structure and mechanism in organic chemistry, 2nd ed. Cornell University Press, Ithaca, N.Y. 1969. pp. 1104–1110.
10. W.F. Reynolds. J. Chem. Soc. Perkin Trans. 2, 985 (1980).
11. J.D. Roberts. The right place and the right time. *Edited by* J.I. Seeman. American Chemical Society, Washington, D.C. 1992. p. 95.
12. G.R. Clemo, W.H. Perkin, and R. Robinson. J. Chem. Soc. 1624 (1927).
13. J.T. Edward and R. Robinson. J. Chem. Soc. 1080 (1952).
14. A.S. Bailey and R. Robinson. J. Chem. Soc. 703 (1948).
15. J.T. Edward, P.G. Farrell, S.A. Samad, R. Wojtowski, and S.C. Wong. Can. J. Chem. **58**, 2380 (1980).
16. J.D. Roberts and W.T. Moreland. J. Am. Chem. Soc. **75**, 2167 (1953).
17. J.T. Edward, S.C. Wong, A.J. Kresge, and M.F. Powell. Can. J. Chem **62**, 2448 (1984).
18. J. Tafel. Justus Liebigs Ann. Chem. **301**, 285 (1898).
19. N. Moufang and J. Tafel. Justus Liebigs Ann. Chem. **304**, 26 (1899).
20. O. Achmatowicz, G.R. Clemo, W.H. Perkin, and R. Robinson. J. Chem. Soc. 267 (1932).
21. A. Kijima and S. Sekiguchi. J. Chem. Soc. Perkin Trans. 2, 1203 (1987).
22. R.H. Dewolfe and R.G. Newcome. J. Org. Chem. **36**, 3876 (1971).
23. L.D. Kershner and R.L. Schowen. J. Am. Chem. Soc. **93**, 2014 (1971).
24. R.S. Brown, A.J. Bennett, and H. Slebocka-Tilk. Acc. Chem. Res. **25**, 481 (1992).
25. R.J.E. Talbot. Comprehensive chemical kinetics. Vol. 10. *Edited by* C.H. Bamford and C.F.H. Tipper. Elsevier, Amsterdam. 1972. Chap. 3.
26. K. Bowden and K. Bromley. J. Chem. Soc. Perkin Trans. 2, 2103 (1990).
27. F.H. Westheimer and M.W. Shookoff. J. Am. Chem. Soc. **62**, 269 (1940); F.H. Westheimer, W.A. Jones, and R.A. Lad. J. Chem. Phys. **10**, 478 (1942).
28. J.H. Smith and F.M. Menger. J. Org. Chem. **34**, 77 (1969).
29. S.S. Biechler and R.W. Taft. J. Am. Chem. Soc. **79**, 4927 (1957).

© 1997 NRC Canada

30. K.J. Laidler. Chemical kinetics. 3rd ed. Harper and Row, New York. 1987. pp. 197–206.
31. L.P. Hammett. Physical organic chemistry. 2nd ed. McGraw–Hill, New York. 1970. pp. 187–201.
32. M.A. Paul. Principles of chemical thermodynamics. McGraw–Hill, New York. 1951. pp. 406–411.
33. A.K. Weller. Prog. React. Kinet. **1**, 204 (1961).
34. B. Perlmutter-Mayman. Prog. React. Kinet. **6**, 237 (1971).
35. G.G. Manov, R.G. Bates, W.J. Hamer, and S.F. Acree. J. Am. Chem. Soc. **65**, 1765 (1943).
36. D.S. Sakegowda, L. Cartz, and C. Natarajan. Acta Crystallogr. Sect. B: Struct. Crystallogr. Cryst. Chem. **B29**, 2760 (1973).
37. F.W. Baker, R.C. Parrish, and L.M. Stock. J. Am. Chem. Soc. **89**, 5677 (1967).
38. C. Tanford. J. Am. Chem. Soc. **79**, 5348 (1957).
39. J.T. Edward, P.G. Farrell, J.L. Job, and B.-L. Poh. Can. J. Chem. **56**, 1122 (1978).
40. L. Pauling. The nature of the chemical bond. 3rd ed. Cornell University Press, Ithaca, N.Y. 1960 p. 260.
41. W.F. Reynolds. Prog. Phys. Org. Chem. **14**, 165 (1983).
42. J.T. Edward. J. Chem. Educ. **47**, 261 (1970).
43. W.J. Chazin, J.T. Edward, and L.D. Colebrook. Can. J. Chem. **61**, 1749 (1983).
44. Tables of interatomic distances and configurations in molecules and ions. Chemical Society Special Publication No. 11, London. 1958. p. M-157.
45. A.L. McClellan. Tables of experimental dipole moments. Vol. 3. Zahara Enterprises, El Cerrito, Calif. 1989. p. 107.
46. P. Rumpf. Bull. Soc. Chim. Fr. **5**, 871 (1938).
47. R.P. Bell. The proton in chemistry. 2nd ed. Chapman and Hall, London. 1973. p. 98.
48. G.F. Smith. The alkaloids. Vol. 8. *Edited by* R.H.F. Manske. Academic Press, New York. 1965. p. 592.
49. S. Ehrenson. J. Am. Chem. Soc. **98**, 7510 (1976).
50. S. Ehrenson. J. Phys. Chem. **81**, 1520 (1977).
51. S. Ehrenson. J. Comput. Chem. **3**, 41 (1981).
52. S. Ehrenson. J. Am. Chem. Soc. **104**, 4793 (1982).
53. S. Ehrenson. J. Org. Chem. **48**, 1884 (1983).
54. W.H. Orttung. J. Am. Chem. Soc. **100**, 4369 (1978).

Can. J. Chem. Downloaded from www.nrcresearchpress.com by 88.146.161.215 on 09/08/12
For personal use only.

© 1997 NRC Canada

Second harmonic generation study of the reconstruction of an Au(110) electrode in $HClO_4$

C. Dale Keefe, Erika Revesz, Michel Dionne, and Mario Morin

Abstract: Second harmonic generation (SHG) was used to carry out an in situ study of the potential-induced reconstruction of an Au(110) single crystal electrode in an aqueous solution of 0.01 M $HClO_4$. In this study, we found that the symmetries of the surface susceptibility of the reconstructed and the unreconstructed Au(110) surfaces have a large component of threefold symmetry. A detailed analysis shows that both surfaces have an overall C_s symmetry giving one-, two-, and threefold symmetries for the surface susceptibility. However, another, different, source of threefold symmetry, perpendicular to the first, is needed to fit the data. We suggest that this extra source of threefold symmetry is due to the (111) microfacets that are present on the open (110) surface.

Key words: electrochemistry, single crystal, reconstruction, second harmonic generation spectroscopy.

Résumé : On a utilisé la génération harmonique secondaire (SHG) pour effectuer, in situ, une étude de la reconstruction d'une électrode Au(110) monocristalline induite par le potentiel dans une solution aqueuse de $HClO_4$ 0,01 M. Dans cette étude, nous avons trouvé que les symétries de la susceptibilité de surface des surfaces de Au(110) reconstruites et non reconstruites sont surtout ternaires. Une analyse détaillée révèle que les deux surfaces ont une symétrie globale de type C_s donnant des symétries simple, binaire et ternaire pour la susceptibilité de surface. Cependant, on doit avoir recours à une autre source différente de symétrie ternaire perpendiculaire à la première pour confirmer les données. Nous suggérons que cette source supplémentaire de symétrie ternaire est due aux microfacettes(111) qui sont présentes sur la surface libre(110).

Mots clés : electrochimie, crystal unique, reconstruction, spectroscopie de génération harmonique de secondaire.

[Traduit par la rédaction]

Can. J. Chem. Downloaded from www.nrcresearchpress.com by 88.146.161.215 on 09/08/12
For personal use only.

Introduction

The electrocatalytic properties of an electrode depend on its surface structure (1, 2). Recent in situ studies (3) with structural probes such as scanning tunneling microscopy (STM), surface X-ray scattering (SXS), and second harmonic generation (SHG) spectroscopy have shown that single crystal electrode surfaces can undergo reconstructions that are induced by the adsorption of molecules or by an applied potential. The surface reconstruction of gold single crystal electrodes has been studied extensively. In situ structural studies (4–14) reveal that when the low-index gold surfaces (100), (110), and (111) reconstruct when they are immersed in a solution containing a weakly adsorbed electrolyte at potentials more negative than the potential of zero charge (pzc). In perchlorate solutions the type of reconstruction depends on the crystallographicaphic orientation. The reconstruction of the densely packed Au(100) and Au(111) surfaces involves long-range order and small atomic displacements and is reversible and slow. In contrast, the more open Au(110) surface undergoes a more local reconstruction in which the atomic displacements are large. Although the Au(110) surface reconstruction is reversible, it leaves a significant amount of defects and islands on the surface because of the large mass transport involved in the reconstruction process.

In situ STM studies (4–6) of the reconstructed and unreconstructed surface of an Au(110) electrode in $HClO_4$ solution showed that the reconstructed surface consists of a mixture of (1×2) and (1×3) local structures at potentials negative to the pzc (−0.050 V (vs. a saturated calomel electrode (SCE)). In the (1×2) structure, half of the rows in the ⟨100⟩ direction have been removed by a missing row process whereas the (1×3) structure has two missing rows. The steps that are parallel to the rows are found to be well ordered and consist of (111) planes or microfacets. The steps across these rows display a lot of kinks. SXS measurements (7) indicate that the reconstructed Au(110) surface in $HClO_4$ forms an incommensurate first layer relative to the bulk. It was suggested that this is due to a random sequence of (1×2) and (1×3) structures. When the potential is more positive than the pzc the reconstruction is lifted. However, the (1×1) unreconstructed surface contains a significant amount of islands and adatoms (4–7).

In this paper, we present an SHG study of the Au(110) sur-

Received May 22, 1996.[1]

C.D. Keefe, E. Revesz, M. Dionne, and M. Morin.[2] Ottawa–Carleton Chemistry Institute and Department of Chemistry, University of Ottawa, Ottawa, ON K1N 6N5, Canada.

[1] Revision received February 20, 1997.

[2] Author to whom correspondence may be addressed. Telephone: (613) 562-5800, ext. 6037. E-mail: mgmorin@science.uottawa.ca

© 1997 NRC Canada

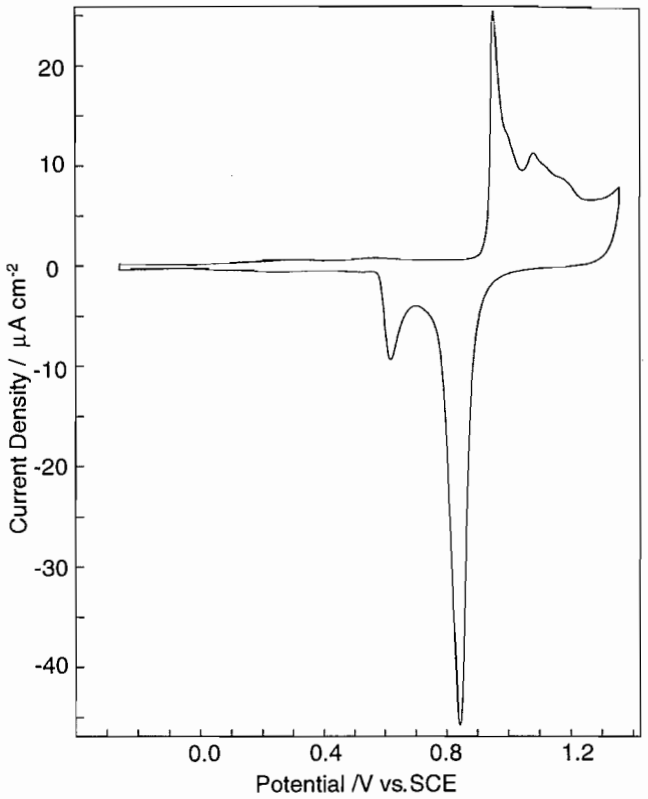
face reconstruction in an aqueous 0.01 M $HClO_4$ solution. Second harmonic generation is a surface-specific technique that has been used to study electrode surface reconstructions (15). The structural sensitivity of SHG spectroscopy arises from the fact that the nonlinear optical response of the surface depends on its symmetry (16). SHG has been shown to be sensitive to a variety of surface reconstructions as well as to the presence of steps and adsorption (11–20). When SHG is used as a structural probe there is, in general, a good correlation of the SHG results with the in situ STM and SXS results (12–20). However, in our in situ study of the Au(110) surface reconstruction in $HClO_4$ we find that the SHG rotational anisotropy curves, from which we obtain information about the surface symmetry, are more complex than predicted from the surface symmetry of the reconstructed and the unreconstructed surfaces. Similar results were observed in a previous SHG study (10) of the Au(110) surface in a 0.1 M $NaClO_4$ solution. Thus, we have done a further analysis to determine the origin of the complex SHG rotational anisotropy using a phenomenological theory (16) in addition to a model suggested earlier (10).

Experimental

The Au(110) sample was aligned to ±0.1° using Laue X-ray back scattering. It was then mechanically polished down to 0.1 μm with a diamond paste and electropolished in $HClO_4$. Before each set of measurements, the sample was annealed in a natural gas flame and then quenched with deionized water (21). The perchloric acid was from Seastar Chemicals (Vancouver, Canada) and the solutions were made with ultrapure deionized water (Milli-Q, Millipore). A three-electrode potentiostat was used for cyclic voltammetry and to control the electrode potential. The Au(111) electrode was mounted in a Teflon holder and used as the working electrode. The counter electrode was a gold foil. The reference electrode was a SCE housed in a separate compartment and linked to the electrochemical cell via a Luggin capillary. All the potential values used in this paper are relative to a SCE. The cyclic voltammogram of the Au(110) in 0.01 M $HClO_4$, obtained by forming a hanging meniscus in order to expose only the Au(110) surface, is presented in Fig. 1. The voltammogram is identical to that obtained in a previous study (22).

We used the fundamental wavelength (1.064 μm) of a picosecond (~35 ps FWHM), active–passive, mode-locked, pulsed Nd:YAG laser as the exciting source. In all the results presented in this paper, the polarization of the fundamental beam is in the plane of incidence (i.e., *p*-polarized). The fundamental light is slightly focused on the surface of the electrode at an angle of incidence of 45° by a 20 cm focal length lens. The energy density at the surface is on the order of 3 mJ/cm^2. In this geometry, the SHG signal generated at the surface is emitted in the same direction as the reflected fundamental (23). The reflected fundamental light and the generated second harmonic signal are collimated by a 15 cm focal length lens. The reflected fundamental is removed by passing it through a dichroic mirror and a low-pass filter. The second harmonic beam then goes through a polarizer so only the *s*-polarized 532 nm light is transmitted. Finally, the second harmonic is focused at the entrance slit of the photomultiplier tube, by a 10 cm focal length lens. The SHG signal is measured using a gated photon counter

Fig. 1. Cyclic voltammogram of Au(110) in 0.01 M $HClO_4$ at 10 mV s^{-1}.



and normalized against the laser power, which is obtained by splitting ~10% of the incident beam. The data presented in this paper are averages of 300 laser shots. The standard deviation of the SHG signal for an average of 300 laser shots is 5% or lower.

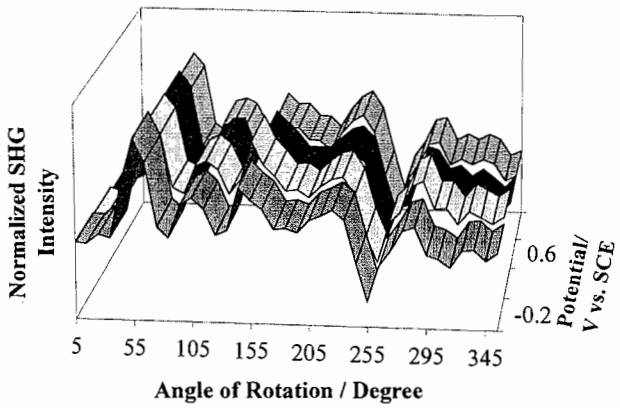
Before the SHG measurements we checked for the presence of contaminants (e.g., organic impurities, Cl^-, etc. ...) by recording a cyclic voltammogram. When the Au(110) surface was clean the potential was held at −0.2, +0.4, +0.6, and +0.8 V (SCE) and the SHG signal was collected. A scan rate of 10 mV/s was used to scan from one potential to the next. The crystal was rotated by 10° and the above procedure was repeated until a full rotation of 360° was achieved. The data shown are the average of four rotational anisotropy curves. Preliminary SHG rotational anisotropy curves obtained on a different Au(110) displayed the same number of peaks located at the same angles and with the same relative intensities. The normalized rotational anisotropy curves had a linear baseline removed before averaging. The angle of rotation is defined as the angle between the plane of incidence of the fundamental light and the ⟨100⟩ direction on the surface. The data were analyzed by a Gauss–Newton method that uses the first partial derivatives of the fitting function (24), i.e., the Levenberg–Marquardt algorithm. We checked the stability of the results by taking a randomly generated starting coefficient and obtaining the same fitted coefficients. The quality of the fit of the different models is based on the standard deviation (24) between the fitted function and the experimental data.

Can. J. Chem. Downloaded from www.nrcresearchpress.com by 88.146.161.215 on 09/08/12
For personal use only.

© 1997 NRC Canada

Can. J. Chem. Downloaded from www.nrcresearchpress.com by 88.146.161.215 on 09/08/12
For personal use only.

Fig. 2. Rotational anisotropy of an Au(110) electrode in 0.01 M $HClO_4$ vs. electrode potential for *p*-polarized fundamental and an *s*-polarized second harmonic. The rotational anisotropy was measured at −0.2, 0.4, 0.6, and 0.8 V (vs. SCE).



Results and discussion

The SHG rotational anisotropy curves at different electrode potentials are shown in Fig. 2. There are six maxima of different intensities on all the curves. No large change in the rotational anisotropy curves occurs over the potential range studied. STM measurements (4) show that the Au(110) surface is unreconstructed at potential more positive than ~0.1 V. Thus a change in the rotational anisotropy curves with the electrode potential is expected since the surface symmetry of the unreconstructed surface is C_{2v} and that of the reconstructed surface is C_s. A surface of C_{2v} symmetry would give either two or four maxima in the rotational anisotropy curves (16). Our results indicate that the nonlinear susceptibility of the Au(110) surface has a symmetry that differs from C_{2v} at all potentials.

A more more detailed analysis was done to find the origin of the complex shape of SHG anisotropy curves of the Au(110) electrode using a phenomenological theory (16). Our models are based on the results of previous STM (4–6) and, SXS (7). We also used a model suggested earlier (10).

The intensity of the SHG signal (23) can be expressed by

$$[1] \quad I^{(2\omega)} \propto |\chi^{(2)}:E^{(\omega)}E^{(\omega)}|^2$$

The SHG intensity is proportional to the square of the magnitude of the product of the third-order susceptibility tensor, $\chi^{(2)}$, and the incident electric field, $E^{(\omega)}$. The structural sensitivity of the SHG spectroscopy arises from the form of the susceptibility matrix, which depends on the surface symmetry (16). In the dipolar approximation, for centrosymmetric solids such as gold, the SHG anisotropy arises only from the surface. Experimental results have shown that the dipolar approximation is adequate for the gold surfaces (20).

Models for the rotational anisotropy of the SH signal

We have used a phenomenological theory developed by Sipe et al. (16) to analyze our data. We applied three different models to fit the experimental data. The first model was developed by Pettinger et al. (10) to take account of the (111) microfacets that appear on the reconstructed (110) surface. The second model was derived using the procedure described in ref. 16 for a reconstructed Au(110) surface that has C_s symmetry. The last model is a modified C_s model, that has two threefold components.

(111) Microfacetting model

Pettinger et al. (10) give the following equation for the second harmonic intensity from Au(110) for a *p*-polarized fundamental and *s*-polarized second harmonic.

$$[2] \quad I^{ps} \propto |b \sin(\phi + \alpha_1) + c \sin 2\phi + d \sin(3\phi + \alpha_3)|^2$$

In eq. [2], b and c are complex parameters while d is a real parameter. We define ϕ as the angle between the plane of the incident beam and the ⟨100⟩ axis on the (110) surface. α_1, and α_3 are angles added to take into account the fact that the (111) microfacets have a crystallographic orientation that is different than the $\langle 1\bar{1}0 \rangle$ axis. α_1 and α_3 are adjustable parameters. In this model, the onefold and threefold sine terms are associated with the pseudo-C_{3v} symmetry of the (111) microfacets.

Equation [2] can be rearranged to

$$[3] \quad I^{ps} \propto |a' \sin\phi + b' \cos\phi + c \sin 2\phi + d' \sin 3\phi + e' \cos 3\phi|^2$$

where $a' = a \cos\alpha_1$, $b' = \sin\alpha_1$, $d' = d \cos\alpha_3$, and $e' = e \sin\alpha_3$. The addition of α_1 and α_3 introduces cos ϕ and cos 3ϕ terms.

C_s model

The C_s model is based on the in situ STM studies (4–6), which showed that the reconstructed surface is formed from long chains of atoms in the $\langle 1\bar{1}0 \rangle$ direction and is highly corrugated in the ⟨100⟩ direction. The large corrugation across the rows (i.e., in the ⟨100⟩ direction) is due to a mixture of (1 × 2) and (1 × 3) local structures. The in situ SXS results (7) also show that there is a random sequence of (1 × 2) and (1 × 3) structures in the ⟨100⟩ direction giving rise to an incommensurate overlayer for the reconstructed Au(110) surface. These results indicate that the reconstructed Au(110) surface has a C_s symmetry with a mirror plane in the ⟨100⟩ direction. Thus the C_s surface in our model has a mirror plane along the ⟨100⟩ direction and perpendicular to the surface plane. The system of coordinates is defined as follow: the $\langle 1\bar{1}0 \rangle$ axis is the x direction, the y direction is along the ⟨100⟩ direction, and z is the direction perpendicular to the surface. In this case, the third-order susceptibility tensor is

$$[4] \quad \chi^{(2)} = \begin{pmatrix} 0 & 0 & 0 & 0 & \chi_{xxz} & \chi_{xxy} \\ \chi_{yxx} & \chi_{yyy} & \chi_{yzz} & \chi_{yyz} & 0 & 0 \\ \chi_{zxx} & \chi_{zyy} & \chi_{zzz} & \chi_{zyz} & 0 & 0 \end{pmatrix}$$

In eq. [4], $\chi^{(2)}$ is expressed in terms of the surface coordinates $(\hat{x}', \hat{y}', \hat{z}')$. These are transformed to the beam coordinates $(\hat{s}, \hat{k}, \hat{z})$ and, the tensor Δ' is obtained (16). The elements of Δ' are given in Table 1. From the elements of the third-order susceptibility tensor, Δ', the intensity of the second harmonic for a C_s surface is calculated to be

$$[5] \quad I^{ps} \propto |e \sin 2\phi + f \cos\phi + g \cos 3\phi|^2$$

© 1997 NRC Canada

Can. J. Chem. Downloaded from www.nrcresearchpress.com by 88.146.161.215 on 09/08/12
For personal use only.

Table 1. Elements of the second-order susceptibility tensor in terms of beam coordinates for a C_s surface.

$$\Delta'^{(2)}_{xxx} = -\frac{1}{2}\left(\chi_{xxy} + \frac{\chi_{yxx} + 3\chi_{yyy}}{2}\right)\cos\phi + \frac{1}{2}\left(\chi_{xxy} + \frac{\chi_{yxx} - \chi_{yyy}}{2}\right)\cos 3\phi$$

$$\Delta'^{(2)}_{xxy} = \Delta'^{(2)}_{xyx} = \frac{1}{2}\left(\chi_{xxy} - \frac{\chi_{yxx} - \chi_{yyy}}{2}\right)\sin\phi - \frac{1}{2}\left(\chi_{xxy} + \frac{\chi_{yxx} - \chi_{yyy}}{2}\right)\sin 3\phi$$

$$\Delta'^{(2)}_{xxz} = \Delta'^{(2)}_{xzx} = \left(\frac{\chi_{xxz} + \chi_{yyz}}{2}\right) - \left(\frac{\chi_{xxz} - \chi_{yyz}}{2}\right)\cos 2\phi$$

$$\Delta'^{(2)}_{xyy} = \frac{1}{2}\left(\chi_{xxy} - \frac{3\chi_{yxx} + \chi_{yyy}}{2}\right)\cos\phi - \frac{1}{2}\left(\chi_{xxy} - \frac{\chi_{yxx} - \chi_{yyy}}{2}\right)\cos 3\phi$$

$$\Delta'^{(2)}_{xyz} = \Delta'^{(2)}_{xzy} = \left(\frac{\chi_{xxz} - \chi_{yyz}}{2}\right)\sin 2\phi$$

$$\Delta'^{(2)}_{xzz} = -\cos\phi\chi_{yzz}$$

$$\Delta'^{(2)}_{yxx} = -\frac{1}{2}\left(\chi_{yxy} - \frac{3\chi_{yxx} + \chi_{yyy}}{2}\right)\sin\phi - \frac{1}{2}\left(\chi_{yxy} + \frac{\chi_{yxx} - \chi_{yyy}}{2}\right)\sin 3\phi$$

$$\Delta'^{(2)}_{yxy} = \Delta'^{(2)}_{yyx} = -\frac{1}{2}\left(\chi_{xxy} - \frac{\chi_{yxx} - \chi_{yyy}}{2}\right)\cos\phi + \frac{1}{2}\left(\chi_{xxy} + \frac{\chi_{yxx} - \chi_{yyy}}{2}\right)\cos 3\phi$$

$$\Delta'^{(2)}_{yxz} = \Delta'^{(2)}_{yzx} = \left(\frac{\chi_{xxz} - \chi_{yyz}}{2}\right)\sin 2\phi$$

$$\Delta'^{(2)}_{xyy} = \frac{1}{2}\left(\chi_{xxy} + \frac{\chi_{yxx} + 3\chi_{yyy}}{2}\right)\sin\phi + \frac{1}{2}\left(\chi_{xxy} + \frac{\chi_{yxx} - \chi_{yyy}}{2}\right)\sin 3\phi$$

$$\Delta'^{(2)}_{yyz} = \Delta'^{(2)}_{yzy} = \left(\frac{\chi_{xxz} + \chi_{yyz}}{2}\right) + \left(\frac{\chi_{xxz} - \chi_{yyz}}{2}\right)\cos 2\phi$$

$$\Delta'^{(2)}_{yzz} = \sin\phi\chi_{yzz}$$

$$\Delta'^{(2)}_{zxx} = \left(\frac{\chi_{zxx} + \chi_{zyy}}{2}\right) - \left(\frac{\chi_{zxx} - \chi_{zyy}}{2}\right)\cos 2\phi$$

$$\Delta'^{(2)}_{zxy} = \Delta'^{(2)}_{zyx} = \left(\frac{\chi_{zxx} - \chi_{zyy}}{2}\right)\sin 2\phi$$

$$\Delta'^{(2)}_{zxz} = \Delta'^{(2)}_{zzx} = -\cos\phi\chi_{zyz}$$

$$\Delta'^{(2)}_{zyy} = \left(\frac{\chi_{zxx} + \chi_{zyy}}{2}\right) + \left(\frac{\chi_{zxx} - \chi_{zyy}}{2}\right)\cos 2\phi$$

$$\Delta'^{(2)}_{zyz} = \Delta'^{(2)}_{zzy} = \sin\phi\chi_{zyz}$$

$$\Delta'^{(2)}_{zzz} = \chi_{zzz}$$

© 1997 NRC Canada

Can. J. Chem. Downloaded from www.nrcresearchpress.com by 88.146.161.215 on 09/08/12
For personal use only.

where ϕ has the same definition as for the (111) microfacetting model and

$$e = f_c f_s(\chi_{xxz} - \chi_{yyz})$$

$$f = \frac{1}{2} f_c^2\left(\chi_{xxy} - \frac{3\chi_{yxx} + \chi_{yyy}}{2}\right) - f_s^2\chi_{yzz}$$

and

$$g = -\frac{1}{2} f_c^2\left(\chi_{xxy} - \frac{\chi_{yxx} - \chi_{yyy}}{2}\right)$$

f_c and f_s are the complex Fresnel factors (16). e, f, and g are complex quantities. For fitting purposes we take e and f as complex quantities and g as a real quantity.

Modified C_s *model*

In the modified C_s model, we account for the possibility of a second source of threefold symmetry for the surface nonlinear susceptibility. This modification is based on the fact that the (110) surface is very open. In the TLK (Terrace, Ledge, Kink) notation the (110) surface of a face-centered cubic metal is a combination of a one-atom (111) ledge and a two-atoms wide (111) terrace. The atoms in the (111) planes are in the grooves between the rows and can be excited by the fundamental light and generate a second harmonic signal. The symmetry of the second harmonic signal originating from these (111) planes is C_{3v}. However, there is a surface relaxation that accompanies the surface reconstruction and modifies the (111) microfacets so they do not have a perfect C_{3v} symmetry (4–6). When taking into account this relaxation, the (111) facets have two mirror planes. One of the mirror planes is coincident with the mirror plane in the C_s model and the other is at 90° to it. The modified C_s model thus consists of eq. [5] to which we added an extra threefold sine component perpendicular to the threefold cosine component. The extra threefold sine component is associated with the (111) microfacets as in the microfacetting model but the angle between the threefold components is fixed. The intensity of the SHG signal, for this model, is given by

$$[6] \quad I^{ps} \propto |h \sin 2\phi + i \cos \phi + j \sin 3\phi + k \cos 3\phi|^2$$

where h, i, j, and k are complex quantities. ϕ has the same definition as for the (111) microfacetting model. For fitting purposes we take h, i, and j as complex quantities and k as a real quantity.

Fitting of the experimental results

The SHG rotational anisotropy data at −0.2 V for the Au(110) electrode and the nonlinear least-squares fits (24) of eqs. [3], [5], and [6] are shown in Fig. 3. The parameters of the fitted equations are given in Table 2. From Fig. 3*B* it is clear that the C_s models cannot reproduce the SHG data. The number of peaks and their positions differ from the observed rotational anisotropy curve in Fig. 3*A*. It is not possible with the C_s model to have only one peak more intense than the others, as we and

Fig. 3. Rotational anisotropy of an Au(110) electrode in 0.01 M $HClO_4$ at −0.2 V (vs. SCE). (*A*) Experimental data. (*B*) Least-squares fit of C_s model (eq. [5]) to data shown in box *A*. (*C*) Least-squares fit of microfacetting model (eq. [3]) to data shown in box *A*. (*D*) Least-squares fit of modified microfacetting model (eq. [6]) to data shown in box *A*.

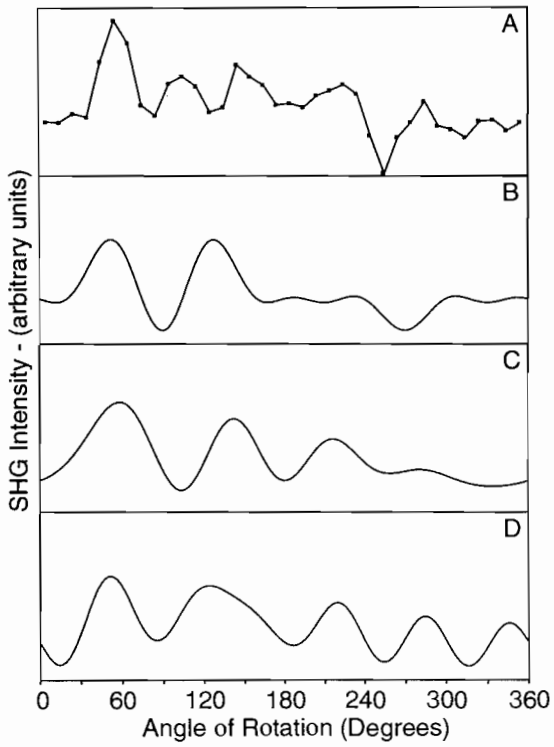


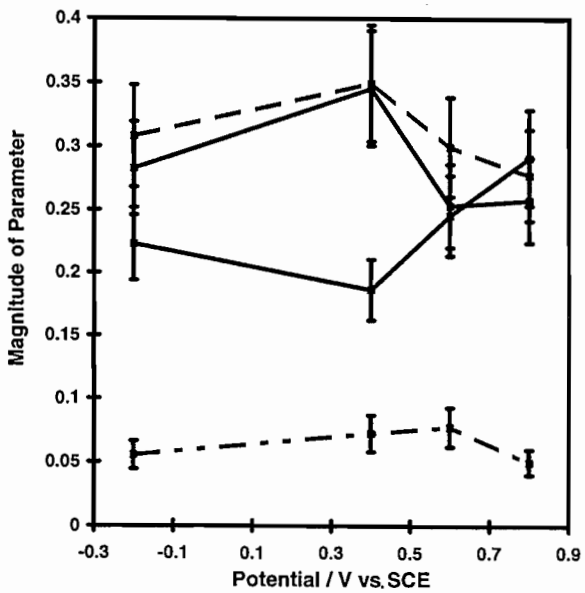
Table 2. Parameters of the nonlinear least-squares fit of the SHG rotational anisotropy curve of Au(110) in 0.01 M $HClO_4$ at −0.2 V.

Parameter	Value
Microfacetting model	
a'	−0.1017 + i 0.1718
b'^a	−0.1248 + i 0.2108
c'	−0.3210 − i 0.0635
d'	0.1147
e'	0.0517
Standard deviation	0.073
C_s model	
e	−0.1266 + i 0.3473
f	0.0338 + i 0.0667
g	0.2558
Standard deviation	0.083
Modified C_s model	
h	−0.1257 + i 0.1839
i	−0.0515 + i 0.0202
j	−0.1470 − i 0.2414
k	0.3080
Standard deviation	0.065

[a]Note that from eqs. [2] and [3], b'_i was held fixed to $b'_i = \frac{a'_i b'_r}{a'_r}$.

© 1997 NRC Canada

Fig. 4. Magnitudes of the fitted components of the modified C_s model (eq. [6]) at different electrode potentials. Solid line: sin 2ϕ; long broken line: cos 3ϕ; short broken line: sin 3ϕ; long/short broken line: cos ϕ. The error bars represent the confidence limit of 75% (*t* test).



others (10) observed for a Au(110) electrode in weakly interacting electrolyte solutions. The microfacetting model suggested previously (10) provides an adequate fit of the rotational anisotropy curve at −0.2 V. The position and the relative intensity of the peaks are reproduced. The extra one- and threefold anisotropy sources provide enough flexibility to the fitting functions to have peaks of different intensities. The meaning of the angles α_1 and α_3 as the extra sources of anisotropy is not clear since they are adjustable parameters.

Our modified C_s model in Fig. 3*D* also reproduces the data adequately. In Fig. 4 we have the magnitude of the components of eq. [6] for the modified C_s model for all the potentials. We see that at −0.2 V the symmetry of the SHG rotational anisotropy is mainly threefold. The two perpendicular sources of threefold symmetry have similar magnitudes. The twofold component is also important; its magnitude is about 2/3 of one of the threefold components. In the modified C_s model the twofold component is assigned to domains of pseudo-C_{2v} symmetry. The onefold contribution to the rotational anisotropy is significantly smaller than the two- and threefold components due to the asymmetry of the SHG rotational anisotropy curve. The magnitude of the parameters of the fitted modified C_s model indicates that the surface nonlinear response of the reconstructed Au(110) could originate from two types of structures having a pseudo-C_{2v} and a pseudo-C_{3v} symmetry. However, our model shows that the presence of two- and threefold symmetry components can arise from a surface with C_s symmetry. This conclusion was also reached in a previous SHG study of the reconstruction of a Au(111) electrode (14). The magnitude of the threefold component cannot be clearly related to the (111) microfacetting. Nevertheless, it is likely that the (111) microfacets are the main source of the threefold anisotropy.

There is no large change in the magnitudes of the parameters over the potential range studied as shown in Fig. 4. This is similar to the reconstructed Au(110) electrode in a 0.1 M $NaClO_4$ solution (10) where the rotational anisotropy curves did not change significantly over a large potential range from −0.2 V to the beginning of the formation of the surface oxide. We see that the magnitudes of the threefold components are almost the same at −0.2 and 0.4 V. If the threefold components originate mainly from the atoms in the (111) microfacets or planes, this result indicates that the number of atoms in the (111) planes does not vary significantly between −0.2 and 0.4 V where the reconstruction is lifted according to STM (4, 5). There is a small decrease in the magnitude of the two threefold symmetry components from 0.4 to 0.8 V. This decrease is not significant at a degree of confidence of 75% (*t* test) represented by the error bars on Fig. 4. The magnitude of the twofold component that is related to the unreconstructed (110) surface or well-ordered (1 × 2) and (1 × 3) domains increases slightly from 0.4 to 0.8 V. This increase is significant at a degree of confidence of 75% (*t* test). We relate the increase of the twofold component to a small increase in the fraction of the surface forming (1 × 1) domains.

Capacitance measurements (5, 22) support the suggestion of a gradual reconstruction. The capacitance measurements show that in the double layer region the capacitance curve has a complex sigmoidal shape. A large hysteresis in the capacitance curve of the positive and negative direction potential sweeps between the pzc (−0.050 V) to 0.6 V is observed (4). If the hysteresis in the capacitance data is related to the surface reconstruction process then the reconstruction occurs gradually. This interpretation of the capacitance data and our observation of a small change of surface symmetry from 0.4 to 0.8 V do not agree with STM measurements (4), which indicate that at 0.1 V the surface has mainly a (1 × 1) (i.e., unreconstructed) structure. Based on the STM measurements, the hysteresis in the capacitance data must then be related to the presence of steps, defects, islands, and microfacetting (22). However, a gradual reconstruction of the Au(110) surface in aqueous 0.1 M H_2SO_4 and 0.1 M $HClO_4$ solutions was observed in another in situ STM (5) study. The reconstruction from a (1 × 2)/(1 × 3) to a (1 × 1) surface occurs between −0.1 and 0.25 V. In this potential range the three different structures are observed simultaneously on the surface. These STM measurements (5) and the capacitance data in 0.1 M H_2SO_4 show a good correlation in contrast to the STM results obtained in perchloric acid solutions (4).

The discrepancy between our, and other, results (5, 10, 22) and an STM study (4) reflects the complexity of the reconstruction of Au(110) in background electrolyte. The differences between the studies could arise from the different surface properties that are measured and from the dimension of the probed surface. SHG spectroscopy must be sensitive to the steps, defects, islands, and (111) microfacets that are present on the unreconstructed (1 × 1) surface. The amount of such defects is of the order of a few percent according to STM (5). Thus we do not expect that the surface defects are the only source of SHG rotational anisotropy. Larger (111) microfacetting can be observed depending on the quality of the flame-annealing process as well as on the purity of the perchloric acid solution used (22). Our analysis shows that SHG spectroscopy is sensitive to the presence of (111) microfacets that have a threefold symmetry (4, 5). Thus, part of the measured

© 1997 NRC Canada

Can. J. Chem. Downloaded from www.nrcresearchpress.com by 88.146.161.215 on 09/08/12
For personal use only.

Can. J. Chem. Downloaded from www.nrcresearchpress.com by 88.146.161.215 on 09/08/12
For personal use only.

rotational anisotropy signal could be due to the slow removal of the defects on the poorly ordered (1 × 1) surface. For strongly adsorbed halogen anions, the SHG rotational anisotropy and STM measurements are in close agreement for the surface symmetry. In the presence of adsorbed bromine anions in a neutral solution, the SHG rotational anisotropy curve (10) shows a clear transition to a C_{2v} symmetry over the range of potential measured in the STM studies (5) for a solution containing chlorine anions. Based on these results, we believe that SHG is monitoring the slow transition from a reconstructed to an unreconstructed Au(110) surface in aqueous perchloric acid solution. The comparison between the SHG and the STM results illustrates the limitations of SHG for studying the reconstruction of open, corrugated surfaces that undergo a local reconstruction. The complex SHG rotational anisotropy curve does not give a straightforward interpretation of the surface reconstruction as is the case for the STM results. Nevertheless, SHG spectroscopy is a useful tool to probe surface reconstructions that are potential induced because it is less invasive than STM, which requires the application of bias potential and a tunneling current.

The slow transition from a reconstructed to an unreconstructed surface suggested by the SHG and capacitance measurements could be due to the low mobility of the surface gold atom in a solution of weakly adsorbed electrolyte. The reason for the gradual transition between reconstructed (1 × 2) or (1 × 3) and unreconstructed (1 × 1) Au(110) surface in weakly adsorbed electrolyte solutions is not well understood. It seems that in a weakly interacting electrolyte the (1 × 1) surface cannot be stabilized by removal of electronic charge from the surface to the extent that the (1 × 1) structure becomes significantly more stable than the (1 × 2) and (1 × 3) structures. The relative stability of these structures is supported by recent first principles calculations (25) of the total energy of the equilibrium geometry of the (1 × 1), (1 × 2), and (1 × 3) structures. This theoretical study suggests that the (1 × 2) and (1 × 3) surfaces have similar energies and that they are more stable than the (1 × 1) surface in the absence of an electric field. This calculation supports our results as well as those of previous studies (5, 10, 22) that indicate that the potential-induced lifting of the Au(110) reconstruction in $HClO_4$ is gradual.

In summary, our results show that the SHG rotational anisotropy of an Au(110) electrode in perchloric acid varies very weakly with the applied potential. The analysis of the rotational anisotropy curves reveals important threefold symmetry components. We assign these components to the presence of (111) microfacets. The small variation of the rotational anisotropy with electrode potential is suggested to be due to the gradual removal of the reconstruction of the Au(110) as the potential is made more positive.

Acknowledgments

The financial support of the Natural Sciences and Engineering Research Council of Canada (NSERC) and the Centre of Excellence in Molecular and Interfacial Dynamics (CEMAID) is acknowledged, as are a postdoctoral (C.D.K.) and a summer (M.D.) fellowship from NSERC. Dr. D.-F. Yang is thanked for the preparation of the Au(110) crystals and for useful discussions. Prof. J. Lipkowski is thanked for the use of his equipment for making the single crystals used in this study.

References

1. J.O'M. Bockris and S.U.M. Khan. Surface electrochemistry: a molecular level approach. Plenum Press, New York. 1993.
2. D. Kolb. *In* Structure of electrified interfaces. *Edited by* J. Lipkowski and P.N. Ross. VCH Publishers, New York. 1993.
3. J. Electroanal. Chem. **376** (1994), special issue in honor of Antoinette Hamelin.
4. X. Gao, G.J. Edens, A. Hamelin, and M.J. Weaver. Surf. Sci. **318**, 1 (1994).
5. O.M. Magnussen, J. Weichers, and R.J. Behm. Surf. Sci. **289**, 139 (1993).
6. X. Gao, G.J. Edens, and M.J. Weaver. J. Electroanal. Chem. **376**, 21 (1994).
7. B.M. Ocko, G. Helgesen, B. Schardt, J. Wang, and A. Hamelin. Phys. Rev. Lett. **69**, 3350 (1992).
8. J. Wang, A.J. Davenport, H.S. Isaacs, and B.M. Ocko. Science, **255**, 1416 (1992).
9. B.M. Ocko, J. Wang, A. Davenport, and H. Isaacs. Phys. Rev. Lett. **65**, 1466 (1990).
10. B. Pettinger, S. Mirwald, and J. Lipkowski. Appl. Phys. A: Solids Surf. **A60**, 121 (1995).
11. D.A. Koos and G.L. Richmond. J. Phys. Chem. **96**, 3770 (1992).
12. A. Freidrich, B. Pettinger, D.M. Kolb, G. Lupke, R. Steinhoff, and G. Marowsky. Chem. Phys. Lett. **163**, 123 (1989).
13. B. Pettinger, J. Lipkowski, and S. Mirwald. Electrochim. Acta, **40**, 133 (1995).
14. J. Lipkowski, L. Stolberg, D.Y. Fang, B. Pettinger, S. Mirwald, F. Henglein, and D.M. Kolb. Electrochim. Acta, **39**, 1045 (1994).
15. G.L. Richmond, J.M. Robinson, and V.L. Shannon. Prog. Surf. Sci. **28**, 1 (1988).
16. J.E. Sipe, D.J. Moss, and H.M. van Driel. Phys. Rev. B: Condens. Matter, **35**, 1129 (1987).
17. K.A. Freidrich and G.L. Richmond. Chem. Phys. Lett. **213**, 491 (1993).
18. C. Jakobsen, D. Podenas, and K. Pedersen. Surf. Sci. **312**, 1 (1994).
19. M.A. Verheijen, C.W. van Hasselt, and T. Rasing. Surf. Sci. **251/252**, 467 (1991).
20. D.A. Koos, V.L. Shannon, and G.L. Richmond. Phys. Rev. B: Condens. Matter, **47**, 4730 (1993).
21. J. Clavilier, R. Faure, G. Guinet, and R. Durand. J. Electroanal. Chem. **107**, 205 (1980).
22. A. Hamelin. J. Electroanal. Chem. **329**, 247 (1992).
23. Y R. Shen. The principles of nonlinear optics. John Wiley & Sons, New York. 1984.
24. A.F. Seber and C.J. Wild. Nonlinear regression. John Wiley & Sons, New York. 1989. Chap. 14.
25. K.P. Bohnen and K.M. Ho. Electrochim. Acta, **40**, 129 (1995).

© 1997 NRC Canada

Modeling of transfer properties using revised HKF theory: thermodynamics of transfer of an amino acid and small peptides from water to urea–water solutions at 298.15 K

Andrew W. Hakin, Lori L. Groft, Jocelyn L. Marty, and Matthew L. Rushfeldt

Abstract: Relative densities, $(\rho - \rho_1^0)$, and heat capacity ratios, $(c_p\rho/(c_{p1}^0\rho_1^0) - 1)$, have been measured for aqueous solutions of glycine, glycylglycine, and glycylglycylglycine in aqueous urea solutions containing 1–13 mol kg^{-1} urea. These data have been used to calculate apparent molar volumes, $V_{2,\phi}$, and apparent molar heat capacities, $C_{p2,\phi}$, which in turn have been used to obtain standard state volumes, $\overline{V}_2^0$, and standard state heat capacities, $\overline{C}_{p2}^0$. Volumes and heat capacities of transfer from water to urea have been calculated from our reported standard state data. Heat capacities of transfer of the investigated systems have been modeled using a procedure developed from the semiempirical calculation procedures proposed by Helgeson, Kirkham, and Flowers.

Key words: amino acids, peptides, calorimetry, transfer thermodynamics, HKF theory.

Résumé : On a mesuré les densités relatives $(\rho - \rho_1^0)$ et les rapports des capacités calorifiques $(c_p\rho/(c_{p1}^0\rho_1^0) - 1)$ pour des solutions aqueuses de glycine, de glycylglycine et de glycylglycylglycine dans des solutions aqueuses d'urée contenant 1–13 mol kg^{-1} d'urée. On a utilisé ces données pour calculer les volumes molaires apparents $V_{2,\phi}$, et les capacités calorifiques molaires apparentes, $C_{p2,\phi}$, à partir desquels on a obtenu les volumes à l'état standard, $\overline{V}_2^0$, et les capacités calorifiques de l'état standard $\overline{C}_{p2}^0$. On a calculé les volumes et les capacités calorifiques de transfert à partir de l'eau vers l'urée, à partir de nos données rapportées pour l'état standard. On a modélisé les capacités calorifiques de transfert des systèmes étudiés en utilisant une méthode développée à partir des méthodes de calcul semi-empiriques proposées par Helgeson, Kirkham et Flowers.

Mots clés : acides aminés, peptides, calorimétrie, transfert thermodynamique, théorie HKF.

[Traduit par la rédaction]

Introduction

The precise role of urea in the denaturation of protein systems appears to remain unclear in spite of extensive investigation (1–3). However, a common thread in many discussions identifies urea's structure-breaking tendencies in water as being of prime importance. Two processes by which urea can interact with proteins have been described. In the first, the presence of urea is thought to diminish the hydrophobic hydration of protein apolar groups. In this way the apolar groups become more repulsive to each other, thus opening up the protein structure. In the second description, which may or may not work in cooperation with the first, urea is thought to preferentially solvate the peptide groups of proteins. This preferential solvation, sometimes referred to as binding, is thought to disrupt intramolecular hydrogen bonding, thus disrupting the native conformation of the protein. Although it appears clear that peptide groups in proteins play a central role in the urea-induced denaturation process, their exact role remains the subject of debate. In their investigation of the interactions of urea and guanidine hydrochloride with lysozyme, ribonuclease, and cyctochrome C, Makhatadze and Privalov (4) found a good correlation between the number of denaturant binding sites and the number of H-bonding groups exposed in the folded or unfolded protein. This finding is supported by the more recent work of Zolkiewski, Nosworthy, and Ginsburg who looked at the urea-induced dissociation and unfolding of dodecameric glutamine synthetase (5). Common to these two investigations is the contention that urea molecules H-bond to available peptide sites in the protein. Unfortunately, the preferential solvation model, which is based on calorimetric data that yield enthalpic pair interaction coefficients, does not support an H-bonding explanation.

Many denaturation protocols recommend the use of urea at a concentration of 8 mol L^{-1} (approximately 13 mol kg^{-1} at 25°C) to ensure complete protein denaturation. Urea at this concentration is thought to destroy the majority of structural organization within the protein molecule. Though disruption is most certainly significant at this concentration, whether the forces contributing to secondary and tertiary structure of a protein have been completely eliminated at this stage cannot be certain. In many cases, a protein's thoroughly denatured conformation, as judged by its hydrodynamic properties, may

Received December 2, 1996.

A.W. Hakin,[1] L.L. Groft, J.L. Marty, and M.L. Rushfeldt.
Department of Chemistry, University of Lethbridge,
4401 University Drive, Lethbridge, AB T1K 3M4, Canada.

[1] Author to whom correspondence may be addressed.
Telephone: (403) 329-2083. Fax: (403) 329-2057.
E-mail: hakin@hg.uleth.ca

© 1997 NRC Canada

Can. J. Chem. Downloaded from www.nrcresearchpress.com by 88.146.161.215 on 09/08/12
For personal use only.

Can. J. Chem. Downloaded from www.nrcresearchpress.com by 88.146.161.215 on 09/08/12
For personal use only.

be unattainable due to the limited solubility of urea in water. An example of such behaviour was found by Kawahara et al. (6) in the case of co-hemoglobin. Therefore, to better predict the actions of urea on secondary and tertiary protein conformation, one must first develop an understanding of the interactions of urea with less complicated molecules that model protein side chains, e.g., amino acids or simple oligopeptides.

To further probe this ongoing puzzle of urea-based protein denaturation, we have investigated the thermochemical and volumetric properties of glycine (gly), glycylglycine (digly), and glycylglycylglycine (trigly) in aqueous urea solutions (in the range 1–13 mol kg^{-1}). Apparent molar volumes and heat capacities for the investigated systems have been used to calculate standard state volumes and heat capacities, which in turn have been used to calculate the relevant extensive thermodynamic properties of transfer.

In addition, the semiempirical modeling procedures of Helgeson, Kirkham, and Flowers (7) have been applied to the calculated heat capacities of transfer from water to urea of gly, digly, and trigly. The methodology presented in this paper shows how calculated heat capacities of transfer may be subdivided into structural and solvation components. Trends in these contributions as a function of urea concentration are examined and discussed.

Experimental

Glycine (99+%), glycylglycine (99.5+%), and glycylglycylglycine (99.5+%), were obtained from Sigma Chemicals Ltd. (catalog numbers G-7126, G-7278, and G-1377, respectively).

All glycyl compounds were purified by repeated recrystallization from water + ethanol mixtures. The purified chemicals were dried and stored over phosphorus pentoxide in a vacuum oven at 50°C. An indication of the purity of the samples was obtained using NMR spectroscopy. The recorded spectra were in excellent agreement with those reported in the literature (8).

Samples of urea (reagent grade) were obtained from Fisher Scientific and BDH Inc. and were used without further purification.

All solutions used in our investigations were prepared by weight on the molality concentration scale using bidistilled, degassed water. Amino acid and peptide solutions in urea + water mixtures were stored in sealable 125 mL Nalgene bottles. All urea solutions were used within 24 hours of their preparation.

The densities of the prepared solutions were measured relative to the solvent (either water or the relevant aqueous urea solution) with a Sodev O2D vibrating tube, flow densitometer (9). This instrument has a thermal stability of ±0.001°C and routinely measures densities with part per million precision. The volumetric heat capacities of the investigated systems in aqueous urea solutions were measured relative to their respective solvent using a Picker flow microcalorimeter (10). Small residual heat leaks in our calorimeter were accounted for by using a calorimetric heat loss correction factor, or *f* factor (11). This factor was evaluated prior to the start of our investigations as $f = 0.9967$ using standard solutions of sodium chloride in water.

Details of the densitometer, the flow microcalorimeter, and procedures used in their calibration have been described previously (12–14).

Results and analysis

Experimentally determined data, namely, relative densities, $(\rho - \rho_1^0)$, and heat capacity ratios $(c_p\rho/(c_{p_1}{}^0\rho_1^0) - 1)$, for gly, digly, and trigly in various urea–water mixtures are reported in Tables 1, 2, and 3, respectively. These tables also contain apparent molar volume, $V_{2,\phi}$, and heat capacity, $C_{p2,\phi}$, data that were calculated from the experimental data using eqs. [1] and [2],

$$[1] \quad V_{2,\phi} = \left(\frac{M}{\rho}\right) - \left(\frac{\rho - \rho_1^0}{m\rho\rho_1^0}\right)$$

$$[2] \quad C_{p2,\phi} = Mc_p + \left(\frac{c_p - c_{p1}{}^0}{m}\right)$$

In these equations M defines the molar mass of the solute, m is the molality of the solution, ρ and ρ_1^0 are the densities of the sample and of pure water, and c_p and $c_{p1}{}^0$ are the specific heat capacities of the sample and pure water. The densities and heat capacities of pure water, used in our calculations, are those reported by Kell (15, 16). The densities and heat capacities of individual urea solvents were calculated using previously published data from this laboratory (17). Calculated uncertainties (13) in the apparent molar properties have been included in parentheses in Tables 1–3.

Standard state volumes and heat capacities for the three systems investigated were calculated at each experimental concentration of urea by fitting equations of the general form described by eq. [3] to our calculated apparent molar volume and apparent molar heat capacity data. A weighted regression analysis procedure was utilized (13).

$$[3] \quad Y_{2,\phi} = Y_{2,\phi}^0 + S_Y m$$

In eq. [3] Y represents the extensive thermodynamic property of interest, $Y_{2,\phi}^0$ is the value of $Y_{2,\phi}$ at infinite dilution (i.e., the standard state property $\overline{Y}_2^0$), and S_Y is the experimental slope. Calculated standard state volumes and heat capacities for each solvent system are reported in Table 4.

Values for standard state volumes and heat capacities for gly and digly in water have been taken from two of our previous investigations (13, 14). Our value of $\overline{V}_2^0 = 112.06 \pm 0.01$ cm^3 mol^{-1} for trigly in water at 298.15 K is in excellent agreement with the value of Chalikian et al. of 112.1 ± 0.3 cm^3 mol^{-1} (18) and in good agreement with Hedwig's value of 111.92 ± 0.03 cm^3 mol^{-1} (19). Similarly, our reported standard state heat capacity for trigly in water at 298.15 K, $\overline{C}_{p2}^0 = 186.3 \pm 0.9$ J K^{-1} mol^{-1} is in good agreement with Hedwig's value (19) of 188.3 ± 0.7 J K^{-1} mol^{-1} and Jolicoeur and Boileau's value (20) of 189.5 ± 0.9 J K^{-1} mol^{-1}. Compared to these values, Makhatadze and Privalov's (21) value of $\overline{C}_{p2}^0 = 175.3$ J K^{-1} mol^{-1} appears too low.

With respect to standard state volumes and heat capacities for gly, digly, and trigly in aqueous urea solutions, only limited literature data are available for comparison purposes. Enea and Jolicoeur (3) previously measured heat capacities and volumes of several oligopeptides in urea + water mixtures at 25°C; however, the only standard state data they report for gly, digly, and trigly refer to an aqueous urea

© 1997 NRC Canada

Can. J. Chem. Downloaded from www.nrcresearchpress.com by 88.146.161.215 on 09/08/12
For personal use only.

Table 1. Relative densities, $(\rho - \rho_1^0)$, apparent molar volumes, $V_{2,\phi}$, heat capacity ratios, $(c_p\rho/(c_{p1}^0\rho_1^0) - 1)$, and apparent molar heat capacities, $C_{p2,\phi}$, of aqueous solutions of glycine at various concentrations of urea.[a]

m (mol kg^{-1})	$(\rho - \rho_1^0)$ (g cm^{-3})	$V_{2,\phi}$ (cm^3 mol^{-1})	$10^3\left(\frac{c_p\rho}{c_{p1}^0\rho_1^0} - 1\right)$	$C_{p2,\phi}$ (J K^{-1} mol^{-1})
		2 *m* Urea		
0.03478	1.053×10^{-3}	44.37 (0.14)	−0.972	68.7 (2.0)
0.05663	1.701×10^{-3}	43.56 (0.08)	−1.546	71.9 (1.2)
0.10463	3.126×10^{-3}	44.64 (0.05)	−2.846	72.4 (0.7)
0.16248	4.848×10^{-3}	44.61 (0.03)	−4.415	72.1 (0.4)
0.18576	5.537×10^{-3}	44.61 (0.03)	−5.031	72.3(0.4)
0.09110	2.730×10^{-3}	44.58 (0.05)	−2.471	72.5 (0.8)
0.14431	4.309×10^{-3}	44.61 (0.03)	−3.861	73.8 (0.5)
0.22181	6.589×10^{-3}	44.66 (0.02)	−5.954	73.3 (0.3)
		4 *m* Urea		
0.061749	1.802×10^{-3}	44.95 (0.07)	−1.465	79.8 (1.1)
0.088623	2.573×10^{-3}	45.06 (0.05)	−2.037	82.6 (0.8)
0.11842	3.414×10^{-3}	45.20 (0.04)	−2.699	83.6 (0.6)
0.14138	4.059×10^{-3}	45.28 (0.03)	−3.203	84.3 (0.5)
0.17118	4.923×10^{-3}	45.20 (0.03)	−3.837	84.8 (0.4)
0.20715	5.922×10^{-3}	45.31 (0.02)	−4.627	85.3 (0.3)
0.25914	7.345×10^{-3}	45.47 (0.02)	−5.744	86.2 (0.3)
		6 *m* Urea		
0.017698	5.364×10^{-4}	43.67 (0.25)	−0.394	86.5 (4.0)
0.023665	6.766×10^{-4}	45.16 (0.18)	−0.508	94.8 (3.0)
0.049618	1.427×10^{-3}	44.98 (0.09)	−1.033	96.3 (1.4)
0.063034	1.791×10^{-3}	45.27 (0.07)	−1.271	99.7 (1.1)
0.066620	1.873×10^{-3}	45.52 (0.07)	−1.342	100.6 (1.1)
0.10347	2.889×10^{-3}	45.64 (0.04)	−2.031	102.8 (0.7)
0.092323	2.585×10^{-3}	45.60 (0.05)	−1.848	101.3 (0.8)
0.18700	5.153×10^{-3}	45.87 (0.02)	−3.620	104.3 (0.7)
		11 *m* Urea		
0.04528	1.213×10^{-3}	45.87 (0.09)	−0.702	114.2 (1.6)
0.07091	1.865×10^{-3}	46.25 (0.06)	−1.034	118.5 (1.0)
0.12888	3.375×10^{-3}	46.28 (0.03)	−1.837	119.5 (0.5)
0.12904	3.357×10^{-3}	46.41 (0.03)	−1.853	119.7 (0.5)
0.16646	4.318×10^{-3}	46.44 (0.03)	−2.347	120.5 (0.4)
0.20110	4.921×10^{-3}	46.53 (0.02)	−2.795	121.4 (0.4)
0.24410	6.218×10^{-3}	46.74 (0.02)	−3.351	122.6 (0.3)
		13 *m* Urea		
0.07205	1.811×10^{-3}	46.91 (0.06)	−0.903	125.8 (1.0)
0.13267	3.299×10^{-3}	47.06 (0.03)	−1.609	127.5 (0.5)
0.16506	4.094×10^{-3}	47.08 (0.02)	−2.050	126.6 (0.4)
0.21786	5.378×10^{-3}	47.08 (0.02)	−2.626	127.7 (0.3)
0.25389	6.236×10^{-3}	47.17 (0.02)	−3.010	128.5 (0.3)
0.29769	7.276×10^{-3}	47.23 (0.01)	−3.439	129.6 (0.2)
0.36391	8.849×10^{-3}	47.26 (0.01)	−4.282	128.9 (0.2)

[a]Uncertainties are shown in parentheses.

solvent at a concentration of 7 mol L^{-1}. Volume and heat capacity data used in the calculation of transfer properties at other urea concentrations were obtained by averaging apparent molar properties (1–4 data points at each concentration) at solute concentrations somewhat removed from the infinite dilution condition.

As one would expect, when Jolicoeur and Enea's averaged apparent molar volume and heat capacities are compared with

© 1997 NRC Canada

Can. J. Chem. Downloaded from www.nrcresearchpress.com by 88.146.161.215 on 09/08/12
For personal use only.

Table 2. Relative densities, $(\rho - \rho_1^0)$, apparent molar volumes, $V_{2,\phi}$, heat capacity ratios, $(c_p\rho/(c_{p1}^0\rho_1^0) - 1)$, and apparent molar heat capacities, $C_{p2,\phi}$, of aqueous solutions of glycylglycine at various concentrations of urea.[a]

m (mol kg^{-1})	$(\rho - \rho_1^0)$ (g cm^{-3})	$V_{2,\phi}$ (cm^3 mol^{-1})	$10^3\left(\frac{c_p\rho}{c_{p1}^0\rho_1^0} - 1\right)$	$C_{p2,\phi}$ (J K^{-1} mol^{-1})
		2 *m* Urea		
0.051089	2.773×10^{-3}	77.01 (0.09)	−1.396	144.7 (1.4)
0.078628	4.231×10^{-3}	77.33 (0.06)	−3.331	143.7 (0.9)
0.099621	5.312×10^{-3}	77.72 (0.04)	−4.038	152.1 (0.7)
0.11923	6.334×10^{-3}	77.83 (0.04)	−4.801	153.4 (0.6)
0.15034	7.950×10^{-3}	77.93 (0.03)	−6.0726	152.9 (0.5)
0.15876	8.383×10^{-3}	77.98 (0.03)	−6.367	154.1 (0.5)
		3.80 *m* Urea		
0.02187	1.149×10^{-3}	78.20 (0.2)	−0.750	175.5 (3.2)
0.05804	3.032×10^{-3}	78.32 (0.08)	−1.972	176.7 (1.2)
0.1007	5.218×10^{-3}	78.55 (0.05)	−3.410	177.6 (0.7)
0.1437	7.364×10^{-3}	78.89 (0.03)	−4.788	180.5 (0.5)
0.1801	9.191×10^{-3}	78.95 (0.02)	−5.979	180.8 (0.4)
0.2298	11.648×10^{-3}	79.08 (0.02)	−7.573	181.8 (0.3)
0.2630	13.266×10^{-3}	79.18 (0.02)	−8.598	182.8 (0.3)
0.3068	15.400×10^{-3}	79.25 (0.02)	−9.929	183.9 (0.2)
0.3476	17.364×10^{-3}	79.32 (0.01)	−11.184	184.5 (0.2)
0.4059	20.084×10^{-3}	79.54 (0.01)	−12.870	186.6 (0.2)
		6 *m* Urea		
0.018102	9.74×10^{-4}	76.40 (0.24)	−0.648	163.4 (3.9)
0.029988	1.608×10^{-3}	76.51 (0.15)	−1.036	168.1 (2.3)
0.048365	2.464×10^{-3}	78.78 (0.09)	−1.495	189.1 (1.5)
0.060955	3.107×10^{-3}	78.70 (0.07)	−1.863	189.9 (1.2)
0.068185	3.476×10^{-3}	78.68 (0.06)	−2.089	189.4 (1.0)
0.097653	4.860×10^{-3}	79.62 (0.05)	−2.833	198.4 (0.7)
0.12601	6.230×10^{-3}	79.80 (0.04)	−3.628	201.4 (0.6)
0.19877	9.710×10^{-3}	80.05 (0.02)	−5.543	203.1 (0.4)
		8 *m* Urea		
0.04799	2.337×10^{-3}	80.17 (0.09)	−1.249	207.2 (1.5)
0.07858	3.864×10^{-3}	79.66 (0.05)	−1.977	208.0 (0.9)
0.10704	5.228×10^{-3}	79.83 (0.04)	−2.667	209.3 (0.7)
0.12747	6.135×10^{-3}	80.37 (0.03)	−3.155	211.7 (0.6)
0.15275	7.327×10^{-3}	80.41 (0.03)	−3.722	213.0 (0.5)
0.18125	8.672×10^{-3}	80.42 (0.02)	−4.378	213.5 (0.4)
		11 *m* Urea		
0.04538	2.117×10^{-3}	81.09 (0.09)	−0.922	224.7 (1.6)
0.08638	4.037×10^{-3}	80.88 (0.05)	−1.725	224.8 (0.8)
0.11770	5.475×10^{-3}	80.95 (0.03)	−2.326	225.6 (0.6)
0.12382	5.756×10^{-3}	80.96 (0.03)	−2.433	225.9 (0.6)
0.15021	6.953×10^{-3}	81.03 (0.03)	−2.954	226.0 (0.5)
0.17320	7.992×10^{-3}	81.07 (0.02)	−3.390	226.3 (0.4)
0.19473	8.956×10^{-3}	81.12 (0.02)	−3.787	226.8 (0.4)
		13 *m* Urea		
0.04363	2.003×10^{-3}	81.21 (0.09)	−0.774	230.2 (1.6)
0.08249	3.774×10^{-3}	81.21 (0.05)	−1.481	229.4 (0.9)
0.11224	5.134×10^{-3}	81.12 (0.04)	−1.984	229.8 (0.6)
0.12264	5.647×10^{-3}	80.84 (0.03)	−2.221	227.4 (0.6)
0.16548	7.518×10^{-3}	81.19 (0.02)	−2.885	230.6 (0.4)
0.18987	8.591×10^{-3}	81.26 (0.02)	−3.300	230.9 (0.4)

[a]Uncertainties are shown in parentheses.

© 1997 NRC Canada

Can. J. Chem. Downloaded from www.nrcresearchpress.com by 88.146.161.215 on 09/08/12
For personal use only.

Table 3. Relative densities, $(\rho - \rho_1^0)$, apparent molar volumes, $V_{2,\phi}$, heat capacity ratios, $(c_p\rho/(c_{p1}^0\rho_1^0) - 1)$, and apparent molar heat capacities, $C_{p2,\phi}$, of aqueous solutions of glycylglycylglycine at various concentrations of urea.[a]

m (mol kg^{-1})	$(\rho - \rho_1^0)$ (g cm^{-3})	$V_{2,\phi}$ (cm^3 mol^{-1})	$10^3\left(\frac{c_p\rho}{c_{p1}^0\rho_1^0} - 1\right)$	$C_{p2,\phi}$ (J K^{-1} mol^{-1})
		2 *m* Urea		
0.03765	2.770×10^{-3}	114.20 (0.13)	−2.008	248.8 (1.9)
0.06384	4.727×10^{-3}	113.52 (0.01)	−3.342	249.2 (0.1)
0.07001	5.141×10^{-3}	114.05 (0.06)	−3.579	255.9 (1.0)
0.11070	8.087×10^{-3}	114.08 (0.04)	−5.620	256.5 (0.6)
0.12385	9.032×10^{-3}	114.09 (0.04)	−6.618	245.8 (0.6)
0.11158	8.024×10^{-3}	114.08 (0.04)	−5.693	259.8 (0.6)
0.17330	1.2543×10^{-2}	114.23 (0.03)	−8.708	257.7 (0.4)
		5 *m* Urea		
0.01779	1.256×10^{-3}	115.47 (0.25)	−0.807	277.8 (3.9)
0.03647	2.579×10^{-3}	115.25 (0.12)	−1.382	303.5 (1.9)
0.05547	3.908×10^{-3}	115.32 (0.08)	−2.123	302.1 (1.3)
0.06431	4.532×10^{-3}	115.23 (0.07)	−2.461	301.7 (1.1)
0.09976	6.995×10^{-3}	115.29 (0.04)	−3.771	302.9 (0.7)
0.11867	8.270×10^{-3}	115.53 (0.04)	−4.461	304.4 (0.6)
0.06594	4.664×10^{-3}	115.00 (0.07)	−2.534	300.2 (1.1)
0.17027	1.1766×10^{-2}	115.67 (0.03)	−6.343	305.3 (0.4)
		9 *m* Urea		
0.03925	2.679×10^{-3}	115.62 (0.11)	−1.158	323.4 (1.8)
0.07455	4.953×10^{-3}	116.88 (0.06)	−2.038	334.8 (1.0)
0.09776	6.487×10^{-3}	116.78 (0.04)	−2.682	333.9 (0.7)
0.12276	8.082×10^{-3}	117.04 (0.03)	−3.242	338.0 (0.6)
0.13376	8.763×10^{-3}	117.23 (0.03)	−3.529	338.6 (0.5)
0.15897	1.0369×10^{-2}	117.30 (0.03)	−4.174	339.4 (0.5)
		13 *m* Urea		
0.02132	1.418×10^{-3}	115.72 (0.19)	−0.466	338.9 (3.3)
0.08765	5.646×10^{-3}	116.95 (0.05)	−1.779	347.6 (0.8)
0.10354	6.646×10^{-3}	117.03 (0.04)	−2.083	348.4 (0.7)
0.12097	7.718×10^{-3}	117.23 (0.03)	−2.437	348.8 (0.6)
0.16497	1.0426×10^{-2}	117.42 (0.02)	−3.245	350.7 (0.4)

[a]Uncertainties are shown in parentheses.

the standard state data reported in this paper they appear to slightly overestimate the standard state values.

An extensive thermodynamic function of transfer, $\Delta\overline{Y}_{2,t}^0\{X:(1) \rightarrow (2)\}$, for the transfer of an organic molecule, X, from water (1) to an aqueous solution of urea (2) may be defined in terms of thermodynamic standard state data using the equation:

$$[4] \quad \Delta\overline{Y}_{2,t}^0\{X:(1) \rightarrow (2)\} = \overline{Y}_2^0\{X:(2)\} - \overline{Y}_2^0\{X:(1)\}$$

One may estimate the uncertainties assigned to the calculated transfer properties of the bulk salts, $\delta\overline{Y}_{2,t}^0$, using the relationship:

$$[5] \quad \delta\overline{Y}_{2,t}^0(1\rightarrow 2) = \sqrt{\delta\overline{Y}_{2,t}^0(2)^2 + \delta\overline{Y}_{2,t}^0(1)^2}$$

where $\delta\overline{Y}_{2,t}^0(2)$ and $\delta\overline{Y}_{2,t}^0(1)$ are the calculated standard errors associated with our reported standard state data in urea + water and water, respectively. Calculated volumes and heat capacities of transfer for gly, digly, and trigly are reported with their estimated uncertainties in Table 5.

Modeling heat capacities of transfer of amino acids and small peptides using revised HKF theory

The semiempirical modeling procedures of Helgeson, Kirkham, and Flowers permit one to subdivide a standard state extensive thermodynamic property into two contributions: a structural contribution and an electrostatic contribution. These contributions are identified in eq. [6] by the subscripts s and e respectively.

$$[6] \quad \overline{Y}_2^0 = \overline{Y}_s^0 + \overline{Y}_e^0$$

The structural contribution in this equation is, in turn, the sum of two contributions: an intrinsic term and a term that reflects

© 1997 NRC Canada

Can. J. Chem. Downloaded from www.nrcresearchpress.com by 88.146.161.215 on 09/08/12
For personal use only.

Table 4. Calculated $\overline{V}_2^0$ and $\overline{C}_{p2}^0$ data for gly, digly, and trigly in water and aqueous solutions at 298.15 K.[a]

Urea (mol/kg)	$\overline{V}_2^0$ ($cm^3\ mol^{-1}$)	S_V ($cm^3\ mol^{-2}\ kg$)	$\overline{C}_{p2}^0$ ($J\ K^{-1}\ mol^{-1}$)	S_{C_p} ($J\ K^{-1}\ mol^{-2}\ kg$)
		gly		
Water	43.26 (0.08)[b]	0.97 (0.23)	37.6 (0.7)[b]	15.1 (1.8)
2	44.53 (0.04)	0.53 (0.22)	71.6 (1.1)	6.6 (5.9)
4	44.88 (0.07)	2.20 (0.35)	80.9 (0.7)	21.0 (3.2)
6	45.15 (0.12)	3.92 (0.80)	97.7 (1.2)	36.4 (7.8)
11	45.89 (0.085)	3.38 (0.43)	115.8 (0.6)	27.8 (3.1)
13	46.90 (0.04)	1.02 (0.13)	126.0 (1.0)	9.2 (3.4)
		digly		
Water	76.29 (0.07)[c]	2.37 (0.47)[c]	102.6 (0.9)[c]	37.4 (6.5)[c]
2	76.89 (0.19)	7.06 (1.38)	141.8 (4.1)	79.5 (29.9)
3.8	78.43 (0.06)	2.67 (0.19)	176.0 (0.4)	25.7 (1.3)
6	78.35 (0.41)	9.09 (2.59)	186.0 (4.3)	92.1 (27.3)
8	79.44 (0.29)	5.76 (1.95)	204.4 (1.1)	52.1 (7.4)
11	80.76 (0.07)	1.82 (0.44)	223.8 (0.3)	15.0 (1.6)
13	80.86 (0.25)	1.92 (1.59)	227.0 (1.9)	19.6 (12.1)
		trigly		
Water	112.06 (0.01)	3.70 (0.10)	186.3 (0.9)	57.4 (7.4)
2	113.73 (0.17)	2.97 (1.3)	249.1 (7.7)	44.6 (56.6)
5	114.94 (0.11)	4.29 (0.84)	299.0 (2.1)	38.5 (16.0)
9	115.98 (0.31)	8.70 (2.36)	326.3 (3.0)	87.0 (23.0)
13	116.35 (0.20)	6.62 (1.43)	328.4 (7.1)	148.9 (54.7)

[a]Uncertainties are shown in parentheses.
[b]Reference 13.
[c]Reference 14.

the disruption of the solvent structure caused by the presence of the solute in the solution.

With respect to standard state heat capacities for neutral organic species in water, eq. [6] may be rewritten in the form:

$$[7]\quad \overline{C}_{p2}^0 = c_1 + \frac{c_2}{(T-\theta)^2} - \frac{2T}{(T-\theta)^3} \times \left(a_3(P-P_r) + a_4 \ln\left(\frac{\Psi+P}{\Psi+P_r}\right)\right) + \omega_e TX$$

where c_1 and c_2 are species-dependent parameters and θ and Ψ represent solvent-dependent parameters that are assigned values of 228 K and 2600 bar, respectively (22). T, P, and P_r represent the temperature and pressure of interest and the reference pressure (1 bar, or 100 kPa) and ω_e defines the effective Born coefficient for the neutral aqueous organic species of interest. Values of this constant for gly and digly may be estimated from Born Transfer Theory, but in the current calculations they were taken from the compilations reported by Shock (22). With respect to trigly, it was necessary to estimate the effective Born coefficient using the standard entropy relationship described by Shock and Helgeson (23). In turn, a value for the standard state entropy of trigly was estimated using the molecular connectivity index model described by Kim et al. (24).

Under the constant pressure condition of $P = P_r$ eq. [7] may be reduced to the form:

$$[8]\quad \overline{C}_{p2}^0 = c_1 + \frac{c_2}{(T-\theta)^2} + \omega_e TX$$

in which the electrostatic contribution to the standard state heat capacity, $\overline{C}_{ps}^0$, is represented by the term $\omega_e TX$. The Born function X is defined in terms of the temperature dependence of the dielectric constant of the solvent (23).

$$[9]\quad X = \frac{1}{\varepsilon}\left\{\left(\frac{\partial^2 \ln \varepsilon}{\partial T^2}\right)_p - \left(\frac{\partial \ln \varepsilon}{\partial T}\right)_p^2\right\}$$

In utilizing the HKF equations to model transfer properties, we begin by dividing calculated heat capacities of transfer into structural and solvation components.

$$[10]\quad \Delta\overline{C}_{pt}^0\{X:(1)\rightarrow(2)\} = \Delta\overline{C}_{ps}^0\{X:(1)\rightarrow(2)\} + \Delta\overline{C}_{pe}^0\{X:(1)\rightarrow(2)\}$$

Alternatively, as shown by eq. [11], these heat capacities of transfer can be expressed as the sum of the structural and electrostatic contributions to standard state heat capacities.

$$[11]\quad \Delta\overline{C}_{pt}^0\{X:(1)\rightarrow(2)\} = \overline{C}_{ps}^0(2) + \overline{C}_{pe}^0(2) - \overline{C}_{ps}^0(1) - \overline{C}_{pe}^0(1)$$

Introducing eq. [8] into the analysis yields:

© 1997 NRC Canada

Can. J. Chem. Downloaded from www.nrcresearchpress.com by 88.146.161.215 on 09/08/12
For personal use only.

Table 5. Calculated volumes and heat capacities of transfer, and their estimated uncertainties, for the transfer of gly, digly, and trigly from water to aqueous solutions at 298.15 K.[a]

Urea concentration (mol kg^{-1})	$\Delta\overline{V}^0_{2,t}\{X:(1)\rightarrow(2)\}$ (cm^3 mol^{-1})	$\Delta\overline{C}^{\,0}_{p2,t}\{X:(1)\rightarrow(2)\}$ (J K^{-1} mol^{-1})
	gly	
2	1.27 (0.09)	34.0 (1.3)
4	1.63 (0.11)	43.3 (1.0)
6	1.90 (0.14)	60.1 (1.4)
11	2.64 (0.12)	78.2 (0.9)
13	3.65 (0.09)	88.4 (1.2)
	digly	
2	0.60 (0.20)	39.2 (4.2)
3.8	2.14 (0.09)	73.4 (1.0)
6	2.06 (0.42)	83.4 (4.4)
8	3.15 (0.30)	101.8 (1.4)
11	4.47 (0.10)	121.2 (0.9)
13	4.57 (0.26)	124.4 (2.1)
	trigly	
2	1.67 (0.17)	62.8 (7.8)
5	2.88 (0.11)	112.7 (2.3)
9	3.92 (0.31)	140.0 (3.1)
13	4.29 (0.20)	142.1 (7.2)

[a]Uncertainties are shown in parentheses.

$$[12]\quad \Delta\overline{C}^0_{pt}\{X:(1)\rightarrow(2)\} = c_1^* + \frac{c_2^*}{(T-\theta)^2} - c_1 - \frac{c_2}{(T-\theta)^2} + (\omega_e^* TX^* - \omega_e TX)$$

where the asterisk (*) has been used to identify a parameter associated with an aqueous urea solution. At this stage we are forced, by a lack of published thermodynamic data, to adopt the assumption that $\omega_e = \omega_e^*$. This step permits the calculation of both structural and electrostatic contributions to calculated heat capacities of transfer; eqs. [13] and [14].

$$[13]\quad \Delta\overline{C}^0_{ps}\{X:(1)\rightarrow(2)\} = c_1^* + \frac{c_2^*}{(T-\theta)^2} - c_1 - \frac{c_2}{(T-\theta)^2}$$

$$[14]\quad \Delta\overline{C}^0_{pe}\{X:(1)\rightarrow(2)\} = \omega_e T(X^* - X)$$

Wyman's dielectric constant data for urea + water systems (25) at 298.15 K were used to derive values for the Born parameters X^* for the investigated urea + water solutions. Values for c_1 and c_2 were obtained for each system by fitting eq. [8] to standard state heat capacity data for the relevant solute in water obtained as a function of temperature.

Calculated structural and electrostatic contributions to heat capacities of transfer are reported in Table 6.

In a similar fashion, the methodology described above may be applied to the analysis of volumes of transfer to yield:

$$[15]\quad \Delta\overline{V}^0_s\{X:(1)\rightarrow(2)\} = \sigma^* + \frac{\xi^*}{(T-\theta)} - \sigma - \frac{\xi}{(T-\theta)}$$

$$[16]\quad \Delta\overline{V}^0_e\{X:(1)\rightarrow(2)\} = \omega_e(Q - Q^*)$$

Table 6. Calculated structural, $\Delta\overline{C}^0_{ps}\{X:(1)\rightarrow(2)\}$, and electrostatic, $\Delta\overline{C}^0_{pe}\{X:(1)\rightarrow(2)\}$, contributions to heat capacities of transfer, for the transfer of gly, digly, and trigly from water to aqueous urea solutions at 298.15 K.

Urea concentration (mol kg^{-1})	$\Delta\overline{C}^0_{ps}\{X:(1)\rightarrow(2)\}$ (J K^{-1} mol^{-1})	$\Delta\overline{C}^0_{ps}\{X:(1)\rightarrow(2)\}$ (J K^{-1} mol^{-1})
	gly	
2	35.3	−1.3
4	45.6	−2.3
6	63.3	−3.2
11	82.7	−4.5
13	93.1	−4.7
	digly	
2	41.9	−2.7
3.8	78.0	−4.6
6	90.0	−6.6
8	109.8	−8.0
11	130.5	−9.3
13	134.1	−9.7
	trigly	
2	65.6	−2.8
5	118.8	−6.1
9	149.0	−9.0
13	152.3	−10.2

Coefficients required in the calculation of $\Delta\overline{C}^0_{pe}\{X:(1)\rightarrow(2)\}$: gly; $\omega_e = -97\,487$ J mol^{-1}, digly; $\omega_e = -201\,167$ J mol^{-1}, trigly; $\omega_e = -213\,170$ J mol^{-1}. X^* (K^{-2}) = -2.70×10^{-7}, -2.37×10^{-7}, -2.34×10^{-7}, -2.18×10^{-7}, -2.04×10^{-7}, -1.81×10^{-7}, -1.73×10^{-7}, -1.59×10^{-7}, and -1.53×10^{-7} at urea concentrations of m (mol kg^{-1}) = 2, 3.8, 4, 5, 6, 8, 9, 11, and 13, respectively.

Unfortunately, this avenue of exploration cannot be pursued further because we are unable to locate dielectric constants for urea + water solutions as a function of pressure at 298.15 K in the literature. These data are required to calculate the Born Q parameter, eq. [17].

$$[17]\quad Q = \frac{1}{\varepsilon}\left(\frac{\partial \ln \varepsilon}{\partial P}\right)_T$$

Discussion

Calculated volumes and heat capacities of transfer for gly, digly, and trigly are found to be positive at all investigated urea concentrations and are seen to increase in a smooth manner with increasing urea concentration. Such trends are indicative of specific urea–solute interactions. At increased urea concentrations transfer values appear to flatten out.

The reported positive volumes and heat capacities of transfer are consistent with the negative enthalpies of transfer for gly, digly, and trigly reported by Prasad and Ahluwalia (26). Heat capacities of transfer reported by these authors refer to 30°C and are therefore not directly comparable to those reported in this study.

In an attempt to interpret the trends observed in our transfer data we turn to several previous investigations of the thermodynamic properties of structurally similar compounds in aqueous urea solutions.

In their investigation of nucleic acid bases, nucleosides, and

© 1997 NRC Canada

Can. J. Chem. Downloaded from www.nrcresearchpress.com by 88.146.161.215 on 09/08/12
For personal use only.

nucleotides in water and aqueous urea solutions, Kishore and Ahluwalia (27) used the Gurney cosphere model (28) to account for observed trends in volumes and heat capacities of transfer. In brief, negative transfer properties were attributed to interactions of urea molecules with hydrophobic components of solute molecules, whilst positive contributions to transfer properties were attributed to interactions of urea molecules with hydrophilic or polar constituents of solute molecules. In the latter case this interaction was thought to take the form of hydrogen bond formation. In an earlier study of the thermodynamics of transfer of oligopeptides from water to aqueous urea solutions Enea and Jolicoeur (3) were able to successfully explain their results in terms of urea – peptide group interactions. However, they concluded that changes in the solvation of apolar and ionic groups in the presence of urea are key in the process of urea-induced protein unfolding.

Privalov et al. (29), in a study of heat capacities and conformations of proteins in the denatured state, advised caution in the interpretation of thermodynamic properties associated with the denaturation of proteins by guanidine hydrochloride or urea. Previous to their investigation it had been implied that heat capacities associated with thermally induced denaturation differed in value from those associated with guanidine hydrochloride induced denaturation. However, these authors were able to show that for the denaturation of lysozyme the heat capacities were in fact "indistinguishable" if the interactions of the denaturant with the protein were correctly accounted for (30). In another series of papers Makhatadze and Privalov (21, 31) supply data for the calculation of partial heat capacities of unfolded polypeptides. Applying their analysis to trigly results in a standard heat capacity of 276.2 J K^{-1} mol^{-1} for the completely unfolded species, an increase of approximately 90 J K^{-1} mol^{-1} over the standard state heat capacity of trigly in its natural state in water. The heat capacity of transfer of trigly for water to 13 mol kg^{-1} urea (a concentration at which complete "unfolding" may be expected) is 142.1 J K^{-1} mol^{-1}, some 52 J K^{-1} mol^{-1} greater than the Makhatadze and Privalov value. However, if one accepts Makhatadze and Privalov's proposal of H-bonding interactions between urea and peptide groups in trigly, then the two values will be brought closer together because such interactions have been shown to provide positive contributions to heat capacities of transfer.

Turning to our reported heat capacity of transfer data, the observed positive values would appear, from the evidence presented above, to be indicative of hydrophilic group – urea interactions and (or) of ionic group – urea interactions. Alternatively, one could argue that urea – apolar group interactions are small compared to urea – hydrophilic and urea – ionic group interactions.

With respect to our HKF analyses of the transfer data (see Table 6) we note that the electrostatic solvation contributions to reported heat capacities are small and negative. The sign of the contributions indicates that electrostatic solvation contributions to heat capacities are less in aqueous urea solutions than in water. Given that water is more polar than aqueous urea solutions, this result is not surprising.

At this stage it is perhaps prudent to reexamine the effect of our assumption, $\omega_e = \omega_e^*$, on the results of the analyses. Let us consider two possibilities for the behaviour of ω_e^*: (*i*) its value becomes more positive with increasing urea concentration; (*ii*) its value becomes more negative with increasing urea concentration. With respect to case (*i*), using $\omega_e/2$ as estimates for ω_e^* values in solutions containing 13 mol kg^{-1} urea yields electrostatic contributions to heat capacities of transfer of −6.9, −14.3, and −15.1 J K^{-1} mol^{-1} for gly, digly, and trigly, respectively. With respect to case (*ii*) using $2\omega_e$ as estimates for ω_e^* in 13 mol kg^{-1} urea produces electrostatic contributions to heat capacities of transfer of −0.2, −0.5, and −0.5 J K^{-1} mol^{-1} for gly, digly, and trigly. Comparing these results with those reported in Table 6 indicates that the term $T(\omega_e^* X^* - \omega_e X)$ is somewhat insensitive to the magnitude of the effective Born coefficient selected for a given solute in an aqueous solution of urea. Indeed, for reasonable differences between ω_e^* and ω_e values, the dominant factor in determining the electrostatic contribution to the transfer property appears to be linked to the change in the dielectric constant of the medium or, more precisely, the difference $X^* - X$. On this basis, our assumption of $\omega_e = \omega_e^*$ appears justifiable, although we acknowledge the magnitude of the uncertainty introduced into our analysis by the use of such an assumption.

Our analysis indicates that structural contributions appear to dominate reported heat capacities of transfer. Structural contributions increase with increasing urea concentration and also as one goes through the series gly to trigly at a fixed urea concentration. These observations appear to chime with the idea of an increase in the disruption of solvent structure; in other words, specific urea – solute molecule interactions appear to play a major role in determining the magnitude of the transfer property.

In conclusion, the results presented above appear to offer little support for the argument of urea denaturation driven by diminishing hydrophobic hydration of apolar groups. Rather our results appear to identify urea – hydrophilic group and (or) urea – ionic group interactions as being dominant. Unfortunately, our analysis is unable to distinguish between H-bonding interactions and the preferential solvation situation described by Lilley and co-workers (32, 33); however, pair enthalpic interaction coefficients appear to offer compelling evidence in support of the latter description.

Acknowledgments

A.W.H. is grateful to the Natural Sciences and Engineering Research Council of Canada (NSERC) for operating support. L.L.G. and M.L.R. are grateful to NSERC for the award of Undergraduate Student Research Awards.

References

1. J.A. Schellman and N.C. Gassner. Biophys. Chem. **59**, 259 (1996).
2. P.L. Privalov. Crit. Rev. Biochem. Mol. Biol. **25**, 281 (1990).
3. O. Enea and C. Jolicoeur. J. Phys. Chem. **86**, 3870 (1982).
4. G.I. Makhatadze and P.L. Privalov. J. Mol. Biol. **226**, 491 (1992).
5. M. Zolkiewski, N.J. Nosworthy, and A. Ginsburg. Protein Sci. **4**, 1544 (1995).
6. K. Kawahara, A.G. Kirshner, and C. Tanford. Biochemistry, **4**, 1203 (1965).
7. H.C. Helgeson, D.H. Kirkham, and G.C. Flowers. Am. J. Sci. **281**, 1249 (1981).
8. C.J. Pouchert and J.R. Campbell. *In* The Aldrich library of NMR spectra. Vol. III. Aldrich Chemical Co. Inc., Milwaukee, Wis. 1974.

© 1997 NRC Canada

9. P. Picker, E. Tremblay, and C. Jolicoeur. J. Solution Chem. **3**, 377 (1974).
10. P. Picker, P.-A. Leduc, P.R. Philip, and J.E. Desnoyers. J. Chem. Thermodyn. **3**, 631 (1971).
11. J.E. Desnoyers, C. DeVisser, G. Perron, and P. Picker. J. Solution Chem. **5**, 605 (1976).
12. A.W. Hakin, S.A.M. Mudrack, and C.L. Beswick. Can. J. Chem. **71**, 925 (1993).
13. A.W. Hakin, M.M. Duke, S.A. Klassen, R.M. McKay, and K.E. Preuss. Can. J. Chem. **72**, 362 (1994).
14. A.W. Hakin, M.M. Duke, L.L. Groft, J.L. Marty, and M.L. Rushfeldt. Can. J. Chem. **73**, 723 (1995).
15. G.S. Kell. J. Chem. Eng. Data, **12**, 66 (1967).
16. G.S. Kell. *In* Water — a comprehensive treatise. Vol. 1. *Edited by* F. Franks. Plenum Press, New York. 1972.
17. A.W. Hakin and C.L. Beswick. J. Chem. Soc. Faraday Trans. **92**, 207 (1996).
18. T.V. Chalikian, A.P. Saravazyan, T. Funck, and K.J. Breslauer. Biopolymers, **34**, 541 (1994).
19. G.R. Hedwig. J. Solution Chem. **17**, 383 (1988).
20. C. Jolicoeur and J. Boileau. Can. J. Chem. **56**, 2702 (1978).
21. G.I. Makhatadze and P.L. Privalov. J. Mol. Biol. **213**, 375 (1990).
22. E.L. Shock. Geochim. Cosmochim. Acta, **56**, 3481 (1992).
23. E.L. Shock and H.C. Helgeson. Geochim. Cosmochim. Acta, **54**, 915 (1990).
24. U. Kim, K. Min, and B. Jin. Bull. Korean Chem. Soc. **15**, 106 (1994).
25. J. Wyman. J. Am. Chem. Soc. **55**, 4116 (1933).
26. K.P. Prasad and J.C. Ahluwalia. Biopolymers, **19**, 273 (1980).
27. N. Kishore and J.C. Ahluwalia. J. Chem. Soc. Faraday Trans. **86**, 905 (1990).
28. R.W. Gurney. Ionic processes in solution. McGraw–Hill, New York. 1953. p. 251.
29. P.L. Privalov, E.I. Tiktopulo, S.Y. Venyaminov, Y.V. Griko, G.I. Makhatadze, and N.N Khechinashvili. J. Mol. Biol. **205**, 737 (1989).
30. W. Pfeil and P.L. Privalov. Biophys. Chem. **40**, 33 (1976).
31. G.I. Makhatadze and P.L. Privalov. J. Mol. Biol. **213**, 385 (1990).
32. A.H. Sijpkes, G. Somsen, and T.H. Lilley. J. Chem. Soc. Faraday Trans. **86**, 2943 (1990).
33. M. Abbate, G. Barone, G. Castronuovo, P.J. Cheek, C. Giancola, T.E. Leslie, and T.H. Lilley. Thermochim. Acta. **173**, 261 (1990).

Can. J. Chem. Downloaded from www.nrcresearchpress.com by 88.146.161.215 on 09/08/12
For personal use only.

© 1997 NRC Canada

Conversion of methane to ethylene

B.K. Miremadi, K. Colbow, and S. Roy Morrison

Abstract: A lithium aluminate – MgO catalyst has been found to convert methane to ethylene with a high selectivity. The rate of conversion increased when a MoO_3 co-catalyst was used to remove the poisoning products. It is shown that for optimum conversion and selectivity to ethylene, the oxygen pressure should be at an intermediate value, high enough to provide active sites but low enough to avoid ethylene oxidation. Thus the oxygen should be "bled-in" along the catalyst bed. In demonstration of these concepts we have shown a 28.6% CH_4 conversion with 63.2% ethylene selectivity and 9.8% ethane, producing a C_2 yield of about 21.4%.

Key words: methane oxidation, methane conversion, ethylene production, oxidation catalyst, aluminate catalyst.

Résumé : On a trouvé qu'un catalyseur d'aluminate de lithium – MgO permet de transformer le méthane en éthylène avec une grande sélectivité. La vitesse de conversion augmente lorsqu'on utilise un cocatalyseur de MoO_3, pour éliminer les produits provoquant un empoisonnement. On a démontré que, pour obtenir une conversion et une sélectivité optimales en éthylène, on doit utiliser une pression d'oxygène intermédiaire, suffisamment élevée pour fournir des sites actifs, mais suffisamment basse pour éviter l'oxydation de l'éthylène. On doit donc laisser l'oxygène s'écouler le long du lit du catalyseur. Une conversion à 28,6% du méthane, avec une sélectivité à 63,2% d'éthylène et 9,8% d'éthane correspondant à un rendement en produits en C_2 de 21,4%, permet de démontrer l'applicabilité de ces concepts.

Mots clés : oxydation du méthane, conversion du méthane, production d'éthylène, catalyseur d'oxydation, catalyseur d'aluminate.

[Traduit par la rédaction]

1. Introduction

There has been increasing interest in the possible use of oxidative coupling to convert methane to higher hydrocarbons, preferably ethylene. The concept is based on the fact that an oxidative reaction

[1] $2CH_4 + O_2 \rightarrow C_2H_4 + 2H_2O$

is exothermic and has been found to occur on many basic oxide catalysts (1–4). The interest in such a reaction is of course that methane is a relatively low-cost gas compared to ethylene, which is more valuable as a petrochemical or as a raw material for oligomerization to higher hydrocarbons.

Part of the problem has been that high C_2H_4 selectivity is usually accompanied by low CH_4 conversion (5). It has been found that the catalyst must be basic (6–8), that the reaction can proceed at temperatures between 700 and 850°C, and that one can best obtain a high selectivity if the CH_4 conversion rate is slow (6). It has been shown (9–12) that the rate-limiting step is the removal of one hydrogen from the methane, producing CH_3, which has been observed in the gas phase. The gas input can be alternated between air and methane (1, 6), but the reaction goes well with a mixture of the gases, and there seems no advantage in switching back and forth between gases. It has been concluded that the dehydrogenation to produce CH_3 occurs on the catalyst, but the remainder of the reaction occurs in the gas phase (2, 13, 14). The most promising catalysts have been based on manganese oxide, samarium oxide, and bismuth oxide (15), with lead oxide (16) or alkali additives as promoters (6, 13, 14).

We observed originally that a lithium aluminate catalyst we were studying for the Fischer–Tropsch reaction at 300–400°C produced a distribution of hydrocarbons in which the ethylene content was relatively high. We found the same kinetic preference to ethylene at the high temperatures for the methane coupling reaction. This was surprising because alumina has been considered a poor support because of its acidity (2, 6, 7), but presumably the high lithium content suppresses this acidity. Studies were initiated to further improve the catalyst. The catalyst was based on an MoS_2–Fe–Al_2O_3 material, featuring alumina platelets (17) obtained by reacting Li at room temperature, or LiOH at high temperature, with porous alumina. We found this lithium aluminate catalyst caused the preference for ethylene. Because of the higher cost of the platelets, we chose to study the catalyst prepared from LiOH.

2. Experimental

The porous alumina was Alcan AA-101 alumina, an activated porous Chi-alumina of 240 m^2/g in area; MoO_3 (98.5%) and LiOH (99%) were from BDH, and $MgCl_2 \cdot 6H_2O$ (98.5%) from Anachem. A model ISI-DS130 scanning electron microscope (SEM) with EG&G ORTEC energy-dispersive X-ray attach-

Received June 11, 1996[1].

B.K. Miremadi,[2] K. Colbow, and S. Roy Morrison. Energy Research Institute, Simon Fraser University, Burnaby, BC V5A 1S6, Canada.

[1] Revision received February 20, 1997.

[2] Author to whom correspondence may be addressed. Telephone: (604) 291-4807. Fax: (604) 291-3592. E-mail: miremadi@sfu.ca

© 1997 NRC Canada

Can. J. Chem. Downloaded from www.nrcresearchpress.com by 88.146.161.215 on 09/08/12
For personal use only.

Table 1. A comparison of optimized selectivities, conversion, and C_2 yield at 785°C. Total air flow ≈ 140 mL/min. Methane flow ≈ 27.2 mL/min. $O_2/CH_4 \approx 1$.

		Reactor		
		Single bed r_1	Double bed in series $r_1 + r_2$	Double bed in series with MoO_3 in addition to 20 mL/min of air injected between r_1 and r_2
% O_2 used		4.13	7.96	8.44
% CH_4 converted		13.33	16.51	28.62
Product[a]	C_2H_4	53.2	51.4	63.6
	C_2H_6	11.4	10.6	9.8
	C_2H_2	1.3	0.9	1.4
	C_3	2.1	1.4	3.4
	CO_2	27.6	34.2	17.3
	CO	0.4	0.6	0.9
	C_4	<0.5	<0.5	<0.5
C-balance[b] %		96.5	99.6	96.9
% H_2 at exit		1.1	1.4	—
C_2 yield[c]		8.8	10.5	21.4

[a]Percent of converted CH_4 appearing as species indicated.
[b]Percent of converted CH_4 appearing as CO_x and C_n (carbon balance).
[c]Percent of CH_4 flow converted to C_2.

Can. J. Chem. Downloaded from www.nrcresearchpress.com by 88.146.161.215 on 09/08/12
For personal use only.

ment (EDX) was used to analyze the elemental compositions of the sample. For the analysis of elemental Li, laser ablation was employed.

The lithium aluminate was prepared by slurrying LiOH and the porous alumina with the Li and Al in the approximate atomic ratio 1/7. The slurry was dried, other additives (such as Mg and particularly powdered MoO_3) were mixed in if desired, and the powder was calcined for more than 5 h at 880°C. In most of the work to be reported, we have included $MgCl_2$ in the slurry at a Mg atomic ratio of 15–20%, calcining the alumina with the additives at 880°C for 10 h. This high-temperature treatment ensured that no trace of Cl^- ions remained in the catalyst. Calcination of the catalysts, for example, at 650°C resulted in poor catalytic activity and residual Cl^- ions of less than 0.4 atomic percent as measured by the Kα Auger line. The catalyst composition was in the approximate atomic ratio of Li:Al:Mg = 1:7:2. The as-received alumina had originally a BET area of 237.6 m^2/g. After the heat treatment the surface area was reduced to 156.8 m^2/g. Addition of Li and Mg produced a further reduction in area to 56.3 m^2/g.

The reactor was a single-pass quartz reactor, generally held at an optimum operating temperature of 785°C (±0.7%). The heating system used was limited to a maximum temperature of 825°C. The temperature was measured with a thermocouple placed in a narrow quartz tube inserted into the catalyst bed. At about 800°C most CH_4 was oxidized to CO_2, with poor selectivity for other products. About 0.1 g of catalyst was dispersed as a powder in quartz wool, held between quartz wool plugs, with the catalyst bed about 0.2 cm in length and 0.8 cm^2 in area. For some of our investigations two such identical catalyst beds were mounted in series 50 cm apart with the option of introducing more gas to the mixture before the second bed. Only one reactor was used except where indicated. The air–methane mixture was not preheated before entering the reactor except where so indicated, although the length of the heating zone was about 6 cm, compared to a length of 0.2 cm for the catalyst bed.

At a pressure of 1 atmosphere (101.3 kPa) the gas mixtures used were air and methane. When the methane flow was reduced, He gas flow was added to keep the total flow rate constant. A Varian gas chromatograph (model 6000), featuring a thermal conductivity and a flame ionization (1) detector, using a 13 X molecular sieve in series with a Porapak-N column was used to sample the gas mixture. The gas flow (air, methane, and helium) was monitored with mass flow meters calibrated against a bubble flow meter installed at the exit of the reactor. Good carbon balance was obtained, as will be noted later in discussion of Table 1. Nitrogen lost in mass balance, $(1 - N_{out}/N_{in})$, was obtained to within 2×10^{-2}. The calibrating gas used to convert the GC data to percent products was from Lil Squirt Ideal Gas Products provided by Varian Corp. It contained a mixture of all possible gases used and produced in our experiments.

3. Results

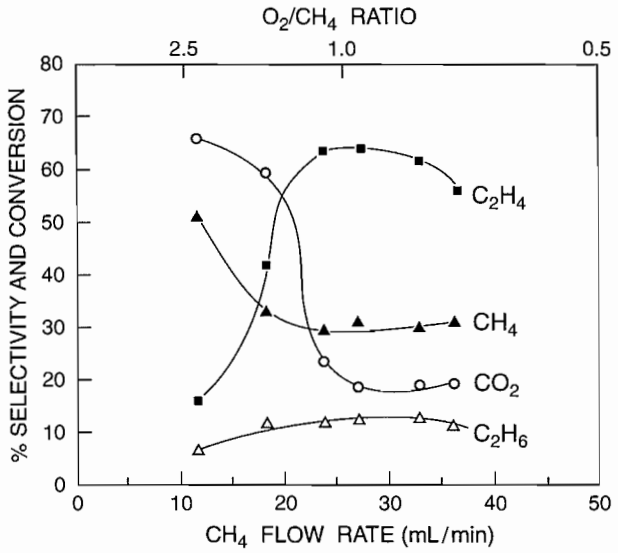
3.1 Lithium aluminate

Table 1 shows a comparison of selectivities and CH_4 conversion. In this experiment we had two identical quartz reactors r_1 and r_2 in series 50 cm apart. As far as was possible the reactors were held at the same temperature. From the results for a single reactor there was ample partial pressure of methane and air reaching the second reactor. However, we observed that the second reactor did not contribute appreciably to the ethylene production, except for an increase in CH_4 conversion (16.5%), which in turn increased the CO_2 production (34.2%). As will be discussed in the next section, a substantial increase in the conversion was observed by addition of 100 mg MoO_3 co-cat-

© 1997 NRC Canada

Can. J. Chem. Downloaded from www.nrcresearchpress.com by 88.146.161.215 on 09/08/12
For personal use only.

Fig. 1. Percent of products as a function of optimized CH_4 flow rate for catalyst and promoter (MoO_3) at 785°C in a double bed reactor with an air flow of 120 mL/min and an injected 20 mL/min of air at the input of the second reactor. At peak conversion methane flow is 27.2 mL/min and $O_2/CH_4 \approx 1$.



alyst powder mixed with the aluminate catalyst in both reactors. MoO_3 oxidizes hydrogen produced in the first reactor (r_1) that was poisoning the second reactor (r_2), thus leading to a further conversion of methane and higher selectivity for ethylene. With addition of MoO3 promoter, at an optimized methane flow rate of 27.2 mL/min and 20 mL/min air injection at the input of the second reactor, the conversion was 28.6%, selectivity was 63.6%, and CO_2 produced reduced to 17.3%. Without addition of MoO_3, the air injection at the input of the second reactor resulted in an increase in both CO_2 and H_2O products.

Figure 1 shows the percent of the products (ethylene and ethane selectivities, methane conversion, and CO_2 produced) of a MoO_3 promoted catalyst against the methane flow rate at a constant air flow of 120 mL/min and with an extra 20 mL/min of air bled-in at the input of the second reactor. The selectivity and conversion peak at a methane flow of 27.2 mL/min, where the oxygen/methane ratio is about 1 and CO_2 produced is a minimum. With high oxygen to methane ratio, conversion is high but most of methane is converted to CO_2. There is evidence of a peak in C_2H_4 conversion at intermediate oxygen-to-methane ratio and low conversion of methane with low oxygen-to-methane ratio.

4. Discussion

4.1 Lithium aluminate catalyst

It was observed that for good conversion of CH_4 and good selectivity to C_2H_4 a high oxygen partial pressure is required, much higher than the stoichiometric ratio (0.5) for

[2] $2CH_4 + O_2 \rightarrow C_2H_4 + 2H_2O$

This is consistent with the currently accepted model with adsorbed O^- as active sites (12); presumably a significant oxygen pressure is required to maintain a high state density. With ample reactive gases still present in the gas stream, no (or negligible) reaction occurred in the second reactor. This observation suggests strongly that the second reactor is poisoned by the products formed in the first reactor, mainly the hydrogen produced. Possible poisons, such as ethylene, carbon dioxide, water, and hydrogen, are all produced during the reaction. These were tested under our "standard" conditions. Addition of C_2H_4 to the input had no effect on the reaction; the ethylene in the output was simply increased by the extra amount added in the input. H_2O added to the input actually increased the yield and selectivity slightly. Added CO_2 at about 5 mL/min also showed no effect. Hydrogen was awkward to introduce in large quantities because of potential explosion, but a small addition of 5 mL/min Forming gas (5% H_2, 95% N_2) was found to lower the selectivity by 10–15%. Since the hydrogen flow from the Forming gas (0.25 mL/min) was lower than hydrogen produced in the reactors, we concluded H_2 was poisoning the active sites and (or) inducing the back reaction:

[3] $2H_2 + C_2H_4 \rightarrow 2CH_4$

With the consideration that such a back reaction is rather unlikely, our suggested model is based on poisoning the active sites.

4.2 MoO_3 and lithium aluminate – Mg as co-catalysts

A search was made for catalysts to remove the H_2, viz. catalysts that would catalyze the oxidation of 5% H_2 in He but not 5% C_2H_4 in He under our normal reaction conditions at 785°C. Of eight oxides tested (Fe_2O_3, Cr_2O_3, Mn_2O, ZnO, SnO_2, TiO_2, ZrO_2, MoO_3), MoO_3 and ZrO_2 were found to be most effective. With 100 mg commercial MoO_3 powder, 95% of the hydrogen but only 18% of the ethylene was oxidized in one pass through the reactor in a ratio of O_2 to reducing agent of 1:6. For this test the lithium aluminate catalyst was not present.

The activity of MoO_3 alone was also tested as a catalyst under our experimental conditions, which indicated a poor selectivity for ethylene production. In comparison to MgO aluminate catalysts, MoO_3 is a poor oxidation catalyst (18, 19), but together with aluminate catalyst (without additional air injection at the input of reactor r_2) it resulted in a 13% increase in selectivity, while the increase with optimized air injection was close to 23%. There is a good possibility that high-temperature calcination of MoO_3 used in this experiment has converted the oxide to some other phases that have become a part of the catalyst itself. Without addition of MoO_3, the air injection at the input of the second reactor resulted in an increase in both CO_2 and H_2O products. A similar test with ZrO_2 showed an overall increase of only 8%. Thus, both MoO_3 and air injection are equally contributing factors in improving ethylene production.

If hydrogen is the poison, the presence of an oxidation catalyst that selectively removes H_2 should (*a*) increase the conversion, either if the back reaction in eq. [3] occurs, or if hydrogen blocks active sites, and (*b*) permit continuing conversion if, as with the second reactor described above, the H_2

© 1997 NRC Canada

produced at the input to the catalyst bed poisons the rest of the catalyst bed and the second reactor.

4.3 Air injection

The conclusion from the above results is that addition of MoO_3 leads to lower hydrogen concentration and higher methane conversion. For such high conversion of methane it appears one must prevent the back reaction of eq. [1] and (or) the blocking of active sites of hydrogen. It also suggests that one must keep the oxygen pressure up, both to provide active sites and to oxidize the hydrogen. However, if the oxygen pressure is too high, there will be a greater tendency to oxidize the ethylene and the selectivity will drop, in addition to an increase in CO_2 product. This effect was also noticed when 20 mL/min air injection was replaced with 10 mL/min pure oxygen to avoid a substantial increase in the total flow. All this leads to the conclusion that oxygen should be admitted in a controlled manner along the catalyst bed, maintaining the oxygen partial pressure at the optimum value as it is consumed, in agreement with the suggestion by Smith and Galuszka (20). To permit somewhat better adjustment of the oxygen partial pressure in the experiments of Fig. 1, we introduced air not only at the input with CH_4, but also between the two reactors r_1 and r_2.

5. Conclusions

We have presented observations regarding the methane oxidative coupling reaction and a possible explanation of the process for the catalyst used. The observations are that lithium aluminate is an excellent catalyst for the reaction, providing a high yield of ethylene and a high conversion per pass of methane. An oxidation catalyst chosen to oxidize hydrogen but not ethylene under the reaction conditions improves the conversion rate substantially. Introducing oxygen along the length of the catalyst bed to replace that used in the reaction leads to a high conversion of methane with a high selectivity to ethylene.

The model suggested for ethylene generation differs from the standard model where the CH_3·radical first dimerizes to C_2H_6 and subsequently the ethane oxidizes to form C_2H_4 + H_2O. A dominant experimental feature suggesting a different role for our catalyst is the low concentration of C_2H_6 as shown in Table 1 and Fig. 1. The poisoning of active sites by hydrogen is the novel result of the analysis. Because the conversion of methane is so strongly limited, it is clear that sites for it must be poisoned, as is observed clearly where the added reactor in series does not affect the product yield, suggesting the sites are poisoned by a product generated in the first reactor.

Considering the confusion in the general behavior of the oxidative methane coupling, it is possible that unnoticed hydrogen poisoned other catalysts as well as ours. The strong effect of MoO_3, which is a comparatively poor catalyst for oxidation of methane (18, 19) as discussed in Sect. 4.2, could be difficult to explain by another model.

It may be possible, by carefully controlled oxygen admission, to further increase CH_4 conversion and the corresponding C_2 products.

Acknowledgments

The authors with to thank T. Cowan and R. Singh for their technical assistance.

References

1. G.E. Keller and M.M. Bhasin. J. Catal. **73**, 9 (1982).
2. J.A. Sofranko, J.J. Leonard, and C. Jones. Catalyst (Philadelphia), **103**, 302 (1987).
3. M.M. Bhasin. *In* Studies in surface science and catalysis. Elsevier, Amsterdam. 1988. pp. 40–65.
4. K. Otsuka, K. Jinno, and A. Morikawa. J. Catal. **100**, 353 (1988).
5. J.S. Lee and S.T. Oyama. Catal. Rev.-Sci. Eng. **30**, 249 (1988).
6. C. Jones, J.J. Leonard, and J.A. Sofranko. J. Catal. **103**, 311 (1987).
7. W. Bytyn and M. Baerns. Appl. Catal. **28**, 199 (1986).
8. K. Asami, S. Hashimoto, S. Shikada, T. Jujimoto and K. Jujimoto. Chem. Lett. 1233 (1986).
9. K.T. Amorebieta and A.J. Colussi. J. Phys. Chem. **92**, 4576 (1988).
10. O.V. Buevskaya, A.I. Suleimanov, S.M. Aliev, and V.D. Sokolovskii. React. Kinet. Catal. Lett. **331**, 223 (1987).
11. N.W. Cant, C.A. Lukey, P.F. Nelson, and R.J. Tyler. Chem. Commun. 766 (1988).
12. K. Otsuka and K. Jinno. Inorg. Chem. Acta, **121**, 237 (1986).
13. C.H. Lin, T. Ito, J.X. Wang, and J.H. Lunsford. J. Am. Chem. Soc. **109**, 4808 (1987).
14. T. Ito, J.X. Wang, C.H. Lin, and J.H. Lunsford. J. Am. Chem. Soc. **107**, 5062 (1985).
15. I.T. Ali-Emesh and Y.J. Amenomiya. J. Phys. Chem. **90**, 4785 (1986).
16. S.K. Agarwal, R.A. Migone, and G. Marcelin. J. Catal. **103**, 302 (1987).
17. B.K. Miremadi and S.R. Morrison. Mater. Res. Bull **25**, 1139 (1990).
18. T.A. Garibyan and L.Ya. Margolis. Cat. Rev.-Sci. Eng. **31**, 355 (1989).
19. J.A. Sofranko, J.J. Leonard, and C.A. Jones. J. Catal. **103**, 302 (1987).
20 K.J. Smith and J.Z. Galuszka. U.S. patent no. 5 132 482 (1992).

Can. J. Chem. Downloaded from www.nrcresearchpress.com by 88.146.161.215 on 09/08/12
For personal use only.

© 1997 NRC Canada

Observation of a single-pot aromatic reductive denitration

Angelo G. Giumanini and Giancarlo Verardo

Abstract: 4,*N*,*N*-Trimethyl-3-nitrobenzenamine gave reductive denitration products (ca. 28%) upon treatment with *n*-butyl nitrite in the presence of catalytic amounts of ammonium chloride and water in an unprecedented one-reagent single-pot process. The three isomeric *N*,*N*-dimethylnitrobenzenamines showed the same behaviour to a much lesser extent; the *ortho* isomer was partially (7%) transformed into 1-methylbenzotriazole.

Key words: aromatic protolytic denitration, nitroaromatics, *n*-butyl nitrite, *E*- and *Z*-nitrosamine.

Résumé : Au cours d'un processus unipot sans précédent, la 4,*N*,*N*-triméthyl-3-benzèneamine fournit des produits de dénitration réductrice (environ 28%) lorsqu'on la soumet à l'action du nitrite de butyle, en présence de quantités catalytiques de chlorure d'ammonium et d'eau. Le trois *N*,*N*-diméthylnitrobenzènamines isomères ont le même comportement, même si le degré est moindre; l'isomère *ortho* se transforme partiellement (7%) en 1-méthylbenzotriazole.

Mots clés : dénitration aromatique protolytique, nitroaromatiques, nitrite de butyle, *E*- et *Z*-nitrosamine.

[Traduit par la rédaction]

One-batch-one reagent aromatic reductive denitration, which could in principle be the reversal of classical nitration by the nitronium ion, is such a rare event that there is no such entry for it in Chemical Abstracts. As a matter of fact, the only way to perform this process appears that of reducing the nitro group to amino, which is subsequently diazotized and reduced by a suitable reagent.

Indeed, a few coherent observations of this one-batch process have been reported (1) as a side reaction in the treatment of a number of tertiary aromatic amines bearing a nitro group in the *ortho* position, with strong acid or photochemically, to yield benzimidazoles and benzimidazole oxides. The envisaged mechanism in the ground state experiment assumed the migration of the nitro group to the amino nitrogen to yield an oximonium nitroso ester, eventually bound for the formation of a Wheland-type intermediate by amino group assisted protonation of the carbon bearing the nitro group, as a final step (route A, Scheme 1), or a more straightforward variation that we would rather like to advance (route B, Scheme 1): both pathways would amount to the reversal of the *ortho*-nitration of an aromatic amine.

Interestingly, this behaviour attributed to the *ortho*-effect (1*a*) was reported only for tertiary amines, inferring that enough steric hindrance is there to cause the phenomenology observed. We now wish to report the observation that stirring 4,*N*,*N*-trimethyl-3-nitrobenzenamine (**1**) at room temperature with *n*-butyl nitrite (BN, 3 mol-equiv.), water (10 mol-equiv.), and ammonium chloride (AC, 0.1 mol-equiv.) during 2 days caused the complete disappearance of **1** and produced two reductive denitration compounds, namely, *N*,4-dimethylbenzenamine (**2**, identified on the basis of its retention properties and mass spectrum) and *N*,4-dimethyl-*N*-nitrosobenzenamine (**3**, in the ratio ca. 5:1), the latter being the GC precursor of the former by pyrolysis in the injector port. The material balance of the volatile fraction was completed by *N*,4-dimethyl-3-nitrobenzenamine (**4**), analogously derived by the thermal decomposition in the GC injector of the corresponding *N*-nitrosamine **5**, as shown in an independent experiment, and two distinct dinitro derivatives of *N*,*N*,4-trimethylbenzenamine (Scheme 2). A suitable work-up of the reaction mixture led to the isolation of **3** and its full identification. In the absence of BN no reaction was observed. The same reaction under the conditions described (2) for the oxidative *N*-demethylation-*N*-nitrosation reaction gave some 81% **5** and 5% **3**.

All of the three isomeric *N*,*N*-dimethylnitrobenzenamines (**6***a–c*), which were found unreactive at room temperature, gave some, but smaller, amounts of reduced denitrated product (**7**) under similar conditions at reflux temperatures and short contact times. The *meta* isomer **6***b* underwent mainly *N*-nitrosation-*N*-demethylation (78%) to *N*-methyl-*N*-nitroso-3-nitrobenzenamine (**8***b*), but some 9% *N*-methyl-*N*-nitrosobenzenamine (**7**) was also present. A similar yield of **6***b* was obtained from the *ortho* isomer **6***a*, which gave only 7% 1-methylbenzotriazole (**9**) but some 58% *N*-methyl-*N*-nitroso-2-nitrobenzenamine (**8***a*). The latter product represented the main course of the process also with the *para* isomer **6***c*, which produced only traces of the reduction product **7**.

The identification of **8***a* was arrived at by elemental analysis, mass spectrometry (the parent ion at *m/z* 181 lost NO to

Received July 2, 1996.[1]

This paper is dedicated to Professor Miha Tisler of the Department of Chemistry and Chemical Sciences of Lubiana University, Slovenia, on the occasion of his 70th birthday.

A.G. Giumanini[2] and G. Verardo. Department of Chemical Sciences and Technologies, University of Udine, I-33100 Udine, Italy.

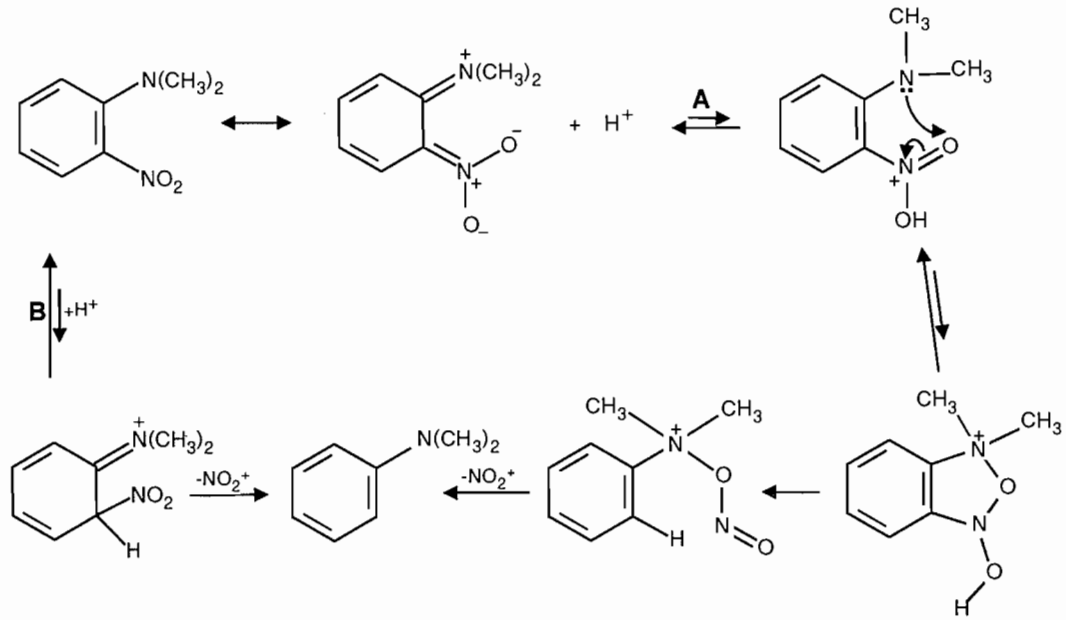
[1] Revision received January 24, 1997.

[2] Author to whom correspondence may be addressed. Telephone: +39-432-558 870 and -558 839. Fax: +39-432-558 803.

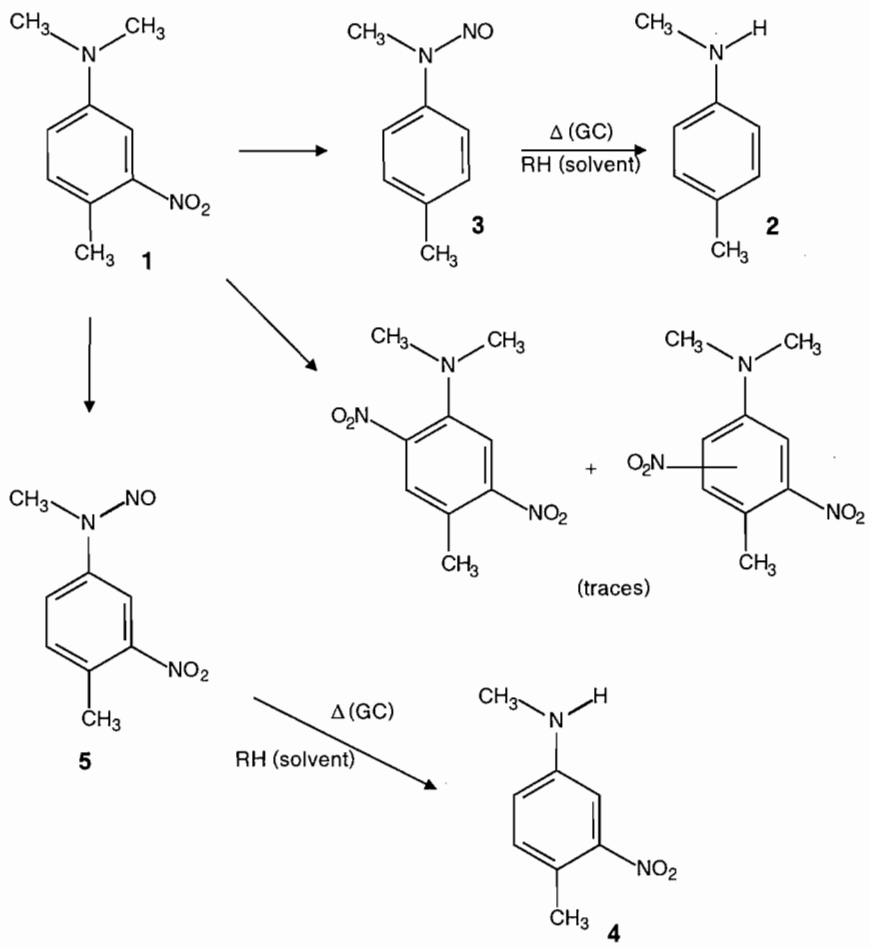
© 1997 NRC Canada

Can. J. Chem. Downloaded from www.nrcresearchpress.com by 88.146.161.215 on 09/08/12
For personal use only.

Scheme 1.



Scheme 2.

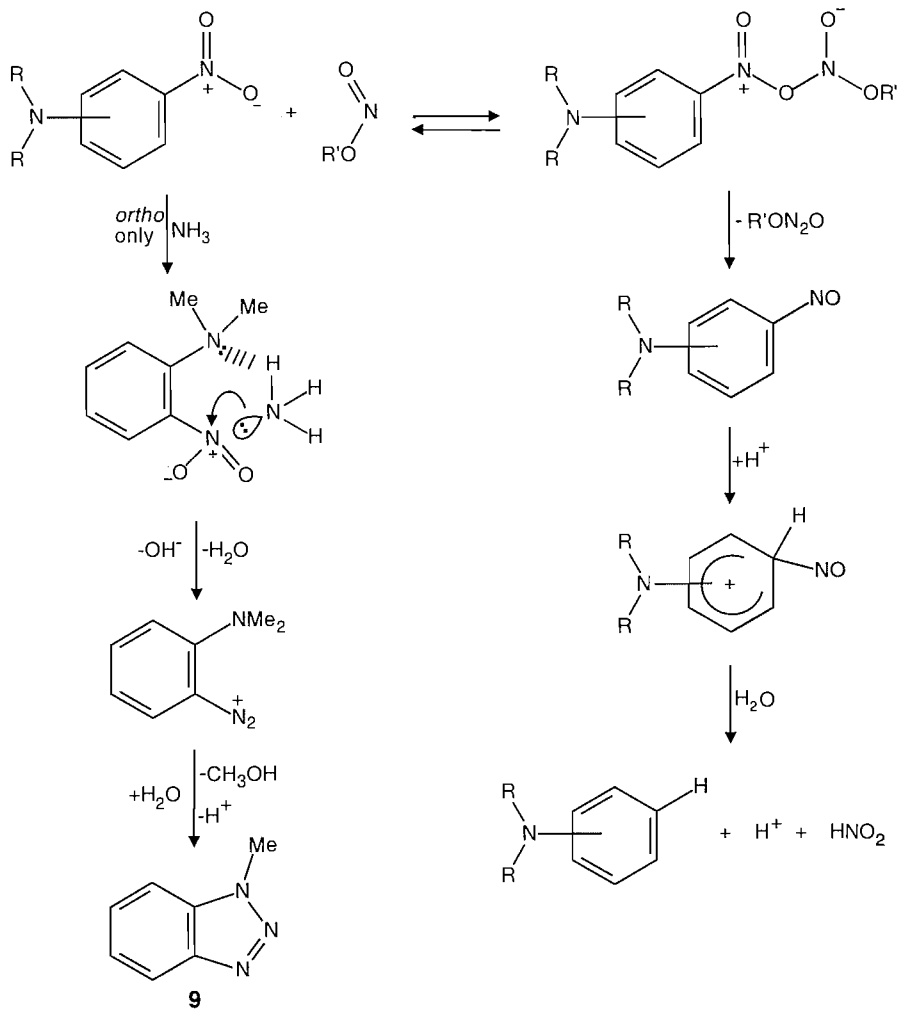


yield the base peak at *m/z* 151, this daughter ion subsequently lost OH, as expected from the location of the nitro group with respect to the methyl group), and infrared (2*a*, 3) ($\nu_{N=O}$ at 1459 cm^{-1}, ν_{N-N} at 961 cm^{-1}, and ν_{C-N} at 1198 cm^{-1}) spectroscopy. The ^1H NMR spectrum of **8***a* was in excellent agreement with what can be expected from a mixture of geometric isomers of a single nitrosamine, showing two sharp singlets for the methyl group. But, curiously, this is at variance with

© 1997 NRC Canada

Can. J. Chem. Downloaded from www.nrcresearchpress.com by 88.146.161.215 on 09/08/12
For personal use only.

Scheme 3.



the spectra of the strictly related nitrosamines **5** (vide infra) and *N*,4-dimethyl-*N*-nitroso-2-nitrobenzenamine **10** ($\delta_{N\text{-}Me}$ at 3.38, singlet, in $CDCl_3$) (*2a*), which exhibited under the same conditions a single peak for the *N*-methyl group, like all of the other *N*-nitroso aromatic nitrosamines investigated by us (*2a*), which are assumed to be in the *E* configuration. Like *N*-methyl-*N*-nitroso-2,6-diisopropylbenzenamine **11** ($\delta_{N\text{-}Me}$ at 3.36 ppm) (*2a*), the phenyl ring is expected to be almost perpendicular to the C-N-N=O plane also in **8***a*, but the ring in the latter case may be prone to some electron charge transfer from the oxygen of the nitro function, thus increasing the stability of the *Z* configuration, which would nonetheless be the lesser represented, showing the methyl resonance at δ 4.50 ppm. When a methyl group is in the *para* position, as is the case for **10**, its electron-releasing effect is allowed to restore a better planarity of the ring (not necessary of the NO_2 group!) and excludes the *Z* form from the equilibrium.

Nitronaphthalene, water, and AC did not yield any naphthalene after long reflux. The addition of BN to the mixture did not change matters. We have repeated the reported (*1b*) reaction between **6***a* and refluxing aqueous hydrochloric acid, but no substantial *N*-methylbenzimidazole-*N*-oxide was detected: denitration proceeded only to a very small extent. Moreover, 2-nitrobenzenamine did not undergo denitration at all under these conditions.

The mechanisms invoked for the reductive denitration of the *ortho*-nitrated tertiary amines cannot be valid here. By and large, the reaction conditions are far from being those for a necessary strong acid catalysis, although at the present time we have no well-grounded rationale for the behaviour of the system described. The formation of **9** indicated the involvement of ammonia (from AC) in the process. Speculations about mechanism are condensed in Scheme 3.

Experimental section

Materials

4,*N*,*N*-Trimethyl-3-nitrobenzenamine (**1**) (4) and 2-, 3-, and 4-nitro-*N*,*N*-dimethylbenzenamine (**6***a*, **6***b*, and **6***c*) (5) as well as *n*-butyl nitrite (BN) (6) were prepared according to described procedures. Compounds for which no references are given were available from previous work (*2a*). Alumina (active neutral Brockmann Grade I) was purchased from BDH (Milan, Italy). Solvents were used as received.

Can. J. Chem. Downloaded from www.nrcresearchpress.com by 88.146.161.215 on 09/08/12
For personal use only.

© 1997 NRC Canada

Can. J. Chem. Downloaded from www.nrcresearchpress.com by 88.146.161.215 on 09/08/12
For personal use only.

Equipment

GC–MS analyses were performed with a Fisons TRIO 2000 gas – chromatograph-mass spectrometer, working in the positive ion 70 eV electron impact mode. Injector temperature was kept at 250°C and column (Supelco® SE-54, 30 m long, 0.32 mm i.d., coated with a 0.25 μm phenyl methyl silicone rubber film) temperature was programmed from 80 to 300°C with a gradient of 10°C/min. Direct inlet mass spectra (DI-MS) were obtained on the same instrument: temperatures between 30 and 70°C were found suitable to volatilize all the compounds into the ion source. IR spectra were obtained with a Nicolet FT-IR Magna 550 spectrophotometer using the KBr technique for solids. ^{1}H NMR spectra were recorded in $CDCl_3$ at room temperature on a Bruker AC-F 200 spectrometer at 200 MHz. NMR peak locations are reported as δ-values from TMS. Some ^{1}H multiplets are characterized by the term *app* (apparent): this refers only to their appearance and may be an oversimplification. Elemental analyses were performed with a Carlo Erba model 1106 elemental analyzer and were in satisfactory agreement with calculated values. Melting points were determined with an automatic Mettler (model FP61) apparatus and are not corrected. Boiling points refer to the center cut of small distillations and are uncorrected.

Physical and spectroscopic properties of materials of common occurrence and (or) commercial origin are not reported.

4,*N*,*N*-Trimethyl-3-nitrobenzenamine (1), BN, AC, and water

Procedure A

The amine **1** (8.1 mmol), BN (24.5 mmol), AC (0.81 mmol), and water (81 mmol) were stirred during 2 days at room temperature. TLC analysis (alumina, hexane–CH_2Cl_2, 70:30 vol/vol) showed the total disappearance of starting material with the formation of two products. GC–MS analysis of the intact mixture from which volatile material was evaporated under vacuum showed the following: *N*,4-dimethylbenzenamine (**2**, 36%); *N*,4-dimethyl-*N*-nitrosobenzenamine (**3**, 8%), showing up as a peak tail of the former, of which it is a thermal decomposition product; *N*,4-dimethyl-3-nitrobenzenamine (**4**, 51%), analogously derived by thermal decomposition of the corresponding *N*-nitrosamine **5** in the injector; and two distinct dinitro derivatives (**12***a*, 1% and **12***b* 4%) of *N*,*N*,4-trimethylbenzenamines, identified on the basis of their mass spectra (**12***a*; MS *m/z*: 225(M^+, 46), 208(36), 180(24), 178(25), 162(48), 161(21), 150(100), 133(46), 132(57), 118(48), 117(28), 91(30), 77(24), 65(25), 51(17), and 42(24); **12***b*, MS *m/z*: 225(M^+, 70), 208(30), 180(5), 178(11), 162(17), 161(27), 150(64), 133(53), 132(100), 118(93), 117(43), 91(32), 77(19), 65(25), 51(10), and 42(24)]. Absorption chromatography, performed on alumina using hexane with increasing concentration of CH_2Cl_2 as eluant, of the total reaction mixture, after evaporation under vacuum of volatile material, yielded only *N*,4-dimethyl-*N*-nitrosobenzenamine (**3**, 28%; mp 56°C (lit. (7) mp 52°C); IR (KBr): 3020w, 2905w, 1510s, 1430vs, 1386vs, 1311s, 1287m, 1218vs, 1205vs, 1098vs, 1017s, 970s, 958s, 818vs, and 533s cm^{-1}; ^{1}H NMR ($CDCl_3$) δ: 2.39 (3H, s, ar-CH_3), 3.43 (3H, s, N-CH_3), 7.15–7.55 (4H, *app* m, ar-H); DI-MS *m/z*: 150(M^+, 34), 120(100), 92(51), 91(76), 77(54), 65(53), and 51(25). Anal. calcd. for $C_8H_{10}N_2O$: C 49.23, H 4.65, N 21.53; found: C 49.20, H 4.61, N 21.56) and *N*,4-dimethyl-*N*-nitroso-3-nitrobenzenamine (**5**, 75%; mp 58°C; IR (KBr): 3060w, 3020w, 1525vs, 1500s, 1460vs, 1400s, 1343vs, 1188vs, 1110s, 975s, 881m, 834s, 790m, 760m, and 708m cm^{-1}; ^{1}H NMR ($CDCl_3$) δ: 2.65 (3H, s, ar-CH_3), 3.46 (3H, s, N-CH_3), 7.22–8.19 (3H, m, ar-H); DI-MS *m/z*: 195(M^+, 19), 165(100), 148(13), 119(49), 118(29), 117(17), and 91(43). Anal. calcd. for $C_8H_9N_3O_3$: C 63.98, H 6.71, N 18.65; found: C 63.91, H 6.71, N 18.63).

Procedure B

A mixture of **1** (18.0 mmol), AC (2.0 mmol), and water (90.0 mmol) was refluxed during 60 min. Absorption chromatography, performed on alumina using hexane with increasing concentration of CH_2Cl_2 as eluant, of the total reaction mixture, after evaporation under vacuum of volatile material, yielded only **3** (5%) and **5** (81%).

N,*N*-Dimethyl-2-nitrobenzenamine (6*a*), BN, AC, and water

A mixture of **6***a* (18.0 mmol), BN (72.3 mmol), AC (2.0 mmol), and water (90.0 mmol) was refluxed during 120 min. Absorption chromatography, performed on alumina using hexane with increasing concentration of CH_2Cl_2 as eluant, of the total reaction mixture, after evaporation under vacuum of volatile material, yielded nitrobenzene (**13**, 1%), unreacted **6***a* (1%), *N*-methyl-2-nitrobenzenamine (**14***a*, 5%), *N*-methyl-*N*-nitrosobenzenamine (**7**, 9%; bp 83°C at 17 Torr (lit. (7) bp 86–87°C at 17 Torr; 1 Torr = 133.3 Pa) IR (neat): 3030w, 2910w, 1618m, 1595m, 1492m, 1467s, 1438vs, 1390m, 1350m, 1330m, 1312m, 1291m, 1263m, 1200s, 1090s, 1028m, 952m, 756s, and 690m cm^{-1}; ^{1}H NMR ($CDCl_3$) δ: 3.44 (3H, s, N-CH_3) and 7.29–7.66 (5H, m, ar-H); DI-MS *m/z*: 136(M^+, 40), 106(100), 105(38), 104(31), 79(73), and 77(92). Anal. calcd. for $C_7H_8N_2O$: C 61.75, H 5.92, N 20.57; found: C 61.72, H 5.92, N 20.58), *N*-methyl-*N*-nitroso-2-nitrobenzenamine (**8***a*, 58%; mp 39°C (lit. (8) mp 36°C); IR (KBr): 3100w, 3077w, 3049w, 1607m, 1528vs, 1459vs, 1441vs, 1358vs, 1277s, 1198s, 1070s, 1016s, 961s, 855m, 820m, 780vs, 748s, 704s, and 647m cm^{-1}; ^{1}H NMR ($CDCl_3$) δ: 3.42 and 4.23 (3H, two s, N-CH_3 in different conformations, % ratio 6.5/1) and 7.17–8.15 (4H, m, ar-H); DI-MS *m/z*: 181(M^+, 29), 151(100), 134(61), 120(8), 106(14), 105(28), 104(32), 93(34), 92(19), 91(22), 79(22), 78(47), 77(61), 76(23), 66(26), 65(31), 63(26), and 51(27). Anal. calcd. for $C_7H_7N_2O_2$: C 55.63, H 4.67, N 18.53; found: C 55.61, H 4.69, N 18.50), and 1–methylbenzotriazole (**9**, 7%; mp 66°C (lit. (9) mp 64–65°C); IR (KBr): 3050w, 2950w, 1498m, 1452m, 1299m, 1268m, 1198s, 1161m, 1024s, 780m, 739vs, and 662m cm^{-1}; ^{1}H NMR ($CDCl_3$) δ: 4.30 (3H, s, N-CH_3), 7.33–7.43 (1H, m, ar-H), 7.48–7.55 (2H, m, ar-H), and 8.06 (1H, *app* dt, J_o = 8.3 Hz, J_m = J_p = 1.1 Hz, ar-H); DI-MS *m/z*: 133(M^+, 100), 105(78), 104(42), 90(55), 78(27), 77(44), 64(27), 63(39), 51(21), and 50(16). Anal. calcd. for $C_7H_7N_3$: C 63.10, H 5.30, N 31.56; found: C 63.13, H 5.28, N 31.59).

N,*N*-Dimethyl-3-nitrobenzenamine (6*b*), BN, AC, and water

A mixture of **6***b* (18.0 mmol), BN (72.3 mmol), AC (2.0 mmol), and water (90.0 mmol) was refluxed during 120 min. Absorption chromatography, performed on alumina using hexane with increasing concentration of CH_2Cl_2 as eluant, of

© 1997 NRC Canada

Can. J. Chem. Downloaded from www.nrcresearchpress.com by 88.146.161.215 on 09/08/12
For personal use only.

the total reaction mixture, after evaporation under vacuum of volatile material, yielded nitrobenzene (**13**, 9%), unreacted **6***b* (3%), *N*-methyl-*N*-nitrosobenzenamine (**7**, 10%), *N*-methyl-3-nitrobenzenamine (**14***b*, 4%; mp 67°C (lit. (10) mp 67.5°C); IR (KBr): 3412s, 3106w, 2896w, 2873w, 2858w, 1627s, 1539vs, 1498s, 1483s, 1345vs, 1278s, 1153m, 1093s, 1082m, 840m, 809s, 731s, and 668s cm^{-1}; ^1H NMR ($CDCl_3$) δ: 2.89 (3H, s, N-CH_3), 4.14 (1H, br s, N-H), 6.86 (1H, ddd, J_o = 8.1 Hz, J_m = 2.4 Hz, $J_{m'}$ = 0.9 Hz, ar-H), 7.27 (1H, *app* t, J = 8.1 Hz, ar-H), 7.37 (1H, *app* t, J = 2.4 Hz, ar-H), and 7.51 (1H, ddd, J_o = 8.1 Hz, J_m = 2.2 Hz, $J_{m'}$ = 1.0 Hz, ar-H); DI-MS *m/z*: 152(M^+, 100), 122(7), 106(41), 105(17), 104(15), 94(11), 91(8), 79(39), 78(23), 77(61), 76(14), and 65(23). Anal. calcd. for $C_7H_8N_2O_2$: C 55.26, H 5.30, N 18.41; found: C 55.24, H 5.30, N 18.39), and *N*-methyl-*N*-nitroso-3-nitrobenzenamine (**8***b*, 78%; mp 78°C (lit. (11) mp 76°C); IR (KBr): 3107m, 3088m, 2942w, 2878w, 1533vs, 1473vs, 1433s, 1405m, 1355vs, 1312s, 1288s, 1201s, 1120vs, 1090s, 1076s, 972vs, 882vs, 813s, 740vs, 728vs, and 672s cm^{-1}; ^1H NMR ($CDCl_3$) δ: 3.52 (3H, s, N-CH_3), 7.71 (1H, *app* t, J = 8.2 Hz, ar-H), 8.00 (1H, ddd, J_o = 8.2 Hz, J_m = 2.2 Hz, $J_{m'}$ = 1.0 Hz, ar-H), 8.21 (1H, ddd, J_o = 8.2 Hz, J_m = 2.1 Hz, $J_{m'}$ = 1.0 Hz, ar-H), and 8.40 (1H, *app* t, J = 2.1 Hz, ar-H); DI-MS *m/z*: 181(M^+, 29), 151(100), 105(73), 104(60), 79(10), 78(25), 77(25), 76(18), and 63(22). Anal. calcd. for $C_7H_7N_2O_2$: C 55.63, H 4.67, N 18.53; found: C 55.60, H 4.67, N 18.56).

N,N-Dimethyl-4-nitrobenzenamine (6*c*), BN, AC, and water

A mixture of **6***c* (18.0 mmol), BN (72.3 mmol), AC (2.0 mmol), and water (90.0 mmol) was refluxed during 120 min. Absorption chromatography, performed on alumina using hexane with increasing concentration of CH_2Cl_2 as eluant, of the total reaction mixture, after evaporation under vacuum of volatile material, yielded nitrobenzene (**13**, 1%), unreacted **6***c* (7%), *N*-methyl-*N*-nitrosobenzenamine (**7**, 2%), *N*-methyl-4-nitrobenzenamine (**14***c*, 4%), and *N*-methyl-*N*-nitroso-4-nitrobenzenamine (**8***c*, 80%; mp 105°C (lit. (12) mp 104°C); IR (KBr): 3095w, 1610m, 1595m, 1510m, 1463m, 1395m, 1338s, 1300s, 1203m, 1175m, 1073s, 943m, 847m, 810m, and 745m cm^{-1}; ^1H NMR ($CDCl_3$) δ: 3.48 (3H, s, N-CH_3), 7.76 (2H, *app* d, J = 9.2 Hz, ar-H), and 8.37 (2H, *app* d, J = 9.2 Hz, ar-H); DI-MS *m/z*: 181(M^+, 32), 151(96), 105(100), 104(30), 90(15), and 63(17). Anal. calcd. for $C_7H_7N_2O_2$: C 55.63, H 4.67, N 18.53; found: C 55.65, H 4.69, N 18.51).

Acknowledgements

This work was supported by Consiglio Nazionale delle Ricerche (CNR) grants (93.03024.CT03 and 94.01556.CT03 to A.G.G.) and the Italian Ministry of University, Science and Technology (MURST 40% and 60% 1993–1994 to A.G.G., MURST 60% 1992–1994 to G.V.). Mr. V. Tosoratti of this department is thanked for his valuable assistance.

References

1. (*a*) O. Meth-Cohn and H. Suschitzky. Adv. Heterocycl. Chem. **14**, 211 (1972); (*b*) R. Fielden, O. Meth-Cohn, and H. Suschitzky. J. Chem. Soc. Perkin Trans. 1, 696 (1973).
2. (*a*) G. Verardo, A.G. Giumanini, and P. Strazzolini. Tetrahedron, **47**, 7845 (1991); (*b*) Tetrahedron, **46**, 4303 (1990).
3. D. Lin-Vien, N.B. Colthup, W.G. Fateley, and J.G. Grasselli. *In* The handbook of infrared and Raman characteristic frequencies of organic molecules. Academic Press, Inc., London. 1991.
4. H.P. Crocker and B.J. Jones. J. Chem. Soc. 1808 (1959).
5. A.G. Giumanini, G. Verardo, M.H. Gei, and L. Lassiani. J. Labelled Compd. Radiopharm. **24**, 255 (1987).
6. A. Vogel, *In* Vogel's textbook of practical organic chemistry, including quantitative organic analysis. 4th ed. *Revised by* B.S. Furniss, A.J. Hannaford, V. Roger, P.W.G. Smith, and A.R. Tatchell. Longman, New York. 1978.
7. E. Schmidt and H. Fischer. Ber. Dtsch. Chem. Ges. **53**, 1529 (1920).
8. A. Hempel. J. Prakt. Chem. **41**, 168 (1890).
9. A. Reissert. Ber. Dtsch. Chem. Ges. **47**, 672 (1914).
10. W.G. Macmillan and T.H. Reade. J. Chem. Soc. 585 (1929).
11. D. Vorlander and E. Siebert. Ber. Dtsch. Chem. Ges. **52**, 283 (1919).
12. W.G. Macmillan and T.H. Reade. J. Chem. Soc. 2863 (1929).

© 1997 NRC Canada

Weak M—H···H—C interactions observed in ruthenium and iridium complexes containing hydride, amine, and bulky phosphine ligands

Wei Xu, Alan J. Lough, and Robert H. Morris

Abstract: New amineruthenium and amineiridium hydride derivatives have been synthesized and characterized with the objective of observing intramolecular MH···HN or MH···HO interactions. These include $RuHCl(CO)(L)(PPr^i_3)_2$ (**1***a*, L = NH_2NH_2; **1***b*, L = NH_3) and $IrCl_2(L)(H)(PCy_3)_2$ (**2***a*, L = $SC(NH_2)_2$; **2***b*, L = NH_3; **2***c*, L = NH_2NH_2; **2***d*, L = $NH_2(CH_2)_3NH_2$; **2***e*, L = NH_2OH). Instead, weak M—H···H—C van der Waals contacts have been detected in the solid state by X-ray analysis and in solution by NMR T_1 measurements and nOe techniques. Both X-ray crystal structure analysis and minimum T_1 measurements indicate that the H···H distances in the M—H···H—C interactions are ca. 2.0–2.2 Å. The weak interactions might influence the course of deuteration of these complexes under D_2 gas. The crystal and molecular structure of $IrCl_2(NH_3)(H)(PCy_3)_2$ **2***a* has been determined by X-ray diffraction at 173 K: monoclinic, space group $P2_1/n$, a = 14.859(2) Å, b = 18.579(3) Å, c = 18.548(3) Å, β = 97.29(1)°, V = 5079.1(13) Å^3, Z = 4, full-matrix least-squares refinement on F^2 for 10 953 independent reflections; $R[F^2 > 4\sigma(F^2)]$ = 0.0283, $wR(F^2)$ = 0.0704.

Key words: ruthenium, iridium, hydride, dihydrogen, complexes, hydrogen bond, NMR, X-ray.

Résumé : On a synthétisé et caractérisé de nouveaux hydrures dérivés de l'amineruthénium et de l'amineiridium pour observer des interactions intramoléculaires MH···HN ou MH···HO. Ils comprennent le $RuHCl(CO)(L)(PiPr_3)_2$ (**1***a*, L = NH_2NH_2; **1***b*, L = NH_3) et $IrCl_2(L)(H)(PCy_3)_2$ (**2***a*, L = $SC(NH_2)_2$; **2***b*, L = NH_3; **2***c*, L = NH_2NH_2; **2***d*, L = $NH_2(CH_2)_3NH_2$; **2***e*, L = NH_2OH). À la place des interactions recherchées, on a observé de faibles contacts de van der Waals MH···HC tant à l'état solide (par diffraction des rayons X) qu'en solution (par des mesures de T_1 et par les techniques d'eOn en RMN). L'analyse des structures cristallines et les minima dans les mesures de T_1 indique que les distances H···H dans les interactions M—H···H—C sont de l'ordre de 2,0–2,2 Å. Ces faibles interactions peuvent influencer le cours de la deutération de ces complexes par le D_2 à l'état gazeux. On a déterminé les structures cristalline et moléculaire du $IrCl_2(NH_3)(H)(PCy_3)_2$ (**2***a*) par diffraction des rayons X à 173 K; les cristaux sont monocliniques, groupe d'espace $P2_1/n$, avec a = 14,859(2), b = 18,579(3) et c = 18,548(3) Å, β = 97,29(1)°, V = 5079,1(13) Å^3, Z = 4, $R[F^2 > 4\sigma(F^2)]$ = 0,0283 et $wR(F^2)$ = 0,0704 pour un affinement par la méthode des moindres carrés sur F^2 pour 10 953 réflexions indépendantes.

Mots clés : ruthénium, iridium, hydrure, dihydrogène, complexes, liaison hydrogène, RMN, rayons X.

[Traduit par la rédaction]

Introduction

Weak hydrogen bonds involving carbon–hydrogen bonds, C—H···X (X = O, N, or Cl), have been found to play a significant role in molecular conformation, molecular assemblies, and crystal engineering (1–3). They sometimes are crucial in structural stabilization of biological systems (4). Such weak interactions are difficult to observe in solution. In our study on intramolecular interactions between iridium hydrides and protons on nitrogen (see Fig. 1(a)), we found that, in addition to the NH proton at about 1.8 Å, some hydrogens of cyclohexyl groups on phosphine ligands contribute to the rate of dipole–dipole relaxation of hydride ligands in iridium complexes containing pyridiniumthiolato and tricyclohexylphosphine ligands (5–7). Desrosiers et al. (8) have already discussed the importance of ligand-hydrogen to metal-hydride dipole–dipole interactions in the analysis of T_1 values of metal hydride and dihydrogen complexes. We find that intramolecular CH···HM interactions also appear to influence the chemistry of the complexes described here.

These observations were made while trying to observe new intramolecular interactions between a metal hydride and an HN or HO hydrogen bond donor as shown in Fig. 1. Amino groups and iminol groups acting as H-bond donors to hydrides have been reported by Crabtree and co-workers (9–12). In all cases but one, a six-membered ring similar to that of (a) in Fig. 1 is involved; the exception is the first intermolecular Re—H···HN interaction (12). Strong evidence for the existence of intermolecular W—H···HO (13) and B—H···HN (14)

Received May 9, 1996.[1]

W. Xu, A.J. Lough, and R.H. Morris.[2] Department of Chemistry, University of Toronto, 80 St. George St., Toronto, ON M5S 3H6, Canada.

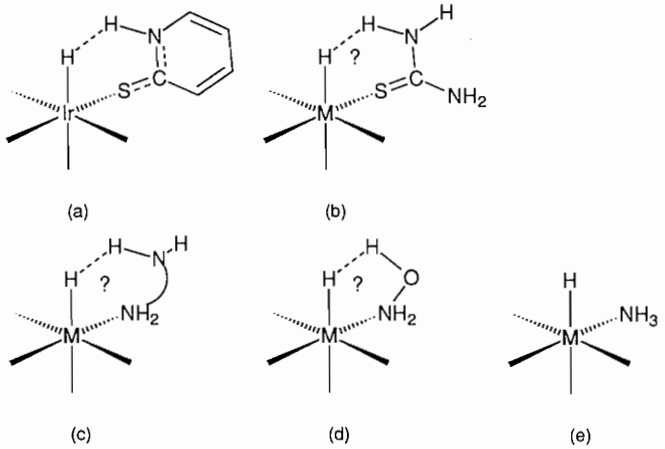
[1] Revision received February 7, 1997.

[2] Author to whom correspondence may be addressed: Telephone and Fax: (416) 978-6962. E-mail: rmorris@chem.utoronto.ca

© 1997 NRC Canada

Can. J. Chem. Downloaded from www.nrcresearchpress.com by 88.146.161.215 on 09/08/12
For personal use only.

Fig. 1. Observed (a) and hypothetical ((b)–(d)) intramolecular proton–hydride interactions between hydrogen bond donors and a metal hydride. The hydrogens in (e) are probably too far apart to interact.



interactions has also been provided recently. We wondered whether five-membered rings (Fig. 1 (c) with NH_2NH_2 ligand or (d) with NH_2OH ligand) would form. The corresponding ammine complexes (e) were prepared for comparison since they were not expected to show such an interaction in a four-membered ring; however, Milstein et al. postulated that there might be a weak attractive interaction between a *cis* hydride and hydroxide hydrogen in such a ring at an H—H distance of 2.4(1) Å in $[Ir(H)(OH)(PMe_3)_4]^+$ (15, 16).

Experimental

General procedures and materials

All operations were conducted in an argon atmosphere by use of Schlenk line techniques, or in a purified nitrogen atmosphere using a Vacuum Atmospheres glove box. Deuterated solvents were dried over Linde type 4 Å molecular sieves and degassed with argon using several evacuate–refill cycles. Reagent-grade chemicals were used as purchased from Aldrich Chemical Company, Inc. unless otherwise stated. Tricyclohexylphosphine (PCy_3) and triisopropylphosphine (PPr^i_3) were purchased from Strem Chemical Co. $IrCl_3{\cdot}3H_2O$ and $RuCl_3{\cdot}3H_2O$ were received as a loan from Johnson–Matthey Co. $IrHCl_2(PCy_3)_2$ was prepared from $IrCl_3{\cdot}3H_2O$–HCl–EtOH and PCy_3 as described elsewhere (17). Methods of preparation starting from other iridium complexes have been described (18). $RuHCl(CO)(PPr^i_3)_2$ was prepared by previously reported methods (19).

NMR spectra were recorded on Varian Unity-400 and Varian Gemini-300 spectrometers. Reported chemical shifts refer to room temperature conditions (20°C) unless specified otherwise. ^{31}P chemical shifts were measured in the proton decoupled mode and referenced externally to 85% H_3PO_4. ^1H chemical shifts were measured relative to partially deuterated solvent peaks, but are reported relative to tetramethylsilane. Fast atom bombardment mass spectrometry (FAB MS) spectra were obtained with a VG 70-250S mass spectrometer using a nitrobenzyl alcohol (NBA) or nitrophenyl octyl ether (NPOE) matrix. Microanalyses were performed by Guelph Chemical Laboratories Ltd.

Preparation of $RuHCl(CO)(L)(PPr^i_3)_2$ (1*a*, L = NH_2NH_2; 1*b*, L = NH_3)

$RuHCl(CO)(PPr^i_3)_2$ (0.5 g, 1 mmol) in toluene (20 mL) and L (L = 90% NH_2NH_2 aq. for **1***a*; L = 30% NH_3 aq. for **1***b*) were vigorously stirred for 20 min. The red toluene suspension of $RuHCl(CO)(PPr^i_3)_2$ turned to a light yellow solution very quickly. When methanol (50 mL) was added to the mixture, a light yellow crystalline compound $RuHCl(CO)(L)(PPr^i_3)_2$ **1** was formed. It was obtained in almost quantitative yield after washing the solid with methanol (2 × 5 mL) and drying under vacuum. $RuHCl(CO)(NH_2NH_2)(PPr^i_3)_2$ **1***a* (light yellow solid, yield 90%): ^1H NMR (CD_2Cl_2, 20°C) δ: −14.5 (br), −15.7 (t, J_{P-H} = 21 Hz). ^1H NMR (CD_2Cl_2, −60°C) δ: −13.6 (t, J_{P-H} = 21 Hz), −13.9 (t, J_{P-H} = 21 Hz), −15.9 (t, J_{P-H} = 21 Hz), 0.9–1.4 (m, 36H, CH_3), 2.56 (m, 6H, $CHMe_2$), 2.09 (br, $RuNH_2NH_2$), 2.36 (br, $RuNH_2NH_2$), 3.46 (br, $RuNH_2NH_2$), 3.60 (br, $RuNH_2NH_2$), 4.8 (s, CH_3OH, 3H). ^{31}P NMR δ: 45.6 (s), 43.0 (s). FAB MS: calcd. for $C_{19}H_{47}{}^{35}ClN_2OP_2{}^{101}Ru$: 517; observed: 517 ($M^+$). Anal. calcd. for $C_{19}H_{47}ClN_2OP_2Ru{\cdot}CH_3OH$: C 43.7, H 9.3, N 5.1; found: C 43.5, H 8.9, N 5.1. $RuHCl(CO)(NH_3)(PPr^i_3)_2$ **1***b* (light yellow solid, yield 88%): ^1H NMR (CD_2Cl_2, 20°C) δ: −14.1 (t, J_{P-H} = 21 Hz, relative int. 10), −14.4 (t, J_{P-H} = 20.5 Hz, relative int. 1), −15.9 (t, J_{P-H} = 20.6 Hz, relative int. 1), 0.9–1.4 (m, 36H, CH_3), 2.56 (m, 6H, $CHMe_2$), 2.3 (br, $RuNH_3$). ^{31}P NMR δ: 49.3 (s, relative int. 1), 49.1 (s, relative int. 10), 48.3 (d, J_{HP} = 20 Hz, relative int. 1). FAB MS: calcd. for $C_{19}H_{46}{}^{35}ClNOP_2{}^{101}Ru$: 502; observed: 502 ($M^+$). Anal. calcd. for $C_{19}H_{46}ClNOP_2Ru$: C 45.4, H 9.2, N 2.8; found: C 45.1, H 9.2, N 2.6.

Preparation of $IrCl_2(L)(H)(PCy_3)_2$ (2*a*, L = $SC(NH_2)_2$; 2*b*, L = NH_3; 2*c*, L = NH_2NH_2; 2*d*, L = $NH_2(CH_2)_3NH_2$; 2*e*, L = NH_2OH)

$Ir(H)Cl_2(PCy_3)_2$ (0.5 g, 0.6 mmol) in toluene (20 mL) and L (L = $SC(NH_2)_2$, 0.1 g, 0.6 mmol for **2***a*; L = NH_3, 5 mL of 30% aq., for **2***b*; L = NH_2NH_2, 5 mL of 90% aq. for **2***c*; L = $NH_2(CH_2)_3NH_2$, 5 mL for **2***d*, L = NH_2OH, 0.1 g of $NH_2OH{\cdot}HCl$ and 1 g KOH dissolved in 1 mL water for **2***e*) were vigorously stirred for 24 h. The red toluene solutions turned slowly into light yellow solutions and then pale yellow solids precipitated from the solutions. The products were filtered off, washed with methanol several times, and dried under vacuum. **2***a* (light yellow solid, 88% yield): ^1H NMR (CD_2Cl_2, 20°C) δ: −24.04 (t, $^2J_{HP}$ = 15.9 Hz, Ir-H), −24.07 (t, $^2J_{HP}$ = 18 Hz, Ir-H), 1.0–3.0 (m, C_6H_{11}), 4.8 (s, CH_3OH, 3H). ^{31}P NMR δ: −4.0 (s), −6.0 (s). FAB MS: calcd. for $C_{37}H_{71}{}^{35}Cl_2{}^{193}IrN_2SP_2$: 900; observed: 863 ($M^+$ − HCl − H), 823 (M^+ − $SC(NH_2)_2$ − H). Anal. calcd. for $C_{37}H_{71}Cl_2IrN_2SP_2{\cdot}CH_3OH$: C 48.9, H 8.1, N 3.0; found: C 48.6, H 8.2, N 3.1. **2***b* (light yellow solid, 100% yield): ^1H NMR (CD_2Cl_2, 20°C) δ: −24.4 (br, 1H), 1.0–3.0 (m, C_6H_{11}). ^1H NMR (CD_2Cl_2, −40°C) δ: −24.4 (t, $^2J_{HP}$ = 25.9 Hz, 1H). ^{31}P NMR δ: −6.2 (s). Anal. calcd. for $C_{36}H_{70}Cl_2IrNP_2$: C 51.4, H 8.4, N 1.7; found: C 51.2, H 8.6, N 1.6. **2***c* (light yellow solid, 100% yield): ^1H NMR (CD_2Cl_2, 20°C) δ: 3.83 (br, $IrNH_2NH_2$, 2H), 5.01 (br, $IrNH_2NH_2$, 2H), −24.1 (br, Ir-H, 1H). ^1H NMR (CD_2Cl_2, −40°C) δ: −24.1 (t, $^2J_{HP}$ = 25.9 Hz, 1H). ^{31}P NMR δ: −6.5 (s). FAB MS: calcd. for $C_{36}H_{71}{}^{35}Cl_2{}^{193}IrN_2P_2$: 856; observed: 819 ($M^+$ − HCl − H). Anal. calcd. for $C_{36}H_{71}Cl_2IrN_2P_2$: C 50.5, H 8.4, N 3.3; found:

© 1997 NRC Canada

Can. J. Chem. Downloaded from www.nrcresearchpress.com by 88.146.161.215 on 09/08/12
For personal use only.

Can. J. Chem. Downloaded from www.nrcresearchpress.com by 88.146.161.215 on 09/08/12
For personal use only.

Table 1. Summary of crystal data, details of intensity collection, and least-squares refinement parameters for **2*b***.

Empirical formula	$[C_{36}H_{70}Cl_2IrNP_2]\cdot 3(C_4H_8O)$
M_r	1058.28
Crystal size, mm	0.23 × 0.24 × 0.18
Crystal class	Monoclinic
Space group	$P2_1/n$
Temperature, K	173(2)
a, Å	14.859(2)
b, Å	18.579(2)
c, Å	18.548(3)
β, °	97.29(1)
V, A^3	5079.1(13)
Z	4
D_{calc}, g cm^{-3}	1.385
μ(MoKα), cm^{-1}	28.35
F(000)	2216
ω scan width, °	0.53
Range θ collected, °	3.05–27.01
Absorption correction	Empirical (ref. 20)
Min. and max. transmission	0.3790, 0.8114
No. reflections collected	11365
Independent reflections	10953
R_{int}	0.0209
No. observed data ($I > 2\sigma(I)$)	7559
R_1 ($I > 2\sigma(I)$)	0.0283
wR_2 (all data)	0.0704
Weighting a,b	0.0382, 0.00
Goodness of fit	0.927
Parameters refined	530
Max density in ΔF map, e/A^3	0.937

Definition of R indices: $R_1 = \Sigma(F_o - F_c)/\Sigma(F_o)$, $wR_2 = [\Sigma[w(F_o^2 - F_c^2)^2]/\Sigma[w(F_o^2)^2]]^{1/2}$.

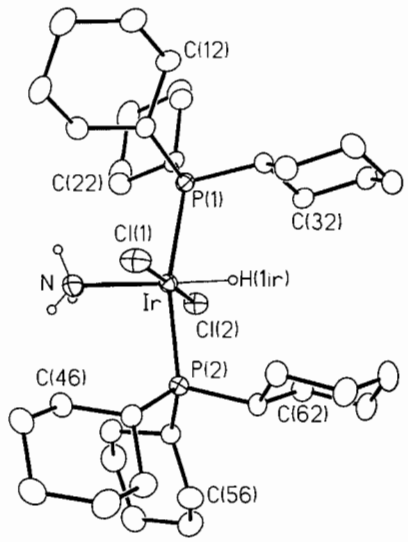
C 50.0, H 8.4, N 2.4. **2*d*** (light yellow solid, yield 95%): ^{1}H NMR (CD_2Cl_2, 20°C) δ: −24.8 (br, 1H). ^{31}P NMR δ: −6.2 (s). Anal. calcd. for $C_{39}H_{77}Cl_2IrN_2P_2$: C 52.1, H 8.6, N 3.1; found: C 51.9, H 8.3, N 3.1. **2*e*** (light yellow solid, yield 100%): ^{1}H NMR (CD_2Cl_2, −40°C) δ: 7.4 (s, OH, 1H), 6.7 (s, 2H, NH_2), −24.8 (t, $^2J_{HP}$ = 14 Hz, Ir-H, 1H). ^{31}P NMR δ: −5.2 ppm (s). Anal. calcd. for $C_{36}H_{70}Cl_2IrNOP_2\cdot CH_3OH$: C 49.9, H 8.4, N 1.6; found: C 49.7, H 8.2, N 1.2.

X-ray crystal structure determination of 2*b*

A summary of selected crystallographic data for **2*b*** is given in Table 1. Crystals were prepared by slow diffusion of methanol into a THF (2 mL) solution of complex **2*b*** (50 mg) under 1 atm (101.3 kPa) Ar. A suitable pale yellow crystal was mounted on a glass fiber. Data were collected on an Siemens P4 diffractometer using graphite-monochromated MoKα radiation (λ = 0.71073 Å). The intensities of three standard reflections measured every 97 reflections showed no decay. The data were corrected for Lorentz and polarization effects and for absorption (20).

The structure was solved using the SHELXTL PC V5.0 (21) package and refined by full-matrix least squares on F^2 using all data (negative intensities included). The weighting scheme was $w = 1/[\sigma^2(F_o^2) + (aP)^2 + bP]$ where $P = (F_o^2 + 2F_c^2)/3$. Hydrogen atoms were included in calculated positions and

Fig. 2. The molecular structure of **2*b*** as determined by single crystal X-ray diffraction at 173 K.



treated as riding atoms. The hydride atom was refined with an isotropic thermal parameter. The hydrogen atoms of the -NH_3 group were visible from a difference Fourier map as a torus of electron density and these atoms were included in the refinement as six half-occupancy H atoms riding on N. The structure contains three THF molecules of solvation and in one of these molecules the oxygen is disordered over two sites (0.76/0.24). The structure of **2*b***, including the crystallographic labelling scheme, is shown in Fig. 2. Selected bond lengths and angles are listed in Table 2. A complete set of crystallographic tables have been deposited as supplementary material.[3]

Results and discussion

Synthesis

The yellow, air-sensitive complexes $RuCl(CO)H(L)(PPr^i_3)_2$ (**1*a***, L = NH_2NH_2; **1*b***, L = NH_3) can be obtained by reaction of $RuH(Cl)(CO)(PPr^i_3)_2$ with an excess of hydrazine (90% aq.) or amine (30% aq.) in toluene. There are a total of three possible isomers of the complexes **1** when the two bulky phosphine ligands stay in *trans* positions (Fig. 3). The ^{1}H and ^{31}P NMR spectra of $RuH(Cl)(CO)(NH_3)(PPr^i3)_2$ **1*b*** show three different hydride and ^{31}P resonances in a 10:1:1 ratio by integration corresponding to three isomers. The exact assignments are not certain. The ^{1}H and ^{31}P NMR spectra of the complex **1*a*** have only two hydride resonances at −14.5 and −15.7 ppm and ^{31}P

[3] Copies of material on deposit may be purchased from: The Depository of Unpublished Data, Document Delivery, CISTI, National Research Council Canada, Ottawa, Canada K1A 0S2. With the exception of thermal parameters, these data have also been deposited with the Cambridge Crystallographic Data Centre, and can be obtained on request from the Director, Cambridge Crystallographic Data Centre, University Chemical Laboratory, 12 Union Road, Cambridge, CB2 1EZ, U.K. Structure factor amplitudes are no longer being deposited and may be obtained directly from the author.

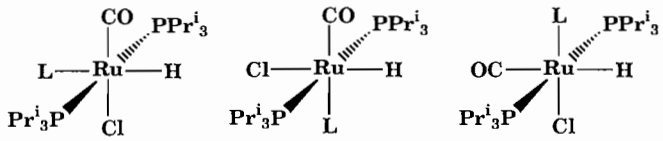
© 1997 NRC Canada

Can. J. Chem. Downloaded from www.nrcresearchpress.com by 88.146.161.215 on 09/08/12
For personal use only.

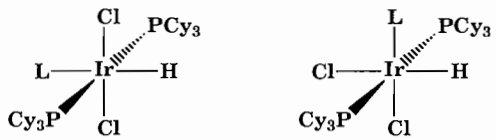
Table 2. Selected bond lengths (Å) and angles (°) for **2***b*.

Ir—N	2.259(3)	Ir—H(1IR)	1.49(4)
H(Ir)···H(C32)	2.235(10)	H(Ir)···H(C36)	2.208(10)
H(Ir)···H(C62)	2.223(10)	H(Ir)···H(C66)	2.351(10)
Ir—P(2)	2.3473(10)	Ir—P(1)	2.3486(10)
Ir—Cl(1)	2.3676(9)	Ir—Cl(2)	2.3761(9)
N-Ir-P(2)	98.03(8)	N-Ir-P(1)	97.68(8)
P(2)-Ir-P(1)	164.28(3)	N-Ir-Cl(1)	88.81(8)
P(2)-Ir-Cl(1)	89.52(3)	P(1)-Ir-Cl(1)	90.54(3)
N-Ir-Cl(2)	90.22(8)	P(2)-Ir-Cl(2)	90.50(3)
P(1)-Ir-Cl(2)	89.70(3)	Cl(1)-Ir-Cl(2)	179.02(3)
N-Ir-H(1IR)	178(2)	P(2)-Ir-H(1IR)	83.7(13)
P(1)-Ir-H(1IR)	80.6(13)	Cl(1)-Ir-H(1IR)	93(2)
Cl(2)-Ir-H(1IR)	88(2)		

Fig. 3. Possible isomers of complexes **1** and **2**.



1*a*: L = NH_2NH_2; **1***b*: L = NH_3



2*a*: L = $(NH_2)_2CS$; **2***b*: L = NH_3; **2***c*: L = NH_2NH_2;
2*d*: L = $H_2N(CH_2)_3NH_2$; **2***e*: L - NH_2OH

resonances at 45.6 and 43.0 ppm in a 2:1 ratio at room temperature. The broad peak at −14.5 ppm in the ^{1}H NMR spectrum splits into two triplets at −80°C (see Fig. 4(*a*)). Therefore there appear to be three isomers of this complex as well. However, we do not have a definitive explanation for the spectral changes that occur with the change in temperature.

The air-stable iridium derivatives $IrH(Cl)_2(L)(PCy_3)_2$ (**2***a*, L = $(NH_2)_2CS$; **2***b*, L = NH_3; **2***c*, L = NH_2NH_2; **2***d*, L = $NH_2(CH_2)_3NH_2$; **2***e*, L = NH_2OH) were prepared by the addition of excess L to a toluene suspension of $IrH(Cl)_2(PCy_3)_2$. There are two possible isomers for the complexes **2** (see Fig. 3). The ^{1}H and ^{31}P NMR spectra of complex **2***a* do show two different hydride and ^{31}P resonances in approximately equal amounts at room temperature. Complexes **2***b–d* have one broad hydride resonance in the ^{1}H NMR spectrum and one singlet in the ^{31}P NMR spectrum. The broad hydride resonance becomes a sharp triplet at temperatures of less than 0°C. The broadening is apparently caused by the dissociation and reassociation of the ligand L, which is labilized by a high *trans*-influence ligand, probably the hydride. The structure determination of crystalline **2***b* (see below) confirms that the ammine is *trans* to hydride. A broad triplet is observed for the hydride resonance of **2***e* at 20°C.

The hydride resonance of **2***b* in CD_2Cl_2 as a function of temperature is shown in Fig. 4(*b*). At least two exchange processes are apparent. The sharpening of the peak with cooling to around 0°C is probably due to the slowing of dissociation of the NH_3 ligand. The resonance for the five-coordinate product of this reaction is not visible in the ^{1}H NMR spectrum at low temperature and this indicates that the equilibrium greatly favors the six-coordinate complex **2***b*. There is no evidence for an isomer with ammine *cis* to hydride. In contrast, the complex $Ir(H_2)H(Cl)_2(P^iPr_3)_2$ is thermodynamically more stable with the π-acid dihydrogen ligand located *cis* to the hydride (22). A second broadening and then decoalescence occurs as the temperature is lowered below −60°C. The triplet at −24.4 ppm reappears along with an incompletely decoalesced, small, broad signal at −24.0 ppm. This might be due to the cyclohexyl groups taking up preferred positions in the complex, with the major species at −24.4 ppm having the conformation observed in the solid state (see the crystal structure presented below). No other isomers of **2***c–e* have been observed at low temperatures.

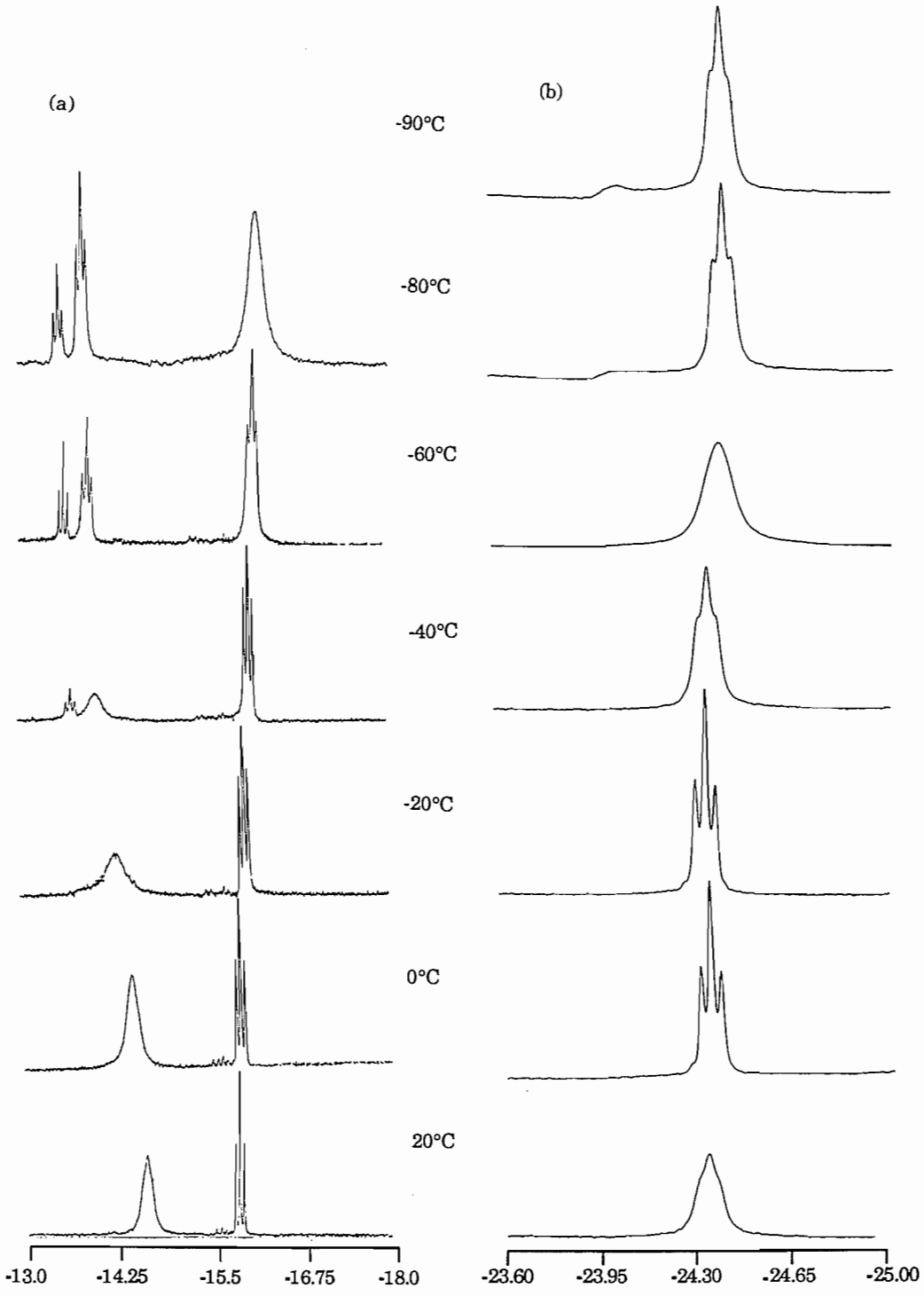
The complexes $IrH(Cl)_2(PCy_3)_2(OCMeNMe_2)$ and $IrH(Cl)_2(PCy_3)_2(CO)$ with structures related to those of **2** have been reported (18). The first complex, which was only characterized as a solid, appears to exist as one isomer since only one IR absorption due to CO stretching is observed. The second complex formed as the isomer with *trans* PCy_3 groups and CO *trans* to hydride in the reaction of $IrH(Cl)_2(PCy_3)_2$ with CO. This compound, with a structure similar to **2***b*, isomerized to a second isomer and also eliminated HCl to give *trans*-$IrCl(CO)(PCy_3)_2$. Complexes **2** in solution do not readily eliminate HCl considering that they are prepared in the presence of excess amine base. Complexes **2***a* and **2***c* do appear to eliminate HCl in the gas phase under the conditions of FAB mass spectroscopy.

X-ray analysis of complex 2*b*

The X-ray diffraction study at 173 K reveals that the iridium atom of **2***b* is in a distorted octahedral environment surrounded by two *trans* PCy_3 ligands, two *trans* chlorine atoms, and one ammine *trans* to the hydride. Selected bond lengths and angles are listed in Table 2. The two tricyclohexylphosphine ligands are bent toward the hydride (P-Ir-P, 164.28(3)°). The Ir-H hydride and hydrogens on cyclohexyl groups are well defined in electron difference maps. The iridium–hydride distance of 1.49(4) Å is reasonable on the basis of distances determined by neutron diffraction studies (23). Interestingly, two cyclohexyl groups tilt toward the hydride and their four H-C protons embrace the Ir-H hydride with close CH···H(Ir) distances that fall between 2.21(1) and 2.35(1) Å (Fig. 5). Similarly the CH···HN distances from six hydrogens on two half-occupancy ammine ligands to cyclohexyl hydrogens in the structure have short contacts of 2.0–2.4 Å. Considering that the van der Waals radius of hydrogen is about 1.2 Å (24), these contacts, at less than twice this radius, might be weakly attractive. Such MH···HC interactions might be energetically favorable considering that CH···O (H···O at 2.1–2.4 Å) hydrogen bonds have been confirmed by neutron diffraction

© 1997 NRC Canada

Fig. 4. Variable temperature 400 MHz ^{1}H NMR spectra. (*a*) Spectra of **1***a* in CD_2Cl_2 in the hydride region (−13 to −18 ppm) and (*b*) spectra of **2***b* in CD_2Cl_2 in the hydride region (−23 to −25 ppm).



studies, and that NH···HIr (H···H at 1.7 Å) interactions have also been shown to be surprisingly strong (11). However, a more likely interpretation is that these short contacts are enforced by the steric bulk of the tricyclohexylphosphine ligands.

NMR studies

Complexes **1** and **2** were tested for the presence of intramolecular NH···HM or OH···HM interactions by use of ^{1}H NMR nOe difference experiments. Irradiation of the hydride resonance did not produce an enhancement in the NH resonance of

Can. J. Chem. Downloaded from www.nrcresearchpress.com by 88.146.161.215 on 09/08/12
For personal use only.

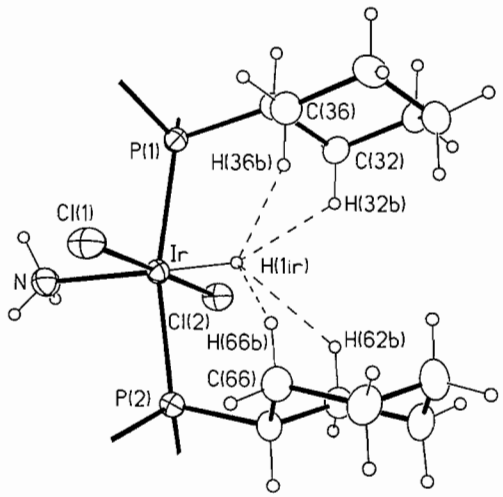
© 1997 NRC Canada

Table 3. List of minimum T_1 values (s, at 400 MHz), calculated H···H distances of four CH···HM interactions, and nOe enhancement of the hydride of complexes **1** and **2** when the isopropyl or cyclohexyl ^{1}H resonances around 1.8 ppm are irradiated.

Complexes	$T_{1\,min}$ s, IrH (Temp. K)	Calcd. $d_{CH\cdots HM}$ (Å)	nOe enhancement (%) of hydride
1*a*	0.17 ± 0.01 (183)[a]	2.0	12.5
2*b*	0.23 ± 0.01 (213)	2.1	13.5
2*c*	0.22 ± 0.01 (223)	2.1	11.5

[a]δ(H) −15.6.

Fig. 5. Part of the molecular structure of **2***b* showing the CH···HIr interactions. The non-interacting cyclohexyl groups are omitted for clarity.



any of the complexes. However, weak CH···HM interactions, as observed in the complex **2***b* by X-ray analysis, are detectable in ^{1}H NMR nOe difference experiments.

Selective irradiation of the hydride resonance of **2***b* leads to an nOe enhancement of C-H proton resonances at 1.8 and 1.9 ppm, but the magnitude of specific interactions could not be calculated due to the large number of non-interacting protons of the cyclohexyl groups that appear in the same region of the ^{1}H NMR spectrum. When the whole region of cyclohexyl resonances is saturated, an nOe enhancement of the hydride signal of over 10% is observed. The hydride of **2***b* has an unusually short minimum T_1 value of 0.23 s at 400 MHz and 213 K that is caused by the presence of CH···HIr interactions. An average H···H distance from the hydride to the closest H-C groups is calculated to be 2.1 ± 0.1 Å when the rate of dipole–dipole relaxation of the hydride is assumed to be made up of contributions from four cyclohexyl protons. The distance estimated by the T_1 method is slightly less than the average H···H distance revealed by the X-ray structure analysis.

The same CH···HM interactions have been observed for the other complexes **1** and **2** in solution. The T_1 and nOe data for selected complexes are listed in Table 3. In each case the minimum T_1 value can be interpreted in terms of a structure containing four CH···HM at 2.0–2.1 Å.

H/D exchange study

When a solution of complex **2***b* in CD_2Cl_2 is exposed to D_2 (1 atm), slow H–D exchange at the ammine and hydride sites is observed by use of ^{2}H NMR. The NH protons exchange with D_2 faster than does the hydride. After 24 h ca. 90% of both (N)H and (Ir)H positions have been deuterated. Since the dihydrogen complexes *trans*- and *cis*-$Ir(H)(H_2)Cl_2(PPr^i_3)_2$ (23, 25, 26) have been reported, it is quite possible that the deuteration is initiated by a short-lived, dideuterium intermediate *trans*-$Ir(H)(D_2)Cl_2(PCy_3)_2$, in spite of the fact that no trace of this complex or the H_2 analogue in solution is detected by NMR spectroscopy. The fast exchange between the acidic dideuterium ligand and the active protons of amines could result in the deuteration as suggested in Scheme 1 (5). The slower H–D exchange of the hydride might involve an initial intermolecular interaction between *trans*-$[Ir(H)_2(Cl)_2(PCy_3)_2]^-$ and NH_3D^+ as indicated. The CH···HIr interactions might make this exchange a slower process than expected because of steric interactions.

^{2}H NMR experiments indicate that the deuteration not only occurs at the hydride and ammine sites, but also at the cyclohexyl groups. When the amine ligand dissociates from complex **2***b* to generate a 16-electron intermediate, certain CH bonds could coordinate to the metal (27). Coordination of the CH bond makes it acidic and susceptible to proton exchange with the deuterated ammine as proposed in Scheme 2. An intramolecular example of H–D exchange between ammine and C—H bonds has also been reported (28) but the stereochemistry of the complexes involved is different than that of **2***b*. Another possible mechanism could involve the oxidative addition of carbon–hydrogen bonds of cyclohexyl groups to the complex $IrCl(PCy_3)_2$ (29). The latter complex might be produced from **2***b* by reductive elimination of NH_4Cl but we do not have evidence to support this idea.

Conclusions

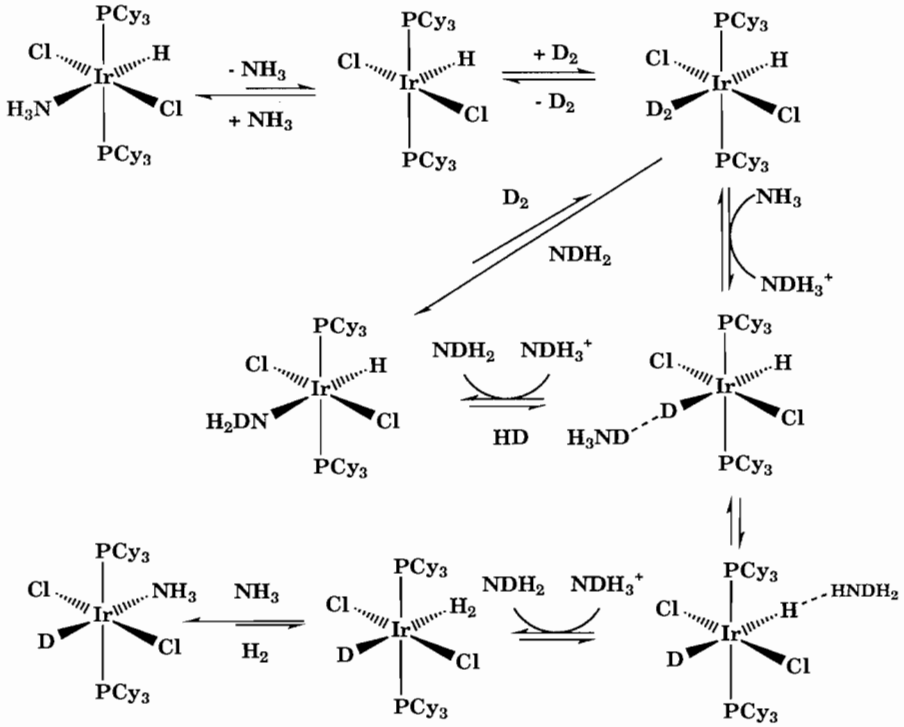
X-ray structural analysis and minimum T_1 and nOe techniques have revealed the presence of short CH···HM van der Waals contacts in complexes **1** and **2**. The H···H distances of 2.1–2.3 Å are less than the sum of the van der Waals radii of two hydrogens (2.4 Å), which might suggest that these interactions are favorable and might be similar to other hydrogen bonds formed by C-H hydrogen bond donors. However even in the absence of attractive interactions, the bulky cyclohexyl groups will probably occupy positions close to the small and polarizable hydride ligand for steric reasons alone. Therefore caution

© 1997 NRC Canada

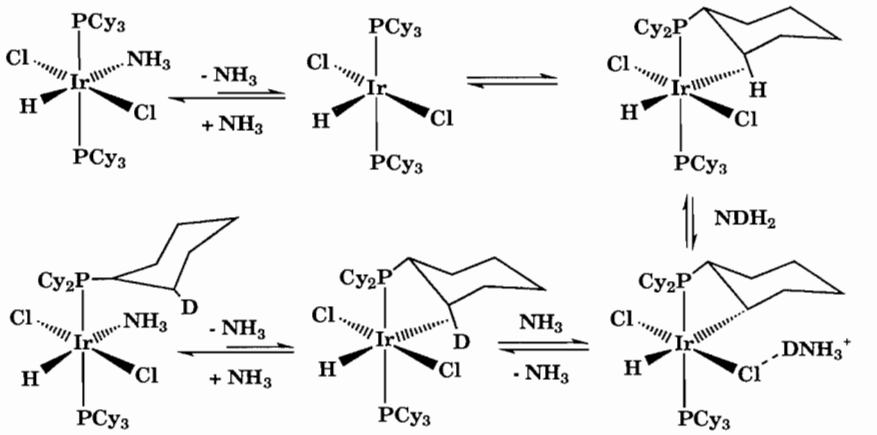
Can. J. Chem. Downloaded from www.nrcresearchpress.com by 88.146.161.215 on 09/08/12
For personal use only.

Can. J. Chem. Downloaded from www.nrcresearchpress.com by 88.146.161.215 on 09/08/12
For personal use only.

Scheme 1.



Scheme 2.



is needed in claiming that CH···HM bonding is present because the size of van der Waals contact distances might vary depending on the steric pressures around the complex. Certainly the contributions of ligand hydrogens to hydride relaxation can be quite important, as suggested previously (8). Tricyclohexylphosphine ligands, when *cis* to a hydride, are likely to make a significant contribution to the relaxation. Such CH···H(Ir) interactions may also play an important role in H–D exchange and CH bond activation reactions. After the submission of this work, Crabtree's group reported that, on the basis of a survey of the Cambridge Crystallographic Database, CH...HM contacts (1.6–2.1 Å) commonly occur between arene CH bonds of phosphine ligands and hydride ligands and that such weak hydrogen bonds might influence the mechanism of cyclometallation of arenes (30).

No intramolecular NH···HIr interactions were observed for complexes **1** and **2**. Such interactions have been observed for ligands that can form six-membered HMXYZH rings. Only the thiourea ligand has the correct geometry to form such a ring; all the other amines would have to form four- (NH_3), five- (NH_2NH_2), or eight- ($NH_2CH_2CH_2CH_2NH_2$) membered rings. Thiourea and the other ligands might form stronger hydrogen bonds to the chloride ligand than to the hydride in these complexes.

Acknowledgment

This work was supported by grants to R.H.M. from the Natural Sciences and Engineering Research Council of Canada (NSERC) and the Petroleum Research Fund, as administered

© 1997 NRC Canada

by the American Chemical Society, by a loan of iridium salts from Johnson Matthey Ltd., and by an NSERC postdoctoral fellowship to W.X. Thanks to Tanya Bartucz for helpful suggestions.

References

1. S. Subramanian and M.J. Zaworotko. Coord. Chem. Rev. **137**, 357 (1994).
2. G.R. Desiraju. Acc. Chem. Res. **24**, 290 (1991).
3. D. Braga, F. Grepioni, K. Biradha, V.R. Pedireddi, and G.R. Desiraju. J. Am. Chem. Soc. **117**, 3156 (1995).
4. T. Steiner, G. Koellner, K. Gessler, and W. Saenger. J. Chem. Soc. Chem. Commun. 511 (1995).
5. W. Xu, A.J. Lough, and R.H. Morris. Inorg. Chem. **35**, 1549 (1995).
6. S.H. Park, R. Ramachandran, A.J. Lough, and R.H. Morris. J. Chem. Soc. Chem. Commun. 2201 (1994).
7. A.J. Lough, S. Park, R. Ramachandran, and R.H. Morris. J. Am. Chem. Soc. **116**, 8356 (1994).
8. P.J. Desrosiers, L. Cai, Z. Lin, R. Richards, and J. Halpern. J. Am. Chem. Soc. **113**, 4173 (1991).
9. J.C. Lee, E. Peris, A.L. Rheingold, and R.H. Crabtree. J. Am. Chem. Soc. **116**, 11014 (1994).
10. E. Peris, J.C. Lee, and R.H. Crabtree. J. Chem. Soc. Chem. Commun. 2573 (1994).
11. E. Peris, J.C. Lee, J.R. Rambo, O. Eisenstein, and R.H. Crabtree. J. Am. Chem. Soc. **117**, 3485 (1995).
12. J. Wessel, J.C. Lee, E. Peris, G.P.A. Yap, J.B. Fortin, J.S. Ricci, G. Sini, A. Albinati, T.F. Koetzle, O. Eisenstein, A.L. Rheingold, and R.H. Crabtree. Angew. Chem. Int. Ed. Engl. **34**, 2507 (1995).
13. E.S. Shubina, N.V. Belkova, A.N. Krylov, E.V. Vorontsov, L.M. Epstein, D.G. Gusev, M. Niedermann, and H. Berke. J. Am. Chem. Soc. **118**, 1105 (1996).
14. T.B. Richardson, S. Degala, R.H. Crabtree, and P.E.M. Siegbahn. J. Am. Chem. Soc. **117**, 12875 (1995).
15. D. Milstein, J.C. Calabrese, and I.D. Williams. J. Am. Chem. Soc. **108**, 6387 (1986).
16. R.C. Stevens, R. Bau, D. Milstein, O. Blum, and T.F. Koetzle. J. Chem. Soc. Dalton Trans. 1429 (1990).
17. S. Brinkmann, R. Ramachandran, R.H. Morris, and S. Park. Inorg. Synth. In press.
18. B.R. James, M. Preece, and S.D. Robinson. *In* Catalytic aspects of metal phosphine complexes. *Edited by* E.C. Alyea and D.W. Meek. Adv. Chem. Ser. **196**, 145 (1982).
19. M.A. Esteruelas and H. Werner. J. Organomet. Chem. **303**, 221 (1986).
20. G.M. Sheldrick. SHELXA-90, University of Göttingen, Germany. 1990.
21. G.M. Sheldrick. SHELXTL PC. V. 5.0, Madison, Wis., U.S.A. 1995.
22. D.G. Gusev, R. Kuhlman, J.R. Rambo, H. Berke, O. Eisenstein, and K.G. Caulton. J. Am. Chem. Soc. **117**, 281 (1995).
23. A. Albinati, V.I. Bakhmutov, K.G. Caulton, E. Clot, J. Eckert, O. Eisenstein, D.G. Gusev, V.V. Grushin, B.E. Hauger, W.T. Klooster, T.F. Koetzle, R.K. McMullan, T.J. O'Loughlin, M. Pelissier, R.S. Ricci, M.P. Sigalas, and A.B. Vymenits. J. Am. Chem. Soc. **115**, 7300 (1993).
24. A. Bondi. J. Phys. Chem. **68**, 441 (1964).
25. V.I. Bakhmutov, A.B. Vymenits, and V.V. Grushin. Inorg. Chem. **33**, 4413 (1994).
26. V.I. Bakhmutov, E.V. Vorontsov, and A.B. Vymenits. Inorg. Chem. **34**, 214 (1995).
27. R.H. Crabtree. Angew. Chem. Int. Ed. Engl. **32**, 789 (1993).
28. R. Koelliker and D. Milstein. J. Am. Chem. Soc. **113**, 8524 (1991).
29. S. Hietkamp, D.J. Stufkens, and K. Vrieze. J. Organomet. Chem. **152**, 347 (1978).
30. T.B. Richardson, T.F. Koetzle, and R.H. Crabtree. Inorg. Chim. Acta, **250**, 69 (1996).

Can. J. Chem. Downloaded from www.nrcresearchpress.com by 88.146.161.215 on 09/08/12
For personal use only.

© 1997 NRC Canada

Spectroscopic and thermochemical investigation of alkaline earth metal salts of 2-oximinopropionate

A.W. Apblett, G.D. Georgieva, and J.T. Mague

Abstract: Alkaline earth metal 2-oximinopropionates were prepared by the reaction of sodium 2-oximinopropionate with the respective metal nitrates or chlorides in water at room temperature. These compounds were characterized by infrared and multinuclear NMR spectroscopy and thermogravimetric analysis. The thermal decomposition of the salts occurs in the range 144–188°C and exhibits a trend towards lower temperature with increasing size of the cation. In all cases, the decomposition yields a metal carbonate. The molecular structure of calcium 2-oximinopropionate hydrate was determined by single-crystal X-ray crystallography. Crystal data: $C_6H_{10}N_2O_7Ca$, MW = 262.24 g/mol, triclinic, space group $P\bar{1}$ (No.2), a = 8.954(1) Å, b = 9.3851(7) Å, c = 6.2445(7) Å, α = 97.209(8)°, β = 104.917(9)°, γ = 87.250(8)°, V = 503.0(2) Å^3, Z = 2, D_{calc} = 1.73 g cm^{-3}, R = 0.03 and R_w = 0.04.

Key words: crystal structure, alkaline earth, 2-oximinopropionate, thermal decomposition.

Résumé : On a préparé les 2-oximinopropionates de métaux alcalino-terreux par réaction du 2-oximinopropionate de sodium avec les nitrates (ou les chlorures) métalliques appropriés, en solution aqueuse, à la température ambiante. On a caractérisé ces composés par spectroscopies infrarouge et RMN multinucléaire et par analyse thermogravimétrique. La décomposition thermale de ces sels se produit entre 144 et 188°C; cette température diminue avec une augmentation de la grosseur du cation. Dans tous les cas, la décomposition conduit à un carbonate métallique. La structure moléculaire de l'hydrate du 2-oximinopropionate de calcium a été déterminée par diffraction des rayons X sur un cristal unique. Les cristaux de $C_6H_{10}N_2O_7Ca$, PM = 262,24 g/mol, sont tricliniques, groupe d'espace $P\bar{1}$ (No.2), avec a = 8,954(1), b = 9,3851(7) et c = 6,2445(7) Å, α = 97,209(8)°, β = 104,917(9)° et γ = 87,250(8)°, V = 503.0(2) Å^3, Z = 2, D_{calc} = 1,73 g cm^{-3}, R = 0,03 et R_w = 0,04.

Mots clés : structure cristalline, alcalino-terreux, 2-oximinopropionate, décomposition thermique.

[Traduit par la rédaction]

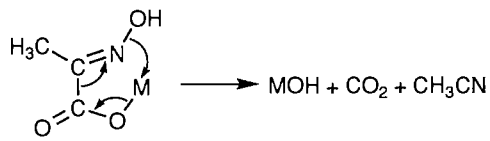
Introduction

Salts of 2-oximinopropionate or pyruvic acid oxime (PAO) are promising candidates for use as low-temperature precursors for metal oxide ceramics (1, 2). These compounds undergo a low-temperature decomposition to yield acetonitrile, carbon dioxide, water, and a metal carbonate, oxide, or hydroxide depending on the nature of the metal (Scheme 1). Typically, these salts are readily prepared via ligand exchange reactions of a metal chloride or nitrate with sodium pyruvic acid oxime (NaPAO). Since most PAO salts of multivalent elements are sparingly soluble in water, this approach generally leads to the ready isolation of the PAO complexes as a precipitate or well-formed crystals.

Very few structural studies of metal PAO complexes have been reported. Previous reports have described the complexation of Cu(II), Ni(II), Co(II), Mn(II), Cr(III), Co(III), Zn(II), and alkali metals with PAO (3–5). However, the only crystal structures reported were for the complexes NaPAO (5) and [BH][M(HL)L] (M = Cu, B = pyridine and M = Co, B = imidazole) where HL is the PAO anion while L is the dianion of PAO in which both the carboxylate and the oxime are deprotonated (6, 7).

The thermal instability of 2-oximinocarboxylate complexes has been remarked upon in previous studies and they have been used for quantitative determination of Cu(II) ions via their precipitation from solution and subsequent pyrolysis to CuO (8). Similar reactions have also been used to prepare metal oxide ceramics (1, 2) and catalysts (9). As well, the thermal decomposition of 2-oximinocarboxylic acids is a useful synthetic route for the preparation of functionalized nitriles (10).

Scheme 1.



Received October 4, 1996.

A.W. Apblett,[1] G.D. Georgieva, and J.T. Mague. Department of Chemistry, Tulane University, 6823 St. Charles Avenue, New Orleans, LA 70118, U.S.A.

[1] Author to whom correspondence may be addressed. Telephone: (504) 862-8943. Fax: (504) 865-5596. E-mail: apblett@mailhost.tcs.tulane.edu

© 1997 NRC Canada

Can. J. Chem. Downloaded from www.nrcresearchpress.com by 88.146.161.215 on 09/08/12
For personal use only.

Can. J. Chem. Downloaded from www.nrcresearchpress.com by 88.146.161.215 on 09/08/12
For personal use only.

In this investigation, the thermal behavior of the alkaline earth metal salts of pyruvic acid oxime has been determined. The results of this study as well as the spectroscopic characterization of the complexes and the crystal structure of $Ca(PAO)_2\cdot(H_2O)$ are reported herein.

Experimental

Sodium pyruvic acid oxime was prepared by treatment of sodium pyruvate with hydroxylamine using a procedure described in a related paper concerning Group 1 2-oximinopropionates (5). $MgCl_2\cdot 6(H_2O)$, $CaCl_2\cdot 2(H_2O)$, $Sr(NO_3)_2$, and $BaCl_2\cdot 2(H_2O)$ were commercial reagents and were used without further purification. Water was distilled and deionized before use. Infrared spectra were obtained as KBr pellets on a Mattson Cygnus 100 FT-IR spectrometer. ^1H and $^{13}C\{^1H\}$ NMR spectra were recorded on either a GE 400 NMR spectrometer or Bruker AC 200 spectrometer and were referenced to TMS. Solid state ^{13}C CPMAS spectra were recorded on a Bruker DSX 300 spectrometer and are referenced to TMS using a hexamethylbenzene secondary standard. Thermogravimetric studies were performed using 20–30 mg samples in a Seiko TG/DTA 220 instrument under a 100 mL/min flow of dry air. The temperature was ramped from 25°C to 625°C at a rate of 2°C per min while the off-gases were analyzed on a Fisons Thermolab mass spectrometer. Bulk pyrolyses at various temperatures were performed in ambient air in a temperature-programmable muffle furnace using ca. 2 g samples, a temperature ramp of 5°C/min, and a hold time of 12 h. X-ray powder diffraction patterns were obtained on a Scintag XDS 2000 diffractometer using copper K_α radiation. Microanalysis for C, H, and N content was performed by Oneida Research Services or Tulane's Coordinated Instrument Facility.

Preparation of $Mg(PAO)_2\cdot 2(H_2O)$

A solution of $MgCl_2\cdot 6(H_2O)$ (2.03 g, 10.0 mmol) in 25 mL of water was added to a solution of $NaPAO\cdot(H_2O)$ (3.30 g, 23.0 mmol) in 25 mL of H_2O. The resulting solution gradually precipitated a white solid. After 48 h, the solid was filtered off, washed with water (2 × 10 mL) and acetone (3 × 10 mL), and then air dried to provide a yield of 1.89 g (72%) of $Mg(PAO)_2\cdot 2(H_2O)$, mp (dec.) 188°C. IR (cm^{-1})(KBr): 3448(s, br), 3399(s, br), 3041(s, br), 2906(s), 2812(s, br), 2283(m), 1750(m, sh), 1674(m, sh), 1674(s), 1647(s), 1483(s), 1394(s), 1367(s), 1219(s), 1045(s), 925(w), 858(s), 769(s, sh), 752(s), 744(m), 686(m), 553(m). ^1H NMR (d_6-DMSO) δ(ppm): 1.87(s, 3H, CH_3), 12.79(br s, ^1H, NOH). $^{13}C\{^1H\}$ NMR (d_6-DMSO) δ(ppm): 11.1 (CH_3), 152.8 (C═N), 167.2 (COO). Anal. calcd. for $C_6H_{12}N_2O_8Mg$ (%): C 27.25, H 4.57, N 10.59; found: C 27.42, H 4.45, N 10.42.

Preparation of $Ca(PAO)_2\cdot(H_2O)$

$Ca(PAO)_2\cdot(H_2O)$ was obtained as large white cubic crystals from the reaction of a solution of $CaCl_2\cdot 2(H_2O)$ (7.35 g, 50.0 mmol) in 50 mL of water with a solution of $NaPAO\cdot(H_2O)$ (14.30 g, 100.0 mmol) in 50 mL of H_2O. Filtration followed by washing with water (2 × 25 mL) and acetone (3 × 25 mL) and then drying in vacuo yielded 11.07 g (81%) of $Ca(PAO)_2\cdot(H_2O)$, mp (dec.) 165.6°C. CHN IR (cm^{-1})(KBr): 3422(s), 3249(s, sh), 3069(s, sh), 2992(m, sh), 2858(m, sh), 1675(s), 1640(s, sh), 1617(s), 1596(s, sh), 1465(s), 1418(m), 1389(m), 1364(m), 1256(m), 1216(s), 1109(m), 1038(s, sh), 1021(s), 980(w), 873(m), 846(m), 814(w), 780(m), 737(s), 617(s), 552(w), 470(w), 424(w). ^1H NMR (d_2O) δ(ppm): 1.83(s, 3H, CH_3), $^{13}C\{^1H\}$ NMR (d_6-DMSO) δ(ppm): 11.0 (CH_3), 153.0 (C═N), 166.1 (COO). Anal. calcd. for $C_6H_{10}N_2O_7Ca$ (%): C 27.48, H 3.84, N 10.66; found: C 27.40, H 3.84, N 10.75.

Preparation of $Sr(PAO)_2$

A solution of $Sr(NO_3)_2$ (6.33 g, 30.0 mmol) in 25 mL H_2O was added to a solution of $NaPAO\cdot(H_2O)$ (8.58 g, 60.0 mmol) in 50 mL of water. Immediate precipitation of a white solid occurred. After 12 h, the precipitate was isolated by filtration and was washed with water (2 × 25 mL) and acetone (3 × 25 mL). Drying in vacuo yielded 7.02 g (80%) of $Sr(PAO)_2$, mp (dec.) 156°C. IR (cm^{-1})(KBr): 3261(s, br), 3131(s, sh), 2945(s, sh), 2696(w), 1658(m, sh), 1674(s), 1594(s), 1479(s), 1393(s), 1358(s), 1203(s), 1023(s), 973(m), 945(m), 843(s), 727(s), 689(m, sh), 549(w). ^1H NMR (D_2O) δ(ppm): 1.85(s, 3H, CH_3). $^{13}C\{^1H\}$ NMR (D_2O) δ(ppm): 11.9 (CH_3), 156.8 (C═N), 171.8 (COO). Anal. calcd. for $C_6H_8N_2O_6Sr$ (%): C 24.70, H 2.76, N 9.60; found: C 24.76, H 2.83, N 9.75.

Preparation of $Ba(PAO)_2$

$Ba(PAO)_2$ was obtained as a white precipitate from the reaction of $BaCl_2\cdot 2(H_2O)$ (7.32 g, 30.0 mmol) in 50 mL of water with a 50 mL aqueous solution of $NaPAO\cdot(H_2O)$ (8.58 g, 60.0 mmol). After 12 h, the solid was isolated by filtration and was washed with water (2 × 25 mL) and acetone (3 × 25 mL). Drying in vacuo yielded 7.84 g (77%) of $Ba(PAO)_2$, mp (dec.) 144°C. IR (cm^{-1})(KBr): 3553(m, sh), 3474(s, sh), 3415(s), 3257(m, sh), 2929(m, br), 1684(s, sh), 1617(s), 1576(s), 1541(s), 1457(s), 1385(s), 1232(m), 1013(s), 842(m), 784(m), 748(m), 729(w), 689(m), 627(w), 518(w). ^1H NMR (D_2O) δ(ppm): 1.83(s, 3H, CH_3). $^{13}C\{1H\}$ NMRn (d_6- DMSO) δ(ppm): 11.7 (CH_3), 154.6 (C═N), 167.7 (COO). Anal. calcd. for $C_6H_8N_2O_6Ba$ (%): C 21.10, H 2.36, N 8.20; found: C 21.03, H 2.41, N 8.33.

X-ray structure determination of $Ca(PAO)_2\cdot(H_2O)$

Crystals of $Ca(PAO)_2\cdot(H_2O)$ suitable for X-ray analysis were obtained by slow evaporation of a saturated aqueous solution. A colorless crystal measuring 0.2 × 0.2 × 0.33 mm was mounted on a thin glass fiber and coated with a thin film of epoxy cement. General procedures for crystal alignment, unit cell determination, and data collection on the CAD4 diffractometer have been published (11) and details of the present study appear in Table 1. No higher symmetry than triclinic was indicated by the CAD4 software or by a check of the Laue symmetry of several reflections of medium to strong intensity. The consequent choice of $P\bar{1}$ as the space group was confirmed by the successful refinement. The data were corrected for Lorentz and polarization effects, for a 2.3% linear decay in intensity monitors, and for absorption using ψ scans on several reflections with χ near 90°. The calcium atom was readily located from an origin-removed Patterson map and the remainder of the structure developed by successive cycles of full-matrix, least-squares refinement followed by difference Fourier synthesis (12). Neutral atom scattering factors include correction for the real and imaginary effects of anomalous

© 1997 NRC Canada

Can. J. Chem. Downloaded from www.nrcresearchpress.com by 88.146.161.215 on 09/08/12
For personal use only.

Table 1. Crystallographic data for $Ca(C_3H_4NO_3)_2 \cdot H_2O$.

Formula	$C_6H_{10}N_2O_7Ca$	T, °C	23
fw	262.24	2θ range, deg	1.0–52.0
Crystal system	Triclinic	Scan type	ω–2θ
Space group	$P\bar{1}$ (No. 2)	Scan range, deg.	0.80 + 0.2 (tanθ)
a, Å	8.954(1)	Scan, speed, deg · min^{-1}	16.4–1.26
b, Å	9.3851(7)	μ, cm^{-1}	6.3
c, Å	6.2445(7)	Range trans. factor	0.962–0.999
α, deg	97.209(8)	No. unique data	2107
β, deg	104.917(9)	No. data $I > 3\sigma(I)$	1673
γ, deg	87.250(8)	No. variables	157
V, Å^3	503.0(2)	Shift/esd. final cycle	0.07
Z	2	R^b	0.027
λ, Å	0.71073[a]	R_w[c]	0.042
d_{calc}, g/cm^3	1.73	GOF[d]	1.53

[a]Mo-K_α, graphite monochromated.
[b]$R = \Sigma||F_o| - |F_c||/\Sigma|F_o|$.
[c]$R_w = [\Sigma w(||F_o| - |F_c||)^2/\Sigma w(|F_o|)^2]^{1/2}$ with $w = 1/(\sigma_F)^2$ where $\sigma_F = \sigma(F^2)/2F$ and $\sigma(F^2) = [(\sigma_I)^2 + (0.04F^2)^2]^{1/2}$.
[d]GOF $= [\Sigma w(||F_o| - |F_c||)^2/(N_o - N_v)]^{1/2}$ where N_o and N_v are, respectively, the number of observations and variables.

dispersion.[2] Towards the end of the refinement, all hydrogen atoms could be located in a difference map. Those of the methyl groups were placed in idealized positions with isotropic thermal parameters 20% larger than the attached carbon atoms and updated periodically while those attached to oxygen were refined with fixed, isotropic thermal parameters 20% larger than the respective oxygen atoms. The final difference map was essentially featureless (residual peaks 0.29 to −0.32 e/Å^3). Bond distances are given in Table 2, and bond angles are provided in Table 3.[3]

Results and discussion

Synthesis of alkaline earth metal PAO salts

The alkaline earth metal salts of pyruvic acid oxime may be readily prepared by reaction of aqueous solutions of the metal ions with an aqueous solution of sodium pyruvic acid oxime (NaPAO) (eq. [1]). Since the Group 2 salts are sparingly soluble, they are readily isolated as precipitates from this reaction. However, since these salts do have a finite solubility in water, the yields are less than quantitative (ca. 71–80%). The yields may be improved by concentrating the filtrate from the precipitation reaction but separation from the sodium nitrate or sodium chloride by-product becomes problematic.

[1] $MX_2 + 2\ CH_3C(=NOH)COONa \rightarrow [CH_3C(=NOH)COO]_2M + 2\ NaX$

[2] All calculations performed on a VAXstation 3100 using the w/MolEN suite of programs (13).

[3] Tables of final atomic positional parameters, anisotropic thermal parameters, calculated hydrogen positions, and calculated and observed structure factors are available from A.A. on request.

Table 2. Bond distances (Å) for $Ca(C_3H_4NO_3)_2 \cdot H_2O$.

Ca—O(1)	2.513(1)	O(4)—C(4)	1.257(2)
Ca—O(1)′	2.387(1)	O(5)—C(4)	1.248(2)
Ca—O(2)	2.465(1)	O(6)—N(2)	1.387(2)
Ca—O(4)	2.451(1)	O(6)—H(6)	0.78(3)
Ca—O(5)	2.557(1)	O(7)—H(7A)	0.89(3)
Ca—O(5)′	2.371(1)	O(7)—H(7B)	0.80(3)
Ca—O(7)	2.477(2)	N(1)—C(2)	1.275(2)
Ca—N(1)	2.503(2)	N(2)—C(5)	1.269(3)
O(1)—C(1)	1.263(2)	C(1)—C(2)	1.624(2)
O(2)′—C(1)	1.247(2)	C(2)—C(3)	1.487(3)
O(3)—N(1)	1.392(2)	C(4)—C(5)	1.518(3)
O(3)—H(3)	0.77(3)	C(5)—C(6)	1.492(3)

Numbers in parentheses are estimated standard deviations in the least significant digits.

If the reaction is performed with less than a stoichiometric amount of NaPAO (e.g., one molar equivalent of NaPAO per metal ion), precipitation does not occur. Instead, slow growth of moderate-sized crystals happens over the course of several days. This may suggest that, under these conditions, complexes of the type $[M(PAO)]^+X^-$ form initially and these subsequently undergo ligand exchange with each other to yield the crystalline bis-PAO complexes (eq. [2]). Unfortunately, ^{13}C and ^1H NMR spectra of the reaction mixtures display only one set of resonances due to a single PAO environment that are not significantly different from those of the isolated bis-PAO salts. Thus, the presence of mono-PAO complexes has not been conclusively demonstrated.

[2] $2\ [CH_3C(=NOH)COOM]^+ \rightarrow [CH_3C(=NOH)COO]_2M + M^{2+}$

Crystal structure of $Ca(PAO)_2 \cdot (H_2O)$

The low solubility of the Group 2 PAO salts in water is in

© 1997 NRC Canada

Can. J. Chem. Downloaded from www.nrcresearchpress.com by 88.146.161.215 on 09/08/12
For personal use only.

Table 3. Interbond angles(deg) for $Ca(C_3H_4NO_3)_2 \cdot H_2O$.

O(1)-Ca-O(1)′	76.63(5)	O(1)′-Ca-N(1)	138.60(5)
O(1)-Ca-O(2)	135.71(4)	O(1)′-Ca-O(5)′	79.33(5)
O(1)-Ca-O(4)	75.24(4)	O(5)′-Ca-N(1)	134.28(5)
O(1)-Ca-O(5)	124.37(4)	Ca-O(1)-Ca″	103.37(5)
O(1)-Ca-O(5)′	135.59(5)	Ca-O(1)-C(1)	122.7(1)
O(1)-Ca-O(7)	71.23(5)	Ca″-O(1)-C(1)	122.8(1)
O(1)-Ca-N(1)	62.28(5)	Ca-O(2)-C(1)′	133.1(1)
O(2)-Ca-O(1)′	146.14(5)	N(1)-O(3)-H(3)	97(2)
O(2)-Ca-O(4)	97.67(5)	Ca-O(4)-C(4)	94.9(1)
O(2)-Ca-O(5)	74.63(5)	Ca-O(5)-Ca′	94.99(5)
O(2)-Ca-O(5)′	79.68(5)	Ca-O(5)-C(4)	90.1(1)
O(2)-Ca-O(7)	108.32(5)	N(2)-O(6)-H(6)	104(2)
O(2)-Ca-N(1)	73.68(5)	Ca-O(7)-H(7A)	104(2)
O(4)-Ca-O(1)′	79.34(5)	Ca-O(7)-H(7B)	104(2)
O(4)-Ca-O(5)	52.07(4)	Ca-N(1)-O(3)	121.4(1)
O(4)-Ca-O(5)′	135.26(5)	Ca-N(1)-C(2)	124.4(1)
O(4)-Ca-O(7)	146.32(5)	O(3)-N(1)-C(2)	113.8(2)
O(4)-Ca-N(1)	85.21(5)	O(6)-N(2)-C(5)	112.3(2)
O(5)-Ca-O(1)′	77.33(5)	O(1)-C(1)-C(2)	116.5(2)
O(5)-Ca-O(7)	155.50(5)	O(1)-C(1)-O(2)′	126.1(2)
O(5)-Ca-N(1)	121.31(5)	O(2)′-C(1)-C(2)	117.4(2)
O(7)-Ca-O(1)′	89.93(5)	N(1)-C(2)-C(1)	113.5(2)
O(7)-Ca-O(5)′	71.98(5)	N(1)-C(2)-C(3)	125.2(2)
O(7)-Ca-N(1)	81.96(5)	C(1)-C(2)-C(3)	121.3(2)
O(4)-C(4)-O(5)	122.9(2)	N(2)-C(5)-C(4)	115.2(2)
O(4)-C(4)-C(5)	116.6(2)	N(2)-C(5)-C(6)	124.9(2)
O(5)-C(4)-C(5)	120.6(2)	C(4)-C(5)-C(6)	119.9(2)

Numbers in parentheses are estimated standard deviations in the least significant digits.

Table 4. Characteristic IR vibrational frequencies (cm^{-1}) of PAO salts.

Compound	ν(C═N)	ν_{as} (COO)	ν_s(COO)	ν(N-O)
HPAO[a]	1652	1696	1420	1048
$NaPAO \cdot H_2O$[a]	1661	1599	1375	1008
$Ni(PAO)_2 \cdot 2H_2O$[b]	1670	1650		1060
$Mg(PAO)_2 \cdot 2H_2O$	1674	1647	1394	1045
$Ca(PAO)_2 \cdot H_2O$	1675	1640, 1617	1418, 1386	1038
$Sr(PAO)_2$	1674	1658, 1594	1393	1023
$Ba(PAO)_2$	1684	1617	1386	1013

[a]From ref. 5.
[b]From ref. 3.

sharp contrast with the high solubility of the Group 1 salts. This suggests that the alkaline earth salts are more polymeric than the alkali metal salts. The structure of $NaPAO \cdot (H_2O)$ was previously (5) found to be composed of chains of NaPAO five-membered metallocycles that are bridged by the carboxylate ions. The PAO ligand is bidentate and coordinates the sodium ions through the oxime nitrogen as well as one of the carboxylate oxygens. The crystal structure of the calcium bis(2-oximinopropionate) hydrate, $Ca(PAO)_2 \cdot (H_2O)$ (Fig. 1) reveals that much more extensive bridging in the solid state does occur for the calcium complex. The structure may be generally described as a three-dimensional polymer based on zigzag $Ca(PAO)_2$ units connected via the sharing of the carboxylate oxygen atoms between neighboring calcium atoms. The calcium ion is eight-coordinate (Fig. 2) with two of its coordination sites occupied by the oxime nitrogen and one of the carboxylate oxygen atoms from one of the PAO ligands. The so-formed N,O-chelate five-membered ring is similar to that observed in the NaPAO structure (5). The Ca—N(1) and Ca—O(1) bond distances are 2.503(2) and 2.513(1) Å, respectively, and are longer than those of the sodium derivative (2.440(2) and 2.490(2) Å, respectively (5)). The second PAO ligand coordinates as an O,O bidentate ligand through both oxygens of the carboxylate group to form a four-membered metallocycle. The Ca—O(4) and Ca—O(5) bond distances within the so-formed chelate are 2.451(1) and 2.557(1) Å, respectively. The inequivalency of these two bond lengths (approximately 0.1 Å) may be attributed to the fact that the O(5) oxygen atom also bridges to an adjacent calcium atom and is, therefore, three-coordinate. The bond distance for this oxygen atom to the second calcium atom, Ca—O(5)′, is 2.371(1) Å and is, therefore, even shorter than the Ca—O(5) bond length. The calcium–oxygen bond distances for the O, O-coordinated PAO ligand, Ca—O(4), Ca—O(5), and Ca—O(5)′, are similar to those found in calcium acetate monohydrate (2.450(2), 2.460(3), and 2.321(3) Å for the analogous bond distances) in which the carboxylate ligand is also coordinated as an O,O chelate through the carboxylate group (14). Two other coordination sites of the calcium ions in $Ca(PAO)_2 \cdot (H_2O)$ are occupied by bridging carboxylate oxygen atoms from PAO ligands coordinated as N,O chelates on two adjacent calcium centers, with the Ca—O(2) and Ca—O(1)′ bond distances being 2.465(1) and 2.387(1) Å. Each of the PAO ligands that form the N,O chelates in $Ca(PAO)_2 \cdot (H_2O)$ is linked to two other calcium centers via the oxygen atoms of its carboxylate group. One of these, the O(1)-type oxygen, bridges two calcium atoms in a similar fashion to O(5).

The coordination sphere of the calcium atom is completed by a solvent water molecule with the Ca—O(7) bond distance of 2.477(2) Å. This water molecule appears to be hydrogen-bonded to the nonbridging carboxylate oxygen atom and to the uncoordinated nitrogen atom of O,O-chelated ligands on adjacent formula units. Thus, the separation O(4)—H(7A)″ of the water molecule bound to Ca″ (Fig. 1) is 1.87(3) Å with an O(4)-H(7A)″-O(7) angle of 164(2)° while the separation N(2)—H(7B)′ of the water molecule bound to Ca′ (Fig. 1) is 1.94(3) Å with an N(2)-H(7B)′-O(7) angle of 172(3)°. In addition, the water molecule is hydrogen-bonded to the hydroxyl group O(6)—H(6) of an adjacent formula unit. Here the O(7)—H(6)′ separation is 1.90(3)Å with an O(7)-H(6)′-O(6)′ angle of 169(3)°.

Presumably, the other alkaline earth salts of PAO also display structures that are highly bridged. However, their X-ray powder diffraction patterns differ from that of $Ca(PAO)_2 \cdot (H_2O)$ and it may be concluded that they are not isomorphous although they may be isostructural.

Spectroscopic characterization of alkaline earth metal PAO salts

Several characteristic infrared vibrational frequencies of the PAO salts are summarized in Table 4. The assignment of these

© 1997 NRC Canada

Fig. 1. A perspective view of a portion of the chain of $Ca(C_3H_4NO_3)_2 \cdot H_2O$ units. Thermal ellipsoids are drawn at the 50% probability level except for non-hydrogen atoms. The methyl hydrogen atoms are omitted for clarity.

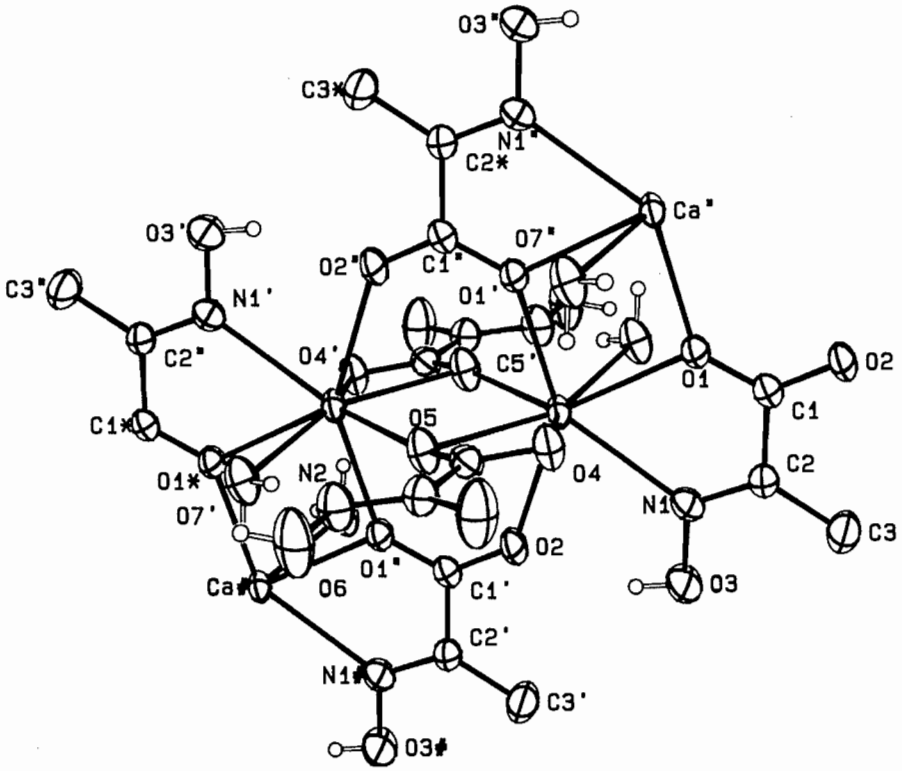


Fig. 2. A view of the coordination about calcium together with the unique ligands. Thermal ellipsoids for the non-hydrogen atoms are drawn at the 65% probability level.

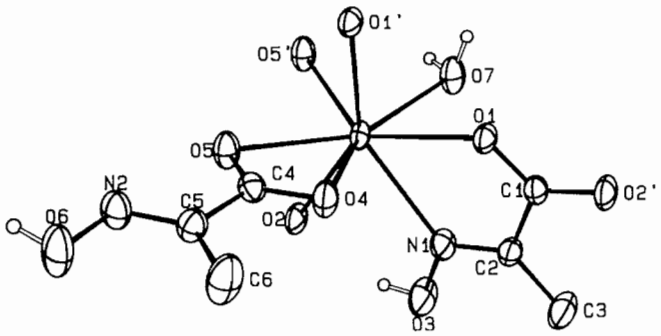


Table 5. ^{1}H and ^{13}C NMR chemical shifts of PAO salts.

	^{1}H NMR		^{13}C NMR		
Compound	CH_3	OH[a]	CH_3	C=N	COO
HPAO	1.88	12.28	10.7	148.9	166.0
$NaPAO \cdot H_2O$	1.84	12.12	11.8	156.4	171.3
$Mg(PAO)_2 \cdot 2H_2O$	1.87	12.79	11.1	152.8	167.2
$Ca(PAO)_2 \cdot H_2O$	1.83		11.0	153.0	166.1
$Sr(PAO)_2$	1.85		11.9	156.8	171.8
$Ba(PAO)_2$	1.83		11.7	154.6	167.7

[a]These chemical shifts were observed in dry d_6-DMSO and are attributable to the oxime protons and those of the waters of crystallization, which undergo rapid exchange.

frequencies is based on literature data for previously reported PAO complexes (3, 4) that utilized ^{15}N isotopic labelling to identify these bands. It may be noted that the IR bands of the alkaline earth PAO complexes more closely resemble those reported for the transition metal complexes than do those of NaPAO. One feature of the IR spectra of the PAO complexes is the significant lowering of the vibrational frequencies of the asymmetric carboxylate stretch by 49–102 cm^{-1} compared to that of the parent acid. These changes in this stretching frequency may be attributed to the deprotonation and delocalization of the negative charge in the carboxylate as well the coordination of the carboxylate to the metal centers and is typical for metal carboxylates (15). The $Ca(PAO)_2 \cdot (H_2O)$ salt displays two bands attributable to each of the asymmetric stretch and symmetric stretch of the carboxylate, reflecting the fact that there are two types of PAO ligand in the solid state. One set, ν_{as} = 1617 cm^{-1} and ν_s = 1386 cm^{-1}, may be assigned to the N,O-chelated PAO ligand due to their similarity to the frequencies of the nickel and sodium salts that contain the same type of chelate. The other set of vibrational frequencies, ν_{as} = 1640 cm^{-1} and ν_s = 1418 cm^{-1}, may then be assigned to the O,O-chelated PAO ligand. Remarkably, the split between ν_{as} and ν_s is approximately the same for the bridging carboxylate (231 cm^{-1}) and the chelating carboxylate (222 cm^{-1}). Usually, this difference is markedly larger for a bridging carboxylate versus a chelating one (16). In this case, the fact that a clear-cut difference is not observed may be due to the fact that the carboxylates are multiply-bridging. Indeed, the observed differences between ν_{as} and ν_s are comparable to those observed for bridging acetates (16).

The coordination of the nitrogen atom of the oximino

Can. J. Chem. Downloaded from www.nrcresearchpress.com by 88.146.161.215 on 09/08/12
For personal use only.

© 1997 NRC Canada

Table 6. Decomposition temperatures of PAO salts.

Group 1 metal	Ionic radius (Å)[a]	Decomposition temperature (°C)[b]	Group 2 metal	Ionic radius (Å)[a]	Decomposition temperature (°C)[b]
Li	0.68	131	Mg	0.66	188
Na	0.97	122	Ca	0.99	166
K	1.33	111	Ba	1.34	144

[a]From ref. 17.
[b]From ref. 5.

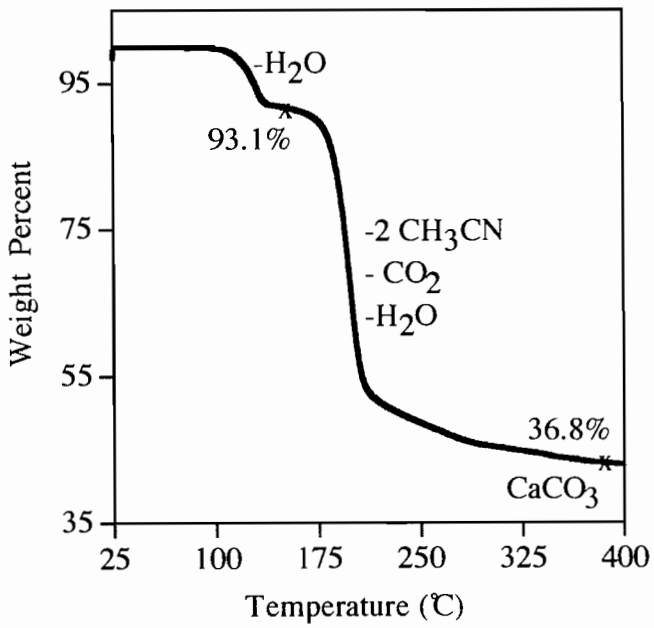
Can. J. Chem. Downloaded from www.nrcresearchpress.com by 88.146.161.215 on 09/08/12
For personal use only.

moiety in the PAO complexes of alkaline earth metals does not significantly affect the vibrational frequency corresponding to the C═N stretch, and is consistent with the data obtained in previous studies (3, 4). The vibrational frequencies attributable to the N-O stretch are lowered by 3–35 cm^{-1} in the Group 2 metal salts of PAO from that observed for the parent acid. This trend is opposite to that observed for transition metal derivatives of PAO, in which an increase in these frequencies was observed (3, 4) but is in the same direction as that observed for the alkali metal PAO salts (5). This difference may be a result of the weak coordination of the nitrogen atom of the oximino group in the alkali and alkaline earth metal salts, as indicated by the elongated Na—N and Ca—N bond distances in $NaPAO{\cdot}H_2O$ (5) and $CaPAO_2{\cdot}H_2O$. It is interesting to note that the frequency of the N-O stretch decreases almost linearly down the group. This phenomenon may be due to either the increase in size of the metal cations or the decrease in electronegativity as the group is descended.

The ^1H and ^{13}C NMR spectral data for these compounds are summarized in Table 6. The ^1H NMR spectra of the PAO salts in D_2O display a single resonance that may be attributed to methyl protons. The chemical shift for these protons is within the range of 1.83 to 1.87 ppm and are similar to those of the alkali metal salts (5). These chemical shifts are not significantly different from the corresponding one for the parent acid since the methyl protons are remote from the carboxylic acid moiety of the PAO ligand and are relatively unaffected by deprotonation. The ^{13}C NMR spectra of the PAO ligands are more indicative in terms of the changes in the local electron density in the ligand as a result of its deprotonation. As expected, the methyl carbon, with a chemical shift in the range 11.0–11.9 ppm, is less affected by the deprotonation and its signal is shifted only about 0.4–1.0 ppm downfield from the corresponding signal of the parent acid (10.7 ppm). The signals of the carbon atoms of the oximino and carboxylate groups undergo more significant downfield shifts from the parent acid upon removal of the proton (3.9–7.9 ppm for C═N and 0.1–11.8 ppm for COO). Since only one set of resonances is observed for $CaPAO_2{\cdot}(H_2O)$, it may be concluded that, as might be expected, the solid state structure is completely degraded upon dissolution in water. The degree of dissociation of individual $M(PAO)_2$ units in solution is difficult to assess but the significant variation of the chemical shifts of the various salts and their deviation from those of NaPAO (which is completely dissociated in water) suggest that complexation does occur to some degree.

The solid state ^{13}C NMR CPMAS spectrum of $CaPAO_2{\cdot}(H_2O)$, on the other hand, shows resolved peaks due to the two different carboxylates: 171.6 and 168.6 ppm for the carboxylate carbon, 153.5 ppm for the oxime carbon, and 12.1 and 11.4 ppm for the methyl protons. The corresponding resonances in NaPAO are 171.7, 153.5, and 12.2 (5). Due to the strong similarity to the NaPAO spectrum, the signals at 171.6 and 12.2 ppm may be assigned to the N,O-chelated PAO ligand while those at 168.6 and 11.4 may be attributed to the O,O-chelated ligand. Unfortunately, due to their high electronic asymmetry, the oxime carbons are broad and are unresolved.

Fig. 3. Thermogravimetric analysis (TGA) trace for $Ca(PAO)_2{\cdot}H_2O$ in dry air with a heating rate of 2°C/min.



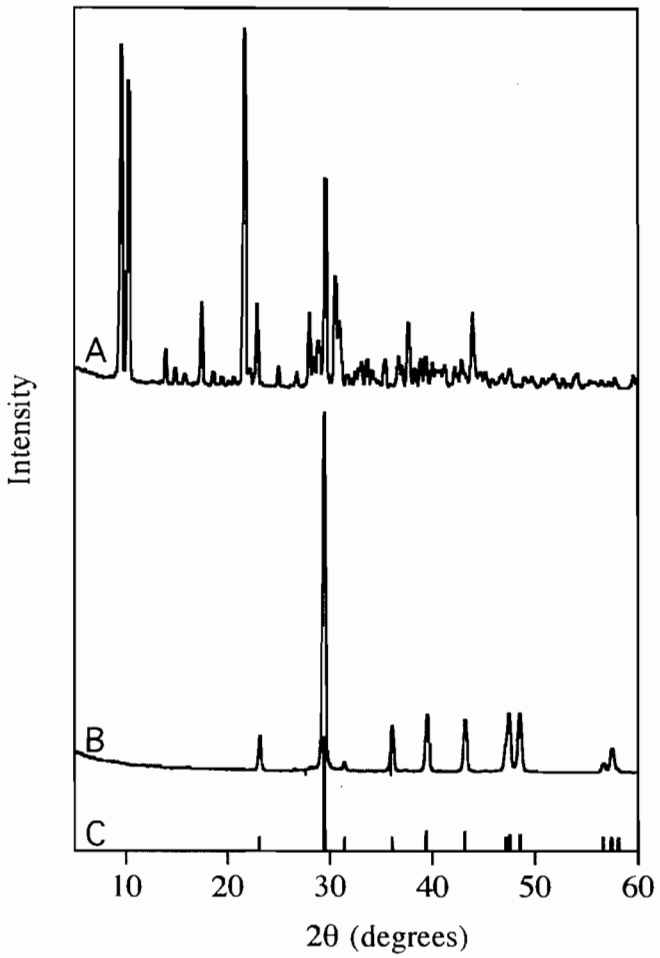
Thermal behaviour of alkaline earth metal PAO salts

The thermogravimetric analysis of $Ca(PAO)_2{\cdot}(H_2O)$ (Fig. 3) exhibits two weight-loss steps. The lower temperature weight change with an onset at 63°C is endothermic and corresponds to the dehydration of the sodium salt. The second weight loss occurs at 166°C and is exothermic. Simultaneous analysis of the off-gases at this temperature by mass spectroscopy indicates that decomposition of the anion is occurring to yield the expected products: water, acetonitrile, and carbon dioxide. The metal-containing residue from this decomposition has a mass that corresponds to formation of calcium carbonate. The

© 1997 NRC Canada

Can. J. Chem. Downloaded from www.nrcresearchpress.com by 88.146.161.215 on 09/08/12
For personal use only.

Fig. 4. X-ray powder diffraction patterns for: (*A*) $Ca(PAO)_2 \cdot H_2O$, (*B*) $Ca(PAO)_2 \cdot H_2O$ pyrolyzed at 200°C for 12 h, and (*C*) calcite.[4]

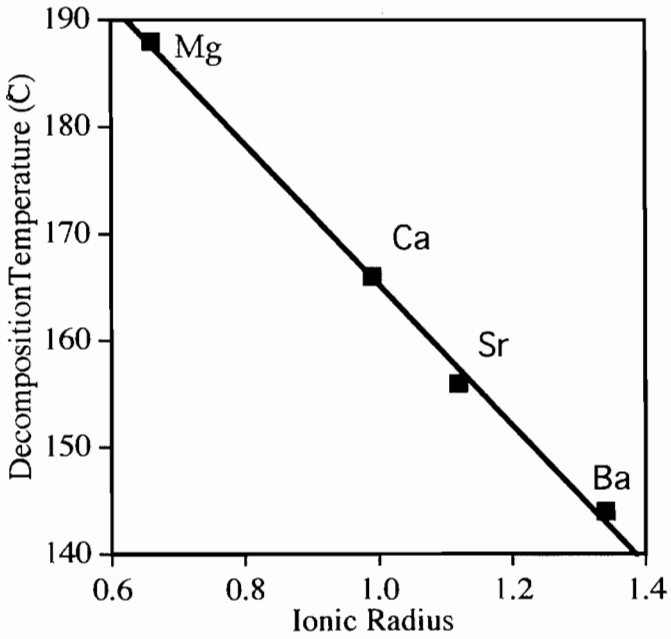


X-ray diffraction pattern of a bulk sample of $Ca(PAO)_2 \cdot (H_2O)$ pyrolyzed at 200°C (Fig. 4) confirms this identification since it matches that reported for calcite.[4]

The results of the thermal analysis of the other PAO salts were similar to that of the calcium salt with the exception of the barium and strontium salts, which do not exhibit a dehydration step since they do not contain waters of crystallization. Like the alkali metal salts, the thermal decomposition temperatures of the alkaline earth metal salts show a surprising decrease with increasing ionic radii of the metal ions (Fig. 5). This is contrary to the predictions of the ionic model based on lattice enthalpies for small cation/large anion lattice enthalpies (17). Indeed, the stabilities of the PAO salts follow a trend opposite to that observed for the alkaline earth metal carbonates. Typically, a failure of the ionic model is attributed to effects of covalent bonding. In the case of the PAO salts the ring strain in the five-membered metallocycles may account for the observed trend in decomposition points. Since the chelated ligand has a small bite angle, the ring strain should increase with increasing ionic radii of the cations and thus lead to destabilization of the complexes in accord with the observed

[4] Powder Diffraction File No. 05-0586. JCPDS (1995).

Fig. 5. Decomposition temperatures versus the ionic radius of alkaline earth metal PAO salts.



experimental data. However, a comparison of the decomposition temperatures of the Group 2 salts to those of the Group 1 salts with similar atomic radii shows that the alkaline earth salts are more stable and have decomposition temperatures 33–57°C higher than their alkali metal counterparts (Table 6). Again, this is contrary to the ionic model, which predicts that the decomposition of the salt with the more highly charged cation will occur at the lower temperature (17). Finally, it should be noted that the XRD patterns indicate that the salts are not isomorphous, so that the decomposition temperatures may also be affected to some degree by differences in the crystalline lattices.

Acknowledgements

We thank the Louisiana Board of Regents for support through the Louisiana Educational Quality Support Fund Contract No. LEQSF(1993-96)-RD-A-26. We also express gratitude to the National Science Foundation, which provided funds for the purchase of the solid state NMR spectrometer used in this investigation (Grant DMR-9407011). The assistance with instrument operation provided by Ray Hoff is also gratefully acknowledged.

References

1. A.W. Apblett, J. Lei, and G.D. Georgieva. Mater. Res. Soc. Symp. Proc. **271**, 77 (1992).
2. A.W. Apblett and G.D. Georgieva. Phosphorus, Sulfur, Silicon, and Relat. Elem. **93–94**, 479 (1994).
3. V.V. Slopenko, R.D. Lampeka, T.Y. Sliva, and D.I. Sakhov. Ukr. Khim. Zh. (Russ. Ed.), **56**, 675 (1990).
4. R.D. Lampeka, V.V. Slopenko, T.Y. Sliva, and K. Khennig. Ukr. Khim. Zh. (Russ. Ed.), **54**, 675 (1988).
5. A.W. Apblett, G.D. Georgieva, and J.T. Mague. Inorg. Chem. In press.

© 1997 NRC Canada

6. Y.A. Simonov, T.Y.Sliva, M.D. Mazus, A.A. Dvorkin, and R.D. Lampeka. Russ. J. Inorg. Chem. **34**, 489 (1989).
7. A.A. Dvorkin, Y.A. Simonov, T.Y. Sliva, R.D. Lampeka, M.D. Mazus, and V.V. Skopenko. Russ. J. Inorg. Chem. **34**, 489 (1989).
8. M. Kathayal and P.R. Singh. Current. Sci. **31**, 373 (1962).
9. A.W. Apblett, G.D. Georgieva, J.T. Mague, and L.E. Reinhardt. Ceram. Trans. In press.
10. A. Ahmad and I.D. Spenser. Can. J. Chem. **39**, 1340 (1961).
11. J.T. Mague and C.L. Lloyd. Organometallics, **7**, 983 (1988).
12. (*a*) D.T. Cromer and J.T. Waber. International tables for X-ray crystallography. Vol. IV. The Kynoch Press, Birmingham, England. 1974. Table 2.2B; (*b*) D.T. Cromer. International tables for X-ray crystallography. Vol. IV. The Kynoch Press, Birmingham, England. 1974. Table 2.3.1.
13. MolEN. An interactive structure solution procedure. Enraf–Nonius, Delft, The Netherlands. 1990.
14. B.E. Klop, A. Schouten, P. Van Der Sluis, and A.L. Spek. Acta. Crystallogr. Sect. C: Cryst. Struct. Commun. **C40**, 51 (1984).
15. A.L. Smith. Applied infrared spectroscopy — fundamentals, techniques and analytical problem-solving. *In* Analysis: a series of monographs on analytical chemistry and its applications. Vol. 54. *Edited by* P.J. Elving, J.D. Winefordner, and I.M. Kolthoff. John Wiley & Sons, New York. 1979.
16. A.I. Grigorev. Russ. J. Inorg. Chem. **8**, 409 (1963).
17. D.F. Shriver, P.W. Atkins, and C.H. Langford. Inorganic chemistry. W.H. Freeman & Co., New York. 1990. pp. 123–133.

Can. J. Chem. Downloaded from www.nrcresearchpress.com by 88.146.161.215 on 09/08/12
For personal use only.

© 1997 NRC Canada

Synthesis and characterization of the mixed valence Cu(I)/Cu(II) 3,5-bis(trifluoromethyl)-pyrazolate complex, $[Cu(II)_2Cu(I)(F_6dmpz)_5]$

Martin K. Ehlert, Alan Storr, David A. Summers, and Robert C. Thompson

Abstract: The reaction of molten 3,5-bis(trifluoromethyl)pyrazole (F_6dmpzH) with copper metal shot under an atmosphere of dioxygen yields the green trimetallic mixed valence $[Cu(II)_2Cu(I)(F_6dmpz)_5]$. Crystals of $[Cu(II)_2Cu(I)(F_6dmpz)_5]$ are triclinic, a = 9.0557(2), b = 9.6164(2), c = 11.8874(3) Å, α = 105.406(1)°, β = 112.317(1)°, γ = 90.662(1)°, Z = 1, space group $P\bar{1}$. The crystal structure was solved by direct methods and was refined by full-matrix least-squares procedures to a final R value of 0.0538 for 2591 reflections with $I \geq 2\sigma(I)$. Magnetic susceptibility studies over the range 2–300 K reveal strong antiferromagnetic exchange coupling between the two copper(II) centers. Fits of the magnetic data to the Bleaney–Bowers equation for two interacting S = ½ centers gives the exchange coupling constant $J = -235$ cm^{-1}.

Key words: trimetallic, copper, 3,5-bis(trifluoromethyl)pyrazolates, X-ray structure, antiferromagnetism.

Résumé : La réaction du 3,5-bis(trifluorométhyl)pyrazole (F_6dmpzH) avec du cuivre métallique projeté sous une atmosphère de dioxygène conduit à un complexe trimétallique vert de valence mixte, $[Cu(II)_2Cu(I)(F_6dmpzH)_5]$. Les cristaux du $[Cu(II)_2Cu(I)(F_6dmpzH)_5]$ sont tricliniques, groupe d'espace $P\bar{1}$, a = 9,0557(2), b = 9,6164(2), c = 11,8874(3) Å, α = 105,406(1)°, β = 112,317(1)°, et γ = 90,662(1)°, Z = 1. On a résolu la structure par des méthodes directes et on l'a affinée par la méthode des moindres carrés jusqu'à une valeur finale de R de 0,0538 pour 2591 réflexions avec $I \geq 2\sigma(I)$. Des études de susceptibilité magnétique à des températures allant de 2 à 300 K ont permis de mettre en évidence un important couplage d'échange antiferromagnétique entre les deux centres de cuivre(II). Un ajustement des données magnétiques à l'aide de l'équation de Bleaney–Bowers pour deux centres interagissant avec S = ½ permet de déterminer la constante de couplage d'échange, $J = -235$ cm^{-1}.

Mots clés : trimétallique, cuivre, 3,5-bis(trifluorométhyl)pyrazolates, structures, diffraction des rayons X, antiferromagnétisme.

[Traduit par la rédaction]

Introduction

Pyrazolate ligands have been used extensively in building polynuclear transition metal systems and this burgeoning field has recently been reviewed (1). Binary copper(II) pyrazolates and substituted pyrazolates have been shown to adopt structures in which the copper ions are doubly bridged by pyrazolate ligands to form extended linear chain polymers (2–5). The compounds show relatively strong antiferromagnetic coupling with values of J, the exchange coupling constant, in the range -58 to -105 cm^{-1}. These values vary with the substitution on the pyrazolate bridging ligands and attempts have been made to correlate structural variations with these numbers. An extension of these earlier studies to include the 3,5-bis(trifluoromethyl)pyrazolate, F_6dmpz^-, bridging ligand, with highly electron-withdrawing trifluoromethyl groups on the heterocyclic rings, is now reported. Interestingly the anticipated polymeric species, $[Cu(F_6dmpz)_2]_x$, was not obtained but instead the dark-green mixed Cu(I)/Cu(II) compound, $[Cu(II)_2Cu(I)(F_6dmpz)_5]$, was isolated. An X-ray structure determination of this complex shows the molecular unit to consist of a triangular arrangement of three copper ions held together by bridging pyrazolate ligands. The magnetic behaviour of the complex over the 2–300 K temperature range is discussed.

Received November 11, 1996.

M.K. Ehlert, A. Storr,[1] D.A. Summers, and R.C. Thompson.[1]
Department of Chemistry, University of British Columbia, 2036 Main Mall, Vancouver, BC V6T 1Z1, Canada.

[1] Authors to whom correspondence may be addressed. Telephone: R.C. Thompson: (604) 822-4979, A. Storr: (604) 822-3962. Fax: (604) 822-2847. E-mail: thompson@chem.ubc.ca, storr@chem.ubc.ca

Experimental

3,5-Bis(trifluoromethyl)pyrazole, F_6dmpzH, was prepared by the method described by Trofimenko (6).

Synthesis of $Cu_3(F_6dmpz)_5$

Clean copper shot (1.954 g, 30.75 mmol) was mixed with F_6dmpzH (1.00 g, 4.90 mmol) and heated, without stirring, under an atmosphere of dioxygen at 95–105°C for 4 days (melting point of F_6dmpzH, 79–81°C). At the cessation of the reaction a dark-green material had formed. Excess F_6dmpzH

© 1997 NRC Canada

Can. J. Chem. Downloaded from www.nrcresearchpress.com by 88.146.161.215 on 09/08/12
For personal use only.

Can. J. Chem. Downloaded from www.nrcresearchpress.com by 88.146.161.215 on 09/08/12
For personal use only.

was sublimed from the product by heating at 60°C under vacuum and finally the dark-green compound was isolated by physical separation from the copper shot. Approximately 0.2 g of $Cu_3(F_6dmpz)_5$ was collected (71% yield based on amount of copper reacted). Anal. calcd. for $C_{25}H_5Cu_3F_{30}N_{10}$: C 24.91, H 0.42, N 11.62; found: C 25.01 H 0.42, N 11.68%.

$Cu_3(F_6dmpz)_5$ melts at 236°C without decomposition and is appreciably volatile at this temperature even at 1 atmosphere (101.3 kPa). It is soluble in dry solvents with a wide range of polarities but is very reactive towards water in solution, the initial green-coloured solution turning blue with the deposition of a purple solid. Upon prolonged exposure to moist air, the compound slowly changes to a purple material. All attempts to identify the purple decomposition product of $Cu_3(F_6dmpz)_5$ have been unsuccessful.

Spectroscopic studies

The electronic spectrum of a Nujol mull of $Cu_3(F_6dmpz)_5$ contained between quartz plates was obtained using a Varian Instruments Cary 5 UV / visible / NIR spectrophotometer. The spectrum consists of an asymmetric absorption band with a maximum at ~14 000 cm^{-1} with a shoulder to higher wave numbers.

An IR spectrum of a KBr pellet of the $Cu_3(F_6dmpz)_5$ was obtained using a Bomem MB-100 spectrometer. The broad band at ~3000 cm^{-1} attributed to the N-H function of the F_6dmpzH starting material was notably absent from the spectrum.

The low-resolution electron impact ionization spectrum of $Cu_3(F_6dmpz)_5$ was obtained using a Kratos MS50 mass spectrometer. The spectrum exhibits a parent ion peak, P^+, at *m/e* ~1206 along with strong signals due to ions arising from consecutive loss of two F_6dmpz ligands, L, from the parent species at *m/e* ~1003 ($P - L^+$) and *m/e* ~800, ($P - 2L^+$). The intensities of the individual lines in these multi-line signals are those expected from the presence of three Cu atoms and the naturally occurring isotopic abundance for the element.

Single crystal X-ray diffraction

Macroscopic well-formed crystals of $Cu_3(F_6dmpz)_5$ were prepared by sublimation of the bulk product under vacuum. Crystal data, data collection, and solution and refinement details are summarized in Table 1.

A single crystal of the compound was attached to a glass fiber and mounted on the Siemens SMART system for a data collection at 173 (2) K. Final cell constants were calculated from a set of 4018 strong reflections from the actual data collection.

The space group $P\bar{1}$ was determined based on systematic absences and intensity statistics.[2] A successful direct-methods solution was calculated that provided most non-hydrogen atoms from the *E*-map. Several full-matrix least-squares / difference Fourier cycles, which located the remainder of the non-hydrogen atoms, were performed. All non-hydrogen atoms were refined with anisotropic displacement parameters unless stated otherwise. All hydrogen atoms were placed in ideal positions and refined as riding atoms with relative ($1.2(U_{iso}$ host carbon)) isotropic displacement parameters.

The complex is disordered by fitting in two possible ways in the lattice. Two half-occupied complexes are related to each other by an inversion center. It is unusual for this to occur, but the criterion for this type of disorder exists with this complex. The equatorial plane contains three Cu atoms in the shape of an isosceles triangle. The two differing Cu···Cu nonbonded distances are due to the presence of one Cu(I) and two Cu(II) ions in the complex. Three F_6dmpz^- groups are equatorially bonded to the Cu atoms. The two Cu atoms in the +2 oxidation state are bridged by two additional F_6dmpz^- groups above and below the equatorial plane. A careful inspection shows that an inversion operation can place the CF_3 groups in the equatorial plane on top of the original ones. The backbones of the two axial F_6dmpz^- groups are superimposed when both images are overlayed. Therefore, regardless of which way the complex fits in the space it looks roughly the same to its environment. To make a more sensible result, 740 restraints were applied to the model. Ten pairs of atoms are close enough to each other to constrain the pairs to a single anisotropic displacement parameter. All F_6dmpz^- groups were restrained to similar bond lengths with the SHELXTL SAME restraint.[2]

Data collection and structure solution were conducted at the X-Ray Crystallographic Laboratory, 160 Kolthoff Hall, Chemistry Department, The University of Minnesota. All calculations were performed using SGI INDY R4400-SC or Pentium computers using the SHELXTL v5.0 suite of programs.

Final atomic coordinates and equivalent isotropic displacement parameters are given in Table 2 and selected bond lengths and angles appear in Tables 3 and 4, respectively. Anisotropic thermal parameters, torsion angles, hydrogen coordinates and isotropic displacement parameters, and least-square planes, together with tables of all bond distances and bond angles and a fully labeled molecular diagram are included as supplementary material.[3]

Magnetic susceptibility studies

Magnetic susceptibilities were measured using a Quantum Design (MPMS) SQUID magnetometer. The sample holder and procedures involving the use of the equipment were described previously (7). Magnetic susceptibilities were corrected for the background signal of the sample holder and for diamagnetic susceptibilities of all atoms (Cu^+, −14; Cu^{2+}, −11; F_6dmpz^-, −82). All corrections are in units of 10^{-6} cm^3mol^{-1}.

Susceptibility versus temperature behaviour (2 to 300 K) was measured at 1.0 and 2.0 T. Magnetization measurements at applied fields ranging from 0 to 5.5 T were made at 2, 50, 100 and 300 K.

[2] SHELXTL-Plus v5.0, Siemens Industrial Automation, Inc. Madison, Wis.

[3] Supplementary material mentioned in the text may be purchased from: The Depository of Unpublished Data, Document Delivery, CISTI, National Research Council Canada, Ottawa, Canada K1A 0S2. Tables of atomic coordinates, bond distances and angles, and a molecular diagram have also been deposited with the Cambridge Crystallographic Data Centre, University Chemical Laboratory, 12 Union Road, Cambridge, CB2 1EZ, UK.

© 1997 NRC Canada

Can. J. Chem. Downloaded from www.nrcresearchpress.com by 88.146.161.215 on 09/08/12
For personal use only.

Table 1. Crystallographic data, data collection, and solution and refinement for $Cu_3(F_6dmpz)_5$.[a]

Formula	$C_{25}H_5Cu_3F_{30}N_{10}$
fw	1206.01
Color, habit	Green, block
Crystal size, mm	0.30 × 0.20 × 0.11
Crystal system	Triclinic
Space group	$P\bar{1}$
a, Å	9.0557(2)
b, Å	9.6164(2)
c, Å	11.8874(3)
α, deg	105.406(1)
β, deg	112.317(1)
γ, deg	90.662(1)
V, Å^3	915.88(4)
Z	1
ρ_{calc}, g/cm^3	2.187
Absorption coefficient, mm^{-1}	1.919
F(000)	582
Diffractometer	Siemens SMART Platform CCD
Radiation	Mo-K_α
Wavelength	λ = 0.71073 Å
Temperature, K	173 (2)
θ range for data collection, °	1.94–25.09
Index ranges	$-10 \le h \le 9$, $-11 \le k \le 11$, $0 \le l \le 14$
Total reflections	5493
Unique reflections	3181 (R_{int} = 0.0282)
System used	SHELXTL-v5.0
Solution	Direct methods
Refinement method	Full-matrix least squares on F^2
Weighting scheme	$w = [\sigma^2(F_o^2) + (AP)^2 + (BP)]^{-1}$, where $P = (F_o^2 + 2Fc^2)/3$, A = 0.0982, and B = 0.6479
Absorption corrections	SADABS (Sheldrick, 1996)
Transmission factors	0.675–1.000
Data / restraints / parameters	3181 / 740 / 547
R indices ($I > 2\sigma(I)$ = 2591)	*R*1 = 0.0538, *wR*2 = 0.1477
R indices (all data)	*R*1 = 0.0654, *wR*2 = 0.1570
Goodness-of-fit on F^2	1.084
Largest diff. peak and hole, e Å^{-3}	0.768 and −0.743

[a]Some equations of interest: $R_{int} = \sum|F_o^2 - \langle F_o^2\rangle|/\sum|F_o^2|$, $R1 = \sum||F_o| - |F_c||/\sum|F_o|$, $wR2 = [\sum[w(F_o^2 - F_c^2)^2]/\sum[w(F_o^2)^2]]^{1/2}$ where $w = q/\sigma^2(F_o^2) + (a*P)^2 + b*P$, GoF = $S = [\sum[w(F_o^2 - F_c^2)^2]/(n-p)]^{1/2}$.

Results and discussion

Attempts to prepare the binary copper(II) 3,5-bis(trifluoromethyl)pyrazolate polymer, $[Cu(F_6dmpz)_2]_x$, by the reaction of copper metal shot with 3,5-bis(trifluoromethyl)pyrazole under an atmosphere of dioxygen at ~100°C led to the formation of a dark-green material of composition $Cu_3(F_6dmpz)_5$. As this synthetic approach had led to the formation of polymeric materials with other pyrazolate ligands (2–5) it was somewhat surprising that no evidence of polymer formation was observed here. Infrared studies established that the green product was devoid of any residual N-H functionalities and mass spectral analysis showed the parent ion, P^+, cluster as the highest *m/e* signals in the spectrum, with strong signals arising from the ions resulting from the consecutive loss of two F_6dmpz ligands $P - L^+$ and $P - 2L^+$.

An X-ray crystal structure determination of well-formed crystals of $Cu_3(F_6dmpz)_5$ shows the three copper ions (two Cu(II) and one Cu(I)) to be arranged in an isosceles triangle with each side of the triangle being occupied by an exobidentate F_6dmpz^- ligand. The two Cu(II) ions, which form the short base of the triangle, are bridged by two additional F_6dmpz^- ligands, one above and one below the trigonal planar array. The molecular arrangement with a selected atom numbering scheme is shown in Fig. 1. The structural array adopted is similar to those arrangements found in the all Cu(I) trimers of formulas $[Cu(tmpz)]_3$ and $[Cu(dmpz)]_3$ (7, 8) with the significant difference arising from the two types of Cu ions found in the present structure. These differences are exemplified by comparing the nonbonded Cu···Cu distances in the trigonal structures. In the title compound the unique Cu(II)···Cu(II) distance is 2.975 Å (sum of van der Waals radii for Cu is 2.86 Å (9)) with the Cu(II)···Cu(I) distances being much longer at 3.236 and 3.250 Å. In the all-Cu(I) trimer species, $[Cu(tmpz)]_3$ (8), the Cu···Cu distance is 3.212 Å and in $[Cu(dmpz)]_3$ (7) the distance is 3.218 Å. Two other structures having the basic central trigonal planar array of Cu ions bridged by pyrazolate ions have been reported. Both are all-Cu(II) systems. In

© 1997 NRC Canada

Can. J. Chem. Downloaded from www.nrcresearchpress.com by 88.146.161.215 on 09/08/12
For personal use only.

Table 2. Atomic coordinates ($\times 10^4$) and equivalent isotopic displacement parameters (Å $\times 10^3$) for $Cu_3(F_6dmpz)_5$.[a]

Atom	*x*	*y*	*z*	*U*(eq)
Cu(1)	4864(1)	6397(1)	6192(1)	29(1)
Cu(2)	4169(1)	4927(1)	3473(1)	29(1)
Cu(3)	6123(1)	3267(1)	5538(1)	32(1)
N(11)	2661(8)	4135(8)	4094(6)	30(1)
N(12)	2968(7)	4801(7)	5343(5)	28(1)
F(11)	−622(20)	1458(22)	1930(20)	62(4)
F(12)	792(21)	2922(17)	1527(17)	62(4)
F(13)	1733(23)	1095(18)	2115(19)	72(4)
C(11)	833(22)	2146(21)	2300(13)	48(1)
C(12)	1461(24)	3043(30)	3662(13)	36(3)
C(13)	911(43)	3060(61)	4585(21)	41(2)
C(14)	1979(26)	4044(32)	5663(14)	41(3)
C(15)	2073(25)	4428(25)	6981(15)	46(2)
F(14)	883(22)	3753(23)	7082(20)	90(6)
F(15)	2138(32)	5854(20)	7490(22)	54(4)
F(16)	3406(25)	4057(31)	7789(19)	69(5)
N(21)	6434(7)	5979(7)	4461(6)	30(1)
N(22)	6762(8)	6606(8)	5722(6)	32(1)
F(21)	9407(19)	5830(22)	3100(19)	66(4)
F(22)	6881(27)	5904(29)	2138(21)	69(5)
F(23)	7741(33)	4031(18)	2691(22)	48(3)
C(21)	7943(26)	5471(24)	3058(16)	46(2)
C(22)	7836(26)	6087(32)	4304(14)	41(3)
C(23)	8988(41)	6962(62)	5404(21)	41(2)
C(24)	8348(24)	7114(30)	6289(13)	36(3)
C(25)	9107(22)	7886(22)	7683(14)	48(1)
F(24)	10396(22)	8764(24)	7960(22)	89(7)
F(25)	8092(20)	8615(19)	8106(16)	63(4)
F(26)	9584(22)	6949(21)	8353(19)	64(4)
N(31)	3326(9)	6803(7)	3770(8)	32(2)
N(32)	3672(8)	7501(7)	5029(6)	30(1)
F(31)	3082(9)	6990(12)	1301(6)	107(3)
F(32)	1024(10)	5891(8)	1163(6)	91(2)
F(33)	1059(18)	8093(12)	1175(8)	135(6)
C(31)	1879(21)	7166(17)	1680(12)	47(5)
C(32)	2473(9)	7637(8)	3093(6)	33(2)
C(33)	2287(10)	8886(8)	3889(7)	41(2)
C(34)	3045(10)	8734(8)	5068(7)	36(2)
C(35)	3274(19)	9773(15)	6322(13)	56(2)
F(34)	2438(29)	10815(19)	6240(13)	220(6)
F(35)	4743(13)	10211(15)	7087(9)	204(8)
F(36)	2724(11)	9187(10)	6995(7)	110(3)
N(41)	5701(7)	2411(6)	3814(6)	32(1)
N(42)	4871(8)	3036(7)	2898(6)	35(1)
F(41)	8292(8)	845(8)	4918(8)	98(3)
F(42)	6179(8)	−554(10)	4323(10)	122(4)
F(43)	7554(27)	−754(18)	3243(12)	220(6)
C(41)	6980(18)	173(14)	3923(14)	56(2)
C(42)	6030(10)	1123(9)	3201(8)	42(2)
C(43)	5483(10)	958(8)	1926(7)	42(2)
C(44)	4768(17)	2159(14)	1790(9)	37(3)
C(45)	3852(33)	2561(21)	598(13)	51(6)
F(44)	3375(34)	3868(17)	864(9)	59(2)

© 1997 NRC Canada

Can. J. Chem. Downloaded from www.nrcresearchpress.com by 88.146.161.215 on 09/08/12
For personal use only.

Table 2 (*concluded*).

Atom	*x*	*y*	*z*	*U*(eq)
F(45)	2609(53)	1631(33)	−235(33)	73(6)
F(46)	4818(62)	2724(59)	5(45)	67(3)
N(51)	6010(7)	5576(7)	7571(5)	32(1)
N(52)	6493(7)	4231(6)	7234(5)	30(1)
F(51)	7286(53)	8290(33)	10374(33)	73(6)
F(52)	5033(62)	7195(59)	10048(45)	67(3)
F(53)	5298(12)	8103(9)	8682(7)	57(2)
C(51)	6014(30)	7366(19)	9492(12)	37(3)
C(52)	6454(68)	5981(34)	8842(17)	59(2)
C(53)	7238(9)	4941(8)	9328(7)	39(2)
C(54)	7238(9)	3897(7)	8327(7)	34(2)
C(55)	7915(20)	2489(16)	8290(13)	43(5)
F(54)	7716(10)	1897(8)	9074(8)	80(2)
F(55)	7320(12)	1529(8)	7165(6)	113(3)
F(56)	9495(9)	2676(10)	8641(10)	93(3)

[a] *U*(eq) is defined as one third of the trace of the orthogonalized U_{ij} tensor. The site occupancy factor (SOF) is 0.5 for all atoms.

Table 3. Selected bond lengths (Å) for $Cu_3(F_6dmpz)_5$, with estimated standard deviations in parentheses.

Bond	Length	Bond	Length
Cu(1)—N(32)	1.969(6)	Cu(1)—N(51)	1.950(6)
Cu(1)—N(12)	2.030(6)	Cu(1)—N(22)	2.022(6)
Cu(2)—N(42)	1.968(6)	Cu(2)—N(31)	1.965(6)
Cu(2)—N(21)	2.026(6)	Cu(2)—N(11)	2.007(6)
Cu(3)—N(41)	1.877(6)	Cu(3)—N(52)	1.877(6)
N(11)—N(12)	1.367(8)	N(21)—N(22)	1.370(8)
N(31)—N(32)	1.376(9)	N(41)—N(42)	1.360(9)
N(51)—N(52)	1.377(8)		

Table 4. Selected bond angles (deg) for $Cu_3(F_6dmpz)_5$, with estimated standard deviations in parentheses.

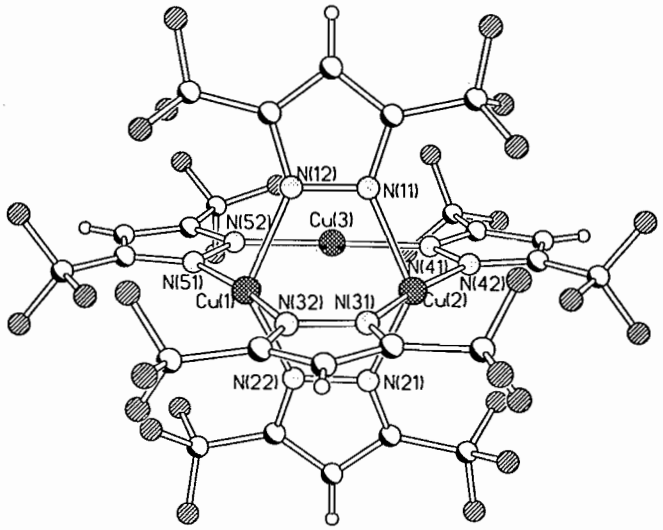
Bond	Angle (deg)	Bond	Angle (deg)
N(51)-Cu(1)-N(22)	94.8(3)	N(51)-Cu(1)-N(32)	170.1(3)
N(51)-Cu(1)-N(12)	94.3(3)	N(32)-Cu(1)-N(22)	89.8(3)
N(22)-Cu(1)-N(12)	128.3(2)	N(32)-Cu(1)-N(12)	89.6(3)
N(31)-Cu(2)-N(11)	89.1(3)	N(31)-Cu(2)-N(42)	171.2(3)
N(31)-Cu(2)-N(21)	89.3(3)	N(42)-Cu(2)-N(11)	94.7(3)
N(11)-Cu(2)-N(21)	129.7(2)	N(42)-Cu(2)-N(21)	94.3(3)
N(12)-N(11)-Cu(2)	113.8(4)	N(52)-Cu(3)-N(41)	176.2(3)
N(21)-N(22)-Cu(1)	114.0(4)	N(11)-N(12)-Cu(1)	113.1(4)
N(32)-N(31)-Cu(2)	114.3(6)	N(22)-N(21)-Cu(2)	112.7(4)
N(41)-N(42)-Cu(2)	116.5(5)	N(31)-N(32)-Cu(1)	113.7(5)
N(52)-N(51)-Cu(1)	116.6(4)	N(42)-N(41)-Cu(3)	122.4(4)
N(51)-N(52)-Cu(3)	121.6(4)		

$[Cu_3(OH)pz_3py_2Cl_2]py$ (10) there is one unique Cu···Cu distance at 3.112 Å and two Cu···Cu distances at 3.321 Å. In this structure there is significant deviation from planarity displayed by the Cu_3pz_3 trigonal core. On the other hand, the central Cu_3pz_3 feature of the complex $[Cu_3(OH)pz_3(Hpz)_2(NO_3)_2]H_2O$ (11) is essentially planar with Cu···Cu distances at 3.324, 3.364, and 3.365 Å. The present structure is completed by two additional bridging 3,5-

© 1997 NRC Canada

Can. J. Chem. Downloaded from www.nrcresearchpress.com by 88.146.161.215 on 09/08/12
For personal use only.

Fig. 1. The structure of $Cu_3(F_6dmpz)_5$ with selected atom numbering scheme.



bis(trifluoromethyl)pyrazolate, F_6dmpz^-, ligands above and below the trigonal planar array and bridging the two Cu(II) ions. These ligands are tilted towards the Cu(I) ion, thereby relieving steric interactions with the pyrazolate ion already bridging the two Cu(II) ions in the trigonal plane. The angle between the least-squares planes of these two bridging groups is ~154°. The coordination about the Cu(I) ion is almost linear (N(52)-Cu(3)-N(41)) at 176.2° whereas the Cu(II) ions display a very distorted square planar environment, (N(42)-Cu(2)-N(31), 171.2°, N(11)-Cu(2)-N(21), 121.7°, N(31)-Cu(2)-N(11), 89.1°, N(31)-Cu(2)-N(21), 89.3°, N(42)-Cu(2)-N(11), 94.7°, N(42)-Cu(2)-N(21), 94.3°).

The nonbonded Cu···Cu distances of the present structure may be compared also with those found in the Cu(II) pyrazolate polymer, $[Cu(pz)_2]_x$. In the latter structure (2) the Cu(II) ions are in a distorted tetrahedral environment created by the two bridging pyrazolate ligands between the Cu centers but the overall linear chain structure allows a much longer Cu···Cu nonbonded distance of 3.889 Å. The two Cu(II) ions of the present structure are in a constrained trigonal environment with the Cu(I) ion and are essentially triply bridged by F_6dmpz^- ligands. The coordination sphere of each of these Cu(II) ions is completed by the F_6dmpz^- ligands being shared with the Cu(I) ion.

The presence of two copper(II) ions triply-bridged by pyrazolate ligands leads to the possibility of strong antiferromagnetic coupling between the two paramagnetic centers. Magnetic susceptibility measurements on powdered samples of $Cu_3(F_6dmpz)_5$ revealed some field dependence over the entire temperature range studied. This observation prompted us to conduct magnetization versus field studies at four different temperatures. These studies revealed linear magnetization versus field behaviour above ~3000 G at all temperatures. Extrapolation of the linear region to zero field gave a non-zero intercept indicative of ferromagnetic impurity, the presence of which made a temperature-independent and field-dependent contribution to the susceptibility data. Subtracting the intercept magnetization from the data corrected for the impurity and gave field-independent susceptibilities. The source of the ferromagnetic impurity is not certain; however, as described above, $Cu_3(F_6dmpz)_5$ is very susceptible to moisture and traces of impurities should not be unexpected.

The magnetic susceptibilities (per mole of copper(II)) are plotted versus temperature for three runs in Fig. 2. The susceptibility decreases from 300 K to about 80 K, then at lower temperatures shows an increase as the temperature is decreased further. This is consistent with strong antiferromagnetic coupling between the copper(II) centers with the upturn in susceptibility at the lowest temperatures arising from trace paramagnetic impurity. To obtain a measure of the strength of the magnetic coupling we fitted the susceptibility data (per mole of Cu(II) for run no. 2 at 1 T) obtained over the entire temperature range to the equation for antiferromagnetic dimeric copper(II) systems developed by Bleaney and Bowers (12), with allowance for a paramagnetic component and for temperature-independent paramagnetism, TIP. The equation used is:

$$[1] \quad \chi = \frac{Ng^2\beta}{kT}\left[[1-P]\left[\frac{e^{2J/kT}}{1+3e^{2J/kT}}\right]+P/4\right]+\text{TIP}$$

where J is the exchange coupling constant and P is the fraction of copper present as paramagnetic impurity. In modelling, the J, g, P, and TIP were allowed to vary. This gave best fit values of $-J$, g, P, and TIP of 235 cm^{-1}, 2.11, 0.0025, and 29×10^{-6} cm^3mol^{-1}, respectively, with the fitting function $F = 0.063$. The function F:

$$[2] \quad F = \left[\frac{1}{n}\sum_{i=1}^{n}\left[\frac{\chi^i_{calc}-\chi^i_{obs}}{\chi^i_{obs}}\right]^2\right]^{1/2}$$

is minimized in the fitting procedure and provides a measure of the agreement between the experimental data and the model. Uncertainties in J and g are estimated to be between ±5% and ±2%, respectively.

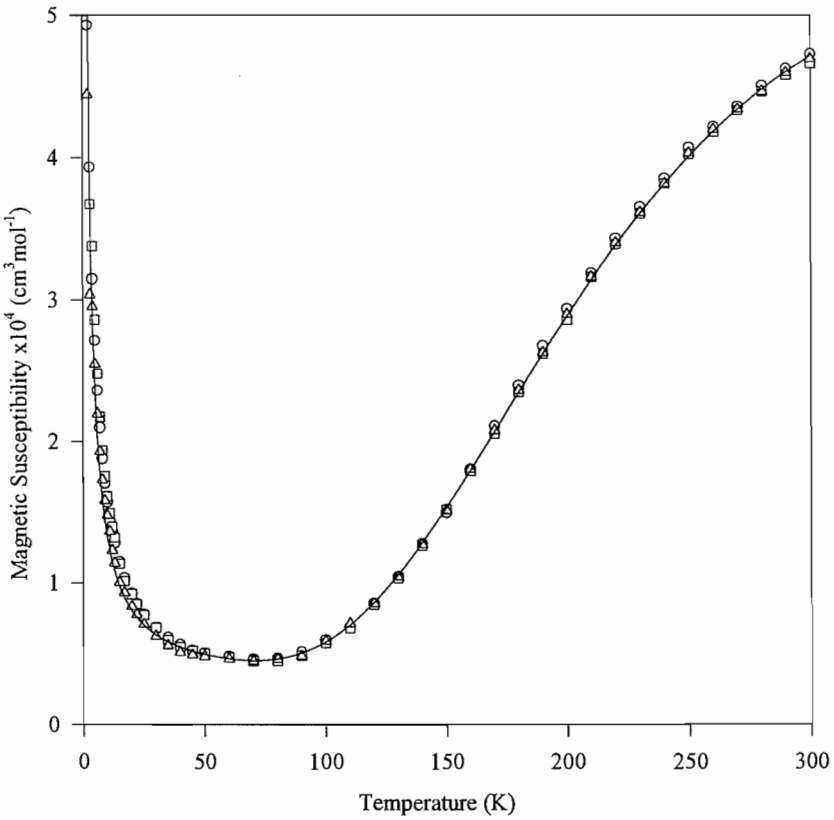
The value of TIP is somewhat low for copper(II); however, it must be realized that the strong coupling in this compound renders the paramagnetism very weak. As a consequence, diamagnetism and TIP contribute a significant amount to the overall susceptibilities, each making a temperature-independent contribution. Diamagnetic corrections were estimated in the usual way (13) and an estimate only 10% greater than the values used here would, for example, not affect the quality of the fit or the other parameters but would lead to a 75% increase in TIP to a value of 51×10^{-6} cm^3mol^{-1}.

$Cu_3(F_6dmpz)_5$ appears to be the first copper compound structurally and magnetically characterized, to have three bridging pyrazolate groups linking two copper(II) centers (tri-μ-pz bridging). The antiferromagnetic exchange in this compound is likely mediated by the ligands as they provide significantly shorter pathways than that involving the copper(I) ion. The unique character of the bridging motif in this compound prevents any detailed discussion of magnetostructural correlations; however, to put the magnitude of the observed exchange coupling ($-J = 235$ cm^{-1}) in perspective, comparisons with related systems are in order.

The binary pyrazolates of copper(II) have polymeric chain structures involving di-μ-pz bridging and compressed tetrahedral MN_4 chromophore geometries (2–5). By virtue of their

© 1997 NRC Canada

Fig. 2. Magnetic susceptibilities (per mole of copper(II)) versus temperature plot. □, Δ, and ○ are data points for run no. 1 at 1 T, run no. 2 at 1 T, and one run at 2 T, respectively. The solid line is calculated from theory as described in the text.



chain structures, the antiferromagnetic exchange in these polymers arises from each metal center interacting with two nearest neighbours rather than one as in the title compound. In view of these differences it is perhaps not surprising that the magnitude of the exchange coupling in the polymers, as determined by $-J$ values in the range 58–105 cm^{-1}, differs significantly from that in the title compound.

More relevant, perhaps, are comparisons with dimetallic copper(II) systems. Structural and magnetic studies have been reported on copper(II) complexes containing binucleating ligands and incorporating singly bridging pyrazolate (1, 14). These compounds, however, also contain other bridging groups that are involved in the exchange, making comparisons with the present system inappropriate. Finally, we refer to a class of compounds that contain dinucleating pyrazolate ligands, which incorporate chelating arms in the 3,5-positions on the pyrazolate ring (15–17). In these compounds two copper(II) centers are bridged by two ligands; each ligand provides one pyrazolate bridge (di-μ-pz bridging) and chelates to each metal via the substituents in the 3,5-positions. The metal–ligand geometry in these systems is square pyramidal and the values of the exchange integral, J, vary from -159 to -214 cm^{-1}. Hence, for these systems the coupling approaches values of the same order of magnitude as that observed for the title compound in spite of the structural differences, including the number of bridging pyrazolate ligands.

Acknowledgements

Funding for the project has been provided by the Natural Sciences and Engineering Research Council of Canada. P. Borda of this department is thanked for the C, H, N analyses. The contribution of Victor G. Young, Jr., of the X-ray Crystallographic Laboratory, Chemistry Department, University of Minnesota, for the X-ray structure determination is gratefully acknowledged. S.J. Rettig is thanked for helpful discussions.

References

1. G. La Monica and G.A. Ardizzoia. Prog. Inorg. Chem. In press. (1997).
2. M.K. Ehlert, S.J. Rettig, A. Storr, R.C. Thompson, and J. Trotter. Can. J. Chem. **67**, 1970 (1989).
3. M.K. Ehlert, S.J. Rettig, A. Storr, R.C. Thompson, and J. Trotter. Can. J. Chem. **69**, 432 (1991).
4. M.K. Ehlert, S.J. Rettig, A. Storr, R.C. Thompson, and J. Trotter. Can. J. Chem. **70**, 1121 (1992).
5. M.K. Ehlert, S.J. Rettig, A. Storr, R.C. Thompson, and J. Trotter. Can. J. Chem. **67**, 331 (1993).
6. S. Trofimenko. J. Am. Chem. Soc. **89**, 3165 (1967).
7. M.K. Ehlert, S.J. Rettig, A. Storr, R.C. Thompson, and J. Trotter. Can. J. Chem. **68**, 1444 (1990).
8. M.K. Ehlert, S.J. Rettig, A. Storr, R.C. Thompson, and J. Trotter. Can. J. Chem. **70**, 2161 (1992).
9. W.W. Porterfield. Inorganic chemistry. A unified approach. Addison – Wesley, Reading, Mass. 1984. p. 168.

© 1997 NRC Canada

Can. J. Chem. Downloaded from www.nrcresearchpress.com by 88.146.161.215 on 09/08/12
For personal use only.

10. M. Angaroni, G.A. Ardizzoia, T. Beringhelli, G. LaMonica, D. Gatteschi, N. Masciocchi, and M. Moret. J. Chem. Soc. Dalton Trans. 3305 (1990).
11. F.B. Hulsbergen, R.W.M. ten Hoedt, G.C. Verschoor, J. Reedijk, and A.L. Spek. J. Chem. Soc. Dalton Trans. 539 (1983).
12. B. Bleaney and K.D. Bowers. Proc. R. Soc. London, Ser. A: **226**, 95 (1952).
13. E. Konig. Landolt–Börnstein numerical data and functional relationships in science and technology. New series, Vol. II/2. *Edited by* K.H. Hellwege and A.M. Hellewege. Springer-Verlag, Berlin. 1966.
14. T.N. Doman, D.E. Williams, J.F. Banks, R.M. Buchanan, H.-R. Chang, R.J. Webb, and D.N. Hendrickson. Inorg. Chem. **29**, 1058 (1990), and refs. therein.
15. T. Kamiusuki, H. Okawa, N. Matsumoto, and S. Kida. J. Chem. Soc. Dalton Trans. 195 (1990).
16. J. Pons, X. López, J. Casabó, F. Teixidor, A. Caubet, J. Ruis, and C. Miravitlles. Inorg. Chim. Acta, **195**, 61 (1992).
17. B. Mernari, F. Abraham, M. Legrenee, M. Drillon, and P. Legoll. J. Chem. Soc Dalton Trans. 1707 (1993).

Can. J. Chem. Downloaded from www.nrcresearchpress.com by 88.146.161.215 on 09/08/12
For personal use only.

© 1997 NRC Canada

The direct electrochemical synthesis of some metal derivatives of lapachol

E.H. de Oliveira, G.E.A. Medeiros, C. Peppe, Martyn A. Brown, and Dennis G. Tuck

Abstract: The electrochemical oxidation of a sacrificial metal anode (M = Zn, Cd, Cu) in an acetonitrile solution of 2-hydroxy-3-(3-methyl-2-butenyl)-1,4-naphthoquinone, lapachol, $C_{15}H_{14}O_3$ (= HL) gives ML_2. The results are in keeping with earlier work on direct electrochemical synthesis in related systems. Adducts with 2,2′-bipyridine (bpy) and *N,N,N′,N′*-tetramethylethanediamine (tmen) have also been prepared. The structure of the 2,2′-bipyridine adduct of Cu(lapacholate)$_2$ has been established by X-ray crystallography. The parameters are triclinic, space group $P\bar{1}$, a = 12.748(59) Å, b = 13.859(49) Å, c = 11.770(59) Å, α = 108.30(4)°, β = 108.08(3)°, γ = 68.94(3)°, Z = 2, R = 0.059 for 2256 unique reflections. The copper atom is in a distorted $CuN_2O_2O_2'$ environment. The mechanism of the formation of this Cu(lapacholate)$_2$ is discussed.

Key words: electrochemical synthesis, lapachol, X-ray crystallography, copper(II) complex.

Résumé : L'oxydation électrochimique de la 2-hydroxy-3-(3-méthylbut-2-ényl)-1,4-naphtoquinone, le lapachol ($C_{15}H_{14}O_3$) (= HL), en solution dans l'acétonitrile, à une anode métallique sacrifiée (M = Zn, Cd, Cu), conduit aux composés ML_2. Ces résultats sont en accord avec ceux obtenus antérieurement à l'occasion de la synthèse électrochimique directe dans des systèmes apparentés. On a aussi préparé les adduits avec la 2,2′-bipyridine (bpy) et avec la *N,N,N′,N′*-tétraméthyléthanediamine (tmen). Faisant appel à la diffraction des rayons-X, on a déterminé la structure de l'adduit Cu(lapacholate)$_2$ avec la 2,2′-bipyridine. Les cristaux sont tricliniques, groupe d'espace $P\bar{1}$, a = 12,748(59), b = 13,859(49) et c = 11,770(59) Å, α = 108,30(4)°, β = 108,08(3)°, γ = 68,94(3)°, Z = 2 et R = 0,059 pour 2256 réflexions uniques. L'atome de cuivre se trouve dans un environnement $CuN_2O_2O_2'$ déformé. On discute du mécanisme de formation de ce Cu(lapacholate)$_2$.

Mots clés : synthèse électrochimique, lapachol, diffraction des rayons-X, complexe du cuivre(II).

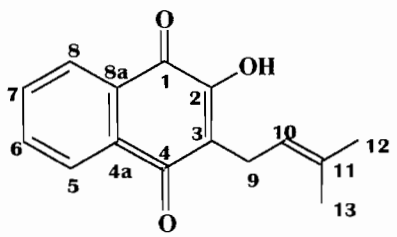
[Traduit par la rédaction]

Introduction

The method of direct electrochemical synthesis consists in oxidizing a sacrificial metal anode in a cell containing a non-aqueous solution of an appropriate ligand, or ligand precursor, and the applications and advantages of this simple and rugged synthetic technique have been reviewed elsewhere (1). It is especially useful for the one-step preparation of derivatives of weak acids, such as metal thiolates (2–5), acetylides (6), dialkylthiocarbamates (7), and substituted catecholates (8). Of special relevance to the present work are recent reports of the synthesis of complexes of bidentate anionic oxygen donors in which a carbonyl group is *ortho* to a phenolate, as in aceto-naphthonate (9), flavonate (9), and pyronate (9, 10), and complexes of several metals have been obtained in this way.

We now report the use of the electrochemical method to prepare some metal derivatives of the naturally occurring compound lapachol, 2-hydroxy-3-(3-methyl-2-butenyl)-1,4-naphtho-quinone (Scheme 1). This interesting substance shows promise as an antibiotic and anti-tumor reagent (11). Its interest as a ligand lies in the unusual combination of a 1,4-quinone structure with the ketoenol function noted above. The results show that coordination to a metal centre may involve each of these functionalities, depending on the metal involved, and upon the oxidation state of that metal.

Scheme 1.



Experimental section

General techniques

Lapachol was obtained from the Institute of Antibiotics of the Universidade Federal da Pernanbuco, Brazil, and recrystallized from ethanol to a constant melting point of 141–143°C. Metals in the form of rods, and 2,2′-bipyridine (bpy) and *N,N,N′*,N′-tetramethylethanediamine (tmen) were used as

Received August 7, 1996.

E.H. de Oliveira, G.E.A. Medeiros, and C. Peppe. Departamento de Química – CCEN, Universidade Federal da Paraíba, Campus I, 58.059-900, João Pessoa – PB, Brazil.
M.A. Brown and D.G. Tuck.[1] Department of Chemistry and Biochemistry, University of Windsor, Windsor, ON N9B 3P4, Canada.

[1] Author to whom correspondence may be addressed. Telephone: (519) 253-4232, ext. 3541. Fax: (519) 973-7098. E-mail: dgtuck@uwindsor.ca

© 1997 NRC Canada

Can. J. Chem. Downloaded from www.nrcresearchpress.com by 88.146.161.215 on 09/08/12
For personal use only.

Table 1. The electrochemical preparation of metal lapacholate compounds.

Compound	LapH (mg)	Current (mA)	Voltage (V)	Time of electrolysis (min)	Mass of metal dissolved (mg)	Mass of product (mg)	Yield (%)	E_F (mol F^{-1})
$Zn(Lap)_2$	540	20	7.0	179	94.0	410	52	0.52
$Cd(Lap)_2$	296	21	9.5	85	76.5	270	75	0.54
$Cu(Lap)_2$	558	20	5.5	185	159.0	419	30	1.08

Table 2. Analytical results for $M(Lap)_2$ compounds and their adducts (Lap = $C_{15}H_{13}O_3^-$).

	Calculated (%)				Found %			
Compound	C	H	N	M	C	H	N	M
$Zn(Lap)_2$	65.7	4.78	—	11.9	64.7	5.50	—	12.5
$Zn(Lap)_2$bpy	68.2	4.87	3.98	9.3	67.3	4.91	3.99	9.3
$Zn(Lap)_2$tmen	65.1	6.37	4.22	9.5	64.8	6.45	4.30	9.8
$Cd(Lap)_2$	60.6	4.40	—	18.9	59.6	4.35	—	19.0
$Cd(Lap)_2$bpy	64.0	4.56	3.73	15.0	63.0	4.45	3.82	15.0
$Cd(Lap)_2$tmen	60.8	5.95	3.94	15.5	60.5	6.08	4.03	15.8
$Cu(Lap)_2$				11.6				12.0
$Cu(Lap)_2$bpy				9.0				9.4
$Cu(Lap)_2$tmen				9.8				9.6

supplied (Aldrich). Tetraethylammonium perchlorate was prepared by mixing aqueous solutions of $NaClO_4$ and Et_4NBr; the product was recrystallized from aqueous ethanol (9:1, v:v). Acetonitrile was refluxed over calcium hydride and distilled before use.

Metal analysis was by complexometric titration with EDTA. Zinc and cadmium complexes (ca. 100 mg) were destroyed in aqueous HCl; the resulting solution was neutralized with NaOH and the pH adjusted to 10 by addition of ammonium hydroxide (1 mL). The resulting solution was titrated with a standard solution of EDTA (10^{-2} M) using Eriochrome Black T as indicator. Copper complexes were destroyed in HCl, and the solution was neutralized and mixed with HCl (0.5 mL) and ammonium acetate (2 g); the resulting solution was titrated with EDTA using 4-(2-pyridylazo)resorcinol, monosodium salt, as indicator.

^1H and ^{13}C nuclear magnetic resonance spectra were recorded on a Bruker AC-300L instrument, and ESR spectra on a Bruker ESP-300 instrument. Elemental analysis was by Canadian Microanalytical Services Ltd., and by the Departamento de Quimica Universidade Federal da Pernanbuco.

Electrochemical procedures

The electrochemical procedures were essentially those described in earlier papers. The electrochemical cell was a 100 mL round-bottomed flask containing the solution phase (~30 mL); the sacrificial metal electrode suspended by a platinum wire through the rubber septum formed the anode of the cell, and a second platinum wire similarly supported was the cathode. All operations were carried out under dry nitrogen, via a Schlenk arm on the flask, using standard vacuum line techniques up to the isolation of the solid products, which are air stable. The details of cell composition, electrical conditions, and electrochemical efficiency are given in Table 1.

The solution phase was degassed by pumping on a vacuum line for 3 min with continuous stirring and the cell was purged with dry nitrogen throughout the electrolysis. As soon as current flowed in the cell, bubbles of H_2 gas were visible at the cathode, and the yellow solution began to turn dark red. The electrolysis was conducted until more than 90% of the lapachol was consumed. Any decrease in the current was corrected by increasing the applied voltage. At the end of the electrolysis the anode was removed, washed, dried, and weighed to obtain the quantity dissolved, and hence the electrochemical efficiency. The dark red solids that precipitated in the cell were collected by filtration, dried under vacuum, and weighed. Analytical results are given in Table 2, and the details for each element are discussed below.

Preparation of adducts

(i) $Zn(Lap)_2$tmen

A suspension of $Zn(Lap)_2$ (118.0 mg, 0.22 mmol) in CH_3CN (8 mL) was treated with excess of tmen (1 mL, 770 mg, 6.64 mmol). The reaction was brought to the boiling point of CH_3CN (82°C) for 10 min and the resultant solution quickly filtered; all the volatiles were removed from the filtrate and the resulting solid washed with diethyl ether (2 mL). This solid was dried under vacuum to yield $Zn(Lap)_2$tmen (140.0 mg, 0.21 mmol, 96%).

© 1997 NRC Canada

Can. J. Chem. Downloaded from www.nrcresearchpress.com by 88.146.161.215 on 09/08/12
For personal use only.

Can. J. Chem. Downloaded from www.nrcresearchpress.com by 88.146.161.215 on 09/08/12
For personal use only.

Table 3. Summary of crystal intensity data, collection, and structural refinement for $Cu(Lap)_2bpy$.

Chemical formula	$C_{40}H_{34}O_6N_2Cu$
M	702.28
Crystal system	Triclinic
Space group	$P\bar{1}$
a (Å)	12.748 (59)
b (Å)	13.859 (49)
c (Å)	11.770 (59)
α (deg)	108.30 (4)
β (deg)	108.08 (3)
γ (deg)	68.94 (3)
V (Å^3)	1796.1 (8)
Z	2
F(000)	738
D_c (g cm^{-3})	1.30
Crystal dimensions (mm)	0.1 × 0.1 × 0.1
μ (cm^{-1})	6.57
2θ (deg (max))	50
Total reflections measured	6624
Unique data used ($I \geq 3\sigma(I)$)	2256
T (°C)	23
No. of parameters	238
R	0.059
R_w	0.049
Maximum shift/error in final cycle	0.01
Maximum, minimum peaks in final difference map (e Å^{-3})	0.46, −0.33

(ii) $Cd(Lap)_2tmen$

A suspension of $Cd(Lap)_2$ (232.2 mg, 0.39 mmol) in CH_3CN (8 mL) was treated with excess of tmen (1 mL, 770 mg, 6.64 mmol). The reaction was brought to the boiling point of CH_3CN for 10 min and the resultant solution quickly filtered; the filtrate was concentrated under vacuum to 50% of its initial volume, and diethyl ether added to the resulting solution. When this was kept at −18°C, $Cd(Lap)_2tmen$ (155.8 mg, 0.22 mmol, 56%) precipitated.

(iii) $M(Lap)_2bpy$ (M= Zn, Cd)

Equimolar amounts of bpy and $M(Lap)_2$ (Cd: 300 mg, 0.5 mmol; Zn: 250 mg, 0.46 mmol) were mixed in acetonitrile (8 mL). The reaction was brought to the boiling point of CH_3CN for 10 min and the resultant solution quickly filtered; the filtrate was concentrated under vacuum to 50% of its initial volume. Diethyl ether was added to the resulting solution, which was kept at −18°C until $M(Lap)_2bpy$ precipitated (Cd: 315 mg, 0.42 mmol, 84%; Zn: 263.0 mg, 37.4 mmol, 81%).

(iv) $Cu(Lap)_2bpy$

$Cu(Lap)_2$ (197 mg, 0.36 mmol) and bpy (60 mg,, 0.38 mmol) were stirred in 10 mL acetonitrile for 24 h; $Cu(Lap)_2bpy$ (116 mg, 0.17 mmol, 47%) was collected by filtration and dried in vacuo. Crystals for X-ray analysis were grown from hot acetonitrile.

(v) $Cu(Lap)_2tmen$

$Cu(Lap)_2$ (301 mg, 0.55 mmol) and excess tmen (0.5 mL, 3.3 mmol) were stirred in 10 mL acetonitrile for 24 h; $Cu(Lap)_2tmen$ (292 mg, 0.44 mmol, 80%) was collected by filtration and dried in vacuo.

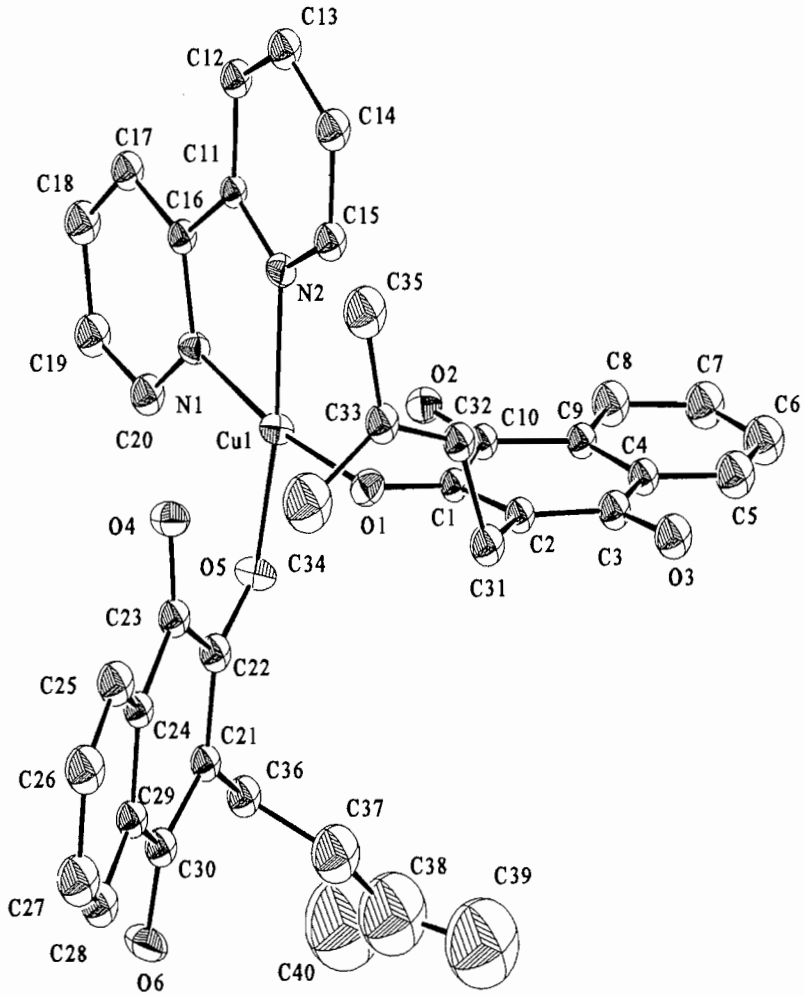
Crystallographic analysis

In the study of $Cu(Lap)_2bpy$, $C_{40}H_{34}O_6N_2Cu$, **1**, a dark-red block crystal on a glass fibre was mounted in a Rigaku AFC6S diffractometer, equipped with graphite monochromated Mo-Kα radiation (λ = 0.71069 Å) and a rotating anode generator. Cell constants and orientation matrices for data collection were obtained from least-squares refinements, using 20 carefully centred reflections in the range $12.61° < 2\theta < 19.62°$. The space group was uniquely identified as $P\bar{1}$ (No. 2) by the lack of systematic absences, and this was confirmed by subsequent solution and refinement of the structure. Details of the intensity collection are given in Table 3.

The intensities of three representative reflections were measured after every 150 reflections. Over the course of data collection, the standards decreased by 0.24%, and a linear correction factor was applied to the results. Absorption corrections were made using Ψ scan (transmission factors 0.9281–1.000), and the values were corrected for Lorentz and polarization effects. The structure was solved by direct methods, and expanded using Fourier techniques. The non-hydrogen atoms were refined isotropically; hydrogen atoms on carbon were included in ideal positions (r = 0.95 Å), but were not refined. The final cycle of full-matrix least-squares refinement was based on 2256 observed reflections ($I > 3\sigma(I)$) and 238 variable parameters, refining the parameters $R = \Sigma||F_o| - |F_c||/\Sigma|F_o|$, $R_w = [\Sigma w(|F_o| - |F_c|)^2/\Sigma wF_o^2]^{1/2}$, $\sigma(F) = \Sigma w\ (|F_o| - |F_c|)^2$, and $p = 0.003$; the solution converged at $R = 0.059$, $R_w = 0.049$. A final Fourier difference map calculation showed no peaks of chemical significance; the maximum and minimum peaks corresponded to 0.46 and −0.33 e Å^{-3}, respectively. The large thermal parameters found for C38–C40 suggest

© 1997 NRC Canada

Fig. 1. Structure of $Cu(Lap)_2bpy$, showing the numbering system; ORTEP diagram, with atoms shown as 30% probability ellipsoids. Hydrogen atoms have been omitted for clarity.



some degree of disorder around the C37—C38 double bond; no correction was applied for this.

Neutral-atom scattering factors were taken from Cromer and Waber (12). Anomalous dispersion effects were included in the calculations (13); the values for $-f'$ and $\Delta f''$ were those published by Cromer (14). All calculations were performed using the TEXSAN (15) crystallographic software package. The structure of the molecule is shown in Fig. 1, the positional parameters are in Table 4, and the important bond distances and angles in Table 5.

Tables of hydrogen-atom coordinates and thermal parameters, anisotropic thermal parameters for other atoms, and least-squares planes are available as supplementary data.[2]

[2] These supplementary data can be purchased from: The Depository of Unpublished Data, Document Delivery, CISTI, National Research Council Canada, Ottawa, Canada K1A 0S2. Tables of hydrogen atom coordinates have also been deposited with the Cambridge Crystallographic Data Centre, and can be obtained on request from The Director, Cambridge Crystallographic Data Centre, University Chemical Laboratory, 12 Union Road, Cambridge, CB2 1EZ, U.K.

Results and discussion

Preparative electrochemistry

The electrochemical synthesis of lapacholate derivatives shows that the chemistry of these systems is more complicated than those studied previously, and this is clearly the result of the presence within the parent molecule of both *para*-quinone and keto-enolate functions. The three metals studied in fact demonstrate two different types of behaviour. For zinc and cadmium, the products are the $M(Lap)_2$ derivatives (Lap = lapacholate anion), which are presumably four-coordinate and accordingly accept bidentate donors to give $M(Lap)_2bpy$ and $M(Lap)_2tmen$, and for these metals the parallels with earlier work are clear. For copper, the primary product is identified as $Cu^{I}(Lap)$, which isomerizes to $Cu^{II}(LapSQ)$ (LapSQ = lapacholate-semiquinone radical dianion), which subsequently reacts in situ to give $Cu^{II}(Lap)_2$ (see below). This in its turn will also form six-coordinate species, and the crystal structure study has confirmed this in the case of $Cu^{II}(Lap)_2bpy$.

The cathodic reduction of lapachol is accompanied by the evolution of hydrogen,

[1] $HLap + e \rightarrow Lap^{-} + 1/2\ H_2$

Can. J. Chem. Downloaded from www.nrcresearchpress.com by 88.146.161.215 on 09/08/12
For personal use only.

© 1997 NRC Canada

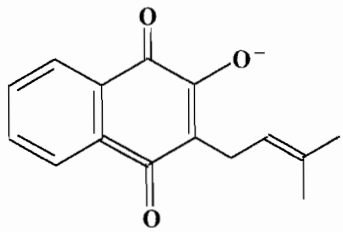
Can. J. Chem. Downloaded from www.nrcresearchpress.com by 88.146.161.215 on 09/08/12
For personal use only.

Table 4. Final fractional coordinates and thermal parameters for the non-hydrogen atoms of $Cu(Lap)_2bpy$, with standard deviations in parentheses.

Atom	*x*	*y*	*z*	*B*(eq)
Cu(1)	0.1821(1)	0.2693(1)	0.8208(1)	3.47(7)
O(1)	0.3147(5)	0.2747(5)	0.7761(6)	3.9(4)
O(2)	0.1116(5)	0.4201(5)	0.7249(6)	4.0(4)
O(3)	0.4828(6)	0.4514(5)	0.6351(6)	5.3(2)
O(4)	0.3052(6)	0.0978(5)	0.8539(6)	4.8(4)
O(5)	0.1379(5)	0.1734(5)	0.6690(6)	4.3(4)
O(6)	0.2399(6)	−0.1679(5)	0.4187(7)	5.9(5)
N(1)	0.0446(6)	0.2854(6)	0.8802(7)	3.3(5)
N(2)	0.2161(6)	0.3628(6)	0.9906(7)	3.0(4)
C(1)	0.3108(8)	0.3473(8)	0.7270(9)	3.0(2)
C(2)	0.4067(8)	0.3589(7)	0.7066(8)	3.3(2)
C(3)	0.3965(9)	0.4408(8)	0.652(1)	4.0(2)
C(4)	0.2834(8)	0.5119(8)	0.6130(9)	3.5(2)
C(5)	0.273(1)	0.590(1)	0.558(1)	5.8(3)
C(6)	0.166(1)	0.660(1)	0.522(1)	6.3(3)
C(7)	0.070(1)	0.657(1)	0.544(1)	5.8(3)
C(8)	0.077(1)	0.580(1)	0.603(1)	5.3(3)
C(9)	0.1857(8)	0.5077(8)	0.6362(9)	3.3(2)
C(10)	0.1939(9)	0.4256(8)	0.6958(9)	3.3(2)
C(11)	0.1356(8)	0.3921(7)	1.0553(8)	2.7(2)
C(12)	0.1458(8)	0.4616(8)	1.170(1)	3.8(2)
C(13)	0.2391(9)	0.4965(8)	1.217(1)	4.3(2)
C(14)	0.3237(9)	0.4657(8)	1.151(1)	4.6(3)
C(15)	0.3087(9)	0.3984(8)	1.036(1)	4.0(2)
C(16)	0.0399(8)	0.3455(7)	0.9939(9)	3.1(2)
C(17)	−0.0529(9)	0.3640(8)	1.0444(9)	3.9(2)
C(18)	−0.137(1)	0.3157(9)	0.978(1)	4.9(3)
C(19)	−0.131(1)	0.2533(9)	0.865(1)	4.9(3)
C(20)	−0.039(1)	0.2390(8)	0.820(1)	4.4(3)
C(21)	0.1848(8)	0.0048(8)	0.5345(9)	3.5(2)
C(22)	0.2032(9)	0.0760(8)	0.646(1)	3.8(2)
C(23)	0.2986(9)	0.0416(8)	0.750(1)	3.8(2)
C(24)	0.3859(8)	−0.0648(8)	0.724(1)	3.3(2)
C(25)	0.488(1)	−0.0915(9)	0.813(1)	5.1(3)
C(26)	0.569(1)	−0.189(1)	0.786(1)	6.1(3)
C(27)	0.546(1)	−0.257(1)	0.670(1)	6.8(3)
C(28)	0.446(1)	−0.2309(9)	0.584(1)	5.2(3)
C(29)	0.3643(8)	−0.1326(8)	0.610(1)	3.7(2)
C(30)	0.2611(9)	−0.1020(9)	0.515(1)	4.0(2)
C(31)	0.524(1)	0.2861(8)	0.753(1)	4.5(3)
C(32)	0.5636(8)	0.3176(8)	0.891(1)	3.9(2)
C(33)	0.5981(9)	0.2587(9)	0.970(1)	4.3(2)
C(34)	0.604(1)	0.147(1)	0.938(1)	9.1(4)
C(35)	0.630(1)	0.306(1)	1.105(1)	7.0(3)
C(36)	0.0853(9)	0.0390(8)	0.431(1)	4.5(3)
C(37)	0.124(1)	0.068(1)	0.341(1)	8.8(4)
C(38)	0.077(2)	0.088(2)	0.226(2)	17.6(8)
C(39)	0.147(2)	0.126(2)	0.180(2)	21(1)
C(40)	−0.045(2)	0.073(2)	0.185(2)	23(1)

Studies of the redox chemistry of lapachol by Bodini and Arancibia (16), using cyclic voltammetry, have established that the anion undergoes no rearrangement at this stage, and is therefore as shown in Scheme 2:

Scheme 2.



With zinc or cadmium, discharge of this anion at the anode will yield the $M(Lap)_2$ species

[2] $2Lap^- + M \rightarrow M(Lap)_2 + 2e$

These compounds are diamagnetic, as shown by the clean NMR spectra obtained for these products and their adducts (see below). This overall mechanism (eqs. [1] + [2]), which is entirely in keeping with earlier results, predicts an electrochemical efficiency of 0.5 mol F^{-1}, as found experimentally (Table 1). The subsequent and separate adduct formation is a common feature of such zinc and cadmium compounds.

The copper system is noticeably different. The electrochemical efficiency is now 1.08 mol F^{-1}, indicating that the primary product is $Cu^I(Lap)$. The significant deviation from the theoretical value of unity is believed to be due to a slow chemical attack on copper by lapachol itself; a piece of clean copper placed in contact with a solution of lapachol in acetonitrile (152 mg, 0.62 mmol) in 5 mL for 48 h lost 34 mg (0.53 mmol) of element. The formation of copper(I) derivatives has been observed in a number of previous direct electrochemical syntheses (17–22), but the most striking feature here is that the final product is paramagnetic; no NMR spectra could be recorded, and the ESR spectrum shows that the anion is in fact the semiquinone, resulting from the sequence of electrochemical oxidation

[3] $Cu + Lap \rightarrow Cu^I(Lap) + e$

followed by an intramolecular electron transfer reaction

[4] $Cu^I(Lap) \rightarrow Cu^{II}(LapSQ)$

The elemental analysis (calcd. for $C_{15}H_{13}O_3Cu$: C 59.1, H 4.30; found: C 58.6, H 4.97) confirms that this is indeed the primary product. The ESR spectrum of this, and other paramagnetic copper derivatives of lapachol, will be discussed elsewhere, but we note here that these results are compatible with the structure of the dianion proposed by Bodini and Arancibia (16) (Scheme 3).

The reaction(s) by which $Cu^{II}(LapSQ)$ is converted to $Cu(Lap)_2$ are difficult to observe, since the reaction mixtures are intensely coloured (dark red) to the point of being virtually opaque. An apparently significant point is that the rate of precipitation of $Cu(Lap)_2$ is dependent on the quantity of excess lapachol in the solution. In the normal procedure 90% of the lapachol was consumed electrolytically, and in such cases the formation of $Cu(Lap)_2$ was slow, and the yield poor (~30%). When a solution of Cu(Lap) was stirred for 24 h with lapachol, the quantity of $Cu(Lap)_2$ that precipitated increased by 50%. We therefore suggest the sequence

© 1997 NRC Canada

Table 5. (*a*) Bond lengths (Å) and (*b*) angles (deg) for $Cu(Lap)_2bpy$, with standard deviations in parentheses.

(*a*) Intramolecular bond lengths.

Atom	Atom	Distance	Atom	Atom	Distance
Cu(1)	O(1)	1.950(6)	C(7)	C(8)	1.40(1)
Cu(1)	O(5)	1.923(6)	C(8)	C(9)	1.42(1)
Cu(1)	N(1)	1.999(7)	C(9)	C(10)	1.47(1)
Cu(1)	N(2)	2.026(7)	C(11)	C(12)	1.39(1)
O(1)	C(1)	1.29(1)	C(11)	C(16)	1.47(1)
O(2)	C(10)	1.23(1)	C(12)	C(13)	1.34(1)
O(3)	C(3)	1.24(1)	C(13)	C(14)	1.38(1)
O(4)	C(23)	1.22(1)	C(14)	C(15)	1.38(1)
O(5)	C(22)	1.30(1)	C(16)	C(17)	1.39(1)
O(6)	C(30)	1.23(1)	C(17)	C(18)	1.37(1)
N(1)	C(16)	1.34(1)	C(18)	C(19)	1.35(1)
N(1)	C(20)	1.34(1)	C(19)	C(20)	1.36(1)
N(2)	C(11)	1.34(1)	C(21)	C(22)	1.38(1)
N(2)	C(15)	1.34(1)	C(21)	C(30)	1.44(1)
C(1)	C(2)	1.39(1)	C(21)	C(36)	1.52(1)
C(1)	C(10)	1.51(1)	C(22)	C(23)	1.50(1)
C(2)	C(3)	1.42(1)	C(23)	C(24)	1.50(1)
C(2)	C(31)	1.52(1)	C(24)	C(25)	1.40(1)
C(3)	C(4)	1.46(1)	C(24)	C(29)	1.39(1)
C(4)	C(5)	1.37(1)	C(25)	C(26)	1.39(1)
C(4)	C(9)	1.38(1)	C(26)	C(27)	1.41(1)
C(5)	C(6)	1.39(1)	C(27)	C(28)	1.37(1)
C(6)	C(7)	1.34(1)	C(28)	C(29)	1.39(1)
C(29)	C(30)	1.46(1)	C(36)	C(37)	1.51(2)
C(31)	C(32)	1.51(1)	C(37)	C(38)	1.36(2)
C(32)	C(33)	1.30(1)	C(38)	C(39)	1.47(3)
C(33)	C(34)	1.45(1)	C(38)	C(40)	1.56(3)
C(33)	C(35)	1.50(1)			

(*b*) Intramolecular bond angles.

Atom	Atom	Atom	Angle	Atom	Atom	Atom	Angle
O(1)	Cu(1)	O(5)	94.1(3)	C(4)	C(5)	C(6)	120(1)
O(1)	Cu(1)	N(1)	171.7(3)	C(5)	C(6)	C(7)	122(1)
O(1)	Cu(1)	N(2)	93.4(3)	C(6)	C(7)	C(8)	120(1)
O(5)	Cu(1)	N(1)	92.9(3)	C(7)	C(8)	C(9)	118(1)
O(5)	Cu(1)	N(2)	171.9(3)	C(4)	C(9)	C(8)	121(1)
N(1)	Cu(1)	N(2)	79.8(3)	C(4)	C(9)	C(10)	119.8(9)
Cu(1)	O(1)	C(1)	123.3(6)	C(8)	C(9)	C(10)	119(1)
Cu(1)	O(5)	C(22)	119.4(6)	O(2)	C(10)	C(1)	118.9(9)
Cu(1)	N(1)	C(16)	115.6(6)	O(2)	C(10)	C(9)	123.4(9)
Cu(1)	N(1)	C(20)	126.4(7)	C(1)	C(10)	C(9)	117.6(9)
C(16)	N(1)	C(20)	117.9(9)	N(2)	C(11)	C(12)	120.5(9)
Cu(1)	N(2)	C(11)	115.3(6)	N(2)	C(11)	C(16)	114.2(8)
Cu(1)	N(2)	C(15)	124.1(7)	C(12)	C(11)	C(16)	125.3(9)
C(11)	N(2)	C(15)	120.5(8)	C(11)	C(12)	C(13)	119(1)
O(1)	C(1)	C(2)	124.0(9)	C(12)	C(13)	C(14)	121(1)
O(1)	C(1)	C(10)	116.2(8)	C(13)	C(14)	C(15)	118(1)
C(2)	C(1)	C(10)	119.8(9)	N(2)	C(15)	C(14)	121(1)

Can. J. Chem. Downloaded from www.nrcresearchpress.com by 88.146.161.215 on 09/08/12
For personal use only.

© 1997 NRC Canada

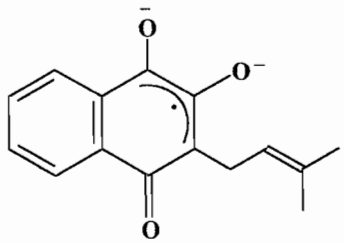
Table 5 (*concluded*).

(*b*) Intramolecular bond angles.

Atom	Atom	Atom	Angle	Atom	Atom	Atom	Angle
C(1)	C(2)	C(3)	121(1)	N(1)	C(16)	C(11)	114.9(9)
C(1)	C(2)	C(31)	117.5(9)	N(1)	C(16)	C(17)	120.8(9)
C(3)	C(2)	C(31)	121.2(9)	C(11)	C(16)	C(17)	124.1(9)
O(3)	C(3)	C(2)	121(1)	C(16)	C(17)	C(18)	119(1)
O(3)	C(3)	C(4)	119(1)	C(17)	C(18)	C(19)	121(1)
C(2)	C(3)	C(4)	120(1)	C(18)	C(19)	C(20)	118(1)
C(3)	C(4)	C(5)	120(1)	N(1)	C(20)	C(19)	124(1)
C(3)	C(4)	C(9)	122(1)	C(22)	C(21)	C(30)	121(1)
C(5)	C(4)	C(9)	119(1)	C(22)	C(21)	C(36)	120.2(9)
C(30)	C(21)	C(36)	119.1(9)	C(28)	C(29)	C(30)	120(1)
O(5)	C(22)	C(21)	123(1)	O(6)	C(30)	C(21)	121(1)
O(5)	C(22)	C(23)	116.0(9)	O(6)	C(30)	C(29)	120(1)
C(21)	C(22)	C(23)	120(1)	C(21)	C(30)	C(29)	120(1)
O(4)	C(23)	C(22)	121(1)	C(2)	C(31)	C(32)	112.1(9)
O(4)	C(23)	C(24)	121(1)	C(31)	C(32)	C(33)	128(1)
C(22)	C(23)	C(24)	117.9(9)	C(32)	C(33)	C(34)	124(1)
C(23)	C(24)	C(25)	119.5(9)	C(32)	C(33)	C(35)	121(1)
C(23)	C(24)	C(29)	118.4(9)	C(34)	C(33)	C(35)	115(1)
C(25)	C(24)	C(29)	122(1)	C(21)	C(36)	C(37)	112(1)
C(24)	C(25)	C(26)	119(1)	C(36)	C(37)	C(38)	136(2)

Can. J. Chem. Downloaded from www.nrcresearchpress.com by 88.146.161.215 on 09/08/12
For personal use only.

Scheme 3.



[5] $Cu^{II}(LapSQ) + HLap \rightarrow Cu(Lap)_2 + H$

[6] $2\,H \rightarrow H_2$

As with zinc and cadmium, adducts of $Cu(Lap)_2$ are readily obtained with bidentate donors, and the structure of $Cu(Lap)_2bpy$ is clearly that of a tetragonal copper (II) complex of a keto-enolate form of the ligand.

The structure of $Cu(Lap)_2bpy$

Figure 1 shows that the bpy adduct of $Cu(Lap)_2$ is a six-coordinate copper(II) complex. The interaction of 2,2′- bipyridine with copper(II) centres has been the subject of a number of previous studies (see ref. 23 for a summary), and the average Cu—N bond lengths in a series of salts of $[Cu(bpy)_2X]^+$ (X = Cl, Br, I) are 1.99 Å (apical) and 2.08 Å (equatorial), in good agreement with the present values of 1.999(7) and 2.026(7) Å. The bite angle of 79.8(3)° is also very close to the previously reported values.

The Cu—O interactions give rise to two distinct sets of bond distances. Those in the CuN_2O_2 plane, which is planar to within +0.054 Å, are 1.950(6) and 1.923(6) Å, and are associated with C—O bonds in the ligand of 1.29(1) and 1.30(1) Å, respectively. These C—O bonds are shorter than those found in catecholate complexes, for which the average r(C—O) = 1.35 Å. The Cu—O bonds orthogonal to the CuN_2O_2 plane are substantially longer (2.40(1), 2.44(1) Å), and here the interaction is clearly with the oxygen atoms of carbonyl groups, for which the r(C═O) values of 1.22(1) and 1.23(1) Å are in fact almost identical with those in the *para*-position of the same rings (1.23(1), 1.24(1) Å. The bond lengths in the quinonoid ring, averaged over both ligands, are shown in Scheme 4 and establish that we are dealing with an *ortho*-enol of a 1,4-quinone, so that the complex is indeed $Cu(Lap)_2bpy$. The distortion from octahedral to tetragonal stereochemistry at copper(II) may be seen as the result of two synergistic factors. One is Jahn–Teller distortion, which has been invoked in many such situations, and the other is the significant electron localization in the appropriate C—O and C—C bonds in the *para*-quinonoid ring.

Zinc and cadmium complexes

As noted bove, the electrochemical oxidation of zinc or cadmium in the presence of lapachol gives the appropriate $M(Lap)_2$ complexes in good yield. These diamagnetic com-

© 1997 NRC Canada

Scheme 4.

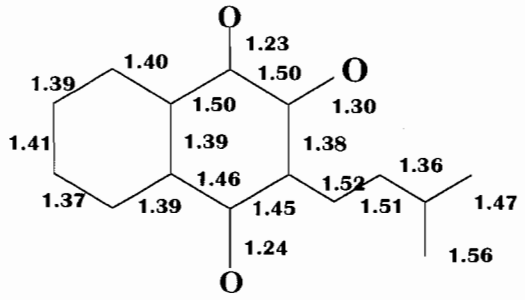


Table 6. ^{13}C NMR results for lapachol and M(Lap)$_2$ (M = Zn,Cd) (ppm) (Me_4Si=O) in DMSO.

C[a]	Lapachol	Zn(Lap)$_2$	Cd(Lap)$_2$
1	181.77	187.17	186.94
2	152.81	162.51	163.59
3	129.52	129.51	129.43
4	186.91	182.41	181.85
4a	134.19	135.22	134.80
5	132.92	131.67	130.00
6	126.12	125.76	125.32
7	126.64	125.86	125.55
8	132.92	131.67	131.34
8a	133.89	134.03	134.51
9	25.84	25.49	25.45
10	119.75	119.78	119.76
11	123.57	123.22	123.14
12*E*	22.70		22.61
13*Z*	17.98	17.64	17.86

[a]Numbering scheme as in Scheme 1.

pounds are clearly derivatives of the lapacholate monoanion (Scheme 2), and are Lewis acids, readily forming adducts with bidentate nitrogen donors. These are presumably six-coordinate, and isostructural with Cu(Lap)$_2$bpy.

The ^1H NMR spectra of these compounds (in d_6-DMSO) show that little change occurs between lapachol and the derivatives, other than the loss of the enol hydrogen, identified at 5.2 ppm (Me_4Si = 0). The ^{13}C spectra are more instructive, and Table 6 compares the results for lapachol and its zinc and cadmium derivatives. The largest changes in the ^{13}C chemical shift are at C2 and C1, corresponding to the transfer of charge to the metal centre and concomitant polarity changes in the C—O bonds. The effects are significantly greater for zinc, suggesting stronger binding of the ligand to this element than to cadmium, in keeping with the known behaviour of these metals with bidentate oxygen donors. Carbon-4, which carries the nonbonding carbonyl oxygen, becomes less shielded on complexation, with changes of ca. −5 ppm. The remaining differences are in the order of 0.5–1.0 ppm. Carbon atoms 5–8 are less shielded, while 4a and 8a show effects in the opposite sense. In general, complexation to zinc or cadmium causes a slight increase in negative charge on the fused aromatic ring, significantly stronger shielding at C1 and C2, and an interesting deshielding at C4. The chemical shifts of the carbon atoms of the side chain at C2 change by less than 0.5 ppm.

Acknowledgement

This work was supported in part by Operating Grants from the Conselho Nacional de Desenvolvimento Cientifico e Technologico, CNPQ, Brazil (to C.P.), and from the Natural Sciences and Engineering Research Council of Canada (to D.G.T.).

References

1. D.G. Tuck. Molecular electrochemistry of inorganic, bioinorganic and organometallic compounds. *Edited* by A.J.L. Pombeiro and J.A. McCleverty. Kluwer, Dordecht. 1992. p. 15.
2. F.F. Said and D.G. Tuck. Inorg. Chim. Acta, **59**, 1 (1982).
3. R.K. Chadha, R. Kumar, and D.G. Tuck. Can. J. Chem. **65**, 1336 (1987).
4. R.K. Chadha, R. Kumar, J.R. Lopez-Grado, and D.G. Tuck. Can. J. Chem. **66**, 2151 (1988).
5. J.H. Green, R. Kumar, N. Seudeal, and D.G. Tuck. Inorg. Chem. **28**, 123 (1989).
6. R. Kumar and D.G. Tuck. J. Organomet. Chem. **281**, C47 (1985).
7. C. Geloso, R. Kumar, J.R. Lopez-Grado, and D.G. Tuck. Can. J. Chem. **65**, 928 (1987).
8. A.E. Mabrouk and D.G. Tuck. J. Chem. Soc. Dalton Trans. 2539 (1988).
9. T.A. Annan, C. Peppe, and D.G. Tuck. Can. J. Chem. **68**, 423 (1990).
10. T.A. Annan, C. Peppe, and D.G. Tuck. Can. J. Chem. **68**, 1598 (1990).
11. S. Budaveri (*Editor*). The Merck index, Merck and Co. Inc., Rahway, N.J. 1989. p. 846.
12. D.T. Cromer and J.T. Waber. International tables for X-ray crystallography. Vol. 4. Kynoch Press, Birmingham. 1974. Table 2.2A.
13. J.H. Ibers and W.C. Hamilton. Acta Crystallogr. **17**, 781 (1964).
14. D.T. Cromer. International tables for X-ray crystallography. Vol. 4. Kynoch Press, Birmingham. 1974. Table 2.3.1.
15. TEXSAN-TEXRAY Structure and analysis package. Molecular Structure Corporation, The Woodlands, Tex. 1985.
16. M.E. Bodini and V. Arancibia. Polyhedron, **8**, 62 (1981).
17. F.F. Said and D.G. Tuck. Can. J. Chem. **59**, 62 (1981).
18. M. Khan, C. Oldham, and D.G. Tuck. Can. J. Chem. **59**, 2714 (1981).
19. R.K. Chadha, R. Kumar, and D.G. Tuck. Can. J. Chem. **65**, 1336 (1987).
20. M.A. Khan, R. Kumar, and D.G. Tuck. Polyhedron, **7**, 49 (1988).
21. T.A. Annan, R. Kumar, and D.G. Tuck. Inorg. Chem. **29**, 2475 (1990).
22. T.A. Annan, J.E. Kickham, and D.G. Tuck. Can. J. Chem. **69**, 251 (1991).
23. M.A. Khan and D.G. Tuck. Acta Crystallogr. Sect. B: Struct. Crystallogr. Cryst. Chem. **B37**, 1409 (1981).

Can. J. Chem. Downloaded from www.nrcresearchpress.com by 88.146.161.215 on 09/08/12
For personal use only.

© 1997 NRC Canada

Quantitative description of analyte migration behavior based on the dynamic complexation model in capillary electrophoresis

Xuejun Peng, Gwendolyn M. Bebault, Stephen L. Sacks, and David D.Y. Chen

Abstract: A theory based on dynamic complexation is used to describe analyte migration behavior in capillary electrophoresis (CE). This theory is based on a one-phase system, instead of the commonly accepted two-phase system. The migration behavior of an analyte is described by three parameters (the electrophoretic mobility of the free analyte, the electrophoretic mobility of the analyte–additive complex, and the equilibrium constant (formation constant) that determines the fractions of the free analyte and the complex at a certain additive concentration). Varying the additive concentration shifts the equilibrium and changes the viscosity of the background electrolyte. Viscosity correction is crucial in interpreting the observed migration behavior of analytes. While electroosmotic flow in a capillary often varies from one capillary to another, the viscosity of a buffer is characteristic of the buffer composition and is constant for each buffer. The electrophoretic mobility of a certain species and the equilibrium constant are intrinsic properties and are less sensitive to changes in the environment. Understanding these relationships is indispensable in CE method development and method validation. A universal resolution equation is proposed, with a separation factor that has taken both the electrophoretic mobilities and equilibria into consideration. This resolution equation gives clear guidance for the optimization of CE separations. A group of nucleosides and their phosphates are used as analytes, and β-cyclodextrin is used as the additive in the model system studied in this paper. Both the observed analyte migration behavior and the resolution of analytes agree well with this theory.

Key words: dynamic complexation capillary electrophoresis, nucleoside and nucleotide separation, capacity factor, resolution equation, viscosity correction.

Résumé : On a utilisé une théorie basée sur la complexation dynamique pour décrire le comportement d'un analyte lors de la migration en électrophorèse capillaire (EC). Cette théorie repose sur un système à une phase, au lieu du système à deux phases communément accepté. Le comportement de l'analyte, lors de la migration, est décrit par trois paramètres (la mobilité électrophorétique de l'analyte libre, la mobilité électrophorétique du complexe analyte–additif, et la constante d'équilibre (constante de formation) qui détermine les fractions de l'analyte libre et du complexe pour certaines concentrations de l'additif). La variation de la concentration de l'additif déplace l'équilibre et change la viscosité de l'électrolyte de support. La correction de la viscosité est vitale pour interpréter le comportement des analytes en migration. Alors que le débit électroosmotique dans un capillaire varie souvent d'un capillaire à l'autre, la viscosité d'un tampon est caractéristique de la composition du tampon et elle est constante pour chaque tampon. La mobilité électrophorétique d'une certaine espèce et la constante d'équilibre sont des propriétés intrinsèques et sont moins sensibles aux changements dans l'environnement. La compréhension de ces relations est indispensable pour le développement de la méthode de l'électrophorèse capillaire et pour la validation de cette méthode. On propose une équation de résolution universelle, avec un facteur de séparation qui tient compte à la fois des mobilités électrophorétiques et des équilibres. Cette équation de résolution donne une orientation claire en vue de l'optimisation des séparations par électrophorèse capillaire. On a utilisé un groupe de nucléosides et leurs phosphates comme analytes et on a utilisé la β-cyclodextrine comme additif dans le système modèle étudié dans cette publication. Le comportement de l'analyte lors de la migration et la résolution de l'analyte sont tous deux en parfait accord avec cette théorie.

Mots clés : électrophorèse capillaire par complexation dynamique; séparation de nucléoside, et de nucléotide; facteur de capacité; équation de résolution; correction de viscosité.

[Traduit par la rédaction]

Received October 18, 1996.

X. Peng, G.M. Bebault, and D.D.Y. Chen.[1] Department of Chemistry, University of British Columbia, Vancouver, BC V6T 1Z1, Canada.
S.L. Sacks. Department of Pharmacology and Therapeutics, University of British Columbia, Vancouver, BC V6T 1Z3, Canada.

[1] Author to whom correspondence may be addressed. Telephone: (604) 822-0878. Fax: (604) 822-2847. E-mail: chen@chem.ubc.ca

© 1997 NRC Canada

Can. J. Chem. Downloaded from www.nrcresearchpress.com by 88.146.161.215 on 09/08/12
For personal use only.

Can. J. Chem. Downloaded from www.nrcresearchpress.com by 88.146.161.215 on 09/08/12
For personal use only.

Introduction

Carrier-free zone electrophoresis was first demonstrated by Hjertén in 1967 (1). Although capillary electrophoresis (CE) for the zone separation of substances was described by Everaerts and Hoving in 1970 (2), this technology was mainly developed after Jorgenson and Lukacs demonstrated the feasibility of achieving high-efficiency zone separations in a simple carrier-free open tube capillary in 1981 (3). The equilibrium process was introduced, through the use of additives in the buffer system, by Terabe et al. in 1984 (4). Terabe's contribution has made CE the most powerful separation technique by combining both field and equilibria in the separation process.

Because the amount of additive used in CE systems is always described by the additive concentration, and that concentration determines the probabilities of collision and reaction between different molecules in a homogeneous solution, it should be considered as a one-phase system. Viscosity is one of the fundamental parameters that determines analyte mobility. Both the electroosmotic mobility and the electrophoretic mobility of an analyte are influenced by the viscosity change when additives are used. However, the additives affect the two mobilities rather differently. Except in a few papers published recently (5–9), most theoretical studies have not included the viscosity change in their fundamental equations.

This paper describes the separation of 20 analytes based on the dynamic complexation equilibria between the analytes and the additive in a CE system. In a one-phase system, the net analyte electrophoretic mobility is determined by three factors: the electrophoretic mobility of the free analyte, the electrophoretic mobility of the analyte–additive complex, and the equilibrium constant that determines the fraction of the analyte in the free or complexed form. The mobility of the free additive does not contribute to the analyte electrophoretic mobility. The relationship between the equilibrium constant and the electrophoretic mobilities can be quantified only when the viscosity change is corrected to the ideal state. This dynamic complexation capillary electrophoresis (DCCE) theory should be applicable to all open tubular CE including micellar electrokinetic capillary chromatography (MECC) (8, 10), affinity CE (11), chiral CE (12, 13), and other types of complexation, e.g., with charged cyclodextrins (10). The migration behavior of all types of analytes and additives, charged or neutral, can be described by this theory.

Theory

Analyte mobilities and the equilibrium constant

The electrophoretic mobility of a charged spherical molecule, μ_{ep}, is described by Debye–Hückel–Henry theory:

$$[1] \quad \mu_{ep} = \frac{Q_{eff}}{6\pi\eta R}$$

where Q_{eff} is the effective charge of the molecule, η is the viscosity of the background electrolyte, and R is the effective radius. It should be noted that μ_{ep} is mostly an intrinsic property determined by the charge-to-size ratio of a molecule, and the viscosity of the background electrolyte.

The electroosmotic mobility, μ_{eo}, was described by Hjertén, also based on the Debye–Hückel–Henry theory (1):

$$[2] \quad \mu_{eo} = \frac{\varepsilon\zeta}{4\pi\eta}$$

where ε is the dielectric constant of the background electrolyte, ζ (zeta potential) is the potential across the diffuse layer at the capillary wall, and η is the viscosity. To an analyte, the electroosmotic flow (EOF) is an external force originating from the capillary wall, and applied equally to all species in the capillary when an electric field is applied. The electroosmotic mobility is affected by many factors. The condition of the capillary wall is never the same from one capillary to another. Any additive used in the buffer system will alter at least one of the parameters that determines the EOF, i.e., the ionic strength, the properties of the diffuse layer and the zeta potential, and the dielectric constant of the background electrolyte. It is apparent that a neutral EOF marker may not accurately reflect the viscosity change in a CE system. In contrast to μ_{ep}, which is a constant in most situations, μ_{eo} changes even when the same capillary and buffer are used.

The prerequisite to separate species A from B in an additive-free CE system is that the charge-to-size ratios, or the electrophoretic mobilities ($\mu_{ep,A}$ and $\mu_{ep,B}$), of the two free analytes are different. If the two free mobilities are the same, an additive can be used to form complexes with the two analytes. The differential complexation and the different complex mobilities can change the net electrophoretic mobility of the analytes (μ_{ep}^{A} and μ_{ep}^{B}).

For analyte A, when an additive C is used in the buffer of a CE system, the equilibrium in a homogenous system can be represented as

$$[3] \quad A + C \rightleftharpoons AC$$

where A is the analyte, C is the additive or complexing agent (such as surfactant, host molecule, polyether, protein, etc.), and AC is the complex. Equation [3] has been used to describe chiral separations (14), affinity CE (11), and analyte–additive pairs with hydrogen-bonding capabilities (15).

The equilibrium constant, K, for eq. [3] is

$$[4] \quad K = \frac{[AC]}{[A][C]}$$

where [AC] is the complex concentration, [A] is the analyte concentration, and [C] is the concentration of the additive.

The capacity factor, k', also called the mass distribution coefficient, is defined in chromatography as the ratio of the amount of the analyte in the stationary phase compared with the amount of analyte in the mobile phase. A similar concept can be used in CE, where we define the capacity factor as the ratio of the amount of complex to the amount of free analyte. Because the additive and the analyte are in the same solution, the capacity factor is

$$[5] \quad k' = \frac{AC}{A} = \frac{[AC]}{[A]} = K[C]$$

In CE, the capacity factor is proportional to the additive concentration. Although [AC] and [A] at the edges of the migration zone may change during the CE separation because

© 1997 NRC Canada

Can. J. Chem. Downloaded from www.nrcresearchpress.com by 88.146.161.215 on 09/08/12
For personal use only.

of band broadening caused by diffusion, it is reasonable to assume that the concentrations are diluted to a similar extent and that this effect is canceled out in eq. [5]. Therefore, the capacity factor will not be affected. The fraction of the free analyte, f, is defined as $[A]/[A]_0$ ($[A]_0$ is the original analyte concentration). When $[C]_0$, the initial additive concentration, is much greater than $[A]_0$, [C] is equal to $[C]_0$. Substituting $[A]_0$ by [A] + [AC] gives:

$$[6] \quad f = \frac{1}{1 + k'}$$

The form of eq. [6] is identical to the fraction of time an analyte spends in the mobile phase as described in chromatographic theories. However, in chromatographic theories,[2] k' is defined as $K(V_S/V_M^0)$, where K is the concentration ratio of the analyte in the stationary phase and the mobile phase, V_S is the volume of the stationary phase, and V_M^0 is the corrected volume of the mobile phase, whereas in CE, k' is equal to K[C].

The net electrophoretic mobility of an analyte A (charged or neutral), μ_{ep}^A, is

$$[7] \quad \mu_{ep}^A = f\mu_{ep,A} + (1-f)\mu_{ep,AC} = \frac{1}{1+k'}\mu_{ep,A} + \frac{k'}{1+k'}\mu_{ep,AC}$$

where $\mu_{ep,AC}$ is the electrophoretic mobility of the complex.

Equation [7] is only valid for the ideal situation when changes in additive concentration do not affect the viscosity. In reality, the viscosity is often changed.

A viscosity correction factor, ν, is therefore introduced to convert the observed net electrophoretic mobility to an ideal state where the additive concentration approaches zero:

$$[8] \quad \nu\mu_{ep}^A = \frac{1}{1+k'}\mu_{ep,A} + \frac{k'}{1+k'}\mu_{ep,AC}$$

The correction factor, ν, is defined as η/η^0, where η is the viscosity of the running buffer at each [C], and η^0 is the viscosity of the solution when [C] is equal to 0. Because of the increase in viscosity, the value of ν is always greater than or equal to one, and the absolute value of the measured electrophoretic mobility is always smaller than or equal to the ideal state mobility. The effect of the correction factor is to convert the apparent electrophoretic mobility to an ideal state where the correction factor approaches one.

The apparent mobility of an analyte μ^A is equal to $\mu_{eo} + \mu_{ep}^A$. Rearranging eq. [8] and substituting μ_{ep}^A by $\mu^A - \mu_{eo}$ gives:

$$[9] \quad \frac{1}{\nu(\mu^A - \mu_{eo}) - \mu_{ep,A}} = \frac{1}{(\mu_{ep,AC} - \mu_{ep,A})K}\frac{1}{[C]} + \frac{1}{(\mu_{ep,AC} - \mu_{ep,A})}$$

Plotting $1/[\nu(\mu^A - \mu_{eo}) - \mu_{ep,A}]$ vs. $1/[C]$ should give a straight line. A similar equation without the correction factor has been proposed (16), however, the equation is only valid when the term $(\mu^A - \mu_{eo})$ is corrected if the viscosity varies with any change in additive concentration.

Note in eq. [9] that the term $\nu(\mu^A - \mu_{eo})$ is equal to net electrophoretic mobility of the analyte in the ideal state. Equations [7]–[9] describe the relationship between the equilibrium constant and the ideal state electrophoretic mobilities, because the analyte–additive interaction has nothing to do with electroosmotic flow.

The capacity factor can be expressed in terms of mobility by rearranging eq. [8]:

$$[10] \quad k' = \frac{\nu\mu_{ep}^A - \mu_{eo,A}}{\mu_{ep,AC} - \nu\mu_{ep}^A}$$

If the additives are large micelles, following the assumption made by Terabe et al. (4), the complex mobility is approximately the same as the mobility of the micelle. Assuming that the electrophoretic mobilities of free neutral analytes ($\mu_{ep,A}$) are zero, eq. [10] can be written as

$$[11] \quad k' = \frac{\nu(\mu^A - \mu_{eo}) - \mu_{ep,A}}{\nu(\mu^{MC} - \mu_{eo}) - \nu(\mu^A - \mu_{eo})} = \frac{\mu^A - \mu_{eo}}{\mu^{MC} - \mu^A}$$

where μ^A is the net mobility of the analyte, μ^{MC} is the mobility of the micelle, and μ_{eo} is the electroosmotic mobility. Equation [11] is identical to the original equation in MECC that was used to derive the k' expressed in terms of migration times. The fundamental difference between MECC theory and DCCE theory is that MECC theory uses the μ^{MC} to describe the analyte mobility, while DCCE theory uses $\mu_{ep,AC}$. It should be noted that, rigorously, μ^{MC} has nothing to do with the analyte mobility. The micelles should be treated as a second additive, and its concentration is related to the first one, the monomers, through the equilibrium of micelle formation. In addition, the MECC equation applies only to neutral analytes and charged micelles, while the theory based on dynamic complexation has no restriction on whether the analytes or additives are charged or not and thus should be applicable to all types of open tubular CE.

A universal resolution equation for open tubular CE

Many attempts have been made to formulate a resolution equation that can be used to describe the differential migration of two analytes. These attempts have been unsuccessful because the separation factor, α, has not been properly defined. In chromatographic theories, α has been known as the ratio of the two capacity factors (k'_B/k'_A).

However, the primary definition of α is $(c_A^M/c_A^S)/(c_B^M/c_B^S)$, where c_A^M, c_A^S, c_B^M, and c_B^S are the concentrations of analyte A and B in the two phases (mobile and stationary), respectively. This definition can not accurately describe the separation process for several reasons. First, the amount of analyte in moles, instead of the concentrations, should be used to describe the difference in the phase distribution of the analytes (even though the volumes will be canceled out in this definition). Secondly, the ratio does not correctly describe the differential migration between A and B, because (c_A^M/c_A^S) and (c_B^M/c_B^S) are not directly related to the migration rates of the analytes.

[2] F.F. Cantwell. University of Alberta Lecture Notes for Chem. 421 (unpublished): available on request, 1995.

© 1997 NRC Canada

Can. J. Chem. Downloaded from www.nrcresearchpress.com by 88.146.161.215 on 09/08/12
For personal use only.

Thirdly, if more than one stationary phase is used in a column, the separation factor will no longer have a clear physical meaning, and can not be used to predict the outcome of a separation. On the other hand, if α is defined as $[n_A^M/(n_A^S + n_A^M)]/[n_B^M/(n_B^S + n_B^M)]$, where $n_A^M/(n_A^S + n_A^M)$ and $n_B^M/(n_B^S + n_B^M)$ are the fractions of the analytes in the mobile phase, then the separation factor will reflect the difference in the migration rates of the two analytes. This is because the migration rate of an analyte is equal to the fraction of the analyte in the mobile phase times the velocity of the mobile phase. This definition can also be used to describe situations when more than one stationary phase is used. It should be noted that the previously defined α implies that the resolution is defined by k'_B/k'_A. In reality, the difference between the migration rates of the two analytes should be described by $(1 + k'_B)/(1 + k'_A)$, which is equal to α when defined as the ratio of the fractions of the analytes in the mobile phase.

In CE without complexation additives, the difference in migration rates is described by the difference in the electrophoretic mobilities of the analytes. Therefore, the separation factor should be defined as the ratio of the two electrophoretic mobilities ($\mu_{ep,A}/\mu_{ep,B}$).

Because both electric field and equilibrium are used in the separation process in DCCE, the separation is governed by both the electrophoretic mobilities and the equilibria involved. The separation factor should be defined as the ratio of the net electrophoretic mobilities (μ_{ep}^A/μ_{ep}^B) when the directions of the two mobilities are the same. This definition takes both mobility and equilibrium into account. When the additive concentration is zero, the separation factor is equal to $\mu_{ep,A}/\mu_{ep,B}$, which is the separation factor for carrier-free CE. A similar definition was suggested for chiral separations by Rawjee et al. (17). This definition should apply to all types of CE.

For two analytes in a one-additive CE system, the separation factor is

$$[12] \quad \alpha = \frac{\mu_{ep}^A}{\mu_{ep}^B} = \frac{\frac{1}{1 + k'_A}\mu_{ep,A} + \frac{k'_A}{1 + k'_A}\mu_{ep,AC}}{\frac{1}{1 + k'_B}\mu_{ep,B} + \frac{k'_B}{1 + k'_B}\mu_{ep,BC}}$$

Some authors have assumed that $K[C] \gg 1$ (i.e., $k' \gg 1$) without knowing the values of the equilibrium constants. This led to the conclusion that $\alpha = K_B/K_A$ (14). Actually, shifting the equilibrium is the most effective way of changing the net analyte mobility when k' is around 1. Others have defined $\alpha = k'_B/k'_A$, which again is equal to K_B/K_A (18). By assuming that α is a constant, it is also assumed that the resolution of two analytes can not be affected by a change in additive concentration. It should be emphasized that equilibrium is not the only factor that governs the separation process in CE. Electric field, which also leads to the differential migration of analytes, should also be included in the separation factor.

Assuming that the peak widths of the closely migrating analytes A and B are similar, the resolution, R_s, of two analytes is defined as

$$[13] \quad R_s = \frac{t_R^B - t_R^A}{\frac{1}{2}(W_A + W_B)} \approx \frac{\sqrt{N}}{4}\left(\frac{t_R^B - t_R^A}{t_R^A}\right)$$

where t_R^B and t_R^A are the migration times of the analytes, W is the average peak width, and N is the number of theoretical plates. Note that for two closely migrating analytes, either t_R^A or t_R^B can be used to calculate the separation efficiency.

Substituting $L_d/(\mu_{eo}^B + \mu_{eo})E$ and $L_d/(\mu_{eo}^A + \mu_{eo})E$ for t_R^B and t_R^A in eq. [13] gives:

$$[14] \quad R_s = \frac{\sqrt{N}}{4}(\mu_{ep}^A + \mu_{eo})\left(\frac{1}{\mu_{ep}^B + \mu_{eo}} - \frac{1}{\mu_{ep}^A + \mu_{eo}}\right)$$

$$= \frac{\sqrt{N}}{4}\left(\frac{1}{\mu_{ep}^B + \mu_{eo}}\right)(\mu_{ep}^A - \mu_{ep}^B)$$

where L_d is the length of the capillary from the inlet to the detector, and E is the electric field applied during the separation (applied voltage divided by the total length of the capillary).

Substituting μ_{ep}^A in eq. [14] by $\alpha\mu_{ep}^B$ (from eq. [12]) gives:

$$[15] \quad R_s = \frac{\sqrt{N}}{4}\frac{\mu_{ep}^B}{(\mu_{ep}^B + \mu_{eo})}(\alpha - 1)$$

Equation [14] is in agreement with the resolution equation proposed by Giddings in 1969 based on the assumption that $\Delta X \ll X$, where X is the migration distance and ΔX is the difference between the migration distances (19). However, there are two major differences between eq. [14] and the equation proposed by Giddings. First, equilibrium was not included in that equation, but is included in the μ_{ep}^A and μ_{ep}^B terms in eq. [14]. Second, there is a retention term in eq. [14] that is not apparent in Giddings' equation because μ_{eo} was not considered then.

Equation [14] can be divided into three distinct sections: the first part describes the column efficiency (N), the second part can be seen as the retention factor (longer migration time gives better resolution), and the third deals with selectivity. These three components give clear guidance for the optimization of CE separations. First, the column efficiency should be optimized. As demonstrated by Hjertén (20), we should not presume that band-broadening in CE is diffusion limited. Injection volume, the aggregation of analytes, wall effects, and electroosmotic flow can also cause significant band-broadening in CE. Second, analyte migration time has a direct impact on resolution because of the retention factor. When the column efficiency is the same, longer migration times give better resolution because the difference in the electrophoretic mobilities of the analytes can contribute longer to the differential migration. This has been demonstrated by Culbertson and Jorgenson (21), using hydrodynamic counter flow, and by Lucy and McDonald (22), and Bowser et al. (23), using EOF to counterbalance the electrophoretic mobility of the analytes, to increase the analyte migration time and achieve better resolution, and by many publications using gel or entangled polymer-filled capillaries. Third, the resolution can be improved by increasing the difference of the net electrophoretic mobilities of the analytes. This can be achieved by selecting an appropriate additive, adjusting the additive concentration, or even using more than one additive in the CE system.

© 1997 NRC Canada

Can. J. Chem. Downloaded from www.nrcresearchpress.com by 88.146.161.215 on 09/08/12
For personal use only.

Experimental section

Apparatus

A Beckman P/ACE 5000 Automated Capillary Electrophoresis System (Beckman Instruments (Canada) Inc., Misssissauga, Ont.) was used for the experiment. The capillary had a 75 μm inner diameter, 375 μm outer diameter, and was 57 cm in length (50 cm to the detector). Uncoated fused silica capillary columns were purchased from Polymicro Technologies (Phoenix, Ariz.). The capillary was cleaned with 1.0 M NaOH for 30 min followed by a 10 min rinse with deionized distilled water, and was equilibrated with electrophoresis running buffer overnight before being used for separation. Absorption was monitored at 254 nm except for benzene. A 0.1% v/v benzene in the buffer solution was used to measure the electroosmotic mobility and was monitored at 214 nm. Samples were introduced by pressure injection for 2 s, and a voltage of 25 kV was used to run the separations. Data were collected using the System Gold software package (Beckman) and a 486 PC computer.

Procedure

The instrument was programmed to rinse the capillary with the electrophoresis buffer at high pressure for 2 min. The buffer (pH 9.1) was prepared with 50 mM $Na_2B_4O_7{\cdot}10H_2O$ (Borax) and 200 mM boric acid. The 200 mM borate buffer was then diluted to 160 mM, which was the buffer used in this experiment. Different concentrations of β-cyclodextrin (β-CD) were added as described in the Results and discussion. The temperature of the capillary was held at 20°C. It should be noted that there will be some temperature gradient between the center of the capillary and the wall, but the average temperature is 20°C. However, because the viscosity is measured as a bulk property, the difference between a liquid of 20°C and a liquid with an average temperature of 20°C is not too great. The viscosity of the running buffer was measured by injecting a plug of thymidine into the capillary, and monitoring the time required for the plug to reach the detector window when a 20 psi (1 psi = 6.9 kPa) pressure was applied to the inlet of the capillary.

Chemicals

The nucleosides, adenosine (A), guanosine(G), uridine(U), thymidine (T), and cytidine (C), were in the form of free bases. Adenosine 5′-mono-, di-, and tri-phosphate (AMP, ADP, ATP); uridine 5′-mono-, di-, and tri-phosphate (UMP, UDP, UTP); cytidine 5′-mono-, di-, and tri-phosphate (CMP, CDP, CTP); guanosine 5′-mono-, di-, and tri-phosphate (GMP, GDP, GTP); thymidine 5′-mono, di-phosphate (TMP, TDP), and deoxythymidine 5′-triphosphate (dTTP) were sodium salts. All the nucleosides and nucleotides were purchased from Sigma (St. Louis, Mo.) and dissolved in water as stock solutions with concentrations ranging from 5.0×10^{-2} M to 1.0×10^{-3} M. Penciclovir (PCV), an acyclic guanosine analog (9-(4-hydroxy-3-hydroxymethylbut-1-yl)guanine), was provided by SmithKline Beecham Pharmaceuticals (Brentford, U.K.). A mixture of nucleosides (2.0×10^{-4} M each) and nucleotides (2.5×10^{-4} M each) was prepared by combining each component from stock solutions. Samples were prepared by adding 20 μL of the mixture to 200 μL of electrophoresis buffer, or by diluting the individual stock solutions to the appropriate concentration with buffer when used as standards for peak identification. β-CD, Borax, and boric acid were purchased from Sigma.

Results and discussion

Viscosity

Accurately measuring the viscosity of the solution in the capillary is necessary to obtain the viscosity correction factor and thus the equilibrium constant. The relationship between the viscosity of a Newtonic liquid and the average linear velocity of the liquid flowing through a capillary under a certain pressure can be described by Poiseuille's equation:

$$[16] \quad U^* = \frac{\Delta P r^2}{8\eta L_c}$$

where U^* is the average linear velocity of the liquid, ΔP is the pressure applied to the capillary, r and L_c are the radius and length of the capillary, respectively, and η is the viscosity of the liquid. Rearranging eq. [16] and replacing U^* with L_d/t gives:

$$[17] \quad \eta = \frac{\Delta P r^2 t}{8 L_c L_d}$$

where L_d is the effective length of the capillary (from the inlet to the detector), and t is the time required for the sample plug to travel from the inlet to the detector when a pressure of ΔP is applied.

Viscosity was measured by injecting a plug of 2×10^{-4} M thymidine into the inlet of a capillary and applying a constant pressure to push the sample plug through the capillary. The Beckman CE system used in this study has a lag period of 0.045 min between when the instruction is given by the computer and when the pressure of 20 psi is fully applied. This time lag must be subtracted from the measured sample migration time.

The viscosity of pure water was measured to be 1.1 cP (1P = 0.1 Pa s) at 20°C. This viscosity value is about 10% higher than the value listed in the CRC Handbook of Chemistry and Physics (1.002 cP) (24). This discrepancy may arise from variations in the capillary diameter, the time required for the pressure to rise to 20 psi, and the uncertainty in the length of the capillary. The accuracy of the pressure and the temperature may also affect the results of the absolute viscosity. The relative viscosity, however, should be unaffected. With a known value for the viscosity of pure water, the viscosity of other solutions can be obtained by:

$$[18] \quad \eta = \frac{\eta_{H_2O} \times t}{t_{H_2O}}$$

where η_{H_2O} and t_{H_2O} are the viscosity and time values for water, and η and t are the viscosity and time values of the solution to be measured. Table 1 is a list of the viscosity values for buffer solutions at different β-CD concentrations. The results were obtained from five measurements with two different capillaries. Using these viscosity values, the correction factor ν in eq. [8] can be calculated.

© 1997 NRC Canada

Can. J. Chem. Downloaded from www.nrcresearchpress.com by 88.146.161.215 on 09/08/12
For personal use only.

Table 1. Viscosity values for the 160 mM borate buffer solutions with different β-CD concentrations.[a]

β-CD Concentration (mM)	Viscosity (cP)
0	1.05 ± 0.01
5.0	1.06 ± 0.01
7.5	1.07 ± 0.01
10.0	1.08 ± 0.01
12.5	1.08 ± 0.01
15.0	1.09 ± 0.01
20.0	1.11 ± 0.01

[a]The Viscosity was measured in a 160 mM borate buffer (pH 9.1).

Although the electric current changes when the buffer viscosity is varied, the viscosity change is not the only factor that produces a change in the current. For example, addition of sodium dodecyl sulfate (SDS) increases the viscosity of a solution as well as the current. In other cases when nonionic species such as β-CD are added, the current decreases. Some interactions between species in the solution may also affect the current. Current ratio can be used as a correction factor only when it is proven experimentally that it changes at the same rate as the viscosity (7), thus eventually the viscosity ratio has to be obtained from direct viscosity measurements.

Calculating the equilibrium constants

Substituting the mobility μ with L_d/tE, where E is the electric field, and t is the migration time, eq. [9] can be rearranged to:

$$[19]\quad \frac{1}{\nu\left(\frac{1}{t}-\frac{1}{t_{eo}}\right)-\frac{1}{t_{ep,A}}} = \frac{1}{\left(\frac{1}{t_{ep,AC}}-\frac{1}{t_{ep,A}}\right)K}\frac{1}{[C]}+\frac{1}{\frac{1}{t_{ep,AC}}-\frac{1}{t_{ep,A}}}$$

The equilibrium constant was calculated by plotting $1\Big/\left[\nu\left(\frac{1}{t}-\frac{1}{t_e}\right)-\frac{1}{t_{ep,A}}\right]$ vs. 1/[C]. Electroosmotic flow rates were obtained by measuring the migration time of a benzene plug through the capillary at different additive concentrations. The neutral molecules, benzene, acetone, and dimethyl formamide, were tested and any of them can be used as the EOF marker in this case because the additive is neutral. The migration times of the analytes were measured from each electropherogram, and the electroosmotic flow rate was measured separately at each β-CD concentration using benzene as a marker. The $1/t_{ep,A}$ value was calculated from $[(1/t_A^0) - (1/t_{eo}^0)]$, where t_A^0 and t_{eo}^0 are the migration time of analyte A and the migration time of the EOF marker, respectively, when there is no additive added to the buffer solution. The migration times of the analytes and the EOF marker were then measured at different β-CD concentrations.

The K for each nucleoside and nucleotide with β-CD was obtained by dividing the intercept by the slope of the linear fitted line. When experiments were repeated with a different capillary and a different batch of buffer solution (same borate concentration), the migration times of the marker and the analytes changed by about 15% because of the change in the EOF. The K values, however, are nearly identical from the two experiments. The average K values, the standard deviations of the two sets of data, and the R^2 values for the curve fittings of both experiments are listed in Table 2. The standard deviations were calculated from the differences in the values obtained from independent measurements. When the change in viscosity is not significant, the K values will be affected less; when there is a significant change in viscosity because of the change in additive concentration, the effect of the correction factor may be very large. For example, when the β-CD concentrations range from 0 to 20 mM, and when the viscosity change is corrected for, the equilibrium constants (K) obtained for ADP and CMP are 50.7 ± 2.8 and 79.5 ± 4.2, respectively. Under the same conditions without the viscosity correction, the values are 21.6 ± 1.8 and 34.2 ± 3.3, respectively.

Table 2. Complexation equilibrium constants for five nucleosides and their phosphates with β-CD.[a]

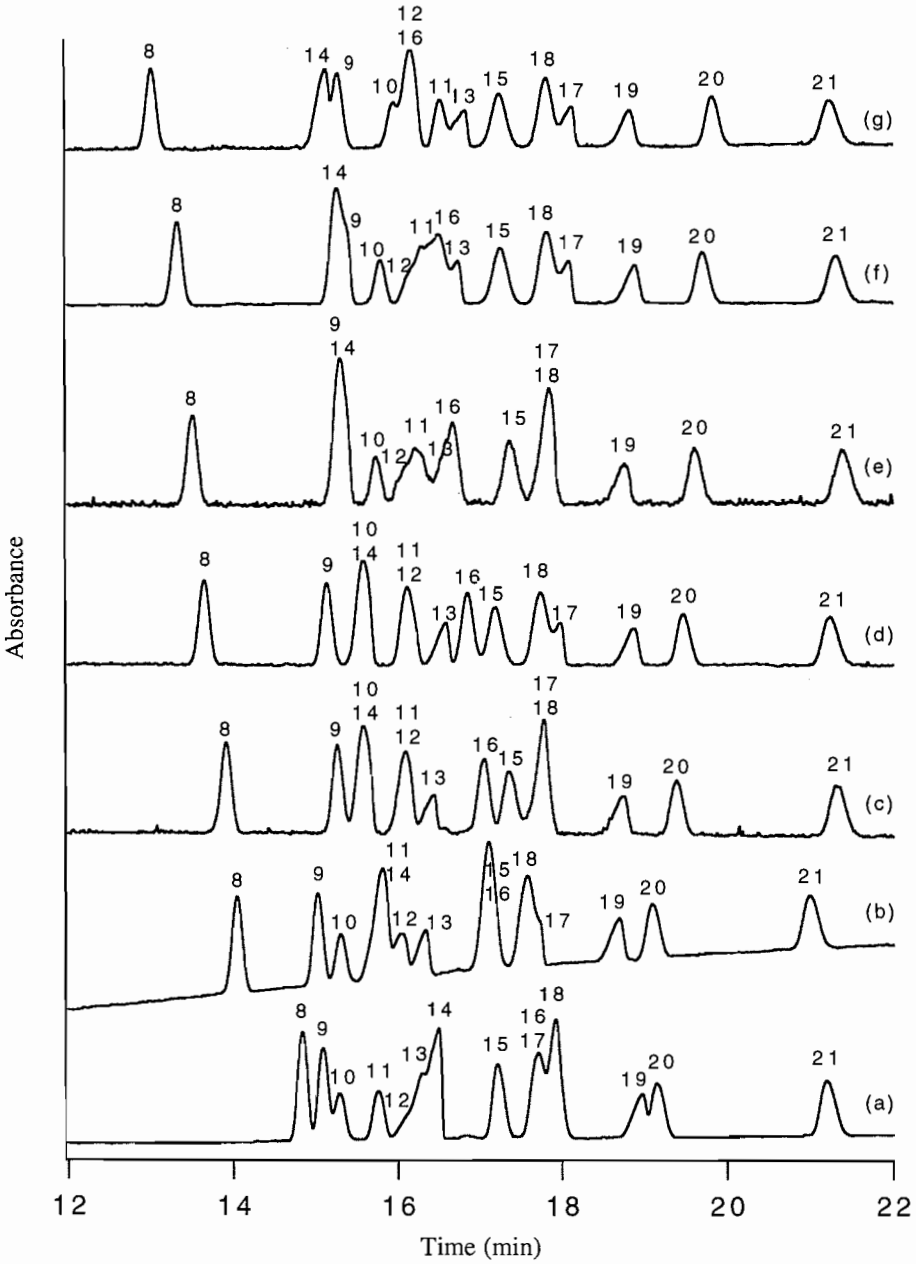
Analyte	K (M^{-1})	R_1^2	R_2^2
A	21.0 ± 2.3	0.958	0.966
C	44.4 ± 1.5	0.968	0.959
G	12.3 ± 1.1	0.959	0.952
U	13.1 ± 0.9	0.950	0.960
T	17.1 ± 0.7	0.953	0.970
AMP	21.4 ± 3.3	0.996	0.986
CMP	79.5 ± 4.2	0.956	0.962
GMP	20.2 ± 1.6	0.987	0.946
UMP	18.6 ± 1.8	0.988	0.957
TMP	27.8 ± 0.2	0.981	0.941
ADP	50.7 ± 2.8	0.971	0.984
CDP	31.8 ± 1.9	0.969	0.959
GDP	13.5 ± 2.7	0.962	0.955
UDP	22.9 ± 0.9	0.984	0.951
TDP	16.6 ± 1.9	0.950	0.931
ATP	31.0 ± 2.6	0.978	0.954
CTP	15.5 ± 1.9	0.962	0.950
GTP	35.8 ± 3.7	0.953	0.984
UTP	25.3 ± 0.04	0.963	0.943
TTP	35.0 ± 0.8	0.960	0.926

[a]The formation constants are measured in 160 mM borate buffer at pH 9.1.

It should be emphasized that the purpose of obtaining the K value is to describe the analyte migration behavior. When the difference in the free and complex mobilities is small, a slight change in viscosity (even if it is less than 1%) will cause significant change in the K values. The error range obtained from regression analysis alone can be underestimated. However, in this situation, the effect of K values on the change in analyte mobility is also reduced because the equilibrium does not play as important a role as when there is a large difference in the free and complex mobilities. Another possibility for the error in the reported K values being underestimated is the influence of temperature. The temperature at the center of the capillary can be quite different from

© 1997 NRC Canada

Fig. 1. The electropherograms of nucleosides and their phosphates in 160 mM borate buffer at pH 9.1 with different amounts of β-CD added to the solution. The concentrations (mM) of β-CD are (a) 0, (b) 5, (c) 7.5, (d) 10, (e) 12.5, (f) 15, and (g) 20. The analytes are: 8. AMP, 9. GMP, 10. ATP, 11. TTP, 12. GTP, 13. TDP, 14. CMP, 15. UMP, 16. ADP, 17. GDP, 18. CTP, 19. UTP, 20. CDP, 21. UDP.



that of the region close to the capillary wall. However, for the purpose of predicting the migration behavior of the analytes, as our results show, the temperature difference does not introduce a significant amount of error. This is because it is the trend of the viscosity change that determines the accuracy of the K value, and it is the averaged macroscopic K value throughout the capillary that determines the analyte migration behavior, not the microscopic K value at a particular spot in the capillary.

It was suggested by Hoffman and Bock in 1970 that β-CD specifically complexes with adenosine nucleotides, and the formation constants were measured by UV spectroscopy (25). Formoso further investigated nucleotide–cyclodextrin complexation by circular dichroism, and indicated that β-CD also forms complexes with other nucleotides (26, 27). The formation constants obtained by DCCE are reasonably close to the values listed in these papers but exhibit much better precision. Because borate buffer was used in the separation media, the K values also reflect the effect of possible complexation between borate and the ribose hydroxyls. One should expect slight differences in the K values when a different buffer system is used. Equations [3]–[9] only describe the migration behavior of the analytes when the interaction between the additive and the analyte is (or can be considered) a simple 1:1 complex. Those equations can be modified to describe other types of interactions.

Can. J. Chem. Downloaded from www.nrcresearchpress.com by 88.146.161.215 on 09/08/12
For personal use only.

© 1997 NRC Canada

Can. J. Chem. Downloaded from www.nrcresearchpress.com by 88.146.161.215 on 09/08/12
For personal use only.

Changes in analyte mobilities

Borate buffer (160 mM, pH 9.1) with 0, 5, 7.5, 10, 12.5, 15, and 20 mM β-CD added to the solution was used in this study. The mobility of an analyte can be changed by changing the β-CD concentration. Figure 1 shows sections of electropherograms from separations of a mixture of nucleosides and their mono-, di-, and tri-phosphates at different β-CD concentrations. The differential migration of this group of analytes arises from their differences in size and charge, as well as the differences in their equilibrium constants with the additive. Similar phenomena have been discussed for chiral compounds (13).

Usually when an additive with a larger molecular weight is added to the buffer, the solution becomes more viscous. One would expect the analytes to migrate more slowly in the more viscous solution, especially in the presence of complexation equilibria. However, as shown in Fig. 1, there is no significant trend of increased migration times as the concentration of β-CD is increased from 0 to 20 mM. This phenomena is explained by eq. [8]. In the 160 mM borate buffer (pH = 9.1), all of the nucleosides and nucleotides have negative electrophoretic mobilities. When an analyte forms a complex with a neutral additive (β-CD), the electrophoretic mobility of the complex will be smaller than that of a free ion because of the smaller charge-to-size ratio. The complex should actually move faster with a reduced negative electrophoretic mobility. There was no significant reduction in the migration time either, except for a few analytes (e.g., AMP and CMP), because the increased viscosity impeded the movement of the analytes. AMP, CMP, and all other analytes would have moved faster if there were no viscosity changes. Without considering the viscosity correction factor, a smaller K would be obtained for this group of analyte–additive interactions because the apparent mobilities did not increase as much as they would have increased if there were no change in viscosity.

There are two factors that affect the electrophoretic mobility of an analyte: the difference between the mobilities of the free analyte and the complex ($\mu_{ep,AC} - \mu_{ep,A}$), and k'. Peak 8 (AMP) has a relatively large change in mobility when different concentrations of β-CD are added to the buffer because of the large difference between the $\mu_{ep,A}$ and the $\mu_{ep,AC}$ of AMP. Peaks 14 and 16 (CMP and ADP) demonstrate large mobility changes mainly because they have relatively large K values. Peaks 17 and 18 (GDP and CTP) have relatively smaller changes in mobilities because their K values are small. An analyte (e.g., peak 14, CMP) could overlap with or be separated from the other analytes by changing the additive concentration.

Optimizing separation conditions

As discussed in the theory section, the net electrophoretic mobility in the ideal state is described by $\mu_{ep,A}$, $\mu_{ep,AC}$, and the equilibrium constant, K. The effect of viscosity has to be included in order to interpret the real experimental results.

From electropherograms obtained without using β-CD, the electrophoretic mobilities of the free analytes can be obtained. The complex electrophoretic mobility can be calculated from the intercept of eq. [9]. These values are listed in Table 3. Based on the values in Tables 2 and 3, the net electrophoretic mobility of each analyte can be described by eq. [8]. Figure 2*a* shows the plots of the ideal state net electrophoretic mobilities for some of the harder-to-separate nucleotides in this buffer system. The curves in Fig. 2*b* are the net electrophoretic mobilities of the same group of nucleotides with the viscosity change taken into consideration (the ideal state mobility divided by the viscosity correction factor as a function of additive concentration). The symbols (e.g., +, x, etc.) are the μ_{ep}^{A} values measured experimentally. The experimental data agree well with the values predicted by DCCE theory. The experimental values are systematically higher than predicted at 12.5 mM β-CD, and lower at 20 mM. This may be due to the error introduced from measuring the EOF in separate runs.

Table 3. List of ideal state ([C] → 0) electrophoretic mobilities of the free analytes and the electrophoretic mobilities of the analyte–β-CD complexes.

Analyte	$\mu_{ep,A}$ ($\times 10^{-4}$ cm^2 V^{-1} s^{-1})	$\mu_{ep,AC}$ ($\times 10^{-4}$ cm^2 V^{-1} s^{-1})
A	−0.143	−0.064
AMP	−0.297	−0.158
ADP	−0.317	−0.254
ATP	−0.301	−0.250
C	−0.143	−0.110
CMP	−0.310	−0.257
CDP	−0.326	−0.270
CTP	−0.319	−0.195
G	−0.171	−0.081
GMP	−0.300	−0.219
GDP	−0.317	−0.189
GTP	−0.308	−0.251
U	−0.177	−0.099
UMP	−0.314	−0.216
UDP	−0.335	−0.258
UTP	−0.325	−0.248
T	−0.026	−0.017
TMP	−0.254	−0.198
TDP	−0.304	−0.220
TTP	−0.308	−0.261

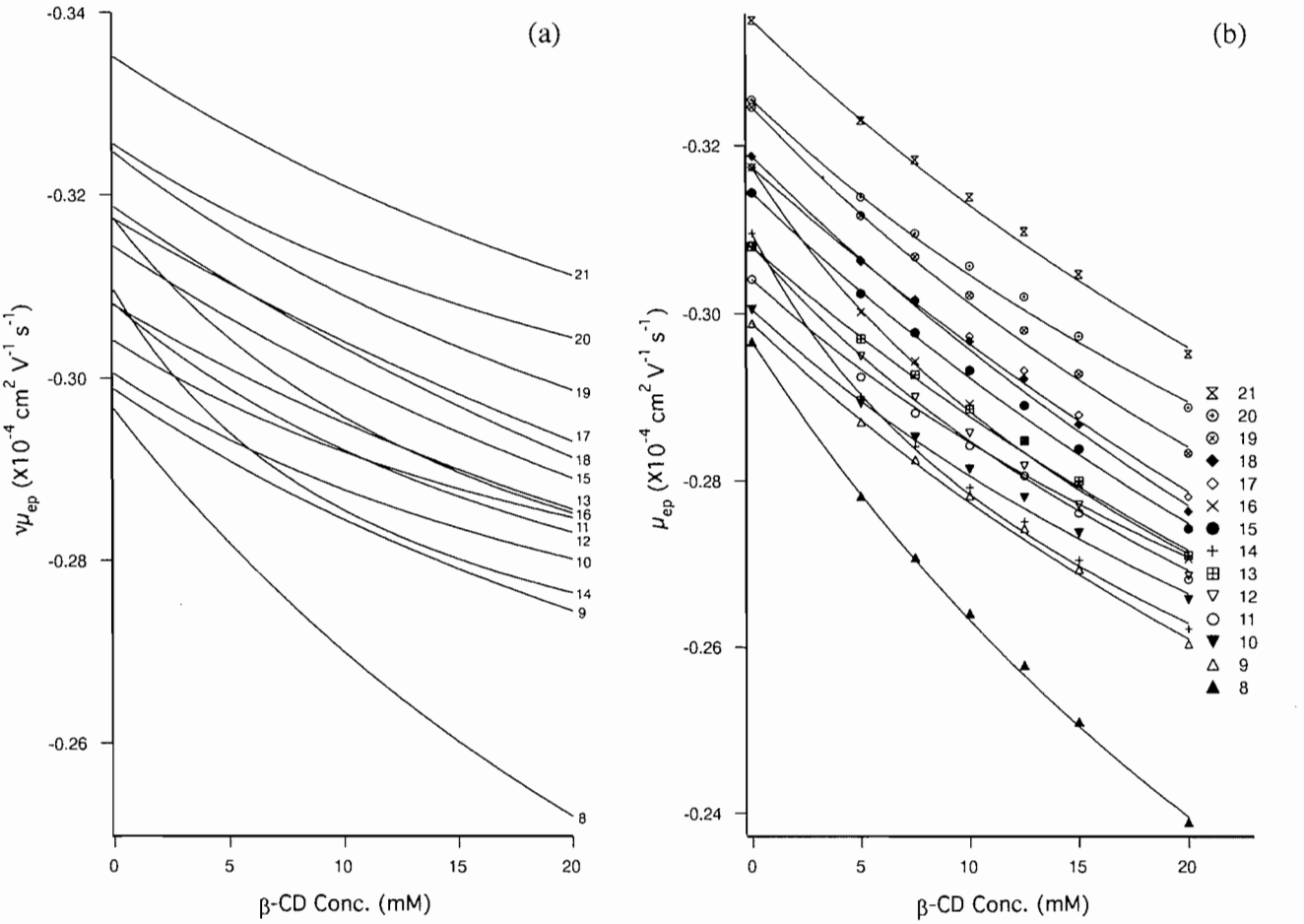
The y intercepts of the curves in Fig. 2 are the electrophoretic mobilities of the free analytes in additive-free solutions. Depending on the K value, the electrophoretic mobility of each analyte changes differently. An optimum additive concentration can be found based on the electrophoretic mobility vs. concentration plot. The optimum condition is at the additive concentration where the overlap of the corrected electrophoretic mobility curves is minimal. The effect of mobility difference on peak resolution can be observed by comparing the μ_{ep} vs. [C] plot in Fig. 2 with the electropherograms in Fig. 1.

The resolution equation

When the separation factor is defined as the ratio of the electrophoretic mobilities of two analytes, the resolution of two peaks can be calculated from eq. [15] based on the analyte electrophoretic mobility, the migration time, and the separation factor. Figure 3 demonstrates the separation of nucleosides A and C at different β-CD concentrations. The measured resolution is obtained from eq. [13] using the average peak width and the difference in migration time measured from the

© 1997 NRC Canada

Fig. 2. The electrophoretic mobilities of analytes as a function of additive concentration. Figure 2*a* shows the changes in the net electrophoretic mobilities of different analytes in the ideal state. All curves are simulated using eq. [8] with the $\mu_{ep,A}$, the $\mu_{ep,AC}$, and the K values from Tables 2 and 3. The curves in Fig. 2*a* are numbered according to the numbers assigned to the compounds in Fig. 1. Figure 2*b* shows the changes in the measured net electrophoretic mobilities (μ_{ep}^{A}) of different analytes at different additive concentrations. The smooth curves (solid lines) are the calculated results with the viscosity change taken into consideration. The number beside each symbol represents the same analyte as in Fig. 1 and Fig. 2*a*. The symbols (e.g., +, x, etc.) are the μ_{ep}^{A} values measured experimentally.



electropherogram. Because it is not possible to accurately measure the peak widths of the overlapped A and C peaks when the concentration of β-CD is 0, 5.0, or 7.5 mM, the average peak width of PCV and G is used as the average peak width of A and C. At other concentrations, the average peak width of A and C is used to obtain the measured resolution. When eq. [15] is used to calculate the resolution, the theoretical plate number N is calculated from $5.54(t_r/W_{1/2})^2$, where the peak width at half maximum (PWHM, $W_{1/2}$) is obtained from a Gaussian fit of the analyte peak. For 0 and 5 mM β-CD, the number of theoretical plates is taken from the average of the PCV and the G peaks, while for other concentrations the C peaks are used. Both the measured and the calculated resolution values are listed in Table 4. The proposed resolution equation (eq. [15]) can accurately predict the resolution of two closely migrating analytes.

Conclusion

CE theory based on dynamic complexation describes the migration behavior of analytes at the molecular level. It is applied to the separation of 20 nucleosides and nucleotides when β-CD is used as an additive. Three parameters (K, $\mu_{ep,A}$, and $\mu_{ep,AC}$) and viscosity determine the net electrophoretic mobility of an analyte at any given additive concentration. Clarification of these fundamental relationships has tremendous impact on method development, separation optimization, and method validation. While the EOF is difficult to control, the electrophoretic mobility of an analyte, which is the real reflection of the intrinsic properties of a species, is reproducible. The μ_{ep} values, not the migration times, should be used as the comparison parameters in method validation. The equilibrium constant of an analyte–additive interaction and the viscosity of a solution with certain composition are also constants. More $\mu_{ep,A}$, $\mu_{ep,AC}$, K, and ν values should be collected to make CE a predictable systematic science.

A universal resolution equation is derived from DCCE theory. This resolution equation is verified by its ability to accurately predict separation results. The separation factor takes both analyte electrophoretic mobilities (free and complexed) and the analyte–additive interaction into account. The resolution equation gives clear guidance for method development.

Can. J. Chem. Downloaded from www.nrcresearchpress.com by 88.146.161.215 on 09/08/12
For personal use only.

© 1997 NRC Canada

Fig. 3. The change in the resolution of A and C as the additive concentration increases. The β-CD concentrations for electropherograms (a)–(g) are the same as the concentrations in Fig. 1.

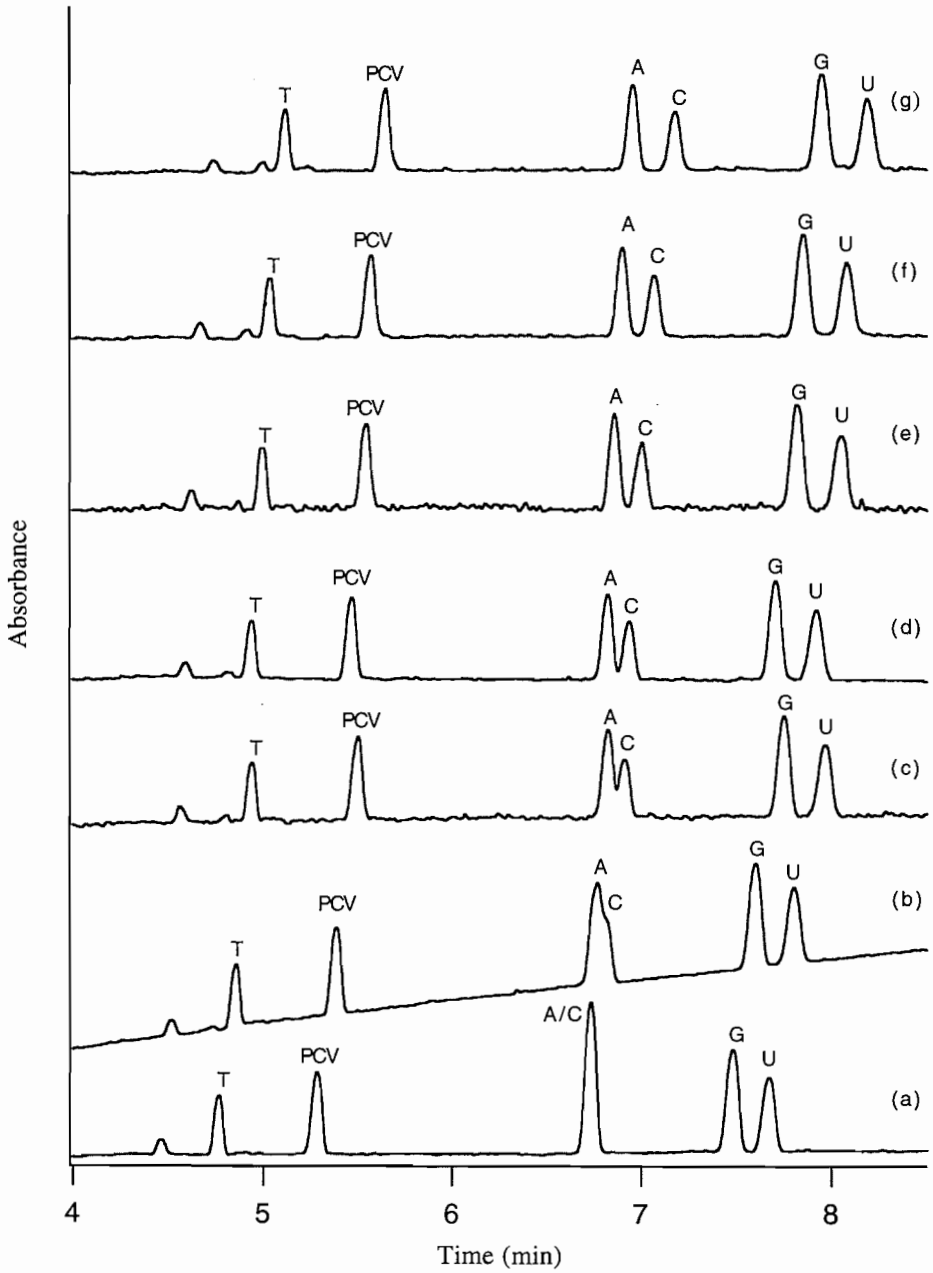


Table 4. List of the measured and calculated resolution values for nucleosides A and C at different β-CD concentrations.

β-CD concentration (mM)	0	5.0	7.5	10.0	12.5	15.0	20.0
R_s, measured	0	0.42	0.69	1.01	1.20	1.49	2.03
R_s, calculated	0	0.42	0.62	0.96	1.10	1.47	1.93

Can. J. Chem. Downloaded from www.nrcresearchpress.com by 88.146.161.215 on 09/08/12
For personal use only.

© 1997 NRC Canada

Acknowledgments

The authors thank Professor Richard A. Wall of the Department of Pharmacology and Therapeutics, University of British Columbia, and Dr. Richard Palmieri of Beckman Instruments, Inc., Fullerton, California, for their insightful discussions. This work is supported by the Department of Chemistry of the University of British Columbia, the Natural Sciences and Engineering Research Council of Canada, and Viridae Clinical Sciences Inc.

References

1. S. Hjertén. Chromatogr. Rev. **9**, 122 (1967).
2. F.M. Everaerts and K.W.M.L. Hoving. Sci. Tools, **17**, 25 (1970).
3. J.W. Jorgenson and K.D. Lukacs. Anal. Chem. **53**, 1298 (1981).
4. S. Terabe, K. Otsuka, K. Ichikawa, A. Tsuchiya, and T. Ando. Anal. Chem. **56**, 111 (1984).
5. A. Shibukawa, D.K. Lloyd, and I.W. Wainer. Chromatographia, **35**, 419 (1993).
6. S.G. Penn, D.M. Goodall, and J.S. Loran. J. Chromatogr. **636**, 149 (1993).
7. S.G. Penn, E.T. Bergstrom, I. Knights, G. Liu, A. Ruddick, and D.M. Goodall. J. Phys. Chem. **99**, 3875 (1995).
8. K.L. Rundlett and D.W. Armstrong. J. Chromatogr. A, **721**, 173 (1996).
9. M.R. Schure and R.E. Merphy. Electrophoresis, **16**, 2074 (1995).
10. S. Terabe, H. Ozaki, K. Otsuka, and T. Ando. J. Chromatogr. **332**, 211 (1985).
11. R. Kuhn, R. Frei, and M. Christen. Anal. Biochem. **218**, 131 (1994).
12. R. Kuhn and S. Hoffstetter-Kuhn. Chromatographia, **34**, 505 (1992).
13. S.A.C. Wren and R.C. Rowe. J. Chromatogr. **603**, 235 (1992).
14. A. Guttman, A. Paulus, A.S. Cohen, N. Grinberg, and B.L. Karger. J. Chromatogr. **448**, 41 (1988).
15. Y. Esaka, Y. Yamaguchi, K. Kano, G. Masashi, H. Haraguchi, and J.-I. Takahashi. Anal. Chem. **66**, 2441 (1994).
16. R. Kuhn and S. Hoffstetter-Kuhn. Capillary electrophoresis: principles and practice. Springer-Verlag, New York. 1993. pp. 91–93.
17. Y.Y. Rawjee, R.L. Williams, and G. Vigh. J. Chromatogr. **635**, 291 (1993).
18. J.R. Mazzeo, M.E. Swartz, and E.R. Grover. Anal. Chem. **67**, 2966 (1995).
19. J.C. Giddings. Sep. Sci. **4**, 181 (1969).
20. S. Hjertén. Electrophoresis, **11**, 665 (1990).
21. C.T. Culbertson and J.W. Jorgenson. Anal. Chem. **66**, 955 (1994).
22. C.A. Lucy and T.L. McDonald. Anal. Chem. **67**, 1074 (1995).
23. M.T. Bowser, E.D. Sternberg, and D.D.Y. Chen. Anal. Biochem. **241**, 143 (1996).
24. R.W. Weast (*Editor*). CRC handbook of chemistry and physics. 68 ed. CRC Press Inc., Boca Raton, Fla. 1987.
25. J.L. Hoffman and R.M. Bock. Biochemistry, **9**, 3542 (1970).
26. C. Formoso. Biochem. Biophys. Res. Commun. **50**, 999 (1973).
27. C. Formoso. Biopolymers, **13**, 909 (1974).

Can. J. Chem. Downloaded from www.nrcresearchpress.com by 88.146.161.215 on 09/08/12
For personal use only.

© 1997 NRC Canada

Photodecarbonylation of chiral cyclobutanones

Jailall Ramnauth and Edward Lee-Ruff

Abstract: Triplet photosensitized irradiation of 2(*S*),3(*R*)-bis[(benzoyloxy)methyl]cyclobutanone gave optically pure (−) *E*-1(*S*),2(*S*)-bis(benzoyloxymethyl)cyclopropane as a major product in the nonpolar fraction along with its stereoisomer and cycloelimination products. The absolute stereochemistry of the chiral cyclopropane was established by independent synthesis and X-ray crystal structure determination of a synthetic precursor. The distribution of decarbonylation and cycloelimination products was inversely dependent on the concentration of the substrate. Irradiation of the same ketone in tetrahydrofuran or benzene gave mostly cycloelimination products. Addition of Michler's ketone increased the ratio of photodecarbonylation, suggesting a triplet state pathway for this process. This was corroborated by the addition of dicyanoethylene, which showed significant quenching of photodecarbonylation. Irradiation of 2(*S*)-[(benzoyloxy)methyl]cyclobutane in acetone gave the corresponding cyclopropane as the principal product.

Key words: photodecarbonylation, chiral cyclopropanes, cyclobutanones, triplet sensitization.

Résumé : L'irradiation triplet photosensibilisée de la 2(*S*),3(*R*)-bis[(benzoyloxy)méthyl]cyclobutanone conduit au (−)-*E*-1(*S*),2(*S*)-bis(benzoyloxyméthyl)cyclopropane comme produit majeur de la fraction non polaire avec son stéréoisomère et des produits de cycloélimination. La stéréochimie absolue du cyclopropane chiral a été déterminée par une synthèse indépendante et par diffraction des rayons X d'un précurseur de synthèse. La distribution des produits de décarbonylation et de cycloélimination varie d'une façon inverse de la concentration du substrat. L'irradiation de la même cétone dans du tétrahydrofurane ou le benzène conduit principalement à des produits de cycloélimination. L'addition de la cétone de Michler augmente le rapport de photodécarbonylation; ceci suggère que le processus se produit par le biais d'un état triplet. Cette conclusion est corroborée par l'addition de dicyanoéthylène qui provoque une désactivation importante de la photodécarbonylation. L'irradiation du 2(*S*)-[(benzoyloxy)méthyl]cyclobutane dans l'acétone conduit au cyclopropane correspondant comme produit principal.

Mots clés : photodécarbonylation, cyclopropanes chiraux, cyclobutanones, sensibilisation triplet.

[Traduit par la rédaction]

Introduction

The photochemistry of cyclobutanones has been thoroughly investigated during the last three decades (1, 2). The primary process involves α-cleavage to a short-lived 1,4-acylalkyl diradical that can undergo one of three independent transformations: cycloelimination to ketene and olefin; ring expansion to a cyclic oxacarbene (2-tetrahydrofuranylidene); and decarbonylation, the latter normally representing a minor process unless structural features permit stabilization of a 1,3-diradical (e.g., presence of a 3-alkylidene group). Furthermore, sensitization experiments with simple cyclobutanones suggest that cyclopropane formation is a dominant pathway from the triplet state (3). Of the three photodecomposition pathways, the solution photodecarbonylation of cyclobutanones has received scant attention. This is largely due to the inefficiency of this process from direct irradiation, with singlet excited states giving rise to efficient cycloelimination and ring expansion as the result of strain effects. Triplet sensitized photochemistry of cyclobutanones appears to take a completely different course of events and is an area that has been relatively unexplored. The triplet sensitized photochemistry of a series of α-vinylcyclobutanones using either acetone or Michler's ketone (4,4′-bis(dimethylamino)benzophenone) as triplet sensitizers gave products derived from a 1,4-acyl alkyl diradical but different from the direct irradiation, in which case the usual cycloelimination and ring expansion pathways are observed (4). Chiral cyclobutanones are now readily accessible by a number of routes (5). The decarbonylation of these derivatives would involve a 1,4-acyl alkyl diradical whose lifetime would influence the extent of epimerization of the resultant cyclopropanes formed. It was of interest to investigate conditions under which chiral cyclopropanes could be produced from photodecarbonylation of chiral cyclobutanones. Chiral cyclopropanes are important intermediates in natural product synthesis and a variety of methods are available for their synthesis (6); however, only a few of these have been reported from ring contraction of chiral cyclobutane derivatives. With the availability of 2(*S*),3(*R*)-bis[(benzoyloxy)methyl] cyclobutanone **1**(*a*) and 2(*S*)-[(benzoyloxy)methyl]cyclobutanone **1**(*b*) in optically pure form (7, 8), we were interested in carrying out exploratory studies on the conditions under which cyclopropanes are efficiently produced by sensitized photodecarbonylation. We

Received July 16, 1996.[1]

J. Ramnauth and E. Lee-Ruff.[2] Department of Chemistry, York University, North York, ON M3J 1P3, Canada.

[1] Revision received January 20, 1997.

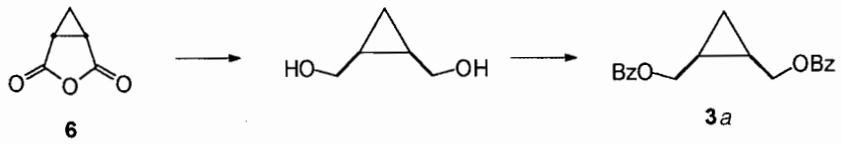
[2] Author to whom correspondence may be addressed. Telephone: (416) 736-5443. Fax: (416) 736-5936.

© 1997 NRC Canada

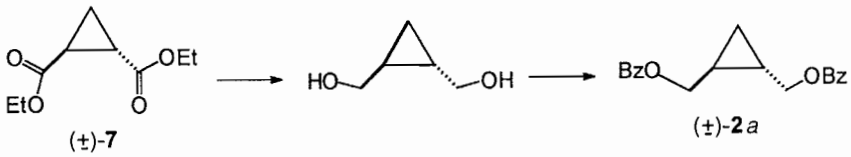
Can. J. Chem. Downloaded from www.nrcresearchpress.com by 88.146.161.215 on 09/08/12
For personal use only.

Can. J. Chem. Downloaded from www.nrcresearchpress.com by 88.146.161.215 on 09/08/12
For personal use only.

Scheme 1.



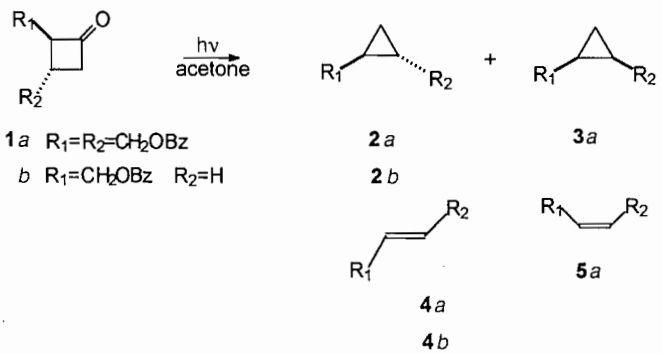
Scheme 2.



have reported the photochemistry of these derivatives under direct irradiation in the presence of purine bases as a novel method for producing ribonucleosides (8, 9). Decarbonylation of **1**(*a*) would produce two diastereomeric cyclopropanes **2**(*a*) and **3**(*a*), the latter derived from epimerization. The *E* isomer **2**(*a*) would be expected to be optically pure. Decarbonylation of **1**(*b*) would give achiral cyclopropane **2**(*b*).

Results and discussion

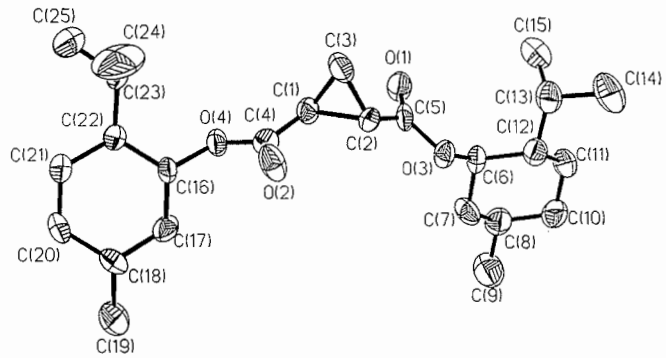
Cyclobutanone derivatives **1**(*a*) and **1**(*b*) were prepared according to literature methods (7, 8). The key step for the asymmetric synthesis of **1**(*a*) was the cycloaddition of dimen-



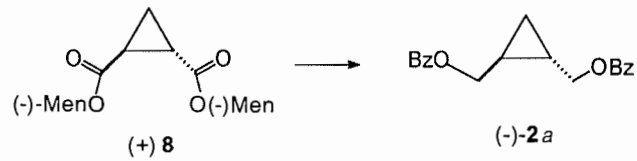
thyl fumarate with 1,1-dimethoxyethylene in the presence of a Lewis acid catalyst (7) giving greater than 98% diastereomeric enrichment. The preparation of optically pure **1**(*b*) was based on the enantioselective synthesis of a cyclobutane precursor from cycloaddition of 3-acryloyl-1,3-oxazolidin-2-one with 1,1-bis(methylthio) ethylene using a chiral titanium catalyst (10). This step occurred with an enantiomeric excess of greater than 98% (10).

Irradiation of a 6×10^{-3} M solution of **1**(*a*) in acetone for 4 h using a medium-pressure mercury lamp with unfiltered light gave a 25% conversion to a mixture of nonpolar compounds consisting of cyclopropanes **2**(*a*) (53%), **3**(*a*) (17%) and olefins **4**(*a*) (19%) and **5**(*a*) (11%). The structures of all photoproducts were assigned based on spectral data, elemental analysis, and independent synthesis. Olefin **5**(*a*) was prepared from benzoylation of *Z*-2-butene-1,4-diol. Its isomer **4**(*a*) was prepared by double nucleophilic substitution of *E*-1,4-dibromo-2-butene with potassium benzoate. Preparation of *Z*-1,2-bis(benzoyloxymethyl) cyclopropane (**3**(*a*))was based on

Fig. 1. X-ray crystal structure of (−) dimenthyl 1(*S*),2(*S*)-cyclopropanedicarboxylate (**+8**).



reduction of 1,2-cyclopropanedicarboxylic acid anhydride (**6**) followed by benzoylation (Scheme 1), whereas the racemic *E* isomer **2**(*a*) was prepared from commercially available diethyl *E*-cyclopropane-1,2-dicarboxylate (**7**) according to Scheme 2. That optically pure cyclopropane **2**(*a*) was produced in the photolysis of **1**(*a*) was established by the observed optical rotation of the nonpolar fraction. The measured specific rotation of **2**(*a*) was −7.5. To confirm the absolute configuration, cyclopropane (−)-**2**(*a*) was prepared from the known (−)-dimenthyl 1(*S*),2(*S*)-cyclopropane-1,2-dicarboxylate (**8**) (11).



We were not able to reproduce the literature procedure for the preparation of (+)-**8** from the methylenation of dimenthyl succinate with bromochloromethane under basic conditions (11). Our method for preparing (+)-**8** was based on the esterification of (±)-cyclopropane-1,2-dicarboxylic acid via the diacid chloride and separation of the diastereomeric diester by recrystallization from methanol. The optical purity of (+)-**8** was verified by matching the specific rotation ($[\alpha]_D$ = +17.5) with that reported in the literature ($[\alpha]_D$ = +17.8). Furthermore, the absolute configuration of (+)-**8** was confirmed by X-ray crystallographic analysis (Fig. 1). Reduction of (+)-**8** with lithium aluminum hydride followed by benzoylation gave

© 1997 NRC Canada

Can. J. Chem. Downloaded from www.nrcresearchpress.com by 88.146.161.215 on 09/08/12
For personal use only.

Table 1. Concentration dependence on the distribution (%) of products in acetone[a]

Conc. (10^{-3} M)	**2**(*a*)	**3**(*a*)	**4**(*a*)	**5**(*a*)	Cycl./olefin
5.6	12.4	3.9	4.4	2.8	2.3
3.0	16.5	5.1	3.4	3.4	3.2
1.5	20.3	5.1	3.3	1.6	5.2

[a]Yields were determined by HPLC analysis and calibration with standard solutions.

(±)-**2**(*a*) having identical spectral features with racemic (α)-**2**(*a*) and a specific rotation $[\alpha]_D = -7.5$ that was identical with the specific rotation for the sample obtained from photolysis.

A photostability study of each of the nonpolar photoproducts **2**(*a*)–**5**(*a*) under the irradiation conditions for **1**(*a*) indicated that cyclopropanes **2**(*a*) and **3**(*a*) were inert whereas olefins **4**(*a*) and **5**(*a*) underwent photoisomerization to give a 60:40 photoequilibrium mixture of **4**(*a*) and **5**(*a*). Thus olefin **5**(*a*) is a likely secondary photoproduct from the initially formed *E* isomer **4**(*a*). This photoequilibrium distribution of **4**(*a*) and **5**(*a*) was observed for all photolysis of **1**(*a*), indicating that photoequilibration competes with the primary photodecomposition.

The extent of photodecarbonylation as affected by substrate concentrations and nature of solvent was investigated. Decreasing concentrations led to increasing yields of cyclopropanes as seen in Table 1. This trend is what would be expected for solvent photosensitized processes. Direct excitation of ketone **1**(*a*) would be minimized under dilute conditions favouring triplet sensitized processes. Photolysis of **1**(*a*) in either tetrahydrofuran or benzene gave predominantly cycloelimination products **4**(*a*) and **5**(*a*) in the nonpolar fraction (Table 2). This latter observation further supports the speculation that decarbonylation of cyclobutanone is the consequence of triplet state decomposition. The formation of *cis*-olefin **5**(*a*) was somewhat surprising in view of the stereoselectivity of photocycloeliminations observed in other cyclobutanone derivatives (1). Further evidence for the intervention of the triplet state in the decarbonylation was obtained from irradiation of **1**(*a*) in THF in the presence of Michler's ketone (4,4′-dimethylamino)benzophenone) a known triplet photosensitizer for cyclobutanones (4). A significant increase in cyclopropane formation was observed under the photosensitized conditions (Table 2).[3] Quenching studies using dicyanoethylene (DCE) (13) showed significant reduction of photodecarbonylation dependent on the DCE concentration in the acetone photolysis (see Table 2). However, addition of DCE under the nonsensitized photolysis in THF did not supress the small amounts of cyclopropanes, indicating a minor singlet state route for photodecarbonylation.

Irradiation of ketone **1**(*b*) in acetone (6×10^{-3} M) gave efficient conversion to cyclopropane **2**(*b*) (86%) and olefin **4**(*b*) (10%). The identity of cyclopropane **2**(*b*) was established from its spectral data and independent synthesis from cyclopropane carboxylic acid as outlined in Scheme 3. The predominance for photodecarbonylation in ketone **1**(*b*) is probably associated with inefficient cycloelimination from β-cleavage of a secondary C—C bond as compared to a tertiary C—C bond in **1**(*a*).

Table 2. Solvent dependence on distribution (%) of products[a]

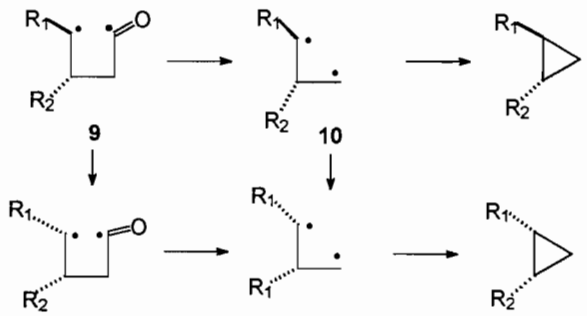
Solvent	**2**(*a*)	**3**(*a*)	**4**(*a*)	**5**(*a*)	Cycl./olefin
Acetone	12.4	3.9	4.4	2.8	2.3
Acetone + 6×10^{-3} M DCE	10.2	3.6	6.2	3.5	1.43
Acetone + 2×10^{-2} M DCE	5.3	1.9	11.5	4.7	0.44
THF	1.8	0.2	8.7	6.4	0.13
Benzene	2.6	0.81	19.3	11.1	0.11
THF + MK[b]	5.4	2.2	8.1	5.2	0.57

[a]Yields were detemined by HPLC analysis and calibration with standard solutions. Concentration of **1**(*a*) was 5.6×10^{-3} M for all solutions.
[b]MK = Michler's ketone.

Scheme 3.



Scheme 4.



It has been shown that chiral cyclopropanes can be prepared from chiral cyclobutanones using acetone as a triplet sensitizer and solvent. The extent of epimerization at the α-carbon in the decarbonylation of cyclobutanones will depend on the lifetimes of the intermediate acyl-alkyl diradical **9** and the 1,3-diradical **10** (Scheme 4). Thermodynamic equilibration of these intermediates would give an epimeric mixture of cyclopropanes. However, 1,3-diradicals (trimethylene) generated from other precursors such as optically active pyrazolines retain their optical activity in the products (14, 15). These observations are rationalized in terms of the stereoselective ring-closure of these triplet trimethylenes. It would be expected that diradical **10** would be formed in the triplet state by spin conservation. Our results show that some epimerization takes place at the stereogenic radical site. Further studies on the triplet sensitized photochemistry of other chiral 2,4-disubstituted cyclobutanones are in progress.

[3] Although triplet-type photoreactions have been reported for cyclobutanones in the presence of Michler's ketone, energy transfer is endothermic. Evidence suggests an electron transfer process operating under these conditions (12).

© 1997 NRC Canada

Can. J. Chem. Downloaded from www.nrcresearchpress.com by 88.146.161.215 on 09/08/12
For personal use only.

Experimental

Melting points (mp) were determined on a Reichert melting point apparatus and are uncorrected. ^{1}H NMR spectra were recorded on a Bruker ARX 400 (400 MHz) spectrometer in $CDCl_3$ solutions containing 1% TMS. Optical rotations were measured using a Perkin–Elmer 241 polarimeter. HPLC analysis was performed on a Waters M-6000A instrument with a Lambda-Max model 481 LC detector using UV detection (254 mm), a Hewlett–Packard integrator, and a Spherisorb Silica analytical column from Sigma–Aldrich. Photolyses were carried out using a Hanovia 450 W medium-pressure mercury arc lamp in a water-cooled immersion well. Quartz tubes containing the samples were strapped around this well and the assembly immersed in an ice–water bath. The samples were degassed with argon for 30 min prior to irradiation. The X-ray crystal structure was performed on a Siemens R 3 m/v diffractometer using 1591 observed reflections. All solvents used in these reactions were dried and distilled. Analytical thin-layer chromatography (TLC) was done on commercially prepared silica gel 60F 254 plastic sheets (E. Merck & Co.). Preparative TLC was conducted on Aldrich silica gel 60F 254 precoated glass plates. Elemental analyses were performed by Guelph Chemical Laboratories Limited. The starting cyclobutanones **1**(*a*) and **1**(*b*) were synthesized according to literature methods (7, 8).

General photolysis procedures

A solution of ketone **1**(*a*) or **1**(*b*) in 70 mL of solvent ($\sim 10^{-3}$ M) was irradiated for 4 h (13 h for **1**(*b*)). The solvent was removed by rotoevaporation under reduced pressure. The residue was chromatographed on TLC plates (hexane:ethyl acetate, 95:5) to give a nonpolar fraction. The polar fraction was not analyzed but consisted of unreacted ketone and products containing an alcohol function. The nonpolar fraction was analyzed by analytical HPLC and comparison with synthesized samples as detailed below. Quenching studies with DCE were carried out under the same conditions using 6×10^{-3} M and 1.2×10^{-2} M solutions of DCE.

(±) E-1,2-Bis(benzoyloxymethyl)cyclopropane ((±) 2(a))

To a stirred suspension of $LiAlH_4$ (0.25 g, 6.44 mmol) in anhydrous ether (15 mL) at 0°C under argon was added diethyl *E*-1,2-cyclopropanedicarboxylate ((±)-**7**) (0.5 g, 2.7 mmol) in 20 mL ether. After 1 h, 3 mL of water was added and the solution filtered. To the filtrate was added anhydrous $MgSO_4$ and the solution was concentrated. ^{1}H NMR analysis of the residue showed the presence of the diol. Most of the diol remained in the filter cake. To the dry filter cake was added pyridine (10 mL), and benzoyl chloride (0.9 g, 6.0 mmol) was added dropwise with constant stirring. After 2 h, water (10 mL) was added to the reaction mixture and the organic layer was extracted with 50 mL ether, dried over anhydrous $MgSO_4$, and concentrated under reduced pressure. The residue was subjected to preparative TLC (benzene) to yield 70 mg (8.4%) of a white solid; mp 48–50°C; IR (KBr): 1715, 1600 cm^{-1}; ^{1}H NMR δ: 8.01–7.34 (m, 10H), 4.40–4.36 (dd, 2H, J = 5.8, 5.5 Hz), 4.48–4.04 (dd, 2H, J = 7.8, 4.0 Hz), 1.42–1.37 (m, 2H), 0.77–0.73 (t, 2H, J = 6.9 Hz). Anal. calcd. for $C_{19}H_{18}O_4$: C 73.55, H 5.81; found: C 73.42, H 5.71.

(−) Dimenthyl E-1(S), 2(S)-cyclopropanedicarboxylate ((+)8)

The title compound was prepared from (±)-cyclopropanedicarbonyl chloride which was prepared using the following procedures. A solution of diethyl *E*-1,2-cyclopropanedicarboxylate (±)-**7** (10 g, 53.7 mmol) in 100 mL of an aqueous methanol solution (9:1 methanol: H_2O) of 10% KOH was heated to reflux for 4 h. After cooling to room temperature, the mixture was diluted with 20 mL of H_2O and acidified with 50 mL of cold 6 M HCl. The solution was saturated with NaCl and extracted with 5 × 40 mL ether. The ether extract was dried over Na_2SO_4 and evaporated to yield 5.7 g of a white crystalline solid, mp 175–177°C (lit. (16) mp for *E*-1,2-cyclopropanedicarboxylic acid 175–177°C). To 4.6 g (38.4 mmol) of the dicarboxylic acid in 15 mL benzene was added 17 g (143 mmol) of $SOCl_2$. The mixture was heated to reflux for 4 h. The mixture was evaporated under reduced pressure. The residue was distilled (88°C, 10 Torr (1 Torr = 133.3 Pa) to give a colourless liquid of the acid chloride. ^{1}H NMR δ: 2.93–2.89 (t, 2H, J = 7.0 Hz), 1.91–1.88 (t, 2H, J = 7.2 Hz).

A solution of (−)-menthol (4.0 g, 25 mmol) in 3 g pyridine and 20 mL benzene was cooled in an ice–water bath. To this solution was added *E*-1,2-cyclopropanedicarbonyl chloride (2.0 g, 12.0 mmol) over a period of 20 min. The mixture was stirred for an additional 20 min at this temperature and for another 2 h at room temperature. After this time 50 mL of H_2O was added. The organic layer was extracted with 50 mL of ether and washed with 100 mL H_2O, dried over Na_2SO_4, and evaporated to yield 3 g (61%) of a white solid. This solid was dissolved in 50 mL of warm methanol. Colourless needles were obtained (1.2 g). An additional three recrystallizations gave optically pure (+)-**8** in 0.82 g (16.7%) yield; mp 94–95°C; $[\alpha]_D$ = +17.5 ($CHCl_3$, *c* 0.1), (lit. (11) $[\alpha]_D$ = +17.8 ($CHCl_3$, *c* 1.0)); IR (KBr): 1724 cm^{-1}. The absolute structure was confirmed by X-ray crystallography (Fig. 1).

(−) E-1(S),2(S)-Bis(benzoyloxymethyl)cyclopropane ((−)-2(a))

To a stirred suspension of $LiAlH_4$ (0.27 g, 1.1 mmol) in 20 mL of dry THF at 0°C under argon was added (−) dimenthyl *E*-1(*S*),2(*S*)-cyclopropanedicarboxylate ((+)-**8**) (0.7 g, 1.7 mmol) in 20 mL THF, dropwise over a period of 20 min. The reaction mixture was then heated to reflux for 4 h. After cooling in an ice–water bath the following were added sequentially:(1) 0.7 mL H_2O, (2) 0.7 mL of 15% aqueous NaOH, and (3) 2.1 mL of H_2O. The mixture was filtered and the precipitate washed with 200 mL of ether. The precipitate was subjected overnight to Soxhlet extraction with ether. The ether extracts were combined and evaporated and to the residue was added 20 mL H_2O, 1 mL methanol, and 20 mL hexane. The organic layer was separated and the aqueous layer was extracted with additional hexane (4 × 20 mL). The combined organic fractions were then washed with 10 mL H_2O. The combined aqueous layers were saturated with NaCl and extracted with ether (5 × 20 mL). The organic extract was dried over Na_2SO_4 and concentrated to give 50 mg (28.4%) of a colourless oil. To this material was added 1 mL of pyridine and the solution cooled to 0°C. Benzoyl chloride (0.25 mL) was added with constant stirring. The reaction mixture was allowed to warm to room temperature and stirred for an additional 2 h. After this time, 20 mL of H_2O was added. The mix-

© 1997 NRC Canada

Can. J. Chem. Downloaded from www.nrcresearchpress.com by 88.146.161.215 on 09/08/12
For personal use only.

ture was extracted with 50 mL ether, and the ether extract was washed with 2 × 40 mL of H_2O, 2 × 40 mL of a 5% aqueous HCl solution, 2 × 40 mL of a saturated $NaHCO_3$ solution, 2 × 100 mL H_2O, and dried over Na_2SO_4. The ether was evaporated to give 70 mg (13.1%) of a white solid identical in all respects (except for specific rotation) with racemic **2**(*a*) prepared above; mp 49–50°C; $[\alpha]_D = -7.5$ ($CHCl_3$, *c* 0.042).

*Z-1,2-Bis(benzoyloxymethyl)cyclopropane (**3**(a))*

To a stirred suspension of $LiAlH_4$ (0.16 g, 4.2 mmol) in 20 mL of THF at 0°C under argon, was added *Z*-1,2-cyclopropanedicarboxylic acid anhydride (**6**) (0.14 g, 1.25 mmol) in 10 mL THF, dropwise over a period of 20 min. The reaction mixture was stirred for an additional 20 min at this temperature and then heated to reflux for 3 h. After cooling to 0°C, the following were added sequentially: (1) 0.17 mL H_2O, (2) 0.17 mL of 15% aqueous NaOH, (3) 0.51 mL H_2O. The mixture was stirred for 20 min. To this mixture was added dropwise 10 mL of pyridine and 1.0 g of benzoyl chloride over a period of 10 min. The mixture was stirred at room temperature for 24 h. After this time, 20 mL of H_2O was added to quench the excess benzoyl chloride. The reaction mixture was then filtered and the filter cake was washed with 50 mL of ethyl acetate. The filtrate was washed with 200 mL of H_2O, 200 mL of saturated $NaHCO_3$, 200 mL of a 5% aqueous HCl solution, and 200 mL of H_2O. The organic layer was dried over Na_2SO_4 and evaporated to give 0.2 g (52%) of a yellow oil. The residue was chromatographed on two preparative TLC plates to give 0.1 g of an oil (benzene); IR: 1717, 1602 cm^{-1}; ^1H NMR δ: 8.10–7.41 (m, 10H), 4.66–4.62 (dd, 2H, *J* = 6.1, 6.8 Hz), 4.23–4.18 (dd, 2H *J* = 8.6, 3.0 Hz), 1.57–1.51 (m, 2H). Anal. calcd. for $C_{19}H_{18}O_4$: C 73.55, H 5.81; found: C 73.21, H 5.77.

E-*1,4-Bis(benzoyloxy)-2-butene (**4**(a))*

Potassium benzoate (8.0 g, 50 mmol) was dissolved in 25 mL of 0.1 M NaOH and 200 mL acetonitrile. The solution was heated to reflux. To this solution was added *E*-1,4-diromo-2-butene (5.0 g, 23 mmol) in one portion. The mixture was heated under reflux with constant stirring for 4 h. After this time, the mixture was poured into 25 mL of a 0.1 M HCl solution with constant stirring. The diester was filtered off and washed several times with a 5% $NaHCO_3$ aqueous solution. The solid was recrystallized from methanol to afford 3.4 g (50%) of a white crystalline solid; mp 102–103°C (lit. (17) mp 100–101°C); ^1H NMR δ: 8.08–7.43 (m, 10H), 6.08–6.07 (t, 2H), 4.88–4.87 (d, 4H).

*Z-1,4-Bis(benzoyloxy)-2-butene (**5**(a))*

A solution containing *Z*-2-butene-1,4-diol (3 g, 34 mmol) in pyridine (6 g, 76 mmol) was cooled to 0°C. Benzoyl chloride (10.5 g, 75 mmol) was added dropwise over a period of 30 min. The mixture was allowed to warm to room temperature and stirring continued for an additional 2 h. After this time, 50 mL of water was added. The diester was filtered and recrystallized from 95% ethanol giving 7.0 g (70%) of a white crystalline solid; mp 66–67°C (lit. (17) mp 66–67°C); ^1H NMR δ: 8.06–7.41 (m, 10H), 5.96–5.95 (t, 2H), 5.04–5.00 (d, 4H).

*Benzoyloxymethylcyclopropane (**2**(b))*

A suspension of $LiAlH_4$ (0.57 g, 15.0 mmol) in 50 mL of anhydrous ether was cooled to 5°C. To this suspension was added dropwise a solution of cyclopropanecarboxylic acid (1 g, 11.6 mmol) in 20 mL ether over a period of 30 min. The reaction mixture was stirred at this temperature for an additional 30 min, then heated to reflux for 2 h. After cooling to 5°C the following were added sequentially: (1) 0.6 mL H_2O, (2) 0.6 mL of 15% aqueous NaOH, (3) 1.8 mL of water. The mixture was stirred for an additional 30 min and filtered. The precipitate was washed with 200 mL ether. The combined ether solution was concentrated to give 0.78 g of cyclopropane-methanol, which was used for the next step without purification. The crude alcohol was dissolved in 15 mL pyridine and cooled to 5°C. To this solution was added dropwise 2.3 g (16.4 mmol) of benzoyl chloride over a period of 15 min. This mixture was allowed to warm to room temperature and stirred overnight. After this time, 2 mL of H_2O was added. The solution was concentrated under reduced pressure and partitioned using 100 mL ethyl acetate and 200 mL H_2O. The organic layer was washed with 2 × 100 mL H_2O, 4 × 100 mL saturated $NaHCO_3$, and 2 × 100 mL of water. After drying over Na_2SO_4 the organic layer was concentrated under reduced pressure to give 1.4 g (68%) of the title compound as an oil; IR: 1718, 1602 cm^{-1}; ^1H NMR δ: 8.08–7.41 (m, 5H), 4.16 (d, 2H, *J* = 7.4 Hz), 1.28–1.24 (m, 1H), 0.63–0.59 (m, 2H), 0.38–0.35 (m, 2H). Anal. calcd. for $C_{11}H_{12}O_2$: C 74.97, H 6.86; found: C 75.00, H 6.97.

Acknowledgements

We would like to thank the Natural Sciences and Engineering Research Council of Canada (NSERC) for financial support.

References

1. D.R. Morton and N.J. Turro. Adv. Photochem. **9**, 197 (1974).
2. E. Lee-Ruff. *In* Advances in strain in organic chemistry. Vol. 1. *Edited by* B. Halton. JAI Press, London. 1991. p. 167.
3. H.O. Denschlag and E.K.C. Lee. J. Am. Chem. Soc. **90**, 3628 (1968).
4. T. Lyle, H.B. Mereyala, A. Pascual, and B. Frei. Helv. Chim. Acta, **67**, 774 (1984).
5. E. Lee-Ruff. *In* Methods in organic chemistry. Vol. E17. *Edited by* A. De Meijere. Houben-Weyl, G. Thieme Verlag, Stuttgart. 1997. Chap. 1.3.4.3. p. 179.
6. J. Salaün. Chem. Rev. **89**, 1247 (1989).
7. S. Ahmad. Tetrahedron Lett. **32**, 6997 (1991).
8. E. Lee-Ruff, F.-D. Xi, and J.H. Qie. J. Org. Chem. **61**, 1547 (1996).
9. E. Lee-Ruff, W.Q. Wan, and J.L. Jiang. J. Org. Chem. **59**, 2114 (1994).
10. K. Narasaka, H. Kusama, and Y. Hayoshi. Bull Chem. Soc. Jpn. **64**, 1471 (1991).
11. K. Furuta, K. Iwanaga, and H. Yamamoto. Org. Synth. Collect. Vol. **67**, 77 (1988).
12. C.C. Wamser, G.S. Hammond, C.T. Chang, and C. Baylor, Jr. J. Am. Chem. Soc. **92**, 6362 (1970).
13. R.O. Loutfy, S.K. Dogra, and R.W. Yip. Can. J. Chem. **57**, 342 (1979).
14. M.P. Schneider and H. Bippi. J. Am. Chem. Soc. **102**, 7363 (1980).
15. T.C. Clarke, L.A. Wendling, and R.G. Bergman. J. Am. Chem. Soc. **97**, 5638 (1975).
16. V.J. Heintz and T.A. Keiderling. J. Am. Chem. Soc. **103**, 2395 (1981).
17. D.A. Thomas and W.K. Warburton. J. Chem. Soc. 2988 (1965).

© 1997 NRC Canada

Réactivité dipolaire-1,3 du 4,4,4-trichloro-3-éthoxycarbonylamino-2-diazobutyrate d'éthyle issu de l'action du diazoacétate d'éthyle sur la *N*-éthoxycarbonyl-*N*-(2,2,2-trichloroéthylidène)amine

Abdelhak Belaissaoui, Sandrine Jacquot, Claude Morpain, Gérard Schmitt, Joël Vebrel et Bernard Laude

Résumé : La réaction du diazoacétate d'éthyle avec la *N*-éthoxycarbonyl-*N*-(2,2,2-trichloroéthylidène)amine conduit, via une réaction d'addition nucléophile, à un nouveau diazocomposé qui a manifesté ensuite une réactivité dipolaire-1,3 vis-à-vis des esters acétylèniques et des maléimides. Dans le cas des esters acétyléniques, la réaction de cycloaddition s'accompagne d'une évolution qui conduit à des pyrazoles très substitués par suite de transpositions sigmatropiques [1,5]. Avec les maléimides, on observe une réaction de cycloaddition diastéréospécifique suivie d'une élimination d'azote conduisant à un maléimidocyclopropane. La diastéréospécificité observée a été rationalisée en faisant appel à un mode d'approche des réactants du type *endo-anti*.

Mots clés : *N*-éthoxycarbonyl-*N*-(2,2,2-trichloroéthylidène)amine, diazoacétate d'éthyle, addition nucléophile, cycloaddition dipolaire-1,3, transposition sigmatropique, diastéréosélectivité.

Abstract: The reaction of ethyl diazoacetate with the *N*-ethoxycarbonyl-*N*-(2,2,2-trichloroethylidene)amine yields, by a nucleophilic addition, a new diazo compound that gives 1,3-dipolar cycloaddition reactions with acetylenic esters and maleimides. With acetylenic esters, the cycloadduct leads to substituted pyrazoles by [1,5] sigmatropic rearrangements. With maleimides, we observe a diastereospecific cycloaddition reaction. The intermediary cycloadduct evolves by nitrogen elimination to give a maleimidocyclopropane. The diastereospecificity was explained by an *endo-anti* approach of the reactants.

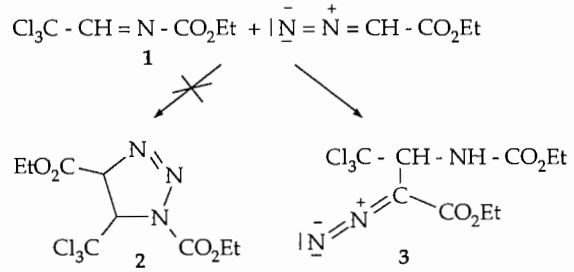
Key words: *N*-ethoxycarbonyl-*N*-(2,2,2-trichloroethylidene)amine, ethyl diazoacetate, nucleophilic addition, 1,3-dipolar cycloaddition, sigmatropic rearrangement, diastereoselectivity.

Introduction

La synthèse des anhydrochloraluréthanes a été rapportée pour la première fois par Moscheles en 1891 (1). Mais Feist a montré ultérieurement qu'il s'agissait de produits de structure $(ROOC\text{-}NH\text{-}CH(CCl_3))_2O$ (2) et c'est en 1968 que la première préparation de la *N*-éthoxycarbonyl-*N*-(2,2,2-trichloroéthylidène)amine **1** a été menée à bien en trois étapes par Ulrich et coll. (3). Les auteurs indiquent un rendement global de 45% que nous avons réussi à porter à 83% (cf. partie expérimentale).

Cette imine est un substrat fortement électrophile et de nombreuses réactions d'addition nucléophile ont été décrites (3). L'imine **1** est aussi un diénophile qui a été engagé dans des réactions de type Diels–Alder avec le cyclohexène (4). La seule réaction de cycloaddition dipolaire-1,3 concerne les nitrones et a été récemment décrite par Consonni et coll. (5) Pour notre part et après avoir étudié le comportement de la *N*-éthoxycarbonyl-*N*-(2,2,2-trichloroéthylidène)amine **1** avec quelques diarylnitrilimines et arylnitriloxydes (6), nous présentons ici les résultats obtenus en engageant le diazoacétate d'éthyle avec l'imine **1**. Dans la littérature (7–16), c'est essentiellement avec le diazométhane que diverses imines ont été mises en réaction, et les travaux décrits font tous état d'une réaction régiospécifique conduisant à une

Schéma 1.



Reçu le 2 novembre 1995.[1]

A. Belaissaoui, S. Jacquot, C. Morpain, G. Schmitt, J. Vebrel et B. Laude.[2] Laboratoire de chimie organique, Université de Franche-Comté, 16 Route de Gray, 25030 Besançon, France.

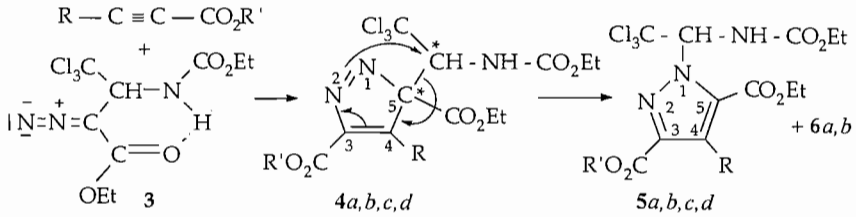
[1] Revision reçu le 20 janvier 1997.

[2] Auteur à qui adresser toute correspondance. Téléphone : 03 81 66 62 70. Fax : 03 81 66 62 30.

© 1997 NRC Canada

Can. J. Chem. Downloaded from www.nrcresearchpress.com by 88.146.161.215 on 09/08/12
For personal use only.

Schéma 2.



a : R = CO_2Me, R' = Me
b : R = H, R' = Me
c : R = CO_2Et, R' = Et
d : R = H, R' = Et

Δ^2-1,2,3-triazoline **2** qui dans le cas présent pourrait éventuellement s'isomériser en une Δ^3-1,2,3-triazoline (schéma 1).

Mais l'examen en spectrométrie IR du produit **3** obtenu ici permet d'observer la présence d'une bande intense à 2104 cm^{-1} caractéristique de la présence du groupe diazo. On obtient donc le 4,4,4-trichloro-3-éthoxycarbonylamino-2-diazobutyrate d'éthyle **3**. Cette structure est en bon accord avec les résultats de l'analyse élémentaire et les paramètres de RMN ^1H et ^{13}C. Ainsi on n'observe pas de signaux correspondant à la présence de deux chainons -CH- vicinaux mais à celle d'un seul groupe -CH- voisin d'un reste -NH- (J_{CH-NH} = 9,8 Hz). Il n'est pas étonnant que la réaction observée soit une addition nucléophile du diazoacétate d'éthyle puisque l'hydrogène fixé sur le carbone porteur du groupe diazo est rendu très mobile par la présence des deux groupes accepteurs liés à cet atome de carbone. On obtient donc un nouveau diazocomposé dont nous avons voulu tester l'activité dipolaire-1,3.

Compte-tenu des observations décrites ultérieurement, nous avons aussi examiné quelle pouvait être sa structure spatiale. À cet effet, nous avons effectué une étude en spectrométrie IR de solutions dans CCl_4 du produit d'addition **3** à différentes concentrations. La variation de la concentration de la solution dans CCl_4 n'entraîne aucune variation de la position et de l'intensité relative des bandes d'absorption $\nu_{(N-H)}$ situées à 3401 et 3436 cm^{-1}. Ce phénomène est caractéristique de l'existence d'une liaison hydrogène intramoléculaire lorsque la concentration est inférieure à 10^{-2} mol L^{-1} (17). On peut donc envisager l'existence de ce composé sous forme quasi-cyclique (Schéma 2).

Réaction du nouveau diazocomposé avec des dipolarophiles acétyléniques

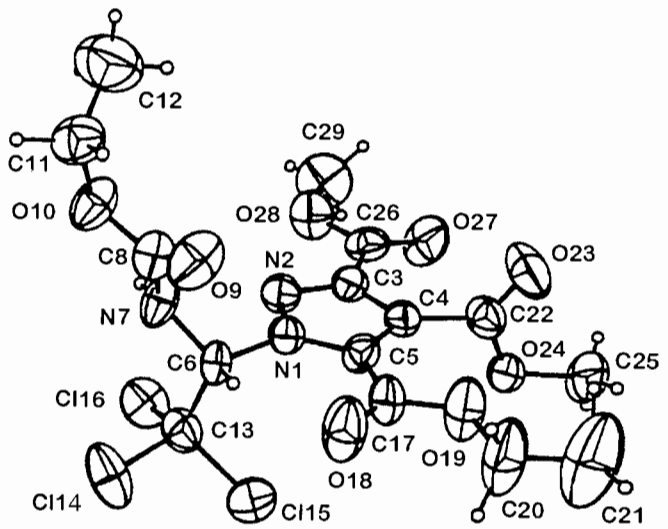
Le diazocomposé **3** n'est pas stable dans le toluène à ébullition où il se dégrade peu à peu, aussi les réactions ont-elles été effectuées à une température de 60°C et suivies par CCM et IR (disparition de la bande $\nu_{(N_2)}$). Dans ces conditions les réactions sont lentes (60–100 h).

1. Cas de l'acétylènedicarboxylate de diméthyle et du propiolate de méthyle

Ce sont les premiers dipolarophiles acétyléniques que nous avons testés. Après départ du solvant, on obtient un résidu qui est purifié par chromatographie sur plaques préparatives.

L'examen en RMN ^1H de chacun des produits ainsi purifiés (une seule tache en CCM) nous a permis d'observer le

Fig. 1. Structure du produit **5***a* (18*a*).



dédoublement de certains signaux. Ainsi dans le cas de l'acétylènedicarboxylate de diméthyle où un seul régioisomère peut être obtenu, on attendait le produit de structure **4***a* (schéma 2).

Nous avons envisagé l'existence de deux diastéréoisomères résultant de la présence de deux centres chiraux dans la structure **4**. Mais nous avons abandonné cette hypothèse parce que le spectre de RMN ^{13}C ne présentait aucun signal attribuable au carbone sp^3 quaternaire C(5) de la structure **4**. Nous avons donc fait appel à une détermination de structure par radiocristallographie X de chaque produit isolé à partir de l'acétylènedicarboxylate de diméthyle (18*a*) (figure 1) d'une part et du propiolate de méthyle (18*b*) (figure 2) d'autre part. Les monocristaux utilisés pour cette étude ont été prélevés au sein du dépôt solide obtenu après évaporation lente d'une solution éthanolique de chaque produit purifié par chromatographie sur plaques préparatives.

Ces structures montrent à l'évidence qu'il ne s'agit pas des cycloadduits **4** attendus mais que chaque produit **5** provient de l'isomérisation du cycloadduit initial (schéma 2).

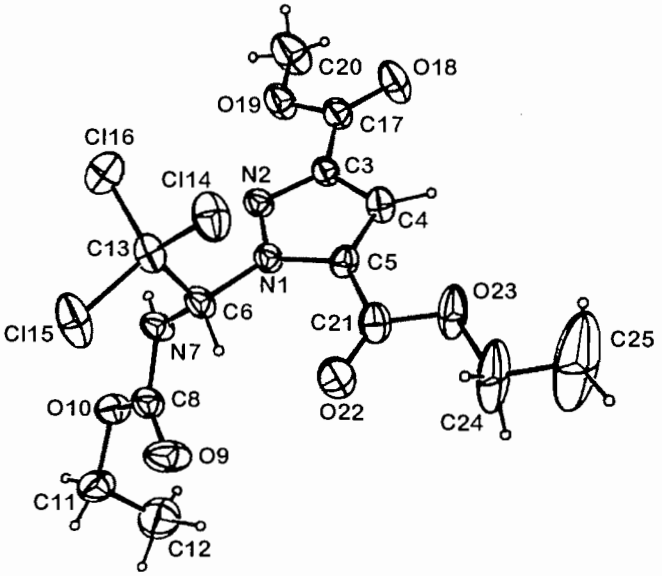
Cette isomérisation peut s'expliquer par une transposition sigmatropique [1,5] dont la force motrice est l'aromaticité du dérivé pyrazolique **5**. De plus, dans le cas du produit **5***b*, la détermination radiocristallographique de sa structure permet

© 1997 NRC Canada

Can. J. Chem. Downloaded from www.nrcresearchpress.com by 88.146.161.215 on 09/08/12
For personal use only.

Can. J. Chem. Downloaded from www.nrcresearchpress.com by 88.146.161.215 on 09/08/12
For personal use only.

Fig. 2. Structure du produit **5***b* (18*b*).



de fixer la régiochimie unique de la réaction de cycloaddition initiale.

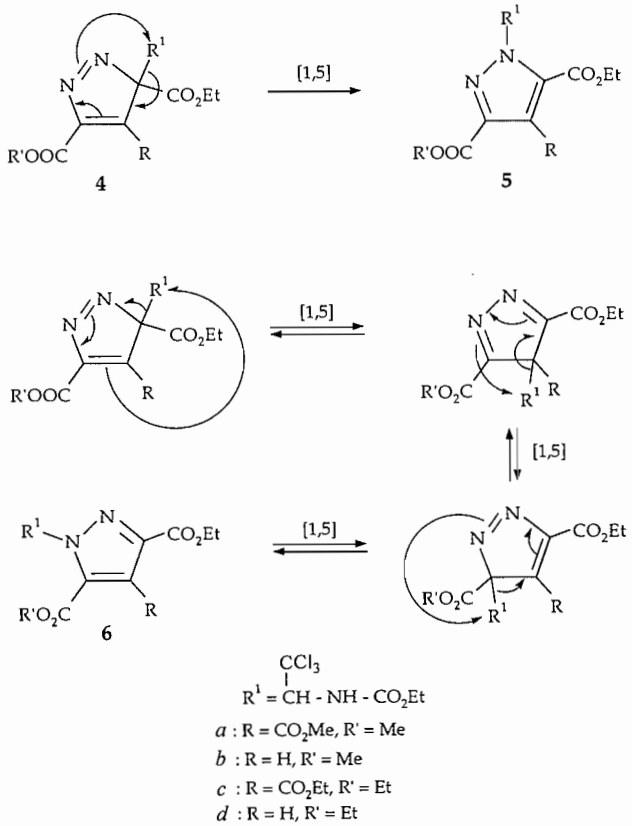
Pour tenter d'expliquer l'origine du dédoublement de certains signaux sur les spectres de RMN ^{1}H et ^{13}C des produits purifiés par chromatographie sur plaques préparatives, nous avons tracé les spectres de RMN ^{1}H et ^{13}C à partir d'une solution dans $CDCl_3$ des monocristaux séparés pour l'étude radiocristallographique. Ces derniers spectres ne présentent plus de dédoublement des signaux. Cette différence est illustrée par les spectres de RMN ^{1}H (figures 3 et 4) dans le cas du produit **5***b*.

Par ailleurs, dans le cas des spectres dédoublés, une étude en RMN à température variable (jusqu'à 213 K dans $CDCl_3$ et 383 K dans DMSO-d_6) ne nous a pas permis d'observer de phénomène de coalescence des signaux dédoublés. À basse température, les signaux sont légèrement élargis par suite d'une augmentation de la viscosité du solvant. Ce résultat nous permet de ne pas retenir l'existence éventuelle de rotamères résultant de la proximité du groupement 2,2,2-trichloro-1-éthoxycarbonylaminoéthyle sur l'azote-1 et du reste ester sur le carbone C-5 du cycle pyrazolique. La construction d'un modèle Dreiding confirme l'inexistence d'une rotation restreinte.

L'analyse élémentaire quantitative des produits isolés par chromatographie étant en excellent accord avec la structure **5** proposée, nous avons alors envisagé l'existence de deux isomères de constitution **5** et **6** non séparés par chromatographie sur plaques préparatives. Une étude en chromatographie HPLC analytique ne nous a encore pas permis de les séparer quelle que soit la polarité de l'éluant (mélange hexane–chloroforme en proportions variables). Néanmoins, l'hypothèse de l'existence de deux isomères de constitution **5** et **6** très difficiles à séparer peut être retenue et sur la suggestion d'un rapporteur[3] nous avons effectué les mêmes réactions entre le diazocomposé **3** et les esters éthyliques des acides butynedioïque et propiolique.

[3] Nous remercions vivement le rapporteur pour cette féconde suggestion.

Schéma 3.



2. Cas de l'acétylènedicarboxylate de diéthyle et du propiolate d'éthyle

Après départ du solvant, l'examen en RMN ^{1}H du brut réactionnel ne fait apparaître qu'un seul produit d'évolution **5** du cycloadduit initial **4** (schéma 2).

Dans le cas présent tous les groupes esters des réactants sont des esters éthyliques et il faut donc admettre que la différence entre ces deux résultats est due au fait que dans le cas précédent, les groupes esters des dipolarophiles étaient des esters méthyliques.

On peut donc proposer que l'évolution du cycloadduit **4** initial peut se faire de deux façons concurrentes (schéma 3). Une première voie consiste dans la transposition sigmatropique [1,5] — déjà explicitée sur le schéma 2 — qui conduit au produit **5**. La seconde voie peut être représentée par trois transpositions sigmatropiques [1,5] successives qui permettent d'aboutir au produit **6**.

Si R′ = Et, les produits **5** et **6** sont identiques et c'est ce que nous observons dans le cas des esters dipolarophiliques éthyliques (**5***c* ≡ **6***c*, **5***d* ≡ **6***d*).

Si R′ = Me, les produits **5** et **6** sont des isomères de constitution (**5***a* ≠ **6***a*, **5***b* ≠ **6***b*) dont les comportements chromatographiques et les paramètres spectroscopiques seront évidemment très voisins ce qui rend compte des dédoublements observés sur les spectres de RMN ^{1}H et ^{13}C du mélange des composés **5***a,b* et **6***a,b*.

On peut de plus noter que dans le cas des composés *a* et *b* les proportions relatives de ces isomères de constitution sont de l'ordre : 65% de composé **5** pour 35% de composé **6**.

© 1997 NRC Canada

Fig. 3. Spectre tracé à partir d'une solution dans $CDCl_3$ des monocristaux de **5***b*.

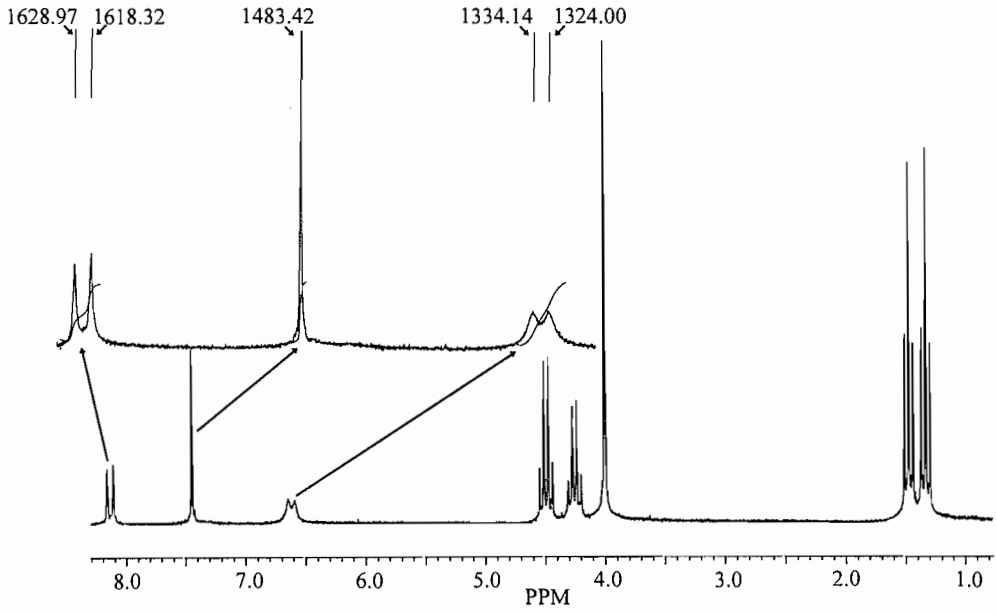
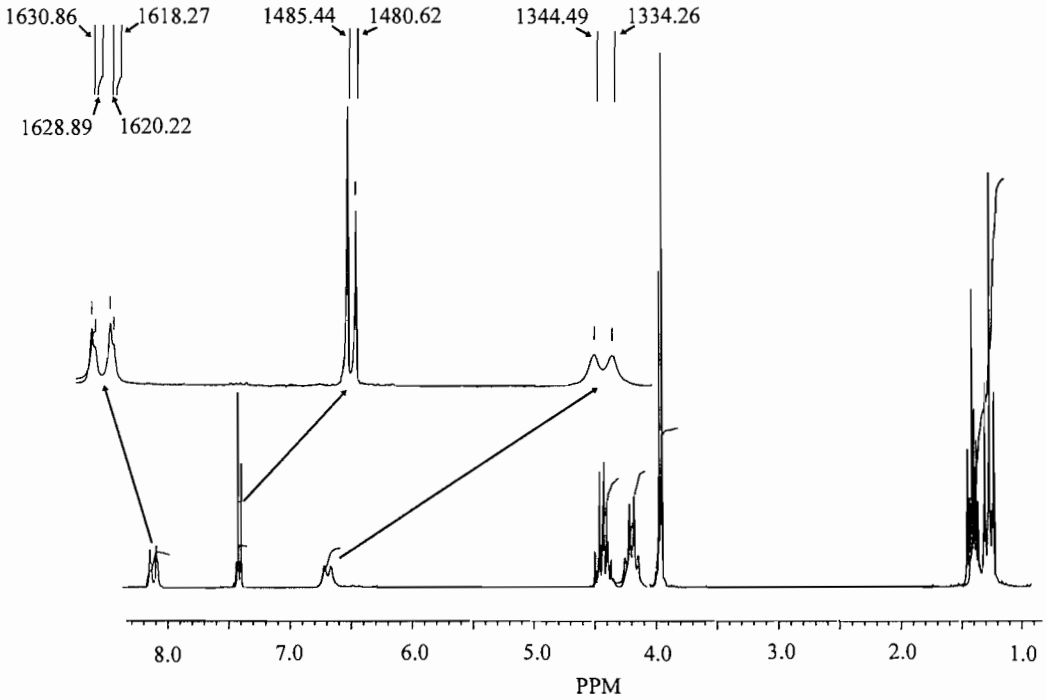


Fig. 4. Spectre tracé à partir d'une solution dans $CDCl_3$ du produit issu du propiolate de méthyle et chromatographié sur plaques préparatives.



D'autres tentatives d'obtention d'un cycloadduit avec d'autres dipolarophiles acétyléniques tels que le phénylacétylène ou le phénylpropiolate de méthyle n'ont donné aucune réaction.

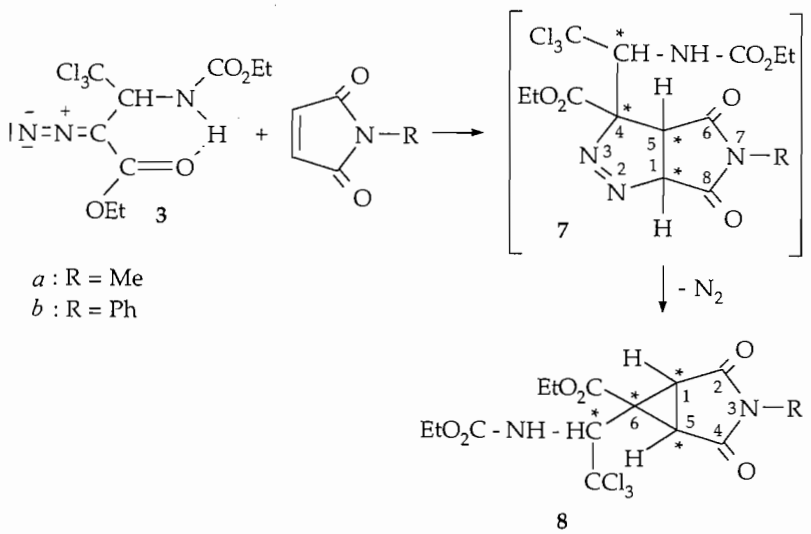
Réaction du nouveau diazocomposé avec les *N*-méthyl et *N*-phénylmaléimides

Nous avons testé divers dipolarophiles éthyléniques et notamment les esters acrylique, maléique et fumarique sans observer une réaction. Seuls les *N*-méthyl et *N*-phénylmaléimides ont permis d'obtenir un cycloadduit avec des rendements modestes (30 et 40%) vraisemblablement dûs au fait que la réaction étant effectuée au reflux du toluène, il y a compétition entre la dégradation du dipôle **3** et sa réaction de cycloaddition. Après retour à la température ambiante, le cycloadduit cristallise dans le toluène. L'analyse élémentaire et les paramètres spectroscopiques (IR, RMN et masse) permettent de retenir la structure de dérivés du maléimidocyclopropane ou 3-méthyl (ou phényl)-3-aza-6-éthoxycarbonyl-6-(2,2,2-

© 1997 NRC Canada

Can. J. Chem. Downloaded from www.nrcresearchpress.com by 88.146.161.215 on 09/08/12
For personal use only.

Schéma 4.



a : R = Me
b : R = Ph

trichloro-1-éthoxycarbonylaminoéthyl)bicyclo[3.1.0]hexane-2,4-dione **8** résultant de la perte d'azote du cycloadduit initial **7** qui est un dérivé d'une maléimido-1-pyrazoline (schéma 4).

Dans les deux cas, nous n'avons obtenu qu'un seul produit alors que la structure du cycloadduit intermédiaire **7** présente quatre centres de chiralité ce qui permettrait d'envisager a priori l'existence de quatre diastéréoisomères puisque les deux atomes d'hydrogène en positions 1 et 5 seront nécessairement dans une disposition *cis* par suite de la stéréochimie *cis* des réactions de cycloaddition. Pour expliquer cette remarquable diastéréospécificité nous pouvons invoquer successivement deux phénomènes :

1. La structure quasi-cyclique du dipôle-1,3 par suite de l'existence de la liaison hydrogène intramoléculaire caractérisée en spectrométrie IR permet de distinguer deux faces diastéréotopiques pour ce dipôle. L'un des « hémisphères » comporte le groupement trichlorométhyle beaucoup plus encombrant que l'atome d'hydrogène situé dans l'autre hémisphère et il est raisonnable d'envisager que l'approche dipôle–dipolarophile s'effectue sur la face la moins encombrée du dipôle-1,3.

2. Il subsiste alors deux approches possibles qui conduiront à des cycloadduits de stéréochimie relative différente entre les atomes C(1)–C(5) et l'atome C(4) dans le cycloadduit **7** qui devient C(6) dans **8** après perte d'azote. Ces deux approches A et B sont représentées sur la figure 5.

On peut désigner l'approche A comme étant une approche « *endo* » du maléimide par rapport au groupement ester du dipôle **3**, groupe ester qu'on retrouve fixé sur le carbone C(4) du cycloadduit **7** et C(6) du produit d'évolution **8**. Elle conduit à un produit où le groupe le plus encombrant (2,2,2-trichloro-1-ethoxycarbonylaminoéthyl) est en « *exo* » par rapport au reste maléimido, donc thermodynamiquement favorisé au contraire de celui qui résulterait de l'approche B.

Pour élucider cette structure nous avons d'abord vérifié que le produit obtenu présentait encore une liaison hydrogène intramoléculaire par une étude spectrométrique IR en dilution : alors que le produit dispersé dans KBr présente deux bandes $\nu_{(NH)}$ à 3345 et 3430 cm^{-1}, une solution dans CCl_4 de plus en plus diluée montre une diminution de l'intensité relative de la bande située à 3345 cm^{-1} jusqu'à sa disparition à la concentration de 10^{-2} mol L^{-1} et le maintien de la bande à 3430 cm^{-1}. Cette observation conforte l'existence d'une liaison hydrogène intramoléculaire.

Chacun des produits obtenus **8** (R = Me, Ph) a été soumis à une étude de NOE-différence en RMN ^1H. L'irradiation du proton H(1′) se traduit par une augmentation de l'intensité des signaux des protons H(1) et H(5) de 10 et 16% ce qui est un argument en faveur de la structure résultant de l'approche A. Il nous semble raisonnable de penser que cette approche « *endo* » pour le groupe ester fixé sur le carbone C(4) du cycloadduit intermédiaire puisse être dûe à des interactions orbitalaires secondaires entre l'un des groupes carbonyle du maléimide et ce groupe ester, ce qui contrôlerait alors la stéréochimie de l'approche pour donner lieu à une très grande diastéréosélectivité de la réaction.

Il faut noter que cette approche préférentielle via l'état de transition cinétiquement favorisé conduit alors au produit thermodynamique et il n'est pas étonnant d'observer la formation unique du produit **8**.

Conclusion

La réaction du diazoacétate d'éthyle sur la *N*-éthoxycarbonyl-*N*-(2,2,2-trichloroéthylidène)amine conduit à un nouveau diazocomposé qui manifeste une réactivité dipolaire-1,3 vis-à-vis des esters acétyléniques et des maléimides.

Dans le cas des esters acétyléniques, la réaction de cycloaddition s'accompagne d'une évolution qui conduit à des pyrazoles par suite de transpositions sigmatropiques [1,5].

Avec les maléimides, on observe une réaction de cycloaddition dipolaire-1,3 diastéréospécifique suivie d'une élimination d'azote qui conduit à un maléimidocyclopropane. La diastéréospécificité observée a été rationnalisée en faisant appel à un mode d'approche des réactants de type *endo-anti*.

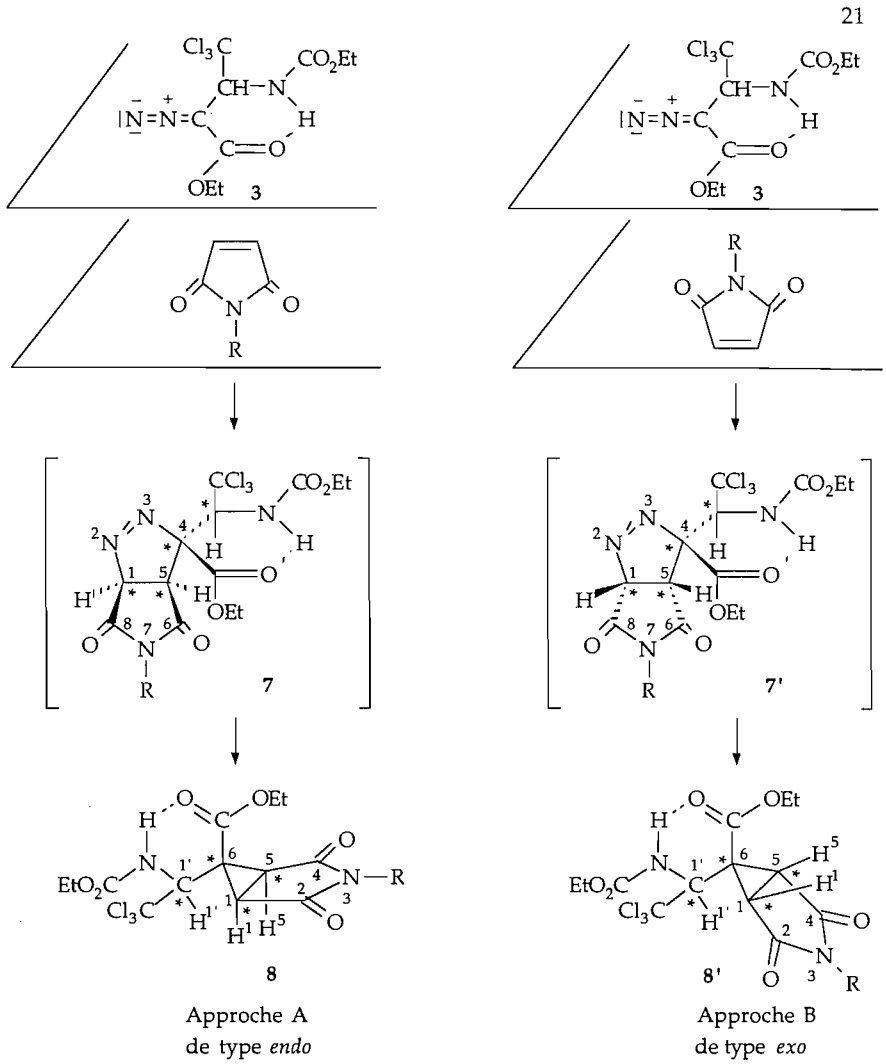
Partie experimentale

Toutes les matières premières sont préparées selon des méthodes déjà décrites dans la littérature et que nous avons

© 1997 NRC Canada

Can. J. Chem. Downloaded from www.nrcresearchpress.com by 88.146.161.215 on 09/08/12
For personal use only.

Fig. 5.



optimisées. Les points de fusion sont mesurés par projection sur banc Kofler et non corrigés. Les spectres d'absorption IR ont été tracés sur un spectrophotomètre Bio-Rad FTS-7, les produits étant dispersés en phase solide dans KBr à 5‰ ou examinés entre deux fenêtres de NaCl dans le cas des liquides. Les études en solution dans CCl_4 sont effectuées dans une cuve. Les spectres de RMN ^1H et ^{13}C ont été obtenus avec un spectromètre Bruker-Spectrospin AC200 (200 MHz pour ^1H et 50 MHz pour ^{13}C), les produits étant dissous dans $CDCl_3$ ou DMSO-d_6 (référence interne TMS). La chromatographie préparative sur plaques a été effectuée à partir de plaques préparées au laboratoire. Elles sont en verre Pyrex (20 × 20 ou 20 × 40) et recouvertes de gel de silice Merck 7747 (60 PF_{254}) (épaisseur 3 mm). Les microanalyses élémentaires ont été effectuées par le Service Central de Microanalyse du CNRS à Vernaison.

Synthèse de la *N*-éthoxycarbonyl-*N*-(2,2,2-trichloroéthylidène)amine 1

Cette imine est préparée selon Ulrich et coll. (3) mais ayant réussi à en améliorer le rendement, nous décrivons ici nos résultats expérimentaux.

1.1 Préparation de la 1-hydroxy-2,2,2-trichloroéthylcarbamate d'éthyle (19)

Dans un erlen rodé de 500 mL, 49,9 g (0,56 mol) d'uréthane sont mélangés à 82,7 g (0,5 mol) de chloral hydraté. Progressivement, une phase liquide se forme. La réaction endothermique est activée par un léger chauffage. On obtient une seule phase homogène qui est diluée avec 40 mL d'acide chlorhydrique concentré. Après 20 min, un bloc cristallin se forme avec un léger échauffement. Il est essoré, lavé à l'eau glacée jusqu'à pH 7. La poudre blanche est séchée à l'étuve à 50°C. Rdt = 94% ; P.F. = 106°C. IR : ν(OH) = 3400 cm^{-1}, ν(NH) = 3260 cm^{-1}, ν(C=O) = 1710 cm^{-1}. RMN ^1H ($CDCl_3$) : 1,20 (t, 3H, J = 7,15 Hz), 4,10 (q, 2H, J = 7,15 Hz), 5,70 (dd, 1H, J = 5,90 Hz et J = 9,70 Hz, CH), 6,60 (d, J = 5,90 Hz, OH), 7,10 (d, J = 9,70 Hz, NH). RMN ^{13}C ($CDCl_3$) : 14,2 (CH_3), 61,0 (OCH_2), 84,0 (CHOH), 102,3 (CCl_3), 155,7 (C=O ester).

1.2 Préparation du 1,2,2,2-tétrachloroéthylcarbamate d'éthyle

Dans un erlen tricol de 2 L équipé d'un réfrigérant et d'un tube à $CaCl_2$, une solution de 119 g de chlorure de thionyle (1 mol) et 2,2 g de pyridine, est additionnée à une suspension de 222,5

© 1997 NRC Canada

Can. J. Chem. Downloaded from www.nrcresearchpress.com by 88.146.161.215 on 09/08/12
For personal use only.

Can. J. Chem. Downloaded from www.nrcresearchpress.com by 88.146.161.215 on 09/08/12
For personal use only.

g (1 mol) de 1-hydroxy-2,2,2-trichloroéthylcarbamate d'éthyle dans 1200 mL de chlorure de méthylène. Après un reflux de 60 min, une solution claire est obtenue. Après évaporation du solvant, le résidu est distillé sous vide. Rdt = 99% (litt. (3) 97%), $Eb_{0,05\ Torr}$ (1 Torr = 133,3 Pa) = 90°C, P.F. = 67°C (litt. (3) 63°C). IR : ν(NH) = 3320 cm^{-1}, ν(C=O) = 1730 cm^{-1}. RMN ^1H (DMSO-d_6) : 1,20 (t, 3H, J = 7,15 Hz), 4,20 (q, 2H, J = 7,15 Hz), 6,50 (s, 1H). RMN ^{13}C (DMSO-d_6) : 14,0 (CH_3), 63,3 (OCH_2), 79,5 (CHCl), 101,2 (CCl_3), 154,8 (C=O ester).

1.3 Préparation du N-éthoxycarbonyl-N-(,2,2,2-trichloroéthylidène)amine ***1***

Dans un erlen tricol de 500 mL muni d'un réfrigérant, d'un tube à $CaCl_2$ et d'une ampoule à brome, on ajoute lentement une solution de 48,2 g (0,2 mol) de 1,2,2,2-tétrachloroéthylcarbamate d'éthyle dans 200 mL de benzène anhydre à une solution de 20,2 g (0,2 mol) de triéthylamine anhydre et fraichement distillée dans 200 mL de benzène anhydre. À la fin de l'addition, le chlorhydrate de triéthylamine est filtré. Après évaporation du solvant à l'évaporateur rotatif, le résidu est distillé sous vide. Rdt = 89% (litt. (3) 47,7%), $Eb_{0,3\ Torr}$ = 65°C (litt. (3) 70°C sous 1,1 Torr). IR : ν(C=O) = 1710 cm^{-1}, ν(C=N) = 1650 cm^{-1}. RMN ^1H ($CDCl_3$) : 1,30 (t, 3H, J = 7,15 Hz), 4,30 (q, 2H, J = 7,15 Hz), 8,20 (s, 1H). RMN ^{13}C ($CDCl_3$) : 13,8 (q, CH_3, J = 127,5 Hz), 63,9 (t, OCH_2, J = 149,0 Hz), 92,4 (s, CCl_3), 160,0 (s, C=O ester), 161,7 (d, CH=N, J = 186,5 Hz).

Réaction du diazoacétate d'éthyle avec la *N*-éthoxycarbonyl-*N*-(2,2,2-trichloroéthylidène)amine : obtention du 3-éthoxycarbonylamino-4,4,4-trichloro-2-diazobutyrate d'éthyle 3

Mode opératoire

Dans un ballon de 100 mL, muni d'un réfrigérant et d'un tube à $CaCl_2$, on introduit 4,37 g (2×10^{-2} mol) de *N*-éthoxycarbonyl-*N*-(2,2,2-trichloroéthylidène) amine **1**, 50 mL de toluène anhydre et 2,28 g (2×10^{-2} mol) de diazoacétate d'éthyle. Le mélange est chauffé à 60°C pendant 44 h. La réaction est suivie par CCM (éluant : chloroforme). Le solvant est éliminé à l'évaporateur rotatif. Le solide jaune obtenu est recristallisé dans l'hexane. Rdt = 83% ; P.F. = 70°C. IR : $\nu_{(NH)}$ = 3401 et 3436 cm^{-1}, $\nu_{(N_2)}$ = 2105 cm^{-1}, $\nu_{(C=O)}$ = 1695 et 1740 cm^{-1}. RMN ^1H ($CDCl_3$) : 1,29 (t, 3H, J = 7,25 Hz, CH_3), 1,31 (t, 3H, J = 7,10 Hz, CH_3), 4,20 (q, 2H, J = 7,10 Hz, CH_2), 4,24 (q, 2H, J = 7,25 Hz, CH_2), 5,50 (d, 1H, J = 9,8 Hz, CH), 6,50 (sl, NH). RMN ^{13}C ($CDCl_3$) : 14,3 (q, CH_3, J = 126,0 Hz), 14,4 (q, CH_3, J = 126,0 Hz), 61,5 (t, CH_2, J = 146,5 Hz), 62,2 (t, CH_2, J = 148,0 Hz), 63,0 (d, CH, J = 146,0 Hz), 102,9 (s, CCl_3), 164,8 (s, C=O ester), 164,9 (s, C=O ester). Analyse pour $C_9H_{12}Cl_3N_3O_4$ calculé : C 32,5%, H 3,64%, N 12,63%, Cl 31,58%, trouvé : C 32,5%, H 3,68%, N 12,38%, Cl 32,25%.

Réactions du 3-éthoxycarbonylamino-4,4,4-trichloro-2-diazobutyrate d'éthyle avec les dipolarophiles acétyléniques

Mode opératoire général

Dans un ballon rodé de 100 mL équipé d'un réfrigérant et d'un tube à $CaCl_2$, on introduit 1,66 g (5 mmol) de 3-éthoxycarbonylamino-4,4,4-trichloro-2-diazobutyrate d'éthyle **3**, 15 mL de toluène anhydre et 5 mmol d'ester acétylénique. Sous agitation magnétique, le mélange réactionnel est chauffé entre 60 et 70°C pendant 60–100 h. La réaction est suivie par CCM et IR (l'avancement de la réaction va dans le même sens que la disparition de la bande $\nu_{(N2)}$ à 2104 cm^{-1}). Le solvant est éliminé à l'évaporateur rotatif. On obtient une huile qui est purifiée par chromatographie préparative sur plaques de gel de silice (éluant : chloroforme) dans le cas des esters méthyliques ou par cristallisation dans l'éthanol dans le cas des esters éthyliques.

Cas des esters méthyliques

La chromatographie permet d'isoler les mélanges des composés **5** et **6**.

(*a*) Produits **5***a* et **6***a* issus de l'acétylènedicarboxylate de diméthyle. Rendement global : 80%. IR : $\nu_{(NH)}$ = 3367 et 3334 cm^{-1}, $\nu_{(C=O)}$ = 1732 cm^{-1}. RMN ^{13}C (DMSO-d_6) : tracé à partir du mélange **5***a* + **6***a*, l'existence des deux isomères de constitution entraîne le dédoublement de certains signaux indiqués par un astérisque. 13,9 et 14,0 (CH_3)*, 14,8 (CH_3), 52,9 et 53,9 (OCH_3)*, 53,1 (OCH_3), 61,7 (OCH_2), 61,9 et 63, (OCH_2)*, 73,5 (CH), 97,2 (CCl_3), 121,7 et 121,8 (Cq)*, 135,4 et 133,5 (Cq)*, 140,4 (Cq), 156,0 (Cq), 158,0 et 158,4 (Cq)*, 159,8 et 160,3 (Cq)*, 162,9 (Cq). Analyse pour $C_{15}H_{18}Cl_3N_3O_8$ calculé : C 37,94%, H 3,82%, N 8,86%, Cl 22,43%, trouvé : C 38,12%, H 3,67%, N 8,95%, Cl 22,37%.

3,4-Diméthoxycarbonyl-5-éthoxycarbonyl-1-(2,2,2-trichloro-1-*N*-éthoxycarbonylaminoéthyl)pyrazole **5***a* séparé par cristallisation fractionnée de l'éthanol. Rdt = 52% ; P.F. = 137°C (monocristaux de l'éthanol). IR : $\nu_{(NH)}$ = 3367 et 3334 cm^{-1}, $\nu_{(C=O)}$ = 1732 cm^{-1}. RMN ^1H (DMSO-d_6) : 1,20 (t, 3H, J = 7,10 Hz), 1,30 (t, 3H, J = 7,10 Hz), 3,90 (s, 3H), 3,99 (s, 3H), 4,20 (q, 2H, J = 7,10 Hz), 4,35 (partie AB d'un système ABX_3, J_{AB} = 11,7 Hz, $J_{AX_3} = J_{BX_3}$ = 7,10 Hz), 7,97 (d, 1H, J = 9,90 Hz), 9,34 (dl, NH, J = 9,90 Hz). Structure radiocristallographique (18*a*).

4,5-Diméthoxycarbonyl-3-éthoxycarbonyl-1-(2,2,2-trichloro-1-*N*-éthoxycarbonylaminoéthyl)pyrazole **6***a* non isolé. Rdt = 28%. RMN ^1H (DMSO-d_6) : 1,20 (t, 3H, J = 7,10 Hz), 1,28 (t, 3H, J = 7,10 Hz), 3,90 (s, 3H), 3,99 (s, 3H), 4,20 (q, 2H, J = 7,10 Hz), 4,35 (q, 2H, J = 7,10 Hz), 7,95 (d, 1H, J = 9,90 Hz), 9,34 (dl, NH, J = 9,90 Hz).

(*b*) Produits **5***b* et **6***b* issus du propiolate de méthyle. Rendement global : 63%; IR : $\nu_{(NH)}$ = 3320 et 3420 cm^{-1}, $\nu_{(C=O)}$ = 1730 cm^{-1}. RMN ^{13}C ($CDCl_3$) : tracé à partir du mélange **5***b* + **6***b*; l'existence des deux isomères de constitution entraîne le dédoublement de certains signaux indiqués par un astérisque. 14,0 (CH_3), 14,3 (CH_3), 52,4 et 52,7 (OCH_3)*, 61,5 (OCH_2), 62,2 et 62,4 (OCH_2)*, 73,5 (CH), 98,3 (CCl_3), 113,9 et 114,1 (CH)*, 135,9 (Cq), 143,6 (Cq), 154,8 (Cq), 158,7 (Cq), 160,9 et 161,5 (Cq)*. Analyse pour $C_{13}H_{16}Cl_3N_3O_6$ calculé : C 37,46%, H 3,97%, N 10,08%, Cl 25,55%, trouvé : C 37,58%, H 4,12%, N 9,87%, Cl 25,68%.

3-Méthoxycarbonyl-5-éthoxycarbonyl-1-(2,2,2-trichloro-1-*N*-éthoxycarbonylaminoéthyl)pyrazole **5***b* séparé par cristallisation fractionnée de l'éthanol. Rdt = 41% ; P.F. = 142°C (monocristaux de l'éthanol). RMN ^1H : 1,35 (t, 3H, J = 7,10 Hz), 1,45 (t, 3H, J = 7,15 Hz), 3,92 (s, 3H, OCH_3), 4,25 (q, 2H, J = 7,15 Hz), 4,50 (q, 2H, J = 7,10 Hz), 6,60 (dl, 1H, J = 10,6 Hz, NH), 7,39 (s, 1H, H-4), 8,10 (d, 1H, J = 10,6 Hz, CH). Structure radiocristallographique (18*b*).

5-Méthoxycarbonyl-3-éthoxycarbonyl-1-(2,2,2-trichloro-

© 1997 NRC Canada

Can. J. Chem. Downloaded from www.nrcresearchpress.com by 88.146.161.215 on 09/08/12
For personal use only.

1-*N*-éthoxycarbonylaminoéthyl)pyrazole **6***b*, non isolé. Rdt = 22%. RMN ^{1}H : 1,30 (t, 3H, J = 7,10 Hz), 1,38 (t, 3H, J = 7,15 Hz), 3,94 (s, 3H, OCH_3), 4,20 (q, 2H, J = 7,15 Hz), 4,40 (q, 2H, J = 7,10 Hz), 6,60 (dl, 1H, J = 10,6 Hz, NH), 7,36 (s, 1H, H-4), 8,09 (d, 1H, J = 10,6 Hz, CH).

Cas des esters éthyliques

(*a*) 3,4,5-Triéthoxycarbonyl-1-(2,2,2-trichloro-1-*N*-éthoxycarbonylaminoéthyl)pyrazole **5***c*. Rdt = 56% ; P.F. = 83°C (éthanol). IR : $\nu_{(NH)}$ = 3354 cm^{-1}, $\nu_{(C=O)}$ = 1739 cm^{-1}. RMN ^{1}H ($CDCl_3$) : 1,27 (t, 3H, J = 7,15 Hz), 1,34 (t, 3H, J = 6,9 Hz), 1,36 (t, 3H, J = 7,15 Hz), 1,38 (t, 3H, J = 7,0 Hz), 4,19 (q, 2H, J = 7,0 Hz), 4,39 (q, 6H, J = 7,10 Hz), 6,62 (dl, 1H, J = 10,5 Hz, NH), 8,05 (d, 1H, J = 10,5 Hz). RMN ^{13}C ($CDCl_3$) : 13,8 (q, J = 128 Hz), 13,9 (q, J = 127 Hz), 14,0 (q, J = 128 Hz), 14,2 (q, J = 127 Hz), 61,9 (t, J = 149 Hz), 62,1 (t, J = 148 Hz), 62,5 (t, J = 149 Hz), 62,7 (t, J = 148 Hz), 73,7 (d, J = 159 Hz), 97,8 (s, CCl_3), 121,9 (s, Cq), 133,2 (s, Cq), 140,9 (s, Cq), 154,7 (s, CO), 157,6 (s, CO), 159,9 (s, CO), 162,7 (s, CO). Analyse pour $C_{17}H_{22}Cl_3N_3O_8$ calculé : C 40,62%, H 4,41%, N 8,36%, Cl 25,46%, trouvé : C 40,48%, H 4,62%, N 8,27%, Cl 25,60%

(*b*) 3,5-Diéthoxycarbonyl-1-(2,2,2-trichloro-1-*N*-éthoxycarbonylaminoéthyl)pyrazole **5***d*. Rdt = 47% ; P.F. = 122°C (éthanol). IR : $\nu_{(NH)}$ = 3421 cm^{-1}, $\nu_{(C=O)}$ = 1734 cm^{-1}. RMN ^{1}H ($CDCl_3$) : 1,28 (t, 3H, J = 7,15 Hz), 1,40 (t, 3H, J = 7,15 Hz), 1,42 (t, 3H, J = 7,05 Hz), 4,20 (q, 2H, J = 7,05 Hz), 4,42 (q, 2H, J = 7,15 Hz), 4,44 (q, 2H, J = 7,15 Hz), 6,68 (dl, 1H, J = 10,6 Hz, NH), 7,40 (s, 1H, H-4), 8,11 (d, 1H, J = 10,6 Hz). RMN ^{13}C ($CDCl_3$) : 14,0 (q, J = 128 Hz), 14,2 (q, J = 126 Hz), 61,4 (t, J = 144 Hz), 62,0 (t, J = 152 Hz), 62,3 (t, J = 152 Hz), 73,4 (d, J = 160 Hz), 98,3 (s, CCl_3), 113,8 (d, J = 168 Hz), 135,7 (s, Cq), 143,8 (s, Cq), 154,8 (s, CO), 158,66 (s, CO), 160,9 (s, CO). Analyse pour $C_{14}H_{18}Cl_3N_3O_6$ calculé : C 39,04%, H 4,21%, N 9,77%, Cl 24,70%, trouvé : C 39,22%, H 4,13%, N 9,82%, Cl 24,57%.

Réactions du 3-éthoxycarbonylamino-4,4,4-trichloro-2-diazobutyrate d'éthyle avec les *N*-méthyl et *N*-phénylmaléimides

Mode opératoire

Dans un erlen rodé de 100 mL, surmonté d'un réfrigérant et d'un tube à $CaCl_2$, on introduit 5×10^{-3} mol de 3-éthoxycarbonylamino-4,4,4-trichloro-2-diazobutyrate d'éthyle **3**, 15 mL de toluène anhydre, et 5×10^{-3} mol de *N*-phényl ou *N*-méthylmaléimide. Sous agitation magnétique, le mélange est porté à reflux pendant 4 jours. La réaction a été contrôlée par IR en suivant la disparition de la bande du groupement diazo à 2104 cm^{-1}. On laisse revenir la solution à température ambiante. Après 1 nuit, un solide cristallise dans le toluène.

3-Méthyl-6-éthoxycarbonyl-6-(2,2,2-trichloro-1-éthoxycarbonylaminoéthyl)-3-azabicyclo[3.1.0]hexane-2,4-dione **8**a : Rdt = 30% ; P.F. = 188°C. IR : $\nu_{(NH)}$ = 3345 cm^{-1}, $\nu_{(C=O)}$ = 1722 et 1781 cm^{-1}. RMN ^{1}H ($CDCl_3$) : 1,25 (t, 3H, ^3J = 7,15 Hz), 1,35 (t, 3H, ^3J = 7,10 Hz), 2,83 (s, 3H), 2,90 (d, 1H, J = 5,40 Hz), 3,20 (d, 1H, J = 5,40 Hz), 4,25 (q et (q + ABX_3), 4H, Jq = 7,15 Hz (J_{AB} = 10,75 Hz, $J_{AX_3} \approx J_{BX_3}$ = 7,10 Hz), 4,28 (d, 1H, J = 10,4 Hz), 6,14 (d, 1H, NH, J = 10,4 Hz). RMN ^{13}C ($CDCl_3$) : 13,6 (q, CH_3, J = 127,5 Hz), 14,3 (q, CH_3, J = 127,0 Hz), 24,4 (q, CH_3, J = 141,5 Hz), 30,0 (d, CH, J = 185,5 Hz), 33,9 (d, CH, J = 185,5 Hz), 44,9 (s, Cq), 62,5 (t, CH_2, J = 148,0 Hz), 63,5 (t, CH_2, J = 149,5 Hz), 68,6 (d, CH, J = 147,0 Hz), 99,2 (s, CCl_3), 155,9 (C=O), 165,2 (C=O), 169,9 (C=O), 170,4 (C=O). Analyse pour $C_{14}H_{17}Cl_3N_2O_6$ calculé : C 40,45%, H 4,12%, N 6,74%, Cl 25,59%, trouvé : C 40,98%, H 4,30%, N 6,67%, Cl 25,58%

3-Phényl-6-éthoxycarbonyl-6-(2,2,2-trichloro-1-éthoxycarbonylaminoéthyl)-3-azabicyclo[3.1.0]hexane-2,4-dione **8**b : Rdt = 40%; P.F. = 165°C. IR : $\nu_{(NH)}$ = 3392 et 3358 cm^{-1}, $\nu_{(C=O)}$ = 1725 cm^{-1}. RMN ^{1}H ($CDCl_3$) : 1,25 (t, 3H, ^3J = 7,10 Hz), 1,35 (t, 3H, J = 7,10 Hz), 3,05 (d, 1H, J = 5,50 Hz), 3,30 (d, 1H, J = 5,50 Hz), 4,00–4,40 (d + q + (ABX_3, q), 5H, Jd = 10,45 Hz, Jq = 7,10 Hz (J_{AB} = 10,80 Hz, $J_{AX} \approx J_{BX}$ = 7,10 Hz, Jq = 7,10 Hz)), 6,15 (d, NH, J = 10,45 Hz), 7,20–7,50 (m, C_6H_5). RMN ^{13}C ($CDCl_3$) : 13,5 (q, CH_3, J = 128,0 Hz), 14,3 (q, CH_3, J = 127,0 Hz), 29,8 (d, CH, J = 186,0 Hz), 33,8 (d, CH, J = 186,0 Hz), 44,5 (s, Cq), 62,6 (t, CH_2, J = 150,0 Hz), 63,4 (t, CH_2, J = 150,0 Hz), 68,7 (d, CH, J = 144,0 Hz), 99,2 (s, CCl_3), 125,9 (d, 2CH, J = 157,0 Hz), 128,6 (d, CH, J = 162,0 Hz), 129,1 (d, 2CH, J = 159,0 Hz), 130,9 (s, Cq), 156,0 (s, Cq), 164,9 (s, Cq), 168,8 (s, Cq), 169,1 (s, Cq). Analyse pour $C_{19}H_{19}Cl_3N_2O_6$ calculé : C 47,75%, H 4,01%, N 5,86%, Cl 22,29%, trouvé : C 47,93%, H 3,92%, N 5,77%, Cl 22,37%.

Bibliographie

1. R. Moscheles. Chem. Ber. **24**, 1803 (1891).
2. F. Feist. Chem. Ber. **45**, 945 (1912).
3. H. Ulrich, B. Tucker et A.A.R. Sayigh. J. Org. Chem. **33**, 2887 (1968).
4. G.R. Krow, C. Johnson et M. Boyle. Tetrahedron Lett. 1978, (1971).
5. R. Consonni, P. Dalla Croce, R. Ferraccioli et C. La Rosa. J. Chem. Res. (S), 32 (1992).
6. A. Belaissaoui, C. Morpain et B. Laude. Bull. Soc. Chim. Belg. **104**, 491 (1995).
7. P.W. Manley, R. Somanathan, D.L.R. Reeves et R.C. Stoor. J. Chem. Soc. Chem. Commun. 396 (1978).
8. A. Mustafa. J. Chem. Soc. 234 (1949).
9. G.D. Buckley. J. Chem. Soc. 1850 (1954).
10. J.M. Stewart, R.L. Clark et P.E. Pike. J. Chem. Eng. Data, **16**, 99 (1971).
11. P.K. Kadaba. Synthesis. 71 (1973).
12. F. Roelants et A. Bruylants. Tetrahedron, **34**, 2229 (1978).
13. K. Burger, J. Fehn et A. Gieren. Liebigs Ann. Chem. **757**, 9 (1972).
14. K. Burger, W. Thenn, J. Fehn, A. Gieren et P. Narayanan. Chem. Ber. **107**, 1526 (1974).
15. A.L. Logothetis. J. Org. Chem. **29**, 3049 (1964).
16. T.C. Callagher et R.C. Storr. Tetrahedron Lett. **22**, 2909 (1981).
17. M. Tichy. Adv. Org. Chem. **5**, 115 (1966).
18. N. Rodier, A. Belaissaoui, C. Morpain et B. Laude. (*a*) Acta Crystallogr. Sect. C: Cryst. Struct. Commun. **C50**, 1171 (1994); (*b*) Acta Crystallogr. Sect C: Cryst. Struct. Commun. **C50**, 1762 (1994).
19. O. Diels et C. Seib. Chem. Ber. **42**, 4062 (1909).

© 1997 NRC Canada

Arene–manganese and arene–rhenium compounds of formula (arene)$M(CO)_2(SiCl_3)$

Valerie M. Hansen, Jonathan L. Male, and Roland K. Pomeroy

Abstract: Derivatives of formula (arene)$M(CO)_2(SiCl_3)$ (M = Mn, Re) have been prepared in moderate to good yield by the reaction of $M(CO)_5(SiCl_3)$ and the appropriate arene (with heptane in those cases where the arene was a solid) in an evacuated sealed tube at 230–260°C for 12–24 h, depending on the arene and the metal. Carefully purified reagents were necessary to obtain satisfactory yields. The (η^6-1,4-$C_6H_4Bu^t_2$)$M(CO)_2(SiCl_3)$ complexes in solution exhibit free rotation of the arene ring about the metal atom to −120°C as ascertained by ^{1}H NMR spectroscopy. The manganese compound did show the onset of decoalescence of two of the signals due to the arene ligand in the $^{13}C\{^1H\}$ NMR spectrum in CD_2Cl_2 solution below −90°C. This, however, is interpreted in terms of restricted rotation of the *tert*-butyl substituent rather than restricted rotation of the arene ring.

Key words: arene, manganese, rhenium, restricted rotation.

Résumé : On a préparé les dérivés de formule (arène)$M(CO)_2(SiCl_3)$ (M = Mn, Re) avec des rendements allant de modérés à bons en faisant réagir du $M(CO)_5(SiCl_3)$ avec l'arène approprié (en présence d'heptane lorsque l'arène est solide), sous vide, dans un tube scellé, à des températures allant de 230 à 260°C pendant 12–24 h suivant la nature de l'arène et du métal. L'utilisation de réactifs purifiés avec soin est nécessaire pour obtenir des rendements satisfaisants. En se basant sur les résultats de la spectroscopie RMN du ^{1}H, les complexes (η^6-1,4-$C_6H_4tBu_2$)$M(CO)_2(SiCl_3)$ en solution présentent de la rotation libre du noyau arène autour de l'atome métallique, jusqu'à −120°C. Dans le cas du spectre RMN $^{13}C\{^1H\}$ du dérivé du manganèse en solution dans le CD_2Cl_2, une décoalescence des deux signaux dus au coordinat arène commence à se produire en dessous de −90°C. Toutefois, on interprète ce résultat en fonction d'une rotation restreinte du substituant *tert*-butyle plutôt que d'une rotation restreinte du noyau arène.

Mots clés : arène, manganèse, rhénium, rotation restreinte.

[Traduit par la rédaction]

Introduction

In 1980, work from this laboratory reported the restricted rotation of the arene ring about the metal atom of (η^6-1,4-$C_6H_4Bu^t_2$)$Ru(CO)(SiCl_3)_2$ in solution as detected by NMR line-broadening techniques (1). This was one of the first cases where this type of restricted rotation had been observed. At the time we were unable to synthesize iron complexes of the type (η^6-$C_6H_{6-x}R_x$)$Fe(CO)(SiCl_3)_2$ in order to compare the barriers to arene–metal rotation with those in the ruthenium analogues. More recently, however, we have found that with carefully purified reagents the iron complexes can indeed be prepared. Not surprisingly, the iron derivatives have large barriers to arene–metal rotation that are the highest so far observed (2).

In this study we report the application of the procedure used for the preparation of the Fe compounds to the synthesis of complexes of formula (arene)$M(CO)_2(SiCl_3)$ (M = Mn, Re) and an attempt to measure the barrier to arene–M rotation in the 1,4-$C_6H_4Bu^t_2$ derivatives. (A brief report of the ^{1}H NMR study of (η^6-1,4-$C_6H_4Bu^t_2$)$Re(CO)_2(SiCl_3)$ has appeared in a communication (3).) Arene–Mn and arene–Re complexes are also of interest since they are far less common than arene derivatives of the group 6 metals (4). Arene derivatives of transition metals, especially those of chromium, have found considerable use in organic synthesis particularly in the area of aromatic nucleophilic substitution (5). Furthermore, a recent review has illustrated the interesting and useful chemistry exhibited by the air-stable [(η^6-arene)$Mn(CO)_3$]$^+$ cations (6).

Experimental section

Unless otherwise stated, manipulations of starting materials and products were carried out under a nitrogen atmosphere with the use of standard Schlenk techniques. Heptane and the liquid arenes were refluxed over potassium, distilled, and stored over molecular sieves before use; olefins had been previously removed from the heptane by the accepted procedure (7). Dichloromethane and $CFCl_3$ were dried in a similar manner to the hydrocarbons except that P_2O_5 was employed as the drying agent. The $CDFCl_2$ was prepared by a literature method (8). Solid arene reagents were recrystallized from hexane and sublimed before use. The precursory complexes, $M(CO)_5(SiCl_3)$ (M = Mn, Re) were prepared by a literature procedure (9); they were also freshly sublimed before use. The

Received December 19, 1996.

V.M. Hansen, J.L. Male, and R.K. Pomeroy.[1] Department of Chemistry, Simon Fraser University, Burnaby, BC V5A 1S6, Canada.

[1] Author to whom correspondence may be addressed. Telephone: (604) 291-3347. Fax: (604) 291-3765. E-mail: pomeroy@sfu.ca

© 1997 NRC Canada

Can. J. Chem. Downloaded from www.nrcresearchpress.com by 88.146.161.215 on 09/08/12
For personal use only.

Can. J. Chem. Downloaded from www.nrcresearchpress.com by 88.146.161.215 on 09/08/12
For personal use only.

Table 1. Analytical and IR data[a] for the (arene)$M(CO)_2(SiCl_3)$ (M = Mn, Re) complexes.

Arene	MS[b]	%C (calcd.)	%H (calcd.)	ν(CO) cm^{-1}
		M = Mn		
C_6H_6	322	29.94(29.70)	2.10(1.87)	1999, 1960.5
C_6H_5Me	336	32.11(32.03)	2.37(2.39)	1994, 1955
$C_6H_5Bu^t$	378	38.16(37.97)	3.73(3.72)	1991, 1951
1,2-$C_6H_4Me_2$	350	34.25(34.16)	2.90(2.87)	1989, 1949.5
1,4-$C_6H_4Me_2$	350	34.40(34.16)	3.02(2.87)	1989.5, 1951
1,4-$C_6H_4Bu^t_2$	434	43.64(44.10)	4.81(5.09)	1984.5, 1943.5
1,3,5-$C_6H_3Me_3$	364	36.00(36.14)	3.18(3.31)	1986, 1946
		M = Re		
C_6H_6	454	21.36(21.13)	1.56(1.33)	1993.5, 1941
C_6H_5Me	468	23.22(23.06)	1.74(1.72)	1989, 1937.5
$C_6H_5Bu^t$	510	28.02(28.21)	2.79(2.76)	1988.5, 1934.5
1,4-$C_6H_4Me_2$	482	24.99(24.88)	2.14(2.09)	1985.5, 1932
1,4-$C_6H_4Pr^i_2$	538	31.45(31.20)	3.52(3.37)	1984, 1931
1,4-$C_6H_4Bu^t_2$	566	33.90(33.89)	3.89(3.91)	1983,1928
1,3,5-$C_6H_3Me_3$	496	26.61(26.59)	2.27(2.43)	1981.5, 1928.5
1,2,3,4,-$C_6H_2Me_4$	510	28.34(28.21)	2.74(2.76)	1976, 1922
1,2,4,5-$C_6H_2Me_4$	510	28.27(28.21)	2.81(2.76)	1976.5, 1924.5
C_6HMe_5	524	30.00(29.74)	3.09(3.07)	1973.5, 1917.5
C_6Me_6	538	31.34(31.20)	3.32(3.37)	1968, 1914.5

[a]In hexane for the Mn complexes; in CH_2Cl_2 for the Re complexes.
[b]Parent ion in each case.

reactions were carried out in thick-walled Carius tubes of approximate volume of 100 mL and fitted with a Teflon valve: the tubes were immersed in the temperature baths to a point only just above that of the reaction solution. Although no problems were experienced with this procedure, precautions against explosion were taken since the reaction temperatures were far above the boiling points of the solvent and most of the arene reagents employed.

Infrared spectra were recorded on a Perkin Elmer 983 spectrometer; electron-impact (70 eV) mass spectra were obtained with a Hewlett–Packard 5985 GC–MS instrument; NMR spectra were recorded on a Bruker WM400 or Bruker SY-100 spectrometer; microanalyses were determined by M. K. Yang of the Microanalytical Laboratory of Simon Fraser University. Infrared and mass spectroscopic data, and elemental analyses for the new compounds are given in Table 1; ^1H and $^{13}C\{^1H\}$ NMR data are given in Table 2.

Preparation of (η^6-arene)$Mn(CO)_2(SiCl_3)$ compounds

A Carius tube was charged with $Mn(CO)_5(SiCl_3)$ (100 mg, 0.304 mmol) and either the liquid arene (10 mL) or olefin-free heptane (1 mL) and the solid arene (1.0 g). The vessel and contents were cooled to −196 °C and evacuated; the solution was rigorously degassed with three freeze–pump–thaw cycles. The vessel was warmed to room temperature and placed in an oil-bath at 230 °C (located behind a protective shield) for 12 h (24 h for the preparation that involved benzene). For the reactions that involved liquid arenes, the vessel was cooled and volatiles removed on the vacuum line (with heating for reactions that involved arenes with high boiling points). The remaining solid was extracted with CH_2Cl_2 (3 × 10 mL); the extracts were filtered through Celite and the solvent was removed on the vacuum line. The crude product remaining after this procedure was recrystallized from the minimum amount of hot hexane to give the desired product. For reactions that involved solid arenes, the reaction mixtures (after cooling) were extracted with CH_2Cl_2 (3 × 10 mL); the extracts were filtered through Celite and all volatiles removed on the vacuum line. The arene was removed by sublimation at elevated temperatures (<0.02 Torr; 1 Torr = 133.3 Pa). The remaining crude product was recrystallized from hexane as described above. The yields in both procedures were 20–70%; the compounds are air-sensitive, pale-yellow crystals. The analytical samples were obtained from a second crystallization from hexane. The compounds may also be sublimed at >80°C (<0.02 Torr) to a probe cooled with cold water.

Preparation of (η^6-arene)$Re(CO)_2(SiCl_3)$ compounds

The methods employed were essentially those used to prepare the Mn complexes, but with the following differences: A reaction temperature of 240°C was employed except in the case of the benzene derivative where a temperature of 230°C and a reaction time of 24 h was used, and the C_6Me_6 derivative where a temperature of 260°C and a reaction time of 24 h was required. After the extraction step, the CH_2Cl_2 extracts were concentrated to ~10 mL, an equal volume of hexane was added, and the resulting solution was stored overnight at −20°C. The resulting crystals were separated from the mother solution, washed with hexane, and dried on the vacuum line. The analytical samples were obtained by heating in hot CH_2Cl_2 with decolorizing charcoal, followed by recrystallization from CH_2Cl_2–hexane. Yields ranged from 20 to 80%. The compounds are colorless, air-sensitive solids that, unlike the

© 1997 NRC Canada

Can. J. Chem. Downloaded from www.nrcresearchpress.com by 88.146.161.215 on 09/08/12
For personal use only.

Table 2. NMR data for the (arene)$M(CO)_2(SiCl_3)$ (M = Mn, Re) complexes.

Arene	^{1}H NMR[a] δ	^{13}C NMR δ		
		CO	Arene-C	Alkyl-C
		M = Mn		
C_6H_6	5.72	220.3	95.3	
C_6H_5Me	5.40(t), 5.60(d, J = ~6 Hz), 5.86(t), 2.31	221.0	111.6, 97.3, 95.2, 92.7	20.7
$C_6H_5Bu^t$	5.65(m),[c] 1.39	221.4	125.3, 96.6, 94.4, 93.8	34.9, 31.1
1,2-$C_6H_4Me_2$	5.59(m),[c] 2.30	221.7	109.9, 97.4, 95.1	19.0
1,4-$C_6H_4Me_2$	5.65, 2.20	221.9	108.2, 97.0	19.8
1,4-$C_6H_4Bu^t_2$	5.85, 1.35	223.3	124.8, 93.0	34.7, 31.0
1,3,5-$C_6H_3Me_3$	5.22, 2.34	222.3	112.6, 94.6	20.5
		M = Re		
C_6H_6	5.81	191.9	92.8	
C_6H_5Me	5.56(t),5.74(d, J = ~6 Hz)), 5.92(t), 2.54	192.9	111.0, 94.7, 92.7, 90.1	20.5
$C_6H_5Bu^t$	5.86(m),[c] 1.35	193.1	125.8, 93.8, 92.8, 90.6	34.9, 31.2
1,4-$C_6H_4Me_2$	5.81, 2.44	193.9	108.4, 94.4	19.8
1,4-$C_6H_4Pr^i_2$	5.87, 2.78,[d] 1.31(d)	194.4	120.4, 91.9	32.5, 23.7
1,4-$C_6H_4Bu^t_2$	5.94, 1.30	194.4	125.6, 90.5	34.7, 31.2
1,3,5-$C_6H_3Me_3$	5.50, 2.60	194.6	113.3, 91.8,	20.3
1,2,3,4,-$C_6H_2Me_4$	5.75, 2.52, 2.48	195.3	109.0, 108.5, 95.2	19.9, 16.3,
1,2,4,5-$C_6H_2Me_4$	5.89, 2.37	195.5	108.2, 98.5	18.2
C_6HMe_5	5.73, 2.58, 2.51, 2.40	196.1	110.8, 109.7, 107.0, 96.8	19.8, 17.0, 16.1
C_6Me_6	2.48	196.7	108.3	17.3

[a]In CD_2Cl_2.
[b]In CH_2Cl_2/CD_2Cl_2 (4/1).
[c]Not resolved at 100 MHz operating frequency.
[d]Heptet, J = 7.0 Hz.

Mn compounds, are insoluble in hexane; they are, however, soluble in CH_2Cl_2.

Preparation of (η^6-C_6Me_6)$Re(CO)_2(SiCl_3)$ from (η^6-C_6H_5Me)$Re(CO)_2(SiCl_3)$

A Carius tube was charged with (η^6-C_6H_5Me)$Re(CO)_2(SiCl_3)$ (20 mg), hexamethylbenzene (0.2 g), and olefin-free heptane (1 mL). The reaction mixture was cooled to −196°C and degassed with three freeze–pump–thaw cycles. The vessel and its contents were heated at 240°C for 12 h. The solution was cooled and extracted with hexane (3 × 5 mL) and the remaining solid dissolved in CH_2Cl_2. An infrared spectrum in the carbonyl stretching region indicated only the presence of product, (η^6-C_6Me_6)$Re(CO)_2(SiCl_3)$.

Results and discussion

Preparation of the (η^6-arene)$M(CO)_2(SiCl_3)$ (M = Mn, Re) compounds

The compounds were prepared in moderate to good yield by heating the appropriate arene with $M(CO)_5(SiCl_3)$ (M = Mn, Re) in an evacuated sealed tube at temperatures in the range 230–260°C, depending on the arene and the metal (eq. [1]). Analytical and spectroscopic data for the new compounds are

$$[1]\quad \text{arene} + M(CO)_5(SiCl_3) \xrightarrow{230\text{–}260^\circ C} (\eta^6\text{-arene})M(CO)_2(SiCl_3)$$

(M = Mn, Re; arene = $C_6H_{6-x}Me_x$ (x = 1–6), 1,4-$C_6H_4Bu^t_2$, etc.)

given in Tables 1 and 2. It was also found that under the same conditions C_6Me_6 displaced toluene from (η^6-C_6H_5Me)$Re(CO)_2(SiCl_3)$ to give (η^6-C_6Me_6)$Re(CO)_2(SiCl_3)$. In all preparations the reagents had to be meticulously purified and all traces of oxygen removed from the reaction. Failure to do this resulted in drastically reduced yields, which for some of the manganese compounds were essentially zero. Furthermore , in those syntheses that involved $Re(CO)_5(SiCl_3)$, when trace oxygen was not removed from the reaction a second product was formed that exhibited four carbonyl stretches in the solution infrared spectrum. Only two of these bands

© 1997 NRC Canada

Can. J. Chem. Downloaded from www.nrcresearchpress.com by 88.146.161.215 on 09/08/12
For personal use only.

changed in frequency with a change of the arene reagent. For example, the product from the reaction that involved benzene exhibited CO-stretches at 2085, ~2024, 2024, and 1915.5 cm^{-1} in CH_2Cl_2 whereas the corresponding hexamethylbenzene product had bands at 2063.5, 2024, 1993.5, and 1916 cm^{-1}. The second product is tentatively identified as $[(arene)Re(CO)_3]^+[Re_2(\mu\text{-}Cl)_3(CO)_6]^-$ by comparison of the carbonyl stretches with those reported in the literature for the individual cation (10) and anion (11). The ionic product could not be readily separated from the $(\eta^6\text{-arene})Re(CO)_2(SiCl_3)$ derivatives and therefore they were not characterized further. It was found, however, for the reaction of C_6Me_6 and $Re(CO)_5(SiCl_3)$ in heptane, that when trace oxygen was deliberately not removed from the reaction (the solution was not degassed) the only detectable product was "$[(\eta^6\text{-}C_6Me_6)Re(CO)_3][Re_2(\mu\text{-}Cl)_3(CO)_6]$."

The crystal structures of two derivatives related to the current arene derivatives have been reported, namely, the structure of $(\eta^6\text{-}1,4\text{-}C_6H_4Bu^t_2)Ru(CO)(SiCl_3)_2$ (12) and that of $(\eta^6\text{-}1,4\text{-}C_6H_4Pr^i_2)Fe(CO)(SiCl_3)_2$ (2). In these complexes, the arene ligand is coordinated to the metal atom, in an η^6-mode with the carbonyl and silyl ligands occupying three sites about the metal atom, which is presumed to have approximate octahedral coordination. The arene compounds reported here are thought to have a similar piano-stool geometry. The $(\eta^6\text{-arene})Mn(CO)_2(SiCl_3)$ compounds are pale-yellow, air-sensitive solids that are soluble in hexane. The Re derivatives, although air-sensitive, are more robust than the Mn analogues; they are colorless solids that are insoluble in hexane (but soluble in dichloromethane). These physical properties may indicate stronger bonding of the arene ring to the metal atom in the Re complexes than that in the Mn complexes. A stronger bonding interaction in the Re complexes might be expected to lead to a larger HOMO–LUMO gap, giving rise to electronic transitions outside the visible region. A stronger bonding interaction could also lead to a greater charge separation between the arene and the rest of the molecule that in turn could give rise to lower solubility in nonpolar solvents of the Re derivatives.

Spectroscopic properties of the $(\eta^6\text{-arene})M(CO)_2(SiCl_3)$ compounds

The carbonyl stretching frequencies in the solution infrared spectra of the $(\eta^6\text{-arene})M(CO)_2(SiCl_3)$ compounds are given in Table 1. The stretches show the typical shift to lower frequencies with increasing methyl (or alkyl) substitution of the arene ring. The more electron-donating methyl groups increase the electron density at the metal atom, which in turn increases the backbonding to the π^* orbitals on the carbonyl ligands. The compound $(\eta\text{-}C_5H_5)Fe(CO)_2(SiMeCl_2)$ exhibits four, rather than two, IR-active carbonyl stretches in hexane solution which is attributed to the presence of two conformers arising from different orientations of the $SiMeCl_2$ group with respect to the Fe—Si bond (9). There was, however, no evidence for more than one conformer for $(\eta^6\text{-arene})Mn(CO)_2(SiCl_3)$ complexes in hexane solution where the arene (rather than the silyl ligand) was asymmetrically substituted: all the Mn complexes exhibited just two sharp CO stretches in hexane consistent with the presence of only one conformer in solution (Table 1).

As mentioned in the Introduction, the $(\eta^6\text{-}1,4\text{-}C_6H_4Bu^t_2)M'(CO)(SiCl_3)_2$ (M′ = Ru, Os) complexes are rare examples of molecules that exhibit restricted rotation of the arene ring about the metal atom as ascertained by NMR line-broadening techniques (1, 3). The slightly broadened singlet observed in the ^1H NMR spectrum (400 MHz) for the arene protons of these complexes in CD_2Cl_2 at ambient temperature decoalesces at lower temperatures such that at −60°C two sharp resonances (with H–H coupling) are observed (1, 3). In view of this behavior, the ^1H NMR spectra of $(\eta^6\text{-}1,4\text{-}C_6H_4Bu^t_2)Mn(CO)_2(SiCl_3)$ (**1**) in $CDFCl_2$–CD_2Cl_2, and its Re analogue (**2**) in $CFCl_3$–CD_2Cl_2, were recorded at low temperatures. In both cases, only a singlet, which did not appear significantly broadened even at −120°C, was obtained for the aromatic protons. As we have previously pointed out for $(\eta^6\text{-}1,4\text{-}C_6H_4Pr^i_2)Ru(CO)(SiCl_3)_2$ (2), from the observation that a sharp singlet is observed for the aromatic protons in the solution ^1H NMR spectrum to −120°C, an upper limit of approximately 5.3 kcal mol^{-1} for the barrier may be estimated for arene–metal rotation in the $(\eta^6\text{-}1,4\text{-}C_6H_4Bu^t_2)M(CO)_2(SiCl_3)$ complexes.

The iron compound, $(\eta^6\text{-}1,4\text{-}C_6H_4Bu^t_2)Fe(CO)(SiCl_3)_2$, could not be prepared, but the corresponding barriers (at 25°C) in the Ru (**3**) and Os analogues are 12.8 and 13.6 kcal mol^{-1}, respectively (1, 3).[2] This is therefore some 7.5–8.3 kcal mol^{-1} higher than the barrier in **1** and **2**. We initially attributed the lower barrier in **2** (compared to that in **3**) to the presence of only one bulky silyl ligand, which allowed the arene ring to tilt as the bulky *tert*-butyl substituents passed over the silyl ligand during the rotation of the arene ring about the metal atom. This tilting was thought to be severely restricted in **3** because of the presence of two bulky substituents on the arene ring and two bulky ligands attached to the metal atom (3). Subsequent studies on the $(\eta^6\text{-arene})Fe(CO)(SiCl_3)_2$ complexes have clearly shown that ground-state effects are also important in determining the barrier to arene rotation in these compounds (2). It is difficult to visualize, however, how the destabilization of the ground state of **2** could be sufficiently large to account for the much lower barrier to arene rotation in **2** compared to that in **3** and its Os congener. We therefore believe that the origin of the decrease in the barrier in **1** and **2** lies predominantly in transition-state stabilization arising from ring tilting that may be combined with more facile compression of the $M(CO)_2(SiCl_3)$ moiety compared to that of the $M'(CO)(SiCl_3)_2$ grouping. Detailed molecular mechanics calculations might resolve which factors are most important in determining the magnitude of barriers to arene–metal rotation in these complexes.

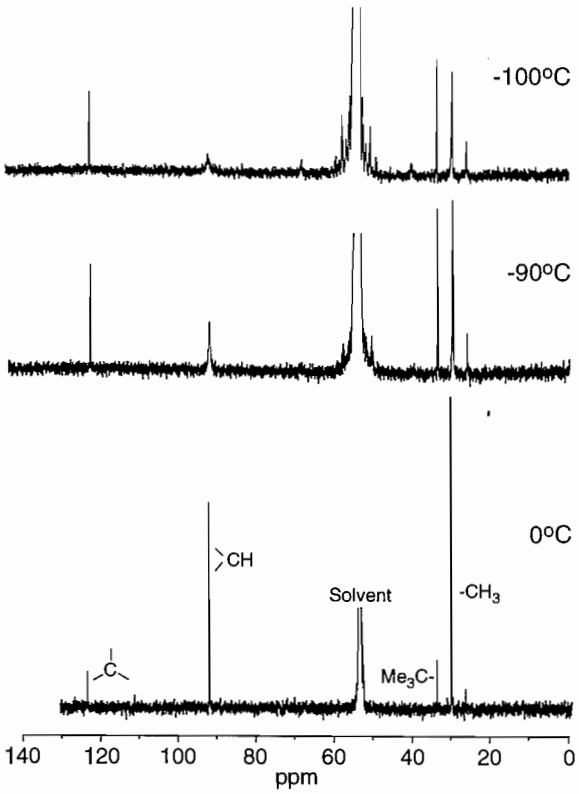
The onset of decoalescence of signals due to the slowing of a fluxional process is more likely to be detected by ^{13}C NMR spectroscopy than by ^1H NMR spectroscopy since the chemical shift separation between the signals due to each site undergoing exchange is invariably much larger in the ^{13}C NMR spectrum. For this reason and because of its favorable solubility, the ^{13}C NMR spectrum of **1** in CD_2Cl_2 was studied to low temperatures. At −90°C and below there were unmistakable signs of decoalescence of the resonance due to the methyl sub-

[2] Also, X. Hu, J. Duchowski, and R.K. Pomeroy. Unpublished results.

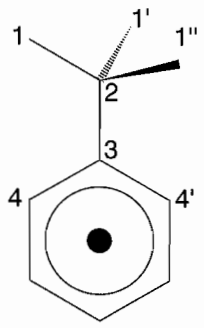
© 1997 NRC Canada

Can. J. Chem. Downloaded from www.nrcresearchpress.com by 88.146.161.215 on 09/08/12
For personal use only.

Fig. 1. Variable temperature $^{13}C\{^1H\}$ NMR spectra (100.6 MHz operating frequency) of (η^6-1,4-$C_6H_4Bu'_2$)$Mn(CO)_2(SiCl)_3$) (**1**) in CD_2Cl_2–CH_2Cl_2.



stituents and that due to the CH carbons of the arene ligand, but the other two signals attributed to the arene ligand remained sharp (Fig. 1). This behavior is consistent with restricted rotation of the *tert*-butyl substituent on the NMR time scale, rather than restricted rotation about the arene–Mn bond. As depicted in **A**, restricted rotation about the C—CMe_3



A

bond causes only the carbon atoms labeled 1 and 4 in **A** to become inequivalent, as is observed for **1**. Restricted rotation about the arene–Mn bond, on the other hand, would cause all four ^{13}C NMR resonances of the arene ligand to split into doublets; this is observed in complexes such as (η^6-1,4-$C_6H_4Bu^t2$)$Ru(CO)(SiCl_3)_2$ (1). The fluxional process in **1** is not detected by ^1H NMR spectroscopy, presumably because the chemical shift difference between the protons at the 1 and 1′ (1″), or between the protons at the 4 and 4′, sites are too small to cause significant line broadening.

In conclusion, a general route to molecules of formula (η^6-arene)$M(CO)_2(SiCl_3)$ (M = Mn, Re) has been established. (Because of the reactivity of the $SiCl_3$ ligands these derivatives are probably of little value for use in organic synthesis without further modification.) The barriers to arene–metal rotation in the manganese complexes are surprisingly low. For example, whereas the barrier to arene–Fe rotation in (η^6-1,4-$C_6H_4Me_2$)$Fe(CO)(SiCl_3)_2$ is 9.6 ± 0.1 kcal mol^{-1} ($\Delta G^{\ddagger}_{298}$) determined from an NMR line-shape analysis (2), in (η^6-1,4-$C_6H_4Bu'_2$)$Mn(CO)_2(SiCl_3)$ there is no evidence in the ^1H NMR spectrum of the compound in solution to −120°C for slowing of the rotation of the arene ring about the Mn atom. The latter observation indicates a barrier to arene–Mn rotation in the complex of no more than 5.3 kcal mol^{-1}.

Acknowledgment

We thank the Natural Sciences and Engineering Research Council of Canada for financial support.

References

1. R.K. Pomeroy and D.J. Harrison. J. Chem. Soc. Chem. Commun. 661 (1980).
2. V.M. Hansen, R.J. Batchelor, F.W.B. Einstein, J.L. Male, R.K. Pomeroy, and M.J. Zaworotko. Organometallics. In press.
3. X. Hu, J. Duchowski, and R. K. Pomeroy. J. Chem. Soc. Chem. Commun. 362 (1988).
4. M.J. Morris. *In* Comprehensive organometallic chemistry II. Vol. 5. *Edited by* G. Wilkinson, F.G.A. Stone, and E.W. Abel. Pergamon Press, Oxford. 1995. p. 471; K.F. McDaniel. *In* Comprehensive organometallic chemistry II. Vol. 6. *Edited by* G. Wilkinson, F.G.A. Stone, and E.W. Abel. Pergamon Press, Oxford. 1995. p. 93; J.M. O'Conner. *In* Comprehensive organometallic chemistry II. Vol. 6. *Edited by* G. Wilkinson, F.G.A. Stone, and E.W. Abel. Pergamon Press, Oxford. 1995. p. 167.
5. M.F. Semmelhack. *In* Comprehensive organometallic chemistry II. Vol. 12. *Edited by* G. Wilkinson, F.G.A. Stone, and E.W. Abel. Pergamon Press, Oxford. 1995. p. 979; S.G. Davis and T.D. McCarthy. *In* Comprehensive organometallic chemistry II. Vol. 12. *Edited by* G. Wilkinson, F.G.A. Stone, and E.W. Abel. Pergamon Press, Oxford. 1995. p. 1039.
6. S. Sun, C.A. Dullaghan, and D.A. Sweigart. J. Chem. Soc. Dalton Trans. 4493 (1996).
7. D.D. Perrin, W.L.F. Armarego, and D.R. Perrin. Purification of laboratory chemicals. 2nd ed. Pergamon Press, New York. 1980. p. 279.
8. J.S. Siegel and F.A.L. Anet. J. Org. Chem. **53**, 2629 (1988).
9. W. Jetz and W.A.G. Graham. J. Am. Chem. Soc. **89**, 2773 (1967).
10. L.A.P. Kane-Maguire and D.A. Sweigart. Inorg. Chem. **18**, 700 (1979); Y.K. Chung, E.D. Honig, and D.A. Sweigart. J. Organomet. Chem. **256**, 277 (1983); F. Calderazzo, R. Poli, A. Barbati, and P.F. Zanazzi. J. Chem. Soc. Dalton Trans. 1059 (1984).
11. B.J. Brisdon, D.A. Edwards, and J.W. White. J. Organomet. Chem. **161**, 233 (1978); F.W.B. Einstein, P.G. Glavina, R.K. Pomeroy, P. Rushman, and A.C. Willis. J. Organomet. Chem. **317**, 255 (1986).
12. F.W.B. Einstein and T. Jones. Inorg. Chem. **21**, 987 (1982).

© 1997 NRC Canada

Metal hydride mediated reduction of 3-(alkylthio)oxindoles containing other potentially reducible groups

Terrence J. Connolly and Tony Durst

Can. J. Chem. Downloaded from www.nrcresearchpress.com by 88.146.161.215 on 09/08/12
For personal use only.

Abstract: The reduction of several 3-(methylthio)oxindoles bearing ester groups on the benzene ring has been studied. The reaction is very dependent on the substitution of the oxindole, and the position of the ester group. Deprotonation of the C3 center by the metal hydride is the major initial pathway. This deprotonation plays a role in the reduction of the pendant ester group. Ester groups *ortho*, and presumably *para*, to C3 are very difficult to reduce, reaction only occurring with excess $LiAlH_4$ at elevated temperatures. Once reduction starts, it is very difficult to stop, with reduction of the ester to a methyl group being observed. When deprotonation at this center is blocked, ester reduction becomes straightforward and can be accomplished at room temperature with $LiEt_3BH$.

Key words: oxindole, reduction, anion.

Résumé : On a étudié la réduction de plusieurs 3-(méthylthio)oxindoles portant des groupes esters sur le noyau benzénique. La réaction varie grandement suivant la nature et la position du substituant présent sur l'oxindole. La déprotonation du centre C3 par l'hydrure métallique est le principal chemin réactionnel initial. Cette déprotonation joue un rôle important dans la réduction du groupe ester. Il est très difficile de réduire les groupes esters *ortho*, et probablement *para*, par rapport au centre C3; la réaction ne se produit qu'avec du $LiAlH_4$, à températures élevées. Lorsque la réduction est induite, il est difficile de l'arrêter; on observe alors la réduction de l'ester en groupe méthyle. Lorsqu'on bloque la déprotonation de ce centre, la réduction de l'ester redevient normale et on peut la réaliser à la température ambiante avec du $LiEt_3BH$.

Mots clés : oxindole, réduction, anion.

[Traduit par la rédaction]

Introduction

The chemistry of oxindoles continues to attract considerable attention, possibly due to the biological activity of substituted oxindoles (1). Given the importance of these molecules, studies of fundamental reactions will lead to a greater understanding of their reactivity, and will be of general interest to those planning multistep syntheses.

Although the reaction of oxindole with $LiAlH_4$ has been known for quite some time, there is little mention in the literature of metal hydride reductions of oxindoles bearing other potentially reducible groups. Julian and Printy reported the reduction of 1-methyloxindoles to form 1-methylindoles and indolines with $LiAlH_4$ (2). This group also noted that oxindoles that were not substituted on nitrogen were not reactive towards $LiAlH_4$. Other studies supported these findings or showed that very little reduction occurs (3, 4). Based on numerous other studies, the conclusion was reached that oxindoles having a single 3-substituent undergo $LiAlH_4$ reduction to afford indoles whereas 3,3-disubstituted oxindoles are reduced to indolines when the reductions are carried out in refluxing dioxane (5–8). Nishio et al. have recently reexamined some of this chemistry, and the use of Dibal-H as a reducing agent (9). Their findings suggest that N-unsubstituted oxindoles, regardless of further substitution, are not reduced with Dibal-H. In addition, when reduction with Dibal-H occurred, indoles rather than indolines were obtained as the major products. Although a comprehensive study was conducted, very little speculation was made regarding the mechanism.

Even less is known regarding the mechanism of metal hydride mediated reductions of oxindoles carrying other potentially reducible groups. Brossi and co-workers, in a series of publications, showed that the nitrile group of 1,3,3-trisubstituted oxindoles with cyanomethyl groups at the 3 position could be reduced without reaction at the oxindole carbonyl (10–12). Pierce et al. studied in detail the reduction of 3-(methylene)oxindoles with $NaBH_4$ (13). Plieninger and Allen examined the reductions of oxindoles with borane (14, 15). To the best of our knowledge, there have not been any studies on the reduction of oxindoles that have pendant ester groups on the benzene ring. In the course of research in our laboratory, we recently had the opportunity to study this reaction in detail. An explanation of these results, and an extension to generalize such reductions by employing several isomers and various reduction conditions, is the subject of this paper.

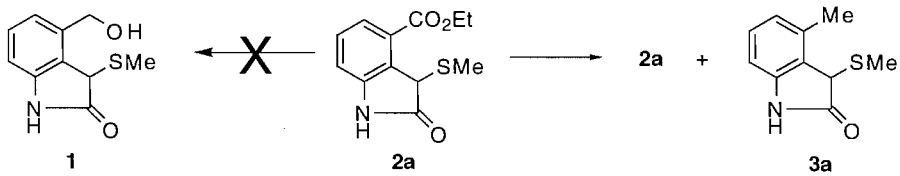
Received November 13, 1996.

T.J. Connolly and T. Durst.[1] Department of Chemistry, University of Ottawa, 10 Marie Curie, Ottawa, ON K1N 6N5, Canada.

[1] Author to whom correspondence may be addressed. Telephone: (613) 562-5800, ext. 5728. Fax: (613) 562-5170. E-mail: tdurst@oreo.uottawa.ca

© 1997 NRC Canada

Scheme 1.



Results

Recent synthetic studies in our laboratory required an efficient synthesis of oxindole **1**. Due to the literature precedent arguing that reduction of the oxindole carbonyl with metal hydrides is difficult when the oxindole has a free N-H, we believed that reduction of the pendant ester group of **2a** would afford the desired 4-hydroxymethyl group. Due to the pioneering work of Gassman and van Bergen (16, 17), oxindoles with the desired framework as shown in **2a** are available in a one-pot synthesis from substituted anilines via a rearrangement of the intermediate aza-sulfonium salts. Oxindole **2a** was prepared from ethyl (3-amino)benzoate in a yield consistently above 75%. However, reduction of **2a** with up to five equivalents of Dibal-H in THF returned starting material in a quantitative yield. Likewise, use of other reducing agents like $LiBH_4$, $LiEt_3BH$, Red-Al, and even $LiAlH_4$ in THF at room temperature resulted in the recovery of starting material. When more forcing reduction conditions were used (10 equivalents $LiAlH_4$, refluxing THF, 18 h), a 1:1.2 mixture of starting material and the completely reduced product **3a** was obtained.

In an attempt to gain more mechanistic insight into these results, a systematic study of various related isomers and analogs of **2** was undertaken. All of the desired starting oxindoles were prepared via Gassman's method (16, 17), or via the modified Gassman method reported by Wierenga et al. (18). All of the substrates in this paper were screened under two different reduction conditions: the reaction with $LiEt_3BH$ was done in THF at room temperature whereas reduction with $LiAlH_4$ was done in refluxing THF. Shown in Table 1 are the results from a series of reductions.

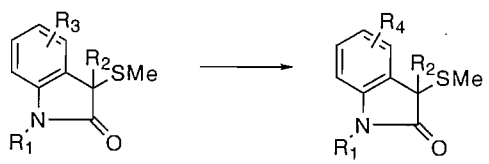


Table 1. Summary of reduction results for oxindoles **2a–2d**.

Entry	R_1	R_2	R_3	R_4	Yield	Conditions[a]
a	H	H	4-CO_2Et	4-CO_2Et	>95%	A
a	H	H	4-CO_2Et	4-CH_3	90%[b]	B
b	Me	H	4-CO_2Et	4-CH_3	90%	B
c	H	Me	6-CO_2Et	6-CH_2OH	88%	A[c]
d	H	H	7-CO_2Et	7-CH_2OH	~84%	A,B[c]

[a]A: $LiEt_3BH$, THF, RT; B: $LiAlH_4$, THF, Δ.
[b]Based on recovered starting material.
[c]Could not be reduced further on exposure to conditions B.

Examination of the table shows a number of trends. Under both $LiEt_3BH$ and $LiAlH_4$ reduction conditions, the oxindole carbonyl group was quite inert to reduction (typically, less than 5% of the product mass was composed of indole and indoline products). It is also evident from substrates **2a** and **2b** that, for oxindoles having a proton on C3 and the ester group *ortho* to this position, initial reduction of the ester group is quite difficult. However, in both cases, once reduction is initiated, it is difficult to stop at the benzylic alcohol stage. For both substrates, which differed only in the N-methyl group, reduction did not occur until excess $LiAlH_4$ was used and the reaction mixture was exposed to harsh conditions, i.e., refluxing THF for prolonged periods of time.

In the case of substrate **2c**, the oxindole was methylated at C3 and had the ester group *para* to C3. Reduction proceeded smoothly with both $LiEt_3BH$ and $LiAlH_4$ to afford the benzylic alcohols. Isolation of the alcohol and its exposure to the forcing conditions ($LiAlH_4$, THF, Δ) resulted in the recovery of starting material. Similarly oxindole **2d**, which was not methylated at C3 and had the ester group *meta* to C3, was also smoothly reduced to the benzylic alcohol with both $LiEt_3BH$ at room temperature and $LiAlH_4$ in refluxing THF. Again, isolation of the benzylic alcohol **3d** and attempted further reduction with $LiAlH_4$ in refluxing THF did not lead to further reduction of the alcohol. Instead, reduction of the oxindole carbonyl group occurred, although this was only about 5% of the mass balance even after 12 h.

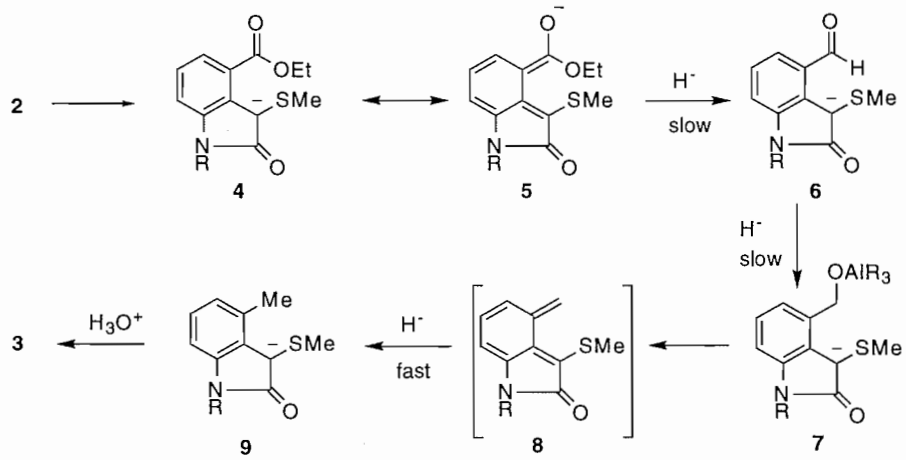
Discussion

It is clear from the results discussed that both the position of the ester group and the substitution pattern at C3 play an important role in the results of the reduction. It seems reasonable that the problem of over-reduction observed for **2a** and **2b** may be ascribed to the presumably high acidity of the proton on C3. Although p*K*a data for these compounds are not available, Gassman has commented on the high acidity of the C3 methine proton, and taken advantage of it in his isatin syntheses (19, 20). Taylor has also commented on problems encountered during ester hydroysis of related structures due to the C3 proton (21). In the case of both **2a** and **2b**, initial deprotonation of the C3 proton would lead to an anion adjacent to the oxindole carbonyl. This increased electron density and enolate character militates against reduction of the oxindole carbonyl group, similar to that reported by Marshall et al. for malonic enolates (22). This C3 anion may also increase the electron density of the ester groups *ortho* or *para* to it by delocalization through the benzene ring, as shown by **4** and **5**. The vinylogous enolate **5** is also quite resistant to addition of hydride. However, once one hydride has added, the aldehyde product **6** is more susceptible to further hydride attack. The next hydride addition results in the benzyloxyaluminate **7**, and the C3 anion, which initially made hydride addition slow, now facil-

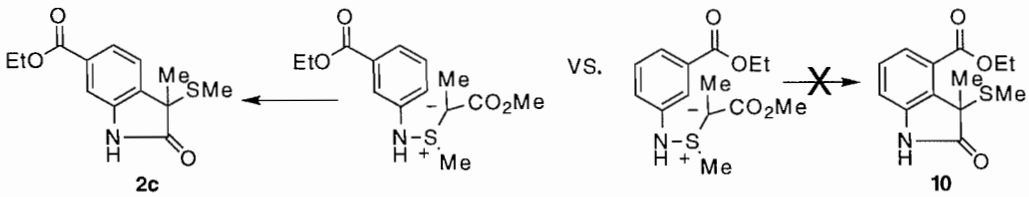
Can. J. Chem. Downloaded from www.nrcresearchpress.com by 88.146.161.215 on 09/08/12
For personal use only.

© 1997 NRC Canada

Scheme 2.



Scheme 3.



itates over-reduction, perhaps via the *ortho*-quinodimethane **8**. The end result is the 4-methyl oxindole, **3a** or **3b**.

To test the proposed mechanism shown in Scheme 2, **10** was an appealing target. This substrate had the ester at the 4 position and an additional methyl group at C3. Attempted monoalkylation of **2** always resulted in a mixture of products that included starting material, N-alkyl and N,C-dialkylated products.[2] An alternative synthesis relied on the Gassman technique. However, when ethyl (3-amino)benzoate was reacted with methyl (2-thiomethyl)propionate under standard Gassman conditions, the isomeric oxindole **2c** was formed. Although both 4- and 6-substituted oxindoles are possible products from *meta*-substituted anilines, only 4-substituted oxindoles were formed up to this point. As suggested in Scheme **3**, the increased steric demand of the branched sulfide-ester may be responsible for this switch in regiochemistry.

The ester groups of **2c** and **10**, which are *ortho* and *para*, respectively, to the C3 position, are electronically quite similar. Results of the reduction of oxindole **2c** also support the proposed mechanism. The additional methyl group at C3 does not allow enolate formation so the electron density of the ester group *para* to C3 is normal. The free NH still protects the oxindole carbonyl group from reduction. With both $LiEt_3BH$ and $LiAlH_4$, reduction of the ester **2c** to benzylic alcohol **3c** proceeded smoothly.

To finish our study on this series, we examined the reduction of oxindole **2d**. This substrate has a proton on C3, but to which the ester is *meta* (**11**). Although not expecting any interference from the C3 anion, we were interested in seeing what effect the nitrogen would have when placed *ortho* to the ester group. Reduction with $LiAlH_4$ in refluxing THF smoothly afforded the benzylic alcohol, which was inert to further reduction by $LiAlH_4$; no evidence was found to support over-reduction of the C7-benzylic alcohol. Reduction also occurred with $LiEt_3BH$ as the reducing agent. From these results, it seems that delocalization of the nitrogen electron density into the benzene (**12**) ring is probably not favored, since it would result in the loss of any resonance energy associated with the amide resonance (**13**).

Conclusion

In this paper, we have examined the reduction of a series of 3-(methylthio)oxindoles that had ester groups on the benzene ring. It was found that having a free proton α to the oxindole carbonyl group protects this group from any significant reduction by metal hydrides like $LiEt_3BH$ and $LiAlH_4$. This protection presumably occurs through deprotonation of the amide NH or the methine proton of the oxindole. This resistance to reduction is reminiscent of the situation reported by Marshall, who showed that malonic enolates are not reduced by $LiAlH_4$ (22). Deprotonation of the methine hydrogen also results in donation of significant electron density into the benzene ring. If the ester group is in a position to accept some of this electron density (*ortho* or *para* to C3) then initial reduction is difficult, resulting in the recovery of starting material when mild conditions are used, and in over-reduction of the ester to a methyl group when more vigorous conditions are used.

Experimental

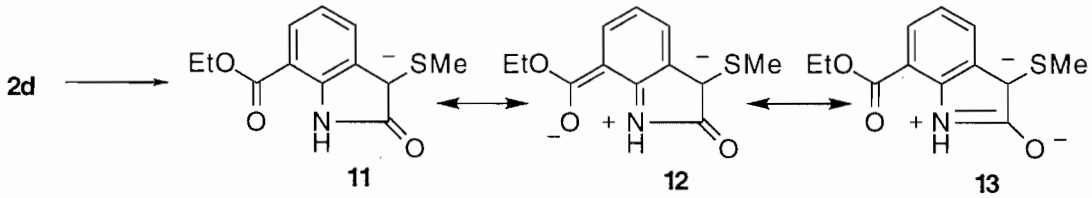
General

All reactions were conducted under an inert atmosphere in flame-dried glassware that had been cooled under a stream of

[2] Reduction of the N-methyl analogue of **10** with $LiAlH_4$ and $LiEt_3BH$ leads to four different products. See accompanying paper.

Can. J. Chem. Downloaded from www.nrcresearchpress.com by 88.146.161.215 on 09/08/12
For personal use only.

© 1997 NRC Canada



dry nitrogen. Melting points were determined on a Fisher–Johns Unimelt melting point apparatus and are uncorrected. Infrared spectra were recorded with a Bomem MB 101 FT-IR spectrometer with solution cells using the highest grade of methylene chloride available unless otherwise stated. Proton and carbon nuclear magnetic resonance were recorded on either a Bruker AMX-500, Varian XL-300, or Varian Gemini 200 operating at frequencies of 500, 300, and 200 MHz for proton and 125, 75, and 50 MHz for carbon, using the specified solvent, and are reported relative to TMS = 0.00 ppm. Low- and high-resolution mass spectra were recorded on a VG 7070 mass spectrometer or a Concept II instrument. Peak intensities are reported as a percentage of the base peak.

The phrase "usual work-up" refers to drying the solvent over anhydrous magnesium sulfate, filtering, and removing the solvent under reduced pressure using a Buchi Rotovapor. The term chromatography refers to flash chromatography performed using 230–400 mesh silica gel supplied by Terochem Laboratories in the solvent specified. All solvents were routinely distilled prior to use. All starting materials were used as received from commercial sources except for the following: triethylamine was distilled from CaH_2 and THF was dried and distilled from sodium with benzophenone as an indicator; methylene chloride was distilled from P_2O_5 prior to use. *tert*-Butyl hypochlorite was prepared according to the literature immediately before use (23). All manipulations involving *t*-BuOCl, including the preparation, were conducted in the dark. The synthesis of all oxindole starting materials was conducted following the general procedure of Gassman or the modified Gassman approach of Wierenga (16–18). No attempt was made to optimize the syntheses of starting oxindoles.

3-(Methylthio)-4-(carboethoxy)oxindole 2a

Oxindole **2a** was prepared according to the general procedure of Gassman (17). A solution of freshly prepared *t*BuOCl (3.30 g, 30.4 mmol) in CH_2Cl_2 (15 mL) was added dropwise to a cooled (−78°C) solution of ethyl 3-aminobenzoate (5.00 g, 30.3 mmol) in CH_2Cl_2 (100 mL). The resulting bright yellow mixture was stirred at this temperature for 10 min, at which point a solution of methyl (methylthio)acetate (3.65 g, 30.4 mmol) in CH_2Cl_2 (15 mL) was added and stirring continued for 2.5 h. A solution of triethylamine (3.10 g, 30.7 mmol) in CH_2Cl_2 (15 mL) was then added, and the initially yellow solution was allowed to warm to room temperature (RT) over 12 h. The reddish solution that resulted was poured into a solution of H_2O (200 mL); the organic phase separated and was worked up in the usual manner to provide an orange solid. Recrystallization from CH_2Cl_2–hexanes afforded the title compound as colorless plates (5.70 g, 75%); mp 150–151°C; IR (CH_2Cl_2): 1613, 1723, 3424 cm^{-1}; ^1H NMR (200 MHz, $CDCl_3$) δ: 1.40 (t, 3H, J = 8.0 Hz), 2.51 (s, 3H), 4.38 (q, 2H, J = 8.0 Hz), 4.68 (s, 1H), 7.02 (d, 1H, J = 8.0 Hz), 7.31 (t, 1H, J = 8.0 Hz), 7.62 (d, 1H, J = 8.0 Hz), 8.05 (br, 1H); ^{13}C NMR (125 MHz, $CDCl_3$) δ: 12.15, 14.05, 46.74, 61.33, 113.39, 124.26, 127.89, 128.19, 129.00, 142.04, 165.52, 177.46; EI-MS *m/z* (%): 251 (2.2, M^+), 205 (100), 176 (13.2), 160 (36.6); HRMS calcd. for $C_{12}H_{13}NO_3S$: 251.06162; found: 251.06118.

Reduction of oxindole 2a with $LiAlH_4$: 3-(methylthio)-4-methyloxindole 3a

A solution of oxindole **2a** (100 mg, 0.40 mmol) in THF (10 mL) was added dropwise to a suspension of $LiAlH_4$ (150 mg, 3.95 mmol) in THF (10 mL). The resulting gray, cloudy solution was refluxed for 18 h, poured into a saturated solution of potassium sodium tartrate (50 mL) and EtOAc (50 mL), and stirred for 4 h. The organic phase was separated and subjected to normal work-up followed by column chromatography (2:1 hex:EtOAc), providing two compounds: recovered starting material (35 mg, 35%) and a less polar compound, **3a**, isolated as an off-white solid (30 mg, 43%); mp 154–155°C; IR (CH_2Cl_2): 1724 cm^{-1}; ^1H NMR (200 MHz, $CDCl_3$) δ: 2.10 (s, 3H), 2.50 (s, 3H), 4.25 (s, 1H), 6.70 (d, 1H, J = 8.0 Hz), 6.80 (d, 1H, J = 8.0 Hz), 7.20 (t, 1H, J = 8.0 Hz); ^{13}C NMR (75 MHz, $CDCl_3$) δ: 11.45, 17.85, 45.52, 107.17, 123.27, 124.31, 128.69, 135.96, 140.98, 177.17; EI-MS *m/z* (%): 193 (26.5, M^+), 146 (100), 118 (4.2); HRMS calcd. for $C_{10}H_{11}NOS$: 193.05614; found: 193.05684.

Ethyl 3-(methylamino)benzoate

Adapted from the procedure of Krishnamurthy (24). A round-bottom flask containing a toluene (50 mL) solution of ethyl (3-amino)benzoate (5 g, 30.30 mmol) and formic acid (5 mL, 98%) was equipped with a Dean–Stark trap and heated to reflux for 12 h. The solvent was removed and the resulting purple residue was suspended in CH_2Cl_2 (50 mL), and washed sequentially with H_2O (2 × 20 mL), HCl (10%, 2 × 20 mL), and $NaHCO_3$ (5%, 2 × 20 mL). The organic phase was worked up in the usual manner, affording a dark solid that was triturated with Et_2O, and filtered. The purplish solid was recrystallized from CH_2Cl_2–hexanes and filtered, affording 3.12 g of ethyl 3-(formyl amino)benzoate (53%) as white cubes.

The resulting N-formyl derivative (3.0 g, 15.54 mmol) was dissolved in THF (50 mL), and heated to reflux, at which point a solution of borane – methyl sulfide complex was added (3.0 mL, 10 M, 30.00 mmol) dropwise via syringe. After 12 h at reflux, the solution was cooled to RT, and MeOH (20 mL) was added slowly (**Caution**: H_2 evolution!). Stirring was continued until hydrogen evolution stopped, and then for 15 min longer, after which time the solution was concentrated to dryness, and the residue purified by column chromatography (2:1 hex:EtOAc), affording the title compound as a clear oil (2.5 g, 90%); IR (CH_2Cl_2): 3435, 1713 cm^{-1}; ^1H NMR (500 MHz, $CDCl_3$) δ: 1.35 (t, 3H, J = 6.8 Hz), 2.82 (s, 3H), 3.80 (br, 1H), 4.32 (q, 2H, J = 6.8 Hz), 6.74 (d, 1H, J = 6.5 Hz), 7.20 (t, 1H,

© 1997 NRC Canada

Can. J. Chem. Downloaded from www.nrcresearchpress.com by 88.146.161.215 on 09/08/12
For personal use only.

Can. J. Chem. Downloaded from www.nrcresearchpress.com by 88.146.161.215 on 09/08/12
For personal use only.

J = 6.5 Hz), 7.25 (d, 1H, J = 6.5 Hz), 7.35 (d, 1H, J = 6.5 Hz); ^{13}C NMR (125 MHz, $CDCl_3$) δ: 14.32, 30.62, 60.79, 112.84, 116.77, 118.23, 129.04, 131.35, 149.34, 167.13; EI-MS *m/z* (%): 179 (100, M^+), 150 (76.0), 134 (40.3), 106 (58.5), 77 (23.2); HRMS calcd. for $C_{10}H_{13}NO_2$: 179.09463; found: 179.09484.

1-Methyl-3-methylthio-4-(carboethoxy)oxindole 2b

Prepared from ethyl (3-*N*-methylamino)benzoate (0.98 g, 5.47 mmol) using the standard Gassman methodology. The orange solid obtained after usual work-up was recrystallized from CH_2Cl_2–hexanes and afforded the title compound as a white solid (175 mg, 12%); mp 82–83°C; IR (CH_2Cl_2): 1717 cm^{-1}; ^{1}H NMR (200 MHz, $CDCl_3$) δ: 1.40 (t, 3H, J = 7.1 Hz), 1.97 (s, 3H), 3.22 (s, 3H), 4.36 (m, 2H), 4.66 (s, 1H), 6.96 (d, 1H, J = 7.1 Hz), 7.41 (t, 1H, J = 7.1 Hz), 7.65 (d, 1H, J = 7.1 Hz); ^{13}C NMR (75 MHz, $CDCl_3$) δ: 12.32, 14.04, 26.33, 46.01, 61.30, 111.40, 124.02, 127.33, 127.86, 128.99, 144.72, 165.55, 174.86; EI-MS *m/z* (%): 265 (5.2, M^+), 219 (100), 190 (18.6), 174 (33.8); HRMS calcd. for $C_{13}H_{15}NO_3S$: 265.07727; found: 265.08194.

Reduction of oxindole 2b with $LiAlH_4$; 1-methyl-3-methylthio-4-methyl oxindole 3b

The general procedure outlined above from **2a** was followed. Oxindole **2b** (40 mg, 0.15 mmol) provided, after usual work-up and column chromatography (1:1 hex:EtOAc), compound **3b** as off-white needles (28 mg, 90%); mp 100–101°C; IR (CH_2Cl_2): 1712 cm^{-1}; ^{1}H NMR (200 MHz, $CDCl_3$) δ: 2.01 (s, 3H), 2.43 (s, 3H), 3.21 (s, 3H), 4.18 (s, 1H), 6.66 (d, 1H, J = 7.5 Hz), 6.88 (d, 1H, J = 7.5 Hz), 7.21 (t, 1H, J = 7.5 Hz); ^{13}C NMR (75 MHz, $CDCl_3$) δ: 11.66, 17.78, 26.01, 44.79, 105.27, 122.54, 124.31, 128.58, 135.53, 143.77, 174.81; EI-MS *m/z* (%): 207 (14.2, M^+), 160 (100), 130 (9.4), 117 (10.4), 77 (7.9); HRMS calcd. for $C_{11}H_{13}NOS$: 207.07179; found: 207.07322.

3-Methyl-3-methylthio-6-(carboethoxy)oxindole 2c

Standard Gassman methodology as reported for the synthesis of **2a** using ethyl (3-amino)benzoate and methyl (2-thiomethyl)propionate afforded, after purification via column chromatography (4:1 hex:EtOAc) and recrystallization from CH_2Cl_2–hexanes, the title compound **2c** as a white solid (24%); mp 135–136°C; IR (CH_2Cl_2): 3421, 1722, 1730 cm^{-1}; ^{1}H NMR (200 MHz, $CDCl_3$) δ: 1.30 (t, 3H, J = 7.2 Hz), 1.59 (s, 3H), 1.80 (s, 3H), 4.28 (q, 2H, J = 7.2 Hz), 7.29 (d, 1H, J = 7.9 Hz), 7.50 (d, 1H, J = 1.4 Hz), 7.73 (dd, 1H, J = 7.9, 1.4 Hz), 8.38 (br, 1H); ^{13}C NMR (75 MHz, $CDCl_3$) δ: 11.82, 14.01, 21.16, 50.19, 60.98, 110.29, 123.53, 124.53, 130.91, 136.38, 139.61, 165.63, 178.90; EI-MS *m/z* (%): 265 (2.9, M^+), 218 (100), 190 (34.5); HRMS calcd. for $C_{13}H_{15}NO_3S$: 265.07727; found: 265.07661.

Reduction of oxindole 2c with $LiEt_3BH$: 3-methyl-3-methylthio-6-(hydroxymethyl)oxindole 3c

A solution of $LiEt_3BH$ (0.45 mL, 1.0 M in THF, 0.45 mmol) was added dropwise to a cooled (0°C) solution of oxindole **2c** (45 mg, 0.17 mmol) in THF (5 mL). Stirring was continued at 0°C for 1 h, after which time the pale yellow solution was poured into a solution of H_2O (10 mL) and made acidic by the dropwise addition of HCl (10%). Extraction with EtOAc (4 × 20 mL), followed by normal work-up and chromatography (2:3 hex:EtOAc) afforded, in addition to returned starting material (7.8 mg), the title compound **3c**, which was recrystallized from CH_2Cl_2–hexanes as white prisms (27.4 mg, 88%); mp 167–168°C; IR (CH_2Cl_2): 3604, 1729 cm^{-1}; ^{1}H NMR (200 MHz, $CDCl_3$) δ: 1.54 (s, 3H), 1.80 (s, 3H), 4.60 (s, 2H), 6.85 (s, 1H), 6.95 (d, 1H, J = 7.5 Hz), 7.19 (d, 1H, J = 7.5 Hz), 8.10 (br, 1H); ^{13}C NMR (75 MHz, $CDCl_3$) δ: 11.79, 21.29, 49.98, 64.77, 108.11, 121.13, 123.71, 130.72, 139.78, 141.78, 179.22; EI-MS *m/z* (%): 223 (6.7, M^+), 176 (100), 148 (2.8); HRMS calcd. for $C_{11}H_{13}NO_2S$: 223.06670; found: 223.06858.

3-Methylthio-7-(carboethoxy)oxindole 2d

The modified Gassman conditions of Wierenga et al. were followed (18). A solution of sulfuryl chloride (2.26 g, 16.7 mmol) in CH_2Cl_2 (5 mL) was added dropwise to a cooled solution (−78°C) of methyl (methylthio)acetate (1.83 g, 15.3 mmol) in CH_2Cl_2 (50 mL), resulting in the slow formation of a white precipitate. After stirring for 1 h, a solution of ethyl (2-amino)benzoate (2.50 g, 15.1 mmol) in CH_2Cl_2 (50 mL) was added dropwise, resulting in slow dissolution of the white precipitate with the solution slowly turning pale yellow. After stirring for 2 h, triethylamine (1.59 g, 15.8 mmol) was added, and the solution was allowed to warm to RT overnight. Water (50 mL) was added, and the aqueous layer was separated and subjected to normal work-up conditions, resulting in a yellow semi-solid, which was dissolved in Et_2O (50 mL) and HCl (10%, 10 mL). The two-phase mixture was refluxed for 12 h, cooled, and the organic phase was separated and worked up in the usual manner. Column chromatography (5:1 hex:EtOAc) afforded a yellow solid, which was recrystallized from CH_2Cl_2–hexanes, affording the title compound **2d** as white flakes (383.8 mg, 10.1%); mp 87–88°C; IR (CH_2Cl_2): 3403, 1721, 1697 cm^{-1}; ^{1}H NMR (500 MHz, $CDCl_3$) δ: 1.39 (t, 3H, J = 7.0 Hz), 2.02 (s, 3H), 4.23 (s, 1H), 4.38 (q, 2H, J = 7.0 Hz), 7.08 (t, 1H, J = 7.5 Hz), 7.50 (d, 1H, J = 7.5 Hz), 7.81 (d, 1H, J = 7.5 Hz), 9.20 (br, 1H); ^{13}C NMR (125 MHz, $CDCl_3$) δ: 12.23, 14.32, 45.32, 61.39, 111.73, 122.14, 127.57, 129.58, 129.66, 143.79, 165.85, 175.92; EI-MS *m/z* (%): 251 (3.4, M^+), 205 (100), 158 (40.9), 130 (14.1); HRMS calcd. for $C_{12}H_{13}NO_3S$: 251.06162; found: 251.06239.

Reduction of oxindole 2d with $LiAlH_4$: 3-methylthio-7-(hydroxymethyl) oxindole 3d

Following the procedure described for **3a**, oxindole **2d** (50 mg, 19.9 mg) afforded, after usual work-up and column chromatography (1:1 hex:EtOAc), **3d** as a white crystalline solid (35 mg, 84%); mp 148–149°C; IR (CH_2Cl_2): 3620, 1721 cm^{-1}; ^{1}H NMR (500 MHz, $CDCl_3$) δ: 2.00 (s, 3H), 4.30 (s, 1H), 4.80 (s, 2H), 7.02 (m, 2H), 7.28 (d, 1H, J = 7.5 Hz), 8.50 (br, 1H); ^{13}C NMR (125 MHz, $CDCl_3$) δ: 12.33, 45.79, 63.43, 120.20, 122.56, 124.54, 127.24, 138.76, 142.36, 168.20; EI-MS *m/z* (%): 209 (7.6, M^+), 163 (100), 144 (42.0), 116 (48.6); HRMS calcd. for $C_{10}H_{11}NO_2S$: 209.05105; found: 209.04985.

Acknowledgments

We are grateful to the Natural Sciences and Engineering Research Council of Canada for continued financial support.

References

1. G.M. Karp. Org. Prep. Proced. Int. **25**, 481 (1993).
2. P.L. Julian and H.C. Printy. J. Am. Chem. Soc. **71**, 3206 (1949).

© 1997 NRC Canada

3. C.B. Hudson and A.V. Robertson. Aust. J. Chem. **20**, 1699 (1967).
4. C.S. Franklin and A.C. White. J. Chem. Soc. 1335 (1963).
5. J.C. Seaton and L. Marion. Can. J. Chem. **35**, 1102 (1957).
6. J.C. Seaton, R. Tondeur, and L. Marion. Can. J. Chem. **36**, 1031 (1958).
7. M. Kates and L. Marion. Can. J. Chem. **29**, 37 (1951).
8. R. Goutarel, M.M. Janot, V. Prelog, R. Sneeden, and W.I. Taylor. Helv. Chim. Acta, **34**, (1951).
9. T. Nishio, N. Okuda, and C. Kashima. Helv. Chim. Acta, **73**, 1719 (1990).
10. B. Schonenberger and A. Brossi. Helv. Chim. Acta, **69**, 1486 (1986).
11. Q.-S. Yu and A. Brossi. Heterocycles, **27**, 1709 (1988).
12. Q.-S. Yu, W.M. Luo, Y.Q. Li, and A. Brossi. Heterocycles, **36**, 1279 (1993).
13. M.E. Pierce, G.F. Huhn, J.H. Jensen, K.W. Sigvardson, Q. Islam, and Y. Xing. J. Heterocycl. Chem. **31**, 17 (1994).
14. F.J. McEvoy and G.R. Allen, Jr. J. Org. Chem. **38**, 3350 (1973).
15. H. Shirowej, S.A. Khan, and H. Plieninger. Synthesis, 84 (1972).
16. P.G. Gassman and T.J. van Bergen. J. Am. Chem. Soc. **95**, 2718 (1973).
17. P.G. Gassman and T.J. van Bergen. J. Am. Chem. Soc. **96**, 5508 (1974).
18. W. Wierenga, J. Griffin, and M.A. Warpehoski. Tetrahedron Lett. **24**, 2437 (1983).
19. P.G. Gassman, B.W. Cue, Jr. and T.-Y. Luh. J. Org. Chem. **42**, 1944 (1977).
20. P.G. Gassman and K.M. Halweg. J. Org. Chem. **44**, 628 (1979).
21. A. Taylor. J. Chem. Res. Synop. 347 (1980).
22. J.A. Marshall, N.H. Andersen, and A.R. Hochstetler. J. Org. Chem. **32**, 113 (1967).
23. M.J. Mintz and C. Walling. Org. Synth. Collect. Vol. **V**, 184 (1973).
24. S. Krishnamurthy. Tetrahedron Lett. **23**, 3315 (1982).

Can. J. Chem. Downloaded from www.nrcresearchpress.com by 88.146.161.215 on 09/08/12
For personal use only.

© 1997 NRC Canada

Metal hydride mediated reduction of 1,3-dimethyl-3(methylthio)oxindole

Terrence J. Connolly and Tony Durst

Abstract: The metal hydride mediated reduction of 4-carboethoxy-1,3-dimethyl-3-(methylthio)oxindole with lithium aluminum hydride and lithium triethylborohydride was studied. The results show that reduction of the oxindole carbonyl group is competitive with reduction of the pendant ester. The hemi-aminal that results from initial addition of hydride to the oxindole carbonyl may follow a number of reaction pathways, one of which is an unprecedented rearrangement. A mechanism is proposed that accounts for all observed products.

Key words: oxindole, reduction, rearrangement.

Résumé : On a étudié la réduction du 4-carboéthoxy-1,3-diméthyl-3-(méthylthio)oxindole par $LiAlH_4$ et par le triéthylborohydrure de lithium. Les résultats montrent que la réduction du groupe carbonyle de l'oxindole est en compétition avec la réduction du groupe ester exocyclique. L'hémi-aminal qui résulte de l'addition initiale d'hydrure sur le groupe carbonyle de l'oxindole peut donner lieu à un certain nombre de réactions subséquentes; l'une d'elle est une transposition sans précédent. On propose un mécanisme pour expliquer la formation de tous les produits observés.

Mots clés : oxindole, réduction, transposition.

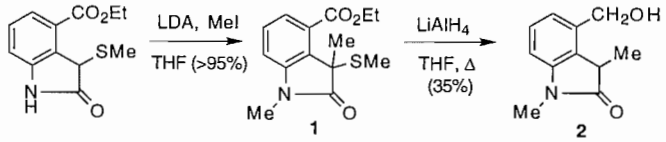
[Traduit par la rédaction]

Can. J. Chem. Downloaded from www.nrcresearchpress.com by 88.146.161.215 on 09/08/12
For personal use only.

Introduction

The biological activity of some compounds possessing the oxindole nucleus and their structural relationship to indoles continue to make these compounds attractive targets in synthetic organic chemistry (1). In particular, the chemistry of 3-(alkylthio)oxindoles is of great interest. Much of this interest may be traced to the reliable yields and ease of preparation of this class of compounds, primarily due to the pioneering works of Gassman and van Bergen (2, 3). A number of notable variations of the original Gassman methodology have been published recently (4, 5). The fact that these advances and improvements have come primarily from industrial pharmaceutical laboratories lends credence to the importance of these compounds. In addition to the improvements in preparative methods, Karp has recently described conditions that allow for the selective alkylation of this nucleus, thus providing a method for the preparation of 1-, 3-, and 1,3-substituted oxindoles (6), a notable achievement given the difficulty associated with oxindole alkylation. Our contribution to this field has focused on a new, mild, and general nonreductive desulfenylation protocol allowing for the selective removal of the 3-alkylthio group always present if the Gassman approach is utilized (7). In the preceding paper, we described the results of a study dealing with the metal hydride mediated reduction of 3-(alkylthio)oxindoles bearing pendant ester groups on the aromatic ring (8). This study concluded that in this series of compounds the presence of a proton α to the oxindole carbonyl group protects it from reduction, presumably via deprotonation by the metal hydride. We also noted the complications involved in the reduction of ester groups attached at various positions on the benzene ring and ascribed these to the formation of a C3 anion. In continuing our studies in this area, we were interested in seeing what effect blocking both of the positions α to the oxindole carbonyl would have on the course of the reaction. The results of this chemistry, and a postulated mechanism regarding the unusual rearrangement we observed, are the focus of this publication.

Scheme 1.



Results

The required 1,3-(dimethylated)oxindole **1** was prepared by treating 4-carboethoxy-3-(methylthio)oxindole (8) with 2 equivalents of LDA at −78°C followed by the addition of excess MeI and allowing the reaction mixture to warm to room temperature. The product oxindole **1**, prepared in a yield of >95%, was readily identified based on the appearance of three equally intense singlets in the ^1H NMR spectrum, accounting for the three methyl groups. Reduction of oxindole **1** with excess $LiAlH_4$ in refluxing THF led to the formation of oxindole **2** as the major polar material in a yield of 35% after column chromatography (Scheme 1).

Received November 13, 1996.

T.J. Connolly and T. Durst.[1] Department of Chemistry, University of Ottawa, 10 Marie Curie, Ottawa, ON K1N 6N5 Canada

[1] Author to whom correspondence may be addressed. Telephone: (613) 562-5800, ext. 5728. Fax: (613) 562-5170. E-mail: tdurst@oreo.uottawa.ca

© 1997 NRC Canada

Can. J. Chem. Downloaded from www.nrcresearchpress.com by 88.146.161.215 on 09/08/12
For personal use only.

To gain insight into the reaction mechanism, the reaction was repeated with a controlled amount of $LiAlD_4$ at room temperature. Quenching the reaction mixture with a saturated solution of potassium sodium tartrate followed by careful chromatography led to the isolation of three products (Scheme 2). The most polar compound (**2-*d***), isolated as a pale yellow solid (mp 100–101°C) in 41% yield, was identical to **2** except that two atoms of deuterium had been incorporated at the benzylic alcohol position. The second compound, also obtained as a pale yellow solid (mp 81–82°C) in 30% yield, proved to be indole **3-*d***. Key spectral evidence included the absence of carbonyl and presence of alcohol functional groups (3391 cm^{-1}) and an aromatic region in the ^1H NMR spectrum that failed to show the fine structure associated with an oxindole. Additionally, ^2H NMR showed that two deuterium atoms had been incorporated into the molecule at chemical shifts of 4.68 and 6.78 ppm in a ratio of 2:1. These chemical shifts correspond to deuterium incorporation at the C4 benzylic and the C2 position of the indole, respectively. The third compound, isolated as a yellow solid (mp 106–107°C) in 25% yield, was confirmed as being **4-*d*** by converting it to **3** via desulfurization with Ni_2B (9–11).

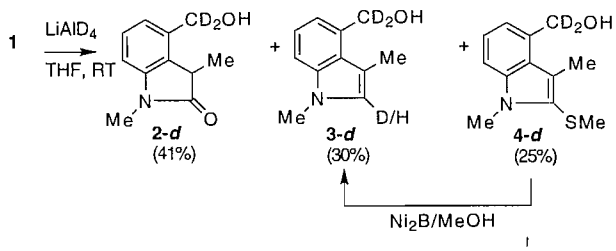
Reduction with $LiEt_3BH$ in THF at room temperature followed by careful chromatography afforded *four* products (Scheme 3). The isolation of **4** and **5** indicates that reduction of the oxindole carbonyl is competitive with reduction of the C4 ester group.

Discussion

The ease of reduction of the oxindole carbonyl group in **1** as compared to oxindoles lacking the 1,3-dimethyl groups (8) proves that an adjacent proton indeed protects it from reduction. In the case of **1**, reduction of the oxindole carbonyl group occurs and leads to either dethiomethylation or an interesting rearrangement. A proposed mechanism to account for all of the isolated products is shown in Scheme 4.

Although it was not possible to determine which carbonyl group was reduced first, it is apparent that reduction of the oxindole carbonyl is facile. Addition of one equivalent of hydride to the oxindole carbonyl results in the formation of hemi-aminal **7**. Further addition of hydride to **7** in a manner reminiscent of amide to amine reduction may occur through **8** to give indoline **9**. We have found that these 3-methylthioindolines are extremely susceptible to dethiomethylation, and readily afford indoles.[2] An analogous transformation on substrate **9** would account for **10**. Reduction of the ester group of **1** prior to or following oxindole reduction accounts for **3**.

Scheme 2.



To account for indole **4**, C3 to C2 migration of the methylthio group of **8** via an episulfonium salt **11** has been invoked. Migrations of alkylthio groups from the 3 to 2 position are known to occur for indoles. Ottenheijm and co-workers first proposed the intermediacy of episulfonium salts to account for this transformation (12). Hamel, Girard, and Atkinson (13, 14) have since shown that a complex intermolecular process can occur, although a concomitant intramolecular rearrangement via an episulfonium species remains a distinct possibility (15). The similarities between intermediate **8** and the intermediates formed in the acid catalyzed rearrangement of 3-alkylthioindoles is striking.

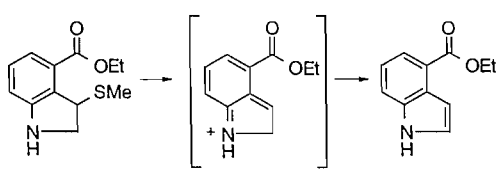
Finally, hemi-aminal **7** may lose MeS, possibly via a nitrogen-assisted 1,4-elimination giving **12**, which may re-aromatize to give enol **13**, which could then re-enolize, accounting for **7**. In this case, ester reduction *must* precede reduction of the oxindole. We have previously shown that C4 esters are difficult to reduce when a C3 anion is formed (8), which is the case for **13a**, and could be the case for **7**, which has a highly acidic C3 proton. We have also shown that reduction of **7** does not lead to the formation of **2**.

Alternatively, **12** may undergo a 1,2-hydride shift that would afford **7** or **2** directly. This latter 1,2-shift is not favored, since we could not detect any deuterium incorporation at this center when conducting the reductions with $LiAlD_4$. However, the high acidity of this C3 proton may cause exchange on work-up, thereby causing scrambling and facilitating against deuterium incorporation in the product.

In an extension of this work, oxygen analogs of the thioethers were prepared. Reduction of oxindole **15**, prepared in three steps from isatin, did not lead to **17**. This, indirectly, lends support to the intermediacy of the episulfonium salt **11** since the longer C—S bond may allow the formation of compounds like **11**, whereas oxonium salt **16** is not accessible due to the shorter C—O bond (Scheme 5).

In related work, the reactive carbonyl group of isatin was transformed into a dithiane and a dithiolane as in **18**. Reaction of **18** with $LiEt_3BH$ or $LiAlH_4$ did not result in the formation of **20** (Scheme 6). The failure to form **20** is probably the result of the rather unlikely nature of forming intermediate **19**, an idea which again supports the intermediary of an episulfonium salt in the migration of SMe from the 3 to 2 position reported earlier. It is also worth noting that this also supports the intermediacy of episulfonium salts in the acid-catalyzed isomerization of indole-3-sulfides to indole-2-sulfides.

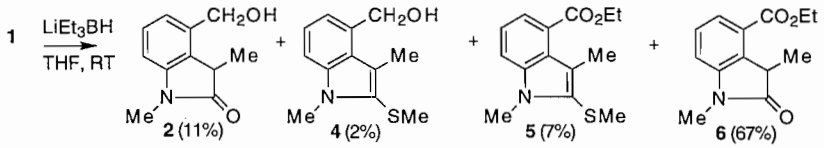
[2] We found that 3-methylthio-4-carboethoxyindolines readily dethioalkylate to afford 4-carboethoxyindole. Although this transformation readily occurs by treatment with reducing agents, including $NaBH_4$, a sample of the pure indoline is slowly converted to the indole, in the absence of other reagents. This observation has led us to propose a nitrogen-assisted 1,4-elimination, followed by re-aromatization as shown below.



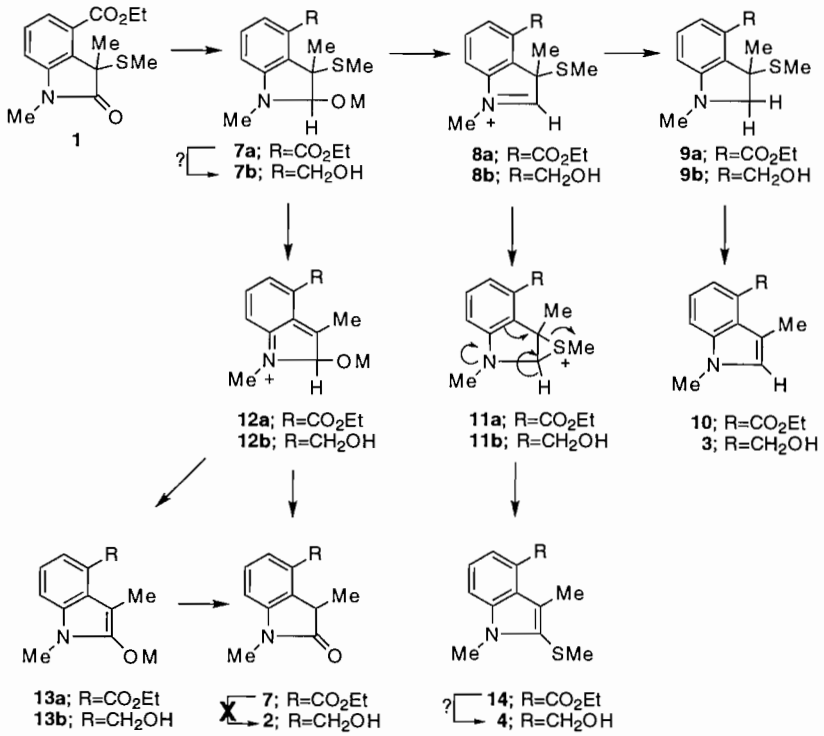
© 1997 NRC Canada

Can. J. Chem. Downloaded from www.nrcresearchpress.com by 88.146.161.215 on 09/08/12
For personal use only.

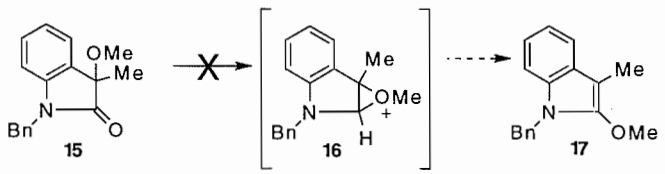
Scheme 3.



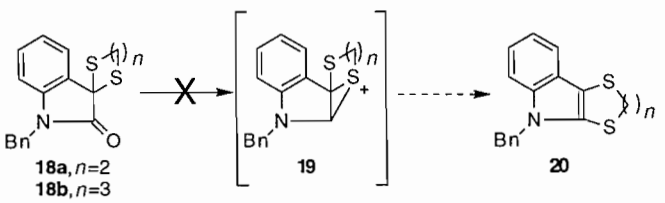
Scheme 4.



Scheme 5.



Scheme 6.



Conclusion

We have shown that the reduction of substituted 3-(methylthio)oxindoles with metal hydrides is a complicated reaction. In the case of 1,3-dialkyl derivatives, oxindole carbonyl reduction is facile, and competitive with the reduction of remote ester groups. The hemi-aminal that results from the first addition of hydride to the oxindole carbonyl affords a number of products. Two dethiomethylation routes compete for oxindole and indole formation. The other observed products, 1,3-dimethyl-2-(methylthio)indoles, seem to be the result of an unusual rearrangement. To the best of our knowledge, this is the first example of such a rearrangement from oxindoles under reductive conditions.

Experimental

General experimental procedures have been described previously (8). In addition to this, ^2H NMR spectra were recorded in CH_2Cl_2 solutions on a Varian XL-300 spectrometer, operating at a frequency of 46.06 MHz, and are referenced to the natural abundance of CD_2Cl_2 at 5.20 ppm.

1,3-Dimethyl-3-(methylthio)oxindole (1)

A solution of freshly prepared LDA (2.1 equiv.) in THF was added dropwise to a cooled (0°C) solution of oxindole 7 (500 mg, 1.99 mmol) in THF (20 mL). Stirring was continued for 1 h, after which time a solution of MeI (631 mg, 4.38 mmol) in THF (5 mL) was added dropwise. The ice bath was removed and the temperature of the resulting solution was allowed to slowly rise to room temperature (RT) over 12 h; the solution was then poured into H_2O (50 mL) and extracted with Et_2O (4 × 20 mL). The combined organic extracts were worked up in the usual manner, affording, after chromatography (2:1

© 1997 NRC Canada

Can. J. Chem. Downloaded from www.nrcresearchpress.com by 88.146.161.215 on 09/08/12
For personal use only.

hex:EtOAc), the title compound **14** as a pale yellow oil (540 mg, <95%); ^{1}H NMR (200 MHz, $CDCl_3$) δ: 1.40 (t, 3H, J = 7.5 Hz), 1.80 (s, 3H), 2.02 (s, 3H), 3.21 (s, 3H), 4.40 (q, 2H, J = 7.5 Hz), 6.98 (dd, 1H, J = 7.0, 1.0 Hz), 7.38 (t, 1H, J = 7.0 Hz), 7.59 (dd, 1H, J = 7.0, 1.0 Hz) ppm; ^{13}C NMR (75 MHz, $CDCl_3$) δ: 12.29, 14.20, 21.32, 26.55, 51.59, 61.40, 111.28, 124.61, 128.70, 129.09, 130.93, 143.62, 165.99, 177.25 ppm; EI-MS *m/z* (%): 279 (12.2, M^+), 233 (100); HRMS calcd. for $C_{14}H_{17}NO_3S$: 279.09292; found: 279.09141.

Reduction of oxindole 1 with $LiAlD_4$ (2-*d*, 3-*d*, 4-*d*)

A solution of oxindole **1** (200 mg, 0.72 mmol) was added dropwise to a suspension of $LiAlD_4$ (50 mg, 1.19 mmol) in THF (10 mL) at RT. After stirring at RT for 7 h, the resulting gray cloudy solution was poured into a solution (50 mL) of saturated potassium sodium tartrate and EtOAc (20 mL). After stirring for 4 h, the organic phase was separated and subjected to normal work-up, affording 180 mg of a pale yellow oil. Chromatography with a gradient of 2:1 to 1:1 hex:EtOAc provided three compounds.

Indole ***4*-d**: 40.3 mg (25.0%), R_f = 0.5 (1:1 hex:EtOAc), pale yellow solid; mp 106–107°C; IR (CH_2Cl_2): 3392 cm^{-1}; ^{1}H NMR (200 MHz, $CDCl_3$) δ: 2.12 (s, 3H), 2.58 (s, 3H), 3.75 (s, 3H), 6.95 (d, 1H, J = 7.5 Hz), 7.10 (m, 2H) ppm; ^{2}H NMR (46 MHz, CH_2Cl_2) δ: 4.87 (s) ppm; ^{13}C NMR (75 MHz, $CDCl_3$) δ: 12.03, 19.61, 29.89, 63.80 (quintet), 109.45, 116.38, 119.24, 122.11, 124.65, 130.10, 132.91, 137.88 ppm; EI-MS *m/z* (%): 223 (100) (M^+), 205 (15.0), 190 (48.5), 175 (28.5); HRMS calcd. for $C_{12}H_{13}NOSD_2$: 223.10309; found: 223.09989.

Indole ***3*-d**: 38.4 mg (30.1%), R_f = 0.40 (1:1 hex:EtOAc), pale yellow solid; mp 80–81°C; IR (CH_2Cl_2): 3391 cm^{-1}; ^{1}H NMR (500 MHz, $CDCl_3$) δ: 2.41 (s, 3H), 3.62 (s, 3H), 6.90 (d, 1H, J = 7.5 Hz), 7.15 (t, 1H, J = 7.5 Hz), 7.23 (d, 1H, J = 7.5 Hz); ^{2}H NMR (46 MHz, CH_2Cl_2) δ: 4.86 (s, 2D), 6.78 (s, 1D); ^{13}C NMR (125 MHz, $CDCl_3$) δ: 12.14, 32.54, 63.80 (quintet), 109.42, 109.75, 119.42, 121.36, 122.86, 128.72, 132.48, 138.62 (doublet); EI-MS *m/z* (%): 178 (96.3) (M^+), 160 (100).

Oxindole ***2*-d**: 56.0 mg (40.5%), R_f = 0.1 (1:1 hex:EtOAc), pale yellow solid; mp 99–101.3°C; IR (CH_2Cl_2): 3603, 1710 cm^{-1}; ^{1}H NMR (200 MHz, $CDCl_3$) δ: 1.38 (d, 3H, J = 7.5 Hz), 3.08 (s, 3H), 3.42 (q, 1H, J = 7.5 Hz), 6.65 (d, 1H, J = 7.5 Hz), 6.98 (d, 1H, J = 7.5 Hz), 7.18 (t, 1H, J = 7.5 Hz); ^{2}H NMR (46 MHz CH_2Cl_2) δ: 4.56 (s, 1D), 4.63 (s, 1D); EI-MS m/z (%): 193 (45.6, M^+), 175 (32.9), 160 (23.9), 43 (100); HRMS calcd. for $C_{11}H_{11}NO_2D_2$: 193.11028; found: 193.10784.

Reduction of oxindole 1 with $LiEt_3BH$ (2, 4, 5, 6)

A solution of $LiEt_3BH$ (2.80 mL, 2.80 mmol, 1.0 M in THF) was added dropwise via syringe to a solution of oxindole **3** (156.3 mg, 0.56 mmol) in THF (15 mL) at RT. The resulting bright yellow solution was stirred at RT for 3 h, after which time the yellow solution was poured into H_2O (20 mL), adjusted to pH 3 by the dropwise addition of HCl (10%), and extracted with EtOAc (4 × 20 mL). The combined organic extracts were worked up as usual, affording a pale yellow oil (120 mg) that was chromatographed with a gradient of 2:1 to 1:1 hex:EtOAc and afforded four compounds.

Indole ***5***: yellow oil, 9.8 mg (6.6%), R_f = 0.9 (1:1 hex:EtOAc); ^{1}H NMR (200 MHz, $CDCl_3$) δ: 1.40 (t, 3H, J = 7.5 Hz), 2.25 (s, 3H), 2.51 (s, 3H), 3.88 (s, 3H), 4.42 (q, 2H, J = 7.5 Hz), 7.20 (t, 1H, J = 7.5 Hz), 7.41 (d, 1H, J = 7.5 Hz), 7.52 (d, 1H, J = 7.5 Hz); EI-MS *m/z* (%): 263 (57.3, M^+), 248 (12.6), 234 (14.0), 219 (24.3), 205 (53.3), 57.0 (100); HRMS calcd. for $C_{14}H_{17}NO_2S$: 263.09800; found: 263.09847.

Indole ***4***: white solid, 2.4 mg (1.9%), R_f = 0.75 (1:1 hex:EtOAc); mp 115–116°C; ^{1}H NMR (200 MHz, $CDCl_3$) δ: 2.21 (s, 3H), 2.68 (s, 3H), 3.85 (s, 3H), 5.05 (s, 2H), 7.04 (d, 1H, J = 7.5 Hz), 7.20 (m, 2H); EI-MS *m/z* (%): 221 (100, M^+), 188 (43.3), 173 (32.2), 145 (36.5); HRMS calcd. for $C_{12}H_{15}NOS$: 221.08744; found: 221.08616.

Oxindole ***6***: pale yellow solid, 88.2 mg (67.6%), R_f = 0.50 (1:1 hex:EtOAc); mp 70–70.5°C; IR (CH_2Cl_2): 1714 cm^{-1}; ^{1}H NMR (200 MHz, $CDCl_3$) δ: 1.38 (t, 3H, J = 7.5 Hz), 1.48 (d, 3H, J = 7.5 Hz), 3.22 (s, 3H), 3.86 (q, 1H, J = 7.5 Hz), 4.38 (q, 2H, J = 7.5 Hz), 6.98 (d, 1H, J = 7.5 Hz), 7.32 (t, 1H, J = 7.5 Hz), 7.68 (d, 1H, J = 7.5 Hz); ^{13}C NMR (75 MHz, $CDCl_3$) δ: 13.89, 15.93, 26.00, 41.65, 60.86, 111.36, 123.46, 126.58, 127.59, 132.41, 144.66, 165.55, 178.66; EI-MS *m/z* (%): 233 (100, M^+), 204 (40.3), 188 (29.7), 160 (83.7); HRMS calcd. for $C_{13}H_{15}NO_3$: 233.10519; found: 233.10495.

Oxindole ***2***: pale yellow solid, 11.8 mg (11.0 %), R_f = 0.10 (1:1 hex:EtOAc); mp 99–100°C; IR (CH_2Cl_2): 3603, 1710 cm^{-1}; ^{1}H NMR (500 MHz, $CDCl_3$) δ: 1.44 (d, 3H, J = 7.6 Hz), 2.70 (br, 1H), 3.14 (s, 3H), 3.44 (q, 1H, J = 7.6 Hz), 4.65 (d, 1H, J = 13.0 Hz), 4.73 (d, 1H, J = 13.0 Hz), 6.72 (d, 1H, J = 8.0 Hz), 7.05 (d, 1H, J = 8.0 Hz), 7.24 (t, 1H, J = 8.0 Hz); ^{13}C NMR (125 MHz, $CDCl_3$) δ: 15.43, 26.29, 40.11, 62.26, 107.42, 121.62, 127.93, 128.12, 137.15, 144.10, 178.81; HRMS calcd. for $C_{11}H_{13}NO_2$: 191.09463; found: 191.09650.

N-(Benzyl)isatin

To a solution of isatin (5.00 g, 33.98 mmol) in CH_2Cl_2 (25 mL) was added benzyl bromide (5.81 g, 33.98 mmol), an aqueous solution of NaOH (10 mL, 20%), and benzyl triethylammonium bromide (100 mg). The dark-red solution was stirred at RT for 4 h, after which time the organic phase was separated and worked up in the usual manner, affording the title compound as an orange solid (6.85 g, 85%); mp 124–125°C; ^{1}H NMR (200 MHz, $CDCl_3$) δ: 4.82 (s, 2H), 6.68 (d, 1H, J = 8.0 Hz), 6.98 (t, 1H, J = 8.0 Hz), 7.20 (s, 1H), 7.35 (td, 1H, J = 8.0, 1.0 Hz), 7.50 (dd, 1H, J = 8.0 1.0 Hz) ppm; ^{13}C NMR (75 MHz, $CDCl_3$) δ: 50.62, 110.68, 117.39, 123.54, 125.11, 127.11, 127.86, 128.74, 134.19, 137.98, 150.43, 157.96, 182.91 ppm; EI-MS *m/z* (%): 237 (62.2, M^+), 180 (38.4), 146 (100); HRMS calcd. for $C_{15}H_{11}NO_2$: 237.07898; found: 237.07912.

1-Benzyl-3-methyl-3-(hydroxy)oxindole

A solution of MeMgBr (0.85 mL, 3.0 M in Et_2O, 2.55 mmol) was added dropwise to a cooled (0°C) solution of *N*-benzylisatin (500 mg, 2.11 mmol) in THF (20 mL). The resulting yellow solution was allowed to warm to RT over 12 h, and the red solution that resulted was poured into a solution of NH_4Cl (10%, 20 mL) and extracted with EtOAc (4 × 10 mL). Usual work-up afforded a reddish oil that was subjected to column

© 1997 NRC Canada

chromatography (2:1 hex:EtOAc), providing the title compound as a yellow solid (346.2 mg, 65%); ^{1}H NMR (200 MHz, $CDCl_3$) δ: 1.63 (s, 3H), 4.80 (d, 1H, J = 15.0 Hz), 4.95 (d, 1H, J = 15.0 Hz), 6.70 (d, 1H, J = 8.0 Hz), 7.05 (t, 1H, J = 8.0 Hz), 7.18 (dd, 1H, J = 8.0, 1.0 Hz), 7.30 (s, 5H), 7.42 (dd, 1H, J = 8.0, 1.0 Hz) ppm; ^{13}C NMR (50 MHz, $CDCl_3$) δ: 24.78, 43.44, 73.41, 109.28, 122.96, 123.21, 126.90, 127.43, 128.56, 129.26, 131.01, 135.16, 141.63, 178.30 ppm; EI-MS *m/z* (%): 253 (24.7, M^+), 235 (20.5), 149 (38.3), 91 (100); HRMS calcd. for $C_{16}H_{15}NO_2$: 253.11078; found: 253.11042.

1-Benzyl-3-methyl-3-(methoxy)oxindole (15)

A THF solution (10 mL) of *N*-benzyl-3-methyl-3-(hydroxy)oxindole (150 mg, 0.59 mmol) was added dropwise to a suspension of NaH (20 mg, 0.83 mmol) in THF (5 mL). The pale yellow solution was stirred at RT for 1 h, excess MeI was added, and the still pale yellow solution was stirred at RT for 18 h, after which time it was evaporated to dryness, leaving a pale yellow solid that was recrystallized from CH_2Cl_2–hexanes, affording the title compound as a bright yellow solid (81.2 mg, 51%); ^{1}H NMR (200 MHz, $CDCl_3$) δ: 1.60 (s, 3H), 3.06 (s, 3H), 4.91 (d, 1H, J = 16.0 Hz), 4.92 (d, 1H, J = 16.0 Hz), 6.70 (d, 1H, J = 8.0 Hz), 7.05 (t, 1H, J = 8.0 Hz), 7.20–7.40 (m, 7H) ppm; ^{13}C NMR (50 MHz, $CDCl_3$) δ: 23.83, 43.44, 52.87, 79.33, 109.21, 122.82, 123.51, 126.93, 127.44, 128.29, 128.55, 129.31, 135.37, 142.23, 176.31 ppm; EI-MS *m/z* (%): 267 (23.4, M^+), 237 (25.3), 176 (14.5), 144 (28.6), 91 (100); HRMS calcd. for $C_{17}H_{17}NO_2$: 267.12593; found: 267.12731.

1-Benzyl-3,3-(ethylenedithio)oxindole (18a)

A solution of *N*-benzylisatin (250 mg, 1.05 mmol) in CH_2Cl_2 (15 mL) containing ethane-1,2-dithiol (119 mg, 1.27 mmol) was stirred at RT while $BF_3{\cdot}OEt_2$ (1 mL) was added dropwise. The resulting solution was stirred at RT for 2 h, then quenched by the addition of H_2O (20 mL), washed with sodium carbonate (10%, 3 × 20 mL), and worked up in the usual manner. Chromatography (5:1 hex:EtOAc) afforded the title compound as a pale yellow solid (222 mg, 67%); mp 107–108°C; IR (CH_2Cl_2): 1717 cm^{-1}; ^{1}H NMR (200 MHz, $CDCl_3$) δ: 3.65 (m, 2H), 3.95 (m, 2H), 4.90 (s, 2H), 6.65 (d, 1H, J = 8.0 Hz), 7.10 (t, 1H, J = 8.0 Hz), 7.15 (t, 1H, J = 8.0 Hz), 7.30 (s, 5H), 7.55 (d, 1H, J = 8.0 Hz) ppm; ^{13}C NMR (50 MHz, $CDCl_3$) δ: 40.34, 43.82, 109.22, 123.13, 125.34, 125.94, 126.99, 127.54, 128.54, 128.69, 129.73, 135.31, 142.22, 177.96 ppm; EI-MS *m/z* (%): 313 (33.1, M^+), 254 (54.2), 222 (53.2), 162 (51.0), 91 (100); HRMS calcd. for $C_{17}H_{15}NOS_2$: 313.05951; found: 313.06144.

1-Benzyl-3,3-(propylenedithio)oxindole (18b)

The title compound was prepared as above, except that propane-1,3–dithiol was used in the place of ethane-1,2-dithiol. Chromatography (6:1 hex:EtOAc) afforded the title compound as a pale yellow solid (241.8 mg, 70.1%); mp 148–149°C; IR (CH_2Cl_2): 1708 cm^{-1}; ^{1}H NMR (200 MHz, $CDCl_3$) δ: 2.0–2.3 (m, 2H), 2.65 (dt, 2H, J = 14.0, 2.0 Hz), 4.09 (td, 2H, J = 14.0, 2.0 Hz), 4.85 (s, 2H), 6.63 (d, 1H, J = 7.6 Hz), 7.00 (t, 1H, J = 7.6 Hz), 7.15 (t, 1H, J = 7.6 Hz), 7.30 (s, 5H), 7.45 (d, 1H, J = 7.6 Hz) ppm; ^{13}C NMR (50 MHz, $CDCl_3$) δ: 24.18, 25.88, 43.16, 109.17, 122.94, 124.99, 126.80, 127.48, 128.71, 129.90, 135.39, 141.43, 175.67 ppm; EI-MS *m/z* (%): 327 (M^+, 23.2), 294 (22.0), 254 (39.5), 162 (61.5), 91 (100); HRMS calcd. for $C_{18}H_{17}NOS_2$: 327.07516; found: 327.07519.

Acknowledgments

We are grateful to the Natural Sciences and Engineering Research Council of Canada for continued financial support.

References

1. G.M. Karp. Org. Prep. Proced. Int. **25**, 481 (1993).
2. P.G. Gassman and T.J. van Bergen. J. Am. Chem. Soc. **95**, 2718 (1973).
3. P.G. Gassman and T.J. van Bergen. J. Am. Chem. Soc. **96**, 5508 (1974).
4. W. Wierenga, J. Griffin, and M.A. Warpehoski. Tetrahedron Lett. **24**, 2437 (1983).
5. S.W. Wright, L.D. McClure, and D.L. Hageman. Tetrahedron Lett. **37**, 4631 (1996).
6. G.M. Karp. J. Org. Chem. **57**, 4765 (1992).
7. T.J. Connolly and T. Durst. Synlett, 663 (1996).
8. T.J. Connolly and T. Durst. Can. J. Chem. **75**, 536 (1997).
9. T.G. Back. J. Chem. Soc. Chem. Commun. 1417 (1984).
10. T.G. Back, K. Yang, and H.R. Krouse. J. Org. Chem. **57**, 1986 (1992).
11. B. Ganem and J. Osby. Chem. Rev. **86**, 763 (1986).
12. R. Plate, R.J.F. Nivard, and H.C.J. Ottenheijm. Tetrahedron, **42**, 4503 (1986).
13. P. Hamel, Y. Girard, and J.G. Atkinson. J. Chem. Soc. Chem. Commun. 63 (1989).
14. P. Hamel, Y. Girard, and J.G. Atkinson. J. Org. Chem. **57**, 2694 (1992).
15. P. Hamel and P. Preville. J. Org. Chem. **61**, 1573 (1996).

Can. J. Chem. Downloaded from www.nrcresearchpress.com by 88.146.161.215 on 09/08/12
For personal use only.

© 1997 NRC Canada

Influence of working electrodes in Belousov–Zhabotinsky oscillatory system

V. Jayalakshmi and R. Ramaswamy

Abstract: The potential oscillatory profiles recorded simultaneously in the same B–Z system using platinum, glassy carbon, and graphite electrodes are different in their characteristics. The variance in the amplitude and potential range is a result of the difference in the potential response of the electrode to the different redox couples. The results obtained by employing cyanoacetic acid, syringic acid, malonic acid, citric acid, methylacetoacetate, or vanillin as the substrate and Ce(III), Mn(II), or Ferroin as the catalyst are presented. The response of the working electrode to the various redox couples is correlated to the value of the exchange current density.

Key words: potential oscillatory profile, redox couple, working electrode, potential response, exchange current density.

Résumé : Les profils de potentiel oscillatoire enregistrés simultanément dans le même système B–Z, en utilisant des électrodes de platine, de carbone vitreux et de graphite présentent des caractéristiques différentes. La variation dans l'amplitude et la plage de potentiel résultent de différences dans la réponse du potential de l'électrode aux différents couples rédox. On présente les résultats obtenus lors de l'utilisation des acides cyanoacétique, syringique, malonique et citrique ou de l'acétoacétate de méthyle ou de la vanilline comme substrats et du Ce(III), du Mn(II) ou de la ferroïne comme catalyseurs. On a établi une corrélation entre la réponse de l'électrode de travail à divers couples rédox et la valeur de l'échange de la densité de courant.

Mots clés : profile de potentiel oscillatoire, couple rédox, électrode de travail, réponse au potentiel, échange de la densité de courant.

[Traduit par la rédaction]

Introduction

The most extensively investigated oscillatory Belousov–Zhabotinsky (B–Z) reactions (1–9) fall into two major classes, namely, catalyzed and uncatalyzed systems. Catalyzed systems contain a metal ion catalyst and an organic substrate and the oscillations are usually registered by potentiometry, spectrophotometry (10), and EPR techniques (11, 12). The oscillations in redox potential measurements are mainly due to the metal ion catalyst and bromine. Uncatalyzed systems contain a highly reactive organic substrate and there is no metal ion catalyst. Oscillations observed in redox potential measurements are mainly due to bromine. The technique most widely used for investigating B–Z reactions is redox potential measurement employing a platinum working electrode. The issue regarding the species monitored in a complex oscillating reaction mixture containing several redox couples has not so far been satisfactorily resolved. The Ce(III) system with malonic acid as the substrate has been studied, employing working electrodes other than platinum (13). In the present paper we focus on the correlation among the potential oscillatory profiles recorded employing different working electrodes, namely, graphite, platinum, glassy carbon, and the Br^- selective electrode. Experiments were carried out by employing cyanoacetic acid, syringic acid, malonic acid, citric acid, vanillin or methylacetoacetate as the substrate and Mn(II), Ce(III), or Ferroin as the catalyst. The sensitivities of different working electrodes to the different redox couples present in the same mixture may vary with the chemical system. A critical examination of the oscillatory profiles with different electrodes represents a qualitative measure of such sensitivity. The conclusions resulting from such studies have been discussed in terms of the value of exchange current density of the redox couples involved.

Experimental

The batch reactor employed in the present investigation contained sulphuric acid, metal ion catalyst, and an organic substrate. Requisite volumes of the constituents were drawn from the stock solution. This was kept well stirred and thermostated at 30 ± 0.1°C in a polythene beaker. The system commences to oscillate after the addition of the last constituent, namely,

Table 1. The standard reduction potentials of the different redox reactions involved.

Redox reaction	$E°$ (V vs. NHE)	$E°$ (V vs. SCE)
$Br_2 + 2e \rightleftharpoons 2Br^-$	1.067	0.825
Ferrin + e ⇌ Ferroin	1.060	0.818
Mn(III) + e ⇌ Mn(II)	1.510	1.268
Ce(IV) + e ⇌ Ce(III)	1.440	1.198
$HOBr + H^+ + e \rightleftharpoons \frac{1}{2}Br_2 + H_2O$	1.595	1.353

Received June 12, 1996.[1]

V. Jayalakshmi and R. Ramaswamy.[2] Department of Chemistry, Indian Institute of Technology, Madras–600 036, India.

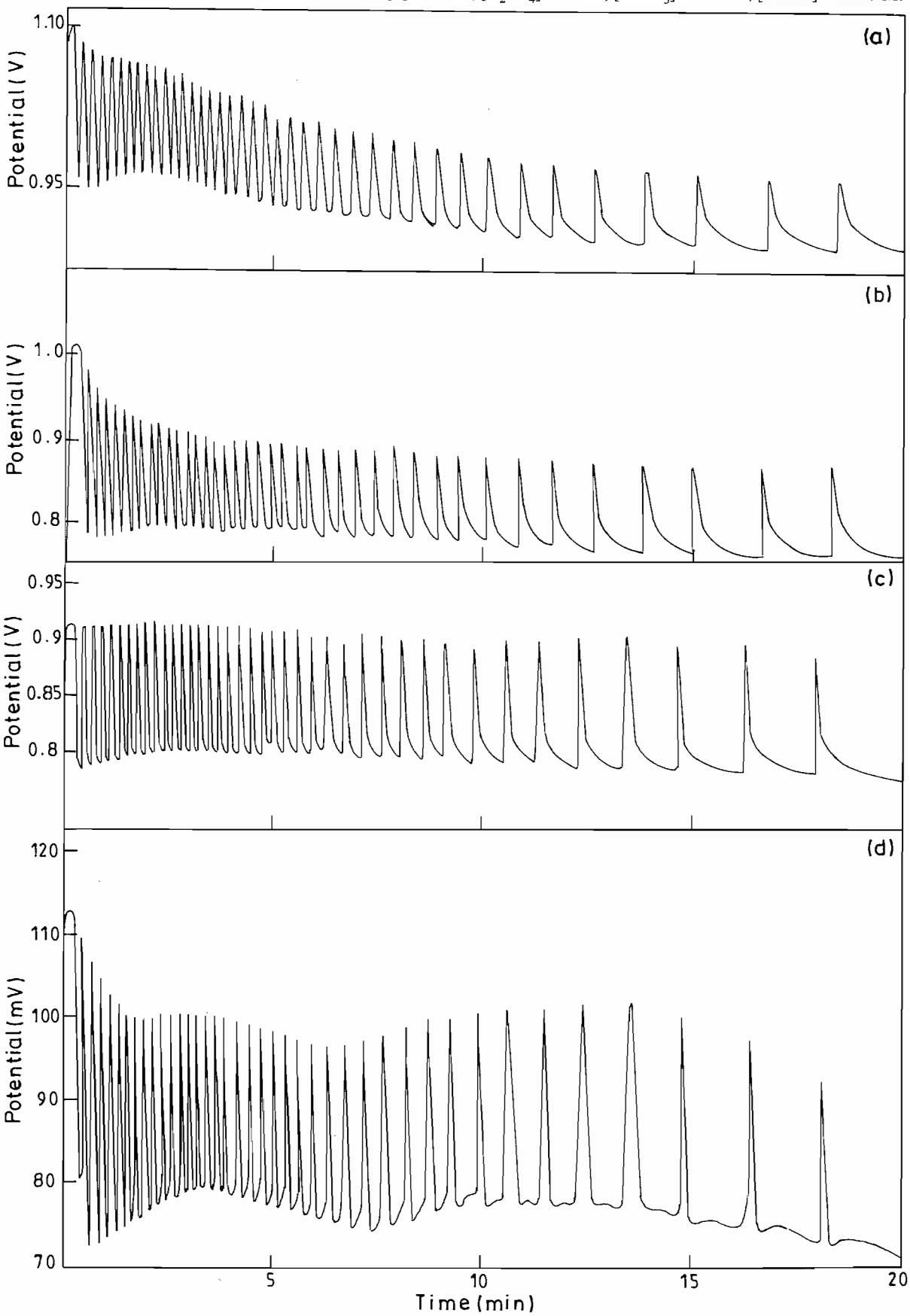
[1] Revision received February 18, 1997.

[2] Author to whom correspondence may be addressed. Fax: 044:2350509. E-mail: Chem2@iitm.ernet.in

© 1997 NRC Canada

Can. J. Chem. Downloaded from www.nrcresearchpress.com by 88.146.161.215 on 09/08/12
For personal use only.

Fig. 1. Potential oscillatory profile of Ferroin – cyanoacetic acid with (*a*) graphite, (*b*) platinum, (*c*) glassy carbon, and (*d*) Br^- selective electrodes. The concentrations of the various constituents are [S] = 0.2 M; [H_2SO_4] = 1.0 M; [$KBrO_3$] = 0.08 M; [ferroin] = 0.005 M.



Can. J. Chem. Downloaded from www.nrcresearchpress.com by 88.146.161.215 on 09/08/12
For personal use only.

© 1997 NRC Canada

Can. J. Chem. Downloaded from www.nrcresearchpress.com by 88.146.161.215 on 09/08/12
For personal use only.

Table 2. Oscillatory characteristics of the Ferroin system (temperature = 30 ± 0.1°C).

Substrate	[S] M	[H_2SO_4] M	[$KBrO_3$] M	[Ferroin] M	Electrode	Initial potential (V) Base	Initial potential (V) Peak	Amplitude (mV)	Number of oscillations	Duration (min)	Average time per oscillation (min)
Cyano acetic acid	0.2	1.0	0.08	0.005	Graphite	0.950	1.090	140	40	20.0	0.50
					Platinum	0.790	0.950	160	40	20.0	0.50
					Glassy carbon	0.780	0.920	140	40	20.0	0.50
					Br^- selective electrode	0.073	0.105	32	40	20.0	0.50
Syringic acid	0.027	0.50	0.05	0.0007	Graphite	0.650	0.900	250	7	5.7	0.68
						0.930	0.980	50	3	5.7–7	
					Platinum	0.350	0.800	450	7	5.7	0.68
						0.750	0.810	60	3	5.7–7	
Vanillin	0.03	0.65	1.0	0.001	Graphite	0.750	0.810	60	13	1.5	0.12
					Platinum	0.610	0.780	170	13	1.5	0.12

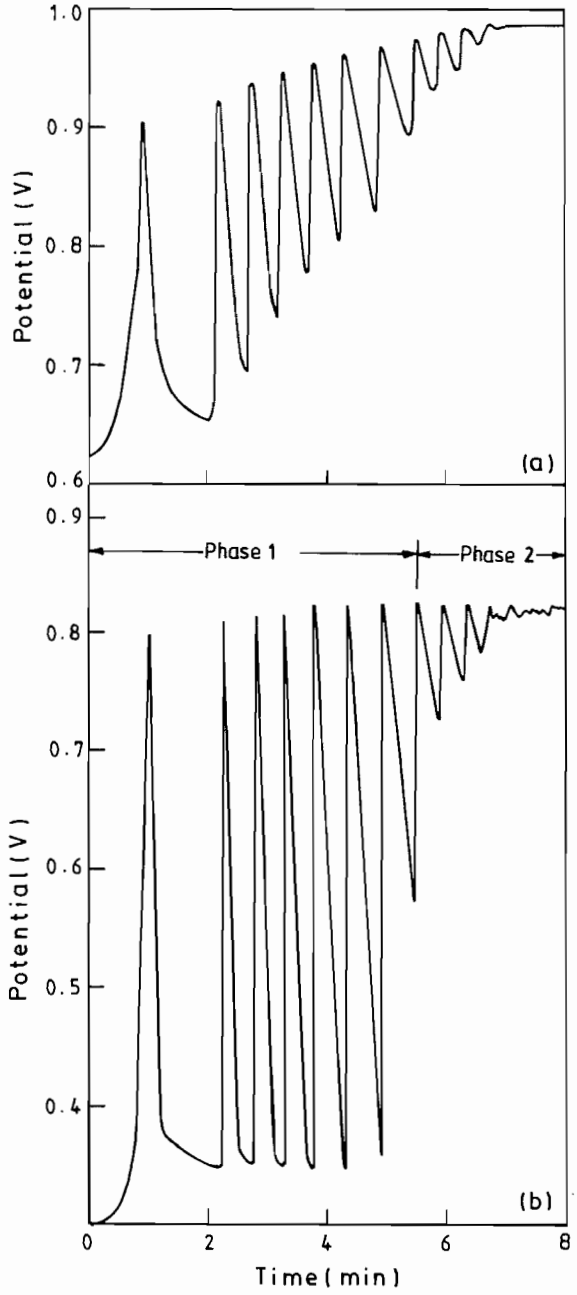
Table 3. Oscillatory characteristics of the Mn(II) system (temperature = 30 ± 0.1°C).

Substrate	[S] M	[H_2SO_4] M	[$KBrO_3$] M	[Mn(II)] M	Electrode	Initial potential (V) Base	Initial potential (V) Peak	Amplitude (mV)	Number of oscillations	Duration (min)	Average time per oscillation (min)
Syringic acid	0.02	0.34	0.085	0.017	Graphite	0.930	1.000	70	11	5.2	0.5
					Platinum	0.250	0.650	400	16	6.3	0.4
Methylacetoacetate	0.06	1.0	0.15	0.010	Graphite	1.105	1.110	5	46	7.6	0.17
					Platinum	0.800	0.950	150	46	7.6	0.17
					Glassy carbon	0.410	0.760	350	46	7.6	0.17
					Br^- selective electrode	0.050	0.065	15	46	7.6	0.17
Malonic acid	0.05	1.0	0.05	0.010	Graphite	1.050	1.100	50	73	42.0	0.57
					Platinum	0.650	0.980	330	73	42.0	0.57
					Glassy carbon	0.480	0.750	270	73	42.0	0.57
					Br^- selective electrode	1.110	0.125	15	73	42.0	0.57
Vanillin	0.03	0.65	1.0	0.02	Graphite	0.780	0.790	10	7	1.2	0.17
						1.100	1.150	50	3	1.2–5	1.27
					Platinum	0.630	0.730	100	7	1.2	0.17
						0.875	0.975	100	3	1.2–5	1.27
					Glassy carbon	0.610	0.650	40	7	1.2	0.17
						0.800	1.020	220	3	1.2–5	1.27

© 1997 NRC Canada

Can. J. Chem. Downloaded from www.nrcresearchpress.com by 88.146.161.215 on 09/08/12
For personal use only.

Fig. 2. Potential oscillatory profile of Ferroin – syringic acid with (*a*) graphite and (*b*) platinum electrodes. The concentrations of the various constituents are [S] = 0.027 M; [H_2SO_4] = 0.5 M; [$KBrO_3$] = 0.05 M; [ferroin] = 0.0007 M.



potassium bromate. The potential oscillatory profile was recorded using different working electrodes, namely, graphite, platinum, glassy carbon, and bromide ion selective electrodes. The reference electrode was a saturated calomel electrode (SCE).

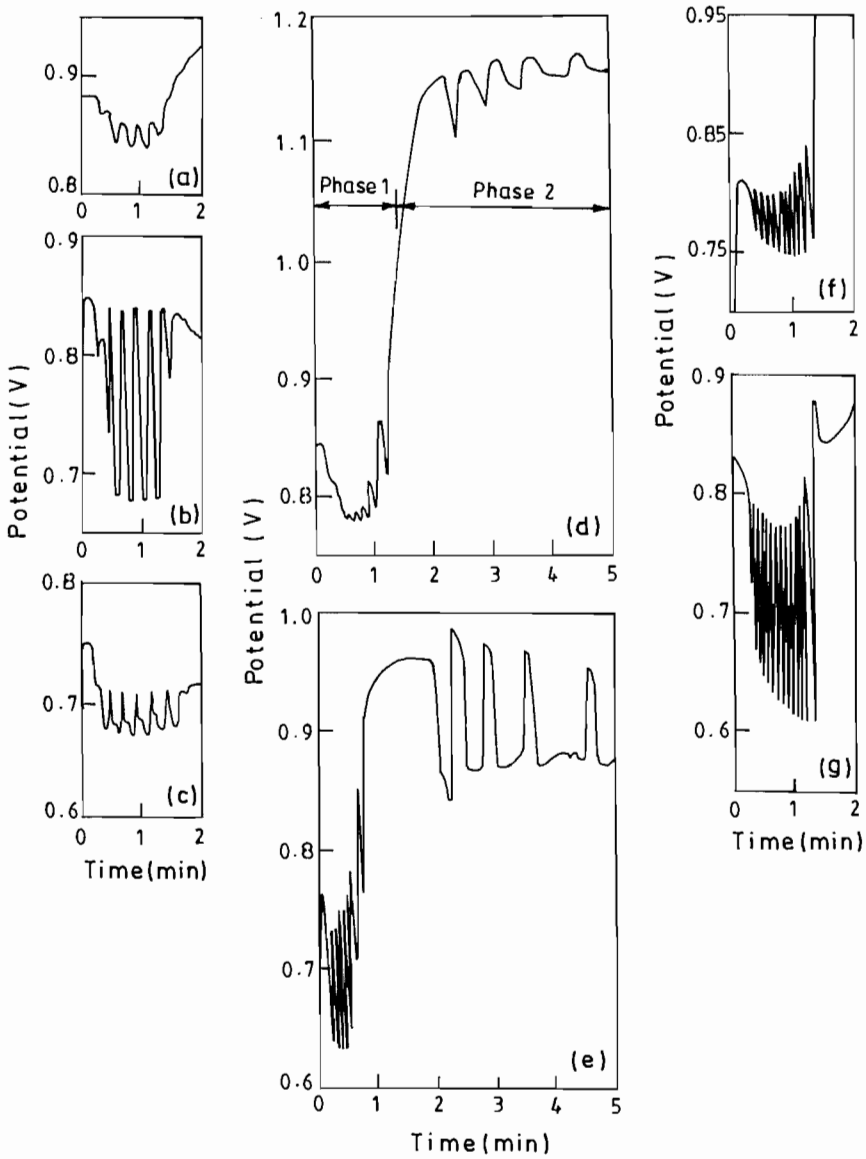
The values of the exchange current density with different electrodes and redox couples at a definite concentration (0.015 M each) and H_2SO_4 (1 M) were determined by obtaining Tafel plots using the electrochemical system BAS 100, USA.

Table 4. Oscillatory characteristics of the Ce(IV) system (temperature = 30 ± 0.1°C).

Substrate	[S] M	[H_2SO_4] M	[$KBrO_3$] M	[Ce(IV)] M	Electrode	Initial potential (V)		Amplitude (mV)	Number of oscillations	Duration (min)	Average time per oscillation (min)
						Base	Peak				
Malonic acid (3.1)	0.16	1.8	0.1	0.002	Graphite	1.140	1.150	10	90	20.1	0.21
					Platinum	1.020	1.100	80	90	20.1	0.21
					Glassy carbon	0.950	1.050	100	90	20.1	0.21
Malonic acid (3.2)	0.05	2.0	0.05	0.005	Graphite	1.190	1.200	10	38	41.5	1.1
					Platinum	1.070	1.110	40	38	41.5	1.1
					Glassy carbon	1.075	1.110	35	38	41.5	1.1
Citric acid	0.05	1.8	0.05	0.004	Graphite	1.260	1.280	20	28	72.0	2.6
					Platinum	1.170	1.220	50	28	72.0	2.6
					Glassy carbon	0.945	1.015	90	28	72.0	2.6

© 1997 NRC Canada

Fig. 3. Potential oscillatory profile of vanillin. The concentrations of the various constituents are [S] = 0.02 M; [H_2SO_4] = 0.6 M; [$KBrO_3$] = 0.09 M for (*a*), (*b*), (*c*); [S] = 0.03 M; [H_2SO_4] = 0.65 M; [$KBrO_3$] = 1.0 M; [Mn(II)] = 0.02 M for (*d*), (*e*); [S] = 0.03 M; [H_2SO_4] = 0.65 M; [$KBrO_3$] = 1.0 M; [ferroin] = 0.001 M for (*f*), (*g*). The oscillatory profile (*a*), (*d*), (*f*) graphite; (*b*), (*e*), (*g*) platinum; and (*c*) glassy carbon.



Results and discussion

(A) Oscillatory potential profile

The potential range of the oscillatory profile recorded using different working electrodes has a bearing on the E° value of the redox couple to which that particular electrode is responding. The values of the exchange current density for various electrode processes cover a wide range, from 10^{-18} to 10^{-2} A/cm^2. If the value of the exchange current density is lower than 10^{-7} A/cm^2, the potential of the electrode process cannot be attained and an alternative process capable of sustaining a greater current density assumes control of the electrode potential (14). The E° values of the different redox couples involved in the study are presented in Table 1.

The potential range of the oscillations is an index of the redox couple mainly controlling the oscillatory potential profile. The E° values of the redox couples (Table 1) of the ions of manganese and cerium are relatively large and comparable to that involving HOBr. It should therefore be expected that the peak potential values of the oscillations of the uncatalyzed bromate system should reach those observed in the catalyzed system if the redox couple involving HOBr contributed to the observed potential. However, the highest peak potential recorded in the uncatalyzed system is less than 1 V (vs. SCE) (15) whereas the peak potential in the catalyzed system reaches values larger than 1 V (vs. SCE). The peak potential value of the catalyzed system is higher than that of the uncatalyzed bromate system by at least 200 mV. It would therefore

© 1997 NRC Canada

Can. J. Chem. Downloaded from www.nrcresearchpress.com by 88.146.161.215 on 09/08/12
For personal use only.

Can. J. Chem. Downloaded from www.nrcresearchpress.com by 88.146.161.215 on 09/08/12
For personal use only.

Fig. 4. Potential oscillatory profile of Mn(II) – syringic acid system with (*a*) graphite and (*b*) platinum electrodes. The concentrations of the various constituents are [S] = 0.02 M; [H_2SO_4] = 0.34 M; [$KBrO_3$] = 0.085 M; [Mn(II)] = 0.017 M.

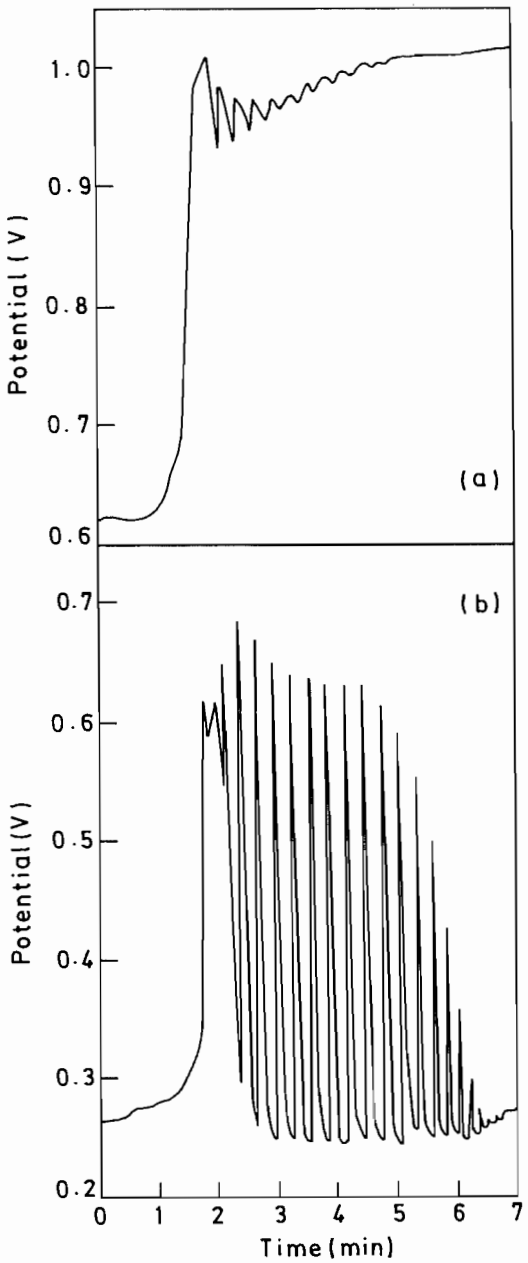
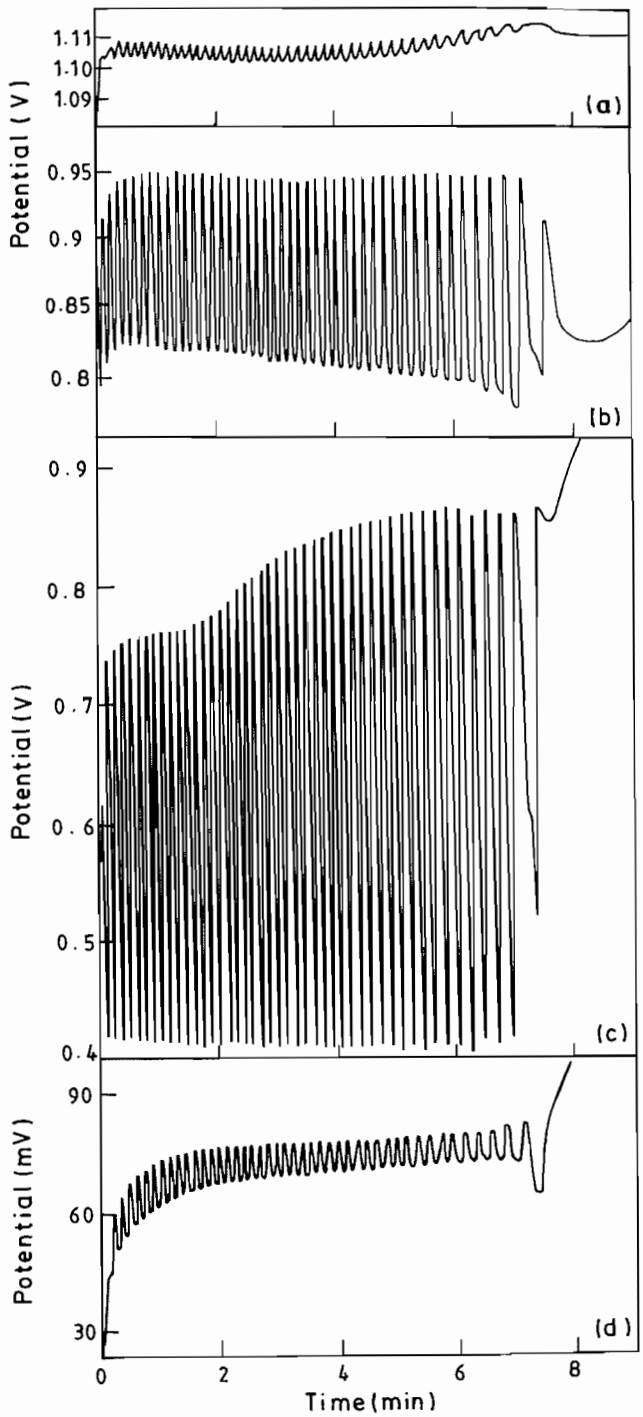


Fig. 5. Potential oscillatory profile of Mn(II) – methylacetoacetate system with (*a*) graphite, (*b*) platinum, (*c*) glassy carbon, and (*d*) Br^- selective electrodes. The concentrations of the various constituents are [S] = 0.06 M; [H_2SO_4] = 1.0 M; [$KBrO_3$] = 0.15 M; [Mn(II)] = 0.01 M.



be logical not to consider contributions to the potential from a redox reaction involving HOBr. It is also well known (16) that the concentration of HOBr in a medium containing 1 M H_2SO_4 would be smaller than 10^{-7} M. The equilibrium constant for the reaction $Br_2 + H_2O \rightleftharpoons H^+ + Br^- + HOBr$ is 7.2×10^{-9} at 298 K. A species existing in solution in such low concentration can hardly contribute to the potential of the electrode system. Likewise, the concentration of $HBrO_2$ in solution would be too insignificant to contribute to the potential. Thus the contribution from the Br_2/Br^- redox couple with its relatively lower value of $E°$ has to be considered as most significant in the uncatalyzed system. However, the catalyzed oscillatory system should be discussed by taking into account the role of the metal ion redox couple in addition to Br_2/Br^-.

The results obtained with Ferroin, Mn(II), and Ce(III) with different organic substrates employing graphite, platinum,

© 1997 NRC Canada

Table 5. Value of the exchange current density. $[H_2SO_4]$ = 1.0 M; [redox couple] = 0.01 5 M each.

Redox couple	Electrode	Exchange current density A/cm^2
Br_2, Br^-	Graphite	5×10^{-6}
	Platinum	1×10^{-5}
	Glassy carbon	2×10^{-4}
Ce(IV), Ce(III)	Graphite	2.5×10^{-4}
	Platinum	5×10^{-5}
	Glassy carbon	2×10^{-6}
Mn(III), Mn(II)	Graphite	5.6×10^{-5}
	Platinum	1.0×10^{-5}
	Glassy carbon	1.3×10^{-5}
Ferrin, Ferroin	Graphite	9×10^{-5}
	Platinum	1×10^{-3}
	Glassy carbon	8×10^{-5}

glassy carbon, and bromide selective electrodes are presented in Tables 2–4.

Ferroin system

It is observed from the oscillatory profile of cyanoacetic acid (Fig. 1) that the potential range with a graphite electrode is the highest (0.95–1.09 V vs. SCE), indicative of oscillations in [Ferrin]/[Ferroin] exclusively. However, the potential range with platinum (0.79–0.95 V) and glassy carbon is lower, indicative of predominant control of potential by [Ferrin]/[Ferroin] and some contribution to the potential by $[Br_2]/[Br^-]$.

The oscillatory profile of syringic acid (Fig. 2) under the concentration conditions indicated in Table 2 is characterized by a dual behaviour. The potential range of the oscillatory profile recorded employing a platinum electrode indicates that the high-amplitude oscillations in Phase 1 are under mixed control of potential by both redox couples, namely, Ferrin/Ferroin and Br_2/Br^-. The small-amplitude oscillations in Phase 2 are mainly due to the Ferrin/Ferroin redox couple. The oscillations recorded with the graphite electrode are controlled by the Ferrin/Ferroin redox couple, predominantly in Phase 1 and exclusively in Phase 2. It is also interesting to note that the oscillations of both profiles in Phase 2 are of almost the same amplitude.

The potential range of oscillations in the vanillin system with the platinum working electrode is 0.610–0.780 V. This is indicative of oscillations predominantly in Br_2/Br^- even though it is a Ferroin-catalyzed system. The potential range with the graphite electrode is 0.75–0.81 V. Such behaviour establishes the fact that under the concentration conditions employed the system behaves as an uncatalyzed bromate oscillator, presumably because of considerable buildup of bromine due to the high reactivity of the substrate. Under these conditions the graphite electrode registers oscillations in $[Br_2]$. This is further supported by the fact that in the catalyzed (Fig. 3*f* and 3*g*) and uncatalyzed bromate systems (Fig. 3*a*, *b* and *c*), with vanillin as the substrate, the potential ranges of the oscillations are almost the same individually for the platinum and graphite electrodes.

Mn(II) system

The concentration conditions employed for the Mn(II) system with syringic acid as the substrate are presented in Table 3. The oscillatory profile with the platinum working electrode is characterized by 11 large-amplitude oscillations (400 mV) in the potential range 0.25–0.65 V followed by 5 damped oscillations for the subsequent 1.2 min (Fig. 4). This indicates that the platinum working electrode is mainly responsive towards Br_2/Br^-. On the other hand the small-amplitude oscillations (11 oscillations in 5 min) with the graphite electrode in the range 0.93–1.0 V are indicative of exclusive control by the metal ion redox couple. It is noteworthy that the graphite electrode does not sense beyond the 11th oscillation at the 5th minute.

The concentration condition with methylacetoacetate is given in Table 3. The oscillatory profile (Fig. 5) indicates that the small-amplitude oscillations in the range 1.105–1.110 V are characteristic of oscillations in [Mn(III)]/[Mn(II)]. The potential range of oscillations with the platinum electrode is 0.8–0.95 V, indicative of mixed control of potential by both redox couples, namely, Mn(III)/Mn(II) and Br_2/Br^-. On the other hand the potential profile with the glassy carbon electrode is characterized by large-amplitude oscillations in the range 0.41–0.86 V. Such behaviour indicates that the glassy carbon electrode is more sensitive to oscillations in $[Br_2]$ than is the platinum electrode, and the buildup of bromine is to an optimum level.

The concentration conditions employed with malonic acid as the substrate are presented in Table 3 and Fig. 6. The response of the graphite electrode in the malonic acid system is similar to that with methylacetoacetate as the substrate. The potential range of oscillations with the platinum electrode (0.65–0.98 V) is indicative of mixed control by both redox couples. However, glassy carbon is responsive mainly to $[Br_2]$, as indicated by the potential range (0.48–0.75 V).

The potential oscillatory profile (Fig. 3*d*, *e*) recorded with the graphite electrode in the Mn(II)–vanillin system is characterized by oscillations in Phase 1 and Phase 2 separated by about 300 mV. The potential range of oscillations in Phase 1 (0.780–0.800 V) matches with the oscillatory phase in the Ferroin – vanillin system and is characteristic of $[Br_2]$ oscillation. The profile in Phase 2 (1.130–1.160 V) represents oscillations in [Mn(III)]/[Mn(II)]. The oscillatory profile recorded simultaneously with the platinum electrode is also characterized by Phase 1 and Phase 2. However, the oscillations in Phase 1 and Phase 2 are of larger amplitude. It is interesting to note that, with the glassy carbon electrode, although the amplitude of the oscillation in Phase 1 is almost of the same magnitude as that recorded with the graphite electrode, the amplitude of the oscillations in Phase 2 are much larger, indicating better sensitivity of the glassy carbon electrode towards bromine.

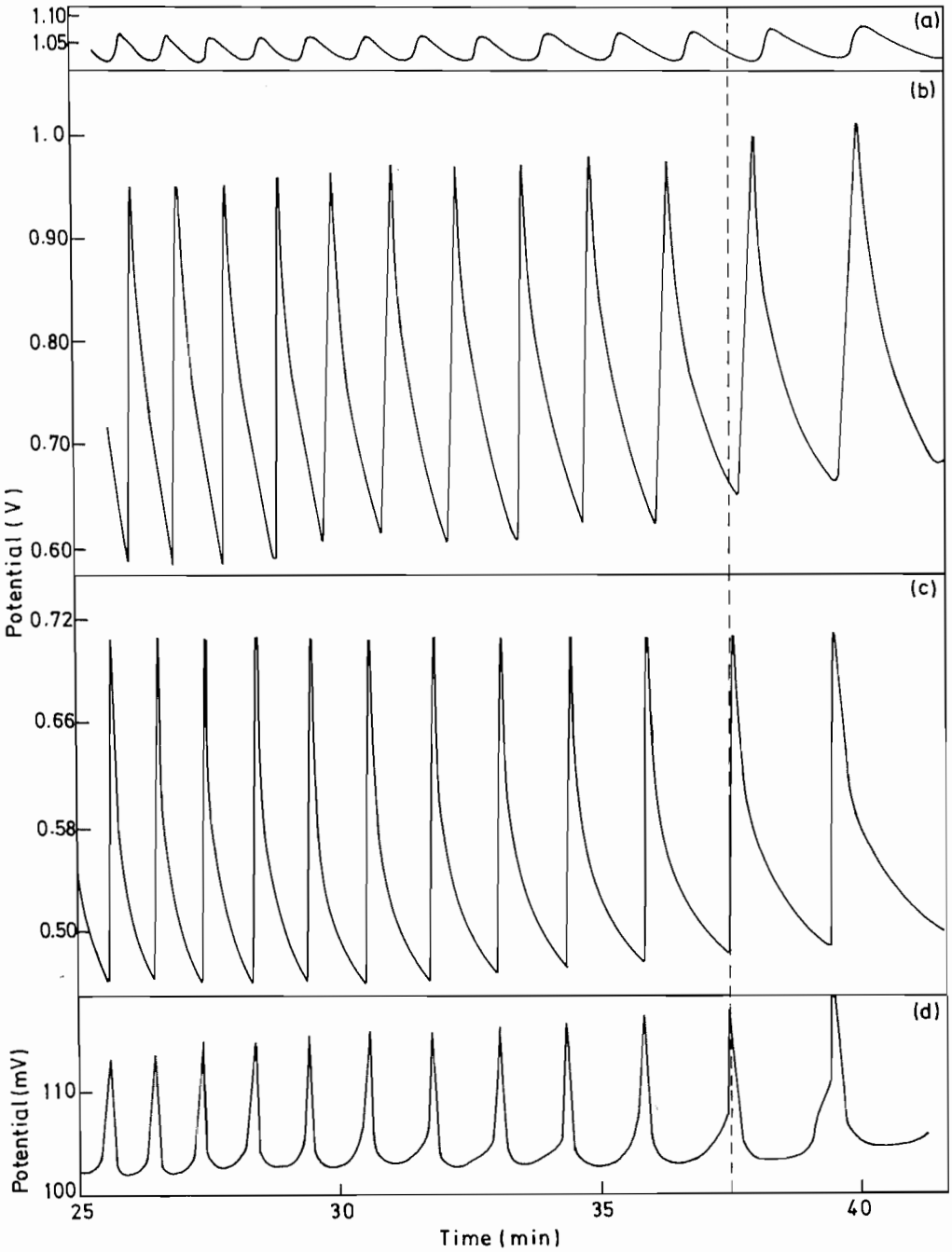
Ce(III) system

The malonic acid system has been studied under two different concentration conditions. The oscillatory profile (Fig. 7) obtained under the concentration condition 3.1 (Table 4) shows that with a platinum electrode the system oscillates in the potential range 1.02–1.10 V indicative of predominant control of metal ion at the initial stage. The potential profile with the graphite electrode indicates exclusive control of

© 1997 NRC Canada

Can. J. Chem. Downloaded from www.nrcresearchpress.com by 88.146.161.215 on 09/08/12
For personal use only.

Fig. 6. Potential oscillatory profile of Mn(II) – malonic acid system with (*a*) graphite, (*b*) platinum, (*c*) glassy carbon, and (*d*) Br^- selective electrodes. The concentrations of the various constituents are [S] = 0.05 M; [H_2SO_4] = 1.0 M; [$KBrO_3$] = 0.05 M; [Mn(II)] = 0.01 M.



potential by the metal ion redox couple. It is interesting to note that initially the amplitude is very small and it increases gradually with the progress of the reaction. The amplitude of oscillation with the glassy carbon electrode is of considerable magnitude even in the beginning and there is a further increase in the amplitude simultaneously with a lowering of the potential range, indicating that the prevailing concentration of bromine gradually increases with the progress of the reaction.

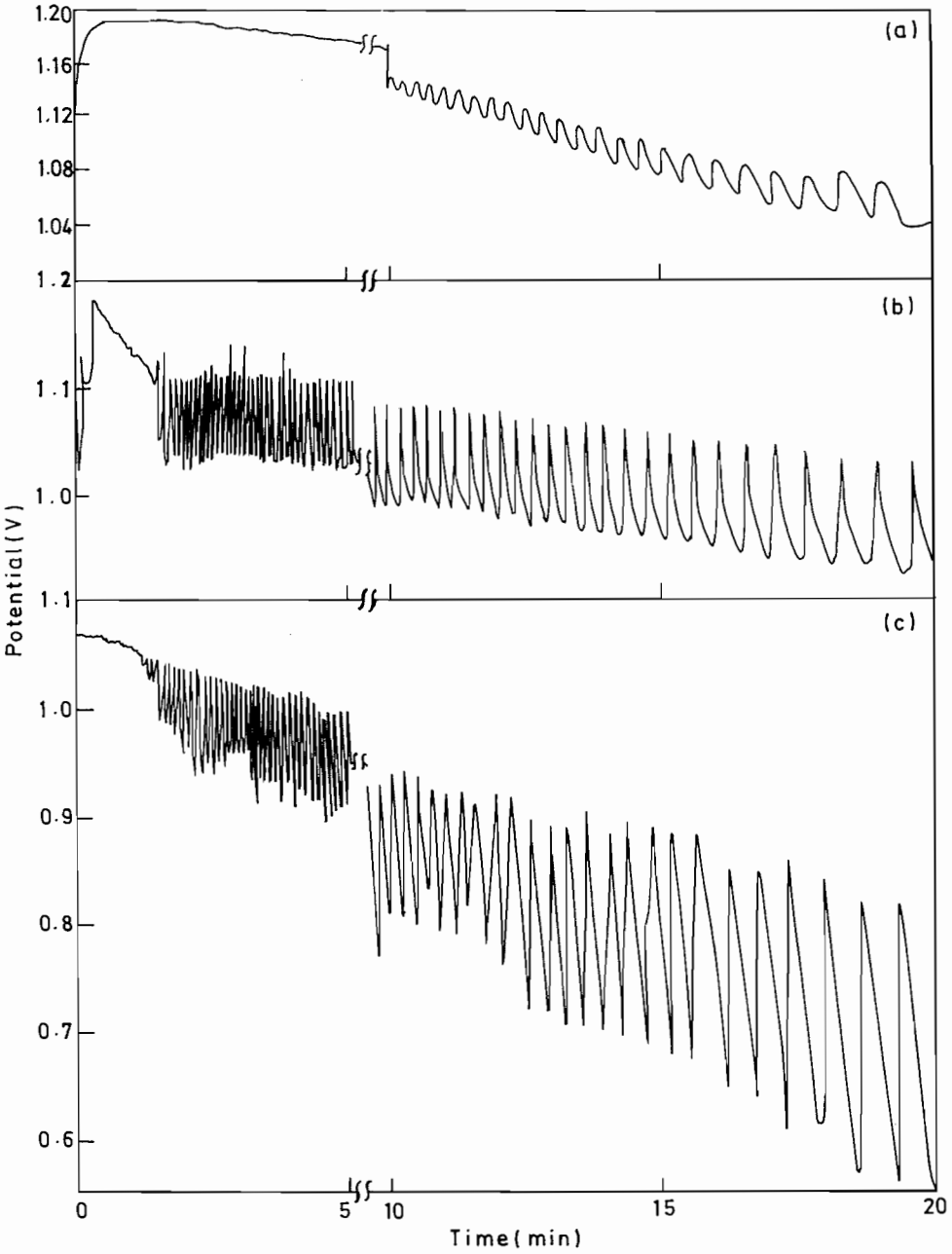
The oscillatory parameters corresponding to the concentration conditions (3.2) given in Table 4 establish that with all three electrodes the oscillatory profile corresponds to change in [Ce(IV)]/[Ce(III)]. This is presumably due to a relatively large concentration of Ce(IV) (5×10^{-3} M) and the high ratio of bromate to substrate (1:1).

The concentration conditions with citric acid as the substrate are also given in Table 4. The potential range is indicative of an exclusive metal ion control with the graphite as well as the platinum electrode. However, an amplitude of 90 mV in the potential range 0.875–0.965 V in the case of the glassy carbon electrode indicates oscillations in the [Br_2]/[Br^-] redox couple as well, especially towards the end of the reaction.

© 1997 NRC Canada

Can. J. Chem. Downloaded from www.nrcresearchpress.com by 88.146.161.215 on 09/08/12
For personal use only.

Fig. 7. Potential oscillatory profile of Ce(IV) – malonic acid system with (*a*) graphite, (*b*) platinum, and (*c*) glassy carbon electrodes. The concentrations of the various constituents are [S] = 0.16 M; [H_2SO_4] = 1.8 M; [$KBrO_3$] = 0.1 M; [Ce(IV)] = 0.002 M.



Can. J. Chem. Downloaded from www.nrcresearchpress.com by 88.146.161.215 on 09/08/12
For personal use only.

(B) Potential response of the different electrodes

These oscillatory systems are characterized by periodic change in the concentration ratio of the metal ion redox couple as well as that of Br_2/Br^-. The formation and consumption of Br_2,Br^- as well as the oxidized and reduced form of the metal ion redox couple can be represented by the following individual steps involved in the overall reaction (17).

Sequence 1

[1.1] $HBrO_2 + Br^- + H^+ \rightleftharpoons 2\,HOBr$
[1.2] $HOBr + Br^- + H^+ \rightleftharpoons Br_2 + H_2O$

Sequence 2

[2.1] $HBrO_2 + BrO_3^- + H^+ \rightleftharpoons 2BrO_2^{\cdot} + H_2O$
[2.2] $BrO_2^{\cdot} + M^{n+} + H^+ \rightleftharpoons M^{(n+1)+} + HBrO_2$

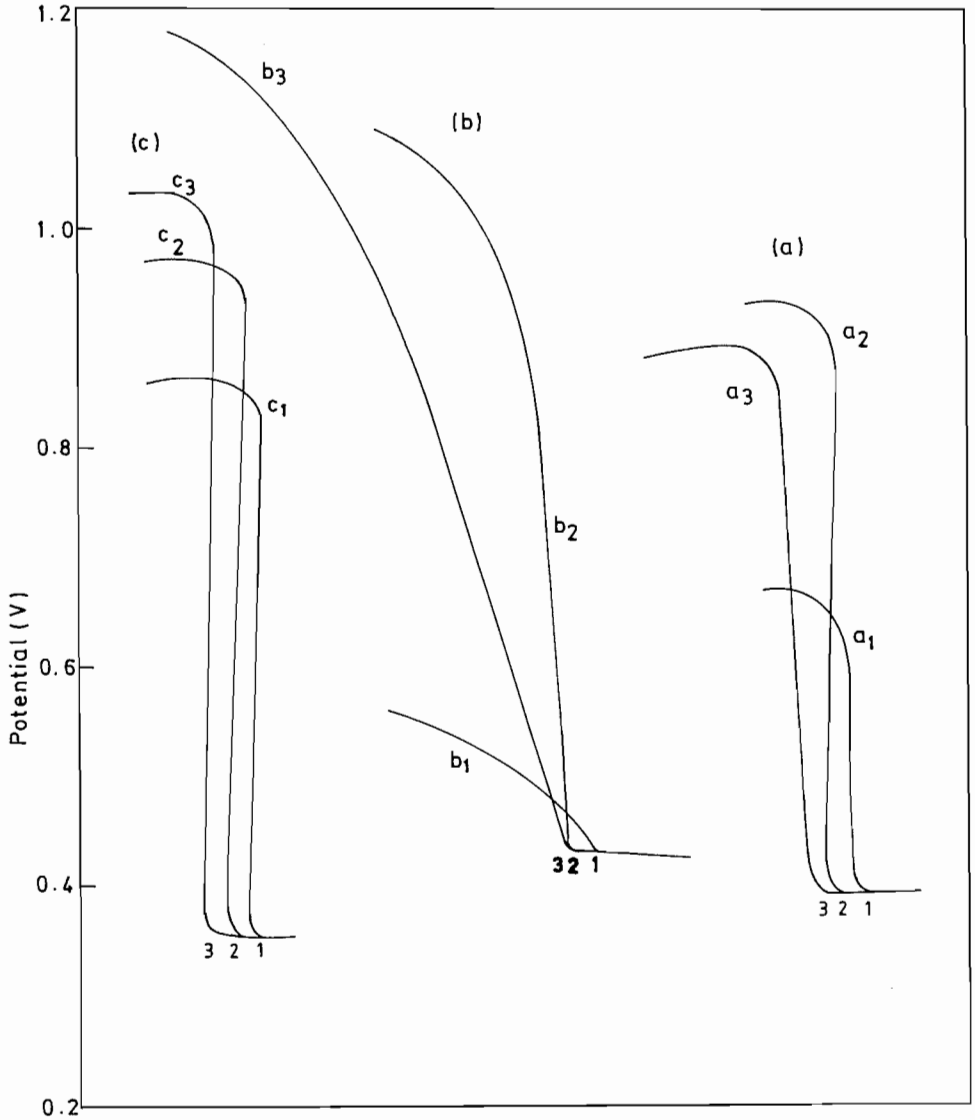
Sequence 3

[3.1] $S + Br_2 \rightleftharpoons Br.S + Br^- + H^+$
[3.2] $S + M^{(n+1)+} \rightleftharpoons M^{n+} + Product$
[3.3] $Br.S + M^{(n+1)+} \rightleftharpoons M^{n+} + Br^- + Product$

Any difference in the response of the working electrode

© 1997 NRC Canada

Fig. 8. The potential response of the working electrode immersed in 0.1 M sulphuric acid with (*a*) platinum, (*b*) graphite, and (*c*) glassy carbon electrodes. The concentration, of the redox couples included are (1) $[Br_2] = [Br^-] = 1 \times 10^{-4}$ M; (2) [Ce(III)] = [Ce(IV)] = 0.001 M; and (3) [Mn(II)] = [Mn(III)] = 0.01 M.



employed to the two redox systems would be manifested as a shift in the position of the peak value of the potential oscillatory profile.

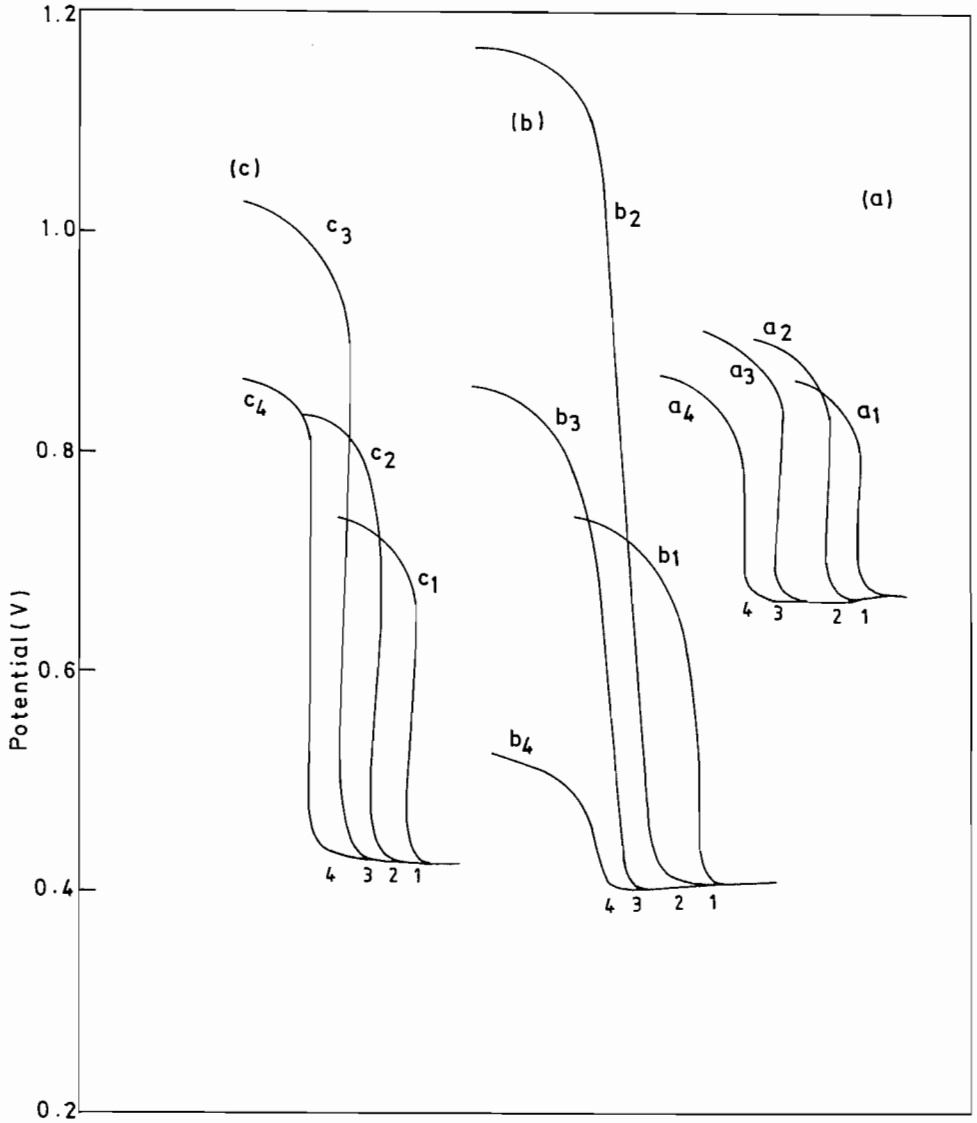
The oscillatory profiles recorded simultaneously in the Mn(II) – malonic acid system employing graphite, platinum, glassy carbon, and Br^- selective electrodes are presented in Fig. 6. It is observed that the peak of the oscillatory profile with the glassy carbon electrode corresponding to maximum $[Br_2]$ almost coincides with the peak of the Br^- profile corresponding to low $[Br^-]$. There is a time lag before the oscillatory potential profile with the platinum electrode reaches the peak value. Such a time lag is a consequence of the fact that the platinum electrode responds to both redox couples, namely, Mn(III), Mn(II) and Br_2, Br^-. Further, the peak value with the graphite electrode is reached with an additional time lag and the response of the graphite electrode is exclusively towards [Mn(III)]/[Mn(II)] under these conditions. Such behaviour is also observed in the Ferroin system with cyanoacetic acid as the substrate (Fig. 1).

The experimental results obtained in oscillatory systems employing different metal ions and substrates establish that the oscillatory profiles recorded simultaneously differ from each other in many of their oscillatory characteristics, including a phase shift. Such behaviour is a direct consequence of the response of the working electrodes to the different redox couples involved. The response of a working electrode towards any redox couple depends upon the value of the exchange current densities and concentration. For this purpose the exchange current densities of Br_2/Br^-, Mn(III)/Mn(II), Ce(IV)/Ce(III), and Ferrin/Ferroin have been determined for each working electrode (platinum, graphite, and glassy carbon) in 1 M sulphuric acid and 0.015 M of the oxidized as well as the reduced species (using BAS 100, USA). The values of the exchange current density are given in Table 5. Thus the

Can. J. Chem. Downloaded from www.nrcresearchpress.com by 88.146.161.215 on 09/08/12
For personal use only.

© 1997 NRC Canada

Fig. 9. The potential response of the working electrode immersed in 0.05 M potassium bromate with (*a*) platinum, (*b*) graphite, and (*c*) glassy carbon electrodes. The concentrations of the various species included are (1) $[H^+]$ = 0.1 M; (2) $[H^+]$ = 0.1 M and Ce(III) = 0.002 M; (3) $[H^+]$ = 0.1 M and Mn(II) = 0.01 M; and (4) $[H^+]$ = 0.1 M and [ferroin] = 0.001 M.



better response of the glassy carbon electrode towards the Br_2/Br^- redox couple with its high value of exchange current density (2×10^{-4} A/cm^2) and the poor response of the graphite electrode with its low value of exchange current density (5×10^{-6} A/cm^2) are reflected in the oscillatory profiles obtained with these electrodes.

The response of the electrodes to the different individual redox systems was determined by the following procedure. In one set of experiments the platinum electrode was dipped in a solution of potassium bromate (0.05 M). The variation of the potential of each working electrode (vs. SCE) was recorded after including different species of known concentration in the experimental solution. In another set of experiments the solution initially contained sulphuric acid (0.1 M) and the variation in potential was followed by including different redox couples. The potential profiles are presented in Figs. 8 and 9.

The following general conclusions can be drawn from these experimental results. The response of the platinum electrode is good towards Br_2/Br^-, Mn(III)/Mn(II), and Ce(IV)/Ce(III). However, the final potential value reached with Br_2/Br^- is of lower magnitude. The response of the glassy carbon electrode is also good. Further, the response of the glassy carbon electrode extends over a larger range of potential than that of platinum. On the contrary, the response of the graphite electrode towards $[Br_2]/[Br^-]$ is poor and it shows a better response towards metal ion redox couples, especially Ce(IV)/Ce(III).

Conclusion

The oscillatory profiles recorded simultaneously with different electrodes differ in their oscillatory characteristics especially with respect to amplitude and potential range. Such a

© 1997 NRC Canada

Can. J. Chem. Downloaded from www.nrcresearchpress.com by 88.146.161.215 on 09/08/12
For personal use only.

difference is caused by the fact that the electrodes respond differently to Br_2/Br^- and metal ion redox couples. The difference in response is obvious from the potential developed at each electrode in the presence of the individual redox couples. The potential response of the electrode depends upon the relative magnitude of the exchange current density of the redox system.

References

1. R.J. Field and M. Burger (*Editors*). Oscillations and travelling waves in chemical systems. Vol. 118. John Wiley and Sons, New York. 1985.
2. K. Bar Eli and S. Haddad. J. Phys. Chem. **83**, 2952 (1979).
3. A. Mittal, P.K.R. Nair, and K. Srinivasulu. Int. J. Chem. Kinet. **13**, 321 (1981).
4. B.P. Belousov. Radiats. Med., Moscow. 1959. p. 145.
5. A.M. Zhabotinsky. Dokl. Akad. Nauk SSSR, **157**, 392 (1964).
6. V. Jayalakshmi and R. Ramaswamy. Int. J. Chem. Kinet. **27**, 197 (1995).
7. P.V. Lalitha and R. Ramaswamy. React. Kinet. Catal. Lett. **51**, 431 (1993).
8. V. Jayalakshmi and R. Ramaswamy. Bull. Electrochem. **11**, 153 (1995).
9. R. Ramaswamy, S. Jaya, and N. Ganapathisubramanian. Proc. Indian Acad. Sci. **89**, 65 (1980).
10. L. Kuhnert and K.W. Pehl. Chem. Phys. Lett. **84**, 159 (1981).
11. P.V. Lalitha, P. Sambasiva Rao, and R. Ramaswamy. Curr. Sci. **61**, 352 (1991).
12. P.V. Lalitha and R. Ramaswamy. J. Phys. Chem. **96**, 7679 (1992).
13. A.S. Kovalenko and L.P. Tikhonova. Teor. Eksp. Khim. **16**, 317 (1979).
14. E.C. Potter. Electrochemistry, principles and application. Cleaver–Hume Press, London. 1956. p. 130.
15. R. Ramaswamy and M. Krishnaratnam. Indian J. Tech. **24**, 510 (1986).
16. F.A. Cotton and F.R.S.G. Wilkinson. Advanced inorganic chemistry. John Wiley and Sons, New York. 1966. pp. 568–569.
17. R.M. Noyes, R.J. Field, and E. Koros. J. Am. Chem. Soc. **94**, 1394 (1972).

Can. J. Chem. Downloaded from www.nrcresearchpress.com by 88.146.161.215 on 09/08/12
For personal use only.

© 1997 NRC Canada

Solvent structure effects on electrical conductivities of small-ion salts compared to large-ion salts in C_1–C_4 alcohols and water

Yixing Zhao and Gordon R. Freeman

Can. J. Chem. Downloaded from www.nrcresearchpress.com by 88.146.161.215 on 09/08/12
For personal use only.

Abstract: The electrical conductances of the small-ion salts LiI and $LiNO_3$ in water and C_1–C_4 alcohols were measured at different temperatures. At the concentrations used, ion association was negligible except when $\varepsilon T < 4200$ K, where ε is the relative permittivity of the solvent at temperature T. Consistent with Walden's rule, the values of $\eta\Lambda_0$ in each solvent are nearly constant as the temperature is increased; the value for LiI in each solvent is slightly higher than that for $LiNO_3$. Ion association occurs in *tert*-butanol and is more extensive for $LiNO_3$ than that for LiI; the planar NO_3^- ions fit less well than the spherical I^- ions into the packing of the rigid, spherical *tert*-butanol molecules. The effective radius of solvated ions in C_N primary alcohols increases approximately as the length of the randomly folded chain, $(N+1)^{1/2}$. For secondary alcohols this factor is somewhat too small for small-ions and too large for large tetraphenyl ions. The values of $E_{\Lambda 0}$ are close to the values of E_η in the corresponding alcohols.

Key words: electrical conductivity, large ions, small-ions, alcohols, solvent effects.

Résumé : Opérant à diverses températures, on a mesuré les conductivités électriques des sels de LiI et $LiNO_3$, à petits ions, dans l'eau ainsi que dans des alcools contenant de un à quatre carbones. Aux concentrations utilisées, l'association ionique est négligeable, excepté lorsque $\varepsilon T < 4200$ K, dans laquelle ε est la permittivité relative du solvant à la température T. En accord avec la règle de Walden, les valeurs de $\eta\Lambda_0$ dans chaque solvant sont pratiquement constantes lorsqu'on augmente la température; la valeur pour LiI dans chacun des solvants est légèrement supérieure à celle pour $LiNO_3$. Il se produit une association d'ions dans le *tert*-butanol qui est plus importante pour le $LiNO_3$ que pour le LiI; dans l'arrangement rigide des molécules de *tert*-butanol sphériques, les ions NO_3^- plans s'insèrent moins bien que les ions I^- sphériques. Les rayons effectifs des ions dans les alcools primaires en C_N augmentent, en première approximation, en fonction de la longueur de la chaîne repliée au hasard, $(N+1)^{1/2}$. Dans le cas des alcools secondaires, ce facteur est légèrement trop petit pour les petits ions et légèrement trop grand pour les gros ions du type tétraphényle. Dans les alcools correspondants, les valeurs de $E_{\Lambda 0}$ se rapprochent des valeurs de E_η.

Mots clés : conductivité électrique, ions volumineux, petits ions, alcools, effets de solvant.

[Traduit par la rédaction]

Introduction

The study of electrical conductivities of electrolytes in different solvents elucidates properties of ions and solvents (1, 2), and provides reference data for solvent effects on the mobilities of solvated electrons (3–6). For the molar conductivity Λ_0 of $LiNO_3$ in C_1–C_8 primary alcohols (4), and of the large-ion salts tetraphenylphosphonium chloride (TPPC), tetraphenylphosphonium bromide (TPPB), and sodium tetraphenylboride (STPB), in C_1–C_4 alcohols (7), it has been found that the value of $(N+1)^{1/2}\eta\Lambda_0$ is nearly constant, with about 15% decrease toward large N, where N is the number of carbon atoms in the alcohol and η is the solvent viscosity. For the separate ionic molar conductivities of the large ions (TPP^+ and TPB^-) in C_1–C_4 primary alcohols, $(N+1)^{1/2}\eta\Lambda_0$ = constant (7). The activation energies of shear viscosities of the butanols (8–10) increase from 1-butanol (19 kJ mol^{-1}) to *tert*-butanol (31 kJ mol^{-1}), whereas the activation energies of mobility of the large tetraphenyl ion salts through the butanols (mostly 20–23 kJ mol^{-1}) are relatively insensitive to the structure and packing of the molecules in the liquid butanols (7).

The value of $(N+1)^{1/2}$ represents the randomly folded chain length of an alcohol molecule, which increases the effective radius of an ion to which it adheres. Lithium nitrate contains small-ions whose sizes are smaller than those of C_1–C_4 alcohol molecules. It is expected that the solvent structure effect on the solvation and mobility of smaller-than-solvent ions will be greater than that on larger-than-solvent tetraphenyl ion salts such as TPPC, TPPB, and STPB. Therefore, it is interesting to compare the solvent structure effect on the electrical conductivities of small-ion salts with those of the large-ion salts in C_1–C_4 alcohols.

Received January 22, 1997.

Y. Zhao and G.R. Freeman.[1] Department of Chemistry, University of Alberta, Edmonton, AB T6G 2G2, Canada.

[1] Author to whom correspondence may be addressed. Telephone: (403) 492-3468. Fax: (403) 492-8231. E-mail: k.np@ualberta.ca

© 1997 NRC Canada

Can. J. Chem. Downloaded from www.nrcresearchpress.com by 88.146.161.215 on 09/08/12
For personal use only.

In the present work, the electrical conductance of lithium iodide was measured in water and C_1–C_4 alcohols at different temperatures. The electrical conductance of lithium nitrate was also remeasured in C_1–C_4 alcohols at lower salt concentrations than previously used, to minimize the ion atmosphere effect and ion association (2, 11, 12). Iodide ion has a spherical shape, and nitrate ion has a planar shape. Solvent -O-H hydrogen-bonding to the spherical I^- would not have a favored orientation, but the -O-Hs would tend to be directed toward the oxygen atoms at the corners of the triangular NO_3^-, which might strain the packing of the solvent molecules. Therefore, smaller amounts of ion pairing or clustering might be expected for iodide than for nitrate ions in alcohols, because the planar nitrate ions more easily form ion clusters or ion-pair aggregates (2).

Although there have been many studies of the conductivities of alkali halides (13) and hydrogen halides (14) in nonaqueous solvents, there are few conductivity data for LiI in C_1–C_4 alcohols except in methanol and ethanol (15).

Experimental

Lithium iodide (Aldrich, anhydrous, 99%) and lithium nitrate (Aldrich, 99.99%) were used as received. The iodide was kept under argon atmosphere in the dark to avoid oxidation of I^-.

The purification of the alcohols and the experimental techniques were described previously (7).

Results and discussion

Specific conductances of LiI and $LiNO_3$

Both salts dissolve easily in water. In alcohols, on going from methanol to butanols, both LiI and $LiNO_3$ are progressively slower to dissolve. In *tert*-butanol, LiI dissolved overnight with stirring, whereas $LiNO_3$ dissolved in about 2 h. The electrical conductances of each salt were measured at least twice in each solvent at different temperatures. The reproducibility of all the measurements at 298 K was better than ±1%.

To avoid or minimize curvature of plots of specific conductance against solute concentration, caused by the ion atmosphere effect (11) or ion association (12), low concentrations were used in the measurements. For LiI, the concentration range 0.025–0.125 mol m^{-3} was used in most measurements, except for those in water and 2-butanol, 0.1–0.5 mol m^{-3}; isobutanol, 0.0125–0.0625 mol m^{-3}. For $LiNO_3$, the concentration range used in the remeasurements in C_1–C_4 alcohols was 0.01–0.05 mol m^{-3}. For the few curved lines obtained with LiI and $LiNO_3$ in some alcohols, the measurement was repeated by using freshly prepared solutions at each temperature.

Figures 1 and 2 show the plots of the measured specific conductance (κ) against the salt concentration (C) of LiI in C_1–C_4 alcohols. On going from methanol to 1-butanol, the lines are straight; in isobutanol, the κ–C plot was slightly curved only at the highest temperature, 343 K, and in 2-butanol the line at 343 is more curved (Fig. 2). In *tert*-butanol, the lines at 318 and 328 K (Fig. 2) were so bent that the conductance values at higher concentrations actually overlapped or were lower than those at lower temperatures (299 K and 308 K).

Figure 3 shows the plots for $LiNO_3$ in propanols and iso and 2-butanols. The lines for $LiNO_3$ in 1-propanol, 2-propanol, and isobutanol are straight, except at the highest temperature (343 K) in 2-propanol and isobutanol; in 2-butanol the line is already curved at 308 K.

The ionic atmosphere effect and ion association vary inversely as the product of the relative permittivity and temperature (εT) (2, 11, 16). The value of εT at a given temperature decreases on going from methanol to butanols (Fig. 4). In methanol, ethanol, and 1-propanol εT is relatively high and the ionic atmosphere effect and ion association are negligible. However, in 2-propanol and butanols, the values of εT are lower, and the effects become significant.

In Fig. 4 the log scale is used to show the relative changes of εT with temperature in C_1–C_4 alcohols. As temperature is increased the values of εT decrease. Plots of κ against C start to bend at values of $\varepsilon T < 4200$ K, because the Coulombic attraction of the ions increases faster than the thermal agitation energy. The values of εT in *tert*-butanol are lower than those in the other alcohols, and decrease relatively rapidly with increasing temperature. Therefore, as temperature increases there is a larger increase of ion association in *tert*-butanol than in other alcohols (Fig. 2).

Another reason that ion association is more extensive in *tert*-butanol is that *tert*-butanol has rigid, globular molecules, and has the poorest ability to solvate small-ions, as we know from the optical spectra of solvated electrons in alcohols (17, 18); the energy of optical absorption of solvated electrons in *tert*-butanol is the lowest among the C_1–C_4 alcohols.

Comparing LiI and $LiNO_3$ in *tert*-butanol, the κ–C plot for LiI (Fig. 2) starts to bend at 318 K, whereas the κ–C plot for $LiNO_3$ (2) starts to bend at 299 K. This indicates that in *tert*-butanol, ion clustering of LiI is not as severe as that of $LiNO_3$. The planar NO_3^- ions fit less well than the spherical I^- ions into the packing of the rigid, spherical *tert*-butanol molecules, and more easily form ion clusters in that liquid (2).

Molar conductivities of LiI and $LiNO_3$

Table 1 lists the low concentration limits of the molar conductivities (Λ_0) of LiI and $LiNO_3$ in C_1–C_4 alcohols and water at different temperatures, along with the solvent viscosities and the relative permittivities. The measured values of molar conductivity limits of LiI and $LiNO_3$ in water, methanol, and ethanol at 298 K are close to those reported earlier (15). Λ_0 values of both LiI and $LiNO_3$ at 298 K decrease on going from water to butanols, and the values for LiI are slightly higher than those for $LiNO_3$.

The molar conductivity Λ(LiI) in *tert*-butanol at 298 K is only $0.23\Lambda_0$(LiI) in isobutanol, whereas the viscosity of *tert*-butanol is only 1.3η (isobutanol), so $\eta\Lambda$ in *tert*-butanol is $0.30\eta\Lambda_0$ in isobutanol (Table 1). Thus the value of Λ(LiI) in *tert*-butanol is not Λ_o(LiI) despite the linear κ–C plots at 299 and 308 K (Fig. 2). The values of εT in *tert*-butanol are below 4200 K (Fig. 4), so complex multiple-ion association causes the low Λ values (2).

The values of Λ(LiI) in 2- and isobutanol, and $\Lambda(LiNO_3)$ in 2-propanol and in 2- and isobutanol at the highest temperatures, were obtained from the initial slopes of the curved lines in the κ–C plots (Figs. 2 and 3); εT is <4200 K at these temperatures, so the ionic atmosphere effect and ion association are significant and these Λ values may not be the low concentration limits of molar conductivity Λ_0 (Table 1).

In water and C_1–C_4 alcohols, except *tert*-butanol, the values of $\eta\Lambda$ for LiI or $LiNO_3$ in each solvent are nearly constant as

© 1997 NRC Canada

Fig. 1. Measured specific conductances κ of LiI against concentrations *C* at different temperatures from methanol to 2-propanol, respectively. ○, 273 K; ●, 298 K; □, 308 K; ■, 313 K; △, 318 K (or 320 K in methanol); ▲, 328 K (or 330 K in methanol); ◇, 343.

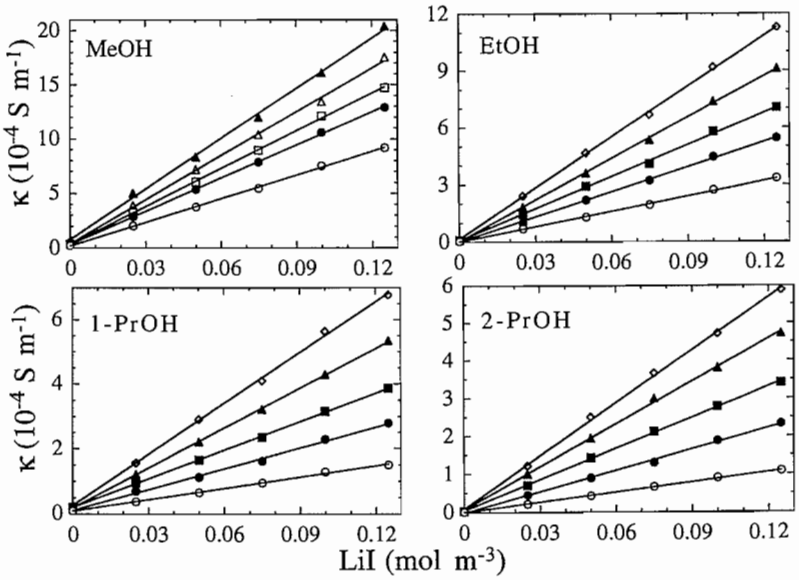
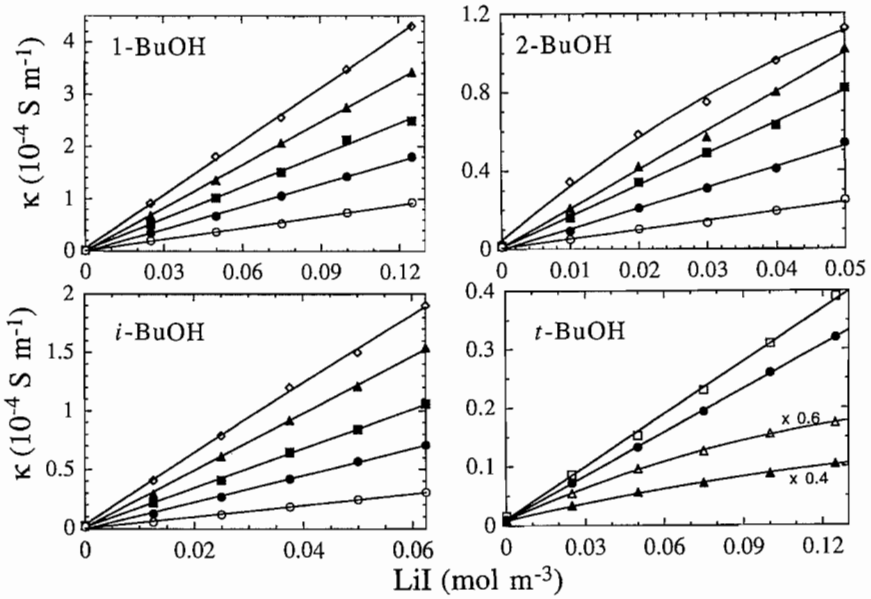


Fig. 2. Measured specific conductances κ of LiI against concentrations *C* at different temperatures in four butanols, respectively. The symbols are the same as in Fig. 1 except for ●, 299 K in *tert*-butanol.



the temperature is increased. This is consistent with Walden's rule (11). The value of ηΛ for LiI in *tert*-butanol decreases with increasing temperature due to increasing ion association. In isobutanol, ηΛ of $LiNO_3$ at 328 K is lower than the average ηΛ at other temperatures (Table 1). This indicates that the value of 20.4×10^{-4} S m^2 mol^{-1} is not $\Lambda_0(LiNO_3)$ in isobutanol at 328 K, despite the linear κ–C plot (Fig. 3).

Solvent structure effects on molar conductivities of different salts

In our previous studies of the molar conductivities of $LiNO_3$ in C_1–C_8 *n*-alcohols (4) and of large-ion salts in C_1–C_4 alcohols (7), the values $(N + 1)^{1/2}\eta\Lambda_0$ were approximately constant, where *N* is the number of carbon atoms in an alcohol molecule and $(N + 1)^{1/2}$ represents the randomly folded chain length of the alcohol. Figure 5 displays the correlations of $(N + 1)^{1/2}\eta\Lambda_0$, and $(N + 1)^{1/2}\eta\Lambda$ in *tert*-butanol, against $1/\eta$ at 298 K for the small-ion salts LiI and $LiNO_3$ (*A*), compared with those for the large-ion salts tetraphenylphosphonium bromide (TPPB) and sodium tetraphenylboride (STPB) (*B*), in C_1–C_4 alcohols. Diffusion behavior of a salt in a solvent depends on (*i*) the solvent molecular structure (4, 7), and (*ii*) the molecular shape and size of each ion (2, 7). These two factors are reflected in Figs. 5 *A* and *B*.

© 1997 NRC Canada

Can. J. Chem. Downloaded from www.nrcresearchpress.com by 88.146.161.215 on 09/08/12
For personal use only.

Can. J. Chem. Downloaded from www.nrcresearchpress.com by 88.146.161.215 on 09/08/12
For personal use only.

Fig. 3. Measured specific conductances κ of $LiNO_3$ against concentrations C at different temperatures in 1-, and 2-propanol, iso- and 2-butanol, respectively. The symbols are the same as in Fig. 1.

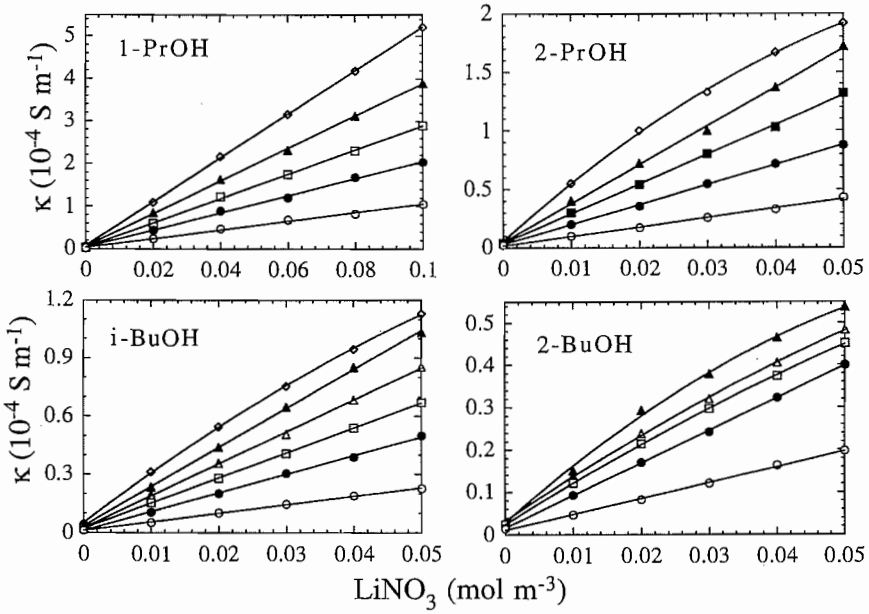
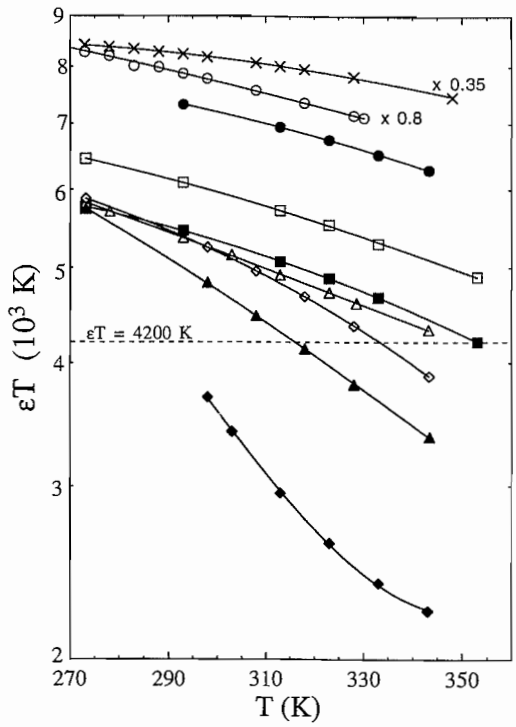
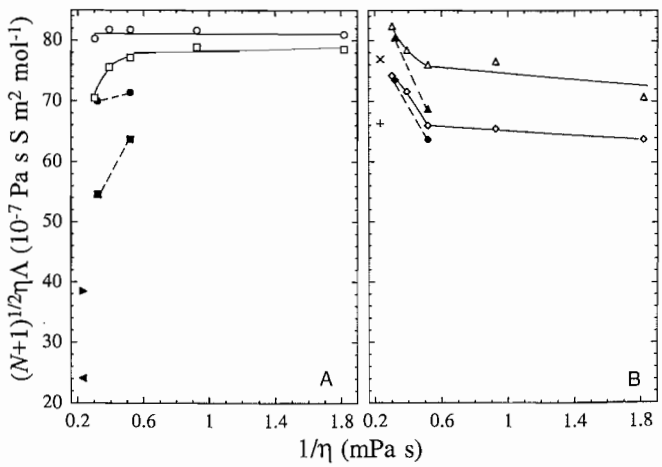


Fig. 4. The change of the product of the relative permittivity and the temperature, εT, with temperature in C_1–C_4 alcohols and water. ×, water; ○, methanol; ●, ethanol; □, 1-propanol; ■, 2-propanol; △, 1-butanol; ◇, isobutanol; ▲, 2-butanol; ◆, *tert*-butanol.



Firstly, for each salt the values of $(N + 1)^{1/2}\eta\Lambda$ in C_1–C_4 alcohols depend on the type of alcohol: primary, secondary, or tertiary. In primary *n*-alcohols, the value of $(N + 1)^{1/2}\eta\Lambda_0$ for LiI is constant at 81 ± 1 (10^{-7} Pa s S m^2 mol^{-1}) and in

Fig. 5. Correlations of $(N + 1)^{1/2}\eta\Lambda$ of salts with fluidity ($1/\eta$) of C_1–C_4 alcohols at 298 K. *A*: *Small-ion salts* LiI: ○, in 1-alcohols, ●, in 2-alcohols, and ◀, in *tert*-butanol; $LiNO_3$ □, in 1-alcohols, ■, in 2-alcohols, and ▶, in *tert*-butanol. *B*: *Large-ion salts* TPPB △, in 1-alcohols, ▲, in 2-alcohols, and ×, in *tert*-butanol; STPB ◇, in 1-alcohols, ◆, in 2-alcohols, and +, in *tert*-butanol. Decreasing $1/\eta$: primary alcohols (solid lines) methanol, ethanol, 1-propanol, 1-butanol, isobutanol; secondary alcohols (broken lines) 2-propanol, 2-butanol.



isobutanol the value is 80, and for $LiNO_3$ in *n*-C_1–C_4 alcohols the value is also constant at 78 ± 1 (Fig. 5*A*).

In the secondary alcohols, for LiI the average value of $(N + 1)^{1/2}\eta\Lambda_0$ in the two secondary alcohols is 12% lower than that in primary alcohols, because the secondary alcohol contains a nonrandom permanent fold and the factor $(N + 1)^{1/2}$ underestimates the effective chain length of the molecules ligated to the ion. The value difference between secondary and primary alcohols for $LiNO_3$ is even larger than that for LiI.

© 1997 NRC Canada

Can. J. Chem. Downloaded from www.nrcresearchpress.com by 88.146.161.215 on 09/08/12
For personal use only.

Furthermore, the decrease on going from 2-propanol to 2-butanol is greater for the nitrate than for the iodide (Fig. 5). Thus the normalization factor $(N + 1)^{1/2}$ is too small for secondary alcohols.

The value of $(N + 1)^{1/2}\eta\Lambda$ for LiI in *tert*-butanol is only 35% of that in 2-butanol, probably due to multiple-ion association in *tert*-butanol, despite the fact that the κ–C plots were straight at 299 and 308 K (Fig. 2). The value of $(N + 1)^{1/2}\eta\Lambda$ for $LiNO_3$ in *tert*-butanol is very low due to the low value of Λ caused by ion clustering (2). In *tert*-butanol the three methyl groups on the α-carbon atom increase the steric hindrance for the alcohol molecules to pack around an ion, and decrease the solvation energy of the ions, thereby leaving it easier for them to agglomerate in clusters.

Secondly, on going from NO_3^-, I^- to large tetraphenyl ions, NO_3^- has a planar shape, the I^- ion is spherical, and the large tetraphenyl ions have low surface charge densities. Thus the solvation of an ion is progressively less sensitive to the solvent molecular structure change on going from NO_3^-, I^- to large tetraphenyl ions.

For the large-ion salts TPPB and STPB, both in primary and secondary alcohols, the value of $(N + 1)^{1/2}\eta\Lambda_0$ increases with increase of chain length of the alcohol molecule (Fig. 5*B*). This indicates that the normalization factor $(N + 1)^{1/2}$ is too high, especially for 1-, 2-, and isobutanols. A tetraphenyl ion is much larger than a molecule of C_1–C_4 alcohols, so the mobility of a large ion is less sensitive to the solvent molecule chain length and structure change.

In *tert*-butanol the value of $(N + 1)^{1/2}\eta\Lambda_0$ for a large-ion salt is about the same as in 1-propanol (Fig. 5*B*). The value is much higher than that for LiI or $LiNO_3$ in *tert*-butanol. This indicates that ion association of the large-ion salt is negligible; the charge density on the surface of a large-ion is low and the electrical attraction between the ions is weak.

Activation energies $E_{\Lambda 0}$ and E_η

Values of the activation energies $E_{\Lambda 0}$ for the small-ion salts LiI (Fig. 6) and $LiNO_3$ (Fig. 7), and for the large-ion salts TPPB and STPB (7), are listed in Table 2, along with the activation energies of shear viscosity (E_η) for comparison. Ion conductance and shear viscosity are both driven by external forces, electrical and gravitational or applied pressure, respectively. Activation energies of diffusion of the ions, driven by thermal energy, are larger than $E_{\Lambda 0}$ by $RT \approx 2$–3 kJ mol^{-1}.

In the calculation of $E_{\Lambda 0}$ of LiI and $LiNO_3$ in 2- and isobutanol, the values of Λ at the highest measured temperatures (labelled * in Figs. 6 and 7) are not taken into account, since the values of Λ are estimates of the initial slopes of the corresponding curved lines in κ–C plots (Figs. 2 and 3) and they may not be the limiting molar conductivities Λ_0.

In *tert*-butanol, values of Λ_0, and hence of $E_{\Lambda 0}$, were not obtained. At temperatures above 318 K for LiI or 308 K for $LiNO_3$ (2), Λ decreases with the increase of temperature, because εT decreases so rapidly that multi-ion clustering or ion-pair aggregation (2) increases more rapidly than does the mobility of Li^+ and NO_3^- ions.

The values of $E_{\Lambda 0}$ (Table 2) for both small-ion salts and large-ion salts are close to the values of E_η in water and the corresponding alcohols, except that in *tert*-butanol. In *tert*-butanol $E_{\Lambda 0}$ of large-ion salts is about 10 kJ mol^{-1} lower than E_η; the latter is unusually high because the rigid, globular *tert*-

Fig. 6. Arrhenius plots of molar conductivities of LiI in C_1–C_4 alcohols and water. The symbols are the same as in Fig. 4. *indicates the initial slopes of the curved lines.

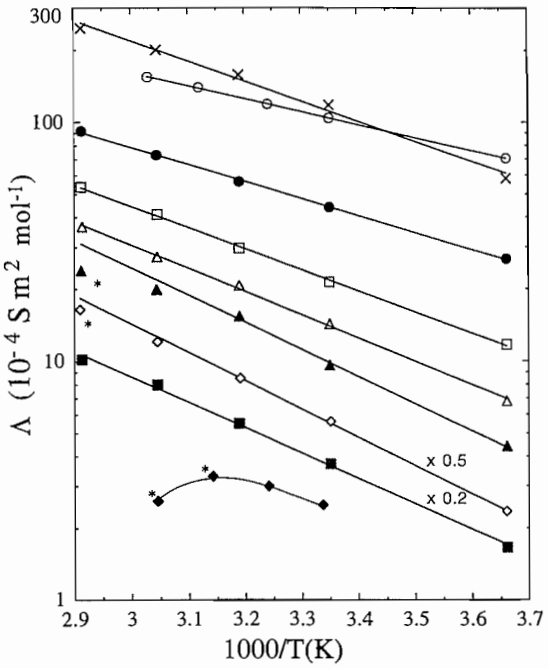
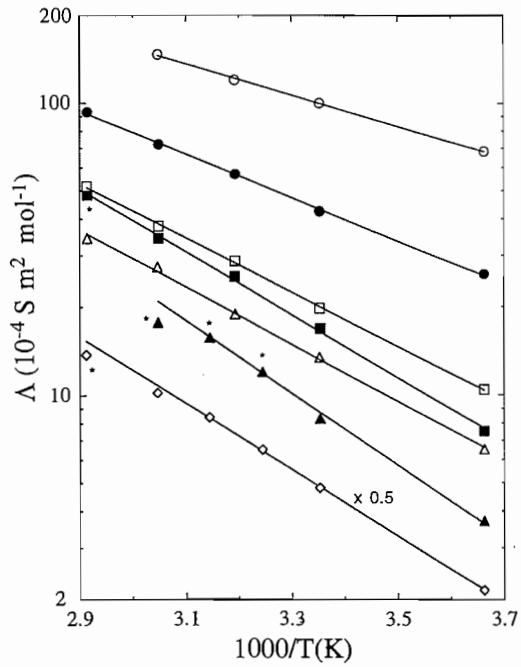


Fig. 7. Arrhenius plots of molar conductivities of $LiNO_3$ in methanol, ethanol, 1- and 2-propanol, 2- and isobutanol. The symbols are the same as in Fig. 4. *indicates the initial slopes of the curved lines.



© 1997 NRC Canada

Table 1. Molar conductivities of LiI and $LiNO_3$, and solvent parameters in C_1–C_4 alcohols and water.

				LiI		$LiNO_3$	
Solvent	T (K)	η^a	ε^b	Λ_0^c	$\eta\Lambda_0^d$	Λ_0^c	$\eta\Lambda_0^d$
Water	273.2	1.79	88.0	58	104		
	278.2	1.52	86.1			68	103
	298.2	0.890	78.5	114(115.6[e])	101	112(110[e])	100
	313.3	0.651	73.3			148	96
	313.5	0.649	73.1	158	103		
	328.5	0.502	68.2	201	101	183	92
	343.2	0.404	63.6	247	99		
	343.6	0.402	62.8			224	90
MeOH	273.2	0.85	37.9	70	60	68	58
	298.2	0.55	32.6	104(102.4[e])	57	101(100.5[e])	56
	308.2	0.47	30.7	119	56		
	313.3	0.44	29.8			120	53
	320.6	0.40	28.5	140	56		
	328.3	0.37	27.1			147	54
	330.1	0.37	26.9*	155	57		
EtOH	273.2	1.67	28.3	27	45	26	43
	298.2	1.08	24.3	43.7(43.6[e])	47	42.2(42.8[e])	46
	313.3	0.85	22.2	56	48	57	48
	328.3	0.66	20.2	73	48	72	48
	343.3	0.50	18.3*	92	46	93	47
1-PrOH	273.2	3.84	23.6*	11.7	45	10.4	40
	298.2	1.93	20.2	21.2	41	20.0	39
	313.5	1.33	18.3	29.7	40	28.7	38
	328.4	0.98	16.5	41.2	40	37.9	37
	343.4	0.73	14.8	53.6	39	51.9	38
2-PrOH	273.2	4.45	21.1*	8.3	37	7.5	33
	298.2	1.93	18.4	18.5	36	16.5	32
	313.5	1.30	16.2	27.5	36	25.4	33
	328.4	0.90	14.5	40	36	34.4	31
	343.3	0.65	13.0	51	33	49**	32
1-BuOH	273.2	5.31	21.3*	6.8	36	6.5	35
	298.2	2.56	17.5	14.2	37	13.2	34
	313.5	1.77	15.7	20.7	37	18.9	33
	328.3	1.24	14.0*	27.4	34	27.4	34
	343.2	0.93	12.6	36.6	34	34.3	32
2-BuOH	273.2	6.24	21.0*	4.6	29	3.6	23
	298.2	3.13	16.2	10.0	31	7.8	24
	308.2	2.47	14.5			10.3**	25
	313.5	2.22	13.8	14.5	32		
	318.1	2.00	13.0			11.4**	23
	328.5	1.63	11.6*	20.0	33	13.5**	22
	343.4	1.27	9.8*	24**	30		
i-BuOH	273.2	8.02	21.5*	4.7	38	4.3	34
	298.2	3.32	17.6	10.8	36	9.5	32
	308.3	2.46	16.1			13.0	32
	313.5	2.06	15.4	16.8	35		
	318.1	1.82	14.7			16.8	31
	328.4	1.41	13.3	24.7	35	20.4	29
	343.3	1.00	11.3*	32**	32	27.5**	28

Can. J. Chem. Downloaded from www.nrcresearchpress.com by 88.146.161.215 on 09/08/12
For personal use only.

© 1997 NRC Canada

Table 1 (*concluded*).

Solvent	T (K)	η^a	ε^b	LiI		$LiNO_3$	
				$\Lambda_0{}^c$	$\eta\Lambda_0{}^d$	$\Lambda_0{}^c$	$\eta\Lambda_0{}^d$
				Λ	$\eta\Lambda$		
t-BuOH	298.2	4.30	12.4	2.5***	10.8	~4[f]	
	299.4	4.10	12.0	2.6	10.7		
	308.4	2.65	10.4	3.0	8.0	ref. 2	
	318.2	1.80	8.7	3.3**	5.9		
	328.3	1.20	7.6	2.7**	3.4		

[a]Shear viscosity (mPa s), water, ref. 19; alcohols, ref. 20.
[b]Relative permittivity, ref. 21.
[c]Unit: 10^{-4} S m^2 mol^{-1}.
[d]Unit: 10^{-7} Pa s S m^2 mol^{-1}.
[e]Reference 15.
[f]Estimated value, ref. 2.
*Extrapolated values from the literature data.
**Initial slope from the curved line in the measurement of the freshly prepared solution.
***Extrapolated from higher temperatures, because freezing point is 298.7 K.

Table 2. Comparison of activation energies[a] of ionic conductance and viscosity in C_1–C_4 alcohols and water near 300 K.

Solvent	$E_\eta{}^b$	$E_{\Lambda 0}$(LiI)	$E_{\Lambda 0}(LiNO_3)$	$E_{\Lambda 0}$(TPPB)[e]	$E_{\Lambda 0}$(STPB)[e]
Water	15.4	16	15[d]	15	16
MeOH	11	10	9.9	9.7	9.6
EtOH	14	14	14	13	13
1-PrOH	18	18	18	17	17
2-PrOH	22	21	21	20	20
1-BuOH	19	18	19	20	20
2-BuOH	26	24	23	24	23
i-BuOH	24	23	22	23	22
t-BuOH	31	~14[c]	~7[c]	21	19

[a]In kJ mol^{-1}.
[b]Arrhenius temperature coefficients for shear viscosity of solvents. Water: refs. 8 and 9; methanol and ethanol: ref. 8; 1-propanol and 2-propanol: ref. 10; butanols, ref. 9.
[c]Not $E_{\Lambda 0}$; temperature coefficients between 299 and 308 K (Fig. 2 and Fig. 6 for LiI and ref. 2 for $LiNO_3$). Above 318 K for LiI or 308 K for $LiNO_3$ the molar conductivity decreases with increase of temperature.
[d]Reference 3.
[e]Reference 7.

butanol molecules cannot efficiently move past each other in the liquid. Space-filling molecular models indicate that the large tetraphenyl ions would break the local structure of liquid *tert*-butanol, which would perhaps lower the activation energies of mobility and diffusion of the ions.

Acknowledgement

We thank the Natural Sciences and Engineering Research Council of Canada for financial assistance and Mr. Ronald Gardner for maintaining the electric equipment.

References

1. M.C. Blanco and D.C. Champeny. Phys. Chem. Liq. **23**, 93 (1991).
2. Y. Zhao and G.R. Freeman. Can. J. Chem. **73**, 2131 (1995).
3. Y. Zhao and G.R. Freeman. Can. J. Chem. **73**, 392 (1995).
4. R. Chen and G.R. Freeman. J. Phys. Chem. **99**, 4970 (1995).
5. K.H. Schmidt, P. Han, and D.M. Bartels. J. Phys. Chem. **96**, 199 (1992).
6. R. Chen and G.R. Freeman. Can. J. Chem. **71**, 1303 (1995).
7. Y. Zhao and G.R. Freeman. J. Phys. Chem. **100**, 17568 (1996).
8. C.C. Lai and G.R. Freeman. J. Phys. Chem. **94**, 302 (1990).
9. P.C. Senanayake and G.R. Freeman. Can. J. Chem. **65**, 2441 (1987).
10. A.P. Sedigallage and G.R. Freeman. Can. J. Phys. **68**, 940 (1990).
11. P.W. Atkins. Physical chemistry. 4th ed. W.H. Freeman and Company, New York. 1990. pp. 251, 752, 760–766.
12. J.O'M. Bockris and A.K.N. Reddy. Modern electrochemistry. Vol. 1. Plenum Press, New York. 1975. p. 450.
13. R.L. Kay. J. Am. Chem. Soc. **82**, 2099 (1960).

Can. J. Chem. Downloaded from www.nrcresearchpress.com by 88.146.161.215 on 09/08/12
For personal use only.

© 1997 NRC Canada

14. G.J. Janz and S.S. Danyluk. Chem. Rev. **60**, 209 (1960).
15. D. Dobos. Electrochemical data. Scientific Publishing, New York. 1975. pp. 87–89.
16. J.E. Gordon. The organic chemistry of electrolyte solutions. John Wiley & Sons, New York. 1975. p. 372.
17. Y. Zhao and G.R. Freeman. Can. J. Chem. **73**, 284 (1995).
18. A.D. Leu, K.N. Jha, and G.R. Freeman. Can. J. Chem. **60**, 2342 (1982).
19. R.C. Weast (*Editor*). Handbook of chemistry and physics. 70th ed. CRC Press, Boca Raton, Fla. 1989. F40.
20. R.W. Gallant. Physical properties of hydrocarbons. Vol. 1. Gulf Publishing Company, Houston, Tex. 1968. Chaps. 8 and 10.
21. Y.Y. Akhadov. Dielectric properties of binary solutions. Pergamon Press, New York. 1980. Chaps. II, III, and IV.

Can. J. Chem. Downloaded from www.nrcresearchpress.com by 88.146.161.215 on 09/08/12
For personal use only.

© 1997 NRC Canada

Electrochemical investigation of some potential antibacterials, II

Rajeev Jain, P. Padmaja, and Seema Gupta

Abstract: The electrochemical behaviour of 2-(4′-sulphonamoyl)hydrazonobutyrate-1,3-diones and sulphonamoylazoaminobenzenes has been studied over a wide range of pH at dropping mercury as well as glassy carbon electrodes. Both types of compounds exhibited a $4e^-$ reduction reaction at both electrodes. At pH > 4.5, 2-(4′-sulphonamoyl)hydrazonobutyrate-1,3-diones exhibited a $2e^-$ reduction wave at higher potentials. Both compounds undergo a $2e^-$ oxidation reaction. On the basis of polarography, linear and cyclic voltammetry, controlled potential electrolysis, coulometry, and spectral analysis, a detailed mechanism has been postulated for the reduction as well as the oxidation.

Key words: electrochemistry, sulphonamides, polarography, cyclic voltammetry, coulometry.

Résumé : Opérant sur une très large plage de pH et utilisant une électrode tombante de mercure ainsi qu'une électrode de carbone vitreux, on a étudié le comportement électrochimique de 2-(4′-sulfonamoyl)hydrazonobutyrate-1,3-diones et de sulfonamoylazoaminobenzènes. Les deux types de composés présentent une réaction de réduction à $4e^-$ avec les deux électrodes. À des pH supérieurs à 4,5, les 2-(4′-sulfonamoyl)hydrazonobutyrate-1,3-diones présentent une réduction à $2e^-$ à des potentiels plus élevés. Les deux types de composés subissent une réaction d'oxydation à $2e^-$. Sur la base des résultats obtenus par polarographie, voltammétrie linéaire et cyclique, électrolyse à potentiel contrôlé, coulométrie et analyse spectrale, on propose un mécanisme détaillé tant pour la réduction que pour l'oxydation.

Mots clés : électrochimie, sulfonamides, polarographie, voltammétrie cyclique, coulométrie.

[Traduit par la rédaction]

Sulphonamides were the first effective chemotherapeutic agents to be employed systematically for the prevention and cure of bacterial infections. Sulphonamides are widely used in the treatment of urinary tract infection, burn therapy, conjunctivitis, and chloroquine-resistant malaria and are also drugs of choice for the treatment of nocardiosis, toxoplasmosis, severe travellers diarrhoea, and meningococcal infections (1, 2).

Keeping in view the medicinal importance of sulphonamides (3), some new derivatives of sulphonamides have been synthesized. The redox behaviour (4, 5) of hydrazones has attracted considerable attention due to their importance as precursors (6) of various antineoplastic and antidiabetic compounds. However, no reference has been found dealing with those compounds bearing a -NH-N=N- group. This group of compounds having a -NH-N- as well as a -N=N- grouping in a single molecule deserve an extensive electrochemical study. In view of the importance of redox phenomena in reactions of physiological importance, it is considered worthwhile to study the mechanism and nature of the end products resulting from the reduction/oxidation of compounds of potential medicinal importance.

Received February 8, 1995.[1]

R. Jain,[1] P. Padmaja, and S. Gupta. School of Studies in Chemistry, Jiwaji University, Gwalior – 474 011, India.

[1] Revision received February 14, 1997.
[2] Author to whom correspondence may be addressed. Telephone: 91-751-340216. Fax: 91-751-341450.

In continuation of our work (7–9) in exploring the redox behaviour of potential antibacterials, we have selected some hydrazono derivatives of sulphonamides, viz., 2-(4′-sulphonamoyl)hydrazonobutyrate-1,3-diones (A) and sulphonamoylazoaminobenzenes (B) for a comprehensive and comparative study taking into consideration such pertinent aspects of redox phenomena as the nature of the waves, characterization of the end products, and mechanism of the electrode process. These studies have been augmented, wherever possible, by results of controlled potential electrolysis, coulometry, and product analysis.

Experimental

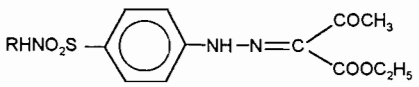
Some representatives of both classes of compounds, viz., 2-(4′-sulphonamoyl)hydrazonobutyrate-1,3-diones (A) and sulphonamoylphenyl azoaminobenzenes (B), as represented in Scheme 1, were selected.

Compounds A and derivatives were synthesized by the literature method (10). Compounds B were synthesized and characterized in the following manner. Sulphanilamide (0.01 mol, 1.72 g) was dissolved in a mixture of concentrated hydrochloric acid (5 mL) and water (5 mL) and cooled to 0°C in an ice bath. To this, a cold aqueous solution of sodium nitrite (0.01 mol, 0.69 g) was added. The diazonium salt so obtained was filtered into an already cooled solution mixture of sodium acetate (8.0 g) and sulphanilamide in alcohol. A yellow precipitate of sulphonamoylphenylazoaminobenzene appeared immediately. The precipitate was filtered, washed with water, and recrystallized from light petroleum, mp 91°C, yield 68%. IR ν_{max}^{KBR}: 3370 ($NH\text{-}C_6H_5$), 3220, 3180 (NH_2SO_2), 1520

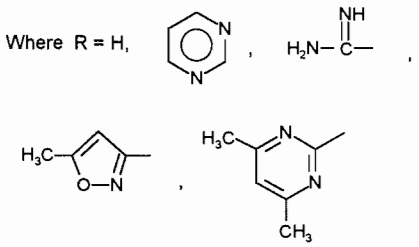
© 1997 NRC Canada

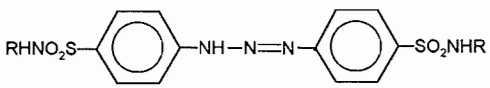
Can. J. Chem. Downloaded from www.nrcresearchpress.com by 88.146.161.215 on 09/08/12
For personal use only.

Scheme 1.

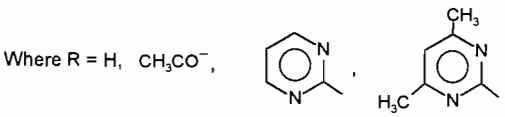


(A)





(B)



(-N=N-), 1340 (SO_2) cm^{-1}; ^1H NMR δ ($CDCl_3$): 2.2 (2H, -NH_2), 7.4 (5H, pH), 9.3 (H, NH). Anal. calcd. for $C_{12}H_{13}N_5S_2O_4$: C 40.56%, H 3.66%, N 19.70%; found: C 40.20%, H 3.5%, N 19.40%.

Similarly, other substituted sulphonamoylphenylazoaminobenzenes were synthesized and duly characterized.

Apparatus and technique

Polarographic measurements were carried out on an ELICO DC CL-25 polarograph. Potentiometric studies were carried out on an expanded-scale pH meter with a glass electrode that was previously standardized with buffer of known pH. All potentials reported are with reference to the SCE. Triply distilled mercury was used for the dropping mercury electrode (DME).

Cyclic voltammetric studies were carried out on a BAS CV-27 cyclic voltammograph in connection with a digital electronic 2000 Omnigraph X-Y/t recorder. A three-electrode cell was used for the purpose. The cell consists of a glass cylinder with a cap having holes for introducing electrodes and tubing for nitrogen gas. Oxygen was removed from the solution by passing nitrogen gas through the solution for about 10 min and then a blanket of nitrogen was maintained throughout the experiment. In the present study, glassy carbon (GC) was used as the working electrode, 1.0 M Ag/AgCl as the reference electrode, and platinum wire was used as the auxillary electrode. The working electrode was polished with fine-grade emery paper, followed by polishing with alumina (0.5 μm), then was washed and activated by triangular voltage sweeps from +1.0 V to −1.6 V at a rate of 5–200 mV/s for 15 min. The activity of the electrode was tested (11) using a ferricyanide–ferrocyanide redox couple in 0.01 M KCl.

For the purpose of cyclic voltammetric and polarographic measurements, solutions were prepared by mixing a 2.0 mL solution of the compound, 2.0 mL of DMF (which is necessary to keep the compound in solution), 1.0 mL of 1.0 M KCl, and 5.0 mL of appropriate Britton–Robinson buffers (12). Britton–Robinson buffers in the pH range 2.0–11.8 were prepared by adding suitable amounts of 0.2 M NaOH solution to a stock B.R. buffer solution (pH 1.8). B.R. buffer stock was prepared by mixing boric acid, phosphoric acid, and glacial acetic acid (mixture contains 2.472 g of boric acid, 2.14 mL of phosphoric acid, 2.30 mL of glacial acetic acid made up to 1000 mL).

For the coulometric determination (13) of the number of electrons transferred in the electrode process, 2.0 mL of the solution of the compound containing buffer, solvent, and supporting electrolyte in the same ratio as used for CV studies was electrolyzed at a slightly more negative potential than the peak potential for the respective peaks. From the decrease in current with time, the number of electrons transferred was calculated. The progress of electrolysis was monitored by recording voltammograms at regular intervals of time. The products of electrolysis were identified by comparison of their properties with authentic products using TLC.

Results and discussion

DC polarography

All the 2-(4′-sulphonamoyl)hydrazonobutyrate-1,3-diones (A) reduced in a single, $4e^-$, well-defined wave in the pH range 2.0–12.0. However, an additional $2e^-$ wave was observed at pH > 4.5 (Table 1). The first wave over the entire pH range was found to be the diffusion-controlled, irreversible reduction of hydrazono group. The diffusion-controlled nature of the limiting current was established on the basis of linear plots of i_d vs. concentration and i_d vs. $h^{1/2}$ (where h is the height of the mercury column). Sulphonamoylphenylazoaminobenzenes (B) exhibited one four-electron, diffusion-controlled irreversible reduction wave over the entire pH range 2.0–12.0 (Table 2). In these compounds, no additional wave was observed at pH > 4.5. The number of electrons involved in the polarographic wave was found, by coulometry, to be four. The value of n was also determined by controlled potential electrolysis using the following formula (14).

$$n = \frac{i_0}{2.30\, C_0 F u(\Delta \log i/\Delta t)}$$

where i_0 is the current at $t = 0$ when $C = C_0$, u is the volume of the solution and $\Delta\log i/\Delta t$ is the slope of the plot of log i against log t. This estimate provided support for the value obtained by the millicoulometric method. The controlled potential electrolysis was carried out at a potential corresponding to the plateau of the wave.

The half-wave potentials of both compounds A and B are a linear function of pH. The plot of $E_{1/2}$ vs. pH was linear up to 7.5 for A and to 9.2 for B and thereafter there is little change in $E_{1/2}$ with pH (Fig. 1). This suggests that protons are involved in the reduction process. However, in alkaline solution, the half-wave potential did not change with pH. Irreversibility of

Can. J. Chem. Downloaded from www.nrcresearchpress.com by 88.146.161.215 on 09/08/12
For personal use only.

© 1997 NRC Canada

Can. J. Chem. Downloaded from www.nrcresearchpress.com by 88.146.161.215 on 09/08/12
For personal use only.

Table 1. Voltammetric characteristics of 2-(4′-sulphonamoyl)hydrazonobutyrate-1,3-diones at pH 4.5, concentration = 1.0×10^{-4} M.

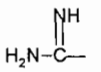
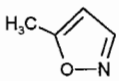
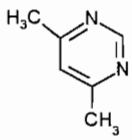
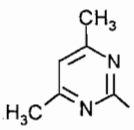
Scan no.	R	$-E_{1/2}$, V	i_d, μA	$-E_p$, V	i_p, μA	Current density $i_p/ACv^{1/2}$
1.	H	0.82	0.80	1.25	5.9	0.12×10^3
2.		0.84	0.88	1.10	5.7	0.11×10^3
3.		0.78	0.92	1.17	5.3	0.11×10^3
4.		0.92	0.92	1.12	6.2	0.12×10^3
5.		0.76	0.80	1.13	6.8	0.18×10^3

Table 2. Polarographic characteristics of sulphonamoylphenylazoaminobenzene at pH 6.70, concentration 2.0×10^{-4} M.

Scan no.	Substituent	Melting point, °C	$-E_{1/2}$, V	Standard deviation	i_d, μA	Standard deviation
1.	H	91	0.82	±0.017	2.32	±0.014
2.	CH_3—CO—	98	0.84	±0.013	2.40	±0.018
3.		101	0.83	±0.015	2.45	±0.020
4.		107	0.81	±0.016	2.41	±0.012

the electrode process was confirmed by plotting $E_{d.e.}$ against $(i/i_d - i)$. It was found that the value of slope exceeded $59.2/n$ mV. The values of αn_a (product of transfer coefficient and number of electrons transferred in the rate-determining step) and p (number of protons involved in rate-determining step) were determined by using the following expressions (15, 16). The values of αn_a determined by logarithmic analysis of the polarographic wave are comparable with those values determined from the expressions given below. The value of p obtained from the expressions was nearly equal to 1.0.

$$E_{3/4} - E_{1/4} = \frac{0.0517}{\alpha n_a}$$

$$\frac{dE_{1/2}}{dpH} = \frac{0.0591}{\alpha n_a} p$$

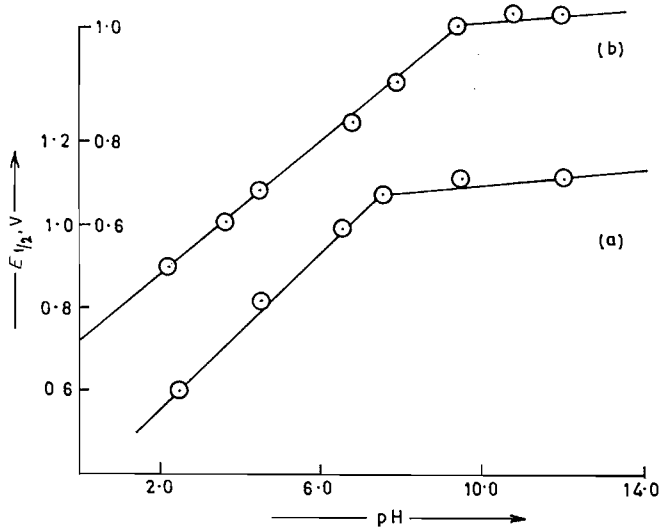
Linear sweep and cyclic voltammetry

Cyclic voltammograms of 2-(4-sulphonamoyl)hydrazonobutyrate-1,3-diones (A) and sulphonamoylazoaminobenzenes (B) were recorded at different scan rates and concentrations using the glassy carbon electrode. Typical cyclic voltammograms are incorporated in Fig. 2. The cyclic voltammogram of compound A exhibited one well-defined cathodic peak in the pH range 2.5–12.0 (Table 1). One more peak, II_c, at higher negative potentials was observed at pH > 4.5. In sulphonamoylazoaminobenzene (B) two well-defined two-electron

© 1997 NRC Canada

Can. J. Chem. Downloaded from www.nrcresearchpress.com by 88.146.161.215 on 09/08/12
For personal use only.

Fig. 1. Plot of $-E_{1/2}$ vs. pH for (*a*) 2-(4′-sulphonamoyl)-hydrazonobutyrate-1,3-diones; (*b*) sulphonamoylphenyl-azoaminobenzene.



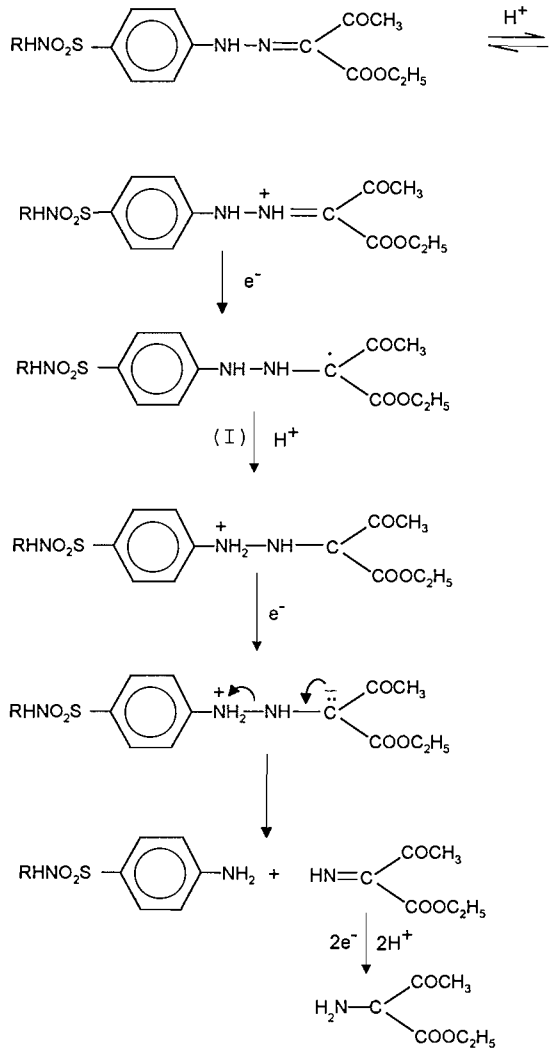
reduction peaks were observed over the entire pH range (Table 3). The peak currents were measured from the direct reading shown on the digital display of the potentiostat. A cyclic voltammogram of the solvent and the supporting electrolyte was recorded after flushing with nitrogen gas for about 10 min. The current of the blank was considered as the base line (c) as indicated in Fig. 2. The peak currents (i_p) of the compound A were comparable to those of the compound B. The linear plots of peak current i_p vs. the square root of the scan rate (Fig. 3) and i_p vs. concentration of the depolarizer show a slight deviation from the origin, indicating adsorption (17) of the depolarizer in both waves, in acidic as well as in alkaline media. The peak potential was found to shift cathodically with scan rate. The peak potentials also shifted to negative values with the concentration of the compound.

The peak potential was dependent on pH and shifted towards more negative potentials with an increase in pH up to 7.5 for compound A and 9.2 for compound B. On reversing the scan, only a small peak was observed at very high positive potentials, indicating that the processes corresponding to both peaks are irreversible. However, this small hump (I_a) in Fig. 2 at positive potentials indicates that these hydrazones and azoaminobenzenes also undergo oxidation at the glassy carbon electrode. To ascertain whether the peak is due to oxidation of hydrazones, voltammograms were initiated in the positive direction. It was found that the oxidation peak appeared at the same potential. Thus it can be safely concluded that the oxidation peak is due to the independent oxidation of hydrazones and azoaminobenzenes. No corresponding peak was observed in the reverse scan, indicating that the oxidation process in both cases is irreversible. The number of electrons involved in the oxidation process was calculated from coulometric measurements and found to be 2.0.

Coulometry and controlled potential electrolysis

At pH 2.5–4.0 at −1.0 V, 2-(4′-sulphonamoyl)hydrazonobutyrate-1,3-diones (A) undergo a four-electron reduction reac-

Scheme 2.



tion. The TLC of the electrolyzed solution on a silica-gel G-plate resulted in two spots. One of the separated compounds exhibited bands corresponding to primary amino stretching bands at 3210 cm^{-1}, C—H linkage at 2650 cm^{-1}, and a peak for the C=O group at 1695 cm^{-1}. The other compound was identified as sulphanilamide by comparison with standard sulphanilamide. It was also verified using different solvent mixtures.

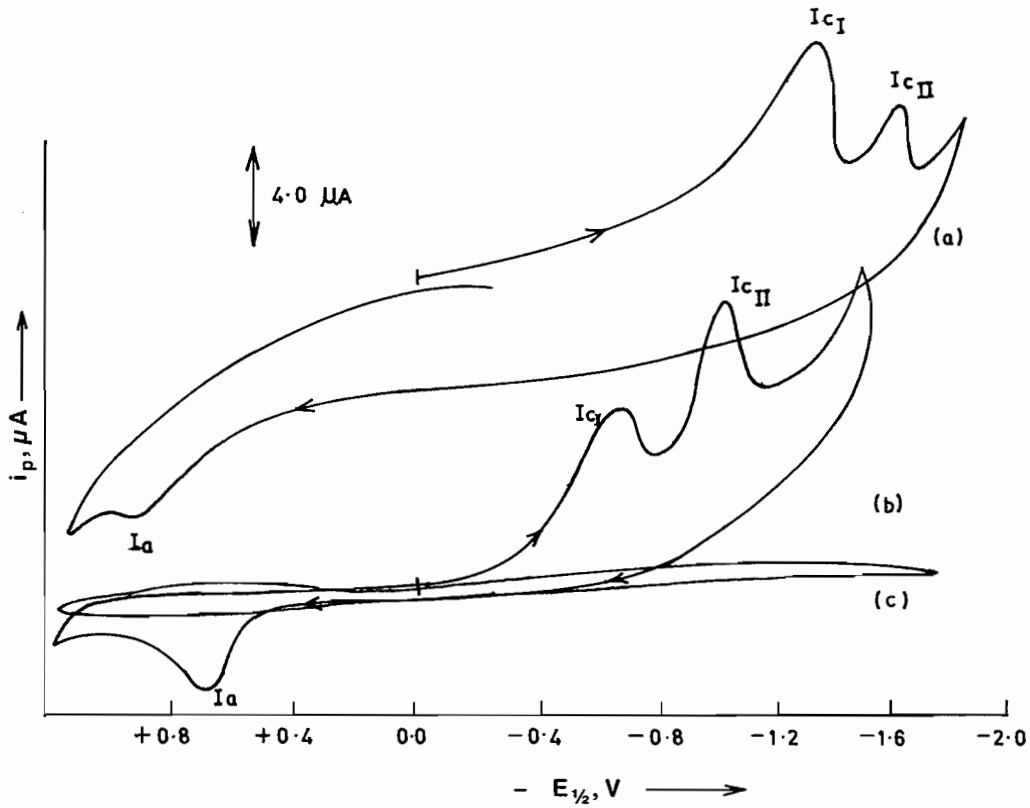
Controlled potential electrolysis at pH 6.2 and 10.5 at −1.5 V and subsequent product analysis confirms the presence of sulphanilamide, ethyl acetoacetate, and ammonia. The presence of ethyl acetoacetate was proved by comparing with authentic ethyl acetoacetate using GLC, and ammonia was detected by Nessler's reagent. The number of electrons involved in the entire overall process was found to be 6.0 + 0.25. A detailed mechanism is given in Scheme 2 in the pH range 2.0–12.0 and at pH > 4.0 in Scheme 3, while azoaminobenzenes over the entire pH range studied consumed four electrons. Each peak required a two-electron process. Controlled potential electrolysis resulted in two products, as separated by TLC on silica gel G plates of 0.25 cm thickness

© 1997 NRC Canada

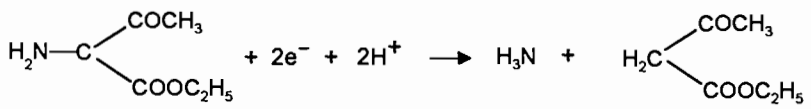
Table 3. Voltammetric characteristics of sulphonamoylphenylazoaminobenzene at GC electrode. Conc. 2.0×10^{-4} M; scan rate (v) 50 mV s^{-1}.

Scan no.	pH	$-E_{pc}$, I	i_{pc}, I	Current density $i_p/Acv^{1/2}$ $\times 10^2$	$-E_{pc}$, II	i_{pc}, II	Current density $i_p/Acv^{1/2}$ $\times 10^2$	E_{pa}I, V	i_{pa}, μA	Current density $i_p/Acv^{1/2}$ $\times 10^2$
1.	2.30	0.70	4.6	0.46	0.82	4.5	0.46	0.66	4.5	0.46
2.	4.60	0.75	5.2	0.52	0.88	5.2	0.52	0.67	4.8	0.48
3.	6.70	0.84	4.8	0.48	0.98	4.9	0.48	0.38	5.0	0.50
4.	7.75	0.80	4.9	0.49	1.03	5.3	0.53	0.30	4.5	0.46
5.	9.20	1.10	5.3	0.53	1.18	5.0	0.50	0.26	5.2	0.52
6.	11.40	1.11	5.0	0.50	1.18	5.2	0.52	0.25	5.0	0.50

Fig. 2. Cyclic voltammograms of (*a*) 2-[4′-(4″-6″-dimethyl)pyrimidinyl sulphonamoyl)hydrazonobutyrate-1,3-dione at pH 7.2, $v = 50$ mV/s, concentration = 1.0×10^{-4} M; (*b*) sulphonamylphenylazoaminobenzene at pH 4.7, $v = 50$ mV/s, concentration = 1.0×10^{-4} M; (*c*) base line in DMF.



Scheme 3.



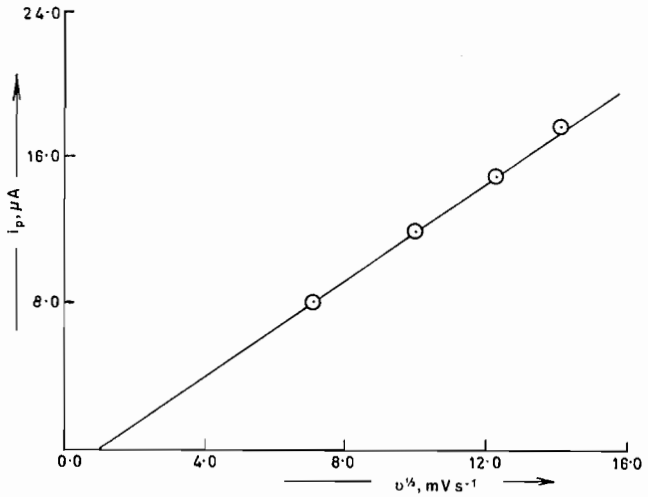
(chloroform and carbon tetrachloride in the ratio 1:1), $R_f = 0.8$ and 0.2. One of the spots is matched with an authentic sample of sulphanilamide (Anal. calcd. for $C_6H_8N_2SO_2$: C 41.86, H 4.65, N 16.27%; found: C 42.52, H 4.92, N 16.5%. IR ν_{max}^{KBr}: 1260 (C-N), 1340 (SO_2); 3180, 3210 (NH_2SO_2) cm^{-1}). The IR spectra could be superimposed on the IR spectra of an authentic sample, confirming that one of the products formed after electrolysis is sulphanilamide. The other product is identified as sulphonamoylphenylhydrazine by comparison of its R_f values with those of related compounds. Keeping these facts in view, the reduction may be proposed to be as given in Scheme 4 for compounds B.

© 1997 NRC Canada

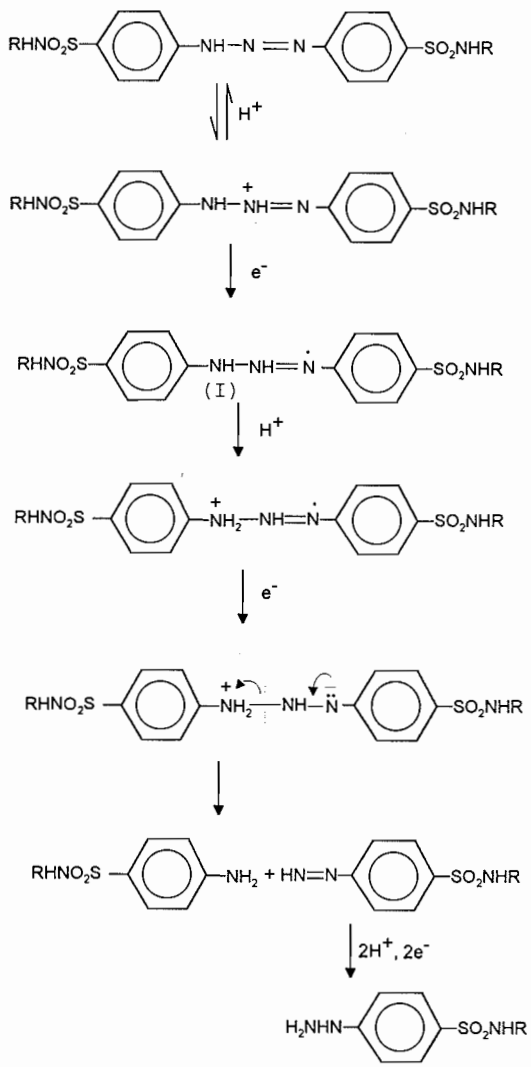
Can. J. Chem. Downloaded from www.nrcresearchpress.com by 88.146.161.215 on 09/08/12
For personal use only.

Can. J. Chem. Downloaded from www.nrcresearchpress.com by 88.146.161.215 on 09/08/12
For personal use only.

Fig. 3. Plot of i_p (μA) vs. $\nu^{1/2}$ for 2-[4′-(4″-6″-dimethyl)pyrimidinyl sulphonamoyl]hydrazonobutyrate-1,3-dione at pH 4.5, concentration = 1.0×10^{-4} M.



Scheme 4.



The above mechanism is supported by the shift of $E_{1/2}$ towards more negative values with pH as protons are consumed in the reduction. As the equilibrium shifts towards the unprotonated forms, $E_{1/2}$ becomes constant. In this mechanism (Schemes 2 and 4), the radical (I) could also combine with an electron instead of a proton, but this possibility is ruled out because such a mechanism involves only two electrons, whereas coulometric data clearly indicate a four-electron reduction process.

However, in compounds A, further reduction of the product formed at the four-electron stage takes place in a second 2e reduction wave at pH > 4.5. The peak/wave has been assigned to the reduction of the activated C—N bond, as shown in Scheme 3. Other workers have also reported a similar mechanism for the activated C—N bond (18, 19). Coulometric data for compounds A and B at the oxidation peak potential resulted in two electrons for each compound. Controlled potential electrolysis of these compounds resulted in two spots, indicating the formation of the different compounds.

Controlled potential electrolysis (CPE) of hydrazono compounds A was carried out to determine the number of products. For CPE, hydrazone was electrochemically oxidized at the GC electrode using 1.0 M tetraethylammonium bromide at 1.2 V. A cyclic voltammogram was recorded using the solvent and supporting electrolyte without depolarizer to determine whether or not oxidation is due to depolarizer. No peak was observed in the range of the hydrazone group. This observation ruled out the possibility of oxidation of any other component than the hydrazono group.

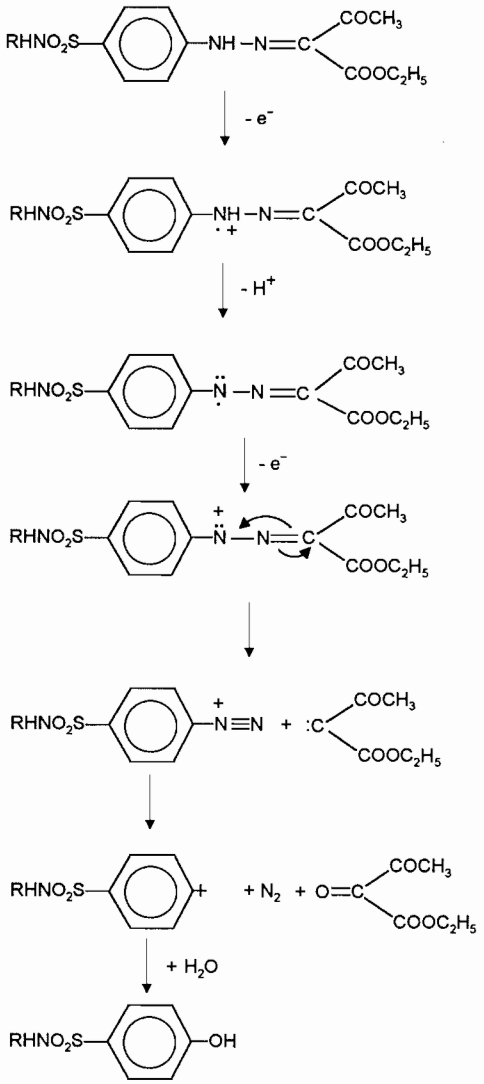
UV–visible spectra of the solution were recorded at different time intervals during electrolysis. λ_{max} at 390 nm due to the -NH-N=C- grouping showed a systematic decrease in the absorption maxima after each time interval and finally disappeared. Disappearance of the peak indicated cleavage of the NH-N=C- group during oxidation. After complete CPE, the analyte was subjected to product analysis. The electrolyzed solution, on separation by TLC using hexane + methanol (70:30 V/V), gave two products. One of the products was identified by TLC as *p*-hydroxy benzenesulphonamide by comparison with an authentic sample. The second product was characterized by spectral analysis, i.e., IR ν_{max}^{KBr} : 1720 cm^{-1}, characteristic of the >C=O group, and ^{1}H NMR δ ($CDCl_3$): 1.39 (t, 3H, -CH_3), 4.24 (q, 2H, -CH_2), clearly indicating that the second product is an α,β-diketoester. The α,β-diketoester was obtained in fairly good yield (20–45%).

The product was confirmed by its reaction with 2,4-dinitrophenylhydrazine. When the product of the electrooxidation was treated with an excess of 2,4-dinitrophenylhydrazine, it readily formed hydrazone, which was isolated and identified by elemental and spectral analysis. Keeping these products in view, a probable mechanism may be proposed, as depicted in Scheme 5. This mechanism is also supported by the work of others (20, 21), whereas in sulphonamoylazoaminobenzene (B), controlled potential electrolysis of the compound resulted in two spots on separation by TLC on alumina using benzene + chloroform (60:40 V/V). The products were identified by comparing with authentic compounds. The probable mechanism for the oxidation of this compound is given in Scheme 6. The products are expected to result from the cleavage of the diazonium cation and by the rearrangement of nitrene formed during the oxidation. The radical cation obtained after

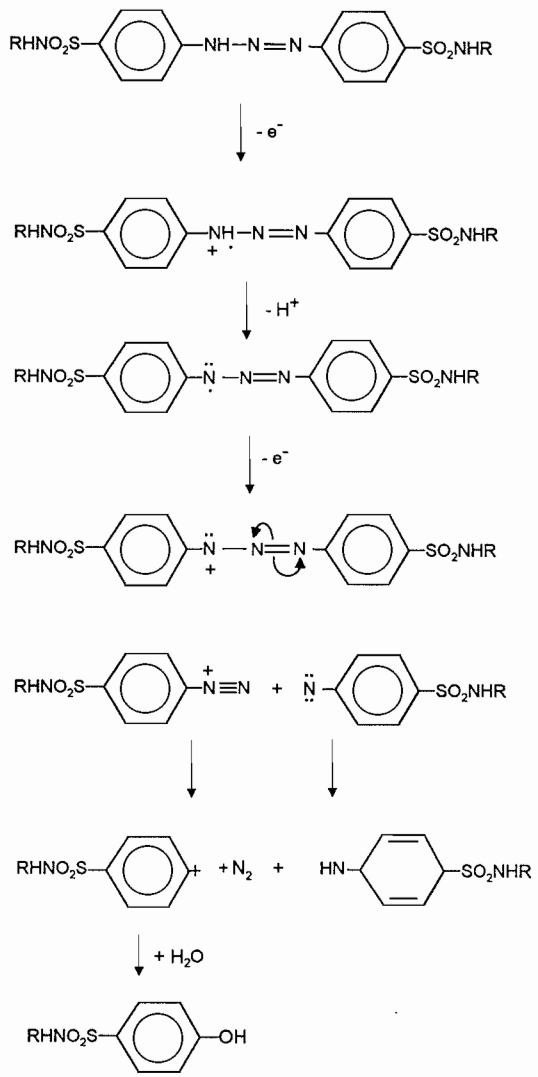
© 1997 NRC Canada

Can. J. Chem. Downloaded from www.nrcresearchpress.com by 88.146.161.215 on 09/08/12
For personal use only.

Scheme 5.



Scheme 6.



abstraction of an electron undergoes two main reactions, viz., loss of a proton from the α-position to the azo group and cleavage of the arylazo group, forming a diazonium cation. The diazonium cation disproportionates into nitrogen and an aryl cation, which loses a proton when a water molecule is added. This compound is matched with an authentic sample. The nitrene formed undergoes tautomerism. This type of mechanism has been proposed by Fasani et al. (22) for the oxidation of azo benzenes.

Finally, it was observed that both reduction and oxidation proceed through the same pathways, although the products are different. In the case of hydrazones at higher pH, i.e., pH > 4.5, the product obtained at the $4e^-$ stage undergoes further reduction due to the activated C—N bond. Lack of electron-withdrawing groups in azoaminobenzene may be the reason why further reduction of hydrazine is hindered, whereas oxidation of hydrazones, as well as azominobenzenes, follows the same path. In hydrazones, carbene formed is flanked by electron-withdrawing groups and hence readily adds a water molecule and is converted into a ketone, while in azoaminobenzene the nitrene obtained readily undergoes tautomerism.

References

1. M.E. Kommos and E.M. Emara. Analyst, **113**, 133 (1988).
2. R.F. Doerge (*Editor*). Wilson and Gisvold's textbook of organic medicinal and pharmaceutical chemistry. 8th ed. John Wiley & Sons, New York. 1983. p. 312.
3. L.S. Goodoman and A. Gilman. The pharmacological basis of therapeutics. 4th ed. Academic Press, 1972. p. 512.
4. G. Dusinsky. Pharmazie, **8**, 897 (1953).
5. W.U. Malik, R.N. Goyal, V.K. Mahesh, and V. Verma. J. Electroanal. Chem. **62**, 451 (1975).
6. H.G. Garg and R.A. Sharma. J. Med. Chem. **12**, 1122 (1969).
7. R. Jain, D.D. Agarwal, and R.K. Shrivastava. J. Chem. Soc. Perkin Trans. **2**, 1353 (1990).
8. R. Jain, D.D. Agarwal, and R.K. Shrivastava. J. Electroanal. Chem. **305**, 313 (1991).
9. R. Jain and M. Damodaran. Can. J. Chem. **73**, 176 (1995).
10. R. Jain and S. Gupta. Indian J. Heterocycl. Chem. **2**, 267 (1993).
11. M. Noel and P. Anantharaman. Analyst, **110**, 1095 (1985).
12. H.T.S. Britton. Hydrogen Ions. Vol. 1. D. Van Nostrand Company, New York. 1956.
13. C. Manousek, O. Exner, and P. Zuman. Collect. Czech. Chem. Commun. **33**, 3989 (1968).

© 1997 NRC Canada

14. G.A. Gilbert and A.K. Rideal. Trans. Faraday Soc. **47**, 396 (1901).
15. L. Meites. Polarographic techniques. Interscience Publishers, New York. 1967.
16. B. Janik and P.J. Eluing. J. Electrochem. Soc. **116**, 1087 (1969).
17. R.S. Nicholson and I. Shain. Anal. Chem. **36**, 722 (1984).
18. P. Zuman and V. Horak. Collect. Czech. Chem. Commun. **26**, 176 (1961).
19. P. Zuman, O. Manousek, and U. Horak. Collect. Czech. Chem. Commun. **29**, 2906 (1964).
20. S.B. Shim, K. Kim, and Y.A. Kim. Tetrahedron Lett. **28**, 645 (1987).
21. M. Okimoto and T. Chiba. J. Org. Chem. **55**, 1070 (1990).
22. E. Fasani, T. Soldi, A. Albini, and S. Pietra. Gazz. Chim. Ital. **120**, 109 (1990).

Can. J. Chem. Downloaded from www.nrcresearchpress.com by 88.146.161.215 on 09/08/12
For personal use only.

© 1997 NRC Canada

Étude expérimentale et modélisation des réactions d'oxydation du *n*-pentane et du cyclopentane

V. Simon, Y. Simon, G. Scacchi et F. Baronnet

Résumé : La réduction des émissions et la reformulation des carburants nécessitent une meilleure compréhension du mécanisme de combustion, en particulier afin de déterminer les processus importants responsables du phénomène de cliquetis dans les moteurs à allumage commandé. Nous avons donc étudié les mécanismes d'oxydation de deux hydrocarbures d'indices d'octane différents : le *n*-pentane (62) et le cyclopentane (100). Cette étude fait suite aux travaux déjà effectués sur l'oxydation du *n*-heptane et de l'isooctane. L'étude expérimentale a été effectuée, à 873 K, en utilisant un réacteur continu autoagité par jets gazeux. Les mécanismes réactionnels du *n*-pentane et du cyclopentane ont alors été analysés en utilisant des considérations purement cinétiques, basées sur les résultats expérimentaux, puis modélisés grâce à un logiciel de simulation de mécanismes réactionnels. La différence de comportement entre ces deux hydrocarbures, vis à vis des phénomènes d'autoinflammation, a été essentiellement attribuée à la concentration relative, dans le milieu réactionnel, de radicaux stabilisés par résonance.

Mots clés : réaction d'oxydation, *n*-pentane, cyclopentane, modélisation, autoinflammation.

Abstract: The reduction of automotive emissions and the reformulation of gasoline composition require a better understanding of the combustion mechanism, in particular aiming at the determination of the influential reactions which are responsible for the onset of knock in spark ignition engines. We have studied the oxidation mechanism of two hydrocarbons of different research octane number: *n*-pentane (62) and cyclopentane (100). This work follows a previous study on the oxidation of *n*-heptane and isooctane. The experimental study was performed at 873 K in a jet-stirred flow reaction vessel. The reaction mechanisms of *n*-pentane and cyclopentane were analysed on a purely kinetic basis, derived from our experimental results, and were finally modelled by using a programme of simulation of reaction mechanisms. The different behaviour of these two hydrocarbons with respect to autoignition phenomena is mainly dependent on the relative concentration of resonance-stabilized radicals in the reaction medium.

Key words: oxidation reaction, *n*-pentane, cyclopentane, modelling, autoignition.

Introduction

L'existence des phénomènes d'autoinflammation dans les moteurs à allumage commandé est connue depuis plus de 50 ans; à cet égard les travaux de P. Dumanois (1) sont particulièrement intéressants et peuvent être considérés comme les précurseurs des travaux et interprétations modernes. Plusieurs expériences, réalisées dans les années trente, ont en effet mis en évidence l'augmentation brutale de pression accompagnant ces phénomènes de cliquetis. Cependant, la découverte de substances antidétonantes, en particulier le plomb tétraéthyle, a résolu ce problème de façon empirique pendant de longues années.

Reçu le 13 novembre 1996.

V. Simon, Y. Simon,[1] G. Scacchi et F. Baronnet. Département de chimie-physique des réactions, Unité de recherche associée n° 328 du Centre national de la recherche scientifique, Institut national polytechnique de Lorraine, École nationale supérieure des industries chimiques, 1, rue Grandville, BP 451, 54001 Nancy Cedex, France.

1. Auteur à qui adresser toute correspondance. Téléphone : 33 (0)3 83 17 51 22. Fax : 33 (0)3 83 37 81 20. E-mail : dcpr@ensic.u-nancy.fr

Pourtant, l'étude du mécanisme de la réaction d'oxydation des hydrocarbures (alcanes en premier lieu) a pris ces dernières années une importance croissante dans le but de déterminer les processus importants responsables du phénomène de cliquetis dans les moteurs à allumage commandé (2) et d'établir des corrélations entre structure des hydrocarbures et indice d'octane (3, 4). En effet, le développement de l'essence sans plomb implique l'utilisation de nouvelles substances à indice d'octane élevé (substances oxygénées par exemple) et la recherche de ces nouveaux composés nécessite une meilleure compréhension du mécanisme de combustion.

C'est pourquoi nous avons étudié les mécanismes d'oxydation d'hydrocarbures d'indice d'octane différent : le *n*-heptane et de l'isooctane (5) puis le *n*-pentane (indice recherche : 62) et le cyclopentane (indice recherche : 100). Cette étude, qui se poursuit actuellement sur l'oxydation de l'isopentane et du néopentane, couplée aux résultats précédents doit permettre l'approfondissement de l'effet de deux paramètres : (*i*) la longueur de la chaîne carbonée et (*ii*) la ramification de celle-ci.

La détermination des mécanismes d'oxydation du *n*-pentane et du cyclopentane est présentée en utilisant deux approches différentes. La première approche est une étude cinétique classique basée sur les résultats expérimentaux bruts

© 1997 NRC Canada

Can. J. Chem. Downloaded from www.nrcresearchpress.com by 88.146.161.215 on 09/08/12
For personal use only.

Can. J. Chem. Downloaded from www.nrcresearchpress.com by 88.146.161.215 on 09/08/12
For personal use only.

et plus particulièrement sur l'analyse des caractères primaire[2] ou secondaire des produits de réaction. La deuxième approche consiste en une simulation des résultats expérimentaux et une analyse de sensibilité qui permet de détecter les processus négligeables et donc de simplifier un mécanisme réactionnel écrit a priori.

Conditions expérimentales

L'étude de l'oxydation du *n*-pentane et du cyclopentane a été réalisée en utilisant un réacteur continu autoagité par jets gazeux en silice. L'injection de l'hydrocarbure liquide dans le réacteur est assurée par un pousse-seringue. Les caractéristiques de l'appareillage expérimental ont déjà été exposées précédemment (5).

Les expériences ont été réalisées à une température de 873 K. Afin d'éviter des problèmes de vaporisation de l'hydrocarbure au niveau du système d'injection, la pression totale au sein du réacteur a été fixée à 540 Torr (1 Torr = 133,3 Pa) dans le cas du *n*-pentane et à 400 Torr dans celui du cyclopentane, valeurs supérieures aux pressions de vapeur saturante (à température ambiante) des composés étudiés. Les pressions partielles d'oxygène et d'hydrocarbure ont été choisies de façon à obtenir un rapport HC/O_2 de 1/4, ce qui correspond à une richesse 2, les conditions stoechiométriques de la réaction d'oxydation totale étant :

$$C_5H_{12} + 8\ O_2 \longrightarrow 5\ CO_2 + 6\ H_2O$$

$$cy\text{-}C_5H_{10} + 15/2\ O_2 \longrightarrow 5\ CO_2 + 5\ H_2O$$

Les produits de réaction formés ont été analysés par chromatographie en phase gazeuse.

Résultats expérimentaux

Cas de l'oxydation du *n*-pentane

La réaction d'oxydation du *n*-pentane a été étudiée pour des temps de passage dans le réacteur variant de 0,2 à 0,6 s, ce qui correspond à un avancement de réaction, par rapport au *n*-pentane, compris entre 4% et 15% (1% correspond à 0,27 Torr). La consommation en oxygène varie de 1% à 10% (1% représente 1 Torr).

L'analyse chromatographique a permis d'identifier 10 produits de réaction différents : H_2, CH_4, C_2H_4, C_3H_6, 1-C_4H_8, 1-C_5H_{10}, H_2O, CO_2, CH_3CHO et C_2H_5CHO. On peut remarquer l'absence de CO, ou tout au moins une présence inférieure à la limite de détection du chromatographe utilisé (environ 0,1 Torr). De même, il faut noter que les aldéhydes identifiés ici sont présents en quantité insuffisante pour pouvoir être dosés. L'hydrogène a été dosé, mais sa courbe de formation n'a pu être tracée pour des raisons d'irreproductibilité. Les courbes de formation des produits de réaction sont représentées sur les figures 1 et 2.

2. Un produit de réaction est dit «primaire» lorsqu'il est formé à partir des réactifs ou radicaux libres uniquement. Il est dit «secondaire» lorsqu'il est formé à partir des produits primaires. Un produit primaire se caractérise par une vitesse de formation initiale non nulle, alors qu'un produit secondaire possède une vitesse de formation initiale nulle.

Fig. 1. Oxydation du *n*-pentane à 873 K. Courbes de formation de C_2H_4, CH_4, CO_2 et H_2O.

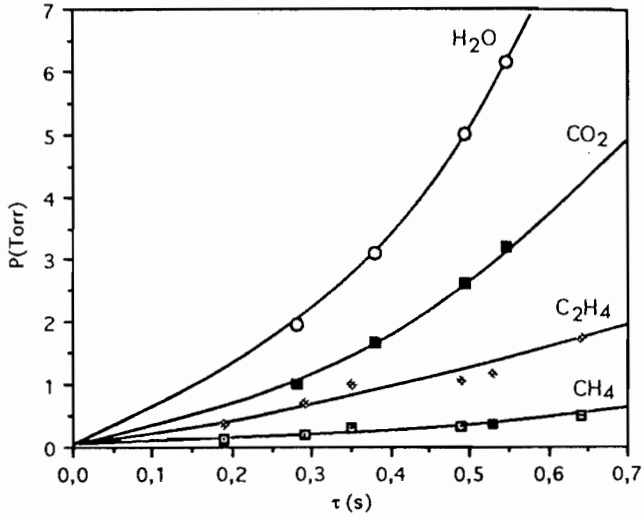
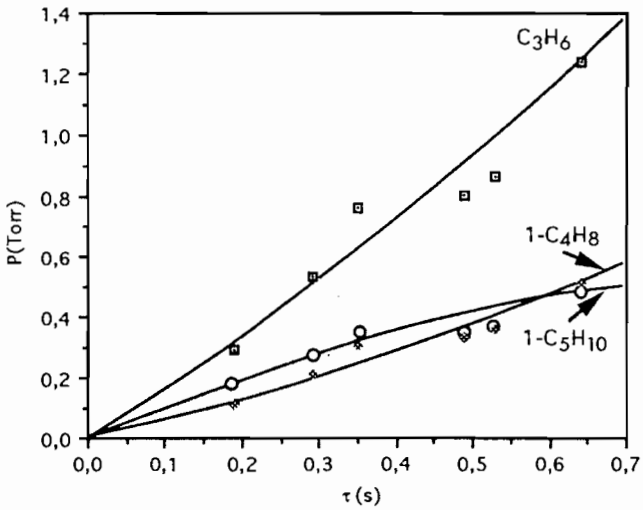


Fig. 2. Oxydation du *n*-pentane à 873 K. Courbes de formation de C_3H_6, 1-C_4H_8 et 1-C_5H_{10}.



Les «diagrammes horizontaux» correspondants à ces produits de réaction sont représentés sur les figures 3 et 4. Ces diagrammes sont tracés en portant le pourcentage molaire du produit considéré par rapport à l'ensemble des produits dosés (réactifs et H_2 non compris) en fonction du temps de passage. Le caractère primaire de la formation d'un composé est alors caractérisé par une courbe ne passant pas par l'origine. On observe donc que tous les produits représentés sont de caractère primaire.

Cas de l'oxydation du cyclopentane

La réaction d'oxydation du cyclopentane a été étudiée pour des temps de passage dans le réacteur variant entre 0,1 et 0,5 s, ce qui correspond à des avancements de réaction, par rapport au cyclopentane, compris entre 2% et 24% (1% représente 0,2 Torr). La consommation en oxygène, par contre, ne dépasse pas 1% (0,8 Torr) pour le temps de passage le plus élevé.

© 1997 NRC Canada

Can. J. Chem. Downloaded from www.nrcresearchpress.com by 88.146.161.215 on 09/08/12
For personal use only.

Fig. 3. Oxydation du *n*-pentane à 873 K. Répartition des produits majoritaires de la réaction en fonction du temps de passage.

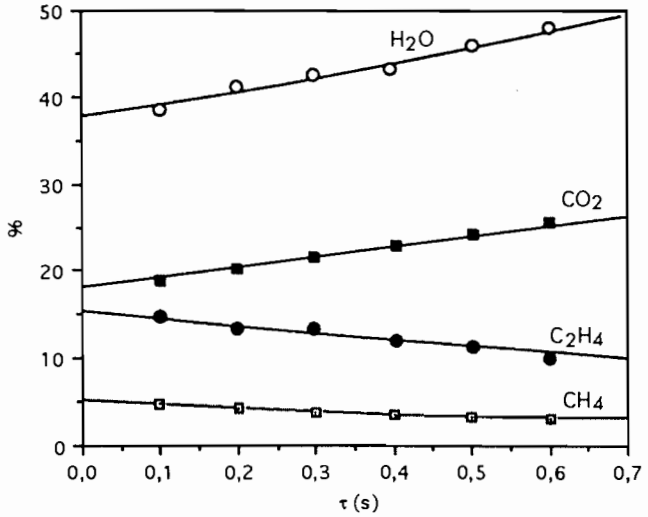
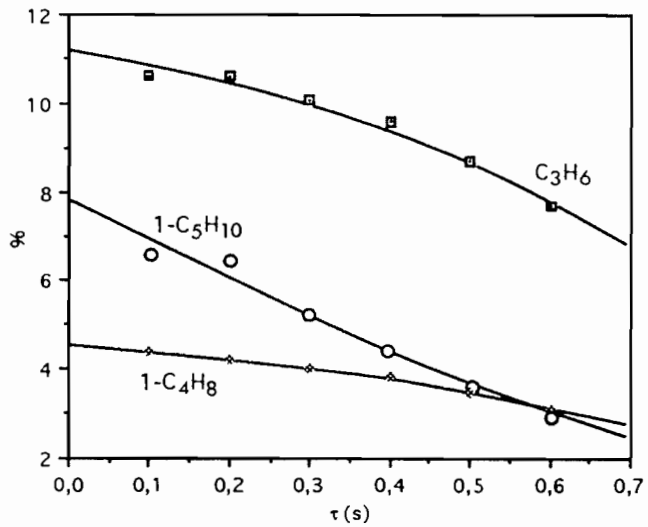


Fig. 4. Oxydation du *n*-pentane à 873 K. Répartition des produits minoritaires de la réaction en fonction du temps de passage.



Cette étude a permis d'identifier les produits de réaction suivants : H_2, CH_4, C_2H_4, C_3H_6, 1,3-C_4H_6, cy-C_5H_6, cy-C_5H_8, CO_2 et H_2O. Le monoxyde de carbone ainsi que les aldéhydes n'ont pu être détectés. Les courbes de formation de ces produits sont représentées sur les figures 5 et 6 et les «diagrammes horizontaux» correspondants sur les figures 7 et 8. Comme dans le cas du *n*-pentane, la courbe de formation de H_2 n'est pas représentée en raison des irreproductibilités. On notera que seul cy-C_5H_6 présente un caractère non primaire.

Interprétation des résultats expérimentaux

L'amorçage des réactions d'oxydation d'hydrocarbures se fait par arrachement d'un atome H· de la molécule d'alcane RH par une molécule d'oxygène :

$$RH + O_2 \longrightarrow R^{\cdot} + HO_2^{\cdot}$$

Fig. 5. Oxydation du cyclopentane à 873 K. Courbes de formation de H_2O, CO_2, cy-C_5H_8, C_2H_4 et cy-C_5H_6.

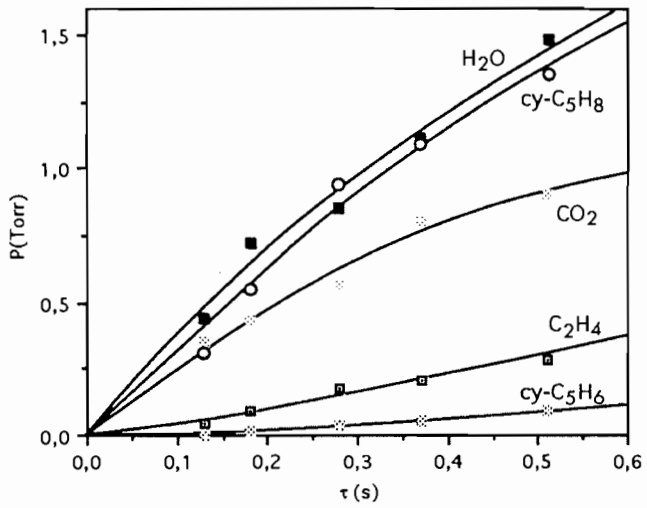


Fig. 6. Oxydation du cyclopentane à 873 K. Courbes de formation de C_3H_6, CH_4 et 1,3-C_4H_6.

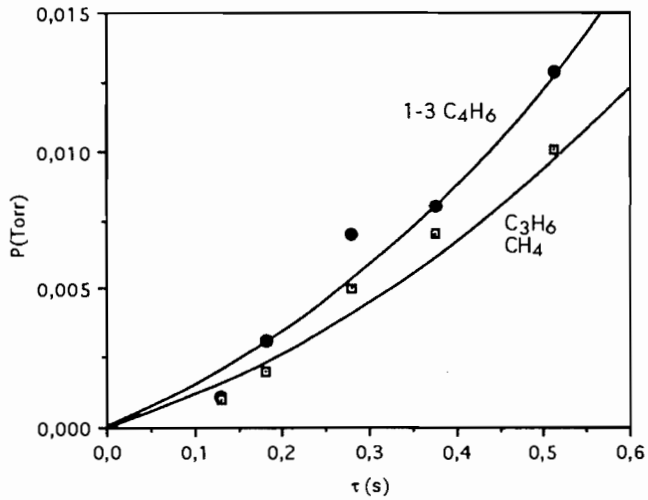
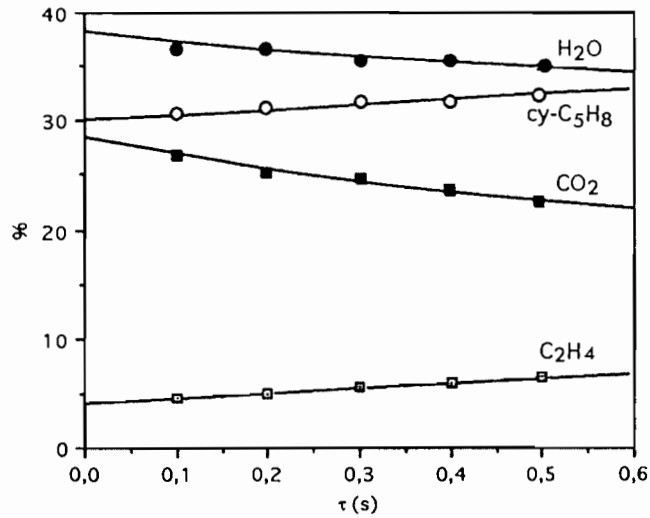


Fig. 7. Oxydation du cyclopentane à 873 K. Répartition des produits majoritaires de la réaction en fonction du temps de passage.



© 1997 NRC Canada

Le radical alcoyle R· peut alors réagir suivant deux mécanismes différents en fonction du domaine de température exploré.

Le radical R· peut se décomposer par rupture de liaisons C—C jusqu'à l'obtention de petits radicaux, qui seuls s'oxydent. Ce mécanisme, dit de *«haute température»*, valable au-dessus de 1000 K, a été proposé par Westbrook, Pitz et al. (6–15) ainsi que par Warnatz (16–19).

Ce radical R· peut aussi réagir avec une molécule d'oxygène pour former le radical peroxyalcoyle RO_2· qui est susceptible de s'isomériser par transfert interne d'atomes H· et conduire aux produits d'oxydation correspondants. Ce mécanisme, dit de *«basse température»*, est valable au-dessous de 800 K et constitue l'aboutissement des travaux de Fish (20–23) dans les années 60, puis de Quinn et Halstead (24) dans les années 70 et enfin de Cox et Cole (25) en 1985.

L'étude de l'oxydation du *n*-pentane et du cyclopentane ayant été réalisée à 873 K, les deux mécanismes précédents doivent être pris en compte. Le mécanisme général de l'oxydation de ces deux alcanes peut donc être schématisé de la façon suivante (Schéma 1) :

Schéma 1. Mécanisme général de l'oxydation des alcanes.

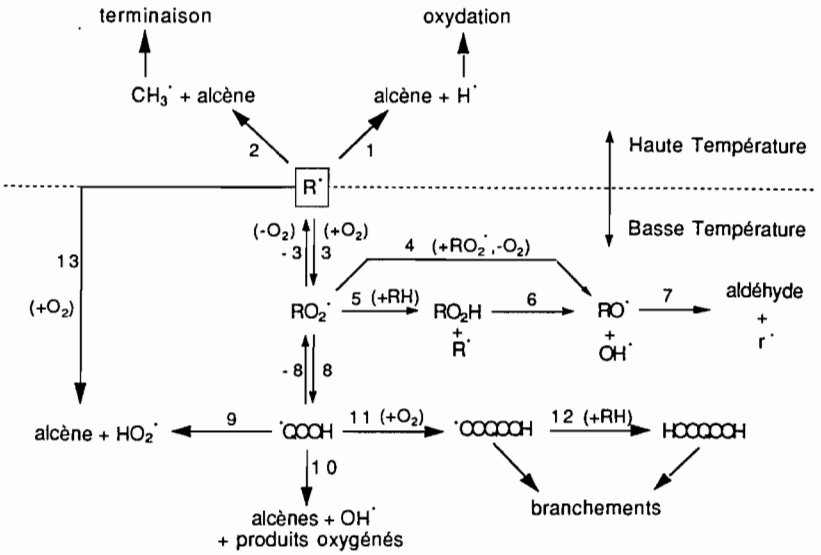
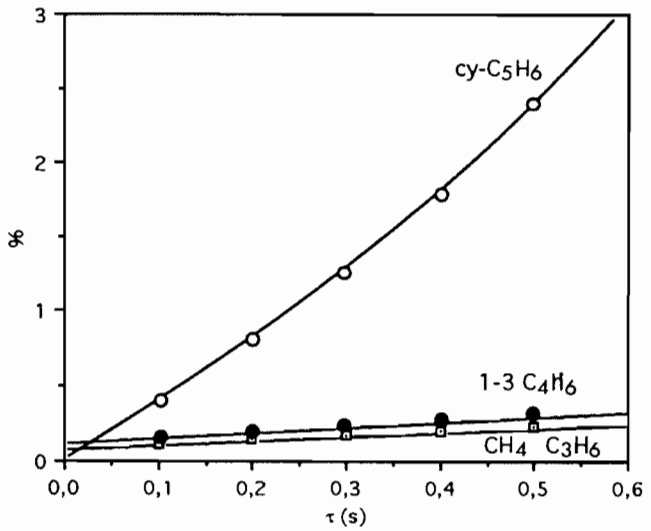
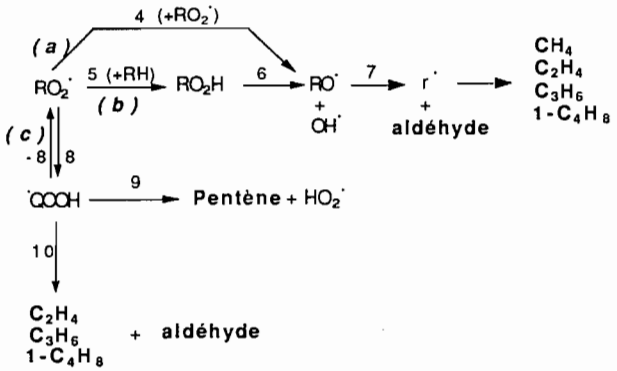


Fig. 8. Oxydation du cyclopentane à 873 K. Répartition des produits minoritaires de la réaction en fonction du temps de passage.



Ce mécanisme général est en fait une synthèse des deux mécanismes de *«haute et basse températures»*. Les différentes parties de ce mécanisme seront analysées en détail dans ce qui suit.

Schéma 2. Oxydation du *n*-pentane : mécanisme de *«basse température»*.



Cas de l'oxydation du *n*-pentane

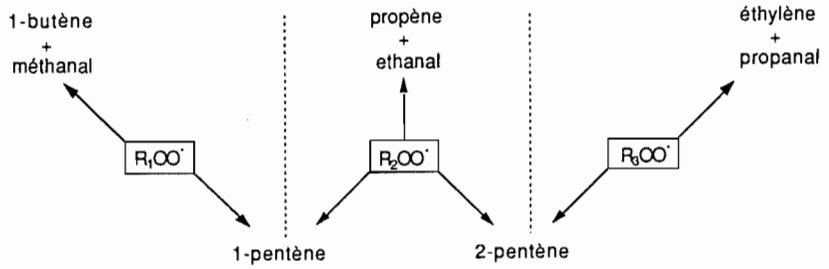
L'amorçage de la réaction d'oxydation du *n*-pentane (noté : RH) conduit à la formation de trois radicaux alcoyles R· différents ; ce sont les radicaux : pentyl-1, pentyl-2 et pentyl-3. Ces radicaux peuvent alors réagir suivant le mécanisme représenté sur le schéma 1. Nous allons tenter de simplifier ce mécanisme en utilisant les résultats expérimentaux et plus particulièrement le caractère primaire ou secondaire des produits formés.

Suivant le mécanisme de *«basse température»*, le radical R· s'oxyde en radical peroxyalcoyle ROO· qui peut réagir de trois manières différentes (Schéma 2).

© 1997 NRC Canada

Can. J. Chem. Downloaded from www.nrcresearchpress.com by 88.146.161.215 on 09/08/12
For personal use only.

Schéma 3. Oxydation du *n*-pentane : isomérisation des radicaux ROO·



Séquence réactionnelle (a)
Dans ce cas, le mécanisme prévoit la formation primaire de CH_4, C_2H_4, C_3H_6 et 1-C_4H_8, ce qui est compatible avec l'expérience (Figs. 3 et 4). Cependant, les aldéhydes sont formés expérimentalement à l'état de traces, alors que la formation des alcènes et même du méthane est beaucoup plus importante. Ces composés ne sont donc manifestement pas formés par la voie (*a*) qui pourra être considérée comme minoritaire, mais qui peut cependant rendre compte de la formation des aldéhydes.

Séquence réactionnelle (b)
Tous les produits de réaction formés par cette voie sont secondaires, puisqu'ils proviennent de la décomposition d'un produit primaire ROOH. Or l'examen des diagrammes horizontaux (Figs. 3 et 4) montre très clairement que CH_4, C_2H_4, C_3H_6 et 1-C_4H_8 sont primaires. La voie (*b*) peut donc être considérée comme négligeable.

Séquence réactionnelle (c)
Soient R_1·, R_2· et R_3· respectivement les radicaux pentyl-1, 2 et 3. La formation d'alcènes à partir du radical ROO· peut être schématisée de la façon suivante (Schéma 3).

D'après les séquences réactionnelles développées ci-dessus, on peut établir un certain nombre de relations entre les concentrations des divers produits formés :

[1] $(C_2H_4) = (C_2H_5CHO)$

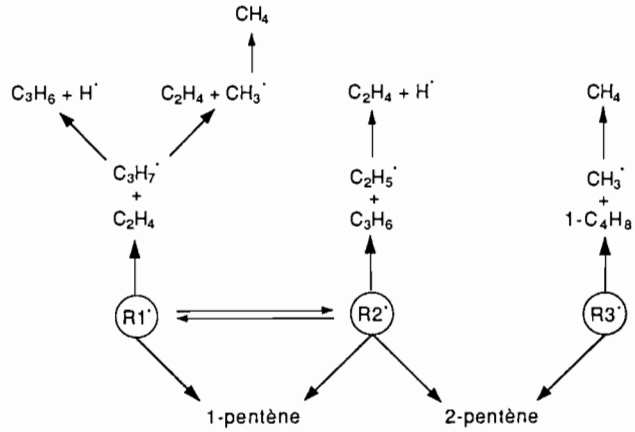
[2] $(C_3H_6) = (CH_3CHO)$

[3] $(1\text{-}C_4H_8) = (CH_2O)$

Or, les pourcentages initiaux (Fig. 4) des alcènes sont respectivement : 11,2; 4,5 et 7,8 pour C_3H_6; 1-C_4H_8 et 1-C_5H_{10} alors que ceux des aldéhydes (présents à l'état de traces) sont proches de 0. Manifestement, cette voie réactionnelle (*c*) ne rend pas compte des résultats expérimentaux. Le mécanisme d'oxydation de «*basse température*» semblerait donc être d'importance minoritaire en ce qui concerne la formation du butène-1, du propène et de l'éthylène. On ne peut, cependant, rien conclure sur l'importance des processus de formation des pentènes.

Si on considère maintenant le mécanisme de «*haute température*», le radical pentyle R· se décompose par cassure de liaisons C—C ou éventuellement C—H pour conduire au schéma réactionnel suivant (Schéma 4) :

Schéma 4. Oxydation du *n*-pentane : mécanisme de «*haute température*».



Si ce mécanisme est effectivement majoritaire, la répartition des produits d'oxydation doit vérifier la relation :

[4] $(C_3H_6) + 2[(CH_4) - (1\text{-}C_4H_8)] = (C_2H_4)$

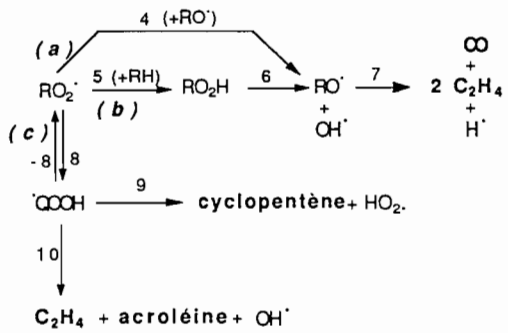
Or, aux premiers instants de la réaction (Figs. 4 et 5) : (C_2H_4) = 15% et $(C_3H_6) + 2[(CH_4) - (1\text{-}C_4H_8)]$ = 13,2%.

En tenant compte des erreurs expérimentales, l'égalité précédente peut-être considérée comme assez bien vérifiée. Il semblerait donc que la réaction d'oxydation du *n*-pentane s'effectue de façon préférentielle suivant le mécanisme de «*haute température*».

Cas de l'oxydation du cyclopentane

L'amorçage de la réaction d'oxydation du cyclopentane conduit à la formation d'un seul type de radical R·, le radical cyclopentyle. L'oxydation de ce radical suivant le mécanisme de «*basse température*» conduit au schéma réactionnel suivant (Schéma 5) :

Schéma 5. Oxydation du cyclopentane : mécanisme de «*basse température*».



© 1997 NRC Canada

Can. J. Chem. Downloaded from www.nrcresearchpress.com by 88.146.161.215 on 09/08/12
For personal use only.

Can. J. Chem. Downloaded from www.nrcresearchpress.com by 88.146.161.215 on 09/08/12
For personal use only.

Séquence réactionnelle (a)
Les produits de réaction formés par cette voie sont de nature primaire, ce qui est le cas, expérimentalement, pour l'éthylène (Fig. 7). Cependant, l'éthylène est formé en grande quantité, alors que le monoxyde de carbone est présent à l'état de traces dans le milieu réactionnel. Cette séquence de processus (*a*) n'a probablement que très peu d'effet sur la production de l'éthylène et pourra donc être considérée comme minoritaire.

Séquence réactionnelle (b)
Cette voie conduit à la formation de composés de caractère secondaire. Or expérimentalement, l'éthylène est de nature primaire, comme le montrent les diagrammes horizontaux de la figure 7. Cette séquence réactionnelle semble donc être minoritaire dans l'oxydation du cyclopentane.

Séquence réactionnelle (c)
Cette voie conduit à la formation d'éthylène, d'acroléine et de cyclopentène primaires (Fig. 8). Expérimentalement, l'éthylène et le cyclopentène sont effectivement de nature primaire, alors que l'acroléine n'a pu être détectée. Les résultats expérimentaux ne permettent donc pas de conclure sur l'importance relative de cette séquence de processus.

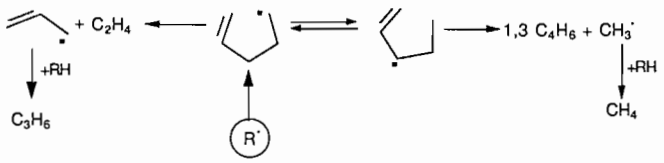
Cependant, l'application de l'AEQS au radical ·QOOH (à 873 K) conduit aux relations suivantes :

$$[5] \quad V_9 = 7 \times 10^5 \, V_{10}$$

Les constantes de vitesse utilisées dans ce calcul étant estimées selon les méthodes de la cinétique thermochimique (26), ce résultat quantitatif ne peut être considéré que comme une approximation. Qualitativement, on peut considérer que la vitesse du processus 9 est beaucoup plus grande que celle du processus 10 et donc que le radical ·QOOH se décompose préférentiellement en formant du cyclopentène.

Si on considère, maintenant, le mécanisme de *«haute température»*, le radical cyclopentyle réagit suivant le schéma 6 :

Schéma 6. Oxydation du cyclopentane : mécanisme de *«haute température»*.



D'après ce mécanisme les concentrations en éthylène et propène ainsi que celles en méthane et butadiène doivent être égales. Or, si le méthane est bien formé en quantité voisine de celle du butadiène, la concentration en éthylène est, quant à elle, cinq fois plus importante que celle du propène. Ce mécanisme ne rend pas compte à lui seul de la formation de l'éthylène qui est probablement formé en quantité non négligeable par le mécanisme de *«basse température»* à partir de l'oxydation des radicaux pentyles.

Modélisation des réactions d'oxydation du *n*-pentane et du cyclopentane

Les mécanismes d'oxydation du *n*-pentane et du cyclopentane ont été simulés grâce au logiciel de simulation de mécanismes réactionnels Morse (27). Cette simulation permet de simplifier les mécanismes d'oxydation des deux hydrocarbures étudiés en identifiant les processus négligeables et ainsi de vérifier la validité des suppositions faites au paragraphe précédent.

Fig. 9. Oxydation du *n*-pentane à 873 K. Courbes de formation simulées de H_2O, C_2H_4 et CH_4.

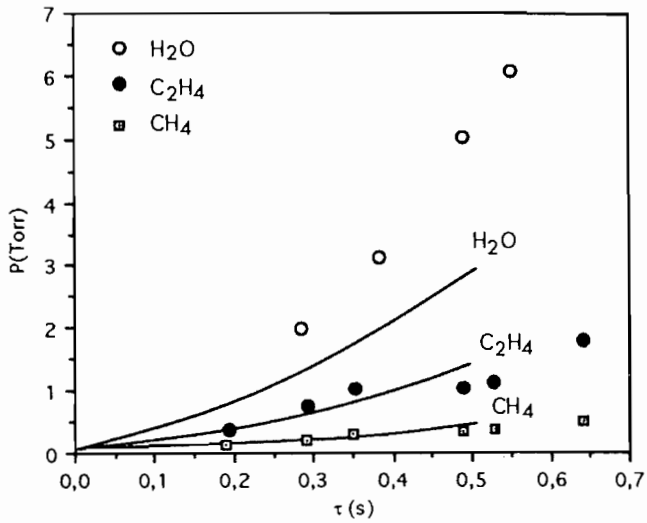
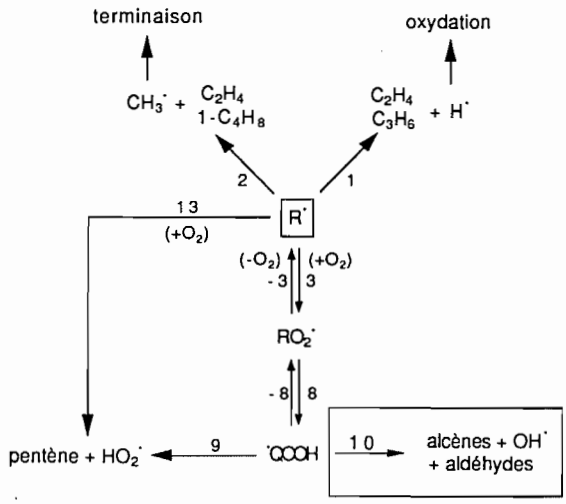


Schéma 7. Mécanisme final de l'oxydation du *n*-pentane (R· représente les radicaux R1·, R2· et R3·).



Cas de l'oxydation du *n*-pentane

Le mécanisme utilisé pour modéliser la réaction d'oxydation du *n*-pentane comporte 168 processus élémentaires représentant les mécanismes primaires de *«haute et basse température»*. De façon à ne pas travailler avec des mécanisme de tailles démesurées, seuls les processus conduisant à la formation de composés identifiés expérimentalement ont été conservés.

Les constantes de vitesse ont été ajustées, dans des limites raisonnables compte tenu de la précision existant sur les paramètres cinétiques, de manière à obtenir, pour les produits d'oxydation dosés, des courbes de formation théoriques aussi proches que possible des courbes expérimentales. La figure 9 montre cet ajustement dans le cas de CH_4, C_2H_4 et H_2O.

© 1997 NRC Canada

Can. J. Chem. Downloaded from www.nrcresearchpress.com by 88.146.161.215 on 09/08/12
For personal use only.

Tableau 1. Mécanisme d'oxydation du *n*-pentane à 873 K.

Processus	k (cm^3, mol, s)
$RH + O_2 \rightarrow R1^{\cdot} + HO_2^{\cdot}$	$1,6 \times 10$
$RH + O_2 \rightarrow R2^{\cdot} + HO_2^{\cdot}$	$5,8 \times 10^2$
$RH + O_2 \rightarrow R3^{\cdot} + HO_2^{\cdot}$	$2,9 \times 10$
$R1^{\cdot} \rightarrow R2^{\cdot}$	$1,1 \times 10^8$
$R2^{\cdot} \rightarrow R1^{\cdot}$	$7,1 \times 10^7$
$R1^{\cdot} + O_2 \rightarrow R1OO^{\cdot}$	$9,9 \times 10^{11}$
$R2^{\cdot} + O_2 \rightarrow R2OO^{\cdot}$	$3,2 \times 10^{12}$
$R3^{\cdot} + O_2 \rightarrow R3OO^{\cdot}$	$3,2 \times 10^{12}$
$R1OO^{\cdot} \rightarrow R1^{\cdot} + O_2$	$4,4 \times 10^7$
$R2OO^{\cdot} \rightarrow R2^{\cdot} + O_2$	$2,2 \times 10^7$
$R3OO^{\cdot} \rightarrow R3^{\cdot} + O_2$	$2,2 \times 10^7$
$R1OO^{\cdot} \rightarrow Q1OOH(^{\cdot}2)$	$2,5 \times 10^7$
$R1OO^{\cdot} \rightarrow Q1OOH(^{\cdot}3)$	$1,6 \times 10^8$
$R2OO^{\cdot} \rightarrow Q2OOH(^{\cdot}3)$	$2,5 \times 10^7$
$R2OO^{\cdot} \rightarrow Q2OOH(^{\cdot}4)$	$1,6 \times 10^8$
$R3OO^{\cdot} \rightarrow Q3OOH(^{\cdot}1)$	$9,6 \times 10^7$
$R3OO^{\cdot} \rightarrow Q3OOH(^{\cdot}2)$	$5,6 \times 10^6$
$Q1OOH(^{\cdot}2) \rightarrow R1OO^{\cdot}$	$1,7 \times 10^8$
$Q1OOH(^{\cdot}3) \rightarrow R1OO^{\cdot}$	$1,1 \times 10^9$
$Q2OOH(^{\cdot}3) \rightarrow R2OO^{\cdot}$	$1,5 \times 10^8$
$Q2OOH(^{\cdot}4) \rightarrow R2OO^{\cdot}$	$9,7 \times 10^8$
$Q3OOH(^{\cdot}1) \rightarrow R3OO^{\cdot}$	$1,2 \times 10^9$
$Q3OOH(^{\cdot}2) \rightarrow R3OO^{\cdot}$	$1,7 \times 10^8$
$Q1OOH(^{\cdot}3) \rightarrow 1\text{-}C_4H_8 + CH_2(^{\cdot})OOH$	$2,9 \times 10^7$
$Q2OOH(^{\cdot}4) \rightarrow C_3H_6 + CH_3CH(^{\cdot})OOH$	$9,6 \times 10^7$
$Q3OOH(^{\cdot}1) \rightarrow C_2H_4 + C_2H_5CH(^{\cdot})OOH$	$3,4 \times 10^7$
$CH_2(^{\cdot})OOH \rightarrow CH_2O + OH^{\cdot}$	$1,7 \times 10^{12}$
$CH_3CH(^{\cdot})OOH \rightarrow CH_3CHO + OH^{\cdot}$	$1,1 \times 10^{12}$
$C_2H_5CH(^{\cdot})OOH \rightarrow CH_3CH_2CHO + OH^{\cdot}$	$1,4 \times 10^{12}$
$Q1OOH(^{\cdot}2) \rightarrow 1\text{-}C_5H_{10} + HO_2^{\cdot}$	$4,0 \times 10^{10}$
$Q2OOH(^{\cdot}3) \rightarrow 2\text{-}C_5H_{10} + HO_2^{\cdot}$	$3,1 \times 10^{10}$
$Q3OOH(^{\cdot}2) \rightarrow 1\text{-}C_5H_{10} + HO_2^{\cdot}$	$5,5 \times 10^{10}$
$R1^{\cdot} + O_2 \rightarrow 1\text{-}C_5H_{10} + HO_2^{\cdot}$	$3,2 \times 10^{10}$
$R2^{\cdot} + O_2 \rightarrow 1\text{-}C_5H_{10} + HO_2^{\cdot}$	$7,6 \times 10^{10}$
$R2^{\cdot} + O_2 \rightarrow 2\text{-}C_5H_{10} + HO_2^{\cdot}$	$1,8 \times 10^{11}$
$R3^{\cdot} + O_2 \rightarrow 2\text{-}C_5H_{10} + HO_2^{\cdot}$	$1,8 \times 10^{11}$
$CH_2O + HO_2^{\cdot} \rightarrow HCO^{\cdot} + H_2O_2$	$1,8 \times 10^9$
$CH_3CHO + HO_2^{\cdot} \rightarrow CH_3CO^{\cdot} + H_2O_2$	$1,8 \times 10^9$
$CH_3CH_2CHO + HO_2^{\cdot} \rightarrow C_2H_5CO^{\cdot} + H_2O_2$	$1,8 \times 10^9$
$CH_2O + OH^{\cdot} \rightarrow HCO^{\cdot} + H_2O$	$4,0 \times 10^{13}$
$CH_3CHO + OH^{\cdot} \rightarrow CH_3CO^{\cdot} + H_2O$	$1,0 \times 10^{13}$
$CH_3CH_2CHO + OH^{\cdot} \rightarrow C_2H_5CO^{\cdot} + H_2O$	$1,0 \times 10^{13}$
$HCO^{\cdot} \rightarrow H^{\cdot} + CO$	$1,6 \times 10^{10}$
$CH_3CO^{\cdot} \rightarrow CH_3^{\cdot} + CO$	$2,0 \times 10^8$
$C_2H_5CO^{\cdot} \rightarrow C_2H_5^{\cdot} + CO$	$2,0 \times 10^8$
$R1^{\cdot} \rightarrow C_2H_4 + 1\text{-}C_3H7^{\cdot}$	$8,6 \times 10^5$
$R2^{\cdot} \rightarrow C_3H_6 + C_2H_5^{\cdot}$	$1,2 \times 10^5$
$R3^{\cdot} \rightarrow 1\text{-}C_4H_8 + CH_3^{\cdot}$	$9,8 \times 10^5$
$1\text{-}C_3H_7^{\cdot} \rightarrow C_3H_6 + H^{\cdot}$	$4,0 \times 10^3$
$C_2H_5^{\cdot} \rightarrow C_2H_4 + H^{\cdot}$	$4,0 \times 10^3$
$1\text{-}C_3H_7^{\cdot} \rightarrow C_2H_4 + CH_3^{\cdot}$	$1,2 \times 10^6$
$RH + H^{\cdot} \rightarrow R1^{\cdot} + H2$	$5,2 \times 10^{11}$
$RH + H^{\cdot} \rightarrow R2^{\cdot} + H2$	$7,9 \times 10^{11}$
$RH + H^{\cdot} \rightarrow R3^{\cdot} + H2$	$3,9 \times 10^{11}$
$RH + CH_3^{\cdot} \rightarrow R1^{\cdot} + CH_4$	$1,7 \times 10^9$
$RH + CH_3^{\cdot} \rightarrow R2^{\cdot} + CH_4$	$3,4 \times 10^9$

Tableau 1 (*suite et fin*).

Processus	k (cm^3, mol, s)
$RH + CH_3^{\cdot} \rightarrow R3^{\cdot} + CH_4$	$1,7 \times 10^9$
$RH + HO_2^{\cdot} \rightarrow R1^{\cdot} + H_2O_2$	$1,7 \times 10^9$
$RH + HO_2^{\cdot} \rightarrow R2^{\cdot} + H_2O_2$	$4,0 \times 10^9$
$RH + HO_2^{\cdot} \rightarrow R3^{\cdot} + H_2O_2$	$2,0 \times 10^9$
$RH + OH^{\cdot} \rightarrow R1^{\cdot} + H_2O$	$3,0 \times 10^{12}$
$RH + OH^{\cdot} \rightarrow R2^{\cdot} + H_2O$	$5,0 \times 10^{12}$
$RH + OH^{\cdot} \rightarrow R3^{\cdot} + H_2O$	$5,0 \times 10^{12}$
$H^{\cdot} + O_2 \rightarrow OH^{\cdot} + .O^{\cdot}$	$2,0 \times 10^{10}$
$HO_2^{\cdot} + H^{\cdot} \rightarrow OH^{\cdot} + OH^{\cdot}$	$8,4 \times 10^{13}$
$HO_2^{\cdot} + {}^{\cdot}O^{\cdot} \rightarrow OH + O_2$	$2,0 \times 10^{13}$
$CH_3^{\cdot} + {}^{\cdot}O^{\cdot} \rightarrow CH_2O + H^{\cdot}$	$7,0 \times 10^{13}$
$CH_3^{\cdot} + O_2 \rightarrow CH_2O + OH^{\cdot}$	$1,8 \times 10^9$
$CH_2O + H^{\cdot} \rightarrow HCO^{\cdot} + H2$	$2,5 \times 10^{12}$
$CH_2O + {}^{\cdot}O^{\cdot} \rightarrow HCO^{\cdot} + OH^{\cdot}$	$4,6 \times 10^{12}$
$CH_2O + O_2 \rightarrow HCO^{\cdot} + HO_2^{\cdot}$	$4,2 \times 10^5$
$HCO^{\cdot} + O_2 \rightarrow CO + HO_2^{\cdot}$	$3,0 \times 10^{13}$
$C_2H_5^{\cdot} + O_2 \rightarrow C_2H_4 + HO_2^{\cdot}$	$9,1 \times 10^{10}$
$CH_3CHO + H^{\cdot} \rightarrow CH_3^{\cdot} + CO + H2$	$3,5 \times 10^{12}$
$CH_3CHO + {}^{\cdot}O^{\cdot} \rightarrow CH_3^{\cdot} + CO + OH^{\cdot}$	$1,5 \times 10^{12}$
$CO + OH^{\cdot} \rightarrow CO_2 + H^{\cdot}$	$1,2 \times 10^{14}$
$CO + HO_2^{\cdot} \rightarrow CO_2 + OH^{\cdot}$	$1,1 \times 10^{11}$
$HO_2^{\cdot} + HO_2^{\cdot} \rightarrow H_2O_2 + O_2$	$2,0 \times 10^{12}$
$CH_3^{\cdot} + H^{\cdot} \rightarrow CH_4$	$6,9 \times 10^{13}$
$CH_3^{\cdot} + CH_3^{\cdot} \rightarrow C_2H_6$	$1,6 \times 10^{13}$
$HO_2^{\cdot} + H^{\cdot} \rightarrow H2 + O_2$	$2,5 \times 10^{13}$
$HO_2^{\cdot} + OH^{\cdot} \rightarrow H_2O + O_2$	$2,0 \times 10^{13}$

NOTA : RH représente la molécule de *n*-pentane. R1$^{\cdot}$, R2$^{\cdot}$ et R3$^{\cdot}$ sont respectivement les radicaux pentyles 1, 2 et 3. Q*p*OOH($^{\cdot}n$) représente le radical hydroperoxyalcoyle issu du radical R*p*$^{\cdot}$ et dont l'électron célibataire se positionne sur le $n^{ème}$ carbone de la chaîne.

L'analyse de sensibilité, effectuée sur les constantes de vitesse, a permis de simplifier considérablement ce mécanisme, en détectant les processus négligeables. Le mécanisme ne comprend plus, après cette simplification, que 82 processus élémentaires (Tableau 1).

Cette simulation a effectivement permis de vérifier les simplifications faites par des considérations d'ordre expérimental.

La réaction d'oxydation du *n*-pentane relève donc des mécanismes de *«haute et basse températures»*. Le processus 10 n'a été conservé que pour rendre compte de la formation des aldéhydes, présents, rappelons-le, à l'état de traces dans le milieu réactionnel. Ce mécanisme, représenté sur le Schéma 7, regroupe les Schémas 2 et 4 après simplification.

Cas de l'oxydation du cyclopentane

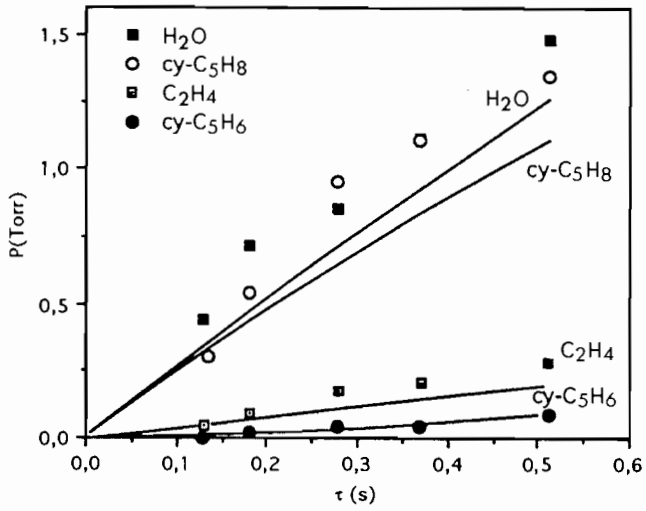
Le mécanisme de départ utilisé pour simuler la réaction d'oxydation du cyclopentane comporte 94 processus élémentaires. Comme pour l'oxydation du *n*-pentane, seuls ont été pris en compte les processus donnant lieu à la formation de composés identifiés expérimentalement.

L'ajustement des constantes de vitesse a permis d'obtenir des courbes de formation théoriques très proches des courbes expérimentales comme le montre la figure 10 dans le cas de l'eau, du cyclopentène, du cyclopentadiène et de l'éthylène. L'éloignement croissant, avec l'augmentation du temps de

© 1997 NRC Canada

Can. J. Chem. Downloaded from www.nrcresearchpress.com by 88.146.161.215 on 09/08/12
For personal use only.

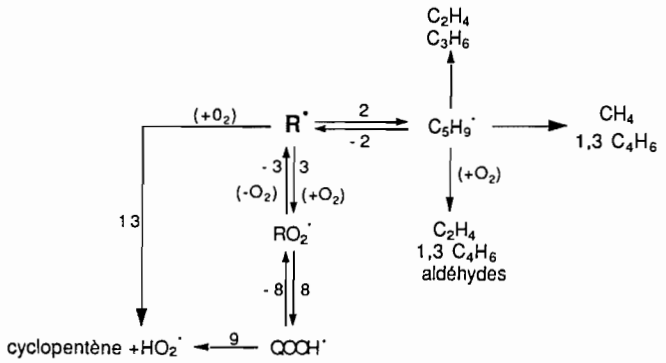
Fig. 10. Oxydation du cyclopentane à 873 K. Courbes de formation simulées de H_2O, cy-C_5H_8, C_2H_4 et cy-C_5H_6.



passage, entre les courbes théoriques et expérimentales peut être interprété par l'intervention de processus secondaires.

Après analyse de sensibilité, le mécanisme d'oxydation du cyclopentane ne comporte plus que 47 processus élémentaires (Tableau 2). La réaction semble partagée entre une évolution suivant le mécanisme de *«haute température»* et une évolution suivant le mécanisme de *«basse température»*, ce qui avait déjà été pressenti dans le paragraphe précédent. Ce mécanisme, qui est une synthèse des Schémas 5 et 6, peut être schématisé de la façon suivante (Schéma 8) :

Schéma 8. Mécanisme final de l'oxydation du cyclopentane (C5H9. représente les deux formes isomères du radical pentènyle)



Interprétation et discussion

La comparaison des mécanismes d'oxydation du *n*-pentane et du cyclopentane montre que ces deux réactions évoluent de manière similaire. En effet, l'oxydation du *n*-pentane, comme celle du cyclopentane, fait intervenir les mécanismes de *«haute et de basse température»*, la part du mécanisme de *«haute température»* semblant cependant être un peu plus importante dans le cas du *n*-pentane.

La différence de comportement de ces deux hydrocarbures vis à vis des phénomènes d'autoinflammation ne peut être interprétée par la seule étude des mécanismes primaires d'oxydation.

Tableau 2. Mécanisme d'oxydation du cyclopentane.

Processus	k (cm^3, mol, s)
$RH + O_2 \rightarrow R^\cdot + HO_2^\cdot$	$9{,}0 \times 10^3$
$R^\cdot + O_2 \rightarrow RO_2^\cdot$	$3{,}2 \times 10^{12}$
$RO_2^\cdot \rightarrow R^\cdot + O_2$	$2{,}2 \times 10^7$
$RO_2^\cdot \rightarrow$ cy-C_5H_8(OOH-1)(·2)	$1{,}6 \times 10^8$
cy-C_5H_8(OOH-1)(·2) $\rightarrow$ cy-$C_5H_8 + HO_2^\cdot$	$1{,}4 \times 10^{11}$
$R^\cdot +$ cy-$C_5H_8 \rightarrow$ cy-$C_5H_8 + HO_2^\cdot$	$4{,}0 \times 10^{10}$
$R^\cdot \rightarrow$ 1-C_5H_9(·5)	$4{,}0 \times 10^5$
1-C_5H_9(·5) $\rightarrow R^\cdot$	$6{,}6 \times 10^6$
1-C_5H_9(·5) $\rightarrow$ 1-C_5H_9(·3)	$1{,}8 \times 10^9$
1-C_5H_9(·3) $\rightarrow$ 1-C_5H_9(·5)	$4{,}1 \times 10^8$
1-C_5H_9(·3) $\rightarrow$ 1,3-$C_4H_6 + CH_3^\cdot$	$1{,}0 \times 10^6$
1-C_5H_9(·5) $\rightarrow C_2H_4 + C_3H_5^\cdot$	$3{,}5 \times 10^6$
1-C_5H_9(·5) $+ O_2 \rightarrow$ 1-C_5H_9(OO·-5)	$3{,}2 \times 10^{11}$
1-C_5H_9(·3) $+ O_2 \rightarrow$ 1-C_5H_9(OO·-3)	$1{,}1 \times 10^{13}$
1-C_5H_9(OO·-5) $\rightarrow$ 1-C_5H_9(·5) $+ O_2$	$2{,}2 \times 10^7$
1-C_5H_9(OO·-3) $\rightarrow$ 1-C_5H_9(·3) $+ O_2$	$2{,}2 \times 10^7$
1-C_5H_9(OO·-5) $\rightarrow$ 1-C_5H_8(OOH-5)(·3)	$1{,}6 \times 10^8$
1-C_5H_9(OO·-3) $\rightarrow$ 1-C_5H_8(OOH-3)(·5)	$9{,}6 \times 10^7$
cy-$C_5H_8 +$ cy-$C_5H_7^\cdot \rightarrow$ cy-$C_5H_7^\cdot + HO_2^\cdot$	$1{,}1 \times 10^5$
cy-$C_5H_7^\cdot \rightarrow$ cy-$C_5H_6 + H^\cdot$	$2{,}0 \times 10^4$
cy-$C_5H_7^\cdot + O_2 \rightarrow$ cy-$C_5H_6 + HO_2^\cdot$	$4{,}0 \times 10^{10}$
1-C_5H_8(OOH-5)(·3) $\rightarrow$ 1,3-$C_4H_6 + CH_2$(·)OOH	$2{,}9 \times 10^7$
1-C_5H_8(OOH-3)(·5) $\rightarrow C_2H_4 + C_2H_3CH$(·)OOH	$3{,}4 \times 10^7$
1-C_5H_8(OOH-3)(·5) $\rightarrow$ cy-C_5H_8(OOH-1)(·2)	$6{,}6 \times 10^6$
CH_2(·)OOH $\rightarrow CH_2O + OH^\cdot$	$1{,}7 \times 10^{12}$
C_2H_3CH(·)OOH $\rightarrow C_2H_3CHO + OH^\cdot$	$1{,}4 \times 10^{12}$
$CH_2O + OH^\cdot \rightarrow HCO^\cdot + H_2O$	$1{,}5 \times 10^{13}$
$C_2H_3CHO + OH^\cdot \rightarrow C_2H_3CO^\cdot + H_2O$	$1{,}0 \times 10^{13}$
$HCO^\cdot \rightarrow H^\cdot + CO$	$1{,}6 \times 10^{10}$
$C_2H_3CO^\cdot \rightarrow C_2H_3^\cdot + CO$	$2{,}0 \times 10^8$
$RH + H^\cdot \rightarrow H_2 + R^\cdot$	$2{,}0 \times 10^{12}$
$RH + CH_3^\cdot \rightarrow CH_4 + R^\cdot$	$2{,}6 \times 10^{10}$
$RH + C_2H_3^\cdot \rightarrow C_2H_4 + R^\cdot$	$7{,}9 \times 10^{11}$
$RH + C_3H_5^\cdot \rightarrow C_3H_6 + R^\cdot$	$7{,}9 \times 10^{11}$
$RH + HO_2^\cdot \rightarrow H_2O_2 + R^\cdot$	$9{,}9 \times 10^7$
$RH + OH^\cdot \rightarrow H_2O + R^\cdot$	$2{,}1 \times 10^{10}$
$H^\cdot + O_2 \rightarrow OH^\cdot + {}^\cdot O^\cdot$	$2{,}0 \times 10^{10}$
$OH^\cdot + OH^\cdot \rightarrow H_2O + {}^\cdot O^\cdot$	$3{,}3 \times 10^{12}$
$HO_2^\cdot + H^\cdot \rightarrow OH^\cdot + OH^\cdot$	$8{,}4 \times 10^{13}$
$HO_2^\cdot + {}^\cdot O^\cdot \rightarrow OH^\cdot + O_2$	$2{,}0 \times 10^{13}$
$CH_3^\cdot + O_2 \rightarrow CH_2O + OH^\cdot$	$1{,}8 \times 10^9$
$C_3H_5^\cdot + O_2 \rightarrow C_3H_4 + HO_2^\cdot$	$2{,}0 \times 10^9$
$CO + OH^\cdot \rightarrow CO_2 + H^\cdot$	$1{,}2 \times 10^{13}$
$HO_2^\cdot + HO_2^\cdot \rightarrow H_2O_2 + O_2$	$2{,}0 \times 10^{12}$
$HO_2^\cdot + H^\cdot \rightarrow H_2 + O_2$	$2{,}5 \times 10^{13}$
$HO_2^\cdot + OH^\cdot \rightarrow H_2O + O_2$	$2{,}0 \times 10^{13}$
$H_2O_2 \rightarrow OH^\cdot + OH^\cdot$	$3{,}0 \times 10^6$

NOTA : RH représente la molécule de cyclopentane et R· le radical cyclopentyle. 1-C_5H_8(OOH-*p*)(·*q*) représente le radical hydroperoxyalcoyle portant le groupement OOH sur le carbone n° *p* et l'électron célibataire sur le carbone n° *q*.

Ces résultats sont, par ailleurs, identiques à ceux obtenus lors de l'étude des réactions d'oxydation du *n*-heptane et de l'isooctane pour lesquels les mécanismes d'oxydation, déterminés dans des conditions expérimentales identiques, étaient également tout à fait similaires (5, 28).

© 1997 NRC Canada

Tableau 3. Indices d'octane recherche de mélange et % initiaux des principaux produits d'oxydation.

	BRON (réf. 29)	*n*-Heptane (RON : 0)	*n*-Pentane (RON : 61,7)	Isooctane (RON : 100)	cy-Pentane (RON : 100)
		0	62	100	141
Éthylène	—	20	15	—	5
Propène	—	8	12	7	—
Isobutène	170	—	—	31	—
cy-Pentène	171	—	—	—	30

Comme dans le cas du *n*-heptane et de l'isooctane, la seule différence existant entre les réactions d'oxydation du *n*-pentane et du cyclopentane réside dans la nature des produits formés et plus particulièrement des alcènes.

En effet, les alcènes formés par les réactions d'oxydation pourraient, par l'intermédiaire de processus secondaires, former, dans certains cas, des radicaux stabilisés par résonance qui inhiberaient la réaction. Ces alcènes se comporteraient, en fait, comme des substances antidétonantes.

L'analyse des produits de réaction formés lors de l'oxydation du *n*-pentane et celle du cyclopentane montre effectivement que le cyclopentane conduit essentiellement à la formation de cyclopentène, précurseur du radical cyclopentényle, stabilisé par résonance.

Le tableau 3 résume les résultats obtenus pour les réactions d'oxydation du *n*-pentane, du cyclopentane, du *n*-heptane et de l'isooctane .

Parmi les produits principaux d'oxydation de ces quatre hydrocarbures, seul l'éthylène ne conduit pas à la formation de radicaux stabilisés. On remarque que plus l'indice d'octane de recherche de l'hydrocarbure (RON) augmente, plus la production d'alcènes précurseurs de radicaux stabilisés par résonance est importante; ceci est également vérifié pour l'indice d'octane recherche de mélange (BRON). L'étude des réactions d'oxydation du *n*-pentane et du cyclopentane confirme donc bien l'hypothèse émise pour expliquer la différence d'indice d'octane entre le *n*-heptane et l'isooctane.

La différence d'indice d'octane entre le *n*-pentane (RON : 62) et le cyclopentane (RON : 100) s'expliquerait donc par la formation, suivant un mécanisme secondaire, de radicaux stabilisés par résonance qui inhiberaient la réaction d'oxydation du cyclopentane.

Cette explication est en concordance avec les études faites sur le caractère antidétonant de certains éthers : le méthyl *tert*-butyléther (MTBE), l'éthyl *tert*-butyléther (ETBE) et le tertio-amylméthyléther (TAME). En effet, les réactions d'oxydation du MTBE et de l'ETBE génèrent de l'isobutène et celle du TAME forme du méthyl-2 butène-1 (BRON : 146) et du méthyl-2 butène-2 (BRON : 176) précurseurs de radicaux stabilisés par résonance (30–32).

Il faut toutefois noter que cette tentative d'explication de la différence d'indice d'octane des hydrocarbures ne peut encore être considérée que comme une hypothèse basée sur l'étude de seulement quatre hydrocarbures différents.

Références

1. J. Weissmann. Carburants et combustibles pour moteurs à combustion interne. Technip, Paris. 1970. p. 224.
2. C.K. Westbrook, J. Warnatz et W.J. Pitz. Symp. (Int.) Combust. 22nd, The Combustion Institute, Pittsburgh, Pa. 1988. p. 893.
3. P.G. Lignola et E. Reverchon. Oxid. Commun. **14**, 81 (1991).
4. C. Chevalier, W.J. Pitz, J. Warnatz, C.K. Westbrook et H. Melenk. Symp. (Int.) Combust. 24th, The Combustion Institute, Pittsburgh, Pa. 1992. p. 93.
5. Y. Simon, G. Scacchi et F. Baronnet. Can. J. Chem. **74**, 1391 (1996).
6. C.K. Westbrook et F.L. Dryer. Symp. (Int.) Combust. 18th, The Combustion Institute, Pittsburgh, Pa. 1981. 749.
7. C.K. Westbrook et W.J. Pitz. Combust. Flame, **63**, 113 (1986).
8. C.K. Westbrook, W.J. Pitz et M.M. Thornton. Combust. Flame, **72**, 45 (1988).
9. N.P. Cernansky, R.M. Green, W.J. Pitz et C.K. Westbrook. Combust. Sci. Technol. **50**, 3 (1986).
10. C.K. Westbrook. A.I.A.A. Aerospace Science Meeting, 24th, Reno, Nev. 1986.
11. W.J. Pitz, C.K. Westbrook, W.M. Proscia et F.L. Dryer. Symp. (Int.) Combust. 20th, The Combustion Institute, Pittsburgh, Pa. 1984. p. 831.
12. C.K. Westbrook et W.J. Pitz. S.A.E. Paper, 872 107 (1987).
13. C.K. Westbrook et W.J. Pitz. Workshop Modell. Chem. React. Syst. (Proc.) 2nd, Heidelberg, Germany. 1986. *Edité par* J. Warnatz et W. Jager. Springer Ser. Chem. Phys. **39**, 1987.
14. E.I. Axelsson, K. Brezinsky, F.L. Dryer, W.J. Pitz et C.K. Westbrook. Symp. (Int.) Combust. 21st, The Combustion Institute, Pittsburgh, Pa. 1986. p. 783.
15. C.K. Westbrook et W.J. Pitz. Communication, A.C.S. Natl. Meeting, Division of Petroleum Chemistry, Miami Beach, Fla. prepr. 1985. p. 321.
16. J. Warnatz. Symp. (Int.) Combust. 20th, The Combustion Institute, Pittsburgh, Pa. 1984. p. 845.
17. J. Warnatz. Symposium on numerical simulation of combustion phenomena, Sophia Antipolis, France. 1985.
18. C. Esser, U. Maas et J. Warnatz. 10th Int. Colloq. Gas Dynamics of Explosions and Reactive Systems (ICODERS) 10th, Berkeley, Calif. 1985.
19. J. Warnatz. Ber. Bunsen-ges. Phys. Chem. **87**, 1008 (1983).
20. W.S. Affleck et A. Fish. Combust. Flame, **12**, 243 (1968).
21. A. Fish. Proc. R. Soc. London, Ser. A: **293**, 378 (1966).
22. A. Fish. Proc. R. Soc. London, Ser. A: **298**, 204 (1967).
23. A. Fish. Angew. Chem. **7**, 45 (1968).
24. M.P. Halstead, L.J. Kirsch, A. Prothero et C.P. Quinn. Proc. R. Soc. London, Ser. A: **346**, 515 (1975).
25. R.A. Cox et J.A. Cole. Combust. Flame, **60**, 109 (1985).

© 1997 NRC Canada

Can. J. Chem. Downloaded from www.nrcresearchpress.com by 88.146.161.215 on 09/08/12
For personal use only.

26. S.W. Benson. Thermochemical kinetics. 2nd ed. John Wiley, New York. 1976.
27. G.M. Côme, G. Scacchi, C. Muller et P.M. Marquaire. J. Chim. Phys. **85**, 201 (1988).
28. Y. Simon, V. Simon, G. Scacchi et F. Baronnet. Oxid. Commun. **17**, 1 (1994).
29. A.S.T.M. Knocking characteristics of pure hydrocarbons information from API Research Project 45. ASTM, Spec. Pub. 225 (1958).
30. J.C. Brocard, F. Baronnet et H.E. O'Neal. Combust. Flame, **52**, 25 (1983).
31. B. El Kadi. Thèse de Doctorat, INPL, Nancy (1990).
32. B. El Kadi et F. Baronnet. J. Chim. Phys. **92**, 706 (1995).

Can. J. Chem. Downloaded from www.nrcresearchpress.com by 88.146.161.215 on 09/08/12
For personal use only.

© 1997 NRC Canada

An examination of sodium alginate from *Sargassum* by NMR spectroscopy

Francisco Llanes, Françoise Sauriol, Frederick G. Morin, and Arthur S. Perlin

Abstract: Alginic acid, obtained from *Sargassum* brown algae that drift from the Sargasso Sea to beaches in Cuba, has been examined as an aqueous solution by ^{1}H and ^{13}C NMR spectroscopy, and also in the solid state by MAS ^{13}C NMR spectroscopy. Its composition is distinctive, relative to that for alginic acid from most other brown algae, in having a lower content of β-D-mannopyranosyluronic acid residues (M) than of α-L-gulopyranosyluronic acid residues (G). That is, M/G is ~0.6, whereas ratios of >1 have been reported for many other species, including *Macrocystis pyrifera*, which was examined here as well. In acquiring the high-resolution spectra, partial depolymerization was used to give solutions of reduced viscosity; as is well known, this procedure may cause separation into fractions and the formation of sediments, examples of which are cited. Proton resonances of the reducing end units of chain-shortened segments of the polymers exhibited unusual, marked, line broadening at elevated temperature, which may reflect thermal dehydration. MAS ^{13}C experiments offered the advantage of information about the intact alginate samples. Although the spectra consisted of broad, heavily overlapping peaks, curve-fitting analysis afforded qualitative and quantitative data that supplement those obtained with solutions of the polymers.

Key words: *Sargassum* alginate, ^{1}H NMR of fractions, M/G constituent ratios, MAS ^{13}C NMR, curve-fitting analysis.

Résumé : On a fait appel à la RMN du ^{1}H et du ^{13}C en solutions aqueuses et de la RMN « MAS » du ^{13}C à l'état solide pour étudier l'acide alginique obtenu d'algues brunes du type *Sargassum* qui vont à la dérive de la mer des Sargasses jusqu'aux plages de Cuba. Sa composition se distingue de celle de l'acide alginique obtenu à partir de la plupart des autres algues brunes. Il contient moins de résidus d'acide β-D-mannopyranosyluronique (M) que de résidus d'acide α-L-gulopyranosyluronique (G); le rapport M/G ≈ 0,6 alors que l'on observe généralement des rapports >1 avec la plupart des autres espèces, y compris *Macrocystis pyrifera* que nous avons étudié antérieurement. Alors de l'obtention des spectres à haute résolution, on a provoqué une dépolymérisation partielle afin de réduire la viscosité; il est bien connu que cette procédure peut provoquer une séparation en fractions et la formation de sédiments et plusieurs exemples sont cités. À température élevée, les résonances du proton des unités réductrices en bout de chaîne des segments de polymères raccourcis présentent un important élargissement de bande inhabituel qui est peut-être le reflet d'une déshydratation thermique. Les expériences de RMN « MAS » du ^{13}C fournissent plus d'information concernant les échantillons intacts d'alginate. Même si les spectres sont composés de pics larges qui se recouvrent fortement, une analyse par ajustement de courbe a permis d'obtenir des données tant qualitatives que quantitatives qui servent de supplément à celles obtenues avec les solutions de polymère.

Mots clés : alginate de *Sargassum*, RMN du ^{1}H, RMN « MAS » du ^{13}C, rapport M/G des constituants, analyse par ajustement de courbe.

[Traduit par la rédaction]

Introduction

Alginic acid is the major structural polysaccharide of marine brown algae (*Phaeophyceae*). Although brown algae are its most important source (1), similar types of polysaccharide are found in bacteria (2–5). Alginic acid is a (1 → 4)-linked copolymer of β-D-mannopyranuronosyl (M) and α-L-gulopyranuronosyl (G) residues. Individual seaweed species characteristically differ from each other in their relative proportions (M/G ratios) of these two constituent sugar acids, as well as in their sequencing within the polymer chain (6–9) structural elements that have a bearing on physical properties. Also, for a given species, the polysaccharide composition and yield vary considerably depending upon the season, age, and the part of the plant used for extraction (10–14). Consequently, the term "alginic acid" covers a range of chemically distinct compounds.

Currently, most of the alginic acid used commercially is obtained from Lessoniaceae (*Macrocystis pyrifera*, *Laminaria digitata*, *Laminaria hyperborea*, *Laminaria japonica*), and *Fucaceae* (*Ascophyllum nodosum*, *Fucus serratus*), whereas *Sargassaceae* (*Sargassum* and *Turbinaria* species)(15–17) are of lesser importance. A unique source of *Sargassum* seaweed is material originating from the Sargasso Sea of the south-west Atlantic Ocean, and carried by tides to the shores of Cuba, where it accumulates in large quantities along beaches.

Received October 30, 1996.

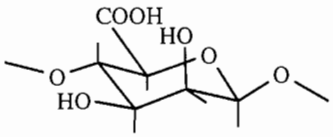
F. Llanes. Biomaterials Center, University of Havana, 10400 Cuba.
F. Sauriol, F.G. Morin, and A.S. Perlin.[1] Pulp and Paper Research Centre and Department of Chemistry, McGill University, Montreal, QC H3A 2A7, Canada.

[1] Author to whom correspondence may be addressed. Telephone: (514) 398-6188. Fax: (514) 398-7249.

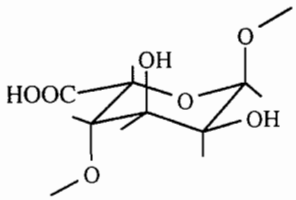
© 1997 NRC Canada

Can. J. Chem. Downloaded from www.nrcresearchpress.com by 88.146.161.215 on 09/08/12
For personal use only.

Alginic acid extracted from specimens of that *Sargassum* is the subject of this report.



(M)



(G)

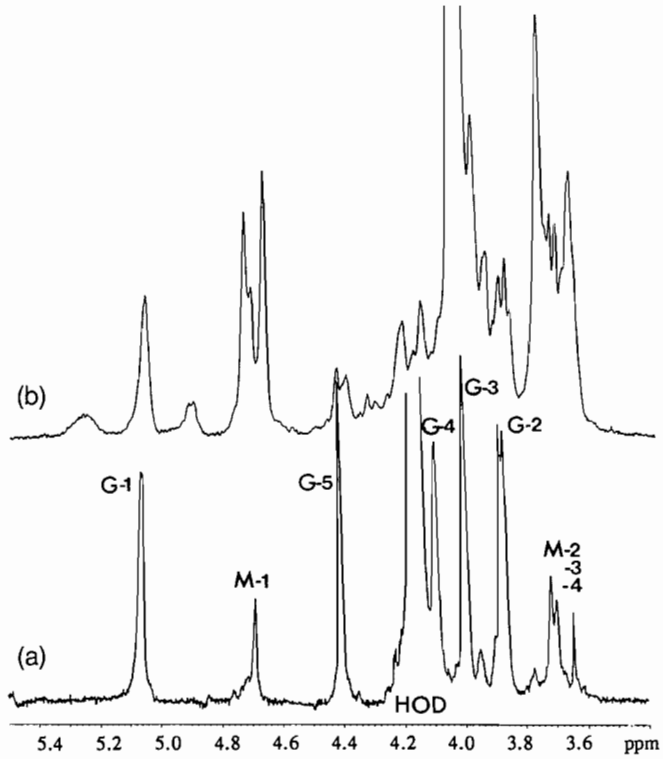
Results and discussion

Estimation of M/G ratios by ^{1}H NMR spectroscopy

NMR spectroscopy has proven (8, 9, 18–21) to be highly effective in the characterization of alginates. Although solutions of these polymers are usually too viscous to give well-resolved spectra, early workers showed (18) that the viscosity can be lowered to satisfactory levels by careful partial acid hydrolysis. Pretreatment in that way was adopted here, i.e., in 0.5 N hydrochloric acid at ~100°C for 1 h, to obtain ^{1}H spectra of the *Sargassum* alginate, as represented in Fig. 1*a*. Signals due to the anomeric protons of the D-mannuronosyl (M) and L-guluronosyl (G) residues, well separated at δ 4.70 and 5.08, respectively, have relative intensities corresponding to an M/G ratio of 0.4. However, this appeared unlikely to be the composition of the unmodified alginate, because there was material in suspension during the pretreatment, and more sedimented out following neutralization. Also, reproducibility was unsatisfactory, as the M/G ratios obtained from several, seemingly comparable, runs ranged from 0.25 to 0.52. Nevertheless, the data suggested that L-guluronic acid is the major constituent. A more valid indication of this feature was obtained by subjecting the alginate to longer prehydrolysis periods. At 4 h, for example, there was less sediment and, hence, a higher percentage of solubilized material in the NMR sample. (As discoloration also occurred, longer reaction times were deemed unsuitable.) The spectrum recorded in this instance (see Fig. 2) afforded an M/G value of 0.5. However, allowance had to be made for the presence of minor H-1 resonances due to reducing end units (which receive further attention below). As the most prominent of these were attributable to species of α,β-mannuronic acid, we estimated that the M/G ratio for the *Sargassum* alginate is close to 0.6.

For comparative purposes, we also examined sodium alginate from *Macrocystis pyrifera*, which has been well characterized by other workers and, in contrast to *Sargassum*, has a higher content of D-mannuronic acid than of L-guluronic acid. Through numerous studies (13, 17–19), M/G ratios ranging from 1.2 to >2.0 have been found, depending on such variables as location, age, season, and the part of the plant analysed. Following prehydrolysis of the *Macrocystis* sample for 1 h and the removal of insoluble material, the ^{1}H NMR spectrum recorded

Fig. 1. ^{1}H NMR spectra (500 MHz) for solutions in D_2O at 90°C of sodium alginate from (*a*) *Sargassum* sp. and (*b*) *Macrocystis pyrifera*. Each alginate had been subjected to prehydrolysis with 0.5 N HCl at ~100°C for 1 h. (Signal assignments are given in Table 1.)



(see Fig. 1*b*) was found to contain a strong cluster of anomeric resonances centered at δ 5.07, their relative intensities corresponding to an M/G ratio of 2.5. Although this is consistent with the mannuronic acid-rich nature of *Macrocystis*, the solution that it represents probably (9, 18, 19) constitutes a fraction of the alginate having relatively fewer residues of guluronic acid than did the intact sample. Evidence supporting this assumption is presented below.

Many alginates possess relatively high M/G ratios, such as those obtained (9, 18, 20, 22–25) from *A. nodosum* (~1.2), *L. japonica* (~2.2), as well as from (12) some other *Sargassum* species (0.8–1.4). Hence, the monosaccharide composition of the polymer extracted from the *Sargassum* seaweed collected on beaches in Cuba is relatively unusual among alginates. Whether or not this composition is also characteristic of the plant in the Sargasso Sea from which the Cuban harvest originates remains to be determined, as are possible variations with age and season.

^{1}H and ^{13}C NMR parameters

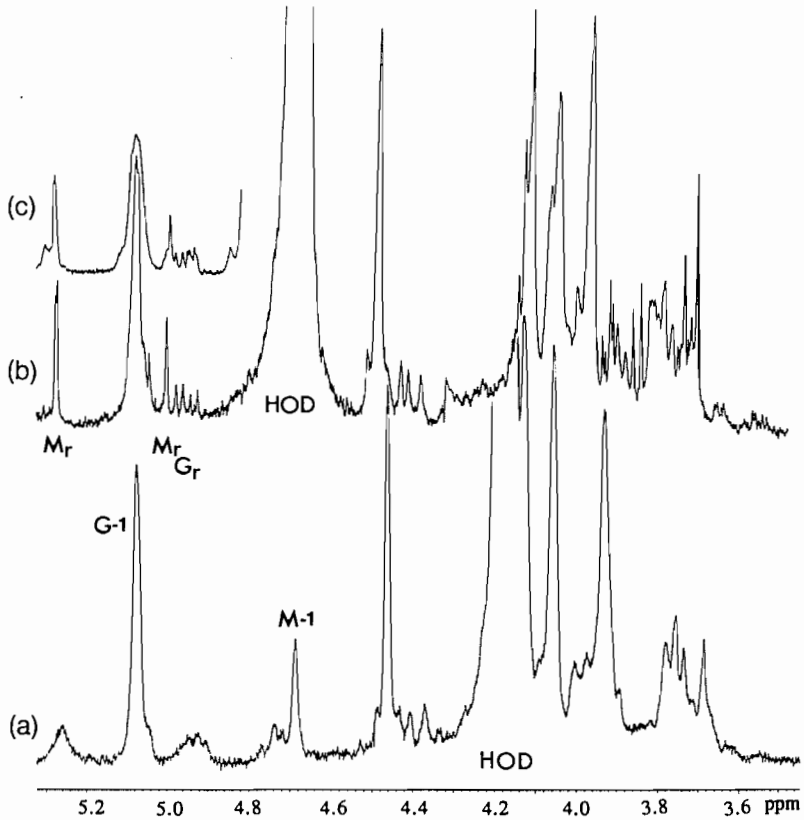
Partial depolymerization of alginates by acid allows, not only for better solubility, but also for fractionation into materials having widely different compositions. This fact has been utilized in several studies (9, 18–20) to provide impressively detailed information about a variety of mixed sequences of the monomeric residues, both by ^{1}H and ^{13}C NMR spectroscopy. For example (20), an alginate from *A. nodosum*, in which the M and G components are close to equimolar, exhibited eight anomeric ^{13}C signals (δ 103.0 ± 0.8) each of which was attributed to a unique triad sequence (MMG, GMG, etc.). By con-

© 1997 NRC Canada

Can. J. Chem. Downloaded from www.nrcresearchpress.com by 88.146.161.215 on 09/08/12
For personal use only.

Can. J. Chem. Downloaded from www.nrcresearchpress.com by 88.146.161.215 on 09/08/12
For personal use only.

Fig. 2. ^{1}H NMR spectra (500 MHz) for solutions in D_2O of sodium alginate from *Sargassum* sp. (*a*) subjected to prehydrolysis for 4 h, recorded at 90°C, and (*b*) the same sample at 25°C. Inset, (*c*) downfield region for the *Macrocystis* sample (1 h prehydrolysis) recorded at 25°C; the corresponding region at 90°C is displayed in Fig. 1*b* (*r* = reducing end).



trast, the anomeric (as well as the other) ^{13}C signals in spectra of the *Sargassum* preparations were not resolved into distinctly separate component lines. This indicated, therefore, that little of the solubilized material contained M and G residues in close proximity to each other, and that the polymeric segments comprised primarily *either* M or G residues.

Assignments for the ^{1}H signals of α-L-guluronic acid residues in Fig. 1*a* were readily obtained from an ^{1}H 2-D COSY spectrum. In turn, the identity of the resonances detected in the corresponding ^{13}C NMR spectrum was determined by ^{13}C–^{1}H 2D correlation spectroscopy. Both sets of data, listed in Table 1, were fully in agreement with earlier ^{1}H and ^{13}C assignments (9, 18–20) for polymeric α-L-guluronic acid residues. Additional information contained in Fig. 1*a*, derived from the COSY spectrum, concerns protons-2, -3, and -4 of D-mannuronic acid residues, which resonate within a narrow region centered at δ 3.7. An ^{1}H-coupled ^{13}C spectrum afforded a value of 169 (±2) Hz for $^1J_{CH}$ of the C-1—H-1 bond of the α-L-guluronosyl residues. As this magnitude of coupling is characteristic (26) of an equatorial anomeric C—H bond (axial C—O glycosidic linkage), it supports earlier proposals (18, 20, 27) that these residues possess the $^1C_4$ (L) conformation.

An unusual effect of temperature change on some ^{1}H resonances

The absence from Fig. 1*a* of signals in the regions of δ 5.2–5.3 and δ 4.8–4.9, expected (9) for the anomeric protons, respectively, of α and β reducing end units liberated, shows that only limited hydrolysis of the *Sargassum* alginate could have occurred. By contrast, according to the readily detectable signals in those regions in Fig. 1*b*, the *Macrocystis* alginate had undergone substantial depolymerization under analogous conditions. That those minor signals are, indeed, due to reducing end units was confirmed by introducing sodium borodeuteride to the solution, whereupon the signals were rapidly eliminated. Although it is not evident from Fig. 1*b* that anomeric protons of both D-mannuronic and L-guluronic acid end units are represented, because they have comparable chemical shifts, this point is clarified later.

By extending the period of acid hydrolysis of the *Sargassum* alginate from 1 to 4 h, as already mentioned, minor resonances attributable to low molecular weight species were generated (see Fig. 2*a*). Polyguluronic acid segments were still in preponderance, as the main signals of the spectrum were not markedly altered from those in Fig. 1*a*; i.e., the patterns of the H-1 to H-5 resonances are closely similar in the two spectra. In addition, however, this more extensively depolymerized alginate produced a group of broad, minor signals centered at δ 5.26 and 4.95. By analogy with the minor peaks for *Macrocystis* at the same positions (in Fig. 1*b*), these signals may also be attributed to the anomeric protons of reducing end units. The fact that they are exceptionally broad is related to the elevated experimental temperature (90°C), because it was found that when the spectrum was recorded at 25°C (see Fig. 2*b*), they were replaced by well-resolved sig-

© 1997 NRC Canada

Can. J. Chem. Downloaded from www.nrcresearchpress.com by 88.146.161.215 on 09/08/12
For personal use only.

nals. Considering literature values of δ, *J*, and anomeric equilibria, the signals at δ 5.28 and 5.02 are compatible (9) with those of α- and β-*manno* anomers ($J_{1,2}$ < 2 Hz; α:β ≃ 2:1), respectively, whereas the doublets at δ 4.98 and 4.92 ($J_{1,2}$ 8.3 Hz) are taken to be those of β-*gulo* reducing end units (probably (9) in MG and GG diads). Not only these anomeric protons, but some secondary protons as well, are highly sensitive to the temperature change, which is seen in the marked line broadening of the group of peaks centered at δ 3.9 in Fig. 2*b* (a COSY spectrum shows that H-2, e.g., of the α-*manno* anomer, resonates there).

Similarly striking temperature effects on lineshape also occurred with the *Macrocystis* alginate. That is, the broad reducing-end ^{1}H signals observed at 90°C, at δ 5.26 and δ 4.92 in Fig. 1*b*, were replaced at 25°C by a group of far better resolved peaks (see Fig. 2*c*, inset), which closely resemble those in Fig. 2*b* for α,β-mannuronic and β-guluronic acid anomeric protons.

As these changes in peak width are observed only with the reducing end units, one possibility is that they originate from tautomeric exchange during equilibration of the α and β anomeric forms of the units. Nevertheless, the well-resolved anomeric ^{1}H signals observed at 25°C are characteristic of aqueous solutions of reducing sugars at equilibrium under conditions of slow exchange. Normally, their appearance should not be altered materially at such a temperature as 90°C because there would be an accompanying increase in the rate of proton exchange. It appears more likely that the thermally induced line broadening is caused by a qualitative effect on molecular motion. This would apply only to relatively short chains, because the major resonances, attributable to "intact" polymer molecules, exhibit little change in lineshape. Perhaps the oligomeric fragments are relatively easily dehydrated as the temperature is raised, which specifically permits them to aggregate, or to become rigid rods, and thereby induces broadening of their ^{1}H resonances.

Solid state ^{13}C NMR spectra

As already mentioned, it was difficult to obtain alginate solutions free of sediment for use in the NMR experiments, a complication also encountered by earlier workers. In such circumstances, an NMR spectrum of the solubilized portion of a given alginate specimen need not have been representative of the total sample. This kind of limitation would be less likely to arise if the intact sodium alginate powder were to be examined directly by MAS ^{13}C spectroscopy, and hence it appeared worthwhile to compare data obtained by this technique with the data reported above for solutions of alginate.

In the spectrum of the *Sargassum* polymer (Fig. 3*a*) there are (at least) two overlapping anomeric ^{13}C signals, centered at δ 103. This corresponds closely to the location of signals of the anomeric carbons of the β-D-mannuronic and α-L-guluronic residues of alginates in solution, i.e., at δ 102.6 and 103.7, respectively (Table 1). As to their assignments in Fig. 3*a*, we assume that the stronger, downfield peak is due to the main constituent, i.e., α-L-guluronic acid. A curve-fitting analysis suggests, however, that these two peaks, which together correspond to an M/G ratio of 0.78, overlay a far broader peak comprising 20% of the total signal intensity (see Fig. 4*a* (inset)), and hence may not give a close estimate of composition.

Fig. 3. Solid state ^{13}C NMR spectra of sodium alginate from (*a*) *Sargassum* sp., and (*b*) *Macrocystis pyrifera*.

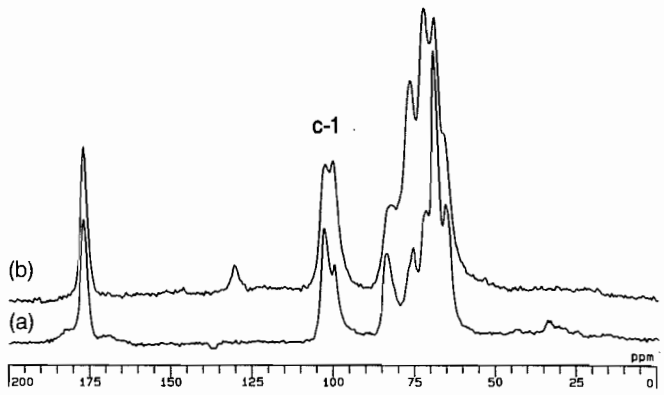


Table 1. ^{13}C and ^{1}H chemical shifts (δ) for residues of α-L-gulopyranosyluronic acid (G) and β-D-mannopyranosyluronic acid (M) in *Sargassum* sodium alginate.

	Carbon Atom					
Residue	1	2	3	4	5	6
G	103.7[a]	67.5	71.6	83.0	69.8	178.3
M	102.8	73.0[b]	74.0[b]	80.7	78.9	177.1
	Proton					
G	5.07	3.89	4.02	4.12	4.45	
M	4.68		3.70–3.74[c]			

[a] $^1J_{CH}$ from ^{13}C–^{1}H coupled spectrum, 169 ± 2 Hz.
[b]May be interchanged.
[c]H-2, -3, -4 unresolved.

Another concern, which arises from observations (20) of ^{13}C spectra of alginates in solution, is the identification of the ^{13}C-1 signals of M and G residues in mixed sequences. As the anomeric carbons of β-mannuronic and α-guluronic acid resonate at close to the same frequency, small inequalities in the effects of neighbouring residues on their chemical shifts in diads, triads, etc., of mixed composition become important (20) in determining the actual chemical shifts found. Hence, a given peak could consist of contributions from both types of uronic acid residues. If signals were to converge similarly in the solid state spectra, then the origins of the overlapping peaks in Fig. 4*a* (inset) are uncertain.

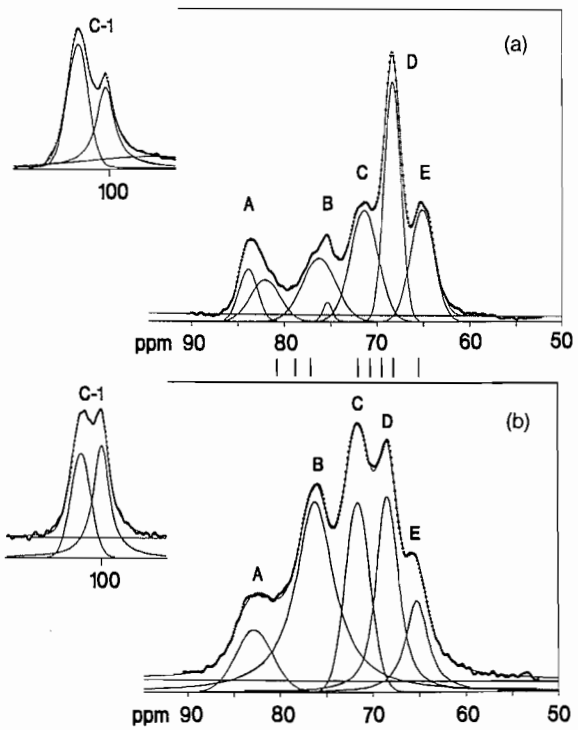
Curve-fitting analysis of the two ^{13}C-1 peaks of the *Macrocystis* alginate (see Fig. 4*b*, inset) afforded an M/G ratio of 1.2 The fact that this value differs widely from the results (M/G = 2.5) obtained from the ^{1}H spectrum is of little consequence, however, because the same uncertainty about the origins of the ^{13}C-1 signals applies here as well.

By contrast, resonances of the secondary ^{13}C nuclei may offer a less equivocal basis for comparison. In solution, according to the data in Table 1 and complementary information (20) about diad and triad mixed sequences of residues, all of these nuclei differ appreciably in chemical shift. A contributing factor (28) is the presence of more axial C—O

© 1997 NRC Canada

Can. J. Chem. Downloaded from www.nrcresearchpress.com by 88.146.161.215 on 09/08/12
For personal use only.

Fig. 4. Curve-fitting analysis (inner lines) of peaks (outer lines) in the solid state ^{13}C NMR spectra (Fig. 3) of sodium alginate from (*a*) *Sargassum* sp. and (*b*) *Macrocystis pyrifera*. Peaks designated A–E are attributed, respectively, to resonances due to guluronic acid C-4 (A), C-3 and C-5 (overlapping, D), and C-2 (E); and due to mannuronic acid C-4 and C-5 (overlapping, B), and C-3 and C-2 (overlapping, C). Inset, anomeric ^{13}C peaks. The corresponding ^{13}C chemical shifts in solution are represented by the row of eight vertical bars (positioned upfield by 2 ppm; see text), attributed (left to right) to carbons G-2, G-5,G-3, M-2 and M-3, M-5, M-4, G-4 (see Table 1).



bonds in the α-*gulo* than in the β-*manno* residues (i.e., at C-1, -3, and -4, vs. C-2, respectively) that specifically induce upfield shifts for C-2, -3, and -5 of the guluronide (C-4 resonates downfield owing to its involvement in the glycosidic bond). To compare the solution ^{13}C data with those of the solid state spectrum, the chemical shifts in Table 1 for individual carbons have been represented by eight vertical lines in Figs. 4*a* and 4*b* (which are expanded portions of Figs. 3*a* and 3*b*). In fact, these lines have been positioned upfield by 2 ppm, which, we assumed, is an allowable adjustment for the "solvent" effect on chemical shift. It then appears that the lines coincide with the MAS peaks (or shoulders) in such a manner that guluronic acid accounts for peaks A (C-4), D (overlapping C-3 and C-5), and E (C-2), whereas mannuronic acid produces peaks B (overlapping C-4 and C-5) and C (overlapping C-3 and C-2). That is, the two sets of five peaks in Figs. 4*a* and 4*b* are both accounted for equitably. As well, it is particularly noteworthy that the peak intensities vary in accord with this analysis of the signals. For example, the far greater prominence of peaks B and C in Fig. 4*b* than in 4*a* is consistent with the known enrichment of *Macrocystes* alginate in mannuronic acid. In principle, then, one may account for the difference in composition between the two types of alginate examined here by comparing the total area of A + D + E (*gulo*) with that for B + C (*manno*).

Analysis conducted on the basis of these considerations afforded the M/G ratios listed in Table 2. As the curve-fitting procedure involved the testing of different types of lineshapes, it afforded a set of different values for each alginate, ranging from 0.57 to 0.61 for *Sargassum* and from 1.3 to 1.4 for *Macrocystis*. The latter values suggest a far different composition than does the ratio (M/G = 2.5) obtained for the *Macrocystis* alginate by ^{1}H NMR spectroscopy. As noted earlier, however, there is precedence (9, 18–20), for the probability that the solution spectrum had not represented the entire sample, but rather, a fraction enriched in mannuronic acid.

As to the *Sargassum* alginate, these MAS ^{13}C ratios are in good agreement with the value (M/G ≈ 0.6) estimated from integrals of the anomeric ^{1}H signals recorded with the 4 h pre-hydrolysis preparation. It appears reasonable to conclude, then, that this alginate contains substantially more guluronic than mannuronic acid, which makes it relatively unique among this class of polymers.

Experimental

Materials

Samples of sodium alginate from *Sargassum* sp. were supplied by the Biomaterials Center of the University of Havana, Cuba. Sodium alginate of *Macrocystis pyrifera* was obtained from commercial sources.

High-resolution NMR spectroscopy

Solutions of sodium alginate examined by NMR spectroscopy were prepared as follows: the alginate (100 mg) was subjected to mild hydrolysis in 0.5 N hydrochloric acid (10 mL) at ~ 100°C for 1 h. After cooling, neutralization, and filtration of the solution, an aliquot was concentrated and exchanged with deuterium oxide, followed, when required, by a second filtration. Ethylene dinitrilotetraacetic acid, disodium salt (EDTA) (Anachemia) was included to avoid signal broadening by divalent cations, and sodium 3-trimethylsilylpropionate-2,2,3,3-d_4 (TSP) (Anachemia) was used as internal reference. The ^{1}H spectra were recorded with a Varian Unity 500 spectrometer, using a temperature of 90°C (or 25°C), a sweep width (SW) of 8000 Hz, a 45° pulse, and an acquisition time of 1.892 s. For COSY spectra, the spectral window was 2333.6 Hz, number of points 1024, number of increments 256, with zero-filling along the evolution domain to provide a 1K × 1K matrix. For HMQC spectra, the SW (^{1}H) was 3237.6 Hz, acquisition time 0.158 s, no. of points 1024, and no. of transients 16; and the SW (^{13}C) was 10 055.8 Hz, number of increments 125; processing was Gaussian in both domains, and the ^{13}C-evolution domain was zero-filled to provide a 1K × 1K matrix. The ^{13}C NMR spectra were recorded with a Varian XL-300 spectrometer operating at 75.42 MHZ, using a temperature of 90°C (or 25°C), a SW of 16 501.7 Hz, a 60° pulse, and an acquisition time of 0.909 s.

Solid state (MAS) ^{13}C spectroscopy

Solid state ^{13}C CPMAS NMR spectra of the sodium alginate powders were obtained using a Chemagnetics CMX-300 spec-

© 1997 NRC Canada

Table 2. Peak areas (%) obtained by curve-fitting analysis of the MAS ^{13}C resonances attributed to residues of α-L-gulopyranosyluronic acid (G) and β-D-mannopyranosyluronic acid (M) in sodium alginate of *Sargassum* and of *Macrocystis pyrifera*.

	G peaks			M peaks		
Lineshape	A(C-4)	D(C-3,5)	E(C-2)	B(C-4,5)	C(C-3,2)	M/G
			Sargassum			
Gaussian	16.2	28.5	18.8	16.9	19.6	0.57
Voigt	15.4	27.4	18.9	16.4	21.7	0.61
			Macrocystes pyrifera			
Voigt	9.8	25.6	8.0	33.5	23.2	1.30
Lorentzian	13.7	19.8	8.2	27.5	30.9	1.41

trometer at 75.3 MHz. The spectral width was 30 kHz, the acquisition time was 17 ms, and 512 points were acquired in the FID and zero-filled to 4096 before Fourier transformation. An ^1H decoupling field of 60 kHz was used. Samples were held in 7.5 mm Zirconia Pencil rotors and spun at 3–4 kHz. The contact time and pulse delay were 1.5 ms and 3s, respectively. No differences in the spectra were noticed when the contact time was varied between 1 and 3 ms or when the recycle delay was varied between 2 and 10 s, except for changes in the overall signal intensity. Nor were changes observed when the spinning rate was changed, even when the spectra were obtained with the TOSS (*To*tal *S*uppression of *S*idebands) pulse sequence. Deconvolutions of the spectra were performed using the program PEAKFIT from Jandel Scientific. A number of fits were performed, each employing such different lineshape types as Lorentzian or Gaussian (or combinations thereof). It was found that although different results may have been obtained for the area of a given peak, depending on the choice of lineshape, the ratios of M/G calculated from the fitted areas were quite consistent (see Table 2).

Acknowledgements

One of us (F.L.) expresses thanks to the Seagram Fellowship Program, McGill University, for generous support. Helpful discussions with R.H. Marchessault are gratefully acknowledged.

References

1. M.J. Winne. *In* The biology of seaweeds. *Edited by* C.S. Lobban and M. Winne. Blackwell Scientific, Oxford. 1981. p. 52.
2. A. Linker and L.R. Jones. J. Biol. Chem. **291**, 3845 (1966).
3. P.A.J. Gorin and J.F.T. Spencer. Can. J. Chem. **44**, 993 (1966).
4. J.R.W. Govan, J.A.M. Fyfe, and T.R. Jarman. J. Gen. Microbiol. **125**, 217 (1981).
5. W.F. Fett, S.F. Osman, M.L. Fishman, and T.S. Siebles. Appl. Environ. Microbiol. **52**, 466 (1986).
6. A. Haug, B. Larsen, and O. Smidsrod. Acta Chem. Scand. **20**, 183 (1966).
7. B. Larsen, O. Smidsrod, T.J. Painter, and A. Haug. Acta Chem. Scand. **24**, 726 (1970).
8. A. Haug, B. Larsen, and O. Smidsrod. Carbohydr. Res. **32**, 217 (1974).
9. H. Grasdalen. Carbohydr. Res. **118**, 255 (1983).
10. R.J. Waaland. *In* The biology of seaweeds. *Edited by* C.S. Lobban and M. Winne. Blackwell Scientific, Oxford. 1981. p. 726.
11. V.S.K. Chennubhotla, N. Kaliaperuman, S. Kalimuthu, M. Selvaraj, J.R. Ramalingam, and M. Najmuddin. Indian J. Mar. Sci. **11**, 195 (1982).
12. Ji Minghou, M.H. Chi, Wang Yujin, Xu Zukong, and Guo Yucai. Hydrobiologia, **116**, 554 (1984).
13. J.W.A. McKee, L. Kavalieris, D.J. Brasch, M.T. Brown, and L.D. Melton. J. Appl. Phycol. **4**, 357 (1992).
14. I.C. Mody and V.D. Chauhan. Res. Ind. **37**, 118 (1992).
15. J. Gorham and S.A. Lewey. Mar. Biol. **80**, 103 (1984).
16. P.C. Thomas and K. Subbaramaiah. Indian J. Mar. Sci. **20**, 169 (1991).
17. B.A. Fasihuddin, D.J. Wedlock, Siraj Omar, and G.O. Phillips. Gums and stabilisers for the food industry. Vol. 4. IRL Press, Oxford. 1988. p. 89.
18. A. Penman and G.R. Sanderson. Carbohydr. Res. **25**, 273 (1972).
19. H. Grasdalen, B. Larsen, and O. Smidsrod. Carbohydr. Res. **68**, 23 (1979).
20. H. Grasdalen, B. Larsen, and O. Smidsrod. Carbohydr. Res. **89**, 179 (1981).
21. O. Smidsrod. Faraday Discuss. Chem. Soc. **57**, 263 (1974).
22. G. Amison, N.V.H. Cheetan, and I.Couperwhite. J. Chromatogr. **264**, 137 (1983).
23. A. Heyraud and C. Leonard. Food Hydrocolloids, **4**, 59 (1990).
24. V.J. Chapman and D.J. Chapman. Seaweeds and their uses. Chapman and Hall, London. 1980. p. 334.
25. E.R. Morris, D.A. Rees, and D. Thom. Carbohydr. Res. **81**, 305 (1980).
26. A.S. Perlin and B. Casu. Tetrahedron Lett. 2921 (1969); S. Wolfe, B.M. Pinto, V. Varma, and R.Y.N. Leung. Can. J. Chem. **68**, 1051 (1990).
27. E.D.T. Atkins, W. Mackie, and E.E. Smolko. Nature, **225**, 626 (1970).
28. A.S. Perlin, B. Casu, and H.J. Koch. Can. J. Chem. **48**, 2596 (1970).

Can. J. Chem. Downloaded from www.nrcresearchpress.com by 88.146.161.215 on 09/08/12
For personal use only.

© 1997 NRC Canada

Design of ligands for the complexation of Fe(II)/Fe(III) in the catalytic oxidation of H_2S to sulfur

Robert D. Hancock, Arthur E. Martell, Dian Chen, Ramunas J. Motekaitis, and Derek McManus

Can. J. Chem. Downloaded from www.nrcresearchpress.com by 88.146.161.215 on 09/08/12
For personal use only.

Abstract: Examination of the stability constants of Fe(II) and Fe(III) chelates of a wide variety of ligands that contain only acetate and amino groups shows a linear correlation. A separate linear correlation displaced toward the ferric ion was obtained for those ligands that contain more basic phenolate donor groups. The ligands of the latter group generally are unsuited to the oxidation of H_2S to sulfur, while ligands in the first correlation are suitable for that purpose. Ligands that do not contain α-methylene groups are relatively resistant to oxidative degradation. Molecular mechanics is employed to compare the Fe(III) complexes of three such ligands, dipicolinic acid (DIPIC), pyridine-2-phosphonic-6-carboxylic acid (2PP6C), and 2-carboxy-8-hydroxyquinoline (CHOX). The calculations show that there is considerable strain in the formation of the Fe(II) and Fe(III) complexes of these ligands, both with respect to the O–O distance and the O-Fe-O angle. The relatively high stability of the CHOX complex compared to that of DIPIC, therefore, is due mainly to the higher basicity of the phenolate oxygen compared to the carboxylate groups of DIPIC. The higher stability of the Fe(III) complex of 2PP6C relative to that of DIPIC is due to the higher basicity and charge of the phosphonate group compared to a carboxylate group of DIPIC that it replaces. In spite of the lack of α-methylene groups in CHOX, the ligand undergoes rapid oxidative degradation when its iron chelate is used as a catalyst for the oxidation of H_2S to sulfur by air. However, the oxidation products were found to also be effective catalysts for this process.

Key words: hydrogen sulfide, oxidation catalysis, dipicolinic acid, pyridine-2-phosphonic-6-carboyxlic acid, 2-carboxy-8-hydroxyquinoline.

Résumé : L'examen des constantes de stabilité de chélates du Fe(II) et du Fe(III) avec une grande variété de coordinats ne contenant que des groupes acétate et amino présente une corrélation linéaire. Avec des coordinats contenant des groupes donneurs plus basiques, des phénolates, on a obtenu une autre corrélation linéaire, déplacée vers l'ion ferrique. Les coordinats de ce dernier groupe ne sont généralement pas appropriés pour l'oxydation du H_2S en soufre alors que les coordinats de la première corrélation peuvent être utilisés à cette fin. Les coordinats qui ne contiennent pas de groupe α-méthylène sont relativement résistants à la dégradation oxydante. On a fait appel à la mécanique moléculaire pour comparer les complexes du Fe(III) de trois de ces ligands, l'acide dipicolinique (DIPIC), l'acide pyridine-2-phosphonique-6-carboxylique (2PP6C) et la 2-carboxy-8-hydroxyquinoléine (CHOX). Les calculs montrent que la formation des complexes de Fe(II) et de Fe(III) de ces coordinats impliquent une grande tension, tant par rapport à la longueur de la liaison O–O que par rapport à l'angle O-Fe-O. La stabilité relativement grande du complexe avec la CHOX par rapport à celle du complexe avec le DIPIC découle donc principalement de la plus grande basicité de l'oxygène du phénolate par rapport aux groupes carboxylates du DIPIC. La plus grande stabilité du complexe du Fe(III) du 2PP6C par rapport à celui du DIPIC découle de la plus grande basicité et de la charge du groupe phosphonate par rapport au groupe carboxylate du DIPIC qu'il remplace. Même si la CHOX ne comporte pas de groupe α-méthylène, ce coordinat subit une rapide dégradation oxydante lorsqu'on utilise son chélate de fer comme catalyseur pour l'oxydation du H_2S en soufre par l'air. Toutefois, on a trouvé que les produits d'oxydation sont aussi des catalyseurs efficaces pour ce processus.

Mots clés : sulfure d'hydrogène, catalyseur d'oxydation, acide dipicolinique, acide pyridine-2-phosphonique-6-carboxylique, 2-carboxy-8-hydroxyquinoléine.

[Traduit par la rédaction]

Received November 27, 1996.

R.D. Hancock. IBC Technologies, Provo, UT 84606, U.S.A.
A.E. Martell,[1] **D. Chen, and R.J. Motekaitis.** Department of Chemistry, Texas A&M University, College Station, TX 77843-3255, U.S.A.
D. McManus. Wheelabrator Clean Air Systems, Inc., Plainfield, IL 60544, U.S.A.

[1] Author to whom correspondence may be addressed. Telephone: (409) 845-2011. Fax: (409) 845-4719.

© 1997 NRC Canada

Can. J. Chem. Downloaded from www.nrcresearchpress.com by 88.146.161.215 on 09/08/12
For personal use only.

Introduction

There are several features necessary in a ligand for the complexation of Fe(II)/Fe(III) in the catalytic oxidation of H_2S to sulfur: (*i*) H_2S is best absorbed at higher pH values where HS^- ion is formed, and so the pH should be at least 8.5 (p*K*a of H_2S = 7.02 (1). (*ii*) The stability of the Fe(II) complex should be high enough to prevent precipitation of FeS(s) (log K_{sp} = −18.1 (1) at the pH employed. (*iii*) The stability of the Fe(III) complex should be high enough to prevent precipitation of $Fe(OH)_3$(s) (log K_{sp} = −38.8 (1) at the operating pH of 8.5. (*iv*) The relative stabilities of the Fe(II) and Fe(III) complexes with the ligand should produce a reduction potential ($E°$) that is of the right range of values. ($E°$ for: $Fe^{III}L_n + e = Fe^{II}L_n$.) If the relative stability of the Fe(III) complex is too high, then the reduction potential will be too low, and H_2S will not be oxidized to S(s). (*v*) The ligand should be resistant to attack by oxidizing species such as the hydroxyl radical ($OH^•$), which is generated in the Fe(III)/Fe(II) systems used for oxidation of H_2S (2). This is the most serious deficiency in the currently used NTA (nitrilotriacetate) ligand for the oxidation of H_2S (3). NTA degrades rapidly in the system, ultimately forming CO_2 and NH_3. The rate of degradation can be slowed considerably by the addition of $Na_2S_2O_3$, which is an effective scavenger for the hydroxyl radical. However, the rate of degradation of NTA has been an obstacle to the use of this system in large installations for the removal of H_2S by catalytic oxidation, and a major aim of this study has been to find a ligand that is considerably more resistant to degradation. It has been found empirically that ligands such as dipicolinic acid (DIPIC) that contain no methylenic carbons (-CH_2-) survive in the presence of the hydroxyl radical much longer than those currently used, such as NTA, that do contain methylenic carbons (2).

Recently two pyridine phosphonic acids, pyridine-2-phosphonic-6-carboxylic acid (2PP6C) and 2,6-pyridinediphosphonic acid (2,6PDPA), which do not have α-methylene groups, were reported to undergo negligibly slow degradation when their iron chelates were used as catalysts in the oxidation of H_2S to S_8 by air (4, 5). To better understand the requirements of iron chelates to be used in this process, the structures of the Fe(II) and Fe(III) chelates of DIPIC and 2PP6C were simulated by molecular mechanics, and compared with the structure of the iron(II,III) chelates of a new ligand, 2-carboxy-8-hydroxyquinoline (CHOX).

Experimental

The molecular mechanics procedure employed

In the MM approach, the structure of molecules and complexes of metal ions can be reproduced using a simple model where the total strain energy of the complex (ΣU) is considered to be the sum of various contributions, typically bond length deformation (U_B), bond angle deformation (U_θ), torsional strain (U_ϕ), and nonbonded (van der Waals) interactions (U_{NB}).

$$[1] \quad \Sigma U = U_B + U_\theta + U_\phi + U_{NB}$$

The energy of deformation of bond lengths is reproduced with a simple Hooke's law expression.

$$[2] \quad U_B = \tfrac{1}{2}K_B(r - r°)^2$$

In eq. [2] U_B is the energy of bond length deformation, K_B is the bond length deformation force constant, r is the observed bond length, and $r°$ is the ideal bond length. The value of $r°$ is determined by fitting calculated to observed structures, which are usually those determined by X-ray crystallography. For a study of Fe(III) and Fe(II) it is necessary here to examine crystal structures of complexes of these ions to obtain values of $r°$ for the Fe—N and Fe—O bonds applicable to Fe(II) and Fe(III).

The energy of deformation of bond angles is reproduced using a similar expression:

$$[3] \quad U_\theta = \tfrac{1}{2}K_\theta(\theta - \theta°)^2$$

Here U_θ is the energy of bond angle deformation, K_θ is the bond angle force constant, θ is the observed bond angle, and θ° is the ideal bond angle. The value of θ° for angles around the metal ion is set to be those appropriate for the geometry found for the metal ion, i.e., O-Fe-O angles would be 90° for octahedral Fe(II) or Fe(III).

Torsional strain energy (U) is given by the expression:

$$[4] \quad U\phi = V/n(1 - 3\cos\phi)$$

where φ is the torsion angle about the particular bond in consideration, and V is the torsional constant for the particular type of torsional interaction being considered, e.g., for H-C-C-H torsion around the C—C bond in a hydrocarbon, for which n = 3. The torsional interactions around M—L bonds such as the Fe—N bond are likely to be small, and so are usually omitted in modeling complexes of metal ions.

The nonbonded interactions (U_{NB}) between atoms that are not bonded to each other are very important, and are usually modeled with the expression:

$$[5] \quad U_{NB} = A\exp(-Br) - C/r^6$$

where A, B, and C are constants typical of the type of nonbonded interaction being modeled, and r is the internuclear separation between the two-bonded atoms.

MM calculations are a powerful tool for modeling the structures of complexes. Computer programs locate the minimum energy structure by perturbing the atomic coordinates for the molecule, and using a minimization routine such as the Newton–Raphson approach to minimize the strain energy of the molecule. The strain energy is an unfavorable contribution to complex formation and, in a series of ligands with the same donor set, where one may consider the energy of formation of the M—L bonds to be the same, differences in energies of complex formation should relate to the changes in strain energy on complex formation, ΔU.

$$[6] \quad \Delta U = U_{ML_n} - nU_L - U_M$$

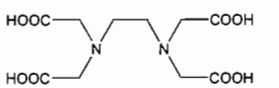
where U_{ML_n}, U_L, and U_M are the strain energies, respectively, of the complex ML_n, the free ligand L, and the metal ion M. For a series of ligands with the same M, U_M will be constant, and can therefore be ignored.

To evaluate steric aspects of the complexation of ligands

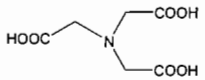
© 1997 NRC Canada

Can. J. Chem. Downloaded from www.nrcresearchpress.com by 88.146.161.215 on 09/08/12
For personal use only.

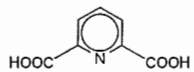
Chart 1. Ligands used in this paper.



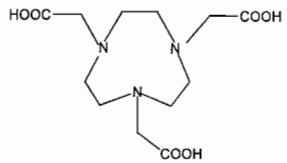
EDTA



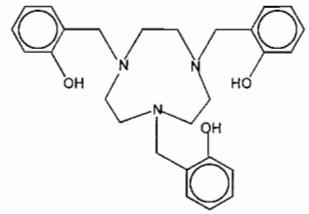
NTA



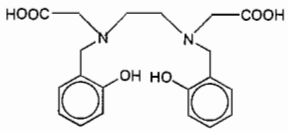
DIPIC



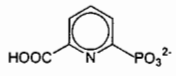
TACN-TA



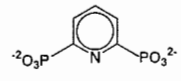
TACN-TB



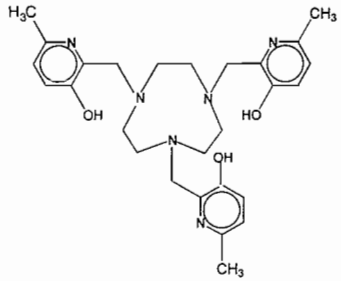
HBED



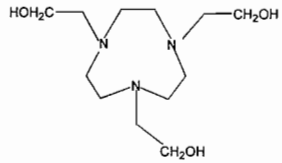
2PP6C



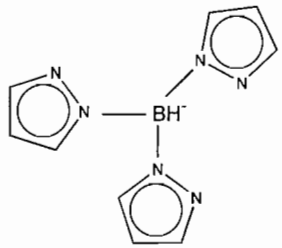
2,6PDPA



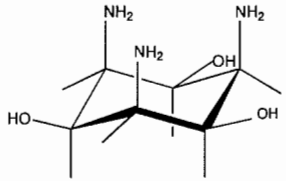
TACN-HP



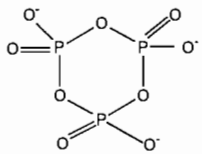
THETACN



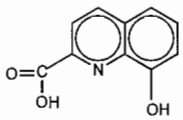
TPB



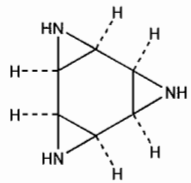
taci



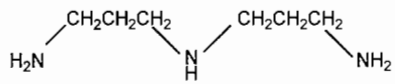
TMP



CHOX



TAB



dptn

© 1997 NRC Canada

Can. J. Chem. Downloaded from www.nrcresearchpress.com by 88.146.161.215 on 09/08/12
For personal use only.

DIPIC, 2PP6C, and CHOX with Fe(III) and Fe(II), we need to develop parameters for the Fe—N and Fe-O bonds involved. The calculations were carried out using the program SYBYL (6). To the TAFF force field (6), which has all the parameters necessary for modeling organic molecules, were added parameters to describe the Fe(II) and Fe(III) complexes of linear NO_2 donor set ligands DIPIC, 2PP6C, and CHOX. The Fe(III) Fe—N and Fe—O ideal bond lengths were taken to be 2.08 and 2.01 Å, respectively, while Fe—N and Fe—O for Fe(II) were taken to be 2.24 and 2.20 Å, respectively, with force constants of 100 kcal mol^{-1} $Å^{-1}$. The L-Fe-L and Fe-L-C angle (where L represents O or N donor atoms of the ligand) bending force constants were set to 0.005 kcal mol^{-1} deg^{-1} with ideal angles of 90° and 120°, respectively.

Oxidative degradation of ligands

The rate of oxidative degradation of CHOX when used as the Fe(III) chelate in the oxidation of H_2S by air was determined under simulated industrial conditions in the continuous glass apparatus described previously for degradation studies of NTA (3). The pH was maintained at 8.5 with a 2.0 molar ratio of ligand to metal and the temperature was 25.0°C. The H_2S flow rate was 2.0 mL/min. The Fe(III) solution was 0.018 M and the CHOX concentration was 0.036 M, and the volume of the test solution was 1.00 L.

HPLC Analysis of CHOX

Preparation of iron-free sample

To 5.0 mL of solution taken from the continuous reactor, 125 mg of NaOH in 30 mL water was added dropwise with stirring. The mixture was heated to 80–90°C for 40 min. The $Fe(OH)_3$ that precipitated was carefully filtered off and was washed several times with water. The filtrate was combined with the washing and was transferred to a 50 mL volumetric flask. To this was added 10.0 mL 1 M KCl solution and the solution was then diluted with distilled water to 50 mL. (The HPLC peak seemed to be improved by the addition of KCl.)

Operating conditions

IB-SIL 5 C8 reverse phase HPLC columns 4.5 × 150 mm; column temperature, ambient; mobile phase, 18% methanol, 77.9 water, 4.1% acetic acid; flow rate 1.5 mL/min; detector UV 250 nm, sample 20 μL; recorder 100 mV full scale, chart speed 0l5 cm/min. The height of the chromatographic peak was taken as a measure of the molar concentration of CHOX. The analytical method was calibrated with known samples of ligand and a linear calibration was obtained for ligand concentrations of 5–0.5 M.

Results and discussion

Types of ligands that meet specified requirements

We may gain an idea of what types of ligands will be suitable for this purpose by examining the relationship between log K_1 for Fe(II) and Fe(III) in Fig. 1. Figure 1 shows a typical relationship found (7) for pairs of metal ions. Fe(III) is considerably harder than Fe(II) in the hard and soft acids and bases (HSAB) classification of Pearson (8). The effect that this has on diagrams such as Fig. 1 is that ligands are separated into different correlations by their hardness in the HSAB sense. Thus, Fig. 1 shows that a single correlation occurs which contains all of the ligands that contain only acetate and amino groups. This group of ligands includes NTA and DIPIC, which have, respectively, saturated nitrogens and pyridine nitrogens as donors, in addition to acetate groups. A separate correlation exists for those ligands that contain the more basic phenolate oxygen groups. The correlation for the phenolate donors is displaced in the direction of the Fe(III) ion, showing a much greater preference for Fe(III) relative to Fe(II). This is illustrated by the log K_1 values (1) for EDTA and HBED.

	Fe(II)	Fe(III)	Δ log K_1 (Fe(III) – VFe(II))
log K_1 EDTA	14.27	25.0	10.7
log K_1 HBED	17.3	39.68	22.4

The large difference between Fe(III) and Fe(II) for HBED above would produce much too unfavorable an oxidation potential for the Fe(II)/Fe(III) couple, and so HBED would not be active as a catalyst for the oxidation of H_2S (9).

Ligands that have proved useful in complexing Fe(II) and Fe(III) to give satisfactory catalysts for oxidation of H_2S to sulfur are EDTA, NTA, and dipicolinic acid. The use of these ligands has been described in several patents, only a few of which are cited here (10–13).

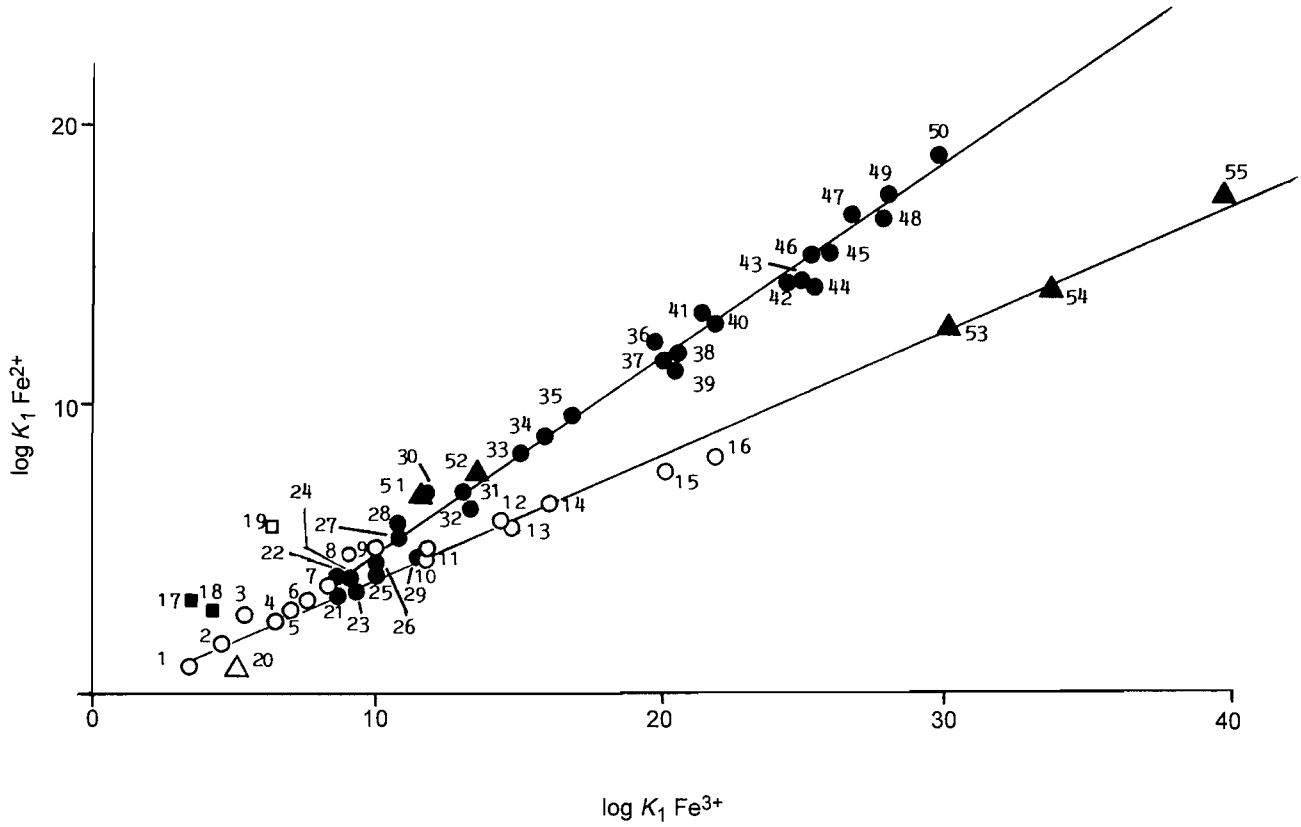
New ligand systems

It has recently been shown that pyridine-2-phosphonic-6-carboxylic acid (2PP6C) and 2,6-pyridinediphosphonic acid (2,6-PDPA) are effective ligands for use in Fe(II)/Fe(III) systems for catalyzing the oxidation of H_2S to sulfur (4, 5). The logic here is that DIPIC has been shown to be resistant to attack by the hydroxyl radical. It appears that ligands with no saturated carbons, especially α-methylene carbons such as DIPIC, may be more resistant to attack by hydroxyl radicals because the aromatic ring is less affected by attack by hydroxyl radical. DIPIC suffers from formation constants with Fe(II) and Fe(III) that are too low, so that the system can operate only at pH 6.5 if precipitation of $Fe(OH)_3$(s) and FeS(s) is to be avoided. The ligands 2PP6C and 2,6-PDPA resemble DIPIC in having no methylene carbon atoms, but the phosphonate donor group (p*K*a about 8.0 rather than 4.8 for a carboxylic acid) is a much stronger base, so that 2PP6C and 2,6-PDPA should be much stronger ligands than DIPIC, but share the important feature of DIPIC in having no methylene carbons. As discussed, both 2PP6C and 2,6-PDPA are successful ligands for the catalytic oxidation of H_2S.

In a search for further ligand systems, it seemed possible that the ligand 2-carboxy-8-hydroxyquinoline (CHOX) described below would resemble DIPIC very closely in its bonding properties with Fe(II) and Fe(III). The hydroxy group of 8-hydroxyquinoline has a protonation constant (1) of 9.81, which means that it will resemble DIPIC in having no methylenic protons, but is a stronger ligand because of the much more basic oxygen donor group. A problem that might arise with ligands such as CHOX is that they are fairly rigid, and there might be problems in relation to the steric fit of such a ligand when coordinating Fe(II) and Fe(III). To gain some insight into the metal ion coordinating properties of the ligands containing pyridyl groups, a Molecular Mechanics

© 1997 NRC Canada

Fig. 1. The relationship between log K_1 for Fe(II)complexes and log K_1 for the corresponding Fe(III) complexes. Key to ligands: ligands with oxygen donors only, ○; (1) CH_3COO^-, (2) squarate, (3) oxydiacetate, (4) D-tartaric acid, (5) malonate, (6) oxalate, (7) HPO_4^{2-}, (8) kojate, (9) acetylacetonate, (10) OH^-, (11) citrate, (12) 5-nitrosalicylate, (13) 5-sulfosalicylate, (14) salicylate, (15) tiron (1,2-dihydroxybenzene-3,5-disulfonic acid), (16) catchol (1,2-hydroxybenzene). Ligands with thioether and acetate donors, ■; (17) ethylenedithiodiacetate, (18) thiodiacetate. Ligand with only nitrogen donors, □; (19) 1,10-phenanthroline. A halide ligand, Δ, (20) fluoride. Ligands with carboxylate and nitrogen donor groups, ●; (21) arginine, (22) threonine, (23) methionine, (24) serine, (25) proline, (26) glycine, (27) picolinate, (28) iminodiacetate, (29) aspartate, (30) HIDA (*N*-2-hydroxyethyliminodiacetate), (31) dipicolinate, (32) *N,N'*-bis(2-carboxyethylethylenediamine, (33) *N,N'*-bis(1-carboxyethyl)ethylenediamine, (34) NTA (nitrilotriacetate), (35) *N*-2-aminoethyliminodiacetate, (36) HEDTA (*N*-2-hydroxyethylethylenediamine-*N,N',N'*-triacetate), (37) 1,3-diaminopropane-2-hydroxy-*N,N,N',N'*-tetraacetate, (38) EGTA (ethylenebis(oxyethylenenitrilo)tetraacetate), (39) thiobis(ethylenenitrilo)tetraacetate, (40) ethylenedinitrilo-*N,N'*-diacethydroxamate-*N,N'*-diacetate, (41) TMDTA (trimethylenediaminetetraacetate), (42) EEDTA (oxybis(ethylenenitrilo)tetraacetate), (43) EDTA (ethylenediaminetetraacetate), (44) DL-ethylenedinitrilo-*N,N'*-di(2-propionato)-*N,N'*-(diacetate), (45) *meso*-1,2-diaminobutanetetraacetate, (46) PDTA (1,2-diaminopropanetetraacetate), (47) 1,4,7,10-tetraazadecanehexaacetate, (48) DTPA (diethylenetriaminepentaacetate), (49) D, L-1,2-diaminobutanetetraacetate, (50) CDTA (*trans*-1,2-diaminotetraacetate. Ligands with phenolate oxygen donor groups, Δ; (51) 5-sulfo-8-hydroxyquinoline, (52) 8-hydroxyquinoline, (53) *N,N'*-bis(2-hydroxybenzyl)ethylenediamine-*N,N'*-bis(methylenephosphonic acid methylester), (54) EHPG (ethylenediiminobis(2-hydroxyphenyl)acetic acid), (55) HBED (*N,N'*-bis(hydroxybenzyl)ethylenediamine-*N,N'*-diacetic acid).



Complex	$[Co(TAB)_2]^{3+}$	$Co(NH_3)_6]^{3+}$	$[Co(en)_3]^{3+}$	$[Co(dptn)_2]^{3+}$
Å, Co—N (calcd.)	1.91	1.97	1.96	2.05
Å, Co—N (obsd.)	1.91	1.97	1.96	2.04

(MM) analysis of the Fe(II) and Fe(III) complexes of DIPIC, 2PP6C, and CHOX was undertaken.

The role of p_π–d_π π-bonding in complexes of Fe(III)

The mechanical model of molecules and complexes employed in MM accounts very well for many types of effects. In the first instance, it accounts, for example, for changes in M—L bond lengths that are caused by steric forces within the molecule. This is seen (14) for complexes of Co(III) with N6 donor groups where the Co—N bond lengths cover a considerable range:

This change of bond length over a wide range is reproduced by MM calculations with no reference to any electronic effects. In contrast, in carrying out MM calculations on organic molecules, it is found that the C—C bond length may vary in a way that is caused by electronic effects due to the electronegativity of the atoms attached to the carbons. Thus, the C—C bond in $HOCH_2CH_2OH$ is only 1.51 Å, in contrast to the C—C bond in ethane, which is 1.54 Å. This is not reproduced in calculations of $HOCH_2CH_2OH$ where $r°$for the C—C bond of 1.54 Å is used, and an extra term to correct for the change in $r°$as a

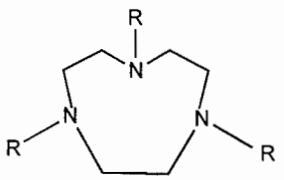
© 1997 NRC Canada

Can. J. Chem. Downloaded from www.nrcresearchpress.com by 88.146.161.215 on 09/08/12
For personal use only.

Can. J. Chem. Downloaded from www.nrcresearchpress.com by 88.146.161.215 on 09/08/12
For personal use only.

function of the electronegativity of the groups attached to the carbon atom has to be introduced. This is usually done only in MM programs such as MM3, where the interest is modeling the structures and energies of organic molecules with maximum accuracy. In approaches such as that adopted here, where the interest lies in the geometry around the metal ion, such extra terms are not included. However, one must be alert for structural and energetic effects that might arise in the bonds involving the metal ions that are due to electronic rather than steric effects. For the Fe(III) ion, it is clear that dramatic electron effects are present in complexes containing mixtures of neutral nitrogen and charged oxygen donors. This can be illustrated by considering complexes of Fe(III) with N_3O_3 sets of donor atoms, as an example, but appears to be a general phenomenon for all complexes of Fe(III) containing both N and O donors.

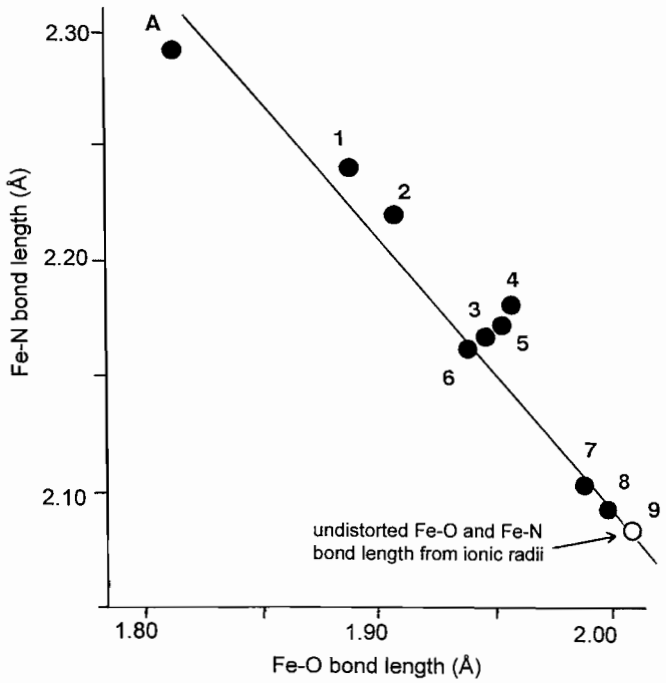
The ligands with N_3O_3 sets of donor atoms considered are as follows:



R = CH_2COOH = TACN-TA
R = Me = Me_3-[9]aneN_3
R = CH_2CH_2OH = THETACN
R = 2-hydroxybenzyl = TACN-HB
R = (3-hydroxy-6-methyl-2-pyridylmethylene) = TACN-HP

The structures (15–22) of the Fe(III) complexes with these ligands reveal an inverse relationship between Fe—N and Fe—O bond lengths, which is shown in Fig. 2. The interpretation of the shortening of the Fe—O bonds (14,18) is that p_π–d_π π-bonding involving the *p*-oribtals on the oxygen, and the half-filled t_{2g} level of the Fe(III), leads to the shortening observed. The longer Fe—N bonds are caused by a *trans* effect, which is demonstrated by the inverse relationship between the Fe—N and Fe—O bonds observed in Fig. 2. The question posed by Fig. 2 is the importance of this π-bonding in the present study. Figure 2 shows that the two complexes that demonstrate almost normal Fe—O and Fe—N bond lengths are those involving the tris-pyrazolylborate ligand (TPB). One sees here that where the nitrogen donors are sp^2 hybridized and capable of competing with the oxygen donors as π-bonders, in the tris-pyrazolylborate ligands, the nearly normal Fe—O and Fe—N bond lengths are observed (points 7 and 8 in Fig. 2). This result indicates therefore, that in modeling complexes of Fe(III) with negative oxygen donor atoms, such as the carboxylate and phenolate present on CHOX, one must be aware that π-bonding could lead to a distortion of the Fe—N and Fe—O bond lengths. However, since (*a*) the nitrogens in such a ligand can only coordinate to each other in a *trans* fashion, and cannot be *trans* to any oxygen donors, and (*b*) the nitrogen of a pyridine should, like those in TPB, be capable of p_π–d_π π-bonding, and therefore minimize shortening of the Fe—N bond due to a *trans* effect from negative oxygen donors, it is concluded that π-bonding distortions do not take place in the Fe(III) complexes of the present ligands.

Fig. 2. The relationship between Fe—N and Fe—O bond lengths in complexes of Fe(III) with N_3O_3 donor sets. The complexes are (1) [Fe(TACN-TB)], (2) [Fe(TACN-HP)], (3) [$(Fe(TPB))_2$-μ-O-μ-$(CH_3COO)_2$], (4) [Fe(TACN-TA)], (5) [$Fe(taci)_2$], (6) [Fe(THETACN)H_{-3}], (7) [(Fe(TPB))2-μ-OH-μ-$(CH_3COO)_2]^+$, (8) [Fe(TPB(TMP)]. Point 9 is for the hypothetical undistorted Fe(III) complex with N_3O_3 donor set, where the Fe—O and Fe—N bonds are as expected from the sum of the ionic radii (14). The point at A is for the very long Fe—N bond found *trans* to the bridging oxide in [(Fe(Me_3-[9]-aneN_3))2-μ-O-μ-$(CH_3COO)_2$], where a very short Fe—O bond is present.



The distortion of complexes of Fe(III) towards trigonal prismatic coordination

Most six-coordinate complexes of trivalent metal ions of the first row of transition metals (Sc^{3+} through Ga^{3+}) show a preference for maintaining a regular octahedral (O_h) coordination geometry, and in metal ions such as Cr(III) and Co(III), where a loss in ligand field stabilization energy (LFSE) results in distortion of the geometry away from O_h, this preference can be very strong. The high-spin Fe(III) ion has the d^5 electronic configuration, which means that LFSE is zero, and preference for O_h geometry should be much weaker. One thus finds, for example, that in the complexes of TACN-TA, where the pendant acetate donor arms of the ligand are too short to wrap effectively around the Fe(III) and achieve regular octahedral coordination geometry, distortion towards trigonal prismatic coordination occurs (Fig. 3). In contrast, the ligand TACN-HP has longer donor groups, and forms six-membered chelate rings on complex formation, and so (Fig. 3) has nearly regular coordination geometry. The extent of distortion toward trigonal prismatic coordination in the TACN-TA complex can be modeled only if the L-Fe-L angle bending force constants around the Fe(III) are set to zero. The available evidence suggests, however, that this loss of maintenance of the ability to maintain O_h geometry is coupled with the distortion of the

© 1997 NRC Canada

Can. J. Chem. Downloaded from www.nrcresearchpress.com by 88.146.161.215 on 09/08/12
For personal use only.

Fig. 3. The structures of (*a*) the complex [Fe(TACN-TA)], showing the distortion of the coordination geometry toward trigonal prismatic, and (*b*) the more nearly regular octahedral coordination geometry found with the complex [Fe(TACN-HP)]. The twist angle, which is defined as the projection of the Fe—L bond angles onto a plane at right angles to the C_3 axis of the complex, is 60° for a regular octahedron, and 0° for the trigonal prism. In (*a*) the twist angle is 25°, while in (*b*) it is 54°.

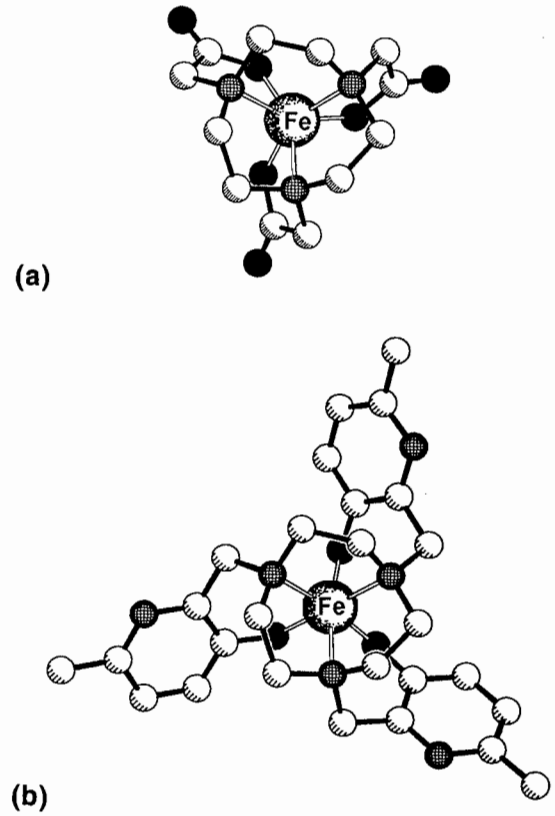
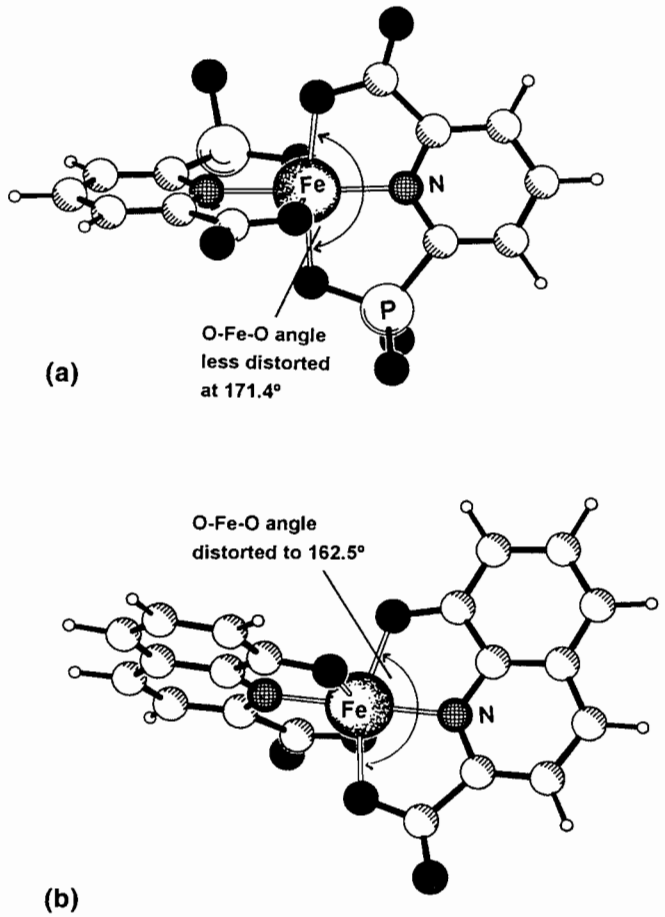


Fig. 4. The structure generated by MM calculation for [Fe(CHOX)]. The structure illustrates the steric difficulty for coordination of this ligand to metal ions in an octahedral fashion, since the O-Fe-O angles are distorted away from the ideal value of 180°.



Fe—N and Fe—O bond lengths, and so where such distortion is not present, it should be assumed that octahedral geometry will be maintained.

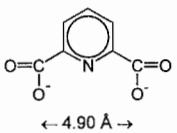
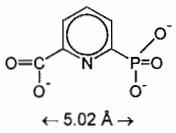
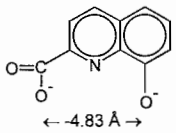
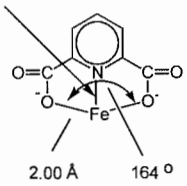
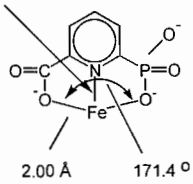
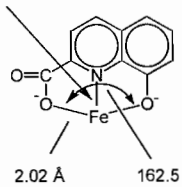
MM analysis of Fe(III) and Fe(II) complexes of CHOX, 2PP6C, and DIPIC

The ligand DIPIC complexes Fe(II) and Fe(III) too weakly, with resulting precipitation of FeS and $Fe(OH)_3$. A solution to this problem, which retains the resistance of DIPIC to attack by hydroxyl radicals, is the ligand CHOX, discussed above. The latter ligand is stronger since it contains a more basic phenolate donor in place of one of the weakly basic carboxylates of DIPIC. A problem with CHOX is its rigidity, which might lead to complexes of Fe(III) and Fe(II) that are not sufficiently stable because of the steric difficulty of coordination to the metal ion. We therefore report here the strain energies of the free ligands DIPIC and CHOX, and of the complexes of these ligands with Fe(III) and Fe(II).

In Fig. 4 are shown the energy minimized structures of $[Fe(2PP6C)_2]^-$ and $[Fe(CHOX)_2]^-$. Figure 4 shows the distortion of the O-Fe-O angle produced by the steric difficulty of coordinating in an octahedral fashion to these ligands. The MM calculations show that all three ligands, CHOX, 2PP6C, and DIPIC, have steric difficulty in coordinating to metal ions. In Table 1 are shown the free ligands CHOX, 2PP6C, and DIPIC. In all three ligands, the O–O distance is shown by MM calculation to be close to 5.0 Å, which is more than double the ideal Fe—O distance for either Fe(II) (2.20 Å) or Fe(III) (2.01 Å). Thus metal ions should experience steric difficulty because the O--O distance is too great. A second problem is that, if the O-Fe-O angles are 180°, then the Fe—N distance in these complexes will be very short, of the order of 1.8 Å. The MM calculations show that the strain energy of $[Fe(CHOX)_2]^-$ is somewhat higher than that of $[Fe(2PP6C)_2]^-$, and $[Fe(DIPIC)_2]^-$. This arises from the greater rigidity of CHOX, which means that stronger distortion of the O-Fe-O angle, as seen in Fig. 4, occurs in $[Fe(CHOX)_2]^-$; the higher strain energy is caused by the greater rigidity, which worsens the problems of coordinating a metal ion to the two oxygens and nitrogen of the ligand, with the Fe—O distances required by the ligand being too long, and the Fe—N distances required being too short. The problem is less serious for the 2PP6C complexes. The long bonds involving the phosphorus (P—C and P—O) of the phosphonate groups mean that the ligand

© 1997 NRC Canada

Table 1. Strain energies of free ligands and complexes with Fe(III) and Fe(II) of the complexes of DIPIC and CHOX.[a]

	DIPIC	2PP6C	CHOX
Strain energy (U_L) of ligand	–0.3	2.8	0.4
O--O distance from MM	 ← 4.90 Å →	 ← 5.02 Å →	 ← 4.83 Å →
Strain energy of $Fe(III)L_2$ complex (U_{ML_2})	19.8	19.6	25.8
Increase in U $U_{ML_2} - 2U_L$	20.4	14.0	25.0
Important dimensions of $Fe(III)L_2$ complexes	1.935 Å  2.00 Å 164 °	1.97 Å  2.00 Å 171.4 °	1.92 Å  2.02 Å 162.5 °
Strain energy of $Fe(II)L_2$ complexes	23.0	21.3	28.5
Change in U_{ML_2} for $Fe(II)L_2 - Fe(III)L_2$	3.2	1.7	2.7

[a]Calculated using the program SYBYL (5). Units for strain energies (U) in kcal mol^{-1}.

requires a somewhat longer M—N bond than does DIPIC and CHOX, and so, sterically, 2PP6C is better suited to complexing the Fe(III) ion. The strain energies calculated for the Fe(II) complexes show that the increase in strain energies that occurs for the complexes of both ligands on passing from the Fe(III) to the Fe(II) complex is fairly similar, so that we should expect the steric contributions to the oxidizing power of these complexes to be similar.

Degradation of the Fe(III)–CHOX complex at pH 8.5

CHOX forms sufficiently stable complexes with Fe(III) so that $Fe(OH)_3$ does not precipitate until the pH is above 10.0 when a 2:1 molar ratio of ligand to Fe(III) ion is used (Fe(III) 0.018 M; CHOX 0.030 M). A precipitate is formed above pH 9.0 when a 1.5:1 molar ratio of ligand to Fe(III) is employed (Fe(III) 0.018 M, CHOX 0.027 M, Fe(III):CHOX = 1:1.5).

The degradation of Fe(III)-CHOX at pH 8.5, with a 2:1 ratio of ligand to Fe(III) ion, is shown in Table 2 and Fig. 5. The results show that the ligand degrades very rapidly during the redox reaction in the continuous reaction apparatus. After the redox reaction was carried out for 52.5 h, about 96% of CHOX

Table 2. Degradation of CHOX at pH 8.5 (Fe(III) 0.018 M, CHOX 0.030 M); H_2S flow 2.0 mL/min, 25.0°C.

Time, h	CHOX, M
0	3.0×10^{-2}
20.	1.0×10^{-2}
35.5	3.9×10^{-3}
52.5	1.2×10^{-3}

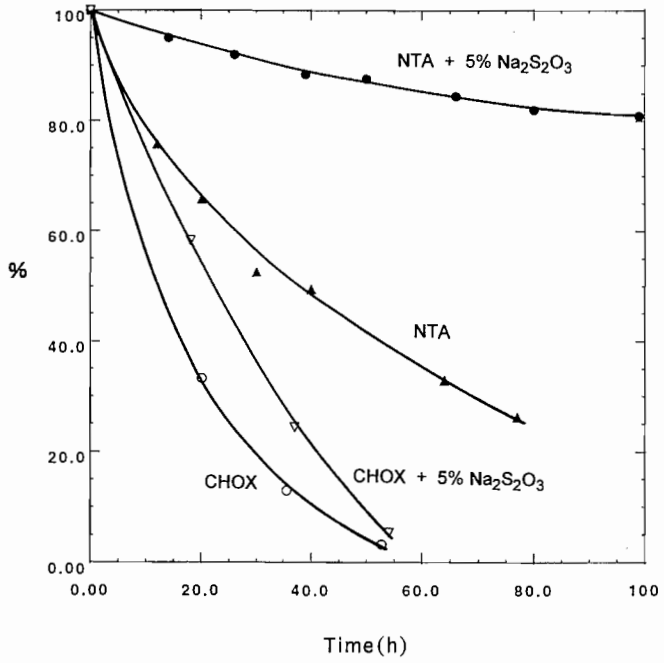
Table 3. Degradation of Fe(III)–CHOX, 5% $Na_2S_2O_3$ (Fe(III) 0.018 M, CHOX 0.036 M); H_2S flow 2.0 mL/min, 25.0°C.

Time, h	CHOX, M
0	3.6×10^{-2}
18	2.1×10^{-2}
37	8.8×10^{-3}
54	2.3×10^{-3}

Can. J. Chem. Downloaded from www.nrcresearchpress.com by 88.146.161.215 on 09/08/12
For personal use only.

© 1997 NRC Canada

Fig. 5. Comparison of degradation of CHOX and of NTA at pH 8.5: ○, CHOX; ▽, CHOX + 5% $Na_2S_2O_3$; ▲, NTA; ●, NTA + 5% $Na_2S_2O_3$; Fe(III) = 0.018 M; ligand = 0.036 M. % is percent of 0.036 M ligand left in reaction mixture.



was lost. The redox reaction was continued for 160 h and no precipitate of $Fe(OH)_3$ was observed during this period of time. This observation, together with the evidence in Fig. 5 for the rapid degradation of CHOX, indicates that the degradation product of CHOX is also a strong ligand for Fe(III).

The degradation of Fe(III)-CHOX with 5% $Na_2S_2O_3$, when used as a redox catalyst in the continuous flow apparatus, is shown in Table 3 and Fig. 5. The results show that CHOX degrades so rapidly that in 54 h about 94% of the ligand was lost, presumably by hydroxylation. The presence of 5% $Na_2S_2O_3$ does not stabilize this ligand from oxidation by the hydroxyl radical. The relative concentrations of CHOX and thiosulfate in Table 3 and Fig. 5 lead one to believe that the ligand has a much greater affinity for $^{\cdot}OH$ than does $S_2O_3^{2-}$.

Sodium thiosulfate is a free-radical scavenger that is used industrially as an additive to slow down the oxidative degradation of chelating agents such as NTA and EDTA when used in this redox process. Its properties and use in this process have been described (2).

The rate of degradation of NTA, with and without thiosulfate, under the same conditions (2), is also shown in Fig. 5 for comparison. It is seen that NTA degrades much less rapidly than CHOX, and is greatly stabilized against oxidative degradation by thiosulfate. The oxidative degradation of CHOX, on the other hand, is much more rapid, and is not stabilized very much by thiosulfate. However, the most remarkable characteristic of this system, and of the degradation tests that have been carried out, is that the degradation product, the nature of which is still to be determined, is also a good catalyst for the redox reaction, because the production of sulfur from H_2S continues at about the initial rate, even after the ligand, CHOX, has been completely degraded. Therefore the product of oxidative attack of the initial ligand is probably a polyhydroxy compound, produced by hydroxylation of CHOX. Such a polyhydroxy compound would probably be a catechol, which would have high affinity for Fe(III), and its iron chelate would be expected to be a good redox catalyst for the oxidation of H_2S to sulfur.

Research is now in progress on the isolation, identification, and purification of the oxidation product of CHOX that seems to be effective (in the form of its Fe(III)/Fe(II) complexes) as a redox catalyst for the oxidation of H_2S. It is hoped to describe this catalyst in a subsequent report.

Conclusions

Therefore the absence of easily oxidized α-methylene groups does not guarantee against oxidative degradation. Also in some cases, as in CHOX, the initially formed chelating agent derivatives may also be effective ligands for Fe(II)/Fe(III) and may form effective catalysts for the oxidation of H_2S to elemental sulfur. Additional work on the tridentate phosphates 2PP6C and 2,6PDPA is now in progress, and will be reported later.

Acknowledgments

This research was supported by grants from Wheelabrator Clean Air Systems, Inc., and the Texas Advanced Technology Program.

References

1. (*a*) A.E. Martell and R.M. Smith. Critical stability constants. Vols. 1–6. Plenum Press, New York. 1974, 1975, 1976, 1977, 1978, 1982; (*b*) R.M. Smith, A.E. Martell, and R.J. Motekaitis. Critical stability constants database. NIST Standard Reference Data No. 46, Version 3, Gaithersburg, Md. 1996.
2. D. Chen, A.E. Martell, and D. McManus. Can. J. Chem. **73**, 264 (1995).
3. D. Chen, R.J. Motekaitis, A.E. Martell, and D. McManus. Can. J. Chem. **71**, 1524 (1993).
4. D. McManus, D. Chen, and A.E. Martell. U.S. Patent 5,591,419, Jan. 1997.
5. A.E. Martell, D. Chen, D. McManus, and R.J. Motekaitis. Can. J. Chem. Submitted.
6. M. Clarke, R.D. Cramer, and N. VanopdenBosch. J. Comput. Chem. **10**, 982 (1989).
7. R.D. Hancock and A.E. Martell. Chem. Rev. **89**, 1875 (1989).
8. R.G. Pearson. J. Am. Chem. Soc. **85**, 3533 (1963).
9. A.E. Martell, R.J. Motekaitis, D. Chen, R.D. Hancock, and D. McManus. Can. J. Chem. **74**, 1872 (1996).
10. J. Diaz. U.S. Patent No. 4,388,239, June 14, 1983.
11. D. McManus and F.R. Kin, U.S. Patent No. 4,622,212, Nov. 11, 1986.
12. S.A. Bedell. U.S. Patent No. 4,891,205, Jan. 24, 1994.
13. D.T. Sawyer and A. Sobkowiak. U.S. Patent No. 5,273,734, Dec. 28, 1993.
14. R.D. Hancock. Prog. Inorg. Chem. **37**, 187 (1989).
15. K. Wieghardt, U. Bossek, P. Chaudhuri, W. Herrman, B.C. Manke, and J. Weiss. Inorg. Chem. **21**, 4308 (1982).
16. U. Auerbach, T. Weyermuller, K. Wieghardt, B. Nuber, E. Bill, C. Burzlaff, and Z.X. Trautwein. Inorg. Chem. **32**, 508 (1993).
17. Y. Sun, L. Hu, A.E. Martell, and A. Clearfield. J. Coord. Chem. **36**, 23 (1995).
18. K. Hegetschweiler, M. Chisletta, L. Hausherr-Primo, and T. Kradolfer. Inorg. Chem. **34**, 1950 (1995).

© 1997 NRC Canada

Can. J. Chem. Downloaded from www.nrcresearchpress.com by 88.146.161.215 on 09/08/12
For personal use only.

19. K.N. Han, D. Wang, H.-J. Lee, Y. Do, and K. Kim. Inorg. Chem. **32**, 2597 (1993).
20. W.H. Armstrong and S.J. Lippard. J. Am. Chem. Soc. **106**, 46732 (1984).
21. R. Luckay, R.D. Hancock, I. Cukrowski, and J.H. Reibenspies. Inorg. Chim. Acta, **246**, 139 (1996).
22. S. Drucke, K. Wieghardt, B. Nuber, and J. Weiss. Inorg. Chem. **28**, 1414 (1989).

List of abbreviations

CHOX	2-Carboxy-8-hydroxyquinoline
DIPIC	Pyridine-2,6-dicarboxylic acid
dptn	1,5,9-Triazanonane
EDTA	Ethylenediaminetetraacetic acid
en	Ethylenediamine
HBED	*N*,*N*′-Bis(2-hydroxybenzyl)ethylene-diamine-*N*,*N*′-diacetic acid
Me_3-[9]aneN_3	*N*,*N*′,*N*″-Trimethyltriazacyclononane
NTA	Nitrilotriacetic acid
2-PP6C	Pyridine-2-phosphonic-6-carboxylic acid
2,6PDPA	2,6-Pyridinediphosphonic acid
TAB	1,4,7-Triaziridinobenzene
taci	*cis*,*cis*-1,3,5-Triamino-*cis*,*cis*-2,4,6-trihydroxycyclohexane
TACN-TA	Triazacyclononane-*N*,*N*′,*N*″-triacetic acid
TACN-TB	*N*,*N*′,*N*″-Tris(2-hydroxybenzyl)triaza-cyclononane
TACN-TP	*N*,*N*′,*N*″-Tris(3-hydroxy-6-methyl-2-pyridylmethylene) triazacyclononane
THETAC	*N*,*N*′,*N*″-Tris(2-hydroxyethyl)triaza-cyclononane
TMP	Trimetaphosphate
TPB	Trispyrazoylborate

Can. J. Chem. Downloaded from www.nrcresearchpress.com by 88.146.161.215 on 09/08/12
For personal use only.

© 1997 NRC Canada

Synthesis of 4,4-bis(2-methylphenyl)-3-butenyl (and butyl) analogs of 4-phenyl-1,4- and 6-phenyl-1,6-dihydropyridine-3-carboxylic acids and their evaluation as neuronal GABA-uptake inhibitors

Nadeem Iqbal, Zhong-Yong Wei, Glen B. Baker, and Edward E. Knaus

Can. J. Chem. Downloaded from www.nrcresearchpress.com by 88.146.161.215 on 09/08/12
For personal use only.

Abstract: Treatment of 3-[2-(4,4-dimethyl-4,5-dihydrooxazolin-2-yl)]-4-phenyl-1,4-dihydropyridine (**13**) with NaH–DMSO, and then reaction with 1,1-bis(2-methylphenyl)-4-bromobutane (**12***c*) afforded 1-[4,4-bis(2-methylphenyl)butyl]-3-[2-(4,4-dimethyl-4,5-dihydrooxazolin-2-yl)]-4-phenyl-1,4-dihydropyridine (**14**). Reaction of methyl nicotinate with 2.1 equivalents **12***c* or 1,1-bis(2-methylphenyl)-4-bromo-1-butene (**11***b*) afforded 4,4-bis(2-methylphenyl)butyl 1-[4,4-bis(2-methylphenyl)butyl]pyridinium-3-carboxylate bromide (**17**) or 4,4-bis(2-methylphenyl)-3-butenyl 1-[4,4-bis(2-methylphenyl)-3-butenyl]pyridinium-3-carboxylate bromide (**18**), respectively. The nonregioselective reaction of the pyridinium salts (**17/18**) with PhMgCl in THF at −23°C using a catalytic amount of CuI afforded a mixture of isomeric 4-phenyl-1,4-dihydropyridyl (**21** or **22**) and 6-phenyl-1,6-dihydropyridyl (**27** or **28**) products in a ratio of approximately 1:1. All attempts to hydrolyze the 4,4-bis(2-methylphenyl)butyl or 3-butenyl ester moiety of **21/22** or **27/28** to a carboxyl group resulted in decomposition products. In contrast, the corresponding 3-(2-cyanoethyl) esters (**23**, **24**, **29**, **30**) were readily converted to the corresponding carboxyl analogs (**25**, **26**, **31**, **32**) via a β-elimination reaction of acrylonitrile using the non-nucleophilic base DBU. The 4-phenyl-1,4-dihydropyridyl (**14**, **25**, **26**) and 6-phenyl-1,6-dihydropyridyl (**27/28** or **31/32**) compounds inhibited the in vitro uptake of [^{3}H]GABA into striatal prisms in the 21–44% range at a 10^{-4} M test compound concentration, relative to the reference drug nipecotic acid (87% inhibition). Structure–activity correlations showed the dihydropyridyl C-3 substituent was a determinant of [^{3}H]GABA uptake where the potency order was CO_2H > 2-(4,4-dimethyl-4,5-dihydrooxazolin-2-yl) > $CO_2(CH_2)_3CH$-(*o*-tolyl)$_2$ and $CO_2(CH_2)_2CH{=}C$-(*o*-tolyl)$_2$. Compounds possessing C-3 and (or) N-1 $CO_2(CH_2)_3CH$-(*o*-tolyl)$_2$ substituents were generally more potent than analogs having $CO_2(CH_2)_2CH{=}C$-(*o*-tolyl)$_2$ substituents. In general, 1,6-dihydropyridyl compounds were more potent than the corresponding 1,4-dihydropyridyl isomers.

Key words: 1,4- and 1,6-dihydropyridines, GABA-uptake inhibitors.

Résumé : Le traitement de la 3-[2-(4,4-diméthyl-4,5-dihydrooxazolin-2-yl)]-4-phényl-1,4-dihydropyridine (**13**) par du NaH–DMSO, suivi d'une réaction avec du 1,1-bis(2-méthylphényl)-4-bromobutane (**12***c*) conduit à la 1-[4,4-bis(2-méthylphényl)butyl]-3-[2-(4,4-diméthyl-4,5-dihydrooxazolin-2-yl)]-4-phényl-1,4-dihydropyridine (**14**). La réaction du nicotinate de méthyle avec 2,1 équivalents de **12***c* ou du 1,1-bis(2-méthylphényl)-4-bromobut-1-ène (**11***b*) fournit le bromure du 1-[4,4-bis(2-méthylphényl)butyl]pyridinium-3-carboxylate de 4,4-bis(2)-méthylphényl)butyle (**17**) ou le bromure du 1-[4-4-bis(2-méthylphényl)but-3-énYl]pyridinium-3-carboxylate de 4,4-bis(2-méthylphényl)but-3-ényle, respectivement. La réaction non régiosélective des sels de pyridinium (**17/18**) avec le PhMgCl dans le THF, à 23°C, en présence d'une quantité catalytique de CuI conduit à un mélange de produits isomères 4-phényl-1,4-dihydropyridylés (**21** ou **22**) et 6-phényl-1,6-dihydropyridylés (**27** ou **28**) dans un rapport approximativement 1 : 1. Tous les essais d'hydrolyser les portions 4,4-bis(2-méthylphényl)butyles ou but-3-énYles des esters **21/22** ou **27/28** en groupe carboxylique n'ont conduit qu'à des produits de décomposition. Par opposition, l'utilisation de la base non nucléophilique DBU permet de transformer facilement les esters 3-(2-cyanoéthylés) (**23**, **24**, **29**, **30**) en analogues carboxylés correspondants (**25**, **26**, **31**, **32**) par une réaction d'élimination-β d'acrylonitrile. Lors d'essais à des concentrations de 10^{-4} M des composés 4-phényl-1,4-dihydropyridylés (**14**, **25**, **26**) et 6-phényl-1,6-dihydropyridylés (**27/28** ou

Received September 3, 1996.

This paper is dedicated to Professor William A. Ayer on the occasion of his 65th birthday.

N. Iqbal, Z.-Y. Wei,[1] G.B. Baker, and E.E. Knaus.[2] Faculty of Pharmacy and Pharmaceutical Sciences, and Department of Psychiatry, Neurochemical Research Unit, University of Alberta, Edmonton, AB T6G 2N8, Canada.

[1] Current address: Astra Pain Research Unit, Bld 3000, 275 Bis Armand-Frappier, Laval, QC H7V 4A7.
[2] Author to whom correspondence may be addressed. Telephone: (403) 492-5993. Fax: (403) 492-1217. E-mail: eknaus@pharmacy.ualberta.ca

© 1997 NRC Canada

31/32), ceux-ci inhibent l'assimilation in vitro du [^{3}H]-«GABA» dans des prismes striataux par des facteurs de 21–44% alors que le médicament de référence, l'acide nopécotique, provoque une inhibition de 87%. Des corrélations structure–activité ont permis de démontrer que le substituant en C-3 du dihydropyridyle est déterminant dans l'assimilation du [^{3}H]-«GABA» et que l'importance de l'activité de ces substituants varie dans l'ordre CO_2H > 2-(4,4-diméthyl-4,5-dihydrooxazon-2-yl) > $CO_2(CH_2)_3CH$-(*o*-tolyl)$_2$ et $CO_2(CH_2)_2CH{=}C$-(*o*-tolyl)$_2$. Les composés comportant des substituants $CO_2(CH_2)_3CH$-(*o*-tolyl)$_2$ en C-3 ou en N-1 sont généralement plus actifs que les analogues possédant des substituants $CO_2(CH_2)_2CH{=}C$-(*o*-tolyl)$_2$. En général, les composés 1,6-dihydropyridylés sont plus actifs que les isomères correspondants 1,4-dihydropyridylés.

Mots clés : 1,4- et 1,6-dihydropyridines, inhibiteurs de l'assimilation de «GABA».

[Traduit par la rédaction]

Can. J. Chem. Downloaded from www.nrcresearchpress.com by 88.146.161.215 on 09/08/12
For personal use only.

Introduction

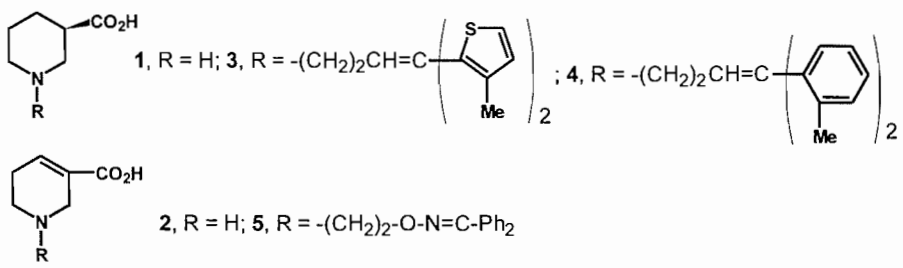
γ-Aminobutyric acid (GABA), the major inhibitory neurotransmitter in the central nervous system (CNS) (1), has been estimated to be present in 60–70% of all synapses within the CNS (2). GABA-mediated neurotransmission is terminated by its rapid uptake via specific, high-affinity transporters located in the presynaptic terminal and (or) surrounding glial cells (3). A reduction in GABA neurotransmission has been implicated in the etiology of a variety of neurological disorders including epilepsy, anxiety, and pain (1). One mechanistic approach to elevate GABA neurotransmission in the CNS involves the inhibition of GABA uptake into neurons and glia. Conventional GABA-uptake inhibitors such as the cyclic amino acids nipecotic acid (**1**) and guvacine (**2**), which can be viewed as conformationally restricted analogs, display in vitro activity as GABA-uptake inhibitors. However, **1** and **2** do not readily cross the blood–brain barrier (BBB), presumably due to their hydrophilic nature (4–6), which precludes their therapeutic usefulness. To overcome this problem, lipophilic side chains were attached to the nitrogen atom of nipecotic acid (**1**) and guvacine (**2**). Thus, tiagabine (**3**), the 4,4-bis(2-methylphenyl)-3-butenyl compound (**4**), and NNC-711 (**5**) were found to be potent GABA-uptake inhibitors that possessed in vivo efficacy as anticonvulsant agents (1, 7, 8). Compounds **3** and **4** having a substituent in an "*ortho*" position in one or both aromatic/heteroaromatic groups exhibited the most potent in vitro GABA-uptake inhibition (7). It was anticipated that coupling a lipophilic 4,4-bis(2-methylphenyl)-3-butenyl or 4,4-bis(2-methylphenyl)butyl moiety to the N-1 position of a 3-carboxy-4-phenyl-1,4-dihydropyridyl moiety would provide agents that inhibit GABA uptake into neurons. This postulate was based on the fact that (*i*) 1-alkyl-1,4-dihydronicotinate esters and related nicotinic acid derivatives exhibit potent anticonvulsant activity in the maximal electroshock screen (9, 10), and (*ii*) that a substituent at the C-4 position of nipecotic acid (**1**) possessing a 1-(4-CF_3-C_6H_4)$_2$-$CHOCH_2CH_2$- substituent is tolerated with respect to GABA-uptake inhibition (11). We now report the synthesis of 4,4-bis(2-methylphenyl)-3-butenyl- and 4,4-bis(2-methylphenyl)butyl analogs of 4-phenyl-1,4- and 6-phenyl-1,6-dihydropyridine-3-carboxylates and their evaluation as neuronal GABA-uptake inhibitors.

Chemistry

Our intitial attempt to prepare 1,1-bis(2-methylphenyl)-4-bromo-1-butene (**11***b*) by reaction of *ortho*-tolylmagnesium bromide with ethyl 4-bromobutyrate afforded a mixture of 2,2-bis(2-methylphenyl)tetrahydrofuran (**7**, 14%) and 1,1-bis(2-methylphenyl)-1,4-butanediol (**8**, 10%), which are likely produced by the respective cyclization and hydrolysis of the intermediate product (*ortho*-tolyl)$_2$-$C(OH)(CH_2)_3Br$ as illustrated in Scheme 1. Since the 1,4-butanediol product **8** was readily converted to 1,1-bis(2-methylphenyl)-1-buten-4-ol (**9**, 94%) using HCl, an alternate preparation of 1,1-bis(2-methylphenyl)-1,4-butanediol (**8**) was investigated. Accordingly, reaction of *ortho*-tolylmagnesium bromide with γ-butyrolactone (**10**) afforded **8** (90%), which was readily converted to 1,1-bis(2-methylphenyl)-1-buten-4-ol (**9**, 90%) by acid-catalyzed dehydration using HCl. Elaboration of **9** to the tosylate analog (**11***a*) and subsequent reaction with either LiBr or NaI in acetone afforded the respective 1,1-bis(2-methylphenyl)-4-bromo-1-butene (**11***b*, 88%) or iodide (**11***c*, 85%). Hydrogenation of 1,1-bis(2-methylphenyl)-1-buten-4-ol (**9**) using 10% Pd/C and H_2 gas at 60 psi (1 psi = 6.9 kPa) gave 1,1-bis(2-methylphenyl)-4-hydroxybutane (**12***a*, 94%), which was elaborated to the tosylate analog (**12***b*, 83%) and then to 1,1-bis(2-methylphenyl)-4-bromobutane (**12***c*, 83%).

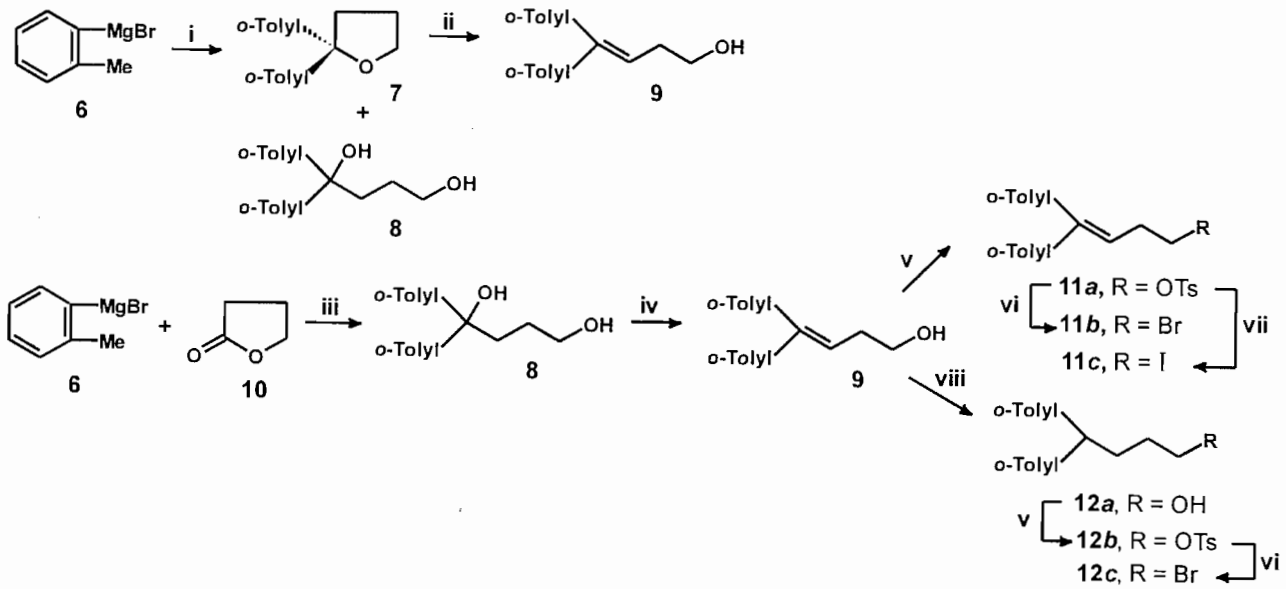
The reaction of 3-[2-(4,4-dimethyl-4,5-dihydrooxazolin-2-yl)]-4-phenyl-1,4-dihydropyridine (**13**) (12) with NaH in DMSO, followed by reaction with 1,1-bis(2-methylphenyl)-4-bromobutane (**12***c*), afforded the *N*-alkylated product **14** (19%) as illustrated in Scheme 2.

Reaction of methyl nicotinate with 2.1 equivalents of 1,1-



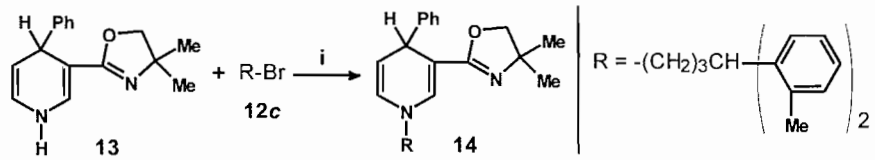
© 1997 NRC Canada

Scheme 1.



Reagents: i, $EtO_2C(CH_2)_3Br$, THF, 0°C → 25°C, 4 h and then aqueous NH_4Cl hydrolysis; ii, 6 N HCl, EtOH, THF, reflux, 4 h; iii, THF, 25°C, 2 h and then aqueous NH_4Cl hydrolysis; iv, 4 N HCl, EtOH, reflux, 6 h; v, 4-Me-C_6H_4-SO_2Cl, pyridine, CH_2Cl_2, 25°C, 12 h and then aqueous NH_4Cl hydrolysis; vi, LiBr, acetone, reflux, 12 h; vii, NaI, acetone, reflux, 12 h; viii, 10% Pd/C, EtOH, H_2 gas, 60 psi, 4 h, 25°C.

Scheme 2.



Reagents: i, NaH/DMSO, 25°C, 12 h.

bis(2-methylphenyl)-4-bromobutane (**12***c*) afforded the pyridinium salt (**17**, 74%) (see Scheme 3). When 1.1 equivalents of **12***c* were employed, **12***c* was all consumed but a considerable amount of methyl nicotinate remained. Similar results were observed in the synthesis of **18** (67%) using a similar reaction with 1,1-bis(2-methylphenyl)-4-bromo-1-butene (**11***b*). A plausible explanation for the replacement of the methyl R^1 substituent by a 4,4-bis(2-methylphenyl)butyl (**17**) or a 4,4-bis(2-methylphenyl)-3-butenyl (**18**) substituent is shown in Scheme 4. This replacement of the Me R^1 substituent proceeds to completion since the volatile by-product MeBr (bp 4°C) would escape from the reaction mixture (reflux in MeCN for 48 h). No product resulting from replacement of the cyanoethyl moiety of **16** was isolated for similar reactions of **16** with either **11***b* or **12***c*.

The nonregioselective reaction of the pyridinium salts (**17**–**20**) with PhMgCl in THF at −23°C using a catalytic amount of CuI afforded a mixture of isomeric 4-phenyl-1,4-dihydropyridyl and 6-phenyl-1,6-dihydropyridyl products in a ratio of approximately 1:1 (**17** → **21** (22%) + **27** (18%); **18** → **22** (24%) + **28** (19%); **19** → **23** (22%) + **29** (20%); **20** → **24** (20%) + **30** (21%)). No product resulting from reaction of the Grignard reagent with the methyl ester moiety was detected. Comins et al. (13) observed that the CuI-catalyzed reaction of methyl nicotinate with phenyl chloroformate in THF – methyl sulfide (3 equiv.) at −20°C resulted in regioselective attack at C-4 (1,4-dihydropyridine : 1,6-dihydropyridine = 95:5).

All attempts to hydrolyze the 4,4-bis(2-methylphenyl)butyl (**21**, **27**), or 4,4-bis(2-methylphenyl)-3-butenyl (**22**, **28**), ester moiety to the corresponding acid using ethanolic NaOH or LiOH were unsuccessful since only decomposition products were produced. In contrast, the cyanoethyl esters were readily converted to the carboxyl analog using the non-nucleophilic base 1,8-diazabicyclo[5.4.0]undec-7-ene (DBU), which proceeds via a β-elimination reaction of acrylonitrile (14) (**23** → **25** (70%); **24** → **26** (56%); **29** → **31** (62%); **30** → **32** (50%)). 2-Cyanoethyl nicotinate (**16**), required for the preparation of the pyridinium salts (**19**, **20**), was prepared by the condensation of nicotinoyl chloride with 2-cyanoethanol in the presence of Et_3N (85%).

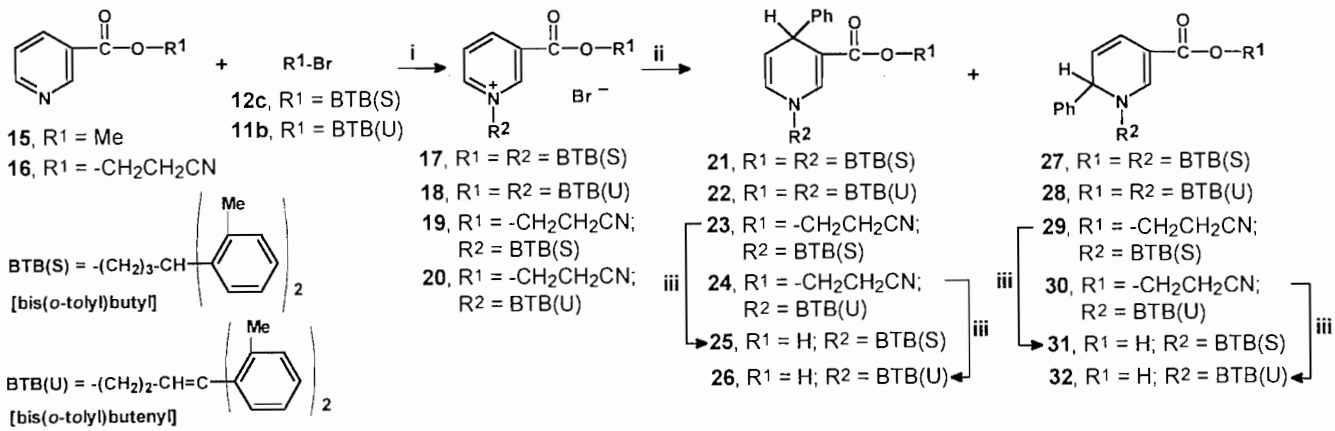
Biological evaluation as GABA-uptake inhibitors

The 1,4-dihydropyridyl (DHP) (**21**–**26**) and 1,6-dihydropyridyl (**27**–**32**) ring systems possess conformational and steric features that are distinctly different from those present in nipecotic acid (**1**), which exists in a chair conformation. Hoffman

© 1997 NRC Canada

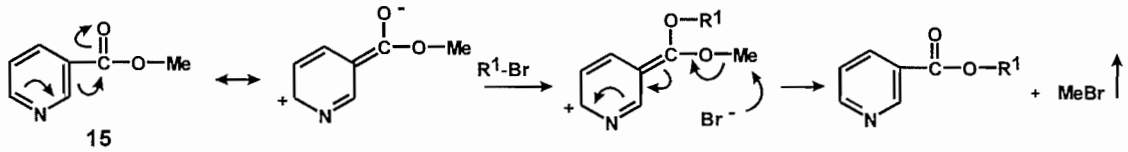
Can. J. Chem. Downloaded from www.nrcresearchpress.com by 88.146.161.215 on 09/08/12
For personal use only.

Scheme 3.



Reagents: i, dry MeCN, reflux, 48 h; ii, dry THF, CuI, PhMgCl, −23°C, 30 min; iii, 1,8-diazabicyclo[5.4.0]undec-7-ene (DBU), MeOH, 25°C, 14 h.

Scheme 4.



and Cimeraglia (15) reported, based on ab initio STO-3G calculations for 4-phenyl-3,5-dicarboxy-1,4-dihydropyridine, that the boat conformation of the 1,4-dihydropyridine ring is favored over a planar ring arrangement, that ring distortion was greater at C-4 than at N-1, and that the C-4 phenyl substituent on the 1,4-DHP ring having a pseudoaxial orientation relative to the plane of the olefinic bonds was unequivocally favored (16). Related theoretical calculations indicated that 1,4-dihydronicotinamide (17) and 1,4-DHP calcium channel antagonists (18) also exist in a boat conformation. The 1,6-DHP ring system is less puckered that the boat-shaped 1,4-DHP ring system, or the chair-shaped piperidine ring system. While the diene (C=C-C=C) moiety of the 1,6-DHP ring system is quasi-planar, there is distortion at the C-6 and N-1 positions. These differences, together with the steric effects due to the ester, N-1, and the 1,4-DHP C-4 and 1,6-DHP C-6, substituents (**21–32**) are expected to alter the overall volume of the molecule, the in vivo biodistribution of the drug between hydrophobic and hydrophilic tissues, and their affinity for a brain GABA transporter(s) (19).

All of the compounds evaluated in the in vitro [^{3}H]GABA-uptake inhibition striatal tissue assay, except for **21** and **22**, which were inactive, inhibited uptake in the 21–44% range, relative to the reference drug nipecotic acid (87% inhibition), at a test compound concentration of 10^{-4} M (see Table 1). All compounds (**14**, **21/22**, **25/28**, and **31/32**) were inactive inhibitors at a test compound concentration of 10^{-5} M relative to nipecotic acid (48% inhibition). Although the differences in percent inhibition of [^{3}H]GABA uptake were sometimes small, some structure–activity correlations are evident. In the 1,4-DHP series of compounds the C-3 R^1 substituent was a determinant of activity where the relative potency order was CO_2H (**25**) > 4,4-dimethyl-4,5-dihydrooxazolin-2-yl) (**14**) > CO_2BTB(S) (**21**, inactive), and CO_2H (**26**) > CO_2BTB(U) (**22**, inactive). These results indicate the 2-(4,4-dimethyl-4,5-dihydrooxazolin-2-yl) ring system (**14**) is a bioisostere of a carboxyl group (**25**) with respect to [^{3}H]GABA-uptake inhibition. A similar activity profile was observed in the 1,6-DHP series of compounds where CO_2H (**31**) ≥ CO_2BTB(S) (**27**) and CO_2H (**32**) > CO_2BTB(U) (**28**). A comparison of compounds having C-3 and (or) N-1 CO_2BTB(S) and CO_2BTB(U) substituents indicated that the relative activity order was generally CO_2BTB(S) > CO_2BTB(U) (**26** > **25** and **27** > **28**), although **31** and **32** were equipotent. In general, the relative potency order was 1,6-DHP > 1,4-DHP (**27** > **21** (inactive), **28** > **22** (inactive), **32** > **26** and **31** ≈ **25**). Although this class of 1,4- and 1,6-DHP compounds are less effective in vitro inhibitors of [^{3}H]GABA uptake than the hydrophilic cyclic amino acid nipecotic acid, which does not readily cross the blood–brain barrier, their enhanced lipohilicity, and potentially more favorable brain uptake, could result in a greater inhibition of neuronal GABA uptake in vivo, and hence therapeutic efficacy.

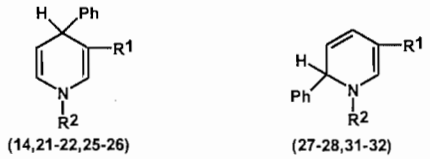
The stability of the 1,4- (**14**, **21/22**, **25/26**) and 1,6- (**27/28**, **31/32**) dihydropyridine analogs during the in vitro [^{3}H]GABA-uptake inhibition assay in striatal tissue was not determined. These 1,4- and 1,6-dihydropyridine analogs could undergo partial oxidation to an inactive pyridinium species (20, 21), whereas the 1,4-dihydropyridine analogs could undergo hydration to yield the corresponding 6-hydroxy-1,4,5,6-tetrahydropyridine analog (20, 22), which may also conceivably act as a GABA-uptake inhibitor. The 4- or 6-

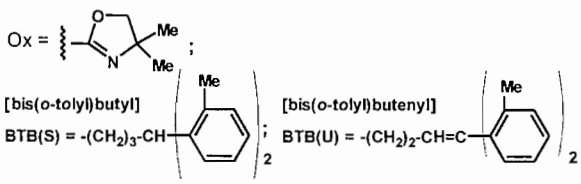
© 1997 NRC Canada

Can. J. Chem. Downloaded from www.nrcresearchpress.com by 88.146.161.215 on 09/08/12
For personal use only.

Can. J. Chem. Downloaded from www.nrcresearchpress.com by 88.146.161.215 on 09/08/12
For personal use only.

Table 1. In vitro inhibition of [^{3}H]GABA uptake in striatal tissue by 1,4- (**14**, **21/22**, **25/26**) and 1,6- (**27/28**, **31/32**) dihydropyridine analogs.





Compound	R^1	R^2	% Inhibition, 10^{-4} M[a]
14	-Ox	BTB(S)	34.6 ± 6.7 (4)
21	-CO_2BTB(S)	BTB(S)	Inactive (4)
22	-CO_2BTB(U)	BTB(U)	Inactive (4)
25	-CO_2H	BTB(S)	44.1 ± 3.3 (5)
26	-CO_2H	BTB(U)	27.2 ± 7.0 (5)
27	-CO_2BTB(S)	BTB(S)	31.4 ± 1.8 (4)
28	-CO_2BTB(U)	BTB(U)	21.1 ± 10.6 (4)
31	-CO_2H	BTB(S)	38.8 ± 7.8 (5)
32	-CO_2H	BTB(U)	40.4 ± 3.0 (5)
Nipecotic acid[b]			87.1 ± 1.6 (11)

[a]The result is presented as the mean ± S.E.M. with the number of experiments shown in parentheses.

[b]At a concentration of 10^{-5} M, nipecotic acid inhibited [^{3}H]GABA uptake by 48.5 ± 6.1% (n = 5).

phenyl substituent is expected to alter the redox potential of these dihydropyridine compounds. The longer N substituents (BTB(S), BTB(U)) are expected to decrease the oxidation rate, which is potentially attributed to steric crowding and a lower degree of solvation for lipophilic derivatives (21). On the basis of previous in vitro and in vivo studies for 3-[2-[[(1-methyl-1,4-dihydropyrid-3-yl)carbonyl]oxy]-ethyl] 5-methyl 1,4-dihydro-2,6-dimethyl-4-(2,3-dichlorophenyl)-3,5-pyridinedicarboxylate (23), it is not expected that oxidative and (or) hydration transformations had a significant effect under the incubation conditions employed in the in vitro [^{3}H]GABA-uptake inhibition assay.

Experimental

Melting points were determined using a Buchi capilliary apparatus and are uncorrected. Nuclear magnetic resonance spectra (^{1}H NMR, ^{13}C NMR) were determined on a Bruker AM-300 spectrometer. The assignment of exchangeable protons (O*H*, N*H*) was confirmed by the addition of D_2O. ^{13}C NMR spectra were acquired using the *J* modulated spin echo technique where methyl and methine carbon resonances appear as positive peaks, and methylene and quaternary carbon resonances appear as negative peaks. High-resolution electron impact (EI) mass spectra were determined using an AEI-MS-50 mass spectrometer. Infrared (IR) spectra were acquired using a Nicolet 550 Series II Magna FT-IR spectrometer. Silica gel column chromatography was carried out using Merck 7734 silica gel (60–200 mesh). 3-[2-(4,4-Dimethyl-4,5-dihydrooxazolin-2-yl)]-4-phenyl-1,4-dihydropyridine (**13**) was prepared using a literature procedure (12). γ-Butyrolactone was purchased from the Aldrich Co. [^{3}H]GABA (specific activity 36.8 Ci/mmol) was purchased from New England Nuclear.

2,2-Bis(2-methylphenyl)tetrahydrofuran (7) and 1,1-bis(2-methylphenyl)-1,4-butanediol (8, Method A)

A solution of *o*-tolylmagnesium chloride in THF (0.1 mol, 100 mL of 1 M) was added dropwise to a solution of ethyl 4-bromobutyrate (9.75 g, 50 mmol) in THF (150 mL) at 0°C with stirring. The reaction was allowed to proceed at 25°C for 4 h, the reaction mixture was cooled to 0°C, and a saturated aqueous solution of NH_4Cl (100 mL) was added. The aqueous fraction was extracted with EtOAc (3 × 100 mL), the combined organic solutions were washed with brine (100 mL), and the organic solution was dried ($MgSO_4$). Removal of the solvent in vacuo gave a residue that was purified by silica gel flash chromatography. Elution with EtOAc–hexane (1:49, v/v) afforded **7** (1.76 g, 14%). Continued elution with EtOAc–hexane (2:3, v/v) gave **8** (1.35 g, 10%).

Fraction 1 (7): mp 120–121°C (recrystallized from hexane); ^{1}H NMR ($CDCl_3$) δ: 1.97 (s, 6H, tolyl *Me*'s), 2.04 (m, 2H, tetrahydrofuranyl H-4), 2.60 (t, J = 7.2 Hz, 2H, tetrahydrofuranyl H-3), 4.04 (t, J = 7.2 Hz, 2H, tetrahydrofuranyl H-5), 7.03 (dd,

© 1997 NRC Canada

Can. J. Chem. Downloaded from www.nrcresearchpress.com by 88.146.161.215 on 09/08/12
For personal use only.

J = 6.8, J = 1.7 Hz, 2H, tolyl H-3), 7.17 (m, 4H, tolyl H-4, H-5), 7.63 (dd, J = 7.2, J = 1.8 Hz, 2H, tolyl H-6); ^{13}C NMR ($CDCl_3$) δ: 21.5, 25.7, 36.3, 67.4, 88.7, 124.9, 126.7, 127.0, 132.1, 136.2, 143.1. Anal. calcd. for $C_{18}H_{20}O$: C 85.67, H 7.99; found: C 85.30, H 7.90.

*Fraction 2 (**8**)*: mp 161–163°C (recrystallized from EtOAc); ^{1}H NMR (CD_3COCD_3) δ: 1.47 (m, 2H, CH_2CH_2OH), 1.86 (s, 6H, tolyl *Me*'s), 2.44 (m, 2H, C(OH)CH_2), 2.86 and 2.89 (two s, 1H each, O*H*'s), 3.52 (m, 2H, CH_2OH), 6.98 (d, J = 7.2 Hz, 2H, tolyl H-3), 7.14 (m, 4H, tolyl H-4, H-5), 7.73 (dd, J = 7.6, J = 1.0 Hz, 2H, tolyl H-6); ^{13}C NMR (CD_3COCD_3) δ: 21.6, 28.2, 37.9, 62.9, 78.0, 125.6, 127.4, 128.0, 132.6, 136.9, 145.7. Anal. calcd. for $C_{18}H_{22}O_2$: C 79.96, H 8.20; found: C 79.73, H 8.28.

1,1-Bis(2-methylphenyl)-1-buten-4-ol (9, Method A)
A solution of **7** (1.25 g, 5 mmol) in THF (5 mL), EtOH (5 mL), and 6 N HCl (5 mL) was refluxed for 4 h; the reaction mixture was cooled to 25°C, and extracted with EtOAc (3 × 50 mL). The combined organic fractions were washed with brine (40 mL) and dried ($MgSO_4$). Removal of the solvent in vacuo gave a residue that was purified by silica gel flash chromatography using EtOAc–hexane (1:4, v/v) as eluant to yield **9** as an oil (1.18 g, 94%); ^{1}H NMR ($CDCl_3$) δ: 2.07 (m, 1H, O*H*), 2.14 and 2.31 (two s, 3H each, tolyl *Me*'s), 2.35 (m, 2H, CH_2CH_2OH), 3.70 (t, J = 6.7 Hz, 2H, CH_2OH), 5.83 (t, J = 7.2 Hz, 1H, C═C*H*), 7.10–7.25 (m, 8H, tolyl H-3, H-4, H-5, H-6).

1,1-Bis(2-methylphenyl)-1,4-butanediol (8, Method B)
A solution of **6** in THF (110 mL of a 1 M solution, 0.11 mol) was added to a solution of γ-butyrolactone (4.3 g, 50 mmol) in THF (150 mL) at 0°C with stirring, and the reaction was allowed to proceed at 25°C for 2 h. The reaction mixture was cooled to 0°C, saturated aqueous NH_4Cl (100 mL) was added, and the aqueous fraction was extracted with EtOAc (3 × 100 mL). The combined organic fractions were washed with brine (50 mL), the organic solution was dried ($MgSO_4$), and the solvent was removed in vacuo. Purification of the residue obtained by silica gel flash column chromatography using EtOAc–hexane (2:3, v/v) as eluant afforded **8** (12.15 g, 90%), which was identical (mp, ^{1}H NMR) to **8** prepared according to Method A. Product **8**, required for all subsequent reactions, was prepared according to Method B.

1,1-Bis(2-methylphenyl)-1-buten-4-ol (9, Method B)
A solution of **8** (8.1 g, 30 mmol, from Method B) in EtOH (30 mL) and 4 N HCl (30 mL) was heated at reflux for 6 h; the reaction mixture was cooled to 25°C, and extracted with EtOAc (3 × 100 mL). The combined organic extracts were washed with brine (60 mL), the organic fraction was dried ($MgSO_4$), and the solvent was removed in vacuo. Purification of the residue by silica gel flash column chromatography using EtOAc–hexane (1:4, v/v) as eluant yielded **9** as an oil (6.8 g, 90%), which was identical to **9** prepared according to Method A).

1,1-Bis(2-methylphenyl)-4-(4-methylbenzenesulfonyloxy)-1-butene (11*a*)
p-Toluensulfonyl chloride (9.5 g, 50 mmol) was added to a solution of **9** (6.3 g, 25 mmol) in pyridine (4.75 g, 60 mmol) and CH_2Cl_2 (100 mL) at 0°C with stirring, and the reaction was allowed to proceed at 25°C for 12 h. Saturated aqueous NH_4Cl (100 mL) was added, the mixture was extracted with EtOAc (3 × 100 mL), the combined organic extracts were washed with brine (2 × 50 mL), and the organic fraction was dried ($MgSO_4$). Removal of the solvent in vacuo gave a residue that was purified by silica gel column chromatography using EtOAc–hexane (1:9, v/v) as eluant to give **11*a*** (9.2 g, 92%); ^{1}H NMR ($CDCl_3$) δ: 2.03 (s, 3H, tosyl *Me*), 2.10 and 2.28 (two s, 3H each, tolyl *Me*'s), 2.39 (m, 2H, butenyl H-3), 4.12 (t, J = 6.7 Hz, 2H, CH_2OTs), 5.76 (t, J = 7.2 Hz, 1H, C═C*H*), 7.05–7.20 (m, 12H, phenyl hydrogens). Product **11*a*** was used immediately in subsequent reactions for the preparation of **11*b*** and **11*c***.

1,1-Bis(2-methylphenyl)-4-bromo-1-butene (11*b*)
A mixture of **11*a*** (4.1 g, 10 mmol) and LiBr (3.48 g, 40 mmol) in acetone (80 mL) was refluxed for 12 h; the reaction mixture was cooled to 25°C, and then poured onto saturated aqueous NH_4Cl (50 mL). Extraction with EtOAc (3 × 50 mL), washing the combined EtOAc extracts with brine (50 mL), drying the EtOAc fraction ($MgSO_4$), and removal of the solvent in vacuo gave a residue. Purification by silica gel column chromatography using EtOAc–hexane (1:99, v/v) as eluant yielded **11*b*** (2.77 g, 88%); ^{1}H NMR ($CDCl_3$) δ: 2.19 and 2.40 (two s, 3H each, tolyl *Me*'s), 2.70 (m, 2H, butenyl H-3), 3.49 (t, J = 6.7 Hz, 2H, CH_2Br), 5.87 (t, J = 7.1 Hz, 1H, C═C*H*), 7.15–7.30 (m, 8H, phenyl hydrogens); ^{13}C NMR ($CDCl_3$) δ: 19.9, 21.1, 32.5, 32.7, 125.3, 125.5, 126.8, 127.2, 129.8, 130.3, 130.8, 135.4, 136.1, 139.5, 141.8, 143.0. Product **11*b*** was used immediately in subsequent reactions.

1,1-Bis(2-methylphenyl)-4-iodo-1-butene (11*c*)
A mixture of **11*a*** (4.1 g, 10 mmol) and NaI (3.0 g, 20 mmol) in acetone (80 mL) was refluxed for 12 h, the reaction was completed, and the product purified according to the procedure described for the preparation of **11*b*** above, to yield **11*c*** (3.08 g, 85%); ^{1}H NMR ($CDCl_3$) δ: 2.12 and 2.32 (two s, 3H each, tolyl *Me*'s), 2.65 (m, 2H, butenyl H-3), 3.20 (t, J = 6.9 Hz, 2H, CH_2I), 5.75 (t, J = 7.1 Hz, 1H, C═C*H*), 7.10–7.25 (m, 8H, phenyl hydrogens).

1,1-Bis(2-methylphenyl)-4-hydroxybutane (12*a*)
10% Palladium-on-charcoal (800 mg) was added to a solution of **9** (8.0 g, 31.7 mmol) in ethanol (40 mL) and the mixture was agitated at 25°C for 4 h under hydrogen gas at 60 psi. The reaction mixture was filtered, the solvent was removed in vacuo, and the residue was purified by silica gel column chromatography using EtOAc–hexane (1:4, v/v) as eluant to yield **12*a*** as an oil (7.6 g, 95%); IR (film): 3360 (OH) cm^{-1}; ^{1}H NMR ($CDCl_3$) δ: 1.60–1.70 (m, 2H, $CH_2CH_2CH_2$), 2.0–2.08 (m, 2H, $CH_2CH_2CH_2OH$), 2.31 (s, 6H, tolyl *Me*'s), 3.67 (t, J = 7.0 Hz, 2H, OCH_2), 4.29 (t, J = 7.0 Hz, 1H, $CHCH_2$), 7.08–7.20 (m, 8H, phenyl hydrogens). Product **12*a*** was used immediately in the subsequent reaction.

1,1-Bis(2-methylphenyl)-4-(4-methylbenzensulfonyloxy)-butane (12*b*)
p-Toluenesulfonyl chloride (9.5 g, 50 mmol) was added to a solution of **12*a*** (6.35 g, 25 mmol) in pyridine (4.75 g, 60 mmol) and CH_2Cl_2 (100 mL) at 0°C with stirring. The reaction

© 1997 NRC Canada

Can. J. Chem. Downloaded from www.nrcresearchpress.com by 88.146.161.215 on 09/08/12
For personal use only.

was allowed to proceed at 25°C for 12 h and the reaction mixture was poured onto a solution of saturated aqueous NH_4Cl (100 mL). Extraction with EtOAc (3 × 100 mL), washing the combined extracts with brine (50 mL), drying the organic fraction ($MgSO_4$), and removal of the solvent in vacuo gave a residue. Purification by silica gel column chromatography using EtOAc–hexane as eluant (1:9, v/v) gave **12***b* (9.0 g, 83%) as a solid; mp 103°C (recrystallized from EtOAc–hexane); ^{1}H NMR ($CDCl_3$) δ: 1.66–1.76 (m, 2H, CH_2CH_2OH), 1.92–2.0 (m, 2H, $CHCH_2CH_2$), 2.26 (s, 6H, tolyl *Me*'s), 2.46 (s, 3H, *p*-tosyl *Me*), 4.05 (t, *J* = 7.0 Hz, 2H, OCH_2), 4.21 (t, *J* = 7.0 Hz, 1H, $CHCH_2$), 7.06–7.16 (m, 8H, *o*-tolyl ring hydrogens), 7.34 and 7.79 (two d, *J* = 8.0 Hz, 2H each, tosyl ring hydrogens). Product **12***b* was used immediately in the subsequent reaction.

1,1-Bis(2-methylphenyl)-4-bromobutane (12*c*)

A mixture of **12***b* (4.08 g, 10 mmol) and LiBr (3.41 g, 40 mmol) in acetone (80 mL) was refluxed for 12h. The reaction mixture was cooled to 25°C, and the mixture was poured onto an aqueous solution of saturated NH_4Cl (50 mL). Extraction with EtOAc (3 × 50 mL), drying the EtOAc extract ($MgSO_4$), and removal of the solvent in vacuo gave a residue. Purification by silica gel column chromatography using EtOAc–hexane (1:99, v/v) as eluant afforded **12***c* as an oil (2.8 g, 83%); ^{1}H NMR ($CDCl_3$) δ: 1.90–2.01 (m, 2H, CH_2CH_2Br), 2.08–2.16 (m, 2H, $CHCH_2$), 2.30 (s, 6H, *o*-tolyl *Me*'s), 3.44 (t, *J* = 7.0 Hz, 2H, CH_2Br), 4.29 (t, *J* = 7.0 Hz, 1H, $CHCH_2$), 7.10–7.22 (m, 8H, phenyl hydrogens).

1-[4,4-Bis(2-methylphenyl)butyl]-3-[2-(4,4-dimethyl-4,5-dihydrooxazolin-2-yl)]-4-phenyl-1,4-dihydropyridine (14)

Sodium hydride (100 mg, 3.26 mmol, 80% suspension in mineral oil) was washed with dry hexane and dried under a nitrogen atmosphere prior to addition of DMSO (5 mL). A solution of **13** (1.37 g, 2.8 mmol) in DMSO (30 mL) was added dropwise at 25°C during 30 min under a nitrogen atmosphere with stirring. The reaction mixture was maintained at 50°C for 30 min, and then at 25°C for 1.5 h at which time no further evolution of hydrogen gas was observed. A solution of **12***c* (0.88 g, 2.8 mmol) in DMSO (2 mL) was added during a 10 min period, and the reaction was allowed to proceed at 25°C for 12 h. Excess DMSO was partially removed in vacuo, the reaction mixture was poured onto ice-water (5 mL), extracted with ether (3 × 100 mL), the ether extract was dried (Na_2SO_4), and the solvent was removed in vacuo to give a residue. Purification by silica gel column chromatography using EtOAc–hexane (1:1, v/v) as eluant gave **14** as an oil (0.5 g, 19%); IR (film): 1589, 1491, 1458 cm^{-1}; ^{1}H NMR ($CDCl_3$) δ: 1.12 and 1.26 (two s, 3H each, oxazolinyl *Me*'s), 1.60–1.80 (m, 2H, $CHCH_2CH_2$), 1.90–2.10 (m, 2H, $CHCH_2$), 2.30 and 2.32 (two s, 3H each, tolyl *Me*'s), 3.24 (t, *J* = 7.0 Hz, 2H, NCH_2), 3.82 (m, 2H, OCH_2), 4.27 (t, *J* = 7.0 Hz, 1H, $CHCH_2$), 4.68 (d, $J_{4,5}$ = 5.0 Hz, 1H, H-4), 4.88 (dd, $J_{5,6}$ = 8.0, $J_{4,5}$ = 5.0 Hz, 1H, H-5), 5.92 (d, $J_{5,6}$ = 8.0 Hz, 1H, H-6), 6.98 (s, 1H, H-2), 7.10–7.40 (m, 13H, phenyl hydrogens). Anal. calcd. for $C_{34}H_{38}N_2O\cdot 1H_2O$: C 80.27, H 7.92, N 5.50; found: C 79.92, H 8.10, N 5.13.

4,4-Bis(2-methylphenyl)butyl 1-[4,4-bis(2-methylphenyl)-butyl]pyridinium-3-carboxylate bromide (17)

A mixture of methyl nicotinate (137 mg, 1.0 mmol) and **12***c* (350 mg, 1.1 mmol) in dry MeCN (20 mL) was refluxed for 24 h. TLC analysis indicated that **12***c* was all consumed, but a considerable amount of methyl nicotinate was still present. Additional **12***c* (317 mg, 1 mmol) was added and the reaction was continued at reflux for 24 h at which time TLC showed the reaction was nearly complete. After cooling to 25°C, the solid product was filtered, washed with ether, and dried (Na_2SO_4) to afford **17** (0.5 g, 74%); mp 80°C; IR (KBr): 1737, 1638 cm^{-1}; ^{1}H NMR (DMSO-d_6) δ: 1.72–2.10 (m, 8H, $-CH_2CH_2CH-$), 2.21 and 2.23 (two s, 6H each, tolyl *Me*'s), 4.20–4.30 (m, 2H, CH_2CH), 4.41 (t, *J* = 7.0 Hz, 2H, OCH_2), 4.66–4.78 (m, 2H, NCH_2), 7.04–7.24 (m, 16H, phenyl hydrogens), 8.26 (dd, $J_{4,5}$ = 8.0 Hz, $J_{5,6}$ = 6.0 Hz, 1H, H-5), 8.96 (d, $J_{4,5}$ = 8.0 Hz, 1H, H-4), 9.30 (d, $J_{5,6}$ = 6.0 Hz, 1H, H-6), 9.58 (s, 1H, H-2). The pyridinium salts **18** (from reaction of **15** with 2.1 equivalents of **11***b*), **19** (from reaction of **16** with 1.1 equivalents of **12***c*) and **20** (from reaction of **16** with 1.1 equivalents of **11***b*) were prepared using a similar procedure.

4,4-Bis(2-methylphenyl)-3-butenyl 1-[4,4-bis(2-methylphenyl)-3-butenyl]pyridinium-3-carboxylate bromide (18)

Yield: 67%; mp 75°C; IR (KBr): 1738, 1639, 1490 cm^{-1}; ^{1}H NMR (DMSO-d_6) δ: 1.86, 2.0, 2.06, and 2.22 (four s, 3H each, tolyl *Me*'s), 2.42–2.58 and 2.60–2.78 (two m, 2H each, OCH_2CH_2, NCH_2CH_2), 4.48 (t, *J* = 7.0 Hz, 2H, OCH_2), 4.82–4.90 (m, 2H, NCH_2), 5.92–5.94 (m, 1H, $CH{=}C$), 6.54 (t, *J* = 7.0 Hz, 1H, $CH{=}C$), 6.92–7.30 (m, 16H, phenyl hydrogens), 8.30 (dd, $J_{4,5}$ = 8.0, $J_{5,6}$ = 6.0 Hz, 1H, H-5), 8.98 (d, $J_{4,5}$ = 8.0 Hz, 1H, H-4), 9.29 (d, $J_{5,6}$ = 6.0 Hz, 1H, H-6), 9.56 (s, 1H, H-2).

2-Cyanoethyl 1-[4,4-bis(2-methylphenyl)butyl]pyridinium-3-carboxylate bromide (19)

Yield: 72%; mp 180–183°C; IR (KBr): 2253 (CN), 1737, 1638 cm^{-1}; ^{1}H NMR (DMSO-d_6) δ: 1.90–2.04 (m, 4H, $CH_2CH_2CH_2CH$), 2.24 (s, 6H, tolyl *Me*'s), 3.11 (t, *J* = 6.0 Hz, 2H, CH_2CN), 4.25 (t, *J* = 7.0 Hz, 1H, CH_2CH), 4.60 (t, *J* = 6.0 Hz, 2H, OCH_2), 4.72–4.82 (m, 2H, NCH_2), 7.06–7.20 (m, 8H, phenyl hydrogens), 8.32 (dd, $J_{4,5}$ = 8.0, $J_{5,6}$ = 6.0 Hz, 1H, H-5), 8.98 (d, $J_{4,5}$ = 8.0 Hz, 1H, H-4), 9.34 (d, $J_{5,6}$ = 6.0 Hz, 1H, H-6), 9.66 (s, 1H, H-2).

2-Cyanoethyl 1-[4,4-bis(2-methylphenyl)-3-butenyl]pyridinium-3-carboxylate bromide (20)

Yield: 60%; mp 75–79°C; IR (KBr): 2250 (CN), 1740 (CO_2); ^{1}H NMR (DMSO-d_6) δ: 1.90 and 2.04 (two s, 3H each, tolyl *Me*'s), 2.64–2.76 (m, 2H, CH_2CH_2CH), 3.10 (t, *J* = 6.0 Hz, 2H, CH_2CN), 4.60 (t, *J* = 6.0 Hz, 2H, OCH_2), 4.88 (t, *J* = 7.0 Hz, 2H, NCH_2), 5.86 (t, *J* = 7.0 Hz, 1H, $CH_2{=}CH$), 6.92–7.20 (m, 8H, phenyl hydrogens), 8.32 (dd, $J_{4,5}$ = 8.0, $J_{5,6}$ = 6.0 Hz, 1H, H-5), 9.0 (d, $J_{4,5}$ = 8.0 Hz, 1H, H-4), 9.32 (d, $J_{5,6}$ = 6.0 Hz, 1H, H-6), 9.61 (s, 1H, H-2).

2-Cyanoethyl nicotinate (16)

A solution of 2-cyanoethanol (0.71 g, 10 mmol) in dry CH_2Cl_2 (5 mL) was added, during 10 min with stirring, to a solution of nicotinoyl chloride (1.78 g, 10 mmol) in dry CH_2Cl_2 (20 mL) at 0°C under a nitrogen atmosphere. The reaction was allowed to proceed at 0°C for 30 min and then at 25°C for 14 h. Water (20 mL) was added, the mixture was extracted with EtOAc (3 × 50 mL), the EtOAc extracts were washed with brine (2 × 50

© 1997 NRC Canada

Can. J. Chem. Downloaded from www.nrcresearchpress.com by 88.146.161.215 on 09/08/12
For personal use only.

mL), and the EtOAc solution was dried (Na_2SO_4). Removal of the solvent in vacuo gave a residue that was purified by silica gel column chromatography using EtOAc–hexane (1:4, v/v) as eluant to yield **16** (1.5 g, 85%) as an oil; IR (film): 2253 (CN), 1728 (CO_2) cm^{-1}; ^1H NMR ($CDCl_3$) δ: 2.88 (t, J = 6.0 Hz, 2H, CH_2CN), 4.58 (t, J = 6.0 Hz, 2H, OCH_2), 7.44 (dd, $J_{4,5}$ = 8.0, $J_{5,6}$ = 6.0 Hz, 1H, H-5), 8.32 (dt, $J_{4,5}$ = 8.0, $J_{4,6}$ = $J_{2,4}$ = 2.0 Hz, 1H, H-4), 8.85 (dd, $J_{5,6}$ = 6.0, $J_{4,6}$ = 2.0 Hz, 1H, H-6), 9.26 (d, $J_{2,4}$ = 2.0 Hz, 1H, H-2).

4,4-Bis(2-methylphenyl)butyl 1-[4,4-bis(2-methylphenyl)-butyl]-4-phenyl-1,4-dihydropyridine-3-carboxylate (21) and 4,4-bis(2-methylphenyl)butyl 1-[4,4-bis(2-methylphenyl)butyl]-6-phenyl-1,6-dihydropyridine-3-carboxylate (27). General method for the synthesis of 1,2- and 1,6-dihydropyridines

A solution of the pyridinium salt **17** (0.675 g, 1 mmol) in dry THF (20 mL) and CuI (35 mg) was stirred under a nitrogen atmosphere until a homogeneous solution was obtained. This solution was cooled to −23°C (Dry Ice – CCl_4 bath), PhMgCl (0.6 mL of a 2 M solution in THF, 1.2 mmol) was added dropwise with stirring, and the reaction mixture was maintained at −23°C for 30 min prior to warming to 25°C. Quenching the reaction with saturated aqueous NH_4Cl (5 mL), extraction with EtOAc (3 × 30 mL), washing the combined EtOAc extracts with brine (2 × 30 mL), drying the EtOAc solution ($MgSO_4$), and removal of the solvent in vacuo afforded a residue. Purification of the residue by silica gel column chromatography using EtOAc–hexane (3:7, v/v) as eluant gave **21** as an amorphous solid. Continued elution afforded **27** as an oil. Attempts to recrystallize **21** and **27** resulted in partial decomposition. Compounds **22** (amorphous solid) and **28** (oil), **23** (oil) and **29** (oil), **24** (oil) and **30** (oil) were also prepared using this general procedure (same molar quantities of reactants).

*Product **21***: (150 mg, 22%); mp 48°C; IR (KBr): 1687, 1589 cm^{-1}; ^1H NMR ($CDCl_3$) δ: 1.52–1.64, 1.66–1.72, 1.80–1.90, and 1.96–2.06 (four m, 2H each, $OCH_2CH_2CH_2CH$, $NCH_2CH_2CH_2CH$), 2.25, 2.26, 2.30, and 2.32 (four s, 3H each, tolyl *Me*'s), 3.26 (t, J = 7.0 Hz, 2H, NCH_2), 3.93–4.09 (m, 2H, OCH_2), 4.18 and 4.27 (two t, J = 7.0 Hz, 1H each, CH_2CH), 4.52 (d, $J_{4,5}$ = 4.5 Hz, 1H, H-4), 4.90 (dd, $J_{5,6}$ = 8.0, $J_{4,5}$ = 4.5 Hz, 1H, H-5), 5.85 (d, $J_{5,6}$ = 8.0 Hz, 1H, H-6), 7.05–7.15 (m, 22H, H-2, phenyl hydrogens). Exact Mass calcd. for $C_{48}H_{51}NO_2$: 673.3919; found: 673.3904.

*Product **27***: (120 mg, 18%); IR (film): 1687, 1589 cm^{-1}; ^1H NMR (DMSO-d_6) δ: 1.42–1.64 and 1.96–2.0 (two m, 4H each, $OCH_2CH_2CH_2CH$, $NCH_2CH_2CH_2CH$), 2.18 and 2.20 (two s, 3H each, tolyl *Me*'s), 2.22 (s, 6H, tolyl *Me*'s), 3.3–3.4 (m, 2H, NCH_2), 4.04 (t, J = 7.0 Hz, 2H, OCH_2), 4.18 and 4.25 (two t, J = 7.0 Hz, 1H each, CH_2CH), 5.08 (dd, $J_{4,5}$ = 9.5, $J_{5,6}$ = 5.0 Hz, 1H, H-5), 5.18 (d, $J_{5,6}$ = 5.0 Hz, 1H, H-6), 6.24 (d, $J_{4,5}$ = 9.5 Hz, 1H, H-4), 7.07–7.40 (m, 21H, phenyl hydrogens), 7.48 (s, 1H, H-2). Exact Mass calcd. for $C_{48}H_{51}NO_2$: 673.3919; found: 673.3907.

4,4-Bis(2-methylphenyl)-3-butenyl 1-[4,4-bis(2-methylphenyl)-3-butenyl]-4-phenyl-1,4-dihydropyridine-3-carboxylate (22)

Yield: 165 mg, 24%; mp 35°C; IR (KBr): 1687, 1589 cm^{-1}; ^1H NMR ($CDCl_3$) δ: 2.09, 2.10, 2.21, and 2.24 (four s, 3H each, tolyl *Me*'s), 2.22–2.40 (m, 4H, $CH_2CH{=}C$), 3.31 (t, J = 7.0 Hz, 2H, NCH_2), 4.04 (t, J = 7.0 Hz, 2H, OCH_2), 4.50 (d, $J_{4,5}$ = 4.5 Hz, 1H, H-4), 4.86 (dd, $J_{5,6}$ = 8.0, $J_{4,5}$ = 4.5 Hz, 1H, H-5), 5.64 (t, J = 7.0 Hz, 1H, $CH_2CH{=}C$), 5.72–5.80 (m, 2H, $CH_2CH{=}C$, H-6), 7.02–7.30 (m, 22H, H-2, phenyl hydrogens). Exact Mass calcd. for $C_{48}H_{47}NO_2$: 669.3607; found: 669.3606.

4,4-Bis(2-methylphenyl)-3-butenyl 1-[4,4-bis(2-methylphenyl)-3-butenyl]-6-phenyl-1,6-dihydropyridine-3-carboxylate (28)

Yield: 125 mg, 19%; IR (film): 1687, 1638, 1573 cm^{-1}; ^1H NMR ($CDCl_3$) δ: 2.10, 2.16, 2.24, and 2.30 (four s, 3H each, tolyl *Me*'s), 2.40–2.50 (m, 4H, $CH_2CH{=}C$), 3.02–3.20 (m, 2H, NCH_2), 4.20–4.30 (m, 2H, OCH_2), 4.95 (dd, $J_{4,5}$ = 9.5, $J_{5,6}$ = 5.0 Hz, 1H, H-5), 5.01 (d, $J_{5,6}$ = 5.0 H, 1H, H-6), 5.70 and 5.88 (two t, J = 7.0 Hz, 1H each, $CH_2CH{=}C$), 6.43 (d, $J_{4,5}$ = 9.5 Hz, 1H, H-4), 7.08–7.37 (m, 21H, phenyl hydrogens), 7.39 (s 1H, H-2). Exact Mass calcd. for $C_{48}H_{47}NO_2$: 669.3607; found: 669.3580.

*2-Cyanoethyl 1-[4,4-bis(2-methylphenyl)butyl]-4-phenyl-1,4-dihydropyridine-3-carboxylate (**23**)*

Yield: 110 mg, 22%; IR (film): 2395 (CN), 1687, 1589 cm^{-1}; ^1H NMR (DMSO-d_6) δ: 1.50–1.62 (m, 2H, $CH_2CH_2CH_2$), 1.80–1.98 (m, 2H, $NCH_2CH_2CH_2CH$), 2.24 and 2.26 (two s, 3H each, tolyl *Me*'s), 2.70–2.80 (m, 2H, CH_2CN), 3.30–3.46 (m, 2H, NCH_2), 4.09–4.14 (m, 2H, OCH_2), 4.24 (t, J = 7.0 Hz, 1H, CH_2CH), 4.38 (d, $J_{4,5}$ = 4.5 Hz, 1H, H-4), 4.88 (dd, $J_{5,6}$ = 8.0, $J_{4,5}$ = 4.5 Hz, 1H, H-5), 6.12 (d, $J_{5,6}$ = 8.0 Hz, 1H, H-6), 7.04–7.28 (m, 13H, phenyl hydrogens), 7.38 (s, 1H, H-2). Product **23** was used immediately for the preparation of **25**.

*2-Cyanoethyl 1-[4,4-bis(2-methylphenyl)butyl]-6-phenyl-1,6-dihydropyridine-3-carboxylate (**29**)*

Yield: 100 mg, 20%; IR (film): 2385 (CN), 1679, 1638 cm^{-1}; ^1H NMR (DMSO-d_6) δ: 1.42–1.60 (m, 2H, CH_2CH_2CH), 1.70–1.80 (m, 2H, CH_2CH_2CH), 2.18 and 2.20 (two s, 3H each, tolyl *Me*'s), 2.86 (t, J = 6.0 Hz, 2H, CH_2CN), 3.30–3.40 (m, 2H, NCH_2), 4.26 (t, J = 7.0 Hz, 3H total, OCH_2, CH_2CH), 5.09 (dd, $J_{4,5}$ = 9.5, $J_{5,6}$ = 5.0 Hz, 1H, H-5), 5.20 (d, $J_{5,6}$ = 5.0 Hz, 1H, H-6), 6.26 (d, $J_{5,6}$ = 9.5 Hz, 1H, H-4), 7.07–7.40 (m, 13H, phenyl hydrogens), 7.54 (s, 1H, H-2). Product **29** was used immediately for the synthesis of **31**.

*2-Cyanoethyl 1-[4,4-bis(2-methylphenyl)-3-butenyl]-4-phenyl-1,4-dihydropyridine-3-carboxylate (**24**)*

Yield: 100 mg, 20%; IR (film): 2196 (CN), 1671, 1638 cm^{-1}; ^1H NMR (DMSO-d_6) δ: 2.02 and 2.06 (two s, 3H each, tolyl *Me*'s), 2.18–2.28 (m, 2H, $CH_2CH{=}$), 2.68–2.76 (m, 2H, CH_2CN), 3.43 (t, J = 7.0 Hz, 2H, NCH_2), 4.08 (t, J = 6.0 Hz, 2H, OCH_2), 4.33 (d, $J_{4,5}$ = 4.5 Hz, 1H, H-4), 4.74 (dd, $J_{5,6}$ = 8.0, $J_{4,5}$ = 4.5 Hz, 1H, H-5), 5.77 (t, J = 7.0 Hz, 1H, $CH_2CH{=}$), 5.96 (d, $J_{5,6}$ = 8.0 Hz, 1H, H-6), 7.0–7.24 (m, 13H, phenyl hydrogens), 7.29 (s, 1H, H-2). Product **24** was used immediately for the synthesis of **26**.

*2-Cyanoethyl 1-[4,4-bis(2-methylphenyl)-3-butenyl]-6-phenyl-1,6-dihydropyridine-3-carboxylate (**30**)*

Yield: 105 mg, 21%; IR (film): 2368 (CN), 1687, 1581 cm^{-1};

© 1997 NRC Canada

Can. J. Chem. Downloaded from www.nrcresearchpress.com by 88.146.161.215 on 09/08/12
For personal use only.

^{1}H NMR ($CDCl_3$) δ: 2.10 and 2.24 (two s, 3H each, tolyl *Me*'s), 2.30–2.40 (m, 2H, CH_2CH), 2.74 (t, J = 6.0 Hz, 2H, CH_2CN), 3.02–3.20 (m, 2H, NCH_2), 4.26–4.40 (m, 2H, OCH_2), 4.96 (dd, $J_{4,5}$ = 9.5, $J_{5,6}$ = 5.0 Hz, 1H, H-5), 5.02 (d, $J_{5,6}$ = 5.0 Hz, 1H, H-6), 5.69 (t, J = 7.0 Hz, 1H, CH_2CH=), 6.69 (d, $J_{4,5}$ = 9.5 Hz, 1H, H-4), 7.04–7.36 (m, 13H, phenyl hydrogens), 7.43 (s, 1H, H-2). Product **30** was used immediately for the synthesis of **32**.

1-[4,4-Bis(2-methylphenyl)butyl]-4-phenyl-1,4-dihydropyridine-3-carboxylic acid (25). General procedure

A solution of **23** (100 mg, 0.2 mmol) and DBU (91 mg, 0.6 mmol) in MeOH (10 mL) was stirred at 25°C for 14 h, and the solvent was removed in vacuo to give an oil residue. Addition of 0.5 N HCl to the oil (pH 1–2) precipitated **25** as a solid, which was filtered and recrystallized from Et_2O–hexane (62 mg, 70%); mp 101–102°C; IR (KBr): 2551–2942 (CO_2H), 1638, 1564 cm^{-1}; ^{1}H NMR (DMSO-d_6) δ: 1.46–1.62 (m, 2H, CH_2CH_2CH), 1.82–1.98 (m, 2H, CH_2CH_2CH), 2.23 and 2.26 (two s, 3H each, tolyl *Me*'s), 3.30–3.42 (m, 2H, NCH_2), 4.24 (t, J = 7.0 Hz, 1H, CH_2CH), 4.34 (d, $J_{4,5}$ = 4.5 Hz, 1H, H-4), 4.80 (dd, $J_{5,6}$ = 8.0, $J_{4,5}$ = 4.5 Hz, 1H, H-5), 6.06 (d, $J_{5,6}$ = 8.0 Hz, 1H, H-6), 7.04–7.24 (m, 13H, phenyl hydrogens), 7.30 (s, 1H, H-2), 11.14 (s, 1H, CO_2H). Anal. calcd. for $C_{30}H_{31}NO_2 \cdot 3/4H_2O$: C 79.88, H 7.26, N 3.10; found: C 79.80, H 7.41, N 3.00. A similar procedure was used for the reactions **29** → **31**, **24** → **26**, and **30** → **32** using the same molar quantities of reactants.

*1-[4,4-Bis(2-methylphenyl)butyl]-6-phenyl-1,6-dihydropyridine-3-carboxylic acid (**31**)*

Yield: 55 mg, 62%; mp 85°C; IR (KBr): 3543–2951 (CO_2H), 1630, 1573 cm^{-1}; ^{1}H NMR (DMSO-d_6) δ: 1.42–1.56 (m, 2H, CH_2CH_2CH), 1.74–1.88 (m, 2H, CH_2CH_2CH), 2.18 and 2.20 (two s, 3H each, tolyl *Me*'s), 3.32–3.50 (m, 2H, NCH_2), 4.16 (t, J = 7.0 Hz, 1H, CH_2CH), 5.04 (dd, $J_{4,5}$ = 9.5, $J_{5,6}$ = 5.0 Hz, 1H, H-5), 5.15 (d, $J_{5,6}$ = 5.0 Hz, 1H, H-6), 6.24 (d, $J_{4,5}$ = 9.5 Hz, 1H, H-4), 7.07–7.34 (m, 13H, phenyl hydrogens), 7.44 (s, 1H, H-2), 11.0 (s, 1H, CO_2H). Anal. calcd. for $C_{30}H_{31}NO_2$: C 82.35, H 7.14, N 3.20; found: C 81.97, H 7.23, N 3.17.

*1-[4,4-Bis(2-methylphenyl)-3-butenyl]-4-phenyl-1,4-dihydropyridine-3-carboxylic acid (**26**)*

Yield: 50 mg, 56%; mp 130–131°C; IR (KBr): 3518–2992 (CO_2H), 1671, 1646, 1589 cm^{-1}; ^{1}H NMR (DMSO-d_6): δ: 2.04 and 2.16 (two s, 3H each, tolyl *Me*'s), 2.17–2.28 (m, 2H, CH_2CH=), 3.43 (t, J = 7.0 Hz, 2H, NCH_2), 4.32 (d, $J_{4,5}$ = 4.5 Hz, 1H, H-4), 474 (d, $J_{5,6}$ = 8.0, $J_{4,5}$ = 4.5 Hz, 1H, H-5), 5.77 (t, J = 7.0 Hz, 1H, CH_2CH=), 5.96 (d, $J_{5,6}$ = 8.0 Hz, 1H, H-6), 7.04–7.22 (m, 13H, phenyl hydrogens), 7.28 (s, 1H, H-2), 11.1 (s, 1H, CO_{2H}). Anal. calcd. for $C_{30}H_{29}NO_2$: C 82.73, H 6.71, N 3.22; found: C 82.48, H 6.83, N 3.32.

*1-[4,4-Bis(2-methylphenyl)-3-butenyl]-6-phenyl-1,6-dihydropyridine-3-carboxylic acid (**32**)*

Yield: (45 mg, 50%); mp 80–82°C; IR (KBr): 3567–2959 (CO_2H), 1630, 1564 cm^{-1}; ^{1}H NMR (DMSO-d_6) δ: 2.01 and 2.17 (two s, 3H each, tolyl *Me*'s), 2.20–2.30 (m, 2H, CH_2CH=), 3.34–3.50 (m, 2H, NCH_2), 4.90–5.0 (m, 2H, H-5, H-6), 5.72 (t, J = 7.0 Hz, 1H, CH_2CH=), 6.20 (d, $J_{4,5}$ = 9.5 Hz, 1H, H-4), 7.0–7.34 (m, 13H, phenyl hydrogens), 7.45 (s, 1H, H-2), 11.0 (s, 1H, CO_2H). Anal. calcd. for $C_{30}H_{29}NO_2$: C 82.73, H 6.71, N 3.22; found: C 82.50, H 6.79, N 3.41.

[^{3}H]GABA-uptake inhibition assay

Male Sprague–Dawley rats were sacrificed by decapitation and the brains were immediately removed and cooled in ice-cold incubation medium. The brains were then transferred to Petri dishs on ice, and the striata were dissected out and chopped into prisms (0.1 mm × 0.1 mm × approximately 2 mm) using a McIlwain tissue chopper. These prisms were suspended in incubation medium that was used for the [^{3}H]GABA-uptake experiments, essentially using the procedure of Iversen and Neal (24). Aminooxyacetic acid (100 mM) was added to the incubation medium to inhibit GABA-transaminase. [^{3}H]GABA (specific activity 36.8 Ci/mmol, which was mixed with unlabeled GABA to give a final concentration of 1.0 mM) was added to the flasks, after a 15 min preincubation of the the prisms at 37°C, in the presence or absence (control) of the test compound. Incubation was continued at 37°C for 5 min, and the contents of the flasks were transferred to a Millipore filter apparatus containing 12 wells with paper filters, and connected to a vacuum line. The samples were rapidly washed twice with incubation medium at 37°C, and the filters added to scintillation vials containing Ready-Safe® scintillation fluid. The amount of radioactivity in the test sample was measured using a liquid scintillation counter, and the % inhibition of [^{3}H]GABA uptake by the test compound (relative to the control) was calculated.

Acknowledgments

We are grateful to the Medical Research Council of Canada (Grant No. MT-8892) for financial support of this research.

References

1. P.D. Suzdak. Drugs Future, **18**, 1129 (1993), and refs. cited therein.
2. S. Fahn. *In* GABA in nervous system function. *Edited by* T. Chase and D. Tower. Raven Press, New York. 1976. pp. 169–183.
3. B.J. Kanner and S. Schuldiner. Mechanism of transport and storage of neurotransmitters. Critical review of biochemistry. Vol. 22. CRC Press, Boca Raton, Fla. 1987. pp. 1–38.
4. D. Lodge, G.A. Johnston, D.R. Curtis, and S.J. Brand. Brain Res. **136**, 513 (1977).
5. H.H. Frey, C. Popp, and W. Loscher. Neuropharmacology, **18**, 581 (1979).
6. M.J. Croucher, B.S. Meldrum, and P. Krogsgaard. Eur. J. Pharmacol. **89**, 217 (1983).
7. K.E. Andersen, C. Braestrup, F.C. Gronwald, A.S. Jorgensen, E.B. Nielsen, U. Sonnewald, P.O. Sorensen, P.D. Suzdak, and L.J. Knutsen. J. Med. Chem. **36**, 1716 (1993).
8. P.D. Suzdak, K. Frederiksen, K.E. Andersen, P.O. Sorensen, L.J. Knutsen, and E.B. Nielsen. Eur. J. Pharmacol. **223**, 189 (1992).
9. E. Pop, M.E. Brewster, and N. Bodor. Drugs Future, **16**, 221 (1991).
10. M. Brewster. Abstract No. 133, 201st ACS National Meeting, Medicinal Chemistry Division, Atlanta, Ga., April 14–19, 1991.
11. M.R. Pavia, S.J. Lobbestael, D. Nugiel, D.R. Mayhugh, V.E. Gregor, C.P. Taylor, R.D. Schwarz, L. Brahce, and M.G. Vartanian. J. Med. Chem. **35**, 4238 (1992).
12. S.K. Dubey and E.E. Knaus. Heterocycles, **22**, 1091 (1984).

© 1997 NRC Canada

13. D.L. Comins, E.D. Stroud, and J.J. Herrick. Heterocycles, **22**, 151 (1984).
14. S.-H. Yiu and E.E. Knaus. Org. Prep. Proced. Int. **28**, 91 (1996).
15. H.J. Hoffmann and R. Cimeraglia. FEBS Lett. **241**, 38 (1988).
16. H.J. Hoffmann and R. Cimiraglia. J. Mol. Struct. (Theochem), **205**, 1 (1990).
17. Y.-D. Wu and K.N. Houk. J. Org. Chem. **58**, 2043 (1993).
18. P.P. Mager, R.A. Coburn, A.J. Solo, D.J. Triggle, and H. Roth. Drug Des. Discovery, **8**, 273 (1992).
19. T.G. Murali Dhar, L.A. Borden, S. Tyagarajan, K.E. Smith, T.A. Branchek, R.L. Weinshank, and C. Gluchowski. J. Med. Chem. **37**, 2334 (1994).
20. E. Pop, M.E. Brewster, and N. Bodor. Drugs Future, **16**, 221 (1991).
21. M.E. Brewster, A. Simay, K. Czako, D. Winwood, H. Farag, and N. Bodor. J. Org. Chem. **54**, 3721 (1989).
22. E. Pop, Z.Z. Liu, J. Vlasak, W.R. Anderson, M.E. Brewster, and N. Bodor. Pharm. Sci. **1**, 265 (1995), and refs. cited therein.
23. S.-H. Yiu and E.E. Knaus. J. Med. Chem. **39**, 4576 (1996).
24. L.L. Iversen and M.J. Neal. J. Neurochem. **15**, 1141 (1968).

Can. J. Chem. Downloaded from www.nrcresearchpress.com by 88.146.161.215 on 09/08/12
For personal use only.

© 1997 NRC Canada

An annulene TCNQ derivative with rather weak acceptor properties

Reginald H. Mitchell, Xin Jin, Tetsuo Otsubo, and Kazuo Takimiya

Abstract: Reaction of the bridged [14]annulenequinone, *trans*-10b,10c-dimethyl-10b,10c-dihydropyrene-2,7-quinone (**12**), with malononitrile in the presence of pyridine and $TiCl_4$ gave 68% of the deep-purple extended TCNQ derivative, α,α,α′,α′-tetracyano-*trans*–10b,10c-dimethyl-10b,10c-dihydropyrene-2,7-quinodimethide (**13**). In solution, quinodimethide **13** appears to form a complex with diethylamine, but is too weak an electron acceptor to form complexes with tetrathiafulvalene, TTF, and related donors. The reduction potential of **13** was substantially lower than that found for TCNQ itself, and in properties **13** behaves more like a benzannelated TCNQ derivative, e.g., α,α,α′,α′-tetracyanopentacene-7,14-quinodimethide (**11**), than a pyrene derivative, e.g., α,α,α′,α′-tetracyanopyrene-2,7-quinodimethide (**6**). This is in agreement with molecular orbital calculations, which indicate that the LUMOs of **13** and **11** are approximately 0.6 eV higher in energy than those for **6** and TCNQ.

Key words: TCNQ — extended, TCNQ-pyrene derivative, reduction potential, annulene-quinodimethide, electron acceptor — weak.

Résumé : La réaction de la [14]annulènequinone pontée, *trans*-10b,10c-diméthyl-10b,10c-dihydropyrène-2,7-quinone (**12**), avec le malononitrile, en présence de pyridine et de $TiCl_4$, conduit à un rendement de 68% du dérivé TCNQ étendu violet foncé α,α,α′,α′-tétracyano-*trans*-10b,10c-diméthyl-10b,10c-dihydropyrène-2,7-quinodiméthane (**13**). En solution, il semble que le composé **13** forme un complexe avec la diéthylamine; c'est toutefois un accepteur d'électron trop faible pour former des complexes avec le tétrathiafulvalène, TTF, et les donneurs apparentés. Le potentiel de réduction du composé **13** est beaucoup plus faible que celui observé pour le TCNQ lui-même et ses propriétés s'apparentent plus à celles d'un dérivé TCNQ ayant subit une annelation avec le benzène, comme l'α,α,α′,α′-tétracyanopentacène-7,14-quinodiméthane (**11**), qu'à celles d'un dérivé pyrène, comme l'α,α,α′,α′-tétracyanopyrène-2,7-quinodiméthane (**6**). Cette constatation est en accord avec les calculs d'orbitales moléculaires qui suggèrent que les énergies des BV des composés **11** et **13** sont approximativement 0,6 eV plus élevées que celles du composé **6** et du TCNQ.

Mots clés : TCNQ étendue, dérivé TCNQ-pyrène, potentiel de réduction, annulène-quinodiméthane, faible accepteur d'électron.

[Traduit par la rédaction]

Introduction

Tetracyano-*p*-quinodimethane (TCNQ) (**1**) has become a very well-known molecule because its charge transfer (CT) salts exhibit a wide array of electrical properties ranging from insulating to "organic metal" (1, 2). Soon after the initial reports (3) on TCNQ itself in the early 1960s, extended π-systems were investigated, for example, the naphthalene derivative TNAP (**2**) (4). Then following the 1973 report (5) of metallic conductivity in TTF–TCNQ (TTF = tetrathiafulvalene), extension of the π-system again became of interest since theoretical studies (6) suggested that extending the π-system of TCNQ would result in a lowering of the intramolecular Coulomb repulsion and lead to highly conducting CT complexes. Weiler and co-workers (7) investigated the biphenyl compound TCNDQ (**3**) and Wudl et al. (8) the tetra-azapyrene TCQQ (**4**). The tetrahydropyrene TCNTP (**5**) and the pyrene TCNP (**6**) were finally made in 1979 and 1980, respectively (9–11), and the anthracene compound TANT (**7**) in 1993 (12). At the same time considerable effort went into studying the benzo-annelated derivatives, e.g., (**8**) (13), (**9**) (14, 15), (**10**) (15, 16), and (**11**) (17). However, quinomethide derivatives in which the quinoid partial structure is *not* derived from a benzenoid aromatic, or equivalent 5-ring heterocycle (18), seem to be rather rare (19), perhaps in part due to the sparsity of annulene quinones (19–21) from which they would be derived. Our recent route (22) to the [14]annulene quinone **12** provided an opportunity to explore the synthesis and properties of the novel π-extended TCNQ derivative **13**. This paper reports the results of this investigation.

Received September 10, 1996.

This paper is dedicated to Professor William A. Ayer on the occasion of his 65th birthday.

R.H. Mitchell[1] **and X. Jin.** Department of Chemistry, University of Victoria, PO Box 3065, Victoria, BC V8W 3V6, Canada.
T. Otsubo and K. Takimiya. Department of Applied Chemistry, Faculty of Engineering, Hiroshima University, Kagamiyama 1-4-1, Higashi-Hiroshima 724, Japan.

[1] Author to whom correspondence may be addressed. Telephone: (250) 721-7159. Fax: (250) 721-7147. E-mail: regmitch@uvvm.uvic.ca

Results and discussion

Synthesis and properties of TCNQ derivative 13

Quinone **12** was converted to **13** using Lehnert's reagent (23)

© 1997 NRC Canada

Can. J. Chem. Downloaded from www.nrcresearchpress.com by 88.146.161.215 on 09/08/12
For personal use only.

Table 1. Half-wave reduction potentials[a] (V) of TCNQ derivatives.

Compound	$E_{1/2}(1)$	$E_{1/2}(2)$	$\Delta E = E_{1/2}(1) - E_{1/2}(2)$
13	−0.34	−0.60	0.26
TCNQ	+0.19	−0.43	0.62
$(MeO)_2$TCNQ (**19**)	+0.01	−0.52	0.53
20	+0.07	−0.54	0.61

[a]Measured in benzonitrile using Pt electrodes and Ag/AgCl as reference (see Experimental).

Table 2. LUMO and SOMO energies (eV) and $E_{1/2}(1)$ and $E_{1/2}(2)$ values (V) for selected TCNQ derivatives.

		LUMO				SOMO
Compound	$E_{1/2}(1)$[a]	AM1[b]	MM2PI[c]	HMO[d]	$E_{1/2}(2)$[a]	AM1[e]
6	+0.13[f]	−3.49	−5.18	−11.13	−0.18	−4.02
1	+0.08	−2.92	−4.46	−10.91	−0.48	−4.47
8	−0.04	−2.70	−4.20	−10.78	−0.41	−4.31
10	−0.18	−2.57	−4.03	−10.71	−0.48	−4.08
21	−0.44	−2.39	−3.89	−10.61	−0.93	−4.28
13	−0.45[g]	−2.35	−3.93	−10.37	−0.65	−3.94
11	−0.57	−2.27	−3.72	−10.53	−0.91	−4.08

[a]Measured in CH_3CN relative to SCE (17).
[b]Calculated using Hyperchem (v.4.5 for Windows, Hypercube Inc., 419 Phillip St., Waterloo, ON N2L 3X2, Canada).
[c]An MM2 + SCF calculation using PCMODEL (v.5.13 for Windows, Serena Software, Box 3076, Bloomington, IN 47402-3076, U.S.A.).
[d]Extended Hückel calculation using Hyperchem.
[e]A UHF calculation using Hyperchem.
[f]Estimated from the BuCN value (11, 14).
[g]Estimated from the PhCN value (see Table 1).

(malononitrile, $TiCl_4$, and pyridine in refluxing chloroform) in 68% yield. It was obtained as dark-purple metallic-looking crystals, which decompose above 350°C, and gave a correct mass spectrum and elemental analysis for **13**. In its IR spectrum, the intense carbonyl absorption of **12** at 1640 cm^{-1} was replaced by the -CN absorption at 2215 cm^{-1} in **13**. In their ^1H NMR spectra, the vinyl protons of **13** at δ 6.84 and 6.56 are more deshielded than those of **12**, δ 6.30 and 6.07, while the internal methyl protons at δ 1.40 are more shielded than those of **12**, δ 1.87. The UV absorption maximum of quinone **12** at 333 nm is red shifted to 460 nm in **13**.

Complexation

Stirring a mixture of the TCNQ **13** and diethylamine in dichloromethane or acetonitrile causes a color change from purple to dark green, with a resultant change in the absorption spectrum, in which the absorption at 460 nm is replaced by a maximum at 770 nm, presumably due to formation of a charge transfer complex. Isolation of the complex was, however, not successful.

Because of the interest in TTF–TCNQ complexes mentioned above, we also attempted formation of complexes of our TCNQ derivative **13** with TTF (**14**) (24), and four stronger donors: tetrathiotetracene, TTT (**15**) (25), tetraselenotetracene, TST (**16**) (26), tetraphenylbipyranylidene, TPBP (**17**) (27), and tetraphenylbithiopyranylidene, TPTP (**18**) (27), by mixing hot solutions of donor and acceptor in chlorobenzene. Collection of the solid material after cooling, and IR analysis indicated only a physical mixture of compounds to be present.

Reduction potential

To understand these rather disappointing results, we measured the reduction potential of **13** in benzonitrile (better solubility than acetonitrile) and found reversible redox waves with half-wave reduction potentials of −0.34 V and −0.60 V, substantially lower than those found for TCNQ itself, and comparable derivatives, see Table 1.

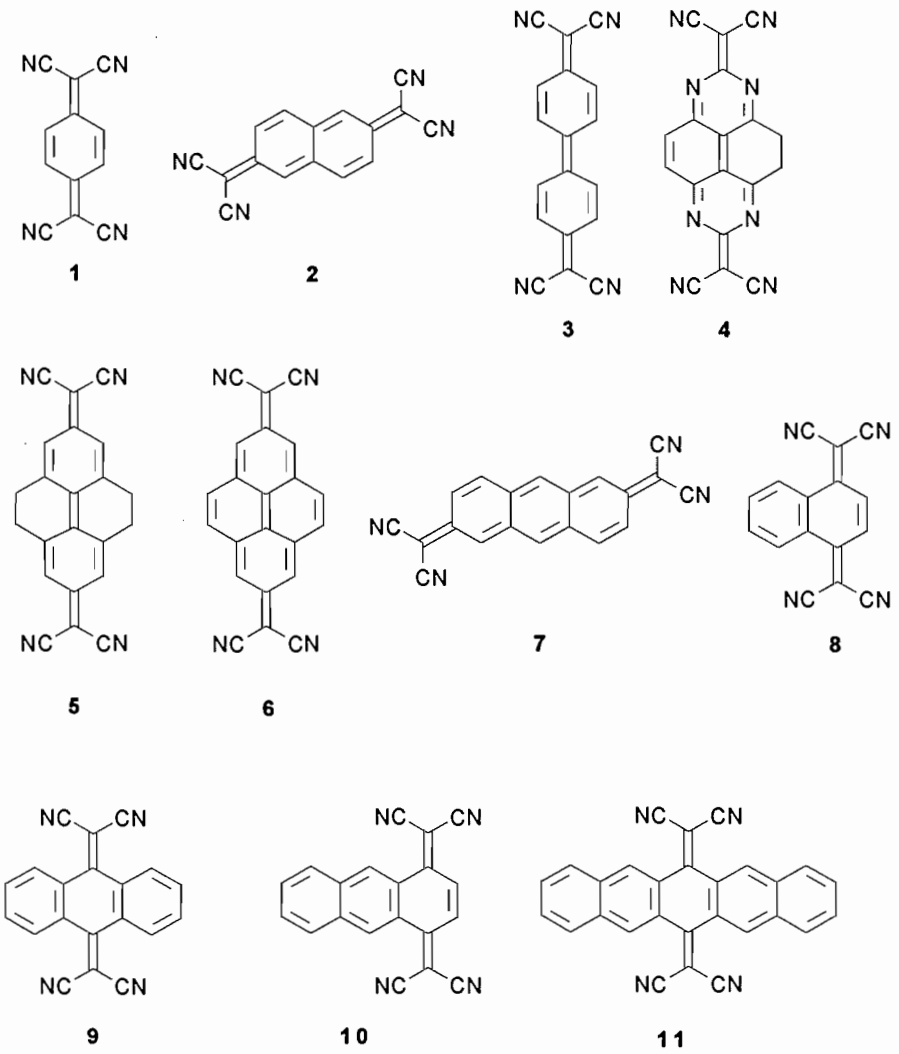
Evidentially, compound **13** is a rather weak acceptor with ΔE much lower than that found for TCNQ itself, and even with the stronger donors (**15–18**) with first oxidation potentials of 0.19, 0.21, 0.12, and 0.19 V, respectively, the accepting ability of **13** is not enough to form a CT complex. When the difference between the donor's oxidation potential and acceptor's reduction potential is beyond the range −0.05 to 0.32 V, conducting CT complexes are not obtained (28).

To better understand the low reduction potential of **13**, we

© 1997 NRC Canada

Can. J. Chem. Downloaded from www.nrcresearchpress.com by 88.146.161.215 on 09/08/12
For personal use only.

Can. J. Chem. Downloaded from www.nrcresearchpress.com by 88.146.161.215 on 09/08/12
For personal use only.



carried out some molecular orbital calculations on **13** and several π-extended TCNQs. These are arranged in decreasing reduction potential order (increasing LUMO energies) and are reported in Table 2. It is well known (29) that the electrode reduction potentials of many aromatic hydrocarbons correlate well with the Hückel LUMO energies. This appears to be approximately true for the TCNQ derivatives studied in Table 2. The AM1 values reported in Table 2 could be obtained for the larger systems, e.g., **11**, in a few hours on a 486 PC, while the PCMODEL calculations only take a few minutes. In either case the trend is remarkably evident, the reduction potential decreases with increasing LUMO energy, and the compound becomes a worse electron acceptor as the table is descended. In terms of electron-accepting ability, annulene derivative **13** is more like the benzannelated TCNQs **21** and **11** than like the pyrene **6**. This is not because of a lack of planarity. The π-systems of **12** and **13** are calculated to be planar (MM2-SCF, AM1, PM3), like that found for the parent bridged [14]annulene (30). The internal bridge atoms are above and below the plane of the 14-π periphery, and serve to keep the latter rigid and planar. Addition of one and then two electrons, to give the radical anion and then the dianion, also leads to planar calculated structures. We believe the main difference between **13** and **6** is that the latter system on reduction gives two distinct 6π circuits, with the top and bottom ring bond lengths becoming more equal on addition of one and then two electrons, i.e., more aromatic (the pyrene 4–5 and 9–10 bonds remain distinctly olefinic). The annulene **13** can also form a more delocalized π-system on reduction, but this time it has to involve the whole 14-π periphery (no 6-π circuits are possible), and this is energetically less favourable. It thus accepts electrons much less willingly than pyrene **6** or TCNQ itself. The benzannelated annulenes, e.g., **11**, become aromatic in the central ring, but the annelating rings remain relatively alternating, i.e., only one 6π circuit is formed.

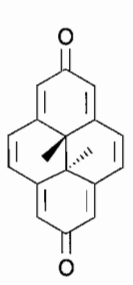
In properties then, extended TCNQ **13** behaves rather like the benzannelated TCNQs **9**–**11**, which also have high negative first reduction potentials and do not form TTF complexes (17), and unlike compounds **2**, **6**, and **7**, which are stronger acceptors than TCNQ (4, 11, 12).

Conclusions

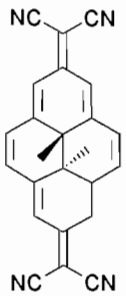
The unusual annulene TCNQ **13** was synthesized in 68% yield from quinone **12**. Even though it has conjugation considerably extended from that of TCNQ itself, it shows (to us) unexpect-

© 1997 NRC Canada

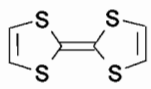
Can. J. Chem. Downloaded from www.nrcresearchpress.com by 88.146.161.215 on 09/08/12
For personal use only.



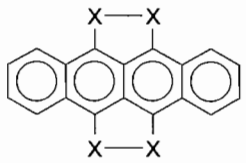
12



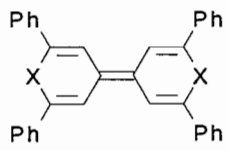
13



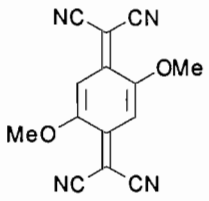
14



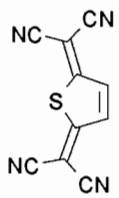
15 X=S
16 X=Se



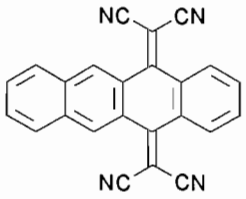
17 X=O
18 X=S



19



20



21

edly weak acceptor properties and does not form a TTF complex. In these properties **13** behaves more like the benzannelated derivatives of TCNQ, e.g., **11**, than the π-extended pyrene derivative **6**.

Experimental

Melting points were determined on a Reichert 7905 melting point apparatus integrated to a chrome–alumel thermocouple. Infrared spectra, major peaks only, calibrated with polystyrene, were recorded on a Bruker IFS25 FT-IR spectrometer as KBr disks. Ultraviolet–visible spectra were recorded on a Cary 5 or a Perkin–Elmer Lambda-4B spectrometer in dichloromethane. Proton NMR spectra were recorded at 360 MHz on a Bruker AMX 360 using $CDCl_3$ as solvent and either TMS as internal standard or the $CHCl_3$ peak at 7.24 ppm. Carbon NMR spectra were recorded at 90.6 MHz in $CDCl_3$, using the solvent peak at 77.0 ppm for calibration. Exact Mass measurements used a Kratos Concept-H instrument with perfluorokerosene as calibrant. Elemental analyses were carried out by Canadian Microanalytical Services Ltd, Vancouver, B.C. All evaporations were carried out under reduced pressure on a rotary evaporator, and all organic extracts were washed with water and dried over anhydrous $MgSO_4$. SiGel refers to Merck Silica Gel, 70–230 mesh. PE refers to distilled petroleum ether, bp 30–60°C.

trans-*10b,10c-Dimethyl-10b,10c-dihydropyrene-2,7-quinone (12)*

Dimethyldihydropyrene (31) (531 mg, 2.3 mmol) in dry DMF (40 mL) was added over 5 h to pyridinium dichromate (32) (4.30 g, 11.4 mmol) in dry DMF (50 mL) at −5°C. After a further 3 h at 0°C, ice-water and CH_2Cl_2 were added and were stirred well to extract the brown precipitate. The organic layer was washed, dried, and evaporated and the residue was dissolved in CH_2Cl_2 and chromatographed over SiGel using CH_2Cl_2–ether (7:3) to yield 455 mg (75%) of quinone **12**. Recrystallization from benzene returned 90% as yellow needles with mp 267–269°C (lit. (33) mp 252°C (dec.)). IR: 1636, 1605, 1555, 1442, 1367, 1291, 930, 915, 905 cm^{-1}; UV λ_{max} nm (ϵ_{max}): 273 (57 900), 317 sh (20 400), 333 (24 600), 348 sh (17 800), 399 (9000). ^1H NMR δ: 6.30 (4H, s, H-4,5,9,10), 6.07 (4H, s, H-1,3,6,8), 1.87 (6H, s, int-CH_3); ^{13}C NMR δ: 186.2, 157.1, 131.6, 128.4, 47.4, 28.5.

α,α,α′,α′-*Tetracyano*-trans-*10b,10c-dimethyl-10b,10c-dihydropyrene-2,7-quinodimethide (13)*

$TiCl_4$ (0.2 mL, 2 mmol) was added dropwise to a well-stirred solution of quinone **12** (131 mg, 0.5 mmol) in dry $CHCl_3$ (20 mL) at 0°C. The resultant brown suspension was stirred for 10 min without further cooling. A solution of malononitrile (0.6 mL, 5 mmol) and pyridine (0.8 mL, 10 mmol) in dry $CHCl_3$ (5 mL) was then added, and the mixture was heated under reflux for 12 h and then cooled. The reddish precipitate was filtered, washed well with water, and was dried under vacuum to give 103 mg (68%) of **13**. This sample was purified further by Soxhlet extraction using CH_2Cl_2, and concentrated to give purple crystals, mp > 350°C (dec.). IR: 2215, 1626, 1509, 1400, 1358, 981, 915 cm^{-1}; UV λ_{max} nm (ϵ_{max}): 296 (47 700), 460 (41 000), 485 sh (32 900); ^1H NMR (CD_2Cl_2) δ: 6.84 (4H, s, H-4,5,9,10), 6.56 (4H, s, H-1,3,6,8), 1.40 (6H, s, int-CH_3); ^{13}C NMR: too insoluble, but CH peaks at 132.1 and 123.6 ppm were just visible; HRMS calcd. for $C_{24}H_{14}N_4$: 358.122; found: 358.124. Anal. calcd: C 80.43, H 3.94; found: C 80.51, H 3.96.

*Complexation of **13** with* N,N-*diethylamine*

Quinodimethide **13** (3.5 mg, 0.01 mmol) was dissolved in dry CH_2Cl_2 (30 mL), freshly distilled Et_2NH (0.7 mg, 0.01 mmol) was added, and the mixture was stirred under N_2 for 8 h, during which time the colour changed from orange to dark green. Evaporation caused disappearance of the green colour. The UV spectrum of the green solution showed broad absorption between 350 and 450 nm and then a strong absorption at 770 nm (ε about 50 000).

*Measurement of reduction potential of **13***

The reduction potential of **13** was measured using a 10^{-3} M solution of **13** in benzonitrile in the presence of 0.1 M tetra-*n*-butylammonium perchlorate as supporting electrolyte, using Pt rods as both working and counter electrode, and Ag/AgCl as reference. The sample showed reversible redox waves with half-wave reduction potentials of −0.34 and −0.60 V. Cyclic voltammetry was carried out on a Hokuto Denko HA-301 using a scan rate of 100 mV s^{-1}. TCNQ was measured under identical conditions (see Table 1).

Acknowledgements

We thank the Natural Sciences and Engineering Research

© 1997 NRC Canada

Council of Canada, The University of Victoria, and Hiroshima University for financial support.

References

1. M.R. Bryce. Chem. Soc. Rev. **20**, 355 (1991).
2. F. Ogura, T. Otsubo, and Y. Aso. Sulphur Rep. **11**, 439 (1992).
3. J. Dieckmann, W.R. Hertler, and R.E. Benson. J. Org. Chem. **28**, 2719 (1963).
4. D.S. Acker and W.R. Hertler. J. Am. Chem. Soc. **84**, 3370 (1962).
5. J. Ferraris, D.O. Cowan, V. Walatka, and J.H. Perlstein. J. Am. Chem. Soc. **95**, 948 (1973).
6. A.F. Garito and A.J. Heeger. Acc. Chem. Res. **7**, 232 (1974).
7. A.W. Addison, N.S. Dalal, Y. Hoyano, S. Huizinga, and L. Weiler. Can. J. Chem. **55**, 4191 (1977).
8. F. Wudl, M.L. Kaplan, B.K. Teo, and J. Marshall. J. Org. Chem. **42**, 1666 (1977).
9. M. Maxfield, D.O. Cowan, A.N. Bloch, and T.O. Poehler. Nouv. J. Chim. **3**, 647 (1979).
10. M. Maxfield, S.M. Willi, D.O. Cowan, A.N. Bloch, and T.O. Poehler. J. Chem. Soc. Chem. Commun. 947 (1980).
11. M. Maxfield, A.N. Bloch, and D.O. Cowan. J. Org. Chem. **50**, 1789 (1985).
12. T. Yanagimoto, K. Takimiya, T. Otsubo, and F. Ogura. J. Chem. Soc. Chem. Commun. 519 (1993).
13. S. Chatterjee. J. Chem. Soc. B, 1170 (1967).
14. A. Aumüller and S. Hünig. Liebigs Ann. Chem. 618 (1984); B.S. Ong and B. Keoshkerian. J. Org. Chem. **49**, 5002 (1984); A.M. Kini, D.O. Cowan, F. Gerson, and R. Mockel. J. Am. Chem. Soc. **107**, 556 (1985).
15. S. Yamaguchi, H. Tatemitsu, Y. Sakata, and S. Misumi. Chem. Lett. 1229 (1983).
16. N. Martin, J.L. Segura, and C. Seoane. J. Org. Chem. **60**, 4077 (1995).
17. N. Martin, R. Behnisch, and M. Hanack. J. Org. Chem. **54**, 2563 (1989).
18. K. Yui, Y. Aso, T. Otsubo, and F. Ogura. Bull. Chem. Soc. Jpn. **62**, 1539 (1989).
19. R. Neidlen and H. Zeiner. Angew. Chem. Int. Ed. Engl. **20**, 1032 (1981).
20. E. Vogel, S. Bohm, A. Hedwig, B.O. Hergarten, J. Lex, J. Uschmann, and R. Gleiter. Angew. Chem. Int. Ed. Engl. **25**, 1000 (1986).
21. E. Vogel, L. Schmalstieg, P. Henk, O. Wilmes, J. Lex, R. Gleiter, and M. Langler. Angew. Chem. Int. Ed. Engl. **30**, 681 (1991).
22. R.H. Mitchell and X. Jin. Tetrahedron Lett. **36**, 4357 (1995).
23. W. Lehnert. Synthesis, 667 (1974).
24. L.R. Melby, H.D. Hartzler, and W.A. Sheppard. J. Org. Chem. **39**, 2456 (1974).
25. E.P. Goodings, D.A. Mitchard, and G. Owen. J. Chem. Soc. Perkin Trans. 1, 1310 (1972).
26. K.A. Balodis, A.D. Livdane, R.S. Medne, and O.Y. Neiland. J. Org. Chem. U.S.S.R. **15**, 343 (1979) .
27. G.A. Reynolds, C.H. Chen, and J.A. Van Allan. J. Org. Chem. **44**, 4456 (1979).
28. G. Saito and J.P. Ferraris. Bull. Chem. Soc. Jpn. **53**, 2141 (1980).
29. A. Streitweiser, Jr. Molecular orbital theory for organic chemists. John Wiley, New York. 1961. p. 177.
30. R.H. Mitchell, V.S. Iyer, N. Khalifa, R. Mahadevan, S. Venugopalan, S.A. Weerawarna, and P. Zhou. J. Am. Chem. Soc. **117**, 1514 (1995).
31. R.H. Mitchell and V. Boekelheide. J. Am. Chem. Soc. **96**, 1547 (1974).
32. M. Fieser, R.L. Danheiser, and W.R. Roush. Reagents for organic synthesis. Vol. 9. Wiley–Interscience, New York. 1981. p. 399.
33. V. Boekelheide and J.B. Phillips. J. Am. Chem. Soc. **89**, 1695 (1967).

Can. J. Chem. Downloaded from www.nrcresearchpress.com by 88.146.161.215 on 09/08/12
For personal use only.

© 1997 NRC Canada

A simple synthesis of (±)-1,2,3,6-tetrahydro-2,3′-bipyridine (anatabine) and (±)-3-(2-piperidinyl)pyridine (anabasine) from lithium aluminum hydride and pyridine

Chi-Ming Yang and Dennis D. Tanner

Abstract: The hydrolysis of a pyridine solution of lithium tetrakis(*N*-dihydropyridyl)aluminate (LDPA), which was prepared at 0°C, yields a mixture of 1,4-, 1,2-, and 2,5-dihydropyridines (DHPs) in a ratio of 26:37:38. The subsequent reversible base-catalyzed condensation of a 1:1 mixture of 1,2- and 2,5-DHPs carried out in the presence of oxygen affords an 89% yield of (±)-anatabine. When the reaction mixture is allowed to stand in the presence of oxygen, anabasine is slowly formed from anatabine by the reaction of the residual DHPs. Anatabine can also be converted into (±)-anabasine by catalytic hydrogenation.

Key words: lithium aluminum hydride, pyridine, anatabine, anabasine.

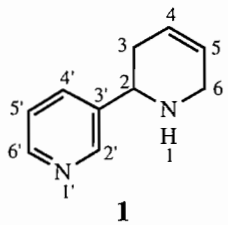
Résumé : L'hydrolyse d'une solution dans la pyridine du tétrakis(*N*-dihydropyridyl)aluminate de lithium («LDPA»), préparée à 0°C, conduit à un mélange de 1,4-, 1,2- et 2,5-dihydropyridines (DHP) dans un rapport de 26 : 37 : 38. Opérant en présence d'oxygène, on a effectué par la suite une condensation réversible, catalysée par les bases, d'un mélange 1 : 1 de 1,2- et 2,5-DHP qui conduit à un rendement de 89% de (±)-anatabine. Quand on laisse le mélange réactionnel en présence d'oxygène, l'anatabine conduit lentement à de l'anabasine par le biais de la réaction des DHP résiduelles. On peut aussi transformer l'anatabine en (±)-anabasine par hydrogénation catalytique.

Mots clés : hydrure de lithium et d'aluminium, pyridine, anatabine, anabasine.

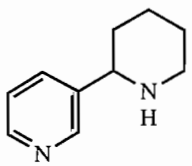
[Traduit par la rédaction]

Introduction

Anatabine (**1**) is the most abundant of the minor alkaloids of tobacco plants (1). In fresh *Nicotiana tabacum L.*, the plant from which it was first isolated (2), the alkaloid mixture consisted of 93% nicotine, 3.9% anatabine, 2.4% nornicotine, and 0.5% anabasine (**2**) (1).



1



2

The total synthesis of anatabine has been reported by three groups of workers (3–5). These syntheses yielded racemic anatabine, which is also isolated from tobacco (2). Two of the synthetic routes (3, 5) proposed, as transient intermediates, 2,5-dihydropyridine like structures.

Four syntheses of anabasine, **2**, have been reported (2, 6–8). The first report was the conversion of (−)-anatabine to (−)-anabasine by catalytic hydrogenation (2).

Recently we observed that the hydrolysis, in the absence of oxygen, of lithium tetrakis(*N*-dihydropyridyl)aluminate (LDPA), **3**, yields a mixture of three dihydropyridines, **4–6** (9). The ratio of 1,4-/1,2-dihydropyridyl ligands in **3** was dependent on the temperature and time of "aging" at which **3** was synthesized (9). When LDPA is formed by mixing lithium aluminum hydride and pyridine at 0°C and "aged" for 2 days the average ratio of 1,4-/1,2-dihydropyridyl ligands, *n*/*m*, in the isomeric mixture of LDPAs, **3a–e** (**3a** $m = 4$, $n = 0$; **3b** $m = 3$, $n = 1$; **3c** $m = 2$, $n = 2$; **3d** $m = 1$, $n = 3$; and **3e** $m = 0$, $n = 4$) was 0.35. The hydrolysis of LDPA formed at 0°C yields a mixture of three isomeric dihydropyridines: **4**, **5**, and **6** in a ratio of 26:37:38. The ratio of $n'/(m' + m'')$ was equal to the original 1,4-/1,2-ratio of ligands in the LDPA before hydrolysis (9).[2]

The biosynthetic pathway established for the synthesis of anatabine (1) suggested that two molecules of nicotinic acid, **7**, undergo 2,5-reduction to form **8**, which then decarboxylates to form the anion, **i**. The same anion, **i**, was derived in this work from the heretofore uncharacterized dihydropyridine, **5**.

Received September 13, 1996.

This paper is dedicated to Professor William A. Ayer on the occasion of his 65th birthday.

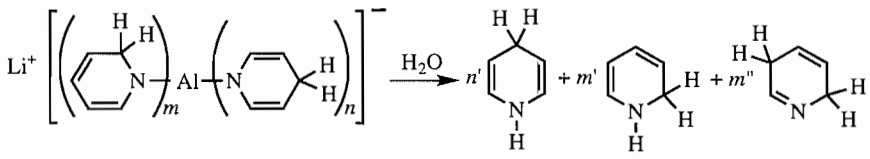
C.-M. Yang and D.D. Tanner.[1] Department of Chemistry, The University of Alberta, Edmonton, AB T6G 2G2, Canada.

[1] Author to whom correspondence may be addressed. Telephone: (403) 492-3512. Fax: (403) 492-3891. E-mail: dennis.tanner@ualberta.ca

[2] To maximize the yield of **5** and **6** the reaction of LAH and pyridine was carried out at 0°C and aged for 2 days.

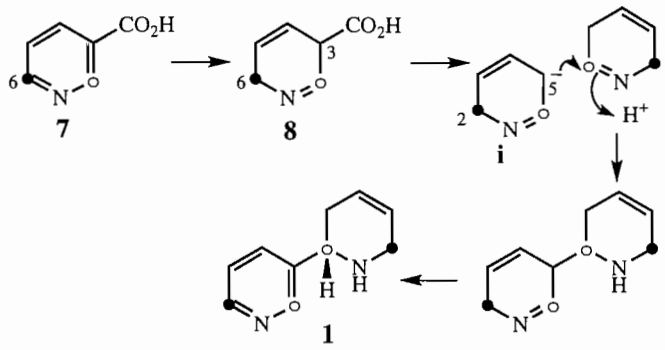
© 1997 NRC Canada

Can. J. Chem. Downloaded from www.nrcresearchpress.com by 88.146.161.215 on 09/08/12
For personal use only.



3 4 5 6

Scheme 1. The suggested biosynthetic pathway for the synthesis of anatabine from [6-^{14}C], ●, and [2-^{14}C], ○, nicotinic acid (refs. 1, 3).



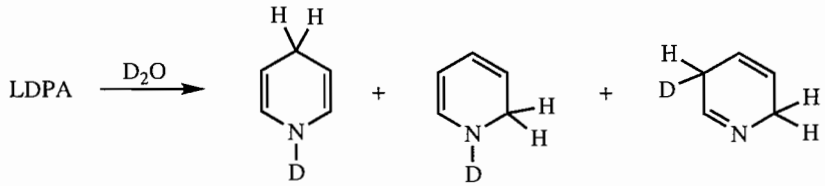
7 8 i 1

In the proposed biosynthetic path, a condensation of **i** and one mole of **6** presumably yields anatabine, **1**, see Scheme 1. The biosynthetic pathway proposed for the synthesis of **1** was suggested on the basis of incorporation studies using [6-^{14}C] and [2-^{14}C] nicotinic acid and upon the expectation that the intermediate, 3,6-dihydronicotinic acid (**8**), a β-imino acid, would readily decarboxylate to form **i** (Scheme 1). Both the decarboxylation of **8** and its subsequent condensation with **6** are reasonable pathways for the formation of anatabine from [6-^{14}C]- or [2-^{14}C]nicotinic acid.

Protonation of **i** yields both tautomers, **6** and **5**, and the condensation of **i** with **5** also yields **1**. Since the hydrolysate of LDPA (formed at low temperature) yields an almost equimolar mixture of **5** and **6**, it was reasonable to suspect that a basic solution (pyridine, $Al(OH)_4$) of the hydrolysate would yield, after oxidation, anatabine. The mixture of dihydropyridines, **4–6**, was stable in the presence of base (>14 days) in the absence of oxygen (9). However, in the presence of oxygen, **1** was slowly formed.

A consistent mechanism for the formation of **1** from a basic solution of **4**, **5**, and **6** (26:37:38) must accommodate the experimental observations that: (*a*) the mixture after hydrolysis is stable for extended periods of time; (*b*) only in the presence of oxygen is **1** slowly formed; (*c*) **2** is slowly formed at the expense of **1**; and (*d*) when LDPA is synthesized using $LiAlD_4$ the deuterated DHPs yield 6,6′-dideuteroanatabene. A mechanistic pathway can be suggested that accommodates these experimental observations: a reversible base-catalyzed condensation followed by a subsequent radical chain autoxidation, followed by a base-catalyzed elimination (Scheme 2). A chain autoxidation is a likely pathway which accounts for the high yield and its chemical specificity although the chain nature of oxidation is only speculative.

The proposed condensation pathway was investigated. When LDPA was hydrolyzed in D_2O, the 1,4-dihydropyridyl ligands yielded **9** while the 1,2-ligands yielded **10** and **11**.

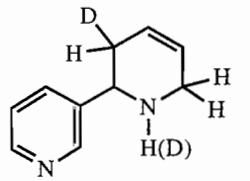


9 10 11

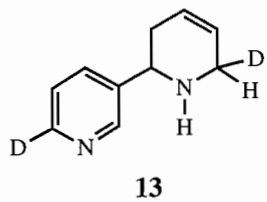
The formation of **1** from **10** and **11** by Scheme 2 yields **12**. Since only **12** is formed, Scheme 2 appears to be the most reasonable pathway that describes the synthesis of **1**.

When **3** is synthesized using $LiAlD_4$ (LAD), the LDPAs formed have ligands with 4-deuterated 1,4-dihydropyridyl ligands and 2-deuterated 1,2-dihydropyridyl ligands. Upon hydrolysis, the dihydropyridines formed are deuterated in the 2- and 4-positions (9). When anatabine is formed from the deuterated DHPs, only 6,6′-dideuteroanatabine (**13**) is found.

The absence of either 6,4′- or 4,4′-dideuterated **1** clearly rules out the involvement of **4** in the formation of **1**. The high yield of **1** from the condensation of **5** (0.68 M) and **6** (0.7 M) attests to the high efficiency of the reaction and confirms that **1** is formed from both **5** and **6**. If **5** is used as the limiting



12

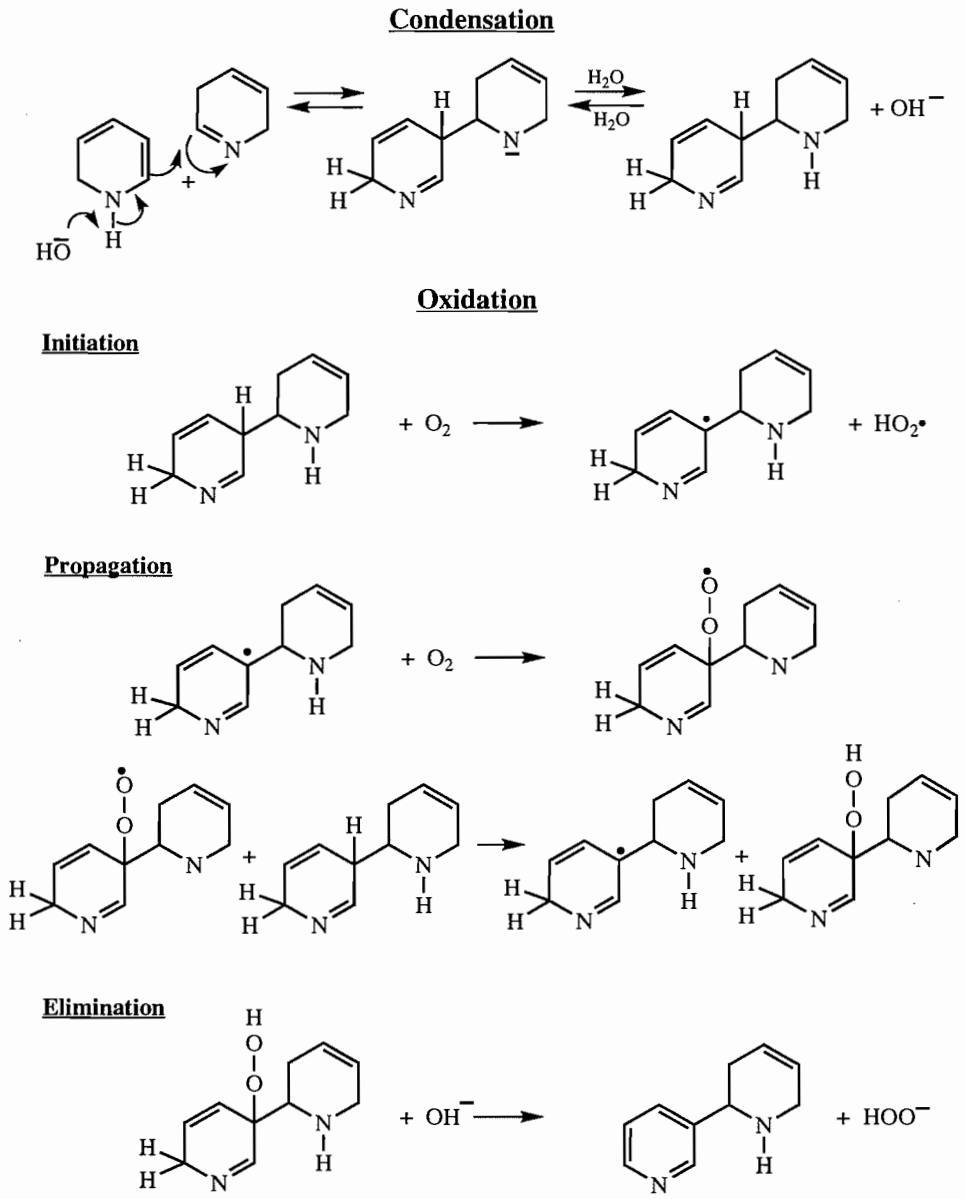


13

Can. J. Chem. Downloaded from www.nrcresearchpress.com by 88.146.161.215 on 09/08/12
For personal use only.

© 1997 NRC Canada

Scheme 2.



reagent, when LDPA is hydrolyzed, then the 59% isolated yield accounts for an 89% yield of **1**, i.e., for a 1:1 condensation of **5** and **6**.[3]

After the mixture of hydrolysates stood at room temperature for more than 3 days during the formation of **1**, a minor amount (~10%) of anabasine, **2**, was formed. Since the LAH and LDPA had been hydrolyzed, the only active reducing agents present in the reaction mixture are the three dihydropyridines, **4**–**6**. Presumably these hydride reagents are responsible for the reduction of **1** and formation of **2.** Unlike the biosynthetic pathway to anabasine, which is formed from nicotinic acid and lysine (10), the precursor of **2** under our reaction conditions must be anatabine.

Experimental

Materials

Pyridine (certified reagent grade, ACS or Caledon Laboratories Ltd.) was freshly distilled over barium oxide and potassium hydroxide pellets prior to use. Lithium aluminum hydride (General Intermediates of Canada) was purified by recovering from ether after filtration (11). D_2O (99.8%, General Intermediates of Canada), and lithium aluminum deuteride (Aldrich, 98% atom D) were used as supplied.

Instrumentation

The ^1H, ^2H, and ^{13}C NMR spectra were obtained using either a Bruker AM-400 (400 MHz) or Bruker AM-300 (300 MHz)

[3] The calculation of the concentration of **5** and **6** was based on the assumption that LAH was converted quantitatively to LDPA (^{27}Al NMR) (9), and that LDPA was hydrolyzed quantitatively to the three dihydropyridines (^1H NMR) (9).

© 1997 NRC Canada

Can. J. Chem. Downloaded from www.nrcresearchpress.com by 88.146.161.215 on 09/08/12
For personal use only.

Can. J. Chem. Downloaded from www.nrcresearchpress.com by 88.146.161.215 on 09/08/12
For personal use only.

NMR spectrometer. Unless otherwise noted, the ^{1}H NMR spectra are referenced to tetramethylsilane as an internal standard at 0.00 ppm or to $CHCl_3$ as an internal standard at 7.26 ppm. The ^{13}C NMR chemical shifts were reported in δ (ppm) relative to chloroform (δ $CDCl_3$ = 77.0). The ^{13}C spectra were studied by APT (attached proton test) to determine the number of protons attached to each carbon.

High-resolution mass spectra were obtained with a Kratos MS50 high-resolution EI$^+$ spectrometer connected to a DS 55 data system. GC analysis was performed with a HP 5840A gas chromatograph equipped with a hydrogen flame ionization detector using a stainless steel column 15 ft. × 1/4 in. packed with 10% SE-30 on Chromosorb W (100–200 mesh) and interfaced with a HP5840A integrator.

GC–IR analysis was performed using an HP-5965 GC/FTIR analytical system; GC–MS were run using a VG 70E mass spectrometer interfaced to a 11–250 data system.

Synthesis of (±)-anatabine, 1

A pyridine solution of LDPA or tetra deutero-LDPA (0.5 or 0.45 M) was treated with H_2O or D_2O (9). While the solution was stirred (3 days) at room temperature, and while it was exposed to atmospheric oxygen the solution was analyzed periodically by GC (10% SE-30 on Chromosorb W). After 3 days, chloroform was added to dilute the slurry and the solution was filtered through sintered glass. After filtration the solvent was evaporated under reduced pressure and the residue was dissolved in a mixture of chloroform/methanol/concentrated ammonium hydroxide (90:10:1)[3] and subjected to silica gel chromatography. The eluate was subjected to vacuum distillation and an isolated yield, 59%, was achieved (3).

(±)-Anatabine: bp 116–117°C/1 Torr (lit. (2) bp 145–156°C/10 Torr; 1 Torr = 133.3 Pa), IR (gas phase) ν: 3043(vs), 2924(s), 2800(s), 1901(w), 1657(w), 1579(m), 1429(s), 1315(m), 1190(m), 1108(s), 1019(m), 946(w), 783(m), 714(s) cm^{-1} (ref. 12). ^{1}H NMR ($CDCl_3$, 400 MHz) δ: 8.54 (d, 1H, $J_{2'4'}$ = 2.0 Hz, H-2′), 8.42 (dd, 1H, $J_{6'5'}$ = 5.0, $J_{6'4'}$ = 1.8 Hz, H-6′), 7.67 (dt, 1H, $J_{4'5'}$ = 8.0, $J_{4'6'}$ = 1.8, $J_{4'2'}$ = 2.0 Hz, H-4′), 7.20 (ddd, 1H, $J_{4'5'}$ = 8.0, $J_{5'6'}$ = 5.0, $J_{5'2'}$ = 0.8 Hz, H-5′), 5.78 (A of AB type, 1H, J_{AB} = 10.0 Hz, H-4), 5.72 (B of AB type, 1H, J_{AB} = 10.0 Hz, J_{56ax} = 4.0 Hz, J_{56eq} = 2.0 Hz, H-5), 3.80 (t, 1H, J_{23} = 7.0 Hz, H-2), 3.53 (dm, 1H, J_{ae} = 17.0 Hz, J_{56eq} = 2.0 Hz, H-′6eq), 3.40 (dm, 1H, J_{ae} = 17.0 Hz, J_{56ax} = 4.0 Hz, H-6 ax), 2.22 (m, N-H), 2.18 (m, 2H, H-3) (refs. 3, 4, 13). ^{13}C NMR ($CDCl_3$, 100.6 MHz) δ: 148.35(C-2′), 148.25(C-6′), 139.79(C-3′), 134.17(C-4′), 126.09(C-5′), 124.89(C-4), 123.49(C-5), 55.04(C-2), 45.71(C-6), 33.58(C-3) (refs. 3, 11); EI$^+$ mass spectrum, m/z^+ (relative intensity): 160 (M$^+$, 100), 159(29), 156(25), 155(16), 149(196), 131(18), 118(12), 107(23), 106(35), 105(42), 95(33), 54(42); high-resolution mass spectrum, m/z obsd.: 160.0996 (M$^+$, calcd. for $C_{10}H_{12}N_2$: 160.1000). Anal. calcd. for $C_{10}H_{12}N_2$: C 74.97, H 7.55, N 17.48; found: C 75.02, H 7.47, N 17.39.

(±)-6,6′-Dideuteroanatabine((±)-[6,6′-$^2H_2$]anatabine) 13

^{1}H NMR ($CDCl_3$, 400 MHz) δ: 8.54 (d, 1H, $J_{2'4'}$ = 2.0 Hz, H-2′), 8.42 (dd, 0.27H, partially deuterated, $J_{5'6'}$ = 5.0 Hz, $J_{4'6'}$ = 1.8 Hz, H-6′), 7.67 (dd, 1H, $J_{4'5'}$ = 8.0, $J_{4'2'}$ = 2.0 Hz, H-4′), 7.20 (d, 1H, $J_{5'4'}$ = 8.0 Hz, H-5′), 5.78–5.65 (AB, 2H, J_{45} = 11.0 Hz, H-4,5), 3.80 (t, 1H, J_{23} = 7.0 Hz, H-2), 3.53 (eq) and 3.40 (ax) (two broad singlets, 1H in total, 0.5H for axial, 0.5 H for equatorial, H-6), 2.22 (m, N-H), 2.18 (m, 2H, H-3). ^{13}C NMR ($CDCl_3$, 100.6 MHz) δ: 148.46(C-2′), 148.40(C-6′), 139.80(C-3′), 133.99(C-4′), 126.12(C-5′), 124.96(C-4), 123.38, 123.24, and 122.95(C-5), 55.03(C-2), 45.64, 45.54, 45.43, 45.34, 45.22, 45.14(C-6, -CDH-), 33.60(C-3). ^{2}H NMR ($CHCl_3$, 30.7 MHz) δ: 8.42 (s, 0.75D, D-6′), 7.26 ($CDCl_3$), 3.53 (s, 0.5D, D-6 eq), 3.40 (s, 0.5D, D-6 ax). ^{2}H NMR (CH_2Cl_2, 400 MHz) δ: 8.50 (s, 0.75D, D-6′), 5.32 (CD_2Cl_2), 3.58 (s, 0.5D, D-6 eq), 3.44 (s, 0.5D, D-6′ax). EI$^+$ mass spectrum, m/z^+ (relative intensity): 162 (M$^+$, 93), 161(100), 151(21), 132(22), 108(41), 107(63), 106(75), 80(44), 55(100); high-resolution EI$^+$ mass spectrum (GC–MS, VG 70E) m/z^+ obsd.: 162.1120 (M$^+$, calcd. for : $C_{10}H_{10}D_2N_2$: 162.1126).

(±)-1′,3′-Dideuteroanatabine((±)-[1′,3′-$^2H_2$]anatabine) 12

The deuterated isomer was obtained from the mixture of products **9**, **10**, and **11** after condensation. ^{1}H NMR ($CDCl_3$, 400 MHz) δ: 8.54 (d, 1H, $J_{2'4'}$ = 2.0 Hz, H-2′), 8.42 (dd, 1H, $J_{6'5'}$ = 5.0, $J_{6'4'}$ = 1.8 Hz, H-6′), 7.67 (ddd, 1H, $J_{4'5'}$ = 8.0, $J_{4'6'}$ = 1.8, $J_{4'2'}$ = 2.0 Hz, H-4′), 7.20 (ddd, 1H, $J_{4'5'}$ = 8.0, $J_{6'5'}$ = 5.0, $J_{5'2'}$ = 0.8 Hz, H-5′), 5.78–5.63 (AB quartet of multiplets, 5.68 (dm br, H-4), 5.63 (dm, H-5), J_{AB} = 11.0 Hz, 2H), 3.80 (a doublet (J_{23} = 7.0 Hz) covered by a small amount of triplet (J_{23} = 7.0 Hz), H-2), 3.53 (dm, 1H, J_{ae} = 17.0 Hz, H-6$_{eq}$), 3.40 (dm, 1H, J_{ae} = 17.0 Hz, H-6$_{ax}$), 2.22 (m, N-H), 2.18 (m, 1H, H-3). ^{2}H NMR ($CHCl_3$, 30.7 MHz) δ: 7.26 ($CDCl_3$), 2.22 (m, N-D), 2.18 (s, 1D, D-3). ^{13}C NMR ($CDCl_3$, 100.6 MHz) δ: 148.15(C-2′), 148.12(C-6′), 139.56(C-3′), 133.77(C-4′), 125.94(C-5′), 124.55(C-4), 123.11(C-5), 54.75, 54.68, and 54.61 (C-2), 45.47(C-6), 33.41(-CH_2-, undeuterated C-3), 33.25, 33.00, and 32.79(C-3). EI$^+$ mass spectrum, m/z^+ (relative intensity): 162 (M$^+$, 41), 161(100), 160(75), 159(17), 149(12), 145(15), 132(14), 131(24), 118(21), 107(41), 106(65), 105(67), 55(87), 54(60); E1$^+$ mass spectrum (GC–MS, VG 70), m/z^+ obsd.: 162.1114 (M$^+$, calcd. for $C_{10}H_{10}D_2N_2$: 162.1126).

(±)-Anabasine from the hydrogenation of (±)-anatabine

(±)-Anatabine (200 mg, 1.25 mmol) in anhydrous ethanol (25 mL) was hydrogenated over 100 mg Pd/C (50 psi H_2 (1 psi = 6.9 kPa) , 2 h, 23°C). The solution was filtered, the solvent evaporated, and the crude (±)-anabasine was subjected to column chromatography (silica gel) followed by vacuum distillation.

(±)-Anabasine: bp 106–108°C/2 Torr (lit. (2) bp 104–105°C/2 Torr). IR (gas phase) ν 3052(w), 2944(vs), 2864(m), 2803(m), 1575(w), 1428(m), 1322(m), 1112(m), 1020(m), 797(w), 716(m) cm^{-1}. ^{1}H NMR ($CDCl_3$, 400 MHz) δ: 8.58 (d, 1H, J_{42} = 2.6 Hz, H-2), 8.46 (dd, 1H, J_{56} = 4.9, J_{46} = 1.5 Hz, H-6), 7.76 (dt, 1H, J_{45} = 8.0, J_{46} = J_{42} = 1.8 Hz, H-4), 7.25 (dd, 1H, J_{45} = 8.0, J_{56} = 4.9 Hz, H-5), 3.66 (dd, 1H, $J_{2'3'}$ = 11.0, $J_{2'1'}$ = 2.2 Hz, H-2′), 3.25 (ddm, 1H, $J_{5'6'}$ = 11 Hz, H-6′), 2.80 (dt, 1H, $J_{5'6'}$ = 11.0, $J_{1'6'}$ = 2.9 Hz, H-6′$_{ax}$), 1.90–1.50 (m, 7H) (14,6). ^{13}C NMR ($CDCl_3$, 75.4 MHz) δ: 148.55(C-2, 6), 140.15(C-3), 134.59(C-4), 123.63(C-5), 59.75(C-2′), 47.51(C-6′), 34.42(C-3′), 25.38(C-5′), 25.06(C-4′) (ref. 4); EI$^+$ mass spectrum, m/z^+ (relative intensity): 162 (M$^+$, 32), 161(22), 133(40), 119(28), 106(36), 105(45), 92(15), 84(100); high-resolution EI$^+$ mass spectrum, m/z^+ obsd.: 162.1155 (M$^+$,

© 1997 NRC Canada

calcd. for $C_{10}H_{14}N_2$: 162.1153). Anal. calcd. for $C_{10}H_{14}N_2$: C, 74.03, H, 8.70, N, 17.27; found: C, 73.74, H, 8.62, N, 17.19.

The vapor phase IR (GC–IR) spectra (14) of the (±)-anabasine formed in the autoxidation reaction of the mixture of the **5** and **6** was identical to that of the (±)-anabasine obtained from the hydrogenation of anatabine or the GC–IR spectra obtained from the commercial sample (15).

(±)-6,6′-Dideuteroanabasine ((±)-[6,6′-$^2H_2$]anabasine) ^{1}H NMR ($CDCl_3$, 400 MHz) δ: 8.58 (d, 1H, J_{24} = 2.6 Hz, H-2), 8.46 (dd, 0.25 H, J_{65} = 4.9, J_{64} = 1.5 Hz, H-6), 7.76 (dd, 1H, J_{45} = 8.0 Hz, J_{42} = 1.8 Hz, H-4), 7.25 (d, 1H, J_{45} = 8.0 Hz, H-5), 3.66 (t, 1H, H-2′), 3.25 (s, br, 0.5H, H-6′eq), 2.80 (s, br, 0.5H, H-6′$_{ax}$), 1.90–1.50 (m, 7H). ^{2}H NMR ($CHCl_3$, 30.7 MHz) δ: 8.58 (s, 0.75D, D-6), 7.26 ($CDCl_3$), 3.25 (s, 0.5D, D-6′$_{eq}$), 2.81 (s, 0.5D, C-6′$_{ax}$). (It was reported by Robins and co-workers (16) that for anabasine, δ: 1.52 (H-3′$_{ax}$), 1.75 (H-3′$_{eq}$), 2.76 (H-6′$_{ax}$), 3.15 (H-6′$_{eq}$).) ^{13}C NMR ($CHCl_3$, 75.4 MHz) δ: 148.48(C-2), 148.38(C-6), 140.63(C-3), 134.12(C-4), 123.33, 123.19, 123.02(C-5), 59.65(C-2′), 47.40, 47.30, 47.19, 47.11, 46.98, 46.91(C-6′), 34.72(C-3′), 25.51(C-5′), 25.08(C-4′). EI$^+$ mass spectrum, m/z^+ (relative intensity): 164 (M^+, 17), 163(14), 162(4), 135(10), 134(11), 133(19), 121(11), 120(10), 119(26), 107(74), 106(100), 105(26), 94(20), 92(12), 86(7), 85(34); high-resolution EI$^+$ mass spectrum, m/z^+ obsd.: 164.1277 (M^+, calcd. for $C_{10}H_{12}D_2N_2$: 164.1284).

(±)-1′,3′-Dideuteroanabasine ((±)-[1′,3′-$^2H_2$]anabasine) ^{1}H NMR ($CDCl_3$, 400 MHz) δ: 8.58 (d, 1H, H-2), 8.46 (dd, 1H, H-6), 7.76 (dt, 1H, H-4), 7.25 (dd, 1H, H-5), 3.66 (s, 1H, H-2′), 3.25 (dm br, 1H, H-6′$_{eq}$), 2.80 (m, 1H, H-6′$_{ax}$), 2.16(N-H), 1.90–1.50 (m, 5H). ^{2}H NMR ($CHCl_3$, 30.7 MHz) δ: 7.26 ($CDCl_3$), 2.17 (bs, N′-D), 1.58 (s, 0.5D, D-3′$_{eq}$), 1.30 (s, 0.5D, D-3′$_{ax}$) (ref. 16). ^{13}C NMR ($CDCl_3$, 75.4 MHz) δ: 148.36(C-2), 148.23(C-6), 140.50(C-3), 133.91(C-4), 123.13(C-5), 59.49, 59.42, 59.35(C-2′), 47.35(C-6′), 34.62(C-3′ undeuterated), 34.44, 34.23, 34.18, 33.97, 33.92(C-3′), 25.45(C-5′), 24.79, 24.86, 24.75(C-4′). EI$^+$ mass spectrum, m/z^+ (relative intensity): 164 (M^+, 27), 163(67), 162(58), 161(18), 135(9), 134(24), 133(66), 121(19), 120(29), 119(53), 107(29), 106(73), 105(74), 95(35), 86(37), 85(100), 84(66). EI$^+$ mass spectrum (GC-MS, VG70), m/z^+ obsd.: 164.1271 (M^+, calcd. for $C_{10}H_{12}D_2N_2$: 164.1284).

Acknowledgment

The authors wish to thank the Natural Sciences and Engineering Research Council of Canada and the University of Alberta for their generous support of this work. C.M.Y. thanks the Alberta Heritage Foundation for Medical Research for a portion of his financial support.

References

1. (*a*) E. Leete and S.A. Slattery. J. Am. Chem. Soc. **98**, 6326 (1976); (*b*) E. Leete. J. Chem. Soc. Chem. Commun. 610 (1978).
2. E. Spath and F. Kesztler. Ber. Dtsch. Chem. Gas. **70**, 239 (1937); **70**, 704 (1937); **70**, 2450 (1937).
3. E. Leete and M.E. Mueller. J. Am. Chem. Soc. **104**, 6440 (1982).
4. P.M. Quan, T.K.B Karns, and L.D. Quin. J. Org. Chem. **30**, 2769 (1965).
5. M. Mehmandoust, C. Marazano, and B.C. Das. J. Chem. Soc. Chem. Commun. 1185 (1989).
6. G.F. Alberici, J. Andrieux, G. Adam, and M.M. Plat. Tetrahedron Lett. **24**, 1937 (1983).
7. F.E. Scully, Jr. J. Org. Chem. **45**, 1515 (1980).
8. H. Kunz and W. Pfrengle. Angew. Chem. Int. Ed. Engl. **28**, 1067 (1989).
9. D.D. Tanner and C.-M. Yang. J. Org. Chem. **58**, 1840 (1993).
10. (*a*) E. Leete, E.G. Gros, and T.J. Gilbertson. J. Am. Chem. Soc. **86**, 3907 (1964); (*b*) E. Leete, K. C. Rambom, and R.M. Riddle. Phytochemistry, **18**, 75 (1979); (*c*) E. Leete. Biosynthesis, 5, (1977).
11. E. Leete. Bioorg. Chem. **6**, 273 (1977).
12. E. Wada, T. Kisaki, and M. Ihida. Arch. Biochem. Biophys. **80**, 258 (1959).
13. I. Yamamoto, H. Kamimura, and R. Yamamoto. Mem. Tokyo Univ. Agric. **7**, 67 (1963).
14. A.M. Duffield, H. Budzikiewicz, and C. Djerassi. J. Am. Chem. Soc. **87**, 2926 (1965).
15. C.J. Pouchert. *In* The Aldrich library of FT-IR spectra. Vol. 1. 1537D, Aldrich Chemical Company, Inc., Milwaukee, Wis. 1985.
16. A.B. Watson, A.M. Brown, I.J. Colquhoun, N.J. Walton, and D.J. Robins. J. Chem. Soc. Perkin Trans. 1, 2607 (1990).

Can. J. Chem. Downloaded from www.nrcresearchpress.com by 88.146.161.215 on 09/08/12
For personal use only.

© 1997 NRC Canada

A synthesis of α-cuparenone based on symmetry considerations

Tse-Lok Ho and May-Hua Chang

Abstract: A ring expansion approach to α-cuparenone was accomplished in 5 or 6 steps. The key intermediate is 3-methyl-3-(4-methylphenyl)cyclobutanone, which was derived from a [2+2]cycloaddition of dichloroketene on a styrene derivative, followed by dechlorination.

Key words: symmetry, α-cuparenone, ring expansion, sesquiterpene.

Résumé : On a réalisé une synthèse de l'α-cuparénone en 5 ou 6 étapes par le biais d'une extension de cycle. L'intermédiaire clé est la 3-méthyl-3-(4-méthylphényl)cyclobutanone obtenue par une cycloaddition [2+2] du dichlorocétène sur un dérivé du styrène, suivie d'une déchloration.

Mots clés : symétrie, α-cuparénone, extension de cycle, sesquiterpène.

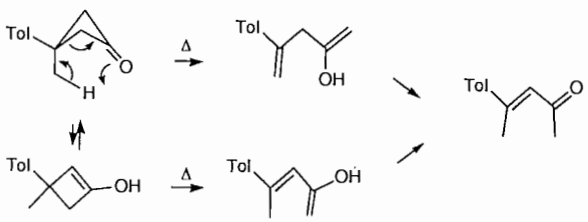
[Traduit par la rédaction]

Can. J. Chem. Downloaded from www.nrcresearchpress.com by 88.146.161.215 on 09/08/12
For personal use only.

Cuparene (**1**) is one of the simplest sesquiterpenes. Its synthetic challenge lies in the presence of two contiguous quaternary carbon centers on a cyclopentane unit. Our interest in the pursuit of a cuparene synthesis stemmed from symmetry considerations (1).

The ring expansion theme formed the basis of several previous approaches (for details, see ref. 2). However, we thought that routes traversing a symmetrical cyclobutanone intermediate would offer distinct advantages by avoiding any regiochemical problems due to indiscriminate C—C bond migration in the ring expansion step. In other words, extra caution of design is not needed to avoid production of regioisomeric cyclopentane derivatives. Accordingly, we started our work by a [2+2]cycloaddition of α,*p*-dimethylstyrene with dichloroketene under ultrasonic irradiation. The adduct **2**, obtained in 76% yield, was dechlorinated with zinc dust and sodium iodide in glacial acetic acid at 80–90°C to afford 3-methyl-3-(4-methylphenyl)cyclobutanone (**3**) in 84% yield. Originally we failed to achieve this transformation using zinc dust alone, zinc–copper couple, or aluminum amalgam as reducing agent; therefore sodium iodide appears to have played a critical role in the reduction. Interesting also is an adventitious observation of ring cleavage to provide dehydrocurcumone on heating **3** to temperatures above 190°C. We can attribute this transformation either to a bond reorganization reminiscent of a McLafferty rearrangement, the driving force being relief of ring strain, or to an electrocyclic reversion via the enol species (eq. [1]). With the symmetrical ketone **3** at hand, the stage was set for ring expansion (3). Reaction of **3**

[1]



with [tris(methylthio)methyl]lithium afforded a mixture of *cis* and *trans* hydroxythioorthoesters **4A/4B**, in a combined yield of 94%. The more polar isomer was considered to have the tolyl and the tris(methylthio)methyl groups disposed in a *trans* relationship because 2D-NMR indicated a nuclear Overhauser effect of the *S*-methyl substituents with the benzylic methyl. Both **4A** and **4B** were elaborated with equal efficiency to the same product **5** on treatment of the corresponding lithium alkoxide with copper(I) perchlorate – acetonitrile complex; therefore in the preparative routine we could perform this step using the stereoisomeric mixture.

At the outset, it was our intention to exploit the blocking of the appropriate α-methylene group by the bis(methythio) unit in **5** to achieve the desired *gem*-dimethylation in a regioselective fashion. Several attempts were made to perform the transformation with various bases (NaH, *t*-BuOK, LDA) and methylating agents (MeI, Me_2SO_4) but, unfortunately, the desired product could not be obtained in acceptable yield. The reaction was complicated by elimination of one methanethiol molecule, presumably after *S*-methylation, and also by enol methylation. In hindsight it may be reasonable to attribute this behavior to steric hindrance by a methylthio group to the approach of the electrophile. Both faces of the cyclic enolate intermediate were shielded by substituents of two quaternary centers. The pathway involving methanethiol elimination apparently did not fare any better, the enolate species being a *cisoid* 2,3-disubstituted diene in which the bulky groups are

Received October 24, 1996.

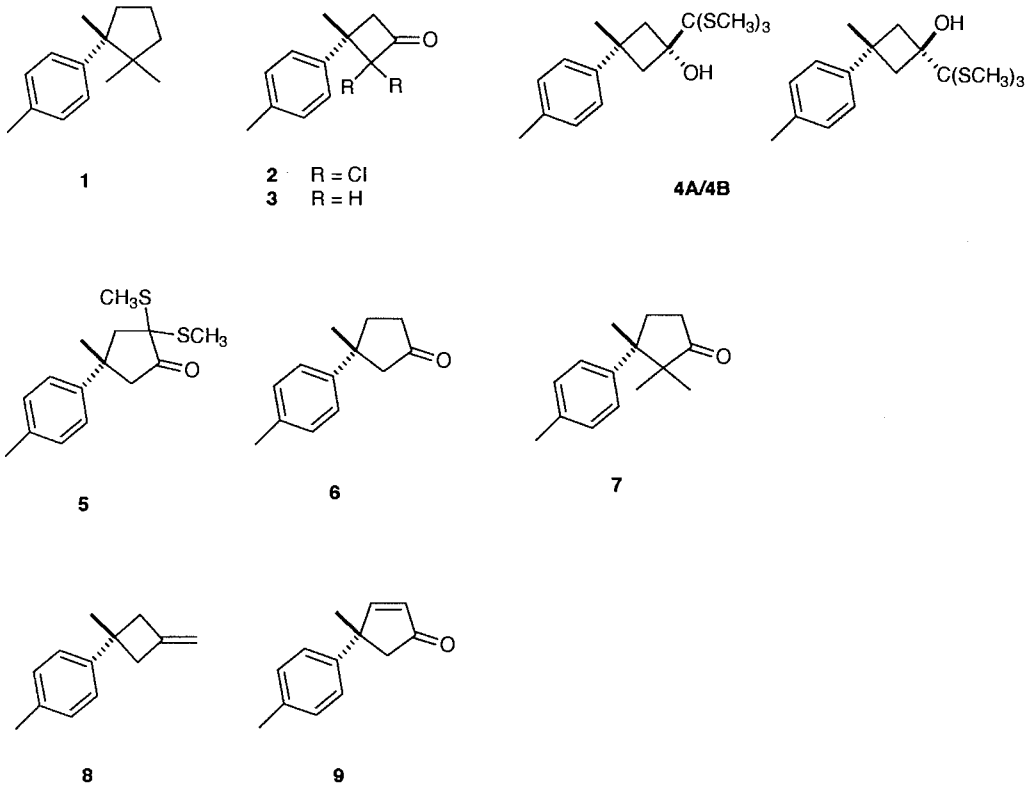
This paper is dedicated to Professor William A. Ayer on the occasion of his 65th birthday.

T.-L. Ho[1] and M.-H. Chang. Department of Applied Chemistry, National Chiao Tung University, Hsinchu, Taiwan, Republic of China.

[1] Author to whom correspondence may be addressed. Telephone: 886-35-712121, ext. 56538. Fax: 886-35-723764.

© 1997 NRC Canada

Can. J. Chem. Downloaded from www.nrcresearchpress.com by 88.146.161.215 on 09/08/12
For personal use only.

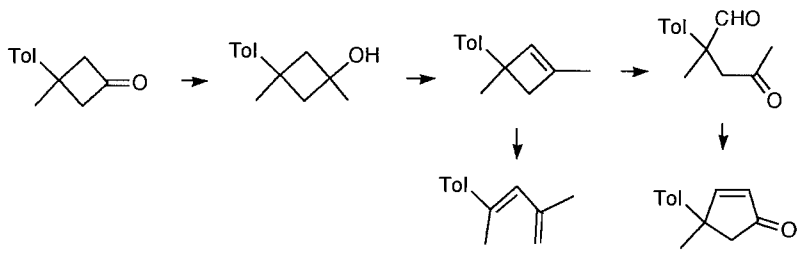


forced to adopt a coplanar conformation. Formation of such an enolate must be quite unfavorable.

Reports (4) that 3-methyl-3-arylcyclopentanones undergo methylation at C-2 with good selectivity ensured us an escape, although the yield was low (26%) and we were still disappointed at the failure of our original design. Desulfurization of **5** with Raney nickel in refluxing ethanol furnished ketone **6** in 85% yield, and the methylation proceeded to give α-cuparenone (**7**). α-Cuparenone is a well-known synthetic precursor of cuparene; therefore our work also represents a formal synthesis of the hydrocarbon.

An alternative and more direct method for the conversion of **3** to **6** is by Wittig reaction followed by treatment of the methylenecyclobutane derivative **8** with thallium(III) nitrate trihydrate (5). We also considered a route in which **3** was subjected to reaction with methylmagnesium iodide, dehydration, ozonolysis, and aldolization (eq. [2]) to reach another known precursor **9** of α-cuparenone. On preliminary investigations we found this last reaction sequence to be much inferior, the cyclobutene intermediate being rather prone to ring opening by electrocyclic reversion.

In conclusion, we have evaluated the concept of symmetry by an expedient route to α-cuparenone.



[2]

Experimental

General

Infrared spectra (IR) were obtained from neat film on KBr disks using a Jasco FT/IR-200 spectrometer. Mass spectra were measured with a TRIO-2000 or JEOL JMS-HX110 instrument. Proton and carbon nuclear magnetic resonance spectra in deuterochloroform solutions were determined by a Varian Unity-300 spectrometer. The following abbreviations were indicated: s = singlet, d = doublet, t = triplet, q = quartet, m = multiplet.

Materials

Anhydrous sodium sulfate was used for drying organic solutions during work-up of reactions. Thin-layer chromatography was performed on aluminum-backed silica gel plates with fluorescent coating. Separation by column chromatography was performed on silica gel 60 as supplied by E. Merck.

2,2-Dichloro-3-methyl-3-(4-methylphenyl)cyclobutanone (2)

A two-necked round-bottom flask was charged with α,*p*-dimethylstyrene (2.26 g, 17.1 mmol) and zinc dust (2.4 g, 36.7 mg-atm) in anhydrous ether (50 mL). The flask, equipped with a rubber septum and a condenser topped with a drying

© 1997 NRC Canada

Can. J. Chem. Downloaded from www.nrcresearchpress.com by 88.146.161.215 on 09/08/12
For personal use only.

tube, was placed in an ultrasonic cleaning bath. While maintaining the temperature of the bath water below 20°C by occasional addition of ice during irradiation, trichloroacetyl chloride (3.0 mL, 26.9 mmol) was introduced slowly into the flask via a syringe. At the end of 3 h, the reaction mixture was diluted with more ether, filtered through Celite, and washed with sodium carbonate solution. Removal of the ether from the dried solution and evaporative distillation gave **2** (3.16 g, 76% yield). IR: 1811 cm^{-1}. ^1H NMR (300 MHz, $CDCl_3$ δ: 1.63 (s, 3H), 2.37 (s, 3H), 3.05 (d, 1H, J = 16 Hz), 3.96 (d, 1H, J = 16 Hz), 7.16 (d, 1H, J = 8 Hz), 7.22 (d, 2H, J = 8 Hz). HRMS, *m/z*: 242.0271, 244.0236, 246.0203 (calcd. for $C_{12}H_{12}OCl_2$: 242.0257, 244.0227, 246.0197).

3-Methyl-3-(4-methylphenyl)cyclobutanone (3)

A mixture of dichloroketone **2** (0.50 g, 2.06 mmol), sodium iodide (0.77 g, 5.14 mmol), and zinc dust (0.34 g, 5.2 mg-atm) in glacial acetic acid (6 mL) was magnetically stirred and maintained between 80 and 90°C for 11 h. On cooling to room temperature, water and dichloromethane were added to the reaction mixture. The organic layer was washed with sodium carbonate solution, dried, and evaporated to give a residue that was filtered through a short column of silica gel, affording **3** (0.30 g, 84% yield). IR: 1795 cm^{-1}. ^1H NMR (300 MHz, $CDCl_3$) δ: 1.58 (s, 3H), 2.36 (s, 3H), 3.07 (d, 2H, J = 16 Hz), 3.42 (d, 2H, J = 16 Hz), 7.16 (d, 2H, J = 8.4 Hz), 7.18 (d, 2H, J = 8.4 Hz). ^{13}C NMR (75 MHz, $CDCl_3$) δ: 20.9 (q), 31.0 (q), 33.5 (s), 59.15 (t), 125.4 (d), 129.1 (d), 135.5 (s), 145.2 (s), 205.4 (s). HRMS, *m/z*: 174.1027 (calcd. for $C_{12}H_{14}O$: 174.1045).

3-Methyl-3-(4-methylphenyl)-1-[tris(methylthio)]-methylcyclobutanols (4A/4B)

A magnetically stirred solution of tris(methylthio)methane (1.40 g, 9.1 mmol) in dry THF (15 mL) at −78°C was treated with *n*-butyllithium (2.5 M in hexane, 3.6 mL, 9.0 mmol). After 0.5 h, ketone **3** (1.06 g, 6.1 mmol) was introduced via a syringe. The reaction was allowed to proceed for 1.5 h, quenched with a mixture of glacial acetic acid (0.6 mL) and ethanol (6 mL), and the cooling bath was removed. When room temperature was reached, the reaction mixture was distributed between CH_2Cl_2 and water; the organic solution was washed with aqueous sodium bicarbonate, dried, and concentrated in vacuo to provide a 1:1 mixture of products **4A** and **4B** (1.87 g, 94% yield), which were separated by silica gel chromatography.

The less polar isomer: IR: 3481 cm^{-1}. ^1H NMR (300 MHz, $CDCl_3$) δ: 1.56 (s, 3H), 2.23 (s, 9H), 2.34 (s, 3H), 2.35 (d, 2H, J = 18.6 Hz), 2.93 (d, 2H, J = 18.6 Hz), 3.64 (s, 1H, OH), 7.25 (s, 4H). ^{13}C NMR (75 MHz, $CDCl_3$) δ: 14.0 (q), 20.8 (q), 27.1 (q), 41.7 (t), 42.4. (s), 75.7 (s), 81.1 (s), 124.1 (d), 128.8 (d), 135.1 (s), 146.0) (s). HRMS, *m/z*: 328.0946, 281.1066 (calcd. for $C_{16}H_{24}OS_3$: 328.0991, for $C_{15}H_{21}OS_2$: 281.1035).

The more polar isomer: IR: 3480 cm^{-1}. ^1H NMR (300 MHz, $CDCl_3$) δ: 1.36 (s, 3H), 2.17 (s, 9H), 2.25 (s, 3H), 2.46 (dd, 2H, J = 13.2, 2.7 Hz), 2.77 (dd, 2H, J = 13.2, 2.7 Hz), 3.02 (s, 1H, OH), 7.07 (d, 2H, J = 8.1 Hz), 7.19 (d, 2H, J = 8.1 Hz). ^{13}C NMR (75 MHz, $CDCl_3$) δ: 14.9 (q), 20.9 (q), 32.7 (q), 35.9 (s), 47.1 (t), 76.6 (s), 79.1 (s), 125.5 (d), 128.9 (d), 134.7 (s), 147.3 (s). EIMS, *m/z*: 328 ($M^{+\cdot}$).

2,2-Bis(methylthio)-3-methyl-3-(4-methylphenyl)-cyclopentanone (5)

To a solution of **4A/4B** (0.25 g, 0.76 mmol) in toluene (40 mL) cooled to −78°C was added by syringe *n*-butyllithium (1.6 M in hexane, 0.6 mL, 0.94 mmol). After 0.5 h, tetrakis(acetonitrile)copper(I) perchlorate (0.55 g, 1.68 mmol) was added in one portion, and the cooling bath was then removed to allow the reaction to proceed at room temperature for 1.5 h, after which it was heated to 78°C for 2 h. The reaction mixture was quenched with a mixture of aqueous NH_4Cl–NH_4OH (pH 8), cooled to room temperature, filtered, and extracted with ether. After washing with water, drying, concentration, and chromatography, **5** was obtained (0.14 g, 64% yield). IR: 1730 cm^{-1}. ^1H NMR (300 MHz, $CDCl_3$) δ: 1.44 (s, 3H), 1.99 (s, 3H), 2.10 (s, 3H), 2.26 (s, 3H), 2.45 (d, 2H, J = 16.8 Hz), 2.59 (d, 2H, J = 7.5 Hz), 2.60 (d, 2H, J = 7.5 Hz), 3.21 (d, 2H, J = 16.8 Hz), 7.08 (s, 4H). ^{13}C NMR (75 MHz, $CDCl_3$) δ: 12.4 (q), 13.0 (q), 20.9 (q), 31.5 (q), 40.5 (s), 49.1 (t), 51.5 (t), 62.5 (s), 125.0 (d), 129.2 (d), 135.9 (s), 145.8 (s), 207.4 (s). HRMS, *m/z*: 280.0949 (calcd. for $C_{15}H_{20}OS_2$: 280.0957).

3-Methyl-3-(4-methylphenyl)-1-methylenecyclobutane (8)

A solution of ketone **3** (0.94 g, 5.4 mmol) in ether (2 mL) was added to the Wittig reagent prepared from methyltriphenylphosphonium bromide (1.785 g, 5 mmol) in anhydrous ether (10 mL) by treatment with *n*-butyllithium (1.43 M, 3.5 mL, 5 mmol) for 5 min at room temperature. The mixture was stirred overnight, filtered, and the residue was triturated with ether. The organic solution was evaporated, and the product was purified by silica gel chromatography to afford **8** (0.865 g, 93% yield). IR: 1687, 876, 816 cm^{-1}. ^1H NMR (300 MHz, $CDCl_3$) δ: 1.53 (s, 3H), 2.37 (s, 3H), 2.73 (d, 2H, J = 13.5 Hz), 3.08 (d, 2H, J = 13.5 Hz), 4.90 (s, 2H), 7.12 (s, 4H). ^{13}C NMR (75 MHz, $CDCl_3$) δ: 21.1 (q), 30.5 (q), 38.3 (s), 44.9 (t), 107.3 (t), 125.8 (d), 128.7 (d), 134.7 (s), 144.6 (s), 147.7 (s). EIMS; *m/z*: 172 ($M^{+\cdot}$).

3-Methyl-3-(4-methylphenyl)cyclopentanone (6)

From 5

A suspension of Raney nickel (ca. 2 mL) was washed three times with ethanol. A solution of **5** (114 mg, 0.41 mmol) in ethanol (6 mL) was added and the mixture was refluxed under nitrogen overnight. The metal was filtered, the filtrate was evaporated, and the residue was chromatographed to provide ketone **6** (65 mg, 85% yield). IR: 1741 cm^{-1}. ^1H NMR (300 MHz, $CDCl_3$ δ: 1.33 (s, 3H), 2.18–2.33 (m, 4H), 2.30 (s, 3H), 2.40 (d, 1H, J = 18 Hz), 2.58 (d, 1H, J = 18 Hz), 7.11 (d, 2H, J = 6 Hz) 7.14 (d, 2H, J = 6 Hz). ^{13}C NMR (75 MHz, $CDCl_3$) δ: 20.7 (q), 29.2 (q), 35.7 (t), 36.5 (t), 43.2 (s), 52.1 (t), 125.1 (d), 129.0 (d), 135.5 (s), 145.2 (s), 218.5 (s). HRMS, *m/z*: 188.1185 (calcd. for $C_{13}H_{16}O$: 188.1202).

From 8

A mixture of the methylenecyclobutane **8** (0.10 g, 0.58 mmol) and thallium(III) nitrate trihydrate (0.26 g, 0.58 mmol) in methanol (6 mL) was stirred at room temperature for 12 h. At this point solid NaCl (0.17 g) was added, the solid was filtered after 10 min, and the filtrate was evaporated in vacuo, redissolved in CH_2Cl_2, washed with brine, then water, dried, and concentrated. The product was purified by silica gel chromatography to give **6** (0.074 g, 68% yield).

© 1997 NRC Canada

α-Cuparenone (7)

Prepared in 26% yield by methylation according to ref. 4. IR: 1741 cm^{-1}. ^1H NMR (300 MHz, $CDCl_3$) δ: 0.60 (s, 3H), 1.16 (s, 3H), 1.25 (s, 3H), 1.85 (m, 1H), 2.33 (s, 3H), 2.3–2.7 (m, 3H), 7.06 (d, 2H, J = 7.8 Hz), 7.18 (d, 2H, J = 7.8 Hz). ^{13}C NMR (75 MHz, $CDCl_3$) δ: 18.4 (q), 20.8 (q), 22.1 (q), 25.3 (q), 29.6 (t), 33.6 (t), 48.3 (s), 53.1 (s), 126.3 (d), 128.9 (d), 135.6 (s), 141.8 (s), 221.9 (s). EIMS, *m/z*: 216 ($M^{+\cdot}$).

Acknowledgment

We thank the National Science Council of the Republic of China (ROC) for financial support of the project.

References

1. T.-L. Ho. Symmetry. A basis for synthesis design. Wiley, New York. 1995.
2. T.-L. Ho. Evolution of synthetic pathways. Parallax and calibration. World Scientific Publ., Singapore. 1996. pp. 61–63.
3. S. Knapp, A.F. Trope, M.S. Theodore, N. Hirata, and J. Barchi. J. Org. Chem. **49**, 608 (1984).
4. G.H. Posner and C.M. Lentz. J. Am. Chem. Soc. **101**, 934 (1979); T. Kametani, K. Kawamura, M. Tsubuki, and T. Honda. Chem. Pharm. Bull. **33**, 4821 (1985); M. Asaoka, K. Takenouchi, and H. Takei. Tetrahedron Lett. **29**, 325 (1988).
5. D. Farcasiu, P.v.R. Schleyer, and D.B. Ledlie. J. Org. Chem. **38**, 3455 (1973).

Can. J. Chem. Downloaded from www.nrcresearchpress.com by 88.146.161.215 on 09/08/12
For personal use only.

© 1997 NRC Canada

Bisindolylbenzenoids from ascostromata of *Petromyces muricatus*

Mikiko Ooike, Koohei Nozawa, Shun-ichi Udagawa, and Ken-ichi Kawai

Abstract: New bisindolylbenzenoids designated petromurins A (**1**), B (**2**), C (**3**), and D (**4**) were isolated from the ascostromata of *Petromyces muricatus*. These structures were determined by chemical and spectroscopic methods.

Key words: *Petromyces muricatus*; bisindolylbenzenoids; petromurin A, B, C, and D; ascostromata; *Aspergillus muricatus*.

Résumé : On a isolé de nouveaux bisindolylbenzénoïdes, appelés pétromurines A (**1**), B (**2**), C (**3**) et D (**4**), à partir des ascostromates du *Petromyces muricatus*. On a déterminé les structures par des méthodes chimiques et spectroscopiques.

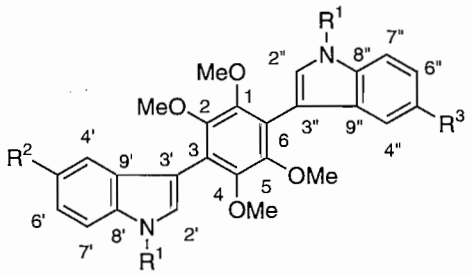
Mots clés : *Petromyces muricatus*; bisindolybenzénoïdes; pétromurines A, B, C et D; ascostromates; *Aspergillus muricatus*.

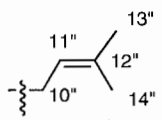
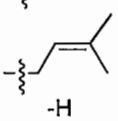
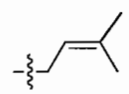
[Traduit par la rédaction]

Introduction

Petromyces muricatus Udagawa et al., the teleomorph of *Aspergillus muricatus* Udagawa et al. in the section *Circumdati*, subgenus *Circumdati* (= *A. ochraceus* group sensu Raper and Fennell), is characterized by producing pale yellow sclerotiodal bodies that may be converted slowly into an ascostroma. This fungus is the third *Petromyces* isolated from grassland soil of the Philippines in 1993 (1).

In the course of chemical studies on the indoloditerpenic metabolites of sclerotium-producing fungi, we previously reported the isolation of nominine, an anti-insectan indoloditerpene originally isolated from sclerotia of *Aspergillus nomius* Kurtzman et al. by Gloer et al. (2), and from ascostromata of *Petromyces alliaceus* Malloch et Cain, along with bicoumarins (3). This is the first case of isolation of sclerotial metabolites from the genus *Petromyces*. It is, therefore, of great interest to compare a profile of sclerotial metabolites of *P. muricatus* with that of taxonomically related species such as sclerotium-forming members of the sect. *Circumdati* of *Aspergillus*, e.g., *A. ochraceus* Wilhelm, *A. sclerotiorum* Huber, and *A. sulphureus* (Fres.) Thom et Church. As a result of an investigation of metabolites that showed positive colorations with Ehrlich's reagent (4), four indole derivatives designated as petromurins A (**1**), B (**2**), C (**3**), and D (**4**) were isolated from ascostromata of *P. muricatus*. The structures of **1**, **2**, **3**, and **4** are now reported in this paper.



	R^1	R^2	R^3
1	-H	-OH	
2	-H	-H	
3	-H	-OH	-H
4	-H	-OH	-OMe
5	-Me	-OMe	

Results and discussion

The molecular formulae of petromurins A (**1**), B (**2**), C (**3**), and D (**4**) were determined by high-resolution mass spectrometry as $C_{31}H_{32}N_2O_5$, $C_{31}H_{32}N_2O_4$, $C_{26}H_{24}N_2O_5$, and $C_{27}H_{26}N_2O_6$, respectively. All of these compounds showed positive coloration (purple) with Ehrlich's reagent. Compounds **1**, **3**, and **4** were also positive with iron(III) chloride reagent. These results suggested the presence of an indole group in **1**–**4** and a phenolic OH in **1**, **3**, and **4**. The ^{1}H NMR spectrum of **1** revealed the presence of two isolated 1,2,4-trisubstituted benzene rings (δ_H 6.99, 6.75, and 7.29, and 7.36, 6.98, and 7.37), four OMe groups (δ_H 3.49, 6H and 3.50, 6H),

Received September 12, 1996.

This paper is dedicated to Professor William A. Ayer on the occasion of his 65th birthday.

M. Ooike, K. Nozawa,[1] **and K. Kawai.** Faculty of Pharmaceutical Sciences, Hoshi University, Ebara 2-4-41, Shinagawa-ku, Tokyo 142, Japan.
S. Udagawa. Nodai Research Institute, Tokyo University of Agriculture, Sakuragaoka 1-1-1, Setagaya-ku, Tokyo 156, Japan.

[1] Author to whom correspondence may be addressed. Telephone: +81-3-5498-5789. Fax: +81-3-3787-0036. E-mail: nozawa@hoshi.ac.jp

© 1997 NRC Canada

Can. J. Chem. Downloaded from www.nrcresearchpress.com by 88.146.161.215 on 09/08/12
For personal use only.

Fig. 1. Difference NOE experiments of trimethylpetromurin A (**5**).

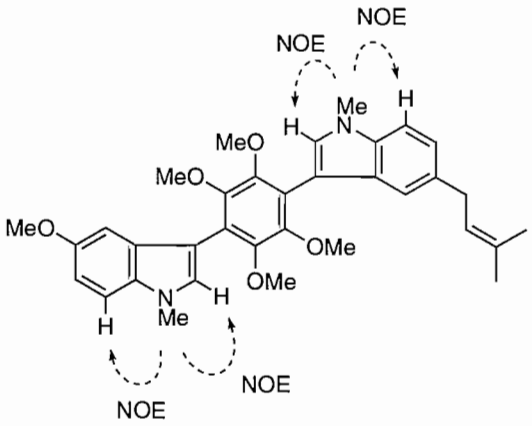
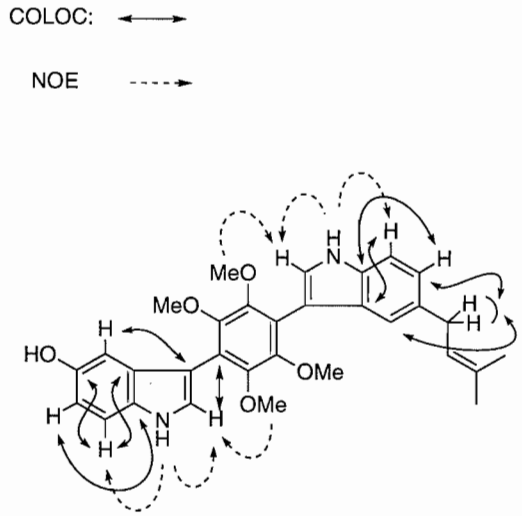


Fig. 2. ^{13}C–^{1}H correlation in COLOC and difference NOE for petromurin A (**1**).



and a 3-methyl-2-butenyl side chain. Each doublet signal at δ_H 7.44 and 7.45 in **1** changed into a singlet when D_2O was added, along with the disappearance of three signals at δ_H 7.55 (phenolic OH), 10.17 (NH), and 10.28 (NH). Petromurin A (**1**) thus contains two 3,5- or 3,6-disubstituted indole units. From these results and the consideration of the molecular formula, the remaining atoms in **1** were assigned to a hexasubstituted benzene ring. To confirm the substitution pattern of the two indole units in petromurin A (**1**), trimethylpetromurin A (**5**) was prepared from **1**. Irradiation of the signal at δ_H3.91 in **5**, attributed to the overlap of two NMe groups, brought about strong enhancements of signals at δ_H 7.38 (1H, br s, H-2″), 7.36 (1H, br s, H-2′), 7.34 (1H, d, J = 8.3 Hz, H-7″), and 7.33 (1H, d, J = 8.8 Hz, H-7′) (Fig. 1). These data coupled with other NMR data (see below) established that **1** had two 3,5-disubstituted indole groups.

The ^{1}H and ^{13}C NMR assignments of **1** and the substitution pattern of the benzene ring in **1** were established on the basis of long-range ^{13}C–^{1}H COSY (COLOC) spectra and difference NOE experiments on petromurin A (**1**) (Fig. 2). The signals at δ_C 121.2 (C-4″) and 123.4 (C-6″) showed COLOC correlations with the methylene proton signals of the 3-methyl-2-butenyl group at δ_H 3.42. The carbon signal at δ_C 136.1 (C-8″) showed a COLOC correlation with a proton at δ_H 6.98 (H-6″), along with correlations to protons at H-2″ and H-4″. The carbon signals at δ_C 129.1 (C-9″) and 133.2 (C-5″) were correlated with a proton at δ_H 7.37 (H-7″). On the other hand, the carbon at δ_C 108.6 (C-3′) in the other indole showed COLOC correlations with a proton at δ_H 6.99 (H-4′). The carbon signal at δ_C 132.3 (C-8′) was correlated with protons at δ_H 6.75 (H-6′) and 6.99 (H-4′). The carbon signals at δ_C 129.7 (C-9′) and 152.0 (C-5′), which were not correlated to any OMe proton signal, showed COLOC correlation with a proton at δ_H 7.29 (H-7′). These results indicated that the 3-methyl-2-butenyl group was situated at C-5 of one indole unit and the phenolic OH at C-5 of the other indole unit of **1**. The six carbons of the hexasubstituted benzene ring in **1** appeared as four signals comprised of signals at δ_C 149.4 (2C) and 149.5 (2C), which were correlated with OMe proton signals at δ_H 3.49 and 3.50, respectively, and signals at 123.9 (C-3) and 123.6 (C-6). Irradiation of the OMe protons at δ_H 3.49 and 3.50 in **1** caused weak enhancements of the signals at δ_H 7.44 (H-2′) and 7.45 (H-2″), respectively. We therefore concluded that the petromurin A (**1**) had a 1,2,4,5-tetramethoxylbenzene ring. Furthermore, a COLOC peak was observed between the carbon at δ_C 123.9 (C-3) and the proton at δ_H 7.44 (H-2′) when the COLOC spectrum of **1** was optimized for J_{CH} = 4 Hz. The structure of petromurin A (**1**), consequently, was assigned as depicted in structure **1** and the ^{13}C NMR assignments of **1** are provided in Table 1.

The ultraviolet (UV) spectra of petromurins B (**2**), C (**3**), and D (**4**) were essentially superimposable on those of petromurin A (**1**). The ^{1}H NMR spectrum of petromurin B (**2**) was similar to that of **1**, except for the presence in **2** of a 1,2-disubstituted benzene ring (δ_H 7.00 (H-5′), 7.09 (H-6′), 7.43 (H-7′), and 7.51 (H-4′)) instead of the 1,2,4-trisubstituted benzene ring of **1** that carried the hydroxyl group. Petromurin C (**3**) also has a 1,2-disubstituted benzene ring (δ_H 7.04 (H-5″), 7.14 (H-6″), 7.47 (H-7″), and 7.55 (H-4″)) lacking the 3-methyl-2-butenyl group present in **1**. The ^{1}H and ^{13}C NMR assignments of **2** and **3** were established by NOE difference experiments and analyses of the ^{13}C–^{1}H COSY and the COLOC spectra. The signals at δ_C121.2 (C-4″) and 123.5 (C-6″) assigned to one of the indole units in **2** showed COLOC correlations with the methylene proton signals (δ_H 3.37) of the 3-methyl-2-butenyl side-chain. The carbons at C-3″ (δ_C 109.2) in **2** and C-3′ (δ_C 108.7) in **3** were correlated with the protons at H-4″ (δ_H 7.31) and H-4′ (δ_H 6.99) in COLOC spectra, respectively. Irradiation of the NH protons (δ_H 10.25, 1″-NH) in **2** and the NH (δ_H 10.17, 1′-NH) in **3** caused strong enhancements of the signals at δ_H 7.32 (H-7″) and 7.41 (H-2″), and 7.29 (H-7′) and δ_H 7.44 (H-2′), respectively. The protons of the four methoxyl groups in **2** and **3** were correlated with the carbons in the central benzene ring. Thus, it is clear that petromurins B and C possess a substituent at C-5 in one indole ring, leading to assignments of the structures as **2** and **3**, respectively.

The ^{1}H NMR spectrum of petromurin D (**4**) was also similar to that of **1**, except for the absence of the 3-methyl-2-butenyl side chain and the appearance of an additional methoxyl group at δ_H 3.77. The ^{1}H and ^{13}C NMR assignments of **4** were established on the basis of the ^{1}H–^{1}H and ^{13}C–^{1}H COSY, and ^{1}H-detected heteronuclear multiple bond connectivity (HMBC) spectra. The substitution pattern of two indoles in **4** was

Can. J. Chem. Downloaded from www.nrcresearchpress.com by 88.146.161.215 on 09/08/12
For personal use only.

© 1997 NRC Canada

Can. J. Chem. Downloaded from www.nrcresearchpress.com by 88.146.161.215 on 09/08/12
For personal use only.

Table 1. ^{13}C NMR chemical shifts of petromurin A (**1**), B (**2**), C (**3**), and D (**4**) in acetone-d_6.

Carbon no.	1	2	3	4
1	149.5	149.6[a]	149.5	149.4
1-OMe	61.1	61.2	61.2	61.1[a]
2	149.4	149.5[a]	149.5	149.4
2-OMe	61.2	61.2	61.2	61.2[a]
3	123.9	124.0[b]	124.1[a]	123.9[b]
4	149.4	149.5[a]	149.5	149.4
4-OMe	61.2	61.2	61.2	61.2[a]
5	149.5	149.6[a]	149.5	149.4
5-OMe	61.1	61.2	61.2	61.1[a]
6	123.6	123.7[b]	123.5[a]	123.5[b]
2′	126.9	126.5	126.4	127.1
3′	108.6	109.5	108.7	108.7
4′	106.4	122.2	106.4	106.5
5′	152.0	120.2	152.2	152.1
6′	112.6	122.4	112.7	112.7
7′	112.6	112.5	112.7	112.7
8′	132.3	137.8	132.5	132.5
9′	129.7	129.0	129.8	129.8
2″	126.4	126.6	127.1	127.2
3″	109.1	109.2	109.5	109.3
4″	121.2	121.2	122.2	104.1
5″	133.2	133.3	120.2	155.3
6″	123.4	123.5	122.4	112.7
7″	112.2	112.3	112.5	113.0
8″	136.1	136.4	137.8	132.9
8″-OMe	—	—	—	56.3
9″	129.1	129.2	129.0	129.4
10″	35.7	35.7	—	—
11″	126.3	126.3	—	—
12″	131.9	132.0	—	—
13″	26.4	26.4	—	—
14″	18.3	18.4	—	—

[a,b,c]Assignments may be reversed.

assigned from the HMBC spectrum. The HMBC spectrum of **4** indicated a cross peak between the carbon at C-5″ and the methoxyl protons at δ_H3.77. On the basis of these results, the structure of petromurin D was proposed as shown in **4**.

Members of this general structural class (5) have been previously reported as fungal metabolites, e.g., cochliodinol from *Chaetomium* spp. (6) and asterriquinones from *Aspergillus terreus* (7). The known compounds commonly contain prenyl groups at various positions on the indole moieties, except for the ochrindoles A–D from sclerotia of *A. ochraceus* Thom, in which the prenyl side chain was located on the central benzenoid ring (8). Petromurins A, C, and D (**1**, **3**, and **4**) are the first examples where O functional group(s) have been observed on the indole moiety in the bisindolylbenzenoids.

Experimental

General procedure

Melting points were determined on a Yanagimoto micro-melting point apparatus and are uncorrected. Mass spectra were taken with a Jeol JMS-D-300 spectrometer. UV and IR spectra were recorded on a Hitachi U-3210 spectrophotometer and a Jasco IR-810 spectrophotometer, respectively. ^1H NMR and ^{13}C NMR spectra were recorded on a Jeol JNM-GX-400 spectrometer at 399.78 and 100.43 MHz, respectively, using tetramethylsilane as internal standard. The HMBC experiment of petromurin D was taken with a Jeol Lambda-500 spectrometer at 500.00 MHz. The coupling patterns are indicated as follows: singlet = s, doublet = d, triplet = t, multiplet = m, and broad = br. Column chromatography was performed using Kieselgel 60 (Art. 7734; Merck). Low-pressure liquid chromatography (LPLC) was performed on a Chemco Low-Prep 81-M-2 pump and glass column (10 mm i.d. × 300 mm) packed with silica gel CQ-3 (30–50 μm; Wako). TLC was conducted on precoated Kieselgel 60 F_{254} plates (Art. 5715; Merck). Spots on TLC plates were detected on the basis of their absorption of UV light, and (or) by spraying Ehrlich's reagent (4) and then heating.

Isolation of metabolites

Petromyces muricatus, strain IMI 368521, was cultivated at 35°C for 3 weeks in 480 Petri dish plates (i.d. 90 mm) containing 25 mL of melted Czapek yeast extract agar (CYA) per dish. The fresh ascostromata were collected and extracted with chloroform at room temperature. The evaporated residue (1.8 g) was separated by silica gel column chromatography into five fractions: cyclohexane – ethyl acetate (10:1), cyclohexane – ethyl acetate (5:1), cyclohexane – ethyl acetate (2:1), acetone, and EtOH. The second fraction was subjected to LPLC using cyclohexane–acetone (5:1) to give petromurin B (**2**) (80 mg). The third fraction was separated by LPLC using cyclohexane–acetone (2:1) to give petromurin A (**1**) (315 mg), petromurin C (**3**) (227 mg), petromurin D (**4**) (113 mg) in that order.

*Petromurin A (**1**)*: Colorless microcrystals; mp (dec.) 100°C (from $CDCl_3$); UV λ_{max}^{MeOH} nm (log ε): 225 (4.66), 278 (4.32); IR ν_{max}^{KBr} cm^{-1}: 3400 (NH), 3000, 1630, 1585, 1560, 1460, 1400, 1200 1060, 960, 800, 765; ^1H NMR (400 MHz, acetone-d_6) δ: 10.28 (1H, br s, 1″-NH), 10.17 (1H, br s, 1′-NH), 7.55 (1H, br s, 5′-OH), 7.45 (1H, d, J = 2.5 Hz, H-2″), 7.44 (1H, d, J = 2.5 Hz, H-2′), 7.37 (1H, d, J = 8.2 Hz, H-7″), 7.36 (1H, br s, H-4″), 7.29 (1H, d, J = 8.6 Hz, H-7′), 6.99 (1H, d, J = 2.4 Hz, H-4′), 6.98 (1H, dd, J = 8.2, 1.6 Hz, H-6″), 6.75 (1H, dd, J = 8.6, 2.4 Hz, H-6′), 5.28 (1H, br t, J = 7.3 Hz, H-11″), 3.50 (2 × OMe), 3.49 (2 × OMe), 3.42 (2H, br d, H-10″), 1.73 (3H, br s, Me), 1.70 (3H, br s, Me); COLOC correlations (acetone-d_6; C/H's): C-1 and C-5 / OMe (δ_H 3.50); C-2 and C-4 / OMe (δ_H 3.49); C-3′ / H-4′; C-4′ / H-6′; C-5′ / H-7′; C-6′ / H-4′; C-8′ / H-2′, H-4′, H-6′; C-9′ / H-2′, H-7′; C-4″ / H-6″, H-10″; C-5″ / H-7″; C-6″ / H-4″, H-10″; C-8″ / H-2″, H-4″, H-6″; C-9″ / H-2″, H-7″; C-10″ / H-4″,H-6″; C-11″ / H-10″, H-13″, H-14″; C-12″ / H-10″, H-13″, H-14″; ^1H NMR (400 MHz, THF-d_8) δ: 10.13 (1H, br s, 1″-NH), 10.00 (1H, br s, 1′-NH), 7.34 (1H, d, J = 2.5 Hz, H-2″), 7.33 (1H, d, J = 2.4 Hz, H-2′), 7.23 (1H, d, J = 8.5Hz, H-7″), 7.36 (1H, br s, H-4″), 7.13 (1H, d, J = 8.7 Hz, H-7′), 6.91 (1H, d, J = 2.4 Hz, H-4′), 6.91 (1H, dd, J = 8.5, 2.5 Hz, H-6″), 6.62 (1H, dd, J = 8.7, 2.4 Hz, H-6′), 5.37 (1H, br t, J = 7.3 Hz, H-11″), 3.44 (2 × OMe), 3.44 (2 × OMe), 3.40 (2H, br d, H-10″), 1.72 (3H, br s, Me), 1.69 (3H, br s, Me); ^{13}C NMR (100 MHz, acetone-d_6), see Table 1;

© 1997 NRC Canada

^{13}C NMR (100 MHz, THF-d_8) δ: 152.0 (C-5′), 149.1 (C-1 and C-5)[*a], 148.9 (C-2 and C-4)[*a], 136.0 (C-8″), 132.5 (C-5″), 132.0 (C-8′), 131.1 (C-12″), 129.2 (C-9′), 128.6 (C-9″), 126.7 (C-2′), 126.2 (C-2″), 126.1 (C-11″), 123.5 (C-3)[*b], 123.0 (C-6)[*b], 122.6 (C-6″), 121.2 (C-4″), 112.1 (C-6′), 111.6 (C-7′), 111.3 (C-7″), 108.8 (C-3″), 108.2 (C-3′), 106.2 (C-4′), 60.5 (2-OMe and 4-OMe)[*c], 60.4 (1-OMe and 5-OMe)[*c], 35.5 (C-10″), 26.0 (Me), 17.9 (Me); ([*a, *b, and *c] indicates that assignments for these carbon atoms may be interchanged.) EI-MS *m/z*: 512.2309 (M^+, 512.2309 calcd. for $C_{31}H_{32}N_2O_5$).

*Petromurin B (**2**)*: Colorless microcrystals; mp 200°C (from MeOH); UV λ_{max}^{MeOH} nm (log ε): 224 (4.76), 282 (4.39); IR ν_{max}^{KBr} cm^{-1}: 3360 (NH), 3000, 1630, 1460, 1400, 1100, 1060,1040, 890, 800, 740; ^{1}H NMR (400 MHz, acetone-d_6) δ: 10.37 (1H, br s, 1′-NH), 10.25 (1H, br s, 1″-NH), 7.51 (1H, br d, *J* = 7.9 Hz, H-4′), 7.46 (1H, d, *J* = 2.3 Hz, H-2′), 7.43 (1H, br d, *J* = 7.9 Hz, H-7′), 7.41 (1H, d, *J* = 2.5 Hz, H-2″), 7.32 (1H, d, *J* = 8.2 Hz, H-7″), 7.31 (1H, br s, H-4″), 7.09 (1H, td, *J* = 7.9, 1.2 Hz, H-6′), 7.00 (1H, td, *J* = 7.9, 1.2 Hz, H-5′), 6.94 (1H, dd, *J* = 8.2, 1.4 Hz, H-6″), 5.34 (1H, br t, *J* = 7.3 Hz, H-11″), 3.46 (2 × OMe), 3.44 (2 × OMe), 3.37 (2H, br d, *J* = 7.3 Hz, H-10″), 1.68 (3H, br s, Me), 1.65 (3H, br s, Me); COLOC correlations (acetone-d_6; C/H's): C-3′ / H-4′; C-4′ / H-6′; C-5′ / H-7′; C-6′ / H-4′; C-8′ / H-2′, H-4′, H-6′; C-9′ / H-2′, H-7′; C-3″ / H-4″; C-4″ / H-6″, H-10″; C-5″ / H-7″; C-6″ / H-4″, H-10″; C-8″ / H-2″, H-4″, H-6″; C-9″ / H-2″, H-7″; C-10″ / H-4″,H-6″; C-11″ / H-10″, H-13″, H-14″; C-12″ / H-10″, H-13″, H-14″; EI-MS *m/z*: 496.2362 (M^+, 496.2362 calcd. for $C_{31}H_{32}N_2O_4$).

*Petromurin C (**3**)*: Colorless microcrystals; mp (dec.) 240°C (from $CDCl_3$); UV λ_{max}^{MeOH} nm (log ε): 223 (4.76), 281 (4.33); IRν_{max}^{KBr} cm^{-1}: 3420 (NH), 2950, 1490, 1460, 1400, 1190, 1060, 1040, 990, 750; ^{1}H NMR (400 MHz, acetone-d_6) δ: 10.40 (1H, br s, 1″-NH), 10.17 (1H, br s, 1′-NH), 7.56 (1H, s, 5′-OH), 7.55 (1H, d, *J* = 7.9 Hz, H-4″), 7.49 (1H, d, *J* = 2.5 Hz, H-2″), 7.47 (1H, br d, *J* = 7.9 Hz, H-7″), 7.44 (1H, d, *J* = 2.5 Hz, H-2′), 7.29 (1H, d, *J* = 8.8 Hz, H-7′), 7.14 (1H, td, *J* = 7.9, 1.2 Hz, H-6″), 7.04 (1H, td, *J* = 7.9, 1.2 Hz, H-5″), 6.99 (1H, br d, *J* = 2.3 Hz, H-4′), 6.75 (1H, dd, *J* = 8.8, 2.3 Hz, H-6′), 3.49 (2 × OMe), 3.49 (2 × OMe); COLOC correlations (acetone-d_6; C/H's): C-3′ / H-4′; C-4′ / H-6′; C-5′ / H-7′; C-6′ / H-4′; C-8′ / H-2′, H-4′, H-6′; C-9′ / H-2′, H-7′; C-3″ / H-4″; C-4″ / H-6″; C-5″ / H-7″; C-6″ / H-4″; C-8″ / H-2″, H-4″, H-6″; C-9″ / H-2″, H-7″; EI-MS *m/z*: 444.1685 (M^+, 444.1685 calcd. for $C_{26}H_{24}N_2O_5$).

*Petromurin D (**4**)*: Colorless microcrystals; mp 127–128°C (from $CDCl_3$); UV λ_{max}^{MeOH} nm (log ε): 223 (4.70), 278 (4.36); IR ν_{max}^{KBr} cm^{-1}: 3400 (NH), 2940, 1620 , 1580, 1480, 1460, 1390, 1210, 1060, 1000, 960, 800, 760; ^{1}H NMR (400 MHz, acetone-d_6) δ: 10.25 (1H, br s, 1″-NH), 10.15 (1H, br s, 1′-NH), 7.54 (1H, s, 5′-OH), 7.46 (1H, d, *J* = 2.4 Hz, H-2″), 7.43 (1H, d, *J* = 2.5 Hz, H-2′), 7.28 (1H, d, *J* = 8.5 Hz, H-7′), 7.35 (1H, d, *J* = 8.8 Hz, H-7″), 7.04 (1H, d, *J* = 2.3 Hz, H-4″), 6.99 (1H, d, *J* = 2.2 Hz, H-4′), 6.75 (1H, dd, *J* = 8.5, 2.2 Hz, H-6′), 6.80 (1H, dd, *J* = 8.8, 2.3 Hz, H-6″), 3.77 (OMe), 3.51 (2 × OMe), 3.50 (2 × OMe); HMBC correlations (acetone-d_6; H/C's): H-2′ / C-8′, C-9′; H-2″ / C-8″, C-9″; H-4′ / C-3′, C-5′, C-8′; H-4″ / C-3″, C-5″, C-8″; H-6′ / C-4′, C-8′; H-6″ / C-4″, C-8″; H-7′ / C-5′, C-9′; H-7″ / C-5″, C-9″; 5-OH / C-4′, C-5′; EI-MS *m/z*: 474.1792 (M^+, 474.1791 calcd. for $C_{27}H_{26}N_2O_6$).

*Methylation of petromurin A (**1**) with methyl iodide – sodium hydride*

A mixture of **1** (25 mg), 60% sodium hydride (10 mg), and methyl iodide (100 mg) in dimethylformamide (3 mL) was stirred at room temperature for 14 h. Work-up in the usual manner provided a crude product, which was purified by LPLC. Elution with cyclohexane–acetone (5:1) gave the trimethylpetromurin A (**5**) (12 mg), which was crystallized from $CDCl_3$ as microcrystals; mp 100°C; ^{1}H NMR (270 MHz, acetone-d_6) δ: 7.38 (1H, br s, H-2″), 7.36 (1H, br s, H-2′), 7.36 (1H, br s, H-4″), 7.34 (1H, , d, *J* = 8.3 Hz, H-7″), 7.33 (1H, d, *J* = 8.8 Hz, H-7′), 7.04 (1H, d, *J* = 2.5 Hz, H-4′), 7.04 (1H, dd, *J* = 8.3, 1.9 Hz, H-6″), 6.86 (1H, dd, *J* = 8.8, 2.5 Hz, H-6′), 5.38 (1H, br t, H-11″), 3.91 (2 × NMe), 3.78 (OMe), 3.51 (4 × OMe), 3.43 (2H, br d, H-10″), 1.73 (3H, br s, Me), 1.70 (3H, br s, Me); EI-MS *m/z*: 554 (M^+).

Acknowledgments

We are grateful to Mrs. Y. Kawada and Mr. Komiya of Hoshi University for NMR and mass measurements. This work was supported in part by a Grant-in-Aid for Scientific Research (No. 07672296) from the Ministry of Education, Science, Sports and Culture, Japan.

References

1. S. Udagawa, S. Uchiyama, and S. Kamiya. Mycotaxon, **52**, 207 (1994).
2. (*a*) J.B. Gloer, B.L. Rinderknecht, D.T. Wicklow, and P.F. Dowd. J. Org. Chem. **54**, 2530 (1989); (*b*) D.T. Wicklow, P.F. Dowd, and J.B. Gloer. *In* The genus aspergillus. *Edited by* K.A. Powell, A. Renwick, and J.F. Peberdy. Plenum Press, New York. 1994. pp. 93–114.
3. K. Nozawa, S. Nakajima, K. Kawai, S. Udagawa, and M. Miyaji. Phytochemistry, **35**, 1049 (1994).
4. R.A. Heacock and M.E. Mahon. J. Chromatogr. **17**, 338 (1965).
5. W.B. Turner and D.C. Aldridge. Fungal metabolites II. Academic Press, London. 1983.
6. W.A. Jerram, A.G. McInnes, W.S.G. Maass, D.G. Smith, A. Taylor, and J.A. Walter. Can. J. Chem. **53**, 727 (1975).
7. Y. Yamamoto, K. Nishimura, and N. Kiriyama. Chem. Pharm. Bull. **24**, 1853 (1976).
8. F.S. de Guzman, D.R. Bruss, J.M. Rippentrop, K.B. Gloer, J.B. Gloer, D.T. Wicklow, and P.F. Dowd. J. Nat. Prod. **57**, 634 (1994).

Can. J. Chem. Downloaded from www.nrcresearchpress.com by 88.146.161.215 on 09/08/12
For personal use only.

© 1997 NRC Canada

C_3 Symmetric oxazolinyl ligand as catalyst in the enantioselective addition of diethylzinc to aldehydes

T.H. Chan and G.Z. Zheng

Abstract: The C_3 symmetric oxazolinyl ligand **1** has been synthesized. Compound **1** catalyzed the addition of diethylzinc to aromatic aldehydes to give secondary alcohols with high enantiomeric excesses (up to 90%).

Key words: diethylzinc, enantioselective synthesis, C_3 symmetric ligands, enantioselective addition reactions, oxazolinyl ligands.

Résumé : On a synthétisé le coordinat oxazolinyle **1**, de symétrie C_3. Le composé **1** catalyse l'addition du diéthylzinc sur les aldéhydes aromatiques qui conduit à des alcools secondaires avec des excès énantiomériques élevés (jusqu'à 90%).

Mots clés : diéthylzinc, synthèse énantiosélective, coordinats de symétrie C_3, réactions d'addition énantiosélective, coordinats oxazolinyles.

[Traduit par la rédaction]

Can. J. Chem. Downloaded from www.nrcresearchpress.com by 88.146.161.215 on 09/08/12
For personal use only.

Introduction

The success of many C_2 symmetric ligands as catalyst in a number of highly enantioselective chemical transformations (1) has underscored the important role that symmetry could play in the stereocontrol of these reactions. It has been suggested that the C_2 ligand enhances the optical yield of the reaction by reducing the number of competing diastereomeric pathways due to the homotopic nature of the remaining coordination sites of the complexes formed by the ligand (1). As a consequence, considerable efforts have been directed to prepare higher order symmetrical compounds (2), such as C_3 symmetric ligands, to see if they can be useful reagents to induce high enantioselectivity in chemical reactions. Although C_3 symmetric phosphine ligands (2*a*), pyrazolyl compounds (2*c*,*d*,*e*), pyridinyl compounds (2*f*), and tris-alkoxides (2*b*) have been made previously, there have been few reports on the use of these ligands in asymmetric synthesis. One example (2*a*) is the asymmetric hydrogenation of dimethyl itaconate using a C_3 phospine ligand giving high ee (95%). On the other hand, for carbon–carbon bond formation, the single report on the use of a chiral C_3 copper complex that catalyzed the cyclopropanation of styrene with diazoacetates gave maximum ee's of only 60% (2*d*). We report here the synthesis of a C_3 symmetric tris(oxazolinyl) compound **1** and its application in asymmetric synthesis.

Received July 12, 1996.

This paper is dedicated to Professor William A. Ayer on the occasion of his 65th birthday.

T.H. Chan[1] **and G.Z. Zheng.** Department of Chemistry, McGill University, Montreal, QC H3A 2K6, Canada.

[1] Author to whom correspondence may be addressed. Telephone: (514) 398-4177. Fax: (514) 398-4768. E-mail: chan@ums1.lan.mcgill.ca

Synthesis

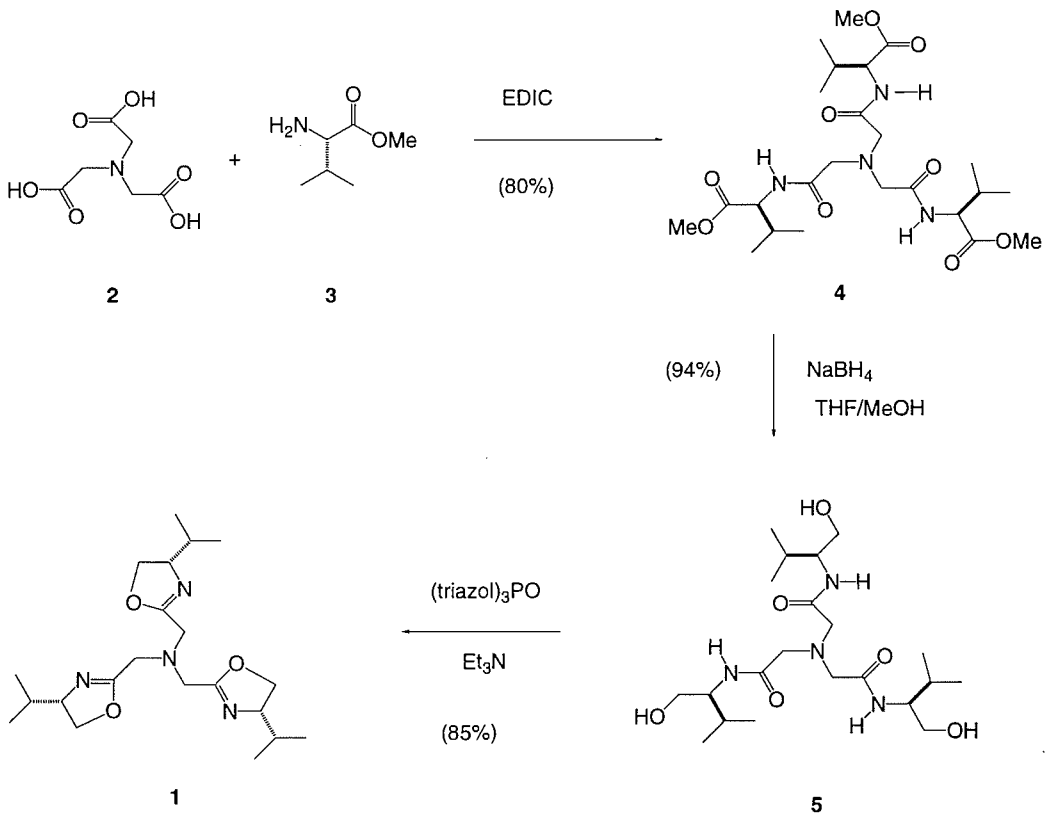
Compound **1** was prepared via the coupling of the triacid **2** with (*S*)-valine methyl ester (**3**) mediated by the coupling agent *N*-(3-dimethylaminopropyl)-*N'*-ethylcarbodiimide hydrochloride (EDCI) (3) (80% yield, Scheme 1). As three chiral centers have been implanted into compound **4**, any racemization during the coupling step should be easily detected by ^{1}H NMR spectroscopy of **4**. The results showed that there was no significant racemization at any of the chiral centres, with or without the presence of 1-hydroxybenzotriazole (HOBT), a reagent reported to prevent racemization during such coupling reactions (4). Selective reduction of the ester functions of **4** to the alcohol **5** was achieved using sodium borohydride (5). The reaction had to be carried out in a mixed solvent system (MeOH:THF = 50:50), and a large excess (5–10 equiv.) of sodium borohydride was used to drive the reduction to completion (94%). The alcohol **5** was subsequently cyclized with the assistance of tris(triazole)phosphine oxide (6) to give the final C_3 product **1** with high yield (85%; Scheme 1). Other cyclization reagents, such as thionyl chloride (7), $(CF_3CO)_2O$–Et_3N (8), *N,N*-dimethylchloromethyleneammonium chloride (9), and $(CF_3SO_2)_2O$–Ph_3PO (10) gave a mixture of products with no significant amount of **1**. Compound **1** could be obtained pure using gel (Sephadex LH-20) filtration (11). It was reasonably stable when stored as a solution of benzene at low temperature. Since the completion of our work, another synthesis of **1** has been reported in the literature (12), using a somewhat different synthetic scheme with lower overall yield.

Enantioselective addition of diethylzinc to aldehydes

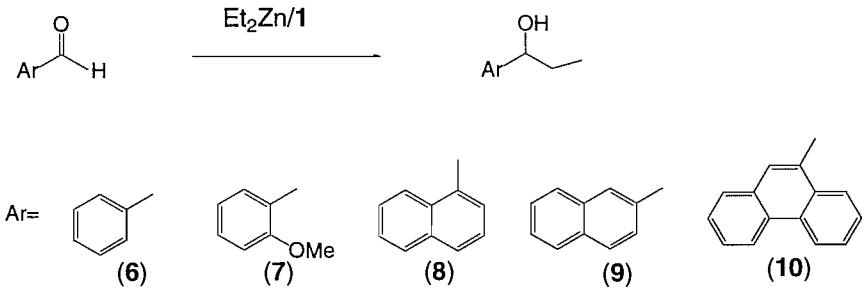
The C_3 symmetric ligand **1** was used as catalyst in the addition of diethylzinc to aromatic aldehydes **6**–**10** (Scheme 2). The results were encouraging in that the enantiomeric excesses of the alcohols obtained were quite high (up to 90% ee), even

© 1997 NRC Canada

Scheme 1.



Scheme 2.



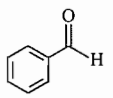
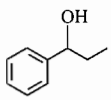
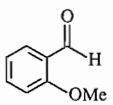
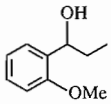
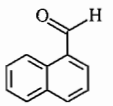
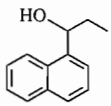
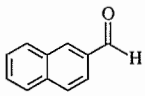
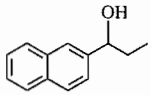
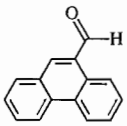
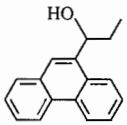
though slightly lower than the best results reported for the same reaction using other types of chiral ligands (13). The results are summarized in Table 1. The optical purity and the absolute configuration of the product were determined by conversion to the corresponding Mosher ester and analysed by NMR. The reaction was carried out in toluene as solvent and gave excellent chemical yield in general, with good to high optical yield (72–90% ee). Similar chemical yields were obtained in hexane as solvent, but with somewhat lower enantiomeric excesses for the products. Even in toluene, the amounts of compound **1** in the reaction mixture were crucial for good stereochemical outcome. Relatively large amounts of **1** (>2% mol) were required to produce high ee. However, over 20% mol concentration of catalyst **1** in the reaction mixture did not enhance the enantiomeric excess significantly. When using 26% mol of the catalyst in the reaction, similar enantiomeric excess was obtained (82% ee (*R*); 90% yield) when the substrate was benzaldehyde (**6**). Reducing the amounts of diethylzinc from 6 equivalents (substrate/Et_2Zn = 1 mmol: 3 mmol) to 4 equivalents (substrate/Et_2Zn = 1 mmol:2 mmol) reduced the enantiomeric excess of the product (to 68% ee (*R*) (82% yield) for **6**). Upon further reduction of the relative amount of diethylzinc to 2 equivalents, the enantiomeric excess decreased even further (to 54% (*R*) (70% yield) for **6**). Such concentration dependence is in agreement with the proposed mechanism in which a dinuclear zinc species involving a second molecule of diethylzinc has been postulated as the reactive intermediate in the critical alkyl transfer step (13).

It is interesting to note that under identical reaction conditions, the use of a similar C_2 symmetric ligand **11**, prepared according to literature procedures (14), as the catalyst gave much lower ee's (<20%) for the reaction of diethylzinc with benzaldehyde. We conclude therefore that the C_3 symmetric ligand **1** is an effective catalyst in promoting high enantioselective addition of diethylzinc to aromatic aldehydes. The results justify the search for other C_3 symmetric ligands, as

© 1997 NRC Canada

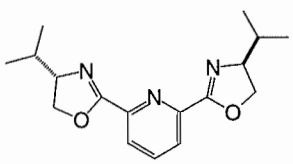
Can. J. Chem. Downloaded from www.nrcresearchpress.com by 88.146.161.215 on 09/08/12
For personal use only.

Table 1. Addition of diethylzinc to aldehydes catalyzed by **1**.

Entry	Substrate	Product	Yield[a] (%)	%ee[b]
1	 **(6)**		92	82 (*R*)
2	 **(7)**		95	72 (*R*)
3	 **(8)**		95	84 (*R*)
4	 **(9)**		90	78 (*R*)
5	 **(10)**		81	90 (*R*)

[a]Purified yield.

[b]The absolute configurations were assigned by NMR analysis of the corresponding Mosher esters.



11

well as further exploration of these ligands in asymmetric synthesis.

Experimental section

General

THF was distilled over sodium – benzophenone ketyl radical prior to use. Hexanes, ethyl acetate, dichloromethane, triethylamine, pyridine, DMF, and acetonitrile were distilled over calcium hydride. 1,2,4-Triazole was recrystallized from CH_2Cl_2–*n*-pentane. Thionyl chloride, phosphoryl chloride, and oxalyl chloride were distilled prior to use. Nuclear magnetic resonance spectra were recorded on Varian Gemini 200 (^{1}H 200 MHz, ^{13}C 50 MHz), XL-200 (^{1}H 200 MHz, ^{13}C 50 MHz), XL-300 (^{1}H 300 MHz, ^{13}C 75 MHz), and Unity 500 (^{1}H 500 MHz, ^{13}C 125 MHz) spectrometers. Chemical shifts are expressed in parts per million (ppm) and the references are the residual proton signals of $CDCl_3$ (δ = 7.24 ppm for ^{1}H, δ = 77.00 ppm for ^{13}C NMR). The following abbreviations were used for NMR spectra: s = singlet; d = doublet; t = triplet; q = quartet; m = multiplet; br = broad. IR spectra were recorded on an Analet FT A25-18 spectrometer between NaCl plates (neat liquids), a film on a NaCl plate, or as a KBr disk. Mass spectra were recorded on a Kratos MS25RFA mass spectrometer.

All the solvents, liquid reagents, and substrates used in asymmetric hydrosilation were degassed via a freeze–thaw cycle under argon prior to use. All asymmetric addition reactions were carried out under an inert atmosphere (argon). The glassware, syringes, needles, and magnetic stirring bars (Teflon coated) were dried at 120°C overnight or longer and were then allowed to cool over Drierite in a glass desiccator. Enantiomeric excess was determined via the (*S*) Mosher's esters of the products using ^{1}H NMR. The corresponding (*R*)-α-methoxy-α-trifluoromethylphenylacetyl chloride was prepared from (*S*)-α-methoxy-α-trifluoromethylphenylacetic acid and thionyl chloride.

Flash column chromatographic separations were performed with Merck Kieselgel 60 (230–400 mesh ASTM) under air pressure. All thin-layer chromatography (TLC) was carried out using precoated cellular plates with Silica Gel 60 F254. The spots were detected by using UV light, or phosphomolybdic acid – Ce_2SO_4 solution followed by charring with a hot-air gun. Gel filtration was performed using Sephadex LH-20.

Low-temperature reactions were carried out in a Dry Ice – acetone bath (−78°C), and in methanol baths cooled by Neslab Cryocool CC-100 II (−20°C to −100°C) and Cryocool PBC-75 II (20°C to −20°C).

N,N,N-Tris[1-((*S*)-1-methoxycarbonyl-2-methylpropyl)]-nitrilotriacetamide (4)

L-Valine methyl ester hydrochloride (7.50 g, 44.7 mmol), nitrilotriacetic acid (2.48 g, 13.0 mmol), 1-(3′-dimethylaminopropyl)-3-ethylcarbodiimide hydrochloride (7.5 g, 39.1 mmol), and DMAP (0.12 g, 0.1 mmol) were dissolved in CH_2Cl_2 (250 mL) in a 500 mL flask under argon. 4-Methylmorpholine (6 mL, 5.52 g, 55 mmol) was added dropwise at room temperature. The reaction mixture was stirred at room temperature for 2 days. To the clear, light-yellow solution, saturated aqueous ammonium chloride solution was added. The organic layer was washed with water (2 × 30 mL) and dried over Na_2SO_4. Removal of solvent gave a reasonably pure product (5.51 g, 80%). IR (film): 1116, 1154, 1210, 1530, 1535, 1543, 1649, 1656, 1742, 2938, 2964, 3263 cm^{-1}; ^{1}H NMR (200 MHz, $CDCl_3$) δ: 7.63 (d, J = 8.9 Hz, 3H), 4.53 (dd, J = 8.9, 5.2 Hz, 3H), 3.72 (s, 9H), 3.44 (d, J = 15.2 Hz, 3H), 3.28 (d, J = 15.2 Hz, 3H), 2.20 (m, 3H), 0.96 (d, J = 6.3 Hz, 9H), 0.92 (d, J = 6.6 Hz, 9H); ^{13}C NMR (50 MHz, $CDCl_3$) δ: 172.1, 169.4, 58.3, 57.6, 52.4, 30.6, 19.7, 18.5; MS *m/z* calcd. for $C_{24}H_{42}O_9N_4$: 530.2952; found: 530.2959; $[\alpha]_D^{20}$ +9.1 (c = 0.0527 g/mL, MeOH).

N,N,N-Tris[2-((*S*)-1-hydroxy-3-methylbutyl)]-nitrilotriacetamide (5)

In a 500 mL, three-neck flask equipped with a condenser, *N,N,N*-tris[1-((*S*)-1-methoxycarbonyl-2-methylpropyl)]nitrilotriacetamide (**4**, 5.40 g, 10.2 mmol) was dissolved in methanol

Can. J. Chem. Downloaded from www.nrcresearchpress.com by 88.146.161.215 on 09/08/12
For personal use only.

© 1997 NRC Canada

Can. J. Chem. Downloaded from www.nrcresearchpress.com by 88.146.161.215 on 09/08/12
For personal use only.

(50 mL) and THF (50 mL) under argon. $NaBH_4$ (3.0 g, 78.9 mmol) was added in small portions to the solution at room temperature. Another portion of $NaBH_4$ (3.0 g, 78.9 mmol) was added to the reaction mixture 2 h later at room temperature. The reaction mixture was stirred at room temperature for 3 h before being quenched with saturated aqueous ammonium chloride solution at 0°C. A clear solution was obtained after HCl (2 N, 30 mL) was added at 0°C. The latter was then neutralized by saturated aqueous K_2CO_3 solution. The organic solvents were removed via rotary evaporator, and the aqueous residue was extracted with ethyl acetate (10 × 40 mL). The combined organic layers were washed with saturated aqueous K_2CO_3 solution (2 mL), water (3 × 10 mL), and then dried over Na_2SO_4. Removal of solvent gave a reasonably pure product (4.33 g, 96%). The product can be purified by flash chromatography on silica gel (ethyl acetate:methanol = 10:1). IR (film): 1076, 1371, 1389, 1466, 1558, 1657, 2934, 2963, 3280, 3294, 3318 cm^{-1}; ^1H NMR (200 MHz, $CDCl_3$) δ: 7.69 (d, 3H), 4.21 (br, 3H), 3.73 (m, 6H), 3.52 (dd, J = 10.1, 8.3 Hz, 3H), 3.39 (d, J = 5.9 Hz, 6H), 1.77 (m, 3H), 0.91 (d, J = 5.1 Hz, 9H), 0.88 (d, J = 5.1 Hz, 9H); ^{13}C NMR (50 MHz, $CDCl_3$) δ: 170.5, 62.9, 59.9, 57.3, 29.9, 20.1, 19.6; MS *m/z* calcd. for $C_{21}H_{40}O_5N_4-(M-H_2O)$: 428.2999; found: 428.3003; $[\alpha]_D^{20}$ −13.7 (c = 0.0648 g/mL, MeOH).

N,N,N-Tris[((4*S*)-isopropyl-2-oxazolin-2-yl)methyl]-amine (1)

1,2,4-Triazole (21.9 g, 317 mmol) was dissolved in acetonitrile (425 mL) in an 1 L flask furnished with a Drierite drying tube. Phosphorus oxychloride (9.7 mL, 15.96 g, 104 mmol) was added at 0°C, followed by triethylamine (50 mL, 36.3 g, 359 mmol) dropwise. The reaction mixture was then stirred at 0°C for 2 h. The mixture was siphonated through a cannula to a sealed sintered glass filter, which was placed in the neck of a 2 L flask, so that the clear filtrate could be added directly to the solution of *N,N,N*-tris[2-((*S*)-1-hydroxy-3-methylbutyl)]nitrilotriacetamide (**5**, 4.07 g, 9.1 mmol) in triethylamine (900 mL) and acetonitrile (100 mL). After the addition was finished, the reaction mixture was stirred another 20 min before saturated aqueous $NaHCO_3$ solution (100 mL) was introduced to the reaction flask. The organic solvents were removed via a rotary evaporator, and the remaining mixture was extracted with CH_2Cl_2 (10 × 50 mL). The combined organic layers were washed with water (3 × 40 mL) and then dried over Na_2SO_4. Removal of solvent gave a reasonably pure product (3.04 g, 85%). The product could be further purified using a gel filtration method (Sephadex LH-20, ethyl acetate). IR (film): 983, 1145, 1194, 1386, 1468, 1672, 2873, 2963, 33.52 cm^{-1}; ^1H NMR (200 MHz, $CDCl_3$) δ: 4.21 (m, 3H), 3.89 (m, 6H), 3.59 (s, 6H), 1.69 (m, 3H), 0.91 (d, J = 6.7 Hz, 9H), 0.83 (d, J = 6.8 Hz, 9H); ^{13}C NMR (125 MHz, $CDCl_3$) δ: 163.9, 72.0, 67.0, 50.3, 32.4, 18.7, 18.1; MS *m/z* calcd. for $C_{21}H_{36}N_4O_3$: 392.2787; found: 392.2785; $[\alpha]_D^{20}$ −73.7 (c = 0.1191 g/mL, CH_2Cl_2).

General procedure for addition of diethylzinc to aldehydes

Benzaldehyde (106 mg, 1.0 mmol) was placed in a 25 mL round-bottom flask furnished with a magnetic stir bar and sealed with a rubber septum under argon. Diethylzinc (2.7 mL, 1.1 M in toluene, 3.0 mmol) was added to this flask at 0°C followed by compound **1** (80 mg, 0.20 mmol) in toluene (1 mL). The reaction mixture was maintained at 0°C for 2 days before quenching with saturated ammonium chloride in aqueous solution.

The reaction mixture was then acidified with HCl (2 N), followed by sodium carbonate (saturated aqueous solution). The mixture was extracted with dichloromethane (3 × 5 mL), and the combined organic layers were dried over Na_2SO_4. After removal of solvent, the crude product was purified via a Kugelröhr apparatus (80°C/5 Torr (1 Torr = 133.3 Pa); 125 mg, 92%). IR (neat): 3400, 3000, 2950, 1500, 1100, 1000, 800 cm^{-1}; ^1H NMR (500 MHz) δ: 7.34 (m, 3H), 7.26 (m, 2H), 4.58 (t, J = 7.0 Hz, 1H), 1.84 (br, 1H), 1.75–1.80 (m, 2H), 0.90 (t, J = 7.0 Hz, 3H); ^{13}C (125 MHz) δ: 144.6, 128.4, 127.5, 126.0, 76.0, 31.9, 10.1; MS (*m/z*): 77 (16.5), 79 (35.2), 92 (13.1), 107 (100.0), 108 (9.1), 136 (14.5, M), 137 (3.0).

1-(2′-Methoxyphenyl)-1-propanol: IR (neat): 753, 1029, 1046, 1089, 1237, 1458, 1464, 1491, 1494, 1588, 1601, 2838, 2936, 2968, 3386 cm^{-1}; ^1H NMR (500 MHz) δ: 7.27 (dd, J = 8.0, 2.0 Hz, 1H), 7.22 (td, J = 7.5, 2.0 Hz, 1H), 6.94 (t, J = 7.5 Hz, 1H), 6.86 (d, J = 8.0 Hz, 1H), 4.76 (t, J = 6.5 Hz, 1H), 3.83 (s, 3H), 1.80 (m, 2H), 0.94 (t, J = 7.5 Hz, 3H); ^{13}C (125 MHz): 156.6, 132.3, 128.2, 127.1, 120.7, 110.5, 72.5, 55.2, 30.1, 10.5; MS (*m/z*): 77 (19.5), 94 (10.0), 107 (58.7), 109 (14.0), 121 (14.0), 137 (100.0), 138 (13.6), 166 (8.9, M).

1-(1′-Naphthyl)-1-propanol: IR (neat): 777, 800, 1029, 1168, 1259, 1458, 1511, 1598, 2875, 2965, 2280 cm^{-1}; ^1H (500 MHz) δ: 7.81 (m, 3H), 7.77 (s, 1H), 7.45 (m, 3H), 4.76 (t, J = 5.0 Hz, 1H), 1.87 (m, 2H), 0.93 (t, J = 8.0 Hz, 3H); ^{13}C (125 MHz) δ: 141.9, 133.2, 132.9, 128.2, 127.9, 127.6, 126.1, 125.7, 124.7, 124.1, 76.1, 31.7, 10.1; MS (*m/z*): 127 (25.6), 128 (39.5), 129 (76.3), 157 (100.0), 158 (15.2), 186 (37.8, M), 187 (5.4).

1-(2′-Naphthyl)-1-propanol: IR (neat): 748, 819, 856, 1018, 1126, 1455, 1463, 2875, 2931, 2965, 3378 cm^{-1}; ^1H (500 MHz) δ: 8.11 (d, J = 8.0 Hz, 1H), 7.86 (d, J = 9.0 Hz, 1H), 7.77 (d, J = 8.0 Hz, 1H), 7.63 (d, J = 7.0 Hz, 1H), 7.48 (m, 3H), 5.39 (dd, J = 7.5, 5.0 Hz, 1H), 2.02 (m, 1H), 1.92 (m, 1H), 1.02 (t, J = 7.5 Hz, 3H); ^{13}C (125 MHz) δ: 140.1, 133.7, 130.3, 128.7, 127.7, 125.8, 125.3, 125.2, 123.1, 122.7, 72.5, 30.9, 10.4; MS (*m/z*): 127 (36.2), 128 (49.2), 129 (100.0), 130 (12.8), 157 (97.5), 158 (14.2), 186 (32.2, M), 187 (4.7).

1-(9′-Phenanthrenyl)-1-propanol: IR (neat): 763, 807, 970, 1046, 1450, 1496, 1654, 2875, 2963, 3301 cm^{-1}; ^1H (500 MHz) δ: 8.74 (dd, J = 8.0, 1.5 Hz, 1H), 8.65 (d, J = 8.0 Hz, 1H), 8.15 (dd, J = 7.5, 1.5 Hz, 1H), 7.89 (s, 1H), 7.88, dd, J = 8.5, 1.5 Hz, 1H), 7.62 (m, 4H), 5.42 (dd, J = 8.0, 5.0 Hz, 1H), 1.96–2.11 (m, 2H), 1.08 (t, J = 7.0 Hz, 3H); ^{13}C (125 MHz): 138.3, 131.4, 130.8, 130.0, 129.7, 128.8, 126.7, 126.6, 126.5, 126.3, 123.9, 123.7, 123.4, 122.4, 72.8, 30.8, 10.5; MS (*m/z*): 177 (21.9), 178 (59.5), 179 (94.2), 180 (13.9), 207 (100.0), 208 (16.7), 236 (32.1, M), 237 (6.1).

Acknowledgement

We thank the Natural Sciences and Engineering Research Council (NSERC) of Canada and le Fonds pour la formation

© 1997 NRC Canada

de chercheurs et l'aide à la recherche (FCAR) of Quebec for financial support.

References

1. J.K. Whitesell. Chem. Rev. **89**, 7 (1989); R.S. Ward. Chem. Soc. Rev. **19**, 1 (1990).
2. (*a*) M.J. Burk and R.L. Harlow. Angew. Chem. Int. Ed. Engl. **29**, 1462 (1990); (*b*) W.A. Nugent and R.L. Harlow. J. Am. Chem. Soc. **116**, 6142 (1994); (*c*) D.D. Le Cloux and W.B. Tolman. J. Am. Chem. Soc. **115**, 1153 (1993); (*d*) C.J. Tokar, P.B. Kettler, and W.B. Tolman. Organometallics, **11**, 2737 (1992); (*e*) D.D. Lecoux, C.J. Tokar, M. Osawa, R.P. Houser, M. Keyes, and W.B. Tolman. Organometallics, **13**, 2855 (1994); (*f*) H. Adolfsson, K. Wärnmark, and C. Moberg. J. Chem. Soc. Chem. Commun. 1054 (1992); 1698 (1992).
3. M.S. Newman and H. Boden. J. Org. Chem. **26**, 2525 (1961).
4. (*a*) W. König and R. Geiger. Chem. Ber. **103**, 788 (1970); (*b*) G.C. Windridge and E.C. Jorgensen. J. Am. Chem. Soc. **93**, 6318 (1971); (*c*) H.R. Bosshard, I. Schechter, and A. Berger. Helv. Chim. Acta, **56**, 717 (1973).
5. J.D. Prugh and A.A. Deana. Tetrahedron Lett. **29**, 37 (1988).
6. C. Sund, J. Ylikoski, and M. Kwiatkowski. Synthesis, 853 (1987).
7. H. Nishiyama, H. Sakaguchi, T. Nakamura, M. Horikata, M. Kondo, and K. Itoh. Organometallics, **8**, 846 (1989).
8. T. Fujisawa, T. Mori, S. Tsuge, and T. Sato. Tetrahedron Lett. **24**, 1543 (1989).
9. T. Fujisawa and T. Sato. Org. Synth. **66**, 121 (1988).
10. J.B. Hendrickson and M.S. Hussoin. J. Org. Chem. **52**, 4137 (1987).
11. (*a*) K. Beijer and E. Nyström. Anal. Biochem. **48**, 1 (1972); (*b*) T. Chojnacki, W. Jankowski, and T. Mankowski. Anal. Biochem. **69**, 114 (1975); (*c*) J. Ellingboe, E. Nystrom, and J. Sjovall. J. Lipid. Res. **11**, 266 (1970).
12. K. Kawasaki, S. Tsumura, and T. Katsuki. Synlett, 1245 (1995).
13. M. Kitamura, S. Okada, S. Suga, and R. Noyori. J. Am. Chem. Soc. **111**, 4028 (1989); R. Noyori. Asymmetric catalysis in organic synthesis. John Wiley & Sons, Inc., New York. 1994.
14. H. Nishiyama, S. Yamaguchi, M. Kondo, and K. Itoh. J. Org. Chem. **57**, 4306 (1992).

Can. J. Chem. Downloaded from www.nrcresearchpress.com by 88.146.161.215 on 09/08/12
For personal use only.

© 1997 NRC Canada

Isolation, structure, and synthesis of chenopodanol and the absolute configuration of chenopodene and chenopodanol

Motoo Tori, Tomonobu Hamaguchi, Mamiko Aoki, Masakazu Sono, and Yoshinori Asakawa

Abstract: (−)-Chenopodanol (**2**) has been isolated from the liverwort *Marchantia chenopoda* and its structure determined by spectroscopic techniques as well as by total synthesis. Chenopodene (**1**) has also been synthesized in an optically active form, resulting in revision of the originally assigned absolute configuration.

Key words: chenopodanol, chenopodene, liverwort, *Marchantia chenopoda*, sesquiterpene.

Résumé : On a isolé du (−)-chénopodanol (**2**) de l'hépatique trilobée *Marchantia chenopoda*; on en a déterminé la structure par des techniques spectroscopiques ainsi que par une synthèse totale. On a aussi synthétisé le chénopodène (**1**) sous forme optiquement active; il en résulte que l'on doit réviser la configuration absolue qui lui avait été originalement attribuée.

Mots clés : chénopodanol, chénopodène, hépatique trilobée, *Marchantia chenopoda*, sesquiterpène.

[Traduit par la rédaction]

Introduction

The absolute configuration of terpenoids isolated from liverworts is very interesting and important (1). In connection with our synthetic studies on liverwort terpenoids in optically active form, we undertook the synthesis of chenopodene (**1**), whose structure, including the absolute configuration, has already been reported (2). At the same time, we further searched for new compounds in the extract of *Marchantia chenopoda* collected in Venezuela and found (−)-chenopodanol (**2**) as a minor constituent. Because **2** is not chemically related to **1**, we decided to prepare both **1** and **2** in optically active forms. We are currently engaged in synthetic studies using the chiral Michael reaction product (+)-**3** to prepare several liverwort sesquiterpenoids (3). This kind of substance could be prepared through the intermediate **4** by introduction of a cyclopropane ring *cis* to the methyl group as shown in Scheme 1. We now describe the details of structure elucidation and the synthesis of **1** and **2**.

Results and discussion

Isolation and structure of chenopodanol

A slightly more polar fraction than (+)-chenopodene (**1**) was further separated by HPLC to afford (−)-chenopodanol (**2**) (see Experimental). The molecular formula of **2** was determined by HRMS to be $C_{15}H_{26}O$, and its IR spectrum indicated the presence of a hydroxyl group (3400 cm^{-1}), which was supported by the ^{13}C NMR (δ 68.5). The presence of a cyclopropane ring and a trisubstituted double bond was indicated by the ^1H NMR spectrum (δ: 5.12 (1H, t, J = 6.8 Hz), 0.44 (1H, ddd, J = 7.4, 7.4, 4.4 Hz), 0.34 (1H, ddd, J = 4.4, 4.4, 4.4 Hz)). The chenopodane skeleton was deduced by HMBC along with the HSQC spectra as shown in Fig. 1. The stereochemistry was inferred by the NOESY spectrum as shown in Fig. 2. Thus the structure of chenopodanol was determined as depicted in formula **2**. The isolation of a compound having the chenopodane skeleton is the second example from nature (2). However, the absolute configuration could not be verified due to the minute quantity of the compound. Because the absolute configuration of (+)-chenopodene (**1**) was deduced by the CD spectrum as reported (2), **2** was temporarily assigned to have the same configuration.

Synthesis of chenopodanol and chenopodene

Chiral keto ester (+)-**3** was easily prepared by the Michael reaction between the imine, prepared from 2-methylcyclohexanone and (*S*)-(−)-1-phenylethylamine and methyl acrylate (96% ee) (4). The absolute configuration was already determined by the original workers by conversion into the known substance (4) and also by our independent work (3). Ketone (+)-**3** was reduced and the primary alcohol **5** was selectively protected by TBDMS to afford a monoprotected alcohol **6**. The alcohol was dehydrated to give olefin **7**, which was oxidized by PDC and *t*BuOOH to afford enone **4**. Attempted cyclopropanation using trimethylsulfoxonium iodide and dimsyl anion (5) failed due to deprotection of the TBDMS group, followed by etherification to the α,β-unsaturated double bond. Methylation (MeLi) and Simmons–Smith cyclopropanation (6) resulted mainly in dehydration of the tertiary hydroxyl group. Therefore, enone **4** was first reduced and the isomeric

Received October 23, 1996.

This paper is dedicated to Professor William A. Ayer on the occasion of his 65th birthday.

M. Tori,[1] T. Hamaguchi, M. Aoki, M. Sono, and Y. Asakawa. Faculty of Pharmaceutical Sciences, Tokushima Bunri University, Yamashiro cho, Tokushima 770, Japan.

[1] Author to whom correspondence may be addressed. Telephone: +81-886-22-9611, ext. 5631. Fax: +81-886-55-3051. E-mail: tori@mxs.meshnet.or.jp

© 1997 NRC Canada

Can. J. Chem. Downloaded from www.nrcresearchpress.com by 88.146.161.215 on 09/08/12
For personal use only.

Scheme 1.

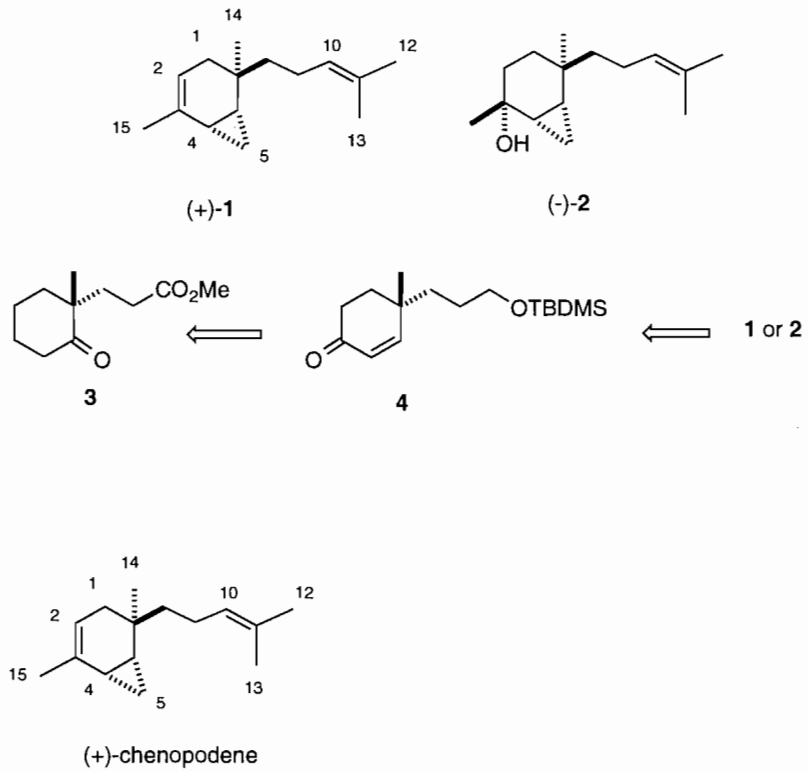


Fig. 1. HMBC correlations for (−)-chenopodanol (**2**).

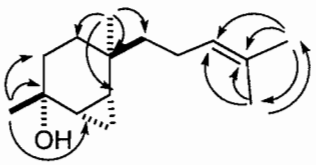
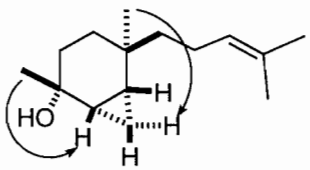
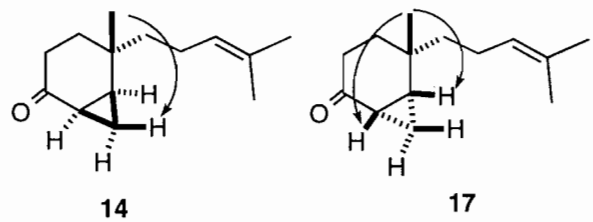


Fig. 2. NOEs detected for (−)-chenopodanol (**2**).



alcohols were separated to give **8** and **9**, although the stereochemistry was not clear at this stage. Simmons–Smith cyclopropanation (6) of alcohols **8** and **9** occurred smoothly to give a sole product, **10** and **11**, respectively, each of which must be a *cis* product, considering the cyclopropane and hydroxyl groups from the mechanistic standpoint (Scheme 2) (7). They were further oxidized by PDC to give the ketones **12** and **15**, respectively. The side chain was formed by a three-step conversion ((*i*) TBAF, (*ii*) PDC, (*iii*) Wittig) to afford **14** and **17**. The stereochemical assignment of the resulting ketones **14** and **17** was determined by the CD spectra as well as NOESY experiments (Fig. 3.). In the case of the α,β-cyclopropyl ketones, the expected Cotton effect is opposite to those for normal ketones as discussed by Djerassi et al. (8). Ketone **14**

Fig. 3. NOEs for ketones **14** and **17**.



14 **17**

showed a positive Cotton effect, while ketone **17** showed a negative effect. Therefore, the stereochemistries were assigned as depicted in Scheme 3.

When ketone **14** was methylated with MeLi, the major product was (+)-**18**, while the desired chenopodanol (**2**) was the minor one. The stereochemistry for the alkylation of the cycloalkanone having a cyclopropane ring in its α,β-position has been discussed by Mash et al. (9). Thus there was poor selectivity for the alkylation of **14** or **17**. The spectral data for product **2** were completely identical with those of the natural product. However, the specific rotation of the synthetic **2** was $[\alpha]_D$ +56.0, while that of the natural product was $[\alpha]_D$ −59.1. Thus the synthetic **2** was the enantiomer and the absolute configuration of the natural chenopodanol ((−)-**2**) must be as depicted in Scheme 1.

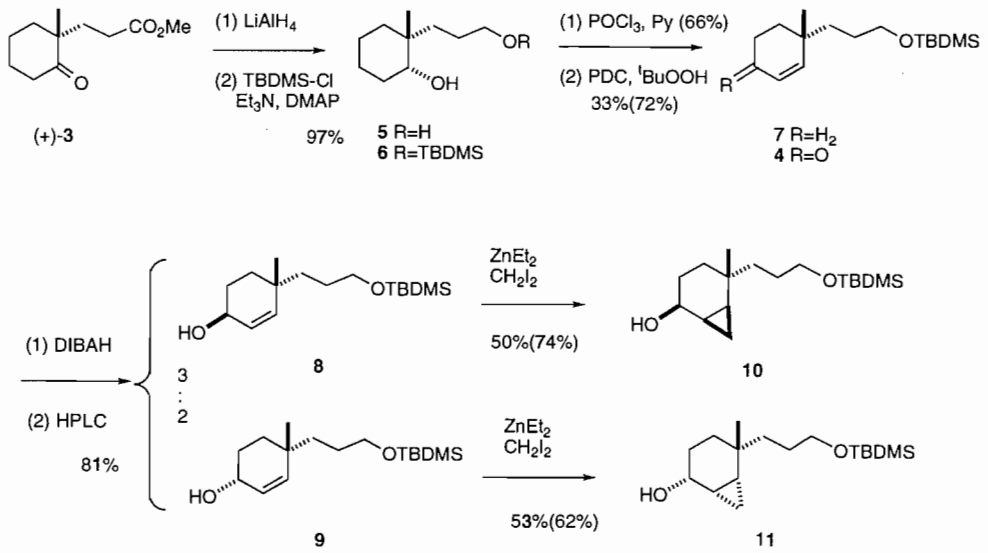
Ketone **17** was similarly methylated to afford **19** and **20**, neither of which was identical to chenopodanol. The stereochemistry of these products was determined by the NOESY spectra.

Compound (+)-**18** was dehydrated by $SOCl_2$ to afford chenopodene (−)-(**1**), which showed the specific rotation $[\alpha]_D$

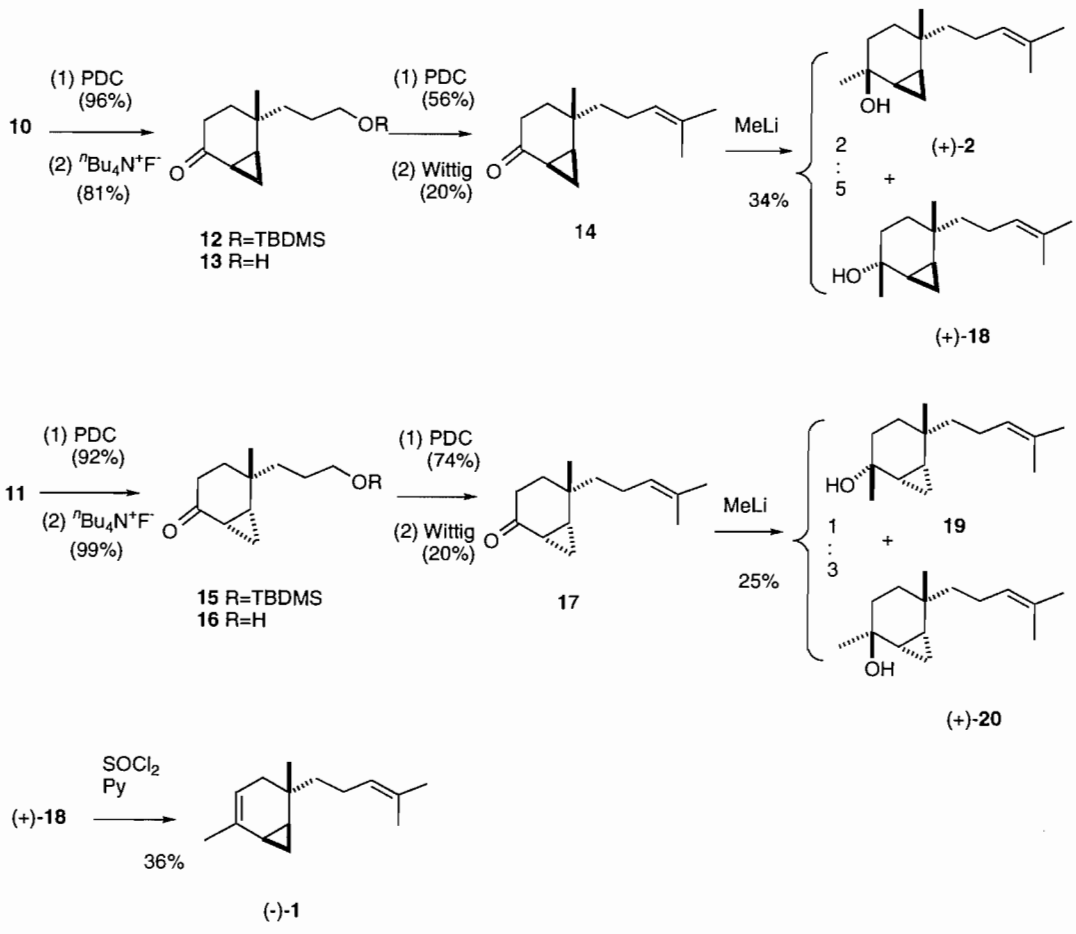
Can. J. Chem. Downloaded from www.nrcresearchpress.com by 88.146.161.215 on 09/08/12
For personal use only.

© 1997 NRC Canada

Scheme 2.



Scheme 3.



-31.0 (lit. $[\alpha]_D(2)$ +32.0). These results established the absolute configuration for both chenopodanol and chenopodene (Scheme 1). The absolute configuration of chenopodene ((+)-**1**) was originally deduced by the CD spectrum to be the enantiomer (2). This was based on the empirical rule proposed by Itô et al. (10). However, this rule was highly dependent upon the molecular conformation and, as pointed out in the literature (10), there is an exception. This must be one of the ambiguous cases for this rule. In such a case, the synthesis is really necessary.

© 1997 NRC Canada

Can. J. Chem. Downloaded from www.nrcresearchpress.com by 88.146.161.215 on 09/08/12
For personal use only.

Can. J. Chem. Downloaded from www.nrcresearchpress.com by 88.146.161.215 on 09/08/12
For personal use only.

Experimental

General

IR spectra were measured on a Jasco FTIR 500 spectrophotometer. ^1H and ^{13}C NMR spectra were recorded on a Varian Unity 600, a JEOL JNM GX-400, a Varian Unity 200, or a Gemini 200 spectrometer. The solvent used for NMR spectra was $CDCl_3$ unless otherwise stated. Mass spectra were measured on a JEOL JMS HX-100 or a JEOL AX-500 spectrometer. The specific rotation and the CD spectra were taken on a JASCO DIP-140 polarimeter and a JASCO J- 500 spectrometer, respectively. Chemcopak Nucleosil 50-5 (10 × 250 mm), (4.6 × 250 mm), and Develosil 60-10 (20 × 250 mm) columns were used for HPLC (JASCO pump system). Silica gel 60 for column chromatography was purchased from Merck.

Isolation of chenopodanol

The crude ether extract of *M. chenopoda*, collected in Venezuela, was separated by Sephadex LH-20 ($CHCl_3$–MeOH) followed by silica gel column chromatography (hexane–EtOAc) to afford chenopodene (**1**) as described in ref. 2. A slightly more polar fraction (101 mg) than **1** was further purified by silica gel column chromatography (hexane-EtOAc) to give a mixture of several compounds (43 mg). This fraction was then separated by HPLC (Nucleosil 50-5, 10 × 250 mm, hexane–EtOAc 9:1, 3.5 mL/min) to give marchantin P (2) and impure chenopodanol (9.6 mg), which was again purified by HPLC (Nucleosil 50-5, 4.6 × 250 mm, hexane–EtOAc 95/5, 3.5 mL/min) to isolate pure (−)-chenopodanol (**2**) (1.0 mg).

(−)-Chenopodanol (2): oil; $[\alpha]_D^{20}$ −59.1 (*c* 0.1, $CHCl_3$); IR: 3400 cm^{-1}; ^1H NMR (600 MHz) δ: 0.34 (1H, ddd, *J* = 4.4, 4.4, 4.4 Hz, H-5), 0.44 (1H, ddd, *J* = 7.4, 7.4, 4.4 Hz, H-5), 0.92 (1H, m, H-6), 0.94 (3H, s, H-14), 1.05 (1H, ddd, *J* = 11, 8, 2.3 Hz, H-1 or H-2), 1.10 (1H, ddd, *J* = 7.4, 7.4, 4.4 Hz, H-4), 1.20 (1H, m, H-1 or H-2), 1.27 (1H, m, H-1 or H-2), 1.33 (1H, m, H-8b), 1.35 (1H, m, H-1 or H-2), 1.41 (3H, s, H-15), 1.43 (1H, m, H-8a), 1.62 (3H, s, H-12), 1.69 (3H, s, H-13), 1.98 (2H, m, H-9), 5.12 (1H, t, *J* = 6.8 Hz, H-10); ^{13}C NMR (150 MHz) δ: 5.1 (C-5), 17.6 (C-12), 22.7 (C-9), 24.4 (C-4), 25.1 (C-6), 25.7 (C-13), 26.7 (C-14), 30.0 (C-7), 30.1 (C-2 or C-1), 31.6 (C-15), 33.2 (C-1 or C-2), 42.9 (C-8), 68.5 (C-3), 125.0 (C-10), 131.2 (C-11); MS *m/z*: 222 $(M)^+$, 207, 204, 189, 179, 161, 151, 135, 121, 107, 93 (base), 81, 69, 55; HRMS *m/z* calcd. for $C_{15}H_{26}O$ 222.1944; found: 222.1955.

Preparation of diol 5

A solution of keto ester **3** (9.0 g, 37.5 mmol) in dry ether (100 mL) was added slowly to a stirred suspension of $LiAlH_4$ (4.1 g, 0.107 mol) in dry ether (300 mL), and the mixture was stirred at room temperature for 3 h. Ethyl acetate (40 mL), H_2O (4 mL), 15% NaOH solution (4 mL), and H_2O (12.0 mL) were added successively, and filtration followed by evaporation afforded diol **5** (7.8 g, quant.); oil; FTIR: 3350 cm^{-1}; ^1H NMR (200 MHz, $CDCl_3$) δ: 0.77 (s), 0.83 (s), 1.0–1.8 (m), 2.80 (br s), 3.3–3.4 (m), 3.5–3.6 (m); MS (CI) *m/z*: 173 $(M + H)^+$, 155, 137, 129, 109, 95 (base), 81, 69, 55; CI-HRMS *m/z* calcd. for $C_{10}H_{21}O_2$: 173.1542; found: 173.1538.

Preparation of monosilyl ether 6

A mixture of diol **5** (4.54 g, 27.48 mmol), triethylamine (5.9 mL, 42.3 mmol), 4-DMAP (0.43 g), and TBDMSCl (6.3 g, 41.8 mmol) in CH_2Cl_2 (180 mL) was stirred at 0°C for 10 min and was kept at room temperature overnight. Water was added and the mixture was extracted with CH_2Cl_2. The organic phase was washed with water, HCl (1.0 M), saturated $NaHCO_3$ solution and brine, dried ($MgSO_4$), and evaporated to give a residue. The residue was purified by silica gel column chromatography (hexane–EtOAc, 0-20%) to afford monosilyl ether **6** (7.33 g, two steps, 97%); oil; FTIR: 3460 cm^{-1}; ^1H NMR (200 MHz) δ: 0.09 (6H, s), 0.90 (12H, s), 1.2–1.8 (12H, m), 1.65 (1H, br s), 3.4 (1H, m), 3.5–3.7 (2H, m); MS (CI) *m/z*: 287 $(M + H)^+$, 269, 253, 153, 137 (base), 109, 95, 81; CI-HRMS *m/z* calcd. for $C_{16}H_{35}O_2Si$: 287.2406; found: 287.2408.

Preparation of olefin 7

A solution of mono silyl ether **6** (18.7 g, 65.38 mmol) in pyridine (150 mL) was treated with $POCl_3$ (20.0 mL, 0.22 mol) at 0°C in the presence of 4A molecular sieves (900 mg). The mixture was stirred at room temperature overnight. Saturated $NaHCO_3$ solution was added and the mixture was extracted with ether. The organic phase was washed with water, dried ($MgSO_4$), and evaporated to give a residue, which was purified by silica gel column chromatography (hexane–EtOAc, 0–20%) to afford olefin **7** (11.5 g, 66%); oil; $[\alpha]_D^{21}$ −9.7 (*c* 0.94, $CHCl_3$); FTIR: 1650, 1460, 780 cm^{-1}; ^1H NMR (200 MHz) δ: 0.05 (6H, s), 0.89 (9H, s), 0.92 (3H, s), 1.2–2.0 (10H, m), 3.57 (2H, t, *J* = 6.6 Hz), 5.39 (1H, br dt, *J* = 10.0, 1.8 Hz), 5.58 (1H, dt, *J* = 10.0, 3.6 Hz); ^{13}C NMR (50 MHz) δ: −5.22 (q × 2), 19.3 (t), 25.2 (t), 26.0 (q × 3), 27.3 (q), 27.6 (t), 29.7 (s), 33.9 (s), 34.8 (t), 38.7 (t), 64.1 (t), 125.3 (d), 136.8 (d); MS (CI) *m/z*: 269 $(M + H)^+$, 267, 253, 211 (base), 137, 135, 109, 95, 81; CI-HRMS *m/z* calcd. for $C_{16}H_{33}OSi$: 269.2301; found: 269.2272.

A solution of the olefin **7** (11.4 g, 42.5 mmol) in PhH (800 mL) was treated with PDC (23.2 g, 63.2 mmol), Celite (89.0 g), and 70% *t*BuOOH (27 mL) at 0°C. The mixture was stirred at room temperature overnight. The mixture was filtered under reduced pressure and the solvent was almost evaporated. The residue was extracted with ether, and the ethereal solution was washed with 10% KOH solution. The residue was purified by silica gel column chromatography (hexane–EtOAc, 0–20%) to afford enone **4** (4.0 g, 33%, 72% based on consumed **7**) and the recovered olefin **7** (6.1 g).

4: oil; $[\alpha]_D^{22}$ −22.2 (*c* 0.90, $CHCl_3$); CD (EtOH) [θ]: −290 (311 nm), −3940 (245 nm); FTIR: 1690, 1620 cm^{-1}; ^1H NMR (200 MHz) δ: 0.03 (6H, s), 0.88 (9H, s), 1.13 (3H, s), 1.4–1.6 (4H, m), 1.7–1.8 (1H, m), 1.95 (1H, m), 2.35–2.45 (2H, m), 3.60 (2H, dd, *J* = 5.8, 4.8 Hz), 5.86 (1H, d, *J* = 10.2 Hz), 6.63 (1H, d, *J* = 10.2 Hz); ^{13}C NMR (50 MHz) δ: −5.4 (q × 2), 18.2 (s), 24.8 (q), 25.9 (q × 3), 27.5 (t), 33.4 (t), 34.1 (t), 35.2 (s), 37.0 (t), 63.2 (t), 127.3 (d), 159.2 (d), 199.5 (s); MS (CI) *m/z*: 283 $(M + H)^+$, 267, 225 (base), 165, 151, 133, 123, 105; CI-HRMS *m/z* calcd. for $C_{16}H_{31}O_2Si$: 283.2093; found: 283.2086.

Reduction of ketone 4

A solution of ketone **4** (1.5 g, 5.32 mmol) in THF (120 mL) was treated with DIBAH (1.0 M in toluene, 16.5 mL, 16.5 mmol) at room temperature for 4 h. Water was added and THF

© 1997 NRC Canada

Can. J. Chem. Downloaded from www.nrcresearchpress.com by 88.146.161.215 on 09/08/12
For personal use only.

was evaporated. The residue was extracted with ether and the ethereal solution was washed with water, dried ($MgSO_4$), and evaporated. The residue was purified by silica gel column chromatography (hexane–EtOAc, 0–50%) and HPLC (hexane–EtOAc 85:15, Nucleosil 50-5, 10 × 250 mm) to afford alcohols **8** (723 mg, 48%) and **9** (494 mg, 33%).

8: oil; $[\alpha]_D^{21}$ −42.3 (*c*, 1.0, $CHCl_3$); FTIR: 3350 cm^{-1}; ^1H NMR (200 MHz) δ: 0.04 (6H, s), 0.88 (9H, s), 0.99 (3H, s), 1.2–2.0 (8H, m), 3.56 (2H, t, *J* = 6.5 Hz), 4.15 (1H, m), 5.48 (1H, d, *J* = 10.6 Hz), 5.61 (1H, dd, *J* = 10.6, 2.1 Hz); ^{13}C NMR (50 MHz) δ: −5.2 (q × 2), 18.4 (s), 26.0 (q × 3), 26.7 (q), 27.5 (t), 29.3 (t), 31.5 (t), 34.4 (s), 38.2 (t), 63.8 (t), 66.6 (d), 128.6 (d), 139.2 (d); MS (CI) *m/z*: 285 $(M + H)^+$, 283, 267, 251, 227, 211, 171, 151, 135 (base); CI-HRMS *m/z* calcd. for $C_{16}H_{33}O_2Si$: 285.2250; found: 285.2245.

9: oil; $[\alpha]_D^{21}$ +18.9 (*c* 1.0, $CHCl_3$); FTIR: 3350 cm^{-1}; ^1H NMR (200 MHz) δ: 0.04 (6H, s), 0.89 (9H, s), 0.93 (3H, s), 1.2–2.0 (8H, m), 3.57 (2H, t, *J* = 6.1 Hz), 4.15 (1H, m), 5.53 (1H, d, *J* = 10.0 Hz), 5.66 (1H, dd, *J* = 10.0, 3.4 Hz); ^{13}C NMR (50 MHz) δ: −5.2 (q × 2), 18.4 (s), 26.0 (q × 3), 26.2 (q), 27.7 (t), 28.7 (t), 30.6 (t), 34.3 (s), 38.0 (t), 63.9 (t), 65.3 (d), 127.5 (d), 140.0 (d); MS (CI) *m/z*: 285 $(M+H)^+$, 283, 267, 251, 227, 209, 171, 151, 135 (base); CI-HRMS *m/z* calcd. for $C_{16}H_{33}O_2Si$ $(M + H)^+$: 285.2250; found: 285.2223; *m/z* calcd. for $C_{16}H_{31}O_2Si$ $(M - H)^+$: 283.2094; found: 283.2101.

Cyclopropanation of alcohol 8

Diethylzinc (1.0 M in hexane, 6.5 mL, 6.5 mmol) was added to a solution of the alcohol **8** (723 mg, 2.55 mmol) in CH_2Cl_2 (68 mL) at 0°C under Ar atmosphere. Diiodomethane (0.4 mL, 4.97 mmol) was slowly added, and the mixture was stirred for 30 min at this temperature and at room temperature for 5 h. Water was added and the mixture was extracted with CH_2Cl_2. The organic phase was washed with water, 10% H_2SO_4, and brine, dried ($MgSO_4$), and evaporated. The residue was purified by silica gel column chromatography (hexane–EtOAc, 0–30%) to afford **10** (382 mg, 50%, 74% based on consumed **8**) and the recovered **8** (230 mg).

10: oil; $[\alpha]_D^{21}$ −1.30 (*c* 1.3, $CHCl_3$); FTIR: 3400 cm^{-1}; ^1H NMR (200 MHz) δ: 0.05 (6H, s), 0.3–0.5 (2H, m), 0.90 (12H, s), 0.8–1.7 (10H, m), 3.58 (2H, t, *J* = 6.5 Hz), 4.15 (1H, m); ^{13}C NMR (50 MHz) δ: −5.3 (q × 2), 3.5 (t), 18.4 (s), 18.6 (d), 24.5 (d), 26.0 (q × 3), 26.1 (q), 26.4 (t), 27.6 (t), 29.5 (s), 32.1 (t), 39.8 (t), 63.9 (t), 66.8 (d); MS (CI) *m/z*: 299 $(M + H)^+$, 297, 281, 265, 241, 223, 167, 149 (base); CI-HRMS *m/z* calcd. for $C_{17}H_{35}O_2Si$ $(M + H)^+$: 299.2407; found: 299.2374; *m/z* calcd. for $C_{17}H_{33}O_2Si$ $(M - H)^+$: 297.2250; found: 297.2268.

Cyclopropanation of alcohol 9

Alcohol **9** (889 mg, 3.13 mmol) was similarly treated with Et_2Zn (8 mL, 8 mmol) and CH_2I_2 (0.55 mL, 1.09 mmol) in CH_2Cl_2 (85 mL). Work-up and chromatography (hexane–EtOAc, 0–30%) afforded **11** (495 mg, 53%, 62% based on consumed **9**) and the recovered **9** (131 mg).

11: oil; $[\alpha]_D^{21}$ +26.1 (*c* 0.88, $CHCl_3$); FTIR: 3400 cm^{-1}; ^1H NMR (200 MHz, $CDCl_3$) δ: 0.05 (6H, s), 0.3–0.6 (2H, m), 0.89 (9H, s), 0.8–1.7 (8H, m), 1.02 (3H, s), 3.60 (2H, t, *J* = 6.6 Hz), 4.23 (1H, ddd, *J* = 6.0, 5.5, 5.8 Hz); ^{13}C NMR (50 MHz) δ: −5.2 (q × 2), 3.5 (t), 18.4 (s), 18.5 (d), 23.8 (d), 26.0 (q × 3), 26.7 (t), 27.6 (t), 27.8 (q), 29.6 (s), 32.4 (t), 38.0 (t), 64.1 (t), 66.2 (d); MS (CI) *m/z*: 299 $(M + H)^+$, 297, 281, 265, 241, 223, 167, 149 (base); CI-HRMS *m/z* calcd. for $C_{17}H_{35}O_2Si$ $(M + H)^+$: 299.2407; found: 299.2377; *m/z* calcd. for $C_{17}H_{33}O_2Si$ $(M - H)^+$: 297.2250; found: 297.2254.

Oxidation of alcohol 10

A solution of alcohol **10** (382 mg, 1.28 mmol) in CH_2Cl_2 (40 mL) was treated with PDC (975.0 mg, 2.66 mmol) and 4A molecular sieves (318.0 mg) for 12 h at room temperature. The mixture was filtered through Celite and passed through a short column of silica gel (elution with ether). Evaporation of the solvents afforded a ketone **12** (363 mg, 96%); oil; $[\alpha]_D^{21}$ −1.85 (*c* 1.0, $CHCl_3$); CD ($CHCl_3$) [θ]: +2020 (298 nm); FTIR: 1700 cm^{-1}; ^1H NMR (200 MHz) δ: 0.04 (6H, s), 0.7–1.6 (9H, m), 0.90 (9H, s), 1.06 (3H, s), 1.85 (1H, m), 2.1–2.2 (2H, m), 3.59 (2H, t, *J* = 5.9 Hz); ^{13}C NMR (50 MHz) δ: −5.2 (q × 2), 10.0 (t), 18.3 (s), 26.0 (q × 3), 26.5 (q), 26.6 (d), 27.3 (t), 28.1 (t), 29.8 (d), 31.0 (s), 32.7 (t), 35.3 (t), 63.6 (t), 209.4 (s); MS (CI) *m/z*: 297 $(M + H)^+$, 281, 239 (base), 193, 165, 147; CI-HRMS *m/z* calcd. for $C_{17}H_{33}O_2Si$: 297.2250; found: 297.2245.

Oxidation of alcohol 11

Alcohol **11** (195 mg, 0.65 mmol) was treated with PDC (517.0 mg, 1.41 mmol) and molecular sieves (168 mg) in CH_2Cl_2 (20 mL) for 12 h at room temperature. Work-up as above afforded a ketone **15** (178 mg, 92%); oil; $[\alpha]_D^{21}$ −18.0 (*c* 1.3, $CHCl_3$); CD ($CHCl_3$) [θ]: −2340 (297 nm); FTIR: 1700 cm^{-1}; ^1H NMR (200 MHz) δ: 0.04 (6H, s), 0.88 (9H, s), 1.06 (3H, s), 1.0–1.8 (10H, m), 2.19 (2H, q, *J* = 5.1 Hz), 3.60 (2H, t, *J* = 6.3 Hz); ^{13}C NMR (50 MHz) δ: −5.3 (q × 2), 10.5 (t), 18.3 (s), 24.6 (q), 25.9 (q × 3), 26.1 (d), 27.3 (t), 28.7 (t), 29.0 (d), 30.9 (s), 32.9 (t), 39.1 (t), 63.7 (t), 209.6 (s); MS (CI) *m/z*: 297 $(M + H)^+$, 281, 239 (base), 193, 165, 147; CI-HRMS *m/z* calcd. for $C_{17}H_{33}O_2Si$: 297.2250; found: 297.2242.

Deprotection of silyl ether 12

A solution of silyl ether **12** (363 mg, 0.99 mmol) in THF (5 mL) was treated with TBAF (1.0 mol/L, 1.5 mL, 1.5 mmol) at 0°C for 4 h. Water was added and the mixture was extracted with ether. The organic phase was washed with water and brine, dried ($MgSO_4$), and evaporated. The residue was purified by silica gel column chromatography (hexane–EtOAc, 0–100%) to afford alcohol **13** (181 mg, 81%); oil; $[\alpha]_D^{21}$ +9.4 (*c* 1.2, $CHCl_3$); CD ($CHCl_3$) [θ]: +1820 (297 nm); FTIR: 3440, 1690 cm^{-1}; ^1H NMR (200 MHz) δ: 1.06 (3H, s), 1.2–2.2 (12H, m), 3.63 (2H, t, *J* = 6.0 Hz); ^{13}C NMR (50 MHz) δ: 10.1 (t), 26.5 (q), 26.6 (d), 27.1 (t), 28.1 (t), 29.8 (d), 31.0 (s), 32.7 (t), 35.4 (t), 63.3 (t), 209.6 (s); MS (CI) *m/z*: 183 $((M + H)^+$ (base), 165, 147, 137, 123, 111, 95; CI-HRMS *m/z* calcd. for $C_{11}H_{19}O_2$: 183.1385; found: 183.1373.

Deprotection of silyl ether 15

Silyl ether **15** (178 mg, 0.60 mmol) in THF (2 mL) was similarly treated with TBAF (1.0 M, 0.71 mL, 0.71 mmol) and work-up afforded alcohol **16** (108 mg, 99%); oil; $[\alpha]_D^{21}$ −23.9 (*c* 1.0, $CHCl_3$); CD ($CHCl_3$) [θ]: −2040 (296 nm); FTIR: 3450, 1690 cm^{-1}; ^1H NMR (200 MHz) δ: 1.10 (3H, s), 1.0–1.8 (10H, m), 2.22 (2H, m), 3.65 (2H, t, *J* = 6.4 Hz); ^{13}C NMR

© 1997 NRC Canada

Can. J. Chem. Downloaded from www.nrcresearchpress.com by 88.146.161.215 on 09/08/12
For personal use only.

(50 MHz) δ: 10.5 (t), 24.5 (q), 26.0 (d), 27.0 (t), 28.4 (t), 29.0 (d), 30.8 (s), 32.7 (t), 39.0 (t), 63.0 (t), 210.0 (s); MS (CI) *m/z*: 183 ((M + H)$^+$ (base), 165, 147, 123, 111, 95, 81; CI-HRMS *m/z* calcd. for $C_{11}H_{19}O_2$: 183.1385; found: 183.1385.

Preparation of ketone 14

A solution of alcohol **13** (181 mg, 0.99 mmol) in CH_2Cl_2 (20 mL) was treated with PDC (703.0 mg, 1.91 mmol) and 4A molecular sieves (120 mg) at room temperature for 2 h. The mixture was filtered through Celite and passed through a short column of silica gel (elution with ether) to afford the aldehyde (101 mg, 56%); oil; $[\alpha]_D^{21}$ +7.0 (*c* 1.0, $CHCl_3$); CD ($CHCl_3$) [θ]: +1870 (297 nm); FTIR: 1720, 1690 cm^{-1}; ^{1}H NMR (200 MHz) δ: 1.08 (3H, s), 1.1 (1H, m), 1.29 (1H, td, *J* = 5.5, 4.6 Hz), 1.4–1.6 (3H, m), 1.7–1.9 (3H, m), 2.1–2.2 (2H, m), 2.45–2.60 (2H, m), 9.81 (1H, t, *J* = 1.6 Hz); ^{13}C NMR (50 MHz) δ: 9.7 (t), 26.1 (q), 26.4 (d), 28.0 (t), 29.0 (d), 30.6 (s), 30.7 (t), 32.3 (t), 38.6 (t), 201.7 (d), 208.5 (s); MS (EI) *m/z*: 180 (M$^+$), 165, 137, 123 (base), 107, 95, 81; CI-HRMS *m/z* calcd. for $C_{11}H_{16}O_2$: 180.1150; found: 180.1148.

Butyllithium (1.69 M, 1.0 mL, 1.69 mmol) was added to a suspension of isopropyltriphenylphosphonium iodide (730 mg, 1.69 mmol) in ether (25 mL) at room temperature, and the mixture was stirred for 1 h. A solution of the aldehyde (101 mg, 0.56 mmol) in ether (3 mL) was added, and the mixture was stirred for 50 min. Water was added and the mixture was extracted with ether. The organic phase was washed with brine, dried ($MgSO_4$), and evaporated. The residue was purified by silica gel column chromatography (hexane–EtOAc, 0-100%) to afford olefin **14** (23.2 mg, 20.1%) and the recovered aldehyde (39.7 mg).

14: oil; $[\alpha]_D^{22}$ −5.0 (*c* 1.0, $CHCl_3$); CD ($CHCl_3$) [θ]: +1550 (304 nm); FTIR: 1700 cm^{-1}; ^{1}H NMR (200 MHz) δ: 1.09 (3H, s), 1.09 (1H, m), 1.28 (1H, m), 1.4–1.6 (5H, m), 1.61 (3H, s), 1.68 (3H, s), 1.80 (1H, m), 1.96–2.05 (2H, m), 2.14–2.19 (2H, m), 5.11 (1H, tsept., *J* = 7.0, 1.4 Hz); ^{13}C NMR (50 MHz) δ: 10.0 (t), 17.6 (q), 22.4 (t), 25.7 (q), 26.4 (q), 26.6 (d), 28.1 (t), 29.8 (d), 31.2 (s), 32.7 (t), 39.4 (t), 124.3 (d), 131.6 (s), 209.6 (s); MS (EI) *m/z*: 206 (M$^+$), 191, 163, 149, 137, 123 (base), 109, 95, 81; EI-HRMS *m/z* calcd. for $C_{14}H_{22}O$: 206.1671; found: 206.1653.

Preparation of ketone 17

Alcohol **16** (108 mg, 0.59 mmol) was similarly treated with PDC (426 mg, 1.16 mmol) and 4A molecular sieves (86 mg) in CH_2Cl_2. Work-up as above afforded aldehyde (78.8 mg, 74%); oil; $[\alpha]_D^{21}$ −32.0 (*c* 0.72, $CHCl_3$); CD ($CHCl_3$) [θ]: −3020 (296 nm); FTIR: 1720, 1690 cm^{-1}; ^{1}H NMR (200 MHz) δ: 1.04 (3H, s), 1.0−1.8 (8H, m), 2.1−2.2 (2H, m), 2.4−2.6 (2H, m), 9.77 (1H, t, *J* = 1.6 Hz); ^{13}C NMR (50 MHz) δ: 10.3 (t), 24.5 (q), 25.9 (d), 28.3 (d), 28.4 (t), 30.7 (s), 32.6 (t), 34.4 (t), 38.9 (t), 202.1 (d), 208.7 (s); MS (CI) *m/z*: 181 (M + H)$^+$ (base), 163, 145, 135, 121, 107, 93, 81. CI-HRMS *m/z* calcd. for $C_{11}H_{17}O_2$: 181.1229; found: 181.1209.

The aldehyde (78.8 mg, 0.44 mmol) was similarly treated with Wittig reagent and work-up afforded olefin **17** (18.0 mg, 20%) and the recovered aldehyde (4.1 mg).

17: oil; $[\alpha]_D^{22}$ −22.1 (*c* 0.8, $CHCl_3$); CD ($CHCl_3$) [θ]: −2240 (304 nm); FTIR: 1700 cm^{-1}; ^{1}H NMR (200 MHz) δ: 1.10 (3H, s), 1.08–1.23 (2H, m), 1.34–1.56 (5H, m), 1.62 (3H, s), 1.70 (3H, s), 1.79 (1H, m), 2.03–2.07 (2H, m), 2.20–2.22 (2H, m), 5.13 (1H, tsept., *J* = 7.0, 1.4 Hz); ^{13}C NMR (50 MHz) δ: 10.5 (t), 17.6 (q), 22.5 (t), 24.5 (q), 25.7 (q), 26.1 (d), 28.6 (t), 29.0 (d), 31.2 (s), 32.9 (t), 43.2 (t), 124.6 (d), 131.5 (s), 209.6 (s); MS (EI) *m/z*: 206 (M$^+$), 191, 173, 163, 149, 135, 123 (base), 110, 95, 81; EI-HRMS *m/z* calcd. for $C_{14}H_{22}O$: 206.1671; found: 206.1677.

Methylation of ketone 14

MeLi (1.10 M, 0.6 mL, 0.66 mmol) was added to a solution of the ketone **14** (20.4 mg, 0.1 mmol) in ether (3 mL) at 0°C, and the mixture was stirred for 2 h. Water was added and the mixture was extracted with ether. The organic phase was washed with brine, dried ($MgSO_4$), and evaporated. The residue was purified by HPLC (hexane–EtOAc 95:5, Nucleosil 50-5, 4.5 × 250 mm) to afford alcohol **2** (2.2 mg, 10.0%), **18** (5.3 mg, 24.1%), and the recovered **14** (3.1 mg).

2: oil; $[\alpha]_D^{20}$ +56.0 (*c* 0.3, $CHCl_3$); FTIR: 3400 cm^{-1}; ^{1}H NMR (400 MHz) δ: 0.34 (1H, q, *J* = 4.4 Hz), 0.44 (1H, td, *J* = 8.0, 4.4 Hz), 0.92 (1H, m), 0.94 (3H, s), 1.00–1.15 (2H, m), 1.20–1.45 (5H, m), 1.41 (3H, s), 1.62 (3H, s), 1.70 (3H, s), 1.96–1.98 (2H, m), 5.12 (1H, t, *J* = 7.0 Hz); ^{13}C NMR (100 MHz) δ: 5.1 (t), 17.6 (q), 22.8 (t), 24.4 (d), 25.1 (d), 25.7 (q), 26.8 (q), 30.0 (s), 30.1 (t), 31.6 (q), 33.3 (t), 42.9 (t), 68.6 (s), 125.0 (d), 131.2 (s); MS (EI) *m/z*: 222 (M$^+$), 204, 189, 175, 161, 147, 135, 133, 122, 107, 105, 93 (base); EI-HRMS *m/z* calcd. for $C_{15}H_{26}O$: 222.1984; found: 222.2013.

18: oil; $[\alpha]_D^{21}$ +20.6 (*c* 0.2, $CHCl_3$); FTIR: 3400 cm^{-1}; ^{1}H NMR (600 MHz) δ: −0.07 (1H, q, *J* = 5.4 Hz), 0.49 (1H, td, *J* = 9.3, 5.4 Hz), 0.84 (1H, td, *J* = 9.3, 5.4 Hz), 0.88 (3H, s), 0.93 (1H, ddd, *J* = 13.9, 5.1, 2.9 Hz), 1.01 (1H, m), 1.21 (1H, ddd, *J* = 14.2, 13.2, 2.9 Hz), 1.15 (1H, m), 1.29 (3H, s), 1.30 (1H, m), 1.38–1.50 (3H, m), 1.62 (3H, s), 1.69 (3H, s), 2.05 (2H, m), 5.12 (1H, tsept., *J* = 7.2, 1.3 Hz); ^{13}C NMR (100 MHz) δ: 6.8 (t), 17.6 (q), 22.4 (d), 24.8 (t), 24.1 (d), 25.7 (q), 26.3 (q), 29.2 (s), 29.9 (q), 30.6 (t), 31.6 (t), 45.7 (t), 69.2 (s), 125.1 (d), 131.1 (s); MS (EI) *m/z*: 222 (M)$^+$, 204, 189, 176, 161, 147, 135, 133, 122, 107, 105, 93 (base); CI-HRMS *m/z* calcd. for $C_{15}H_{25}$: 205.1956; found: 205.1941 (M − H_2O + H)$^+$.

Methylation of ketone 17

Ketone **17** (15.0 mg, 0.07 mmol) was similarly methylated with MeLi (1.10 M, 0.4 mL, 0.44 mmol) to afford a mixture of alcohol **19** (1.0 mg, 9.6%, a small amount of the recovered **17** was included) and the alcohol **20** (3.0 mg, 21.9%).

19: oil; ^{1}H NMR (200 MHz) δ: 0.34 (1H, q, *J* = 5.4 Hz), 0.47 (1H, td, *J* = 8.3, 4.8 Hz), 0.8–1.8 (8H, m), 1.04 (3H, s), 1.42 (3H, s), 1.61 (3H, s), 1.69 (3H, s), 1.9–2.1 (2H, m), 5.12 (1H, m); MS (CI) *m/z*: 205 (M − H_2O + H)$^+$ (base), 189, 161, 147, 135, 123, 121, 107, 95, 81; CI-HRMS *m/z* calcd. for $C_{15}H_{25}$: 205.1956; found 205.1961 (M − H_2O + H)$^+$.

20: oil; $[\alpha]_D^{21}$ +51.5 (*c* 0.3, $CHCl_3$); FTIR: 3400 cm^{-1}; ^{1}H NMR (600 MHz) δ: −0.07 (1H, q, *J* = 5.4 Hz), 0.54 (1H, td, *J* = 9.3, 5.4 Hz), 0.76 (1H, td, *J* = 9.3, 5.4 Hz), 1.0–1.1 (3H, m), 1.13 (3H, s), 1.2–1.4 (4H, m), 1.28 (3H, s), 1.62 (3H, s), 1.69

© 1997 NRC Canada

(3H, s), 2.00 (1H, m), 2.10 (1H, m), 5.13 (1H, tsept., J = 7.1, 1.5 Hz); ^{13}C NMR (50 MHz) δ: 6.8 (t), 17.6 (q), 21.9 (d), 22.7 (t), 24.3 (d), 25.8 (q), 29.3 (s), 29.4 (q), 29.9 (q), 32.1 (t), 32.3 (t), 41.7 (t), 69.5 (s), 125.3 (d), 130.9 (s); MS (EI) *m/z*: 222 (M^+), 204, 189, 175, 161 (base), 147, 135, 133, 123, 107, 105, 93; EI-HRMS *m/z* $C_{15}H_{26}O$: calcd. for 222.1983; found: 222.1976.

Preparation of chenopodene (1)

A solution of alcohol **18** (4.2 mg, 0.02 mmol) in pyridine (0.5 mL) was treated with $SOCl_2$ (0.02 mL, 0.27 mmol) at 0°C for 30 min under stirring. Water was added and the mixture was extracted with ether. The organic phase was washed with water and brine, dried ($MgSO_4$), and evaporated. The residue was purified by silica gel column chromatography (hexane–EtOAc, 0–100%) to afford chenopodene (**1**) (1.4 mg, 36.3%); oil; $[\alpha]_D^{21}$ −31.0 (*c* 0.1, $CHCl_3$); CD (MeOH) [θ]: −580 (227 nm); ^{1}H NMR (400 MHz) δ: 0.51 (1H, dt, J = 6.0, 4.2 Hz), 0.72 (1H, td, J = 8.4, 4.2 Hz), 0.8–1.8 (6H, m), 1.03 (3H, s), 1.60 (3H, s), 1.67 (3H, s), 1.80 (3H, br s), 1.85–2.00 (2H, m), 4.98 (1H, dq, J = 7.0, 1.4 Hz), 5.12 (1H, tsept., J = 7.0, 1.4 Hz); ^{13}C NMR (100 MHz) δ: 9.6 (t), 15.6 (d), 17.6 (q), 23.0 (t), 23.5 (q), 25.5 (q), 25.7 (d), 27.4 (q), 29.5 (s), 33.2 (t), 40.8 (t), 114.3 (d), 125.5 (d), 130.8 (s), 136.1 (s); MS (EI) *m/z*: 204 (M^+), 189, 161, 133, 107, 93, 55.

Acknowledgements

We thank Drs. R. Gradstein, Göttingen University, Germany, for identification of the liverwort, and T. Nakano, IVIC, Caracas, Venezuela, for help in the collection of the liverwort. The 600 MHz NMR and MS spectra were measured in this University by Ms. Y. Kan and Y. Okamoto, to whom many thanks are due. This work is partly supported by a Grant-in-Aid from the Ministry of Health and Welfare, Japan (to Y.A.).

References

1. Y. Asakawa. Prog. Chem. Org. Nat. Prod. **42**, 1 (1982); **65**, 1 (1995).
2. M. Tori, M. Aoki, and Y. Asakawa. Phytochemistry, **36**, 73 (1994).
3. M. Tori, T. Hamaguchi, R. Shirai, M. Sono, and Y. Asakawa. Proc. 37th Tennen Yuki Kagobutsu Toronkai, Tokushima, Japan, October 1995, p. 295; M. Tori, T. Hamaguchi, K. Sagawa, M. Sono, and Y. Asakawa. J. Org. Chem. **61**, 5362 (1996), and refs. cited therein.
4. M. Pfau, G. Revial, A. Guigant, and J. d'Angelo. J. Am. Chem. Soc. **107**, 273 (1985).
5. E.J. Corey and M. Chaykovsky. J. Am. Chem. Soc. **87**, 1353 (1965).
6. H.E. Simmons and R.D. Smith. J. Am. Chem. Soc. **81**, 4256 (1959).
7. C.D. Poulter, E.C. Friedrich, and S. Winstein. J. Am. Chem. Soc. **91**, 6892 (1969).
8. C. Djerassi, W. Klyne, T. Norin, G. Ohloff, and E. Klein. Tetrahedron, **21**, 163 (1965).
9. E.A. Mash, M.A. Kaczynski, and S.P. Dolata. Tetrahedron Lett. **31**, 4565 (1990).
10. S. Itô, K. Kuriyama, T. Norin, and G. Snatzke. Israel J. Chem. **22**, 59 (1982).

Can. J. Chem. Downloaded from www.nrcresearchpress.com by 88.146.161.215 on 09/08/12
For personal use only.

© 1997 NRC Canada

Total synthesis of mycophenolic acid

Ricardo A. de la Cruz, Francisco X. Talamás, Alfredo Vázquez, and Joseph M. Muchowski

Abstract: A total synthesis of mycophenolic acid is reported. Diels–Alder reaction of [5-methoxy-3-(1-methoxypropenyl)-4,5-dihydrofuran-2-yloxy]-trimethylsilane with 3-benzenesulfinyl-5*H*-furan-2-one afforded the hexasubstituted nucleus. The side chain was constructed from the unveiled aldehyde.

Key words: mycophenolic acid, Diels–Alder reaction, pentasubstituted diene.

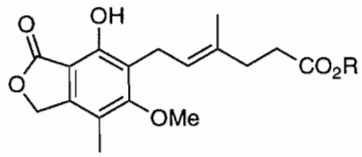
Résumé : On a effectué une synthèse totale de l'acide mycophénolique. Une réaction de Diels–Alder du [5-méthoxy-3-(1-méthoxypropényl)-4,5-dihydrofuran-2-yloxy]-triméthylsilane avec la 3-benzènesulfinyl-5*H*-furan-2-one a permis d'obtenir le noyau hexasubstitué. On a créé la chaîne latérale à partir de l'aldéhyde déprotégé.

Mots clés : acide mycophénoliquie, réaction de Diels–Alder, diène pentasubstitué.

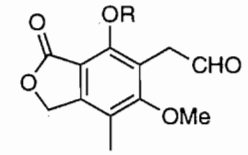
[Traduit par la rédaction]

Introduction

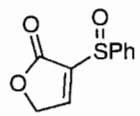
Mycophenolic acid (**1***a*), a metabolite of several Penicillium species (1), has been known as a potent inhibitor of inosine monophosphate dehydrogenase (IMPDH; EC 1.1.1.205) for over 25 years (2). It has recently become of importance in organ transplant rejection due to its immunosuppressive activity and low degree of toxicity (3). As a consequence of the pharmacological activity of **1***a*, much effort has been devoted to the preparation of congeners thereof (4) as well as to its total synthesis (5). The known (5b) phthalide **2***b* was chosen as a synthetic target because it is a useful precursor of mycophenolic acid itself and of several highly active side-chain-modified derivatives (4). This article describes a new synthesis of the phthalides **2***a*-**2***c* and the conversion of **2***c* into mycophenolic acid using the process of Patterson and Huang (5*b*, 6). Like others (5) who have utilized phthalides as precursors of **1***a*, we chose to use a Diels–Alder strategy, as did Watanabe et al. (5*d*), as the first step en route to **2***b*. Of several processes studied, the most successful involved the use of the dienophile **3** and the pentasubstituted diene **4**.



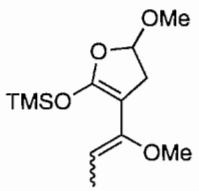
1*a* R = H
1*b* R = Et



2*a* R = H
2*b* R = $SiMe_2t$-Bu
2*c* R = $CH_2O(CH_2)_2OCH_3$



3



4

Results and discussion

Compound **3** was prepared (98% yield) by *m*-chloroperbenzoic acid oxidation from the corresponding (7) sulfide. The starting material for the diene **4** was 5-methoxy-2(3H)-dihydrofuranone **5** (8), which was deprotonated with lithium bis(trimethylsilyl)amide (2.1 equiv.) in anhydrous THF (−78°C) and treated with propionyl chloride (1.1 equiv., −78°C) to give the β-ketolactone **6** (68%). The extra equivalent of base used was required to drive the reaction to completion. When lithium diisopropylamide (LDA) was used as the base in this reaction, the yield decreased considerably. Attempts to transform **6** into the enol ether **7** under different basic conditions (e.g., KH, MeI, HMPA) resulted in complex mixtures. Better results were obtained when acid catalysis was used for this transformation. Reaction of **6** with trimethyl orthoformate (2.0 equiv.), containing a catalytic quantity of concentrated H_2SO_4 (r.t.) (9) gave the enol ether **7** (63% yield after flash chromatography, SiO_2) contaminated by a minor amount (ca 10%) of its geometric isomer (10). This compound was converted into the diene **4** (60% yield after distillation) by lithiation with LDA (THF, −78°C) followed by reaction with chlorotrimethylsilane (TMSCl) (−78°C to r.t.) (11).

The optimum conditions for the [4π + 2π] cycloaddition

Received November 1, 1996.

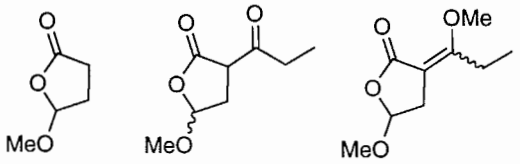
This paper is dedicated to Professor William A. Ayer on the occasion of his 65th birthday.

R.A. de la Cruz, F.X. Talamás,[1] **A. Vázquez.** Syntex S.A. de C.V., División de Investigación, Apartado Postal 272 (CIVAC), Jiutepec, Morelos, México cp 62500.
J.M. Muchowski. Syntex Research, Institute of Organic Chemistry, 3401 Hillview Avenue, Palo Alto, CA 94304, U.S.A.

[1] Author to whom correspondence may be addressed. Present address: Roche Bioscience, 3401 Hillview Ave., Palo Alto, CA 94304, U.S.A. Telephone: (415) 354-2511. Fax: (415) 354-2442. Internet: francisco.talamas@roche.com

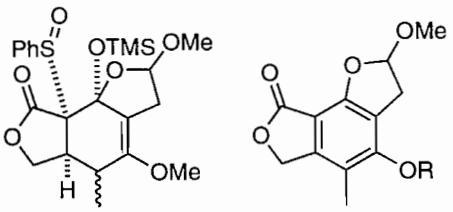
© 1997 NRC Canada

Can. J. Chem. Downloaded from www.nrcresearchpress.com by 88.146.161.215 on 09/08/12
For personal use only.



5 6 7

and subsequent aromatization involved reaction of **3** with 2.0 equivalents of the diene **4** in toluene solution under mild conditions (0°C, 1 h; r.t., 1 h) followed by thermolysis of the putative adduct **8** at reflux temperature (30 min). Column chromatography separation (SiO_2) of the reaction mixture provided the expected phthalide derivative **9***a* as well as the phenol **9***b* in 33 and 14% yields, respectively. Since **9***b* is readily and efficiently (89%) methylated (MeI, NaH, DMF), **9***a* is thus obtained in 45% combined yield. When the reaction was carried out under the same reaction conditions but with the sulfoxide **3** as the excess reagent (2.0 equiv.), compound **9***a* was obtained in only 13% yield. To convert **9***a* into the desired phthalide, deprotection with 89% formic acid (r.t., 20 min, quant.) to the phenolic aldehyde **2***a* was carried out. The most notable feature of this process is that a hexasubstituted benzenoid derivative containing all the functionality required for conversion into mycophenolic acid, or side-chain congeners thereof, is produced with a considerable economy in steps and reasonable efficiency.

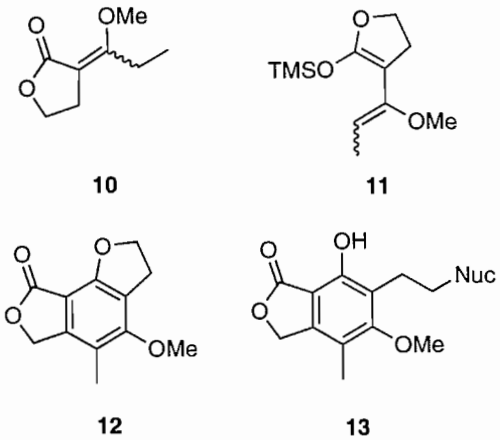


8 **9***a* R = Me
9*b* R = H

Protection of the latent aldehyde protected as an acetal through the synthesis up to this point solved the problem encountered in an early attempt as described in Scheme 1. Thus, 3-propionyldihydrofuran-2-one was converted into the enol ether **10** (10) under acid conditions (H_2SO_4, trimethyl orthoformate). Compound **10** was converted to the diene **11** in 75% yield, using the conditions employed for the transformation of **7** to **4**. Reaction of sulfoxide **3** and diene **11** (2.0 equiv.) in toluene solution (0°C–reflux, 2.5 h) afforded, after column chromatography, the phthalide **12** in 46% yield. Attempts to obtain the phenol **13** by opening of the dihydrofuran moiety on **12** with nucleophiles were unsuccessful. Although transient formation of **13** presumably occurred, closure back to the starting material or loss of the methoxy group was observed. Extensive studies were carried out before it was decided to start with the desired oxidation state on an early intermediate as described above.

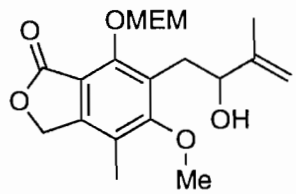
The synthesis was completed as follows. Treatment of compound **2***a* with *tert*-butyldimethylsilyl chloride (TBDMSCl) (imidazole, DMF) (12) afforded the desired aldehyde **2***b* in only 18% yield along with other by-products. Although the aldehyde **2***b* could not be generated with acceptable efficiency under a wide variety of conditions (13), the ether **2***c* was easily

Scheme 1.



10 11 12 13

prepared (86%) from **2***a* and 2-methoxyethoxymethyl chloride (MEMCl) by the procedure of Corey et al. (*i*-Pr_2NEt–CH_2Cl_2) (14). This compound was reacted with prop-2-enyl magnesium bromide (THF, −40°C) and the allylic alcohol **14** so obtained (67%) was subjected to the *ortho*-ester Claisen conditions of Patterson (5*b*, 6). Removal of the MEM group from the product (PPTS, *t*-BuOH, 80°C, 6 h) gave ethyl mycophenolate **1***b* (60% from **14**), which on saponification provided mycophenolic acid (**1***a*) in near quantitative yield.



14

The process described herein could without doubt be applied to the synthesis of a wide variety of nucleus- and side-chain-modified analogs of mycophenolic acid.

Experimental

General methods

Unless otherwise noted, materials were obtained from commercial suppliers and were used without further purification. Tetrahydrofuran (THF) was distilled under argon atmosphere from sodium–benzophenone directly before use. Hexamethyldisilazane and diisopropylamine were distilled from CaH_2 before use. Toluene was degassed by bubbling argon and applying ultrasound for 5 min. Reactions and chromatography fractions were monitored by thin-layer chromatography. Chromatography was carried out using Merck 60 (230–400 mesh) silica gel. Melting points are uncorrected. IR spectra were recorded as $CHCl_3$ solution using a Perkin–Elmer 1720-X instrument. ^1H NMR measurements were recorded at 200.0 MHz and ^{13}C NMR measurements were recorded at 50.0 MHz using a Varian Gemini-200 instrument. Spectra are reported in ppm downfield from tetramethylsilane as the internal standard. Unless otherwise noted, NMR spectra were measured in $CDCl_3$ solution. Low-resolution mass spectra (LRMS) were

© 1997 NRC Canada

Can. J. Chem. Downloaded from www.nrcresearchpress.com by 88.146.161.215 on 09/08/12
For personal use only.

Can. J. Chem. Downloaded from www.nrcresearchpress.com by 88.146.161.215 on 09/08/12
For personal use only.

recorded on a Finnigan MAT-INCOS XL instrument. Elemental analyses were performed using a Fison EA-1108 instrument or were done at Midwest-Microlab, 7212N Shadeland Ave. Indianapolis, IN 46250, U.S.A.

3-Benzenesulfinyl-5*H*-furan-2-one (3)

Sulfoxide **3** was prepared as reported (*7a*) to obtain an oil, which was crystallized to obtain yellow needles; mp 87–88.5°C (EtOH); IR: 3014, 1766, 1216, 1052 cm^{-1}; ^1H NMR δ: 8.05 (t, J = 1.6 Hz, 1H), 7.89–7.76 (m, 2H), 7.59–7.48 (m, 3H), 5.05 (dd, J = 19.0, 1.7 Hz, 1H), 4.89 (dd, J = 19.0, 1.6 Hz, 1H); ^{13}C NMR δ: 167.2, 151.6, 141.6, 141.3, 132.2, 129.6, 124.9, 71.3; LRMS (EI), *m/z* (relative intensity): 208 (M^+, 14), 51 (100). Anal. calcd. for $C_{10}H_8O_3S$: C 57.67, H 3.87, S 15.39; found: C 57.52, H 3.81, S 15.19.

5-Methoxy-3-propionyl-dihydrofuran-2-one (6)

A 1.38 M solution of *n*-BuLi–hexanes (145.0 ml, 0.2 mol) was added to hexamethyldisilazane (42.3 mL, 0.2 mol) in THF (195.0 ml) at 0°C under argon. The reaction was stirred for 20 min, cooled to −78°C, and **5** (11.1 g, 0.095 mol) was added in THF (27.0 ml). After 30 min, propionyl chloride (9.14 mL, 0.105 mol) was added and the mixture was stirred for 15 min at −78°C and then allowed to reach room temperature. The reaction was quenched with 10% NH_4Cl (50.0 mL), diluted with EtOAc, and the organic phase was washed with 10% NH_4Cl (2 × 50.0 mL) and dried over anhydrous Na_2SO_4. The solvent was removed under vacuum and the residue (14.5 g) purified by flash chromatography (SiO_2, hex–EtOAc 85:15) to obtain **6** as an oil (11.1 g, 68%). The NMR spectra show **6** as a 1:1 mixture of two diastereoisomers: IR: 3025, 1774, 1724, 1355, 1110, 932 cm^{-1}; ^1H NMR δ: 5.45 (dd, J = 5.8, 1.7 Hz, 1H), 3.88 (t, J = 8.8 Hz, 0.5H), 3.50 (s, 3H), 3.25–2.82 (m, 2H), 2.81–2.38 (m, 2H), 2.14 (ddd, J = 13.8, 9.0, 1.9 Hz, 0.5 H), 1.10 (t, J = 7.1 Hz, 3H); LRMS (EI), *m/z* (relative intensity): 173 (M^+, 11), 57 (100). Anal. calcd. for $C_8H_{12}O_4$: C 55.80, H 7.03; found: C 55.72, H 7.10.

5-Methoxy-3-(1-methoxypropylidene)-dihydrofuran-2-one (7)

To a solution of the β-keto lactone **6** (11.2 g, 0.065 mol) in trimethyl orthoformate (14.2 mL, 0.13 mol) at 0°C under argon was slowly added concentrated H_2SO_4 (0.18 mL, 3.24 mmol); the mixture was stirred for 15 min at the same temperature and then for 3.5 h at room temperature. The reaction was diluted with CH_2Cl_2, washed with 10% $NaHCO_3$ (2 × 50.0 mL) and brine, and dried over anhydrous Na_2SO_4. After removal of the solvent, the residue (12.2 g) was purified by flash chromatography (SiO_2, hex–EtOAc 85:15) to obtain the enol ether **7** as an oil (7.69 g, 63%). IR: 3020, 1738, 1654, 1229, 1074, 1014, 915 cm^{-1}; ^1H NMR δ: 5.32 (dd, J = 6.5, 2.2 Hz, 1H), 3.81 (s, 3H), 3.49 (s, 3H), 3.05–2.80 (m, 3H), 2.71 (dd, J = 16.7, 2.1 Hz, 1H), 1.15 (t, J = 7.5 Hz, 3H); ^{13}C NMR δ: 171.4, 170.3, 101.0, 98.7, 56.1, 54.6, 32.8, 19.0, 12.2; LRMS (EI), *m/z* (relative intensity): 186 (M^+, 28), 57 (100). Anal. calcd. for $C_9H_{14}O_4$: C 58.05, H 7.58; found: C 57.66, H 7.74.

[5-Methoxy-3-(1-methoxypropenyl)-4,5-dihydrofuran-2-yloxy]-trimethylsilane (4)

A 1.38 M solution of *n*-BuLi–hexanes (18.0 mL, 24.9 mmol) was added to diisopropylamine (3.8 mL, 27.1 mmol) in THF (44.0 mL) at 0°C under argon. The reaction was stirred for 20 min, cooled to −78°C, and **7** (4.1 g, 21.9 mmol) was added in THF (22.0 mL). After 30 min, chlorotrimethylsilane (3.4 mL, 27.1 mmol) was added; the mixture was stirred for 15 min at −78°C and then allowed to reach room temperature. The reaction mixture was concentrated until a precipitate formed, then diluted with hexane, filtered through Celite®, and concentrated to dryness to obtain an oil. The crude product was distilled to obtain the diene **4** (3.39 g, 60%) as a colorless liquid; bp 74–76°C (0.37 Torr; 1 Torr = 133.3 Pa); IR: 3014, 2938, 1694, 1255, 855 cm^{-1}; ^1H NMR δ: 5.29 (dd, J = 7.2, 2.4 Hz, 1H), 4.53 (q, J = 7.0 Hz, 1H), 3.46 (s, 3H), 3.45 (s, 3H), 2.99 (dd, J = 15.0, 7.2 Hz, 1H), 2.56 (dd, J = 15.0, 2.2 Hz, 1H), 1.56 (d, J = 6.8 Hz, 3H), 0.26 (s, 9H); ^{13}C NMR δ: 152.3, 150.1, 103.8, 103.1, 93.7, 55.3, 54.5, 37.0, 12.7, 0.24; LRMS (EI), *m/z* (relative intensity): 258 (M^+, 4), 73 (100).

2,4-Dimethoxy-5-methyl-3,6-dihydro-2*H*-1,7-dioxa-*as*-indacen-8-one (9*a*) and 4-hydroxy-2-methoxy-5-methyl-3,6-dihydro-2*H*-1,7-dioxa-*as*-indacen-8-one (9*b*)

To a solution of the sulfoxide **3** (1.24 g, 6.0 mmol) in degassed toluene (10.0 mL) at 0°C under argon was added dropwise the diene **4** (3.27 g, 12.65 mmol). The reaction was stirred for 1 h at 0°C, 1 h at room temperature, and for 30 min at reflux. The solvent was removed and the crude product purified by flash chromatography (SiO_2, CH_2Cl_2–acetone 98:2) to obtain **9*a*** (489 mg, 33%) and **9*b*** (199 mg, 14%). Compound **9*a***, mp 135–137°C (hex–EtOAc), presents the following spectroscopic data: IR: 3023, 1759, 1639, 1615, 951 cm^{-1}; ^1H NMR δ: 5.83 (dd, J = 6.4, 2.1 Hz, 1H), 5.14 (s, 2H), 3.97 (s, 3H), 3.59 (s, 3H), 3.49 (dd, J = 16.3, 6.5 Hz, 1H), 3.25 (dd, J = 16.1, 2.0 Hz 1H), 2.06 (s, 3H); ^{13}C NMR δ: 168.8, 159.7, 155.8, 146.8, 115.1, 114.1, 109.0, 102.8, 69.0, 59.0, 56.3, 35.3, 10.9; LRMS (EI), *m/z* (relative intensity): 250 (M^+, 100). Anal. calcd. for $C_{13}H_{14}O_5$: C 62.39, H 5.64; found: C 62.01, H 5.70. Compound **9*b***, mp 168–170°C (hex–EtOAc), presents the following spectroscopic data: IR: 3588, 3250, 3019, 1757, 1625, 950 cm^{-1}; ^1H NMR ($CDCl_3$ + DMSO-d_6) δ: 9.08 (s, 1H, D_2O exchange), 5.82 (dd, J = 6.4, 2.3 Hz, 1H), 5.13 (s, 2H), 3.57 (s, 3H), 3.26 (dd, J = 16.5, 6.5 Hz, 1H), 3.07 (dd, J = 16.6, 2.1 Hz, 1H), 2.06 (s, 3H); ^{13}C NMR (DMSO-d_6) δ: 168.2, 157.2, 154.5, 147.4, 111.8, 110.9, 109.4, 99.3, 68.7, 55.6, 33.4, 10.5; LRMS (EI), *m/z* (relative intensity): 236 (M^+, 57), 43 (100). Anal. calcd. for $C_{12}H_{12}O_5$: C 61.01, H 5.12; found: C 60.83, H 5.14.

Conversion of 9*b* to 9*a*

To a solution of **9*b*** (100 mg, 0.42 mmol) in DMF (5.0 mL) at 0°C under argon was added 60% NaH–oil (20 mg, 0.5 mmol) The reaction was stirred for 15 min and then CH_3I (0.06 mL, 1.05 mmol) was added. The reaction was stirred for 30 min at 0°C and 30 min at room temperature, then poured on water and the product extracted with EtOAc (3×). The organic phase was washed with water, brine, and dried over anhydrous Na_2SO_4. The solvent was removed and the residue purified by flash chromatography (SiO_2, hex–EtOAc 6:4) to obtain **9*a*** (94 mg, 89%).

(4-Hydroxy-6-methoxy-7-methyl-3-oxo-1,3-dihydroisobenzofuran-5-yl)-acetaldehyde (2*a*)

A solution of **9*a*** (73 mg, 0.29 mmol) in 89% formic acid (2.0 mL) was stirred at room temperature for 20 min and con-

© 1997 NRC Canada

Can. J. Chem. Downloaded from www.nrcresearchpress.com by 88.146.161.215 on 09/08/12
For personal use only.

centrated to dryness. The residue was azeotroped with toluene (3×) to remove traces of acid. The aldehyde **2***a* (66 mg, quantitative) was obtained as a white solid in pure form. The NMR spectra shows the phenol-aldehyde **2***a* to be in equilibrium with the corresponding cyclic hemiacetal in solution; mp 144–145°C (hex–CH_2Cl_2); IR: 3417, 1755, 1640, 1612 cm^{-1}; ^1H NMR δ: 9.75 (t, J = 1.5 Hz, 0.18H, aldehyde), 7.70 (s, 1H, D_2O exchange), 6.29 (dd, J = 6.5, 2.6 Hz, 0.82H, hemiacetal), 5.24 (s, 0.36H), 5.14 (s, 1.64H), 3.98 (s, 2.46H), 3.80 (d, J = 1.4 Hz, 0.36 H), 3.73 (s, 0.54H), 3.49 (dd, J = 16.0, 6.5 Hz, 0.82H), 3.22 (dd, J = 16.1, 2.5 Hz, 0.82H), 2.17(s, 0.54H), 2.05 (s, 2.46H); LRMS (EI), *m/z* (relative intensity): 236 (M^+, 2), 208 (55), 159 (100). Anal. calcd. for $C_{12}H_{12}O_5$: C 61.01, H 5.12; found: C 61.29, H 5.03.

3-(1-Methoxypropylidene)-dihydrofuran-2-one (10)

To a solution of 3-propionyl-dihydrofuran-2-one (16.8 g, 0.12 mol) in trimethyl orthoformate (19.4 mL, 0.17 mol) at 0°C was added concentrated H_2SO_4 (0.3 mL). The reaction was allowed to reach room temperature and was stirred for 15 h. The solution was concentrated and quinoline (0.8 mL) added. The crude product was distilled to give **10** as the *E* isomer (10) (2.76 g) and *Z* isomer (10.9 g) as colorless liquids in 74% yield. The *E* isomer, bp 68–70°C (3.0 Torr), presents the following spectroscopic data: IR: 1689, 1640 cm^{-1}; ^1H NMR δ: 4.41 (t, J = 9.7 Hz, 2H), 3.71 (s, 3H), 2.89 (tt, J = 9.6, 1.0 Hz, 2H), 2.66 (qt, J = 7.6, 1.0 Hz, 2H), 1.12 (t, J = 7.5 Hz, 3H); LRMS (EI), *m/z* (relative intensity): 155 ($M^+ - 1$). The *Z* isomer, bp 120–122°C (3.0 Torr), presents the following spectroscopic data: IR: 1728, 1653 cm^{-1}; ^1H NMR δ: 4.25 (t, J = 7.7 Hz, 2H), 3.82 (s, 3H), 3.03–2.80 (m, 4H), 1.15 (t, J = 7.5 Hz, 3H); LRMS (EI), *m/z* (relative intensity): 156 (M^+).

[3-(1-Methoxypropenyl)-4,5-dihydrofuran-2-yloxy]-trimethylsilane (11)

Enol ether **10** (3.0 g, 19.2 mmol) was converted to the diene **11** (3.28 g) in 75% yield as described for **4**; bp 75–81°C (0.35 Torr); IR: 1691, 860 cm^{-1}; ^1H NMR δ: 4.51 (q, J = 6.7 Hz, 1H), 4.27 (dd, J = 9.1, 8.6 Hz, 2H), 3.46 (s, 3H), 2.75 (t, J = 0.9 Hz, 2H), 1.55 (d, J = 6.9 Hz, 3H), 0.21 (s, 9H); LRMS (EI), *m/z* (relative intensity): 228 (M^+).

4-Methoxy-5-methyl-3,6-dihydro-2*H*-1,7-dioxa-*as*-indacen-8-one (12)

Diels–Alder reaction of **11** (1.21 g, 5.0 mmol) and **3** (0.54 g, 2.6 mmol) as described for **9** afforded compound **12** (0.26 g) in 46% yield; mp 141–142°C (hex–CH_2Cl_2); IR: 1749 cm^{-1}; ^1H NMR δ: 5.13 (s, 2H), 4.78 (t, J = 8.8 Hz, 2H), 3.98 (s, 3H), 3.41 (t, J = 8.8 Hz, 2H), 2.06 (s, 3H); LRMS (EI), *m/z* (relative intensity): 220 (M^+).

[4-(*tert*-Butyldimethylsilanyloxy)-6-methoxy-7-methyl-3-oxo-1,3-dihydroisobenzofuran-5-yl]-acetaldehyde (2*b*)

To a solution of **2***a* (200 mg, 0.85 mmol) and imidazole (116 mg, 1.7 mmol) in DMF (10.0 mL) was added TBDMSCl (153 mg, 1.02 mmol). The reaction was stirred at room temperature overnight, then diluted with water and EtOAc. The organic phase was separated and washed with 10% HCl, 10% $NaHCO_3$, and brine, and dried over anhydrous Na_2SO_4. After removal of the solvent the residue was purified by flash chromatography (SiO_2, hex–EtOAc 4:1) to give **2***b* (53 mg, 18%) as a white solid (4*a*). 1H NMR δ: 9.62 (m, 1H), 5.10 (s, 2H), 3.72 (s, 5H), 2.18 (s, 3H), 1.01 (s, 9H), 0.21 (s, 6H); LRMS (EI), *m/z* (relative intensity): 350 (M^+).

[6-Methoxy-4-(2-methoxyethoxymethoxy)-7-methyl-3-oxo-1,3-dihydroisobenzofuran-5-yl]-acetaldehyde (2*c*)

A solution of the phenol **2***a* (1.76 g, 7.45 mmol), *N,N*-diisopropylethylamine (3.24 mL, 18.6 mmol), and 2-methoxyethoxymethyl chloride (1.1 g, 8.9 mmol) in CH_2Cl_2 (50.0 mL) was stirred for 2 h at room temperature. The reaction was diluted with CH_2Cl_2 and washed with 10% $NaHCO_3$, water, and brine, and dried over anhydrous Na_2SO_4. The solvent was removed and the residue purified by flash chromatography (SiO_2, hex–acetone 7:3) to obtain the MEM ether **2***c* (1.98 g, 86%) as a solid; mp 45–50°C; IR: 3021, 1760, 1724, 1130, 1069, 961 cm^{-1}; ^1H NMR δ: 9.72 (t, J = 1.5 Hz, 1H), 5.44 (s, 2H), 5.17 (s, 2H), 3.92–3.84 (m, 4H), 3.74 (s, 3H), 3.60–3.52 (m, 2H), 3.37 (s, 3H), 2.21 (s, 3H); ^{13}C NMR δ: 199.0, 168.7, 162.9, 154.0, 148.3, 121.1, 120.4, 112.2, 100.2, 71.5, 69.4, 68.3, 60.8, 59.0, 39.7, 11.6; LRMS (EI), *m/z* (relative intensity): 324 (M^+, 1), 59 (100). Anal. calcd. for $C_{16}H_{20}O_7$: C 59.25, H 6.21; found: C 59.42; H, 6.35.

6-(2-Hydroxy-3-methylbut-3-enyl)-5-methoxy-7-(2-methoxyethoxymethoxy)-4-methyl-3*H*-isobenzofuran-2-one (14)

To a solution of the aldehyde **2***c* (1.4 g, 4.3 mmol) in THF (40.0 mL) at −40°C under argon was added freshly prepared prop-2-enyl magnesium bromide (0.58 M in THF, 15 mL) and stirred for 40 min. The reaction was diluted with EtOAc and 50% NH_4Cl and allowed to reach room temperature. The organic phase was washed with 10% NH_4Cl and brine, and dried over anhydrous Na_2SO_4. The solvent was evaporated and the residue purified by flash chromatography (SiO_2, hex–EtOAc 7:3) to obtain the MEM alcohol **14** (949 mg, 67%) as an oil. IR: 1758, 1604, 1129, 1068 cm^{-1}; ^1H NMR δ: 5.45 (q, J = 6.7 Hz, 2H), 5.14 (s, 2H), 4.99 (br t, J = 0.82 Hz, 1H), 4.84 (br t, J = 1.2 Hz, 1H), 4.32 (dd, J = 8.2, 5.0 Hz, 1H), 4.06–3.86 (m, 2H), 3.82 (s, 3H), 3.59 (t, J = 4.7 Hz, 2H), 3.37 (s, 3H), 3.12–2.92 (m, 2H), 2.20 (s, 3H), 1.86 (s, 3H); ^{13}C NMR δ: 169.0, 163.1, 154.3, 147.7, 147.2, 126.8, 120.5, 112.3, 110.4, 100.4, 75.5, 71.5, 69.4, 68.2, 60.9, 59.0, 31.3, 18.0, 11.7; LRMS (EI), *m/z* (relative intensity): 366 (M^+, 1), 220 (25), 59 (100). Anal. calcd. for $C_{19}H_{26}O_7$: C 62.27, H 7.53; found: C 61.95, H 7.49.

6(4-Hydroxy-6-methoxy-7-methyl-3-oxo-1,3-dihydroisobenzofuran-5-yl)-4-methyl-hex-4-enoic acid ethyl ester (1*b*)

A solution of the allylic alcohol **14** (930 mg, 2.56 mmol), freshly distilled triethyl orthoformate (8.0 mL, 43.6 mmol), and pivalic acid (6 mg, 0.05 mmol) in xylene (45.0 mL) was heated in an oil bath at 135–140°C for 6 h. The solvent was removed, the residue dissolved in *t*-BuOH (70.0 mL), PPTS (700 mg, 2.8 mmol) was added, and the solution stirred at 80°C for 6 h. The reaction was diluted with EtOAc, washed with 10% $NaHCO_3$, and water, and dried over anhydrous Na_2SO_4. The solvent was removed and the residue (1.34 g) was purified by flash chromatography (SiO_2, hex–acetone 85:15) to give the ester **1***b* (516 mg, 60% from **14**); mp 95–96°C (hex–CH_2Cl_2); IR: 3454, 1735, 1628, 1138 cm^{-1};

© 1997 NRC Canada

^{1}H NMR δ: 7.66 (s, 1H, D_2O exchange), 5.24 (t, J = 6.9 Hz, 1H), 5.20 (s, 2H), 4.07 (q, J = 7.1 Hz, 2H), 3.76 (s, 3H), 3.38 (d, J = 6.8 Hz, 2H), 2.44–2.22 (m, 4H), 2.14 (s, 3H), 1.80 (s, 3H), 1.20 (t, J = 7.1 Hz, 3H); ^{13}C NMR δ: 173.3, 163.6, 153.6, 143.9, 134.2, 122.6, 122.1, 116.7, 106.3, 70.0, 60.9, 60.1, 34.6, 33.1, 22.5, 16.1, 14.1, 11.5; LRMS (EI), *m/z* (relative intensity): 348 (M^+, 6), 207 (100). Anal. calcd. for $C_{19}H_{24}O_6$: C 65.50, H 6.94; found: C 65.41, H 7.00.

Mycophenolic acid (1*a*)

A solution of the ester **1***b* (100 mg, 0.28 mmol) in methanol (3 mL) was treated with LiOH (34 mg, 0.81 mmol) in water (0.5 mL). The reaction was stirred for 12 h, diluted with EtOAc, and washed with water. The aqueous phase was cooled on ice and 10% HCl was added to pH = 1, extracted with EtOAc, dried over anhydrous Na_2SO_4 and concentrated to give **1***a* (119 mg, 98%) as a white solid; mp 140°C (hex–CH_2Cl_2) (5).

References

1. J.H. Birkinshaw, H. Raistrick, and D.G. Ross. Biochem. J. **50**, 630 (1952); A.E. Oxford and H. Raistrick. Biochem. J. **26**, 1441 (1932); **26**, 1902 (1932); Biochem. J. **27**, 1176 (1933); **27**, 1473 (1933).
2. TJ. Franklin and J.M. Cook. Biochem. J. **113**, 515 (1969).
3. A.C. Allison and E.M. Eugui. Clin. Transplant. **7**, 96 (1993); Immunol. Rev. **136**, 5 (1993).
4. (*a*) P.H. Nelson, S.F. Carr, B.H. Devens, E.M. Eugui, F. Franco, C. González, R.C. Hawley, D.G. Loughhead, D.J. Milan, E. Papp, J.W. Patterson, S. Rouhafza, E.B. Sjogren, D.B. Smith, R.A. Stephenson, F.X. Talamás, A.M. Waltos, R.J. Weikert, and J.C. Wu. J. Med. Chem. **39**, 4181 (1996); (*b*) D.B. Smith, A.M. Waltos, D.G. Loughhead, R.J. Weikert, D.J. Morgans, Jr., J.C. Rohloff, J.O. Link, and R.R. Zhu. J. Org. Chem. **61**, 2236 (1996); (*c*) J.C. Rohloff, J.O Gardner, and R.W. Towne. Tetrahedron Lett. **36**, 7803 (1995); (*d*) J.W. Patterson. J. Org. Chem. **60**, 560 (1995); (*e*) J.W. Patterson, D.J. Morgans, Jr., D.B. Smith, F.X. Talamás, D.R. Artis, A. Cervantes, T.R. Elworthy, M. Fernández, F. Franco, R.C. Hawley, T. Lara, D.G. Loughhead, P.H. Nelson, E.B. Sjogren, A. Trejo, A.M. Waltos, and R.J. Weikert. U.S. Patent 5,444,072, 1995; (*f*) D.J. Morgans, Jr., D.B. Smith, F.X. Talamás, D.R. Artis, A. Cervantes, T.R. Elworthy, M. Fernández, F. Franco, R.C. Hawley, T. Lara, D.G. Loughhead, P.H. Nelson, J.W. Patterson, J.C. Rohloff, E.B. Sjogren, A. Trejo, A.M. Waltos, and R.J. Weikert. U.S. Patent 5,493,070, 1996; (*g*) P.H. Nelson, E. Eugui, C.C. Wang, and A.C. Allison. J. Med. Chem. **33**, 833 (1990); (*h*) D.F. Jones and S.D. Mills. J. Med. Chem., **14**, 305 (1971); (*i*) D.F. Jones, R.H. Moore, and G.C. Crawley. J. Chem. Soc. 1725 (1970).
5. (*a*) G.M. Makara and W.K. Anderson. J. Org. Chem. **60**, 5717 (1995); (*b*) J.W. Patterson. Tetrahedron, **49**, 4789 (1993); (*c*) K. Kobayashi, H. Shimizu, M. Itoh, and H. Suginome. Bull. Chem. Soc. Jpn. **63**, 2435 (1990); (*d*) M. Watanabe, M. Tsukazaki, Y. Hamada, M. Iwao, and S. Furuka. Chem. Pharm. Bull. **37**, 2948 (1989); (*e*) R.L. Danheiser, S.K. Gee, and J.J. Perez. J. Am. Chem. Soc. **108**, 806 (1986); (*f*) S. Auricchio, A. Ricca, and O.V. de Pava. J. Org. Chem. **48**, 602 (1983); (*g*) L. Colombo, B. Rindone, E. Santaniello, and C. Scolastico. Tetrahedron, **28**, 4395 (1972); (*h*) A.J. Birch and J.J. Wright. Aust. J. Chem. **22**, 2635 (1969).
6. J.W. Patterson and G.T. Huang. J. Chem. Soc. Chem. Commun. 1579 (1991).
7. (*a*) M. Watanabe, M. Tsukazaki, Y. Hirakawa, M. Iwao, and S. Furukawa. Chem. Pharm. Bull. **37**, 2914 (1989); (*b*) K. Iwai, H. Kosugi, H. Uda, and M. Kawai. Bull. Chem. Soc. Jpn. **50**, 242 (1977); (*c*) H.J. Monteiro and A.L. Gemal. Synthesis, 437 (1975).
8. J.C. de Jong, F. van Bolhuis, and B.L. Feringa. Tetrahedron Asymmetry, **2**, 1247 (1991).
9. E.E. Smissman and A.N. Voldeng. J. Org. Chem. **29**, 3161 (1964).
10. (*a*) Y. Tamaru, M. Hojo, and Z.I. Yoshida. J. Org. Chem. **56**, 1099 (1991); (*b*) E. Taskinen. Acta Chem. Scand. B, **39**, 489 (1985).
11. P. Brassard and J. Savard. Tetrahedron, **40**, 3455 (1984).
12. E.J. Corey and A. Venkateswarlu. J. Am. Chem. Soc. **94**, 6190 (1972).
13. (*a*) Y. Tanabe, M. Murakami, K. Kitaichi, and Y. Yoshida. Tetrahedron Lett. **35**, 8409 (1994); (*b*) Y. Tanabe, H. Okumura, A. Marda, and M. Murakami. Tetrahedron Lett. **35**, 8413 (1994); (*c*) T.W. Greene and P.G. Wuts. Protective groups in organic synthesis. 2nd ed. John Wiley, New York. 1991. pp. 68–87.
14. E.J. Corey, J.-L. Gras, and P. Ulrich. Tetrahedron Lett. **17**, 809 (1976).

Can. J. Chem. Downloaded from www.nrcresearchpress.com by 88.146.161.215 on 09/08/12
For personal use only.

© 1997 NRC Canada

Synthetic studies on clerodane diterpenoids. The total synthesis of (±)-2-oxo-5α,8α-13,14,15,16-tetranorclerod-3-en-12-oic acid

Hsing-Jang Liu, Kak-Shan Shia, Yongxin Han, Daqing Sun, and Yu Wang

Abstract: A general synthetic approach to diterpenoids of the *cis*-clerodane family has been developed, leading to the first total synthesis, in racemic form, of 2-oxo-5α,8α-13,14,15,16-tetranorclerod-3-en-12-oic acid (**2**). The key operation involved is the face-selective Diels–Alder reaction of dienone ester **10** with *trans*-piperylene, giving rise to adduct **11** containing the decalin nucleus and correct stereogenic centers common to many *cis*-clerodane diterpenoids.

Key words: *cis*-clerodanes, general synthetic approach, total synthesis, face-selective Diels–Alder reaction.

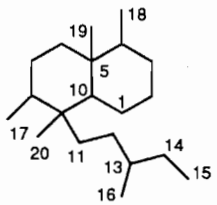
Résumé : On a développé une méthode générale de synthèse des diterpénoïdes de la famille du *cis*-clérodane qui a conduit à la première synthèse totale de l'acide 2-oxo-5α,8α-13,14,15,16-tétranorclérod-3-én-12-oïque (**2**) sous forme racémique. L'opération clé implique une réaction de Diels–Alder face spécifique de la diénone-ester **10** avec le *trans*-pipérylène qui conduit à l'adduit **11** contenant le noyau décaline et les centres stéréogéniques corrects pour plusieurs diterpénoïdes du *cis*-clérodane.

Mots clés : *cis*-clérodanes, méthode générale de synthèse totale, réaction de Diels–Alder face sélective.

[Traduit par la rédaction]

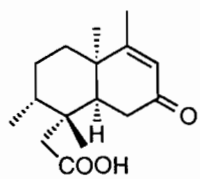
Introduction

Diterpenoids possessing the clerodane (**1**) carbon skeleton are widely distributed in nature and constitute one of the largest and, yet, still rapidly growing family of secondary metabolites. To date, more than 800 compounds have been isolated and structurally characterized from various natural sources, about one quarter in the last four years (1). Clerodanes are best



1

known for their antifeedant properties. Of the relatively few tested for biological activity, many were also found to possess interesting medicinal properties and are potentially useful as antiviral, antitumor, antifungal, antibiotic, anti-peptic ulcer, and psychotropic agents (1, 2). The structural complexity and biological activity associated with this class of natural products have attracted extensive effort towards their total syntheses. More than 15 successful syntheses have been reported for the sub-series of *trans*-clerodanes (Fig. 1) (3). Relatively few syntheses, however, are known for the *cis* sub-series of compounds (Fig. 1) (4). In virtually all of the reported syntheses, a linear approach to the specific target molecule is involved. Since naturally occurring clerodanes are vast in number and their structural differences are mainly due to stereochemistry, oxidation level, and oxygen contents of various centers, it is highly desirable to develop a general nonlinear synthetic approach, whereby a large number of target molecules can be synthesized by a common strategy with minor adjustments. We wish to demonstrate herein such an approach highlighted by the first total synthesis, in racemic form, of the title carboxylic acid **2**, which was recently isolated from *vellozia bicolor* L.B. Smith by Garcez and co-workers (5).



2

Results and discussion

In recent years, an extensive study of the Diels–Alder chemistry of 4,4-dimethyl-2-cyclohexenones and several closely related cross-conjugated cyclic unsaturated β-dicarbonyl compounds has been carried out in our laboratories (6–12). On the basis of these studies, a general synthetic scheme

Received July 2, 1996.

This paper is dedicated to Professor William A. Ayer on the occasion of his 65th birthday.

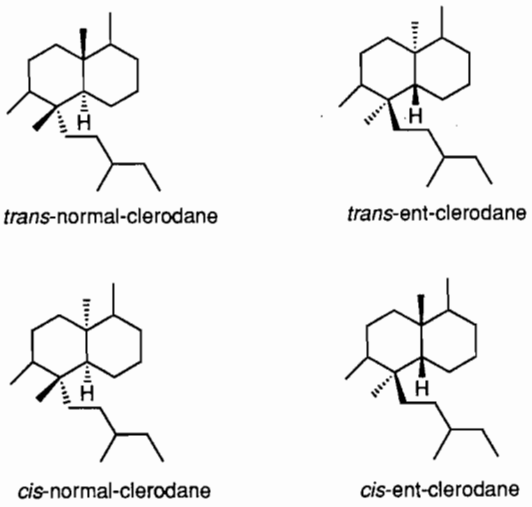
H.J. Liu,[1] K.S. Shia, Y. Han, and D. Sun. Department of Chemistry, University of Alberta, Edmonton, AB T6G 2G2, Canada.
Y. Wang. Department of Chemistry, National Taiwan University, Taipei, Taiwan, Republic of China.

[1] Author to whom correspondence may be addressed. Telephone: (403) 492-3477. Fax: (403) 492-8231.

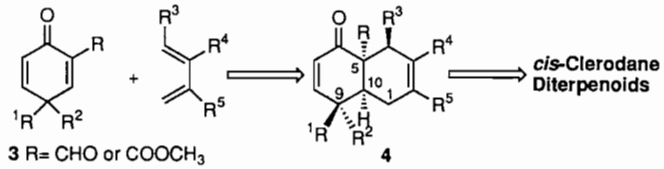
© 1997 NRC Canada

Can. J. Chem. Downloaded from www.nrcresearchpress.com by 88.146.161.215 on 09/08/12
For personal use only.

Fig. 1. Major structural types of clerodane diterpenoids.



Scheme 1.

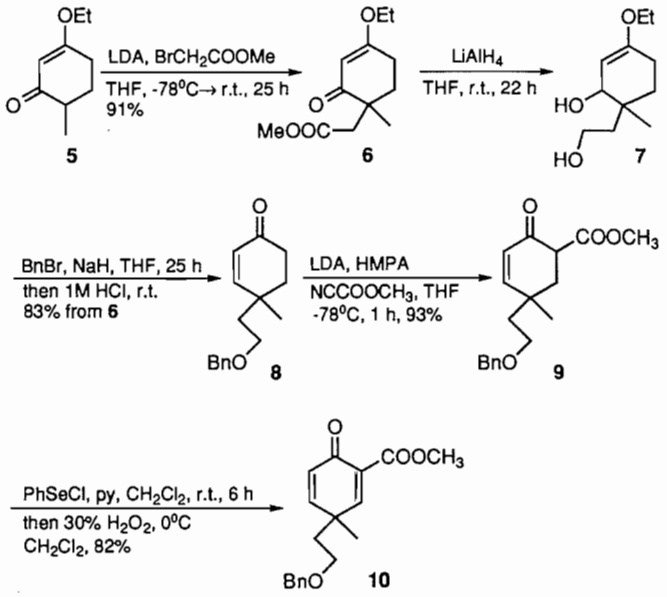


(Scheme 1) that would facilitate the rapid assembly of a variety of *cis*-clerodane diterpenes, especially the highly oxygenated ones, via a general intermediate **4** has been conceived. By this Diels–Alder approach, the relative stereochemistry of the three contiguous chiral centers C_5, C_9, and C_{10} (clerodane numbering) of **4** is expected to be arranged in the same manner as those of the natural *cis*-clerodanes based mainly on the following steric consideration. It is highly conceivable that, if R^2 is bulkier than R^1, addition of the diene to dienophile **3** will occur preferentially from the sterically less hindered R^1 face. This approach has now been experimentally realized, culminating in the total synthesis of 2-oxo-5α,8α-13,14,15,16-tetranorclerod-3-en-12-oic acid (**2**) in racemic form and the formation of several advanced intermediates potentially useful for the preparation of a variety of *cis*-clerodanes.

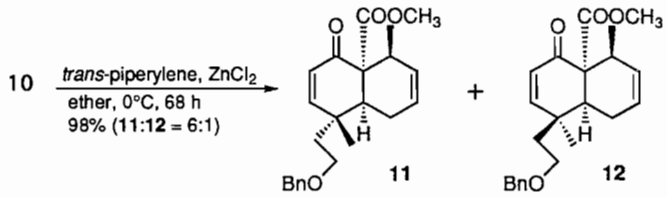
During the preliminary investigation, several dienophiles of formula **3** have been synthesized and explored. The outcome revealed that Diels–Alder adducts obtained with an angular aldehyde moiety α to the ketone carbonyl were not stable enough for further elaboration. A more practical dienophile **10**, a dienone with an α-ester group, was finally adopted.

Compound **10** was readily prepared from 3-ethoxy-6-methyl-2-cyclohexenone (**5**) (13) according to the synthetic sequence shown in Scheme 2. Stork–Danheiser alkylation (14) of **5** with methyl bromoacetate gave enone ester **6** in 91% yield. This compound was reduced with lithium aluminum hydride to give a mixture of two diastereomeric diols **7** in nearly equal amounts. Without further purification, the mixture of the unstable diols **7** was immediately subjected to selective benzylation with a slight excess of sodium hydride and benzyl bromide. Treatment of the crude product with dilute hydrochloric acid afforded enone **8** in 83% yield from **6**. Later,

Scheme 2.



Scheme 3.



it was found that, even if benzylation occurred at both hydroxyls when excess benzyl bromide and base were applied, the *bis*-benzylated product could also be easily converted into **8** under the same hydrolysis conditions. Enone **8** was subjected to carbomethoxylation using lithium diisopropylamide and methyl cyanoformate (15) to give keto ester **9** as a mixture of three isomers (a pair of epimers and an enol ester) in a ratio of 2:1.4:1 as indicated by the ^{1}H nmr spectrum. Keto ester **9** was then treated with phenylselenenyl chloride in the presence of pyridine (16). Oxidative elimination of the resulting selenide with hydrogen peroxide gave the required dienone ester **10** in 82% yield.

Dienone ester **10** proved to be an excellent dienophile. Under zinc chloride catalysis, it underwent cycloaddition with *trans*-piperylene to furnish adducts **11** (from the sterically less hindered methyl face) and **12** in 84% and 14% yield, respectively (Scheme 3). Slightly inferior results (95% yield; **11**:**12** = 5.3:1) were obtained when ferric chloride was used as a catalyst (CH_2Cl_2, −55°C, 21 h). The Diels–Alder adducts were readily separated by flash chromatography, and their regiochemistries were deduced by the following evidences. For the less polar major isomer **11**, the splitting pattern (ddd, J = 10, 7, 2 Hz) of the ring junction C_6 proton at δ 2.75 in the ^{1}H nmr spectrum clearly demonstrated that it was an *ortho* adduct. In a similar fashion, the minor isomer **12** showed a doublet of doublet of doublets (J = 10, 7, 2 Hz) for the C_6 proton at δ 2.68 suggesting that it was also an *ortho*-addition product. To determine the relative stereochemistry of each, extensive NOE

© 1997 NRC Canada

Can. J. Chem. Downloaded from www.nrcresearchpress.com by 88.146.161.215 on 09/08/12
For personal use only.

Fig. 2. NOE effects for **11**.

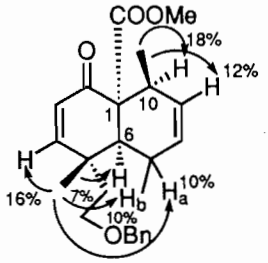
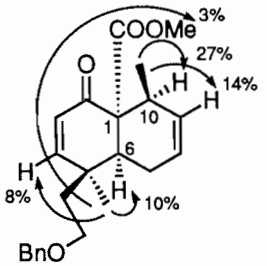


Fig. 3. NOE effects for **12**.

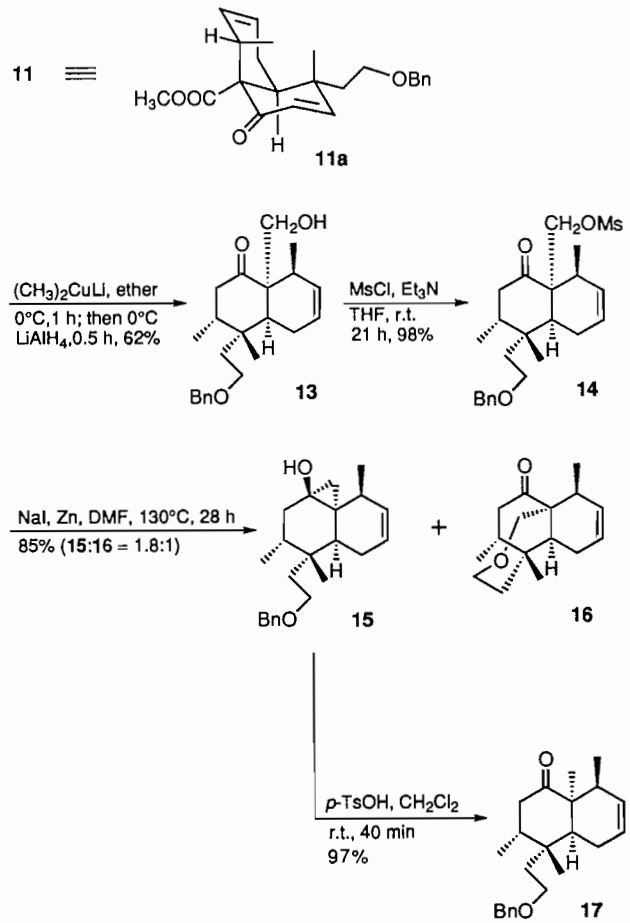


experiments were carried out for both compounds. For the major isomer, irradiation of the C_5 methyl at δ 1.10 resulted in enhancements for H_4 (16%), H_6 (6.9%), H_{7a} (10.2%), and H_{7b} (10.2%) (Fig. 2). On the other hand, irradiation of the C_5 methyl (δ 1.15) of the minor isomer gave enhancements for the methoxy methyl (2.8%), the C_4 vinylic proton (8.4%), and the C_6 proton (10%) (Fig. 3). No enhancements were observed for H_{7a} and H_{7b}. Therefore, structures **11** and **12** were assigned to the major and minor products, respectively.

Although, at this stage, the relative stereochemistry at each C_{10} position of **11** and **12** could not be confirmed based on the NOE studies, the configuration of this center in each case was tentatively assigned based on the previously observed preferential *endo*-to-ketone addition of *trans*-piperylene to several dienophiles resembling compound **10** (6). These structural assignments were later substantiated by the X-ray crystallographic analysis of a more advanced intermediate **16** (*vide* infra).

Adduct **11** possesses four contiguous stereogenic centers incorporated simultaneously in a correct sense for many naturally occurring *cis*-clerodanes. The remaining crucial stereogenic center was introduced via a conjugate addition process (Scheme 4). Treatment of adduct **11** with lithium dimethylcuprate followed by reduction of the resulting enolate with lithium aluminum hydride afforded keto alcohol **13** in 62% yield by a single operation. In this transformation, the enolate resulting from the conjugate addition served as an effective protecting group for the more reactive ketone carbonyl; thereby the desired reduction of the less reactive ester carbonyl could be achieved without further elaboration. Compound **13** was formed as the only stereoisomer, presumably via preferential axial addition of the cuprate to the sterically less hindered side of the conformer **11a**. To remove its hydroxy group, keto alcohol **13** was converted to the corresponding mesylate in quantitative yield using methanesulfonyl chloride and triethylamine. Reduction of mesylate **14** with sodium iodide and zinc dust (17) in DMF at 130°C gave rise to a 55% yield of cyclopropanol **15** and a 30% yield of the crystalline tricyclic ketone **16**, mp 74.5–76.0°C. The former product was likely formed via the addition of the intermediate carbanion resulting from the reductive removal of the methanesulfonyloxy group to the ketone carbonyl, and the latter via the displacement of the mesylate with the benzyl ether followed by debenzylation. Ketone **16** was subjected to X-ray crystallographic analysis. The crystal structure of **16** as shown in Fig. 4 made unambiguous the assignment of the five contiguous stereogenic centers along C_1, C_4, C_5, C_6, and C_{10} present in **16** and its precursors. Cyclopropanol **15** was found to be a suitable intermediate for the formation of the desired ketone **17** (Scheme 4). Upon exposure to a catalytic amount of *p*-toluenesulfonic acid in methylene chloride, it underwent rapid ring cleavage to give ketone **17** in 97% yield.

Scheme 4.



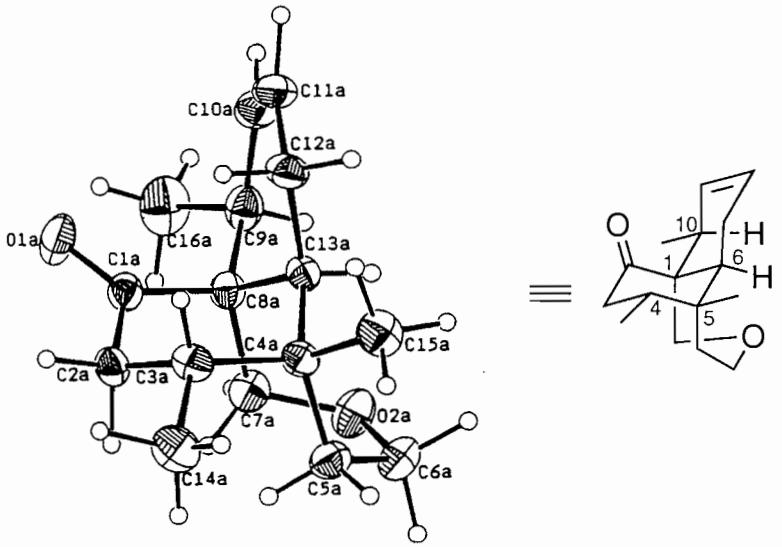
Several other methods were explored in attempts to produce the desired ketone **17** more efficiently. These efforts, however, were not fruitful. Reduction of mesylate **14** with an excess of lithium triethylborohydride in tetrahydrofuran gave rise to alcohol **18** as a result of the reduction of the ketone carbonyl followed by a Grob fragmentation and further reduction of the ensuing aldehyde. In another approach, keto alcohol **13** was transformed to thiocarbonate **19** in 72% yield by treatment with phenyl chlorothionoformate and pyridine in dichloromethane at room temperature. Unfortunately, other functionalities present in **19** were shown to be incompatible with

Can. J. Chem. Downloaded from www.nrcresearchpress.com by 88.146.161.215 on 09/08/12
For personal use only.

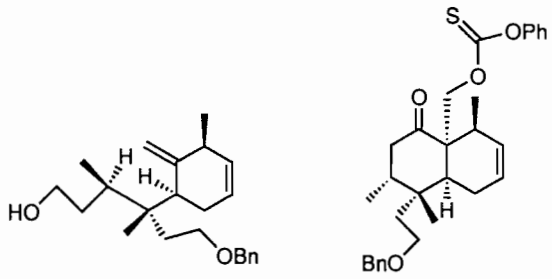
© 1997 NRC Canada

Can. J. Chem. Downloaded from www.nrcresearchpress.com by 88.146.161.215 on 09/08/12
For personal use only.

Fig. 4. The three-dimensional X-ray crystallographical strucutre of **16**.



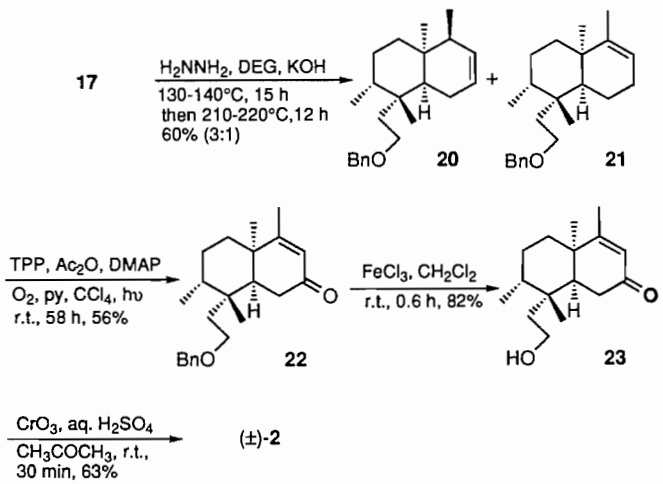
the reaction conditions required to remove the thiocarbonate moiety using tri-*n*-butyltin hydride.



18 **19**

Ketone **17** can, in principle, serve as a key intermediate for two groups of *cis*-clerodane diterpenes, one with an oxygen atom at C_6 (clerodane numbering), such as solidagolactones II–VIII (18–21), 6β-acetoxy-2-oxokolavenool (22), etc., and the other without an oxygen atom at C_6, such as solidagoic acid A (23, 24), tinotufolin B (25), 2-oxo-5α,8α-13,14,15,16-tetranorclerod-3-en-12-oic acid (**2**), etc. The total synthesis of **2** has been accomplished as follows (Scheme 5). The ketone carbonyl of **17** was removed by a Wolff–Kishner reduction using hydrazine, and potassium hydroxide in diethylene glycol at ~210°C. Two isomeric products **20** and **21** were formed in 3:1 ratio (^{1}H nmr analysis) and in a total yield of 60%. Subsequent irradiation (tungsten lamps) of this inseparable mixture in carbon tetrachloride in the presence of oxygen, 5,10,15,20-tetraphenyl-21*H*,23*H*-porphine, acetic anhydride, pyridine, and 4-dimethylaminopyridine (26) gave rise to enone **22** (56% yield based on **20**) along with an unidentified product. The regioselectivity observed for the photooxygenation reaction was somewhat unusual. Instead of forming an enone system with a less substituted double bond following the "normal" regiochemical course of photooxygenation, the double bond moved towards the carbon center possessing a greater number of substituents. The unusual regiochemistry in the present case was nevertheless quite predictable based on the studies on several structurally closely related compounds in this series (27–29). However, exactly what controls the regiochemistry is

Scheme 5.



not fully understood. Enone **22** was subjected to treatment with ferric chloride (30) to effect the removal of the benzyl protecting group. Finally, alcohol **23** thus obtained in 82% yield was oxidized using Jones reagent (31) to afford the target clerodenoic acid **2** (63% yield) in racemic form, m.p. 226–227°C (236°C for the optically active natural **2** (5)). The spectral data (^{1}H nmr, ^{13}C nmr, and mass) of the synthetic material are in good agreement with those reported for the natural product.

Conclusion

The foregoing describes a simple nonlinear, general synthetic approach to diterpenoids of the clerodane family. Several advanced synthetic molecules, e.g., **13**, **17**, and **23**, are potentially useful for the preparation of a variety of naturally occurring compounds. Furthermore, by careful selection of the starting diene involved in the early Diels–Alder cycloaddition, oxygen functionalities can, in principle, also be directly incorporated to C_1, C_2, C_3, and C_{18}. Thus, by a small adjustment, the

© 1997 NRC Canada

Can. J. Chem. Downloaded from www.nrcresearchpress.com by 88.146.161.215 on 09/08/12
For personal use only.

demonstrated scheme should also facilitate the synthesis of those clerodanes oxygenated at one or more of these positions. The validity of this synthetic approach is illustrated with the total synthesis of (±)-2-oxo-5α,8α-13,14,15,16-tetranorclerod-3-en-12-oic acid (**2**).

Experimental

General

Melting points were recorded on a Kofler hot stage apparatus and are not corrected. Combustion elemental analyses were performed by the microanalytical laboratory of this department. Fourier transform infrared spectra (ir) were recorded on a Nicolet 7199 or Nicolet MX-1 FTIR spectrophotometer. Proton nuclear magnetic resonance (^{1}H nmr) spectra were recorded on a Bruker WH-80, Bruker WH-200, Bruker WH-300, Bruker WH-400, or Bruker AM-400 spectrometer using deuteriochloroform ($CDCl_3$) as solvent unless otherwise stated. Tetramethylsilane (TMS) was used as an internal reference. Coupling constants are reported to ±0.5 Hz. Chemical shift measurements are reported in ppm downfield from TMS in delta (δ) units. The following abbreviations are used: s = singlet, d = doublet, t = triplet, q = quartet, m = multiplet, and br = broad. Carbon-13 nuclear magnetic resonance (^{13}C nmr) spectra were recorded on a Varian Unity-500 (125 MHz) spectrometer or a Bruker WH-300 (75 MHz) NMR spectrometer, and were obtained as solutions in deuteriochloroform as the internal standard setting the central peak at 77.00 ppm. Carbon-13 multiplicities were derived from Carr–Purcell–Meiboom–Gill spin echo *J*-modulated experiments (APT or Attached Proton Test) (32, 33). Methyl and methine groups are shown as signals possessing an antiphase (a) with respect to the deuteriochloroform signal, whereas methylene groups, quaternary carbons, and carbonyl groups appear in phase (p) with it. Nuclear Overhauser enhancement (nOe) experiments were determined in the difference mode in which a control (undecoupled) spectrum was computer subtracted from the irradiated spectrum after Fourier transformation. Positive enhancements are defined as signals possessing an antiphase with respect to the irradiated signal. Samples for nOe measurements were deoxygenated with argon for 10 min prior to use. High-resolution electron impact mass spectra (hrms) were recorded using an A.E.I. model MS-50 mass spectrometer. Chemical ionization mass spectra (cims) were recorded on an A.E.I. model MS-12 mass spectrometer, using ammonia as the reagent gas. Spectral data are reported as *m/z* values.

All reactions were carried out under slight positive pressure of argon. Bulb-to-bulb distillation was performed using a Kugelrohr distillation apparatus. Flash chromatography developed by Still et al. (34) was used routinely for purification and separation of product mixtures, using silica gel (Merck) of 230–400 mesh. All solvents for chromatography were distilled prior to use. Concentrations of solvent systems used in column chromatography are given by volume, e.g., 20% ethyl acetate in petroleum ether means 20 parts of ethyl acetate by volume to 80 parts of petroleum ether by volume. Analytical thin-layer chromatography (tlc) was carried out on aluminum sheets precoated (0.2 mm layer thickness) with silica gel 60 F_{254} (E. Merck, Darmstadt). Ultraviolet-active materials were detected by visualization under a uv lamp (254 or 350 nm). For tlc, the visualization of the chromatograms was completed by dipping in an ethanol solution of vanillin (5%, w/v) and sulfuric acid (5%, v/v), followed by careful charring on a hot plate. Alternatively, an aqueous solution of phosphomolybdic acid (3%, w/v) containing ceric sulfate (0.5%,w/v) and sulfuric acid (3%, v/v) was used as the dipping solution, followed by charring on a hot plate.

Materials

Unless otherwise stated, all materials used are commercially available. All compounds made are racemic. Solvents used were distilled under an argon atmosphere from appropriate drying agents. Tetrahydrofuran (THF), diethyl ether, toluene, and 1,2-dimethoxyethane (DME) were dried with sodium and benzophenone. Acetone was predried with potassium carbonate, and then distilled from potassium permanganate. Diisopropylamine was obtained by distillation from sodium hydroxide or potassium hydroxide. Pyridine, benzene, dichloromethane, carbon tetrachloride, and triethylamine (TEA) were distilled from calcium hydride. Reactions requiring anhydrous conditions were performed in oven- or flame-dried glassware that was assembled and allowed to cool while being purged with argon. Argon was passed through a column of 4 Å molecular sieves and self-indicating silica gel.

6-(Carbomethoxymethyl)-3-ethoxy-6-methyl-2-cyclohexenone (6)

To a solution of diisopropylamine (8.3 mL, 59 mmol) in THF (17 mL) at 0°C under an argon atmosphere, was added *n*-BuLi (34 mL, 1.6 M in hexane) slowly. The mixture was stirred at 0°C for 15 min and then cooled down to −78°C. A solution of 3-ethoxy-6-methyl-2-cyclohexenone (**5**) (7.65 g, 49 mmol) in THF (20 mL) was added dropwise over a period of 15 min. The resulting mixture was stirred at −78°C for 1 h, and methyl bromoacetate (9.6 mL, 98 mmol) was added in one portion. The mixture was allowed to warm up slowly to room temperature and stirred overnight. Saturated ammonium chloride was added and the mixture was extracted with ether (3 × 40 mL). The extracts were combined, washed with water, brine, and dried over magnesium sulfate. Filtration and concentration followed by bulb-to-bulb distillation at 128–130°C/0.7 Torr (1 Torr = 133.3 Pa) gave rise to the alkylation product **6** (10.2 g, 91% yield) as a light yellow oil: ir (CH_2Cl_2 cast): 1737 (C=O, ester) and 1654 (C=O, enone) cm^{-1}; ^{1}H nmr (200 MHz) δ: 5.29 (d, *J* = 1 Hz, 1 H, -C=C**H**-C=O), 3.91 (q, *J* = 7 Hz, 1 H, CH_3C**H**HO-), 3.90 (q, *J* = 7 Hz, 1 H, CH_3CH**H**O-), 3.62 (s, 3 H, -COOC**H**$_3$), 2.79 (d, *J* = 15.5 Hz, 1 H, -C**H**HCOOCH$_3$), 2.35 (d, *J* = 15.5 Hz, 1 H, -CH**H**COOCH$_3$), 2.60–2.19 (m, 3 H), 1.81–1.67 (m, 1 H), 1.35 (t, *J* = 7 Hz, 3 H, C**H**$_3$CH$_2$O-), and 1.16 (s, 3 H, -C**H**$_3$); ^{13}C nmr (75 MHz) δ: 200.18 (p), 174.54 (p), 171.64 (p), 101.31 (a), 63.87 (p), 50.84 (a), 42.33 (p), 41.76 (p), 31.56 (p), 26.08 (p), 22.33 (a), and 13.98 (a); hrms M$^+$: 226.1200 (calcd. for $C_{12}H_{18}O_4$: 226.1205). Anal. calcd. for $C_{12}H_{18}O_4$: C 63.70, H 8.02; found: C 63.70, H 8.39.

4-(2-Benzyloxyethyl)-4-methyl-2-cyclohexenone (8)

To a suspension of lithium aluminium hydride (0.81 g, 21.3 mmol) in THF (20 mL) at 0°C under an argon atmosphere, was added dropwise a solution of enone ester **6** (2.1 g, 9.3 mmol) in THF (20 mL). The resulting mixture was stirred at 0°C for 1 h and then at room temperature for 21 h. To the mixture cooled to 0°C and diluted with ether (30 mL), were added alternately

© 1997 NRC Canada

Can. J. Chem. Downloaded from www.nrcresearchpress.com by 88.146.161.215 on 09/08/12
For personal use only.

portions of water (0.12 mL) and 3 N NaOH (0.12 mL) over a period of 1 h. The resulting grey suspension was stirred for another hour and filtered. The residue was washed thoroughly with ether. The filtrate was concentrated to give the crude product (1.9 g), which, without purification, was dissolved in THF (18 mL) and added to a suspension of sodium hydride (0.48 g, 11.4 mmol) in THF (20 mL) at 0°C under argon. The mixture was stirred for 1 h (0°C→room temperature), and then benzyl bromide (3.25 g, 19 mmol) was introduced at 0°C. After stirring at room temperature for 25 h, the solution was acidified to pH = 1-1.5 with 1 N HCl, and the resulting solution stirred for 2 h. After the hydrolysis was complete, the mixture was extracted with ether (3 × 40 mL). The extracts were combined and washed with saturated sodium bicarbonate, water, and brine. After being dried over magnesium sulfate, the solution was filtered and concentrated to give the crude product. Flash chromatography using ethyl acetate and hexane (20:80) gave compound **8** (1.88 g, 83% yield from **6**) as a light yellow oil. Alternatively, it could be distilled at 175°C/1 torr to give the product as a colorless oil: ir ($CHCl_3$ cast): 1680 (C═O, enone), 738 and 698 (C-H bending, aromatic) cm^{-1}; ^1H nmr (300 MHz) δ: 7.32 (m, 5 H, aromatic **H**), 6.75 (d, J = 10 Hz, 1 H, -C**H**═CH-C═O), 5.86 (d, J = 10 Hz, 1 H, -CH═C**H**-C═O), 4.49 (s, 2 H, -OC**H**$_2$Ph), 3.51–3.64 (m, 2 H, -C**H**$_2$OBn), 2.47 (m, 2 H), 2.02 (ddd, J = 15, 7, 7 Hz , 1 H, -C**H**HC═O), 1.73–1.90 (complex, 3 H), and 1.18 (s, 3 H, -C**H**$_3$); ^{13}C nmr (75 MHz) δ: 199.27 (p), 158.75 (a), 138.11 (p), 128.31 (a, 2 × aromatic **C**), 127.54 (a), 127.49 (a, 2 × aromatic **C**), 127.12 (a), 73.04 (p), 66.59 (p), 40.20 (p), 34.92 (p), 34.05 (p, 2 × -**C**H$_2$-), and 25.19 (a); hrms M^+: 244.1459 (calcd. for $C_{16}H_{20}O_2$: 244.1463). Anal. calcd. for $C_{16}H_{20}O_2$: C 78.65, H 8.25; found: C 78.93, H 8.52.

4-(2-Benzyloxyethyl)-6-carbomethoxy-4-methyl-2-cyclohexenone (9)

To a suspension of sodium hydride (60% dispersion in mineral oil, 4.21 g, 105 mmol) in THF (20 mL) under an argon atmosphere, was added dimethyl carbonate (17 mL, 180 mmol). The mixture was brought to boiling, and then a solution of enone **8** (11.3 g, 46 mmol) in THF (20 mL) was added dropwise over a period of 30 min. The resulting mixture was heated under reflux for 24 h and then cooled to 0°C. Ice-cold 1 N HCl (35 mL) was added cautiously to the mixture, and the resulting solution extracted with ether (3 × 50 mL). The extracts were combined and washed with water and brine. After being dried over magnesium sulfate, the solution was filtered and concentrated to give the crude product. Flash chromatography using ethyl acetate and hexane (10:90) gave keto ester **9** (7.56 g, 54% yield) as a yellowish oil: ir ($CHCl_3$ cast): 1744 (C═O, ester), 1681 (C═O, enone), 1626 and 1592 (C═C, enol ester), 738 and 698 (C-H bending, aromatic) cm^{-1}; ^1H nmr (300 MHz), three isomers in a ratio of 2:1.4:1; isomer 1: δ: 7.32 (m, 5 H, aromatic **H**), 6.81 (dd, J = 10, 2 Hz, 1 H, -C**H**═CHCO), 5.90 (d, J = 10 Hz, 1 H, -CH═C**H**CO), 4.48 (s, 2 H, -OC**H**$_2$Ph), 3.78 (s, 3 H, -COOC**H**$_3$), 3.50–3.65 (m, 2 H, -C**H**$_2$OBn), 1.64–2.50 (m), and 1.21 (s, 3 H, -C**H**$_3$); isomer 2: δ: 6.72 (dd, J = 10, 1.5 Hz, 1 H, -C**H**═CHCO), 5.92 (d, J = 10 Hz, 1 H, -CH═C**H**CO), 4.49 (s, 2 H, -OC**H**$_2$Ph), 3.74 (s, 3 H, -COOC**H**$_3$), and 1.18 (s, 3 H, -C**H**$_3$); isomer 3: δ: 11.87 (s, 1 H, -C═C-O**H**), 6.11 (d, J = 10 Hz, 1 H, -C**H**═CHCO), 5.88 (d, J = 10 Hz, 1 H, -CH═C**H**CO), 4.47 (s, 2 H, -OC**H**$_2$Ph), 3.73 (s, 3 H, -COOC**H**$_3$), and 1.07 (s, 3 H, -C**H**$_3$); hrms M^+: 302.1515 (calcd. for $C_{18}H_{22}O_4$: 302.1518). Anal. calcd. for $C_{18}H_{22}O_4$: C 71.49, H 7.34; found: C 71.41, H 7.39.

Alternatively, the above carbomethoxylation could be achieved by the following method in higher yield. *n*-Butyllithium (6.06 mL, 2.5 M in hexane) was added to a stirred solution of anhydrous diisopropylamine (2.25 mL, 15.9 mmol) in THF (20 mL) at 0°C under an atmosphere of argon. After 30 min, the temperature was lowered to −78°C, a solution of enone **8** (1.85 g, 7.58 mmol) in THF (10 mL) was added dropwise to the mixture over a period of 15 min, and stirring continued at 0°C for 1 h. The temperature was lowered again to −78°C, and then HMPA (1.45 mL, 8.34 mmol) was added, followed by the addition of methyl cyanoformate (0.91 mL, 11.4 mmol) in one portion. After stirring for 1 h at −78°C, the mixture was warmed up to room temperature and quenched with cold water (10 mL). The product was extracted into ether (3 × 20 mL), dried ($MgSO_4$), filtered, concentrated, and chromatographed on silica gel (10% ethyl acetate in hexane) to afford compound **9** (2.1 g, 93% yield) as a yellowish oil.

4-(2-Benzyloxyethyl)-2-carbomethoxy-4-methyl-2,5-cyclohexadienone (10)

Pyridine (0.51 mL, 5.9 mmol) was added slowly to a solution of phenylselenenyl chloride (1.10 g, 5.7 mmol) in dichloromethane (25 mL) at 0°C. After 20 min, keto ester **9** (1.4 g, 4.6 mmol) in dichloromethane (10 mL) was added. The mixture was stirred at 0°C for 1 h and then at room temperature for 6 h. The organic layer was separated, washed with 10% HCl (2 × 10 mL), and cooled again to 0°C. A solution of 30% H_2O_2 was added successively (0.2 mL every 5 min) until the white precipitate was formed. After an additional 20 min, H_2O (5 mL) was added. The organic layer was separated, and the aqueous solution extracted with dichloromethane (2 × 20 mL). The combined extracts were washed with water, saturated aqueous sodium bicarbonate, and brine. After being dried over $MgSO_4$, the solution was filtered and concentrated. The residue was subjected to flash chromatography using ethyl acetate and hexane (30:70) as the eluant to give dienone ester **10** (1.14 g, 82% yield) as a light yellow oil: ir (CH_2Cl_2 cast): 1741 (C═O, ester), 1664 (C═O, enone), 739 and 699 (C-H bending, aromatic) cm^{-1}; ^1H nmr (300 MHz) δ: 7.59 (d, J = 3 Hz, 1 H, -C**H**═C-COOCH$_3$), 7.21–7.36 (m, 5 H, aromatic **H**), 6.78 (dd, J = 10, 3 Hz, 1 H, -C**H**═CHC═O), 6.29 (d, J = 10 Hz, 1 H, -CH═C**H**C═O), 4.35 (s, 2 H, -OC**H**$_2$Ph), 3.80 (s, 3 H, -COOC**H**$_3$), 3.26–3.41 (m, 2 H, -C**H**$_2$OBn), 1.97–2.13 (m, 2 H, -C**H**$_2$CH$_2$OBn), and 1.32 (s, 3 H, -C**H**$_3$); ^{13}C nmr (75 MHz) δ: 181.59 (p), 165.03 (p), 160.88 (a), 153.52 (a), 137.77 (p), 130.53 (p), 129.19 (a), 128.34 (a, 2 × aromatic **C**), 127.62 (a, 2 × aromatic **C**), 73.15 (p), 66.66 (p), 52.18 (a), 41.05 (p), 40.54 (p), and 25.98 (a); hrms M^+: 300.1353 (calcd. for $C_{18}H_{20}O_4$: 300.1361). Anal. calcd. for $C_{18}H_{20}O_4$: C 71.98, H 6.71; found: C 71.81, H 6.76.

(1*R**,5*R**,6*S**,10*S**)-5-(2-Benzyloxyethyl)-1-carbomethoxy-5,10-dimethylbicyclo[4.4.0]deca-3,8-dien-2-one (11) and (1*R**,5*S**,6*S**,10*S**)-5-(2-benzyloxyethyl)-1-carbomethoxy-5,10-dimethylbicyclo[4.4.0]deca-3,8-dien-2-one (12)

$ZnCl_2$ (1.0 g, 7.5 mmol) in a three-neck round bottom flask was fused under argon and then cooled to room temperature.

© 1997 NRC Canada

Can. J. Chem. Downloaded from www.nrcresearchpress.com by 88.146.161.215 on 09/08/12
For personal use only.

Dry ether (25 mL) was added and the $ZnCl_2$ was crushed to small pieces using a spatula. The mixture was stirred for 15 min until a fine suspension was formed. It was then cooled to 0°C and a solution of dienone ester **10** (0.75 g, 2.5 mmol) in ether (20 mL) was added dropwise. After the addition, the cloudy suspension turned clear, presumably due to the complexation of the dienophile and $ZnCl_2$. *trans*-Piperylene (3.75 mL, 7.52 mmol) was added and the resulting mixture was stirred under argon at 0°C for 68 h. The solution was quenched by addition of water and made basic with saturated aqueous sodium bicarbonate. The aqueous solution was extracted with ether (2 × 15 mL) and the combined extracts were washed with water, saturated sodium bicarbonate, and brine. Drying ($MgSO_4$), filtration, concentration, and flash chromatography using ethyl acetate and petroleum ether (5:95) gave adduct **11** (0.77 g, 84% yield) as a colorless oil: ir ($CHCl_3$ cast): 1725 (C=O, ester), 1690 (C=O, enone), 734 and 699 (C-H bending, aromatic) cm^{-1}; ^1H nmr (300 MHz) δ: 7.32 (m, 5 H, aromatic **H**), 6.29 (dd, *J* = 10, 2 Hz, 1 H, -C**H**=CHC=O), 5.92 (d, *J* = 10 Hz, 1 H, -CH=C**H**C=O), 5.57 (ddd, *J* = 10, 4, 2 Hz, 1 H, C-9 **H**), 5.50 (ddd, *J* = 10, 7, 3 Hz, 1 H, C-8 **H**), 4.52 (d, *J* = 14 Hz, 1 H, -OC**H**HPh), 4.48 (d, *J* = 14 Hz, 1 H, -OCH**H**Ph), 3.69 (s, 3 H, -COOC$\mathbf{H}_3$), 3.58–3.66 (m, 2 H, -C$\mathbf{H}_2$OBn), 2.83 (m, 1 H, C-10 **H**), 2.75 (ddd, *J* = 10, 7, 2 Hz, 1 H, C-6 **H**), 2.16 (dm, *J* = 18 Hz, 1 H, C-7 $\mathbf{H}_a$), 1.95 (dm, *J* = 18 Hz, 1 H, C-7 $\mathbf{H}_b$), 1.78 (dd, *J* = 14, 7 Hz, 1 H, -C**H**HCH$_2$OBn), 1.72 (dd, *J* = 14, 7 Hz, 1 H, -CH**H**CH$_2$OBn), 1.22 (d, *J* = 7 Hz, 3 H, C-10 C$\mathbf{H}_3$), and 1.10 (s, 3 H, C-5 C$\mathbf{H}_3$); ^{13}C nmr (75 MHz) δ: 196.33 (p), 174.54 (p), 152.27 (a), 138.37 (p), 130.62 (a), 128.42 (a, 2 × aromatic **C**), 127.57 (a, 2 × aromatic **C**), 127.32 (a), 123.36 (a), 73.12 (p), 66.64 (p), 59.29 (p), 52.37 (a), 43.07 (a), 39.61 (p), 39.10 (p), 37.66 (a), 26.62 (p), 24.22 (a), and 16.87 (a); hrms M^+: 368.1980 (calcd. for $C_{23}H_{28}O_4$: 368.1987). Anal. calcd. for $C_{23}H_{28}O_4$: C 74.97, H 7.66; found: C 75.03, H 7.81.

Further elution gave adduct **12** (0.13 g, 14% yield) as a colorless oil: ir ($CHCl_3$ cast): 1726 (C=O, ester), 1689 (C=O, enone), 735 and 699 (C-H bending, aromatic) cm^{-1}; ^1H nmr (300 MHz) δ: 7.33 (m, 5 H, aromatic **H**), 6.29 (dd, *J* = 10, 2 Hz, 1 H, -C**H**=CHC=O), 5.85 (d, *J* = 10 Hz, 1 H, -CH=C**H**C=O), 5.56 (ddd, *J* = 10, 4, 2 Hz, 1 H, C-9 **H**), 5.47 (ddd, *J* = 10, 7, 3 Hz, 1 H, C-8 **H**), 4.51 (d, *J* = 14 Hz, 1 H, -OC**H**HPh), 4.49 (d, *J* = 14 Hz, 1 H, -OCH**H**Ph), 3.71 (s, 3 H, -COOC$\mathbf{H}_3$), 3.54–3.66 (m, 2 H, -C$\mathbf{H}_2$OBn), 2.75 (m, 1 H, C-10 **H**), 2.68 (ddd, *J* = 10, 7, 2 Hz, 1 H, C-6 **H**), 2.30 (dddd, *J* = 19, 7, 4, 3 Hz, 1 H, C-7 $\mathbf{H}_a$), 2.02 (dm, *J* = 19 Hz, 1 H, C-7 $\mathbf{H}_b$), 1.93 (ddd, *J* = 14, 8, 6 Hz, 1 H, -C**H**HCH$_2$OBn), 1.64 (ddd, *J* = 14, 8, 6 Hz, 1 H, -CH**H**CH$_2$OBn), 1.26 (d, *J* = 7 Hz, 3 H, C-10 C$\mathbf{H}_3$), and 1.15 (s, 3 H, C-5 C$\mathbf{H}_3$); ^{13}C nmr (75 MHz) δ: 196.23 (p), 174.65 (p), 152.03 (a), 138.16 (p), 130.55 (a), 128.46 (a, 2 × aromatic **C**), 127.71 (a), 127.58 (a, 2 × aromatic **C**), 127.04 (a), 123.37 (a), 73.26 (p), 65.67 (p), 59.22 (p), 52.20 (a), 46.27 (a), 39.81 (p), 38.75 (a), 38.69 (p), 27.04 (p), 24.78 (a), and 16.69 (a); hrms M^+: 368.1984 (calcd. for $C_{23}H_{28}O_4$: 368.1987).

(1*S**,4*R**,5*R**,6*S**,10*S**)-5-(2-Benzyloxyethyl)-1-(1-hydroxymethyl)-4,5,10-trimethylbicyclo[4.4.0]dec-8-en-2-one (13)

A suspension of CuI (1.4 g, 7.3 mmol) in ether (20 mL) in a flame-dried round bottom flask was cooled to 0°C under argon. Methyllithium (10.5 mL, 1.4 M in ether) was added dropwise over a period of 5 min, and the resulting solution was stirred at 0°C for 1 h. Enone ester **11** (900 mg, 2.44 mmol) in ether (5 mL) was then introduced slowly over a period of 25 min. After the resulting yellow mixture was stirred for 1 h, lithium aluminium hydride (0.28 g, 7.3 mmol) was added. The reaction mixture turned into a dark suspension immediately after the addition of lithium aluminium hydride. This dark suspension was stirred for 30 min. Saturated aqueous ammonium chloride (10 mL) was added carefully until gas evolution ceased, followed by the addition of 3 N HCl (18 mL). The mixture was extracted with ether (4 × 20 mL). The combined extracts were washed with water (2 × 10 mL), saturated aqueous sodium bicarbonate, and brine. Drying (magnesium sulfate), filtration, and concentration gave the crude product, which was subjected to chromatography. Elution with ethyl acetate and hexane (20:80) gave alcohol **13** (501 mg, 61% yield) as a colorless oil: ir (CH_2Cl_2 cast): 3448 (br, OH), 1692 (C=O, ketone), 736 and 698 (C-H bending, aromatic) cm^{-1}; ^1H nmr (500 MHz) δ: 7.31 (m, 5 H, aromatic **H**), 5.85 (dt, *J* = 10, 4.5 Hz, 1 H, C-8 **H**), 5.75 (dd, *J* = 10, 5 Hz, 1 H, C-9 **H**), 4.49 (s, 2 H, -OC$\mathbf{H}_2$Ph), 3.58 (d, *J* = 11 Hz, 1 H, -C**H**HOH), 3.55 (t, *J* = 7 Hz, 2 H, -C$\mathbf{H}_2$OBn), 3.45 (d, *J* = 11 Hz, 1 H, -CH**H**OH), 3.26 (br s, 1 H, -O**H**), 2.50 (m, 1 H, C-10 **H**), 2.36 (dd, *J* = 10.5, 10.5 Hz, 1 H, C-3 **H**), 2.00–2.19 (complex, 5 H), 1.60 (m, 2 H), 1.10 (d, *J* = 7 Hz, 3 H, C-10 C$\mathbf{H}_3$), 0.97 (s, 3 H, C-5 C$\mathbf{H}_3$), and 0.89 (d, *J* = 6.5 Hz, 3 H, C-4 C$\mathbf{H}_3$); ^{13}C nmr (125 MHz) δ: 219.94 (p), 138.30 (p), 132.36 (a), 132.20 (a), 128.21 (a, 2 × aromatic **C**), 127.65 (a, 2 × aromatic **C**), 126.60 (a), 73.25 (p), 69.36 (p), 67.01 (p), 55.24 (p), 45.95 (p), 41.63 (a), 37.32 (p), 35.07 (a), 34.84 (p), 33.03 (a), 22.67 (p), 22.53 (a), 17.31 (a), and 15.53 (a); cims $[M+NH_4]^+$: 374. Anal. calcd. for $C_{23}H_{32}O_3$: C 77.49, H 9.05; found: C 77.29, H 9.26.

(1*S**,4*R**,5*R**,6*S**,10*S**)-5-(2-Benzyloxyethyl)-1-(1-mesyloxymethyl)-4,5,10-trimethylbicyclo[4.4.0]dec-8-en-2-one (14)

To a solution of alcohol **13** (110 mg, 0.31 mmol) and triethylamine (0.22 mL, 1.5 mmol) in THF (8 mL) at 0°C under an argon atmosphere, mesyl chloride (0.12 mL, 1.5 mmol) was added slowly. The reaction mixture was stirred at room temperature for 21 h, at which time 1 N HCl (3 mL) was added. The mixture was extracted with ether (3 × 15 mL), and the extracts were combined and washed with saturated aqueous sodium bicarbonate, water, and brine. The solution was dried over magnesium sulfate, filtered, and concentrated to afford the crude product, which was purified by flash chromatography on silica gel. Elution with ethyl acetate and hexane (5:95) gave mesylate **14** (131 mg, 98% yield) as a colorless oil: ir (CH_2Cl_2 cast): 1701 (C=O, ketone), 1357 and 1176 (S=O), 737 and 699 (C-H bending, aromatic) cm^{-1}; ^1H nmr (300 MHz) δ: 7.35 (m, 5 H, aromatic **H**), 5.91 (m, 1 H, -C**H**=CH-), 5.67 (m, 1 H, -CH=C**H**-), 4.54 (d, *J* = 12 Hz, 1 H, -OC**H**HPh), 4.51 (d, *J* = 9.5 Hz, 1 H, -C**H**HOMs), 4.44 (d, *J* = 12 Hz, 1 H, -OCH**H**Ph), 4.04 (d, *J* = 9.5 Hz, 1 H, -CH**H**OMs), 3.57 (m, 2 H, -C$\mathbf{H}_2$OBn), 2.96 (s, 3 H, -OSO$_2$C$\mathbf{H}_3$), 2.43 (dd, *J* = 7.5, 4.5 Hz, 1 H), 2.31 (dd, *J* = 16, 6 Hz, 1 H), 1.96–2.03 (complex, 5 H), 1.50–1.72 (complex, 2 H), 1.03 (d, *J* = 7 Hz, 3 H, C-10 C$\mathbf{H}_3$), 1.00 (s, 3 H, C-5 C$\mathbf{H}_3$), and 0.91 (d, *J* = 6.5 Hz, 3 H, C-4 C$\mathbf{H}_3$); ^{13}C nmr (75 MHz) δ: 213.39 (p), 138.45 (p), 130.93 (a), 128.43 (a, 2 × aromatic **C**), 127.80 (a, 2 × aromatic

© 1997 NRC Canada

Can. J. Chem. Downloaded from www.nrcresearchpress.com by 88.146.161.215 on 09/08/12
For personal use only.

C), 127.61 (a), 127.40 (a), 74.05 (p), 73.25 (p), 67.04 (p), 54.20 (p), 45.24, (p), 39.60 (a), 37.28 (p), 37.09 (a), 35.60 (a), 35.23 (p), 34.36 (a), 22.88 (p), 22.76 (a), 17.13 (a), and 15.70 (a); hrms M^+: 434.2127 (calcd. for $C_{24}H_{34}O_5S$: 434.2127).

(1*S,3*S**,5*R**,6*R**,7*S**,11*S**)-6-(2-Benzyloxyethyl)-5,6,11-trimethyltricyclo[5.4.0.0^{1,3}]undec-9-en-3-ol (15) and (1*S**,2*S**,6*S**,7*R**,14*R**)-2,7,14-trimethyl-10-oxatricyclo[5.4.3.0^{1,6}]tetradec-3-en-12-one (16)**

To a stirred solution of mesylate **14** (0.11 g, 0.25 mmol) in DMF (10 mL with 0.15% H_2O), were added sodium iodide (0.36 g, 2.5 mmol) and zinc powder (0.33 g, 5.0 mmol). The reaction mixture was immersed in a preheated oil bath at 130°C and maintained at that temperature for 28 h. The mixture was then filtered to remove excess sodium iodide and zinc powder. The filtrate was poured into water (6 mL) and extracted with 15% ethyl acetate in hexane (3 × 15 mL). The combined organic layers were then washed with water and brine, dried over $MgSO_4$, and concentrated under reduced pressure. The residual oil was purified by flash chromatography using ethyl acetate and hexane (6:94) to give tricyclic ketone **16** (19 mg, 30% yield) as a white solid, which was recrystallized from ethyl acetate and *n*-hexane to form a crystalline compound: mp 74.5–76.0°C; ir ($CHCl_3$ cast): 1704 (C=O, ketone) cm^{-1}; ^1H nmr (300 MHz) δ: 5.53 (m, 2 H, -C**H**=C**H**-), 4.21 (d, *J* = 13.5 Hz, 1 H, -C**H**HO-), 4.00 (m, 2 H, -CH_2C$\mathbf{H}_2$O-), 3.61 (d, *J* = 13.5 Hz, 1 H, -CH**H**O-), 2.63 (dd, *J* = 16.5, 8.5 Hz, 1 H, -C**H**HC=O), 2.10–2.36 (complex, 5 H), 1.92 (m, 1 H), 1.57 (dd, *J* = 5.5, 4.5 Hz, 1 H), 1.51 (dd, *J* = 5.5, 4.5 Hz, 1 H), 1.26 (d, *J* = 7.5 Hz, 3 H, C-2 C$\mathbf{H}_3$), 1.05 (s, 3 H, C-7 C$\mathbf{H}_3$), and 0.98 (d, *J* = 6.5 Hz, 3 H, C-14 C$\mathbf{H}_3$); ^{13}C nmr (APT) δ: 211.87 (p), 131.85 (a), 123.00 (a), 69.54 (p), 65.68 (p), 58.11 (p), 49.81 (a), 46.78 (p), 38.79 (p), 38.75 (a), 36.59 (a), 35.52 (p), 27.23 (a), 25.22 (p), 16.72 (a), and 15.92 (a); hrms M^+: 248.1788 (calcd. for $C_{16}H_{24}O_2$: 248.1778). Anal. calcd. for $C_{16}H_{24}O_2$: C 77.38, H 9.74; found: C 77.34, H 9.63.

Further elution gave compound **15** (47 mg, 55% yield) as a colorless oil: ir (CH_2Cl_2 cast): 3436 (br, OH), 735 and 696 (C-H bending, aromatic) cm^{-1}; ^1H nmr (300 MHz) δ: 7.32 (m, 5 H, aromatic **H**), 6.22 (m, 1 H, -C**H**=CH-), 5.96 (m, 1 H, -CH=C**H**-), 4.50 (s, 2 H, -OC$\mathbf{H}_2$Ph), 3.49 (t, *J* = 8 Hz, 2 H, -C$\mathbf{H}_2$OBn), 1.92–2.23 (complex, 6 H), 1.56–1.72 (complex, 3 H), 1.46 (m, 1 H), 1.08 (s, 3 H, C-7 C$\mathbf{H}_3$), 1.06 (d, *J* = 7 Hz, 3 H, C-2 C$\mathbf{H}_3$), 0.83 (d, *J* = 7 Hz, 3 H, C-8 C$\mathbf{H}_3$), 0.58 (dd, *J* = 5, 1.5 Hz, 1 H, cyclopropyl **H**), 0.52 (d, *J* = 5 Hz, 1 H, cyclopropyl **H**); hrms M^+: 340.2393 (calcd. for $C_{23}H_{32}O_2$: 340.2402).

(1*S,4*R**,5*R**,6*S**,10*S**)-5-(2-Benzyloxyethyl)-1,4,5,10-tetramethylbicyclo[4.4.0]dec-8-en-2-one (17)**

To a solution of compound **15** (60 mg, 0.18 mmol) in dichloromethane (5 mL) at room temperature, was added a crystal of *p*-toluenesulfonic acid. After stirring for 40 min, the reaction mixture was diluted with dichloromethane (6 mL) and then washed with saturated aqueous sodium bicarbonate, water, and brine. The organic solution was dried over $MgSO_4$, filtered, and concentrated. Flash chromatography of the residue with 10% ethyl acetate in hexane gave **17** (58 mg, 97% yield) as a colorless oil: ir ($CHCl_3$ cast): 1695 (C=O, ketone), 735 and 698 (C-H bending, aromatic) cm^{-1}; ^1H nmr (300 MHz) δ: 7.31 (m, 5 H, aromatic **H**), 5.85 (m, 1 H, -C**H**=CH-), 5.72 (m, 1 H, -CH=C**H**-), 4.52 (d, *J* = 12 Hz, 1 H, -OC**H**HPh), 4.48 (d, *J* = 12 Hz, 1 H, -OCH**H**Ph), 3.57 (m, 2 H, -C$\mathbf{H}_2$OBn), 2.23 (dd, *J* = 13, 9 Hz, 1 H, -C**H**HC=O), 2.21 (dd, *J* = 8, 4 Hz, 1 H), 2.04–2.18 (complex, 3 H), 1.96 (t, *J* = 7 Hz, 1 H), 1.58–1.71 (complex, 3 H), 1.27 (s, 3 H, C-1 C$\mathbf{H}_3$), 1.00 (d, *J* = 7 Hz, 3 H, C-10 C$\mathbf{H}_3$), 0.98 (s, 3 H, C-5 C$\mathbf{H}_3$), and 0.91 (d, *J* = 6.5 Hz, 3 H, C-4 C$\mathbf{H}_3$); ^{13}C nmr (75 MHz) δ: 217.10 (p), 138.44 (p), 132.67 (a), 129.61 (a, 2 × aromatic **C**), 128.44 (a, 2 × aromatic **C**), 127.62 (a), 126.70 (a), 73.19 (p), 67.13 (p), 51.05 (p), 47.53 (a), 45.07 (p), 39.43 (a), 37.70 (p), 35.87 (a), 35.18 (p), 29.50 (a), 23.70 (p), 23.14 (a), 17.08 (a), and 16.05 (a); hrms M^+: 340.2395 (calcd. for $C_{23}H_{32}O_2$: 340.2402).

(3*R,4*R**)-6-Benzyloxy-3,4-dimethyl-4-((1*S**,5*S**)-5-methyl-6-methylene-3-cyclohexenyl)-1-hexanol (18)**

To a solution of compound **14** (0.15 g, 0.35 mmol) in dry THF (8 mL) at 0°C under an argon atmosphere, was added lithium triethylborohydride (1.38 mL, 1.0 M in THF). After the mixture was stirred at 0°C for 30 min and then at room temperature for 3 h, the reaction was quenched with water (3 mL), and the aqueous phase was extracted with ether (2 × 10 mL). The combined organic layers were washed with brine, dried over magnesium sulfate, filtered, and concentrated under reduced pressure to give an oil, which was purified by flash chromatography using 10% ethyl acetate in hexane as eluant to yield **18** (0.1 g, 82% yield) as a colorless oil: ir (CH_2Cl_2 cast): 3342 (OH, broad) cm^{-1}; ^1H nmr (300 MHz) δ: 7.35 (m, 5 H, aromatic **H**), 5.62 (m, 1 H, -C**H**=CH-), 5.41 (m, 1 H, -CH=C**H**-), 4.97 (br s, 1 H, **H**HC=C), 4.88 (d, *J* = 1.5 Hz, 1 H, H**H**C=C), 4.42 (s, 2H, -OC$\mathbf{H}_2$Ph), 3.65 (m, 1H), 3.45–3.56 (complex, 3 H), 2.88 (m, 1 H), 2.45 (dd, *J* = 10, 5 Hz, 1H), 2.05–2.31 (complex, 2 H), 1.95 (m, 1 H), 1.85 (dd, *J* = 10, 7 Hz, 1 H), 1.62–1.75 (complex, 2 H), 1.35 (br s, 1 H, -O**H**), 1.18 (m, 1 H), 1.09 (d, J = 7 Hz, 3 H, -C$\mathbf{H}_3$), 1.0 (s, 3 H, -C$\mathbf{H}_3$), 0.89 (d, *J* = 7 Hz, 3 H, -C$\mathbf{H}_3$); hrms [M − C_5H_8]$^+$: 274.1934 (calcd. for $C_{18}H_{26}O_2$: 274.1933); cims [M+H]$^+$: 343, [M+NH_4]$^+$: 360.

(1*S,4*R**,5*R**,6*S**,10*S**)-5-(2-Benzyloxyethyl)-1-(1-phenoxythiocarbonyloxymethyl)-4,5,10-trimethylbicyclo[4.4.0]dec-8-en-2-one (19)**

Keto alcohol **13** (0.12 g, 0.34 mmol) was dissolved in dichloromethane (10 mL) and cooled to 0°C under an atmosphere of argon. 4-Dimethylaminopyridine (5 mg), pyridine (0.05 mL, 0.68 mmol), and phenyl chlorothionoformate (0.08 mL, 0.64 mmol) were introduced sequentially to the stirred solution. After stirring at room temperature for 20 h, the reaction mixture was poured into ice-cold 1 M hydrochloric acid and extracted with ether (3 × 10 mL). The extracts were washed with ice-cold 1 M hydrochloric acid, water, dried ($MgSO_4$), filtered, and concentrated. The residue was subjected to flash chromatography on silica gel, eluting with 10% ethyl acetate in hexane to give **19** (0.1 g, 70% yield) as a light yellow oil: ir (CH_2Cl_2 cast): 1703 (C=O, ketone), 1590 (C=C stretching, aromatic),1290 and 1200 (C=S) cm^{-1}; ^1H nmr (300 MHz) δ: 7.16–7.39 (complex, 8 H, aromatic **H**), 7.00 (m, 2 H, aromatic **H**), 5.82 (m, 1 H, -C**H**=CH-), 5.61 (m, 1 H, -CH=C**H**-), 4.67 (d, *J* = 10.5 Hz, 1 H, -C**H**HOCSOPh), 4.43 (s, 2 H, -OC$\mathbf{H}_2$Ph), 4.41 (d, *J* = 10.5 Hz, 1 H, -CH**H**OCSOPh), 3.53 (m, 2 H, -C$\mathbf{H}_2$OBn), 2.34 (dd, *J* = 8, 3.5 Hz, 1 H), 2.24 (dd, *J* = 17, 6 Hz, 1 H, -C**H**HCO-), 1.93–2.19 (complex, 6 H), 1.61 (ddd, *J* =

© 1997 NRC Canada

Can. J. Chem. Downloaded from www.nrcresearchpress.com by 88.146.161.215 on 09/08/12
For personal use only.

8, 8, 2 Hz, 1 H), 1.00 (d, J = 7 Hz, 3 H, C-10 C**H**$_3$), 0.98 (s, 3 H, C-5 C**H**$_3$), and 0.86 (d, J = 7 Hz, 3 H, C-4 C**H**$_3$); cims [M+NH$_4$]$^+$: 494.

(1*S,2*S**,6*R**,7*R**,8*R**)-7-(2-Benzyloxyethyl)-1,2,7.8-tetramethylbicyclo[4.4.0]dec-3-ene (20) and (1*R**,6*S**,7*R**,8*R**)-7-(2-Benzyloxyethyl)-1,2,7,8-tetramethylbicyclo[4.4.0]dec-2-ene (21)**

To a solution of ketone **17** (28 mg, 0.08 mmol) in diethylene glycol (7 mL) at room temperature, were added potassium hydroxide (32 mg, 0.56 mmol) and anhydrous hydrazine (0.2 mL, 4.0 mmol). The mixture was heated at 130–140°C for 12 h under argon. The temperature was then raised to 220°C to remove water and excess hydrazine using a Dean–Stark apparatus, and maintained at 210-220°C for 10 h. The reaction mixture was then cooled, diluted with water (6 mL), acidified with aqueous NH_4Cl, and extracted with ethyl acetate (3 × 10 mL). The combined extracts were dried ($MgSO_4$), filtered, and concentrated to give a yellow oil, which was chromatographed using 5% ethyl acetate in hexane to furnish an inseparable 3:1 mixture of compounds **20** and **21** (16 mg, 60% yield) as a colorless oil: ir (CH_2Cl_2 cast): 736 and 697 (C-H bending, aromatic) cm^{-1}; ^{1}H nmr (300 MHz) δ: **20**: 5.57 (m, 1 H, -C**H**=CH-), 5.29 (m, 1 H, -CH=C**H**-), 4.57 (d, J = 12 Hz, 1 H, -OC**H**HPh), 4.50 (d, J = 12 Hz, 1 H, -OCH**H**Ph), 3.54 (m, 2 H, -C**H**$_2$OBn), 1.14 (s, 3 H, -C**H**$_3$), 0.93 (s, 3 H, -C**H**$_3$), 0.87 (d, J = 7 Hz, 3 H, -C**H**$_3$), and 0.85 (d, J = 7 Hz, 3 H, -C**H**$_3$); **21**: 5.32 (m, 1 H, -C=C**H**-), 4.52 (s, 2 H, -OC**H**$_2$Ph), 3.70 (m, 2 H, -C**H**$_2$OBn), 1.61 (s, 3 H, -CH=CC**H**$_3$), 1.17 (s, 3 H, -C**H**$_3$), 0.93 (d, J = 7 Hz, 3 H, C-8 C**H**$_3$), and 0.81 (s, 3 H, -C**H**$_3$); hrms [M-C$_5$H$_8$]$^+$: 258.1984 (calcd. for $C_{18}H_{26}O$: 258.1983); cims [M + NH$_4$]$^+$: 344.

(1*S,6*R**,9*R**,10*R**)-10-(2-Benzyloxyethyl)-5,6,9,10-tetramethylbicyclo[4.4.0]dec-4-en-3-one (22)**

A solution of the 3:1 mixture of **20** and **21** (25 mg, 0.07 mmol), acetic anhydride (0.06 mL, 0.5 mmol), pyridine (0.05 mL, 0.5 mmol), a catalytic amount of 4-dimethylaminopyridine, and 5,10,15,20-tetraphenyl-21*H*,23*H*-porphine (2 mg) in dry carbon tetrachloride (40 mL) was saturated with oxygen for 10 min and then irradiated with two 200 W tungsten lamps for 58 h. During this period a gentle stream of oxygen was bubbled through the reaction mixture. After 58 h, irradiation was stopped and oxygen was bubbled through the solution for another 10 h. The reaction mixture was washed sequentially with saturated aqueous sodium bicarbonate (2 × 5 mL), 1 M hydrochloric acid (2 × 5 mL), saturated aqueous copper sulfate (1 × 5 mL), and saturated aqueous sodium chloride. After being dried over $MgSO_4$, the organic solution was filtered and concentrated. The resulting residue was subjected to flash chromatography using 5–15% ethyl acetate in hexane as the eluant to give **22** (11 mg, 56% yield based on **20**) as a colorless oil as well as an unidentified uv-active product (6.2 mg). For compound **22**: ir (CH_2Cl_2 cast): 1661 (C=O, enone), 736 and 697 (C-H bending, aromatic) cm^{-1}; ^{1}H nmr (300 MHz) δ: 7.32 (m, 5 H, aromatic, **H**), 5.88 (br s, 1 H, -C=C**H**C=O), 4.48 (s, 2 H, -OC**H**$_2$Ph), 3.50 (m, 2 H, -C**H**$_2$OBn), 2.73 (dd, J = 18, 6 Hz, 1 H, -C**H**HC=O), 2.60 (dd, J = 18, 3 Hz, 1 H, -C**H**HC=O), 1.95 (d, J = 1.5 Hz, 3 H, C-5 C**H**$_3$), 1.91 (dd, J = 6, 3 Hz, 1 H, C-1 **H**), 1.78–1.86 (complex, 2 H), 1.40–1.65 (complex, 5 H), 1.25 (s, 3 H, C-6 C**H**$_3$), 0.97 (d, J = 7 Hz, 3 H, C-9 C**H**$_3$), and 0.86 (s, 3 H, C-10 C**H**$_3$); hrms M$^+$: 340.2400 (calcd. for $C_{23}H_{32}O_2$: 340.2402).

(1*S,6*R**,9*R**,10*R**)-10-(2-Hydroxyethyl)-5,6,9,10-tetramethylbicyclo[4.4.0]dec-4-en-3-one (23)**

To a solution of compound **22** (4.0 mg, 0.012 mmol) in dry dichloromethane (6 mL) under an atmosphere of argon, was added anhydrous $FeCl_3$ (7 mg, 0.04 mmol) in one portion. After stirring for 50 min at room temperature, the reaction was quenched by addition of water (1 mL). The aqueous solution was separated and extracted with dichloromethane (2 × 6 mL). The combined organic layers were washed with brine, dried ($MgSO_4$), filtered, and concentrated to give the crude product, which was purified by flash chromatography with ethyl acetate and hexane (50:50) to afford **23** (2.4 mg, 82% yield) as a colorless oil: ir (CH_2Cl_2 cast): 3439 (OH, broad) and 1651 (C=O, enone) cm^{-1}; ^{1}H nmr (300 MHz) δ: 5.89 (br s, 1 H, -C=C**H**C=O), 3.69 (t, J = 7.5 Hz, 2 H, -C**H**$_2$OH), 2.75 (dd, J = 18, 6 Hz, 1 H, -C**H**HC=O), 2.59 (dd, J = 18, 3 Hz, 1 H, -CH**H**C=O), 1.96 (br s, 3 H, C-5 C**H**$_3$), 1.92 (dd, J = 6, 3 Hz, 1 H, C-1 **H**), 1.79–1.88 (complex, 2 H), 1.40–1.68 (complex, 6 H), 1.27 (s, 3 H, C-6 C**H**$_3$), 1.11 (d, J = 7 Hz, 3 H, C-9 C**H**$_3$) and 0.89 (s, 3 H, C-10 C**H**$_3$); hrms M$^+$: 250.1931 (calcd. for $C_{16}H_{26}O_2$: 250.1932), [M − H$_2$O]$^+$: 232.1825 (calcd. for $C_{16}H_{24}O$ 232.1827).

(±)-2-Oxo-5α,8α-13,14,15,16-tetranorclerod-3-en-12-oic acid (2)

Enone **23** (1.6 mg, 0.006 mmol) was dissolved in acetone (4 mL, distilled over $KMnO_4$) and the solution was cooled to 10°C. Freshly prepared Jones reagent (0.02 mL) was added dropwise, and the resulting solution stirred for 30 min at room temperature. Water was added to dissolve all green precipitates and the aqueous layer was extracted with dichloromethane (3 × 5 mL). The combined extracts were washed with brine, dried over $MgSO_4$, filtered, and concentrated to give the crude product, which was subjected to flash chromatography using ethyl acetate and hexane (50:50) as the eluant to afford pure acid (1.1 mg, 63% yield) as a white powder: mp 226–227°C; ir (CH_2Cl_2 cast): 3300–2450 (OH, carboxylic acid), 1725 (C=O, carboxylic acid), and 1628 (C=O, enone) cm^{-1}; ^{1}H nmr (300 MHz, $CDCl_3$) δ: 8.7 (br s, 1 H, -COO**H**), 5.90 (br s, 1 H, -C=C**H**C=O), 2.79 (dd, J = 18, 6.5 Hz, 1 H, -C**H**HC=O), 2.56 (d, J = 15 Hz, 1 H, -C**H**HCOOH), 2.48 (dd, J = 18, 2.5 Hz, 1 H, -CH**H**C=O), 2.21 (d, J = 15 Hz, 1 H, -CH**H**COOH), 2.07 (dd, J = 6.5, 2.5 Hz, 1 H, C-10 **H**), 2.00 (m, 1 H), 1.97 (d, J = 1 Hz, 3 H, C-4 C**H**$_3$), 1.85 (dm, J = 14 Hz, 1 H), 1.45–1.70 (m, 2 H), 1.30–1.36 (m, 1 H), 1.28 (s, 3 H, C-5 C**H**$_3$), 1.06 (s, 3 H, C-9 C**H**$_3$), and 1.05 (d, J = 7.5 Hz, 3 H, C-8 C**H**$_3$); ^{1}H nmr (200 MHz, $CDCl_3$–C_5D_5N) δ: 5.90 (br s, 1 H,-C=C**H**C=O), 3.06 (br s, 1 H, -COO$^-$C$_5$D$_5$N$^+$H), 2.79 (dd, J = 18, 6.5 Hz, 1 H, -C**H**HC=O), 2.59 (d, J = 15 Hz, 1 H, -C**H**HCOOH), 2.54 (dd, J = 18, 2.5 Hz, 1 H, -CH**H**C=O), 2.24 (d, J = 15 Hz, 1 H, -CH**H**COOH), 2.13 (dd, J = 6.5, 2.5 Hz, 1 H, C-10 **H**), 2.11 (m, 1 H), 1.97 (d, J = 1 Hz, 3 H, C-4 C**H**$_3$), 1.85 (dm, J = 14 Hz, 1 H), 1.50–1.75 (m, 3 H), 1.29 (s, 3 H, C-5 C**H**$_3$), 1.13 (s, 3 H, C-9 C**H**$_3$), and 1.09 (d, J = 7.5 Hz, 3 H, C-8 C**H**$_3$); ^{13}C nmr (125 MHz, $CDCl_3$) δ: 198.5, 176.1, 168.6, 128.6, 45.9, 42.2, 39.8, 39.6, 35.7, 35.5, 31.0, 29.6, 26.6, 23.5, 20.9, and 15.0; hrms M$^+$: 264.1721 (calcd. for

© 1997 NRC Canada

$C_{16}H_{24}O_3$: 264.1725), $[M - CH_3]^+$: 249.1488 (calcd. for $C_{15}H_{21}O_3$: 249.1490), $[M - CH_3COOH]^+$: 204.1509 (calcd. for $C_{14}H_{20}O$: 204.1514).

Acknowledgments

We are grateful to the Natural Sciences and Engineering Research Council of Canada and the National Science Council of the Republic of China for financial support.

References

1. T. Tokoroyama. J. Synth. Org. Chem. Jpn. **51**, 1164 (1993).
2. A.T. Merritt and S.V. Ley. Nat. Prod. Rep. **9**, 243 (1992).
3. (*a*) H. Hagiwara, K. Inome, and H. Uda. J. Chem. Soc. Perkin Trans. 1, 757 (1995); Tetrahedron Lett. **35**, 8189 (1994); (*b*) P.S. Jones, S.V. Ley, N.S. Simpkins, and A.J. Whittle. Tetrahedron, **42**, 6519 (1986); S.V. Ley, N.S. Simpkins, A.J. Whittle. J. Chem. Soc. Chem. Commun. 503 (1983); (*c*) S.D. Bruner, H.S. Radeke, J.A. Tallarico, and M.L. Snapper. J. Org. Chem. **60**, 1114 (1995); (*d*) J.M. Luteijn and Ae. de Groot. Tetrahedron Lett. **23**, 3421 (1982); (*e*) E. Piers and J.Y. Roberge. Tetrahedron Lett. **33**, 6923 (1992); (*f*) H. Iio, M. Monder, K. Okada, and T. Tokoroyama. J. Chem. Soc. Chem. Commun. 358 (1987); (*g*) E. Piers and J.S.M. Wai. Can. J. Chem. **72**, 146 (1994); E. Piers and J.S.M. Wai. J. Chem. Soc. Chem. Commun. 1342 (1987); (*h*) S. Takahashi, T. Kusumi, and H. Kakisawa. Chem. Lett. 515 (1979); (*i*) A.S. Kende, B. Roth, and I. Kubo. Tetrahedron Lett. **23**, 1751 (1982); (*j*) D.J. Goldsmith and R. Deshpande. Synlett, 495 (1995); (*k*) A.S. Sharma, and A.K. Gayen. Tetrahedron, **41**, 4581 (1985); (*l*) A.S. Sarma and P. Chattopadhyay. J. Org. Chem. **47**, 1727 (1982); (*m*) E. Piers and J.S.M. Wai. J. Chem. Soc. Chem. Commun. 1245 (1988).
4. (*a*) T. Tokoroyama, K. Fujimori, T. Shimizu, Y. Yamagiwa, M. Monden, and H. Iio. J. Chem. Soc. Chem. Commun. 1516 (1983); T. Tokoroyama, R. Kanazawa, S. Yamamoto, T. Kamikawa, H. Suenaga, and M. Miyabe. Bull. Chem. Soc. Jpn. **63**, 1720 (1990); T. Tokoroyama, K. Matsuo, and T. Kubota. Tetrahedron, **34**, 1907 (1978); T. Tokoroyama, K. Matsuo, H. Kotsuki, and R. Kanazawa. Tetrahedron, **36**, 3377 (1980); (*b*) T. Tokoroyama, M. Tsukamoto, T. Asada, and H. Iio. Tetrahedron Lett. **28**, 6645 (1987); (*c*) E. Piers, M.L. Breau, Y. Han, G.L. Plourde, and W.L. Yeh. J. Chem. Soc. Perkin Trans. 1, 963 (1995).
5. A.C. Pinto, W.S. Garcez, P.P.S. Queiroz, and N.G. Fiorani. Phytochemistry, **37**, 1115 (1994).
6. H.J. Liu and E.N.C. Browne. Can. J. Chem. **65**, 1262 (1987).
7. H.J. Liu and E.N.C. Browne. Can. J. Chem. **57**, 377 (1979).
8. H.J. Liu and E.N.C. Browne. Tetrahedron Lett. 2929 (1977).
9. H.J. Liu and E.N.C. Browne. Can. J. Chem. **59**, 601 (1981).
10. H.J. Liu, E.N.C. Browne, and S.Y. Chew. Can. J. Chem. **66**, 2345 (1988).
11. H.J. Liu and Y. Han. Tetrahedron Lett. **34**, 423 (1993).
12. H.J. Liu, Y. Li, and E.N.C. Browne. Can. J. Chem. **72**, 1883 (1994).
13. A.S. Kende and P. Fludzinski. Org. Synth. **64**, 68 (1985).
14. G. Stork and R. Danheiser. J. Org. Chem. **38**, 1775 (1973).
15. L.N. Mander and S.P. Sethi. Tetrahedron Lett. **24**, 5425 (1983).
16. D. Liotta, C. Barnum, R. Puleo, G. Zima, C. Bayer, and H. S. Kezar III. J. Org. Chem. **46**, 2920 (1981).
17. Y. Fujimoto and T. Tatsuno. Tetrahedron Lett. 3325 (1976).
18. A. Goswami, R.N. Barua, R.P. Sharma, J.N. Baruah, P. Kulanthaivel, and W. Herz. Phytochemistry, **23**, 837 (1984).
19. S. Manabe and C. Nishino. Tetrahedron, **42**, 3461 (1986).
20. M. Niwa and S. Yamamura. Tetrahedron Lett. **22**, 2789 (1981).
21. C. Nishino, S. Manabe, M. Kazui, and T. Matsuzaki. Tetrahedron Lett. **25**, 2809 (1984).
22. F. Bohlmann and C. Zdero. Liebigs Ann. Chem. 1764 (1985).
23. T. Anthonsen, M.S. Henderson, A. Martin, R.D.H. Murray, R. McCrindle, and D. McMaster. Can. J. Chem. **51**, 1332 (1973).
24. M.S. Henderson, R. McCrindle, and D. McMaster. Can. J. Chem. **51**, 1346 (1973).
25. N. Fukuda, M. Nakamura, M. Yonemitsu, T. Kimura, R. Isobe, and T. Komori. Liebigs Ann. Chem. 325 (1993).
26. E.D. Mihelich and D.J. Eickhoff. J. Org. Chem. **48**, 4135 (1983).
27. H.J. Liu, K.S. Shia, Y. Han, and Y. Wang. Synlett. 545 (1995).
28. H.J. Liu, G. Ulibarri, and E.N.C. Browne. Can. J. Chem. **70**, 1545 (1992).
29. H.J. Liu, W.L. Yeh, and S.Y. Chew. Tetrahedron Lett. **34**, 4435 (1993).
30. J.I. Padron and J.T. Vazquez. Tetrahedron: Asymmetry, **6**, 857 (1995).
31 C. Djerassi, R.R. Engle, and A. Bowers. J. Org. Chem. **21**, 1547 (1956).
32. D.R. Rabenstein and T.T. Nakashima. Anal. Chem. **51**, 1465A (1979).
33. S.L. Patt and J.N. Shoolery. J. Magn. Reson. **46**, 535 (1982).
34. W.C. Still, M. Kahn, and A. Mitra. J. Org. Chem. **43**, 2923 (1978).

Can. J. Chem. Downloaded from www.nrcresearchpress.com by 88.146.161.215 on 09/08/12
For personal use only.

© 1997 NRC Canada

Assembly of tricyclic compounds that include the spiro[4.4]nonane subunit

Pei-Ying Liu, Yong-Jin Wu, and D. Jean Burnell

Abstract: Spiroannulation of ketals derived from unsaturated cyclohexenone derivatives by the Lewis acid-catalyzed reaction of 1,2-bis((trimethylsilyl)oxy)cyclobutene **5** led to spiro[4.5]decene-diones **9** and **30**. These were transformed into spiro[4.4]nonene derivatives **25** and **35/36** via similar sequences involving ozonolysis and aldol ring reclosure. Reduction of an annular double bond allowed facile closure of a third ring, also by an aldol reaction. This work led to a single oxygenated angular triquinane **28** from **9**, and to the tricyclo[6.2.1.$0^{1,5}$]undecane derivative **41** from **30**. An oxatricyclo[5.3.1.$0^{1,5}$]undecane derivative **19** was also obtained from **9**.

Key words: spiroannulation, geminal acylation, sesquiterpene synthesis.

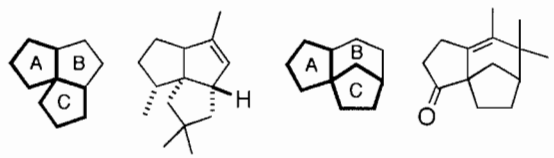
Résumé : La spiroannelation de cétals a été réalisée à partir de dérivés insaturés de la cyclohexénone en effectuant une réaction catalysée par les acides de Lewis avec du 1,2-bis((triméthylsilyl)oxy)cyclobutène (**5**); elle conduit aux spiro[4.5]décènediones **9** et **30**. Ces cétones ont été transformées en dérivés spiro[4.4]nonène **25** et **35/36** par le biais d'une séquence de réactions impliquant une ozonolyse et une refermeture aldolique de cycle. La réduction d'une des doubles liaisons annulaires permet de former facilement un troisième cycle par une autre réaction aldolique. Ce travail a permis de transformer le produit **9** en un seul triquinane angulaire oxygéné, **28**, alors que le produit **30** conduit au dérivé tricyclo[6.2.1.$0^{1,5}$]undécane **41**. On a aussi obtenu un dérivé oxatricyclo[5.3.1.$0^{1,5}$]undécane, **19**, à partir du produit **9**.

Mots clés : spiroannelation, acylation géminée, synthèse de sesquiterpène.

[Traduit par la rédaction]

Introduction

In a large number of tricyclic natural products, two cyclopentane rings (rings A and C) are joined in a spirocyclic manner, with the third ring (ring B) being a two-carbon bridge joining rings A and C. The angular triquinane system **1** is the result of bridging between carbons on rings A and C that are α to the spirocyclic center, and **1** is found in sesquiterpenes such as pentalenene (**2**), silphinene, silphiperfolene, isocomene, β-isocomene, and subergorgic acid. On the other hand, bridging between carbons that are α and β to the spirocyclic center gives the tricyclo[6.2.1.$0^{1,5}$]undecane system **3**, which is the ring system of sesquiterpenes such as isokhusimone (**4**), zizanoic acid, and prezizanol. Natural products with ring systems **1** and **3** have been the targets of a large number of synthetic studies (1), but very few of these have employed spiroannulation to establish rings A and C.[2]



1 **2** **3** **4**

The Lewis acid-catalyzed geminal acylation of acetals with 1,2-bis((trimethylsilyl)oxy)cyclobutene (**5**) (2), shown in its simplest form in Scheme 1, can be a method of considerable utility for the synthesis of spirocyclic compounds. Kuwajima's original procedure involved the isolation of the cyclobutanone **6**, followed by a separate rearrangement step with trifluoroacetic acid to the cyclopentanedione **7** (3). We improved the process such that the cyclopentanedione derivative can be obtained from the acetal in a single operation in higher overall yield (4–6). More recently, we showed that geminal acylation can also be carried out directly on a ketone (7). The geminal acylation on acetals has been exploited successfully in a number of synthetic applications (8, 9) but, to our knowledge, only our own syntheses of pentalenene (**2**) (10) and isokhusimone (**4**) (6) have targeted molecules with ring systems **1** and **3**.

Retention of an oxygen function in ring A would be a significant improvement in our spiroannualtion approach to **1** because this oxygen would be well positioned for elaboration or extension of the tricyclic system. This characteristic would not be available by a simple modification of the previously reported synthesis of pentalenene (10) because functionality in ring A is lost fairly early in that reaction sequence. Also, an extension of this strategy for the assembly of the ring system **3**

Received August 15, 1996.

This paper is dedicated to Professor William A. Ayer on the occasion of his 65th birthday.

P.-Y. Liu, Y.-J. Wu, and D.J. Burnell.[1] Department of Chemistry, Memorial University of Newfoundland, St. John's, NF A1B 3X7, Canada

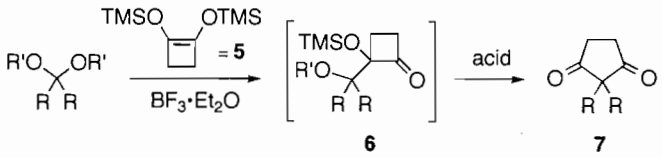
[1] Author to whom correspondence may be addressed. Telephone: (709) 737-8535. Fax: (709) 737-3702. E-mail: jburnell@plato.ucs.mun.ca

[2] For the synthesis of angular triquinanes prior to 1990, see ref. 1*e*. For synthesis of the tricyclo[6.2.1.$0^{1,5}$]undecane system prior to 1990, see ref. 6.

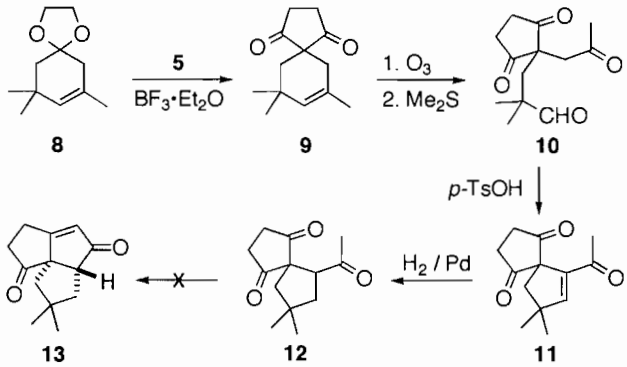
© 1997 NRC Canada

Can. J. Chem. Downloaded from www.nrcresearchpress.com by 88.146.161.215 on 09/08/12
For personal use only.

Scheme 1.



Scheme 2.



has been examined. Progress in both of these directions is described in this paper.

Results and discussion

Synthesis of the angular triquinane skeleton

During the development of the geminal acylation methodology it was shown that a substituent α to the acetal or ketone markedly reduces the yield of the reaction (4, 7). Therefore, the present strategy involved spiroannulation with an unencumbered cyclohexenone derivative and subsequent ring cleavage followed by recyclization to the required spiro[4.4]nonanedione system. Isophorone was the starting compound for the approach to **1** because its *gem*-dimethyl groups could serve as the *gem*-dimethyl groups of a number of natural products including the more highly oxygenated congeners of **2**. The strategy necessitated isomerization of the double bond of isophorone. This was accomplished concomitantly with its acetalization to **8**, and **8** underwent geminal acylation with **5** under catalysis by $BF_3 \cdot Et_2O$ to provide **9**, as we described previously (4, 10).

Ozonolysis of **9** gave an unstable tetracarbonyl compound **10**, but this was recyclized immediately under acidic conditions to the spiro[4.4]nonene derivative **11** in 52% yield (Scheme 2). It was not surprising that a second aldol to close ring B was not obtained, because the annular double bond would have imparted considerable strain. However, it was disappointing that the hydrogenated compound **12** was destroyed much more rapidly than it would cyclize to the tricyclic enone **13** under either acidic or basic conditions.

This failure could be attributed to the sensitivity of the 1,3-cyclopentanedione moiety of **12**. In the pentalenene synthesis (10) this problem was avoided by the conversion of one of the ketones to a C=C double bond. Therefore, for the present application, one of the ketones in **9** was reduced to the secondary alcohol and protected (see below). The reduction of **9** with sodium borohydride, followed by work-up with 10% aqueous HCl, gave a 1:1 mixture of isomeric mono-alcohols. Although production of the diastereomeric compounds **14** and **15** might have been expected, significant differences in the mass spectra of the two products suggested that the difference between them was not one of relative stereochemistry. Sodium borohydride reduction of **9** with neutral work-up gave only one of the mono-alcohol products, which later proved to be **14**. However, attempts to establish the relative stereochemistry of this mono-alcohol from nuclear Overhauser effect (NOE) measurements were inconclusive. Reduction of the diketone **16**, which is a double-bond isomer of **9** and which was the result of geminal acylation directly on isophorone (7), with neutral work-up provided exclusively the second mono-alcohol. NOE measurements unequivocally established its relative stereochemistry at C-4 and C-5 as that of **17** (Scheme 3). The relative stereochemistry of **14** must have been the same because treatment of mono-alcohol **14** with HCl in methanol once again gave the same 1:1 mixture of **14** and **17**. The genuine epimeric mono-alcohol **15** could be produced by reduction of **14** to the *trans*-diol **18**, followed by partial reoxidation with PCC to a mixutre of **14** and **15**. It was interesting that **18** very cleanly gave the tricyclic ether **19** in acidic solutions. Only one of the alcohols can cyclize to give *cis*-fused five-membered rings so the relative stereochemistry for **19** must be as shown. (The NOE data for **19** were not helpful in conclusively corroborating this relative stereochemistry, nor were the NOE data for the corresponding acetate **20**.) On the other hand, the mono-alcohol **15** would not cyclize at all to **21** in acid. Ketone **21** was available for comparison by PCC oxidation of **19**, and reduction of **21** with sodium borohydride yielded **22**, the carbinol epimer of **19**.

There was a very high degree of facial selectivity in the reduction of **9** to **14**. We have synthesized a number of diketones related to **9**, and the results of reactions with sodium borohydride and with methyllithium point to a stereoelectronic phenomenon as the factor governing the facial selectivity in these reactions (9).

Protection of the alcohol function **14** as the *tert*-butyldimethylsilyl ether **23** was straightforward. As before, ozonolysis gave a somewhat unstable product **24** that was cyclized without delay (Scheme 4). In this instance an acidic medium gave a very poor yield of enone, but, in contrast with **10**, methoxide did effect the cyclization to **25**. Also, a small amount of the deprotected, but cyclized, product **26** was isolated. Catalytic hydrogenation of the double bond of **25** afforded **27** as a homogeneous compound, but the relative stereochemistry at C-6 was not determined. Nevertheless, it was very gratifying that base-induced cyclization of ring B proceeded to give the triquinane **28** in 83% yield.

In the synthesis of pentalenene there was only modest control of the relative stereochemistry of the methyl group at C-9 (10), but the short route to **28** described above exploited the extremely high selectivity in the $NaBH_4$ reduction step (**9** → **14**) to ultimately provide only one epimer at C-9.

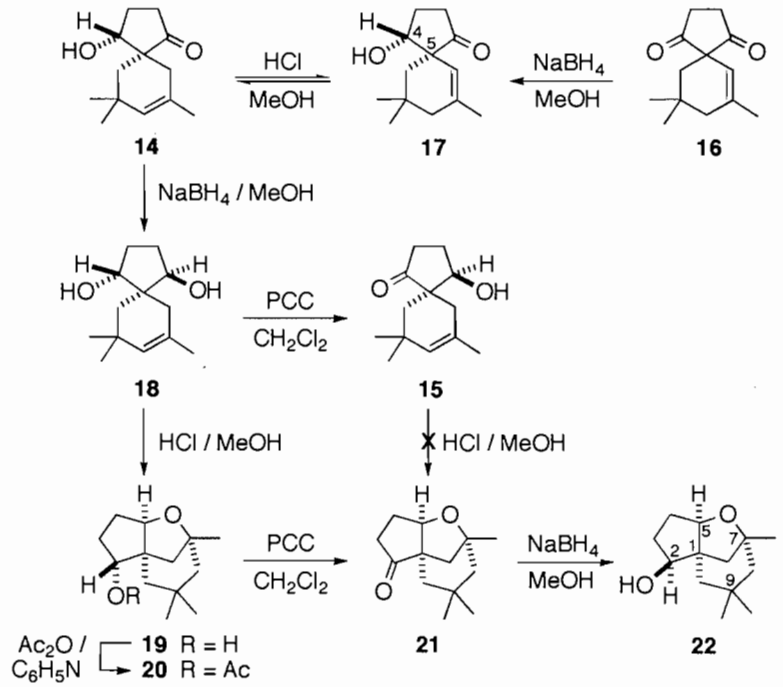
Synthesis of the tricyclo[6.2.1.$0^{1,5}$]undecane system

Treatment of the mono-acetal of 1,4-cyclohexanedione **26** with methyllithium gave a tertiary alcohol, and spiroannulation with **5** catalyzed by $BF_3 \cdot Et_2O$ proceeded with concomitant dehydration of the alcohol to give the desired diketone **30** in 71% yield from **29** (Scheme 5). Addition of excess methyl-

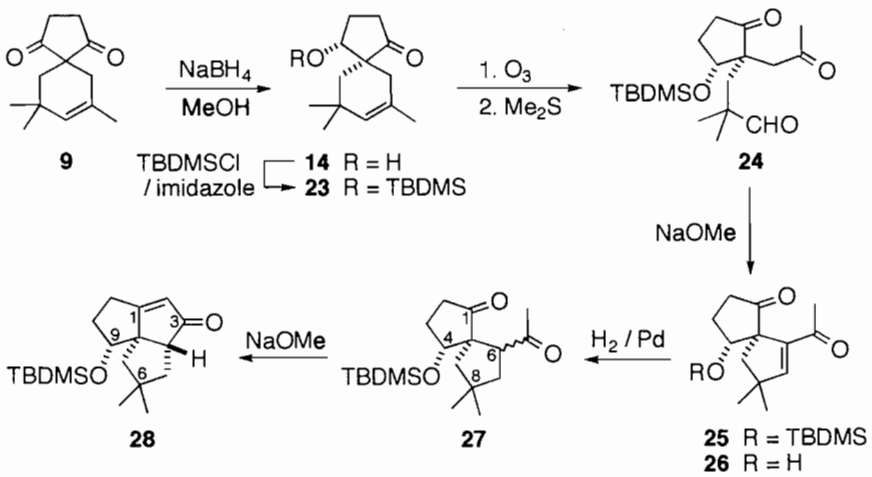
Can. J. Chem. Downloaded from www.nrcresearchpress.com by 88.146.161.215 on 09/08/12
For personal use only.

© 1997 NRC Canada

Scheme 3.



Scheme 4.



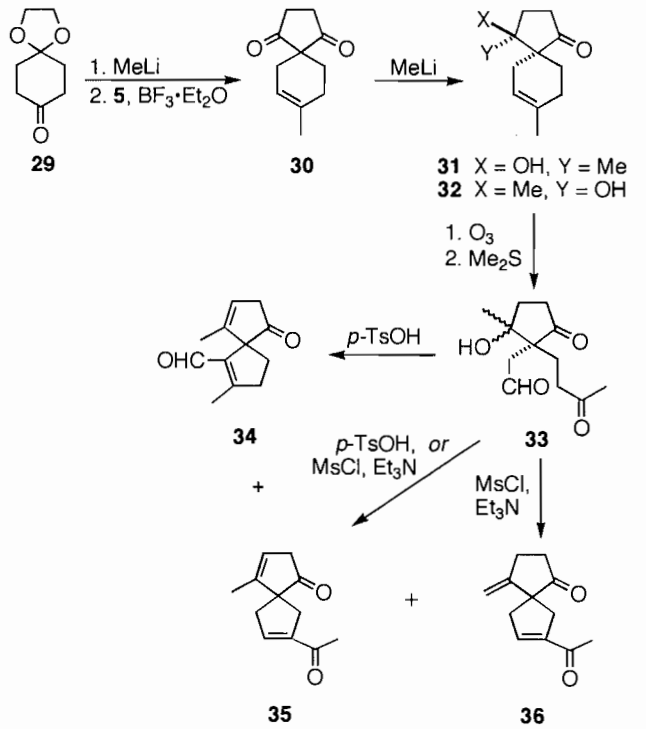
lithium to **30** gave only two mono-alcohols in a 4:1 ratio. Some of the major one was obtained by painstaking chromatography, and NOE measurements established its relative stereochemistry as that of **31**. However, separation of **31** and **32** was unnecessary. Ozonolysis of the mixture gave unstable **33**, which was introduced immediately into a solution of *p*-toluenesulfonic acid in benzene. The major product was the keto-aldehyde **34** rather than the desired diketone **35**, which was a minor component of the product mixture. Addition of methoxide to **33** led to rapid decomposition, but treatment with mesyl chloride in triethylamine resulted in aldol cyclization only in the desired direction and elimination of the tertiary alcohol. Nevertheless, this still gave a 1:1 mixture of the endocyclic and exocyclic double-bond isomers **35** and **36**. Catalytic hydrogenation of this mixture gave the saturated diketone **37** as a mixture of four isomers. Chromatography yielded two pairs of (inseparable) compounds in a 7:3 ratio. Each pair could be cyclized independently and in good yield with *tert*-butoxide, but each pair yielded **38** and **39** in the same ratio of 1:1.2, respectively. Hence, the chromatographic process could effectively separate C-7 epimers, but not C-4 epimers. This was unfortunate as C-7 was epimerizable whereas C-4 was not. In the pentalenene synthesis (10), the ratio of cyclized products analogous to **38** and **39** could be reversed (from 1:3.5 to 2:1 with a methyl substituent, and from 1:5 to 4:1 with an ethyl substituent) by ensuring that the conjugated double bond be reduced first. In this instance the change in ratio was very modest. Dissolving metal reduction of the mixture of **35** and **36** followed by catalytic hydrogenation and then cyclization gave **38** and **39** in a ratio of 1.2:1, albeit in a reasonable yield of 63% over the three steps (Scheme 6). Separation of the epimers **38** and **39** was carried out over $AgNO_3$-impregnated silica gel, but NOE measurements did not give unequivocal evidence for their relative

Can. J. Chem. Downloaded from www.nrcresearchpress.com by 88.146.161.215 on 09/08/12
For personal use only.

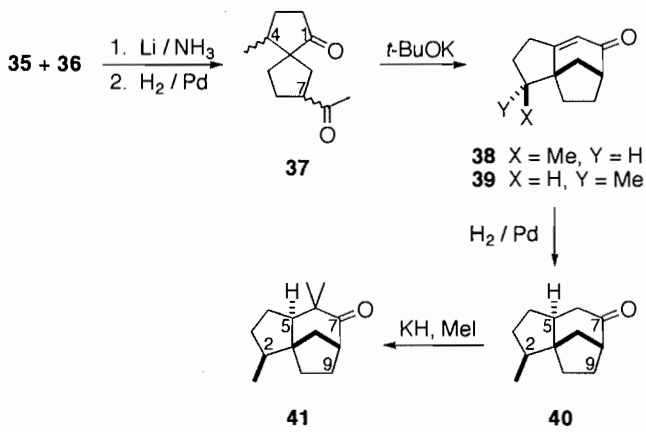
© 1997 NRC Canada

Can. J. Chem. Downloaded from www.nrcresearchpress.com by 88.146.161.215 on 09/08/12
For personal use only.

Scheme 5.



Scheme 6.



stereochemistry at C-2. This was determined by conversion to known tricyclic ketones. Reduction of the double bond of **38** under dissolving metal conditions or by catalytic hydrogenation gave the same product **40**, which had ^{1}H NMR data similar to those given by Weisner and co-workers (11). This was corroborated by double methylation of **40** to provide **41**, for which NMR spectra were reported by Mori and co-workers (12).

Experimental

General

Melting points (mp) were determined on a Fisher–Johns apparatus and are uncorrected. Infrared (IR) spectra were recorded on a Mattson FT instrument as thin films. Nuclear magnetic resonance (NMR) spectra were obtained on a General Electric GE 300-NB instrument as $CDCl_3$ solutions; ^{1}H shifts were calibrated relative to internal tetramethylsilane; ^{13}C shifts were calibrated relative to the solvent resonance (δ 77.0). Each ^{13}C chemical shift is followed in parentheses by the number of attached protons, as determined by APT and heteronuclear correlation spectra. Nuclear Overhauser effect (NOE) measurements were made by the difference method, as described previously (13). Mass spectral (MS) data were obtained with a V.G. Micromass 7070HS instrument, except in some instances in which data were from a Hewlett–Packard 5970 mass selective detector (GC–MS). MS data have this form: *m/z* (% of base peak). 1,2-Bis((trimethylsilyl)oxy)cyclobutene (**5**) was prepared by the method of Bloomfield and Nelke (2), and the diketone **9** was obtained from **8** following our own procedure (4, 10). Reactions were run under N_2. Solvents and boron trifluoride etherate were distilled. Flash chromatography ("chromatography") used 230–400 mesh silica gel; eluents were either "actone" = acetone in petroleum ether (30–60°C boiling fraction) or "EtOAc" = ethyl acetate in hexanes.

6-Acetyl-8,8-dimethylspiro[4.4]non-6-ene-1,4-dione 11

Ozone was passed through a solution of **9** (200 mg, 0.97 mmol) in CH_2Cl_2 at −78°C until the blue color persisted. Excess O_3 was removed by bubbling O_2 through the solution for 5 min, then N_2 for 10 min. After addition of Me_2S (3.0 mL), the solution was stirred overnight while it was allowed to rise to room temperature. Concentration under vacuum provided crude **10**. MS (from GC–MS): no M^+, 210 (2), 195 (2), 178 (4), 167 (13), 154 (23), 139 (13), 125 (15), 112 (30), 111 (17), 107 (14), 97 (10), 55 (19), 43 (100), 41 (19). A solution of the crude **10** and *p*-TsOH (200 mg) in C_6H_6 was heated at reflux with azeotropic removal of H_2O for 2 h. After cooling, the solution was washed with saturated $NaHCO_3$, and the aqueous layer was re-extracted with ether (×3). The combined organic solutions were washed with saturated $NaHCO_3$ and brine (×2), then dried over $MgSO_4$, and concentrated under vacuum. Chromatography (3% acetone) of the residue provided **11** (113 mg, 52% from **9**) as a colorless oil: IR: 1725, 1665, 1625 cm^{-1}; ^{1}H NMR δ: 6.76 (1H, s), 3.08 (2H, m), 2.73 (2H, m), 2.25 (3H, s), 1.89 (2H, s), 1.32 (6H, s); MS: 220 (13, M^+), 205 (5), 201 (6), 192 (44), 177 (33), 163 (24), 135 (28), 55 (25), 43 (100). Exact Mass calcd. for $C_{13}H_{16}O_3$: 220.1098; found: 220.1087.

6-Acetyl-8,8-dimethylspiro[4.4]nonane-1,4-dione 12

A solution of **11** (55 mg, 0.25 mmol) in dry MeOH (30 mL) was shaken with 5% Pd on carbon (30 mg) under 300 kPa of H_2 for 1 h. After filtration and concentration, **12** (55 mg, 100%) was obtained as a colorless oil: IR: 1715 (br) cm^{-1}; ^{1}H NMR δ: 3.64 (1H, dd, J = 7.0, 13.8 Hz), 3.00–2.60 (4H, m), 2.35 (1H, dd, J = 11.7, 13.8 Hz), 2.09 (3H, s), 2.00 (1H, dd, J = 7.0, 11.7 Hz), 1.72 (1H, d, J = 13.4 Hz), 1.56 (1H, d, J = 13.4 Hz), 1.19 (3H, s), 1.17 (3H, s); ^{13}C NMR δ: 217.9 (0), 216.3 (0), 208.2 (0), 65.4 (1), 62.3 (0), 48.9 (2), 43.5 (2), 40.2 (0), 35.6 (2C, 2), 30.0 (3), 29.6 (3), 27.8 (3); MS: 222 (2, M^+), 179 (100), 165 (5), 161 (4), 137 (38), 43 (52). Exact Mass calcd. for $C_{13}H_{18}O_3$: 222.1256; found: 222.1273.

(4*R**,5*R**)-4-Hydroxy-7,9,9-trimethylspiro[4.5]dec-7-en-1-one 14

To a solution of **9** (300 mg, 1.46 mmol) in MeOH (10 mL) at 0°C was added $NaBH_4$ (14 mg, 0.37 mmol) in small portions.

© 1997 NRC Canada

Can. J. Chem. Downloaded from www.nrcresearchpress.com by 88.146.161.215 on 09/08/12
For personal use only.

The mixture was stirred for a further 30 min before H_2O was added. Much of the MeOH was removed under vacuum before extraction with ether (×3). The combined organic solutions were washed with brine (×2), dried over $MgSO_4$, and concentrated under vacuum. Chromatography of the residue (2% acetone) provided **14** (243 mg, 80%) as a colorless oil, and 28 mg (9%) of **9** was recovered. For **14**: IR: 3460 (br), 1730 cm^{-1}; ^1H NMR δ: 5.23 (1H, br s), 4.23 (1H, m), 2.64–1.51 (9H, m), 1.64 (3H, s), 1.04 (3H, s), 1.02 (3H, s); ^{13}C NMR δ: 222.0 (0), 131.8 (1), 127.3 (0), 74.5 (1), 54.4 (0), 35.0 (2), 34.8 (2), 33.2 (2), 32.0 (3), 31.2 (0), 30.3 (3), 28.0 (2), 27.3 (3); MS: 208 (52, M^+), 193 (13), 175 (87), 149 (78), 133 (86), 131 (32), 121 (42), 119 (55), 107 (50), 105 (38), 91 (62), 81 (32), 79 (34), 77 (37), 55 (47), 53 (33), 43 (74), 41 (100). Exact Mass calcd. for $C_{13}H_{20}O_2$: 208.1462; found: 208.1462. Treatment of **14** with PCC gave only **9**.

(4*R**,5*S**)-4-Hydroxy-7,9,9-trimethylspiro[4.5]dec-6-en-1-one 17

*By equilibration of **14***

To a MeOH solution of **14** (42 mg, 0.20 mmol) was added 10% HCl, and the mixture was stirred at room temperature for 10 min. After addition of H_2O, much of the MeOH was removed under vacuum, and the mixture was extracted with ether (×3). The combined organic solutions were washed with H_2O (×2), saturated $NaHCO_3$ (×2), and brine (×2). The solution was dried over $MgSO_4$, then concentrated under vacuum to give a 1:1 mixture of **14** and **17** (42 mg, 100%).

*By reduction of **16***

To a solution of **16** (15.1 mg, 0.073 mmol) in MeOH at 0°C was added $NaBH_4$ (1.0 mg, 0.026 mmol). The mixture was stirred for a further 30 min before H_2O was added. Much of the MeOH was removed under vacuum before extraction with ether (×3). The combined organic extracts were washed with brine (×2), dried over $MgSO_4$, and concentrated under vacuum. Chromatography of the residue (2% acetone) provided **17** (10.4 mg, 69%) as a colorless oil: IR: 3464 (br), 1731 cm^{-1}; ^1H NMR δ: 4.96 (1H, br s, irradiation gave a 1.4% NOE at 4.22), 4.22 (1H, narrow m, irradiation gave a 4.4% NOE at 4.96), 2.55–2.17 (4H, m), 2.02 (1H, m), 1.88 (1H, br d, J = 17.3 Hz), 1.68 (2H, s), 1.63 (3H, s), 1.02 (3H, s), 0.97 (3H, s), and the signal to which δ 1.88 is coupled must be buried δ 1.68–1.62; ^{13}C NMR δ: 219.1.(0), 137.7 (0), 116.4 (1), 76.5 (1), 58.3 (0), 43.8 (2), 33.7 (2), 32.8 (2), 30.8 (3), 29.4 (0), 27.5 (3), 27.4 (2), 24.5 (3); MS: 208 (28, M^+), 175 (72), 149 (100), 137 (26), 133 (30), 123 (28), 121 (69), 119 (33), 109 (21), 107 (74), 105 (30), 93 (44), 91 (51), 81 (28), 79 (43), 77 (38), 69 (28), 57 (29), 55 (47), 41 (70). Exact Mass calcd. for $C_{13}H_{20}O_2$: 208.1462; found: 208.1462. Treatment of **17** with PCC gave only **16**.

trans-7,9,9-Trimethylspiro[4.5]dec-7-ene-1,4-diol 18

$NaBH_4$ (23 mg, 0.62 mmol) was added in portions to a solution of **14** (64 mg, 0.31 mmol) in MeOH (20 mL) at 0°C. The mixture was stirred for another 30 min at 0°C, then H_2O was added and much of the MeOH was removed under vacuum. The product was extracted into ether (×3), and the combined organic solutions were washed with brine (×2), then dried over $MgSO_4$ and concentrated under vacuum. Chromatography (5% acetone) of the residue provided **18** (65 mg, 100%) as a colorless oil: IR: 3340 (very br) cm^{-1}; ^1H NMR δ: 5.19 (1H, s), 4.10 (1H, t, J = 7.9 Hz), 3.97 (1H, dd, J = 0.9, 5.2 Hz), 2.23–2.10 (3H, m), 1.66 (3H, s), 1.66–1.20 (7H, m), 1.06 (3H, s), 1.03 (3H, s); ^{13}C NMR δ: 131.3 (1), 129.4 (0), 77.4 (1), 76.7 (1), 48.5 (0), 38.6 (2), 32.0 (2C, 0 and 3), 31.1 (2C, 2 and 3), 29.6 (2), 29.0 (2), 24.1 (3); MS: 210 (6, M^+), 195 (26), 192 (21), 177 (36), 159 (70), 149 (21), 148 (20), 136 (29), 135 (32), 133 (100), 123 (35), 121 (25), 119 (33), 109 (20), 107 (38), 105 (39), 93 (27), 91 (38), 81 (29), 55 (32), 43 (64), 41 (70). Exact Mass calcd. for $C_{12}H_{19}O_2$ ($M^+ - CH_3$): 195.1384; found: 195.1379.

(4*R**,5*S**)-4-Hydroxy-7,9,9-trimethylspiro[4.5]dec-7-en-1-one 15

PCC (11 mg, 0.05 mmol) was added to a solution of **18** (11 mg, 0.05 mmol) in CH_2Cl_2 at room temperature, and the solution was stirred for a further 3 h. Filtration through a Florisil pad removed a black precipitate, and ether was passed through the pad. The combined organic solutions were concentrated under vacuum, and chromatography (3% acetone) of the residue provided a 1:1 mixture of **14** and **15** (7.2 mg, 67%). For **15** (from the mixture): ^1H NMR δ: 5.24 (1H, br s), 4.32 (1H, t, J = 5.8 Hz), 2.57–1.45 (8H, m), 1.06 (3H, s), 0.98 (3H, s); MS (from GC–MS): 208 (18, M^+), 175 (78), 149 (87), 133 (100), 131 (40), 121 (62), 119 (63), 107 (60), 105 (51), 93 (31), 91 (71), 85 (23), 81 (37), 79 (42), 77 (46), 69 (37), 67 (26), 65 (32), 57 (31), 55 (61), 53 (33), 44 (36), 43 (82), 41 (97). Further oxidation of this mixture gave **9** cleanly.

(1*R**,2*S**,5*S**,7*S**)-7,9,9-Trimethyl-6-oxatricyclo[5.3.1.0^{1,5}]undecan-2-ol 19

A solution of **18** (56 mg, 0.27 mmol) in MeOH was adjusted to pH 2 by addition of 10% HCl, and the mixture was stirred at room temperature for 30 min. Much of the MeOH was removed under vacuum, and the product was extracted with ether (×3). The combined organic solutions were washed with H_2O (×2), saturated $NaHCO_3$ (×2), and brine (×2), then dried over $MgSO_4$ and concentrated under vacuum. Chromatography (20% acetone) of the residue provided **19** (53 mg, 100%) as a colorless solid: mp 82–83°C; IR: 3405 (br), 1463 cm^{-1}; ^1H NMR δ: 4.52 (1H, dd, J = 4.4, 8.6 Hz), 4.03 (1H, dd, J = 1.4, 5.0 Hz), 2.34 (1H, br m), 2.16 (1H, br m), 1.89 (1H, br dd, J = 1.8, 13.4 Hz), 1.76–1.24 (8H, m), 1.28 (3H, s), 1.21 (3H, s), 1.00 (3H, s); ^{13}C NMR δ: 84.4 (1), 83.1 (0), 77.0 (1), 57.6 (0), 51.0 (2), 46.3 (2), 42.5 (2), 36.6 (3), 32.5 (2C, 2 and 3), 31.5 (2), 30.4 (0), 26.8 (3); MS: 210 (40, M^+), 195 (10), 165 (11), 154 (16), 153 (24), 109 (100), 95 (32), 57 (29), 43 (84), 41 (43). Exact Mass calcd. for $C_{13}H_{22}O_2$: 210.1619; found: 210.1602.

(1*R**,2*S**,5*S**,7*S**)-2-Acetyloxy-7,9,9-trimethyl-6-oxatricyclo[5.3.1.0^{1,5}]undecane 20

Acetic anhydride (0.5 mL) was added to a solution of **19** (7.8 mg, 0.037 mmol) in pyridine (0.5 mL), and the solution was stirred at room temperature for 30 min. After addition of H_2O, the product was extracted with ether (×3). The combined organic solutions were washed with water (×2), 5% HCl (×3), and brine (×2), then dried over $MgSO_4$ and concentrated under vacuum. Chromatography (5% acetone) of the residue provided **20** (8.3 mg, 89%) as a colorless oil: IR: 1746 cm^{-1}; ^1H

© 1997 NRC Canada

Can. J. Chem. Downloaded from www.nrcresearchpress.com by 88.146.161.215 on 09/08/12
For personal use only.

NMR δ: 5.08 (1H, dd, J = 2.1, 5.5 Hz), 4.50 (1H, dd, J = 4.9, 8.4 Hz), 2.35 (1H, br m), 2.10 (1H, br m), 2.06 (3H, s), 1.75–1.53 (4H, m), 1.45 (1H, d, J = 11.5 Hz), 1.41 (1H, d, J = 8.6 Hz), 1.35 (1H, d, J = 8.6 Hz), 1.29 (3H, s), 1.27 (1H, d, J = 11.5 Hz), 1.20 (3H, s), 0.96 (3H, s); MS: 252 (10, M^+), 237 (3), 192 (34), 165 (19), 136 (27), 135 (54), 109 (24), 57 (49), 56 (27), 43 (100), 42 (21), 41 (64).

(1*R,5*S**,7*S**)-7,9,9-Trimethyl-6-oxatricyclo[5.3.1.0^{1,5}]undecan-2-one 21**

PCC (39 mg, 0.18 mmol) was added to a solution of **19** (25 mg, 0.12 mmol) in CH_2Cl_2, and the solution was stirred at room temperature for 14 h. Filtration through a Florisil pad removed a black precipitate, and ether was passed through the pad. The combined organic solutions were concentrated under vacuum to provide **21** (25 mg, 100%) as a colorless solid: mp 25°C; IR: 1740 cm^{-1}; ^{1}H NMR δ: 4.60 (1H, t, J = 7.6 Hz), 2.64 (1H, br m), 2.37–2.17 (2H, m), 1.96 (1H, dt, J = 2.4, 11.2 Hz), 1.87 (1H, d, J = 14.0 Hz), 1.76 (1H, br m), 1.64 (1H, br d, J = 13.9 Hz), 1.49 (1H, br d, J = 14.0 Hz), 1.37 (1H, d, J = 11.2 Hz), 1.36 (3H, s), 1.32 (1H, d, J = 13.9 Hz), 1.20 (3H, s), 1.01 (3H, s); ^{13}C NMR δ: 216.3 (0), 85.5 (0), 83.8 (1), 58.5 (0), 50.7 (2), 44.0 (2), 41.9 (2), 37.3 (2), 35.9 (3), 32.2 (3), 30.2 (0), 28.5 (2), 26.3 (3); MS: 208 (13, M^+), 180 (14), 165 (13), 152 (38), 96 (100), 95 (17), 57 (17), 43 (39), 41 (23). Exact Mass calcd. for $C_{13}H_{20}O_2$: 208.1462; found: 208.1463.

(1*R,2*R**,5*S**,7*S**)-7,9,9-Trimethyl-6-oxatricyclo-[5.3.1.0^{1,5}]undecan-2-ol 22**

$NaBH_4$ (15 mg, 0.40 mmol) was added in small portions to a solution of **21** (81 mg, 0.39 mmol) in MeOH at 0°C. The mixture was stirred for 30 min before water was added and much of the MeOH was removed under vacuum. The product was extracted with ether (×3), and the combined organic solutions were washed with water, then brine (×2), dried over $MgSO_4$, and concentrated under vacuum. Chromatography (5% acetone) of the residue provided **22** (78 mg, 96%) as a colorless oil: IR: 3420 cm^{-1}; ^{1}H NMR δ: 4.27 (1H, dd, J = 4.8, 7.9 Hz), 3.85 (1H, t, J = 7.9 Hz), 2.13 (1H, br, O*H*), 2.00–1.78 (4H, m), 1.60 (1H, partially overlapped d, J = 14.4 Hz), 1.44 (1H, br dd, J = 1.9, 13.4 Hz), 1.323 (3H, s), 1.320 (1H, d, J = 14.4 Hz), 1.27 (1H, d, J = 11.1 Hz), 1.19 (3H, s), 0.98 (3H, s); ^{13}C NMR δ: 84.4 (0), 83.8 (1), 77.0 (1), 56.7 (0), 51.1 (2), 46.7 (2), 41.7 (2), 36.3 (3), 32.6 (3), 30.8 (2), 30.5 (0), 29.2 (2), 26.9 (3); MS: 210 (33, M^+), 195 (8), 165 (10), 154 (15), 153 (24), 109 (100), 95 (28), 57 (26), 43 (53), 41 (27). Exact Mass calcd. for $C_{13}H_{22}O_2$: 210.1619; found: 210.1619.

(4*R,5*R**)-4-((*tert*-Butyldimethylsilyl)oxy)-7,9,9-trimethylspiro[4.5]dec-7-en-1-one 23**

A solution of **14** (161 mg, 0.77 mmol), *tert*-butylchlorodimethylsilane (232 mg, 1.54 mmol), imidazole (157 mg, 2.31 mmol), and 4-dimethylaminopyridine (10 mg) in dry DMF (7.0 mL) was heated at 80°C for 15 h. Ether and water were added to the cooled solution. The aqueous layer was re-extracted with ether (×3), and the combined organic solutions were washed with water (×2) and brine (×2), then dried over $MgSO_4$, and concentrated under vacuum. Chromatography (5% acetone) of the residue provided **23** (113 mg, 46%) as a colorless oil, and 76 mg (47%) of **14** was recovered. For **23**: IR: 1740 cm^{-1}; ^{1}H NMR δ: 5.18 (1H, br s, $W_{1/2}$ = 5.4 Hz), 3.99 (1H, br t, J = 5.6 Hz), 2.42 (1H, br m), 2.22–1.93 (3H, m), 1.82–1.70 (3H, m), 1.67 (3H, br s), 1.56 (1H, d, J = 14.3 Hz), 0.96 (3H, s), 0.91 (3H, s), 0.88 (9H, s), 0.09 (3H, s), 0.05 (3H, s); ^{13}C NMR δ: 220.1 (0), 131.7 (1), 128.2 (0), 76.6 (1), 54.2 (0), 35.1 (2), 33.7 (2), 33.5 (2), 32.2 (3), 31.7 (0), 30.0 (3), 27.7 (2), 25.9 (3C, 3), 23.7 (3), 18.1 (0), −3.8 (3), −4.6 (3); MS: 322 (43, M^+), 265 (33), 179 (17), 175 (18), 173 (45), 164 (28), 149 (31), 147 (45), 133 (27), 131 (26), 129 (45), 119 (22), 105 (22), 101 (23), 91 (22), 75 (100), 73 (90), 59 (31), 57 (26), 41 (45). Exact Mass calcd. for $C_{19}H_{34}O_2Si$: 322.2326; found: 322.2293.

(4*R,5*S**)-6-Acetyl-4-((*tert*-butyldimethylsilyl)oxy)-8,8-dimethylspiro[4.4]non-6-en-1-one 25 and (4*R**,5*S**)-6-acetyl-4-hydroxy-8,8-dimethylspiro[4.4]non-6-en-1-one 26**

Ozone was passed through a solution of **23** (113 mg, 0.35 mmol) in MeOH (15 mL) at −78°C until the blue color persisted. Excess O_3 was removed by bubbling O_2 through the solution for 5 min, then N_2 for 10 min. After addition of Me_2S (2.0 mL), the solution was stirred overnight while it was allowed to rise to room temperature. Concentration under vacuum provided crude **24**: MS (from GC–MS): no M^+, 297 (15), 279 (14), 239 (12), 225 (13), 213 (13), 211 (15), 205 (18), 197 (16), 195 (18), 169 (34), 163 (27), 151 (18), 145 (12), 139 (17), 75 (100), 73 (78), 43 (92), 41 (32). To dry MeOH (10 mL) at 0°C was added sodium metal (24.2 mg, 1.05 mmol), followed a few min later by a solution of the crude **24** in MeOH. This solution was stirred at 0°C for 8 min. Water was added and much of the MeOH was removed under vacuum before extraction with ether (×3). The combined organic extracts were washed with brine (×2), dried over $MgSO_4$, and concentrated under vacuum. Chromatography (2% acetone) provided **25** (25 mg, 21%) as a colorless oil and 2.0 mg (3%) of **26**.

For 25: IR: 1745, 1670, 1625 cm^{-1}; ^{1}H NMR δ: 6.69 (1H, s), 4.69 (1H, dd, J = 6.4, 10.6 Hz), 2.52–2.32 (3H, m), 2.28 (3H, s), 2.16 (1H, m), 1.58 (1H, m), 1.44 (1H, d, J = 13.2 Hz), 1.21 (6H, s), 0.88 (9H, s), 0.02 (3H, s), −0.05 (3H, s); ^{13}C NMR δ: 217.2 (0), 196.0 (0), 158.4 (1), 141.8 (0), 72.9 (1), 67.6 (0), 45.8 (0), 39.9 (2), 35.6 (2), 30.0 (2), 29.7 (3), 28.9 (3), 26.7 (3), 25.9 (3C, 3), 18.0 (0), −4.5 (3), −4.7 (3); MS: 336 (4, M^+), 321 (2), 303 (5), 280 (23), 279 (100), 261 (23), 237 (40), 235 (15), 193 (17), 189 (11), 161 (14), 159 (14), 145 (16), 75 (34), 73 (37), 43 (42).

For 26: ^{1}H NMR δ: 6.72 (1H, s), 4.69 (1H, dd, J = 4.0, 6.5 Hz), 2.65–2.26 (3H, m), 2.298 (3H, s), 2.296 (1H, d, J = 13.3 Hz), 1.80 (1H, br), 1.62 (1H, m), 1.53 (1H, d, J = 13.3 Hz), 1.24 (6H, s); MS: 222 (4, M^+), 207 (4), 204 (10), 189 (7), 179 (10), 176 (17), 163 (17), 162 (32), 161 (42), 147 (37), 133 (15), 121 (14), 119 (25), 43 (100). Treatment of **26** with PCC provided **11**.

(4*R,5*S**,6ξ)-6-Acetyl-4-((*tert*-butyldimethylsilyl)oxy)-8,8-dimethylspiro[4.4]nonan-1-one 27**

A solution of **25** (40 mg, 0.12 mmol) in dry MeOH (25 mL) was shaken with 5% Pd on carbon (30 mg) under 300 kPa of H_2 for 1 h. After filtration and concentration, **27** (41 mg, 100%) was obtained as a colorless solid: mp 77–77.5°C; IR:

© 1997 NRC Canada

Can. J. Chem. Downloaded from www.nrcresearchpress.com by 88.146.161.215 on 09/08/12
For personal use only.

1740, 1690 cm^{-1}; ^1H NMR δ: 4.39 (1H, dd, J = 6.2, 10.0 Hz), 2.95 (1H, dd, J = 6.9, 13.5 Hz), 2.33 (2H, m), 2.25 (1H, dd, J = 11.6, 13.5 Hz), 2.13 (3H, s), 2.11 (1H, m), 2.04 (1H, br d, J = 13.5 Hz), 1.86 (1H, dd, J = 6.9, 11.6 Hz), 1.53 (1H, m), 1.28 (1H, d, J = 13.5 Hz), 1.11 (3H, s), 1.06 (3H, s), 0.90 (9H, s), 0.08 (3H, s), 0.05 (3H, s); ^{13}C NMR δ: 219.4 (0), 209.9 (0), 75.0 (1), 62.4 (0), 57.7 (1), 44.4 (2), 41.2 (2), 37.9 (0), 36.0 (2), 30.2 (3), 30.0 (2C, 2 and 3), 29.4 (3), 25.8 (3C, 3), 18.0 (0), −4.3 (3), −4.7 (3); MS: no M^+, 323 (0.3), 295 (5), 281 (61), 263 (16), 239 (10), 189 (22), 161 (17), 147 (34), 75 (100), 73 (88), 62 (25), 45 (71), 43 (79). Exact Mass calcd. for $C_{15}H_{25}O_3Si$ ($M^+ - (CH_3)_3C$): 281.1573; found: 281.1573.

(4*R,8*R**,9*R**)-9-((*tert*-Butyldimethylsilyl)oxy)-6,6-dimethyltricyclo[6.3.0.0^{4,8}]undec-1-en-3-one 28**

To dry MeOH (10 mL) at 0°C was added sodium metal (6.1 mg, 0.27 mmol), followed a few minutes later by a solution of **27** (30 mg, 0.089 mmol) in MeOH. This solution was stirred at 0°C for 10 min. Water was added and much of the MeOH was removed under vacuum before extraction with ether (×3). The combined organic solutions were washed with brine (×2), dried over $MgSO_4$, and concentrated under vacuum. Chromatography (4% acetone) of the residue provided **28** (24 mg, 83%) as a colorless oil: IR: 1741, 1711, 1630 cm^{-1}; ^1H NMR δ: 5.81 (1H, br s), 3.82 (1H, dd, J = 7.9, 9.6 Hz), 2.83–1.03 (9H, m), 1.04 (3H, s), 0.90 (9H, s), 0.87 (3H, s), 0.05 (6H, s); MS: no M^+, 305 (3), 281 (14), 263 (100), 235 (6), 207 (6), 189 (7), 161 (12), 147 (10), 145 (12), 105 (15), 91 (19), 77 (15), 75 (94), 73 (71), 59 (21), 43 (26), 41 (30). Exact Mass calcd. for $C_{15}H_{23}O_2Si$ ($M^+ - (CH_3)_3C$): 263.1466; found: 263.1464.

8-Methylspiro[4.5]dec-7-ene-1,4-dione 30

To a solution of **29** (2.40 g, 15.6 mmol) in ether (80 mL) at −78°C was added 13.4 mL (18.7 mmol) of 1.4 M CH_3Li in ether. The mixture was stirred for 2 h before it was allowed to warm above 0°C and water was added. The product was extracted with ether (×3), and the combined organic solutions were washed with water and brine (×2), then dried over $MgSO_4$ and concentrated under vacuum. Chromatography (8% EtOAc) of the residue provided 0.19 g (7%) of recovered **29** and *8-methyl-1,4-dioxaspiro[4.5]decan-8-ol* (2.43 g, 91%) as colorless crystals: mp 68–69°C; IR: 3300 (br), 3263 cm^{-1}; ^1H NMR δ: 3.94 (4H, m), 1.94–1.84 (2H, m), 1.80 (1H, s, O*H*), 1.72–1.54 (6H, m), 1.25 (3H, s); ^{13}C NMR δ: 108.6 (0), 68.6 (0), 64.0 (2C, 2), 36.5 (2C, 2), 30.6 (2C, 2), 29.6 (3); MS: 172 (0.5, M^+), 100 (85), 99 (100), 86 (56), 71 (13), 55 (24), 42 (15). A solution of this alcohol (1.53 g, 9.94 mmol) in CH_2Cl_2 (100 mL) was cooled to −78°C before freshly distilled $BF_3 \cdot Et_2O$ (18.3 mL, 149 mmol) was added, followed over 20 min by a solution of **5** (7.9 mL, 30 mmol) in CH_2Cl_2 (25 mL). The mixture was stirred overnight while it attained room temperature. After pouring into ice-cold saturated $NaHCO_3$ solution, the aqueous layer was extracted with CH_2Cl_2. The combined organic solutions were washed with saturated $NaHCO_3$ and brine (×2), then dried over $MgSO_4$ and concentrated under vacuum. Chromatography (5% EtOAc) of the residue afforded **30** (1.23 g, 78% from the hydroxy-acetal, 71% from **29**) as colorless crystals: mp 76–77°C (lit.(14) mp 81.5–83°C); IR: 1716, 1410 cm^{-1}; ^1H NMR δ: 5.40 (1H, m), 3.00–2.61 (4H, m), 2.13 (2H, sextet, J = 2.1 Hz), 2.02 (2H, apparent t, J = 5.7 Hz), 1.75 (2H, t, J = 6.3 Hz), 1.70 (3H, br s); ^{13}C NMR δ: 214.7 (2C, 0), 132.8 (0), 116.7 (1), 55.1 (0), 34.2 (2C, 2), 27.6 (2), 26.7 (2), 25.7 (2), 23.3 (3); MS: 178 (62, M^+), 149 (25), 136 (22), 135 (100), 121 (34), 107 (31), 94 (21), 93 (35), 91 (45), 57 (21), 55 (43), 51 (29), 43 (24), 41 (39). Exact Mass calcd. for $C_{11}H_{14}O_2$: 178.0993; found: 178.0991. Anal. calcd. for $C_{11}H_{14}O_2$: C 74.13, H 7.92; found: C 74.23, H 7.99.

(4*R,5*S**)-31 and (4*R**,5*R**)-4-Hydroxy-4,8-dimethylspiro[4.5]dec-7-en-1-one 32**

To a solution of diketone **30** (603 mg, 3.39 mmol) in ether (40 mL) at −78°C was added 4.8 mL (6.8 mmol) of 1.4 M CH_3Li in ether. The mixture was stirred for 2 h before it was allowed to warm above 0°C and water was added. The aqueous layer was extracted with ether (×3), and the combined organic solutions were washed with water and brine (×2), then dried over $MgSO_4$ and concentrated under vacuum. Chromatography (6% EtOAc) of the residue gave 454 mg (69%) of **31**, 131 mg (20%) of **32**, and 42 mg (6%) of recovered **30**.

For 31: mp 67–68°C; IR: 3480 (br), 1728 cm^{-1}; ^1H NMR δ: 5.31 (1H, narrow d, J = 1.5 Hz, irradiation gave a 2% NOE at 1.92, 1% NOE at 1.67), 2.46 (1H, br m), 2.24–2.00 (3H, m), 2.04–1.68 (7H, m including O*H*), 1.67 (3H, br s, irradiation gave a 9% NOE at 5.31), 1.27 (3H, s, irradiation gave a 3% NOE at 1.92); ^{13}C NMR δ: 220.6 (0), 134.0 (0), 117.7 (1), 79.6 (0), 53.7 (0), 34.3 (2), 34.0 (2), 28.5 (2), 27.0 (2), 24.5 (3), 23.3 (3), 23.0 (2); MS: 194 (10, M^+), 136 (57), 121 (26), 119 (18), 118 (37), 93 (25), 91 (24), 79 (23), 77 (25), 55 (23), 43 (100), 41 (25). Exact Mass calcd. for $C_{12}H_{18}O_2$: 194.1306; found: 194.1310.

For 32: mp 98–99°C; IR: 3499 (br), 1723 cm^{-1}; ^1H NMR δ: 5.46 (1H, m), 2.40–2.34 (2H, m), 2.18–1.86 (7H, m including O*H*), 1.68 (3H, br s), 1.65–1.48 (2H, m), 1.28 (3H, s); ^{13}C NMR δ: 219.9 (0), 133.2 (0), 118.8 (1), 85.5 (1), 54.3 (0), 33.6 (2), 33.3 (2), 33.3 (2), 26.8 (2), 25.2 (2), 23.3 (3), 22.6 (3); MS essentially the same as for **31**. Exact Mass calcd. for $C_{12}H_{18}O_2$: 194.1306; found: 194.1307.

6-Formyl-4,7-dimethylspiro[4.5]nona-3,6-dien-1-one 34 and 7-acetyl-4-methylspiro[4.4]nona-3,7-dien-1-one 35

Ozone was passed through a solution of the keto-alcohols **31** and **32** (254 mg, 1.31 mmol) in CH_2Cl_2 (40 mL) at −78°C until the blue color persisted. The excess ozone was removed by bubbling O_2, then N_2, through the solution. Me_2S (3.0 mL) was introduced, and the mixture was stirred overnight during which time the mixture attained room temperature. The solvent was evaporated under vacuum to give crude *3-hydroxy-3-methyl-2-(3-oxobutyl)-2-(2-oxoethyl)cyclopentanone* **33** as a yellow oil (91% by GC–MS), which was used without further purification: MS: 226 (1, M^+), 165 (12), 147 (10), 141 (11), 110 (10), 109 (18), 99 (39), 71 (11), 55 (14), 43 (100). A solution of this crude **33** and 50 mg of *p*-TsOH in C_6H_6 (40 mL) was heated at reflux for 2 h with azeotropic removal of water. After cooling, saturated $NaHCO_3$ was added to the reaction mixture. The aqueous layer was extracted with ether (×3). The combined organic solutions were washed with $NaHCO_3$, water, and brine, then dried over $MgSO_4$ and concentrated under vacuum. Chromatography (4% EtOAc) of the residue provided **34** (77 mg, 31%) as an oil and 113 mg (45%) of a 1:1.2 mixture of **34** and **35**, respectively. For **34**: IR: 1739,

© 1997 NRC Canada

Can. J. Chem. Downloaded from www.nrcresearchpress.com by 88.146.161.215 on 09/08/12
For personal use only.

1654, 1620 cm^{-1}; ^1H NMR δ: 9.08 (1H, s), 5.74 (1H, q, J = 1.8 Hz), 3.24 (1H, dt, J = 2.4, 22.9 Hz), 2.86 (1H, dt, J = 3.3, 22.9 Hz), 2.69 (2H, m), 2.23 (3H, s), 2.17–1.80 (2H, m), 1.63 (3H, dd, J = 1.7, 2.4 Hz); ^{13}C NMR δ: 221.4 (0), 187.3 (1), 167.6 (0), 143.4 (0), 139.9 (0), 122.3 (1), 69.2 (2), 43.5 (2), 40.7 (2), 33.0 (2), 16.0 (3), 15.3 (3); MS: 190 (55, M^+), 147 (73), 133 (21), 119 (100), 105 (40), 91 (73), 79 (31), 77 (54), 65 (28), 53 (33), 51 (42), 50 (14), 41 (46). Exact Mass calcd. for $C_{12}H_{14}O_2$: 190.0993; found: 190.0984. Anal. calcd. for $C_{12}H_{14}O_2$: C 75.76, H 7.42; found: C 75.59, H 7.33. (For **35** see below.)

7-Acetyl-4-methylspiro[4.4]nona-3,7-dien-1-one 35 and 7-acetyl-4-methylenespiro[4.4]non-7-en-1-one 36

To a solution of crude **33**, derived as above from 206 mg (1.06 mmol) of a mixture of **31** and **32**, in CH_2Cl_2 (20 mL) at 0°C was added Et_3N (3.0 mL), followed dropwise by an excess (0.5 mL) of MsCl. The mixture was warmed to room temperature and stirred for 1 h. The mixture was poured into water, and this was extracted with CH_2Cl_2(×2). The combined organic solutions were washed with 1 M HCl, water, and brine, then dried over $MgSO_4$ and concentrated under vacuum. Chromatography on silica gel failed to separate **35** and **36**, but 138 mg (68% from **31** and **32**) of the 1:1 mixture was obtained as a colorless oil: IR: 1742, 1664, 1630 cm^{-1}. Exact Mass calcd. for $C_{12}H_{14}O_2$: 190.0993; found 190.0993.

*For **35*** (from the mixture): ^1H NMR δ: 6.65 (1H, m), 5.67 (1H, t, J = 1.8 Hz), 3.42–2.40 (6H, m), 2.35 (3H, s), 1.71 (3H, q, J = 2.4 Hz); ^{13}C NMR δ: 218.7 (0), 195.4 (0), 153.4 (0), 143.1 (0), 140.7 (1), 119.5 (1), 57.5 (0), 41.4 (2), 38.2 (2), 27.3 (2), 26.3 (3), 13.5 (3); MS (from GC–MS): 190 (0.2, M^+), 162 (15), 119 (23), 91 (24), 43 (100), 41 (15).

*For **36*** (from the mixture): ^1H NMR δ: 6.66 (1H, m), 5.01 (1H, t, J = 1.8 Hz), 4.90 (1H, t, J = 1.8 Hz), 3.42–2.40 (8H, m), 2.34 (3H, s); ^{13}C NMR δ: 220.5 (0), 195.4 (0), 144.1 (0), 142.1 (0), 140.9 (1), 106.2 (2), 58.6 (0), 43.2 (2), 42.2 (2), 41.0 (2), 39.0 (2), 27.7 (3); MS: essentially the same as for **35**.

7-Acetyl-4-methylspiro[4.4]nonan-1-one 37

Excess lithium (40 mg) was added to ammonia (30 mL) at −78°C followed by a solution of **35** and **36** (142 mg, 0.749 mmol) in dry THF (5.0 mL). The temperature of the reaction was raised to −35°C, and this was stirred for 30 min. Solid NH_4Cl was added until the blue color disappeared, and the ammonia was allowed to evaporate at room temperature. Water was added, and this was extracted with ether (×3). The combined organic solutions were washed with water and brine (×2), then dried over $MgSO_4$ and concentrated under vacuum. The resulting crude product showed NMR signals for alcohols, so the product was stirred with PCC (0.65 g, 3.0 mmol) in CH_2Cl_2 (30 mL) overnight. The solution was filtered through a Florisil pad to remove a black precipitate, and the pad was washed with ether. Concentration of the filtrate and the organic extracts provided 126 mg of an oily product, *(5*R*, 7*S*)- and (5*R*, 7*R*)-7-acetyl-4-methylspiro[4.4]non-3-en-1-one*: MS: 192 (22, M^+), 164 (35), 149 (30), 121 (51), 119 (23), 105 (26), 93 (41), 91 (36), 79 (44), 77 (31), 55 (25), 43 (100), 41 (24). A MeOH (30 mL) solution of this crude product was maintained under 300 kPa of H_2 for 1 h in the presence of 10% palladium on charcoal (50 mg). Filtration removed the catalyst, and the filtrate was concentrated under vacuum. Chromatography (6% EtOAc) of the residue provided 31 mg (24%) of **37a/b** and 80 mg (63%) of **37c/d**.

*For **37a/b***: IR: 1733, 1709 cm^{-1}; ^1H NMR (selected signals) δ: 3.22–3.08 (2H, m), 2.18 (3H, s), 2.17 (3H, s), 1.01 (6H, d, J = 2.6 Hz); MS: 194 (6, M^+), 137 (17), 133 (16), 123 (15), 111 (57), 95 (21), 79 (16), 67 (22), 55 (25), 43 (100), 41 (30). Exact Mass calcd. for $C_{12}H_{18}O_2$: 194.1306; found: 194.1306.

*For **37c/d***: IR: 1732, 1709 cm^{-1}; ^1H NMR (selected signals) δ: 2.90–2.78 (2H, m), 2.19 (3H, s), 2.17 (3H, s), 1.03 (3H, d, J = 2.4 Hz), 1.01 (3H, d, J = 2.7 Hz); MS essentially the same as for **37a/b**. Exact Mass calcd. for $C_{12}H_{18}O_2$: 194.1306; found: 194.1299.

(1*R**,2*R**,8*R**)- 38 and (1*R**,2*S**,8*R**)-2-Methyltricyclo[6.2.1.0^{1,5}]undec-5-en-7-one 39

Potassium *tert*-butoxide (114 mg, 1.01 mmol) was added to a solution of **37a–d** (98 mg, 0.51 mmol) in C_6H_6 (30 mL) at room temperature. After stirring for 20 min, TLC revealed essentially complete conversion so water was added. The aqueous layer was extracted with ether (×3). The combined organic solutions were washed with water and brine (×2), then dried over $MgSO_4$ and concentrated under vacuum. Chromatography (5% EtOAc) of the residue gave a mixture of the tricyclic enones **38** and **39** (64 mg, 72% combined) in a 1.2:1 ratio, respectively. For spectra of **38** and **39**, see below.

Separation of 38 and 39

Chromatography of a 1.2:1 mixture of enones **38** and **39** (148 mg) on 25% silver nitrate-impregnated silica gel with 2% ethyl acetate in hexane as the eluent provided homogeneous samples of **38** (48 mg, 32%) and **39** (29 mg, 20%) with the remainder of the fractions being a mixture of **38** and **39**.

*For **38***: IR: 1677 cm^{-1}; ^1H NMR δ: 5.74 (1H, q, J = 1.8 Hz), 2.90 (1H, m), 2.62–2.56 (2H, m), 2.20–1.99 (3H, m), 1.82–1.71 (3H, m), 1.62–1.47 (3H, m), 0.94 (3H, d, J = 6.9 Hz); ^{13}C NMR δ: 204.3 (0), 180.7 (0), 119.6 (0), 57.0 (0), 50.2 (1), 40.3 (2), 39.5 (1), 36.0 (2), 32.6 (2), 30.4 (2), 25.5 (2), 16.7 (3); MS: 176 (42, M^+), 135 (100), 134 (17), 133 (22), 107 (15), 105 (17), 91 (35), 79 (22), 77 (16), 41 (15). Exact Mass calcd. for $C_{12}H_{16}O$: 176.1200; found: 176.1204. Anal. calcd. for $C_{12}H_{16}O$: C 81.77, H 9.15; found: C 81.65, H 9.17.

*For **39***: IR: 1678 cm^{-1}; ^1H NMR δ: 5.72 (1H, q, J = 1.8 Hz), 2.85 (1H, m), 2.66–2.42 (2H, m), 2.17–1.98 (3H, m), 1.84–1.71 (3H, m), 1.63–1.37 (3H, m), 1.04 (3H, d, J = 6.6 Hz); ^{13}C NMR δ: 204.1 (0), 180.9 (0), 119.4 (0), 56.2 (0), 49.5 (1), 42.0 (2), 38.8 (1), 32.4 (2), 32.3 (2), 26.0 (2), 25.3 (2), 16.6 (3); MS: essentially the same as for **38**. Exact Mass calcd. for $C_{12}H_{16}O$: 176.1200; found: 176.1206.

(1*R**,2*R**,5*R**,8*R**)-2-Methyltricyclo[6.2.1.0^{1,5}]undecan-7-one 40

10% Palladium on carbon (50 mg) was added to a solution of enone **38** (88 mg, 0.50 mmol) in dry C_6H_6 (30 mL), and this was shaken for 1 h under 300 kPa of H_2. After filtration through a silica gel plug, the solution was concentrated under

© 1997 NRC Canada

vacuum, and chromatography (6% EtOAc) of the residue provided **40** (80 mg, 91%) as a colorless oil: IR: 1714 cm^{-1}; ^1H NMR δ: 2.66 (1H, dd, J = 5.1, 7.8 Hz), 2.52 (1H, dd, J = 8.4, 17.7 Hz), 2.13 (1H, dd, J = 4.5, 17.4 Hz), 2.42–1.67 (7H, m), 1.60–1.26 (5H, m), 0.92 (3H, d, J = 6.6 Hz); ^{13}C NMR δ: 215.7 (0), 52.5 (0), 49.3 (1), 44.9 (1), 39.7 (2), 38.5 (1), 32.8 (2), 32.1 (2), 32.0 (2), 30.3 (2), 26.6 (2), 14.0 (3); MS: 178 (23, M^+), 135 (24), 134 (36), 108 (21), 107 (46), 95 (30), 94 (43), 93 (75), 91 (43), 81 (36), 80 (33), 79 (77), 77 (46), 68 (40), 67 (81), 65 (26), 55 (65), 53 (36), 41 (100). Exact Mass calcd. for $C_{12}H_{18}O$: 178.1357; found: 178.1353. Anal. calcd. for $C_{12}H_{18}O$: C 80.85, H 10.18; found: C 80.78, H 10.21.

(1*R,2*R**,5*R**,8*R**)-2,6,6-Trimethyltricyclo[6.2.1.0^{1,5}]undecan-7-one 41**

Following the method of Szmant and Nanjundiah (15), to a suspension of KH (155 mg, 1.36 mmol) in THF (30 mL) at 25°C was added dropwise a solution of **40** (80 mg, 0.45 mmol) in THF (4.0 mL). After 5 min an excess (0.5 mL) of CH_3I was added dropwise. After 30 min, water (5.0 mL) was added cautiously. The mixture was partitioned between ether and water, and the aqueous layer was extracted with ether (×3). The combined organic slutions were washed with brine (×2), dried over anhydrous K_2CO_3, and concentrated under vacuum. Chromatography (4% EtOAc) of the residue provided **41** (77 mg, 82%) as a colorless oil: IR: 1704 cm^{-1}; ^1H NMR δ: 2.73 (1H, m), 1.99–1.21 (12H, m), 1.17 (3H, s), 1.05 (3H, s), 0.90 (3H, d, J = 6.9 Hz); ^{13}C NMR δ: 220.0 (0), 57.3 (1), 53.5 (0), 50.1 (1), 38.6 (1), 37.1 (2), 32.9 (3), 31.7 (0), 31.1 (2), 30.6 (2), 27.2 (2), 25.9 (2), 24.5 (3), 14.5 (3); MS: 206 (12, M^+), 135 (23), 95 (21), 94 (46), 93 (34), 91 (25), 82 (26), 81 (22), 79 (41), 77 (26), 69 (36), 67 (51), 55 (46), 53 (23), 43 (22), 41 (100). Exact Mass calcd. for $C_{14}H_{22}O$: 206.1670; found: 206.1686. Anal. calcd. for $C_{14}H_{22}O$: C 81.50, H 10.75; found: C 81.59, H 10.68.

Acknowledgements

We thank Ms. N. Brunet and Dr. C.R. Jablonski for NMR spectra, and Miss M. Baggs and Dr. B. Gregory for mass spectra. Financial support from the Natural Sciences and Engineering Research Council of Canada is gratefully acknowledged.

References

1. (*a*) M. Klobus, L.J. Zhu, and R.M. Coates. J. Org. Chem. **57**, 4327 (1992); (*b*) E.G. Rowley and N.E. Schore. J. Org. Chem. **57**, 6853 (1992); (*c*) L.A. Paquette, P.G. Meister, D. Friedrich, and D.R. Sauer. J. Am. Chem. Soc. **115**, 49 (1993); (*d*) D.J. Norris, J.F. Corrigan, Y. Sun, N.J. Taylor, and S. Collins. Can. J. Chem. **71**, 1029 (1993); (*e*) L. Fitjer and H. Monzó-Oltra. J. Org. Chem. **58**, 6171 (1993), and refs. therein; (*f*) H.A. Patel, J.B. Stothers, and S.E. Thomas. Can. J. Chem. **72**, 56 (1994); (*g*) N. Selvakumar and G.S.R.S. Rao. J. Chem. Soc. Perkin Trans. 1, 3217 (1994); (*h*) V.H. Rawal, C. Dufour, and A. Eschbach. J. Chem. Soc. Chem. Commun. 1797 (1994); (*i*) G.J. Hollingworth, G. Pattenden, and D.J. Schultz. Aust. J. Chem. **48**, 381 (1995).
2. J.J. Bloomfield and J.M. Nelke. Org. Synth. Collect. Vol. VI. Wiley, New York. 1988. p. 167.
3. (*a*) E. Nakamura and I. Kuwajima. J. Am. Chem. Soc. **99**, 961 (1977); (*b*) J. Shimada, K. Hashimoto, B.H. Kim, E. Nakamura, and I. Kuwajima. J. Am. Chem. Soc. **106**, 1759 (1984).
4. Y.-J. Wu, D.W. Strickland, T.J. Jenkins, P.-Y. Liu, and D.J. Burnell. Can. J. Chem. **71**, 1311 (1993).
5. Y.-J. Wu and D.J. Burnell. Tetrahedron Lett. **30**, 1021 (1989).
6. D.J. Burnell and Y.-J. Wu. Can. J. Chem. **68**, 804 (1990).
7. T.J. Jenkins and D.J. Burnell. J. Org. Chem. **59**, 1485 (1994).
8. (*a*) D.J. Burnell and Y.-J. Wu. Can. J. Chem. **67**, 816 (1989), and refs. therein; (*b*) B. Pandey, U.R. Khire, and N.R. Ayyangar. Synth. Commun. **19**, 2741 (1989); (*c*) M. Julia, L. Saint-Jalmes, C. Lila, J.Z. Xu, L. Moreau, B. Pfeiffer, G. Eck, L. Pelsez, and C. Rolando. Bull. Soc. Chim. Fr. **130**, 447 (1993); (*d*) J.A. Wendt, P.J. Gauvreau, and R.D. Bach. J. Am. Chem. Soc. **116**, 9921 (1994); (*e*) A. Balog and D.P. Curran. J. Org. Chem. **60**, 337 (1995); (*f*) A. Balog, S.J. Geib, and D.P. Curran. J. Org. Chem. **60**, 345 (1995).
9. P.-Y. Liu and D.J. Burnell. J. Chem. Soc. Chem. Commun. 1183 (1994).
10. Y.-J. Wu, Y.-Y. Zhu, and D.J. Burnell. J. Org. Chem. **59**, 104 (1994).
11. A. Deljac, W.D. MacKay, C.S.J. Pan, K.J. Wiesner, and K. Wiesner. Can. J. Chem. **50**, 726 (1972).
12. K. Sakurai, T. Kitahara, and K. Mori. Tetrahedron, **46**, 761 (1990).
13. J.R. Gillard and D.J. Burnell. Can. J. Chem. **70**, 1296 (1992).
14. P.E. Eaton, W.H. Bunnelle, and P. Engel. Can. J. Chem. **62**, 2612 (1984).
15. H.H. Szmant and R. Nanjundiah. J. Org. Chem. **43**, 1835 (1978).

Can. J. Chem. Downloaded from www.nrcresearchpress.com by 88.146.161.215 on 09/08/12
For personal use only.

© 1997 NRC Canada

Regio- and stereoselective ring openings of unsymmetrical oxatricyclo adducts

Simon Woo, Masood Parvez, and Brian A. Keay

Abstract: S_N2' ring-opening reactions of a number of substituted 11-oxatricyclo[6.2.1.$0^{1,6}$]undec-9-en-5-ones prepared via the intramolecular Diels–Alder reaction employing a furan diene (IMDAF) are reported. Primary, secondary, and tertiary organolithium reagents were capable of effecting the ring-opening reaction, while methyllithium required activation before any ring opening was observed. Hydride reagents, organocuprates, and Grignard reagents were generally ineffective. The ring-opening reaction was highly regio- and stereoselective for attack at C_9 *syn* to the bridging oxygen atom provided that C_8 was not substituted. A highly stereoselective nucleophilic addition to the carbonyl group *anti* to the bridging oxygen was also observed. The high selectivity appears to be due to a combination of steric and electronic effects.

Key words: S_N2' reactions, oxatricyclo adducts, Diels–Alder reaction, ring opening.

Résumé : On a effectué des réactions d'ouverture de cycles S_N2' sur un certain nombre de 11-oxatricyclo[6.2.1.$0^{1,6}$]undéc-9-én-5-ones substituées préparées par une réaction de Diels–Alder intramoléculaire à l'aide d'une furane diène («IMDAF»). Les réactifs organolithiens primaires, secondaires et tertiaires permettent d'effectuer la réaction d'ouverture de cycle; toutefois, avec le méthyllithium, il est nécessaire de procéder à une activation avant de pouvoir observer une ouverture. Les hydrures, les organocuprates et les réactifs de Grignard sont généralement inefficaces. Lorsque le carbone en C-8 n'est pas substitué, la réaction d'ouverture de cycle est extrêmement régio- et stéréosélective par rapport aux attaques en C-9 *syn* relatives à l'atome d'oxygène format le pont. On a aussi observé une réaction d'addition extrêmement stéréosélective sur le groupe carbonyle en *anti* par rapport à l'atome d'oxygène formant le pont. La sélectivité élevée semble être due à une combinaison d'effets stériques et électroniques.

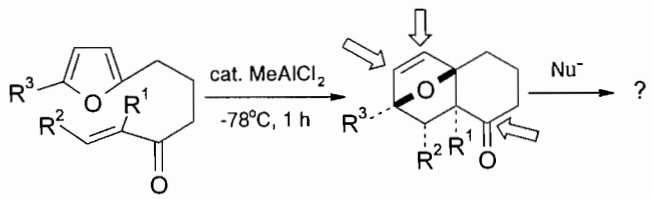
Mots clés : réactions S_N2', adduits oxatricyclo, réaction de Diels–Alder, ouverture de cycle.

[Traduit par la rédaction]

Introduction

The intramolecular Diels–Alder reaction with a furan diene (IMDAF) is capable of forming oxatricyclo adducts (Scheme 1) with a great deal of stereocontrol, producing only *exo* products with the sidearm oriented *syn* relative to the bridging oxygen atom (1). Preliminary experiments with DIBAL-H in 1986 had suggested that these cycloadducts may be amenable to ring openings; however, at that time, the methodology for preparing the cycloadducts had not been fully developed. By 1990, the oxatricyclo adducts were readily accessible using methodology developed in our laboratory (1), and the S_N2' ring-opening studies were initiated. At that time, ring openings on oxatricyclo adducts had not been attempted (2). In addition, when these studies were first started in 1990, little was known about the factors affecting the regioselectivity of the S_N2' ring openings of unsymmetrical oxabicyclo systems, as only the group of Arjona and Plumet (3) had observed a large degree of regioselectivity at that time. Lautens et al. had also reported a regioselective opening of some oxabicyclo adducts but the regioselectivity was reported to be marginal (60:40) (4). More recently, however, many groups have reported on several advances in the S_N2' ring-opening reactions of oxa-*n*-cyclic compounds and a review on this topic has recently been published (2).

Scheme 1.



A number of questions about the reactivity of the IMDAF cycloadducts with regard to the S_N2' ring-opening reactions therefore remained unanswered in 1990. These questions included:

1. What conditions were required to effect an S_N2' ring opening of the IMDAF cycloadducts?
2. What was the chemoselectivity with respect to nucleophilic addition to the ketone carbonyl group versus the S_N2' ring opening (arrows in Scheme 1)?
3. What degree of regioselectivity would be observed in the ring opening-reactions of the unsymmetrical IMDAF cycloadducts?

Received October 21, 1996.

This paper is dedicated to Professor William A. Ayer on the occasion of his 65th birthday.

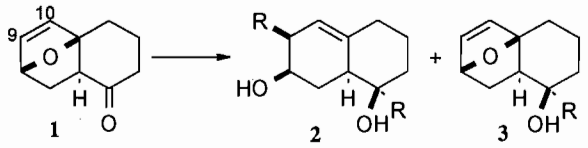
S. Woo, M. Parvez, and B.A. Keay.[1] Department of Chemistry, University of Calgary, Calgary, AB T2N 1N4, Canada.

[1] Author to whom correspondence may be addressed. Telephone: (403) 220-5354. Fax: (403) 284-1372. E-mail: keay@chem.ucalgary.ca

© 1997 NRC Canada

Can. J. Chem. Downloaded from www.nrcresearchpress.com by 88.146.161.215 on 09/08/12
For personal use only.

Table 1. Reaction of **1** with various organometallic reagents.



R	Reagent/conditions	Product	% Yield
1 *n*-Bu	3 eq. *n*-BuLi, Et_2O, −78°C → r.t., 16 h	**2***a*	66
2 i-Pr	3 eq. i-PrLi, Et_2O, −78°C → r.t., 16 h	**2***b*	68
3 *t*-Bu	3 eq. *t*-BuLi, Et_2O, −78°C → 0°C, 2 h	**2***c*	90
4 Vinyl	3 eq. vinyl MgBr, Et_2O, −78°C → r.t., 20 h	**3***d*	73
5 Me	2 eq. $Me_2CuLi{\cdot}LiCN$, THF, 0°C → r.t., 25 h	**3***e*	95
6 Me	2 eq. $Me_2CuLi{\cdot}LiI$, THF, 0°C → r.t., 19 h	**3***e*	100
7 Ph	3 eq. PhLi, Et_2O, −78°C → r.t., 18 h	**3***f*	87
8 Me	2 eq. MeLi, Et_2O, −78°C → r.t., 22 h	**3***e*	64
9 Me	8 eq. MeLi, Et_2O, reflux, 22 h	**2***e*:**3***e*	27:59
10 Me	3 eq. MeLi, 1:1 TMEDA:Et_2O, 0°C → r.t., 48 h	**2***e*:**3***e*	30:33[a]
11 Me	40 eq. MeLi, DME, −20°C → r.t., 22 h	**2***e*	73
12 H	1.5 eq. LiAl(*t*-Bu)(i-Bu)$_2$H, THF, 0°C, 1 h	**3***g*	83

[a]Other unidentified side-products produced as well.

4. What degree of stereoselectivity would be observed with both the nucleophilic addition to the carbonyl group and the ring opening, and from which face would nucleophilic attack predominantly occur?
5. What effect would the presence of other substituents on the IMDAF cycloadducts have on these variables, if any?

With these questions answered, an assessment of the applicability of an IMDAF ring-opening reaction sequence for the synthesis of natural products would be possible. As a result, a study of the scope and limitations of the S_N2' ring-opening reactions of the IMDAF cycloadducts was undertaken and our initial results communicated (5, 1*c*). Recently, an application illustrating the usefulness of the IMDAF ring-opening sequence towards the C_{15}–C_{23} fragment of venturicidin A was described (6). In this paper, a full account of the S_N2' ring openings of the IMDAF oxatricyclo adducts is reported.

Results

Oxatricyclo adducts **1**, **14**, **29**, and **35** with methyl substituents at various positions were prepared as previously described (1*d*, 1*e*) and subjected to a number of reaction conditions to investigate the scope and limitations of the ring-opening reaction.

The simplest of these systems, **1**, was chosen for initial study to determine the conditions required for the S_N2' ring openings. Compound **1** was treated with a variety of organometallic reagents, and the results are summarized in Table 1. Primary (*n*-butyllithium), secondary (isopropyllithium (7)), and tertiary (*tert*-butyllithium) organolithium reagents were capable of effecting a highly regio- and stereoselective ring opening of **1** and a highly stereoselective nucleophilic addition to the ketone carbonyl group, so that only one diastereomer **2** was produced in good to excellent yields (Table 1, entries 1–3). *sec*-Butyllithium reacted similarly, but a mixture of diastereomers was formed due to the presence of an additional stereogenic centre in the nucleophile.

The direction of regioselectivity was evident from the integration of the ^{1}H NMR spectrum, since the broadened signal at 5.3–5.5 ppm, assigned to the alkene proton of **2**, integrated to one proton instead of the two alkene protons required for the regioisomer. The stereochemistry of the resulting products was not easily determined by ^{1}H NMR, so a suitable crystal of **2***a*, produced by recrystallization from hexane, was subjected to X-ray crystallographic analysis.[2] The ORTEP plot (Fig. 1) clearly shows that *n*-butyllithium attacked the ketone carbonyl from the α-face, and had effected a ring-opening reaction by attacking C_9 from the β-face.[3]

The crystal structure of **2***a* also aided in the explanation of the appearance of the alkene proton as a broadened signal in the ^{1}H NMR spectrum rather than a doublet with additional coupling. The solution structure should also show the intramolecular hydrogen bonding in an aprotic solvent such as deuteriochloroform, and should therefore resemble the crystal structure. Examination of molecular models shows that, in this conformation, the dihedral angle between H_7 and H_8 is close to

[2] Details of the X-ray crystal analysis, including tables of atomic coordinates, bond lengths and angles, anisotropic displacement parameters, torsion angles, and nonbonded contacts, have been deposited as supplementary material and can be purchased from: The Depository of Unpublished Data, Document Delivery, CISTI, National Research Council Canada, Ottawa, Canada K1A 0S2. Except for the tables of anisotropic displacement parameters, torsion angles, and nonbonded contacts, this material has also been deposited with the Cambridge Crystallographic Data Centre, and can be obtained on request from The Director, Cambridge Crystallographic Data Centre, University Chemical Laboratory, 12 Union Road, Cambridge, CB2 1EZ, U.K.

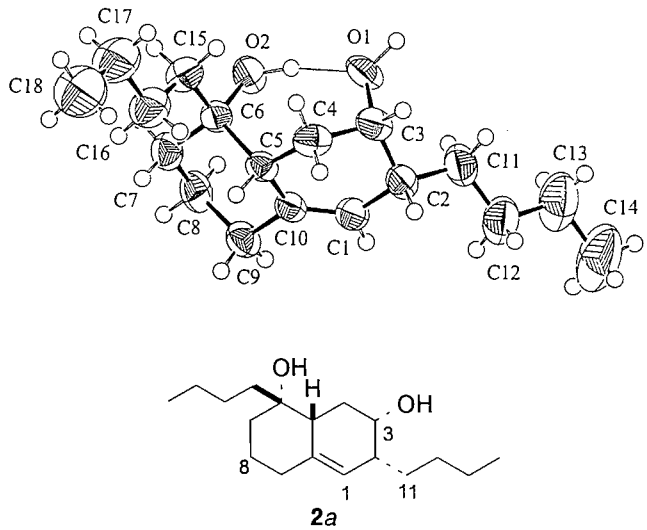
[3] The numbering of atoms in the compounds will reflect the numbering required to name the compound by IUPAC rules. As a result, the number of a particular atom may be different in the reactants versus the products.

© 1997 NRC Canada

Can. J. Chem. Downloaded from www.nrcresearchpress.com by 88.146.161.215 on 09/08/12
For personal use only.

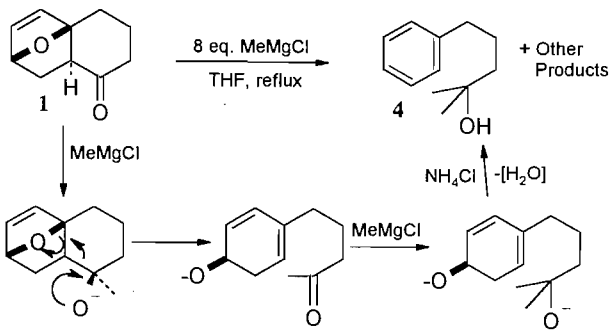
Can. J. Chem. Downloaded from www.nrcresearchpress.com by 88.146.161.215 on 09/08/12
For personal use only.

Fig. 1. X-ray crystal structure of compound **2***a*.



2*a*

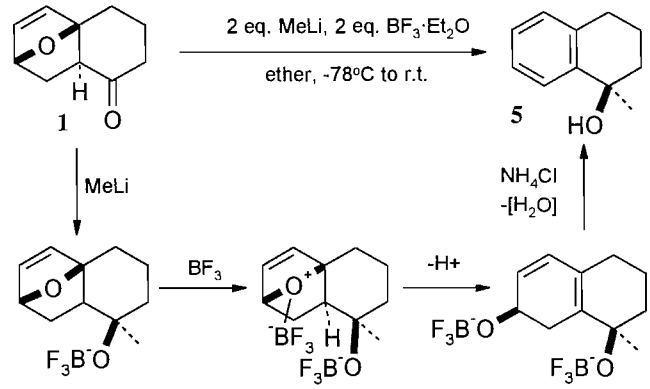
Scheme 2.



90° so that the vicinal coupling between these protons should be small. When this small coupling is combined with the several small allylic couplings between H_8 and the protons on C_1 and C_5, the net result is expected to be a broadened signal. Since the ^{1}H NMR signals for the alkene protons of **2***b* and **2***c* were similar to that of **2***a* in appearance, the same analysis holds and the stereochemistry of all three products should be the same.

Other less reactive organometallic reagents did not cause any ring opening, but did react stereoselectivity with the ketone carbonyl group to generate **3**, indicating that nucleophilic addition to the ketone carbonyl was more facile than the ring opening. Reagents in this category included Grignard reagents, organocuprate reagents ($Me_2CuLi{\cdot}LiCN$ (8) and $Me_2CuLi{\cdot}LiI$ (9)), and the less reactive organolithium reagents phenyllithium and methyllithium (Table 1, entries 4–8). Although some ring opening was observed with methyllithium when the reaction was carried out in refluxing diethyl ether (Table 1, entry 9), the reaction was slow. Increasing the reaction temperature further was not an option, since the reaction of **1** with methylmagnesium chloride in refluxing THF had produced some of the fragmentation product **4** (Scheme 2). This product likely resulted from a Grob-type fragmentation (10) of the intermediate alkoxide. Addition of a second equivalent of methylmagnesium chloride to the resulting alkoxyketone, followed by aromatization by dehydration on work-up, would generate **4**. The inability to easily cause an S_N2' ring opening with methyllithium was disappointing so methods for assisting the ring opening or enhancing the reactivity of the methyllithium were therefore investigated.

Scheme 3.



The use of lithium salts for increasing the rate of nucleophilic addition of methyllithium to ketones has been reported (11). This effect has been attributed to the complexation of the lithium salt with the ketone carbonyl group, allowing the lithium salt to act as a Lewis acid catalyst. A similar assistance in the S_N2' ring openings could result from the complexation of a lithium salt to the bridging oxygen atom. The addition of excess lithium iodide or lithium perchlorate to a mixture of **1** and methyllithium, however, produced less than 10% of the ring-opened product based on integration of the ^{1}H NMR spectrum of the crude reaction mixture. Boron trifluoride etherate has also been employed in the reaction of organolithium reagents with epoxides and oxetanes (12). Only **3***e* was produced when **1** was treated with methyllithium and boron trifluoride etherate at −78°C. Slowly increasing the reaction temperature to 25°C produced **5** (Scheme 3). This product presumably arose from cleavage of the oxygen bridge via a Lewis acid assisted β-elimination followed by aromatization on work-up. The addition of the methyl moiety to the carbonyl group could either precede, as drawn, or succeed the elimination step.

Since the attempts to facilitate the ring opening were unsuccessful, altering the reactivity of the methyllithium was tried next. Electron-donating solvents or additives such as HMPA and TMEDA have been reported to increase the nucleophilicity of organolithium reagents (13). This higher reactivity has traditionally been attributed to the formation of more reactive lower aggregates of the organolithium in the presence of electron donors, but this explanation was questioned recently by Collum (14). He argued that the lability of the organolithium–ligand complex may be more important, or that the stabilization of transition states by the additive may be the source of increased reactivity. Regardless of the reason for the effect, the increase in reactivity could allow for the S_N2' ring opening of **1** to be accomplished at room temperature. Although the addition of HMPA to the reaction mixture still resulted in the production of only **3***e*, a substantial amount of **2***e* was observed in addition to **3***e* (Table 1, entry 10) when TMEDA was employed as a cosolvent with diethyl ether. The ^{1}H NMR

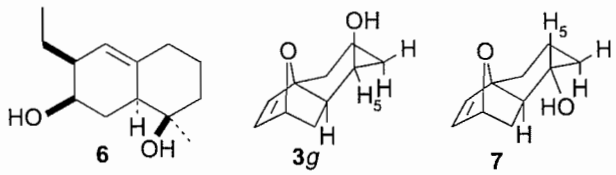
© 1997 NRC Canada

Can. J. Chem. Downloaded from www.nrcresearchpress.com by 88.146.161.215 on 09/08/12
For personal use only.

spectrum of the crude reaction mixture, however, showed the presence of a significant amount of unidentified side products as well.

DME has been reported to be a slightly weaker activator than TMEDA (see ref. 13, p. 7). The use of DME as the electron-donating reaction solvent provided the best results since **2***e* was formed in good yield and fewer side products were observed (Table 1, entry 11). Unfortunately, since organolithium reagents react with DME (15) at the higher reaction temperatures required for the ring-opening reaction, a large excess of methyllithium was required to ensure enough reagent was present to drive the reaction to completion. The use of less methyllithium resulted in the production of a mixture of **2***e* and **3***e*. DME that was freshly distilled from benzophenone ketyl was essential for the success of the reaction, since the use of Aldrich Sure-Seal® DME gave only **3***e*. The only observed side product was tentatively identified as **6**. This structural assignment was based on the ^{13}C NMR spectrum, which was very similar to the ^{13}C NMR spectrum **2***e* but contained an additional signal at 24.3 ppm resulting from a methylene carbon based on DEPT experiments. A similar product resulting from the reaction of methyllithium with another oxatricyclo adduct in DME has also been characterized by X-ray crystallography. This X-ray crystal structure and a possible mechanism for the formation of these side products will be discussed later.

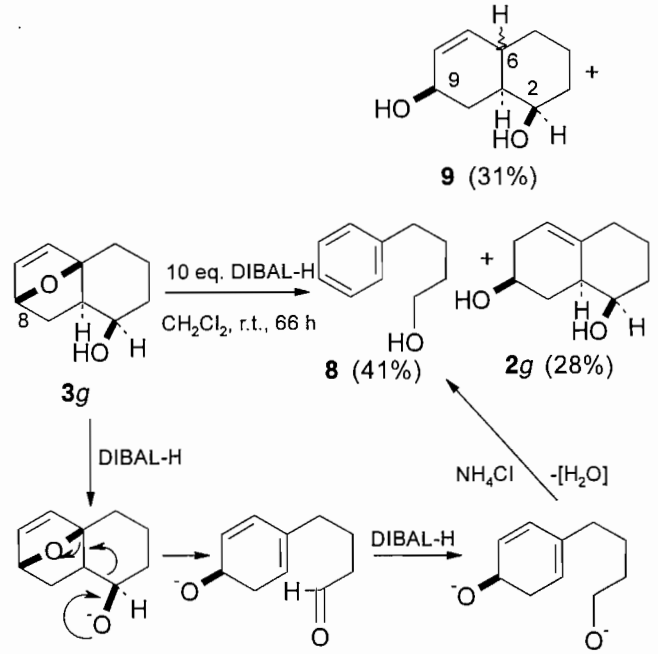
The treatment of **1** with DIBAL-H (16), in an attempt to effect a reductive ring opening, produced a complex mixture of products. The isolation of both **3***g* and the epimeric alcohol **7** from the reaction mixture indicated that the complexity of the mixture was due, in part, to the fact that the reduction of the ketone carbonyl group was not stereoselective.



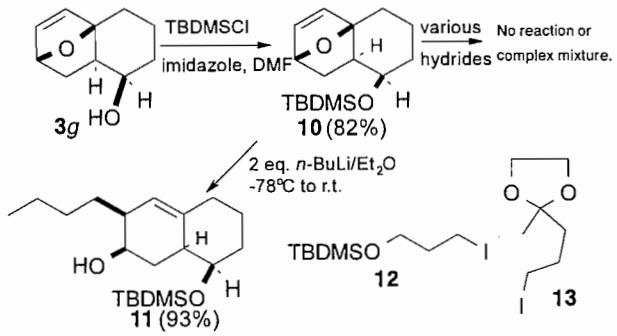
This problem of a non-stereoselective ketone reduction was circumvented by reducing the ketone in a separate step with a bulkier hydride reagent, lithium *tert*-butyldiisobutylaluminohydride (17), to form the axial alcohol **3***g* exclusively (Table 1, entry 12). When **3***g* was treated with DIBAL-H, a mixture of three products was formed (Scheme 4). The ring-opened product **2***g* was accompanied by a considerable amount of 4-phenyl-1-butanol (**8**). This product was possibly formed via a Grob-type fragmentation (10) of the initially formed alkoxide, and reduction of the resulting alkoxyaldehyde to produce a dialkoxide, followed by aromatization upon work-up with saturated ammonium chloride as illustrated in Scheme 4. The third product, which could not be completely separated from **2***g*, was tentatively identified as **9** with unknown stereochemistry at C_6. This product may have been formed from a direct reduction of the oxygen bridge. If the reduction had occurred via an S_N2-like process, attack should have occurred at the less hindered carbon atom, C_8, of **3***g*. Due to the Lewis acidic nature of DIBAL-H, however, the reduction may be more S_N1-like so that **9** was produced.

In an attempt to suppress the fragmentation reaction, compound **3***g* was converted to its *tert*-butyldimethylsilyl ether **10**

Scheme 4.



Scheme 5.



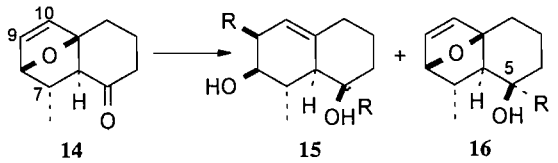
under standard conditions (18) (Scheme 5). When the protected compound was treated with DIBAL-H, however, no reaction was observed. A number of other reducing agents, including 9-BBN (19), sodium amalgam (16), lithium di-*tert*-butylbiphenyl (LiDBB) radical anion (20), and Super-Hydride® (21), also returned only unreacted starting material. Both lithium aluminum hydride (22) and DIBAL-H in hexanes produced a complex mixture of products in which the unprotected alcohol **3***g* was the major component. Although the reducing agents were unable to effect an S_N2' ring opening of compound **10**, *n*-butyllithium reacted in a highly regio- and stereoselective manner to produce **11** in high yield. This reaction illustrated that a free alkoxide was not required for the regiochemical control and that two different groups could be introduced due to the difference in the rates of the ring-opening reaction and nucleophilic attack at the ketone carbonyl. Unfortunately, attempts to extend this reaction to the functionalized nucleophiles derived from lithium–halogen exchange of the iodides **12** and **13** were unsuccessful, and only unreacted starting material was isolated.

The initial studies with **1** provided some idea of the condi-

© 1997 NRC Canada

Can. J. Chem. Downloaded from www.nrcresearchpress.com by 88.146.161.215 on 09/08/12
For personal use only.

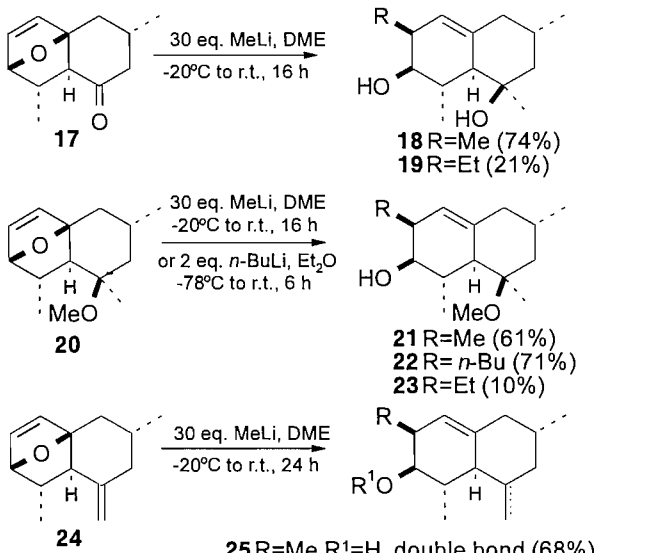
Table 2. Reaction of **14** with various organometallic reagents.



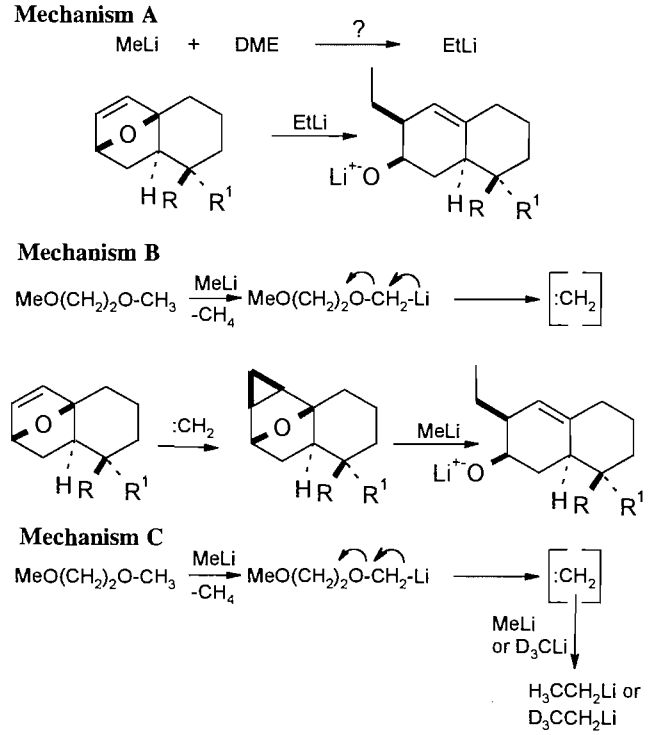
14 **15** **16**

R	Reagent/conditions	Product	% Yield
n-Bu	3 eq. *n*-BuLi, Et_2O, –78°C → r.t., 16 h	**15***a*	72
Me	3 eq. MeLi, 1:1 TMEDA:Et_2O, 0°C → r.t., 312 h	**16***b*	95
H	1.5 eq. LiAl(*t*-Bu)(i-Bu)$_2$H, THF, 0°C, 1 h	**16***c*	100

Scheme 6.



Scheme 7.



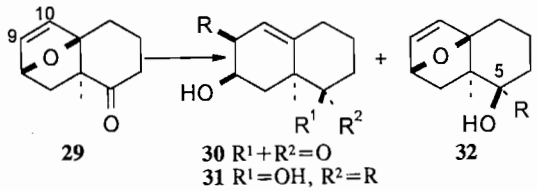
tions required to induce the S_N2' ring openings of the IMDAF cycloadducts. The effect of methyl substituents was examined next. Compound **14**, with a methyl group at C_7, was subjected to some of the reaction conditions that were successful with **1**. The results of these experiments are presented in Table 2.

n-Butyllithium smoothly reacted with **14** to generate **15***a* exclusively, showing that a C_7 methyl group had no effect on the regioselectivity of the ring-opening reaction. Surprisingly, however, the methyllithium–TMEDA system did not successfully cleave the bridging ether linkage. While the methyllithium–DME reagent was not tried with **14**, it was successful with the related compounds **17**, **20**, and **24**, giving **18**, **21**, and **25**, respectively (Scheme 6). Compounds **17**, **20**, and **24** were prepared as previously described (1). In each of these reactions, varying amounts of the ethyl derivatives **19**, **23**, and **26** were formed as side products. All three compounds were detected by GC–MS, and the *p*-nitrobenzoate ester **27**, prepared from the hydrogenation product of **26**, was characterized by X-ray crystallography. While the X-ray diffraction data were not good enough to allow for complete refinement of the crystal structure (R = 0.108), the identity and relative stereochemistry of the compound was still clearly established. Compound **20** also reacted cleanly with *n*-butyllithium, providing **22** in good yield. The reactions of **20** and **24** provided additional proof that the regioselectivity was not dependent on the presence of a free alkoxide.

Since the formation of the ethyl derivatives was both unexpected and intriguing, possible mechanisms for their formation were investigated further. The fact that the reaction was observed with **20** and **24** in addition to **17** suggested that a free alkoxide at C_5 was not involved in the reaction mechanism. Several possible mechanisms are illustrated in Scheme 7. The first possibility, mechanism A, requires the presence of ethyllithium as an impurity in the methyllithium or the formation, in some way, of ethyllithium under the reaction conditions. The homologation of secondary and tertiary organolithium reagents, usually by two carbon atoms, due to reaction with diethyl ether at room temperature is known (23). An S_N2' ring-opening reaction by the ethyllithium would then produce the

© 1997 NRC Canada

Table 3. Reaction of **29** with various organometallic reagents.



29 **30** $R^1+R^2=O$ **31** $R^1=OH$, $R^2=R$ **32**

R	Reagent/conditions	Product(s)	% Yield
n-Bu	3 eq. *n*-BuLi, Et_2O, −78°C → r.t., 16 h	**30***a*:**31***a*	62:8
Me	3 eq. MeLi, 1:1 TMEDA:Et_2O, 0°C → r.t., 312 h	**32***b*	61
H	1.5 eq. LiAl(*t*-Bu)(i-Bu)$_2$H, THF, 0°C, 1 h	**32***c*	100

observed products. A second potential mechanism, mechanism B, involves an α-elimination from the DME-derived primary anion to produce a carbene or carbenoid. The decomposition of α-haloorganolithium (see ref. 13, pp. 169–172) and α-phenoxyorganolithium (24) reagents to carbenes or carbenoids has been reported and, while an alkoxide is a poorer leaving group than either a halide or a phenoxide, the proposed α-elimination is still reasonable. The carbene or carbenoid could then react with the strained double bond of the IMDAF cycloadducts to introduce a cyclopropane ring. Attack of methyllithium to cleave the cyclopropane ring and effect the ring opening would then furnish the observed product. The chemical reactivity of cyclopropanes is similar to that of alkenes (25), and this type of reaction leading to the cleavage of the cyclopropane ring in 1-cyclopropyl-1-bromoalkanes by organocuprates (26) or piperidine (27) is known. Several experiments were performed on both the cycloadducts and on model compounds in an attempt to find support for these mechanisms.

One of the first experiments involved treatment of acetophenone with methyllithium, but no product of ethyl addition to acetophenone was detected. In addition, only 2-phenyl-2-propanol was formed when acetophenone was treated with an aliquot of a mixture of methyllithium and DME that had been stirred at room temperature for 1.5, 8.5, or 25 h. There was a possibility that any other organolithium reagents formed were simply behaving as bases with acetophenone and causing enolate formation rather than reacting with the carbonyl group. This possibility was addressed by carrying out the same experiment with benzaldehyde since benzaldehyde cannot enolize. Once again, however, only 1-phenylethanol, resulting from the addition of methyllithium to benzaldehyde, was observed. These experiments appeared to refute mechanism A since products resulting from the addition of the ethyl anion required for this mechanism should have occurred.

The treatment of **1** with trideuteriomethyllithium in DME provided **28** (Scheme 6). The mass spectrum of the reaction mixture showed that three deuterium atoms had been incorporated into **28** (M^- = 223). This result provided support for mechanism B (Scheme 7) since, in this mechanism, the methylene and methyl groups of the ethyl moiety originate from the DME and MeLi, respectively. An attempt to provide additional support for mechanism B involved performing a Simmons–Smith cyclopropanation (28) on compound **1** to introduce a cyclopropane ring on the strained double bond. Treatment of this compound with methyllithium in DME, however, returned only the cyclopropanated product, suggesting that mechanism B was not operating.

A potential explanation using a combination of mechanisms A and B is shown in mechanism C (Scheme 7). This involves the formation of ethyllithium from methyllithium and a carbene or carbenoid species generated from DME. The ethyllithium formed could then react with the oxatricyclo compound (mechanism A). In the absence of the oxatricyclo compound to immediately trap the ethyllithium formed, however, the ethyllithium could decompose the DME by the more conventional route of deprotonation of one of the methylene groups followed by β-elimination. As a result, none of the products resulting from the addition of ethyllithium to acetophenone or benzaldehyde was observed in the quenching experiments. This last explanation is purely speculative, and the possibility of a different mechanism has not been refuted.

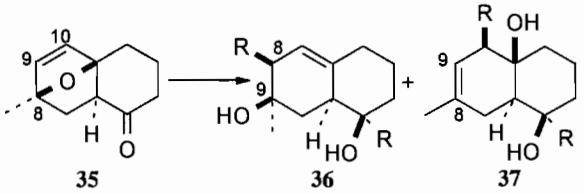
Compound **14** reacted with lithium *tert*-butyldiisobutylaluminohydride to produce the axial alcohol **16***c* exclusively in excellent yield (Table 2). The proton on C_5 appeared as a broadened multiplet at 3.99 ppm, establishing the stereochemistry of the hydroxyl group. This result also confirmed that the ketone carbonyl group of **14** was still biased towards attack from the α-face. When **16***c* was treated with DIBAL-H, a complex mixture of compounds was produced. As the production of the complex mixture meant that the reaction would not be synthetically useful, no attempt was made to characterize any of the compounds in the mixture.

The effect of a methyl group adjacent to the carbonyl group in the IMDAF cycloadducts was probed with **29** and the results are shown in Table 3. *n*-Butyllithium once again caused a regioselective S_N2' ring opening; however, the major product isolated was **30***a*, in which nucleophilic addition to the carbonyl group had *not* occurred. A small amount of the "normal" product **31***a* was also isolated. The methyl group adjacent to the carbonyl group was apparently hindering nucleophilic attack at the carbonyl group from the α-face so that the ring-opening reaction became comparatively more facile. However, slightly less bulky alkyl groups, such as methyllithium, could still attack the carbonyl group. In fact, the methyllithium–TMEDA mixture attacked the carbonyl group, producing only **32***b*, and did not produce any ring-opened products. The production of the axial alcohol **32***c* exclusively upon treatment of **29** with lithium *tert*-butyldiisobutylaluminohydride illustrated that reaction at the carbo-

Can. J. Chem. Downloaded from www.nrcresearchpress.com by 88.146.161.215 on 09/08/12
For personal use only.

© 1997 NRC Canada

Table 4. Reaction of **35** with various organometallic reagents.

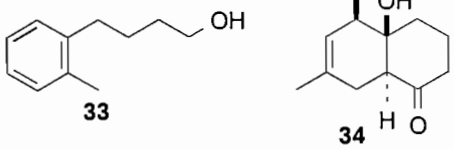


35 **36** **37**

R	Reagent/conditions	Ratio of **36**:**37**	Combined yield (%)
n-Bu	3 eq. *n*-BuLi, Et_2O, −78°C → r.t., 16 h	1.7:1	80
i-Pr	3 eq. i-PrLi/Et_2O, −78°C → r.t., 16 h	1.5:1	95
t-Bu	3 eq. *t*-BuLi, Et_2O, −78°C → 0°C, 3 h	2.2:1	55

nyl group was still biased towards attack from the α-face. Treatment of **32***c* with DIBAL-H produced predominantly the fragmentation product **33**. The formation of **33** could occur via the same mechanism for the formation of **8** from **3***g* (Scheme 4) under the same conditions.

Finally, compound **35** was used to investigate the effect of a methyl group on the bridgehead position of the IMDAF cycloadducts. The results of these experiments are summarized in Table 4. Although the ring-opening reaction could be effected with organolithium reagents, the presence of the bridgehead methyl group caused a dramatic decrease in the regioselectivity so that both **36** and **37** were formed in ratios varying from 1.5:1 to 2.2:1. In the case of the reaction with *tert*-butyllithium, a small amount (12%) of **34** was isolated as



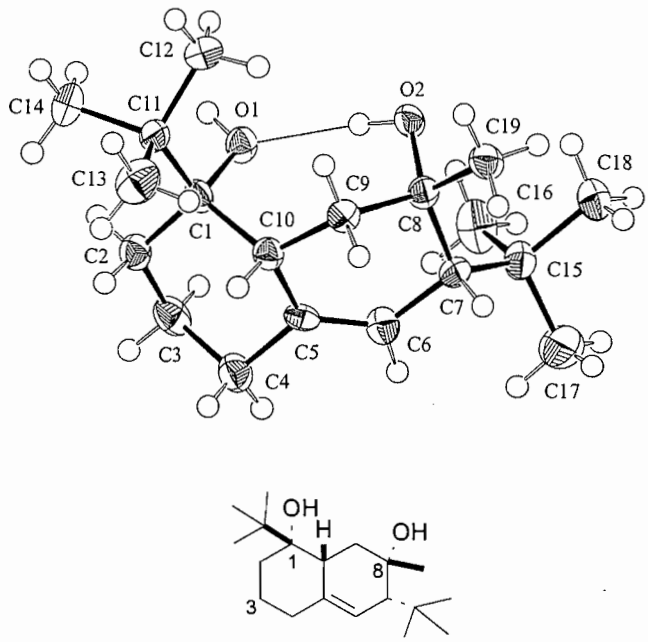
well. Because the two regioisomers were not easily separated by column chromatography and only the regioisomer that eluted first could be cleanly isolated, the ratios of products were determined by integration of the alkene protons. The major isomer from the reaction with *t*-BuLi was confirmed by an X-ray crystal structure (Fig. 2) and assigned structure **36***c*.[2] The X-ray crystal structure also established the facial selectivity of both the ring-opening reaction and the nucleophilic addition to the carbonyl group.

None of the normal S_N2' ring-opened products was observed when **35** was treated with the methyllithium–TMEDA reagent. Instead, a mixture of the non-ring-opened product **38** and the diene **39** was isolated (Scheme 8). Compound **39** was presumably formed via a β-elimination reaction as shown in Scheme 8. A similar reaction has been reported by Arjona et al. (29). This compound was somewhat unstable, and decomposed overnight upon storage in deuteriochloroform.

Discussion

Three items regarding the selectivity of the reaction of the organolithium reagents with the IMDAF cycloadducts need to be addressed. These items are the regioselectivity of the ring-opening reactions, the stereoselectivity of the ring-opening reactions, and the stereoselectivity of the nucleophilic addition to the ketone carbonyl group.

Fig. 2. X-ray crystal structure of compound **36***c*.



36*c*

Since the nucleophile would be donating electrons into the lowest unoccupied molecular orbital (LUMO) of the IMDAF cycloadducts, a difference in the lobe sizes at C_9 and C_{10} of the LUMO could be used to explain the regioselectivity. The LUMOs of several IMDAF cycloadducts, calculated at the AM1 semiemperical level using the SPARTAN molecular modelling program,[4] did not show a noticeable variation in the C_9 and C_{10} lobe sizes. Other explanations were therefore investigated.

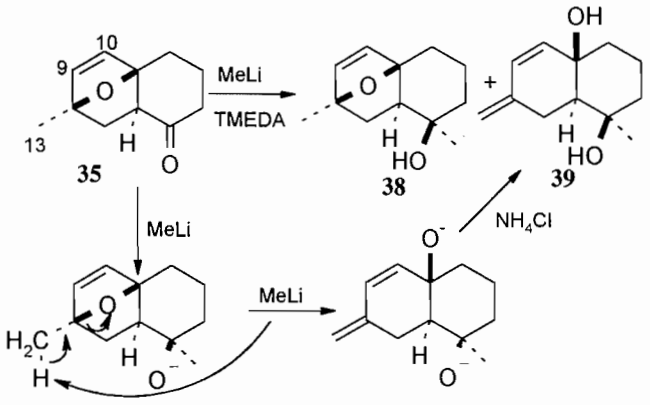
The regioselectivity could be rationalized by electronic effects. Because the organolithium reagents also behave as Lewis acids, coordination of the lithium to the bridging oxygen atom likely occurs first. The developing positive charge

[4] SPARTAN 3.0, Wavefunction, Inc., Irvine, Calif.

© 1997 NRC Canada

Can. J. Chem. Downloaded from www.nrcresearchpress.com by 88.146.161.215 on 09/08/12
For personal use only.

Scheme 8.



Scheme 9.

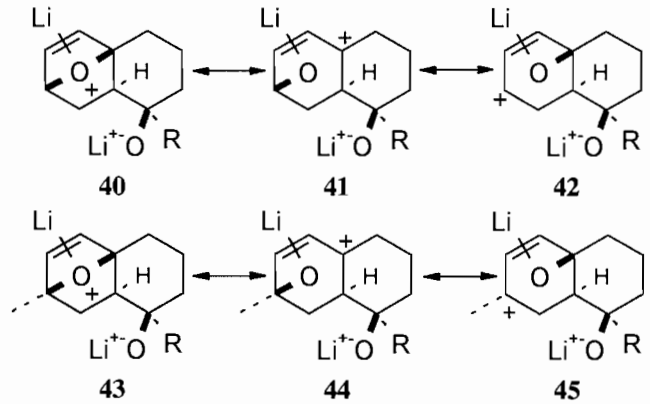


Table 5. Carbon–oxygen bond lengths of 3-21G(*) optimized structures of intermediates **40** and **43**.

Bond lengths for **40** (Å)		Bond lengths for **43** (Å)	
C_1–oxygen	1.5430	C_1–oxygen	1.5366
C_8–oxygen	1.5144	C_8–oxygen	1.5230
Difference	0.0286	Difference	0.0136

on the oxygen atom could be stabilized by resonance structures **41** or **42** for the intermediate **40** or structures **44** or **45** for the intermediate **43** (Scheme 9). For **40**, the resonance structure **41** should make a greater contribution to the resonance hybrid since the positive charge resides on a tertiary allylic carbon atom as opposed to a secondary allylic carbon atom in **42**. As a consequence, the C_1—O bond should be longer and weaker than the C_8—O bond, so that attack of a nucleophile at C_9 of **40** in an S_N2' fashion should be more facile than attack at C_{10}. On the other hand, the positive charge resides on a tertiary allylic carbon atom in both resonance structures **44** and **45**, so that these two structures should contribute equally to the resonance hybrid. As a result, the carbon–oxygen bond lengths should be more similar, and attack at C_9 or C_{10} of **43** should have more similar energy barriers. This argument was supported by the calculated structures of the intermediates **40** and **43** at the 3-21G(*) level using the SPARTAN molecular modelling program[3] (Table 5). The C_1—O bond length is longer than the C_8—O bond length in **40** and **43**; however, the difference is smaller in **43**. The slightly longer C_1_O bond length in **43** could also account for the slight preference for attack at C_9 in **35**. A similar argument has been used to rationalize the regioselectivity of acid-catalyzed ring openings of epoxides (30).

Steric arguments could also be used to rationalized the observed regioselectivity. The space-filling model of the 3-12G(*) optimized structure of **1** indicated that one of the hydrogen atoms on C_2 hinders attack at C_{10}, while attack at C_9 is less encumbered. The space-filling model of **35** indicated the same hindrance at C_{10}, but attack at C_9 is also obstructed by the hydrogen atoms (H_{13}) of the methyl group on C_8. As a result, the steric environments are more similar, leading to a corresponding decrease in the regioselectivity. A combination of steric and electronic effects is likely responsible for the observed regioselectivity.

The stereoselectivity of the S_N2' ring opening may be the result of the approach of the nucleophile from the less sterically hindered *exo* face of the oxatricyclic system (31). Coordination of the organolithium to the bridging oxygen atom or stereoelectronic effects favouring a *syn* S_N2' attack (32) are other possible contributing factors.

Steric effects are likely responsible for the stereoselective nucleophilic addition to the ketone carbonyl group. A steric argument is the classical explanation for the preference for equatorial attack at the carbonyl group of cyclohexanone when larger nucleophiles are employed (33). A different view of the space-filling model of **1** (optimized at the 3-21G(*) level) illustrated that the face of the carbonyl group opposite the bridging oxygen atom is more accessible to an attacking nucleophile.

Conclusions

The IMDAF cycloadducts are amenable to S_N2' ring openings by organolithium reagents. The minimum reactivity of the organolithium reagent required to effect the ring-opening reaction appeared to lie somewhere between that of *n*-butyllithium and methyllithium, since the former reagent and more reactive secondary and tertiary organolithium reagents were able to cause the ring opening, while methyllithium required activation by DME before any ring opening was observed. Less reactive organometallic reagents provided no ring-opened products. The reaction showed high facial selectivity for attack *syn* to the bridging oxygen atom, and was highly regioselective for attack at C_9 providing that the bridgehead position (C_8) of the IMDAF cycloadducted was not substituted. A combination of steric and electronic effects may be responsible for the high degree of selectivity. Substituents at other positions (C_3, C_6, and C_7) of the IMDAF cycloadducts were tolerated, and had no effect on the regioselectivity or stereoselectivity of the reaction.

Nucleophilic addition to the ketone carbonyl group of the IMDAF cycloadducts was generally more facile than the S_N2' ring-opening reaction unless the carbon atom adjacent to the carbonyl group bore a substituent. This addition was also highly stereoselective, providing products resulting from nucleophilic attack at the carbonyl group from the face opposite to the bridging oxygen atom. The IMDAF–S_N2' ring-opening reaction sequence provided products with up to five contiguous asymmetric centres of known relative stereochemistry in good to excellent yields.

© 1997 NRC Canada

Can. J. Chem. Downloaded from www.nrcresearchpress.com by 88.146.161.215 on 09/08/12
For personal use only.

Can. J. Chem. Downloaded from www.nrcresearchpress.com by 88.146.161.215 on 09/08/12
For personal use only.

All of the questions posed at the beginning of this article were answered by this study. With the viability of the S_N2' ring-openings established, we are continuing to apply this methodology to the enantioselective synthesis of natural products (6).

Experimental section

General experimental

Melting points were determined on solids purified by column chromatography using an Electrothermal® melting point apparatus and are uncorrected. Boiling points are uncorrected and refer to air-bath temperatures using a Kugelrohr short-path distillation apparatus. Optical rotations were measured with a Rudolph Research Autopol® III polarimeter using a 1 cm path length cell. Infrared spectra were recorded using a Mattson Galaxy Series 4030 FT-IR spectrophotometer. Solid samples were handled as pressed KBr discs, while liquid samples were placed neat between NaCl plates. Nuclear magnetic resonance spectra were obtained on either a Bruker ACE-200 (^{1}H 200 MHz, ^{13}C 50 MHz) or Bruker AM-400 (^{1}H 400 MHz, ^{13}C 100 MHz) spectrometer using deuteriochloroform as solvent. ^{13}C NMR spectra were referenced to the ^{13}C resonance of deuteriochloroform (δ 77.0), while ^{1}H NMR spectra were referenced to the ^{1}H resonance of residual chloroform (δ 7.27). Low-resolution mass spectra were either obtained using a Hewlett Packard 5890 Series II gas chromatograph interfaced to a Hewlett Packard 5971A mass selective detector or acquired by Mrs. Q. Wu (University of Calgary) using a VG-7070 spectrometer. High-resolution mass spectra were obtained by Mrs. D. Fox (University of Calgary) on a Kratos MS-80 spectrometer. Elemental analyses were also performed by Mrs. D. Fox using a Control Equipment Corporation 440 elemental analyzer. Chiral phase gas–liquid chromatography was performed on a Shimadzu GC-9A gas chromatograph equipped with a flame ionization detector using a 25 m × 0.33 mm (i.d.) × 0.25 μm (film thickness) Cydex-B (Scientific Glass Engineering) fused silica column. Analytical gas–liquid chromatography was performed on the same instrument using a 25 m × 0.53 mm (i.d.) × 3 μm (film thickness) 007 Series Methyl Silicone (Quadrex Corporation) fused silica column. Helium was used as the carrier gas in both cases. Flash column chromatography was accomplished with silica gel 60 (E. Merck, 0.04–0.063 mm, 230–400 mesh). Radial plate chromatography was performed with a Chromatotron (Harrison Research, model 7924T) with plates bearing 1, 2, or 4 mm thicknesses of silica gel (EM Science silica gel 60 PF_{254} with gypsum binder). Solvent systems refer to mixtures, by volume, of hexanes and ethyl acetate unless otherwise specified.

General procedure 1 for the S_N2' ring openings

A N_2-purged three-neck round-bottom flask equipped with an addition funnel containing a solution of the oxatricyclo compound (0.32 mmol) in anhydrous Et_2O (6 mL) was cooled with a −78°C bath. The flask was charged with anhydrous Et_2O (4 mL) and the organometallic reagent (1.0 mmol), and the solution of the oxatricyclo compound was added dropwise from the addition funnel. The mixture was warmed to 0°C and, if the reaction was not complete within 2 h, was then warmed to room temperature and stirred overnight. Wet Et_2O (10 mL) and saturated aqueous NH_4Cl (10 mL) were added sequentially, and the aqueous layer was extracted with Et_2O (4 × 10 mL). After the combined organic layers had been dried over anhydrous Na_2SO_4 and filtered, the solvent was removed in vacuo to provide the crude product. Purification was effected by flash column chromatography.

General procedure 2 for the S_N2' ring openings with methyllithium

A solution of the oxatricyclo compound (1.1 mmol) in anhydrous DME (29 mL) in a N_2-purged three-neck round-bottom flask was cooled with a −23°C bath. Methyllithium (33 mmol, 1.4 M in Et_2O) was added to the cooled reaction mixture, which was then warmed to 0°C and allowed to slowly reach room temperature overnight. The reaction was cooled back down to −23°C, and wet Et_2O (30 mL) and saturated aqueous NH_4Cl (30 mL) were cautiously added sequentially. The aqueous layer was extracted with Et_2O (4 × 30 mL), and the combined organic layers were dried over anhydrous Na_2SO_4. The dried solution was filtered, and the solvent was removed in vacuo to provide the crude product. Purification was effected by flash column chromatography.

(1*RS*,2*SR*,8*RS*,9*SR*)-2,8-Dibutylbicyclo[4.4.0]dec-6-en-2,9-diol (2*a*)

General procedure 1 was used to prepare compound **2***a*. Cycloadduct **1** (52.7 mg, 0.321 mmol) was treated with *n*-butyllithium (0.40 mL of 2.5 M in hexanes, 1.00 mmol) for 16 h to give diol **2***a* (59.4 mg, 0.212 mmol) as a white solid in 66% yield following purification by flash column chromatography (5:1); mp 104–105°C; IR (KBr): 3192 cm^{-1}; ^{1}H NMR (400 MHz): 0.92 and 0.93 (overlapping t, 6H, J = 7.0 Hz), 1.23–1.42 (m, 10H), 1.48–1.70 (m, 7H), 1.79 (ddd, 1H, J = 3.1 Hz, J = 8.8 Hz, J = 14.4 Hz), 1.96–2.05 (m, 2H), 2.13 (ddd, 1H, J = 3.4 Hz, J = 6.0 Hz, J = 14.4 Hz), 2.20–2.25 (m, 2H), 2.86 (br s, 1H), 3.88 (m, 1H), 5.36 (br s, 1H); ^{13}C NMR (50 MHz): 2 × 14.1, 22.5, 23.0, 23.3, 26.3, 28.1, 29.4, 31.0, 35.4, 36.6, 40.1, 40.3, 42.6, 66.4, 74.2, 124.5, 136.3; MS: 280 (8, M^+), 113 (100). Anal. calcd. for $C_{18}H_{32}O_2$: C 77.09, H 11.50; found: C 77.43, H 11.12.

X-ray crystal data for compound 2*a*

A sample of **2***a* was recrystallized from hexane to give colorless needles that were submitted for X-ray crystallographic analysis. See Fig. 1 for the X-ray crystal structure. Crystal data: empirical formula $C_{18}H_{32}O_2$; space group $P2_1/n$; a = 12.566(2) Å; b = 8.617(3) Å; c = 16.227(2) Å; β = 90.50(1)°; V = 1757.0 Å^3; Z = 4; d = 1.06 g/cm^3; Mo-Kα radiation (22°C); total of 3564 reflections in the range $2° < \theta < 25°$, of which 2247 were used ($I > 3\sigma(I)$) in the structure solution; R = 0.0516 and Rw = 0.0575.

(1*RS*,2*RS*,8*RS*,9*SR*)-2,8-Di(1-methylethyl)bicyclo[4.4.0]dec-6-en-2,9-diol (2*b*)

A solution of isopropyllithium was prepared using the method of Gilman et al. (7). An argon-purged three-neck round-bottom flask equipped with a glass-coated stirring bar and a dropping funnel containing a solution of freshly distilled 2-chloropropane (1.60 g, 2.04 mmol) in dry pentane (7 mL) was charged with dry penatane (13 mL). Freshly cut pieces of high-sodium (1%) lithium wire (0.2 g, 28.8 mmol) were added to the three-neck flask and the 2-chloropropane solution was

© 1997 NRC Canada

Can. J. Chem. Downloaded from www.nrcresearchpress.com by 88.146.161.215 on 09/08/12
For personal use only.

added dropwise to the reaction mixture. The addition funnel was replaced with a condenser and the solution was heated at reflux overnight. The resulting purple suspension was allowed to settle, and the supernatant was withdrawn and used. Standardization against 2,5-dimethoxybenzyl alcohol (34) indicated that the supernatant was 0.33 M in isopropyllithium.

General procedure 1 was used to prepare compound **2***b*. Cycloadduct **1** (48.2 mg, 0.294 mmol) was treated with the prepared solution of isopropyllithium (3.1 mL of 0.33 M in pentane, 1.02 mmol) for 16 h to give diol **2***b* (50.3 mg, 0.199 mmol) as a white solid in 68% yield following purification by flash column chromatography (5:1); mp 140–141.5°C; IR (KBr): 3250, 3117, 1385, 1363 cm^{-1}; ^1H NMR (200 MHz): 0.89 (d, 3H, J = 7.0 Hz), 0.95 (d, 3H, J = 6.8 Hz), 1.02 (d, 6H, J = 6.0 Hz), 1.35–1.83 (m, 7H), 1.98–2.37 (m, 5H), 2.97 (br s, 2H), 4.01 (m, 1H), 5.48 (br t, 1H, J = 1.6 Hz); ^{13}C NMR (50 MHz): 16.6, 17.6, 20.8, 20.8, 22.4, 28.3, 28.6, 29.5, 34.1, 34.1, 40.8, 47.1, 64.3, 76.3, 121.7, 137.1; MS: 252 (11, $M^{+\cdot}$), 131 (100). Exact Mass calcd. for $C_{16}H_{28}O_2$: 252.2089; found: 252.2084.

(1*RS*,2*SR*,8*SR*,9*SR*)-2,8-Di(1,1-dimethylethyl)bicyclo[4.4.0]dec-6-en-2,9-diol (2*c*)

General procedure 1 was used to prepare compound **2***c*. Cycloadduct **1** (49.8 mg, 0.303 mmol) was treated with *tert*-butyllithium (0.40 mL of 1.7 M in hexanes, 0.68 mmol) for 2 h at 0°C to give diol **2***c* (76.8 mg, 0.274 mmol) as a white solid in 90% yield following purification by flash column chromatography (9:1; mp 144–145.5°C; IR (KBr): 3231, 1395, 1365 cm^{-1}; ^1H NMR (400 MHz): 1.04 and 1.09 (two s, 9H each), 1.59–1.87 (m, 6H), 1.95–2.06 (m, 1H), 2.22–2.27 (m, 1H), 2.44 (br d, 1H, J = 7.1 Hz), 2.69 (dd, 1H, J = 4.2 Hz, J = 15.1 Hz), 2.82 (br s, 1H), 3.96 (br s, 1H), 4.16 (m, 1H), 5.49 (br t, 1H, J = 1.7 Hz); ^{13}C NMR (50 MHz): 23.8, 27.8, 28.2, 32.3, 32.7, 34.3, 36.9, 38.6, 42.5, 49.7, 65.4, 78.4, 121.7, 137.9; MS: 280 (4, $M^{+\cdot}$), 57 (100). Exact Mass calcd. for $C_{18}H_{32}O_2$: 280.2402; found: 280.2412.

(1*RS*,5*SR*,6*RS*,8*RS*)-5-Ethenyl-11-oxatricyclo[6.2.1.0^{1,6}]undec-9-en-5-ol (3*d*)

General procedure 1 was used to prepare compound **3***d*. Cycloadduct **1** (45.6 mg, 0.278 mmol) was treated with vinylmagnesium bromide (0.83 mL of 1.0 M in THF, 0.83 mmol) for 20 h to give alcohol **3***d* (39.2 mg, 0.204 mmol) as a slightly yellow oil in 73% yield following purification by flash column chromatography (3:1); bp 40–45°C/0.06 Torr (1 Torr = 133.3 Pa); IR (neat): 3478, 1630 cm^{-1}; ^1H NMR (200 MHz): 1.26 (dd, 1H, J = 8.0 Hz, J = 11.8 Hz), 1.42–1.67 (m, 3H), 1.72–2.32 (m, 5H), 3.52 (br s, 1H), 4.88 (dd, 1H, J = 1.7 Hz, J = 4.9 Hz), 5.00 (dd, 1H, J = 1.9 Hz, J = 10.6 Hz), 5.26 (dd, 1H, J = 1.9 Hz, J = 17.2 Hz), 5.75 (dd, 1H, J = 10.6 Hz, J = 17.2 Hz), 5.93 (d, 1H, J = 5.7 Hz), 6.47 (dd, 1H, J = 1.7 Hz, J = 5.7 Hz); ^{13}C NMR (50 MHz): 16.4, 27.6, 28.4, 36.9, 41.1, 71.9, 78.4, 87.7, 112.0, 137.2, 139.1, 144.0; MS: 192 (1, $M^{+\cdot}$), 94 (100). Exact Mass calcd. for $C_{12}H_{16}O_2$: 192.1150; found: 192.1138.

(1*RS*,5*RS*,6*RS*,8*RS*)-5-Methyl-11-oxatricyclo[6.2.1.0^{1,6}]undec-9-en-5-ol (3*e*)

General procedure 1 was used to prepare compound **3***e*. Cycloadduct **1** (48.6 mg, 0.296 mmol) was treated with methyllithium (0.46 mL of 1.4 M in Et_2O, 0.64 mmol) for 22 h to give alcohol **3***e* (34.1 mg, 0.189 mmol) as a colorless oil in 64% yield following purification by flash column chromatography (20:1 benzene:acetone); bp 50–60°C/0.07 Torr; IR (neat): 3497 cm^{-1}; ^1H NMR (200 MHz): 1.12 (s, 3H), 1.25–1.63 (m, 4H), 1.67–2.01 (m, 3H), 2.17–2.30 (m, 2H), 3.36 (br s, 1H), 4.89 (dd, 1H, J = 1.7 Hz, J = 4.9 Hz), 5.93 (d, 1H, J = 5.7 Hz), 6.47 (dd, 1H, J = 1.7 Hz, J = 5.7 Hz); ^{13}C NMR (50 MHz): 16.7, 27.8, 28.5, 28.9, 38.6, 42.7, 69.5, 78.5, 88.0, 137.5, 138.8; MS: 180 (weak, $M^{+\cdot}$), 94 (100). Exact Mass calcd. for $C_{11}H_{16}O_2$: 180.1150; found: 180.1154.

(1*RS*,5*RS*,6*SR*,8*RS*)-5-Phenyl-11-oxatricyclo[6.2.1.0^{1,6}]undec-9-en-5-ol (3*f*)

General procedure 1 was used to prepare compound **3***f*. Cycloadduct **1** (47.3 mg, 0.288 mmol) was treated with phenyllithium (0.45 mL of 2.0 M in cyclohexane–Et_2O, 0.90 mmol) for 18 h to give alcohol **3***f* (60.6 mg, 0.250 mmol) as a yellow solid in 87% yield following purification by flash column chromatography (5:1); mp 114–115°C; IR (KBr): 3459, 1491, 1451 cm^{-1}; ^1H NMR (200 MHz): 1.11 (dd, 1H, J = 7.8 Hz, J = 11.7 Hz), 1.67–1.76 (m, 1H), 1.87–2.13 (m, 6H), 2.36–2.42 (m, 1H), 4.13 (s, 1H), 4.91 (dd, 1H, J = 1.7 Hz, J = 4.7 Hz), 6.00 (d, 1H, J = 5.7 Hz), 6.48 (dd, 1H, J = 1.7 Hz, J = 5.7 Hz), 7.19–7.52 (m, 5H); ^{13}C NMR (50 MHz): 17.2, 27.6, 28.5, 39.1, 43.4, 73.3, 78.5, 88.2, 124.8, 126.2, 127.9, 137.2, 139.1, 147.7; MS: 242 (1, $M^{+\cdot}$), 94 (100). Exact Mass calcd. for $C_{16}H_{18}O_2$: 242.1307; found: 242.1305.

(1*RS*,2*SR*,8*RS*,9*SR*)-2,8-Dimethylbicyclo[4.4.0]dec-6-en-2,9-diol (2*e*) and (1*RS*,2*SR*,8*RS*,9*SR*)-8-ethyl-2-methylbicyclo[4.4.0]dec-6-en-2,9-diol (6)

(a) Using methyllithium–TMEDA

Anhydrous Et_2O (2 mL) was placed in a N_2-purged three-neck round-bottom flask equipped with an addition funnel containing a solution of cycloadduct **1** (48.0 mg, 0.292 mmol) in anhydrous Et_2O (5 mL). The flask was cooled with an ice bath, and methyllithium (0.80 mL of 1.4 M in Et_2O, 1.12 mmol) and dry TMEDA (7.8 mL) was added. The solution of **1** was added dropwise from the addition funnel, and the reaction was warmed to room temperature and stirred for 48 h. Wet Et_2O (10 mL) and saturated aqueous NH_4Cl (10 mL) were then added sequentially, and the aqueous layer was extracted with Et_2O (4 × 10 mL). The combined organic layers were washed with 10% aqueous $CuSO_4$ (2 × 30 mL), dried over anhydrous Na_2SO_4, and filtered. The solvent was removed from the filtrate in vacuo. The crude product contained a mixture of **2***e*:**3***e* in a ratio of approximately 1:1. Flash column chromatography (3:1) provided **3***e* (17.5 mg, 0.0971 mmol) and **2***e* (16.9 mg, 0.0861 mmol) in yields of 33 and 30%, respectively.

(b) Using methyllithium–DME

Cycloadduct **1** (36.0 mg, 0.219 mmol) was treated with methyllithium (6.30 mL of 1.4 M in Et_2O, 8.82 mmol) for 22 h according to general procedure 2. Flash column chromatography (3:1) provided diol **2***e* (31.6 mg, 0.161 mmol) and a compound tentatively identified as **6** (12.0 mg, 0.0570 mmol) in yields of 74 and 26%, respectively. Compound **2***e* was characterized as a white solid, mp 124–125°C; IR (KBr): 3244 cm^{-1}; ^1H NMR (200 MHz): 1.05 (d, 3H, J = 7.2 Hz), 1.26 (s, 3H), 1.44–2.35 (m, 10H), 2.89 (br s, 2H), 3.84 (m, 1H), 5.33 (br s,

© 1997 NRC Canada

Can. J. Chem. Downloaded from www.nrcresearchpress.com by 88.146.161.215 on 09/08/12
For personal use only.

1H); ^{13}C NMR (50 MHz): 16.0, 22.6, 27.7, 28.1, 35.0, 35.1, 40.3, 45.2, 67.9, 72.0, 126.1, 136.0; MS: 196 (6, $M^{+\cdot}$), 120 (100). Anal. calcd. for $C_{12}H_{20}O_2$: C 73.41, H 10.29; found: C 73.27, H 10.10.

The second compound (**6**) was also a white solid, but was contaminated. ^{1}H NMR (200 MHz): 1.00 (t, 3H, J = 7.3 Hz), 1.27 (s, 3H), 1.32–2.33 (m, 18H, high due to contaminant), 3.00 (br s, 2H), 3.91 (br m, 1H), 5.34 (br s, 1H); ^{13}C NMR (50 MHz): 12.0, 22.7, 24.3, 28.0, 28.7, 35.4, 40.4, 42.1, 44.9, 66.0, 72.2, 124.0, 136.2; MS: No $M^{+\cdot}$, 192 (27, $M^{+\cdot} - H_2O$).

(1*RS*,5*RS*,6*RS*,8*RS*)-11-Oxatricyclo[6.2.1.0^{1,6}[undec-9-en-5-ol (3*g*) and (1*RS*,5*SR*,6*RS*,8*RS*)-11-oxatricyclo[6.2.1.0^{1,6}]undec-9-en-5-ol (7)

(a) Using DIBAL-H

Cycloadduct **1** (77.3 mg, 0.471 mmol) was placed in a N_2-purged three-neck round-bottom flask and dissolved in CH_2Cl_2 (10 mL). The solution was cooled using a −78°C cold bath, and DIBAL-H (1.10 mL of 1.0 M in THF, 1.10 mmol) was added by syringe. The reaction was warmed to 0°C, and then slowly warmed to room temperature and stirred for 22 h. Wet Et_2O (10 mL) and saturated aqueous NH_4Cl (10 mL) were then added to quench the reaction, and the mixture was filtered through Celite.® The Celite® was washed well with several portions of Et_2O. The aqueous layer was extracted with Et_2O (4 × 10 mL) and the combined organic layers were dried with anhydrous Na_2SO_4. The drying agent was removed by filtration, and the solvent was removed in vacuo to provide a crude reaction product. Flash column chromatography (3:1, then 1:1) provided **3***g* (13.2 mg, 0.0794 mmol) and **7** (29.0 mg, 0.174 mmol) in yields of 17 and 37%, respectively. A mixture of uncharacterized compounds (29.9 mg) was also isolated.

(b) Using lithium tert-butyldiisobutylaluminohydride

Cycloadduct **1** (71.0 mg, 0.432 mmol) was placed in a N_2-purged three-neck round-bottom flask and dissolved in THF (6 mL). The solution was cooled using a −78°C cold bath, and lithium *tert*-butyldiisobutylaluminohydride (0.65 mL of 1.0 M in THF, 0.65 mmol) was added by syringe. The mixture was stirred at −78°C until analysis by TLC indicated that the starting material had been consumed (15 min). Solid $Na_2SO_4 \cdot 10H_2O$ (274 mg, 0.850 mmol) was added, and the reaction was poured into a mixture of 0.5 M aqueous $KHSO_4$ (8 mL) and $CHCl_3$ (6 mL) and stirred for 15 min. The aqueous layer was extracted with $CHCl_3$ (4 × 10 mL). After the combined organic layers had been dried with anhydrous Na_2SO_4 and filtered, the solvent was removed in vacuo to give **3***g* (59.9 mg, 0.360 mmol) exclusively in 83% yield after purification by flash column chromatography (3:1). Compound **3***g* was characterized as a colorless oil, bp 44–50°C/0.08 Torr; IR (neat): 3493 cm^{-1}; ^{1}H NMR (200 MHz): 1.38 (dd, 1H, J = 8.1 Hz, J = 11.5 Hz), 1.43–2.08 (m, 6H), 2.17–2.33 (m, 2H), 3.08 (d, 1H, J = 8.2 Hz), 3.82–3.99 (br m, 1H), 4.90 (dd, 1H, J = 1.7 Hz, J = 4.9 Hz), 5.91 (d, 1H, J = 5.7 Hz), 6.47 (dd, 1H, J = 1.7 Hz, J = 5.7 Hz); ^{13}C NMR (50 MHz): 14.7, 27.9, 29.5, 32.0, 37.5, 67.2, 78.1, 87.6, 137.2, 138.8; MS: 166 (1, $M^{+\cdot}$), 94 (100). Exact Mass calcd. for $C_{10}H_{14}O_2$: 166.0994; found: 166.0980.

Compound **7** was characterized as a colorless oil, bp 40–50°C/0.08 Torr; IR (neat): 3392 cm^{-1}; ^{1}H NMR (200 MHz): 1.29–1.98 (m, 9H), 2.16–2.26 (m, 1H), 3.39 (ddd, 1H, J = 3.8 Hz, J = 9.2 Hz, J = 11.2 Hz), 4.95 (dd, 1H, J = 1.7 Hz, J = 4.5 Hz), 5.99 (d, 1H, J = 5.7 Hz), 6.38 (dd, 1H, J = 1.7 Hz, J = 5.7 Hz); ^{13}C NMR (50 MHz): 20.5, 28.2, 33.8, 34.8, 44.0, 76.0, 78.9, 88.3, 137.5, 137.8; MS: 166 (1, $M^{+\cdot}$), 94 (100). Exact Mass calcd. for $C_{10}H_{14}O_2$: 166.0994; found: 166.0996.

(1*RS*,2*SR*,9*RS*)-Bicyclo[4.4.0]dec-6-en-2,9-diol (2*g*) and (1*RS*,2*SR*,6*SR*,9*SR*)- or (1*RS*,2*SR*,6*RS*,9*SR*)-bicyclo[4.4.0]dec-7-en-2,9-diol (9)

Compound **3***g* (51.8 mg, 0.312 mmol) was placed in a N_2-purged three-neck round-bottom flask and dissolved in CH_2Cl_2 (10 mL). The solution was cooled using a −78°C cold bath, and DIBAL-H (3.20 mL of 1.0 M in THF, 3.20 mmol) was added by syringe. The reaction was warmed to 0°C, and then slowly warmed to room temperature and stirred for 66.5 h. Wet Et_2O (10 mL) and saturated aqueous NH_4Cl (10 mL) were then added to quench the reaction, and the mixture was filtered through Celite.® The Celite® was washed well with several portions of Et_2O. The aqueous layer was extracted with Et_2O (4 × 10 mL) and the combined organic layers were dried with anhydrous Na_2SO_4. The drying agent was removed by filtration, and the solvent was removed in vacuo to provide a crude reaction product. Flash column chromatography (1:5) provided 4-phenyl-1-butanol **8** (19.1 mg, 0.127 mmol), **2***g* (14.8 mg, 0.0880 mmol), and a third compound tentatively identified as **9** (16.2 mg, 0.0963 mmol, contaminated by **2***g*) in yields of 41, 28, and 31%, respectively. Compound **2***g* was characterized as a white solid. IR (KBr): 3395 cm^{-1}; ^{1}H NMR (200 MHz): 1.53–2.40 (m, 11H), 2.74 (br s, 2H), 3.89 (br s, 1H), 4.03 (m, 1H), 5.45 (br s, 1H); ^{13}C NMR (50 MHz): 20.9, 33.2, 2 × 33.8, 34.9, 40.8, 64.5, 71.3, 118.5, 136.0; MS: 168 (23, $M^{+\cdot}$), 55 (100). Exact Mass calcd. for $C_{10}H_{16}O_2$: 168.1150; found: 168.1148.

The impure sample of **9** was partially characterized. ^{13}C NMR (50 MHz) following elimination of signals due to **2***g*: 20.6, 32.2, 33.4, 34.5, 36.9, 44.1, 69.1, 70.3, 130.0, 134.7. 4-Phenyl-1-butanol **8** exhibited ^{1}H NMR (200 MHz): 1.30 (br s, 1H) 1.40–1.85 (m, 4H), 2.63 (t, 2H, J = 7 Hz), 3.69 (t, 2H, J = 7 Hz), 7.11–7.36 (m, 5H).

(1*RS*,5*RS*,6*RS*,8*RS*)-5-(*tert*-Butyldimethylsiloxy)-11-oxatricyclo[6.2.1.0^{1,6}]undec-9-ene (10)

Compound **3***g* (0.112 g, 0.676 mmol) was dissolved in dry DMF (2 mL) in a N_2-purged three-neck round-bottom flask. Freshly distilled TBDMSCl (0.369 g, 2.45 mmol) and imidazole (0.349 g, 5.13 mmol) were added, and the reaction was stirred at room temperature for 16 h. When analysis by TLC indicated that the reaction was complete, Et_2O (10 mL) and saturated aqueous NaCl (3 mL) was added. The organic layer was separated and washed with additional saturated aqueous NaCl (3 × 3 mL). After the organic phase had been dried with anhydrous Na_2SO_4 and filtered, the solvent was removed in vacuo. Purification by flash column chromatography (20:1) provided **10** (0.156 g, 0.554 mmol) as a colorless liquid in 82% yield; bp 50–60°C/0.06 Torr; IR (neat): 2900 cm^{-1}; ^{1}H NMR (200 MHz): 0.04 (s, 6H), 0.91 (s, 9H), 1.23 (dd, 1H, J = 8.3 Hz, J = 10.7 Hz), 1.35–1.57 (m, 3H), 1.80–2.12 (m, 4H), 2.22–2.28 (m, 1H), 4.03 (br m, 1H), 4.83 (dd, 1H, J = 1.6 Hz, J = 4.7 Hz), 5.96 (d, 1H, J = 5.6 Hz), 6.33 (dd, 1H, J = 1.6 Hz, J = 5.6 Hz); ^{13}C NMR (50 MHz): −5.2, −4.3, 15.1, 18.1, 25.8,

© 1997 NRC Canada

Can. J. Chem. Downloaded from www.nrcresearchpress.com by 88.146.161.215 on 09/08/12
For personal use only.

28.4, 28.5, 32.8, 39.8, 66.9, 77.9, 85.8, 137.7, 139.4; MS: 280 (0.4, $M^{+\cdot}$), 75 (100). Exact Mass calcd. for $C_{16}H_{28}O_2Si$: 280.1859; found: 280.1850.

(1*RS*,3*SR*,4*RS*,10*SR*)-4-Butyl-10-(*tert*-butyldimethylsiloxy)bicyclo[4.4.0]dec-5-en-3-ol (11)

Compound **10** (58.2 mg, 0.207 mmol) was treated with *n*-butyllithium (0.17 mL of 2.5 M in hexanes, 0.425 mmol) for 18 h according to general procedure 1 to give compound **11** (65.0 mg, 0.192 mmol) as a white solid in 93% yield following purification by flash column chromatography (9:1); mp 44–46°C; IR (KBr): 3345 cm^{-1}; ^1H NMR (200 MHz): 0.09, 0.13 (two s, 3H each), 0.91 (overlapping t and s, 12h), 1.21–2.05 (m, 15H), 2.18–2.35 (m, 2H), 3.81 (m, 1H), 3.89 (br s, 1H), 5.29 (br s, 1H); ^{13}C NMR (50 MHz): −4.6, −4.2, 14.1, 18.3, 20.5, 23.0, 26.0, 29.6, 31.0, 32.6, 33.7, 34.9, 40.7, 41.3, 67.1, 72.5, 85.8, 124.1, 135.4; MS: 338 (0.1, $M^{+\cdot}$), 189 (100). Exact Mass calcd. for $C_{16}H_{29}O_2Si$ $M^{+\cdot}$ − *t*-Bu): 281.1936; found: 281.1911.

(1*RS*,2*SR*,8*RS*,9*RS*,10*RS*)-2,8-Dibutyl-10-methylbicyclo[4.4.0]dec-6-en-2,9-diol (15*a*)

General procedure 1 was used to prepare compound **15***a*. Cycloadduct **14** (30.3 mg, 0.170 mmol) was treated with *n*-butyllithium (0.20 mL of 2.5 M in hexanes, 0.50 mmol) for 16 h to give diol **15***a* (36.1 mg, 0.123 mmol) as a white solid in 72% yield following purification by flash column chromatography (5:1); mp 122–123°C; IR (KBr): 3198 cm^{-1}; ^1H NMR (200 MHz): 0.93–0.97 (d and two overlapping t, 9H, J = 7.3 Hz (for d)), 1.22–2.18 (m, 19H), 2.21–2.28 (m, 1H), 2.37 (dq, 1H, J = 2.7 Hz, J = 7.3 Hz), 3.55 (2 overlapping br s, 3H), 5.23 (br s, 1H); ^{13}C NMR (50 MHz): 14.1, 14.1, 20.5, 22.9, 23.0, 23.4, 26.5, 29.3, 31.1, 32.7, 35.6, 36.3, 37.2, 40.8, 50.1, 70.7, 74.7, 122.3, 135.0; MS: 294 (1, $M^{+\cdot}$), 174 (100). Exact Mass calcd. for $C_{19}H_{34}O_2$: 294.2559; found: 294.2566.

(1*RS*,5*RS*,6*RS*,7*SR*,8*SR*)-5,7-Dimethyl-11-oxatricyclo[6.2.1.0^{1,6}]undec-9-en-5-ol (16*b*)

Anhydrous Et_2O (2 mL) was placed in a N_2-purged three-neck round-bottom flask equipped with an addition funnel containing a solution of cycloadduct **14** (56.7 mg, 0.318 mmol) in anhydrous Et_2O (5 mL). The flask was cooled with an ice bath, and methyllithium (0.70 mL of 1.4 M in Et_2O, 0.98 mmol) and dry TMEDA (7.7 mL) were added. The solution of **14** was added dropwise from the addition funnel, and the reaction was warmed to room temperature and stirred for 312 h. Wet Et_2O (10 mL) and saturated aqueous NH_4Cl (10 mL) were added sequentially, and the aqueous layer was extracted with Et_2O (4 × 10 mL). The combined organic layers were washed with 10% aqueous $CuSO_4$ (2 × 30 mL), dried over anhydrous Na_2SO_4, and filtered. The solvent was removed from the filtrate in vacuo. Flash column chromatography (20:1 benzene:acetone) provided **16***b* (58.5 mg, 0.301 mmol) as a white solid in 95% yield; mp 41–42°C; IR (KBr): 3492 cm^{-1}; ^1H NMR (200 MHz): 0.92 (d, 3H, J = 7.1 Hz), 1.03 (d, 1H, J = 3.0 Hz), 1.18 (s, 3H), 1.30–1.97 (m, 5H), 2.10–2.24 (m, 1H), 2.71 (m, 1H), 3.33 (s, 1H), 4.72 (dd, 1H, J = 1.7 Hz, J = 4.9 Hz), 6.05 (d, 1H, J = 5.8 Hz), 6.43 (dd, 1H, J = 1.7 Hz, J = 5.8 Hz); ^{13}C NMR (50 MHz): 16.6, 18.1, 28.1, 29.0, 35.3, 38.5, 51.6, 69.7, 81.9, 88.9, 136.4, 138.7; MS: 194 (weak, $M^{+\cdot}$), 94 (100). Exact Mass calcd. for $C_{12}H_{18}O_2$: 194.1307; found: 194.1312.

(1*RS*,5*RS*,6*RS*,7*SR*,8*SR*)-7-Methyl-11-oxatricyclo[6.2.1.0^{1,6}]undec-9-en-5-ol (16*c*)

Cycloadduct **14** (51.0 mg, 0.286 mmol) was placed in a N_2-purged three-neck round-bottom flask and dissolved in THF (4 mL). The solution was cooled using a −78°C cold bath, and lithium *tert*-butyldiisobutylaluminohydride (0.43 mL of 1.0 M in THF, 0.43 mmol) was added by syringe. The mixture was stirred at −78°C until analysis by TLC indicated that the starting material had been consumed (50 min). Solid $Na_2SO_4 \cdot 10H_2O$ (150 mg, 0.466 mmol) was added, and the reaction was poured into a mixture of 0.5 M aqueous $KHSO_4$ (10 mL) and $CHCl_3$ (5 mL) and stirred for 30 min. The aqueous layer was extracted with $CHCl_3$ (4 × 10 mL). After the combined organic layers had been dried with anhydrous Na_2SO_4 and filtered, the solvent was removed in vacuo to give **16***c* (51.5 mg, 0.286 mmol) exclusively in 100% yield after purification by flash column chromatography (5:1). Compound **16***c* was characterized as a colorless oil, bp 45–50°C/0.05 Torr; IR (neat): 3501 cm^{-1}; ^1H NMR (200 MHz): 0.86 (d, 3H, J = 7.0 Hz), 1.14 (t, 1H, J = 3.6 Hz), 1.20–1.52 (m, 2H), 1.69–2.01 (m, 3H), 2.17–2.24 (m, 1H), 2.64–2.90 (overlapping m and br s, 2H), 3.99 (br t, 1H), 4.71 (dd, 1H, J = 0.9 Hz, J = 4.6 Hz), 6.01 (d, 1H, J = 5.8 Hz), 6.41 (dd, 1H, J = 0.9 Hz, J = 5.8 Hz); ^{13}C NMR (50 MHz): 14.5, 16.6, 28.2, 31.8, 35.7, 46.7, 66.1, 81.7, 88.3, 136.2, 138.5; MS: 180 (1, $M^{+\cdot}$), 94 (100). Exact Mass calcd. for $C_{11}H_{16}O_2$: 180.1150; found: 180.1151.

(1*S*,2*R*,4*S*,8*S*,9*S*,10*S*)-2,4,8,10-Tetramethylbicyclo[4.4.0]dec-6-en-2,9-diol ((+)-18)

Cycloadduct (−)-**17** (prepared according to ref. 1*c*) (123.8 mg, 0.644 mmol) was treated with methyllithium (14.0 mL of 1.4 M in Et_2O, 20 mmol) for 16 h according to general procedure 2. Integration of the alkene signals of the ^1H NMR spectrum of the crude reaction mixture showed the presence of (+)-**18** and a compound tentatively identified as the ethyl derivative **19** in a 3.5:1 ratio. Flash column chromatography (3:1) provided diol (+)-**18** (106.6 mg, 0.4751 mmol) as a white solid in 74% yield; mp 139.5–141°C; $[\alpha]_D^{23}$ +40.7 (*c* 3.08, $CHCl_3$); IR (KBr): 3253 cm^{-1}; ^1H NMR (200 MHz): 0.89, 0.98, and 1.07 (d, 3H each, J = 6.4 Hz, J = 7.3 Hz, J = 7.3 Hz), 1.22 (dd, 1H, J = 12.1 Hz, J = 13.5 Hz), 1.28 (s, 3H), 1.55–1.78 (m, 3H), 1.80–1.97 (m, 1H), 2.17–2.30 (m, 2H), 2.39 (dq, 1H, J = 3.2 Hz, J = 7.3 Hz), 3.47 (br m, 1H), 3.72 (br s, 2H), 5.14 (br s, 1H); ^{13}C NMR (50 MHz): 16.8, 20.7, 21.9, 28.3, 29.2, 30.3, 33.2, 44.7, 49.7, 51.7, 72.3, 72.5, 123.3, 134.8; MS: 224 (5, $M^{+\cdot}$), 107 (100). Exact Mass calcd. for $C_{14}H_{24}O_2$: 224.1776; found: 224.1774.

Compound **19** was detected by GC–MS. MS: 238 (3, $M^{+\cdot}$), 220 (15, $M^{+\cdot}$ − H_2O), 180 (31, retro Diels–Alder), 133 (100).

(1*RS*,2*RS*,3*RS*,4*RS*,8*RS*,10*SR*)-10-Methoxy-2,4,8,10-tetramethylbicyclo[4.4.0]-dec-5-en-3-ol (21)

Cycloadduct **20** (174.7 mg, 0.786 mmol) was treated with methyllithium (17.0 mL of 1.4 M in Et_2O, 24 mmol) for 16 h according to general procedure 2. Integration of the alkene signals of the ^1H NMR spectrum of the crude reaction mixture showed the presence of **21** and a compound tentatively identified as the ethyl derivative **23** in a 6.25:1 ratio. Flash column chromatography (3:1) provided **21** (114.5 mg, 0.480 mmol) as a viscous colorless oil in 61% yield. Since this compound was

© 1997 NRC Canada

Can. J. Chem. Downloaded from www.nrcresearchpress.com by 88.146.161.215 on 09/08/12
For personal use only.

prone to decomposition, it was not fully characterized; bp 70–80°C/0.05 Torr; ^{1}H NMR (200 MHz): 0.89, 0.98, and 1.08 (three d, 3H each, J = 6.1 Hz, J = 7.4 Hz, J = 7.3 Hz), 1.03 (overlapping with doublets, 1H), 1.24 (s, 3H), 1.58–1.74 (m, 3H), 1.95–2.04 (m, 1H), 2.16–2.27 (m, 2H), 2.39 (dq, 1H, J = 3.2 Hz, J = 7.4 Hz), 3.15 (s, 3H), 3.35 (br s, 1H), 4.83 (br s, 1H), 5.11 (br m, 1H); ^{13}C NMR (50 MHz): 17.2, 21.4, 21.8, 22.1, 28.4, 30.5, 33.6, 42.9, 44.6, 48.6, 52.5, 71.9, 77.2, 124.1, 133.8; MS: 238 (3, $M^{+\cdot}$), 99 (100).

Compound **23** was detected by GC–MS. MS: 252 (1, $M^{+\cdot}$), 237 (weak, $M^{+\cdot} - CH_3$), 220 (4, $M^{+\cdot}$ − MeOH), 202 (2, $M^{+\cdot}$ − MeOH − H_2O), 191 (6, $M^{+\cdot} - CH_3OH - CH_2CH_3$), 163 (7, $M^{+\cdot} - CH_3O$ retro Diels–Alder), 99 (100).

(1*RS*,2*RS*,3*RS*,4*RS*,8*RS*,10*SR*)-4-Butyl-10-methoxy-2,8,10-trimethylbicyclo[4.4.0]dec-5-en-3-ol (22)

Cycloadduct **20** (39.3 mg, 0.177 mmol) was treated with *n*-butyllithium (0.15 mL of 2.5 M in Et_2O, 0.38 mmol) for 6 h according to general procedure 1. Flash column chromatography (3:1) provided **22** (35.2 mg, 0.125 mmol) as a viscous colorless oil in 71% yield; bp 85–95°C/0.08 Torr; IR (neat): 3368 cm^{-1}; ^{1}H NMR (200 MHz): 0.89, 0.92, and 0.97 (overlapping d, t, and d, 9H, coupling for doublets J = 6.0 Hz, J = 7.4 Hz), 1.03 (dd, 1H, J = 11.6 Hz, J = 14.2 Hz), 1.24 (s, 3H), 1.29–1.74 (m, 9H), 1.96–2.05 (m, 2H), 2.21–2.27 (m, 1H), 2.36 (dq, 1H, J = 2.9 Hz, J = 7.4 Hz), 3.15 (s, 3H), 3.45 (dm, 1H, J = 9.2 Hz), 4.91 (d, 1H, J = 9.2 Hz), 5.18 (br s, 1H); ^{13}C NMR (50 MHz): 14.1, 21.4, 21.8, 22.1, 23.0, 28.4, 29.4, 31.4, 33.5, 35.8, 42.8, 44.7, 48.6, 52.8, 70.2, 77.2, 122.9, 133.8; MS: 280 (1, $M^{+\cdot}$), 99 (100). Exact Mass calcd. for $C_{18}H_{32}O_2$: 280.2402; found: 280.2410.

(1*RS*,2*SR*,3*SR*,4*SR*,8*SR*)-2,4,8-Trimethyl-10-methylidenebicyclo[4.4.0]dec-5-en-3-ol (25) and (1*RS*,2*SR*,3*SR*,4*SR*,8*SR*)-4-ethyl-2,8-dimethyl-10-methylidenebicyclo-[4.4.0]dec-5-en-3-ol (26)

Compound **24** (6) (1.027 g, 5.40 mmol) was treated with methyllithium (116 mL of 1.4 M in Et_2O, 162 mmol) for 24 h according to general procedure 2. Flash column chromatography (9:1) provided **25** (0.755 g, 3.66 mmol) and **26** (0.136 g, 0.615 mmol) in yields of 68 and 11%, respectively. Both compounds were relatively unstable and were therefore not fully characterized. Compound **25** was a viscous colorless oil that sometimes crystallized upon storage in the refrigerator; mp 61–62.5°C; ^{1}H NMR (200 MHz): 0.94, 0.98, and 1.08 (d, 3H each, J = 6.2 Hz, J = 7.0 Hz, J = 6.3 Hz), 1.36–1.61 (m, 2H), 1.75 (apparent br t composed of 2 overlapping br d at 1.72 and 1.78, 2H, J = 12.6 Hz, J = 12.2 Hz), 2.12–2.42 (m, 5H), 3.60 (dd, 1H, J = 4.8 Hz, J = 8.8 Hz), 4.76–4.79 (m, 2H), 5.28 (m, 1H); ^{13}C NMR (50 MHz): 14.9, 17.7, 22.1, 31.3, 33.8, 35.7, 44.1, 45.9, 50.1, 74.8, 106.1, 123.2, 137.6, 149.4; MS: 206 (2, $M^{+\cdot}$), 188 (27, $M^{+\cdot} - H_2O$), 173 (35, $M^{+\cdot} - H_2O - CH_3$), 148 (100, retro Diels–Alder).

Compound **26** was a viscous colorless oil. ^{1}H NMR (200 MHz): 0.98 and 1.05 (overlapping d and t, d, 9H, J = 6.2 Hz, J = 6.2 Hz, J = 6.3 Hz), 1.12–1.32 (m, 1H), 1.33–1.89 (m, 5H), 1.97–2.15 (br s, 1H), 2.20–2.48 (m, 4H), 3.65 (br s, 1H), 4.80 (br s, 2H), 5.33 (m, 1H); ^{13}C NMR (50 MHz): 11.9, 18.1, 22.1, 23.3, 31.9, 35.8, 40.1, 44.4, 46.0, 49.6, 73.9, 106.2, 121.2, 137.7, 149.7; MS: 220 (2, $M^{+\cdot}$), 202 (27, $M^{+\cdot} - H_2O$), 162 (100, retro Diels–Alder).

(1*RS*,2*RS*,3*RS*,4*RS*,8*SR*,10*SR*)-4-Ethyl-2,8,10-trimethylbicyclo[4.4.0]dec-5-en-3-ol from hydrogenation of 26

Compound **26** (51.8 mg, 0.235 mmol) was dissolved in a mixture of EtOH (10 mL) and benzene (1 mL) in a round-bottom flask. Platinum oxide hydrate (10 mg) was added, and the reaction vessel was evacuated with a water aspirator and back-purged with hydrogen three times. After the reaction had been stirred under a balloon atmosphere of hydrogen for 50 min at room temperature, the catalyst was removed by filtration and the reaction flask and catalyst were washed well with additional ethanol. The solvent was removed from the combined organic phases in vacuo to give the hydrogenated compound (52.2 mg, 0.235 mmol) as a white solid in 100% yield following purification by flash column chromatography (5:1). Sublimation point 64–70°C/0.05 Torr; IR (KBr): 3393 cm^{-1}; ^{1}H NMR (200 MHz): 0.80, 0.86, and 1.01 (d, 3H each, J = 7.0 Hz, J = 6.0 Hz, J = 6.2 Hz), 0.98 (t, 3H, J = 6.9 Hz), 1.05–1.27 (m, 2H), 1.42–1.82 (m, 7H), 2.03–2.22 (m, 3H), 3.50 (dd, 1H, J = 5.3 Hz, J = 10.7 Hz), 5.57 (dt, 1H, J = 1.7 Hz, J = 6.2 Hz); ^{13}C NMR (50 MHz): 12.2, 14.4, 15.9, 22.5, 22.8, 26.9, 30.3, 32.5, 42.4, 42.8, 44.0, 49.2, 75.5, 123.7, 136.9; MS: 222 (23, $M^{+\cdot}$), 204 (9, $M^{+\cdot} - H_2O$) 135 (100, $M^{+\cdot} - CH_2CH_3$ retro Diels–Alder). Exact Mass calcd. for $C_{15}H_{26}O$: 222.1984; found: 222.1975.

(1*RS*,2*RS*,3*RS*,4*RS*,8*SR*,10*SR*)-4-Ethyl-2,8,10-trimethylbicyclo-[4.4.0]dec-5-en-3-yl *p*-nitrobenzoate (27)

The hydrogenated compound produced above (33.3 mg, 0.150 mmol) was sublimed under reduced pressure (0.05 Torr) and dissolved in dry CH_2Cl_2 (5 mL) in a N_2-purged round-bottom flask. DMAP (27.9 mg, 0.228 mmol) and *para*-nitrobenzoyl chloride (41.7 mg, 0.225 mmol) were added to the flask and the reaction mixture was stirred at room temperature for 19 h. Et_2O (20 mL) and H_2O (5 mL) were added to the reaction, and the organic layer was washed with 1% aqueous HCl (3 mL) and 5% aqueous $NaHCO_3$ (5 mL). After the organic layer had been dried with anhydrous Na_2SO_4 and filtered, the solvent was removed in vacuo to provide ester **27** (55.5 mg, 0.149 mmol) as a slightly yellow solid in 99% yield after purification by flash column chromatography (9:1); mp 141–142°C; ^{1}H NMR (200 MHz): 0.85 and 0.87 (overlapping d and t, 6H, J = 6.8 Hz, J = 7.0 Hz), 0.97 (d, 6H, J = 6.6 Hz), 1.18–1.37 (m, 2H), 1.57–1.74 (m, 4H), 1.89–2.30 (m, 2H), 2.30–2.49 (m, 1H), 5.03 (dd, 1H, J = 5.4 Hz, J = 11.3 Hz), 5.59 (br d, 1H, J = 6.3 Hz), 8.21–8.34 (AA′BB′ m, 4H); ^{13}C NMR (50 MHz): 12.0, 14.4, 15.8, 22.5, 23.7, 26.8, 30.1, 30.4, 39.4, 42.6, 43.7, 48.9, 79.9, 122.8, 123.6, 130.6, 136.2, 137.1, 150.5, 164.2.

X-ray crystal structure data for compound 27

A sample of **27** was recrystallized from pentane to give slightly yellow plates, which were submitted for X-ray crystallographic analysis. Crystal data: empirical formula $C_{22}H_{29}NO_4$; space group $C2/c$ (no. 15); a = 10.678(7) Å, b = 9.076(8) Å; c = 42.37(2) Å; β = 93.24(5)°; V = 4099(4) Å^3; Z = 8; d = 1.204 g/cm^3; Mo-Kα radiation (−73°C); total of 3046 reflections in the range $0 < 2\theta < 50.1°$, of which 517 were used ($I > 3\sigma(I)$) in the structure solution; R = 0.108 and Rw = 0.119.

© 1997 NRC Canada

Can. J. Chem. Downloaded from www.nrcresearchpress.com by 88.146.161.215 on 09/08/12
For personal use only.

(1*RS*,8*RS*,9*SR*)-8-Butyl-9-hydroxy-1-methylbicyclo[4.4.0]dec-6-en-2-one (30*a*) and (1*RS*,2*SR*,8*RS*,9*SR*)-2,8-dibutyl-1-methylbicyclo[4.4.0]dec-6-en-2,9-diol (31*a*)

General procedure 1 was used to prepare compounds **30*a*** and **31*a***. Cycloadduct **29** (55.3 mg, 0.310 mmol) was treated with *n*-butyllithium (0.37 mL of 2.5 M in hexanes, 0.93 mmol) for 89 h to give ketone **30*a*** (45.1 mg, 0.191 mmol) and diol **31*a*** (7.6 mg, 0.026 mmol) in yields of 6 and 8%, respectively, following purification by flash column chromatography (3:1). Compound **30*a*** was a white solid, mp 55–57°C; IR (KBr): 3445, 1707, 1659 cm^{-1}; ^1H NMR (200 MHz): 0.88 (br m, 3H), 1.10–1.40 (m, 5H), 1.33 (s, 3H), 1.46 (dd, 1H, J = 2.6 Hz, J = 14.1 Hz), 1.50–1.80 (m, 2H), 1.78 (br s, 1H), 1.98–2.15 (m, 2H), 2.16–2.41 (m, 2H), 2.44–2.74 (overlapping m, 3H), 3.95–4.02 (m, 1H), 5.36 (poorly resolved dd, 1H, J = 1.4 Hz, J = 3.0 Hz); ^{13}C NMR (50 MHz): 14.0, 22.9, 26.0, 26.5, 29.4, 30.0, 30.5, 36.4, 37.7, 40.3, 51.0, 66.7, 125.6, 139.0, 214.5; MS: 236 (17, $M^{+\cdot}$), 192 (28, retro Diels–Alder), 137 (100). Exact Mass calcd. for $C_{15}H_{24}O_2$: 236.1776; found: 236.1768.

Compound **31*a*** was characterized as a white solid, mp 104–106°C; IR (KBr): 3348 cm^{-1}; ^1H NMR (200 MHz): 0.91 and 0.92 (two overlapping br t, 6H), 1.15 (s, 3H), 1.22–1.74 (m, 18H), 1.90–2.38 (m, 4H), 2.33 (dd, 1H, J = 8.0 Hz, J = 13.9), 3.89 (m, 1H), 5.41 (poorly resolved dd, 1H, J = 1.7 Hz, J = 3.8 Hz); ^{13}C NMR (50 MHz): 14.1, 14.2, 22.3, 23.0, 23.6, 25.4, 25.5, 29.6, 30.4, 31.3, 31.4, 34.6, 36.7, 40.4, 44.6, 67.3, 76.2, 125.5, 141.9; MS: 294 (1, $M^{+\cdot}$), 276 (8, $M^{+\cdot} - H_2O$), 41 (100). Exact Mass calcd. for $C_{19}H_{34}O_2$: 294.2559; found: 294.2534.

(1*RS*,5*RS*,6*RS*,8*RS*)-5,6-Dimethyl-11-oxatricyclo[6.2.1.0^{1,6}]undec-9-en-5-ol (32*b*)

Anhydrous Et_2O (2 mL) was placed in a N_2-purged three-neck round-bottom flask equipped with an addition funnel containing a solution of cycloadduct **29** (67.7 mg, 0.380 mmol) in anhydrous Et_2O (5 mL). The flask was cooled with an ice bath, and methyllithium (0.80 mL of 1.4 M in Et_2O, 1.1 mmol) and dry TMEDA (7.8 mL) were added. The solution of **29** was added dropwise from the addition funnel, and the reaction was warmed to room temperature and stirred for 312 h. Wet Et_2O (10 mL) and saturated aqueous NH_4Cl (10 mL), were then added sequentially, and the aqueous layer was extracted with Et_2O (4 × 10 mL). The combined organic layers were washed with 10% aqueous $CuSO_4$ (2 × 30 mL), dried over anhydrous Na_2SO_4, and filtered. The solvent was removed from the filtrate in vacuo. Flash column chromatography (20:1 benzene:acetone) provided **32*b*** (44.9 mg, 0.231 mmol) as a colorless oil in 61% yield; bp 40–50°C /0.07 Torr; IR (neat): 3457 cm^{-1}; ^1H NMR (200 MHz): 0.91 (d, 1H, J = 11.5 Hz), 0.96 (s, 3H), 1.10 (d, 3H, J = 1.1 Hz), 1.51–2.25 (m, 6H), 2.66 (dd, 1H, J = 5.2 Hz, J = 11.5 Hz), 4.42 (d, 1H, J = 1.1 Hz), 4.84 (dd, 1H, J = 1.7 Hz, J = 5.2 Hz), 6.04 (d, 1H, J = 5.8 Hz), 6.48 (dd, 1H, J = 1.7 Hz, J = 5.8 Hz); ^{13}C NMR (50 MHz): 16.7, 21.3, 25.5, 26.7, 34.7, 35.7, 44.3, 73.1, 78.6, 91.6, 137.6, 138.0; MS: 194 (weak, $M^{+\cdot}$), 176 (4, $M^{+\cdot} - H_2O$), 94 (100). Exact Mass calcd. for $C_{12}H_{18}O_2$: 194.1307; found: 194.1294.

(1*RS*,5*RS*,6*RS*,8*RS*)-6-Methyl-11-oxatricyclo[6.2.1.0^{1,6}]undec-9-en-5-ol (32*c*)

Cycloadduct **29** (56.4 mg, 0.316 mmol) was placed in a N_2-purged three-neck round-bottom flask and dissolved in THF (4 mL). The solution was cooled using a −78°C cold bath, and lithium *tert*-butyldiisobutylaluminohydride (0.48 mL of 1.0 M in THF, 0.48 mmol) was added by syringe. The mixture was stirred at −78°C until analysis by TLC indicated that the starting material had been consumed (30 min). Solid $Na_2SO_4 \cdot 10H_2O$ (150 mg, 0.466 mmol) was added, and the reaction was poured into a mixture of 0.5 M aqueous $KHSO_4$ (10 mL) and $CHCl_3$ (5 mL) and stirred for 30 min. The aqueous layer was extracted with $CHCl_3$ (4 × 10 mL). After the combined organic layers had been dried with anhydrous Na_2SO_4 and filtered, the solvent was removed in vacuo to give **32*c*** (57.0 mg, 0.316 mmol) exclusively in 100% yield after purification by flash column chromatography (5:1). Compound **32*c*** was characterized as a colorless oil, bp 45–50°C/0.05 Torr; IR (neat): 3488 cm^{-1}; ^1H NMR (200 MHz): 0.95 (overlapping s and d, 4 H, J = 11.4 Hz for d), 1.46–1.52 (m, 1H), 1.72–2.19 (m, 5H), 2.66 (dd, 1H, J = 5.2 Hz, J = 11.4 Hz), 3.27 (br s, 1H), 3.58 (br s, 1H), 4.82 (dd, 1H, J = 1.6 Hz, J = 5.2 Hz), 5.98 (d, 1H, J = 5.8 Hz), 6.50 (dd, 1H, J = 1.6 Hz, J = 5.8 Hz); ^{13}C NMR (50 MHz): 15.0, 22.4, 25.5, 28.5, 37.5, 40.5, 73.4, 78.2, 90.5, 136.6, 138.7; MS: 180 (1, $M^{+\cdot}$), 162 (3, $M^{+\cdot} - H_2O$), 94 (100). Exact Mass calcd. for $C_{11}H_{16}O_2$: 180.1150; found: 180.1154.

(1*RS*,2*SR*,8*RS*,9*SR*)-2,8-Dibutyl-9-methylbicyclo[4.4.0]dec-6-en-2,9-diol (36*a*) and (1*RS*,5*RS*,6*RS*,10*RS*)-5,10-dibutyl-8-methylbicyclo[4.4.0]dec-8-en-1,5-diol (37*a*)

General procedure 1 was used to prepare a mixture of compounds **36*a*** and **37*a***. Cycloadduct **35** (69.5 mg, 0.390 mmol) was treated with *n*-butyllithium (0.47 mL of 2.5 M in hexanes, 1.2 mmol) for 16 h to give compounds **36*a*** and **37*a*** in a 1.7:1 ratio based on the integration of the alkene signals at 5.50 and 5.23 ppm, respectively, in the crude ^1H NMR spectrum. These two compounds could not be separated by column chromatography. Fortunately, compound **36*a*** was slightly less soluble in a mixture of 1:1 petroleum ether:Et_2O so that washing the mixture of compounds with this solvent system provided a pure sample of **36*a*** (25.6 mg, 0.0869 mmol) along with a mixture of both compounds (66.0 mg, 0.224 mmol) in a combined yield of 80%. Attempts to secure a pure sample of **37*a*** through recrystallization were not successful.

Compound **36*a*** was characterized as a white solid, mp 132–133°C; IR (KBr): 3230 cm^{-1}; ^1H NMR (200 MHz): 0.92 and 0.93 (overlapping t, 6H, J = 7.0 Hz), 1.22 (s, 3H), 1.11–1.78 (m, 18H), 1.79–2.04 (overlapping m and dd, 3H, J = 4.7 Hz, J = 13.9 Hz for dd), 2.11–2.28 (m, 2H), 2.63 (br s, 1H), 5.50 (br s, 1H); ^{13}C NMR (50 MHz): 14.1, 14.1, 22.5, 23.0, 23.3, 26.2, 28.3, 29.9, 30.1, 30.1, 34.4, 35.0, 36.5, 43.5, 45.2, 69.7, 74.3, 125.2, 135.3; MS: 294 (3, $M^{+\cdot}$), 276 (49, $M^{+\cdot} - H_2O$), 174 (100). Exact Mass calcd. for $C_{19}H_{34}O_2$: 294.2559; found: 294.2559.

Since compound **37*a*** could not be purified, it was not characterized. The ^1H NMR spectrum showed signals at 1.75 (br s, 3H) and 5.23 (br s, 1H). The compound was detected by GC–MS. MS: 294 (100, $M^{+\cdot}$), 276 (78, $M^{+\cdot} - H_2O$), 258 (13, $M^{+\cdot} - 2H_2O$), 237 (17, $M^{+\cdot} - n$-Bu), 219 (41, $M^{+\cdot} - H_2O - n$-Bu), 201 (39, $M^{+\cdot} - 2H_2O - n$-Bu).

(1*RS*,2*RS*,8*RS*,9*SR*)-9-Methyl-2,8-di-(1-methylethyl)bicyclo[4.4.0]dec-6-en-2,9-diol (36*b*) and

© 1997 NRC Canada

Can. J. Chem. Downloaded from www.nrcresearchpress.com by 88.146.161.215 on 09/08/12
For personal use only.

(1*RS*,5*SR*,6*RS*,10*RS*)-8-methyl-5,10-di-(1-methylethyl)bicyclo[4.4.0]dec-8-en-1,5-diol (37*b*)

A solution of isopropyllithium was prepared using the method of Gilman et al. (7) as described for compound **2***b*. Standardization against 2,5-dimethoxybenzyl alcohol (34) indicated that the supernatant was 0.22 M in isopropyllithium.

General procedure 1 was used to prepare a mixture of compounds **36***b* and **37***b*. Cycloadduct **35** (51.2 mg, 0.287 mmol) was treated with the prepared solution of isopropyllithium (5.6 mL of 0.22 M in pentane, 1.2 mmol) for 16 h to give compounds **36***b* and **37***b* in a 1.5:1 ratio based on the integration of the alkene signals at 5.43 and 5.23 ppm, respectively, in the crude ^{1}H NMR spectrum. Flash column chromatography (5:1) provided a pure sample of **37***b* (18.6 mg, 0.0698 mmol) and a mixture of **36***b* and **37***b* (54.2 mg, 0.203 mmol) in a combined yield of 95%.

An impure mixture of **36***b* containing approximately 15% of **37***b* was partially characterized. ^{1}H NMR (200 MHz, not including signals due to **37***b*): 0.88 (d, 3H, J = 7.1 Hz), 0.93 (d, 6H, J = 6.7 Hz), 1.01 (d, 3H, J = 7.0 Hz), 1.22 (s, 3H), 1.24–2.50 (m, 13H), 2.82 (br s, 1H), 5.43 (br s, 1H); ^{13}C NMR (50 MHz, not including signals due to **37***b*): 16.4, 17.4, 19.3, 22.4, 23.9, 26.8, 29.2, 29.5, 33.6, 34.9, 35.3, 42.4, 50.2, 70.1, 76.4, 121.9, 136.6; MS: 266 (1, $M^{+\cdot}$), 248 (7, $M^{+\cdot} - H_2O$), 230 (0.3, $M^{+\cdot} - 2H_2O$), 223 (1, $M^{+\cdot} - (CH_3)_2CH$), 43 (100).

Compound **37***b* was characterized as a white solid, mp 109–111°C; IR (KBr): 3430, 3373 cm^{-1}; ^{1}H NMR (200 MHz): 0.80, (d, 3H, J = 7.0 Hz), 0.88 (d, 3H, J = 6.6 Hz), 0.91 (d, 3H, J = 6.6 Hz), 0.96 (d, 3H, J = 7.0 Hz), 1.05–1.30 (m, 3H), 1.51–2.02 (m, 7H), 1.77 (br s, 3H), 2.02–2.41 (m, 3H), 3.95 (br s, 1H), 5.23 (br s, 1H); ^{13}C NMR (50 MHz): 15.7, 16.4, 17.4, 18.0, 23.4, 23.7, 25.3, 26.2, 29.0, 33.3, 35.0, 42.7, 51.8, 74.2, 75.8, 118.1, 135.1; MS: 266 (8, $M^{+\cdot}$), 248 (1, $M^{+\cdot} - H_2O$), 230 (0.3, $M^{+\cdot} - 2H_2O$), 223 (1, $M^{+\cdot} - (CH_3)_2CH$), 113 (100). Exact Mass calcd. for $C_{17}H_{30}O_2$: 266.2246; found: 266.2243.

(1*RS*,2*SR*,8*SR*,9*SR*)-2,8-Di(1,1-dimethylethyl)-9-methylbicyclo[4.4.0]dec-6-en-2,9-diol (36*c*), (1*RS*,5*RS*,6*SR*,10*SR*)-5,10-di-(1,1-dimethylethyl)-8-methylbicyclo[4.4.0]dec-8-en-1,5-diol (37*c*), and (1*RS*,6*SR*,7*RS*)-7-(1,1-dimethylethyl)-6-hydroxy-9-methylbicyclo[4.4.0]dec-8-en-2-one (34)

General procedure 1 was used to prepare a mixture of compounds **36***c*, **37***c*, and **34**. Cycloadduct **35** (56.4 mg, 0.316 mmol) was treated with *tert*-butyllithium (0.56 mL of 1.7 M in hexanes, 0.95 mmol) for 3 h at 0°C to give compounds **36***c*, **37***c*, and **34**. The ratio of **36***c*:(**37***c* and **34**) was 2.2:1 based on the integration of the alkene signals at 5.54 and 5.35 ppm, respectively, in the crude ^{1}H NMR spectrum. Flash column chromatography (9:1) provided a pure sample of **36***c* (31.7 mg, 0.108 mmol) and a mixture of **36***c* and **37***c* (19.1 mg, 0.0648 mmol) in a combined yield of 55%. Compound **34** (8.8 mg, 0.037 mmol) was also isolated in 12% yield.

Compound **36***c* was characterized as a white solid, mp 128–129°C; IR (KBr): 3439, 3362 cm^{-1}; ^{1}H NMR (200 MHz): 1.07 and 1.11 (two s, 9H each), 1.30 (s, 3H), 1.26–1.73 (m, 6H), 1.80–2.05 (m, 3H), 2.13–2.41 (m, 3H), 5.54 (m, 1H); ^{13}C NMR (50 MHz): 23.4, 27.7, 30.3, 32.6, 33.7, 35.2, 36.1, 38.6, 39.6, 44.2, 53.7, 72.8, 78.1, 125.5, 136.8; MS: no $M^{+\cdot}$, 276 (8, $M^{+\cdot} - H_2O$), 261 (0.5, $M^{+\cdot} - H_2O - CH_3$), 237 (0.5, $M^{+\cdot} - t$-Bu), 57 (100). Anal. calcd. for $C_{19}H_{34}O_2$: C 77.48, H 11.66; found: C 77.39, H 11.21.

X-ray crystal structure data for compound 36*c*

A sample of **36***c* was recrystallized from pentane to give colorless prisms that were submitted for X-ray crystallographic analysis. See Fig. 2 for the X-ray crystal structure. Crystal data: empirical formula $C_{19}H_{34}O_2$; space group $P2_1/c$ (no. 14); a = 8.715(3) Å; b = 20.215(4) Å; c = 9.866(3) Å; β = 94.01(2)°; V = 1733.9(8) Å^3; Z = 4; d = 1.128 g/cm^3; Mo-Kα radiation (−123°C); total of 3396 reflections in the range $0 < 2\theta < 50.1°$, of which 1941 were used ($I > 3\sigma(I)$) in the structure solution; R = 0.066 and Rw = 0.091.

Since compound **37***c* could not be purified, it was not characterized. The ^{1}H NMR spectrum showed signals at 1.02 and 1.08 (two s, 9H each), 1.78 (br s, 3H), and 5.35(br s, 1H).

Compound **34** was characterized as a white solid, mp 80–82.5°C; IR (KBr): 3501, 1703 cm^{-1}; ^{1}H NMR (200 MHz): 1.10 (s, 9H), 1.51–1.80 (m, 2H), 1.77 (br s, 3H), 1.88–2.56 (m, 8H), 2.67–2.81 (dm, 1H, J = 13.7 Hz), 5.35 (br s, 1H); ^{13}C NMR (50 MHz): 21.8, 23.8, 25.3, 30.6, 35.4, 37.7, 41.4, 54.8, 55.9, 78.6, 122.2, 133.0, 211.0; MS: 236 (2, $M^{+\cdot}$), 221 (1, $M^{+\cdot} - CH_3$), 218 (1, $M^{+\cdot} - H_2O$), 180 (15, $M^{+\cdot} - C_4H_8$), 109 (100). Exact Mass calcd. for $C_{15}H_{24}O_2$: 236.1776; found: 236.1774.

(1*RS*,5*RS*,6*RS*,8*RS*)-5,8-Dimethyl-11-oxatricyclo[6.2.1.0^{1,6}]undec-9-en-5-ol(38) and (1*RS*,5*RS*,6*RS*)-5-methyl-8-methylidenebicyclo[4.4.0]dec-9-en-1,5-diol (39)

Anhydrous Et_2O (2 mL) was placed in a N_2-purged three-neck round-bottom flask equipped with an addition funnel containing a solution of cycloadduct **35** (59.9 mg, 0.366 mmol) in anhydrous Et_2O (5 mL). The flask was cooled with an ice bath, and methyllithium (0.70 mL of 1.4 M in Et_2O, 0.98 mmol) and dry TMEDA (7.8 mL) were added. The solution of **35** was added dropwise from the addition funnel, and the reaction was warmed to room temperature and stirred for 53 h. Wet Et_2O (10 mL) and saturated aqueous NH_4Cl (10 mL) were then added sequentially, and the aqueous layer was extracted with Et_2O (4 × 10 mL). The combined organic layers were washed with 10% aqueous $CuSO_4$ (2 × 30 mL), dried over anhydrous Na_2SO_4, and filtered. The solvent was removed from the filtrate in vacuo. Flash column chromatography (5:1) provided **38** (22.1 mg, 0.114 mmol) and **39** (25.8 mg, 0.133 mmol) in yields of 31 and 36%, respectively.

Compound **38** was characterized as a colorless oil, bp 40–50°C/0.07 Torr; IR (neat): 3485 cm^{-1}; ^{1}H NMR (200 mHz): 1.12 (s, 3H), 1.15–1.62 (m, 4H), 1.63–1.98 (m, 3H), 1.61 (s, 3H), 2.21–2.34 (m, 2H), 3.46 (br s, 1H), 5.95 (d, 1H, J = 5.6 Hz), 6.30 (d, 1H, J = 5.6 Hz); ^{13}C NMR (50 MHz): 16.7, 28.2, 35.1, 38.6, 18.7, 28.9, 46.2, 69.4, 86.5, 88.2, 138.2, 141.8; MS: 194 (1, $M^{+\cdot}$), 176 (1, $M^{+\cdot} - H_2O$), 161 (1, $M^{+\cdot} - H_2O - CH_3$), 108 (100). Exact Mass calcd. for $C_{12}H_{18}O_2$: 194.1307; found: 194.1293.

Compound **39** was characterized as a light tan solid, mp 129–135°C (dec.); IR (KBr): 3456, 1634, 1597 cm^{-1}; ^{1}H NMR (200 MHz): 1.20 (s, 3H), 1.31–1.59 (m, 4H), 1.71–2.11 (m, 3H), 2.20–3.10 (overlapping m and br s, 4H), 4.96–4.99 (m, 2H), 5.64 and 6.16 (d, 1H each, J = 9.5 Hz); ^{13}C NMR (50 MHz): 17.1, 25.3, 38.2, 40.6, 27.6, 47.2, 69.8, 71.9, 114.2, 131.4, 134.2, 142.9; MS: 194 (4, $M^{+\cdot}$), 176 (17, $M^{+\cdot} - H_2O$),

© 1997 NRC Canada

118 (100). Exact Mass calcd. for $C_{12}H_{18}O_2$: 194.1307; found: 194.1318.

Acknowledgements

We thank the Natural Sciences and Engineering Research Council of Canada (NSERC) and the University of Calgary for financial support. In addition, we thank NSERC, the Killam Trusts, and the Alberta Heritage Scholarship Fund for graduate scholarships (to S.W.).

References

1. (*a*) I.R. Hunt, A. Rauk, and B.A. Keay. J. Org. Chem. **61**, 751 (1996); (*b*) I.R. Hunt, C. Rogers, S. Woo, A. Rauk, and B.A. Keay. J. Am. Chem. Soc. **117**, 1049 (1995); (*c*) S. Woo and B.A. Keay. Tetrahedron Asymmetry, **5**, 1411 (1994); (*d*) C. Rogers and B.A. Keay. Can. J. Chem. **71**, 611 (1993); (*e*) Can. J. Chem. **70**, 2929 (1992); (*f*) S. Yu, G. Beese, and B.A. Keay. J. Chem. Soc. Perkin Trans. 1, 2729 (1992); (*g*) C. Rogers and B.A. Keay. Tetrahedron Lett. **32**, 6477 (1991); (*h*) Synlett, 353 (1991); (*i*) Tetrahedron Lett. **30**, 1349 (1989); (*j*) B.A. Keay and P.W. Dibble. Tetrahedron Lett. **30**, 1045 (1989); (*k*) B.A. Keay. J. Chem. Soc. Chem. Commun. 419 (1987).
2. S. Woo and B.A. Keay. Synthesis, 669 (1996).
3. (*a*) O. Arjona, R. Fernández de la Pradilla, E. Garcia, A. Martin-Domenech, and J. Plumet. Tetrahedron Lett. **30**, 6437 (1989); (*b*) O. Arjona, R. Fernández de la Pradilla, S. Pérez, and J. Plumet. Tetrahedron Lett. **28**, 5547 (1987); (*c*) O. Arjona, R. Fernández de la Pradilla, A. Mallo, S. Pérez, and J. Plumet. J. Org. Chem. **54**, 4158 (1989).
4. M. Lautens, A.C. Smith, A.S. Abd-El-Aziz, and A.H. Huboux. Tetrahedron Lett. **31**, 3253 (1990).
5. S. Woo and B.A. Keay. Tetrahedron Lett. **33**, 2661 (1992).
6. S. Woo and B.A. Keay. Synlett, 135 (1996).
7. H. Gilman, W. Langham, and F.W. Moore. J. Am. Chem. Soc. **62**, 2327 (1940).
8. B.H. Lipshutz. Synthesis, 325 (1987).
9. H. Gilman, R.G. Jones, and L.A. Woods. J. Org. Chem. **17**, 1630 (1952).
10. M. Kato, H. Kurihara, and A. Yoshikoshi. J. Chem. Soc. Perkin Trans. 1, 2740 (1979).
11. E.C. Ashby and S.A. Noding. J. Org. Chem. **44**, 4371 (1979).
12. M.J. Eis, J.E. Wrobel, and B. Ganem. J. Am. Chem. Soc. **106**, 3693 (1984).
13. B.J. Wakefield. *In* Organolithium methods. Academic Press, Toronto. 1988. pp. 4 and 36.
14. D.B. Collum. Acc. Chem. Res. **25**, 448 (1992).
15. J.J. Fitt and H.W. Gschwend. J. Org. Chem. **49**, 209 (1984).
16. R.S. Lenox and J.A. Katzenellenbogen. J. Am. Chem. Soc. **95**, 957 (1973).
17. S. Kim, K.H. Ahn, and Y.W. Chung. J. Org. Chem. **47**, 4581 (1982).
18. E.J. Corey and A. Venkateswarlu. J. Am. Chem. Soc. **94**, 6190 (1972).
19. H.C. Brown and J.V.N.V. Prasad. J. Org. Chem. **50**, 3002 (1985).
20. (*a*) P.K. Freeman and L.L. Hutchinson. J. Org. Chem. **45**, 1924 (1980); (*b*) S.G. Cauwbergs and P.J. De Clercq. Tetrahedron Lett. **29**, 6501 (1988).
21. E.J. Parish and G.J. Schroepfer, Jr. Tetrahedron Lett. 3775 (1976).
22. B. Fraser-Reid, S.Y.-K. Tam, and B. Radatus. Can. J. Chem. **53**, 2005 (1975).
23. (*a*) P.D. Bartlett, S. Friedman, and M. Stiles. J. Am. Chem. Soc. **75**, 1771 (1953); (*b*) L. Spialter and C.W. Harris. J. Org. Chem. **31**, 4263 (1966).
24. U. Schollkopf and M. Eisert. Angew. Chem. **72**, 349 (1960).
25. H.-U. Reissig. *In* The chemistry of the cyclopropyl group. Vol. 1. *Edited by* Z. Rappoport. John Wiley and Sons, Ltd., Toronto. 1987. p. 377.
26. R.T. Hrubiec and M.B. Smith. Tetrahedron, **40**, 1457 (1984).
27. R.T. Hrubiec and M.B. Smith. Tetrahedron Lett. **24**, 5031 (1983).
28. I. Arai, A. Mori, and H. Yamamoto. J. Am. Chem. Soc. **107**, 8254 (1985).
29. O. Arjona, S. Conde, J. Plumet, and A. Viso. Tetrahedron Lett. **36**, 6157 (1995).
30. W.J. Hehre, L.D. Burke, A.J. Shusterman, and W.J. Pietro. *In* Experiments in computational organic chemistry. Wavefunction, Inc., Irvine, Calif. 1993.
31. F.A. Carey and R.J. Sundberg. *In* Advanced organic chemistry. Part A: structure and mechanisms. 3rd ed. Plenum Press, New York. 1990. p. 171.
32. P. Deslongchamps. *In* Stereoelectronic effects in organic chemistry. Pergamon Press, Toronto. 1983. pp. 174–178, and refs. cited therein.
33. W.G. Dauben, G. Fonken, and D.S. Noyce. J. Am. Chem. Soc. **92**, 709 (1970).
34. M.R. Winkle, J.M. Lansinger, and R.C. Ronald. J. Chem. Soc. Chem. Commun. 87 (1980).

Can. J. Chem. Downloaded from www.nrcresearchpress.com by 88.146.161.215 on 09/08/12
For personal use only.

© 1997 NRC Canada

Synthesis of 10-methyl-Δ^4-octalins by Diels–Alder reactions of 2*H*-thiopyran surrogates for 1-ethenyl-2-methylcyclohexene

Dale E. Ward and Yuanzhu Gai

Can. J. Chem. Downloaded from www.nrcresearchpress.com by 88.146.161.215 on 09/08/12
For personal use only.

Abstract: Diels–Alder reactions of 1-ethenyl-2-methylcyclohexene derivatives could be a versatile route to a variety of natural product skeletons that possess a 10-methyldecalin substructure with additional substitution at C-8 and C-9. These dienes are unreactive due (in part) to the presence of the vinyl methyl group, which destabilizes the necessary s-*cis* conformation. The use of 2*H*-thiopyran diene surrogates for 1-ethenyl-2-methylcyclohexene is investigated. The desired Diels–Alder adducts were not obtained by reaction of 6,7,8,8a-tetrahydro-5,5-dimethyl-3-tris(1-methylethyl)silyloxy-1*H*-2-benzothiopyran (**7***c*) or 1,5,7,8-tetrahydrospiro[6*H*-2-benzothiopyran-6,2′-[1,3]dioxolane] (**17**) with *N*-phenylmaleimide. Reactions of 3-[2-(2-methyl-1,3-dioxolan-2-yl)ethyl]-4-[(tris(1-methylethyl)silyl)oxy]-2*H*-thiopyran (**19**) with maleimide, *N*-methylmaleimide, and *N*-phenylmaleimide under thermal conditions and with *N*-methylmaleimide, *N*-phenylmaleimide, 3-(propenoyl)-2-oxazolidinone, and methyl acrylate under Lewis acid mediated conditions ($EtAlCl_2$, $TiCl_4$) gave Diels–Alder adducts in moderate to good yields. In each case, those adducts were readily converted into products that are synthetically equivalent to Diels–Alder adducts of **17** with the same dienophiles. Desulfurization of those products gives 10-methyl-Δ^4-octalins (2,3,4,4a,5,6,7,8-octahydro-4a-methylnapthalenes) that are synthetically equivalent to hypothetical Diels–Alder adducts of 1-ethenyl-2-methylcyclohexene-5-one.

Key words: Diels–Alder, 2*H*-thiopyran, *cis*-substituted 1,3-diene surrogate, 1-ethenyl-2-methylcyclohexene, octahydro-4a-methylnapthalene derivatives.

Résumé : Les réactions de Diels–Alder des dérivés du 1-éthényl-2-méthylcyclohexène pourraient être des voies versatiles pour atteindre les squelettes de produits naturels comportant une sous-structure 10-méthyldécaline et des substituants additionnels en C-8 et en C-9. Ces diènes ne sont pas réactifs à cause (en partie) de la présence du groupe vinyle qui déstabilise la conformation s-*cis* nécessaire. On a étudié la possibilité d'utiliser un diène du 2*H*-thiopyrane comme substitut du 1-éthényl-2-méthylcyclohexène. On n'a pas obtenu les adduits de Diels–Alder désirés lors de la réaction de la *N*-phénylmaléimide avec le 6,7,8,8a-tétrahydro-5,5-diméthyl-3-tris(1-méthylethyl)silyloxy-1*H*-2-benzothiopyrane (**7***c*) ou avec le 1,5,7,8-tétrahydrospiro[6*H*-2-benzothiopyrane-6,2′-[1,3]dioxolane] (**17**). Les réactions du 3-[2-(2-méthyl-1,3-dioxolan-2-yl)éthyl]-4-[(tris(1-méthyléthyl)silyl)oxy]-2*H*-thiopyrane (**19**) avec les maléimide, *N*-méthylmaléimide et *N*-phénylmaléimide dans des conditions thermiques et avec les *N*-méthylmaléimide et *N*-phénylmaléimide, la 3-(propénoyl)-2-oxazolidinone et l'acrylate de méthyle dans des conditions catalysées par un acide de Lewis ($EtAlCl_2$, $TiCl_4$) ont permis d'obtenir des adduits de Diels–Alder avec de bons rendements. Dans chacun des cas, il a été possible de transformer facilement ces adduits en produits synthétiquement équivalents aux adduits de Diels–Alder du produit **17** avec les mêmes diénophiles. La désulfurisation de ces produits fournit les 10-methyl-Δ^4-octalines (2,3,4,4a,5,6,7,8-octahydro-4a-méthylnapthalenes) qui sont synthétiquement équivalentes aux adduits hypothétiques de Diels–Alder de la 1-éthényl-2-méthylcyclohexèn-5-one.

Mots clés : Diels–Alder, 2*H*-thiopyrane, substitut d'un 1,3-diène *cis*-substitué, 1-éthényl-2-méthylcyclohexène, dérivés octahydro-4a-méthylnapthalènes.

[Traduit par la rédaction]

Received November 21, 1996.

This paper is dedicated to Professor William A. Ayer on the occasion of his 65th birthday.

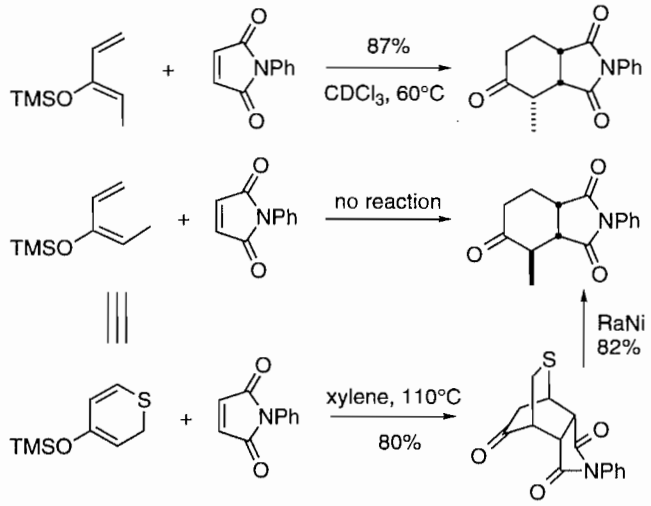
D.E. Ward[1] and Y. Gai. Department of Chemistry, University of Saskatchewan, 110 Science Place, Saskatoon, SK S7N 5C9, Canada.

[1] Author to whom correspondence may be addressed. Telephone: (306) 966-4656. Fax: (306) 966-4730. E-mail: dale.ward@usask.ca

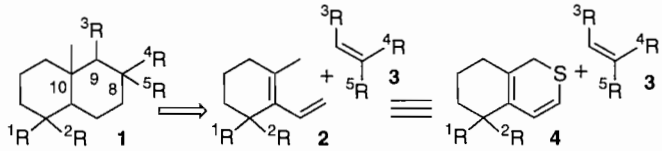
© 1997 NRC Canada

Can. J. Chem. Downloaded from www.nrcresearchpress.com by 88.146.161.215 on 09/08/12
For personal use only.

Scheme 1.



Scheme 2.

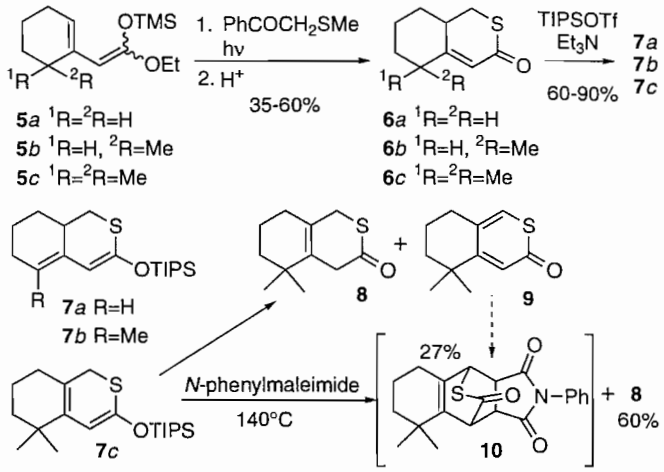


Introduction

The Diels–Alder reaction is perhaps the most powerful and versatile reaction in the synthetic chemist's arsenal (1). The increase in molecular complexity resulting from the simultaneous formation of two σ-bonds and up to four stereogenic centers coupled with the attributes of wide generality, atom economy, and predictable regio- and stereoselectivity contribute to the unrivaled synthetic utility of this reaction. The scope of this process is often limited by the poor reactivity associated with *cis*-substituted dienes (2) (Scheme 1). Recently, we have investigated the potential of 2*H*-thiopyrans to act as surrogates for *cis*-dienes in a strategy to overcome this limitation and thereby expand the scope of the Diels–Alder reaction (3). We have developed methods for the preparation of various substituted 2*H*-thiopyrans and have systematically investigated their Diels–Alder reactivity under a variety of conditions in both inter- (3*b*, 3*d*) and intra-molecular cases (3*g*). Adducts resulting from reactions of 2*H*-thiopyrans with dienophiles are, after desulfurization, synthetically equivalent to adducts from unreactive *cis*-dienes (3*a*, 3*g*).

Several structurally and biologically interesting natural products have substructures that incorporate a fused decalin ring system with a C-10 angular methyl group and alkyl substitution at C-8 and C-9 (**1**; e.g., drimanes, labdanes, triterpenes, steroids, etc.) (4). The most commonly employed synthetic approaches to this type of structure include Robinson annulation, polyene cyclization, or Diels–Alder reaction (5). These methods are not always compatible with the required substitution pattern of many of the target structures, often necessitating a linear multistep adjustment (5). For example, a Diels–Alder reaction of the generalized diene and dienophiles **2** and **3** could provide a versatile approach to these structures (Scheme 2). However, despite several attempts (6), this approach is successful only when $^1R = {}^2R$ =Me and only with certain dienophiles (e.g., dimethyl acetylenedicarboxylate, quinone). By contrast, to the best of our knowledge, there are no reports of successful Diels–Alder reaction of the diene **2** with $^1R = {}^2R$ = H. Dienes such as **2** can be regarded as *cis*-substituted and, as such, their low Diels–Alder reactivity can be attributed (in part) to the steric destabilization of the s-*cis* conformation. The modest success observed with **2** ($^1R = {}^2R$ = Me) is presumably due to the destabilization of the s-*trans* conformation by the geminal dimethyl group. We considered that the low reactivity of dienes such as **2** could be overcome by exploiting the chemistry of 2*H*-thiopyrans (e.g., **4**). Herein we report our preliminary results on the synthesis of 10-methyloctalins by Diels–Alder reactions of 2*H*-thiopyran surrogates of **2**.

Scheme 3.



Results and discussion

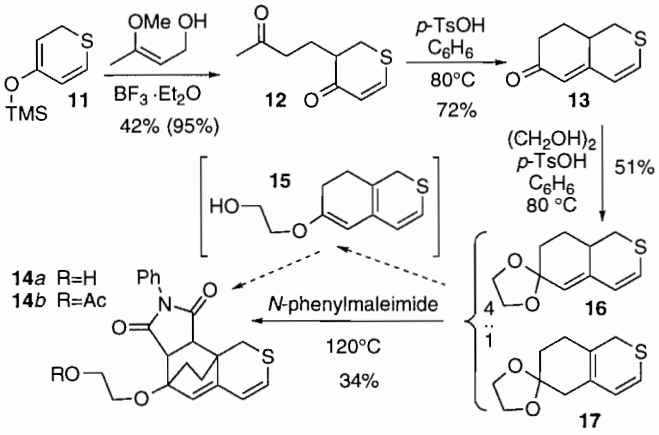
Our initial attempts at the synthesis of a 5,6,7,8-tetrahydro-1*H*-2-benzothiopyran (**4**) derivative involved the Diels–Alder reaction of the trimethylsilyl dienolate of cyclohexylideneacetate (**5***a*) with thioformaldehyde generated in situ according to the method of Vedejs et al. (7) to give the benzothiopyranone **6***a* after work-up (Scheme 3). Enolsilylation of **6***a* according to the usual protocol (3*b*) gave only the exocyclic diene **7***a*. The 5-methylbenzothiopyranone **6***b* was similarly prepared as a 1:1 mixture of diastereomers but also gave the exocyclic diene **7***b* upon enolsilylation. Reactions of the dienes **7***a* and **7***b* with *N*-phenylmaleimide in the presence of dichloromaleimide (8)[2] failed to give Diels–Alder adducts. Finally, treatment of the 5,5-dimethylbenzothiopyranone derivative **6***c* with triisopropylsilyl trifluoromethansulfonate (TIPSOTf) and Et_3N gave the unstable endocyclic diene **7***c*. Attempted Diels–Alder reaction of **7***c* with *N*-phenylmaleimide did not produce the expected product but gave an adduct tentatively identified as **10** in low yield. Subsequently, we found that **7***c* is rapidly converted into a mixture of **8** and **9** on standing and therefore presume that **10** resulted from the reaction of **9** (formed from **7***c* in situ) with the dienophile.

[2] Dichloromaleimide promotes diene isomerization (8) (cf. ref. 3*b*).

© 1997 NRC Canada

Can. J. Chem. Downloaded from www.nrcresearchpress.com by 88.146.161.215 on 09/08/12
For personal use only.

Scheme 4.



In an effort to form a more stable benzothiopyran derivative, the diene **11** (3b) was treated with 3-methoxy-2-butenol (9) and $BF_3{\cdot}Et_2O$ to give **12** (10) (Scheme 4). Cyclization of **12** under acidic conditions gave the dienone **13**, which, after reaction with ethylene glycol and 4-methylbenzenesulfonic acid (*p*-TsOH), gave a 4:1 mixture of the exocyclic and endocyclic dienes **16** and **17**, respectively. Reaction of the **16/17** mixture with *N*-phenylmaleimide again did not produce the expected adduct but gave **14***a* in 34% yield.[3] Although the mechanism is uncertain, the structure of **14***a* is consistent with a Diels–Alder reaction of the dienophile and the putative diene (i.e., **15**) resulting from elimination of the ethylene ketal in **16** and (or) **17**.

The failure of our 5,6,7,8-tetrahydro-1*H*-2-benzothiopyran derivatives **7***c* and **17** to undergo the expected Diels–Alder reactions led us to consider an alternative scenario where the desired adduct would result from an initial Diels–Alder reaction of a suitably substituted thiopyran diene followed by closure of the second carbocyclic ring (Scheme 5). Towards this end, the dione **12** was converted into the monoketal **18**, which, upon treatment with TIPSOTf and Et_3N, gave the diene **19**. Reaction of **19** with maleimide or *N*-substituted derivatives in benzene solution at 130–140°C gave ca. 7–10:1 mixtures (^{1}H NMR) of *endo* and *exo* Diels–Alder adducts **20** and **21**, respectively, in 30–35% yield.[4] The stereochemistry of the adducts was readily assigned, as previously (3*b*,*d*,*g*), based on the characteristic magnitudes of the H–H coupling constants observed for 2-thiabicyclo[2.2.2]octanes (see Fig. 1). Treatment of **20***a* with aqueous HF in acetonitrile provided the dione **22***a*, which, gratifyingly, underwent acid-catalyzed cyclization to **23***a* on heating with *p*-TsOH. The enone **23***b* was prepared analogously. Diels–Alder reactions of **19** with *N*-phenyl- and *N*-methylmaleimide in the presence of $EtAlCl_2$ gave the diones **22***a* and **22***b*, respectively, in good yields after acidic work-up (3*d*). Lewis acid mediated reactions of **19** with 3-propenoyl-2-oxazolidinone and with

Scheme 5.

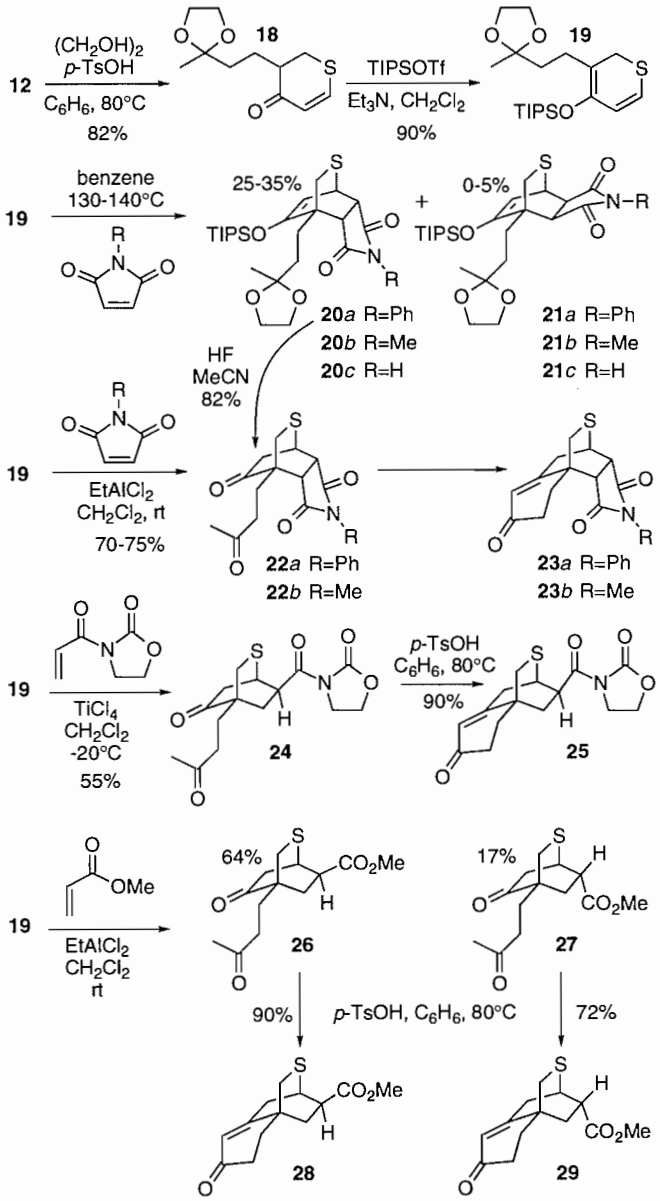
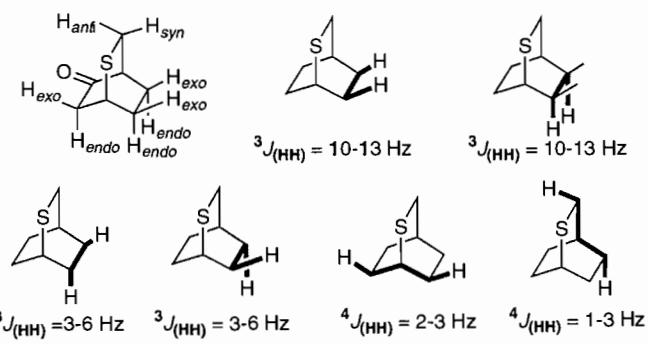


Fig. 1. Typical $^3J_{(HH)}$ and $^4J_{(HH)}$ coupling constants for 2-thiabicyclo[2.2.2]octan-5-ones.

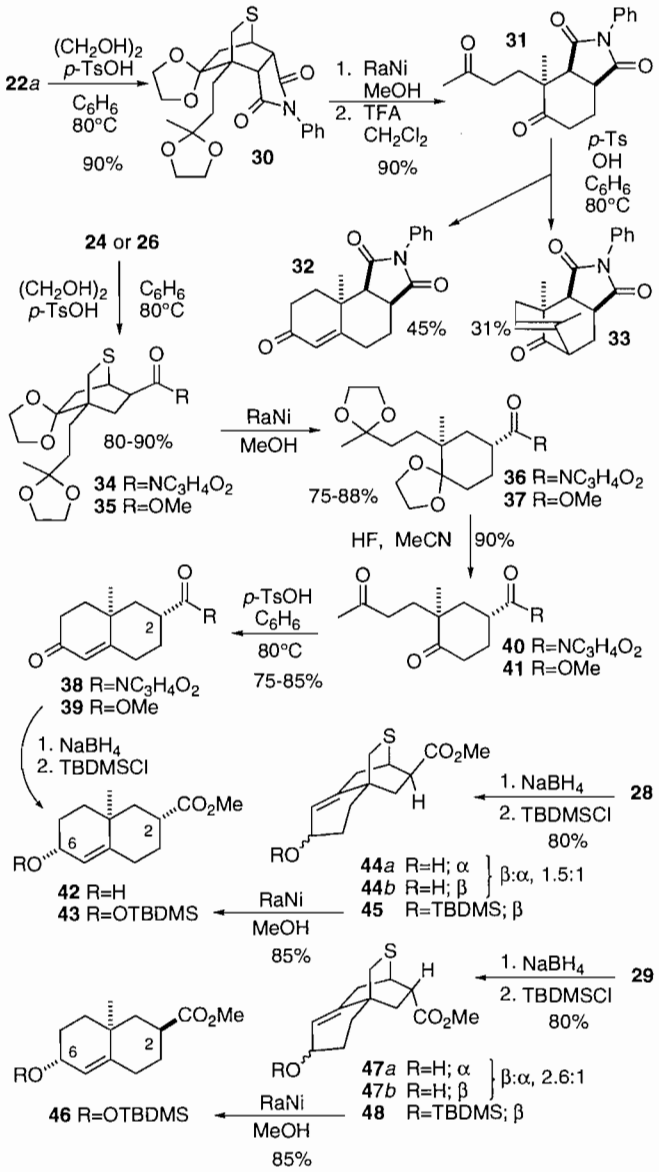


[3] The corresponding acetate **14***b* was also characterized.

[4] The *endo* adducts **20***a*,*b*,*c* were isolated and characterized. In each case, the corresponding *exo* adducts could be detected in the ^{1}H NMR spectra of the reaction mixtures (*endo*:*exo* ca. 7–10:1) but only **21***a* was isolated and characterized.

© 1997 NRC Canada

Scheme 6.



methyl acrylate were highly *exo*-selective in analogy with similar reactions with a less substituted thiopyran diene (cf. **11**) (3*d*). The product diones **24**, **26**, and **27** readily cyclized to the corresponding enones **25**, **28**, and **29**. The enones **23**, **25**, **28**, and **29** can be regarded as synthetically equivalent to Diels–Alder adducts of the 5,6,7,8-tetrahydro-1*H*-2-benzothiopyran derivative **17**.

Despite considerable experimentation, we were unable to cleanly obtain 10-methyl-Δ^4-octalin-3-one derivatives by direct desulfurization of the enones **23**, **25**, **28**, and **29** with Raney nickel or with nickel boride (11). In each case, a mixture of products was obtained in which reduction or migration of the double bond and (or) reduction or deoxygenation of the ketone had occurred in addition to desulfurization. This problem could be avoided by effecting desulfurization prior to the aldol cyclization (Scheme 6). Thus, acid-catalyzed reaction of **22***a* (or **20***a*) with ethylene glycol gave the bisketal **30**, which was smoothly desulfurized on treatment with Raney Ni to give the diketone **31** after an acidic work-up. Aldol condensation of **31** gave the desired **32** along with a substantial amount of the regioisomeric product **33**. Similarly, the diones **24** and **26** were subjected to the same series of reactions to obtain the desired 10-methyl-Δ^4-octalin-3-one derivatives **38** and **39**.[5] The expected *cis* stereochemistry for **38** and **39** was confirmed by the small vicinal coupling constants for HC-2 (numbering according to formal nomenclature)[5] in the respective ^{1}H NMR spectra, which clearly indicated an equatorial proton.[5]

Alternatively, the enones **28** and **29** were reduced with $NaBH_4$ in methanol to give, in each case, a diastereoisomeric mixture of alcohols **44***a*,*b* and **47***a*,*b*, respectively. The major alcohol isomers **44***b* and **47***b* were each converted into the corresponding *tert*-butyldimethylsilyl (TBDMS) ethers (**45** and **48**) and then desulfurized by treatment with Raney nickel to give the desired 10-methyl-Δ^4-octalin-3-one derivatives **43** and **46**,[5] respectively (Scheme 6).[6] The expected relative stereochemistry between the methyl and methoxycarbonyl groups was confirmed as *cis* for **43** and *trans* for **46** by the vicinal coupling constants observed for HC-2 in the ^{1}H NMR spectra; this proton was clearly equatorial in **43** and axial in **46**. The relative stereochemistry at C-6 in **43** (and thus in **45** and **44***a*,*b*) was determined by $NaBH_4$ reduction of **39** followed by formation of the TBDMS ether which gave a product (**43**) identical to that obtained from desulfurization of **45**. Ample literature precedent suggests that hydride reduction of Δ^4-octalin-3-one derivatives like **39** should selectively produce the alcohol with the hydroxyl group *cis* to the substituent at the ring junction (i.e., Me) (12). The stereochemistry at C-6 in **46** was assigned based on the close similarity of the HC-6 protons in the NMR spectra of **43** and **46** and on the assumption that the reductions of **28** and **29** occur with the same diastereofacial selectivity.

In summary, the 5,6,7,8-tetrahydro-1*H*-2-benzothiopyran derivatives **7***c* and **17**, prepared as surrogates for the unreactive 1-ethenyl-2-methylcyclohexene, failed to produce the desired Diels–Alder adducts. By contrast, the protected 2-oxobutyl-2*H*-thiopyran diene **19** reacted with maleimide and acrylate dienophiles to give adducts (**20**, **22**, **24**, **26**) in modest to good yields. The observed stereoselectivities, *endo* with maleimides and *exo* with acrylate dienophiles, are in accord with previous results obtained with less substituted 2*H*-thiopyran dienes like **11**. The Diels–Alder adducts are easily and efficiently converted into products that are synthetically equivalent to Diels–Alder adducts of **17**. Desulfurization of those products gives 10-methyl-Δ^4-octalin derivatives that are synthetically equivalent to hypothetical Diels–Alder adducts of 3-ethenyl-4-methyl-3-cyclohexenone. Depending on the scope and stereoselectivity of the Diels–Alder reactions of **19** and analogues, this approach should be applicable to the synthesis of a variety of natural product skeletons. We are actively investigating this strategy.

[5] Formally these are 1,2,3,4,6,7,8,8a-octahydro-8a-methyl-6-oxonaphthalene-2-carboxylic acid derivatives.

[6] Similar reaction of the minor alcohol isomers proceeded analogously; however, the products were not fully characterized in these cases.

© 1997 NRC Canada

Can. J. Chem. Downloaded from www.nrcresearchpress.com by 88.146.161.215 on 09/08/12
For personal use only.

Can. J. Chem. Downloaded from www.nrcresearchpress.com by 88.146.161.215 on 09/08/12
For personal use only.

Experimental

General methods

All solvents were distilled prior to use. Pyridine and Et_3N were distilled from CaH_2 and stored over KOH pellets. i-Pr_2NH was freshly distilled from CaH_2. Anhydrous solvents were distilled under argon as follows: ether and tetrahydrofuran (THF) from benzophenone potassium ketyl; benzene, toluene, and CH_2Cl_2 from P_2O_5 and stored over 3Å molecular sieves; MeOH from $Mg(OMe)_2$. Benzene solutions for Diels–Alder reactions were degassed by bubbling argon through the solvent (solution) followed by three freeze–thaw cycles under high vacuum (0.01 Torr; 1 Torr = 133.3 Pa). Unless otherwise noted, reactions were carried out under an atmosphere of argon and reaction temperatures refer to the bath. Concentration refers to removal of volatiles at water aspirator pressure on a rotary evaporator.

Preparative TLC was carried out on glass plates (20 × 20 cm) precoated (0.25 mm) with silica gel 60 F_{254}. Materials were detected by visualization under an ultraviolet lamp (254 nm) and (or) by treating a 1 cm vertical strip removed from the plate with a solution of phosphomolybdic acid (5%) containing a trace of ceric sulfate in aqueous sulfuric acid (5% v/v), followed by charring on a hot plate. Flash column chromatography (FCC) was performed according to the method of Still et al. (13) with Merck Silica Gel 60 (40–63 μm). Medium-pressure chromatography (MPC) was performed with minor modifications of the procedure reported by Taber (14). All mixed solvent eluents are reported as v/v solutions.

Spectral data

Low-resolution mass spectra (LRMS) were recorded on a magnetic scanning MS-12 instrument. EI ionization was accomplished at 70 eV and CI at 50 eV with ammonia as the reagent gas; only partial data are reported. IR spectra were recorded on a Fourier transform interferometer using a diffuse reflectance cell; only diagnostic peaks are reported. Unless otherwise noted, NMR spectra were measured in $CDCl_3$ solution at 300 MHz for ^1H and 75 MHz for ^{13}C. For ^1H NMR, residual $CHCl_3$ in $CDCl_3$ was employed as the internal standard (7.26 δ); for ^{13}C NMR, $CDCl_3$ was employed (77.0 δ). The ^1H NMR chemical shifts and coupling constants were determined assuming first-order behavior. Multiplicity is indicated by one or more of the following: s (singlet), d (doublet), t (triplet), q (quartet), m (multiplet), br (broad), ap (apparent); the list of coupling constants (J) corresponds to the order of the multiplicity assignment. ^1H NMR spectra were normally obtained with a digital resolution of 0.244 Hz/pt (sweep width = 4000 Hz, FID = 32 K data points) and coupling constants are reported to the nearest 0.5 Hz. The ^1H NMR assignments were made on the basis of chemical shift and multiplicity and were confirmed, where necessary, by homonuclear decoupling and (or) NOE experiments. The multiplicity of ^{13}C NMR signals refers to the number of attached H's (i.e., s = C, d = CH, t = CH_2, q = CH_3) and was determined by J-modulation (15). The ^{13}C assignments were made on the basis of chemical shift, multiplicity, and consistency within a series of similar structures. Assignments for ^{13}C signals of the same multiplicity and similar chemical shift (i.e., $\Delta\delta < 1$ ppm) are tentative. Elemental analyses were performed using a Perkin–Elmer 2400 CHN elemental analyzer.

Materials

2,2-Dimethylcyclohexanone (16), methyl phenacyl sulfide (17), 3-methoxy-2-butenol (9), **11** (3b), 3-propenoyl-2-oxazolidinone (18) were prepared as reported. Methyl acrylate was freshly distilled. All other reagents were commercially available and, unless otherwise noted, were used as received.

General procedure for preparation of ***5***

Ethyl cyclohexylidenethanoate and the 2′-methyl and 2′,2′-dimethyl derivatives were prepared in 60–70% yields by reactions of triethyl phosphonoacetate with the corresponding cyclohexanones according to the procedure of Wood and coworkers (19). Vinyl ketene acetals were prepared according to the procedure of Savard and Brassard (20): The esters (1–1.5 g) were added dropwise to a stirred solution of LDA (prepared from i-Pr_2NH (1.1 equiv.) and n-BuLi (1 equiv.)) in dry THF (1 mL/mmol of ester) at −78°C. After 1 h, TMSCl (1.5 equiv.) was added to the mixture at −78°C. The reaction mixture was allowed to slowly warm to room temperature (rt) and then was concentrated and the residue distilled to give the products.

*1-[2-Ethoxy-2-(trimethylsilyloxy)ethenyl]cyclohexene (****5****a)* (1 g, 80% yield): bp 95–100°C (3 Torr). ^1H NMR δ: 5.56 (1H, dd, J = 3, 3 Hz, HC-2), 4.08 (1H, s, HC-1′), 3.75 (2H, q, J = 7 Hz, H_2CO), 2.28–220 (2H, m), 2.12–2.00 (2H, m), 1.70–1.48 (4H, m), 1.28 (3H, t, J = 7 Hz, H_3CC), 0.22 (9H, s, H_3CSi).

*1-[2-Ethoxy-2-(trimethylsilyloxy)ethenyl]-6-methylcyclohexene, (****5****b)* (1.4 g, 75% yield): bp 95–100°C (2 Torr). ^1H NMR δ: 5.12 (1H, dd, J = 4, 4 Hz, HC-2), 3.98 (1H, s, HC-1′), 3.77 (2H, q, J = 7 Hz, H_2CO), 2.50–2.40 (1H, m), 2.07–1.98 (2H, m), 1.80–1.40 (4H, m), 1.26 (3H, t, J = 7 Hz, H_3CCH_2), 1.15 (3H, d, J = 7 Hz, H_3CC-6), 0.23 (9H, s, H_3CSi).

*1-[2-Ethoxy-2-(trimethylsilyloxy)ethenyl]-6,6-dimethylcyclohexene (****5****c)* (0.72 g, 62% yield): bp 92–95°C (3 Torr). ^1H NMR δ: 5.87 (1H, t, J = 4 Hz, HC-2), 4.00 (1H, s, HC-2′), 3.77 (2H, q, J = 7 Hz, H_2CO), 2.10–2.00 (2H, m, H_2C-3), 1.70–1.40 (6H, m), 1.29 (3H, t, H_3CCH_2), 1.02 (6H, s, H_3CC-6), 0.22 (9H, s, H_3CSi).

General procedure for the preparation of ***6***

A degassed solution of methyl phenacyl sulphide (19) (1 equiv.) and the ketene acetal **5** (2 equiv.) in dry benzene (5 mL/mmol of **5**) was irradiated at rt for 2 h through a 6% aqueous $CuSO_4$ filter using a 100 W sun lamp. Trifluoroacetic acid (TFA; several drops) was added to the mixture and, after stirring for 1.5 h at rt, the reaction mixture was concentrated and fractionated by FCC (15–30% ether in hexane) to give the products.

*1,5,6,7,8,8a-Hexahydro-3*H*-2-benzothiopyran-3-one, (****6****a)* (100 mg, 60% yield): IR ν_{max}: 2931, 1639, 1207, 1156 cm^{-1}; ^1H NMR δ: 5.93 (1H, dd, J = 2, 2 Hz, HC-4), 3.08–3.02 (2H, m, HC-1), 2.60–2.40 (2H, m, HC-5), 2.32–2.18 (1H, m, HC-8a), 2.08–1.83 (3H, m), 1.61–1.25 (3H, m); ^{13}C NMR δ: 189.9 (s, C-3), 163.9 (s, C-4a), 123.7 (d, C-4), 36.7 (d, C-8a), 36.1 (t, C-5), 33.1 (t), 33.0 (t), 26.4 (t), 25.2 (t); LRMS (EI), m/z (relative intensity): 168 ([M]$^+$, 15), 140 (100), 111 (28), 97 (24), 79 (26). Elemental anal. calcd. for $C_9H_{12}OS$: C 64.25, H 7.19; found: C 64.10, H 7.07.

© 1997 NRC Canada

Can. J. Chem. Downloaded from www.nrcresearchpress.com by 88.146.161.215 on 09/08/12
For personal use only.

*1,5,6,7,8,8a-Hexahydro-5-methyl-3*H*-2-benzothiopyran-3-one (**6**b)* (342 mg, 34%): IR ν_{max}: 2930, 1639, 1177 cm^{-1}; ^1H NMR δ: 5.97 (0.5H, d, J = 1.5 Hz), 5.94 (0.5H, s), 3.35 (0.5H, dd, J = 5, 13.5 Hz), 2.99 (1.5H, m), 2.80–2.60 (1H, m), 2.51–2.41 (0.5H, m), 2.32–2.22 (0.5H, m), 2.02–1.75 (2H, m), 1.75–1.50 (1H, m), 1.64 (2.5H, m), 1.38–1.25 (0.5H, m), 1.18 (1.5H, d, J = 7 Hz), 1.10 (1.5H, d, J = 7 Hz); LRMS (EI), *m/z* (relative intensity): 182 ($[M]^+$, 37), 154 (100), 139 (46), 111 (35).

*1,5,6,7,8,8a-Hexahydro-5,5-dimethyl-3*H*-2-benzothiopyran-3-one (**6**c)* (187 mg, 37%): IR ν_{max}: 2930, 1636, 1160 cm^{-1}; ^1H NMR δ: 6.08 (1H, d, J = 1.5 Hz, HC-4), 3.05–2.95 (2H, m, H_2C-1), 2.78–2.66 (1H, m, HC-8a), 2.00–1.90 (1H, m), 1.80–1.55 (3H, m), 1.50–1.25 (2H, m), 1.16 (3H, s, H_3C), 1.12 (3H, s, H_3C); LRMS (EI), *m/z* (relative intensity): 196 ($[M]^+$, 17), 168 (91), 153 (100).

General procedure for enolsilylation of thiopyranones
A solution of thiopyranone (1 equiv.), Et_3N (2.5 equiv.), and TIPSOTf (1.25 equiv.) in CH_2Cl_2 (ca. 10 mL/mmol of thiopyranone) was stirred under argon at rt for 0.5–3 h. The mixture was poured onto 5% Na_2CO_3 and extracted with ether (×3). The combined organic layers were dried over Na_2SO_4, concentrated, and fractionated by FCC (hexane; SiO_2 pretreated with Et_3N in hexane) to give the product. The dienol silyl ethers were freshly prepared and used immediately and the proposed structures were characterized only by ^1H NMR.

*6,7,8,8a-Tetrahydro-3-tris(1-methylethyl)silyloxy-1*H*-2-benzothiopyran (7*a*)* (3 h; 64 mg, 98%): ^1H NMR δ: 5.61 (1H, s, HC-4), 5.28 (1H, br s, HC-5), 2.73 (1H, dd, J = 11, 12 Hz, HC-1), 2.66 (1H, dd, J = 3.5, 12 Hz, HC-1), 2.48–2.33 (1H, m, HC-8a), 2.12–2.05 (2H, m, HC-6), 1.95–1.78 (2H, m), 1.68–1.51 (1H, m), 1.25–1.05 (21H, m).

*6,7,8,8a-Tetrahydro-5-methyl-3-tris(1-methylethyl)silyloxy-1*H*-2-benzothiopyran (7*b*)* (2 h; 15 mg, 72%): ^1H NMR δ: 5.90 (1H, s, HC-4), 2.72 (1H, dd, J = 12, 12 Hz, HC-1), 2.62 (1H, dd, J = 3.5, 12 Hz, HC-1), 2.42–2.38 (1H, m, HC-8a), 2.15–1.50 (6H, m), 1.66 (3H, br s, H_3CC-5).

*6,7,8,8a-Tetrahydro-5,5-dimethyl-3-tris(1-methylethyl)silyloxy-1H-2-benzothiopyran (7*c*)*
This diene was particularly unstable. Work-up of a reaction of **6***c* (5 mg, 0.025 mmol), Et_3N (0.02 mL, 0.15 mmol), and TIPSOTf (0.015 mL, 0.05 mmol) after 20 min gave a crude product that was a 1.8:1 mixture of **7***c* and **6***c*, respectively; ^1H NMR δ for **7***c*: 5.58 (1H, s, HC-4), 3.24 (1H, s, HC-1), 2.07 (2H, br t, J = 6 Hz, HC-8), 1.75–1.55 (2H, m), 1.48–1.40 (2H, m), 1.30–1.00 (21H, m, H_3CCHSi), 0.96 (6H, s, H_3CC-5). Fractionation by PTLC (66% ether in hexane) of the residue after concentration gave 5,6,7,8-tetrahydro-5,5-dimethyl-1*H*-2-benzothiopyran-3(4*H*)-one (**8**; 1.2 mg, 24%): ^1H NMR δ: 3.45 (2H, s, HC-1), 3.12 (2H, s, HC-4), 2.15 (2H, br t, J = 6 Hz, HC-8), 1.71–1.60 (2H, m), 1.52–1.45 (2H, m), 1.00 (6H, s, H_3C); and 5,6,7,8-tetrahydro-5,5-dimethyl-3*H*-2-benzothiopyran-3-one (**9**; 1.4 mg, 29%): ^1H NMR δ: 7.00 (1H, s, HC-1), 6.65 (1H, s, HC-4), 2.68 (2H, br t, J = 6 Hz, HC-8), 1.80–1.70 (2H, m), 1.67–1.57 (2H, m), 1.26 (6H, s, H_3C).

*Attempted Diels–Alder reaction of 7*c
Enolsilylation of **6***b* (8.8 mg, 0.045 mmol) for 30 min at rt gave an oil (14 mg) after work-up and fractionation. A solution of the oil and *N*-phenylmaleimide (8 mg, 0.045 mmol) in $C_6D_5CD_3$ (0.4 mL) was sealed in a NMR tube and heated at 140°C for 72 h. The mixture was concentrated and fractionated by PTLC (66% ether in hexane) to give **8** (4.7 mg, 60%) and a product tentatively indentified as 3a,4,5,6,7,8,9,9a-octahydro-5,5-dimethyl-2-phenyl-9,4-epithiomethano-1*H*-benz[*e*]isoindole-1,3(2*H*),11-trione (**10**; 4 mg, 27%): ^1H NMR δ: 7.16–7.50 (5H, m, Ar-H), 4.36 (1H, d, J = 4 Hz, HC-9), 4.20 (1H, d, J = 3 Hz, HC-4), 3.75 (1H, dd, J = 4, 9 Hz, HC-9a), 3.50 (1H, dd, J = 3, 9 Hz, HC-3a), 2.35–2.12 (2H, m, H_2C-8), 1.80–1.55 (2H, m), 1.50–1.40 (2H, m), 1.02 (3H, s, H_3C), 0.86 (3H, s, H_3C).

*3,4-Dihydro-3-(3-oxobutyl)-4*H*-thiopyran-4-one (**12**)*
A solution of $BF_3{\cdot}Et_2O$ (0.35 mL, 2.7 mmol) in dry ether (0.4 mL) was added dropwise to a stirred solution of **11** (2.8 g, 15 mmol) and 3-methoxy-2-butenol (9) (1.02 g, 10 mmol) in CH_3NO_2 (28 mL) at −20°C under argon. After 1 h, the reaction mixture was quenched by addition of saturated $NaHCO_3$ and was extracted with CH_2Cl_2 (×3). The combined organic layers were dried over Na_2SO_4, concentrated, and fractionated by FCC (75% ether in hexane) to give recovered starting material as 2,3-dihydro-4*H*-thiopyran-4-one (1 g, 58%) and **12** (10) (0.78 g, 42%): IR ν_{max}: 3033, 1712, 1657, 1583, 1551 cm^{-1}; ^1H NMR δ: 7.37 (1H, dd, J = 10 Hz, HC-6), 6.10 (1H, d, J = 10 Hz, HC-5), 3.33 (1H, dd, J = 4, 13.5 Hz, HC-2), 3.07 (1H, dd, J = 9, 13.5 Hz, HC-2), 2.58 (2H, t, J = 7.5 Hz, H_2C-2′), 2.59–2.50 (1H, m, HC-3), 2.16 (3H, s, H_3C-4′), 2.16–2.07 (1H, m, HC-1′), 1.88–1.79 (1H, m, HC-1′); ^{13}C NMR δ: 208.1 (s, C-3′), 195.5 (s, C-4), 145.4 (d, C-6), 122.9 (d, C-5), 44.3 (d, C-3), 40.8 (t, C-2′), 32.4 (t, C-2), 30.0 (q, C-4′), 22.8 (t, C-1′); LRMS (CI, NH_3), *m/z* (relative intensity): 185 ($[M+1]^+$, 100), 167 (34), 113 (18).

*1,7,8,8a-Tetrahydro-6*H*-2-benzothiopyran-6-one (**13**)*
A solution of **12** (0.184 g, 1 mmol) and *p*-TsOH (10 mg, 0.05 mmol) in benzene (10 mL) was heated under reflux for 4.5 h. The cooled (rt) reaction mixture was washed with 5% Na_2CO_3 and water, dried over Na_2SO_4, concentrated, and fractionated by FCC (75% ether in hexane) to give recovered **12** (26 mg, 14%) and **13** (0.12 g, 72%): IR ν_{max}: 3038, 1641, 1583, 1548 cm^{-1}; ^1H NMR δ: 6.73 (1H, d, J = 10 Hz, HC-3), 6.34 (1H, d, J = 10 Hz, HC-4), 5.78 (1H, s, HC-5), 2.85–2.75 (3H, m, H_2C-1, HC-8a), 2.56 (1H, ddd, J = 2.5, 4.5, 17 Hz, HC-7), 2.43 (1H, ddd, J = 5, 14, 17 Hz, HC-7), 2.22–2.12 (1H, m, HC-8), 1.82–1.68 (1H, m, HC-8); ^{13}C NMR δ: 198.7 (s, C-6), 153.6 (s, C-4a), 132.9 (d, C-3), 124.6 (d, C-4), 123.2 (d, C-5), 37.9 (t, C-7), 35.9 (d, C-8a), 31.3 (t, C-1 or C-8), 30.6 (t, C-8 or C-1); LRMS (EI), *m/z* (relative intensity): 166 ($[M]^+$, 100), 138 (36), 110 (98).

*3a,9b-Dihydro-4-[(2-hydroxyethyl)oxy]-9*H*-4,9a-ethanothiopyrano[3,4-e]isoindole-1,3(2*H*,4*H*)-trione (**14***a*)*
A solution of the 4:1 mixture of **16** and **17** (18 mg, 0.085 mmol) and *N*-phenylmaleimide (15 mg, 0.085 mmol) in C_6D_6 (0.5 mL) was sealed in a NMR tube and heated at 120°C. After 87 h, ^1H NMR revealed the absence of **16** and **17**. The solution was concentrated and fractionated by FCC (ethyl acetate) to

© 1997 NRC Canada

Can. J. Chem. Downloaded from www.nrcresearchpress.com by 88.146.161.215 on 09/08/12
For personal use only.

give **13** (4 mg, 28%) and **14***a* (11 mg, 34%): IR ν_{max}: 3411, 1703, 1497 cm^{-1}; ^1H NMR δ: 7.38–7.29 (3H, m, Ar-H), 7.05–7.00 (2H, m, Ar-H), 6.30 (1H, d, *J* = 9.5 Hz, HC-7), 6.23 (1H, d, *J* = 9.5 Hz, HC-6), 5.87 (1H, s, HC-5), 4.16 (1H, d, *J* = 13 Hz, HC-3b), 3.90–3.68 (4H, m, H_2CO), 3.34 (1H, d, *J* = 8.5 Hz, HC-9), 2.99 (1H, d, *J* = 8.5 Hz, HC-9), 2.49 (1H, d, *J* = 13 Hz, HC-9b), 2.33–2.20 (1H, m, HC-10 or HC-11), 2.10–1.95 (1H, m, HC-10 or HC-11), 1.65–1.48 (2H, m, HC-10, HC-11); ^{13}C NMR δ: 175.4 (s, C=O), 174.0 (s, C=O), 135.4 (s, C-5a), 131.9 (s, C_6H_5), 128.5 (d ×2, C_6H_5), 128.0 (d, C_6H_5), 126.6 (d ×2, C_6H_5), 126.6 (d, C-7), 123.5 (d, C-5 or C-6), 123.4 (d, C-5 or C-6), 78.3 (s, C-4), 64.1 (t, CH_2O), 60.5 (t, CH_2O), 48.2 (d, C-3a), 44.6 (d, C-9b), 40.6 (s, C-9a), 30.4 (t, C-9), 27.9 (d, C-10 or C-11), 27.5 (t, C-10 or C-11); LRMS (CI, NH_3), *m/z* (relative intensity): 384 ($[M+1]^+$, 100), 210 (38).

*2-[(1,2,3,3a,4,9b-Hexahydro-1,3-dioxo-9*H*-4,9a-ethanothiopyrano[3,4-*e*]isoindol-4-yl)oxy]ethyl ethanoate (**14***b*)*

A solution of **14***a* (9 mg, 0.023 mmol), pyridine (1 drop), and acetic anhydride (2 drops) in CH_2Cl_2 (ca. 1 mL) was stirred at rt for 38 h. The mixture was diluted with CH_2Cl_2, washed with 1 N HCl and water, dried over Na_2SO_4, and concentrated from toluene (×2) to give **14***b* (9 mg, 92%); IR ν_{max}: 3062, 1773, 1735, 1701, 1596, 1497 cm^{-1}; ^1H NMR δ: 7.46–7.30 (3H, m, Ar-H), 7.18–7.11 (2H, m, Ar-H), 6.38 (1H, d, *J* = 10 Hz, HC-7), 6.30 (1H, d, *J* = 10 Hz, HC-6), 5.97 (1H, s, HC-5), 4.36 (1H, d, *J* = 13 Hz, HC-3a), 4.34–4.28 (2H, m, H_2COCO), 4.07–4.00 (1H, m, HCO), 3.85–3.77 (1H, m, HCO), 3.35 (1H, d, *J* = 8.5 Hz, HC-9), 3.02 (1H, d, *J* = 8.5 Hz, HC-9), 2.54 (1H, d, *J* = 13 Hz, HC-9b), 2.33–2.24 (1H, m, HC-10 or HC-11), 2.08 (3H, s, H_3CCO), 2.06–1.95 (1H, m, HC-10 or HC-11), 1.62–1.45 (2H, m, HC-10, HC-11); ^{13}C NMR δ: 175.3 (s, C=O), 173.3 (s, C=O), 171.3 (s, O=CCH_3), 136.2 (s, C-4a), 131.7 (s, C_6H_5), 129.1 (d ×2, C_6H_5), 128.6 (d, C_6H_5), 126.5 (d ×2, C_6H_5), 126.3 (d, C-7), 124.9 (d, C-5 or C-6), 123.5 (d, C-5 or C-6), 79.1 (t, CH_2O), 63.7 (t, CH_2O), 61.3 (s, C-4), 49.0 (d, C-3a), 45.4 (d, C-9b), 41.5 (s, C-9a), 32.0 (t, C-9), 28.9 (t, C-10 or C-11), 28.4 (t, C-10 or C-11), 21.0 (q, CH_3CO); LRMS (CI, NH_3), *m/z* (relative intensity): 426 ($[M+1]^+$, 24), 87 (100).

*1,7,8,8a-Tetrahydrospiro[6*H*-2-benzothiopyran-6,2′-[1,3]dioxolane] (**16**) and 1,5,7,8-tetrahydrospiro[6*H*-2-benzothiopyran-6,2′-[1,3]dioxolane] (**17**)*

A solution of **13** (50 mg, 0.3 mmol), ethylene glycol (ca. 0.1 mL), and pyridinium *p*-toluenesulfonate (PPTS, 3 mg) in benzene (1 mL) was heated under reflux for 2 h. The cooled (rt) reaction mixture was diluted with benzene, washed with 5% Na_2CO_3 and water, dried over Na_2SO_4, concentrated, and fractionated by FCC (75% ether in hexane) to give recovered **13** (12 mg, 24%) and product as a 4:1 mixture of **16** and **17** (32 mg, 51%): IR ν_{max}: 3019, 1629, 1373, 1124 cm^{-1}; ^1H NMR δ for **16**: 6.24 (1H, dd, *J* = 1.5, 10 Hz, HC-3), 6.14 (1H, d, *J* = 10 Hz, HC-4), 5.36 (1H, br s, HC-5), 4.05–3.85 (4H, m, H_2CO), 2.77 (1H, d, *J* = 12.5 Hz, HC-1), 2.66 (1H, ddd, *J* = 1.5, 3.5, 12.5 Hz, HC-1), 2.58–2.46 (1H, m, HC-8a), 2.03–1.78 (3H, m, H_2C-7, HC-8), 1.57 (1H, m, HC-8); δ for **17**: 6.15 (1H, d, *J* = 10 Hz, HC-3), 5.89 (1H, d, *J* = 10 Hz, HC-4), 3.18 (2H, br s, H_2C-1), 2.71 (2H, s, H_2C-5); ^{13}C NMR δ for **16**: 138.4 (s, C-4a), 124.0 (d, C-3), 123.8 (d, C4 or C-5), 123.6 (d, C5 or C-4), 106.3 (s, C-6), 64.9 (t, CH_2O), 64.4 (t, CH_2O), 36.3 (d, C-8a), 34.0 (t, C-1), 31.6 (t, C-7), 28.8 (t, C-8); LRMS (CI, NH_3), *m/z* (relative intensity): 211 ($[M+1]^+$, 100), 182 (20), 163 (8), 138 (22), 110 (15).

*3,4-Dihydro-3-[2-(2-methyl-1,3-dioxolan-2-yl)ethyl]-4*H*-thiopyran-4-one (**18**)*

A solution of **12** (230 mg, 1.25 mmol), ethylene glycol (0.5 mL, excess), and PPTS (20 mg) in benzene (15 mL) was heated under reflux for 2 h. The cooled (rt) reaction mixture was washed with 5% Na_2CO_3 and water, dried over Na_2SO_4, and concentrated to give an oil (this was a mixture of mono- and bis-ketals). The oil was dissolved in acetone that contained several drops of water and stirred with PPTS (20 mg) for 2 h. The mixture was concentrated, diluted with ether, washed with 5% Na_2CO_3 and water, dried over Na_2SO_4, concentrated, and fractionated by FCC (75% ether in hexane) to give **18** (234 mg, 82%): IR ν_{max}: 1658, 1551, 1060 cm^{-1}; ^1H NMR δ: 7.45 (1H, d, *J* = 10 Hz, HC-6), 6.12 (1H, d, *J* = 10 Hz, HC-5), 3.99–3.87 (4H, m, H_2CO), 3.31 (1H, dd, *J* = 3.5, 13.5 Hz, HC-2), 3.05 (1H, dd, *J* = 9, 13.5 Hz, HC-2), 2.58–2.48 (1H, m, HC-3), 2.02–1.92 (1H, m, HC-1′), 1.80–1.55 (3H, m, HC-1′,H_2C-2′), 1.24 (3H, s, H_3C); ^{13}C NMR δ: 195.9 (s, C-4), 145.1 (d, C-6), 123.0 (d, C-5), 109.6 (s, C-2″), 64.7 (t, CH_2O), 64.6 (t, CH_2O), 45.1 (d, C-3), 36.2 (t, C-2), 31.8 (t, C-2′), 23.9 (q, CH_3), 22.7 (t, C-1′); LRMS (CI, NH_3), *m/z* (relative intensity): 229 ($[M+1]^+$, 100), 87 (66). Elemental anal. calcd. for $C_{11}H_{16}O_3S$: C 57.87, H 7.06, found: C 58.06, H 7.05.

*3-[2-(2-Methyl-1,3-dioxolan-2-yl)ethyl]-4-[(tris(1-methylethyl)silyl)oxy]-2*H*-thiopyran (**19**)*

TIPSOTf (0.24 mL, 0.90 mmol) was added to a stirred solution of **18** (171 mg, 0.75 mmol) and Et_3N (0.32 mL, 2.2 mmol) in CH_2Cl_2 (8 mL) at rt. After 20 min, the reaction mixture was concentrated and fractionated by FCC (pentane; silica gel pretreated with 10% v/v Et_3N in pentane) to give **19** (260 mg, 90%): IR ν_{max}: 1657, 1611, 1463, 1223 cm^{-1}; ^1H NMR δ: 6.18 (1H, d, *J* = 9.75 Hz, HC-6), 5.94 (1H, d, *J* = 9.75 Hz, HC-5), 3.99–3.90 (4H, m, H_2CO), 3.30 (2H, s, H_2C-2), 2.39–2.30 (2H, m, H_2C-1′), 1.80–1.70 (2H, m, H_2C-2′), 1.16 (3H, s, H_3CC-2″), 1.20–1.00 (21H, m, $(H_3C)_2CHSi$); ^{13}C NMR δ: 144.0 (s, C-4), 122.9 (d, C-6), 122.3 (d, C-5), 109.8 (s, C-3′), 107.0 (s, C-3), 64.7 (t ×2, CH_2O), 37.0 (t, C-2), 29.4 (t, C-1′), 24.6 (t, C-2′), 23.9 (q, CH_3C-2″), 18.0 (q, CH_3CHSi), 13.2 (d, CHSi); LRMS (CI, NH_3), *m/z* (relative intensity): 385 ($[M+1]^+$, 100), 227 (76).

*General procedure for thermal Diels–Alder reactions of **19** with maleimides*

A solution of **19** (0.07–0.15 g), BHT (0.1 equiv.), and the maleimide derivative (1.2 equiv.) in C_6D_6 or C_6H_6 (0.5–1 mL) was sealed in an NMR tube and heated at 130–140°C for 48–72 h. ^1H NMR of the reaction mixture indicated the presence of a 7–10:1 mixture of *endo*:*exo* adducts. The cooled (rt) solution was concentrated and fractionated by FCC (50% ethyl acetate in hexane) to give the adduct(s).

*General procedure for $EtAlCl_2$ mediated Diels–Alder reactions of **19** with maleimides*

$EtAlCl_2$ (1 M solution in hexane; 1 equiv.) was added to a stirred solution of the dienophile (1.2 equiv.) in dry CH_2Cl_2 (20 mL/mmol of **19**) at rt. A solution of **19** (20–50 mg; 1 equiv.) in CH_2Cl_2 (10 mL/mmol of **19**) was added via a

© 1997 NRC Canada

Can. J. Chem. Downloaded from www.nrcresearchpress.com by 88.146.161.215 on 09/08/12
For personal use only.

syringe to the mixture and, after 1 h, the reaction was quenched by addition of saturated aqueous $NaHCO_3$. The mixture was extracted with CH_2Cl_2 and the combined organic layers were dried over Na_2SO_4 and concentrated. The enol ethers **20** could be obtained by fractionation of the residue by FCC (75% ether in hexane); however, because some hydrolysis could usually be detected at this point, it was convenient to complete the hydrolysis by dissolving the residue in CH_2Cl_2 (2 mL) containing TFA (2 drops). After stirring overnight, the mixture was concentrated and fractionated by FCC (ether) to provide **22**.

*(3a*S*, 4*R*, 7*R*, 7a*S*)-3a,4,7,7a-Tetrahydro-7-[2-(2-methyl-1,3-dioxolan-2-yl)ethyl]-8-[(tris(1-methylethyl)silyl)oxy]-1,3-dioxo-2-phenyl-4,7-ethenothiopyrano[3,4-c]pyrrole-1,3(2H,-6H)-dione (**20**a)* (28% from thermal reaction of **19** with *N*-phenylmaleimide): IR ν_{max}: 3066, 1774, 1711, 1626, 1598 cm^{-1}; ^1H NMR δ: 7.18–7.47 (5H, m, Ar-H), 5.35 (1H, d, *J* = 7.5 Hz, HC-9), 4.08 (1H, dd, *J* = 3, 7.5 Hz, HC-4), 3.96 (4H, br s, H_2CO), 3.53 (1H, dd, *J* = 3, 8.5 Hz, HC-3a), 3.19 (1H, d, *J* = 11 Hz, HC-6_{syn}), 3.08 (1H, d, *J* = 8.5 Hz, HC-7a), 2.62 (1H, dt, *J* = 4.5, 13.5 Hz, HC-1′), 2.52 (1H, d, *J* = 11 Hz, HC-6_{anti}), 2.17 (1H, dd, *J* = 4.5, 13 Hz, HC-2′), 1.92 (1H, dt, *J* = 3, 13.5 Hz, HC-1′), 1.76 (1H, dt, *J* = 3, 13 Hz, HC-2′), 1.41 (3H, s, H_3CC-2″), 1.20–1.00 (21H, m, $(CH_3)_2CHSi$); ^{13}C NMR δ: 175.4 (s, C═O), 175.0 (s, C═O), 154.8 (s, C-8), 131.6 (s, C_6H_5), 129.2 (d ×2, C_6H_5), 128.5 (s, C_6H_5), 126.3 (d ×2, C_6H_5), 110.1 (s, C-2″), 102.2 (d, C-9), 64.8 (t, CH_2O), 64.7 (t, CH_2O), 49.8 (d, C-3a), 44.1 (s, C-7), 44.1 (d, C-7a), 35.9 (t, C-6), 35.7 (d, C-4), 33.3 (t, C-2′), 26.5 (t, C-1′), 23.9 (q, CH_3C-2″), 18.1 (q, CH_3CHSi), 12.6 (d, CHSi); LRMS (EI), *m/z* (relative intensity): 557 ($[M]^+$, 22), 470 (8), 424 (9), 340 (16), 87 (100), 73 (28), 59 (57).

*(3a*S*, 4*R*, 7*R*, 7a*S*)-3a,4,7,7a-Tetrahydro-2-methyl-1,3-dioxo-7-[2-(2-methyl-1,3-dioxolan-2-yl)ethyl]-8-[(tris(1-methylethyl)silyl)oxy]-4,7-ethenothiopyrano[3,4-c]pyrrole-1,3-(2H,6H)-dione (**20**b)* (35% from thermal reaction of **19** with *N*-methylmaleimide): IR ν_{max}: 1775, 1703, 1626, 1463, 1434 cm^{-1}; ^1H NMR δ: 5.21 (1H, d, *J* = 7.5 Hz, HC-9), 3.96 (5H, m, HC-4, H_2CO), 3.35 (1H, dd, *J* = 3, 8.5 Hz, HC-3a), 3.10 (1H, d, *J* = 10.5 Hz, HC-6_{syn}), 2.90 (1H, d, *J* = 8.5 Hz, HC-7a), 2.83 (3H, s, H_3CN), 2.52 (1H, dt, *J* = 4.5, 13.5 Hz, HC-1′), 2.48 (1H, d, *J* = 10.5 Hz, HC-6_{anti}), 2.13 (1H, dt, *J* = 4.5, 13 Hz, HC-2′), 1.89 (1H, dt, *J* = 3.5, 13.5 Hz, HC-1′), 1.73 (1H, dt, *J* = 3.5, 13 Hz, HC-2′), 1.41 (3H, s, H_3CC), 1.20–1.00 (21H, m, $(H_3C)_2CHSi$); ^{13}C NMR δ: 176.5 (s, C═O), 176.2 (s, C═O), 154.6 (s, C-8), 110.1 (s, C-2″), 101.6 (d, C-9), 64.8 (t, CH_2O), 64.7 (t , CH_2O), 49.9 (d, C-3a), 44.1 (d, C-7a), 43.7 (s, C-7), 35.7 (t, C-6), 35.3 (d, C-4), 33.4 (t, C-2′), 26.5 (t, C-1′), 24.6 (q, CH_3N), 24.0 (q, CH_3), 17.9 (q, CH_3CSi), 12.5 (d, CHSi); LRMS (EI), *m/z* (relative intensity): 495 ($[M]^+$, 10), 383 (17), 278 (9), 115 (19), 88 (100), 73 (30), 59 (63).

*(3a*S*, 4*R*, 7*R*, 7a*S*)-3a,4,7,7a-Tetrahydro-7-[2-(2-methyl-1,3-dioxolan-2-yl)ethyl]-8-[(tris(1-methylethyl)silyl)oxy]-1,3-dioxo-4,7-ethenothiopyrano[3,4-c]pyrrole-1,3(2H,6H)-dione (**20**c)* (36% from thermal reaction of **19** with maleimide): IR ν_{max}: 3213, 3080, 2944, 1778, 1720, 1712, 1627 cm^{-1}; ^1H NMR δ: 7.93 (1H, s br, HN), 5.29 (1H, d, *J* = 7.5 Hz, HC-9), 3.96 (5H, m, HC-3a, CH_2O), 3.41 (1H, dd, *J* = 3, 8.5 Hz, HC-4), 3.09 (1H, d, *J* = 11 Hz, HC-6_{syn}), 2.94 (1H, d, *J* = 8.5 Hz, HC-7a), 2.49 (1H, d, *J* = 11 Hz, HC-6_{anti}), 2.49 (1H, dt, *J* = 4.5, 13.5 Hz, HC-1′), 2.10 (1H, dt, *J* = 4.5, 13 Hz, HC-2′), 1.90 (1H, dt, *J* = 3, 13.5 Hz, HC-1′), 1.72 (1H, dt, *J* = 3, 13 Hz, HC-2′), 1.42 (3H, s, H_3CC-2″), 1.20–1.00 (21H, m, $(CH_3)_2CHSi$); ^{13}C NMR δ: 176.6 (s, C═O), 176.0 (s, C═O), 156.7 (s, C-8), 110.2 (s, C-2″), 101.7 (d, C-9), 64.8 (t, CH_2O), 64.7 (t, OCH_2), 51.2 (d, C-3a), 45.4 (d, C-7a), 43.7 (s, C-7), 35.6 (t, C-6), 35.1 (d, C-4), 33.3 (t, C-2″), 26.4 (t, C-1″), 23.9 (q, CH_3C-2″), 17.9 (q, CH_3CHSi), 12.6 (d, CHSi); LRMS (EI), *m/z* (relative intensity): 481 ($[M]^+$, 27), 394 (11), 348 (13), 264 (23), 171 (13), 115 (21), 87 (100), 59 (48).

*(3a*R*, 4*R*, 7*R*, 7a*R*)-3a,4,7,7a-Tetrahydro-7-[2-(2-methyl-1,3-dioxolan-2-yl)ethyl]-8-[(tris(1-methylethyl)silyl)oxy]-1,3-dioxo-2-phenyl-4,7-ethenothiopyrano[3,4-c]pyrrole-1,3(2H,-6H)-dione (**21**a)* (5% from thermal reaction of **19** with *N*-phenylmaleimide): IR ν_{max}: 1778, 1712, 1625, 1499 cm^{-1}; ^1H NMR δ: 7.26–7.50 (5H, m, Ar-H), 5.52 (1H, d, *J* = 7.5 Hz, HC-9), 3.99 (1H, dd, *J* = 3.5, 7.5 Hz, HC-4), 3.94 (4H, m, H_2CO), 3.25 (1H, dd, *J* = 3.5, 10 Hz, HC-3a), 3.10 (1H, dd, *J* = 2, 10 Hz, HC-7a), 3.00 (1H, d, *J* = 11 Hz, HC-6_{syn}), 2.56 (1H, dd, *J* = 2, 11 Hz, HC-6_{anti}), 2.30 (1H, dt, *J* = 5, 13 Hz, HC-1′), 2.03 (3H, m, HC-1′, HC-2′), 1.38 (3H, s, H_3CC-2″), 1.09 (21H, m, $(CH_3)_2CHSi$); ^{13}C NMR δ: 176.0 (s, C═O), 175.5 (s, C═O), 157.6 (s, C-8), 132.1 (s, C_6H_5), 129.2 (d ×2, C_6H_5), 128.8 (d, C_6H_5), 126.6 (d ×2, C_6H_5), 110.0 (s, C-2″), 104.3 (d, C-9), 64.7 (t ×2, OCH_2), 49.6 (d, C-3a), 44.0 (d, C-7a), 43.6 (s, C-7), 36.8 (d, C-4), 35.7 (t, C-6), 35.3 (t, C-2′), 27.5 (t, C-1′), 23.8 (q, CH_3C-2″), 18.0 (q, CH_3CHSi), 12.9 (d, CHSi); LRMS (EI), *m/z* (relative intensity): 557 ($[M]^+$, 14), 383 (15), 282 (13), 115 (27), 87 (100), 73 (36), 59 (60).

*(3a*S*, 4*R*, 7*R*, 7a*S*)-3a,4,7,7a-Tetrahydro-1,3,8-trioxo-7-(3-oxobutyl)-2-phenyl-4,7-ethanothiopyrano[3,4-c]pyrrole-1,3(2H,6H)-dione (**22**a)* (72% from $EtAlCl_2$ mediated reaction of **19** with *N*-phenylmaleimide): IR ν_{max}: 1776, 1712, 1664 cm^{-1}; ^1H NMR δ: 7.49–7.12 (5H, m, Ar-H), 3.82 (1H, ddd, *J* = 2, 3, 9.5 Hz, HC-3a), 3.69 (1H, ddd, *J* = 3, 3, 6 Hz, HC-4), 3.36 (1H, d, *J* = 9.5 Hz, HC-7a), 3.06 (1H, d, *J* = 12 Hz, HC-6_{syn}), 2.92 (1H, ddd, *J* = 2, 2, 18.5 Hz, HC-9_{exo}), 2.87 (1H, d, *J* = 12 Hz, HC-6_{anti}), 2.78–2.65 (2H, m, HC-2′, HC-9_{endo}), 2.50 (1H, ddd, *J* = 5.5, 10, 15.5 Hz, HC-2′), 2.35 (1H, ddd, *J* = 5.5, 10, 15.5 Hz, HC-1′), 2.29–2.15 (1H, m, HC-1′), 2.20 (3H, s, H_3C-4′); ^{13}C NMR δ: 207.7 (s, C═O), 207.4 (s, C═O), 174.5 (s, C═O), 174.1 (s, C═O), 131.1 (s, C_6H_5), 129.3 (d ×2, C_6H_5), 129.2 (d, C_6H_5), 126.3 (d ×2, C_6H_5), 47.7 (s, C-7), 47.4 (d, C-3a), 45.0 (t, C-9), 44.1 (d, C-7a), 38.2 (t, C-2′), 34.0 (d, C-4), 29.9 (q, C-4′), 29.9 (t, C-6), 25.4 (t, C-1′); LRMS (EI), *m/z* (relative intensity): 357 ($[M]^+$, 6), 339 (100), 300 (33), 183 (60), 174 (35), 165 (22), 141 (30), 126 (36). Elemental anal. calcd. for $C_{19}H_{19}NO_4S$: C 63.85, H 5.36, N 3.92; found: C 63.71, H 5.50, N 3.83.

*(3a*S*, 4*R*, 7*R*, 7a*S*)-3a,4,7,7a-Tetrahydro-2-methyl-1,3,8-trioxo-7-(3-oxobutyl)-4,7-ethanothiopyrano[3,4-c]pyrrole-1,3(2H,6H)-dione (**22**b)* (71% from $EtAlCl_2$ mediated reaction of **19** with *N*-methylmaleimide): IR ν_{max}: 1775, 1721, 1692 cm^{-1}; ^1H NMR δ: 3.67–3.57 (2H, m, HC-3a, HC-4), 3.19 (1H, d, *J* = 9 Hz, HC-7a), 3.00 (1H, d, *J* = 12 Hz, HC-6_{syn}), 2.95 (3H, s, H_3CN), 2.81 (1H, d, *J* = 12 Hz, HC-6_{anti}), 2.82

© 1997 NRC Canada

Can. J. Chem. Downloaded from www.nrcresearchpress.com by 88.146.161.215 on 09/08/12
For personal use only.

(1H, ddd, J = 2.5, 2.5, 20 Hz, HC-9$_{exo}$), 2.67 (1H, ddd, J = 6, 10, 17 Hz, HC-2′), 2.55–2.43 (2H, m, HC-2′, HC-9$_{endo}$), 2.33–2.15 (2H, m, HC-1′), 2.21 (3H, s, H_3C-4′); ^{13}C NMR δ: 207.7 (s, C=O), 207.4 (s, C=O), 175.0 (s, C=O), 174.9 (s, C=O), 47.6 (s, C-7), 47.4 (d, C-3a), 44.8 (t, C-9), 44.1 (d, C-7a), 38.2 (t, C-2′), 33.7 (d, C-4), 30.1 (t, C-6), 29.8 (q, C-4′), 25.4 (t, C-1′), 25.1 (q, CH_3N); LRMS (EI), *m/z* (relative intensity): 295 ([M]$^+$, 6), 277 ([M−H_2O]$^+$, 100), 262 (21), 238 (42), 210 (15), 183 (77), 141 (39), 126 (46).

General procedure for aldol cyclodehydration of 1,5-diones

A solution of dione and *p*-TsOH (0.05–0.15 equiv.) in C_6H_6 (ca. 20 mL/mmol of dione) was heated under reflux. When the reaction was complete (TLC), the cooled (rt) mixture was diluted with C_6H_6, washed with 5% Na_2CO_3 and water, dried over Na_2SO_4, concentrated, and fractionated by FCC (25–50% ethyl acetate in hexane or ether) to provide the product.

*3a*S*, *4*R*, *9a*R* *9b*S*)-3a,4,5,8,9,9b-Hexahydro-3-oxo-2-phenyl-1*H*,7*H*-9a,4-(epithiomethano)benz[e]indole-1,3(2*H*),-7-trione (**23**a)* (30 mg, 88% from aldol cyclodehydration of **22***a* for 41 h): IR ν_{max}: 1774, 1710, 1671, 1496 cm^{-1}; ^{1}H NMR δ: 7.17–7.50 (5H, m, Ar-H), 6.04 (1H, br s, HC-6), 3.75 (1H, ddd, J = 2, 5, 9.5 Hz, HC-3a), 3.47 (1H, ddd, J = 2.5, 2.5, 5 Hz, HC-4), 3.41 (1H, m, HC-9), 3.27 (1H, d, J = 11 Hz, HC-10), 3.09 (1H, d, J = 9.5 Hz, HC-9b), 2.98 (1H, d, J = 19.5 Hz, HC-5$_{endo}$), 2.87 (1H, d, J = 11 Hz, HC-10), 2.79 (1H, ddd, J = 2, 2.5, 19.5 Hz, HC-5$_{exo}$), 2.53 (2H, m, HC-8), 1.88 (1H, ddd, J = 5, 14.5, 14.5 Hz, HC-9); ^{13}C NMR δ: 196.5 (s, C-7), 175.3 (s, C=O), 175.1 (s, C=O), 158.2 (s, C-5a), 131.2 (s, C_6H_5), 129.4 (d ×2, C_6H_5), 129.1 (d, C_6H_5), 126.2 (d ×2, C_6H_5), 129.0 (d, C-6), 48.1 (d, C-3a), 46.3 (d, C-9b), 37.3 (s, C-9a), 35.3 (t, C-8), 33.9 (t, C-5), 33.5 (t, C-10), 32.8 (d, C-4), 29.3 (t, C-9); LRMS (EI), *m/z* (relative intensity): 339 ([M]$^+$, 10), 175 (100), 165 (22).

*3a*S*, *4*R*, *9a*R* *9b*S*)-3a,4,5,8,9,9b-Hexahydro-2-methyl-3-oxo-1*H*,7*H*-9a,4-(epithiomethano)benz[e]indole-1,3(2*H*),-7-trione (**23**b)* (10 mg, 70% from aldol cyclodehydration of **22***b* for 45 h): IR ν_{max}: 1773, 1693, 1667, 1434, 1381, 1284 cm^{-1}; ^{1}H NMR δ: 5.97 (1H, dd, J = 2, 2 Hz, HC-6), 3.59 (1H, ddd, J = 2, 2.5, 9.5 Hz, HC-3a), 3.48–3.35 (2H, m, HC-4, HC-9), 3.24 (1H, d, J = 11 Hz, HC-10), 2.99 (3H, s, H_3CN), 2.94 (1H, d, J = 6 Hz, HC-9b), 2.91–2.84 (1H, m, HC-5), 2.82 (1H, d, J = 11 Hz, HC-10), 2.60–2.45 (3H, m, HC-5, H_2C-8), 1.85 (1H, ddd, J = 5, 14.5, 14.5 Hz, HC-9); ^{13}C NMR δ: 196.5 (s, C-7), 176.0 (s ×2, C=O), 158.3 (s, C-5a), 128.9 (d, C-6), 48.1 (d, C-3a), 46.2 (d, C-9b), 37.1 (s, C-9a), 35.2 (t), 33.9 (t), 33.4 (t), 32.6 (d, C-4), 29.2 (t), 25.1 (q, CH_3N); LRMS (CI, NH_3), *m/z* (relative intensity): 295 ([M+18]$^+$, 47), 278 ([M+1]$^+$, 100), 113 (54).

*(1′*R*, *4′*R*, *6′*R*)-3-[(8-Oxo-4-(3-oxobutyl)-2-thiabicyclo-[2.2.2]oct-6-yl)carbonyl]-2-oxazolidinone (**24**)*

To a stirred solution of 3-propenoyl-2-oxazolidinone (40 mg, 0.03 mmol) in CH_2Cl_2 (2 mL) at −20°C was added $TiCl_4$ (0.2 M solution in CH_2Cl_2; 1 mL, 0.2 mmol). A solution of **19** (92 mg, 0.24 mmol) in CH_2Cl_2 (2 mL) was added to the mixture. After 1 h, the reaction was quenched by addition of 1 N HCl. The mixture was diluted with CH_2Cl_2, washed with saturated $NaHCO_3$, dried over Na_2SO_4, concentrated, and fractionated by FCC (50% ethyl acetate in hexane) to give **12** (9 mg, 20%), the Michael adduct 3-[3,4-dihydro-3-(3-oxobutyl)-4-oxo-2*H*-thiopyran-3-yl]propanoyl-2-oxazolidinone (5 mg, 6%):[7] IR ν_{max}: 1775, 1707, 1698, 1652, 1560, 1388 cm^{-1}; ^{1}H NMR δ: 7.30 (1H, dd, J = 1, 10 Hz, HC-6″), 6.03 (1H, d, J = 10 Hz, HC-5″), 4.41 (2H, ap t, J = 8 Hz, H_2C-5), 4.00 (2H, ap t, J = 8 Hz, H_2C-4), 3.27 (1H, d, J = 13.5 Hz, HC-2″), 3.03 (1H, dd, J = 1, 13.5 Hz, HC-2″), 2.98–2.75 (2H, m, H_2C-2′), 2.56–2.28 (2H, m, H_2C-2‴), 2.17–2.05 (2H, m, H_2C-1‴), 2.13 (3H, s, H_3C-4‴), 1.99–1.82 (2H, m, H_2C-1′); ^{13}C NMR δ: 207.7 (s, C-3‴), 196.4 (s, C-4″), 172.7 (s, C-1′), 153.5 (s, C-2), 144.9 (d, C-6″), 122.8 (d, C-5″), 62.1 (t, C-5), 44.9 (s, C-3″), 42.6 (t, C-4), 38.0 (t, C-2‴), 36.1 (t, C-2′), 30.0 (t, C-2″), 27.7 (t, C-1‴ or C-3′), 26.3 (t, C-1‴ or C-3′); LRMS (CI, NH_3), *m/z* (relative intensity): 343 ([M+18]$^+$, 25), 326 ([M+1]$^+$, 100), 254 (29), 239 (28), 183 (71); and the *exo* Diels–Alder adduct **24** (43 mg, 55%): IR ν_{max}: 2919, 1775, 1768, 1721, 1692, 1650 cm^{-1}; ^{1}H NMR δ: 4.47 (2H, ap t, J = 8.5 Hz, H_2C-5), 4.22–4.00 (3H, m, H_2C-4, HC-6′), 3.52 (1H, ddd, J = 3, 3, 6.5 Hz, HC-1′), 2.93 (1H, d, J = 11 Hz, HC-3′$_{syn}$), 2.85 (2H, d, J = 3 Hz, HC-7′), 2.71 (1H, dd, J = 3, 11 Hz, HC-3′$_{anti}$), 2.61 (1H, dd, J = 5, 14 Hz, HC-5′$_{exo}$), 2.51 (2H, ap t, J = 8 Hz, HC-2″), 2.16 (3H, s, H_3C-4″), 1.93–1.80 (2H, m, HC-1″), 1.73 (1H, ddd, J = 3, 10.5, 14 Hz, HC-5′$_{endo}$); ^{13}C NMR δ: 211.8 (s, C-8′), 207.8 (s, C-3″), 172.0 (s, O=CC-6′), 153.4 (s, C-2), 62.4 (t, C-5), 48.5 (t, C-4), 44.2 (s, C-4′), 43.8 (d, C-6′), 43.1 (t, C-7′), 38.4 (t, C-2″), 36.7 (d, C-1′), 31.6 (t, C-3′), 29.9 (q, CH_3), 28.3 (t, C-1′), 28.1 (t, C-5); LRMS (EI), *m/z* (relative intensity): 325 ([M]$^+$, 44), 307 ([M−H_2O]$^+$, 11), 267 (46), 191 (28), 88 (39), 43 (100).

*(3′*R*, *8a′*R*, *10′*R*)-3-[(3,4,7,8-Tetrahydro-6-oxo-6*H*-3,8a-ethano-1*H*-2-benzothiopyran-10-yl)carbonyl]-2-oxazolidinone (**25**)* (135 mg, 90% from aldol cyclodehydration of **24** for 33 h): IR ν_{max}: 2921, 1774, 1770, 1703, 1665, 1631 cm^{-1}; ^{1}H NMR δ: 5.97 (1H, br s, HC-5′), 4.47 (2H, ap t, J = 7 Hz, H_2C-5), 4.20–4.00 (3H, m, H_2C-4, HC-10′), 3.39 (1H, ddd, J = 3, 3, 3 Hz, HC-3′), 3.05–3.00 (2H, m, H_2C-4′), 2.95 (1H, dd, J = 3, 10 Hz, HC-1′$_{anti}$), 2.83 (1H, d, J = 10 Hz, HC-1′$_{syn}$), 2.55–2.38 (3H, m, H_2C-7′, HC-9′$_{exo}$), 1.97–1.89 (2H, m, H_2C-8′), 1.67 (1H, ddd, J = 3, 10.5, 13.5 Hz, HC-9′$_{endo}$); ^{13}C NMR δ: 197.5 (s, C-6′), 172.6 (s, C-2), 165.0 (s, O=CC-10′), 153.4 (s, C-4a), 126.2 (d, C-5′), 62.4 (t, C-5), 44.6 (d, C-10′), 43.1 (t, C-4), 39.7 (t, C-7′), 34.6 (d, C-3′), 33.7 (t, C-1′), 33.7 (s, C-8a), 33.4 (t, C-4′), 32.6 (t), 31.1 (t); LRMS (EI), *m/z* (relative intensity): 307 ([M]$^+$, 69), 260 (40), 220 (43), 192 (43), 173 (100), 166 (55), 146 (23), 117 (32).

*Methyl (1*R*, *4*R*, *6*R*)-8-oxo-4-(3-oxobutyl)-2-thiabicyclo[2.2.2]octane-6-carboxylate (**26**)* (64% from $EtAlCl_2$ mediated reaction of **19** with methyl acrylate): IR ν_{max}: 1721, 1662, 1435, 1357, 1204, 1167 cm^{-1}; ^{1}H NMR δ: 3.78 (3H, s, H_3CO), 3.51 (1H, ddd, J = 3, 3, 6.5 Hz, HC-1), 3.09 (1H, ddd, J = 3.5, 5.5, 11 Hz, HC-6), 2.86 (1H, dd, J = 3, 20 Hz, HC-7$_{exo}$), 2.85 (1H, d, J = 11 Hz, HC-3$_{syn}$), 2.73 (1H, dd, J = 2.5, 11 Hz, HC-3$_{anti}$), 2.71 (1H, dd, J = 3, 20 Hz, HC-7$_{endo}$), 2.52-

[7] This is the first occasion where we have isolated a Michael adduct from a Lewis acid mediated reaction of a 2*H*-thiopyran diene with a dienophile (cf. refs. 3*d* and 10).

© 1997 NRC Canada

Can. J. Chem. Downloaded from www.nrcresearchpress.com by 88.146.161.215 on 09/08/12
For personal use only.

2.45 (3H, m, H_2C-2′, HC-5_{exo}), 2.15 (3H, s, H_3C-4′), 1.90–1.75 (3H, m, HC-1′, HC-5_{endo}); ^{13}C NMR δ: 211.7 (s, C-8), 207.8 (s, C-3′), 172.7 (s, O═CO), 52.5 (q, CH_3O), 48.1 (t, C-7), 44.1 (d, C-6), 38.4 (t, C-2′), 36.6 (d, C-1), 31.3 (t, C-3), 29.9 (q, C-4′), 29.2 (t, C-5), 28.3 (t, C-1′); LRMS (EI), *m/z* (relative intensity): 270 ($[M]^+$, 56), 252 ($[M-H_2O]^+$, 16), 212 (65), 199 (31), 184 (28), 183 (26), 125 (25), 43 (100).

*Methyl (1*R**, 4*R**, 6*S**)-8-oxo-4-(3-oxobutyl)-2-thiabicyclo[2.2.2]octane-6-carboxylate (**27**)* (17% from $EtAlCl_2$ mediated reaction of **19** with methyl acrylate): IR ν_{max}: 2952, 1721, 1224, 1174 cm^{-1}; ^1H NMR δ: 3.73 (3H, s, CH_3O), 3.46–3.37 (2H, m, HC-1, HC-6), 2.87 (1H, d, J = 11 Hz, HC-3_{syn}), 2.78 (1H, dd, J = 2.5, 11 Hz, HC-3_{anti}), 2.72 (2H, br s, H_2C-7), 2.60–2.46 (2H, m, H_2C-2′), 2.20–2.15 (2H, m, HC-5_{endo}), 2.16 (3H, s, H_3C-4′), 2.00 (1H, dd, J = 11, 14 Hz, HC-5_{exo}), 1.92 (1H, ddd, J = 6.5, 9, 14 Hz, HC-1′), 1.70 (1H, ddd, J = 6.5, 9, 14 Hz, HC-1′); ^{13}C NMR δ: 211.2 (s, C-8), 207.9 (s, C-3′), 173.3 (s, O═CO), 52.4 (q, CH_3O), 45.2 (t, C-7), 45.0 (s, C-4), 44.7 (d, C-6), 38.5 (t, C-2′), 35.5 (d, C-1), 32.0 (t, C-3), 29.9 (t, C-5), 29.9 (q, C-4′), 28.3 (t, C-1′); LRMS (EI), *m/z* (relative intensity): 270 ($[M]^+$, 72), 212 (55), 184 (29), 183 (27), 165 (20), 125 (30), 91 (25), 43 (100).

*Methyl (3*R**, 8a*R**, 10*R**)-3,4,7,8-tetrahydro-6-oxo-6*H*-3,8a-ethano-1*H*-2-benzothiopyran-10-carboxylate (**28**)* (80 mg, 95% from aldol cyclodehydration of **26** for 48 h): IR ν_{max}: 1736, 1667, 1630, 1200 cm^{-1}; ^1H NMR δ: 5.98 (1H, dd, J = 1.5, 1.5 Hz, HC-5), 3.78 (3H, s, H_3CO), 3.33 (1H, ddd, J = 3, 3.5, 3.5 Hz, HC-3), 3.10 (1H, ddd, J = 3.5, 4, 11 Hz, HC-10), 3.03 (1H, ddd, J = 1.5, 3.5, 18 Hz, HC-4), 2.94 (1H, dd, J = 3, 10.5 Hz, HC-1_{anti}), 2.91 (1H, ddd, J = 1.5, 3, 18 Hz, HC-4), 2.74 (1H, d, J = 10.5 Hz, HC-1_{syn}), 2.45 (3H, m, H_2C-7, HC-9_{exo}), 1.93 (2H, m, H_2C-8), 1.78 (1H, ddd, J = 3, 11, 14 Hz, HC-9_{endo}); ^{13}C NMR δ: 197.5 (s, C-6), 173.1 (s, OC═O), 164.9 (s, C-4a), 126.1 (d, C-5), 52.3 (q, CH_3O), 44.7 (d, C-10), 39.3 (t, C-7), 34.6 (d, C-3), 33.7 (t), 33.6 (s, C-8a), 33.4 (t), 31.9 (t), 31.3 (t); LRMS (EI), *m/z* (relative intensity): 252 ($[M]^+$, 100), 166 (72), 147 (45), 146 (83), 145 (94), 117 (68), 91 (67).

*Methyl (3*R**, 8a*R**, 10*S**)-3,4,7,8-tetrahydro-6-oxo-6*H*-3,8a-ethano-1*H*-2-benzothiopyran-10-carboxylate (**29**)* (25 mg, 72% from aldol cyclodehydration of **27** for 48 h): IR ν_{max}: 1730, 1667, 1631, 1434, 1196, 1171 cm^{-1}; ^1H NMR δ: 5.94 (1H, dd, J = 1.5, 2 Hz, HC-5), 3.71 (3H, s, H_3CO), 3.36 (1H, dddd, J = 2, 2, 3.5, 10 Hz, HC-10), 3.23 (1H, ddd, J = 2, 2.5, 3.5 Hz, HC-3), 3.07 (1H, dd, J = 2.5, 10.5 Hz, HC-1_{anti}), 2.94 (1H, ddd, J = 2, 2.5, 18.5 Hz, HC-4_{endo}), 2.81 (1H, dddd, J = 1.5, 2, 3.5, 18.5 Hz, H-4_{exo}), 2.73 (1H, d, J = 10.5 Hz, HC-1_{syn}), 2.55–2.35 (2H, m, H_2C-7), 2.00 (3H, m, H_2C-9, HC-8), 1.83 (1H, ddd, J = 4, 5.5, 14 Hz, HC-8); ^{13}C NMR δ: 201.5 (s, C-6), 173.4 (s, OC═O), 165.1 (s, C-4a), 126.1 (d, C-5), 52.3 (q, CH_3O), 45.5 (d, C-10), 36.0 (t), 34.3 (s, C-8a), 33.7 (t), 33.5 (t), 33.5 (d, C-3), 33.4 (t), 32.3 (t); LRMS (EI), *m/z* (relative intensity): 252 ($[M]^+$, 100), 205 (51), 166 (89), 147 (28), 146 (35), 145 (54), 117 (60), 91 (50).

*General procedure for preparation of bisketals **30**, **34**, and **35***
A solution of the dione, ethylene glycol (10–25 equiv.), and *p*-TsOH (0.05–0.15 equiv.) in benzene (ca. 25 mL/mmol of dione) was heated under reflux for 1.5–2 h. When the reaction was complete (TLC), the cooled (rt) mixture was diluted with C_6H_6, washed with 5% Na_2CO_3 and water, dried over Na_2SO_4, concentrated, and fractionated by FCC (10–20% ethyl acetate in hexane) to give product.

*(3a*S**, 4*R**, 7*R**, 7a*S**)-1,2,3,3a,4,6,7,7a-Octahydro-7-[2-(2-methyl-1,3-dioxolan-2-yl)ethyl]-1,3-dioxo-2-phenylspiro-[4,7-ethanothiopyrano[3,4-c]pyrrole-8,2′-*[1,3]dioxolane] (**30**) (70 mg, 93% from **22***a*): IR ν_{max}: 2980, 1775, 1710, 1597, 1498, 1382, 1183 cm^{-1}; ^1H NMR δ: 7.48–7.20 (5H, m, C_6H_5), 3.95–3.83 (8H, m, H_2CO), 3.53 (1H, ddd, J = 1.5, 3, 10 Hz, HC-3a), 3.38 (1H, ddd, J = 3, 3, 3 Hz, HC-4), 3.08 (1H, d, J = 10 Hz, HC-7a), 2.99 (1H, d, J = 11.5 Hz, HC-6_{syn}), 2.84 (1H, d, J = 11.5 Hz, HC-6_{anti}), 2.45–2.10 (4H, m, H_2C-2′, H_2C-9), 1.65–1.55 (2H, m, H_2C-1′), 1.38 (3H, s, H_3C); ^{13}C NMR δ: 175.8 (s ×2, C═O), 132.3 (s, C_6H_5), 129.2 (d ×2, C_6H_5), 128.6 (d, C_6H_5), 126.6 (d ×2, C_6H_5), 110.2 (s, C-8 or C-2′), 108.5 (s, C-8 or C-2′), 65.5 (t, CH_2O), 65.0 (t, CH_2O), 64.6 (t ×2, CH_2O), 47.1 (d, C-3a), 43.6 (t, C-9), 42.7 (s, C-7), 41.9 (d, C-7a), 32.8 (t), 31.9 (d, C-4), 28.1 (t), 24.1 (t), 23.7 (q, CH_3); LRMS (EI), *m/z* (relative intensity): 445 ($[M]^+$, 63), 430 (23), 400 (65), 383 (100), 358 (20).

General procedure for Raney Ni desulfurization
A suspension of sulfide and W2 Raney Ni (21) (ca. 1–3 mL/mmol of sulfide) in methanol (ca. 20 mL/mmol of sulfide) was heated under reflux for 2–4 h. When the reaction was complete (TLC), the mixture was filtered through Celite and the combined filtrate and washings were concentrated and, if necessary, fractionated FCC (ethyl acetate in hexane or ether) to give the product.

*(3a*S**,4*S**,7a*S**)-3a,6, 7,7a-Tetrahydro-4-methyl-4-(3-oxobutyl)-2-phenylisoindole-1,3,5(2*H*,4*H*)-trione (**31**)* The crude product from desulfurization of **30** (55 mg, 0.12 mmol) was dissolved in CH_2Cl_2 (3 mL) containing TFA (several drops) and stirred at rt overnight. The mixture was concentrated and fractionated by FCC (10% ethyl acetate in ether) to give **31** (36 mg, 92%): IR ν_{max}: 2972, 1774, 1708, 1497, 1380, 1193 cm^{-1}; ^1H NMR δ: 7.53–7.26 (5H, m, Ar-H), 3.38–3.28 (1H, m, HC-7a), 3.12 (1H, d, J = 10 Hz, HC-3a), 2.70–2.40 (5H, m), 2.40–2.20 (1H, m), 2.20–2.05 (1H, m), 2.09 (3H, s, H_3C-4′), 1.70–1.60 (1H, m), 1.39 (3H, s, H_3CC-4); ^{13}C NMR δ: 211.5 (s, C-5), 209.0 (s, C-3′), 177.5 (s, C═O), 175.7 (s, C═O), 131.7 (s, C_6H_5), 129.3 (d ×2, C_6H_5), 128.9 (d, C_6H_5), 126.5 (d ×2, C_6H_5), 48.4 (s, C-4), 48.0 (d, C-3a), 38.6 (d, C-7a), 37.7 (t), 36.7 (t), 30.1 (q, C-4′), 27.4 (t), 21.5 (q, CH_3C-4), 19.7 (t); LRMS (EI), *m/z* (relative intensity): 327 ($[M]^+$, 21), 299 (17), 271 (20), 270 (21), 257 (33), 187 (44), 110 (46), 95 (29), 43 (100).

*(3a*S**, 9a*S**, 9b*S**)-4,5,8,9,9a,9b-Hexahydro-9a-methyl-2-phenylbenz[e]isoindole-1,3,7(2*H*,3a*H*)-trione (**32**)* (5.1 mg, 45% from aldol cyclodehydration of **31** for 7 h): IR ν_{max}: 2949, 1776, 1708, 1664, 1496, 1381 cm^{-1}; ^1H NMR δ: 7.50–7.20 (5H, m, Ar-H), 5.84 (1H, br s, HC-6), 3.42 (1H, ddd, J = 3, 7, 8.5 Hz, HC-3a), 3.31 (1H, ddd, J = 5.5, 13.5, 13.5 Hz, HC-8), 3.06 (1H, d, J = 8.5 Hz, HC-9b), 2.67 (1H, ddd, J = 5, 13.5, 18 Hz, HC-9), 2.53 (1H, ddd, J = 3, 5.5, 18 Hz, HC-9), 2.43 (1H, ddd, J = 2, 5, 12 Hz, HC-5), 2.38–2.15 (3H, m, H_2C-4, HC-5), 1.92 (1H, ddd, J = 3, 5, 13.5 Hz, HC-8), 1.54 (3H, s,

© 1997 NRC Canada

Can. J. Chem. Downloaded from www.nrcresearchpress.com by 88.146.161.215 on 09/08/12
For personal use only.

H_3C); ^{13}C NMR δ: 198.0 (s, C-7), 177.8 (s, NC═O), 175.8 (s, NC═O), 164.4 (s, C-5a), 131.6 (s, C_6H_5), 129.3 (d ×2, C_6H_5), 128.9 (d, C_6H_5), 126.6 (d, C-1), 126.4 (d ×2, C_6H_5), 48.3 (d, C-9b), 39.6 (d, C-3a), 34.0 (s, C-9a), 34.0 (t), 33.6 (t), 28.2 (q, CH_3), 28.1 (t), 22.7 (t); LRMS (CI, NH_3), *m/z* (relative intensity): 327 ([M+18]$^+$, 81), 310 ([M+1]$^+$, 100).

(3aS, 4S*, 6S*, 7aS*)-3a,6,7,7a-Tetrahydro-4,8-dimethyl-2-phenyl-6,4-propeno-1H-isoindole-1,3,5(2H,4H)-trione (**33**)* (3.5 mg, 31% from aldol cyclodehydration of **31** for 7 h): IR ν_{max}: 1777, 1710, 1500, 1381, 1157 cm^{-1}; ^1H NMR δ: 7.53–7.26 (5H, m, Ar-H), 5.46 (1H, br d, *J* = 4.5 Hz, HC-9), 3.24 (1H, d, *J* = 9 Hz, HC-3a), 3.14 (1H, dd, *J* = 2.5, 14.5 Hz, HC-7), 3.01 (1H, dd, *J* = 8, 8.5 Hz, HC-7a), 2.80 (1H, br s, HC-6), 2.55 (1H, dd, *J* = 5, 19 Hz, HC-10), 2.20–2.19 (2H, m, HC-7, HC-10), 1.75 (3H, s, H_3CC-8), 1.38 (3H, s, H_3CC-4); LRMS (CI, NH_3), *m/z* (relative intensity): 327 ([M+18]$^+$, 100), 310 ([M+1]$^+$, 27), 187 (17).

(1R, 4R*, 7R*)-4-[2-(2-Methyl-1,3-dioxolan-2-yl)ethyl]-7-[(2-oxazolidinone-3-yl)carbonyl]spiro[2-thiabicyclo[2.2.2]-octane-5,2′-[1,3]dioxolane] (**34**)* (45 mg, 84% from bisketalization of **24**): IR ν_{max}: 1774, 1700, 1386 cm^{-1}; ^1H NMR δ: 4.39 (2H, ap t, *J* = 8 Hz, H_2COCO), 4.10–3.82 (11H, m, H_2CO (×4), H_2CN, HC-7), 3.16 (1H, ddd, *J* = 3, 3, 3 Hz, HC-1), 2.80 (1H, dd, *J* = 1.5, 11 Hz, HC-3$_{anti}$), 2.67 (1H, d, *J* = 11 Hz, HC-3$_{syn}$), 2.42–2.25 (3H, m), 1.70–1.45 (5H, m), 1.29 (3H, s, H_3C); ^{13}C NMR δ: 173.2 (s, O═CC-7), 153 (s, O═CO), 110.3 (s, C-5 or C-2″), 110.2 (s, C-5 or C-2″), 64.8 (t, CH_2O), 64.7 (t ×2, CH_2O), 64.4 (t, CH_2O), 62.2 (t, C-5), 46.1 (t, CH_2N), 43.2 (d, C-7), 43.1 (t, C-6), 37.8 (s, C-4), 35.3 (d, C-1), 33.2 (t), 28.4 (t), 27.0 (t), 26.8 (t), 23.9 (q, CH_3); LRMS (CI, NH_3), *m/z* (relative intensity): 414 ([M+1]$^+$, 61), 370 (12), 354 (12), 87 (100).

(6′S, 8′R*)-3-[(6-methyl-6-(2-(2-Methyl-1,3-dioxolan-2-yl)-ethyl)-1,4-dioxaspiro[4.5]decan-8-yl)carbonyl]-2-oxazolidinone (**36**)* (13 mg, 66% from desulfurization of **34**):[8] IR ν_{max}: 2967, 1777, 1697, 1388 cm^{-1}; ^1H NMR δ: 4.38 (2H, ap t, *J* = 8 Hz, HC-5), 4.01–3.80 (11H, m, H_2CO, H_2C-4), 1.92–1.55 (10H, m), 1.35 (3H, s, H_3CC-2‴), 0.84 (3H, s, H_3CC-6); LRMS (CI, NH_3), *m/z* (relative intensity): 401 ([M+18]$^+$, 16), 384 ([M+1]$^+$, 72), 357 (75), 340 (76), 322 (100), 227 (32), 105 (35), 99 (75).

Methyl (6S, 8R*)-6-methyl-6-[2-(2-methyl-1,3-dioxolan-2-yl)ethyl]-1,4-dioxaspiro[4.5]decan-8-carboxylate (**37**)*
Bisketalization of **26** (22 mg, 0.08 mmol) gave **35** (26 mg, 89%): ^1H NMR δ: 3.95–3.80 (8H, m, H_2CO (×4), H_2CN, HC-7), 3.19 (1H, ddd, *J* = 2.5, 3, 4 Hz, HC-1), 2.96 (1H, ddd, *J* = 2.5, 6, 10 Hz, HC-7), 2.80 (1H, dd, *J* = 2, 11 Hz, HC-3$_{anti}$), 2.60 (1H, d, *J* = 11 Hz, HC-3$_{syn}$), 2.30 (1H, dd, *J* = 3, 12 Hz, HC-6), 2.20 (1H, dd, *J* = 4, 12 Hz), 2.12 (1H, dd, *J* = 6, 14 Hz, HC-8$_{exo}$), 1.80 (1H, ddd, *J* = 2.5, 10, 14 Hz, HC-8$_{endo}$), 1.70-1.40 (4H, m), 1.28 (3H, s, H_3C). Desulfurization of **35** (26 mg, 0.073 mmol) gave **37** (21 mg, 88%): IR ν_{max}: 2953, 1735, 1202, 1168, 1087 cm^{-1}; ^1H NMR δ: 3.92 (8H, m, H_2CO), 3.65 (3H, s, H_3CO), 2.55–2.43 (1H, m, HC-8), 1.91–1.82 (1H, m), 1.80–1.65 (3H, m), 1.65–1.55 (6H, m), 1.33 (3H, s, H_3CC-2″), 0.83 (3H, s, H_3CC-6); LRMS (EI), *m/z* (relative intensity): 328 ([M]$^+$, 47), 313 (21), 297 (24), 285 (27), 284 (25), 243 (28), 253 (30), 241 (27), 227 (100).

(2′R, 8a′S*)-3-[1,2,3,4,6,7,8,8a-Octahydro-8a-methyl-6-oxonaphthalene-2-carbonyl]-2-oxazolidinone (**38**)* (7 mg, 83% from aldol cyclodehydration of **40**): IR ν_{max}: 2929, 1775, 1693, 1666, 1388, 1225 cm^{-1}; ^1H NMR δ: 5.80 (1H, br s, HC-5′), 4.46-4.37 (2H, m, HC-5), 4.12–3.94 (2H, m, HC-4), 3.75–3.65 (1H, m, HC-2′), 2.84–2.72 (1H, m, HC-4′), 2.53 (1H, ddd, *J* = 5, 14, 17.5 Hz, HC-7′), 2.39 (1H, ddd, *J* = 2, 4.5, 17.5 Hz, HC-7′), 2.31–2.20 (2H, m, H_2C-3′), 2.11 (1H, ddd, *J* = 5, 13.5, 14 Hz, HC-8′), 1.98 (1H, dd, *J* = 7.5, 14 Hz, HC-1′), 1.88–1.75 (1H, m, HC-4′), 1.75 (1H, dd, *J* = 4.5, 14 Hz, HC-1′), 1.69 (1H, ddd, *J* = 2.5, 5, 13.5 Hz, HC-8′); ^{13}C NMR δ: 199.1 (s, C-6′), 176.2 (s, O═CC-2′), 170.3 (s, C-4′a), 153.0 (s, C-2), 125.1 (d, C-5′), 62.1 (t, C-5), 43.0 (t, C-4), 41.6 (t, C-1′), 36.3 (t, C-7′), 36.1 (s, C-8a), 35.9 (d, C-2′), 34.1 (t), 28.7 (t), 26.2 (t), 23.6 (q, CH_3); LRMS (CI, NH_3), *m/z* (relative intensity): 295 ([M+18]$^+$, 21), 278 ([M+1]$^+$, 100).

Methyl (2R, 8aS*)-1,2,3,4,6,7,8,8a-octahydro-8a-methyl-6-oxonaphthalene-2-carboxylate* (**39**) (9 mg, 78% from aldol-cyclodehydration of **41**): IR ν_{max}: 2948, 1730, 1672, 1619, 1437, 1208 cm^{-1}; ^1H NMR δ: 5.76 (1H, br s, HC-5), 3.73 (3H, s, H_3CO), 2.75–2.63 (2H, m, HC-2, HC-4), 2.50 (1H, ddd, *J* = 6, 13.5, 17.5 Hz, HC-7), 2.40–2.28 (2H, m, HC-1, HC-7), 2.28–2.15 (2H, m, HC-3, HC-4), 1.82 (1H, ddd, *J* = 5, 13.5, 13.5 Hz, HC-8), 1.79 (1H, ddd, *J* = 3, 6, 13.5 Hz, HC-8), 1.72–1.58 (2H, m, HC-1, HC-3), 1.14 (3H, s, H_3CC); ^{13}C NMR δ: 199.2 (s, C-6), 175.4 (s, OC═O), 169.7 (s, C-4a), 124.7 (d, C-5), 51.9 (q, CH_3O), 41.7 (t), 37.4 (t), 37.1 (d, C-2), 36.0 (s, C-8a), 33.8 (t), 29.1 (t), 26.7 (t), 22.6 (q, CH_3C); LRMS (EI), *m/z* (relative intensity): 222 ([M]$^+$, 49), 194 (37), 180 (50), 163 (36), 121 (100).

(1′R, 3′S*)-3-[(3-Methyl-3-(3-oxobutyl)-4-oxo-cyclohexan-1-yl)carbonyl]-2-oxazolidinone (**40**)* A solution of **36** (13 mg, 0.034 mmol) and 5% HF (0.1 mL) in CH_3CN (2 mL) was stirred at rt for 30 min. The mixture was diluted with CH_2Cl_2, washed with 5% $NaHCO_3$ and water, dried over Na_2SO_4, concentrated, and fractionated by PTLC (10% ethyl acetate in ether) to give **40** (9 mg, 90%): IR ν_{max}: 2964, 1773, 1700, 1388, 1224 cm^{-1}; ^1H NMR δ: 4.44 (2H, ap t, *J* = 8 Hz, HC-5), 4.17 (1H, dddd, *J* = 3.5, 3.5, 12.5, 12.5 Hz, HC-1′), 4.02 (2H, m, HC-4), 2.66 (1H, ddd, *J* = 6, 14.5, 14.5 Hz, HC-5′), 2.55–2.40 (1H, m, HC-2″), 2.34 (1H, ddd, *J* = 2.5, 4.5, 14.5 Hz, HC-5′), 2.28–2.00 (4H, m), 2.12 (3H, s, H_3C-4″), 1.91 (1H, dddd, *J* = 4.5, 12.5, 13, 14.5 Hz, HC-6′), 1.74 (2H, m, HC-1″, HC-2′); ^{13}C NMR δ: 213.5 (s, C-4′), 207.6 (s, C-3″), 174.8 (s, O═CC-1′), 153.2 (s, C-2), 62.1 (t, C-5), 47.3 (s, C-3′), 42.8 (t, C-4), 41.6 (t), 37.8 (t), 37.3 (t), 37.0 (d, C-1′), 30.5 (t), 30.1 (q, C-4″), 28.9 (t), 21.9 (q, CH_3C-3′); LRMS (CI, NH_3), *m/z* (relative intensity): 313 ([M+18]$^+$, 84), 296 ([M+1]$^+$, 100), 183 (80).

Methyl (1R, 3S*)-3-methyl-3-(3-oxobutyl)-4-oxo-cyclohexan-1-carboxylate (**41**)*
A solution of **37** (21 mg, 0.064 mmol) and 5% HF (0.1 mL) in

[8] This reaction also gave **37** (2 mg, 13%).

© 1997 NRC Canada

Can. J. Chem. Downloaded from www.nrcresearchpress.com by 88.146.161.215 on 09/08/12
For personal use only.

CH_3CN (2 mL) was stirred at rt for 30 min. The mixture was diluted with CH_2Cl_2, washed with 5% Na_2CO_3 and water, dried over Na_2SO_4, concentrated, and fractionated by PTLC (10% ethyl acetate in ether) to give **41** (14 mg, 94%): IR ν_{max}: 2954, 1732, 1709, 1435, 1200 cm^{-1}; ^1H NMR δ: 3.68 (3H, s, J = 3.5, 12.5 Hz, H_3CO), 3.00 (1H, dddd, J = 3.5, 3.5, 12.5, 12.5 Hz, HC-1), 2.60–2.00 (7H, m), 2.11 (3H, s, H_3C-4′), 1.90–1.70 (2H, m), 1.66–1.54 (1H, m), 1.00 (3H, s, H_3CC-3); ^{13}C NMR δ: 213.5 (s, C-4), 207.6 (s, C-3′), 174.9 (s, OC═O), 52.0 (q, CH_3O), 47.1 (s, C-3), 42.0 (t), 37.9 (t), 37.8 (d, C-1), 37.2 (t), 30.7 (t), 30.1 (q, C-4′), 29.2 (t), 21.9 (q, CH_3C-3′); LRMS (CI, NH_3), *m/z* (relative intensity): 258 ([M+18]$^+$, 33), 241 ([M+1]$^+$, 100).

*Methyl (2*R**, 6*R**, 8a*S**)-1,2,3,4,6,7,8,8a-octahydro-8a-methyl-6-[(dimethyl(1,1-dimethylethyl)silyl)oxy]naphthalene-2-carboxylate (**43**)*

Method A: $NaBH_4$ (2 mg, 0.05 mmol) was added to a solution of **39** (2 mg, 0.009 mmol) in 50% CH_3OH – CH_2Cl_2 (0.8 mL) and the mixture was stirred at rt for 30 min. The mixture was diluted with CH_2Cl_2, washed with water, dried over Na_2SO_4, and concentrated to give the crude alcohol (2 mg). A solution of the alcohol, TBDMSCl (3.4 mg, 0.022 mmol), and imidazole (1.2 mg, 0.018 mmol) in CH_2Cl_2 (0.6 mL) was stirred at rt for 16 h. The mixture was diluted with CH_2Cl_2, washed with water, dried over Na_2SO_4, and concentrated to give the crude TBDMS ether (3 mg), which was identical by TLC and by ^1H NMR with the product obtained from **45** as described below.

Method B: (16 mg, 85% from desulfurization of **45**): IR ν_{max}: 2932, 1735, 1471, 1204, 1158, 1130 cm^{-1}; ^1H NMR δ: 5.26 (1H, br s, HC-5), 4.25–4.18 (1H, m, HC-6), 3.69 (3H, s, H_3CO), 2.65–2.58 (1H, m, HC-2), 2.52–2.38 (1H, m, HC-4), 2.26 (1H, dddd, J = 2.5, 2.5, 2.5, 13 Hz, HC-3), 2.14 (1H, ddd, J = 2.5, 2.5, 13.5 Hz, HC-1), 1.95–1.85 (1H, m, HC-4), 1.81–1.70 (1H, m, HC-7), 1.60–1.25 (5H, m), 0.98 (3H, s, H_3CC), 0.90 (9H, s, $(H_3C)_3$), 0.08 (3H, s, H_3CSi), 0.07 (3H, s, H_3CSi); ^{13}C NMR δ: 176.1 (s, C═O), 144.2 (s, C-4a), 125.3 (d, C-5), 69.0 (d, C-6), 51.5 (q, CH_3O), 42.9 (t, C-1), 37.8 (d, C-2), 37.4 (t), 35.0 (s, C-8a), 29.0 (t), 28.8 (t), 28.0 (t), 26.0 (q, $(CH_3)_3$), 23.9 (q, CH_3C), 18.4 (s, CSi), −4.4 (q, CH_3Si), −4.5 (q, CH_3Si); LRMS (EI), *m/z* (relative intensity): 338 ([M]$^+$, 14), 281 (54), 207 (20), 147 (100), 105 (36), 91 (35), 75 (54).

*Methyl (3*R**, 6*S**, 8a*R**, 10*R**)-3,4,7,8-tetrahydro-6-hydroxy-6H-3,8a-ethano-1H-2-benzothiopyran-10-carboxylate (**44**a)*

$NaBH_4$ (ca. 10 mg, 0.26 mmol) was added in one portion to a stirred solution of **26** (32 mg, 0.13 mmol) in 50% CH_3OH in CH_2Cl_2 (3 mL) at rt. The mixture was stirred for 30 min and then was diluted with CH_2Cl_2, washed with water, dried over Na_2SO_4, concentrated, and fractionated by MPC (40% ethyl acetate in hexane) to give **44***b* (17.5 mg, 54%) and **44***a* (12 mg, 37%): IR ν_{max}: 3388, 2930, 1736, 1666, 1434, 1203, 1180 cm^{-1}; ^1H NMR δ: 5.63 (1H, ddd, J = 2, 2, 3.5 Hz, HC-5), 4.21–4.15 (1H, m, HC-6), 3.74 (3H, s, CH_3O), 3.21 (1H, ddd, J = 3, 3, 3 Hz, HC-3), 2.96 (1H, ddd, J = 3, 6, 11 Hz, HC-10), 2.85–2.75 (2H, m, H_2C-4), 2.70 (1H, dd, J = 2.5, 10.5 Hz, HC-1_{anti}), 2.56 (1H, d, J = 10.5 Hz, HC-1_{syn}), 2.23 (1H, dd, J = 6, 13.5 Hz, HC-9_{exo}), 1.90 (1H, m, HC-7), 1.79 (1H, ddd, J = 3, 11, 13.5 Hz, HC-9_{endo}), 1.68–1.54 (2H, m, HC-7, HC-8), 1.47–1.34 (1H, m, HC-8); ^{13}C NMR δ: 173.8 (s, OC═O), 141.1 (s, C-4a), 125.3 (d, C-5), 65.2 (d, C-6), 52.1 (q, CH_3O), 44.9 (d, C-10), 38.5 (t, C-4), 34.9 (d, C-3), 34.4 (t, C-1), 33.3 (t), 32.3 (s, C-8a), 31.2 (t), 28.8 (t); LRMS (EI), *m/z* (relative intensity): 254 ([M]$^+$, 52), 223 (11), 192 (12), 175 (21), 147 (100), 134 (76), 131 (38), 91 (74).

*Methyl (3*R**, 6*R**, 8a*R**, 10*R**)-3,4,7,8-tetrahydro-6-hydroxy-6H-3,8a-ethano-1H-2-benzothiopyran-10-carboxylate (**44**b)*: IR ν_{max}: 3383, 2931, 1731, 1666, 1433, 1201, 1012 cm^{-1}; ^1H NMR δ: 5.62 (1H, br s, HC-5), 4.22–4.13 (1H, m, HC-6), 3.74 (3H, s, H_3CO), 3.20 (1H, ddd, J = 3, 3, 3 Hz, HC-3), 2.97 (1H, ddd, J = 3, 5, 11 Hz, HC-10), 2.85 (1H, br d, J = 17.5 Hz, HC-4), 2.70–2.65 (2H, m, HC-1_{anti}, HC-4), 2.61 (1H, d, J = 10 Hz, HC-1_{syn}), 2.21 (1H, dd, J = 5.5,13.5 Hz, HC-5_{exo}), 1.95–1.84 (1H, m, HC-7), 1.58 (4H, m, HC-5_{endo}, HC-7, H_2C-8); ^{13}C NMR δ: 173.8 (s, OC═O), 140.9 (s, C-4a), 125.7 (d, C-5), 65.9 (d, C-6), 52.0 (q, CH_3O), 45.0 (d, C-10), 38.5 (t), 34.7 (d, C-3), 34.6 (t), 33.2 (t), 32.2 (s, C-8a), 32.0 (t), 29.0 (t); LRMS (EI), *m/z* (relative intensity): 254 ([M]$^+$, 70), 236 (78), 223 (19), 147 (87), 129 (93), 91 (100).

*Methyl (3*R**, 6*R**, 8a*R**, 10*R**)-3,4,7,8-tetrahydro-6-[(dimethyl(1,1-dimethylethyl)silyl)oxy]-6H-3,8a-ethano-1H-2-benzothiopyran-10-carboxylate (**45**)*

A solution of **44***b* (17 mg, 0.067 mmol), TBDMSCl (25 mg, 0.17 mmol), and imidazole (9 mg, 0.13 mmol) in CH_2Cl_2 (3 mL) was stirred at rt for 20 h. The mixture was diluted with CH_2Cl_2, washed with water, dried over Na_2SO_4, concentrated, and fractionated by FCC (10% ether in hexane) to give **45** (21.5 mg, 87%). IR ν_{max}: 2949, 1741, 1666, 1434, 1213, 1109, 1071 cm^{-1}; ^1H NMR δ: 5.49 (1H, br s, HC-5), 4.22–4.13 (1H, m, HC-6), 3.74 (3H, s, H_3CO), 3.17 (1H, ddd, J = 3, 3, 3 Hz, HC-3), 2.99 (1H, ddd, J = 3, 5, 11 Hz, HC-10), 2.90–2.80 (2H, m, HC-1_{anti}, HC-4), 2.69 (1H, ddd, J = 3, 5, 17 Hz, HC-4), 2.58 (1H, d, J = 10 Hz, HC-1_{syn}), 2.23 (1H, dd, J = 5, 13.5 Hz, HC-9_{exo}), 1.85–1.74 (1H, m, HC-7), 1.65–1.38 (4H, m, HC-7, H_2C-8, HC-9_{endo}), 0.89 (9H, s, $(H_3C)_3C$), 0.07 (3H, s, H_3CSi), 0.07 (3H, s, H_3CSi); ^{13}C NMR δ: 173.9 (s, OC═O), 138.8 (s, C-4a), 127.1 (d, C-5), 67.1 (d, C-6), 52.1 (q, CH_3O), 45.3 (d, C-10), 38.4 (t), 34.8 (d, C-4), 34.7 (t), 33.6 (t), 32.8 (t), 32.0 (t, C-8a), 29.4 (t), 26.0 (q, $(CH_3)_3$), 18.3 (s, $C(CH_3)_3$), −4.5 (q, CH_3Si); LRMS (EI), *m/z* (relative intensity): 368 ([M]$^+$, 17), 353 (32), 337 (100).

*Methyl (2*S**, 6*R**, 8a*S**)-1,2,3,4,6,7,8,8a-octahydro-8a-methyl-6-[(dimethyl(1,1-dimethylethyl)silyl)oxy]naphthalene-2-carboxylate (**46**)* (5 mg, 87% from desulfurization of **48**): IR ν_{max}: 2933, 1738, 1471, 1435, 1251, 1160, 1078 cm^{-1}; ^1H NMR δ: 5.26 (1H, br s, HC-5), 4.26–4.18 (1H, m, HC-6), 3.66 (3H, s, H_3CO), 2.67 (1H, dddd, J = 3.5, 3.5, 12.5, 12.5 Hz, HC-2), 2.28–2.12 (1H, m, HC-4), 2.10–1.95 (2H, m, HC-1, HC-4), 1.85–170 (2H, m, HC-1, HC-3), 1.65–1.30 (5H, m), 1.12 (3H, s, H_3CC), 0.90 (9H, s, $(H_3C)_3$), 0.09 (3H, s, CH_3Si), 0.08 (3H, s, CH_3Si); ^{13}C NMR δ: 176.2 (s, C═O), 142.8 (s, C-4a), 125.8 (d, C-5), 68.9 (d, C-6), 51.6 (q, CH_3O), 44.4 (t, C-1), 39.4 (d, C-2), 37.4 (t), 34.7 (s, C-8a), 31.1 (t), 30.6 (t), 29.2 (t), 26.0 (q, $(CH_3)_3$), 23.8 (q, CH_3C), 18.4 (s, CSi), −4.4 (q, CH_3Si), −4.6 (q, CH_3Si); LRMS (CI, NH_3), *m/z* (relative intensity): 339 ([M+1]$^+$, 2), 282 (5), 208 (100).

© 1997 NRC Canada

Can. J. Chem. Downloaded from www.nrcresearchpress.com by 88.146.161.215 on 09/08/12
For personal use only.

Methyl (3R, 6R*, 8aR*, 10S*)-3,4,7,8-tetrahydro-6-hydroxy-6H-3,8a-ethano-1H-2-benzothiopyran-10-carboxylate (**47**b)*

$NaBH_4$ (ca. 5 mg, 0.13 mmol) was added in one portion to a stirred solution of **29** (20 mg, 0.079 mmol) in 50% CH_3OH in CH_2Cl_2 (2 mL) at rt. The mixture was stirred for 30 min and then was diluted with CH_2Cl_2, washed with water, dried over Na_2SO_4, concentrated, and fractionated by MPC (40% ethyl acetate in hexane) to give **47***a* (5 mg, 25%) and **47***b* (13 mg, 65%): IR ν_{max}: 3384, 2930, 1732, 1450, 1433, 1226, 1196 cm^{-1}; ^1H NMR δ: 5.55 (1H, br s, HC-5), 4.22–4.14 (1H, m, HC-6), 3.69 (3H, s, H_3CO), 3.28 (1H, dddd, J = 2, 2, 7, 10.5 Hz, HC-10), 3.12 (1H, ddd, J = 3, 3, 3 Hz, HC-3), 2.90 (1H, dd, J = 2.5, 10.5 Hz, HC-1_{anti}), 2.75–2.58 (2H, m, H_2C-4), 2.60 (1H, d, J = 10.5 Hz, HC-1_{syn}), 2.20–1.95 (1H, m, HC-7), 1.94 (1H, ddd, J = 2.5, 7, 13.5 Hz, HC-9_{exo}), 1.80 (1H, dd, J = 10.5, 13.5 Hz, HC-9_{endo}), 1.54 (3H, m, HC-7, H_2C-8); ^{13}C NMR δ: 173.9 (s, OC=O), 140.3 (s, C-4a), 126.0 (d, C-5), 66.6 (d, C-6), 52.1 (q, CH_3O), 45.8 (d, C-10), 34.8 (t), 34.5 (t), 34.4 (t), 33.6 (d, C-3), 32.8 (s, C-8a), 32.6 (t), 29.3 (t); LRMS (EI), *m/z* (relative intensity): 254 ([M]$^+$, 38), 236 (38), 195 (23), 150 (40), 147 (84), 129 (55), 91 (100).

Methyl (3R, 6R*, 8aR*, 10S*)-3,4,7,8-tetrahydro-6-[(dimethyl(1,1-dimethylethyl)silyl)oxy]-6H-3,8a-ethano-1H-2-benzothiopyran-10-carboxylate (**48**)*

A solution of **47***b* (10 mg,0.039 mmol), TBDMSCl (15 mg, 0.098 mmol), and imidazole (3.4 mg, 0.05 mmol) in CH_2Cl_2 (3 mL) was stirred at rt for 20 h. The mixture was diluted with CH_2Cl_2, washed with water, dried over Na_2SO_4, concentrated, and fractionated by FCC (5% ether in hexane) to give **48** (12.8 mg, 89%): IR ν_{max}: 2950, 2930, 1735, 1471, 1434, 1094, 1068 cm^{-1}; ^1H NMR δ: 5.42 (1H, br s, HC-5), 4.22–4.13 (1H, m, HC-6), 3.69 (3H, s, H_3CO), 3.28 (1H, br dd, J = 7, 10 Hz, HC-10), 3.10 (1H, ddd, J = 2.5, 3, 3 Hz, HC-3), 2.95 (1H, dd, J = 2, 10 Hz, HC-1_{anti}), 2.72–2.58 (2H, m, H_2C-4), 2.58 (1H, d, J = 10 Hz, HC-1_{syn}), 1.90 (1H, ddd, J = 2, 7, 13.5 Hz, HC-9_{endo}), 1.83–1.74 (2H, m, HC-4, HC-9_{exo}), 1.65–1.40 (3H, m, H_2C-7, HC-8), 0.89 (9H, s, $(H_3C)_3C$), 0.07 (6H, s, H_3CSi); ^{13}C NMR δ: 174.0 (s, OC=O), 138.4 (s, C-4a), 127.3 (d, C-5), 67.7 (d, C-6), 52.1 (q, CH_3O), 46.0 (d, C-10), 34.9 (t), 34.6 (t), 34.4 (t), 33.6 (d, C-3), 33.2 (t), 32.6 (s, C-8a), 29.5 (t), 26.0 (q, $(CH_3)_3C$), 18.3 (s, CSi), −4.5 (q, CH_3Si); LRMS (EI), *m/z* (relative intensity): 368 ([M]$^+$, 2), 312 (64), 280 (17), 238 (29), 237 (81), 178 (26), 162 (63), 143 (54), 75 (100).

Acknowledgements

Financial support from the Natural Sciences and Engineering Research Council of Canada is gratefully acknowledged.

References

1. (*a*) F. Fringuelli and A. Taticchi. *In* Dienes in the Diels–Alder reaction. Wiley, New York. 1990; (*b*) W. Carruthers. *In* Cycloaddition reactions in organic synthesis. Pergamon, Oxford. 1990; (*c*) G. Desimoni, G. Tacconi, A. Barcoa, and G. P. Pollini. *In* Natural product synthesis through pericyclic reactions. ACS Mongraph 180. American Chemical Society, Washington. 1983; (*d*) B.M. Trost and I. Fleming (*Editors*). Comprehensive organic synthesis. Vol. 5. Pergamon Press, Oxford. 1991. Chap. 4.
2. (*a*) J.G. Martin and R.K. Hill. Chem. Rev. **61**, 537 (1961); (*b*) J. Sauer. Angew. Chem. Int. Ed. Engl. **6**, 16 (1967).
3. (*a*) D.E. Ward, W.M. Zoghaib, C.K. Rhee, and Y. Gai. Tetrahedron Lett. **31**, 845 (1990); (*b*) D.E. Ward, Y. Gai, and W.M. Zoghaib. Can. J. Chem. **69**, 1487 (1991); (*c*) D.E. Ward and Y. Gai. Tetrahedron Lett. **33**, 1851 (1992); (*d*) Can. J. Chem. **70**, 2627 (1992); (*e*) D.E. Ward and T.E. Nixey. Tetrahedron Lett. **34**, 947 (1993); (*f*) D.E. Ward, Y. Gai, and Y. Lai. Synlett, 261 (1996); (*g*) D.E. Ward, T.E. Nixey, Y. Gai, M.J. Hrapchak, and M.S. Abaee. Can. J. Chem. **74**, 1418 (1996).
4. T.K. Devon and A.I. Scott. Handbook of naturally occurring compounds. Vol. 2. Academic Press, New York. 1975.
5. J. Apsimon (*Editor*). Total synthesis of natural products. Wiley, New York. Vol. 2. 1973; Vol. 5. 1983; Vol. 6. 1984.
6. T.A. Engler, U. Sampath, S. Naganathan, D. Vander Velde, and F. Takusagawa. J. Org. Chem. **54**, 2712 (1989).
7. E. Vedejs, T.H. Eberlein, D.J. Mazur, C.K. McClure, D.A. Perry, R. Ruggeri, E. Schwartz, J.S. Stults, D.L. Varie, R.G. Wilde, and S. Wittenberger. J. Org. Chem. **51**, 1556 (1986).
8. A.J. Birch and K.P. Dastur. J. Chem. Soc. Perkin Trans. 1, 1650 (1973).
9. P. Duhamel, L. Hennequin, J.M. Poirier, G. Tavel, and C. Vottero. Tetrahedron, **42**, 4777 (1986).
10. T. Harayama and M. Otsuyama. Yagugaku Zasshi, **103**, 1096 (1983).
11. T.G. Back, D.L. Baron, and K. Yang. J. Org. Chem. **58**, 2407 (1993).
12. J. Malek. Org. React. **34**, 1 (1985).
13. W.C. Still, M. Kahn, and A. Mitra. J. Org. Chem. **43**, 2923 (1978).
14. D.F. Taber. J. Org. Chem. **47**, 1351 (1982).
15. D.W. Brown, T.T. Nakashima, and D.L. Rabenstein. J. Magn. Reson. **45**, 302 (1981).
16. I. Paterson and I. Fleming. Tetrahedron Lett. 995 (1979).
17. A.J.H. Labuschagne, J.S. Malherbe, C.J. Meyer, and D.F. Schneider. J. Chem. Soc. Perkin Trans. 1, 955 (1978).
18. D.A. Evans, K.T. Chapman, and J. Bisaha. J. Am. Chem. Soc. **110**, 1238 (1988).
19. S.S. Al-Hassan, R.J. Cameron, A.W.C. Curran, W.J.S. Lyall, S.N. Nicholson, D.R. Robinson, A. Stuart, C.J. Suckling, I. Stirling, and H.C.S. Wood. J. Chem. Soc. Perkin Trans. 1, 1645 (1985).
20. J. Savard and P. Brassard. Tetrahedron, **40**, 3455, (1984).
21. R. Mozingo. Org. Synth. Collect. Vol. **3**, 181 (1955).

© 1997 NRC Canada

Copper(I) chloride-mediated oxidative coupling of alkenyltrialkylstannyl functions: efficient stereocontrolled syntheses of uniquely functionalized conjugated diene systems

Edward Piers, Ernest J. McEachern, Miguel A. Romero, and Patricia L. Gladstone

Abstract: Treatment of the β-trialkylstannyl α,β-unsaturated esters **1–9** with 2.5 equivalents of copper(I) chloride in *N,N*-dimethylformamide at room temperature results in the efficient, stereocontrolled production of the highly functionalized conjugated dienes **10–18**, respectively. In each of these oxidative couplings, production of 1 equivalent of product is accompanied by the formation of 2 equivalents of both the trialkylstannyl chloride and copper metal.

Key words: alkenyltrialkylstannanes, copper(I) chloride, transmetalation, conjugated dienes, oxidative coupling, β-trialkylstannyl α,β-unsaturated esters, substituted dialkyl muconates, organostannane, organocopper.

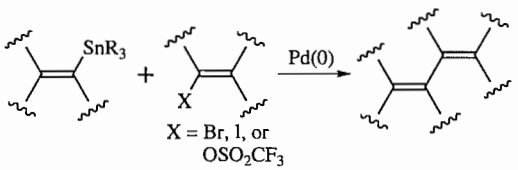
Résumé : La réaction des esters β-trialkylstannyl-α,β-insaturés **1–9** avec 2,5 équivalents de chlorure cuivreux, dans le *N,N*-diméthylformamide, à la température ambiante, conduit à la formation efficace et stéréocontrôlée des dienes conjugués hautement fonctionnalisés **10–18** respectivement. Dans chacun de ces couplages oxydants, la production d'un équivalent de produit s'accompagne de la formation de deux équivalents respectivement de chlorure de trialkylstannyle et de cuivre métallique.

Mots clés : alcénytrialkylstannanes, chlorure cuivreux, transmétalation, dienes conjugués, couplage oxydant, esters β-trialkylstannyl-α,β-insaturés, muconates de dialkyle substitués, organostannane, organocuivre.

[Traduit par la rédaction]

Introduction

The palladium(0)-catalyzed intermolecular cross-couplings represented in general terms by eq. [1], collectively known as the Stille coupling, are now well known protocols for the stereospecific syntheses of conjugated diene systems (1–5). Indeed, both the inter- and intramolecular versions of this process have been employed effectively in the synthesis of a wide variety of structurally complex organic compounds (1–5). In 1990, an important paper by Liebeskind and Fengl (6) disclosed that Pd(0)-catalyzed cross-couplings of alkenyltrialkylstannanes with alkenyl bromides and iodides are cocatalyzed by Cu(I) salts. This modified protocol, which generally leads to increased reaction rates and higher product yields, has been employed to advantage in a number of different contexts (see references 7–10 and citations therein) and has proven to be particularly good for successfully carrying out Stille-type couplings that are sluggish or inefficient under the "conventional" experimental conditions. A recent detailed study of this process led to very reasonable proposals regarding the cocatalytic role of Cu(I) in the overall coupling reaction (11).

[1] 

In 1993, a report (12) from this laboratory disclosed that *intra*molecular couplings of alkenyltrimethylstannane and alkenyl halide (I, Br) functions can be accomplished smoothly and efficiently by treatment of the requisite substrates with copper(I) chloride (~2–3 equivalents) in *N,N*-dimethylformamide (DMF). Examples are shown in eqs. [2] and [3]. The presence of a palladium(0) catalyst is not required and, in fact, we have subsequently found[2] that the CuCl-mediated processes are, in some instances, cleaner and more efficient than the corresponding Pd(0)-catalyzed transformations.

Very recently, a synthetically valuable extension to this

Received November 12, 1996.

This paper is dedicated to Professor William A. Ayer on the occasion of his 65th birthday.

E. Piers,[1] E.J. McEachern, M.A. Romero, and P.L. Gladstone. Department of Chemistry, University of British Columbia, 2036 Main Mall, University Campus, Vancouver, BC V6T 1Z1, Canada.

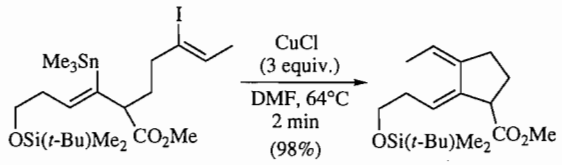
[1] Author to whom correspondence may be addressed. Telephone: (604) 822-3219. Fax: (604) 822-2847. E-mail: epier@unixg.ubc.ca

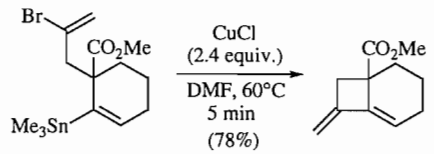
[2] E. Piers, T. Wong, and K.E. Ellis. Unpublished results.

© 1997 NRC Canada

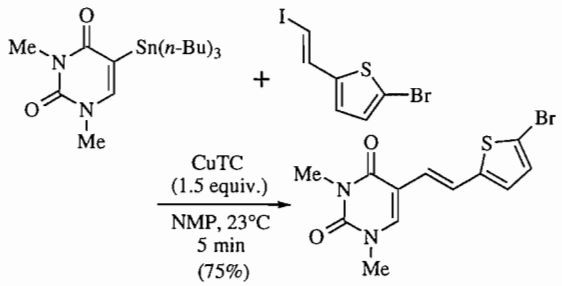
Can. J. Chem. Downloaded from www.nrcresearchpress.com by 88.146.161.215 on 09/08/12
For personal use only.

Can. J. Chem. Downloaded from www.nrcresearchpress.com by 88.146.161.215 on 09/08/12
For personal use only.

[2] 

[3] 

methodology was described by Allred and Liebeskind (13), who found that *inter*molecular cross-couplings of alkenyl- and aryltributylstannanes with alkenyl and aryl iodides can be successfully mediated by copper(I) thiophene-2-carboxylate (CuTC) in *N*-methylpyrrolidone (NMP). An example is provided in eq. [4].

[4] 

Further research in our laboratory related to the use of Cu(I)-mediated processes in organic synthesis has led to the discovery that CuCl also effects the inter- (14) and intramolecular (15) coupling of two alkenyltrimethylstannane functions. We report herein the details of a study (14) that revealed that treatment of alkyl 3-trialkylstannyl-2-alkenoates and alkyl 2-trimethylstannyl-1-cycloalkenecarboxylates with 2.5 equivalents of CuCl in DMF at room temperature results in the assembly of structurally novel, highly functionalized conjugated diene systems via the stereospecific coupling of the vinylic carbons bearing the R_3Sn function.

In connection with the results described in this paper, recent reports (16–21) emanating from other laboratories should be mentioned. Four of these reports (16–19) describe the *copper(II) nitrate*-mediated intermolecular coupling of alkenyltributylstannane functions, although the papers by Kyler and co-workers (16), Zhang et al. (17), and Crisp and Glink (18) collectively give a total of only seven examples. On the other hand, in the work by Quayle and co-workers (19), the carbon atom bearing the Bu_3Sn group was, in each of the substrates, also attached to a heteroatom (oxygen or sulfur) and, therefore, all the products possess either vinyl ether or vinyl sulfide linkages. The recent publications by Falck et al. (20) and Takeda et al. (21) describe the copper(I) salt-mediated cross-coupling of α-heteroatom-substituted *alkyl*tributylstannane functions with a variety of organic halides and the CuI-promoted *allylation* of alkenyltributylstannanes, respectively.

Results and discussion

The coupling reactions

The structural formulas of the substrates (**1–9**) employed in this study are shown in Table 1. In connection with our continuing investigations into the preparation and synthetic uses of alkenyltrialkylstannanes, compounds **1** (22), **2** (23), **3** (23), **4** (24), **5** (25), **6** (23), and **7** (26) have been reported previously. The cyclic unsaturated esters **8** and **9** were prepared via a method modified from that described by Piers and Tse (26). Thus, sequential treatment of each of the keto esters **19** and **20** with potassium hydride and *N*-phenyltrifluoromethanesulfonimide in dry tetrahydrofuran (THF) provided excellent yields of the corresponding alkenyl trifluoromethanesulfonates **21** and **22** (eq. [5]). When the latter two compounds were allowed to react with lithium (phenylthio)(trimethylstannyl)cuprate (27) in THF containing hexamethylphosphoramide (HMPA), the substrates **8** and **9** were obtained in yields of 90 and 82%, respectively.

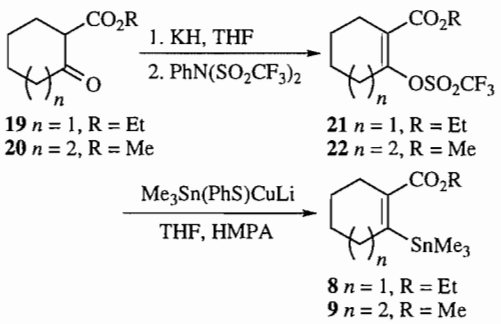
[5] 

Table 1 contains a summary of the coupling processes that were carried out during the course of this investigation. Addition of solid copper(I) chloride (2.5 equivalents) to a solution of ethyl (*Z*)-5-methyl-3-trimethylstannyl-2-hexenoate (**1**) in DMF, followed by stirring of the reaction mixture at room temperature for 1 h, provided diethyl (*Z*,*Z*)-3,4-bis(2-methylpropyl)muconate (**10**) in 96% yield (entry 1). In a very similar fashion, the β-trimethylstannyl α,β-unsaturated esters **2**, **3**, and **5–9** were transformed cleanly and efficiently into the corresponding functionalized dienes **11**, **12**, and **14–18** (entries 2, 3, and 5–9). Although we have not studied extensively the use of tributylstannanes in this research, the conversion of **4** into **13** (entry 4) indicates that this type of substrate can also be successfully employed in this coupling protocol.

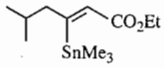
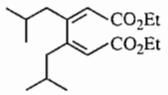
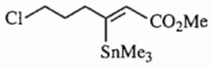
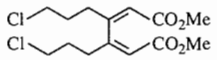
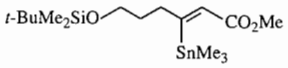
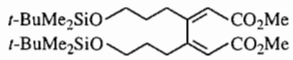
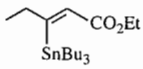
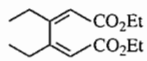
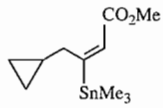
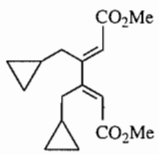
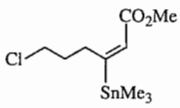
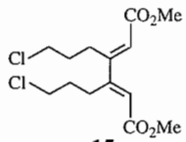
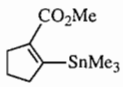
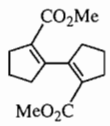
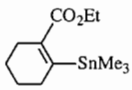
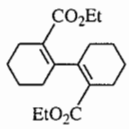
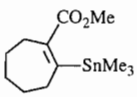
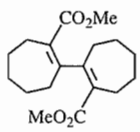
The results summarized in Table 1 show that the new coupling method is efficient and tolerates a variety of functional groups. From the viewpoint of synthesis, it is particularly noteworthy that the process occurs without loss of configurational integrity. Indeed, the data given in Table 1 show that the coupling process is stereospecific and that each of the reactions proceeds with retention of configuration at the alkenyl centers that are being coupled.

Of the products listed in Table 1, ethyl 2-(2-ethoxycarbonyl-1-cyclohexen-1-yl)-1-cyclohexenecarboxylate (**17**) (28) has been reported previously. The geometric configurations of the products **10–15** were established by use of nuclear magnetic resonance (NMR) spectroscopy. An examination of the ^1H and ^{13}C NMR spectra of the substances **10–15** shows clearly that each of the products possesses an element of symmetry. For example, the ^1H NMR spectrum of the diester **11** displays a 6-proton singlet for the two methoxy groups, a 2-proton triplet (J = 1 Hz) for the two olefinic hydrogens, and three 4-proton multiplets derived from the three magnetically different methylene units of the two 3-chloropropyl groups. In a similar vein, the ^{13}C NMR spectrum of **11** contains reso-

© 1997 NRC Canada

Can. J. Chem. Downloaded from www.nrcresearchpress.com by 88.146.161.215 on 09/08/12
For personal use only.

Table 1. Intermolecular coupling of alkenyltrialkylstannane functions.[a]

Entry	Starting material	Product (yield, %)	
1	 **1**	 **10**	(96)
2	 **2**	 **11**	(90)
3	 **3**	 **12**	(86)
4	 **4**	 **13**	(97)
5	 **5**	 **14**	(92)
6	 **6**	 **15**	(82)
7	 **7**	 **16**	(99)
8	 **8**	 **17**	(80)
9	 **9**	 **18**	(86)

[a]All the coupling reactions were carried out with 2.5 equivalents of CuCl in *N,N*-dimethylformamide at room temperature. The reaction time was 1 h in each case, except for the experiment summarized in entry 5; in this case, the reaction time was 2 h.

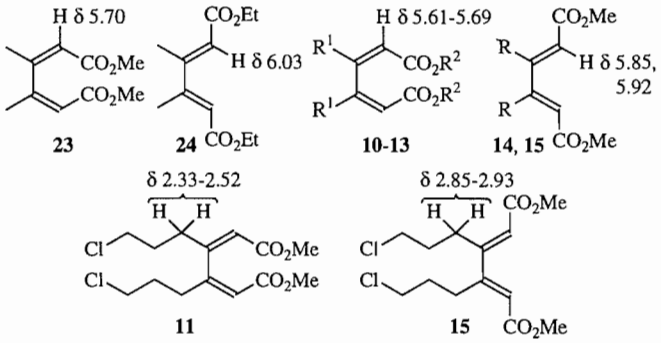
nances for only seven magnetically different carbon atoms. The ^{1}H and ^{13}C NMR spectra of the other acyclic products listed in Table 1 exhibit analogous characteristics.

In the ^{1}H NMR spectra ($CDCl_3$) of the known diesters **23** (29) and **24** (30), the olefinic protons resonate at δ 5.70 and 6.03, respectively. In the same solvent, the signals due to the olefinic hydrogens of compounds **10**–**13** appear at δ 5.63, 5.69, 5.68, and 5.61, respectively. On the other hand, the corresponding resonances in the spectra of **14** and **15** are found at δ 5.85 and 5.92, respectively. These data provide strong evi-

© 1997 NRC Canada

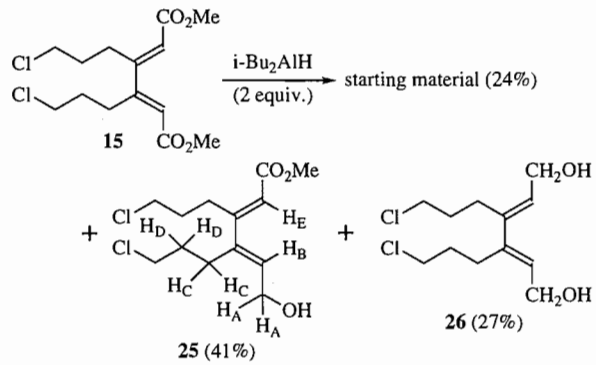
Can. J. Chem. Downloaded from www.nrcresearchpress.com by 88.146.161.215 on 09/08/12
For personal use only.

dence for the configurational assignments. It should also be noted that the protons of the allylic CH_2 groups in the (*Z,Z*)-diene **11** resonate at δ 2.33–2.52 (multiplet), while the corresponding protons of the (*E,E*)-diene **15** give rise to a multiplet at δ 2.85–2.93.[3] Since, in compounds **11** and **15**, the CH_2 groups in question are *trans* and *cis*, respectively, to the methoxycarbonyl group, the relative chemical shifts are as expected. Similar chemical shift patterns can be observed in the ^{1}H NMR spectra of substances **10** and **12–14**.



Further evidence for the structure of the diester **15** was obtained as follows. Treatment of this material with 2 equivalents of diisobutylaluminum hydride in diethyl ether at −78°C afforded a mixture consisting of the starting material **15**, the ester alcohol **25**, and the diol **26** (eq. [6]). Flash chromatography of this mixture on silica gel (31) provided, in addition to recovered **15** (24%), the two products **25** and **26** in yields of 41 and 27%, respectively. Key ^{1}H NMR nuclear Overhauser enhancement difference experiments were carried out on compound **25**. Thus, irradiation at δ 4.32 (doublet due to H_A protons)[3] caused enhancement of the signals derived from the olefinic proton H_B (triplet at δ 5.94) and the allylic protons H_C (triplet at δ 2.42). On the other hand, irradiation at δ 2.42 caused an increase in the intensity of each of the resonances at δ 1.74–1.83 (multiplet, H_D protons), 4.32, and 5.86 (singlet, H_E). These experiments clearly establish the configuration of **25** and confirm the earlier conclusions regarding the stereochemistry of the diester **15**.

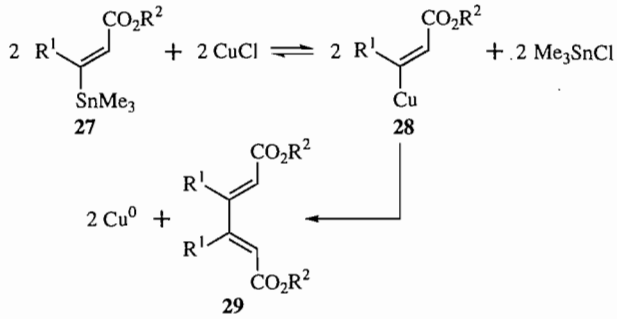
[6]



Mechanistic considerations

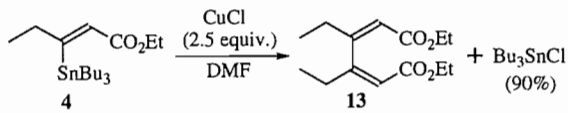
Detailed mechanistic studies related to the new coupling method have not been carried out. However, on the basis of observations derived from previous investigations (11, 13, 32), along with the results of experiments described below, it seems reasonable to propose, in a rather sketchy fashion, that the oxidative couplings take place via the pathway outlined in Scheme 1.

Scheme 1.



Liebeskind and co-workers (11) have shown that, in polar solvents, alkenyltrialkylstannanes undergo transmetalation with copper(I) halides to produce trialkylstannyl halides and, presumably, the corresponding alkenylcopper(I) derivatives. It has also been proposed that these reactions are reversible (13). The postulate that the overall coupling process is initiated by such a transmetalation process (initial equilibrium step shown in Scheme 1) was supported by an experiment involving the conversion of **4** into **13** (eq. [7]). Thus, flash chromatography (31) of the crude product derived from treatment of **4** with 2.5 equivalents of CuCl gave, in addition to the coupled product **13**, a 90% yield of tributylstannyl chloride.

[7]



Support for the reversible nature of the transmetalation step was obtained from a number of experiments. Scheme 1 suggests that the conversion of starting material to product should proceed to completion by treatment of the former with 1 equivalent of CuCl. However, experiments show that when this quantity of the reagent is employed, the reaction is initially quite facile but becomes very sluggish with time. For example, a solution of **1** in DMF was treated with 1 equivalent of CuCl and the progress of the reaction was monitored by periodic removal of aliquots, which were subjected to an appropriate work-up procedure and analysis by gas–liquid chromatography (GLC). After a period of 30 min, approximately 50% of the starting material **1** had been converted to the product **10**. However, a reaction time of ~14 h was required for complete consumption of the starting material.[4] On the other hand, use of 2.5 equivalents of CuCl alleviates this problem and the reaction proceeds to completion within a relatively short reaction time (Table 1, entry 1). The same is true of the other coupling reactions summarized in Table 1. Presumably, the function of the excess reagent (CuCl) is to push the equilibrium between **27** and **28** (Scheme 1) to the right.

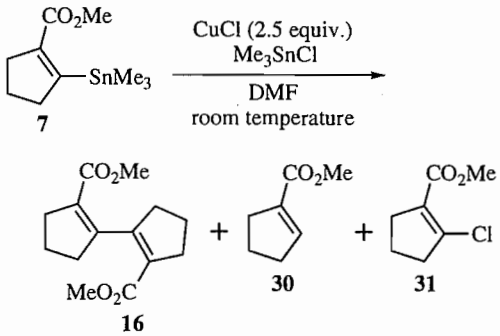
In connection with the conversion of substrate **7** into the diene diester **16**, it was demonstrated that addition of trimethylstannyl chloride to the reaction mixture prior to addi-

[3] The resonance assignments were readily confirmed by ^{1}H NMR COSY experiments.

[4] The isolated yield of the product **10** at this stage was ~90%.

© 1997 NRC Canada

tion of the CuCl reagent is also deleterious to the reaction efficiency (eq. [8]). In the absence of added Me_3SnCl, the reaction

[8] 

affords the product cleanly and efficiently (Table 1, entry 7). However, addition of the stannyl chloride decreased significantly the rate of consumption of the starting material **7**. Furthermore, under these conditions, the formation of the coupled product **16** was accompanied by the production of the protio- and chlorodestannylated products **30** and **31**, respectively.[5] For example, treatment of a solution of **7** in DMF with 1 equivalent of Me_3SnCl prior to the addition of 2.5 equivalents of CuCl increased the time necessary for consumption of the starting material from 1 h (Table 1, entry 7) to ~9 h. The product **16**, which was isolated in a yield of 75%, was accompanied by ~20% of a mixture of **30** and **31** in a ratio (GLC) of ~1:2, respectively. In a separate experiment, it was found that disappearance of the starting material **7** after addition of 2.5 equivalents of Me_3SnCl required ~20 h. In this case, the crude product consisted of **16** (isolated yield 57%) and a mixture (~35%) of **30** and **31** (ratio ~1:1.5). Although the overall role(s) that the added Me_3SnCl plays in these reactions is probably complex, it is reasonable to conclude that its function in decreasing the rate of starting material consumption is related primarily to shifting the equilibrium reaction shown in Scheme 1 to the left.

Observation of the reaction mixtures derived from the coupling processes summarized in Table 1 indicated that, in each case, copper metal was produced. The amount of Cu^0 formed per mmol of substrate employed was quantified by an experiment involving conversion of **1** into **10** (Table 1, entry 1). Suitable work-up of the reaction mixture derived from treatment of 1 equivalent of **1** with 2.5 equivalents of CuCl in DMF, followed by an appropriate analytical procedure (33), showed that 0.92 equivalents of Cu^0 had been produced. Thus, the coupling of two molecules of the alkenyltrimethylstannane **27** to produce one molecule of the diene **29** is accompanied by the production of two copper atoms (Scheme 1). Although, as discussed above, it seems likely that this process proceeds via the intermediacy of the alkenylcopper(I) species **28**, the mechanistic details of the transformation of **28** into **29** remain obscure.

[5] The presence of **30** and **31**, indicated by the ^1H NMR spectrum of the crude product, was confirmed by analysis of the mixture by GLC – high-resolution mass spectrometry, which showed the presence of three components with molecular masses 126.0684 (**30**, calcd. for $C_7H_{10}O_2$: 126.0681), 160.0291 (**31**, calcd. for $C_7H_9{}^{35}ClO_2$: 160.0291), and 250.1208 (**16**, calcd. for $C_{14}H_{18}O_4$: 250.1205).

Conclusion

The investigations described above show that copper(I) chloride effectively mediates the oxidative dimerization of β-trialkylstannyl α,β-unsaturated esters. This new coupling method should be of considerable value for the concise synthesis of usefully functionalized conjugated diene systems. Alkenyltrialkylstannanes possessing a wide variety of functionalized carbon skeletons are readily prepared (12, 22–27, 32, 34) and, therefore, several extensions to this work can be envisaged. A number of possibilities are currently being pursued.

Experimental

General information

Melting points and distillation temperatures (short-path Kugelrohr distillations) are uncorrected. Infrared (IR) spectra were recorded using potassium bromide pellets or liquid films on sodium chloride discs. Proton (^1H) and carbon (^{13}C) nuclear magnetic resonance (NMR) spectra were recorded using $CDCl_3$ solutions. Signal positions in ^1H NMR spectra were measured relative to signals for Me_4Si (δ 0) (internal standard) or $CHCl_3$ (δ 7.24), while resonances in ^{13}C NMR spectra were recorded relative to the signal for $CDCl_3$ (δ 77.0). Tin–hydrogen coupling constants (J_{Sn-H}) are given as the average of the ^{117}Sn and ^{119}Sn values. Molecular mass determinations (high-resolution mass spectrometry) for substances containing Me_3Sn are based on ^{120}Sn. Flash chromatography (31) was carried out with 230–400 mesh silica gel (E. Merck). Thin-layer chromatography (TLC) was accomplished with commercial aluminum-backed plates (E. Merck, Type 5554). Gas–liquid chromatography (GLC) was performed on instruments equipped with flame ionization detectors and 25 m × 0.20 mm fused silica columns coated with HP-5 (cross-linked 5% phenyl methyl silicone).

Petroleum ether refers to a mixture of alkanes with bp 35–60°C. Commercial copper(I) chloride (99.995%) and *N*-phenyltrifluoromethanesulfonimide were used without further purification.

Aqueous NH_4Cl–NH_4OH (pH 8) was prepared by the addition of ~50 mL of aqueous ammonia (58%) to ~950 mL of saturated aqueous NH_4Cl.

Note: Unless otherwise stated, all reactions were carried out under an atmosphere of dry argon in oven- (110°C) or flame-dried glassware.

General procedure 1. Preparation of the alkenyl trifluoromethanesulfonates 21 and 22

A suspension of KH (1.1 equiv.) in dry THF (~5 mL per mmol of substrate) was cooled to 0°C and the neat β-keto ester (**19** or **20**) (1 equiv.) was added dropwise. After the mixture had been stirred for 30 min, *N*-phenyltrifluoromethanesulfonimide (1.2 equiv.) was added as a solid in one portion and stirring was continued for 30 min at 0°C and for 1 h at room temperature. Petroleum ether (~1.5 mL per mmol of substrate) was added and the mixture was filtered through a plug of silica gel (~1.5 g per mmol substrate) presoaked with 1:1 petroleum ether – Et_2O. The silica gel was eluted with the same solvent mixture. The filtrate was concentrated and the crude oil was purified by flash chromatography on silica gel.

© 1997 NRC Canada

Can. J. Chem. Downloaded from www.nrcresearchpress.com by 88.146.161.215 on 09/08/12
For personal use only.

Can. J. Chem. Downloaded from www.nrcresearchpress.com by 88.146.161.215 on 09/08/12
For personal use only.

The following compounds were prepared via this general procedure.

*Ethyl 2-(trifluoromethanesulfonyloxy)-1-cyclohexene-carboxylate (**21**)*

Purification (flash chromatography, 230 g of silica gel, 95:5 to 3:1 petroleum ether – Et_2O) of the crude product obtained from 2-ethoxycarbonylcyclohexanone (5.32 g, 31.3 mmol) and *N*-phenyltrifluoromethanesulfonimide (12.8 g, 1.2 equiv.) gave 8.90 g (94%) of the alkenyl trifluoromethanesulfonate **21**, a colourless oil that displayed IR (neat): 1719, 1672, 1287, 1142, 1094, 1044, 916 cm^{-1}; ^1H NMR (400 MHz, $CDCl_3$) δ: 1.30 (t, 3H, J = 7 Hz), 1.60–1.70 (m, 2H), 1.71–1.85 (m, 2H), 2.35–2.42 (m, 2H), 2.43–2.50 (m, 2H), 4.25 (q, 2H, J = 7 Hz); ^{13}C NMR (75 MHz, $CDCl_3$) δ: 14.0. 21.0, 22.2, 26.1, 28.5, 61.6, 120.4, 123.2, 151.3, 164.8. Exact Mass calcd. for $C_{10}H_{13}F_3O_5S$: 302.0436; found: 302.0435.

*Methyl 2-(trifluoromethanesulfonyloxy)-1-cycloheptene-carboxylate (**22**)*

This compound was prepared from 2-methoxycarbonylcycloheptanone (2.94 g, 17.3 mmol) and *N*-phenyltrifluoromethanesulfonimide (7.62 g, 1.2 equiv.). Flash chromatography of the crude product on silica gel (150 g, petroleum ether to 95:5 petroleum ether – Et_2O) gave 4.94 g (95%) of **22** as a colourless oil that exhibited IR (neat): 1728, 1659, 1423, 1249, 1212, 1141, 1003, 867 cm^{-1}; ^1H NMR (400 MHz, $CDCl_3$) δ: 1.60–1.79 (m, 6H), 2.49–2.59 (m, 4H), 3.78 (s, 3H); ^{13}C NMR (75 MHz, $CDCl_3$) δ: 23.7, 25.2, 28.0, 30.7, 34.0, 52.3, 118.3, 127.8, 155.0, 166.1. Exact Mass calcd. for $C_{10}H_{13}F_3O_5S$: 302.0436; found: 302.0431. Anal. calcd. for $C_{10}H_{13}F_3O_5S$: C 39.74, H 4.33, S 10.61; found: C 39.97, H 4.41, S 10.57.

General procedure 2. Preparation of the alkenyltrimethylstannanes 8 and 9

To a cold (−20°C), stirred solution of lithium (phenylthio)(trimethylstannyl)cuprate (27) (1.5 equiv.) in dry THF (~15 mL per mmol of substrate) was added a solution of the alkenyl trifluoromethanesulfonate (**21** or **22**) (1 equiv.) in dry THF (~0.7 mL per mmol of substrate). After the mixture had been stirred at −20°C for 1 h, dry HMPA (2 equiv.) was added, the mixture was allowed to warm to 0°C, and was stirred for an additional 1 h. Saturated aqueous ammonium chloride (~14 mL per mmol of substrate) and 4:1 petroleum ether – Et_2O (~14 mL per mmol substrate) were added and the mixture was stirred until the organic layer was colourless. The mixture was filtered to remove the solid material. The filtrate was washed (saturated aqueous copper(II) sulfate, water, brine), dried ($MgSO_4$), and concentrated. The crude product was purified by flash chromatography on silica gel followed, for compound **8**, by distillation.

The following compounds were prepared via this general procedure.

*Ethyl 2-(trimethylstannyl)-1-cyclohexenecarboxylate (**8**)*

Flash chromatography (220 g of silica gel, 4:1 petroleum ether – benzene) of the crude product derived from the alkenyl trifluoromethanesulfonate **21** (8.90 g, 29.5 mmol), followed by distillation (85–95°C/0.1 Torr) of the derived oil, provided 8.41 g (90%) of **8** as a colourless oil that showed IR (neat): 1694, 1593, 1448, 1367, 1250, 1056, 768 cm^{-1}; ^1H NMR (400 MHz, $CDCl_3$) δ: 0.08 (s, 9H, $^2J_{Sn-H}$ = 54 Hz), 1.26 (t, 3H, J = 7 Hz), 1.50–1.69 (m, 4H), 2.26–2.43 (m, 4H), 4.16 (q, 2H, J = 7 Hz); ^{13}C NMR (75 MHz, $CDCl_3$) δ: −7.4, 14.3, 22.2, 22.8, 26.4, 33.9, 60.6, 136.0, 163.1, 169.0. Exact Mass calcd. for $C_{11}H_{19}O_2Sn$ (M^+ − Me): 303.0407; found: 303.0401. Anal. calcd. for $C_{12}H_{22}O_2Sn$: C 45.27, H 7.00; found: C 45.39, H 7.16.

*Methyl 2-(trimethylstannyl)-1-cycloheptenecarboxylate (**9**)*

This substance was prepared from the alkenyl trifluoromethanesulfonate **22** (2.52 g, 8.34 mmol). Flash chromatography of the crude product on silica gel (53 g, petroleum ether to 30:1 petroleum ether – Et_2O) afforded 2.17 g (82%) of **9** as a colourless oil that exhibited IR (neat): 1694, 1583, 1435, 1281, 1259, 1205, 1156, 1071, 769 cm^{-1}; ^1H NMR (400 MHz, $CDCl_3$) δ: 0.09 (s, 9H, $^2J_{Sn-H}$ = 53 Hz), 1.38–1.45 (m, 4H), 1.75–1.81 (m, 2H), 2.53–2.63 (m, 4H), 3.70 (s, 3H); ^{13}C NMR (75 MHz, $CDCl_3$) δ: −6.8, 24.8, 26.0, 28.3, 32.6, 34.8, 51.9, 143.5, 169.7, 170.0. Exact Mass calcd. for $C_{11}H_{19}O_2Sn$ (M^+ − Me): 303.0407; found: 303.0407. Anal. calcd. for $C_{12}H_{22}O_2Sn$: C 45.27, H 7.00; found: C 45.35, H 6.97.

General procedure 3. Copper(I) chloride–mediated coupling reactions

To a stirred solution of the alkenyltrialkylstannane in DMF (~0.5 mL per mmol of substrate) at room temperature was added solid copper(I) chloride (2.5 equiv.) and the resulting brown solution was stirred for 1 h. Aqueous NH_4Cl–NH_4OH (pH 8, the same volume as DMF) was added and the mixture was stirred, open to the atmosphere, until the aqueous phase turned deep blue. The phases were separated and the aqueous layer was extracted three times with Et_2O. The combined organic extracts were washed (water, brine), dried ($MgSO_4$), and concentrated. The crude product was purified by flash chromatography on silica gel.

The following compounds were prepared via this general procedure.

*Diethyl (Z,Z)-3,4-bis(2-methylpropyl)muconate (**10**)*

This material was synthesized from ethyl (*Z*)-5-methyl-3-trimethylstannyl-2-hexenoate (**1**) (250 mg, 0.78 mmol). Flash chromatography of the crude oil on silica gel (10 g, 4:1 pentane–Et_2O) afforded 117 mg (96%) of **10**, a colourless oil that displayed IR (neat): 1724, 1653, 1619, 1467, 1176, 1063 cm^{-1}; ^1H NMR (400 MHz, $CDCl_3$) δ: 0.94 (br signal, 12H), 1.20 (t, 6H, J = 7 Hz), 1.87 (m, 2H, J = 7 Hz), 1.95–2.08 (br m, 2H), 2.22–2.35 (br m, 2H), 4.06 (q, 4H, J = 7 Hz), 5.63 (t, 2H, J = 1 Hz); ^{13}C NMR (50.3 MHz, $CDCl_3$) δ: 14.2, 22.7, 25.5, 46.4, 59.7, 115.1, 159.9, 165.4. Exact Mass calcd. for $C_{18}H_{30}O_4$: 310.2144; found: 310.2148. Anal. calcd. for $C_{18}H_{30}O_4$: C 69.64, H 9.74; found: C 69.86, H 9.74.

*Dimethyl (Z,Z)-3,4-bis(3-chloropropyl)muconate (**11**)*

This compound was prepared from methyl (*Z*)-6-chloro-3-trimethylstannyl-2-hexenoate (**2**) (140 mg, 0.43 mmol). Flash chromatography of the crude product on silica gel (10 g, 4:1 pentane–Et_2O) afforded 63 mg (90%) of **11**, a colourless oil that showed IR (neat): 1724, 1621, 1435, 1176, 1040, 871, 654 cm^{-1}; ^1H NMR (400 MHz, $CDCl_3$) δ: 1.91–2.05 (br m, 4H), 2.33–2.52 (br m, 4H), 3.50–3.59 (br m, 4H), 3.60 (s, 6H), 5.69 (t, 2H, J = 1 Hz); ^{13}C NMR (50.3 MHz, $CDCl_3$) δ: 29.7, 34.2,

© 1997 NRC Canada

Can. J. Chem. Downloaded from www.nrcresearchpress.com by 88.146.161.215 on 09/08/12
For personal use only.

44.2, 51.2, 114.9, 159.4, 165.6. Exact Mass calcd. for $C_{14}H_{20}{}^{35}Cl_2O_4$: 322.0739; found: 322.0731. Anal. calcd. for $C_{14}H_{20}Cl_2O_4$: C 52.03, H 6.24; found: C 52.20, H 6.24.

*Dimethyl (Z,Z)-3,4-bis(3-(*tert*-butyldimethylsiloxy)propyl)-muconate (**12**)*

Flash chromatography (2 g of silica gel, 9:1 to 3:2 pentane–Et_2O) of the crude oil obtained from methyl (*Z*)-6-(*tert*-butyldimethylsiloxy)-3-trimethylstannyl-2-hexenoate (**3**) (104 mg, 0.25 mmol) provided 55 mg (86%) of **12**, a colourless oil that exhibited IR (neat): 1732, 1655, 1621, 1473, 1436, 1256, 1105, 836 cm^{-1}; ^1H NMR (400 MHz, $CDCl_3$) δ: 0.01 (s, 12H), 0.85 (s, 18H), 1.65–1.80 (m, 4H), 2.21–2.46 (m, 4H), 3.51–3.70 (m, 4H), 3.60 (s, 6H), 5.68 (s, 2H); ^{13}C NMR (50.3 MHz, $CDCl_3$) δ: −5.3, 18.2, 25.9, 30.1, 33.8, 51.0, 62.3, 113.8, 161.9, 165.8. Exact Mass calcd. for $C_{26}H_{50}O_6Si_2$: 514.3146; found: 514.3146. Anal. calcd. for $C_{26}H_{50}O_6Si_2$: C 60.66, H 9.80; found: C 60.76, H 9.76.

*Diethyl (Z,Z)-3,4-diethylmuconate (**13**)*

Purification (flash chromatography, 10 g of silica gel, 4:1 pentane–Et_2O) of the crude product obtained from ethyl (*Z*)-3-tributylstannyl-2-pentenoate (**4**) (207 mg, 0.50 mmol) gave 74 mg (97%) of **13**, a colourless oil that displayed IR (neat): 1719, 1655, 1620, 1300, 1176, 811 cm^{-1}; ^1H NMR (400 MHz, $CDCl_3$) δ: 1.08 (t, 6H, *J* = 7 Hz), 1.18 (t, 6H, *J* = 7 Hz), 2.08–2.46 (br m, 4H), 4.04 (q, 4H, *J* = 7 Hz), 5.61 (t, 2H, *J* = 1 Hz); ^{13}C NMR (50.3 MHz, $CDCl_3$) δ: 11.2, 14.1, 30.2, 59.7, 113.2, 163.5, 165.6. Exact Mass calcd. for $C_{14}H_{22}O_4$: 254.1518; found: 254.1512. Anal. calcd. for $C_{14}H_{22}O_4$: C 66.12, H 8.72; found: C 66.33, H 8.84.

*Dimethyl (E,E)-3,4-bis(cyclopropylmethyl)muconate (**14**)*

Note: The reaction time in this case was 2 h. Flash chromatography (10 g of silica gel, 4:1 pentane–Et_2O) of the crude product derived from methyl (*E*)-4-cyclopropyl-3-trimethylstannyl-2-butenoate (**5**) (250 mg, 0.83 mmol) afforded 106 mg (92%) of **14**, a colourless oil that showed IR (neat): 1719, 1629, 1340, 1173, 1020, 872 cm^{-1}; ^1H NMR (400 MHz, $CDCl_3$) δ: 0.10–0.20 (m, 4H), 0.33–0.41 (m, 4H), 0.69–0.81 (m, 2H), 2.75 (d, 4H, *J* = 7 Hz), 3.66 (s, 6H), 5.85 (s, 2H); ^{13}C NMR (50.3 MHz, $CDCl_3$) δ: 4.8, 10.0, 33.3, 51.2, 117.5, 161.2, 166.5. Exact Mass calcd. for $C_{16}H_{22}O_4$: 278.1518; found: 278.1519. Anal. calcd. for $C_{16}H_{22}O_4$: C 69.04, H 7.97; found: C 69.15, H 8.02.

*Dimethyl (E,E)-3,4-bis(3-chloropropyl)muconate (**15**)*

This compound was derived from methyl (*E*)-6-chloro-3-trimethylstannyl-2-hexenoate (**6**) (250 mg, 0.77 mmol). Flash chromatography (10 g of silica gel, 4:1 pentane–Et_2O) of the crude oil afforded 102 mg (82%) of **15**, a colourless, crystalline solid (mp 52–53° C) that exhibited IR (KBr): 1709, 1601, 1438, 1340, 1178, 869, 539 cm^{-1}; ^1H NMR (400 MHz, $CDCl_3$) δ: 1.79–1.89 (m, 4H), 2.85–2.93 (m, 4H), 3.52 (t, 4H, *J* = 6 Hz), 3.69 (s, 6H), 5.92 (s, 2H); ^{13}C NMR (50.3 MHz, $CDCl_3$) δ: 26.5, 31.5, 44.5, 51.4, 119.3, 158.5, 166.1. Exact Mass calcd. for $C_{14}H_{20}{}^{35}Cl_2O_4$: 322.0739; found: 322.0739. Anal. calcd. for $C_{14}H_{20}Cl_2O_4$: C 52.03, H 6.24; found: C 52.02, H 6.40.

*Methyl 2-(2-methoxycarbonyl-1-cyclopenten-1-yl)-1-cyclopentenecarboxylate (**16**)*

This substance was prepared from methyl 2-(trimethylstannyl)-1-cyclopentenecarboxylate (**7**) (57 mg, 0.20 mmol). Flash chromatography of the crude product on silica gel (1 g, 9:1 to 3:2 pentane–Et_2O) afforded 25 mg (99%) of **16**, a colourless solid (mp 78–79°C) that displayed IR (KBr): 1718, 1667, 1604, 1439, 1257, 1050, 773 cm^{-1}; ^1H NMR (400 MHz, $CDCl_3$) δ: 1.94 (quintet, 4H, *J* = 8 Hz), 2.58–2.72 (m, 8H), 3.54 (s, 6H); ^{13}C NMR (50.3 MHz, $CDCl_3$) δ: 22.5, 33.4, 38.1, 51.2, 128.4, 154.4, 165.4. Exact Mass calcd. for $C_{14}H_{18}O_4$: 250.1205; found: 250.1200. Anal. calcd. for $C_{14}H_{18}O_4$: C 67.17, H 7.25; found: C 67.46, H 7.45.

*Ethyl 2-(2-ethoxycarbonyl-1-cyclohexen-1-yl)-1-cyclohexenecarboxylate (**17**)*

Flash chromatography (2 g of silica gel, 9:1 to 3:2 pentane–Et_2O) of the crude product derived from ethyl 2-(trimethylstannyl)-1-cyclohexenecarboxylate (**8**) (100 mg, 0.315 mmol) gave 38 mg (80%) of **17**, a colourless oil that exhibited IR (neat): 1715, 1650, 1615, 1449, 1230, 1050, 967 cm^{-1}; ^1H NMR (400 MHz, $CDCl_3$) δ: 1.18 (t, 6H, *J* = 7 Hz), 1.64 (br signal, 8H), 2.16 (br signal, 4H), 2.29 (br signal, 4H), 4.05 (q, 4H, *J* = 7 Hz); ^{13}C NMR (75 MHz, $CDCl_3$) δ: 14.3, 22.0, 22.2, 25.6, 31.0, 59.8, 122.0, 152.6, 167.7. Exact Mass calcd. for $C_{18}H_{26}O_4$: 306.1831; found: 306.1828. Anal. calcd. for $C_{18}H_{26}O_4$: C 70.55, H 8.56; found: C 70.32, H 8.47.

*Methyl 2-(2-methoxycarbonyl-1-cycloheptenyl-1-yl)-1-cycloheptenecarboxylate (**18**)*

This compound was derived from methyl 2-(trimethylstannyl)-1-cycloheptenecarboxylate (**9**) (68 mg, 0.21 mmol). Flash chromatography of the crude product on silica gel (5 g, 4:1 petroleum ether – Et_2O) provided 28 mg (86%) of **18** as a colourless oil that exhibited IR (neat): 1713, 1640, 1621, 1435, 1260, 1208, 1117, 1015 cm^{-1}; ^1H NMR (400 MHz, $CDCl_3$) δ: 1.38–1.85 (m, 12H), 2.22–2.54 (m, 8H), 3.59 (s, 6H); ^{13}C NMR (50.3 MHz, $CDCl_3$) δ: 25.7, 26.2, 29.8, 32.3, 35.2, 51.3, 128.4, 155.7, 169.8. Exact Mass calcd. for $C_{18}H_{26}O_4$: 306.1831; found: 306.1830. Anal. calcd. for $C_{18}H_{26}O_4$: C 70.55, H 8.56; found: C 70.62, H 8.67.

Methyl (*E,E*)-3,4-bis(3-chloropropyl)-6-hydroxy-2,4-hexadienoate (25) and (*E,E*)-3,4-bis(3-chloropropyl)-2,4-hexadiene-1,6-diol (26)

To a cold (−78°C), stirred solution of dimethyl (*E,E*)-3,4-bis(3-chloropropyl)muconate (**15**) (75 mg, 0.23 mmol) in dry Et_2O (2 mL) was added a 1.0 M solution of diisobutylaluminum hydride in hexanes (0.46 mL, 0.46 mmol). After 1 h, the solution was warmed to room temperature, saturated aqueous sodium potassium tartrate (2 mL) was added, and the resultant gelatinous emulsion was stirred for 2 h. The aqueous phase was extracted with Et_2O (3 × 10 mL). The combined organic layers were washed (brine, 10 mL), dried ($MgSO_4$), and concentrated. Flash chromatography (5 g of silica gel, 1:1 pentane–Et_2O) of the crude oil afforded 18 mg (24%) of the starting material **15**, 17 mg (27%) of the diol **26**, and 28 mg (41%) of the partial reduction product **25**, a colourless crystalline solid (mp 87–88°C) that displayed IR (KBr): 3437, 1714, 1607, 1437, 1175, 1025, 875 cm^{-1}; ^1H NMR (400 MHz, $CDCl_3$) δ: 1.54 (br s, 1H), 1.74–1.83 (m, 2H), 1.83–1.92 (m, 2H), 2.42 (t, 2H, *J* = 8 Hz), 2.88–2.95 (m, 2H), 3.49 (t, 2H, *J* = 6 Hz), 3.56 (t, 2H, *J* = 7 Hz), 3.69 (s, 3H), 4.32 (d, 2H, *J* = 6 Hz), 5.86 (s, 1H), 5.94 (t, 1H, *J* = 6 Hz); ^{13}C NMR (50.3 MHz,

© 1997 NRC Canada

$CDCl_3$) δ: 25.1, 26.4, 31.1, 32.0, 44.3, 44.8, 51.2, 59.5, 116.9, 131.7, 140.7, 159.1, 166.8. Exact Mass calcd. for $C_{13}H_{20}{}^{35}Cl_2O_3$: 294.0790; found: 294.0781. Anal. calcd. for $C_{13}H_{20}Cl_2O_3$: C 52.89, H 6.83; found: C 53.14, H 7.00.

The diol **26**, a colourless crystalline solid (mp 92–93°C), showed IR (KBr): 3369, 1616, 1419, 1032, 844, 780, 648 cm^{-1}; ^1H NMR (400 MHz, $CDCl_3$) δ: 1.37 (br s, 2H), 1.75–1.84 (m, 4H), 2.39 (t, 4H, J = 8 Hz), 3.49 (t, 4H, J = 6 Hz), 4.28 (d, 4H, J = 7 Hz), 5.73 (t, 2H, J = 7 Hz); ^{13}C NMR (50.3 MHz, $CDCl_3$) δ: 25.0, 31.3, 44.5, 59.4, 127.8, 141.2. Exact Mass calcd. for $C_{12}H_{20}{}^{35}Cl_2O_2$: 266.0841; found: 266.0839. Anal. calcd. for $C_{12}H_{20}Cl_2O_2$: C 53.94, H 7.54; found: C 53.63, H 7.43.

Oxidative coupling of 4: determination of the amount of Bu_3SnCl produced

Following general procedure 3, ethyl (*Z*)-3-tributylstannyl-2-pentenoate (**4**) (30 mg, 0.072 mmol) was treated with CuCl (18 mg, 2.5 equiv.) in DMF (0.5 mL). Flash chromatography (3 g of silica gel, Et_2O) of the resulting crude oil afforded 21 mg (0.90 equiv., 90%) of Bu_3SnCl. This material exhibited a ^1H NMR spectrum identical with that of an authentic sample and displayed in a low resolution mass spectrum a peak for the molecular ion at *m/e* = 326.

Oxidative coupling of 1: determination of the amount of copper metal produced

To a stirred solution of ethyl (*Z*)-5-methyl-3-trimethylstannyl-2-hexenoate (**1**) (244 mg, 0.76 mmol) in DMF (5 mL) at room temperature was added solid copper(I) chloride (189 mg, 2.5 equiv.) and the resulting brown solution was stirred for 1 h. Diethyl ether (3 mL) and saturated aqueous NH_4Cl (3 mL) were added and the resulting mixture was stirred, open to the atmosphere, for 10 min. The mixture was filtered through a medium-frit sintered glass funnel and the reaction flask and the collected material were washed successively with DMF (2 mL), hot distilled deionized water (20 mL), and diethyl ether (30 mL). The filtrate flask was replaced by a clean flask and the copper residue on the walls of the reaction flask was dissolved in 50% v/v aqueous HNO_3 (2 mL). This acidic solution was also used to dissolve the copper deposited on the funnel. The reaction flask and funnel were washed successively with 10% v/v aqueous HNO_3 (8 mL) and distilled, deionized water (15 mL). The collected acidic filtrate was neutralized with concentrated aqueous NH_4OH until a dark blue colour persisted, then the filtrate was reacidified to pH ~5 with a few drops of 50% v/v aqueous acetic acid. To the resulting solution was added solid urea (125 mg, 2.1 mmol), followed by a 50% w/w aqueous solution of KI (6 mL). The dark brown solution was immediately titrated with a 0.1073 M solution of $Na_2S_2O_3$ until the brown iodine colour had almost dissipated, then a freshly prepared 0.5% w/w aqueous solution of starch (1 mL) was added, and the titration was continued until the blue starch–iodine colour was discharged. The total volume of the $Na_2S_2O_3$ solution used in the titration was 6.52 mL. Thus, the amount of copper metal produced was determined to be 44.5 mg (0.92 equiv., 92% yield).

Acknowledgements

We thank the Natural Sciences and Engineering Research Council (NSERC) of Canada and Merck Frosst Canada Inc. for financial support. An NSERC Postgraduate Scholarship (to E.J.M.) and an NSERC Postdoctoral Fellowship (to P.L.G.) are gratefully acknowledged.

References

1. J.K. Stille. Angew. Chem. Int. Ed. Engl. **25**, 508 (1986).
2. W.J. Scott, G.T. Crisp, and J.K. Stille. Org. Synth. **68**, 116 (1990).
3. T.N. Mitchell. Synthesis, 803 (1992).
4. L.S. Hegedus. *In* Organometallics in organic synthesis. *Edited by* M. Schlosser. Wiley, Chichester. 1994. pp. 413–417.
5. V. Farina. *In* Comprehensive organometallic chemistry II. *Edited by* E.W. Abel, E.G.A. Stone, and G. Wilkinson. Vol. 12. *Edited by* L.S. Hegedus. Elsevier, Oxford. 1995. pp. 200–220.
6. L.S. Liebeskind and R.W. Fengl. J. Org. Chem. **55**, 5359 (1990).
7. C.R. Johnson, J.P. Adams, M.P. Braun, and C.B.W. Senanayake. Tetrahedron Lett. **33**, 919 (1992).
8. L.S. Liebeskind and S.W. Rissinger. J. Org. Chem. **58**, 408 (1993).
9. J. Ye, R.K. Bhatt, and J.R. Falck. J. Am. Chem. Soc. **116**, 1 (1994).
10. G.P. Roth, V. Farina, L.S. Liebeskind, and E. Peña-Cabera. Tetrahedron Lett. **36**, 2191 (1995).
11. V. Farina, S. Kapadia, B. Krishnan, C. Wang, and L.S. Liebeskind. J. Org. Chem. **59**, 5905 (1994).
12. E. Piers and T. Wong. J. Org. Chem. **58**, 3609 (1993).
13. G.D. Allred and L.S. Liebeskind. J. Am. Chem. Soc. **118**, 2748 (1996).
14. E. Piers, E.J. McEachern, and M.A. Romero. Tetrahedron Lett. **37**, 1173 (1996).
15. E. Piers and M.A. Romero. J. Am. Chem. Soc. **118**, 1215 (1996).
16. S. Ghosal, G.P. Luke, and K.S. Kyler. J. Org. Chem. **52**, 4296 (1987).
17. H.X. Zhang, F. Guibé, and G. Balavoine. J. Org. Chem. **55**, 1857 (1990).
18. G.T. Crisp and P.T. Glink. Tetrahedron Lett. **32**, 4649 (1992).
19. R.L. Beddoes, T. Cheeseright, J. Wang, and P. Quayle. Tetrahedron Lett. **36**, 283 (1995).
20. J.R. Falck, R.K. Bhatt, and J. Ye. J. Am. Chem. Soc. **117**, 5973 (1995).
21. T. Takeda, K. Matsunaga, Y. Kabasawa, and T. Fujiwara. Chem. Lett. 771 (1995).
22. E. Piers and K.A. Ellis. Tetrahedron Lett. **34**, 1875 (1993).
23. E. Piers, T. Wong, and K.A. Ellis. Can. J. Chem. **70**, 2058 (1992).
24. E. Piers, J.M. Chong, K. Gustafson, and R.J. Andersen. Can. J. Chem. **62**, 1 (1984).
25. E. Piers and A.V. Gavai. J. Org. Chem. **55**, 2374 (1990).
26. E. Piers and H.L.A. Tse. Can. J. Chem. **71**, 983 (1993).
27. E. Piers, H.E. Morton, and J.M. Chong. Can. J. Chem. **65**, 78 (1987).
28. I.N. Houpis, L. DiMichele, and A. Molina. Synlett, 365 (1993).
29. M. Wiessler. Tetrahedron Lett. 233 (1977).
30. R.J.K. Taylor. Synthesis, 564 (1977).
31. W.C. Still, M. Kahn, and A. Mitra. J. Org. Chem. **43**, 2923 (1978).
32. E. Piers, E.J. McEachern, and P.A. Burns. J. Org. Chem. **60**, 2322 (1995).
33. W.T. Elwell and D. Price. *In* Comprehensive analytical chemistry. Vol. 1C. *Edited by* C.L. Wilson and D.W. Wilson. Elsevier, Amsterdam. 1962. pp. 371–373.
34. M. Pereyre, J.-P. Quintard, and A. Rahm. Tin in organic synthesis. Butterworths, London. 1987.

Can. J. Chem. Downloaded from www.nrcresearchpress.com by 88.146.161.215 on 09/08/12
For personal use only.

© 1997 NRC Canada

Synthesis and characterization of organometallic hydro-tris-pyrazolylborate derivatives of scandium via alkane elimination

James Blackwell, Corinne Lehr, Yimin Sun, Warren E. Piers, Susan D. Pearce-Batchilder, Michael J. Zaworotko, and Victor G. Young, Jr.

Abstract: Reaction between the potassium salts of the hydro-tris-pyrazolylborate ligands $Tp^{Me,Me}$ and $Tp^{tBu,Me}$ and the tris THF adduct of scandium trichloride lead to isolation of the scandium complexes $(Tp^{Me,Me})ScCl_2(THF)$, **1***a*, and $(Tp^{tBu,Me})ScCl_2$, **1***b*, in 65 and 49% yield, respectively. Subsequent reactions between **1***a* and **1***b* and alkyl lithium reagents RLi (R = Me, CH_2SiMe_3, and $CH(SiMe_3)_2$) gave the lithium salts of the Tp ligands as the major isolated products in all cases but one. The complex $(Tp^{Me,Me})Sc(CH_2SiMe_3)_2(THF)$, **2***a*, could be obtained contaminated with at least 10% $Tp^{Me,Me}Li$ via this methodology. A salt-free alkane elimination route to bis-trimethylsilylmethyl complexes **2***a* and the THF-free $(Tp^{tBu,Me})Sc(CH_2SiMe_3)_2$, **2***b*, involving reaction between in situ generated $Sc(CH_2SiMe_3)_3(THF)_2$ and the protonated ligands, $Tp^{R,Me}H$, gave samples of the desired bis-alkyl derivatives in 67 and 87% yield, respectively. In solution, complexes **2***a* and **2***b* are both fluxional at room temperature. These dynamic processes were frozen out on the NMR time scale at lower temperatures and interpreted on the basis of the ^1H NMR spectra obtained as well as information obtained from the solid state structures of both compounds. **2***a*: monoclinic, space group $P2_1/c$, a = 11.765(4) Å, b = 14.8311(20) Å, c = 20.891(5) Å, β = 105.69(3)°, V = 3509.4(15) Å^3, Z = 4, R = 0.088, R_w = 0.082. **2***b*: triclinic, space group $P\bar{1}$, a = 11.9427(2) Å, b = 20.3641(3) Å, c = 26.5602(2) Å, α = 112.192(1)°, β = 100.569(1)°, γ = 92.928(1)°, V = 5830.38(14) Å^3, Z = 6, R = 0.0500, R_w = 0.1137.

Key words: organoscandium complexes, hydro-tris-pyrazolylborate ligands, alkane elimination.

Résumé : La réaction des sels de potassium des coordinats hydro-tris-pyrazolylborate $Tp^{Me,Me}$ et $Tp^{tBu,Me}$ et l'adduit tris THF du trichlorure de scandium permet d'isoler les complexes du scandium $(Tp^{Me,Me})ScCl_2(THF)$, **1***a*, et $(Tp^{tBu,Me})ScCl_2$, **1***b*, avec des rendements respectivement de 65 et 49%. Dans tous les cas, à l'exception d'un, des réactions subséquentes des produits **1***a* et **1***b* avec des réactifs alkyllithium, RLi (R = Me, CH_2SiMe_3 et $CH(SiMe_3)_2$), conduisent aux sels de lithium des coordinats Tp comme produits principaux. Par le biais de cette méthodologie, il a été possible d'obtenir le complexe $(Tp^{Me,Me})Sc(CH_2SiMe_3)_2(THF)$, **2***a*, contaminé par au moins 10% du $Tp^{Me,Me}Li$. Une voie d'élimination d'alcane sans sel conduisant aux complexes bis-triméthylsilylméthyles **2***a* et $(Tp^{tBu,Me})Sc(CH_2SiMe_3)_2$, sans THF, **2***b*, et impliquant une réaction entre du $Sc(CH_2SiMe_3)_3(THF)_2$ généré in situ et les coordinats protonés, $Tp^{R,Me}H$, ont permis d'obtenir des échantillons des dérivés bis-alkylés désirés avec des rendements respectifs de 67 et 87%. En solution, à la température ambiante, les complexes **2***a* et **2***b* sont tous les deux en fluxion. En opérant à des températures plus faibles, ces processus dynamiques ont pu être figés à l'échelle de temps de la RMN et on a pu les interpréter sur la base des spectres RMN du ^1H obtenus ainsi que des informations obtenues à partir des structures des deux composés à l'état solide. Le composé **2***a* est monoclinique, groupe d'espace $P2_1/c$, a = 11,765(4), b = 14,8311(20) et c = 20,891(5) Å, β = 105,69(3)°, V = 3509,4(15) Å^3, Z = 4, R = 0,088 et R_w = 0,082. Le composé **2***b* est triclinique, groupe d'espace $P\bar{1}$, a = 11,9427(2), b = 20,3641(3) et c = 26,5602(2) Å, α = 112,192(1)°, β = 100,569(1)° et γ = 92,928(1)°, V = 5830,38(14) Å^3, Z = 6, R = 0,0500 et R_w = 0,1137.

Mots clés : complexes organoscandium, coordinats hydro-tris-pyrazolylborate, élimination d'alcane.

[Traduit par la rédaction]

Received September 16, 1996.

This paper is dedicated to Professor William A. Ayer on the occasion of his 65th birthday.

J. Blackwell, C. Lehr, Y. Sun, and W.E. Piers.[1] Department of Chemistry, University of Calgary, 2500 University Dr. N.W., Calgary, AB T2N 1N4, Canada.
S.D. Pearce-Batchilder and M.J. Zaworotko. Department of Chemistry, Saint Mary's University, Halifax, NS B3H 3C3, Canada.
V.G. Young, Jr. Department of Chemistry, The University of Minnesota, 207 Pleasant St. S.E. Minneapolis, MN 55455, U.S.A.

[1] Author to whom correspondence may be addressed. Fellow of the Alfred P. Sloan Foundation, 1996–1998. Fax: (403)-289-9488. E-mail: wpiers@chem.ucalgary.ca

© 1997 NRC Canada

Can. J. Chem. Downloaded from www.nrcresearchpress.com by 88.146.161.215 on 09/08/12
For personal use only.

Can. J. Chem. Downloaded from www.nrcresearchpress.com by 88.146.161.215 on 09/08/12
For personal use only.

Hydro-tris-pyrazolylborate ("$Tp^{R,R'}$")[2] ligands are among the most versatile and ubiquitous supporting ligands in inorganic chemistry (1). This versatility is in part due to the tunability of these ligands, particularly from a steric point of view, via modification of substitution patterns on the pyrazolyl rings. Atoms or ions of varying size can be bound in a range of coordination environments depending on the steric properties of the groups in the 3 and 5 positions of the pyrazolyl ring. Thus, complexes of almost every transition metal exist and several examples each of Tp complexes with *s* and *p*-block elements (2), the lanthanides (3), and actinides (1*b*) are known.

Despite the maturity of Tp coordination chemistry, scandium complexes of these ligands are, to our knowledge, unreported in the chemical literature.[3] Examples of related yttrium (4), lanthanum (5), aluminum (6), gallium (7), and indium (7, 8) Tp complexes have been reported but scandium appears to have been neglected. This was a surprise to us when we settled on the hydro-tris-pyrazolylborate ancillary to begin studying the chemistry of bis-alkyl derivatives of scandium, which until recently (9) have also been overlooked. As reported herein, $Tp^{R,Me}$ (R = Me, *t*Bu) complexes of scandium are readily prepared using an alkane elimination protocol that we recently developed (10).

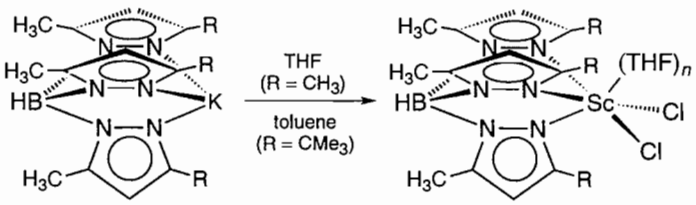
Results and discussion

Reactions between one equivalent of the potassium salts of the hydro-tris-pyrazolylborate ligands $Tp^{Me,Me}$ and $Tp^{tBu,Me}$ and $ScCl_3{\cdot}THF_3$ in THF or toluene yields the dichloride complexes $(Tp^{Me,Me})ScCl_2(THF)$, **1***a*, and $(Tp^{tBu,Me})ScCl_2$, **1***b* (eq. [1]). Longer reaction time is required for the bulkier $Tp^{tBu,Me}$ ligand but both complexes were prepared in good yield. The less bulky $Tp^{Me,Me}$ ligand allows one THF ligand to remain in the scandium coordination sphere, as indicated by the solution NMR spectra (see Table 1); resonances for the pyrazolyl ring substituents in **1***a* are split into two sets in a 2:1 ratio as would be predicted for a six-coordinate, octahedral complex. Although the five-coordinate complex **1***b* would be expected to also have inequivalent pyrazolyl rings in a static structure, by ^1H and $^{13}C\{^1H\}$ NMR spectroscopy, all three rings are equivalent. The ^1H NMR spectra of **1***b* at lower temperatures exhibits broadening and changes in the observed chemical shifts but the process responsible for exchanging the substituents on the pyrazolyl rings could not be frozen out at accessible temperatures.

As starting materials for bis-alkyl derivatives of scandium, **1***a* and **1***b* have limited utility. As shown in eq. [2], when treated with two equivalents of trimethylsilylmethyl lithium, a bis-alkyl derivative of **1***a* could be generated but the isolated product was contaminated with variable amounts of an impurity identified as the lithium salt of the $Tp^{Me,Me}$ ligand. Under certain reaction conditions (see Experimental section) followed by careful fractional crystallization, 90% pure samples of **2***a* could be obtained but the procedure was unsatisfying and tedious. The situation was worse for derivatization of **1***b*; only small amounts of the desired alkyl derivative **2***b* were observed and the major product in all reactions performed was $Tp^{tBu,Me}Li$. Use of other alkylating agents, including MeLi, $LiCH(SiMe_3)_2$, and $KCH_2C_6H_5$, for both **1***a* and **1***b* gave even less satisfactory results.

Clearly, other routes to **2***a* and **2***b* were necessary. Recently we have reported on alkane elimination protocols for attaching cyclopentadienyl-amido type ligands to both scandium (10) and zirconium (11). These procedures involve treatment of in situ generated metal alkyl complexes with proteo ligands; the elimination of alkanes provides the driving force for the reaction and yields organometallic compounds directly. Since proton salts of hydro-tris-pyrazolylborate ligands are available (12), adaptation of our alkane elimination procedure seemed promising for the synthesis of **2***a* and **2***b* in a "salt-free" manner.

Accordingly, in situ generated $Sc(CH_2SiMe_3)_3{\cdot}THF_2$ (13), when treated with $Tp^{Me,Me}H$ or $Tp^{tBu,Me}H$, led directly to bis-alkyl compound **2***a* and **2***b* in good to excellent yields (eq. [3]). The products were completely free of the lithium salts of the

[1] $ScCl_3{\cdot}THF_3$ + 

ligand, provided the solutions of $Sc(CH_2SiMe_3)_3{\cdot}THF_2$ were filtered prior to treatment with the $Tp^{R,Me}H$ reagents.

Access to pure samples of bis-alkyls **2** allowed us to fully characterize these compounds both in solution and in the solid state (vide infra). In solution, both compounds exhibit dynamic behavior that serves to exchange related pyrazolyl substituent groups rapidly at room temperature. In the case of **2***a*, this behavior appears to be driven by a more labile THF ligand in comparison to the dichloride **1***a*, perhaps because of the moderately bulky trimethylsilylmethyl ligands. Although the THF cannot be removed from **2***a* even upon exposure to high vacuum for several hours, variable temperature ^1H NMR spectra suggest that **2***a* is in equilibrium with a fluxional five-coordinate species. Upon cooling, the singlets for each of the C-3, -4, and -5 substituents on the pyrazolyl ring coalesced and reappeared in patterns similar to those found for the static

[2] The abbreviation convention introduced in ref. 1*b* is employed in this paper.

[3] The synthesis of $(Tp^{Me,Me})ScCl_2(THF)$ (**1***a* in this paper) was, however, disclosed publically at an ACS meeting several years ago: R. Ball, J.G. Matisons, and J. Takats. Abstract 291, 190th Meeting of the American Chemical Society, Chicago (1985).

© 1997 NRC Canada

[2]

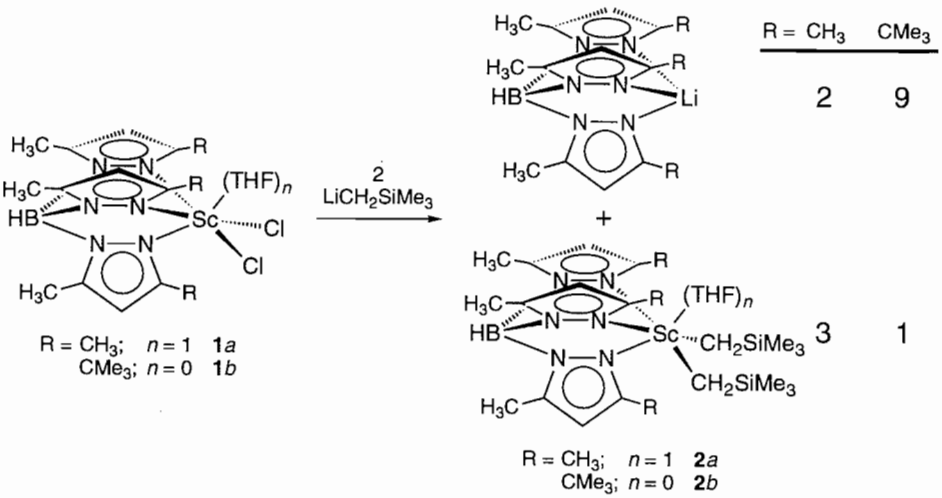
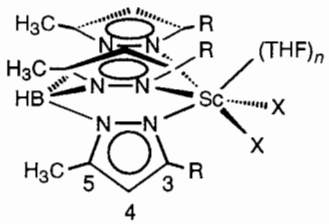


Table 1. ^{1}H and $^{13}C\{^{1}H\}$ NMR data for isolated new compounds.[a]



4

Compound	no.		C-3 R	C-3	CH-4	C-5 CH_3	C-5	X	THF
n = 1		^{1}H	2.99 (3H)		5.49 (2H)	2.09 (6H)			3.93 (4H)
			2.46 (6H)		5.30 (1H)	2.04 (3H)			1.16 (4H)
X = Cl	**1***a*								
R = CH_3		^{13}C	15.1	152.6	106.7 (2)	12.7 (2)	144.5 (2)		73.0
			15.0 (2)	150.9 (2)	106.6	12.5	144.0		25.4
n = 1		^{1}H	2.45 (9H)		5.57 (3H)	2.13 (9H)		0.42 (4H)	3.79 (4H)
X = CH_2SiMe_3	**2***a*							0.21 (18H)	1.26 (4H)
R = CH_3		^{1}H	2.88 (3H)		5.58 (2H)	2.12 (6H)		0.60 (2H)[b]	Broad
		–50°C	2.24 (6H)		5.52 (1H)	2.13 (3H)		0.24 (2H)	
								0.29 (18H)	
		^{13}C	15.4	149.7	106.2	12.9	144.2	4.4	71.2
									25.3
n = 0		^{1}H	1.60 (27H)		5.60 (3H)	1.92 (9H)			
X = Cl	**1***b*	^{13}C	33.0	147.0	105.0	13.2	166.6		
R = CMe_3			31.6 (3)						
n = 0		^{1}H	1.52 (27H)		5.65 (3H)	2.09 (9H)		0.82 (4H)	
X = CH_2SiMe_3	**2***b*							0.13 (18H)	
R = CMe_3		^{1}H	1.54 (27H)		5.55 (2H)	2.20 (6H)		1.09, 0.71	
		–78°C			5.31 (1H)	1.51 (3H)		0.72, –0.19	
		^{13}C	32.7	146.5	104.5	13.6	164.6	53.5 (br)	
			32.2 (3)					3.9	

[a]All room temperature spectra recorded in C_6D_6. Low-temperature spectra recorded in C_7D_8.
[b]^{2}J = 5.8 Hz.

Can. J. Chem. Downloaded from www.nrcresearchpress.com by 88.146.161.215 on 09/08/12
For personal use only.

© 1997 NRC Canada

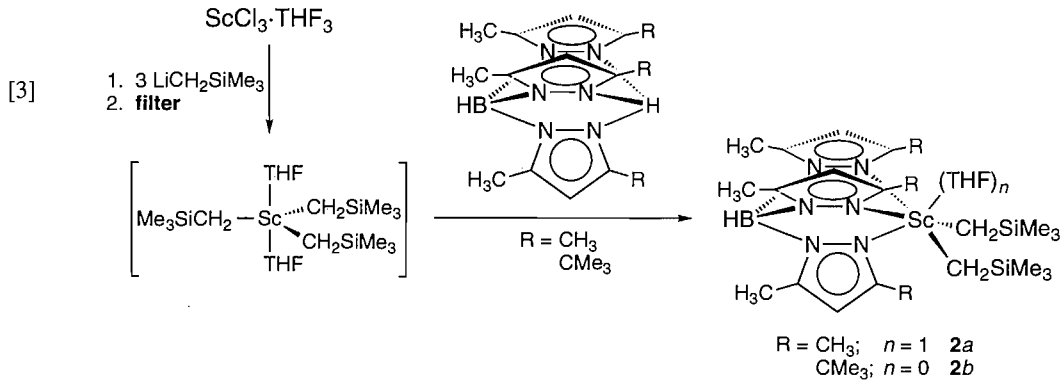
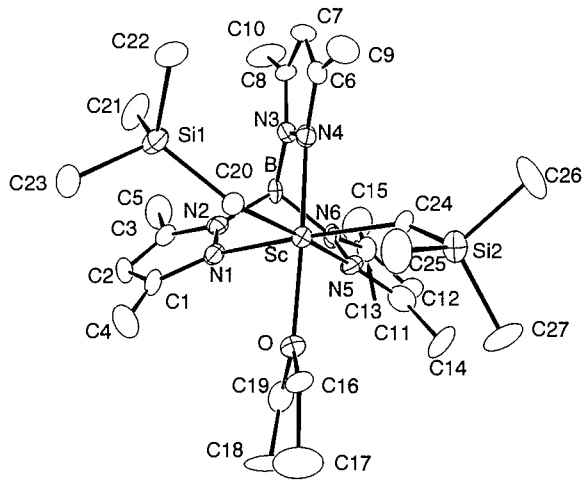


Fig. 1. ORTEP drawing of $(Tp^{Me,Me})Sc(CH_2SiMe_3)_2(THF)$, **2***a*.



six-coordinate dichloride, consistent with the observed solid state structure (vide infra). Curiously, the signals for the THF protons also coalesce, which perhaps implies a separate exchange process involving free and bound THF[4] or restricted rotation of the THF ligand at lower temperatures, resulting in different environments for the two halves of the ligand.

X-ray quality crystals of **2***a* were obtained from benzene; an ORTEP representation of the compound is given in Fig. 1 and molecular coordinates and selected metrical parameters can be found in Tables 2 and 3, respectively. The formally 12-electron scandium center is octahedrally coordinated with distortions from the ideal attributable to the contraints of the chelating $Tp^{Me,Me}$ ligand. The Sc—C20 and Sc—C24 distances are virtually identical and closely compare with the Sc—C distance in $Cp^*_2ScCH_3$ of 2.243(11) Å (14). The THF ligand contains an sp^2 hybridized, trigonal planar oxygen atom, the plane of which bisects the C20-Sc-C24 angle. Thus, the filled unhybridized *p* orbital on oxygen is potentially available to π donate to an empty *d* orbital not involved in σ bonding to the alkyl and pyrazolylborate ligands. The Sc—O distance of 2.206(10) Å is comparable to analogous bond lengths in $ScCl_3(THF)_3$ (2.236(8), 2.147(7), and 2.164(7) Å) and $Cp_2Sc(THF)Si(SiMe_3)_3$ (2.216(3) Å) (15).

The steric properties of the $Tp^{tBu,Me}$ ligand are sufficient to preclude coordination of THF to the scandium center; by NMR spectroscopy, **2***b* is completely THF free (Table 1). A static five-coordinate structure would be expected to exhibit inequivalent pyrazolyl rings in a 2:1 ratio but at room temperature all rings are equivalent; however, as the sample was cooled, coalescence behavior was observed. A series of ^1H NMR spectra at various temperatures is shown in Fig. 2. As can be seen, the C-3 methyl and C-4 H resonances, which are singlets at room temperature, coalesce at about 242 K and reappear as two singlets in a 2:1 ratio. The resonances associated with the trimethylsilylmethyl ligands also collapse at about 242 K and in the low-temperature limit give distinct resonances for each group.

This spectrum is consistent with the solid state structural results in which one of the pyrazolyl rings is only weakly bound to the scandium center in this extremely sterically crowded molecule. Crystals of **2***b* were obtained from toluene–hexanes and, upon analysis, three independent molecules were discovered in the unit cell. Since the metrical parameters for these independent molecules were very similar, data for molecule A only are presented herein (Tables 4 and 5); full details on the other molecules are included in the deposited material.

Figure 3 shows an ORTEP diagram of molecule A of **2***b*. The scandium center is trigonal bipyramidal in geometry with N2, N6, and C25 occupying the equatorial positions and N4 and C29 the apical sites. Although **2***b* is formally only a 10-electron complex, clearly the scandium center is sterically saturated. Indeed, the $Tp^{tBu,Me}$ ligand has been termed a "tetrahedral enforcer" (16) because of its steric bulk and five-coordinate structures of complexes incorporating this ligand are rare outside of the lanthanides. Examination of the Sc—N bond distances reveals that the apical Sc—N4 distance of 2.493(2) Å is more than 0.2 Å longer than the other two Sc—N bond lengths. This lengthening is probably a result of the steric interaction between this ring's C-3 *tert*-butyl group and the equatorial alkyl group. Alternation of this more weakly bound ring between the three pyrazolyl groups is a plausible fluxional process (Scheme 1) that accounts for the observed temperature dependence of the ^1H NMR spectra. Similar behaviour has been observed in the related compound $(Tp^{Me,Me})GaMe_2$ (17). In this compound, the tris-pyrazolylborate ligands are η^2 bound to a tetrahedral gallium center in the solid state but the

[4] Although the observed solid state structure of **2***a* shows the presence of only one THF molecule in the crystal, integration of the THF resonances in the ^1H NMR spectra were always slightly higher than expected.

Can. J. Chem. Downloaded from www.nrcresearchpress.com by 88.146.161.215 on 09/08/12
For personal use only.

© 1997 NRC Canada

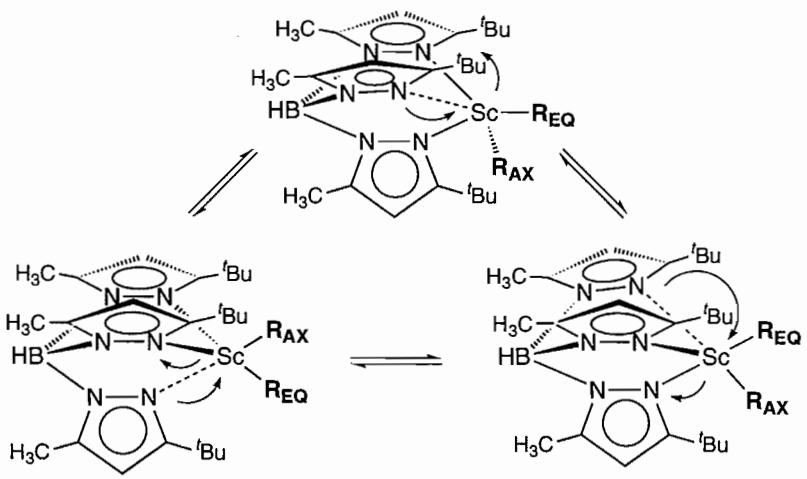
Can. J. Chem. Downloaded from www.nrcresearchpress.com by 88.146.161.215 on 09/08/12
For personal use only.

Table 2. Atomic parameters x, y, z and B_{iso} for $(Tp^{Me,Me})Sc(CH_2SiMe_3)_2(THF)$, **2***a*.

Atom	x	y	z	B_{iso}[a]
Sc	0.62462(24)	0.40536(18)	0.19850(15)	3.07(16)
Si1	0.8639(4)	0.4221(3)	0.1119(3)	4.4(3)
Si2	0.3839(4)	0.2626(3)	0.0831(3)	4.4(3)
O	0.4993(9)	0.5185(6)	0.1700(6)	3.2(6)
N1	0.7480(10)	0.5188(8)	0.2611(7)	2.8(8)
N2	0.8112(12)	0.5002(8)	0.3249(7)	2.9(7)
N3	0.7621(12)	0.3077(8)	0.2579(7)	3.0(8)
N4	0.8244(12)	0.3315(8)	0.3213(8)	3.4(8)
N5	0.5708(11)	0.4064(8)	0.2973(6)	3.2(7)
N6	0.6560(10)	0.4055(8)	0.3575(6)	3.1(7)
C1	0.7862(14)	0.6001(11)	0.2438(9)	3.5(10)
C2	0.8687(15)	0.6325(9)	0.2986(10)	3.6(9)
C3	0.8837(14)	0.5692(10)	0.3505(9)	3.1(10)
C4	0.7430(15)	0.6481(10)	0.1772(8)	4.8(10)
C5	0.9632(14)	0.5666(10)	0.4185(8)	5.1(9)
C6	0.8104(17)	0.2314(11)	0.2431(9)	3.5(10)
C7	0.9058(17)	0.2072(10)	0.2968(11)	4.2(11)
C8	0.9122(14)	0.2708(12)	0.3476(9)	3.6(10)
C9	0.7726(15)	0.1817(10)	0.1813(9)	5.1(11)
C10	0.9999(16)	0.2805(11)	0.4114(10)	6.5(12)
C11	0.4708(15)	0.3975(11)	0.3176(9)	4.0(10)
C12	0.4917(16)	0.3908(11)	0.3834(10)	4.2(10)
C13	0.6111(17)	0.3944(11)	0.4110(9)	4.0(10)
C14	0.3493(15)	0.3975(12)	0.2647(8)	6.3(11)
C15	0.6834(16)	0.3902(12)	0.4800(9)	6.4(12)
C16	0.4280(14)	0.5288(10)	0.1037(9)	4.3(10)
C17	0.3428(20)	0.6074(15)	0.1017(12)	9.1(16)
C18	0.3942(20)	0.6562(13)	0.1592(13)	9.2(16)
C19	0.4724(13)	0.5928(12)	0.2100(7)	4.5(10)
C20	0.7032(11)	0.4171(9)	0.1118(6)	3.1(8)
C21	0.9749(13)	0.4297(11)	0.1938(8)	5.9(11)
C22	0.9076(16)	0.3241(9)	0.0693(9)	6.0(12)
C23	0.8947(14)	0.5227(9)	0.0623(8)	5.2(11)
C24	0.4966(13)	0.2934(9)	0.1574(8)	3.5(9)
C25	0.4167(16)	0.3034(10)	0.0054(8)	5.8(10)
C26	0.3656(19)	0.1391(10)	0.0734(11)	8.8(14)
C27	0.2301(13)	0.3079(11)	0.0835(9)	6.2(11)
B	0.7947(15)	0.4141(12)	0.3643(9)	3.8(11)

[a] B_{iso} is the mean of the principal axes of the thermal ellipsoid.

Scheme 1.



© 1997 NRC Canada

Can. J. Chem. Downloaded from www.nrcresearchpress.com by 88.146.161.215 on 09/08/12
For personal use only.

Table 3. Selected bond distances and angles for **2***a*.

Bond lengths (Å)			
Sc—O	2.206(10)	N1—N2	1.367(20)
Sc—N1	2.372(12)	N1—C1	1.368(21)
Sc—N3	2.273(13)	N2—C3	1.347(21)
Sc—N5	2.318(12)	N2—B	1.560(21)
Sc—C20	2.253(13)	N3—N4	1.376(22)
Sc—C24	2.250(14)	N3—C6	1.340(23)
Si1—C20	1.891(13)	C1—C2	1.37(3)
Si2—C24	1.806(16)	C1—C4	1.524(24)
O—C16	1.420(22)	C2—C3	1.408(25)
O—C19	1.468(20)	C3—C5	1.476(24)
Bond angles (°)			
O-Sc-N1	82.8(4)	Sc-N1-N2	119.0(9)
O-Sc-N3	163.1(5)	Sc-N1-C1	132.5(11)
O-Sc-N5	84.9(4)	N2-N1-C1	107.7(12)
O-Sc-C20	96.6(4)	N1-N2-C3	110.6(12)
O-Sc-C24	97.4(4)	N1-N2-B	124.6(13)
N1-Sc-N3	84.9(5)	C3-N2-B	124.6(14)
N1-Sc-N5	77.2(5)	N1-C1-C2	107.3(15)
N1-Sc-C20	93.8(5)	N1-C1-C4	126.9(15)
N1-Sc-C24	168.8(5)	C2-C1-C4	125.8(15)
N3-Sc-N5	81.0(5)	C1-C2-C3	108.8(14)
N3-Sc-C20	95.8(5)	N2-C3-C2	105.5(15)
N3-Sc-C24	92.4(5)	N2-C3-C5	122.1(15)
N5-Sc-C20	170.6(5)	C2-C3-C5	132.4(15)
N5-Sc-C24	91.7(5)	Sc-C20-Si1	129.0(7)
C20-Sc-C24	97.3(5)	Sc-C24-Si2	140.8(8)
Sc-O-C16	121.4(9)	N2-B-N4	104.6(12)
Sc-O-C19	130.4(9)	N2-B-N6	106.7(12)
C16-O-C19	108.2(11)	N4-B-N6	105.0(12)

rings and the two alkyl groups exchange rapidly on the NMR time scale in solution at room temperature.

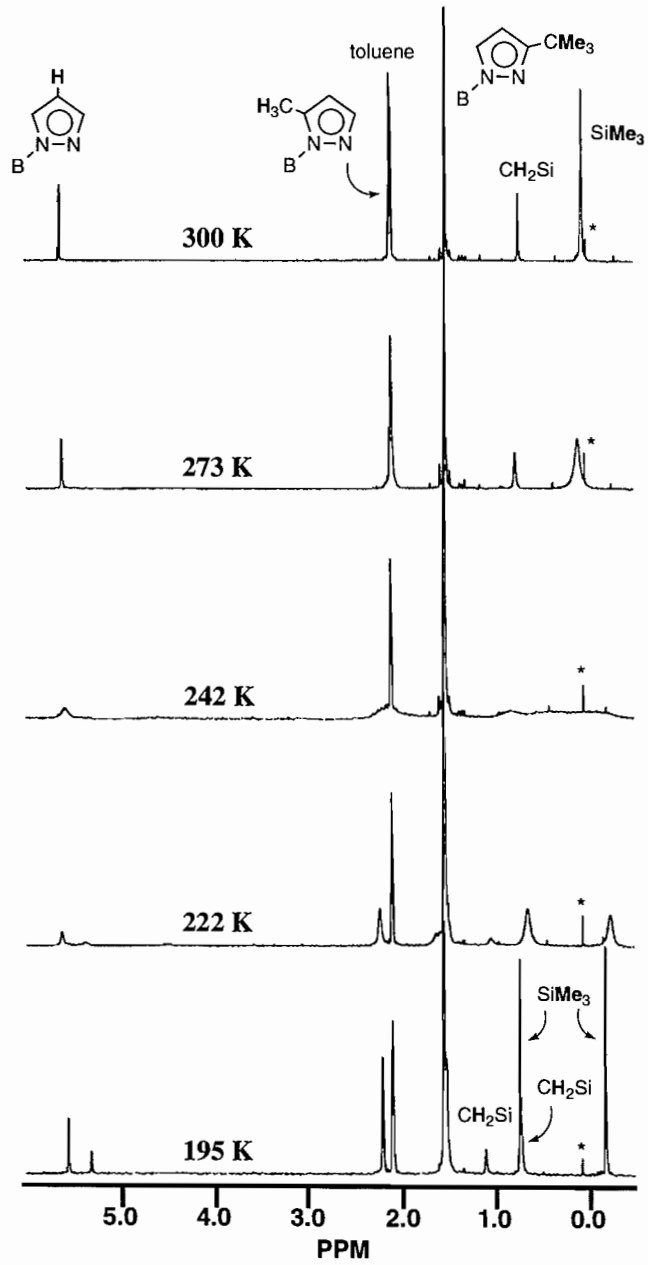
These structural features help to explain some of the observations we have made in preliminary reactivity studies of **2***b* in which the $Tp^{tBu,Me}$ ligand is readily removed from the metal. For example, the compound is extremely sensitive to water but protonolysis of the $Tp^{tBu,Me}$ ligand is competitive with loss of Me_4Si as evidenced by the presence of $Tp^{tBu,Me}H$ in samples intentionally treated with fractional equivalents of water. Furthermore, stirring a THF solution of **2***b* with an excess of dry LiCl led to slow formation of $Tp^{tBu,Me}Li$ and an unidentified scandium product, emphasizing the need to filter away the LiCl by-product from $Sc(CH_2SiMe_3)_3 \cdot THF_2$ before treating with $Tp^{tBu,Me}H$ (see eq. [3] above). These observations suggest that the more weakly bound (or dissociated) pyrazolyl nitrogen is the kinetically favoured site for reactivity with incoming electrophiles. We are currently probing the reactivity of these hydro-tris-pyrazolylborate scandium bis-trimethylsilylmethyl complexes in more detail and will report on this chemistry in due course.

Experimental section

General

All operations were performed under a purified argon atmosphere using glove box or high vacuum lines using standard techniques (18). Solvents were purified as follows: toluene

Fig. 2. ^1H NMR spectra of $(Tp^{tBu,Me})Sc(CH_2SiMe_3)_2$, **2***b*, in C_7D_8 at various temperatures. The peak marked by an asterisk (*) is due to an impurity.



was distilled from sodium benzophenone ketyl and stored over "titanocene" (19); tetrahydrofuran (THF) was predried with activated (10^{-4} Torr (1 Torr = 133.3 Pa), 200°C, 3 h) 3Å molecular sieves, distilled from, and stored over, sodium benzophenone ketyl; hexanes were distilled from lithium aluminum hydride (Aldrich) and stored over "titanocene"; dichloromethane was distilled from CaH_2; d_6-benzene was dried sequentially over activated 3Å sieves and "titanocene" and stored in the glove box; other NMR solvents were dried analogously to the perprotio solvents. ^1H and $^{13}C\{^1H\}$ NMR spectra were recorded on Bruker AC-200 and WH-400 MHz spectrometers. Elemental analyses were performed by Oneida Research Services, Inc., One Halsey Road, Whitesboro, NY

© 1997 NRC Canada

Can. J. Chem. Downloaded from www.nrcresearchpress.com by 88.146.161.215 on 09/08/12
For personal use only.

Table 4. Atomic parameters x, y, z ($\times 10^4$) and U_{eq} for $(Tp^{Me,tBu})Sc(CH_2SiMe_3)_2$, **2***b* (molelcule A).

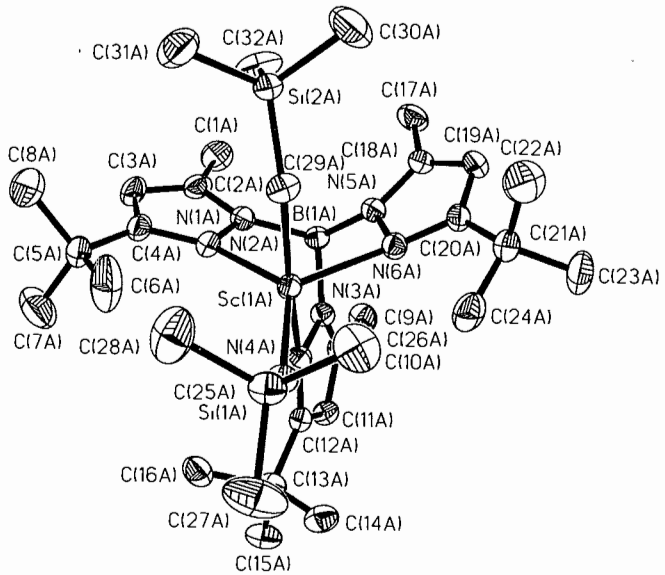
Atom	x	y	z	U_{eq}[a]
Sc(1A)	5040(1)	2295(1)	1512(1)	23(1)
B(1A)	3342(2)	852(2)	944(1)	25(1)
N(1A)	3324(2)	1196(1)	1574(1)	26(1)
N(2A)	4147(2)	1747(1)	1956(1)	27(1)
C(1A)	1711(3)	349(2)	1563(1)	46(1)
C(2A)	2679(2)	941(2)	1849(1)	32(1)
C(3A)	3095(3)	1323(2)	2411(1)	37(1)
C(4A)	4012(2)	1820(2)	2467(1)	30(1)
C(5A)	4803(3)	2334(2)	3003(1)	36(1)
C(6A)	5569(4)	2862(2)	2899(2)	71(1)
C(7A)	5546(3)	1896(2)	3252(2)	64(1)
C(8A)	4080(3)	2742(2)	3413(2)	71(1)
N(3A)	4525(2)	607(1)	882(1)	24(1)
N(4A)	5540(2)	1051(1)	1184(1)	24(1)
C(9A)	3831(3)	−676(2)	248(1)	37(1)
C(10A)	4740(2)	−70(1)	611(1)	26(1)
C(11A)	5905(2)	−73(1)	746(1)	28(1)
C(12A)	6381(2)	626(1)	1107(1)	24(1)
C(13A)	7632(2)	869(1)	1407(1)	30(1)
C(14A)	8258(2)	1318(2)	1165(1)	37(1)
C(15A)	8248(3)	206(2)	1346(1)	42(1)
C(16A)	7694(2)	1283(2)	2032(1)	37(1)
N(5A)	3086(2)	1359(1)	635(1)	25(1)
N(6A)	3951(2)	1835(1)	632(1)	25(1)
C(17A)	1058(2)	824(2)	140(1)	39(1)
C(18A)	2148(2)	1293(1)	238(1)	28(1)
C(19A)	2410(2)	1725(2)	−29(1)	31(1)
C(20A)	3531(2)	2053(1)	223(1)	26(1)
C(21A)	4227(2)	2554(2)	62(1)	33(1)
C(22A)	3638(3)	3224(2)	119(2)	58(1)
C(23A)	4307(3)	2157(2)	−550(1)	52(1)
C(24A)	5440(3)	2770(2)	421(1)	42(1)
C(25A)	6799(2)	2872(1)	1734(1)	30(1)
Si(1A)	7420(1)	3829(1)	2050(1)	35(1)
C(26A)	6959(3)	4316(2)	1589(2)	54(1)
C(27A)	9027(3)	3922(2)	2191(2)	72(1)
C(28A)	7023(4)	4319(2)	2733(2)	67(1)
C(29A)	4057(2)	3231(1)	1727(1)	33(1)
Si(2A)	2563(1)	3358(1)	1811(1)	29(1)
C(30A)	1814(3)	3730(2)	1320(2)	66(1)
C(31A)	2550(3)	4003(2)	2534(1)	59(1)
C(32)A	1621(3)	2521(2)	1677(2)	52(1)

[a] U_{eq} is one third of the trace of the orthogonalized U_{ij} tensor.

13492, or in house using a Control Equipment Corporation model 440 elemental analyzer. Materials were purchased from Aldrich Chemical Company and used as received or purified using standard procedures (20). The compounds $ScCl_3 \cdot THF_3$ (21), $Tp^{R,Me}K$ (12, 22), and $Tp^{R,Me}Tl$ (22) were synthesized according to published procedures. Protonated ligands $Tp^{R,Me}H$ were prepared by treating the thallium salts with excess hydrogen sulfide (Matheson).[5]

[5] G. Parkin, personal communication.

Fig. 3. ORTEP drawing of $(Tp^{tBu,Me})Sc(CH_2SiMe_3)_2$, **2***b*.



Synthesis of $(Tp^{Me,Me})ScCl_2(THF)$, 1*a*

$ScCl_3 \cdot THF_3$ (5.0 g, 13.6 mmol) and $Tp^{Me,Me}K$ (4.41 g, 13.1 mmol) were combined in a flask and attached to a swivel frit apparatus. The assemblage was evacuated and THF (150 mL) was vacuum transferred into the vessel at −78°C. The reaction was stirred for 4 h at room temperature at which time the THF was removed in vacuo and replaced by toluene (150 mL). After sufficient extraction, the white suspension was filtered, the solution was concentrated, and hexanes were added. The resulting precipitate was isolated by filtration and washed with cold hexanes. Yield: 4.3 g, 65%. Anal. calcd. for $C_{19}H_{30}N_6Cl_2BOSc$: C 47.04, H 6.23, N 17.32; found: C 47.91, H 6.03, N 16.86.

Synthesis of $(Tp^{tBu,Me})ScCl_2$, 1*b*

$ScCl_3 \cdot THF$ (4.3 g, 11.8 mmol) and $Tp^{Me,tBu}K$ (5.02 g, 11.8 mmol) were combined in a flask and attached to a swivel frit apparatus. The assemblage was evacuated and toluene (50 mL) was vacuum transferred into the vessel at −78°C. The reaction was stirred for 24 h at room temperature at which time the toluene was removed in vacuo and replaced by methylene chloride (50 mL). After sufficient extraction, the white suspension was filtered and the methylene chloride was completely removed. The resulting white solid was triturated with hexanes and isolated by filtration. Yield: 3.1 g, 49%. Anal. calcd. for $C_{24}H_{40}N_6Cl_2BSc$: C 53.72, H 7.53, N 15.65; found: C 53.02, H 7.25, N 15.38.

Synthesis of $(Tp^{Me,Me})Sc(CH_2SiMe_3)_2(THF)$, 2*a* by metathesis

$(Tp^{Me,Me})ScCl_2(THF)$ (0.98 g, mmol) and solid $LiCH_2SiMe_3$ (1.95 equiv.) were combined in a flask and attached to a swivel frit apparatus. The assemblage was evacuated and toluene (≈25 mL) was vacuum transferred into the vessel at −78°C. The reaction was stirred at −78°C for 30 min and warmed gradually to room temperature. The suspension was filtered and concentrated; hexanes were added (toluene:hexanes, 1:4). The white precipitate was isolated by filtration. Yield: 0.85 g

© 1997 NRC Canada

Can. J. Chem. Downloaded from www.nrcresearchpress.com by 88.146.161.215 on 09/08/12
For personal use only.

Table 5. Selected bond distances and angles for **2*b*** (molecule A).

Bond lengths (Å)			
Sc(1)—C(25)	2.217(3)	C(1)—C(2)	1.488(4)
Sc(1)—C(29)	2.232(3)	C(2)—C(3)	1.375(4)
Sc(1)—N(2)	2.260(2)	C(3)—C(4)	1.399(4)
Sc(1)—N(6)	2.267(2)	C(4)—C(5)	1.515(4)
Sc(1)—N(4)	2.493(2)	C(5)—C(6)	1.512(5)
B(1)—N(1)	1.556(4)	C(5)—C(7)	1.528(4)
N(1)—C(2)	1.360(3)	C(5)—C(8)	1.534(4)
N(1)—N(2)	1.386(3)	C(25)—Si(1)	1.856(3)
N(2)—C(4)	1.349(3)	C(29)—Si(2)	1.858(3)
Bond angles (°)			
C(25)-Sc(1)-C(29)	99.28(10)	C(4)-N(2)-N(1)	106.9(2)
C(25)-Sc(1)-N(2)	130.90(9)	C(4)-N(2)-Sc(1)	142.2(2)
C(29)-Sc(1)-N(2)	94.68(9)	N(1)-N(2)-Sc(1)	110.02(14)
C(25)-Sc(1)-N(6)	123.24(9)	N(1)-C(2)-C(3)	107.7(2)
C(29)-Sc(1)-N(6)	90.03(9)	N(1)-C(2)-C(1)	123.4(3)
N(2)-Sc(1)-N(6)	103.44(8)	C(3)-C(2)-C(1)	128.9(3)
C(25)-Sc(1)-N(4)	98.07(8)	C(2)-C(3)-C(4)	107.0(2)
C(29)-Sc(1)-N(4)	162.64(9)	N(2)-C(4)-C(3)	109.0(2)
N(2)-Sc(1)-N(4)	74.27(7)	N(2)-C(4)-C(5)	123.5(2)
N(6)-Sc(1)-N(4)	79.88(7)	C(12)-N(4)-Sc(1)	147.1(2)
N(3)-B(1)-N(5)	109.2(2)	N(3)-N(4)-Sc(1)	106.28(14)
N(3)-B(1)-N(1)	108.9(2)	C(20)-N(6)-Sc(1)	139.3(2)
N(5)-B(1)-N(1)	113.8(2)	N(5)-N(6)-Sc(1)	105.35(14)
C(2)-N(1)-N(2)	109.4(2)	Si(1)-C(25)-Sc(1)	134.42(14)
C(2)-N(1)-B(1)	127.1(2)	Si(2)-C(29)-Sc(1)	134.8(2)
N(2)-N(1)-B(1)	122.4(2)		

(71%) of a ≈90% pure material. Further recrystallizations failed to improve the purity.

Synthesis of $(Tp^{Me,Me})Sc(CH_2SiMe_3)_2(THF)$, 2*a*, by alkane elimination

$ScCl_3(THF)_3$ (0.62 g, 1.7 mmol) and $LiCH_2SiMe_3$ (0.47 g, 5.0 mmol) were combined in a flask and attached to a swivel frit apparatus. The assemblage was evacuated and hexanes (≈25 mL) were vacuum transferred into the vessel at −78°C. The mixture was stirred at 0°C for 2 h, then filtered to remove LiCl. To the filtrate was added a solution of $Tp^{Me,Me}H$ (0.5 g, 1.7 mmol) in 10 mL of toluene at 0°C. The reaction solution was stirred at room temperature for 30 min, then reduced in volume to 5 mL and diluted with hexanes. The solid product (0.64 g, 67%) was collected on a frit, washed with cold hexanes, and dried under vacuum. Satisfactory microanalytical data could not be obtained on this compound, despite several attempts.

Synthesis of $(Tp^{tBu,Me})Sc(CH_2SiMe_3)_2$, 2*b*

$ScCl_3(THF)_3$ (0.50 g, 1.4 mmol) and $LiCH_2SiMe_3$ (0.38 g, 4.1 mmol) were combined in a flask and attached to a swivel frit apparatus. The assemblage was evacuated and hexanes (≈25 mL) were vacuum transferred into the vessel at −78°C. The mixture was stirred at 0°C for 2 h, then filtered to remove LiCl. To the filtrate was added a slurry of $Tp^{tBu,Me}H$ (0.57 g, 1.4 mmol) in 10 mL of hexanes at 0°C. The reaction solution was stirred at room temperature for 18 h, then reduced in volume to 5 mL and cooled to −35°C. Two crops of microcrystalline product (0.76 g, 87%) were collected by decanting away the mother liquor, then were washed with cold hexanes and dried under vacuum. Anal. calcd. for $C_{32}H_{62}N_6Si_2BSc$: C 59.79, H 9.72, N 13.04; found: C 55.61, H 9.44, N 12.84. This was the best of several microanalyses. The low carbon value is due either to incomplete combustion or the presence of a minor (<3%) unidentified impurity that could not be completely removed (see Fig. 2).

Identification of $Tp^{R,Me}Li$

$Tp^{R,Me}H$ (≈20 mg) was dissolved in 0.3 mL of C_6D_6. To this was added a solution of one equivalent of $LiCH_2SiMe_3$ in 0.4 mL of C_6D_6 in a dropwise fashion. The resulting cloudy solution was loaded into an NMR tube and the ^1H NMR spectrum was recorded. ^1H NMR spectrum for $Tp^{Me,Me}Li$ (200 MHz, C_6D_6, ppm): 5.78 (s, C*H*); 2.35 (s, C5-CH_3); 1.76 (C3-CH_3). ^1H NMR spectrum for $Tp^{tBu,Me}Li$ (200 MHz, C_6D_6, ppm): 5.71 (s, C*H*); 2.32 (s, C5-CH_3); 1.30 (s, C3-C(CH_3)$_3$.

X-ray crystallographic analysis of $(Tp^{Me,Me})Sc(CH_2SiMe_3)_2(THF)$, 2*a*

Single crystals suitable for X-ray crystallography were mounted in thin-walled glass capillaries and optically centered in the X-ray beam of an Enraf Nonius CAD-4 diffractometer. Unit cell dimensions were determined via least-squares refinement of the setting angles of 24 high-angle reflections and intensity data were collected using the ω–2θ scan mode. Data were corrected for Lorentz, polarization, and absorption effects but not for extinction. Pertinent data collection and structure refinement parameters are presented in Table 6. The

© 1997 NRC Canada

Can. J. Chem. Downloaded from www.nrcresearchpress.com by 88.146.161.215 on 09/08/12
For personal use only.

Table 6. Summary of data collection and structure refinement details for **2***a* and **2***b*.

Empirical formula	$C_{27}H_{42}N_6Si_2OBSc$	$C_{32}H_{62}N_6Si_2BSc$
fw	578.60	642.83
Crystal system	Monoclinic	Triclinic
Space group	$P2_1/c$	$P\bar{1}$
Crystal dimensions, mm	0.20 × 0.30 × 0.40	0.45 × 0.40 × 0.40
Temp, °K	294	173(2)
a, Å	11.765(4)	11.9427(2)
b, Å	14.8311(20)	20.3641(3)
c, Å	20.891(5)	26.5602(2)
α, °		112.192(1)
β, °	105.69(3)	100.569(1)
γ, °		92.928(1)
V, Å^3	3509.4(15)	5830.38(14)
Z	4	6
F(000)	1233.84	2100
d_{calc}, g cm^{-3}	1.095	1.098
μ, cm^{-1}	0.30	
h, k, l ranges	−12, 12; 0, 15; 0, 22	−14, 9; 22, −24; 31, −31
No. unique reflections	4592	19666
No. observed reflections ($I > 3.0\sigma$)	1912	
No. of parameters	343	1189
k value	0.000050	
Min/Max transmission	0.453/0.965	0.835/0.887
Max residual density, e Å^{-3}	0.520	0.739
Min residual density, e Å^{-3}	−0.590	−0.417
R, R_w	0.088, 0.082	0.0500, 0.1137
gof	3.46	1.038

structure was solved using direct methods. All non-hydrogen atoms were refined with anisotropic thermal parameters. Aryl and methylene hydrogens were placed in calculated positions (D_{C-H} = 1.00 and 1.08 Å, respectively) whereas methyl hydrogen atoms were located via inspection of difference Fourier maps. Hydrogen atoms were given isotropic temperature factors based upon the atom to which they are bonded and fixed during least-squares refinement. A weighting scheme based upon counting statistics was used with the weight modifier *k* in kF_o^2 being determined via evaluation of variation in the standard reflections that were collected during the course of data collection. Neutral atom scattering factors were taken from *International tables for X-ray crystallography* (23). Values of *R* and R_w are given by $R = (F_o - F_c)/EF_o$ and $R_w = [E(w(F_o - F_c))^2/E(wF_o^2)]^{1/2}$. All crystallographic calculations were conducted with the PC version of the NRCVAX program package (24) locally implemented on an IBM-compatible 80486 computer. Anisotropic thermal parameters and hydrogen atom parameters are available as supplementary material.[6]

[6] Copies of material on deposit may be purchased from: The Depository of Unpublished Data, Document Delivery, CISTI, National Research Council Canada, Ottawa, Canada K1A 0S2. Tables of atomic coordinates and of bond lengths and angles have also been deposited with the Cambridge Crystallographic Data Centre, and can be obtained on request from The Director, Cambridge Crystallographic Data Centre, University Chemical Laboratory, 12 Union Road, Cambridge, CB2 1EZ, U.K.

X-ray crystallographic analysis of $(Tp^{tBu,Me})Sc(CH_2SiMe_3)_2$, 2*b*

A crystal of **2***b* was attached to a glass fiber and mounted on the Siemens SMART system for a data collection at 173(2) K. An initial set of cell constants was calculated from reflections harvested from three sets of 30 frames. Final cell constants were calculated from a set of 8082 strong reflections from the actual data collection. See Table 6 for additional crystal and refinement information.

In the hemisphere collection technique employed here, a randomly oriented region of reciprocal space is surveyed to the extent of 1.3 hemispheres to a resolution of 0.84 Å. Three major swaths of frames are collected with 0.30° steps in ω. This collection strategy provides a high degree of redundancy in the data, providing good ψ input in the event that an empirical absorption correction is applied (see Table 6). Frames were 45 s in duration.

The space group $P\bar{1}$ was determined based on systematic absences and intensity statistics. A successful direct-methods solution was calculated that provided most non-hydrogen atoms from the *E*-map. Several full-matrix least-squares difference/Fourier cycles were performed that located the remainder of the non-hydrogen atoms. All non-hydrogen atoms were refined with anisotropic displacement parameters. All hydrogen atoms were placed in ideal positions and refined as riding atoms with individual (or group, if appropriate) isotropic displacement parameters. In the space group $P\bar{1}$, $Z = 6$, so three independent molecules were found in the asymmetric unit. All calculations were performed using SGI INDY

© 1997 NRC Canada

R4400-SC or Pentium computers using the SHELXTL V5.0 suite of programs.[7]

Acknowledgments

Financial support for this work was provided by the Natural Sciences and Engineering Research Council of Canada. W.E.P. thanks Professor Ged Parkin (Columbia University) for providing details on the unpublished preparations for the protonated tris-pyrazolylborate reagents and Professor Joe Takats (University of Alberta) for helpful discussions and access to his unpublished results concerning compound **1***a*.

References

1. (*a*) N. Kitajima and W.B. Tolman. Prog. Inorg. Chem. **43**, 419 (1995); (*b*) S. Trofimenko. Chem. Rev. **93**, 943 (1993); (*c*) P.K. Byers, A.J. Canty, and R.T. Honeyman. Adv. Organomet. Chem. **34**, 1 (1992).
2. G. Parkin. Adv. Inorg. Chem. **42**, 291 (1995).
3. L. Hasinoff, J. Takats, X.W. Zhang, A.H. Bond, and R.D. Rogers. J. Am. Chem. Soc. **116**, 8833 (1994).
4. D.L. Reger, J.A. Lindeman, and L. Lebioda. Inorg. Chem. **27**, 1890 (1988).
5. D.L. Reger, J.A. Lindeman, and L. Lebioda. Inorg. Chim. Acta, **139**, 71 (1987).
6. (*a*) R. Han, A. Looney, and G. Parkin. J. Am. Chem. Soc. **111**, 7276 (1989); (*b*) A. Looney and G. Parkin. Polyhedron, **9**, 265 (1990).
7. D.L. Reger. Coord. Chem. Rev. **147**, 571 (1996).
8. (*a*) M.C. Kuchta and G. Parkin. J. Am. Chem. Soc. **117**, 12651 (1995); (*b*) M.C. Kuchta, H.V.R. Dias, S.G. Bott, and G. Parkin. Inorg. Chem. **35**, 943 (1996).
9. M.D. Fryzuk, G. Giesbrecht, and S.J. Rettig. Organometallics, **15**, 3329 (1996).
10. Y. Mu, W.E. Piers, D.C. MacQuarrie, M.J. Zaworotko, and V.G. Young, Jr. Organometallics, **15**, 2720 (1996).
11. Y. Mu, W.E. Piers, D.C. MacQuarrie, and M.J. Zaworotko. Can. J. Chem. **74**, 1696 (1996).
12. S. Trofimenko. J. Am. Chem. Soc. **89**, 3170 (1967).
13. M.F. Lappert and R. Pearce. J. Chem. Soc. Chem. Commun. 126 (1973).
14. M.E. Thompson, S.M. Baxter, A.R. Bulls, B.J. Burger, M.C. Nolan, B.D. Santarsiero, W.P. Schaefer, and J.E. Bercaw. J. Am. Chem. Soc. **109**, 203 (1987).
15. (*a*) J.L. Atwood and K.D. Smith. J. Chem. Soc. Dalton Trans. 921 (1974); (*b*) B.K. Campion, R.H. Heyn, and T.D. Tilley. Organometallics, **12**, 2584 (1993).
16. S. Trofimenko, J.C. Calabrese, J.K. Kochi, S. Wolowiec, F.B. Hulsbergen, and J. Reedijk. Inorg. Chem. **31**, 3943 (1992).
17. D.L. Reger and Y. Ding. Organometallics, **12**, 4485 (1993).
18. B.J. Burger and J.E. Bercaw. ACS Symp. Ser. **357** (1987).
19. R.H. Marvich and H.H. Brintzinger. J. Am. Chem. Soc. **93**, 2046 (1971).
20. D.D. Perrin and W.L.F. Armarego. Purification of laboratory chemicals. 3rd ed. Pergamon Press, New York. 1988.
21. L.E. Manzer. Inorg. Synth. **21**, 135 (1982).
22. (*a*) S. Trofimenko. J. Am. Chem. Soc. **89**, 6288 (1967); (*b*) S. Trofimenko, J.C. Calabrese, and J.S. Thompson. Inorg. Chem. **26**, 1507 (1987).
23. International tables for X-ray crystallography. Vol. IV. Kynoch Press, Birmingham, England. 1974.
24. E.J. Gabe, Y. Le Page, J.-P. Charland, F.L. Lee, and P.S. White. J. Appl. Crystallogr. **22**, 384 (1989).

[7] SHELXTL-Plus V5.0, Siemens Industrial Automation, Inc., Madison, Wis.

Can. J. Chem. Downloaded from www.nrcresearchpress.com by 88.146.161.215 on 09/08/12
For personal use only.

© 1997 NRC Canada

Synthesis of 1-*N*-hydroxyhydantoin 5-phosphates as potential fungicides

Stephen Hanessian, Rui-Yang Yang, and Jean-Yves Sancéau

Abstract: Two hydantoin analogs were synthesized utilizing an organometallic allylation reaction in aqueous solution as a key step. One of the derivatives showed weak fungicidal activity.

Key words: hydantoin, fungicide, phosphate.

Résumé : Deux dérivés hydantoïniques ont été synthétisés utilisant une allylation organométallique en milieux aqueux comme réaction clé. L'un des dérivés a démontré une activité fongicidale faible.

Mots clés : hydantoïne, fongicide, phosphate.

Can. J. Chem. Downloaded from www.nrcresearchpress.com by 88.146.161.215 on 09/08/12
For personal use only.

Since the discovery of hydantocidin **1** (1), a potent nontoxic herbicide, a number of syntheses of this unusual compound (2) together with modifications of both the hydantoin ring (3) and the sugar unit (4) have been reported (5). Detailed investigations on its mode of action have recently shown that a phosphorylation occurs at the 5′-position to form the active principle **2** (6). In a previous paper, we described the synthesis of a prototype structure that incorporates an 1-*N*-hydroxyhydantoin motif as shown in express ion **3** (7). Continuing our interest in the design and synthesis of structurally novel 1-*N*-hydroxy hydantoins, we describe herein new target molecules of type **4**, in which the carbohydrate moiety of the parent hydantocidin **1** has been replaced by an acyclic chain terminating with a phosphate ester (Fig. 1).

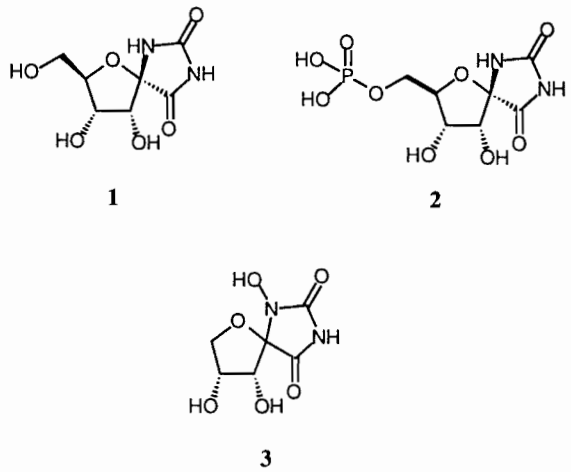
The retrosynthetic route of **4** is shown in Fig. 2, and relies on a recently published method from our laboratory for the asymmetric synthesis of L-allylglycine (8). Variations in the length of the acyclic chain at C-5 of the heterocycle can be easily obtained from the allyl group via simple chemical transformations.

The target molecules were prepared as shown in Schemes 1 and 2. Thus, reaction of allyl bromide, the *O*-benzyl oxime of 2-propyl glyoxylate **5**, and commercial zinc powder in aqueous NH_4Cl–THF solution gave the allylglycine derivative **6** in 98% yield. The crude product **6** was pure enough for the next reaction, where it was reacted with chlorosulfonyl isocyanate in CH_2Cl_2 at −78°C to afford the *N*-benzyloxy urea derivative **7**. The latter was treated with TBAF in refluxing THF to give the key intermediate 1-*N*-benzyloxy-5-allylhydantoin **8**. Hydroboration with 2 equivalents of 9-BBN, followed by oxidation with 30% H_2O_2 in 3 M NaOAc aqueous solution at 50°C provided the hydroxy compound **9** in 63% yield. These oxidation conditions were crucial for the success of this reaction, since other conditions (for example, 30% H_2O_2 in NaOH, MCPBA, etc.) resulted in unacceptably low yields. Treatment of **9** under Mitsunobu conditions gave the corresponding dibenzyl phosphate ester, which upon hydrogenolysis led to the target compound **4a**.

The two-carbon chain analog **4b** was obtained from the common intermediate **8** (Scheme 2). Thus, ozonolysis followed by reduction with $NaBH_4$ afforded **11**. A Mitsunobu reaction with dibenzylphosphoric acid and hydrogenolysis of the product **12** gave *N*-hydroxy hydantoin 5-phosphate **4b**.

Compounds **4a** and **4b** were tested for fungicidal activity. Interestingly, weak but reproducible inhibitory activity was found against *Erysiphe graminis* (mildew) by foliar application for compound **4a**, but not for the two-carbon chain analog **4b**. Thus, structural and functional features present in hydantoin motifs such as **4a** are of interest, and further exploration of this venerable heterocycle in connection to fungicidal and related activities are worthy of further study.

Fig. 1.



Received December 12, 1996.

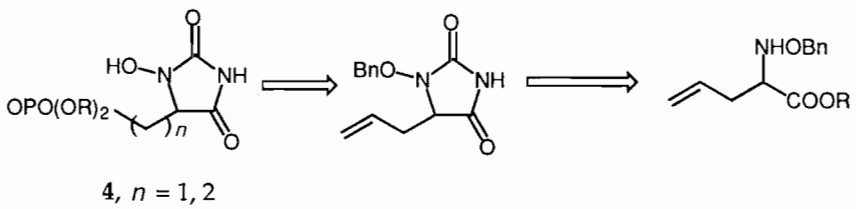
This paper is dedicated to Professor William A. Ayer on the occasion of his 65th birthday.

S. Hanessian,[1] R.-Y. Yang, and J.-Y. Sancéau. Department of Chemistry, Université de Montréal, C.P. 6128, Succursale A, Montréal, QC H3T 3J7, Canada.

[1] Author to whom correspondence may be addressed. Telephone: (514) 343-6738. Fax: (514) 343-5728. E-mail: hanessia@ere.umontreal.ca

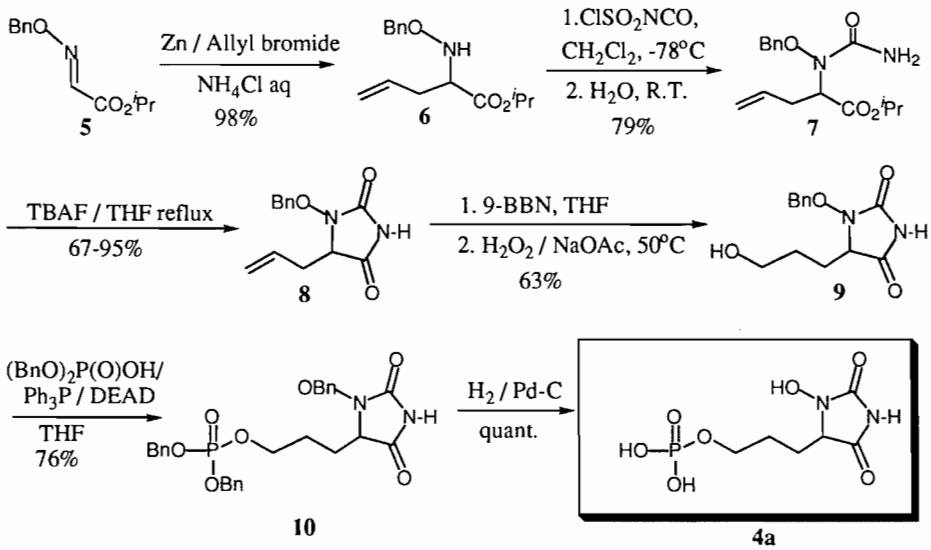
© 1997 NRC Canada

Fig. 2.

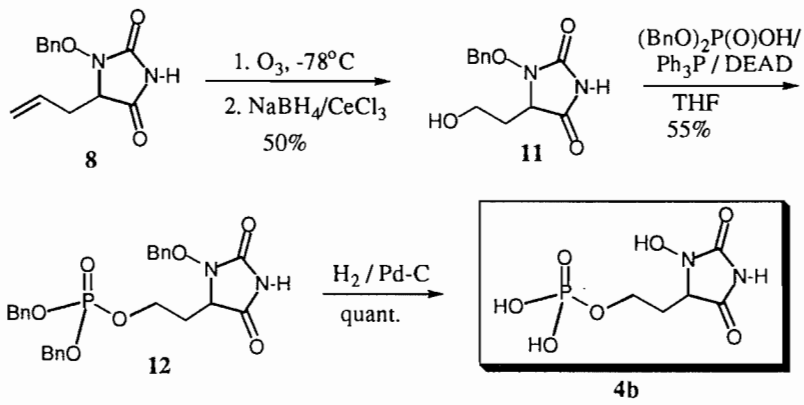


4, $n = 1, 2$

Scheme 1.



Scheme 2.



Experimental

Tetrahydrofuran was distilled over benzophenone and potassium prior to use. Analytical thin-layer chromatography (TLC) was carried out on Merck Kieselgel silica gel 60 F_{254} glass plates. ^{1}H nuclear magnetic resonance spectra were obtained on a Bruker WH-400 spectrometer. ^{1}H multiplicities are recorded by use of the following abbreviations: s, singlet; d, doublet; m, multiplet; br, broad; *J*, coupling constant (Hz). High-resolution mass spectra were recorded by means of Kratos MS5OTCTA and AEI-MS 902 spectrometers at l'Université de Montréal. Melting points were measured on a Buchi apparatus and are uncorrected. Column chromatography was done using the flash technique (9).

Can. J. Chem. Downloaded from www.nrcresearchpress.com by 88.146.161.215 on 09/08/12
For personal use only.

© 1997 NRC Canada

Can. J. Chem. Downloaded from www.nrcresearchpress.com by 88.146.161.215 on 09/08/12
For personal use only.

N-Benzyloxy-allylglycine 2-propyl ester (6)

Commercial zinc powder (114 mg, 1.8 mmol) was added portionwise to a biphasic solution containing oxime **5** (221 mg, 1.0 mmol), allyl bromide (1.4 mmol) in THF (1 mL), and aqueous NH_4Cl (2 mL) at room temperature (rt). The mixture was stirred for 5 min, the reaction mixture was extracted with ethyl acetate (10 mL × 3), and dried over $MgSO_4$. After concentration, the crude product was purified by column chromatography on silica gel with 10% ethyl acetate in hexanes as eluent to give pure product **6** as an oil (258 mg, 98%). ^1H NMR ($CDCl_3$) δ: 1.26 (d, J = 6.3 Hz, 3H), 1.29 (d, J = 6.3 Hz, 3H), 2.32–2.37 (m, 2H), 3.66 (t, J = 6.8 Hz, 1H), 4.74 (s, 2H), 5.06–5.16 (m, 2H), 5.68–5.82 (m, 1H), 7.27–7.36 (m, 5H). ^{13}C NMR ($CDCl_3$) δ: 21.78, 21.81, 33.85, 63.20, 68.44, 76.08, 117.98, 127.70, 128.22, 128.29, 133.08, 137.70, 172.55 ppm. MS (FAB) *m/z*: 264(M+H, 100), 222(10), 176(7). HRMS calcd. for $C_{15}H_{22}NO_3$ (M+H): 264.1600; found: 264.1585.

N-Benzyloxy-N-ureido allylglycine 2-propyl ester (7)

To a solution of **6** (263 mg, 1.0 mmol) in CH_2Cl_2 at −78°C was added chlorosulfonylisocyanate (212 mg, 1.5 mmol) under argon, and the resulting solution was stirred for 2 h at that temperature. Water (10 mL) was added and the reaction mixture was allowed to slowly warm to rt. After stirring overnight, the reaction mixture was extracted with CH_2Cl_2 (3 × 10 mL), the combined organic phase was dried over Na_2SO_4 and concentrated. The residue was purified by column chromatography on silica gel (30% EtOAc – hexanes) to give 243 mg of a white solid **7** (79%), mp 64–66°C. ^1H NMR ($CDCl_3$) δ: 1.24 (d, J = 5.2 Hz, 3H), 1.26 (d, J = 5.2 Hz, 3H), 2.67–2.87 (m, 2H), 4.86 (dd, J = 5.6 Hz, J' = 9.6 Hz, 1H), 4.90–4.98 (m, 2H), 5.05 (sept, 1H), 5.10–5.19 (m, 2H), 5.45 (br, 2H), 5.83–5.97 (m, 1H), 7.37 (s, 5H). ^{13}C NMR ($CDCl_3$) δ: 21.70, 32.08, 62.04, 69.01, 78.27, 117.73, 128.67, 128.77, 128.86, 134.29, 134.96, 169.59 ppm. MS (FAB) *m/z*: 307(M+H, 100), 264(92), 222(27), 176(20). HRMS calcd. for $C_{16}H_{23}N_2O_4$ (M+H): 307.1658; found: 307.1668.

1-N-Benzyloxy-5-allylhydantoin (8)

To a solution of **7** (0.955 g, 3.11 mmol) in THF (5 mL) was added tetra-*n*-butylammonium fluoride (TBAF) in THF (1 M, 4.5 mL), and the resulting mixture was brought to reflux until all the starting material was consumed. After cooling to rt, water (10 mL) was added, the resulting mixture was then extracted with ethyl acetate (10 mL × 3), and the combined organic phase was washed throughly with water to remove TBAF. The organic phase was dried with Na_2SO_4 and concentrated, and the residue was purified by column chromatography on silica gel (20% EtOAc – hexanes) to give **8** in 87–90% yield. ^1H NMR ($CDCl_3$) δ: 2.46–2.64 (m, 2H), 3.97 (t, J = 4.8Hz, 1H), 5.05 (AB, J = 10.7 Hz, J = 16.4 Hz, 2H), 5.16–5.20 (m, 2H), 5.61–5.74 (m, 1H), 7.27–7.46 (m, 5H). ^{13}C NMR ($CDCl_3$) δ: 32.52, 64.22, 79.16, 120.36, 128.61, 129.05, 129.43, 130.47, 134.89, 157.47, 169.55 ppm. MS (FAB) *m/z*: 247.1(M+H, 100). HRMS calcd. for $C_{13}H_{15}N_2O_3$: 247.1083; found: 247.1094.

1-N-Benzyloxy-5-(3-hydroxypropyl)-hydantoin (9)

To a solution of **8** (437 mg, 1.78 mmol) in THF (8 mL) was added 7.8 mL of a THF solution of 9-BBN (0.5 M, 3.9 mmol), at 10°C to 0°C and the resulting solution was stirred for 2.5 h below −5°C. A solution of 30% H_2O_2 (3 mL) was added, followed by 5 mL of 3 M aqueous sodium acetate, and the resulting mixture was heated at 50°C for 4 h. After cooling to rt, the reaction mixture was extracted with EtOAc (15 mL × 4), and the combined organic phase was dried over Na_2SO_4 and concentrated. The residue was purified by column chromatography on silica gel (70% EtOAc – hexanes) to give a white solid **9** (297 mg, 63%), mp 87–89°C. ^1H NMR ($CDCl_3$) δ: 1.38–1.59 (m, 2H), 1.68–1.93 (m, 2H), 2.40 (br, 1H), 3.54 (t, J = 6.3 Hz, 2H), 3.96 (dd, J = 4.1 Hz, J' = 5.6 Hz, 1H), 5.03 (AB, quart. J = 11.0 Hz, J' = 18.5 Hz, 2H), 7.27–7.45 (m, 5H), 8.97 (s, 1H). ^{13}C NMR ($CDCl_3$) δ: 24.56, 26.52, 61.64, 63.86, 79.01, 128.59, 129.01, 129.55, 135.03, 158.37, 171.31 ppm. MS *m/z*: 266(M+2, 20), 265(M+H, 100), 181(12). HRMS calcd. for $C_{13}H_{17}N_2O_4$ (M+H): 265.1188; found: 265.1179.

1-N-Benzyloxy-5-(3-dibenzylphosphorylpropyl)-hydantoin (10)

To a solution of **9** (132 mg, 0.5 mmol), dibenzylphosphoric acid (140 mg, 0.5 mmol), and PPh_3 (131 mg, 0.5 mmol) in THF (6 mL) was added dropwise DEAD (0.17 mL, 1.0 mmol) under argon at rt. After 2 h, another portion of dibenzylphosphoric acid (140 mg, 0.5 mmol) and PPh_3 (131 mg, 0.5 mmol) was added, followed by 0.16 mL DEAD (1.0 mmol), dropwise, and the resulting mixture was stirred overnight. The reaction mixture was quenched with water, extracted with EtOAc (15 mL × 3), and the combined organic phase was dried over Na_2SO_4 and concentrated. The residue was purified by column chromatogarphy on silica gel (60% EtOAc – hexanes) to give **10** as a white solid (200 mg, 76%), mp 78–80°C. ^1H NMR ($CDCl_3$) δ: 1.51–1.70 (m, 3H), 1.76–1.85 (m, 1H), 3.84–3.93 (m, 3H), 4.94–5.10 (m, 6H), 7.35–7.42 (m, 15H), 8.98 (s, 1H). ^{13}C NMR ($CDCl_3$) δ: 24.47, 24.57, 63.65, 66.87, 69.27, 69.34, 79.05, 127.91, 128.50, 128.53, 128.58, 129.02, 129.51, 135.00, 135.66, 135.75, 158.00, 169.94 ppm. MS *m/z*: 525(M+H, 26), 417(5), 247(43), 181(51), 91(100). HRMS calcd. for $C_{27}H_{29}N_2O_7P$ (M+H): 525.1791; found: 525.1808.

1-N-Hydroxy-5-(3-dihydrophosphorylpropyl)-hydantoin (4a)

A solution of **10** (131 mg, 0.25 mmol) in MeOH (5 mL) was subjected to hydrogenolysis under H_2 (1 atm (= 101.3 kPa)) in the presence of 5% Pd–C (10 mg) at rt overnight. After filtration, the filtrate was concentrated to give **4a** in quantitative yield. ^1H NMR (CD_3OD) δ: 1.67–2.05 (m, 4H), 3.99–4.03 (m, 2H), 4.18 (t, J = 3.0 Hz, 1H). ^{13}C NMR (CD_3OD) δ: 25.97, 26.28 (d), 65.66, 67.10 (d), 160.37, 173.14 ppm. HRMS calcd. for $C_6H_{12}N_2O_7P$ (M+H): 254.0279; found: 254.0280.

1-N-Benzyloxy-5-(2-hydroxyethyl)-hyantoin (11)

A stream of ozone was passed through a solution of **8** (121 mg, 0.5 mmol) in a mixture of CH_2Cl_2–MeOH (10 mL, 1/1) at −78°C until a blue color persisted (10 min). A solution of $CeCl_3 \cdot 7H_2O$ (465 mg, 1.2 mmol) was added, followed by $NaBH_4$ (50 mg, 1.2 mmol). The cooling bath was removed and the mixture was allowed to warm to 0°C. After 1 h of stirring, it was neutralized with 5% aqueous acetic acid, then concentrated. The aqueous solution was extracted several times with EtOAc, and the organic phase was washed with brine, dried (Na_2SO_4), and concentrated. The residue was purified by column chromatography on silica gel (EtOAc – hexanes, 1/1) to

© 1997 NRC Canada

Can. J. Chem. Downloaded from www.nrcresearchpress.com by 88.146.161.215 on 09/08/12
For personal use only.

give the alcohol **11** as a white solid (81 mg, 66%), mp 62°C. ^{1}H NMR ($CDCl_3$) δ: 1.84–2.06 (m, 2H), 3.66–3.71 (m, 2H), 4.01 (t, J = 6.6 Hz, 1H), 5.05 (dd, 2H), 7.40–7.46 (m, 5H), 7.70 (s, 1H). ^{13}C NMR ($CDCl_3$) δ: 30.73, 57.79, 61.84, 78.99, 128.58, 128.99, 129.35, 134.98, 158.33, 172.10 ppm. HRMS calcd. for $C_{12}H_{14}N_2O_4$ (M+H): 251.1032; found: 251.1045.

1-*N*-Benzyloxy-5-(2-dibenzylphosphorylethyl)-hydantoin (12)

Triphenylphosphine (162 mg, 0.62 mmol), and dibenzylphosphate (166.3 mg, 0.62 mmol) were added to a solution of alcohol **11** (75 mg, 0.31 mmol) in dry THF (2 mL). DEAD (0.195 μL, 1.24 mmol) was slowly added to the solution and, after 5 h of stirring, the solvent was evaporated. The crude product was chromatographed (EtOAc – hexanes, 4/1) to yield **12** (85 mg, 55%). ^{1}H NMR ($CDCl_3$) δ: 1.75–2.05 (m, 2H), 3.85–3.97 (m, 4H), 4.85–4.98 (m, 6H), 7.18–7.29 (m, 15H). ^{13}C NMR ($CDCl_3$) δ: 29.00(d), 60.60, 62.97(d), 69.29(d), 77.32, 78.82, 127.85, 128.41, 128.45, 128.89, 129.43, 134.80, 135.41, 135.50, 158.14, 170.00 ppm. HRMS calcd. for $C_{26}H_{28}N_2O_7P$ (M+H): 510.1678; found: 510.1584.

1-*N*-Hydroxy-5-(2-dihydrophosphorylethyl)-hydantoin (4b)

The dibenzylphosphate hydantoin **12** (80 mg, 0.156 mmol) in MeOH (10 mL) was hydrogenolyzed in the presence of 10% Pd–C (10 mg) under atmospheric pressure for 5 h. The catalyst was filtered off and the solvent was evaporated to give **4b** in 95% yield (35 mg). ^{1}H NMR (CD_3OD) δ: 1.95 (m, 2H), 3.90 (m, 2H), 3.97 (t, J = 5.8 Hz, 1H). ^{13}C NMR (CD_3OD) δ: 31.3(d), 63.1, 63.56(d), 160.59, 173.12 ppm. HRMS calcd. for $C_5H_{10}N_2O_7P$ (M+H): 240.0123; found 240.0156.

Acknowledgments

We thank the Natural Sciences and Engineering Research Council of Canada (NSERC) for financial support through the University–Industry collaborative program. We are also extremely grateful to Dr. Philippe Chemla and colleagues at Ciba-Agro for the biological tests and for stimulating discussions.

References

1. (*a*) M. Nakajima, K. Itoi, Y. Takamatsu, T. Kinoshita, T. Okazaki, K. Kawakubo, M. Shindo, T. Honma, M. Tohjigamori, and T. Haneishi. J. Antibiot. **44**, 293 (1991); (*b*) H. Haruyama, T. Takayama, T. Kinoshita, M. Kondo, M. Nakajima, and T. Haneishi. J. Chem. Soc. Perkin Trans. 1, 1637 (1991).
2. (*a*) C. Lamberth and S. Blarer. Synth. Commun. **26**, 75 (1996); (*b*) N. Nakajima, M. Kirihara, M. Hashimoto, T. Katoh, and S. Terashima. Tetrahedron, **52**, 1177 (1996); (*c*) N. Nakajima, M. Kirihara, M. Hashimoto, and T. Katoh. Heterocycles, **42**, 503 (1996); (*d*) T.H. Fruh, P. Chemla, J. Enrler, and S. Faraaq. Pestic. Sci. **46**, 37 (1996); (*e*) H. Sano, S. Mio, M. Hamura, J. Kitagawa, M. Shindou, T. Honma, and S. Sugai. Biosci. Biotechnol. Biochem. **59**, 2247 (1995); (*f*) P.M. Harrington and M.E. Jung. Tetrahedron Lett. **35**, 5145 (1994); (*g*) P. Chemla. Tetrahedron Lett. **34**, 7391 (1993); (*h*) M. Matsumoto, M. Kirihara, T. Yoshino, T. Katoh, and S. Terashima. Tetrahedron Lett. **34**, 6289 (1993); (*i*) S. Mio, Y. Kumagawa, and S. Sugai. Tetrahedron, **47**, 2133 (1991); (*j*) S. Mio, R. Ichinose, K. Goto, and S. Sugai. Tetrahedron, **47**, 2111 (1991).
3. (*a*) H. Sano, S. Mio, J. Kitagawa, M. Shindou, T. Honma, and S. Sugai. Tetrahedron, **51**, 12563 (1995); (*b*) A.J. Fairbanks and G.W.J. Fleet. Tetrahedron, **51**, 3881 (1995); (*c*) H. Sano, S. Mio, J. Kitagawa, and S. Sugai. Tetrahedron: Asymmetry, **5**, 2233 (1994); (*d*) S. Mio, H. Sano, M. Shindou, T. Honma, and S. Sugai. Agric. Biol. Chem. **55**, 1105 (1991); (*e*) S. Mio, M. Ueda, M. Hamura, J. Kitagawa, and S. Sugai. Tetrahedron, **47**, 2145 (1991).
4. (*a*) T.W. Brandstetter, C. Fuente, Y. Kim, L.N. Johnson, S. Crook, P.M.Q. Lilley, D.J. Watkin, K.F. Tsitsanou, S.E. Zographos, E.D. Chrysina, N.G. Oikonomakos, and G.W.J. Fleet. Tetrahedron, **52**, 10721 (1996); (*b*) T.W. Brandstetter, M.R. Wormald, R.A. Dwek, T.D. Butters, F.M. Platt, K.E. Tsitsanou, S.E. Zographos, N.G. Oikonomakos, and G.W.J. Fleet. Tetrahedron: Asymmetry, **7**, 157 (1996); (*c*) C.J.F. Bichard, E.P. Mitchell, M.R. Wormald, K.A. Watson, L.N. Johnson, S.E. Zographos, D.D. Koutra, N.G. Oikonpmakos, and G.W.J. Fleet. Tetrahedron Lett. **36**, 2145 (1995).
5. (*a*) J.C. Estevez, M.D. Smith, M.R. Wormald, G.S. Besra, P.J. Brennan, R.J. Nash, and G.W.J. Fleet. Tetrahedron: Asymmetry, **7**, 391 (1996); (*b*) J.C. Estevez, M.D. Smith, A.L. Lane, S. Crook, D.J. Watkin, G.S. Besra, P.J. Brennan, R.J. Nash, and G.W.J. Fleet. Tetrahedron: Asymmetry, **7**, 387 (1996); (*c*) T.M. Krulle, K.A. Watson, M. Gregoriou, L.N. Johnson, S. Crook, D.J. Watkin, R.C. Griffiths, R.J. Nash, K.E. Tsitsanou, S.E. Zographos, N.G. Oikonomakos, and G.W.J. Fleet. Tetrahedron Lett. **36**, 8291 (1995); (*d*) J.C. Estevez, D.D. Long, M.R. Wormald, R.A. Dwek, and G.W.J. Fleet. Tetrahedron Lett. **36**, 8287 (1995); (*e*) T.W. Brandstetter, Y. Kim, J.C. Son, H.M. Tayor, P.M.Q. Lilley, D.J. Watkin, L.N. Johnson, N.G. Oikonomakos, and G.W.J. Fleet. Tetrahedron Lett. **36**, 2149 (1995).
6. R. Fonné-Pfister, P. Chemla, E. Ward, M. Girardet, K.E. Kreutz, R.B. Honzatko, H.J. Fromm, H.-P. Schär, M.G. Grütter, and S.W. Cowan-Jacob. Proc. Natl. Acad. Sci. USA, **93**, 9431 (1996).
7. S. Hanessian, J.-Y. Sanceau, and P. Chemla. Tetrahedron, **51**, 6669 (1995).
8. S. Hanessian and R.-Y. Yang. Tetrahedron Lett. **37**, 5273 (1996).
9. W.C. Still, M. Kahn, and A. Mitra. J. Org. Chem. **43**, 2923 (1978).

© 1997 NRC Canada

Bioactive compounds from an endophytic fungus from eastern larch (*Larix laricina*) needles

John A. Findlay, Guoqiang Li, and John A. Johnson

Abstract: The structures of two novel metabolites isolated from cultures of an unidentified endophytic fungus obtained from an eastern larch (*Larix laricina* (Du Roi) K. Koch) needle were shown to be 8,1′,5′-trihydroxy-3′,4′dihydro-1′*H*-[2,4′]binaphthalenyl-1,4,2′-trione, **1**, and 2-methyloctanoic acid 6-oxo-2-propenyl-3,6-dihydro-2*H*-pyran-3-yl ester, **2**. Structures were determined by spectroscopic means. Compound **1** was toxic to spruce budworm (*Choristoneura fumiferana Clem.*) larvae while **2** was active against *Vibrio salmonicida*, *Pseudomonas aeruginosa*, and *Staphylococcus aureus*.

Key words: insect toxin, *Larix laricina* endophyte, antimicrobial, endophyte metabolite.

Résumé : On a établi les structures de deux nouveaux métabolites isolés de cultures d'un champignon endophytique non identifié des aiguilles d'un mélèze de l'Est (*Larix laricina* (Du Roi) K. Koch); il s'agit de la 8,1′,5′-trihydroxy-3′,4′dihydro-1′*H*-[2,4′]binaphthalényl-1,4,2′-trione, **1**, et de l'ester 2-méthyloctanoic de 6-oxoprop-2-ényl-3,6-dihydro-2*H*-pyran-3-yle ester, **2**. On a déterminé les structures par des méthodes spectroscopiques. Le composé **1** est toxique pour les larves de la tordeuse des bourgeons d'épinette (*Choristoneura fumiferana Clem.*) alors que le composé **2** est actif contre les *Vibrio salmonicida*, *Pseudomonas aeruginosa* et *Staphylococcus aureus*.

Mots clés : insecticide, endophyte *Larix laricina*, antimicrobien, métabolite d'endophyte.

[Traduit par la rédaction]

In the past we reported on the isolation of several insect toxins from cultures of endophytic fungi originating from conifer needles. Thus, by bioassay-guided fractionation, rugulosin was isolated as the toxic agent produced by a strain of *Hormonema dermatioides*, and heptelidic acid and two novel derivatives were isolated from cultures of a *Phyllosticta* sp. strain (1). More recently we characterized two novel isopimarane diterpenoids responsible for the insect toxicity of an unidentified endophyte from balsam fir (*Abies. balsamea* (L.) Mill.)(2) and two toxic isocoumarins from a culture of *Conoplea elegantula* originating from black spruce (*Picea mariana* BSP) needles (3).

Continuing our search for bioactive agents from conifer needle endophytes, we have examined the constituents of cultures of an unidentified endophyte L1930 obtained from an eastern larch (*Larix laricina* (Du Roi) K. Koch) needle. This endophyte displayed significant inhibition of the salmon pathogen *Vibrio salmonicida*, as well as *Pseudomonas aeruginora* and *Staphylococcus aureus* in agar diffusion assays (4). We now report the isolation and structure elucidation of two novel bioactive agents from cultures of L1930.

Compound **1** was isolated as an optically active ($[\alpha]_D$ +178), yellow crystalline (mp 214–216°C), UV-active (λ max 212, 256, 334, 418 nm) substance of composition $C_{20}H_{14}O_6$ as revealed by HREIMS. Strong absorptions in the IR spectrum (3500, 1635, 1610 cm^{-1}) were indicative of hydroxyl, conjugated carbonyl, and aromatic features. Due to low solubility in $CDCl_3$ and overlap of some aromatic signals in methanol-d_4 and acetone-d_6, the NMR data (Table 1) were recorded in pyridine-d_5 despite slow decomposition of **1** in this medium. In the ^1H NMR spectrum in acetone-d_6, three signals exchange in D_2O, two of which are attributed to phenolic (δ12.43, 12.00) features and the other (δ4.88) to a secondary hydroxyl, in view of its coupling (J = 4.8 Hz) to a methine proton at δ5.03 as revealed by the COSY spectrum in acetone-d_6.

The ^1H NMR and COSY spectra (pyridine-d_5) showed the presence of an AMX system comprising methylene protons at δ3.77 and δ2.82 coupled with a methine at δ4.11. In addition, two AMX systems, typical of 1,2,3-trisubstituted benzene rings, gave rise to mutually coupled signals at δ7.63 (dd, J = 7.4, 1.0 Hz), 7.54 (dd, J = 8.6, 7.4 Hz), 7.30 (dd, J = 8.6, 1.0 Hz) and δ7.06 (dd, J = 8.6, 1.0 Hz), 7.48 (dd, J = 8.6, 7.6 Hz), 7.09 (bd, J = 7.6 Hz). A small (allylic) coupling (J = 1.2 Hz) also exists between the methine signals at δ4.11 and δ5.35 and between δ4.11 and δ7.39 noted in the COSY spectrum and confirmed by decoupling experiments. Thus the ^1H NMR spectral data support the structural feature -CH═C-CH(CH_2)C═C-CHOH in addition to two 1,2,3-trisubstituted benzene rings.

The presence of these moieties together with three ketonic

Received October 30, 1996.

This paper is dedicated to Professor William A. Ayer on the occasion of his 65th birthday.

J.A. Findlay[1] **and G. Li.** Chemistry Department, University of New Brunswick, Fredericton, NB E3B 6E2, Canada.
J.A. Johnson. Department of Biology, University of New Brunswick, Saint John, NB E2L 4L5, Canada.

[1] Author to whom correspondence may be addressed. Telephone: (506) 453-4868. Fax: (506) 453-4981.

© 1997 NRC Canada

Can. J. Chem. Downloaded from www.nrcresearchpress.com by 88.146.161.215 on 09/08/12
For personal use only.

Can. J. Chem. Downloaded from www.nrcresearchpress.com by 88.146.161.215 on 09/08/12
For personal use only.

Table 1. NMR data for compound **1** (pyr-d_5).

Position	^{13}C (δ, ppm)	DEPT	^{1}H(δ, ppm)[a]	*J*(Hz)
1	190.3	C		
2	149.2	C		
3	137.6	CH	7.39d	1.2
4	184.4	C		
4a	132.5	C		
5	118.7	CH	7.63dd	7.4, 1.0
6	136.9	CH	7.54dd	8.6, 7.4
7	124.3	CH	7.30dd	8.6, 1.0
8	161.8	C		
8a	115.7	C		
1′	68.6	CH	5.35s	
2′	204.9	C		
3′	36.7	CH_2	α,2.82ddt	16.8,3.6,1.2
			β,3.77ddd	16.8,13.2,0.8
4′	38.7	CH	4.11dm	13.2
4′a	115.7	C		
5′	163.1	C		
6′	118.1	CH	7.06dd	8.6, 0.8
7′	137.4	CH	7.48dd	8.6, 7.6
8′	120.1	CH	7.09bd	7.6
8′a	146.4	C		

[a]Assignments facilitated by COSY, HMQC, and HMBC data.

carbonyls and two phenolic OHs was confirmed by the ^{13}C NMR (Table 1), HMBC, HMQC, and DEPT spectra. The ^{13}C chemical shifts of the 8-hydroxy-1,4-naphthoquinone moiety closely resemble those of juglone (5). Analysis of HMBC correlations (Table 2) allowed us to extend the structure to **1**. The attachment of the hydroxy naphthoquinone moiety from C2 to C4′ of the 2-tetralone moiety is supported by the observation that the signals for protons H-1′, H-3′α, H-3′β, and H-4′ undergo deuterium exchange when a sample of **1** is equilibrated in pyridine-d_5–D_2O.

The relative stereochemistry was established by NOE difference spectroscopy, the results of which are summarized in Table 2. In particular, the strong NOEs between H-1′ and H-4′ indicate a *cis* relationship while the 20.3% enhancement of the signal for H-3 when H-3′β is irradiated indicates their close proximity.

Thus we conclude that **1** is 8,1′,5′-trihydroxy-3′,4′-dihydro-1′*H*-[2,4′]binaphthalenyl-1,4,2′-trione, and its preferred conformation is as depicted.

While decaketides featuring substituted 5-hydroxy-1,4-naphthoquinone moieties have been reported (6) as fungal metabolites, they are generally derivatives of extended 9,10-anthraquinone systems, for example, 6-deoxyversicolorin C from *Dothistoma pini* (7) or bipolarin from *Bipolarus sp* (8). On the other hand 1,1′ binaphthyl-type dimeric pentaketides of fungal origin are known (9) as well as naphthoquinone derivatives such as 2,7-dimethoxy-5-hydroxy-4-naphthoquinone from an Actinomycete (10). We are not aware of any dimeric 1,2′ binaphthyl-type pentaketides and thus compound **1** represents a new skeletal type of probable pentaketide dimerization biogenesis.

This compound displayed significant insect toxicity (96% mortality) when fed to spruce budworm larvae at 0.0004 g/g diet in a feeding assay (1).

Table 2. HMBC and NOE correlations for **1** (pyr-d_5).

Position	δH(ppm)	HMBC Carbon no.	NOE Proton no. (%)
3	7.39	2, 1, 4′, 4a	4′(0.9), 3′$_β$(6.4)
5	7.63	7, 4, 8a	6(4.4)
6	7.54	8, 4a	5(11.3), 7(25.3)
7	7.30	8, 5, 8a	6(6.3)
1′	5.35	8′, 3′, 4′a	4′(7.9), 8′(10.5)
3′$_α$	2.82	1′, 2′, 2, 4′, 4′a	3(2.1), 3′(23.2), 4′(11.6)
3′$_β$	3.77	1′, 2′, 2, 4′, 4′a	3(20.3), 3′α(25.1)
4′	4.11	1, 1′, 2, 2′, 3, 3′	1′(3.4), 3′α(5.2)
6′	7.06	4′a, 5′, 8′	7′(21.5)
7′	7.48	5′, 8′a	6′(19.5), 8′(27.1)
8′	7.09	1′, 5′, 6′, 4′a	1′(8.5), 7′(31.3)

Table 3. NMR data for compound **2** ($CDCl_3$).

Position	^{13}C, δ(ppm)	DEPT	^{1}H, δ(ppm)[a]	*J*(Hz)
1	175.8	C		
2	39.4	CH	2.45m	6.4, 6.8
3	33.6	CH_2	1.39m, 1.60m	
4	27.1	CH_2	1.24bs	
5	29.1	CH_2	1.24bs	
6	31.7	CH_2	1.24bs	
7	22.6	CH_2	1.24bs	
8	14.0	CH_3	0.86t	6.4
9	17.1	CH_3	1.12d	6.8
2′	79.4	CH	4.94dd	3.2, 7.2
3′	63.9	CH	5.22dd	3.2, 5.6
4′	140.7	CH	6.92dd	5.6, 9.6
5′	124.6	CH	6.18d	9.6
6′	162.6	C		
7′	123.5	CH	5.57ddq	1.6, 7.2, 15.6
8′	132.7	CH	5.92ddq	1.2, 6.8, 15.6
9′	17.9	CH_3	1.74dd	1.6, 6.8

[a]Assignments facilitated by COSY, HMQC, and HMBC data.

Compound **2** was isolated as an optically active ($[\alpha]_D$ +264) oil and displayed strong IR absorptions at 1730 and 1739 cm^{-1} attributed to α,β-unsaturated and saturated ester moieties, respectively. The ^{13}C NMR spectrum shows a total of 17 carbons comprising 3 methyls, 5 methylenes, 7 methines, and 2 quaternary carbonyl carbons as revealed by DEPT analysis. Four of the methine carbons are sp^2 hybridized while two others are oxygen bearing in view of their chemical shifts (Table 3).

The ^{1}H NMR, ^{1}H–^{1}H COSY, and HMBC spectra revealed the coupling sequence H_3-8 to H-7 to H-6 to H-5 to H-4 to H-3 to H-2 as contained in structure **2**. Another coupling sequence supports the unsaturated alkyl side chain and ring proton connectivity (H-5′ → H_3-9′).

The ^{1}H–^{13}C long-range correlations revealed by the HMBC experiment are contained in Table 4 and allowed us to derive

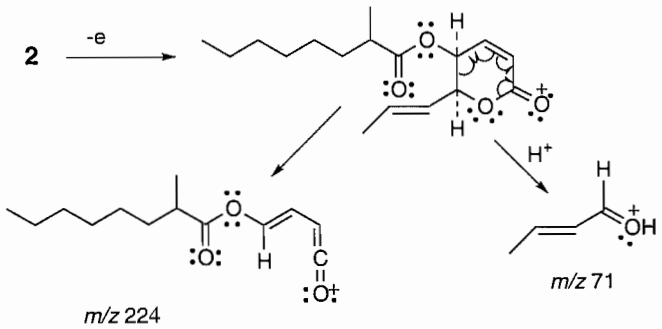
© 1997 NRC Canada

Can. J. Chem. Downloaded from www.nrcresearchpress.com by 88.146.161.215 on 09/08/12
For personal use only.

Table 4. HMBC and NOE correlations for **2** ($CDCl_3$).

Position	δH(ppm)	HMBC Carbon no.	NOE Proton no. (%)
2	2.45	1, 3, 4, 9	3(2.2), 4(4.3), 9(4.5)
3a	1.39	1, 2, 4.5, 9	2(4.2), 3b(15.2)
3b	1.60	1, 2, 4, 5, 9	2(1.8), 3a(6.9), 4(4.1)
8	0.86	6, 7	
9	1.12	1, 2, 3	
2′	4.94	3′, 7′, 8′	3′(12.9), 7′(2.9), 8′(6.8)
3′	5.23	1, 2′, 4′, 5′, 7′	2′(12.1), 4′(7.9)
4′	6.92	2′, 3′, 5′, 6′	3′(7.0), 5′(11.0)
5′	6.18	3′, 6′	4′ (9.4)
7′	5.57	2′, 8′, 9′	2′(1.7), 8′(-0.1), 9′(2.8)
8′	5.92	2′, 9′	2′(5.7), 7′(0.6), 9′(4.9)
9′	1.74	7′, 8′	7′(3.0), 8′(3.7)

Scheme 1.



the complete structure **2**. Compound **2** does not provide a molecular ion in HREIMS due to its propensity to undergo both (*a*) cleavage at the ester ethereal bond to give a base peak corresponding to the side chain $C_9H_{17}O$ and (*b*) reverse Diels–Alder to afford the major fragment $C_{13}H_{20}O_3^+$ and the complementary fragment C_4H_7O in Scheme 1. The *cis* relationship of H-2′ and H-3′ is inferred by the small coupling ($J = 3.2$ Hz) and confirmed by strong NOEs between these signals (Table 4). Thus we conclude that compound **2** is 2-methyloctanoic acid 6-oxo-2-propenyl-3,6-dihydro-2*H*-pyran-3-yl ester.

Compound **2** is closely related to several antimicrobial metabolites previously isolated from *Aspergillus crespitosus*, such as 5, 6-dihydro-5(*S*)-acetoxy-6(*S*)-(1,2-*trans* propenyl)-2*H*-pyran-2-one, **3**, whose published (11) ^{1}H NMR data for the pyranone and propenyl side-chain moieties are virtually coincident with those for **2** except for H-4′, which is at δ6.69 instead of δ6.92 in **2**. The strong +'ve optical rotations of **3** ($[\alpha]_D$ +311.8) and **2** imply that they possess the same absolute configuration.

Compound **2** displayed significant inhibitory activity in disk assays at 100 μg against the bacteria *Vibrio salmonicida*, and *Staphylococcus aureus* and at 500 μg against *Pseudomonas aeruginosa*.

Experimental

General

High-resolution mass spectra were recorded on a Kratos MS-50 instrument. Optical rotations were measured on a Perkin–Elmer 241 polarimeter. Melting points were taken with a Kofler hot-stage apparatus and are uncorrected. The IR spectra were recorded as films on a Bruker IF-S25 spectrometer. PTLC was performed with precoated Si gel F_{254} (0.5 or 0.25 mm) plates. NMR data were recorded on a Varian Unity 400 spectrometer, using the solvent as reference. All 2D NMR spectra were recorded non-spinning at 25°C. The UV spectra were measured on a Hewlett Packard 8452A diode array spectrophotometer.

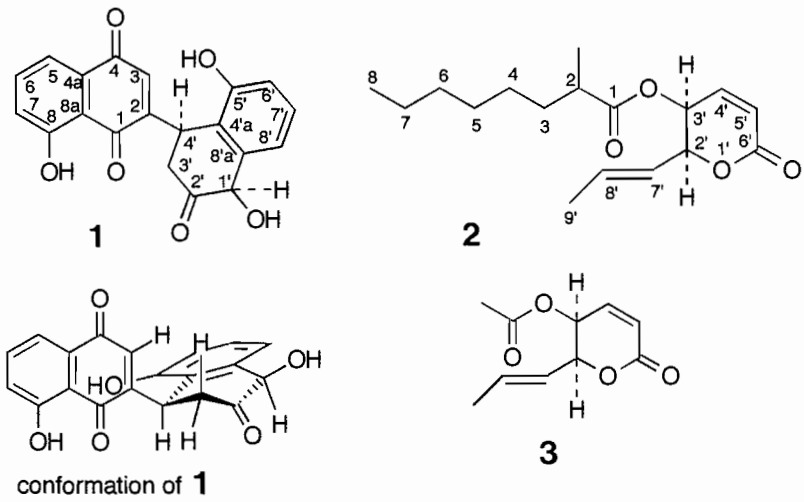
Fungal strain

The endophyte strain L1930 was isolated from eastern larch (*Larix laricina* (Du Roi) K. Koch) needles from trees in Rockwood Park, Saint John, N.B., Canada (12). This isolate failed to produce spores, other structures, or cultural features to permit identification. L1930 was grown on 2% malt extract agar (MEA), potato dextrose agar (PDA), cornmeal agar (CA), Czapex-*d*ox, and tap water agar. It is deposited in the Herbarium Collection, Forestry Canada, Quebec Region (1055 du P.E.P.S., P. O. Box 3800, Saint Foy, QC G1V 4C7).

This endophyte was cultured as previously described (1, 4). After filtration the hyphae and medium were freeze-dried and kept in cold storage until used.

Disk assays

Vibrio salmonicida cultures were grown on brain heart infu-



© 1997 NRC Canada

Can. J. Chem. Downloaded from www.nrcresearchpress.com by 88.146.161.215 on 09/08/12
For personal use only.

sion agar (BHIA) (37 g of Lab M (Amersham) brain heart infusion medium/L, 15 g of Difco bactoagar/L) at 17°C. *Pseudomonas aeruginosa* and *Staphylococcus aureus* were grown on tryptic soy agar (TSA) (40 g of Difco tryptic soy agar/L) at 37°C. Controls consisted of 10 μL of methanol, 100 units of Penicillin G, and 100 units of Streptomycin in water. The assays were carried out with test material at 50, 100, and 500 μg/disk delivered in 10 μL of solvent.

Isolation

The freeze-dried medium (68.9 g) from cultures (8 L) of endophyte L1930 was extracted with acetone (3 × 350 mL) yielding a crude extract (0.10 g) after solvent evaporation. This extract was chromatographed on a silica gel column (Kieselgel 60G, 3.0 × 3.3 cm) and eluted with a discontinuous gradient of $CHCl_3$–CH_3OH (1:0 → 4:1) to give 14 fractions (40 mL each). Evaporation of fractions 4 and 5 gave crude **1**, which was further purified by PTLC using $CHCl_3$ (R_f = 0.16) followed by PTLC using nC_6H_{14}:C_6H_6: EtOAc (3:5:2), to give pure **1** (7.1 mg, R_f = 0.38).

The freeze-dried hyphae (2.2 g) from cultures (5 L) of endophyte L1930 was extracted with acetone (3 × 30 mL) yielding a crude extract (0.09 g) after solvent evaporation. This extract was subjected to chromatography on a short silica gel column (Kieselgel 60G, 2.2 × 2.5 cm) eluting with $CHCl_3$, giving eight fractions (35 mL each). Fractions 2–5 were combined (15 mg) and purified by PTLC using C_6H_6: $CHCl_3$ (2:3) to yield pure **2** (1.7 mg, R_f = 0.35).

Compound 1

Yellow powdery solid, mp 214–216°C (sublimes 190°C), $[\alpha]_D$ +178 (acetone, c = 0.0075). UV, $\lambda_{max}(\varepsilon)$: 212 (84 800), 256 (36 700), 334 (9 590), 418 (7 250) nm. IR ($CHCl_3$): 3469 (br), 3113 (m), 3042 (m), 2924 (m), 1664 (m), 1635 (s), 1612 (s), 1452 (s), 1337 (s), 829 (m), 737 (m) cm^{-1}. HREIMS *m/z*: 350.0795 (73.7), (M^+) (calcd. for $C_{20}H_{14}O_6$: 350.0790), 332 (100)($M - H_2O)^+$, 304 (9.0), 287(6.9), 202 (42.1), 149 (23.4), 121 (15.4).

Compound 2

Oil, $[\alpha]_D$ +264 ($CHCl_3$, c = 0.0009). IR ($CHCl_3$): 2954 (m), 1739(s), 1730(s), 1200 (m) cm^{-1}. HREIMS *m/z*: 224.14203 (26.9, $M^+ - C_4H_5O$) (calcd. for $C_{13}H_{20}O_3$: 224.14125), 141 (100, $C_9H_{17}O$), 113 (21.9), 71 (52.8, C_4H_6O), 57 (41.3).

Acknowledgements

Thanks are due to the Natural Sciences and Engineering Research Council of Canada and the Forestry Canada Green Plan (Research Network for the Discovery and Development of Natural Products for Integrated Forest Pest Management) for financial assistance, to Dan Drummond for recording mass spectra, and to Jason Dobranic for assistance with the endophyte cultures and bioassays.

References

1. L.A. Calhoun, J.A. Findlay, J.D. Miller, and N.J. Whitney. Mycol. Res. **96**, 281 (1992).
2. J.A. Findlay, G. Li, P.E. Penner, and J.D. Miller. J. Nat. Prod. **58**, 197 (1995).
3. J.A. Findlay, S. Buthelezi, R. Lavoie, L. Peña-Rodriguez, and J.D. Miller. J. Nat. Prod. **58**, 1759 (1995).
4. J.K. Dobranic. M.Sc. thesis, University of New Brunswick (1995).
5. M. Kobayashi, Y. Terui, K. Tori, and N. Tsuji. Tetrehedron Lett. 619 (1976).
6. W.B. Turner and D.C. Aldridge. Fungal Metabolites II. Academic Press, New York. 1983.
7. A.V. Danks and R. Hodges. Aust. J. Chem. **27**, 1603 (1974).
8. P.J. Auchamp and J.S. Holzapfel. Agric. Chem. Inst. **23**, 40 (1970).
9. W.B. Turner. Fungal metabolites. Academic Press, New York. 1971.
10. J. E. Davies, F.E. King, and J.C. Roberts. Chem. Ind. 1110 (1954).
11. S. Mizuba, K. Lee, and J. Jiu. Can. J. Microbiol. **21**, 1781 (1975).
12. J.K. Dobranic, J.A. Johnson, and Q.R. Alikan. Can. J. Microbiol. **41**, 194 (1995).

© 1997 NRC Canada

Further examples of photocycloadditions of 1,3-diketonatoboron difluorides to olefins: a description of the reaction pattern and mechanism

Yuan L. Chow, Xianen Cheng, Shi S. Wang, and Susan P. Wu

Abstract: The photocycloaddition of dibenzoylmethanatoboron difluoride ($DBMBF_2$) with conjugated nitriles, ketones, and esters occurs more slowly than that with simple olefins and with fair regioselectivity. For these electron-deficient olefins, the cyclic analogues react more slowly than the acyclic ones and the cyano analogues react more slowly than all others; also a β-methyl substituent reverses the regioselectivity in adduct formation. Benzoylacetonatoboron difluoride ($BABF_2$) photocycloadds to simple cyclic olefins from the excited state isomer in which the double bond is conjugated with the phenyl group, and occurs more slowly than that of the corresponding reaction of $DBMBF_2$. The efficiency and regiochemistry of these cycloadditions have been explained with respect to the exciplex as the immediate intermediate.

Key words: photocycloaddition, dibenzoylmethanatoboron difluoride, benzoylacetonatoboron difluoride, exciplex.

Résumé : Les photocycloadditions du difluorure de dibenzoylméthanabore ($DBMBF_2$) sur les nitriles, cétones et esters conjugués s'effectuent plus lentement que celles sur les oléfines simples et leurs régiosélectivités sont correctes. Dans le cas de ces oléfines électrodéficientes, les analogues cycliques réagissent plus lentement que les acycliques et les analogues cyanés réagissent plus lentement que tous les autres; de plus, une substitution par un groupe β-méthyle inverse la régiosélectivité lors de la formation de l'adduit. Le difluorure de benzoylacétonatobore ($BABF_2$) conduit à une réaction de photocycloaddition sur les oléfines cycliques simples par le biais de l'isomère de l'état excité dans lequel la double liaison est conjuguée au groupe phényle; cette réaction est plus lente que la réaction correspondante du $DBMBF_2$. On a expliqué l'efficacité et la régiochimie de ces cycloadditions par le biais de l'exciplexe comme intermédiaire immédiat.

Mots clés : photocycloaddition, difluorure de dibenzoylméthanabore, difluorure de benzoylacétonabore, exciplexe.

[Traduit par la rédaction]

Introduction

Photochemistry of 1,3-diketonatoboron difluorides has been investigated (1–7) in order to remedy the low quantum yields of the de Mayo reaction (i.e., the photoaddition of 1,3-diketones with olefins)(8), and been shown not only to give good quantum yields in the photocycloaddition (1–4) but also to possess electron transfer reactivities (4, 7) and to show interesting photophysical phenomena (5, 6). The singlet excited state of these boron difluorides interacts with various types of electron-rich as well as electron-poor π-bond substrates. Both dibenzoylmethanatoboron difluoride ($DBMBF_2$, **1***a*) (1) and acetylacetonatoboron difluoride ($AABF_2$, **1***c*) (2) have been used as models to show that their singlet excited state either undergoes electron transfer with a substrate at the collision complex distance (ca. 7 Å) to form solvent-separated radical ion pairs, or approaches further to collapse to exciplexes (6, 7). The former radical ion pairs are preferentially formed in the interaction with electron-rich olefins or arenes, such as conjugated dienes, anethole, quadricyclane, etc., and constitute the initiation of observed radical cation reactions from such substrates (4). The formation of exciplexes can be observed with arenes through their fluorescence spectra, particularly in nonpolar solvent (6); exciplexes with olefins are assumed to be formed and act as the discrete intermediates in the photocycloaddition, although the corresponding exciplex fluorescence bands have not been detected.

Photocycloaddition of $DBMBF_2$ can occur with olefins ranging from electron-rich conjugated dienes and enol ethers (4) to electron-deficient conjugated ketones and esters (3), although the reaction with substituted benzenes has not been observed and is replaced instead by exciplex fluorescence in many cases (6, 7). It is noteworthy that, in the reaction with electron-rich olefins, solvent polarity can be adjusted to manipulate the reaction in favor of either the cation radical reaction or cycloaddition in a continuous pattern (4). In con-

Received September 15, 1996.

This paper is dedicated to Professor William A. Ayer on the occasion of his 65th birthday.

Y.L. Chow,[1] X. Cheng, S. S. Wang, and S.P. Wu. Department of Chemistry, Simon Fraser University, Burnaby, BC V5A 1S6, Canada.

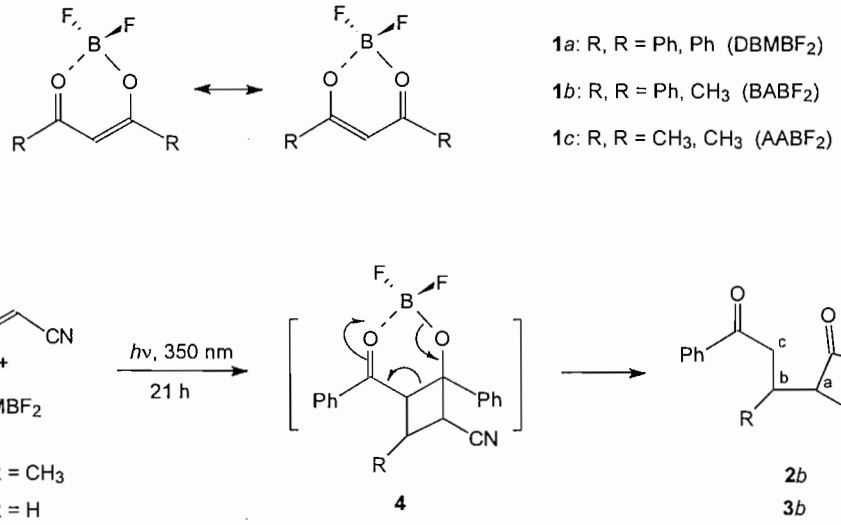
[1] Author to whom correspondence may be addressed. Telephone: (604) 291–3352. Fax: (604) 291–3765. E-mail: ychow@sfu.ca

© 1997 NRC Canada

Can. J. Chem. Downloaded from www.nrcresearchpress.com by 88.146.161.215 on 09/08/12
For personal use only.

Can. J. Chem. Downloaded from www.nrcresearchpress.com by 88.146.161.215 on 09/08/12
For personal use only.

Scheme 1.

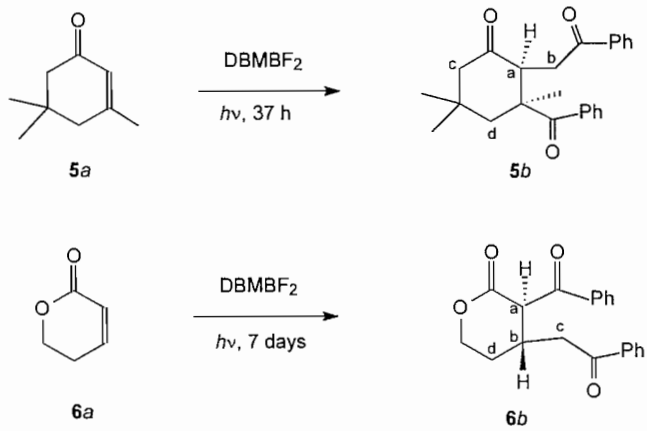


trast, $AABF_2$ does undergo photocycloaddition with substituted benzenes and simple olefins (2), but shows no photoreactivity toward enol ethers or conjugated dienes even in nonpolar solvent. Mechanistic studies using $DBMBF_2$ as the model compound have yielded sufficient information to allow us to describe the basic pattern of photoreactions of the boron compounds and substrates (6). This paper attempts to clarify some pockets left unexplored previously, and to reconfirm certain unusual conclusions made before. It will be discussed in the light of the overall mechanism recently proposed (6).

Results

We wish to report, first of all, the photocycloaddition of $DBMBF_2$ to olefins whose C=C bond is conjugated with a nitrile, ester, or ketone group, followed by the addition of benzoylacetonatoboron difluoride ($BABF_2$, **1***b*) to simple olefins. Some examples of the former addition to the conjugated esters and ketones were reported in 1993 (3) to occur more slowly than comparable simple olefins; similar photoreaction with the conjugated cyano derivatives, crotononitrile (**2***a*) and acrylonitrile (**3***a*), was found to be even less efficient. The photoreaction was carried out by the method and conditions similar to those reported before (1–3); a solution of $DBMBF_2$ (0.05 M) and a substrate (0.5 M) in acetonitrile was distributed in Pyrex tubes and irradiated with Rayonet 350 nm lamps. The progress of the reaction was monitored with GC analysis. The products were isolated by silica gel chromatography. The photoaddition to acrylonitrile **3***a* gave polymeric precipitate and was stopped when $DBMBF_2$ was only 25% consumed; single product **3***b* was isolated in 59% yield based on consumed $DBMBF_2$ (% yields for others were calculated the same way unless specified otherwise). Similar reaction with crotononitrile **2***a* did not give precipitates, and gave 41% of *threo*-**2***b* on nearly 50% conversion (Scheme 1). Both reactions followed the regiospecific orientation of substrates shown in **4** (arbitrarily defined as head-to-head) to give single products; as there were unisolated minor products, the regioselectivity was good but not complete. The sample of **2***b* contained the major compound (90%) showing a NMR spectrum with the H_a signal at 4.81 ppm (J_{ab} 3.6 Hz), and a weak signal at 4.64 ppm (J_{ab} 4.8 Hz); the latter

Scheme 2.

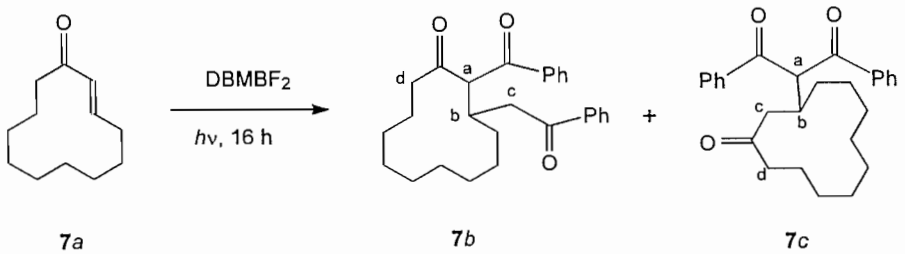


must arise from the minor component of the isomer at the "a"-position. Although, on the basis of the well-established concerted *cis*-photocycloaddition, this reaction should result in *erythro*-**2***b*, the stereochemistry of the isolated compound could not be defined for certain due to the facile isomerization. Such an isomerization at the "a"-position is facile because of double activations by two electron-withdrawing groups and has also been reported in a previous paper (3). Both products **2***b* and **3***b* exhibited pertinent IR, MS, and NMR (^1H and ^{13}C) parameters as shown in the experimental. The presence of cyano group was indicated by the ^{13}C NMR signal at 117.21 and 115.93 ppm and IR absorptions at 2251 and 2248 cm^{-1}, respectively.

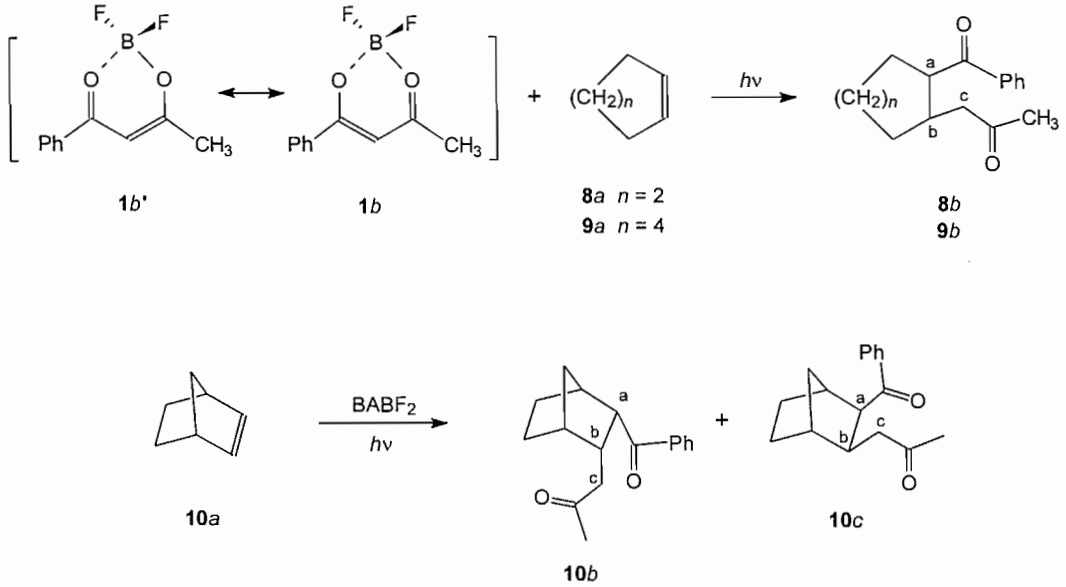
The photoaddition of $DBMBF_2$ to isophorone was carried out to completion to give amorphous product **5***b* (44%) (Scheme 2), which was derived from the alternative orientation (head-to-tail) (3) in the first cycloaddition step; similar reversal of the orientation caused by a β-methyl group was observed before in allied photocycloadditions to mesityl oxide and crotonates (3). The structure was proven by the well-defined ABX system of H_a and H_b in **5***b*; the stereochemistry should be as shown since an isomerization at the "a"-position is not rapid. A similar photocycloaddition to the cyclic lactonic

© 1997 NRC Canada

Scheme 3.



Scheme 4.



olefin **6***a* (9) was very slow, consuming 70% of $DBMBF_2$ in 7 days to give the adduct *trans*-**6***b* (37%) from the regular head-to-head cycloaddition; the adduct must be the more stable *trans* configuration as shown by the coupling constant J_{ab} 8.2 Hz (1, 3) for H_a at 4.59 ppm. The initial product was no doubt *cis*-**6***b*, which must be isomerized in the slow photoreaction and decreased during isolation to about 10% as shown by the weak ^1H NMR signal at 5.07 ppm with J_{ab} 4.6 Hz.

E-2-Cyclododecenone **7***a* was prepared by the known method (10) and underwent the photocycloaddition readily to give adducts **7***b* (42%) and **7***c* (14%), which were formed from the regular head-to-head addition (Scheme 3). In addition to this, a mixture fraction (about 20%) of more than 10 dimers of enone **7***a* was also formed as shown by GC–MS (with M^+ 360). The sample of **7***b* was contaminated with 8% of its isomer at the "a"-position as shown by a weak NMR signal at 5.21 ppm (J_{ab} 3.5 Hz); the stereochemistry could not be defined easily owing to the facile isomerization. The *cis* cycloaddition of $DBMBF_2$ to the *trans* olefinic bond must lead to the *erythro* configuration, which should converge to the more stable isomer by such an isomerization. The NMR spectrum of **7***b* showed J_{ab} 11.1 Hz for the H_a at 4.92 ppm; these data unfortunately could not be interpreted unambiguously to define the *erytho–threo* configuration. Compound **7***c* was derived from the alternate electronic shifts in the intermediate stage (e.g., **4**) involving the other carbonyl as the sink (3). The sample was not obtained in a pure state, but the structure was supported by the low-field doublet H_a at 6.14 ppm, in analogy to the similar photoreaction with other enones.

Using the same apparatus and conditions described before, the quantum yields of 2-cyclopentenone, 2-cyclohexenone, **5***a*, 2-cyclooctenone, and **7***a* were determined to be 0.003, 0.007, 0.006, 0.052, and 0.057, respectively. It was noteworthy that, in contrast to low quantum yields of five- and six-membered cyclic enones, the larger ring enones gave reasonably good yields. The quantum yields of photocycloadditions to **2***a*, **3***a*, and **6***a* were too low for determination.

The photocycloaddition of $BABF_2$ to cyclohexene (**8***a*) and cyclooctene (**9***a*) (Scheme 4) was not as fast as that of $DBMBF_2$, and was terminated in 15 h to give about 50% of the $BABF_2$ consumption; the products **8***b* and **9***b* were isomerized during the reaction and isolation, which led to difficulty in purification and low isolated yields of 19 and 59%, respectively. The isomerization was faster with **8***b*, the isolated sample of which obviously possessed the *trans* configuration as shown by J_{ab} 8 Hz (1) obtained by decoupling experiments of H_a at 3.64 ppm. The corresponding J_{ab} in **9***b* was also ascertained to be 4.0 Hz by decoupling, which indicated the *cis* configuration for **9***b* in analogy to the allied eight-membered ring adducts reported before (1, 3).

© 1997 NRC Canada

Can. J. Chem. Downloaded from www.nrcresearchpress.com by 88.146.161.215 on 09/08/12
For personal use only.

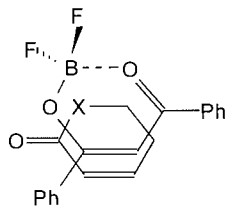
Can. J. Chem. Downloaded from www.nrcresearchpress.com by 88.146.161.215 on 09/08/12
For personal use only.

A similar photoreaction with norbornene consumed all $BABF_2$ in 10 h to give *cis,endo*-adduct **10***b* (68%) and an impure sample of *cis-exo*-**10***c* (8%); the formation of the former *cis-endo*-**10***b* as the major product was analogous to the case of $DBMBF_2$ photoreaction (1), and its structure was suggested by the lack of long-range coupling of H_a with the vicinal bridge and *anti* bridgehead protons. Both compounds had a strong *m/e* 199 derived from the elimination of the CH_3COCH_2 fragment. The H_a signal of **10***b* at 3.35 ppm with J_{ab} 9.1 Hz was easily located by decoupling with H_b (2.78 ppm). Irradiation of H_a caused a strong NOE effect on the H_b and *syn* bridgehead proton that unambiguously determined the *endo-cis* configuration. It is interesting to mention that irradiation of H_b did not cause NOE effects on the *syn* bridgehead proton, probably owing to twisting of the ring. The structure of **10***c* was suggested from MS showing a stronger *m/e* 189 peak than did **10***b*; this fragment must be derived from a McLafferty rearrangement and elimination. The same fragmentation pattern was also observed with the allied adduct of $DBMBF_2$, and used as evidence for the structural assignment (1).

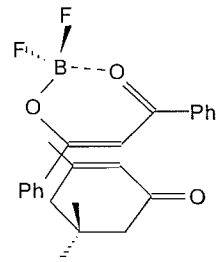
Discussion

First of all, the $DBMBF_2$ photocycloaddition will be discussed. The examples of addition to conjugated nitriles, cyclic ketones, and esters described above extend the observations in our previous publication and reinforce those conclusions (3). They are as follows: (*i*) the effect of the β-methyl group is to reverse the orientation; (*ii*) cyclic enones and esters (lactones) tend to undergo photoreaction much more slowly than their acyclic analogues; (*iii*) conjugated nitriles react most slowly but still give the expected products, and finally; (*iv*) the adducts isomerize under the reaction conditions. As an exciplex is assumed to be the immediate precursor of the cycloaddition, the results summarized above, except the last, must originate from and be controlled by the properties of exciplexes, that is, the nature and configuration of exciplexes govern the orientation and efficiency of the cycloaddition. Owing to the short lifetimes of exciplexes, their nature is not known in detail and probably will not be readily available for some time. At present the properties and nature of exciplexes are elucidated from their spectroscopic data (6) and may be augmented by reverse reasoning from the product data. The studies from our laboratory have established that the BF_2 exciplexes possess charge transfer (CT) and locally excited (LE) contributions (6). Further, we have come to the conclusion that, while the LE component provides the driving force for exciplex formation (and therefore, cycloaddition), the CT component determines the regiospecificity of the cycloaddition by generating the dipoles (6). These conclusions will be used for discussion here.

Whereas five- or six-membered cyclic conjugated esters and ketones have mandatory *cis* configuration, acyclic analogues are more likely to have the *trans* configuration under the photolysis conditions. The slower photocycloaddition of the former (particularly cyclohexenone, cyclopentenone, and **6***a*) as compared with that of the latter suggests that such an exciplex formation is crowded to the extent that the cyclobutane bond formation is counteracted. Taking the head-to-head orientation as a requirement, complex **11** shows the approach of cyclohexenone (X = CH_2) and a probable hindrance from the *cis* double bond. For the approach of lactone **6***a* (X = O), the crowding may arise from the lone pair electrons of the heteroatoms. In the presence of the β-methyl group (**5***a* or mesityl



11



12

oxide), the steric factor should force a drastic reorientation of the exciplex partners to avoid excessive hindrance as suggested by the product regiochemistry. In particular, as enone **5***a* must avoid the crowding of the 5,5′-dimethyl group, **12** is proposed as a possible exciplex conformation. As a cyano group is a powerful electron withdrawer, in conjugation with an olefin it may accumulate a high electron density terminal to create a repulsive force against the BF_2 group. These represent only speculations to rationalize the results and, unavoidably, must remain imprecise until more knowledge on exciplexes becomes available.

The X-ray analysis of $BABF_2$ (11) has proven that the chelate ring shows extensive delocalization of the electrons so that both C—C and B—O bonds are equidistant. The product pattern suggests that singlet excited $BABF_2$ reacts from the structure **1***b* in Scheme 4, so that the adducts have the benzoyl and acetonyl groups attached to the original double bond. Addition products from the alternative structure **1***b*′, if formed at all, are probably in small yields as shown by small GC peaks. Using the concept of exciplexes as the cycloaddition intermediate, $*BABF_2$ may form a less tight intermediate with substrates, in general, than $*DBMBF_2$, and therefore shows a lesser tendency to undergo cycloaddition. This is caused by weaker LE interactions (i.e., weaker electronic coupling matrix element) generated by $*BABF_2$ than by $*DBMBF_2$ in forming exciplexes. The dipoles of $*BABF_2$–olefin exciplexes (generated by the CT interactions) can be dependent on the C=C position in the borate ring, which in turn directs the location of the cycloaddition. In contrast to the generally observed *exo* approach of addenda to a norbornene ring, it is unusual that $*BABF_2$ reacts with norbornene preferentially from the *endo* face to give the *cis-endo* configuration in analogy to that observed in the $DBMBF_2$ case (1); such a reaction pattern with norbornene is rare and, so far as we are aware, has not been previously found. This again must arise from the preferred geometry in the exciplexes, which have different electronic and steric factors than the corresponding ground state complexes.

Experimental section

Materials, apparatus, and conditions were the same as those published in the previous reports (1, 3).

General conditions of the photocycloaddition of $DBMBF_2$

The method of the photocycloaddition of $DBMBF_2$ to conjugated nitriles, ketones, and esters was the same as that

© 1997 NRC Canada

Can. J. Chem. Downloaded from www.nrcresearchpress.com by 88.146.161.215 on 09/08/12
For personal use only.

Table 1. IR data.

Compound	ν (cm^{-1}) in neat film
2*b*	3064, 2970, 2935, 2248, 1688, 1682, 1597, 1581, 1448, 1409, 1367, 1312, 1274, 1220, 1183, 1001, 956, 912, 766, 692
3*b*	3064, 2935, 2251, 1693, 1682, 1597, 1581, 1449, 1412, 1368, 1283, 1261, 1219, 1182, 1160, 1002, 973, 912, 690
5*b*	3060, 2958, 2908, 2873, 1714, 1683, 1597, 1579, 1461, 1448, 1392, 1368, 1324, 1286, 1254, 1212, 1178, 1103, 1003, 968, 955, 910, 751, 730, 691
6*b*	3062, 2967, 2913, 1731, 1682, 1597, 1581, 1478, 1448, 1407, 1359, 1364, 1201, 1078, 1001, 955, 912, 754, 690, 648
7*b*	3064, 2994, 2862, 1711, 1682, 1670, 1596, 1579, 1467, 1448, 1413, 1359, 1271, 1200, 1181, 1120, 981, 960
7*c*	3604, 2933, 2864, 1698, 1667, 1596, 1580, 1469, 1448, 1352, 1321, 1279, 1266, 1207, 1180
8*b*	3060, 2930, 2857, 1714, 1675, 1596, 1580, 1448, 1410, 1371, 1357, 1254, 1216, 1178, 1162, 1002, 977, 946, 795, 760, 702, 661
9*b*	2936, 2874, 1720, 1684, 1603, 1588, 1454, 1363, 1226, 1209, 1188, 1170
10*b*	3012, 2963, 2866, 1718, 1683, 1456, 1376, 1233, 1171

Table 2. ^{13}C NMR parameters of the products.

Compound	δ (ppm) in $CDCl_3$
2*b*	16.32, 30.29, 43.46, 46.43, 115.93, 128.17, 128.94, 129.24 (2C), 133.90, 134.48, 134.06, 136.52, 191.42, 198.77
3*b*	24.44, 34.91, 39.31, 117.21, 128.14, 128.89, 129.10, 129.26, 133.76, 134.68, 134.02, 136.43, 190.90, 198.52
5*b*	27.19, 27.39, 34.09, 34.16, 34.87, 51.06, 53.40, 54.82, 55.72, 128.27, 128.40, 128.45, 128.83, 132.10, 132.92, 137.12, 137.35, 199.43, 205.45, 206.93
6*b*	27.54, 30.85, 42.55, 54.32, 68.19, 127.95, 128.69, 128.71, 129.15, 133.49, 133.73, 136.36, 136.45, 167.79, 195.48, 197.66
7*b*	21.48, 22.66, 23.85 (3C), 24.72, 25.88, 28.65, 34.76, 37.60, 40.39, 68.04, 128.09, 128.53, 128.83 (2C), 132.91, 133.72, 136.99, 137.19, 196.13, 199.28, 206.09
7*c*	22.76, 22.82, 23.44, 24.19, 24.38, 25.71, 26.07, 28.38, 36.05, 41.40, 42.71, 59.78, 128.50, 128.65, 128.77, 128.86, 133.39, 133.45, 137.16(2C), 195.80, 195.99, 212.58
8*b*	22.75, 23.66, 25.62, 29.53, 30.45, 32.71, 43.97, 46.15, 128.09 (2C), 128.61 (2C), 132.76, 136.95, 203.45, 207.85
9*b*	26.18, 26.37, 27.29, 27.48, 28.38, 29.79, 31.69, 33.76, 45.75, 46.78, 128.39, 128.78, 132.60, 137.98, 203.49, 205.77 (in C_6D_6)
10*b*	29.60, 29.70, 29.80, 35.04, 41.77, 42.16, 42.84, 45.15, 51.95, 128.48, 128.64, 132.47, 139.03, 201.62, 205.98 (in C_6D_6)

described by Chow et al. (3). A 30 mL acetonitrile solution of $DBMBF_2$ (0.05 M) and freshly distilled α,β-unsaturated ketone or ester (0.5 M) was distributed into six Pyrex test tubes (100 x 13 mm). The solution was purged with dry nitrogen and then placed in the Rayonet photoreactor for irradiation with a 350 nm light source. The photoreaction was monitored by GC or TLC to follow the disappearance of $DBMBF_2$. The yellowish or brownish solution was evaporated in vacuo and the residue was chromatographed on silica gel. Some typical runs were described below. The spectral data are collected in Tables 1–4.

Photoaddition to acrylonitrile (3*a*) and crotononitrile (2*a*)

$DBMBF_2$ (340 mg, 1.25 mmol) and **3***a* (663 mg, 12.5 mmol) were dissolved in 25 mL of *p*-dioxane. After irradiation for 26 h, some polymer had precipitated in the test tubes. This was collected (0.1 g, insoluble in acetone and water). The filtrate contained one major product by GC and TLC analysis. Evaporation and addition of ether:hexane (1:2) gave $DBMBF_2$ as a yellow precipitate, 0.29 g (25% conversion). The filtrate was chromatographed on silica gel using hexane:dichloromethane:ether (5:0.8:0.2–3.5:0.8:0.2). The pale-yellow oil **3***b* was isolated (66 mg, 59% based on the consumed $DBMBF_2$): R_f 0.074 (SiO_2, hexane:dichloromethane:ether = 3.5:0.8:0.2.

Similar photolysis of a 25 mL *p*-dioxane solution of $DBMBF_2$ (340 mg, 1.25 mmol) and **2***a* (839 mg, 12.5 mmol) for 26 h yielded no polymer. The $DBMBF_2$ was recovered as a yellow powder, 0.16 g (47% conversion). Chromatography (hexane:ethyl acetate = 8:1) produced 100 mg of **2***b* (41%), mp 98–99°C, R_f 0.21 (SiO_2, hexane:dichloromethane:ether = 5:0.8:0.2). Anal. calcd. for $C_{19}H_{17}O_2N$: C 78.35, H 5.84, N 4.81; found: C 78.30, H 5.89, N 4.69.

Photoaddition to isophorone (5*a*)

$DBMBF_2$ (204 mg, 0.75 mmol) and **5***a* (1.04 g, 7.5 mmol) were dissolved in 15 mL of acetonitrile. After 37 h of irradiation, GC analysis showed that $DBMBF_2$ had almost disappeared. One product spot was observed by TLC at R_f 0.18 (SiO_2, hexane:ethyl acetate = 6:1). The photolysate was

© 1997 NRC Canada

Can. J. Chem. Downloaded from www.nrcresearchpress.com by 88.146.161.215 on 09/08/12
For personal use only.

Table 3. ^{1}H NMR parameters of the products.

Compound	δ (ppm) and J (Hz) in $CDCl_3$
2*b*	1.13 (CH_3, d, J = 6.9 Hz), 3.02 (H_b, m), 3.15 (H_c, dd, J = 18.6, 3.4 Hz), 3.44 ($H_{c'}$, dd, J = 18.6, 10.2 Hz), 5.12 (H_a, d, J = 3.6 Hz), 7.40–8.25 (10H, m, phenyl). Also show a weak signal at 4.64 (d, J = 4.8 Hz)
3*b*	2.28 (H_b, dddd, J = 14.1, 9.7, 5.4, 5.4 Hz), 2.58 ($H_{b'}$, dddd, J = 14.1, 9.0, 5.3, 5.3 Hz), 3.29 (H_c, ddd, J = 18.4, 5.4, 5.3 Hz), 3.42 ($H_{c'}$, ddd, J = 18.4, 9.0, 5.4 Hz), 4.81 (H_a, dd, J = 9.7, 5.3 Hz), 7.45–8.30 (10H, m, phenyl)
5*b*	0.74 (CH_3, s), 1.10 (CH_3, s), 1.55 (CH_3, s), 2.20 (H_c, d, J = 14.7 Hz), 2.30 (H_d, d, J = 14.8 Hz), 2.38 ($H_{d'}$, d, J = 14.8 Hz), 2.65 (H_b, dd, J = 18.4, 2.7 Hz), 2.71 ($H_{c'}$, d, J = 14.7 Hz), 3.20 (H_a, dd, J = 7.6, 2.7 Hz), 4.34 ($H_{b'}$, dd, J = 18.4, 7.6 Hz), 7.30–8.10 (10H, m, phenyl)
6*b*	1.82, 2.27 (H_d and $H_{d'}$, m), 3.00 (H_c, dd, J = 17.2, 7.4 Hz), 3.13 ($H_{c'}$, dd, J = 17.2, 5.3 Hz), 3.29 (H_b, m), 4.53 (OCH_2, m), 4.59 (H_a, d, J = 8.2 Hz), 7.25–8.00 (10H, m, phenyl). A weak signal at 5.07 (d, J = 4.6 Hz)
7*b*	1.20–1.50 ($8CH_2$, m), 1.89 (H_d, m), 2.10 ($H_{d'}$, m), 2.86 (H_c, dd, J = 16.2, 7.3 Hz), 3.03 ($H_{c'}$, dd, J = 16.2, 3.7 Hz), 3.31 (H_b, m), 4.92 (H_a, d, J = 11.1 Hz), 7.30–8.00 (10H, m, phenyl). A weak signal at 5.21 (d, J = 3.5 Hz)
7*c*	1.20–1.80 ($8CH_2$, m), 2.21 (H_d, ddd, J = 13.9, 9.1, 3.7 Hz), 2.48 (H_c, dd, J = 17.3, 6.0 Hz), 2.58 ($H_{d'}$, ddd, J = 13.9, 8.9, 3.5 Hz), 2.90 ($H_{c'}$, dd, J = 17.3, 4.0 Hz), 3.09 (H_b, m), 6.14 (H_a, d, J = 9.1 Hz), 7.30–8.10 (10H, m, phenyl)
8*b*	1.40–1.69 (6H, m), 1.81 (1H, m), 1.83 (1H, m), 2.01 (3H, s), 2.45 ($H_{c'}$, dd, J = 16, 7.5 Hz), 2.53 (H_c, dd, J = 16, 5.0 Hz), 2.55 (H_b, m, J = 8 Hz), 3.64 (H_a, m, J = 8 Hz), 7.44–7.92 (5H, m, phenyl)
9*b*	1.50–1.90 (12H, m), 1.57 (3H, s), 2.04 (H_c, dd, J = 17.6, 8.3 Hz), 2.40 ($H_{c'}$, dd, J = 17.6, 4.9 Hz), 2.78 (H_b, ddddd, J = 8.3, 8.3, 4.9, 4.0, 4.0 Hz), 3.75 (H_a, ddd, J = 9.2, 4.0, 4.0 Hz), 7.1–8.0 (5H, m)
10*b*	1.09 (1H, dm, J = 10 Hz), 1.25–1.55 (4H, m), 1.47 (3H, s), 1.91 (1H, m, J = 3.7 Hz), 2.08 (H_c, dd, J = 17.6, 8.3 Hz), 2.13 (1H, dm, J = 10 Hz), 2.41 (1H, m), 2.45 ($H_{c'}$, dd, J = 17.6, 6.5 Hz), 2.57 (H_b, ddd, J = 9.1, 6.5, 8.3 Hz), 3.35 (H_a, d, J = 9.1 Hz), 7.15 (3H, m), 7.97 (2H, dd)

mixed with 50 mL ether and washed twice with saturated sodium bicarbonate solution. The resulting solution was adsorbed onto 4 g of silica gel and chromatographed on a 27 × 3 cm silica gel column with hexane:ethyl acetate (9:1) to yield 0.12 g (44%) of a pale-yellow powder **5***b*, mp 37–40°C. Anal. calcd. for $C_{24}H_{26}O_3$: C 79.56, H 7.18, found: C 79.19, H 7.50.

Table 4. GC–MS data.

Compound	Mode	*m/z* (%)
2*b*	EI	291 (M^+, 6), 223 (2), 184 (2), 175 (1), 149 (4), 147 (5), 120 (10), 105 (100), 77 (51)
3*b*	EI	277 (M^+, 7), 171 (2), 161 (3), 149 (7), 105 (100), 77 (45)
5*b*	EI	362 (M^+. 25), 344 (M – 18, 27), 329 (16), 257 (57), 243 (13), 224 (10), 137 (10), 105 (100), 77 (55)
6*b*	CI	323 (M + 1, 46), 203 (100), 159 (50)
7*b*	CI	405 (M + 1, 100), 387 (12), 285 (8), 225 (12), 181 (10)
7*c*	CI	405 (M + 1, 24), 387 (5), 299 (5), 225 (100), 197 (20), 181 (10)
8*b*	CI	245 (M + 1)
	EI	187 (15), 105 (100), 77 (35)
9*b*	EI	272 (M^+, 22), 254 (16), 215 (20), 105 (100), 77 (58), 43 (72)
10*b*	EI	256 (M^+, 35), 238 (10), 213 (55), 199 (35), 189 (28), 105 (100), 77 (80), 43 (85)
10*c*	EI	256 (M^+, 44), 238 (20), 213 (18), 199 (40), 189 (41), 105 (88), 77 (86), 43 (100)

Photoaddition to 5,6-dihydro-2*H*-pyran-2-one (6*a*)

5,6-Dihydro-2*H*-pyran-2-one was prepared by refluxing of vinylacetic acid (31.6 g, 1 mol) with paraformaldehyde (43 g, 0.5 mol) in 125 mL of acetic acid containing 3 mL concentrated sulfuric acid (9). The distillation of the crude product at ~115°C/18 Torr (1 Torr = 133.3 Pa) gave 5.6 g of **6***a* (11%). The GC purity was 98% with RT 3.32 min at 80°C (on a 15 m OV–1 capillary column); ^{1}H NMR (100 MHz, $CDCl_3$) δ: 2.33–2.54 (2H, m), 4.40 (2H, t), 5.98 (H, dt), 6.93 (H, m) ppm; MS (EI) *m/z*: 98 (M^+, 23), 68 (M-18, 100).

$DBMBF_2$ (272 mg, 1 mmol) and **6***a* (981 mg, 10 mmol) were dissolved in 20 mL of acetonitrile. After a 9 day irradiation, GC analysis showed that $DBMBF_2$ conversion had reached 70%, and on TLC one product spot was found at R_f 0.11 (SiO_2, hexane:ethyl acetate = 4:1). The clear brown photolysate was mixed with 60 mL ether and washed with saturated aqueous sodium bicarbonate. The solution was adsorbed onto 3 g of silica gel and chromatographed on a 20 × 3 cm column with hexane:ethyl acetate (6:1–4:1) to give 0.11 g of a yellow oil. Further purification was performed by preparative TLC with hexane:dichloromethane:acetone (2:0.9:0.1) to yield 84 mg of a oil (37%) identified as *trans*-**6***b* (R_f 0.09).

© 1997 NRC Canada

cis-**6***b* was also observed in the ^{1}H NMR spectrum as a ~5% impurity in the isolated product.

Photoaddition to *E*-2-cyclododecenone (7*a*)

E-2-Cyclododecenone was prepared from cyclododecanone according to the published procedure, and showed the reported spectral properties (10). $DBMBF_2$ (204 mg, 0.75 mmol) and **7***a* (540 mg, 3 mmol) were dissolved in 15 mL of acetonitrile. After a 16 h irradiation, GC analysis showed nearly complete disappearance of $DBMBF_2$. TLC showed products at R_f 0.18 and at 0.13 (hexane:acetone = 15:1).

The dark-red solution was mixed with ether, washed with saturated aqueous sodium bicarbonate, and chromatographed on a 30 x 3 cm silica gel column. Elution with hexanes gave 0.1 g of an oil containing more than 10 components. Most of these showed similar dimer fragmentation on GC–MS (EI): *m/z*: 360 (M^+, 18), 342 (4), 275 (3), 233 (5), 222 (8), 207 (10), 193 (9), 181 (23), 180 (14), 162 (29), 152 (10), 135 (15), 121 (24), 109 (29), 95 (47), 81 (80), 79 (46), 69 (50), 67 (81), 55 (100).

Further elution with hexane:acetone (20:1) produced 0.17 g of a yellow solid (56%), as two components at R_f 0.18 and 0.13 in the ratio ~74:26. Recrystallization from hexanes yielded 109 mg of the major adduct **7***b* (R_f 0.18), mp 155–157°C. Anal. calcd. for $C_{27}H_{32}O_3$: C 80.20, H 7.92, found: C 79.94, H 8.01. The mother liquor was chromatographed on a 20 × 20 cm TLC plate with hexanes:acetone (15:1) to yield 14 mg of the minor adduct **7***c* (R_f 0.13).

Photocycloaddition of $BABF_2$ with simple olefins

The photocycloaddition of $BABF_2$ to simple olefins was carried out according to the procedure described in ref. 1. A solution of $BABF_2$ (0.05 M, 210 mg) and an olefin (0.5 M) in acetonitrile was kept under nitrogen in Pyrex tubes that were irradiated with the same apparatus as above. The photoreaction with **8***a* and **9***a* consumed 50% $BABF_2$ in 15 h. The crude adduct from **8***a* decreased and became more complex during the chromatography, from which **8***b* was obtained in 19% yield. Under similar conditions and operation **9***b* was isolated in 59% yield.

A similar reaction with norbornene consumed >90% of $BABF_2$ in 18 h and afforded **10***b* in 68% isolated yield and an impure fraction containing **10***b* and **10***c*. The yield of **10***c* was estimated from GC analysis to be 8%.

Acknowledgment

The authors are grateful to the Natural Sciences and Engineering Research Council of Canada for generous financial support of this project.

References

1. Y.L. Chow and X.E. Cheng. Can. J. Chem. **69**, 1331, 1575 (1991); X.E. Cheng. Ph.D. Thesis, Simon Fraser University, 1990
2. Y.L. Chow and X.X. Ouyang. Can. J. Chem. **69**, 423 (1991); Y.L. Chow, S.P. Wu, and X.X. Ouyang. J. Org. Chem. **59**, 421 (1994).
3. Y.L. Chow, S.-S. Wang, and X.E. Cheng. Can. J. Chem. **71**, 846 (1993).
4. Y.L. Chow, M. Vanossi, and S.-S. Wang. J. Photochem. Photobiol. A: **88**, 125 (1995); Y.L. Chow and S.-S. Wang. Tetrahedron Lett. **35**, 9661 (1994); Y.L. Chow, S.-S. Wang, Z.L. Liu, V. Wintgens, P. Valat, and J. Kossanyi. New J. Chem. **18**, 923 (1994).
5. Y.L. Chow, X.E. Cheng, and C.I. Johansson. J. Photochem. Photobiol. A: **51**, 247 (1990); Y.L. Chow, Y.H. Zhang, R. Gautron, L. Yang, A. Rassat, and S.Z. Yang. J. Phys. Org. Chem. **9**, 7 (1996).
6. Y.L. Chow, S.-S. Wang, C.I. Johansson, and Z.L. Liu. J. Am. Chem. Soc. **118**, 11725 (1996): Y.L. Chow and C.I. Johansson. J. Phys. Chem. **99**, 17558 (1995); **99**, 17566 (1995).
7. L. Yang, M. Zhang, Y.C. Liu, Z.L. Liu, and Y.L. Chow. J. Chem. Soc. Chem. Commun. 1055 (1995); Y.L. Chow and C.I. Johansson. Chem. Phys. Lett. **231**, 541 (1994).
8. A.C. Weedon. *In* Synthetic organic photochemistry. *Edited by* W.M. Horspool. Plenum, New York. 1984. p. 61.
9. M. Nakagawa, J. Saegusa, M. Tonozuka, M. Obi, M. Kiuchi, T. Hino, and Y. Ban. Org. Synth. **56**, 49 (1977); B.M. Trost, T.N. Salzmann, and K. Hiroi. J. Am. Chem. Soc. **98**, 4887 (1976); I. Shimizu, I. Minami, and J. Tsuji. Tetrahedron Lett. **24**, 1797 (1983).
10. S. Fujita, T. Kawaguti, and H. Nozaki. Bull. Soc. Chem. Jpn. **43**, 2596 (1970).
11. A.W. Hanson and E.W. MacAuley. Acta Crystallogr. Sect. B: Struct. Crystallogr. Cryst. Chem. **B28**, 1961 (1972).

Can. J. Chem. Downloaded from www.nrcresearchpress.com by 88.146.161.215 on 09/08/12
For personal use only.

© 1997 NRC Canada

Four new hydrolyzable tannins and an acylated flavonol glycoside from *Euphorbia maculata*

Yoshiaki Amakura, Keita Kawada, Tsutomu Hatano, Isao Agata, Takeshi Sugaya, Sansei Nishibe, Takuo Okuda, and Takashi Yoshida

Abstract: The structure of a new acylated flavonol glycoside from the leaf extract of *Euphorbia maculata* was characterized as quercetin 3-*O*-(2″,3″-di-*O*-galloyl)-β-D-glucopyranoside. Four new hydrolyzable tannins together with twelve known tannins were also isolated and their structures were established by spectral and chemical means as 1,2,6-tri-*O*-galloyl-α-D-glucose, 1-*O*-galloyl-2,4;3,6-di-*O*-chebuloyl-β-D-glucose (eumaculin E), and dimers (eumaculins B and D) having a tergalloyl and a macaranoyl group as the linking unit of monomers, respectively.

Key words: *Euphorbia maculata*, Euphorbiaceae, tannin, eumaculin B, eumaculin E.

Résumé : On a déterminé la structure d'un nouveau glycoside acylé du flavonol extrait de la feuille d'*Euphorbia maculata*; il s'agit du 3-*O*-(2″,3″-di-*O*-galloyl)-β-D-glucopyranoside de quercétine. On a aussi isolé quatre nouveaux tannins hydrolysables ainsi que douze tannins connus et on a déterminé leurs structures à l'aide de méthodes tant spectrales que chimiques; il s'agit du 1,2,6-tri-*O*-galloyl-α-D-glucose, du 1-*O*-galloyl-2,4;3,6-di-*O*-chébuloyl-β-D-glucose (eumaculine E) et de dimères (eumaculines B et D) comportant respectivement un groupe tergalloyle et un groupe macaranoyle pour relier les unités de monomère.

Mots clés : *Euphorbia maculata*, Euphorbiaceae, tannin, eumaculine B, eumaculine E.

[Traduit par la rédaction]

Introduction

Many plants of the family Euphorbiaceae that grow in warm and temperate climates have been widely used as folk medicines in various areas of the world including East Africa, Southeast Asia, China, and Japan. The plants in this family, particularly *Euphorbia*, *Phyllanthus*, and *Macaranga* species, have been recognized to produce the ellagitannins with a vast structural diversity as represented by the geraniin metabolites (1–5). Amongst them, euphorbin A (**1**) and its analogous dimers possessing the geraniin unit as a constructing component were characterized as the abundant constituent of chemotaxonomical significance in many euphorbiaceous plants (5).

We previously examined the tannins of *Euphorbia maculata* L. (Euphorbiaceae), which has been used as a folk medicine for wound treatment in Mexico and China (6), and as an antidiarrheal in China (7), and isolated a new dimeric hydrolyzable tannin, eumaculin A (**11**), which contains the $^1C_4$ and $^4C_1$ glucopyranose cores linked through a valoneoyl group (8). Further investigation on the polyphenolic constituents in the leaf extract of the plant has revealed the presence of euphorbin A (**1**) and its analogs, euphorbins B (1) and D (9). In addition to these dimers together with eight known tannins, a new digalloylated flavonol glycoside (**2**) and four new hydrolyzable tannins (**3**, **4**, **9**, **10**) have also been isolated. This paper describes the structural elucidation of the new compounds.

Results and discussion

The aqueous acetone homogenate of dried leaves of *E. maculata* was extracted successively with ether, EtOAc, and *n*-BuOH. The EtOAc extract was chromatographed over Toyopearl HW-40 and MCI-gel CHP-20P to yield 17 polyphenolics including new compounds **2**–**4**, **9**, and **10**. Among them, 12 were identified as 1,3,6-tri-*O*-galloyl-β-D-glucose, 3,4,6-tri-*O*-galloyl-D-glucose, 1,2,3,4,6-penta-*O*-galloyl-β-D-glucose (10), euphormisin M_3 (2), chebulanin (11), chebulagic acid (**8**) (12), tercatain (13), granatin B (14), excoecarianin (15), and euphorbins A (**1**) (16, 17), B (1, 16, 17), and D (9), by direct comparisons with authentic specimens or by comparisons of their physical data with those reported in the literature.

Compound **2** showed UV absorption bands characteristic of a flavonol derivative. The ^{1}H NMR spectrum of **2** indicated the presence of a quercetin moiety as revealed by 1,3,4-trisubstituted benzene proton signals at δ 7.78 (d, J = 2.5 Hz), 7.59 (d, J = 2.5, 8.5 Hz), and 6.94 (d, J = 8.5 Hz) and *meta*-coupled signals at δ 6.45 (d, J = 2 Hz) and 6.22 (d, J = 2 Hz). Besides these signals, two singlets attributable to two galloyl

Received October 31, 1996.

This paper is dedicated to Professor William A. Ayer on the occasion of his 65th birthday.

Y. Amakura, K. Kawada, T. Hatano, T. Okuda, and T. Yoshida.[1] Faculty of Pharmaceutical Sciences, Okayama University, Tsushima, Okayama 700, Japan.
I. Agata, T. Sugaya, and S. Nishibe. Faculty of Pharmaceutical Sciences, Health Sciences University of Hokkaido, Ishikari-Tobetsu, Hokkaido 061-02, Japan.

[1] Author to whom correspondence may be addressed. Telephone: (086) 251-7936. Fax: (086) 255-7456. E-mail: yoshida@pheasant.pharm.okayama-u.ac.jp

© 1997 NRC Canada

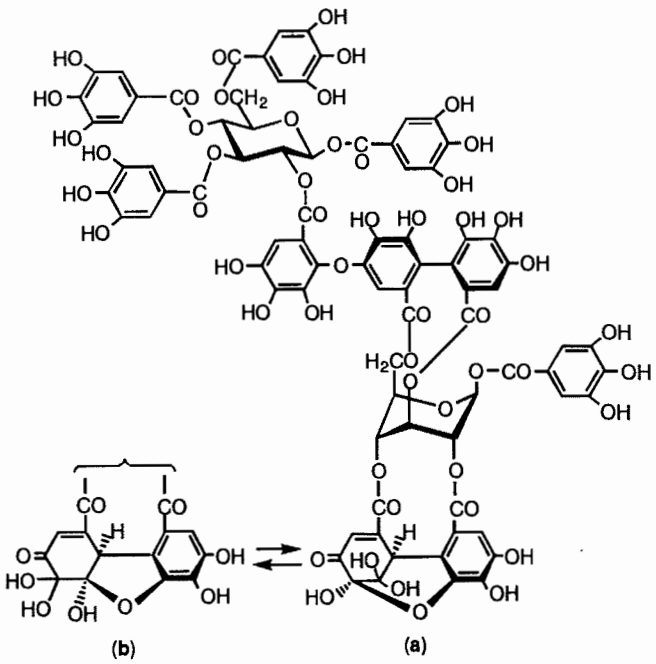
Can. J. Chem. Downloaded from www.nrcresearchpress.com by 88.146.161.215 on 09/08/12
For personal use only.

Can. J. Chem. Downloaded from www.nrcresearchpress.com by 88.146.161.215 on 09/08/12
For personal use only.

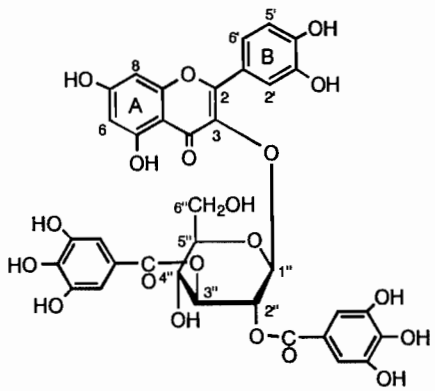
groups (δ 7.04, 7.10, each 2H) were observed in the aromatic region. The coupling patterns of the aliphatic proton signals, which were assigned with the aid of ^{1}H–^{1}H shift correlation spectroscopy (COSY), were consistent with those of $^4C_1$ glucopyranose. The ^{13}C NMR resonances of the aglycone moiety were also in agreement with those of isoquercitrin (18). These data coupled with the FABMS data (*m/z* 791 $(M+Na)^+$) indicated that **2** is a digallate of isoquercitrin. The galloyl groups in **2** were located at O-2 and O-3 of the glucose residue based on the remarkable downfield shifts of the H-2″ (δ 5.39) and H-3″ (δ 5.51) signals. Enzymatic hydrolysis of **2** with tannase yielded gallic acid, isoquercitrin, and quercetin 3-*O*-(2″-*O*-galloyl)-β-D-glucopyranoside (19). The compound **2** was thus characterized as quercetin 3-*O*-(2″,3″-di-*O*-galloyl)-β-D-glucopyranoside (**2**). Although various acylated flavonol glycosides are found widely in the plant kingdom (20), digallates such as **2** are quite rare, and to our knowledge compound **2** is the first example of a natural flavonol glycoside galloylated at O-3 of the glucose residue.

Compound **3** gave an $(M+Na)^+$ ion peak at *m/z* 659 corresponding to the molecular formula $C_{27}H_{24}O_{18}$ in the FABMS. Its ^{1}H NMR spectrum showed signals attributable to three galloyl groups (δ 7.16, 7.12, 7.06, each 2H singlet) and seven aliphatic protons characteristic of a $^4C_1$ glucopyranose residue. The glucose H-3 and H-4 signals were observed at higher field (δ 4.26, 3.83) than the other proton signals, indicating that the hydroxyl groups at C-3 and C-4 are not acylated, while the others are all acylated. The α-configuration of the galloyloxy group at the anomeric center was apparent from the small coupling constant (J = 3.5 Hz) of the H-1 signal. Compound **3** was thus characterized as 1,2,6-tri-*O*-galloyl-α-D-glucose[2] (**3**).

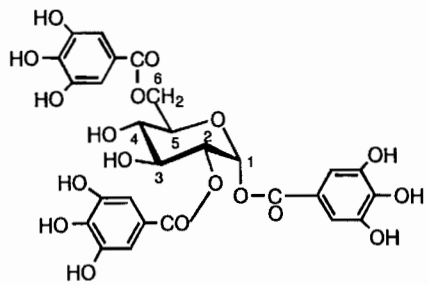
A new compound (**4**), which was designated as eumaculin E, showed an ion peak $(M+H)^+$ at *m/z* 973 in the FABMS. The ^{1}H NMR spectrum of **4** displayed a two-proton singlet at δ 7.22 due to a galloyl group, and signals assignable to two chebuloyl groups (12) (δ 2.18 (2H, m), 2.26 (dd, J = 3.5, 17 Hz), 2.18 (dd, J = 12, 17 Hz) (H-5); 3.87 (ddd, J = 1.5, 5, 11 Hz), 3.80 (ddd, J = 2, 3.5, 12 Hz) (H-4); 5.10 (dd, J = 1.5, 7 Hz), 4.94 (dd, J = 2,7 Hz), (H-3); 4.87 (d, J = 7 Hz), 4.82 (d, J = 7 Hz) (H-2); 7.52 (s) and 7.48 (s) (H-3′)). The presence of the chebuloyl groups in **4** was also substantiated by the ^{13}C NMR spectrum (δ 66.4 (2C, C-2), 39.9, 41.1 (C-3), 39.3, 39.6 (C-4), 30.5, 30.7 (C-5) and eight carbonyl carbon resonances), and by the formation of trimethyl tri-*O*-methylchebulate (**6**) (23) and methyl tri-*O*-methylgallate (**5**) on methanolysis of the methylated derivative of **4**. The coupling patterns of the sugar proton signals were characteristic of glucopyranose adopting a skew-boat conformation (24). The positions of the acyl groups in **4** were determined by HMBC measurement ($^{2,3}J_{C-H}$ = 8 Hz). The presence of the galloyl group at O-1 was indicated by correlation of the galloyl proton signal through three-bond coupling with an ester carbonyl carbon signal at δ 165.1 that also showed a cross peak with the anomeric proton. The signals at δ 7.52 and δ 7.48 (chebuloyl H-3′) showed correlations with the H-6 and H-2 signals through common ester carbonyl carbon signals at δ 167.5 and 165.6, respectively (Fig. 1), establishing the orientation of the chebuloyl groups at O-2/O-4 and O-3/O-6 of the glucose core. Although the stereochemistry of the chebuloyl moieties is apparent from the CD spectrum of **6**, which is identical with that of authentic specimens (23),



1



2

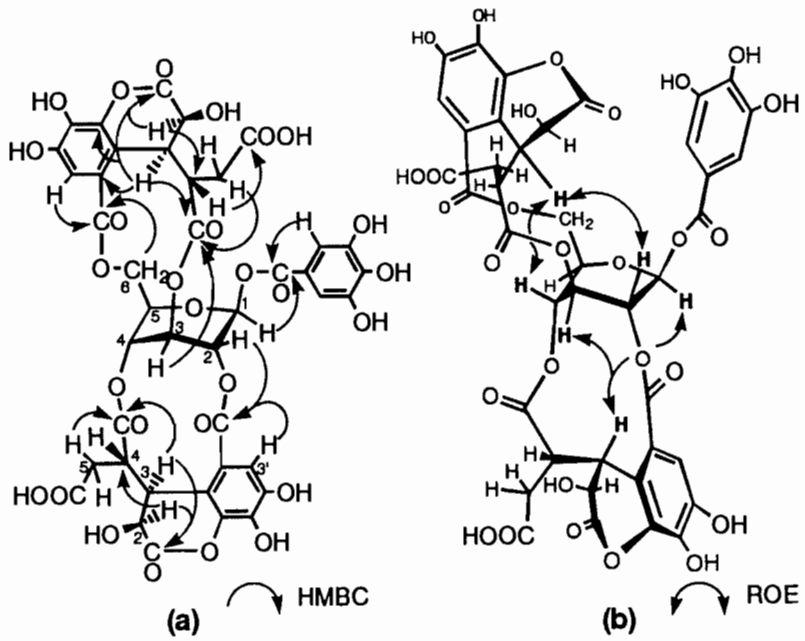


3

[2] Although the structure **3** was once assigned to a constituent of *Nuphar japonicum* (21), it was later revised to 1,2,4-tri-*O*-galloyl-α-D-glucose (22), and thus **3** is a new compound.

© 1997 NRC Canada

Fig. 1. (*a*) HMBC and (*b*) ROE correlations of **4**.



Can. J. Chem. Downloaded from www.nrcresearchpress.com by 88.146.161.215 on 09/08/12
For personal use only.

further evidence for the absolute configuration at C-3 of each chebuloyl group in **4** was provided by ROE's between the chebuloyl H-3 signals (δ 5.10, 4.94) and the glucose proton signals (H-1, H-3 and H-2, H-4, respectively), in rotating-frame nuclear Overhauser enhancement spectroscopy (ROESY). On the basis of these results, the structure of eumaculin E was established as 1-*O*-galloyl-2,4;3,6-di-*O*-chebuloyl-β-D-glucopyranose (**4**). Tannin **4** might be regarded as a metabolite which can be produced via chebulagic acid (**8**) by structural modifications of geraniin (**7**) .

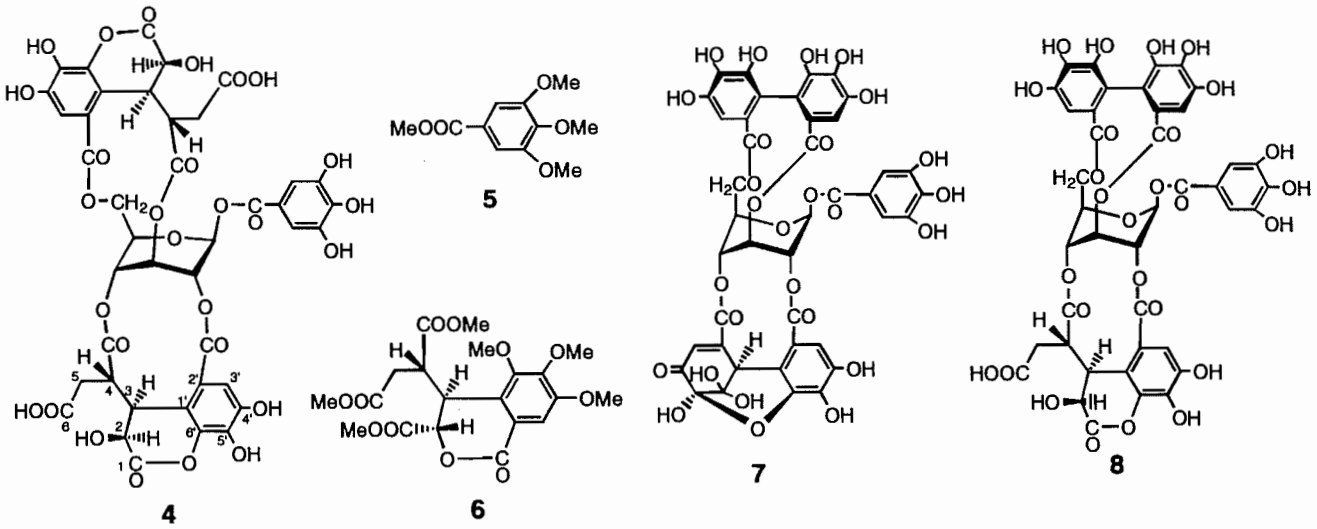
Compounds **9** and **10** were shown to be new dimers analogous to eumaculin A (**11**) as described below, and thus named eumaculins B and D, respectively. The molecular formula of eumaculin B (**9**), $C_{68}H_{52}O_{44}$, was deduced from an $(M+Na)^+$ ion peak at *m/z* 1595 in the FABMS. The ^1H NMR spectrum of **9** disclosed signals due to five galloyl groups (δ 7.17, 7.13, 7.11, 7.05, 7.02 (each 2H, s)), three aromatic protons (δ 6.98, 6.84, 6.48 (each 1H, s)), and two glucose cores (see Table 1). The coupling patterns of the glucose protons are typical for those of $^4C_1$ and $^1C_4$ glucopyranoses. The hydroxyl groups on the $^4C_1$ glucopyranose core are fully acylated as revealed by the chemical shifts of the H-1–H-4 and H-6 signals, whereas the hydroxyl groups at C-2′ and C-4′ in the $^1C_4$ glucose core were shown to be unacylated by the appearance of H-2′ (δ 4.12) and H-4′ (δ 4.60) in the high-field region. These NMR features of **9** were similar to those of eumaculin A (8), indicating that **9** is a dimer composed of corilagin and pentagalloylglucose units like **11**. A spectral difference between **9** and **11** includes a remarkable downfield shift of one of the aromatic 1H-singlets (δ 6.19 in **11** → δ 6.48 in **9**), which suggested that the linking unit of the monomers in eumaculin B (**9**) differs from that (valoneoyl group) of eumaculin A (**11**). Methylation of **9** with dimethyl sulphate and potassium carbonate in acetone and subsequent methanolysis yielded methyl tri-*O*-

Table 1. ^1H NMR spectral data for the glucose moieties of compounds **11**, **9**, and **10**[a] (500 MHz in acetone-d_6 + D_2O, *J* in Hz).

Proton	**11**	**9**	**10**
Glucose-I			
H-1	6.27 d	6.28 d	5.89 d
	(*J* = 8)	(*J* = 8.5)	(*J* = 8.5)
H-2	5.69 dd	5.73 dd	5.69 dd
	(*J* = 8, 9.5)	(*J* = 8.5, 10)	(*J* = 8.5, 9)
H-3	5.56 m[b]	6.05 t	5.93 t
		(*J* = 10)	(*J* = 9)
H-4	5.56 m[b]	5.67 t	5.53 t,
		(*J* = 10)	(*J* = 9)
H-5	4.40 m	4.55 m[c]	4.68 m
H-6	4.54 dd	4.55 m[c]	4.51 dd
	(*J* = 2, 12.5)		(*J* = 1.5, 12.5)
	4.27 dd	4.37 dd	4.36 dd
	(*J* = 5, 12.5)	(*J* = 4.5, 13)	(*J* = 3, 12.5)
Glucose-II			
H-1′	6.33 d	6.39 br s	6.42 br s
	(*J* = 2)		
H-2′	4.07 br s	4.12 br s	4.32 br s
H-3′	4.81 br s	4.84 br s	5.09 br s
H-4′	4.38 br s	4.60 br s	4.85 br s
H-5′	4.43 t-like	4.55 m[c]	4.41 m
	(*J* = 9.5)		
H-6′	4.72 t	4.92 t	4.90 t
	(*J* = 11)	(*J* = 11)	(*J* = 10)
	4.07 dd	4.15 dd	4.24 dd
	(*J* = 8, 11)	(*J* = 8.5, 11)	(*J* = 8, 10)

[a]Measured in CD_3OD.
[b,c]Overlapped with each other.

© 1997 NRC Canada



methylgallate (**5**) and trimethyl octa-*O*-methyltergallate (**14**) (1, 25), as major products. The linking unit of the monomers in eumaculin B (**9**) was thus confirmed to be a tergalloyl group. Dimethyl hexamethoxydiphenate (**12**) and trimethyl octa-*O*-methylvaloneate (**13**) were also obtained as minor products in the above reaction. These two products were regarded as secondary products derived from the tergalloyl moiety in **9** by cleavage of the biphenyl ether bond and Smiles-type rearrangement, respectively (1). The HMBC ($^{2,3}J_{C-H}$ = 8 Hz) of **9** showed a cross peak by three-bond coupling between the glucose H-6′ signal (δ 4.92 (t, J = 11 Hz)) and the ester carbonyl carbon resonance at δ 168.3, which, in turn, correlated with the aromatic proton signal at δ 6.48. This aromatic proton signal was assigned to H_B of the tergalloyl group based on its correlation through two-bond coupling with the signal attributed to C-4′ (δ 149.1) of the tergalloyl B-ring (4), and also through three-bond coupling with C-1′ (δ 115.3). The connectivity between the tergalloyl B-ring and C-6′ of the glucose core-II was thus established. The structure **9** thus proposed for eumaculin B was substantiated by chemical transformation of eumaculin B (**9**) into eumaculin A (**11**) through Smiles-type rearrangement (1, 25). Namely, an aqueous solution of **9** containing a small amount of phosphate buffer (pH 7.4) was left at room temperature for 5 h to give an isomerized product identical with **11**. Based on these findings, the structure of eumaculin B including the orientation and absolute configuration of the tergalloyl group at O-3/O-6 of glucose was represented by the formula **9**.

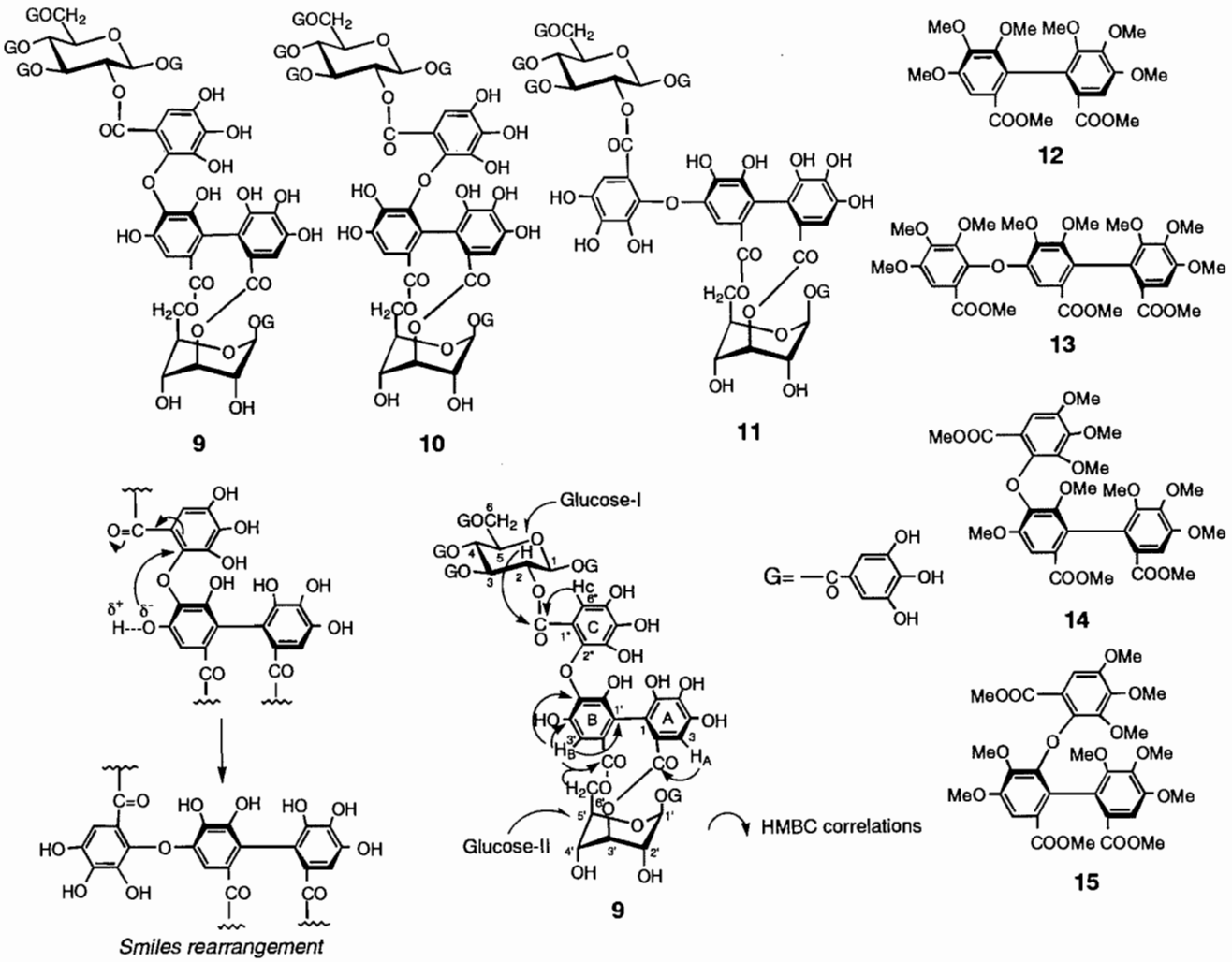
Eumaculin D (**10**) showed an ion peak at *m/z* 1595 ascribable to $(M+Na)^+$ in the FABMS, and gave a large retention volume on normal-phase HPLC, like **11** and **9**, suggesting it to be a dimeric hydrolyzable tannin (5). The ^{1}H NMR spectrum of **10** measured in acetone-d_6 and D_2O at ambient temperature showed duplicate signals for each proton, probably due to the presence of rotamers resulting from restricted rotation about the ether linkage of a macaranoyl group. The spectrum of **10** measured in MeOH-d_4, which was simplified by enhanced ratio of one rotamer, was similar to those of **11** and **9**, particularly in the chemical shifts and coupling patterns of the sugar moieties. A significant difference in the ^{1}H NMR spectra among **10**, **9**, and **11** was a downfield shift of one of the aromatic 1H singlets in **10** (δ 6.19 in **11**; δ 6.48 in **9** → δ 6.67 in **10**), which suggested that the linking unit of two monomers in **10** is different from that in both **11** and **9**. Methylation of eumaculin D (**10**) with dimethyl sulphate and potassium carbonate in acetone, followed by methanolysis with sodium methoxide, yielded methyl tri-*O*-methylgallate (**5**) and trimethyl octa-*O*-methylmacaranate (**15**) (1), as major products, accompanied by the minor products **12**, **13**, and **14**. The latter three were regarded as secondary products formed from the macaranoyl group in a similar manner to that from the tergalloyl group in **9**. The position and orientation of the macaranoyl group were based on the HMBC measurement ($^{2,3}J_{C-H}$ = 8 Hz) of **10**, which revealed the connectivity between glucose H-6 and the macaranoyl H_B signal through three-bond couplings with an ester carbonyl carbon signal at δ 170.1. The assignment of the macaranoyl H_B signal was based on two- and three-bond couplings with the macaranoyl C-4′ and C-1′ signals. Eumaculin D (**10**) was thus concluded to be an isomer of **11** and **9** differing only in the structure of the linking unit of the monomeric constituents. The structure **10** for eumaculin D was finally substantiated by chemical correlation between **10** and **11**. The isomerized product obtained by the Smiles-type rearrangement upon treatment of **10** with phosphate buffer (pH 7.4) was identical in all respects with eumaculin A (**11**).

Experimental

^{1}H and ^{13}C NMR spectra were recorded on a Varian VXR-500 instrument at 500 MHz and 126 MHz, respectively, and chemical shifts are given in δ values (ppm), based on the ^{1}H and ^{13}C signals of solvents (acetone-d_6 (δ_H 2.04; δ_C 29.8) or CD_3OD (δ_H 3.30; δ_C 49.0)) on a TMS scale. EI and FAB mass spectra were measured on a JEOL GMS HX-100 or a VG 70-SE mass spectrometer. ESI mass spectra were carried out with a Micromass AutoSpec OA-Tof mass spectrometer (solvent: MeOH-H_2O (1:1) + 0.1% $AcONH_4$, flow rate: 20 μL/min). Optical rotations were obtained on a JASCO DIP-1000 digital polarimeter, CD spectra on a JASCO J-720W spectropolarimeter, and UV spectra on a Shimadzu UV-180 spectrophotometer. Normal-phase HPLC was carried out with a Shimadzu LC-6A using a YMC-Pack SILA-003 column (4.6 × 250 mm) devel-

© 1997 NRC Canada

Can. J. Chem. Downloaded from www.nrcresearchpress.com by 88.146.161.215 on 09/08/12
For personal use only.



oped with *n*-hexane–MeOH–THF – formic acid (60:45:15:1, v/v) containing oxalic acid (500 mg/1.2 L) (flow rate, 1.5 mL/min; detection 280 nm) at room temperature. Reversed-phase HPLC was performed on a YMC-Pack A312 (ODS) column (4.6 × 150 mm) developed with 0.01 M H_3PO_4 – 0.01 M KH_2PO_4 – CH_3CN (41:41:18, v/v) (flow rate, 1.0 mL/min; detection 280 nm) at 40°C. TLC was conducted on Kieselgel 60 PF_{254} (Merck) plates with *n*-hexane–$CHCl_3$–acetone (4:6:1). Column chromatography was performed on Toyopearl HW-40 (coarse and fine grades, Tosoh), Sephadex LH-20 (Pharmacia Fine Chemicals), Dia-ion HP-20, and MCI-gel CHP-20P (Mitsubishi Kasei Industry).

Plant material

The leaves of *E. maculata* L. were collected at the campus of Okayama University in summer 1992 and a voucher specimen has been deposited at the Herbal Garden of the Faculty of Pharmaceutical Sciences, Okayama University.

Extraction and isolation

The dried leaves (2.0 kg) were homogenized (× 3) in acetone–H_2O (7: 3) (12 L × 3) and the homogenate was filtered. The filtrate was concentrated and further extracted with Et_2O (3 L × 3), EtOAc (3 L × 6), and *n*-BuOH saturated with H_2O (3 L × 6). A part (6.0 g) of the EtOAc extract (124.5 g) was chromatographed over Toyopearl HW-40 (fine) (2.2 cm i.d. × 35 cm) with MeOH–H_2O (5:5 → 6:4 → 7:3) → MeOH–H_2O–acetone (7:2:1 → 6:2:2) → acetone–H_2O (7:3) in a stepwise gradient mode. The fractions showing similar HPLC patterns were combined and further purified by rechromatography over Sephadex LH-20 with EtOH and (or) MCI-gel CHP-20P with aqueous MeOH to afford 3,4,6-tri-*O*-galloyl-D-glucose (1.7 mg), 1,3,6-tri-*O*-galloyl-β-D-glucose, euphormisin M_3 (1.3 mg), 1,2,3,4,6-penta-*O*-galloyl-β-D-glucose (8 mg), chebulanin (16 mg), chebulagic acid (**8**) (3 mg), tercatain (5 mg), granatin B (4 mg), excoecarianin (14 mg), euphorbin A (**1**) (53 mg), euphorbin B (5 mg), euphorbin D (99 mg), quercetin 3-*O*-(2″,3″-di-*O*-galloyl)-β-D-glucopyranoside (**2**) (7.6 mg), 1,2,6-tri-*O*-gallyl-α-D-glucose (**3**) (2 mg), eumaculin E (**4**) (4.8 mg), eumaculin B (**9**) (30 mg), and eumaculin D (**10**) (45 mg). To obtain additional crops of the new tannins, the other part (10 g) of the EtOAc extract was similarly fractionated by repeated column chromatographies over Toyopearl HW-40 (fine), Sephadex LH-20, and MCI-gel CHP-20P to give eumaculin E (**4**) (25 mg), eumaculin B (**9**) (50 mg), and eumaculin D (**10**) (55 mg).

Quercetin 3-O-(2″,3″-di-O-galloyl)-β-D-glucopyranoside (**2**):

© 1997 NRC Canada

Can. J. Chem. Downloaded from www.nrcresearchpress.com by 88.146.161.215 on 09/08/12
For personal use only.

Can. J. Chem. Downloaded from www.nrcresearchpress.com by 88.146.161.215 on 09/08/12
For personal use only.

yellow amorphous powder; $[\alpha]_D$ −18 (*c* 1.0, MeOH); UV λ_{max} MeOH nm (log ε): 215 (5.75), 254sh (5.31), 265 (5.43), 292sh (5.39), 357 (5.39); ^{1}H NMR (500 MHz, acetone-d_6 + D_2O) δ: 7.10, 7.04 (each 2H, s, galloyl), 7.78 (1H, d, *J* = 2.5, B-ring H-2′), 7.59 (1H, dd, *J* = 2.5, 8.5 Hz, B-ring H-6′), 6.94 (1H, d, *J* = 8.5 Hz, B-ring H-5′), 6.45 (1H, d, *J* = 2 Hz, A-ring H-8), 6.22 (1H, d, *J* = 2 Hz, A-ring H-6), 6.04 (1H, d, *J* = 8 Hz, Glc H-1″), 5.39 (1H, dd, *J* = 8, 10 Hz, Glc H-2″), 5.51 (1H, t, *J* = 10 Hz, Glc H-3″), 3.90 (1H, t, *J* = 10 Hz, Glc H-4″), 3.60 (1H, ddd, *J* = 2.5, 5, 10 Hz, Glc H-5″), 3.78 (1H, dd, *J* = 2.5, 12 Hz, Glc H-6″), 3.70 (1H, dd, *J* = 5, 12 Hz, Glc H-6″); ^{13}C NMR (126 MHz, acetone-d_6 + D_2O) δ: 157.7 (C-2), 134.2 (C-3), 178.4 (C-4), 162.6 (C-5), 99.4 (C-6), 166.7 (C-7), 94.4 (C-8), 157.8 (C-9), 105.4 (C-10), 122.8 (C-1′), 115.8 (C-2′), 145.4 (C-3′), 149.1 (C-4′), 117.1 (C-5′), 122.7 (C-6′) (quercetin moiety), 121.2, 121.0 (galloyl C-1), 110.2, 110.0 (each 2C, galloyl C-2,6), 145.8, 145.9 (each 2C, galloyl C-3,5), 138.9, 139.0 (galloyl C-4), 165.1, 166.3 (galloyl C-7), 99.8 (Glc C-1″), 73.3 (Glc C-2″), 76.4 (Glc C-3″), 69.2 (Glc C-4″), 78.0 (Glc C-5″), 61.7 (Glc C-6″). FABMS: *m/z* 791 $(M+Na)^+$; HRESIMS: *m/z* 769.1223 (calcd. for $C_{35}H_{29}O_{20}$: 769.1252 $(M+H)^+$).

Enzymatic hydrolysis of ***2***

An aqueous solution of **2** (5 mg/ 3 mL) was incubated at 37°C with tannase that was prepared from *Aspergillus niger* (26), and the progress of the reaction was monitored by HPLC. The formation of isoquercitrin and quercetin 3-*O*-(2″-*O*-galloyl)-β-D-glucopyranoside, together with gallic acid, was observed by the accompanying disappearance of the starting material, and these products were identified by co-chromatography on HPLC with authentic samples.

1,2,6-Tri-O-*galloyl*-α-D-glucose (**3**): off-white amorphous powder; $[\alpha]_D$ +31 (*c* 0.5, MeOH); UV λ_{max} MeOH nm (log ε): 218 (4.79), 277 (4.42); ^{1}H NMR (500 MHz, acetone-d_6 + D_2O) δ: 7.16, 7.12, 7.06 (each 2H, s, galloyl), 6.50 (1H, d, *J* = 3.5 Hz, Glc H-1), 5.02 (1H, dd, *J* = 3.5, 10 Hz, Glc H-2), 4.26 (1H, t, *J* = 10 Hz, Glc H-3), 3.83 (1H, t, *J* = 10 Hz, Glc H-4), 4.16 (1H, m, Glc H-5), 4.52 (1H, dd, *J* = 2, 12 Hz, Glc H-6), 4.12 (1H, dd, *J* = 4, 12 Hz, Glc H-6). FABMS: *m/z* 659 $(M+Na)^+$.

Eumaculin E ***(4)***: light-brown amorphous powder; $[\alpha]_D$ +5 (*c* 1.0, MeOH); UV λ_{max} MeOH nm (log ε): 220 (4.83), 278 (4.48); CD: $[\theta]_{216}$ +186 000, $[\theta]_{242}$ −62 300, $[\theta]_{267}$ +38 200, $[\theta]_{294}$ −66 700 (MeOH); ^{1}H NMR (500 MHz, acetone-d_6 + D_2O) δ: 7.22 (2H, s, galloyl), 7.52, 7.48 (each 1H, s, chebuloyl H-3′), 5.10 (1H, dd, *J* = 1.5, 7 Hz), 4.94 (1H, dd, *J* = 2, 7 Hz) (chebuloyl H-3), 4.87 (1H, d, *J* = 7 Hz), 4.82 (1H, d, *J* = 7 Hz) (chebuloyl H-2), 3.87 (1H, ddd, *J* = 1.5, 5, 11 Hz), 3.80 (1H, ddd, *J* = 2, 3.5, 12 Hz) (chebuloyl H-4), 2.18 (2H, m), 2.26 (1H, dd, *J* = 3.5, 17 Hz), 2.18 (1H, dd, *J* = 12, 17 Hz) (chebuloyl H-5), 6.38 (1H, d, *J* = 5 Hz, Glc H-1), 5.45 (1H, dd, *J* = 1.5, 5 Hz, Glc H-2), 5.65 (1H, dd, *J* = 1.5, 3.5 Hz, Glc H-3), 5.30 (1H, brd, *J* = 3.5 Hz, Glc H-4), 4.73 (1H, brt, *J* = 3.5 Hz, Glc H-5), 5.42 (1H, dd, *J* = 3.5, 13.5 Hz, Glc H-6), 4.21 (1H, brd, *J* = 13.5 Hz, Glc H-6); ^{13}C NMR (126 MHz, acetone-d_6 + D_2O) δ: 119.6 (galloyl C-1), 110.2 (2C, galloyl C-2, 6), 146.2 (2C, galloyl C-3, 5), 139.9 (galloyl C-4), 66.4 (2C, chebuloyl C-2), 39.9, 41.1 (chebuloyl C-3), 39.3, 39.6 (chebuloyl C-4), 30.5, 30.7 (chebuloyl C-5), 115.3, 115.8 (chebuloyl C-1′), 116.9, 117.1 (chebuloyl C-2′), 110.2 (2C, chebuloyl C-3′), 146.4, 146.5 (chebuloyl C-4′), 139.0, 139.7 (chebuloyl C-5′), 140.7, 141.1 (chebuloyl C-6′), 94.2 (Glc C-1), 74.7 (Glc C-2), 66.6 (Glc C-3), 69.7 (Glc C-4), 78.6 (Glc C-5), 65.7 (Glc C-6), 173.6, 173.1, 172.8, 172.7, 169.9, 169.6, 167.5, 165.6, 165.1 (ester carbonyl). Anal. calcd. for $C_{41}H_{32}O_{28}\cdot 6H_2O$: C 45.56, H 4.10; found: C 45.87, H, 4.19. FABMS: *m/z* 973 $(M+H)^+$.

Methylation of ***4*** *followed by methanolysis*

A mixture of **4** (8 mg), K_2CO_3 (150 mg), and $(CH_3)_2SO_4$ (0.02 mL) in acetone (2.5 mL) was stirred overnight at room temperature, and then heated at reflux for 2 h. After removal of the inorganic material by centrifugation, the resulting supernatant was evaporated to dryness. The residue was directly methanolyzed with 1% NaOMe in MeOH (1 mL), and subjected to preparative TLC (Kieselgel PF_{254}, toluene–acetone, 4:1) to give methyl tri-*O*-methylgallate (**5**) (2 mg; EIMS: *m/z* 226 $(M)^+$) and trimethyl tri-*O*-methylchebulate (**6**) (2.5 mg; CD (MeOH): $[\theta]_{210}$ −34 000, $[\theta]_{227}$ +31 000, $[\theta]_{244}$ −5000, $[\theta]_{271}$ +28 000 (MeOH); ^{1}H NMR (500 MHz, acetone-d_6) δ: 7.32 (1H, s), 5.35 (1H, d, *J* = 1 Hz), 3.85 (1H, dd *J* = 1, 9.5 Hz), 3.22 (1H, dt, *J* = 5.5, 9.5 Hz), 2.75 (1H, dd, *J* = 9.5, 17 Hz), 2.49 (1H, dd, *J* = 5.5, 17 Hz), 3.93, 3.91, 3.87, 3.68, 3.62, 3.50 (each 3H, s); EIMS: *m/z* 440 $(M)^+$), which were identical with those of authentic samples in all respects.

Eumaculin B ***(9)***: light-brown amorphous powder; $[\alpha]_D$ −50 (*c* 1.0, MeOH); UV λ_{max} MeOH nm (log ε): 220 (5.28), 278 (4.92); CD (MeOH): $[\theta]_{204}$ +99 000, $[\theta]_{217}$ −26 000, $[\theta]_{236}$ −64 000, $[\theta]_{263}$ +36 000, $[\theta]_{293}$ −56 000; ^{1}H NMR (500 MHz, acetone-d_6 + D_2O) δ: 7.17, 7.13, 7.11, 7.05, 7.02 (each 2H, s, galloyl), 6.92, 6.84, 6.48 (each 1H, s, tergalloyl), glucose protons see Table 1; ^{13}C NMR (126 MHz, acetone-d_6 + D_2O) δ: 93.2 (Glc C-1), 94.3 (Glc C-1′), 72.3 (Glc C-2), 69.0 (Glc C-2′) , 73.3 (Glc C-3), 71.1 (Glc C-3′), 69.3 (Glc C-4), 62.0 (Glc C-4′), 73.7 (Glc C-5), 75.3 (Glc C-5′), 62.7 (Glc C-6), 64.6 (Glc C-6′), 110.1, 110.3, 110.5 (each 2C), 109.8 (4C) (galloyl C-2,6), 119.5, 119.96, 120.02, 120.05, 121.0 (galloyl C-1), 139.0, 139.2, 139.37, 139.42 (2C) (galloyl C-4), 145.80, 145.82 (each 2C), 145.87, 145.9 (each 4C) (galloyl C-3,5), 165.2, 165.3, 165.74, 166.42, 166.45 (galloyl C-7), 108.3, 108.5, 110.1, 113.1, 115.3, 117.1, 124.7, 130.8, 136.6, 137.0, 140.0, 140.6, 140.7, 142.1, 144.7 (2C), 149.1, 149.4, 167.3, 167.8, 168.3 (tergalloyl-C). Anal. calcd. for $C_{68}H_{52}O_{44}\cdot 8H_2O$: C 47.56, H 3.99; found: C 47.65, H 4.12. FABMS: *m/z* 1595 $(M+Na)^+$.

Methylation of ***9*** *followed by methanolysis*

A mixture of **9** (5 mg), K_2CO_3 (100 mg), and $(CH_3)_2SO_4$ (0.01 mL) in acetone (2 mL) was stirred overnight at room temperature and then heated at reflux for 2.5 h. After removal of K_2CO_3 by centrifugation followed by evaporation of the solvent, the residue was directly subjected to methanolysis with 1% NaOMe in MeOH (1 mL) at room temperature overnight. After acidification with AcOH and evaporation of the solvent, the residue was submitted to preparative TLC (Kieselgel PF_{254}, *n*-hexane–$CHCl_3$–acetone, 3:7:1) to give **5** (0.9 mg), trimethyl octa-*O*-methyltergallate (**14**) (0.6 mg, EIMS *m/z* 660 $(M)^+$), dimethyl hexamethoxydiphenate (**12**) (0.2 mg), and trimethyl octa-*O*-methylvaloneate (**13**) (0.1 mg).

Eumaculin D ***(10)***: off-white amorphous powder; $[\alpha]_D$ −6 (*c* 1.2, MeOH); UV λ_{max} MeOH nm (log ε): 218 (5.20),

© 1997 NRC Canada

Can. J. Chem. Downloaded from www.nrcresearchpress.com by 88.146.161.215 on 09/08/12
For personal use only.

278 (4.85); CD (MeOH): $[\theta]_{216}$ −110 000, $[\theta]_{241}$ −22 000, $[\theta]_{263}$ +89 000, $[\theta]_{290}$ −92 000, $[\theta]_{320}$ +19 000; ^{1}H NMR (500 MHz, MeOH-d_4) δ: 7.10, 7.07, 7.05, 6.94, 6.81 (each 2H, s, galloyl), 7.06, 7.01, 6.67 (each 1H, s, macaranoyl), glucose protons see Table 1; (500 MHz, acetone-d_6 + D_2O) δ: 5.90, 6.29 (each d, J = 8 Hz, Glc H-1), 5.73, 5.69 (each dd, J = 8, 9.5 Hz, Glc H-2), 6.01, 6.12 (each t, J = 9.5 Hz, Glc H-3), 5.57, 5.68 (each t, J = 9.5 Hz, Glc H-4), 4.55–4.64 (Glc H-5, 6), 4.27, 4.30 (each dd, J = 5, 13 Hz, Glc H-6), 6.43, 6.37 (each br s, Glc H-1′), 4.38, 4.13 (each br s, Glc H-2′), 5.16, 4.85 (each br s, Glc H-3′), 4.87, 4.44 (each br s, Glc H-4′), 4.51, 4.57 (each t, J = 11 Hz, Glc H-5′), 4.80, 4.82 (each t, J = 11 Hz, Glc H-6′), 4.22, 4.15 (each dd, J = 8.5, 11 Hz, Glc H-6′); ^{13}C NMR (126 MHz, MeOH-d_4) δ: 93.8 (Glc C-1), 95.1 (Glc C-1′), 72.0 (Glc C-2), 69.3 (Glc C-2′) , 74.5 (Glc C-3), 71.9 (Glc C-3′), 70.4 (Glc C-4), 62.1 (Glc C-4′), 73.0 (Glc C-5), 76.3 (Glc C-5′), 63.3 (Glc C-6), 65.2 (Glc C-6′), 110.4, 110.9, 111.0 (each 2C), 110.3 (4C) (galloyl C-2,6), 120.6 (2C), 120.7, 121.0, 121.1 (galloyl C-1), 139.0, 139.5, 139.9, 140.0, 140.3 (galloyl C-4), 146.0, 146.2 (each 2C), 146.31, 146.32 (each 4C) (galloyl C-3,5), 166.0, 166.7, 166.8, 166.9, 167.3 (galloyl C-7), 108.2, 110.0, 111.0, 113.4, 118.7, 119.1, 124.6, 125.6, 138.4, 138.6, 140.3, 140.4, 141.3, 142.1, 142.3, 143.2, 143.7, 146.8, 168.0, 168.4, 170.6 (macaranoyl-C). Anal. calcd. for $C_{68}H_{52}O_{44}\cdot 6H_2O$: C 48.58, H 3.83; found: C 48.60, H, 4.16. FABMS: m/z 1595 $(M+Na)^+$; HRESIMS: m/z 1590.2370 (calcd. for $C_{68}H_{56}NO_{44}$: 1590.2175 $(M+NH_4)^+$).

*Methylation of **10** followed by methanolysis*

A solution of **10** (10 mg), K_2CO_3 (200 mg), and $(CH_3)_2SO_4$ (0.02 mL) in acetone (3 mL) was stirred overnight at room temperature, and then heated at reflux for 4 h. After removal of the inorganic material by centrifugation, the supernatant was evaporated to dryness. The residue was directly methanolyzed with 1% NaOMe in MeOH (1 mL) at room temperature overnight. After acidification with AcOH and evaporation, the residue was subjected to preparative TLC (Kieselgel PF_{254}, *n*-hexane–$CHCl_3$–acetone, 3:7:1) to give **5** (2.2 mg), trimethyl octa-*O*-methylmacaranate (**15**) (1.0 mg, EIMS m/z 660 $(M)^+$), **12** (0.2 mg), **13** (0.5 mg), and **14** (0.3 mg), which were identical in all respects by direct comparison with authentic samples.

*Isomerization of **9** and **10** to **11***

A solution of **10** (3 mg) (or **9** (3 mg)) in 0.02 M phosphate buffer (KH_2PO_4–Na_2PO_4, pH 7.4) (2 mL) was left standing at room temperature and the progress of reaction was monitored by HPLC. After disappearance of the starting material (3 h) (or 5 h for eumaculin B), the reaction mixture was acidified with dilute HCl, and applied to a Sep-Pak cartridge (Waters). After washing with H_2O, the products were eluted with MeOH to yield **11** (2.8 mg from **10**; 2.5 mg from **9**), which was identical with an authentic sample by ^{1}H NMR spectral comparison.

Acknowledgements

We are grateful to the SC-NMR Laboratory of Okayama University for the NMR experiments.

References

1. Y. Amakura and T. Yoshida. Chem. Pharm. Bull. **44**, 1293 (1996).
2. T. Yoshida, Y. Amakura, Y.-Z. Liu, and T. Okuda. Chem. Pharm. Bull. **42**, 1803 (1994).
3. T. Yoshida, H. Itoh, S. Matsunaga, R. Tanaka, and T. Okuda. Chem. Pharm. Bull. **40**, 53 (1992).
4. J.-H. Lin, M. Ishimatsu, T. Tanaka, G. Nonaka, and I. Nishioka. Chem. Pharm. Bull. **38**, 1844 (1990).
5. T. Okuda, T. Yoshida, and T. Hatano. *In* Progress in the chemistry of organic natural products. Vol. 66. *Edited by* W. Herz, G.W. Kirby, R.E. Moore, W. Steglich, and Ch. Tamm. Springer-Verlag, New York. 1995. p. 1.
6. S. v. R. Altschul. *In* Drugs and foods from little-known plants, Notes in Harvard University Herbaria. Harvard University Press, Cambridge. 1973. p. 167.
7. *In* Dictionary of traditional Chinese drugs. *Edited by* Chiang Su New Medicinal College. Shanghai Scientific Technologic Publishers, Shanghai. 1977. p. 4732.
8. I. Agata, T. Hatano, Y. Nakaya, T. Sugaya, S. Nishibe, T. Yoshida, and T. Okuda. Chem. Pharm. Bull. **39**, 881 (1991).
9. T. Yoshida, O. Namba, K. Yokoyama, and T. Okuda. Abstracts of Papers, the 31st Symposium of the Chemistry of Natural Products, Nagoya. 1989. p. 601.
10. E.A. Haddock, R.K. Gupta, S.M.K. Al-Shafi, E. Haslam, and D. Magnolato. J. Chem. Soc. Perkin Trans. 1, 2515 (1982).
11. J.-H. Lin, T. Tanaka, G. Nonaka, and I. Nishioka. Abstracts of Papers, 108th Annual Meeting of the Pharmaceutical Society of Japan, Hiroshima. 1988. p. 278.
12. T. Yoshida, R. Fujii, and T. Okuda. Chem. Pharm. Bull. **28**, 3713 (1980).
13. T. Tanaka, G. Nonaka, and I. Nishioka. Chem. Pharm. Bull. **34**, 1039 (1986).
14. T. Okuda, T. Yoshida, K. Mori, and T. Hatano. Heterocycles, **15**, 1323 (1981).
15. J.-H. Lin, T. Tanaka, G. Nonaka, I. Nishioka, and I.-S. Chen. Chem. Pharm. Bull. **38**, 2162 (1990).
16. T. Yoshida, L. Chen, T. Shingu, and T. Okuda. Chem. Pharm. Bull. **36**, 2940 (1988).
17. T. Yoshida, K. Yokoyama, O. Namba, and T. Okuda. Chem. Pharm. Bull. **39**, 1137 (1991).
18. K.R. Markham, B. Ternai, R. Stanley, H. Geiger, and T.J. Mabry. Tetrahedron, **34**, 1389 (1978).
19. K. Kameda, T. Takatsu, H. Okuda, Y. Kimura, T. Okuda, T. Hatano, I. Agata, and S. Arichi. J. Nat. Prod. **50**, 680.
20. J.B. Harborne and R.J. Grayer. *In* The flavonoids, advances in research since 1986. *Edited by* J. B. Harborne. Chapman and Hall, London. 1990.
21. M. Nishizawa, T. Yamagishi, G. Nonaka, I. Nishioka, and H. Bando. Chem. Pharm. Bull. **30**, 1094 (1982).
22. M. Ishimatsu, T. Tanaka, G. Nonaka, I. Nishioka, M. Nishizawa, and T. Yamagishi. Chem. Pharm. Bull. **37**, 129 (1989).
23. T. Yoshida, T. Okuda, T. Koga, and N. Toh. Chem. Pharm. Bull. **30**, 2655 (1982).
24. T. Okuda, T. Yoshida, and T. Hatano. J. Chem. Soc. Perkin Trans. 1, 9 (1982).
25. T. Yoshida, T. Maruyama, A. Nitta, and T. Okuda. Chem. Pharm. Bull. **40**, 1750 (1992).
26. T. Yoshida, K. Tanaka, X.-M. Chen, and T. Okuda. Chem. Pharm. Bull. **37**, 920 (1989).

© 1997 NRC Canada

Identification of iridals as piscicidal components of Iridaceous plants and their conformations associated with CD spectra

Yoko Miyake, Hideyuki Ito, and Takashi Yoshida

Abstract: Upon toxicity-guided fractionation of the extractives of the *Iris germanica* rhizomes and *I. japonica* roots using killie-fish (*Oryzias latipes*), 12 iridal-type triterpenoids including three new iridals were isolated as piscicidal constituents. Of these, iriflorental, iripallidal, and γ-irigermanal exhibited a potent activity at a concentration of less than 1 μg/mL. The structures of new iridals, irisgermanicals A (**7**), B (**10**), and C (**11**), from *I. germanica* were elucidated based on the spectral analysis. The absolute configuration at C-13 of the known spiroiridal (**15**) from *I. japonica*, which remained to be solved, was defined as *R* on the basis of NOE measurement. The hitherto unreported correlation between the Cotton effects in the CD spectra of some iridals and their conformations was also discussed on the basis of molecular modeling.

Key words: *Iris germanica*, *Iris japonica*, iridal-type triterpenoid, piscicidal activity, CD spectra.

Résumé : Faisant appel à des poissons (*Oryzias latipes*), on a fractionné des extraits de rhizomes de l'*Iris germanica* et de racines de l'*I. japonica*, guidé par la toxicité, et on a isolé 12 triterpénoïdes du type iridal, y compris trois nouveaux iridals, à partir des constituants présentant une activité piscicide. Parmi ceux-ci, l'iriflorental, l'iripallidal et le γ-irigermanal présentent une grande activité à des concentrations inférieures à 1 μg/mL. On a élucidé les structures des nouveaux iridals, les irisgermanicals A (**7**), B (**10**) et C (**11**) isolés de l'*I. germanica*, en se basant sur des analyses spectrales. La configuration absolue en C-13 du spiroiridal connu (**15**) isolé de l'*I. japonica*, qui n'avait pas encore été déterminée, a été définie comme *R* en se basant sur des mesures d'EON. En se basant sur du modelage moléculaire, on discute aussi de la corrélation, qui n'avait pas été rapportée antérieurement, entre les effets Cotton des spectres de DC de quelques iridals et leurs conformations.

Mots clés : *Iris germanica*, *Iris japonica*, triterpénoïde de type iridal, activité comme piscicide, spectres de DC.

[Traduit par la rédaction]

Introduction

Among numerous biologically active natural products, the piscicidal substances have often been found to show such various other biological activities as exemplified by the insecticidal, aphrodisiac, and antitumor promoting activities (1) of piscicidal rotenone, potent tumor-promoting activity (2) of phorbol-type diterpenoids (3), antifungal activity of 5-*O*-methylembelin (4), and antitumor and inflammatory activities (unpublished data) of buddledin A (5), etc. In a continuing study on biologically active natural products using piscicidal bioassay as a primary screening, MeOH extracts of *Iris germanica* and *I. japonica* (Iridaceae) were found to exhibit potent toxicity to *Oryzias latipes* (killie-fish; Japanese name, medaka). Many isoflavonoids (6), quinones (7) and iridals (8–11) are reportedly contained in the rhizomes of Iridaceous plants. Amongst them, iridals, which are biogenetically interesting mono- and bicyclic triterpenoids discovered first by Marner et al. (8, 9), have been recognized during the last decade as the metabolites characteristic of Iridaceae (8–11). Some possible roles in living plant cells, such as antioxidant function (12) and drought-resistant activity (13), are suggested for the iridals. The biological activities of these components have, however, been little known except for antiulcer activity in experimental stress ulcers (14), and differentiation-inducing activity in HL-60 promyelocytic leukemia cells (15) for some iridals. Toxicity-guided fractionation has resulted in the isolation of eight piscicidal substances including three new compounds named irisgermanicals A (**7**), B (**10**), and C (**11**), from *I. germanica*, and four from *I. japonica*. This paper describes the isolation and characterization of the piscicidal components of both *Iris* species.

Received October 31, 1996.

This paper is dedicated to Professor William A. Ayer on the occasion of his 65th birthday.

Y. Miyake, H. Ito, and T. Yoshida.[1] Faculty of Pharmaceutical Sciences, Okayama University, Tsushima, Okayama 700, Japan.

[1] Author to whom correspondence may be addressed. Telephone and Fax: 086-251-7936. E-mail: yoshida@pheasant.pharm.okayama-u.ac.jp

Results and discussion

The rhizomes of *I. germanica* were percolated with MeOH. The concentrated solution was extracted with *n*-hexane, EtOAc, and *n*-BuOH to give the respective extracts and the residue obtained after concentration of the water-soluble portion. Of these, the *n*-hexane and EtOAc extracts exhibited a potent toxicity to killie-fish with a lethal concentration of 20 μg/mL, giving no survivors after 1.5–2.5 h among five fishes tested. Toxicity-guided fractionation of the active extract by

© 1997 NRC Canada

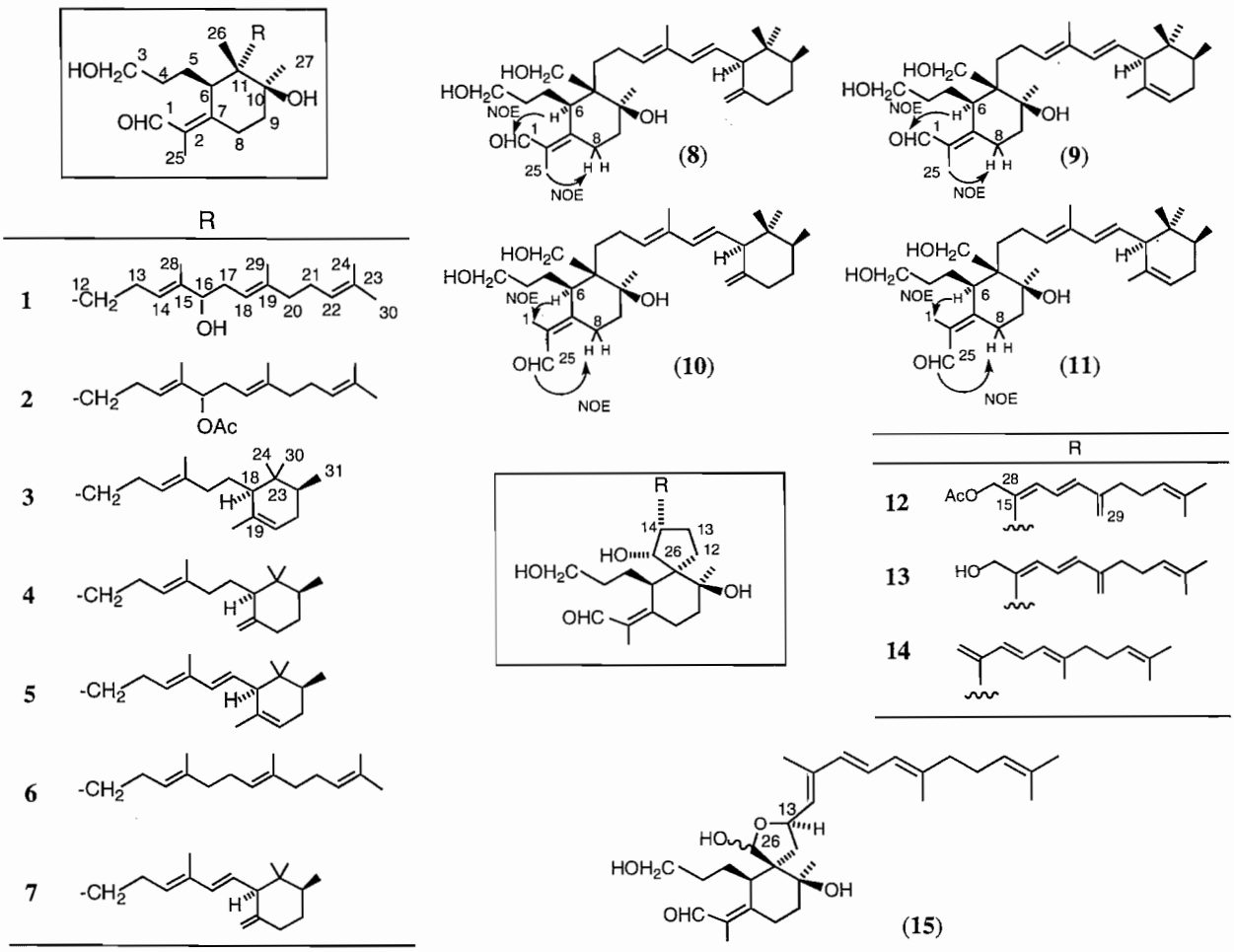
Can. J. Chem. Downloaded from www.nrcresearchpress.com by 88.146.161.215 on 09/08/12
For personal use only.

column chromatography over silicic acid and subsequent purification by preparative HPLC afforded 11 compounds including irisgermanicals A (**7**), B (**10**), and C (**11**). Eight of these were identified as the known iridal-type triterpenoids, isoiridogermanal (**1**) (8), 16-*O*-acetylisoiridogermanal (**2**) (11), α-irigermanal (**3**) (8), γ-irigermanal (**4**) (8), α-dehydroirigermanal (**5**) (9), iridal (**6**) (9), iriflorental (**8**) (9), and iripallidal (**9**) (9), by comparison of their spectral data with the literature values. The active Et_2O extract of *I. japonica* roots was similarly fractionated by a combination of normal and reversed-phase column chromatographies to yield six iridals, which were identical with belamcandal (**12**) (11), 28-deacetylbelamcandal (**13**) (11), isoiridogermanal (**1**), iridal (**6**), (+)-(6*R*,10*S*,11*S*,14*S*,26*R*)-26-hydroxy-15-methylidenespiroirid-16-enal (**14**) (16), and (6*R*,10*S*,11*R*)-26-ζ-hydroxy-13ζ-oxaspiroirid-16-enal (**15**) (17), by comparison of their physical data with those already reported. This is the first report of the isolation of **2** and **6** from *I. germanica*, and also of **6** and **15** from *I. japonica*.

Structures of irisgermanicals A, B, and C

A new compound, irisgermanical A (**7**), showed the presence of an α,β-unsaturated aldehyde group in the ^1H and ^{13}C NMR spectra (δ_H 10.19 (1H, s), δ_C 190.0, 133.3, and 162.7). The ^1H NMR spectrum also showed signals for a secondary methyl and six tertiary methyl groups, an exomethylene (δ 4.49 and 4.72), a primary alcohol function (δ 3.61 (2H, t, J = 6 Hz)), and three olefinic protons at δ 5.20, 5.64, and 5.94. These spectral features, together with 9 sp^2 and 22 sp^3 carbon resonances in the ^{13}C NMR, suggested that **7** is an analog of γ-type bicyclic iridal. The ^1H and ^{13}C NMR spectra of **7** were closely similar to those of iriflorental (**8**), except for the presence of a tertiary methyl signal at δ_H 1.10, δ_C 18.0 and absence of the primary alcohol group (δ_C 68.3) (see Experimental), indicating **7** to be 26-deoxyiriflorental. The appearance of an $(M+H)^+$ ion peak at *m/z* 471 in the FABMS supported this structure. The CD spectrum of **7** showed a positive Cotton effect at 230 nm (Δε +8.5) and a negative one at 260 nm (Δε −8.5), which were almost superimposable on those of **8**, indicating that the absolute stereochemistry of **7** should be the same as that of **8**.

Irisgermanical B (**10**) was determined to have the molecular formula $C_{31}H_{50}O_4$ (HRFABMS). The ^1H NMR (Table 1) and ^{13}C NMR spectra of **10** displayed close resemblance with those of iriflorental (**8**), particularly in the chemical shifts and coupling patterns of the signals due to the C-11 side chain in the ^1H NMR spectrum. Hence, **10** also has a bicyclic iridal skeleton. However, the H-6 methine and one of the H-8 methylene proton signals in the ^1H NMR spectrum were shifted to higher (Δδ 0.57 ppm) and lower field (Δδ 0.69 ppm), respectively, than the corresponding signals of **8**. Furthermore, a remarkable difference was observed in the chemical shift of the C-6 resonance between the ^{13}C NMR spectra



Can. J. Chem. Downloaded from www.nrcresearchpress.com by 88.146.161.215 on 09/08/12
For personal use only.

© 1997 NRC Canada

Can. J. Chem. Downloaded from www.nrcresearchpress.com by 88.146.161.215 on 09/08/12
For personal use only.

Table 1. The ^{1}H NMR data for **7**–**11** (500 MHz, in $CDCl_3$).

	7	8	10	9	11
H-1	10.19 s	10.22 s	1.82 brs	10.22 s	1.83 brs
H-3	3.61 t (6)	3.69, 3.57 m	3.71, 3.58 m	3.60, 3.67 m	3.67, 3.60 m
H-4	1.58–1.38 m	1.57–1.39 m	1.58–1.38 m	1.46–1.41 m	1.48–1.36 m
H-5	2.25 m	2.25 m	2.25 q (7.5)	2.22–2.15 m	2.23 q (7)
H-6	3.32 brd (10)	3.61 m	3.04 t (7.5)	3.67 m	3.04 t (7)
H-8	2.60 dt (5, 14)	2.69 dt (5, 14)[a]	2.70 td (5, 14)	2.70 dt (6, 14)	2.70 brt (7)
	2.53 brd (14)	2.54 brd (14)	3.23 brd (14)	2.54 brd (14)	3.23 brd (14)
H-9	1.82–1.58 m	1.80–1.60 m	1.82–1.58 m	1.76–1.68 m	1.90–1.60 m
H-12	1.30–1.21 m	1.38–1.21 m	1.30–1.21 m	1.21 m	1.30–1.25 m
H-13	2.10 m	2.01–1.97 m	2.10 m	1.96 dd (7, 16)	2.05 m
H-14	5.20 t (6.5)	5.16 dd (7.5, 14)	5.15 m	5.16 t (7.5)	5.17 t (7.5)
H-16	5.94 d (15.5)	5.93 d (16)	5.94 d (16)	5.95 d (15.5)	5.97 d (15.5)
H-17	5.64 dd (10, 15.5)	5.64 dd (10, 16)	5.65 dd (10, 16)	5.33 dd (10.5, 15.5)	5.34 dd (10.5, 15.5)
H-18	2.37 brd (10)	2.37 brd (10)	2.40 brd (10)	2.37 brd (10.5)	2.37 brd (10.5)
H-20	2.30 dq (2, 11.5)	2.24–2.04 m	2.37–2.10 m	5.43 brs	5.43 brs
H-21	1.58–1.39 m	1.57–1.38 m	1.58–1.38 m	1.96–1.85 m	1.90–1.60 m
H-22	1.48–1.39 m	1.42–1.38 m	1.42–1.38 m	1.48–1.39 m	1.48–1.36 m
H-24	0.64 s	0.63 s	0.64 s	0.63 s	0.63 s
H-25	1.82 brs	1.84 brs	10.24 s	1.85 brs	10.25 s
H-26	1.10 s	4.09, 3.96 d (11)	4.09, 3.96 d (11)	4.09, 3.96 d (11)	4.08, 3.96 d (11.5)
H-27	1.16 s	1.32 s	1.33 s	1.32 s	1.33 s
H-28	1.74 s	1.68 brs	1.74 brs	1.68 brs	1.69 brs
H-29	4.72, 4.49 brs	4.72, 4.48 brs	4.72, 4.48 brs	1.50 brs	1.50 brs
H-30	0.85 s	0.85 s	0.85 s	0.83 s	0.83 s
H-31	0.84 d (7.5)	0.84 d (7)	0.84 d (7.5)	0.84 d (7)	0.85 d (7)

[a]The *J* values (Hz) are in parentheses.

of **8** and **10**. All the above data clearly indicated that compound **10** is the geometrical isomer of **8** at the conjugated aldehyde system. The relevant evidence for the structure of **10** was obtained from the NOESY measurement. Compound **8** exhibited NOEs between the aldehyde proton (δ 10.22) and H-6 proton (δ 3.61) and between the vinyl methyl (δ 1.84) and H-8 proton (δ 2.54) in the NOESY spectrum, while the aldehyde proton (δ 10.22) and vinyl methyl (δ 1.82) signals of **10** showed NOE correlations with one of the C-8 methylene protons (δ 3.23) and H-6, respectively.

Irisgermanical C (**11**), $C_{31}H_{50}O_4$, showed ^{1}H NMR (Table 1) and ^{13}C NMR spectra closely similar to those of iripallidal (**9**). However, the ^{1}H NMR signals for the H-6 proton and one of the C-8 methylene protons in **11** were shifted to higher and lower field, respectively, in comparison with those of **9**, as in the case of **10**. It became evident from the observed differences between the NOESY spectra of **11** and **9** that compound **11** is a geometrical isomer of **9** at the α,β-unsaturated aldehyde moiety. The CD spectra of **10** and **11** showed Cotton effects similar to those of **8** and **9**, although their amplitudes were somewhat different from each other. The dihydro derivatives (**10***a* and **11***a*) prepared by $NaBH_4$ reduction of **10** and **11** also showed CD spectra similar to those of the corresponding derivatives (**8***a* and **9***a*) of **8** and **9**, clearly indicating that these compounds have the same stereostructures.

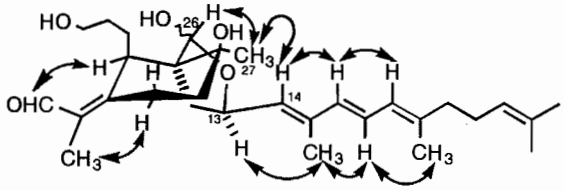
Irisgermanicals B (**10**) and C (**11**) seem to be generated from the keto–enol tautomerization of **8** and **9**, respectively. Therefore, the isomerization of the iridals under a variety of conditions was examined. Treatment of the mono- and bicyclic iridals with *p*-toluenesulfonic acid (TsOH) or MeOH–HCl revealed a formation of the corresponding geometrical isomers at the α,β-unsaturated aldehyde moiety. For example, α-irigermanal (**3**) partly transformed into its geometrical isomer (**3***a*) upon treatment with TsOH at room temperature for several hours. The structure of **3***a* was proved by analyzing its ^{1}H NMR and NOESY data. The corresponding isomers from iridal (**6**) and γ-irigermanal (**4**) were also detected on HPLC of the reaction mixture. Similarly, tautomerization of **8** and **9** was shown by HPLC, which showed identical peaks with those of **10** and **11**. Although α-irigermanal (**3**) and iridal (**6**) are abundant constituents of *I. germanica* and their yields were much higher than that of iripallidal (**9**), the corresponding geometrical isomers of the former two have never been detected even in a trace amount from the extracts and any fractions on HPLC. The isolation of irisgermanicals B and C was reproducible, as also confirmed by extraction from both the fresh and dried rhizomes of *I. germanica*. These two iridals are thus most likely to be genuine natural products. However, the possibility that they are artifacts arising from tautomerization of **8** and **9** during the isolation procedure might not be completely ruled out.

Absolute configuration at C-13 of spiroiridal (15)

Spiroiridal (**15**), which exists as an equilibrium mixture of epimers at the hemiacetal carbon (C-26), had first been isolated from *Iris pseudacorus* and the structure was proposed as **15** without assigning the configuration at C-13 (17). The absolute configuration at C-13 has now been proposed to be *R* by the NOESY spectrum of **15**. The C-27 methyl signals showed

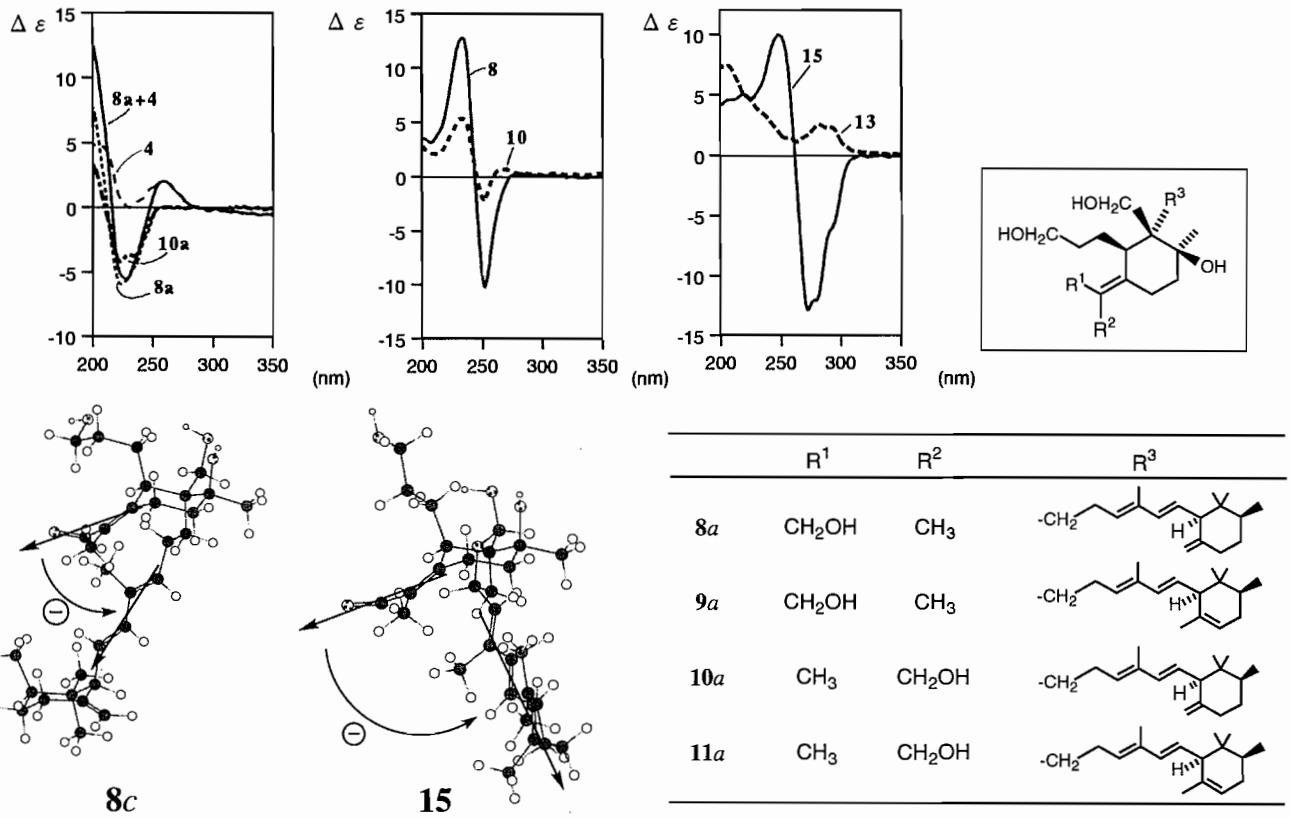
© 1997 NRC Canada

Fig. 1. NOEs observed for **15**.



15

Fig. 2. CD spectra of iridals in MeOH or MeCN and stereostructures of **8***c* and **15**.



	R^1	R^2	R^3
8*a*	CH_2OH	CH_3	
9*a*	CH_2OH	CH_3	
10*a*	CH_3	CH_2OH	
11*a*	CH_3	CH_2OH	

cross peaks with H-26 and H-14, while H-13 disclosed an NOE with one of the vinyl methyl signals at δ 1.80. The other NOE correlations are shown by arrows in Fig. 1, and are consistent with the proposed structure **15**, including an (all-*E*)-triene chain.

CD spectra of iridals and their correlation with conformations

Iridal-type triterpenoids characterized so far are classified largely into three groups according to their structures: monocyclic- (e.g., **1**, **2**, and **6**), bicyclic- (e.g., **3**–**5** and **7**–**11**), and spiroiridals (e.g., **12**–**15**). Although the CD spectral data of a series of iridals have been reported in the individual structural determinations, little has been hitherto discussed on the nature of each Cotton effect. This fact prompted us to examine the correlation between their Cotton effects and stereostructures. The CD spectra of mono- and bicyclic iridals (e.g., **3** and **4**) having only an α,β-unsaturated chromophore as the conjugated system show an intense positive Cotton effect at about 254 nm and a weakly negative multiple one at nearly 340 nm, which are typically associated with π–π* (conjugated carbonyl group) and *n*–π* (carbonyl group) transitions in an asymmetric surrounding, respectively (18) (Fig. 2). On the other hand, the bicyclic iridals (e.g., **7**–**11**) with a conjugated diene chromophore in the side chain at C-11 exhibited intense Cotton effects of opposite sign centered at around 245 nm (Fig. 2). These CD bands have been indicated to result from exciton-coupling interaction between the conjugated aldehyde and apparently remote side-chain chromophores by the following observations. Dihydro derivatives **8***a*–**11***a* showed negative CD bands at 238 nm associated with their UV absorption maxima due to the conjugated diene chromophore. The CD curves calculated by simple summation of the curves of **8***a* and **4** were definitely different from the observed curve of **8** as shown in Fig. 2, indicating that the two chromophores in **8** electrically interact with each other. To ascertain the conformation of

Can. J. Chem. Downloaded from www.nrcresearchpress.com by 88.146.161.215 on 09/08/12
For personal use only.

© 1997 NRC Canada

Can. J. Chem. Downloaded from www.nrcresearchpress.com by 88.146.161.215 on 09/08/12
For personal use only.

Table 2. Piscicidal activity of iridals.

Compounds	TLm (μg/mL)[a]
Bicyclic iridals	
8	0.10
3	0.53
5	0.57
9	0.72
7	0.76
4	0.92
10	3.0
11	3.0
Spiroiridals	
14	1.6
12	1.8
13	2.5
15	3.5
Monocyclic iridals	
2	>8
1	>8
6	>8

[a]TLm: Median tolerance limit after 24 h.

these iridals, their structures were calculated using the Insight II molecular modeling program with the Consistent Valence force field. The side chain with the diene chromophore in the lowest energy conformation (**8***c*) of iriflorental as shown in Fig. 2 is in a favorable position to allow a π–π* stacking interaction with the conjugated aldehyde chromophore at a distance of 5.8 Å.

The right-handed chirality is consistent with the observed negative first Cotton effect of **8** according to the exciton chirality rule (19). Similar analysis and interpretation were possible for spiroiridal (**15**) (Fig. 2). Interestingly, the energy minimization revealed that the iridals having no conjugated diene function at the side chain at C-11 adopt a different conformation with the long side chain expanded far from the cyclohexane ring, which is similar to that in the solid state as revealed by X-ray crystallographic analysis of **4** (8).

Piscicidal activity

Piscicidal activity of the compounds isolated in the present study was evaluated using medaka according to the method previously reported (3). As shown in Table 2, iriflorental (**8**) exhibited the most potent activity with 0.1 μg/mL of median tolerance limit (TLm) value after 24 h. The other bicyclic iridals, except for **10** and **11**, showed the activity of TLm 0.5–0.9 μg/mL. Spiro-type iridals exhibited moderate activity (TLm 1–2.5 μg/mL), while the TLm values of **10**, **11**, and **15** were 3–3.5 μg/mL. The monocyclic iridals were all inactive, indicating that the strength of the piscicidal activity seems to depend largely on the structure of the substituent (side chain) at C-11 and also on the geometry of the α,β-unsaturated aldehyde moiety.

It is noteworthy that iridal (**6**), iriflorental (**8**), iripallidal (**9**), and irigermanals (**3**, **4**), which were reported to exhibit an in vivo antiulcer activity in several experimental mouse ulcers (14), have also been isolated as potent active principles upon piscicide-directed fractionation. This finding provides additional evidence to the supposition that piscicidal assay may play the part of useful primary screening in making a survey of bioactive natural products. In fact, regarding investigation of the other biological activities of iridals, some piscicidal compounds were found to exhibit significant inhibitory effects on activation of TPA-induced Epstein-Barr virus early antigen and on protein kinase C, which might be associated with antitumor promoting activity.[2]

Experimental

UV spectra and optical rotations were taken on a Hitachi 100-10 spectrophotometer and on a Jasco DIP-1000 polarimeter. ^1H and ^{13}C NMR spectra were measured in $CDCl_3$ on a Varian VXR-500 instrument (500 MHz for ^1H NMR and 126 MHz for ^{13}C NMR) and chemical shifts are given in δ values (ppm) relative to that of solvent (residual $CHCl_3$ (δH 7.26; δC 77.0)) on a TMS scale. FABMS were recorded on VG 70-SE and Micromass AutoSpec OA-Tof mass spectrometers using 3-nitrobenzyl alcohol as the matrix agent, and CD spectra were measured on a Jasco J-720W spectrometer. Reversed-phase HPLC was performed on a LiChrospher RP-18 (4 × 250 mm) or a Superspher RP-18 (4 × 250 mm) column developed with MeOH-H_2O (9:1 (A) or 85:15 (B)) (flow rate, 1 mL/min; detection 254 nm) at 40°C using a Shimadzu SPD-6A or Union Giken MCPD-350 detector. Analytical and preparative TLC were carried out on Kieselgel PF_{254} with toluene–MeCN–AcOEt (1:1:9). Solvent was evaporated under reduced pressure below 40°C.

Extraction and isolation

The fresh rhizomes of *I. germanica* (2.6 kg), collected in July 1995, were cut off, soaked in MeOH (9 L × 3), and filtered. The concentrated solution (ca. 150 mL) was diluted with H_2O (100 mL) and extracted successively with *n*-hexane (250 mL × 4), EtOAc (250 mL × 4), and *n*-BuOH saturated with H_2O (250 mL × 4). The *n*-hexane extract (21.5 g), which showed potent piscicidal activity to killie-fish, was chromatographed over silica gel with *n*-hexane→*n*-hexane–EtOAc(9:1→8:2→7:3→6:4→1:1→4:6) →EtOAc → EtOAc–acetone (4:1→1:1)→ acetone → acetone – MeOH (4 : 1). The toxic fractions were purified by repeated column chromatography over silica gel, Chromatorex ODS, and (or) YMC-GEL ODS-AQ 120-S50 using MeOH–H_2O (8 : 2 → 95 : 5) as eluant to yield iriflorental (**8**, 56.3 mg), iripallidal (**9**, 9.1mg), α-irigermanal (**3**, 164.3 mg), γ-irigermanal (**4**, 20.7 mg), isoiridogermanal (**1**, 1.2 mg), 16-*O*-acetylisoiridogermanal (**2**, 4.8 mg), iridal (**6**, 39.1 mg), irisgermanical A (**7**, 6.7 mg), irisgermanical B (**10**, 3.3 mg), and irisgermanical C (**11**, 2.9 mg).

The bark of dried rhizomes of *I. germanica* (765 g), collected in March 1994, was treated as mentioned above. The EtOAc extract (1.4 g) was subjected to column chromatography over silica gel with $CHCl_3$ → $CHCl_3$–acetone (20:1→5:4)→ acetone. The toxic fractions to killie-fish were purified by preparative HPLC (reversed-phase) with MeOH–H_2O (85:15) to give iriflorental (**8**, 6.3 mg), iripallidal (**9**, 9.5 mg), α-irigermanal (**3**, 14.8 mg), γ-irigermanal (**4**, 8.4 mg), α-

[2] Details will be reported elsewhere.

© 1997 NRC Canada

Can. J. Chem. Downloaded from www.nrcresearchpress.com by 88.146.161.215 on 09/08/12
For personal use only.

dehydroirigermanal (**5**, 3.1 mg), isoiridogermanal (**1**, 26.3 mg), 16-*O*-acetylisoiridogermanal (**2**, 11.3 mg), irisgermanical A (**7**, 8.1 mg), irisgermanical B (**10**, 3.6 mg), and irisgermanical C (**11**, 5.3 mg).

The chipped fresh roots of *I. japonica* (1.34 kg), collected in November 1995, were soaked in *n*-hexane (3 L × 2) and filtered. The solvent was removed to give the *n*-hexane extract (2.23 g). The residue was then extracted with MeOH (3 L × 3) and filtered. After removal of an oil (17 g) deposited upon concentration of the filtrate, the concentrated solution was extracted successively with Et_2O and *n*-BuOH saturated with H_2O. A part (10 g) of the oil was subjected to column chromatography over silica gel with $CHCl_3$ → $CHCl_3$–acetone (20:1→1:9)→ acetone. The toxic fractions were further chromatographed over Chromatorex ODS and YMC-GEL ODS-AQ 120-S50 with MeOH–H_2O (8:2→ 95:5) to yield six known iridals, which were identical with belamcandal (**12**, 30 mg), 28-deacetylbelamcandal (**13**, 210 mg), isoiridogermanal (**1**, 330 mg), iridal (**6**, 80 mg), (+)-(6*R*,10*S*,11*S*,14*S*,26*R*)-26-hydroxy-15-methylidene-spiroirid-16-enal (**14**, 20 mg), and (6*R*,10*S*,11*R*)-26-ζ-hydroxy-13*R*-oxaspiroirid-16-enal (**15**, 25 mg), respectively, by comparison of their physical data with the reported values.

*Iriflorental (**8**)*: glassy solid, $[\alpha]_D$ +29.7 (*c* 1.0, CH_2Cl_2); UV λ_{max} (EtOH) nm (log ε): 237 nm (4.98); CD (MeCN, Δε) nm: 223 (+12.8), 251 (−10.2), 282 (+0.3), 336 (−0.1); ^{1}H NMR: see Table 1. ^{13}C NMR δ: 189.9 (C-1), 162.2 (C-7), 150.5 (C-19), 136.7 (C-16), 134.2 (C-15), 133.2 (C-2), 129.6 (C-17), 126.7 (C-14), 107.9 (C-29), 76.2 (C-10), 68.3 (C-26), 62.6 (C-3), 58.2 (C-18), 46.8 (C-11), 42.5 (C-6), 42.2 (C-22), 38.7 (C-23), 37.2 (CH_2), 36.5 (CH_2), 35.5 (CH_2), 32.2 (CH_2), 32.2 (CH_2), 27.7 (C-31), 27.1 (CH_2), 26.5 (C-27), 23.9 (CH_2), 21.6 (CH_2), 16.1 (C-28), 14.2 (C-24), 12.6 (C-30), 11.0 (C-25); FABMS, *m/z*: 509 $(M+Na)^+$, 487 $(M+H)^+$.

*Iripallidal (**9**)*: glassy solid, $[\alpha]_D$ +22.4 (*c* 1.0, CH_2Cl_2); UV λ_{max} (EtOH) nm (log ε) : 238 (4.92); CD (MeCN, Δε) nm : 234 (+15.5), 253 (−7.7), 276 (+0.3), 336 (−0.1); ^{1}H NMR: see Table 1. ^{13}C NMR δ: 190.1 (C-1), 162.5 (C-7), 137.3 (C-16), 134.6 (C-19), 134.0 (C-15), 133.3 (C-2), 129.3 (C-17), 128.6 (C-14), 121.7 (C-29), 76.3 (C-10), 68.5 (C-26), 62.6 (C-3), 56.4 (C-18), 46.8 (C-11), 42.7 (C-6), 38.2 (C-22), 37.2 (CH_2), 35.7 (CH_2), 35.6 (C-23), 32.2 (CH_2), 32.0 (CH_2), 27.2 (CH_2), 26.5 (C-27), 26.6 (C-31), 24.0 (CH_2), 23.2 (C-29), 21.7 (CH_2), 15.7 (C-28), 14.7 (C-24), 12.7 (C-30), 12.0 (C-25); FABMS, *m/z*: 487 $(M+H)^+$.

*(6R,10S,11R)-26-ζ-Hydroxy-13R-oxaspiroirid-16-enal (**15**)*: glassy solid, $[\alpha]_D$ +31.7 (*c* 1.0, MeOH); UV λ_{max} (MeOH) nm (log ε): 204 (4.62), 254 (5.05), 281sh (4.75), 290sh (4.61); CD (MeCN, Δε) nm: 248 (+10.0), 272 (−12.9); ^{1}H NMR ($CDCl_3$) (data of second anomer, if different, are found in parentheses) δ: 10.27 (10.20) (s, H-1), 6.42 (1H, dd, *J* = 11, 15 Hz, H-17), 6.13 (6.10) (d, *J* = 15 Hz, H-16), 5.86 (1H, d, *J* = 11 Hz, H-18), 5.71 (5.16) (s), 5.48 (1H, d, *J* = 8 Hz, H-14), 5.17 (4.58) (dd, *J* = 8, 15.5 Hz, H-13), 5.08 (1H, t, *J* = 6.5 Hz, H-22), 3.66 (3.27) (brt, H-6), 3.66, 3.54 (2H in total, m, H-3), 2.68, 2.50 (2H, m, H-8), 2.09 (2H, m, H-21), 2.09, 1.93 (2H in total, m, H-5), 2.09 (2H in total, m, H-20), 1.83 (3H, s, H-25), 1.78 (1.81, 1.80) (brs, H-28, 29), 1.67 (3H, s, H-24), 1.59 (3H, s, H-30), 1.21 (1.45) (s); ^{13}C NMR δ: 191.1 (190.4) (C-1), 162.5 (161.7) (C-7), 139.9 (139.8) (C-19), 137.2 (137.0) (C-16), 134.0 (133.9) (C-15), 132.9 (132.5) (C-2), 131.7 (130.0) (C-23), 129.3 (C-14), 125.3 (125.5) (C-17), 124.9 (C-18), 123.8 (C-22), 99.0 (105.0) (C-26), 73.7 (74.8) (C-10), 73.4 (69.2) (C-13), 62.0 (62.1) (C-3), 59.7 (54.2) (C-11), 42.6 (46.5) (C-6), 40.1 (C-20), 38.1 (37.9) (C-9), 31.9 (CH_2), 31.1 (CH_2), 28.8 (27.0) (CH_2), 27.7 (27.6) (C-27), 26.6 (C-21), 25.6 (C-24), 23.9 (23.8) (C-8), 17.6 (C-30), 16.8 (C-29), 13.2 (13.1) (C-28), 11.1 (11.0) (C-25); FABMS, *m/z*: 509 $(M+Na)^+$, 487 $(M+H)^+$, 469 $(M-H_2O+H)^+$, 451$(M-2H_2O+H)^+$, 69 $(C_5H_9)^+$.

*Irisgermanical A (**7**)*: glassy solid, $[\alpha]_D$ +46.2 (*c* 0.5, CH_2Cl_2); UV λ_{max} (EtOH) nm (log ε): 237 (4.43); CD (MeCN, Δε) nm: 234 (+13.2), 251 (−11.5), 278 (+0.3), 337 (−0.4); ^{1}H NMR; see Table 1. ^{13}C NMR δ: 190.0 (C-1), 162.7 (C-7), 150.7 (C-19), 136.9 (C-16), 134.1 (C-15), 133.3 (C-2), 130.1 (C-17), 126.5 (C-14), 107.9 (C-29), 75.1 (C-10), 63.1 (C-3), 58.3 (C-18), 44.8 (C-11), 43.5 (C-6), 42.3 (C-22), 38.8 (C-23), 37.1 (CH_2), 37.1 (CH_2), 36.6 (CH_2), 32.8 (CH_2), 32.3 (CH_2), 27.8 (C-31), 26.7 (CH_2), 26.4 (C-27), 23.9 (CH_2), 22.4 (CH_2), 18.0 (C-26), 16.2 (C-28), 14.3 (C-24), 12.7 (C-30), 11.1 (C-25); HRFABMS: 471.3839 $(M+H)^+$ (calcd. for $C_{31}H_{51}O_3$: 471.3838).

*Irisgermanical B (**10**)*: glassy solid, $[\alpha]_D$ +69.8 (*c* 1.0, CH_2Cl_2); UV λ_{max} (EtOH) nm (log ε): 237 (4.90); CD (MeCN, Δε) nm : 233 (+5.4), 250 (−2.1); ^{1}H NMR: see Table 1. ^{13}C NMR δ: 190.8 (C-25), 162.7 (C-7), 150.5 (C-19), 136.7 (C-16), 134.1 (C-15), 133.0 (C-2), 129.8 (C-17), 126.7 (C-14), 107.9 (C-29), 76.4 (C-10), 68.2 (C-26), 62.8(C-3), 58.2 (C-18), 47.3 (C-11), 46.6 (C-6), 42.2 (C-22), 38.7 (C-23), 38.2 (CH_2), 35.7 (CH_2), 35.5 (CH_2), 32.2 (CH_2), 31.8 (CH_2), 27.7 (C-31), 27.6 (CH_2), 26.6 (C-27), 22.6 (CH_2), 20.0 (CH_2), 16.1 (C-28), 14.3 (C-24), 12.7 (C-30), 12.0 (C-1); HRFABMS: 487.3722 $(M+H)^+$ (calcd. for $C_{31}H_{51}O_4$: 487.3787).

*Irisgermanical C (**11**)*: glassy solid, $[\alpha]_D$ + 37.4 (*c* 1.0, CH_2Cl_2); UV λ_{max} (EtOH) nm (log ε): 238 (4.92); CD (MeCN, Δε) nm: 235 (+16.5), 256 (−2.7); ^{1}H NMR ($CDCl_3$); see Table 1. ^{13}C NMR δ: 190.9 (C-25), 162.8 (C-7), 137.2 (C-16), 134.5 (C-19), 134.0 (C-15), 133.0 (C-2), 129.4 (C-17), 128.6 (C-14), 121.7 (C-29), 76.4 (C-10), 68.3 (C-26), 62.8 (C-3), 56.3 (C-18), 47.3 (C-11), 46.6 (C-6), 38.2 (C-22), 38.2 (CH_2), 35.5 (CH_2), 35.6 (C-23), 31.9 (CH_2), 31.8 (CH_2), 27.2 (CH_2), 26.5 (C-27), 26.6 (C-31), 23.2 (CH_2), 22.6 (C-29), 20.0 (CH_2), 15.6 (C-28), 14.7 (C-24), 12.7 (C-30), 12.0 (C-1); HRFABMS: 487.3757 $(M+H)^+$ (calcd. for $C_{31}H_{51}O_4$: 487.3787).

*Reduction of iriflorental (**8**), iripallidal (**9**), irisgermanical B (**10**), and irisgermanical C (**11**)*

A mixture of the compound (1–4 mg) and $NaBH_4$ (7–15 mg) in EtOH (1–4 mL) was left standing for 30 min at room temperature. After excess of $NaBH_4$ was quenched with acetone, solvents were dispersed with N_2. The residue was partitioned with dilute HCl and $CHCl_3$, and the $CHCl_3$ layer was evaporated to give the corresponding dihydro derivatives, **8***a* (3.5 mg) from **8** (3.6 mg); **9***a* (1.0 mg) from **9** (1.1 mg); **10***a* (1.0 mg) from **10** (1.1 mg); and **11***a* (0.8 mg) from **11** (0.9 mg).

© 1997 NRC Canada

Can. J. Chem. Downloaded from www.nrcresearchpress.com by 88.146.161.215 on 09/08/12
For personal use only.

*Dihydroiriflorental (**8**a)*: glassy oil, $[\alpha]_D$ +28.9 (*c* 1.0, CH_2Cl_2); UV λ_{max} (EtOH) nm (log ε): 205 (4.25), 236 (4.46); CD (MeOH, $\Delta\varepsilon$) nm: 223 (−5.9); ^{1}H NMR ($CDCl_3$) δ: 5.95 (1H, d, *J* = 16 Hz, H-16), 5.66 (1H, dd, *J* = 10, 15.5 Hz, H-17), 5.19 (1H, d, *J* = 7.5, 14 Hz, H-14), 4.73, 4.49 (each 1H, brs, H-29), 4.16 (1H, d, *J* = 11 Hz, H-1), 4.09 (1H, d, *J* = 11 Hz, H-1), 4.10 (1H, d, *J* = 11.5 Hz, H-26), 3.85 (1H, d, *J* = 11.5 Hz, H-26), 3.92–3.55 (2H, m, H-3), 2.82 (1H, td, *J* = 3, 10.5 Hz, H-8), 2.75 (1H, d, *J* = 11.5 Hz, H-8), 2.38 (1H, brd, *J* = 13.5 Hz, H-18), 2.38 (1H, brd, *J* = 13.5, 5 Hz, H-18), 1.77 (3H, brs, H-28), 1.58 (3H, overlap, H-25), 1.25 (3H, s, H-27), 0.85 (3H, s, H-30), 0.84 (3H, d, *J* = 7 Hz, H-30), 0.64 (3H, s, H-24), 2.0–1.2 (14H); FABMS *m/z*: 489(M+H)$^+$.

*Dihydroiripallidal (**9**a)*: glassy oil, $[\alpha]_D$ +53.1 (*c* 1.0, CH_2Cl_2); UV λ_{max} (EtOH) nm (log ε): 206 (4.12), 237 (4.23); CD (MeOH, $\Delta\varepsilon$) nm: 231 (−2.6); ^{1}H NMR ($CDCl_3$) δ: 6.00 (1H, d, *J* = 15 Hz, H-16), 5.44 (1H, brs, H-20), 5.35 (1H, dd, *J* = 10, 15 Hz, H-17), 5.22 (1H, t, H-14, *J* = 6.5 Hz), 4.28 (2H, brs, H-1), 4.04 (1H, d, *J* = 11.5 Hz, H-26), 3.93 (1H, d, *J* = 11.5 Hz, H-26), 3.65 (2H, m, H-3), 2.82 (2H, dd, *J* = 3.5, 7 Hz, H-8), 2.36 (4H, brt, *J* = 3.5 Hz), 2.04 (2H, m, H-5), 1.72 (3H, s, H-28), 1.57 (3H, overlap, H-25), 1.51 (3H, s, H-29), 1.30 (3H, s, H-27), 0.85 (3H, d, *J* = 7 Hz, H-31), 0.83 (3H, s, H-30), 0.61 (3H, s, H-24); FABMS *m/z*: 489 (M+H)$^+$.

*Dihydroirisgermanical B (**10**a)*: glassy oil, $[\alpha]_D$ +24.1 (*c* 1.0, CH_2Cl_2); UV λ_{max} (EtOH) nm (log ε): 204 (4.69), 236 (4.31); CD (MeOH, $\Delta\varepsilon$) nm: 225 (−4.1); ^{1}H NMR ($CDCl_3$) δ: 5.95 (1H, d, *J* = 16 Hz, H-16), 5.66 (1H, dd, *J* = 11, 15.5 Hz, H-17), 5.19 (1H, brd, *J* = 16 Hz, H-14), 4.73, 4.49 (each 1H, brs, H-29), 4.10 (1H, d, *J* = 8 Hz, H-5), 3.85 (1H, d, *J* = 8 Hz, H-5), 4.10 (1H, d, *J* = 11.5 Hz, H-26), 3.85 (1H, d, *J* = 11.5 Hz, H-26), 3.92–3.55 (2H, m, H-3), 2.82 (1H, td, *J* = 3, 10.5 Hz, H-8), 2.75 (1H, d, *J* = 11.5 Hz, H-8), 2.38 (1H, d, *J* = 10 Hz, H-18), 2.33 (1H, brd, *J* = 13.5 Hz, H-20), 2.08 (1H, td, *J* = 13.5, 5 Hz, H-20), 1.77 (3H, brs, H-28), 1.58 (overlap, 3H, H-1), 1.25 (3H, s, H-27), 0.85 (3H, s, H-30), 0.84 (3H, d, *J* = 7.5 Hz, H-31), 0.64 (3H, s, H-24), 2.0–1.2 (2H, m, H-12); FABMS *m/z*: 511 (M+Na)$^+$.

*Dihydroirisgermanical C (**11**a)*: glassy oil, $[\alpha]_D$ +37.4 (*c* 1.0, CH_2Cl_2); UV λ_{max} (EtOH) nm (log ε): 204 (4.05), 238 (3.96); CD (MeOH, $\Delta\varepsilon$) nm: 231 (−6,4); ^{1}H NMR ($CDCl_3$) δ: 6.01 (1H, d, *J* = 15.5 Hz, H-16), 5.44 (1H, m, H-20), 5.35 (1H, dd, *J* = 10, 15.5 Hz, H-17), 5.23 (1H, t, H-14, *J* = 7.0 Hz), 4.24 (1H, d, *J* = 11.5 Hz, H-25), 4.13 (1H, d, *J* = 11.5 Hz, H-25), 4.06 (1H, d, *J* = 11 Hz, H-26), 3.93 (1H, d, *J* = 11 Hz, H-26), 3.80–3.40 (2H, m, H-3), 2.83 (1H, m, H-8), 2.80 (1H, dd, *J* = 10.5, 3.5 Hz, H-8), 2.45 (1H, m), 2.36 (1H, brd, *J* = 10 Hz, H-18), 2.05 (2H, m, H-5), 1.71 (3H, brs, H-28), 1.55 (3H, overlap, H-1), 1.49 (3H, s, H-29), 1.29 (3H, s, H-27), 0.91 (3H, d, *J* = 10.5 Hz, H-31), 0.84 (3H, s, H-30), 0.64 (3H, s, H-24); FABMS *m/z*: 489 (M+H)$^+$.

Tautomerization of iridals

A solution of α-irigermanal (**3**) (9.8 mg) and *p*-toluenesulfonic acid (2.0 mg) in $CHCl_3$ (5 mL) was kept at room temperature for 2 h. The reaction mixture was diluted with $CHCl_3$ (5 mL), and washed with saturated aqueous $NaHCO_3$ (5 mL × 2) and then with H_2O (5 mL). The $CHCl_3$ layer was evaporated to dryness to give crude products (9.0 mg), HPLC of which showed two peaks of close retention times (t_R 17.08 and 17.63 min, solvent A). The mixture was chromatographed over YMC-GEL ODS-AQ 120-S50 with MeOH–H_2O (85:15) as eluent to give α-irigermanal (**3**) (2.5 mg) and its isomer (**3***a*) (3.0 mg). **3***a*: glassy solid, $[\alpha]_D$ +31.8 (*c* 0.5, CH_2Cl_2); UV λ_{max} (MeOH) nm (log ε): 257 (4.10); 1H NMR ($CDCl_3$) δ: 10.24 (s, H-25), 5.31 (1H, brs, H-20), 4.97 (1H, t, *J* = 6 Hz, H-14), 3.61 (1H, t, *J* = 6 Hz, H-3), 3.2 (1H, brd, *J* = 13.5 Hz, H-8), 2.80 (1H, brd, *J* = 12 Hz, H-6), 2.60 (^{1}H, brt, *J* = 14, H-8), 1.81 (3H, d, *J* = 1.5 Hz, H-1), 1.69 (3H, brs, H-28), 1.59 (3H, s, H-29), 1.17 (3H, s, H-27), 1.01 (3H, s, H-26), 0.87 (3H, s, H-30), 0.83 (3H, d, *J* = 6.5 Hz, H-31), 0.62 (3H, s, H-24).

Similar tautomerization was observed for **4**, **8**, and **6**. HPLC peaks (solvent A) of each reaction mixture were as follows: t_R 15.35 (**4**) and 15.78 min (isomer) for **4**; t_R 8.69 (**8**) and 8.22 (isomer (**10**)) for **8**; t_R 11.92 (**6**) and 12.20 (isomer) for **6**.

Piscicidal activity

The assay was conducted essentially in the same way as reported previously (3), using the medaka (killie-fish; *Oryzias latipes*) (170–350 mg in weight and 2.5–3.5 cm in length) as the test fish. A test solution was prepared by adding an acetone or a MeOH solution (0.5 mL) of the compounds of known concentration into aerated H_2O (100 mL). The median tolerance limit (TLm) after 24 h was evaluated for five fish/group by straight-line graphical interpolation. A control experiment was carried out under the same conditions, adding only acetone or MeOH (0.5 mL).

Acknowledgements

The authors are grateful to Prof. F.-J. Manner, Köln University, for his valuable discussion, and to the SC NMR Laboratory of Okayama University for NMR measurements.

References

1. L. Luyengi, I.-S. Lee, W. Mar, H.H.S. Fong, J.M. Pezzuto, and A.D. Kinghorn. Phytochemistry, **36**, 1523 (1994).
2. Y. Ito, S. Yanase, H. Tokuda, M. Kishishita, H. Ohigashi, M. Hirota, and K. Koshimizu. Cancer Lett. **18**, 87 (1983).
3. T. Okuda, T. Yoshida, S. Koike, and N. Toh. Phytochemistry, **14**, 509 (1975).
4. E. Gomez, O.C. Giron, A.A. Cruz, B.S. Joshi, V. Chittawong, and D.H. Miles. J. Nat. Prod. **52**, 649 (1989).
5. T. Yoshida, J. Nobuhara, M. Uchida, and T. Okuda. Chem. Pharm. Bull. **26**, 2535 (1978).
6. (*a*) A.A. Ali, N.A. E.-Emary, M.A. E.-Moghazi, F.M. Darwish, and W. Frahm. Phytochemistry, **22**, 2061 (1983); (*b*) H. Minami, A. Okubo, M. Kodama, and Y. Fukuyama. Phytochemistry, **41**, 1219 (1996), and refs. cited therein.
7. F.-J. Marner and W.W. Horper. Helv. Chim. Acta, **75**, 1557 (1992).
8. F.-J. Marner, W. Krick, B. Gellrich, and L. Jaenicke. J. Org. Chem. **47**, 2531 (1982)
9. (*a*) W. Krick, F.-J. Marner, and L. Jaenicke. Z. Naturforsch. C: Biosci. **38C**, 179 (1983); (*b*) Z. Naturforsch. C: Biosci. **38C**, 689 (1983); (*c*) L. Jaenicke and F.-J Marner. Prog. Chem. Org. Nat. Prod. **50**, 1 (1986); (*d*) F.-J. Marner and I. Longerch. Liebigs Ann. Chem. 269 (1992); (*e*) A. Littek and F.-J. Marner. Helv. Chim. Acta, **74**, 2035 (1991).
10. (*a*) K. Seki, T. Tomihari, K. Haga, and R. Kaneko. Phytochemistry, **36**, 433 (1994); (*b*) Phytochemistry, **36**, 425 (1994).

© 1997 NRC Canada

11. F. Abe, R.-F. Chen, and T. Yamauchi. Phytochemistry, **30**, 3379 (1991).
12. F.-J. Marner and B. Kerp. Z. Naturforsch. C: Biosci. **47C**, 21 (1992)
13. J.-P. Bonfils, Y. Sauvaire, Y. Baissac, and F.-J. Marner. Phytochemistry, **37**, 701 (1994).
14. Y. Muto, H. Ichikawa, O. Kitagawa, K. Kumagai, M. Watanabe, E. Ogawa, M. Seiki, Y. Shirataki, I. Yokoe, and M. Komatu. Yakugaku Zasshi, **114**, 980 (1994).
15. K. Takahashi, M. Ishino, Y. Hoshino, Y. Tokumaru, and S. Suzuki. Yakugaku Zasshi, **113**, 647 (1993).
16. F.-J. Marner, Y. Karimi-Nejad, and L. Jaenicke. Helv. Chim. Acta, **73**, 433 (1990).
17. F.-J. Marner, A. Littek, R. Arold, K. Seferiadis, and L. Jaenicke. Liebigs Ann. Chem. 563 (1990).
18. P. Crabbe. ORD and CD in chemistry and biochemistry. Academic Press, New York. 1972. p. 43.
19. N. Harada and K. Nakanishi. Acc. Chem. Res. **5**, 257 (1972).

Can. J. Chem. Downloaded from www.nrcresearchpress.com by 88.146.161.215 on 09/08/12
For personal use only.

© 1997 NRC Canada

On a new synthesis of sterpurene and the bioactivity of some related *Chondrostereum purpureum* sesquiterpene metabolites

George M. Strunz, Richard Bethell, Michael T. Dumas, and Nick Boyonoski

Abstract: Sterpurene, a sesquiterpene hydrocarbon metabolite of *Chondrostereum purpureum*, a plant pathogen and potential mycoherbicide, was synthesized by a six-step sequence, in 33% overall yield. The key steps were a thermal [4 + 2] (Diels–Alder) cycloaddition of a ketene acetal diene with a conjugated ester dienophile, and a remarkably stereoselective [2 + 2] photocycloaddition of ethylene with the resulting conjugated ketone. Several related, more highly oxygenated, metabolites isolated from culture filtrates of *C. purpureum* (cf. Ayer) were tested for toxicity to cells of a hybrid aspen, *Populus deltoides* X *nigra*. Their phytotoxicity, at concentrations as low as 10 ppm, suggests that, like the *endo*-polygalacturonase produced by the fungus, these sesquiterpenes may be partially responsible for the foliar lesions associated with infection of deciduous species by the pathogen.

Key words : *Chondrostereum purpureum*, mycoherbicide, metabolites, sterpurenes, synthesis, Diels–Alder, photocycloaddition, pyramidalization, phytotoxicity.

Résumé : Nous avons synthétisé, en six étapes et avec un rendement global de 33%, la sterpurène, un métabolite sesquiterpénique hydrocarbonique de la *Chondrostereum purpureum*, qui est un pathogène des plantes et qui a du potentiel en tant que mycoherbicide. Les étapes clés étaient une cycloaddition [4 + 2] thermale (Diels–Alder) entre un acétal céténique diénique avec un ester conjugué diénophilique, et une photocycloaddition [2 + 2] entre la cétone conjuguée résultante avec l'éthylène, qui se produit avec une stéréosélectivité remarquable. Nous avons fait plusieurs épreuves sur des métabolites apparentés plus oxygénés, isolés (d'après Ayer) de cultures de *C. purpureum*, pour évaluer leur toxicité contre les cellules de *Populus deltoides* X *nigra*. Leur phytotoxicité, à des concentrations aussi basses que 10 ppm, suggère que, tout comme l'*endo*-polygalacturonase produite par le champignon, ces sesquiterpènes seraient en partie responsables des lésions des feuilles associées à l'infection par la pathogène des espèces décidues.

Mots clés : *Chondrostereum purpureum*, mycoherbicide, métabolites, sterpurènes, synthèse, Diels–Alder, photocycloaddition, pyramidalisation, phytotoxicité.

Introduction

The fungus *Chondrostereum purpureum* (Pers. ex Fr.) Pouz. (= *Stereum purpureum* (Pers. ex Fr.) Fr.) is widespread in North American forests and fruit orchards. The organism is a pathogen of a variety of deciduous species, causing, in fruit trees, a destructive condition designated silver leaf disease (1, 2). The foliar "silvering" symptoms result from reflection of light from leaf surfaces in which the epidermal cells have separated from the palisade cells (2), and the disease can lead to death of the host tree. *Chondrostereum purpureum* can colonize coniferous wood as a saprophyte but, in contrast to its pathogenicity to hardwoods, it is not known to cause any disease of conifers (1).

Concerns about non-target effects of synthetic herbicides have led to major constraints on the use of these compounds in forestry operations, and biological control is emerging as an attractive alternative for suppressing the development of competing vegetation in the early growth stages of crop trees. During 1995 and 1996, extensive field trials were conducted by Canadian Forest Service scientists and cooperators to test the efficacy of *C. purpureum* as a mycoherbicide in preventing regrowth of hardwood stump sprouts. The promising results of these trials have kindled our interest in examining chemical aspects of the bioactivity of this pathogen.

Pioneering studies by Ayer in the early 1980s on metabolites of *C. purpureum* led to the discovery of a novel class of sesquiterpenes that embody the carbon skeleton of sterpurene, **1**, at various states of oxidation (3). The hydrocarbon **1** was found in the mycelium of *C. purpureum* (3), while sterpuric acid **2** and sterpurene-3,12,14 triol **4** were the major components of the broth extract, which also contained **3** (3, 4). In addition, the biogenetically related isolactaranes, sterepolide **5**

Received October 21, 1996.

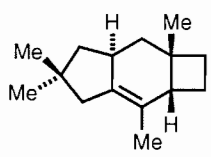
This paper is dedicated to Professor William A. Ayer, champion of natural products chemistry and champion natural products chemist (!), on the occasion of his 65th birthday.

G.M. Strunz[1] **and R. Bethell**. Canadian Forest Service–Atlantic Forestry Centre, Natural Resources Canada, P.O. Box 4000, Fredericton, NB E3B 5P7, Canada.
M.T. Dumas and N. Boyonoski. Canadian Forest Service–Ontario, Natural Resources Canada, P.O. Box 490, Sault Ste. Marie, ON P6A 5M7, Canada.

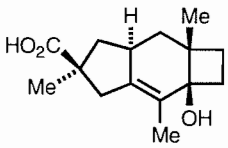
[1] Author to whom correspondence may be addressed. Telephone: (506) 452-3531. Fax: (506) 452-3525. E-mail: gstrunz@fcmr.forestry.ca

© 1997 NRC Canada

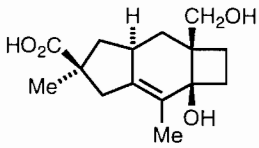
Can. J. Chem. Downloaded from www.nrcresearchpress.com by 88.146.161.215 on 09/08/12
For personal use only.



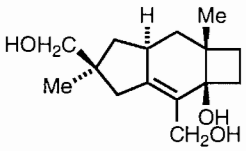
1



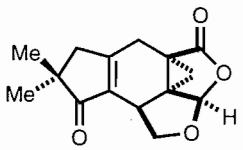
2



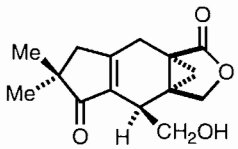
3



4



5



6

Can. J. Chem. Downloaded from www.nrcresearchpress.com by 88.146.161.215 on 09/08/12
For personal use only.

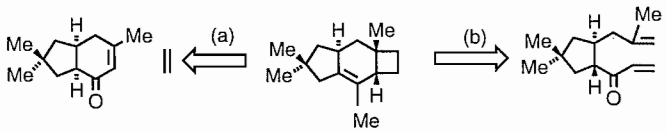
and dihydro sterepolide **6**, were produced by *C. purpureum* (5, 6). Other related metabolites of *C. purpureum* were later identified (7), and sterpurene-type sesquiterpenes were also found to be elaborated by other microorganisms (8).

Miyaire et al. (2, 9) identified an *endo*-polygalacturonase from filtrates of *C. purpureum* that induced silver leaf symptoms when injected at low doses into apple trees (~25 μg per tree). On the other hand, crude material from ethyl acetate extracts of *C. purpureum* culture broths also caused the symptoms (4), although the purified sesquiterpenes were never tested individually for phytotoxicity.[2] In an attempt to clarify chemical aspects of the interaction between pathogen and host, we reisolated a number of the sesquiterpene metabolites described by Ayer, and tested them for phytotoxicity, using cells of a hybrid aspen, *Populus deltoides* X *nigra*, for the bioassay. Another component of our research program on *C. purpureum* metabolites was the exploration and development of an efficient strategy for synthesis of sterpurene, with the potential for modification to give access to the more highly oxygenated congeners of the sesquiterpene.

The first synthesis of sterpurene, a biomimetic route from humulene, was reported in 1981 (10, cf. refs. 6, 11). This was followed by several elegant routes, each designed to exploit novel synthetic methodology (12–15).

The simplest retrosynthetic analysis, Scheme 1, suggests two formal routes, each having, as the key step, construction of a cyclobutane ring, in principle feasible by a photocycloaddition process. Inspection of models and mechanistic considerations indicated that the success of the intramolecular cyclization process (path (b) in Scheme 1), leading to simultaneous formation of six- and four-membered rings with appropriate stereochemistry, was by no means assured. Indeed, in considering products (e.g., **8**, **9**, or **9′**) that might result from photoirradiation of **7** (Scheme 2), **8** (derived by "head-to-tail" cycloaddition (16)) seemed the more probable outcome. The latter product was not, however, devoid of interest, as its reaction with methyl Grignard reagent should afford carbinol **10**,

Scheme 1.



which, on protonation, could be expected to rearrange to **11** (**11′**). An intermediate embodying the same carbon skeleton has been postulated in the biosynthesis of sterpurene (6, 11) (Scheme 2), giving us some incentive for exploring briefly the photochemistry of **7**.

The more promising intermolecular photocycloaddition strategy, path (a) (Scheme 1) was employed by Little and co-workers (12) and Paquette et al. (17) in the synthesis of sterpurene, **1**, and sterpuric acid, **2**, respectively. In the course of both these syntheses, interesting stereochemical effects were observed that seemed to warrant further investigation.

This paper reports our contributions to date in the arena of bioactivity and synthesis of *C. purpureum* metabolites.

Results and discussion

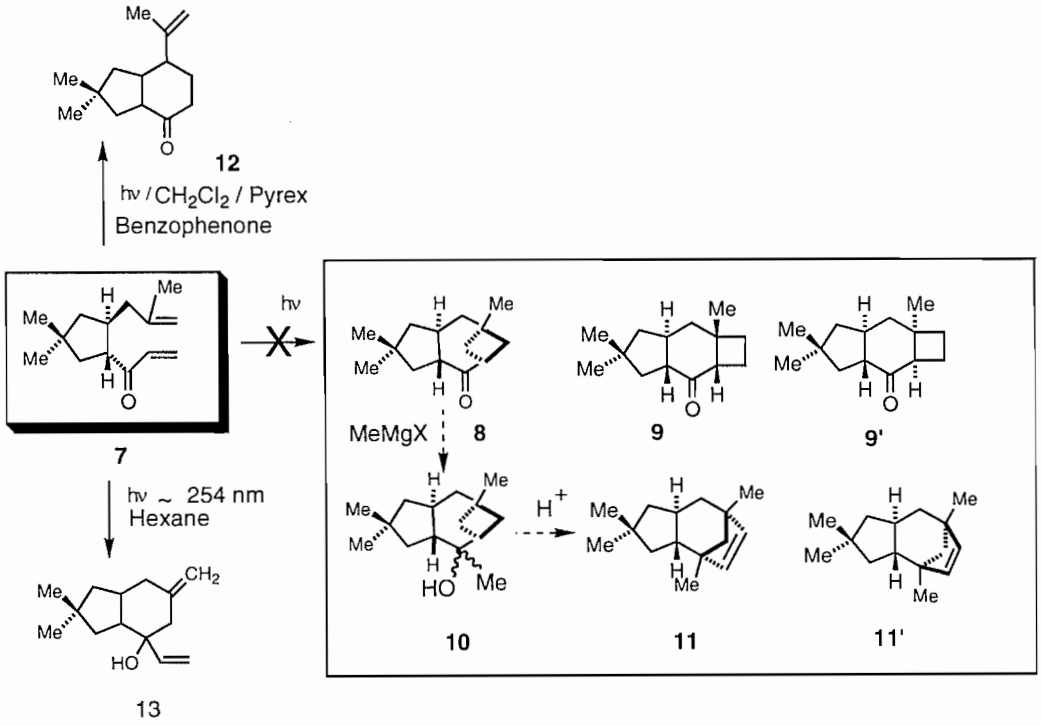
The starting material for both inter- and intramolecular photocycloaddition routes, methyl 4,4-dimethylcyclopent-1-ene carboxylate **14** (Scheme 3), was readily prepared from commercially available 4,4-dimethyl-2-cyclohexen-1-one by hydrogenation to 4,4-dimethylcyclohexanone, α-carboxymethylation (18), and chlorination. Dehydrochlorination–decarbonylation of the α-chloro-β-ketoester product, by treatment with sodium carbonate in boiling xylene according to Buchi et al. (19), gave the desired conjugated ester **14**. The overall yield of **14** from 4,4-dimethyl-2-cyclohexen-1-one (Scheme 3) was 52%, making this route a useful alternative to an earlier synthesis, via photoirradiation of diazodimedone (20).

Ester **15** was prepared in 40% (not optimized) yield by conjugate addition of isobutenyltrimethyl silane to **14**, catalyzed by tetrabutylammonium fluoride according to Majetich et al.

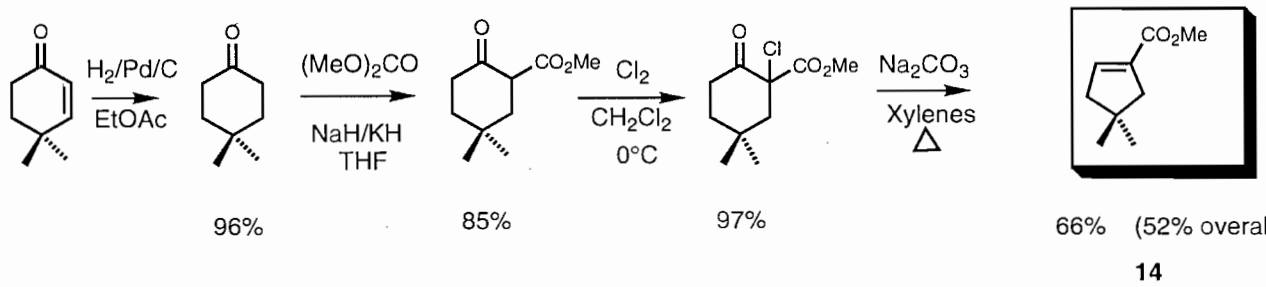
[2] W.A. Ayer. Personal communication.

© 1997 NRC Canada

Scheme 2.



Scheme 3.



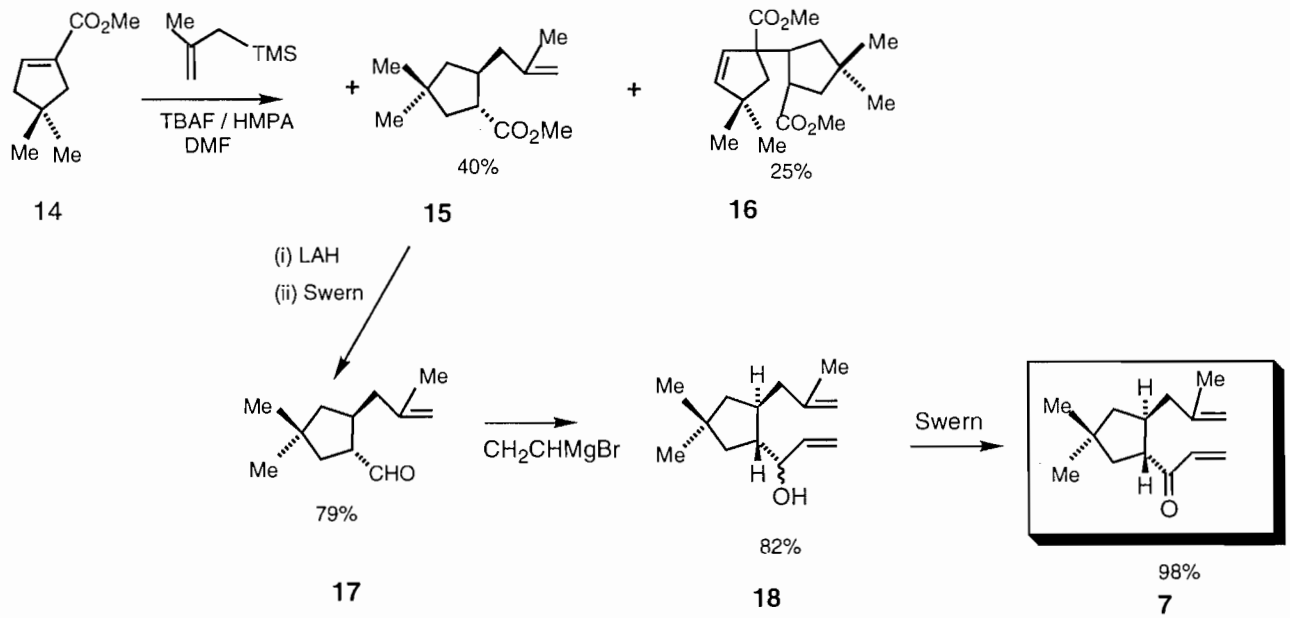
(21) (Scheme 4). (A by-product (25%) of this process was the dimeric ester product **16**, which was accessible in preparatively useful yield (~75%) when the silane was omitted. Synthetic applications of this fluoride-catalyzed dimerization and related processes are being investigated independently.) Conversion of ester **15** to the aldehyde **17** was effected in two steps, via reduction to the alcohol and reoxidation using the Swern procedure (22). Addition of vinyl magnesium bromide to the aldehyde afforded **18**, in 82% yield, and the synthesis of the desired conjugated ketone **7** (98%) was completed by Swern oxidation of the carbinol. (A minor by-product (<10%), not readily separable from **7**, was tentatively identified as the corresponding *cis* isomer.) Enone **7**, prepared thus, exhibited an ultraviolet absorption maximum (in cyclohexane solution) at 221 nm (ε 2145). The low extinction coefficient of this absorption band suggests deviation from coplanarity in the conjugated system (23).

In preliminary experiments, external irradiation (Hanovia 200 W mercury arc lamp) of a dichloromethane solution of **7** at room temperature for several hours through Pyrex (λ > 280 nm) or Corex (λ > 260 nm) filters led to recovery of unchanged starting material, (along with a small amount of presumably polymeric material, which was immobile on silica gel chromatography). Irradiation of a solution of **7** in the same solvent for 1 h at 0°C through a Vycor filter (5% transmission at 220 nm, 45% at 240 nm) led to extensive decomposition, but allowed recovery of ~4% of an isomeric product. The latter was obtained in a somewhat more satisfactory yield (39%) by photoirradiation of a dichloromethane solution of **7** at 0°C through Pyrex for 30 min, using benzophenone as sensitizer. The photoproduct was identified as **12** (Schemes 2 and 5) on the basis of its spectroscopic characteristics, especially aspects of the ^{1}H NMR spectrum. The three signals between δ 6.38 and 5.74, characteristic of the vinyl ketone, were no longer present, whereas signals at δ 4.63 and 1.65, corresponding, respectively, to the *geminal* vinyl methylene and allylic methyl hydrogens of the isopropenyl group, were retained. A multiplet at δ 2.75–2.60 could be assigned to the three protons α to the carbonyl group. Peaks attributable to a minor diastereomer were also observed (see Experimental). Infrared

© 1997 NRC Canada

Can. J. Chem. Downloaded from www.nrcresearchpress.com by 88.146.161.215 on 09/08/12
For personal use only.

Scheme 4.

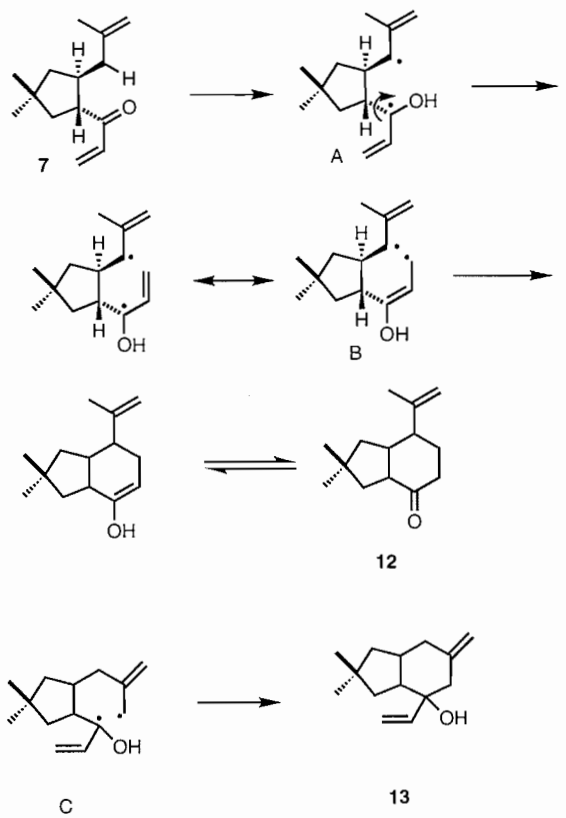


absorption at 1705 cm^{-1}, associated with the (nonconjugated) ketone group, was consistent with structure **12**.

In another experiment, a dilute hexane solution of **7** at room temperature in a quartz cell was irradiated (externally) at 254 nm for 48 h with a 4 W Spectroline E-Series UV lamp. Starting material was consumed, with concomitant formation of a complex product mixture. Separation attempts afforded material (ca. 20%) that was apparently homogeneous by TLC, but resolved by GC on a capillary column into two major products in the approximate ratio 2:3. These were shown by GC–MS to be isomers (and isomeric with the starting material), *m/z* 206. Whereas the available data were insufficient for rigorous identification of these products, they suggested the vinyl alcohol **13** and a tricyclic ketone (lacking olefinic protons) (cf. Scheme 2). Thus, the NMR spectrum of the mixture was free of signals below δ 3.0, other than a clean pattern for five vinylic protons that was fully consistent with the vinyl carbinol structure **13**. Major ions in the mass spectrum of the smaller GC peak with lower retention time supported this tentative assignment. All hydrogens of the second isomer must be assigned among the abundant NMR signals in the region above δ 3.0, not inconsistent with a tricyclic product. Significant absorptions in the infrared spectrum of the mixture are comparable to peaks in the spectrum of **29**. Ions at *m/z* 178 and 82, which are abundant in the mass spectrum of the major GC peak (and insignificant in the smaller peak), corresponding in the HREIMS of the mixture to $(M - C_2H_4)^+$ and $(C_5H_6O)^+$, can be rationalized in terms of structure **9** or **9′** (or corresponding diastereomeric structures[3] arising from photocyclization of the minor *cis* isomer (<10%) accompanying **7**) (cf. spectrum of **29**, experimental section).

A reasonable mechanism for formation of **12** from the photoirradiation of **7** might involve γ-hydrogen transfer (24, 25) producing the diradical **A**, which, after bond rotation, could cyclize to the enol form of **12**, as depicted in Scheme 5. Under different conditions, appropriate hydrogen transfer in either **7** or the diradical **A** could afford diradical **C**, suitably disposed for cyclization to **13**.

Scheme 5.

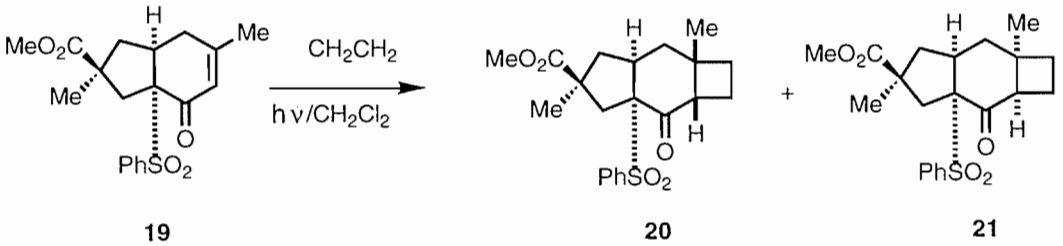


[3] A referee has pointed out that a photoproduct obtained in a yield of this magnitude could well arise not from **7**, but from the small amount of *cis* isomer accompanying it.

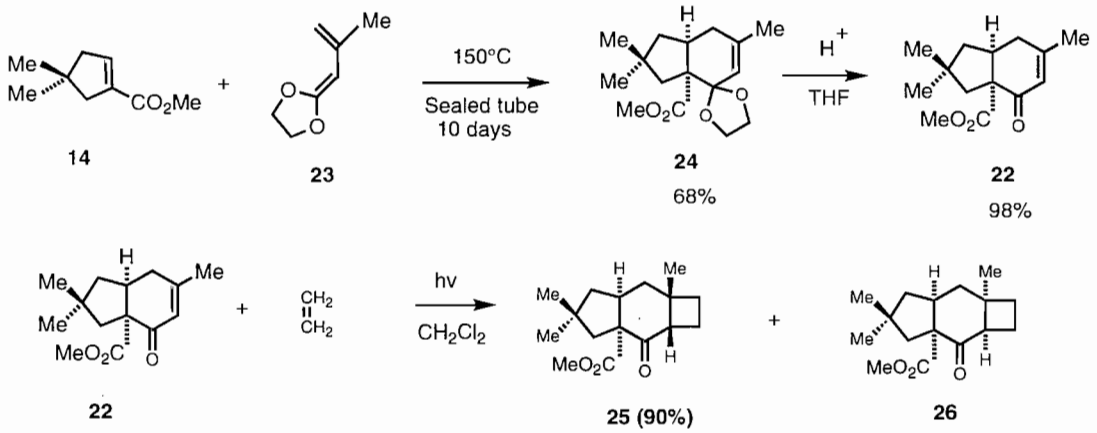
Can. J. Chem. Downloaded from www.nrcresearchpress.com by 88.146.161.215 on 09/08/12
For personal use only.

© 1997 NRC Canada

Scheme 6.



Scheme 7.



This cursory preliminary examination of the photochemical behavior of **7**, in which tricyclic product(s) were produced, if at all, in very low yield, did little to allay our reservations about path (b) (Scheme 1), and we refocussed our attention on the intermolecular photocycloaddition strategy, path (a).

In the synthesis of sterpuric acid, **2**, Paquette et al. (17) observed that photocycloaddition of ethylene to the sulfone **19** occurred with only modest stereoselectivity, affording a mixture of the desired product **20** and the diastereomeric **21,** in a ratio of 3:1 (Scheme 6). As it appeared highly probable that the sulfone and methyl ester functionalities in the *cis*-fused ring system **19** were playing a significant role in determining the stereochemical outcome of the ethylene photocycloaddition (cf. ref. 12), it was of some interest to examine the stereochemistry of photocycloaddition to the *cis*-indane-ester-enone **22** (Scheme 7), which is a logical intermediate for the synthesis of sterpurene.

Bicyclic enone **22** was readily synthesized, in 67% yield, by thermal Diels–Alder reaction of methyl 4,4-dimethylcyclopent-1-ene carboxylate **14** (prepared above) with ketene acetal **23** (26), and deprotection of the acetal product **24** (Scheme 7). Irradiation of **22** in methylene chloride solution in the presence of a large excess of ethylene at −78°C was conducted to approximately 50% conversion of enone (cf. ref. 17) using a Hanovia 200 W mercury arc lamp. The total yield of cycloaddition product, based on consumed starting material, was 97%, and it was gratifying to observe that the ratio of desired product **25** to its diastereomer **26** (Scheme 7) was 12:1 !

An empirical model for predicting stereoselectivity in photocycloaddition of olefins to cyclic α,β-unsaturated ketones was advanced by Wiesner some 20 years ago (27). This was based on the concept that "the preferred configuration of the excited state determined the configuration of the major photoadduct." It was proposed that, in the excited state, the α-carbon could be considered trigonal and that the most stable configuration of a *pyramidalized* β-carbon would determine the facial selectivity of the photoaddition (27). Notwithstanding the manifestly empirical nature of these ideas, which Wiesner was at pains to emphasize, and although the model has encountered some skepticism (28), its ability to predict stereoselectivity in photocycloadditions of olefins to enones has been impressive. Insofar as it can be applied in the present case, the stereoselectivity predicted seems to be in accord with our observed results. Thus, according to the model, the excited state of **22** may be regarded as resembling one of the conformers **A** or **B** (R = CO_2CH_3), with the methyl group in the more stable pseudoequatorial configuration (Fig. 1). Inspection of molecular models and simple MM2 calculations (29) on conformers of a formally similar (ground state) structure[4] suggest that both conformers, **A** and **B** (R = CO_2CH_3), could be present under the reaction conditions, with the former predominating. For steric reasons, reaction at the α-face of **A** (R = CO_2CH_3), giving the observed major product **25**, would then appear to be more favorable than attack at the β-face of **B** (R = CO_2CH_3) (cf. ref. 12).

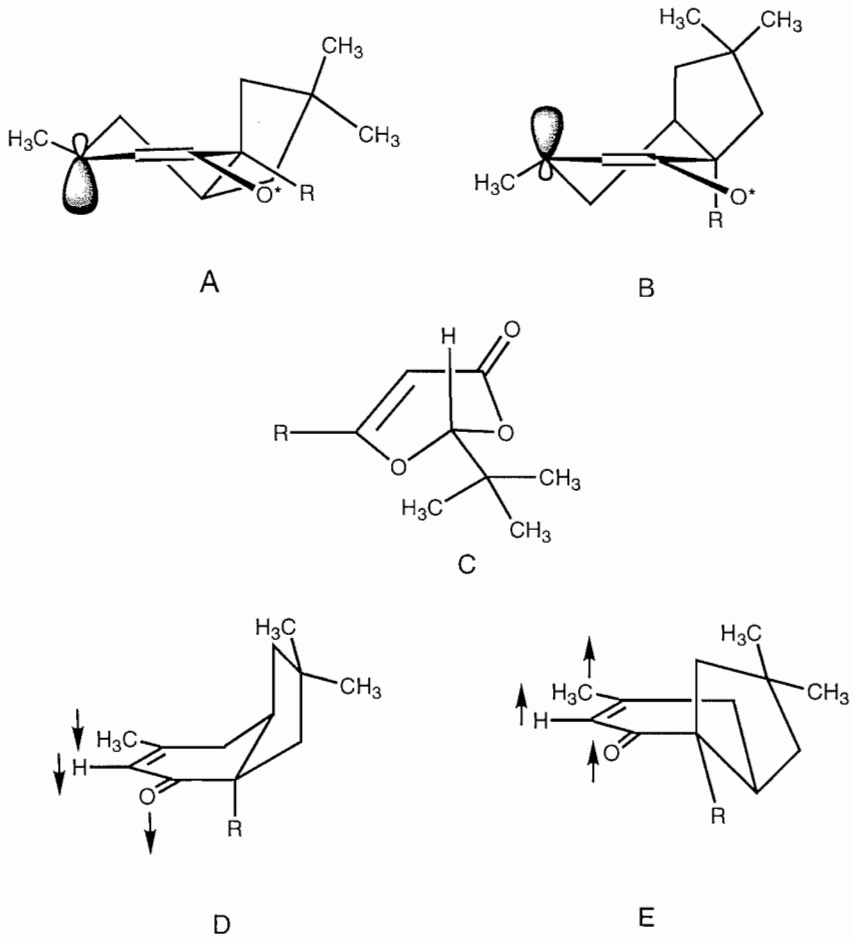
More recently, attempts have been made to understand the stereoselectivity of ground state and excited state additions to enones in the context of pyramidalization of the three trigonal carbon atoms of the conjugated system, predicted on the basis of X-ray crystallographic structures and theoretical calcula-

[4] The enol of the saturated ketone corresponding to **22** was used for modeling, approximately, the Wiesner empirical representation of the excited state.

Can. J. Chem. Downloaded from www.nrcresearchpress.com by 88.146.161.215 on 09/08/12
For personal use only.

© 1997 NRC Canada

Fig. 1.



tions. Thus, Seebach et al. (30) analyzed factors controlling or associated with facial selectivity in addition of organocuprates to (and catalytic hydrogenation of) dioxinones containing a stereogenic acetal center, e.g., **C** (Fig. 1). He noted that "the stereoselectivities of thermal and photochemical additions to dioxinones and other systems are correlated with pyramidalizations of the reacting centers," suggesting that "the steric course of attack on a trigonal center can be predicted from the direction of its pyramidalization." (30). There is strong pyramidalization in the excited state, with two of the three computed triplet states pyramidalized in the direction opposite to that in the ground state (30), which could account for the observation that ground state conjugate additions and photocycloadditions have opposite facial selectivity (31, 32).[5]

Lange and co-workers (33) reported further studies on the facial selectivity of ground state and excited state reactions of related systems, in the context of enone pyramidalization. In the course of this work, he observed that some simple cyclohexenones also displayed pyramidalization of trigonal carbons in the ground state, though to a lesser extent. It was noted that "in those systems where there is significant pyramidalization, the groups at C-4 to C-6 are always bent below the plane, i.e., away from the pucker at C-2" (33), (numbering as for 1,3-dioxin-4-one).

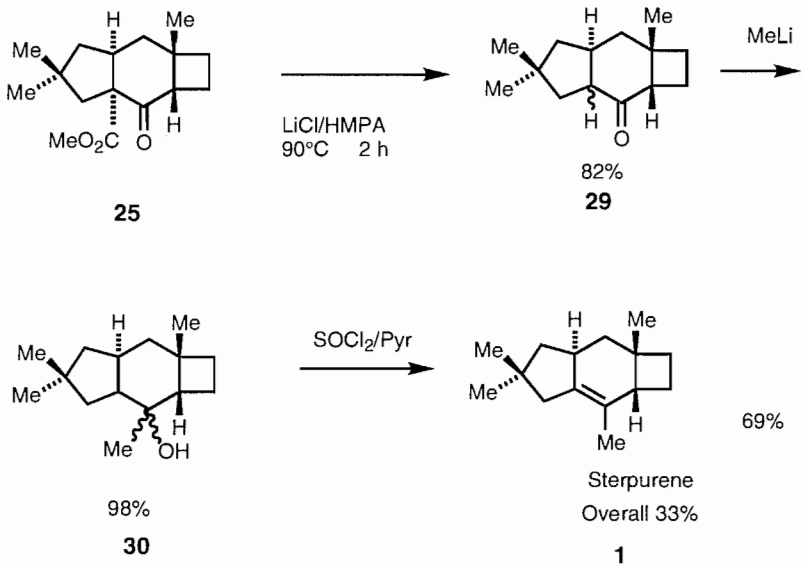
Simple molecular mechanics calculations (MM2* force field using MacroModel 4.5) (29) suggest that of the sofa conformations of our bicyclic enone **22**, represented approximately as **D** (R = CO_2CH_3) and **E** (R = CO_2CH_3) (Fig. 1), the former are all more stable than the latter, with an average energy difference of ~2 kcal/mol (signifying a significant preponderance of the former conformers at −78°C). In the absence of high-level calculations, an attempt to extend Lange's findings on ground state pyramidalization in simple cyclohexenones to the excited state of a system such as **D** (R = CO_2CH_3) is clearly fraught with pitfalls! It may, nevertheless, be more than coincidence that an analysis, based roughly on the observations of Lange and Seebach, appears to point to the observed facial selectivity for photocycloaddition of ethylene to **22**. Thus, the three trigonal carbon atoms of the preferred conformers **D** (R = CO_2CH_3) might be slightly pyramidalized

[5] The calculated opposite pyramidalization for enone ground and excited states (30) does not, however, appear to account adequately for the fact that facial selectivity was the *same for Diels–Alder reactions and photocycloadditions* (32). In Sato's view, cycloaddition reactions occur at the less hindered face of dioxinone enones in the sofa conformation "irrespective of the electronic states of the substrates," whereas the facial selectivity of "rather exceptional" thermal reactions occurring under kinetic control at the opposite face may be associated with pyramidalization (32).

Can. J. Chem. Downloaded from www.nrcresearchpress.com by 88.146.161.215 on 09/08/12
For personal use only.

© 1997 NRC Canada

Scheme 8.

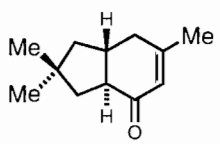


25 **29** **30** **1**

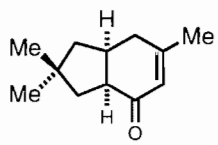
in the ground state, with displacement of the attached groups below the approximate plane formed by five of the ring carbons (away from the "pucker") as shown by the arrows (33) (Fig. 1). If, then, pyramidalization is reversed in the excited state, in accordance with Seebach's proposal (30), reaction at the bottom face of **D** (R = CO_2CH_3) would indeed be preferred.

The fact that the stereoselectivity observed by Paquette et al. (17) was somewhat lower in photocycloaddition of ethylene with **19** could be due to differences in conformation associated with the large sulfone group and the ester on the five-membered ring, and other steric effects.

Little and co-workers reported (12) that, whereas photocycloaddition of ethylene to the *trans*-fused enone **27** (lacking substitution at the ring junction) proceeded smoothly, the *cis*-fused isomer **28** *was unreactive under the same conditions*. This result is surprising. Molecular mechanics calculations indicate that the two sofa conformations of **28**, **D** (R = H) and **E** (R = H) (Fig. 1), do not differ significantly in energy. The former, which should be reactive in photocycloaddition, is more stable by ~0.3 kcal/mol. In the light of the above discussion, it does not seem obvious why **22** and **28** should differ so dramatically in their reactivity with respect to photocycloaddition.



27



28

Whatever the basis for the satisfactory stereoselectivity of the photocycloaddition of **22** with ethylene, the stage was now set for completion of the synthesis of racemic sterpurene (Scheme 8). Demethoxycarbonylation of **25**, by Krapcho's procedure, using LiCl–HMPA (34), afforded a mixture of two epimeric ketones **29** (82%) that, without separation, was treated with methyllithium to give a diastereoisomeric mixture of methyl carbinols **30** in a total yield of 98%. Finally, treatment of **30** with thionyl chloride and pyridine (12) effected dehydration, affording a 69% yield (33% overall from **14**) of racemic sterpurene **1**, whose spectra were in accord with those in the literature (3) and with data kindly supplied by Professor Ayer. (The structure of synthetic **1** and NMR assignments were confirmed by 2-D NMR experiments.)

Biological activity of some *C. purpureum* sesquiterpene metabolites

Several metabolites, previously described by Ayer et al. (3–6), were reisolated from culture filtrates of *C. purpureum*, and sterpuric acid **2**, sterepolide **5**, and dihydrosterepolide **6**, as well as synthetic sterpurene **1**, were assayed for phytotoxicity to cells of hybrid aspen, *Populus deltoides X nigra*. The results in Table 1 show that, of the compounds tested, sterpuric acid **2** is the most toxic to the aspen cells, but that the dose response curve for **2** is steeper in the concentration range studied (50–10 ppm) than for sterepolide **5** and dihydrosterepolide **6**. Sterpurene **1** was devoid of phytotoxicity to *P. deltoides X nigra* cells at the levels tested. The crude methylene chloride extract at 500 ppm exhibited approximately the same degree of phytotoxicity as sterpuric acid at 50 ppm.

Conclusions

We have synthesized the *C. purpureum* sesquiterpene metabolite, sterpurene **1** by a six-step pathway including a relatively stereoselective [2 + 2] photocycloaddition process, in an overall yield of 33% (the highest yield for any synthesis of the hydrocarbon reported to date).

Some metabolites of *C. purpureum,* previously described by Ayer, were reisolated, and bioassays of sterpuric acid **2**, sterepolide **5**, and dihydrosterepolide **6** showed them to be toxic to cells of hybrid aspen, *P. deltoides X nigra* at concentrations as low as 10 ppm. This suggests that sesquiterpene metabolites may play a role, along with the *endo*-polygalacturonase described by Miyaire et al. (2, 9), in the pathogenicity of *C. purpureum* to hardwood trees.

© 1997 NRC Canada

Can. J. Chem. Downloaded from www.nrcresearchpress.com by 88.146.161.215 on 09/08/12
For personal use only.

Table 1: Percent viability of *Populus tremuloides* cells treated with *C. purpureum* sesquiterpenes. Values within a column followed by the same letter do not differ significantly at $p < 0.05$ (Student Neuman Keuls test).

Treatment		% Viability
Control		89.9 a
C. purpureum extract	(1000 ppm)	0 b
	(750 ppm)	10.8 c
	(500 ppm)	26.8 d
	(250 ppm)	54.2 ef
	(100 ppm)	80.3 a
Sterpuric acid, **2**	(50 ppm)	24.6 d
Sterpuric acid, **2**	(10 ppm)	61.4 f
Sterepolide, **5**	(50 ppm)	56.6 ef
Sterepolide, **5**	(10 ppm)	55.2 ef
Dihydrosterepolide, **6**	(50 ppm)	51.9 ef
Dihydrosterepolide, **6**	(10 ppm)	45.8 e
Sterpurene, **1**	(50 ppm)	90.8 a
Sterpurene, **1**	(10 ppm)	90.7 a

Experimental

General

Melting points were determined on a hot-stage apparatus and are uncorrected. Infrared spectra were recorded on a Philips Pye Unicam PU9516 infrared spectrophotometer and the ultraviolet spectra on a Philips PU 8800 UV–VIS spectrophotometer. Accurate mass measurements were made on a Kratos MS-50 instrument, which was also used for obtaining the FAB spectra. The GC–MS analysis was conducted using a HP 5989A (Engine). (The sample, in methanol solution, was injected onto a 30 m DB-1ht column (injection temperature 250°C, temperature program 60–300°C at 20°C/min). Source and transfer line temperatures were 275°C and 280°C, respectively, and data were acquired in full scan, EI mode, over the range 40–359 amu, 1.65 scans/s). NMR spectra were recorded in $CDCl_3$ on a Varian XL-200 spectrometer operating at a frequency of 200.068 MHz for ^1H, and on a Varian Unity 400 operating at a frequency of 399.946 MHz for ^1H and 100.564 MHz for ^{13}C.

2-Carbomethoxy-4,4-dimethyl-1-cyclohexanone

2-Carbomethoxy-4,4-dimethyl-1-cyclohexanone was prepared, in two steps from commercially available 4,4-dimethyl-2-cyclohexene-1-one, essentially according to Liu's procedure (35). Hydrogenation of the starting material at atmospheric pressure (101.3 kPa) (rather than at 15 psi (1 psi = 6.9 kPa) (35)), and the addition of a catalytic amount of potassium hydride with the sodium hydride in the carboxymethylation step (18), did not affect the yields (overall 82%).

2-Chloro-2-carbomethoxy-4,4-dimethyl-1-cyclohexanone

Chlorine gas was passed into a vigorously stirred solution of 2-carbomethoxy-4,4-dimethyl-1-cyclohexanone (23.5 g, 128 mmol) in freshly distilled CH_2Cl_2 maintained at 0°C. During a period of 10–20 min, color changes from pale yellow to dark green to pale orange occurred, at which time chlorine addition was discontinued. (Thin-layer chromatography indicated that all starting material had been consumed at this stage.) The mixture was purged with argon, and solvent was removed in vacuo. The crude oily residue was purified by flash chromatography on a column of silica gel, eluting with hexane–EtOAc (10:1) to furnish the oily chloro ketoester (27.0 g, 97%); IR ($CHCl_3$): 3100–2800, 1730, and 1435 cm^{-1}; ^1H NMR ($CDCl_3$, 200 MHz) δ: 3.81 (3H, s), 2.82–2.65 (3H, m), 2.07–2.00 (1H, m), 1.77–1.69 (2H, m), 1.09 (3H, s), 1.04 (3H, s); EIMS, *m/z* (relative intensity) (ion): 220 (8) $(M + 2)^+$, 219 (6) $(M + 1)^+$, 218 (18) (M^+).

Methyl 4,4-dimethyl-1-cyclopentenecarboxylate, 14 (cf. refs. 19, 20)

A solution of the chloro ketoester (315 mg, 1.44 mmol) in distilled xylenes (10 mL) was heated under reflux in an atmosphere of argon with anhydrous sodium carbonate (160 mg, 1.51 mmol) for 24 h. The mixture was cooled, filtered, and concentrated under reduced pressure. Flash chromatography of the crude residue on a silica gel column (hexane–EtOAc, 10:1) afforded 147 mg (66%) of the oily conjugated ester, **14**; IR ($CHCl_3$): 3100–2800, 1705, 1630, 1500–1400 cm^{-1}; ^1H NMR ($CDCl_3$, 200 MHz) δ: 6.64 (1H, m), 3.70 (3H, s), 2.37–2.28 (4H, m), 1.08 (6H, s); EIMS, *m/z* (relative intensity) (ion): 154 (15) (M^+), 139 (10) $(M - CH_3)^+$, 126 (34) $(M - CO)^+$, 111 (15), 95 (30) $(M - CO_2CH_3)^+$, 79 (25) , 71 (100) $(C_5H_{11})^+$, 70 (31) $C_5H_{10})^+$.

Methyl 2-(2′-methyl-2′-propenyl)-4,4-dimethylcyclopentanecarboxylate, 15

Tetrabutylammonium fluoride (trihydrate) (460 mg, 1.46 mmol: previously dried under high vacuum for 1 h) in anhydrous DMF (3.0 mL) was treated in a flame-dried flask with activated 4 Å molecular sieves at ambient temperature for 30 min. The solution was transferred to another flame-dried flask containing activated 4 Å molecular sieves, and conjugated ester **14** (1.0 g, 6.49 mmol) in anhydrous DMF (5.0 mL) was added, followed by dropwise addition of a solution of isobutenyltrimethylsilane (2.50 g, 19.5 mmol) and distilled HMPA (3.4 mL, 19.5 mmol) in anhydrous DMF (5 mL) (cf. ref. 21). The reaction mixture was stirred at ambient temperature for 1 h, when additional isobutenyltrimethylsilane (831 mg, 6.49 mmol) was added and stirring continued for 4 h. Work-up consisted of addition of methanol, then water, followed by thorough ether extraction. The combined extracts were washed with water and brine, dried over $MgSO_4$, and concentrated in vacuo. Flash chromatography of the crude product on a silica gel column (hexane–EtOAc, 10:1) afforded the desired ester **15** (550 mg, 40%) as an oil; IR ($CHCl_3$): 3100–2800, 1725, 1650, 1440, and 1370 cm^{-1}; ^1H NMR ($CDCl_3$, 200 MHz) δ: 4.63 (2H, br), 3.63 (3H, s), 2.50 (2H, m), 2.12 (1H, m), 2.0–1.88 (1H, m), 1.78–1.63 (3H, m), 1.67 (3H, s), 1.15–1.07 (1H, m), 1.02 (3H, s), 1.00 (3H,s); HREIMS, *m/z* (relative intensity) (ion): 210.1634 (10) (M^+) (calcd. for $C_{13}H_{22}O_2$: 210.1620), 195 (100) $(C_{12}H_{19}O_2)$ $(M - CH_3)^+$, 155 (24) $(C_9H_{15}O_2)$ $(M - C_4H_7)^+$, 150 (25) $(C_{11}H_{18})$ $(M - H/CO_2CH_3)^+$, 139 (36) $(C_8H_{11}O_2)$ $(M - C_5H_{11})$, 135 (39) $(C_{10}H_{15})$, 123 (11) $(C_8H_{11}O)$, 109 (19) (C_8H_{13}), 107 (10) (C_7H_7O), 95 (74) (C_7H_{11}), 93 (16) (C_7H_9).

A by-product of the reaction was the dimer **16** (350 mg), IR ($CHCl_3$) 2960, 2875, 1725, and 1480–1410 cm^{-1}; ^1H NMR ($CDCl_3$, 200 MHz) δ: 5.51 (1H, m), 5.42 (1H, m), 3.62 (6H, s),

Can. J. Chem. Downloaded from www.nrcresearchpress.com by 88.146.161.215 on 09/08/12
For personal use only.

© 1997 NRC Canada

Can. J. Chem. Downloaded from www.nrcresearchpress.com by 88.146.161.215 on 09/08/12
For personal use only.

3.08–3.00 (1H, m), 2.68–2.63 (1H, m), 2.33–2.27 (1H, dd), 1,75–1.62 (2H, m), 1.54–1.46 (2H, m), 1.22–1.13 (1H, m), 1.11–0.99 (12 H, m); ^{13}C NMR (100 MHz, $CDCl_3$) (two stereoisomers) δ: 176.8/176.7 (s), 176.7/176.4 (s), 143.0/142.8 (d), 128.9/128.8 (d), 62.9/62.5 (s), 51.9/51.8 (q), 51.6/51.6 (q), 48.1/48.1 (d), 45.8/45.8 (t), 45.5/45.4 (d), 44.9/44.8 (s), 44.0/43.6 (t), 43.5/43.4 (t), 38.2/38.0 (s), 29.9/29.8 (q), 29.5/29.3 (q), 29.3/29.2 (q), 29.0/28.9 (q) . HREIMS, *m/z* (relative intensity) (ion): 249.1855 (100) $(M - CO_2CH_3)^+$ (calcd. for $C_{16}H_{25}O_2$: 249.1854), 233 (8) ($C_{15}H_{21}O_2$), 217 (15) ($C_{15}H_{21}O$), 189 (94) ($C_{14}H_{21}$), 173 (9) ($C_{13}H_{17}$), 154 (33) ($C_9H_{14}O_2$), 139 (20) ($C_8H_{11}O_2$).

1-Formyl-2-(2′-methyl-2′-propenyl)-4,4-dimethylcyclopentane, 17

Ester **16** (500 mg, 2.62 mmol) was added to 95% LAH (105 mg, 2.62 mmol) in anhydrous THF (15 mL) under an argon atmosphere at 0°C. The mixture was allowed to attain ambient temperature and was set aside with stirring for 3 h. Work-up consisted of addition of water (1 equiv.) followed by aqueous NaOH (1 equiv. 15% solution), and then water (3 equiv.). The mixture was filtered and the filtrates evaporated under reduced pressure. Flash chromatography of the residue on silica gel with hexane–EtOAc (10:1) as eluent afforded the corresponding amorphous alcohol (389 mg, 90%); IR ($CHCl_3$): 3625 (sharp), 3100–2800, 1650, 1480–1410, 1405–1345, and 900 cm^{-1}; ^{1}H NMR ($CDCl_3$, 200 MHz) δ: 4.67 (2H, br s), 3.66 (1H, dd, J = 10.4 and 4.7 Hz), 3.48 (1H, dd, J = 10.5 and 6.5 Hz), 2.25–2.21 (1H, m), 1.93–1.80 (3H, m), 1.72–1.57 (2H, m), 1.68 (3H, s), 1.40 (1H, s), 1.29–1.04 (2H, m), 1.00 (3H, s), and 0.98 (3H, s); EIMS, *m/z* (relative intensity) (ion): 182 (9) (M^+), 167 (52) $(M - CH_3)^+$, 164 (23) $(M - H_2O)^+$, 125 (100) $(M - C_4H_9)^+$.

Anhydrous DMSO (0.77 mL, 10.9 mmol) in freshly distilled dichloromethane (5.0 mL) was added to a solution of oxalyl chloride (0.47 mL, 5.40 mmol) in dichloromethane (20 mL) at −78°C under an argon atmosphere. After 2 min, the alcohol prepared as above (660 mg, 3.63 mmol) in dichloromethane (5 mL) was added dropwise at −78°C during a 5 min period. Stirring was continued at this temperature for 30 min and, after addition of dry triethylamine (2.52 mL, 18.1 mmol), for a further 5 min, when the mixture was allowed to warm to ambient temperature. After addition of water and dichloromethane extraction, the extracts were washed with water and brine, dried over $MgSO_4$, and concentrated in vacuo. Flash chromatography of the residue, eluting with hexane–EtOAc (10:1), afforded aldehyde **17** (625 mg, 96%) as an oil: IR ($CHCl_3$): 2950, 2870, 1715, 1650, and 1480–1400 cm^{-1}; ^{1}H NMR ($CDCl_3$, 200 MHz) δ: 9.58 (1H, d, J = 2.3 Hz), 4.67 (2H, br s), 2.53–1.71 (4H, m), 1.68 (3H,s), 1.65–1.09 (4H, m), 1.02 (3H, t), and 0.96 (3H, s); EIMS, *m/z* (relative intensity) (ion): 181 (54) ($M^+ + 1$), 180 (16) (M^+), 165 (31) $(M - CH_3)^+$, 151 (11) $(M - CHO)^+$, 136 (15) $(M - CHO - CH_3)^+$, 125 (37) $(M - C_4H_7)^+$, 124 (27) $(M - C_4H_8)^+$, 123 (77) $(M - C_4H_9)^+$ or $(M - C_3H_5O)^+$, 122 (36), 121 (18), 111 (10), 109 (27), 107 (30), and 96 (100) $(C_7H_{12})^+$.

1-(1′-Hydroxy-2′-propenyl)-2-(2″-methyl-2″-propenyl)-4,4-dimethylcyclopentane, 18

Vinyl magnesium bromide (2.0 mL 1.0 M solution in THF, 2.00 mmol) was added at 0°C under anhydrous conditions and an argon atmosphere to the aldehyde **17** (325 mg, 1.80 mmol) in freshly distilled THF (30 mL). The mixture was allowed to attain ambient temperature and was set aside with stirring for 1.5 h. After addition of saturated NH_4Cl solution, the mixture was extracted with ether, and the extracts were dried over $MgSO_4$ and concentrated in vacuo. Flash chromatography of the residue, eluting with hexane–EtOAc (10:1), afforded vinyl carbinol **18** (310 mg, 82%) as an oil; IR ($CHCl_3$) 3600 (sharp), 2950, 2940, 2865, 1650, 1600 and 1480–1400 cm^{-1}; ^{1}H NMR ($CDCl_3$, 200 MHz) δ: 5.94–5.76 (1H, m), 5.25–5.05 (2H, m), 4.65 (2H, br s), 4.14–4.00 (1H, m), 2.39–2.25 (1H, m), 2.13–1.72 (2H, m), 1.68 (3H,s), 1.65–1.03 (5H, m), and 0.98 (6H, overlapping singlets); EIMS, *m/z* (relative intensity) (ion): 208 (8) (M^+), 193 (13) $(M - CH_3)^+$, 190 (15) $(M - H_2O)^+$, 175 (24) $(M - CH_3 - H_2O)^+$, 165 (20), 152 (29) $(M - C_4H_8)^+$, or $(M - C_3H_4O)^+$, 151 (100) $(M - C_4H_9)^+$ or $(M - C_3H_5O)^+$, 147 (29) , 136 (27), and 135 (19).

1-(1′-Oxo-2′-propenyl)-2-(2″-methyl-2″-propenyl)-4,4-dimethylcyclopentane, 7

The Swern oxidation (22) of vinyl carbinol **18** was conducted as described above using oxalyl chloride (0.19 mL, 2.18 mmol), anhydrous DMSO (0.31 mL, 4.37 mmol), and triethylamine (1.0 mL, 7.2 mmol) for oxidation of the alcohol (300 mg, 1.44 mmol). The yield of product **7**, after work-up and chromatography, was 290 mg, 98%; IR ($CHCl_3$): 2950, 2865, 1690, 1670, 1610, 1450, 1405, and 1370 cm^{-1}; UV λ_{max} (cyclohexane): 221 nm (ε 2145); ^{1}H NMR ($CDCl_3$, 200 MHz) δ: 6.38 (1H, dd, J = 10.2 and 18.1 Hz), 6.13 (1H, dd, J = 1.7 and 17.6 Hz), 5.74 (1H, dd, J = 1.7 and 10.1 Hz), 4.61 (2H, br), 2.98–2.85 (1H, m), 2.78–2.63 (1H, m), 2.12–1.44 (5H, m), 1.65 (3H, s), 1.21–1.10 (1H, m), 1.03 (3H, s), and 1.00 (3H,s); HREIMS, *m/z* (relative intensity) (ion): 191.1426 (29) $(M - CH_3)^+$, (calcd. for $C_{13}H_{19}O$: 191.1436), 173 (14) ($C_{13}H_{17}$), 138 (23) ($C_9H_{14}O$), and 95 (100) (C_7H_{11}) (in the GC–MS (total ion current), a small shoulder (<10%) on the longer retention side of the main peak, whose MS was very similar to that of **7**, is presumed to represent the corresponding *cis* isomer).

Photoirradiation of 7

(*i*) In a cylindrical Pyrex vessel, a solution of ene-enone **7** (31 mg, 0.15 mmol) in freshly distilled dichloromethane (11.0 mL) containing benzophenone (7 mg, 0.038 mmol) was purged with argon for 30 min. The solution at ~0°C was irradiated (externally) for 30 min using a Hanovia 200 W mercury arc lamp in a quartz well, the latter apparatus and the contiguous reaction vessel being cooled in an ice bath. At this stage, TLC analysis indicated that no unchanged starting material remained. The solution was allowed to attain ambient temperature, and the solvent was removed under reduced pressure. Chromatography of the product on a preparative TLC plate, eluting with hexane–EtOAc (10:1), afforded 12 mg (39%) of photoproduct **12**; IR ($CHCl_3$): 3050–2800, 1705, 1600, 1480–1400, 1390–1360, and 900 cm^{-1}; ^{1}H NMR ($CDCl_3$, 200 MHz) δ: 4.63 (2H, narrow m), 2.75–2.60 (3H, m), 2.10–1.65 (6H m), 1.65 (~0.75 Me, s), 1.54 (~0.25 Me), 1.55–1.05 (2H, m), 1.04 (s), 1.02 (s), and 0.99 (s) (6H) (peaks at δ: 1.54 and 1.04 attributed to methyl groups of minor diastereomer); LREIMS, *m/z* (relative intensity) (ion): 206 (20) (M^+), 191 (29) $(M - CH_3)^+$, 163 (43) $(M - CH_3 - C_2H_4)^+$, or $(M - CH_3 - CO)^+$, 151 (84)

© 1997 NRC Canada

Can. J. Chem. Downloaded from www.nrcresearchpress.com by 88.146.161.215 on 09/08/12
For personal use only.

$(M - C_4H_7)^+$ or $(M - C_3H_3O)^+$, 136 (29) $(M - C_5H_{10})^+$, 123 (80) $(M - C_6H_{11})^+$, 109 (45) $(C_7H_9O)^+$, 95 (100) $(C_7H_{11})^+$, 81 (84) $(C_6H_9)^+$, 67 (25) $C_5H_7)^+$, 55 (59) $(C_3H_3O)^+$ or $(C_4H_7)^+$; HREIMS, *m/z* (relative intensity) (ion): 206.1676 (38) (M^+) (calcd. for $C_{14}H_{22}O$: 206.1671).

(*ii*) A solution of ene-enone **7** (38 mg, 0.184 mmol) in distilled hexane (3.0 mL) (0.0615 M) at ambient temperature in a quartz cell was irradiated at 254 nm for 71 h using a 4 W Spectroline E-Series UV lamp. The solution was concentrated and the residue subjected to preparative TLC on a silica gel plate (hexane–EtOAc, 10:1). Material (8 mg, ca 20%) from an apparently homogeneous band on the plate was found by GC–MS to consist of two isomeric products in the approximate ratio 2:3. The spectra of the mixture contained features in accord with structure **13**; IR ($CHCl_3$): 3600, 2940, 2870, 1690, and 1455 cm^{-1}; ^1H NMR ($CDCl_3$, 200 MHz) δ: 5.86 (1H, dd, J = 17.4 and 10.7 Hz), 5.26 (1H, dd, J = 17.2 and 1.5 Hz), 5.05 (1H, dd, J = 10.7 and 1.4 Hz), 4.86 (1H, br), 4.77 (1H,br), and 2.80–0.85 (~60 H, m); GC–MS (minor peak: (**13**) (4.41 min)) *m/z* (proposed ion): 206 $(M)^+$ $(C_{14}H_{22}O)^+$, 151 $(M - C_4H_7)^+$, 109 $(C_7H_9O)^+$, 95 $(C_7H_{11})^+$, 81 $(C_6H_9)^+$, 55 $(C_4H_7)^+$ or $(C_3H_3O)^+$; (major peak: (**9** or **9′**?) (5.12 min)) *m/z*: 206 $(M)^+$ $(C_{14}H_{22}O)^+$, 191 $(M - CH_3)^+$, 178 $(C_{12}H_{18}O)^+$, $(M - C_2H_4)^+$, 163 $(M - CH_3 - C_2H_4)^+$, 122 $(C_8H_{10}O)^+$, 95 $(C_7H_{11})^+$, 82 $(C_5H_6O)^+$, and 55 $(C_4H_7)^+$.

Diels–Alder addition of conjugated ester, 14, and ketene acetal, 23

A mixture of ester **14** (130 mg, 0.84 mmol) and ketene acetal **23** (650 mg, crude, ca. 5.15 mmol, prepared according to Boehler and Konopelski (26)) with K_2CO_3 (10 mg) was heated under argon in a sealed tube at 150°C for 10 days. Flash chromatography of the product, eluting with hexane–EtOAc (10:1), afforded the Diels–Alder adduct **24** (160 mg, 68 %); IR ($CHCl_3$): 3100–2800, 1720, and 1500–1400 cm^{-1}; ^1H NMR ($CDCl_3$, 200 MHz) δ: 5.40 (1H, s), 3.98–3.79 (4H, m), 3.67 (3H, s), 3.00 (1H, m), 2.40–2.15 (2H, m), 1.83–1.69 (5H, m), 1.63–1.52 (1H, m), 1.31–1.20 (1H, m), 1.01 (3H, s), and 0.86 (3H, s); HREIMS, *m/z* (relative intensity) (ion): 280.1668 (13) $(M)^+$ (calcd. for $C_{16}H_{24}O_4$, 280.1674), 249 (15) $(C_{15}H_{21}O_3)$ $(M - OCH_3)^+$, 221 (48) $(C_{14}H_{21}O_2)$ $(M - CO_2CH_3)^+$, 191 (14) $(C_{13}H_{19}O)$, 177 (15) $(C_{12}H_{17}O)$, 176 (14) $(C_{12}H_{16}O)$, 161 (17) $(C_{11}H_{13}O)$, 142 (13) $(C_7H_{10}O_3)$, 127 (100) $(C_7H_{11}O_2)$, 123 (16) $(C_8H_{11}O)$, 121 (12) (C_8H_9O), 111 (15) (C_6H_7O), 105 (12) (C_8H_9), 99 (22) $(C_5H_7O_2)$, 93 (11) (C_7H_9), 91 (20) (C_7H_7).

Deprotection of Diels–Alder adduct

Acetal **24** (320 mg, 1.14 mmol), from the Diels–Alder reaction, was stirred in THF (6.0 mL) containing 5% aqueous HCl (2.4 mL) at ambient temperature for 36 h. Work-up afforded the chromatographically homogeneous bicyclic enone ester **22** in a yield of 265 mg (98%); IR ($CHCl_3$): 3150–2800, 1720, 1660, and 1440 cm^{-1}; ^1H NMR ($CDCl_3$, 400 MHz) δ: 5.95 (1H, s), 3.65 (3H, s), 3.00–2.94 (1H, m), 2.72 (1H, dd, J = 19.3 and 6.2 Hz), 2.50 (1H, d, J = 13.7 Hz), 2.14 (1H, d, J = 19.3 Hz), 1.96 (1H, d, J = 13.8 Hz), 1.93 (3H, s), 1.58 (1H, dd, J = 12.6 and 6.8 Hz), 1.41 (1H, t, J = 13.0 Hz), 1.06 (3H, s), 0.95 (3H, s); HREIMS, *m/z* (relative intensity) (ion): 236.1399 (8) $(M)^+$, (calcd. for $C_{14}H_{20}O_3$, 236.1412), 221 (1) $(C_{13}H_{17}O_3)$ $(M - CH_3)^+$, 205 (2) $(C_{13}H_{17}O_2)$ $(M - OCH_3)^+$, 204 (2) $(C_{13}H_{16}O_2)$, 177 (14) $(C_{12}H_{17}O)$, 176 (4) $(C_{12}H_{16}O)$, 161 (6) $(C_{11}H_{13}O)$, 123 (2) $(C_8H_{11}O)$, 121 (3) (C_8H_9O), 82 (100) (C_5H_6O).

Photocycloaddition of ethylene to 22

A solution of enone ester **22** (117 mg, 0.496 mmol) in freshly distilled dichloromethane (20 mL) contained in a cylindrical Pyrex vessel was purged with argon for 30 min. As ethylene (excess) was bubbled in, the solution was irradiated (externally) for 2 h using a Hanovia 200 W mercury arc lamp in a quartz well, the latter apparatus and the contiguous reaction vessel being cooled in a Dry Ice – acetone bath. After the photocycloaddition, the solution was allowed to attain ambient temperature, and the solvent was removed under reduced pressure. Preparative thin-layer chromatography of the crude product (132 mg) on a silica gel plate, eluting with hexane–EtOAc (10:1), afforded unreacted enone ester **22** (50 mg) and 73 mg (97% based on consumed starting material) of a mixture of isomeric photoadducts **25** and **26** in the ratio (by NMR) 12:1. The isomers were separated chromatographically with the major (desired) product, **25**, eluting more slowly than its stereoisomer. Photoadduct **25**, mp 49°C, displayed the following spectroscopic properties: IR ($CHCl_3$) 3000–2800, 1730, 1690, and 1480–1400 cm^{-1}; ^1H NMR ($CDCl_3$, 400 MHz) δ: 3.73 (3H, s), 3.53–3.43 (1H, m), 2.75–2.71 (1H, dd, J = 10.2 and 6.6 Hz), 2.22–2.00 (5H, m), 1.90–1.85 (1H, dd, J = 13.0 and 7.7 Hz), 1.82–1.75 (2H, m), 1.41–1.36 (1H, dd, J = 13.0 and 6.7 Hz), 1.33–1.25 (1H, m), 1.22 (3H, s), 1.05 (3H, s), and 0.98 (3H, s); ^{13}C NMR (100 MHz, $CDCl_3$) δ: 210.4 (s), 173.4 (s), 65.8 (s), 52.7 (q), 51.2 (d), 48.0 (t), 47.7 (t), 42.3 (d), 41.0 (s), 39.2 (t), 37.5 (s), 31.5 (q), 30.9 (t), 30.5 (q), 29.9 (q), and 17.9 (t); HREIMS, *m/z* (relative intensity) (ion): 264.1712 (8) $(M)^+$ (calcd. for $C_{16}H_{24}O_3$, 264.1725), 249 (3) $(C_{15}H_{21}O_3)$ $(M - CH_3)^+$, 233 (5) $(C_{15}H_{21}O_2)$ $(M - OCH_3)^+$, 232 (9) $(C_{15}H_{20}O_2)$, 217 (5) $(C_{14}H_{17}O_2)$, 193 (9) $(C_{12}H_{17}O_2)$, 177 (27) $(C_{12}H_{17}O)$, 155 (15) $(C_9H_{15}O_2)$, 82 (100) (C_5H_6O).

Minor photoadduct **26** displayed the following spectroscopic properties: IR ($CHCl_3$): 2960, 2875, 1705, and 1480–1405 cm^{-1}; ^1H NMR ($CDCl_3$, 400 MHz) δ: 3.68 (3H, s), 3.64–3.54 (1H, m), 2.75–2.71 (1H, m), 2.46 (1H, d, J = 13.8 Hz), 2.31–2.22 (1H, m), 2.16–2.07 (1H, m), 1.84–1.61 (5H, m), 1.33 (3H, m), 1.31–1.21 (1H, m), 1.15–1.09 (1H, m), 1.04 (3H, s), and 0.95 (3H, s); ^{13}C NMR (100 MHz, $CDCl_3$) δ: 211.0 (s), 174.0 (s), 64.5 (s), 52.6 (q), 49.4 (t), 48.9 (d), 45.4 (t), 44.2 (d), 43.7 (s), 40.9 (t), 38.4 (s), 32.9 (t), 29.3 (q), 27.5 (q), 26.4 (q), and 17.4 (t); HREIMS, *m/z* (relative intensity) (ion): 264.1725 (18) $(M)^+$ (calcd. for $C_{16}H_{24}O_3$, 264.1725), 249 (12) $(C_{15}H_{21}O_3)$ $(M - CH_3)^+$, 233 (9) $(C_{15}H_{21}O_2)$ $(M - OCH_3)^+$, 232 (11) $(C_{15}H_{20}O_2)$, 217 (7) $(C_{14}H_{17}O_2)$, 177 (29) $(C_{12}H_{17}O)$, 176 (19) $(C_{12}H_{16}O)$, 155 (15) $(C_9H_{15}O_2)$, 123 (20) $(C_8H_{11}O)$, 110 (27) $(C_7H_{10}O)$, and 82 (100) (C_5H_6O).

Demethoxycarbonylation of 25: tricyclic ketone, 29

The major photoadduct **25** (295 mg, 1.12 mmol) dissolved in distilled HMPA (10 mL) was heated at 100°C with LiCl (95 mg, 2.24 mmol) in an argon atmosphere under anhydrous conditions for 20 h (cf. ref. 34). Work-up and flash chromatography in the normal manner afforded the desired tricyclic ketone, **29** (188 mg, 82%), IR ($CHCl_3$): 2940, 2870, 1680, 1455, and 1370 cm^{-1}; ^1H NMR ($CDCl_3$, 400 MHz) δ: 3.29–3.21 (1H, m), 3.13–3.06 (1H, m), 2.66–2.62 (1H, m), 2.27–

© 1997 NRC Canada

2.14 (2H, m), 2.04–1.95 (1H, m), 1.90–1.81 (2H, m), 1.64–1.59 (3H, m), 1.16 (3H, s), 1.11–1.06 (1H, m), 1.07 (3H, s), 0.99 (3H, s), and 0.93–0.87 (1H, m); HREIMS, *m/z* (relative intensity) (ion): 206.1682 (21) $(M)^+$ (calcd. for $C_{14}H_{22}O$, 206.1671), 191 (38) $(C_{13}H_{19}O)$ $(M - CH_3)^+$, 178 (64) $(C_{12}H_{18}O)$ $(M - C_2H_4)^+$,123 (23) $(C_8H_{11}O)$, 82 (100) (C_5H_6O).

Tricyclic carbinol 30

A solution of methyllithium in ether (0.65 mL, containing 0.909 mmol) was added to tricyclic ketone **29** (170 mg, 0.825 mmol) in freshly distilled ether (10 mL) at 0°C in an atmosphere of argon under anhydrous conditions. The reaction mixture was set aside at 0°C with stirring for 10 min, after which saturated NH_4Cl solution was added. Ether extraction and standard work-up afforded, without chromatography, 179 mg (98%) of a mixture of stereoisomeric alcohols **30**; IR ($CHCl_3$): 3600 (sharp), 2940, 2870, 1690, 1455, and 1375 cm^{-1}; ^1H NMR ($CDCl_3$, 200 MHz) δ: 2.52–1.05 (13 H, m), 1.12 (3H, s), 1.07 (3H, s), 0.98 (3H, s), and 0.97 (3H, m); HREIMS, *m/z* (relative intensity) (ion): 204.1892 (15) $(M - H_2O)^+$ (calcd. for $C_{15}H_{24}$, 204.1878), 189 (9) $(C_{14}H_{21})$ $(M - H_2O - CH_3)^+$, 176 (100) $(C_{13}H_{20})$, 175 (51) $(C_{13}H_{19})$, 161 (78) $(C_{12}H_{17})$, 149 (6) $(C_{11}H_{17})$, 121 (22) (C_9H_{13}), 120 (31) (C_9H_{12}), 119 (28) (C_9H_{11}), 107 (21) (C_8H_{11}), 105 (45) (C_8H_9), 95 (5) (C_7H_{11}), and 91 (17) (C_7H_7).

Sterpurene, 1

Carbinol (mixture) **30** (39 mg, 0.176 mmol) was stirred with thionyl chloride (0.03 mL, 0.411 mmol) and dry pyridine (0.2 mL) at 0°C in an atmosphere of argon under anhydrous conditions for 1.5 h. After addition of water, the mixture was extracted with ether and worked up in the conventional manner. Flash chromatography of the crude product on a silica gel column eluting with *n*-pentane afforded pure racemic sterpurene (23.4 mg, 69%); IR ($CHCl_3$): 3025–2800, 1480–1400, and 1400–1345 cm^{-1}; ^1H NMR ($CDCl_3$, 400 MHz) δ: 2.63 (1H, m), 2.41–2.31 (1H, m), 2.12–2.06 (3H, m), 1.96–1.88 (1H, m), 1.68–1.64 (1H, m), 1.55–1.51 (4H, m), 1.47–1.38 (2H, m), 1.20 (3H, s), 1.11–1.05 (1H, m), 1.07 (3H, s), 1.05 (3H, s), and 0.70–0.64 (1H, m); ^{13}C NMR (100 MHz, $CDCl_3$) δ: 136.5 (s), 127.7 (s), 48.6 (t), 44.6 (d), 44.4 (t), 39.3 (t), 38.0 (s), 37.6 (d), 36.5 (s), 30.2 (q), 29.4 (q), 29.3 (q), 27.9 (t), 24.7 (t), and 17.8 (q); HREIMS, *m/z* (relative intensity) (ion): 204.1892 (15) $(M)^+$ (calcd. for $C_{15}H_{24}$, 204.1878), 189 (9) $(C_{14}H_{21})$ $(M - CH_3)^+$, 176 (100) $(C_{13}H_{20})$, 175 (51) $(C_{13}H_{19})$, 161 (78) $(C_{12}H_{17})$, 149 (6) $(C_{11}H_{17})$, 121 (22) (C_9H_{13}), 120 (31) (C_9H_{12}), 119 (28) (C_9H_{11}), 107 (21) (C_8H_{11}), 105 (45) (C_8H_9), 95 (5) (C_7H_{11}), and 91 (17) (C_7H_7).

Natural products

Isolation of sterpuric acid **2**, sterepolide **5**, and dihydrosterepolide **6** from culture filtrates of *C. purpureum* was previously described by Ayer et al. (3–6). Physical properties and spectroscopic characteristics of these metabolites, isolated in the present study from 30-day-old cultures, were in agreement with the literature data.

Bioassays

A callus line was initiated from a bud of *P. deltoides X nigra* (DN17) and maintained on half-strength Gamborg medium at 25°C in the dark. Ten-day-old cells were removed using a sterile bacteriological loop and approximately 5 mg (fresh weight) was added to 2 mL of the above medium (minus agar) containing the test compound dissolved in 25 μL 50% aqueous acetone. The cells were incubated in this mixture at 25°C in the dark with shaking (100 rpm) for 2 h. Viable cells could be distinguished from dead cells by their fluorescence under UV after adding fluorescein diacetate (2 μL of solution containing 5 mg/mL). For each treatment, 100 cells were examined and the ratio of living to dead cells gave the % viability.

Acknowledgements

Financial support from the Canadian Forest Service Green Plan BICOVER Network, the Ontario Ministry of Natural Resources (ARIO), and the Natural Sciences and Engineering Research Council of Canada is gratefully acknowledged. We thank Dr. J.A. McLaughlin for providing us with the *C. purpureum* culture. We are grateful to a referee for a constructive criticism of our original disussion on the facial selectivity of the photocycloaddition. His comments engendered the discussion as presented herewith in the revised version. We wish also to thank Professors Z. Valenta and G. Deslongchamps for an exchange of ideas on this subject, and we are particularly indebted to the latter colleague for conducting the MM2 calculations. We thank Professor G. Lange for reading the manuscript and for his comments. We are grateful to Mr. Dan Drummond and Dr. Larry Calhoun, University of New Brunswick, for recording the mass spectra and some of the NMR spectra, respectively, and to Ms. Linda MacDonald, Canadian Forest Service, Sault Ste. Marie, for the GC–MS analysis.

References

1. R.E. Wall. North. J. Appl. For. **7**, 17 (1990).
2. K. Miyairi, K. Fujita, T. Okuno, and K. Sawai. Agric. Biol. Chem. **41**, 1897 (1977).
3. W.A. Ayer and M.H. Saeedi-Ghomi. Can. J. Chem. **59**, 2536 (1981).
4. W.A. Ayer, M.H. Saeedi-Ghomi, D. van Engen, B. Tagle, and J. Clardy. Tetrahedron, **37**, Suppl. No. 1, 379 (1981).
5. W.A. Ayer and M.H. Saeedi-Ghomi. Tetrahedron Lett. **22**, 2071 (1981).
6. W.A. Ayer, T.T. Nakashima, and M.H. Saeedi-Ghomi. Can. J. Chem. **62**, 531 (1984).
7. J.L. Xie, L.-P. Li, and Z.-Q. Dai. J.Org. Chem. **57**, 2313 (1992).
8. G. Cimino, A. De Giulio, S. De Rosa, and S. De Stefano. Tetrahedron, **45**, 6479 (1989).
9. K. Miyairi, T. Okuno, and K. Sawai. Bull. Fac. Hirosaki Univ. **31**, 1 (1979).
10. Y. Murata, T. Ohtsuka, H. Shirahama, and T. Matsumoto. Tetrahedron Lett. **22**, 4313 (1981).
11. C. Abell and A.P. Leech. Tetrahedron Lett. **28**, 4887 (1987).
12. L. Moens, M.M. Baizer, and R.D. Little. J. Org. Chem. **51**, 4497 (1986).
13. R.A. Gibbs and W.H. Okamura. J. Am. Chem. Soc. **110**, 4062 (1988).
14. S-.K. Zhao and P. Helquist. J. Org. Chem. **55**, 5820 (1990).
15. N. Krause. Justus Liebigs Ann. Chem. 521 (1993).
16. E.J. Corey, J.D. Bass, R. Le Mahieu, and R.B. Mitra. J. Am. Chem. Soc. **86**, 5570 (1964).
17. L.A. Paquette, H.-S. Lin, and M.J. Coghlan. Tetrahedron Lett. **28**, 5017 (1987).
18. L. Ruest, G. Blouin, and P. Deslongchamps. Synth. Commun. **6**, 169 (1976).

Can. J. Chem. Downloaded from www.nrcresearchpress.com by 88.146.161.215 on 09/08/12
For personal use only.

© 1997 NRC Canada

19. G. Buchi, U. Hochstrasser, and W. Pawlak. J. Org. Chem. **38**, 4348 (1973).
20. P. Magnus and D. Quagliato. J. Org. Chem. **50**, 1621 (1985).
21. G. Majetich, A. Casares, D. Chapman, and M. Behnke. J. Org. Chem. **51**, 1745 (1986).
22. K. Omura and D. Swern. Tetrahedron, **34**, 1651 (1978).
23. A.I. Scott. Interpretation of the ultraviolet spectra of natural products. Pergamon Press, New York. 1964.
24. J. March. Advanced organic chemistry. 3rd ed. John Wiley and Sons, New York. 1985.
25. R.O. Kan. Organic photochemistry. McGraw–Hill, New York. (1966)
26. M.A. Boehler and J.P. Konopelski. Tetrahedron, **47**, 4519 (1991).
27. (*a*) K. Wiesner. Tetrahedron, **31**, 1655 (1975); (*b*). G. Marini-Bettolo, S.P. Sahoo, G.A. Poulton, T.Y.R. Tsai, and K. Wiesner. Tetrahedron, **36**, 719 (1980).
28. R.O. Loufty and P. de Mayo. J. Am. Chem. Soc. **99**, 3559 (1977).
29. F. Mohamadi, N.G.J. Richards, W.C. Guida, R. Liskamp, M. Lipton, C. Caufield, G. Chang, T. Hendrickson, and W.C. Still. J. Comput. Chem. **11**, 440 (1990).
30. D. Seebach, J. Zimmermann, U. Gysel. R. Ziegler, and T.-K. Ha. J. Am. Chem. Soc. **110**, 4763 (1988).
31. M. Demuth, A. Palomer, H.-D Sluma, A.K. Dey, C. Krüger, and Y.-H. Tsay. Angew. Chem. Int. Ed. Engl. **25**, 1117 (1986).
32. M. Sato, Y. Abe, and C. Kaneko. J. Chem. Soc. Perkin Trans. 1779 (1990).
33. M.G. Organ, R.D.J. Froese, J.T. Goddard, N.J. Taylor, and G.L. Lange. J. Am. Chem. Soc. **116**, 3312 (1994).
34. A.P. Krapcho. Synthesis, 893 (1982).
35. H.-J. Liu, E.N.C. Browne, and S.Y. Chew. Can. J. Chem. **66**, 2345 (1988).

Can. J. Chem. Downloaded from www.nrcresearchpress.com by 88.146.161.215 on 09/08/12
For personal use only.

© 1997 NRC Canada

Enantioselective ring opening of tropinone. A new entry into tropane alkaloids

Marek Majewski, Ryszard Lazny, and Agnieszka Ulaczyk

Abstract: The lithium enolate of tropinone reacts with alkyl chloroformates to give 6-*N*-carboalkoxy-*N*-methyl-2-cycloheptenones (**4**). These compounds can be produced enantioselectively, in up to 95% ee, if chiral lithium amides (derived from optically pure amines **5**–**7**) are used for deprotonation of tropinone in the presence of additives. The effect of additives such as LiCl, LiBr, LiF, $LiClO_4$, $CeCl_3$, $ZnCl_2$, LiOH, TMEDA, HMPA, and DMPU on enantioselectivity of this deprotonation – ring opening sequence varies from slight to very large depending on the chiral amide – additive combination. Especially large increases in enantioselectivity are observed when the chiral, C2 symmetrical, lithium bis-α,α′-methylbenzylamide (Li-**5***a*) is used with one equivalent of LiCl. This reagent is best generated in situ from the corresponding amine hydrochloride and *n*-BuLi (2 equiv.). The ring-opening reaction combined with transposition of the carbonyl group (via Wharton reaction or allylic oxidation) provides a new method of stereoselective synthesis of tropane alkaloids having a protected hydroxyl at C-6 or C-7 (6β- and 7β-acetoxytropanes **14***a*, *b*) and physoperuvine (**19**).

Key words: enantioselective deprotonation, tropane alkaloids.

Résumé : L'énolate de lithium de la tropinone réagit avec les chloroformiates d'alkyles pour conduire à 6-*N*-carboalkoxy-*N*-méthylcyclopent-2-énones (**4**). Il est possible de produire ces composés avec une énantiosélectivité allant jusqu'à 95% ee si l'on utilise des amides de lithium chiraux (obtenus à partir des amines optiquement pures, **5**–**7**) pour effectuer la déprotonation de la tropinone, en présence d'additifs. L'effet de ces additifs, tels que LiCl, LiBr, LiF, $LiClO_4$, $CeCl_3$, $ZnCl_2$, LiOH, TMEDA, HMPA et DMPU, sur l'énantiosélectivité de cette séquence de déprotonation et d'ouverture de cycle peut être léger ou important suivant la nature de la combinaison de l'amide chiral et de l'additif. On observe des augmentations d'énantiosélectivité particulièrement importantes lorsqu'on utilise du bis-α,α′-méthylbenzylamide de lithium chiral, symétrique en C2 (Li-**5***a*), avec un équivalent de LiCl. Les meilleurs résultats sont obtenus en générant ce réactif in situ à partir du chlorhydrate de l'amine correspondant et du *n*-BuLi (2 équiv.). La réaction d'ouverture de cycle combinée avec la transposition du groupe carbonyle (via une réaction de Wharton ou une oxydation allylique) fournit une nouvelle méthode de synthèse stéréosélective des alcaloïdes du tropane comportant un groupe hydroxyle protégé en position C-6 ou C-7 (6β- ou 7β-acétoxytropanes, **14***a*, *b*) et de la physopéruvine (**19**).

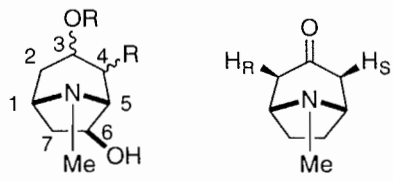
Mots clés : déprotonation énantiosélective, alcaloïdes du tropane.

[Traduit par la rédaction]

Introduction

Tropane alkaloids are a group of natural products isolated from plants (mainly of the *Solanaceae* family) and comprise over 200 compounds of which some 30% are chiral (1). This family of alkaloids includes some species famous (or infamous) for their biological activity, e.g., cocaine, atropine, scopolamine. Structurally, all tropane alkaloids contain the tropane (8-methyl-8-azabicyclo[3.2.1]octane) skeleton and a number of functional groups that, most often, are: a functionalized hydroxyl at C-3 (α or β), a side chain at C-2 or C-4 (α or β; the side chain is usually carbonyl based or is either an alkyl or a hydroxyalkyl group), and a β-hydroxyl at C-6 or C-7 (Fig. 1).

Fig. 1. Tropane alkaloids (**1**, generalized structure) and tropinone (**2**).



1 **2**

Tropinone (**2**) could be envisaged as a convenient starting material for synthesis of diverse tropane alkaloids provided that several stereoselectivity problems can be solved. A few years ago we began studying the enolate chemistry of tropinone with the aim of using this readily available symmetrical ketone as the starting material for synthesis of tropane alkaloids (2). During the early studies we established that tropinone lithium enolate (**3**), resulting from deprotonation of tropinone with LDA, undergoes a novel ring-opening reaction

Received December 11, 1996.

This paper is dedicated to Professor William A. Ayer on the occasion of his 65th birthday.

M. Majewski,[1] R. Lazny, and A. Ulaczyk. Department of Chemistry, University of Saskatchewan, 110 Science Pl., Saskatoon, SK S7N 5C9, Canada.

[1] Author to whom correspondence may be addressed. Telephone: (306) 966-4671. Fax: (306) 966-4730. E-mail: MAJEWSKI@sask.usask.ca

© 1997 NRC Canada

Can. J. Chem. Downloaded from www.nrcresearchpress.com by 88.146.161.215 on 09/08/12
For personal use only.

Scheme 1.

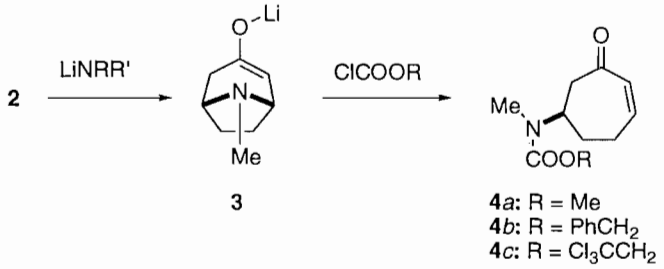
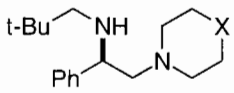


Fig. 2. Chiral amines used as precursors of the lithium amide bases.



5a: R'= Me; R"= Ph
5b: R'= R"= Me
5c: R'= R"= Ph
5d: R'=Me; R"= 1- naphtyl

6a: R = cyclohexyl
6b: R = 1-naphtyl



7a: X = CH_2
7b: X = NMe

upon treatment with a chloroformate (2*e*,*f*) to yield the substituted cycloheptenone **4** (Scheme 1). This compound can be produced enantioselectively when chiral lithium amides are used for deprotonation (3). Below, we describe the effects of additives on the enantioselectivity in this system and applications of the ring opening to the synthesis of physoperuvine and dihydroxytropanes.

Results and discussion

Our initial experiments with the deprotonation of tropinone using chiral lithium amides gave products in low enantioselectivity. We decided to evaluate several different bases and, since deprotonation reactions are often strongly affected by organic or inorganic additives (4) like lithium halides, amines (e.g., TMEDA), or by small amounts of polar cosolvents (e.g., HMPA, DMPU), we also used the chiral lithium amides in the presence of such additives.

Structures of chiral amines used as precursors for the chiral lithium amide bases in this study are shown in Fig. 2 and the experiments that involved deprotonation of **2** with these bases, followed by treatment of the resulting enolate with trichloroethyl chloroformate to give **4***c*, are summarized in Table 1. The dextrarotoatory isomer of **4***c* was the major product in all cases; the absolute stereochemistry of this isomer was established by correlation with anhydroecgonine (2*a*) and is as shown in Scheme 1. Most of the lithium amides tested gave low enantioselectivity in the absence of additives. The two exceptions were the lithiated bidentate amines **7***a*, *b* developed by Koga (5) that gave **4***c* in over 80% ee when the reaction was

Table 1. Formation of compound **4***c* (cf Scheme 1) using chiral lithium amides derived from chiral amines **5**, **6**, or **7**.

Entry	Lithium amide	Additive	ee[a] (%)	Yield[b] of **4***c* (%)
1	Li-**5***a*	—	44	80
2	Li-**5***a*	LiCl[c]	96	92
3	Li-**5***b*	—	29	80
4	Li-**5***c*	—	78	86
5	Li-**5***c*	LiCl[c]	87	65
6	Li-**5***d*	—	48	50
7	Li-**5***d*	LiCl[d]	88	89
8	Li-**6***a*	—	17	22
9	Li-**6***a*	LiCl[d]	72	60
10	Li-**6***b*	LiCl[d]	74	71
11	Li-**7***a*	—	83	82
12	Li-**7***a*	LiCl[c]	95	88
13	Li-**7***b*	—	87	80
14	Li-**7***b*	LiCl[c]	95	87

[a]The enantiomeric excess was determined by HPLC; cf. the experimental section.
[b]Yield of the purified compound **4***c* after column chromatography.
[c]One molar equivalent of LiCl with respect to **2** was used.
[d]Amine hydrochloride was used to generate the 1:1 Li-amide–LiCl complex.

run in THF (Table 1, entries 11 and 13). Addition of one equivalent of lithium chloride prior to enolization resulted in great enhancement of enantioselectivity when lithiated monodentate amines, and especially the C2 symmetrical amide Li-**a***a*, were used (Table 1, entries 1 and 2). Lithium chloride had a much smaller effect on the already efficient reactions involving the bidentate amides **7***a* and **7***b* (Table 1, entries 11 and 12, 13 and 14), but still caused the reaction selectivity, i.e., the k_{HS}/k_{HR} ratio, to increase by a factor of 2 (or greater).

Lithium amide derived from the C2 symmetrical amine **5***a* appeared to be the base of choice; the reagent used in the presence of LiCl was as efficient as Li-**7***a* or Li-**7***a*. The parent amines of the two latter compounds are much more difficult, and expensive, to make. We decided to investigate the effect of additives on the behavior of Li-**5***a* in greater detail: variable amounts of LiCl were tried as well as different lithium salts, salts of other metals, and also organic additives: TMEDA and cosolvents such as HMPA and DMPU. The results are summarized in Table 2.

Addition of even small amounts of LiCl or LiBr resulted in an increase of enantioselectivity. The salt effects leveled off after one (LiCl) or two (LiBr) equivalents of the halide were added. The dependence of enantioselectivity on the number of equivalents of LiCl and LiBr is shown in Fig. 3. Lithium iodide, fluoride, or perchlorate had no effect on the selectivity of deprotonation. Cerium trichloride and zinc chloride showed salt effects similar to LiCl or LiBr but it should be noted that all our experiments with $ZnCl_2$ resulted in low yields. Organic additives, i.e., TMEDA, HMPA, and DMPU, had little effect. Interestingly, deliberate addition of water followed by the addition of the corresponding excess of BuLi (Table 2, entries 20 and 21; water and BuLi should translate into addition of 0.05 or 0.20 molar equivalent of LiOH, respectively) essen-

Can. J. Chem. Downloaded from www.nrcresearchpress.com by 88.146.161.215 on 09/08/12
For personal use only.

© 1997 NRC Canada

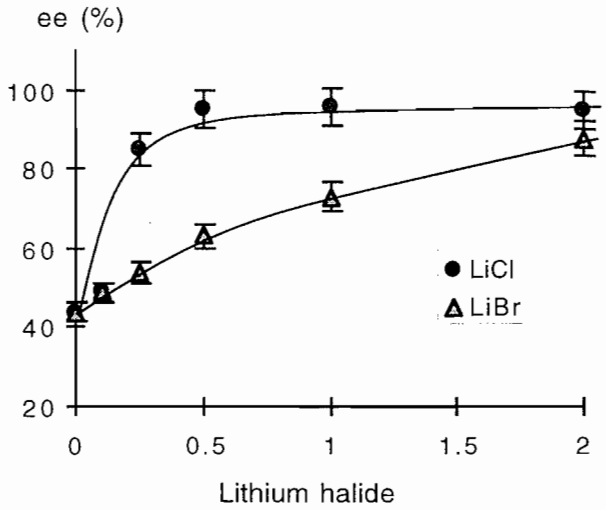
Can. J. Chem. Downloaded from www.nrcresearchpress.com by 88.146.161.215 on 09/08/12
For personal use only.

Table 2. The effect of additives on enantioselectivity of deprotonation of **2** with Li-**5***a*.

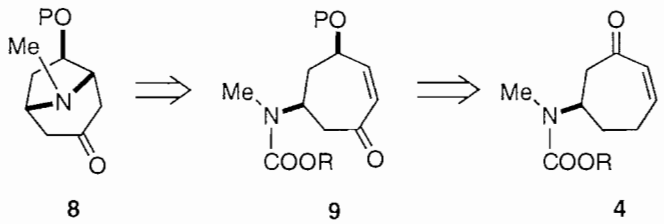
Entry	Additive (equiv.)	ee[a] (%)	Yield[b] of **4***c* (%)
1	—	44	80
2	LiCl (0.10)	49	84
3	LiCl (0.25)	85	92
4	LiCl (0.50)	95	90
5	LiCl (1.0)	96	92
6	LiCl (2.0)	95	94
7	LiBr (0.10)	49	78
8	LiBr (0.25)	54	82
9	LiBr (0.50)	63	88
10	LiBr (1.0)	73	93
11	LiBr (2.0)	88	85
12	LiF (1.0)	38	70
13	LiI (2.0)	41	78
14	$LiClO_4$ (1.0)	45	85
15	$CeCl_3$	80	70
16	$ZnCl_2$ (1.0)	87	40
17	TMEDA (1.0)	40	45
18	HMPA (1.0)	39	71
19	DMPU (1.0)	52	65
20	H_2O (0.05)[c]	24	48
21	H_2O (0.20)[c]	5	13

[a,b]See footnotes to Table 1.
[c]Excess BuLi (5% or 20%) was used in these experiments.

Fig. 3. Effect of LiCl and LiBr on enantioselectivity of formation of **4***c* (curves were fitted arbitrarily).



Scheme 2.



tially destroyed reaction selectivity and resulted in low yields. In all cases the yields were much lower than would be indicated by a simple assumption that a certain percentage of the base or the enolate was quenched. This underscores the need for thorough drying of the reagents and also the fact that it is not enough to titrate *n*-BuLi prior to use; if the reagent is contaminated with appreciable quantities of LiOH it will not work despite the reasonably high concentration of BuLi present. The great change in the reaction selectivity when a small amount of LiCl or LiBr was added precipitated the question of how halide-free was the commercial *n*-BuLi solution used in these experiments. This question was addressed by cyclic voltammetry: the amount of halide ions in a sample of *n*-BuLi hydrolyzed with MeOH was found to be smaller than 0.003 mole per mole of *n*-BuLi and thus could be assumed to have no effect on deprotonation.

It appeared that some salts, and especially LiCl and LiBr, had a strong influence on enantioselectivity of deprotonation of tropinone with the amide Li-**5***a*. A similar (but shorter) study with the lithium amide Li-**7***a* revealed that addition of LiCl resulted in some increase in selectivity that was independent of the amount of LiCl in the 0.1–2.0 equivalent range (using 0.1 or 2.0 equiv. LiCl gave **4***c* in 94% ee in both cases); addition of HMPA had no effect (variable amounts of HMPA from 0.1 to 3.0 molar equivalents were tried) and addition of 0.20 molar equivalents of H_2O resulted in loss of selectivity and very low yields (6% ee and 8% yield of **4***c*).

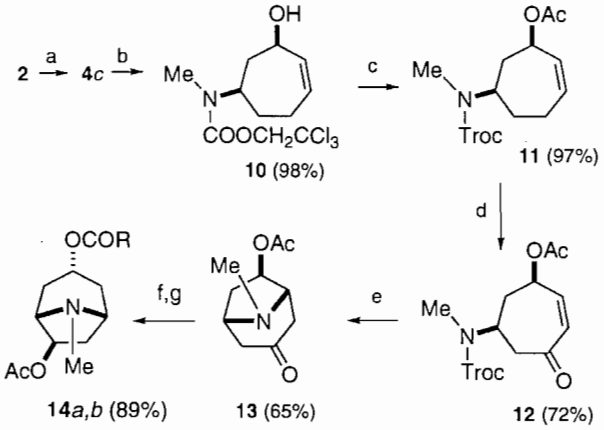
It can be concluded that addition of one equivalent of LiCl greatly increases enantioselectivity of deprotonation of tropinone with some lithium amides. The amide Li-**5***a* used in the presence of one molar equivalent of LiCl is a very efficient reagent in this system. Lithium chloride can be easily generated in situ, and its is usually better to use the hydrochloride of the amine (e.g., **5***a*-HCl) with 2 molar equivalents of *n*-BuLi to obtain the required 1:1 amide–LiCl complex. In many cases the crystalline hydrochloride salts are easier to purify and to dry than the viscous liquid amines. The hydrochlorides are also much more stable than the parent amines (longer shelf life, especially in the presence of moisture, oxygen, and CO_2) and can be easily manipulated.

After elaborating the optimal conditions for the enantioselective ring-opening reaction the stage was set for applications of this method to synthesis of tropane alkaloids. A number of these natural products have a hydroxy group at C-6 (or C-7; alkaloid numbering) of the tropane skeleton (cf Scheme 1) and we thought that the ring opening could provide a good enantioselective entry into these systems. It should be noted that the amine **5***a* is available in both enantiomeric forms and thus the enantioselective ring-opening reaction, described above, provides a way to render either C-6 or C-7 allylic. However, we quickly found out that we were unable to either hydroxylate or brominate the γ position in the enone functional group of compound **4**, even after protecting the C=O groups as an acetal. In the end we developed a strategy for synthesis of 7β-acetoxy tropanes based on the 1,4-transposition of the carbonyl group in compound **4** (Scheme 2).

Enantioselective syntheses of two natural products, 7β-acetoxy-3α-tigloyloxytropane and 3α,7β-diacetoxytropane, are shown in Scheme 3. Reduction of the substituted cyclo-

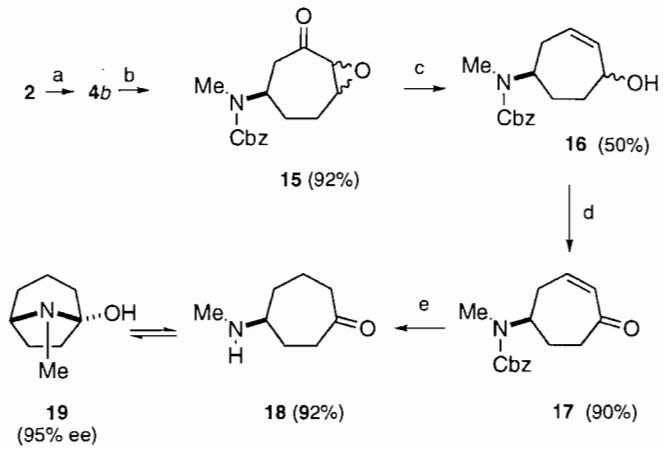
© 1997 NRC Canada

Scheme 3.



a. (i) LiCl, **5***a*; (ii) ClCOOCHcCCl$_3$; b. NaBH$_4$, CeCl$_3$; c. Ac$_2$O, Et$_3$N, DMAP; d. (i) H$_2$SeO$_3$, (ii) PDC; e. Zn, EtOH; f. H2/PtO2; g. Ac$_2$O or Tg$_2$O

Scheme 4.



a. (i) LiCl, 5*a*; (ii) CbzCl; b. H$_2$O$_2$, KOH; c. NH$_2$NH$_2$; d. PDC; e. H$_2$/Pd

heptenone **4***c* proceeded selectively under conditions developed by Luche (6), i.e., with $CeCl_3$–$NaBH_4$. The allylic alcohol product **10** had to be protected before the oxidation was attempted. Several groups (e.g., 1-methoxy-1-methylethyl, TBDMS) were tried but failed to provide sufficient protection under typical allylic oxidation conditions (*t*-BuOOH–PDC, SeO_2). Finally the acetate **11**, which could lead directly to 7-acetoxy alkaloids, proved stable under these conditions. Another serious problem, however, was that none of the oxidants mentioned above was sufficiently effective. Best results were obtained with H_2SeO_3 in wet dioxane, but the reaction did not proceed beyond 15% conversion and produced a complex mixture of three oxidation products (two diasteroisomeric allylic alcohols and the enone **12**) and several unidentified byproducts. Increasing the reaction time, using an excess of the oxidant or adding the selenium reagent in small portions over a long time, did not improve the effectiveness of this process. However, after observing that substantial amounts of selenium were produced as a colloidal suspension, scavenging the selenium with Celite increased in the reaction yield significantly. To avoid dealing with the mixtures of allylic alcohols and the ketone **12** we decided on an oxidative work-up. Transformation of the acetate **11** to the enone **12** was finally accomplished in 72% yield by oxidation with H_2SeO_3–Celite followed by PDC (Scheme 3). Removal of the 2,2,2-trichloroethylcarbamate group from **12** with zinc in ethanol was followed by an immediate cyclization to give 7β-acetoxytropinone **13** in 95% ee. Scalemic **13** served as the key intermediate in the synthesis of two optically active tropane alkaloids: (+)-3α,7β-diacetoxytropane (**14***a*) and (−)-7β-acetoxy-3α-tigloyloxytropane (**14***b*). Stereoselective reduction of the carbonyl group in **13** was accomplished by hydrogenation over Adams' catalyst (Scheme 3).

A different transposition of the C=O group in **4** was used in the synthesis of physoperuvine **19** (Scheme 4). The cyclic hemiaminal functional group in this alkaloid can readily open (in fact physoperuvine exists in equilibrium with the ring-open form **18**) and, thus protected, 6-aminocycloheptenone **4** could be a precursor to **19** via a 1,3-transposition of the carbonyl group in the enone system. The Wharton reaction (7) provided a successful solution to this problem. Thus, after enantioselective deprotonation of tropinone with Li-**5***a*–LiCl (the lithium amide was generated in situ from the hydrochloride of **5***a*) and ring opening using benzyl chloroformate (CbzCl), the double bond in compound **4***b* was epoxidized using alkaline hydrogen peroxide. Although methanol is typically used as the solvent for epoxidation of enones, aqueous THF had to be used in this case to avoid the competing conjugate addition of methanol to **4***b*. The Wharton rearrangement was done by treatment of the mixture of two isomeric epoxides **15** with hydrazine and a catalytic amount of acetic acid. The rearranged allylic alcohol **16** was easily oxidized to the corresponding enone **17** using PDC. The ^{1}H NMR spectrum of this product is very similar to the spectrum of the enone **4***b*; however, a close examination of the spectra showed small differences in chemical shifts of the vinylic hydrogens, indicating that the two enones, **4***b* and **17**, are regioisomers. The transformation of this enone to physoperuvine (**19**) was precedented in the literature (8) but no experimental details were given. Hydrogenation of **17** provided the natural alkaloid, which exists predominantly in its hemiaminal form **19** (9).

Conclusions

Opening the five-membered ring of tropinone by deprotonation with a lithium amide base followed by treatment with a chloroformate was the source of protected 6-aminocycloheptenone **4**. The ketone can be produced enantioselectively by using chiral, nonracemic lithium amide bases for enantioselective deprotonation. The selectivity of this reaction depends on the structure of the base and on the reaction conditions (additives, cosolvents). The C2 symmetrical lithium amide Li-**a***a* generated in situ from the hydrochloride salt of the corresponding amine **5***a* and *n*-BuLi (2 equivalents) is the best reagent for this transformation. The ring-opening reaction was used for synthesis of physoperuvine **19** and two natural products from the 7β-acetoxytropane group (**14**).

Experimental part

All air-sensitive reactions were carried out under argon (10). Tetrahydrofuran was distilled under nitrogen from sodium and benzophenone. Diisopropylamine and other amines used as a

© 1997 NRC Canada

Can. J. Chem. Downloaded from www.nrcresearchpress.com by 88.146.161.215 on 09/08/12
For personal use only.

Can. J. Chem. Downloaded from www.nrcresearchpress.com by 88.146.161.215 on 09/08/12
For personal use only.

precursors for lithium amides were distilled from calcium hydride and stored over 4 Å molecular sieves. Chiral amines were prepared as described previously (11). Lithium chloride, bromide, and iodide were dried at 130–150°C under vacuum for 12 h and lithium perchlorate was dried (melted) at 200°C in an over for 12 h. The salts were then dissolved in THF and stored under argon. Butyllithium (*n*-BuLi solution in hexanes, Aldrich) was periodically titrated using 2,5-dimethoxybenzyl alcohol as the indicator. Tetramethylethylenediamine (TMEDA), hexamethylphosphoric triamide (HMPA), and 1,3-dimethyl-3,4,5,6-tetrahydro-2(1*H*)-pyrimidinone (DMPU) were distilled from calcium hydride.

Flash column chromatography (FCC) (12) and dry-column flash chromatography (DFC) (13) were carried out using Merck silica gel 60 (230–400 mesh) and Sigma silica gel type H (10–40 μm), respectively, and thin-layer chromatography (TLC) was performed on precoated glass plates (Merck, silica gel 60, F254). The spots were detected using UV light (254 nm), the Dragendorff reagent (14), or with a developing solution of phosphomolybdic acid and ceric sulfate followed by charring on a hot plate.

Optical rotation was measured on a Perkin Elmer 241 polarimeter (1 dm cell); all concentrations are given in g/100 mL. Mass spectra are reported as *m/z* ratio (relative intensity); electron impact (EI) ionization was accomplished at 70 eV and chemical ionization (CI) at 50 eV. Infrared (IR) spectra were recorded on a Biorad FTS-40 Fourier Transform interferometer by a diffuse reflectance cell method; only diagnostic peaks are reported. Gas chromatography was performed using a Hewlett Packard 5890A instrument fitted with a methyl silicone gum column (HP-1, 5 m × 0.53 mm) unless otherwise stated.

Chromatographic analyses of enantiomeric purity of compound **4***c* were done on a chiralpack AD column. The solvent used was 15:1 hexane:isopropanol at 0.8 mL/min flow rate, and the sample concentration was 1 mg/mL. Statistically estimated error was ±1% ee. It should be noted, however, that differences between any two different experiments could be larger; the critical parameter for good reproducibility (and higher ee) seems to be slow rate of addition of the ketone to the lithium amide.

To obtain a high signal-to-noise ratio, ^{1}H NMR spectra for analysis of the ee were recorded on 20–25 mg samples in 0.4 mL $CDCl_3$ in the presence of 20 mg of *S*-(+)-2,2,2-trifluoro-1-(9-anthryl)ethanol (*S*-(+)-TFAE). Statistically estimated error of the measurement was ±2% ee.

Generation of nonracemic tropinone lithium enolate using chiral amine hydrochloride

A solution of *n*-BuLi in hexanes (2.49 M, 7.12 mL, 17.7 mmol) was added to a suspension of (*S,S*)-(−)-*N,N*-bis(1-phenylethyl)amine hydrochloride (2.307 g, 8.80 mmol) in THF (80 mL) at 0°C and the mixture was stirred for 45 min. After cooling to −78°C for 20 min, tropinone (1.112 g, 8 mmol) in THF (8 mL) was added via a syringe pump (over 105 min) and the resulting solution was stirred for 120 min.

6-[*N*-(2,2,2-Trichloroethoxy)carbonyl-*N*-methyl]amino-2-cyclohepten-1-one (4*c*)

2,2,2-Trichloroethyl chloroformate (0.16 mL, 0.246 g, 1.16 mmol) was added to a solution of tropinone lithium enolate (1 mmol) at −78°C and the mixture was stirred for 30 min. After quenching with 40% K_2CO_3 (4 mL) and warming to room temperature (rt), the reaction mixture was extracted with ether (3 × 10 mL). The extracts were washed with 5% H_2SO_4 (to remove the chiral amine, 98% recovery) and brine, and were then dried ($MgSO_4$). The solvent was removed under vacuum to give the crude scalemic product, which was purified by crystallization from 5 mL of hexane (white solid, 0.289 g, 92%). The chiral amine was left in the mother liquor; mp (racemic): 59–61°C; mp (scalemic): 89–90°C; $[\alpha]_D^{26}$ +55.4 (*c* 1.05, MeOH), second crystallization +56.5 (*c* 1.04, MeOH); IR: 1713 (C=O), 1666 (C=O) cm^{-1}; ^{1}H NMR: 6.64 (ddd, *J* = 12 Hz, *J* = 6 Hz, *J* = 5 Hz, 1H), 6.05 (d, *J* = 12 Hz, 1H), 4.75 (s, 2H), 4.55 (br, 1H), 2.90 (s, 3H), 2.92–2.82 (m, 2H), 2.68–2.45 (m, 2H), 2.20–1.90 (m, 2H); ^{13}C NMR: 200.0, 154.0, 146.4, 132.4, 95.5, 75.0, 51.8, 47.9, 30.6, 29.3, 27.7 (some signals appeared as two peaks of unequal height due to amide isomerism); MS (EI): 315 (4), 313 (4), 124 (29), 108 (100), 109 (38), 82 (59), 81 (31), 80 (20). Anal. calcd. for $C_{11}H_{14}NO_3Cl_3$: C 41.99, H 4.48, N 4.45; found: C 42.-0, H 4.37, N 4.26.

(1*R*,6*R*)-6-[*N*-(2,2,2-Trichloroethoxy)carbonyl-*N*-methyl]amino-2-cyclohepten-1-ol (10)

A solution of $CeCl_3 \cdot 7H_2O$ (2.73 g, 7.32 mmol) in MeOH (15 mL) was added to an ice-cooled solution of the enone **4***c* (2.302 g, 7.33 mmol) in MeOH (25 mL). Solid $NaBH_4$ (0.280 g, 7.37 mmol) was added in small portions to the solution over 45 min. The reaction mixture was warmed up to rt (TLC showed absence of the starting material) and most of the solvent was removed under vacuum. The residue was treated with aqueous K_2CO_3 (2 g in 200 mL) and was extracted with CH_2Cl_2 (3 × 30 mL). The extracts were washed with water and brine, and were dried ($MgSO_4$). The solvent was removed under vacuum and the crude product (2.293 g, 99%) was used in the next step. An analytical sample was obtained by DFC (4:1 hexane–AcOEt). Properties: colorless oil, R_f = 0.56 (1:1 hexane–AcOEt); $[\alpha]_D^{26}$ +17.4 (*c* 1.32, MeOH); IR: 3453 (OH), 1711 (CO) cm^{-1}; ^{1}H NMR: 5.82–5.68 (m, 2H), 4.80–4.70 (m, 2H), 4.45–4.38 (m, 1H), 4.30–4.12 (m, 1H), 2.88 (s, 3H), 2.35–2.18 (m, 1H), 2.10–1.68 (m, 4H), 1.62–1.45 (m, 1H); ^{13}C NMR: 153/7, 138.6, 127.7, 95.4, 74.7, 68.1, 55.8, 40.5, 30.2, 28.4, 24.7; MS (EI): 300 (3), 397 (11), 234 (11), 232 (12), 149 (14), 110 (28), 92 (37), 84 (100). Anal. calcd.: C 41.72, H 5.09, N 4.42; found: C 41.97, H 5.13, N 4.31.

(1*R*,6*R*)-1-Acetoxy-6-[*N*-(2,2,2-trichloroethoxy)carbonyl-*N*-methyl]amino-2-cycloheptene (11)

A solution of the allylic alcohol **10** (2.200 g, 6.96 mmol) in CH_2Cl_2 (6 mL) and Et_3N (4 mL) containing DMAP (0.02 g) was cooled to 0°C. Acetic anhydride (1.0 mL, 10.6 mmol) was added and the reaction mixture was left at rt for 24 h. The reaction mixture was then shaken with aqueous K_2CO_3 (1.5 g in 20 mL) for 20 min, diluted with water (30 mL), and extracted with CH_2Cl_2 (3 × 30 mL). The combined extracts were washed with water (90 mL), dried ($MgSO_4$), and concentrated under vacuum. The residue was subjected to DFC (5–10% AcOEt–hexane), which gave the pure product as a colorless oil (2.410 g, 97%); R_f = 0.79 (1:1 hexane–AcOEt); $[\alpha]_D^{26}$ +16.7 (*c* 1.05, MeOH); IR: 1714, 1739 cm^{-1}; ^{1}H NMR: 5.88–5.25 (m, 1H), 5.65 (d, *J* = 12 Hz, 1H), 5.48–5.37 (m, 1H), 4.90–4.68 (m, 2H), 4.45–4.15 (m, 1H), 2.88 (s, 3H), 2.39–2.20 (m, 1H), 2.07

© 1997 NRC Canada

Can. J. Chem. Downloaded from www.nrcresearchpress.com by 88.146.161.215 on 09/08/12
For personal use only.

(s, 3H), 2.18–1.72 (m, 4H), 1.68–1.48 (m, 1H); ^{13}C NMR: 169.9, 153.8, 134.7, 129.4, 95.8, 75.0, 71.1, 56.2, 37.1, 30.5, 28.9, 24.9, 21.2; MS (EI): 359 (5), 357 (5), 324 (65), 322 (100), 318 (31), 317 (28), 316 (86), 315 (34), 314 (88). Anal. calcd.: C 43.53, H 5.06, N 3.90; found: C 43.56, H 5.13, N 3.92.

(4*R*,6*S*)-4-Acetoxy-6-[*N*-(2,2,2-trichloroethoxy)carbonyl-*N*-methyl]amino-2-cyclohepten-1-one (12)

A solution of H_2SeO_3 (0.942 g, 7.32 mmol) in wet dioxane (35 mL dioxane + 0.4 mL water) was added to a stirred mixture of allylic acetic **11** (2.399 g, 6.70 mmol), Celite (9 g), and dioxane (30 mL). The resulting mixture was refluxed with stirring for 18 h, diluted with EtOH (30 mL), and refluxed for a further 10 min. The black mixture was then filtered through Celite and the solvents were removed under vacuum. The residue was dissolved in 10% MeOH – CH_2Cl_2 and filtered through TLC-grade silica. Solvents were thoroughly removed from the filtrate and the residue was treated with CH_2Cl_2 (45 mL) and PDC (5.64 g, 15 mmol) for 12 h. The reaction mixture was then diluted with Et_2O (100 mL) and filtered through Celite/Florisil. The solvents were removed under vacuum and the residue was subjected to DFC (15–20% AcOEt – hexane), which provided the recovered starting material (0.963 g, 40%) and the product (1.086 g, 44%, 73% yield based on recovered starting material). Properties: colorless oil, R_f = 0.62 (1:1 hexane–AcOEt); $[\alpha]_D^{26}$ +22.5 (*c* 1.52, MeOH); IR: 1739, 1715, 1670 cm^{-1}; ^{1}H NMR: 6.48 (dd, *J* = 12.5 Hz *J* = 4 Hz, 1H), 6.03 (dd, *J* = 12 Hz, *J* = 4 Hz, 1H), 5.55 (br d, *J* = 12 Hz, 1H), 4.65 (s, 2H), 4.65–4.50 (m, 1H), 2.87 (s, 3H), 2.98–2.75 (m, 2H), 2.35–2.08 (m, 2H), 2.05 (s, 3H); ^{13}C NMR: 198.3, 169.5, 153.8, 144.9, 131.2, 95.3, 75.0, 69.2, 48.7, 47.5, 36.7, 29.6, 20.8; MS (CI-NH_3): 374 (10), 372 (10), 282 (34), 280 (54), 279 (30), 198 (44), 140 (100), 107 (50), 61)50). Anal. calcd.: C 41.90, H 4.38, N 3.76; found: C 41.77, H 4.28, N 3.63.

(−)-7β-Acetoxytropinone (13) (ref. 15)

A mixture of the enone **12** (1.030 g, 2.77 mmol) and zinc powder (3.9 g) in 95% EtOH (60 mL) was refluxed for 2 h (TLC showed the absence of the starting material). Most of the solvent was removed under vacuum and the residue was treated with 25% aqueous NH_3 (2 mL), CH_2Cl_2 (80 mL), Celite, and $MgSO_4$. The resulting suspension was filtered, the solvent was evaporated under vacuum, and the residue was subjected to DFC (2% MeOH – CH_2Cl_2). A yellowish oil was obtained (0.382 g, 70%). Kugelrohr distillation (at 120°C/0.5 Torr (lit. (16) bp 110°C/0.03 Torr); 1 Torr = 133.3 Pa) gave the pure product (0.354 g, 65%); R_f = 0.35 (3% MeOH in CH_2Cl_2), R_f = 0.60 (10% MeOH in CH_2Cl_2); $[\alpha]_D^{26}$ −20.2 (*c* 1.10, MeOH), 95% ee *S*-(+)-TFAE; IR: 1713, 1732 cm^{-1}; ^{1}H NMR: 4.88 (dd, *J* = 4, 6.5 Hz, 1H), 3.60 (br s, 1H), 3.46 (br d, 1H), 2.70 (d, *J* = 5 Hz, 1H), 2.64 (d, *J* = 5 Hz, 1H), 2.60 (s, 3H), 2.30 (d, *J* = 16.5 Hz, 1H), 2.18–2.08 (m, 3H), 2.01 (s, 3H); ^{13}C NMR: 206.9, 170.3, 77.6, 65.6, 59.3, 44.2, 42.0, 37.3, 35.8, 20.8.

(+)-7β-Acetoxy-3α-hydroxytropane (13*a*) (ref. 15)

A solution of the ketone **14** (0.298 g, 1.51 mmol) in 95% EtOH (18 mL) with PtO_2 (0.03 g) was hydrogenated in a Paar apparatus at 50 psi (1 psi = 6.9 kPa) and at rt for 12 h. The mixture was filtered through Celite and the solvent was removed under vacuum. A yellowish oil was obtained (0.290 g, 97%). An analytical sample was purified through DFC; R_f = 0.13 (10% MeOH in CH_2Cl_2); $[\alpha]_D^{26}$ +21.3 (*c* 1.05, MeOH); IR: 3162, 1733 cm^{-1}; ^{1}H NMR: 5.63 (dd, *J* = 3, 7.5 Hz, 1H), 4.09 (t, *J* = 5 Hz, 1H), 3.39–3.30 (m, 1H), 3.18 (br s, 1H), 2.90 (br, 1H), 2.74 (dd, *J* = 7.5, *J* = 14 Hz, 1H), 2.53 (s, 3H), 2.26–2.03 (m, 3H), 2.06 (s, 3H), 1.79 (d, *J* = 15 Hz, 1H), 1.58 (d, *J* = 15 Hz, 1H); ^{13}C NMR: 171.0, 79.3, 65.4, 63.5, 59.3, 38.3, 36.0, 35.0, 34.1, 21.2.

(+)-3α,7β-Diacetoxytropane (14*a*) (refs. 16, 17)

A solution of the alcohol **13*a*** (0.127 g, 0.638 mmol) in CH_2Cl_2 (0.5 mL) and Et_3N (0.5 mL) containing DMAP (0.005 g) was treated with Ac_2O (0.097 g, 0.95 mmol) and the reaction mixture was left at rt for 24 h. The reaction mixture was then shaken with aqueous K_2CO_3 for 10 min, diluted with water (10 mL), and extracted with CH_2Cl_2 (3 × 15 mL). The extracts were dried ($MgSO_4$) and evaporated under vacuum. The residue was subjected to DFC (3–6% MeOH – CH_2Cl_2), which gave the pure product as a colorless oil (0.143 g, 93%); R_f = 0.42 (10% MeOH – CH_2Cl_2); $[\alpha]_D^{26}$ +15.5 (*c* 1.04 EtOH) (lit. (16) $[\alpha]_D^{26}$ (enantiomer) −16.6; 96% optical purity); IR: 1734 cm^{-1}; ^{1}H NMR: 5.45 (dd, *J* = 3, 7.5 Hz, 1H), 5.04 (t, *J* = 5 Hz, 1H), 3.43–3.34 (m, 1H), 3.22 (s br, 1H), 2.57 (dd, *J* = 7.5, 14 Hz, 1H), 2.55 (s, 3H), 2.32–2.05 (m, 3H), 2.09 (s, 3H), 2.08 (s, 3H), 1.83 (d, *J* = 15.5 Hz, 1H), 1.61 (d, *J* = 15.5 Hz, 1H); ^{13}C NMR: 170.4, 169.5, 78.5, 66.4, 64.6, 58.7, 38.0, 35.7, 32.2, 30.6, 21.0, 20.8.

(−)-7β-Acetoxy-3α-tigloyloxytropane (14*b*) (refs. 18, 19)

The alcohol **13*a*** (0.100 g, 0.502 mmol) was dissolved in dry pyridine (1.2 mL) and dry benzene (0.6 mL), and treated with DMAP (0.026 g) and tigloic anhydride (Tg_2O; 0.2 g, 1.1 mmol) for 3.5 days. The mixture was then diluted with $CHCl_3$ shaken with aqueous K_2CO_3 solution, and extracted with $CHCl_3$ (3 × 20 mL). The extracts were washed with water, dried ($MgSO_4$), and the solvent was removed under vacuum. The residue was subjected to DFC (1% MeOH – CH_2Cl_2 eluted unreacted anhydride, 3% eluted with product), which gave the pure product as a colorless oil (0.130 g, 92%); R_f = 0.47 (10% MeOH – CH_2Cl_2); $[\alpha]_D^{25}$ −14.6 (*c* 2.03, EtOH) (lit. (18) $[\alpha]^{20}$D −11.5 (*c* 12.4, EtOH); −9.0 (*c* 1.55, $CHCl_3$) (lit. (19) $[\alpha]_D^{19}$ −13 ($CHCl_3$); IR: 1734, 1707, 1650 cm^{-1}; ^{1}H NMR: 6.91 (tt, *J* = 1, 7 Hz, 1H), 5.50 (dd, *J* = 3, 7.5 Hz, 1H), 5.23 (t, *J* = 5 Hz, 1H), 3.45–3.36 (m, 1H), 3.26 (s br, 1H), 2.63 (dd, *J* = 14, *J* = 7.5 Hz, 1H), 2.57 (s, 3H), 2.36–2.22 (m, 2H), 2.20–2.10 (m, 1H), 2.08 (s, 3H), 1.89 (s, 3H), 1.84 (dd, *J* = 7 Hz, *J* = 1 Hz, 3H), 1.65 (br d, *J* = 15 Hz, 1H); ^{13}C NMR: 170.4, 166.5, 137.2, 128.3, 78.5, 66.2, 64.5, 58.8, 38.1, 36.1, 32.4, 30.9, 20.8, 14.1, 11.6.

5-(*N*-Benzyloxycarbonyl-*N*-methyl)amino-2-cyclohepten-1-one (4*b*)

Benzyl chloroformate (0.17 mL, 0.204 g, 1.20 mmol) was added to a solution of tropinone lithium enolate (1 mmol) at −78°C and the mixture was stirred for 30 min. After quenching with 40% K_2CO_3 (4 mL) and warming to rt, the reaction mixture was extracted with ether (3 × 10 mL). The extracts were washed with 5% H_2SO_4 (to remove the chiral amine, 98% recovery) and brine, and were dried ($MgSO_4$). The solvent was removed under vacuum to give the crude product, which was subjected to chromatographic purification by DFC

© 1997 NRC Canada

Can. J. Chem. Downloaded from www.nrcresearchpress.com by 88.146.161.215 on 09/08/12
For personal use only.

(5–50% hexane – AcOEt, R_f = 0.43 in 1:1 hexane–AcOEt). The product was obtained as a colorless oil (0.232 g, 85%); $[\alpha]_D^{24}$ +70.0 (*c* 1.04, MeOH); IR: 1697, 1666 cm^{-1}; ^1H NMR: 7.35–7.20 (m, 5H), 6.64 (ddd, *J* = 12 Hz, *J* = 6 Hz, *J* = 5 Hz, 1H), 6.05 (d, *J* = 12 Hz, 1H), 5.13 (s, 2H), 4.50 (br, 1H), 2.90–2.80 (m, 2H), 2.85 (s, 3H), 2.65–2.40 (m, 2H), 2.12–1.88 (m, 2H); ^{13}C NMR: 200.2, 155.5, 146.2, 136.5, 132.3, 128.3, 127.8, 127.6, 67.0, 51.2, 48.0, 30.8, 29.2, 27.6; MS (EI): 273 (1), 167 (11), 138 (23), 110 (20), 107 (11), 92 (21), 91 (100), 65 (17). Anal. calcd. for $C_{16}H_{19}NO_3$: C 70.31, H 7.01, N 5.12; found: C 70.16, H 7.83, N 5.07.

(−)-6-(*N*-Benzoyloxycarbonyl-*N*-methyl)amino-2,3-epoxycycloheptan-1-one (15)

Compound **4***b* (1.215 g, 4.45 mmol) was dissolved in a mixture of THF (20 mL) and water (5 mL), and the solution was cooled to ca. −10°C (ice–acetone bath). A hydrogen peroxide solution (30%, 3 mL, 26 mmol), followed by a solution of KOH (0.05 g, 0.9 mmol) in water (2 mL), was added to the stirred mixture. After min the reaction mixture was warmed to rt and was further stirred for 15 min. TLC showed absence of the starting material. The reaction mixture was diluted with water (80 mL) and was extracted with $CHCl_3$ (4 × 40 mL). The extracts were dried ($MgSO_4$), the solvent removed under vacuum, and the residue was subjected to DFC. a mixture of two isomeric epoxides (3:1) was obtained (1.20 g, 93%) as a colorless oil (major isomer R_f = 0.53, minor isomer R_f = 0.44 in 1:1 hexane–AcOEt); $[\alpha]_D^{24}$ −48 (*c* 1.1, MeOH), major isomer; IR: 1703 cm^{-1}; ^1H NMR: 7.43–7.30 (m, 5H), 5.16 (s, 2H), 4.05–3.75 (m, br, 1H), 3.46–3.42 (m, 2H), 3.20 (t, *J* = 12 Hz, 1H), 2.85 (s, 3H), 2.44–2.40 (m, 1H), 2.34 (d, *J* = 10 Hz, 1H), 2.28–2.22 (m, 1H), 2.10–1.90 (m, 1H), 1.70–1.60 (m, 1H); ^{13}C NMR: 206.7, 155.0, 136.2, 128.0, 127.6, 127.4, 66.8, 58.8, 55.3, 51.8, 44.2, 28.0, 27.0, 24.3; MS (EI): 289 (4), 146 (30), 111 (9), 92 (100), 83 (12), 65 (11), 57 (11), 55 (7); HRMS: 289.132 (M^+); calcd. for $C_{16}H_{19}NO_4$: 289.131.

(−)-5-(*N*-Benzyloxycarbonyl-*N*-methyl)amino-2-cyclohepten-1-ol (16)

The epoxide **15** (1.00 g, 3.46 mmol) was dissolved in dry MeOH and a solution of hydrazine (0.34 g, 19.6 mmol in 5 mL of MeOH dried with 3Å molecular sieves) was added at rt with stirring. After addition of glacial AcOH (2 drops), stirring was continued for another 2 h (N_2 evolved and the reaction mixture warmed up slightly). The resulting solution was then diluted with $CHCl_3$ (25 mL) and was washed with 5% H_2SO_4. The acid washings were extracted with $CHCl_3$ (3 × 20 mL). The combined extracts were dried ($MgSO_4$), filtered through a small pad of TLC-grade silica, and the solvent was removed under vacuum. The resulting residue was subjected to DFC (35–50% AcOEt in hexane). A mixture of two isomers was obtained (0.476 g, 50%). Major isomer R_f = 0.32, minor isomer R_f = 0.27 (1:1 hexane–AcOEt); $[\alpha]_D^{24}$ −66 (*c* 1.1, MeOH), major isomer; IR: 3415, 1695, 1677 cm^{-1}; ^1H NMR: 7.40–7.25 (m, 5H), 5.85–5.10 (m, 2H), 5.13 (s, 2H), 4.50–4.10 (m, 1H), 2.80 (s, 3H), 2.52–2.45 (m, 2H), 2.35 (d, *J* = 10 Hz, 1H), 2.20–2.08 (m, 1H), 2.07–1.70 (m, 4H); ^{13}C NMR: 155.7, 135.0, 128.3, 127.8, 127.7, 127.6, 124.9, 71.5, 68.5, 66.9, 54.2, 53.7, 35.4, 32.3; MS ($CI0NH_3$): 276 (20), 274 (11), 259 (18), 258 (100), 168 (17), 166 (27), 108 (28), 91 (65); HRMS: 275.152 (M^+); calcd. for $C_{16}H_{21}NO_3$: 275.152.

(5*R*)-5-(*N*-Benzyloxycarbonyl-*N*-methyl)amino-2-cyclohepten-1-one (17) (ref. 8)

A solution of the alcohol **16** (0.448 g, 1.63 mmol) in CH_2Cl_2 (25 mL) was treated with PDC (0.94 g, 2.50 mmol) for 12 h at rt. The reaction mixture was diluted with Et_2O (75 mL) and filtered through a pad of Celite and TLC-grade silica (washed with 1:1 hexane–AcOEt). After removing the solvents the crude product was obtained as a colorless oil (0.400 g, 90%); R_f = 0.35 (1:1 hexane–AcOEt); $[\alpha]_D^{25}$ +93 (*c* 1.0, MeOH); IR: 1693, 1679 cm^{-1}; ^1H NMR: 7.42–7.25 (m, 5H), 6.57 (ddd, *J* = 12 Hz, *J* = 6.5 Hz, *J* = 5 Hz, 1H), 6.07 (d, *J* = 12 Hz, 1H), 5.13 (s, 2H), 4.50 (br, 1H), 2.89 (s, 3H), 2.80–2.53 (m, 4H), 2.09–1.85 (m, 2H); ^{13}C NMR: 201.7, 155.1, 142.2, 136.2, 132.1, 128.0, 127.5, 127.3, 66.6, 54.2, 39.8, 33.3, 29.0, 25.0.

(+)-Physoperuvine (19) (refs. 4*c*, 4*d*, 20)

A solution of the enone **17** (0.340 g, 1.24 mmol) in MeOH (12 mL) was hydrogenated in the presence of 30% Pd/C (0.026 g) over 2 h at 30 psi in a Paar apparatus. The mixture was filtered through Celite and the solvent was removed under vacuum to provide an off-white solid (0.163 g, 92%). Analytically pure material was obtained through Kugelrohr sublimation (at 100–120°C/0.5 Torr). Properties: white solid, R_f = 0.66 (5:4:1 $CHCl_3$–MeOH – 25% aqueous NH_3); mp (racemic) 72–73°C (acetone) (lit. (21) mp 75°C); $[\alpha]_D^{25}$ +17.9 (*c* 1.30, H_2O), 95% ee with (*S*)-(+)-TFAE (lit. (21) $[\alpha]_D$ +1.2 (*c* 1.3, H_2O); mp (opt. active) 48–50°C (sublimed) (lit. (20) mp 47°48°C); IR: 3099 (OH) cm^{-1}; ^1H NMR: 3.13 (br s, 1H), 2.38 (s, 3H), 2.15–1.87 (m, 4H), 1.82–1.52 (m, 5H), 1.34–1.20 (m, 1H).

Acknowledgements

We thank Professor A. Baranski for help with the cyclic voltammetry experiments. We also thank the Natural Sciences and Engineering Research Council of Canada and the University of Saskatchewan for financial support.

References

1. (*a*) Recent review: M. Lounasmaa and T. Tamminen. The alkaloids **44**, 1 (1993); Physoperuvine: (*b*) A.T. McPhail and A.R. Pinder. Tetrahedron, **40**, 1661 (1984); (*c*) A.R. Pinder. J. Org. Chem. **47**, 3607 (1982); (*d*) M. Sahai and A.B. Ray. J. Org. Chem. **45**, 3265 (1980).
2. (*a*) M. Majewski and R. Lazny. J. Org. Chem. **60**, 5825 (1995); (*b*) Synlett, 785 (1996); (*c*) Tetrahedron Lett. **35**, 3653 (1994); (*d*) M. Majewski and G.-Z. Zheng. Can. J. Chem. **70**, 2618 (1992); (*e*). Synlett, 173 (1991); (*f*) This reaction had also been independently reported in a lecture: N.S. Simpkins. Chem. Soc. Rev. **19**, 335 (1990).
3. Enantioselective deprotonation was reviewed: (*a*) P.J. Cox and N.S. Simpkins. Tetrahedron: Asymmetry, **2**, 1 (1991); (*b*) M. Majewski. *In* Advances in carbanion synthesis. Vol. 3. *Edited by* V. Snieckus. JAI Press, Greenwich, Connt. In press.
4. (*a*) E. Juaristi, A.K. Beck, J. Hansen, T. Matt, T. Mukhopadhyay, M. Simson, and D. Seebach. Synthesis, 1271 (1993); (*b*) P.L. Hall, J.H. Gilchrist, and D.B. Collum. J. Am. Chem. Soc. **113**, 9571 (1991); (*c*) A. Loupy and B. Tchoubar. Salt effects in organic and organometallic chemistry. VCH, New York. 1991; (*d*) D. Seebach. Angew. Chem. Int. Ed. Engl. **27**, 1624 (1988), (*e*) D. Seebach, A.K. Beck, and A. Studer. *In* Modern synthetic methods. Vol. 7. *Edited by* B. Ernst and C.

© 1997 NRC Canada

Leumann. VCH, Weinheim. 1995; (*f*) P. Coggins, S. Gaur, and N.S. Simpkins. Tetrahedron Lett. **36**, 1545 (1995); (*g*) M. Majewski, R. Lazny, and P. Nowak. Tetrahedron Lett. **36**, 5465 (1995); (*h*) M. Toriyama, K. Sugasawa, M. Shindo, N. Tokutake, and K. Koga. Tetrahedron Lett. **38**, 567 (1997).
5. K. Koga. Pure Appl. Chem. **66**, 1487 (1994).
6. J.-L. Luche. J. Am. Chem. Soc. **100**, 2226 (1978).
7. P.S. Wharton and D.H. Bohlen. J. Org. Chem. **26**, 3615 (1961).
8. F.-D. Boyer, P.-H. Ducrot, V. Henryon, and J.-Y. Lallemand. Synlett, 357 (1992).
9. A.B. Ray, Y. Oshima, H. Hikino, and C. Kabuto. Heterocycles, **19**, 1233 (1982).
10. J. Leonard, B. Lygo, and G. Procter. Advanced practical organic chemistry. Chapman & Hall, New York. 1995.
11. (*a*) R. Shirai, K. Aoki, D. Sato, H.-D. Kim, M. Murakata, T. Yasukata, and K. Koga. Chem. Pharm. Bull. **42**, 690 (1994); (*b*) C.G. Overberger, N.P. Marullo, and R.G. Hiskey. J. Am. Chem. Soc. **83**, 1374 (1961); (*c*) H.M.R. Hoffmann, K. Haase, Z.M. Ismail, S. Preftitsi, and A. Weber. Chem. Ber. **115**, 3880 (1982); (*d*) J.F. Normant and C. Piechucki. Bull. Soc. Chim. Fr. **6**, 2402 (1972).
12. W.C. Still, M. Khan, and A. Mitra. J. Org. Chem. **43**, 2923 (1978).
13. L.M. Harwood. Aldrichimica Acta, **18**, 25 (1985).
14. G. Zweig and J. Sherma. Handbook of chromatography. Vol. 2. CRC Press, Boca Raton, Fla. 1972.
15. Y.Y. Lin and J.B. Jones. J. Org. Chem. **38**, 3575 (1973).
16. G. Fodor and F. Soti. Tetrahedron Lett. 1917 (1964).
17. A.J. Parr, J. Payne, J. Eagles, B.T. Chapman, R.J. Robins, and M. Rhodes. Phytochemistry, **29**, 2545 (1990).
18. W.C. Evans and A. Major. J. Chem. Soc. (C), 1621 (1966).
19. I.R.C. Bick, J.W. Gillard, H.-M. Leow, and N.W. Preston. Aust. J. Chem. **32**, 2071 (1979).
20. A.T. McPhail and A.R. Pinder. Tetrahedron, **40**, 1661 (1984).

Can. J. Chem. Downloaded from www.nrcresearchpress.com by 88.146.161.215 on 09/08/12
For personal use only.

© 1997 NRC Canada

Synthesis of sugar-modified 2,6-diaminopurine and guanine nucleosides from guanosine via transformations of 2-aminoadenosine and enzymatic deamination with adenosine deaminase[1]

Morris J. Robins, Ruiming Zou, Fritz Hansske, and Stanislaw F. Wnuk

Abstract: Treatment of 2,6-diaminopurine riboside (2-aminoadenosine) with α-acetoxyisobutyryl bromide in acetonitrile gave mixtures of the *trans* 2′,3′-bromohydrin acetates **2**. Treatment of **2** with zinc–copper couple effected reductive elimination, and deprotection gave 2,6-diamino-9-(2,3-dideoxy-β-D-*erythro*-pent-2-enofuranosyl)purine (**3***a*). Treatment of **2** with Dowex 1 × 2 (OH^-) resin in methanol gave the 2′,3′-anhydro derivative **4**. Stannyl radical-mediated hydrogenolysis of **2** and deprotection gave the 2′-deoxy **6***a* and 3′-deoxy **7***a* nucleosides. Treatment of the 3′,5′-*O*-(tetraisopropyldisiloxanyl) derivative (**5***a*) with trifluoromethanesulfonyl chloride – 4-(dimethylamino)pyridine gave 2′-triflate **5***c*. Displacement with lithium azide – dimethylformamide and deprotection gave the arabino 2′-azido derivative **8***a*, which was reduced to give 2,6-diamino-9-(2-amino-2-deoxy-β-D-arabinofuranosyl)purine (**8***b*). Sugar-modified 2,6-diaminopurine nucleosides were treated with adenosine deaminase to give the corresponding guanine analogues.

Key words: adenosine deaminase, 2,6-diaminopurine nucleosides, deoxygenation, guanine nucleosides, nucleosides.

Résumé : Le traitement du riboside de 2,6-diaminopurine (2-aminoadénosine) par du bromure d'α-acétoxyisobutyryle, dans l'acétonitrile, conduit à un mélange des acétates de la *trans*-2′,3′-bromohydrine (**2**). Le traitement de **2** par le couple zinc–cuivre provoque une élimination réductrice et une déprotection subséquente conduit à la 2,6-diamino-9-(2,3-didésoxy-β-D-*érythro*-pent-2-énofuranosyl)purine (**3***a*). Le traitement de **2** par de la résine Dowex 1 × 2 (OH^-) dans le méthanol conduit au dérivé 2′,3′-anhydro (**4**). Une hydrogénolyse du composé **2** catalysée par le radical stannyle, suivie d'une déprotection, fournit les nucléosides 2′-désoxy (**6***a*) et 3′-désoxy (**7***a*). Le traitement du dérivé 3′,5′-*O*-(tétraisopropyldisiloxanyl) (**5***a*) par du chlorure de trifluorométhanesulfonyle dans la 4-(diméthylamino)pyridine conduit au 2′-triflate (**5***c*). Un déplacement par de l'azoture de lithium dans le diméthylformamide, suivi d'une déprotection, conduit au dérivé 2′-azido-arabino (**8***a*) qui, par réduction, conduit à la 2,6-diamino-9-(2-amino-2-désoxy-β-D-arabinofuranosyl)purine (**8***b*). Les nucléosides de la 2,6-diaminopurine comportant des sucres modifiés ont été traités par de la désaminase d'adénosine pour conduire aux analogues guanines correspondantes.

Mots clés : désaminase d'adénosine, nucléosides de la 2,6-diaminopurine, désoxygénation, nucléosides de la guanine, nucléosides.

(Traduit par la rédaction)

Received October 21, 1996.

This paper is dedicated to Professor William A. Ayer, a most congenial, helpful, and knowledgable colleague, on the occasion of his 65th birthday.

M.J. Robins,[2] R. Zou,[3] F. Hansske,[4] and S.F. Wnuk.[5] Department of Chemistry, University of Alberta, Edmonton, AB T6G 2G2, Canada, and Department of Chemistry and Biochemistry, Brigham Young University, Provo, UT 84602-5700, U.S.A.

[1] This paper is Nucleic acid related compounds. 96. Paper 95 is ref. 1.
[2] Author to whom correspondence may be addressed at Brigham Young University. Telephone: (801) 378-6272. Fax: (801) 378-5474.
[3] Present address: Gilead Sciences, Foster City, California, U.S.A.
[4] Present address: Boehringer Mannheim GmbH, Mannheim, Germany.
[5] On faculty leave from the Department of Chemistry, University of Agriculture, Poznan, Poland.

© 1997 NRC Canada

Can. J. Chem. Downloaded from www.nrcresearchpress.com by 88.146.161.215 on 09/08/12
For personal use only.

Can. J. Chem. Downloaded from www.nrcresearchpress.com by 88.146.161.215 on 09/08/12
For personal use only.

Introduction

Transformations of adenosine to give sugar-modified adenine nucleosides are well known (2, 3). However, analogous transformations of guanosine are plagued by experimental problems including poor solubility, instability, and formation of gels (4, 5). Vorbrüggen and Krolikiewicz reported an efficient transformation of the lactam functionality of guanosine into the cyclic amidine of 2,6-diamino-9-(β-D-ribofuranosyl)purine (**1**, 2,6-diaminopurine riboside, DAPR) (6), and DAPR (2-aminoadenosine) is a substrate (7) of calf intestinal adenosine deaminase (ADA; adenosine aminohydrolase, EC 3.5.4.4). Thus, conversion of the troublesome guanosine system into a chemical analogue of adenosine and subsequent enzymatic conversion of modified 2,6-diaminopurine nucleosides to their guanine counterparts allows convenient use of DAPR as a "masked guanosine" precursor for modifications of the sugar moiety (8). ADA also effects hydrolytic replacement of chloro and methoxy groups from 2-amino-6-chloropurine (9*a*) and 2-amino-6-methoxypurine (9*b*) nucleosides to give the corresponding guanine derivatives. The scope of such chemical/enzymatic syntheses is not limited to the specificity of mammalian ADA (10*a*) since this enzyme activity from *Aspergillus oryzae* has less stringent substrate requirements at C5′ (10*b*) and adenylic acid deaminase has broad tolerance for conversions to 6-oxopurine nucleosides (10*c*).

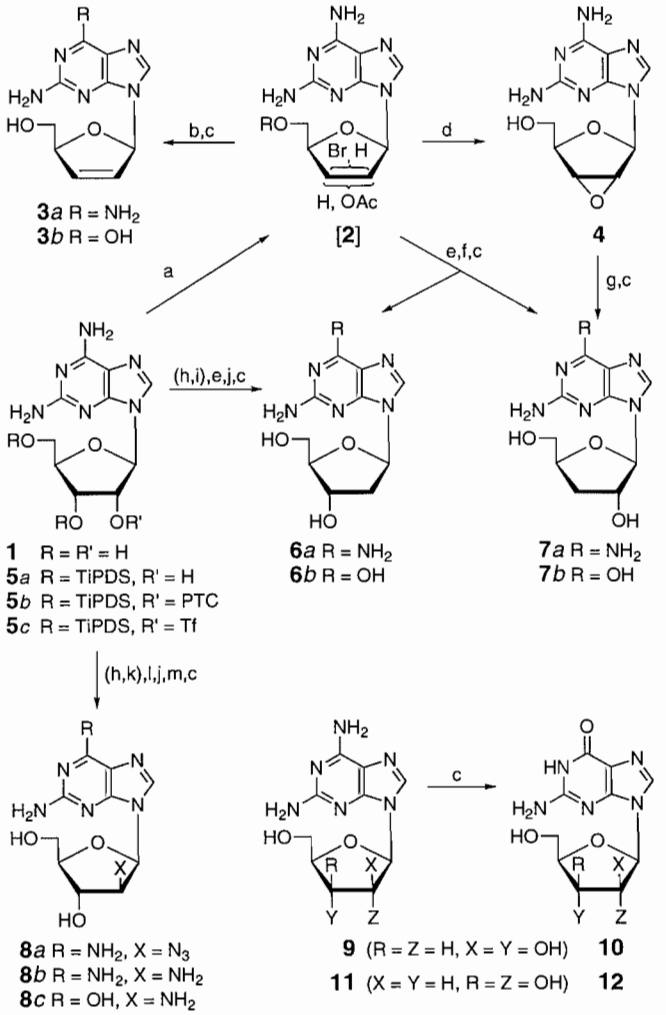
ADA is an ubiquitous human enzyme and sugar-modified 2,6-diaminopurine nucleosides are prodrugs of sugar-modified guanine nucleosides (11–13). Thus, 2,6-diamino-9-(2,3-dideoxy-β-D-*glycero*-pentofuranosyl)purine (2,6-diaminopurine 2′,3′-dideoxyriboside, ddDAPR) is an effective inhibitor of hepatitis B virus (11) and also has anti-HIV activity (12). We now report sugar modifications with DAPR and deaminations with ADA to give their guanine counterparts.

Results and discussion

DAPR (**1**, Scheme 1) was prepared from guanosine by modification (14) of the known method (6). Treatment of **1** with α-acetoxyisobutyryl bromide gave a mixture of *trans* bromo acetates **2** (R = H or 2,5,5-trimethyldioxolan-4-on-2-yl) (3, 15). Treatment of **2** with Dowex 1 × 2 (OH^-) resin in MeOH gave the 2′,3′-anhydro nucleoside **4** (81% from **1**). Lithium triethylborohydride effected selective cleavage (3, 16) of the epoxide O—C3′ bond of **4** to give 3′-deoxyDAPR (**7***a*, 85%). Treatment of **2** with tributyltin hydride and deprotection (NH_3–MeOH) gave 2′-deoxyDAPR (**6***a*, 16%) and 3′-deoxyDAPR (**7***a*, 59%), which were separated by ion-exchange chromatography with Dowex 1 × 2 (OH^-).

Treatment of **2** with zinc–copper couple in *N,N*-dimethylformamide (DMF) effected reductive elimination of bromide and acetate to give 2′,3′-didehydro-2′,3′-dideoxyDAPR (**3***a*), which was hydrogenated to give ddDAPR (3, 15*b*). A sample of DAPR containing 2′*R*[^{2}H] (~20% 2′[^{2}H]-**1**, obtained as the minor product from oxidation of **5***a* and reduction ($NaBD_4$) of the 2′-ketone (17)) was subjected to the sequence **1** → **2** → **3***a*. The product (containing 2′[^{2}H]-**3***a*) was analyzed by ^{1}H (3) and ^{13}C (Table 1) NMR. The higher field ^{1}H NMR signal at δ 6.10 (H2′) was diminished by ~20% relative to the signal at δ 6.42 (H3′) in agreement with the inverted signal positions observed with 3′[^{2}H]-adenosine as starting material (3, 15*a*). Also, the higher field vinyl ^{13}C signal was assigned to C2′ (δ 125.9) on the basis of selective ^{13}C–^{1}H decoupling and its reduced intensity relative to the signal at δ 134.5 (C3′).

Scheme 1.



(a) $(CH_3)_2C(OAc)COBr/CH_3CN/H_2O$; (b) Zn-Cu/DMF; (c) ADA/buffer; (d) Dowex 1 × 2 (OH^-)/MeOH; (e) Bu_3SnH/AIBN/toluene/Δ; (f) NH_3/MeOH; (g) $LiEt_3BH$/THF/DMSO; (h) $TiPDSCl_2$/pyridine; (i) PTCCl/DMAP/CH_3CN; (j) TBAF/THF; (k) TfCl/DMAP/CH_2Cl_2; (l) LiN_3/DMF; (m) N_2H_4/Raney Ni/EtOH.

Treatment of **1** with 1,3-dichloro-1,1,3,3-tetraisopropyldisiloxane ($TiPDSCl_2$) gave **5***a*, which was acylated with phenoxythiocarbonyl (PTC) chloride (18). Thionocarbonate **5***b* was reduced (tributyltin hydride) and deprotected (tetrabutylammonium fluoride, TBAF) to give 2′-deoxyDAPR (**6***a*, 41% from **1**). Triflation of **5***a* gave **5***c*, which was treated with lithium azide and deprotected (TBAF) to give the arabino 2′-azido analogue **8***a* (59%). Hydrogenolysis (Raney nickel) of **8***a* gave 2,6-diamino-9-(2-amino-2-deoxy-β-D-arabinofuranosyl)purine (**8***b*, 85%). Triflation of an analogously protected guanosine derivative had given a 2′,6-bis-*O*-(trifluoromethanesulfonyl) by-product (19) and other 6-*O*-triflyl derivatives of 2-deoxyguanosine have been reported (13*b*).

Enzymatic conversion of **3***a*, **6***a*, **7***a*, and **8***b* to their guanine counterparts **3***b*, **6***b*, **7***b*, and **8***c*, respectively, was effected with ADA in aqueous sodium phosphate buffer. Isolated

© 1997 NRC Canada

Table 1. ^{13}C NMR spectral data.[a,b]

Compound	C2	C4	C5	C6	C8	C1′	C2′	C3′	C4′	C5′
3*a*	156.3	151.6	113.2	160.5	136.5	88.1	125.9	134.5	87.9	63.2
3*b*	153.7	150.8	116.4	156.7	135.2	87.8	125.3	134.2	87.2	62.9
4	156.2	157.5	113.0	160.3	135.6	81.5	57.8	58.7	80.9	61.0
6*a*	156.1	151.2	113.5	160.0	135.7	83.1	39.4	71.0	87.6	61.9
6*b*	153.4	150.8	116.6	156.7	135.4	82.7	39.6	70.6	87.4	61.6
7*a*	156.2	151.2	113.4	160.1	135.8	90.2	74.4	34.5	80.2	62.9
7*b*	153.6	150.7	116.7	156.7	135.2	90.0	74.8	34.5	80.4	62.7
8*a*	156.1	151.6	112.8	160.4	136.2	81.1	67.5	71.9	83.4	59.8
8*b*	156.0	151.6	112.9	160.2	137.1	84.0	60.3	75.4	84.3	60.7
8*c*	153.4	150.9	116.2	156.8	136.5	84.0	60.0	75.1	84.1	60.4
9	155.9	151.6	112.4	160.1	136.9	83.1	75.5[c]	75.5	84.1	61.1
10	153.5	150.9	113.6	156.7	136.8	83.3	75.4	75.3	84.2	60.9
11	156.1	150.8	113.0	159.9	136.6	89.0	80.8	75.3	82.9	59.4
12	154.1	151.4	116.8	157.5	137.1	89.3	81.5	75.6	83.8	60.0

[a]Chemical shifts (δ) at 50 or 100 MHz (Me_4Si/Me_2SO-d_6).
[b]Proton-decoupled singlets.
[c]Signal absent in 2′*S*[^{2}H]-**9**.

yields of the guanine nucleosides were >80%, except for the 2′,3′-unsaturated nucleoside **3***b*. Complete deamination of **3***a* (a potent inhibitor of ADA (12)) required 10 days and the somewhat unstable **3***b* partially decomposed during the extended reaction period, which makes this route to **3***b* less appealing than direct deoxygenation of guanosine (3, 20). The arabino **9** and xylo **11** epimers of DAPR were subjected to deamination to give AraG (**10**) and XyloG (**12**), respectively, in high yields. An oxidation–reduction sequence at C2′ of protected guanosine (17) had given 9-(β-D-arabinofuranosyl)guanine (**10**). Coupling of 2-amino-6-chloropurine (followed by 7/9 isomer separation and base conversion to guanine (21*a*)) or 2-*N*-acetylguanine (followed by 7/9 isomer separation (21*b*)) (8) with xylofuranose derivatives had been employed to prepare 9-(β-D-xylofuranosyl)guanine (**12**).

In summary, this indirect approach (conversion of guanosine to DAPR, modification of the sugar, and enzymatic deamination to give the guanine nucleoside) is more experimentally convenient in many instances than direct sugar transformations with guanosine. Separation of isomers and purification of intermediates can be achieved readily since 2,6-diaminopurine nucleosides are amenable to ion-exchange chromatography with Dowex 1 × 2 (OH^-) resin and usually crystallize without difficulty.

Experimental

Uncorrected melting points were obtained with a hotstage apparatus. UV spectra were determined with solutions in MeOH unless otherwise noted. ^1H (200 or 400 MHz) and ^{13}C (50 or 100 MHz, Table 1) NMR spectra (Me_4Si–Me_2SO-*d6*) were recorded with Bruker spectrometers. Mass spectra (EI MS, CI, FAB) were determined at 20 or 70 eV. Solvents were purified, dried (CaH_2 or $LiAlH_4$), and distilled before use. Pyridine was dried by refluxing with and distillation from CaH_2. Reagent grade chemicals were used without further purification. TLC was performed with silica gel 60 F_{254} sheets, and silica gel (200–425 mesh) was used for column chromatography. Elemental analyses were determined by the Microanalytical Laboratory at the University of Alberta. Calf intestinal adenosine deaminase (ADA, 2.7 units/mg protein) was obtained from Sigma.

2,6-Diamino-9-(2,3-anhydro-β-D-ribofuranosyl)purine 4

Amorphous solid **2** (prepared (3, 15*b*) from **1** (2 mmol)) was dissolved in a minimal volume of MeOH and the solution was applied to a column of Dowex 1 × 2 (OH^-) resin previously soaked in and washed with MeOH. The column was allowed to stand for 1 h at ambient temperature and the product was eluted with MeOH (crystallization occurred in early fraction-collecting tubes). Evaporation of appropriate fractions and recrystallization (MeOH) gave **4** (427 mg, 81% from **1**); mp ~180°C (dec.); UV max: 255, 280 nm (ε 9900, 10 300); ^1H NMR δ: 3.55 (m, *J* = 11.5, 5.5, 5.0 Hz, 2H), 4.15 (t, *J* = 5.0 Hz, 1H), 4.17 (d, *J* = 2.5 Hz, 1H), 4.37 (d, *J* = 2.5 Hz, 1H), 5.09 (t, *J* = 5.0 Hz, 1H), 5.85 (s, 2H), 6.01 (s, 1H), 6.77 (s, 2H), 7.92 (s, 1H); MS *m/z*: 264.0968 (23, M^+ = 264.0971). Anal. calcd. for $C_{10}H_{12}N_6O_3$: C 45.45, H 4.58, N 31.80; found: C 45.35, H 4.75, N 31.48.

2,6-Diamino-9-(2-deoxy-β-D-*erythro*-pentofuranosyl)-purine 6*a* and 2,6-diamino-9-(3-deoxy-β-D-*erythro*-pentofuranosyl)purine 7*a*

Amorphous solid **2** (prepared (3, 15*b*) from **1** (2 mmol)) was dissolved in deoxygenated toluene (80 mL), AIBN (64 mg, 0.4 mmol) and Bu_3SnH (2.2 mL, 2.38 g, 8.2 mmol) were added, and the solution was refluxed for 1 h. Volatiles were evaporated, the residue was dissolved in CH_3CN–H_2O (100 mL, 1:1), and this solution was washed with pentane (100 mL) and then evaporated. The residue was stirred with NH_3–MeOH (50 mL, saturated at −10°C) at ambient temperature for 4 h and volatiles were evaporated. The residue was chromatographed (Dowex 1 × 2 (OH^-), H_2O) and recrystallized (MeOH) to give **6***a* (85 mg, 16% from **1**); mp 154–155°C (lit. (22) mp 147–149°C); UV max: 256, 280 nm (ε 10 100, 10 600); ^1H NMR δ: 2.20 (m, *J* = 13.0, 6.0, 3.0 Hz, 1H); 2.62 (m, *J* = 13.0, 8.0, 5.5

© 1997 NRC Canada

Can. J. Chem. Downloaded from www.nrcresearchpress.com by 88.146.161.215 on 09/08/12
For personal use only.

Can. J. Chem. Downloaded from www.nrcresearchpress.com by 88.146.161.215 on 09/08/12
For personal use only.

Hz, 1H), 3.54 (m, J = 12.0, 6.0, 4.0 Hz, 1H), 3.60 (m, J = 12.0, 5.0 Hz, 1H), 3.86 (m, J = 2.0 Hz, 1H), 4.37 (m, J = 4.0 Hz, 1H), 5.26 (d, J = 4.0 Hz, 1H), 5.29 (dd, J = 6.0, 5.0 Hz, 1H), 5.76 (s, 2H), 6.19 (dd, J = 8.0, 6.0 Hz, 1H), 6.76 (s, 2H), 7.92 (s, 1H); MS *m/z*: 266.1128 (12, M^+ = 266.1127). Anal. calcd. for $C_{10}H_{14}N_6O_3$: C 45.11, H 5.30, N 31.56; found: C 45.01, H 5.41, N 31.31.

Further elution of the ion-exchange column (30% MeOH–H_2O) and recrystallization of the residue (MeOH) gave **7***a* (316 mg, 59% from **1**); mp 198–199°C; MS *m/z*: 266.1129 (11, M^+ = 266.1127); other data identical to those with **7***a* prepared by the following reduction of **4**.

2,6-Diamino-9-(3-deoxy-β-D-*erythro*-pentofuranosyl)-purine 7*a*

$LiEt_3BH$–THF (1 M; 25 mL, 25 mmol) was added dropwise to a stirred solution of **4** (528 mg, 2 mmol) in DMSO (40 mL) at 10°C under N_2. The cooling bath was removed after 1 h and the reaction mixture was stirred at ambient temperature for 3 days. H_2O (60 mL) was added carefully and the solution was purged vigorously with N_2 to remove *pyrophoric* triethylborane. Volatiles were evaporated in vacuo (~0.5 Torr; 1 Torr = 133.3 Pa) at <60°C and the residue was chromatographed (Dowex 1 × 2 (OH^-), H_2O followed by 30% MeOH–H_2O) and recrystallized (MeOH) to give **7***a* (453 mg, 85%), mp 198–199°C, mp 122–123°C (from H_2O) (lit. (23) mp 120–121°C (from H_2O)); UV max: 255, 280 nm (ε 10 200, 10 700); ^{1}H NMR δ: 1.92 (m, J = 13.0, 6.5, 3.5 Hz, 1H), 2.24 (m, J = 13.0, 8.0, 6.0 Hz, 1H), 3.50 (m, J = 11.5, 5.5, 4.0 Hz, 1H), 3.65 (m, J = 11.5, 5.5, 3.5 Hz, 1H), 4.30 (m, 1H), 4.51 (m, J = 4.5, 2.5 Hz, 1H), 5.18 (t, J = 5.5 Hz, 1H), 5.56 (d, J = 4.5 Hz, 1H), 5.70 (d, J = 2.5 Hz, 1H), 5.78 (s, 2H), 6.75 (s, 2H), 7.92 (s, 1H); MS *m/z*: 266.1124 (16, M^+ = 266.1127). Anal. calcd. for $C_{10}H_{14}N_6O_3$: C 45.11, H 5.30, N 31.56; found: C 44.90, H5.31, N 31.52.

2,6-Diamino-9-(3,5-*O*-(1,1,3,3-tetraisopropyldisilox-1,3-diyl)-β-D-ribofuranosyl)purine 5*a*

$TiPDSCl_2$ (4 mL, 3.88 g, 12.3 mmol) was added to a stirred suspension of **1** (2.82 g, 10 mmol) in dried pyridine (50 mL) at ambient temperature. EtOH (5 mL) was added after 6 h and volatiles were evaporated. Toluene was added and evaporated several times and the residue was partitioned ($CHCl_3$–H_2O, 1:1; 600 mL). The organic layer was concentrated and chromatographed (silica gel, 10% MeOH–$CHCl_3$) to give **5***a* (5.12 g, 97%) as an amorphous solid with data as reported (24); ^{1}H NMR δ: 1.94–2.14 (m, 28H), 3.90–4.14 (m, 3H), 4.31 (m, J = 5.0, 1.5 Hz, 1H), 4.45 (dd, J = 8.0, 5.0 Hz, 1H), 5.61 (d, J = 5.0 Hz, 1H), 5.72 (d, J = 1.5 Hz, 1H), 5.79 (s, 2H), 6.79 (s, 2H), 7.78 (s, 1H); MS *m/z*: 524.2602 (8, M^+ ($C_{22}H_{40}N_6O_5Si_2$) = 524.2599).

2,6-Diamino-9-(2-deoxy-β-D-*erythro*-pentofuranosyl)-purine 6*a*

PTCCl (0.40 mL, 380 mg, 2.2 mmol) was added to a suspension of **5**a (obtained from **1** (2 mmol)) in dried CH_3CN (20 mL) containing DMAP (489 mg, 4 mmol) at ambient temperature. Stirring was continued for 1 h and the resulting solution was diluted (EtOAc, 100 mL), washed (AcOH–H_2O, $NaHCO_3$–H_2O), dried (Na_2SO_4), evaporated, and coevaporated successively with toluene, $CHCl_3$, and Et_2O. The resulting amorphous **5***b* was dried in vacuo at ambient temperature for 2 h and dissolved in toluene (20 mL). AIBN (66 mg, 0.4 mmol) and Bu_3SnH (0.85 mL, 920 mg, 3.2 mmol) were added and the solution was deoxygenated (N_2, 30 min) and heated at 80°C overnight. TBAF–THF (1 M; 4 mL, 4 mmol) was added and heating was continued for 3 h. Volatiles were evaporated and the residue was partitioned (H_2O–Et_2O, 1:1; 200 mL). The aqueous phase was concentrated and applied to a column of Dowex 1 × 2 (OH^-). Elution (H_2O) and recrystallization (MeOH) of the residue gave **6***a* (216 mg, 41% from **1**); mp 154–155°C; MS *m/z*: 266.1124 (15, M^+ = 266.1127) with data identical to those with **6***a* from debromination of **2**.

2,6-Diamino-9-(2-azido-2-deoxy-β-D-arabinofuranosyl)-purine 8*a*

CF_3SO_2Cl (0.15 mL, 237 mg, 1.4 mmol) was added to a cold (~0°C) stirred suspension of **5***a* (525 mg, 1 mmol) and DMAP (367 mg, 3 mmol) in dried CH_2Cl_2 (10 mL). $CHCl_3$ (50 mL) was added after 30 min and the solution was washed (2% HOAc–H_2O, brine), dried (Na_2SO_4), and evaporated. The residue was successively coevaporated with toluene, $CHCl_3$, and Et_2O to give amorphous **5***c*, which was dried in vacuo at ambient temperature for 4 h. A solution of this **5***c* and dried LiN_3 (196 mg, 4 mmol) in dried DMF (10 mL) was stirred at ambient temperature overnight and volatiles were evaporated. The residue was dissolved (EtOAc, 50 mL) and the solution was washed (brine) and evaporated. The residue was dissolved (THF, 10 mL) and stirred with TBAF–THF (1 M; 3 mL, 3 mmol) at ambient temperature overnight. Evaporation of volatiles and chromatography of the residue (Dowex 1 × 2 (OH^-), H_2O and then 20% MeOH–H_2O) gave crystalline **8***a* (181 mg, 59%); mp ~262°C (dec.); UV max: 255, 280 nm (ε 10 300, 10 800); ^{1}H NMR δ: 3.64 (m, J = 12.0, 5.5, 4.5 Hz, 1H), 3.72 (m, J = 12.0, 5.5, 3.0 Hz, 1H), 3.76 (m, J = 7.5 Hz, 1H), 4.35 (m, J = 7.5, 5.5 Hz, 1H), 4.49 (dd, J = 7.5, 6.5 Hz, 1H), 5.20 (t, J = 5.5 Hz, 1H), 5.83 (s, 2H), 5.99 (d, J = 5.5 Hz, 1H), 6.19 (d, J = 6.5 Hz, 1H), 6.78 (s, 2H), 7.90 (s, 1H); MS *m/z*: 307.1141 (13, M^+ = 307.1141). Anal. calcd. for $C_{10}H_{13}N_9O_3$: C 39.09, H 4.25, N 41.03; found: C 38.85, H 4.35, N 40.63.

2,6-Diamino-9-(2-amino-2-deoxy-β-D-arabinofuranosyl)-purine 8*b*

Hydrazine (95%, 1 mL) was added to a stirred suspension of **8***a* (307 mg, 1 mmol) in EtOH–H_2O (3:1, 20 mL) containing Raney Ni (100 mg) at ambient temperature. The reaction mixture was filtered after 6 h and the solid was washed (EtOH–H_2O, 8:2). The filtrate and washings were combined, concentrated, and chromatographed (Dowex 1 × 2 (OH^-), H_2O) to give crystalline **8***b* (238 mg, 85%); mp 289–292°C; UV (H_2O) max: 255, 280 nm (ε 9 800, 10 300); ^{1}H NMR δ: 1.20–1.80 (br s, 2H), 3.40 (t, J = 6.5 Hz, 1H), 3.58 (dd, J = 12.5, 4.5 Hz, 1H), 3.68 (dd, J = 12.5, 2.5 Hz, 1H), 3.70 (m, 1H), 4.01 (m, 1H), 4.60–5.60 (br s, 1H), 5.39 (d, J = 4.5 Hz, 1H), 5.76 (s, 2H), 6.02 (d, J = 6.5 Hz, 1H), 6.68 (s, 2H), 7.88 (s, 1H); MS *m/z*: 281.1232 (10, M^+ = 281.1236). Anal. calcd. for $C_{10}H_{15}N_7O_3$: C 42.70, H 5.38, N 34.86; found: C 42.56, H 5.38, N 34.87.

2′-Deoxyguanosine 6*b* (deamination procedure)

ADA (10 mg; Sigma, 2.7 units/mg protein) was added to a solution of **6***a* (266 mg, 1 mmol) in DMSO (5 mL) and aque-

© 1997 NRC Canada

Can. J. Chem. Downloaded from www.nrcresearchpress.com by 88.146.161.215 on 09/08/12
For personal use only.

ous sodium phosphate buffer (0.1 M, 25 mL; pH 7.4) and stirring was continued at ambient temperature overnight (reaction progress was monitored by thin-layer electrophoresis). Volatiles were evaporated in vacuo and the residue was applied to a column of Dowex 1 × 2 (OH^-), which was washed successively with H_2O, 80% MeOH–H_2O, and H_2O. The product was then eluted (30 mM aqueous $Et_3NH{\cdot}HCO_3$) and fractions were evaporated, coevaporated several times with H_2O, and recrystallized (H_2O) to give **6***b* (250 mg, 91%); mp ~250°C (dec.) (lit. (18) mp 251–252°C); UV (H_2O) max: 252 nm (ε 13 400); ^1H NMR δ: 2.20 (m, J = 13.0, 6.0, 3.0 Hz, 1H), 2.50 (m, J = 13.0, 7.5, 5.5 Hz, 1H), 3.52 (m, J = 12.0, 5.5, 4.5, Hz, 2H), 3.80 (m, 1H), 4.34 (m, 1H), 4.95 (t, J = 5.5 Hz, 1H), 5.26 (d, J = 4.0 Hz, 1H), 6.12 (dd, J = 7.5, 6.0 Hz, 1H), 6.46 (s, 2H), 7.92 (s, 1H), 10.64 (s, 1H); MS (FAB) *m/z*: 268 (6, MH^+). Anal. calcd. for $C_{10}H_{13}N_5O_4{\cdot}0.5H_2O$: C 43.48, H 5.11, N 25.35; found: C 43.42, H 4.90, N 25.62.

3′-Deoxyguanosine 7*b*

Treatment of **7***a* (266 mg, 1 mmol) with ADA (as described for **6***b*) and recrystallization (H_2O) gave **7***b* (239 mg, 87%) as a hemihydrate; mp ~250°C (dec.) (lit. (25) mp >300°C (dec.)); UV (H_2O) max: 252 nm (ε 13 600); ^1H NMR δ: 1.89 (m, J = 13.5, 6.5, 3.0 Hz, 1H), 2.20 (m, J = 13.5, 9.0, 5.5 Hz, 1H), 3.51 (dd, J = 12.0, 4.5 Hz, 1H), 3.64 (dd, J = 12.0, 3.5 Hz, 1H), 4.31 (m, 1H), 4.46 (m, 1H), 4.60–5.90 (br s, 2H), 5.70 (d, J = 2.0 Hz, 1H), 6.49 (s, 2H), 7.94 (s, 1H), 10.65 (s, 1H); MS (FAB) *m/z*: 268 (6, MH^+). Anal. calcd. for $C_{10}H_{13}N_5O_4{\cdot}0.5H_2O$: C 43.48, H 5.11, N 25.35; found: C 43.38, H 4.89, N 25.39.

9-(2,3-Dideoxy-β-D-*glycero*-pent-2-enofuranosyl)guanine 3*b*

Treatment of **3***a* (248 mg, 1 mmol; prepared as described (3, 15b)) with ADA (reaction mixture stirred at ambient temperature for 10 days with additions of ADA (20 mg) every second day) gave a residue that was chromatographed (Dowex 1 × 2 (OH^-), $Et_3NH{\cdot}HCO_3$–H_2O) and recrystallized (H_2O (gentle heating)) to give **3***b* (130 mg, 50%) with data as reported (3, 20); mp ~200°C (dec.); UV (H_2O) max: 252 nm (ε 13 800); MS (FAB) *m/z*: 250 (16, MH^+). Anal. calcd. for $C_{10}H_{11}N_5O_3{\cdot}0.5H_2O$: C 46.51, H 4.68, N 27.12; found: C 46.20, H 4.58, N 27.07.

9-(2-Amino-2-deoxy-β-D-arabinofuranosyl)guanine 8*c*

Treatment of **8***b* (141 mg, 0.5 mmol) with ADA (pH 6.5, stirred at ambient temperature for 15 days with addition of ADA (8 mg) every second day) gave a residue that was chromatographed (Dowex 1 × 2 (OH^-), $Et_3NH{\cdot}HCO_3$–H_2O) to give **8***c* as a mixed salt and free 2′-amine. Further ion-exchange chromatography and recrystallization (H_2O) gave **8***c* (131 mg, 90%) with data as reported (26); mp ~230°C (dec.) (lit. (26) mp 193–196°C (dec.)); UV (H_2O) max: 252 nm (ε 13 000); MS (FAB) *m/z*: 283 (57, MH^+). Anal. calcd. for $C_{10}H_{14}N_6O_4{\cdot}0.5H_2O$: C 41.24, H 5.19, N 28.85; found: C 41.38, H 4.93, N 28.68.

9-(β-D-Xylofuranosyl)guanine 12

Treatment of **11** (282, 1 mmol) (prepared by coupling ($SnCl_4$–CH_3CN (27)) 2,6-diacetamidopurine (28*a*) with 1,2,3,5-tetra-*O*-acetyl-D-xylofuranose and deprotection (NH_3–MeOH), with data as reported (28*b*, 29); mp 159-161°C (lit. (28*b*) mp 160–163°C); MS *m/z*: 282.1080 (8, M^+ ($C_{10}H_{14}N_6O_4$) = 282.1076)) with ADA (stirred at ambient temperature for 3 days with addition of ADA (20 mg) each day) gave a residue that was chromatographed (Dowex 1 × 2 (OH^-), $Et_3NH{\cdot}HCO_3$–H_2O) and recrystallized (H_2O) to give **12** (242 mg, 83%); mp ~250°C (dec.) (lit. (21*a*) mp 236–240°C); UV (H_2O) max: 252 nm (ε 13 300); MS (FAB) *m/z*: 284 (28, MH^+); and other data as reported (21*a*). Anal. calcd. for $C_{10}H_{13}N_5O_5{\cdot}0.5H_2O$: C 41.10, H 4.83, N 23.96; found: C 41.01, H 4.63, N 23.63.

9-(β-D-Arabinofuranosyl)guanine 10

Deamination of **9** (17) proceeded analogously to give **10** with data identical to those of a sample prepared previously (17).

Acknowledgements

We thank the Natural Sciences and Engineering Research Council, the University of Alberta, and Brigham Young University for support and Mrs. Jeanny K. Gordon for assistance with the manuscript.

References

1. M.J. Robins, Z. Guo, and S.F. Wnuk. J. Am. Chem. Soc. **119**, 3637 (1997).
2. (*a*) J.G. Moffatt. *In* Nucleoside analogues: chemistry, biology, and medical applications. *Edited by* R.T. Walker, E. De Clercq, and F. Eckstein. Plenum Press, New York. 1979. pp. 71–164; (*b*) P.C. Srivastava, R.K. Robins, and R.B. Meyer, Jr. *In* Chemistry of nucleosides and nucleotides. Vol. 1. *Edited by* L.B. Townsend. Plenum Press, New York. 1988. pp. 113–281.
3. M.J. Robins, J.S. Wilson, D. Madej, N.H. Low, F. Hansske, and S.F. Wnuk. J. Org. Chem. **60**, 7902 (1995).
4. R. Mengel and W. Muhs. Chem. Ber. **112**, 625 (1979).
5. T.C. Jain, I.D. Jenkins, A.F. Russell, J.P.H. Verheyden, and J.G. Moffatt. J. Org. Chem. **39**, 30 (1974).
6. H. Vorbrüggen and K. Krolikiewicz. Liebigs Ann. Chem. 745 (1976).
7. H.-P. Baer, G.I. Drummond, and E.L. Duncan. Mol. Pharmacol. **2**, 67 (1966).
8. M.J. Robins, R. Zou, F. Hansske, D. Madej, and D.L.J. Tyrrell. Nucleosides Nucleotides, **8**, 725 (1989).
9. (*a*) V. Nair and T.B. Sells. Synlett, 753 (1991); (*b*) M.R. Almond, J.L. Collins, B.E. Reitter, J.L. Rideout, G.A. Freeman, and M.H. St. Clair. Tetrahedron Lett. **32**, 5745 (1991).
10. (*a*) A. Bloch, M.J. Robins, and J.R. McCarthy, Jr. J. Med. Chem. **10**, 908 (1967); (*b*) S.F. Wnuk, J.D. Stoeckler, and M.J. Robins. Nucleosides Nucleotides, **13**, 389 (1994); (*c*) A.L. Margolin, D.R. Borcherding, D. Wolf-Kugel, and N. Margolin. J. Org. Chem. **59**, 7214 (1994).
11. (*a*) S. Suzuki, B. Lee, W. Luo, D. Tovell, M.J. Robins, and D.L.J. Tyrrell. Biochem. Biophys. Res. Commun. **156**, 1144 (1988); (*b*) B. Lee, W. Luo, S. Suzuki, M.J. Robins, and D.L.J. Tyrrell. Antimicrob. Agents Chemother. **33**, 336 (1989).
12. (*a*) J. Balzarini, R. Pauwels, M. Baba, M.J. Robins, R. Zou, P. Herdewijn, and E. De Clercq. Biochem. Biophys. Res. Commun. **145**, 269 (1987); (*b*) J. Balzarini, M.J. Robins, R. Zou, P. Herdewijn, and E. De Clercq. Biochem. Biophys. Res. Commun. **145**, 277 (1987); (*c*) R. Pauwels, M. Baba, J. Balzarini, P. Herdewijn, J. Desmyter, M.J. Robins, R. Zou, D. Madej, and E. De Clercq. Biochem. Pharmacol. **37**, 1317 (1988).
13. (*a*) J. Balzarini, M. Baba, R. Pauwels, P. Herdewijn, S.G. Wood, M.J. Robins, and E. De Clercq. Mol. Pharmacol. **33**, 243 (1988); (*b*) P. Herdewijn and A. Van Aerschot. Tetrahedron

© 1997 NRC Canada

Lett. **30**, 855 (1989); (*c*) M.J. Robins, S.G. Wood, N.K. Dalley, P. Herdewijn, J. Balzarini, and E. De Clercq. J. Med. Chem. **32**, 1763 (1989).
14. M.J. Robins, F. Hansske, and S.E. Bernier. Can. J. Chem. **59**, 3360 (1981).
15. (*a*) M.J. Robins, F. Hansske, N.H. Low, and J.I. Park. Tetrahedron Lett. **25**, 367 (1984); (*b*) M.J. Robins, D. Madej, N.H. Low, F. Hansske, and R. Zou. *In* Nucleic acid chemistry: improved and new synthetic procedures, methods and techniques. Vol 4. *Edited by* L.B. Townsend and R.S. Tipson. John Wiley & Sons, New York. 1991. pp. 211–219.
16. F. Hansske and M.J. Robins. Tetrahedron Lett. **26**, 4295 (1985).
17. F. Hansske, D. Madej, and M.J. Robins. Tetrahedron, **40**, 125 (1984).
18. M.J. Robins, J.S. Wilson, and F. Hansske. J. Am. Chem. Soc. **105**, 4059 (1983).
19. M.J. Robins, S.D. Hawrelak, A.E. Hernández, and S.F. Wnuk. Nucleosides Nucleotides, **11**, 821 (1992).
20. C.K. Chu, V.S. Bhadti, B. Doboszewski, Z.P. Gu, Y. Kosugi, K.C. Pullaiah, and P. Van Roey. J. Org. Chem. **54**, 2217 (1989).
21. (*a*) G. Gosselin, M.-C. Bergogne, J. De Rudder, E. De Clercq, and J.-L. Imbach. J. Med. Chem. **29**, 203 (1986); (*b*) J. Med. Chem. **30**, 982 (1987).
22. L.F. Christensen, A.D. Broom, M.J. Robins, and A. Bloch. J. Med. Chem. **15**, 735 (1972).
23. E. Walton, F.W. Holly, G.E. Boxer, R.F. Nutt, and S.R. Jenkins. J. Med. Chem. **8**, 659 (1965).
24. M.J. Robins, J.S. Wilson, L. Sawyer, and M.N.G. James. Can. J. Chem. **61**, 1911 (1983).
25. G.L. Tong, K.J. Ryan, W.W. Lee, E.M. Acton, and L. Goodman. J. Org. Chem. **32**, 859 (1967).
26. A. Sato, R. Imai, N. Nakamizo, and T. Hirata. Chem. Pharm. Bull. **27**, 821 (1979).
27. M. Saneyoshi and E. Satoh. Chem. Pharm. Bull. **27**, 2518 (1979).
28. (*a*) J. Davoll and B.A. Lowy. J. Am. Chem. Soc. **73**, 1650 (1951); (*b*) J. Am. Chem. Soc. **74**, 1563 (1952).
29. J.A. Montgomery and K. Hewson. J. Org. Chem. **34**, 1396 (1969).

Can. J. Chem. Downloaded from www.nrcresearchpress.com by 88.146.161.215 on 09/08/12
For personal use only.

© 1997 NRC Canada

New antifungal metabolites from the coprophilous fungus *Cercophora sordarioides*

Authrine C. Whyte, Katherine B. Gloer, James B. Gloer, Brenda Koster, and David Malloch

Abstract: A chemical investigation of the coprophilous fungus *Cercophora sordarioides* has led to the isolation of arthrinone (**1**), a known fungal metabolite, and three new related compounds: 1-dehydroxyarthrinone (**2**), 3a,9a-deoxy-3a-hydroxy-1-dehydroxyarthrinone (**3**), and cerdarin (**4**). These metabolites were obtained from antifungal ethyl acetate extracts of liquid cultures of *C. sordarioides* through bioassay-guided fractionation, and their structures were assigned on the basis of 1D-NMR, HMQC, and HMBC results. Compounds **2** and **4** exhibited anti-*Candida* activity.

Key words: antifungal, fungal metabolite, natural product, *Cercophora sordarioides.*

Résumé : Une investigation chimique du champignon coprophileux *Cercophora sordarioides* a permis d'isoler l'arthrinone (**1**), une métabolite connu de champignons, et trois nouveaux composés qui lui sont apparentés : la 1-déshydroxyarthrinone (**2**) la 3a,9a-déoxy-3a-hydroxy-1-déshydroxyarthrinone (**3**) et la cerdarine (**4**). On a isolé ces métabolites à partir des extraits à l'acétate d'éthyle des antifongicides des cultures liquides du *C. sordarioides*, par un fractionnement guidé par des bioessais, et on en a attribué les structures sur la base de résultats de RMN en 1D, de « HMCQ » et de « HMBC ». Les composés **2** et **4** présentent une activité anti-*Candida.*

Mots clés : antifongicide, métabolite de champignons, produit naturel, *Cercophora sordarioides.*

[Traduit par la rédaction]

Antagonistic interactions among coprophilous (dung-colonizing) fungi often involve the production of a chemical agent by one species that inhibits the growth of another (1, 2). Our studies of these fungi have led to the discovery of a variety of new antifungal agents (3, 4). Recently, we reported the isolation of several new cytotoxic and antifungal metabolites from *Cercophora areolata* (5). As part of a continuing study of coprophilous fungi of this genus, we investigated the chemistry of an isolate of *C. sordarioides* that displayed antifungal activity. This investigation led to the isolation of the known fungal metabolite arthrinone (**1**) (6) and three new related compounds: 1-dehydroxyarthrinone (**2**), 3a,9a-deoxy-3a-hydroxy-1-dehydroxyarthrinone (**3**), and cerdarin (**4**). Compounds **2** and **4** exhibited anti-*Candida* activity. This report describes the isolation, structure elucidation, and biological activities of these metabolites.

Results and discussion

An isolate of *C. sordarioides* (JS 271 = UAMH 7495) obtained from cow dung was grown in liquid shake culture for 30 days. The EtOAc extract of the resulting broth was fractionated directly by reversed-phase HPLC to afford arthrinone (**1**) and three related metabolites (**2–4**).

Arthrinone (**1**) was originally reported as a metabolite of an *Arthrinium* sp., and its structure and relative stereochemistry were confirmed by X-ray crystallographic analysis (6). The sample obtained from *C. sordarioides* was identified through analysis of HREIMS and NMR data, and by comparison of these and other data with literature values (6). This assignment was confirmed by ^{1}H NMR analysis of a 1:1 mixture of the sample with an authentic standard of **1**, which revealed that all signals were coincident.

The HREIMS and NMR data for compound **2** indicated that it is closely related to **1**, but contains one less oxygen atom. ^{1}H NMR (Table 1), ^{13}C NMR (Table 2), and DEPT data revealed the presence of a pair of *meta*-coupled aromatic protons, two oxygenated methylene groups, an oxygenated sp^3 methine carbon, two oxygenated quaternary carbons, a conjugated ketone, a methoxy group, and two hydroxy signals, one of which (11.6 ppm) was consistent with the presence of an intramolecularly hydrogen-bonded phenol moiety. The absence of an oxygenated methine signal near 95 ppm and the appearance of a new oxygenated methylene resonance at 66.6 ppm in the ^{13}C NMR spectrum suggested that the hemiacetal group present in **1** was replaced by an oxygenated methylene unit in **2**.

HMBC correlations (Table 3) observed for the aryl protons (H-5 and H-7), the oxymethine proton (H-4), the methoxy group (H_3-10), and the hydrogen-bonded phenolic proton (OH-8) in **2** were consistent with correlations noted for arthrinone (**1**) (6). Reciprocal HMBC correlations observed for the oxymethylene groups (H_2-1 and H_2-3), and correlations linking these groups with C-3a and C-9a, provided evidence

Received November 1, 1996.

This paper is dedicated to Professor William A. Ayer on the occasion of his 65th birthday.

A.C. Whyte, K.B. Gloer, and J.B. Gloer.[1] Department of Chemistry, University of Iowa, Iowa City, IA 52242, U.S.A.
B. Koster and D. Malloch. Department of Botany, University of Toronto, Toronto, ON M5S 1A1, Canada.

[1] Author to whom correspondence may be addressed. Telephone: (319) 335-1361. Fax: (319) 335-1270. E-mail: james-gloer@uiowa.edu

© 1997 NRC Canada

Can. J. Chem. Downloaded from www.nrcresearchpress.com by 88.146.161.215 on 09/08/12
For personal use only.

Can. J. Chem. Downloaded from www.nrcresearchpress.com by 88.146.161.215 on 09/08/12
For personal use only.

Table 1. ^{1}H NMR data for 1-dehydroxyarthrinone (**2**), 3a,9a-deoxy-3a-hydroxy-1-dehydroxyarthrinone (**3**), and cerdarin (**4**) (δ_H (multiplicity; J_{HH})).

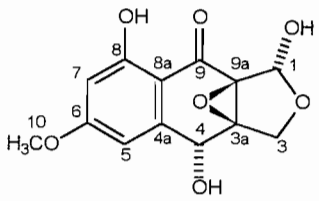
Position	**2**[a]	**3**[b]	**4**[a]
1	4.30 (d; 10)[c]	4.32 (dd; 8.0, 1.2)	5.08 (dd; 17, 4.0)
	4.11 (d; 10)[d]	4.23 (dd; 8.0, 5.8)	4.97 (dd; 17, 0.8)
3	4.15 (d; 11)[c]	3.79 (d; 9.9)	6.18 (dd; 4.0, 0.8)
	4.04 (d; 11)[d]	3.73 (d; 9.9)	
3a	—	4.82 (br s; OH)[e]	—
4	5.27 (d; 8.0)	5.18 (br s)	—
4-OH	5.24 (d; 8.0)	5.30 (br s)[e]	—
5	6.65 (d; 2.4)	6.85 (dd; 2.4, 1.4)	7.12 (d; 2.5)
7	6.46 (d; 2.4)	6.37 (d; 2.4)	6.79 (d; 2.5)
8-OH	11.6 (s)	12.8 (s)	12.2 (s)
9a	—	3.06 (dd; 5.8, 1.2)	—
10	3.89 (s)	3.91 (s)	3.99 (s)
11	—	—	3.46 (s)

[a]Recorded at 300 MHz.
[b]Recorded at 600 MHz.
[c–e]Identical superscripts represent interchangeable assignments.

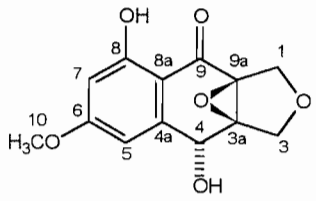
Table 2. ^{13}C NMR data[a] for 1-dehydroxyarthrinone (**2**), 3a,9a-deoxy-3a-hydroxy-1-dehydroxyarthrinone (**3**), and cerdarin (**4**) (δ_C).

Position	**2**	**3**[b]	**4**
1	66.6[c]	71.9	72.1
3	65.6[c]	76.0	108.1
3a	71.0	82.5	150.9[d]
4	66.3	72.7	181.5
4a	146.7	147.5	135.8
5	111.0	105.8	109.0
6	167.9	168.2	167.1
7	101.6	100.0	106.8
8	165.6	166.3	165.7
8a	107.5[b]	110.1	110.8
9	196.1	202.3	185.6
9a	65.5	58.5	143.5[d]
10	56.3	56.2	56.8
11	—	—	55.2

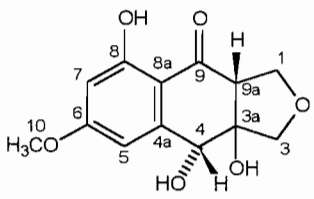
[a]Recorded at 75 MHz.
[b]These ^{13}C NMR chemical shifts were obtained from HMQC and HMBC results.
[c,d]Identical superscripts represent interchangeable assignments.



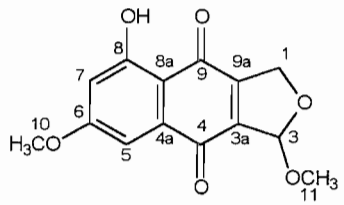
1



2



3



4

for the epoxy-tetrahydrofuran system. An additional HMBC correlation of OH-4 (5.24 ppm) with C-3a (71.0 ppm) and a selective INEPT correlation of H-4 with C-9a (65.5 ppm) established the NMR assignments for the oxygenated quaternary carbons in **2**. Compound **2** was therefore determined to be 1-dehydroxyarthrinone.

The absolute stereochemistry at C-4 of **2** was assigned by application of Helmchen's rules (7). Treatment of a sample of **2** with (*R*)-2-phenylbutyric acid (PBA) and dicyclohexylcarbodiimide (DCC) resulted in monoacylation at the 4-OH group. The (*S*)-PBA monoester was obtained by similar treatment of **2** with racemic PBA–DCC, followed by HPLC separation of the resulting diastereomeric mixture. Independent confirmation of the chemical shift assignments for the *R*-PBA

© 1997 NRC Canada

Table 3. HMBC data[a] for 1-dehydroxyarthrinone (**2**), 3a,9a-Deoxy-3a-hydroxy-1-dehydroxyarthrinone (**3**), and cerdarin (**4**).

^{1}H Position	**2** (C-#)	**3** (C-#)	**4** (C-#)
1	C-3, 3a	C-3, 3a, 9	C-3, 3a, 9,[c] 9a
3	C-1, 3a, 9a	C-1, 3a, 4	C-1, 3a,[c] 11
4	C-3a, 4a, 5, 8a, 9a[b]	C-3, 3a, 4a	—
4-OH	C-3a, 4, 4a	—	—
5	C-4, 6, 7, 8a	C-4, 7, 8a	C-4, 4a,[b,c] 6,[c] 7, 8a, 9[c,d]
7	C-5, 6, 8, 8a	C-5, 6, 8, 8a	C-5, 6, 8, 8a, 9[c,d]
8-OH	C-7, 8, 8a	C-7, 8, 8a	C-7, 8, 8a
9a	—	C-3, 3a, 9	—
10	C-6	C-6	C-6
11	—	—	C-3

[a]Recorded at 600 MHz (^{1}H dimension).
[b]These correlations were also observed in selective INEPT experiments optimized for J = 4 Hz.
[c]These correlations were observed in a D-HMBC experiment optimized for J = 4 Hz.
[d]Represents a four-bond correlation.

ester was achieved through analysis of COSY, HMQC, and HMBC data for this derivative. The absolute configuration at C-4 was deduced to be (*R*), based on downfield shifts of the H-5, H-7, OH-8, and H_3-10 signals and upfield shifts of the H_2-1 and H_2-3 signals in the spectrum of the (*R*)-PBA ester relative to those in the spectrum of the (*S*) derivative. Assuming a similar biosynthetic pathway for **1** and **2**, and considering the close NMR similarities, the relative stereochemistry for **2** is proposed to be the same as that reported for arthrinone (**1**). Therefore, the absolute configurations at C-3a and C-9a are each proposed to be (*S*) in **2**.

The molecular formula of a third related metabolite (compound **3**) was established as $C_{13}H_{14}O_6$ (seven unsaturations) by analysis of HREIMS and ^{13}C NMR data. The presence of a ketone carbonyl and six olefinic or aromatic carbons in the ^{13}C NMR spectrum indicated a tricyclic structure for **3**, and changes in several NMR signals (Tables 1 and 2) clearly indicated the absence of an epoxy group in this case. HMBC results (Table 3) confirmed that the 1,2,3,5-tetrasubstituted benzene subunit found in **1** and **2** was also present in **3**.

COSY data revealed that the C-1 oxymethylene protons are vicinally coupled with H-9a. In contrast to the data for **1** and **2**, the H_2-1 signals showed HMBC correlations with the aryl ketone carbonyl carbon (C-9), thereby unambiguously placing C-9a between C-9 and C-1. HMBC correlations of the benzylic H-4 signal with the second oxygenated methylene carbon (C-3) and the oxygenated quaternary carbon C-3a, together with the lack of COSY correlations between H-4 and H_2-3, indicated that C-3a (82.5 ppm) is located between C-4 and C-3. Correlations of H-9a with C-3, and of H_2-3 with C-1 and C-3a, provided evidence for the presence of a tetrahydrofuran ring. On the basis of these and other correlations (Table 3), as well as the molecular formula, C-3a must be attached to C-9a, and must bear a hydroxy group. The structure of **3** was therefore assigned as 3a,9a-deoxy-3a-hydroxy-1-dehydroxyarthrinone.

The relative stereochemistry at positions C-4 and C-9a of **3** was proposed on the basis of a NOESY correlation observed between the signals for H-4 and H-9a. To accommodate this correlation, Dreiding molecular models suggest that the C-3a to C-9a ring fusion is most likely *trans*; however, the lack of other useful NOESY correlations renders this assignment inconclusive, so the relative configuration at position C-3a remains undefined.

The HREIMS, ^{13}C NMR (Table 2), and DEPT data for cerdarin (**4**) suggested a molecular formula of $C_{14}H_{12}O_6$ (nine unsaturations) for this metabolite. Signals for two methoxy groups, an oxygenated methylene group, two *meta*-coupled aromatic protons, an intramolecularly hydrogen-bonded phenolic proton, and a downfield-shifted signal (6.18 ppm) consistent with an olefinic proton or an acetal moiety were observed in the ^{1}H NMR spectrum of **4** (Table 1). The ^{13}C NMR spectrum contained two conjugated ketone carbonyl signals (185.6 and 181.5 ppm), and nine additional signals consistent with the presence of a benzenoid ring, a tetrasubstituted olefinic unit, and an acetal carbon. These data satisfied seven of the unsaturations required by the molecular formula, leaving two more rings to be established.

HMBC correlations for H-5, H-7, OH-8, and H_3-10 were analogous to those observed for the aromatic subunit of **1–3**, except that H-5 showed a correlation to the carbonyl signal at 181.5 ppm (C-4) rather than to an oxymethine signal, requiring that this carbonyl be attached to C-4a. As in **1–3**, the remaining ketone carbonyl signal at 185.6 ppm (C-9) in **4** must be attached to C-8a to account for the downfield chemical shift of OH-8.

The chemical shifts of 6.18/108.1 ppm for the C-3 methine unit, together with reciprocal HMBC correlations observed between this unit and OCH_3-11, indicated that C-3 is part of an acetal functionality. Further reciprocal correlations between this unit and the oxygenated methylene group (CH_2-1) required that C-1 and C-3 share the only remaining oxygen atom through an ether linkage. Additional HMBC correlations between H_2-1 and the sp^2 carbon signals at 143.5 and 150.9 ppm (C-3a and C-9a), and between H-3 and the signal at 150.9 ppm, permitted construction of a dihydrofuran ring. Interestingly, an unusually large homoallylic coupling (4.0 Hz) was observed between H_a-1 and one of the protons on C-3.

The final ring in cerdarin (**4**) must result from connection of

© 1997 NRC Canada

Can. J. Chem. Downloaded from www.nrcresearchpress.com by 88.146.161.215 on 09/08/12
For personal use only.

Can. J. Chem. Downloaded from www.nrcresearchpress.com by 88.146.161.215 on 09/08/12
For personal use only.

the dihydrofuran ring with carbonyl carbons C-4 and C-9 to form a quinone subunit. The ^{13}C NMR chemical shifts of these carbons are consistent with the presence of a naphthoquinone moiety (8). However, a question remained regarding the regiochemistry of the dihydrofuran ring (i.e., the positioning of the CH_3O substituent at C-1 vs. C-3) because the HMBC experiment showed no correlations of either H-1 or H-3 with C-4 or C-9. Compounds **1–4** appear to be closely related hexaketide-type metabolites, and the regiochemistry of the furan ring in **4** was intially presumed to be analogous to that of **1** based on simple biogenetic analogy. However, one could also envision formation of the alternative regioisomer via a process involving additional reduction and (or) allylic oxidation steps. Therefore, in an effort to make an unambiguous assignment, a D-HMBC (9) experiment optimized for J = 4 Hz was conducted. This experiment revealed correlations of both C-1 protons with the carbonyl resonance at 185.6 ppm (C-9), strongly suggesting placement of the oxymethylene group adjacent to C-9 on the quinone ring. Four-bond heteronuclear correlations are possible, and although molecular models indicate that neither proton can adopt a coplanar W-relationship with C-4, one could envision observation of heteronuclear allylic coupling in such a system. Ultimately, however, the presence of correlations of C-9 with *both* methylene protons, together with the lack of possible conformations that would place both protons at ca. 90° vicinal angles with respect to C-9, argues for their assignment as three-bond correlations. Thus, the structure of cerdarin is proposed as shown in **4**, with the furanoid ring regiochemistry opposite to that of **1**. The absolute stereochemistry at C-3 was not determined.

Signals consistent with those observed for compounds **1–4** were present in the ^1H NMR spectrum of the unprocessed extract, indicating that these compounds are not artifacts of the isolation process. Compounds **1**, **2**, and **4** caused complete growth inhibition of the early successional coprophilous fungus *Ascobolus furfuraceus* in centerpoint disk inoculation assays at 200 μg/disk. Cerdarin (**4**) also completely inhibited the growth of *Sordaria fimicola* at the same level, but arthrinone (**1**) and dehydroxyarthrinone (**2**) showed only modest activity against this coprophilous fungal competitor. Compounds **1** and **2** also exhibited antibacterial activity against *B. subtilis* (21 and 25 mm zones of inhibition, respectively) and *S. aureus* (17 mm zones of inhibition), and **2** displayed activity against *Candida albicans* (11 mm zone of inhibition) at 200 μg/disk. Cerdarin displayed more significant anti-*Candida* and antibacterial activity in disk assays at the same level (20, 35, and 23 mm zones of inhibition against *C. albicans*, *B. subtilis*, and *S. aureus*, respectively). Compounds **1** and **2** exhibited limited cytotoxicity in the NCI 60-tumor cell line bioassay panel, displaying average GI_{50} values of 1.0 and 9.4 μg/mL, respectively.

Experimental section

General experimental procedures

Semipreparative HPLC purifications employed a Beckman Ultrasphere C_8 column (5-μm particles, 25 × 1.0 cm) at a flow rate of 2.0 mL/min with UV detection at 215 nm, with a gradient solvent system of 50–100% MeOH – H_2O, unless otherwise indicated. HPLC retention times are reported for an isocratic solvent system of 50% MeOH – H_2O. NMR spectra were recorded in Me_2CO-d_6 solutions, and chemical shifts were referenced relative to the corresponding solvent signals (2.04 ppm/29.8 ppm). Carbon multiplicities were established by DEPT experiments, and are consistent with the assignments. Specific rotations were measured on a Jasco model DIP-1000 digital polarimeter. Descriptions of NMR parameters, as well as NMR, MS, UV, IR, and mp instrumentation (10), and details of the antifungal bioassays (11), have been provided elsewhere. Chemical reagents were used as purchased without further purification. The THF employed in the esterification of **2** was freshly distilled from Na–benzophenone.

Cultivation of *C. sordarioides*

The isolate of *C. sordarioides* (JS 271) was obtained from a sample of cow dung collected by B. Koster in Issy l'Eveque, France, in August, 1994. A subculture has been deposited at the University of Alberta Mycological Herbarium Collection and was assigned the accession number UAMH 7495. Four 2-L Erlenmeyer flasks, each containing 400 mL of potato dextrose broth (Difco), were each inoculated with two 1-cm^2 agar plugs taken from stock cultures of *C. sordarioides*. Flask cultures were incubated at 25–28°C and aerated by agitation on an orbital shaker at 160 rpm for 30 days.

Isolation and characterization of arthrinone (1), 1-dehydroxyarthrinone (2), 3a,9a-deoxy-3a-hydroxy-1-dehydroxyarthrinone (3), and cerdarin (4)

The mycelia and culture broth from the fermentation of *C. sordarioides* (1600 mL) were together extracted with EtOAc (3 × 1000 mL), and the organic phase was dried ($MgSO_4$) and concentrated to yield 434 mg of a dark red solid. A portion of the extract (237 mg) was directly subjected to semipreparative reversed-phase HPLC to afford arthrinone (**1**; 58 mg), 1-dehydroxyarthrinone (**2**; 14 mg), and cerdarin (**4**; 3.7 mg).

To obtain an additional sample of **2** for stereochemical studies, a second liquid fermentation culture of *C. sordarioides* was generated using the conditions described. The broth (400 mL) and mycelia from this fermentation were together extracted using EtOAc (2 × 400 mL), and the organic phase was dried ($MgSO_4$) and concentrated to yield 37 mg of a brown solid. This extract was subjected to semipreparative reversed-phase HPLC to yield 1-dehydroxyarthrinone (**2**; 18 mg) and 3a,9a-deoxy-3a-hydroxy-1-dehydroxyarthrinone (**3**; 1.4 mg).

Arthrinone (1): $[\alpha]_D$ −5.3 (*c* 0.0019 g/mL). Spectral data and other physical properties for **1** have been previously reported (6).

1-Dehydroxyarthrinone (2): amber solid; mp 193–195°C; $[\alpha]_D$ +2.3 (*c* 0.001 g/mL, MeOH); HPLC t_R: 15.3 min; UV (MeOH) λ_{max}: 331 (ε 3400), 303 (3500), 257 (4700), 241 (3500) nm; IR (NaCl) ν_{max}: 3590, 2927, 1627, 1382, 1295, 1206, 1155 cm^{-1}; EIMS (70 ev) *m/z*: 264 (M^+, rel. int. 100), 246 (9), 206 (19), 177 (15), 151 (47); ^1H NMR, ^{13}C NMR, and HMBC data, see Tables 1, 2, and 3; HREIMS *m/z* calcd. for $C_{13}H_{12}O_6$: 264.0634; found: 264.0626 (M^+).

© 1997 NRC Canada

Can. J. Chem. Downloaded from www.nrcresearchpress.com by 88.146.161.215 on 09/08/12
For personal use only.

Esterification of 1-deoxyarthrinone (2)

A solution of (*R/S*)-2-phenylbutyric acid (PBA; 4.8 mg; 0.03 mmol) in 1 mL THF was added to a stirred solution of 1,3-dicyclohexylcarbodiimide (DCC; 6.2 mg; 0.03 mmol in 1 mL THF). A solution of compound **2** (4.0 mg; 0.015 mmol) in 1 mL THF was then added, followed by dimethylaminopyridine (40 μg), and the resulting mixture was allowed to stir at room temperature for 24 h. A white precipitate (DCC-urea) was formed. The THF was evaporated under N_2 flow, and the residue was redissolved in 3 mL of Et_2O. The organic solution was washed successively with 4 mL of 2% HOAc solution, 5 mL H_2O, and 5 mL of 3% $NaHCO_3$, and was then dried with $MgSO_4$. After removal of the solvent in vacuo, the organic residue was subjected to reversed-phase semipreparative HPLC using a gradient system of 80–100% MeOH – H_2O for 15 min to afford the acylated products (2.7 mg (*R*)-ester and 2.1 mg (*S*)-ester; 78% yield). Similar treatment of **2** with (*R*)-PBA/DCC yielded a sample of the (*R*) diastereomer.

(R)-2-Phenylbutyryl ester of 2: ^{1}H NMR ($CDCl_3$): 11.6 (s, OH-8), 7.30 (m, 2H, Ar), 7.26 (m, 1H, Ar), 7.19 (m, 2H, Ar), 6.49 (d, 2.4, H-5), 6.43 (d, 2.4, H-7), 6.40 (br s, H-4), 4.20 (d, 11, H_a-3), 3.94 (d, 11, H_b-3), 3.80 (s, H_3-10), 3.77 (d, 10, H_a-1), 3.38 (t, 7.7, ester CH), 3.17 (d, 10, H_b-1), 2.06 (dq, 21, 7.5, ester CH_2), 1.79 (br dq, 21, 7.5, ester CH_2), 0.82 (t, 7.4 Hz, ester CH_3) ppm; ^{13}C NMR ($CDCl_3$): 193.7 (C-9), 172.9 (ester C=O), 166.8 (C-6), 165.1 (C-8), 139.6 (C-4a), 137.8 (phenyl), 128.8 (phenyl), 127.8 (2) (phenyl), 111.0 (C-5), 107.6 (C-8a), 102.0 (C-7), 67.5 (C-3a), 66.0 (C-4), 65.4 (C-1), 64.9 (C-3), 64.1 (C-9a), 55.8 (C-10), 53.1 (ester CH), 26.0 (ester CH_2), 11.9 (ester CH_3) ppm; EIMS (70 eV) *m/z*: 410 (M^+, rel. int. 11), 264 (4), 246 (4), 218 (4), 205 (5), 189 (28), 119 (69), 91 (100).

(S)-2-Phenylbutyryl ester of 2: ^{1}H NMR ($CDCl_3$): 11.5 (s, OH-8), 7.24 (m, Ar), 7.17 (m, Ar), 6.37 (d, 2.5, H-5), 6.35 (br s, H-4), 6.24 (d, 2.3, H-7), 4.28 (d, 11, H_a-3), 4.06 (d, 11, H_b-3), 4.03 (d, 10, H_a-1), 3.72 (s, H_3-10), 3.65 (d, 10, H_b-1), 3.43 (t, 7.6, ester CH), 2.04 (m, ester CH_2), 1.78 (m, ester CH_2), 0.85 (t, 7.6 Hz, ester CH_3) ppm.

3a,9a-Deoxy-3a-hydroxy-1-dehydroxyarthrinone (3): amber solid; mp 159–163°C (dec.); $[\alpha]_D$ +3.0 (*c* 0.001 g/mL, MeOH); HPLC t_R: 22.5 min; UV (MeOH) λ_{max}: 326 (ε 1400), 288 (2200), 224 (1900) nm; EIMS (70 eV) *m/z*: 266 (M^+, rel. int. 61), 248 (11), 218 (19), 178 (40), 151 (100); ^{1}H NMR, ^{13}C NMR, and HMBC data, see Tables 1, 2, and 3; HREIMS *m/z* calcd. for $C_{13}H_{14}O_6$: 266.0790; found: 266.0799 (M^+).

Cerdarin (4): bright orange solid; mp 142–144°C; $[\alpha]_D$ +1.0 (*c* 0.001 g/mL, MeOH); HPLC t_R: 31.6 min; UV (MeOH) λ_{max}: 439 (ε 480), 353 (300), 265 (1700), 237 (1600), 219 (3000) nm; EIMS (70 eV) *m/z*: 276 (M^+, rel. int. 23), 245 (75), 244 (39), 216 (21); ^{1}H NMR, ^{13}C NMR, and HMBC data, see Tables 1, 2, and 3; HREIMS *m/z* calcd. for $C_{14}H_{12}O_6$: 276.0634; found: 276.0647 (M^+).

Acknowledgments

Support for this work from the U.S. National Institutes of Health (R01 AI 27036) is gratefully acknowledged. We also thank Dr. J. Qian-Cutrone of the Bristol-Myers Squibb Pharmaceutical Research Institute for providing an authentic sample of arthrinone (**1**), and the National Cancer Institute for cytotoxicity data.

References

1. D.T. Wicklow and B.J. Hirschfield. Can. J. Microbiol. **25**, 855 (1979).
2. N. Singh and J. Webster. Trans. Br. Mycol. Soc. **61**, 487 (1973).
3. J.B. Gloer. Can. J. Bot. **73**, S1265 (1995).
4. H.-J. Wang, J.B. Gloer, J.A. Scott, and D. Malloch. Tetrahedron Lett. **36**, 5847 (1995).
5. A.C. Whyte, J.B. Gloer, J.A. Scott, and D. Malloch. J. Nat. Prod. **59**, 765 (1996).
6. J. Qian-Cutrone, Q. Gao, S. Huang, S.E. Klohr, J.A. Veitch, and Y. Shu. J. Nat. Prod. **57**, 1656 (1994).
7. G. Helmchen. Tetrahedron Lett. **12**, 1527 (1974).
8. E. Pretsch, T. Clerc, J. Seibl, and W. Simon. Tables of spectral data for structure determination of organic compounds. Springer-Verlag, New York. 1983.
9. K. Furihata and H. Setoa. Tetrahedron Lett. **36**, 2817 (1995).
10. A.A. Alfatafta, J.B. Gloer, J.A. Scott, and D. Malloch. J. Nat. Prod. **57**, 1696 (1994).
11. P.F. Dowd. Entomol. Exp. Appl. **47**, 69 (1988).

© 1997 NRC Canada

New terpenoid metabolites from the skin extracts, an egg mass, and dietary sponges of the Northeastern Pacific dorid nudibranch *Cadlina luteomarginata*

Eric J. Dumdei, Julia Kubanek, John E. Coleman, Jana Pika, Raymond J. Andersen, Jorge Rios Steiner, and Jon Clardy

Abstract: Chemical investigations of *Cadlina luteomarginata* skin extracts, egg masses, and dietary sponges have led to the identification of the novel terpenoids cadlinaldehyde (**30**), spongian **32**, seco-spongian **35**, 20-acetoxy-12-marginatone (**38**), and lutenolide (**39**) from the nudibranch skin extracts, the new drimane sesquiterpenoid 1α,2α-diacetoxyalbicanyl acetate (**40**) from the nudibranch's egg mass, and the new sesquiterpenoids *O*-methyl-9-oxofurodysininlactone (**47**), 2-oxomicrocionin-2-lactone (**48**), and *O*-methyl-2-oxomicrocionin-2-lactone (**49**), from the dietary sponge *Pleraplysilla* sp. The known terpenoids furodysinin (**1**), furodysin (**16**), marginatafuran (**21**), and 9,11-dihydrogracillin A (**37**), which have been frequently isolated from *C. luteomarginata* skin extracts, were found for the first time in extracts of the dietary sponges *Pleraplysilla* sp. and *Aplysilla* sp. One of the new terpenoids, cadlinaldehyde (**30**), has an unprecedented degraded sesterterpenoid skeleton.

Key words: nudibranch, sponge, terpenoids, structure elucidation.

Résumé : Des investigations chimiques d'extraits de peau, de masses des oeufs et d'éponges alimentaires du *Cadlina luteomarginata* ont permis d'identifier la présence des terpénoïdes cadlinaldéhyde (**30**), spongiane **32**, séco-spongiane **35**, 20-acétoxy-12-marginatone (**38**) et luténolide (**39**) dans les extraits de peau du nudibranche, du nouveau sesquiterpénoïde du drimane, l'acétate de 1α,2α-diacétoxyalbicanyle (**40**), à partir de la masse des oeufs du nudibranche ainsi que les nouveaux sesquiterpénoïdes *O*-méthyl-9-oxofurodysininlactone (**47**), 2-oxomicrocionine-2-lactone (**48**) et *O*-méthyl-2-oxomicrocionine-2-lactone (**49**) à partir des éponges alimentaires de l'espèce *Pleraplysilla*. Les terpénoïdes connus furodysinine (**1**), furodysine (**16**), marginatafurane (**21**) et 9,11-dihydrogracilline A (**37**), fréquemment isolés des extraits de peau du *C. luteomarginata*, ont été retrouvés pour la première fois dans les extraits d'éponges alimentaires des espèces *Pleraplysilla* et *Aplysilla*. L'un des nouveaux terpénoïdes, le cadlinaldéhyde (**30**), présente un squelette de sesterterpénoïde dégradé jamais rencontré antérieurement.

Mots clés : nudibranch, sponge, terpenoids, structure elucidation.

[Traduit par la rédaction]

Introduction

Cadlina luteomarginata is a relatively common dorid nudibranch that is found in rocky intertidal and shallow subtidal habitats all along the west coast of North America from Auke Bay, Alaska, to Point Eugenia, Mexico. Skin extracts of *C. luteomarginata* have proven to be an extremely rich source of terpenoid metabolites that in some instances apparently play a role in defending these shell-less molluscs from predation (1–7). Many of the terpenoids obtained from *C. luteomarginata* have been shown to be sequestered unchanged by the molluscs from the marine sponges that make up their diets (2, 5–7). It has also been found that the terpenoid content of skin extracts of specimens of *C. luteomarginata* can vary dramatically from collecting site to collecting site, reflecting the different terpenoid constituents present in the dietary sponges available at each site. The initial discovery of geographic variability in *C. luteomarginta* terpenoid constituents prompted investigations of geographic variance in metabolite content of other species and led ultimately to the general proposal that geographic invariance of metabolite content in nudibranch skin extracts was a good predictor of de novo biosynthesis of the metabolites (8). Recently, a number of biosynthetic investigations of nudibranch terpenoids and polyketides have provided support for this proposal (9–11).

The terpenoid constituents present in skin extracts of *C. luteomarginata* have been identified for specimens collected

Received December 2, 1996.

This manuscript is dedicated to Professor William Ayer, an inspirational teacher, mentor, and role model, on the occasion of his 65th birthday.

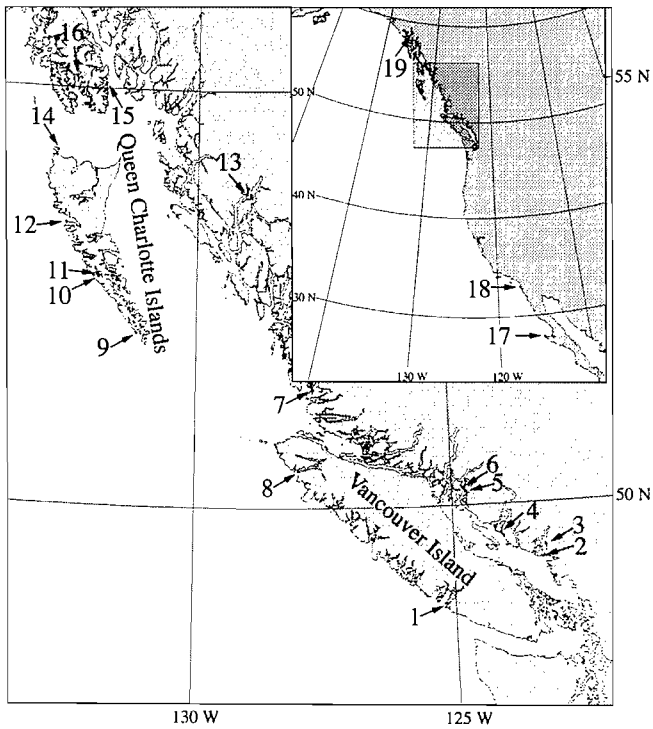
E.J. Dumdei, J. Kubanek, J.E. Coleman, J. Pika, and R.J. Andersen.[1] Departments of Chemistry and Oceanography – Earth and Ocean Sciences, University of British Columbia, Vancouver, BC V6T 1Z1, Canada.
J.R. Steiner and J. Clardy.[1] Department of Chemistry – Baker Laboratory, Cornell University, Ithaca, NY 14853-1301, U.S.A.

[1] Authors to whom correspondence may be addressed. RJA: Telephone: (604) 822-4511. Fax: (604) 822-6091. E-mail: randersn@unixg.ubc.ca

© 1997 NRC Canada

Can. J. Chem. Downloaded from www.nrcresearchpress.com by 88.146.161.215 on 09/08/12
For personal use only.

Fig. 1. Sites along the western coast of North America where the terpenoid constituents of *C. luteomarginata* have been studied.



1. Sanford Island, Barkley Sound, BC
2. Passage Island, Howe Sound, BC
3. Kelvin Grove, Howe Sound, BC
4. Agamemnon Channel, BC
5. East Redonda Island, BC
6. Pendrell Sound, BC
7. Rivers Inlet, Bull Island, BC
8. Quatsino Sound, BC
9. Anthony Island, BC
10. Tasu Narrows, BC
11. Tasu Sound, BC
12. Rennell Sound, BC
13. Emilia Island, BC
14. Langara Island, BC
15. Moira Sound, Alaska
16. Hetta Inlet, Alaska
17. Point Eugenia, Mexico
18. La Jolla, California
19. Auke Bay, Alaska

at both the southern and northern extremes of their geographic range (Fig. 1). Shown in Fig. 2 are the metabolites **1–15** that have been isolated from specimens collected in Southern California along with the dietary sponge source where it is known (2). As illustrated, the Southern California specimens yielded sesquiterpenoid and sesterterpenoid furans along with a number of sesquiterpenoid isonitriles, isothiocyanates, and formamides. Shown in Fig. 3 are the terpenoids **1**, **7**, **9**, and **16–29**, which have been reported to date from *C. luteomarginata* specimens collected at various sites along the coast of British Columbia all the way from Vancouver to the Alaskan border (1, 3–7). There are some similarities and some clear differences between the terpenoids reported from the B.C. and California populations of *C. luteomarginata*. Both groups of nudibranchs yielded sesquiterpenoid furans, isonitriles, isothiocyanates, and formamides; however, only three specific compounds, furodysinin (**1**), isonitrile **7**, and formamide **9**, have been reported from both populations. The B.C. specimens are unique in that they contain the drimane sesquiterpenoid albicanyl acetate (**19**) as the major constituent and the degraded sesterterpenoid luteone (**20**) as a minor constituent in their extracts at nearly all locations from Vancouver to Alaska. A group of degraded and rearranged spongian diterpenoids (i.e., **22–24**) and a marginatane diterpenoid (**21**), whose occurrence is very site dependent, have also been found in the B.C. specimens but have not been reported from the California specimens.

The terpenoid chemistry of *C. luteomarginata* has continued to attract our attention for a number of reasons. First, *C. luteomarginata*'s capacity for feeding on and efficiently sequestering terpenoid metabolites from a wide variety of sponge species makes it a useful surrogate for investigations of the terpenoid constituents of many sponges in B.C. waters that are rare and, therefore, not readily collectable in sufficient quantities for direct chemical studies. Thus, we have continued to collect specimens from as many different B.C. sites as possible in an attempt to identify novel terpenoids. Second, the true origin of *C. luteomarginata* terpenoids is of considerable interest. There is indirect evidence that *C. luteomarginata* might have the capability of making some terpenoids via de novo biosynthesis or perhaps even modifying some sequestered metabolites. Thus, we have attempted to link as many *C. luteomarginata* skin metabolites as possible directly to a sponge source. Finally, there has been an ongoing interest in understanding what ecological role if any the terpenoids might play. An opportunity to examine the terpenoid constituents in a *C. luteomarginata* egg mass has helped to identify one possible ecological role as well as shedding some light on the question of de novo biosynthesis. Presented below are the results of our recent chemical investigations of *C. luteomarginata* skin extracts, egg masses, and dietary sponges. These studies have led to the identification of the novel terpenoids **30**, **32**, **35**, **38**, and **39** from the nudibranch skin extracts, the new drimane sesquiterpenoid **40** from the nudibranch's egg mass, the new sesquiterpenoids **47** – **49** from the dietary sponge *Pleraplysilla* sp., and the known terpenoids **21** and **37** from the dietary sponge *Aplysilla* sp. One of the new terpenoids, cadlinaldehyde (**30**), has a unprecedented degraded sesterterpenoid skeleton.

Results

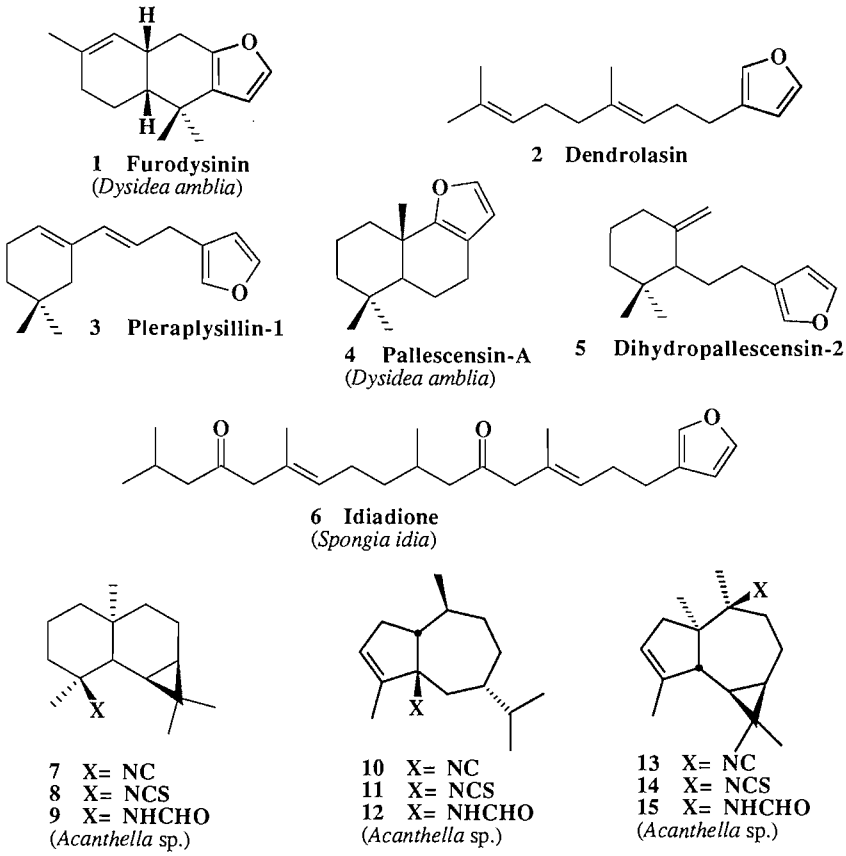
Figure 1 shows the sites along the B.C. coast from which specimens of *C. luteomarginata* have been collected. Animals collected at the Agamemnon Channel, Jervis Inlet site, yielded the known terpenoids albicanyl acetate (**19**) (3), luteone (**20**) (1), and the spongian **31** (12) as well as the new terpenoids cadlinaldehyde (**30**) and the spongian derivative **32**. The known compounds **19** and **31** were identified by comparing their spectroscopic data with literature values. Luteone (**20**), an extremely volatile compound that is largely responsible for the pleasant odor of B.C. specimens of *C. luteomarginata*, was originally isolated in trace amounts only as its nonvolatile dinitrophenylhydrazone derivative (1). The Agamemnon Channel collection of *C. luteomarginata* provided sufficient quantities of the underivatized luteone (**20**) to permit for the first time a complete assignment of its ^{1}H and ^{13}C NMR spectra as presented in Table 1.

Cadlinaldehyde (**30**) was obtained as optically active colorless needles (mp 65°C) that gave a parent ion in the HREIMS at *m/z* 318.2489 corresponding to a molecular formula of $C_{21}H_{34}O_2$. The ^{13}C/APT and HMQC spectra (Table 1) of **30** identified resonances for all 21 carbons (4 × C, 4 × CH, 9 × CH_2, 4 × CH_3) and they further showed that all of the protons

Can. J. Chem. Downloaded from www.nrcresearchpress.com by 88.146.161.215 on 09/08/12
For personal use only.

© 1997 NRC Canada

Fig. 2. Terpenoids isolated from Southern California specimens of *Cadlina luteomarginata* (2).



in the molecule were attached to carbon atoms. Only one site of unsaturation, represented by an aldehyde functionality (^{13}C δ 206.4: ^{1}H δ 10.7), could be directly identified from the NMR data, indicating that cadlinaldehyde had to be tetracyclic in order to satisfy the unsaturation number of five required by the molecular formula. A quaternary carbon at δ 79.5 (C13) and a methylene carbon at δ 64.9 (C16) could be assigned to the attachment points of the remaining oxygen atom in **30**, which had to be present as an ether. One of the methylene protons (H16: δ 3.80) attached to the carbon at δ 64.9 (C16) showed a strong HMBC correlation to the carbon at δ 79.5 (C13) confirming the ether linkage. COSY correlations observed between both of the geminal methylene proton resonances at δ 3.80 (H16) and 3.88 (H16′) and a pair of geminal methylene proton resonances at δ 1.70 (H15) and 1.80 (H15′), and between the methylene resonance at δ 1.70 (H15) and a methine proton resonance at δ 1.39 (H14), identified an -O-CH_2-CH_2-CH- fragment. A singlet methyl proton resonance at δ 0.98 (Me21) showed HMBC correlations to a methylene carbon resonance at δ 39.2 (C12), to the quaternary ether carbon resonance at δ 79.5 (C13), and to a methine carbon resonance at δ 59.5 (C14), which in turn showed a HMQC correlation to the proton resonance at δ 1.39 (H14). The latter pair of HMBC correlations indicated that the ether was part of a tetrahydrofuran fragment that was joined to the rest of the molecule through the vicinal quaternary ether (C13: δ 79.5) and methine (C14: δ 59.5) carbons.

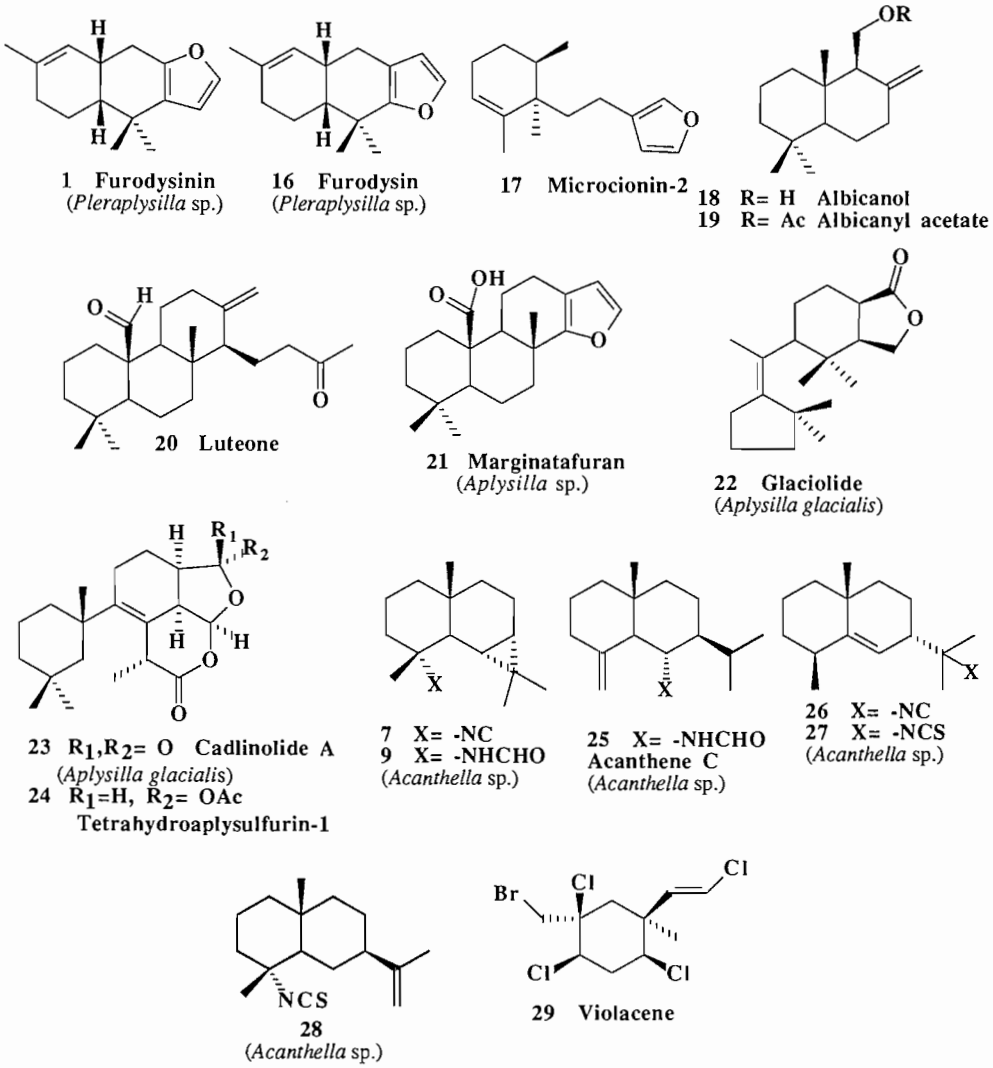
Comparison of the remaining NMR data for cadlinaldehyde (**30**) (Table 1) with the NMR data for luteone (**20**) suggested that the two molecules contained identically substituted *trans* decalin A/B ring systems. Three methyl singlets at δ 0.70, 0.77 and 0.92, assigned to Me19, Me18, and Me17, respectively, along with the aldehyde resonance at δ 10.07 in the ^{1}H NMR spectrum of cadlinaldehyde (**30**) served as useful HMBC antennae to confirm the nature of the A/B ring system. The Me18 ^{1}H resonance at δ 0.77 showed HMBC correlations to ^{13}C resonances assigned to Me17 (δ 31.9), C3 (41.7), C4 (33.6), and C5 (55.6), while the aldehyde ^{1}H resonance at δ 10.07 showed HMBC correlations to ^{13}C resonances assigned to C10 (δ 53.4) and C1 (34.4). A proton resonance at δ 2.49 ($H1_{eq}$), which showed a HMQC correlation to the methylene carbon at δ 34.4 (C1), gave HMBC correlations to ^{13}C resonances assigned to C5 (δ 55.6) and C3 (41.7). The $H1_{eq}$ resonance at δ 2.49 also showed COSY correlations to its geminal partner at δ 0.70 ($H1_{ax}$) and to the H2/H2′ geminal methylene proton resonances at δ 1.26 and 1.42, which in turn showed HMBC correlations to the C3 resonance at δ 41.7. A HMQC correlation between the H2/H2′ resonances at δ 1.26 and 1.42 and a methylene carbon resonance at δ 19.3 completed the assignments for the A ring of cadlinaldehyde (**30**) and, along with the HMBC and COSY correlations described above, confirmed the proposed connectivity.

The Me19 ^{1}H resonance at δ 0.70 showed HMBC correlations to ^{13}C resonances assigned to C7 (δ 40.4), C8 (36.5), C9 (61.4), and the methine carbon (C14: 59.5) of the tetrahydrofuran ring. An HMQC correlation showed that the methine carbon resonance at δ 61.4, assigned to C9, was attached to a proton with a chemical shift of δ 1.22 (H9). The H9 proton

Can. J. Chem. Downloaded from www.nrcresearchpress.com by 88.146.161.215 on 09/08/12
For personal use only.

© 1997 NRC Canada

Fig. 3. Terpenoids isolated from British Columbia specimens of *Cadlina luteomarginata* and already reported in the literature (1, 3–7) along with the dietary sponge source where it is known.



resonance (δ 1.22) in turn showed HMBC correlations to the ^{13}C resonances assigned to Me19 (δ 16.6) and C20 (206.4), thereby establishing the C8/C9/C10 connectivity. COSY correlations between H5 (δ 1.24) and $H6_{ax}$ (δ 1.10) confirmed the C5/C6 connectivity and HMBC correlations between the $H7_{eq}$ (δ 1.70) and C5 (δ 55.6), and the $H6_{eq}$ (δ 1.84) and C7 (δ 40.4) and C8 (δ 36.5) resonances, confirmed the presence of the -CH_2-CH_2- bridge between C5 and C8. The Me19 to C14 HMBC correlation described above required that the Me19 bearing quaternary carbon C8 be bonded directly to the tetrahydrofuran methine carbon C14. HMQC correlations were observed between the ^{13}C resonance for the methylene carbon (C12: δ 39.2) attached to the quaternary carbon (C13) of the tetrahydrofuran ring and a pair of proton resonances at δ 1.30 ($H12_{ax}$) and 1.88 ($H12_{eq}$). One of these methylene proton resonances ($H12_{eq}$: δ 1.88) showed a COSY correlation to a vicinal methylene proton resonance at δ 1.77 ($H11_{ax}$), which in turn showed a COSY correlation to a resonance at δ 1.90 ($H11_{eq}$), assigned to its geminal partner, and an HMQC correlation to a methylene carbon resonance at δ 17.4 (C11). An HMBC correlation between the $H12_{eq}$ resonance at δ 1.88 and the C9 resonance at δ 61.4, in conjunction with the COSY, HMQC, and HMBC correlations described above, confirmed the connectivity between C9 and C11.

A series of nOe difference experiments established the relative stereochemistries of the A/B and B/C ring junctions in **30**. Irradiation of H20 (δ 10.07) induced nOes in the Me18 (δ 0.77), Me19 (δ 0.70), and $H6_{ax}$ (δ 1.10) resonances demonstrating that the A and B rings were in chair conformations, that the A/B ring junction was *trans*, and that Me18, Me19, and C20 were all axial. Irradiation of the Me21 resonance at δ 0.98 induced an nOe in the Me19 resonance at δ 0.70 indicating that the B/C ring junction was also *trans*, that ring C was in a chair conformation, and that Me21 was axial. The relative configuration at C14 could not be determined by nOe experiments. To determine the relative configuration at C14 and to confirm the connectivity determined by NMR analysis, cadlinaldehyde (**30**) was subjected to single crystal X-ray diffraction analysis. Figure 5 shows a computer-generated perspective drawing of cadlinaldehyde (**30**) that confirms the

© 1997 NRC Canada

Can. J. Chem. Downloaded from www.nrcresearchpress.com by 88.146.161.215 on 09/08/12
For personal use only.

Can. J. Chem. Downloaded from www.nrcresearchpress.com by 88.146.161.215 on 09/08/12
For personal use only.

Table 1. NMR data recorded in $CDCl_3$ for luteone (**20**) and cadlinaldehyde (**30**).

	20		**30**	
Carbon no.	δ ^{1}H	δ ^{13}C	δ ^{1}H	δ ^{13}C
1 H_{ax}	0.65 m	34.4	0.70 m	34.4
H_{eq}	2.47 br d (J = 13)		2.49 br d (J = 13)	
2 H_{ax}	1.28 m	19.4	1.26 m	19.3
H_{eq}	1.83 m		1.42 m	
3 H_{ax}	1.16 m	41.7	1.17 m	41.7
H_{eq}	1.34 m		1.36 m	
4		33.6		33.6
5	1.25 m	55.1	1.24 m	55.6
6 H_{ax}	1.80 m	18.4	1.10 m	19.9
H_{eq}	1.80 m		1.84 m	
7 H_{ax}	1.20 m	39.5	1.27 m	40.4
H_{eq}	2.03 m		1.70 m	
8		39.8		36.5
9	1.38 m	60.2	1.22 m	61.4
10		53.8		53.4
11 H_{ax}	1.07 m	23.5	1.77 m	17.4
H_{eq}	1.80 m		1.90 m	
12 H_{ax}	1.87 m	37.7	1.30 m	39.2
H_{eq}	2.34 m		1.88 m	
13		147.1		79.5
14	1.60 d (J = 12)	55.2	1.39 m	59.5
15 H	1.48 m	17.6	1.70 m	22.9
H′	1.88 m		1.80 m	
16 H	2.30 m	42.6	3.80 dd (J = 17, 8)	64.9
H′	2.57 ddd (J = 18, 8, 5)		3.88 dt (J = 9, 3)	
17		209.2	0.92 s	31.9
18	2.09 s	30.1	0.77 s	20.8
19	0.91 s	31.9	0.70 s	16.6
20	0.74 s	20.7	10.07 br s	206.4
21	0.57 s	16.2	0.98 s	20.8
22	10.07 d (J = 1)	206.3		
23 H	4.40 br s	106.9		
H′	4.79 d (J = 1)			

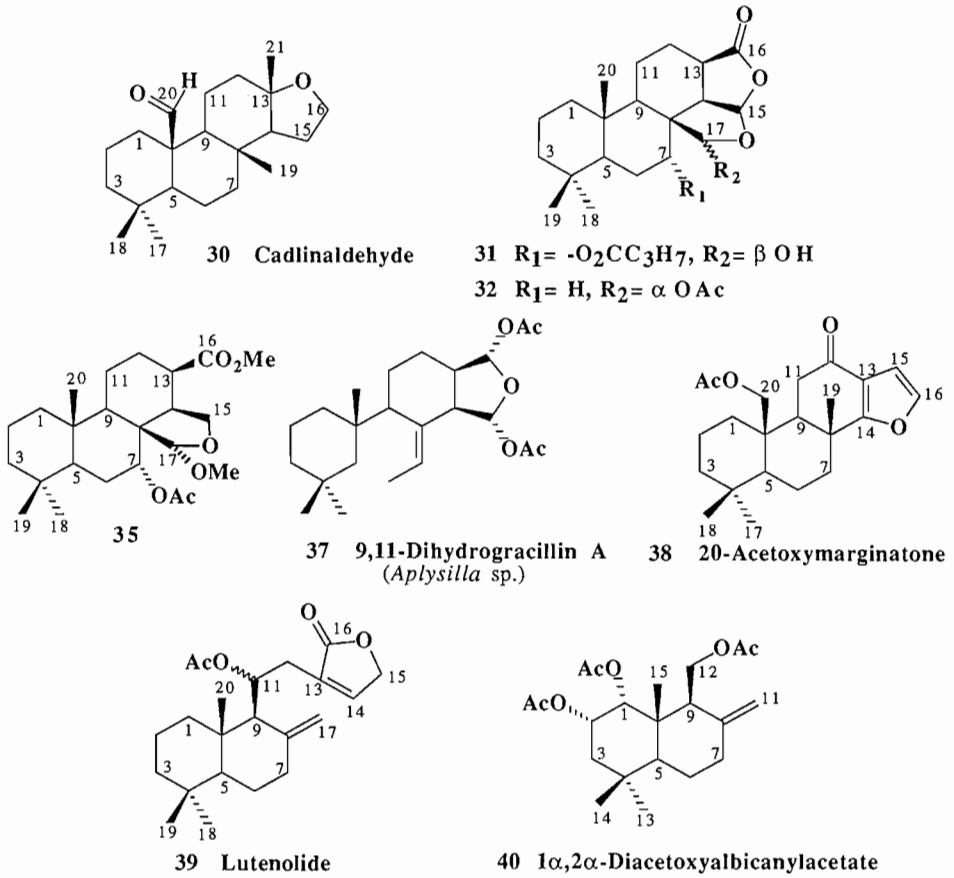
proposed constitution and establishes the relative stereochemistry at C14. Cadlinaldehyde (**30**) has an unprecedented 21 carbon terpenoid skeleton that we have named the cadlinalane skeleton. It seems most likely that cadlinaldehyde (**30**) and luteone (**20**) are degraded sesterterpenoids (Scheme 1).

Spongian **32** was isolated as a colorless oil that gave a parent ion in the HREIMS at *m/z* 376.2249 appropriate for a molecular formula of $C_{22}H_{32}O_5$. Comparison of the ^{1}H and ^{13}C NMR data (Table 2) obtained for **32** with that for the co-occurring known metabolite **31** (12) showed that the two molecules were closely related. Further detailed analysis of the NMR data for **32** showed that it was simply the acetate of the known compound **33**, which was previously isolated from the Australian nudibranch *Ceratosoma brevicaudatum* and the sponge *Dendrilla rosea* (13). The main differences in the ^{1}H NMR data of **32** and **33** are the presence of the acetate resonance (δ 2.04, s, 3H) in **32** and the downfield shift of H17 (**32** δ 6.29: **33** δ 5.50). The α-acetoxy stereochemistry at C17 of **32** was assigned on the basis of the similarity in chemical shift of H17 in **32** (δ 6.29 s) and the known analog **34** (δ 6.20) (13).

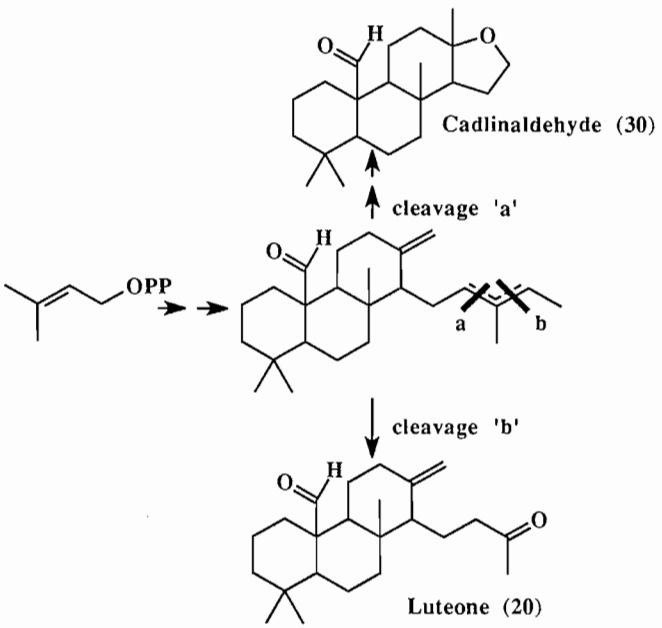
Specimens of *C. luteomarginata* collected at Sanford Island in Barkley Sound yielded the known compounds albicanyl acetate (**19**), luteone (**20**), glaciolide (**22**), and cadlinaldehyde (**30**) along with a new seco-spongian derivative **35**. Seco-spongian **35** was isolated as a colorless oil that gave a parent ion in the HRCIMS at *m/z* 422.26805 appropriate for a molecular formula of $C_{24}H_{38}O_6$. The ^{13}C NMR spectrum of **35** contained resolved resonances for all 24 carbon atoms (Table 2) and the HMQC data indicated that all of the hydrogen atoms were bonded to carbon. Only two sites of unsaturation, represented by ester carbonyls (δ 170.3 and 175.7), could be identified from the ^{13}C NMR data, indicating that **35** was tetracyclic. Comparison of the ^{1}H and ^{13}C NMR data (Table 2) obtained for the seco-spongian **35** with the literature data for the spongian derivative **36** (12) suggested that the two molecules were closely related, even though **36** was pentacyclic and **35** was tetracyclic. The HMBC, HMQC, and COSY data for **35** confirmed that the A, B, and C rings in **35** were identical to those present in **36** and they identified the regions of difference in the two molecules.

© 1997 NRC Canada

Fig. 4. Terpenoids isolated from skin extracts and an egg mass of British Columbia specimens of *Cadlina luteomarginata* during the current study.



Scheme 1. Proposed biogenesis of the luteane and cadlinalane carbon skeletons.



HMBC correlations between a methyl resonance at δ 2.06 (Me22) and a carbonyl resonance at δ 170.3 (C21), and between a deshielded methyl resonance at δ 3.62 (Me23) and a carbonyl resonance at δ 175.7 (C16), identified acetate and methyl ester functionalities in **35**. Additional HMBC correlations between a second deshielded methyl resonance at δ 3.30 (Me24) and a methine carbon resonance at δ 105.2 (C17), and between the H9 (δ1.67) resonance and the same methine carbon resonance (δ 105.2: C18) identified a methyl acetal functionality and tentatively located it at C17. The acetal methine proton resonance (δ 5.16: H17) showed an HMBC correlation to an oxygen-bearing methylene carbon resonance at δ 66.1 assigned to C15, which identified the second alkoxy component of the acetal functionality. HMQC data showed that C15 (δ 66.1) was attached to a pair of protons that gave resonances at δ 3.64 (H15β) and 3.80 (H15α). In the COSY spectrum, the H15 resonances gave correlations to a methine resonance at δ 2.46, assigned to H14 (HMQC to δ 44.4), which was in turn correlated to a methine resonance at δ 2.71, assigned to H13 (HMQC to δ 39.0), thereby identifying an -O-CH_2-CH-CH- fragment. The methine resonance assigned to H13 (δ 2.71) and the carbon it was attached to (C13: δ 39.0) had chemical shifts nearly identical to those assigned to H13 (δ 2.74) and C13 (δ 37.6) in **36**, suggesting that the methyl ester functionality in **35** was attached to C13.

© 1997 NRC Canada

Can. J. Chem. Downloaded from www.nrcresearchpress.com by 88.146.161.215 on 09/08/12
For personal use only.

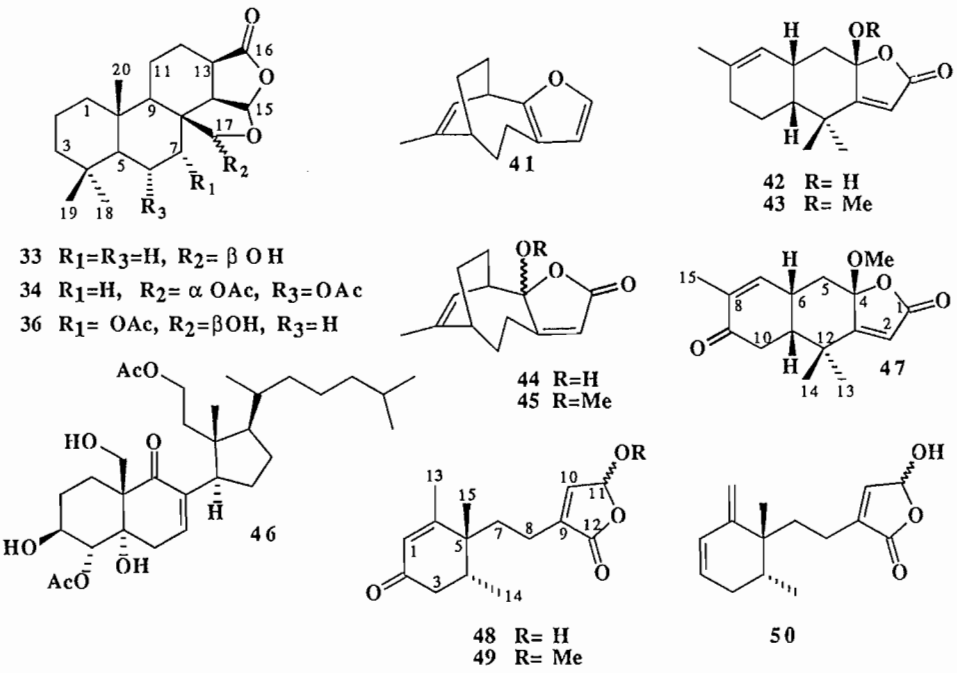
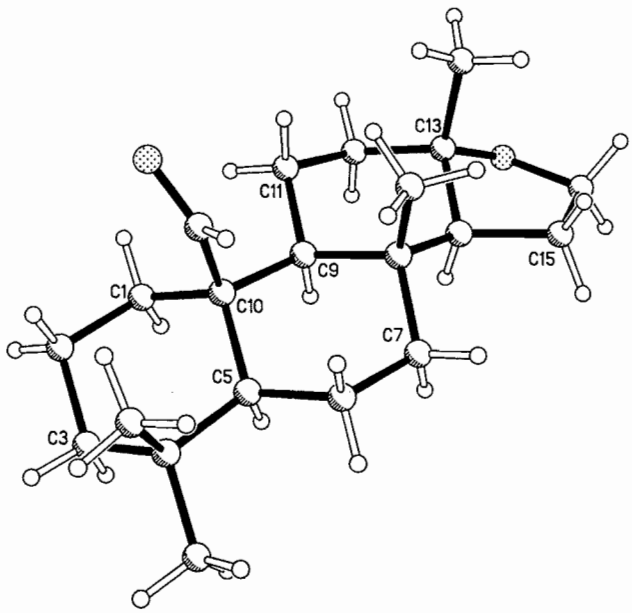


Fig. 5. Computer-generated perspective drawing of cadlinaldehyde (**30**).



A series of difference nOe experiments established the relative stereochemistry in the seco-spongian **35**. Irradiation of H7 (δ 5.28) induced an nOe in H14 (δ 2.46) indicating that H14 was α and H7 was β; irradiation of H17 (δ 5.16) induced an nOe in Me20 (δ 0.87) demonstrating that C17 was axial and that H17 was β; and irradiation of H13 (δ 2.71) induced an nOe in H9 (δ 1.67) that showed that ring C was in a boat conformation with H13 α. The downfield shift of H7 (δ 5.28) in **35** relative to H7 in **36** (δ 4.73) was consistent with the expected deshielding influence of the α-oriented C17 methoxy substituent in **35** relative to the influence on H7 of the β-oriented C17 hydroxyl substituent in **36**.

Specimens of *C. luteomarginata* collected on the eastern side of Anthony Island yielded the known diterpenoids marginatafuran (**21**) and 9,11-dihydrogracillin A (**37**) along with the two new diterpenoids 20-acetoxy-12-marginatone (**38**) and lutenolide (**39**). 9,11-Dihydrogracillin A (**37**) had been previously isolated from the Antarctic sponge *Dendrilla membranosa* (14) and marginatafuran (**21**) had been previously isolated from *C. luteomarginata* (4). Both compounds were identified by comparing their spectroscopic data with the literature values. 20-Acetoxy-12-marginatone (**38**) was isolated as a colorless oil that gave a molecular ion at *m/z* 358.2144 in the HREIMS corresponding to a molecular formula of $C_{22}H_{30}O_4$. The ^{13}C NMR spectrum of **38** showed resolved resonances for all 22 carbon atoms and an APT spectrum indicated that all the protons were attached to carbon (4 × CH_3, 7 × CH_2, 4 × CH, 7 × C) (Table 3). Resonances at δ 193.6 and 174.4 in the ^{13}C NMR spectrum were assigned to ketone and ester carbonyls, respectively, while four deshielded resonances at δ 106.7 (CH), 118.9 (C), 142.3 (CH), and 170.0 (C) were assigned to sp^2 hybridized carbons, accounting for a total of four sites of unsaturation. The remaining four sites of unsaturation required by the molecular formula of **38** had to be present as rings.

A number of features of the NMR data obtained for **38** suggested that it was closely related to the co-occurring diterpenoid marginatafuran (**21**) (Table 3). Thus, the four sp^2 carbons (δ 106.7 (C15), 118.9 (C13), 142.3 (C16), and 170.0 (C14)) and the two attached protons (δ 6.65 (H15) and 6.84 (H16)) could be assigned to an α,β-disubstituted furan ring system identical to the one present in **21**. In addition, the ^1H NMR spectrum of **38** contained three methyl singlet resonances (δ 0.67 (Me18), 0.71 (Me17), and 1.10 (Me19)) as well as a pair of deshielded geminal methylene proton resonances at δ 4.05 (dd, J = 12, 2 Hz: H20) and 4.67 (d, J = 12 Hz: H20′), that made up an isolated spin system assigned to an acetoxymethyl

Can. J. Chem. Downloaded from www.nrcresearchpress.com by 88.146.161.215 on 09/08/12
For personal use only.

© 1997 NRC Canada

Can. J. Chem. Downloaded from www.nrcresearchpress.com by 88.146.161.215 on 09/08/12
For personal use only.

Table 2. NMR data for the spongian diterpenoids **31** ($CDCl_3$), **32** (C_6D_6), **33** ($CDCl_3$), **34** ($CDCl_3$), **35** ($CDCl_3$), and **36** ($CDCl_3$).

Carbon no.	**31** δ ^{1}H	**32** δ ^{1}H	**32** δ ^{13}C	**33** δ ^{1}H	**34** δ ^{1}H	**35** δ ^{1}H	**35** δ ^{13}C	**36** δ ^{1}H
1 H_{ax}		0.9 m	39.0			0.93 m	39.0[b]	
H_{eq}		1.69 m				1.66 m		
2 H_{ax}		1.42 m	18.7			1.43 m	18.5	
H_{eq}		1.5 m				1.65 m		
3 H_{ax}		1.1 m	41.8			1.16 m	41.8	
H_{eq}		1.4 m				1.40 m		
4			[a]				32.6	
5	1.28 dd (J = 15, 2)	0.9 m	55.3		1.13 d (J = 12)	1.30 m	48.5	1.28 dd (J = 15, 2)
6 H_{ax}	1.64 td (J = 15, 2)	1.57 m	19.9	1.34 qd (J = 12, 3)	5.39 td (J = 12, 4)	1.57 m	24.9	
H_{eq}	1.85 dt (J = 15, 2)	1.6 m		1.62 m		1.80 m		1.85 dt (J = 15, 2)
7 H_{ax}	4.76 t (J = 3)	1.13 m	41.7	1.08 td (J = 12, 4)	2.61 dd (J = 12, 4)			
H_{eq}		1.9 m		1.87 dt (J = 12, 3)	1.15 t (J = 12)	5.28 t (J = 5)	73.6	4.75 t (J = 3)
8			[a]				52.6	
9		1.3 dd (J = 12, 3)	56.8	1.46 br d (J = 13)		1.67 m	44.8	
10			[a]				38.2	
11 H_{ax}	1.5 m	1.19 td (J = 15, 3)	16.6	1.64 m		1.40 m	14.7	1.5 m
H_{eq}	1.99 qd (J = 13, 4)	1.94 dt (J = 14, 3)		1.93 qd (J = 12, 4)		1.65 m		1.95 qd (J = 13, 4)
12 H_{ax}	1.6 m	1.6 m	23.7	1.60 m	1.92 m	1.81 m (2H)	19.0	1.6 m
H_{eq}	2.38 dm (J = 14)	2.45 br d (J = 13)		2.40 br dt (J = 12, 2)	2.03 m			2.37 dm (J = 14)
13	2.74 br dd (J = 12, 7)	2.76 dd (J = 11, 7)	37.5	2.72 br dd (J = 12, 8)	2.61 m	2.71 m	39.1[b]	2.74 dd (J = 11, 8)
14	2.85 dd (J = 12, 6)	2.65 dd (J = 11, 6)	49.2	2.58 dd (J = 12, 6)	2.82 dd (J = 9, 5)	2.46 m	44.4	2.87 dd (J = 12, 6)
15 H	6.04 d (J = 6)	6.10 d (J = 6)	104.2	6.08 d (J = 6)	6.02 d (J = 5)	3.64 dd (J = 10, 2)	66.1	6.03 d (J = 6)
H′						3.80 dd (J = 10, 7)		
16			[a]				175.7	
17	5.48 s	6.29 s	100.6	5.50 br s	6.20 s	5.16 s	105.2	5.48 s
18	0.75 s	0.86 s	33.4	0.82 s[b]	1.02 s	0.75 s	33.3	0.77 s
19	0.78 s	0.80 s	21.3	0.86 s[b]	0.87 s	0.77 s	21.3[c]	0.81 s
20	0.93 s	0.72 s	15.6	0.92 s[b]	0.79 s	0.87 s	14.7	0.93 s
21			[a]				170.3	
22	2.37 t	2.04 s	21.5		2.06 s	2.06 s	21.4[c]	2.14 s
23	1.67m					3.62 s	51.6	
24	0.99 m				2.28 s	3.30 s	55.0	

[a]Signal not seen due to sample size.
[b,c]Assignments in the same column may be interchanged.

© 1997 NRC Canada

Can. J. Chem. Downloaded from www.nrcresearchpress.com by 88.146.161.215 on 09/08/12
For personal use only.

Table 3. NMR data for marginatafuran (**21**) (C_6D_6), 20-acetoxy-12-marginatone (**38**) ($CDCl_3$), and lutenolide (**39**) ($CDCl_3$).

Carbon no.	21		38		39	
	δ ^{1}H	δ ^{13}C	δ ^{1}H	δ ^{13}C	δ ^{1}H	δ ^{13}C
1 H_{ax}	0.64 dd (J = 13, 4)	38.6	0.41 m	34.2	1.07 m	39.0
H_{eq}	2.53 d (J = 13)		1.79 br d (J = 13)		1.75 m	
2 H_{ax}	1.40 m (2H)	20.5	1.5 m	17.9	1.5 m	19.1
H_{eq}			1.27 m			
3 H_{ax}	1.00 m	42.5	0.94 dd (J = 14, 4)	41.5	1.14 m	41.9
H_{eq}	2.29 m		1.25 m		1.37 m	
4		33.8		32.8		[a]
5	0.79 dd (J = 8, 4)	56.5	0.62 dd (J = 13, 4)	56.3	0.99 m	56.2
6 H_{ax}	1.54 m	19.1	1.16 m	18.3	1.34 m	24.4
H_{eq}	2.35 dm (J = 12)		1.35 m		1.69 m	
7 H_{ax}	1.40 m	37.3	1.24 m	36.0	1.96 m	39.2
H_{eq}	2.34 m		2.08 dd (J = 13, 3)		2.35 dm (J = 12)	
8		37.4		37.4		144.8
9	1.36 m	56.0	1.5 m	55.1	1.82 m	59.6
10		48.6		40.6		[a]
11 H_{ax}	1.74 dd (J = 13, 6)	20.9	2.75 m (2H)	38.4	5.59 t (J = 8)	70.2
H_{eq}	2.06 ddd (J = 13, 12, 6)					
12 H_{ax}	2.21 ddd (J = 16, 12, 6)	23.3		193.6	H 2.61 dd (J = 15, 5)	30.5
H_{eq}	2.35 m				H′ 2.83 dd (J = 15, 8)	
13		113.9		118.9		130
14		159.5		170.0	7.19 s	145.8
15	5.99 d (J = 2)	110.2	6.65 d (J = 2)	106.7	4.74 d (J = 2) (2H)	70.2
16	7.08 d (J = 2)	140.5	6.84 d (J = 2)	142.3		[a]
17 H	0.87 s	33.7	0.71 s	33.5	5.00 br s	110.4
H′					5.12 s	
18	1.02 s	22.9	0.67 s	20.4	0.83 s	33.7
19	1.31 s	20.0	1.10 s	19.2	0.79 s	21.7
20 H		182.4	4.05 dd (J = 12, 2)	64.2	0.81 s	15.8
H′			4.67 d (J = 12)			
21				174.4		171
22			1.58 s	21.6	1.99 s	21.5

[a]Signal not seen due to small sample size.

residue, thereby accounting for the four quaternary methyl appendages required by the marginatane diterpenoid skeleton. The acetoxy, ketone, and furan functionalities accounted for all four oxygen atoms present in the molecular formula of **38**. What remained was to identify the location of the ketone and acetoxy functionalities on the marginatane skeleton. The relatively shielded chemical shift of the ketone carbonyl (δ 193.6) indicated that it was conjugated and, therefore, it had to be situated at C12 in **38**. COSY and HMQC data identified an isolated spin system consisting of a methine proton resonance at δ 1.5 (H9) and a pair of methylene protons resonances at δ 2.75 (H11, H11′). The only position on the 12-ketomarginatane skeleton to situate an isolated -CH-CH_2- spin system was at C9/C11. In support of this assignment was the observed chemical shift of the methylene protons (δ 2.75: H11, H11′), which was consistent with a placement adjacent to the C12 ketone functionality.

A series of difference nOe experiments and long-range COSY correlations identified the location of the acetoxymethyl group and established the relative stereochemistry of **38**. Irradiation of the H11/H11′ resonance at δ 2.75 induced nOe's in resonances assigned to $H1_{eq}$ (δ 1.79), H9 (1.5), Me19 (1.10), and the acetate methyl (1.58); irradiation of the H20′ resonance at δ 4.67 induced nOe's in resonances assigned to H20 (δ 4.05), Me18 (0.67), and $H2_{ax}$ (1.5); irradiation of the H20 resonance at δ 4.05 induced nOe's in resonances assigned to H20′ (δ 4.67), Me19 (1.10), and $H6_{ax}$ (1.16). This set of nOe's was only consistent with the *trans/anti/trans* stereochemistry of the A/B/C rings and the placement of the acetoxymethyl group at C20 as shown in **38**. COSY correlations, assigned to W coupling, observed between H20′ (δ 4.67) and H9 (1.5) and between H20 (δ 4.05) and $H1_{ax}$ (δ 0.41) were consistent with this assignment.

Lutenolide (**39**) was isolated as a colorless oil that failed to give a parent ion in the HREIMS. The highest mass peak observed in the HREIMS was at *m/z* 300.2091 corresponding to a molecular formula of $C_{20}H_{28}O_2$. Analysis of the NMR data for **39** (Table 3) indicated that this peak corresponded to loss of acetic acid from the molecular ion of an acetoxy diterpenoid, leading to the molecular formula $C_{22}H_{32}O_4$ for the intact natural product. A (M + NH_4) peak observed at *m/z* 378 in the LRCIMS of **39** confirmed this interpretation. The limited

© 1997 NRC Canada

Can. J. Chem. Downloaded from www.nrcresearchpress.com by 88.146.161.215 on 09/08/12
For personal use only.

quantity of lutenolide that was available gave a very weak ^{13}C NMR spectrum that showed resonances for all of the carbons except the two ester carbonyls (C16 and C21) and the two aliphatic quaternary carbons (C4 and C10). Resonances were present in the ^1H NMR spectrum of **39** that could be assigned to a pair of olefinic methylene protons (δ 5.00, bs, H17 and 5.12, bs H17': HMQC correlation to δ 110.4), to an acetoxy methine (δ 5.59, H11 and 1.99, s, 3H, Me22), to three quaternary methyls (δ 0.79, s, 3H, Me19; 0.81, s, 3H, Me20; 0.83, s, 3H, Me18), to a proton on a trisubsituted olefin (δ 7.19, H14), and to a pair of oxymethylene protons (δ 4.74, m, 2H, H15/H15'). The IR spectrum contained two carbonyl stretching bands at 1735 and 1752 cm^{-1} that were both assigned to ester functionalities, accounting for the four oxygen atoms in the molecular formula. An HMBC correlation between the acetate methyl proton resonance at δ 1.99 and a carbon resonance at δ 171 confirmed the presence of the acetoxy group. The strongly deshielded chemical shift of the olefinic methine proton resonance (δ 7.19: H14) and of the corresponding carbon resonance (δ 145.8: C14) indicated that the proton was on the β carbon of an α,β-unsaturated ester substructure. A strong COSY correlation between the olefinic methine proton resonance (δ 7.19: H14) and the two proton oxymethylene resonances at δ 4.74 (H15/H15') indicated that olefin and methylene protons were vicinal to each other. Linking the carbonyl of the α,β-unsaturated ester to the oxygen atom of the oxymethylene group attached to the β carbon of the unsaturated ester system identified a butenolide substructure in **39** as shown.

The butenolide, acetoxy, and olefinic methylene functionalities accounted for five of the seven sites of unsaturation required by the molecular formula of lutenolide, indicating that the remainder of the structure had to be bicyclic. COSY data helped elucidate the remaining portion of the molecule and link it to the already identified fragments. The acetoxy methine proton resonance at δ 5.59 (H11) showed COSY correlations to a pair of geminal methylene proton resonances at δ 2.61 (H12) and 2.83 (H12') that were in turn correlated to each other. Correlations in the long-range COSY spectrum between both the methylene proton resonances (δ 2.61 (H12) and 2.83 (H12')) and the butenolide olefinic methine proton resonance at δ 7.19 (H14) could be assigned to homoallylic coupling, thereby linking the methylene carbon of the -CH_2-CHOAc- fragment to the α carbon (C13) of the butenolide. Additional correlations in the long-range COSY spectrum between the acetoxy methine resonance (δ 5.59, H11) and a methine proton resonance at δ 1.82 (H9), and between this methine resonance (H9) and the olefinic methylene proton resonance at δ 5.12 (H17'), linked the methine carbon (C11) of the -CH_2-CHOAc- fragment to the quaternary carbon of the olefin (C8) via an intermediate methine carbon (C9).

Comparison of the remaining NMR data for lutenolide (Table 3) with the NMR data for albicanyl acetate (**19**) (1) (Table 4) revealed a close correspondence, suggesting that the two molecules had identical A/B ring systems and leading to the proposed overall structure **39** for lutenolide. COSY, HMBC, and difference nOe data supported this assignment. The long-range COSY spectrum showed correlations between the olefinic methylene proton resonance at δ 5.00 (H17) and a methylene proton resonance at δ 1.96 that was assigned to $H7_{ax}$. In the normal COSY spectrum, the $H7_{ax}$ resonance (δ 1.96) showed correlations to resonances at δ 2.35, assigned to $H7_{eq}$, and to δ 1.34 and 1.69, assigned to $H6_{ax}$ and $H6_{eq}$, respectively. The $H6_{ax}$ (δ 1.34) and $H6_{eq}$ (1.69) resonances showed further COSY correlations to a methine resonance at δ 0.99 that was assigned to H5. HMBC correlations consistent with the proposed structure **39** were observed between the Me20 proton resonance at δ 0.81 and carbon resonances assigned to C1 (δ 39.0) and C9 (δ 59.6); between the Me19 proton resonance at δ 0.79 and carbon resonances assigned to C3 (δ 41.9) and Me18 (δ 33.7); between the Me18 proton resonance at δ 0.83 and carbon resonances assigned to C3 (δ 41.9), C5 (δ 56.2), and Me19 (δ 21.7); between the H17 and H17' proton resonances at δ 5.00 and 5.12 and carbon resonances assigned to C9 (δ 59.6) and C7 (δ 39.2); and between both the H12 and H15/H15' proton resonances at δ 2.83 and 4.74, respectively, and a carbon resonance at δ 130, assigned to C13. The similarity in the ^{13}C NMR chemical shifts assigned to the A/B rings of lutenolide and those of the corresponding carbons in albicanyl acetate (**19**) indicated that the A/B rings and substituents in lutenolide had the relative stereochemistry shown in the proposed structure **39**. Irradiation of the H5 resonance at δ 0.99 induced a difference nOe in the H9 resonance at δ 1.82 in agreement with this stereochemical assignment. The relative stereochemistry at C11 in **39** remains undetermined.

A chance encounter with a specimen of *C. luteomarginata* that was laying eggs at a dive site in Rennell Sound provided us with an opportunity to examine the egg mass for the presence of terpenoids. Extracts of the single egg mass yielded small samples of two drimane terpenoids whose ^1H NMR data indicated that they were mono- and diacetoxy derivatives of albicanyl acetate (**19**). Only one of the albicanyl acetate derivatives, 1α,2α-diacetoxyalbicanylacetate (**40**), was obtained in sufficient quantity to permit complete structural characterization. Compound **40** was isolated as a colorless oil that failed to show a molecular ion in the HREIMS. The highest mass observed in the HREIMS of **40** was at *m/z* 320.1985 corresponding to an elemental composition of $C_{19}H_{28}O_4$. Complete analysis of the NMR data for **40** revealed that it was a diacetoxy derivative of albicanyl acetate (**19**) and, therefore, the MS peak at *m/z* 320.1985 could be assigned to a fragment ion formed by loss of acetic acid from the natural product.

The ^1H NMR spectrum of **40** (Table 4) contained three deshielded resonances at δ 1.94 (s, 3H), 1.96 (s, 3H), and 2.16 (s, 3H) that were assigned to acetate methyls; two deshielded methine proton resonances at δ 5.18 (ddd, J = 12, 5, 3 Hz: H2) and 5.25 (bs: H1), assigned to acetoxy methine protons; a pair of deshielded geminal methylene protons resonances at δ 4.08 (dd, J = 11, 10 Hz : H12) and 4.18 (dd, J = 11, 3 Hz: H12'), assigned to an acetoxy methyl residue; a pair of deshielded resonances at δ 4.65 (bs: H11) and 4.95 (bs: H11'), assigned to a pair of olefinic methylene protons; and three shielded methyl resonances at δ 0.92 (s, 3H: Me15), 0.93 (s, 3H: Me14), and 1.02 (s, 3H: Me13), assigned to three quaternary methyl groups. COSY correlations were observed between both of the acetoxy methyl resonances at δ 4.08 (H12) and 4.18 (H12') and an aliphatic methine resonance at δ 2.48, assigned to H9, and between the aliphatic methine resonance (δ 2.48: H9) and the olefinic methylene proton resonances at δ 4.65 (H11) and 4.95 (H11'). The fragment defined by the above COSY correlations in **40** corresponded to the C11/C8/C9/C12 substructure

© 1997 NRC Canada

Can. J. Chem. Downloaded from www.nrcresearchpress.com by 88.146.161.215 on 09/08/12
For personal use only.

Table 4. NMR data recorded in $CDCl_3$ for albicanylacetate (**19**) and 1α,2α-diacetoxyalbicanylacetate (**40**).

Carbon no.	**19**		**40**	
	δ ^{1}H	δ ^{13}C	δ ^{1}H	δ ^{13}C
1 H	1.25 m	39.0	5.25 br s	73.2
H′	1.68 m			
2 H	1.45 m	19.2	5.18 ddd (*J* = 12, 5, 3)	68.4
H′	1.52 qt (*J* = 14, 3)			
3 H	1.19 m	41.9	1.42 dd (*J* = 12, 4)	40.0
H′	1.37 dm (*J* = 13)		1.80 t (*J* = 12)	
4		33.5		[a]
5	1.09 dd (*J* = 13, 3)	55.1	1.59 dd (*J* = 11, 4)	48.5
6 H	1.29 qd (*J* = 13, 4)	23.9	1.33 m	22.7
H′	1.68 m		1.75 dm (*J* = 13)	
7 H	1.99 m	37.8	2.00 m	37.4
H′	2.36 ddd (*J* = 13, 4, 2)		2.40 dm (*J* = 12)	
8		146.8		145.4
9	2.00 m	54.7	2.48 dm (*J* = 10)	48.4
10 H		38.9		
H′				[a]
11 H	4.47 d (*J* = 1)	107.1	4.65 br s	109.6
H′	4.81 d (*J* = 1)		4.95 br s	
12 H	4.14 dd (*J* = 11, 9)	61.6	4.08 dd (*J* = 11, 10)	60.8
H′	4.29 dd (*J* = 11, 4)		4.18 dd (*J* = 11, 3)	
13	0.84 s	33.6	1.02 s	33.4
14	0.77 s	21.7	0.93 s	23.4
15	0.71 s	15.1	0.92 s	14.7
16		171.4		[a]
17	1.97 s	21.1	2.16 s[b]	21.0[b]
18				[a]
19			1.96 s[b]	20.9[b]
20				[a]
21			1.94 s[b]	20.5[b]

[a]Not seen due to small sample size.
[b]Assignments in the same column may be interchanged.

present in albicanyl acetate (**19**). Long-range COSY correlations were observed between the olefinic methylene proton resonances at δ 4.65 (H11) and 4.95 (H11′) and an aliphatic resonance at δ 2.00, assigned to H7. The H7 resonance showed additional COSY correlations to a resonance at δ 2.40, assigned to its geminal partner H7′, and to a pair of resonances at δ 1.33 and 1.75, assigned to $H6_{ax}$ and $H6_{eq}$, respectively. Both the $H6_{ax}$ (δ 1.33) and $H6_{eq}$ (δ 1.75) resonances showed COSY correlations to a resonance at δ 1.59, assigned to H5. This latter set of COSY correlations confirmed that the C5/C6/C7 portion of the B ring of **40** was identical to that in **19**.

What remained was to locate the positions of the two acetoxy substituents on the available sites at C1, C2, and C3 of ring A in **40**. COSY correlations were observed between the acetoxy methine proton resonance at δ 5.18 (H2) and a pair of geminal methylene proton resonances at δ 1.42 ($H3_{ax}$) and 1.80 ($H3_{eq}$). The second acetoxy methine proton resonance at δ 5.25 (H1) failed to show COSY correlations to either the other acetoxy methine resonance (δ 5.18: H2) or the geminal methylene proton resonances (δ 1.42, $H3_{ax}$: 1.80, $H3_{eq}$). Fortunately, a pair of double resonance experiments involving independent selective irradiation of the two acetoxy methine proton resonances at δ 5.18 (H2) and 5.25 (H1) showed that they were indeed coupled to each other with a very small coupling constant. Therefore, **40** had to contain the substructure -CH_2-CHOAc-CHOAc-. A series of difference nOe experiments, conducted in C_6D_6 for increased dispersion, provided evidence for the placement of the two acetoxy substituents at C1/C2 as well as establishing the relative stereochemistry of **40**. Thus, irradiation of the H1 resonance at δ 5.52 induced nOe's in the H2 (δ 5.34), H12′ (δ 4.45), and Me15 (δ 0.78) resonances; irradiation of the H2 resonance at δ 5.34 induced nOe's in the H1 (δ 5.52), Me14 (δ 0.71), and Me15 (δ 0.78) resonances; irradiation of the Me15 resonance at δ 0.78 induced nOe's in the H1 (δ 5.52), H2 (δ 5.34), H12 (δ 3.94), and Me14 (δ 0.71) resonances; and irradiation of the Me14 resonanace at δ 0.71 induced nOe's in the H2 (δ 5.34), $H3_{eq}$ (δ 1.4), $H6_{ax}$ (δ 1.1), Me13 (δ 0.83), and Me15 (δ 0.78) resonances. The above set of nOe's were consistent only with the regio- and stereochemistry shown for **40**.

Part of our ongoing investigation of *C. luteomarginata* terpenoid chemistry has involved an attempt to determine the

© 1997 NRC Canada

Table 5. NMR data recorded in $CDCl_3$ for the sesquiterpenoids **42**, **47**, **48**, and **49**.

Carbon no.	**42** δ ^{1}H	**42** δ ^{13}C	**47** δ ^{1}H	**47** δ ^{13}C	**48** δ ^{1}H	**48** δ ^{13}C	**49** δ ^{1}H	**49** δ ^{13}C
1		174.8		168.8	5.91 s	128.8	5.90 s	128.8
2	5.67 s	115.3	5.92 s	118.7		198.8		198.4
3 H		169.8		171.0	2.29 m	41.8	2.26 m	41.9
H′					2.37 m		2.35 m	
4		104.9		106.8	2.33 m	33.8	2.30 m	33.6
5 H	1.57 dd (J = 14, 13)	41.2	1.64 dd (J = 14, 13)	38.6		42.1		42.1
H′	2.28 dd (J = 14, 4)		2.47 m					
6	2.80 m	30.4	3.09 m	31.0		167.3		167
7 H	5.36 br dd (J = 6, 2)	123.5	6.74 br d (J = 6)	146.5	1.81 m (2H)	33.9	1.77 m	33.9
H′							1.83 m	
8 H		134.5		135.8	2.03 m	20.5	2.03 m	20.2
H′					2.33 m		2.31 m	
9	1.96 m (2H)	31.0		198.1		138.2		129
10 H	1.12 br ddd (J = 13, 13, 10)	18.7	2.05 dd (J = 17, 15)	35.0	6.87 d (J = 1)	143.1	6.79 br s	142.0
H′	1.70 br ddd (J = 13, 4, 3)		2.47 m					
11	1.63 m	47.3	2.25 dt (J = 15, 4)	47.1	6.11 d (J = 8)	96.4	5.73 br s	102.5
12		38.5		37.6		170.9		[a]
13	1.38 s[b]	25.3[b]	1.22 s[b]	24.7[b]	1.98 s	20.2	1.97 br s	20.5
14	1.21 s[b]	26.8[b]	1.40 s[b]	25.0[b]	1.00 d (J = 6)	15.4	0.99 d (J = 6)	15.4
15	1.61 br s	23.0	1.77 s	15.6	1.06 s	19.4	1.06	19.4
16			3.20 s	50.6			3.58 br s	57.2
O*H*	3.5 br s				3.50 d (J = 8)			

[a]Not seen due to small sample size.
[b]Assignments in the same column may be interchanged.

true origin of the metabolites. Consequently, chemical investigations of sponges collected at the same sites as specimens of *C. luteomarginata* previously resulted in the identification of dietary sponge origins for a number of terpenoids found in skin extracts of B.C. specimens of *C. luteomarginata* (i.e., **22** and **24** from *Aplysilla glacialis* and **25–29** from *Acanthella* sp.). Continuing chemical investigations of sponges found in the same habitats as *C. luteomarginata* have identified two additional undescribed species, a *Pleraplysilla* sp. and an *Aplysilla* sp., which contain terpenoids that have also been found in the nudibranch skin extracts.

Samples of *Pleraplysilla* sp. were collected at Checleset Bay and Botanical Beach, B.C. Extracts of *Pleraplysilla* sp. yielded a number of known terpenoids, including furodysinin (**1**) (15), furodysin (**16**) (15), nakafuran-8 (**41**) (16), furodysinin lactone (**42**) (17), its methoxybutenolide derivative **43** (17), nakafuran-8 lactone (**44**) (16), its methoxy butenolide derivative **45** (16), and blancasterol (**46**) (18), that were identified by comparison of their spectroscopic data to the literature values. The *Pleraplysilla* sp. metabolites furodysinin (**1**) and furodysin (**16**) are two of the more commonly encountered terpenoids in skin extracts of B.C. specimens of *C. luteomarginata*. Three new terpenoids, *O*-methyl-9-oxofurodysininlactone (**47**), 2-oxomicrocionin-2-lactone (**48**), and *O*-methyl-2-oxomicrocionin-2-lactone (**49**), were also isolated from the *Pleraplysilla* sp. extracts.

O-Methyl-9-oxofurodysinin lactone (**47**) was isolated as a colorless glass that gave a parent ion in the HREIMS at *m/z* 276.1371 corresponding to a molecular formula of $C_{16}H_{20}O_4$. Comparison of the ^{1}H NMR data obtained for **47** with those obtained for the co-occurring known metabolites furodysinin lactone (**42**) and *O*-methylfurodysinin lactone (**43**) (17) (Table 5) revealed that the three metabolites were closely related. The major difference in the spectroscopic data for the molecules was ^{13}C NMR (δ 198.1) and IR (1665 cm^{-1}) evidence for the presence of an α,β-unsaturated ketone functionality in **47**. COSY correlations between an olefinic methine proton resonance at δ 6.74, assigned to H7, and olefinic methyl (δ 1.77) and allylic methine (δ 3.09) proton resonances assigned to Me15 and H6, respectively, confirmed the presence of a $\Delta^{7,8}$ olefin in **47**. HMBC correlations between the H7 (δ 6.74) and Me15 (δ 1.77) proton resonances and the ketone carbonyl resonance at δ 198.1 supported the placement of the ketone functionality at C9. All of the remaining COSY, HMBC, HMQC, and difference nOe data obtained for **47** were consistent with the structure shown.

2-Oxomicrocionin-2-lactone (**48**) was obtained as a colorless oil that gave a molecular ion in the HREIMS at *m/z* 264.1317 appropriate for a molecular formula of $C_{15}H_{20}O_4$ requiring six sites of unsaturation. The IR spectrum of **48** contained absorption bands at 1650, 1758, and 3317 cm^{-1} that were assigned to α,β-unsaturated ketone, α,β-unsaturated γ-lactone, and hydroxyl functionalities, respectively, by comparison with the IR data for **47**. ^{13}C NMR resonances at δ 198.8 and 170.9 were assigned to the α,β-unsaturated ketone and α,β-unsaturated γ-lactone carbonyls, respectively, and four deshielded resonances at δ 128.8 (CH), 167.3 (C), 138.2 (C), and 143.1 (CH) accounted for the two olefinic functionalities

© 1997 NRC Canada

Can. J. Chem. Downloaded from www.nrcresearchpress.com by 88.146.161.215 on 09/08/12
For personal use only.

Can. J. Chem. Downloaded from www.nrcresearchpress.com by 88.146.161.215 on 09/08/12
For personal use only.

conjugated to the carbonyls (Table 5). The remaining two sites of unsaturation required by the molecular formula of **48** had to be present as rings. A series of NMR experiments further elaborated the γ-lactone fragment. HMBC correlations were observed between an olefinic methine proton resonance at δ 6.87 (H10) and the lactone carbonyl resonance at δ 170.9 (C12) and an acetal carbon resonance at δ 96.4 (C11). The acetal resonance at δ 96.4 (C11) showed a HMQC correlation to a proton resonance at δ 6.11 (bs: H11) that in turn showed COSY correlations to the olefinic methine proton resonance at δ 6.87 (H10) and to an exchangable proton resonance at δ 3.50 (OH). Additional COSY correlations were observed between the olefinic methine proton resonance at δ 6.11 (H10) and a pair of geminal allylic methylene proton resonances at δ 2.03 (H8) and 2.33 (H8′). The above data suggested the presence of an α-methylene-substituted γ-hydroxy-α,β-butenolide fragment in **48**. Comparison of the data listed above for this fragment in **48** with the data reported for the identical fragment in the known compound **50** (^{1}H NMR δ: 6.1 (C*H*OH), 6.8 (O=C-C=C*H*); ^{13}C NMR δ: 172.5, s, 143.5, d, 138.5, s, 97.3, d; IR: 3380 and 1755 cm^{-1}) confirmed the assignment.

COSY correlations between the allylic methylene proton resonances at δ 2.03 (H8) and 2.33 (H8′) and a two-proton multiplet at δ 1.81, assigned via HMQC data to a pair of geminal methylene protons (H7, H7′: C7 δ 33.9) that showed no additional COSY correlations, expanded the α substituent on the hydroxybutenolide fragment to a -CH_2-CH_2- residue. HMBC, HMQC, and COSY data provided evidence for the remaining cyclohexenone fragment of **48** and linked it to the already identified hydroxybutenolide fragment. Thus, HMBC correlations were observed between a methyl proton resonance at δ 1.06 (s, Me15) and carbon resonances assigned to C4 (δ 33.8), C5 (δ 42.1), C6 (δ 167.3), and C7 (δ 33.9); between a methyl proton resonance at δ 1.00 (d, J = 6 Hz, Me14) and carbon resonances assigned to C3 (δ 41.8), C4 (δ 33.8), and C5 (δ 42.1); between a methyl proton resonance at δ 1.98 (s, Me13) and carbon resonances assigned to C1 (δ 128.8), C5 (δ 42.1), and C6 (δ 167.3); between an olefinic methine proton resonance at δ 5.91 (H1) and carbon resonances assigned to C3 (δ 41.8) and Me13 (δ 20.2); and between a methylene proton resonance at δ 2.29 (H3) and a carbon resonance at δ 198.8 assigned to C2. COSY correlations observed between the H1 resonance (δ 5.91) and the Me13 resonance (δ 1.98), and between the H4 resonance (δ 2.33) and both the H3 (δ 2.29) and H3′ (δ 2.37) resonances, were consistent with the proposed structure **48**. Difference nOe's were observed between H4 (δ 2.33) and Me15 (δ 1.06) and between Me14 (δ 1.00) and H7/H7′ (δ 1.81), indicating that the relative stereochemistry at C4 and C5 was as shown in **48**. 2-Oxomicrocionin-2-lactone (**48**) is closely related to microcionin-2 (**17**) (19), which is frequently encountered in skin extracts of B.C. specimens of *C. luteomarginata*.

O-Methyl-2-oxomicrocionin-2-lactone (**49**) was isolated as a clear glass that gave a molecular ion in the HREIMS at *m/z* 278.1508, corresponding to a molecular formula of $C_{16}H_{22}O_4$. Examination of the NMR data obtained for **49** (Table 5) readily showed that it was simply the C12 methoxy analog of **48**. Since methanol was used in the extraction of terpenoids from *Pleraplysilla* sp. it is likely that **49** is an artifact formed from **48** during the extraction process. Similarly, the -OMe residues in compounds **35**, **45**, **43**, and **47** are also probably artifacts introduced during extraction of *C. luteomarginata* and *Pleraplysilla* sp. specimens with methanol.

Samples of an undescribed species of *Aplysilla* were collected in the high intertidal zone at Botanical Beach on Vancouver Island, B.C. Examination of the terpenoids present in the methanol extracts of the *Aplysilla* sp. revealed the presence of the two known compounds marginatafuran (**21**) and 9,11-dihydrogracillin A (**37**) that have both been found repeatedly in *C. luteomarginata* skin extracts. Compounds **21** and **37** were identified by comparison of their spectroscopic data with the literature values (4, 14). A number of additional unknown terpenoids were also encountered in the extracts of *Aplysilla* sp., and their structures, which are currently under investigation, will be reported elsewhere.

Discussion

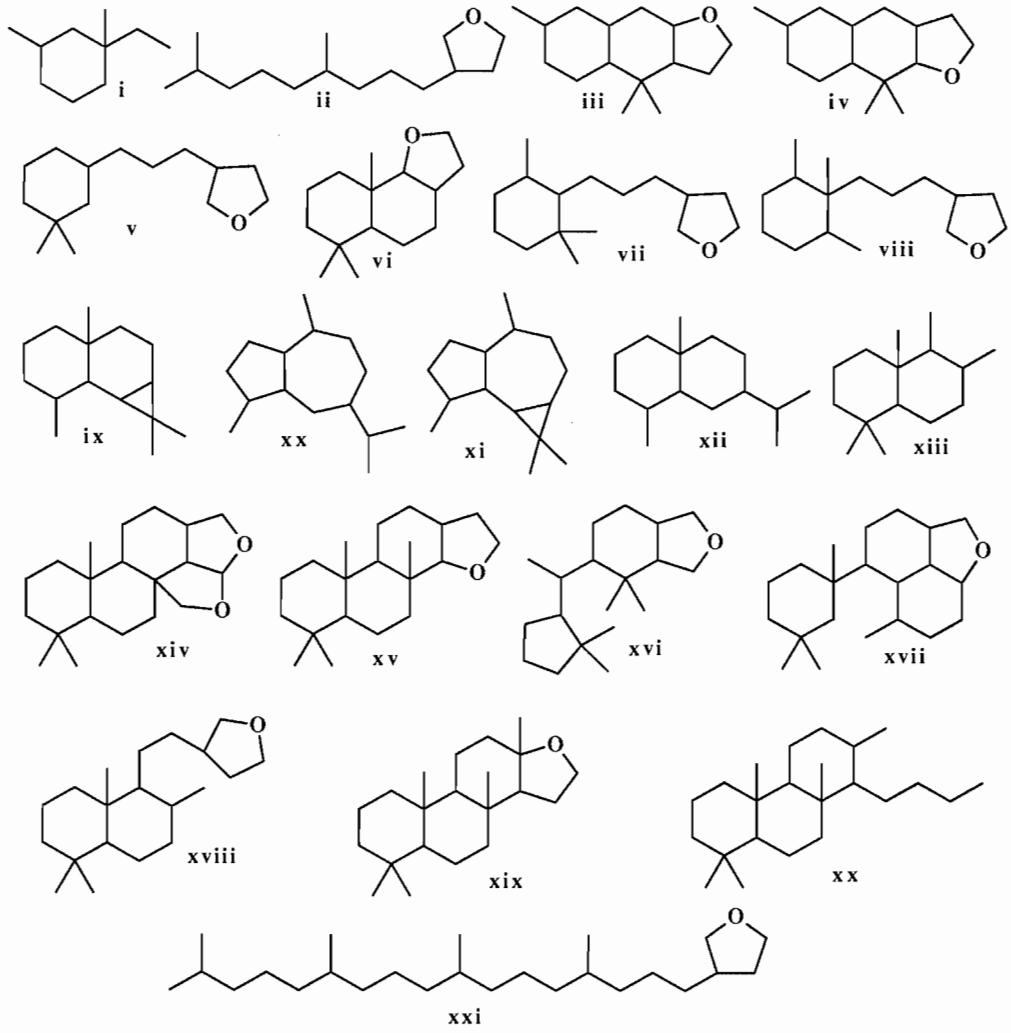
Chemical investigations of *C. luteomarginata* have resulted in the identification of a truly remarkable collection of terpenoid metabolites. To date, a total of 37 terpenoids representing twenty-one different carbon skeletons (Fig. 6) have been isolated from *C. luteomarginata* skin and egg mass extracts. The 21 carbon skeletons include monoterpenoid, sesquiterpenoid, diterpenoid, sesterterpenoid, degraded diterpenoid, and degraded sesterterpenoid representatives. Four of these skeletons, the marginatane (**xv**) (4), glaciane (**xvi**) (5), cadlinalane (**xx**), and luteane (**xxi**) (1) skeletons, were first encountered in *C. luteomarginata* metabolites. The *C. luteomarginata* terpenoids represent a rarely encountered range of biosynthetic diversity in the secondary metabolites obtained from a single living organism. This great metabolite diversity results primarily from *C. luteromarginata*'s highly developed capabilities for sequestering terpenoids from sponges in its diet. Thus, *C. luteomarginata* has not had to develop the biosynthetic capabilities required to make this wide range of compounds de novo.

A number of interesting observations emerge from a more detailed analysis of the relationship between terpenoids isolated from *C. luteomarginata* and terpenoids isolated from putative dietary sponges. The monoterpenoid violacene (**29**) was found in the sponge *Acanthella* sp. collected in the Queen Charlotte Islands. Violacene (**29**) is a known metabolite of red algae in the genus *Plocamium* (20) and its presence in the sponge *Acanthella* sp. can be best explained by the sponge concentrating the compound from exudates of specimens of *Plocamium* species living near to the sponge. A related observation has been reported by Giordano et al. who isolated halogenated metabolites typical of *Laurencia* species of red algae from the Mediterranean sponge *Mycale rotilis* (21). If this scenario is correct, it represents an interesting example of metabolite transfer from a red alga to a sponge and then to a nudibranch. *Acanthella* sp. collected in both the Queen Charlotte Islands and in Southern California contained the isonitrile (i.e., **7**, **10**, **13**, **26**), isothiocyanate (i.e., **8**, **11**, **14**, **27**), and formamide (i.e., **9**, **12**, **15**, **25**) sesquiterpenoids found in skin extracts of specimens of *C. luteomarginata* collected in both locations.

A major group of *C. luteomarginata* metabolites are sesquiterpenoids, diterpenoids, degraded diterpenoids, and sesterterpenoids that appear to have a common biogenetic origin from linear furanoterpenoid precursors. In California

© 1997 NRC Canada

Fig. 6. Carbon skeletons represented in the terpenoids isolated to date from *Cadlina luteomarginata*.



Can. J. Chem. Downloaded from www.nrcresearchpress.com by 88.146.161.215 on 09/08/12
For personal use only.

waters, two of the furanosesquiterpenoids, furodysinin (**1**) and pallescensin-A (**4**), have been found in the dietary sponge *Dysidea amblia*. Idiadione (**6**), the lone furanoseterterpenoid isolated to date from *C. luteromarginata*, has been also found in the California sponge *Spongia idia*. In B.C. waters, the furanosesquiterpenoids furodysinin (**1**) and furodysin (**16**) have now been found in the sponge *Pleraplysilla* sp. The same *Pleraplysilla* sp. contains 2-oxomicrocionin-2-lactone (**48**), an oxidized analog of microcionin-2 (**17**) that has been isolated from B.C. specimens of *C. luteomarginata*. A number of the diterpenoids and degraded diterpenoids isolated from B.C. specimens of *C. luteomarginata* have also been found in two *Aplysilla* sp. collected at the same locales. Thus, *Aplysilla glacialis* has yielded glaciolide (**22**) and cadlinolide A (**23**), while an undescribed species of *Aplysilla* has yielded marginatafuran (**21**) and 9,11-dihydrogracillin A (**37**). Another group of diterpenoids, including tetrahydroaplysulfurin-1 (**24**), the spongians **31**, **32**, **35**, and 20-acetoxy-12-marginatone (**38**), are closely related to known *Aplysilla* metabolites but they have not yet been found in B.C. sponges.

Five terpenoids isolated from B.C. specimens of *C. luteomarginata* do not fit the profile of sequestered metabolites. These are the drimane sesquiterpenoids albicanol (**18**) and albicanyl acetate (**19**) obtained from skin extracts, 1α, 2α-diacetoxyalbicanyl acetate (**40**) obtained from the egg mass, and luteone (**20**) and cadlinaldehyde (**30**) also obtained from skin extracts. Albicanyl acetate (**19**) is the major metabolite found in *C. luteomarginata* extracts at all locations in B.C. and its occurrence over the range of B.C. sites does not show the geographic variation typical of the terpenoids such as furodysinin (**1**) or cadlinolide A (**23**) that are known to be sequestered from sponges. Furthermore, the derivative 1α,2α-diacetoxyalbicanyl acetate (**40**), which was found in the egg mass, has never been found in skin extracts or whole body extracts and, therefore, it seems likely that it is being made in whole or in part by *C. luteomarginata*. Albicanyl acetate (**19**) is a reasonably potent fish antifeedant (2). Therefore, the presence of acetoxy derivatives of **19** in the nudibranch's egg mass suggests a protective role for these compounds and, from an evolutionary perspective, it perhaps makes sense for the nudibranch to produce these compounds de novo in order to have complete control over the critical issue of protection of their egg masses. The possibility of de novo biosynthesis of **18**, **19**, and **40** by *C.*

© 1997 NRC Canada

Can. J. Chem. Downloaded from www.nrcresearchpress.com by 88.146.161.215 on 09/08/12
For personal use only.

luteomarginata has precedent in the literature reports that several other species of dorid nudibranchs, including *Dendrodoris limbata* (22) and *Archidoris montereyensis* (10), are capable of de novo biosynthesis of drimane sesquiterpenoids. It has also been reported that *Dendrodoris grandiflora* sequesters sponge metabolites (23) as well as making drimane sesquiterpenoids via de novo biosynthesis (24) and depositing them in its egg masses.

Luteone (**20**) and cadlinaldehyde (**30**) have unprecedented degraded skeletons comprising 23 and 21 carbon atoms, respectively. The luteane and cadlinalane skeletons can be envisaged to arise from degradation of a common tricyclic sesterterpenoid skeleton as shown in Scheme 1. To date, terpenoids related to **20** and **30** have not been detected in extracts of sponges collected in B.C. Since discovering these two compounds and developing competent analytical methodology for detecting them, it has been found that they are present in skin extracts of all B.C. specimens of *C. luteomarginata*, regardless of collection site. Therefore, luteone (**20**) and cadlinaldehyde (**30**) also fail to show the geographic variation within B.C. collecting sites typical of sequestered metabolites, suggesting that they may be biosynthesized de novo by *C. luteomarginata*. Prompted by the above arguments concerning the true origin of compounds **19**, **20**, and **30**, biosynthetic studies have been initiated with *C. luteomarginata* using the stable isotope methodology recently applied to other dorids found in B.C. waters (9–11). Initial results are consistent with de novo biosynthesis of all three compounds. Full details of these experiments will be published elsewhere.

Experimental

General methods

High-performance liquid chromatography was performed on a Waters 501 system using a Perkin–Elmer LC25 refractive index detector. Optical rotations were determined on a Perkin–Elmer 241MC polarimeter. Ultraviolet spectra were recorded using a Hewlett–Packard 8452A diode array spectrophotometer and IR spectra with a Perkin–Elmer 1710 FTIR instrument. ^{1}H, COSY, and nOe NMR experiments were run on a Bruker WH-400 spectrometer and are recorded in ppm referenced to $CDCl_3$ (δ 7.24) or C_6D_6 (δ 7.15). ^{13}C, HMQC, and HMBC NMR experiments were run on a Bruker AMX-500 spectrometer.

Isolation of luteone (20), cadlinaldehyde (30), spongian 32, and secospongian 35

Specimens of *Cadlina luteomarginata* were collected by SCUBA at depths of 10–50 feet in Agamemnon Channel, Jervis Inlet, and in Barkley Sound, B.C. Each collection of animals was processed separately following the same protocol outlined below. The animals were immersed in methanol immediately upon collection and extracted exhaustively with methanol (two times) and methanol/methylene chloride (1:1) (three times). The extracts were combined, reduced in vacuo, and partitioned between water and ethyl acetate. The ethyl acetate extracts were dried over anhydrous magnesium sulfate, combined, and reduced in vacuo to yield a fragrant yellow oil (≈ 500 mg per 20 animals). This oil was fractionated on a silica gel flash column using a gradient eluent system (9:1 hexanes/ethyl acetate to ethyl acetate). Fractions were further purified by C_{18} reversed-phase high-performance liquid chromatography (9:1 methanol/water) to yield pure albicanyl acetate (**19**), luteone (**20**), cadlinaldehyde (**30**), spongian **31**, and spongian **32** from the Agamemnon Channel specimens and albicanyl acetate (**19**), luteone (**20**), cadlinaldehyde (**30**), and seco-spongian **35** from the Barkley Sound specimens.

Luteone (20): white crystalline solid; $[\alpha]^{25}_D$ ($CHCl_3$) +12; UV ($CHCl_3$) λ_{max}: 244 (log ε = 2.42) nm; IR (film) ν_{max}: 3078, 2931, 2849, 2750, 1708, 1646, 1457, 1363, 1161 cm^{-1}; ^{1}H NMR (see Table 1); ^{13}C NMR (see Table 1); HREIMS *m/z*: 344.2717 ($C_{23}H_{36}O_2$ requires 344.2715).

Cadlinaldehyde (30): white amorphous solid subsequently recrystallized from methanol to yield white needles; $[\alpha]^{25}_D$ ($CHCl_3$) +25; UV ($CHCl_3$) λ_{max}: 246 (log ε = 2.66), 250sh (log ε = 2.59) nm; IR (film) ν_{max}: 2926, 2750, 1705, 1457, 1377 cm^{-1}; ^{1}H NMR (see Table 1); ^{13}C NMR (see Table 1); HREIMS *m/z*: 318.2489 ($C_{21}H_{38}O_2$ requires 318.2589).

Spongian 32: colorless oil; IR (film) ν_{max}: 1784, 1755 cm^{-1}; ^{1}H NMR (see Table 2); ^{13}C NMR (see Table 2); HREIMS *m/z*: 376.2249 ($C_{22}H_{32}O_5$ requires 376.2249).

Seco-spongian 35: clear colorless oil; $[\alpha]^{25}_D$ ($CHCl_3$) −5.5; UV ($CHCl_3$) λ_{max}: 248sh (log ε = 2.64), 252 (log ε = 2.68) nm; IR (film) ν_{max}: 2926, 1737, 1464, 1374, 1241 cm^{-1}; ^{1}H NMR (see Table 2); ^{13}C NMR (see Table 2); HRCIMS *m/z*: 422.26805 ($C_{24}H_{38}O_2$ requires 422.26685); HREIMS *m/z*: 391.24876 (M − MeO $C_{23}H_{35}O_5$ requires 391.24844).

Isolation of 20-acetoxymarginatone (38) and lutenenolide (39)

Specimens of *C. luteomarginata* collected at Anthony Island (Queen Charlotte Islands, B.C.) were immersed in methanol immediately upon collection. After one further extraction, the combined methanol extracts were concentrated in vacuo to give an aqueous suspension that was partitioned between water and methanol/methylene chloride (1:1). The water layer was further extracted with methylene chloride and the organic layers combined, dried over magnesium sulfate, and reduced to dryness in vacuo. The resulting oil was fractionated by sequential application of silica gel flash column chromatography, silica gel radial thin-layer chromatography, and normal phase high-performance liquid chromatography, resulting in pure samples of 20-acetoxymarginatone (**38**) (1.8 mg per animal) and lutenenolide (**39**) (0.05 mg per animal).

20-Acetoxymarginatone (38): clear colorless oil; IR (film) ν_{max}: 2937, 2870, 1738, 1681, 1455, 1441, 1234, 1047 cm^{-1}; ^{1}H NMR (see Table 3); ^{13}C NMR (see Table 3); HREIMS *m/z*: 358.2144 ($C_{22}H_{30}O_4$ requires 358.2144).

Lutenolide (39): clear colorless oil; IR (film) ν_{max}: 2928, 1752, 1735, 1654, 1235, 1061 cm^{-1}; ^{1}H NMR (see Table 3); ^{13}C NMR (see Table 3); LRDCIMS (NH_3) *m/z* 378; HREIMS *m/z*: 300.2091 (M − HOAc $C_{20}H_{28}O_2$ requires 300.2089).

Isolation of monoacetoxyalbicanyl diacetate and 1α,2α-diacetoxyalbicanylacetate (40)

During a SCUBA dive in Rennell Sound, Queen Charlotte

© 1997 NRC Canada

Can. J. Chem. Downloaded from www.nrcresearchpress.com by 88.146.161.215 on 09/08/12
For personal use only.

Islands, B.C., a specimen of *C. luteomarginata* was found to be laying eggs. The egg mass was collected and worked up as described above for the isolation of 20-acetoxymarginatone (**38**) and lutenenolide (**39**). The egg mass extract yielded the pure compounds monoacetoxyalbicanylacetate (0.3 mg) and 1α,2α-diacetoxyalbicanylacetate (**40**) (1.5 mg). The quantity of monoacetoxyalbicanylacetate that was obtained was not sufficient to permit complete characterization.

Monoacetoxyalbicanylacetate: clear colorless oil; ^{1}H NMR (C_6D_6) δ: 0.64 (s, 3H), 0.75 (s, 3H), 0.88 (s, 3H), 1.75 (s, 3H), 2.06 (s, 3H), 2.30 (m, 1H), 2.68 (m, 1H), 4.15 (t, J = 11.6 Hz, 1H), 4.49 (dd, J = 4,0, 11.6 Hz, 1H), 4.81 (bs, 1H), 4.95 (bs, 2H); HREIMS *m/z*: 322.2140 ($C_{19}H_{30}O_4$ requires 320.1988).

*1*α,2α-Diacetoxyalbicanylacetate (**40**): clear colorless oil; IR (film) ν_{max}: 2937, 1736, 1702, 1458, 1364, 1248, 1039 cm^{-1}; ^{1}H NMR (see Table 4); ^{13}C NMR (see Table 4); HREIMS *m/z*: 320.1985 (M − HOAc $C_{19}H_{28}O_4$ requires 320.1988).

Isolation of terpenoids from *Pleraplysilla* sp.

Samples of *Pleraplysilla* sp. were collected from exposed pools during low tide at Botanical Beach on Vancouver Island, B.C. A voucher sample of *Pleraplysilla* sp. was submitted to Professor Rob van Soest at the University of Amsterdam for identification and archival purposes. The sponge specimens were identified as an undescribed species belonging to the genus *Pleraplysilla*. Freshly collected specimens of *Pleraplysilla* sp. (20 g) were soaked in methanol (30 mL) and stored at 7°C for 5 weeks. The extract was filtered and the methanol filtrate was concentrated in vacuo. The resultant dark oil was partitioned between brine (50 mL) and ethyl acetate (4 × 25 mL). The ethyl acetate extracts were pooled, dried over anhydrous sodium sulfate, and evaporated in vacuo to yield a brown oil (68 mg). This oil was fractionated using Sephadex LH-20 size-exclusion chromatography with ethyl acetate/methanol/water (20:5:2) as the eluent. Terpenoid-rich fractions were pooled and further partitioned using silica gel gradient flash chromatography (diethyl ether/dichloromethane (1:19) to ethyl acetate) followed by normal phase high-performance liquid chromatography (hexane/dichloromethane (3:7)) to yield pure furodysinin lactone (**42**) (2 mg), *O*-methyl furodysinin lactone (**43**) (1 mg), nakafuran-8 lactone (**44**) (1 mg), *O*-methyl nakafuran-8 lactone (**45**) (0.2 mg), blancasterol (**46**) (1 mg), *O*-methyl 9-oxofurodysinin lactone (**47**) (0.5 mg), 2-oxomicrocionin-2 lactone (**48**) (0.8 mg), and *O*-methyl 2-oxomicrocionin-2 lactone (**49**).

O-*Methyl 9-oxofurodysinin lactone (**47**)*: colorless glass; UV λ_{max} (hexane): 220 nm (log ε = 3.43); IR (film) ν_{max}: 1767, 1665 cm^{-1}; CD (hexane) $(\Theta)_{223}$ −31 000; ^{1}H NMR (see Table 5); ^{13}C NMR (see Table 5); HREIMS *m/z*: 276.1371 ($C_{16}H_{20}O_4$ requires 276.1362).

*2-Oxomicrocionin-2 lactone (**48**)*: colorless oil; IR (film) ν_{max}: 3317, 1758, 1650 cm^{-1}; ^{1}H NMR (see Table 5); ^{13}C NMR (see Table 5); HREIMS *m/z*: 264.1317 ($C_{15}H_{20}O_4$ requires 264.1322)

O-*Methyl 2-oxomicrocionin-2 lactone (**49**)*: translucent white glass; IR (film) ν_{max}: 1764, 1663 cm^{-1}; ^{1}H NMR (see Table 5); ^{13}C NMR (see Table 5); HREIMS *m/z*: 278.1508 ($C_{16}H_{22}O_4$ requires 278.1509).

Isolation of terpenoids from *Aplysilla* sp.

Samples of a second sponge, distinct from *Pleraplysilla* sp., were also collected during low tides at Botanical Beach on Vancouver Island, B.C. A voucher sample was submitted to Professor Patricia Berquist, University of Auckland, for taxonomic and archival purposes. The sponge was identified as an undescribed species belonging to the genus *Aplysilla*. A repetition of the extraction procedure described above for *Pleraplysilla* sp. yielded a crude oil from the *Aplysilla* sp. that after fractionation by reversed-phase HPLC gave pure samples of marginatafuran (**21**) (8 mg) and 9,11-dihydrogracillin A (**37**) (2 mg) along with several other unknown diterpenoids.

X-ray diffraction analaysis of cadlinaldehyde (30)

All pertinent crystallographic data are summarized in Table 1 of the Supplementary Material.[2] Data were collected at room temperature on a Siemans R3m/V diffractometer (Cu K_α, λ = 1.54178 Å, graphite monochromator) using ω/2Θ scan mode. Unit-cell parameters were obtained from 25 reflections in the range of 25°–45°. Data were corrected for Lorentz and polarization effects. The structure was solved by direct methods (25) that revealed the presence of two molecules in an asymmetric unit. Hydrogen atoms were introduced geometrically and were given displacement parameters based on the carbon atom to which they were bonded. The structure was refined anisotropically with riding H atoms (26). The two symmetrically independent molecules have essentially the same geometry: weighted r.m.s. deviation is equal 0.021 Å. All calculations were effected on a Pentium IBM compatible computer. Fractional atomic coordinates and isotropic thermal parameters are given in Table 2 of the Supplementary Material. A full table of bond lengths and angles and a table of anisotropic displacement parameters have also been deposited.

Acknowledgements

Funding was provided by grants to R.J.A. from the Natural Sciences and Engineering Research Council of Canada and to J.C. from the National Institues of Health (CA 24487). The authors wish to thank Mike LeBlanc, the staff of the Bamfield Marine Station, and the crew of the J.P. Tulley for assisting the collections of *C. luteomarginata*, and Professor Rob Van Soest, Professor Patricia Bergquist, and Dr. Bill Austin for sponge taxonomy.

References

1. J. Hellou, R.J. Andersen, S. Rafii, E. Arnold, and J. Clardy. Tetrahedron Lett. **22**, 4173 (1981).

[2] The above supplementary material can be purchased from: The Depository of Unpublished Data, Document Delivery, CISTI, National Research Council Canada, Ottawa, Canada K1A 0S2. With the exception of the anisotropic displacement parameters, these data have also been deposited with the Cambridge Crystallographic Data Centre, and can be obtained on request from The Director, Cambridge Crystallographic Data Centre, University Chemical Laboratory, 12 Union Road, Cambridge, CB2 1EZ, U.K.

© 1997 NRC Canada

2. J.E. Thompson, R.P. Walker, S.J. Wratten, and D.J. Faulkner. Tetrahedron, **38**, 1865 (1982).
3. J. Hellou, R.J. Andersen, and J.E. Thompson. Tetrahedron, **38**, 1875 (1982).
4. K. Gustafson, R.J. Andersen, H. Cun-heng, and J. Clardy. Tetrahedron Lett. **26**, 2581 (1985).
5. M. Tischler and R.J. Andersen. Tetrahedron, Lett. **30**, 5717 (1989).
6. M. Tischler, R.J. Andersen, M.I. Choudhary, and J. Clardy. J. Org. Chem. **56**, 42 (1991).
7. D.L. Burgoyne, E. Dumdei, and R.J. Andersen. Tetrahedron, **49**, 4503 (1993).
8. D.J. Faulkner, T.F. Molinski, R.J. Andersen, E.J. Dumdei, and E.D. de Silva. Comp. Biochem. Physiol. C: Comp. Pharmacol. **97C,** 233 (1990).
9. E.I. Graziani and R.J. Andersen. J. Am. Chem. Soc. **118**, 4701 (1996).
10. E.I. Graziani, R.J. Andersen, P.J. Krug, and D.J. Faulkner. Tetrahedron, **52**, 6869 (1996).
11. E.I Graziani and R.J. Andersen. Chem. Commun. 2377 (1996).
12. F.J. Schmitz, J.S. Chang, M.B. Hossain, and D. van der Helm. J. Org. Chem. **50**, 2862 (1985).
13. M.B. Ksebati and F.J. Schmitz. J. Org. Chem. **52**, 3766 (1987).
14. T.F. Molinski and D.J. Faulkner. J. Org. Chem. **52**, 296 (1987).
15. R. Kazlauskas, P.T. Murphy, R.J. Wells, J.J. Daly, and P. Schonholzer. Tetrahedron Lett. 4951 (1978).
16. G. Shulte, P.J. Scheuer, and O.J. McConnell. Helv. Chim. Acta, **63**, 2159 (1980).
17. S.H. Grode and J.H. Cardellina. J. Nat. Prod. **47**, 76 (1984).
18. J. Pika and R.J. Andersen. Tetrahedron, **49**, 8757 (1993).
19. G. Cimino, S. De Stephano, A. Guerriero, and L. Minale. Tetrahedron Lett. 3723 (1975).
20. D. Van Engen, J. Clardy, E. Kho Wiseman, P. Crews, M.D. Higgs, and D.J. Faulkner. Tetrahedron Lett. 29 (1978).
21. F. Giordano, L. Mayol, G. Notaro, V. Piccialli, and D. Sica. Chem. Commun. 1559 (1990).
22. G. Cimino, S. de Rosa, S. de Stephano, G. Sodano, and G. Villani. Science, **219**, 1237 (1983).
23. G. Cimino, S. De Rosa, S. De Stephano, R. Morrone, and G. Sodano. Tetrahedron, **41**, 1093 (1985).
24. C. Avila, G. Cimino, A. Crispino, and A. Spinella. Experientia, **47**, 306 (1991).
25. G.M. Sheldrick. SHELX-86. A computer program for crystal structure determination. University of Gottingen, Germany. 1986.
26. G.M. Sheldrick. SHELX-93. Program for the refinement of crystal structures. University of Gottingen, Germany. 1993.

Can. J. Chem. Downloaded from www.nrcresearchpress.com by 88.146.161.215 on 09/08/12
For personal use only.

© 1997 NRC Canada

Synthesis and evaluation of thio-trisaccharides as acceptors for *N*-acetylglucosaminyltransferase-V

Pu-Ping Lu, Ole Hindsgaul, Hong Li, and Monica M. Palcic

Abstract: *N*-Acetylglucosaminyltransferase-V (GlcNAcT-V) transfers a β-linked GlcNAc residue from UDP-GlcNAc to the 6-OH group of the αMan residue in oligosaccharides terminating in the sequence β-D-Glc*p*NAc-(1→2)-α-D-Man*p*-(1→6)-β-D-Glc*p*-OR (**5**, R = $(CH_2)_7CH_3$). The terminal GlcNAc moiety may be replaced by a Glc residue to produce trisaccharide **6**. Two thio analogs (**7**, **8**) of trisaccharide **6**, where the oxygen atoms in the glycosidic linkages between sugar residues were replaced by sulfur, were prepared by multistep chemical synthesis that made use of the key intermediates 1,2-anhydro-3,4,6-tri-*O*-benzyl-α-D-glucose (**10**) and 1,2-anhydro-3,4,6-tri-*O*-benzyl-β-D-mannose (**13**) as donors for the glycosylations. The thio analogs (**7**, **8**) were kinetically evaluated as substrates for GlcNAcT-V and found to be acceptors with two- to three-fold increase in V_{max} but higher K_m values (**7**, K_m = 376 μM; **8**, K_m = 300 μM) than their parent compound **6** (K_m = 111 μM), which has the natural oxygen linkage. The thio analogs **7** and **8** could be quantitatively converted into the expected product tetrasaccharides (**27**, **28**) by incubation with GlcNAcT-V and UDP-GlcNAc. The enzymatic results indicate that GlcNAcT-V tolerates the substitution of the natural oxygen linkage of the acceptor by a sulfur linkage.

Key words: *N*-acetylglucosaminyltransferase-V, enzyme acceptors, trisaccharide analogs, thioglycosides.

Résumé : La *N*-acétylglucosaminyltransférase-V (GlcNAcT-V) permet de transférer un résidu GlcNAc lié en β d'un UDP-GlcNAc à un groupe 6-OH d'un résidu α-Man d'oligosaccharides se terminant par une séquence β-D-Glc*p*NAc-(1→2)-α-D-Man*p*-(1→6)-β-D-Glc*p*-OR (**5**, R = $(CH_2)_7CH_3$). On peut remplacer la portion GlcNAc terminale par un résidu Glc pour produire le trisaccharide **6**. En procédant à une synthèse en plusieurs étapes faisant appel aux intermédiaires clés 1,2-anhydro-3,4,6-tri-*O*-benzyl-α-D-glucose (**10**) et 1,2-anhydro-3,4,6-tri-*O*-benzyl-β-D-mannose (**13**) comme donneurs lors des glycosylations, on a préparé deux analogues thio (**7**, **8**) du trisaccharide **6**, dans lesquels les atomes d'oxygène des liaisons glycosidiques entre les unités de sucre ont été remplacés par des atomes de soufre. On a évalué le comportement cinétique des dérivés thio (**7**, **8**) comme substrats de la GlcNAcT-V et on a trouvé qu'ils sont de meilleurs accepteurs avec des augmentations par des facteurs de 2 à 3 dans les valeurs de V_{max}; les valeurs de K_m sont toutefois plus élevées (**7**, K_m = 376 μM; **8**, K_m = 300 μM) que celle de leur composé parent (**6**, K_m = 111 μM) comportant la liaison oxygénée normale. Par incubation avec de la GlcNAcT-V et du UDP-GlcNAc, on peut transformer quantitativement les analogues thio en tétrasaccharides attendus (**27**, **28**). Les résultats enzymatiques indiquent que la GlcNAcT-V tolère la substitution de la liaison oxygène naturelle de l'accepteur par une liaison sulfurée.

Mots clés : *N*-acétylglucosaminyltransférase-V, accepteurs d'enzyme, analogues trisaccharides, thioglycosides.

[Traduit par la rédaction]

Introduction

UDP-GlcNAc: α-mannoside β (1→6)-*N*-acetylglucosaminyltransferase-V (GlcNAcT-V, EC 2.4.1.155) transfers an *N*-acetyl-D-glucosamine (GlcNAc) residue from uridine 5′-diphospho-GlcNAc (UDP-GlcNAc) to natural glycopeptide acceptors bearing the minimum heptasaccharide sequence **1** (Scheme 1), converting it to the octasaccharide **2** (1, 2). This enzyme plays a key role in the biosynthesis of highly branched asparagine-linked oligosaccharides (1, 2). A strong correlation between an increase in the activity of this enzyme and the increased metastatic potential of several cancer cell lines has been demonstrated (3–5). This enzyme has, therefore, become a target for the development of glycosyltransferase inhibitors.

Knowledge of the detailed substrate specificity of GlcNAcT-V is essential for a rational approach to inhibitor design. We previously found that the much simpler synthetic trisaccharide **3**, a partial structure of **1**, is also an effective substrate for the enzyme, yielding the expected tetrasaccharide **4** (6). The enzyme tolerates the substitution of the βMan residue in **3** by a βGlc residue since trisaccharide **5** was found to be an excellent acceptor (7). The enzyme further tolerates the substitution of the terminal GlcNAc moiety by a βGlc

Received January 23, 1997.

This paper is dedicated to Professor William A. Ayer on the occasion of his 65th birthday.

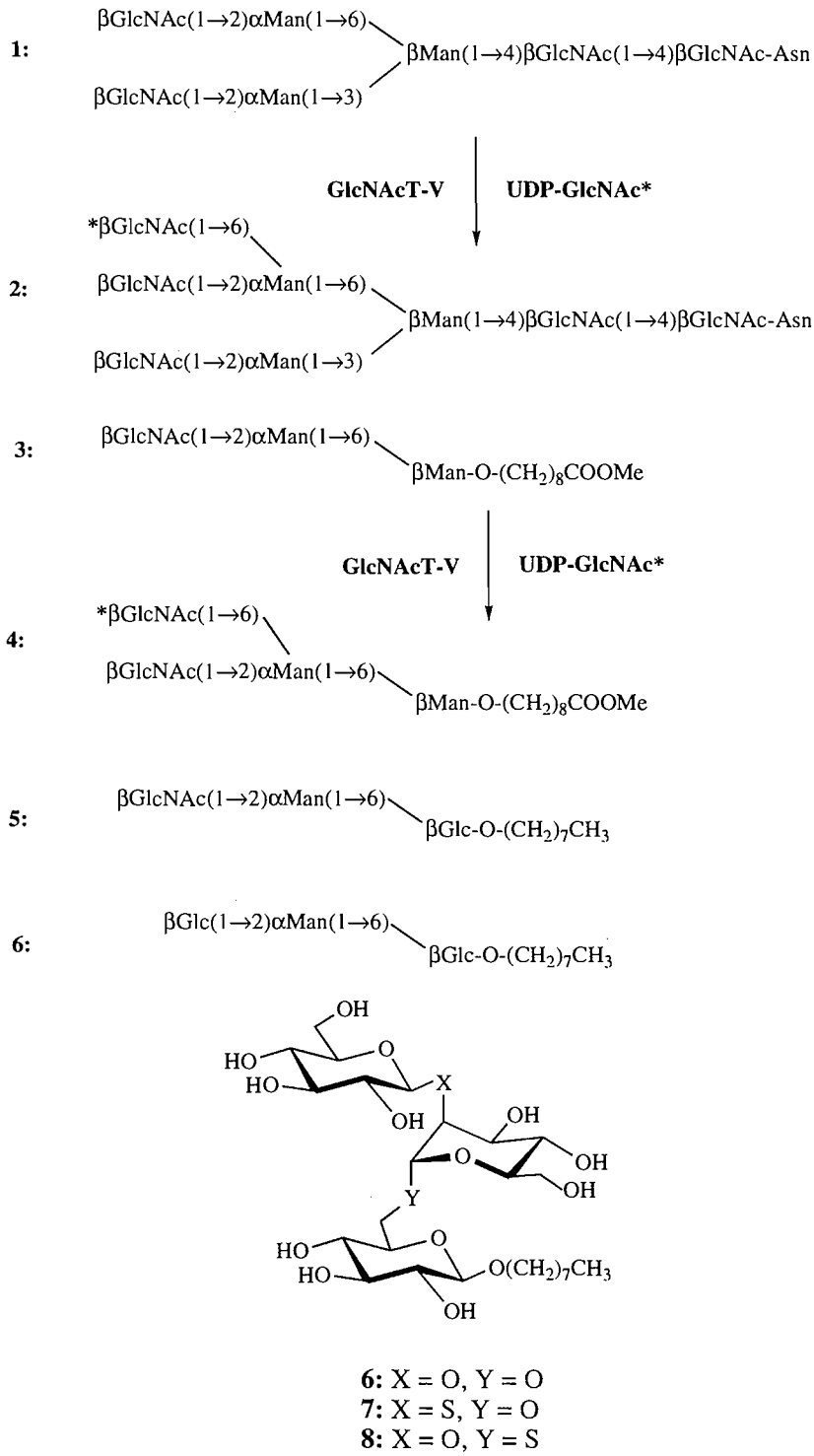
P.-P. Lu, O. Hingsgaul,[1] H. Li, and M.M. Palcic.[1] Department of Chemistry, University of Alberta, Edmonton, AB T6G 2G2 Canada.

[1] Authors to whom correspondence may be addressed.
OH, Telephone: (403) 492-4171. Fax: (403) 492-7705.
E-mail: ole.hindsgaul@ualberta.ca
M.M.P. Telephone: (403) 492-0377. Fax: (403) 492-7705.
E-mail: monica.palcic@ualberta.ca

© 1997 NRC Canada

Can. J. Chem. Downloaded from www.nrcresearchpress.com by 88.146.161.215 on 09/08/12
For personal use only.

Scheme 1. Glycosylation reactions catalyzed by GlcNAcT-V.



6: X = O, Y = O
7: X = S, Y = O
8: X = O, Y = S

residue, since the trisaccharide **6** was also found to be a good acceptor (8). The aliphatic aglycons in **3** and **5** were incorporated into these structures in order to facilitate the enzyme assay procedures (9). We report here a continuation of these enzyme-specificity studies where the requirement of the natural intra-residue oxygen linkage of **6** in substrate recognition by GlcNAcT-V is probed through the synthesis and enzymatic analysis of the two thio analogs **7** and **8**, which have an intersaccharidic sulfur atom. The use of the 1,2-anhydro sugars (glycal epoxides) as building blocks provided short synthetic routes to these thio-linked trisaccharides.

Can. J. Chem. Downloaded from www.nrcresearchpress.com by 88.146.161.215 on 09/08/12
For personal use only.

© 1997 NRC Canada

Can. J. Chem. Downloaded from www.nrcresearchpress.com by 88.146.161.215 on 09/08/12
For personal use only.

Results and discussion

Since only small (mg) quantities of **7** and **8** were required, the synthetic plan was to devise short reaction sequences even if yields were found to be low by normal synthetic criteria. The retrosynthetic analysis for the preparation of **7** and **8** is shown in Scheme 2. In designing the synthesis of **7**, we chose 1,2-anhydro-3,4,6-tri-*O*-benzyl-α-D-glucopyranose (**10**) as the central building block. The opening of epoxide **10** by **9** was expected to produce an α/β mixture of disaccharides with OH-2′ free. After conversion of OH-2′ into a leaving group, S_N2 displacement using a protected 1-thio-D-glucose (**11**) was then envisioned to produce the desired trisaccharide. In designing the synthesis of **8**, we chose 1,2-anhydro-3,4,6-tri-*O*-benzyl-β-D-mannopyranose (**13**) as the central building block. The opening of the epoxide **13** by highly nucleophilic **12** would provide a disaccharide with OH-2′ free for further coupling to give the desired trisaccharide.

The three building blocks required for the synthesis of **7** were prepared according to published procedures (**9** (7), **10** (10), **11** (11)). The coupling of **10** with alcohol **9** was carried out in THF at −78°C using trifluoromethanesulfonic acid as catalyst, to afford the desired α-linked disaccharide **15** along with the β-linked disaccharide **16** in 24% and 47% yield, respectively (based on consumed alcohol). Treatment of **15** with excess trifluoromethanesulfonic anhydride in anhydrous pyridine gave the 2′-triflate (**17**) in quantitative yield. The S_N2 displacement of **17** was carried out by using the sodium salt of the 1-thio-D-glucose derivative (**11**) in DMF. The sodium salt was made by treating **11** with sodium hydride in THF. The trisaccharide **18** was obtained in 25% yield. Zemplén deacetylation of **18** yielded **19**. Final debenzylation of **19** by treatment with Na/liquid NH_3 afforded target trisaccharide **7** in 79% yield (Scheme 3).

For the synthesis of **8**, compound **13** was prepared by treatment of 3,4,6-tri-*O*-benzyl-D-mannopyranose (12) with hydrogen chloride in ether, followed by work-up with NH_3 (13). Mesylation of **9**, followed by reaction with potassium thioacetate and deacetylation, provided **12** with the required free 6-thiol group (Scheme 4). Imidate (**14**) was prepared from hemiacetal **23** by reaction with trichloroacetonitrile and sodium hydride in dichloromethane according to standard procedures (14). Compound **23** was prepared by treating **22** (15) with silver carbonate in wet acetone (Scheme 4). The opening of the epoxide **13** by the sodium salt of **12** gave the α-linked disaccharide **24** (63%) with OH-2′ for subsequent coupling. Using *O*-(2-*O*-acetyl-3,4,6-tri-*O*-benzyl-α-D-glucopyranosyl)-trichloroacetimidate (**14**) as donor, glycosylation of **24** afforded the desired β-linked trisaccharide in 88% yield. After Zemplén deacetylation (92%), debenzylation with Na/liquid NH_3 furnished the target trisaccharide in 82% yield (Scheme 5).

Compounds **7** and **8** were characterized by ^1H NMR, ^1H–^1H 2D COSY, ^{13}C NMR (APT), HMQC, and high-resolution FAB mass spectrometry. The anomeric configurations of the mannopyranosyl and glucopyranosyl linkages were further verified by measurement of the ^1J heteronuclear coupling constants (16) of the anomeric carbon atoms for compounds **7** and **8**.

Evaluation of thioglycoside analogs as acceptors for GlcNAcT-V

Compounds **7** and **8** and the unmodified structure **6** were kinetically evaluated as acceptors for GlcNAcT-V using the cloned rat kidney enzyme (17). The enzyme experiments were performed according to a well-established radioactive "Sep-Pak assay" method (9, 18–20). The results of the kinetic evaluations are reported in Table I. Both compounds (**7**, **8**) are relatively good substrates for GlcNAcT-V. The V_{max} values are two- to three-fold higher than those of their parent compound (**6**); however, their binding is likely weaker as reflected in the higher K_m values for the analogs. Trisaccharide **8** was also evaluated with GlcNAcT-V isolated from hamster kidney (18–20). As was previous found (21), both sources of GlcNAcT-V have essentially identical substrate specificity.

To confirm that the thio analogs **7** and **8** were indeed acceptors of GlcNAcT-V, preparative enzymatic syntheses were performed. When the acceptors were incubated with UDP-GlcNAc and GlcNAcT-V, the enzyme transferred a β-D-GlcNAc residue to the 6-OH of the core D-Man*p* unit of the acceptors, converting **7** and **8** into the expected tetrasaccharides **27** and **28**, respectively (Scheme 6). The structures of tetrasaccharides **27** and **28** were confirmed by ^1H NMR and FAB mass spectrometry.

This work indicates that neither of the intersaccharidic oxygen atoms in the trisaccharide acceptor are involved in specific recognition by GlcNAcT-V. The enzyme tolerates the substitution of the natural intersaccharidic oxygen linkages by sulfur. Since thioglycosides are resistant to cleavage by glycosidases, these structures should prove useful as metabolically stable acceptors for assaying GlcNAcT-V.

Experimental

General methods

TLC was performed on Silica Gel 60-F254 (E. Merck) with detection by quenching of fluorescence, and (or) by charring

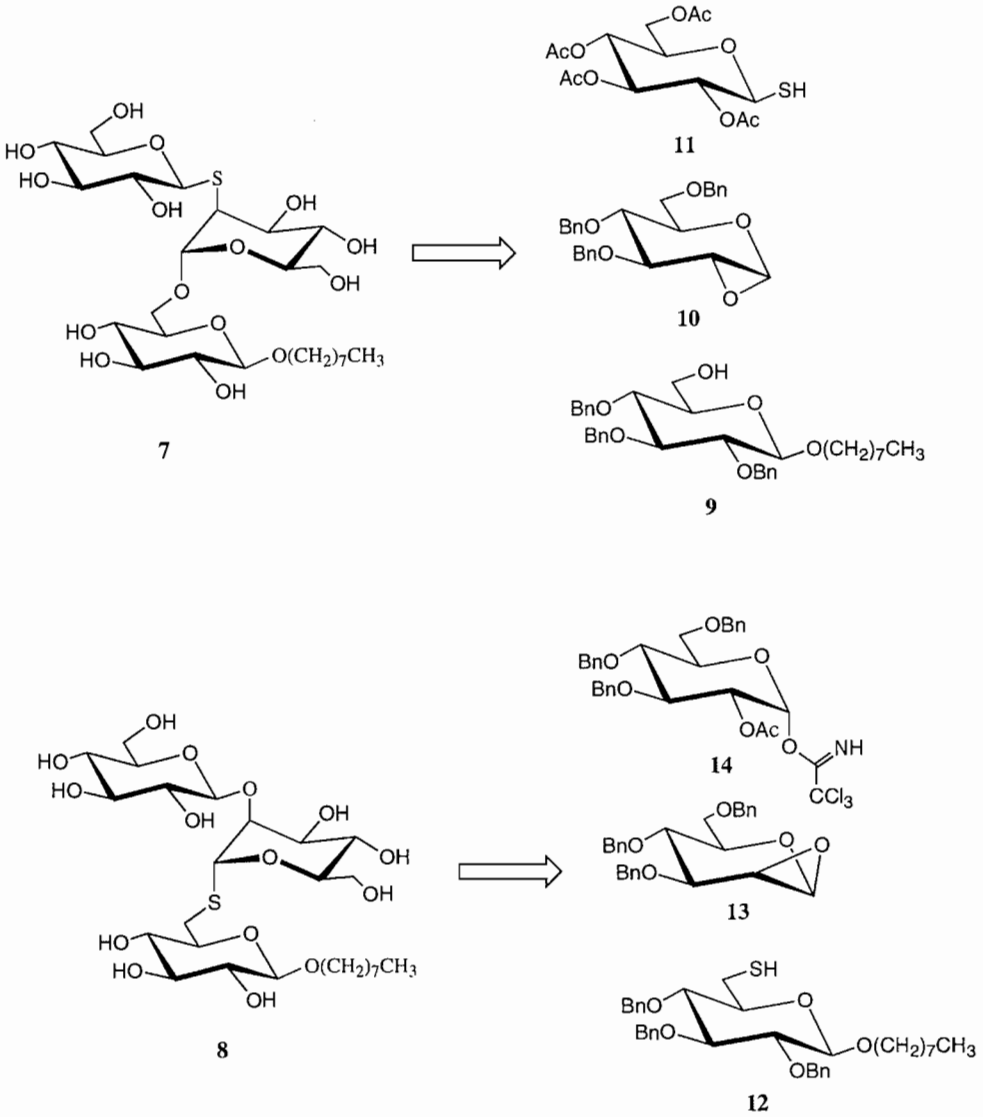
Table 1. Kinetic parameters for GlcNAcT-V acceptor analogs.

Acceptor	GlcNAcT-V	K_m (μM)	V_{max} (pmol/min)	V_{max}, rel[a]
6	Cloned	111±7	2.1	100
7	Cloned	376±16	3.5	167
8	Cloned	300±24	6.1	290
8	Isolated	256±12	9.0	—

[a]The value for compound **6** is arbitrarily set to 100.

© 1997 NRC Canada

Scheme 2. Synthetic strategy for the synthesis of **7** and **8**.



with H_2SO_4. Unless otherwise noted, column chromatography was performed on Silica Gel 60 (E. Merck, 40–63 mm). Iatrobeads were from Iatron Laboratories, Inc. (Japan). C-18 Sep-Pak sample preparation cartridges were from Waters Associates. Millex-GV (0.22 μm) filter units were from Millipore. Optical rotations were measured with a Perkin–Elmer 241 polarimeter at 22°C. IR spectra were recorded with a Nicolet SX-20 FTIR by the spectral services laboratory of the Chemistry Department. ^{1}H NMR spectra were recorded at 360 MHz (Bruker AMR 360), at 400 MHz (Bruker AM 400), or at 500 MHz (Varian UNITY 500) on solutions in $CDCl_3$ (internal Me_4Si, δ 0) or D_2O. ^{13}C NMR spectra were recorded at 75.5 MHz, 100.6 MHz, or 125 MHz, respectively, on the same instruments in $CDCl_3$ (internal Me_4Si δ 0) or D_2O (internal 1,4-dioxane, δ 67.4). The assignments of ^{13}C NMR are tentative. FAB mass spectra (FAB MS) were obtained on a Kratos AEIMS9 instrument using glycerol as matrix. Electrospray ionization mass spectra (ESI MS) were obtained from a Micromass ZabSpec Hybrid Sector-TOF instrument using methanol–toluene as liquid carrier. Elemental analyses were carried out on a Carlo Erba EA1108. For the enzyme experiments, cloned rat kidney GlcNAcT-V was a generous gift from Dr. M. Pierce (17); partially purified GlcNAcT-V was isolated from hamster kidney by a modification (20) of published procedures (18, 19). UDP-^{3}H-GlcNAc was from American Radiolabeled Chemicals, Inc. (specific activity 40–60 Ci/mmol). UDP-GlcNAc (disodium salt) was from Sigma.

Octyl 3,4,6-tri-*O*-benzyl-α-D-glucopyranosyl-(1→6)-2,3,4-tri-*O*-benzyl-β-D-glucopyranoside (15)

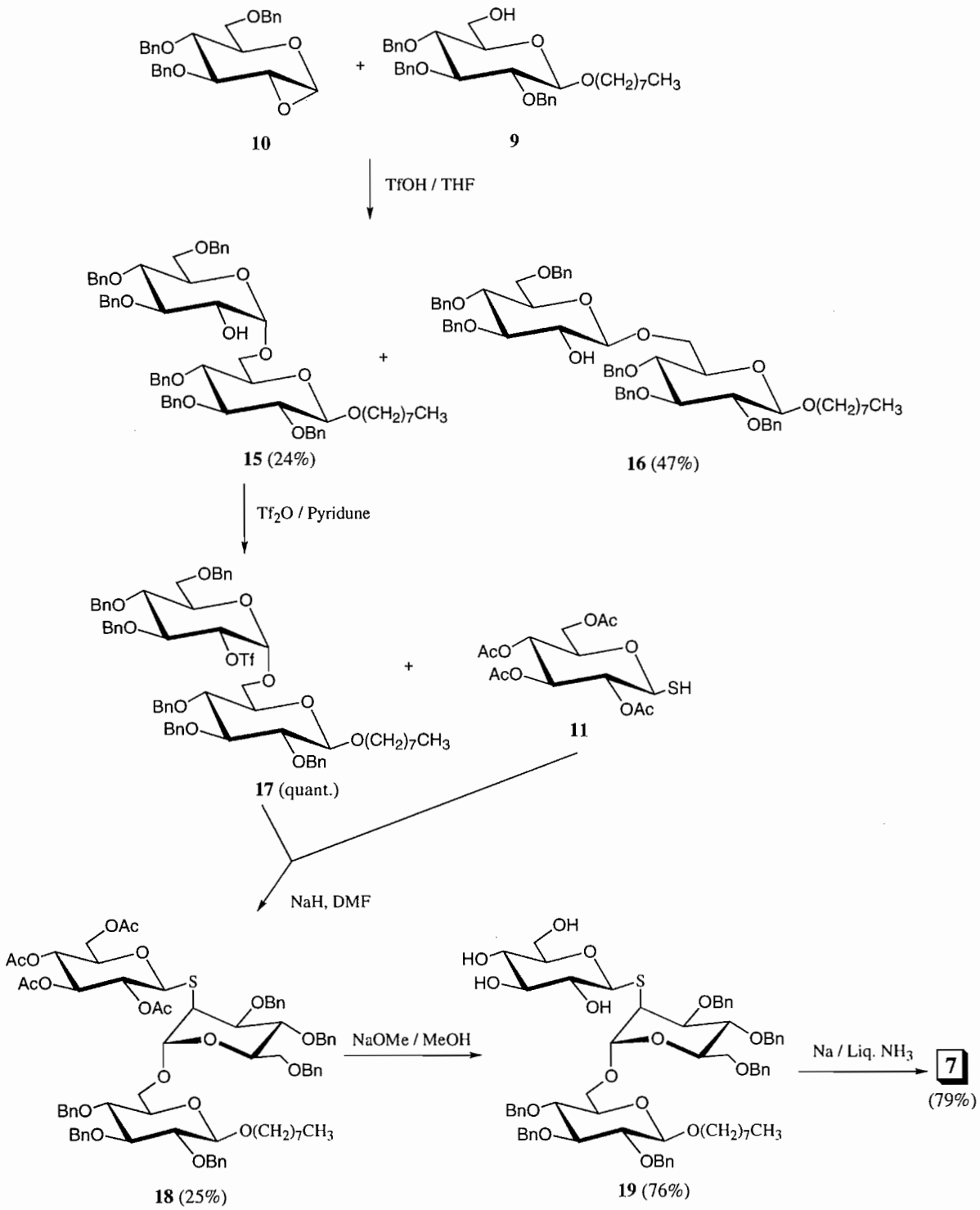
A mixture of **9** (7) (600 mg, 1.07 mmol) and trifluoromethanesulfonic acid (17.6 μL, 0.2 mmol) in dry THF (20 mL) was cooled to −78°C. To the resulting mixture was added dropwise a solution of 1,2-anhydro-3,4,6-tri-*O*-benzyl-α-D-glucopyranose **10** (432 mg, 1.0 mmol) in dry THF (10 mL). The reaction mixture was stirred at −78°C for 2 h, then warmed to room temperature (r.t.) and stirred for 10 h. The reaction mixture was then concentrated and the residue was dissolved in

Can. J. Chem. Downloaded from www.nrcresearchpress.com by 88.146.161.215 on 09/08/12
For personal use only.

© 1997 NRC Canada

Can. J. Chem. Downloaded from www.nrcresearchpress.com by 88.146.161.215 on 09/08/12
For personal use only.

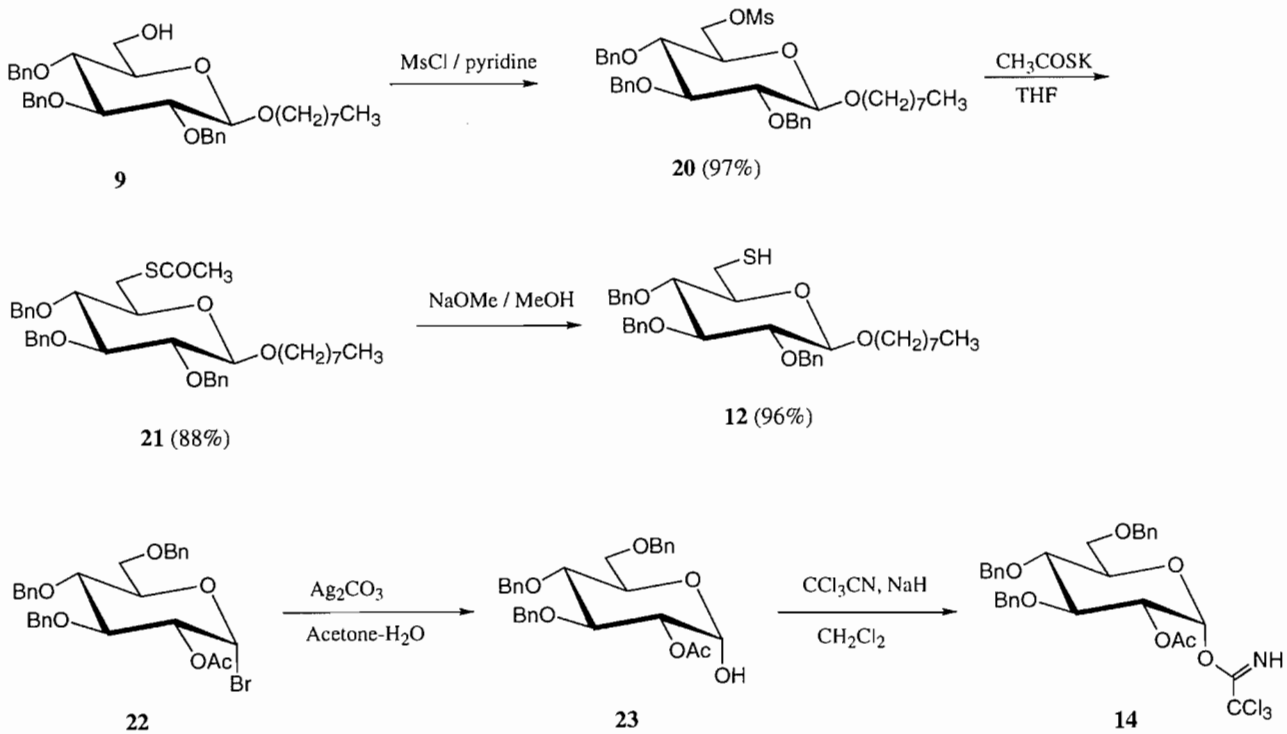
Scheme 3.



CH_2Cl_2 (20 mL). The CH_2Cl_2 solution was washed with saturated $NaHCO_3$ and water, then dried over anhydrous $MgSO_4$, filtered, and concentrated. The purification of the residue by column chromatography (hexane–EtOAc 2:1) provided **15** (170 mg, 24% based on consumed alcohol), **16** (330 mg, 47%), and recovered alcohol **9** (200 mg, 33%); $[\alpha]_D$ +57.3 (*c* 0.7, CH_2Cl_2); ^1H NMR (400 MHz, $CDCl_3$) δ: 7.40–7.10 (m, 30H, Ar-H), 4.97, 4.96, 4.95 (3d, each 1H, J_{gem} 11.0 Hz, $PhCH_2$), 4.95 (d, 1H, $J_{1',2'}$ 3.5 Hz, H-1′), 4.88 (d, 1H J_{gem} 11.0 Hz, $PhCH_2$), 4.84 (d, 2H, J_{gem} 10.8 Hz, $PhCH_2$), 4.78, 4.72 (2d, each 1H, J_{gem} 10.8 Hz, $PhCH_2$), 4.61, 4.57 (2d, each 1H, J_{gem} 11.0 Hz, $PhCH_2$), 4.48 (d, 1H, J_{gem} 10.1 Hz, $PhCH_2$), 4.45 (d, 1H, J_{gem} 11.0 Hz, $PhCH_2$), 4.41 (d, 1H $J_{1,2}$ 7.8 Hz, H-1), 3.82 (ddd, 1H, $J_{2',3'}$ 10.0 Hz, $J_{2',OH}$ 2.0 Hz, H-2′), 3.42 (dd, 1H, $J_{2,3}$

© 1997 NRC Canada

Scheme 4.



9.5 Hz, H-2), 0.87 (t, 3H, J_{vic} 7.0 Hz, octyl CH_3); ^{13}C NMR (100.6 MHz) δ: 138.5, 138.4, 138.0 (benzyl C1), 128.4, 128.4, 128.3, 128.1, 128.0, 127.9, 127.8, 127.7, 127.64, 127.59, 127.5 (Ar), 103.5 (C-1), 99.2 (C-1′), 75.7, 75.2, 74.94, 74.86, 74.83, 73.4 (Ph*C*H_2), 70.2 (octyl C1), 68.4 (C-6″), 67.0 (C-6), 31.8, 29.8, 29.4, 29.2, 26.2, 22.6 (octyl C2–C7), 14.1 (octyl CH_3). Anal. calcd. for $C_{62}H_{74}O_{11}$ (995.27): C 74.82, H 7.49; found: C 74.90, H 7.61.

Octyl 3,4,6-tri-*O*-benzyl-2-*O*-trifluoromethanesulfonyl-α-D-glucopyranosyl-(1→6)-2,3,4-tri-*O*-benzyl-β-D-glucopyranoside (17)

To a mixture of compound **15** (115 mg, 0.116 mmol) in dry pyridine (2 mL) at −22°C was added trifluoromethanesulfonic anhydride (85 μL, 0.505 mmol). The reaction mixture was allowed to warm to r.t. and then stirred for 1 h. After addition of ice-cold 1 M HCl (10 mL), the reaction mixture was stirred for 30 min and extracted with CH_2Cl_2. The CH_2Cl_2 solution was washed with saturated $NaHCO_3$ and water, and dried over anhydrous $MgSO_4$. Filtration followed by evaporation of the CH_2Cl_2 gave the title product (130 mg, 100%) as a syrup. ^1H NMR (360 MHz, $CDCl_3$) δ: 7.40–7.05 (m, 30H, Ar-H), 5.175 (d, 1H, $J_{1',2'}$ 3.5 Hz, H-1′), 4.96, 4.95, 4.94, 4.89, 4.85, 4.78, 4.78, 4.76 (8d, each 1H, J_{gem} 11.0 Hz, $PhCH_2$), 4.74 (dd, 1H, $J_{2',3'}$ 9.5 Hz, H-2′), 4.71 (d, 1H, J_{gem} 11.0 Hz, $PhCH_2$), 4.60 (d, 1H, J_{gem} 12.0 Hz, $PhCH_2$), 4.58 (d, 1H, J_{gem} 11.0 Hz, $PhCH_2$), 4.45 (d, 1H, J_{gem} 12.0 Hz, $PhCH_2$), 4.39 (d, 1H, $J_{1,2}$ 7.8 Hz, H-1), 4.05 (dd, 1H, $J_{3',4'}$ 9.5 Hz, H-3′), 0.87 (t, 3H, J_{vic} 7.0 Hz, octyl CH_3).

Octyl 2,3,4,6-tetra-*O*-acetyl-β-D-glucopyranosyl-(1→2)-3,4,6-tri-*O*-benzyl-2-deoxy-2-thio-α-D-mannopyranosyl-(1→6)-2,3,4-tri-*O*-benzyl-β-D-glucopyranoside (18)

To a solution of 2,3,4,6-tetra-*O*-acetyl-1-thio-β-D-glucopyranose **11** (11) (105 mg, 0.288 mmol) in dry THF (2 mL) was added sodium hydride (60% suspension in oil, 13 mg, 0.318 mmol). The mixture was stirred, resulting in the evolution of bubbles. After the sodium salt (white solid in THF) was produced, the THF was evaporated using a stream of argon. To the resulting residue was added a solution of **17** (130 mg, 0.115 mmol) in dry DMF (2 mL). The reaction mixture was stirred at r.t. for 12 h, and methanol (2 mL) was added to quench the reaction. The reaction mixture was concentrated to dryness and the residue was dissolved in CH_2Cl_2 (10 mL). The CH_2Cl_2 solution was washed with water, dried over $MgSO_4$, filtered, and concentrated. Purification of the residue by column chromatography using hexane–EtOAc (2:1) as eluant gave the title compound (38 mg, 25%); ^1H NMR (360 MHz, $CDCl_3$) δ: 5.24 (dd, 1H, $J_{2'',3''}$, $J_{3'',4''}$ 9.2 Hz, H-3″), 5.14 (dd, 1H, $J_{1',2'}$ 2.0 Hz, H-1′), 5.10 (dd, 1H, $J_{4'',5''}$ 9.5 Hz, H-4″), 5.06 (dd, 1H, $J_{1'',2''}$ 9.6 Hz, H-2″), 4.98, 4.95, 4.86, 4.82, 4.81, 4.80. 4.78, 4.71 (8d, each 1H, J_{gem} 11.0 Hz, $PhCH_2$), 4.48 (d, 1H, H-1″), 4.40 (d, 1H, $J_{1,2}$ 8.0 Hz, H-1), 4.37 (d, 1H, J_{gem} 10.5 Hz, $PhCH_2$), 4.22 (dd, 1H, J_{gem} 12.5 Hz, $J_{5'',6''a}$ 5.5 Hz, H-6″a), 4.14 (dd, 1H, $J_{5'',6''b}$ 2.0 Hz, H-6″b), 3.38 (dd, 1H, $J_{2,3}$ 9.0 Hz, H-2), 2.01, 1.98, 1.97, 1.96 (4s, each 3H, 4 Ac), 0.87 (t, 3H, J_{vic} 7.0 Hz, octyl CH_3); ^{13}C NMR (75.5 MHz) δ: 174.2, 170.6, 170.1, 169.4 (C═O), 138.5, 138.4, 138.2, 138.1, 137.9 (benzyl C1), 128.5, 128.4, 128.3, 128.2, 128.1, 128.0, 127.9, 127.9, 127.8, 127.6, 127.5 (Ar), 103.7 (C-1), 101.3 (C-1″), 87.6 (C-1′), 70.5 (octyl C1), 68.8 (C-6″), 66.1 (C-6), 62.3 (C-6′), 47.0 (C-2′), 31.7, 29.7, 29.5, 29.3, 26.2, 22.7 (octyl C2–C7), 20.7 (*C*H_3CO), 14.10 (octyl CH_3). ESI MS *m/z*: 1363.7 $(M+Na)^+$.

Octyl β-D-glucopyranosyl-(1→2)-3,4,6-tri-*O*-benzyl-2-deoxy-2-thio-α-D-mannopyranosyl-(1→6)-2,3,4-tri-*O*-benzyl-β-D-glucopyranoside (19)

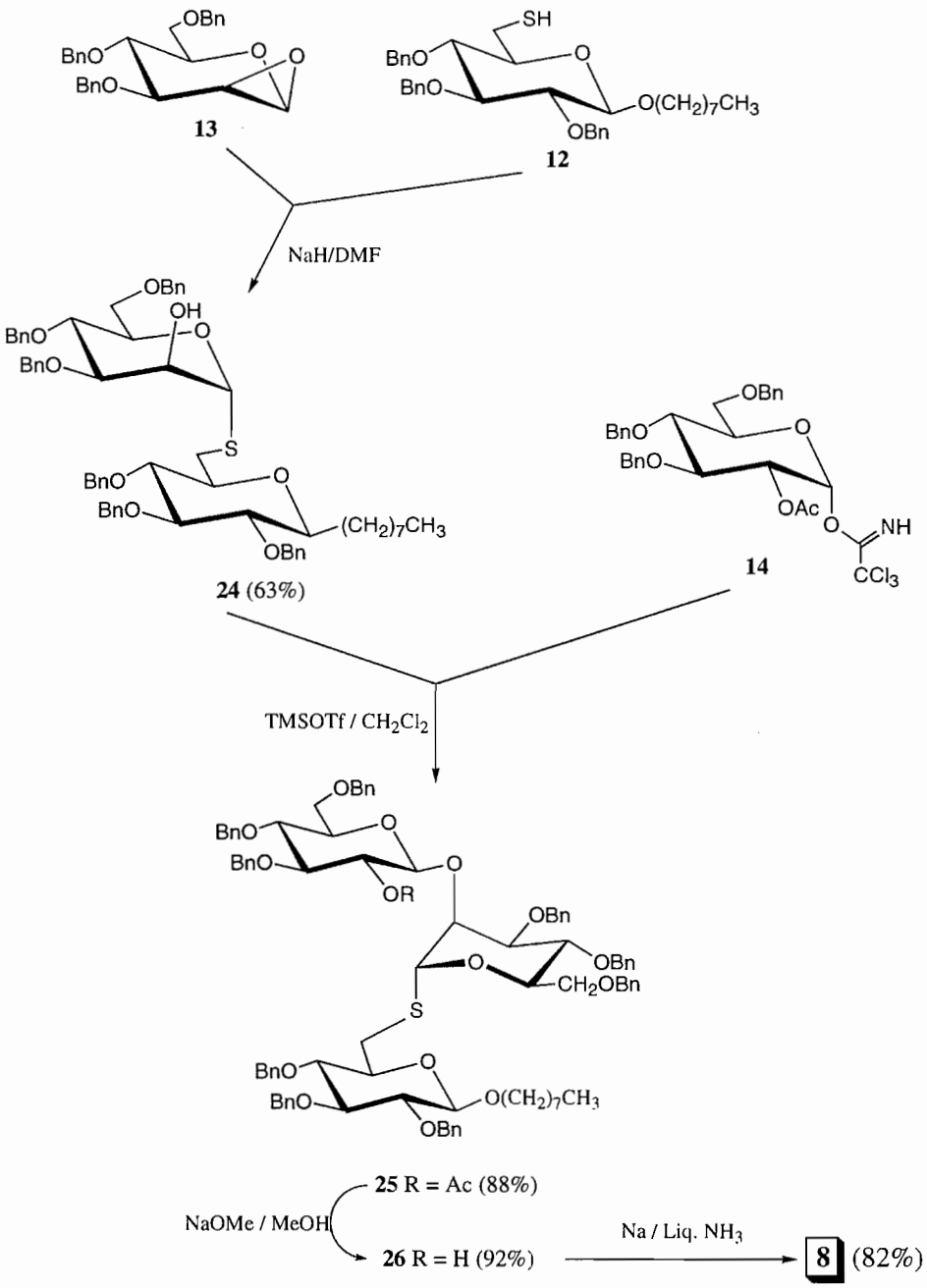
Compound **18** (30 mg, 22.4 μmol) was treated with methan-

© 1997 NRC Canada

Can. J. Chem. Downloaded from www.nrcresearchpress.com by 88.146.161.215 on 09/08/12
For personal use only.

Can. J. Chem. Downloaded from www.nrcresearchpress.com by 88.146.161.215 on 09/08/12
For personal use only.

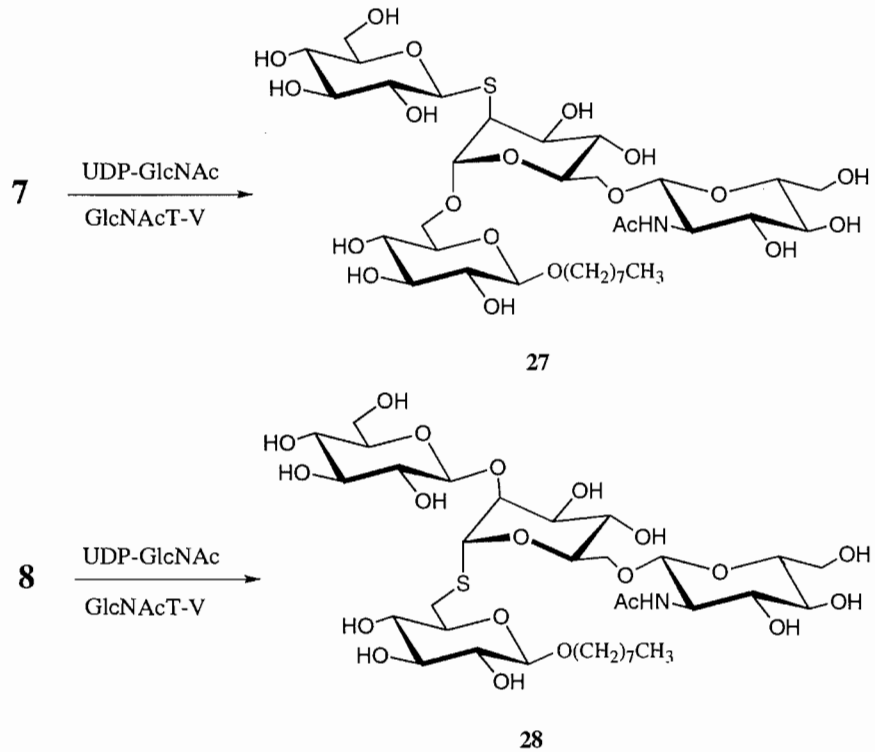
Scheme 5.



olic NaOMe (0.05 N, 3 mL) at r.t. for 12 h. Neutralization with Amberlite IR-120 (H^+) resin, removal of the resin by filtration, and concentration left a residue that was purified by column chromatography (5% MeOH in CH_2Cl_2) and preparative TLC (5% MeOH in CH_2Cl_2) to give compound **19** as a syrup (20 mg, 76%); $[\alpha]_D$ +30.9 (*c* 1.3, CH_2Cl_2); ^1H NMR (400 MHz, $CDCl_3$) δ: 5.10 (d, 1H, $J_{1',2'}$ 2.0 Hz, H-1′), 4.97, 4.96, 4.88, 4.81, 4.79, 4.78, 4.74, 4.70 (8d, each 1H, J_{gem} 11.0 Hz, $PhCH_2$), 4.42 (d, 1H, J_{gem} 12.5 Hz, $PhCH_2$), 4.39 (d, 1H, $J_{1,2}$ 8.0 Hz, H-1), 4.29 (d, 1H, $J_{1'',2''}$ 9.5 Hz, H-1″), 4.16 (dd, 1H, $J_{2',3'}$ 4.0 Hz, $J_{3',4'}$ 8.5 Hz, H-3′), 3.94 (dt, 1H, J_{gem} 10.0 Hz, J_{vic} 6.2 Hz, octyl C1-H_a), 3.45 (dd, 1H, H-2′), 2.58 (d, 1H, *J* 1.0 Hz, OH), 2.52 (s, 1H, OH), 2.51 (d, 1H, *J* 1.2 Hz, OH), 2.32 (dd, 1H, *J* 6.0, 5.5 Hz, C6″-OH), 0.87 (t, 3H, J_{vic} 7.0 Hz, octyl CH_3); ^{13}C NMR (100.6 MHz) δ: 138.4, 138.2, 138.0, 137.0 (benzyl C1), 128.7, 128.6, 128.4, 128.4, 128.3, 128.1, 127.9, 127.70, 127.66, 127.5 (Ar), 103.7 (C-1), 101.9 (C-1″), 85.1 (C-1′), 75.8, 74.9, 74.8, 74.6, 73.7, 73.3 ($PhCH_2$), 71.99 (octyl C_1), 68.5 (C-6′), 65.7 (C-6), 62.4 (C-6″), 45.9 (C-2′), 31.8, 29.68, 29.42, 29.24, 26.12, 22.64 (octyl C2–C7), 14.07 (octyl CH_3): FAB MS *m/z*: 1211.3 $(M+K)^+$, 1196.4 $(M+Na)^+$.

© 1997 NRC Canada

Scheme 6. Enzymatic synthesis of **27** and **28**.



27

28

Can. J. Chem. Downloaded from www.nrcresearchpress.com by 88.146.161.215 on 09/08/12
For personal use only.

Octyl β-D-glucopyranosyl-(1→2)-2-deoxy-2-thio-α-D-mannopyranosyl-(1→6)-β-D-glucopyranoside (7)

A solution of **19** (13 mg, 11.1 μmol) in THF (0.5 mL) was added to a mixture of liquid NH_3 (10 mL, distilled over Na) and *tert*-butanol (50 μL) at −78°C. Small pieces of sodium were added until the reaction mixture remained blue, and the mixture was stirred at −78°C for 4 h. Ammonium chloride (solid) was then added until the blue color disappeared. The liquid NH_3 was allowed to evaporate slowly and the remaining solution was concentrated to dryness. The residue was dissolved with Milli-Q water. The aqueous solution was loaded onto a C-18 Sep-Pak cartridge. The cartridge was washed with water (2 × 10 mL) followed by methanol (10 mL). The methanolic eluate was concentrated to dryness. The residue was dissolved with Milli-Q water, passed through a Millex filter, and the filtrate was lyophilized to give **7** (5.5 mg, 79%); $[\alpha]_D$ +1.1 (*c* 0.7, CH_3OH); ^1H NMR (500 MHz, D_2O) δ: 5.15 (d, 1H, $J_{1',2'}$ 1.0 Hz, H-1′), 4.55 (d, 1H, $J_{1'',2''}$ 10.0 Hz, H-1″), 4.45 (d, 1H, $J_{1,2}$ 8.0 Hz, H-1), 4.18 (dd, 1H, $J_{2',3'}$ 4.5 Hz, $J_{3',4'}$ 9.5 Hz, H-3′), 3.91 (dd, 1H, J_{gem} 11.2 Hz, $J_{5,6a}$ 5.4 Hz, H-6a), 3.88 (dd, 1H, J_{gem} 12.5 Hz, $J_{5',6'a}$ 2.2 Hz, H-6′a), 3.84 (dd, 1H, J_{gem} 11.9 Hz, $J_{5'',6''a}$ 2.5 Hz, H-6″a), 3.78 (dd, 1H, $J_{5,6b}$ 2.0 Hz, H-6b), 3.72 (dd, 1H, $J_{5',6'b}$ 6.9 Hz, H-6′b), 3.67 (dt, 1H, J_{gem} 10.5 Hz, J_{vic} 7.0 Hz, octyl C1-H_b), 3.63 (dd, 1H, H-2′), 3.58 (m, 1H, H-5), 3.51 (dd, 1H, $J_{4',5'}$ 9.6 Hz, H-4′), 3.48 (dd, 1H, $J_{2'',3''}$, $J_{3'',4''}$ 9.6 Hz, H-3″), 3.45 (dd, 1H, $J_{2,3}$, $J_{3,4}$ 9.5 Hz, H-3), 3.42 (dd, 1H, $J_{4'',5''}$ 9.5 Hz, H-4″), 3.36 (dd, 1H, H-2″), 3.25 (dd, 1H, H-2), 1.62 (p, 2H, J_{vic} 7.0 Hz, octyl C2-H), 1.38–1.24 (m, 10H, octyl CH_2), 0.86 (t, 3H, J_{vic} 7.0 Hz, octyl CH_3); ^{13}C NMR (125.7 MHz, D_2O) δ: 103.2 (C-1, $J_{C\text{-}1,H\text{-}1}$ 160.4 Hz), 101.3 (C-1′, $J_{C\text{-}1',H\text{-}1'}$ 174.3 Hz), 86.0 (C-1″, $J_{C\text{-}1'',H\text{-}1''}$ 156.4 Hz), 80.8 (C-3), 77.84 (C-5″), 76.9 (C-3″), 74.9 (C-5), 74.0 (C-5′), 73.8 (C-2), 73.1 (C-2″), 71.6 (octyl C1), 70.4 (C-4), 70.2 (C-4″), 69.7 (C-3′), 68.6 (C-4′), 66.7 (C-6), 61.6 (C-6′), 61.4 (C-6″), 51.1 (C-2′), 31.9, 29.6, 29.3, 29.2, 25.9, 22.9 (octyl C2–C7), 14.3 (octyl CH_3): FAB MS *m/z*: 671.0 $(M+K)^+$, 655.0 $(M+Na)^+$, 633.0 $(M+H)^+$.

Octyl 2,3,4-tri-*O*-benzyl-6-*O*-methanesulfonyl-β-D-glucopyranoside (20)

To a solution of **9** (213 mg, 0.370 mmol) in pyridine at −25°C was added dropwise methanesulfonyl chloride (292 μL, 3.79 mmol). The reaction mixture was warmed to r.t. over 30 min and stirred at r.t. for 4 h. The mixture was then poured into ice-cold 0.5 N aqueous HCl and extracted with CH_2Cl_2. The CH_2Cl_2 solution was washed by saturated $NaHCO_3$ and water. Concentration gave **20** (234 mg, 97%). ^1H NMR (360 MHz, $CDCl_3$) δ: 7.35–7.10 (m, 15H, Ar-H), 4.96, 4.94, 4.89, 4.80, 4.71, 4.62 (6d, each 1H, J_{gem} 11.0 Hz, $PhCH_2$), 4.46 (dd, 1H, J_{gem} 11.5 Hz, $J_{5,6a}$ 1.0 Hz, H-6a), 4.41 (d, 1H, $J_{1,2}$ 7.8 Hz, H-1), 4.33 (dd, 1H, $J_{5,6b}$ 4.0 Hz, H-6b), 3.90 (dt, 1H, J_{gem} 10.0 Hz, J_{vic} 6.5 Hz, octyl C1-H_a), 3.67 (ddd, 1H, $J_{4,5}$ 9.5 Hz, H-5), 3.59 (dt, 1H, octyl C1-H_b), 3.42 (dd, 1H, $J_{2,3}$ 9.2 Hz, H-2), 3.03 (s, 3H, mesyl CH_3), 1.63 (p, 2H, J_{vic} 7.0 Hz, octyl C2-H), 1.41–1.19 (m, 10 H, octyl CH_2), 0.88 (t, 3H, J_{vic} 7.0 Hz, octyl CH_3).

Octyl 6-*S*-acetyl-2,3,4-tri-*O*-benzyl-6-deoxy-6-thio-β-D-glucopyranoside (21)

A mixture of **20** (230 mg, 0.359 mmol) and potassium thioacetate (433 mg, 3.79 mmol) in dry DMF (15 mL) was stirred at r.t. for 16 h. TLC showed incomplete reaction. The reaction mixture was then stirred at 40°C for an additional 2 h and concentrated to dryness. The residue was dissolved in CH_2Cl_2,

© 1997 NRC Canada

Can. J. Chem. Downloaded from www.nrcresearchpress.com by 88.146.161.215 on 09/08/12
For personal use only.

washed with water, and concentrated. The residue was purified by silica gel chromatography using hexane–EtOAc (6:1) as eluant to afford **21** (195 mg, 88%). ^{1}H NMR (360 MHz, $CDCl_3$) δ: 7.35–7.10 (m, 15H, Ar-H), 4.95, 4.93, 4.88, 4.78, 4.70, 4.64 (6d, each 1H, J_{gem} 11.0 Hz, $PhCH_2$), 4.36 (d, 1H, $J_{1,2}$ 8.0 Hz, H-1), 3.91 (dt, 1H, J_{gem} 9.8 Hz, J_{vic} 7.0 Hz, octyl C1-H_a), 3.63 (dd, 1H, $J_{2,3}$, $J_{3,4}$ 9.5 Hz, H-3), 3.60 (dd, 1H, J_{gem} 14.0 Hz, $J_{5,6a}$ 2.7 Hz, H-6a), 3.57 (dt, 1H, octyl C1-H_b), 3.46–3.31 (m, 3H, H-2, H-4, H-5), 2.97 (dd, 1H, $J_{5,6b}$ 7.5 Hz, H-6b), 2.36 (s, 3H, CH_3CO), 1.65 (p, 2H, J_{vic} 7.0 Hz, octyl C2-H), 0.89 (t, 3H, J_{vic} 7.0 Hz, octyl CH_3); ^{13}C NMR (75.5 MHz, $CDCl_3$) δ: 194.9 (C=O), 138.5, 138.4, 137.8 (benzyl C1), 128.5, 128.4, 128.34, 128.26, 128.1, 127.9, 127.6 (Ar), 103.5 (C-1), 75.7, 75.1, 74.8 (Ph*C*H_2), 31.8 (C-6), 31.1 (octyl C2), 30.5 (*C*H_3CO), 29.8, 29.4, 29.2, 26.2, 22.7 (octyl C3–C7), 14.1 (octyl CH_3). Anal. calcd. for $C_{37}H_{48}O_6S$ (620.84): C 71.58, H 7.79, S 5.16; found: C 71.27, H 8.15, S 5.52.

Octyl 2,3,4-tri-*O*-benzyl-6-deoxy-6-thio-β-D-glucopyranoside (12)

Compound **21** (133 mg, 0.214 mmol) was treated with methanolic NaOMe (0.05 N, 45 mL) at r.t. for 30 min. Neutralization with Amberlite IR-120 (H^+) resin, removal of the resin by filtration, and concentration gave **12** (124 mg, 96%); ^{1}H NMR (360 MHz, $CDCl_3$) δ: 7.40–7.10 (m, 15H, Ar-H), 4.96, 4.95, 4.89, 4.79, 4.72, 4.62 (6d, each 1H, J_{gem} 11.0 Hz, $PhCH_2$), 4.42 (d, 1H, $J_{1,2}$ 8.0 Hz, H-1), 3.95 (dt, 1H, J_{gem} 9.6 Hz, J_{vic} 6.5 Hz, octyl C1-H_a), 3.66 (dd, 1H, $J_{2,3}$, $J_{3,4}$ 9.5 Hz, H-3), 3.56 (dt, 1H, octyl C1-H_b), 3.47 (dd, 1H, $J_{4,5}$ 9.5 Hz, H-4), 3.43 (dd, 1H, $J_{2,3}$ 9.5 Hz, H-2), 3.37 (ddd, 1H, $J_{5,6a}$ 2.8 Hz, $J_{5,6b}$ 7.5 Hz, H-5), 2.89 (ddd, 1H, J_{gem} 14.0 Hz, $J_{6a,SH}$ 9.5 Hz, H-6a), 2.63 (ddd, 1H, $J_{6b,SH}$ 7.6 Hz, H-6b), 1.70 (dd, 1H, SH, D_2O exchangeable), 1.66 (p, 2H, J_{vic} 7.0 Hz, octyl C2-H), 0.88 (t, 3H, J_{vic} 7.0 Hz, CH_3).

2-*O*-Acetyl-3,4,6-tri-*O*-benzyl-α-D-glucose (23)

To a solution of 2-*O*-acetyl-3,4,6-tri-*O*-benzyl-α-D-glucopyranosyl bromide (**22**) (15) (313 mg, 0.563 mmol) in acetone (4 mL) at 0°C was added water (1 drop) and silver carbonate (192 mg, 0.698 mmol). The reaction mixture was vigorously stirred, warmed to r.t., and stirred overnight. The reaction mixture was filtered through a Celite bed that was washed with acetone. The acetone filtrate was concentrated, and the residue was purified by chromatography using hexane–EtOAc (2:1) as eluant to afford **23**. Compound **23** was not characterized but was used directly for the preparation of imidate **14**.

***O*-(2-*O*-Acetyl-3,4,6-tri-*O*-benzyl-α-D-glucopyranosyl)-trichloroacetimidate (14)**

To a solution of **23** (64 mg, 0.130 mmol) in dry CH_2Cl_2 was added NaH (60% suspension in oil, 5.2 mg, 0.130 mmol) and trichloroacetonitrile (60 μL). The reaction mixture was stirred at r.t. for 2 h and was concentrated. The residue was purified by chromatography using hexane–ether–Et_3N (50:50:1) as eluant to afford imidate **14** (50 mg, 60%); ^{1}H NMR (360 MHz, $CDCl_3$) δ: 8.58 (s, 1H, NH), 7.30–7.10 (m, 15H, Ar-H), 6.53 (d, 1H, $J_{1,2}$ 3.5 Hz, H-1), 5.07 (dd, 1H, $J_{2,3}$ 9.6 Hz, H-2), 4.86 (d, 1H, J_{gem} 11.5 Hz, $PhCH_2$), 4.84 (d, 1H, J_{gem} 10.8 Hz, $PhCH_2$), 4.77 (d, 1H, J_{gem} 11.5 Hz, $PhCH_2$), 4.64 (d, 1H, J_{gem} 11.8 Hz, $PhCH_2$), 4.58 (d, 1H, J_{gem} 10.8 Hz, $PhCH_2$), 4.50 (d, 1H, J_{gem} 11.8 Hz, $PhCH_2$), 4.10 (dd, 1H, $J_{3,4}$ 9.5 Hz, H-3), 4.02 (ddd, 1H, $J_{4,5}$ 9.5 Hz, H-5), 3.88 (dd, 1H, H-4), 3.82 (dd, 1H, J_{gem} 11.2 Hz, $J_{5,6a}$ 3.5 Hz, H-6a), 3.70 (dd, 1H, $J_{5,6b}$ 2.0 Hz, H-6b), 1.92 (s, 3H, Ac).

Octyl 3,4,6-tri-*O*-benzyl-α-D-mannopyranosyl-(1→6)-2,3,4-tri-*O*-benzyl-6-deoxy-6-thio-β-D-glucopyranoside (24)

To a solution of **12** (124 mg, 0.214 mmol) in dry THF (5 mL) was added sodium hydride (60% suspension in oil, 13 mg, 0.321 mmol). The resulting mixture was stirred at r.t. for 30 min. After the sodium salt (white precipitate) was produced, THF was removed using a stream of argon. The residuum sodium salt was dissolved with DMF (2 mL) and was added dropwise to a solution of 1,2-anhydro-3,4,6-tri-*O*-benzyl-β-D-mannose **13** (13) (85 mg, 0.195 mmol) in DMF (1 mL). The reaction mixture was stirred at r.t. for 1 h. Methanol (1 mL) was added to the reaction mixture; the reaction mixture was then concentrated and the residue was purified by column chromatography using hexane–EtOAc (3:1) as eluant to give **24** (94 mg, 63%); $[\alpha]_D$ +83.4 (*c* 0.5, CH_2Cl_2); ^{1}H NMR (360 MHz, $CDCl_3$) δ: 5.44 (d, 1H, $J_{1',2'}$ 1.5 Hz, H-1′), 4.96, 4.94, 4.85, 4.82, 4.76, 4.71 (6d, each 1H, J_{gem} 11.0 Hz, $PhCH_2$), 4.62 (d, 1H, J_{gem} 12.2 Hz, $PhCH_2$), 4.57, 4.51 (2d, each 1H, J_{gem} 11.0 Hz, $PhCH_2$), 4.44 (d, 1H, J_{gem} 12.2 Hz, $PhCH_2$), 4.38 (d, 1H, $J_{1,2}$ 8.0 Hz, H-1), 4.14 (ddd, 1H, $J_{2',3'}$ 3.2 Hz, $J_{2',OH}$ 2.7 Hz, H-2′), 4.12 (ddd, 1H, H-5′), 3.93 (dt, J_{gem} 10.0 Hz, J_{vic} 6.5 Hz, octyl C1-H_a), 3.91 (dd, 1H, $J_{4',5'}$, $J_{3',4'}$ 9.5 Hz, H-4′), 3.85 (dd, 1H, H-3′), 3.75 (dd, 1H, J_{gem} 11.8 Hz, $J_{5',6'a}$ 4.5 Hz, H-6′a), 3.63 (dd, 1H, $J_{2,3}$, $J_{3,4}$ 9.5 Hz, H-3), 3.61 (dd, 1H, $J_{5',6'b}$ 2.0 Hz, H-6′b), 3.50 (dt, 1H, octyl C1-H_b), 3.48 (dd, 1H, $J_{4,5}$ 9.5 Hz, H-4), 3.48 (m, 1H, H-5), 3.41 (dd, 1H, H-2), 3.07 (dd, J_{gem} 14.0 Hz, $J_{5,6a}$ 2.5 Hz, H-6a), 2.78 (dd, 1H, $J_{5,6b}$ 6.0 Hz, H-6b), 2.57 (d, 1H, C2′-OH), 0.87 (t, 3H, J_{vic} 7.0 Hz, octyl CH_3); ^{13}C NMR (100.6 MHz, $CDCl_3$) δ: 138.6, 138.5, 138.4, 138.2, 137.7 (benzyl C1), 128.6, 128.4, 128.3, 128.1, 128.0, 127.91, 127.86, 127.6, 127.5 (Ar), 103.5 (C-1), 84.5 (C-1′), 75.6, 75.2, 75.1, 74.8, 73.4, 72.0 (Ph*C*H_2), 70.2 (octyl C1), 68.9 (C-6′), 31.9 (C-6), 31.8, 29.8, 29.4, 29.3, 26.2, 22.7 (octyl C2–C7), 14.1 (octyl CH_3). Anal. calcd. for $C_{62}H_{74}O_{10}S$ (1011.33): C 73.63, H 7.38, S 3.17; found: C 73.18, H 7.44, S 3.30.

Octyl 2-*O*-acetyl-3,4,6-tri-*O*-benzyl-β-D-glucopyranosyl-(1→2)-3,4,6-tri-*O*-benzyl-α-D-mannopyranosyl-(1→6)-2,3,4-tri-*O*-benzyl-6-deoxy-6-thio-β-D-glucopyranoside (25)

A mixture of **14** (48 mg, 75.4 μmol), **24** (66 mg, 65.2 μmol), powdered molecular sieve 4Å (60 mg), and CH_2Cl_2 (3 mL) was stirred at r.t. for 30 min. To the mixture was added a solution of TMSOTf (1.45 μL, 7.5 μmol) in CH_2Cl_2 (150 μL) under argon. After stirring for 1 h, Et_3N (0.1 mL) was added and the mixture was filtered through Celite and concentrated. The residue was purified by chromatography using hexane–EtOAc (3:1) as eluant to afford **25** (44 mg, 88% based on consumed alcohol) and recovered alcohol **24** (32 mg, 49%); $[\alpha]_D$ +37.7 (*c* 1.2, CH_2Cl_2): ^{1}H NMR (360 MHz, $CDCl_3$) δ: 5.40 (d, 1H, $J_{1',2'}$ 1.2 Hz, H-1′), 5.15 (dd, 1H, $J_{1'',2''}$ 8.5 Hz, $J_{2'',3''}$ 9.0 Hz, H-2″), 4.47 (d, 1H, H-1″), 4.39 (d, 1H, $J_{1,2}$ 8.0 Hz, H-1), 4.27 (dd, 1H, $J_{2',3'}$ 3.2 Hz, H-2′), 4.08 (ddd, 1H, $J_{4',5'}$ 9.6 Hz, $J_{5',6'a}$ 6.4 Hz, $J_{5',6'b}$ 2.0 Hz, H-5′), 3.97 (dt, 1H, J_{gem} 10.0 Hz, J_{vic} 6.5 Hz, octyl C1-H_a), 3.82 (dd, 1H, $J_{3',4'}$ 9.5 Hz, H-3′), 3.62 (dd, 1H, $J_{3,4}$ 9.5 Hz, H-3), 3.53 (dt, 1H, octyl C1-H_b), 3.44 (dd, $J_{2,3}$

© 1997 NRC Canada

Can. J. Chem. Downloaded from www.nrcresearchpress.com by 88.146.161.215 on 09/08/12
For personal use only.

9.2 Hz, H-2), 3.10 (dd, 1H, J_{gem} 14.2 Hz, $J_{5,6a}$ 2.2 Hz, H-6a), 2.82 (dd, 1H, $J_{5,6b}$ 5.4 Hz, H-6b), 1.92 (s, 3H, Ac), 0.86 (t, 3H, J_{vic} 7.0 Hz, octyl CH_3); ^{13}C NMR (100.6 MHz, $CDCl_3$) δ: 169.4 (C=O), 138.58, 138.56, 138.5, 138.33, 138.27, 138.1, 138.0, 137.9 (benzyl C1), 128.4, 128.37, 128.34, 128.28, 128.2, 128.1, 127.99, 127.97, 127.87, 127.81, 127.69, 127.66, 127.6, 127.4 (Ar), 103.7 (C-1), 99.0 (C-1″), 84.6 (C-1′), 75.6, 75.3, 75.1, 75.0, 74.83, 74.81, 73.6, 72.9, 70.5 (PhCH$_2$), 70.3 (octyl C1), 69.7 (C-6″), 69.5 (C-6′), 31.82 (C-6), 31.81, 29.8, 29.5, 29.3, 26.2, 22.6 (octyl C2–C7), 20.9 (CH_3CO), 14.1 (octyl CH_3). Anal. calcd. for $C_{91}H_{104}O_{16}S$ (1485.99): C 73.56, H 7.05, S 2.16; found: C 73.59, H 7.14, S 2.10.

Octyl 3,4,6-tri-*O*-benzyl-β-D-glucopyranosyl-(1→2)-3,4,6-tri-*O*-benzyl-α-D-mannopyranosyl-(1→6)-2,3,4-tri-*O*-benzyl-6-deoxy-6-thio-β-D-glucopyranoside (26)

Compound **25** (24 mg, 16.2 μmol) was treated with methanolic NaOMe (0.05 N, 25 mL) at r.t. for 8 h. Neutralization with Amberlite IR-120 (H^+) resin, removal of the resin by filtration, and concentration left a residue that was purified by column chromatography (hexane–EtOAc 2:1) to give **26** as a syrup (21 mg, 92%); ^{1}H NMR (400 MHz, $CDCl_3$) δ: 5.54 (d, 1H, $J_{1',2'}$ 1.8 Hz, H-1′), 4.44 (d, 1H, $J_{1'',2''}$ 7.8 Hz, H-1″), 4.37 (d, 1H, $J_{1,2}$ 8.0 Hz, H-1), 4.33 (dd, 1H, $J_{2',3'}$ 3.2 Hz, H-2′), 4.12 (dd, 1H, $J_{3',4'}$, $J_{4',5'}$ 9.5 Hz, H-4′), 4.03 (ddd, 1H, $J_{5',6'a}$ 4.5 Hz, $J_{5',6'b}$ 2.0 Hz, H-5′), 3.98 (dt, 1H, J_{gem} 10.0 Hz, J_{vic} 6.5 Hz, octyl C1-H$_a$), 3.88 (dd, 1H, H-3′), 3.43 (dd, 1H, $J_{2,3}$ 9.0 Hz, H-2), 3.38 (br s, 1H, C2″-OH), 3.06 (dd, 1H, J_{gem} 14.5 Hz, $J_{5,6a}$ 2.0 Hz, H-6a), 2.83 (dd, 1H, $J_{5,6b}$ 5.0 Hz, H-6b), 0.85 (t, 3H, J_{vic} 7.0 Hz, octyl CH_3); ^{13}C NMR (100.6 MHz, $CDCl_3$) δ: 139.0, 138.6, 138.52, 138.47, 138.3, 138.2, 138.0, 137.97, 137.7 (benzyl C1), 128.46, 128.34, 128.28, 128.25, 128.01, 127.93, 127.87, 127.81, 127.76, 127.64, 127.58, 127.54, 127.42 (Ar), 103.7 (C-1), 100.6 (C-1″), 84.5 (C-1′), 75.6, 75.1, 75.1, 75.0, 74.9, 74.8, 73.5, 73.3, 71.7 (PhCH$_2$), 70.4 (octyl C1), 69.5 (C-6″), 68.7 (C-6′), 32.4 (C-6), 31.8, 29.8, 19.5, 29.2, 26.2, 22.6 (octyl C2–C7), 14.1 (octyl CH_3).

Octyl β-D-glucopyranosyl-(1→2)-α-D-mannopyranosyl-(1→6)-6-deoxy-6-thio-β-D-glucopyranoside (8)

The benzyl ether protecting groups in **26** (18 mg, 12.5 μmol) were removed by treatment with Na/liquid NH_3, and then purified as described for the preparation of **7**. Lyophilization from water gave **8** as a white powder (6.5 mg, 82%); $[\alpha]_D$ +54.6 (*c* 0.5, CH_3OH); ^{1}H NMR (500 MHz, D_2O) δ: 5.50 (d, 1H, $J_{1',2'}$ 1.0 Hz, H-1′), 4.50 (d, 1H, $J_{1'',2''}$ 8.0 Hz, H-1″), 4.46 (d, 1H, $J_{1,2}$ 8.0 Hz, H-1), 4.24 (dd, 1H, $J_{2',3'}$ 3.5 Hz, H-2′), 4.01 (ddd, 1H, $J_{4',5'}$ 9.5 Hz, $J_{5',6'a}$ 3.2 Hz, $J_{5',6'b}$ 6.0 Hz, H-5′), 3.90 (dd, 1H, J_{gem} 12.0 Hz, $J_{5'',6''a}$ 2.0 Hz, H-6″a), 3.89 (dd, 1H, J_{gem} 12.0 Hz, $J_{5',6'a}$ 6.5 Hz, H-6′a), 3.87 (dd, 1H, $J_{5',6'b}$ 2.5 Hz, H-6′b), 3.87 (dd, 1H, $J_{3',4'}$ 9.5 Hz, H-3′), 3.85 (dt, 1H, J_{gem} 10.5 Hz, J_{vic} 6.5 Hz, octyl C1-H$_a$), 3.75 (dd, 1H, $J_{5'',6''b}$ 5.4 Hz, H-6″b), 3.74 (dd, 1H, $J_{3',4'}$, $J_{4',5'}$ 9.5 Hz, H-4′), 3.71 (dt, 1H, octyl C1-H$_b$), 3.61 (ddd, 1H, $J_{4,5}$ 9.5 Hz, $J_{5,6a}$ 2.7 Hz, $J_{5,6b}$ 8.0 Hz, H-5), 3.49 (ddd, 1H, $J_{4'',5''}$ 9.5 Hz, H-5″), 3.47 (dd, $J_{2,3}$, $J_{3,4}$ 9.5 Hz, H-3), 3.43 (dd, 1H, H-4″), 3.39 (dd, 1H, H-4), 3.36 (dd, 1H, $J_{2'',3''}$ 9.5 Hz, H-2″), 3.26 (dd, 1H, $J_{2,3}$ 9.5 Hz, H-2), 3.20 (dd, J_{gem} 14.4 Hz, $J_{5,6a}$ 2.7 Hz, H-6a), 2.80 (dd, 1H, $J_{5,6b}$ 8.0 Hz, H-6b), 1.64 (p, 2H, J_{vic} 7.0 Hz, octyl C2-H), 1.40–1.25 (m, 10H, 5 octyl CH_2), 0.87 (t, 3H, J_{vic} 7.0 Hz, octyl CH_3); ^{13}C NMR (100.6 MHz) δ: 103.2 (C-1, $J_{C\text{-}1,H\text{-}1}$ 160.6 Hz), 101.8 (C-1″, $J_{C\text{-}1'',H\text{-}1''}$ 161.1 Hz), 82.7 (C-1′, $J_{C\text{-}1',H\text{-}1'}$ 167.9 Hz, C-1′), 79.4 (C-2′), 76.8 (C-3), 76.5 (C-5″), 76.3 (C-3″), 74.9 (C-5), 74.1 (C-2), 73.9 (C-5′), 73.5 (C-2″), 73.1 (C-4), 71.8 (octyl C1), 71.1 (C-3′), 70.1 (C-4″), 67.9 (C-4′), 61.5 (C-6″), 61.2 (C-6′), 32.4 (C-6), 31.9, 29.7, 29.3, 29.2, 25.9, 22.8 (octyl C2–C7), 14.2 (octyl CH_3); FAB MS *m/z*: 671.1 $(M+K)^+$, 655.2 $(M+Na)^+$, 633.3 $(M+H)^+$. Exact FAB MS for $C_{26}H_{48}O_{15}SNa$, theoretical MS: 655.2612; found: 655.2620 (std. deviation 1.3).

Evaluation of trisaccharide analogs as acceptors for GlcNAcT-V

Materials

The cloned rat kidney GlcNAcT-V was from Dr. M. Pierce. Partially purified GlcNAcT-V was prepared by a modification (20) of published procedures (18, 19). The activity of cloned GlcNAcT-V was 10 mU/mL with **5** as acceptor (protein content = 0.286 mg/mL, specific activity = 35 mU/mg). The activity of isolated GlcNAcT-V was 1.0 mU/mL with **5** as acceptor. Enzyme was stored at 4°C in 50 mM MES buffer, pH 6.5, containing 300 mM NaCl, and 5 mM EDTA.

Methods

A standard assay contained final concentrations of 40 μM **5** as acceptor, 550 μM UDP GlcNAc including UDP-^{3}H-GlcNAc (~200 000 dpm) as donor substrates, 5–9 μU cloned GlcNAcT-V (0.5–0.9 μL), in 25 mM sodium cacodylate buffer, pH 6.5, 0.05% Triton X-100, 10% glycerol, 5 mM EDTA, and 0.5 mg/mL BSA, in a total volume of 20 μL. Assay tubes were incubated for 30–60 min at 37°C, then quenched with 0.5 mL water. Radiolabeled product was separated from unreacted donor on Sep-Pak C-18 reversed-phase cartridge and quantitated by liquid scintillation counting in 10 mL of Ecolite cocktail (ICN) (9, 18–20).

Kinetics

Kinetic parameters for acceptors were determined with the radiochemical assay described above. Assays contained buffer, donor, ^{3}H donor, and enzyme concentrations as for the standard assay. Assays were performed in duplicate with six different acceptor concentrations. Tubes were incubated at 37°C for 60 or 30 min and processed on C-18 Sep-Pak cartridges as for the standard assay. Kinetic data (K_m and V_{max}) listed in Table 1 were obtained by fitting the initial rate data to the Michaelis-Menten equation using nonlinear regression analysis (Sigma Plot 4.10) (9).

Preparative enzymatic synthesis of octyl β-D-glucopyranosyl-(1→2)-[2-acetamido-2-deoxy-β-D-glucopyranosyl-(1→6)]-2-deoxy-2-thio-α-D-mannopyranosyl-(1→6)-β-D-glucopyranoside (27)

A mixture of **7** (0.49 mg, 0.774 μmol), UDP-GlcNAc (2 mg, 3 μmol), cloned rat kidney GlcNAcT-V (17) (0.5 mL, 1.48 mU/mL), and buffer (170 mM sodium cacodylate buffer, pH 6.5, 70% glycerol, 35 mM EDTA, and 3.5 mg/mL BSA, in a total volume of 200 μL) was incubated at r.t. for 48 h. The mixture was diluted with Milli-Q water and loaded onto a C-18 Sep-Pak cartridge. The cartridge was eluted with water (3 × 10 mL) followed by methanol (10 mL). The methanolic eluate was concentrated to dryness, and the residue was dissolved in Milli-Q water and passed through a Millex filter. Compound

© 1997 NRC Canada

27 was obtained as a white powder in 100% yield after lyophilization of the filtrate. ^{1}H NMR (500 MHz, D_2O) δ: 5.13 (d, 1H, $J_{1',2'}$ 0.5 Hz, H-1′), 4.53 (d, 1H, $J_{1'',2''}$ 10.5 Hz, H-1″), 4.45 (d, 1H, $J_{1,2}$ 8.0 Hz, H-1), 4.52 (d, 1H, $J_{1''',2'''}$ 8.0 Hz, H-1‴), 4.17 (dd, 1H, $J_{2',3'}$ 4.5 Hz, $J_{3',4'}$ 9.8 Hz, H-3′), 3.61 (dd, 1H, H-2′), 3.38 (dd, 1H, $J_{2'',3''}$ 9.5 Hz, H-2″), 3.26 (dd, 1H, $J_{2,3}$ 9.5 Hz, H-2), 2.09 (s, 3H, Ac), 1.63 (p, 2H, J_{vic} 7.0 Hz, octyl C2-H), 1.40–1.24 (m, 10H, octyl CH_2), 0.86 (t, 3H, J_{vic} 7.0 Hz, octyl CH_3); FAB MS *m/z*: 858.1 $(M+Na)^+$.

Preparative enzymatic synthesis of octyl β-D-glucopyranosyl-(1→2)-[2-acetamido-2-deoxy-β-D-glucopyranosyl-(1→6)]-α-D-mannopyranosyl-(1→6)-6-deoxy-6-thio-β-D-glucopyranoside (28)

A mixture of **8** (0.50 mg, 0.789 μmol), UDP-GlcNAc (1.5 mg, 2.3 μmol), partially purified GlcNAcT-V (1.5 mL, 1 mU/mL) from hamster kidneys (18–20), and buffer (150 mM sodium cacodylate buffer, pH 6.5, 60% glycerol, 30 mM EDTA, and 3 mg/mL BSA, in a total volume of 500 μL) was incubated at r.t. for 72 h. The mixture was diluted with Milli-Q water and loaded onto a C-18 Sep-Pak cartridge. The cartridge was eluted with water (3 × 10 mL) followed by methanol (10 mL). The methanolic eluate was concentrated to dryness, and the residue was purified by chromatography on Iatrobeads using $CHCl_3$–MeOH–H_2O (65:35:8) as eluant to give the crude product. The crude product was dissolved in Milli-Q water and was loaded onto a C-18 Sep-Pak cartridge. The cartridge was washed with water (10 mL) followed by methanol (10 mL). The methanolic eluate was concentrated to dryness, the residue was dissolved in Milli-Q water and passed through a Millex filter. Compound **28** was obtained as a white powder in 100% yield after lyophilization of the filtrate. ^{1}H NMR (500 MHz, D_2O) δ: 5.48 (d, 1H, $J_{1',2'}$ 1.0 Hz, H-1′), 4.52 (d, 1H, $J_{1'',2''}$ 8.4 Hz, H-1″), 4.48 (d, 1H, $J_{1''',2'''}$ 7.6 Hz, H-1‴), 4.45 (d, 1H, $J_{1,2}$ 8.1 Hz, H-1), 4.22 (dd, 1H, $J_{2',3'}$ 3.5 Hz, H-2′), 4.15 (dd, 1H, J_{gem} 11.0 Hz, $J_{5',6'a}$ 2.4 Hz, H-6′a), 4.11 (ddd, 1H, $J_{4',5'}$ 9.5 Hz, $J_{5',6'b}$ 4.8 Hz, H-5′), 3.94 (d, 1H, J_{gem} 12.0 Hz, $J_{5'',6''a}$ 2.0 Hz, H-6″a), 3.83 (dd, 1H, $J_{3',4'}$ 9.5 Hz, H-3′), 3.61 (ddd, 1H, $J_{4,5}$ 9.6 Hz, $J_{5,6a}$ 3.0 Hz, $J_{5,6b}$ 8.0 Hz, H-5), 3.26 (dd, 1H, $J_{2,3}$ 9.5 Hz, H-2), 3.17 (dd, 1H, J_{gem} 14.3 Hz, $J_{5,6a}$ 3.0 Hz, H-6a), 2.80 (dd, 1H, $J_{5,6b}$ 8.0 Hz, H-6b), 2.07 (s, 3H, Ac), 1.64 (p, 2H, J_{vic} 7.0 Hz, octyl C2-H), 0.87 (t, 3H, J_{vic} 7.0 Hz, octyl CH_3); FAB MS *m/z*: 874.2 $(M+K)^+$, 858.2 $(M+Na)^+$, 836.3 $(M+H)^+$.

Acknowledgments

We thank Ms. C.A. Compston for performing some of the enzyme experiments and Dr. Albin Otter for recording the 500 MHz NMR spectra of **7**, **8**, **27**, and **28**. The cloned GlcNAcT-V was a generous gift from Dr. M. Pierce, University of Georgia. This work was supported by grants from the Medical Research Council of Canada (M.M.P.) and the Natural Sciences and Engineering Research Council of Canada (O.H.). Pu-Ping Lu is the recipient of a scholarship from Alberta Heritage Foundation for Medical Research.

References

1. R.D. Cummings and I.S. Trowbridge. J. Biol. Chem. **257**, 13421 (1982).
2. H. Schachter. Biochem. Cell. Biol. **64**, 163 (1986).
3. J.W. Dennis, S. Laferte, C. Waghorne, M.L. Breitman, and R.S. Kerbel. Science, **236**, 236582 (1987).
4. J.W. Dennis. Cancer Surv. **7**, 573 (1988).
5. J.W. Dennis. *In* Cell surface carbohydrates and cell development. *Edited by* M. Fukuda. CRC press, Boca Raton, Fla. 1991. pp. 161-194.
6. O. Hindsgaul, S.H. Tahir, O.P. Srivastava, and M. Pierce. Carbohydr. Res. **173**, 263 (1988).
7. O.P. Srivastava, O. Hindsgaul, M. Shoreibah, and M. Pierce. Carbohydr. Res. **179**, 137 (1988).
8. O. Kanie, M. Palcic, and O. Hindsgaul. RIKEN Rev. 853 (1995).
9. M.M. Palcic, L.D. Heerze, M. Pierce, and O. Hindsgaul. Glycoconjugate J. **5**, 49 (1988).
10. R.L. Halcomb and S.J. Danishefsky. J. Am. Chem. Soc. **111**, 6661 (1989).
11. D. Horton. Methods Carbohydr. Chem. **2**, 433 (1963).
12. N.E. Franks and R. Montgomery. Carbohydr. Res. **6**, 286 (1968).
13. S.J. Sondheimer, H. Yamaguchi, and C. Schuerch. Carbohydr. Res. **74**, 327 (1979).
14. R.R. Schmidt and J. Michel. Angew. Chem. Int. Ed. Engl. **19**, 731 (1980).
15. O. Hindsgaul, T. Norberg, J.Le Pendu, and R.U. Lemieux. Carbohydr. Res. **109**, 109 (1982).
16. K. Bock and C. Pedersen. J. Chem. Soc. Perkin Trans. 2, 293 (1974).
17. M. Shoreibah, G.S. Perng, B. Adler, J. Weinstein, R. Cuddles, D. Wen, J.K. Browne, P. Buckhaults, N. Fregien, and M. Pierce. J. Biol. Chem. **268**, 5381 (1993).
18. S.H. Khan, S.C. Crawley, O. Kanie, and O. Hindsgaul. J. Biol. Chem. **268**, 2468 (1993).
19. O. Kanie, S.C. Crawley, M.M. Palcic, and O. Hindsgaul. Carbohydr. Res. **243**, 139 (1993).
20. P.-P. Lu, O. Hindsgaul, C.A. Compston, and M.M. Palcic. Bioorg. Med. Chem. **4**, 2011 (1996).
21. S. Ogawa, T. Furuya, H. Tsunoda, O. Hindsgaul, K. Stangier, and M.M. Palcic. Carbohydr. Res. **271**, 197 (1995).

Can. J. Chem. Downloaded from www.nrcresearchpress.com by 88.146.161.215 on 09/08/12
For personal use only.

© 1997 NRC Canada

A new *ent*-kaurane from the root extract of *Chiococca alba*

Rocío Borges-Argáez, Leticia Medina-Baizabál, Filogonio May-Pat, and Luis M. Peña-Rodríguez

Abstract: A bioassay-guided purification of the methanolic crude extract obtained from the roots of *Chiococca alba* (L.) Hitchc. resulted in the isolation of a new, bioactive, metabolite identified as *ent*-17-hydroxy-16α-kauran-3-one (**1**). Elucidation of the new structure was based on analyses of the results obtained from various spectroscopic methods (IR, MS, ^{1}H NMR, and ^{13}C NMR) and chemical transformations. The stereochemistry at C16 was assigned by comparing both the proton and carbon chemical shifts of C17 with those reported in the literature. The new kaurane showed weak antimicrobial activity when tested against *Staphylococcus aureus*.

Key words: medicinal plants, *Chiococca alba*, Rubiaceae, kaurane, diterpene, antimicrobial.

Résumé : Une purification orientée par des bioessais d'extraits méthanoliques bruts obtenus des racines du *Chiococca alba* (L.) Hitchc. a permis d'isoler un nouveau métabolite bioactif identifié comme l'*ent*-17-hydroxy-16α-kauran-3-one (**1**). L'élucidation de la nouvelle structure est basée sur l'analyse des résultats obtenus par diverses méthodes spectroscopiques (IR, SM, RMN du ^{1}H et du ^{13}C) et transformations chimiques. La stéréochimie en C-16 a été attribuée par comparaison des déplacements chimiques tant du proton que du carbone du C-17 avec ceux rapportés dans la littérature. Le nouveau kaurane présente une faible activité antimicrobienne contre le *Staphylococcus aureus*.

Mots clés : plantes médicinales, *Chiococca alba*, Rubiaceae, kaurane, diterpène, antimicrobien.

[Traduit par la rédaction]

Introduction

As part of our continuing search for bioactive metabolites from Yucatecan medicinal plants, we have investigated the components present in the roots of *Chiococca alba* (L.) Hitchc. (Rubiaceae). This plant is one of the 10 most popular species used by the people of the Yucatan peninsula where it is commonly known as "t'unche'" or "kanchakche'" (1–4). The root decoction of *C. alba* is used in Yucatecan traditional medicine to cure dysentery, as a diuretic and cathartic, and against snake bites (5). The leaf infusion is used to alleviate a number of ailments such as asthma, headaches, and diarrhea, and a decoction of the whole plant is reported to be effective as a laxative and against gonorrhea, skin infections, and rheumatism (1, 3).

Although there are a number of phytochemical studies on the constituents of rubiaceus plants (6–11), there is limited knowledge about the chemical constituents of *C. alba*. Recent studies report the isolation and identification of two biologically active quinoline alkaloids (12) and a new oleanane-type triterpene (13) from the root extract of the plant, while two new ketoalcohols have been reported from the leaf extract (14). We wish to report here the isolation and identification of a new, biologically active, *ent*-kaurane derivative (**1**) from the root extract of *C. alba*.

Received December 10, 1996.

This paper is dedicated to Professor William A. Ayer on the occasion of his 65th birthday.

R. Borges-Argáez, L. Medina-Baizabál, F. May-Pat, and L.M. Peña-Rodríguez.[1] Departamento de Química Orgánica, Centro de Investigación Científica de Yucatán, A.C., Apartado Postal 87 Cordemex, Mérida, Yucatán, México 97310.

[1] Author to whom correspondence may be addressed. Telephone: (99) 81-07-70. Fax: (99) 81-39-00. E-mail: lmanuel@cicy.cicy.mx

Results and discussion

During our investigation we found that the methanolic extract of the roots of *C. alba* showed antimicrobial activity when tested against *Staphylococcus aureus* (15). A bioassay-directed fractionation of the crude extract, using both an initial solvent partition procedure and successive chromatographic purifications, yielded a biologically active fraction showing a single component by TLC and GC. The bioactive metabolite **1** was obtained as an amorphous, wax-like, solid that could not be induced to crystallize. The parent ion peak at *m/z* 304 in the HREIMS of **1** corresponded to the molecular formula $C_{20}H_{32}O_2$, suggesting a diterpene structure. Two intense absorptions at 3430 and 1690 cm^{-1} in the IR spectrum indicated the presence of both an alcohol and keto groups in the structure of **1** and allowed for the assignment of the two oxygen atoms in the molecular formula. The primary nature of the alcohol group was evident from a fragment ion peak at *m/z* 273 (M^+-31) in the HREIMS of **1** and the presence of an AB quartet having two one-proton doublets of doublets at 3.42 (J = 12.0 and 3.2 Hz) and 3.37 ppm (J = 11.2 and 2.4 Hz) in its ^{1}H NMR spectrum. Treatment of **1** with acetic anhydride and pyridine yielded the expected monoacetate **2** showing a parent

© 1997 NRC Canada

Can. J. Chem. Downloaded from www.nrcresearchpress.com by 88.146.161.215 on 09/08/12
For personal use only.

Can. J. Chem. Downloaded from www.nrcresearchpress.com by 88.146.161.215 on 09/08/12
For personal use only.

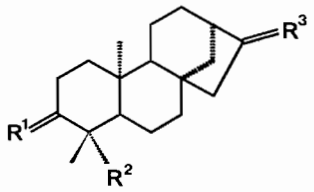
ion peak at *m/z* 346 in its HREIMS, a lack of absorption bands in the hydroxyl region of the IR spectrum, and the expected downfield shift for the hydroxymethylene protons, to a two-proton doublet at 3.83 ppm (J_{AB} = 7.6 Hz), in its ^{1}H NMR spectrum. In the same manner, treatment of **1** with pyridinium chlorochromate (16) resulted in the obtention of aldehyde **3**, which showed, in its ^{1}H NMR spectrum, a characteristic one-proton doublet at 9.65 ppm (J = 1.2 Hz).

A careful analysis of the ^{13}C NMR spectrum and of the results from DEPT and HETCOR experiments permitted the assignment of all carbons in the structure of **1** as three methyl groups, nine methylenes, four methines, and four quaternary carbons. The three methyl singlets at 1.05, 1.04, and 1.01 ppm in the ^{1}H NMR of **1** further indicated their all being bonded to quaternary carbons. Since the only sp^2 carbon observed in the ^{13}C NMR of **1** corresponded to that of the ketone carbonyl group, the four remaining unsaturation sites implied by the molecular formula of **1** were assigned to four carbocyclic rings. A diterpene structure having four rings, four methines, and three methyl groups in quaternary carbons could only be accommodated in a kaurane skeleton having a primary alcohol and a keto group.

A closer analysis of both the ^{1}H NMR and the ^{1}H–^{1}H COSY spectra of **1** permitted the correct assignment of the location of the keto group in the structure. A two-proton doublet of doublets at 2.45 ppm (J = 6.4 and 8.4 Hz) showed cross peaks with two signals at 1.40 and 2.00 ppm, indicating a partial structure of two methylene groups in positions α and β to a carbonyl group. This type of partial structure could only be fitted in the kaurane skeleton if the ketone group was located in either position 1 or 3 of the structure. It could be argued that location of the carbonyl group at C3 is favored on biogenetic grounds, via the catalyzed cyclization of an epoxy-geranyl geranyl pyrophosphate unit, following a similar biosynthetic pathway to that of squalene leading to triterpenes (17, 18). Final confirmation of a C3 carbonyl group in the structure of **1** came from comparison of its virtually identical carbon chemical shift values with those reported for *ent*-17-norkaurane-3,16-dione (**4**) (Table 1) (19).

The additional coupling to a methine proton at 1.90 ppm shown by the hydroxymethyl group in the ^{1}H–^{1}H COSY spectrum of **1** allowed for the correct placement of the primary alcohol group at C17. Assignment of the stereochemistry at C16 was made by comparing both the proton and carbon chemical shift values of C17 in the corresponding spectra of **1** with those reported in the literature for C16α and β *ent*-kauranes. While the hydroxymethyl group protons and carbon chemical shift values in methyl 17-hydroxy-16β-(−)-kauran-19-oate (**5**) (20) appear at 3.70 ppm (d, J = 7 Hz) and 64.1 ppm, respectively, in the 16α epimer (**6**), as is the case for **1**, the C17 methylene protons and carbon appear at higher (3.40 ppm) and lower (67.4 ppm) fields, respectively (20). This effect is also observed in the corresponding acetylated derivatives **7** and **8**, as well as in other structurally similar *ent*-kauranes (**9**–**12**) (20–22). On this basis **1** was identified as the new bioactive metabolite *ent*-17-hydroxy-16α-kauran-3-one.

Although there are reports of kaurane diterpenes having been isolated from plants of the Rubiaceae family (11), little is known about their biological activity. Recent investigations have resulted in the isolation of several *ent*-kauranoids showing cytotoxic (23, 24) and anti-HIV (21, 25) activities. This is the first report of an *ent*-kaurane showing antimicrobial activity.



	R^1	R^2	R^3
1	O	CH_3	β-H, α-CH_2OH
2	O	CH_3	β-H, α-CH_2OAc
3	O	CH_3	β-H, α-CHO
4	O	CH_3	O
5	H_2	COOMe	β-CH_2OH, α-H
6	H_2	COOMe	β-H, α-CH_2OH
7	H_2	COOMe	β-CH_2OAc, α-H
8	H_2	COOMe	β-H, α-CH_2OAc
9	H_2	COOH	β-CH_2OH, α-H
10	H_2	COOH	β-H, α-CH_2OH
11	H_2	CH_3	β-CH_2OH, α-OH
12	H_2	CH_3	β-OH, α-CH_2OH

Experimental

General methods

IR spectra were recorded in $CHCl_3$ using a Perkin–Elmer 683 spectrophotometer. GC–MS analyses were performed on a Hewlett–Packard 5890 gas chromatograph (1.0 μL of 3% sample in $CHCl_3$, HP Ultra 2 column (crosslinked 5% Ph Me Silicone, 25 m × 0.32 mm × 0.52 μm film thickness), temperature program: T_1 = 150°C, T_2 = 300°C, gradient = 10°C/min, injector temperature = 300°C, detector temperature = 290°C) coupled to a Hewlett–Packard 5971A mass selective detector. HREIMS and CIMS spectra were recorded on Kratos AEI MS-50 and AEI MS-12 mass spectrometers, respectively. ^{1}H NMR (400 MHz) and ^{13}C NMR (100 MHz) spectra were obtained in $CDCl_3$ on a Varian Unity 400 spectrometer using the $CHCl_3$ signal (7.29 and 77.48 ppm, respectively) as reference. The strains used in the antimicrobial assay: *Bacillus subtilis* (ATCC 6633), *Candida albicans* (ATCC 10231), *Escherichia coli* (ATCC 10538), *Pseudomonas aeruginosa* (ATCC 15442), *Saccharomyces cerevisiae* (ATCC 9763), and *Staphylococcus aureus* (ATCC 6538) were obtained from the American Type Culture Collection. Analytical TLC analyses and preparative TLC purifications were carried out using precoated silica gel aluminum and glass plates, respectively (E.M. Merck DC Alufolien, Kieselgel 60 F254, 0.20 mm thickness and E.M. Merck DC Fertigplatten, Kieselgel 60 F254, 0.25 mm thickness). Chromatograms were examined under UV light in a UV-viewing cabinet (Spectroline model CX-20) and visualized by dipping in 4% phosphomolybdic acid solution containing a trace of ceric sulfate in 5% sulfuric acid, followed by drying and gentle heating. Medium-pressure

© 1997 NRC Canada

Can. J. Chem. Downloaded from www.nrcresearchpress.com by 88.146.161.215 on 09/08/12
For personal use only.

column chromatography (flash cc) purifications were run according to Still et al. (26) using silica gel 60 (230–400 mesh) from Aldrich Chemical Co.

Plant material

The roots of *C. alba* were collected in July 1992 from plants growing on a field located at km 24 of the Merida-Progreso highway. A voucher specimen has been deposited in the herbarium of the Natural Resources Department of Centro de Investigación Científica de Yucatán (CICY) under the collection number 696. The plant material was washed with tap water and dried, first for a week at room temperature and then for 72 h in an oven at 55°C. The dry roots were ground using a Brabender Dusiburg (880804 type) mill and collected using a No. 2 sieve.

Extraction and isolation

Soxhlet extraction of the ground plant material (195.12 g) using methanol (2 L) resulted in the obtention of 16.01 g of crude methanolic extract. Testing of a 5% solution of the crude extract in the antimicrobial assay showed a 1 mm inhibition zone against *Staphylococcus aureus*. The biologically active extract was suspended in a 3:2 mixture of water/methanol (ca. 100 mL of solution/300 mg of crude extract) and the resulting suspension was partitioned successively between hexane, dichloromethane, and ethyl acetate to yield the low-polarity (0.31 g), medium-low polarity (2.45 g), and medium polarity fractions (1.19 g), respectively. Successive flash cc (dichloromethane/acetone, 98:2) and preparative TLC (multiple elution, four times, hexane/acetone, 80:20) purifications of the bioactive low-polarity fraction yielded 15.0 mg (0.008%) of **1** in pure form. The isolated metabolite showed a 2 mm inhibition zone when tested at 1% against *Staphylococcus aureus*, but no activity was observed when **1** was evaluated against *B. subtilis*, *C. albicans*, *E. coli*, *P. aeruginosa*, and *S. cerevisiae*.

ent-*17-Hydroxy-16α-kauran-3-one (1)*

Obtained as an amorphous solid (mp 104–107°C) that could not be induced to crystallize. TLC: R_f 0.32 (hexane/acetone, 80:20); IR ν_{max} (KBr): 3430 (OH stretch), 2940 (CH_3 and CH_2, asymmetric stretch), 2860 (CH_3 and CH_2, symmetric stretch), 1690 (C=O stretch), 1370 and 1365 (*gem*-dimethyl, C-H bending) cm^{-1}; ^1H NMR ($CDCl_3$): 3.42 (1H, dd, J = 3.2, 12.0 Hz, H17a), 3.37 (1H, dd, J = 2.4, 11.2 Hz, H17b), 2.45 (2H, dd, J = 6.4, 8.4 Hz, H2), 2.00 (1H, m, H1a), 1.90 (1H, m, H13), 1.40 (1H, m, H1b), 1.05 (3H, s, H19), 1.04 (3H, s, H18), 1.01 (3H, s, H20) ppm; ^{13}C NMR ($CDCl_3$): see Table 1; HREIMS, *m/z* (relative intensity) calcd. for $C_{20}H_{32}O_2$: 304.2402; found: 304.2411 (M^+, 87.3), 286 (M^+-18, 10.4), 273 (M^+-31, 4.7); CIMS (NH_3), *m/z* (relative intensity): 322 (M^++18, 96.3), 305 (M^++1, 100.0).

ent-*17-Acetoxy-16α-kauran-3-one (2)*

A mixture of **1** (3.0 mg), acetic anhydride (1 mL), and pyridine (0.5 mL) was allowed to stir overnight at room temperature. The reaction mixture was poured over water (30 mL) and the resulting suspension extracted with ethyl acetate (3 times, 1:1, v/v). The organic layer was washed (1:1, v/v) successively with water, 5% HCl, 2.5% KOH, and a NaCl saturated solution; treatment of the solvent with anhydrous Na_2SO_4 followed by filtration and evaporation yielded 3.12 mg (91.5%) of **2**.

Table 1. ^{13}C NMR data of **1**, **4**, **5**, and **6**.

	ent-Kauranoids			
Carbon no.	**1**	**4** (19)	**5** (20)	**6** (20)
1	39.3 (t)[a]	39.0	41.6	42.0
2	34.1 (t)	33.9	19.0	19.0
3	208.0 (s)	217.1	38.0	38.0
4	47.1 (s)	47.0	44.1	44.6
5	54.4 (d)	53.6	56.6	56.9
6	21.9 (t)	20.3	22.1	22.4
7	40.5 (t)	39.9	40.7	40.8
8	44.5 (s)	42.2	43.6	43.7
9	54.9 (d)	54.2	55.3	56.4
10	38.4 (s)	38.5	39.3	39.8
11	19.1 (t)	19.0	18.3	18.8
12	31.2 (t)	29.3	26.0	28.9
13	38.1 (d)	47.6	37.1	37.1
14	36.8 (t)	36.9	38.1	40.3
15	44.7 (d)	54.6	43.6	44.9
16	43.2 (d)	221.5	43.2	42.3
17	67.4 (t)	—	64.1	67.4
18	27.3 (q)	27.3	31.3	31.3
19	20.9 (q)	21.0	177.9	177.9
20	17.6 (q)	18.1	18.7	18.7

[a]Multiplicities determined from DEPT and HETCOR experiments.

TLC: R_f 0.57 (hexane/acetone, 80:20); IR ν_{max} ($CHCl_3$): 1725 (ester C=O stretch), 1700 (ketone C=O stretch) cm^{-1}; ^1H NMR ($CDCl_3$): 3.83 (2H, d, J_{AB} = 7.6 Hz, H17), 2.45 (2H, dd, J = 6.4, 8.4, Hz, H2), 2.03 (3H, s, CH_3COO), 1.05 (3H, s, H19), 1.03 (3H, s, H18), 1.01 (3H, s, H20) ppm; HRMS, *m/z* (relative intensity) calcd. for $C_{22}H_{34}O_3$: 346.2508; found: 346.2518 (M^+, 94.7), 303 (M^+-43, 6.3), 286 (M^+-60, 25.8).

ent-*16α-Kauran-17-al-3-one (3)*

A solution of **1** (2.0 mg) in dichloromethane was treated with an excess of pyridinium chlorochromate dissolved in 2 mL of the same solvent. The reaction mixture was left to stir overnight at room temperature and then diluted with 5 mL of dichloromethane. The resulting solution was filtered through a 2 cm bed of silica gel 60 followed by evaporation of the solvent to produce 1.3 mg (65.7%) of **3**. TLC: R_f 0.55 (hexane/acetone, 80:20); IR ν_{max} ($CHCl_3$): 2860 (aldehyde C-H stretch), 1700 (aldehyde/ketone C=O stretch) cm^{-1}; ^1H NMR ($CDCl_3$): 9.65 (1H, d, J = 1.2 Hz, H17), 2.54 (1H, m, H16), 2.42 (2H, dd, J = 6.0, 8.0 Hz, H2), 1.02 (3H, s, H19), 0.98 (3H, s, H18), 0.96 (3H, s, H20); HRMS, *m/z* (relative intensity) calcd. for $C_{20}H_{30}O_2$: 302.2246; found: 302.2245 (M^+, 66.6), 273 (M^+-29, 3.7).

Acknowledgements

We thank Dr. Javier Flores Abuxapqui, CIR "Hideyo Noguchi," Mérida, Yucatán, México, for initial antimicrobial assays; Dr. Francisco Talamás Murra, Syntex S.A., Cuernavaca, Morelos, México, for the inital ^1H NMR spectra; Drs. William A. Ayer and Lois M. Browne, The University of

© 1997 NRC Canada

Alberta, Edmonton, Alberta, Canada, for HRMS and CIMS spectra; Drs. John A. Findlay and Peter Penner, University of New Brunswick, Fredericton, New Brunswick, Canada, for ^{1}H and ^{13}C NMR spectra as well as COSY, DEPT, and HETCOR experiments; Ms. Fabiola Escalante Erosa for determining IR spectra and running GC–MS analyses; Mr. Irving Ramírez Erosa and Ms. Isela Flores Montenegro for technical assistance; and Mr. Sergio Peraza Sánchez and Ms. Marcela Gamboa Angulo for helpful discussions. This work was supported by grants F/1744-1 and F/1744-2 from the International Foundation for Science.

References

1. R.M. Mendieta and R.S. del Amo. Plantas medicinales del estado de Yucatán. Editorial CECSA, Xalapa, Veracruz. 1981. p. 98.
2. M. Martínez. Catálogo de nombres vulgares y científicos de plantas mexicanas. Fondo de Cultura Económica, México, D.F. 1979. pp. 148, 1043.
3. Enciclopedia Yucatanense. Vol. 1. Introducción, Geografía Física, Fauna y Flora. Edición oficial del Gobierno del Estado de Yucatán, Mérida, Yucatán. 1977. p. 487.
4. R.S. del Amo and A.L. Anaya. Biotica, **7**, 293 (1982).
5. Atlas de las plantas de la medicina tradicional mexicana. Vol. 2. Edición del Instituto Nacional Indigenista, México, D.F. 1984. p. 1082.
6. The New Encyclopaedia Britannica. 15th ed. Vol. 10. University of Chicago, Chicago, Ill. 1990. p. 226.
7. G.E. Trease and W.C. Evans. Tratado de farmacognosia. 13a Edición. Nueva Editorial Interamericana–McGraw–Hill, México, D.F. 1989. pp. 9, 177, 221.
8. X.A. Domínguez. Métodos de investigación fitoquímica. Editorial Limusa, México, D.F. 1973. pp. 39, 162.
9. H. Inouye, Y. Takeda, H. Nishimura, A. Kanomi, T. Okuda, and C. Puff. Phytochemistry, **27**, 2591 (1988).
10. S. Sankara and A.G.R. Nair. Phytochemistry, **10**, 2125 (1971).
11. C. Albor Calderón. Tesis de Maestría, Facultad de Química, UNAM. México, D.F. 1989.
12. N. El Abbadi, B. Weniger, A. Lobstein, J.C. Quirion, and R. Anton. Planta Med. **55**, 603 (1989).
13. J. Bhattcharyya and E.V.L. Cunha. Phytochemistry, **31**, 2546 (1992).
14. M.A. Abd El-Hafiz, B. Weniger, J.C. Quirion, and R. Anton. Phytochemistry, **30**, 2029 (1991).
15. A.M. Clark. Antimicrobial screening. *In* Workshop on simple bioassays: An introduction. Proceedings of the Thirtieth Annual Meeting of the American Society of Pharmacognosy, San Juan, Puerto Rico. August 1989.
16. E.J. Corey and J.W. Suggs. Tetrahedron Lett. **31**, 2647 (1975).
17. K. Nakanishi, T. Goto, S. Ito, S. Natori, and S. Nozoe. Natural products chemistry. Vols. 1 and 3. Academic Press, New York. 1974. pp. 112 and 327.
18. A. Crozier. The biochemistry and physiology of gibberellins. Vol. 1. Praeger Publishers, New York. 1983. p. 76.
19. J.R. Hanson, M. Siverns, F. Piozzi, and G. Savona. J. Chem. Soc. Perkin Trans. 1, 114 (1976).
20. J.T. Etse, A.I. Gray, and P.G. Waterman. J. Nat. Prod. **50**, 979 (1987).
21. Y.-C. Wu, Y.-C. Hung, F.-R. Chang, M. Cosentino, H.-K. Wang, and K.-H. Lee. J. Nat. Prod. **59**, 635 (1996).
22. Y.-L. Ding and Z.-J. Jia. Phytochemistry, **30**, 2413 (1991).
23. M.O. Fatope, O.T. Audu, Y. Takeda, L. Zeng, G. Shi, H. Shimada, and J.L. McLaughlin. J. Nat. Prod. **59**, 301 (1996).
24. H.-D. Sun, Z.-W. Lin, F.-D. Niu, Q.-T. Zhen, B. Wu, L.-Z. Lin, and G.A. Cordell. Phytochemistry, **40**, 1461 (1995).
25. K.R. Gustafson, M.H.G. Munro, J.W. Blunt, J.H. Cardellina II, J.B. McMahon, R.J. Gulakowski, G.M. Cragg, P.A. Cox, L.S. Brinen, J. Clardy, and M.R. Boyd. Tetrahedron, **47**, 4547 (1991).
26. W.C. Still, M. Kahn, and A. Mitra. J. Org. Chem. **43**, 2923 (1978).

Can. J. Chem. Downloaded from www.nrcresearchpress.com by 88.146.161.215 on 09/08/12
For personal use only.

© 1997 NRC Canada

Diels–Alder adducts of *ortho*-benzoquinones: rearrangements and further transformations

Rina Carlini, Kerianne Higgs, Nicholas Taylor, and Russell Rodrigo

Abstract: *ortho*-Benzoquinones substituted with an electron-withdrawing group (EWG = CO_2Me, COSMe, $COCH_3$, CHO) at C-3 or C-4 react as dienophiles at the C3—C4 double bond in Diels–Alder reactions with several dienes, with predictable regiochemistry. The adducts undergo migration of the "angular" EWG substituent with concomitant aromatization to produce substituted catechols. The bicyclic products can be oxidized in situ and annelated by a further Diels–Alder reaction to yield 9,10-phenanthraquinone systems. When (2*E*)-2,4-pentadienol is employed as the diene in the second cycloaddition, reaction of the alcoholic hydroxyl group with one of the quinone carbonyl groups results in the production of tetracyclic lactols **22a**, **22b**, and **23**.

Key words: benzoquinone, Diels–Alder, rearrangement, phenanthraquinone, phenanthrofuran.

Résumé : Lors de réactions de Diels–Alder avec divers dienes, les *ortho*-benzoquinones substituées en positions C-3 ou C-4 par un groupe électroattracteur (GEA = CO_2Me, COSMe, $COCH_3$, CHO) réagissent comme diénophiles au niveau de la double liaison C3—C4 et la régiochimie de ces réactions peut être prédite. Les adduits subissent une migration du GEA «angulaire» avec une aromatisation concomitante conduisant à des catéchols substitués. Les produits bicycliques peuvent être oxydés in situ et subir une nouvelle annelation, par réaction de Diels–Alder, pour conduire aux systèmes de la 9,10-phénanthraquinone. Lorsqu'on utilise du (2*E*)-penta-2,4-diénol comme diène dans la deuxième cycloaddition, la réaction du groupe hydroxyle de l'alcool avec l'un des groupes carbonyles de la quinone conduit à la formation des lactols tétracycliques **22a**, **22b** et **23**.

Mots clés : benzoquinone, Diels–Alder, phénanthraquinone, phénanthrofurane.

[Traduit par la rédaction]

With some elegant exceptions (1), the notorious instability of *ortho*-benzoquinones has limited their employment as intermediates in the synthesis of complex natural products. In a recent paper (2) we reported the initial results of our attempts to generate substituted *o*-benzoquinones in situ and to investigate the regiochemistry of the intermolecular Diels–Alder reaction of these dienophilic intermediates with nonsymmetrical dienes. Effective regiocontrol at both components of the cycloaddition reaction was achieved by the placement of an electron-withdrawing group (EWG = CO_2H, CO_2Me, COSMe, CHO) at C-3 or C-4 of the *o*-benzoquinone. In the course of those investigations, we uncovered several interesting rearrangements of the initial adducts. Some of them, we believe, were responsible for the formation of mixtures of products, but others proceeded with greater efficiency and possessed much synthetic potential. Such rearrangements of *o*-benzoquinonoid adducts have not been reported before although a successful oxy-Cope rearrangement of a bridged intramolecular Diels–Alder adduct of an *o*-benzoquinonoid species has been reported (3) very recently.

Our initial investigations were conducted with the Diels–Alder adducts **1a**–**1d** and **3** (Table 1). The preparation of these compounds, with the exception of **1c** (26% yield) and **1d** (23% yield), from *o*-benzoquinones substituted at C-4 with carbomethoxy (CO_2Me) and carbothiomethyl (COSMe) has previously been described (2). Rearrangements were effected by stirring in neat trifluoroacetic acid (TFA) at ambient temperature for ca. 2 h. The first two adducts (**1a** and **1b**) underwent a smooth [1,2]-shift (a dienone–phenol rearrangement) of the C-4a ester groups to C-4 to yield 1,2-dihydroxynaphthalenes **2a** and **2b** almost quantitatively. No trace of any materials arising from shifts of ring carbon atoms C-5 or C-8 could be detected. Migrations of angular ester substituents in similar reactions have not been common but rearrangement of the dienone **4** by acid treatment to phenol **5** has been reported (4) to proceed in moderate yield. The presence of a methyl substituent at C-4 blocked the rearrangement process completely and the starting materials were recovered unchanged after extended treatment of **1c**, **1d**, and **3** with TFA.

Compounds **6a** and **6b**, derived from diketoadduct **7** (2) by enolization (**6a**) and subsequent O-methylation (**6b**), were examined next for susceptibility to rearrangement. Stirring these precursors in TFA at room temperature resulted in the

Received November 6, 1996.

This paper is dedicated to Professor William A. Ayer on the occasion of his 65th birthday for his many years of outstanding service to research and education in Organic Chemistry.

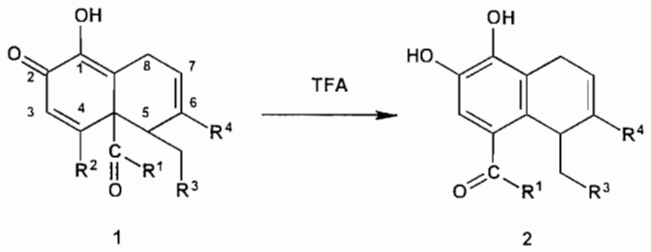
R. Carlini, K. Higgs, and N. Taylor. Department of Chemistry, Guelph–Waterloo Center for Graduate Work in Chemistry, University of Waterloo, Waterloo, ON N2L 3G1, Canada.
R. Rodrigo.[1] Department of Chemistry, Wilfrid Laurier University, Waterloo, ON N2L 3C5, Canada.

[1] Author to whom correspondence may be addressed. Telephone: (519) 885-1211, ext. 2844. Fax: (519) 746-0435. E-mail: rrodrigo@mach1.wlu.ca

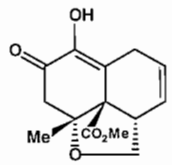
© 1997 NRC Canada

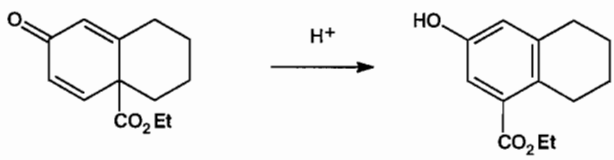
Can. J. Chem. Downloaded from www.nrcresearchpress.com by 88.146.161.215 on 09/08/12
For personal use only.

Table 1. Acid-catalyzed rearrangements of Diels–Alder adducts **1a–1d** and **3**.



1 2

	Diels–Alder adduct	Product (% yield)
1a	(R^1 = OMe, R^2 = R^4 = H, R^3 = CH_2CO_2Me,)	**2a** (90)
1b	(R^1 = SMe, R^2 = H R^3 = CO_2Et, R^4 = Me)	**2b** (98)
1c	(R^1 = SMe, R^2 = Me R^3 = CO_2Et, R^4 = H)	No reaction
1d	(R^1 = OMe, R^2 = Me R^3 = CO_2Me, R^4 = H)	No reaction
3		No reaction

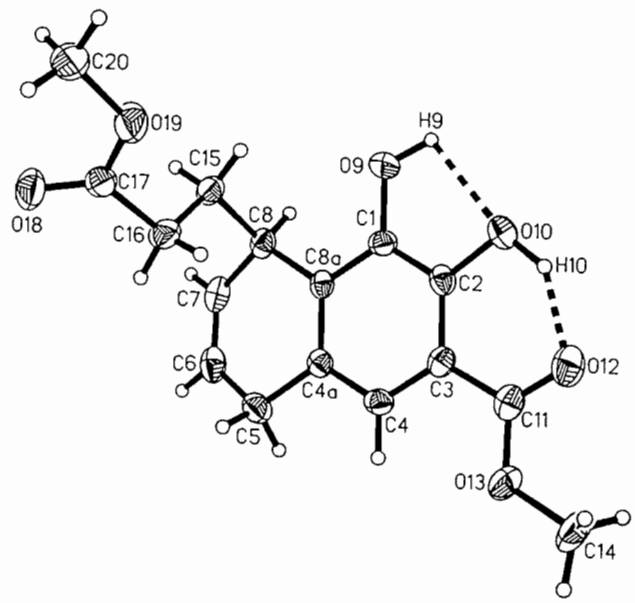


4 5

slow but complete conversion to aromatic esters (Table 2). The ^{1}H NMR spectrum of the product obtained from **6a** contained one aromatic proton at 7.16, one hydrogen-bonded hydroxyl proton at 10.6, and a second hydroxyl proton at 5.8 ppm. The regioisomeric structures **8a**, **9a**, and **10a** are consistent with these data. Structures **9a** and **10a** (Scheme 1) might have arisen from migration of C-8 to form a spiro intermediate (5) followed by a [1,2]-shift of C-5 or C-8, and this mechanism would have resulted in a product mixture. Since only one product was isolated from rearrangement of **6a**, structures **9a** and **10a** appear to be unlikely. Support for structure **8a** was obtained by NMR correlation methods (NOEDS, TOCSY, HMBC) but unequivocal proof of its identity was sought and obtained by a single-crystal X-ray analysis (Fig. 1). Rearrangement of **6b** gave an aromatic ester **8b** with the methoxyl group intact and no hydrogen-bonded hydroxyl proton in the ^{1}H NMR spectrum, a result that was consistent with structure **8b** but not with **9b** or **10b**.

The formation of **8a-b** from **6a-b** by migration of the C-8a ester to C-3 is unprecedented for *o*-benzoquinone adducts. Two mechanistic pathways can be postulated (Scheme 2) and a method for deciding between them became available when it was discovered that identical rearrangement products were obtained in comparable yields with trimethyloxonium tetrafluoroborate in methylene chloride. If pathway **B** operated, then treatment of **6a** or **6b** with triethyloxonium tetrafluoroborate should have produced at least some ethyl ester. However, no ethyl ester products were observed; only **8a** and **8b**

Fig. 1. Molecular plot of **8a**.

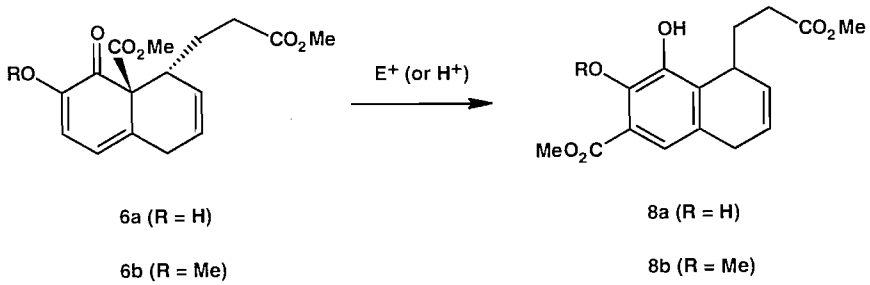


were obtained as in the TFA-catalyzed rearrangements. Rearrangements of *p*-benzoquinone adducts involving the migration of angular acetyl and carbomethoxy groups were studied earlier and a mechanism involving a [1,5]-shift of the acetyl group in the enol tautomer followed by a [1,2]-shift and

© 1997 NRC Canada

Can. J. Chem. Downloaded from www.nrcresearchpress.com by 88.146.161.215 on 09/08/12
For personal use only.

Table 2. Rearrangements of **6a** and **6b** with TFA, Me_3OBF_4, and Et_3OBF_4.



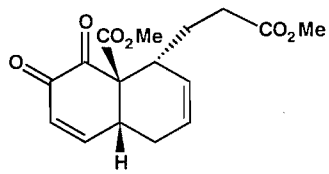
6a (R = H)

6b (R = Me)

8a (R = H)

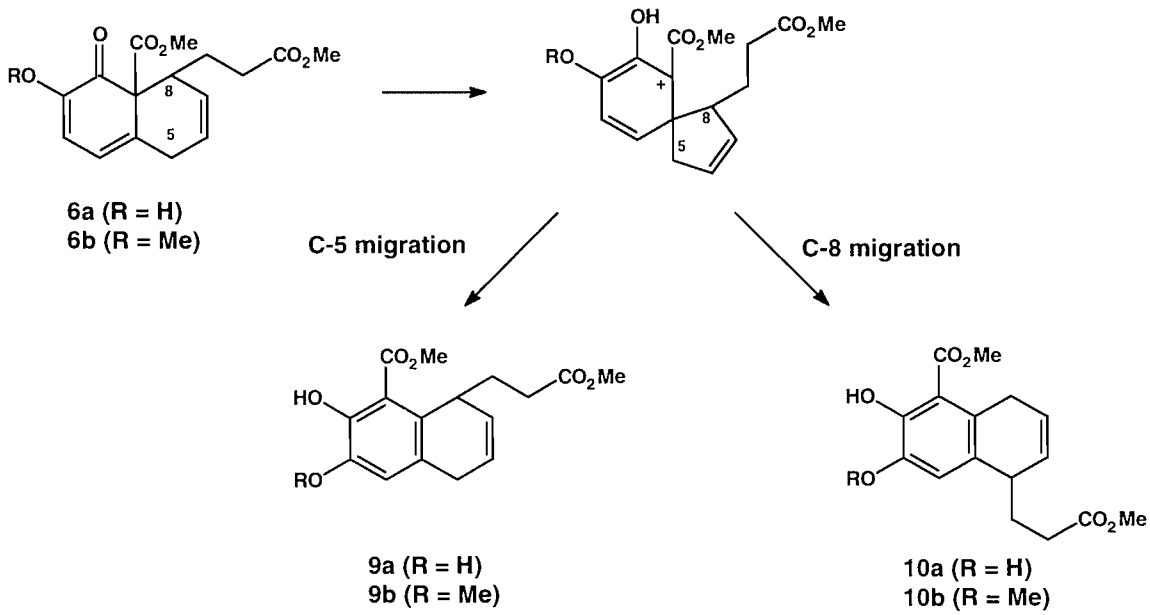
8b (R = Me)

E^+	Substrate	Time (h)	Product (% yield)
H^+ (TFA)	**6a**	18	**8a** (65)
	6b	12	**8b** (74)
Me^+ (Me_3OBF_4)	**6a**	24	**8a** (60)
	6b	48	**8b** (60)
Et^+ (Et_3OBF_4)	**6a**	10	**8a** (59)
	6b	18	**8b** (62)



7

Scheme 1.

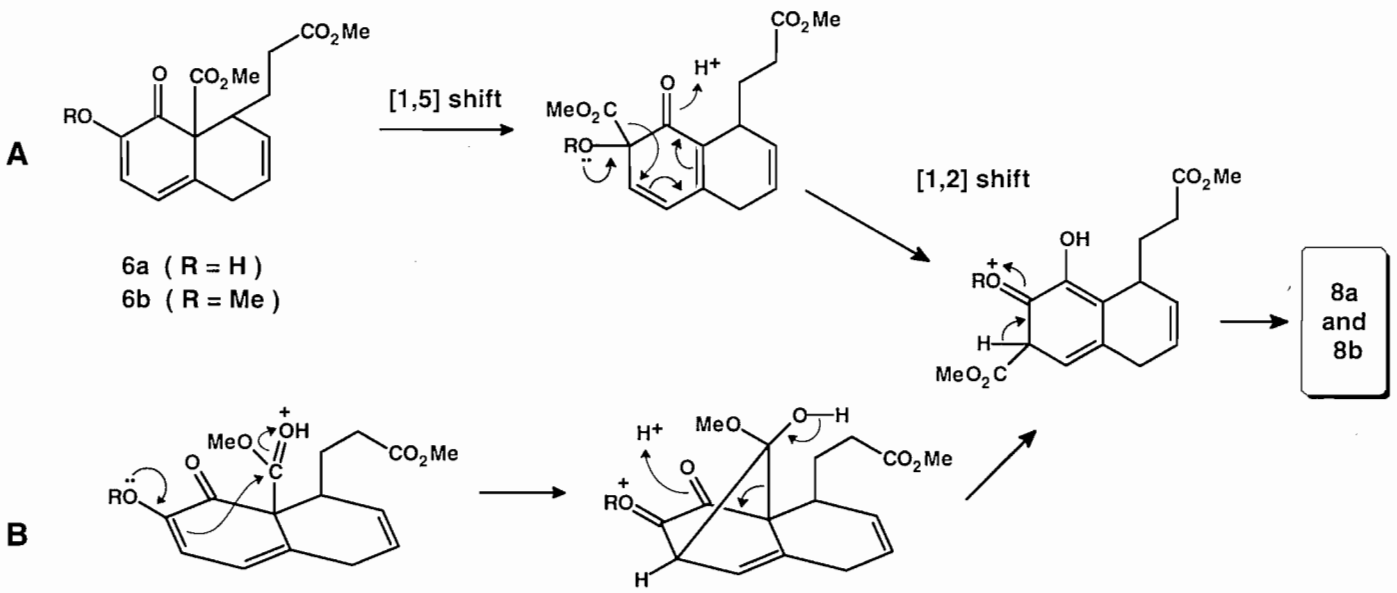


subsequent aromatization was proposed (6) (Scheme 3). The analogous methoxycarbonyl adduct did not rearrange under similar conditions, but heating with acetic anhydride and sodium acetate (140°C, 4 h) provoked a different migration of the ester, resulting in the isolation of the diacetate **11** (Scheme 3) in moderate yield. The pathway **A** in Scheme 2 also involves a [1,5]-shift of the ester followed by a [1,2]-shift in the second step. The latter is promoted by the C-2 oxygen sub-

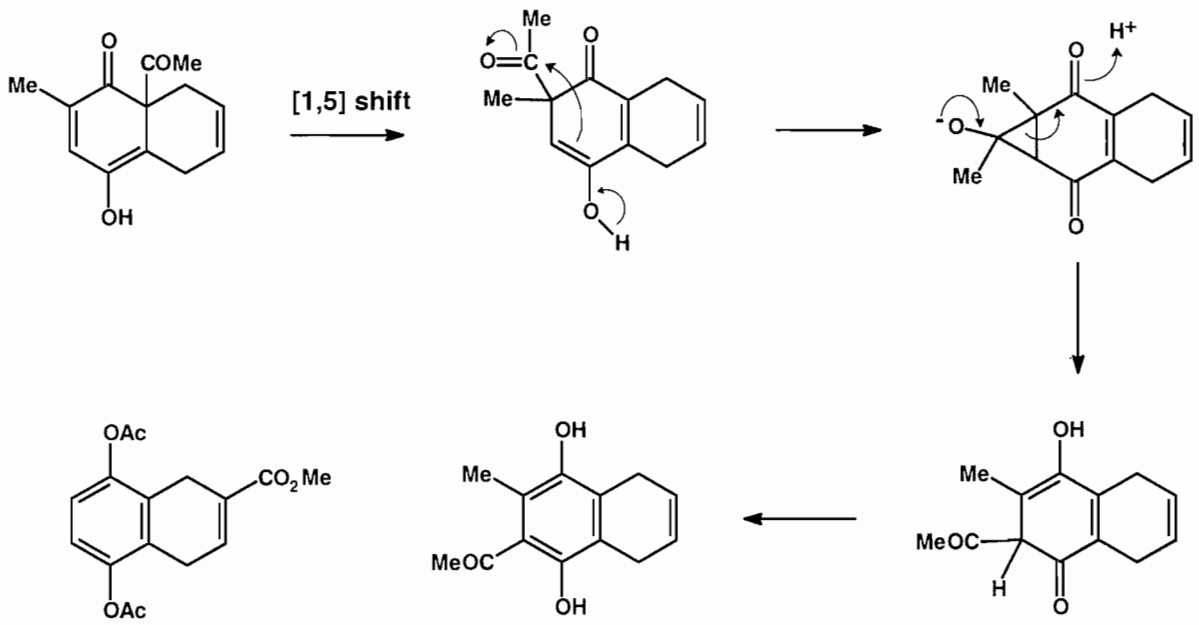
© 1997 NRC Canada

Can. J. Chem. Downloaded from www.nrcresearchpress.com by 88.146.161.215 on 09/08/12
For personal use only.

Scheme 2.



Scheme 3.



stituent, and this step bears resemblance to both the α-ketol and dienone–phenol rearrangements. Migration of the hydroxyl or methoxyl group instead of the ester group is obviously disfavoured by the fact that a positive charge would have to be generated between the two carbonyl groups.

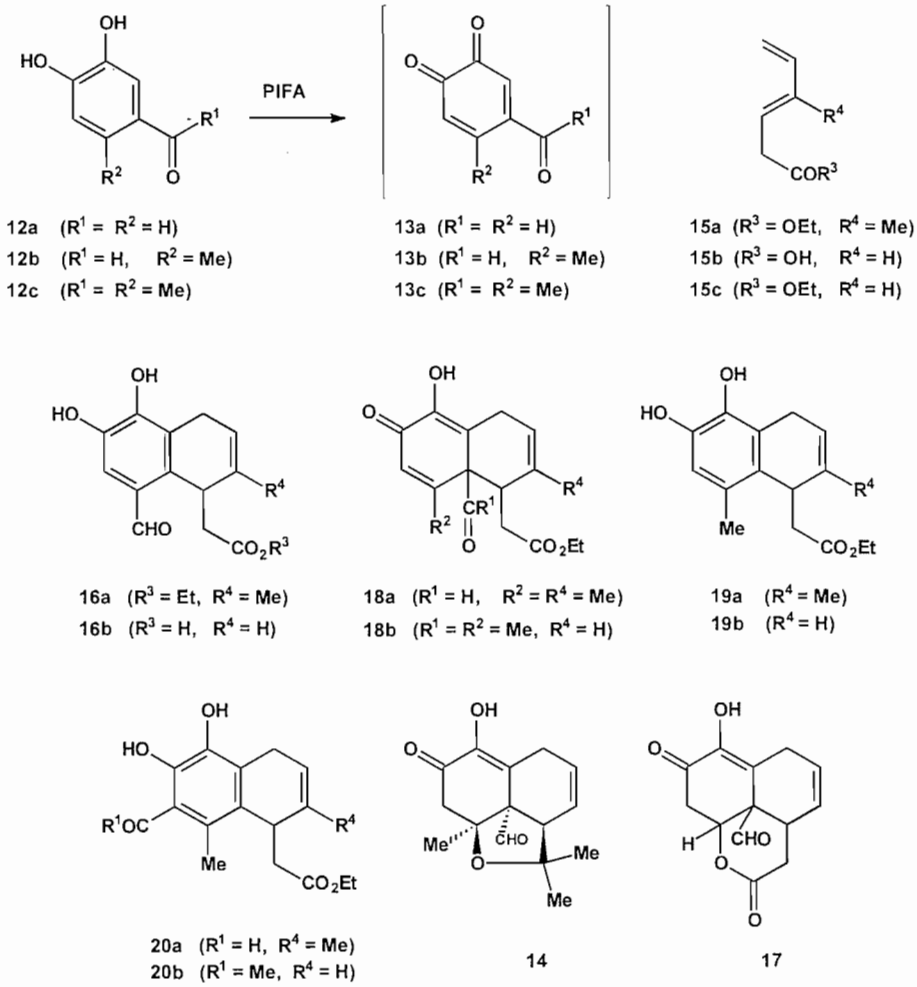
Migratory aptitudes of substituents in these types of reactions had been previously estimated (7) to be in the order CHO > COMe > CO_2Me. We therefore turned our attention to the catechol aldehydes **12a** and **12b**, which were oxidized to *ortho*-benzoquinones **13a** and **13b** with phenyliodosyl bis(trifluoroacetate) (PIFA) in the presence of various dienes (8).[2] As reported earlier (2), naphthofuran **14**, a prospective intermediate for the synthesis of the tricyclic diterpene nardonoxide (9), was produced in one step from **12b** and (2*E*)-1,1-

[2] For the preparation of dienes, see: CH_2=CHC(CH_3)=$CHCH_2$-CO_2Et : ref. 8*a*; CH_2=CHCH=$CHCH_2CO_2Et$: ref. 8*b*; CH_2=CHCH=$CHCH_2OH$: ref. 8*c*; CH_2=CHCH=$CHCH_2CO_2R$, R = Me, H: ref. 8*d*.

© 1997 NRC Canada

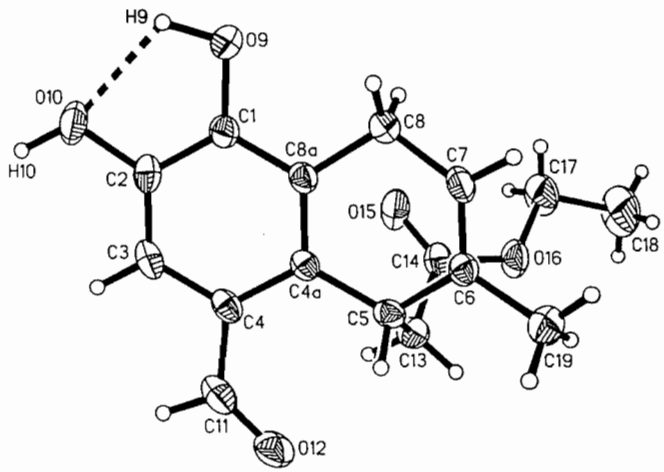
Can. J. Chem. Downloaded from www.nrcresearchpress.com by 88.146.161.215 on 09/08/12
For personal use only.

Can. J. Chem. Downloaded from www.nrcresearchpress.com by 88.146.161.215 on 09/08/12
For personal use only.



dimethyl-2,4-pentadienol, albeit in low yield. Reaction of **13a** with dienes **15a** and **15b**, where naphthofuran formation was not possible, gave adducts **16a** and **16b**, resulting from apparent addition to the less activated C5—C6 double bond of the *o*-quinone **13a**. To confirm this result an X-ray structure of **16a** was obtained (Fig. 2). In our opinion, products **16a** and **16b**, isolated in yields of 23% and 39%, respectively, were formed by Diels–Alder addition to the more dienophilic C3–C4 double bond of **13a** followed by rapid [1,2]-migration of the formyl group in the acidic medium of the reaction. The dienoic acid **15b** was investigated in the hope that the cycloaddition would be followed by cyclization to produce the δ-lactone **17**, thus saturating C-4 of the adduct and forestalling the migration of the aldehyde group. Unfortunately, this expectation was not realized and a probable explanation is that the 1,4-addition step was reversible and that the migration was followed by aromatization to give **16b** from which there could be no return. Another way of blocking the migration of the angular carbonyl group and subsequent aromatization was demonstrated with esters **1c** and **1d** where methyl groups are situated at C-4, the prospective terminus of the migration. Catechol aldehyde **12b** was expected to give an analogous adduct **18a** with a C-4 methyl substituent present to block the migration of the formyl group. However, oxidation in situ to *o*-quinone **13b** and subsequent reaction with diene **15a** did not

Fig. 2. Molecular plot of **16a**.



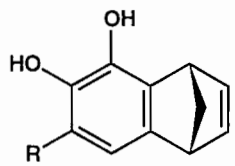
give the expected adduct **18a**, but rather compounds derived from that adduct in low yields, namely, the deformylated dihydroxynaphthalene **19a** and the product **20a** of an apparent [1,3]-migration of the formyl group. The aldehyde **20a** must have arisen from the initial adduct **18a** by two successive

© 1997 NRC Canada

Can. J. Chem. Downloaded from www.nrcresearchpress.com by 88.146.161.215 on 09/08/12
For personal use only.

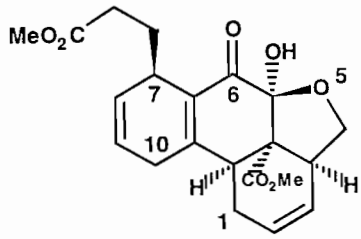
[1,2]-migrations of the formyl group. The second [1,2]-migration could proceed by a mechanism similar to that suggested by Bruce and co-workers (6) (Scheme 3). In view of these facile aromatizations of the aldehyde adducts, we decided to investigate the cycloaddition of the *o*-quinone **13c** (from oxidation of catechol **12c** (10)) with diene **15c**, expecting that the adduct **18b** would be isolable because of the lower migratory aptitude of the acetyl group. Adduct **18b** was isolated in low yield along with the major product, which was the deacetylated dihydroxynaphthalene **19b**. The adduct **18b** rearranged upon standing to the product **20b**, again by an apparent [1,3]-shift of the acetyl group analogous to that proposed for the formation of aldehyde **20a** from **18a**. It therefore appears that in these vinylogous β-diketo systems the push to aromatization can be just as easily satisfied by decarbonylation processes as by [1,2]-migrations.

In view of the ease of the various rearrangements that end in aromatization and formation of substituted catechols, it is most likely that the Diels–Alder adducts represented by **21** do not arise by the "abnormal" addition of cyclopentadiene to the less dienophilic C5–C6 double bond of the C3-EWG substituted *o*-benzoquinone as claimed (11). Instead, the formation of the expected adduct at C3—C4 followed by rearrangements akin to the conversion of **6a** to **8a** must be responsible for the apparent anomaly.



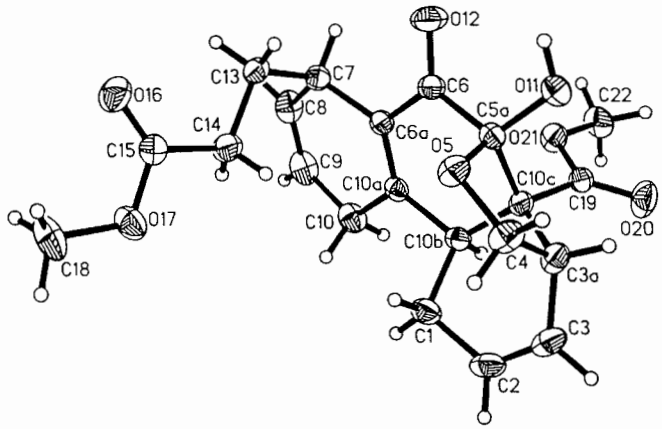
21 (R = CHO, COMe, CO_2Me, CN)

Migrations of the ester group (e.g., **1a**→**2a** and **6a**→**8a**) discussed herein result in the formation of catechols bearing such substituents at C-3 or C-4. Thus, just as the dienophilic double bonds of *p*-quinones permit successive Diels–Alder additions to produce linear tricyclic compounds, the rearrangement products **2a** and **8a** offer the possibility of generating angular tricyclic systems by oxidation and cycloaddition with a second diene. Treatment of **8a** with PIFA and (2*E*)-2,4-pentadienol[3] using conditions described earlier (2) resulted in a moderate yield (56%) of two diastereomeric adducts **22a** and **22b** in equal amounts. The diastereomers were separable by chromatography, but assignment of relative stereochemistry to each product, by analysis of NMR spectra alone, could not be accomplished with certainty. An X-ray crystallographic structure determination was therefore undertaken and the structure and relative configuration of one diastereomer was firmly established as **22a** (Fig. 3). Compounds **22a** and **22b** (Fig. 4) are phenanthrofurans, diastereomeric at C-7; the regiochemistry of the cycloaddition is controlled by the ester substitutent at C-3 of the *o*-quinonoid species and both are



22a

Fig. 3. Molecular plot of **22a**.



endo[4] adducts. *endo*-Cycloadducts are usually found (2) in intermolecular Diels–Alder reactions of *o*-benzoquinones, and this generalization appears to hold for these *o*-quinones as well.

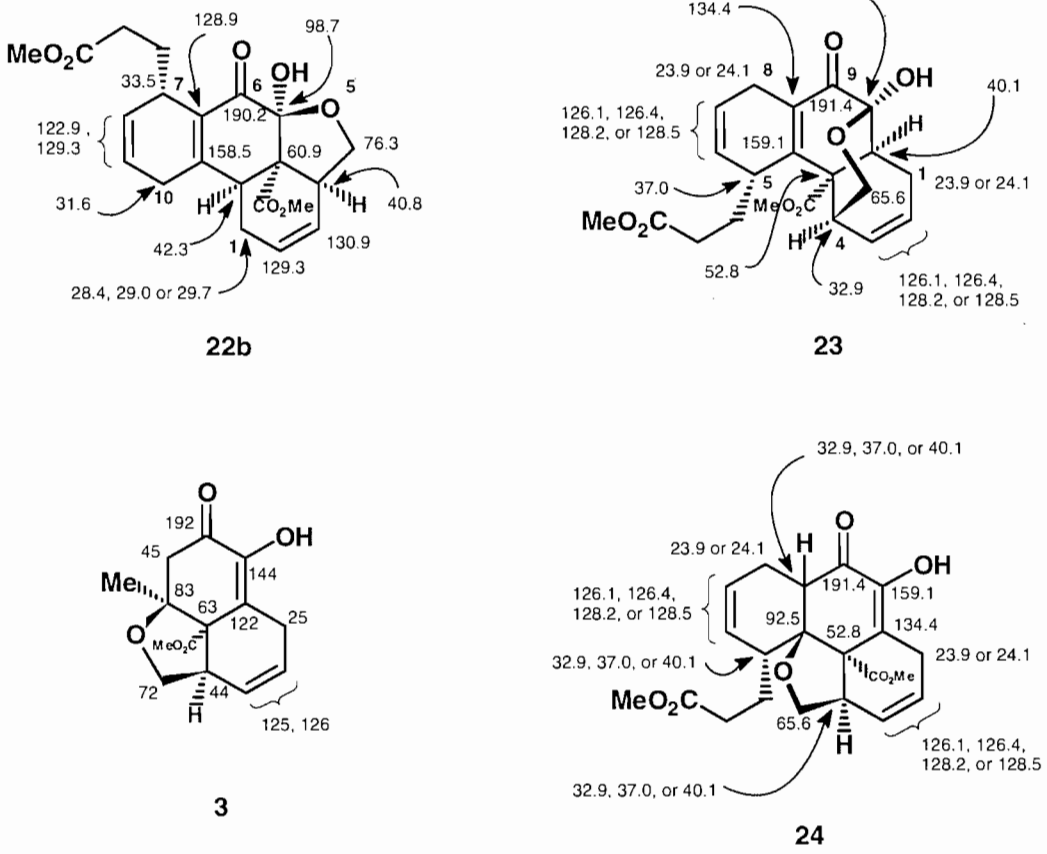
The reaction was next attempted with **2a**, a case where the ester substituent is at C-4 rather than C-3. Only a single adduct could be isolated in low yield (ca. 11%). Its mass spectrum (at low and high resolution), as well as its ^1H and ^{13}C NMR spectra, was consistent with the structure and relative stereochemistry represented by the 4,10-methyleneoxy bridged phenanthrene **23** (Fig. 4). High-field ^1H and ^{13}C assignments were confirmed by HMQC as well as by homonuclear (^1H) decoupling experiments. However, an alternative structure **24**, analogous to the known naphthofuran **3** (2), also had to be considered. In Fig. 4, some important ^{13}C chemical shifts of the adduct (illustrated in possible structures **23** and **24**) were compared to spectral data for the known compounds **22b** and **3**. The data indicated that the assignments made for structure **23** bear a greater similarity to those of **22b** than the assignments for **24** do to naphthofuran **3**. In addition, the geminal coupling constant of the methylene group adjacent to oxygen, measured at 11.9 Hz, is more in keeping (12) with its presence in tetrahydropyran as in structure **23** rather than in a tetrahydrofuran ($J_{gem} \approx 8.0$–9.5 Hz) as required by structure **24**. The relative stereochemistry at C-4, C-4a, C-10, and C-10a in compound **23** was established by the cycloaddition (*endo*) and subsequent methyleneoxy bridging, while that of C-5 became evident from the detection of a small NOE in the difference spectrum between H-4 and H-5β.

[3] The preparation of (2*E*)-2,4-pentadienol from commercially available 1,4-pentadien-3-ol was accomplished in one step in 60.5% yield. This procedure is a more efficient method than that previously cited in the literature (8*c*). See experimental section.

[4] *endo*-Stereochemistry refers to the *o*-quininoid ring.

© 1997 NRC Canada

Fig. 4. Comparison of ^{13}C NMR assignments for ring carbon atoms of known compounds, **22b** and **3** (2), with hypothetical structures for adducts **23** and **24**.



The Diels–Alder→aromatization–rearrangement→Diels–Alder sequence outlined here with substituted *o*-benzoquinones generated in situ thus permits the rational construction of angular tricyclic and tetracyclic systems with complete control of regiochemistry at each step. This synthetic sequence has the potential for the elaboration of functionalized phenanthrene and phenanthrofuran ring systems found in complex natural products.

Experimental

Melting points were measured using a Gallenkamp melting point apparatus and are uncorrected. Infrared spectra were obtained with a Bomem FTIR spectrometer. Nuclear magnetic resonance spectra were performed on Bruker AM-250 and AMX-500 or Varian XL-200 spectrometers at 298 K, and coupling constants were measured directly from the spectra by first-order analysis and are approximate by ±0.3 Hz. NMR spectral assignments were confirmed by common 2D techniques (TOCSY, HMQC, NOESY). All spectra were run in $CDCl_3$ with tetramethylsilane as an internal standard unless otherwise indicated. Low- and high-resolution mass spectra were determined at the Southwestern Ontario Regional Mass Spectrometry Center at McMaster University, Hamilton, Ontario. Elemental analyses were determined by MHW Laboratories in Phoenix, Arizona. The dienes **15a**, **15b**, **15c**, and (*E*)-methyl-3,5-hexadienoate (for preparation of **1d**) were prepared as described in the literature (8) and were freshly distilled prior to use in a reaction. PIFA refers to the commercially available oxidant phenyliodosyl bis(trifluoroacetate), or bis(trifluoroacetoxy)iodobenzene (Aldrich®). Column chromatography was performed using Merck 230–400 mesh silica gel 60 with ethyl acetate – hexane (typically 1:4) used as eluant unless otherwise stated. Anhydrous sodium sulfate was used as the drying agent.

X-ray crystal structure determinations

A summary of crystallographic data is reported in Table 3. Crystal structure analyses were performed on an LT2 equipped Siemens P4 diffractometer using MoKα radiation (λ = 0.71073 Å). In each case, unit cell dimensions were obtained from 25 reflections well dispersed in reciprocal space. Data were collected by the ω-scan method with a scan width of 1.2° using variable scan speeds, the scan rate being determined by a fast prescan. Background measurements were made at the beginning and end of each scan for a total of half the scan time. Data were corrected for Lorentz and polarization effects and by face-indexed analytical absorption methods. The structures were solved by direct methods and refined by full-matrix least-squares methods using Siemens SHELXTL IRIS software. The function minimized in the least-squares process was $w(F_o - F_c)^2$. Hydrogen atoms were easily found by difference Fourier syntheses and were included in the refinements with refined isotropic thermal parameters. In the final

© 1997 NRC Canada

Can. J. Chem. Downloaded from www.nrcresearchpress.com by 88.146.161.215 on 09/08/12
For personal use only.

Can. J. Chem. Downloaded from www.nrcresearchpress.com by 88.146.161.215 on 09/08/12
For personal use only.

cycles of refinement, weighting schemes of the form $w^{-1} = \sigma^2(F)$ as well as extinction coefficients were employed. Final difference maps revealed no anomalous electron density peaks or holes. Supplementary data include a complete listing of atomic coordinates, bond lengths and angles, and anisotropic thermal parameters.[5]

General method A: rearrangements with trifluoroacetic acid (TFA)

Compounds were mixed with an excess amount of TFA (10–20 equivalents) and stirred at room temperature under an argon atmosphere for time periods ranging from 0.5 to 18 h, as monitored by thin-layer chromatography. The solution was concentrated in vacuo and the crude residue extracted into ether, and washed with either brine or dilute aqueous $NaHCO_3$ solution. The ether layer was dried and concentrated in vacuo. The resulting product was further purified either by recrystallization in ether and/or ether-hexane, or by column chromatography.

General method B: rearrangements with trialkyloxonium tetrafluoroborates

Compounds **6a** and **6b** were dissolved in dry CH_2Cl_2 and cooled to 0°C for 10 min. Approximately 1.2 equivalents of R_3OBF_4, either as a solution in dry CH_2Cl_2 (for Et_3OBF_4) or as a neat crystalline solid (for Me_3OBF_4), was added to the cooled solution of **6a** or **6b** under an argon atmosphere. The resulting brown mixture was stirred at 0°C for 30 min and then at room temperature for 10–48 h. The reaction was quenched with a saturated solution of NH_4Cl, and the CH_2Cl_2 layer was separated, washed with brine, dried, filtered, and concentrated in vacuo to a black oil. The product was purified by column chromatography.

General Procedure C: Diels–Alder reactions of 12a, 12b, and 12c, and preparation of 1c and 1d

To a cooled solution (0°C) of the catechol and the diene (7–10 equivalents) in dry THF was added PIFA (1.2 equivalents) in small portions under an argon atmosphere. Solid $NaHCO_3$ (2.4 equivalents) was added to neutralize the TFA produced upon catechol oxidation. The solution was stirred at room temperature for 1–12 h; then THF was removed in vacuo. The crude residue was dissolved in ethyl acetate, washed with brine, dried (Na_2SO_4), and concentrated in vacuo. The excess diene was removed by reduced pressure distillation and the product purified by column chromatography.

*5-Carbethoxymethyl-4a-carbothiomethyl-1-hydroxy-4-methyl-2,4a,5,8-tetrahydronaphthalene-2-one (**1c**)*: 26%, colorless microcrystals from ether–hexane; mp 96°C; IR (KBr): 3366 (OH), 1730 (CO), 1645 (C=C) cm^{-1}; ^1H NMR (250 MHz) δ: 1.22 (t, $CO_2CH_2CH_3$, J = 7.1 Hz), 1.90 (dd, 1H, CH_2CO_2Et, J = 15.5, 10.6 Hz), 1.98 (d, 4-CH_3, J = 1.1 Hz), 2.05 (dd, 1H, CH_2CO_2Et, J = 15.5, 4.4 Hz), 2.22 (s, SMe), 3.08 (ddd, 1H, H-8, J = 22.7, 3.5, 2.4 Hz), 3.43 (m, 1H, H-8, J = 22.7 Hz), 3.76 (ddd, H-5, J = 10.6, 5.7, 4.4 Hz), 4.10 (q, OCH_2CH_3, J = 7.1 Hz), 5.70 (dt, H-7, J = 9.8, 3.5 Hz), 5.97 (ddt, H-6, J = 9.8, 5.7, 2.4 Hz), 6.42 (q, H-3, J = 1.1 Hz), 6.82 (s, OH); ^{13}C NMR (50 MHz) δ: 12.0 (SCH_3), 14.1 (OCH_2CH_3) 19.1 (4-CH_3), 25.9 (CH_2CO_2Et), 36.2 (C-8), 37.4 (C-5), 60.6 (OCH_2CH_3), 65.7 (C-4a), 122.3 (C-8a), 124.6 (C-7), 128.4, 128.6 (C-3, C-6), 146.5 (C-1), 157.4 (C-4), 171.0 (CO_2Et), 179.5 (C-2), 196.5 (COSMe); MS(EI) *m/z* (relative %): 336 (M, 1), 291 (8), 248 (39), 173 (100). HRMS calcd. for $C_{17}H_{20}O_5S$: 336.1031; found: 336.1031.

*5-Carbomethoxymethyl-4a-carbomethoxy-1-hydroxy-4-methyl-2,4a,5,8-tetrahydronaphthalene-2-one (**1d**)*: 23%, colorless plates from ether–hexane; mp 151°C; IR (KBr): 3357 (OH), 1729 (CO), 1643 (C=C) cm^{-1}; ^1H NMR (250 MHz) δ: 2.42 (dd, 1H, CH_2CO_2Me, J = 15.6, 10.9 Hz), 2.01 (d, 4-CH_3, J = 1.3 Hz), 2.02 (dd, 1H, CH_2CO_2Me, J = 15.6, 4.2 Hz), 2.85 (m, 1H, H-8, J = 22.1 Hz), 3.45 (m, 1H, H-8, J = 22.1 Hz), 3.63, 3.66 (s, 6H, 2 × CO_2CH_3), 3.68 (m H-5), 5.72 (dt, H-7, J = 9.8, 3.4 Hz), 5.97 (ddt, H-6, J = 9.8, 5.7, 2.4 Hz), 6.39 (q, H-3, J = 1.3 Hz), 6.60 (s, OH); ^{13}C NMR (50 MHz) δ: 19.4 (4-CH_3), 25.9 (CH_2CO_2Me), 35.7 (C-8), 38.6 (C-5), 51.5, 53.1 (2 × CO_2CH_3), 58.5 (C-4a), 123.7 (C-8a), 124.9 (C-7), 128.5, 128.6 (C-3, C-6), 144.7 (C-1), 156.6 (C-4), 170.0, 171.2 (2 × CO_2Me), 179.9 (C-2); MS(EI) *m/z* (relative %): 306 (M, 9), 275 (10), 247 (35), 187 (98) 173 (100). Anal. calcd. for $C_{16}H_{18}O_6$: C 62.73, H 5.92; found: C 62.76, H 6.16.

*5-Carbomethoxyethyl-4-carbomethoxy-1,2-dihydroxy-5,8-dihydronaphthalene (**2a**)*: 90%, colorless microcrystals from ether; mp 121°C; IR (KBr): 3459 (OH, sharp), 3281 (OH, broad), 1701 (CO, broad), 1602 (C=C) cm^{-1}; ^1H NMR (250 MHz) δ: 1.94 (m, 2H, $CH_2CH_2CO_2CH_3$, J = 9.7, 5.6 Hz), 2.13 (m, 1H, $CH_2CH_2CO_2CH_3$, J = 15.8, 9.9, 6.0 Hz), 2.34 (m, 1H, $CH_2CH_2CO_2CH_3$, J = 15.6, 10.0, 5.6 Hz), 3.12 (m, 1H, H-8, J = 21.9 Hz), 3.44 (m, 1H, H-8, J = 21.8, 4.8 Hz), 3.59, 3.82 (s, 6H, 2 × CO_2CH_3), 4.51 (m, 1H, H-5), 5.91 (ddd, 1H, H-6, J = 9.9, 5.2, 2.6 Hz), 6.02 (ddd, 1H, H-7, J = 9.9, 4.8, 2.1 Hz), 7.41 (s, 1H, H-4); ^{13}C NMR (63 MHz) δ: 24.7 ($CH_2CH_2CO_2CH_3$), 30.6 ($CH_2CH_2CO_2CH_3$), 33.1 (C-8), 35.1 (C-5), 51.6, 51.9 (2 × CO_2CH_3), 116.7 (C-3), 119.2 (C-4), 123.9 (C-8a), 124.4 (C-7), 128.9 (C-6), 135.2 (C-4a), 139.9 (C-2), 146.2 (C-1), 168.9 (CO_2CH_3 at C-4), 175.3 ($CH_2CH_2CO_2CH_3$); MS(CI) *m/z* (relative %): 324 ($M^+ + NH_4$, 17), 307 ($M^+ + H$, 5), 292 (100), 275 ($M^+ - CH_3O$, 17); HRMS calcd. for $C_{16}H_{18}O_6$: 306.1103; found: 306.1102. Anal. calcd. for $C_{16}H_{18}O_6$: C 62.73, H 5.92; found: C 62.75, H 5.78.

*5-Carbethoxymethyl-4-carbothiomethyl-1,2-dihydroxy-6-methyl-5,8-dihydronaphthalene (**2b**)*: 98% from **1b**, colorless microcrystals from hexane–ether; mp 148°C; IR (KBr): 3274 (OH), 1698 (CO), 1656 (C=C) cm^{-1}; ^1H NMR (acetone-d_6, 250 MHz) δ: 1.11 (t, OCH_2CH_3, J = 7.2 Hz), 1.81 (br s, 6-CH_3), 2.37 (s, SCH_3), 2.42 (dd, 1H, CH_2CO_2Et, J = 13.9, 7.0 Hz), 2.59 (dd, 1H, CH_2CO_2Et, J = 13.9, 4.8 Hz), 2.92 (br s, OH), 3.03 (m, 1H, H-8), 3.44 (dd, 1H, H-8, J = 21.3, 5.7 Hz), 3.95 (q, OCH_2CH_3, J = 7.2 Hz), 4.31 (m, H-5), 5.72 (m, H-7), 7.37 (s, H-3), 8.40 (br s, OH); ^{13}C NMR (acetone-d_6, 50 MHz)

[5] These data can be purchased from: The Depository of Unpublished Data, Document Delivery, CISTI, National Research Council Canada, Ottawa, Canada K1A 0S2. Tables of atomic coordinates, bond lengths and angles have also been deposited with the Cambridge Crystallographic Data Centre, and can be obtained on request from The Director, Cambridge Crystallographic Data Centre, University Chemical Laboratory, 12 Union Road, Cambridge, BB2 1EZ, U.K.

© 1997 NRC Canada

Table 3. Crystal structure determination summary.

Compound		8a	16a	22a
Empirical formula		$C_{16}H_{18}O_6$	$C_{16}H_{18}O_5$	$C_{21}H_{24}O_7$
Color		Colorless	Colorless	Colorless
Habit		Plate fragment	Needle prism fragment	Prism fragment
Crystal size (mm)		0.40 × 0.38 × 0.28	0.24 × 0.22 × 0.40	0.56 × 0.44 × 0.42
Crystal system		Monoclinic	Monoclinic	Triclinic
Space group		$P2_1/c$	$P2_1/c$	$P1$
Unit cell dimensions	a (Å)	9.775(1)	11.561(1)	7.720(1)
	b (Å)	15.658(2)	16.115(2)	10.036(1)
	c (Å)	9.707(1)	7.8693(7)	13.052(1)
	α (deg)			100.826(9)
	β (deg)	93.233(6)	90.642(7)	98.998(9)
	γ (deg)			105.222(7)
Volume (Å^3)		1483.4(5)	1466.0(3)	935.6(3)
Z		4	4	2
Formula weight		306.3	290.3	388.4
Density (calcd.) (g/cm^3)		1.372	1.315	1.379
Absorption coefficient (cm^{-1})		1.05	0.98	1.03
F (000)		648	616	412
Temperature (K)		160	295	295
2θ Range (deg)		4.0–50	4.0–50	4.0–52
Min./max. transmission		0.9600 / 0.9721	0.9731 / 0.9798	0.9553 / 0.9662
Extinction correction[a] χ		0.00113(11)	0.0039(2)	0.0117(8)
Final R indices (%) R / wR		3.18 / 3.37	3.66 / 3.62	3.99 / 4.95
Goodness-of-fit		2.37	2.05	2.79
Largest difference peak (e Å^{-3})		0.17	0.16	0.19
Largest difference hole (e Å^{-3})		–0.14	–0.14	–0.16

[a]Where $F^* = F[1 + 0.002\chi F^2/\sin(2\theta)]^{-1/4}$.

δ: 12.4, (SCH_3), 14.4 (OCH_2CH_3), 22.5 (6-CH_3), 25.6 (CH_2CO_2Et), 38.7 (C-5), 41.2 (C-8), 60.4 (OCH_2CH_3), 115.1 (C-3), 121.4 (C-7), 125.6, 127.8, 131.9 (C-4, C4a, and C-8a), 136.8 (C-6), 142.1 (C-2), 146.6 (C-1), 171.8 (CO_2Et), 193.3 (COSMe); MS(EI) *m/z* (relative %): 336 (M, <1), 248 (13), 201 (100); HRMS calcd. for $C_{17}H_{20}O_5S$: 336.1031; found: 336.1034.

*(8α,8aβ)-8-Carbomethoxyethyl-8a-carbomethoxy-2-hydroxy-1,5,8,8a-tetrahydronaphthalene-1-one (**6a**)*

A solution of diketoadduct **7** (2) (0.408 g, 1.33 mmol) in dry DME (30 mL) was heated at reflux for 8 h in the presence of solid $NaHCO_3$ (0.195 g, 2.33 mmol). The reaction was quenched at 0°C with 3 N HCl until the aqueous phase was mildly acidic (pH 4). The crude product was extracted into ether (100 mL), washed twice with brine solution, dried, filtered, and concentrated in vacuo to a brown oil. The product **6a** was purified by column chromatography, which gave a bright yellow solid (0.352 g) in 86% yield. Yields were variable due to the instability of **6a**, which was typically methylated to **6b** upon isolation. IR (neat): 3418 (OH, broad), 1736 (CO, ester), 1645 (CO, enone), 1216 cm^{-1}; ^{1}H NMR (500 MHz) δ: 1.33 (m, 1H, $CH_2CH_2CO_2CH_3$, J = 13.2, 6.0 Hz), 1.58 (m, 1H, $CH_2CH_2CO_2CH_3$, J = 12.7, 6.5, 5.8 Hz), 2.27 (m, 2H, $CH_2CH_2CO_2CH_3$, J = 14.6, 9.7 Hz), 3.00 (m, 2H, H-5, J = 20.9 Hz), 3.45 (m, 1H, H-8, J = 10.7, 5.3, 4.8 Hz), 3.63, 3.66 (s, 6H, 2 × CO_2CH_3), 5.68 (dt, 1H, H-6, J = 9.9, 3.4 Hz), 5.85 (m, 1H, H-7, J = 9.8, 5.3 Hz), 6.13 (s, OH), 6.25 (dd, 1H, H-4, J = 6.9, 2.0 Hz), 6.48 (d, 1H, H-3, J = 6.9 Hz); ^{13}C NMR (50 MHz) δ: 26.2 (C-8), 31.4, 32.8 ($CH_2CH_2CO_2CH_3$), 45.6 (C-5), 51.7, 53.4 (2 × CO_2CH_3), 65.9 (C-8a), 116.3, 119.0, 126.2, 128.4 (C-3, C-4, C-6, and C-7), 138.4 (C-4a), 145.9 (C-2), 167.8 (CO_2CH_3 at C-8a), 173.4 ($CH_2CH_2CO_2CH_3$), 193.7 (C-1); MS(EI) *m/z* (relative %): 306 (M$^+$, 1.5), 275 (M$^+$ − OCH_3, 4), 247 (M$^+$ − CO_2CH_3, 16), 215 (46), 187 (26), 173 (100), 143 (23), 115 (31).

*(8α,8aβ)-8-Carbomethoxyethyl-8a-carbomethoxy-2-methoxy-1,5,8,8a-tetrahydronaphthalene-1-one (**6b**)*

The pure product **6a** (0.43 g, 1.4 mmol) was dissolved in ether (20 mL) and stirred in ice while a freshly prepared ethereal solution of CH_2N_2 (ca. 4.2 mmol in 30 mL ether) was added dropwise over 30 min. The excess CH_2N_2 was neutralized with glacial acetic acid, and the product crystallized from ether as white needles (0.39 g) in 87% yield (an X-ray crystal structure has been reported (2)); mp 116–117°C; IR (KBr): 2961 (CH), 1744 (CO, esters), 1671 (CO, enone), 1642 (C=C) cm^{-1}; ^{1}H NMR (500 MHz) δ: 1.33 (m, 1H, $CH_2CH_2CO_2CH_3$, J = 13.2, 10.7, 5.7 Hz), 1.63 (m, 1H, $CH_2CH_2CO_2CH_3$, J = 13.1, 6.0, 4.3 Hz), 2.24 (m, 2H, $CH_2CH_2CO_2CH_3$, J = 16.3, 6.1 Hz), 2.95 (dm, 2H, H-5, J = 21.0 Hz), 3.39 (m, 1H, H-8, J = 10.8, 5.3, 4.8 Hz), 3.58 (s, 3H, $CH_2CH_2CO_2CH_3$), 3.62 (s, 3H, CO_2CH_3 at C-8a), 3.69 (s, 3H, OCH_3), 5.63 (dt, 1H, H-6, J = 9.8, 6.7 Hz), 5.83 (m, 1H, H-7,

© 1997 NRC Canada

Can. J. Chem. Downloaded from www.nrcresearchpress.com by 88.146.161.215 on 09/08/12
For personal use only.

Can. J. Chem. Downloaded from www.nrcresearchpress.com by 88.146.161.215 on 09/08/12
For personal use only.

J = 9.8, 5.3 Hz), 6.18 (d, 1H, H-3, J = 7.1 Hz), 6.21 (dd, 1H, H-4, J = 7.1, 1.2 Hz); ^{13}C NMR (63 MHz) δ: 26.2 (C-8), 31.4, 32.5 ($CH_2CH_2CO_2CH_3$), 45.3 (C-5), 51.5, 53.1 ($2 \times CO_2CH_3$), 55.4 (OCH_3), 66.3 (C-8a), 113.7, 118.2, 125.8, 128.7 (C-3, C-4, C-6, and C-7), 138.2 (C-4a), 149.7 (C-2), 167.9 (CO_2CH_3 at C-8a), 173.4 ($CH_2CH_2CO_2CH_3$), 192.3 (C-1); MS(CI) *m/z* (relative %): 338 ($M^+ + NH_4^+$, 7), 321 ($M^+ + H$, 20), 289 (100), 187 (6); HRMS calcd. for $C_{17}H_{20}O_6$: 320.1259; found: 320.1267.

*8-Carbomethoxyethyl-3-carbomethoxy-1,2-dihydroxy-5,8-dihydronaphthalene (**8a**)*: 59–65% yield from **6a**, grey prisms from ether; mp 74–76°C; IR (KBr): 3410 (OH), 1720 (CO of esters), 1674 (C═C) cm^{-1}; ^{1}H NMR (500 MHz). δ: 2.00 (m, 1H, $CH_2CH_2CO_2CH_3$, J = 5.3, 4.5 Hz), 2.16 (m, 2H, $CH_2CH_2CO_2CH_3$, J = 5.3 Hz), 2.30 (m, 1H, $CH_2CH_2CO_2CH_3$, J = 9.6 Hz), 3.28 (m, 2H, H-5, J = 20.9 Hz). 3.60 (s, 3H, $CH_2CH_2CO_2CH_3$), 3.83 (narrow m, 1H, H-8), 3.94 (s, 3H, CO_2CH_3 at C-3), 5.78 (s, OH at C-1), 5.89 (m, 1H, H-7, J = 9.9, 3.3 Hz), 6.00 (ddd, 1H, H-6, J = 9.9, 4.8 Hz), 7.16 (s, 1H, H-4), 10.6 (s, 1H, H-bonded OH at C-2); ^{13}C NMR (63 MHz) δ: 29.2, 29.6, 30.4 (C-5, $CH_2CH_2CO_2CH_3$), 33.8 (C-8), 51.4 ($CH_2CH_2CO_2CH_3$), 52.2 (CO_2CH_3 at C-3), 110.3 (C-3), 118.9 (C-4), 125.8 (C-6), 128.0 (C-7), 126.6 (C-4a), 130.7 (C-8a), 141.7 (C-1), 146.1 (C-2), 170.6 (CO_2CH_3 at C-3), 174.3 ($CH_2CH_2CO_2CH_3$); MS(EI) *m/z* (relative %): 306 (M^+, 13), 274 ($M^+ - CH_3OH$, 15), 219 (23), 187 (100), 84 (25). Anal. calcd. for $C_{16}H_{18}O_6$: C 62.73, H 5.92; found: C 62.92, H 5.94.

*8-Carbomethoxyethyl-3-carbomethoxy-1-hydroxy-2-methoxy-5,8-dihydronaphthalene (**8b**)*: 60–74% from **6b**, pale golden oil; IR (neat): 3419 (OH, broad), 1723 (CO), 1250 (OCH_3) cm^{-1}; ^{1}H NMR (500 MHz) δ: 2.01 (m, 1H, $CH_2CH_2CO_2CH_3$, J = 12.6 Hz), 2.15 (m, 2H, $CH_2CH_2CO_2CH_3$, J = 12.5, 5.6 Hz); 2.31 (m, 1H, $CH_2CH_2CO_2CH_3$, J = 12.4, 6.2 Hz), 3.34 (m, 2H, H-5, J = 21.2, 2.2 Hz), 3.59 (s, 3H, $CH_2CH_2CO_2CH_3$), 3.79 (s, 1H, H-8), 3.89, 3.91 (s, 3H, Ar-CO_2CH_3 and OCH_3), 6.18 (s, 1H, OH), 5.89 (m, 1H, H-7, J = 9.8, 3.6 Hz), 6.00 (ddd, 1H, H-6, J = 9.9, 4.5, 2.3 Hz), 7.21 (s, 1H, H-4); ^{13}C NMR (63 MHz) δ: 29.5, 29.8, 30.4 (C-5, $CH_2CH_2CO_2CH_3$), 34.0 (C-8), 51.4, 52.0 ($2 \times CO_2CH_3$), 62.3 (Ar-OCH_3), 120.9 (C-3), 121.7 (C-4), 125.6 (C-6), 128.1 (C-7), 129.9, 131.7 (C-4a and C-8a), 144.8 (C-1), 146.9 (C-2), 165.9 (CO_2CH_3 at C-3), 174.3 ($CH_2CH_2CO_2CH_3$); MS(EI) *m/z* (relative %): 320 (M^+, 5), 288 ($M^+ - CH_3OH$, 17), 257 (11), 233 (18), 201 (100), 157 (15), 115 (17); HRMS calcd. for $C_{17}H_{20}O_6$: 320.1259; found: 320.1266.

*5-Carbethoxymethyl-4-formyl-1,2-dihydroxy-6-methyl-5,8-dihydronaphthalene (**16a**)*: 23%, colorless prisms from ether–hexane; mp 161°C; IR (KBr): 3283 (OH), 1698 (CO), 1668 (C═C) cm^{-1}; ^{1}H NMR (acetone-d_6, 250 MHz) δ: 1.08 (t, OCH_2CH_3, J = 7.2 Hz), 1.86 (d, 6-CH_3, J = 1.2 Hz), 2.54 (d, 2H, CH_2CO_2Et, J = 6.1 Hz), 2.83 (s, OH), 3.06 (m, 1H, H-8), 3.44 (dd, 1H, H-8, J = 21.4, 5.6 Hz), 4.10 (q, OCH_2CH_3, J = 7.2 Hz), 4.57 (m, H-5), 5.75 (m H-7), 7.30 (s, H-3), 10.09 (s, CHO); ^{13}C NMR (acetone-d_6, 50 MHz) δ: 14.3 (OCH_2CH_3), 22.2 (6-CH_3), 25.3 (CH_2CO_2Et), 37.2 (C-5), 41.5 (C-8), 60.6 (OCH_2CH_3), 116.7 (C-3), 121.7 (C-7), 124.9, 125.7, 135.9 (C-4, C-4a, and C-8a), 136.3 (C-6), 143.1 (C-2), 148.7 (C-1), 172.0 (CO_2Et), 190.8 (CHO); MS(EI) *m/z* (relative %): 291 (M + 1, 100), 262 (13), 245 (8), 203 (45); HRMS calcd. for $C_{16}H_{18}O_5$: M + 1, 291.1232; found: 291.1241.

*5-Carboxymethyl-4-formyl-1,2-dihydroxy-5,8-dihydronaphthalene (**16b**)*: 39%, tan solid from ether; mp 181°C; IR (KBr): 3207 (OH), 1708 (CO), 1633 (C═C) cm^{-1}; ^{1}H NMR (acetone-d_6, 250 MHz) δ: 2.33 (dd, 1H, CH_2CO_2H, J = 15.8, 10.1 Hz), 2.65 (dd, 1H, CH_2CO_2H, J = 15.8, 3.8 Hz), 2.81 (s, OH), 3.15 (br d, 1H, H-8, J = 21.9 Hz), 3.47 (m, 1H, H-8), 4.68 (m, H-5), 6.00, 6.13 (m, each 1H, H-6, H-7), 7.31 (s, H-3), 10.03 (s, CHO); ^{13}C NMR (acetone-d_6, 63 MHz) δ: 24.9 (CH_2CO_2H), 32.4 (C-5), 43.6 (C-8), 118.9 (C-3), 124.6, 125.7, 134.9 (C-4, C-4a, and C-8a), 125.6 (C-7), 129.3 (C-6), 143.1 (C-2), 148.9 (C-1), 173.2 (CO_2H), 191.4 (CHO). MS(EI) *m/z* (relative %): 249 (M + 1, <1), 93 (100); HRMS calcd. for $C_{13}H_{12}O_5$: M + 1, 249.0763; found: 249.0747.

*Reaction of **12b** to give **19a** and **20a***

Reaction according to general procedure C and purification by column chromatography gave **19a** (10%) and **20a** (14%).

*5-Carbethoxymethyl-1,2-dihydroxy-4,6-dimethyl-5,8-dihydronaphthalene (**19a**)*: 10%, pale yellow oil; IR (neat): 3447 (OH), 1711 (CO) cm^{-1}; ^{1}H NMR (250 MHz) δ: 1.15 (t, OCH_2CH_3, J = 7.2 Hz), 1.76 (d, 6-CH_3, J = 1.1 Hz), 2.16 (s, 4-CH_3), 2.28 (dd, 1H, CH_2CO_2Et, J = 14.1, 8.2 Hz), 2.38 (dd, 1H, CH_2CO_2Et, J = 14.1, 4.3 Hz), 2.99 (dd, 1H, H-8, J = 21.3, 2.4 Hz), 3.37 (dd, 1H, H-8, J = 21.3, 5.8 Hz), 3.69 (m, H-5), 4.02 (q, OCH_2CH_3, J = 7.2 Hz) 5.66 (br d, H-7, J = 5.8 Hz), 6.55 (s, H-3); ^{13}C NMR (50 MHz) δ: 13.7 (OCH_2CH_3), 18.0 (4-CH_3), 21.9 (6-CH_3), 24.6 (CH_2CO_2Et), 38.6 (C-5), 40.6 (C-8), 59.8 (OCH_2CH_3), 114.9 (C-3), 120.5 (C-7), 122.6, 125.2, 129.5 (C-4, C-4a, and C-8), 136.3 (C-6), 139.2, 141.1 (C-1, C-2), 171.8 (CO_2Et); MS(FAB) *m/z* (relative %): 277 (M + 1, <1), 188 (100); HRMS calcd. for $C_{16}H_{20}O_4$: M + 1, 277.1440; found: 277.1432.

*5-Carbethoxymethyl-3-formyl-1,2-dihydroxy-4,6-dimethyl-5,8-dihydronaphthalene (**20a**)*: 14%, yellow microcrystals from ether–hexane; mp 90°C; IR (KBr): 3316 (OH), 1714 (CO), 1632 (C═C) cm^{-1}; ^{1}H NMR (250 MHz) δ: 1.22 (t, OCH_2CH_3, J = 7.2 Hz), 1.86 (s, 6-CH_3), 2.42 (d, 2H, CH_2CO_2Et, J = 5.8 Hz), 2.55 (s, 4-CH_3), 3.11 (m, 1H, H-8, J = 22.2 Hz), 3.55 (dd, 1H, H-8, J = 22.2, 5.7 Hz), 3.88 (t, H-5, J = 5.8 Hz), 4.10 (q, OCH_2CH_3, J = 7.2 Hz), 5.68 (s, 1-OH), 5.72 (m, H-7), 10.36 (s, CHO), 12.16 (s, 2-OH); ^{13}C NMR (50 MHz) δ: 14.1 (OCH_2CH_3), 15.7 (4-CH_3), 23.9 (6-CH_3), 27.1 (CH_2CO_2Et), 39.8 (C-5), 42.2 (C-8), 62.1 (OCH_2CH_3), 118.7 (C-3), 121.7 (C-7), 129.6, 131.4, 133.0 (C-4, C-4a, and C-8a), 138.1 (C-6), 141.2 (C-1), 149.3 (C-2), 173.4 (CO_2Et), 197.1 (CHO); MS(EI) *m/z* (relative %): 304 (M, 4), 216 (100), 171 (38), 143 (17); HRMS calcd. for $C_{17}H_{20}O_5$: 306.1311; found: 304.1306.

*Reaction of **12c** to give **18b**, **19b**, and **20b***

Reaction according to general procedure **C** and purification by column chromatography gave **18b** (5%) and **19b** (12%); the former rearranged on standing to **20b**.

4a-Acetyl-5-carbethoxymethyl-1-hydroxy-4-methyl-2,4a,5,8-

© 1997 NRC Canada

Can. J. Chem. Downloaded from www.nrcresearchpress.com by 88.146.161.215 on 09/08/12
For personal use only.

*tetrahydronaphthalene-2-one (**18b**)*: 5%, yellow oil; ^{1}H NMR (250 MHz) δ: 1.23 (t, $CO_2CH_2CH_3$, J = 7.1 Hz), 1.88 (partially obscured dd, 1H, CH_2CO_2Et, J = 15.4 Hz) 1.92 (d, 4-CH_3, J = 1.1 Hz), 1.93 (s, $COCH_3$), 1.99 (dd, 1H, CH_2CO_2Et, J = 15.4, 4.2 Hz), 2.74 (dt, 1H, H-8, J = 22.4, 2.9 Hz), 3.53 (m, 1H, H-8), 3.68 (m, H-5), 4.10 (q, OCH_2CH_3, J = 7.1 Hz), 5.64 (dt, H-7, J = 9.8, 3.5 Hz), 5.99 (m, H-6), 6.55 (q, H-3, J = 1.1 Hz), 6.78 (s, OH). This compound was not characterized further since it rearranged to **20c** rapidly on standing.

5-Carbethoxymethyl-1,2-dihydroxy-4-methyl-5,8-dihydronaphthalene (**19b**): 12%, yellow oil; IR (neat): 3403 (OH), 1716 (CO), 1714 (CO) cm^{-1}; ^{1}H NMR (250 MHz) δ: 1.26 (t, OCH_2CH_3, J = 7.1 Hz), 2.22 (s, 4-CH_3), 2.28 (dd, 1H, CH_2CO_2Et, J = 15.1, 10.7 Hz), 2.60 (dd, 1H, CH_2CO_2Et, J = 15.1, 3.5 Hz), 3.11 (br d, 1H, H-8, J = 21.6 Hz), 3.42 (ddd, 1H, H-8, J = 21.6, 4.5, 2.2 Hz), 3.87 (m, H-5), 4.15 (q, OCH_2CH_3, J = 7.1 Hz), 5.42 (s, OH), 5.88 (s, OH), 6.04 (m, 2H, H-6, H-7), 6.59 (s, H-3); ^{13}C NMR (50 MHz) δ: 14.2 (OCH_2CH_3), 18.3 (4-CH_3), 24.5 (CH_2CO_2Et), 33.5 (C-5), 41.9 (C-8), 60.4 (OCH_2CH_3), 115.5 (C-3), 122.7 126.5 128.9 (C-4, C-4a, and C-8a), 125.1 (C-7), 128.8 (C-6), 139.3, 140.9 (C-1, C-2), 172.2 (CO_2Et); MS(FAB) *m/z* (relative %): 263 (M + 1, <1), 217 (20) 187 (25), 174 (100); HRMS calcd. for $C_{15}H_{18}O_4$: M + 1 263.1283; found: 263.1246.

*3-Acetyl-5-carbethoxymethyl-1,2-dihydroxy-4-methyl-5,8-dihydronaphthalene (**20c**)*: brown oil from **18b** on standing. IR (neat): 3416 (OH), 1721 (br CO) cm^{-1}; ^{1}H NMR (250 MHz) δ: 1.27 (t, OCH_2CH_3, J = 7.1 Hz), 2.29 (dd, 1H, CH_2CO_2Et, J = 15.3, 10.8 Hz), 2.47, 2.65 (s, each 3H, 4-CH_3, $COCH_3$), 2.52 (dd, 1H, CH_2CO_2Et, J = 15.3, 3.5 Hz), 3.11 (m, 1H, H-8, J = 22.5 Hz), 3.55 (m, 1H, H-8, J = 22.5 Hz), 4.00 (m, H-5), 4.17 (q, OCH_2CH_3, J = 7.1 Hz) 5.78 (s, 1-OH), 6.02 (ddd, 1H, H-7, J = 9.9, 4.9, 1.8 Hz), 6.11 (ddd, 1H, H-6, J = 9.9, 5.3, 2.8 Hz), 11.62 (s, 2-OH); ^{13}C NMR (50 MHz) δ: 14.2 (OCH_2CH_3), 17.8 (4-CH_3), 24.8 (CH_2CO_2Et), 33.0 ($COCH_3$), 33.4 (C-5), 41.8 (C-8), 60.4 (OCH_2CH_3), 122.1, 122.2, 125.1, 127.4 (C-3, C-4. C-4a, and C-8a), 124.8 (C-7), 128.8 (C-6), 140.3 (C-1), 145.5 (C-2), 171.5 (CO_2Et), 206.4 (COMe); MS(EI) *m/z* (relative %): 304 (M, 5), 217 (20), 216 (58), 43 (100); HRMS calcd. for $C_{17}H_{20}O_5$: M$^+$, 304.1311; found: 304.1325.

Synthesis of (2E)-2,4-pentadienol

Commercially available 1,4-pentadien-3-ol (25 g, 0.297 mol) was distilled (bp 36°C/20 Torr; 1 Torr = 133.3 Pa) and dissolved in dry THF (20 mL). To this solution was added 10 mL of 1:1 conc. H_2SO_4–H_2O, and the mixture was stirred for 24–48 h at room temperature. The resulting yellow solution was neutralized with solid $NaHCO_3$, and extracted into ether (300 mL). The ether layer was washed with dilute aqueous $NaHCO_3$, and then brine, until the pH of the washings was 6–7. The ether layer was dried and the ether removed in vacuo, leaving the crude dienol product, which was distilled under reduced pressure (using a small amount of hydroquinone as stabilizer) to afford 15.12 g (60.5% yield) of pure (2*E*)-2,4-pentadienol (bp 62°C/20 Torr). The ^{1}H NMR spectral data were in accordance with values cited in the literature (8*c*).

*Diels–Alder reaction of **8a** and (2E)-2,4-pentadienol (adducts **22a** and **22b**)*

A solution of **8a** (0.2 g, 0.683 mmol) in dry THF (10 mL) was cooled to 0°C for 10 min, after which was added excess (2*E*)-2,4-pentadienol (0.4 g, 4.78 mmol) followed by PIFA (0.35 g, 0.82 mmol) in small portions. The reaction was stirred under an atmosphere of argon for 8 h, while warming to room temperature, to give a yellow-orange solution. The solution was concentrated in vacuo and the resulting orange oil purified by flash column chromatography to furnish a white solid (0.148 g, 56% yield) consisting of a 1:1 diastereomeric mixture of products **22a** and **22b**. The diastereomers were further resolved by column chromatography using 1:9 ether–CH_2Cl_2 as eluant.

*7β-Carbomethoxyethyl-10cα-carbomethoxy-5aα-hydroxy-1,3aα,4,5a,7,10,10bα,10c-octahydrophenanthro[10,1-bc]furan-6-one (**22a**)*: colorless prisms from ether; mp 122–123°C; IR (KBr): 3462 (OH, sharp), 1739 (CO, ester), 1677 (CO, enone) cm^{-1}; ^{1}H NMR (500 MHz) δ: 1.87 (m, 2H, $CH_2CH_2CO_2CH_3$, J = 15.4, 8.9 Hz), 2.06 (ddd, 1H, H-1, J = 18.2, 11.7, 3.1 Hz), 2.21 (m, 2H, $CH_2CH_2CO_2CH_3$), 2.35 (dd, 1H, H-10b, J = 11.6, 4.2 Hz), 2.47 (ddd, 1H, H-1, J = 15.1, 7.5, 4.9 Hz), 2.74 (dt, 1H, H-10, J = 23.1, 4.1 Hz), 3.12 (dd, 1H, H-10, J = 23.1, 5.4 Hz), 3.59 (dd, 1H, H-4, J = 8.0, 7.1 Hz), 3.60, 3.62 (s, 6H, 2 × CO_2CH_3), 3.62 (m, 1H, H-7), 4.00 (m, 1H, H-3a, J = 9.8, 7.0 Hz), 4.48 (dd, 1H, H-4, J = 9.8, 8.0 Hz), 4.71 (s, 1H, OH), 5.81 (narrow m, 2H, H-8 and H-9, J = 9.3, 6.1 Hz), 6.10 (ddd, 1H, H-2, J = 9.1, 7.5, 3.3 Hz), 6.24 (ddd, 1H, H-3, J = 9.1, 7.0, 3.0 Hz); MS(EI) *m/z* (relative %): 388 (M$^+$, 2), 371 (M$^+$ − OH, 100), 338 (33), 237 (13), 195 (24), 165 (30); HRMS calcd. for $C_{21}H_{24}O_7$: 388.1522; found: 388.1530 .

*7α-Carbomethoxyethyl-10cα-carbomethoxy-5aα-hydroxy-1,3aα,4,5a,7,10,10bα,10c-octahydrophenanthro[10,1-bc]furan-6-one (**22b**)*: white microcrystals from ether–hexane; mp 126°C; IR (KBr): 3446 (OH, sharp), 1745, 1715 (CO for each CO_2CH_3), 1622 cm^{-1}; ^{1}H NMR (500 MHz) δ: 1.93 (m, 1H, $CH_2CH_2CO_2CH_3$), 2.04 (ddd, 1H, H-1, J = 15.1, 11.8, 3.1 Hz), 2.12–2.28 (m, 3H, $CH_2CH_2CO_2CH_3$), 2.35 (dd, 1H, H-10b, J = 11.8, 4.4 Hz), 2.45 (ddd, 1H, H-1, J = 15.1, 7.6, 3.1 Hz), 2.83 (dd, 1H, H-10, J = 23.1, 5.6 Hz), 3.05 (dt, 1H, H-10, J = 23.1, 4.1 Hz), 3.51 (narrow m, 1H, H-7), 3.60 (dd, 1H, H-4, J = 8.0, 6.0 Hz), 3.63, 3.66 (s, 6H, 2 × CO_2CH_3), 4.01 (ddd, 1H, H-3a, J = 9.6, 6.7, 6.5 Hz), 4.32 (s, 1H, OH), 4.51 (dd, 1H, H-4, J = 9.6, 8.1 Hz); 5.81 (narrow m, 2H, H-8 and H-9), 6.09 (m, 1H, H-2, J = 9.3, 7.6, 3.1 Hz), 6.22 (m, 1H, H-3, J = 9.2, 7.0, 3.0 Hz); ^{13}C NMR (125 MHz) δ: 28.4, 29.0, 29.7 (C-1, $CH_2CH_2CO_2CH_3$), 31.6 (C-10), 33.5 (C-7), 40.8 (C-3a), 42.3 (C-10b), 51.6, 52.7 (2 × CO_2CH_3), 60.9 (C-10c), 76.3 (C-4), 98.7 (C-5a), 122.9 (C-8 or C-9), 128.9 (C-6a), 129.28, 129.32 (C-2, and C-8 or C-9), 130.9 (C-3), 158.5 (C-10a), 171.9, 174.4 (2 × CO_2CH_3), 190.2 (C-6); MS(EI) *m/z* (relative %): 388 (M$^+$, 2), 371 (M$^+$ − OH, 100), 357 (M$^+$ − OCH_3, 9), 338 (16), 301 (M$^+$ − $CH_2CH_2CO_2CH_3$, 34), 195 (27), 165 (36); HRMS calcd. for $C_{21}H_{24}O_7$: 388.1522; found: 388.1534 .

*Diels–Alder reaction of **2a** and (2E)-2,4-pentadienol (adduct **23**)*

A solution of **2a** (0.35 g, 1.16 mmol) in dry THF (10 mL) was cooled to 0°C, after which was added excess (2*E*)-2,4-penta-

© 1997 NRC Canada

dienol (0.8 g, 9.5 mmol) followed by PIFA (0.6 g, 1.39 mmol) in small portions. The solution was stirred under argon atmosphere for 24 h at room temperature, and then concentrated in vacuo. The resulting yellow oil was purified by column chromatography and gave **23** (51 mg, 11%) as a colorless oil.

*5α-Carbomethoxyethyl-4aα-carbomethoxy-10α-hydroxy-4β, 10β-methyleneoxy-1,4α,4aα,5,8,9,10,10aα-octahydrophenanthrene-9-one (**23**)*: IR (neat): 3442 (OH), 1733 (CO), 1679 (CO), 1437, 733 cm^{-1}; ^1H NMR (500 MHz) δ: 1.54 (m, 1H, $CH_2CH_2CO_2CH_3$, J = 14.4, 7.2 Hz), 1.73 (m, 1H, $CH_2CH_2CO_2CH_3$), 2.25 (br t, 2H, $CH_2CH_2CO_2CH_3$, J = 8.5 and 7.7 Hz), 2.38 (dd, 1H, H-1, J = 19.5, 7.2 Hz), 2.54 (br s, 1H, H-4), 2.69 (br d, 1H, H-8, J = 21.5 Hz), 2.75 (br d, 1H, H-1, J = 19.5 Hz), 2.85 (d, 1H, H-10a, J = 7.2 Hz), 3.26 (br s, 1H, H-5), 3.31 (ddd, 1H, H-8, J = 21.6, 5.4, 2.0 Hz), 3.63 (d, 1H, CH_2O, J = 11.8 Hz), 3.65 (s, 3H, CO_2CH_3), 3.73 (dd, 1H, CH_2O, J = 11.9, 2.6 Hz), 3.79 (s, 3H, CO_2CH_3), 4.92 (s, 1H, OH), 5.86 (m, 3H, H-2, H-3 and H-7, J = 10.5 Hz), 6.02 (m, 1H, H-6, J = 9.4, 5.5 Hz); ^{13}C NMR (63 MHz) δ: 23.9 and 24.1 (C-1, C-8), 29.8, 30.5 ($CH_2CH_2CO_2CH_3$), 32.9 (C-4), 37.0 (C-5), 40.1 (C-10a), 51.6, 52.5 (2 × CO_2CH_3), 52.8 (C-4a), 65.6 (CH_2O), 92.5 (C-10), 126.1, 126.4, 128.2, 128.5 (C-2, C-3, C-6, and C-7), 134.4 (C-8a), 159.1 (C-4b), 172.1, 173.2 (2 × CO_2CH_3), 191.4 (C-9); MS(EI) *m/z* (relative %): 389 (M^+ + H, 82), 388 (M^+, 24), 370 ($M^+ - H_2O$, 26), 357 ($M^+ - OCH_3$, 25), 301 (52), 195 (60), 165 (100); HRMS calcd. for $C_{21}H_{24}O_7$: 388.1522; found: 388.1512.

Acknowledgments

The authors would like to thank Kevin Turnbull for his assistance in the laboratory, Janet Venne for performing many of the high-field NOEDS and 2D NMR experiments, and the Natural Sciences and Engineering Research Council of Canada (NSERC) for financial support of this work.

References

1. (*a*) P. Deslongchamps. Pure Appl. Chem. **49**, 1329 (1977); (*b*) A.C. Bazan, J.H. Edwards, and U. Weiss. Tetrahedron Lett. 147 (1977); (*c*) S. Yamamura, Y. Shizuri, H. Shigemori, Y. Okhuno, and M. Okhubo. Tetrahedron, **47**, 635 (1991).
2. R. Carlini, C-L. Fang, D. Herrington, K. Higgs, R.Rodrigo, and N. Taylor. Aust. J. Chem. **50**, 271 (1997).
3. T.H. Lee, C.-C. Liao, and N.-C. Liu. Tetrahedron Lett. **37**, 5897 (1996).
4. S. Inayama and Y. Yanagita. J. Org. Chem. **27**, 1465 (1962).
5. A. Planas, J. Tomas, and J.-J. Bonet. Tetrahedron Lett. **28**, 471 (1987).
6. (*a*) F.B.H. Ahmad, J.M. Bruce, J. Khalafy, V. Pejanovic, K. Sabetian, and I. Watt. J. Chem. Soc. Chem. Commum. 166 (1981); (*b*) F.B.H. Ahmad, J.M. Bruce, J. Khalafy, and K. Sabetian. J. Chem. Soc. Chem. Commun. 169 (1981); (*c*) M.U. Akpuaka, R.L. Beddoes, J.M. Bruce, S. Fitzjohn, and O. Mills. J. Chem. Soc. Chem. Commun. 686 (1982).
7. S.C. Cooper and P.G. Sammes. J. Chem. Soc. Chem. Commun. 633 (1980).
8. (*a*) G. Vidari, S. Ferrino, and P.A. Grieco. J. Am. Chem. Soc. **106**, 3539 (1984); (*b*) T.R. Hoye, A.S. Magee, and W.S. Trumper. Synth. Commun. **12**, 183 (1987); (*c*) K. Mori. Tetrahedron, **30**, 3807 (1974); (*d*) R.K. Boeckmann and D.M. Demko. J. Org. Chem. **47**, 1789 (1982).
9. L. Shide, R. Mayer, and G. Rucker. Planta Med. **53**, 332 (1987).
10. J.M. Bruce. J. Chem. Soc. 360 (1960).
11. R. Al-Hamdany and S. Salih. J. Iraqi Chem. Soc. **6–7**, 61 (1982): Chem. Abstr. **101**, 210214c (1984).
12. R.C. Cookson, T.A. Crabb, J.J. Frankel, and J. Hudec. Tetrahedron, Suppl. 7, **355** (1966).

Can. J. Chem. Downloaded from www.nrcresearchpress.com by 88.146.161.215 on 09/08/12
For personal use only.

© 1997 NRC Canada

Synthesis of regiospecifically substituted 2-hydroxybenzocyclobutenones

Yvonne Lear and Tony Durst

Abstract: Regiospecifically substituted 2-hydroxybenzocyclobutenones were synthesized from the corresponding TBS protected 2-bromo-mandelate esters via halogen–metal exchange, cyclization, and subsequent deprotection.

Key words: 2-hydroxybenzocyclobutenones, halogen–metal exchange, benzocyclobutenediones, 2-bromomandelate esters.

Résumé : Opérant à partir des esters correspondants de l'acide 2-bromomandélique protégés par du «TBS» et procédant par le biais d'un échange halogène–métal, d'une cyclisation et d'une déprotection subséquente, on a réalisé la synthèse de 2-hydroxybenzocyclobuténones régiospécifiquement substituées.

Mots clés : 2-hydroxybenzocyclobuténones, échange halogène–métal, benzocyclobutènediones, esters de l'acide 2-bromomandélique.

[Traduit par la réduction]

Can. J. Chem. Downloaded from www.nrcresearchpress.com by 88.146.161.215 on 09/08/12
For personal use only.

Introduction

Benzocyclobutenediones have been shown to be useful intermediates in the synthesis of polycyclic natural products, in particular naphtha- and anthraquinones (1, 2) (Scheme 1). In general, the benzocyclobutenedione **1** is treated with a Grignard reagent to generate a 2-hydroxybenzocyclobutenone **2**. The thermal opening of the 2-hydroxybenzocyclobutenone **2** occurs at about 110°C and is governed by the torquoselectivity rules described by Houk and co-workers (3). This results exclusively in the formation of the intermediate **3** in which the aryl or vinyl substituent is suitably placed for an intramolecular acylation process. Thus anthraquinones or naphthaquinones are obtained, depending on whether an aryl or a vinyl Grignard reagent is used in the addition reaction. The regioselectivity of the addition of Grignard reagents to **1** is difficult to control except when R in **1** is a large *ortho* substituent (4). To have a general synthesis of specifically substituted anthraquinones **4**, based on such a reaction sequence, access to unsymmetrically substituted benzocyclobutenediones with one of the carbonyl moieties masked is needed. Ideally, such compounds would allow for the addition of an organometallic reagent at one of the carbonyl groups, followed by unmasking of the second carbonyl group, and the thermolysis reactions described above.

Previous efforts in this group involved the synthesis of 2-benzylidene-benzocyclobutenone **5** as an unsymmetrical benzocyclobuten-1,2-dione equivalent (5) (Scheme 2). Addition of organolithiums or Grignard reagents occurred exclusively by a 1,2 pathway to give **6** (R′ = aryl). The usefulness of **6** as a synthetic intermediate to anthraquinones suffered greatly since it was oxidized to **7** in only poor yields. Furthermore, thermolysis of **6**, prior to oxidation of the benzylidene group to a carbonyl function, led to a variety of ring enlargement products. The possibility of first protecting the ketone in **5** as a ketal to give **8**, then ozonolyzing the benzylidene group to reveal the other carbonyl group to give **9**, was also considered; again the oxidation step proceeded in only poor yield (6).

Since it had already been shown that benzocyclobutenols could be made by halogen–metal exchange in *o*-bromophenylacetone followed by cyclization (7), it was envisioned that this method could also be applied to the synthesis of benzocyclobutenones. It was necessary to generate a substrate that had a halogen *ortho* to a "functionalized arm" containing two oxygen functionalities: one as an ester to serve as an electrophile in the cyclization process and generate the benzocyclobutenone and the other a potential carbonyl group, for example, a protected hydroxy group (Scheme 3). The realization of such a process is described below.

Results and discussion

The known 6-bromopiperonal **12a** (8) (Scheme 4) was converted to the cyanohydrin **13a** using trimethylsilyl cyanide in dichloromethane with catalytic zinc iodide (9). Further treatment with hydrochloric acid in refluxing ethanol for 1 h afforded the hydroxy ester **14a**. The changes described were easily followed by NMR spectroscopy.

Gallagher and Beak have shown that, under halogen–metal exchange conditions, acidic protons are removed before the exchange reaction takes place (10). To avoid this complication, the hydroxy ester **14a** was protected using *tert*-butyldimethylsilyl chloride in DMF using imidazole as base. When the protected ester **15a** was treated with 2 equivalents of *tert*-

Received November 22, 1996.

This paper is dedicated to Professor William A. Ayer on the occasion of his 65th birthday.

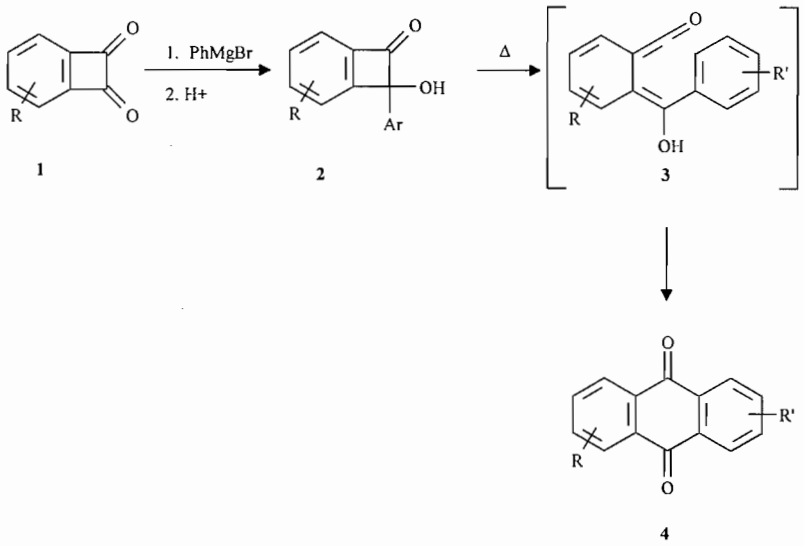
Y. Lear and T. Durst.[1] Ottawa-Carleton Chemistry Institute, Department of Chemistry, University of Ottawa, Ottawa, ON K1N 6N5, Canada.

[1] Author to whom correspondence may be addressed. Telephone: (613) 562-5800, ext. 6072. Fax: (613) 562-5170. E-mail: tdurst@oreo.chem.uottawa.ca

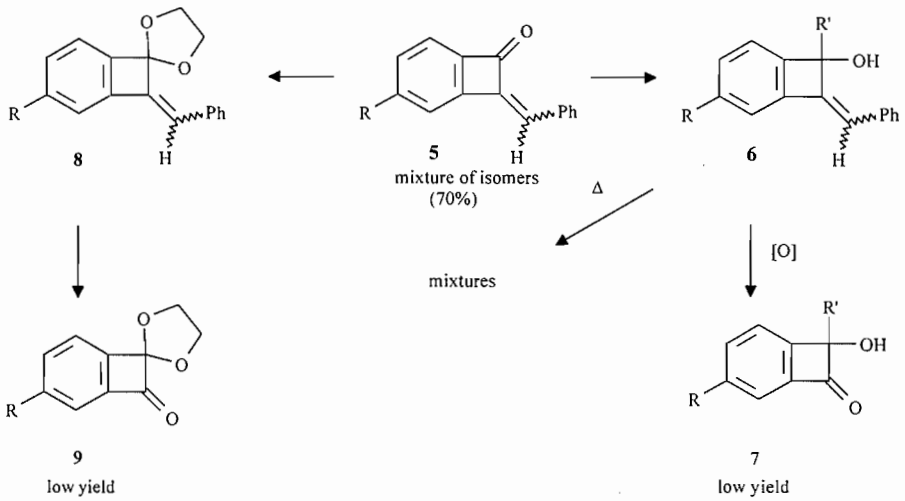
© 1997 NRC Canada

Can. J. Chem. Downloaded from www.nrcresearchpress.com by 88.146.161.215 on 09/08/12
For personal use only.

Scheme 1.



Scheme 2.



butyllitium at −78°C,[2] the desired cyclobutenone **16a** was formed but was accompanied by the tertiary alcohol **18a** (Scheme 5). Use of 1.1 equivalents of *tert*-butyllithium afforded a crude reaction mixture whose ^{1}H NMR spectrum indicated that approximately 60% of the starting material had been converted to the desired benzocyclobutenone. Reaction of **15a** with 1.5 equivalents of *tert*-butyllithium at −78°C for 15 min, followed by quenching of the reaction mixture with saturated ammonium chloride at that temperature, led to a 95% yield of the desired benzocyclobutenone. The compound could be purified by silica gel chromatography, or by simple recrystallization from hexanes – ethyl acetate. The ^{1}H NMR spectrum showed the disappearance of the ethyl group of the ester and the shift of the benzylic proton from 5.48 to 5.56 ppm

Scheme 3.



P=protecting group, L=leaving group, X=halogen

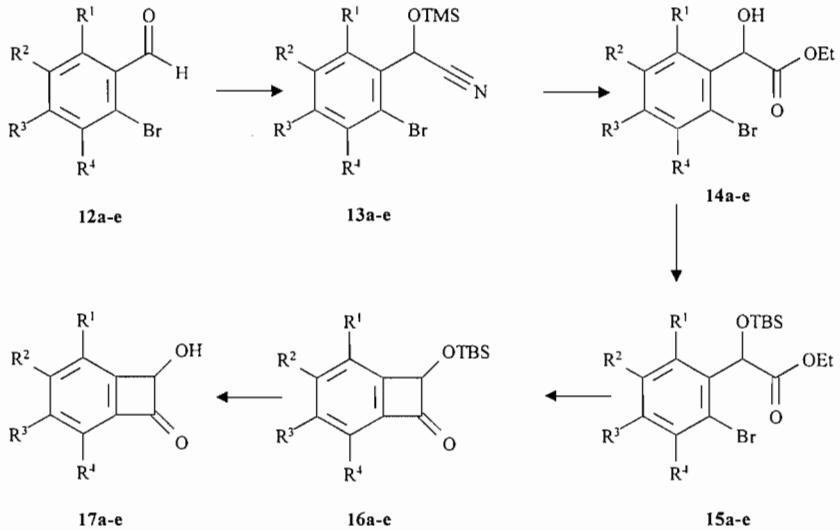
in going from **15a** to **16a**. The ^{13}C NMR peak at 187.5 ppm and the IR absorbtion at 1757 cm^{-1} are values associated with the carbonyl group in other benzocyclobutenones (5). Deprotection using tetra-*n*-butylammonium fluoride in THF afforded the hydroxybenzocyclobutenone **17a** in 80% yield.

The starting materials for the remaining cyclization precursors were the commercially available 2-bromobenzaldehyde, *m*-anisaldehyde, *p*-anisaldehyde, and 3-bromophenol. *m*-Anisaldehyde was brominated at the 2 position using the same method as for piperonal to give **12d**. *p*-Anisaldehyde was

[2] Halogen–metal exchange reactions are generally carried out using two equivalents of butyllithium, one to do the exchange reaction and the other consumed as base, causing an elimination from the butyl bromide formed from the reaction (11).

© 1997 NRC Canada

Scheme 4.



a $R^1=R^4=H$ $R^2,R^3=OCH_2O$

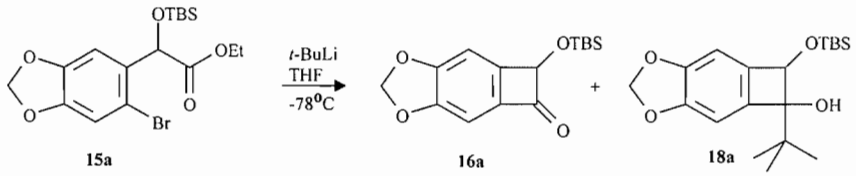
b $R^1=R^2=R^3=R^4=H$

c $R^1=OCH_3$ $R^2=R^3=R^4=H$

d $R^2=OCH_3$ $R^1=R^3=R^4=H$

e $R^3=OCH_3$ $R^1=R^2=R^4=H$

Scheme 5.



halogenated using Comins' procedure to afford **12e** (12, 13). *m*-Bromophenol was formylated under Reimer–Tiemann conditions (14) and methylated using potassium carbonate and methyl iodide in acetone to give **12c**.

The above *ortho*-bromobenzaldehydes were converted in >95% yield to the corresponding trimethylsilyl protected cyanohydrins **13a–e** using trimethylsilyl cyanide as previously described and were then converted to the ethyl esters. The reactivities of these cyanohydrins toward ethanolysis were variable. When the cyanohydrin **13e** was reacted under the conditions previously described for the piperonal system, a 1:1 mixture of the hydroxy ester **14e** and the corresponding α-ethoxy ester was obtained. This difference in reactivity is likely due to the methoxy group *para* to the benzylic alcohol that makes the benzylic hydroxyl group susceptible to exchange with the solvent ethanol. This reaction was suppressed by using hydrogen chloride gas bubbled through anhydrous ethanol instead of concentrated aqueous hydrochloric acid. This led to the exclusive formation of the desired hydroxy ester in 87% yield. The formation of the other hydroxy esters was carried out using aqueous acid in ethanol with yields ranging from 60 to 90%. (See Experimental section)

The α-hydroxy esters were protected as *tert*-butyldimethylsilyl (TBS) ethers using either TBSCl with imidazole as base, or *tert*-butyldimethylsilyl trifluoromethane sulfonate with 2,6-lutidine as base. For the hydroxy ester **14c**, protection using TBSCl with imidazole was incomplete after 3 days, necessitating the use of the triflate, which gave **15c** in >95% yield in 30 min.

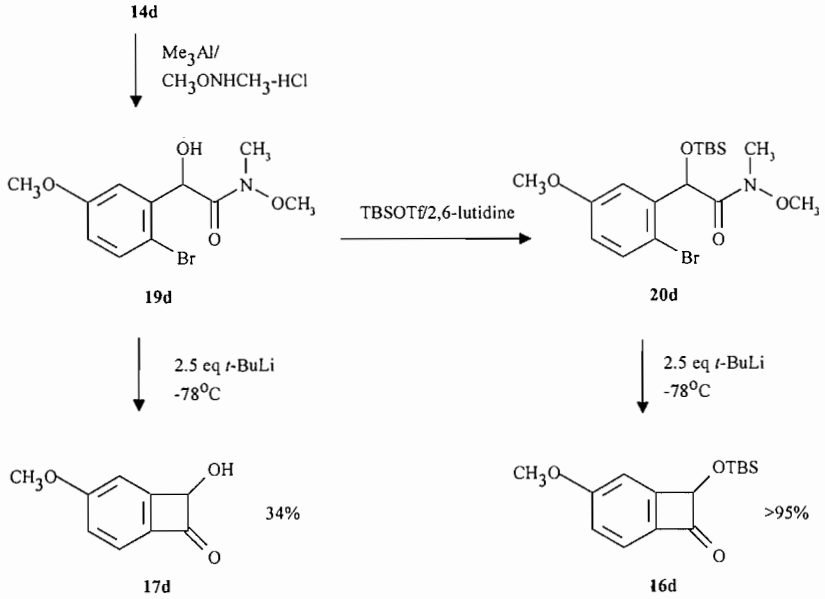
As in the case of **15a** it was necessary to determine the appropriate amount of *tert*-butyllithium for optimum yields in the cyclization of **15b–e**. When the *ortho*-bromo ester **13d** was treated with two equivalents of *tert*-butyllithium at −78°C, the cyclized product **16b** was obtained in 90% isolated yield. Compounds such as **14e–16e** bearing an aryl methoxy group required only 1.2–1.5 equivalents of *tert*-butyllithium, as did the piperonal derivative **16a**.

When cyclization reactions were carried out on mandelic esters **15d** and **15e,** the ^{1}H NMR spectrum of the crude reaction mixtures generally showed mixtures of the starting material, the desired benzocyclobutenone, and a third compound in

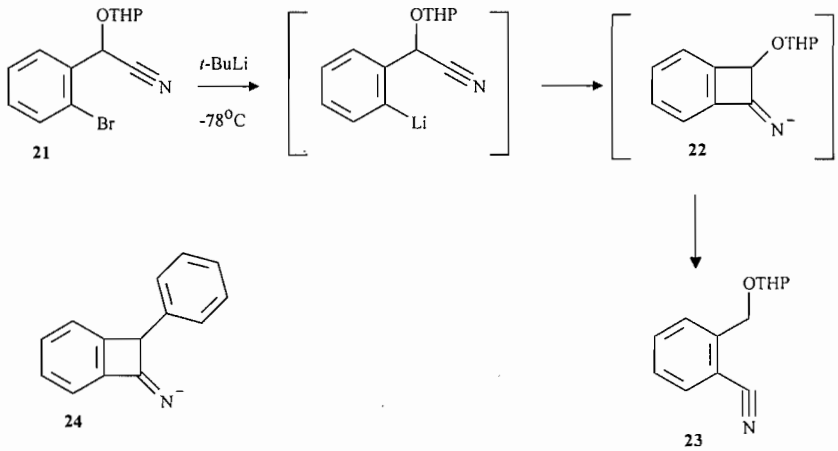
Can. J. Chem. Downloaded from www.nrcresearchpress.com by 88.146.161.215 on 09/08/12
For personal use only.

© 1997 NRC Canada

Scheme 6.



Scheme 7.



which *tert*-butyllithium had added to the benzocyclobutenone. This indicated that the addition of *tert*-butyllithium to the benzocyclobutenone product begins before halogen–metal exchange is complete. Slower addition of *tert*-butyllithium and (or) lowering the reaction temperature did not improve the selectivity. The reactions were optimized with yields in the 60–70% range. This problem was overcome by converting the mandelic ester **14d** to the corresponding Weinreb amide **19d** (15, 16), which was protected using TBSOTf to give **20d**. When the protected hydroxy amide **20d** was reacted with 2.5 equivalents of *tert*-butyllithium at −78°C, the desired benzocyclobutenone **16d** was produced in essentially quantitative yield (Scheme 6). Attempts to shorten the sequence by direct cyclization of the unprotected hydroxy ester **19d** using 2.5 equivalents of *tert*-butyllithium at −78°C led to the cyclized product **17d** in only 34% yield, along with four other side products that were not identified.

Deprotection of the TBS derivatives **16** using tetra-*n*-butylammonium fluoride afforded the 2-hydroxybenzocyclobutenones **17** in 65–90% isolated yields. For the preparation of benzocyclobutenone **17e**, it was necessary to add acetic acid in the deprotection step in order to avoid base-catalyzed ring opening (17).

To try to shorten the reaction sequence, cyclization was attempted directly on the protected cyanohydrin **21** rather than the hydrolyzed cyanohydrin (Scheme 7). It was anticipated that halogen–metal exchange followed by cyclization would yield the iminium ion **22** as an intermediate and the benzocyclobutenone **11** upon aqueous work-up.

The cyanohydrin **21**, when treated with 1 equivalent of *t*-BuLi at −78°C for 5 min, afforded the rearranged nitrile **23** as the major product. The expected cyclization to **22** did occur but this intermediate underwent [2+2] ring opening even at −78°C; subsequent protonation afforded **23**. Biehl and co-workers had earlier noted the instability of the iminium ion of 2–phenylbenzocyclobutenone (18). We anticipated that cycloreversion of **22** would be considerably less favourable than **24** but unfortunately were unable to intercept it prior to ring opening.

© 1997 NRC Canada

Can. J. Chem. Downloaded from www.nrcresearchpress.com by 88.146.161.215 on 09/08/12
For personal use only.

Can. J. Chem. Downloaded from www.nrcresearchpress.com by 88.146.161.215 on 09/08/12
For personal use only.

Experimental section

General

Tetrahydrofuran (THF) was freshly distilled from sodium and benzophenone before use. Hexanes and ethyl acetate used for chromatography and distillation were routinely distilled before use. Melting points were determined using a Thomas Scientific melting point apparatus and are uncorrected. ^{1}H NMR and ^{13}C NMR spectra were recorded on either a Varian Gemini 200, Varian XL-300, or Bruker AMX 500 spectrometer in deuterated chloroform unless otherwise stated. IR spectra were recorded on a Bomem Michelson FTIR as solutions in CH_2Cl_2; then the solvent spectrum was subtracted.

Preparation of 6-bromopiperonal 12a

Piperonal (15 g, 0.10 mol) was stirred with 100 mL glacial acetic acid and bromine (6 mL, 0.12 mol) for 18 h. Water (300 mL) was added to precipitate the product. The solid was collected on a Buchner funnel and recrystallized from ethanol as colorless needles of **12a** (14.3 g, 63 mmol, 63% yield), mp 126–128°C (lit. (8) mp 127–129°C). ^{1}H NMR δ: 6.10 (s, 2H), 7.13 (s, 1H), 7.35 (s, 1H), 10.15 (s, 1H).

Preparation of 6-bromo-2-methoxybenzaldehyde 12c

A mixture of *m*-bromophenol (5 g, 29 mmol), calcium hydroxide (14 g, 0.19 mol), sodium carbonate (16 g, 0.13 mol), and 100 mL water was stirred and heated to 70°C. Chloroform (7 mL, 10.4 g, 87 mmol) was added at a rate such that a gentle reflux was maintained, about 90 min. Stirring was continued for 2 h. The mixture was acidified with concentrated sulfuric acid, extracted with CH_2Cl_2, dried with $MgSO_4$, and the solvent evaporated. Chromatography on silica gel (9:1 hexane/ethyl acetate) gave 6-bromo-2-hydroxybenzaldehyde (660 mg, 3.3 mmol, 12% yield), 600 mg of the other isomer, 2-hydroxy-4-bromobenzaldehyde, and about 1.2 g of starting material; mp 50–51°C (lit. (19) mp 52.5°C) ^{1}H NMR δ: 6.92 (dt, J = 8.9, 0.8 Hz, 1H), 7.14 (dd, J = 6.7, 0.8 Hz, 1H), 7.30 (dd, 6.7, 8.9 Hz, 1H), 10.31 (s, 1H), 11.96 (s, 1H). A mixture of 6-bromo-2-hydroxybenzaldehyde (380 mg, 2 mmol), potassium carbonate (1 g, 7.2 mmol), methyl iodide (2 mL, 4.56 g, 32 mmol), and 10 mL acetone was stirred for 20 h, diluted with 20 mL water, and extracted with ether. The organic extracts were dried with anhydrous $MgSO_4$ and evaporated to afford 400 mg crystalline **12c** (2 mmol, >95% yield), which was pure by ^{1}H NMR. mp 52–53°C. IR: 1585, 1697 cm^{-1}. ^{1}H NMR δ: 3.87 (s, 3H), 6.89 (dd, J = 1.1, 8.1 Hz, 1H), 7.16–7.32 (m, 2H), 10.36 (s, 1H). ^{13}C NMR δ: 55.86, 110.71, 124.29, 126.08, 131.07, 134.58, 161.61, 190.29. HRMS, calcd. for $C_8H_7O_2Br$: 213.9629; found: 213.9631.

Preparation of 2-bromo-5-methoxybenzaldehyde 12d

The procedure was the same as that used to prepare **12a** except the starting material was *m*-anisaldehyde. Isolated yield of **12d**: 16.5 g (70% yield), mp 71–73°C (lit. (20) mp 74°C). ^{1}H NMR δ: 3.83 (s, 3H), 7.01 (dd, J = 8.8, 3.0 Hz, 1H), 7.40 (d, J = 3.0 Hz, 1H), 7.45 (d, J = 3.0 Hz, 1H), 10.29 (s, 1H).

Preparation of 2-bromo-4-methoxybenzaldehyde 12e

To a stirred solution of trimethylethylenediamine (4.6 mL, 3.7 g, 36 mmol) in 80 mL THF at −20°C was added dropwise *n*-BuLi (13 mL 2.5 M, 32 mmol). The solution was stirred for 15 min, then *p*-anisaldehyde (3.7 mL, 4.4 g, 33 mmol) was added and stirred for 15 min. *n*-BuLi (39 mL, 2.5 M, 97.5 mmol) was added and the solution stirred, then let stand in a freezer (0°C) for 22 h. The solution was cooled to −78°C, carbon tetrabromide (30 g, 90 mmol) was added, and the solution allowed to warm to 25°C. A 10% HCl solution (300 mL) was added and extraction carried out with CH_2Cl_2. The combined organic extracts were washed with sodium thiosulfate until no cloudiness was imparted to the aqueous layer, then washed with water and brine. The organic solution was dried with anhydrous $MgSO_4$ and the solvent evaporated. The product was isolated by silica gel column chromatography (9:1 hexanes/ethyl acetate) and recrystallized from ethanol to afford 350 mg **12e** (54% yield), mp 70–71°C. IR: 1595, 1686 cm^{-1}. ^{1}H NMR δ: 3.79 (s, 3H), 6.82 (dd, 1H), 7.12 (d, 1H), 7.80 (d, 1H), 10.11 (s, 1H). ^{13}C NMR δ: 55.52, 113.74, 118.13, 126.59, 128.32, 130.93, 164.13, 190.12. HRMS, calcd. for $C_8H_7O_2Br$: 213.9629; found: 213.9622.

Preparation of cyanohydrins 13a–e

The cyanohydrins were prepared according to Gassman's procedure (9). The cyanohydrin was stirred for 1 h with 1.2 equivalents of trimethylsilyl cyanide in CH_2Cl_2. The product was isolated either by evaporating the solvent and using the crude product directly or by passing the reaction mixture through a short silica gel plug to remove the catalyst and then evaporating the solvent. The yield for all cyanohydrins was >95%, on scales from 100 mg to 15 g. **13a**: ^{1}H NMR δ: 0.23 (s, 9H), 5.67 (s, 1H), 6.01 (s, 2H), 6.98 (s, 1H), 7.16 (s, 1H). **13b**: ^{1}H NMR δ: 0.18 (s, 9H), 5.68 (s, 1H), 7.16 (dd, 1H), 7.32 (dd, 1H), 7.48 (d, 1H), 7.65 (d, 1H). **13c**: ^{1}H NMR δ: 0.18 (s, 9H), 3.91 (s, 3H), 6.16 (s, 1H), 6.87–6.91 (m, 1H), 7.18–7.21 (m, 2H). **13d**: ^{1}H NMR δ: 0.16 (s, 9H), 3.72 (s, 3H), 5.61 (s, 1H), 6.71 (dd, 1H), 7.15 (d, 1H), 7.34 (d, 1H). **13e**: ^{1}H NMR δ: 0.22 (s, 9H), 3.80 (s, 3H), 5.72 (s, 1H), 6.94 (dd, J = 2.6, 8.7 Hz, 1H), 7.10 (d, J = 2.6, 8.7 Hz, 1H).

Preparation of 2-bromohydroxy esters 14a–e

Procedure A

The cyanohydrin **13** in a solution of 3:2 ethanol/concentrated hydrochloric acid (1 g **13** in 15 mL acid solution) was refluxed for 1 h, the solution neutralized with sodium bicarbonate or sodium hydroxide, the ethanol evaporated, and extraction carried out with ether. The organic extracts were combined, dried with anhydrous $MgSO_4$, and the solvent was evaporated.

Procedure B

As for procedure A except reflux was continued for 20 h.

Procedure C

Anhydrous hydrogen chloride was bubbled through a solution of **13** in absolute ethanol for 30 min. Work-up was as for procedure A.

The crude product was generally clean by ^{1}H NMR, but could be purified by silica gel column chromatography (9:1 hexanes/ethyl acetate). The reactions were carried out on scales from 100 mg to 15 g with no decrease in yield.

14a: The compound was prepared by procedure A starting with 7.2 g **13a** (22 mmol); the yield of **14a** was 4.9 g

© 1997 NRC Canada

Can. J. Chem. Downloaded from www.nrcresearchpress.com by 88.146.161.215 on 09/08/12
For personal use only.

(16 mmol, 73% yield), mp 56–58°C. IR: 1731, 3528 cm^{-1}. ^1H NMR δ: 1.22 (t, J = 7.1 Hz, 2H), 3.49 (d, J = 4.7 Hz, 1H), 4.21 (m, 2H), 5.47 (d, J = 4.7 Hz, 1H), 5.96 (s, 2H), 6.82 (s, 1H), 6.99 (s, 1H). ^{13}C NMR δ: 14.0, 62.5, 72.1, 102.0, 108.0, 112.9, 114.4, 131.0, 147.7, 148.5, 173.3. HRMS, calcd. for $C_{11}H_{11}O_5Br$: 301.9789; found: 301.9779.

14b: This compound was prepared by procedure A starting with 1.42 g **13b** (5 mmol); the yield of **14b** was 1.13 g (4.3 mmol, 87% yield), oil. IR: 3693, 1703 cm^{-1}. ^1H NMR δ: 1.11 (t, J = 7.1 Hz, 3H), 3.40–3.60 (br, 1H), 3.95–4.25 (m, 2H), 5.45 (s, 1H), 7.06–7.11 (m, 1H), 7.15–7.35 (m, 2H), 7.46 (dd, J = 8.7 Hz, 1H). ^{13}C NMR δ: 13.6, 62.0, 72.0, 123.2, 127.4, 128.4, 129.5, 132.8, 137.5, 172.8. HRMS, calcd. for $C_{10}H_{11}O_3Br$: 257.9891; found: 257.9890.

14c: The compound was prepared by procedure B from 540 mg **13c** (1.7 mmol); the yield of **14c** was 280 mg (0.97 mmol, 57% yield), mp 102–103°C. IR: 1737 cm^{-1}. ^1H NMR δ: 1.19 (t, J = 7.6 Hz, 3H), 3.62 (d, J = 1.7, 6.8 Hz, 1H), 3.79 (s, 3H), 4.21 (q, J = 7.6 Hz, 2H), 5.66 (d, J = 6.8 Hz, 1H), 6.81 (dd, J = 1.7, 7.7 Hz, 1H), 7.10–7.24 (m, 2H). ^{13}C NMR δ: 14.1, 55.9, 61.8, 70.7, 110.4, 125.5, 127.2, 130.4, 158.3, 173.2 (two of the aromatic carbon signals apparently overlap). LRMS (CI,M+1), calcd. for $C_{11}H_{13}O_4Br$: 289.0; found: 288.9

14d: The compound was prepared by procedure A from 13.9 g **13d** (44 mmol); the yield of **14d** was 10.9 g (38 mmol, 86% yield), mp 60–62°C. IR: 3517, 1732 cm^{-1}. ^1H NMR δ: 1.19 (t, J = 7.1 Hz, 3H), 3.70 (br, 1H), 3.73 (s, 3H), 4.09–4.31 (m, 2H), 5.60 (s, 1H), 6.70 (dd, J = 3.0, 8.8 Hz, 1H), 6.88 (d, J = 3.0 Hz, 1H), 7.40 (d, J = 8.8 Hz, 1H). ^{13}C NMR δ: 13.6, 55.1, 62.1, 72.0, 113.4, 113.5, 115.7, 133.4, 138.3, 158.8, 172.7. HRMS, calcd. for $C_{11}H_{13}O_2Br$: 287.9997; found: 287.9998.

14e: The compound was prepared by procedure C from 100 mg **13e** (0.32 mmol); the yield of **14e** was 81 mg (0.28 mmol, 88% yield), mp 58–59°C. IR: 3519, 1732 cm^{-1}. ^1H NMR δ: 1.23 (t, J = 7.1 Hz, 3H), 3.48 (d, J = 5.0 Hz, 1H), 3.78 (s, 3H), 4.21 (m, 2H), 5.46, (d, J = 5.0 Hz, 1H), 6.84 (dd, J = 2.7, 8.7 Hz, 1H), 7.10 (d, J = 2.7 Hz, 1H), 7.24 (d, J = 8.7 Hz, 1H). ^{13}C NMR δ: 13.6, 55.2, 61.9, 71.6, 113.4, 117.9, 129.0, 129.6, 159.6, 173.1, 190.3. HRMS, calcd. for $C_{11}H_{13}O_2Br$: 287.9997; found: 287.9985.

Preparation of TBS protected esters 15a–e

Procedure A

The hydroxy ester was treated with 1.2 equivalents of *tert*-butyldimethylsilyl chloride and 2.2 equivalents of imidazole in DMF and stirred at 25°C for 24 h. The reaction mixture was diluted with water, extracted with CH_2Cl_2, and the organic extracts were washed with water until no concentration gradients were visible when water was added. The organic extracts were dried with anhydrous $MgSO_4$ and the solvent was evaporated. The compounds were isolated and purified by either silica gel column chromatography or reduced pressure distillation as indicated. This reaction was carried out on scales from 100 mg to 15 g with no effect on the yield.

Procedure B

The hydroxy ester was stirred with 1.5 equivalents of *tert*-butyldimethylsilyl trifluoromethanesulfonate and 2 equivalents of 2,6–lutidine in CH_2Cl_2 at 25°C for 30 min. Water was added and extraction carried out with CH_2Cl_2. The organic extracts were dried with anhydrous $MgSO_4$ and the solvent was evaporated. The crude material was purified by flash chromatography on silica gel (9:1 hexane/ethyl acetate).

15a: The compound was prepared by procedure A from 2.65 g **14a** (8.7 mmol); the yield of **15a** was 3.19 g (7.5 mmol, 87% yield), oil. IR: 1743 cm^{-1}. ^1H NMR δ: 0.03 (s, 3H), 0.11 (s, 3H), 0.89 (s, 9H), 1.21 (t, J = 7.1 Hz, 3H), 4.13 (q, J = 7.1 Hz, 2H), 5.48 (s, 1H), 5.96 (s, 1H), 6.94 (s, 1H), 7.07 (s, 1H). ^{13}C NMR δ: −5.1, −5.0, 14.1, 18.2, 25.7, 25.8, 61.2, 73.4, 101.8, 108.4, 112.2, 113.0, 132.4, 148.2, 171.2. LRMS (M^+ − t-Bu), calcd. for $C_{13}H_{16}O_5BrSi$: 359.0; found: 358.8.

15b: The compound was prepared by procedure A from 2.90 g **14b** (11 mmol); the yield of **15b** was 3.74 g (9.9 mmol, 90% yield), oil. IR: 3661, 1738 cm^{-1}. ^1H NMR δ: 0.03 (s, 3H), 0.12 (s, 3H), 0.89 (s, 9H), 1.20 (t, J = 7.1 Hz, 3H), 4.13 (q, J = 7.1 Hz, 2H), 5.57 (s, 1H), 7.15 (dd, J = 1.8, 9.4 Hz, 1H), 7.31 (m, 1H), 7.49 (d, J = 1.3, 9.4 Hz, 1H), 7.59 (dd, J = 1.8, 7.8 Hz, 1H). ^{13}C NMR δ: −4.7, −4.6, 13.6, 17.9, 25.2, 25.3, 60.8, 73.1, 122.1, 127.2, 128.5, 129.1, 132.1, 138.7, 170.8. LRMS (M^+ − t-Bu), calcd. for $C_{12}H_{16}O_3BrSi$: 315.0; found: 315.0.

15c: This compound was prepared by procedure B from 60 mg **14c** (0.2 mmol); 60 mg of **15c** (0.15 mmol, 75% yield) was isolated after flash chromatography on silica gel (9:1 hexanes/ethyl acetate as eluent), oil. IR: 1753 cm^{-1}. ^1H NMR δ: -0.05 (s, 3H), 0.14 (s, 3H), 0.85 (s, 9H), 1.18 (t, J = 7.1 Hz, 3H), 3.77 (s, 3H), 4.16 (dq, J = 3.2, 7.1 Hz, 2H), 5.74 (s, 1H), 6.80 (dd, J = 2.0, 7.6 Hz, 1H), 7.08–7.20 (m, 2H). ^{13}C NMR δ: −4.9, −4.6,14.3, 18.3, 25.8, 56.4, 61.0, 70.1, 110.9, 125.0, 125.6, 129.2, 130.1, 158.6, 172.6. MS (CI,M^++1), calcd. for $C_{17}H_{27}O_4BrSi$: 403.1; found: 402.9.

15d: This compound was prepared by procedure A from 1.25 g **14d** (4.3 mmol), the yield of **15d** was 1.59 g (3.9 mmol, 89% yield) after silica gel column chromatography, oil. IR: 1742 cm^{-1}. ^1H NMR δ: 0.04 (s, 3H), 0.12 (s, 3H), 0.90 (s, 9H), 1.21 (t, J = 7.1 Hz, 3H), 3.77 (s, 3H), 4.08–4.18 (dq, J = 7.1, 0.8 Hz, 2H), 5.50 (s, 1H), 6.71 (dd, J = 3.3, 8.8 Hz, 1H), 7.15 (d, J = 3.3 Hz, 1H), 7.38 (d, J = 8.8 Hz, 1H). ^{13}C NMR δ: −5.0, −5.1, 13.6, 17.9, 24.8, 25.3, 55.0, 60.8, 73.1, 112.4, 113.1, 115.7, 132.6, 139.5, 158.7, 170.6. HRMS (M^+ − t-Bu), calcd. for $C_{13}H_{18}O_4BrSi$: 345.0157; found: 345.0163.

15e: The compound was prepared by procedure B from 130 mg **14e** (0.45 mmol); the yield of **15e** was 180 mg (0.45 mmol, >95% yield) after flash chromatography on silica gel, oil. IR: 1722 cm^{-1}. ^1H NMR δ: 0.01 (s, 1H), 0.10 (s, 3H), 0.88 (s, 9H), 1.20 (t, J = 7.1 Hz, 3H), 3.77 (s, 3H), 4.12 (q, J = 7.1 Hz, 2H), 5.50 (s, 1H), 6.86 (dd, J = 2.6, 8.8 Hz, 1H), 7.04 (d, J = 2.6 Hz, 1H), 7.48 (d, J = 8.8 Hz, 1H). ^{13}C NMR δ: −4.9, −4.7, 14.0, 18.2, 25.5, 25.6, 55.4, 61.0, 73.0, 113.8, 117.4, 122.7, 129.4, 131.1, 159.7, 171.4. MS calcd. for $C_{17}H_{27}O_4SiBr$: 402.1(M^+), 345.0 for M^+−t-Bu; found CI (M^++1): 403.0; EI (M^+−t-Bu): 345.0.

© 1997 NRC Canada

Can. J. Chem. Downloaded from www.nrcresearchpress.com by 88.146.161.215 on 09/08/12
For personal use only.

Preparation of 2-tert-Butyldimethylsilyloxybenzocyclobutenones 16a–e

General method

tert-Butyllithium (equivalents as indicated for each compound) was added to a solution of ester **15** in THF under nitrogen atmosphere at −78°C and stirred for 15 min. The solution was quenched with saturated NH_4Cl solution and allowed to warm to room temperature. Extraction was carried out with diethyl ether, the organic extracts were dried with anhydrous $MgSO_4$, and the solvent was evaporated. Purification was carried out using flash chromatography on silica gel (9:1 hexanes/ethyl acetate as eluent). Recrystallization was carried out as noted for each compound.

16a: The compound was prepared by the general method using 1.5 equivalents of *tert*-butyllithium and 1.9 g of **15a** (4.5 mmol) as starting material; the yield of **16a** was 1.35 g (4.5 mmol, >95% yield), isolated as colorless prisms after recrystallization from hexanes – ethyl acetate, mp 104–105°C. IR: 1757 cm^{-1}. ^1H NMR δ: 0.15 (s, 3H), 0.17 (s, 3H), 0.92 (s, 9H), 5.56 (s, 1H), 6.07 (s, 2H), 6.80 (s, 1H), 6.99 (s, 1H). ^{13}C NMR δ: −4.7, −4.5, 18.3, 25.8, 83.9, 100.7, 102.2, 103.4, 140.5, 151.5, 154.4, 155.5, 187.5. HRMS, calcd. for $C_{15}H_{20}O_4Si$: 292.1131; found: 292.1108. Anal. calcd. for $C_{15}H_{20}O_4Si$: C 61.61, H 6.90%; found: C 61.48, H 6.86%.

16b: This compound was prepared by the general method using 2 equivalents of *tert*-butyllithium and 1.0 g **15b** (2.6 mmol); the yield of **16b** was 0.62 g (2.5 mmol, 96% yield) after purification by radial chromatography (9:1 hexanes/ethyl acetate), oil. IR: 1765 cm^{-1}. ^1H NMR δ: 0.20 (s, 3H), 0.22 (s, 3H), 0.96 (s, 9H), 5.78 (s, 1H), 7.44–7.68 (m, 4H). ^{13}C NMR δ: −4.8, −4.5, 18.3, 25.8, 86.2, 121.6, 123.6, 131.0, 135.4, 146.9, 158.0, 190.7. HRMS, calcd. for $C_{14}H_{20}O_2Si$: 248.1233; found: 248.1204.

16c: The compound was prepared by the general method using 1.2 equivalents *tert*-butyllithium and 750 mg **15c** (1.6 mmol), 386 mg **16c** (1.4 mmol, 88% yield) was isolated after purification by silica gel chromatography (9:1 hexanes/ethyl acetate), oil. IR: 1769 cm^{-1}. ^1H NMR δ: 0.18 (s, 3H), 0.19 (s, 3H), 0.91 (s, 9H), 4.00 (s, 3H), 5.83 (s, 1H), 7.01 (m, 2H), 7.41 (m, 1H). ^{13}C NMR δ: −4.5, −3.8, 18.8, 26.3, 57.8, 86.6, 112.9, 113.9, 121.8, 133.6, 142.6, 149.3, 157.1, 191.4. HRMS, calcd. for $C_{15}H_{22}O_3Si$: 278.1329; found: 278.1350.

16d: This compound was prepared by the general method using 1.5 equivalents of *tert*-butyllithium and 1 g **15d** (2.5 mmol); the yield of **16d** was 470 mg (1.7 mmol, 68% yield). Purification was carried out by flash chromatography on silica gel (9:1 hexanes/ethyl acetate), mp 43–44°C. IR: 1754 cm^{-1}. ^1H NMR δ: 0.18 (s, 3H), 0.21 (s, 3H), 0.95 (s, 9H), 3.91 (s, 3H), 5.68 (s, 1H), 7.00–7.08 (m, 1H), 7.05 (s, 1H), 7.36 (dd, J = 1.7, 7.5 Hz, 1H). ^{13}C NMR: δ: −4.8, −4.5, 18.3, 25.7, 55.8, 85.1, 105.9, 120.7, 123.6, 138.9, 160.4, 165.6, 188.1. HRMS, calcd. for $C_{15}H_{22}O_3Si$: 278.1329; found: 278.1315.

16e: The compound was prepared by the general method using 1.5 equivalents of *tert*-butyllithium and 120 mg **15e** (3.0 mmol); the yield of **16e** was 50 mg (1.8 mmol, 60% yield) after flash chromatography on silica gel, oil. IR: 1762 cm^{-1}. ^1H NMR δ: 0.15 (s, 3H), 0.17 (s, 3H), 0.92 (s, 9H), 3.80 (s, 3H), 5.67 (s, 1H), 6.87 (d, J = 2.0 Hz, 1H), 7.13 (dd, J = 2.0, 8.2 Hz, 1H), 7.53 (d, J = 8.2 Hz, 1H). ^{13}C NMR δ: −4.7, −4.5, 18.3, 25.8, 55.7, 85.0, 102.6, 124.6, 125.4, 148.3, 151.3, 162.3, 190.2. HRMS, calcd. for $C_{15}H_{22}O_3Si$: 278.1329; found: 278.1352.

Preparation of 2-hydroxybenzocyclobutenones 17a–e

General method

Tetra-*n*-butylammonium fluoride solution in THF (1 equivalent) was added to a stirred solution of the benzocyclobutenone in THF and immediately quenched with saturated aqueous NH_4Cl. The mixture was extracted with diethyl ether, the organic extracts were dried with anhydrous magnesium sulfate, and the solvent was evaporated. The compounds were purified by flash chromatography on silica gel (1:1 hexanes/ethyl acetate as eluent).

17a: This compound was prepared by the general method using 420 mg **16a** (1.4 mmol); the yield of **17a** was 190 mg (1.1 mmol, 79% yield) after silica gel column chromatography, mp 155–157°C. IR: 1756, 3581 cm^{-1}. ^1H NMR (d_6 acetone) δ: 5.35 (br, 1H), 5.50 (s, 1H), 6.19 (s, 2H), 6.86 (s, 1H), 7.16 (s, 1H). ^{13}C NMR (d_6 acetone) δ: 84.6, 100.6, 103.5, 104.2, 141.4, 152.5, 155.3, 157.1, 188.8. HRMS, calcd. for $C_9H_6O_4$: 178.0266; found: 178.0279. Anal. calcd. for $C_9H_6O_4$: C 60.68, H 3.39%; found: C 60.49, H 3.25%.

17b: This compound was prepared by the general method using 380 mg **16b** (1.5 mmol); the yield of **17b** was 132 mg (0.99 mmol, 66% yield) after silica gel column chromatography, mp 52.5–53.5°C. IR: 1766, 3582 cm^{-1}. ^1H NMR δ: 3.05 (br, 1H), 5.79 (s, 1H), 7.49–7.62 (m, 3H), 7.75 (m, 1H). ^{13}C NMR (d_6 acetone) δ: 87.1, 121.7, 124.6, 131.8, 136.2, 148.0, 159.6, 192.2. HRMS, calcd. for $C_8H_6O_2$: 134.0368; found: 134.0379. Anal. calcd. for $C_8H_6O_2$: C 71.64, H 4.51%; found: C 71.93, H 4.29%.

17c: The reaction was performed on 50 mg **16c** (0.18 mmol); isolated after column chromatography was 20 mg **17c** (0.12 mmol, 67% yield), which crystallized on standing, mp 70–72°C. IR: 1767, 3575 cm^{-1}. ^1H NMR δ: 3.50 (br, 1H), 4.03 (s, 3H), 5.85 (br, 1H), 7.01–7.07 (m, 2H), 7.45 (m, 1H). ^{13}C NMR δ: 57.3, 85.7, 113.5, 121.7, 133.4, 141.3, 148.9, 156.6, 191.3. HRMS, calcd. for $C_9H_8O_3$: 164.0473; found: 164.0487.

17d: This compound was prepared using the general method on 470 mg **16d** (1.7 mmol); the yield of **17d** was 240 mg (1.5 mmol, 88% yield) after silica gel column chromatography, mp 95.0–95.5°C. IR: 1758, 3587 cm^{-1}. ^1H NMR (d_6 acetone) δ: 3.95 (s, 3H), 5.63 (s, 1H), 7.12 (dd, J = 2.0, 8.5 Hz, 1H), 7.27 (d, J = 2.0 Hz, 1H), 7.38 (dd, J = 0.7, 8.5 Hz, 1H). ^{13}C NMR (d_6 acetone) δ: 56.4, 86.0, 107.1, 121.3, 123.7, 139.9, 162.2, 166.5, 189.5. HRMS, calcd. for $C_9H_8O_3$: 164.0473; found: 164.0453.

17e: TBAF (1 M, 0.16 mL, 0.16 mmol) was added to a solution of 11 mg **16e** (0.040 mmol) and 100 μL acetic acid in 5 mL THF. The solution was stirred for 1 h, washed with

© 1997 NRC Canada

saturated NH_4Cl, saturated $NaHCO_3$, and brine, then dried with anhydrous $MgSO_4$, and the solvent evaporated. Column chromatography on silica gel (ethyl acetate needed to remove **17e**) afforded approximately 2 mg of the desired hydroxy ketone **17e** (0.012 mmol, ~30% yield). ^{1}H NMR δ: 3.82 (s, 3H), 5.69 (br s, 1H), 6.88 (dd, J = 2.2, 0.4 Hz, 1H), 7.19 (dd, J = 8.3, 2.2 Hz, 1H), 7.62 (dd, J = 8.3, 0.4 Hz, 1H). ^{13}C NMR δ: 55.8, 85.1, 102.7, 124.9, 125.8, 148.8, 150.5, 162.7, 189.2. HRMS, calcd. for $C_9H_8O_3$: 164.0473; found: 164.0453.

Preparation of Weinreb amide 19d

Trimethylaluminum (4.3 mL, 2.0 M, 8.6 mmol) was added to a solution of *N,O*-dimethylhydroxylamine hydrochloride (370 mg, 3.8 mmol) in 10 mL dry CH_2Cl_2 under nitrogen atmosphere and the solution stirred for 15 min at 25°C. A solution of **14d** (1 g, 3.5 mmol) in dry CH_2Cl_2 was added and the solution refluxed for 24 h. Dilute HCl(aq) was **slowly and carefully** added dropwise through the condenser until gas evolution ceased and all remaining white precipitate had dissolved. The layers were separated and the aqueous layer extracted with CH_2Cl_2. The organic extracts were combined, washed with water and brine, dried with anhydrous $MgSO_4$, and the solvent was evaporated. Yield: ^{1}H NMR spectrum showed 60% conversion, 450 mg isolated, 73% based on conversion of starting material; mp 71.0–71.5°C. IR: 1662, 3447 cm^{-1}. ^{1}H NMR δ: 3.20 (s, 3H), 3.29 (s, 3H), 3.73 (s, 3H), 4.28 (br, 1H), 5.71 (br, 1H), 6.68–6.76 (m, 2H), 7.44 (d, J = 8.6 Hz, 1H). ^{13}C NMR δ: 55.1, 60.5, 70.4, 89.2, 113.2, 114.3, 115.6, 133.3, 139.3, 159.0, 172.7. HRMS, calcd. for $C_{11}H_{14}NO_4$ (M^+ − Br) 224.0923; found: 224.0914.

Preparation of 20d

A solution of **19d** (135 mg, 0.44 mmol), *tert*-butyldimethylsilyl triflate (154 μL, 0.66 mmol), and 2,6–lutidine (105 μL, 0.88 mmol) in 10 mL dry CH_2Cl_2 was stirred for 30 min at 25°C. The solution was diluted with water (10 mL) and extracted with CH_2Cl_2. The combined organic extracts were dried with anhydrous $MgSO_4$ and the solvent was evaporated leaving 179 mg **20d** (0.43 mmol, >95% yield), a pale yellow crystalline solid that was pure by ^{1}H NMR, mp 81.0–81.5°C. IR: 1677 cm^{-1}. ^{1}H NMR δ: −0.01 (s, 3H), 0.12 (s, 3H), 0.86 (s, 9H), 3.13 (s, 3H), 3.48 (s, 3H), 3.75 (s, 3H), 5.83 (s, 1H), 6.68–6.71 (m, 1H), 7.09–7.11 (m, 1H), 7.35–7.38 (m, 1H). ^{13}C NMR δ: −4.8, −4.6, 18.2, 25.8, 32.7, 55.5, 61.0, 71.8, 113.3, 114.5, 116.3, 132.9, 140.0, 159.1, 171.9. HRMS, calcd. for $C_{13}H_{19}BrNO_4Si$ (M^+ − *t*-Bu): 360.0267; found: 360.0279.

Preparation of 23

Compound **21** (300 mg, 0.88 mmol) in 10 mL THF was cooled to −78°C and *tert*-butyllithium (550 μL, 1.7 M, 0.94 mmol) was added and stirred for 15 min. The reaction was quenched with saturated NH_4Cl solution and allowed to warm to 25°C. Extraction was carried out with CH_2Cl_2, the solvent dried with anhydrous $MgSO_4$, and the solvent evaporated. The major compound isolated after chromatography on silica gel was **23**, oil. ^{1}H NMR δ: 1.4–1.9 (m, 6H), 3.45–3.63 (m, 1H), 3.82–3.97 (m, 1H), 4.58 (d, J = 18 Hz, 1H), 4.72–4.78 (m, 1H), 4.82 (d, J = 18 Hz, 1H), 5.98 (s, 1H), 6.04 (s, 2H), 6.98 (s, 1H), 7.02 (s, 1H). HRMS, calcd. for $C_{14}H_{15}O_4N$: 261.1002; found: 261.1008.

Acknowledgements

The authors acknowledge the financial support of the Natural Sciences and Engineering Research Council of Canada (NSERC).

References

1. D.K. Jackson, L. Narasimhan, and J.S. Swenton. J. Am. Chem. Soc. **101**, 3989 (1979).
2. J.P. Edwards, D.J. Krysan, and L.S. Liebeskind. J. Org. Chem. **58**, 3942 (1993), and references cited therein.
3. C.W. Jefford, G. Bernardienelli, Y. Wang, D.C. Spellmeyer, A.B. Buda, and K.N. Houk. J. Am. Chem. Soc. **114**, 1157 (1992).
4. T. Hosoya, T. Hasegawa, Y. Kuriyama, and K. Suzuki. Tetrahedron Lett. **36**, 3377 (1995).
5. J.-C. Bradley and T. Durst. J. Org. Chem. **56**, 5459 (1991).
6. J.-C. Bradley. PhD Thesis, University of Ottawa, 1993.
7. I.S. Aidhen and N.S. Narasimhan. Tetrahedron Lett. **32**, 2171 (1991).
8. M.E. Jung, P.Y.-S. Lam, M.M. Mansuri, and L.M. Speltz. J. Org. Chem. **50**, 1087 (1985).
9. P.G. Gassman and J.J. Talley. Tetrahedron Lett. 3773 (1978).
10. D.J. Gallagher and P. Beak. J. Am. Chem. Soc. **113**, 7984 (1991).
11. M.B. Smith. Organic synthesis. McGraw-Hill, New York. 1994. p. 725.
12. D.L. Comins and M.O. Killpack. J. Org. Chem. **52**, 104 (1987).
13. D.L. Comins and J.D. Brown. J. Org. Chem. **49**, 1078 (1984).
14. H.H. Hodgson, and T.A. Jenkinson. J. Chem. Soc. 3041 (1927).
15. A. Basha, M. Lipton, and S. Weinreb. Tetrahedron Lett. **48**, 4171 (1978).
16. S. Nahm and S. Weinreb. Tetrahedron Lett. **22**, 3815 (1981).
17. R.C. Ronald, J.M. Lansinger, T.S. Lillie, and C.J. Wheeler. J. Org. Chem. **47**, 2541 (1982).
18. M. Dutt, B. Fravel, G.P. Ford, and E.R. Biehl. J. Org. Chem. **59**, 497 (1994).
19. K.A. Thakar and D.D. Goswami. J. Indian Chem. Soc. **49**, 9 (1972).
20. T. Inokuchi, S. Matsumoto, M. Fukushima, and S. Torii. Bull. Chem. Soc. Jpn. **64**, 796 (1991).

Can. J. Chem. Downloaded from www.nrcresearchpress.com by 88.146.161.215 on 09/08/12
For personal use only.

© 1997 NRC Canada

Preparation, biotransformation, and antifungal activity of methyl benzyldithiocarbamates

M. Soledade C. Pedras, Abdul Q. Khan, Kevin C. Smith, and Shawndra L. Stettner

Abstract: The biotransformation of three methyl benzyldithiocarbamates by the blackleg fungus (*Leptosphaeria maculans* (Desm.) Ces. et de Not., asexual stage *Phoma lingam* (Tode ex Fr.) Desm) was investigated. The main biotransformation products were isolated and their chemical structures were determined by spectroscopic methods. Similarly to our previous studies with the phytoalexin brassinin, these results suggest that virulent blackleg isolates are significantly more effective in metabolizing benzyldithiocarbamates than the related avirulent isolates.

Key words: benzyldithiocarbamates, brassinin, *Leptosphaeria maculans*, *Phoma lingam*, phytoalexins.

Résumé : On a étudié la biotransformation de trois benzyldithiocarbamates de méthyle par le champignon à jambe noire (*Leptosphaeria maculans* (Desm.) Ces. et de Not., stage asexué du *Phoma lingam* (Tode ex Fr.) Desm). On a isolé les principaux produits de biotransformation et on a déterminé leurs structures chimiques par des méthodes spectroscopiques. Comme ce fût le cas dans nos études antérieures sur la phytoalexine brassinine, ces résultats suggèrent que les souches virulents du champignon à jambe noire sont beaucoup plus efficaces à métaboliser les benzyldithiocarbamates que les souches avirulentes.

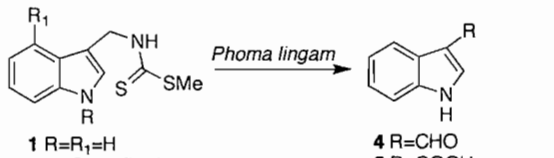
Mots clés : benzyldithiocarbamates, brassinine, *Lestosphaeria maculans*, *Phoma lingam*, phytoalexines.

[Traduit par la rédaction]

Although dithiocarbamates have long been known as a very important class of bioactive products (1), only recently were they reported to occur in plants. A group of phytoalexins containing a dithiocarbamate group attached to a 3-methylindolyl moiety, as, for example, the brassinins **1–3**, is produced by plants from diverse *Brassica* species (e.g., canola, rapeseed, broccoli, cabbage, turnip, etc.) in response to stress (2). In general, the production of phytoalexins is an important defense mechanism in plants (3). On the other hand, phytoalexin metabolism can be used by phytopathogens as a detoxification mechanism to overcome the plants' chemical defenses (4). Our studies to elucidate the metabolism of brassica phytoalexins by their pathogenic fungi suggest that detoxification mechanisms are related to fungal virulence (5, 6). In fact, detoxification of brassinin (**1**) appears to be one of the mechanisms by which the blackleg fungus (*Phoma lingam* (Tode ex Fr.) Desm., perfect stage *Leptosphaeria maculans* (Desm.) Ces. et de Not.) overcomes rapeseed/canola (*Brassica napus, B. rapa*) defenses (5). We established that the metabolism of brassinin (**1**) by diverse virulent isolates of *P. lingam* yields the aldehyde **4** and the significantly less toxic carboxylic acid **5**. Importantly, we determined that avirulent isolates of *P. lingam*[2] (7) follow a different metabolic pathway from that of virulent isolates, yielding mostly acetylamine **6** (5). It is noteworthy that other phytopathogens of brassicas, as, for example, *Alternaria brassicae* (blackspot disease), follow a pathway similar to that of avirulent isolates of *P. lingam*.[3] Because brassinin (**1**) is a biogenetic precursor of several other phytoalexins (8), its metabolism by fungi could deprive the plant of other important phytoalexins. The overall result would be a plant more susceptible to further fungal colonization.

We are currently investigating phytoalexin detoxification by fungal and bacterial pathogens of brassicas with the goal of devising new strategies for controlling plant fungal diseases (2*a*, 6). One important aspect of our investigation requires the isolation of the fungal enzymes and (or) genes involved in the detoxification of these phytolexins. An approach to isolate the fungal genes responsible for the detoxification of brassinin

Scheme 1.



1 R=R$_1$=H
2 R=OMe; R$_1$=H
3 R=H; R$_1$=OMe

4 R=CHO
5 R=COOH
6 R=CH$_2$NHC(O)Me

Received November 21, 1996.

This paper is dedicated to Professor William A. Ayer on the occasion of his 65th birthday.

M.S.C. Pedras,[1] A.Q. Khan, K.C. Smith, and S.L. Stettner. Department of Chemistry, University of Saskatchewan, 110 Science Place, Saskatoon, SK S7N 5C9, Canada.

[1] Author to whom correspondence may be addressed. Telephone: (306) 966-4772. Fax: (306) 966-4730. E-mail: pedras@sask.usask.ca

[2] Avirulent isolates of *P. lingam* are a different species, see ref. 7.

[3] M.S.C. Pedras, unpublished work.

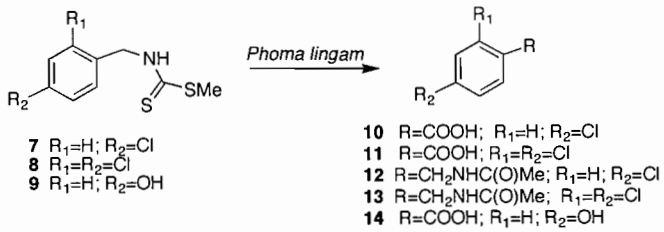
© 1997 NRC Canada

Can. J. Chem. Downloaded from www.nrcresearchpress.com by 88.146.161.215 on 09/08/12
For personal use only.

Table 1. Metabolism of dithiocarbamates **7–9** by *Phoma lingam* isolates BJ-125 (virulent to canola) and Unity (avirulent to canola).

Fungal isolate (virulence)	Compound (concentration in fungal culture)	Products of metabolism, incubation time
BJ-125 (virulent)	Me 4-chlorobenzyldithiocarbamate (**7**) (10^{-4} M)	4-Chlorobenzoic acid, complete transformation in 6 h
	Me 2,4-dichlorobenzyldithiocarbamate (**8**) (10^{-4} M)	*N*-(2,4-Dichlorobenzyl)acetamide, complete transformation in 24 h
	Me 4-hydroxybenzyldithiocarbamate (**9**) (4×10^{-4} M)	Polar product(s), complete transformation in 10 h
	N-(2,4-Dichlorobenzyl)acetamide (**13**) (10^{-4} M)	No detectable transformation in 48 h
	4-Hydroxybenzoic acid (**14**) (4×10^{-4} M)	Polar product(s), 80% transformation in 8 h
Unity (avirulent)	Me 4-chlorobenzyldithiocarbamate (**7**) (6×10^{-5} M)	4-Chlorobenzoic acid, <10% in 48 h
	Me 2,4-dichlorobenzyldithiocarbamate (**8**) (6×10^{-5} M)	*N*-(2,4-Dichlorobenzyl)acetamide, <10% in 48 h
	Me 4-hydroxybenzyldithiocarbamate (**9**) (4×10^{-4} M)	Polar product(s), 70% transformation in 10 h

Scheme 2.



7 R_1=H; R_2=Cl
8 R_1=R_2=Cl
9 R_1=H; R_2=OH

10 R=COOH; R_1=H; R_2=Cl
11 R=COOH; R_1=R_2=Cl
12 R=$CH_2NHC(O)Me$; R_1=H; R_2=Cl
13 R=$CH_2NHC(O)Me$; R_1=R_2=Cl
14 R=COOH; R_1=H; R_2=OH

involves genetic transformation followed by selection of these transformants with brassinin. However, because of the low solubility of brassinin in the selection medium, it would be useful to have at hand brassinin analogs having stronger antifungal activity and (or) higher solubility in the selection medium. Towards this end we evaluated several dithiocarbamates and now wish to report the biotransformation of benzyldithiocarbamates **7**, **8**, and **9** by blackleg fungi.

Results and discussion

Benzyldithiocarbamates **7–9** were prepared from the corresponding benzylamines to investigate their antifungal activity and metabolism by isolates of *P. lingam*. Isolates BJ-125 (virulent to canola) and Unity (avirulent to canola) were grown in shake cultures. After 42–44 h, solutions of methyl 4-chlorobenzyldithiocarbamate (**7**) (various concentrations, 6×10^{-5} M to 4×10^{-4} M) in DMSO were added to fungal cultures and to uninoculated media. Control cultures of the fungus were grown separately. Cultures were incubated and samples were withdrawn at 2–24 h intervals (up to 6 days), extracted first with Et_2O, and then acidified and reextracted. Comparison of the HPLC chromatograms of extracts of control cultures and extracts of fungal cultures incubated with **7** indicated that the later extracts contained possible biotransformation products. The optimum incubation time for isolation of the putative products was determined by TLC and (or) HPLC analysis of each extract. Subsequently, the components of the neutral Et_2O extracts obtained from larger scale cultures (200 mL or more) were separated by preparative TLC and each constituent analyzed by ^1H and ^{13}C NMR, FTIR, and MS. Similar experiments were carried out for methyl 2,4-dichlorobenzyldithiocarbamate (**8**) and methyl 4-hydroxybenzyldithiocarbamate (**9**).

The rate and products of biotransformation of the two chlorobenzyldithiocarbamates differed significantly (Table 1); while the monochloro derivative **7** was metabolized by virulent isolate BJ-125 in less than 6 h to the corresponding 4-chlorobenzoic acid, the dichloro derivative **8** was metabolized to the corresponding 2,4-dichlorobenzylacetamide (**13**, R_1 = R_2 = Cl) in ca. 24 h. The corresponding carboxylic acid **11** (R_1 = R_2 = Cl), although a minor component, was also detected in the cultures incubated with dichloro derivative **8**; however no 2-chlorobenzylacetamide was detected in cultures incubated with the monochloro derivative **7**. The structure of 2,4-dichlorobenzylacetamide was deduced from spectroscopic data and corroborated by acetylation (Ac_2O) of 2,4-dichlorobenzylamine. 2,4-Dichlorobenzylacetamide was stable in fungal cultures and in uninoculated medium for at least 6 days. The structures of 2,4-dichloro and 4-chlorobenzoic acids were readily determined by comparison of their spectroscopic data with those of authentic samples and confirmed by methylation of each acid with diazomethane.[4] Furthermore, the dichlorobenzyldithiocarbamate **8** was significantly more toxic to isolate BJ-125 than the monochlorobenzyldithiocarbamate **7**. The latter compound **7**, even at a concentration of 4×10^{-4} M, was metabolized to the corresponding benzoic acid by this virulent isolate, whereas **8** at a similar concentration did not give biotransformation products (up to 6 days) and appeared to inhibit completely the growth of the fungal mycelium. On the other hand, the 4-hydroxybenzyldithiocarbamate (**9**) did not appear to have a detectable toxic effect even at a concentration of 4×10^{-4} M, as it was metabolized by the virulent isolate BJ-125 to unidentified polar product(s) in less than 10 h. The corresponding 4-hydroxybenzoic acid (**14**) was not detected either in neutral or acidic extracts of cultures incubated with **9**. However, the biotransformation of **9** is also likely to occur via the corresponding acid since the fungus metabolized 4-hydroxybenzoic acid (**14**) very rapidly to unidentified polar product(s).

The avirulent isolate Unity was also incubated with dithiocarbamates **7** and **8**; in contrast with the results obtained for the virulent isolate, the biotransformation appeared to be significantly slower. As shown in Table 1, less than 10% of each

[4] The methyl esters of both acids give well-resolved peaks by HPLC analysis.

© 1997 NRC Canada

Can. J. Chem. Downloaded from www.nrcresearchpress.com by 88.146.161.215 on 09/08/12
For personal use only.

Can. J. Chem. Downloaded from www.nrcresearchpress.com by 88.146.161.215 on 09/08/12
For personal use only.

Table 2. HPLC retention times (for conditions see experimental section) of dithiocarbamates **7–9**, their biotransformation products, and derivatives.

Compound	Retention time (min)
Me 4-chlorobenzyldithiocarbamate (**7**)	23.6
Me 2,4-dichlorobenzyldithiocarbamate (**8**)	27.3
Me 4-hydroxybenzyldithiocarbamate (**9**)	11.6
4-Chlorobenzoic acid (**10**)	ca. 5 (broad)
2,4-Dichlorobenzoic acid (**11**)	ca. 4 (broad)
N-(4-Chlorobenzyl)acetamide (**12**)	8.2
N-(2,4-Dichlorobenzyl)acetamide (**13**)	11.6
4-Hydroxybenzoic acid (**14**)	ca. 2 (broad)
Me 4-chlorobenzoate	20.4
Me 2,4-dichlorobenzoate	23.2

dithiocarbamate was metabolized in 48 h to either the corresponding 4-chlorobenzoic acid (**10**) or to the 2,4-dichloroacetamide (**13**), similar to the virulent isolate BJ-125. The 4-hydroxybenzyldithiocarbamate (**9**) did not appear to have a significant toxic effect on isolate Unity, even at a concentration of 4×10^{-4} M, as it was metabolized rapidly to unidentified polar product(s), although at a lower rate than the virulent isolate BJ-125 (Table 1).

As in our previous studies with brassinin (5) and brassicanal A (6), these results suggest that virulent blackleg isolates are significantly more effective in detoxifying benzyldithiocarbamates than the related avirulent isolates. However, we found an unexpected difference between the biotransformation of dithiocarbamates **7** and **8**. In contrast with our previous work on metabolism of brassinin (**1**) (5) and methyl 4-methylbenzyldithiocarbamate (9), this virulent isolate of *P. lingam* metabolized the dichlorinated dithiocarbamate **8** to the acetamide **13**. As expected, the metabolism of the monochlorinated dithiocarbamate **7** proceeded to give the corresponding carboxylic acid. On the other hand, the hydroxy dithiocarbamate **9** appeared to be rapidly transformed by both virulent and avirulent isolates to polar metabolite(s) via the corresponding 4-hydroxybenzoic acid (**14**). It is worth noting that the same virulent isolate BJ-125 metabolized brassinin to the corresponding nontoxic carboxylic acid.

Although our data are insufficient for a definite conclusion, it is not surprising to find that the chlorinated benzyldithiocarbamates **7** and **8** are more toxic than the hydroxybenzyldithiocarbamate **9**, as chlorinated compounds are known to have diverse toxic effects (10). The puzzling difference between the metabolism of the two chlorinated compounds may reflect in fact the higher toxicity of the dichlorobenzyldithiocarbamate. Nonetheless, both biotransformations yield products that are much less toxic to the fungal cells than any of the chlorinated dithiocarbamates **7** or **8**. A better understanding of these detoxification processes might be obtained with cell-free systems of virulent and avirulent fungal isolates.

Experimental

General

All chemicals were purchased from Aldrich Chemical Company, Inc., Madison, Wis., or Sigma Chemical Company, St. Louis, Mo. All solvents were HPLC grade and used as such. Preparative TLC: Merck, Kieselgel 60 F_{254}, 20 × 20 cm × 0.25 mm; analytical TLC: Merck, Kieselgel 60 F_{254}, aluminum sheets, 5 × 2 cm × 0.2 mm; compounds were visualized by exposure to UV and by dipping the plates in a 5% aqueous (w/v) phosphomolybdic acid solution containing a trace of ceric sulfate and 4% (v/v) H_2SO_4, followed by heating at 200°C. Flash column chromatography (FCC): silica gel Merck, grade 60, mesh size 230–400, 60 Å. HPLC analysis was carried out with a high-performance Hewlett Packard liquid chromatograph equipped with quaternary pump, automatic injector, and diode array detector (wavelength range 190–600 nm), degasser, and a Hypersil ODS column (5 μm particle size silica, 4.6 i.d. × 200 mm). HPLC mobile phase: 75% H_2O – 25% CH_3CN to 100% CH_3CN, for 35 min, linear gradient, and a flow rate 1.0 mL/min. Samples for HPLC analysis were dissolved in acetonitrile (ca. 0.5 mg/mL) and filtered through a cotton plug. NMR spectra were recorded on a Bruker AMX 500 or AM 300 spectrometer; for ^1H (300 or 500 MHz), δ values were referenced to $CHCl_3$ (7.24 ppm) and for ^{13}C (75.5 or 125.8 MHz), referenced to $CDCl_3$ (77.0 ppm). Fourier transform infrared (FTIR) spectra were obtained on a Bio-Rad FTS-40 spectrometer using a diffuse reflectance cell. Mass spectra (MS) were obtained on a VG 70 SE mass spectrometer (high resolution (HR), electron impact (EI)], employing a solids probe.

Fungal cultures

Phoma lingam virulent isolate BJ-125 and avirulent isolate Unity were obtained from Séguin-Swartz (Agriculture Canada Research Station, Saskatoon, Saskatchewan). The fungal isolates were grown on V8 agar (20% (v/v) V8 juice, 0.75 g/L $CaCO_3$, 100 mg/L streptomycin sulfate, 40 mg/L Rose Bengal, 15 g/L agar) plates at 21°C, 12 h photoperiod for 10 days. Spore suspensions of each isolate were prepared by overlaying the V8 agar plates with 10 mL sterile distill water and the plate surfaces were rubbed with a flamed glass rod to dislodge the spores. The suspension was transferred to centrifuge tubes and the spores were pelleted by centrifugation at 3000 g for 10 min. After washing once, the spores were stored in sterile distilled water at −20°C. Liquid cultures were initiated by inoculating fungal spores in sterile minimal medium (15 g/L glucose, 3.12 g/L KNO_3, 750 mg/L K_2HPO_4, 750 mg/L KH_2PO_4, 100 mg/L NaCl, 280 mg/L asparagine, 0.4 mg/L $ZnSO_4 \cdot 7\ H_2O$, 79 μg/L $CuSO_4 \cdot 5\ H_2O$, 41 μg/L $MnSO_4 \cdot 4\ H_2O$, 18 μg/L MoO_3, 0.5 mg/L ferric citrate, 38 μg/L $Na_2B_4O_7 \cdot 10\ H_2O$, 100 mg/L $CaCl_2 \cdot 2\ H_2O$, 0.5 g/L $MgSO_4 \cdot 7\ H_2O$, 0.1 mg/L thiamin, in distilled water).

Biotransformation of dithiocarbamates by blackleg isolates

Liquid shake cultures (100 mL media in 250 mL Erlenmeyer flasks) inoculated with fungal spores (2×10^7 spores per mL) of the two isolates listed above were used throughout the biotransformation studies. Control cultures of each isolate were grown separately. Solutions of Me 4-chlorobenzyldithiocarbamate (final concentrations $4 \times 10^{-4} - 6 \times 10^{-5}$ M) or Me 2,4-dichlorobenzyldithiocarbamate (10^{-4} and 6×10^{-5} M), Me 4-hydroxybenzyldithiocarbamate (final concentrations $4 \times 10^{-4} - 6 \times 10^{-5}$ M) in DMSO were administered to 42- to 44-hour-old fungal cultures and to uninoculated media and incu-

© 1997 NRC Canada

Can. J. Chem. Downloaded from www.nrcresearchpress.com by 88.146.161.215 on 09/08/12
For personal use only.

bated at 25 ± 2°C Samples (15 mL) were withdrawn at 2–24 h intervals up to 6 days, and were either frozen at −20°C, or immediately filtered and extracted with diethyl ether (20 mL); the aqueous phase was then acidified to pH of 1–2 (conc. HCl) and extracted with diethyl ether (2 × 20 mL). The extracts were dried (Na_2SO_4), concentrated, and analyzed by TLC and HPLC. The purification of metabolites resulting from the fungal transformation of dithiocarbamates **7** and **8** was carried out by PTLC (CH_2Cl_2–MeOH, 97:3). Compounds **7**–**14** were stable in uninoculated control cultures.

Preparation of 4-hydroxybenzylamine

4-Hydroxybenzylamine was obtained from 4-(benzyloxy)benzonitrile by reduction with $LiAlH_4$–$AlCl_3$ (11) followed by debenzylation of the resulting amine, as follows. Benzyl chloride (1.52 g, 12 mmol), K_2CO_3 (1.66 g, 12 mmol), and KI (33 mg, 0.2 mmol) were added to a solution of 4-hydroxybenzonitrile (1.19 g, 10 mmol) in DMF (10 mL) at 25°C. After 2 h the reaction mixture was diluted with H_2O (25 mL), extracted with Et_2O (2 × 30 mL), and the combined organic layers concentrated at reduced pressure. The crude product was crystallized from hexane–Et_2O to give 4-benzyloxybenzonitrile (2.03 g, 97%). The crystalline product (1.05 g, 5 mmol) was dissolved in Et_2O (10 mL) and added dropwise to a solution of $LiAlH_4$–$AlCl_3$ (228 mg, 6 mmol/800 mg, 6 mmol) in Et_2O (20 mL) and kept at 25°C for 2 h. Water (25 mL) was added dropwise to the reaction mixture and the aqueous layer was extracted with Et_2O (2 × 30 mL). The combined organic layers were dried over sodium sulfate and concentrated under reduced pressure to yield crude amine (1.04, 97%). A suspension of the crude amine (200 mg) and 10% Pd/C (50 mg) in EtOH–NH_4OH (10 mL:3 mL) was stirred under H_2 (1 atm (= 101.3 kPa)) for 1 h at 0°C. The reaction mixture was filtered, concentrated under reduced pressure, and the crude product purified by FCC (CH_2Cl_2–MeOH–NH_4OH, 90:10:1) to give 4-hydroxybenzylamine (96 mg, 83%).

Preparation of methyl benzyldithiocarbamates 7–9

Dithiocarbamates **7**–**9** were synthesized from the corresponding primary amines, similarly to brassinin (5). Typically, CS_2 (2.3 mmol) was added to a solution of the amine (2.3 mmol) in pyridine (1.2 mL) and triethylamine (2.3 mmol) at 0°C. After 60 min at 0°C, MeI (2.3 mmol) was added to the reaction mixture, and after further 12 h at 0°C the reaction mixture was poured onto 1.5 M sulfuric acid (35 mL) and extracted with Et_2O (2 × 140 mL); the combined organic layers were dried over sodium sulfate and concentrated under reduced pressure. After purification by FCC (CH_2Cl_2–hexane, 1:1) and crystallization (CH_2Cl_2–hexane) the products were obtained as colorless solids.

4-Hydroxybenzylamine: white powder, 83% yield; ^{1}H NMR (CD_3OH) δ: 7.14 (m, 2H), 6.73 (m, 2H), 3.68 (s, CH_2); ^{13}C NMR (CD_3OH) δ: 46.2 (t), 116.5 (d), 129.9 (d), 134.1 (s), 158.0 (s).

Methyl 2,4-dichlorobenzyldithiocarbamate: white powder, 75% yield; R_f 0.54, CH_2Cl_2–hexane (60:40); FTIR ν_{max}: 3212, 1498, 1368, 1327, 1102, 1048, 926 cm^{-1}; ^{1}H NMR ($CDCl_3$) δ: 7.5 (br s, 1H, D_2O exchangeable), 7.42–7.40 (m, 2H), 7.23 (m, 1H), 5.00 (d, J = 4.8 Hz, CH_2), 2.65 (s, SCH_3); ^{13}C NMR ($CDCl_3$) δ: 18.6 (q), 48.0 (t), 127.6 (d), 129.7 (d), 131.9 (d), 132.7 (s), 134.7 (s), 134.9 (s), 199.9 (s); HREIMS *m/z* (% relative abundance) measured: 264.9556 (264.9553 calcd. for $C_9H_9{}^{35}Cl_2NS_2$); EIMS *m/z* (% relative abundance): 265 $[M]^+$ (2), 232 (30), 230 (72), 161 (64), 159 (100).

Methyl 4-chlorobenzyldithiocarbamate: white powder, 82% yield; R_f 0.52, CH_2Cl_2–hexane, (60:40); FTIR ν_{max}: 3258, 1491, 1376, 1328, 1236, 1090, 1014, 922, 800 cm^{-1}; ^{1}H NMR ($CDCl_3$) δ: 7.9 (br s, 1H, D_2O exchangeable), 7.34–7.21 (m, 4H), 4.87 (d, J = 5.1 Hz, CH_2), 2.63 (s, SCH_3); ^{13}C NMR ($CDCl_3$) δ: 18.2 (q), 49.6 (t), 129.0 (d), 129.4 (d), 133.7 (s), 134.6 (s), 199.5 (s); HREIMS *m/z* (% relative abundance) measured: 230.9945 (230.9943 calcd. for $C_9H_{10}{}^{35}ClNS_2$); EIMS *m/z* (% relative abundance): 233 $[M]^{2+}$ (9), 231 $[M]^+$ (23), 127 (42), 125 (100).

Methyl 4-hydroxybenzyldithiocarbamate: yellowish powder, 98% yield; R_f 0.35, CH_2Cl_2–MeOH, (95:5); FTIR ν_{max}: 3330, 1515, 1380, 1328, 1214, 916 cm^{-1}; ^{1}H NMR (CD_3CN) δ: 7.15 (m, 2H), 6.91 (s, 1H, D_2O exchangeable), 6.75 (m, 2H), 4.75 (d, J = 5.6 Hz, CH_2), 2.53 (s, SCH_3); ^{13}C NMR (CD_3CN) δ: 18.3 (q), 50.5 (t), 118.4 (d), 129.4 (s), 130.6 (d), 157.3 (s), 199.6 (s); HREIMS *m/z* (% relative abundance) measured: 213.0282 (213.0282 calcd. for $C_9H_{11}NOS_2$); EIMS *m/z* (% relative abundance): 213·$[M]^+$ (35), 107 (100).

Acknowledgments

We gratefully acknowledge the financial support of the University of Saskatchewan and the Natural Sciences and Engineering Research Council of Canada (research and equipment grants to M.S.C.P.). We would like to thank G. Séguin-Swartz, Agricultural and Agri-Food Canada Research Station, Saskatoon, for kindly providing isolates of *Phoma lingam* (virulent isolate BJ-125, and avirulent isolate Unity).

References

1. G.D. Thorn and R.A. Ludwig. The dithiocarbamates and related compounds. Elsevier Publishing Company, New York. 1962. pp. 169–276.
2. (*a*) M.S.C. Pedras, A.Q. Khan, and J.L. Taylor. *In* Phytochemicals for pest control. *Edited by* P. Hedin, P.A. Hollingworth, R.M. Masler, E.P. Miyamoto, and D.G. Thompson. ACS Symp. Ser. **658**, 155 (1997); (*b*) T. Rouxel, A. Kolman, and M.H. Ballesdent. *In* Handbook of phytoalexin metabolism and action. *Edited by* M. Daniel and R.P. Purkayastha. Marcel Dekker, Inc., New York. 1995. pp. 229–261.
3. C.J. Smith. New Phytol. **132**, 1 (1996).
4. H.D. Van Etten, D.E. Mathews, and P.S. Mathews. Annu. Rev. Phytopathol. **27**, 143 (1989).
5. M.S.C. Pedras and J.L. Taylor. J. Nat. Prod. **56**, 731 (1993).
6. M.S.C. Pedras and A.Q. Khan. J. Agric. Food Chem. **44**, 3403 (1996).
7. M.S.C. Pedras, J.L. Taylor, and V.M. Morales. Phytochemistry, **38**, 1215 (1995).
8. K. Monde, M. Takasugi, and T. Ohnishi. J. Am. Chem. Soc. **116**, 6650 (1994).
9. M.S.C. Pedras, I. Borgmann, and J.L. Taylor. Life Sci. Adv.: Phytochem. **11**, 1 (1992).
10. J.R. Corbett, K. Wright, and A.C. Baillie. *In* The biochemical mode of action of pesticides. Academic Press, Inc., London. 1984.
11. R.F. Nystrom. J. Am. Chem. Soc. **77**, 2544 (1954).

© 1997 NRC Canada

The design, production, purification, and testing of a chimeric antigen protein to be used as an immunosterilant in domestic animals

J.G. Manns, C. Barker, and S.K. Attah-Poku

Abstract: A method is described for the design of a protein that incorporates a carrier molecule fused to a novel tandem repeat configuration of a 10 amino acid peptide, Gonadotrophin Releasing Hormone (GnRH), which normally would not be immunogenic because it is a self-antigen. This molecule can be produced with adequate yield in *E. coli* bacteria and purified to homogeneity using standard chromatographic procedures. When low doses of the molecule are injected with an appropriate adjuvant, rats and pigs respond by producing high antibody titres to GnRH. The immunization results in a dramatic reduction of pituitary gonadotrophin secretion and, as a consequence, reduces steroid secretion and causes gonadal atrophy.

Key words: GnRH, fusion protein, immunosterilant, vaccine

Résumé : On décrit une méthode permettant de mettre au point une protéine incorporant une molécule porteuse attachée à une nouvelle configuration répétitive en tandem d'un peptide à 10 acides aminés, la gonadolibérine (GN-RH), qui ne serait normalement pas immunogène puisqu'elle est auto-antigène. Il est possible de produire cette molécule avec un rendement raisonnable à l'aide de la bactérie *E. coli*; les méthodes chromatographiques standards permettent de la purifier jusqu'à ce qu'elle soit homogène. Lorsqu'on injecte de faibles doses de la molécule en présence d'un adjuvant approprié, les rats et les cochons réagissent en produisant des titres élevés d'anticorps au GN-RH. L'immunisation provoque une réduction dramatique de sécrétion de la gonadotraphine pituitaire et, par voie de conséquence, une réduction de la sécrétion de stéroïde conduisant à une atrophie gonadale.

Mots clés : GN-RH, fusion de protéine, immunostérilisant, vaccine.

[Traduit par la rédaction]

Introduction

Except in countries such as England, Australia, and Spain, male pigs are castrated surgically shortly after birth. This is done despite the fact that intact males utilize feed more efficiently and have a superior carcass (1, 2). Boars are not raised for meat production because at typical market weights some boars may reach sexual maturity, and androstenone (5α-androst-16-ene-3-one), a volatile, unpleasant smelling steroid, may be produced by the maturing testes and be present in edible tissues. This condition is called boar taint.

Steroid secretion by the testes is regulated principally by luteinizing hormone (LH), a pituitary glycoprotein that is controlled by the hypothalamic peptide, gonadotrophin releasing hormone (GnRH) (3–5). Therefore, it should be possible to block testicular steroid production by eliminating the secretion or neutralizing the effect of GnRH. One possible strategy would be to immunize animals against GnRH (1, 2, 6) with the goal of producing antibodies that could bind to GnRH and thereby block its effects.

Developing an efficacious, yet practical, GnRH antigen has proven to be problematic for a variety of reasons. GnRH is a 10 amino acid peptide that is structurally identical among mammals, and therefore immunization with the peptide alone is not effective because it is not recognized as a foreign molecule. Secondly, in animal health and human medical applications, antigens must be well characterized and produced with high purity at minimum cost. However, most antigens are large protein molecules that are not practical to synthesize by defined chemical processes. Furthermore, except for short peptides, chemical synthesis is expensive.

One strategy for preparing antigens against small self-peptides is to synthesize the peptide chemically and then conjugate it to a larger carrier protein using a coupling reagent such as carbodiimide (7). However, such methods generally create a number of reaction products that require extensive purification to provide a homogenous protein. Furthermore, the cost of peptide synthesis and other reagents adds considerably to

Received November 4, 1996.

This paper is dedicated to Professor William A. Ayer on the occasion of his 65th birthday.

J.G. Manns[1] **and C. Barker.** BIOSTAR Inc., 343 - 111 Research Drive, Saskatoon, SK S7N 3R2, Canada.
S.K. Attah-Poku. Veterinary Infectious Disease Organization, 120 Veterinary Road, University of Saskatchewan, Saskatoon, SK S7N 5E3, Canada.

[1] Author to whom correspondence may be addressed. Telephone: (306) 931-7500. Fax: (306) 242-9010. E-mail: jmanns@innovplace.saskatoon.sk.ca

© 1997 NRC Canada

Can. J. Chem. Downloaded from www.nrcresearchpress.com by 88.146.161.215 on 09/08/12
For personal use only.

Can. J. Chem. Downloaded from www.nrcresearchpress.com by 88.146.161.215 on 09/08/12
For personal use only.

the cost of utilizing this method in the commercial production of vaccines.

An alternative strategy is to select a gene that codes for a carrier protein that contains a diverse population of T helper cell epitopes and therefore can generate a strong antibody response (8). Then, an oligonucleotide is synthesized that codes for the peptide against which an immune response is desired, and that piece of DNA is ligated to the gene for the carrier protein by placing it at the amino or carboxyl ends, or at internal positions as dictated by specific restriction sites in the DNA sequence coding for the carrier protein. Such a DNA sequence coding for a chimeric protein could then be transferred to a highly regulated bacterial expression system and identical copies of the antigen could be produced in high yield. A carrier protein molecule that meets such criteria is the bacterial protein called leukotoxin (LKT) from *Pasteurella haemolytica.* The present study describes a practical method for designing such a chimeric molecule, a simple but effective purification process, and experimental results that document the efficacy of a vaccine using this approach.

Materials and methods

Antigen design and production

Plasmid constructs

The plasmid pAA352, which carries a 96 kDa version of LKT under the Tac promoter, was used as the base plasmid for all GnRH fusion constructs (9). A complementary set of 154bp oligonucleotides coding for four copies of GnRH were synthesized and inserted into the BamHI site at the carboxyl end of the LKT gene. An additional four copies were added to provide eight copies, thereby creating the plasmid referred to as pCB112. To increase the amount of GnRH epitope per mole of protein, the LKT carrier was shortened to preserve the putative T-cell epitopes in the first 350 amino acids predicted by the method of Margalit et al. (8). pCB112 was digested with NaeI and BstBI; the ends were blunted with mungbean nuclease and allowed to self-ligate to create the plasmid pCB114. This plasmid codes for a 52 kDa LKT protein with eight copies of GnRH. This shortened version of LKT was used to produce a plasmid derived from pCB114 but containing eight additional copies of GnRH in the BglII site at the amino terminal region of the 52 kDa LKT. This gene, which codes for a 73 800 MW protein designated LKT.16GnRH, is present in the plasmid pCB122.

Protein production

Protein inclusion bodies of LKT:16GnRH were produced in *E. coli* strain W1485 transformed with the plasmid pCB122. A single colony was used to inoculate 10 mL of Terrific Broth (TB) (12 g tryptone, 24 g yeast extract, 4 mL glycerol, 2.31 g KH_2PO_4, and 12.54 g K_2HPO_4 in 1 L of H_2O) containing ampicillin at a final concentration of 100 μg/mL. The culture was incubated overnight on a rotary shaker at 37°C and was used to inoculate 1 L of TB containing ampicillin. This culture was incubated on a rotary shaker at 37°C until it reached an optical density of 0.6 at 660 nanometers. When it reached that cell density, the culture was induced to produce the recombinant protein by addition of 10 mL of 0.1 M isopropylthio-β-D-galactoside. The culture was incubated for 2 h longer and the cells were then harvested by centrifugation. The cell pellet was suspended in 20 mL of a 25% sucrose 0.05 M Tris pH 8.0 solution and frozen at −70°C until required for further processing.

The cells obtained from a 1 L culture were thawed, mixed with 100 mg of lysozyme, and incubated at room temperature for 30 min. Triton X-100 and ethylene diamine tetraacetic acid (EDTA) were then added to give a final concentration of 2% and 0.05 M, respectively, and the cells were vortexed and sonicated at full power for 3 × 30 s bursts. The disruptate was then centrifuged to collect the protein inclusion bodies, which were washed twice with water and stored at 4°C.

For further processing, the inclusion bodies were dissolved in 4 M guanidine HCl and centrifuged to remove any undissolved material. The clarified protein solution was dialyzed against water for 48 h at 4°C and the protein, which precipitates out as the guanidine concentration decreases, was collected and lyophilized.

Purification of recombinant LKT-GnRH fusion protein

The first trials were conducted with a LKT-GnRH-8 produced from plasmid pCB114 and the following purification scheme, which was developed for that molecule, was also used to purify LKT-16 GnRH.

The crude protein sample containing LKT-16 GnRH was dissolved in 8 M guanidine and then diluted to 6 M guanidine with the elution buffer (4 M guanidine, 50 mM sodium phosphate, 50 mM sodium chloride, 1 mM disodium EDTA, 1 mM dithiothreitol pH 7.5) to give a protein concentration of 25 mg/mL. The solution was centrifuged at 10 000*g* for 10 min and the supernatant was filtered through a 0.45 μm filter. The filtrate was loaded on a Sephacryl S400HR size exclusion column (XK26/100, 100 cm long × 2.6 cm i.d., Pharmacia Biotechnology, Uppsala, Sweden) equilibrated with the elution buffer. The proteins were eluted with the elution buffer at a flow rate of 2 mL/min; protein concentration in the column effluent was monitored at 280 nm.

Purity of the various fractions was evaluated by sodium dodecyl sulfate polyacrylamide gel electrophoresis; an example is shown in Fig. 1. A Western blot analysis using polyclonal antibodies against the GnRH portion of the molecule was used (Fig. 2) to confirm that the protein band with the appropriate molecular weight contained GnRH.

Additional confirmation was obtained by determining the molecular weight of the purified antigen using MALDI-TOF mass spectrometry. The analysis was conducted using standard methods in the Department of Biochemistry, Mass Spectrometry Facility, University of Washington, Seattle.

Vaccine formulation and immunization trials

The LKT-GnRH vaccines were prepared by dissolving the antigen in 4 M guanidine HCl at a concentration of approximately 20 mg/mL and adding an appropriate volume of that solution, with agitation, to a commercially available oil-in-water based emulsion (MVP Laboratories, Ralston, Nebraska) along with 0.9% NaCl to give the desired antigen concentration. Although numerous antigens were evaluated, data from only the 8 and 16 copy molecules are presented.

The assay for GnRH antibody utilized monoiodinated GnRH-I^{125} in a competitive binding assay (2). This in vitro assay was conducted by adding 0.1 mL (10 000 – 15 000 cpm)

© 1997 NRC Canada

Fig. 1. Impure LKT-16 GnRH protein and a purified fraction were applied to a 10% sodium dodecyl sulfate polyacrylimide gel. Lane 1, molecular weight standards; lane 2, purified LKT-16 GnRH; lane 3, crude LKT-16 GnRH protein; lane 4, purified LKT-16 GnRH as for lane 2 except a smaller mass was applied to the gel.

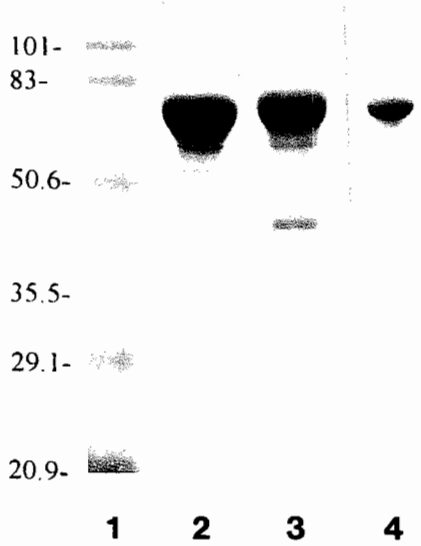
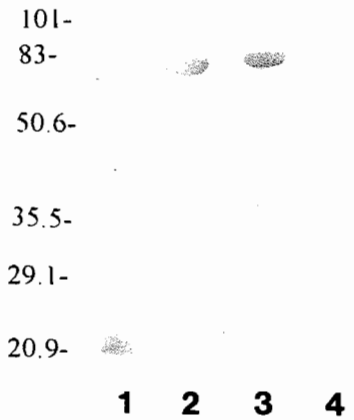


Fig. 2. Western blot of the gel in Fig. 1 probed with a polyclonal antibody to GnRH. Lane 1, molecular weight standards; lane 2, purified LKT-16 GnRH; lane 3, crude LKT-16 GnRH; lane 4, purified LKT-16 GnRH. The mass of antigen in lane 4 was not sufficient to be visible in the photograph of the gel.



of iodinated GnRH to a series of tubes. An appropriate dilution of sera to be tested was added and the volume brought to 0.7 mL. After incubating for 48 h at 5°C the free GnRH-I^{125} was separated from antibody-bound material by adding 0.75 mL of a 0.5% charcoal suspension. After vortexing, the mixture was centrifuged, the supernatant was decanted, and the precipitate containing free GnRH-I^{125} was counted. These data along with the knowledge of the amount of GnRH-I^{125} added were used to calculate the per cent binding at a specific serum dilution.

Trial 1: At day 0 of the experiment 10 male Sprague Dawley rats were immunized with a single injection of 50 μg LKT-8 GnRH in 1.0 mL adjuvant and 10 male rats were injected with adjuvant only. Blood was collected at approximately 21 day intervals and assayed for GnRH antibodies and serum testosterone. Serum testosterone was measured using a standard radioummunoassay method in kits provided by Diagnostic Products Corp., Los Angeles. Assay sensitivity was approximately 0.1 ng/mL and coefficient of variation was less than 6%.

Trial 2: Twenty weanling pigs (10 male and 10 female) 21 days of age and weighing 3–5 kg were assigned to each treatment. They were injected with 1.0 mL of vaccine containing 0–160 μg of highly purified LKT-16 GnRH antigen at day 0 of the experiment. At day 35, a booster immunization with a similar dose was given and blood was collected 14, 33, and 49 days thereafter and assayed for serum antibody titres and serum LH. The LH assay used iodinated bovine LH and porcine LH as reference standard and has been validated for use in sera from pigs (10).

Results and discussion

The SDS-PAGE gel in Fig. 1 shows that the relatively impure protein prepared by dissolving inclusion bodies in 4 M guanidine HCl (lane 3) had several minor components. A large mass of protein purified using the chromagraphic procedure was run in lane 2 to highlight any minor impurities that might be present. A much smaller sample was applied in lane 4; it appears as a single band and we believe the protein is at least 90% pure. MALDI-TOF mass spectrometry gave a single peak with molecular weight of 73 600, which is nearly identical to the 73 800 MW estimated by the amino acid composition predicted by the known DNA base sequence. Figure 2 shows that the purified protein reacts with polyclonal antibodies directed against the GnRH portion of the molecule, thus confirming the identity of the molecule.

pCB114 derived protein (50 μg) injected into rats (Fig. 3) gave a remarkable response. The normal response to a single injection of an antigen in an oil-in-water adjuvant in most mammals would be to cause a short-lived, modest increase in antibody titres that would not result in observable biological effects (i.e., no neutralization of GnRH). However, in this species we observed a dramatic and sustained increase in antibody titres that resulted in serum testosterone concentrations similar to values expected in castrate males. When these animals were killed 224 days after the single injection, the immunized animals had testes which weighed 1.48 ± 0.24 g (mean ± s.d.) compared to 7.30 ± 0.10 g for control animals.

Doses as low as 1 μg of LKT-16 GnRH stimulated strong antibody production in pigs (Fig. 4). When a dose of 10 μg or greater was given 35 days after the primary immunization, all animals responded with antibody titres of at least 20% binding of GnRH-I^{125} when measured in a 1:5000 dilution of serum. Serum LH in 10 control castrate males had higher LH than 10 intact females (Fig. 5). This is expected since the negative arm of the feedback loop is absent in castrate animals. Serum LH

Can. J. Chem. Downloaded from www.nrcresearchpress.com by 88.146.161.215 on 09/08/12
For personal use only.

© 1997 NRC Canada

Can. J. Chem. Downloaded from www.nrcresearchpress.com by 88.146.161.215 on 09/08/12
For personal use only.

Fig. 3. Serum GnRH antibody titres (top panel) in immunized rats (1:5000 dilution) and placebo injected controls (1:100 dilution). Serum testosterone values (mean ± SE) are shown in the bottom panel.

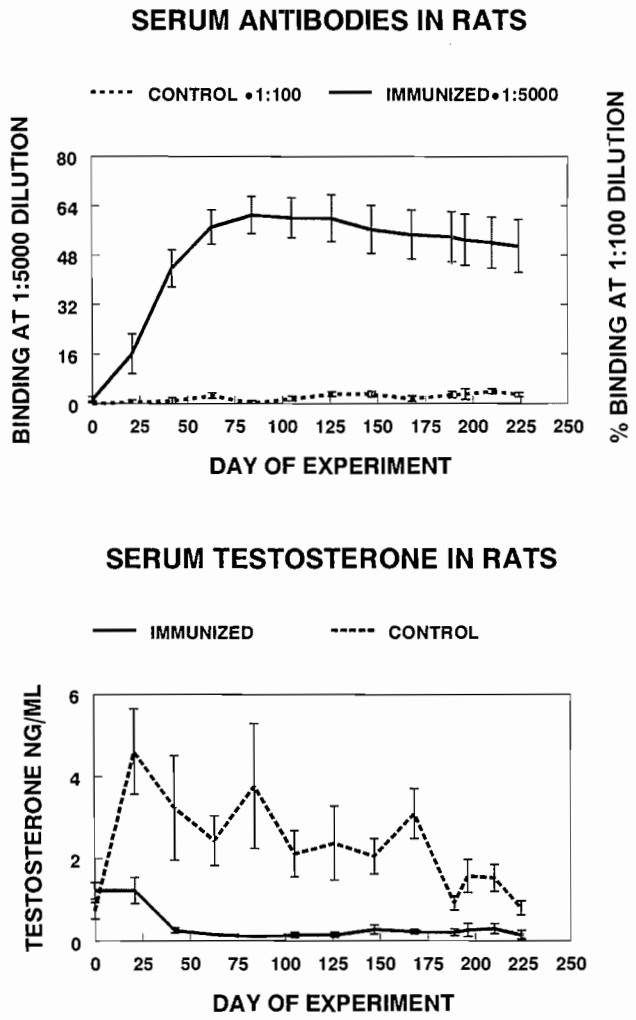


Fig. 4. Serum GnRH antibody titres (means ± SE) 14 days after the booster injection of 0–160 µg of pCB122 protein. There were 20 animals per group. The ratio at the top of each column indicates the proportion of animals responding with titres greater than 20% binding at 1:5000 serum dilution.

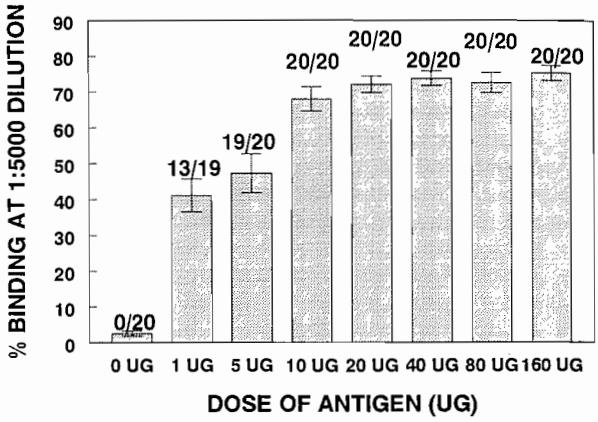
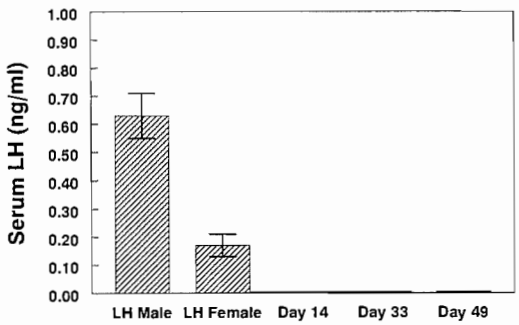


Fig. 5. Serum LH (ng/mL) in barrows (LH male) and gilts (LH female) injected with adjuvant only (control) compared to the pooled results for animals receiving 20, 40, or 80 µg of LKT-16 GnRH antigen. There were 10 animals in each of the LH male and LH female columns and 60 animals (30 male and 30 female) in each of the day 14, 33, and 49 columns.



was assayed in individual samples from all animals given 20, 40, and 80 µg of antigen; the results for each bleeding date were pooled and the mean is shown at 14, 33, and 49 days after the booster injection. Serum LH was not detectable in any of the samples, indicating that the antibodies had a powerful neutralizing effect on secreted GnRH.

Designing a protein with a desired molecular weight and a diverse population of strong T helper cell epitopes while incorporating tandem repeats of unique peptide sequences at various locations in the molecule is a useful strategy for constructing well-defined antigens. Such proteins can be produced from a single gene in a carefully controlled bacterial system, which ensures adequate yields of a homogeneous protein. The insolubility of the bacterial aggregate (inclusion bodies) can facilitate early stage purification using simple washing procedures. A single pass through a molecular sieving column of appropriate size provides a protein of high purity.

These studies indicate that production of proteins from DNA molecules that are engineered to contain two functional components is practical for commercial applications. Such an approach is useful where it is essential to have well-defined molecules that can be produced cheaply, reproducibly, and with high purity.

Acknowledgments

The technical assistance of H. Liu is acknowledged; Trenna Derdall helped in the preparation of the manuscript.

References

1. M. Bonneau and W.J. Enright. Livest. Prod. Sci. **42**, 193 (1995).
2. R.H. Meloen, J.A. Turkstra, H. Lankhof, W.C. Puijk, W.M.M. Schaaper, G. Dijkstra, C.J.G. Wensing, and R.B. Oonk. Vaccine, **12**, 741 (1994).
3. H. Matsuo, A. Arimura, R.M.G. Nair, and A.V. Schally. Biochem. Biophys. Res. Commun. **45**, 822 (1971).
4. A. Arimura, H. Sator, T. Kumasaka, R.B. Worobec, L. Debeljuk, J. Dunn, and A.V. Schally. Endocrinology, **93**, 1092 (1973).
5. R. Gillemin. Contraceptions, **5**, 1 (1971).

© 1997 NRC Canada

6. R. Aitken and T.R. Hirst. Livest. Prod. Sci. **42**, 163 (1995).
7. H.M. Fraser, A. Gunn, S.L. Jeffcoate, and D.T. Holland. J. Endocrinol. **63**, 399 (1974).
8. H. Margalit, J.L. Sprouge, J.L. Cornette, K.B. Cease, C. DeLisi, and J.A. Berzofsky. J. Immunol. **138**, 2213 (1987).
9. A.W. Potter, M. Campos, and H.W. Hughes. U.S. Patent 5,238,823 (1993).
10. D.L. Kingsbury and N.C. Rawlings. J. Reprod. Fertil. **98**, 245 (1993).

Can. J. Chem. Downloaded from www.nrcresearchpress.com by 88.146.161.215 on 09/08/12
For personal use only.

© 1997 NRC Canada

The biosynthesis of the new tremulane sesquiterpenes isolated from *Phellinus tremulae*

Elizabete R. Cruz

Abstract: The tremulane sesquiterpenes isolated from the wood-rotting fungus *Phellinus tremulae* are irregular isoprenoids derived from the cyclization and rearrangement of farnesyl pyrophosphate (FPP). The most interesting feature in the formation of the tremulane skeleton seems to involve the migration of a methyl group from one of the isoprene units. To investigate the biosynthetic origin of this unique sesquiterpene skeleton, labelling experiments were carried out by adding ^{13}C-labelled sodium acetate to liquid cultures of *Phellinus tremulae*. The labelling pattern was determined by ^{13}C NMR spectral analysis of labelled tremulenediol A, which was purified as its di-*p*-bromobenzoate. A possible route to the tremulane skeleton, which accounts for the observed labelling pattern, proceeds from FPP, via humulene. The stereochemical course of the tremulane biosynthesis is discussed.

Key words: fungal metabolites, aspen, perhydroazulene sesquiterpenes, labelling experiments.

Résumé : Les sesquiterpènes dérivés du trémulane extraits du champignon *Phellinus tremulae*, qui provoquent le pourrissement du bois, sont des isoprénoïdes irréguliers produits par une cyclisation, accompagnée d'une transposition, du pyrophosphate de farnésyle (PPF). La caractéristique la plus intéressante de la formation du squelette du trémulane semble impliquer la migration d'un groupe méthyle de l'une des unités isopréniques. Dans le but d'étudier l'origine biosynthétique de ce squelette unique de sesquiterpène, on a réalisé des expériences de marquage en ajoutant de l'acétate de sodium marqué au ^{13}C aux liquides de culture du *Phellinus tremulae*. On a déterminé la distribution des marqueurs par une analyse des spectres RMN du ^{13}C du trémulènediol A marqué, purifié sous la forme de di-*p*-bromobenzoate. L'une des voies possibles de formation du squelette du trémulane, qui permet d'expliquer la distribution des marqueurs, procède du PPF par le biais de l'humulène. On discute des aspects stéréochimiques de la biosynthèse du trémulane.

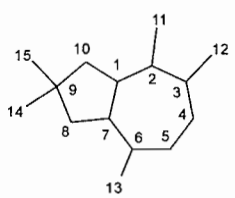
Mots clés : métabolites de champignons, peuplier, sesquiterpènes du perhydroazulène, expériences de marquage.

[Traduit par la rédaction]

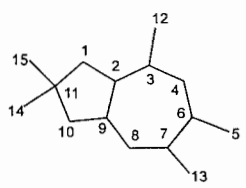
Introduction

We recently reported the isolation of a new family of sesquiterpenes possessing a previously unreported carbon skeleton, which we call tremulane (**1**), produced by the wood-rotting fungus *Phellinus tremulae* (1, 2).[2] This fungus is the most serious fungal pathogen of aspen (*Populus tremuloides* Michx.) and greatly reduces the economic value of this resource in Canada (3).

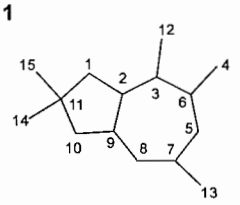
Tremulane is a positional isomer of two other perhydroazulene-type carbon skeletons called lactarane (**2**) and merulane (**3**) (4, 5). The lactarane skeleton **2** and, presumably, the merulane skeleton **3** are formed from farnesyl pyrophosphate (FPP) via the humulene pathway (4). Since the tremulane (**1**) family could also be formed via this pathway through different rearrangement reactions, it was of interest to study the biosynthesis of this unique sesquiterpene skeleton. Labelling experiments were carried out using singly and doubly labelled sodium acetate, added periodically to liquid cultures of



1



2



3

Received November 7, 1996.

This paper is dedicated to Professor William A. Ayer on the occasion of his 65th birthday.

Elizabete R. Cruz.[1] Department of Chemistry, University of Alberta, Edmonton, AB T6G 2G2, Canada.

[1] Present address: Institute of Biological Chemistry, Washington State University, Pullman, WA 99164-6340, U.S.A. Telephone: (509) 335-3435. E-mail: betecruz@mail.wsu.edu

[2] An overview of part of this work was presented by Professor W.A. Ayer in the 1994 E.W.R. Steacie Award Lecture delivered at the Annual Conference of the Canadian Society for Chemistry, Winnipeg, Manitoba, June 1, 1994, and published as ref. 1.

© 1997 NRC Canada

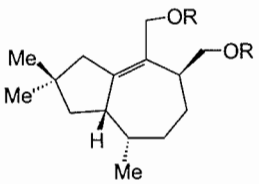
Can. J. Chem. Downloaded from www.nrcresearchpress.com by 88.146.161.215 on 09/08/12
For personal use only.

Can. J. Chem. Downloaded from www.nrcresearchpress.com by 88.146.161.215 on 09/08/12
For personal use only.

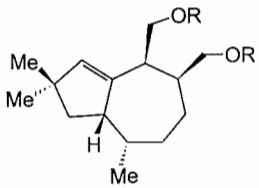
P. tremulae; the acetate incorporation was investigated by ^{13}C NMR spectroscopy. The labelling results are presented for tremulenediol A (**4**), which can be isolated in reasonable amounts and is readily purified as its di-*p*-bromobenzoate.

Results and discussion

Phellinus tremulae was cultivated in shake culture on 2% malt extract broth for 16 days, in the presence of DIAION HP 20® resin,[3] and was periodically supplemented with injections of a sterile solution of labelled sodium acetate: [1-^{13}C], [2-^{13}C], and [1,2-$^{13}C_2$]. The culture broth was filtered and the resin and wet mycelium were extracted with dichloromethane. The tremulanes were isolated as reported previously (2). Since tremulenediol A (**4**) can be isolated in reasonable amounts (> 8 mg/400 mg of crude extract) and in pure form as its di-*p*-bromobenzoate **4a**, it was chosen as the substrate to study the incorporation pattern. The procedure for the separation and purification of **4a** also leads to the isolation of the di-*p*-bromobenzoate of tremulenediol B (**5a**), which was analyzed to confirm the results found for **4a**. The labelled compounds are identified as **4b**, **4c**, and **4d**, corresponding to the tremulenediol A incorporated with [1,2-$^{13}C_2$]acetate, [1-^{13}C]acetate, and [2-^{13}C]acetate, respectively. An equivalent identification is used for the di-*p*-bromobenzoate of tremulenediol B (**5a**).



4 R = H
4a R = OCO*p*BrPh
4b [1,2-$^{13}C_2$]acetate labelled
4c [1-^{13}C]acetate labelled
4d [2-^{13}C]acetate labelled



5 R = H
5a R = OCO*p*BrPh
5b [1,2-$^{13}C_2$]acetate labelled
5c [1-^{13}C]acetate labelled
5d [2-^{13}C]acetate labelled

The ^{13}C NMR spectrum of **4b** exhibits six pairs of spin-coupled doublets appearing as satellites about the enhanced natural abundance singlets, as well as three enhanced singlets. The results are presented in Table 1, along with the data for compound **5b**. Enrichment data are presented in the experimental section. The doublets result from coupling between two adjacent ^{13}C atoms coming from intact acetate units. The enhanced singlets are derived from fragmented acetate units. The fragmentation takes place during the conversion of mevalonate, a product of acetate metabolism, into isopentenyl pyrophosphate (IPP). In this process C-1 of mevalonate is lost and the result is the appearance of enhanced singlets in the ^{13}C NMR spectrum for the carbons derived from C-2 of mevalonate (7, 8). In the case of tremulane these singlet carbons are C-5, C-12, and C-14. An INADEQUATE (9) experiment (Fig. 1) confirms the spin-coupled carbons as the following pairs: C-1,C-10; C-2,C-11; C-3,C-4; C-6,C-13; C-7,C-8; and C-9,C-15. Carbons C-5, C-12, and C-14 do not give rise to cross peaks

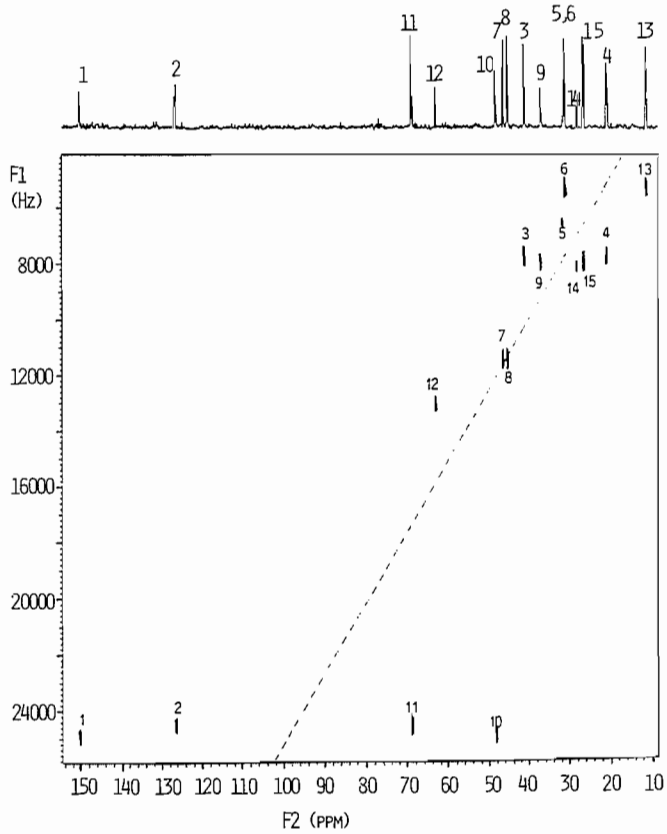
[3] A highly porous styrene–divinylbenzene resin useful in removing nonpolar metabolites from aqueous media, produced by Mitsubishi Chemical Industries Ltd., Tokyo; see also ref. 6.

Table 1. ^{13}C NMR data of doubly labelled tremulenediols A (**4b**) and B (**5b**).

	4b		**5b**	
Carbon	δ_C (mult)[a]	J_{CC}, Hz	δ_C (mult)	J_{CC}, Hz
C-1	150.3 (s)	40	144.2 (s)	70
C-2	126.5 (s)	48	42.4 (d)	39
C-3	41.3 (d)	34	44.7 (d)	33
C-4	21.2 (t)	34	29.7 (t)	33
C-5*	31.7 (t)	—	30.4 (t)	—
C-6	31.4 (d)	36	35.7 (d)	35
C-7	46.6 (d)	35	48.2 (d)	34
C-8	45.3 (t)	35	42.7 (t)	34
C-9	37.2 (s)	36	41.6 (s)	35
C-10	48.3 (t)	40	139.9 (d)	70
C-11	69.0 (t)	48	63.4 (t)	39
C-12*	63.2 (t)	—	68.1 (t)	—
C-13	11.7 (q)	36	19.6 (q)	35
C-14*	28.4 (q)	—	29.2 (q)	—
C-15	26.8 (q)	36	26.4 (q)	35

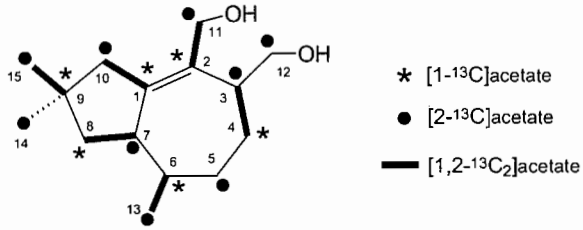
[a]Mult = multiplicity.
*Enriched singlet.

Fig. 1. INADEQUATE spectrum of the doubly labelled tremulenediol A di-*p*-bromobenzoate (**5a**).



© 1997 NRC Canada

Fig. 2. Labelling pattern of tremulenediol A: incorporation of [1-^{13}C]-, [2-^{13}C]-, and [1,2-$^{13}C_2$]acetate.



with other carbon resonances, showing that they are actually singlets. The same coupling pattern is observed for **4b** and **5b**, as indicated in the tremulane skeleton shown in Fig. 2. This result with doubly labelled acetate confirms that tremulane is formed by rearrangement of a methyl group in one of the isoprene units. To elucidate the nature of this rearrangement, singly labelled acetate (1-^{13}C and 2-^{13}C) was added to cultures of *P. tremulae* in the same manner as described above. Singly labelled tremulenediols A and B were isolated as their di-*p*-bromobenzoates **4a** and **5a** and analyzed by ^{13}C NMR spectroscopy. The broad-band ^{13}C spectrum was obtained using the same conditions for unlabelled (**4a**, **5a**), [1-^{13}C]acetate (**4c**, **5c**), and [2-^{13}C]acetate (**4d**, **5d**) labelled compounds. The enriched signals were identified by subtracting the natural abundance spectrum (unlabelled) from the labelled spectra (see experimental section for enrichment data). A summary of the results is presented in Fig. 2.

These results strongly support the previous observation of migration of one of the *geminal* methyl groups in one of the isoprene units. The most plausible mechanism to account for this rearrangement invokes the common pathway of sesquiterpene biosynthesis from *trans,trans*-farnesyl pyrophosphate (10) via humulene[4] (Scheme 1). The stereochemical course of the biosynthesis is based on the work of Cane and Nachbar (7), in which the condensation and cyclizations are related to the absolute stereochemistry at each chiral centre. All the chiral centres in the tremulane sesquiterpenes possess *S*-configuration (2). Cane and Nachbar have demonstrated that the intramolecular cyclization of *trans,trans*-FPP is a result of the electrophilic attack by the C-1 carbinyl carbon at C-11, which may occur on the *re* or *si* face of the terminal double bond. If attack occurs on the *re* face, the methyl group derived from an intact acetate unit becomes the *pro-R* methyl (C-15) of humulene. If the attack is on the *si* face the same methyl becomes *pro-S* (C-14). In the case of tremulane the distinction between the *geminal* methyl groups C-14 and C-15 was based on correlations observed in the NOESY spectrum of compound 4 and by comparison with the NMR data obtained for other tremulanes. It has been established by NMR and X-ray that the hydrogen at C-7 of the tremulane series is β-oriented (2). In the NOESY spectrum of **4**, we observe a cross peak between H-7 (δ 3.10) and the methyl group at δ 0.87, which is consistent with its assignment as H-15 (2). According to HMQC experiments, this hydrogen resonance at δ 0.87 correlates to the carbon at δ 26.9, therefore establishing the assignment of C-15. Since the labelling experiments indicate that C-15 in tremulane comes from an intact acetate unit, we can assume that FPP cyclization occurs on the *re* face of the terminal double bond. The mechanism continues with an intramolecular cyclization to form a *cis*-fused five-membered ring. To account for this stereochemistry the protonation of the 9,10-double bond at C-10 has to be followed by a *si* attack by the 2,3-double bond on C-9, which leads to the carbocation **A**. Then a double [1,2]-H shift takes place. The hydrogen at C-2 migrates to the upper face of the carbocation C-3 (**A**) and the hydrogen at C-9 shifts to the upper face of the newly formed carbocation C-2 (**B**) generating the intermediate **C**. This sets the *S* absolute stereochemistry at C-2 and C-3, which corresponds to the observed *S* stereochemistry at C-7 and C-6 of tremulane, respectively. A few cationic rearrangements are necessary to promote the migration of a methyl group to C-6. A *si* attack by the 6,7-double bond on C-9 leads to the formation of the cyclopropyl carbinyl cation **D**, which rearranges to form the tertiary cyclobutyl cation **E**. The migration of the β-oriented cyclopropyl at C-7 to the top face of the carbocation C-6 is imposed by the required *S* stereochemistry at C-6 of humulene (C-3 of tremulane) and by the fact that C-7,C-13 comes from an intact acetate unit according to experimental results with the doubly labelled acetate incorporation. Therefore, migration of C-13 has been ruled out. Further rearrangement within the cyclopropyl carbinyl-cyclobutyl reaction manifold results in cyclobutyl ring opening to the homoallylic cation **F**, which is quenched by nucleophilic water, affording **G**. Allylic oxidation at C-13 of **G** gives tremulenediol A, whose labelling pattern from humulene is shown in structure **H** (Scheme 1), with the numbering of humulene. This labelling pattern is consistent with that obtained for tremulane (Fig. 2).

The present study shows that the tremulane sesquiterpenes are irregular terpenoids derived from FPP via humulene. The stereochemical course of tremulane biosynthesis leads to the formation of the tremulane skeleton with the appropriate absolute stereochemistry. The migration of one of the methyl groups from one of the isoprene units occurs through a series of carbocationic rearrangements giving rise to the tremulane family.

Experimental

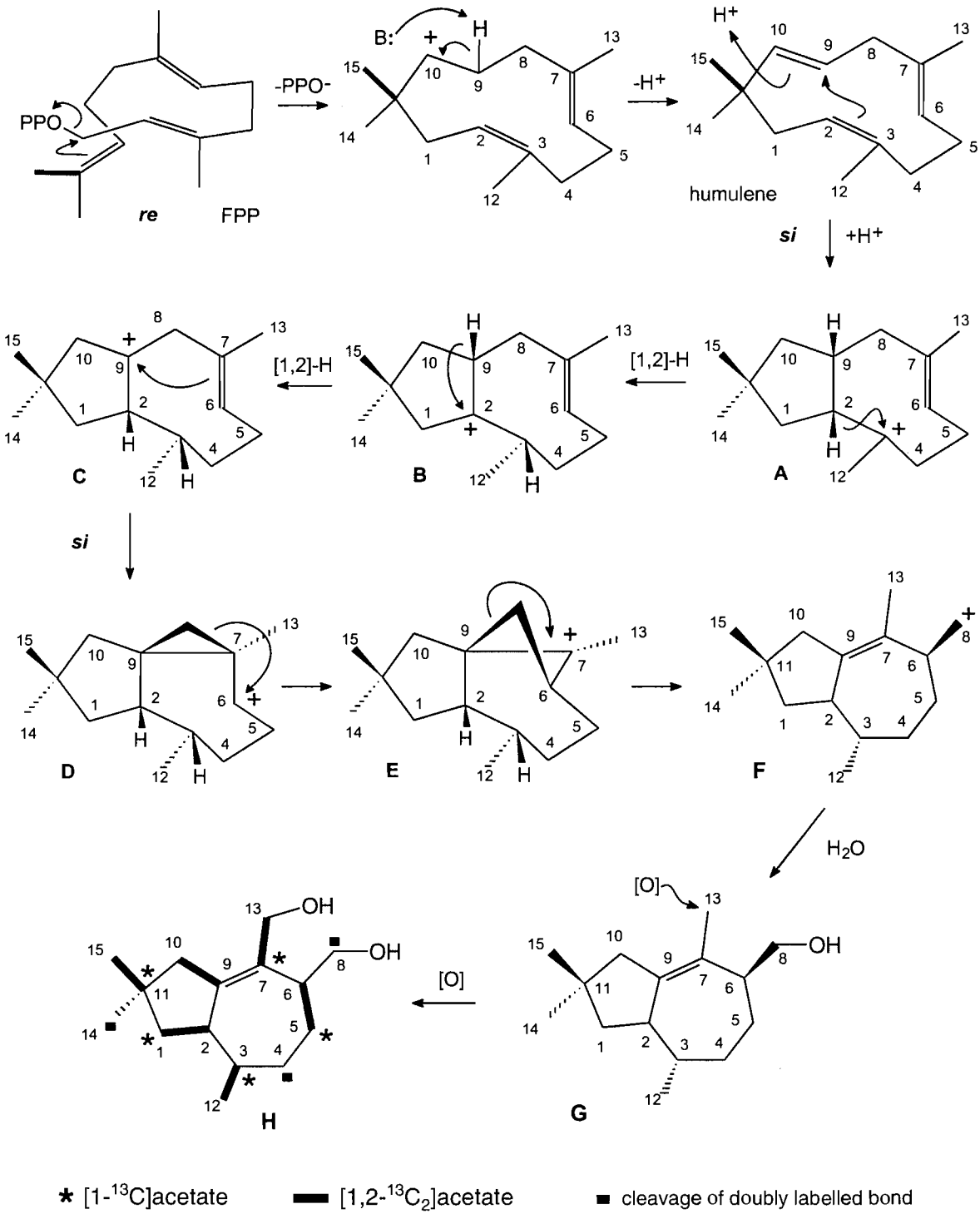
^{13}C nuclear magnetic resonance (NMR) spectra and Incredible Natural Abundance Double Quantum Transfer Experiment (INADEQUATE) for the doubly labelled acetate incorporation were obtained on a Varian Unity-500 spectrometer. The singly labelled acetate incorporation spectra were recorded on a Bruker 400 MHz spectrometer. All NMR spectra were recorded in $CDCl_3$ solution. The $CDCl_3$ chemical shift was used as reference for ^{13}C chemical shifts having tetramethylsilane as an internal standard. Universal Scientific Incorporated silica gel 60 (40 μm) was used for flash chromatography. Preparative thin-layer chromatography (PTLC) was performed on E. Merck precoated 20 × 20 glass plates of silica gel 60 F-254 or on prepared 20 × 20 glass plates using Aldrich silica gel for TLC with a fluorescent indicator. Analytical thin-layer chromatography (TLC) was carried out on cut sections of E. Merck precoated aluminium sheets of silica gel 60 F-254. Ultraviolet-active materials were detected by visualization under a UV lamp (254 nm). Liquid media were prepared

[4] We thank Professor David Cane for first suggesting this pathway.

Can. J. Chem. Downloaded from www.nrcresearchpress.com by 88.146.161.215 on 09/08/12
For personal use only.

© 1997 NRC Canada

Scheme 1.



using Bacto™ malt extract broth (DIFCO Laboratories) and Diaion HP-20® resin (Mitsubishi Chemical Industries Ltd., supplied by TCI America - 9211 N. Harborgate St., Portland, OR 97203, U.S.A.). Feeding experiments were performed with sodium [1-^{13}C]acetate, sodium [2-^{13}C]acetate, and sodium [1,2-$^{13}C_2$]acetate (99 at. %) purchased from ICON Isotopes, ICON Services. All solvents were distilled prior to use.

Growth of *Phellinus tremulae*: administration of ^{13}C-labelled sodium acetate

Cultures of *P. tremulae* (strain NOF 1464) were obtained from Dr. Y. Hiratsuka, Forestry Canada, Northern Forestry Centre, Edmonton, and are deposited at the University of Alberta Microfungus Herbarium (UAMH 7005). Plate cultures of *P. tremulae* were blended in a Waring blender with sterile water and ca. 30 mL aliquots were inoculated into 4-L Erlenmeyer

© 1997 NRC Canada

Can. J. Chem. Downloaded from www.nrcresearchpress.com by 88.146.161.215 on 09/08/12
For personal use only.

Can. J. Chem. Downloaded from www.nrcresearchpress.com by 88.146.161.215 on 09/08/12
For personal use only.

flasks charged with 2 L of sterile malt extract medium (40 g of malt extract broth DIFCO, 40 g of DIAION HP 20® resin (6), and 2 L of redistilled water). A 0.2 M sterile solution of labelled sodium acetate (0.75 g) in redistilled water (45 mL) was periodically added to a *P. tremulae* culture (2 L) by injecting 15 mL after day 1 and 10 mL each after days 3, 5, and 7 of growth. The work-up and separation were performed as described previously (2).

Growth of *Phellinus tremulae*: unlabelled metabolites

Unlabelled metabolites were obtained under the same growth conditions as described above for labelled metabolites but using unlabelled sodium acetate.

NMR spectra of unlabelled and singly labelled acetate metabolites

The NMR spectra were recorded using 40 and 15 mM solution in $CDCl_3$ for tremulenediol A and B, respectively. The spectra were obtained using the same parameters for unlabelled and labelled compounds: 4000 transients with acquisition time of 0.6 s. The transients were doubled for the 15 mM solutions.

[1,2-$^{13}C_2$]acetate-labelled metabolites

Tremulenediol A di-p-*bromobenzoate (**4b**)*: 14 mg. ^{13}C NMR ($CDCl_3$, 125 MHz) spin-coupled carbons, δ: 150.3 (C-1, $J_{1,10}$ = 40 Hz), 126.5 (C-2, $J_{2,11}$ = 48 Hz), 69.0 (C-11, $J_{2,11}$ = 48 Hz), 48.3 (C-10, $J_{1,10}$ = 40 Hz), 46.6 (C-7, $J_{7,8}$ = 35 Hz), 45.3 (C-8, $J_{7,8}$ = 35 Hz), 41.3 (C-3, $J_{3,4}$ = 34 Hz), 37.2 (C-9, $J_{9,15}$ = 36 Hz), 31.4 (C-6, $J_{6,13}$ = 36 Hz), 26.8 (C-15, $J_{9,15}$ = 36 Hz), 21.2 (C-4, $J_{3,4}$ = 34 Hz), 11.7 (C-13, $J_{6,13}$ = 36 Hz); enriched singlets, δ: 63.2 (C-12), 31.7 (C-5), 28.4 (C-14); INADEQUATE ($CDCl_3$, 125 MHz) cross peaks (two double quantum); δ: 150.3 (C-1) ↔ 48.3 (C-10); 126.5 (C-2) ↔ 69.0 (C-11); 41.3 (C-3) ↔ 21.2 (C-4); 31.4 (C-6) ↔ 11.7 (C-13); 46.6 (C-7) ↔ 45.3 (C-8); 37.2 (C-9) ↔ 26.8 (C-15); singlet carbons, δ: 63.2 (C-12), 31.7 (C-5), 28.4 (C-14). Enrichment data (incorporation is equal to 1.1 I_s/I_c where I_s is the sum of the intensities of the two satellite resonances and I_c the intensity of the central peak (11)): C-1 (0.2), C-2 (0.2), C-3 (0.3), C-4 (0.4), C-6 (0.3), C-7 (0.3), C-8 (0.3), C-9 (0.2), C-10 (0.3), C-11 (0.4), C-13 (0.6), C-15 (0.6).

Tremulenediol B di-p-*bromobenzoate (**5b**)*: 10 mg. ^{13}C NMR ($CDCl_3$, 125 MHz) spin-coupled carbons, δ: 144.2 (C-1, $J_{1,10}$ = 70 Hz), 139.9 (C-10, $J_{1,10}$ = 70 Hz), 63.4 (C-11, $J_{2,11}$ = 39 Hz), 48.2 (C-7, $J_{7,8}$ = 34 Hz), 44.7 (C-3, $J_{3,4}$ = 33 Hz), 42.7 (C-8, $J_{7,8}$ = 34 Hz), 42.4 (C-2, $J_{2,11}$ = 39 Hz), 41.6 (C-9, $J_{9,15}$ = 35 Hz), 35.7 (C-6, $J_{6,13}$ = 35 Hz), 29.7 (C-4, $J_{3,4}$ = 33 Hz), 26.4 (C-15, $J_{9,15}$ = 35 Hz), 19.6 (C-13, $J_{6,13}$ = 35 Hz); enriched singlets, δ: 68.1 (C-12), 30.4 (C-5), 29.2 (C-14).

[1-^{13}C]acetate-labelled metabolites

[1-^{13}C]Tremulenediol A di-p-*bromobenzoate (**4c**)*: 12 mg. ^{13}C NMR ($CDCl_3$, 100 MHz) enriched signals, δ: 150.3 (C-1), 126.5 (C-2), 45.3 (C-8), 37.2 (C-9), 31.4 (C-6), 21.2 (C-4); natural abundance signals, δ: 69.0 (C-11), 63.2 (C-12), 48.3 (C-10,), 46.6 (C-7), 41.3 (C-3), 31.7 (C-5), 28.4 (C-14), 26.8 (C-15), 11.7 (C-13). Enrichment data (incorporation is equal to (I_L/I_U) − 1.1 where I_L is the intensity of the peak in the labelled spectrum and I_U the intensity of the peak in the unlabelled spectrum): C-1 (0.6), C-2 (0.6), C-4 (0.8), C-6 (0.7), C-8 (0.6), C-9 (0.7).

[1-^{13}C]Tremulenediol B di-p-*bromobenzoate (**5c**)*: 4 mg. ^{13}C NMR ($CDCl_3$, 100 MHz) enriched signals, δ: 139.9 (C-10), 68.1 (C-12), 63.4 (C-11), 48.2 (C-7), 44.7 (C-3), 30.4 (C-5), 29.2 (C-14), 26.4 (C-15), 19.6 (C-13); natural abundance signals, δ: 144.2 (C-1), 42.7 (C-8), 42.4 (C-2), 41.6 (C-9), 35.7 (C-6), 29.7 (C-4).

[2-^{13}C]acetate-labelled metabolites

[2-^{13}C]Tremulenediol A di-p-*bromobenzoate (**4d**)*: 24 mg. ^{13}C NMR ($CDCl_3$, 100 MHz) enriched signals, δ: 69.0 (C-11), 63.2 (C-12), 48.3 (C-10), 46.6 (C-7), 41.3 (C-3), 31.7 (C-5), 28.4 (C-14), 26.8 (C-15), 11.7 (C-13); natural abundance signals, δ: 150.3 (C-1), 126.5 (C-2), 45.3 (C-8), 37.2 (C-9), 31.4 (C-6), 21.2 (C-4). Enrichment data (incorporation is equal to (I_L/I_U) − 1.1 where I_L is the intensity of the peak in the labelled spectrum and I_U the intensity of the peak in the unlabelled spectrum): C-3 (0.4), C-5 (0.7), C-7 (0.5), C-10 (0.5), C-11 (0.6), C-12 (0.4), C-13 (0.7), C-14 (0.6), C-15 (0.8).

[2-^{13}C]Tremulenediol B di-p-*bromobenzoate (**5d**)*: 10 mg. ^{13}C NMR ($CDCl_3$, 100 MHz) enriched signals, δ: 144.2 (C-1), 42.7 (C-8), 42.4 (C-2), 41.6 (C-9), 35.7 (C-6), 29.7 (C-4); natural abundance signals, δ: 139.9 (C-10), 68.1 (C-12), 63.4 (C-11), 48.2 (C-7), 44.7 (C-3), 30.4 (C-5), 29.2 (C-14), 26.4 (C-15), 19.6 (C-13).

Acknowledgements

I wish to express my profound gratitude to Professor William A. Ayer for his guidance, encouragement, and support during the course of this work. It has been a great privilege to have been associated with such a great man and scientist. I also wish to thank the Natural Sciences and Engineering Research Council of Canada and Conselho Nacional de Desenvolvimento Científico e Tecnológico of Brazil for financial support; Y. Hiratsuka and L. Hutchison, Forestry Canada, Northern Forestry Centre, Edmonton, for cultures of *Phellinus tremulae*; and Drs. T. T. Nakashima and M. G. Pausler for assistance with NMR experiments.

References

1. W.A. Ayer. Can. J. Chem. **73**, 465 (1995).
2. W.A. Ayer and E.R. Cruz. J. Org. Chem. **58**, 7529 (1993).
3. L.S. Trifonov, P. Chakravarty, Y. Hiratsuka, and W.A. Ayer. Eur. J. For. Pathol. *22*, 441 (1992).
4. W.A. Ayer and L.M. Browne. Tetrahedron, **37**, 2199 (1981), and references cited therein.
5. M. Jonassohn, H. Anke, O. Sterner, and C. Svensson. Tetrahedron Lett. **35**, 1593 (1994).
6. (*a*) Y. Tokiwa, M. Miyoshi-saitoh, H. Kobayashi, R. Sunaga, M. Konishi, T. Oki, and S. Iwasaki. J. Am. Chem. Soc. **114**, 4107 (1992); (*b*) K. Ando, T. Ito, and H. Kusano. *In* Ion exchange for industry. *Edited by* M. Streat. Ellis Horwood, England. 1988. pp. 232–238.
7. D.E. Cane and R.B. Nachbar. J. Am. Chem. Soc. **100**, 3208 (1978).
8. J.C. Vederas. Nat. Prod. Rep. **4**, 277 (1987).

© 1997 NRC Canada

9. (*a*) A. Bax, R. Freeman, and S.P. Kempsell. J. Am. Chem. Soc. **102**, 4849 (1980); (*b*) T.H. Mareci and R. Freeman. J. Magn. Reson. **48**, 158 (1982); (*c*) D.L. Turner. J. Magn. Reson. **49**, 175 (1982).
10. J. Mann. Secondary metabolites. 2nd ed. Clarendon, Oxford. 1987. pp. 95–131.
11. G. McInnes, D.G. Smith, J.A. Walter, L.C. Vining, and J.L.C. Wright. J. Chem. Soc. Chem. Commun. 282 (1974).

Can. J. Chem. Downloaded from www.nrcresearchpress.com by 88.146.161.215 on 09/08/12
For personal use only.

© 1997 NRC Canada

Oxygen insertion in *Sesamum indicum* furanofuran lignans. Diastereoselective syntheses of enzyme substrate analogues

Patrice A. Marchand, Jaroslav Zajicek, and Norman G. Lewis

Abstract: The furofuran lignans in sesame seed have an unusual oxygen insertion between their furan and aryl rings. In our continuing investigations on the isolation and characterization of the enzyme(s) involved, the diastereoselective syntheses of various substrate analogues for the oxygen insertion step were developed for future substrate specificity and inhibitor studies. This synthetic strategy also provided entry to so-called furofuranone epoxy-lignans, such as salicifoliol from *Bupleurum* sp., and acuminatolide from *Helichrysum* sp.

Key words: furofuran lignans, sesame, epimers, salicifoliol, acuminatolide.

Resumé : On observe dans les lignanes furanofuraniques des graines de sésame, une insertion d'oxygène typique entre le cycle tétrahydrofuranique et le cycle aromatique. Comme avant propos à l'étude et l'isolation des enzymes responsables de la biosynthèse de la sésamoline à partir du pinorésinol, nous décrivons ici la synthèse diastéréosélective des épimères de ces intermédiaires oxygénés. Une extension de cette voie synthétique nous a fournit la possibilité d'accéder aux furolactones, le salicifoliol et l'acuminatolide.

Mots clés : lignanes furofuraniques, sésame, épimères, salicifoliol, acuminatolide.

Can. J. Chem. Downloaded from www.nrcresearchpress.com by 88.146.161.215 on 09/08/12
For personal use only.

Introduction

The furofuran lignans present in sesame (*Sesamum indicum*) seed have many important roles. They can function as potent antioxidants (1–5), either directly or through conversion to sesaminol **1** (4), thereby enhancing the quality and shelf life of sesame seed oil. Sesame lignans can also act as synergists with pyrethrum insecticides (6, 7), or as cyclic AMP phosphodiesterase (8) and Δ-5 desaturase inhibitors in mammalian species (9). Moreover, addition of sesamin **2** to the diet reduces serum and liver cholesterol levels in rats (10) and has a hypocholesterolemic effect in humans (11). Dietary sesame lignans can protect against EtOH or CCl_4 induced liver damage (12), and enhance vitamin E activities (13) and the bioavailability of γ-tocopherol (14) in vivo.

Chemotaxonomic analyses of *Sesame* seed has established its major lignans as (+)-sesamin **2** and (+)-sesamolin **4** (Scheme 1) with the latter differing only by an oxygen insertion between the furofuran and piperonyl (3,4 methylenedioxyphenyl) groups. Biochemical entry to these furofuran lignans occurs via stereoselective coupling of two molecules of *E*-coniferyl alcohol **5** to give (+)-pinoresinol **3**, an enzymatic conversion of particular interest being the first example of regio- and stereospecific control of bimolecular phenoxy radical coupling (15–17). Although its enzymology of formation was first delineated in *Forsythia* sp. (15–17), (+)-pinoresinol **3** biosynthesis from *E*-coniferyl alcohol **5** in *Sesame* sp. is apparently engendered in a comparable manner (unpublished data).

Depending upon the species involved, (+)-pinoresinol **3** (a central intermediate in lignan biosynthesis) can be metabolized into a wide variety of different furofuran, furano, dibenzyl butane, dibenzyl butyrolactone, and aryl (tetrahydro)-naphthalene lignans (18, 19). For example, in *Forsythia intermedia*, enantiospecific reduction of (+)-pinoresinol **3** gives rise to (+)-lariciresinol **6** and (−)-secoisolariciresinol **7** (20–22), the dehydrogenation of which then affords (−)-matairesinol **8** (23). The NADPH-dependent enzyme catalyzing the sequential reductive steps leading to (−)-secoisolariciresinol **7** has been purified to apparent homogeneity, and the gene encoding the protein cloned (24).

In contrast, the lignan pathway in *Sesame* sp. converts (+)-pinoresinol **3** into (+)-sesamolin **4** via introduction of methylenedioxy bridges and an oxygen insertion between its aryl and furan rings. However, the sequence of oxidative/cyclization steps, and its associated enzymology, are as yet unknown. Scheme 2 shows plausible biosynthetic intermediates in the direct conversion of (+)-pinoresinol **3** to (+)-sesamolin **4**. At this juncture, it is emphasized that the nomenclature system adopted is that of the 8,8′-linked lignans; the other recommended systems (IUPAC and CAS) were not used since they lacked any internal numbering consistency between the

Received January 2, 1997.

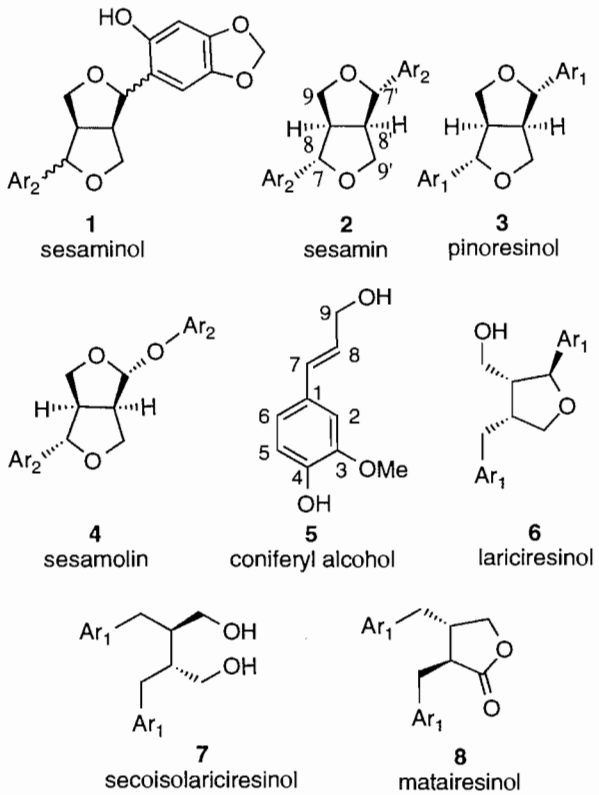
This paper is dedicated to Professor William A. Ayer on the occasion of his 65th birthday.

P.A. Marchand and N.G. Lewis.[1] Institute of Biological Chemistry, Washington State University, Pullman, WA 99164-6340, U.S.A.
J. Zajicek. Department of Chemistry and Biochemistry, University of Notre Dame, Notre Dame, IN 46556, U.S.A.

[1] Author to whom correspondence may be addressed. Telephone: (509) 335-2682. Fax: (509) 335-7643. E-mail: lewisn@wsu.edu

© 1997 NRC Canada

Scheme 1.



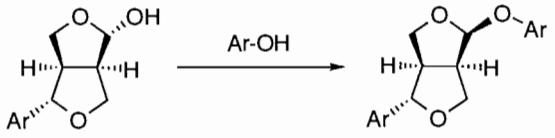
Legend: Ar_1 = 3-methoxy-4-hydroxyphenyl; Ar_2 = 3,4-methylenedioxyphenyl

different classes of lignans (and lignan-derived substances) described in this paper.

As can be seen, oxygen insertion could initially occur with (+)-pinoresinol **3** (route **a**) to give (+)-pinoresinolin **9**, with sequential methylenedioxy bridge formation to afford (+)-piperitolin **10** and (+)-sesamolin **4**, respectively. Oxygen insertion could also either follow or precede methylenedioxy bridge formation, i.e., from (+)-piperitol **11** to give (+)-sesamolinol **12** (route **b**) or from (+)-piperitol **11** to (+)-piperitolin **10** (route **c**), respectively. Perhaps, more unlikely, (+)-sesamin **2** may be directly converted into (+)-sesamolin **4** (route **d**). Synthetic methodology to pinoresinol **3** (22, 25), piperitol **11** (26), sesamin **2** (27), sesamolin **4** (27), pinoresinolin **9**, piperitolin **10**, and sesamolinol **12** (manuscript in preparation) has already been established, thus setting the stage for systematic study of the biosynthetic sequence involved.

The purpose of this investigation was to synthesize "epimers" **13–15** of the plausible aryl-*O*-furofuran biosynthetic intermediates **9, 10**, and **12**, which differ only in their stereochemistry at C-7′ (Scheme 3). These are required to examine both the substrate specificity of the oxygen insertion reaction using epi-pinoresinol **16**, epi-piperitol **17**, and related compounds as enzyme substrate analogues, as well as determining whether they could function as inhibitors of the enzymatic transformation itself. Moreover, given our ongoing interest in the enantiospecificity of lignan biosynthetic conversions, and identification of the *precise* enzymology involved, it was important to obtain these putative substrate analogues in

Fig. 1. General strategy to "oxygenated" lignans.



racemic form. This is because the various enantiomers can readily be separated by chiral column HPLC and, hence, provide the means to probe in detail both the enantiospecificity and diastereoselectivity of the oxygen insertion step. This approach has already been successfully applied to the study of (+)-pinoresinol **3** (15–17), (+)-lariciresinol **6**, (−)-secoisolariciresinol **7**, (−)-matairesinol **8** (20–24), and (−)-arctigenin **18** (28) biosynthesis.

Results and discussion

The main goal of this study was to develop a facile synthesis of the "oxygenated" lignans, epi-pinoresinolin **13**, epi-piperitolin **14**, and epi-sesamolinol **15**. To achieve this goal, we envisaged the best overall strategy to be that of synthesis of lactols of the type shown above, followed by aryl alkyl ether formation with inversion of configuration at C-7′ (see Fig. 1).

We sought first to establish the validity and usefulness of the proposed approach using, as synthon, the lactol samin **19**, which can readily be obtained in either racemic (±), (+), or (−) form (27, 29, 30). For this study, (+)-samin **19** (230 mg) was first conveniently prepared by acid hydrolysis (30, 31) of (+)-sesamolin **4** (527 mg), which in turn had previously been isolated from *S. indicum* seeds (Scheme 4).

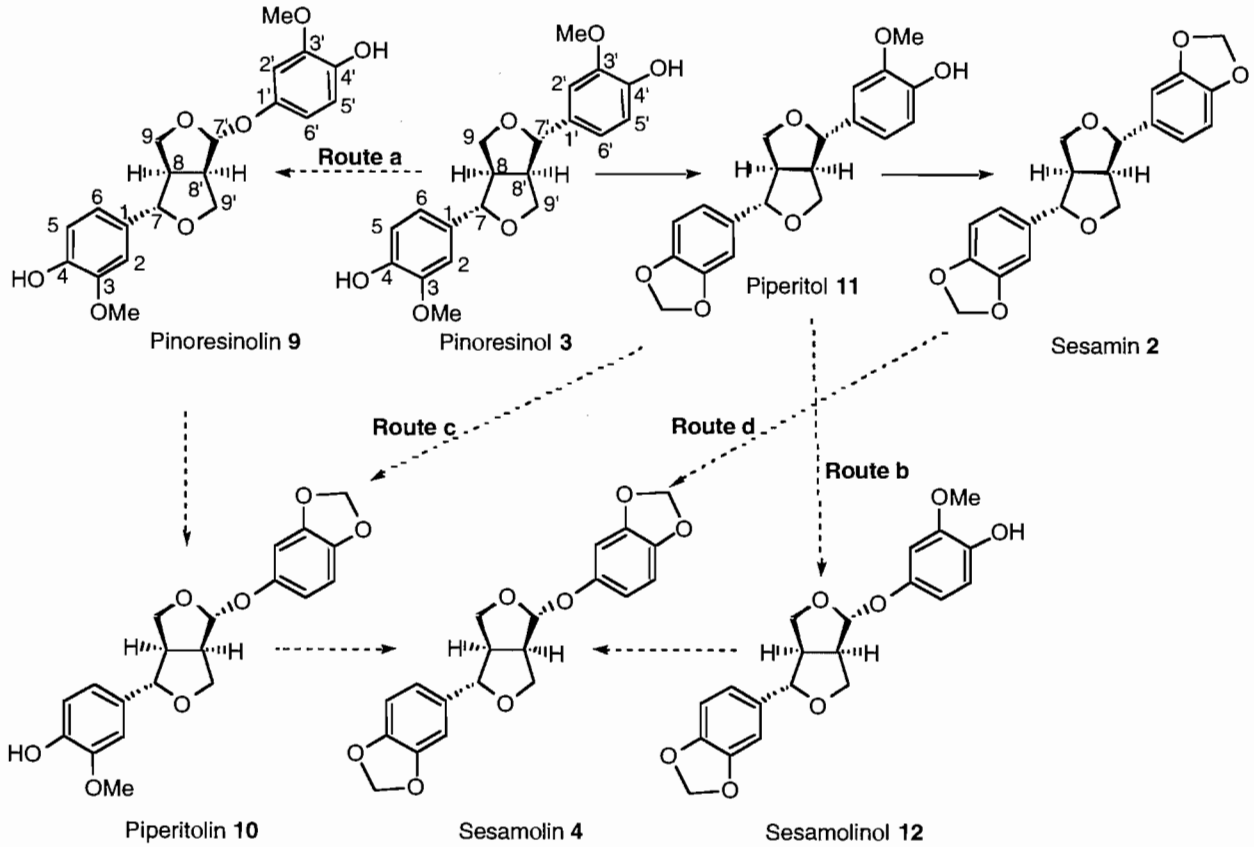
In the ^{1}H NMR spectrum of the starting material, (+)-sesamolin **4**, the H_{ax} proton at C-7′ appears as a singlet resonance at δ 5.47 (32); its absence of coupling with the adjacent bridgehead proton at H-8′ is in agreement with the projected dihedral angle of ~90°. Importantly, the corresponding H_{ax} proton at C-7′ of (+)-samin **19** also gave a singlet at δ 5.45 (data not shown), indicating that the relative stereochemistry in both molecules was the same at this position. Although the (+)-samin **19** thus generated had essentially an identical melting point, as well as IR, UV, and ^{1}H/^{13}C NMR spectra, to that reported previously (29), additional verification of the configuration of the furofuranol skeleton of **19** was determined by its conversion via oxidation with pyridinium dichromate to give the lactone, (+)-acuminatolide **20**. Its (−) antipode had previously been isolated from *Helichrysum acuminatum* (33), as well as obtained by total synthesis (27). Other than its optical rotation, (+)-acuminatolide **20** was identical in every respect to that of the natural product, thus verifying the overall configuration of (+)-samin **19** to be as shown. Moreover, to our knowledge, this is the first (hemi)synthesis of (+)-acuminatolide **20**.

With the configuration of (+)-samin **19** so defined, attention was next directed to the synthesis of (+)-epi-sesamolinol **15**. First, 4-benzyloxy-3-methoxyphenol **22** was obtained by Bayer–Villiger oxidation (34, 35) of *O*-benzyl vanillin **21** (23) via the action of *m*-chloroperoxybenzoic acid (*m*-CPBA) and subsequent NaOH hydrolysis. Phenol **22** was then condensed with (+)-samin **19**, in the presence of PPh_3 and DEAD (36), to give **23**, subsequent deprotection of which with H_2/Pd/C

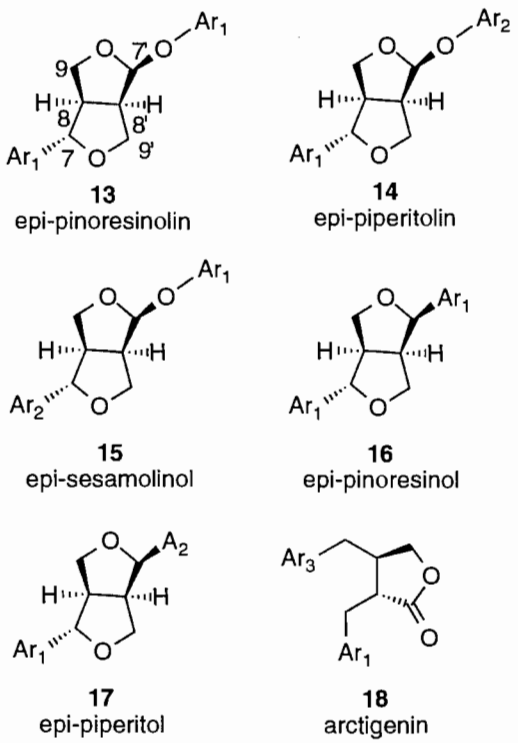
Can. J. Chem. Downloaded from www.nrcresearchpress.com by 88.146.161.215 on 09/08/12
For personal use only.

© 1997 NRC Canada

Scheme 2. Proposed biosynthetic pathways from (+)-pinoresinol **3** to (+)-sesamolin **4**.



Scheme 3.



Legend: Ar_1 = 3-methoxy-4-hydroxyphenyl; Ar_2 = 3,4-methylenedioxyphenyl; Ar_3 = 3,4-dimethoxyphenyl

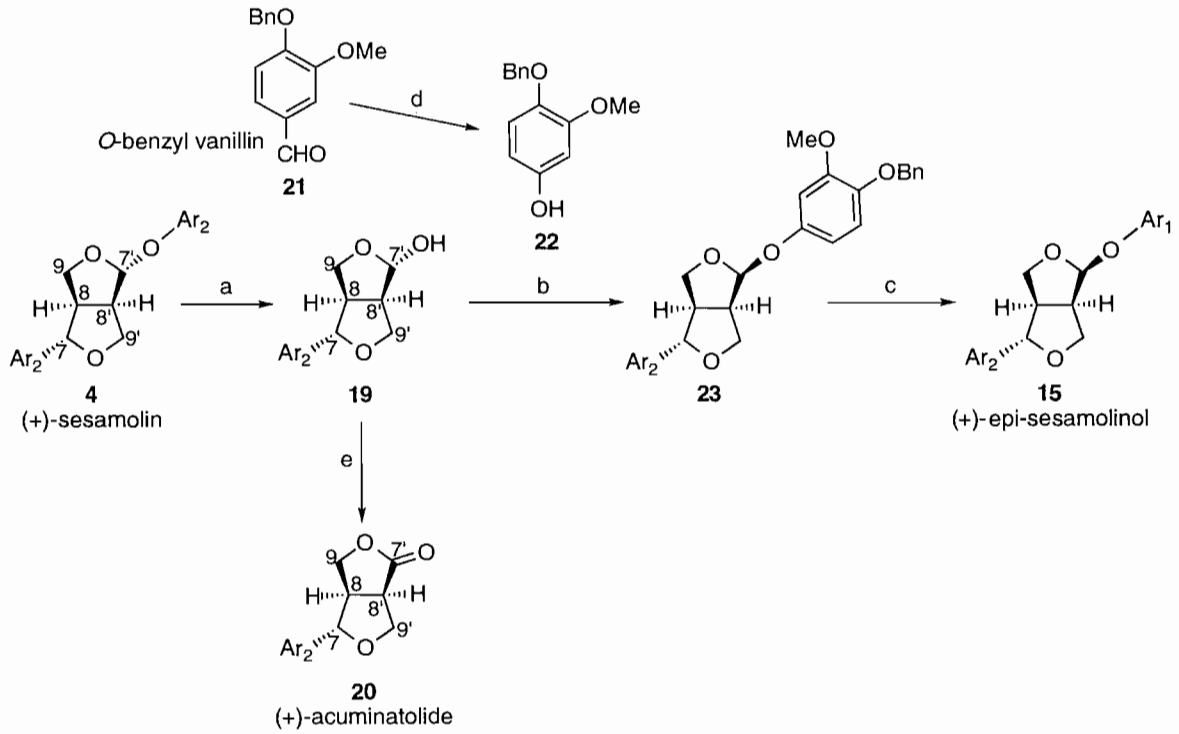
afforded (+)-epi-sesamolinol **15** in 60% overall yield. That the synthetic product so obtained had undergone an inversion of configuration at C-7′ could readily be determined by inspection of the ^{1}H NMR spectrum. The most striking change was the appearance of a doublet (J = 5.6 Hz) at 5.59 ppm, corresponding to the H_{eq} proton at C-7′ coupled to the C-8′ bridgehead proton. (This contrasts with the comparable H-7′$_{ax}$ resonance in (+)-sesamolin **4**, which has a singlet at δ 5.47 ppm.) This downfield shift of 0.15 ppm is consistent with related spectroscopic assignments for the naturally occurring lignan insecticidal agent, haedoxan A (H-7′$_{ax}$), to that of its epimeric synthetic product, isohaedoxan A (H-7′$_{eq}$), which showed a comparable downfield shift of 0.17 ppm (37). All other spectroscopic data supported epi-sesamolinol **15** to have the structure as shown. Consequently, not only does this represent the first (hemi)synthesis of (+)-epi-sesamolinol **15**, but adaptation of this approach using (±)-samin **19** gives a convenient route to racemic (±)-epi-sesamolinol **15**.

With the overall synthetic approach thus validated, attention was next directed to formation of the two other putative substrate analogues/inhibitors, epi-pinoresinolin **13** and epi-piperitolin **14**. In an analogous manner, this required synthesis of the pivotal lactol intermediate **24** (Scheme 5), which differs only from samin **19** by having a 4-benzyloxy-3-methoxyphenyl rather than a piperonyl group. Condensation of lactol **24** with either phenol **22** or its corresponding piperonyl analog would therefore afford (following deprotection) epi-pinoresinolin **13** and epi-piperitolin **14**, respectively (Schemes 5 and 6).

© 1997 NRC Canada

Can. J. Chem. Downloaded from www.nrcresearchpress.com by 88.146.161.215 on 09/08/12
For personal use only.

Scheme 4. Hemisynthesis of (+)-epi-sesamolinol **12** and (+)-acuminatolide **20**.



Legend: Ar_1 = 3-OMe-4-OH-Ph; Ar_2 = 3,4-OCH_2O-Ph; Bn = CH_2-Ph; a: H_3O^+, 65%; b: PPh_3, DEAD, THF, 80%; c: H_2/Pd/EtOAc, 75%; d: *m*-CPBA, CH_2Cl_2, then NaOH, MeOH, 64%; e: PDC, AcOH, 4 Å, CH_2Cl_2, 78%.

Lactol **24** was obtained from 4-vinylbutyrolactone **25** (38) as follows. Treatment of lactone **25** with LDA generated the corresponding lithiated form, which readily underwent diastereoselective addition with *O*-benzylvanillin **21**. This afforded exclusively the *trans* lactonic alcohol **26**, as a mixture of diastereoisomers in 92% yield (Scheme 5), which was used without further purification/resolution. (That the geometry of the pendant groups on the butyrolactone was indeed *trans* was based on a previous report of the configuration of the piperonyl analogue of **26**, prepared in a similar manner, which in turn was employed in the synthesis of the lignan insecticidal agents, haedoxan A, D, E, and their stereoisomers (37).)

Subsequent reduction of lactone **26** with $LiAlH_4$ and reaction of corresponding triol **27** with bromotrimethylsilane gave tetrahydrofuran **28**, presumed to possess both vinyl and hydroxymethyl substituents in a *syn* conformation, in 81% overall yield for both steps (37). Treatment of the vinyl group of alcohol **28** with OsO_4 in catalytic amount then afforded triol **29** as a mixture of diastereoisomers in 79% yield. Subsequent cleavage of its 1,2-diol by $NaIO_4$ gave the corresponding aldehyde, which underwent spontaneous cyclization, to afford lactol **24** in 84% yield. That this possessed a C-7′ H_{ax} was again established by inspection of the ^1H NMR spectrum, which displayed a 1H singlet at δ 5.35 ppm. Additionally, verification that only one stereoisomer resulted from this synthetic scheme was established via two pieces of interlocking evidence. The first involved oxidative conversion to the known lignan-derived furofuranone natural product, salicifoliol **31**, and the second by determination of the configuration of epi-pinoresinolin **13** via a combination of NOESY and HETCOR analyses (see later).

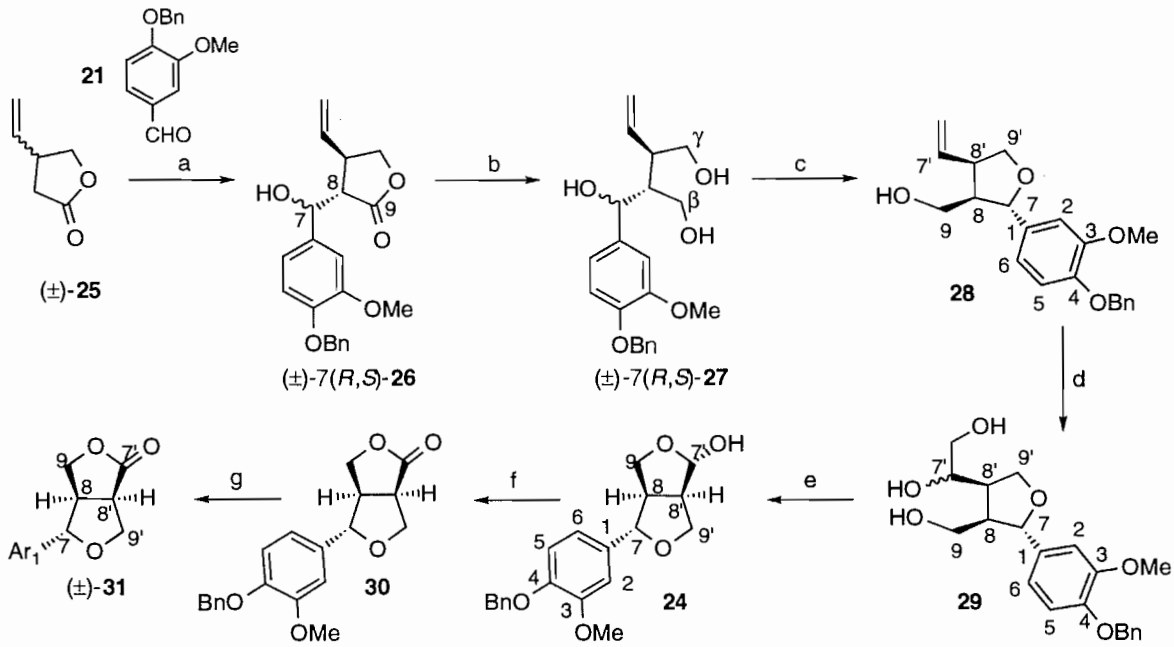
It had previously been established that the aerial portions of *Bupleurum salicifolium* Soland (39) contain salicifoliol **31**, in addition to the lignans (+)-pinoresinol **3**, (+)-eudesmin, and (+)-medioresinol. Thus, to verify the configuration of racemic lactol **24**, it was converted into salicifoliol **31** by oxidation with pyridinium dichromate (PDC) in the presence of AcOH and 4Å molecular sieves as before (40), with subsequent debenzylation (Scheme 5). That the synthetic product was indeed (±)-salicifoliol **31** was determined by its identical melting point to that of the natural product (101–102°C vs. 102–103°C (39)), as well as by comparison of its MS fragmentation patterns, $^1H/^{13}C$ NMR, UV, and IR spectra to those reported for (+)-salicifoliol **31**. Previous COSY experiments had shown that the pendant aryl group of salicifoliol **31** was *exo*, and that the bridgehead hydrogens were *cis* to each other. Thus, with all spectroscopic data identical to the naturally occurring product, with the exception of optical rotation, this represents the first synthesis of (±)-salicifoliol **31**. More importantly, it provided strong evidence that the configuration of lactol **24** was as shown.

With good evidence supporting the structure and configuration of lactol **24** as shown, attention was directed to the formation of (±)-epi-pinoresinolin **13** (Scheme 6). Again, *O*-benzylvanillin **21** was converted into the corresponding phenol **22**, via Bayer–Villiger oxidation with *m*-CPBA and subsequent NaOH hydrolysis. This was then reacted with lactol **24**, in the presence of PPh_3 and DEAD, to give **32**, subsequent

© 1997 NRC Canada

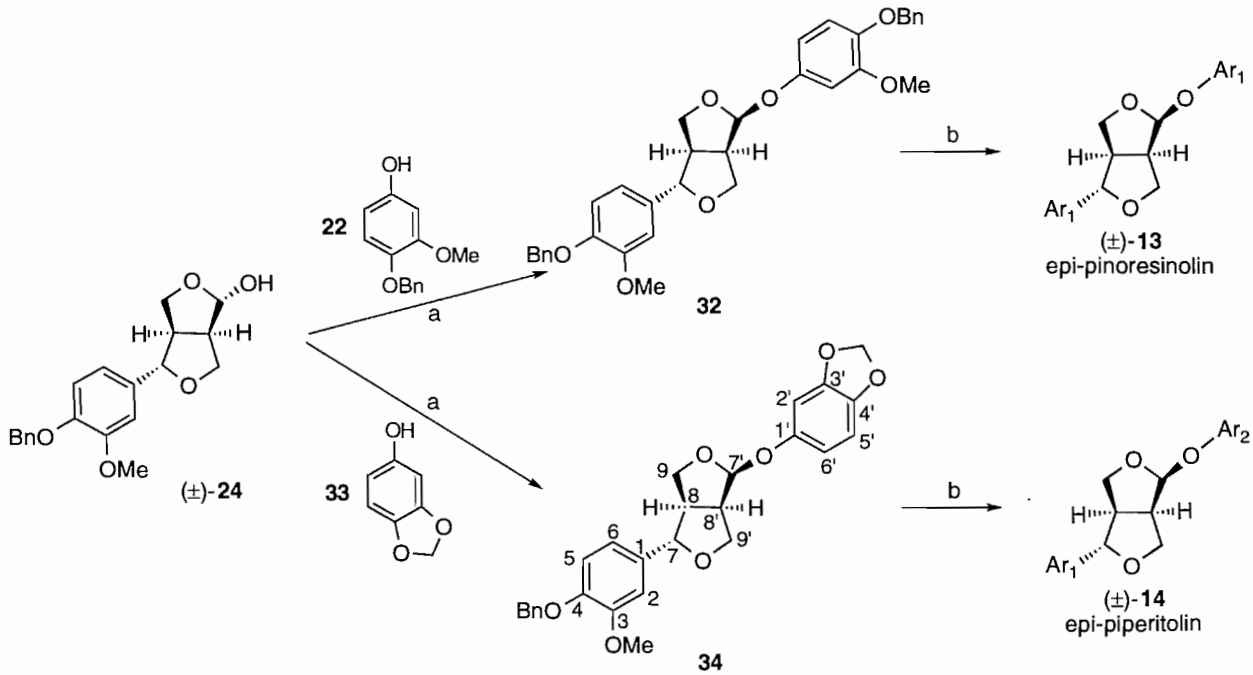
Can. J. Chem. Downloaded from www.nrcresearchpress.com by 88.146.161.215 on 09/08/12
For personal use only.

Scheme 5. Synthesis of (±)-lactol **24** and (±)-salicifoliol **31**.



Legend: Ar_1 = 3-OMe-4-OH-Ph, Bn = CH_2-Ph; a: LDA, THF, **21**, 92%; b: $LiAlH_4$, THF, 89%; c: TMSBr, THF, 89%; d: OsO_4, NMO, THF/H_2O, 79%; e: $NaIO_4$, THF, 89%; f: PDC, AcOH, 4 Å, CH_2Cl_2, 78%; g: H_2/Pd/C, EtOAc, 90%.

Scheme 6. Synthesis of (±)-epi-pinoresinolin **13** and (±)-epi-piperitolin **14**.



Legend: Ar_1 = 3-OMe-4-OH-Ph; Ar_2 = 3,4-OCH_2O-Ph; Bn = CH_2-Ph; a: PPh_3, DEAD, THF, **22**: 89%; **33**: 85%; b: H_2/Pd/C, EtOAc, **13**: 84%; **14**: 88%.

deprotection of which with H_2/Pd/C gave (±)-epi-pinoresinolin **13** in 75% overall yield. Its configuration was next determined by a combination of HETCOR and NOESY spectral analyses, where the ^1H NMR signals of epi-pinoresinolin **13** were assigned to individual protons on the basis of chemical shift, observed multiplicities, and decoupling experiments (Table 1), and all carbons (with directly attached protons) assigned using the HETCOR spectrum. Assignments of sig-

© 1997 NRC Canada

Can. J. Chem. Downloaded from www.nrcresearchpress.com by 88.146.161.215 on 09/08/12
For personal use only.

Can. J. Chem. Downloaded from www.nrcresearchpress.com by 88.146.161.215 on 09/08/12
For personal use only.

Table 1. NMR (600 MHz, ^1H; 150 MHz, ^{13}C; $CDCl_3$) spectral data for epi-pinoresinolin **13**.

	^{13}C	^1H	
Assignment	δ	δ	*J* (Hz)
1	132.69	—	
2	108.53	6.93	d, $J_{2,6}$ = 1.9
3	146.66[a]	—	
4	145.23[a]	—	
5	114.23	6.89	d, $J_{5,6}$ = 8.1
6	118.90	6.83	d,d, $J_{2,6}$ = 1.9, $J_{5,6}$ = 8.1
7	85.30	4.80	d, $J_{7,8}$ = 7.1
8	52.75	3.04	m, $J_{8,9ax}$= 7.6, $J_{8,9eq}$ = 4.7
9	69.30	H_{ax}, 4.12	m, $J_{9ax,eq}$ = 9.1
		H_{eq}, 4.03	
OH	—	5.43	br s
OCH_3	55.87	3.90	s, 3H
1′	150.80	—	
2′	101.75	6.69	d, $J_{2',6'}$ = 2.7
3′	146.83[a]	—	
4′	140.91[a]	—	
5′	114.17	6.84	d, $J_{5',6'}$ = 8.7
6′	108.41	6.64	dd, $J_{6',2'}$ = 2.7, $J_{6',5'}$ = 8.7
7′	102.83	5.60	d, $J_{7',8'}$ = 5.6
8′	51.10	3.33	$J_{8',9'ax}$ = 8.0, $J_{8',9'eq}$ = 4.1, $J_{8',8}$ = 10.0
9′	67.00	H_{ax}, 4.42	$J_{9'ax,eq}$ = 9.1
		H_{eq}, 4.17	
OH	—	5.73	br s
OCH_3	55.91	3.87	s

[a]Assigments are interchangeable for nonprotonated carbons.

nals derived from quaternary carbons were based on comparison with reported chemical shift data for (+)-sesamolin **4** (32).

To summarize, the NOESY spectra (mixing times 300 and 600 ms) showed a strong cross-peak between the H-8 and H-8′ proton signals suggesting that both were *cis* to each other. Moreover, the H-8 signal exhibited a correlation with the H-2 and H-6 proton resonances of the pendant aryl (Ar) group at δ 6.93 and 6.83, respectively, indicating that the 3-OMe-4-OH-phenyl group was attached to C-7 in a *cis* relationship to the H-8 and H-8′ protons. Significantly, although the NOESY spectra also displayed cross peaks between the H-7′ proton resonance and the H-2′ and H-6′ signals, none of the proton signals of the aryl group attached to the C-7′ showed any correlation to the H-8′ signal. In contrast, the H-7′ signal exhibited a correlation to the H-8′ signal, suggesting that the pendant aryl group attached to C-7′ was *trans* to the H-8 and H-8′ protons. The axial "β" configuration of the aryl group at C-7′ was again further supported by the fact that the signal of the H-$7'_{eq}$ proton was a downfield doublet ($J_{7',8'}$ = 5.6 Hz) at δ 5.6 ppm. Thus, via a combination of derivatization and spectroscopic analyses, the configuration of epi-pinoresinolin **13** was as shown.

Lastly, with the configuration of epi-pinoresinolin **13** unambiguously determined, sesamol **33** (3,4-methylenedioxy phenol) was condensed with lactol **24** to afford, after deprotection of **34**, (±)-epi-piperitol **14** in 75% overall yield.

Concluding remarks

This study provides a convenient synthetic strategy to the "oxygenated" lignans epi-pinoresinolin **13**, epi-piperitolin **14**, and epi-sesamolinol **15** in good overall yield. The configuration of each molecule was determined via a number of spectroscopic means as well as by chemical derivatization, the latter proceeding in a manner that also permitted the synthesis of furofuranone lignan-derived substances, such as acuminatolide **20** and salicifoliol **31**. Future studies will be directed to defining the enzymology of the "oxygen" insertion step, with the compounds so obtained used as substrate analogues or inhibitors.

Experimental

Unroasted and unbleached seeds of *Sesamum indicum* were purchased in a local grocery store. IR and UV spectra were recorded on Perkin–Elmer 1720-X FTIR and Lambda 6 UV/VIS spectrophotometers, respectively. NMR studies of epi-pinoresinolin **13** were performed on a Varian UNITY*plus* (599.89 MHz, ^1H) spectrometer, whereas all other $^1H/^{13}C$ spectra were obtained on a Brüker AMX-300 (300.14 MHz, ^1H) instrument. NMR spectra were recorded in $CDCl_3$ solution with TMS as an internal reference, with chemical shifts (δ) expressed in ppm and coupling constants (*J*) in Hz.

© 1997 NRC Canada

Can. J. Chem. Downloaded from www.nrcresearchpress.com by 88.146.161.215 on 09/08/12
For personal use only.

NOESY spectra were recorded using the standard pulse sequence (41), with mixing times, t_m, of 300 and 600 ms. HETCOR spectra were measured using the pulse sequence previously described (42). The ^1H chemical shifts and coupling constants were obtained by first-order analysis of 1D spectra. EIMS were carried out using a Waters Integrity HPLC/MS, whereas HRMS employed a VG 7070 EHF mass spectrometer with a temperature source of 250°C at 70 eV with Ar_1 = 3-methoxy-4-hydroxyphenyl and Ar_2 = 3,4-methylenedioxyphenyl for fragment interpretation. Solvents were either HPLC grade (CH_3CN, MeOH, AcOH, CH_2Cl_2, THF) or ACS grade (EtOAc, hexanes) and were obtained from Baker. Tetrahydrofuran (THF) and methylene chloride (CH_2Cl_2) were distilled over $LiAlH_4$–triphenylmethane and CaH_2, and column and analytical thin-layer chromatographic separations were performed using silica gel 60 (230–400 mesh) and AL SI G/UV 254 (Whatman), respectively.

(+)-Samin 19

This was synthesized as outlined (30, 31) but modified as follows. A suspension of (+)-sesamolin **4** (527 mg, 1.42 mmol), DOWEX 50 X2-200 (545 mg), NaOAc (150 mg, 1.83 mmol), and HCl 10% (1 mL) in CH_3CN (10 mL) was stirred under reflux for 2 h. The suspension was then cooled to room temperature, the resin removed by filtration, and the filtrate evaporated in vacuo, to give a dry solid. The resulting residue was dissolved in a minimum amount of $CHCl_3$ and subjected to silica gel column chromatography, eluted with hexanes:EtOAc 3:1 to 1:1, to give (+)-samin **19** (230.8 mg, 65%); mp 108–109°C (EtOAc:cyclohexane) (lit. (31) mp 106°C; (29) mp 108–109°C); $[\alpha]_D$ +104.65 (*c* 0.516, $CHCl_3$) (lit. $[\alpha]_D$ (30) +103); IR ($CHCl_3$) ν_{max}: 3400 (br, OH), 1610, 1505, 1490, 1446, 1245 cm^{-1}; MS *m/e* (relative %): 250 (M^+, 86), 232 ($M - H_2O^+$, 6), 194 ($M - C_2O_2^+$, 38), 176 (54), 149 (Ar_2CO^+, 100), 135 ($Ar_2CH_2^+$, 58), 122 (Ar_2H^+, 22); HRMS; calcd. for $C_{13}H_{14}O_5$: 250.0841 (M^+), found: 250.0805; for ^1H and ^{13}C NMR spectral analyses: see ref. 29.

(+)-Acuminatolide 20

To a solution of (+)-samin **19** (80 mg, 0.32 mmol) in dry CH_2Cl_2 (50 mL) was added pyridinium dichromate (PDC) (4 equiv., 481 mg), AcOH (1 equiv., 20 μL), and 4Å molecular sieves (500 mg). The resulting suspension was stirred for 6 h at room temperature (r.t.), then filtered through a plug of silica gel and the filtrate removed in vacuo to give a yellow solid. The residue was dissolved in a minimum amount of $CHCl_3$ and subjected to silica gel column chromatography, eluted with hexanes:EtOAc (2:1), to give **20** (61.84 mg, 78%); mp 118°C (EtOAc:hexanes) (lit. (27, 33) mp 118–119°C); $[\alpha]_D$ +100.2 (*c* 0.11, $CHCl_3$) (lit. $[\alpha]_D$ (27) −103.82 (*c* 0.31, $CHCl_3$); $[\alpha]_D$ (33) −37 (*c* 0.11, $CHCl_3$)); IR ($CHCl_3$) ν_{max}: 1775 (C=O), 1610, 1510, 1500 (C=CAr), 1245 (C-O) cm^{-1}; ^1H NMR δ: 6.80 (br s, 1H, H-2), 6.70 (br s, 2H, H-5 and H-6), 5.95 (s, 2H, OCH_2O), 4.57 (d, 1H, $J_{7,8}$ = 6.8, H-7), 4.46 (dd, 1H, $J_{9eq,9ax}$ = 6.8, $J_{8,9eq}$ = 9.7, H-9eq), 4.35–4.25 (m, 2H, H-9′ax and H-9ax), 4.14 (dd, 1H, $J_{9'eq,9'ax}$ = 3.6, $J_{8',9'eq}$ = 9.3, H-9′eq), 3.40 (ddd, 1H, $J_{7,8'}$ = 3.6, $J_{8',9'eq}$ = 9.3, $J_{8',8}$ = 9.0, H-8′), 3.05 (m, 1H, H-8); ^{13}C NMR δ: 178.16 (C-7′), 148.11 (C-3), 147.60 (C-4), 132.73 (C-1), 119.57 (C-6), 108.22 (C-5), 106.27 (C-2), 101.19 (OCH_2O), 85.92 (C-7), 69.93 and 69.77 (C-9/C-9′), 48.86 (C-8), 46.58 (C-8′) ppm; MS *m/e* (relative %): 248 (M^+, 100), 218 ($M - CH_2O^+$, 22), 163 (83), 150 (Ar_2CHO^+, 80), 149 (Ar_2CO^+, 100), 135 ($Ar_2CH_2^+$, 82), 121 (Ar_2^+, 38); HRMS, calcd. for $C_{13}H_{12}O_5$: 248.0685 (M^+); found: 248.0683.

4-Benzyloxy-3-methoxy phenol 22

Phenol **22** (139.5 mg, 0.64 mmol) was prepared from *O*-benzylvanillin **21** (242 mg, 1 mmol) (23) in 64% overall yield exactly as described (34, 35).

O-Benzyl-epi-sesamolinol 23

To a solution of (+)-samin **19** (29.8 mg, 0.12 mmol) in dry THF (10 mL), PPh_3 (31.6 mg, 0.12 mmol), and protected phenol **22** (26.2 mg, 0.12 mmol) was added diethylazodicarboxylate (DEAD) (19 μL, 1 equiv.). The mixture was stirred at r.t. for 24 h and the solvent removed in vacuo. The residue was next subjected to silica gel column chromatography, eluted with hexanes:EtOAc 3:1 (v/v), to give *O*-benzyl epi-sesamolinol **23** (44.8 mg, 80%). IR ($CHCl_3$) ν_{max}: 1600, 1510, 1450 (C=CAr), 1250, 1220 (C-O) cm^{-1}; ^1H NMR δ: 7.50–7.20 (m, 5H, Bn), 6.90–6.55 (m, 6H, C*H*Ar), 5.94 (s, 2H, OCH_2O), 5.62 (d, 1H, $J_{7',8'}$ = 5.6, H-7′), 5.10 (s, 2H, CH_2Ph), 4.80 (d, 1H, $J_{7,8}$ = 6.8, H-7), 4.45–4.38 (m, 1H, H-9′ax), 4.20–4.10 (m, 1H, H-9′eq), 4.15–4.10 (m, 1H, H-9ax), 4.05–3.95 (m, 1H, H-9eq), 3.87 (s, 3H, OCH_3), 3.35–3.25 (m, 1H, H-8′), 3.05–2.90 (m, 1H, H-8); ^{13}C NMR δ: 151.95, 151.14, 150.56, 147.92, 147.13 (C-3, C-4, C-1′, C-3′, C-4′), 134.79 (*C*q/Bn), 143.31 (C-1), 128.42, 128.38, 127.37 (*C*H/Bn), 119.42 (C-6), 115.27 (C-5′), 108.13 (C-5), 107.03 (C-6′), 106.39 (C-2), 102.65 (C-7′), 102.41 (C-2′), 101.02 (OCH_2O), 85.31 (C-7), 71.83 (CH_2Ph), 69.40 (C-9′), 67.08 (C-9), 55.93 (OCH_3), 52.85 (C-8), 51.09 (C-8′); MS *m/e* (relative %): 462 (M^+, 5), 243 (20), 230 (70), 203 (30), 165 (15), 149 (Ar_2CO^+, 15), 135 ($Ar_2CH_2^+$, 100), 121 (Ar_2^+, 70), 105 (15); HRMS, calcd. for $C_{27}H_{26}O_7$: 462.1679; found: 462.1671.

(+)-Epi-sesamolinol 15

(+)-*O*-Benzyl epi-sesamolinol **23** (59.2 mg, 0.13 mmol) in EtOAc (5 mL) was treated with Pd/C 10% (15 mg). The solution was then stirred for 3 h under H_2 atmosphere, following which it was filtered over a short path silica gel column eluted with EtOAc. The filtrate was removed in vacuo, and the resulting residue purified by silica gel column chromatography, eluted with EtOAc:hexanes 2:1 (v/v), to give (+)-epi-sesamolinol **15** (29 mg, 75%). $[\alpha]_D$ +182 (*c* 0.996 g/100 mL in $CHCl_3$); IR ($CHCl_3$) ν_{max}: 3425 (br, OH), 1613, 1510, 1490, 1448 (C=CAr), 1234, 1196 cm^{-1}; UV λ_{max}: 230, 285 nm; ^1H NMR δ: 6.90–6.70 (m, 6H), 5.95 (s, 2H, OCH_2O), 5.59 (d, 1H, $J_{7',8'}$ = 5.6, H-7′), 5.38 (br s, 1H, OH), 4.78 (d, 1H, $J_{7,8}$ = 7, H-7), 4.50–4.35 (m, 1H, H-9′ax), 4.20–4.10 (m, 1H, H-9′eq), 4.10–4.08 (m, 1H, H-9ax), 4.05–3.95 (m, 1H, H-9eq), 3.87 (s, 3H, OCH_3), 3.35–3.20 (m, 1H, H-8′), 3.05-2.95 (m, 1H, H-8); ^{13}C NMR δ: 150.69 (C-1′), 147.88 (C-3), 147.07 (C-4), 146.80 (C-3′), 140.82 (C-4′), 134.90 (C-1), 119.36 (C-6), 114.13 (C-5′), 108.56 (C-5), 108.26 (C-6′), 106.54 (C-2), 101.92 (C-7′), 101.15 (OCH_2O), 100.98 (C-2′), 85.44 (C-7), 69.47 (C-9), 67.23 (C-9′), 56.08 (OCH_3), 53.08 (C-8′), 51.26 (C-8); MS *m/e* (relative %): 372 (M^+, 5), 273 (5), 233 (28), 203 ($Ar_2C_5H_6O^+$, 45), 149 (Ar_2CHO^+, 30), 140 (70), 135 ($Ar_2CH_2^+$, 100), 121 (Ar_2^+, 25), 105 (18); HRMS, calcd. for $C_{20}H_{20}O_7$: 372.1209; found: 372.1194.

© 1997 NRC Canada

Can. J. Chem. Downloaded from www.nrcresearchpress.com by 88.146.161.215 on 09/08/12
For personal use only.

Lactone 26

To a solution of LDA (3.18 mmol, 1.1 equiv.), freshly prepared from diisopropyl amine (0.42 mL) and 1.6 M *n*-BuLi in hexanes (1.99 mL) at −15°C, in dry THF (10 mL) under argon at −78°C (acetone – Dry Ice bath), was added dropwise 4-vinyl butyrolactone **25** (323.5 mg, 2.88 mmol, 1 equiv.) in dry THF (6 mL) over 30 min. The resulting mixture was stirred at −78°C for 30 min, following which *O*-benzylvanillin **21** (578.5 mg, 2.39 mmol) in dry THF (5 mL) was added dropwise over 30 min with the mixture allowed to stir at −78°C for an additional 3.5 h. A saturated solution of $NH_4Cl_{(aq)}$ (0.5 mL) was added, and the resulting mixture was then allowed to warm to r.t. The mixture was sequentially extracted with diethyl ether (2 × 15 mL) and EtOAc (2 × 15 mL), with the combined organic layers dried (Na_2SO_4), evaporated in vacuo, and the resulting residue chromatographed on a silica gel column, eluted with hexanes:EtOAc 2:1 (v/v), to give the diastereoisomeric lactone **26** (779.7 mg, 92%) mixture, which was not resolved further. IR ($CHCl_3$) ν_{max}: 3492 (br, OH), 1762 (C=O), 1593, 1515, 1455 (C=CAr) cm^{-1}; ^1H NMR δ: 7.40–7.18 (m, 5H, Bn), 6.88–6.85 (m, 3H, C*H*Ar), 5.30–5.15 (m, 1H, =C*H*), 4.85–4.55 (m, 1H, C*H*OH), 4.35–4.15 (m, 2H, =CH_2), 4.15–3.90 (m, 2H, CH_2OCO), 3.74 (s, 3H, OCH_3), 3.25–3.10 and 2.85–2.70 (m, 1H, =CH-C*H*), 2.70–2.55 (m, 1H, CO-C*H*); ^{13}C NMR δ: 177.72, 177.46 (*C*O), 149.17, 149.07, 147.42, 146.76 (*C*q-O/Ar), 136.69, 136.65 (*C*q/Bn), 135.78, 134.46 (CH$_2$=*C*H), 134.26, 131.92 (*C*q/Ar), 128.04, 127.38, 126.92 (*C*H/Bn), 118.84, 117.46 (*C*H/Ar), 113.36, 113.16 (*C*H/Ar), 116.96, 116.38 (*C*H$_2$=), 110.05, 109.27 (*C*H/Ar), 72.90, 69.93 (*C*HOH), 70.44, 70.35 (*C*H$_2$O), 70.42 (*C*H$_2$Ph), 55.97 (O*C*H$_3$), 55.47, 51.58 (*C*H$_2$CO), 41.96, 38.58 (*C*H-CH=); MS *m/e* (relative %): 354 (M^+, 90), 337 (65), 336 (27), 315 (30), 243 (100), 151 (Ar_1CO^+, 80), 123 (Ar_1^+, 50); HRMS, calcd. for $C_{21}H_{22}O_5$: 354.1467; found: 354.1486.

Triol 27

To a solution of $LiAlH_4$ (51.2 mg, 1.5 equiv.) in dry THF (10 mL) at 0°C, under an atmosphere of argon, was added dropwise a solution of lactone **26** (302.1 mg, 0.85 mmol) in dry THF (15 mL). The temperature was next raised to 50°C, this being maintained for an additional 1.5 h. After cooling to r.t., the solution was neutralized with saturated $NH_4Cl_{(aq)}$ and extracted with $CHCl_3$ (3 × 10 mL). The organic solubles were combined, dried (Na_2SO_4), evaporated to dryness in vacuo, and the resulting residue purified by chromatography on silica gel, eluted sequentially with hexanes:EtOAc 2:1 (v/v) and EtOAc, to give the diastereoisomeric triol **27** (258 mg, 89%) mixture, which was not resolved further. IR ($CHCl_3$) ν_{max}: 3310 (br, OH), 1640 (C=C), 1606, 1593, 1510, 1455 (C=C, C=CAr), 1261, 1219 (C-O) cm^{-1}; ^1H NMR δ: 7.35–7.20 (m, 5H, Bn), 6.90–6.80 and 6.80–6.70 (m, 3H, C*H*Ar), 5.90–5.50 (m, 1H, =C*H*), 5.20–5.00 (m, 2H, =CH_2), 5.07 (s, 1H) and 5.06 (s, 1H, CH_2-Ph), 5.00–4.70 (m, 1H, C*H*OH), 3.81 (s, 3H, OCH_3), 3.80–3.30 (m, 4H, CH_2OH), 2.60–2.20 (m, 1H, C*H*-CHOH), 2.10–1.60 (m, 1H, =CH-C*H*); ^{13}C NMR δ: 149.29, 149.20 (C-4), 146.99, 146.90 (C-3), 138.52, 138.40 (*C*H=), 136.86, 136.05 (C-1, *C*q/Bn), 128.32, 127.67, 127.15 (*C*H/Bn), 118.40, 117.95 (C-6), 117.24, 116.30 (*C*H$_2$=), 113.59, 113.46 (C-5), 109.87, 109.49 (C-2), 74.55, 72.16 (*C*HOH), 70.82 (*C*H$_2$-Ph), 63.06, 62.50, 59.96, 59.53 (2 × *C*H$_2$OH), 55.77 (O*C*H$_3$), 50.06, 48.07 (=CH-*C*H), 44.87, 43.05 (*C*H-CHOH); MS *m/e* (relative %): 340 ($M^+ - H_2O^+$, 19), 322 (100), 291 (19), 275 (34), 231 (85), 201 (81), 167 (87), 149 (79), 128 (81); HRMS, calcd. for $C_{21}H_{26}O_5$: 340.1675 ($M - H_2O^+$); found: 340.1686.

Tetrahydrofuran 28

To a solution of the diastereoisomeric triol mixture **27** (189 mg, 0.55 mmol) in dry CH_2Cl_2 (5 mL) was added TMSBr (140 μL, 2 equiv.). The resulting solution was then stirred at r.t. for 15 min, neutralized with saturated $NaHCO_{3(aq)}$ (0.5 mL), dried (Na_2SO_4), with the organic solvent evaporated in vacuo and the residue subjected to silica gel column chromatography, eluted with hexanes:EtOAc 2:1 (v/v), to give tetrahydrofuran **28** (159.3 mg, 89%). IR ($CHCl_3$) ν_{max}: 3300 (br, OH), 1640 (C=C), 1606, 1594, 1515, 1465 (C=CAr), 1263, 1225 (C-O) cm^{-1}; ^1H NMR δ: 7.45–7.30 (m, 5H, Bn), 6.93 (d, 1H, J = 1.7, C*H*Ar), 6.84–6.78 (m, 1H, C*H*Ar), 5.97–5.90 (m, 1H, =C*H*), 5.22–5.14 (m, 2H, =CH_2), 5.16 (s, 2H, CH_2-Ph), 4.70 (d, 1H, J = 7.3, ArC*H*O), 4.23 and 3.83 (dd, 2H, J = 6.7, 8.6, CH_2OC), 3.90 (s, 3H, OCH_3), 3.75–3.69 (m, 1H) and 3.64–3.60 (m, 1H, CH_2OH), 3.15–3.05 (m, 1H, =CH-C*H*), 2.40–2.30 (m, 1H, C*H*-CH$_2$OH); ^{13}C NMR δ: 149.63 (C-4), 147.49 (C-3), 137.07 (*C*q/Bn), 135.57 (*C*H=), 135.38 (C-1), 128.44, 127.73, 127.19 (*C*H/Bn), 118.10 (C-6), 117.32 (*C*H$_2$=), 113.72 (C-5), 109.47 (C-2), 82.41 (C-7), 72.61 (C-9′), 70.94 (*C*H$_2$-Ph), 60.76 (C-9), 55.90 (O*C*H$_3$), 53.41 (C-8), 45.62 (C-8′); MS *m/e* (relative %): 322 ($M - H_2O^+$, 100), 293 (10), 268 (5), 231 (95), 201 (73), 171 (55), 149 (63), 123 (Ar_1^+, 65); HRMS, calcd. for $C_{21}H_{24}O_4$ ($M - H_2O^+$): 322.1569; found: 322.1558.

Triol 29

To a solution of tetrahydrofuran **28** (144 mg, 0.45 mmol) in THF (3 mL) was added OsO_4 (2.5% equiv., 108 μL of a 2.5% soln. in *t*-BuOH) and *N*-methylmorpholine-*N*-oxide (NMO) (1.4 equiv., 124 μL of a 60% soln. in H_2O). The suspension was stirred for 2 days at r.t., following which it was extracted with $CHCl_3$ (3 × 10 mL). The organic solubles were combined, dried (Na_2SO_4), the solvent removed in vacuo, and the resulting residue chromatographed on silica gel, eluted with hexanes:EtOAc 2:1 (v/v), to give the triol **29** (132.1 mg, 79%). IR ($CHCl_3$) ν_{max}: 3390 (br, OH), 1607, 1594, 1515, 1455 (C=CAr), 1263, 1217 (C-O) cm^{-1}; ^1H NMR δ: 7.40–7.20 (m, 5H, Bn), 6.90–6.70 (m, 3H, C*H*Ar), 5.14 (s, 2H, CH_2-Ph), 4.79 (d, J = 6.4) and 4.51 (d, J = 3.8, 1H, OC*H*-Ar), 4.10–3.90 (m, 1H, C*H*OH-CH$_2$OH), 3.90–3.30 (m, 6H, CH_2OH and CH_2O), 3.83 (s, 3H, OCH_3), 2.60–2.30 (m, 1H, C*H*CHOH), 2.60–2.35 and 2.30–2.20 (m, 1H, C*H*CH$_2$OH); ^{13}C NMR δ: 149.51 (C-4), 147.47 (C-3), 136.84 (*C*q/Bn), 135.07, 134.98 (C-1), 128.38, 127.73, 127.20 (*C*H/Bn), 117.96, 117.81 (C-6), 113.62 (C-5), 109.41 (C-2), 82.81, 82.11 (C-7), 70.87 (*C*H$_2$-Ph), 70.46, 70.35 (*C*HOH), 68.93, 68.25 (C-7′) 65.71, 65.39 (*C*H$_2$OH), 60.67, 59.53 (C-9), 55.91 (O*C*H$_3$), 51.15, 50.74 (C-8), 43.86, 42.54 (C-8′); MS *m/e* (relative %): 374 (M^+, 83), 356 (80), 338 (50), 295 (50), 283 (20), 265 (90), 175 (78), 151 (Ar_1CO^+, 80), 123 (Ar_1^+, 100), 107 (90); HRMS, calcd. for $C_{21}H_{26}O_6$: 374.1726; found: 374.1741.

Furanofuran-1-ol 24

To a solution of triol **29** (125.1 mg, 0.334 mmol) in MeOH (3 mL) at 0°C was added dropwise a solution of $NaIO_4$ (85.7 mg, 1.2 equiv.) in MeOH–H_2O (6.5 mL, 10:3) over 10 min. The

© 1997 NRC Canada

Can. J. Chem. Downloaded from www.nrcresearchpress.com by 88.146.161.215 on 09/08/12
For personal use only.

temperature was raised to r.t., with the mixture allowed to stir for an additional 12 h, and then filtered. The resulting filtrate was extracted with $CHCl_3$ (3 × 10 mL) with the organic layers combined and dried (Na_2SO_4), and the solution evaporated to dryness in vacuo. The residue was subjected to chromatography on silica gel, eluted with hexanes:EtOAc 2:1 (v/v), to give the furanofuranol **24** (101.8 mg, 89%). IR ($CHCl_3$) ν_{max}: 3410 (br, OH), 1594, 1515, 1455 (C═CAr) cm^{-1}; ^1H NMR δ: 7.45–7.20 (m, 5H, Bn), 6.95 (d, 1H, $J_{2,6}$ = 1.7, H-2), 6.75–6.65 (m, 2H, H-5, H-6), 5.16 (s, 2H, CH_2-Ph), 5.35 (s, 1H, H-7′), 4.38 (d, 1H, $J_{7,8}$ = 7.1, H-7), 4.39 (dd, 1H, $J_{9ax,9eq}$ = 7, $J_{8,9ax}$ = 8.9, H-9ax), 4.25-4.10 (m, 1H, H-9′ax), 3.95–3.85 (m, 1H, H-9′eq), 3.56 (dd, 1H, $J_{9ax,9eq}$ = 7, $J_{8,9eq}$ = 9.1, H-9 eq), 3.91 (s, 3H, OCH_3), 3.76 (br s, 1H, O*H*), 3.11–2.87 (m, 2H, H-8, H-8′), ^{13}C NMR δ: 149.78 (C-3), 147.82 (C-4), 136.99 (*C*q/Bn), 133.51 (C-1), 128.47, 127.78, 127.20 (*C*H/Bn), 118.47 (C-6), 113.69 (C-5), 109.61 (C-2), 102.02 (C-7′), 85.79 (C-7), 71.21 (C-9), 70.93 (*C*H_2Ph), 69.13 (C-9′), 55.95 (OCH_3), 53.51 (C-8′), 52.52 (C-8); MS *m/e* (relative %): 342 (M^+, 20), 251 (10), 223 (10), 193 (5), 151 (Ar_1CO^+, 6), 137 ($Ar_1CH_2^+$, 5), 123 (Ar_1^+, 5), 91 (100); HRMS, calcd. for $C_{20}H_{22}O_5$: 342.1467; found: 342.1475.

Furolactone 30

To a solution of **24** (34.41 mg, 0.1 mmol) in dry CH_2Cl_2 (5 mL) was added pyridinium dichromate (PDC) (4 equiv., 151.4 mg), AcOH (1 equiv., 5.76 μL), and 4Å molecular sieves (150 mg). Following stirring for 6 h at r.t., the suspension was filtered through a short-path silica gel plug and the filtrate removed in vacuo to give a residue that was then subjected to silica gel column chromatography, eluted with hexanes:EtOAc 2:1 (v/v), to give **30** (26.7 mg, 78%); mp 114–115°C; IR ($CHCl_3$) ν_{max}: 1772 (C═O), 1594, 1516, 1456 (C═CAr), 1244 (C-O) cm^{-1}; ^1H NMR δ: 7.45–7.25 (m, 5H, Bn), 6.93 (d, 1H, *J* = 1.8, H-2), 6.87 (d, 1H, $J_{5,6}$ = 8.2, H-5), 6.79 (dd, 1H, $J_{2,6}$ = 1.8, $J_{5,6}$ = 8.2, H-6), 5.17 (s, 2H, Ar-CH_2), 4.62 (d, 1H, $J_{7,8}$ = 6.7, H-7), 4.50 (dd, 1H, $J_{9eq,8}$ = 9.8, $J_{9eq,9ax}$ = 6.8, H-9 eq), 4.40–4.30 (m, 2H, H-9ax and H-9′ax), 4.20 (dd, 1H, $J_{8',9'eq}$ = 9.2, $J_{9'eq,9'ax}$ = 3.8, H-9′ eq), 3.92 (s, 3H, OCH_3), 3.45 (ddd, 1H, $J_{8',9'ax}$ = 9.2, $J_{8',8}$ = 9.2, $J_{8',9'eq}$ = 3.8, H-8′), 3.15–3.10 (m, 1H, H-8); ^{13}C NMR δ: 178.13 (C-7′), 149.94 (C-4), 148.17 (C-5), 136.81 (*C*q/Bn), 131.81 (C-1), 128.49, 127.82, 127.13 (*C*H/Bn), 118.29 (C-6), 113.70 (C-5), 109.43 (C-2), 85.89 (C-7), 70.89 (*C*H_2Ph), 69.93 and 69.77 (C-9 and C-9′), 55.98 (OCH_3), 48.03 (C-8′), 45.92 (C-8); MS *m/e* (relative %): 340 (M^+, 100), 250 (20), 221 (45), 149 (48); HRMS, calcd. for $C_{20}H_{20}O_5$: 340.1311; found: 340.1319.

(±)-Salicifoliol 31

To a solution of **30** (26.7 mg, 0.078 mmol) in EtOAc (5 mL) was added Pd/C 10% (15 mg). The suspension was then stirred under an H_2 atmosphere, as described for epi-(+)-sesamolinol **15**, with salicifoliol **31** purified by silica gel column chromatography, eluted with hexanes:EtOAc (2:1 → 1:1 (v/v)), to give **31** (17.66 mg, 90%); mp 101–102°C (lit. (39) mp 102–103°C); IR ($CHCl_3$) ν_{max}: 3417 (br, OH), 1768 (C═O), 1605, 1519, 1466 (C═CAr), 1241 (C-O) cm^{-1}; UV λ_{max}: 234, 278 nm; ^1H NMR δ: 6.93 (d, 1H, *J* = 6.9, H-5), 6.89 (d, 1H, *J* = 1.6, H-2), 6.80 (dd, 1H, $J_{2,6}$ = 1.6, $J_{5,6}$ = 8, H-6), 5.74 (s, 1H, OH), 4.61 (d, 1H, $J_{7,8}$ = 6.9, H-7), 4.51 (dd, 1H, $J_{9eq,8}$ = 9.8, $J_{9eq,9ax}$ = 6.8, H-9ax), 4.40–4.30 (m, 1H, H-9eq and H-9′ax), 4.19 (dd, 1H, $J_{8',9'eq}$ = 9.2, $J_{9'eq,9'ax}$ = 3.8, H-9′ eq), 3.90 (s, 3H, OCH_3), 3.43 (ddd, $J_{8',9'eq}$ = 9.2, $J_{8',8}$ = 9.2, $J_{8',9'ax}$ = 3.8, 1H, H-8′), 3.18–3.08 (m, 1H, H-8); ^{13}C NMR δ: 178.32 (C-7′), 146.98 (C-3), 145.88 (C-4), 130.63 (C-1), 119.15 (C-6), 114.47 (C-5), 105.51 (C-2), 86.13 (C-7), 70.01 and 69.91 (C-9/C-9′), 56.02 (OCH_3), 48.21 (H-8), 45.99 (H-8′); MS *m/e* (relative %): 250 (M^+, 100), 233 (10), 219 (15), 205 ($Ar_1C_5H_6O^+$, 10), 165 (50), 152 (Ar_1CHO^+, 90), 151 (Ar_1CO^+, 100), 137 ($Ar_1CH_2^+$, 95), 123 (Ar_1^+, 50), 109 (75); HRMS, calcd. for $C_{14}H_{14}O_5$: 250.0841; found: 250.0843.

Furofuran 32

To a solution of lactol **24** (101.1 mg, 0.3 mmol) in dry THF (30 mL), PPh_3 (79 mg, 0.3 mmol), and 4-benzyloxy-3-methoxyphenol **22** (65.4 mg, 0.3 mmol) was added diethylazodicarboxylate (DEAD) (47.5 μL, 1 equiv.), and the mixture was allowed to stir at r.t. for an additional 24 h. The solvent was then removed in vacuo and the residue subjected to silica gel column chromatography, eluted with hexanes:EtOAc (3:1 → 2:1 (v/v)), to give the furofuran lignan **32** (147.9 mg, 89%). IR ($CHCl_3$) ν_{max}: 1597, 1510, 1455 (C═CAr) cm^{-1}; ^1H NMR δ: 7.43–7.25 (m, 10H, Bn), 6.95 (d, 1H, $J_{2,6}$ = 1.5 , H-2), 6.85–6.70 (m, 2H, C*H*Ar), 6.70 (d, 1H, $J_{2',6'}$ = 2.7, H-2′), 6.60 (dd, 1H, *J* = 2.7, H-6′), 5.59 (d, 1H, *J* = 5.6, H-7′), 5.13 (s, 2H, CH_2Ph), 5.08 (s, 2H, CH_2Ph), 4.78 (d, 1H, $J_{7',8'}$ = 6.9, H-7), 4.38 (dd, 1H, $J_{9'ax,8'}$ = 9.1, $J_{9'eq,9'ax}$ = 4.7, H-9′ax), 4.20–4.00 (m, 2H, H-9′eq and H-9ax), 3.95 (dd, $J_{8,9eq}$ = 9.1, $J_{9eq,9ax}$ = 4.7, H-9eq), 3.89 (s, 3H, OCH_3), 3.86 (s, 3H, OCH_3), 3.35-3.20 (m, 1H, H-8′), 3.04 (m, 1H, H-8); ^{13}C NMR δ: 151.95 (C-1′), 150.53 (C-3′), 149.72 (C-3), 147.63 (C-4), 143.27 (C-4′), 137.31 (*C*q/Bn), 137.02 (*C*q/Bn), 133.92 (C-1), 128.47, 128.42, 127.71, 127.70, 127.35, 127.20 (*C*H/Bn), 118.17 (C-6), 115.53 (C-5), 113.80 (C-5′), 109.63 (C-6′), 107.06 (C-2), 102.63 (C-7′), 102.47 (C-2′), 85.21 (C-7), 71.82 (*C*H_2Ph), 70.96 (*C*H_2Ph), 69.38 (C-9), 67.04 (C-9′), 55.93 (OCH_3), 55.92 (OCH_3), 52.78 (C-8), 51.15 (C-8′); MS *m/e* (relative %): 554 (M^+, 5), 464 (3), 445 (2), 429 (2), 325 (10), 295 (30), 243 (50), 230 (100), 139 (75); HRMS, calcd. for $C_{34}H_{34}O_7$: 554.2304; found: 554.2318.

(±)-Epi-pinoresinolin 13

To a solution of the protected furolignan **32** (69.7 mg, 0.125 mmol) in EtOAc (5 mL) was added Pd/C 10% (20 mg). The solution was then stirred for 3 h under an H_2 atmosphere, as for epi-sesamolinol **15**, to give epi-pinoresinolin **13** (39.4 mg, 84%). IR ($CHCl_3$) ν_{max}: 3410 (br, OH), 1613, 1511, 1452 (C═CAr) cm^{-1}; ^1H and ^{13}C NMR spectra (see Table 1); MS *m/e* (relative %): 374 (M^+, 35), 275 (22), 235 (90), 205 ($Ar_1C_5H_6O^+$, 95), 137 ($Ar_1CH_2^+$, 100); HRMS, calcd. for $C_{20}H_{22}O_7$: 374.1366; found: 374.1387.

Furofuran 34

The furanofuranol **24** (17.7 mg, 0.05 mmol) was treated with sesamol **33** (7.01 mg, 0.05 mmol) as described above to give **34** (20.3 mg, 85%). IR ($CHCl_3$) ν_{max}: 1600, 1508, 1466 (C═CAr), 1245, 1217 (C-O) cm^{-1}; ^1H NMR δ: 7.45–7.20 (m, 5H, Bn), 6.90–6.50 (m, 6H, C*H*Ar), 5.93 (s, 2H, OCH_2O), 5.56 (d, 1H, $J_{7',8'}$ = 5.6, H-7′), 5.15 (m, 2H, CH_2Ph), 4.77 (d, 1H, $J_{7,8}$ = 7, H-7), 4.38 (dd, 1H, $J_{9'ax,8'}$ = 9.1, $J_{9'eq,9'ax}$ = 4.2, H-9′ax), 4.20–4.05 (m, 2H, H-9′eq and H-9ax), 3.97 (dd, 1H, $J_{8,9eq}$ = 9.1, $J_{9eq,9ax}$ = 4.8, H-9eq), 3.91 (s, 3H, OCH_3), 3.38–

© 1997 NRC Canada

3.25 (m, 1H, H-8′), 3.10–2.95 (m, 1H, H-8); ^{13}C NMR δ: 152.15 (C-1′), 149.75 (C-3′), 148.03 (C-3), 147.68 (C-4), 143.55 (C-4′), 136.95 (*C*q/Bn), 133.87 (C-1), 128.46, 127.74, 127.16 (*C*H/Bn), 118.13 (C-6), 113.75 (C-5), 109.58 (C-6′), 108.93 (C-5′), 107.95 (C-2), 102.94 (C-7′), 101.18 (O*C*H$_2$O), 100.14 (C-2′), 85.17 (C-7), 70.95 (*C*H$_2$Ph), 69.30 (C-9), 66.96 (C-9′), 55.95 (O*C*H$_3$), 52.70 (C-8), 51.11 (C-8′); MS *m/e* (relative %): 462 (M$^+$, 15), 325 (30), 295 (70), 243 (55), 227 (100), 203 (Ar$_2$C$_5$H$_6$O$^+$, 30), 179 (12), 137 (Ar$_1$CH$_2^+$, 55), 107 (15); HRMS, calcd. for $C_{27}H_{26}O_7$: 462.1678; found: 462.1671.

(±)-Epi-piperitolin 14

O-Benzyl piperitolin **34** (59.2 mg, 0.128 mmol) in EtOAc (5 mL) was treated with Pd/C 10% (15 mg), as described for furofuran **32**, to give (±)-**14** (41.4 mg, 95 %); mp 116–117°C; IR ($CHCl_3$) ν_{max}: 3446 (br, OH), 1612, 1547, 1488 (C=CAr), 1271, 1243 (C-O) cm^{-1}; UV λ_{max}: 230, 285 nm; ^{1}H NMR δ: 6.90 (d, 1H, $J_{2,6}$ = 1.8, H-2), 6.81 (dd, 1H, $J_{6,2}$ = 1.8, $J_{5,6}$ = 8.1, H-6), 6.8 (d, 1H, $J_{5,6}$ = 8.1, H-5), 6.72 (d, 1H, $J_{5',6'}$ = 8.4, H-5′), 6.69 (d, 1H, $J_{2',6}$ = 2.4, H-2′), 6.56 (dd, 1H, $J_{2',6'}$ = 2.4, $J_{5',6'}$ = 8.4, H-6′), 5.92 (s, 2H, OC*H*$_2$O), 5.74 (s, 1H, O*H*), 5.55 (d, 1H, $J_{7',8'}$ = 5.6, H-7′), 4.47 (d, 1H, $J_{7,8}$ = 7, H-7), 4.40–4.36 (m, 1H, H-9′ax), 4.17–4.07 (m, 2H, H-9′eq and H-9ax), 4.02–3.95 (m, 1H, H-9eq), 3.89 (s, 3H, OC*H*3), 3.33–3.28 (m, 1H, H-8′), 3.06–3.00 (m, 1H, H-8); ^{13}C NMR δ: 152.28 (C-1′), 148.15 (C-3′), 146.77 (C-3), 145.33 (C-4′), 142.79 (C-4′), 132.79 (C-1), 118.99 (C-6), 114.34 (C-5), 109.14 (C-6′), 108.64 (C-2), 108.04 (C-5′), 103.07 (C-7′), 100.23 (O*C*H$_2$O), 85.48 (C-7), 69.40 (C-9), 67.04 (C-9′), 55.97 (O*C*H$_3$), 52.87 (C-8′), 51.22 (C-8); MS *m/e* (relative %): 372 (M$^+$, 15), 261 (5), 235 (60), 205 (Ar$_1$C$_5$H$_6$O$^+$, 65), 187 (5), 161 (Ar$_1$C$_3$H$_4^+$, 5), 159 (4), 153 (Ar$_2$CHO$^+$, 30), 151 (Ar$_1$CHO$^+$, 50), 138 (90), 137 (Ar$_2$CH$_2^+$, 100), 115 (30), 107 (60); HRMS, calcd. for $C_{20}H_{20}O_7$: 372.1209; found: 372.1219.

Acknowledgments

The authors wish to thank the United States Department of Agriculture National Research Initiative Competitive Grants Program (U.S.D.A NRICGP) (Grant 94-02968 and 96-03622) and the Arthur M. and Kate Eisig Tode Foundation (to P.A.M.) for generous support of this study, and Dr. W.F. Siems (Department of Chemistry, Washington State University) for high-resolution mass spectra.

References

1. P. Budowski and K.S. Markley. Chem. Rev. **48**, 125 (1951).
2. Y. Fukuda, T. Osawa, M. Namiki, and T. Ozaki. Agric. Biol. Chem. **49**, 301 (1985).
3. T. Osawa, M. Nagata, M. Namiki, and Y. Fukuda. Agric. Biol. Chem. **49**, 3351 (1985).
4. Y. Fukuda, M. Isobe, M. Nagata, T. Osawa, and M. Namiki. Heterocycles, **24**, 923 (1986).
5. H. Katsuzaki, M. Kawasumi, S. Kawakishi, and T. Osawa. Biosci. Biotech. Biochem. **56**, 2087 (1992).
6. H.L. Haller, E.R. McGovran, L.D. Goodhue, and W.N. Sullivan. J. Org. Chem. **7**, 183 (1942).
7. H.L. Haller, F.B. LaForge, and W.N. Sullivan. J. Org. Chem. **7**, 185 (1942).
8. T. Nikaido, T. Ohmoto, T. Kinoshita, U. Sankawa, S. Nishibe, and S. Hisada. Chem. Pharm. Bull. **29**, 3586 (1981).
9. S. Shimizu, K. Akimoto, Y. Shinmen, H. Kawashima, M. Sugano, and H. Yamada. Lipids, **26**, 512 (1991).
10. N. Hirose, T. Inoue, K. Nishihara, M. Sugano, K. Akimoto, S. Shimizu, and H. Yamada. J. Lipid Res. **32**, 629 (1991).
11. F. Hirata, K. Fujita, Y. Ishikura, K. Hosoda, T. Ishikawa, and H. Nakamura. Atherosclerosis, **122**, 135 (1996).
12. K. Akimoto, Y. Kitagawa, T. Akamatsu, N. Hirose, M. Sugano, S. Shimizu, and H. Yamada. Ann. Nutr. Metab. **37**, 218 (1993).
13. K. Yamashita, Y. Iizuka, T. Imai, and M. Namiki. Lipids, **30**, 1019 (1995).
14. A. Kamal-Eldin, D. Pettersson, and L.-Å. Appelqvist. Lipids, **30**, 499 (1995).
15. P. Paré, H.-B. Wang, L.B. Davin, and N.G. Lewis. Tetrahedron Lett. **35**, 4731 (1994).
16. L.B. Davin and N.G. Lewis. An. Acad. Bras. Cienc. **67** (Supl. 3), 363 (1995).
17. L.B. Davin, H-B. Wang, A.L. Crowell, D.L. Bedgar, D.M. Martin, S. Sarkanen, and N.G. Lewis. Science, **375**, 362 (1997).
18. L.B. Davin and N.G. Lewis. ACS Symp. Ser. **562**, 202 (1994).
19. N.G. Lewis, M.J. Kato, N.P. Lopez, and L.B. Davin. ACS Symp. Ser. **588**, 135 (1995).
20. N.G. Lewis, L.B. Davin, T. Katayama, and D.L. Bedgar. Bull. Liaison — Groupe Polyphénols, **16**, 98 (1992).
21. A. Chu, A. Dinkova, L.B. Davin, D.L. Bedgar, and N.G. Lewis. J. Biol. Chem. **268**, 27026 (1993).
22. T. Katayama, L.B. Davin, A. Chu, and N.G. Lewis. Phytochemistry, **33**, 581 (1993).
23. T. Umezawa, L.B. Davin, and N.G. Lewis. J. Biol. Chem. **266**, 10210 (1991).
24. A.T. Dinkova-Kostova, D.R. Gang, L.B. Davin, D.L. Bedgar, A. Chu, and N.G. Lewis. J. Biol. Chem. **271**, 29473 (1996).
25. T. Umezawa, L.B. Davin, E. Yamamoto, D.G.I. Kingston, and N.G. Lewis. J. Chem. Soc. Chem. Commun. 1405 (1990).
26. H. Fujimoto, F. Nakatsubo, and T. Higuchi. Mokuzai Gakkaishi, **28**, 555 (1982).
27. S. Takano, T. Ohkawa, S. Tamori, S. Satoh, and K. Ogasawara. J. Chem. Soc. Chem. Commun. 189 (1988).
28. S. Ozawa, L.B. Davin, and N.G. Lewis. Phytochemistry, **32**, 643 (1993).
29. G. Maiti, S. Adhikari, and S.C. Roy. Tetrahedron, **51**, 8389 (1995).
30. E. Haslam and R.D. Haworth. J. Chem. Soc. 827 (1955).
31. W. Adriani. Z. Unters. Lebensm. **56**, 187 (1928).
32. S.S. Kang, J.S. Kim, J.H. Jung, and Y.H. Kim. Arch. Pharm. Res. **18**, 361 (1995).
33. J. Jakupovic, V.P. Pathak, F. Bohlmann, R.M. King, and H. Robinson. Phytochemistry, **26**, 803 (1987).
34. L. Syper. Synthesis, 167 (1989).
35. I.M. Godfrey, M.V. Sargent, and J.A. Elix. J. Chem. Soc. Perkin Trans. 1, 1353 (1974).
36. M.S. Manhas, W.H. Hoffman, B. Lal, and A.K. Bose. J. Chem. Soc. Perkin Trans. 1, 461 (1975).
37. F. Ishibashi and E. Taniguchi. Agric. Biol. Chem. **53**, 1565 (1989).
38. K. Kondo and F. Mori. Chem. Lett. 741 (1974).
39. A.G. Gonzalez, R. Estévez-Reyes, and C. Mato. J. Nat. Prod. **52**, 1139 (1989).
40. E.J. Corey and W-G. Su. J. Am. Chem. Soc. **109**, 7534 (1987).
41. G. Bodenhausen, H. Kogler, and R.R. Ernst. J. Magn. Reson. **58**, 370 (1984).
42. A. Bax and G.A. Morris. J. Magn. Reson. **42**, 501 (1981).

Can. J. Chem. Downloaded from www.nrcresearchpress.com by 88.146.161.215 on 09/08/12
For personal use only.

© 1997 NRC Canada

Diversity in crystal production by some bird's nest fungi (Nidulariaceae) in culture

Tracy C. Shinners and Jalpa P. Tewari

Abstract: Hyphae of many species of bird's nest fungi (Nidulariaceae) were examined for the presence of crystals. Scanning electron microscopy revealed crystals typical of calcium oxalate associated with hyphae. Crystal depositions included complete hyphal encrustation, organized druses, randomly arranged groups, single crystals, and relatively "clean" hyphae. The majority of crystals could be morphologically classified as styloid, raphide, or bipyramidal type. Energy-dispersive X-ray microanalyses confirmed that all crystal types were rich in calcium, and X-ray diffraction identified both the dihydrate (weddellite) and monohydrate (whewellite) forms of calcium oxalate. Morphological variation of crystals was species and medium specific, with generally more crystals being produced on relatively calcium-rich V8 juice agar than on PDA. No association was found between crystal types and geographic and habitat distribution of species.

Key words: wood rotting fungus, decomposition, calcium oxalate.

Résumé : On a examiné les hyphes de plusieurs espèces de champignons (Nidulariacae) de nids d'oiseau afin d'évaluer la présence de cristaux. La microscopie électronique à balayage a révélé la présence de cristaux typiques d'oxalate de calcium associés aux hyphes. Les dépôts de cristaux comportent des incrustations complètes des hyphes, des maclages organisés, des groupes arrangés au hasard, des cristaux uniques et des hyphes relativement « propres ». D'un point de vue morphologique, la majorité des cristaux peut être classifiée sous les types styloïde, raphide ou bipyramidal. Les microanalyses de rayons X à dispersion d'énergie ont confirmé que tous les types de cristaux sont riches en calcium; la diffraction des rayons X a permis d'identifier les formes dihydratée (weddellite) et monohydratée (whewellite) de l'oxalate de calcium. Les variations morphologiques des cristaux sont spécifiques aux espèces et aux milieux; il y a généralement une plus grande production de cristaux sur le jus V-8, relativement riche en calcium, que sur le « PDA ». On n'a pas observé d'association entre les types de cristaux et la distribution géographique ou de l'habitat des espèces.

Mots clés : champignon du pourissement du bois, décomposition, oxalate de calcium.

[Traduit par la rédaction]

Introduction

The Nidulariaceae are an interesting group of fungi that have attracted much attention due to their beauty, morphology, and unique dispersal mechanisms. From a functional perspective, these fungi are ecologically important as white-wood rotters involved in the decomposition of numerous substrates worldwide. Some are coprophilous, but many are commonly found growing and fruiting on plant residues, twigs, or some type of plant fibre (Table 1) (1). These fungi are aggressive colonizers due to the formation of mycelial cords or rhizomorphs that invade the substrate and travel through the soil. In addition to these physical attributes, the Nidulariaceae are a chemically active group that produce many enzymes (2), an antibiotic complex (3–5), and other specific metabolites (6–8).

Based on these biochemical and plant residue-colonizing capabilities, research has been initiated to evaluate the potential role of some bird's nest fungi in accelerating biodegradation of crop residues, such as that of canola. Crop stubble serves as a habitat for microbes, and hence plays an important role in the epidemiology of many stubble-borne diseases. Research in this area may lead to the development of a microbial inoculant (biological control agent) to accelerate stubble decomposition, and hence reduce disease incidence.

Recently, calcium oxalate crystals have been found to be associated with hyphae of *Cyathus olla* and *C. striatus* (Nidulariaceae) (9). This crystal production is an indicator of oxalic acid biosynthesis and secretion by these fungi. During decomposition, oxalic acid secretion leads to the sequestration of calcium, mostly from the cell walls of the substrate, which subsequently combines with oxalic acid to form insoluble calcium oxalate crystals (10–12). Crystal-forming fungi are important ecosystem inhabitants as they are involved in calcium recycling, nutrient availability for plant growth, and soil genesis (13, 14). To date, other members of the Nidulariaceae have not been studied for crystal development.

Crystals have been described on the hyphae of many members of Basidiomycotina under a given set of conditions (10, 13, 15, 16). However, it is not known if crystal morphology

Received December 19, 1996.

This paper is dedicated to Professor William A. Ayer whose research has significantly contributed to understanding the chemical activities of this group of fungi.

T.C. Shinners and J.P. Tewari.[1] Department of Agricultural, Food and Nutritional Science, University of Alberta, Edmonton, AB T6G 2P5, Canada.

[1] Author to whom correspondence may be addressed. Telephone: (403) 492-4554. Fax: (403) 492-4265. E-mail: jtewari@afns.ualberta.ca

© 1997 NRC Canada

Can. J. Chem. Downloaded from www.nrcresearchpress.com by 88.146.161.215 on 09/08/12
For personal use only.

Table 1. Geographic location and common substrates of some members of the Nidulariaceae.

Species	Location	Common substrate
Crucibulum laeve	Europe North America South America Japan Australia/ New Zealand (temperate zone species)	Stems, twigs, old nut shells, wood fruits, woodchips, manure Primarily lignicolous
Cyathus africanus	Tanzania	Unknown
Cyathus berkeleyanus	Widespread in tropics	Bamboo pots
Cyathus bulleri	Tropics	Unknown
Cyathus canna	Exclusively tropical (Jamaica, Costa Rica, Barbados, Mexico, Mauritius)	Unknown
Cyathus earlei	Tropical/sub-tropical (Cuba, Puerto Rico, Mexico, Hawaii)	Unknown
Cyathus julietae	Jamaica	Unknown
Cyathus olla	Europe North America South America South Africa Australia Not found in warm, moist tropics	Old wood, dead herbaceous plant stems Plant fibres/artifacts
Cyathus pallidus	American tropics West Indies Mexico South America China	Small chips and twigs Compost/mulch
Cyathus pygmaeus	United States	Old dead stems of shrubby plants of arid area Manure
Cyathus stercoreus	Worldwide	Coprophilous Manured soils
Cyathus striatus	Widespread in temperate areas	Small twigs, woody leaf mould Cereal residue Plant fibre/ artifacts
Nidula niveo-tomentosa	Western North America South America Japan New Zealand Jamaica	Associated with bracken fern

Can. J. Chem. Downloaded from www.nrcresearchpress.com by 88.146.161.215 on 09/08/12
For personal use only.

would vary if the conditions were changed. Cultures of these fungi are usually mycelial and fruiting can only be achieved in some cases under special conditions often requiring extended periods of time. It would be advantageous to develop diagnostic criteria for species identification using hyphal morphology.

Hyphae of many species of Nidulariaceae were examined in this investigation with the objective of answering the following questions: (*a*) Do the various species produce different types of crystals? (*b*) Is crystal morphology affected by growth media? (*c*) Do species from various geographical areas and habitats differ in crystal production?

Materials and methods

Fungal cultures were obtained from the University of Alberta Microfungus Collection, Edmonton, and the Canadian Collection of Fungal Cultures, Agriculture and Agri-Food Canada, Ottawa (Table 2). All cultures were subcultured on to V8 agar (V8 juice (Campbell Soup Co.) 200 mL, Difco Bacto-Agar 20 g, $CaCO_3$ 3 g, distilled H_2O to 1 litre) and Difco potato-dextrose agar (PDA) and maintained at room temperature (approx. 22°C) in the dark.

Agar blocks of both V8 and PDA media were excised approximately 1 cm from the original inoculation plug from

© 1997 NRC Canada

Figs. 1–7. Fig. 1. SEM of crystal-free hyphae of *C. pygmaeus*. Bar = 5 μm. **Fig. 2.** SEM of heavily encrusted hyphae of *C. africanus* on V8 juice medium. Bar = 5 μm. **Fig. 3.** SEM of raphide druses produced by *C. olla* on PDA. Bar = 1 μm. **Fig. 4.** SEM of *C. stercoreus* hyphae encrusted with various crystal types. Bar = 2 μm. **Fig. 5.** SEM of typical styloid crystal shapes. Bar = 1 μm. **Fig. 6.** SEM of many raphide crystals. Note the spear-like, tapered ends. Bar = 1 μm. **Fig. 7.** SEM of crystals typical of the dihydrate form of calcium oxalate. Note the bipyramidal ends. Bar = 1 μm.

Can. J. Chem. Downloaded from www.nrcresearchpress.com by 88.146.161.215 on 09/08/12
For personal use only.

3-week-old cultures of *Nidula niveo-tomentosa, Crucibulum laeve, Cyathus olla, C. earlei, C. pygmaeus, C. canna, C. africanus, C. pallidus, C. julietae, C. stercoreus, C. striatus, C. berkeleyanus,* and *C. bulleri.* Each block was placed on a microscope coverslip (7 mm diameter) and secured with double-sided tape. All samples were vapor-fixed with 1% osmium tetroxide in water for 1 h, then air-dried for several days in a fume hood. Samples were mounted onto scanning electron microscope (SEM) stubs and secured with Marivac colloidal carbon paint. The specimens were sputter-coated with approx. 1 nm layer of gold and examined in a Jeol JSM 6301 FXV SEM operated at 5 kV. Energy-dispersive X-ray microanalyses were conducted using a Link eXL energy-dispersive X-ray system with a light element detector. All samples were examined in triplicate.

Crystals for X-ray diffraction analysis were collected by preparing a 10 mL hyphal suspension prepared from the agar plate. The suspension was filtered through four layers of cheesecloth and the filtrate spun at 1750*g* for 10 min at 20°C in a Sorvall GLC-1 table-top centrifuge. The supernatant was discarded and the pellet was resuspended in 5 mL of distilled water. Droplets of the solution were dried down on a quartz plate and examined using a Rigaku-Geigerflex vertical goniometer system with a graphite monochromator. The crystals were exposed to cobalt radiation ($CoK_{\alpha\ 1+2}$ = 1.79026Å) and compared to American Society for Materials (ASTM) X-ray standard file cards for weddellite (17-541) and whewellite (20-231).

Results

In total, 13 species of bird's nest fungi were examined. From this group, 10 were shown to produce crystals rich in calcium. Detailed crystal morphology for each species is presented in Table 3. Crystals were not observed in *C. pygmaeus, N. niveo-tomentosa*, and *C. laeve.* Hyphae of these species appeared "clean" (Fig. 1). In contrast to this, hyphae of *C. earlei, C. stercoreus,* and *C. africanus* (Fig. 2) growing on V8 media were heavily encrusted with variably shaped crystals, typical of both the monohydrate (whewellite) and dihydrate (weddellite) forms of calcium oxalate (17). Encrustation in these species was extremely heavy, rendering hyphae unidentifiable. On PDA, crystals were evident on these species but were considerably sparse compared with hyphae on V8 agar.

Cyathus olla, C. striatus, C. berkeleyanus, C. julietae, C. bulleri, and *C. pallidus* all produced crystals of various morphologies when grown on V8 media. From this group, only *C. olla* and *C. striatus* produced crystals on PDA. *Cyathus canna* was an exception, producing styloids and variably shaped crystals on PDA and none when grown on V8 agar.

Crystals were observed in druses (spherical aggregates) (Fig. 3) or randomly attached to hyphae singly or in groups. Druses produced by *C. olla* and *C. berkeleyanus* on V8 agar were all raphide crystals, but other crystal clusters seen on these species, as well as on many others, contained many different crystal types (Fig. 4).

Crystal types observed during this study were typically styloid- (Fig. 5) and raphide-shaped (monohydrate forms of calcium oxalate) (Fig. 6), or bipyramidal crystals, typical of the dihydrate form (Fig. 7). Styloids and raphides are elongated crystals that are easily distinguished from one another. Both ends of a styloid crystal form a prism, whereas raphide crystals form a tapered, spearlike end (17). Dihydrate forms such as bipyramidal types have a fourfold axis, a plane of symmetry perpendicular to it, and a center of symmetry with no symmetrical planes parallel to the crystal axis (17).

Energy-dispersive X-ray microanalyses of all crystal types produced spectra high in calcium (Fig. 8). Osmium and gold peaks resulted from the fixative and gold coating, respectively. Potassium and chlorine peaks are attributed to components from the V8 juice-based medium. X-ray diffraction results confirmed the presence of both the monohydrate (whewellite) and dihydrate (weddellite) forms of calcium oxalate (Fig. 9). Based on these spectral data, documented calcium oxalate crystal morphology (17), and previous identification of calcium oxalate crystals associated with *C. olla* and *C. striatus* (9), the crystals observed in this study were identified as calcium oxalate. In addition to crystals, many exudate droplets were present on the hyphae of a number of species. Identification of components of this exudate was not performed during this study.

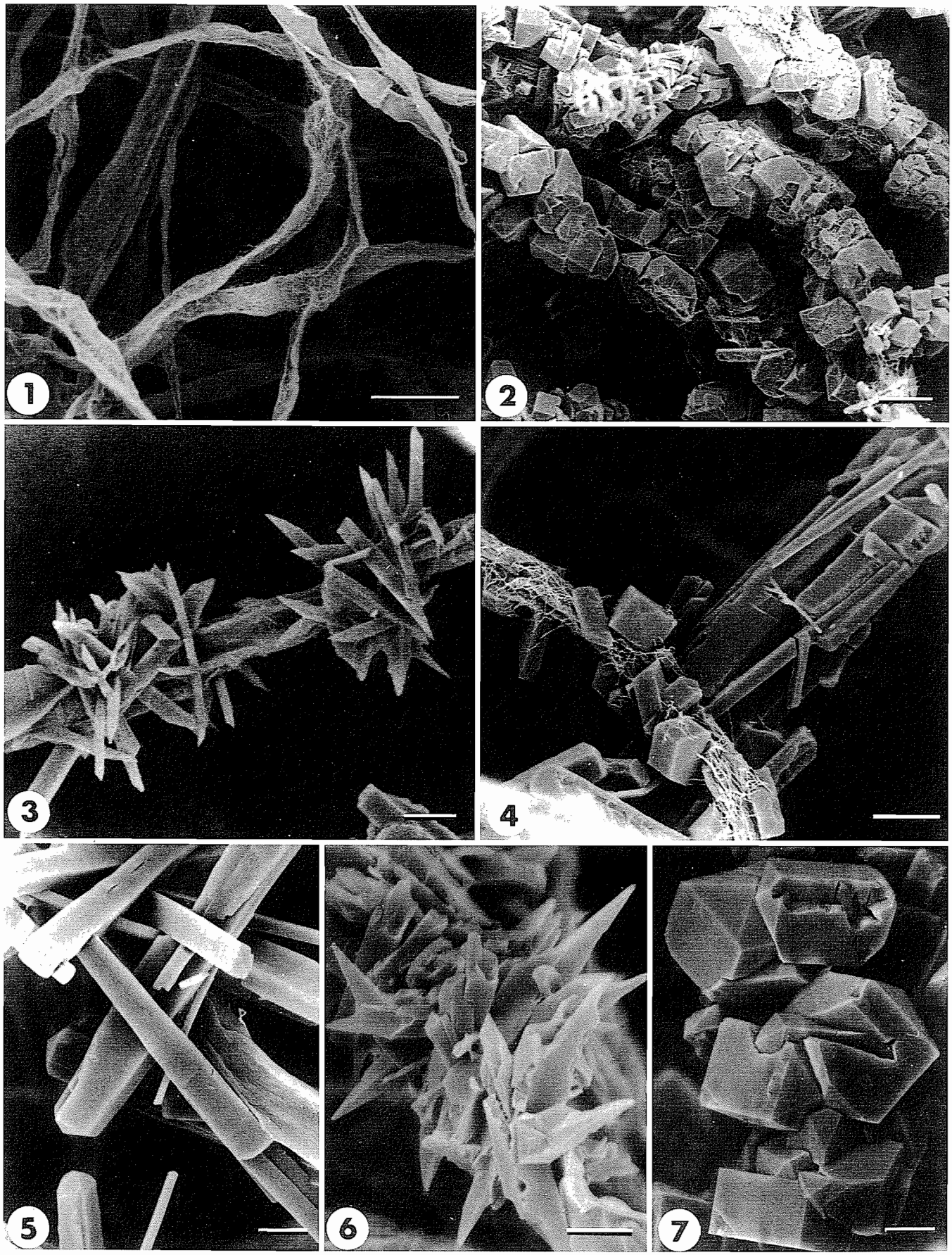
Discussion

Crystal production and morphology may be influenced by many factors including oxalic acid secretion, calcium availability, hydration state, and other environmental factors (11, 17). Diversity among species of Nidulariaceae with respect to crystal production appears to be attributed to species-specific variation since factors such as calcium availability and environmental conditions were consistent throughout this experiment. In many plants, calcium oxalate crystal shape and location are species and tissue specific (18). There are many similar reports for fungi (19); however, with respect to the Nidulariaceae, many more isolates must be examined to confirm these observations.

Crystal production was greatest on the V8 medium (approximately 3.0072 g Ca/ L), which had a greater concentration and availability of calcium than PDA (approximately 30.85–38.85 mg Ca/ L). Calculations of calcium content are based on

© 1997 NRC Canada

Can. J. Chem. Downloaded from www.nrcresearchpress.com by 88.146.161.215 on 09/08/12
For personal use only.



© 1997 NRC Canada

Table 2. Sample source and identification.

Isolate	Source	ID.no.
Crucibulum laeve	CCFC[a]	DAOM 196687
Cyathus africanus	CCFC	DAOM 196686
Cyathus berkeleyanus	CCFC	DAOM 197568
Cyathus bulleri	CCFC	DAOM 195062
Cyathus canna	CCFC	DAOM 196684
Cyathus earlei	UAMH[b]	UAMH 8104
Cyathus julietae	CCFC	DAOM 196681
Cyathus olla	UAMH	UAMH 8276
Cyathus pallidus	CCFC	DAOM 196678
Cyathus pygmaeus	UAMH	UAMH 8020
Cyathus stercoreus	CCFC	DAOM 172472
Cyathus striatus	Tewari[c]	USA
Nidula niveo-tomentosa	UAMH	UAMH 8101

[a]CCFC (Canadian Collection of Fungal Cultures).
[b]UAMH (University of Alberta Microfungus Collection and Herbarium).
[c]Collected by I. Tewari.

Table 3. Crystal morphology on PDA and V8 media.

Species	PDA	V8	Comments
Crucibulum laeve	None	None	
Cyathus africanus	Raphide	Raphide, styloid, bipyramidal, variable	Hyphae on V8 hyphae heavily encrusted
Cyathus berkeleyanus	None	Styloid, raphides, bipyramidal, variable	Exudate droplets present on PDA cultures
Cyathus bulleri	None	Styloid, raphide	Exudate droplets on PDA culture
Cyathus canna	Raphide, variable	None	Exudate droplets on both PDA and V8
Cyathus earlei	Raphide styloid	Raphide bipyramidal, variable	Hyphae completely encrusted
Cyathus julietae	None	Raphide, styloid	Exudate droplets on PDA, hyphae on V8 cultures completely encrusted
Cyathus olla	Raphide	Bipyramidal	
Cyathus pallidus	None	Styloid	Dense mycelial mat
Cyathus pygmaeus	None	None	
Cyathus stercoreus	Styloid	Styloid, bipyramidal, variable	Hyphae on PDA were completely encrusted
Cyathus striatus	Styloid, raphide	Raphide, styloid, bipyramidal, variable	
Nidula niveo-tomentosa	None	None	

Can. J. Chem. Downloaded from www.nrcresearchpress.com by 88.146.161.215 on 09/08/12
For personal use only.

© 1997 NRC Canada

Fig. 8. X-ray spectrum of crystals from *C. earlei*. Note the calcium peaks.

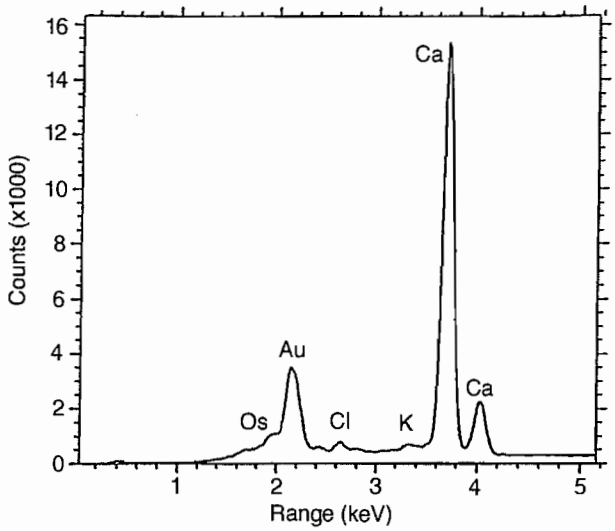
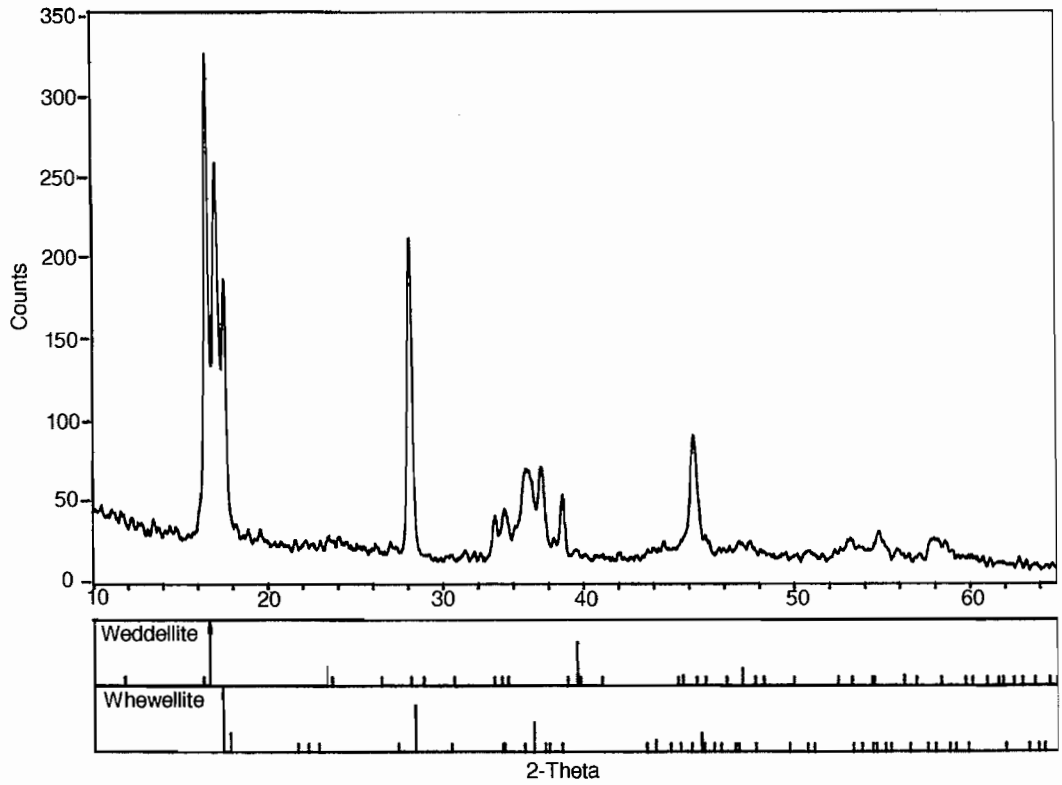


Fig. 9. X-ray diffraction spectrum of crystals from *C. striatus*. Note the spectral comparison to ASTM standard cards for weddellite and whewellite.



media formulation, information, and mineral analyses provided by Campbell's Soup Company, Difco Laboratories, and potato mineral content information (20). The approximate calcium content of PDA does not reflect the actual value since PDA is made from potato infusion. For this preparation, the solid phase, which contains most of the calcium (plant cell walls), is removed. Therefore, the actual value will be significantly lower than the estimate. From this information, it can be assumed that calcium was a limiting factor to crystal production on the PDA medium for most species. It is not clear why *C. canna* produced crystals on PDA and none on the V8 medium. This species may require a starch-rich medium for

© 1997 NRC Canada

Can. J. Chem. Downloaded from www.nrcresearchpress.com by 88.146.161.215 on 09/08/12
For personal use only.

induction of crystals, but this stipulation has to be validated further.

Morphological variation of crystals is a function of hydration state and was species and medium specific. There was no association between crystal types and geographic and habitat distribution of species. *Cyathus stercoreus* is coprophilous whereas all the other species used in this investigation were from woody substrata. These two groups did not differ in crystal morphologies.

Crystal-producing ability of the fungi observed in culture can be extrapolated to natural environments and the ecological niche these fungi inhabit. Many bird's nest fungi are involved in the decomposition of plant residues. Oxalic acid secretion and subsequent sequestration of calcium weakens cell wall stability, and improves access for enzymes involved in decomposition (10, 11). Horner et al. (13) have suggested that crystal-forming fungi are ecologically important for calcium recycling, nutrient availability, and soil genesis. From this study, it can be concluded that many species of the Nidulariaceae play a role in these environmental/ ecological processes. Crystals were not observed in all species examined in this experiment; however, the importance of these species cannot be minimized by these results. Crystal production by these fungi may be induced by natural or environmental factors not provided in this experiment.

Acknowledgments

This research was supported through a research grant (OGP 0491) from the Natural Sciences and Engineering Research Council of Canada (NSERC) to J.P.T. T.C.S. was supported through a postgraduate scholarship, also from NSERC. George Braybrook, Christina Barker, and Diane Caird helped in scanning electron microscopy, energy-dispersive X-ray microanalyses, and X-ray diffraction analyses, respectively.

References

1. H.J. Brodie. The bird's nest fungi. University of Toronto Press, Toronto, Ont. 1975.
2. R.C. Kuhad and B.N. Johri. Indian J. Microbiol. **31**, 291 (1991).
3. A.D. Allbutt, W.A. Ayer, H.J. Brodie, B.N. Johri, and H. Taube. Can. J. Microbiol. **17**, 1401 (1970).
4. W.A Ayer, S.P. Lee, and T.T. Nakashima. Can. J. Chem. **57**, 3338 (1979).
5. W.A Ayer and S.P. Lee. Can. J. Chem. **57**, 3332 (1979).
6. W.A Ayer and P.P. Singer. Phytochemistry, **19**, 2717 (1980).
7. W.A. Ayer and R.H. McAskill. Tetrahedron Lett. **21**, 1917 (1980).
8. W.A. Ayer and R.H. McAskill. Tetrahedron Lett. **21**, 1921 (1980).
9. J.P. Tewari, T.C. Shinners, and K.G. Briggs. Z. Naturforsch. C: Biochem. Biophys. Biol. In press.
10. M.V. Dutton, C.S. Evans, P.T. Akley, and D.A. Wood. Appl. Microbiol. Biotechnol. **39**, 5 (1993).
11. Z.K. Punja and S.F. Jenkins. Can. J. Bot. **62**, 2028 (1984).
12. D.V. Rao and J.P. Tewari. Phytopathology, **77**, 780 (1987).
13. H.T. Horner, L.H. Tiffany, and G. Knaphus. Mycologia, **87**, 34 (1995).
14. W.C. Graustein, K. Cromack, Jr., and P. Sollins. Science, **198**, 1252 (1977).
15. H.J. Arnott and M.A. Webb. Scanning Electron Microsc. **4**, 1747 (1983).
16. K.D. Whitney and H.J. Arnott. Mycologia **72**, 180 (1987).
17. A. Frey-Wyssling. Am. J. Bot. **68**, 130 (1981).
18. H.T. Horner and B.L. Wagner. *In* Calcium oxalate in biological systems. *Edited by* S.R. Khan. CRC Press, Boca Raton, Fla. 1995. pp. 53–72.
19. H.J. Arnott. *In* Calcium oxalate in biological systems. *Edited by* S.R. Khan. CRC Press, Boca Raton, Fla. 1995. pp. 73–111.
20. O. Smith. Potatoes: production, storing, processing. The AVI Publishing Company Inc., Westport, Conn. 1968.

Can. J. Chem. Downloaded from www.nrcresearchpress.com by 88.146.161.215 on 09/08/12
For personal use only.

© 1997 NRC Canada

Thermolysis and photolysis of two steroidal hydroxamic acid methanesulfonates

Oliver E. Edwards, Gunnar Grue-Sørensen, and Barbara A. Blackwell

Abstract: Thermolysis or photolysis of *N*-methanesulfonyloxy-4-aza-5α-cholestan-3-one gave derivatives of 4-azacholestan-3-one, 4-aza-A-nor-B-homocholestan-3-one, 3-aza-A-norcholestane, bis (4-aza-3-oxocholest-5-en-6-yl) methane, and bis(3-aza-A-norcholestan-3-yl) urea. The corresponding 5β-methanesulfonate gave the 5β (coprostane) analogues. Evidence for the mechanism of formation of these products, including a Favorski-like ring contraction and amide oxidation by methanesulfonic acid, is presented. Detailed ^{1}H and ^{13}C assignments are made for many of the products, and ultraviolet absorption for seven steroidal enamides is tabled. Long-range homo- and heteronuclear NMR connectivities were used to confirm the structure of three dimeric compounds and to assign the configuration of the methoxy function of 4-aza-5-methoxy-A-nor-β-homocholestan-3-one to be 5α.

Key words: steroidal enamides, 3-aza-A-norcholestanes, 4-aza-A-nor-B-homocholestanes, aza-Favorskii ring contraction.

Résumé : La thermolyse ou la photolyse de la *N*-méthanesulfonyloxy-4-aza-5α-cholestan-3-one fournit des dérivés de la 4-azacholestan-3-one, de la 4-aza-A-nor-B-homocholestan-3-one, du 3-aza-A-norcholestane, du bis(4-aza-3-oxocholest-5-én-6-yl)méthane et de la bis(3-aza-A-norcholestan-3-yl)urée. Le 5β-méthanesulfonate conduit aux analogues 5β (coprostane). On présente des données relatives au mécanisme de formation de ces produits, y compris une contraction de cycle de type Favorski et une oxydation d'amide par l'aide méthanesulfonique. On a effectué des attributions détaillées des spectres RMN du ^{1}H et du ^{13}C de plusieurs produits et on présente un tableau incorporant les absorptions ultraviolettes de sept énamides stéroïdaux. On a utilisé les connectivités RMN homo- et hétéronucléaires à longue distance pour confirmer les structures de trois composés dimères et pour conclure que la configuration de la fonction méthoxy de la 4-aza-5-méthoxy-A-nor-β-homocholestan-3-one est 5α.

Mots clés : énamides stéroïdaux, 3-aza-A-norcholestanes, 4-aza-A-nor-B-homocholestanes, contraction de cycle d'aza-Favorski.

[Traduit par la rédaction]

Introduction

Considerable interest has been shown in the potential of *N*-acyl imines (**1**) and related carbinolamides (**2**) as biochemical intermediates (1*a*), as possible biological alkylating agents with chemotherapeutic activity (1*b–d*), and as reagents for organic synthesis (1*e*). Three aliphatic *N*-acyl imines have been isolated in our laboratories (1*c*, 2) and showed moderate stability. Thus we were encouraged to attempt preparation of 4-azacholest-4-en-3-one (**3**) and related steroidal *N*-acyl imines.

Received January 15, 1997.

This paper is dedicated to Professor William A. Ayer on the occasion of his 65th birthday.

O.E. Edwards.[1] Chemistry Department, Carleton University, Colonel By Drive, Ottawa, ON K1S 5B6, Canada.
G. Grue-Sørensen. Leo Pharmaceutical Products, Industriparken 55, DK-2750, Ballerup, Denmark. Visiting Fellow, National Research Council of Canada 1982–1984.
B.A. Blackwell. Eastern Cereal and Oilseed Research Centre, Agriculture and Agri-Food Canada, Ottawa, ON K1A 0C6, Canada.

[1] Author to whom correspondence may be addressed. Telephone: (613) 520-3841. Fax: (613) 520–3749.

Attempts to prepare 5α-azido-A-norcholestan-3-one **4** failed,[2] foiling attempts to prepare **3** by the photochemical route discovered in our laboratories (1*c*).

Thermolysis of keto acid **5** (R = H) in ammonia (3*a*) or exposure of the corresponding keto amide or enol lactone to ammonia gave enamide **17** or the corresponding carbinolamide (3*b*). Base-catalysed elimination of HCl from the *N*-chloro lactam **6** also gave **17** as major product[3] (see also recent work on photolysis of **6** by Back and Brunner (1*d*)). Thus it was evident that isomerization of **3** to **17** was facile.

This paper details attempts to observe or obtain **3** by rupture of the relatively weak N—O bond of hydroxamic acid methanesulfonates **13** and **14**. Since this work was initiated, Hoffman et al. (4) have shown that thermolysis of hydroxamic acid triflates gives transient *N*-acyl immonium salts.

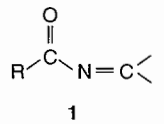
Results

The desired methanesulfonates were prepared from keto acid **5** (R = H) as shown in Scheme 1. After the cyanoborohydride reduction of oximino acid **7** the cyclization to the hydroxamic

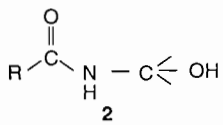
[2] Unpublished experiments by G. Grue-Sørensen, J.L. Douglas, and C. Grieco.
[3] Unpublished experiments with T.G. Back.

© 1997 NRC Canada

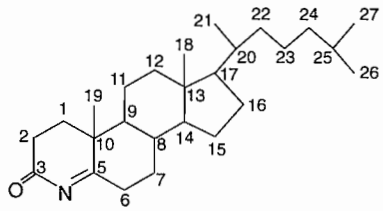
Can. J. Chem. Downloaded from www.nrcresearchpress.com by 88.146.161.215 on 09/08/12
For personal use only.



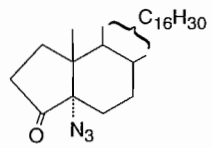
1



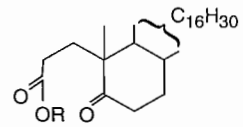
2



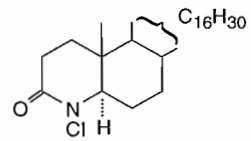
3



4



5



6

Table 1. Steroidal enamides.

Enamide	λ_{max} (EtOH), nm	ε	Reference
8	238.5	14 400	—
15	234	13 500	—
16	240	9 100	—
17	232	13 000	3*a*
31	239	13 700	—
35	232	6 200	1*c*
36	240	6 600	6

acids **9** and **10** was spontaneous. The methyl ethers **11** and **12** were prepared for comparison with subsequent products. The properties and configurations as determined by the ^{1}H NMR signals for the 5-hydrogens agreed well with those reported by Edward and Morand (5) for samples prepared in other ways.

Finally, the methanesulfonates **13** and **14** were prepared using methanesulfonyl chloride in pyridine. Heating of **7** in vacuo gave the enamide *N*-hydroxycholest-5-en-3-one **8**.

Thermolysis of both mesylates **13** and **14** in dry tetramethylurea at 185°C under argon produced at least seven products (TLC), three of which were purified and characterized. The minor one (ca. 6%) was the hitherto unknown enamide 4-aza-A-nor-B-homocholest-5-en-3-one **15**. This had ν_{max} 1690 cm^{-1} (five-membered lactam), no NH, and two vinyl hydrogens. Its ultraviolet absorption (Table 1) indicated an enamide character. This, its chemistry, and the ^{13}C NMR spectrum (see Table 3) left no doubt that it had structure **15**.

A major product (52–57%) was 4-azacholest-5-en-3-one **17**, a known compound.[2] Another was the unexpected coupling product bis(4-aza-3-oxocholest-5-en-6-yl)-methane **16** (7–19%). This was a polar enamide (see Table 1) with NH absorption (ν_{max} 3390 cm^{-1}; δ 7.45). Its EI mass spectrum showed only very weak peaks above *m/z* 427, so it appeared to be a monomer. However a 2D NMR spectrum showed that an apparent one-hydrogen signal at δ 2.6 ppm was actually due to a methylene group, thus suggesting that it was linking two steroid units. The fact that none of the hydrogen or carbon signals were doubled indicated high symmetry. Since the general spectra were similar to those of **17** but the vinyl hydrogen was missing, the structure appeared to be **16**. Partial synthesis from **17** (see below) confirmed this.

To test if the methanesulfonic acid produced in the thermolysis was catalysing the isomerization of preformed **3**, powdered calcium carbonate was added to the reaction mixture before thermolysis. The results were erratic, but the yield of **17** increased at the expense of **16**, reaching as high as 84%. No *N*-acyl imine **3** was detected using ^{13}C NMR.

To reduce the effect of the methanesulfonic acid even further, the thermolysis was conducted in dry collidine. Yields of **17** of 73% (5α) and 80% (5β) were realized. No products derived from the A-nor base **24** were detected from **14** and no **3** was observed despite gentle work-up (expected ^{13}C NMR signals near 180 ppm and ν_{max} near 1700 cm^{-1}).

Thermolysis of **13** and **14** in dry methanol at 180°C in sealed tubes under argon again gave **15** and **17**, as well as **5** (R = CH_3), which undoubtedly arose by acid-catalysed methanolysis of **17** followed by hydrolysis during work-up. Indeed, treatment of **17** with acidic methanol did give **5** (R = CH_3). Additional products of the thermolysis were the methyl carbamates **18** and **19** (eqs. [1] and [2]). Since **19** formed excellent crystals it was submitted for X-ray crystallography. We are grateful to Prof. C. Bensimon for the structure and stereochemistry shown in formula **19**. The analogous spectra of **18** left no doubt as to its identity (Tables 2 and 3).

Photolysis of **13** and **14** in dry methanol gave enamide **17**, the carbamates **18** and **19**, respectively, and a new common product, the carbinolamide ether **20** clearly related to **15**. Indeed the two could be interconverted (see eq. [15]). Apparently pure samples of **20** slowly converted to a crystalline mixture containing **15** and **20** plus methanol, according to NMR results. Approximately 5% of the two lactams **21** and **22** (eqs. [3] and [4]) were formed from **13** and **14**, respectively.

In the hope of obtaining the bases corresponding to carbamates **18** and **19**, the mesylates **13** and **14** were photolyzed in aqueous tetrahydrofuran (eqs. [5] and [6]). The bases **23** and **24** were formed, and were characterized as their hydrochlorides and *N*-acetyl derivatives **27** and **28**. The yield of lactams **21** and **22** increased to 11%.

Photolysis of **13** and **14** in dichloromethane gave spectroscopic evidence for reactive intermediates with ν_{max} 1743 cm^{-1} (see Mechanism section). Depending on work-up conditions the products shown in eqs. [7]–[10] were formed. The reactive intermediates appeared to be the source of the carbamates **18** and **19**, the ureas **25** and **26**, and, as a consequence of traces of water (aqueous work-up), the bases **23** and **24**. The latter were subsequently acetylated, giving **27** and **28**.

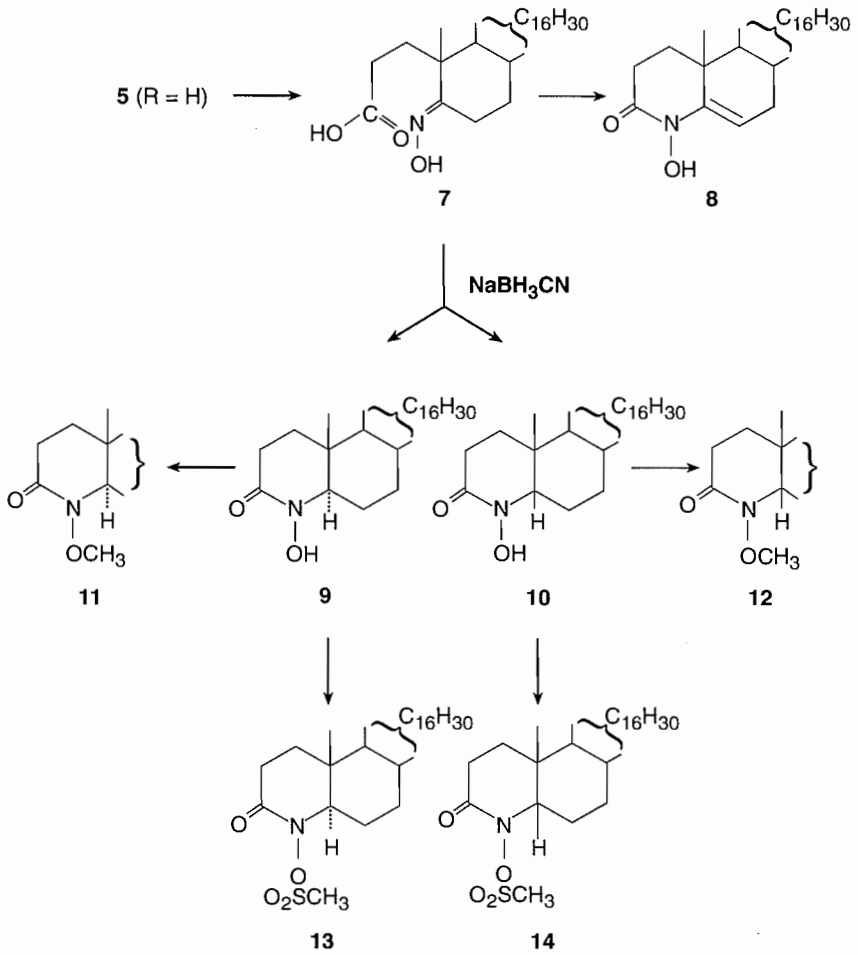
In a last attempt to intercept the *N*-acylimine **3**, a small molar excess of triethylamine was added to a dichloromethane solution of **14** before photolysis. Again a transient species with ν_{max} 1743 cm^{-1} was formed. Treatment of the product with methanol, then acetic anhydride, gave a mixture of

© 1997 NRC Canada

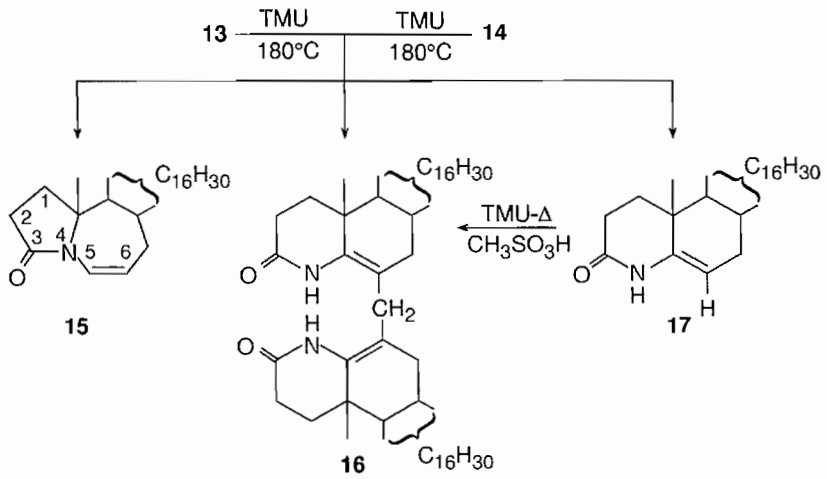
Can. J. Chem. Downloaded from www.nrcresearchpress.com by 88.146.161.215 on 09/08/12
For personal use only.

Can. J. Chem. Downloaded from www.nrcresearchpress.com by 88.146.161.215 on 09/08/12
For personal use only.

Scheme 1.



Scheme 2.



5β-carbamate **19**, enamide **15**, and *N*-acetyl derivative **28**. No evidence for the presence of **3** or the related 5-methoxy or 5-acetoxy lactams **34** was found.

Since methoxy lactam **20** was moderately stable, attempts were made to prepare the 5-acetoxy-4-aza-A-nor-B-homo-cholest-3-one. However, the exposure of enamide **15** to an acetic acid – acetic anhydride mixture in the presence of *p*-toluenesulfonic acid at room temperature or at 68°C gave no isolable acetoxy compound.

Enamides **8**, **15**, **16**, and **17** deteriorated in air, especially in

© 1997 NRC Canada

Can. J. Chem. Downloaded from www.nrcresearchpress.com by 88.146.161.215 on 09/08/12
For personal use only.

Table 2A. 500 MHz ^{1}H NMR assignments of selected azasteroids (δ, ppm from TMS).

	Compound			
Position	**11**	**12**	**15**	**16**
1	1.30; 1.83	1.37; 1.76	1.82; 1.96	1.43; 1.87
2	2.42 (ddd 1.8, 7.0, 18.0)	2.31 (ddd 17.6, 6.0, 1.7)	2.37 (septet)	2.45 (m)
	2.49 (ddd 6.7, 12.7, 18.0)	2.39 (ddd 17.6, 13.6, 5.8)		
5	3.26 (dd 3.5, 12.4)	3.46 (t, 2.7)	6.34 (dd 9.0, 3.0)	—
6	1.45	1.60 (dd 14.7, 3.7);	5.25 (ddd 9.0, 9.1, 3.0)	—
	2.11 (dq 3.6, 7.0, 12.8)	2.12 (dq 14.7, 3.1)		
7	0.92	1.07	1.66	1.52
	1.77	1.46	2.24 (ddd 15.5, 9.1, 2.6)	1.87
8	1.30	1.35	1.38	1.02 (br m)
9	0.76	1.27	1.24	1.52 (br m)
11	1.31; 1.48	1.30	1.35; 1.64	1.40; 1.52
12	1.13; 1.98 (dt 3.4, 12.8)	1.12; 1.96 (dt 12.8; 3.4)	1.20; 1.95	1.15; 2.0 (dt)
14	1.06	1.00	1.09	0.98
15	1.24; 1.82	1.21; 1.81	1.25; 1.81	1.25; 1.83
16	1.05; 1.56	1.01; 1.54	1.09; 1.69	1.03; 1.52
17	0.98	1.02	1.03	1.07
18	0.65 (s)	0.63 (s)	0.65 (s)	0.67 (s)
19	0.81 (s)	1.00 (s)	1.12 (s)	1.03 (s)
NH				7.45
Me	3.68 (s)	3.71 (s)		
$-CH_2-$				2.59 (brs)

Position	**17**	**18**	**19**	**20**
1	1.44; 1.87	1.33; 1.62 (ddd 11.5, 6.2, 1.9)	1.38; 1.78	1.55; 2.28
2	2.44	3.40 (m)	3.36	2.30;
			3.46	2.41 (ddd 7.9, 12.8, 17.0)
5		2.84 (dd 12.3, 3.4)	3.24 (br s)	5.44 (dd 7.7, 10.1)
6	4.84 (dd 2.6, 5.0)	2.56 (brd)	1.45	1.65
		1.46	2.55 (br)	2.29
7	1.63 (dd 2.6, 17.0)	0.85	0.86	0.78 (dd)
	2.07 (dt 5.0, 17.0)	1.70 (dt 13.6, 3.1)	1.38	1.55
8	1.0	1.35	1.16	1.40
9	1.5	0.81	0.96	1.08
11	1.25; 1.40	1.32; 1.43 (ddd 12.7, 3.8)	1.33–1.45	1.40; 1.50
12	1.16; 2.01 (dt 12.7, 3.4)	1.14; 1.95 (dt 12.5; 3.4)	1.11; 1.97 (dt 12.6, 3.3)	1.15; 1.94 (dt 12.7, 3.4)
14	1.00	1.08	0.95-1.05	1.10
15	1.27; 1.82	1.23; 1.80	1.21; 1.80	1.25; 1.80
16	1.10; 1.57	1.04; 1.55	1.07; 1.56	1.10; 1.58
17	1.06	1.00	0.95–1.05	1.10
18	0.68 (s)	0.65 (s)	0.65 (s)	0.68 (s)
19	1.06 (s)	0.81 (s)	0.97 (s)	1.35 (s)
NH	8.0			
Me		3.63 (s)	3.64 (s)	3.22 (s)
$-CH_2-$				

solution. The melting points obtained in evacuated capillaries were higher and sharper than those taken in air.

Partial synthesis of enamide **16** was readily achieved by reaction of enamide **17** with formaldehyde using p-toluenesulfonic acid as catalyst. It was also possible to prepare 6-ethoxymethyl-4-azacholest-5-en-3-one **31** and react this with **17** to give the dimer **16** (eq. [11]).

Hydrogenation of **15** gave the parent lactam **32** (4-aza-A-nor-B-homocholestane-3-one).

Mechanism

The thermolysis of **13** and **14** in tetramethylurea or methanol is readily understood in ionic terms involving ion pair **A**

© 1997 NRC Canada

Table 2A. (*concluded*).

	Compound			
Position	**25**	**26**	**27**	**32**
1	1.40; 1.60 (dd 7.2, 11.5)	1.43; 1.79	1.37; 1.68	1.59 (dt 12.6, 9.6); 2.08 (ddd 3.3, 12.6, 8.7)
2	3.13 (t, 9.4)	3.09 (br m)	3.43	2.23 (ddd 16.8, 3.0, 9.3)
	3.43 (dt 6.7, 10.4)	3.41	3.37	2.39 (dt 16.8, 9.1)
5	2.99 (dd 3.0, 11.7)	3.50 (br m)	2.90 (m)	2.95 (p 14.2, 7.2); 3.82 (p 14.2, 7.2)
6	1.22	1.42	1.45	1.48
	2.40 (dq 12.0, 3.1)	2.25 (br d 13.7)	2.24 (br d)	1.88
7	0.97	0.87	0.98	0.95
	1.65 (dq 13.3)	1.35	1.68	1.67
8	1.38	1.19	1.37	1.15–1.30
9	0.87	0.92	0.80	1.02–1.14
11	1.32; 1.43 (dd)	1.32–1.45	1.34; 1.43	1.37; 1.48
12	1.15; 1.95 (dd)	1.14; 1.98 (dt 12.6; 3)	1.15; 1.95	1.13; 1.94 (dt 12.7, 3.4)
14	1.09	1.10	1.10	1.02–1.14
15	1.21; 1.80	1.22; 1.79	1.22; 1.80	1.24; 1.80
16	1.02; 1.55	1.06; 1.56	1.07; 1.55	1.08; 1.67
17	1.00	0.97	0.98	1.02–1.14
18	0.65 (s)	0.66 (s)	0.65 (s)	0.66 (s)
19	0.86 (s)	1.01 (s)	0.82 (s)	1.20 (s)
NH				
Me				1.97 (s)
$-CH_2-$				

Table 2B. Selected ^1H NMR assignments of some azasteroids (δ, ppm from TMS).

	Compound						
Position	**8**	**21**	**22**	**23**	**24**	**28**	**31**
1	1.45; 1.87 (dt 12.8, 4.1)	1.86; ?	1.85; ?	1.5; 1.8	1.8; ?	1.83; ?	1.42; 1.82
2	2.58 (m)	2.42 (m)	2.3–2.4	3.38 (m)	3.27; 3.45	3.50 (m)	2.44 (m)
5	—	3.05 (dd)	3.3 (t, 3)	2.72 (m)	3.18 (m)	3.40 (br m)	—
6	5.48 (dd 5.2, 2.8)	1.72 (dq); ?	1.87; ?	2.04; ?	2.07; ?	2.6; ?	—
7	1.68 (ddd 2.8, 10.3, 17.0)	—	—	?	—	—	1.5
	2.22 (dt 5.4, 17.0)	—	—	1.80	—	—	2.0
12	1.18; 2.62 (dt 3.5, 12.7)	1.98 (dt); ?	2.00; ?	1.98; ?	1.94 (dt 12, 3); ?	2.0 (dt 12,3); ?	1.15; 2.03
15	1.27; 1.83	1.82; ?	1.82; ?	1.8; 1.2	1.78; ?	1.22; 1.80	1.20; 1.83
16	1.13; 1.58	1.58; ?	—	1.5; ?	—	1.07; 1.56	1.0; 1.5
18	0.69 (s)	0.65 (s)	0.64 (s)	0.64 (s)	0.64 (s)	0.65 (s)	0.67 (s)
19	1.08 (s)	0.89 (s)	1.00 (s)	0.98 (s)	1.03 (s)	0.99 (s)	1.08 (s)
NH	8.97	6.2	6.95	9.2; 10.0	9.05, 10.02		8.38
CH_3						2.14 (s)	1.21 (t)
OCH_2							3.45 (q)
$-CH_2-$							3.70; 4.05 (d 12.2)

Note: "?" denotes resonances where precise chemical shifts are not resolvable.

(Scheme 3). The high yield of **17** in collidine and the effect of calcium carbonate in the other solvents is consistent with a base-catalysed elimination involving the 5-hydrogen, leading to **3** as a metastable intermediate. This must rapidly rearrange to the more thermodynamically stable **17**.

However, since no *N*-methoxy compounds **11** or **12** were formed in methanol we conclude that free nitrenium ions **A** were not involved and that processes (a), (b), or (c) were synchronous with N—O bond rupture.

The formation of the A-nor amine derivatives could follow the ionic pathway (a) through ion pair **B**. However, an alternate ionic process involving an α-lactam could proceed as illustrated in eq. [12], although spectroscopic evidence for a reactive intermediate (ν_{max} 1743 cm^{-1}) in photolysis of **13** and

© 1997 NRC Canada

Can. J. Chem. Downloaded from www.nrcresearchpress.com by 88.146.161.215 on 09/08/12
For personal use only.

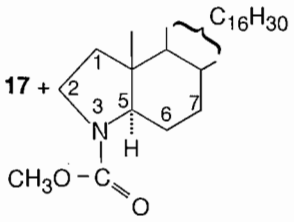
Can. J. Chem. Downloaded from www.nrcresearchpress.com by 88.146.161.215 on 09/08/12
For personal use only.

Table 3. ^{13}C NMR assignments of selected azasteroids (δ, ppm from TMS).

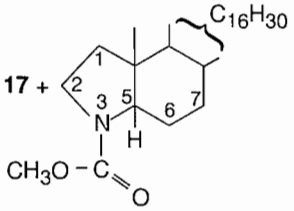
	Compound																		
Position	**8**	**11**	**12**	**15**	**16**	**17**	**18**	**19**	**20**	**21**	**22**	**23**	**24**	**25**	**26**	**27**	**28**	**31**	**32**
1	31.0	33.2	31.7	33.8	31.7	31.5	36.2	35.1	32.9	32.7	31.3	36.5	35.0	37.3	36.2	36.6	35.1	31.7	33.5
2	27.2	*29.5	29.0	28.8	28.2	28.3	46.0	45.6	29.5	29.6	28.2	43.4	41.2	48.7	48.2	47.3	47.2	28.2	29.3
3	161.0	168.6	168.1	175.0	169.6	169.8	—	—	176.7	173.6	174.5	—	—	—	—	—	—	169.0	174.4
5	138.2	69.1	66.3	125.1	135.5	139.9	68.0	65.3	82.3	61.1	59.5	67.5	65.2	68.6	65.0	69.0	66.2	138.1	37.5
6	103.9	23.3	23.1	116.3	109.3	103.9	24.9	23.6	32.7	27.2	25.2	22.9	22.5	25.0	23.7	25.2	23.0	107.9	25.2
7	29.7	*29.9	26.1	33.0	34.8	29.7	30.2	25.8	26.4	27.8	26.8	29.9	24.8	29.9	26.3	30.3	26.1	34.3	30.2
8	48.2	34.6	35.0	33.9	48.0	48.0	35.1	35.5	42.3	35.0	35.0	34.8	35.4	35.6	36.0	35.3	35.2	47.9	39.6
9	31.1	51.7	40.8	55.1	31.4	31.6	52.2	44.0	51.6	51.2	39.2	52.4	42.3	52.5	44.2	52.2	44.6	31.4	53.1
10	36.0	37.7	36.5	66.2	35.0	37.2	44.0	43.2	67.0	35.6	33.9	42.3	42.5	43.1	42.4	43.5	43.3	34.6	66.2
11	20.8	21.1	20.9	24.3	21.0	20.9	23.0	22.8	26.2	21.1	20.8	23.2	22.8	23.2	22.9	23.1	22.9	20.9	25.3
12	39.5	39.7	39.8	39.5	39.4	39.5	39.7	40.2	40.0	39.6	39.8	39.3	39.4	39.8	40.4	39.7	40.1	39.4	39.6
13	42.4	42.7	42.6	42.1	42.4	42.4	43.2	42.7	42.9	42.7	42.6	43.0	42.7	43.2	42.8	43.2	42.7	42.4	42.5
14	56.1	55.9	55.9	56.2	56.4	56.1	56.2	56.3	56.3	55.9	55.7	56.0	54.9	56.2	56.4	56.2	56.3	56.1	56.1
15	28.2	27.9	28.2	27.8	28.2	28.2	28.2	28.3	27.9	28.1	27.4	28.1	28.2	28.1	28.3	28.2	28.2	28.2	27.8
16	24.2	24.0	24.1	25.3	24.1	24.2	24.1	24.1	24.9	24.1	24.1	24.2	24.1	24.3	24.2	24.2	24.1	24.1	25.2
17	56.5	56.2	56.2	55.6	56.1	56.5	55.8	56.4	56.4	56.2	56.2	55.3	55.7	55.9	56.5	55.8	56.6	56.4	56.3
18	11.9	12.1	11.9	11.7	11.9	11.9	12.2	12.1	12.3	11.4	11.9	12.2	12.0	12.3	12.1	12.3	12.0	11.9	12.0
19	19.0	12.5	21.7	16.8	18.4	18.7	14.0	19.5	21.9	12.1	20.8	13.2	18.5	14.4	19.5	14.2	19.6	18.8	21.3
C=0							157.0	156.3						165.4	163.3	171.3	171.3		
OMe		62.7	61.1				51.7	51.9	55.2										
$-CH_2-$					31.5													71.2	
CH_3																23.6	22.8	15.1	
OCH_2																		66.1	

© 1997 NRC Canada

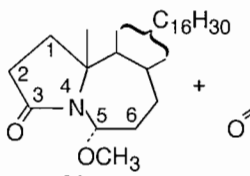
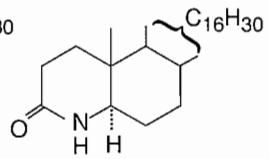
Can. J. Chem. Downloaded from www.nrcresearchpress.com by 88.146.161.215 on 09/08/12
For personal use only.

[1] **13** $\xrightarrow[180°C]{CH_3OH}$ **5** (R=CH_3) + **15** + **17** + 

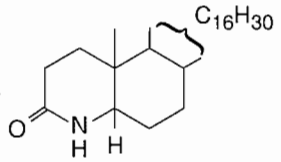
18

[2] **14** $\xrightarrow[180°C]{CH_3OH}$ **5** (R=CH_3) + **15** + **17** + 

19

[3] **13** $\xrightarrow[CH_3OH]{h\nu}$ **17** + **18** +  + 

20 **21**

[4] **14** $\xrightarrow[CH_3OH]{h\nu}$ **15** + **17** + **19** + **20** + 

22

14 in dichloromethane favors **C**[4] since an α-lactam would have absorption near 1850 cm^{-1} (7). Secondly, α-lactam formation as in eq. [12] and subsequent reaction would involve a 2-hydrogen. But thermolysis or photolysis of the mesylates in methanol-*d* gave no more than minor deuterium exchange on C-2 for **18** and **19**. Thirdly, photolysis or thermolysis of **13** and **14** in methanol (acidic) or photolysis in dichloromethane followed by treatment with acidic methanol gave none of the 2-methoxy-4-azacholest-3-one expected for an α-lactam intermediate (*7b*) and no acid **29** or its derivatives were observed[5] under more basic conditions.

Finally, had proton elimination as in eq. [12] been the source of the A-nor derivatives, a base such as collidine for thermolysis, or triethylamine for photolysis in dichloromethane, should have increased the yield of these. Actually the A-nor derivatives could not be detected in thermolysis in collidine and the yields in the photolysis did not change.

We conclude that the mechanisms in Scheme 3 are essentially correct. The formation of the A-nor derivatives is a new type of ring contraction. Since the reaction is closely analogous to the Favorskii-type ring contraction observed in deamination of α-amino ketones when cyclopropanone formation was impossible (8), it can be called an aza-Favorskii reaction.

The high energy available in the photolyses (ca. 250 nm) means that a homolytic fission of the N—O bond as a first step (eq. [13]) is possible. Cadogan and Rowley have produced evidence for such fission for hydroxamic acid toluenesulfonates (9). The only direct evidence for nitrogen-centered radicals in our work is the isolation of lactams **21** and **22** (eqs. [3] and [4]). As expected, the yields of these were highest in the best hydrogen atom donor tetrahydrofuran, lower in methanol, and near zero for dichloromethane.[6] Since most of our

[4] Attempts to make a simple analogue of C failed.

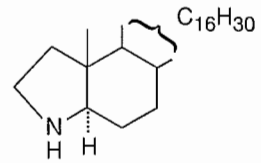
[5] The base-promoted opening of *N-tert*-butyl phenylaziridinones are cases of C—C bond cleavage of α-lactams (*7c*).

[6] The high yield of parent lactams in the photolysis of *N*-chlorolactams (*1d*) contrasts with our experience with the mesylates.

© 1997 NRC Canada

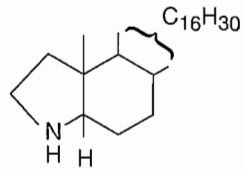
Can. J. Chem. Downloaded from www.nrcresearchpress.com by 88.146.161.215 on 09/08/12
For personal use only.

[5] **13** $\xrightarrow[\text{aq THF}]{h\nu}$ **15** + **17** + **21** +



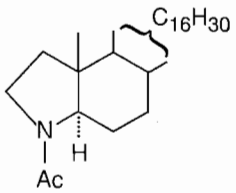
23

[6] **14** $\xrightarrow[\text{aq THF}]{h\nu}$ **15** + **17** + **22** +



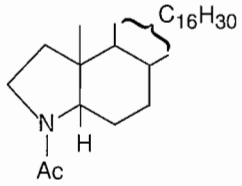
24

[7] **13** $\xrightarrow[(2)\ CH_3OH\ (3)\ Ac_2O]{(1)\ h\nu\ in\ CH_2Cl_2\ (H_2O)}$ **15** + **17** + **20** +



27

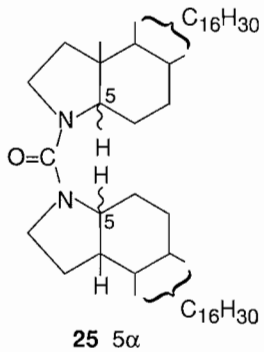
[8] **14** $\xrightarrow[(2)\ Ac_2O,\ pyridine]{(1)\ h\nu\ in\ CH_2Cl_2\ (H_2O)}$ **15** + **26** +



28

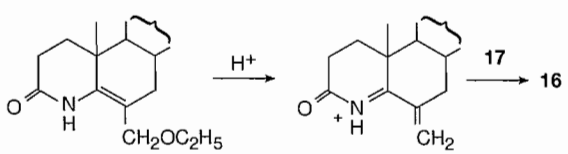
[9] **13** $\xrightarrow[(2)\ Ac_2O,\ pyridine]{(1)\ h\nu\ in\ CH_2Cl_2}$ **15** + **25** + **27**

[10] **14** $\xrightarrow[(2)\ CH_3OH\ (3)\ Ac_2O]{(1)\ h\nu\ in\ CH_2Cl_2}$ **15** + **19**+ **28**



25 5α
26 5β

[11]



31

products seem to be of ionic origin, electron transfer to ion pair **A** would have to occur as a major step (eq. [13]). For similar electron transfer, see ref. 10*a* (see, however, ref. 10*b*).

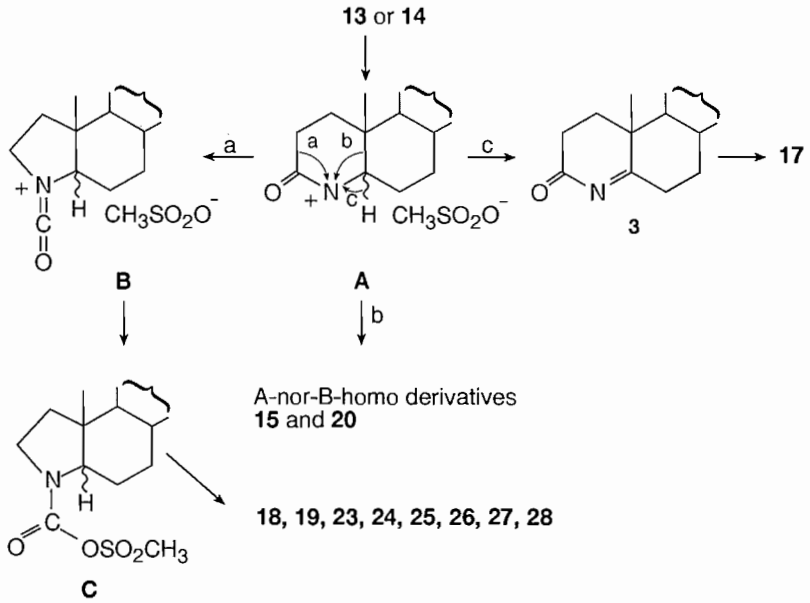
The rearrangement of the proposed *N*-acyl nitrenium ion **A** to the A-nor-B-homo derivatives **15** and **20** (path b, Scheme 3) is plausible. It gave a modest yield of **15** (maximum observed 30% in aqueous tetrahydrofuran). Recently a preparation of 2-alkylated steroids with this skeleton was developed by Back et al. (11).

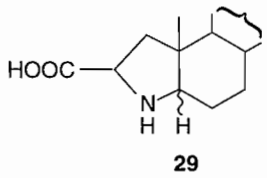
A most surprising result in the photolyses in tetramethyl urea was the formation of the methylene-bridged dimer **16**. When TMU containing methanesulfonic acid was heated at 180°C neither formaldehyde nor trimethyl urea could be detected among the products. However, the formaldehyde required to form the methylene bridge must have arisen from a methyl group of the TMU (eq. [14]). Heating **17** with tetramethyl urea under argon at 180°C gave no **16**, but if methanesulfonic acid was included a 50% yield of **16** was obtained. Thus the methanesulfonic acid formed from the mesylates is the oxidant. The occurrence of products containing both methylamido and steroid units was evident from ^{1}H NMR spectra, but none were characterized. These must arise from reaction

© 1997 NRC Canada

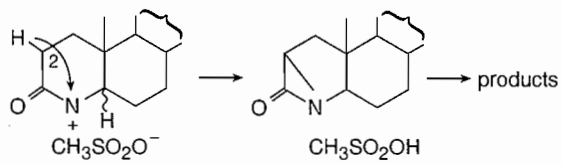
Can. J. Chem. Downloaded from www.nrcresearchpress.com by 88.146.161.215 on 09/08/12
For personal use only.

Scheme 3.

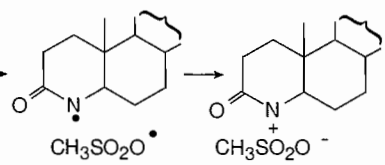




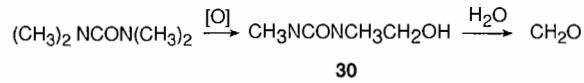
[12]



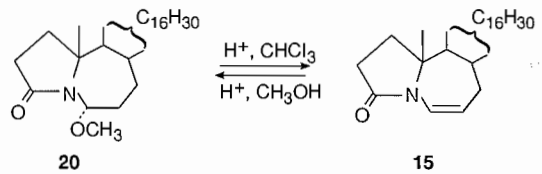
[13]



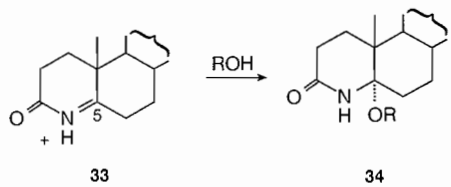
[14]



[15]



[16]



of carbinolamides such as **30** with enamides such as **17**. The acid-catalysed formation of **16** from **17** and formaldehyde or from **17** and the ethoxymethylene compound **31** (eq. [11]) shows the electron-donating potential of enamides. The addition of methanol to enamide **15** undoubtedly involves the same phenomenon: i.e., protonation on C-6 to give the immonium salt, then methanol attack on C-5 (eq. [15]). Attempts to convert **17** to the immonium salt **33** and then to neutralize this using weak base to obtain **3** failed. Acid-catalysed addition of methanol or acetic acid to **17** to give the 5-methoxy or 5-acetoxy compounds **34** (R = OCH_3 or $OCOCH_3$) also failed, probably due to the steric crowding at C-5.

Spectra

Table 1 lists the characteristic ultraviolet absorption spectra of the known steroidal enamides. Detailed NMR spectral assignments for the C-1 to C-19 nuclei of many of the compounds discussed are presented in Tables 2A, 2B, and 3. These constitute either full chemical shift assignments of known compounds or those of the new compounds to determine their structures. Other NMR data to confirm known structures are reported in the Experimental. The assignments reported in Table 2A result from a combination of homo- and heteronuclear correlation experiments so that, even if the multiplets themselves cannot be resolved in the overlapped portion of the proton spectrum (0.8–1.8 ppm), the centres of AB systems can be determined. Selected proton chemical shift assignments for other compounds are reported in Table 2B where more detailed information was not available (i.e., no 2D experiments were performed). The ^{13}C chemical shift assignments were determined from direct and long-range (HMBC) $^{1}H/^{13}C$ correlation experiments for critical or new structures (i.e., **12**, **15**, **16**, **18**, **24**, **26**, and **32**), while assignments for others were made by comparison of related spectra (e.g., **27** and **33** compared to **18** and **25**, **28** and **24** compared to **19** and **26**, etc.). Tables 2 and 3 show that the chemical shifts of positions C-11

© 1997 NRC Canada

Can. J. Chem. Downloaded from www.nrcresearchpress.com by 88.146.161.215 on 09/08/12
For personal use only.

Table 4. ^{13}C and ^{1}H NMR assignments for the C_8H_{17} moiety.

Position	^{1}H	^{13}C
20	1.35 (m)	35.7
21	0.88 (d, 6.6)	18.6
22	0.98; 1.31	36.1
23	1.15; 1.30	23.8
24	1.04–1.17 (br m)	39.4
25	1.49 (dq, 6.6)	28.0
26,27	0.840; 0.836 (d, 6.6)	22.5, 22.8

to C-17 are relatively constant for all compounds, but that positions C-8 and C-9 are strongly influenced by the nature of the B ring (six- or seven-membered, presence of a 5,6 double bond, etc.).

There is some ambiguity regarding the assignment of resonances due to C-14 and C-17. Although similar in chemical shift, these may be distinguished as long as the corresponding proton resonances are resolved. Thus for compounds **12**, **15**, **16**, **18**, **25**, and **26** these resonances may be distinguished by correlation to their respective protons and the proton coupling of H-14 to H-15 or that of H-17 to H-16 and H-20 as seen in the COSY spectrum. However, for compounds such as **19**, **20**, and **32**, where H-14 and H-17 are coincident, the identity of the carbon resonances is not confirmed.

For simplicity, the chemical shift assignments for the C_8H_{17} side chain for all compounds are summarized in Table 4. These figures represent an average of all compounds characterized. Variability between compounds was very slight, amounting to only ± 0.1 ppm for ^{13}C and ± 0.02 ppm for ^{1}H. This indicates that the overall molecular configuration for all compounds studied was very similar, in spite of changes in the A and B rings.

Interesting differences show up between the spectra of the members of the 5α and 5β series of compounds, especially for the A-nor series. Comparison of the ^{13}C chemical shifts of the 5α A-nor compounds (**18**, **23**, **27**, and **25**) with the 5β analogues (**19**, **24**, **28**, and **26**) shows that C-5, C-7, and C-9 are shifted upfield by ca. 3, 3–4, and 8 ppm, respectively, in the 5β compared to the 5α compounds. C-6, however, is unaffected, while the methyl function C-19 is shifted downfield by 5 ppm in the β series. A similar comparison of the spectra of the 6,6-nucleus analogues (**11**, **21** (5H-α) and **12**, **22** (5H-β) yields the same qualitative effects although shift differences are larger for C-9 and C-19 (11 ppm upfield and 8 ppm downfield, respectively). The shift of the C-5 resonance is the same (ca. 3 ppm upfield). Both C-6 and C-7 are relatively unaffected in these compounds by the orientation of the H-5 proton. Concomitant but much smaller shift effects are seen in the proton spectra for all of these compounds. The effects observed in the ^{13}C spectra may be due to a marked increase in the strain of ring A (according to Dreiding models) in the 5α, as compared to the 5β, configurations. There is no evidence for such strain in the 6,6 series. However, for the 5β compounds **12** and **22**, the H-9 and C-9 are in the shielding cone of the amide. In all cases, the 5α proton is distinguished from the 5β proton by the presence of a large *trans* diaxial coupling (ca. 12 Hz) to one of the hydrogens at position 6.

The dimeric compounds **16**, **25**, and **26** yield deceptively simple NMR spectra, in that identical ^{1}H and ^{13}C shifts are observed for both steroid nuclei in these structures. In the absence of clear mass spectrometric evidence (see above), the only clue to the presence of a dimer rather than a monomer for these compounds is the appearance of a carbonyl resonance of reduced intensity in the ^{13}C spectra of **25** and **26** (at 165.4 and 163.3 ppm, respectively) and of an extra methylene carbon (again reduced in intensity) at 31.5 ppm in the spectrum of **16**, which in turn was correlated to a broad singlet at 2.59 ppm in the proton spectrum. The location of this methylene bridge at position C-6 was confirmed by the HMBC experiment, which showed coupling of the methylene singlet at 2.56 ppm in the proton spectrum to C-6 at 109.3 ppm in the carbon spectrum. Weaker couplings were also observed between this proton signal and C-5 and C-7 at 135.5 and 34.8 ppm, respectively. Similarly, couplings were observed between the H-5 protons at 3.0 and 3.5 ppm and H-2 protons at 3.4 and 3.1 ppm in the spectra of **25** and **26** to the carbonyl carbons at 165.4 and 163.3 ppm, respectively, thus supporting other spectroscopic and chemical evidence for the urea structures.

Two explanations are possible for the simplicity of the NMR spectra: either that rotation about the bonds of the bridging function is sufficiently fast on the NMR time scale to average out any effects or that the barrier to rotation is high and only one rotamer exists — one that has a plane of symmetry. The former explanation is preferred in the case of compound **16**, since free rotation about the bridging methylene function would be expected. In the case of the ureas **25** and **26**, the overlap of the two nitrogen lone pairs with the carbonyl function predicts that there is less double bond character than in an ordinary amide and therefore the barrier to rotation should also be relatively low. This is consistent with the fact that tetramethyl urea gives a single signal for both ^{1}H and ^{13}C at room temperature while for the classical example of dimethyl formamide, where the barrier to rotation is quite high, there is doubling of signals (12).

Other motional effects are observed when the spectra of the A-nor series of compounds are compared. In the ^{13}C spectra of the carbamates **18** and **19**, the resonances due to C-2, C-6, and C-10 of the A ring are broadened and reduced in intensity. The C-5 resonance is also affected but to a lesser extent. In the proton spectrum of **19**, the resonance due to H-6α is only barely visible and shifted to 2.6 ppm and the resonances of H-5 and H-2 are also broadened. These effects are also seen in the spectra of **18**. The broadening of these particular resonances was also observed for the *N*-acetyl derivatives **27** and **28** but is not so pronounced, less so for the ureas **25** and **26**, and absent for the salts **23** and **24**. In all cases the effect is more pronounced in the 5β compounds than the 5α. This behavior may be accounted for by the presence of two rotamers with restricted rotation on the NMR time scale. This restricted motion would be maximum in the carbamates, less for the *N*-acetyl compounds, and least for the ureas and the salts. This is supported by the infrared spectra, in which the carbamate frequencies are high (ca. 1695 cm^{-1}) with little overlap while the frequencies for the ureas are low (1626 cm^{-1}). Therefore, the energy required to stretch the C=O bond is lowest in the ureas, where the amount of the double-bond character is the least. The restricted rotation is greater in the 5β compounds since the nonbonded interactions are also maximized.

© 1997 NRC Canada

Can. J. Chem. Downloaded from www.nrcresearchpress.com by 88.146.161.215 on 09/08/12
For personal use only.

Long-range couplings, both homonuclear ($^1H/^1H$) and heteronuclear ($^1H/^{13}C$), that occurred through the nitrogen atom in ring A were observed in several cases in COSY and HMBC spectra. These long-range *J* values are likely enhanced by the partial C=N double-bond character of the amide system. In particular, long-range couplings were observed in the spectra of compounds **32** and **20** that permit the determination of configuration of C-5 in the latter. In the COSY spectrum of **32**, a homoallylic coupling ($^5J_{HH}$) was observed between H-2β at 2.25 ppm and H-5β at 2.95 ppm. Homoallylic coupling is often observed in aromatic systems where the π orbitals of the double bond system are parallel and overlap with the CH bond (13). This would favour a conformation in which the 5β hydrogen is axial. In the spectra of compound **20**, no allylic coupling was observed but NOE measurements show a positive effect both between H-2 at 2.30 ppm and H-5 at 5.44 and H-5 and CH_3-19 at 1.35 ppm. Thus the methoxy function has an α configuration and the conformation of ring β is such that the 5β proton is axial and proximate to the CH_3-19. This conformation minimizes the nonbonded interaction of the 5α methoxy group with the carbonyl function.

The correct assignment of the C-2 proton of the A-nor compounds was critical to the determination of mechanism for the aza-Favorskii reaction (see mechanism section). Integration of the H-2 signals at ca. 3.4 ppm from samples of **18** and **19** formed from methanol-*d* showed that less than 5% exchange of these hydrogens had occurred. As expected (see eq. [15]), both enamides **15** and **17** produced in these reactions showed partial exchange of the C-6 hydrogens (at 5.25 ppm and 4.24 ppm, respectively), while no reduction in the intensity of the H-2 signals at ca. 2.4 ppm was observed.

Summary

Attempts to prepare *N*-acyl imine **3** failed, but it was implicated as a transient intermediate in reactions of hydroxamic acid methanesulfonates **13** and **14**. A new aza-Favorskii reaction was observed, leading to a new route to 3-aza-A-nor steroids. A new preparation of 4-aza-A-nor-B-homocholestane derivatives and a high-yielding synthesis of the enamide 4-azacholest-5-ene-3-one (**17**) were described. Both homolytic and heterolytic reactions were implicated in the photochemistry of the methanesulfonates.

Experimental

Infrared spectra were for dichloromethane solutions, unless otherwise indicated, on a Perkin–Elmer model 683 grating spectrometer, and ultraviolet spectra were taken for 95% ethanol solutions unless otherwise indicated. Routine ^1H NMR spectra were taken on a Varian Gemini instrument at 200 MHz and ^{13}C spectra at 50 MHz. High-resolution ^1H and ^{13}C NMR spectra were recorded in deuterochloroform ($CDCl_3$) at 500.13 and 125.18 MHz, respectively, on a Bruker AM500 NMR spectrometer operating at 303 K. A 5 mm normal geometry $^{13}C/^1H$ probe was used (90° ^{13}C = 18 μs, 90° ^1H = 7 μs). Chemical shifts were referenced to $CDCl_3$ at 77.0 ppm (^{13}C) and 7.24 ppm (^1H) and are reported relative to TMS. The resonance assignments for known compounds were elaborated and for new compounds were determined using a combination of $^1H/^1H$ correlation (COSY, TOCSY), DEPT, ID NOE, and $^1H/^{13}C$ correlation (HETCOR, HMBC) experiments using standard Bruker pulse sequences.

All preparative thin-layer chromatography was done on 20 × 20 cm glass plates with fluorescent indicator and column chromatography on 100–200 mesh silica gel or Woelm neutral alumina. Melting points were corrected using standards. Tetramethyl urea and 2,4,6-collidine were distilled from calcium hydride, tetrahydrofuran from lithium aluminum hydride, methanol from magnesium methoxide, and dichloromethane from phosphorus pentoxide. Yields were calculated based on unrecovered starting material.

Unless otherwise noted, the NMR spectral assignments, both ^1H and ^{13}C, of the following compounds are documented in Tables 2 and 3.

3,5-Seco-A-nor-5-oxocholestan-3-oic acid 5 (R = H)

A modified procedure of Singh and Paul (14) was used to prepare **5** (R = H).

To a stirred solution of 13 g of 4-cholesten-3-one in 600 mL of *tert*-butyl alcohol was added 7 g of potassium carbonate in 150 mL of water, then 45 g of sodium periodate in 350 mL of water, followed by 100 mg of potassium permanganate in 10 mL of water. A cold water bath was used to keep the temperature below 38°C. After 3 h the solid (mostly inorganic) was removed by filtration. Solid sodium hydrogen sulfite was added to the filtrate until only a pale yellow color persisted. The two phases were separated. The aqueous phase was extracted with dichloromethane. The phase rich in *tert*-butyl alcohol was evaporated to a volume of 150 mL. This was made strongly acid using dilute sulfuric acid, then extracted with dichloromethane. The combined dichloromethane extracts were washed with water, dried, and concentrated. Addition of hexane resulted in crystallization of 7.7 g of desired acid with mp as high as 145°C. On recrystallization from methanol this gave 6.9 g (50%), mp 147–152°C (lit. (13) mp 154–154.5°C). A purified specimen had mp 151–153°C, ν_{max}: 1703 cm^{-1}, and ^1H NMR signals at δ 1.13 (3H), 0.93, 0.89, 0.85 (methyl resonances), and 0.73 (3H).

Methyl 3,5-seco-A-nor-5-oxocholestan-3-oate 5 (R = CH_3)

This ester, prepared by action of diazomethane on a methanol solution of **5** (R = H), remained amorphous. It has ν_{max} 1732 and 1700 cm^{-1} and gave ^1H NMR signals at δ 3.66 (3H), 1.12 (3H), 0.93, 0.89, 0.85 (methyl resonances), and 0.73 (3H). ^{13}C NMR: 214.7, 174.3, 56.0, 55.7, 51.5, 50.3, 47.8, 42.5, 39.4, 38.1, 36.1, 35.9, 35.7, 31.3, 29.5, 29.1, 28.0, 24.4, 24.2, 23.8, 22.5, 21.4, 20.5, 18.6, and 12.0 ppm.

3,5-Seco-A-nor-5-oximinocholestan-3-oic acid 7

Acid **5** (2.0 g) and hydroxylamine hydrochloride (2.5 g) were dissolved in 30 mL of ethanol, then 2.0 g of anhydrous sodium acetate was added. The mixture was heated under reflux for 3 h, cooled, then filtered from inorganic salts. The filtrate was evaporated to dryness. The residue was dissolved in 100 mL of dichloromethane. This solution was washed with 1 M sulfuric acid, then water, dried over sodium sulfate, then concentrated (care; the oxime may crystallize at any stage). Three crops of crystals totalling 1.8 g (87%), mp 181°C, were collected. These were purified on 55 g of "flash" silica gel using 5% methanol in chloroform (a red zone just precedes the main eluate, probably an iron chelate) raising the mp to 183–185°C.

© 1997 NRC Canada

Can. J. Chem. Downloaded from www.nrcresearchpress.com by 88.146.161.215 on 09/08/12
For personal use only.

This gave ν_{max}: 3580, 3260, and 1703 cm^{-1} and ^1H NMR signals at δ 3.35 (1H, br d), 1.09, 0.88, 0.85, and 0.69 (sharp methyl signals).

***N*-Hydroxy-4-aza-cholestane-3-ones (hydroxamic acids)**

The oximino seco acid **7** (2.35 g) was dissolved in 45 mL of hot acetic acid. The solution was cooled to room temperature, then 1.1 g of sodium cyanoborohydride was added in portions with stirring during 7 min. Hydrogen was steadily evolved. After 0.5 h a further 250 mg of cyanoborohydride was added. After warming gently to dissolve all solids, the mixture was stirred for 1 h. The acetic acid was then removed on a rotating evaporator under 1 Torr (133.3 Pa), leaving a froth. This was dissolved in dichloromethane and the solution washed with water (emulsion). The dichloromethane layer gave 2.5 g of colorless froth. This was separated on 100 g of flash silica gel using chloroform. The lower melting isomer (5β) eluted first, followed by a sharp orange band (a small amount of iron chelate) and then the higher melting isomer (5α). Both isomers crystallized from ethyl acetate. The yield of **9** (5α) was 402 mg (18%) and of **10** (5β), 608 mg (27%).

***N*-Hydroxy-4-aza-5α-cholestane-3-one 9**

The higher melting isomer after recrystallization from ethyl acetate formed shimmering needles with mp 195°C (lit. (5) mp 185–187°C). It had ν_{max}: 3390, 3250, and 1625 cm^{-1} and gave ^1H NMR signals at δ 8.5 (OH), 3.33 (1H dd, J = 11.6, 3.3 Hz), 2.52 (2H m), 2.25 (1H, m), 0.97, 0.92, 0.88, 0.85, and 0.67 (sharp methyl signals). ^{13}C NMR: 165.6, 68.0, 56.1, 55.9, 51.4, 42.7, 39.6, 39.5, 37.5, 36.1, 35.7, 34.4, 32.6, 29.3, 28.2, 28.0, 27.8, 24.0, 23.8, 23.1, 22.8, 22.5, 21.0, 18.6, 12.5, and 12.1 ppm. Anal. calcd. for $C_{26}H_{45}NO_2$: C 77.36, H 11.24, N 3.47; found: C 77.23, H 11.37, N 3.49.

***N*-Methanesulfonyloxy-4-aza-5α-cholestan-3-one 13**

A solution of 402 mg of hydroxamic acid **9** and 0.3 mL of methanesulfonyl chloride in 2 mL dry pyridine was left at room temperature for 16 h. A crystalline solid separated. The mixture was cooled with ice, then 1 mL of water was added. After 50 min much of the pyridine and water was removed under reduced pressure. The residue was distributed between dichloromethane and dilute sulfuric acid. The dichloromethane yielded 466 mg of light brown gum, which crystallized from ethyl acetate. The product was purified by passage of a dichloromethane solution through a column of 6 g of neutral alumina, activity 1, giving 350 mg of **13**. This crystallized from ethyl acetate as fine needles, mp 158–159°C. It had ν_{max}: 1692, 1373, and 1183 cm^{-1} and gave ^1H NMR signals at δ 3.45 (1H dd, J = 13, 4 Hz), 2.62 (2H m), 1.06, 0.91, 0.88, 0.85, and 0.67 (sharp methyl signals). ^{13}C NMR: 169.5, 71.9, 56.2, 55.8, 51.7, 42.6, 40.3, 39.7, 39.5, 39.2, 36.1, 35.7, 34.4, 33.3, 30.5, 29.3, 28.2, 28.0, 24.5, 24.0, 23.8, 22.8, 22.6, 21.2, 18.7, 12.5, 12.1. Anal. calcd. for $C_{27}H_{47}NO_4S$: C 67.25, H 9.77, N 2.91; found: C 67.40, H 9.89, N 3.08.

***N*-Hydroxy-4-aza-5β-cholestan-3-one 10**

This crystallized from ethyl acetate, mp 125–126°C (lit. (5) mp 122–124°C), recrystallizing and melting at 131°C if heating was very slow. It had ν_{max}: 3670, 3390, 3240, and 1014 cm^{-1} and gave ^1H NMR signals at δ 8.65 (OH), 3.51 (1H s), 2.40 (3H m), 1.04 (3H s), 0.91, 0.88, 0.85 (sharp methyl signals), 0.67 (3H s). ^{13}C NMR: 164.9, 66.0, 56.2, 55.8, 42.6, 41.0, 39.9, 39.5, 36.4, 36.1, 35.8, 35.0, 31.3, 28.2, 28.0, 26.8, 25.7, 24.1, 23.9, 23.1, 22.8, 22.6, 21.4, 21.1, 18.7, 12.0 ppm. Anal. calcd. for $C_{26}H_{45}NO_2$: C 77.36, H 11.24, N 3.47; found: C: 77.18, H 11.40, N 3.53.

***N*-Methanesulfonyloxy-4-aza-5β-cholestan-3-one 14**

The 126°C hydroxamic acid **5** (218 mg) was treated with methanesulfonyl chloride in pyridine as for the 192°C isomer. The product was purified by passage through a column of 4 g of neutral alumina, activity 1. Hexane eluted 31 mg of mesylate containing a small amount of higher R_f impurities (TLC). A 30% ethyl acetate in hexane mixture eluted 211 mg of pure mesylate. This did not crystallize readily, but finally separated from hexane as fine needles, mp 87–88°C. Methanol proved to be the solvent of choice for recrystallization. The crystals had ν_{max}: 1678, 1372, and 1182 cm^{-1} and gave ^1H NMR signals at δ 3.80 (1H, br s), 3.45 (3 H, s), 2.5 (2H, m), 1.07, 0.91, 0.88, 0.85, and 0.67 (sharp methyl signals). ^{13}C NMR: 167.9, 71.2, 56.2, 55.8, 42.6, 40.8, 40.7, 39.8, 39.5, 37.8, 36.1, 35.8, 35.0, 31.2, 29.2, 28.2, 28.0, 25.5, 24.1, 23.8, 23.6, 22.8, 22.6, 21.5, 20.9, 18.7, 12.0. Its CI mass spectrum gave *m/z*: 482(81), 388(100), 387(44), and 386(75); calcd. for $C_{27}H_{47}NO_4S$: 481.

***N*-Methoxy-4-aza-5α-cholestan-3-one 11**

A solution of sodium methoxide in 3 mL of dry methanol was prepared using 104 mg of sodium hydride. To this was added 95 mg of hydroxamic acid **9** and 90 μL of methyl iodide in 5 mL of methanol. After 2 h refluxing a further 80 μL of methyl iodide was added, then the refluxing continued for an extra 2 h. The mixture was evaporated under reduced pressure, water was added, and then the product was extracted into dichloromethane. The 70 mg of **11** recovered from the dichloromethane was recrystallized from hexane. It had mp 146°C and ν_{max} 1668 cm^{-1}.

***N*-Methoxy-4-aza-5β-cholestan-3-one 12**

This was prepared from hydroxamic acid **10** as described for **11**. It crystallized from aqueous methanol as thin plates with mp 115°C (Lit. (5) mp 115°C). It had ν_{max} 1655 cm^{-1}.

***N*-Hydroxy-4-azacholest-5-en-3-one 8**

Oximino acid **7** in an evacuated (0.2 Torr) flask was placed in a bath at 185°C for 20 min. The melt bubbled vigorously. After cooling, the product was dissolved in dichloromethane. After addition of ethyl acetate the bulk of the dichloromethane was evaporated. A gel formed that was slowly transformed into balls of extremely fine needles, mp 196–198°C, in an evacuated capillary (immersed at 180°C). Chromatography over silica gel with chloroform eluant gave an orange zone followed by **8**. Its mp remained the same. It had ν_{max}: 3660, 3380, 3230, and 1617 cm^{-1} and λ_{max} 238.5 nm (Table 1).

Thermolysis of 13

(a) In tetramethyl urea

The 5α mesylate **13** (77 mg) in 2 mL of dry tetramethylurea (TMU) was heated in a bath at 180°C under argon for 5 h. The solvent was then removed at 100°C under 0.5 Torr pressure. A dichloromethane solution of the residue was washed with aqueous sodium carbonate. The 65 mg recovered from the

© 1997 NRC Canada

Can. J. Chem. Downloaded from www.nrcresearchpress.com by 88.146.161.215 on 09/08/12
For personal use only.

dichloromethane crystallized in part from an ethyl acetate – hexane mixture giving 30 mg of enamide **17**. The mother liquor was separated on a 1 mm SiO_2 plate using 80% ethyl acetate – 20% hexane. Of the seven zones visible under UV light, three were characterized as enamide **15** (R_f 0.5, 3 mg, 5%), enamide **17** (R_f 0.33, 4 mg), and dimeric enamide **16** (R_f 0.14, 8 mg, 7%). The total yield of enamide **17** was 34 mg (57%). The yield of **17** and products related to it with the 4-azacholest-5-ene skeleton was 71% (calculated as monomer).

(b) In TMU with $CaCO_3$

For details see the comparable experiment with **14**: 71 mg of **13** and 158 mg of $CaCO_3$ in 2 mL of dry TMU under argon were stirred at 180°C for 3 h. Mesylate (3 mg) was recovered. Crystalline **17** (42 mg, 77%) was obtained, along with small amounts of **15** and **16**.

(c) In collidine

A solution of 5α-mesylate **13** in 0.8 mL of dry 2,4,6-collidine under argon was placed in a bath at 145°C. The temperature was raised to 175°C (1 h), then maintained at that temperature for 2.5 h. The bulk of the collidine was removed under 0.5 Torr pressure, and then the residue was dissolved in dichloromethane. This solution was washed with 1 N sulfuric acid, then with aqueous sodium carbonate. The 65 mg of brown residue recovered from the dichloromethane crystallized from ethyl acetate – hexane mixture, giving 40 mg of enamide **17**. Separation of the contents of the mother liquor as for (*c*) gave 8 mg of **17**; total yield 48 mg (73%).

Thermolysis of 5β-mesylate 14

(a) In tetramethylurea (TMU)

A flask containing 180 mg of mesylate **14** and 4 mL of dry TMU was flushed with argon, then heated in a bath at 180°C for 3 h. The solvent was removed under 0.5 Torr pressure, the residue dissolved in dichloromethane, then this was washed with saturated aqueous sodium bicarbonate. The aqueous layer was evaporated, finally at 60°C under 0.5 Torr pressure, leaving 179 mg of gum. This crystallized in part from 1:1 ethyl acetate/hexane giving 38 mg of **17**. Again the solvents were removed, finally at 120°C, 0.5 Torr. A ^{13}C NMR spectrum of the residue showed the presence of **17** (140.0, 103.4 ppm), **15** (135.3, 109.6 ppm), and **16** (125.1, 116.3 ppm) with carbonyl carbons at 169.7 and 169.6 ppm. No signal corresponding to an *N*-acyl imine was present.

The residue (121 mg) was separated on a 1 mm plate of C-18 coated silica gel using 30% benzene – 70% acetonitrile. The products, in order of decreasing R_f, were **15** (9 mg, 7%), unchanged mesylate (25 mg), unknown (9 mg), **17** (15 mg), and dimer **16** (47 mg, 19%). The total yield of crystalline **17** was 50 mg (41%) but the yield of products with the 4-azacholest-5-ene skeleton was 79%.

(b) In TMU with $CaCO_3$

A solution of 161 mg of **14** in 4 mL of dry TMU and 373 mg of powdered $CaCO_3$ in a flask fitted with a sintered glass funnel was flushed with argon, then heated at 180°C for 3.5 h. The cooled suspension was diluted with dichloromethane, then filtered under pressure. The solid was washed twice with dichloromethane. The filtrate was evaporated, finally at 75°C, 0.5 Torr pressure. The residue crystallized in part from dichloromethane–hexane, giving 88 mg of **17**. The products recovered from the filtrate were separated on a 1 Torr SiO_2 plate using 1:1 ethyl acetate/hexane giving, in order of decreasing R_f, recovered mesylate, 9 mg; enamide **15**, 6 mg (5%), enamide **17**, 7 mg; and enamide **16**, 12 mg (5%). The total yield of crystalline **17** was 95 mg (78%). A zone just ahead of **16** contained 9 mg of a mixture giving two main N-CH_3 or N-CH_2 signals near δ 3.0 and the steroid CH signals, i.e., these were coupling products of **17** with products such as **30**. None of these was characterized further. The use of higher ratios of $CaCO_3$ produced yields of **17** as high as 88%. A ^{13}C NMR spectrum of the total chloroform-soluble product before plating showed only low-field signals due to **17**.

(c) In 2,4,6-collidine

This was carried out as for the 5α-mesylate **13**. The yield of **17** was 80%, averaged over three runs.

(d) In methanol with $CaCO_3$

A mixture of 90 mg of **14**, 273 mg of $CaCO_3$ powder, and 5 mL of dry methanol was sealed in a tube under argon. This was heated at 190 ± 5°C for 3 h. The cooled suspension was filtered and the solid washed with methanol. The filtrate was evaporated in vacuo, finally at 60°C, 0.5 Torr pressure. The residue was suspended in dichloromethane, then filtered, giving 11 mg of insoluble solid. The filtrate yielded 74 mg of gum. The ^1H NMR and ^{13}C NMR of this residue showed only the main products described below. These were separated on a 1 mm SiO_2 plate using 1:1 ethyl acetate/hexane. The products identified were, in order of decreasing R_f, methyl keto ester **5** (R = CH_3), 12 mg (16%); carbamate **19**, 12 mg (15%); enamide **15**, 22 mg (30%); methoxy lactam **20**, 5 mg (6%); enamide **17**, 9 mg (16%).

(e) In methanol-d *with $CaCO_3$*

A solution of 116 mg of **14** in 4 mL of methanol-*d* and 244 mg of $CaCO_3$ was heated as for (*d*) but at 175°C for 4 h. The yields were **5** (R = CH_3), 9 mg (9%); **19**, 24 mg (18%); **15**, 48 mg (38%); **17**, 11 mg (12%).

The ^1H NMR spectrum of carbamate **19** showed less than 5% exchange of the hydrogens on C-2. Both enamides **15** and **17** showed approximately 50% exchange of the 6-hydrogens for deuterium (see the NMR section).

Irradiation of 13

(a) In methanol

A solution of 189 mg of 5α mesylate **13** (warming) in 55 mL of dry methanol was irradiated for 5.5 h using 254 nm Rayonet lamps (cold finger at 15°C). The bulk of the methanol was removed on a rotating evaporator, the residue was dissolved in dichloromethane, and then this solution was washed with 5% sodium carbonate. The organic layer yielded a gum that was separated on two 1 mm plates using 30% hexane – 70% ethyl acetate. The products identified were methyl keto ester **5** (R = CH_3, 4%); carbamate **18**, 57 mg (35%); methoxy lactam **20**, 42 mg (25%); enamide **17**, 12 mg (8%); and lactam **21**, 8 mg (5%).

(b) In methanol-d

A solution of 103 mg of **13** in 42 mL of methanol-*d* was irra-

© 1997 NRC Canada

Can. J. Chem. Downloaded from www.nrcresearchpress.com by 88.146.161.215 on 09/08/12
For personal use only.

diated as for (*a*) with the cold finger at 23°C. The main products and yields were the same as for the photolysis in methanol. Enamide **17** had partial exchange of the vinyl hydrogen (H-6) (see NMR section)

(c) In aqueous tetrahydrofuran

A solution of 114 mg of **13** in 50 mL of tetrahydrofuran and 5 mL of water was flushed with argon. This was irradiated for 4.5 h with the cold finger at 5°C, with mixing at half-hour intervals. The solvent was evaporated on a rotating evaporator, then the product was distributed between 5% sodium carbonate and chloroform. The mixture recovered from the chloroform was dissolved in methanol, then this was titrated to pH 2 with hydrochloric acid in methanol. The solvent was evaporated to dryness and the residue suspended in ethyl acetate. This was filtered, giving 56 mg of solid (mainly **23** hydrochloride). The products in the filtrate were separated on a 0.5 mm plate using 10% ethanol in chloroform. The products identified were: **15**, 27 mg (30%); **17**, 3 mg (5%); **21**, 10 mg (11%); and **23** hydrochloride, 5 mg. The total yield of pure **23** hydrochloride was 34%.

(d) In dichloromethane

13 (103 mg) in 50 mL of dry dichloromethane was irradiated for 4 h with the cold finger at −5°C. The solvent was evaporated (bath at 40°C), then 2 mL of dry dichloromethane was added. This solution had ν_{max}: 1750 (str), 1696 (med), 1625 (wk), and 1215 (str) cm^{-1}. Methanol (2 mL) was added, then the mixture was heated for 10 min, distilling off the dichloromethane. The methanol was removed in a rotating evaporator, dichloromethane was added, then this was shaken with sodium carbonate solution. The organic layers yielded 94 mg of neutral and basic products. Acetic anhydride (1 mL) was added. After 20 h at room temperature the anhydride was removed in vacuo, the residues were heated with methanol, and then the mixture was evaporated again. A dichloromethane solution of the residue was washed with sodium carbonate solution, dried, and then the solvent was distilled, giving 86 mg of gum. This was separated on a 1 mm plate using 10% hexane – 80% ethyl acetate giving, in order of decreasing R_f, carbamate **19**, 21 mg (24%); unknown, 4 mg; unknown, 6 mg; *N*-acetyl derivative **27**, 10 mg (12%); unknown (origin), 11 mg. The estimated yield of products having the A-nor skeleton **23** was 36%.

(e) In moist dichloromethane

A dichloromethane solution (70 mL) of **13** (243 mg) was irradiated (cold finger at 15°C, stirring at intervals) for 5 h. The solution was washed with aqueous sodium carbonate, dried, and evaporated. The residue in 1 mL of acetic anhydride and 1 mL of pyridine was heated to give a clear solution. After 18 h at room temperature the mixture was worked up as in (*d*), giving 228 mg of product. This was separated on three 1 mm plates as for (*d*,) giving in order of decreasing R_f: urea **25**, 30 mg (9%); unchanged **13**, 28 mg; enamide **15**, 29 mg (16%); unknown, 12 mg; an unknown, 10 mg; and *N*-acetyl derivative **27**, 50 mg (29%). The yield of products with the A-nor skeleton **23** was 29% + (2 × 9%) = 47%.

Irradiation of 14

(a) In methanol

Mesylate **14** (188 mg) in 45 mL of dry methanol was irradiated under argon with the cold finger at 10°C for 4.5 h, with mixing at 1 h intervals. The methanol was evaporated and the residue dissolved in dichloromethane, then this solution was washed with aqueous sodium bicarbonate. The 165 mg of colorless oil was separated on two 1 mm plates using 30% hexane – 70% ethyl acetate. Recovered mesylate **14** (17 mg) was followed in order of decreasing R_f by carbamate **19**, 56 mg (38%); methoxy lactam **20**, 47 mg (32%); and enamide **17**, 14 mg (10%).

(b) In methanol-d

A solution of **14** (122 mg) in 30 mL of methanol-*d* was irradiated (cold finger at 23°C) for 4 h. Work-up and separation as for (*a*) gave 14 mg of unchanged **14**; carbamate **19**, 35 mg (32%); enamide **15**, 4 mg (5%); methoxy lactam **20**, 11 mg (12%); and **17**, 9 mg (10%). ^{1}H NMR spectra of **15** and **17** showed partial exchange of H-6 for deuterium. Carbamate **19** showed less than 5% exchange of the 2-hydrogens (see NMR section).

(c) In aqueous tetrahydrofuran

A solution of 212 mg of **14** in 100 mL of tetrahydrofuran and 10 mL of water was irradiated in two equal portions as for **13**. In the work-up, ether was used to precipitate the hydrochloride (50 mg). The filtrate was evaporated and the residue separated on two 1 Torr plates using 15% hexane – 75% ethyl acetate. The products characterized in order of decreasing R_f were enamide **15**, 48 mg (28%); enamide **17**, 11 mg (6%); and lactam **22**, 19 mg (11%). The low R_f zone was extracted with hot methanol in chloroform. After evaporation of the solvent the extract was treated with 1:1 acetic anhydride/pyridine, giving *N*-acetyl derivative **28**, 9 mg (5%). The total yield of products related to A-nor base **24** was 33%.

(d) In dichloromethane

1. Dry, methanol work-up: Following irradiation of 102 mg of **14** as for **13** but at 15°C, 10 mL of methanol was added. After 0.5 h the solvents were evaporated under reduced pressure. The residue was dissolved in dichloromethane, then the solution was washed with aqueous sodium carbonate. The dried solution was evaporated. The residue was suspended in chloroform, filtered from a small amount of inorganic solid, and then separated on a 1 mm plate using 30% hexane – 70% ethyl acetate. The products characterized were carbamate **19**, 15 mg (19%); recovered **14**, 10 mg; and enamide **15**, 9 mg (12%). The low R_f zone was treated as in (*c*) yielding **28**, 8 mg (10%).

2. Dry dichloromethane (55 mL) containing 118 mg of **14** was irradiated for 4 h with the cold finger at 5°C. Moisture was probably introduced during stirring. The solution was shaken with aqueous sodium carbonate, dried, and distilled. The residue was acetylated using acetic anhydride and pyridine (20 h). The product after removal of the reagents under 1 Torr pressure was dissolved in dichloromethane. This solution was washed with 1 N sulfuric acid, then with 5% sodium carbonate. The dried solution gave 100 mg of gum, which was separated on a 1 mm plate using 2% methanol in chloroform. The products identified were urea **26**, 10 mg (6%); recovered mesylate, 11 mg; enamide **16**, 15 mg (17%); and *N*-acetyl derivative **28**, 16 mg (19%).

(e) In dichloromethane with triethylamine

Mesylate **14** (58 mg) and triethylamine (20 mg) in 50 mL of

© 1997 NRC Canada

Can. J. Chem. Downloaded from www.nrcresearchpress.com by 88.146.161.215 on 09/08/12
For personal use only.

dry dichloromethane were irradiated under argon with the cold finger at 20°C for 3 h. The solvent was evaporated on a rotating evaporator in a bath at 40°C, then the residue put under 0.5 Torr pressure at 40°C. The residue had ν_{max}: 1743, 1686, 1614, and 1037 cm^{-1}. Its ^{13}C NMR spectrum (500 MHz) had the olefinic and carbonyl peaks of **15** as dominant, but also minor ones of unknown origin at 175.5, 162.9, 146.3, 144.8, and 136.6. A signal at 89.05, corresponding to a carbon carrying two hetero atoms, is also unassigned.

The product recovered from the $CDCl_3$ was heated briefly in methanol, then left in solution for 2 h at room temperature. After removal of the methanol the infrared spectrum was retaken. The 1743 cm^{-1} band was completely gone but the 1686 and 1614 cm^{-1} peaks remained. A dilute dichloromethane solution was shaken with aqueous sodium carbonate. The organic layer gave 55 mg of brown gum. This was acetylated using acetic anhydride. The neutral products were then separated on a 1 Torr plate using 30% hexane – 70% ethyl acetate. The major components were carbamate **19**, 13 mg (28%); recovered **14**, 4 mg; enamide **15**, 6 mg (14%); and *N*-acetyl derivative **28**, 6 mg (13%).

*Enamide **15***: This crystallized from ethyl acetate – hexane as fine needles, mp 134°C. For its UV spectrum, see Table 1. It gave ν_{max}: 1690 and 1180 cm. Its EI mass spectrum had peaks at *m/z* 385.3345 (M^+), 370, 272, 173, and 137 (base peak); calcd. for $C_{26}H_{43}NO$: 385.3344. Its CI mass spectrum had peaks at *m/z* 386 ($M^+ + 1$) and 370 ($M^+ - CH_3$).

*Bis(4-aza-3-oxocholest-5-en-6-yl)-methane **16***: This remained amorphous. Its UV absorption is listed in Table 1. It had ν_{max}: 3390 and 1667 cm.

*4-Azacholest-5-en-3-one **17***: This crystallized from dichloromethane – ethyl acetate as short needles, mp 253°C (immersed at 243°C), 258–260°C (immersed at 230°C in an evacuated capillary (lit. (3*a*) mp 256°C). Its ultraviolet spectrum is listed in Table 1. It had ν_{max}: 3380, 3185, 1681 (med), and 1661 (str) cm^{-1}.

N-*Methoxycarbonyl 3-aza-A-nor-5α-cholestane **18***: This formed fine needles from methanol, mp 128–129°C. It had ν_{max}: 1695 and 1124 cm^{-1}. The mass spectrum in CI mode showed a strong $M^+ + 1$ ion at *m/z* 418 and in EI mode an M^+ ion at *m/z* 417.

N-*methoxycarbonyl-3-aza-A-nor-5β-cholestane **19***: This crystallized from aqueous methanol as hexagonal plates with mp 88°C. It had ν_{max}: 1691, 1135, and 1105 cm^{-1}. Its CI mass spectrum had peaks at *m/z* 418 ($M^+ + 1$), 402 ($M^+ + 1$) $- CH_4$), and 386 ($M^+ + 1 - CH_3OH$). Its structure was determined by X-ray crystallography (unpublished work by Professor C. Bensimon, University of Ottawa).

*4-Aza-5-methoxy-A-nor-B-homocholestan-3-one **20***: This crystallized as rods from cold hexane, mp 82–83°C. It had ν_{max}: 1682 and 1089 cm^{-1}. Its CI mass spectrum gave *m/z* 387 ($M - 31 + H^+$).

*4-Aza-5α-cholestan-3-one **21***: This crystallized from methanol as short needles, mp 250–252°C (lit. (5) mp 252°C) and had ν_{max}: 3380, 3190, and 1659 cm^{-1}.

*4-Aza-5β-cholestan-3-one **22***: This crystallized from ethyl acetate, mp 189–190°C, which disagrees with the literature value of 151–155°C (5) (dimorphic ?). It had ν_{max}: 3380 and 1658 cm^{-1}.

*3-Aza-5α-A-norcholestane hydrochloride (**23** hydrochloride)*: The hydrochloride of **23** crystallized as fine needles from dichloromethane – ethyl acetate, mp 262°C (dec.) when heating was started at 245°C.

*3-Aza-5β-A-norcholestane hydrochloride (**24** hydrochloride)*: The hydrochloride of **24** crystallized from methanol – ethyl acetate as small plates or needles, mp 258°C (dec.) when heated from 245°C.

*Urea **25***: After purification using a preparative plate and 1:1 dichloromethane/hexane (R_f 0.3) and crystallization from methanol – ethyl acetate, **25** formed fine needles, mp 236–242°C. It had ν_{max} 1627 cm^{-1}.

*Urea **26***: The 5β urea **26** crystallized from dichloromethane – methanol or ethyl acetate, mp 250–252°C. It had ν_{max} 1626 cm^{-1}.

N-*Acetyl-3-aza-5α-A-norcholestane **27***: This was hard to free from a trace of UV – visible contaminant. Recrystallization from methanol gave **27** as fine needles, mp 122–123°C. It had ν_{max} 1642 cm^{-1}.

N-*Acetyl-3-aza-5β-A-norcholestane **28***: Preparative TLC (2% ethanol in chloroform (R_f 0.2), then 80% ethyl acetate – 20% hexane) failed to remove a trace of UV-active impurity. Recrystallization from hexane, then aqueous methanol, gave **28** as flat needles, mp 94°C. It gave ν_{max} 1641 cm^{-1}.

*A-Nor-β-homo-4-azacholestan-3-one **32***
A suspension of 26 mg of 10% Pd on charcoal in 4 mL of 95% ethanol was saturated with hydrogen, then 36 mg of enamide **15** was added. Uptake of 2.5 mL (1.1 mol) of hydrogen was rapid. The filtrate from removal of the catalyst was evaporated. The residue was suspended in hexane, then filtered from a trace of insoluble product. A concentrated hexane solution gave twisted hair-like crystals of **32**, mp 117–118°C. This had ν_{max} 1665 cm^{-1}.

*Action of methanesulfonic acid on **17** in TMU*
A solution of 125 mg of **17** and 98 mg of methanesulfonic acid in 5 mL of tetramethylurea was heated in a bath at 180°C under argon for 3 h. The solvent was removed under 1 Torr pressure in a bath at 60°C, the residue was dissolved in dichloromethane, and this was washed with aqueous sodium carbonate. The dried dichloromethane solution yielded 129 mg of gum after evaporation and heating at 100°C under 0.1 Torr pressure. This crystallized from a hexane–dichloromethane mixture, giving 53 mg of recovered enamide **17**. The mother liquor was evaporated and the residue separated on a 1 Torr silica gel plate using 80% ethyl acetate – 20% hexane mixture. The products in order of decreasing R_f were enamide **17**

© 1997 NRC Canada

(12 mg; total recovered 62 mg), unknown (14 mg), and enamide **16** (30 mg). The yield of **16** was 50% based on unrecovered **17**.

4-Aza-6-ethoxymethylcholest-5-en-3-one 31

A solution of paraformaldehyde (59 mg), *p*-toluenesulfonic acid hydrate (8 mg), and *p*-toluenesulfonic anhydride (14 mg) in 3 mL of dry chloroform and 0.3 mL of absolute ethanol was prepared. After addition of 48 mg of enamide **17** the mixture was heated in a bath at 60°C for 24 h. A crop of crystals was removed by filtration, then the filtrate was evaporated to small volume. The residue was dissolved in chloroform, and the solution was shaken with aqueous sodium carbonate, dried, and distilled, leaving 63 mg of product. This was separated on a 1 mm plate using 5% ethanol in chloroform. The main ultraviolet–visible zone yielded 34 mg of crude **31**, which crystallized from ethyl acetate – hexane to give 26 mg, mp 143°C (47%). Recrystallization of this from hexane gave **31** with mp 146–148°C after sintering at 143°C (heating started at 135°C). It had ν_{max}: 3310 and 1659 cm^{-1}. For λ_{max} see Table 1.

Coupling of 6-ethoxymethyl enamide 31 and enamide 17

A mixture of 16 mg of 4-aza-6-ethoxymethylcholest-5-en-3-one **31**, 4.7 mg of *p*-toluenesulfonic acid hydrate, 7.7 mg of *p*-toluenesulfonic anhydride, and 14 mg of enamide **17** in 3 mL of dry ethanol-free chloroform was left in a bath at 65°C under argon for 4 h. The cooled solution was extracted with aqueous sodium bicarbonate, dried, and distilled. The residue was separated on a 1 mm SiO_2 plate using 5% methanol in ethyl acetate. The main UV – visible zone yielded 26 mg (91%) of product, identified as the dimeric enamide **16** by ^1H and ^{13}C NMR.

Enamide 15 and acetic acid

A solution of **15** (21 mg) in 1 mL of acetic acid and 17 mg of acetic anhydride containing 9 mg of toluenesulfonic acid hydrate was left at room temperature for 2 days. After addition of 21 mg of sodium bicarbonate and 0.05 mL of water the mixture was stirred for 1 h. It was then evaporated to small volume on a rotating evaporator (bath at 55°C), finally under 0.5 Torr pressure. The residue was extracted with dichloromethane, filtered, then the filtrate evaporated, finally under 0.5 Torr. The residue gave an ^1H NMR spectrum identical to that of **15**.

Action of acids on enamide 17

(*a*) Dry hydrogen chloride was bubbled into a solution of 65 mg of **17** in 4 mL of dry ethanol-free chloroform at 0°C for 5 h. The residue from evaporation of the solvent crystallized from ethyl acetate giving 55 mg (84%) of unchanged **17**. The mother liquor contained a mixture of products (TLC) giving ^{13}C NMR signals at 132.5, 130.9, and 128.8 ppm.

(*b*) A solution of 138 mg of **17** and 89 mg of *p*-toluenesulfonic acid hydrate in 10 mL of dry methanol (heat) was left overnight, then refluxed for 6 h. The residue after evaporation of the solvent (rotating evaporator) was dissolved in dichloromethane. After washing with aqueous sodium carbonate and drying (Na_2SO_4), this was evaporated, yielding 140 mg of semi-crystalline solid. This was suspended in methanol and filtered, giving 46 mg of unchanged **17**. The contents of the filtrate were separated on a 1 mm SiO_2 plate using 5% methanol in chloroform. The highest R_f component (53 mg) proved, by IR and ^1H NMR to be **5** (R = CH_3). Other than another 13 mg of **17**, the other minor products were not identified.

Acknowledgements

The authors would like to thank Professor J.W. ApSimon for the opportunity to finish this work at Carleton University, John Nikiforuk for the NMR spectra, Ottawa University mass spectrometry centre and Guy Dupont for the mass spectra, and Professor C. Bensimon for the X-ray structure of **19**. B. Blackwell would like to dedicate this paper to her mother, Joan Blackwell, who succumbed to Parkinson's Syndrome during the final stages of preparing this manuscript. This publication constitutes No. 971130 for the Eastern Cereal and Oilseed Research Centre.

References

1. (*a*) B.W. Bycroft. Nature, **224**, 595 (1969); *In* Comprehensive organic chemistry. Vol. 5. *Edited by* D.H.R. Barton and W.D. Ollis. Pergamon Press, New York. 1979. pp. 241–287; U. Redeker, N. Engel, and W. Steglich. Tetrahedron Lett. **22** 4263 (1981); (*b*) O.E. Edwards and W. Rank. Can. J. Chem. **68**, 1425 (1990), and references therein; (*c*) O.E. Edwards, J.L. Douglas, D.C. Horwell, W. Rank, and T. Sano. Can.J. Chem. **70**, 2405 (1992); (*d*) T.G. Back and K. Brunner. J. Org. Chem. **54**, 1904 (1989), and references therein; (*e*) H. Hiemstra and W.N. Speckamp. *In* Comprehensive organic synthesis. Vol. 2. *Edited by* B.M. Frost. Pergamon Press, London. 1991. pp. 1046–1082; O.E. Edwards, A.M. Greaves, and W.-W. Sy. Can. J. Chem. **66**, 1163 (1988), and references therein.
2. W.A. Court, O.E. Edwards, C. Grieco, W. Rank, and T. Sano. Can. J. Chem. **53**, 463 (1975).
3. (*a*) N.J. Doorenbos, C.L. Huang, C.R. Tamorria, and M.L. Wu. J. Org. Chem. **16**, 2546 (1961); (*b*) M. Uskaković and M. Gut. Helv. Chim. Acta, **42**, 2258 (1959).
4. R.V. Hoffman and N.K. Nayyar. J. Org. Chem. **59**, 3530 (1994); R.V. Hoffman, N.K. Nayyar, J.M. Shankweiler, and B.W. Klinekole III. Tetrahedron Lett. **35**, 3231 (1994).
5. J.T. Edward and P.F. Morand. Can. J. Chem. **38**, 1316 (1960).
6. G. Rosenkranz, O. Mancera, F. Sondheimer, and C. Djerassi. J. Org. Chem. **21**, 520 (1956).
7. (*a*) C.M. Bladon and G.W. Kirby. J. Chem. Soc. Chem. Commun. 1402 (1982); (*b*) J.C. Sheehan. Angew. Chem. Int. Ed. Engl. **8**, 1 (1969); (*c*) H.E. Baumgarten, R.D. Clark, L.S. Endres, L.D. Hagemeier, and V.J. Elia. Tetrahedron Lett. 5053 (1967).
8. O.E. Edwards and M. Lesage. Can. J. Chem. **41**, 1594 (1963).
9. J.D.G. Cadogan and A.G. Rowley. J. Chem. Soc. Perkin Trans. 1, 1069 (1975).
10. (*a*) P.J. Kropp. Acc. Chem. Res. **17**, 131 (1984); O.E. Edwards and P.-T. Ho. Can. J. Chem. **56**, 733 (1979); H.E. Zimmerman. Angew. Chem. Int. Ed. Engl. **8**, 1 (1969); J.A. Pincock. Acc. Chem. Res. **30**, 43 (1997); (*b*) H. Vancik, V. Gabelica, V. Rogan, and D.E. Sunko. J. Chem. Res. (S), 92 (1990).
11. T.G. Back, J.H.-L. Chau, P.W. Codding, P.I. Gladstone, D.H. Jones, J.W. Morzycke, and A.W. Roszak. J. Org. Chem. **57**, 4110 (1992).
12. J.B. Stothers. Carbon-13 NMR spectroscopy. Academic Press, New York. 1972. p. 427, and references therein.
13. R.B. Turner. J. Am. Chem. Soc. **72**, 579 (1950).
14. H. Singh and D. Paul. J. Chem. Soc. Perkin Trans. 1, 1475 (1974).

Can. J. Chem. Downloaded from www.nrcresearchpress.com by 88.146.161.215 on 09/08/12
For personal use only.

© 1997 NRC Canada

Synthesis of thyroxine: biomimetic studies

Natalie V. Bell, W. Russell Bowman, Paul F. Coe, Andrew T. Turner, and Del Whybrow

Abstract: The biomimetic oxidative coupling of the ethyl ester of *N*-acetyl-3,5-diiodotyrosine (**1**) to yield the ethyl ester of *N*-acetylthyroxine (**2**) has been investigated. A putative mechanism involving phenolic coupling to yield an intermediate aryloxydienone (**7**) followed by an E2 elimination for loss of the side chain has been proposed. Oxidative couplings with analogous 4-substituted 3,5-diiodophenols indicate that a number of mechanisms are possible; these include quinone methide intermediates and S_N2 substitutions in the intermediate aryloxydienones. Rearomatization of the intermediate aryloxydienones is a strong driving force for the loss of the side chains. The results indicate that 3,5-diiodo-4-aryloxydienones are good leaving groups in E2 and S_N2 mechanisms. The synthetic method provides a facile synthesis of thyroxine analogues from readily available 4-substituted 3,5-diiodophenols.

Key words: diiodotyrosine, phenolic coupling, phenoxyl radicals, thyroxine.

Résumé : On a étudié le couplage oxydant biomimétique de l'ester éthylique de la *N*-acétyl-3,5-diiodotyrosine (**1**) qui conduit à l'ester éthylique de la *N*-acétylthyroxine (**2**). On propose un mécanisme impliquant un couplage phénolique conduisant à un intermédiaire aryloxydiénone (**7**), suivi d'une élimination E2 impliquant la perte de la chaîne latérale. Des couplages oxydants avec des 3,5-diiodophénols substitués d'une façon analogue en position 4 indiquent qu'un certain nombre de mécanismes possibles incluent des intermédiaires quinométhanes et des substitutions S_N2 dans les aryloxydiénones intermédiaires. La réaromatisation des aryloxydiénones intermédiaires fournit une importante force motrice pour la perte des chaînes latérales. Les résultats indiquent que les 3,5-diiodo-4-aryloxydiénones sont de bons groupes partants dans les mécanismes E2 et S_N2. La méthode de synthèse permet de préparer facilement des analogues de la thyroxine à partir de 3,5-diiodophénols substitués en position 4 facilement disponibles.

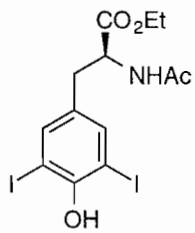
Mots clés : diiodotyrosine, couplage phénolique, radicaux phényloxyles, thyroxine.

[Traduit par la rédaction]

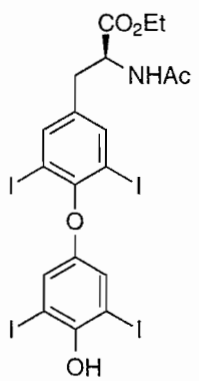
Introduction

Oxidative coupling of phenols is well researched (1), has been known for more than a century, and was first invoked in biosynthesis over 50 years ago. The biomimetic synthesis and biosynthesis of the hormone thyroxine from 3,5-diiodotyrosine provides one of the most interesting and unusual examples of oxidative coupling of phenols. The two diiodotyrosine units make up part of the thyroglobulin protein responsible for thyroxine biosynthesis in the thyroid gland and the coupling is catalyzed by the enzyme, thyroid peroxidase. The coupling of two molecules of 3,5-diiodotyrosine to form thyroxine was first proposed as early as 1927 (2) and biomimetic studies were first carried out in 1942 (3). Study of the biosynthesis continues to produce interesting results in the elucidation of the mechanism (4).

One of the industrial syntheses of thyroxine involves a step in which the ethyl ester of *N*-acetyl-3,5-diiodotyrosine (**1**) is subjected to phenolic coupling to yield the ethyl ester of *N*-acetylthyroxine (**2**) in good yield. While the reaction conditions are obviously different from those in the biological system the crucial coupling step can be regarded as biomimetic. For instance, the phenolate anion is oxidized to phenoxyl radicals, followed by coupling and elimination of one the tyrosine side chains. In this paper we report our studies to elucidate the



(**1**)



(**2**)

Received January 2, 1997.

This paper is dedicated to Professor William A. Ayer on the occasion of his 65th birthday.

N.V. Bell and W.R. Bowman.[1] Department of Chemistry, Loughborough University, Loughborough, Leics. LE11 3TU, U.K.

P.F. Coe, A.T. Turner, and D. Whybrow. Chemical Development Group, Knoll Pharmaceuticals, Pennyfoot Street, Nottingham, Notts. NG1 1GF, U.K.

[1] Author to whom correspondence may be addressed. Telephone: 44 1509 222569. Fax: 44 1509 223925. E-mail: W.R.Bowman@Lboro.ac.uk

© 1997 NRC Canada

Can. J. Chem. Downloaded from www.nrcresearchpress.com by 88.146.161.215 on 09/08/12
For personal use only.

Table 1. Oxidative coupling of the ethyl ester of *N*-acetyl-3,5-diiodotyrosine (**1**).

Experiment	Mn[a]	O_2 or N_2	Pressure[b]	Temperature	Time (h)	% Yield (**2**)[c]	% Unaltered **1**[c]
1	cat. Mn(II)	O_2	5 bar	60–70°C	20	28	72
2	cat. Mn(II)	O_2	Atmos.	Reflux	48	22	78
3	cat. Mn(II)	O_2	5 bar	25°C	48	1	99
4	cat. Mn(II)	N_2	5 bar	60–70°C	20	0	100
5	cat. Mn(II)	N_2	Atmos.	Reflux	48	0	100
6	cat. Mn(II)	O_2	Atmos.	Reflux	48	19, 20	81, 80
7	None	O_2	Atmos.	Reflux	48	10, 16	90, 84
8	$Mn(IV)O_2$	N_2	Atmos.	Reflux	48	0	100
9	$Mn(III)(OAc)_3$	N_2	Atmos.	Reflux	48	0	100
10	$Mn(III)(OAc)_3$[d]	N_2	Atmos.	Reflux	48	0	100

[a]$Mn(II)SO_4$ (10 molar %) and $Mn(IV)O_2$ and $Mn(III)(OAc)_3$ (equimolar amounts).
[b]Atmos. = atmospheric pressure.
[c]Yields were measured using ^1H NMR spectroscopy with an internal standard and by HPLC.
[d]Acetic acid was used in place of aqueous ethanol as the solvent.

mechanism of this coupling/elimination step and to determine the generality of this unusual reaction. A competing non-radical reaction takes place at low pH to yield C—C *ortho-ortho* coupling to give the corresponding dityrosines and will be reported in a future publication. Electrochemical studies of the oxidation of diiodophenols and their phenolates will also be reported in a future publication.

There is growing evidence to suggest that an α,β-dehydroalanine unit is left in the protein chain after elimination of the side chain, which is subsequently hydrolyzed (4–6). An E2 mechanism to explain the loss of side chain has been proposed since 1944 (7) but none of the studies have clearly proven the identity of the eliminated fragment (2–12). This mechanism has replaced an early and well-studied proposal (8–12), which suggested that the side chain was oxidized prior to coupling to the corresponding α-ketoacid, 3,5-diiodo-4-hydroxyphenylpyruvic acid. A number of biological processes, including transamination catalysed by transaminases with the coenzyme pyridoxal phosphate, readily convert α-amino acids to α-ketoacids (8). This proposal was supported by biomimetic reactions with 3,5-diiodo-4-hydroxyphenylpyruvic acid and 3,5-diiodotyrosine, which gave small yields of thyroxine (9–12). No clear mechanism was proposed for loss of the pyruvate side chain.

Oxidative coupling of the ethyl ester of *N*-acetyl-3,5-diiodotyrosine

The reaction conditions employed in the industrial synthesis involve oxidation of the phenolate anion of the ethyl ester of *N*-acetyl-3,5-diiodotyrosine (**1**) in aqueous ethanol solution at ca. 60–65°C and under pressure for 20 h. The oxidant is molecular oxygen. The solution contains catalytic amounts of manganese(II) sulfate and the pH is controlled to 9.2–9.4 by using sodium hydroxide. The reactions were carried out under various conditions to determine the parameters of the reaction and the results are shown in Table 1. The effects of time, temperature, and pressure are as expected (experiments 1–3). Longer reactions gave higher yields. Oxygen was shown to be essential (experiments 4 and 5) with no reaction taking place under an atmosphere of nitrogen.

The effect of the Mn(II) was also tested in concurrent reactions (experiments 6 and 7). The difference in yields between reactions carried out with or without Mn(II) is relatively small and therefore its effect is possibly secondary. Mn(II) is oxidized by oxygen to Mn(III), which could act as an oxidant. However, the use of $Mn(IV)O_2$ or $Mn(III)(OAc)_3$ in place of $Mn(II)SO_4$ in the absence of oxygen (nitrogen atmosphere) gave only unaltered **1**, indicating that Mn(III) is not the primary oxidant in the reaction and is not able to replace oxygen as the oxidant (experiments 8–10). The use of Mn(III) as an oxidant of enols from β-dicarbonyl compounds in radical reactions has been extensively studied in recent years (13) and the diiodophenols could be regarded as suitable substrates for $Mn(III)(OAc)_3$ oxidations. Oxidation of **1** with $Mn(III)(OAc)_3$ in acetic acid also failed to yield any of the thyroxine derivative **2**. Studies of possible oxidation of the amino acid side chain by Mn(III)/Mn(II) were carried out using the ethyl ester of *N*-acetylphenylalanine and also proved negative.

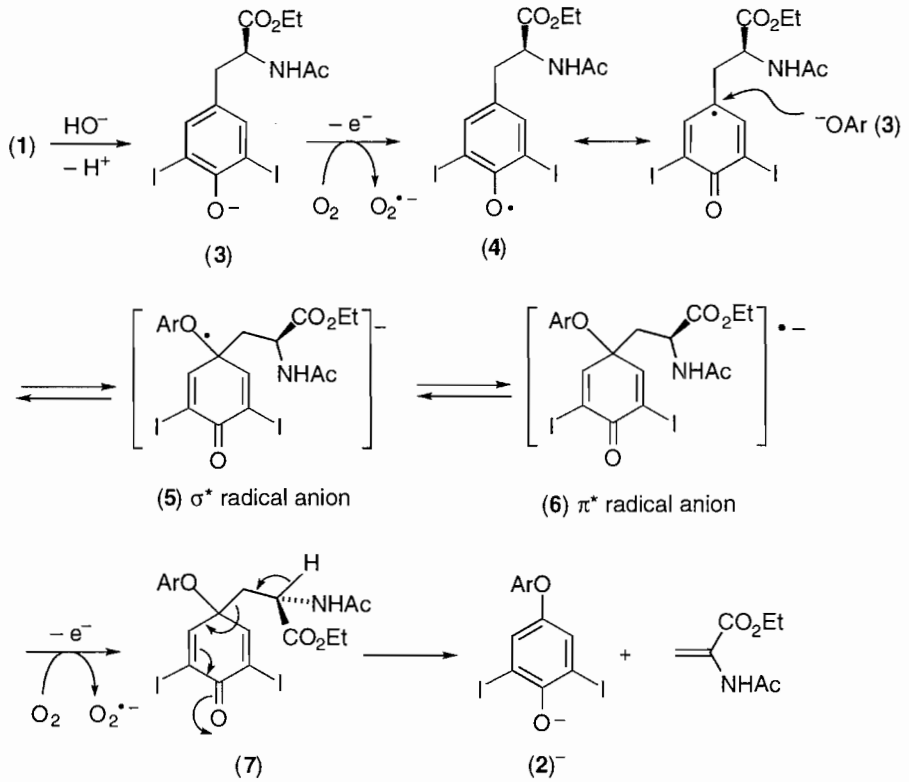
Superoxide is almost certainly formed and could be predicted to attack the starting diiodophenol or intermediate phenoxyl radicals but no evidence of such products was observed. Superoxide has been reported to rapidly add to tyrosine and tyrosinyl radicals (14). All reactions were particularly clean and only contained starting diiodophenol and coupled product.

We propose the mechanism shown in Scheme 1. Our results provide further evidence that oxygen oxidizes the phenolate anion (**3**) to the phenoxyl radical (**4**), which rapidly reacts with further phenolate anion to yield an intermediate radical anion (**5**). Dimerization of the phenoxyl radical (**4**) to yield the dienone (**7**) as suggested in earlier studies (1) for phenolic oxidation is unlikely. The phenoxyl radical is present in low concentration whereas the anion is present in high concentration and, therefore, the rate of reaction between phenoxyl (**4**) and phenolate (**3**) will be much faster than the rate of reaction between two molecules of the phenoxyl radical (**4**). The intermediate radical anion (**5**) will initially hold the unpaired electron in an unstable C—O σ* molecular orbital (MO). Rapid reorganization of MOs will give the more stable π* intermediate (**6**). Loss of the electron to molecular oxygen will be extremely rapid but reversible.

© 1997 NRC Canada

Can. J. Chem. Downloaded from www.nrcresearchpress.com by 88.146.161.215 on 09/08/12
For personal use only.

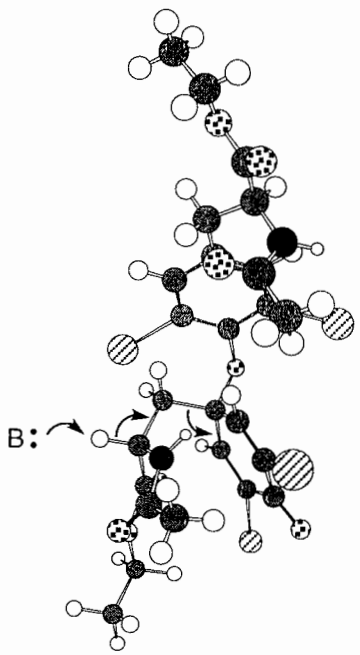
Scheme 1. Putative mechanism for phenolic coupling of the ethyl ester of *N*-acetyltyrosine (**1**).



E2 elimination is the best explanation for loss of the side chain and has been proposed by several research groups (4–7, 15). The elimination must be fast, otherwise the dienone would accumulate in the reaction. E2 elimination with a dienone as a leaving group coupled with rearomatization as a driving force has been known for some time in the biosynthesis of alkaloids that proceed via phenolic coupling. A useful example has been reported in the biosynthesis of erythrina alkaloids (16). Elementary molecular modelling of the intermediate aryloxydienone (**7**) using Chem3D and MM2 packages showed a localized energy minimum with the acetamidoester α-hydrogen lining up at exactly 180° to the dienone leaving group (Fig. 1). This is the correct conformation required for E2 elimination. The predicted product of E2 elimination is ethyl 2-acetamidopropenoate. Another potential product is the ethyl ester of *N*-acetylserine formed by addition of hydroxide to the β-position of the α,β-unsaturated ester. Both were synthesized and used as standards in all the analyses of coupling reactions. Disappointingly, no signs of these products were observed by ^{1}H NMR spectroscopy or TLC and HPLC analysis of product mixtures. However, both were found to be unstable under the vigorous conditions of the reactions, which could explain their absence. Further study is required to ascertain the product of elimination of the side chain.

This unusual reaction and the uncommon presence of iodine in nature deserves some comment. Interestingly, the most active thyroxine hormone species is the triiodo analogue, 3,5,3′-triiodo-L-thyronine. Therefore, for maximum hormone activity, one of the iodine atoms is lost. We propose that the

Fig. 1. E2 elimination in intermediate dienone (**7**). MM2 model.

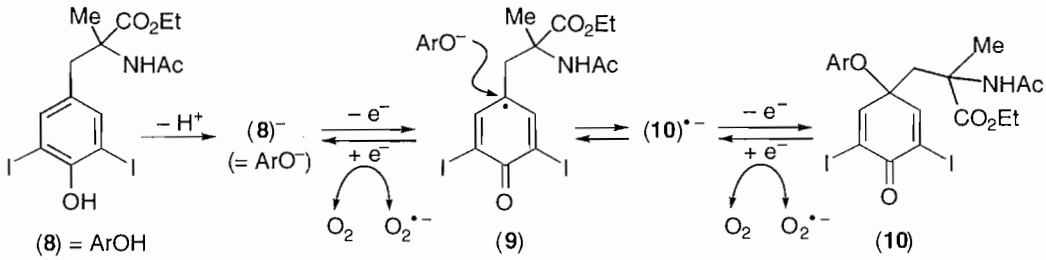


iodine atoms serve a number of functions. Firstly, they are required to encourage the elimination of the side chain by making the dienone a better leaving group. Secondly, the pK_a of 3,5-diiodotyrosine is 6.35 which is ca. 100 times more acidic than 3-iodotyrosine (pK_a = 8.7). Therefore, 3,5-diiodo-

Can. J. Chem. Downloaded from www.nrcresearchpress.com by 88.146.161.215 on 09/08/12
For personal use only.

© 1997 NRC Canada

Scheme 2. Reversible coupling with E2 elimination blocked.



tyrosine is ionized at physiological pH. Phenols are most easily oxidized when ionized as the phenolate anion and would not be oxidized by oxygen in the non-ionized phenol form.

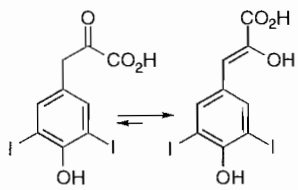
The large size of the iodine atoms may also play a role in sterically directing the coupling to give *para* regioselectivity. Molecular modelling (MM2) indicates that coupling between the oxygen centre of the phenolate and the radical, localized on the *ortho* position of the phenoxyl radical, is sterically hindered. In the attacking phenolate anion, the oxygen centre is sterically hindered by the very large *ortho*-iodine atoms. Both *ortho* positions of the phenoxyl radical also have large iodine substituents that are planar with the ring. The methylene group in the *para* position is much smaller and rotation allows the α-acetamidoester group to swing out of the way. Therefore, this lower steric hindrance may facilitate faster attack by the phenoxide at the *para* position rather than at the *ortho* position. However, this regioselectivity may also be explained by the fact that the electron density in phenoxyl radicals is higher at the *para* position than in the *ortho* position.

Attempted oxidative coupling of ethyl 2-acetamido-3-(3,5-diiodo-4-hydroxyphenyl)-2-methylpropanoate (8)

Isolation of the intermediate aryloxydienone (**7**) would provide strong evidence for the mechanism proposed in Scheme 1. We reasoned that if the α-position of the acetamidoester was substituted by a methyl group instead of a hydrogen, E2 elimination would be blocked and allow isolation of an aryloxydienone intermediate, e.g., **10** in Scheme 2. With this aim in mind, the α-methyl derivative of the ethyl ester of *N*-acetyl-3,5-diiodotyrosine (**1**), ethyl 2-acetamido-3-(3,5-diiodo-4-hydroxyphenyl)-2-methylpropanoate (**8**), was synthesized. The α-methyl analogue **8** was oxidized using the standard conditions under atmospheric pressure for 48 and 96 h. Only unaltered **8** was recovered, in quantitative yield. The α-methyl group is not able to affect the reactivity of the oxidation of the phenolate or the coupling process relative to the phenolate of **1**, only the elimination is blocked. Therefore, to explain the apparent lack of reaction, we propose that all the steps are reversible. Thus, if elimination is blocked, the intermediate aryloxydienone **10** is reduced and reverts to starting phenolate via the radical anion **10**$^{\bullet-}$] and the phenoxyl radical (**9**) (Scheme 2). The reversibility of phenolic coupling has been clearly demonstrated for some of the reactions of 2,4,6-tri(*tert*-butyl)phenol (15). In this coupling E2 elimination from the intermediate aryloxydienone is very slow. In the presence of reductants the dienone reverts to phenolates.

Oxidative coupling between (3,5-diiodo-4-hydroxyphenyl)pyruvic acid (11) and the ethyl ester of *N*-acetyl-3,5-diiodotyrosine (1)

Early proposals (8–12) suggested that the side chain of 3,5-diiodotyrosine was oxidized to the corresponding α-ketoacid, (3,5-diiodo-4-hydroxyphenyl)pyruvic acid (**11**), prior to coupling. To test this hypothesis, equimolar amounts of **1** and **11** were reacted under similar conditions under pressure at 60–70°C and at room temperature. Thyroxine **2** was obtained in 11 and 7% yields, respectively (yield based on **1**), and unaltered **1** was recovered (89, 93%, respectively). A large amount of decomposition products resulting from **11**, which included



(**11**)

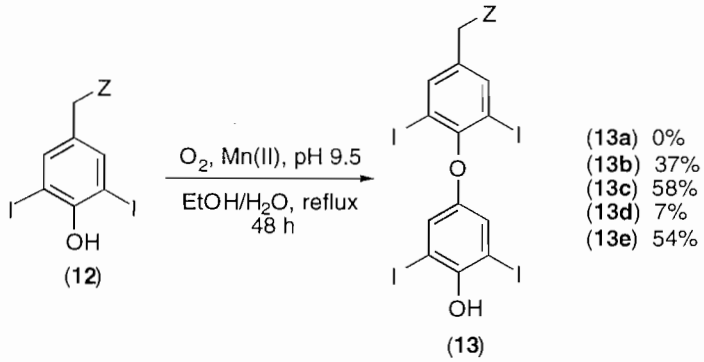
3,5-diiodo-4-hydroxybenzaldehyde, were observed. Reaction between 3,4-diiodotyrosine and **11** at room temperature and pressure in ethanol–water with sodium hydroxide, pH 7–8.5, and oxygen has been reported (11, 15) to give low yields of thyroxine (5–15%). Reaction between **1** and **11** at room temperature and pressure gave similar yields (**2**, 6 and 2%). The ethyl ester of *N*-acetyl-3,5-diiodotyrosine (**1**) does not undergo coupling under these conditions. Considerable attempts were made to improve yields but without success. Our results also confirmed that 3,5-diiodo-4-hydroxyphenylpyruvic acid breaks down rapidly at higher pH to yield 3,5-diiodo-4-hydroxybenzaldehyde and other decomposition products (11, 15).

Studies were also carried out to show that 3,5-diiodo-4-hydroxybenzaldehyde and 3,5-diiodo-4-hydroxybenzoic acid, potential breakdown products from (3,5-diiodo-4-hydroxyphenyl)pyruvic acid **11**, were not involved in the synthesis of **2**. A 2:3 molar ratio of **1** and 3,5-diiodo-4-hydroxybenzaldehyde, and **1** and 3,5-diiodo-4-hydroxybenzoic acid, were reacted under similar conditions under pressure at 60–70°C to yield thyroxine **2** (20 and 18%, respectively) and unaltered **1** (80, 82%) and quantitative recovery of 3,5-diiodo-4-hydroxybenzaldehyde and 3,5-diiodo-4-hydroxybenzoic acid. The yields of **2** (see Table 1) are unaltered by the addition of 3,5-diiodo-4-hydroxybenzaldehyde and 3,5-diiodo-4-hydroxybenzoic acid, indicating that they play no role in the coupling.

© 1997 NRC Canada

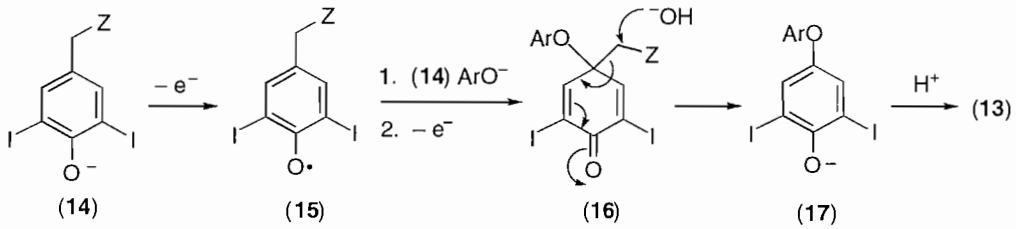
Can. J. Chem. Downloaded from www.nrcresearchpress.com by 88.146.161.215 on 09/08/12
For personal use only.

Scheme 3. Oxidative coupling of 2,6-diiodo-4-substituted phenols.



(**a**), Z = CH_2CO_2Et; (**b**), Z = CH_2NHAc, (**c**), Z = H; (**d**), Z = CH_2CH_3; (**e**), Z = CO_2Et

Scheme 4. Putative S_N2 mechanism for side-chain loss.



The possibility of side-chain oxidation prior to phenolic coupling to yield 3,5-diiodo-4-hydroxyphenylpyruvic acid was investigated using the methyl ester of *N*-acetylphenylalanine as a model without the complication of the phenolic group. A number of oxidative conditions similar to those in the coupling of the ethyl ester of *N*-acetyl-3,5-diiodotyrosine (**1**) were used, including potassium ferricyanide and hydroxide, $Mn[(III)OAc]_3$ or $Mn(III)(acac)_3$ in methanol or acetic acid and under nitrogen or oxygen, and $Mn(II)(OAc)_2 \cdot 2H_2O$ and $Mn(II)SO_4$ in ethanol–water under an atmosphere of oxygen at normal pressure and under 5 bar pressure at 60–65°C for 20 h (1 bar = 100 kPa). While the substrate is not necessarily comparable, the reactions indicate that the side chain is not readily oxidized under the general conditions of the reaction.

In summary, these results indicate that prior oxidation of the side chain is not a route for the oxidative coupling of **1** even though the corresponding pyruvate (**11**) does facilitate a small amount of coupling at room temperature.

Oxidative coupling of 2,6-diiodo-4-substituted phenols

To further investigate the mechanism, the oxidative coupling of a range of 2,6-diiodo-4-substituted phenols (**12a**–**12e**) was investigated (Scheme 3). The same procedure as for the oxidative coupling of the ethyl ester of *N*-acetyl-3,5-diiodotyrosine under atmospheric pressure was used. Yields were not optimized. Analogues **12a** and **12b** were investigated because they have one group removed compared to the tyrosine (**1**). The ester **12a** was predicted to behave like **1** because it has an acidic α-H for E2 elimination whereas **12b** does not and differences in mechanism were expected. However, the tyramine analogue **12b** gave a good yield of the thyroxine analogue **13b** (37%) whereas **12a** yielded ethyl 3-(3,5-diiodo-4-hydroxyphenyl)propenoate (**15**) (53%) and no traces of the corresponding thyroxine analogue **13a**. 2,6-Diiodophenols **12c**, **12d**, and **12e** also gave corresponding thyroxine analogues, **13c** (58%), **13d** (7%), and **13e** (54%). All the reactions were faster than the tyrosine (**1**) reaction, indicating alternative mechanisms with faster rates of reaction.

Ethyl 2-acetamido-3-(3,5-diiodo-4-hydroxyphenyl)propenoate (**21**), 3,5-diiodo-4-hydroxybenzaldehyde, and 3,5-diiodo-4-hydroxybenzoic acid do not undergo coupling under the same reaction conditions and are recovered unaltered.

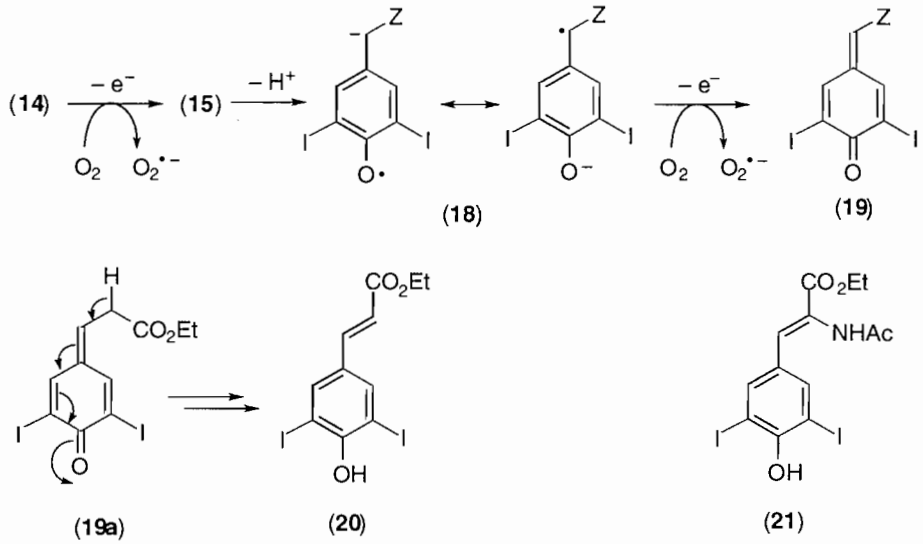
The E2 mechanism shown in Scheme 1 cannot be used to explain the formation of the thyroxine derivatives **13c**–**13e** because the 2,6-diiodophenols **12c**, **12d**, and **12e** do not have a hydrogen β to the aryloxydienone leaving group. The β-hydrogen is required for an E2 elimination for removal of the side chain from the intermediate aryloxydienone. We propose that an S_N2 mechanism is operative (Scheme 4). If the aryloxydienone is a good leaving group in an E2 elimination for the aryloxydienone **7**, then it should also be able to act as a leaving group in S_N2 substitutions. S_N2 substitution is not normally favoured on a "neopentyl" type carbon because of steric hindrance. However, in the "neopentyl" system the bulky group is orthogonal to the incoming nucleophile and leaving group, whereas in this mechanism the bulky group is the leaving group and is at 180° to the nucleophile; therefore steric hindrance is not a major problem.

The S_N2 mechanism (Scheme 4) is also a good explanation for the mechanism of formation of the thyroxine derivative **13b**. The hydrogen α to the acetamido group is not acidic and therefore an E2 elimination, although possible, is not

© 1997 NRC Canada

Can. J. Chem. Downloaded from www.nrcresearchpress.com by 88.146.161.215 on 09/08/12
For personal use only.

Scheme 5. Quinone methide mechanism.



favoured. However, the S_N2 mechanism for the elimination of the side chains from aryloxydienones **7** and **10**, resulting from the tyrosines **1** and **8**, would be unfavourable. The sterically bulky groups α to the carbon center under S_N2 attack would severely hinder S_N2 attack by nucleophiles. The α-"neopentyl" group in the dienone intermediate **10** would make S_N2 substitution very unfavourable. Both S_N2 and E2 mechanisms are unfavourable for the reaction of **8**, which helps to explain the lack of reactivity. The formation of ethyl 3-(3,5-diiodo-4-hydroxyphenyl)propenoate **20** from **12a** has to be explained by a faster competing reaction than coupling followed by S_N2 or E2 mechanisms. A possible mechanism is removal of the acidic proton α to the ester to yield an anion. This would allow oxidation with addition of oxygen to yield an intermediate α-peroxyl ester. E2 elimination would be favoured and yield to the conjugated alkene present in **20**.

An alternative explanation for the formation of ethyl 3-(3,5-diiodo-4-hydroxyphenyl)propenoate **15** from **12a** may be the intermediacy of a quinone methide (**19a**) (Scheme 5). Loss of a proton from the intermediate phenoxyl **15** to form a quinone methide radical anion (**18**) is likely to be fast if planarity can be readily achieved. Loss of a proton from radicals is generally favoured because of enhanced acidity (17), e.g., hydroquinone, pK_a = 9.9, 4-hydoxyphenoxyl, pK_a = 4.1. The benzylic hydrogen in **15a** is more acidic than phenoxyls **15b**–**15d** due to the β-effect of the ester group. Loss of an electron from the radical anion **18** to yield the quinone methide **19** will be extremely fast in the presence of oxygen. Similarly, the rearomatization of the quinone methide **19a** to yield **20** will be fast. Deprotonation in the quinone methides **19b** and **19d** is unlikely and does not take place.

The formation of this unusual unsaturated product (**20**) begs the question why the ethyl ester of *N*-acetyl-3,5-diiodotyrosine (**1**) does not also proceed by this route to ethyl 2-acetamido-3-(3,5-diiodo-4-hydroxyphenyl)propenoate (**21**). If the proposal that prior side chain oxidation (8–12) was important, either via phenolic oxidation or α-amino acid oxidation, then a likely product would be the side-chain unsaturated intermediate **21**. This proposal requires side-chain oxidation, followed by phenolic oxidation of the new intermediate, and then coupling to **1**. The phenolate of **1** would be more nucleophilic than the phenolate of **21** and hence be predicted to react faster in the coupling reaction.

When **21** was reacted under the standard coupling conditions under pressure, the only isolable product was 3,5-diiodo-4-hydroxybenzaldehyde, which is stable under the conditions. This hydrolytic cleavage is explained by hydroxide addition to the β-position of the α,β-unsaturated ester followed by a retro-aldol reaction (11, 15). When **21** was oxidized under the same conditions with the ethyl ester of *N*-acetyl-3,5-diiodotyrosine (**1**) in the same reaction (**21**:**1**, 3:2), only the normal amount (11%) of the thyroxine **2** was observed along with a small amount of 3,5-diiodo-4-hydroxybenzaldehyde (10%). These results suggest that **21** is not an intermediate and breaks down under the conditions of the reaction.

While formation of the α,β-unsaturated ester **21** (see mechanism in Scheme 5) from the phenoxyl radical **4** by loss of a proton requires planarity for quinone methide formation, models indicate that the steric bulk of the α-acetamidoester would make this unfavourable, thereby raising the energy of the transition state (TS). Hence the bimolecular coupling reaction is more favourable than quinone methide formation. Ethyl 2-acetamido-3-(3,5-diiodo-4-hydroxyphenyl)-2-methylpropanoate (**8**) would similarly not be able to form a quinone methide intermediate.

The mechanism for coupling and side-chain loss for 2,6-diiodophenols **12b**, **12c**, **12d**, and **12e** to the corresponding thyroxine analogues is difficult to explain by a quinone methide mechanism. The quinone methides **19b**–**19e**, if formed, would react rapidly with nucleophiles such as phenolate anions or hydroxide and no signs of such products were observed. The reactions were very clean with only starting phenols and thyroxine analogues being observed or isolated. Hydroxide addition would yield benzyl alcohol analogues, which would rapidly form new quinone methides and lose a proton to yield the keto analogues. Ethyl 2-(3,5-diiodo-4-hydroxyphenyl)acetate **12e** should readily form a quinone methide because the benzylic hydrogen in phenoxyl **15e** will

Can. J. Chem. Downloaded from www.nrcresearchpress.com by 88.146.161.215 on 09/08/12
For personal use only.

© 1997 NRC Canada

be very acidic. A possible explanation is that allylic strain inhibits planarity and makes the rate of quinone methide formation slower than the rate of coupling. These explanations are preliminary and may not fully explain the range of mechanisms observed.

In conclusion, we have further elucidated the mechanism of the biomimetic formation of thyroxine analogues. Furthermore, extensive studies need to be undertaken to fully determine the mechanisms, and, in particular, isolation of the "lost" side chain remains a challenge. The facile oxidative coupling provides a useful synthetic protocol for the formation of thyroxine analogues.

Experimental

IR spectra were run as neat samples using a Nicolet 205 FT-IR spectrometer. Elemental analyses were carried out using a Perkin Elmer 2400 CHN elemental analyser. Mass spectra were run on a Kratos MS80 spectrometer or on a VG Analytical ZAB-E spectrometer by the EPSRC Mass Spectrometry Service at the University of Wales, Swansea, Wales. All mass spectra are electron impact (EI) spectra unless otherwise stated. ^{1}H NMR spectra were run at 250 MHz and ^{13}C NMR spectra were run 62.9 MHz using a Bruker AC 250 and (or) DPX400 spectrometer and are quoted at 250 and 62.9 MHz, respectively, unless otherwise stated. $CDCl_3$ was used as the NMR solvent with TMS as internal standard. Light petroleum refers to the bp 40–60°C fraction. Solvents were purified by standard methods. Analytical thin-layer chromatography was carried out using aluminium-backed plates coated with Merck Kieselgel 60 GF_{254} and compounds were visualized by UV light, iodine vapour, or by staining with potassium permanganate dip followed by heating. Flash chromatography was carried out using silica gel as absorbent and light petroleum (bp 40–60°C) and dichloromethane mixtures as eluant unless otherwise stated. HPLC was carried using a Pye Unicam PU4015 pump and Pye Unicam PU4025 UV detector fitted with a Zorbax SB-C8 4.6 mm × 15 cm column.

The ethyl ester of *N*-acetyl-3,5-diiodotyrosine was obtained from Knoll Pharmaceuticals and 3,5-diiodo-4-hydroxybenzoic acid was purchased commercially.

2,6-Diiodo-4-methylphenol (12c). General procedure for the iodination of phenols

A solution of iodine (4.713 g, 18.55 mmol) and potassium iodide (12.521 g, 75.42 mmol) in water (75 mL) was added to a two-phase mixture of *p*-cresol (1.023 g, 9.25 mmol) in dichloromethane (75 mL) and potassium carbonate (1.412 g, 10.08 mmol) in water (100 mL). The reaction was stirred for 14 h, acidified using hydrochloric acid (2 M), and the product was extracted into dichloromethane. The organic extracts were washed with dilute hydrochloric acid, sodium thiosulfate solution, dried, and evaporated to dryness. Flash column chromatography yielded 2,6-diiodo-4-methylphenol (**12c**) as colourless crystals (2.332 g, 70%), mp 55–58°C (lit. (18) mp 62°C). IR (Nujol) cm^{-1}: 3575, 1545, 1250, 852. ^{1}H NMR δ: 2.25 (s, 3H), 5.60 (s, 1H), 7.57 (s, 2H). ^{13}C NMR δ: 19.52, 82.12, 152.08, 139.52, 133.79.

Ethyl 3-(3,5-diiodo-4-hydroxyphenyl)propionate (***12a***): 65%, mp 82–85°C. IR (Nujol) cm^{-1}: 3405, 2977, 1715, 1540, 1414, 872. ^{1}H NMR δ: 1.24 (t, J = 7.1 Hz, 3H), 2.55 (t, J = 7.6 Hz, 2H), 2.81 (t, J = 7.5 Hz, 2H), 4.13 (q, J = 7.1 Hz, 2H), 5.65 (s, 1H, OH), 7.52 (s, 2H). ^{13}C NMR δ: 14.69, 36.16, 52.49, 61.03, 82.66, 129.37, 137.07, 139.47, 172.73. MS (EI) *m/z* (M$^+$, 445.8878. $C_{11}H_{12}I_2O_3$ requires 445.8879), 446 (100, M$^+$), 372 (85, M$^+$ − CO_2Et), 246. Anal. calcd. for $C_{11}H_{12}I_2O_3$: C 29.62, H 2.71; found: C 29.51, H 2.61.

N-*Acetyl-3,5-diiodotyramine* (***12b***): Yellow crystals (52%), mp 143–145°C. IR (Nujol) cm^{-1}: 3298, 2932, 1633, 1556, 1402, 869. ^{1}H NMR (400 MHz, d_6-acetone) δ: 1.86 (s, 3H), 2.68 (t, J = 7.0 Hz, 2H), 3.37 (t, J = 7.0 Hz, 2H), 7.26 (s, 1H), 7.63 (s, 2H), 8.12 (s, 1H,). ^{13}C NMR (100.62 MHz, d_6-acetone) δ: 22.40, 32.84, 40.77, 84.17, 136.38, 140.17, 153.95, 169.68. MS (EI) *m/z* (M$^+$, 430.8874. $C_{10}H_{11}I_2NO_2$ requires 430.8882), 431 (100), 372 (11, M$^+$ −Ac). Anal. calcd. for $C_{10}H_{11}I_2NO_2$: C 27.87, H 2.57, N 3.25; found: C 28.04, H 2.20, N 3.28.

2,6-Diiodo-4-propylphenol (***12d***): 82%. IR (neat) cm^{-1}: 3475, 2956, 1545, 1312, 1154, 884. ^{1}H NMR (400 MHz) δ: 0.95 (t, J = 7.2 Hz, 3H), 1.66–1.56 (m, 2H), 2.48 (t, J = 7.2 Hz, 2H), 5.60 (s, 1H), 7.51 (s, 2H). ^{13}C NMR (100.62 MHz) δ: 13.99 (Me), 24.83, 36.45, 82.45, 139.22, 151.91 (ArCOH), 189.46 (Ar*C*H). MS (EI) *m/z* (M$^+$ 387.8824. $C_9H_{10}I_2O$ requires 387.8824), 388 (82), 359 (100, M$^+$ − Et), 232 (13, M$^+$ − I).

Ethyl 2-(4-hydroxy-3,5-diiodophenyl)acetate (***12e***): 69%, mp 119–121°C. IR (Nujol) cm^{-1}: 3453, 2982, 1722, 1545, 888. ^{1}H NMR (400 MHz) δ: 1.26 (t, J = 7.0 Hz, 3H), 3.46 (s, 2H), 5.72 (s, 1H), 4.16 (q, J = 7.0 Hz, 2H), 7.60 (s, 2H). ^{13}C NMR (100.62 MHz) δ: 14.57, 39.50, 61.58, 130.37, 140.32, 82.51, 153.18, 171.23. MS (EI) *m/z* (M$^+$, 431.8722. $C_{10}H_{10}I_2O_3$ requires 431.8723) 432 (76, M$^+$), 359 (99, M$^+$ − CO_2Et), 232 (21). Anal. calcd. for $C_{10}H_{10}I_2O_3$: C 27.93, H 2.34; found: C 27.80, H 2.08.

3,5-Diiodo-4-hydroxybenzaldehyde: (68%). Colourless crystals, mp 187–189°C (lit. (10) mp 199–200°C). IR (Nujol) cm^{-1}: 3194, 1710, 1675, 1465, 1400. ^{1}H NMR δ: 8.21 (s, 2H), 9.73 (s, 1H). ^{13}C NMR δ: 82.58, 132.85, 140.95, 175.57, 187.56.

Ethyl ester of *N*-acetylserine

N-Acetylserine (2.327 g, 15.83 mmol) was dissolved in ethanol containing a catalytic amount of concentrated sulfuric acid. The solution was refluxed for 6 h, cooled, and evaporated to dryness. The residual oil was taken up in ethyl acetate and concentrated brine solution. The aqueous layer was washed with ethyl acetate, followed by dichloromethane. The organic extracts were dried and evaporated to dryness. Flash column chromatography using dichloromethane:ethyl acetate (1:1) as eluant yielded the ethyl ester of *N*-acetylserine as a colourless oil (1.936 g, 69%). IR (neat) cm^{-1}: 3361, 2925, 1738, 1659, 1377, 1148. ^{1}H NMR δ: 1.27 (t, J = 7.1 Hz, 3H), 2.03 (s, 3H), 3.84–3.95 (m, 2H), 4.20 (q, J = 7.1 Hz, 2H), 4.62–4.58 (m, 1H), 6.83 (d, J = 7.1 Hz, 1H, NH). ^{13}C NMR (100.62 MHz) δ: 14.46, 23.32, 55.23, 62.22, 63.43, 171.02, 171.37. MS (EI) *m/z* (M$^+$, 176.0925. $C_7H_{13}NO_4$ requires 736.0923), 176 (100, MH$^+$), 158 (15, M$^+$ − H_2O), 145 (20), 134 (12), 102 (50), 99 (22).

Can. J. Chem. Downloaded from www.nrcresearchpress.com by 88.146.161.215 on 09/08/12
For personal use only.

© 1997 NRC Canada

Can. J. Chem. Downloaded from www.nrcresearchpress.com by 88.146.161.215 on 09/08/12
For personal use only.

Ethyl 2-acetamidopropenoate

The ethyl ester of *N*-acetylserine (105 mg, 0.60 mmol) was dissolved in acetonitrile (60 mL). To this solution was added 1-(3-dimethylaminopropyl)-3-ethylcarbodiimide hydrochloride (0.135 g, 7.06 mmol) and copper(I) chloride (17 mg, 0.17 mmol), and the reaction was stirred at 40°C for 24 h and evaporated to dryness. The residual oil was taken up in ethyl acetate and the solution washed with sodium hydrogen carbonate solution and water, dried, and evaporated to dryness. Flash column chromatography yielded ethyl 2-acetamidopropenoate as a colourless oil (73 mg, 78%). IR (neat) cm^{-1}: 3365, 3024, 1695, 1630, 1039. ^1H NMR δ: 1.34 (t, J = 7.1 Hz, 3H), 2.12 (s, 3H), 4.29 (q, J = 7.1 Hz, 2H), 5.88 (s, 1H), 6.58 (s, 1H), 7.74 (s, 1H, NH). ^{13}C NMR (100.62 MHz) δ: 13.23, 23.82, 61.37, 107.51, 130.20, 163.30, 167.95. MS (EI) *m/z* (M^+, 157.0739. $C_7H_{11}NO_3$ requires 157.0739), 157 (61, M^+), 115 (100, M^+ − Ac), 71 (98).

Oxidative coupling reactions with the ethyl ester of *N*-acetyl-3,5-diiodotyrosine (1)

The reactions were carried out under a number of different reaction conditions, which included 5 bar and atmospheric pressure. Oxygen gas was replaced by nitrogen as required.

Oxidative coupling under pressure

The ethyl ester of *N*-acetyl-3,5-diiodotyrosine (**1**) (0.75 g, 1.5 mmol) was dissolved in ethanol (90 mL) and water (75 mL). Mn(II) sulfate (18 mg, 0.075 mmol) was added and the pH adjusted to 9.5 using aqueous sodium hydroxide solution (2.0 M). When the pH had stabilized at 9.5 for 10 min the solution was charged to a glass pressure vessel surrounded by a jacket containing oil for heating. The reaction was heated to 60–65°C and pressurized to 5 bar with oxygen, kept under these conditions for 18–24 h (normally 20 h), then cooled, and the pressure released. The final reaction pH was measured and the reaction solution evaporated to dryness. The solid residue was taken up in ethyl acetate and hydrochloric acid (0.01 M). The layers were separated and the aqueous layer was washed with ethyl acetate. The organic extracts were washed twice with hydrochloric acid (0.01 M), dried, and evaporated to dryness to give a mixture of the ethyl esters of *N*-acetyl-3,5-diiodotyrosine and *N*-acetylthyroxine. The combined yields of the ethyl esters of *N*-acetyl-3,5-diiodotyrosine (**1**) and *N*-acetylthyroxine (**2**) were high (>90%) with minor impurities. The ethyl ester of *N*-acetylthyroxine was characterized by comparison with authentic material in a number of experiments after purification using flash column chromatography; mp 206–211°C. IR (Nujol) cm^{-1}: 3401, 3277, 1708, 1636, 1545, 1180, 911. ^1H NMR ($CDCl_3$: d_6-DMSO, 20:1) δ: 1.21 (t, J = 7.1 Hz, 3H), 1.89 (s, 3H), 2.90 (ddd, J = 6.0, 8.5, 15.0, Hz, 2H, ArCH_2), 4.14 (m, 2H), 4.56 (dt, J = 7.5, 8.5 Hz, 1H, α-H), 7.06 (s, 2H), 7.76 (s, 2H), 8.29 (d, J = 7.5 Hz, 1H, NH), 9.08 (s, 1H). ^{13}C NMR (100.62 MHz) δ: 14.35, 23.18, 36.57, 53.20, 62.00, 81.51, 90.56, 126.01, 137.73, 141.22, 149.48, 150.12, 152.57, 169.58, 171.08.

Oxidative coupling of the ethyl ester of N*-acetyl-3,5-diiodotyrosine (1) under atmospheric pressure*

The reaction was carried out and worked up as above except that the reaction was refluxed for 48 h under an atmosphere of oxygen, which was bubbled through the reaction solution. The pH was checked regularly and kept close to 9.5 by the addition of aqueous sodium hydroxide solution (0.5 M) when necessary. In the crude product mixture the combined yields of the ethyl esters of *N*-acetyl-3,5-diiodotyrosine (**1**) and *N*-acetylthyroxine (**2**) were essentially quantitative with no impurities.

Analysis of the extent of reaction

Standards of the pure starting materials and the ethyl ester of *N*-acetylthyroxine (**2**) in acetonitrile:water (9:1) were analysed by HPLC to obtain peak areas at known concentrations. The mobile phase was acetonitrile:water:orthophosphoric acid (520:480:0.5 mL) and compounds were detected by UV light at 225 nm. Samples of the reaction mixtures were dissolved in the sample solution (acetonitrile:water, 9:1) and analysed. From the peak areas the ratios of compounds, and hence relative yield of the ethyl ester of *N*-acetylthyroxine (**2**) could be calculated. The product mixtures were also analysed by ^1H NMR spectroscopy, which confirmed the HPLC results.

(3,5-Diiodo-4-hydroxyphenyl)pyruvic acid (11)

A mixture of hippuric acid (0.359 g, 2.17 mmol), 3,5-diiodo-4-hydroxybenzaldehyde (0.733 g, 1.96 mmol), and sodium acetate (8.432 g, 102.82 mmol) was dissolved in acetic anhydride (150 mL) and refluxed for 2 h. The reaction was cooled, filtered, and washed with water to remove the sodium acetate. The crystals were recrystallized from toluene to give 4-(4-acetoxy-3,5-diiodobenzal)-2-phenyl-5-oxazolone as yellow crystals (0.410 g, 56%), mp 227–232°C (lit. (19) mp 242–242.5°C). IR (Nujol) cm^{-1}: 3050, 1805, 1765, 1660, 1590, 1465, 1360. ^1H NMR δ: 2.38 (s, 3H), 6.96 (s, 1H), 7.57 (m, 3H), 8.59 (s, 2H), 8.10 (dd, J = 1.6, 8.4 Hz, 2H). ^{13}C NMR δ: 21.24, 90.49, 124.93, 126.43, 128.55, 129.00, 133.81, 134.76, 134.90, 142.63, 153.08, 164.83, 166.76, 167.07. Anal. calcd. for $C_{18}H_{11}I_2NO_4$: C 38.67, H 1.98, N 2.51; found: C 38.59, H 1.90, N 2.57.

4-(4-Acetoxy-3,5-diiodobenzal)-2-phenyl-5-oxazolone (0.223 g, 0.42 mmol) was dissolved in glacial acetic acid (160 mL) and hydrochloric acid (6 M, 40 mL). The reaction was refluxed for 5 h, cooled, and placed in an ice bath. The crystals were filtered, washed with water, and dried to give the enol of 3,5-diiodo-4-hydroxyphenylpyruvic acid as a white powder (0.135 g, 78%), mp 222–228°C (lit. (10) mp 215–220°C). IR (Nujol) cm^{-1}: 3525, 3050, 1720, 1675, 1550, 1460, 1260. ^1H NMR (CD_3OD) δ: 6.27 (s, 1H), 8.16 (s, 2H). ^{13}C NMR (CD_3OD) δ: 85.33, 108.76, 133.24, 142.10, 142.73, 143.05, 168.34. MS (EI) *m/z*: 432 (M^+), 306 (M^+ − I).

Oxidative coupling reactions between the ethyl *N*-acetyl-3,5-diiodotyrosine (1) and (3,5-diiodo-4-hydroxyphenyl)pyruvic acid (11)

The ethyl ester of *N*-acetyl-3,5-diiodotyrosine (**1**) (2 mmol) was dissolved in ethanol (50 mL) and phosphate buffer (0.003 M, pH 7.5, 20 mL) or borate buffer (0.1 M, pH 8.3). The pH was adjusted to pH 7.5–8.5 using sodium hydroxide solution (1 M) and oxygen was vigorously bubbled through the solution. The pH was kept between 7.6 and 8.3 throughout the reaction. (3,5-Diiodo-4-hydroxyphenyl)pyruvic acid (**11**) (2 mmol) was added in small portions every 5–10 min over 1 h. The pH was checked regularly during addition and, when necessary, sodium hydroxide solution (1 M) was added to keep the pH between 7.6 and 7.8. After the addition was complete,

© 1997 NRC Canada

Can. J. Chem. Downloaded from www.nrcresearchpress.com by 88.146.161.215 on 09/08/12
For personal use only.

oxygen was bubbled through the solution until the dichloromethane had evaporated and then was stopped. The reaction was left stirring in air for a further 18 h. Hydrochloric acid (4 M) was used to acidify the reaction and the aqueous layer was extracted with ethyl acetate. The organic fractions were washed with saturated ammonium chloride solution, dried, and evaporated to dryness. The products and remaining starting material were characterized by TLC and ^{1}H NMR spectroscopy and the relative yields were calculated from ^{1}H NMR spectroscopy with *p*-dimethoxybenzene as internal standard.

Ethyl 2-acetamido-3-(3,5-diiodo-4-hydroxyphenyl)propenoate (21)

4-(4-Acetoxy-3,5-diiodobenzal)-2-methyl-5-oxazolone was prepared using the same method as used for the synthesis of 4-(4-acetoxy-3,5-diiodobenzal)-2-phenyl-5-oxazolone in the preparation of (3,5-diiodo-4-hydroxyphenyl)pyruvic acid (**11**) except that *N*-acetyl glycine (1.932 g, 16.53 mmol) was used in place of hippuric acid. 4-(4-Acetoxy-3,5-diiodobenzal)-2-methyl-5-oxazolone was isolated as yellow crystals (57%). ^{1}H NMR δ: 2.43 (s, 3H), 2.44 (s, 3H), 6.90 (s, 1H), 8.52 (s, 2H). ^{13}C NMR δ: 16.18, 21.763, 91.11, 126.69, 134.60, 134.72, 142.86, 153.47, 167.33, 167.42, 167.99.

4-(4-Acetoxy-3,5-diiodobenzal)-2-methyl-5-oxazolone (0.305 g, 0.61 mmol) was dissolved in anhydrous ethanol (150 mL) under a nitrogen atmosphere. Sodium hydride (0.034 g, 1.41 mmol) was added and the reaction stirred for 3 h. Water was then added and the reaction evaporated to dryness. The residue was dissolved in ethyl acetate and dilute hydrochloric acid and separated. The organic extracts were washed with water, dried, and evaporated to dryness. Flash column chromatography gave ethyl 2-acetamido-3-(3,5-diiodo-4-hydroxyphenyl)propenoate (**21**) as colourless crystals (0.297 g, 97%), mp 190–194°C. ^{1}H NMR (d_6-acetone) δ: 1.28 (t, J = 7.1 Hz, 3H), 2.09 (s, 3H), 4.21 (q, J = 7.1 Hz, 2H), 7.14 (s, 1H), 8.05 (s, 2H), 8.73 (s, 1H). ^{13}C NMR (d_6-acetone) δ: 14.49, 22.83, 61.77, 83.99, 127.44, 128.89, 131.29, 141.82, 156.64, 165.60, 169.49. MS (EI) *m/z*: 500 (M^+), 459 (M^+ − Ac), 385. Anal. calcd. for $C_{13}H_{13}I_2NO_4$: C 31.16, H 2.61, N 2.79; found: C 31.04, H 2.48, N 2.87.

Ethyl 2-acetamido-3-(3,5-diiodo-4-hydroxyphenyl)-2-methylpropanoate (8)

N-*Acetyl*-O-(tert-*butyldimethylsilyl)-3,5-diiodotyrosine*

The ethyl ester of *N*-acetyltyrosine (2.066 g, 4.10 mmol) was dissolved in dichloromethane (120 mL) under an atmosphere of nitrogen. Imidazole (0.323 g, 4.74 mmol) was added and the reaction was stirred and cooled to 0°C. *tert*-Butyldimethylsilyl chloride (0.617 g, 4.11 mmol) was added and the reaction was stirred for 72 h and allowed to warm to room temperature. The reaction was washed with water, dilute aqueous sodium hydroxide solution, and water, dried, and evaporated to dryness. Flash column chromatography yielded the ethyl ester of *N*-acetyl-*O*-(*tert*-butyldimethylsilyl)tyrosine as a pale yellow solid (1.72 g, 68%), mp 58–61°C. IR (Nujol) cm^{-1}: 3405, 2930, 2120, 1733, 1652, 1548, 1252, 1117, 885. ^{1}H NMR δ: 0.44 (s, 6H), 1.04 (s, 9H), 1.25 (t, J = 7.1 Hz, 3H), 2.00 (s, 3H), 2.94–2.91 (m, 2H, $ArCH_2$), 4.22–4.12 (m, 2H), 4.75–4.70 (m, 1H, α-H), 6.23 (d, J = 7.6 Hz, 1H, NH), 7.52 (s, 2H). ^{13}C NMR (100.62 MHz) δ: 0.00, 14.26, 18.58, 23.08, 26.52, 35.83, 53.19, 61.79, 88.32, 132.85, 141.11, 154.34, 169.71, 171.29. MS (CI) *m/z* (M^+, 616.9954. $C_{19}H_{29}I_2NO_4Si$ requires 616.9954), 618 (44, M^+), 492 (33, M^+ − I), 451 (43, M^+ − I, Ac), 364 (100, M^+ − 2 I).

*Ethyl 2-acetamido-3-[4-(*tert*-butyldimethylsilyloxy)-3,5-diiodophenyl)]-2-methylpropanoate*

Diisopropylamine (2.260 g, 22.43 mmol) was stirred in THF (4 mL) and cooled to −78°C. Butyllithium (1.436 g, 22.43 mmol) was added and the reaction stirred for 30 min. A solution of the ethyl ester of *N*-acetyl-*O*-(*tert*-butyldimethylsilyl)tyrosine (4.621 g, 7.48 mmol) in THF (20 mL) was added slowly and the reaction allowed to warm to −30°C, cooled to −78°C, and stirred for a further 10 min. Methyl iodide (2.818 g, 19.98 mmol) was added, and the reaction was stirred for 30 min and warmed to room temperature. The reaction was quenched by the addition of a few drops of saturated ammonium chloride solution and allowed to stir 5 min, further saturated ammonium chloride solution (50 mL) and diethyl ether (40 mL) were added, and the layers separated. The aqueous layer was extracted with diethyl ether. The organic extracts were washed with water, dried, and evaporated to dryness to yield ethyl 2-acetamido-3-[4-(*tert*-butyldimethylsilyloxy)-3,5-diiodophenyl]-2-methylpropanoate as a white solid (4.186 g, 88%), mp 135–137°C. IR (Nujol) cm^{-1}: 3405, 2930, 2102, 1733, 1652, 1548, 1252, 1117, 885. ^{1}H NMR δ: 0.46 (s, 6H), 1.06 (s, 9H), 1.35 (t, J = 7.1 Hz, 3H), 1.65 (s, 3H), 2.00 (s, 3H), 3.00 (d, J = 13.5 Hz, 1H), 3.51 (d, J = 13.6 Hz, 1H), 4.24 (q, J = 6.9 Hz, 2H), 6.18 (s, 1H), 7.46 (s, 2H). ^{13}C NMR (100.62 MHz) δ: 0.00, 14.23, 18.89, 23.35, 24.01, 26.47, 38.29, 61.34, 62.16, 88.27, 133.45, 141.52, 154.09, 169.67, 173.56. MS (CI) *m/z* (M^+, 631.0110. $C_{20}H_{31}I_2NO_4Si$ requires 631.0110), 632 (100, MH^+), 506 (25, M^+ − I), 465 (22, M^+ − I, Ac), 378 (66, M^+ − 2 I). Anal. calcd. for $C_{20}H_{31}I_2NO_4Si$: C 38.05, H 4.95, N 2.12; found: C 37.75, H 4.84, N 2.36.

Ethyl 2-acetamido-3-(3,5-diiodo-4-hydroxyphenyl)-2-methylpropanoate

Ethyl 2-acetamido-3-[4-(*tert*-butyldimethylsilyl)-3,5-diiodo-4-hydroxyphenyl)]-2-methylpropanoate (4.186 g, 6.63 mmol) was dissolved in THF and tetrabutylammonium fluoride (0.190 g, 6.63 mmol) was added as a solution in THF. The solution was stirred for 2 h, a small amount of water added, and the reaction evaporated to dryness. The resulting solid was separated between dichloromethane and dilute hydrochloric acid and the aqueous layer extracted with dichloromethane. The organic extracts were washed with dilute hydrochloric acid, dried, and evaporated to dryness. Flash column chromatography yielded ethyl 2-acetamido-3-(3,5-diiodo-4-hydroxyphenyl)-2-methylpropanoate as pale yellow crystals (3.263 g, 95 %), mp 66–68°C. IR (Nujol) cm^{-1}: 3381, 2982, 1737, 1657, 1544, 1181, 883. ^{1}H NMR δ: 1.36 (t, J = 7.0 Hz, 3H), 1.65 (s, 3H), 2.00 (s, 3H), 3.03 (d, J = 13.7 Hz, 1H), 3.55 (d, J = 13.7 Hz, 1H), 4.25 (q, J = 7.1 Hz, 2H), 5.69 (s, 1H), 6.18 (s, 1H), 7.37 (s, 2H). ^{13}C NMR (100.62 MHz) δ: 14.68, 23.77, 24.46, 38.86, 61.86, 62.64, 82.30, 133.26, 140.82, 152.93, 170.14, 174.00. MS (CI) *m/z* (M^+, 516.9246. $C_{14}H_{17}I_2NO_4$ requires 516.9253), 518 (22, MH^+), 392 (32, M^+ − I), 266 (100, M^+ − 2I).

© 1997 NRC Canada

Can. J. Chem. Downloaded from www.nrcresearchpress.com by 88.146.161.215 on 09/08/12
For personal use only.

Oxidative coupling of diiodophenols 12a–12e

The procedure for oxidative coupling of the ethyl ester of *N*-acetyl-3,5-diiodotyrosine (**1**) under atmospheric pressure was used for the following diiodophenols except that reaction times were 48 h. Yields were not optimized.

*Ethyl 3-(3,5-diiodo-4-hydroxyphenyl)propenoate (**20**)*

Ethyl 3-(3,5-diiodo-4-hydroxyphenyl)propionate (**12a**) (1.456 g). Flash column chromatography (dichloromethane:ethyl acetate, 9:1) yielded ethyl 3-(3,5-diiodo-4-hydroxyphenyl)propenoate (**20**) as colourless crystals (0.769 g, 53%), mp 104–106°C. IR (Nujol) cm^{-1}: 3460, 1687, 1624, 1577, 1199, 1114, 856. ^1H NMR δ: 1.32 (t, J = 7.1 Hz, 3H), 4.25 (q, J = 7.1 Hz, 2H), 5.94 (s, 1H, OH), 6.29 (d, J = 15.9 Hz, 1H, ArC*H*), 7.45 (d, J = 15.9 Hz, 1H, C*H*CO_2Et), 7.85 (s, 2H). ^{13}C NMR (100.62 MHz) δ: 14.68, 61.03, 82.94, 118.79, 131.48, 139.17, 141.12, 155.35, 166.86. MS (CI) *m/z* (M^+, 443.8719. $C_{11}H_{10}I_2O_3$ requires 443.8719), 445 (5, MH^+), 336 (16), 319 (17), 193 (100).

*4-(2-Acetylaminoethyl)-2,6-diiodo-1-(3,5-diiodo-4-hydroxyphenoxyl)benzene (**13b**)*

N-Acetyl-3,5-diiodotyramine (**12b**) (1.034 g). Trituration of the crude product with ethyl acetate yielded 4-(2-acetylaminoethyl)-2,6-diiodo-1-(3,5-diiodo-4-hydroxyphenoxyl)benzene (**13b**) as colourless crystals (0.327 g, 37%), mp 233–235°C. IR (Nujol) cm^{-1}: 3358, 1637, 1534, 1186. ^1H NMR (400 MHz, d_6-acetone) δ: 7.84 (s, 2H), 7.20 (s, 2H), 7.18 (s, 1H, NH or OH), 3.46–3.41 (m, 2H, CH_2N), 2.80 (t, J = 7.0 Hz, 2H, ArCH_2), 1.84 (s, 3H). ^{13}C NMR (100.62 MHz, d_6-acetone) δ: 21.93, 32.71 (CH_2N), 38.83, 86.99, 191.01, 24.54, 139.63, 140.86, 149.62, 150.34, 150.49, 168.59. MS (CI) *m/z* (M^+, 774.7056. $C_{16}H_{13}I_4NO_3$ requires 774.7075), 776 (30, MH^+), 647 (6, $M^+ - I$), 432 (10).

*2,6-Diiodo-1-(3,5-diiodo-4-hydroxyphenoxyl)-4-methylbenzene (**13c**)*

2,6-Diiodo-4-methylphenol (**12c**) (1.338 g). Flash column chromatography yielded 2,6-diiodo-1-(3,5-diiodo-4-hydroxyphenoxyl)-4-methylbenzene (**13c**) as colourless crystals (0.756 g, 58%), mp 176–178°C. IR (Nujol) cm^{-1}: 3476, 3058, 1586, 1435, 1183, 853. ^1H NMR δ: 2.31 (s, 3H), 5.46 (s, 1H, OH), 7.12 (s, 2H), 7.66 (s, 2H). ^{13}C NMR δ: 20.27, 81.97 (*C*-I), 50.73, 90.82, 126.34, 139.78, 141.35, 149.67, 151.57. MS (CI) *m/z* (M^+, 703.6703. $C_{13}H_8I_4O_2$ requires 703.6694), 703 (21, M^+), 578 (10, $M^+ - I$), 450 (15, $M^+ - 2I$), 324 (4, $M^+ - 3$ I).

*2,6-Diiodo-1-(3,5-diiodo-4-hydroxyphenoxyl)-4-propylbenzene (**13d**)*

2,6-Diiodo-4-propylphenol (**12d**) (1.123 g). Flash column chromatography yielded 2,6-diiodo-1-(3,5-diiodo-4-hydroxyphenoxyl)-4-propylbenzene (**13d**) as a colourless oil (0.074 g, 7%). IR (neat) cm^{-1}: 3486, 2960, 2930, 1585, 1422, 1183, 851. ^1H NMR (400 MHz) δ: 0.90 (t, J = 7.3 Hz, 3H), 1.61–1.51 (m, 2H), 2.46 (t, J = 7.3 Hz, 2H), 5.38 (s, 1H, OH), 7.04 (s, 2H), 7.58 (s, 2H). ^{13}C NMR (100.62 MHz) δ: 14.14, 24.60, 36.78, 81.91 (*C*-I), 90.85, 126.35, 140.64, 144.55, 149.66, 150.73, 151.65. MS (CI) *m/z* (M^+, 731.7016. $C_{15}H_{12}I_4O_2$ requires 731.7016), 732 (7, M^+), 606 (4, $M^+ - I$), 478 (2, $M^+ - 2I$).

*2,6-Diiodo-1-(3,5-diiodo-4-hydroxyphenoxyl)-4-(ethoxycarbonylmethyl)benzene (**13e**)*

Ethyl 2-(3,5-diiodo-4-hydroxyphenyl)acetate (**12e**) (1.761 g). Flash column chromatography (dichloromethane:ethyl acetate, 9:1) yielded 2,6-diiodo-1-(3,5-diiodo-4-hydroxyphenoxyl)-4-(ethoxycarbonylmethyl)benzene (**13e**) as colourless crystals (0.853 g, 54%), mp 72–75°C. IR (Nujol) cm^{-1}: 3471, 3065, 1726, 1585, 1423, 1182, 850. ^1H NMR δ: 1.29 (t, J = 7.1 Hz, 3H), 3.57 (s, 2H), 4.20 (q, J = 7.1 Hz, 2H), 5.47 (s, 1H, OH), 7.11 (s, 2H), 7.81 (s, 2H). ^{13}C NMR (100.62 MHz) δ: 13.92, 39.08, 61.17, 81.32 (*C*-I), 90.11, 125.70, 134.98, 140.97, 149.14, 150.13, 153.52, 170.05. MS (CI) *m/z* (M^+, 775.6914. $C_{16}H_{12}I_4O_4$ requires 775.6917), 793 (100, MNH_4^+), 776 (6, M^+), 668 (61, $MNH_4^+ - I$).

*Ethyl 2-acetamido-3-(3,5-diiodo-4-hydroxyphenyl)-2-methylpropanoate (**8**)*

The starting material was recovered in quantitative yield under the same conditions as all the other phenolic oxidations.

Acknowledgements

We gratefully thank Knoll Pharmaceuticals, Nottingham, U.K., for generous funding and a studentship (N.V.B), the EPSRC for a 400 MHz NMR spectrometer and the Engineering and Physical Sciences Research Council (EPSRC) MS Service at University of Wales, Swansea, Wales.

References

1. D.A. Whiting. *In* Comprehensive organic synthesis. Vol. 3. *Edited by* B.M. Trost and I. Fleming. Pergamon Press, Oxford. 1991. pp. 659–703.
2. C.R. Harrington and G. Barger. Biochem. J. **21**, 169 (1927).
3. T.B. Johnson and L.B. Tewkesbury. Proc. Natl. Acad. Sci. U.S.A. **28**, 73 (1942).
4. Reviews: R. Eckholm. Int. Rev. Cytol. **120**, 243 (1990); A.W. Norman and G. Litwack. *In* Hormones. Academic Press, Orlando, Fla. 1987. pp. 221–262; A. Taurog. *In* Endocrinology. *Edited by* L.J. DeGroot, G.F. Cahill, and L. Martini. Grune and Stratton, New York. 1979. pp. 331–346; Recent leading papers: S. Xiao, H.G. Pollock, A. Taurog, and A.B. Rabwitch. Arch. Biochem. Biophys. **320**, 96 (1995); A. Taurog, M. Dorris, and D.R. Doerge. Arch. Biochem. Biophys. **315**, 82 (1994).
5. Y. Ohmiya, H. Hayashi, T. Kondo, and Y. Kondo. J. Biol. Chem. **265**, 5281 (1990);
6. J.-M. Gavaret, J. Nunez, and H.J. Cahnmann. J. Biol. Chem. **255**, 9066 (1980); J.-M. Gavaret, H.J. Cahnmann, and J. Nunez. J. Biol. Chem. **254**, 11218 (1979).
7. R. Pitt-Rivers and A.T. James. Biochem. J. **70**, 173 (1958); R. Pitt-Rivers. Biochem. J. **43**, 223 (1948); C.R. Harrington. J. Chem. Soc. 193 (1944).
8. S. Ito, M. Kajiwara, Y. Kato, K. Inoue, and T. Kaneko. Arch. Biochem. Biophys. **140**, 90 (1970); S. Ito, K. Seo, K. Sano, and M. Nishikawa. Endrocinol. Jpn. **16**, 129 (1969); T. Shiba and H.J. Cahnmann. Biochim. Biophys. Acta, **58**, 609 (1962).
9. F. Blasi, F. Fragomele, and I. Covelli. Eur. J. Biochem. **5**, 215 (1968); F. Blasi. Biochim. Biophys. Acta, **121**, 204 (1966); A. Nishinaga and T. Matsuura. J. Org. Chem. **29**, 1812 (1964); H.J. Cahnmann and A. Nishinaga. J. Am. Chem. Soc. **82**, 2050 (1960).
10. R.I. Melzter and R.J. Stanaback. J. Org. Chem. **26**, 1977 (1961).
11. T. Shiba and H.J. Cahnmann. J. Org. Chem. **29**, 3061 (1964); **29**, 3063 (1964); **27**, 1773 (1962).

© 1997 NRC Canada

12. A. Nishinaga, H.J. Cahnmann, H. Kon, and T. Matsuura. Biochemistry, **7**, 388 (1968).
13. Review: G.G. Melikyan. Synthesis, 833 (1993).
14. F. Jin, J. Leitich, and C. von Sonntag. J. Chem. Soc. Perkin Trans. 1, 1583 (1993).
15. T. Matsuura, A. Nishinaga, and H.J. Cahnmann. J. Org. Chem. **27**, 3620 (1962); T. Matsuura and A. Nishinaga. J. Org. Chem. **27**, 3072 (1962); T. Matsuura and H.J. Cahnmann. J. Am. Chem. Soc. **82**, 2055 (1960); **81**, 871 (1959).
16. D.H.R. Barton, C.J. Potter, and D.A. Widdowson. J. Chem. Soc. Perkin Trans. 1, 346 (1974).
17. R. Stewart. The proton: applications to organic chemistry. Academic Press, Orlando, Fla. 1985. pp. 217–227.
18. R.L. Datta and N. Prosand. J. Am. Chem. Soc. **39**, 443 (1917).
19. R.A. Pages and A. Burger. J. Med. Chem. **10**, 435 (1967).

Can. J. Chem. Downloaded from www.nrcresearchpress.com by 88.146.161.215 on 09/08/12
For personal use only.

© 1997 NRC Canada

Synthesis of the fatty acid of pramanicin

Christopher Cow, David Valentini, and Paul Harrison

Abstract: The natural product tetradec-2-enoic acid-4,5-epoxide (**2**), which is also a component of the antibiotic pramanicin (**1**), was prepared in racemic form by a glycoluril-template directed approach. Two sequential additions of acetate units to decanoic acid are effected by intramolecular condensations on the template, mimicking the proposed biosynthetic pathway to **1**. Cleavage of the grown *trans,trans*-tetradeca-2,4-dienoyl chain from the template and epoxidation yields **2**. The reaction sequence illustrates the applicability of this biomimetic approach to total synthesis of natural products.

Key words: pramanicin, biomimetic, glycoluril, template.

Résumé : On a préparé la forme racémique de l'acide 4,5-époxy tétradéc-2-énoïque (**2**), un produit naturel qui est également un constituant de l'antibiotique pramanicine (**1**), en utilisant l'approche directe à l'aide d'un modèle glycolurile. On a effectué deux additions séquentielles d'unités acétates sur l'acide décanoïque par condensations intramoléculaires sur le composé modèle, imitant ainsi la voie biosynthétique proposée pour le composé **1**. Le clivage de la chaîne *trans-trans*-tétradéca-2,4-diénoyle en formation à partir du composé modèle et son époxydation subséquente conduisent au composé **2**. La séquence des réactions illustre la validité de cette approche biomimétique lors de la synthèse totale des produits naturels.

Mots clés : pramanicine, biomimétique, glycolurile, modèle.

[Traduit par la rédaction]

Introduction

Pramanicin (**1**) and the related fatty acid **2** (Scheme 1) are co-occurring natural products isolated recently by Schwartz et al. from an unidentified fungus in grass (1). The antibiotic activity of **1** against the fungal pathogen *Cryptococcus neoformans* (1), the causative agent of meningitis in AIDS patients, makes it an interesting target for synthesis. Such a synthesis should allow for the determination of the absolute stereochemistry of the epoxide, as well as for the preparation of analogues for structure–activity correlations.

The glycoluril **3** is being developed in our group as a template to effect intramolecular crossed-Claisen-like condensations between two acyl units (2, 3) in a manner that mimics some of the features of polyketide and fatty acid biosynthesis (4). To utilize this approach in the synthesis of **1**, the fatty acid **2** was chosen as a key intermediate, since a Claisen-like condensation between **2** and an appropriately substituted and protected pyrrolidinone would generate the carbon skeleton of **1** (Scheme 1). Further, **2** could be derived from a series of Claisen-type condensations between acyl units, followed by functional group manipulations. Although the biosynthetic pathway to **1** and **2** has not been investigated, it is probable that this retrosynthetic analysis corresponds to the sequence of events in the biosynthesis of **1**.

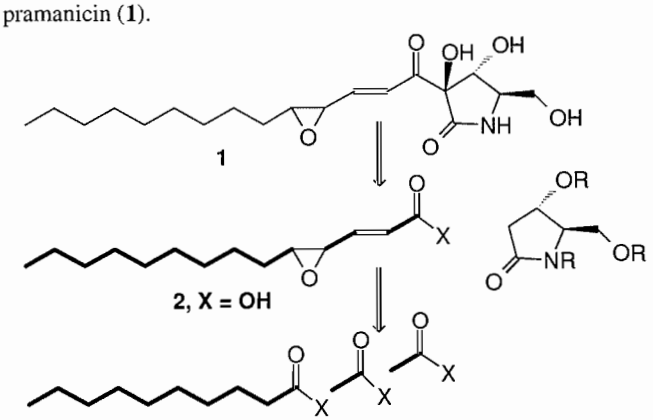
Received October 30, 1996.

This paper is dedicated to Professor William A. Ayer on the occasion of his 65th birthday.

C. Cow, D. Valentini, and P. Harrison.[1] Department of Chemistry, McMaster University, 1280 Main Street West, Hamilton, ON L8S 4M1, Canada.

[1] Author to whom correspondence may be addressed. Telephone: (905) 525-9140, ext. 27290. Fax: (905) 522-2509. E-mail: pharriso@mcmail.cis.mcmaster.ca

Scheme 1. Retrosynthetic, and probable biogenetic, analysis of pramanicin (**1**).



Herein, we describe the application of this methodology to the synthesis of **2** from decanoic acid. Although **2** could in principle be constructed by sequential "head-to-tail" condensations of seven acetate units, we chose to assemble the target from decanoyl chloride, which is the last readily available acid derivative in the proposed synthetic sequence.

Results

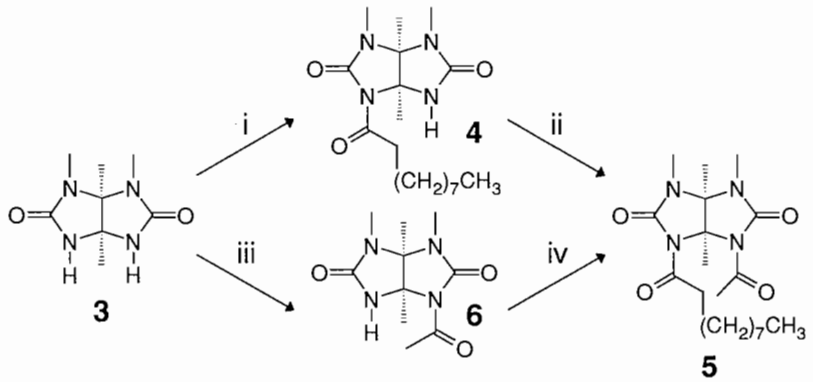
Treatment of glycoluril **3** (5) with *n*-BuLi, then decanoyl chloride, afforded the decanoyl derivative **4** (Scheme 2). As with other acylations of glycoluril **3** (2, 3), only a small amount of didecanoylglycoluril was formed in this reaction; presumably, the steric hindrance provided by the first acyl moiety prevents acylation at the second, free, NH site. Further acylation can be accomplished, however, by treating **4** with *n*-BuLi, then acetyl chloride, to give the decanoyl acetyl derivative **5**. This reaction, which proceeded rather poorly, was not optimized since the yield of **5** was considerably improved by acetylation of

© 1997 NRC Canada

Can. J. Chem. Downloaded from www.nrcresearchpress.com by 88.146.161.215 on 09/08/12
For personal use only.

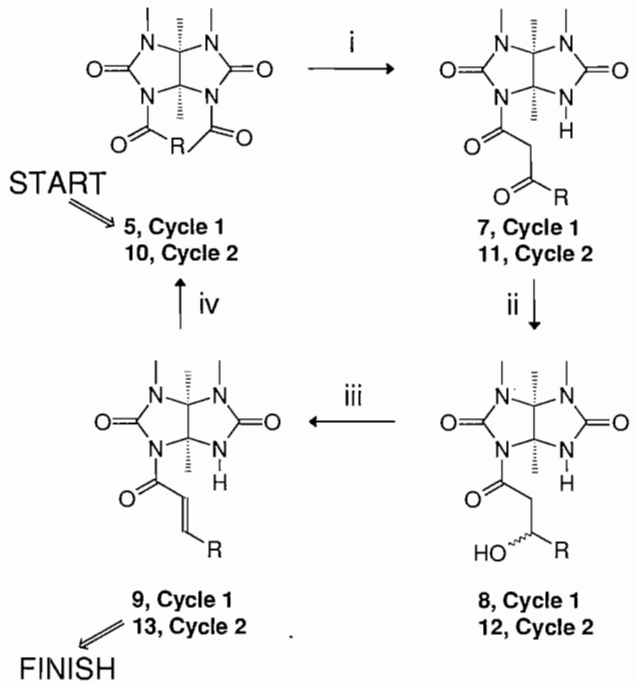
Can. J. Chem. Downloaded from www.nrcresearchpress.com by 88.146.161.215 on 09/08/12
For personal use only.

Scheme 2.



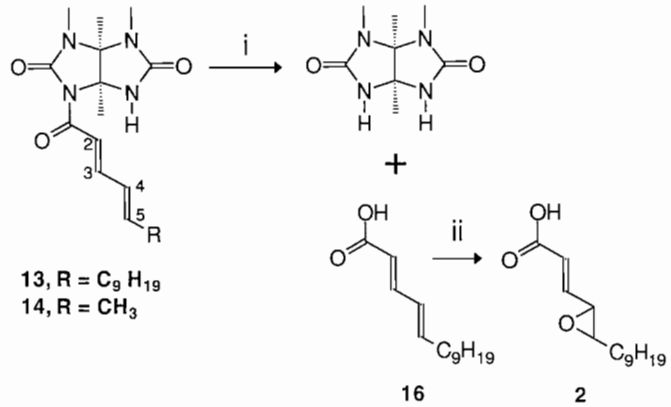
Reagents: (i) *n*-BuLi, THF, reflux, 2 h, then $C_9H_{19}COCl$, r.t., 1 h, 65%; (ii) *n*-BuLi, THF, r.t., 10 min, then CH_3COCl, 1 h, 38%; (iii) $(CH_3CO)_2O$, neat, reflux, 16 h, 78%; (iv) *n*-BuLi, THF, reflux, 2 h, then $C_9H_{19}COCl$, r.t., 1 h, 75%.

Scheme 3.



Reagents: (i) *t*-AmOLi, THF, 0°C, 20 min, then $NaHSO_4$(aq); for **7**: 65%, for **11**: 50%; (ii) $NaBH_4$, MeOH, 0°C, 10 min, then AcOH; for **8**: 79%, for **12**: 24%; (iii) $(CF_3CO)_2O$, 1 h, then excess Et_3N, reflux 20 min; for **9**: 76%, for **13**: 94%; (iv) *n*-BuLi, THF, r.t., 10 min, then CH_3COCl, 1 h, 61%, Cycle 1 to Cycle 2. R = C_9H_{19} for Cycle 1, R = $C_9H_{19}CH{=}CH$ for Cycle 2.

Scheme 4.



Reagents: (i) *t*-BuOK (6 equiv.), H_2O (2 equiv.), Et_2O, r.t., 3 h, 68%; (ii) Oxone, H_2O, PhH, Me_2CO, 18-crown-6, 0°C, pH 7.5, 3 h, 35%.

glycoluril **3** first, to give **6** (2, 3), followed by treatment with *n*-BuLi and decanoyl chloride.

The Claisen-like condensation between the acetyl and decanoyl groups of **5** was effected with lithium *tert*-amylate in THF at 0°C (Scheme 3). As in our previous studies (2, 3), the condensation proceeded rapidly under mild conditions to give **7** as the sole detectable product. Compound **7** was reduced to the β-hydroxydodecanoylglycoluril **8**, from which elimination of water proceeded smoothly to give the unsaturated derivative **9**, which was >99% *trans* by NMR. The sequence of reactions was now repeated: acetylation of **9** gave **10**, and intramolecular Claisen-like condensation afforded ketone **11**. Reduction of **11** yielded alcohol **12**, and elimination of water gave exclusively the *trans,trans* isomer of tetradeca-2,4-dienoylglycoluril (**13**).

It now remained to convert **13** to **2**. It was unclear, however, whether to remove the acyl moiety from the glycoluril template prior to or after the epoxidation of the 4,5 double bond, and we therefore investigated both possible routes using *trans,trans*-hexa-2,4-dienoylglycoluril **14** (3) as a model substrate. Treatment of **14** with *m*CPBA furnished the desired epoxide **15** in good yield and with high selectivity for the 4,5 over the 2,3 double bond. However, when **15** was treated with a variety of reagents that were expected to effect cleavage of the acyl–glycoluril bond (LiOH, LiOMe, LiOBn, or KO*t*Bu–H_2O), in all cases these reactions failed to yield the desired products. In contrast, when either **13** or **14** was treated with potassium *tert*-butoxide–water according to the procedure of

© 1997 NRC Canada

Can. J. Chem. Downloaded from www.nrcresearchpress.com by 88.146.161.215 on 09/08/12
For personal use only.

Gassman et al. (6), the free acids were obtained in good yields (Scheme 4). Subsequent epoxidation of tetradeca-2,4-dienoic acid **16** (7, 8) using oxone (9) required the use of a biphasic mixture of benzene, 18-crown-6, aqueous buffered phosphate, and acetone in order to solubilize the components. This reaction is again highly selective for the 4,5 double bond, affording racemic epoxide **2**, which was spectroscopically identical to the natural product.

Discussion

This sequence of reactions presumably corresponds to the events occurring on the putative polyketide synthase that is responsible for formation of **2** in vivo. After assembly of the decanoyl chain from five acetate units in the conventional manner of fatty acid biosynthesis, the condensing subunit of the enzyme is loaded with the decanoyl moiety, and a malonyl group, which acts as an acetyl enolate equivalent, is then covalently attached. Decarboxylative condensation on the enzyme surface generates a new C—C bond; likewise, covalent attachment of an acetyl group to decanoyl glycoluril **4**, followed by intramolecular Claisen-like condensation, generates a 12-carbon chain. Further, both the β-ketoacyl enzyme and the corresponding glycoluril **7** undergo reductions to β-hydroxyacyl groups, and subsequent eliminations of water. The resulting enoyl derivatives can be reacylated and the sequence repeated, resulting in the iterative growth of long chains on both the enzyme and the mimic. Finally, cleavage of the newly synthesized acyl chain regenerates the glycoluril template or the enzyme, which can in either case be recycled.

Since this methodology parallels the enzymatic events, it should prove useful for the synthesis of natural products, as well as putative precursors for the investigation of biosynthetic pathways. This sequence represents the first application of this methodology to the synthesis of a natural product that is not readily available, and illustrates the potential of the approach for the synthesis of a variety of fatty acid and polyketide natural products, or analogues thereof. The approach provides a useful method for effecting Claisen condensations on α,β-unsaturated acyl groups; no detectable conjugate addition was observed in these cases, presumably due to the orientational effects of the glycoluril template. The preparation of the pyrrolidinone moiety and condensation with **2** to give pramanicin will be described in due course.

Experimental

General

All reactions were performed in flame-dried glassware, under a positive pressure of dry nitrogen, unless otherwise noted. Air- and moisture-sensitive compounds were transferred by syringe. Melting points are uncorrected. Proton and carbon-13 NMR spectra were obtained on a Bruker AC-200 spectrometer. The reference for NMR chemical shifts was TMS. Data are given as chemical shift (integral, multiplicity (s = singlet, d = doublet, t = triplet, q = quartet, m = multiplet), coupling constant(s) (Hz), assignment). Fourier transform infrared (FTIR) spectra were recorded on a Bio-Rad SPC 3200 spectrophotometer. Mass spectra were recorded on a VG analytical ZAB-E machine using electron impact (EIMS). High-resolution mass spectra were also recorded on the same spectrometer. Flash column chromatography was performed with Kieselgel 60 (230–400 mesh ASTM) according to the method of Still et al. (10). THF was freshly distilled under nitrogen protection from potassium–benzophenone. *n*-Butyllithium (*n*-BuLi) was titrated using 2,5-dimethoxybenzyl alcohol in THF (11). Water was obtained from a Millipore purification device.

Preparation of 1-decanoyl-3,4,7,8-tetramethylglycoluril (4)

To a suspension of glycoluril **3** (1 g, 5.1 mmol) in THF (60 mL) at reflux was added *n*-BuLi (3.45 mL of a 1.6 M solution in hexane, 5.5 mmol). The mixture was cooled to room temperature and decanoyl chloride (1.3 mL, 1.2 g, 6.3 mmol) was added. After stirring for 1 h, solid ammonium bicarbonate (2 g) was added. The mixture was filtered, and the residue was washed with chloroform (2 × 30 mL). The filtrate was evaporated, and the product was purified by flash column chromatography in EtOAc to give 1.17 g (3.3 mmol, 65%) of **4** as white crystals. ^{1}H NMR ($CDCl_3$, 200 MHz) δ: 6.09 (1H, br s, N*H*), 2.98 (3H, s, NCH_3), 2.84 (3H, s, NCH_3), 2.81 (2H, m, O=C-CH_2), 1.65 (3H, s, CH_3), 1.56 (2H, pent, J = 7.3 Hz, O=C-CH_2CH_2), 1.52 (3H, s, CH_3), 1.24 (12 H, br s, CH_2), 0.83 (3H, t, J = 6.6 Hz, CH_2CH_3); ^{13}C NMR ($CDCl_3$, 50 MHz) δ: 174.28 (*C*=O), 157.20 (NN*C*=O), 152.94 (NN*C*=O), 78.53 (*C*NN), 77.63 (*C*NN), 36.36, 31.78, 29.33, 29.18 (2C), 29.07, 27.00, 26.34, 24.23, 22.58, 19.60, 15.67, 14.02; EIMS *m/z*: 352 $[M]^+$, 253, 240 (base), 199, 156, 141, 125; HRMS (EI) calcd. for $C_{18}H_{32}N_4O_3$: 352.2474; found: 352.2482.

1-Decanoyl-6-acetyl-3,4,7,8-tetramethylglycoluril (5)

Method 1

A solution of decanoylglycoluril **4** (500 mg, 1.4 mmol) in THF (30 mL) at 0°C was treated with *n*-BuLi (0.88 mL of a 1.6 M solution in hexane, 1.4 mmol). The mixture was stirred for 10 min, then acetyl chloride (0.12 mL, 0.13 g, 1.7 mmol) was added and stirring continued for 1 h, during which time the mixture warmed slowly to room temperature. Aqueous $NaHSO_4$ (5 mL, 1 M) was added, and the mixture was extracted with chloroform (3 × 30 mL). The chloroform layers were combined, washed with water, dried over Na_2SO_4, and concentrated. Flash column chromatography of the residue in EtOAc gave white crystals of **5** (214 mg, 38%) and unreacted **4** (159 mg, 32%).

Method 2

A solution of acetylglycoluril **6** (524 mg, 2.2 mmol) in THF (50 mL) was treated with *n*-BuLi (1.5 mL of a 1.6 M solution in hexane, 2.4 mmol) at 0°C for 30 min. Decanoyl chloride (0.54 mL, 0.50 g, 2.6 mmol) was added and the solution was stirred for 1 h, during which time the mixture warmed slowly to room temperature. Aqueous $NaHSO_4$ (5 mL, 1 M) was added, and the mixture was extracted with chloroform (3 × 30 mL). The chloroform layers were combined, washed with water, dried over Na_2SO_4, and concentrated. Flash column chromatography of the residue in EtOAc gave product **5** (517 mg, 62%) and unreacted **6** (34 mg, 6%). IR (KBr pellet): 2921, 2853 (C-H str.), 1684-1749 (br C=O str.), 1332, 1092, 759, 607; ^{1}H NMR ($CDCl_3$, 200 MHz) δ: 2.92 (6H, s, NCH_3), 2.81 (2H, m, O=CCH_2), 2.44 (3H, s, O=CCH_3), 1.90 (3H, s, CH_3), 1.56 (4H, m, O=CCH_2CH_2 and O=$CH_2CH_2CH_2$),

© 1997 NRC Canada

Can. J. Chem. Downloaded from www.nrcresearchpress.com by 88.146.161.215 on 09/08/12
For personal use only.

1.45 (3H, s, CH_3), 1.22 (10 H, br m, CH_2), 0.83 (3H, t, J = 7 Hz, CH_2CH_3); ^{13}C NMR ($CDCl_3$, 50 MHz) δ: 173.73 (*C*=O), 170.50 (*C*=O), 153.06 (2 NN*C*=O), 80.48 (*C*NN), 77.63 (*C*NN), 37.61, 31.80, 29.37–29.05 (5 C overlapping), 26.70, 26.14, 24.31, 22.60, 19.06, 14.51, 14.04; EIMS *m/z*: 394 $[M]^+$, 353, 295, 282, 253, 241 (base), 199, 168, 141, 125.

1-(3′-Oxododecanoyl)-3,4,7,8-tetramethylglycoluril (7)

Acetyl decanoyl glycoluril **5** (4.7 g, 12 mmol) was dissolved in THF (200 mL). Separately, *n*-BuLi (9.4 mL of a 1.6 M solution in hexane, 15 mmol) was added to *tert*-amyl alcohol (2.6 mL, 24 mmol) in THF (10 mL) at 0°C, and the mixture was stirred for 10 min. The amylate solution was cannulated into the glycoluril solution at 0°C, and the mixture was stirred for 2 h at 0°C. Aqueous $NaHSO_4$ (20 mL, 1 M) was added, and the mixture was extracted into chloroform. The chloroform layers were combined, washed with water, dried over Na_2SO_4, and concentrated. Flash column chromatography of the residue in EtOAc gave **7** (3.0 g, 65%) as white crystals and unreacted **5** (0.92 g, 17%). IR (KBr pellet): 3337 (N-H str.), 2925, 2854 (C-H str.), 1724 (br C=O str.), 1411, 1111, 760; ^{1}H NMR ($CDCl_3$, 200 MHz) δ: 6.05 (1H, s, N*H*), 4.29 (1H, d, J = 16.3 Hz, O=C-CH_aH-C=O), 3.52 (1H, d, J = 16.3 Hz, O=C-CHH_b-C=O), 2.93 (3H, s, NCH_3), 2.83 (3H, s, NCH_3), 2.48 (2H, m, O=CCH_2CH$_2$), 1.71 (3H, s, CH_3), 1.65 (2H, m, O=CCH$_2$CH_2),1.53 (3H, s, CH_3), 1.22 (12 H, br m, CH_2), 0.84 (3H, t, J = 6.0 Hz, CH_3); ^{13}C NMR ($CDCl_3$, 50 MHz) δ: 203.66 (*C*=O), 167.42 (*C*=O), 157.14 (*C*=O), 152.73 (*C*=O), 76.71, 76.60, 51.48, 42.06, 31.80, 29.34 (2C), 29.20, 28.99, 27.06, 26.40, 23.28, 22.60, 19.23, 15.68, 14.04; EIMS *m/z*: 394 $[M]^+$ 352, 295, 282, 253, 240, 199, 183, 138, 125 (base); HRMS (EI) calcd. for $C_{20}H_{34}N_4O_4$: 394.2851; found: 394.2589.

1-(3′-Hydroxydodecanoyl)-3,4,7,8-tetramethylglycoluril (8)

Oxododecanoyl glycoluril **7** (45 mg, 0.11 mmol) was dissolved in MeOH (7 mL) at 0°C. $NaBH_4$ (5 mg, 0.16 mmol) was added and the mixture was stirred for 10 min. Glacial acetic acid (1 mL) was added, then solvents were removed on the rotary evaporator. Flash column chromatography of the residue in EtOAc gave **8** (36 mg, 79%) as a white crystalline solid. ^{1}H NMR ($CDCl_3$, 200 MHz) δ: 6.04 (1H, br m, N*H*), 4.00 (1H, m, C*H*OH), 3.21 (1H, dd, J = 17.0, 2.6 Hz, O=C-CH_aH$_b$), 2.98 (3H, s, NCH$_3$), 2.84 (3H, s, NCH$_3$), 2.84 (1H, m, O=CCH_bH$_a$), 1.67 (3H, s, CH_3), 1.60 (3H, s, CH_3), 1.44 (2H, m, HOCHCH_2), 1.23 (15 H, br s, CH_2 and O*H*), 0.85 (3H, t, J = 6.0 Hz, CH_3); ^{13}C NMR ($CDCl_3$, 50 MHz) δ: 167.42 (*C*=O), 157.14 (*C*=O), 152.73 (*C*=O), 77.63, 76.50, 67.95, 43.34, 31.86, 29.55–29.28 (6C), 27.13, 26.41, 22.60, 19.23, 15.68, 14.04; EIMS *m/z*: 396 $[M]^+$ 378, 269, 240, 199, 156, 138, 125 (base).

1-(*trans*-Dodec-2′-enoyl)-3,4,7,8-tetramethylglycoluril (9)

Compound **8** (720 mg, 1.8 mmol) was dissolved in CH_2Cl_2 (10 mL), then trifluoroacetic anhydride (0.77 mL, 5.4 mmol) was added and the mixture was stirred for 1 h. Triethylamine (0.33 mL, 3.6 mmol) in CH_2Cl_2 (5 mL) was added dropwise. After 10 min, further Et_3N (2 mL) was added and the mixture was heated at reflux for 20 min. Evaporation and flash column chromatography of the residue in EtOAc gave **9** (520 mg, 76%) as a white crystalline solid. IR (KBr pellet): 3337 (N-H str.) 2925, 2854 (C-H str.), 1702–1736 (br C=O str.), 1630 (C=C str.), 1468, 1089, 761; ^{1}H NMR ($CDCl_3$, 200 MHz) δ: 7.28 (1H, dd, J = 15.3, 3.2 Hz, O=CC*H*=CH), 7.09 (1H, dt, J = 15.3, 6.6 Hz, O=C-CH=C*H*), 6.09 (1H, s, N*H*), 3.04 (3H, s, NCH_3), 2.89 (3H, s, NCH_3), 2.27 (2H, dt, J = 6.9, 6.9 Hz, O=CCH=CHCH_2), 1.74 (3H, s, CH_3), 1.59 (3H, s, CH_3), 1.49 (2H, m, CH=CHCH$_2$-CH_2), 1.29 (12H, br s, CH_2), 0.90 (3H, t, J = 6.7 Hz, CH_3); ^{13}C NMR ($CDCl_3$, 50 MHz) δ: 165.90 (*C*=O), 157.25 (*C*=O), 153.02 (*C*=O), 150.60 (*C*=O), 121.74, 78.54, 76.68, 32.60, 31.80, 29.40–29.17 (4C), 28.07, 27.06, 26.33, 22.60, 19.70, 15.71, 14.05; EIMS *m/z*: 378 $[M]^+$, 251, 199, 125 (base). HRMS (EI) calcd. for $C_{20}H_{34}N_4O_3$: 378.2632; found: 378.2618.

1-(*trans*-Dodec-2-enoyl)-6-acetyl-3,4,7,8-tetramethylglycoluril (10)

Dodecenoylglycoluril **9** (416 mg, 1.1 mmol) was dissolved in THF (10 mL). *n*-BuLi (0.73 mL of a 1.6 M solution in hexane, 1.1 mmol) was added at 0°C, the mixture was stirred (10 min), and acetyl chloride (86 μL, 1.2 mmol) was added. After 1 h, aqueous $NaHSO_4$ (1 mL, 1 M) was added, and the mixture was extracted with chloroform (3 × 10 mL). The chloroform layers were combined, washed with water (2 × 10 mL), dried over Na_2SO_4, and concentrated. Flash column chromatography in EtOAc afforded **10** as a white solid (282 mg, 61%) and recovered **9** (98 mg, 24%). ^{1}H NMR ($CDCl_3$, 200 MHz) δ: 6.8–7.1 (2H, m, C*H*=C*H*), 2.90 (3H, s, NCH_3), 2.89 (3H, s, NCH_3), 2.39 (3H, s, O=CCH_3), 2.14 (2H, dt, J = 6.9, 6.9 Hz, O=CCH=CHCH_2), 1.89 (3H, s, CH_3), 1.44 (3H, s, CH_3), 1.44 (2H, m, CH=CHCH$_2$CH_2), 1.17 (12H, br s, CH_2), 0.79 (3H, t, J = 6.7 Hz, CH_3); EIMS *m/z*: 420 $[M]^+$, 336, 293, 282, 241, 225, 199, 168, 125 (base).

1-(3′-Oxo-*trans*-tetradec-4′-enoyl)-3,4,7,8-tetramethylglycoluril (11)

Acetyl dodecenoyl glycoluril **10** (395 mg, 0.94 mmol) was dissolved in THF (20 mL). Separately, *n*-BuLi (0.69 mL of a 1.6 M solution in hexane, 1.1 mmol) was added to *tert*-amyl alcohol (0.21 mL, 2.2 mmol) in 5 mL THF and the mixture was stirred for 10 min at 0°C. The *tert*-amylate solution was cannulated into the glycoluril solution, and the mixture was stirred at 0°C for 2 h. Aqueous $NaHSO_4$ (2 mL, 1 M) was added and the mixture was extracted into chloroform (3 × 20 mL). The chloroform layers were combined, washed with water, dried over Na_2SO_4, and concentrated. Flash column chromatography of the residue in EtOAc gave **11** (197 mg, 50%) as a white crystalline solid, and recovered **10** (140 mg, 35%). IR (KBr pellet): 3237 (N-H str.), 2914, 2851 (C-H str.), 1690–1722 (br C=O str.), 1466, 1412, 1090, 759; ^{1}H NMR ($CDCl_3$, 200 MHz), keto form, δ: 7.03 (1H, m, O=C-C*H*=CH), 6.26 (1H, s, N*H*), 6.05 (1H, d, J = 15.8 Hz, O=CCH=C*H*), 4.46 (1H, d, J = 16.2 Hz, O=C-C*H*H-C=O), 3.69 (1H, d, J = 16.2 Hz, O=C-CH*H*-C=O), 2.97 (3H, s, NCH_3), 2.82 (3H, s, NCH_3), 2.17 (2H, m, O=CCH=CHCH_2), 1.72 (3H, s, CH_3), 1.52 (3H, s, CH_3), 1.42 (2H, br m, CH=CHCH$_2$CH_2), 1.22 (12H, br m, CH_2), 0.84 (3H, t, CH_3); enol form, δ: 13.17 (1H, s, O*H*), 6.72 (1H, m, HOC-C*H*=CH), 6.47 (1H, s, O=C-C*H*=COH), 6.20 (1H s, N*H*), 5.84 (1H, dd, J = 12.3, 1.6 Hz, HOC-CH=C*H*), 2.92 (3H, s, NCH_3), 2.82 (3H, s, NCH_3), 2.17 (2H, m, O=C-

© 1997 NRC Canada

Can. J. Chem. Downloaded from www.nrcresearchpress.com by 88.146.161.215 on 09/08/12
For personal use only.

CH=CH-CH_2), 1.69 (3H, s, CH_3), 1.52 (3H, s, CH_3), 1.42 (2H, br m, CH=CH-CH$_2$-CH_2), 1.22 (12H, br m, CH_2), 0.84 (3H, t, J = 7.0 Hz, CH_3); ^{13}C NMR ($CDCl_3$, 50 MHz) δ: 193.23, 172.67, 171.29, 170.01, 167.76, 165.84, 157.34, 152.70, 151.19, 150.60, 149.30, 129.36, 125.01, 121.70, 120.81, 90.90, 78.69, 78.52, 76.70, 76.35, 48.93, 32.57, 32.45, 32.18, 31.78, 29.39, 29.30, 29.20, 28.31, 28.02, 27.84, 27.04, 26.37, 22.58, 19.97, 19.67, 19.23, 15.67, 14.02; EIMS *m/z*: 420 $[M]^+$ 378, 240, 141, 125 (base); HRMS (EI) calcd. for $C_{22}H_{36}N_4O_4$: 420.2737; found: 420.2732.

1-(3′-Hydroxy-*trans*-tetradec-4′-enoyl)-3,4,7,8-tetramethylglycoluril (12)

Oxotetradecenoyl glycoluril **11** (84 mg, 0.20 mmol) was dissolved in MeOH at 0°C. $NaBH_4$ (11.3 mg, 0.30 mmol) was added and the mixture was stirred for 10 min. Excess glacial acetic acid (0.5 mL) was added, and solvents were removed on the rotary evaporator. Flash column chromatography of the residue in EtOAc gave **17** (20 mg, 24%). ^{1}H NMR ($CDCl_3$, 200 MHz) δ: 6.04 (1H, s, N*H*), 5.70 (1H, td, J = 6.5, 15.5 Hz, HOCH-CH=C*H*), 5.47 (1H, dd, J = 15.5, 5.0 Hz, HOCH-C*H*=CH), 4.51 (1H, m, C*H*OH), 3.23 (1H, m, OCCH_aH$_b$), 3.01 (1H, m, O=CCH$_b$H$_a$), 2.98 (3H, s, NCH_3), 2.84 (3H, s, NCH_3), 1.96 (2H, m, CH=CH-CH_2), 1.70 (3H, s, CH_3), 1.54 (3H, s, CH_3), 1.23 (15H, br s, CH_2 and O*H*), 0.85 (3H, t, J = 6.7 Hz, CH_3); EIMS *m/z*: 422 $[M]^+$ 406, 348, 295, 282, 240, 206, 199, 125 (base); HRMS (EI) calcd. for $C_{22}H_{38}N_4O_4$: 422.2893; found: 422.2889.

1-(*trans*, *trans*-Tetradeca-2′,4′-dienoyl)-3,4,7,8-tetramethylglycoluril (13)

Alcohol **12** (5.5 mg, 0.013 mmol) was dissolved in CH_2Cl_2 (2 mL), and trifluoroacetic anhydride (5.5 μL, 0.039 mmol) was added. The mixture was stirred for 1 h, then Et_3N (1.8 μL, 0.026 mmol) dissolved in CH_2Cl_2 (1 mL) was added dropwise. After 10 min, an additional 0.5 mL Et_3N was added and the mixture was heated at reflux for 20 min. Evaporation followed by flash column chromatography of the residue in EtOAc afforded **13** (4.9 mg, 94%) as a white crystalline solid. ^{1}H NMR ($CDCl_3$, 200 MHz) δ: 7.40 (1H, dd, J = 15.3, 9.2 Hz, O=CCH=C*H*), 7.22 (1H, d, J = 15.2 Hz, O=C-C*H*), 6.20 (2H, m, C*H*=C*H*CH$_2$), 6.09 (1H, s, N*H*), 3.02 (3H, s, NCH_3), 2.86 (3H, s, NCH_3), 2.17 (2H, q, J = 6.6 Hz, CH=CHCH_2), 1.71 (3H, s, CH_3), 1.56 (3H, s, CH_3), 1.37 (2H, br m, CH=CHCH$_2$CH_2), 1.26 (12H, br m, CH_2), 0.87 (3H, t, J = 6.8 Hz, CH_3); ^{13}C NMR ($CDCl_3$, 125 MHz) δ: 166.22 (CH*C*=O), 157.29 (*C*=O), 153.02 (*C*=O), 145.90 (*C*=C), 145.78 (C=*C*), 128.97 (*C*=C), 119.73 (C=*C*), 78.53, 33.00, 31.81, 29.44, 29.36, 29.22, 29.10, 28.60, 27.04, 26.36, 22.59, 19.76, 16.94, 15.71, 14.02; EIMS *m/z*: 404 $[M]^+$, 277, 236, 220, 206, 199, 153, 125 (base), 94, 84, 56, 49; HRMS (EI) calcd. for $C_{22}H_{36}N_4O_3$: 404.2789; found: 404.2795.

trans, *trans*-Tetradeca-2,4-dienoic acid (16)

The tetradecadienoyl adduct **13** (22.7 mg, 0.056 mmol) was added to a slurry of H_2O (2.1 μL, 0.11 mmol) and *t*-BuOK (38 mg, 0.33 mmol) in ether (10 mL). The mixture was stirred at room temperature overnight, then 5% HCl (1 mL) was added and the mixture was extracted with chloroform (3 × 10 mL). The combined extracts were washed with water (10 mL) and brine (10 mL), then dried over Na_2SO_4 and filtered. Concentration of the filtrate gave the title acid as a solid white powder (8.9 mg, 71%). IR (KBr pellet): 3423 (O-H str.), 2924, 2854 (C-H str.), 1686 (C=O str.), 1638 (C=C str.), 1617 (C=C str.), 1466, 1307, 1007, 698; ^{1}H NMR ($CDCl_3$, 200 MHz) δ: 7.34 (1H, m, C*H*=CH), 6.20 (2H, m, 2 C*H*=CH), 5.78 (1H, d, J = 15.22 Hz, O=CC*H*=CH), 2.18 (2H, m, CH=CHCH_2), 1.42 (2H, m, CH=CHCH$_2$-CH_2), 1.26 (12 H, m, CH_2), 0.88 (3H, t, J = 6.12 Hz, CH_3); ^{13}C NMR ($CDCl_3$, 125 MHz) δ: 171.36 (C=O), 147.49 (C=C), 146.23 (C=C), 128.22 (C=C), 117.94 (C=C), 33.05, 31.87, 29.50, 29.41, 29.28, 29.18, 28.64, 22.66, 14.07; EIMS *m/z*: 225 $[MH]^+$, 224 $[M]^+$, 216, 195, 181, 164, 153, 142, 125, 109, 97, 84, 49, 45 (base), 43; HRMS (EI) calcd. for $C_{14}H_{25}O_2$ (MH^+): 225.1856; found: 225.1864.

trans, *trans*-Tetradec-2-enoic acid 4,5-epoxide (2)

Tetradeca-2,4-dienoic acid (**16**) (100 mg, 0.45 mmol) was added to a well-stirred biphasic mixture of benzene (30 mL) and phosphate buffer (15 mL, pH 7.5, 0.5 M) containing acetone (2 mL) and 18-crown-6 (100 mg, 0.38 mmol) as the phase transfer catalyst. A freshly prepared solution of potassium peroxomonosulfate (Oxone) (0.04 M, 20 mL) with $EDTANa_2$ (4×10^{-4} M) was added dropwise over 30 min. at 6–8°C. During addition, the pH was maintained at 7.5 by addition of 0.5 N KOH. The mixture was stirred for 3 h at room temperature, then extracted with benzene (3 × 30 mL) and dried over $MgSO_4$. The combined extracts were concentrated, then purified by flash column chromatography using 30% EtOAc in hexanes as eluant. Evaporation gave a white powder (35%, 37.5 mg) mp 81–81.5°C; IR (KBr pellet): 3420 (O-H str.), 2916, 2851 (C-H str.), 1730 (C=O str.), 1696 (C=C str.), 1308, 857 (epoxide); ^{1}H NMR (CD_3OD, 200 MHz) δ: 6.62 (1H, dd, ^3J = 7.2, 15.7 Hz, O=C-CH=C*H*), 6.11 (1H, d, ^3J = 15.6 Hz, O=C-C*H*=CH), 3.21 (1H, dd, ^3J = 1.6, 7.0 Hz, CH=CH-C*H*-O), 2.90 (1H, dt, ^3J = 5.9, 2.0 Hz, CH=CH-CH-O-C*H*), 1.58 (2H, m, O-CH-CH_2), 1.44 (2H, m, O-CH-CH$_2$-CH_2), 1.29 (12 H, br s, CH$_2$), 0.89 (3H, t, ^3J = 6.7 Hz, CH_3); ^{13}C NMR ($CDCl_3$, 125 MHz) δ: 169.89 (C=O), 147.34 (C=C), 122.56 (C=C), 61.72 (C-O-C), 56.13 (C-O-C), 31.90, 31.86, 29.46, 29.33, 29.26, 25.78, 25.65, 22.65, 14.06 (CH_3); EIMS *m/z*: 241 $[MH]^+$ (v. weak), 240 $[M]^+$ (v. weak), 195, 84 (base).

Acknowledgement

This work was supported by the Natural Sciences and Engineering Research Council of Canada (NSERC).

References

1. R.E. Schwartz, G.L. Helms, E.A. Bolessa, K.E. Wilson, R.A. Giacobbe, J.S. Tkacz, G.F. Bills, J.M. Liesch, D.L. Zink, J.E. Curotto, B. Pramanik, and J.C. Onishi. Tetrahedron, **50**, 1675 (1994).
2. S. Sun and P.H.M. Harrison. Tetrahedron Lett. **33**, 7715 (1992).
3. S. Sun and P. Harrison. J. Chem. Soc. Chem. Commun. 2235 (1994).
4. D. O'Hagan. Nat. Prod. Rep. **10**, 593 (1993).
5. H. Biltz. Chem. Ber. **40**, 4806 (1907).
6. P.G. Gassman, P.K.G. Hodgson, and R.J. Balchunis. J. Am. Chem. Soc. **98**, 1275 (1976).
7. R.S. Burden and L. Crombie. J. Chem. Soc. (C), 2477 (1969).

© 1997 NRC Canada

8. M.A. Guedeau-Boudeville. C. R. Acad. Sci. Ser. II: Mec. Phys. Chim. Astron. **315**, 541 (1992).
9. R. Curci, M. Fiorentino, L. Troisi, J. Edwards, and R. Peter. J. Org. Chem. **45**, 4758 (1980).
10. W.C. Still, M. Kahn, and A. Mitra. J. Org. Chem. **43**, 2923 (1978).
11. W.R. Winkle, J.M. Lansinger, and R.C. Ronald. J. Chem. Soc. Chem. Commun. 124 (1979).

Can. J. Chem. Downloaded from www.nrcresearchpress.com by 88.146.161.215 on 09/08/12
For personal use only.

© 1997 NRC Canada

NMR kinetic study of ligand exchange on a (μ-oxo)bis(μ-acetato)diruthenium(III) complex. A special kinetic case of introduction of a more labile ligand

Joana Mara Santos, Cecília Cipriano, Roberto B. Faria, and J. Daniel Figueroa-Villar

Can. J. Chem. Downloaded from www.nrcresearchpress.com by 88.146.161.215 on 09/08/12
For personal use only.

Abstract: We have prepared the new $[Ru_2(\mu\text{-}O)(\mu\text{-}O_2CCH_3)_2(4\text{-pic})_6](PF_6)_2$ complex and followed the kinetics of exchange of the 4-picoline ligands, *trans* to the oxo bridge, with dimethyl sulfoxide (DMSO-d_6) by ^{1}H NMR at 30, 40, 50, and 60°C. The ^{1}H NMR spectra of this complex in DMSO gradually change in the acetyl methyl region as solvent substitution of the 4-picoline *trans* to the oxo bridge takes place. This substitution is in accordance with the lability of the ligands *trans* to the Ru^{III}-O-Ru^{III} bridge in this kind of complex. The kinetic data fit in a series of double reversible reactions, pseudo first order in the forward direction and second order in the reverse direction, with $\Delta H^{\ddagger}$ = 115, 105, 116, and 106 kJ mol^{-1} and $\Delta S^{\ddagger}$ = 35.7, 17.2, 38.8, and 16.9 J K^{-1} mol^{-1} associated with k_1, k_{-1}, k_2, and k_{-2} rate constants, respectively.

$$\mathbf{A} \underset{k_{-1}}{\overset{k_1}{\rightleftarrows}} \mathbf{B} + \text{4-pic} \qquad \mathbf{B} \underset{k_{-1}}{\overset{k_2}{\rightleftarrows}} \mathbf{C} + \text{4-pic}$$

A, **B** and **C** stand for the nonexchanged, monoexchanged, and diexchanged complexes, respectively. The large $\Delta H^{\ddagger}$ and positive $\Delta S^{\ddagger}$ values agree with the dissociative nature of the mechanism in both forward and reverse reactions. The differences in ^{1}H and ^{13}C NMR chemical shifts of the three complexes are explained in terms of the effect of the ligand exchange on the N—Ru bond lengths and the geometry of the dimetal core. It is evident from our data that the exchange on one metallic site modifies the reactivity at the other site in this kind of dinuclear complex.

Key words: diruthenium complex, variable temperature NMR, ligand exchange kinetics.

Résumé : On a préparé le nouveau complexe $[Ru_2(\mu\text{-}O)(\mu\text{-}O_2CCH_3)_2(4\text{-pic})_6](PF_6)_2$ et on a suivi la cinétique de l'échange des coordinats 4-picoline, *trans* par rapport au pont oxo, avec le diméthylsulfoxyde (DMSO-d_6) par RMN du ^{1}H à 30, 40, 50 et 60°C. Au fur et à mesure que le solvant remplace la 4-picoline *trans* par rapport au pont oxo, le spectre de RMN du ^{1}H de ce complexe dans le DMSO se modifie graduellement dans la région du méthyle de l'acétyle. Cette substitution se fait à cause de la labilité des coordinats *trans* par rapport au pont Ru(III)-O-Ru(III) dans ce genre de complexe. Les données cinétiques s'accordent bien avec une série de doubles réactions réversibles, de pseudo-premier ordre pour la réaction vers l'avant et du deuxième ordre pour la direction inverse, avec $\Delta H^{\ddagger}$ = 115, 105, 116 et 106 kJ mol^{-1} et $\Delta S^{\ddagger}$ = 35,7, 17,2, 38,8, et 16,9 J K^{-1} mol^{-1} associés respectivement avec les constantes de vitesse k_1, k_{-1}, k_2, k_{-2}.

$$\mathbf{A} \underset{k_{-1}}{\overset{k_1}{\rightleftarrows}} \mathbf{B} + \text{4-pic} \qquad \mathbf{B} \underset{k_{-1}}{\overset{k_2}{\rightleftarrows}} \mathbf{C} + \text{4-pic}$$

A, **B** et **C** représentent respectivement les complexes non échangés, monoéchangés et diéchangés. Les valeurs élevées du $\Delta H^{\ddagger}$ et positives $\Delta S^{\ddagger}$ sont en accord avec la nature dissociative du mécanisme tant dans les réactions vers l'avant qu'à l'inverse. Les différences de déplacements chimiques dans les spectres RMN du ^{1}H et du ^{13}C des trois complexes peuvent être expliquées en

Received November 4, 1996.

This paper is dedicated to Professor William A. Ayer on the occasion of his 65th birthday.

J.M. Santos,[1] C. Cipriano,[2] R.B. Faria,[2] and J.D. Figueroa-Villar.[3] *Instituto Militar de Engenharia, Praça General Tibúrcio, 80, CEP 22290-270, Rio de Janeiro, RJ, Brazil, and Instituto de Química, Universidade Federal do Rio de Janeiro, caixa postal 68563, CEP 21945-970, Rio de Janeiro, RJ, Brazil.*

[1] Escola Técnica Federal de Química-RJ. Telephone: (55-021) 5691771. Fax: (55-021) 5698690.
[2] Universidade Federal do Rio de Janeiro. Fax: (55-021) 2904746. E-mail: rfaria@iq.ufrj.br
[3] Author to whom correspondence may be addressed at the Instituto Militar de Engenharia. Fax: (55-021) 2759047. E-mail: figueroa@aquarius.ime.eb.br

© 1997 NRC Canada

fonction de l'effet d'échange du coordinat sur les longueurs des liaisons N—Ru et sur la géométrie du coeur dimétallique. Il est évident sur la base des données obtenues que, dans ce type de complexe dinucléaire, l'échange d'un site métallique modifie la réactivité de l'autre site.

Mots clés : complexe de diruthénium, RMN à température variable, cinétique de l'échange de coordinat.

[Traduit par la rédaction]

Can. J. Chem. Downloaded from www.nrcresearchpress.com by 88.146.161.215 on 09/08/12
For personal use only.

Introduction

The recent discovery of a tribridged (μ-oxo)bis(μ-carboxylato)diiron core as the active site of non-heme iron enzymes, such as methane monooxygenase (MMO) (1), has brought new perspectives to the study and preparation of several interesting artificial low molecular weight transition-metal dinuclear complexes, principally of iron and ruthenium. In spite of the promising results obtained with (μ-oxo)bis(μ-carboxylato)diruthenium complexes, for example, the conversion of cyclohexane into cyclohexanol (2), the solution chemistry of these complexes has rarely been studied as a model for homogeneous catalytic processes. Furthermore, since the chemistry of the terminal ligands is important in understanding the catalytic role of these dinuclear complexes (3), the preparation and study of model ruthenium complexes with exchangeable ligands at terminal positions should contribute to a better understanding of the mechanism of action of these catalysts.

Wilkinson and co-workers were the first to propose ruthenium complexes of the type $Ru_2O(O_2CR)_4(PPh_3)_2$ (4). In recent years, it has been shown that this core can also be stabilized by the presence of other facial ligands, such as pyridine (5), tridentate triazacyclononane (6), tris(1-pyrazolyl)methane (7), (2-pyridylethyl)(2-pyridylmethyl)methylamine (8), or even by two or three different terminal ligands (9, 10). Sasaki et al. have shown that the pyridine ligands *trans* to the oxygen bridge in the $[Ru_2(\mu\text{-}O)(\mu\text{-}O_2CCH_3)_2(py)_6]^{2+}$ complex are exchanged by deuterated pyridine (5).

We have prepared a new $[Ru_2(\mu\text{-}O)(\mu\text{-}O_2CCH_3)_2(4\text{-pic})_6]^{2+}$ complex as its PF_6^- salt in order to study its chemistry in solution, and especially the exchange reaction of the 4-picoline ligands *trans* to the oxygen bridge with dimethyl sulfoxide (DMSO). We present herein a complete kinetic study derived from NMR spectroscopy of the complexes to elucidate the mechanism of this exchange reaction.

Our results also show that the ligands *trans* to the Ru^{III}-O-Ru^{III} bridge are preferentially labile, and their exchange is composed of two reversible reactions.

We have for the first time been able to determine the rate constants and activation parameters for ligand exchange on a (μ-oxo)bis(μ-carboxylato)dimetal complex by NMR spectroscopy. To the best of our knowledge, this is the first time that all the activation parameters for all of the steps in a series of double reversible reactions have been determined for a ligand substitution process on a transition metal complex.

A complete ^1H and ^{13}C NMR assignment for the three complexes involved in the exchange process is presented and these data are used to speculate on the structural modifications of the complexes throughout the reactions.

Experimental section

General

Acetonitrile was distilled over P_2O_5, 4-picoline was distilled over KOH. Double-distilled acetone and ether were used throughout all the work. All other reagents and solvents used were reagent grade quality and used as supplied. The instruments used in the characterization of the complex were a Perkin–Elmer 2400 elementary analysis apparatus, a HP 8452A ultraviolet–visible spectrophotometer, and a Varian Unity-300 NMR spectrometer. All NMR chemical shifts were measured using TMS as internal reference and DMSO-d_6 99.9 at.% D (Aldrich) as solvent.

Preparation of the complex

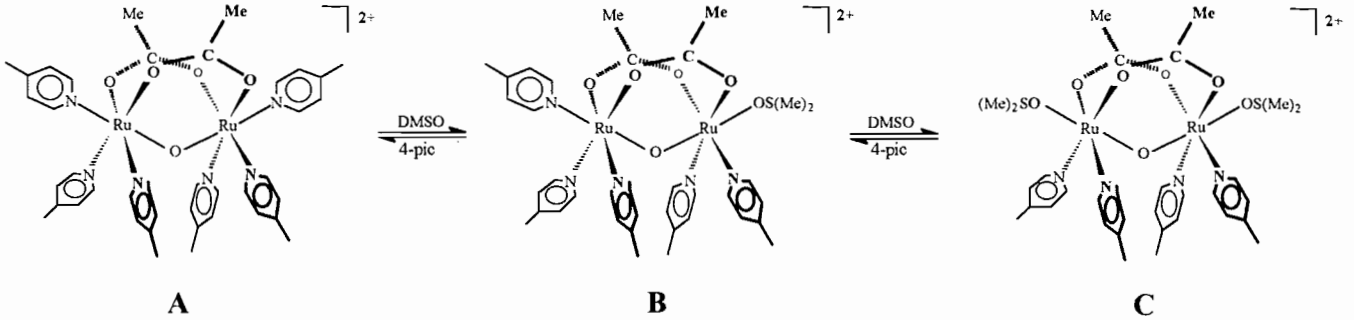
The $Ru_2(\mu\text{-}O)(\mu\text{-}O_2CCH_3)_2(4\text{-pic})_6(PF_6)_2$ complex was prepared according to the procedure described by Sasaki et al. (5). To a solution of $RuCl_3 \cdot nH_2O$ (0.5 g) in acetic acid (40 mL) – water (60 mL) – ethanol (20 mL), preheated for 10 min at 70°C, was added the ligand 4-picoline (3.5 mL). The mixture was refluxed for 1 h at 90°C. The crude product was dissolved in acetonitrile and filtered through an acidic alumina column. After addition of a few drops of 4-picoline, the filtrate was kept at 80°C for 15 min and the solvent removed under reduced pressure. The complex was recrystallized from acetone, by diffusion of gaseous ether, to produce blue crystals of the pure product in 65% overall yield. UV–VIS (CH_3CN) λ_{max}/nm (log ε): 210 (4.6), 242 (4.4), 288 (4.2), 322 (4.3) and 582 (4.0). ^1H NMR (300 MHz, CD_3CN) δ: 1.48 (s, 6H, CH_3 acetate), 2.44 (s, 12H, CH_3 4-pic *cis* to μ-O), 2.85 (s, 6H, CH_3 4-pic *trans* to μ-O), 7.02 (d, 8H, H-3 and H-5 4-pic *cis* to μ-O), 7.35 (d, 8H, H-2 and H-6 4-pic *cis* to μ-O), 8.04 (d, 4H, H-3 and H-5 4-pic *trans* to μ-O), 9.17 (d, 4H, H-2 and H-6 4-pic *trans* to μ-O). ^{13}C NMR (75 MHz, CD_3CN) δ: 18.5 (CH_3 4-pic *cis* to μ-O), 19.2 (CH_3 4-pic *trans* to μ-O), 21.4 (CH_3 acetate), 124.0 (C-3 and C-5 4-pic *cis* to μ-O), 126.6 (C-3 and C-5 4-pic *trans* to μ-O), 151.1 (C-4 4-pic *cis* to μ-O), 151.4 (C-2 and C-6 4-pic *cis* to μ-O), 153.4 (C-4 4-pic *trans* to μ-O), 155.5 (C-2 and C-6 4-pic *trans* to μ-O), 194.0 (CO_2 acetate). Anal. calcd. for $[C_{40}H_{48}N_6O_5Ru_2P_2F_{12}]$: C 40.55, H 4.08, N 7.09%; found: C 40.42, H 4.06, N 6.89%.

NMR kinetic study of the 4-picoline–DMSO exchange reaction

All the ^1H NMR spectra were obtained using 20 mg samples of the complex dissolved in 0.50 mL of 99.9% DMSO-d_6 in 5 mm NMR tubes. The spectra were recorded using a spectral width of 5000 Hz (transmitter offset 500) and 16 transients of 37 440 data points. A series of spectra was recorded at 30, 40,

© 1997 NRC Canada

Scheme 1.



50, and 60°C, with temperature control of ± 0.1°C for different samples. For the experiments carried out at 30°C, the samples were kept in a temperature-controlled oven between measurements. For the other higher temperatures, the samples were kept inside the spectrometer and the interval between measurements was controlled using its preacquisition delay, which was fixed as 120, 30, and 10 min for 40, 50, and 60°C, respectively. The course of the reaction was followed by measuring the integrated area of the singlets at δ 1.55, 1.59, and 1.62, which correspond to the acetate methyl signals of the nonexchanged (**A**), the monoexchanged (**B**), and the diexchanged (**C**) complexes, respectively. The integration interval (in ppm) for each signal was rigorously kept the same for all experiments at a given temperature.

Kinetic modeling

The concentration of each species is defined as [X] which is equal to $[\mathbf{A}]_{total} \cdot I_X/(I_A + I_B + I_C)$, where X = **A**, **B**, or **C**, $[\mathbf{A}]_{total}$ is the summed concentration of the complexes, and I_X is the integrated intensity of the methyl groups of the acetate bridges of the complex under consideration. The concentration vs time curves obtained experimentally were compared with the curves simulated using numerical integration according to the reaction scheme proposed in eqs. [1] and [2] (see ahead). The differential equation system corresponding to the chemical equations was solved by the Euler–Cauchy method using a spreadsheet (11). The integration step was selected by reducing its size until the results did not change with further decrease of the integration step. The numerical integration results for some experiments were checked using Lengyel's Turbo Pascal program, which solves autonomous ordinary differential equation systems using a semi-implicit Runge-Kutta method (12). Exactly the same results were obtained with both methods.

Results and discussion

Syntheses

The complex $Ru_2(\mu\text{-}O)(\mu\text{-}O_2CCH_3)_2(4\text{-pic})_6(PF_6)_2$ was obtained in high yield from $RuCl_3 \cdot nH_2O$ using the procedure described by Sasaki et al. (5). The $Ru_2(\mu\text{-}O)(\mu\text{-}O_2CCH_3)_2$ core is the most likely precursor of the isolated dinuclear complex. Purification by column chromatography followed by recrystallization from acetone afforded a crystalline complex, which was fully characterized by spectroscopic methods. The evidence for a binuclear ruthenium complex containing a (μ-oxo)bis(μ-carboxilato)diruthenium(III) core was the strong absorption at 582 nm in the electronic spectra obtained in acetonitrile. This absorption is attributed to a charge-transfer band involving the Ru^{III}-$d\pi$ and μ-oxo-$p\pi$ orbitals, which is characteristic of this kind of compound (7). The structure of the complex was confirmed by ^{1}H NMR in deuterated acetonitrile. The two 4-picoline ligands *trans* to the Ru-O-Ru bridge appear at different chemical shifts from those of the other four facial ligands.

Exchange of the 4-picolines with DMSO-d_6

The ^{1}H NMR spectrum of the complex at 20°C in DMSO-d_6 shows a well-resolved singlet at δ 1.55, which integrates for six hydrogens corresponding to the two methyl groups of the acetate bridges. The intensity of this singlet at δ 1.55 decreases with time, as the sample is heated, giving rise first to one singlet at δ 1.59 and then to another singlet at δ 1.62 (see Fig. 1). The appearance of these signals at δ 1.59 and δ 1.62 is attributed to the exchange of the labile *trans* 4-picoline ligands with DMSO-d_6. The lability of N-heterocyclic bonded ligands *trans* to the oxygen bridge is known to occur in binuclear Ru clusters (5), and has been observed in trinuclear Ru clusters (13). The signal at δ 1.59 was assigned to the hydrogens of the two equivalent methyl groups in the acetate bridges after the exchange of only one 4-picoline ligand *trans* to the oxo bridge with DMSO-d_6. The singlet at δ 1.62 corresponds to the same methyl hydrogens after the exchange of the two labile 4-picoline ligands with DMSO-d_6.

The ligand exchange is also supported by the gradual decrease of the signals at δ 9.30, 8.22, and 2.90, which correspond to the *ortho* (H2, H6), *meta* (H3, H5), and the methyl hydrogens of the 4-picolines *trans* to the oxygen bridge, respectively. The gradual and almost complete disappearance of these signals is accompanied by a simultaneous appearance of the signals at δ 8.42, 7.21, and 2.31, corresponding to the respective hydrogens of the free 4-picoline. The integration of these signals, shown in Fig. 2, supports these assignments.

Thus, the integration of the NMR singlets at δ 1.55, 1.59, and 1.62, corresponding to the methyl groups of the acetate bridges of the nonexchanged (**A**), the monoexchanged (**B**), and the diexchanged (**C**) complexes, respectively, was used to monitor the concentration of these three species [**A**], [**B**], and [**C**] during the course of the exchange reaction at different temperatures, as illustrated in Fig. 3 for the experiment at 60°C.

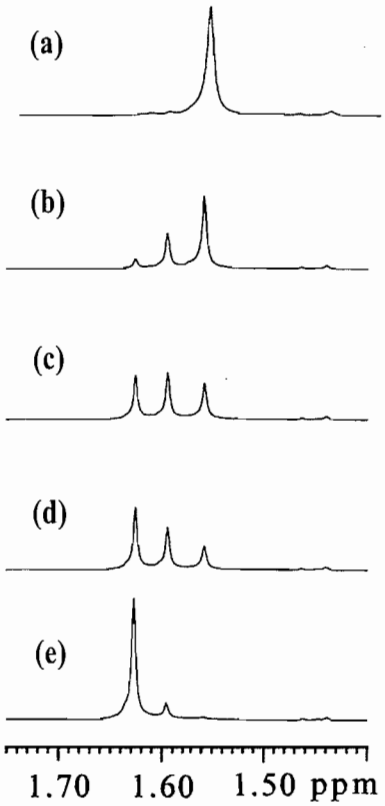
Figure 3 shows that the concentration of the nonexchanged

© 1997 NRC Canada

Can. J. Chem. Downloaded from www.nrcresearchpress.com by 88.146.161.215 on 09/08/12
For personal use only.

Can. J. Chem. Downloaded from www.nrcresearchpress.com by 88.146.161.215 on 09/08/12
For personal use only.

Fig. 1. Time dependence of the ^{1}H NMR spectrum of $Ru_2(\mu\text{-}O)(\mu\text{-}O_2CCH_3)_2(4\text{-pic})_6(PF_6)_2$ in DMSO-d_6 for the acetate methyl region: (*a*) 30 min after dissolution at 20°C, (*b*) 14 min after dissolution at 60°C, (*c*) 37 min at 60°C, (*d*) 70 min at 60°C, (*e*) 140 min at 60°C.



species (**A**) decreases as the concentration of the diexchanged species (**C**) increases until it reaches equilibrium. The concentration of the monoexchanged species (**B**) shows a different behavior. It initially increases to a maximum, and then decreases gradually to a final equilibrium concentration. The same trend is found when the exchange reaction is carried out at 30, 40, and 50°C.

We took advantage of this information to conduct the spectroscopic characterization of the three complexes. The same sample was utilized to obtain the ^{1}H and ^{13}C NMR spectra of the three complexes and the conversion of one species into another was accomplished by temperature manipulation of this sample. Thus, the characterization of the nonexchanged species (**A**) was possible by recording the spectra of a freshly prepared sample of the complex at 20°C. At this temperature no significant exchange is detected by NMR within 3 h, and the recorded NMR spectra could unequivocally be assigned to complex **A**. The sample was then heated to 60°C for 30 min in order to achieve a maximum concentration of the monoexchanged species (**B**). The NMR spectra, recorded after cooling the sample to 20°C, show the presence of all three complexes (**A**, **B**, and **C**) in approximately the same concentration. The assignment of the resonances due to complex **B** was done by subtracting the signals due to complex **A** and complex **C** from the spectra. The spectra corresponding to complex **C** were recorded using the sample treated at 60°C for 3 h and then cooled to 20°C. The recorded ^{1}H and ^{13}C NMR spectra show the presence of complex **C** as the major compound, complex **B** as the minor compound, and traces of complex **A**. The signals due to complexes **A** and **B** did not interfere in the analysis of the spectra, which provided an unambiguous assignment of complex **C**. Table 1 summarizes these assignments. The resonance of the bonded DMSO-d_6 is observed at δ 37.42 in the ^{13}C NMR spectra of **C** (the chemical shift of the central line of free DMSO-d_6 is δ 39.45), which represents additional evidence for the participation of DMSO-d_6 in the exchange reaction.

The data shown in Table 1 along with X-ray diffraction data of a similar diruthenium complex (5), $[Ru_2(\mu\text{-}O)(\mu\text{-}O_2CCH_3)_2(py)_6]^{2+}$, enable us to explore several interesting aspects of this exchange reaction. For example, Sasaki has shown in his study that the Ru—N bond distance *trans* to the oxygen bridge (average 2.185 Å) is larger than that of the *cis* Ru—N bond (average 2.087 Å). We observed that the chemical shifts of all the atoms of the *trans* ligands in complex **A** are deshielded when compared with the atoms of the *cis* ligands. Clearly, when the Ru—N bond is shorter the chemical shifts are smaller. This may be partly due to an increase in electronic density as a consequence of the shortening of the Ru—N bond. On the other hand, analysis of the data in Table 1 indicates that the exchange of the *trans* 4-picoline with DMSO decreases the chemical shifts of C2, C6, and C4 of the *cis* 4-picolines located at the same face of the complex where the exchange took place. Since the atoms affected are the ones in the *ortho* and *para* positions of the 4-picoline, this effect must be due to a change in the electronic density at the nitrogen atom. Possibly the exchange of one 4-picoline for DMSO decreases the steric hindrance between the ligands, allowing the vicinal 4-picolines to bond more tightly to the ruthenium atom. It is even more important to observe that the chemical shifts of the 4-picoline *trans* to the Ru-O-Ru bridge at the face opposite to where the exchange took place are affected. It has usually been accepted that the metallic centers in this kind of complex are chemically independent from one another (13*a*, 14) but from our results in Table 1 it is clear that this is not the case. In fact, the substitution of one of the *trans* 4-picolines by DMSO decreases the chemical shifts of C2, C6, and C4 of the other *trans* 4-picoline remaining in the complex. This suggests that the exchange shortens the bond between the remaining *trans* 4-picoline and ruthenium. According to this, the second forward substitution reaction should be slower than the first one. On the other hand, the chemical shifts of the *cis* 4-picoline ligands at one face of the complex are practically unaffected by the exchange of the *trans* ligand at the other face. This seems to indicate that the effects of changes at one face are transmitted to the other face through the oxygen bridge. The observation that the chemical shift of the sp^2 carbon of the acetate bridges changes from δ 194.50 in **A** to δ 190.88 in **B** and δ 187.97 in **C** may be related to changes in the geometry of the complex as the bulkier 4-picoline ligands are gradually substituted by DMSO. To a lesser extent, the same kind of effect is shown by the ^{13}C NMR of acetate bridge methyl groups.

Kinetics of the exchange reaction

The change in the concentration of the different species involved in the exchange reaction shown in Fig. 3 can be

© 1997 NRC Canada

Fig. 2. Full ^{1}H NMR spectrum at 20°C of $[Ru_2(\mu\text{-}O)(\mu\text{-}O_2CCH_3)_2(4\text{-pic})_6]^{2+}$ in DMSO-d_6: (*a*) immediately after dissolution , (*b*) after 3 h at 60°C.

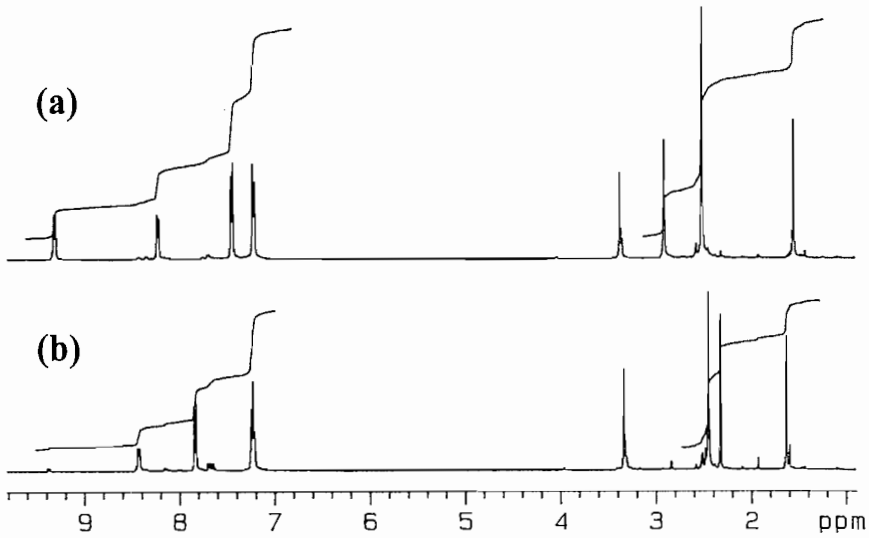


Table 1. ^{1}H and ^{13}C NMR assignments for all the complexes.

	Complex **A**		Complex **B**		Complex **C**		Free 4-picoline	
Assignment[a]	δ ^{13}C	δ ^{1}H	δ ^{13}C	δ ^{1}H	δ ^{13}C	δ ^{1}H	δ ^{13}C	δ ^{1}H
CO_2 acetate	194.50		190.88		187.97			
Me acetate	23.07	1.55	22.83	1.59	22.55	1.62		
cis 2,6	152.26	7.44	152.45	7.69	151.53	7.82	149.22	8.42
cis 3,5	125.10	7.21	125.17	7.44	125.48	7.23	124.56	7.21
cis 4	151.40		151.05		150.63		146.66	
cis Me	19.80	2.51	19.84	2.47	19.93	2.44	20.35	2.31
**cis* 2,6			151.35	7.65				
**cis* 3,5			125.44	7.44				
**cis* 4			150.90					
**cis* Me			19.87	2.45				
trans 2,6	156.62	9.30	155.09	9.38				
trans 3,5	127.77	8.22	127.76	8.15				
trans 4	153.83		153.05					
trans Me	20.57	2.90	20.67	2.82				

[a]*cis* and *trans* refer to the position of the ligand in relation to the Ru-O-Ru bridge, except for free 4-picoline. The numbers 2,6 are the *ortho* CH; 3,5 are the *meta* CH; and 4 is *para* C of the 4-picolines. An asterisk indicates 4-picoline vicinal to the exchanged DMSO-d_6 in **B**.

explained considering the kinetic schemes proposed in eqs. [1] and [2].

$$[1]\quad \mathbf{A} \underset{k_{-1}}{\overset{k_1}{\rightleftarrows}} \mathbf{B} + \mathrm{L}$$

$$[2]\quad \mathbf{B} \underset{k_{-2}}{\overset{k_2}{\rightleftarrows}} \mathbf{C} + \mathrm{L}$$

Where k_1 and k_2 are pseudo-first-order rate constants, which include the DMSO concentration, k_{-1} and k_{-2} are second-order rate constants, and L stands for the 4-picoline ligand.

Evidence for the participation of 4-picoline in the rate law comes from the non-zero areas of ^{1}H NMR signals at δ 1.55 and 1.59 at equilibrium, corresponding to non-zero equilibrium concentrations for **A** and **B**, respectively. When the experiments were carried out in the presence of an initial amount of free 4-picoline, higher equilibrium concentrations of **A** and lower equilibrium concentrations of **C** were found, and the rate of formation of these species changed. These

© 1997 NRC Canada

Can. J. Chem. Downloaded from www.nrcresearchpress.com by 88.146.161.215 on 09/08/12
For personal use only.

Can. J. Chem. Downloaded from www.nrcresearchpress.com by 88.146.161.215 on 09/08/12
For personal use only.

Table 2. Rate constants and corresponding activation parameters for the substitution of the 4-picoline *trans* to the oxo bridge by deuterated dimethyl sulfoxide (DMSO-d_6) in $Ru_2(\mu\text{-}O)(\mu\text{-}O_2CCH_3)_2(4\text{-pic})_6(PF_6)_2$.

Temperature (°C)	k_1 (s^{-1})	k_{-1} (s^{-1} mol^{-1} L)	k_2 (s^{-1})	k_{-2} (s^{-1} mol^{-1} L)	K_1[b]	K_2[b]
30.0	7.50×10^{-6}	4.17×10^{-5}	6.67×10^{-6}	2.92×10^{-5}	0.180	0.228
40.0	3.55×10^{-5}	1.75×10^{-4}	2.92×10^{-5}	1.28×10^{-4}	0.203	0.228
50.0	1.33×10^{-4}	6.33×10^{-4}	1.13×10^{-4}	4.33×10^{-4}	0.210	0.261
60.0	5.08×10^{-4}	1.92×10^{-3}	4.73×10^{-4}	1.42×10^{-3}	0.265	0.333
25.0[a]	3.52×10^{-6}	2.11×10^{-5}	2.97×10^{-6}	1.48×10^{-5}	0.17	0.20
$\Delta H^{\ddagger}$ (kJ mol^{-1})	115 ± 1.3	105 ± 2.1	116 ± 2.1	106 ± 2.0		
$\Delta S^{\ddagger}$ (J mol^{-1} K^{-1})	35.7 ± 4.1	17.2 ± 6.7	38.8 ± 6.6	16,9 ± 6.2		

[a]Rate constants at 25°C calculated from Arrhenius plots.
[b]$K_1 = k_1/k_{-1}$ and $K_2 = k_2/k_{-2}$.

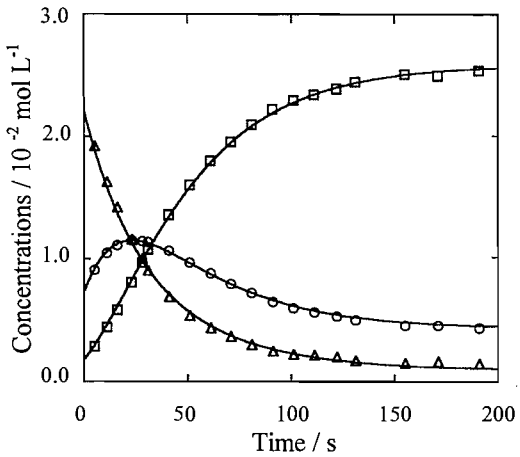
results indicate that the concentration of free 4-picoline affects the rate of formation of **B** and **C** and, consequently, the equilibrium concentration of **A**, **B**, and **C**. This result was the driving force to include the concentration of free 4-picoline in the mechanistic consideration for the reverse reactions. Attempts to use other kinetic mechanistic schemes, for example, a series of two reversible first-order reactions, did not provide good agreement with the experimental data. When only first-order reactions were considered, it was not possible to explain the dependence on the concentration of free 4-picoline in the equilibrium. Moreover, it is clear that as the 4-picoline ligand is exchanged with DMSO the concentration of free 4-picoline increases and it slows the whole process by accelerating the reverse reactions.

Equations [1] and [2] were used as a model to find the rate constant combinations that provide the best fit to the experimental data obtained for the exchange reaction at all four different temperatures. The results are listed in Table 2 and Fig. 3, which present one typical fit of the model given by eqs. [1] and [2] to the experimental data at 60°C. In Fig. 3 we see very good agreement between the calculated (solid line) and the experimental (symbols) data. Similar agreement is observed when the data at 30, 40, and 50°C are considered.

The Arrhenius plots of the rate constants obtained are shown in Fig. 4, and a very good linear behavior is indicated by their correlation coefficients, R^2, which are equal to or greater than 0.9992.

The data shown in Table 2 enable us to explore other interesting aspects of this chemistry. First, even though k_1 and k_2 are very similar, k_1 is consistently larger than k_2, indicating that the substitution of one *trans* 4-picoline by DMSO slightly hinders the substitution of the other one. This is in agreement with the proposed shortening of the N—Ru bond for the *trans* 4-picoline in complex **B**, suggested by the X-ray data and by our NMR results discussed earlier. In perfect accord with these results is the observation that k_{-1} is always larger than k_{-2}, showing that the substitution of one DMSO for 4-picoline in **C** increases the lability of the DMSO ligand left in the complex. This implies that there is a significant difference between the *trans* effect of 4-picoline and DMSO that is transmitted through the Ru^{III}-O-Ru^{III} bridge. In other words, the exchange

Fig. 3. Experimental (symbols) and calculated (solid lines) concentration vs. time dependence of the complexes formed in the reaction between $Ru_2(\mu O)(\mu\text{-}O_2CCH_3)_2(4\text{-pic})_6(PF_6)_2$ and DMSO-d_6 at 60°C: (Δ) $[Ru_2(\mu\text{-}O)(\mu\text{-}O_2CCH_3)_2(4\text{-pic})_6]^{2+}$, **A**; (○) $[Ru_2(\mu\text{-}O)(\mu\text{-}O_2CCH_3)_2(DMSO\text{-}d_6)(4\text{-pic})_5]^{2+}$, **B**; (□) $[Ru_2(\mu\text{-}O)(\mu\text{-}O_2CCH_3)_2(DMSO\text{-}d_6)_2(4\text{-pic})_4]^{2+}$, **C**.



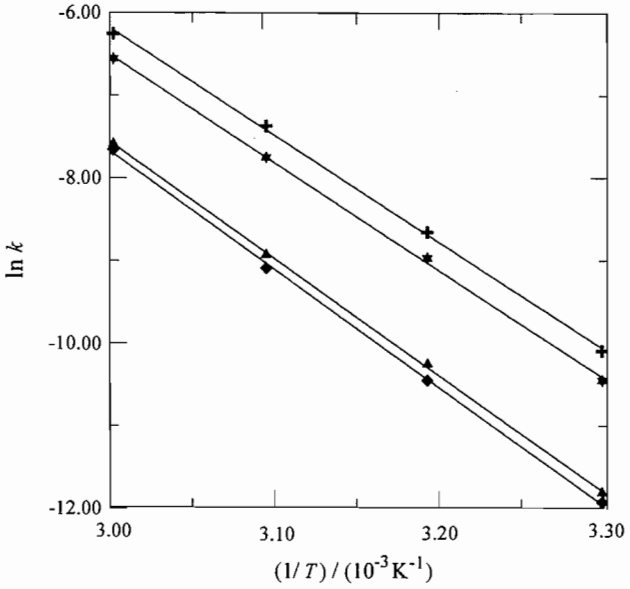
of one *trans*-4-picoline for DMSO in **A** makes more difficult the exchange of the other *trans*-4-picoline, because the *trans* effect of the DMSO is weaker than the 4-picoline *trans* effect, and therefore k_1 is greater than k_2. In the reverse reaction the exchange of one DMSO for 4-picoline in **C** facilitates the exchange of the remaining DMSO, because the *trans* effect of 4-picoline is stronger than the DMSO *trans* effect, and therefore k_{-2} is smaller than k_{-1}. This interpretation contradicts the existing view of independent substitution at each site of trinuclear complexes such as Ru, Mo, and W (13*a*, 14).

Second, it is interesting to note that the forward first-order rate constants k_1 and k_2 are lower than the reverse second-order rate constants k_{-1} and k_{-2}, which makes the equilibrium constant K smaller than unity. This is consistent with the expected lower affinity of DMSO for ruthenium as compared with that of 4-picoline, which is due to the stronger basic char-

© 1997 NRC Canada

Can. J. Chem. Downloaded from www.nrcresearchpress.com by 88.146.161.215 on 09/08/12
For personal use only.

Fig. 4. Arrhenius plots for k_1 (▲), k_{-1} (+), k_2 (◆), and k_{-2} (★) (see eqs. [1] and [2] for model).



acter of nitrogen in relation to oxygen. It has been shown that DMSO binds through its oxygen in some mono- and trinuclear Ru(III) complexes (15).

Another statistical approach to be considered for the analysis of these data is the *per metal ion* rate constants, k_1^M and k_{-2}^M values which are half of the respective k_1 and k_{-2}, values listed in Table 2. When k_1^M values are calculated from the k_1 values listed in Table 1 at all temperatures, we obtain k_1^M values lower than the k_2 values. Contrary to what was postulated using the NMR results, the lower k_1^M values calculated suggest that the DMSO ligand exerts a stronger *trans* effect than the 4-picoline ligand in the forward reaction. Also, a comparison of the k_{-2}^M and k_{-1} values leads to a weaker *trans* effect for the reverse reaction. This implies that either the *trans* effect through the Ru^{III}-O-Ru^{III} bridge is not statistically significant or that this kind of statistical treatment does not apply in this case. The same kind of result was found in a kinetic study on diplatinum(III) complexes (16).

In spite of the possibility of having no significance in this case, the k^M values were used to compare the rate of ligand exchange found for these 4-picoline complexes (**A** and **B**) with rates for other ruthenium complexes (Table 3). We observe that the values are lower for the former (entries 4 and 5). This is expected because of the more labile interaction of DMSO with ruthenium compared to that of 4-picoline. The high k_1^M values observed for the exchange of water with isonicotinamide in trinuclear ruthenium complexes (entries 8 and 9) support this observation.

The rate constant k_1 that we obtained at 50°C is 1.33×10^{-4} s^{-1}, which is almost the same value found by Sasaki et al. for the pyridine exchange reaction in the complex $[Ru_2(\mu\text{-}O)(\mu\text{-}O_2CCH_3)_2(py)_6]^{2+}$ ($k = 2.2 \times 10^{-4}$ s^{-1}) (5). Since the two exchange reactions mentioned involve very different entering ligands, the similarity between these two complexes indicates that the rate constant k_1 is probably independent of the nature of the ligand entering the coordination sphere of the metal. In

Table 3. Rate constants and activation parameters for some selected ligand exchange reactions on ruthenium complexes at 25°C.

Entry	Complex	System	$k^{M\,a}$ (s^{-1})(25°C)	$\Delta H^{\ddagger}$ (kJ mol^{-1})	$\Delta S^{\ddagger}$ (J mol^{-1} K^{-1})	Reference
1	$[Ru(H_2O)_6]^{3+}$	H_2O-exchange	3.5×10^{-6}	89.8 ± 4	–48.3 ± 14	17
2	$[Ru(H_2O)_5(OH)]^{2+}$	H_2O-exchange	5.9×10^{-4}	95.8 ± 7.9	14.9 ± 24.4	17
3	$[Ru(NH_3)_5(H_2O)]^{2+}$	H_2O-exchange	2.3×10^{-4}	91.5 ± 7.9	–7.7 ± 4.4	18
4	$[Ru_2(\mu\text{-}O)(\mu\text{-}O_2CCH_3)_2(4\text{-pic})_6]^{2+}$	4-pic → DMSO-d_6	1.8×10^{-6}	115 ± 1.3	29.9 ± 4.1	This work
5	$[Ru_2(\mu\text{-}O)(\mu\text{-}O_2CCH_3)_2(4\text{-pic})_5(DMSO\text{-}d_6)]^{2+}$	4-pic → DMSO-d_6	3.0×10^{-6}	116 ± 2.1	16.9 ± 6.2	This work
6	$[Ru_3(\mu_3\text{-}O)(\mu\text{-}O_2CCH_3)_6(H_2O)_3]^{+}$	$H_2O \rightarrow CD_3OD$	7.7×10^{-4}	103 ± 6	41 ± 12	13*a*
7	$[Ru_2Rh(\mu_3\text{-}O)(\mu\text{-}O_2CCH_3)_6(H_2O)_3]^{+}$	$H_2O \rightarrow CD_3OD$	9.9×10^{-5}	109 ± 4	44 ± 9	13*a*
8	$[Ru_3(\mu_3\text{-}O)(\mu\text{-}O_2CCH_3)_6(H_2O)_3]^{+}$	$H_2O \rightarrow$ isonicotinamide	5.5×10^{-4}	116.9 ± 11.4	85.1 ± 36.6	13*b*
9	$[Ru_3(\mu_3\text{-}O)(\mu\text{-}O_2CCH_3)_6(H_2O)(OH_2)]^{-}$	$H_2O \rightarrow$ isonicotinamide	9.6×10^{-5}	101.2 ± 7.8	17.8 ± 24.6	13*b*

[a] k^M = rate constants per metal ion. Those not available at 25°C were calculated by using reported data.

© 1997 NRC Canada

Can. J. Chem. Downloaded from www.nrcresearchpress.com by 88.146.161.215 on 09/08/12
For personal use only.

this case the ligand substitution mechanism must be of the dissociative type. Another similarity of our results with Sasaki's pyridine exchange reaction is the absence of *cis*-oxo bridge ligand substitution, as we concluded from our NMR data for the temperature range of 30–60°C (5).

The activation parameters (Table 2) were calculated from the rate constants using transition state theory and 45°C as the average temperature (19). From Table 1 we see that the $\Delta H^{\ddagger}$ values associated with k_1 and k_2 are greater than those associated with k_{-1} and k_{-2}. This is in agreement with the expected stronger bond between Ru and N than between Ru and O, based on the greater basicity of 4-picoline compared to DMSO. The positive $\Delta S^{\ddagger}$ values associated with k_1 are similar to those associated with k_2. The values of $\Delta S^{\ddagger}$ associated with k_{-1} and k_{-2} are also positive and about half the values for the forward reactions. It is generally accepted that positive $\Delta S^{\ddagger}$ and large $\Delta H^{\ddagger}$ values indicate that the ligand substitution is dominated by a dissociative process (20). This, together with the similarity of the rate constants k_1 at 50°C found in our experiments and reported by Sasaki for the pyridine complex (which suggest that the mechanism of exchange is not dependent on the nature of the entering ligand), led us to consider, for the present study, the dissociative mechanism shown below.

$$[3]\quad \mathbf{A} \underset{k_{-a}}{\overset{k_a}{\rightleftarrows}} I_1 + L$$

$$[4]\quad I_1 + S \underset{k_{-b}}{\overset{k_b}{\rightleftarrows}} \mathbf{B}$$

$$[5]\quad \mathbf{B} \underset{k_{-c}}{\overset{k_c}{\rightleftarrows}} I_2 + L$$

$$[6]\quad I_2 + S \underset{k_{-d}}{\overset{k_d}{\rightleftarrows}} \mathbf{C}$$

where L = 4-picoline, S = DMSO-d_6, I_1 is the intermediate lacking one ligand, i.e., with one Ru atom pentacoordinate, and I_2 is another intermediate containing one DMSO-d_6 ligand *trans* to the oxygen bridge bonded to one hexacoordinate ruthenium and with the other ruthenium pentacoordinate.

In this mechanism I_1 and I_2 are reactive intermediates. The second-order nature of the reverse reactions can be explained based on the competition between I_1 (or I_2 for the solvent (DMSO-d_6)) and 4-picoline. As the 4-picoline concentration increases during the reaction, more intermediates are able to react with it and show second-order behavior (first order on 4-picoline).

Although no experiments were carried out with different DMSO concentrations to verify whether they affect the velocity of the forward reaction, it is reasonable to suppose that forward reactions are pseudo first order with [DMSO] included in the rate constants k_1 and k_2. Dividing k_1 and k_2 by [DMSO-d_6] will render two new second-order rate constants k_1' and k_2' with $\Delta S^{\ddagger}$ = 13.7 ± 4.2 and 16.8 ± 6.7 J K^{-1} mol^{-1}, respectively. In this way, all four $\Delta S^{\ddagger}$ (for k_1', k_{-1}, k_2', and k_{-2}) become very close to each other, in agreement with the dissociative mechanism proposed in eqs. [3]–[6]. As expected, the values obtained for $\Delta H^{\ddagger}$ associated with k_1' and k_2' did not suffer any significant change compared to those related to k_1 and k_2.

The activation parameters, $\Delta H^{\ddagger}$ and $\Delta S^{\ddagger}$, associated with the k_1^{M} values are comparable to the values found in the literature (13, 17, 18). From Table 3 it can be seen that the values of $\Delta H^{\ddagger}$ for complexes **A** and **B** (entries 4 and 5) are in good agreement with those for trinuclear Ru complexes (entries 6–9). It should be noted that some of these literature values were obtained assuming different kinetic models, usually direct but not reversible reactions. The $\Delta S^{\ddagger}$ values for complexes **A** and **B** are positive, similar to those reported for the trinuclear complexes. We note that our results for $\Delta H^{\ddagger}$ and $\Delta S^{\ddagger}$ are closer to those for trinuclear than for mononuclear ruthenium complexes. This may be related to the presence of the $Ru_n(\mu\text{-}O)(\mu\text{-}O_2CCH_3)_m$ ($n > 1$) core in the di- and trinuclear complexes. In addition, some mononuclear ruthenium complexes (entries 1 and 3) react by an associative mechanism in ligand exchange reactions as determined by the authors (suggested by their negative $\Delta S^{\ddagger}$ and $\Delta V^{\ddagger}$) (17, 18). The associative mechanism is probably not possible for di- and trinuclear complexes because of steric hindrance. On the other hand, it seems that the dissociative mechanism is favored by steric hindrance and increased lability of the ligand–ruthenium bonds *trans* to the oxo bridge present in the multinuclear ruthenium complexes.

The sequence of four dissociative reversible reactions, eqs. [3] and [4] (or eqs. [5] and [6]), cannot be taken as a final proposition. Other possibilities, such as the formation of outer-sphere complexes, cannot be excluded at this time.

Conclusions

The substitution of 4-picoline by DMSO-d_6 in a $[Ru_2(\mu\text{-}O)(\mu\text{-}O_2CCH_3)_2(4\text{-pic})_6]^{2+}$ complex was followed by ^{1}H NMR at four different temperatures. The ^{1}H NMR data present clear evidence for the lability of the ligands *trans* to the Ru^{III}-O-Ru^{III} bridge when compared to the ligands at other positions.

The kinetics of exchange could also be followed by ^{13}C NMR. The ^{13}C NMR studies allowed the assignment of all carbons in the three complexes involved in the process of exchange. The effect, of the substitution of one 4-picoline by DMSO, on the chemical shifts of the *cis* ligands at the face where the reaction took place, and on the *trans* ligand at the other face, indicates that the Ru—N bonds are shortened after the exchange.

The kinetic results are better explained in terms of a complex mechanism involving a series of two reversible reactions. Pseudo-first-order reactions were considered for the forward direction and second-order reactions for the reverse.

The activation parameters ($\Delta H^{\ddagger}$ and $\Delta S^{\ddagger}$) for each of the two forward substitution steps are very similar. The large $\Delta H^{\ddagger}$ and positive $\Delta S^{\ddagger}$ values suggest a dissociative mechanism for the process in which the rate-controlling step is the breaking of the Ru—N bond.

For the reverse reactions the activation parameters again show identical and large $\Delta H^{\ddagger}$ values and identical and positive $\Delta S^{\ddagger}$ values, also suggesting a dissociative mechanism. The $\Delta H^{\ddagger}$ values for reverse reaction steps are lower than those for the forward steps and correspond to the Ru—O (oxygen from DMSO) bond breaking.

The supposition that the two forward pseudo-first-order rate

© 1997 NRC Canada

constants include the solvent concentration (DMSO) allowed us to calculate the second-order forward rate constants, which have positive $\Delta S^{\ddagger}$ values very similar to those for the second-order reverse rate constants. This supposition, which seems valid, gives additional support to the conclusion that all four steps (two forward and two reverse) are dominated by a dissociative mechanism controlled by bond-breaking steps.

Analysis of the NMR chemical shifts of the three complexes involved in the exchange process, together with the kinetic data, shows that the two metallic sites in these complexes are chemically dependent on one another.

Acknowledgments

We thank Dr. E.R. Cruz for revision of the manuscript and Dr. István Lengyel for allowing us to use his numerical integration computer program. This work was supported by the Conselho Nacional de Desenvolvimento Científico e Tecnológico — CNPq, Financiadora de Estudos e Projetos — FINEP, and Fundação José Bonifácio.

References

1. (*a*) A.L. Feig and S.J. Lippard. Chem. Rev. **94**, 759 (1994); (*b*) R.E. Stenkamp. Chem. Rev. **94**, 715 (1994); (*c*) D.M. Kurtz, Jr. Chem. Rev. **90**, 585 (1990); (*d*) L. Que, Jr. and A.E. True. Prog. Inorg. Chem. **38**, 97 (1990); (*e*) J.B. Vincent, G.L. Olivier-Lilley, and B.A. Averill. Chem. Rev. **90**, 1447 (1990).
2. G. Powell, D.T. Richens, and L. Khan. J. Chem. Res.(S), **12**, 506 (1994).
3. J. Sanders-Loehr. *In* Iron carriers and iron proteins. Vol. 5. *Edited by* T.M. Loehr. VCH, New York. 1989. pp. 373–466.
4. R.W. Mitchell, A. Spencer, and G. Wilkinson. J. Chem. Soc. Dalton Trans. 846 (1973).
5. Y. Sasaki, M. Susuki, A. Nagasawa, A. Tokiwa, M. Ebihara, T. Yamaguchi, C.Kabuto, T. Ochi, and T. Ito. Inorg. Chem. **30**, 4903 (1991).
6. P. Neubold, K. Wieghardt, B. Nuber, and J. Weiss. Inorg. Chem. **28**, 459 (1989).
7. A. Llobet, M.E. Curry, H.T. Evans, and T.J. Meyer. Inorg. Chem. **28**, 3131 (1989).
8. N. Gupta, S. Mukerjee, S. Mahapatra, M. Ray, and R. Mukherjee. Inorg. Chem. **31**, 139 (1992).
9. (*a*) M.C. Barral, and R. Jiménez-Aparicio. Polyhedron, **12**, 903 (1993); (*b*) A. Syamala and A.R. Chakravarty. Polyhedron, **13**, 3079 (1994).
10. A. Syamala and A.R. Chakravarty. Polyhedron, **12**, 273 (1993).
11. D.A. Coe. J. Chem. Educ. **64**, 496 (1987).
12. P. Kaps and P. Rentrop. Numer. Math. **33**, 55 (1979).
13. (*a*) Y. Sasaki, A.Nagasawa, A. Tokiwa-Yamamoto, and T. Ito. Inorg. Chim. Acta, **212**, 175 (1993); (*b*) G. Powell, D.T. Richens, and A.K. Powell. Inorg. Chim. Acta, **213**, 147 (1993).
14. K. Nakata, A. Nagasawa, N. Soyama, Y. Sasaki, and T. Ito. Inorg. Chem. **30**, 1575 (1991).
15. (*a*) A. Yeh, N. Scott, and H. Taube. Inorg. Chem. **21**, 2542 (1982); (*b*) H.E. Toma and A.D.P. Alexiou. Electrochim. Acta, **38**, 975 (1993).
16. R. El-Mehdawi, S.A. Bryan, and D.M. Roundhill. J. Am. Chem. Soc. **107**, 6282 (1985).
17. I. Rapaport, L. Helm, A.E. Merbach, P. Bernhard, and A. Ludi. Inorg. Chem. **27**, 873 (1988).
18. H. Doine, K. Ishihara, H.R. Krouse, and T.W. Swaddle. Inorg. Chem. **26**, 3240 (1987).
19. (*a*) K.A. Connors. Chemical kinetics: the study of reaction rates in solutions. VCH, New York. 1990. pp. 200–216; (*b*) R. Schmid and V.N. Sapunov. Non-formal kinetics: in search for chemical reaction pathways. Verlag Chemie, Weinheim; Deerfield Beach, Florida; Basel, 1982. pp. 107–118.
20. (*a*) F.A. Cotton and G. Wilkinson. Advanced inorganic chemistry. 5th ed. Wiley, New York. 1988. pp. 1283–1334; (*b*) B.E. Douglas, D.H. McDaniel, and J.J. Alexander. Concepts and models of inorganic chemistry. 3rd ed. Wiley, New York. 1994. pp. 490–492; (*c*) R.H.Crabtree. The organometallic chemistry of the transition metals. Wiley, New York. 1988. pp. 74–77.

Can. J. Chem. Downloaded from www.nrcresearchpress.com by 88.146.161.215 on 09/08/12
For personal use only.

© 1997 NRC Canada

Activated cyclooctenones are effective dienophiles[1]

Hsing-Jang Liu, Dan-Xiong Wang, Jeung Bea Kim, Eric N.C. Browne, and Yu Wang

Abstract: The first Diels–Alder addition of a diene to a cyclooctenone dienophile has been observed. Three activated cyclooctenone dienophiles **1**, **2**, and **3** are studied with a variety of simple and functionalized dienes. Diels–Alder adducts are produced in excellent yields under very mild Lewis acid catalyzed conditions. The usual orientation rules are followed and, as predicted, the products are formed for the most part exclusively by ester-*endo* addition. The stereoselectivity is influenced by the substitution pattern of the diene in some cases. The factors influencing the stereochemical selectivity of the addition are discussed in some detail.

Key words: 2-carbalkoxy-2-cyclooctenones, Diels–Alder reaction, six–eight fused ring system.

Résumé : On a observé la première addition de Diels–Alder d'un diène sur une cycloocténone comme diénophile. On a étudié trois diénophiles, des cycloocténones activées **1**, **2** et **3**, avec divers dienes simples et fonctionalisées. On a obtenu les adduits de Diels–Alder avec d'excellents rendements dans des conditions très douces avec des catalyseurs de Lewis. On a suivi les règles usuelles d'orientation et comme prévu, les produits obtenus sont presqu'exclusivement les résultats d'une addition *endo* d'esters. La stéréosélectivité, dans quelques cas, est influencée par le schéma de distribution des dienes. On discute des facteurs qui influencent la sélectivité stéréochimique de l'addition.

Mots clés : 2-carbalkoxy-2-cycloocténones, réaction de Diels–Alder, système à six–huit noyaux condensés.

[Traduit par la rédaction]

Introduction

Our group has continued to expand on our long-standing program of investigation into the Diels–Alder chemistry of cycloalkenone dienophiles.[5] Encouraged by recent successes in applying our discoveries of methodology in this field to the synthesis of structurally challenging and important natural products such as (+)-qinghaoshu (2), (−)-qinghaoshu IV (3), and two diterpenoids of the *cis*-clerodane family (4), we have turned our attention to the more challenging larger ring cycloalkenones as a tool for rapid assembly of less accessible polycyclic ring systems. We recently reported (1) our work on the scarcely precedented Diels–Alder addition to cycloheptenones in which the tactic of activating reactivity by the use of a 2-carbalkoxy substituent aided additions to a variety of substituted derivatives. There are no reports in the literature of intermolecular Diels–Alder additions to 2-cyclooctenones. Yet there is an increasing number of examples in the literature of complex natural products possessing the six–eight fused ring system that could result from such an addition.[6]

This provides a strong challenge for the development of this unprecedented approach and its application to synthesis. We are pleased now to report for the first time on the facile, selective, and highly efficient additions of 1,3-dienes to activated cyclooctenones.

Results and discussion

We examined three activated cyclooctenones **1**, **2**, and **3**, which were selected for their simplicity yet still would serve as probes to the regio- and stereoselectivity of the additions. As outlined in Scheme 1, the unsaturated enone ester **1** was prepared from cycloheptanone via boron trifluoride catalyzed ring expansion with ethyl diazoacetate (9), which gave a 74% yield of keto ester **4** and its enol tautomer **5** in ca. 1.6:1 ratio. This was followed by a phenylselenenylation – oxidative elimination process (10) to furnish **1** in 85% yield.

Two complementary approaches to the substituted enone ester system of **2** and **3**, summarized in Schemes 2 and 3, were

Received February 26, 1997.

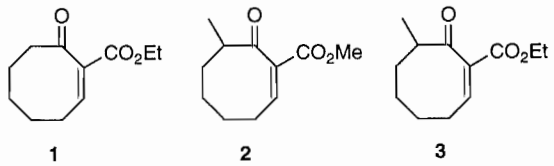
This paper is dedicated to Professor William A. Ayer on the occasion of his 65th birthday.

H.J. Liu,[2] D.-X. Wang, J.B. Kim,[3] E.N.C. Browne.[4] Department of Chemistry, University of Alberta, Edmonton, AB T6G 2G2, Canada.
Y. Wang. Department of Chemistry, National Taiwan University, Taipei, Taiwan, Republic of China.

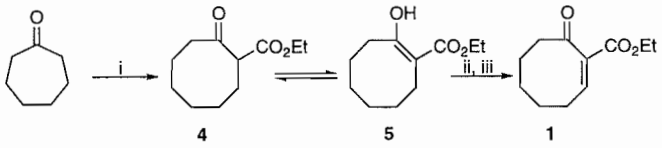
[1] This report is taken in part from the M.Sc. thesis of D.-X. Wang, the University of Alberta, 1997.
[2] Author to whom correspondence may be addressed. Telephone: (403) 492-3477. Fax: (403) 492-8231.
[3] Present address: Department of Environmental Chemistry, Keimyung University, Taegu, 704-701, Korea.
[4] Present address: Wyeth-Ayerst Research Inc., 1025 Marcel Laurin Blvd., St. Laurent, QC H4R 1J6, Canada.
[5] See ref. 1 and the bibliography of ref. 5 therein.
[6] For selected examples see these reports on variecolein (5), taxol (6), aleurodiscal (7), and schisanlignone (8).

© 1997 NRC Canada

Can. J. Chem. Downloaded from www.nrcresearchpress.com by 88.146.161.215 on 09/08/12
For personal use only.

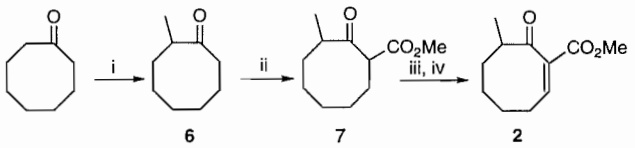


Scheme 1. The preparation of enone ester **1**.



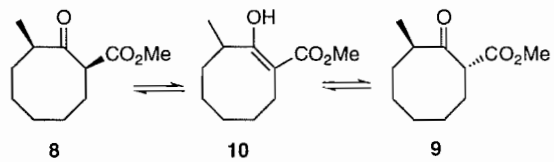
(i) N_2CHCO_2Et, $BF_3{\bullet}OEt_2$, ether, r.t., 24 h, 74%; (ii) PhSeCl, Py, CH_2Cl_2, 0°C, 1 h; (iii) H_2O_2, CH_2Cl_2, 0°C, 40 min, 85% (two steps).

Scheme 2. The preparation of enone ester **2**.



(i) LDA, THF, -78°C, 30 min; then CH_3I, r.t., 40 h, 89%; (ii) NaH, $(CH_3O)_2CO$, DME, reflux, 19 h, 85%; (iii) NaH, PhSeCl, THF, 0°C, 15 min; (iv) H_2O_2, CH_2Cl_2, 0°C → r.t., 40 min, 86% (two steps).

followed. α-Methylation of cyclooctanone with lithium diisopropylamide and methyl iodide (11) gave ketone **6** in 89% yield. Carbomethoxylation of **6** with dimethyl carbonate and sodium hydride (12) gave exclusively keto ester **7** in 85% yield as a mixture of two epimeric keto forms **8** and **9** and the enol tautomer **10** (4:2:3 ratio). The cross-conjugated double bond was introduced by phenylselenenylation and oxidative elimination (10) to give **2** in 86% overall yield.

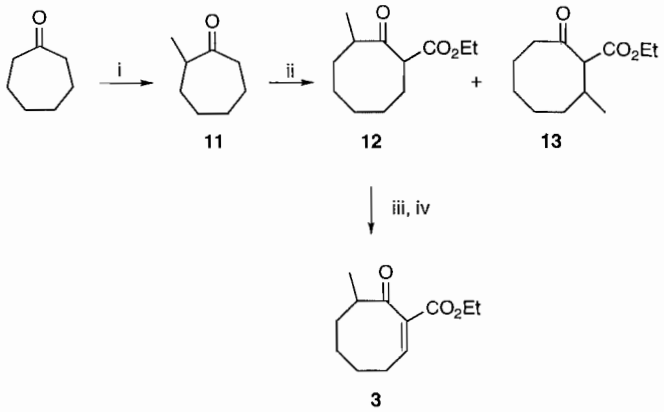


Alternatively, α-methylation of cycloheptanone by the same method used above gave ketone **11** in 70% yield. The keto ester **12** was obtained in this case by ring expansion with ethyl diazoacetate and boron trifluoride etherate (9), giving the product in 56% yield along with a significant quantity (38% yield) of the separable by-product **13**.[7] The keto ester **12** was also obtained as a mixture of epimeric ketones **14** and **15** and the enol tautomer **16** in a ratio of about 3:1:1. The same selenenylation – oxidative elimination approach used previously converted **12** to **3** in 85% yield. A bromination–dehydrobromination approach (13), used in our laboratory in other systems, was unsuccessful as treatment of **12** with *N*-bromosuccinimide gave a complex mixture of products.

The 2-silyloxy-substituted dienes **17**–**20** used in our study

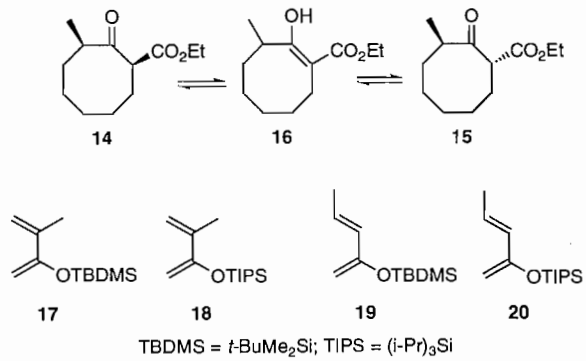
[7] The ethyl diazoacetate – boron trifluoride ring expansion has been used frequently in our laboratories and is usually much more selective than in this case.

Scheme 3. The preparation of enone ester **3**.



(i) LDA, THF, -78°C, 30 min; then CH_3I, r.t., 10 h, 70 %; (ii) N_2CHCO_2Et, $BF_3{\bullet}OEt_2$, ether, r.t., 24 h, 94% (**12** : **13** = 1.5 : 1); (iii) NaH, PhSeCl, THF, 0°C, 30 min; (iv) H_2O_2, CH_2Cl_2, 0°C → r.t., 40 min, 85% (two steps).

were not commercially available and were prepared by the general method of Ireland and Thompson (14) using *tert*-butyldimethylsilyl chloride and triisopropylsilyl chloride to trap the enolates generated from *trans*-3-penten-2-one and 3-methyl-3-buten-2-one with lithium diisopropylamide.



TBDMS = *t*-$BuMe_2Si$; TIPS = $(i\text{-}Pr)_3Si$

Diels–Alder reactions

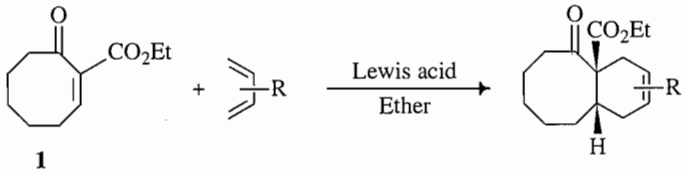
The general procedures for the Diels–Alder cycloaddition were straightforward. For those catalyzed by ferric chloride, stannic chloride, or boron trifluoride etherate, the Lewis acid was simply added to an ether solution of the diene and dienophile. For zinc chloride catalyzed reaction, the Lewis acid was first flame fused and then dissolved in ether. The dienophile was then added as a solution in ether and, after stirring for 30 min to allow for complex formation, the diene was introduced. After complete consumption of the dienophile, the reaction was quenched by addition of aqueous sodium bicarbonate and worked up. The additions to unsubstituted enone ester **1** are summarized in Table 1. At −20°C, both ferric chloride and stannic chloride gave adduct **21** in high yield. Ferric chloride gave a particularly fast conversion to product. Boron trifluoride etherate and zinc chloride gave slow conversions even at higher temperature (0°C). As expected, the uncatalyzed reaction gave virtually no adduct at room temperature. Having thus determined effective conditions and catalysts for this system, we investigated a selected group of examples with simple dienes to give adducts **22** through **27**. The yields were uniformly high. The addition took place as expected with com-

© 1997 NRC Canada

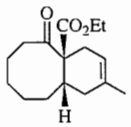
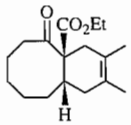
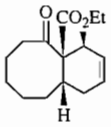
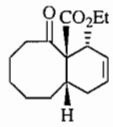
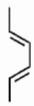
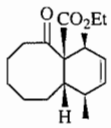
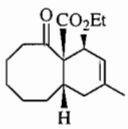
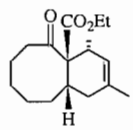
Can. J. Chem. Downloaded from www.nrcresearchpress.com by 88.146.161.215 on 09/08/12
For personal use only.

Can. J. Chem. Downloaded from www.nrcresearchpress.com by 88.146.161.215 on 09/08/12
For personal use only.

Table 1. Diels–Alder reaction of 2-carbethoxy-2-cyclooctenone (**1**).

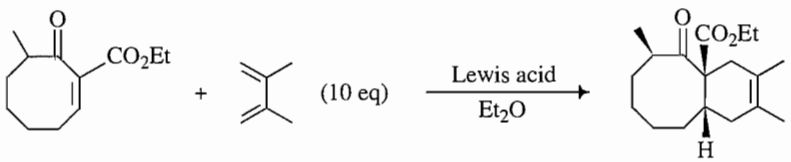


1

Entry	Diene (10 equiv.)	Time (h)	Temp (°C)	Product	Lewis acid[a]	Yield (%)
1		1/3	–20	 **21**	$FeCl_3$	84
		24	–20		$SnCl_4$	86
		72	0		$ZnCl_2$	16
		48	0		$BF_3{\cdot}OEt_2$	35
		72	r.t.		—	2
2		1/3	–20	 **22**	$FeCl_3$	89
3		1/3	–20	 **23** (85:15)  **24**	$FeCl_3$	80
		18	–20		$SnCl_4$	89
4		24	–20	 **25**	$SnCl_4$	95
		10	–78		$FeCl_3$	82
5		1	–20	 **26** (77:23)  **27**	$SnCl_4$	83

[a]Ferric chloride, stannic chloride, and boron trifluoride etherate were used at 1 equivalent. Zinc chloride was used at 2 equivalents.

Table 2. Lewis acid catalyzed Diels–Alder reaction of enone **3** and 2,3-dimethyl-1,3-butadiene.

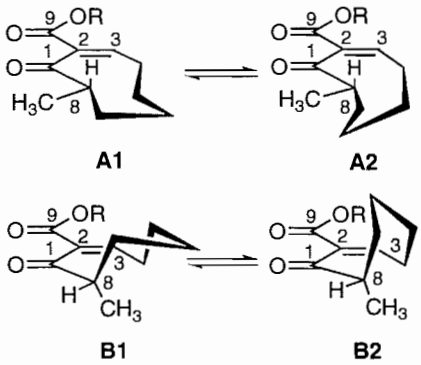


3 **28**

Time (h)	Temp (°C)	Lewis acid[a]	Yield (%)
0.5	–40	$FeCl_3$ (1 equiv.)	96
17	–40	$SnCl_4$ (1 equiv.)	98
101	r.t.	$ZnCl_2$ (2 equiv.)	85
52	r.t.	$BF_3{\cdot}OEt_2$ (1 equiv.)	0

© 1997 NRC Canada

Scheme 4. The conformational equilibrium of cyclooctenones.



plete *ortho*-rule and *para*-rule selectivity and with moderate to good preference for the same ester-*endo* addition as in other systems.[5]

Initial investigations of additions to enone ester **3** are summarized in Table 2. Again ferric chloride and stannic chloride were superior and powerful catalysts. But in this sequence boron trifluoride was completely ineffective. The dienophile was recovered quantitatively. Zinc chloride did in fact produce product **28** in good yield although with a much slower rate than the first two catalysts mentioned. Thus the broader studies on Diels–Alder reactions of **2** and **3** were concentrated on examples with stannic chloride and ferric chloride. The results of these investigations are summarized in Table 3. These reactions too followed the expected regiochemical rules (15). Even for addition of the 2,3-disubstituted diene **18** the expected regio-directing dominance of the electron-donating silyloxy substituent led to complete selection in favor of the adduct **34** with none of the isomeric adduct observed. All of the adducts were formed by preferential ester-*endo* addition except for that with cyclopentadiene, which was at best only slightly selective. A significant proportion of the keto-*endo* adduct **43** was formed. This particular loss of selectivity for cyclopentadiene is not exhibited in other systems we have studied and is not readily explained. The ester-*endo* attack observed for the majority of adducts is expected on the basis of minimum steric interaction between the diene and dienophile in the transition state.

The face selectivity of the additions to the dienophiles with two different diastereotopic faces was less consistent. When the C-2 position of the diene was substituted, addition to **2** and **3** proceeded with preferential addition to the apparently less hindered face (opposite to the methyl substituent). This was expected even though reversed selectivity in favor of the apparently more hindered face had previously been observed for additions to the congener **44** (1). But where the diene had no C-2 substituent, the diene appeared to add to **3** preferentially from the more hindered methyl-substituted face. As noted for additions to **44**, the rationale for this unexpected selectivity is unclear.[8] Several of the additions (Entries 2, 5, and 8) also produced one inseparable minor isomer whose stereochemistry could not be completely assigned. It was therefore impossible to determine if these minor isomers were derived from keto-*endo* addition, which would indicate diminished preference for the established ester-*endo* orientation of addition, giving products epimeric at C-12, or from diminished face selectivity resulting in products that are epimeric at C-3.

We considered the conformational effects of the eight-membered ring on the orientations of the Diels–Alder additions. Using the report of Arshinova (16) and considering the effect of planar fragments (ketone carbonyl and double bond) as constraints on the flexibility of the ring system, we have proposed two conformations around the enone-ester system that are illustrated in Scheme 4. The conformations **A1** and **A2** would clearly present a face opposite to the methyl substituent for relatively unhindered cycloaddition to the enone. Conformations **B1** and **B2** are clearly less suited to additions at the enone double bond since the methyl substituent is pseudo-axial on one face while the remainder of the eight-membered ring occupies the other face of the system. And yet addition to the methyl-substituted face was observed. Further study and a broadened selection of examples may provide a better understanding of the complex stereochemical and conformational relationships that are expressed in this system.

Structural assignments

While the establishment of product structures has by now become fairly routine in our studies of cycloalkenone dienophiles, there are a few elements that warrant particular attention and are discussed below. For the most part, however, the structures were clearly evident on first-order examination of the spectroscopic data.

The stereochemistry of adduct **28** was confirmed by NOE experiments in which irradiation of the C-3 methyl substituent gave enhancement of the signals for the ester methyl (11%) and methylene (1%) protons and for the C-8 ring-junction proton (5%). Irradiation of the C-3 proton gave enhancement of the allylic methyls at C-10 and C-11 (1% each) and one of the C-12 protons (7%). These two results indicated that the methyl substituent was on the same face of the ring as the carbethoxy group. Similar NOE studies were run for other compounds in the series and the results of those experiments are summarized in Table 4.

Proof of the *para*-addition orientation for adduct **29** was made by an INEPT-NMR experiment and by chemical transformation. In the INEPT experiment, when the vinyl proton of **29** at δ 5.30 was irradiated the signal of the quaternary ring junction carbon at C-1 (δ 63.3 in the ^{13}C NMR APT spectrum) was observed in the corresponding INEPT ^{13}C NMR spectrum. If the adduct had the *anti-para* addition structure **45**, this irradiation should cause display of the signal for the tertiary ring junction carbon at C-8.

Chemical derivatization of **29** was achieved by photooxidation (17) to give two products **46** and **47**. In the ^{1}H NMR spectrum of the enone derivative **47** the vinyl proton was observed at δ 6.60 as a quartet of doublets (J = 1, 5.5 Hz) due to coupling with the enone methyl substituent and most importantly with the ring junction proton. In the corresponding derivative **48** of the *anti-para* product **45**, the 5.5 Hz coupling to the ring junction would be absent and the enone proton would appear only as a finely split quartet.

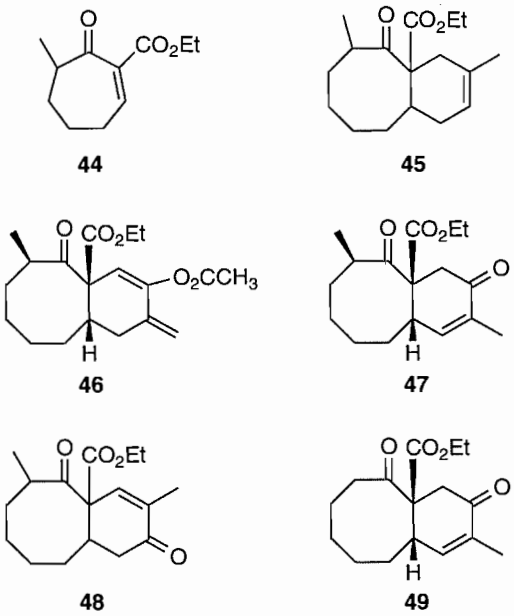
[8] It could be that the C-2 substituted diene reacts in an almost stepwise manner under pseudo-charge control, which has a different steric demand from the C-2 unsubstituted diene that should react in a more concerted manner. We thank the referee for this suggestion.

© 1997 NRC Canada

Can. J. Chem. Downloaded from www.nrcresearchpress.com by 88.146.161.215 on 09/08/12
For personal use only.

Can. J. Chem. Downloaded from www.nrcresearchpress.com by 88.146.161.215 on 09/08/12
For personal use only.

The regiochemistry of adduct **21** was confirmed in a similar manner. Photooxidation of this compound gave enone **49** as the sole product, which showed, in the ^{1}H NMR spectrum, a quartet of doublets (J = 1, 6 Hz) at δ 6.68 for the vinylic proton.

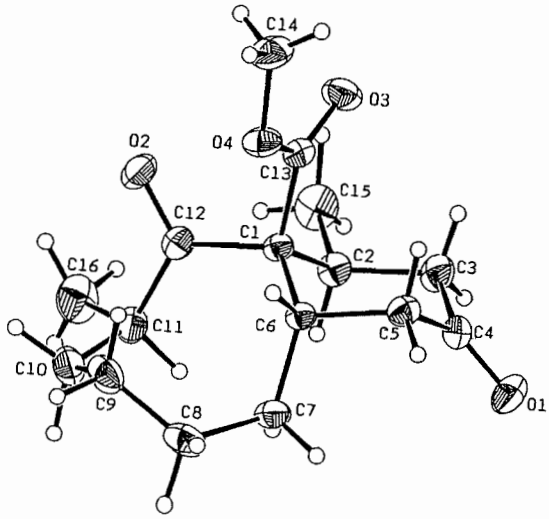


Adducts of **2** and **3** with diene **17** were found to be highly unstable and could not be isolated or characterized. Decomposition occurred in an NMR sample tube in deuteriobenzene within 20 min to give a complex mixture. Even at –22°C extensive decomposition was seen within 24 h. The other functionalized dienes **18**, **19**, and **20** gave stable adducts that could be purified. Nevertheless, addition of **20** to **2** gave primarily the deprotected derivative **37** and only a trace of protected enol ether **38** in which the double bond had migrated. TLC analyses showed that the silyl protecting group was eliminated in the cycloaddition reaction mixture. The structure of **37** was verified by X-ray crystallographic analysis.[9] The X-ray structure is shown in Scheme 5. The regiochemistry of compound **38** was confirmed by ^{1}H NMR decoupling experiments.

Conclusion

The Lewis acid catalyzed Diels–Alder addition of activated cyclooctenones proceeds under mild conditions in high yield and with moderate to high and predictable stereochemistry to give adducts with great potential for synthetic use. Adducts are in use in our laboratory as key intermediates in the synthesis of several natural products and further details on this work will be reported in a future publication.

Scheme 5. The three-dimensional X-ray crystallographical structure of compound **37**.



Experimental

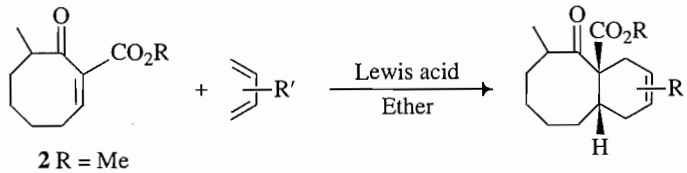
General

Melting points were recorded on a Kofler hot stage apparatus and are not corrected. Combustion elemental analyses were performed by the microanalytical laboratory of this department. Fourier transform infrared (FT-IR) spectra were recorded on a Nicolet 7199 or Nicolet MX-1 FT-IR spectrophotometer. Proton nuclear magnetic resonance (^{1}H NMR) spectra were recorded on a Bruker WH-200, Bruker WH-300, Bruker WH-400, or UNITY-500 using deuteriochloroform ($CDCl_3$) as solvent unless otherwise stated. The chemical shift of the deuterated solvent peak (for $CDCl_3$: δ = 7.25 ppm, for C_6D_6: δ = 7.15 ppm) was used as an internal reference. Coupling constants are reported to ±0.5 Hz. Chemical shift measurements are reported in delta (δ) units. The following abbreviations are used: s = singlet, d= doublet, t = triplet, q = quartet, m = multiplet and br = broad. Carbon-13 nuclear magnetic resonance (^{13}C NMR) spectra were recorded on a Bruker WH-300 (75 MHz) NMR spectrometer as solutions in deuteriochloroform ($CDCl_3$) as the internal standard, setting the central peak at 77.00 ppm. Carbon-13 multiplicities were derived from Carr–Purcell–Meiboom–Gill spin echo J-modulated experiments (APT or Attached Proton Test) (18). Methyl and methine groups are shown as singlets antiphase (a) with respect to the deuteriochloroform signal, whereas methylene groups, quaternary carbons, and carbonyl groups appear in phase (p) with it. Nuclear Overhauser enhancement (NOE) experiments were determined in the difference mode in which a control (undecoupled) spectrum was computer subtracted from the irradiated spectrum after Fourier transformation. Positive enhancements are defined as signals possessing an antiphase with respect to the irradiated signal. Samples for NOE measurements were deoxygenated with argon for 10 min prior to use. Two-dimensional (2D) homonuclear correlation spectrum (COSY) and proton spin decoupling experiments were performed on the Bruker WH-300 MHz NMR machine

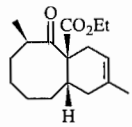
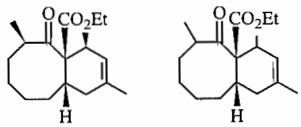
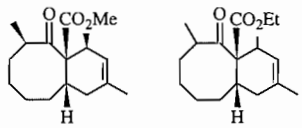
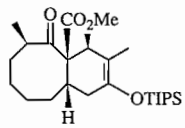
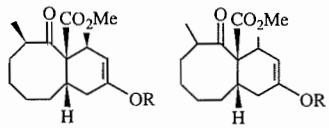
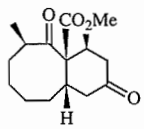
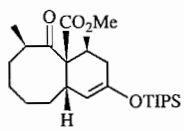
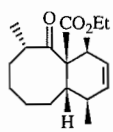
[9] X-ray crystallographic data for **37**, comprising tables of bond distances and angles, atomic parameters, and anisotropic temperature factors, have been deposited and can be purchased from: The Depository of Unpublished Data, Document Delivery, CISTI, National Research Council Canada, Ottawa, Canada K1A 0S2. With the exception of the anisotropic temperature factors, these data have also been deposited with the Cambridge Crystallographic Data Centre, and can be obtained on request from The Director, Cambridge Crystallographic Data Centre, University Chemical Laboratory, 12 Union Road, Cambridge, CB2 1EZ, U.K.

© 1997 NRC Canada

Table 3. Lewis acid catalyzed Diels–Alder reaction of enones **2** and **3**.



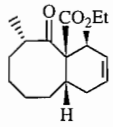
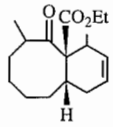
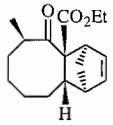
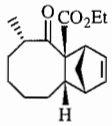
2 R = Me
3 R = Et

Entry	Diene	Time (h)	Temp (°C)	Product(s)	Lewis acid	Yield (%)
1	(10 equiv.)	0.5	–40	 **29**	$FeCl_3$ (1 equiv.)	95
2	(10 equiv.)	0.5 0.5 0.5	–40 –50 –78	 **30** (4:1) **31**	$FeCl_3$ (1 equiv.)	75 80 77
		0.5 24	–78 –78	 **32** (4:1) **33**	$FeCl_3$ (1 equiv.) $SnCl_4$ (1 equiv.)	82 80
3[a]	OTBMS (10 equiv.) **17**			Unstable		
4[a]	OTIPS (2 equiv.) **18**	4	–78	 **34**	$SnCl_4$ (1 equiv.)	90
5[a]	OR **19** R = TBDMS; (10 equiv.)	1	–78	 **35** (2:1) **36**	$SnCl_4$ (1 equiv.)	89
6[a]	OTIPS **20** (2 equiv.)	1	–78	 **37**	$SnCl_4$ (1 equiv.)	98
				 **38**		Trace
7	(10 equiv.)	5.5 2	–40 –20	 **39**	$FeCl_3$ (1 equiv.)	92 68

Can. J. Chem. Downloaded from www.nrcresearchpress.com by 88.146.161.215 on 09/08/12
For personal use only.

© 1997 NRC Canada

Table 3. (*concluded*).

Entry	Diene	Time (h)	Temp (°C)	Product	Lewis acid	Yield (%)
8	 (10 equiv.)	0.4 0.5	–40 –78	 **40** (4:1)  **41**	$FeCl_3$ (1 equiv.)	68 92
9	 (10 equiv.)			 **42**  **43**		
		1	–78	2 : 1	$FeCl_3$	76
				1 : 1	(1 equiv.)	
		78	0 → 20		$ZnCl_2$ (2 equiv.)	91

[a]In this reaction, the diene was added to the solution of the complex of enone **2** and Lewis acid.

Table 4. NOE data for Diels–Alder adducts.

Compound	Irradiation	δ (ppm)	% Enhancement (proton)
28	O=CCHC**H**$_3$	1.04	11.0 ($CO_2CH_2C\mathbf{H}_3$), 1.0 ($CO_2C\mathbf{H}_2CH_3$), 5.0 (C-8 **H**)
	O=CC**H**CH$_3$	3.25	1.0 ($H_3CC{=}CC\mathbf{H}_3$, 7.0 (C-12 **H**)
29	O=CCHC**H**$_3$	1.04	3.1 (C-8 **H**)
	O=CC**H**CH$_3$	3.25	6.0 (C-12 **H**)
30	O=CCHC**H**$_3$	0.95	0.1 (C-8 **H**)
	C=CHCHC**H**$_3$	0.88	1.4 ($CO_2C\mathbf{H}_2CH_3$)
	C-8 **H**	2.60	1.4 ($CO_2C\mathbf{H}_2CH_3$), 1.5 (C=CHCHC**H**$_3$)
32	O=CC**H**CH$_3$	2.50	1.2 (C=CHCHC**H**$_3$), 1.4 (C=C**H**)
	C=CHC**H**CH$_3$	2.07	7.3 (O=CC**H**CH$_3$)
	C=CHCHC**H**$_3$	0.90	3.6 ($CO_2CH_2C\mathbf{H}_3$)
34	O=CCHC**H**$_3$	2.90	5.6 ($CO_2C\mathbf{H}_3$)
35	O=CC**H**CH$_3$	2.93	10.3 (C=C**H**)
	C=CHCHC**H**$_3$	1.17	3.0 ($CO_2C\mathbf{H}_3$)
37	O=CCH$_2$C**H**CH$_3$	2.09	11.8 (O=CC**H**CH$_3$)
38	O=CC**H**CH$_3$	2.70	10.3 ($CH_2C\mathbf{H}CH_3$)
39	O=CCHC**H**$_3$	1.15	0.5 (C-12 **H**)
	C-9 C**H**$_3$	0.95	2.0 (C-8 **H**)
40	O=CCHC**H**$_3$	1.08	1.0 (C-11 **H**), 2.0 (C-12 **H**)
42	O=CCHC**H**$_3$	1.10	1.3 ($CO_2C\mathbf{H}_2CH_3$), 0.3 (C-8 **H**), 1.0 (C-10 **H**)
	C-8 **H**	3.30	1.7 (C-10 **H**)
43	O=CCHC**H**$_3$	1.00	1.0 (C-12 **H**), 5.0 (C-11 **H**), 1.0 (C-10 **H**)
	C-12 **H**	6.23	1.0 (O=CCHC**H**$_3$)
	C-8 **H**	2.90	2.6 (C-13 **H**)
26	C=CHCHC**H**$_3$	1.02	5.8 ($CO_2C\mathbf{H}_2CH_3$)
	C=CHC**H**CH$_3$	2.80	2.4 (O=CC**H**H)

Can. J. Chem. Downloaded from www.nrcresearchpress.com by 88.146.161.215 on 09/08/12
For personal use only.

© 1997 NRC Canada

Can. J. Chem. Downloaded from www.nrcresearchpress.com by 88.146.161.215 on 09/08/12
For personal use only.

using the standard proton parameters. High-resolution electron impact mass spectra (HRMS) were recorded using an A.E.I. model MS-50 mass spectrometer. Chemical ionization mass spectra (CIMS) were recorded on an A.E.I. MS-12 mass spectrometer, using ammonia as the reagent gas. Spectral data are reported as *m/z* values. Bulb-to-bulb distillation was performed using a Kugelrohr distillation apparatus. Concentrations of solvent systems used in column chromatography are given by volumes.

Unless otherwise stated, all materials used were commercially available. All compounds made were racemic. With the exception of photooxidation, all reactions were carried out under a positive pressure of argon. Solvents were distilled under argon from appropriate drying agents before use. Tetrahydrofuran (THF), diethyl ether, toluene, and 1,2-dimethoxyethane (DME) were freshly distilled from solutions of sodium benzophenone ketyl. Diisopropylamine was distilled from sodium hydroxide or potassium hydroxide. Pyridine, benzene, dichloromethane, and triethylamine (TEA) were distilled from calcium hydride. Reactions requiring anhydrous conditions were performed using oven- or flame-dried glassware, assembled, and allowed to cool while being purged with argon. Argon was passed through a column of 4 Å molecular sieves, with a self-indicating silica gel (coarse grained) as the indicator. Flash chromatography was used routinely for purification and separation of product mixtures, using silica gel (Merck) of 230–400 mesh. All solvents were distilled prior to use for chromatography. Skellysolve B (Skelly B) refers to Skelly Oil Company light petroleum, bp 62–70°C. Analytical thin-layer chromatography (TLC) was carried out on aluminum sheets precoated (0.2 mm layer thickness) with silica gel 60 F_{254} (E. Merck, Darmstadt). Ultraviolet-active materials were detected by visualization under a UV lamp (254 or 350 nm). For TLC, the visualization of the chromatograms was completed by dipping in an ethanol solution of vanillin (5%, w/v) and sulfuric acid (5%, v/v), followed by careful charring on a hot plate.

2-Carbethoxycyclooctanone (4)

To a solution of cycloheptanone (1.12 g, 10 mmol) in ether (15 mL) cooled to 0°C was added boron trifluoride etherate (1.85 mL, 15 mmol). A solution of ethyl diazoacetate (1.71 g, 1.57 mL, 15 mmol) in ether (2 mL) was then added dropwise over 10 min. After 24 h at room temperature, the reaction mixture was cooled to 0°C, and a saturated aqueous solution of sodium bicarbonate was added to the mixture until the pH was raised to 7. The aqueous layer was extracted with ether (3 × 10 mL) and the organic layers were combined, washed twice with water (10 mL each), and once with saturated aqueous sodium chloride solution (10 mL), dried over anhydrous magnesium sulfate, filtered, and concentrated. The crude product was subjected to flash chromatography on silica gel. Elution with 5% ethyl acetate in Skelly B gave 2-carbethoxycyclooctanone (**4**) (19) (1.47 g, 74% yield). Compound **4** existed as a mixture of ketone and enol in a ratio of 1:1.56. IR ($CHCl_3$ cast): 1747 (C=O, ester, keto form), 1708 (C=O, ketone), 1644 (C=O, ester, enol form), 1613 (enol C=C) cm^{-1}; ^1H NMR (300 MHz in $CDCl_3$) δ: 12.57 (s, 0.39H, O**H**, enol form), 4.20 (q, 0.78H, J = 7.5 Hz, O**C**$\mathbf{H}_2$, enol form), 4.13 (q, 1.22H, J = 7.5 Hz, O**C**$\mathbf{H}_2$ keto form), 3.55 (dd, 0.61H, J = 5, 10.5 Hz, O=CC**H**CO_2Et), 1.28 (t, 1.17H, J = 7.5 Hz, $OCH_2C\mathbf{H}_3$, enol form), 1.22 (t, 1.83 H, J = 7.5 Hz, $OCH_2C\mathbf{H}_3$ keto form); ^{13}C NMR (APT, 75 MHz in $CDCl_3$) for the keto form δ: 212.2 (p), 176.0 (p), 61.1 (p), 57.0 (a), 41.6 (p), 28.9 (p), 27.0 (p), 26.5 (p), 25.2 (p), 24.5 (p), 14.0 (a), for the enol form δ: 172.9 (p), 170.1 (p), 99.2 (p), 60.1 (p), 32.2 (p), 29.9 (p), 28.7 (p), 26.0 (p), 25.5 (p), 23.8 (p), 14.3 (a); HRMS, *m/z* (M^+) calcd. for $C_{11}H_{18}O_3$: 198.12560; found: 198.12535.

2-Carbethoxy-2-cyclooctenone (1)

At 0°C, to a solution of pyridine (0.27 mL, 3.40 mmol) and phenylselenenyl chloride (651 mg, 3.40 mmol) in dichloromethane (20 mL) was added a dichloromethane solution (5 mL) of 2-carbethoxycyclooctanone (**4**) (562 mg, 2.83 mmol) over 30 min. The mixture was stirred at 0°C for 30 min and then poured into ice-cold 2 N aqueous HCl (10 mL). The organic layer was then separated and cooled to 0°C. Aqueous hydrogen peroxide (30%, 1 mL) was added dropwise till the yellow color of the solution discharged. The mixture was stirred for 30 min and then diluted with water (10 mL). The organic layer was separated, and the aqueous layer extracted with ether (3 × 10 mL). The organic layers were combined, washed with saturated aqueous sodium bicarbonate (10 mL), water (10 mL), and saturated aqueous solution of sodium chloride (10 mL), dried over anhydrous magnesium sulfate, filtered, and concentrated. The crude product was subjected to flash chromatography. Elution with 10% ethyl acetate in Skelly B gave enone **1** (20) (473 mg, 85% yield). IR ($CHCl_3$ cast): 1720 (C=O, ester), 1695 (C=O, ketone), 1640 (C=C) cm^{-1}; ^1H NMR (300 MHz in $CDCl_3$) δ: 7.20 (t, 1H, J = 4.5 Hz, =C**H**), 4.18 (m, 2H, O**C**$\mathbf{H}_2$), 2.55 (m, 2H, O=CC**H**$_2$), 2.38 (m, 1H, =CHC**H**H), 1.25 (t, 3H, J = 7.5 Hz, $OCH_2C\mathbf{H}_3$); ^{13}C NMR (APT, 75 MHz in $CDCl_3$) δ: 208.9 (p), 164.4 (p), 146.4 (a), 131.7 (p), 61.1 (p), 44.53 (p), 30.1 (p), 29.2 (p), 22.1 (p), 21.7 (p), 14.1 (a); HRMS, *m/z* (M^+) calcd. for $C_{11}H_{16}O_3$: 196.10994; found: 196.10952. Anal. calcd. for $C_{11}H_{16}O_3$: C 67.32%, H 8.22%; found: C 67.59%, H 8.17%.

2-Methylcyclooctanone (6)

Diisopropylamine (2.62 mL, 0.02 mol) was dissolved in 12.5 mL of THF and cooled to 0°C while stirring. A solution of *n*-butyllithium (1.6 M in THF, 12.5 mL) was added dropwise over 20 min and the mixture was cooled to −78°C. A solution of cyclooctanone (1.26 g, 0.01 mol) in 5 mL of THF was added dropwise over 30 min. The solution was stirred at −78°C for 30 min followed by rapid addition of methyl iodide (1.24 mL, 0.02 mol). After 5 min, the reaction mixture was allowed to warm to room temperature and was stirred for 40 h. The reaction mixture was quenched with 25 mL of water and the aqueous layer was extracted three times with ether (10 mL each). The organic layers were combined, washed twice with water (10 mL each) and once with saturated aqueous sodium chloride solution (10 mL), dried over anhydrous magnesium sulfate, filtered, and concentrated. The crude was subjected to flash chromatography on silica gel, eluting with 2.5% ethyl acetate in Skelly B, to give 2-methylcyclooctanone (**6**) (21, 22) (0.86 g, 89% yield based on consumed starting material) along with 30% recovery of the starting material. IR ($CHCl_3$ cast): 1701 (C=O), 1376 (CH_3) cm^{-1}; ^1H NMR (300 MHz in $CDCl_3$) δ: 2.55 (m, 1H, C**H**CH_3), 2.35 (m, 2H, C$\mathbf{H}_2$C=O), 1.00 (d, 3H, J = 7 Hz, C$\mathbf{H}_3$); ^{13}C NMR (APT, 75 MHz in $CDCl_3$) δ: 220.3 (p), 45.3 (a), 40.4 (p), 33.2 (p), 26.4 (p), 26.0

© 1997 NRC Canada

Can. J. Chem. Downloaded from www.nrcresearchpress.com by 88.146.161.215 on 09/08/12
For personal use only.

(p), 25.2 (p), 24.1 (p), 6.9 (a); HRMS, *m/z* (M^+) calcd. for $C_9H_{16}O$: 140.12012; found: 140.11977.

2-Methylcycloheptanone (11)

The title compound (23) was prepared from cycloheptanone (5.0 g, 44.6 mmol) in 70% yield using the same procedure as described above.

2-Carbomethoxy-8-methylcyclooctanone (7)

To a suspension of sodium hydride (8.57 g, 0.214 mol, 60% in oil) in 60 mL of DME was added predried dimethyl carbonate (32.17 g, 0.357 mol). The mixture was heated to reflux with stirring. A solution of 2-methylcyclooctanone (**6**) (10 g, 0.0714 mol) in 20 mL of DME was added dropwise and the reaction mixture was refluxed for 19 h, then cooled to 0°C. A 10% aqueous solution of acetic acid was added with stirring until the pH was acidic. The mixture was separated and the aqueous layer was extracted three times with ether (30 mL each). The organic layers were combined, washed with water (30 mL), saturated aqueous solution of sodium bicarbonate (30 mL), water (30 mL), and saturated aqueous solution of sodium chloride (30 mL), dried over magnesium sulfate, filtered, and concentrated. Flash chromatography of the residue on silica gel, eluting with 2.5% ethyl acetate in Skelly B, gave the ß-keto ester **7** (12.0 g, 85% yield) as a colorless oil. This compound was a mixture of two keto forms and an enol form (4:2:3 ratio). IR ($CHCl_3$, cast): 1749 (C═O, ester), 1707 (C═O, ketone), 1640 (C═O, ester, enol form), 1609 (C═C, enol form), 1365 (CH_3) cm^{-1}; ^1H NMR (300 MHz in $CDCl_3$) δ: 13.47 (d, 0.33H, J = 1.5 Hz, **OH**, enol form), 3.46 (dd, 0.22H, J = 5, 10.5 Hz, OCC**H**CO_2Me, minor keto form), 3.29 (dd, 0.45H, J = 3, 15.5 Hz, OCC**H**CO_2Me, major keto form), 3.36 (s, 1.35H, O**C**H_3, ester, major keto form), 3.31 (s, 0.66H, O**C**H_3, ester, minor keto form), 3.25 (s, 0.99H, O**C**H_3, ester, enol form), 1.55 (d, 1.35H, J = 7 Hz, **C**H_3, major keto form), 1.06 (d, 0.99H, J = 7 Hz, **C**H_3, enol form), 1.01 (d, 0.66H, J = 7 Hz, **C**H_3, minor keto form); ^{13}C NMR (75 MHz in $CDCl_3$) for the major keto form, δ: 213.1 (p), 178.5 (p), 56.2 (a), 51.1 (a), 45.2 (a), 37.9 (p), 31.3 (p), 28.2 (p), 26.1 (p), 24.5 (p), 19.1 (a). The following minor ^{13}C NMR signals were observed for the other two isomers: 212.4 (p), 173.8 (p), 170.5 (p), 170.3 (p), 99.6 (p), 54.9 (a), 51.6 (a), 51.5 (a), 46.3 (p), 34.8 (p), 34.4 (a), 31.4 (p), 30.1 (p), 27.4 (p), 26.2 (p), 25.6 (p), 25.0 (p), 24.4 (p), 17.0 (a), 13.9 (a); HRMS, *m/z* (M^+) calcd. for $C_{11}H_{18}O_3$: 198.12560; found: 198.12635. Anal. calcd. for $C_{11}H_{18}O_3$: C 66.64%, H 9.15%; found: C 66.90%, H 9.15%.

2-Carbethoxy-8-methylcyclooctanone (12) and 2-carbethoxy-3-methylcyclooctanone (13)

To a solution of 2-methylcycloheptanone (**11**) (2.56 g, 0.02 mol) in 50 mL of dry ether cooled to 0°C was added boron trifluoride etherate (3.94 mL, 0.032 mol). A solution of ethyl diazoacetate (3.31 mL, 0.032 mol) in 5 mL of dry ether was then added dropwise over 10 min followed by warming to room temperature. After 24 h, the reaction mixture was cooled to 0°C and a saturated aqueous solution of sodium bicarbonate was added to the mixture until the pH was raised to 7. The aqueous layer was extracted three times with ether (10 mL each) and the organic layers were combined, washed twice with water (10 mL each) and once with saturated aqueous sodium chloride solution (10 mL), dried over anhydrous magnesium sulfate, filtered, and concentrated. The crude product was subjected to flash chromatography on silica gel. Elution with 5% ethyl acetate in Skelly B gave first 2-carbethoxy-8-methylcyclooctanone (**12**) (2.4 g, 56% yield) and then 2-carbethoxy-3-methylcyclooctanone (**13**) (1.6 g, 38% yield). Compound **12** was a mixture of two keto forms and an enol form (3:1:1 ratio). IR ($CHCl_3$ cast): 1747 (C═O, ester), 1708 (C═O, ketone), 1638 (C═O, ester, enol form), 1610 (C═C, enol form) cm^{-1}; ^1H NMR (300 MHz in $CDCl_3$) δ: 12.89 (d, 0.22H, J = 1.5 Hz, **OH**, enol form), 4.19 (q, 0.44H, J = 7 Hz, O**C**H_2, enol form), 4.15–4.05 (m, 1.56H, O**C**H_2, two keto forms), 3.85 (dd, 0.2H, J = 4, 11 Hz, COC**H**CO_2Et, minor keto form), 3.50 (dd, 0.58H, J = 3.5, 12 Hz, COC**H**CO_2Et, major keto form), 1.95 (t, 0.6H, J = 7 Hz, $OCH_2C\mathbf{H}_3$, minor keto form), 1.28 (t, 0.66H, J = 7 Hz, $OCH_2C\mathbf{H}_3$, enol form), 1.21 (t, 1.74H, J = 7 Hz, $OCH_2C\mathbf{H}_3$, major keto form), 1.12 (d, 0.66H, J = 7 Hz, **C**H_3, enol form), 1.11 (d, 1.74H, J = 7 Hz, **C**H_3, major keto form), 0.95 (d, 0.6H, J = 7 Hz, **C**H_3, minor keto form); ^{13}C NMR (75 MHz in $CDCl_3$) for the major keto form, δ: 215.0 (p), 170.24 (p) 61.1 (p), 56.4 (a), 45.1 (a), 35.0 (p), 28.5 (p), 25.9 (p), 25.6 (p), 24.2 (p), 19.0 (a), 14.0 (a). The following minor ^{13}C NMR signals were observed for the other two isomers: 213.7 (p), 177.9 (p), 170.15 (p), 99.6 (p), 60.9 (p), 60.1 (p), 55.0 (a), 46.4 (a), 37.7 (p), 34.1 (a), 31.3 (p), 30.9 (p), 30.2 (p), 27.2 (p), 26.0 (p), 24.7 (p), 24.5 (p), 24.4 (p), 16.7 (a), 14.3 (a), 13.7 (a); HRMS, *m/z* (M^+) calcd. for $C_{12}H_{20}O_3$: 212.14125; found: 212.14087. Compound **13** existed completely in the keto form: IR ($CHCl_3$, cast): 1745 (C═O, ester), 1705 (C═O, ketone), 1385 (CH_3) cm^{-1}; ^1H NMR (300 MHz, $CDCl_3$) δ: 4.10 (m, 2H, O**C**H_2), 3.30 (d, 1H, J = 11 Hz, COC**H**CO_2Et), 2.75–2.56 (m, 1H, C**H**HC═O), 2.54–2.23 (m, 1H, CH**H**C═O), 1.20 (t, 3H, J = 7 Hz, $OCH_2C\mathbf{H}_3$), 0.95 (d, 3H, J = 7 Hz, **C**H_3); ^{13}C NMR (APT, 75 MHz, $CDCl_3$) δ: 211.0 (p), 169.4 (p), 64.7 (a), 61.1 (p), 42.0 (p), 34.7 (a), 34.5 (p), 27.3 (p), 25.6 (p), 23.6 (p), 20.7 (a), 14.1 (a); HRMS, *m/z* (M^+) calcd. for $C_{12}H_{20}O_3$: 212.14125; found: 212.14058.

2-Carbomethoxy-8-methyl-2-cyclooctenone (2)

Sodium hydride (1.02 g, 60% in oil, 25.3 mmol) was suspended in 10 mL of THF with stirring and cooled to 0°C. A solution of 2-carbomethoxy-8-methylcyclooctanone (**7**) (1.0 g, 5.05 mmol) in 5 mL of THF was added dropwise to the suspension over 15 min. When formation of the sodium enolate was complete and hydrogen gas evolution had ceased, a thick suspension developed. Stirring and cooling were continued for 20 min. Then a solution of phenylselenenyl chloride (4.86 g, 25.3 mmol) in 10 mL of THF was added. The reaction mixture was stirred at 0°C for another 15 min, then poured into a solution of ether and aqueous saturated sodium bicarbonate. The aqueous layer was extracted three times with ether (10 mL each). All the organic layers were combined, washed with water twice (10 mL each) and saturated aqueous sodium chloride solution once (10 mL), dried over anhydrous magnesium sulfate, filtered, and concentrated. The crude product was dissolved in 20 mL of dichloromethane. The solution was stirred at 0°C and aqueous hydrogen peroxide (30%, 2 mL) was added dropwise to the solution. When oxidation was complete, as indicated by the discharge of the yellow color of the solution, the reaction mixture was warmed to room temperature with vigorous stirring for 20 min and then cooled again to 0°C. After 15 min, the suspension of benzeneselenenic acid

© 1997 NRC Canada

Can. J. Chem. Downloaded from www.nrcresearchpress.com by 88.146.161.215 on 09/08/12
For personal use only.

was filtered off. The filtrate was washed once with 10 mL of saturated aqueous solution of sodium bicarbonate, twice with water (10 mL each), and once with saturated aqueous solution of sodium chloride (10 mL), dried over anhydrous magnesium sulfate, filtered, and concentrated. The crude product was subjected to flash chromatography on silica gel. Elution with 10% ethyl acetate in Skelly B gave 2-carbomethoxy-8-methyl-2-cyclooctenone (**2**) (0.86 g, 86% yield) as a colorless oil. IR ($CHCl_3$ cast): 1723 (C=O, ester), 1695 (C=O, ketone), 1640 (C=C), 1379 (α-CH_3), 1365 (OCH_3) cm^{-1}; ^1H NMR (300 MHz in $CDCl_3$) δ: 7.18 (t, 1H, J = 4.5 Hz, =C**H**), 3.68 (s, 3H, O**C**$\mathbf{H}_3$), 2.60 (m, 1H, C**H**CH_3), 2.34 (m, 2H, =CHC$\mathbf{H}_2$), 1.10 (d, 3H, J = 7 Hz, C$\mathbf{H}_3$); ^{13}C NMR (APT, 75 MHz in $CDCl_3$) δ: 211.0 (p), 165.0 (p), 147.0 (a), 131.4 (p), 52.2 (a), 47.5 (a), 30.2 (p), 29.7 (p), 26.0 (p), 21.5 (p), 15.3 (a); HRMS, *m/z* (M^+) calcd. for $C_{11}H_{16}O_3$: 196.10984; found: 196.11022. Anal. calcd. for $C_{11}H_{16}O_3$: C 67.32%, H 8.22%; found: C 67.23%, H 8.31%.

2-Carbethoxy-8-methyl-2-cyclooctenone (3)

This compound was prepared from keto ester **12** (500 mg, 2.36 mmol) in 85% yield using the phenylselenenylation – oxidative elimination process described above. IR ($CHCl_3$ cast): 1720 (C=O, ester), 1696 (C=O, ketone), 1639 (C=C), 1378 (α-CH_3), 1369 (CH_3, ester) cm^{-1}; ^1H NMR (300 MHz in $CDCl_3$) δ: 7.18 (t, 1H, J = 4.5 Hz, =C**H**), 4.27 (m, 2H, O$\mathbf{CH}_2$), 2.60 (m, 1H, C**H**CH_3), 2.35 (m, 2H, $\mathbf{CH}_2$CH=), 1.23 (t, 3H, J = 7 Hz, $OCH_2\mathbf{CH}_3$), 1.14 (d, 3H, J = 7 Hz, C$\mathbf{H}_3$); ^{13}C NMR (APT, 75 MHz in $CDCl_3$) δ: 211.0 (p), 164.6 (p), 146.0 (a), 131.9 (p), 61.1 (p), 47.7 (a), 30.2 (p), 29.9 (p), 26.1 (p), 21.6 (p), 15.6 (a), 14.1 (a); HRMS, *m/z* (M^+) calcd. for $C_{12}H_{18}O_3$: 210.12560; found: 21.12554. Anal. calcd. for $C_{12}H_{18}O_3$: C 68.55%, H 8.63%; found: C 68.45%, H 8.50%.

General procedure for the preparation of trialkylsilyloxy substituted 1,3-butadienes 17–20

Diisopropylamine (0.25 mL, 1.8 mmol) was dissolved in 5 mL of THF and cooled to 0°C with stirring. A solution of *n*-butyllithium (1.6 M in THF, 1.2 mL, 1.9 mmol) was added dropwise over 20 min. The resulting lithium diisopropylamide solution was then cooled to −78°C followed by dropwise addition of a solution of the corresponding substituted methyl vinyl ketone (100 mg, 1.2 mmol) in 5 mL of THF over 30 min. The solution was stirred at −78°C for 30 min followed by rapid addition of the corresponding trialkylsilyl chloride (1.8 mmol). The reaction mixture was allowed to warm to room temperature after 15 min and stirred at room temperature for 40 h. The reaction mixture was quenched with 10 mL of water and the aqueous layer was extracted three times with Skelly B (10 mL each). The organic solutions were combined, washed twice with water (10 mL each) and once with saturated aqueous sodium chloride solution (10 mL), dried over anhydrous magnesium sulfate, filtered, and concentrated. The crude yellow oil was purified by bulb-to-bulb distillation to give the product.

2-tert-*Butyldimethylsilyloxy-3-methyl-1,3-butadiene (**17**)*

This compound was prepared in an improved yield of 92% yield from 3-methyl-3-buten-2-one using *tert*-butyldimethylsilyl chloride as the trapping reagent according to the reported procedure (14, 24).

*2-Triisopropylsilyloxy-3-methyl-1,3-butadiene (**18**)*

The title compound was prepared from 3-methyl-3-buten-2-one using triisopropylsilyl chloride as the trapping reagent. Bulb-to-bulb distillation of the crude product at 80°C/0.2 Torr (1 Torr = 133.3 Pa) gave the desired diene **18** in 70% yield. IR (hexane cast): 1590 (C=C-O), 1384 (CH_3), 1023, 819 (Si-O-C) cm^{-1}; ^1H NMR (300 MHz in C_6D_6) δ: 5.70 (ddd, 1H, J = 0.5, 0.5, 2.5 Hz, C**H**H=C(CH_3)), 5.00 (s, br, CH**H**=C(CH_3)), 4.45 (s, 1H, C**H**H=C(OTIPS)), 4.35 (s, 1H, CH**H**=C-(OTIPS)), 1.75 (s, 3H, C$\mathbf{H}_3$C=), 1.13–1.11 (m, 21H, C**H**, C$\mathbf{H}_3$ on TIPS); ^{13}C NMR (75 MHz in C_6D_6) δ: 157.2 (p), 140.2 (p), 113.9 (p), 91.7 (p), 19.9 (a), 18.3 (6C, a), 13.2 (3C, a); HRMS, *m/z* (M^+) calcd. for $C_{14}H_{28}OSi$: 240.19095; found: 240.18995.

trans-*2*-tert-*Butyldimethylsilyloxy-1,3-pentadiene (**19**)*

Diene **19** was prepared from *trans*-3-penten-2-one using *tert*-butyldimethylsilyl chloride as the trapping reagent. Bulb-to-bulb distillation of the crude product and collecting the fraction at 70°C/0.5 Torr gave the diene in 85% yield. IR (neat film): 1657 and 1641 (C=C, conjugated), 1593 (C=C-O), 1023, 826 (Si-O-C) cm^{-1}; ^1H NMR (300 MHz, $CDCl_3$) δ: 6.17 (qd, 1H, J = 7, 14 Hz, CH_3C**H**=CH), 5.88 (qd, 1H, J = 2, 14 Hz, CH_3CH=C**H**), 4.29 (s, 1H, =CH**H**), 4.22 (s, 1H, =C**H**H), 1.58 (dd, 3H, J = 2, 7 Hz, C$\mathbf{H}_3$CH=), 0.99 (s, br, 9H, $(\mathbf{CH}_3)_3$C), 0.15 (s, br, 6H, 2 C$\mathbf{H}_3$); ^{13}C NMR (APT, 75 MHz, C_6D_6) δ: 155.4 (p), 129.8 (a), 126.0 (a), 93.4 (p), 25.8 (3C, a), 18.3 (p), 17.3 (a), −4.7 (2C, a); HRMS, *m/z* (M^+) calcd. for $C_{14}H_{28}OSi$: 240.19095; found: 240.18995.

trans-*2-Triisopropylsilyloxy-1,3-pentadiene (**20**)*

The title compound was prepared from 3-penten-2-one using triisopropylsilyl chloride as the trapping reagent. The crude product was purified by bulb-to-bulb distillation. Diene **20** was collected at 40°C/0.5 Torr in 90% yield. ^1H NMR (300 MHz, C_6D_6) δ: 6.25 (qd, 1H, J = 7, 14 Hz, CH_3C**H**=CH), 5.88 (qd, 1H, J = 2, 14 Hz, CH_3CH=C**H**), 4.29 (s, br, 1H, **H**HC=), 4.19 (s, br, 1H, H**H**C=), 1.60 (dd, 3H, J = 2, 7 Hz, =CHC$\mathbf{H}_3$), 1.13 (m, 3H, 3 SiC**H**$(CH_3)_2$), 1.02 (d, 18H, J = 6.5 Hz, 3 CH($\mathbf{CH}_3)_2$); ^{13}C NMR (300 MHz, C_6D_6) δ: 155.8 (p), 130.0 (a), 126.1 (a), 92.8 (p), 18.3 (a), 17.9 (6C, a), 12.6 (3C, a); HRMS, *m/z* (M^+) calcd. for $C_{14}H_{28}OSi$: 240.19095; found: 240.18994.

General procedure for $FeCl_3$, $SnCl_4$, and $BF_3 \cdot OEt_2$ catalyzed Diels–Alder reactions

To an ethereal solution (3 mL) of enone (0.24 mmol) was added the diene (2.4 mmol). Lewis acid (0.24 mmol) was then added and the resulting solution was stirred. The progress of the reaction was monitored by TLC. Upon completion, a saturated aqueous sodium bicarbonate solution was added. The ether layer was separated and the aqueous layer was extracted three times with ether (10 mL each). The combined ether solutions were washed with water (10 mL) and saturated aqueous sodium chloride solution (10 mL), dried over anhydrous magnesium sulfate, filtered, and concentrated. The residue was purified by flash chromatography (ethyl acetate – Skelly B) to give the desired adduct(s). Yield, time, and temperature of each reaction are shown in Tables 1, 2, and 3. When more than one product was obtained, products are presented in order of elution from flash chromatography.

© 1997 NRC Canada

Can. J. Chem. Downloaded from www.nrcresearchpress.com by 88.146.161.215 on 09/08/12
For personal use only.

General procedure for $ZnCl_2$ catalyzed Diels–Alder reactions

Zinc chloride (0.48 mmol) was fused in a reaction flask under an argon atmosphere and dissolved in dry ether (3 mL). A solution of enone (0.24 mmol) in dry ether (1 mL) was added. After stirring at room temperature for 30 min, diene (2.4 mmol) was then added. The resulting mixture was stirred at room temperature. The reaction was monitored with TLC and upon completion was quenched with saturated aqueous sodium bicarbonate solution. The ether layer was separated and the aqueous layer was extracted three times with ether (10 mL each). The combined ether solutions were washed with saturated aqueous sodium chloride solution (10 mL), dried over anhydrous magnesium sulfate, filtered, and concentrated. The residue was purified by flash chromatography (ethyl acetate – Skelly B) to give the desired adduct(s). Yields and reaction conditions are shown in Tables 1, 2, and 3.

(1S, 8S*)-1-Carbethoxy-10-methylbicyclo[6.4.0]dodec-10-en-2-one (**21**)*: IR ($CHCl_3$ cast): 1738 (C=O, ester), 1705 (C=O, ketone) cm^{-1}; ^1H NMR (500 MHz, $CDCl_3$) δ: 5.18 (m, 1H, =C**H**), 4.10 (m, 2H, OC$\mathbf{H}_2$), 3.15 (m, 1H, C**H**, C-8), 3.11 (dm, 1H, J = 12 Hz, CH**H**C=O), 2.80 (ddd, 1H, J = 1.5, 5.5, 18.5 Hz, C**H**H, C-12), 2.54 (dm, 1H, J = 18 Hz, C**H**H, C-9), 2.16 (dddd, 1H, J = 2, 4, 7, 18.5 Hz, CH**H**, C-12), 2.08 (ddd, 1H, J = 3.5, 5, 12 Hz, C**H**HC=O), 1.58 (s, br, 3H, =CC$\mathbf{H}_3$), 1.18 (t, 3H, J = 7 Hz, $OCH_2C\mathbf{H}_3$); ^{13}C (APT, 75 MHz, $CDCl_3$) δ: 212.3 (p), 170.6 (p), 131.6 (p), 118.5 (a), 63.34 (p), 61.5 (p), 37.2 (p), 36.4 (p), 32.8 (a), 32.6 (p), 29.8 (p), 26.2 (p), 25.09 (p), 24.2 (p), 23.4 (a), 14.0 (a); HRMS, *m/z* (M^+) calcd. for $C_{16}H_{24}O_3$: 264.17255; found: 264.17239.

(1S, 8S*)-1-Carbethoxy-10,11-dimethylbicyclo[6.4.0]dodec-10-en-2-one (**22**)*: IR ($CHCl_3$ cast): 1738 (C=O, ester), 1705 (C=O, ketone) cm^{-1}; ^1H NMR (300 MHz, $CDCl_3$) δ: 4.10 (m, 2H, OC$\mathbf{H}_2$), 3.18 (m, 1H, C**H**HC=O), 3.12 (m, 1H, C**H**, ring junction), 2.70 (d, 1H, J = 18 Hz, C**H**H, C-12), 2.55 (d, 1H, J = 18 Hz, C**H**H, C-9), 2.20 (d, 1H, J = 18 Hz, CH**H**, C-12), 2.10 (m, 1H, CH**H**C=O), 1.65 (s, br, 3H, =CC$\mathbf{H}_3$), 1.55 (s, br, 3H, =CC$\mathbf{H}_3$), 1.15 (t, 3H, J = 7 Hz, $OCH_2C\mathbf{H}_3$); ^{13}C (APT, 75 MHz, $CDCl_3$) δ: 212.7 (p), 170.6 (p), 123.3 (p), 122.8 (p), 64.1 (p), 61.4 (p), 38.0 (p), 37.2(p), 33.0 (a), 33.6 (p), 30.7 (p), 29.8 (p), 26.3 (p), 24.3 (p), 19.1 (a), 18.8 (a), 14.0 (a); HRMS, *m/z* (M^+) calcd. for $C_{17}H_{26}O_3$: 278.18820; found: 278.18844.

(1S, 8S*, 12S*)-1-Carbethoxy-12-methylbycyclo[6.4.0.]-dodec-10-en-2-one (23) and (1S*, 8S*, 12R*)-1-carbethoxy-12-methylbicyclo[6.4.0]dodec-10-en-2-one (**24**)*

The products **23** and **24** were obtained as an inseparable mixture in an 85:15 ratio. For the mixture: IR ($CHCl_3$ cast): 1736 (C=O, ester), 1702 (C=O, ketone) cm^{-1}; HRMS, *m/z* (M^+) calcd. for $C_{16}H_{24}O_2$: 264.17255; found: 264.17258. Anal. calcd. for $C_{16}H_{24}O_2$: C 72.69%, H 9.15%; found: C 72.56%, 9.34%. For the major isomer **23**: ^1H NMR (300 MHz, $CDCl_3$) δ: 5.50–5.60 (m, 2H, C**H**=C**H**), 4.15 (m, 2H, OC$\mathbf{H}_2$), 3.00–3.10 (m, 2H, C**H** ring junction, and CH**H**C=O), 2.96 (q, 1H, J = 7.5 Hz, $CH_3C\mathbf{H}$CH=), 2.40 (m, 1H, C**H**HCH=), 2.15 (ddd, 1H, J = 7.5, 8, 13 Hz, C**H**HC=O), 1.90–1.30 (m, 7H, 3 C$\mathbf{H}_2$ and CH**H**CH=), 1.25 (t, 3H, J = 7 Hz, $OCH_2C\mathbf{H}_3$), 1.15 (d, 3H, J = 7.5 Hz, $C\mathbf{H}_3$CHCH=); ^{13}C NMR (APT, 75 MHz, $CDCl_3$) δ: 210.9 (p), 171.8 (p), 131.3 (a), 123.4 (a), 65.4 (p), 61.6 (p), 40.9 (p), 35.0 (a), 34.5 (a), 32.4 (p), 30.2 (p), 27.5 (p), 27.3 (p), 23.3 (p), 16.6 (a), 13.9 (a). For the minor isomer **24**: ^1H NMR δ: 1.07 (d, 3H, J = 7 Hz, C$\mathbf{H}_3$); ^{13}C NMR δ: 211.1 (p), 130.1 (a), 123.6 (a), 63.4 (p), 60.6 (p), 40.3 (p), 32.2 (a), 32.1 (p), 31.8 (p), 29.8 (a), 27.3 (p), 26.2 (p), 24.0 (p), 18.0 (a), 14.1 (a).

(1S, 8S*, 9R*, 12S*)-1-Carbethoxy-9,12-dimethylbicyclo-[6.4.0]dodec-10-en-2-one (**25**)*: IR ($CHCl_3$, cast): 1738 (C=O, ester), 1697 (C=O, ketone) cm^{-1}; ^1H NMR (300 MHz, $CDCl_3$) δ: 5.60 (ddd, 1H, J = 3, 5, 10 Hz, =C**H**, C-11), 5.20 (ddd, 1H, J = 1, 2, 10 Hz, =C**H**, C-10), 4.10 (m, 2H, OC$\mathbf{H}_2$), 3.30 (m, 2H, C**H**, C-12 and CH**H**C=O), 3.10 (m, 1H, C**H** ring junction), 2.60 (m, 1H, C**H**, C-9), 2.22 (m, 1H, C**H**HC=O), 1.20 (t, 3H, J = 7 Hz, $OCH_2C\mathbf{H}_3$), 1.15 (d, 3H, J = 7.5, $C\mathbf{H}_3$CHCH=), 1.00 (d, 3H, J = 7.5 Hz, =CHCHC$\mathbf{H}_3$); ^{13}C NMR (APT, 75 MHz, $CDCl_3$), δ: 211.8 (p), 171.0 (p), 131.9 (a), 127.9 (a), 68.0 (p), 61.9 (p), 39.2 (p), 38.1 (a), 32.5 (a), 31.7 (a), 30.4 (p), 27.2 (p), 27.1 (p), 25.2 (p), 18.0 (a), 17.0 (a), 13.9 (a); HRMS, *m/z* (M^+) calcd. for $C_{17}H_{26}O_3$: 278.18800; found: 278.18800. Anal. calcd. for $C_{17}H_{26}O_3$: C 73.33%, H 9.41%; found: C 73.44%, H 9.78%.

(1S, 8S*, 12S*)-1-Carbethoxy-10,12-dimethylbicyclo-[6.4.0]dodec-10-en-2-one (**26**) and (1S*, 8S*, 12R*)-1-carbethoxy-10,12-dimethylbicyclo[6.4.0]dodec-10-en-2-one (**27**)*

The two isomeric products were obtained as an inseparable 77:23 mixture. For the mixture: IR ($CHCl_3$ cast): 3058 (=CH), 1738 (C=O, ester), 1704 (C=O, ketone) cm^{-1}; HRMS, *m/z* (M^+) calcd. for $C_{17}H_{26}O_3$: 278.18820; found: 278.18587. For the major isomer **26**: ^1H NMR (300 MHz, $CDCl_3$) δ: 5.06 (s, br, 1H, =C**H**), 4.20–4.00 (m, 2H, OC$\mathbf{H}_2$), 3.05–2.95 (m, 2H, C**H** ring junction and HC**H**C=O), 2.80 (m, 1H, C**H**, C-12), 2.28–2.10 (m, 2H, C$\mathbf{H}_2$, C-9), 1.68 (s, 3H, $C\mathbf{H}_3$C=), 1.20 (t, 3H, J = 7.5 Hz, $OCH_2C\mathbf{H}_3$), 1.02 (d, 3H, J = 7 Hz, $C\mathbf{H}_3$CH); ^{13}C NMR (APT, 75 MHz, $CDCl_3$) δ: 211.1 (p), 170.7 (p), 130.7 (p), 124.2 (a), 63.3 (p), 60.5 (p), 40.2 (p), 36.6 (p), 32.8 (a), 32.1 (p), 30.0 (a), 27.6 (p), 26.2 (p), 24.0 (p), 23.5 (a), 18.3 (a), 14.1 (a). For the minor isomer **27**: ^1H NMR (300 MHz, $CDCl_3$) δ: 5.26 (s, br, =C**H**), 2.75–2.65 (m, 2H, C**H**, ring junction and C**H**, C-12), 2.40 (m, 1H, C**H**HC=O), 1.65 (s, 3H, =CC$\mathbf{H}_3$), 1.10 (d, 3H, J = 7 Hz, CHC$\mathbf{H}_3$); ^{13}C NMR (APT, 75 NHz, $CDCl_3$) δ: 210.8 (p), 172.1 (p), 130.5 (p), 125.4 (a), 65.0 (p), 61.5 (p), 41.2 (p), 35.6 (a), 35.1 (a), 34.9 (p), 29.8 (p), 27.6 (p), 27.0 (p), 23.0 (p), 16.9 (a), 14.0 (a).

General procedure for the $SnCl_4$ catalyzed Diels–Alder reaction of trialkylsilyloxy substituted dienes 17–20

Stannic chloride (0.24 mmol) was added to an ether solution (3 mL) of enone **2** (0.24 mmol) at −78°C and stirred for a period of time to allow for the formation of the complex of stannic chloride and the dienophile **2**. Then an ether solution (1 mL) of diene (0.48 mmol for dienes **18** and **20**, 2.4 mmol for dienes **17** and **19**) was added and the reaction was monitored by TLC. Upon completion of the reaction, saturated aqueous sodium bicarbonate solution was added. The ether layer was separated and the aqueous layer was extracted three times with ether (10 mL each). The combined ether solutions were washed with water (10 mL) and saturated aqueous sodium chloride solution (10 mL), dried over anhydrous magnesium

© 1997 NRC Canada

Can. J. Chem. Downloaded from www.nrcresearchpress.com by 88.146.161.215 on 09/08/12
For personal use only.

sulfate, and concentrated. The crude product was purified by flash chromatography to give the desired product(s). Yields of products and individual reaction conditions are shown in Table 3.

(1S, 3R*, 8S*)-1-Carbethoxy-3,10,11-trimethylbicyclo-[6.4.0]dodec-10-en-2-one (**28**)*: IR ($CHCl_3$, cast): 1737 (C=O, ester), 1695 (C=O, ketone), 1374 (CH_3) cm^{-1}; ^1H NMR (300 MHz, $CDCl_3$) δ: 4.15 (m, 2H, OCH_2), 3.25 (m, 1H, CH_3CHC=O), 2.66 (m, 2H, =CCH_2, C-9), 2.59 (s, 2H, CH_2C=, C-12), 1.63 (s, br, 3H, =CCH_3), 1.54 (s, br, 3H, =CCH_3), 1.21 (t, 3H, J = 7 Hz, OCH_2CH_3), 1.04 (d, 3H, J = 7 Hz, $CHCH_3$); ^{13}C NMR (APT, 75 MHz, $CDCl_3$) δ: 216.8 (p), 172.2 (p), 124.0 (p), 121.7 (p), 64.4 (p), 60.9 (p), 42.1 (a), 40.0 (p), 36.50 (a), 36.45 (p), 32.4 (p), 31.9 (p), 26.5 (p), 25.8 (p), 19.4 (a), 19.04 (a), 19.03 (a), 14.1 (a); HRMS, *m/z* (M^+) calcd. for $C_{18}H_{28}O_3$: 292.20386; found: 292.20349. Anal. calcd. for $C_{18}H_{28}O_3$: C 73.93%, H 9.65%; found: C 74.02%, H 9.42%.

(1S, 3R*, 8S*)-1-Carbethoxy-3,10-dimethylbicyclo-[6.4.0]-dodec-10-en-2-one (**29**)*: IR ($CHCl_3$, cast): 1695 (C=O, ketone), 1737 (C=O, ester) cm^{-1}; ^1H NMR (300 MHz, $CDCl_3$) δ: 5.33 (m, 1H, =C**H**), 4.17 (m, 2H, OCH_2), 3.25 (m, 1H, $CHCH_3$), 2.82–2.50 (m, 4H, CH_2CH=$C(CH_3)CH_2$), 1.60 (s, 3H, CH_3C=), 1.23 (t, 3H, OCH_2CH_3), 1.04 (d, 3H, J = 6.5 Hz, CH_3); ^{13}C NMR (APT, 75 MHz in $CDCl_3$) δ: 216.9 (p), 172.2 (p), 132.4 (p), 116.9 (a), 63.3 (p), 61.0 (p), 42.1 (a), 38.4 (p), 36.6 (p), 36.5 (a), 32.4 (p), 26.4 (p), 26.3 (p), 25.9 (p), 23.6 (a), 19.3 (a), 14.0 (a); HRMS, *m/z* (M^+) calcd. for $C_{17}H_{26}O_3$: 278.18820; found: 278.18771. Anal. calcd. for $C_{17}H_{26}O_3$: C 73.35%, H 9.41%; found: C 73.35%, H 9.59%. INPET: irr. H at δ 5.33 (4946 Hz), found C signals from ^{13}C NMR at δ 63.3 (**C**, ring juction), 38.4 (=$CHCH_2$), 26.3 (=$C(CH_3)CH_2$), 23.7 (=CCH_3); irr. H at δ 3.25 (4337.4 Hz), found C signals from ^{13}C NMR at δ 217.0 (**C**=O ketone), 36.6 ($CH_2CH(CH_3)$), 25.9(CH_2), 19.3 ($CHCH_3$); irr. H at δ 1.04 (3679.3 Hz) found C signals from ^{13}C NMR at δ 217.0 (**C**=O ketone), 42.1 ($CH(CH_3)$).

(1R, 3R*, 8S*, 12S*)-1-Carbethoxy-3,10,12-trimethylbicyclo[6.4.0]dodec-10-en-2-one (**30**) and diastereomer **31***

In this Diels–Alder reaction, an inseparable mixture of **30** and **31** was obtained in a ratio of 4:1. For the mixture: IR ($CHCl_3$, cast): 1723 (C=O, ester), 1696 (C=O, ketone) cm^{-1}; HRMS, *m/z* (M^+) calcd. for $C_{18}H_{28}O_3$: 292.20386; found: 292.20374. Anal. calcd. for $C_{18}H_{28}O_3$: C 73.93%, H 9.65%; found: C 73.90%, H 9.69%. For the major isomer **30**: ^1H NMR (300 MHz, $CDCl_3$) δ: 5.08 (m, 1H, =C**H**), 4.15 (m, 2H, OCH_2), 2.85 (m, 1H, CH_3CHCH=), 2.60 (m, 1H, C**H**, ring junction), 2.55 (m, 1H, C**H**C=O), 2.29 (dd, 1H, J = 6, 18 Hz, CH**H**C=), 2.05 (dd, 1H, J = 6, 18 Hz, C**H**HC=), 1.60 (s, 3H, =CCH_3), 1.20 (t, 3H, J = 7 Hz, OCH_2CH_3), 0.95 (d, 3H, J = 6.5 Hz, CH_3CHC=O), 0.88 (d, 3H, J = 7.5 Hz, CH_3CHCH=); ^{13}C NMR (75 MHz, $CDCl_3$) δ: 214.3 (p), 173.5 (p), 132.2 (p), 125.0 (a), 65.3 (p), 60.9 (p), 45.2 (a), 38.8 (a), 38.4 (a), 34.7 (p), 33.5 (p), 31.2 (p), 26.0 (p), 23.3 (a), 21.0 (p), 18.9 (a), 17.9 (a), 14.1 (a). For the minor isomer **31**: ^1H NMR (300 MHz, $CDCl_3$) δ: 5.18 (s, br, =C**H**), 1.26 (t, 3H, J = 7 Hz, OCH_2CH_3), 1.19 (d, 3H, J = 7 Hz, CH_3), 1.12 (d, 3H, J = 7 Hz, CH_3); ^{13}C NMR (APT, 75 MHz, $CDCl_3$) δ: 171.9 (p), 131.4 (p), 124.3 (a), 65.8 (p), 60.4 (p), 41.8 (a), 38.6 (p), 37.0 (a), 36.1 (p), 31.6 (a), 31.2 (p), 26.2 (p), 25.0 (p), 23.3 (a), 20.0 (a), 18.9 (a), 16.1 (a).

(1R, 3R*, 8S*, 12S*)-1-Carbomethoxy-3,10,12-trimethylbicyclo[6.4.0]dodec-10-en-2-one (**32**) and diastereomer **33***

For the mixture of **32** and **33**: IR ($CHCl_3$, cast): 1733 (C=O, ester), 1699 (C=O, ketone) cm^{-1}; HRMS, *m/z* (M^+) calcd. for $C_{17}H_{26}O_3$: 278.18820; found: 278.18799. Anal. calcd. for $C_{17}H_{26}O_3$: C 73.35%, H 9.42%; found: C 73.46%; H 9.35%. For the major isomer **32**: ^1H NMR (300 MHz, $CDCl_3$) δ: 5.13 (m, 1H, =C**H**), 3.72 (s, 3H, OCH_3), 2.84 (m, 1H, CH_3CHCH=), 2.60 (m, 1H, C**H**, ring junction), 2.50 (m, 1H, C**H**C=O), 2.30 (dd, 1H, J = 10.5, 19 Hz, CH**H**C=), 2.07 (dd, 1H, J = 8, 19 Hz, C**H**HC=), 1.67 (s, 3H, =CCH_3), 0.98 (d, 3H, J = 6.5 Hz, CH_3CHC=O), 0.90 (d, 3H, J = 7.0 Hz, CH_3CHCH=); ^{13}C NMR (75 MHz, $CDCl_3$) δ: 214.2 (p), 174.1 (p), 132.2 (p), 125.0 (a), 65.4 (p), 51.9 (a), 45.2 (a), 38.8 (a), 38.46 (a), 34.7 (p), 33.5 (p), 31.0 (p), 26.0 (p), 22.8 (a), 21.1 (p), 18.8 (a), 17.9 (a). For the minor isomer **33**: ^1H NMR (300 MHz, $CDCl_3$) δ: 5.18 (s, br, =C**H**), 3.67 (s, 3H, OCH_3), 3.13 (m, 1H, =$CHCHCH_3$), 2.97 (m, 1H, C**H**C=O), 1.15 (d, 3H, J = 7.5 Hz, CH_3CHC=O), 1.09 (d, 3H, J = 7.5 Hz, CH_3CHCH=); ^{13}C NMR (APT, 75 MHz, $CDCl_3$) δ: 131.3 (p), 124.3 (a), 66.8 (p), 51.5 (a), 41.9 (a), 38.54 (p), 36.6 (a), 36.0 (p), 31.7 (a), 26.1 (p), 24.7 (p), 23.4 (a), 19.9 (a), 18.0 (a).

(1S, 3R*, 8S*)-1-Carbomethoxy-10-triisopropylsilyloxy-3,11-dimethylbicyclo[6.4.0]dodec-10-en-2-one (**34**)*

In this reaction, the solution of dienophile **2** and stannic chloride was stirred for 20 min at −78°C and then the diene **18** was added dropwise. The adduct **34** was obtained as the only isomer in 90% yield. IR ($CHCl_3$, cast): 1744 (C=O, ester), 1696 (C=O, ketone), 1658 (C=C) cm^{-1}; ^1H NMR (300 MHz, C_6D_6) δ: 3.40 (s, 3H, OCH_3), 3.05 (d, br, 1H, J = 18 Hz, C**H**HC(OTIPS)=), 2.95–2.85 (m, 2H, $CHCH_3$ and C**H** ring junction), 2.83 (d, 1H, J = 18 Hz, C**H**HC(CH_3)=), 2.64 (d, br, 1H, J = 18 Hz, CH**H**C(CH_3)=), 1.77 (s, 3H, =CCH_3), 1.73 (d, 1H, J = 18 Hz, CH**H**C(OTIPS)=), 1.25–1.00 (m, 26H, 3 SiC**H**(CH_3)$_2$, 2 CH_2 and C**H**H), 0.97 (d, 3H, J = 7.5 Hz, CH_3); ^{13}C NMR (APT, 75 MHz, C_6D_6) δ: 215.1 (p), 172.1 (p). 142.2 (p), 106.8 (p), 63.8 (p), 51.9 (a), 42.0 (a), 39.0 (p), 37.9 (a), 36.5 (p), 32.6 (p), 31.3 (p), 26.3 (p), 26.1 (p), 19.5 (a), 18.3 (a, 6C), 16.6 (a), 14.2 (a), 13.5 (a, 3C); HRMS, *m/z* (M^+) calcd. for $C_{25}H_{44}O_4Si$: 436.30090; found: 436.30084. Anal. calcd. for $C_{25}H_{44}O_4Si$: C 68.76%, H 10.16%; found: C 68.87%, H 10.30%.

(1R, 3R*, 8S*, 12S*)-10-*tert*-Butyldimethylsilyloxy-1-carbomethoxy-3,12-dimethylbicyclo[6.4.0]dodec-10-en-2-one (**35**) and diastereomer **36***

In this reaction, the solution of enone **2** and stannic chloride was stirred for 20 min at −78°C and then diene **19** was added. The mixture of **35** and **36** was obtained in 89% yield as an inseparable mixture of two isomers in a ratio of 2:1. For the mixture: IR ($CHCl_3$, cast): 1730 (C=O, ester), 1694 (C=O, ketone) cm^{-1}; HRMS, *m/z* (M^+) calcd. for $C_{22}H_{30}O_4Si$: 394.25294; found: 394.25318. For the major isomer **35**: ^1H NMR (300 MHz, C_6D_6) δ: 4.72 (s, br, 1H, =C**H**), 3.32 (s, 3H, OCH_3), 3.15 (m, 1H, CH_3CHCH=), 2.93 (m, 1H, CH_3CHC=O), 2.30 (dddd, 1H, J = 1.5, 3, 9.5, 18 Hz, CH**H**, C-9), 2.10 (dddd, 1H, J = 1.5, 3, 7.5, 18 Hz, C**H**H, C-9), 1.27

© 1997 NRC Canada

Can. J. Chem. Downloaded from www.nrcresearchpress.com by 88.146.161.215 on 09/08/12
For personal use only.

(d, 3H, J = 7 Hz, $CH_3CHC{=}O$), 1.17 (d, 3H, J = 7.5 Hz, $CH_3CHCH{=}$), 1.00 (s, 9H, $SiC(CH_3)_3$), 0.19 (m, 6H, 2 $SiCH_3$); ^{13}C NMR (APT, 75 MHz, C_6D_6) δ: 211.8 (p), 173.4 (p), 148.6 (p), 107.7 (a), 65.4 (p), 51.4 (a), 46.9 (a), 41.4 (a), 39.0 (p), 38,8 (a), 33.6 (p), 31.4 (p), 26.7 (p), 26.5 (a), 25.9 (a, 3C), 21.3 (p), 19.8 (a), 18.8 (a), 18.2 (p), 14.3 (a). For the minor isomer **36**: ^1H NMR (300 MHz, C_6D_6) δ: 4.78 (s, br, 1H, $=CH$), 3.39 (s, 3H, OCH_3), 2.83 (m, 1H, $CH_3CHCH{=}$), 2.55 (m, 1H, $CH_3CHC{=}O$), 1.15 (d, 3H, J = 7.5 Hz, $CH_3CHC{=}O$), 0.99 (s, 9H, $SiC(CH_3)_3$), 0.18 (s, 6H, 2 $SiCH_3$); ^{13}C NMR (APT, 75 MHz, C_6D_6) δ: 215.3 (p), 171.8 (p), 108.2 (a), 67.0 (p), 51.2 (a), 36.5 (p), 37.8 (a), 33.7 (p), 32.3 (p), 31.2 (p), 30.9 (a), 26.0 (a, 3C), 24.9 (p), 22.8 (p), 19.9 (a), 18.9 (a), 14.6 (a), 11.6 (a).

(1R, 3R*, 8S*, 12S*)-1-Carbomethoxy-3,12-dimethylbicyclo[6.4.0]dodecane-2,10-dione (37) and (1R*, 3R*, 8S*, 12S*)-1-carbomethoxy-10-triisopropylsilyloxy-3,12-dimethylbicyclo[6.4.0]dodec-9-en-2-one (38)*

In this reaction, the solution of enone **2** and stannic chloride was stirred for 1 h at −78°C and then diene **20** was added. Ketone **38** (1% yield) and dione **37** (98% yield) were separated by flash chromatography. Compound **38**: IR ($CHCl_3$, cast): 1739 (C=O, ester), 1694 (C=O, ketone), 1674 (C=C) cm^{-1}; ^1H NMR (300 MHz, C_6D_6) δ: 4.92 (dd, 1H, J = 1, 6 Hz, $=CH$), 3.50 (s, 3H, OCH_3), 3.20 (m, br, 1H, CH, ring junction), 2.70 (m, 1H, $CH_3CHC{=}O$), 2.47 (dd, br, 1H, J = 10, 16 Hz, CHHCOTIPS), 2.20 (m, 2H, CHHCOTIPS, $CHCH_3$), 1.22 (d, 3H, J = 6.5 Hz, $CHCH_3$), 1.02 (d, 3H, J = 6 Hz, CH_3CHCO), 1.11 (s, br, 18H, 3 $SiCH(CH_3)_2$), 1.08 (m, 3H, 3 $SiCH(CH_3)_2$); ^{13}C NMR (APT, 75 MHz, C_6D_6) δ: 215.9 (p), 171.7 (p), 149.2 (p), 109.1 (a), 68.4 (p), 51.3 (a), 40.5 (a), 38.9 (a), 37.8 (p), 37.0 (p), 31.2 (p), 29.3 (a), 28.2 (p), 23.6 (p), 20.2 (a), 18.2 (a, 6C), 18.1 (a), 13.0 (a, 3C); HRMS, *m/z* (M^+) calcd. for $C_{25}H_{44}O_4Si$: 436.30090; found: 436.30074. Compound **37**, mp 106–107°C (hexane): IR ($CHCl_3$, cast): 1733 (C=O, ester), 1695 (C=O, ketone) cm^{-1}; ^1H NMR (300 MHz, C_6D_6) δ: 3.42 (s, 3H, OCH_3), 2.73 (m, 1H, $CH_3CHC{=}O$), 2.40 (dd, 1H, J = 14, 14 Hz, $CHHC{=}O$), 2.27 (dd, 1H, J = 5.5, 14 Hz, $CHHC{=}O$), 2.18 (ddd, 1H, J = 2, 4.5, 14 Hz, $CHHC{=}O$), 2.09 (m, 1H, $CHCH_3$), 1.90 (ddd, 1H, J = 2.5, 2.5, 14 Hz, $CHHC{=}O$), 1.02 (d, 3H, J = 6.5 Hz, CH_3CHCO), 0.90 (d, 3H, J = 6.5 Hz, CH_3CH); ^{13}C NMR (APT, 75 MHz, C_6D_6) δ: 214.5 (p), 206.6 (p), 171.8 (p), 68.9 (p), 51.5 (a), 48.6 (p), 46.7 (p), 40.7 (a), 39.9 (a), 37.0 (p), 33.3 (a), 28.5 (p), 27.1 (p), 23.1 (p), 19.9 (a), 18.4(a); HRMS, *m/z* (M^+) calcd. for $C_{16}H_{24}O_3$: 280.16745; found: 280.16707. Anal. calcd. for $C_{16}H_{24}O_3$: C 68.55%, H 8.63%; found: C 68.72%, H 8.89%.

(1R, 3S*, 8S*, 9R*, 12S*)-1-Carbethoxy-3,9,12-trimethylbicyclo[6.4.0]dodec-10-en-2-one (39)*: IR ($CHCl_3$, cast): 3012 (=CH), 1741 (C=O, ester), 1714 (C=O, ketone), 1684 (C=C) cm^{-1}; ^1H NMR (300 MHz, $CDCl_3$) δ: 5.56 (ddd, 1H, J = 3, 4, 10 Hz, $=CH$), 5.21 (ddd, 1H, J = 1, 2, 10 Hz, $=CH$), 4.15 (m, 2H, OCH_2), 3.25 (m, 1H, $CHCH{=}$), 3.15 (dt, 1H, J = 5, 10 Hz, CH, ring junction), 2.81 (qdd, 1H, J = 3, 7, 11 Hz, CH_3CHCO), 2.30 (m, 2H, CHCH= and CHH, C-7), 1.4–1.9 (m, 7H, 3 CH_2 and CHH, C-7), 1.22 (t, 3H, J = 7 Hz, OCH_2CH_3), 1.15 (d, 3H, J = 7 Hz, CH_3CHCO), 1.08 (d, 3H, J = 7 Hz, $CH_3CHCH{=}$), 0.95 (d, 3H, J = 7 Hz, $CH_3CHCH{=}$); ^{13}C NMR (APT, 75 MHz, $CDCl_3$) δ: 214.0 (p), 172.7 (p), 131.5 (a), 128.1 (a), 69.4 (p), 61.5 (p), 49.5 (a), 39.9 (a), 33.4 (a), 32.8 (p), 32.5 (p), 27.0 (p), 25.9 (p), 24.9 (p), 21.1 (a), 18.3 (p), 17.8 (a), 14.0 (a); HRMS, *m/z* (M^+) calcd. for $C_{18}H_{28}O_3$: 292.20386; found: 292.20308. Anal. calcd. for $C_{18}H_{28}O_3$: C 73.93%, H 9.65%; found: C 73.87%, H 9.64%.

(1R, 3S*, 8S*, 12S*)-1-Carbethoxy-3,12-dimethylbicyclo[6.4.0]dodec-10-en-2-one (40) and diastereomer 41*

Compound **40** and its diastereomer **41** were obtained as an inseparable mixture in a ratio of 4:1. For the mixture: IR ($CHCl_3$, cast): 3022 (=CH), 1735 (C=O, ester), 1695 (C=O, ketone) cm^{-1}; HRMS, *m/z* (M^+) calcd. for $C_{17}H_{26}O_3$: 278.39497; found: 278.39497. Anal. calcd. for $C_{17}H_{26}O_3$: C 73.35%, H 9.41%; found: C 73.38%, H 9.40%. For the major isomer **40**: ^1H NMR (500 MHz, $CDCl_3$) δ: 5.70 (ddd, 1H, J = 3.5, 7, 10 Hz, $CH{=}$), 5.46 (ddd, 1H, J = 2, 4.5, 10 Hz, $CH{=}$), 4.24 (m, 2H, OCH_2), 2.87 (m, 1H, $CH_3CHCH{=}$), 2.60 (m, 2H, CH, ring junction, and CH_3CHCO), 2.30 (m, 1H, $CHHCH{=}$), 2.15 (m, 1H, $CHHCH{=}$), 1.25 (t, 3H, J = 7 Hz, OCH_2CH_3), 1.08 (d, 3H, J = 7.5 Hz, $CH_3CHC{=}O$), 0.98 (d, 3H, J = 7.5 Hz, $CH_3CHCH{=}$); ^{13}C NMR (75 MHz, $CDCl_3$) δ: 213.9 (p), 173.3 (p), 130.6 (a), 124.8 (a), 65.2 (p), 61.0 (p), 45.9 (a), 38.2 (a), 38.0 (a), 34.1 (p), 30.1 (p), 28.8 (p), 26.3 (p), 21.0 (p), 19.4 (a), 17.2 (a), 14.1 (a). For the minor isomer **41**: ^1H NMR (500 MHz in $CDCl_3$) δ: 5.58 (m, 1H, =CH), 5.49 (ddd, 1H, J = 2, 4.5, 10 Hz, =CH), 4.18 (m, 2H, OCH_2), 2.54 (m, 1H, $CHHCH{=}$), 1.28 (t, 3H, J = 7.5 Hz, OCH_2CH_3), 1.22 (d, 3H, J = 7.5 Hz, CH_3), 1.14 (d, 3H, J = 6.5 Hz, CH_3); ^{13}C NMR (75 MHz, $CDCl_3$) δ: 213.9 (p), 171.8 (p), 130.2 (a), 124.1 (a), 65.2 (p), 60.5 (p), 41.9 (a), 40.4 (a), 36.2 (a), 33.6 (p), 31.1 (p), 29.7 (p), 26.0 (p), 24.8 (p), 20.0 (a), 18.0 (a), 14.1 (a).

(1R, 2R*, 4R*, 9S*, 10S*)-2-Carbethoxy-4-methyltricyclo[8.2.1.0^{2,9}]tridec-11-en-3-one (42) and (1S*, 2R*, 4S*, 9S*, 10R*)-2-carbethoxy-4-methyltricyclo-[8.2.1.0^{2,9}]tridec-11-en-3- one (43)*

For compound **42**: IR ($CHCl_3$, cast): 3064 (=CH), 1735 (C=O, ester), 1689 (C=O, ketone) cm^{-1}; ^1H NMR (300 MHz, $CDCl_3$) δ: 6.35 (dd, 1H, J = 3, 5.5 Hz, $=CH$, C-11), 5.93 (dd, 1H, J = 3, 5.5 Hz, $=CH$, C-12), 4.15 (qd, 1H, J = 7.5, 11 Hz, OCHH), 3.98 (qd, 1H, J = 7.5, 11 Hz, OCHH), 3.30 (s, br, 1H, CH, ring junction), 2.49–2.60 (m, 3H, $=CHCH$, $CHCH_3$, CHCHH), 2.00 (dddd, 1H, J = 1, 11, 11, 15 Hz, $CHCH{=}$), 1.24 (t, 3H, J = 7.5 Hz, OCH_2CH_3), 1.10 (d, 3H, J = 7 Hz, CH_3); ^{13}C NMR (APT, 75 MHz, $CDCl_3$) δ: 213.3 (p), 172.2 (p), 141.1 (a), 135.5 (a), 60.8 (p), 68.7 (p), 54.1 (a), 53.8 (a), 51.8 (a) 49.1 (a), 47.0 (p), 33.4 (p), 31.4 (p), 31.2 (p), 29.7 (p), 21.9 (a), 13.9 (a); HRMS, *m/z* (M^+) calcd. for $C_{17}H_{24}O_3$: 276.17255; found: 276.17267. Anal. calcd. for $C_{17}H_{24}O_3$: C 73.88%, H 8.75%; found: C 73.69%, H 8.92%. For compound **43**: IR ($CHCl_3$, cast): 3010 (=CH), 1736 (C=O, ester), 1690 (C=O, ketone) cm^{-1}; ^1H NMR (300 MHz, $CDCl_3$) δ: 6.32 (dd, 1H, J = 3, 5.5 Hz, $=CH$, C-11), 6.25 (ddd, 1H, J = 0.5, 3, 5.5 Hz, $=CH$, C-12), 4.20 (m, 2H, OCH_2), 3.37 (s, 1H, $CHCH{=}$), 2.90 (ddd, 1H, J = 3, 3, 12 Hz, CH, ring junction), 2.80 (m, 2H, CHCH= and $CHCH_3$), 1.25 (t, 3H, J = 7 Hz, OCH_2CH_3), 1.00 (d, 3H, J = 7 Hz, CH_3); ^{13}C NMR (APT, 75 MHz, $CDCl_3$) δ: 215.6 (p), 174.0 (p), 137.7 (a), 135.3 (a), 71.3 (p), 61.3 (p), 54.5 (a), 49.9 (a), 49.2 (a), 49.1 (p), 45.8 (a), 33.9 (p), 31.3 (p), 28.3 (p), 25.4 (p), 19.7 (a),

© 1997 NRC Canada

Can. J. Chem. Downloaded from www.nrcresearchpress.com by 88.146.161.215 on 09/08/12
For personal use only.

14.0 (a); HRMS, *m/z* (M^+) calcd. for $C_{17}H_{24}O_3$: 276.17255; found: 276.17242. Anal. calcd. for $C_{17}H_{24}O_3$: C 73.88%, H 8.75%; found: C 74.20%, H 8.90%.

(1R, 3R*, 8S*)-11-Acetoxy-1-carbethoxy-3-methyl-10-methylenebicyclo[6.4.0]dodec-11-en-2-one (**46**) and (1S*, 3R*, 8S*)-1-carbethoxy-3,10-dimethylbicyclo-[6.4.0]dodec-9-ene-2,11-dione (**47**)*

A gentle stream of oxygen was bubbled through a solution of the Diels–Alder adduct **29** (50 mg, 0.18 mmol), acetic anhydride (0.025 mL, 0.27 mmol), pyridine (0.021 mL, 0.27 mmol), 5,10,15,20-tetraphenyl-21*H*, 23*H*-porphine (5 mg), and 4-dimethylaminopyridine (catalytic amount) in 40 mL of carbon tetrachloride for 20 min. The bubbling was continued while the solution was irradiated with two 200-W tungsten light bulbs for 35 h. After turning off the light, bubbling was continued for another 19 h. The solution was diluted with 20 mL of ether and then washed with saturated aqueous sodium bicarbonate (15 mL), aqueous 1 M HCl (15 mL), and saturated aqueous sodium chloride solution (10 mL). The organic layer was separated, dried over anhydrous magnesium sulfate, filtered, and concentrated to give the crude product. This crude product was subjected to flash chromatography. Elution with 5% ethyl acetate in Skelly-B gave first the compound **46** (16.3 mg, 31% yield) and then compound **47** (7 mg, 13% yield). For compound **46**: IR (CH_2Cl_2, cast): 1767 (C=O, acetate), 1761 (C=O, ketone), 1744 (C=O, ester), 1682 (C=C, endocyclic), 1678 (C=C, exocyclic) cm^{-1}; ^1H NMR (300 MHz, $CDCl_3$) δ: 5.70 (s, 1H, =C**H**), 5.10 (m, 1H, =CH**H**), 4.95 (s, 1H, =C**H**H), 4.18 (m, 2H, OC**H**$_2$), 3.12 (m, 1H, C**H**CH$_3$), 2.80 (dddd, 1H, *J* = 2, 2, 4, 15 Hz, C**H**HC=CH$_2$), 2.70 (m, 1H, C**H**, ring junction), 2.30 (s, 3H, COC**H**$_3$), 2.20 (dd, 1H, *J* = 3, 15 Hz, CH**H**C=CH$_2$), 1.20 (t, 3H, *J* = 7 Hz, OCH$_2$C**H**$_3$), 0.90 (d, 3H, *J* = 7 Hz, C**H**$_3$); ^{13}C NMR (APT, 75 MHz, $CDCl_3$) δ: 215.5 (p), 170.4 (p), 169.0 (p), 147.0 (p), 134.7 (p), 114.0 (a), 111.6 (p), 65.5 (p), 61.5 (p), 42.2 (a), 41.3 (a), 38.1 (p), 34.4 (p), 29.8 (p), 29.5 (p), 28.7 (p), 24.9 (p), 20.8 (a), 19.1 (a); HRMS, *m/z* (M^+) calcd. for $C_{19}H_{26}O_5$: 334.17801; found: 334.17771. For compound **47**: IR ($CHCl_3$, cast): 1738 (C=O, ester), 1698 (C=O, ketone), 1682 (C=O, enone) cm^{-1}; ^1H NMR (300 MHz, $CDCl_3$) δ: 6.60 (dq, 1H, *J* = 1, 5.5 Hz, =C**H**), 4.15 (m, 2H, OC**H**$_2$), 3.40 (m, 1H, C**H**CH=), 3.15 (m, 1H, C**H**CH$_3$), 3.05 (s, br, 2H, C**H**$_2$CO), 1.72 (d, 3H, *J* = 1 Hz, =CC**H**$_3$), 1.19 (t, 3H, *J* = 7 Hz, OCH$_2$C**H**$_3$), 1.09 (d, 3H, *J* = 7 Hz, C**H**$_3$); ^{13}C NMR (APT 75 MHz, $CDCl_3$) δ: 213.0 (p), 195.2 (p), 171.1 (p), 148.1 (a), 133.3 (p), 64.5 (p), 61.9 (p), 42.2 (a), 41.6 (a), 38.3 (p), 35.5 (p), 27.9 (p), 26.5 (p), 26.1 (p), 19.5 (a), 15.5 (a), 14.0 (a); HRMS, *m/z* (M^+) calcd. for $C_{17}H_{24}O_4$: 292.16745; found: 292.16791.

(1S, 8S*)-1-Carbethoxy-10-methylbicyclo[6.4.0]dodec-9-ene-2,11-dione (**49**)*

This compound was prepared from adduct **21** in 31% yield using the photooxidation process described above. IR ($CHCl_3$ cast): 1733 (C=O, ester), 1708 (C=O, ketone), 1680 (C=O, conjugated ketone) cm^{-1}; ^1H NMR (300 MHz, $CDCl_3$) δ: 6.68 (dd, 1H, *J* = 1, 6 Hz, =C**H**), 4.13 (m, 2H, OC**H**$_2$), 3.70 (m, 1H, C**H**, ring junction), 3.13 (dd, 1H, *J* = 1, 18 Hz, CH**H**C=O, C-12), 3.04 (ddd, 1H, *J* = 4, 12, 13 Hz, C**H**HC=O, C-3), 2.69 (d, 1H, *J* = 18 Hz, C**H**HC=O, C-12), 2.21 (ddd, 1H, *J* = 4, 5.5, 13 Hz, CH**H**C=O, C-3), 1.57 (s, 3H, =CC**H**$_3$), 1.17 (t, 3H, *J* = 7 Hz, OCH$_2$C**H**$_3$); ^{13}C NMR (APT, 75 MHz $CDCl_3$) δ: 208.4 (p), 196.5 (p), 170.4 (p), 147.0 (a), 134.7 (p), 65.9 (p), 62.3 (p), 38.8 (a), 37.3 (p), 30.2 (p), 29.8 (p), 28.0 (p), 26.1 (p), 25.0 (p), 15.5 (a), 13.9 (a); HRMS, *m/z* (M^+) calcd. for $C_{16}H_{22}O_4$: 278.15179; found: 278.15197.

Acknowledgments

The contribution of Miss J. Yip of this laboratory is gratefully acknowledged for the preparation of diene **17**. We are also grateful to the Natural Sciences and Engineering Research Council of Canada and the National Science Council of the Republic of China for financial support.

References

1. H.J. Liu, W.L. Yeh, and E.N.C. Browne. Can. J. Chem. **73**, 1135 (1995).
2. H.J. Liu, W.L. Yeh, and S.Y. Chew. Tetrahedron Lett. **34**, 4435 (1993).
3. H.J. Liu and W.L. Yeh. Heterocycles, **42**, 493 (1996).
4. K.S. Shia. Ph.D. Dissertation, The University of Alberta, 1995.
5. O.D. Hensens. J. Org. Chem. **56**, 3399 (1991).
6. M.C. Wani, H.L. Taylor, M.E. Wall, P. Coggon, and A.T. McPhail. J. Am. Chem. Soc. **93**, 2325 (1971).
7. U. Leuer and T. Arke. J. Antibiot. **42**, 875 (1989).
8. J.S. Liu and H.X. Zhou. Huaxue Xuebao, **49**, 412 (1991).
9. H.J. Liu and S.P. Majumdar. Synth. Commun. **5**, 125 (1975).
10. J.M. Renga and H.J. Reich. Org. Synth. Coll. Vol. **VI**, 23 (1988).
11. A.S. Kende and P. Fludzinski. Org. Synth. Coll. Vol. **VII**, 208 (1990).
12. H.J. Liu, E.N.C. Browne, and S.Y. Chew. Can. J. Chem. **66**, 2345 (1988).
13. H.J. Liu, G. Ulibarri, and L.A.K. Nelson. Can. J. Chem. **72**, 2416 (1994).
14. R.E. Ireland and W.J. Thompson. J. Org. Chem. **44**, 3041 (1979).
15. H.J. Liu and E.N.C. Browne. Can. J. Chem. **65**, 1262 (1987).
16. R.P. Arshinova. Russ. Chem. Rev. **57**, 1142 (1988).
17. E.D. Mihelich and D.J. Eickhoff. J. Org. Chem. **48**, 4135 (1983).
18. S.L. Patt and J.N. Schoolery. J. Magn. Reson. **46**, 535 (1982).
19. A.P. Krapcho, J. Diamanti, C. Cayen, and R. Bingham. Org. Synth. Coll. Vol. **V**, 198 (1973).
20. R.D. Clark and K.G. Untch. J. Org. Chem. **44**, 248 (1979).
21. B. Milenkov and M. Hesse. Helv. Chim. Acta, **69**, 1323 (1986).
22. Y. Ohtsuka and T. Oishi. Chem. Pharm. Bull. **31**, 454 (1983).
23. J.A. Marshall and J.J. Partridge. J. Org. Chem. **33**, 4090 (1968).
24. H.J. Liu, G. Ulibarri, and E.N.C. Browne. Can. J. Chem. **70**, 1545 (1992).

© 1997 NRC Canada

Preparation and bioactivity of pyrazole derivatives as potential cross-linking agent

H. Katayama and T. Oshiyama

Abstract: A series of pyrazole derivatives with two and three alkylating sites were prepared and their cytotoxicity against cancer cells as well as antitumor activity against L1210 was investigated. The best result of cytotoxicity was obtained with the trichloride **5** and the best antitumor activity (ILS 33%) with the dibromide **3**. These results can provide valuable information for further study of the more effective antitumor agent.

Key words: pyrazole, synthesis, cytotoxicity, antitumor activity, polyalkylator.

Résumé : On a préparé une série de dérivés du pyrazole avec deux et trois sites d'alkylation et on a étudié leur cytotoxicité contre les cellules cancéreuses aussi bien que leur activité antitumorale vis à vis du L1210. On a obtenu les meilleurs résultats de cytotoxicité avec le trichlorure **5** et la meilleure activité antitumorale (ILS 33%) avec le dibromure **3**. Ces résultats peuvent fournir une information valable pour une étude plus poussée de l'agent antitumoral le plus efficace.

Mots clés : pyrazole, synthèse, cytotoxicité, activité antitumorale, polyalkylateur.

[Traduit par la rédaction]

Introduction

Among alkylating agents with antitumor activities, the agents that are able to cross-link DNA are believed to be much more effective than singly alkylating agents (e.g., nitrogen mustard) (1). The degree of DNA cross-linking was correlated with the rate of cell death and it was suggested that the cross-linking of DNA represents the molecular basis for the inhibition of DNA replication and consequent cell death (e.g., mitomycin C) (2). The cross-linking distance is quite important for clinically effective anticancer agents and the distance of four carbons was reported to be quite important for effective clinical treatment as demonstrated in an activated form of mitomycin C (MMC), pyrrolizidine alkaloid, and busulphan (Chart 1) (3). The DNA cross-linking action of the mitomycins remains unique among the known naturally occurring antibiotics (2). This action was confirmed with simplified molecular models such as 2,3-bis(acetoxymethyl)-1-methylpyrrole (BAMP). Similar simplification of the pyrrolizidine alkaloid was also accomplished with the synthesis of dehydroretronecine diacetate (DHRA). These compounds were able to cross-link the DNA with some sequence selectivity (Chart 1, cross-linking sites are marked with full circle) (4). We had planned to introduce the cross-linking distance of these compounds into the skeleton of pyrazolo[1,5-*a*]indole, which has been attracting our interest from the chemical and bioactive standpoint (5), and elaborated the target compounds **A** and **B**. Compound **A** can be regarded as an 3-azamitosene. We are also interested in compound **C**, because it is formed by cleaving the C4—C4a bond of **B** and may provide useful information for evaluating the bioactivities of compound **B**. The nonplanarity of the 1-phenyl group in **C** is also important in this evaluation, because the twist angle between the 1-phenyl and pyrazole rings was estimated to be around 50° (6), but these two rings are planar in **B**. In this article we would like to report the preparation and bioactivity of compound **C**.

Results and discussion

Compounds **1–5** were synthesized according to the scheme summarized in Chart 2. Starting compound **6** was prepared by coupling benzaldehyde phenylhydrazone and ethyl acetoacetate at 120°C for 3.5 h in an open flask (7*a*). Introduction of bromide at the 5-methyl group was carried out by radical bromination with *N*-bromosuccimide (NBS) (8), and the bromide **7** was hydrolyzed with $NaHCO_3$ in aqueous tetrahydrofuran (THF) at refluxing temperature to give hydroxyester **8**. Addition of tetra-*n*-butylammonium salt was essential for this selective reaction. This reaction is analogous with the esterification of carboxylate with alkyl halide catalyzed with phase transfer catalyst (9). Reduction of hydroxyester **8** with lithium aluminum hydride (LAH) in ether yielded diol **9** in 51% yield. Transformation of the diol to the dicarbamate was carried out by the reported method (10). Thus diol **9** was esterified with phenyl chloroformate, and the bis-phenyl carbonate **10** so obtained was treated with ammonia to give the bis-carbamate **1** in good yield. When diol **9** was mesylated with methanesulfonyl chloride and triethylamine in dichloromethane, dimesylate was not obtained but the stable dichloride **2** was formed as a single product. This type of substitution readily takes place when the mesylate is treated with nucleophiles (e.g.,

Received October 18, 1996.

This work is dedicated to Professor William A. Ayer on the occasion of his 65th birthday.

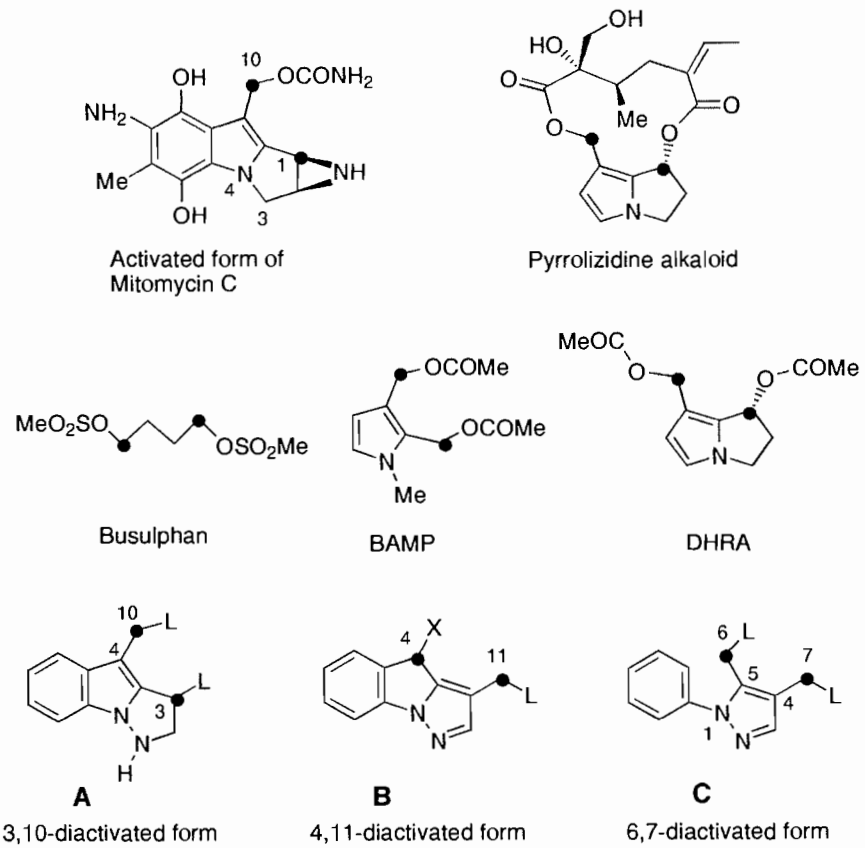
H. Katayama and T. Oshiyama. Niigata College of Pharmacy, 5-13-2 Kamishin'ei-cho, Niigata, 950-21, Japan.

[1] Author to whom correspondence may be addressed. Telephone: (025) 269-3170. Fax: (025) 268-1181. E-mail: Katayama@niigata-pharm.ac.jp

© 1997 NRC Canada

Can. J. Chem. Downloaded from www.nrcresearchpress.com by 88.146.161.215 on 09/08/12
For personal use only.

Chart 1.



LiCl) in polar aprotic solvent (11), and this method is useful even at non-activated positions such as the C-11 of mitomycins (12). In the ^{13}C NMR of **2**, the difference in the chemical shifts of the C-7 (Δ 18.1 ppm) between diol **9** and dichloride **2** was about the same as that of the benzylic site (Δ 18.1 ppm) between benzyl alcohol and benzyl chloride (13). This similarity suggests that the chemical reactivity of **2** is comparable with that of benzyl chloride. As a compound that is more reactive than dichloride **2**, the dibromide **3** was prepared from the dialcohol **9** by refluxing in 48% HBr solution.

In preliminary cytotoxic tests a better level of activity was detected with chloride **2** than with carbamate **1**, so only chlorides were synthesized for the following pyrazole derivatives. Dichloride **4** was required to investigate the effect of the 2-substituent and trichloride **5** to explore the effect of an additional alkylating site on bioactivities. Compound **5** is unique in having three alkylating sites within the same molecule, all in a 1,4 relationship. Few alkylating agents with more than three alkylating sites in the molecule, e.g., polyaziridinyl compounds (14), have been investigated. Compounds **4** and **5** were prepared from triester **11**, which was obtained by the coupling reaction of hydrazonylchloride with the sodium salt of the β-ketoester as shown in Chart 2 (15). Since the formation of anhydride may takes place readily between two carboxyl groups and the removal of the 3-carboxyl group at 120°C was reported with 1-*p*-nitrophenylpyrazole-3,4,5-tricarboxylic acid (15), the triester **11** was converted to the triacid **12** (16) and **12** was reacted with acetic anhydride at the boiling point (138–140°C) for 7 h. During the reaction a stream of argon was introduced to the reaction vessel and CO_2 generation was monitored by bubbling the argon stream into an aqueous solution of barium hydroxide. The reaction was halted when no generation of CO_2 was detected (7 h). The crude reaction product of **14** obtained by the removal of acetic anhydride was dissolved in methanol and methylated by refluxing with sulfuric acid. The diester **15** (16) thus obtained was reduced with LAH to give the diol **16**. In the ^1H NMR spectrum of **16** a characteristic singlet signal for the 3-H (δ 7.62) was observed, which supports the removal of the 3-carboxyl group. The transformation of diol **16** to dichloride **4** was effected with MsCl, *s*-collidine, and LiCl in DMF (11). Triol **13** was prepared by the reduction of the triester **11** with LAH and was transformed to the trichloride **5** by a reaction similar to that used in the preparation of **4**. Special care was taken to isolate the diols **9** and **16** and the triol **13** after LAH reduction. Aqueous work-up of the LAH reduction product caused difficulties in the isolation of these alcohols and resulted in poor yields. Thus the work-up procedure using NaF and a controlled amount of water (17) was adopted and only moderate yields of these alcohols were obtained. An alternative procedure reported for isolating intractable aminodiol by using triethanolamine (18) was not effective in our case. Reduction of **11** with $NaBH_4$ in *t*-BuOH–MeOH (19) was used to avoid this work-up problem but was also not effective in reducing the ester group.

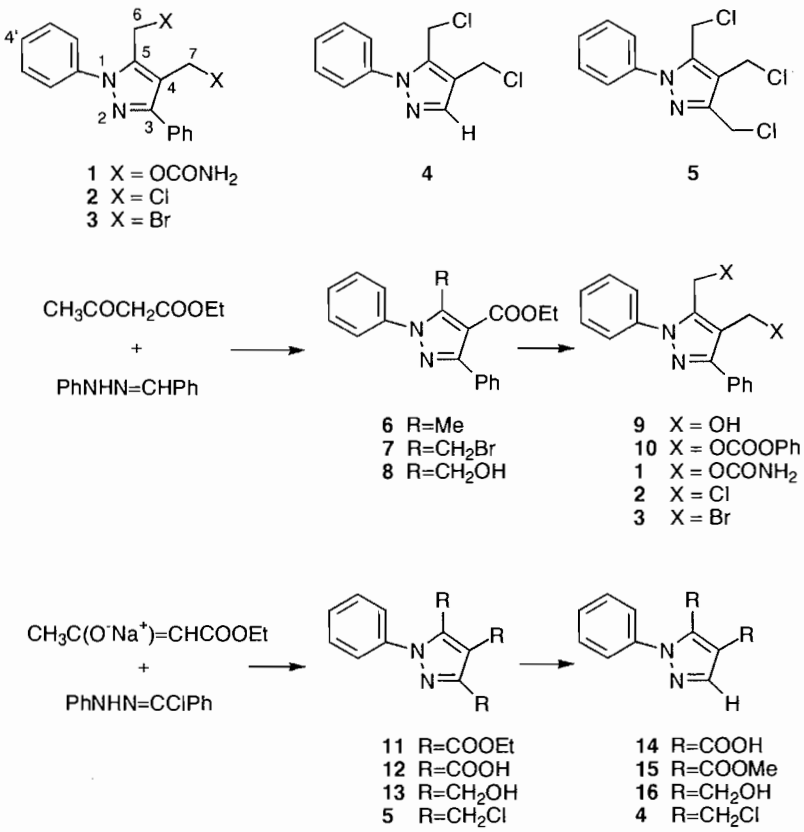
Cytotoxicity was measured by the microculture tetrazolium assay (20). Results for pyrazole derivatives **1–5** against cancer cells are summarized in Table 1. The activities of these compounds are relatively weak compared with the reference compound, MMC. The dichloride **2** was found to be more active than the dicarbamate **1**. The low activity of **1** may be a result of the poor reactivity of carbamate as a leaving group. But the

© 1997 NRC Canada

Can. J. Chem. Downloaded from www.nrcresearchpress.com by 88.146.161.215 on 09/08/12
For personal use only.

Can. J. Chem. Downloaded from www.nrcresearchpress.com by 88.146.161.215 on 09/08/12
For personal use only.

Chart 2.



dibromide **3**, which is chemically more reactive than the dichloride **2**, did not show a higher activity than **2**. The activity of **3** was found to be as low as that of the carbamate **1**. The small difference in activity between the two dichlorides, **2** and **4**, indicates that the contribution of the 2-phenyl group to the cytotoxic activity may be poor. Selectivity of activity against cancer cells was small. Since the trichloride **5** showed the highest activity against cancer cells, the number of alkylating sites may play an important role in the cytotoxicity. The activity of the trichloride **5** against uterus cervical cancer cells (HeLa) was noteworthy, since the increase of the alkylating sites from two to three increased the activity of the trichloride **5** 36 times more than that of the dichloride **2**. The activity of **5** against HeLa cell was found to be 2.8 times stronger than that of MMC.

Antitumor activities of the selected pyrazole derivatives **1–3** and **5** against murine leukemia L1210 are cited in Table 2 and the effect is expressed by ILS (increase of life span in %). The carbamate **1** did not show antitumor activity but it showed toxicity in mice. ILS of the dichloride **2** was proportional to the dose and 25.6% of ILS was obtained when a dose of 200 mg/kg was applied. At the same dose, the dibromide **3** showed a slightly better ILS value of 33.3%, which is thought to be effective. Although these ILS were relatively low compared with mitomycin C (74.4%), this dose dependence suggests that the intrinsic toxic property of the skeleton **C** is small. Contrary to the encouraging effects of **2** and **3**, the ILS of trichloride **5** was disappointingly small (4.8%) at maximum dose (12.5 mg/kg). In **5**, toxic effects became more significant than the desired activity at higher dose. The high chemical reactivity could be the reason for the toxic effect of **5**. Since the electron density at N-1 can control the reactivity of the alkylating sites, it may be possible to explore the desirable properties of the more effective antitumor agent by introducing a proper substituent at the N-1 position. Finally, the trichloride **5** attracted the attention of NCI in its in vitro screening test against 60 cancer cell lines but the potency in the test against prostate cell strains was disappointing. In conclusion, we have prepared a series of 1-phenylpyrazole derivatives with two and three alkylating sites and evaluated their cytotoxicities against cancer cells and antitumor activities against murine leukemia L1210. The best result of cytotoxicity was obtained with the trichloride **5** and the best in vivo result (ILS 33%) was obtained with the dibromide **3**. These results could provide valuable information for the further study of a series of **B** compounds.

Experimental

All melting points (mp) were determined with a Yanaco micro melting point apparatus without correction. Spectra were measured with the following spectrometers: IR (KBr pellet unless otherwise stated), Perkin–Elmer FT-IR 1720; ^{1}H and ^{13}C NMR, JEOL JNM-FT 200 and JNM-ALPHA 400 in $CDCl_3$ (unless otherwise mentioned) at ambient temperature (25–27°C) with tetramethylsilane as an internal standard; MS and high-resolution MS (HRMS), Hitachi RMU-7MG; UV and visible spectra (VIS), Shimadzu UV-200.

Ethyl 1,3-diphenyl-5-methylpyrazole-4-carboxylate 6 (ref. 7*a*)

Benzaldehyde phenylhydrazone (mp 156.0–158°C, 6.0 g, 0.031 mol), ethyl acetoacetate (6.0 g, 0.046 mol), and

© 1997 NRC Canada

Can. J. Chem. Downloaded from www.nrcresearchpress.com by 88.146.161.215 on 09/08/12
For personal use only.

Table 1. Cytotoxicities of pyrazole derivatives **1–5** against cancer cells.

	IC_{50} (μg/mL)[b]					
Compound[a]	L1210	Hela	PC-1	KATOIII	LoVo	MCF-7
MMC	0.085	0.148	0.117	0.333	0.279	0.065
1	>10	9.51	>10	7.09	9.15	>10
2	0.85	1.91	2.25	3.16	3.44	1.72
3	>2.5	>10	>5	>10	>10	>5
4	2.93	1.64	4.59	6.16	0.61	3.78
5	0.36	0.053	0.26	1.46	0.27	0.51

[a]MMC: Mitomycin C.

[b]Activities against cancer cells (L1210, murine leukemia; HeLa, uterus cervical; PC-1, lung; KATOIII, gastric; LoVo, colon; MCF-7, breast) were measured by MTT assay after 3 days of incubation and expressed as concentration for 50% growth inhibition (IC_{50}).

Table 2. Antitumor activities of pyrazole derivatives **1–3** and **5** against murine leukemia L1210

Compound	Dose[a] (mg/kg)	(i.p.)	MST[b] (Day)	ILS[b] (%)
Control			7.8 ± 0.2	
MMC	5	×1	13.6 ± 1.6	74.4
1	50	×1	7.4 ± 0.2	−5.1
	100	×1	7.4 ± 0.2	−5.1
	200	×1	7.2 ± 0.2	−7.7
2	50	×1	9.0 ± 0.6	15.4
	100	×1	9.0 ± 0.6	15.4
	200	×1	9.8 ± 0.8	25.6
Control			7.2 ± 0.2	
3	200	×1	9.6 ± 0.4	33.3
Control			8.4 ± 0.4	
5	12.5	×1	8.8 ± 0.2	4.8

[a]L1210 Cells (1×10^5) were inoculated i.p. into BDF1 mice (male, 6 weeks).

[b]Survival number was monitored daily and the increase in life span (ILS, %) was calculated from [(mean survival time of treated group) / (mean survival time of control group) − 1] × 100.

powdered anhydrous $ZnCl_2$ (0.6 g, 4.4 mmol) were placed in a beaker (100 mL) and the mixture was gradually heated to 120°C with stirring and kept at this temperature for 3.5 h. After cooling, ethanol was added, and the isolated crystals were collected to give **6** (4.15 g, yield: 44.3%), mp 102.5–105.0°C. IR: 3069, 1709, 1599, 1505, 1455, 1427, 1148, 1122, 1092, 772, 702 cm^{-1}. ^1H NMR δ: 1.21 (3H, t, J = 7.3, OCH_2CH_3), 2.58 (3H, s, 5-CH_3), 4.24 (2H, q, J = 7.3, OCH_2Me), 7.65–7.70 (2H, m, Ar-*H*), 7.44–7.52 (5H, m, Ar-*H*), 7.36–7.42 (3H, m, Ar-*H*); ^{13}C NMR δ: 12.7 (C-*9*), 14.1 (C-*6*), 60.0 (C-*8*), 110.6 (C-*4*), 125.8 (2 × C), 127.6 (2 × C), 128.2, 128.6, 129.2 (2 × C), 129.4 (2 × C), 133.1, 138.8 (C-*3*), 144.7 (C-*5*), 153.6, 164.1 (C-*7*). MS *m/e* (relative %): 307 (M^+ + 1, 19), 306 (M^+, 100), 262 (17), 261 (94), 260 (50), 259 (33), 234 (32), 233 (20), 118 (21), 77 (16).

Ethyl 5-bromomethyl-1,3-diphenylpyrazole-4-carboxylate 7

A mixture of **6** (15.0 g, 0.049 mol), *N*-bromosuccimide (13.35 g, 0.075 mol), and benzoylperoxide (4.1 g, 0.017 mol) in dry benzene (150 mL) was refluxed for 3 h. The solution was washed successively, with aqueous 1 M NaOH solution, water, and saturated brine and dried with anhydrous Na_2SO_4. Filtration and evaporation of the filtrate gave the crude product, which was recrystallized from EtOH to give the bromide **7** (17.4 g, 92.3%), mp 98.5–101.5°C. IR: 1717, 1595, 1532, 1496, 1458, 1259, 1147, 766, 694 cm^{-1}. ^1H NMR δ: 1.21 (3H, t, J = 7.1, OCH_2CH_3), 4.24 (2H, q, J = 7.1, OCH_2Me), 4.85 (2H, s, 6-*H*), 7.42–7.45 (3H, m, Ar-*H*), 7.62–7.70 (7H, m, Ar-*H*). ^{13}C NMR δ: 13.7 (C-*9*), 20.8 (C-*6*), 60.2 (C-*8*), 110.2 (C-*4*), 125.4 (2 × C), 127.7 (2 × C), 128.4, 129.0 (2 × C), 129.4, 129.5 (2 × C), 131.9, 137.7 (C-*3*), 143.2 (C-*5*), 152.5, 162.2 (C-*7*). MS *m/e* (relative %): 386 (M^+ + 2, 16), 384 (M^+, 19), 305 (68), 277 (21), 259 (91), 231 (12), 105 (79), 77 (100), 51 (18), 45 (13). Anal. calcd. for $C_{19}H_{17}BrN_2O_2$ (mw 385.25): C 59.24, H 4.45, N 7.27%; found: C 59.33, H 4.46, N 7.25.

Ethyl 5-hydroxymethyl-1,3-diphenylpyrazole-4-carboxylate 8

Bromide **7** (3.00 g, 7.8 mmol) and tetra-*n*-butylammonium bromide (0.75 g, 2.3 mmol; 29 mol%) were dissolved in tetrahydrofuran (THF, 30 mL). To this solution was added saturated aqueous $NaHCO_3$ solution (30 mL) and the mixture was refluxed until the total disappearance of **7** was observed on TLC (27 h). The solution was evaporated and the residue was diluted with water. Following extraction with CH_2Cl_2 (60 mL × 3), usual work-up of the extracts gave the crude product. Purification with flash column chromatography (SiO_2, petroleum ether – ethyl acetate 4:1) yielded the alcohol **8** (2.51 g, 41.0%), mp 80.5–81.5°C (petroleum ether – ethyl acetate 10:1). IR: 3451, 1707, 1598, 1538, 1501, 1216, 1185, 775, 769, 764, 759, 697 cm^{-1}. ^1H NMR δ: 1.20 (3H, t, J = 7.1, OCH_2CH_3), 4.14 (1H, t, J = 7.3, OH), 4.27 (2H, q, J = 7.1, OCH_2Me), 4.77 (2H, d, J = 7.1, 6-*H*; singlet by D_2O addition), 7.36–7.43 (3H, m, Ar-*H*), 7.45–7.61 (5H, m, Ar-*H*), 7.63–7.68 (2H, m, Ar-*H*). ^{13}C NMR δ: 13.9 (C-*9*), 55.3 (C-*6*), 60.9 (C-*8*), 111.7 (C-*4*), 125.6 (2 × C), 127.6 (2 × C), 128.5, 129.0, 129.4 (2 × C), 129.6 (2 × C), 132.7, 138.2 (C-*3*), 147.7 (C-*5*), 153.5,

© 1997 NRC Canada

Can. J. Chem. Downloaded from www.nrcresearchpress.com by 88.146.161.215 on 09/08/12
For personal use only.

165.1 (C-7). MS *m/e* (relative %): 323 (M^+ + 1, 7), 322 (M^+, 45), 276 (36), 275 (100), 247 (4), 104 (7), 77 (55), 43 (78). Anal. calcd. for $C_{19}H_{18}N_2O_3$ (mw 322.36): C 70.79, H 5.63, N 8.69%; found: C 70.84, H 5.63, N 8.66.

4,5-Dihydroxymethyl-1,3-diphenylpyrazole 9

A solution of hydroxyester **8** (0.285 g, 0.88 mmol) in anhydrous ether (60 mL) was added gradually to a solution of lithium aluminum hydride (0.8 g, 21.1 mmol) in dry ether (10 mL) for 1 h. The reaction mixture was stirred overnight. After cooling with an ice-bath, the reaction was successively quenched with NaF (2.5 g, 59.5 mmol) and water (5 mL). The resulting solution was stirred vigorously at room temperature until the inorganic precipitates became totally white. The inorganics were removed by filtration and washed well with ether (50 mL). The filtrate and washings were combined, dried with anhydrous $MgSO_4$ overnight, and evaporated. Chromatographic purification of the crude product gave the diol **9** (0.127 g, 51.3%), mp 167.0–168.0°C (from EtOH). IR: 3379, 3338, 3181, 3060, 1596, 1559, 1503, 1117, 1008, 993, 775, 715 cm^{-1}; ^1H NMR δ: 4.53 (2H, d, *J* = 5.0, 7-H; singlet by irradiation at δ 5.00), 4.54 (2H, d, *J* = 5.2, 6-H; singlet when irradiated at δ 5.44), 5.00 (1H, t, *J* = 5.0, O*H*), 5.44 (1H, t, *J* = 5.2, O*H*), 7.86–7.93 (2H, m, Ar-*H*), 7.74–7.80 (2H, m, Ar-*H*), 7.34–7.60 (6H, m, Ar-*H*). ^{13}C NMR δ: 51.7 (C-*7*), 52.7 (C-*6*), 119.1 (C-*4*), 123.8 (2 × C), 127.4, 127.5 (2 × C), 127.7, 128.4 (2 × C), 129.1 (2 × C), 133.1, 139.4 (C-*3*), 142.0 (C-*5*), 150.3. MS *m/e* (relative %): 281 (M^+ + 1, 14), 280 (M^+, 100), 262 (35), 261 (57), 233 (49), 130 (31), 104 (26), 77 (86). Anal. calcd. for $C_{17}H_{16}N_2O_2$ (mw 280.33): C 72.84, H 5.75, N 9.99%; found: C 72.90, H 5.89, N 9,99.

4,5-Diphenoxycarbonyloxymethyl-1,3-diphenylpyrazole 10

Phenyl chloroformate (2.98 mL, 23.8 mmol) was introduced into a solution of the dialcohol **9** (2.20 g, 7.8 mmol) in dry pyridine (15 mL) that was precooled in an ice-bath. The resulting solution was stirred at room temperature for 46 h. The solution was diluted with water (100 mL), and precipitates were collected. Recrystallization of the crude product from acetone–hexane (1:5) gave **10** (3.797 g, 93.0%), mp 138.5–139.0°C. IR: 1765, 1598, 1501, 1471, 1376, 1257, 1204, 779, 706 cm^{-1}. ^1H NMR δ: 5.45 (4H, s, 6-H_2 + 7-*H*), 7.07–7.58 (16H, m, Ar-*H*), 7.64 (2H, m, Ar-*H*), 7.83 (2H, m, Ar-*H*). ^{13}C NMR δ: 58.5 (C-*7*), 60.5 (C-*6*), 114.6 (C-*4*), 121.0 (2 × C), 121.1 (2 × C), 125.5 (2 × C), 126.0, 126.1, 128.3 (2 × C), 128.6, 128.8 (2 × C), 128.9, 129.4 (4 × C), 132.1, 137.7 (C-*3*), 138.9 (C-*5*), 151.1, 151.2, 152.7, 153.2 (C-*8*), 153.6 (C-*9*). MS *m/e* (relative %): 520 (M^+, <1), 384 (28), 383 (100), 339 (12), 246 (26), 245 (30), 94 (21), 43 (55). Anal. calcd. for $C_{31}H_{24}N_2O_6$: C 71.53, H 4.65, N 5.38%; found: C 71.74, H 4.65, N 5.49.

4,5-Diaminocarbonyloxymethyl-1,3-diphenylpyrazole 1

A solution of **10** (2.00 g, 3.84 mmol) in dry CH_2Cl_2 (100 mL) was cooled to −78°C by Dry Ice – acetone, and dry ammonia was introduced under a stream of nitrogen to this solution to collect about 200 mL of ammonia. The cooling bath was removed and the flask equipped with the Dry Ice condenser was left at room temperature for 5 h. Ammonia was evaporated during this period and the crystals isolated in the residual solution were collected. Usual work-up of the filtrate yielded the second crop of the crystals. The combined crystals were recrystallized from ethanol to give **1** (1.34 g, 95.0%), mp 226.0–227.0°C. IR: 3437, 3339, 3279, 3215, 1703, 1692, 1613, 1504, 1422, 1344, 1339, 1063, 1009, 779, 697, 571 cm^{-1}. ^1H NMR δ: 5.07 (2H, s, 6-*H*), 5.10 (2H, s, 7-*H*), 6.60–6.66 (4H, br s, 2 × NH_2), 7.42–7.65 (8H, m, Ar-*H*), 7.74–7.79 (2H, m, Ar-*H*). ^{13}C NMR δ: 53.8 (C-*6*), 55.1 (C-*7*), 115.2 (C-*4*), 124.8 (2 × C), 127.5 (2 × C), 128.1, 128.3, 128.5 (2 × C), 129.2 (2 × C), 132.3, 138.8 (C-*3*), 138.9 (C-*5*), 150.9, 155.7 (*C*O), 156.4 (*C*O). MS *m/e* (relative %): 366 (M^+, 6), 305 (13), 262 (100), 233 (19), 142 (7), 130 (16), 77 (46), 57 (36), 43 (80). Anal. calcd. for $C_{19}H_{18}N_4O_4$: C 62.29, H 4.95, N 15.29%; found: C 62.09, H 4.89, N 15.32.

4,5-Dichloromethyl-1,3-diphenylpyrazole 2

Methanesulfonyl chloride (0.63 mL, 8.0 mmol) was dropped for 5 min into a solution of the dialcohol **9** (0.84 g, 3.0 mmol) and triethylamine (1.26 mL, 9.1 mmol) in dry CH_2Cl_2 (30 mL) that was cooled in an ice-bath, and the reaction mixture was stirred at room temperature until the solution showed a single spot on TLC (22 h). The solution was washed successively with water, aqueous 10% HCl solution, aqueous $NaHCO_3$-saturated solution, and a saturated brine. The crude product obtained was recrystallized from ether–pentane to give the dichloride **2** (0.51 g, 39%), mp 119.0–120.0°C. IR: 3068, 2968, 1596, 1559, 1503, 1471, 1373, 1284, 1193, 1110, 1075, 1028, 917, 876, 766, 756, 695, 664, 514 cm^{-1}. ^1H NMR δ: 4.69 (2H, s, CH_2Cl), 4.77 (2H, s, CH_2Cl), 7.41–7.58 (6H, m, Ar-*H*), 7.61–7.67 (2H, m, Ar-*H*), 7.75–7.82 (2H, m, Ar-*H*); ^{13}C NMR δ: 33.6 (C-*7*), 36.3 (C-*6*), 116.2 (C-*4*), 125.2 (2 × C), 128.1 (2 × C), 128.5, 128.8 (2 × C), 128.9, 129.5 (2 × C), 131.9, 138.6 (C-*3*), 138.7 (C-*5*), 151.6. MS *m/e* (relative %): 320 (M^+ + 4, 4), 318 (M^++ 2, 26), 316 (M^+, 39), 283 (36), 282 (20), 281 (100), 245 (18), 142 (11), 115 (6), 77 (16). Anal. calcd. for $C_{17}H_{14}N_2Cl_2$: C 64.67, H 4.45, N 8.63%; found: C 64.37, H 4.74, N 8.83.

4,5-Dibromomethyl-1,3-diphenylpyrazole 3

A solution of **9** (500 mg, 1.78 mmol) in aqueous 48% HBr solution (5 mL) was refluxed for 0.5 h. The solution was diluted with water, basified to pH 7–8 with Na_2CO_3, and extracted with ether. The extract was washed with water and aqueous 50% NaBr solution and, following the usual work-up, gave the crude product (0.73 g). Chromatographic purification (silica gel, CH_2Cl_2–hexane 1:1) yielded pure **3** (0.473 g, 65.3%), mp 94.5–95.5°C (hexane–ether 5:2). IR: 1597, 1550, 1503, 1457, 1375, 1212, 1198, 916, 779, 761, 699, 685, 590 cm^{-1}. ^1H NMR δ: 4.58 (2H, s, CH_2Br), 4.69 (2H, s, CH_2Br), 7.42–7.60 (6H, m, Ar-*H*), 7.65–7.69 (2H, m, Ar-*H*), 7.79–7.83 (2H, m, Ar-*H*). ^{13}C NMR δ: 19.3 (C-*7*), 23.5 (C-*6*), 116.3 (C-*4*), 125.1 (2 × C), 128.1 (2 × C), 128.6, 128.8 (2 × C), 128.9, 129.5 (2 × C), 131.9, 138.5 (C-*3*), 138.8 (C-*5*), 151.5. MS *m/e* (relative %): 327 (91), 325 (90), 246 (100), 245 (95), 142 (27), 123 (20), 115 (19), 77 (54), 51 (20). Anal. calcd. for $C_{17}H_{14}Br_2N_2$: C 50.28, H 3.47, N 6.90%; found: C 50.39, H 3.54, N 6.83.

4,5-Bis (hydroxymethyl)-1-phenylpyrazole 16

The triester **11** (2.00 g, 5.55 mmol) was dissolved in the KOH solution prepared from KOH (12.46 g) and aqueous ethanol

© 1997 NRC Canada

Can. J. Chem. Downloaded from www.nrcresearchpress.com by 88.146.161.215 on 09/08/12
For personal use only.

(water-EtOH 1:1, 200 mL), and the resulting solution was refluxed for 4 h. After evaporation the residual solution was acidified with 35% HCl solution and the isolated crystals were collected to give the triacid **12** (1.32 g, 86.1%), mp 228.0–229.0°C (Lit. (14) mp 213.0–214.0°C). IR: 3442 (br), 1718, 1598, 1498, 1429, 1384, 1320, 1132, 1017, 770 cm^{-1}. ^1H NMR δ: 7.46–7.53 (5H, m, Ar-*H*). ^{13}C NMR δ: 118.1, 126.3 (2 × C), 128.6 (2 × C), 129.0, 137.5 (C-*4*), 141.0 (C-*5*), 144.0 (C-*3*), 158.4 (C-*7*), 160.9 (C-*5*), 167.6 (C-*6*).

The triacid **12** (2.00 g, 7.24 mmol) was added to acetic anhydride (50 mL), and the solution was refluxed for 7 h under a stream of argon. Reaction was halted when the stream of argon was introduced to the barium hydroxide solution and no generation of CO_2 was detected. Solvent was removed and the residue containing diacid **14** was dissolved in methanol (50 mL) containing sulfuric acid (3 mL). The solution was refluxed for 5 h, and evaporated. Basification with aqueous 1 M sodium carbonate solution and extraction with ethyl acetate gave, after the usual work-up, 1.41 g of **15** (14).

A solution of the diester **15** (0.30 g, 1.2 mmol) in dry THF (100 mL) was slowly added to a solution of LAH (0.175 g, 4.6 mmol) in dry THF (200 mL) for 30 min. The solution was refluxed for 2.5 h, and the reaction was quenched by the addition of NaF (0.773 g, 18.4 mmol) and water (1 mL). After stirring the solution for 2 h, the inorganic precipitates were removed and the filtrate was evaporated to give the oily dialcohol **16** (0.157 g, 66.8%). IR: 3338, 1599, 1505, 1392, 1017, 757, 692 cm^{-1}. ^1H NMR δ: 4.47 (2H, d, *J* = 5.4, 7-*H*), 4.48 (2H, d, *J* = 5.4, 6-*H*), 4.84 (1H, t, *J* = 5.4, 7-O*H*), 5.35 (1H, t, *J* = 5.4, 6-O*H*), 7.36–7.44 (1H, m, Ar-*H*), 7.48–7.55 (2H, m, Ar-*H*), 7.62 (1H, s, 3-*H*), 7.65–7.69 (2H, m, Ar-*H*). ^{13}C NMR δ: 51.7 (C-*7*), 53.6 (C-*6*), 122.4 (s, C-*4*), 123.7 (d, 2 × C), 127.2 (d), 129.0 (d, 2 × C), 139.2 (s, C-*5*), 139.5 (s + d, *ipso*-C + C-*3*). MS *m/e* (relative %): 204 (M^+, 44), 188 (50), 187 (39), 186 (45), 185 (53), 171 (21), 159 (40).

4,5-Bis (dichloromethyl)-1-phenylpyrazole 4

Under an argon atmosphere, methanesulfonyl chloride (1.13 mL, 8.1 mmol) was gradually dropped into a solution of the dialcohol **16** (0.75 g, 3.7 mmol), *s*-collidine (1.07 mL, 8.8 mmol), and LiCl (0.31 g, 7.6 mmol) in dry dimethylformamide (DMF, 35 mL) at 0°C. The solution was stirred at the same temperature for 1 h, then left at room temperature overnight. Dilution with ice-water and extraction with ether–pentane yielded the crude product (1.17 g), which was crystallized from isopropyl ether – ethyl acetate to give **4** (0.20 g, 22.6%), mp 90.0–91.5°C. IR: 1598, 1570, 1407, 1288, 1260, 1206, 1131, 1070, 987, 911, 868, 772 cm^{-1}. ^1H NMR δ: 4.62 (2H, s, 7-*H*), 4.67 (2H, s, 6-*H*), 7.45–7.60 (5H, m, Ar-*H*), 7.71 (1H, s, 3-*H*). ^{13}C NMR δ: 33.3 (C-*7*), 35.7 (C-*6*), 119.0, 125.1 (2 × C), 128.9, 129.5 (Ar-*H*), 137.0 (C-*4*), 138.7 (C-*5*), 140.4 (C-*3*). MS *m/e* (relative %): 242 (M^+ + 2, 12), 240 (M^+, 19), 207 (35), 206 (14), 205 (100), 170 (11), 169 (20), 142 (11), 115 (7), 77 (23). Anal. calcd. for $C_{11}H_{10}N_2Cl_2$: C 54.79, H 4.18, N 11.62, Cl 29.41%; found: C 54.96, H 4.19, N 11.56.

1-Phenyl-3,4,5-tris (hydroxymethyl)pyrazole 13

A solution of the triester **11** (5.40 g, 15 mmol) in dry THF (400 mL) was slowly dropped into a solution of LAH (2.28 g, 60 mmol) in dry THF (600 mL) at room temperature for 6 h, and the resulting solution was stirred overnight. Under vigorous stirring, NaF (10.08 g, 240 mmol) and water (15 mL) were added and the stirring was resumed until the inorganic precipitates became totally white. The inorganics were removed by filtration and washed with THF. The filtrate and washings were combined and evaporated. The oily product (3.02 g) was purified by column chromatography (silica gel 90 g, CH_2Cl_2 containing 10% methanol) to give 1.02 g (29.1%) of the trialcohol **13**, mp 102.0–103.0°C (ethyl acetate – isopropyl ether). IR: 3310, 3274, 1506, 1402, 1082, 1031, 1003, 830, 769, 701 cm^{-1}. ^1H NMR δ: 4.46 (2H, d, *J* = 5.1, 7-*H*; singlet by D_2O addition), 4.53 (4H, d, *J* = 5.3, 6-*H* and 8-*H*; singlet after addition of D_2O), 4.76 (1H, t, *J* = 5.4, O*H*), 5.05 (1H, t, *J* = 5.6, O*H*), 5.40 (1H, t, *J* = 5.4, O*H*), 7.41 (1H, d, *J* = 7.1, Ar-*H*), 7.52 (2H, t, *J* = 7.4, Ar-*H*), 7.67 (2H, d, *J* = 7.1, Ar-*H*). ^{13}C NMR δ: 51.8 (C-*7*), 52.8 (C-*6*), 56.1 (C-*8*), 120.0, 123.9 (2 × C), 127.3, 129.2 (2 × C), 139.5 (C-*4*), 140.7 (C-*5*), 151.4 (C-*3*). MS *m/e* (relative %): 234 (M^+, 59%), 216 (61), 198 (100), 187 (36), 169 (22), 157 (20), 142 (19), 130 (23), 117 (13), 104 (16), 77 (78), 51 (22). Anal. calcd. for $C_{12}H_{14}H_2O_3$ (mw 234.25): C 61.53, H 6.02, N 11.96%; found: C 61.34, H 6.01, N 12.00.

1-Phenyl-3,4,5-tris (chloromethyl)pyrazole 5

Under an argon atmosphere at ice-cooling temperature, methanesulfonyl chloride (0.924 mL, 6.6 mmol) was gradually dropped into a solution of trialcohol **13** (468 mg, 2.0 mmol), *s*-collidine (0.876 mL, 6.6 mmol), and LiCl (254 mg, 6.0 mmol) in dry DMF (30 mL) for 1 h, and the resulting solution was stirred overnight. The reaction was quenched with addition of ice-water (5 mL), and the solution was extracted with ether–pentane (1:1). The combined extracts were washed once with aqueous Cu $(NO_3)_2$ solution, and the usual work-up was followed. Crystallization of the crude product (436 mg, 75%) from ether–petroleum ether yielded the trichloride **5**, mp 53.0–54.0°C. IR: 3066, 1603, 1578, 1509, 1463, 1402, 1280, 1265, 1230, 1053, 1024, 813, 780, 770, 752 cm^{-1}. ^1H NMR δ: 4.60 (2H, s, 7-*H*), 4.74 (2H, s, 8-*H*), 4.76 (2H, s, 6-*H*), 7.47–7.58 (5H, m, Ar-*H*). ^{13}C NMR δ: 33.1 (C-*7*), 34.5 (C-*8*), 36.9 (C-*6*), 117.3, 125.1 (2 × C), 129.1 (2 × C), 129.5 (2 × C), 138.1 (C-*4*), 138.5 (C-*5*), 148.1 (C-*3*). MS *m/e* (relative %): 292 (M^+ + 4, 6), 290 (M^+ + 2, 18), 288 (M^+, 20), 255 (66), 253 (100), 217 (19), 183 (12), 77 (14), 51 (5). Anal. calcd. for $C_{12}H_{11}C_{l3}N_2$ (mw 289.59): C 49.77, H 3.83, N 9.67; found: C 50.07, H 3.78, N 9.74.

Cytotoxic activities

Cytotoxicity was measured by the microculture tetrazolium assay as described (20). Cancer cell lines of uterus cervical (HeLa), human lung (PC-1), gastric (KATOIII), colon (LoVo), breast (MCF-7), and murine leukemia cell (L1210) were maintained in RPM1 1640 (Nissui Pharmaceutical Co. Ltd., Tokyo) supplemented with 10% fetal bovine serum (Hyclone Laboratories, Inc., Utah, U.S.A.). Growth inhibition experiments were carried out in 96-well (flat bottom) microplates, and the amount of viable cells at the end of the incubation was determined using the MTT assay. Thus, tumor cells (L1210, 5×10^3 cells/well; HeLa, 2×10^3 cells/well, and other cells, 3×10^3 cells/well) were incubated in RPM1-1640 supplemented with 10% fetal calf serum. Drugs were dissolved in DMSO (2 mg/mL), diluted with cultural media (20 μg/mL), and introduced to the cell culture with gradual dilution. The

© 1997 NRC Canada

cells were exposed to drugs for 3 days at 37°C in air containing 5% carbon dioxide.

MTT (10 μL, 5 mg/mL in phosphate-buffered saline) was added to each culture well. The plates were incubated for an additional 4 h, and the medium was removed. The formazan product was dissolved in DMSO (150 μL/well) and the absorbance was measured at 540 nm using a Microplate Reader (Molecular Devices Corporation, California, U.S.A.). Each data point on the growth curves was an average of three wells. The 50% growth inhibitory concentration (IC_{50}) was calculated by the probit method.

Antitumor activity

The assays for L1210 leukemia in mice were performed as specified in the standard NCI protocols (21). L1210 Cells (1×10^5) were inoculated interperitoneally (i.p.) into BDF1 mice (male, 6 weeks old) on day 0 and mice divided into several groups (5 mice per group) on day 1. Test compounds were suspended in 0.5% CMC and given i.p. on days 1. Survival was monitored daily and the increase in life span (ILS) was calculated using the following formula: ILS (%) = [(mean survival time of treated group)/(mean survival time of control group) − 1] × 100.

Acknowledgments

We are grateful to Drs. Y. Ikeda and N. Kondo at the Kanebo Institute for Cancer Research, Kanebo Co., Ltd. (1-5-90 Tomobuchicho, Miyakojima-Ku, Osaka, 534), for biological evaluations and to Dr. A. Kato in our institution for the MS measurements.

References

1. (*a*) I.K. Larsen. *In* A textbook of drug design and development. *Edited by* P. Krogsgaard-Larsen and H. Bundgaard. Harwood Academic, Chur, Switzerland. 1991. Chap. 6; (*b*) R.B. Silvermann. *In* The organic chemistry of drug design and drug action. Academic Press Inc., San Diego, Calif. 1992. Chap. 6.
2. M. Tomasz. *In* Molecular aspects of anticancer drug – DNA interactions. Vol. 2. *Edited by* S. Neidle and M. Waring. The Macmillan Press Ltd., London. 1994. Chap. 8.
3. J.A. Hartley. *In* Molecular aspects of anticancer drug – DNA interactions. Vol. 1. Edited by S. Neidle and M. Waring. The Macmillan Press Ltd., London. 1993. Chap. 1.
4. (*a*) M.F. Weidner, S.Th. Sigurdsson, and P.B. Hopkins. Biochemistry, **29**, 9225 (1990); (*b*) J. Woo, S.Th. Sigurdsson, and P.B. Hopkins. J. Am. Chem. Soc. **115**, 3407 (1993).
5. (*a*) J.-K. Shen, H. Katayama, N. Takatsu, and I. Shiro. J. Chem. Soc. Perkin Trans. 1, 2087 (1993); (*b*) J.-K. Shen and H. Katayama. Chem. Pharm. Bull. **42**, 214 (1994); (*c*) Chem. Pharm. Bull. **42**, 222 (1994); (*d*) J.-K. Shen, H. Katayama, and N. Takatsu. Chem. Pharm. Bull. **42**, 237 (1994); (*e*) H. Katayama, Y. Kawada, T. Oshiyama, and A. Ejima. Chem. Pharm. Bull. **44**, 1276 (1996).
6. I.L. Finar. J. Chem. Soc. (B), 725 (1968).
7. (*a*) G. Minunni. Gazz. Chim. Ital. **55**, 502 (1925); (*b*) R. Huisgen, M. Seidel, G. Wallbillich, and H. Knupfer. Tetrahedron, **17**, 3 (1962).
8. E. Campaigne and B.F. Tullar. Org. Synth. Coll. Vol. **4**, 921 (1963).
9. J. March. *In* Advanced organic chemistry. 3rd ed. Wiley–Interscience, New York. 1985. p. 353.
10. G.R. Allen, Jr., J.F. Poletto, and M.J. Weiss. J. Org. Chem. **30**, 2897 (1965).
11. E.W. Collington and Q.I. Meyers. J. Org. Chem. **36**, 3044 (1971).
12. D. Choi, B. Yoo, K.L. Colson, G.E. Martin, and H. Kohn. J. Org. Chem. **60**, 3391 (1995).
13. W. Bremser, L. Ernst, B. Franke, R. Gerhards, and A. Hardt. *In* Carbon-13 NMR spectral data. Verlag Chemie, Weinheim. 1986.
14. (*a*) R.C. Raynolds. *In* Cancer chemotherapeutic agents. *Edited by* W.O. Foye. American Chemical Society. 1995; p. 186; (*b*) J.A. Maddry. *In* Cancer chemotherapeutic agents. *Edited by* W.O. Foye. American Chemical Society. 1995; p. 201.
15. R. Fusco. Gazz. Chim. Ital. **69**, 344 (1939); Chem. Abstr. **33**, 8609b (1939).
16. (*a*) R.G. Jones and C.W. Whitehead. J. Org. Chem. **20**, 1342 (1955); (*b*) L. Bauer and C.S. Mahajanshetti. J. Heterocycl. Chem. **4**, 325 (1967).
17. S. Sasatani, T. Miyazaki, K. Maruoka, and H. Yamamoto. Tetrahedron Lett. **24**, 4711 (1983).
18. J. Powell, N. James, and S.J. Smith. Synthesis, 338 (1986).
19. M.R. Harnden and R.L. Jarvest. Tetrahedron Lett. **35**, 4265 (1985).
20. M.C. Alley, D.A. Seudiero, A. Monks, M.L. Hursey, M.J. Czerwinski, D.L. Fine, B.J. Abbott, J.G. Mayo, R.M. Shoemaker, and M.R. Byod. Cancer Res. **48**, 589 (1988).
21. R.I. Geran, N.H. Greenberg, M.M. Macdonald, A.M. Schumacher, and B.J. Abbott. Cancer Chemother. Rep. Part 3, **3**, 7 (1972).

Can. J. Chem. Downloaded from www.nrcresearchpress.com by 88.146.161.215 on 09/08/12
For personal use only.

© 1997 NRC Canada

Isolation and structure of spongilipid from the Republic of Singapore marine porifera *Spongia cf. hispida*[1]

George R. Pettit, Timothy J. Bond, Delbert L. Herald, Martin Penny, Dennis L. Doubek, Michael D. Williams, Robin K. Pettit, and John N.A. Hooper

Abstract: Cell growth inhibitory (P388 lymphocytic leukemia) fractions from the purple marine sponge *Spongia cf. hispida* were employed to uncover a new biologically active monogalactosyl monoglyceride designated spongilipid (**5a**). The structure and absolute configuration of spongilipid was established by X-ray crystallography. Spongilipid specifically inhibited growth of the fecal opportunist *Enterococcus faecalis*.

Key words: marine sponge, *Spongia hispida*, spongilipid.

Résumé : On a fait appel à des fractions inhibant la croissance de cellules (leucémie lymphocytique P388) extraites de l'éponge marine pourpre (*Spongia cf. hispida*) pour mettre à jour un nouveau monoglycéride monogalactosylé biologiquement actif appelé spongilipide (**5a**). On a déterminé la structure et la configuration absolue du spongilipide par diffraction des rayons X. Le spongilipide inhibe spécifiquement la croissance de l'opportuniste fécal *Enterococus faecalis*.

Mots clés : éponge marine, *Spongia hispida*, spongilipide.

[Traduit par la rédaction]

Introduction

In 1989, we extended our broad geographic survey (2, 3) of marine animals as new sources of structurally unique antineoplastic substances (4–11) to Republic of Singapore ocean areas. During that expedition, a purple (darkens on exposure to air) colored reef sponge subsequently identified as *Spongia sp.* was collected and found to afford methanol extracts with cancer cell line (murine P388 lymphocytic leukemia) inhibitory activity.

Marine sponges in the genus *Spongia* previously yielded a variety of terpenoids (9–12). Australian specimens of *Spongia hispida* have been found to contain the sesterterpenoids hyrtiosal (**1**) (12, 13), isocalafurans A (**2**) and B (13), the sesterterpene/quinone 5-epi-isospongiaquinone (**3**) (14), and the Mediterranean *Spongia virgultosa* furan (**4**) (15). Hyrtiosal (**1**) was found to show moderate cell growth inhibitory activity against the KB cell line and 5-epi-isospongiaquinone (**3**) displayed antibiotic activity against *Staphyloccus aureus* and a *Micrococcus sp.* No biological data have been reported for terpene **2**. We herein summarize the isolation (P388 bioassay directed), structure elucidation, and preliminary biological activity for the monogalactosyl monoacylglyceride (MGMG) designated spongilipid (**5a**) from *Spongia cf. hispida* collected in the Republic of Singapore.

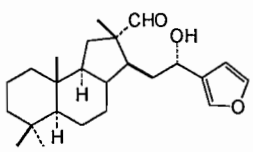
Received March 26, 1997.

This paper is dedicated to Professor William A. Ayer on the occasion of his 65th birthday.

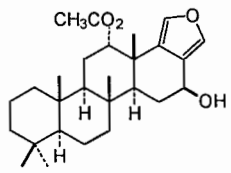
G.R. Pettit,[2] T.J. Bond, D.L. Herald, M. Penny, D.L. Doubek, M.D. Williams, R.K. Pettit, and J.N.A. Hooper. Cancer Research Institute and Department of Chemistry, Arizona State University, Tempe, AZ 85287-1604, U.S.A.

[1] Part 378 of Antineoplastic Agents. For the previous contribution see ref. 1.

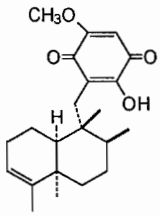
[2] Author to whom correspondence may be addressed. Telephone: (602) 965-3351. Fax: (602) 965-8558.



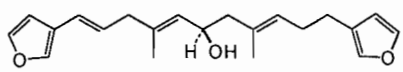
1



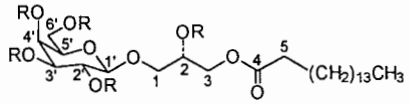
2



3



4



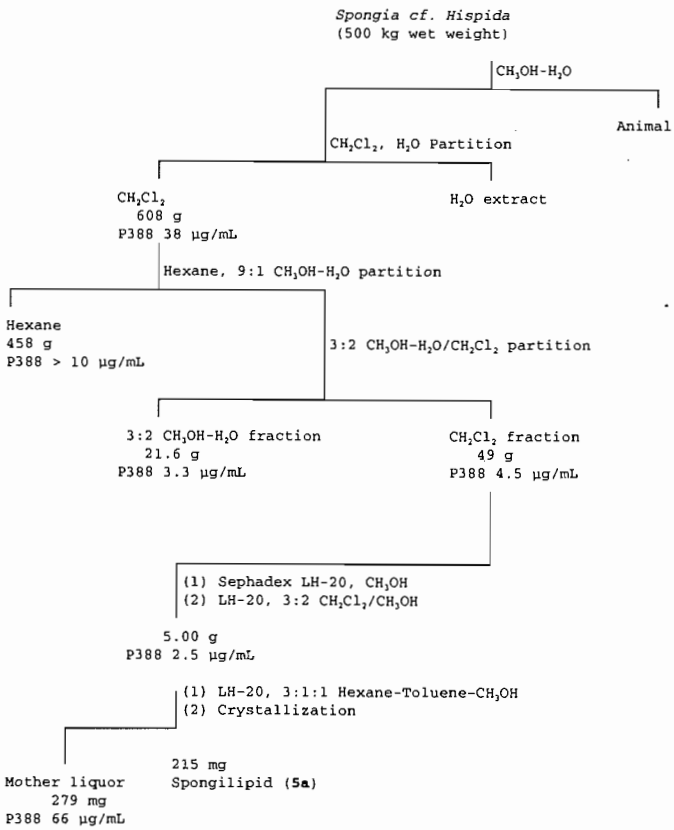
5a, R = H
5b, R = $COCH_3$

© 1997 NRC Canada

Can. J. Chem. Downloaded from www.nrcresearchpress.com by 88.146.161.215 on 09/08/12
For personal use only.

Can. J. Chem. Downloaded from www.nrcresearchpress.com by 88.146.161.215 on 09/08/12
For personal use only.

Scheme 1.



Results

The methanol–water used as preservative during shipment was concentrated to a water fraction and partitioned with methylene chloride. Further partitioning between methanol–water (9:1 → 3:2) and hexane followed by methylene chloride yielded a gummy brown methylene chloride fraction (49 g) that inhibited growth of the P388 (ED_{50} 4.5 µg/mL) murine leukemia cell line. Initial gel-permeation chromatographic separation on a column of Sephadex LH-20 in methanol was followed by another LH-20 chromatography of the resulting active fraction with 3:2 methylene chloride – methanol as eluent, affording a concentration of activity. Further separation was achieved by employment of column partition chromatography on Sephadex LH-20 with 3:1:1 hexane–toluene–methanol as the mobile phase. Slow evaporation of the solvent mixture from one fraction yielded two crops of fine colorless needlelike crystals of a new substance designated spongilipid (**5a**) (Scheme 1). Under standard P388 techniques, the activities of spongilipid ranged from about 2 to >100 µg/mL, presumably owing to difficulties caused by severe solubility problems and suspension formation in the cell media. Further approaches to resolve this problem are ongoing. However, we were able to show unequivocally that this MGMG (**5a**) exhibited antimicrobial activity.

By FAB high-resolution mass spectrometry, spongilipid (**5a**) was found to have molecular formula $C_{25}H_{48}O_9$ (*m/z* 515.3202 for $C_{25}H_{48}O_9Na$ — 1.1 ppm) and two double bond equivalents. The IR spectrum indicated the presence of hydroxyl, ester, and ether groups (3356, 1737, and 1467 cm^{-1}). The ^1H NMR (C_5D_5N) spectrum showed a broad peak at δ5.48 (OH), complex overlapping signals at δ5.00–4.00 ppm, a triplet at δ2.33, multiplets at δ1.63 and 1.27, and a triplet at δ0.87. The multiplet at δ1.24 integrated to at least 24 protons and the triplet at δ0.87 indicated a long-chain aliphatic unit terminating in a methyl group. In the mass spectrum, loss of *m/e* 239 was attributed to the mass fragment $[C_{16}H_{31}O]^+$, thus indicating a C_{16} saturated aliphatic ester (palmitoyl group).

Conversion of alcohol **5a** to acetate **5b** and measurement of the ^1H NMR chemical shifts in benzene-d_6 indicated the presence of five acetate groups and caused spreading of the previously overlapping peaks in the δ5.00–4.00 region to *ca* δ5.80–3.20 ppm. Acetylation allowed the assignment of a signal at δ4.20 ppm to that of an anomeric hydrogen of the sugar. Because of the large coupling constant (J = 9.7 Hz) observed, which is indicative of an axial–axial vicinal relationship, a β-linkage was deemed to be present. The five signals at δ5.33(m), δ4.35(dd), δ4.17(dd), δ3.84(dd), and δ3.54(dd) indicated a glycerol unit. The shift sequence suggested a 1,3 linkage via a C-1 ether and a C-3 ester. An APT NMR experiment for carbon hybridization combined with COSY, HMQC, and HMBC deductions required for determining the connectivities led to overall structure **5b** (and by inference **5a**). The structure of this spongilipid was unequivocally confirmed and the absolute stereochemistry assigned by X-ray analysis.

Figure 1 shows the absolute structure and conformation of spongilipid **5a**. The sugar moiety assumes the preferred $^4C_1$ conformation for a β-D-galactopyranoside with the glycerol ester occupying an equatorial position on the anomeric carbon. A rather striking feature exhibited by this structure is the perfectly linear orientation and nearly perpendicular direction assumed by the long fatty acid side chain with respect to the sugar ring. This phenomenon is fairly typical of that observed in the crystal structures of lipids (16) and emphasizes the amphiphilic nature of these compounds. No apparent twist or turn is discernable in the long side chain of spongilipid, and the molecule thus occupies a much larger volume of space than that which might be anticipated if the side chain were to wrap or curl back toward the sugar moiety. Stabilization for this arrangement of atoms can be seen by examination of the cell packing diagram, shown in Fig. 2. Sheets of the long fatty acid side chains are formed by alignment of alternating molecules of the spongilipid in the unit cell such that the interior of the cell is composed of adjacent and parallel side chains, whereas the ends of the cell are occupied by layers of sugar molecules. The alternating layers of sugar moieties are, in turn, stabilized via H-bonding between the O6′ galactose atom of one layer and the O4′ oxygen of the adjacent galactose layer (O6′ ··· O4′ distance, 2.90 Å). As a consequence, the interior of the cell is very hydrophobic, while the ends of the cell are quite hydrophilic. Finally, it should be noted that the *S* configuration at C2 of the glycerol unit is identical to that of an ether type glycolipid recently isolated from another marine sponge (17). According to the standard nomenclature for lipids, the absolute structure of spongilipid can thus be designated as 1-palmitoyl-3-β-D-galactosyl-*sn*-glycerol (**5a**).

As part of an extended biological evaluation, the antimicrobial activity of spongilipid was assessed. Spongilipid was active against *Enterococcus faecalis*, an opportunist of current

© 1997 NRC Canada

Fig. 1. Crystal structure drawing (50% probability ellipsoids) showing the absolute stereochemistry and X-ray numbering system of spongilipid **5a**.

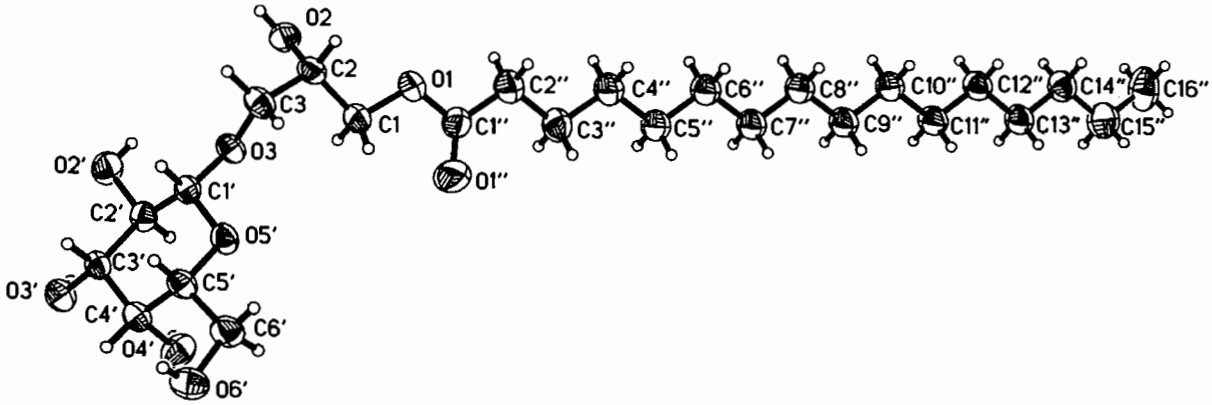
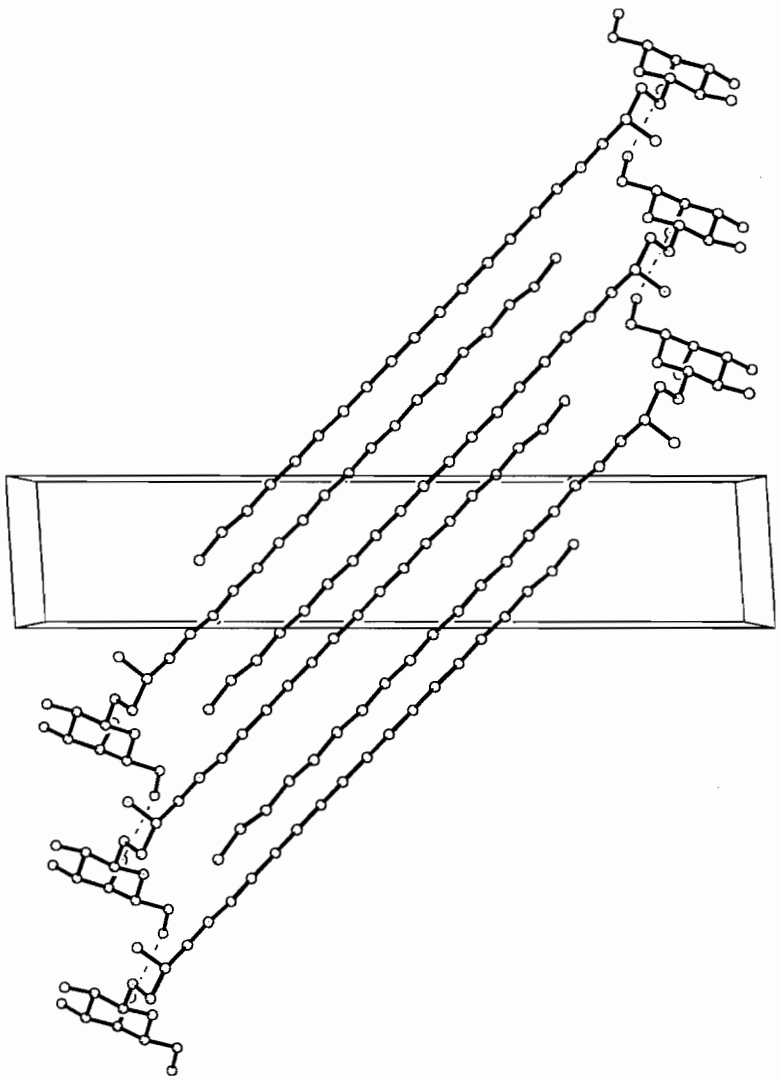


Fig. 2. Cell packing diagram (hydrogen atoms excluded) showing stacking of molecules of spongilipid **5a** and the association of fatty acid side chains (interior of cell) and sugars (ends of cell) forming layers or sheets of molecules. Broken lines indicate H-bonding between sugar hydroxyl groups in adjacent layers.



Can. J. Chem. Downloaded from www.nrcresearchpress.com by 88.146.161.215 on 09/08/12
For personal use only.

© 1997 NRC Canada

Can. J. Chem. Downloaded from www.nrcresearchpress.com by 88.146.161.215 on 09/08/12
For personal use only.

clinical concern due to its innate and acquired resistance to many antibiotics. This Gram-positive bacterium is a normal flora of the large intestine, but can cause urinary tract infections, endocarditis, and abdominal abscesses. The enterococci are also an emerging cause of nosocomial bacteremia. This can be explained in part by a recent study, which showed that the frequency of multiple antibiotic resistant *E. faecalis* blood culture isolates increased significantly during the period 1988–1995 (18).

Other monogalactosyl monoacylglycerides (MGMG) and monogalactosyl diacylglycerides (MGDG) have been isolated from higher plants and bacteria (19–23) and are the predominant lipid components of chloroplast membranes. More recently, microalgae (24) have also yielded related biologically active MGMG, MGDG, and digalactosyl diacylglycerides (DGDG), which have been shown to possess cell growth inhibitory (25) and antimicrobial activities (26). Interestingly, compounds related to structure **5a** have been synthesized using a β-galactosidase to introduce the β-anomeric configuration (27). Because of the hydrophilic galactose unit and lipophilic side chain, glycerol derivatives such as spongilipid are presumed to be important in cellular differentiation mechanisms and in other important aspects of cell chemistry (28–30). The role of spongilipid in Porifera biology and implications for cancer cell growth inhibition and antibiotic development warrant further investigation.

Experimental

General methods

Prior to use, all solvents for chromatographic procedures were redistilled. The Sephadex® LH-20 (25–100 μg) employed for gel permeation and partition chromatography was obtained from Pharmacia Fine Chemicals AB, Uppsala, Sweden. The silica gel GF Uniplates for TLC were from Analtech Inc., Newark, Del. TLC analyses utilized 9:1 CH_2Cl_2–CH_3OH as eluent and the plates were developed with anisaldehyde spray reagent or by exposure to iodine vapor. The IR spectrum was obtained with a Mattson Instruments Galaxy 20/20 FT-IR spectrometer. The ^1H and ^{13}C NMR spectra were recorded using a Varian Unity 500 spectrometer. Melting points are uncorrected. X-ray data collection was performed on an Enraf–Nonius CAD4 diffractionater.

Animal collection

The sponge was collected off the south side of the Terumbu Pempang Jaut reef by SCUBA in 1989 at a depth of 7–10 m. *Spongia cf. hispida* Lamarck, 1814 (class Demospongiae, order Dictyoceratida, family Spongiidae) corresponds to an irregular branching specimen with an exterior purple color, which darkens upon exposure to air, and an interior color of beige. The sample gave a dark green original extract. Voucher samples are maintained at the Cancer Research Institute, Arizona State University, and the Queensland Museum, South Brisbane, Queensland, Australia.

Animal extraction and partitioning

The preserving methanol–water solution (~450 L) was removed from the sponge (~500 kg wet weight) and concentrated to 120 L. The resulting fraction was partitioned with methylene chloride (4 × 60 L). The methylene chloride extract (608 g, P388 ED_{50} 38 μg/mL) was redissolved in methanol–water (9:1) and partitioned with hexane (4 × 20 L each). Water was added to dilute to 3:2 methanol–water and the solution was partitioned (4×) with 20 L of methylene chloride. The methylene chloride fraction (49 g, P388 ED_{50} 4.5 μg/mL) was used for isolation of spongilipid as outlined in Scheme 1.

Isolation of spongilipid (5a)

The 49 g active fraction (Scheme 1) was subjected to three steps of column chromatography on Sephadex® LH-20 with sequential (see Scheme 1) columns eluted with CH_3OH, CH_2Cl_2–CH_3OH (3:2), and *n*-hexane–toluene–CH_3OH (3:1:1) to afford two fractions that, upon standing, gave spongilipid (**5a**) as a crystalline solid (0.55 g): mp 119–121°C; $[\alpha]_D$ 0.0 (*c* 0.3, pyridine); IR (NaCl thin film) ν_{max} (cm^{-1}): 3356(m), 2916(s), 2850(m), 1737(s), 1467(m), 1066(m); NMR, δ^1H (500 MHz, C_5D_5N): 5.48 (4H, br s), 4.90 (1H, d, J = 8 Hz), 4.57 (2H, m), 4.50 (2H, m), 4.45 (2H, d, J = 6 Hz), 4.41 (1H, dd, J = 10.25, 6 Hz), 4.17 (1H, dd, J = 9.5, 3.5 Hz), 4.09 (2H, m), 2.33 (2H, t, J = 7.5 Hz), 1.63 (2H, q, J = 7 Hz), 1.27 (26H, m), 0.87 (3H, t, J = 7 Hz); $\delta^{13}C$ (C_6D_5N): 173.67, 105.95, 77.14, 75.38, 72.61, 72.28, 70.30, 69.06, 66.64, 62.37, 34.35, 32.13, 29.98, (δ29–30 ppm not discrete peaks, overlap), 29.93, 29.78, 29.61, 29.41, 25.28, 22.95, 14.28; FABHRMS *m/z*: 515.3202 for $C_{25}H_{48}O_9Na$ (−1.1 ppm from the calcd. *m/z*).

Acetylation of spongilipid (5b)

To alcohol **5a** (35 mg) in dry pyridine (5 mL) was added freshly distilled acetic anhydride (1 mL) under argon, with stirring at room temperature. After 24 h the reaction mixture was poured into ice water (10 mL) and extracted with ethyl acetate (3 × 10 mL). The combined organic extract was washed sequentially with saturated copper sulfate solution (10 mL) and water (2 × 10 mL), dried over sodium sulfate, and the solvent was removed in vacuo to yield peracetate **5b** as a clear gum (52 mg, 96%); δ^1H (500 MHz, C_6D_6): 5.59 (1H, dd, J = 10.5, 7.5 Hz, H-2′), 5.46 (1H, d, J = 3.5 Hz, H-4′), 5.33 (1H, m, H-2), 5.14 (1H, dd, J = 14, 4 Hz, H-3′), 4.35 (1H, dd, J = 9.5, 4 Hz, H-3a), 4.20 (1H, dd, J = 9.7, 2.5 Hz, H-1′), 4.17 (2H, dd, J = 12.5, 7 Hz, H-6′), 4.13 (1H, d, J = 8.5 Hz, H-3b), 3.84 (1H, dd, J = 13.5, 7 Hz, H-1a), 3.54 (1H, dd, J = 13.5, 6.5 Hz, H-1b), 3.38 (1H, m, H-5′), 2.11 (2H, t, J = 9.5 Hz, H-5), 1.85 (3H, s, OAc), 1.72 (3H, s, OAc), 1.71 (3H, s, OAc), 1.68 (3H, s, OAc), 1.55 (3H, s, OAc), 1.30 (22–26 H, m, CH_2's), 0.9 (3H, t, J = 6.5 Hz, terminal CH_3); $\delta^{13}C$ (C_6D_6): 172.77, 170.06, 169.79, 169.65, 169.58, 168.99, 101.79, 71.23, 71.06, 70.36, 69.00, 67.71, 67.31, 62.53, 61.34, 34.09, 32.29, 30.13 (δ29–31 ppm not discrete peaks, overlap), 30.09, 30.05, 29.88, 29.78, 29.65, 29.40, 25.16, 23.07, 20.49, 20.42, 20.18, 20.13, 19.84, 14.32; FABHRMS *m/z*: 709.3963 ($C_{35}H_{58}O_{14}Li$).

X-ray structure determination of spongilipid (5a)

Very long, slender, colorless needles were obtained by the slow evaporation of a hexane:toluene:methanol solution of the compound obtained via partition chromatography. The thickest crystal specimen was chosen and cleaved to the approximate dimensions of 0.12 × 0.30 × 0.32 mm, then mounted on the tip of a glass fiber. Refined lattice parameters were obtained by least-squares fitting of 25 carefully measured independent reflections in the 35–40° θ range. Data collection was performed at 299 ± 1 K for a monoclinic system. All

© 1997 NRC Canada

Can. J. Chem. Downloaded from www.nrcresearchpress.com by 88.146.161.215 on 09/08/12
For personal use only.

reflections corresponding to a complete quadrant, with $2\theta \leq 130°$, were measured using the ω–2θ scan technique. Friedel reflections were also recorded, whenever possible, after each reflection. Subsequent statistical analysis of the complete reflection data set using the XPREP program,[3] coupled with density measurements, indicated the space group was $P2_1$, the asymmetric unit of the cell containing a single molecule of compound **5a**.

Crystal data

$C_{25}H_{48}O_9$, monoclinic space group $P2_1$, with $a = 5.519(1)$, $b = 8.977(1)$, $c = 27.328(5)$ Å, $\beta = 93.48(2)°$, $V = 1351.4(4)$ Å^3, λ (Cu Kα) = 1.54184 Å, $\rho_c = 1.211$ g cm^{-3}, $\rho_o = 1.181$ g cm^{-3} for $Z = 2$ and F.W. = 390.05, $F(000) = 380$. After Lorentz and polarization corrections, merging of equivalent reflections, and rejection of systematic absences, 4472 unique reflections (R(int) = 0.1220) remained, of which 4217 were considered observed ($I_o > 2\sigma(I_o)$) and were used in the subsequent structure determination and refinement. Linear and anisotropic decay corrections were applied to the intensity data as well as an empirical absorption correction (based on a series of ψ-scans) (31). Structure determination was readily accomplished with the direct-methods program SIR92 (32). All non-hydrogen atom coordinates were located in a routine run using default values in that program. The remaining hydrogen atoms, calculated at optimum positions for **5a** using the program SHELXL-93 (33), were assigned thermal parameters equal to 1.5, the U_{iso} value of the atom to which they were attached, and then both coordinates and thermal values were forced to ride that atom during final cycles of refinement. All non-hydrogen atoms were refined anisotropically in a full-matrix least-squares refinement process with the SHELXL-93 software package. The final standard residual R value for the model shown in Fig. 1[4] was 0.0769 for observed data (4217 reflections) and 0.0802 for all data (4472 reflections). The corresponding Sheldrick R values were wR_2 of 0.1951 and 0.2077, respectively. A final difference Fourier map showed minimal residual electron density; the largest difference peak and hole being 0.330 and −0.494 e/Å^3, respectively. All final bond distances and angles were within acceptable limits.[5]

The structure and absolute stereochemistry of spongilipid (**5a**) is presented in Fig. 1. Refinement of the enantiomer depicted in Fig. 1, in conjunction with the Flack absolute structure parameter χ (34), resulted in a value of −0.08 (e.s.d. 0.25). On the other hand, refinement of the opposite enantiomer of **5a** resulted in a Flack parameter value of 1.07 (e.s.d. 0.26). Nearly identical R values were observed for the refinement of the opposite enantiomer, e.g., $R = 0.0769$, $wR_2 = 0.2081$. Although these results were certainly not conclusive in enabling assignment of the absolute stereochemistry, the relation of the relative stereochemistry of the molecule to the absolute stereochemistry known for the D-galactose sugar moiety contained in spongilipid established the absolute stereochemistry with certainty. As a consequence, the absolute stereochemistry for the six stereogenic centers of the **5a** could be assigned as follows (using the X-ray numbering system): 2*S*, 1′*R*, 2′*R*, 3′*S*, 4′*R*, 5′*R*.

Antimicrobial susceptibility evaluation

Antimicrobial disk susceptibility tests were performed according to the method established by the National Committee for Clinical Laboratory Standards (35). Mueller–Hinton agar was used for susceptibility testing of *Staphylococcus aureus* (ATCC no. 29213), *Enterococcus faecalis* (ATCC no. 29212), and *Escherichia coli* (ATCC no. 25922); Gonococcal Typing agar was used for *Neisseria gonorrhoeae* (ATCC no. 49226); and YM agar for *Candida albicans* (ATCC no. 90028) and *Cryptococcus neoformans* (ATCC no. 90112). Immediately prior to susceptibility assays, spongilipid (**5a**) was reconstituted in sterile DMSO and twofold dilutions were applied to sterile 6-mm disks. Zones of inhibition were read at 16 h for *S. aureus, E. faecalis, E. coli*, and *N. gonorrhoeae* and at 42 h for *M. luteus*, *C. albicans*, and *C. neoformans*. MIC determinations were performed in duplicate. The MIC of spongilipid for *Enterococcus faecalis* was 25–50 μg/disk. At 100 μg/disk, spongilipid had no activity against the other bacteria and fungi tested.

Acknowledgments

The research reported here was supported by Outstanding Investigator Grant CA-443440-1A1-09 awarded by the Division of Cancer Treatment, the U.S. National Cancer Institute, DHHS, The Arizona Disease Control Research Commission, the Fannie E. Rippel Foundation, and the Robert B. Dalton Endowment Fund. We also wish to thank Drs. Fiona Hogan, Michael R. Boyd, and Jean M. Schmidt for other assistance, as well as the Republic of Singapore (Professors T. J. Lam, Chou Loke Ming, and Khoo Hong Woo, Zoology Department, National University of Singapore), Larry Tackett, Denise Nielsen Tackett, and Deanna Hansen.

References

1. D.L. Herald, J.K. Srirangam, and G.R. Pettit. J. Am. Chem. Soc. In press.
2. G.R. Pettit, J.F. Day, J.L. Hartwell, and H.B. Wood. Nature, **227**, 962 (1970).
3. G.R. Pettit, Y. Kamano, Y. Fujii, C.L. Herald, M. Inoue, P. Brown, D. Gust, K. Kitahara, J.M. Schmidt, D.L. Doubek, and C. Michel. J. Nat. Prod. **44**, 482 (1981).
4. G.R. Pettit. *In* Progress in the chemistry of organic natural products. Vol. 57. *Edited by* W. Herz, G.W. Kirby, W. Steglich, and Ch. Tamm. Springer-Verlag, Vienna. 1991. pp. 153–195.

[3] XPREP — The automatic space group determination program in the SHELXTL PC program package.

[4] Preparation of Fig. 1 was done with SHELXTL-PC Version 5.03, (1994), an integrated software system for the determination of crystal structures from diffraction data, Siemens Industrial Automation, Inc., Analytical Instrumentation, Madison, WI 53719, U.S.A.

[5] Tables of crystal data, atomic parameters, bond lengths and angles, and anisotropic displacement parameters have been deposited and may be purchased from: The Depository of Unpublished Data, Document Delivery, CISTI, National Research Council Canada, Ottawa, Canada K1A 0S2. With the exception of the anisotropic displacement parameters, these tables have also been deposited with the Cambridge Crystallographic Data Centre, and can be obtained on request from The Director, Cambridge Crystallogrphic Data Centre, University Chemical Laboratory, 12 Union Road, Cambridge, CB2 1EZ, U.K.

© 1997 NRC Canada

Can. J. Chem. Downloaded from www.nrcresearchpress.com by 88.146.161.215 on 09/08/12
For personal use only.

5. G.R. Pettit. *In* Progress in the chemistry of organic natural products. Vol. 70. *Edited by* W. Herz, G.W. Kirby, R.E. Moore, W. Steglich, and Ch. Tamm. Springer-Verlag, Vienna. 1997. pp. 1–79.
6. G.R. Pettit. J. Nat. Prod. **59**, 812 (1996).
7. G.R. Pettit, J.K. Srirangam, S.B. Singh, M.D. Williams, D.L. Herald, J. Barkoczy, D. Kantoci, and F. Hogan. J. Chem. Soc. Perkin Trans. 1, **8**, 859 (1996).
8. G.R. Pettit. Pure Appl. Chem. **66**, 2271 (1996).
9. G.R. Pettit, Z.A. Cichacz, F. Gao, C.L. Herald, M.R. Boyd, J.M. Schmidt, and J.N.A. Hooper. J. Org. Chem. **58**, 1302 (1993).
10. G.R. Pettit, F. Gao, D.L. Doubek, M.R. Boyd, E. Hamel, R. Bai, J.M. Schmidt, L.P. Tacket, and K. Rhtzler. Gazz. Chim. Ital. **123**, 371 (1993).
11. G.R. Pettit, J. Xu, J.M. Schmidt, and M.R. Boyd. BioMed. Chem. Lett. **5**, 2027 (1995).
12. Y. Iguchi, Y. Shimada, and Y. Yamada. J. Org. Chem. **57**, 522 (1992).
13. R. Davis and R.J. Capon. Aust. J. Chem. **46**, 1259 (1993).
14. S. Urban and R.J. Capon. J. Nat. Prod. **55**, 1638 (1992).
15. A. Fontana, L. Albarella, G. Scognamiglio, M. Uriz, and G. Cimino. J. Nat. Prod. **59**, 869 (1996).
16. D. Marsh. *In* CRC handbook of lipid bilayers. CRC Press, Boca Raton, Fla. 1990.
17. V. Costantino, E. Fattorusso, A. Mangoni, M. Aknin, A. Fall, A. Samb, and J. Miralles. Tetrahedron, **49**, 2711 (1993).
18. P.C. Iwen, D.M. Kelly, J. Linder, S.H. Hinrichs, E.A. Dominguez, M.E. Rupp, and K.D. Patil. Antimicrobial Agents and Chemotherapy **41**, 494 (1997).
19. F.A. Exterkate and J.H. Veerkamp. Biochim. Biophys. Acta, **176**, 65 (1969).
20. T.A. Clayton, T.A. McMurray, and W.R. Morrison. J. Chromatogr. **47**, 277 (1970).
21. H. Meyer and F. Meyer. Biochim. Biophys. Acta, **231**, 93 (1971).
22. O.M.R.A. Heisig and E. Heinz. Phytochemistry, **11**, 815 (1972).
23. P. Baruah, N.C. Baruah, R.P. Sharma, J.N. Baruah, P. Zulanthaivel, and W. Herz. Phytochemistry, **22**, 1741 (1983).
24. Y. Oshima, S-H. Yamada, K. Matsunaga, T. Moriya, and Y. Ohizumi. J. Nat. Prod. **57**, 534 (1994).
25. T. Morimoto, A. Nagatsu, N. Murakami, J. Sakakibara, H. Tokuda, H. Nishino, and A. Iwashima. Phytochemistry, **40**, 1433 (1995).
26. R.T. Williamson and P.J. Seaton. Proc. 211th ACS Natl. Meet. New Orleans, La, March 24–28, 1996.
27. F. Bjorkling and S.E. Godtfredsen. Tetrahedron, **44**, 2957 (1988).
28. V. Costantino, E. Fattorusso, and A. Mangoni. Liebigs Ann. Chem. 2133 (1995).
29. V. Costantino, E. Fattorusso, and A. Mangoni. Liebigs Ann. Chem. 1471 (1995).
30. F. Cafieri, E. Fattorusso, Y. Mahajnah, and A. Mangoni. Liebigs Ann. Chem. 1187 (1994).
31. A.C. North, D.C. Philips, and F.S. Mathews. Acta. Crystallogr. Sect. A: Cryst. Phys. Diffr. Theor. Gen. Crystallogr. **A24**, 351 (1968).
32. A. Altomare, G. Cascarano, C. Giacovazzo, A. Guagliardi, M. Burla, G. Polidori, and M. Camalli. SIR92 — A program for automatic solution of crystal structures by direct methods. Dipartimento Geomineralogico, Univ. of Bari, Italy.
33. G.M. Sheldrick. SHELXL-93. Program for the refinement of crystals structures. Univ. of Göttingen, Germany (1993).
34. H.D. Flack. Acta Crystallogr. Sect. A: Found. Crystallogr. **A39**, 876 (1983).
35. National Committee for Clinical Laboratory Standards (1990). Performance standards for antimicrobial disk susceptibility tests – fourth addition: Approved standard M2-A4. NCCLS, Villanova, Pa.

© 1997 NRC Canada

A spectral displacement study of the binding constants of cyclodextrin–hydrocarbon and –fluorocarbon surfactant inclusion complexes

Lee D. Wilson, Stephanie R. Siddall, and Ronald E. Verrall

Abstract: The spectral displacement technique with phenolphthalein as the chromophore has been used to obtain 1:1 equilibrium binding constants (K_2) for a homologous series of hydrocarbon (hc) ($C_nH_{2n+1}COONa$, n = 5–13) and fluorocarbon (fc) anionic surfactants ($C_nF_{2n+1}COONa$, n = 3–8) with β-cyclodextrin (β-CD). The magnitude of K_2 increases as the alkyl chain length increases in each homologous series. K_2 values in the ranges of 10^2–10^5 M^{-1} and 10^1–10^4 M^{-1} were obtained for the β-CD–fc and for the β-CD–hc surfactant complexes, respectively. The different binding affinity of β-CD with hc and fc surfactants is discussed in terms of such physicochemical properties of the guest species as hydrophobicity, geometrical size, conformational effects, molecular polarizability, and solvation of the head group.

Key words: spectral displacement, phenolphthalein, cyclodextrin, surfactant, binding constant.

Résumé : On a fait appel à la technique du déplacement spectral avec la phénolphtaléine comme chromophore pour déterminer les constantes d'association (K_2) de la β-cyclodextrine avec une série d'agents de surface hydrocarbonés (hc) ($C_nH_{2n+1}COONa$, n = 5–13) et fluorocarbonés (fc) ($C_nF_{2n+1}COONa$, n = 3–8). Dans chacune de ces deux séries, l'amplitude des constantes K_2 augmente avec une augmentation de la longueur de la chaîne alkyle. On a obtenu des valeurs de K_2 de 10^2–10^5 M^{-1} et de 10^1–10^4 M^{-1} respectivement pour les complexes de β-CD – agents de surface fc et β-CD – agents de surface hc. On discute des diverses affinités d'association des β-CD avec les agents de surface hc et fc en fonction des propriétés physicochimiques des espèces incluses, telles que l'hydrophobicité, la taille géométrique, les effets conformationnels, la polarisabilité moléculaire et la solvatation des groupes formant la tête.

Mots clés : déplacement spectral, phénolphtaléine, cyclodextrine, agent de surface, constante d'association.

[Traduit par la rédaction]

Introduction

Cyclodextrins (CDs) show remarkable complexation behaviour with a wide variety of inorganic and organic inclusates (1, 2). The inclusion properties of CDs in aqueous media have attracted considerable attention due to their potential application as controlled-release agents (3). For example, pharmaceutical drugs are generally hydrophobic in nature and of a size that is suitable for their encapsulation by CDs. Of necessity, a rational design of improved drug delivery systems requires a correlation of physicochemical properties and binding affinity between the host and guest molecules. Thus there is a need to carry out systematic studies of a wide variety of CD–inclusate systems and to determine, as accurately as possible, the magnitude of the binding constants and their correlation with the physicochemical nature of the host–guest system. Of further interest is the need to better understand the fundamental nature of these relatively strong binding constants in terms of the weak intermolecular forces that are the basis for the existence of such complexes.

A number of different instrumental methods have been used to study CD–inclusate complexes. Among the most widely used of these techniques are NMR (4), sound velocity (5), conductivity (6), surface tension (7), emf (8), and UV–VIS spectrophotometry (9). The latter two methods involve direct measurement of bound or free inclusate concentrations whereas the other methods involve measurement of a total solution property, essentially a weighted average of two or more states, that is a measure of complex formation. Discrepancies in the literature between binding constants derived from different physical measurements have been attributed to the relative accuracies of the measured variables. Techniques that measure the concentration of free or bound species are expected to yield a more accurate estimate of the binding constant (10).

The spectral displacement technique (11–16), with phenolphthalein (phth) as the chromophoric species, can be used to determine the binding constants of optically transparent compounds to CD. The determination of these binding constants involves measuring the change in absorbance of phth in the presence of CD and a competing non-chromophoric surfactant

Received July 29, 1996.[1]

L.D. Wilson, S.R. Siddall, and R.E. Verrall.[2] Department of Chemistry, Thorvaldson Building, University of Saskatchewan, 110 Science Place, Saskatoon, SK S7N 5C9, Canada.

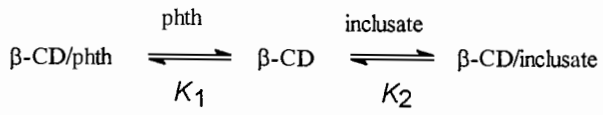
[1] Revision received January 14, 1997.

[2] Author to whom correspondence may be addressed. Telephone: (306) 966-4669. Fax: (306) 966-4730. E-mail: verrallr@sask.usask.ca

© 1997 NRC Canada

Can. J. Chem. Downloaded from www.nrcresearchpress.com by 88.146.161.215 on 09/08/12
For personal use only.

Scheme 1. Competing equilibria involved in the indirect spectral displacement technique, which utilizes phenolphthalein (phth) as a probe molecule.



(S). Scheme 1 illustrates the two competitive equilibria involved in the spectral displacement technique. K_1 and K_2 are the 1:1 binding constants for the CD–phth and CD–S complexes, respectively, as defined in ref. 11.

[1] K_1 = [CD–phth]/[CD] [phth]

[2] K_2 = [CD–S]/[CD] [S]

This technique provides a relatively accurate determination of K_2 since the absorbance changes are generally large and directly related to the amount of unbound inclusate. On the other hand, non-spectroscopic techniques are susceptible to larger error when K_2 is large (>10^4 M^{-1}) since the fraction of unbound species is low and the total solution property does not accurately reflect contributions from species of low concentration.

This paper presents the results of a determination of the binding constants between β-CD and a series of homologous hydrocarbon (hc) ($C_nH_{2n+1}COONa$, n = 5–13) and fluorocarbon (fc) ($C_nF_{2n+1}COONa$, n = 3–8) anionic surfactants at room temperature using the spectral displacement technique with phenolphthalein as the indirect chromophoric probe (11).

Experimental

Absorption measurements in the visible region were obtained using a fixed wavelength spectrophotometer (Milton Roy Spectronic 20) operating at 550 nm and at room temperature (295 ± 0.5 K). A double-beam spectrophotometer (Varian CARY 2315) was used to measure absorption vs. wavelength, when required. All solutions were prepared by volume in a 0.1 M Na_2CO_3 buffer adjusted to pH 10.5. The concentration of phth (C_{phth}) was 2×10^{-5} M in all experiments. For the determination of K_2, the concentration of β-CD (C_{CD}) was fixed at 3×10^{-4} M and the concentration of surfactant (C_S) was varied to exceed the 1:1 mole ratio of CD–S. The concentration of S was always kept below the critical micelle concentration (CMC) and values of the property for the surfactants used in this study are listed in Tables 1 and 2. A stock solution of phth in ethanol was made and aliquots were utilized to prepare ethanol–water (0.04%; v/v) solutions of phth in buffer. All aqueous solutions were freshly prepared and run within 1.5 h to ensure that any small absorbance change arising from instability of phth at pH 10.5 did not contribute to an experimental artifact.

β-CD (Aldrich) was used as received and the water content was determined from a Karl Fischer titration. It was accounted for in the determination of C_{CD}. All hydrocarbon surfactants ($C_nH_{2n+1}COONa$, n = 5–13) (Sigma, 99%) were used as received. All fluorocarbon surfactants ($C_nF_{2n+1}COONa$, n = 3–8) were prepared from the corresponding acids (Fluorochem, 99%) by titration with an equimolar quantity of NaOH (BDH, 99%). The sodium salts were recrystallized several times from methanol–chloroform mixtures. Phenolphthalein (Aldrich) was recrystallized from an ethanol–water mixture but no difference was observed between the molar absorptivities of the purified and unrecrystallized material.

A previously described (11) nonlinear least-squares (NLLS) fitting procedure was used to determine the 1:1 binding constants, K_1 and K_2, for the chromophore and the surfactant, respectively. The method is based on application of the Beer–Lambert law with the assumption that the molar absorptivity of the CD–phth complex is zero (13).

Table 1. 1:1 Binding constants (K_2)[a] obtained from spectral displacement studies of β-CD–hc surfactant systems at 295 K and pH 10.5 in 0.1 M Na_2CO_3 buffer and CMC[b] data in water.

Surfactant	CMC (mol L^{-1})[b]	$K_2(M^{-1})$	ΔG^0(kJ mol^{-1})
$C_8H_{17}SO_3Na$	0.133	$(9.0 \pm 1.1) \times 10^2$	−16.7
$C_{12}H_{25}SO_4Na$	8.3×10^{-3}	$(1.5 \pm 0.2) \times 10^4$	−23.6
$C_5H_{11}CO_2Na$	1.57	$(5.5 \pm 0.7) \times 10^1$	−9.8
$C_6H_{13}CO_2Na$	0.95	$(2.2 \pm 0.3) \times 10^2$	−13.2
$C_7H_{15}CO_2Na$	0.35	$(6.6 \pm 0.8) \times 10^2$	−15.9
$C_8H_{17}CO_2Na$	0.23	$(2.2 \pm 0.3) \times 10^3$	−18.9
$C_9H_{19}CO_2Na$	0.096	$(5.1 \pm 0.6) \times 10^3$	−20.9
$C_{11}H_{23}CO_2Na$	0.024	$(1.6 \pm 0.2) \times 10^4$	−23.7
$C_{13}H_{27}CO_2Na$	6.9×10^{-3}	$(4.8 \pm 0.6) \times 10^4$	−26.4

[a]Estimated precision is between 5 and 15% for each K_2 based on the standard deviation of K_1 for β-CD–phth.
[b]CMC values in water at 293–298 K from ref. 42.

Table 2. 1:1 Binding constants (K_2) obtained from spectral displacement studies of β-CD–fc surfactant systems at 295 K and pH 10.5 in 0.1 M Na_2CO_3 buffer and CMC[a] data in water at pH 10.5.

Surfactant	CMC (mol L^{-1})	$K_2(M^{-1})$	ΔG^0(kJ mol^{-1})
$C_3F_7CO_2Na$	>1.000	$(2.8 \pm 0.4) \times 10^2$	−13.8
$C_4F_9CO_2Na$	0.520	$(2.6 \pm 0.3) \times 10^3$	−19.3
$C_6F_{13}CO_2Na$	0.080	$(3.7 \pm 0.9) \times 10^4$	−25.8
$C_7F_{15}CO_2Na$	0.030	$(3.3 \pm 0.4) \times 10^5$	−31.2
$C_8F_{17}CO_2Na$	0.010	$(9.4 \pm 1.2) \times 10^5$	−33.7

[a]CMC values at 295 K and pH 10.5 obtained from ref. 36.

Results and discussion

The molar absorptivity of phth (ε_{phth}) was studied as a function of pH and water–ethanol composition. The magnitude of ε_{phth} was found to increase with increasing pH but remained constant as a function of ethanol content in the range 0.025–5% v/v. The latter result indicates that phth is fully dissolved at the conditions employed in this study. A low ethanol composition (0.04% v/v) was chosen in order to minimize competitive binding of ethanol with CD and to avoid any solvent effects (17–19) while a pH of 10.5 was used to optimize the optical density and to minimize the possibility of deprotonation of the hydroxyl groups of β-CD ($pK_a \cong 12$) (1). All absorption measurements were carried out at 550 nm since no

© 1997 NRC Canada

Can. J. Chem. Downloaded from www.nrcresearchpress.com by 88.146.161.215 on 09/08/12
For personal use only.

Can. J. Chem. Downloaded from www.nrcresearchpress.com by 88.146.161.215 on 09/08/12
For personal use only.

change in the shape of the VIS absorption band of phth in the presence of CD was observed at this wavelength.

To obtain the best estimates of the 1:1 binding constant (K_2), two essential conditions must be met when using the spectral displacement technique: (*i*) competing ligands must not absorb in the wavelength region of interest or interact with the chromophore and (*ii*) ligands must bind exclusively in a 1:1 stoichiometry. With respect to the first condition, any contribution from micelle–phth interactions was eliminated by carrying out all measurements below the CMC of the surfactants (20). Nevertheless, in a few instances a very small decrease in the absorbance of phth did occur and it is believed to be due to the formation of small clusters of surfactant around phth. An appropriate correction was applied to absorbance data in these cases. Condition (*ii*) is likely met in this study as it has been shown (7, 21) that surfactants possessing alkyl chain lengths (n_c) $\geq$ 16 carbon atoms are required to form 2:1 CD–surfactant complexes. The surfactants examined in this study were restricted to $n_c \leq 14$. Also, from a consideration of mass balance, the range of values of C_S used in this study, when compared to C_{CD}, do not favor the formation of 2:1 complexes. A further condition that should be met is that the competing ligand must fully displace the chromophore and bind as a well-defined CD–ligand inclusion complex. For example, the formation of a ternary (CD–phth–ligand) complex would not fully displace the chromophore and this could affect the magnitude of K_2 (20). However, the monotonic variations in the magnitude of K_2 as a function of the hydrocarbon chain lengths studied in each series seem to militate against this possibility. Finally, a practical requirement is to have $K_1 \geq K_2$ such that phth is displaced over a suitable range of C_S in order to obtain adequate absorbance changes (11). This condition is satisfied for most of the surfactants studied in this work.

Figure 1 illustrates a typical plot of absorbance vs. C_{CD} at a fixed concentration of phth. The line through the experimental data represents the calculated absorbance values obtained by using the NLLS fitting procedure. The rapid falloff of absorbance with increasing C_{CD} represents the formation of the CD–phth complex since the molar absorptivity of the latter is assumed to be zero. Benesi–Hildebrand (22) plots were not utilized to determine values of K_1 since the assumption that $[CD]_{total} >> [CD\text{–phth}]$ is not valid in the present study. As well, such classical double-reciprocal plots (1/Abs against $1/C_{CD}$) improperly weight the data, particularly at lower values of absorbance, i.e., low C_{CD} (11, 21). This is why a NLLS fitting procedure was employed to obtain values of K_1 and K_2 (11). A value of $K_1 = (2.5 \pm 0.3) \times 10^4$ M^{-1} was determined from several independent measurements and is in good agreement with literature values (12–14, 16). However, the value of K_1 reported here is slightly higher than that of Selvidge and Eftink (11). Since a lower concentration of ethanol was used in the present study, this difference may be due to a solvent effect.

Figure 2 shows a representative plot of absorbance vs. C_S for a weak binding CD–S system (β-CD–$C_5H_{11}COONa$). The absorbance exhibits a smooth monotonic increase with increasing C_S corresponding to the displacement of phth from the CD cavity upon inclusion of the surfactant. Table 1 lists the values of K_2 obtained for the β-CD–hc systems. The error in K_2 is based on the standard deviation in K_1 and the error associated with the absorbance measurements. The magnitude of K_2 ranges from 10^1 to 10^4 M^{-1} and increases with increasing hydrocarbon chain length.

Fig. 1. Absorbance (Abs; λ = 550 nm) vs. concentration of β-CD (C_{CD}) in 0.1 M Na_2CO_3 at pH 10.5, [phth] = 2×10^{-5} M and T = 295 K.

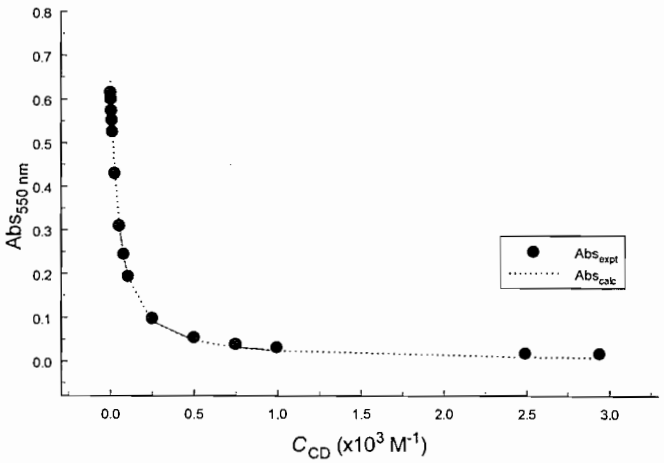


Fig. 2. Absorbance (Abs; λ = 550 nm) vs. concentration of sodium hexanoate (C_S) in 0.1 M Na_2CO_3 at pH 10.5, [β-CD] = 3×10^{-4} M, [Phth] = 2×10^{-5} M, and T = 295 K.

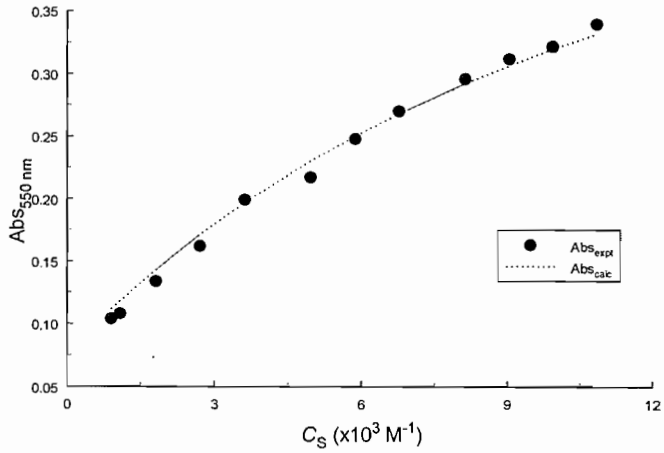


Figure 3 represents a typical plot of absorbance vs. C_S for a strongly bound CD–S system (β-CD–$C_{11}H_{23}COONa$). The absorbance changes sharply as a function of C_S and the shape of the curve becomes increasingly sigmoidal because the displacement of phth by surfactant occurs over a narrower range of C_S than in the case of the system shown in Fig. 2. Values of K_2 were also obtained for β-CD–$C_{12}H_{25}SO_4Na$(SDS) and β-CD–$C_8H_{17}SO_3Na$(SOS) systems in order to compare with known literature values under similar conditions. As seen from Table 1, there is good agreement with previously reported values ($K_2 = 1.8 \times 10^4$ M^{-1} (β-CD–SDS) and $K_2 = 9.0 \times 10^2$ M^{-1} (β-CD–SOS)) (14, 16). It is to be noted that these values of K_2 are similar in magnitude to those obtained for alkyl carboxylates of comparable chain length (see Table 1). These results support previous conclusions that host–guest alkyl chain interactions may play a more important role than

© 1997 NRC Canada

Fig. 3. Absorbance (Abs; λ = 550 nm) vs. concentration of sodium dodecanoate (C_S) in 0.1 M Na_2CO_3 at pH 10.5, [β-CD] = 3×10^{-4} M, [Phth] = 2×10^{-5} M, and T = 295 K.

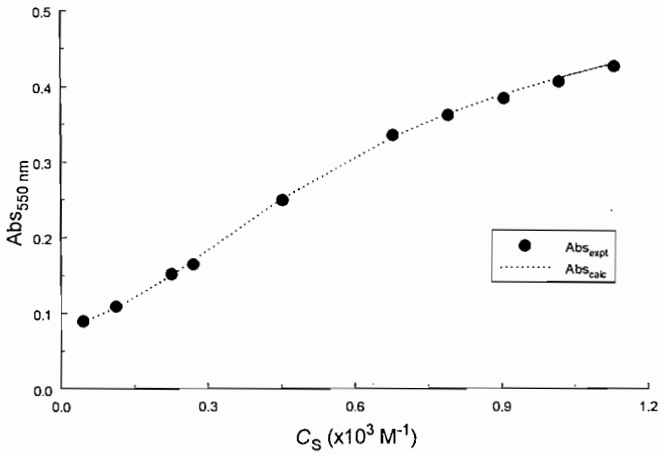
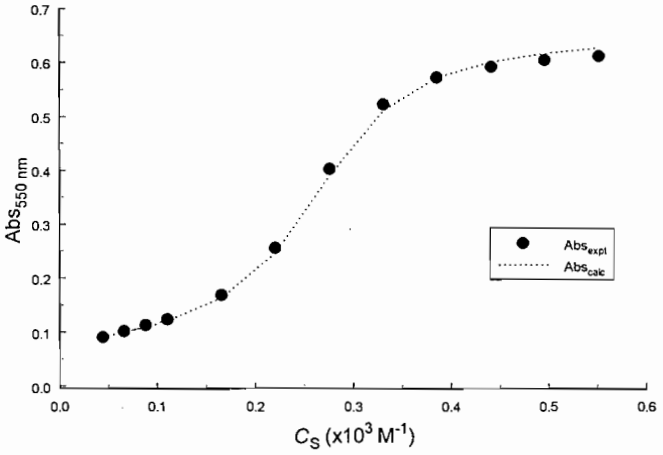


Fig. 4. Absorbance (Abs; λ = 550 nm) vs. concentration of sodium perfluorononanoate (C_S) in 0.1 M Na_2CO_3 at pH 10.5, [β-CD] = 3×10^{-4} M, [Phth] = 2×10^{-5} M, and T = 295 K.



host–guest head group interactions in the binding of surfactants to cyclodextrins.

Figure 4 is a typical plot of absorbance against C_S for a strongly bound CD–S system (β-CD–C_8F_{17}COONa). This curve exhibits a sigmoidal appearance that is more pronounced than that for a strongly bound hc surfactant (cf. Fig. 3). Table 2 lists the values of K_2 for the β-CD–fc surfactant systems investigated. The magnitude of K_2 ranges from 10^2 to 10^5 M^{-1} and increases with increasing hydrocarbon chain length (n_c). Furthermore, the values of K_2 are systematically greater for fc than for hc surfactants possessing similar n_c. Schuette and Warner observed a similar trend in their study of the complexation of low molecular weight hc and fc alcohols with β-CD (18).

Cooperative binding phenomena are often associated with sigmoidal-shaped binding isotherms, as seen in Figs. 3 and 4 (23). Thus it appears that cooperativity becomes more important for CD–S complexes as the hydrocarbon chain length increases for both the fc and hc surfactants. A comment about the cooperativity observed for the 1:1 CD–S complexes is warranted as it does not seem reasonable to attribute it to traditional allosteric arguments.

Lemieux has shown that water plays a critical role in regulating various aspects of molecular recognition, for example, the association of carbohydrates to the surfaces of proteins (24). The importance of the solvent in CD–inclusate binding phenomena has been outlined previously (2). Solvent-mediated cooperative binding processes can be readily appreciated by considering the contributions, shown by the different terms in eq. [3], made by the solvent to the overall Gibbs energy change of complexation (ΔG^0) between a host and guest species

$$[3] \quad \Delta G^0 = \Delta G^0_{H/S} + \Delta G^0_{G/S} + \Delta G^0_{H/G/S} + \Delta G^0_{S/S}$$

where G, H, and S are guest, host, and solvent, respectively. Equation [3] indicates that extensive coupling and, hence, cooperative binding between host and guest can occur due to resolvation of these species during complex formation. Hydration phenomena of this type are consistent with the hydrophobic effect. Such solvent-mediated cooperative binding phenomena should exhibit a dependence on the concentration and size of the apolar guest due to the destruction of hydrophobic hydration during complex formation. Independent support for solvent-based cooperative binding phenomena has been alluded to in a previous study where the binding constant was found to be dependent on the activity of the water (25). Chervenak and Toone argued that solvent reorganization encompasses 25–100% of the enthalpy contribution of ligand binding to macromolecules (26). Thus it would appear that solvent-based cooperativity is a more tenable argument for the molecular origins of the cooperative binding observed here, and further studies are being carried out to clarify this conjecture.

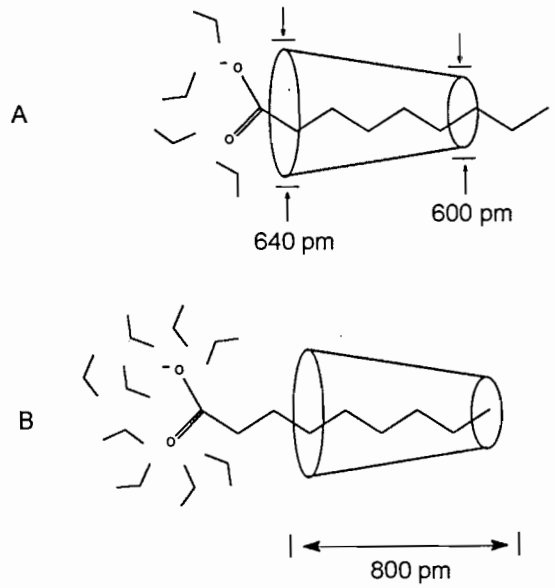
A number of physicochemical properties of the guest species may contribute to the different binding affinities of hc and fc surfactants to β-CD. They are hydrophobicity, geometrical size and conformation, molecular polarizability, and head group solvation. First, the greater hydrophobicity of an fc compared to an hc, as evidenced by lower CMC values and higher surface activities, may contribute to a higher binding affinity of fc surfactants to β-CD (27, 28). Secondly, the size differences between hc and fc alkyl chains are apparent from a comparison of the van der Waals radii for H (145 pm) and F (160 pm) and from the van der Waals volumes of the groups, CF_3 (21.3), CF_2 (15.3), CH_3 (13.7), and CH_2 (10.2), where the volumes are expressed in cm^3 mol^{-1} (29). Because the magnitude of the attractive and repulsive intermolecular potentials ($U_{ij}(R) \approx 1/R^n$) are related to the distance (R) between binding sites, molecular size is an important factor in determining the magnitude of K_2. As well, the contribution of different conformational isomers of the surfactant chain is a factor that affects the apparent size of the guest. Fluorocarbon chains generally exist in an all-*trans* conformation due to a relatively higher *gauche–trans* energy difference (263 J/mol) (30) resulting from unfavorable steric effects between adjacent perfluorinated methylene groups. The lower *gauche–trans* energy difference (170 J/mol) (30) for hc chains results in a higher population of *gauche* conformers relative to fc chains. Consequently, conformational effects as well as van der Waals radii are factors that influence the size of the guest. As the size of

Can. J. Chem. Downloaded from www.nrcresearchpress.com by 88.146.161.215 on 09/08/12
For personal use only.

© 1997 NRC Canada

Can. J. Chem. Downloaded from www.nrcresearchpress.com by 88.146.161.215 on 09/08/12
For personal use only.

Scheme 2. Influence of head group solvation on inclusion geometry of β-CD–surfactant complexes: (*A*) β-CD–fc surfactant complex and (*B*) β-CD–hc surfactant complex. (∧) represents a water molecule.

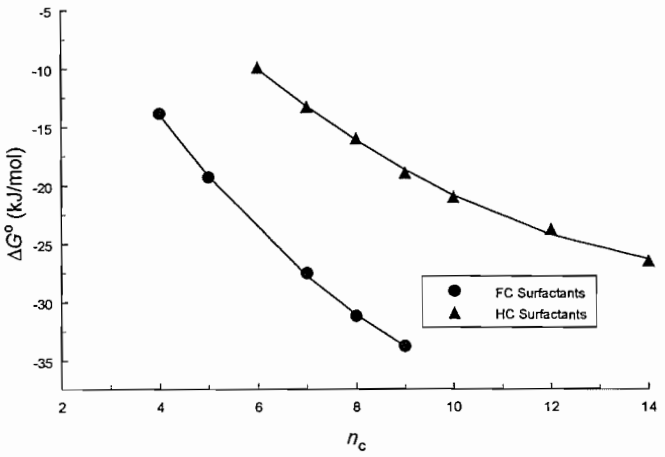


guest increases, more points of interaction may exist between host and guest and thereby affect the binding affinity. The importance of the size of aliphatic guest molecules has been discussed previously (31).

Thirdly, the importance of the polarizability property has been inferred from studies of mixed micelles consisting of fc and hc surfactants where the mixing behaviour is often non-ideal and phase separation is observed at certain concentrations (32). Furthermore, the relative strength of intermolecular interactions has been found to follow the order: fc–fc > hc–hc > fc–hc, based on NMR studies of mixed hc and fc anionic micelles (33). These observations are readily understood in terms of the relative molecular polarizabilities (α) of hc and fc groups, namely, $\alpha(CH_3) > \alpha(CH_2) > \alpha(CF_3) > \alpha(CF_2)$ (34). CDs are microheterogeneous assemblies consisting of C, H, and O atoms that can provide numerous potential atom–atom (O–F, O–H, H–H, H–F) interaction sites for an fc or an hc surfactant. It is expected that dispersive interactions should dominate within the apolar CD interior, whereas dipolar interactions should take place in the hydrophilic annular region of β-CD. The similar polarizabilities (34, 35) of O and F should result in more favorable dispersion interactions between them than between O and H or H and F. Indirect experimental support for this argument derives from the fact that molecular oxygen has a higher solubility in fc than in hc solvents. There are 28 oxygen atoms in the CD interior that may complex with an fc chain. In comparison, there are 14 H atoms in the CD interior that may complex with an hc chain. The hydroxyl group protons are neglected due to their participation in intramolecular H-bonding. Consequently, one might expect that the binding affinity of β-CD to an fc chain will be greater than to an hc chain due to the number and type of available interaction sites.

Fourthly, the importance of the head group solvation can be understood in terms of the dipolar interactions between the

Fig. 5. ΔG^0 vs. alkyl chain length (n_c) for the binding of hc and fc surfactants to β-CD.

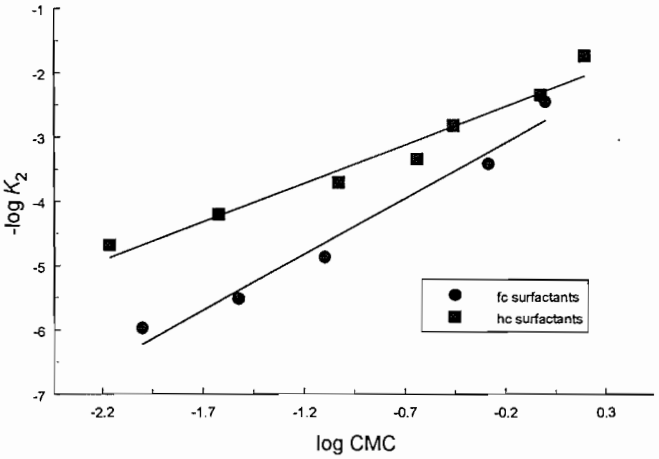


hydroxyl groups of the CD annulus and the carboxylate head group. The inclusion geometry and stoichiometry is dependent on the length of the surfactant chain (21); however, there are subtle differences in the way hc and fc surfactants appear to bind with β-CD. The effects of these differences can be understood from consideration of Scheme 2. Previous ^{19}F NMR studies (36) indicated that the carboxylate head group of fc surfactants interacts strongly with the hydroxyl groups in the annulus region of CD. The occurrence of multipoint (head group and alkyl chain) interactions in β-CD–surfactant complexes may result in greater binding affinity than in complexes where the latter effect is absent (see Scheme 2). The latter scenario could apply to hc surfactants where the highly hydrated head group is sterically restricted from interacting with β-CD and consequently lowers the binding affinity. Significant differences in the relative basicities and hydration of the hc and fc carboxylate anions are anticipated since pK_a (hydrogenated fatty acids) > pK_a (perfluorinated fatty acids) (37). Studies of emf (38, 39) indicate also that sodium ion binding to the β-CD–$C_7F_{15}COO^-$ complex is greater than for the β-CD–$C_9H_{19}COO^-$ complex. These results further support the contention that the carboxylate head group is more hydrated in β-CD–hc than in β-CD–fc complexes. It is important to recognize that β-CD does not form an inclusion complex with the Na^+ ion and, therefore, has no effect on the value of K_2 (38, 39).

Figure 5 shows a plot of ΔG^0 against n_c for binding of both fc and hc surfactants with β-CD. ΔG^0 exhibits a monotonic decrease (more negative) with increasing value of n_c for both surfactant series, with the decrease being more negative for the fc series. This result can be attributed to the physicochemical properties discussed above but it is of interest to compare the changes in ΔG^0 per methylene group determined in this work with values obtained from consideration of incremental free energies, $\Delta\Delta G^0(H_2O \rightarrow$ hc–water), for the transfer of a CF_2 or CH_2 group from water to an hc–water interface. Mukerjee reported $\Delta\Delta G^0(H_2O \rightarrow$ hc–water) = −5.1 kJ/mol (CF_2) and −3.4 kJ/mol (CH_2) (32). These incremental values are in reasonable agreement but slightly greater than the incremental free energies of complexation (−4.4 kJ/mol (CF_2) and −2.7 kJ/mol (CH_2)) obtained from the slopes of the curves in Fig. 5.

© 1997 NRC Canada

Fig. 6. $-\text{Log } K_2$ vs. log CMC for hc and fc surfactants.



However, the hexane–water interface is a crude approximation of the microenviroment of the CD interior and the interfacial region. What is clear from the present results is that the less negative values of $\Delta\Delta G^0$ per methylene moiety are closer to values expected for the transfer of a methylene group from the bulk phase to a micelle ($\Delta\Delta G^0(CH_2) = -2.7$ to -3.0 kJ/mol) (32) where a change in the hydration of the head group may also make a contribution. Nevertheless, the relative difference in the magnitude of $\Delta\Delta G^0$ between fc and hc methylene groups obtained from the slopes in Fig. 5 is consistent with the data of Mukerjee.

The nonlinear dependence of ΔG^0 on n_c for hc and fc chains can be attributed to the degree of inclusion of the surfactant chain within the CD cavity. As the alkyl chain exceeds the depth of the CD cavity, ΔG^0 decreases less due to fewer alkyl groups interacting with the CD interior. Park and Song (40) have suggested that the β-CD interior can accommodate no more than approximately eight CH_2 groups if allowance is made for chain coiling. Because of the all-*trans* conformation of the fc chain, it is likely that fewer CF_2 than CH_2 groups can be included in the CD interior and the fc series will show greater nonlinearity than the hc series, as seen in Fig. 5. While it can also be argued that the nonlinear dependence of ΔG^0 on n_c may be due to the contribution of higher order binding phenomena, the experimental range of C_S chosen in this work was done with the view to minimize, as much as possible, the formation of such complexes. Furthermore, the goodness of fit of the experimental data to a 1:1 binding model does not warrant the consideration of higher order binding phenomena.

The hydrophobic effect has been implicated in various CD–inclusate complexation phenomena (41). Since hydrophobicity can be related to the CMC, there should be a correlation between K_2 and the CMC. A plot of $-\log K_2$ vs. log CMC is shown in Fig. 6. The relationship is approximately linear for both surfactant systems and the slope is greater for the fc surfactants, consistent with their greater hydrophobicity. Fig. 6 provides additional evidence that the hydrophobic effect is a significant contributor to the different binding affinities of hc and fc surfactants to β-CD. The approximately linear relation shown in Fig. 6 offers a useful semiempirical method for estimating a value of K_2, by interpolation, for a complex within a homologous series of inclusates when K_2 values are known for only a few members of the series.

Conclusion

The spectral displacement technique has been used to obtain accurate estimates of the 1:1 binding constants (K_2) for a series of hc surfactants, ($C_nH_{2n+1}COONa$, n = 5–13) and fc surfactants ($C_nF_{2n+1}COONa$, n = 3–8) with β-CD. The values of K_2 for the hc surfactants are in the range 10^1–10^4 M^{-1} and the values of K_2 for the fc surfactants are in the range 10^2–10^5 M^{-1}. The values of K_2 for the fc surfactants are systematically greater than those for the hc surfactants. The stronger binding affinity of fc surfactants compared to that of hc surfactants can be attributed to differences in hydrophobicity, conformational effects, size, polarizability, and solvation of the surfactant head group. The contribution of the hydrophobic effect in these complexation phenomena is supported by the near-linear relation observed between $-\log K_2$ and log CMC as well as the dependence of K_2 on the alkyl chain length.

The spectral displacement technique using phenolphthalein appears to be a good method of obtaining accurate estimates of K_2 for anionic surfactants with strong binding affinities to β-CD. Thermodynamic studies of CD–surfactant systems are in progress to better understand various aspects of the hydrophobic and cooperative solvent effects observed in these systems.

Acknowledgements

Financial assistance provided by the Natural Sciences and Engineering Research Council of Canada is gratefully acknowledged. L.D.W. thanks the University of Saskatchewan for the award of a Graduate Teaching Fellowship.

References

1. M.L. Bender and M. Komiyama. Cyclodextrin chemistry. Springer, Berlin. 1978.
2. R.J. Clarke, J.H. Coates, and S.F. Lincoln. Adv. Carbohydr. Chem. **46**, 205 (1988).
3. K. Uekama, F. Hirayama, and T. Irie. *In* New trends in cyclodextrins and derivatives. *Edited by* D. Duchêne. Éditions de Santé, Paris. 1991. pp. 411–423.
4. D.J. Wood, F.E. Hruska, and W. Saenger. J. Am. Chem. Soc. **17**, 694 (1977).
5. E. Junquera, G. Tardajos, and E. Aicart. Langmuir, **9**, 1213 (1993).
6. E. Saint Aman and D. Serve. J. Colloid Interface Sci. **138**, 365 (1990).
7. U.R. Dharmawardana, S.D. Christian, E.E. Tucker, R.W. Taylor, and J.F. Scamehorn. Langmuir, **9**, 2258 (1993).
8. W.M.Z. Wan Yunus, J. Taylor, D.M. Bloor, D.G. Hall, and E. Wyn-Jones. J. Phys. Chem. **96**, 8979 (1992).
9. R.I. Gelb, L.M. Schwartz, B. Cardelino, and D.A. Laufer. Anal. Biochem. **103**, 362 (1980).
10. H. Mwakibété, R. Cristiantino, D.M. Bloor, E. Wyn-Jones, and J.F. Holzwarth. Langmuir, **11**, 57 (1995).
11. L.A. Selvidge and M.R. Eftink. Anal. Biochem. **154**, 400 (1986).
12. Á. Buvári, J. Szeijtli, and L. Barcza. J. Inclusion Phenom. **1**, 151 (1983).
13. Á. Buvári, L. Barcza, and M. Kajtár. J. Chem. Soc. Perkin Trans. 2, 1627 (1988).
14. K.J. Sasaki, S.D. Christian, and E.E. Tucker. Fluid Phase Equilib. **49**, 281 (1989).
15. Á. Buvári and L. Barcza. Inorg. Chim. Acta, **33**, L179 (1979).
16. J.E. Gray, S.A. MacLean, and V.C. Reinsborough. Aust. J. Chem. **48**, 551 (1995).

© 1997 NRC Canada

Can. J. Chem. Downloaded from www.nrcresearchpress.com by 88.146.161.215 on 09/08/12
For personal use only.

17. C. Donzé, A. Chatjigakis, and A.W. Coleman. J. Inclusion Phenom. Mol. Recognit. Chem. **13**, 155 (1992).
18. J.M. Schuette and I.M. Warner. Anal. Lett. **27**, 1175 (1994).
19. I.M. Warner and J.M. Schuette. Adv. Multidimens. Lumin. **2**, 61 (1993).
20. K.J. Sasaki, S.D. Christian, and E.E. Tucker. J. Colloid Interface Sci. **134**, 412 (1990).
21. N. Funasaki, H. Yodo, S. Hada, and S. Neya. Bull. Chem. Soc. Jpn. **65**, 1323 (1992).
22. H. Benesi and H. Hildebrand. J. Am. Chem. Soc. **71**, 2703 (1949).
23. K.A. Connors. Binding constants. John Wiley, New York. 1987. p. 78.
24. R.U. Lemieux. Acc. Chem. Res. **29**, 373 (1996).
25. W. Gerasimowicz and J. Wodcik. Bioorg. Chem. **11**, 420 (1982).
26. M.C. Chervenak and E.J. Toone. J. Am. Chem. Soc. **116**, 10533 (1994).
27. J.C. Ravey and M.J. Stébé. Colloids Surf. A: **84**, 11 (1994).
28. H. Kunieda and K. Shinoda. J. Phys. Chem. **80**, 2468 (1976).
29. P. Gianni and L. Lepori. J. Solution Chem. **25**, 1 (1996).
30. G.J.T. Tiddy. *In* Modern trends of colloid science in chemistry and biology. *Edited by* E. Eicke. Birkhauser Verlag, Basel. 1985. p. 153.
31. M.R. Eftink, M.L. Andy, K. Bystrom, H.D. Perlmutter, and D.S. Kristol. J. Am. Chem. Soc. **111**, 6765 (1989).
32. P. Mukerjee. Colloids Surf. A: **84**, 1 (1994).
33. T. Asakawa, T. Inoue, S. Ikeda, S. Miyagishi, and M. Nishida. Langmuir, **7**, 262 (1991).
34. K.J. Miller. J. Am. Chem. Soc. **112**, 8533 (1990).
35. A. Maciejewski. J. Photochem. Photobiol. **51**, 87 (1990).
36. W. Guo, B.M. Fung, and S.D. Christian. Langmuir, **8**, 446 (1992).
37. A.L. Henne and C.J. Fox. J. Am. Chem. Soc. **73**, 2323 (1951).
38. R. Palepu and V.C. Reinsborough. Can. J. Chem. **67**, 1550 (1989).
39. Y.E. Macpherson, R. Palepu, and V.C. Reinsborough. J. Inclusion Phenom. Mol. Recog. Chem. **9**, 137 (1990).
40. J.W. Park and H.J. Song. J. Phys. Chem. **93**, 6454 (1989).
41. W. Blokzijl and J.F.B.N. Engberts. Angew. Chem. Int. Ed. Engl. **32**, 1545 (1993).
42. M. Mukerjee and K.J. Mysels. Critical micelle concentration of aqueous surfactant systems. NSRDS-NBS 36, Washington, D.C. 1971.

Can. J. Chem. Downloaded from www.nrcresearchpress.com by 88.146.161.215 on 09/08/12
For personal use only.

© 1997 NRC Canada

The electronic absorption spectra of some *N*-sulfinylanilines. A molecular orbital treatment

R. Abu-Eittah, H. Moustafa, and A.M. Al-Omar

Abstract: The electronic absorption spectra of *N*-sulfinylaniline and some of its derivatives were investigated using different solvents. The spectral behavior of the molecules indicated their planarity and that the NSO group is a strong electron acceptor. All the observed bands correspond to delocalized $\pi \rightarrow \pi^*$ transitions; $n \rightarrow \pi^*$ transition were not observed as discrete bands. Ab initio molecular orbital calculations were performed using four different basis sets. The results showed that the NSO group is nonlinear, the molecules studied are planar, and the *syn* conformer is more stable than the *anti* conformer.

Key words: *N*-sulfinylanilines, spectra and theoretical treatment.

Résumé : On a étudié, dans différents solvants, les spectres d'absorption électronique de la *N*-sulfinylaniline et de certains de ses dérivés. Le comportement spectral des molécules indique qu'elles sont planes et que le groupe NSO est un puissant accepteur d'électrons. Toutes les bandes observées correspondent à des transitions délocalisées $\pi \rightarrow \pi^*$, on n'a pas observé de bandes discrètes correspondant à des transitions $n \rightarrow \pi^*$. On a effectué des calculs d'orbitales moléculaires ab initio en utilisant quatre ensembles de base différents. Les résultats indiquent que le groupe NSO est non linéaire, que les molécules étudiées sont planes et que le conformère *syn* est plus stable que le conformère *anti*.

Mots clés : *N*-sulfinylanilines, spectres et théorie.

[Traduit par la rédaction]

Introduction

Although discovered in 1890–1893, the aryl(ArNSO) (1, 2), alkyl (RNSO) (2, 3), and thionylamines have not been extensively investigated and their electronic spectra are hardly discussed in the literature. *N*-Sulfinylaniline (Ph.N:S:O) is considered to be an interesting potential donor–acceptor system (4). The spectra of fluorinated *N*-sulfinylanilines showed that the -NSO group is a strong electron acceptor (5). The interaction of fluorinated *N*-sulfinylanilines with low-energy electrons leads to the formation of resonant states of the negative molecular ions (6). The infrared and Raman spectra of several substituted *N*-sulfinylanilines showed that no coupling exists between ν(N-S) and ν(S-O) (7–9). Butt et al. (7) showed that the NSO group has little resonance interaction with the benzene ring in the ground state but is capable of resonance donation or acceptance depending on the electron demand of the substituents. Microwave (10, 11) spectra indicated that the molecule is planar. Infrared spectra at low temperature showed two very close components of the NSO group that may be attributed to the existence of two rotational isomers (12).

The NMR spectra of R-C_6H_4NSO (R = *o*, *m*-Me) have shown that the NSO group is nonlinear and its free rotation around the C—N bond is restricted to some extent because of charge delocalization (13). No significant shift or splitting was observed upon cooling from 40 to −60°C, a result that indicates that the molecules have only one conformation (14). Substitution of hydrogen atoms by methyl groups in C_6H_5NSO causes the expected shifts in the NMR spectra. The spectra showed free rotation, even at −60°C, of the aryl ring around the C—N axis. If one *ortho* position of the phenyl ring is occupied by a methyl group the free rotation is hindered. This idea was supported by Waclawek et al. (15) who studied the rotation of the NSO group about the N—C_{ar} bond by dipole moment measurements.

The electronic dipole moment measurements and ^{1}H NMR spectra of a series of *N*-sulfinylanilines have shown that these compounds adopt preferentially a *cis* or *syn* structure with respect to the central -N=S- bond (16); the same result was obtained for alkylsulfinylanilines (17). However, infrared spectroscopic methods as well as dielectric constant measurements have shown that the NSO group, on various aliphatic and aromatic molecules, exists in a stable *anti* conformation and acts as a weak π-electron acceptor (18).

UV spectral studies (19) indicated that the N—S bond can be regarded as a 4-electron bond that is in resonance with the neighboring π-electron system. The X-ray spectra (20) of 4-RC_6H_4NSO (R = H, Me, MeO) indicated the participation of the sulfur 3*d* orbital in bonding.

In this work the electronic absorption spectra of some *N*-sulfinylanilines have been investigated and the results interpreted with respect to the properties of sulfinyl and the attached groups. Gaussian analysis was adapted to the observed spectra to resolve the overlapping bands. A MATHCAD (21) program was used and the best analysis is that which results in a minimum residue between the analyzed spectrum and the experimental one. Molecular orbital calculations with

Received December 2, 1996.

R. Abu-Eittah,[1] H. Moustafa, and A.M. Al-Omar. Department of Chemistry, Faculty of Science, University of Cairo, Giza, Egypt.

[1] Author to whom correspondence may be addressed. E-mail: hilal2@frcu.eun.eg

© 1997 NRC Canada

Can. J. Chem. Downloaded from www.nrcresearchpress.com by 88.146.161.215 on 09/08/12
For personal use only.

Can. J. Chem. Downloaded from www.nrcresearchpress.com by 88.146.161.215 on 09/08/12
For personal use only.

Fig. 1. The electronic spectrum of *N*-sulfinylaniline using heptane as a solvent.

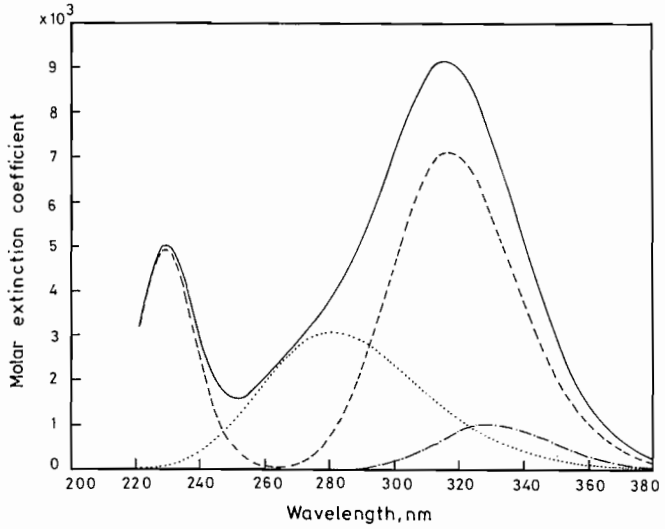
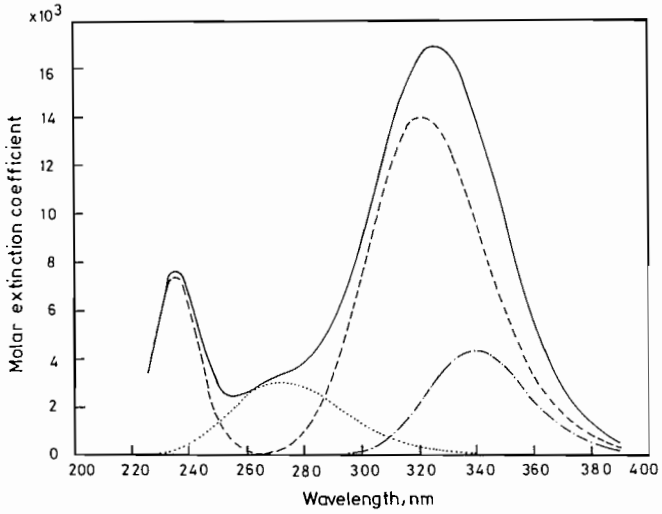


Fig. 2. The electronic spectrum of *p*-methyl-*N*-sulfinylaniline using heptane as a solvent.



geometry optimization were performed on the ground states of the molecules studied, using ab initio procedures through the GAMESS (22) program. Excited states were treated theoretically using the AM1 (23) procedure.

Experimental

Compounds

The compounds studied were prepared and purified by standard procedures cited in the literature (2, 14). The refractive indices for the prepared compounds {X-C_6H_4NSO} are given:

Compounds, X =	Refractive index (this work)	Refractive index (Ref. 19)
H[a]	1.6248(25°C)	1.6259(20°C)
m-CH_3	1.6250(25°C)	1.6132(20°C)
p-CH_3	1.6170(25°C)	1.6241(20°C)
p-OCH_3	1.6480(25°C)	1.6300(20°C)

Solvents

Polar and nonpolar solvents were obtained form Merck, AR-grade, and were used without further purification.

Apparatus

Spectra were scanned on a Perkin Elmer Lambda 4B spectrophotometer using 1.0 cm fused silica cells. The machine records linearly in percent transmittance over the range 190–900 nm.

Results and discussion

I Electronic absorption spectra

I.1 N-*Sulfinylaniline*

The electronic absorption spectrum of *N*-sulfinylaniline consists of two intense and well-separated bands. The long-wavelength band is rather broad, extends from 360 to 250 nm, and is easily resolved (Fig. 1) by Gaussian analysis to three overlapping bands with λ_{max} at 330, 317, and 281 nm. Band intensity varies from $\varepsilon \cong 800$ to 3200 L mol^{-1} cm^{-1}, which indicates that these bands correspond to allowed $\pi \rightarrow \pi^*$ transitions and none of them corresponds to an $n \rightarrow \pi^*$ transition. The spectrum reflects the planarity of the molecule. If the molecule were nonplanar its spectrum would have been the additive spectra of benzene and NSO chromophores. Molecular orbital calculations gave two distinct bands for NSO^-, at 397 and 300 nm, but only the 379 nm band is observed (24).

The variation of λ_{max} with solvent polarity is apparent for the lowest energy transition (Table 1), a result that indicates a contribution of the charge transfer (CT) configuration to the excited states of the molecule.

I.2 p-*Methyl*-N-*sulfinylaniline*

Substitution by a methyl group in the *para* position will enhance the electron donor and acceptor properties in the molecule. The spectrum shows two well-defined separated bands. The long-wavelength band is broad, 360–260 nm, and easily resolved to three overlapping bands corresponding to three transitions with band maxima at 339, 321, and 272 nm (Fig. 2). A red shift of λ_{max} with the polarity of solvent, from 339 nm in heptane to 344 nm in ethanol, is observed (Table 1). The spectra of the molecule have been scanned in different solvents and Gaussian analysis of the bands shows that all the components are strong enough to exclude any $n \rightarrow \pi^*$ transition.

I.3 m-*Methyl*-N-*sulfinylaniline*

The spectrum of this molecule in heptane as a solvent is given in Fig. 3. A comparison of band maxima of the lowest-energy transition shows that for *N*-sulfinylaniline and *p*-methyl and *m*-methyl derivatives the values are 330, 339, and 335 nm, respectively. The perturbation effect of methyl substitution is detected.

I.4 p-*Methoxy*-N-*sulfinylaniline*

The electronic spectrum shows two main bands (Fig. 4), a broad one in the 400–260 nm region and another relatively sharp one with λ_{max} around 246 nm. The long-wavelength

© 1997 NRC Canada

Can. J. Chem. Downloaded from www.nrcresearchpress.com by 88.146.161.215 on 09/08/12
For personal use only.

Table 1. Band maxima and intensities of the studied compounds in different solvents.

Compound	Solvent	λ_{max}(nm)	ε, L mol^{-1} cm^{-1}	*f*
		330	776	0.02
	Heptane	317	7154	0.15
		281	3223	0.10
N-Sulfinylaniline		228	5060	0.08
		332	1440	0.09
	Ethnaol	318	1973	0.45
		278	8030	0.23
		231	2602	0.56
		339	2798	0.03
	Heptane	321	14490	0.34
		272	2814	0.09
		235	7569	0.11
p-Methyl-*N*-sulfinylaniline				
		344	3045	0.37
	Ethanol	334	9848	0.25
		278	2510	0.11
		234	1319	0.22
		335	1302	0.02
	Heptane	317	10650	0.26
		277	3340	0.11
		235	7022	0.11
m-Methyl-*N*-sulfinylaniline				
		337	1001	0.02
	Ethanol	319	6523	0.16
		278	2445	0.06
		236	8857	0.18
		367	1742	0.02
		354	11840	0.16
	Heptane	326	6818	0.12
		282	1619	0.05
p-Methoxy-*N*-sulfinylaniline		246	7016	0.10
		371	1408	0.01
		358	7629	0.12
	Ethanol	326	3947	0.09
		287	1031	0.02
		245	6094	0.14

broad band has been analyzed to four bands with λ_{max} (heptane as solvent) at 367, 354, 326, and 282 nm, (Fig. 4). All obtained bands are sufficiently intense and correspond to $\pi \rightarrow \pi^*$ transitions. A comparison of the values of λ_{max} of the most intense bands of *p*-methoxy-*N*-sulfinylaniline, *N*-sulfinylaniline, *p*-methyl- and *m*-methyl-*N*-sulfinylaniline in heptane as a solvent gives 354, 317, 321, 317 nm, respectively. A significant red shift is observed with *p*-methoxy substitution that, again, confirms the electron-accepting properties of the NSO group.

II Molecular orbital calculations

II.1 N-*Sulfinylaniline*

II.1.a Ground state of N-*sulfinylaniline:* The equilibrium geometry of the molecule in the ground state was predicted by ab initio calculations using the GAMESS program package (version 1995). Several basis sets, namely, STO-3G**, STO-6G**, 3-21G**, and 6-21G**, which are stored in the program, were considered initially to determine the

© 1997 NRC Canada

Can. J. Chem. Downloaded from www.nrcresearchpress.com by 88.146.161.215 on 09/08/12
For personal use only.

Fig. 3. The electronic spectrum of *m*-methyl-*N*-sulfinylaniline using heptane as a solvent.

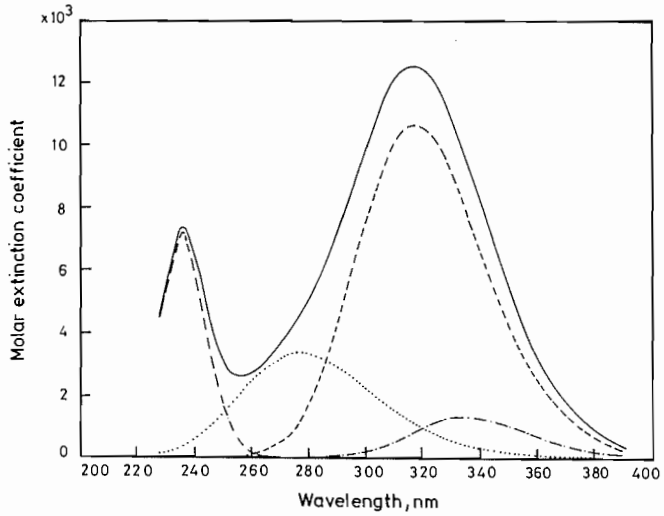
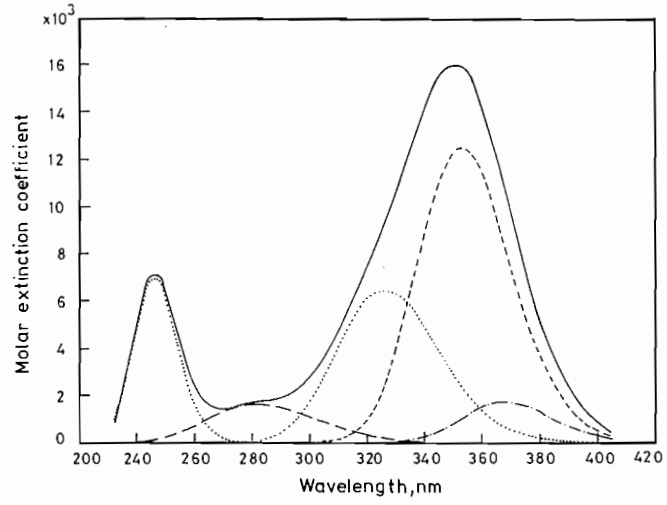


Fig. 4. The electronic spectrum of *p*-methoxy-*N*-sulfinylaniline using heptane as a solvent.

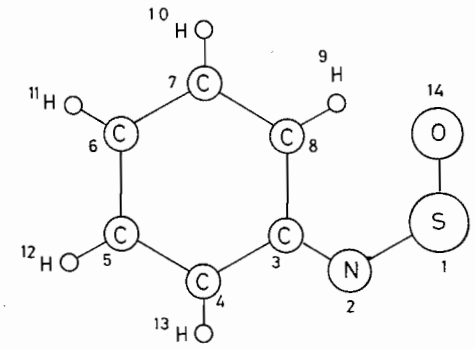


equilibrium geometry of the molecule. In this work explicit MO calculations using the SCF-HF method were performed on both the *syn* (*cis*), I, and the *anti* (*trans*), II, conformers (Fig. 5). The calculated parameters for the optimized geometries, Tables 2 and 3, were used in further calculations. All the basis sets used include *d*-functions for heavy atoms and *p*-functions for the H-atom.

Experimental results indicate that *N*-sulfinylaniline exists in the planar *syn* conformer (8) and molecular orbital calculations performed in this work confirm this result. The *syn* conformer is of lower total energy than the *anti* conformer, with a *syn* ⇒ *anti* conversion energy varying from 6.9 kcal mol^{-1} (STO-6G**) to 10.7 kcal mol^{-1} (6-21G**).

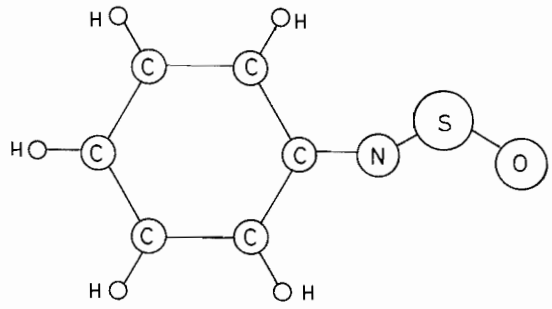
For the *syn* conformer Tables 2 and 3 show that the lowest total energy, −756.453 24 au, is obtained with the split-valence basis set 6-21G**, which was used to calculate all the structural parameters of the molecule. The experimental C—N

Fig. 5. Ab initio optimized geometry and numbering system of the *syn* (*cis*) and the *anti* (*trans*) conformers of *N*-sulfinylaniline.



I

SYN-N-SULFINYLANILINE



II

ANTI-N-SULFINYLANILINE

bond length, Table 2, in CH_3NSO is 1.421 ± 0.005 Å (25); that expected in C_6H_5NSO would be shortened as a result of a partial contribution of resonance structures representing possible delocalization involving the phenyl group. The same reasoning applies to the expected shortening of the N—S and S—O bonds in *N*-sulfinylaniline compared to HNSO or CH_3NSO.

The values of bond angles (Table 2) NSO, CNS, and NC_3C_4 are nicely reproduced by both basis sets 3-21G** and 6-21G**. For the NSO angle a value of 119.01° compares well with a value of 117 ± 2° (25) found for the same angle in CH_3NSO, 120.4° (26) in HNSO, and 123° in C_6H_5NSO (10). In the mean time the bond angle CNS is calculated by the 6-21G** basis set to be 133.6°, which is in good order compared with experimental values 126 ± 2° (25) in CH_3NSO and 130° adjusted to reproduce the rotation spectra of *N*-sulfinylaniline (10).

The difference is bonding between N, S and S, O in *N*-sulfinylaniline is clearly reflected in the calculated values of Mulliken overlap population between the respective atoms using split-valence basis sets. The overlap population between C_{ar}—N, 0.526 (Table 3), is an indication of an essential single bond whereas a value of 1.023–1.058 between the atoms N and S and a value of 0.907–0.938 between the atoms S and O indicate the existence of double bonds but of different degrees. The aromatic double bond character in the benzene ring of *N*-sulfinylaniline gives an overlap population of 0.925–0.927 (Table 3), using split-valence basis sets.

The calculated charge densities are accurate and lead to accurate values of dipole moments. The calculated dipole

© 1997 NRC Canada

Can. J. Chem. Downloaded from www.nrcresearchpress.com by 88.146.161.215 on 09/08/12
For personal use only.

Table 2. Calculated equilibrium geometric parameters for *N*-sulfinylanilines at various theoretical levels.

Compound	Basis sets	Geometrical parameters					
		$r(C_3—N)$,[a] Å	r(N—S), Å	r(S—O), Å	θ(NSO),°	θ(C_3NS),°	θ(NC_3C_4),°
C_6H_5NSO	3-21G**	1.399[b](1.402)	1.485(1.485)	1.451(1.449)	118.9(115.52)	134.50(132.20)	118.30(117.61)
	6-21G**	1.404(1.408)	1.490(1.485)	1.456(1.446)	119.01(115.05)	133.60(130.95)	117.89(117.11)
p-CH_3-C_6H_4NSO	3-21G**	1.402(1.402)	1.484(1.485)	1.452(1.442)	118.90(115.40)	134.70(132.40)	118.20(117.50)
	6-21G**	1.407(1.411)	1.489(1.491)	1.458(1.448)	119.06(115.015)	133.92(131.14)	117.75(117.02)
m-CH_3-C_6H_4NSO	3-21G**	1.403(1.407)	1.484(1.485)	1.450(1.441)	119.07(115.33)	134.76(131.93)	118.10(117.45)
	6-21G**	1.408(1.412)	1.489(1.491)	1.456(1.447)	119.21(115.08)	133.98(130.71)	117.73(116.94)
p-CH_3O-C_6H_4NSO	3-21G**	1.401(1.404)	1.485(1.485)	1.453(1.442)	118.16(115.40)	134.51(132.76)	118.02(117.46)
	6-21G**	1.406(1.410)	1.490(1.492)	1.459(1.449)	118.87(115.16)	133.73(131.49)	117.66(116.96)
Experimental		1.421 ± 0.005[c]	1.525 ± 0.004,[c] 1.512[d]	1.466 ± 0.004,[c] 1.451[d]	120.4,[d] 117 ± 2,[c] 123.0[e]	130.0,[e] 126 ± 2[c]	—

[a]For numbering system, see Fig. 5.
[b]For *syn* conformer; *anti* conformer is in parentheses.
[c]Reference 25, values for CH_3NSO.
[d]Reference 26, values for HNSO.
[e]Reference 10, values for C_2H_5NSO.

Table 3. Calculated properties for *N*-sulfinylanilines at various theoretical levels.

Compound	Basis sets	Energy, au		Total energy, au	Dipole moment,[c] D	Overlap population					Charge density			
		HOMO	LUMO			S—O	S—N	N—C	C_3—C_4	C_4—C_5	N	S	O	Phenyl
C_6H_5NSO	3-21G**	−0.325 92[a]	0.03682	−753.030 22	1.999(2.07)(27)	0.907	1.023	0.503	0.925	0.880	−0.635	0.729	−0.516	0.422
		−0.326 61[b]	0.03694	−753.013 65	4.311	0.962	0.884	0.576	0.925	0.881	−0.610	0.690	−0.480	0.400
	6-21G**	−0.324 32[a]	0.03862	−756.453 24	1.994	0.938	1.058	0.526	0.927	0.900	−0.608	0.702	−0.502	0.408
		−0.324 81[b]	0.03691	−756.436 67	4.330	0.995	0.920	0.598	0.930	0.882	−0.587	0.665	−0.469	0.391
p-CH_3-C_6H_4NSO	3-21G**	−0.314 98[a]	0.04266	−791.845 21	2.429(2.40)(27)	0.905	1.024	0.497	0.935	0.882	−0.629	0.721	−0.522	0.430
		−0.315 97[b]	0.04406	−791.828 76	4.856	0.960	0.884	0.572	0.937	0.865	−0.610	0.683	−0.488	0.415
	6-21G**	−0.312 96[a]	0.04557	−795.439 27	2.435	0.935	1.060	0.520	0.937	0.888	−0.602	0.694	−0.509	0.417
		−0.314 76[b]	0.04428	−795.422 12	4.879	0.992	0.920	0.592	0.940	0.871	−0.581	0.656	−0.475	0.400
p-CH_3O-C_6H_4NSO	3-21G**	−0.305 28[a]	0.04759	−866.284 21	3.890(2.90)(19)	0.903	1.020	0.504	0.912	0.763	−0.626	0.716	−0.526	0.436
	6-21G**	−0.303 26[a]	0.04928	−870.178 32	3.892	0.932	1.056	0.524	0.932	0.761	−0.598	0.688	−0.513	0.423

[a]*syn* Conformer.
[b]*anti* Conformer.
[c]Experimental dipoles and their references are in parentheses.

© 1997 NRC Canada

Can. J. Chem. Downloaded from www.nrcresearchpress.com by 88.146.161.215 on 09/08/12
For personal use only.

Table 4. A comparison between the first ionization potential and ab initio eigenvalues of *syn*-, *anti*-C_6H_5NSO, *syn*- and *anti*-*p*-CH_3-C_6H_4NSO using 6-21G** basis sets.

Compound	MO	Eigenvalue, eV	I. P., eV (28)
C_6H_5NSO	ψ_{36}	−8.825 (−8.839)[a]	9.12
	ψ_{35}	−9.578 (−9.766)	9.65
	ψ_{34}	−11.920 (−11.203)	10.62
	ψ_{33}	−12.264 (−12.274)	11.09
p-CH_3-C_6H_4NSO	ψ_{40}	−8.546 (−8.468)	8.84
	ψ_{39}	−9.548 (−9.744)	0.53
	ψ_{38}	−11.836 (−11.099)	10.60
	ψ_{37}	−11.950 (−11.948)	11.09

[a]Values for *anti* conformer.

moments of *N*-sulfinylaniline are 1.999 D (using 3-21G**) and 1.994 D (using 6-21G**), which agree nicely with the experimental one, 2.07 D (27). The same behavior is observed with *p*-methyl-*N*-sulfinylanine; calculations using the split-valence basis set 6-21G** lead to accurate values of charge density, which in turn give 2.429 D for the dipole moment, corresponding nicely to the experimental value (2.40 D) (27).

He(I) and He(II) photoelectron spectra of some *N*-sulfinylanilines have been reported (28). A comparison between experimental values of the ionization potentials of C_6H_5NSO with the results of ab initio calculations is given in Table 4. The correspondence is quite adequate. The first, lowest, ionization potential for C_6H_5NSO, 9.12 eV, corresponds nicely to the energy of the HOMO (ψ_{36}). This MO is a combination of a $\pi(e_{1g})$ orbital of benzene and a π(N═S) bonding orbital.

The second ionization potential, at 9.65 eV, is assigned to the energy of the molecular orbital ψ_{35}; this orbital is a π-MO and is almost completely localized on the *ortho* and *meta* carbon atoms of the benzene ring of *N*-sulfinylaniline. However, an ionization energy of 9.65 eV is significantly higher than the corresponding value in benzene, indicating a substantial charge flow to the NSO moiety.

The third ionization potential, 10.62 eV, corresponding to the eigenvalue (11.92) of the MO ψ_{34}, this MO is a delocalized σ-MO with a large contribution of N, O, and S atoms. The overlap between the NSO group and the benzene ring, in ψ_{34}, is nil. The overlap between AOs of C-atoms in benzene ring is also nil in ψ_{34} (antibonding MO) and this explains the high eigenvalue of ψ_{34}. The third ionization from a π orbital is harder to identify in the photoelectron spectrum of C_6H_5NSO and, applying the same rule for the three π-orbitals, a value of 11.31 eV was derived for it (28).

II.1.b Excited states of N-*sulfinylaniline:* An appropriate semi-empirical method that reproduces the spectroscopic properties of the molecules is the AM1 method stored in a MOPAC6 (29) program package. The MOs were computed and the CI matrix was solved where electronic transitions were considered between the highest three occupied and the lowest two unoccupied MOs. In the AM1 procedure both α and β spins are considered for the transferred electron.

The electronic transitions and the corresponding assignments of *N*-sulfinylaniline are given in Table 5. For the *syn* conformer, four electronic transitions are calculated and

Table 5. Electronic transition and the corresponding assignments of *N*-sulfinylaniline.

Transition energy, eV		
Calcd.	Exp.	Assignment
***syn* Conformer**		
3.47	—	$n \rightarrow \pi_1^*$: localized on NSO
3.60	3.70	$\pi_2 \rightarrow \pi_1^*$: CT $C_6H_5 \rightarrow$ NSO
3.84	3.91	$\pi_2 \rightarrow \pi_2^*$, $\pi_1 \rightarrow \pi_1^*$: delocalized
4.80	4.42	$\pi_2 \rightarrow \pi_2^*$, $\pi_1 \rightarrow \pi_1^*$: delocalized
5.52	5.43	$\pi_1 \rightarrow \pi_2^*$: localized on C_6H_5
***anti* Conformer**		
3.69		$\pi_2 \rightarrow \pi_1^*$: CT $C_6H_5 \rightarrow$ NSO
3.94		$\pi_2 \rightarrow \pi_2^*$, $\pi_1 \rightarrow \pi_1^*$: delocalized
4.90		$\pi_2 \rightarrow \pi_2^*$, $\pi_1 \rightarrow \pi_1^*$: delocalized
5.53		$\pi_1 \rightarrow \pi_2^*$: localized on C_6H_5

The MOs, ϕ_{21}, ϕ_{22}, and ϕ_{23} are identified as n, π_1, π_2 MOs whereas the MOs ϕ_{24} and ϕ_{25} are identified as π_1^* and π_2^* MOs.

observed in the UV–VIS region. The calculated energy for the lowest transition is 3.47 eV and corresponds to an $n \rightarrow \pi_1^*$ transition, localized over the NSO group. This transition is not observed in the spectrum, Fig. 1, and is obscured by the stronger $\pi_2 \rightarrow \pi_1^*$ transition.

II.2 p-*Methyl*-N-*sulfinylaniline*

Molecular orbital calculations were performed on this molecule following the same steps, and all the basis sets, used with *N*-sulfinylaniline. The calculated results indicate that bond lengths, Table 2, were generally elongated in the *anti* conformer compared to the *syn* conformer; the bond lengths and bond angles calculated for the *syn* conformer are nearer to the experimental values (25). The *syn* conformer is more stable than the *anti* conformer with all the basis sets used, Table 3. The dipole moment calculated for the *syn* conformer, using split-valence basis sets, is 2.429 D, in excellent agreement with the experimental value, 2.40 D (27).

The photoelectron spectrum (28) of the molecule shows an overlap of most of the bands. Table 4 compares the eigenvalues of the highest four occupied MOs of the *syn* and *anti* conformers using the 6-21G** basis sets and the ionization potentials that were measured experimentally.

Excited states were investigated by solving the CI matrix using the AM1 procedure. The CI matrix built from interaction terms between the highest three occupied MOs, ψ_{24}–ψ_{26}, and the lowest two unoccupied MOs, ψ_{27}–ψ_{28}, was solved. It is found that ψ_{24} is a $\sigma(n)$ MO localized over the NSO group where ψ_{25} is a π-MO, localized over the tolyl ring. The MO ψ_{26} is a delocalized π-MO whereas ψ_{27} is a π^*-MO delocalized over the NSO group and ψ_{28} is a π^*-MO localized on the tolyl ring. The calculated $n \rightarrow \pi_1^*$ transition energy, 3.44 eV (Table 6), has no experimental correspondence. The broad band in the spectrum, 275–370 nm (Fig. 2), is resolved into bands with energies 3.65 and 3.86 eV and these corresponding nicely to the calculated transition energies at 3.49 and 3.87 eV, respectively. The highest-energy transition, 5.53 eV, corresponds to a $\pi_1 \rightarrow \pi_2^*$ transition localized over the tolyl ring

© 1997 NRC Canada

Can. J. Chem. Downloaded from www.nrcresearchpress.com by 88.146.161.215 on 09/08/12
For personal use only.

Table 6. Electronic transition of *syn-p*-methyl- and -*m*-methyl-*N*-sulfinylanilines and the corresponding assignments.

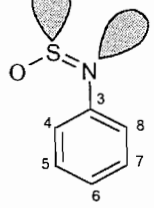
Transition energy, eV		
Calcd.	Exp.	Assignment
***syn-p*-Methyl-*N*-sulfinylaniline**		
3.44	—	$n \rightarrow \pi_1^*$: localized on NSO
3.49	3.65	$\pi_2 \rightarrow \pi_1^*$: CT p-CH_3-$C_6H_4 \rightarrow$ NSO
3.87	3.86	$\pi_1 \rightarrow \pi_1^*$, $\pi_1 \rightarrow \pi_2^*$: delocalized
4.68	4.56	$\pi_2 \rightarrow \pi_2^*$, $\pi_1 \rightarrow \pi_1^*$: delocalized
5.53	5.28	$\pi_1 \rightarrow \pi_2^*$: localized on p-CH_3-C_6H_4
***syn-m*-Methyl-*N*-sulfinylaniline**		
3.43	—	$n \rightarrow \pi_1^*$: localized on NSO
3.54	3.70	$\pi_2 \rightarrow \pi_1^*$: CT m-CH_3-$C_6H_4 \rightarrow$ NSO
3.83	3.90	$\pi_1 \rightarrow \pi_1^*$, $\pi_2 \rightarrow \pi_2^*$: delocalized
4.68	4.48	$\pi_2 \rightarrow \pi_2^*$, $\pi_1 \rightarrow \pi_1^*$: delocalized
5.52	5.27	$\pi_1 \rightarrow \pi_2^*$: localized on m-CH_3-C_6H_4

The MOs ϕ_{24}, ϕ_{25}, and ϕ_{26} are identified as n, π_1, π_2 MOs whereas the MOs ϕ_{27} and ϕ_{28} are identified as π_1^* and π_2^* MOs.

and nicely corresponds to the experimentally observed band with energy 5.28 eV.

II.3 m-*Methyl*-N-*sulfinylaniline*

The optimized equilibrium geometry parameters using the split-valence basis sets, 3-21G** and 6-21G**, are given for the *syn* and *anti* conformers in Table 2. Results show only a slight difference in the bond lengths N—S and S—O, which suggests the existence of the same type of bonding between N and S and between S and O atoms. The values of bond angles NSO and NC_3C_4 indicate sp^2 hybridization on the central atom. The enlargement of angle θSNC_3 must be related to the lone pair – lone pair repulsion.



Excited states of the *syn* conformer of *m*-methyl-*N*-sulfinylaniline were obtained as with the *syn-p*-methyl-*N*-sulfinylaniline. Configuration interaction was allowed between the highest three occupied MOs, ψ_{24}–ψ_{26}, and the lowest two unoccupied MOs, ψ_{27}–ψ_{28}. The AM1 calculations showed that ψ_{24} is a $\sigma(n)$ MO localized over the NSO group, MO ψ_{25} is a π-MO localized over the tolyl group, ψ_{26} is a π delocalized MO, whereas ψ_{27} is a π^*-MO localized over the NSO group and ψ_{28} is a π^*-MO localized over the tolyl group.

Four $\pi \rightarrow \pi^*$ electronic transitions in addition to a low-energy $n \rightarrow \pi^*$ transition are calculated for this molecule in the accessible UV region, Table 6. The $n \rightarrow \pi_1^*$ transition is not observed and is obscured by the stronger, $\pi_2 \rightarrow \pi_1^*$, transition. The correspondence between calculated and experimentally observed transition energies is satisfactory, 3.54 eV versus 3.70, 3.83 versus 3.90, 4.68 versus 4.48, and 5.52 versus 5.27 eV.

Table 7. Electronic transition and the corresponding assignments of *syn-p*-methoxy-*N*-sulfinylanilines.

Transition energy, eV		
Calcd.	Exp.	Assignment
3.34	3.38	$\pi_2 \rightarrow \pi_1^*$: CT p-CH_3O-$C_6H_4 \rightarrow$ NSO
3.40	3.50	$\pi_1 \rightarrow \pi_1^*$, $\pi_2 \rightarrow \pi_2^*$: delocalized
3.44		$n \rightarrow \pi_1^*$: localized on NSO
3.96	3.80	$\pi_1 \rightarrow \pi_1^*$, $\pi_2 \rightarrow \pi_2^*$: delocalized
4.62	4.40	$\pi_1 \rightarrow \pi_1^*$, $\pi_2 \rightarrow \pi_2^*$: delocalized
5.50	5.04	$\pi_1 \rightarrow \pi_2^*$: localized on p-CH_3O-C_6H_4

The MOs ϕ_{27}, ϕ_{28}, and ϕ_{29} are identified as n, π_1, π_2 MOs whereas the MOs ϕ_{30} and ϕ_{31} are identified as π_1^* and π_2^* MOs.

II.4 p-*Methoxy*-N-*sulfinylaniline*

The total energy calculated for the *syn* conformer was always less than that for the *anti* conformer, Table 3. There is a slight elongation of the N—S bond (Table 2) relative to the S—O bond, which is a result of the resonance effect of the *p*-methoxy group.

The AM1 procedure was used to perform MO calculations on the excited states of the *syn* conformer of this molecule. The results showed that the highest occupied MOs ψ_{27}, ψ_{28}, and ψ_{29} are $\sigma(n)$ MO localized on the NSO group, π-MO localized over the p-$OCH_3C_6H_4$ group, and π-MO delocalized over the whole molecule, respectively. The LUMOs, ψ_{30} and ψ_{31} are π^*-MO localized over the NSO group and π^*-MO localized over the p-$OCH_3C_6H_4$ chromophore, respectively. The lowest-energy electronic transition is a $\pi_2 \rightarrow \pi_1^*$ charge transfer transition from the p-$OCH_3C_6H_4$ group to the NSO moiety, Table 7. The $n \rightarrow \pi_1^*$ transition, calculated theoretically with an energy of 3.44 eV, is localized on the NSO group and is submerged under the stronger $\pi_1 \rightarrow \pi_1^*$ transition. Three $\pi \rightarrow \pi^*$ electronic transitions are predicted theoretically and observed experimentally for the molecule; these are delocalized over the whole molecule except for the highest energy transition, which is localized over the p-$CH_3OC_6H_4$ group. The correspondence between calculated and observed transition energies is rather satisfactory, 3.34 versus 3.38, 3.40 versus 3.50, 3.96 versus 3.80, 4.62 versus 4.40, and 5.50 versus 5.04 eV.

Conclusions

The electronic absorption spectra of the *N*-sulfinylanilines studied reflect the planarity of the molecules. The observed spectra were not the additive spectra of the NSO group and the benzene ring. The overlap of the low-energy electronic transitions is a common feature of the observed spectra and no discrete band was observed for any $n \rightarrow \pi^*$ transition. Solvent effect on band maxima is not pronounced, a result that indicates the small contribution of the charge transfer configuration to the wave function of the excited states. The NSO group acts as an electron acceptor, especially in the presence of a

© 1997 NRC Canada

complementary group, methyl or methoxy, which enhances the electron-donor or electron-acceptor properties of the NSO group. Charge transfer transitions become more clear than they are in the parent molecule (C_6H_5NSO).

MO calculations at the levels used indicated the planarity of the molecules studied and that the NSO group is nonlinear. The *syn* conformer is more stable, of lower energy, and the height of the barrier of rotation is 6.9–10.7 kcal mol^{-1}. The calculated dipole moment agrees satisfactorily with the experimental one when using split-valence basis sets. The calculated structural parameters, bond lengths, and bond angles agree nicely with the experimental ones. Also, the calculated energies of the occupied MOs agree with the experimental ionization potentials.

The difference in bonding between the N—S and S—O atoms is reflected in the calculate values of Mulliken overlap population. The results indicated an essential single bond between C_{ar} and N and double bonds between N and S as well as between S and O atoms but with different extents.

Molecular orbital calculations showed the existence of an $n \rightarrow \pi^*$ transition localized on the NSO group. However, this transition is not observed experimentally and is obscured by the neighboring strong $\pi \rightarrow \pi^*$ transition.

References

1. A. Michaelis and R. Hertz. Ber. Dtsch. Chem. Ges. **23**, 3480 (1890).
2. A. Michaelis. Ber. Dtsch. Chem. Ges. **24**, 745 (1891).
3. A. Michaelis. Justus Liebigs Ann. Chem. **274**, 187 (1893).
4. N.C. Collins and W.K. Glass. Spectrochim. Acta, Part A: **30A**, 1335 (1974).
5. A.V. Zibarev, Sh.A. Sultannov, and I.I. Furlei. Izv. Akad. Nauk SSSR. Ser. Khim. **2**, 474 (1986).
6. E.A. Burmistrov, I.I. Furlei, and Sh.A. Sultanov. Khim. Fiz. **9**, 504 (1990).
7. G. Butt, M. Davis, Y.T. Pang, R.D. Topsom, and A.R. Katritzky. J. Chem. Soc. Perkin Trans. 2, 260 (1974).
8. S. Mohan and S. Krishnamurthy. Acta Cienc. Indica, Phys. **16p**, 73 (1990).
9. R. Meij, A. Oskam, and D.J. Stufkens. J. Mol. Struct. **51**, 37 (1979).
10. W. Caminati, A.M. Mirri, and G. Maccagnani. J. Mol. Spectrosc. **66**, 368 (1977).
11. N. Heineking and N.C.L. Gerry. J. Mol. Spectrosc. **158**, 62 (1993).
12. W.K. Glass and A.D.E. Pullin. Trans. Faraday Soc. **57**, 546 (1961).
13. J. Mirek and Z. Czerwiec. Zesz. Nauk. Univ. Jagiellon. Pr. Chem. **18**, 183 (1973).
14. J. Kuyper and K. Vrieze. J. Organomet. Chem. **86**, 127 (1975).
15. W. Waclawek, C. Puchala, and Z. Czerwiec. Bull. Acad. Pol. Sci. Ser. Sci. Chim. **26**, 337 (1978).
16. H.F. Van Woerden and S.H. Bijl-Vlieger. Recl. Trav. Chim. Pays-Bas, **93**, 85 (1974).
17. W.H. Kirchoff. J. Am. Chem. Soc. **91**, 2437 (1986).
18. Yu.P. Egoroy, Yu.Ya. Borovikov, G.S. Fedyuk, and E.S. Levchenko. Zh. Obshch. Khim. **43**, 2470 (1973).
19. G. Kresze and H. Smalla. Chem. Ber. **92**, 1042 (1959).
20. J. Filipecki, Z. Czerwiec, J. Dworakowski, J. Koziol, and J.C. Glassl. Chem. Scr. **25**, 157 (1985).
21. MATHCAD 5.0^{PLUS} from MathSoft © 1986–1994 MathSoft Inc.
22. M.W. Schmidt, K.K. Baldridge, J.A. Boatz, S.T. Elbert, M.S. Gordon, J.H. Jensen, S. Koseki, N. Matsunage, K.A. Nguyen, S.J. Su, T.L. Windus, M. Dupuis, and J.A. Montgomery. J. Comput. Chem. **14**, 1347 (1993).
23. M.J.S. Dewar, E.G. Zoebisch, E.F. Healy, and J.J.P. Stewart. J. Am. Chem. Soc. **107**, 3902 (1985).
24. T. Chivers, A.B.F. Da Silva, O.J. Treu, and M. Trsic. J. Mol. Struct. **162**, 351 (1987).
25. B. Beagley, S.J. Chantrell, R.G. Kirby, and D.G. Schmidling. J. Mol. Struct. **25**, 319 (1975).
26. J. Carbtti, G. Dilonardo, G. Golloni, and A. Tronbetti. J. Mol. Spectrosc. **84**, 155 (1980).
27. L. Lannelli, U. Lamanna, and H. Lumbroso. Bull. Soc. Chim. Fr. **11**, 3626 (1966).
28. J.N. Louwen, H. Van Dam, D.J. Stufkens, A. Oskam, and H.H. Jaffe. J. Electron Spectrosc. Relat. Phenom. **26**, 235 (1982).
29. Quantum Chemistry Program Exchange (QCPE), Department of Chemistry, Indiana University, Bloomington, Indiana 47405, U.S.A.

Can. J. Chem. Downloaded from www.nrcresearchpress.com by 88.146.161.215 on 09/08/12
For personal use only.

© 1997 NRC Canada

5-Hydroxypentane-2,3-dione and 3-amino-1-hydroxypropan-2-one, putative precursors of vitamin B_6

Eckardt Wolf, Isaac A. Kennedy, Klaus Himmeldirk, and Ian D. Spenser

Abstract: New syntheses are described of 5-hydroxypentane-2,3-dione (**7**) (i.e., laurencione (**7** ⇄ **8**)) and of 3-amino-1-hydroxypropan-2-one (3-amino-1-hydroxyacetone) (**5**) hydrochloride, putative precursors of the C_5 unit, C-2′,2,3,4,4′, and of the C_3N unit, N-1,C-6,5,5′, respectively, of pyridoxine (**6**).

Key words: 3-amino-1-hydroxyacetone, 3-amino-1-hydroxypropanone, 5-hydroxypentane-2,3-dione, laurencione, vitamin B_6.

Résumé : On décrit de nouvelles synthèses de la 5-hydroxypentane-2,3-dione (**7**) (c'est-à-dire de la laurencione (**7** ⇄ **8**)) et du chlorhydrate de la 3-amino-1-hydroxypropan-2-one (3-amino-1-hydroxyacétone) (**5**), des précurseurs potentiels respectivement de l'unité en C_5, C-2′,2,3,4,4′, et de l'unité C_3N, N-1,C-6,5,5′, de la pyridoxine (**6**).

Mots clés : 3-amino-1-hydroxypropane-2-one, 3-amino-1-hydroxyacétone, 5-hydroxypentane-2,3-dione, laurencione, vitamine B_6.

[Traduit par la rédaction]

Introduction

Two precursors, one a modified pentose, 1-deoxy-D-xylulose (**1**), the other a non-protein amino acid, 4-hydroxy-L-threonine (**2**), account for the origin of the entire C_8N skeleton of vitamin B_6 (pyridoxol, pyridoxine) (**6**) (1). A hypothetical seven-step reaction sequence was advanced to account for the chemical mechanism of the formation of the pyridoxine skeleton from these two substrates (2). The first step in this sequence was postulated to be the union of the two precursors to form a Schiff base (**3**), which was then primed to generate the bond destined to become C-4—C-5 of pyridoxol, by intramolecular aldol condensation in a multistep reaction sequence. The fragment destined to become C-2′,2,3,4,4′ of pyridoxol, derived from 1-deoxy-D-xylulose (**1**), was modified by dehydration, and the fragment destined to yield N-1,C-6,5,5′, derived from 4-hydroxy-L-threonine (**2**), underwent dehydrogenation and decarboxylation.

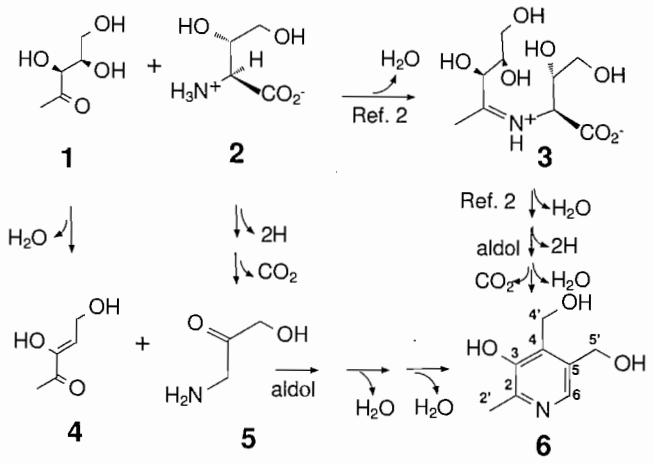
It is equally plausible, however, that the corresponding modifications of the two substrates take place ahead of Schiff base formation, so that the immediate precursors that undergo condensation to form the pyridoxine skeleton are the enol (**4**) of 5-hydroxypentane-2,3-dione (**7**), generated by dehydration of 1-deoxy-D-xylulose (**1**), rather than 1-deoxy-D-xylulose itself, and 3-amino-1-hydroxypropan-2-one (**5**), generated by dehydrogenation and decarboxylation of 4-hydroxy-L-threonine (**2**), rather than the intact amino acid (Scheme 1).

Received February 21, 1997.

E. Wolf, I.A. Kennedy, K. Himmeldirk, and I.D. Spenser.[1]
Department of Chemistry, McMaster University, Hamilton, ON L8S 4M1, Canada.

[1] Author to whom correspondence may be addressed: Telephone: (905) 525-9140, ext 23245. Fax: (905) 522-2509. E-mail: spenser@mcmaster.ca

Scheme 1. Alternative routes for the derivation of pyridoxol (**6**) from 1-deoxy-D-xylulose (**1**) plus 4-hydroxy-L-threonine (**2**).



In an effort to throw further light on the mechanism of formation of pyridoxol, we have prepared synthetic samples of **5** and **7**, the two compounds that incorporate these structural modifications.

5-Hydroxypentane-2,3-dione (**7**), in an equilibrium mixture with the isomeric furanose (**8**), i.e., laurencione (**7** ⇄ **8**) (3), was prepared in five steps from the commercially available pent-3-yn-1-ol (**18**) in an overall yield of 81%. Furthermore, a bond-labeled sample, [2,3-$^{13}C_2$]-5-hydroxypentane-2,3-dione (**7***) (or rather [2,3-$^{13}C_2$]laurencione (**7*** ⇄ **8***)) was prepared from [$^{13}C_2$]acetylene (**15***) in seven steps in an overall yield of 31% (cf. Scheme **4**). Earlier syntheses of laurencione (**7** ⇄ **8**) had given the product in overall yields of 21% (in six steps, starting from γ-butyrolactone), 19% (in eight steps from 2-acetylbutyrolactone) and 17% (in five steps from 1,1-dichloroacetone), respectively (4).

© 1997 NRC Canada

Can. J. Chem. Downloaded from www.nrcresearchpress.com by 88.146.161.215 on 09/08/12
For personal use only.

Can. J. Chem. Downloaded from www.nrcresearchpress.com by 88.146.161.215 on 09/08/12
For personal use only.

3-Amino-1-hydroxypropan-2-one (3-amino-1-hydroxyacetone) (**5**) hydrochloride, the compound derivable from 4-hydroxy-L-threonine (**2**) by dehydrogenation and decarboxylation, was synthesized in four steps from DL-3-aminopropane-1,2-diol (**23**) in an overall yield of 42% (cf. Scheme 5).

A discussion of the rationale for the selection of the two compounds as putative pyridoxine precursors, and of their synthesis follows.

Results and discussion

Rationale for the choice of 5-hydroxypentane-2,3-dione (7) and 3-amino-1-hydroxypropan-2-one (5) as putative pyridoxine precursors

In *Escherichia coli* only two genes, *pdxA* and *pdxJ*, and therefore only two enzyme-catalyzed steps, are implicated in the generation of pyridoxol (**6**) from 1-deoxy-D-xylulose (**1**) plus 4-hydroxy-L-threonine (**2**) (5).

In considering a possible mechanism of this process it is a reasonable assumption that each one of the two substrates is involved in one of these enzymic steps. If these steps occurred before the two substrates interacted, then the products of the two reactions would be intermediates in the formation of pyridoxol (**6**) from **1** plus **2**. Formally, the creation of the pyridoxol skeleton ($C_8H_{11}NO_3$) (**6**) from **1** ($C_5H_{10}O_4$) plus **2** ($C_4H_9NO_4$) requires a decarboxylation ($-CO_2$), the elimination of three molecules of water ($-3\ H_2O$), and a dehydrogenation ($-2H$). If these processes corresponded to the actual mechanistic steps, then two of them must be enzyme catalyzed.

In the formation of pyridoxol from the two acyclic substrates, **1** plus **2**, a new C—N bond and a new C—C bond must be formed. Formation of the new C—N bond, between the keto group, C-2, of **1** and the amino group of **2**, poses no problems. However, since the new C—C bond must be formed by interaction of C-4 of **1** with C-3 of **2**, both of which are secondary carbinols, activation at these sites is required, so that bond formation between them can take place.

One way of achieving activation of C-4 of **1** is by dehydration, to yield the enol (**4**), i.e., a tautomer of the diketone (**7**). This diketone, 5-hydroxypentane-2,3-dione, has recently been found in nature (3), existing as an equilibrium mixture with its furanose isomer (**8**). The mixture **7** ⇄ **8** is referred to as laurencione. The 5-phosphate ester of hydroxypentane-2,3-dione (**7**) had earlier been postulated (6) as the precursor of the C_5 chain, C-4′,4,5,6,7, of the thiazole unit of thiamin (**9**). 1-Deoxy-D-xylulose (**1**), the compound from which 5-hydroxypentane-2,3-dione (**7**) may be derived by dehydration, has been shown to be incorporated into the C_5 chain, C-4′,4,5,6,7, of the thiazole unit of thiamin (7–10) and concurrently also into C-2′,2,3,4,4′ of pyridoxol (10). Furthermore, 1-deoxy-D-xylulose (**1**) has been identified as an intermediate of the nonmevalonic acid route to isoprenoids (e.g., **10**) in *E. coli* (11) and 5-hydroxypentane-2,3-dione (**7**) was again invoked as an intermediate (12).

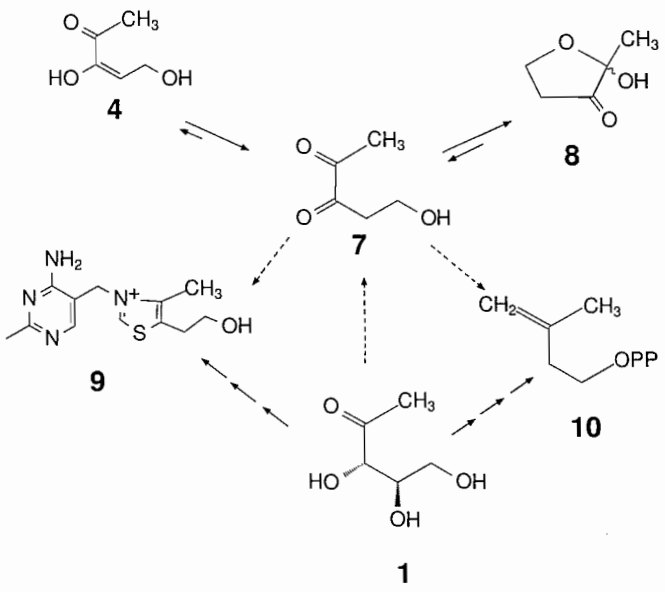
Thus, 5-hydroxypentane-2,3-dione (**7**) appeared to be a prime candidate in the choice of possible intermediates on the route from 1-deoxy-D-xylulose (**1**) into the C_5 unit, C-2′,2,3,4,4′, of pyridoxol (**6**).

In selecting the reaction that might serve to activate the carbinol carbon, C-3, of the other substrate, 4-hydroxy-L-threonine (**2**), for bond formation, we considered dehydrogenation, a process that is formally required in the conversion of the two substrates, **1** plus **2**, into pyridoxol (**6**) (Scheme 1). The product of dehydrogenation at C-3 of 4-hydroxy-L-threonine would be L-2-amino-4-hydroxy-3-oxobutanoic acid (**11**). This compound has not been described. The corresponding dehydrogenation product of threonine (**12**), L-2-amino-3-oxobutanoic acid (**13**), has been prepared (13, 14): It was found that this compound lacks stability, with a half life of ca. 10 min at physiological pH, undergoing spontaneous decarboxylation to yield 1-aminopropan-2-one (**14**) (Scheme 3). It is most likely that the corresponding dehydrogenation of 4-hydroxy-L-threonine (**2**) to the oxoamino acid (**11**) is accompanied by an analogous spontaneous decarboxylation, leading to 3-amino-1-hydroxypropan-2-one (**5**). Such a reaction sequence on the route to pyridoxol would then account not only for the required, presumably enzyme-catalyzed, dehydrogenation, but also for the required, but presumably spontaneous, decarboxylation.

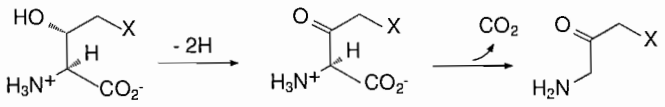
3-Amino-1-hydroxypropan-2-one (**5**) thus appeared to be a promising choice as a possible intermediate on the route from 4-hydroxy-L-threonine (**2**) into the C_3N unit, N-1,C-6,5,5′, of pyridoxol (**6**).

To date we have not been able to obtain evidence that either of the two compounds serves as precursor of pyridoxol in *Escherichia coli*. The reason for this lack of success may be

Scheme 2. 5-Hydroxypentane-2,3-dione (**7**) as a possible intermediate on the routes from 1-deoxy-D-xylulose (**1**) into thiamin (**9**) and into isoprenoids (e.g., **10**).



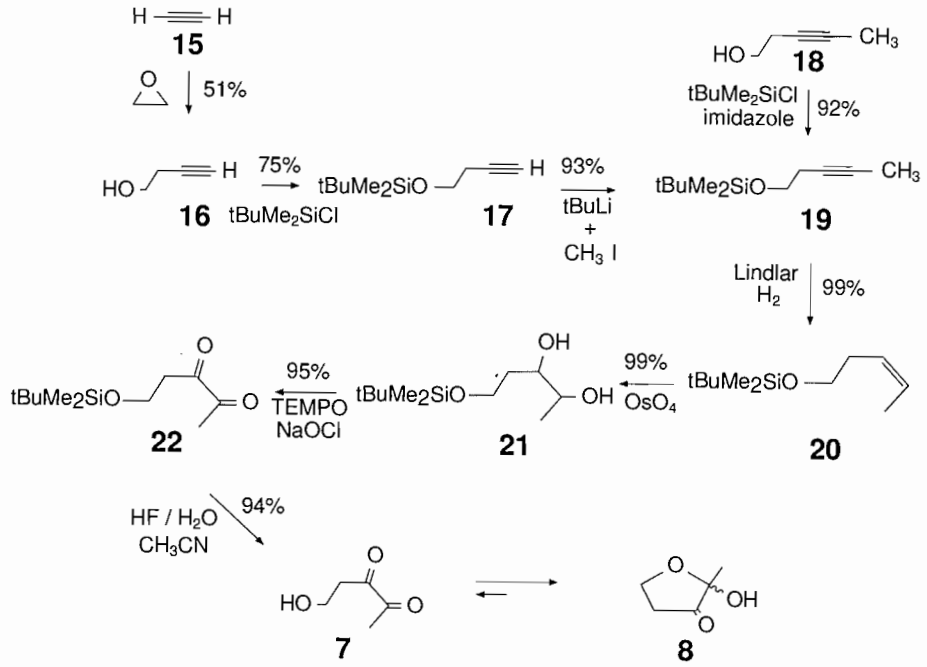
Scheme 3. The oxidative decarboxylation of threonine (**12**).



2 X = OH **11** X = OH **5** X = OH
12 X = H **13** X = H **14** X = H

© 1997 NRC Canada

Scheme 4. Synthesis of laurencione (**7** ⇄ **8**).



that the actual substrates for the enzymic reaction are the 5-phosphate ester of **7** and the 1-phosphate ester of **5**, rather than the non-phosphorylated species.

A discussion of the synthesis of the two putative intermediates of pyridoxol biosynthesis, **5** and **7**, follows.

Synthesis of 5-hydroxypentane-2,3-dione (7) (i.e., laurencione (7 ⇄ 8)) (Scheme 4)

Recent syntheses of laurencione (4) start from γ-butyrolactone, from 2-acetylbutyrolactone or from 1,1-dichloroacetone. These syntheses are not readily adaptable to the preparation of the [2,3-$^{13}C_2$]-labeled sample of 5-hydroxypentane-2,3-dione that we required. Our synthesis starts with [$^{13}C_2$]acetylene, one of the few bond-labeled compounds that are commercially available (Cambridge Isotope Laboratories).

[$^{13}C_2$]Acetylene (**15***) was converted into [3,4-$^{13}C_2$]but-3-yn-1-ol (**16***) by generating the mono lithium salt, which was reacted with ethylene oxide.[2] Reaction with *tert*-butyldimethylsilyl chloride in the presence of imidazole then protected the alcohol group. The resulting silyl ether (**17***) was treated with *tert*-butyllithium, followed by methyl iodide, to yield the silyl ether (**19***) of [3,4-$^{13}C_2$]pent-3-yn-1-ol. The corresponding unlabeled compound (**19**) is accessible by *tert*-butyldimethylsilyl chloride – imidazole treatment of pent-3-yn-1-ol (**18**), which is commercially available. Lindlar hydrogenation of the triple bond of **19*** gave [2,3-$^{13}C_2$]-(*Z*)-5-*tert*-butyldimethylsilyloxypent-2-ene (**20***), which was converted to the corresponding *cis*-diol (**21***) by means of osmium tetroxide. TEMPO oxidation (16) of the diol gave the corresponding dione (**22***), i.e., the silyl ether of the desired product. Removal of the silyl ether group by means of fluoride gave [2,3-$^{13}C_2$]-5-hydroxypentane-2,3-dione (**7***), together with the corresponding cyclic isomer, [2,3-$^{13}C_2$]-(2*RS*)-2-hydroxy-2-methyl-3-oxotetrahydrofuran (**8***), that is, [2,3-$^{13}C_2$]-laurencione. The overall yield in the seven-step synthesis of [2,3-$^{13}C_2$]laurencione (**7*** ⇄ **8***) from [$^{13}C_2$]acetylene (**15***) was 31%. The five-step synthetic route to unlabeled laurencione (**7** ⇄ **8**) from pent-3-yn-1-ol (**18**) gave the product in 81% yield and thus represents a significant improvement on the earlier syntheses (4). The composition of the equilibrium mixture **7** ⇄ **8** of laurencione, as determined by ^{13}C NMR spectroscopy, depends on the solvent. In $CDCl_3$ the ratio, **7** to **8**, was found (3) to be 17:83, whereas in C_6D_6 the **7** to **8** ratio was 40:60. Laurencione is unstable at room temperature, due to oligomerization. It can be stored in benzene (frozen) at ca. 0°C or in aqueous solution at 4°C. From aqueous solution it can be recovered by extraction into chloroform followed by evaporation of the solvent.

Synthesis of 3-amino-1-hydroxypropan-2-one (5) hydrochloride (Scheme 5)

Surprisingly, neither Beilstein nor the Dictionary of Organic Compounds contains an entry for this simple three-carbon compound. Certainly, the compound is not described in the recent chemical literature. A very determined search did uncover a preparation of the compound by a three-step synthesis, in indifferent yield, from *N*-acetonylphthalimide, in connection with an early synthetic approach to ergothioneine (17).

3-Amino-1-hydroxypropan-2-one (**5**) hydrochloride was prepared starting from (±)-3-aminopropane-1,2-diol (**23**), a compound that is available commercially.

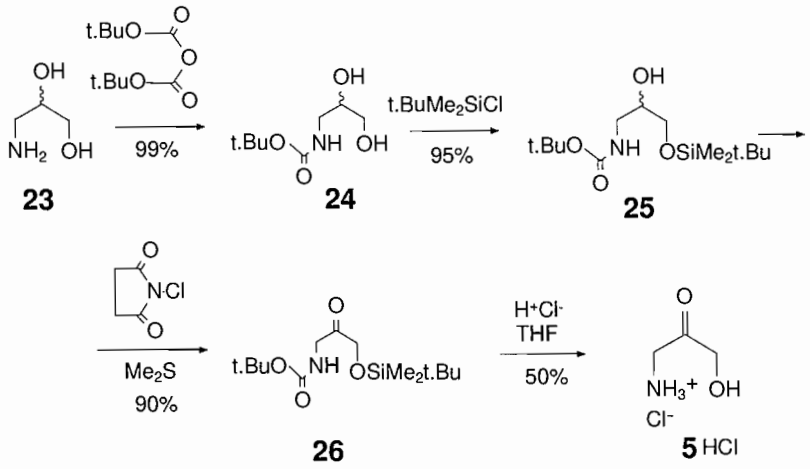
Conversion of (±)-3-aminopropane-1,2-diol (**23**) into the desired product requires preferential oxidation of the secondary alcohol group. To achieve this the primary alcohol and the amino group of the starting material had to be protected.

[2] The preparation of unlabeled but-3-yn-1-ol by this method is described by Verkruijsse and Brandsma (15*a*); see also ref. 15*b*.

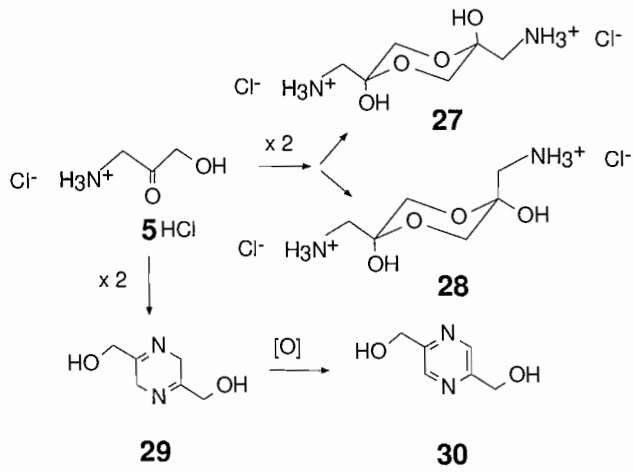
Can. J. Chem. Downloaded from www.nrcresearchpress.com by 88.146.161.215 on 09/08/12
For personal use only.

© 1997 NRC Canada

Scheme 5. Synthesis of 3-amino-1-hydroxypropan-2-one (**5**).



Scheme 6. Dimers of 3-amino-1-hydroxypropan-2-one (**5**).



Protection of the amino group in the presence of the two alcohol functions was implemented by means of di-*tert*-butyl dicarbonate (18), to yield (±)-*N*-*tert*-butyloxycarbonyl-3-aminopropane-1,2-diol (**24**). The primary alcohol group of the latter was protected selectively by means of Corey silylation in the presence of 4-dimethylaminopyridine (19). The resulting doubly protected product (**25**) was then oxidized with *N*-chlorosuccinimide in the presence of dimethyl sulfide (20) to yield the protected aminoketone (**26**), which was deprotected by acid hydrolysis. 3-Amino-1-hydroxyacetone (**5**) hydrochloride was obtained as slightly yellow crystals that darkened on standing.

Slow recrystallization from ethanol-*tert*-butyl methyl ether gave the product as long, slightly yellow needles. X-ray crystallography of a 0.02 mm thick single crystal of the crystalline product shows it to be pure 3-amino-1-hydroxyacetone (**5**) hydrochloride.

However, the ^{1}H NMR spectrum in D_2O of every sample of the product **5** showed, in addition to the COCH_2O (δ 4.35 ppm) and the COCH_2N (δ 4.03 ppm) singlet signals of equal intensity, two additional singlets, each ca. one fifth as intense as the other two, at δ 3.54 and 3.06 ppm, indicating the presence of another component, with which **5** was in equilibrium in aqueous solution. The structure of the minor component was deduced from the ^{13}C NMR spectrum. In addition to the three major signals at δ 204.6 (*C*O), 65.7 (*C*H_2O), 44.9 (*C*H_2N), the spectrum showed a less intense signal at δ 92.7 (ketal). Furthermore, the two *C*H_2 signals show satellites of lower intensity: three satellites (δ 66.2, 65.6, 65.3 ppm) straddle the *C*H_2O signal, two (δ 45.3, 44.2 ppm) appear at the *C*H_2N signal.

We conclude that in aqueous solution the aminoketone exists in equilibrium with the two stereoisomers of a dimer, *trans*- and *cis*-2,5-dihydroxy-2,5-aminomethyl-1,4-dioxane dihydrochloride (**27** and **28**). Since these ring compounds are fluxional, the ^{1}H NMR spectrum does not show evidence of diastereotopic protons. When the D_2O solution of the sample is kept for 3 weeks at room temperature, the COCH_2N signals (δ 4.03 and 3.04 ppm) in the ^{1}H NMR spectrum have almost completely disappeared, indicating deuterium exchange. In addition, weak signals in the aromatic region of the spectrum are observable. These become prominent when the sample is exposed to air for several weeks at elevated temperature. This suggests formation of another dimer (**29**), which eventually oxidizes to the pyrazine (**30**). We did not attempt to isolate samples of the decomposition products.

Experimental

Synthesis of 5-hydroxypentane-2,3-dione (7), in equilibrium with (2*RS*)-2-hydroxy-2-methyl-3-oxotetrahydrofuran [(2*RS*)-2-hydroxy-2-methyl-dihydrofuran-3(2*H*)-one] (8) (i.e., laurencione (7 ⇄ 8)) (Scheme 4)

5-tert-Butyldimethylsilyloxypent-2-yne (19)

Pent-3-yn-1-ol (**18**) (3.21 g, 38.1 mmol) was dissolved in dry *N,N*-dimethylformamide (100 mL). Imidazole (5.71 g, 83.9 mmol) was added, followed by *tert*-butyldimethylsilyl chloride (6.36 g, 42.2 mmol) in small portions. The mixture was stirred overnight at room temperature, was then poured into petroleum ether (150 mL), and the solution was extracted with water (750 mL), aqueous HCl (ca. 5%, 2 × 100 mL), and water. The organic phase was dried ($MgSO_4$) and the solvent distilled off. The residue was distilled at reduced pressure

© 1997 NRC Canada

Can. J. Chem. Downloaded from www.nrcresearchpress.com by 88.146.161.215 on 09/08/12
For personal use only.

Can. J. Chem. Downloaded from www.nrcresearchpress.com by 88.146.161.215 on 09/08/12
For personal use only.

(bp 80–85°C at 10 Torr (1 Torr = 133.3 Pa)) to yield the silyl ether (**19**) (7.00 g, 92.5%). ^{1}H NMR (200 MHz, $CDCl_3$) δ: 3.66 (t, $^3J_{H,H}$ = 7.0 Hz, 2H), 2.31 (tq, $^3J_{H,H}$ = 7.0 Hz, $^5J_{H,H}$ = 2.5 Hz, 2H), 1.74 (t, $^5J_{H,H}$ = 2.5 Hz, 3H), 0.87 (s, 9H), 0.04 (s, 6H).

^{13}C NMR (50.3 MHz, $CDCl_3$) δ: 76.6, 76.1, 62.3, 25.8, 23.1, 18.3, 3.4, −5.3. MS (CI) *m/z*: 199 (100%, m + H$^+$).

*(Z)-5-*tert*-Butyldimethylsilyloxypent-2-ene (**20**)*

Alkyne **19** (3.97 g, 20 mmol) and quinoline (1 mL) were dissolved in ethyl acetate (100 mL). Lindlar catalyst (450 mg, Aldrich) was added and the mixture hydrogenated at ca. 1 atm (101.3 kPa) until uptake of hydrogen ceased. The catalyst was filtered off and washed with ethyl acetate, and the filtrate was extracted with HCl (ca. 5%, 2 × 50 mL) and brine. The organic layer was dried over K_2CO_3, and the solvent was evaporated, to yield the alkene (**20**) (4.00 g, 99%). ^{1}H NMR (200 MHz, $CDCl_3$) δ: 5.33–5.56 (m, 2H), 3.59 (t, $^3J_{H,H}$ = 7.0 Hz, 2H), 2.26 (t, $^3J_{H,H}$ = 7.0 Hz, 2H), 1.60 (d, $^3J_{H,H}$ = 6.5 Hz, 3H), 0.88 (s, 9H), 0.04 (s, 6H). ^{13}C NMR (50.3 MHz, $CDCl_3$) δ: 126.6, 125.7, 62.8, 30.8, 25.9, 18.4, 12.9, −5.3. MS (CI) *m/z*: 201 (80%, m + H$^+$), 135 (100%).

*(3R4S,3S4R)-1-*O*-*tert*-Butyldimethylsilylpentane-1,3,4-triol (**21**)*

Alkene **20** (2.77 g, 13.8 mmol) was dissolved in *tert*-butanol (28 mL) and tetrahydrofuran (12 mL). Water (4 mL) and 4-methylmorpholine-*N*-oxide (NMO) (2.10 g) was added. Air was displaced by passing a stream of nitrogen through the mixture. An aqueous solution of osmium tetroxide (4%, 1 mL) was added and the mixture stirred 5 h at room temperature. An aqueous solution of sodium bisulfite (150 mg in 5 mL water) was added, followed by Florisil R (5.0 g). The mixture was stirred 10 min and then filtered through silica gel, which was then washed with ethyl acetate. Evaporation of the filtrate in vacuo yielded the colourless oily product (**21**) (3.20 g, 99%). ^{1}H NMR (200 MHz, $CDCl_3$) δ: 3.78–3.91 (m, 4H), 2.11 (s (br), 2H), 1.60–1.72 (m, 2H), 1.16 (d, $^3J_{H,H}$ = 6.0 Hz, 3H), 0.89 (s, 9H), 0.07 (s, 6H). ^{13}C NMR (50.3 MHz, $CDCl_3$) δ: 75.7, 70.0, 62.2, 32.5, 25.8, 18.0, 17.7, −5.7. MS (CI) *m/z*: 235 (100%, m + H$^+$).

*5-*tert*-Butyldimethylsilyloxypentane-2,3-dione (**22**)*

Compound **21** (938 mg, 4 mmol) was dissolved in methylene chloride (60 mL). 2,2,6,6-Tetramethyl-1-piperidinyloxy (TEMPO, 30 mg), water (4 mL), and KBr (240 mg) were added and the mixture was cooled in an ice bath. Ice-cold aqueous solutions of saturated $NaHCO_3$ (48 mL) and of NaOCl (Cl_2 content ca. 4%, 48 mL) were added and the mixture, cooled in an ice bath, was stirred 10 min. The layers were separated, the aqueous layer was extracted with methylene chloride (50 mL), and the combined organic phases were dried ($MgSO_4$). The mixture was filtered through silica gel, which was then washed with methylene chloride until the washings emerged colourless. Concentration in vacuo gave the pure product **22** as a yellow liquid (892 mg, 95%). UV–VIS: λ_{max} = 422 nm, $\varepsilon_0 = 1.63 \times 10^6$. ^{1}H NMR (200 MHz, $CDCl_3$) δ: 3.91 (t, $^3J_{H,H}$ = 6.2 Hz, 2H), 2.91 (t, $^3J_{H,H}$ = 6.1 Hz, 2H), 2.29 (s, 3H), 0.83 (s, 9H), 0.02 (s, 6H). ^{13}C NMR (50.3 MHz, $CDCl_3$) δ: 197.8, 196.7, 59.8, 38.5, 25.1, 22.9, 17.5, −6.2. MS (CI) *m/z*: 231 (100%, m + H$^+$).

*5-Hydroxypentane-2,3-dione (**7**), in equilibrium with (2*RS*)-2-hydroxy-2-methyl-3-oxotetrahydrofuran (**8**)*

Freshly distilled (Kugelrohr, bp 120°C at 0.7 Torr) diketone **22** (230 mg, 1 mmol) was dissolved in acetonitrile (10 mL). The solution was cooled in an ice bath and aqueous hydrofluoric acid (49% w/v, 0.6 mL) was added with stirring. The ice bath was removed after 15 min and stirring continued for 45 min. The mixture was poured into chloroform (30 mL), sodium bicarbonate (1.5 g) followed by saturated aqueous bicarbonate solution (1 mL) was added, and the mixture was stirred until evolution of CO_2 had ceased (ca. 10 min). Solid $MgSO_4$ (ca. 5 g) was added to remove water and the mixture was filtered after standing overnight. Evaporation of the solvent in vacuo gave the product as a yellow oily liquid (108 mg, 94%). Fast distillation in vacuo (Kugelrohr, 130°C, 0.5 Torr) gave pure product (92 mg, 80%) consisting of 5-hydroxypentane-2,3-dione (**7**) (17%), in equilibrium with (2*RS*)-2-hydroxy-2-methyl-3-oxotetrahydrofuran (**8**) (83%), as determined on the basis of an NMR spectrum in $CDCl_3$. In C_6D_6 the ratio of **7** to **8** was 40:60.

***7** (cf. ref. 3)*: ^{1}H NMR (200 MHz, $CDCl_3$) δ: ~4.2 (OH, overlapping OCH_2 of **8**), 3.84 (t, $^3J_{H,H}$ = 5.5 Hz, 2H), 2.91 (t, $^3J_{H,H}$ = 5.5 Hz, 2H), 2.24 (s, 3H). ^{13}C NMR (50.3 MHz, $CDCl_3$) δ: 198.4, 197.1, 56.9, 38.2, 23.3.

***8** (cf. ref. 3)*: ^{1}H NMR (200 MHz, $CDCl_3$) δ: 4.00–4.27 (m, ca. 3H; OCH_2 of **8**, overlapped by OH of **7** and **8**), 2.37–2.55 (m, 2H), 1.29 (s, 3H). ^{13}C NMR (50.3 MHz, $CDCl_3$) δ: 210.2, 96.3, 61.6, 33.4, 20.9.

***7** + **8** (cf. ref. 3)*: MS (CI, NH_3) *m/z*: 116 (100%, m − OH + NH_3^+).

Synthesis of [2,3-$^{13}C_2$]-5-hydroxypentane-2,3-dione (7*), in equilibrium with [2,3-$^{13}C_2$]-(2*RS*)-2-hydroxy-2-methyl-3-oxotetrahydrofuran ([2,3-$^{13}C_2$]-(2*RS*)-2-hydroxy-2-methyldihydrofuran-3(2*H*)-one) (8*) (*i.e.*, [$^{13}C_2$]laurencione (7* ⇄ 8*))

*[2,3-$^{13}C_2$]-5-*tert*-Butyldimethylsilyloxypent-2-yne (**19***) from [1,2-$^{13}C_2$]acetylene (**15***)*

*[3,4-$^{13}C_2$]But-3-yn-1-ol (**16***) (cf. ref. 15)*

[$^{13}C_2$]Acetylene (**15***) (0.5 L, ca. 22 mmol) was condensed from the breakseal flask in which it was supplied (Cambridge Isotope Laboratories) into an evacuated 250 mL reaction flask, immersed in a liquid nitrogen bath. After complete transfer (ca. 1 h) the breakseal flask was disconnected and the reaction vessel was flushed with dry nitrogen while still maintained at ca. −180°C. Dry NH_3 (ca. 50 mL) was condensed into the system and $LiNH_2$ (0.55 g, 22.8 mmol) was then added. The liquid nitrogen bath was replaced by an ethanol – solid CO_2 bath that had been precooled to ca. −50°C, and the mixture was refluxed (Dry Ice condenser) for 2 h. Ethylene oxide (ca. 1.5 mL, 30 mmol) was then condensed into the system and the mixture was refluxed for 40 h. NH_3 was evaporated and water (30 mL) and saturated NH_4Cl solution (10 mL) were then added. The aqueous phase was continuously extracted with diethyl ether (2 days); the ether was then evaporated at atmospheric pressure to yield the crude product (823 mg) as a

© 1997 NRC Canada

Can. J. Chem. Downloaded from www.nrcresearchpress.com by 88.146.161.215 on 09/08/12
For personal use only.

mobile liquid. The product from several runs (2.93 g) was pooled and distilled to yield [3,4-$^{13}C_2$]but-3-yn-1-ol (**16***) (2.75 g, 51%, purity >95%, main contaminant diethyl ether); bp 125–130°C (lit. (15) bp of the unenriched compound 128.9°C). IR; ν (cm^{-1}): 3279, 2947, 2889, 1048 (ν_{max}). ^1H NMR (200 MHz, $CDCl_3$) δ: 3.71 (dt(q), $^3J_{H,H} = {}^3J_{C,H} = 6.1$, 2H), 2.36–2.44 (m, 2H), 2.22 (br s), 1H), 2.01 (ddt, $^4J_{H,H} = 2.6$ Hz, $^1J_{C,H} = 244.2$ Hz, $^2J_{C,H} = 54.2$ Hz, 1H). ^{13}C NMR (50.3 MHz, $CDCl_3$) δ: 81.3 (enriched)(d, $^1J_{C,C} = 171$ Hz), 69.7 (enriched)(d, $^1J_{C,C} = 171$ Hz), 60.8, 22.7 (dd, $^1J_{C,C} = 65.4$ Hz, $^2J_{C,C} = 14$ Hz). MS (EI) *m/z*: 73 (5%, m + H^+), 71 (15%), 55 (30%), 45 (100%).

*[1,2-$^{13}C_2$]-4-*tert*-Butyldimethylsilyloxybut-1-yne (**17***)*
[3,4-$^{13}C_2$]But-3-yn-1-ol (**16***) (1.25 g, 17.3 mmol) was dissolved in dry dimethylformamide (40 mL). Imidazole (2.50 g, 36.7 mmol) was added, followed by *tert*-butyldimethylsilyl chloride (3.00 g, 19.9 mmol). The mixture was stirred overnight and was then poured into petroleum ether (40–60°C) (50 mL). The mixture was extracted with water (400 mL), dilute HCl (5% v/v, 2 × 25 mL), and water (50 mL). The petroleum ether solution was then dried (anhydrous $MgSO_4$), the solvent distilled off, and the residue distilled in vacuo. [1,2-$^{13}C_2$]-4-*tert*-Butyldimethylsilyloxybut-1-yne (**17***) (2.65 g, purity 92% by NMR, yield 75%) was obtained from the fraction, bp 65–70°C at 10 Torr. IR (film) ν (cm^{-1}): 2956, 2932, 2859, 1111, 839 (ν_{max}). ^1H NMR (200 MHz, $CDCl_3$) δ: 3.72 (dt, $^3J_{H,H} = 7.1$ Hz, $^3J_{C,H} = 4.3$, 2H), 2.30–2.45 (m, 2H), 1.93 (ddt, $^4J_{H,H} = 2.6$ Hz, $^1J_{C,H} = 244.4$ Hz, $^2J_{C,H} = 53.4$ Hz, 1H), 0.88 (s, 9H), 0.05 (s, 6H). ^{13}C NMR (50.3 MHz, $CDCl_3$) δ: 81.7 (enriched)(d, $^1J_{C,C} = 172$ Hz), 69.0 (enriched) (d, $^1J_{C,C} = 172$ Hz), 61.8, 25.9, 22.8 (dd, $^1J_{C,C} = 64$ Hz, $^2J_{C,C} = 10$ Hz), 18.3, −5.3. MS (CI) *m/z*: 187 (100%, m + H^+), 132 (60%).

*[2,3-$^{13}C_2$]-5-*tert*-Butyldimethylsilyloxypent-2-yne (**19***)*
[1,2-$^{13}C_2$]-4-*tert*-Butyldimethylsilyloxybut-1-yne (**17***) (1.78 g, 8.8 mmol) was dissolved in dry tetrahydrofuran (100 mL). The mixture was cooled to −20°C, a solution of *tert*-butyllithium (5.5 mL, 1.7 M in pentane) was added over a period of 5 min, and the mixture was allowed to stand for 1 h. Methyl iodide (1.0 mL, 16 mmol) was added, the cooling bath was removed after 30 min and stirring was continued for another 30 min. The mixture was poured into petroleum ether (40–60°C, 150 mL), followed by extraction with half-concentrated NaCl solution (2 × 150 mL). The organic phase was dried (anhydrous $MgSO_4$) and the solvent distilled off. The residual liquid was distilled in vacuo (Kugelrohr, 85°C, 10 Torr), yielding [2,3-$^{13}C_2$]-5-*tert*-butyldimethylsilyloxypent-2-yne (**19***) (1.80 g, 93%). IR (film); ν (cm^{-1}): 2956, 2930, 2858, 1103, 837 (ν_{max}). ^1H NMR (200 MHz, $CDCl_3$) δ: 3.76 (dt, $^3J_{H,H} = 7.4$ Hz, $^3J_{C,H} = {}^4J_{C,H} = 1.8$ Hz, 2H), 2.24–2.39 (m, 2H), 1.74 (q, $^4J_{H,H} = 2.5$ Hz, $^2J_{C,H} = 2.5$ Hz, 3H), 0.88 (s, 9H), 0.05 (s, 6H). ^{13}C NMR (50.3 MHz, $CDCl_3$) δ: 78.1 (enriched)(d, $^1J_{C,C} = 176$ Hz), 74.6 (enriched)(d, $^1J_{C,C} = 176$ Hz), 62.3, 25.9 (dd, $^1J_{C,C} = 45$ Hz, $^2J_{C,C} = 34$ Hz), 23.0 (dd, $^1J_{C,C} = 45$ Hz, $^2J_{C,C} = 34$ Hz), 18.3, 3.4, −5.3. MS (CI, NH_3) *m/z*: 218 (20%, m + NH_4^+), 201 (100%, m+H^+), 132 (20%).

The experimental procedure for the conversion of [2,3-$^{13}C_2$]-5-*tert*-butyldimethylsilyloxypent-2-yne (**19***) into [2,3-$^{13}C_2$]-(*Z*)-5-*tert*-butyldimethylsilyloxypent-2-ene (**20***) and thence, via **21*** and **22***, into bond-labeled laurencione (**7*** ⇄ **8***), was similar to that described above for the preparation of the corresponding unenriched compounds. Spectral data for the enriched compounds are given below.

*[2,3-$^{13}C_2$]-(Z)-5-*tert*-Butyldimethylsilyloxypent-2-ene (**20***)*: IR (film), ν (cm^{-1}): 3004, 2956, 2931, 2859, 1255, 1089, 837 (ν_{max}). ^1H NMR (200 MHz, $CDCl_3$) δ: 6.06–4.83 (m, 2H), 3.59 (dt, $^3J_{H,H} = 7.1$ Hz, $^3J_{C,H} = 3.4$ Hz, 2H), 2.20–2.39 (m, 2H), 1.60 (ddd, $^3J_{H,H} = 5.0$ Hz, $^2J_{C,H} = 6.8$ Hz, $^4J_{H,H} = 0.9$ Hz, 3H), 0.86 (s, 9H), 0.04 (s, 6H). ^{13}C NMR (50.3 MHz, $CDCl_3$) δ: 126.9 (enriched)(d, $^1J_{C,C} = 70$ Hz), 125.2 (enriched)(d, $^1J_{C,C} = 70$ Hz), 62.8 (d, $^2J_{C,C} = 3$ Hz), 30.8 (dd, $^1J_{C,C} = 33$ Hz, $^2J_{C,C} = 10$ Hz), 26.0 18.4, 12.9 (dd, $^1J_{C,C} = 32$ Hz, $^2J_{C,C} = 10$ Hz), −5.2. MS (CI), *m/z*: 203 (100%, m + H^+), 162 (20%), 130 (60%).

*[2,3-$^{13}C_2$]-(2R3S,2S3R)-5-*O*-tert-Butyldimethylsilylpentane-2,3,5-triol (**21***)*: IR (film), ν (cm^{-1}): 3385, 2956 (ν_{max}), 2931, 2859, 1256, 1090, 836. ^1H NMR (200 MHz, $CDCl_3$) δ: 4.16–3.33 (m, 2H), 3.77–3.96 (m, 2H), 2.54 (br s), OH, 2H), 1.58–1.78 (m, 2H), 1.15 (dt, $^3J_{H,H} = 6.4$ Hz, $^3J_{C,H} = {}^2J_{C,H} = 2.1$ Hz, 3H), 0.88 (s, 9H), 0.07 (s, 6H). ^{13}C NMR (50.3 MHz, $CDCl_3$) δ: 75.7 (enriched)(d_{AB}, $^1J_{C,C} = 43$ Hz), 70.0 (enriched)(d_{AB}, $^1J_{C,C} = 42$ Hz), 62.5, 31.8 (d, $^1J_{C,C} = 37$ Hz), 25.8, 18.0, 17.7 (d, $^1J_{C,C} = 39$ Hz), −5.7. MS (CI), *m/z*: 237 (100%, m + H^+), 140 (30%).

*[2,3-$^{13}C_2$]-5-*tert*-Butyldimethylsilyloxypentane-2,3-dione (**22***)*: IR (film), ν (cm^{-1}): 2957, 2932, 2887, 2859, 1677 (ν_{max}). ^1H NMR (200 MHz, $CDCl_3$) δ: 3.40 (dt, $^3J_{H,H} = 6.1$ Hz, $^3J_{C,H} = 4.0$ Hz, 2H), 2.91 (q, $^3J_{H,H} = 6.1$ Hz, $^2J_{C,H} = 6.1$ Hz, 2H), 2.30 (d, $^2J_{C,H} = 5.5$ Hz, 3H), 0.83 (s, 9H), 0.01 (s, 6H). ^{13}C NMR (50.3 MHz, $CDCl_3$) δ: 198.7 (enriched)(d_{AB}, $^1J_{C,C} = 46$ Hz), 197.2 (enriched)(d_{AB}, $^1J_{C,C} = 46$ Hz), 58.4, 39.4 (dd, $^1J_{C,C} = 39$ Hz, $^2J_{C,C} = 15$ Hz), 25.8, 22.4 (d, $^1J_{C,C} = 35$ Hz), 18.2, −5.7. MS (CI, NH_3), *m/z*: 250 (100%, m + NH_4^+), 233 (100% m + H^+).

[2,3-$^{13}C_2$]-5-Hydroxypentane-2,3-dione (7*), in equilibrium with [2,3-$^{13}C_2$]-(2*RS*)-2-hydroxy-2-methyldihydrofuran-3(2*H*)-one ([2,3-$^{13}C_2$]-(2*RS*)-2-hydroxy-2-methyl-3-oxotetrahydrofuran) (8*)

7*: ^1H NMR (200 MHz, C_6D_6) δ: 3.69 (q, $^3J_{H,H} = 7.8$ Hz, 2H), 2.55–2.64 (m, 2H), 1.85 (d, $^2J_{C,H} = 4.2$ Hz, 3H). ^{13}C NMR (50.3 MHz, C_6D_6) δ: 196.2 (enriched)(d_{AB}, $^1J_{C,C} = 46$ Hz), 195.2 (enriched)(d_{AB}, $^1J_{C,C} = 46$ Hz), 55.2, 35.2 (dd, $^1J_{C,C} = 31$ Hz, $^2J_{C,C} = 22$ Hz), 21.9 (dd, $^1J_{C,C} = 33$ Hz, $^2J_{C,C} = 24$ Hz).

8*: ^1H NMR (200 MHz, C_6D_6) δ: 3.43–3.60 (m, 2H), 1.70–1.90 (m, 2H), 1.27 (dd, $^2J_{C,H} = 5.0$ Hz, $^3J_{C,H} = 2.8$ Hz, 3H). ^{13}C NMR (50.3 MHz, C_6D_6) δ: 206.0 (enriched)(d, $^1J_{C,C} = 51$ Hz), 98.3 (enriched)(d, $^1J_{C,C} = 51$ Hz), 60.7, 32.1 (dd, $^1J_{C,C} = 39$ Hz, $^2J_{C,C} = 13$ Hz), 15.8 (d, $^1J_{C,C} = 47$ Hz).

7* + 8*: IR (film), ν (cm^{-1}): 3939, 2990, 2900, 1725 (ν_{max}), 1678, 1075. MS (CI, NH_3), *m/z*: 118 (100%, m − OH + NH_3^+).

Synthesis of 3-amino-1-hydroxypropan-2-one (3-amino-1-hydroxyacetone) (5) hydrochloride from (±)-3-aminopropane-1,2-diol (23) (Scheme 5)

*(±)-*N*-tert-Butyloxycarbonyl-3-aminopropane-1,2-diol (**24**)*
Di-*tert*-butyl dicarbonate (18) (25 g, 114.6 mmol), dissolved

© 1997 NRC Canada

Can. J. Chem. Downloaded from www.nrcresearchpress.com by 88.146.161.215 on 09/08/12
For personal use only.

in CH_2Cl_2 (25 mL), was added slowly to a stirred solution of (±)-3-aminopropane-1,2-diol (**23**) (8.7 g, 95.5 mmol) in CH_2Cl_2–MeOH (20 mL, 1:5) and triethylamine (1.3 mL, 9.6 mmol). The reaction, which was followed by TLC, was complete in 2 h. Evaporation of the solvents gave the product **24** (18 g, 99%) as a colourless solid that was used without further purification; mp 55–58°C. ^{1}H NMR (200 MHz, $CDCl_3$) δ: 5.12 (br s, 1H), 3.18–3.76 (m, 5H), 1.39 (s, 9H). ^{13}C NMR (50.3 MHz, $CDCl_3$) δ: 157.4, 80.0, 71.3, 63.6, 42.8, 27.9.

N-tert-*Butyloxycarbonyl-3-amino-1*-tert-*butyldimethylsilyloxy-2-propanol (25)*

N-tert-Butyloxycarbonyl-3-amino-1,2-propanediol (**24**) (18 g, 94.2 mmol) was dissolved in CH_2Cl_2 (150 mL) and *tert*-butyldimethylsilyl chloride (11 g, 103.7 mmol) and triethylamine (15.7 mL, 113 mmol) were added with stirring, followed by 4-dimethylaminopyridine (19) (0.46 g, 3.7 mmol), and stirring was continued overnight. Water (20 mL) was then added to quench the reaction. The layers were separated, the aqueous layer was washed with CH_2Cl_2 (3 × 10 mL), and the combined organic fraction was washed with water (3 × 10 mL) and brine and dried with anhydrous $MgSO_4$. Concentration of the solution gave a light yellow oil that was distilled at reduced pressure to give the product (**25**) (27.3 g, 95%) as a colourless oil. ^{1}H NMR (200 MHz, $CDCl_3$) δ: 5.26 (br s, 1H), 2.80–3.71 (m, 5H), 1.41 (s, 9H), 0.86 (s, 9H), 0.04 (s, 6H). ^{13}C NMR (50.3 MHz, $CDCl_3$) δ: 156.7, 79.4, 71.2, 64.8, 43.3, 28.3, 25.8, 18.2, −5.5. MS (EI), *m/z*: 306 (m + H^+), 250, 232, 206, 148.

N-tert-*Butyloxycarbonyl-3-amino-1*-tert-*butyldimethylsilyloxy-2-propanone (26)*

A suspension of *N*-chlorosuccinimide (16 g, 120.5 mmol) in CH_2Cl_2 (100 mL) was cooled to 0°C, dimethyl sulfide (12.2 mL, 166 mmol) (20) was added, and the mixture was cooled further to −20°C (CCl_4 – Dry Ice). *N-tert*-Butyloxycarbonyl-3-amino-1-*tert*-butyldimethylsilyloxy-2-propanol (**25**) (24.5 g, 80.3 mmol) in CH_2Cl_2 (20 mL) was added and the mixture was stirred at −20°C for 2 h. Triethylamine (16.8 mL, 120.5 mmol) was then added, the cooling mixture was removed, and stirring continued for 1 h. The reaction mixture was then diluted with ether (100 mL), washed with 1 M HCl, water, and brine, and dried with anhydrous $MgSO_4$. The solution was concentrated and the oily residue was chromatographed (5% diethyl ether – hexanes) on silica gel (200–400 mesh). The product **26** (21.9 g, 90%) was obtained as a colourless oil. ^{1}H NMR (200 MHz, $CDCl_3$) δ: 4.19 (s, 4H), 1.39 (s, 9H), 0.86 (s, 9H), 0.04 (s, 6H). ^{13}C NMR (50.3 MHz, $CDCl_3$) δ: 206.7, 115.6, 79.6, 68.2, 48.0, 28.2, 25.7, 18.1, −5.7. MS (EI), *m/z*: 246 (m − *t*.Bu^+), 230, 190, 129. MS (CI, NH_3), *m/z*: 321 (100%, m + NH_4^+).

3-Amino-1-hydroxyacetone (3-amino-1-hydroxypropan-2-one) (5) hydrochloride

N-tert-Butyloxycarbonyl-3-amino-1-*tert*-butyldimethylsilyloxy-2-propanone (**26**) (11.2 g, 37 mmol) was dissolved in a mixture containing aqueous 20% HCl and THF (50 mL, 2:5) and stirred for 24 h. Removal of the solvent gave a brownish crystalline solid that was recrystallized from EtOH-*tert*-butyl methyl ether to afford the product **5** (2.3 g) as light yellow needles; m.p. 134–136°C (lit. (8) mp 136–137°C). ^{1}H NMR (200 MHz, D_2O) δ: 4.35 (s, 2H, CH_2O), 4.03 (s, 2H, $CH_2NH_3^+$), 3.54 (s, CH_2O of dimer, intensity ca. 20% of 4.35 ppm signal), 3.06 (s, CH_2N of dimer, intensity ca. 20% of 4.05 ppm signal). ^{13}C NMR (50.3 MHz, D_2O), major signals δ: 204.6, 65.7, 44.9; minor signals δ: 92.7, 66.2, 65.6, 65.3, 45.3, 44.5. MS (CI, NH_3), *m/z*: 107 (5%, m (of free base) + NH_4^+), 90 (100%, m + H^+).

Acknowledgments

Research grants from the Natural Sciences and Engineering Research Council of Canada and from the National Institute of General Medical Sciences, U.S. Public Health Service, are gratefully acknowledged. We thank Dr. James F. Britten for confirming the structure of the synthetic sample of **5** HCl by X-ray crystallography.

References

1. R.E. Hill, K. Himmeldirk, I.A. Kennedy, R.M. Pauloski, B.G. Sayer, E. Wolf, and I.D. Spenser. J. Biol. Chem. **271**, 30426 (1996).
2. I.D. Spenser and R.E. Hill. Nat. Prod. Rep. **12**, 555 (1995).
3. M.W. Bernart, W.H. Gerwick, E.E. Corcoran, A.Y. Lee, and J. Clardy. Phytochemistry, **31**, 1273 (1992).
4. N. De Kimpe, A. Georgieva, M. Boeykens, and L. Lazar. J. Org. Chem. **60**, 5262 (1995); N. De Kimpe, A. Georgieva, M. Boeykens, I. Kozekov, and W. Aelterman. Synthesis, 1131 (1996).
5. T.-K. Man, G. Zhao, and M.E. Winkler, J. Bacteriol. **178**, 2445 (1996), and refs. cited therein.
6. R.H. White. Biochemistry, **17**, 3833 (1978).
7. S. David, B. Estramareix, J.-C. Fischer, and M. Therisod. J. Am. Chem. Soc. **103**, 7341 (1981).
8. M. Therisod, J.-C. Fischer, and B. Estramareix. Biochem. Biophys. Res. Commun. **98**, 374 (1981).
9. S. David, B. Estramareix, J.-C. Fischer, and M. Therisod. J. Chem. Soc. Perkin Trans. I, 2131 (1982).
10. K. Himmeldirk, I.A. Kennedy, R.E. Hill, B.G. Sayer, and I.D. Spenser. J. Chem. Soc. Chem. Commun. 1187 (1996).
11. S.T.J. Broers. Dissertation Nr. 10978, ETH Zürich, Switzerland. 1994.
12. M.K. Schwarz. Dissertation Nr. 10951, ETH Zürich, Switzerland. 1994.
13. W.G. Laver, A. Neuberger, and J.J. Scott. J. Chem. Soc. 1483 (1959).
14. J.P. Marcus and E.E. Dekker. Biochem. Biophys. Res. Commun. **190**, 1006 (1993).
15. (*a*) H.D. Verkruijsse and L. Brandsma. Synth. Commun. **21**, 235 (1991); (*b*) L. Brandsma. Preparative acetylenic chemistry. Elsevier, Amsterdam. 1971. pp. 60–61.
16. A.E.J. de Nooy, A.C. Besemer, and H. van Bekkum. Synthesis, 1153 (1996).
17. A.O. Jackson and C.S. Marvel. J. Biol. Chem. **103**, 191 (1933).
18. O. Keller, W.E. Keller, G. van Look, and G. Wersin. Org. Synth. **63**, 160 (1985).
19. S.K. Chaudhary and O. Hernandez. Tetrahedron Lett. 99 (1979).
20. K.K. Ogilvie, N. Nguyen-Ba, and R.G. Hamilton. Can. J. Chem. **62**, 1622 (1984).

© 1997 NRC Canada

Transition metal azolates from metallocenes. Part 1: Dimetallic and trimetallic cyclopentadienyl nickel pyrazolates, synthesis and structural studies

Steven J. Rettig, Alan Storr, David A. Summers, Robert C. Thompson, and James Trotter

Can. J. Chem. Downloaded from www.nrcresearchpress.com by 88.146.161.215 on 09/08/12
For personal use only.

Abstract: The reactions of nickelocene with pyrazoles in benzene solution have resulted in the isolation of either dimeric compounds, $[CpNi(\mu\text{-}pz')]_2$, (room temperature conditions) or trimetallic complexes, $[CpNi(\mu\text{-}pz'')_2]_2Ni$, (elevated temperature conditions). Both dimeric and trimetallic species were obtained as red crystalline materials and X-ray structural investigations are reported for representative samples of each type. Structural features are interpreted and compared with similar, previously reported, nickel pyrazolate structures. Crystals of $[CpNi(3,5\text{-diMepz})]_2$ ($C_{20}H_{24}N_4Ni_2$), **1**, are orthorhombic, a = 15.204(1), b = 17.967(2), c = 6.9786(9) Å, Z = 4, space group *Ama*2; those of $[CpNi(4\text{-}NO_2\text{-}3,5\text{-diMepz})]_2$ ($C_{20}H_{22}N_6Ni_2O_2$), **5**, are orthorhombic, a = 17.145(3), b = 17.738(1), c = 7.006(1) Å, Z = 4, space group $P2_12_12_1$; those of $[CpNi(3,5\text{-}F_6\text{diMepz})]_2$ ($C_{20}H_{12}F_{12}N_4Ni_2$), **6**, are orthorhombic, a = 18.7134(8), b = 15.619(2), c = 7.7263(9) Å, Z = 4, space group *Pnma*; those of $[CpNi(3,5\text{-diMepz})_2]_2Ni$ ($C_{30}H_{38}N_8Ni_3$), **7**, are triclinic, a = 10.078(2), b = 16.134(2), c = 9.992(1) Å, α = 91.586(10)°, β = 111.050(9)°, γ = 86.95(1)°, Z = 2, space group $P\bar{1}$; and those of $[CpNi(4\text{-Cl-}3,5\text{-diMepz})_2]_2Ni$ ($C_{30}H_{34}Cl_4N_8Ni_3$), **10**, are monoclinic, a = 10.2201(7), b = 16.174(1), c = 10.7207(9) Å, β = 108.193(5)°, Z = 2, space group $P2_1/a$. The structures were solved by direct (dimetallic species) or Patterson (trimetallic complexes) methods and were refined by full-matrix least-squares procedures to R = 0.035, 0.032, 0.058, 0.032, and 0.033 (R_w = 0.021, 0.026, 0.053, 0.028, and 0.032) for 1157, 1894, 1642, 4499, and 2113 reflections with $I \geq 3\sigma(F^2)$, respectively.

Key words: crystal structures, nickel, nickelocene, pyrazolates, cyclopentadienyl.

Résumé : Les réactions du nickelocène avec les pyrazoles en solution dans le benzène conduisent à la formation de composés de nature dimère, $[CpNi(\mu\text{-}pz')]_2$ (réactions à la température ambiante), ou à des complexes trimétalliques, $[CpNi(\mu\text{-}pz'')_2]_2Ni$ (réactions à température élevée). Les espèces tant dimériques que trimétalliques ont été obtenues sous la forme de matériaux cristallins rouges; on a effectué des déterminations de structure par diffraction des rayons X sur des échantillons représentatifs de chacun des types. On a interprété les caractéristiques structurales et on les compare avec celles rapportées antérieurement pour des structures semblables de pyrazolate de nickel. Les cristaux de $[CpNi(3,5\text{-diMepz})]_2$ ($C_{20}H_{24}N_4Ni_2$), **1**, sont orthorhombiques, groupe d'espace *Ama*2, avec a = 15,204(1), b = 17,967(2) et c = 6,9786(9) Å et Z = 4; ceux du $[CpNi(4\text{-}NO_2\text{-}3,5\text{-diMepz})]_2$ ($C_{20}H_{22}N_6Ni_2O_2$), **5**, sont orthorhombiques, groupe d'espace $P2_12_12_1$, avec a = 17,145(3), b = 17,738(1) et c = 7,006(1) Å, Z = 4; ceux de $[CpNi(3,5\text{-}F_6\text{diMepz})]_2$ ($C_{20}H_{12}F_{12}N_4Ni_2$), **6**, sont orthorhombiques, groupe d'espace *Pnma*, avec a = 18,7134(8), b = 15,619(2) et c = 7,7263(9) Å, Z = 4; ceux de $[CpNi(3,5\text{-diMepz})_2]_2Ni$ ($C_{30}H_{38}N_8Ni_3$), **7**, sont tricliniques, groupe d'espace $P\bar{1}$, avec a = 10,078(2), b = 16,134(2) et c = 9,992(1) Å, α = 91,586(10)°, β =111,050(9)° et γ = 86,95(1)° et Z = 2 et ceux de $[CpNi(4\text{-Cl-}3,5\text{-diMepz})_2]_2Ni$ ($C_{30}H_{34}Cl_4N_8Ni_3$), **10**, sont monocliniques, groupe d'espace $P2_1/a$, avec a = 10,2201(7), b = 16,174(1) et c = 10,7207(9) Å, β = 108,193(5)° et Z = 2. Les structures ont été résolues par des méthodes directes (espèces bimétalliques) ou de Patterson (complexes trimétalliques) et on les a affinées par la méthode des moindres carrés (matrice complète) jusqu'à des valeurs respectives de R de 0,035, 0,032, 0,058, 0,032 et 0,033 (R_w de 0,021, 0,026, 0,053, 0,028 et 0,032) pour 1157, 1894, 1642, 4499 et 2113 réflexions avec $I \geq 3\sigma(F^2)$.

Mots clés : structures cristallines, nickel, nickelocène, pyrazolates, cyclopentadiényle.

[Traduit par la rédaction]

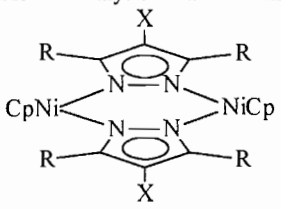
Received February 20, 1997.

S.J. Rettig, A. Storr,[1] D.A. Summers, R.C. Thompson,[1] and J. Trotter. Department of Chemistry, The University of British Columbia, Vancouver, BC V6T 1Z1, Canada.

[1] Authors to whom correspondence may be addressed. Telephone, R.C. Thompson: (604) 822-4979; A. Storr: (604) 822-3962. Fax: (604) 822-2847. E-mail: thompson@chem.ubc.ca, storr@chem.ubc.ca

© 1997 NRC Canada

Table 1. Analytical data for dimeric systems.



Compound			Analysis				δ ppm (C_6D_6 solution)[a]		
Number	R	X		C	H	N	Cp	Me	X
1	Me	H	Found	55.1	5.5	12.7	5.20 s	2.20 s	5.55 s
			Calcd.	54.9	5.5	12.8			
2	Me	Cl	Found	47.8	4.3	11.0	5.00 s	2.10 s	NA
			Calcd.	47.4	4.4	11.0			
3	Me	Br	Found	40.7	3.7	9.4	4.95 s	2.10 s	NA
			Calcd.	40.3	3.7	9.4			
4	Me	Me	Found	57.1	6.3	11.8	5.22 s	2.15 s	1.62 s
			Calcd.	56.7	6.1	12.0			
5	Me	NO_2	Found	45.7	4.2	16.0	5.20 s	2.20 s	NA
			Calcd.	45.5	4.2	15.9			
6	CF_3	H	Found	37.1	2.0	8.6	3.37 s	NA	6.67 s
			Calcd.	36.8	1.9	8.6			

[a]δ (C_6H_6) = 7.20 ppm.
NA = not applicable.

Introduction

In 1977, Blake et al. reported reactions of bis(η-cyclopentadienyl)nickel, nickelocene, with several pyrazoles. In this report the authors describe the isolation of (*i*) polymeric (or, at least, highly oligomeric) nickel complexes incorporating pyrazole and 3-methylpyrazole and (*ii*) dimeric nickel complexes containing doubly bridging 3,5-dialkylpyrazolate ligands and end-capping η-C_5H_5 groups (1). Steric arguments were used in an attempt to explain the lack of polymerization in the reactions involving the 3,5-disubstituted pyrazole. No structures were confirmed by X-ray diffraction studies in this earlier work. Our long-standing interest in transition metal azolate polymers and oligomers (2–6) has prompted further investigations on this system, particularly on the products of reactions involving 3,5-disubstituted pyrazoles. Specifically, we report studies of the reactions of nickelocene with 4-X-3,5-dimethylpyrazole (X = H, Cl, Br, CH_3, and NO_2) and with 3,5-bis(perfluoromethyl)pyrazole that, depending on conditions, have led not only to the isolation of dimeric complexes (analogous to those reported by Blake et al.) but also trimetallic and polymeric materials. This report focuses on the synthesis of the dimeric and trimetallic complexes and their characterization, including the structure determination of five of these by single crystal X-ray diffraction studies. Studies on the polymeric materials are still in progress and will be reported in a future communication.[2]

Experimental

Nickelocene was prepared by the method of R.B. King (7). Pyrazoles were used as supplied (Aldrich) or prepared as described previously (3*a*, 6, 8). Solvents used were reagent grade and were dried and distilled under an atmosphere of dry dinitrogen before use.

Synthesis of $[CpNi(\mu\text{-}pz')]_2$ dimers

where μ-pz′ = 3,5-dimethylpyrazolate, 3,5-diMepz **1**
= 4-chloro-3,5-dimethylpyrazolate, 4-Cl-3,5-diMepz **2**
= 4-bromo-3,5-dimethylpyrazolate, 4-Br-3,5-diMepz **3**
= 3,4,5-trimethylpyrazolate, 3,4,5-triMepz **4**
= 4-nitro-3,5-dimethylpyrazolate, 4-NO_2-3,5-diMepz **5**
= 3,5-bis(trifluoromethyl)pyrazolate, 3,5-F_6diMepz **6**

Nickelocene (1.9 g, 0.010 mol) and the appropriate pyrazole were mixed in equimolar amounts and dissolved in ~150 mL of dry, oxygen-free benzene under a dinitrogen atmosphere. The resulting solution was stirred at room temperature over a period of ~12 h with the initial green colour changing to red within 30 min. The benzene solvent was then removed under vacuum and any remaining reactants were removed by sublimation. This resulted in the isolation of the products as red solid materials in yields of 45–55%. Recrystallization of these products was achieved by dissolving the solids in benzene, followed by slow evaporation of the solvent. Elemental analytical results and ^1H nmr data on recrystallized samples are given in Table 1.

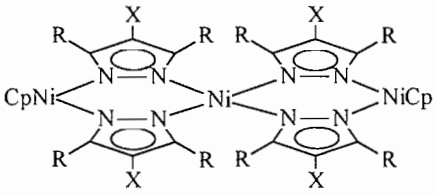
[2] A. Storr, D.A. Summers, and R.C. Thompson. In preparation.

Can. J. Chem. Downloaded from www.nrcresearchpress.com by 88.146.161.215 on 09/08/12
For personal use only.

© 1997 NRC Canada

Can. J. Chem. Downloaded from www.nrcresearchpress.com by 88.146.161.215 on 09/08/12
For personal use only.

Table 2. Analytical data for trimetallic complexes.



Compound			Analysis				δ ppm (C_6D_6 solution)[a]		
Number	R	X		C	H	N	Cp	Me	X
7	Me	H	Found	52.6	5.5	16.2	5.63 s	2.15, 2.20 s	5.40 s
			Calcd.	52.5	5.5	16.3			
8	Me	Br	Found	36.0	3.4	11.3	5.15 s	1.95, 2.10 s	NA
			Calcd.	35.9	3.4	11.1			
9	Me	Me	Found	55.2	6.3	15.0	5.53 s	2.05, 2.23 s	1.55 s
			Calcd.	55.0	6.2	15.1			
10	Me	Cl	Found	43.7	4.2	13.9	5.65 s	2.15, 2.18 s	NA
			Calcd.	43.7	4.2	13.6			

[a]δ (C_6H_6) = 7.20 ppm.
NA = not applicable.

Synthesis of trimetallic $[CpNi(\mu\text{-pz}'')_2]_2Ni$ compounds

where μ-pz″ = 3,5-dimethylpyrazolate, 3,5-diMepz **7**
= 4-bromo-3,5-dimethylpyrazolate, 4-Br-3,5-diMepz **8**
= 3,4,5-trimethylpyrazolate, 3,4,5-triMepz **9**
= 4-chloro-3,5-dimethylpyrazolate, 4-Cl-3,5-diMepz **10**

Nickelocene (0.5 g, 2.7 mmol) and an approximately 10-fold excess of the appropriate pyrazole (~30 mmol) were mixed and dissolved in dry and oxygen-free benzene solvent. The initially green solution was heated at 60–70 °C under a dinitrogen atmosphere. After a very short period of time the solution had turned red and after about 3 h a red precipitate began to deposit in the reaction vessel. After ~18 h the solution was allowed to cool and the red crystalline product was isolated by filtration in yields of 30–35%. The product was subsequently washed with small amounts of the dry benzene to remove any residual ligand. Analytical results and ^{1}H nmr data are given in Table 2.

X-ray crystallographic analyses of $[CpNi(3,5\text{-diMepz})]_2$, **1**, $[CpNi(4\text{-}NO_2\text{-}3,5\text{-diMepz})]_2$, **5**, $[CpNi(3,5\text{-}F_6\text{diMepz})]_2$, **6**, $[CpNi(3,5\text{-diMepz})_2]_2Ni$, **7**, and $[CpNi(4\text{-Cl-}3,5\text{-diMepz})_2]_2Ni$, **10**

Crystallographic data appear in Table 3. The final unit-cell parameters were obtained by least squares on the setting angles for 25 reflections with 2θ = 35.0°–41.5° for **1**, 23.5°–30.9° for **5**, 88.6°–109.5° for **6**, 30.6°–34.0° for **7**, and 46.0°–66.0° for **10**. The intensities of three standard reflections, measured every 200 reflections throughout the data collections, decayed linearly by 2.5% for **5**, by 2.4% for **6**, and showed only small random fluctuations for the three other complexes. The data were processed,[3] corrected for Lorentz and polarization effects, decay (**5** and **6**), and absorption (based on azimuthal scans).

The structures were solved by direct (dimeric complexes) or Patterson (trimetallic complexes) methods. The structure analysis of **1** was initiated in the centrosymmetric space group *Cmcm* but was disordered, prompting a change to the lower symmetry space group *Ama*2. Molecules **1** and **6** have crystallographic mirror symmetry. The asymmetric unit of **7** consists of two crystallographically independent half-molecules, each complete molecule being located at a center of symmetry. Molecule **10** is also located at a centre of symmetry. All nonhydrogen atoms were refined with anisotropic thermal parameters. Hydrogen atoms were fixed in calculated positions (methyl orientations based on difference map peak positions) with C—H = 0.98 Å and $B_H = 1.2\ B_{\text{bonded atom}}$. Corrections for secondary extinction were applied (Zachariasen type, isotropic, Gaussian) for four of the complexes, the final values of the extinction coefficients being $4.60(9) \times 10^{-7}$ for **1**, $2.39(10) \times 10^{-6}$ for **6**, $4.7(2) \times 10^{-7}$ for **7**, and $1.04(8) \times 10^{-6}$ for **10**. No secondary extinction correction was necessary for **5**. In some instances, the cyclopentadienyl ring thermal motion suggests possible disordering. In no case was it possible to refine disordered models. This high thermal motion is probably due to significant libration about the metal–centroid vector, common in sterically unhindered complexes of this type. Neutral atom scattering factors for all atoms and anomalous dispersion corrections for the non-hydrogen atoms were taken from the *International tables for X-ray crystallography* (9). The absolute configuration of **5** (for the particular crystal used for data collection) was determined by a parallel refinement of the mirror image, which resulted in significantly higher residuals, the R and R_w factor ratios being 1.18 and 1.24, respectively. Selected bond lengths and selected bond angles appear in Tables 4 and 5, respectively. Final atomic coordinates and equivalent isotropic thermal parameters, complete listings of bond lengths and angles, hydrogen atom

[3] teXsan: Crystal structure analysis package. Unix version 1.7. Molecular Structure Corporation. The Woodlands, Tex. 1995.

© 1997 NRC Canada

Can. J. Chem. Downloaded from www.nrcresearchpress.com by 88.146.161.215 on 09/08/12
For personal use only.

Table 3. Crystallographic data.[a]

Compound	[CpNi(3,5-diMepz)]$_2$	[CpNi(4-NO$_2$-3,5-diMepz)]$_2$	[CpNi(3,5-F$_6$diMepz)]$_2$	[CpNi(3,5-diMepz)$_2$]$_2$Ni	[CpNi(4-Cl-3,5-diMepz)$_2$]$_2$Ni
	1	**5**	**6**	**7**	**10**
Formula	$C_{20}H_{24}N_4Ni_2$	$C_{20}H_{22}N_6Ni_2O_4$	$C_{20}H_{12}F_{12}N_4Ni_2$	$C_{30}H_{38}N_8Ni_3$	$C_{30}H_{34}Cl_4N_8Ni_3$
fw	431.38	527.83	653.72	686.78	824.56
Crystal system	Orthorhombic	Orthorhombic	Orthorhombic	Triclinic	Monoclinic
Space group	*Ama*2	$P2_12_12_1$	*Pnma*	$P\bar{1}$	$P2_1/a$
a, Å	15.204(1)	17.145(3)	18.7134(8)	10.078(2)	10.2201(7)
b, Å	17.967(2)	17.738(1)	15.619(2)	16.134(2)	16.174(1)
c, Å	6.9786(9)	7.006(1)	7.7263(9)	9.992(1)	10.7207(9)
α, °	90	90	90	91.586(10)	90
β, °	90	90	90	111.050(9)	108.193(5)
γ, °	90	90	90	86.95(1)	90
V, Å^3	1906.4(6)	2130.8(5)	2258.2(6)	1513.9(4)	1683.6(2)
Z	4	4	4	2	2
ρ_{calc}, g/cm^3	1.525	1.645	1.923	1.506	1.626
F(000)	912	1088	1296	716	844
Radiation	Mo	Mo	Cu	Mo	Cu
μ, cm^{-1}	19.86	18.08	31.87	18.81	51.48
Crystal size, mm	0.22 × 0.35 × 0.40	0.13 × 0.25 × 0.25	0.15 × 0.15 × 0.45	0.15 × 0.15 × 0.45	0.10 × 0.25 × 0.30
Transmission factors	0.76–1.00	0.80–1.00	0.93–1.00	0.78–1.00	0.59–1.00
Scan type	ω–2θ	ω–2θ	ω–2θ	ω–2θ	ω–2θ
Scan range, deg in ω	1.42 + 0.35 tan θ	1.00 + 0.35 tan θ	1.00 + 0.20 tan θ	1.47 + 0.35 tan θ	0.85 + 0.20 tan θ
Scan speed, deg/min	32 (up to 9 scans)	16 (up to 9 scans)	16 (up to 9 scans)	32 (up to 9 scans)	16 (up to 9 scans)
Data collected	$+h$, $+k$, $+l$	$+h$, $+k$, $+l$	$+h$, $+k$, $+l$	$+h$, $\pm k$, $\pm l$	$+h$, $+k$, $\pm l$
$2\theta_{max}$, deg	65	60	155	60	155
Crystal decay, %	Negligible	2.5	2.4	Negligible	Negligible
Total reflections	1963	3530	2681	9291	3859
Total unique reflections	1963	3530	2681	8823	3674
R_{merge}	—	—	—	0.029	0.018
Reflections with $I \geq 3\sigma(F^2)$	1157	1894	1642	4499	2113
No. of variables	117	289	179	374	206
R	0.035	0.032	0.058	0.032	0.033
R_w	0.021	0.026	0.053	0.028	0.032
gof	2.24	1.43	1.32	1.61	1.77
Max Δ/σ (final cycle)	0.007	0.002	0.003	0.0008	0.0008
Residual density e/Å^3	–0.66 to 0.58	–0.26 to 0.28	–0.42 to 1.36	–0.28 to 0.25	–0.35 to 0.27

[a]Temperature 294 K, Rigaku AFC6S diffractometer, Mo K_α radiation (λ = 0.71069 Å) or Cu K_α radiation (λ = 1.54178 Å), graphite monochromator, takeoff angle 6.0°, aperture 6.0 × 6.0 mm at a distance of 285 mm from the crystal, stationary background counts at each end of the scan (scan/background time ratio 2:1), $\sigma^2(F^2) = [S^2(C + 4B)]/Lp^2$ (S = scan rate, C = scan count, B = normalized background count), function minimized $\Sigma w(|F_o| - |F_c|)^2$ where $w = 1$ for [CpNi(3,5-F$_6$diMepz)]$_2$ and $w = 4F_o^2/\sigma^2(F_o^2)$ for the other four complexes, $R = \Sigma||F_o| - |F_c||/\Sigma|F_o|$, $R_w = (\Sigma w(|F_o| - |F_c|)^2/\Sigma w|F_o|^2)^{1/2}$, and gof = $[\Sigma w(|F_o| - |F_c|)^2/(m - n)]^{1/2}$. Values given for R, R_w, and gof are based on those reflections with $I \geq 3\sigma(F^2)$.

© 1997 NRC Canada

Table 4. Selected bond lengths (Å) with estimated standard deviations in parentheses.[a]

Bond	Length	Bond	Length
	[CpNi(3,5-diMepz)]$_2$, **1**		
Ni(1)—N(1)	1.905(4)	Ni(1)—C(6)	2.169(8)
Ni(1)—C(7)	2.063(6)	Ni(1)—C(8)	2.183(7)
Ni(1)—Cp(1)	1.78	Ni(2)—N(2)	1.877(4)
Ni(2)—C(9)	2.131(7)	Ni(2)—C(10)	2.101(6)
Ni(2)—C(11)	2.177(6)	Ni(2)—Cp(2)	1.78
N(1)—N(2)	1.370(5)		
	[CpNi(4-NO$_2$-3,5-diMepz)]$_2$, **5**		
Ni(1)—N(1)	1.922(4)	Ni(1)—N(3)	1.908(4)
Ni(1)—C(11)	2.141(9)	Ni(1)—C(12)	2.066(7)
Ni(1)—C(13)	2.119(6)	Ni(1)—C(14)	2.054(7)
Ni(1)—C(15)	2.12(1)	Ni(1)—Cp(1)	1.77
Ni(2)—N(2)	1.884(4)	Ni(2)—N(4)	1.889(4)
Ni(2)—C(16)	2.167(6)	Ni(2)—C(17)	2.084(6)
Ni(2)—C(18)	2.127(5)	Ni(2)—C(19)	2.063(6)
Ni(2)—C(20)	2.167(7)	Ni(2)—Cp(2)	1.76
N(1)—N(2)	1.383(5)	N(3)—N(4)	1.389(6)
	[CpNi(3,5-F$_6$diMepz)]$_2$, **6**		
Ni(1)—N(1)	1.921(4)	Ni(1)—C(6)	2.11(1)
Ni(1)—C(7)	2.077(7)	Ni(1)—C(8)	2.167(7)
Ni(1)—Cp(1)	1.76	Ni(2)—N(2)	1.930(4)
Ni(2)—C(9)	2.09(1)	Ni(2)—C(10)	2.055(8)
Ni(2)—C(11)	2.119(8)	Ni(2)—Cp(2)	1.75
N(1)—N(2)	1.368(5)		
	[CpNi(3,5-diMepz)$_2$]$_2$Ni, **7**		
Ni(1)—N(1)	1.904(2)	Ni(1)—N(3)	1.905(2)
Ni(2)—N(2)	1.882(2)	Ni(2)—N(4)	1.884(2)
Ni(2)—C(11)	2.105(4)	Ni(2)—C(12)	2.183(4)
Ni(2)—C(13)	2.187(3)	Ni(2)—C(14)	2.078(3)
Ni(2)—C(15)	2.138(4)	Ni(2)—Cp(1)	1.77
Ni(3)—N(5)	1.896(2)	Ni(3)—N(7)	1.899(2)
Ni(4)—N(6)	1.892(3)	Ni(4)—N(8)	1.887(2)
Ni(4)—C(26)	2.174(4)	Ni(4)—C(27)	2.069(4)
Ni(4)—C(28)	2.148(4)	Ni(4)—C(29)	2.110(4)
Ni(4)—C(30)	2.188(4)	Ni(4)—Cp(2)	1.77
N(1)—N(2)	1.382(3)	N(3)—N(4)	1.388(3)
N(5)—N(6)	1.375(3)	N(7)—N(8)	1.371(3)
	[CpNi(4-Cl-3,5-diMepz)$_2$]$_2$Ni, **10**		
Ni(1)—N(1)	1.897(3)	Ni(1)—N(3)	1.900(3)
Ni(2)—N(2)	1.894(3)	Ni(2)—N(4)	1.892(3)
Ni(2)—Cp	1.77	Ni(2)—C(11)	2.124(4)
Ni(2)—C(12)	2.088(4)	Ni(2)—C(13)	2.175(4)
Ni(2)—C(14)	2.175(4)	Ni(2)—C(15)	2.094(4)
N(1)—N(2)	1.373(3)	N(3)—N(4)	1.373(3)

[a]Cp refers to the unweighted centroid of the appropriate cyclopentadienyl ring. Symmetry operations: (*) 3/2 – *x*, *y*, *z* (′) *x*, 1/2 – *y*, *z*.

Can. J. Chem. Downloaded from www.nrcresearchpress.com by 88.146.161.215 on 09/08/12
For personal use only.

© 1997 NRC Canada

Can. J. Chem. Downloaded from www.nrcresearchpress.com by 88.146.161.215 on 09/08/12
For personal use only.

Table 5. Selected bond angles (deg) with estimated standard deviations in parentheses.[a]

Bonds	Angle(deg)	Bonds	Angle(deg)
	[CpNi(3,5-diMepz)]$_2$, **1**		
N(1)-Ni(1)-N(1)*	91.7(2)	N(1)-Ni(1)-Cp(1)	133.8
N(2)-Ni(2)-N(2)*	93.6(2)	N(2)-Ni(2)-Cp(2)	132.8
Ni(1)-N(1)-N(2)	117.8(3)	Ni(1)-N(1)-C(1)	133.8(3)
Ni(2)-N(2)-N(1)	118.7(3)	Ni(2)-N(2)-C(3)	133.1(4)
	[CpNi(4-NO$_2$-3,5-diMepz)]$_2$, **5**		
N(1)-Ni(1)-N(3)	94.9(2)	N(1)-Ni(1)-Cp(1)	131.9
N(3)-Ni(1)-Cp(1)	132.6	N(2)-Ni(2)-N(4)	91.0(2)
N(2)-Ni(2)-Cp(2)	134.7	N(4)-Ni(2)-Cp(2)	133.5
Ni(I)-N(1)-N(2)	117.3(3)	Ni(1)-N(1)-C(1)	133.7(4)
Ni(2)-N(2)-N(1)	118.0(3)	Ni(2)-N(2)-C(3)	132.6(4)
Ni(1)-N(3)-N(4)	117.4(3)	Ni(1)-N(3)-C(6)	135.0(4)
Ni(2)-N(4)-N(3)	117.8(3)	Ni(2)-N(4)-C(8)	132.3(4)
	[CpNi(3,5-F$_6$diMepz)]$_2$, **6**		
N(1)-Ni(1)-N(1)′	90.6(3)	N(1)-Ni(1)-Cp(1)	134.6
N(2)-Ni(2)-N(2)′	90.4(2)	N(2)-Ni(2)-Cp(2)	134.6
Ni(1)-N(1)-N(2)	117.3(3)	Ni(1)-N(1)-C(1)	135.5(4)
N(2)-N(1)-C(1)	106.4(4)	Ni(2)-N(2)-N(1)	117.1(3)
Ni(2)-N(2)-C(3)	134.9(3)		
	[CpNi(3,5-diMepz)$_2$]$_2$Ni, **7**		
N(1)-Ni(1)-N(1)′	180.0	N(1)-Ni(1)-N(3)	90.22(10)
N(1)-Ni(1)-N(3)′	89.78(10)	N(3)-Ni(1)-N(3)′	180.0
N(2)-Ni(2)-N(4)	91.23(10)	N(2)-Ni(2)-Cp(1)	136.0
N(4)-Ni(2)-Cp(1)	132.8	N(5)-Ni(3)-N(5)″	180.0
N(5)-Ni(3)-N(7)	88.89(10)	N(5)-Ni(3)-N(7)″	91.11(10)
N(7)-Ni(3)-N(7)″	180.0	N(6)-Ni(4)-N(8)	91.6(1)
N(6)-Ni(4)-Cp(2)	135.7	N(8)-Ni(4)-Cp(2)	132.6
Ni(1)-N(1)-N(2)	120.9(2)	Ni(1)-N(1)-C(1)	131.5(2)
Ni(2)-N(2)-N(1)	119.0(2)	Ni(2)-N(2)-C(3)	132.8(2)
Ni(1)-N(3)-N(4)	120.3(2)	Ni(1)-N(3)-C(6)	131.5(2)
Ni(2)-N(4)-N(3)	119.3(2)	Ni(2)-N(4)-C(8)	132.7(2)
Ni(3)-N(5)-N(6)	120.6(2)	Ni(3)-N(5)-C(16)	130.6(2)
Ni(4)-N(6)-N(5)	119.4(2)	Ni(4)-N(6)-C(18)	133.3(2)
Ni(3)-N(7)-N(8)	120.5(2)	Ni(3)-N(7)-C(21)	131.3(2)
Ni(4)-N(8)-N(7)	119.7(2)	Ni(4)-N(8)-C(23)	132.2(2)
	[CpNi(4-Cl-3,5-diMepz)$_2$]$_2$Ni, **10**		
N(1)-Ni(1)-N(1)*	180.0	N(1)-Ni(1)-N(3)	88.8(1)
N(1)-Ni(1)-N(3)*	91.2(1)	N(3)-Ni(1)-N(3)*	180.0
N(2)-Ni(2)-N(4)	91.1(1)	N(2)-Ni(2)-Cp	133.8
N(4)-Ni(2)-Cp	135.0	Ni(1)-N(1)-N(2)	121.4(2)
Ni(1)-N(1)-C(1)	129.9(2)	N(2)-N(1)-C(1)	108.6(3)
Ni(2)-N(2)-N(1)	119.4(2)	Ni(2)-N(2)-C(3)	132.2(2)
Ni(1)-N(3)-N(4)	121.9(2)	Ni(1)-N(3)-C(6)	128.8(2)
Ni(2)-N(4)-N(3)	119.0(2)	Ni(2)-N(4)-C(8)	133.4(3)

[a]Cp refers to the unweighted centroid of the appropriate cyclopentadienyl ring. Symmetry operations: (*) 3/2 – x, y, z for [CpNi(3,5-diMepz)]$_2$ and 1 – x, 1 – y, 1 – z for [CpNi(4-Cl-3,5-diMepz)$_2$]$_2$Ni (′) x, 1/2 – y, z for [CpNi(3,5-F$_6$diMepz)]$_2$ and –x, –y, –z for [CpNi(3,5-diMepz)$_2$]$_2$Ni (″) 1 – x, 1 – y, –z.

© 1997 NRC Canada

Can. J. Chem. Downloaded from www.nrcresearchpress.com by 88.146.161.215 on 09/08/12
For personal use only.

parameters, anisotropic thermal parameters, torsion angles, intermolecular contacts, and least-squares planes are included as supplementary material.[4]

Physical measurements

The ^{1}H nmr spectra were recorded in C_6D_6 solution using a Bruker AC-200E nmr spectrometer. Magnetic susceptibilities were measured using a Quantum Design (MPMS) SQUID magnetometer. The sample holder and procedures involving the use of the equipment were described previously (2*g*). Magnetic susceptibilities were corrected for the background signal of the sample holder and for diamagnetic susceptibilities of all atoms (10). Susceptibility versus temperature behaviour (2–300 K) was measured at 1.0 T.

Results and discussion

On the basis of their earlier studies Blake et al. suggested that, due to steric restraints, reactions of nickelocene with 3,5-dialkyl-substituted pyrazoles would yield only dimeric complexes of formation $[CpNi(\mu\text{-pz}')]_2$. In the present work we have found that reactions of nickelocene with 3,5-dimethylpyrazoles under mild conditions yield not only dimeric complexes of formulation $[CpNi(\mu\text{-pz}')]_2$ (obtained in benzene solution at room temperature) but also trimetallic species of formulation $[CpNi(\mu\text{-pz}'')_2]_2Ni$ at slightly elevated temperatures. Indeed, reactions at even higher temperatures yield paramagnetic polymeric materials of composition $[Ni(\mu\text{-pz}'')_2]_x$.[2] Both the dimeric and trimetallic complexes can be isolated as crystalline materials and five have been subjected to X-ray crystallographic study in the present work.

Dimeric $[CpNi(\mu\text{-pz}')]_2$ complexes

The analytical data for these complexes are given in Table 1. The ^{1}H nmr results are consistent with a symmetrical structure with equivalent μ-pz′ and Cp groups, the latter exhibiting but one sharp singlet signal indicative of free rotation about the Ni–Cp centroid axis. A planar six-membered Ni-(N-N)$_2$-Ni central ring system with end-capping, freely rotating Cp groups could explain these ^{1}H nmr results, but molecular modeling studies show such an arrangement would lead to severe steric interaction between the methyl substituents on the μ-pz′ rings and the Cp groups. A boat conformation for the Ni-(N-N)$_2$-Ni ring reduces these steric interactions considerably and maintains planarity about the nitrogen atoms of the μ-pz′ rings, thereby retaining the resonance delocalization energy of the system. We have determined the X-ray crystal structures of three of the dimeric complexes and all of them display the predicted boat-like conformation for the Ni-(N-N)$_2$-Ni ring system.

A noteworthy feature in the ^{1}H nmr results is the effect of substituting CF_3 for CH_3 groups on the bridging pyrazolates. This substitution leads to a marked shift in the signals for both the 4-H proton on the pyrazolate rings and the Cp ring protons. The latter signal moves to a higher field position at δ 3.37 whereas the former signal shifts to a lower field position as δ 6.67. Similar shifts in the 4-H proton signal have been reported by Dias et al. for a number of HB(3,5-F_6diMepz)$_3$ containing complexes (11, 12).

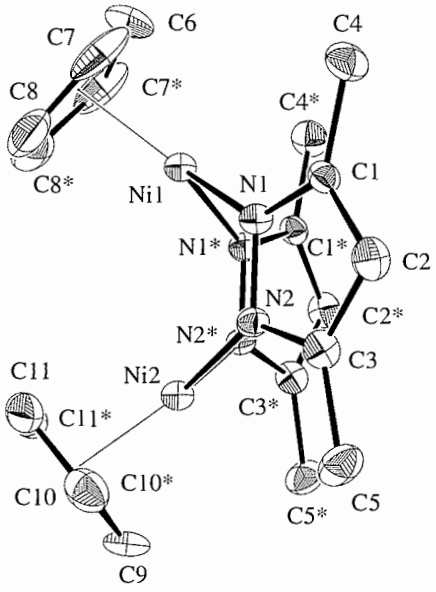


Fig. 1. The molecular structure of $[CpNi(3,5\text{-diMepz})]_2$, **1**, with atom numbering scheme and 33% probability thermal ellipsoids for all non-hydrogen atoms.

The molecular structures of **1**, **5**, and **6** are shown in Figs. 1–3. The internal bond angles and bond lengths in the cyclopentadienyl and pyrazolate ligands are normal for all three complexes. Examination of the nickel(II) coordination spheres of **1** and **5** reveal no significant differences in bond parameters (Tables 4 and 5) and hence no measurable structural effect, on substitution of the hydrogen in the 4-position of the pyrazolate ring by the nitro group. Larger structural effects might be expected with the substitution of the methyl substituents in the 3,5-positions by the significantly more electron-withdrawing and larger trifluoromethyl groups. Comparisons of the average Ni—N bond lengths in the two complexes (1.891(20) for **1** versus 1.926(8) for **6**) indicates a slight lengthening in the complex with the electron-withdrawing substituents. This is accompanied by a small increase in the Ni-N-C bond angles and decrease in the Ni-N-N bond angles in **6** compared to **1** (Tables 4 and 5), a consequence perhaps of increased steric repulsion between the CF_3 groups and the cyclopentadienyl ligands in **6**. This also appears to result in a slightly shorter nonbonded Ni···Ni distance in **6** than in **1** (see below).

It is interesting to compare the nonbonded Ni···Ni separations in these complexes with previously reported values for similar doubly pyrazolate-bridged dinickel systems (13, 14). These values are listed in Table 6. In the three structures reported here the Ni···Ni separations vary very little, with only a slight reduction in the distance observed on substituting CH_3

[4] Copies of material on deposit may be purchased from: The Depository of Unpublished Data, Document Delivery, CISTI, National Research Council Canada, Ottawa, Canada K1A 0S2. Tables of atomic coordinates and bond lengths and angles involving hydrogen atoms have also been deposited with the Cambridge Crystallographic Data Centre and can be obtained on request from The Director, Cambridge Crystallographic Data Centre, University Chemical Laboratory, 12 Union Road, Cambridge CB2 1EZ, UK.

© 1997 NRC Canada

Can. J. Chem. Downloaded from www.nrcresearchpress.com by 88.146.161.215 on 09/08/12
For personal use only.

Fig. 2. The molecular structure of $[CpNi(4\text{-}NO_2\text{-}3,5\text{-}diMepz)]_2$, **5**, with atom numbering scheme and 33% probability thermal ellipsoids for all non-hydrogen atoms.

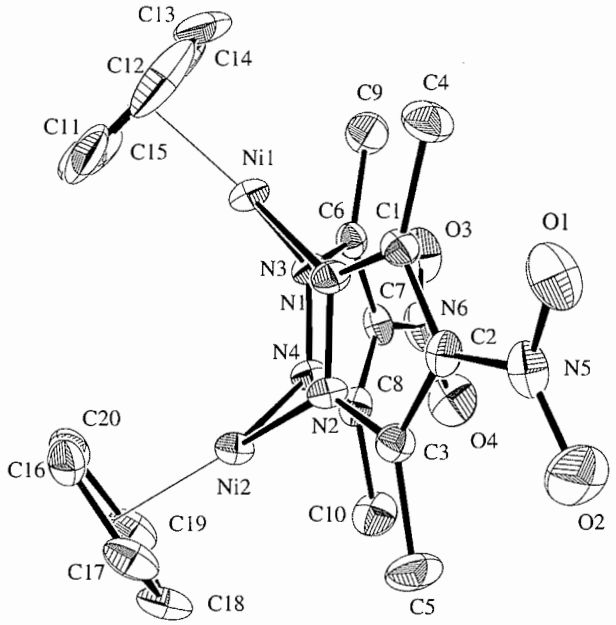
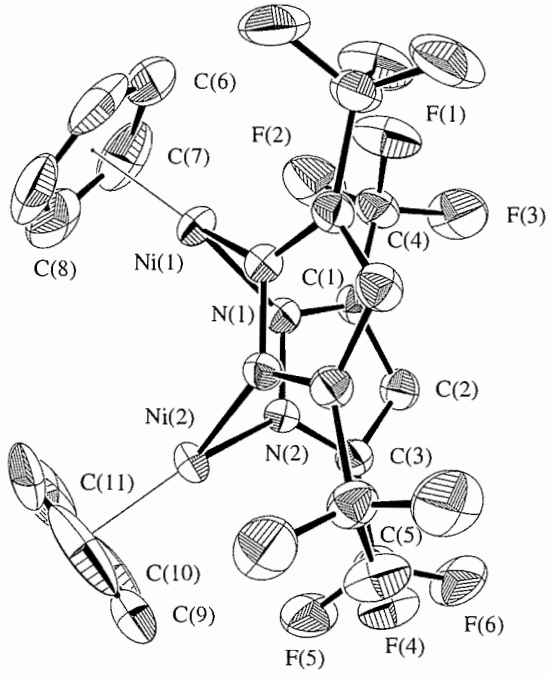
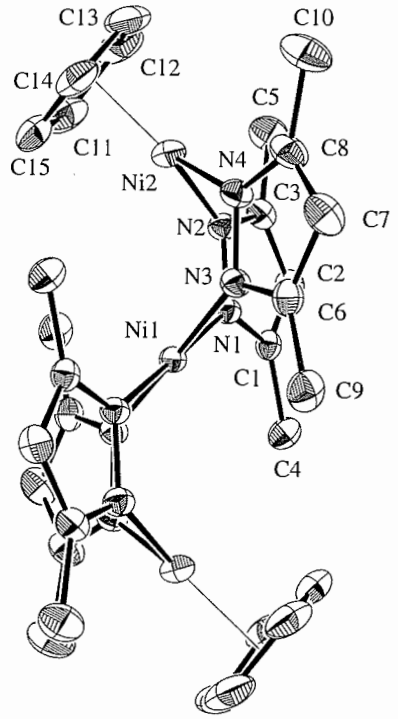


Fig. 3. The molecular structure of $[CpNi(3,5\text{-}F_6diMepz)]_2$, **6**, with atom numbering scheme and 33% probability thermal ellipsoids for all non-hydrogen atoms.



groups by the CF_3 groups on the bridging μ-pz′ moieties. All three of these dimeric compounds are formally 18-electron Ni complexes in contrast to the η^3-allyl and linear nitrosyl complexes listed in the table. These latter complexes are both 16-electron Ni systems and display widely different Ni···Ni separations. The η^3-allyl complex value at 3.00 Å arises from a

Fig. 4. The molecular structure of one of the two independent molecules of $[CpNi(3,5\text{-}diMepz)_2]_2Ni$, **7**, with atom numbering scheme and 33% probability thermal ellipsoids for all non-hydrogen atoms.



severely puckered Ni-$(N\text{-}N)_2$-Ni ring and suggests a possible metal–metal bonding interaction. In contrast, the very long Ni···Ni separation (3.673 Å) in the nitrosyl derivative results from the planar Ni-$(N\text{-}N)_2$-Ni six-membered ring. This arrangement is not disadvantaged sterically since the NO group, unlike the η^3-allyl group, is sterically nondemanding. In addition, it has been suggested that the planar arrangement in the nitrosyl complex may arise from favorable π-bonding between the pyrazolate π-system and the filled *d*-orbitals on the Ni atoms (14).

Trimetallic $[CpNi(\mu\text{-}pz'')_2]_2Ni$ complexes

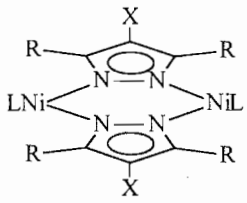
The analytical data for these complexes are given in Table 2. The ^1H nmr data for the complexes in C_6D_6 solution are again consistent with the solid state structures described below. In solution, the two end-capping Cp rings are equivalent and freely rotating about the Ni–Cp axis, giving rise to one sharp singlet at δ 5.6. The 3-Me and 5-Me groups on the μ-pz″ ligands are nonequivalent in these structures and give rise to two closely separated singlets at ~ δ 2.1–2.2. The 4-X substituents, where applicable, give signals that are easily located in the ^1H nmr spectra on the basis of both anticipated intensities and predicted chemical shifts.

The molecular structures of **7** and **10** are shown in Figs. 4 and 5 and, as expected, display the boat conformation for the Ni-$(N\text{-}N)_2$-Ni ring systems. These are favoured over a planar conformation on two counts, to relieve steric interactions between the Cp rings and adjacent Me substituents on the μ-pz″ ligands, and also to relieve steric interaction between the Me substituents of the μ-pz″ rings that are adjacent to the

© 1997 NRC Canada

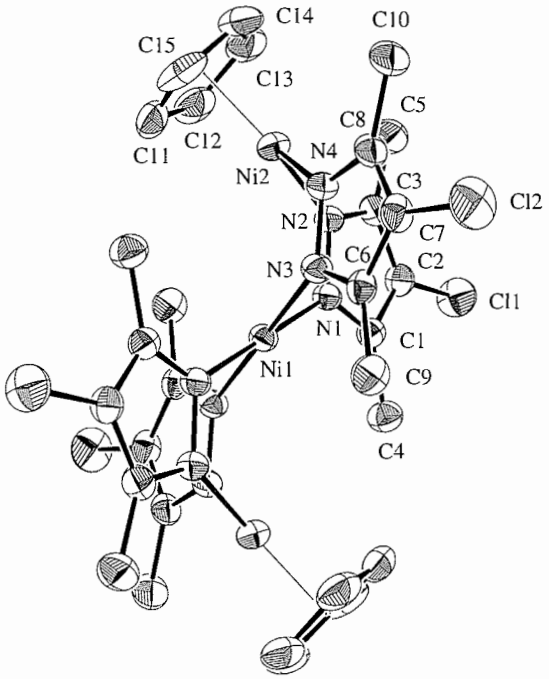
Can. J. Chem. Downloaded from www.nrcresearchpress.com by 88.146.161.215 on 09/08/12
For personal use only.

Table 6. Ni···Ni non-bonded distances in dimeric Ni systems.



Compound				
L	R	X	Ni···Ni Distances (Å)	References
Cp	CH_3	H	3.159	This work, **1**
Cp	CH_3	NO_2	3.156	This work, **5**
Cp	CF_3	H	3.128	This work, **6**
η^3-Allyl	CH_3	H	3.00	13
NO	CH_3	H	3.673	14

Fig. 5. The molecular structure of $[CpNi(4\text{-}Cl\text{-}3,5\text{-}diMepz)_2]_2Ni$, **10**, with atom numbering scheme and 33% probability thermal ellipsoids for all non-hydrogen atoms.

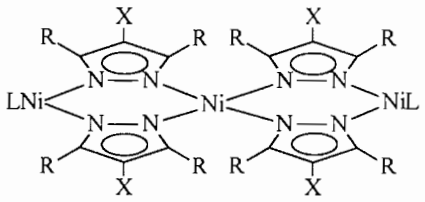


central Ni atom. As observed for the dimeric complexes, the internal bond lengths and angles of the ligands in **7** and **10** are normal. Moreover, bond parameters associated with the nickel coordination sphere are not significantly different in the two complexes, showing, again, that substitution of the hydrogen in the 4-position by a more electron-withdrawing substituent (Cl) has no measurable structural consequence. The Ni···Ni nonbonded distance is slightly greater in **10** than in **7** and this is accompanied by marginally greater Ni-N-N and smaller Ni-N-C bond angles in the former complex (Table 5). There seem no obvious intramolecular steric interactions that could cause these small differences, suggesting that intermolecular packing forces are responsible. In Table 7 we have listed the Ni···Ni nonbonded distances observed in **7** and **10** together with those for related trinickel complexes (13–15). In these systems the values of the Ni···Ni nonbonded distances span a much smaller range of values than in the dimetallic systems discussed above. Even the $[(ON)Ni(\mu\text{-}pz'')_2]_2Ni$ complex displays only a slightly longer Ni···Ni distance than the other complexes listed. The result is not unexpected since a totally planar structure, which might lead to a longer nonbonded nickel–nickel distance (as observed for the dimeric nitrosyl derivative (14)), is not favoured since this would lead to severe steric interactions around the central Ni atom (see above).

The observation of nmr spectra for all complexes is consistent with spin-paired d^8 Ni(II) configurations. To verify this we examined the magnetic susceptibilities at temperatures from 2 to 300 K of two representative dimeric compounds (R = CH_3, X = H and R = CH_3, X = NO_2) and two trimetallic compounds, (R = CH_3, X = H and R = CH_3, X = Cl). All four compounds gave evidence for weak paramagnetism. In the high-temperature region the magnetization could not be measured accurately as it was of the order of that obtained as a background signal for the sample container. The susceptibilities measured below 50 K showed an increase in magnitude with decreasing temperature as expected for paramagnetism. The magnitude of the measured susceptibilities was small, typically of the order of 3% or less than expected for $S = 1$ high-spin nickel(II). These results support the conclusion that the compounds involve diamagnetic spin-paired nickel(II) centers with small amounts of high-spin nickel(II) impurity. In the dimeric systems, Blake et al. (1) concluded that the ligand environment of Ni(II) in the complexes resulted in a low-spin d^8 configuration. Our results confirm this. Moreover, Blake et al. (1) observed weak paramagnetism in their complexes that they ascribe to either the presence of small amounts of paramagnetic pseudotetrahedral monomers or the presence of a thermally accessible excited $S = 1$ state in the dimers. Our results eliminate the second possibility since the observation

© 1997 NRC Canada

Table 7. Ni···Ni non-bonded distances in trimetallic nickel complexes.



Compound				
L	R	X	Ni···Ni distances (Å)	References
L	R	X		
Cp	CH_3	H	3.2739	This work, **7**
Cp	CH_3	Cl	3.2949	This work, **10**
η^3-Allyl	CH_3	H	3.2314	13
NO	CH_3	H	3.3770	14
acac	CH_3	H	3.1972	15

of an increase in susceptibility with decreasing temperature is not consistent with it. In the trimetallic systems the outer Ni(II) ions have the same environment as the Ni(II) ions in the dimeric systems, whereas the central Ni(II) ion is in a regular square planar environment. It is not surprising therefore that the trimetallic species also display diamagnetic behaviour.

Acknowledgements

Funding for the project has been provided by the Natural Sciences and Engineering Research Council of Canada. P. Borda of this department is thanked for the C, H, N analyses.

References

1. A.B. Blake, D.F. Ewing, J.E. Hamlin, and J.M. Lockyer. J. Chem. Soc. Dalton Trans. 1987 (1977).
2. M.K. Ehlert, S.J. Rettig, A. Storr, R.C. Thompson, and J. Trotter. Can. J. Chem. (*a*) **67**, 1970 (1989); (*b*) **68**, 1444 (1990); (*c*) **68**, 1494 (1990); (*d*) **69**, 432 (1991); (*e*) **70**, 2161 (1992); (*f*) **71**, 331 (1993); (*g*) **71**, 1425 (1993).
3. M.K. Ehlert, A. Storr, and R.C. Thompson. Can. J. Chem. (*a*) **70**, 1121 (1992); (*b*) **71**, 1412 (1993).
4. M.K. Ehlert, S.J. Rettig, A. Storr, R.C. Thompson, and J. Trotter. Acta. Crystallogr. Sect. C: Cryst. Struct. Commun. **C50**, 1023 (1994).
5. M.K. Ehlert, S.J. Rettig, A. Storr, R.C. Thompson, and J. Trotter. Inorg. Chem. **32**, 5176 (1993).
6. M.K. Ehlert, A. Storr, D.A. Summers, and R.C. Thompson. Can. J. Chem. Submitted
7. R.B. King. Organometallic synthesis. Academic Press, New York. 1965. p. 71.
8. G.T. Morgan and I. Ackerman. J. Chem. Soc. **123**, 1308 (1923).
9. (*a*) International tables for X-ray crystallography. Vol. IV. Kynoch Press, Birmingham, U.K. (present distributor Kluwer Academic Publishers: Boston, Mass.). 1974. pp. 99–102; (*b*) International tables for crystallography. Vol. C. Kluwer Academic Publishers, Boston, Mass. 1992. pp. 200–206.
10. E. Konig. Landolt–Börnstein numerical data and functional relationships in science and technology. New series, Vol. II/2. *Edited by* K.H. Hellwege and A.M. Hellewege. Springer-Verlag, Berlin. 1966.
11. H.V.R. Dias, W. Jin, H.J. Kim, and H.L. Lu. Inorg. Chem. **35**, 2317 (1996).
12. H.V.R. Dias and W. Jin. Inorg. Chem. **35**, 3687 (1996).
13. K.S. Chong, S.J. Rettig, A. Storr, and J. Trotter. Can. J. Chem. **59**, 996 (1981).
14. K.S. Chong, S.J. Rettig, A. Storr, and J. Trotter. Can. J. Chem. **57**, 3090 (1979).
15. M. Maekawa, M. Munakata, T. Kuroda, and Y. Nozaka. Inorg. Chim. Acta, **208**, 243 (1993).

Can. J. Chem. Downloaded from www.nrcresearchpress.com by 88.146.161.215 on 09/08/12
For personal use only.

© 1997 NRC Canada

Chemoselective intramolecular annulation of 3-alkylindolines into dihydro or tetrahydrofuro[2,3-*b*]indoles

Oscar R. Suárez-Castillo, Manuel García-Velgara, Martha S. Morales-Ríos, and Pedro Joseph-Nathan

Can. J. Chem. Downloaded from www.nrcresearchpress.com by 88.146.161.215 on 09/08/12
For personal use only.

Abstract: 3-Alkyl-2-hydroxyindolines, conveniently prepared from 2-hydroxyindolenines and a Grignard reagent, cyclize in the aprotic solvent tetrahydrofuran to afford tetrahydro-3-cyano-2-oxofuro[2,3-*b*]indoles, while in the protic solvent methanol the chemoselectivity changed to give dihydro-2-amino-3-carbomethoxyfuro[2,3-*b*]indoles. The steric effect of the alkyl group on the reactivity of 3-alkyl-2-hydroxyindolines is discussed for both processes. The ring transformation of tetrahydro-3-cyano-2-oxofuro[2,3-*b*]indoles into dihydro-2-amino-3-carbomethoxyfuro[2,3-*b*]indoles via γ-lactone imines is also discussed.

Key words: furo[2,3-*b*]indoles, α-cyano-γ-lactones, chemoselectivity, ring transformation, β-enamino esters.

Résumé : Les 3-alkyl-2-hydroxyindolines convenablement préparées à partir des 2-hydroxyindolénines et un réactif de Grignard, se cyclisent dans un solvant aprotique, le tétrahydrofuranne, pour donner les tétrahydro-3-cyano-oxofuro[2,3-*b*]-indoles tandis que dans un solvant protique, le méthanol, la chimiosélectivité change pour donner les dihydro-2-amino-3-carbométhoxyfuro[2,3-*b*]indoles. On discute de l'effet stérique du groupe alkyle sur la réactivité des 3-alkyl-2-hydroxyindolines dans les deux réactions étudiées. On discute également de la transformation du cycle des tétrahydro-3-cyano-oxofuro[2,3-*b*]-indoles en dihydro-2-amino-3-carbométhoxyfuro[2,3-*b*]indoles via les imines de γ-lactones.

Mots clés : furo[2,3-*b*]indole, α-cyano-γ-lactones, chimiosélectivité, transformation de cycle, β-énamino-esters.

[Traduit par la rédaction]

Introduction

The reaction of nitriles with alcohols is a standard procedure for preparing imino esters (1). These compounds are important not only because they are versatile intermediates in organic transformations, but also because they or their ketene amino-hemiketal tautomers have been used in the synthesis of nitrogen heterocycles (2). In particular, the alkoxide-catalyzed rearrangement of α-cyano-γ-lactones has attracted significant attention because the β-enamino esters formed represent an access to heterocyclic systems of potential biological interest (3). We recently reported (4) that the conjugate addition of Grignard reagents to the 2-hydroxyindolenine **1** resulted in the formation of 3-alkyl-2-hydroxyindolines **2***a–c* (R = Me, Et, i-Pr) together with the corresponding *cis*-fused tetrahydro-3-cyano-2-oxofuro[2,3-*b*]indoles **3***b–d* (R = Et, i-Pr, *t*-Bu). We also found that, regardless of the existence of two potential paths for intramolecular cyclization, compounds **2***b* and **2***c* cyclized selectively and efficiently to the corresponding tetrahydro-3-cyano-2-oxofuro[2,3-*b*]indoles **3***b* and **3***c* by treatment with triethylamine in anhydrous THF at room temperature. Clearly, under these reaction conditions, intramolecular attack at the nitrile group is not competitive with the lactonization process. Thus, we set out to explore the reaction conditions under which the γ-lactone imines **4** or their tautomeric β-enamino esters **5** could be selectively formed.

Herein, we wish to describe the chemoselective formation of dihydro-2-amino-3-carbomethoxyfuro[2,3-*b*]indoles **5***a–c* from 3-alkyl-2-hydroxyindolines **2***a–c*, as well as the ring transformations of **3***a–d* into **5***a–d* via γ-lactone imines **4***a–d* (Scheme 1). The influence of steric effects as well as that of the base and the temperature has been tested. These reactions provide a useful mild method for the construction of the furo[2,3-*b*]indole ring system, a skeleton frame found in several biologically active natural and synthetic compounds (5).

Results and discussion

Before studying the chemoselective transformation of 3-alkyl-2-hydroxyindolines **2***a–c* into dihydro-2-amino-3-carbomethoxyfuroindoles **5***a–c* we felt the need to refocus our attention on the selective lactonization of **2***a*, since in our previous work we found that diastereomerically pure (2*R**, 3*S**, 8*S**)-3-alkyl-2-hydroxyindolines **2***b* and **2***c* cyclized smoothly to the tetrahydro-3-cyano-2-oxofuroindoles **3***b* and **3***c* in the aprotic solvent THF containing triethylamine (4*a*). In contrast, under these conditions, the less hindered (2*R**, 3*S**, 8*S**)-2-hydroxy-3-methylindoline **2***a* was recovered as an epimeric mixture (ca. 1:1) (4*b*), resulting from a ring–chain tautomerization at the C2 hemiaminalic stereogenic center (6). We now have found that a successful lactonization of **2***a* to afford **3***a* can be achieved by employing the more polar solvent DMSO,

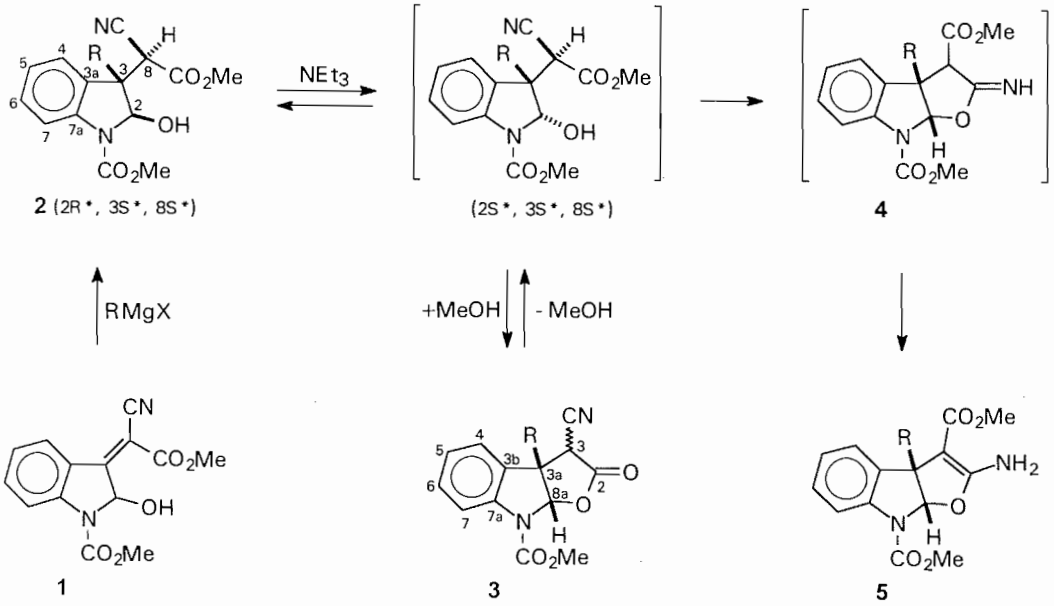
Received December 20, 1996.

O.R. Suárez-Castillo, M. García-Velgara, M.S. Morales-Ríos, and P. Joseph-Nathan.[1] Departamento de Química del Centro de Investigación y de Estudios Avanzados, Instituto Politécnico Nacional, Apartado 14-740, México D.F. 07000 México.

[1] Author to whom correspondence may be addressed. Telephone: (525) 747-7112. Fax: (525) 747-7113.

© 1997 NRC Canada

Scheme 1. Reaction pathways and list of compounds.



2,[a] 3,[b] 4, 5	R
a	Me
b	Et
c	i-Pr
d	*t*-Bu

[a]Isolated by crystallization from the epimeric mixtures, except for **2***d*, which was not isolated or detected.
[b]Epimeric mixtures, except for **3***d*.

and NaCN (25 mol%) as the catalyst (7). Under these conditions, the cyclization of the 2-hydroxy-3-methylindoline **2***a* is completed within 0.5 h at 100°C in 70% yield (Table 1, entry 1). Higher temperatures are ineffective at improving the yield, resulting instead in the formation of decomposition products. The *cis*-fused tetrahydro-3-cyano-2-oxofuroindole **3***a* was obtained in a diastereomerical ratio of 4:1 as determined by ^{1}H NMR spectroscopy (in DMSO-d_6) of the crude reaction product. This result can be rationalized in terms of a partial epimerization at the acidic C3 stereogenic center, as evidenced by fast deuterium exchange with D_2O. A steric hindrance between the methyl and the nitrile groups should favor an *anti* C3/C3a relationship. The *cis*-ring junction of **3***a* was evidenced by an NOE experiment, in which an enhancement of the H8a signal was observed when the angular methyl was irradiated.

Although nitrile carbon atoms are weak electrophilic sites when compared with ester carbonyl carbons, the intramolecular cyclization of 3-alkyl-2-hydroxyindolines **2** might proceed with chemoselectivity in protic solvents to give the desired dihydro-2-amino-3-carbomethoxyfuroindoles **5**, via formation of a γ-lactone imine **4** (8). Thus, the reaction course of **2***a* with the protic solvent methanol was monitored by TLC as a function of the disappearance of the starting material over time (Table 1). The reaction of **2***a* with $NaHCO_3$ (1:1 w/w) at 25°C in methanol furnished compound **5***a* after 2 h in 82% yield, accompanied by trace amounts of **3***a* (<3%, entry 2). When the reaction of **2***a* in methanol was performed under reflux for 0.5 h, a mixture of **3***a* and **5***a* was obtained in slightly lower yield (77%, entry 3), and with poorer chemoselectivity (4:5, from ^{1}H NMR). A more effective procedure involved reaction of **2***a* in refluxing methanol with MeONa (entry 4). In this case, the intramolecular reaction proceeded cleanly at the nitrile group and almost no products derived from attack at the carbonyl ester group were produced. In a similar fashion, the change of solvent from THF to methanol reversed the chemoselectivity of the cyclization in substrates **2***b* and **2***c*, leading to the almost exclusive formation of the dihydro-2-amino-3-carbomethoxyfuroindoles **5***b* and **5***c* in excellent yields (Table 1, entries 5–8). The above experimental results indicate that the nature of the solvent, the base, and reaction temperature exert a dramatic influence on the chemoselectivity regardless of the size of the alkyl group at C3. We noticed that increasing the steric requirement in the substrate by the bulkiness of the alkyl group (R) resulted in a decreased reactivity in the order i-Pr < Et < Me (Table 1, entries 4, 6, and 8). This trend, showing that a larger R group on C3a decreases the reactivity, can be attributed to steric interactions between the R group and the bulky carbonyl ester group in conformer **B**, which governs the for-

© 1997 NRC Canada

Can. J. Chem. Downloaded from www.nrcresearchpress.com by 88.146.161.215 on 09/08/12
For personal use only.

Can. J. Chem. Downloaded from www.nrcresearchpress.com by 88.146.161.215 on 09/08/12
For personal use only.

Table 1. Chemoselective intramolecular annulation of 3-alkylindolines **2***a–c*.

Entry	Compound	Solvent, base	Temp. (°C)	Time (h)	Yield (%)[e] **3**[d] + **5**	Ratio[f] **3/5**
1	**2***a*	DMSO–H_2O NaCN[a]	100	0.5	70	1/0
2	**2***a*	MeOH–H_2O $NaHCO_3$[b]	25	2	82	Traces/1
3	**2***a*	MeOH–H_2O $NaHCO_3$[b]	Reflux	0.5	77	4/5
4	**2***a*	MeOH MeONa[a]	Reflux	1.5	95	Traces/1
5	**2***b*	THF, NEt_3[c]	25	10	96	1/0
6	**2***b*	MeOH MeONa[a]	Reflux	4	93	Traces/1
7	**2***c*	THF, NEt_3[c]	25	10	96	1/0
8	**2***c*	MeOH MeONa[a]	Reflux	11	95	Traces/1

[a]Catalytic amount.
[b]1:1 (w/w).
[c]1:15 (w/w) substrate to amine.
[d]Epimeric *anti*/*syn* mixture.
[e]Yield after crystallization.
[f]Determined from the ^{1}H NMR spectrum of the crude reaction mixture.

mation of dihydro-2-amino-3-carbomethoxyfuroindoles **5***a–c* (Scheme 2). In other words, as the size of R increases, the steric destabilization in conformer **B** also increases. In contraposition, the formation of tetrahydro-3-cyano-2-oxofuroindoles **3***a–c*, which gave a reversed trend regarding the size of the R group (**5***a*), could be rationalized considering that conformer **A** becomes more populated as the size of the R group increases.

We next turned our attention to the possibility of forming dihydro-2-amino-3-carbomethoxyfuroindoles **5***a–d* by ring transformation of tetrahydro-3-cyano-2-oxofuroindoles **3***a–d*. This ring transformation is favored by the presence of the neighboring electron-withdrawing nitrile group, which may strongly activate the carbonyl ring group for addition reactions of nucleophiles such as methoxide (9), thus affording in a first step the bielectrophilic ring-opening α-nitrile esters **2***a–d*. In agreement with our expectation, **3***a* reacted cleanly under reflux with sodium methoxide – methanol, furnishing the desired dihydro-2-amino-3-carbomethoxyfuroindole **5***a* in 90% yield (Table 2, entry 1). The homologous tetrahydro-3-cyano-2-oxofuroindoles **3***b–c* exhibited analogous behavior, affording the dihydro-2-amino-3-carbomethoxyfuroindoles **5***b–c* in excellent yields. However, as can be seen in Table 2, a dramatic decrease in reactivity was observed as the bulkiness of the alkyl group was increased. Thus, on changing the methyl group at C3 for an isopropyl group, the reaction time increased from 9 to 77 h (entries 1 and 3), as determined by TLC. Moreover, the reaction of **3***d* was extremely slow (entry 4), since only a 25% conversion was observed after 17 days under reflux, as determined from the ^{1}H NMR spectrum of the crude reaction mixture, wherein no side-reaction products were detected. The extremely low

Scheme 2. Favored conformations (C8—C3 bond) for the annulation reaction intermediates having the 2*S**, 3*S**, 8*S** configuration.

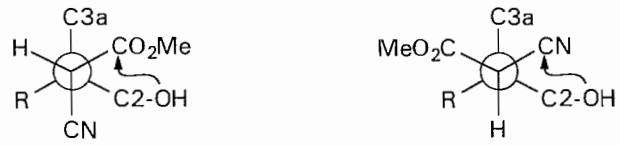


Table 2. Ring transformation of **3***a–d* into **5***a–d*.[a]

Entry	Compound	R	Time	Yield (%)[b] **5**
1	**3***a*	Me	9 h	90
2	**3***b*	Et	36 h	90
3	**3***c*	i-Pr	77 h	95
4	**3***d*	*t*-Bu	17 days	25[c]

[a]At refluxing methanol containing traces of MeONa.
[b]Yield after crystallization.
[c]71% of starting material **3***d*.

reactivity of **3***d* as compared with **3***a* may be ascribed to the bulkier *tert*-butyl group, which introduces a severe steric hindrance unfavorable for ring opening in the first step (**3** → **2**). In fact, comparison of the reaction times given in

© 1997 NRC Canada

Can. J. Chem. Downloaded from www.nrcresearchpress.com by 88.146.161.215 on 09/08/12
For personal use only.

Tables 1 (entries 4, 6, 8) and 2 suggests that the ring-opening step (**3** → **2**) is slower than the intramolecular ring closure (**2** → **4**), irrespective of the bulkiness of the alkyl group at C3.

The sequence involving the intramolecular cyclization of **2** to either **3** or **5** and the ring transformation of **3** into **5**, depicted in Scheme 1, involves the γ-lactone imines **4** as common intermediates (8). From a mechanistic point of view it is clear that lactones **3** are first transformed, in a base-catalyzed ring-opening reaction, to γ-alkoxy esters, which after attack at the cyano carbon atom afford the rearranged γ-imino lactones **4**. In the next step, a tautomerization allows the conversion of the intermediate γ-imino lactones **4** into the β-enamino esters **5**. Under the reaction conditions, neither the 3-alkyl-2-hydroxyindolines **2***a–d* nor the γ-imino lactones **4***a–d* could be isolated or detected in the ^{1}H NMR spectra of the crude material. Thus, the rearranged products **5** were driven by the reversibility between **2** and **3** (see Scheme 1). Implicit in the observed chemoselectivity is that the β-enamino esters **5** are the thermodynamic products.

The versatile 3-alkyl-2-hydroxyindolines **2** can serve as an entry point into either *cis*-fused tetrahydro-3-cyano-2-oxofuroindoles **3** or dihydro-2-amino-3-carbomethoxyfuroindoles **5**. The fact that the 1,3-prototropic rearrangement appears to be an irreversible process under these conditions allowed us to prepare compounds **5***a–c* uncontaminated by either **2***a–c* or **3***a–c*. The IR, ^{1}H and ^{13}C NMR, as well as the EIMS and HRMS, are in agreement with the given structures (see Experimental). ^{1}H NMR assignments were made on the basis of chemical shift and multiplicity and were confirmed, where necessary, by homonuclear decoupling and ^{13}C–^{1}H correlation experiments. The ^{1}H NMR spectra of **5***a–d* show in the aromatic region two triplets, one of which couples to a broad signal (H7, $^3J_{6,7}$ = 7.5 ± 0.2 Hz) and is thus due to H6, leaving the other one for H5 ($^4J_{5,7}$ = 1.0 ± 0.1 Hz). Also, a doublet is identified as the H4 signal by its NOE with the alkyl group at C3a (R = Me, *t*-Bu). In addition, the signal of H8a appears as a singlet and the remaining broad signal is due to the NH_2 group (D_2O exchangeable). The *cis*-ring junction was supported by NOE experiments. In particular, irradiation of the *tert*-butyl singlet (δ = 1.04 ppm) in **5***d* resulted in a strong enhancement (37%) of the H8a signal (δ = 6.34 ppm), demonstrating that the alkyl group and H8a are located in the same half-space. In addition, the C4 hydrogen (δ = 7.79 ppm) in **5***d* also showed a significant NOE (21%) on saturation of the *tert*-butyl singlet.

Summary

Intramolecular carbon–oxygen bond formation was achieved using 3-hydroxyindolines **2**, from which either products **3** or **5** can be obtained with total chemoselectivity in good to excellent yields by the proper choice of base and solvent. Formation of dihydro-2-amino-3-carbomethoxyfuroindoles **5** is also possible via ring transformation of tetrahydro-3-cyano-2-oxofuroindoles **3**. The success of these processes relies on the irreversibility of the 1,3-prototropic rearrangement of the intermediate γ-lactone imines **4**. The steric hindrance of the alkyl group on C3 has an important effect on the reaction times. These new transformations provide access to the dihydrofuro[2,3-*b*]indole ring system.

Experimental

Starting 3-alkyl-2-hydroxyindolines **2***a–c* and tetrahydro-3-cyano-2-oxofuro[2,3-*b*]indoles **3***b–d* were prepared from the corresponding 2-hydroxyindolenine **1** according to a previously published procedure (4). Melting points were determined on a Fisher–Johns apparatus and are uncorrected. UV spectra were obtained on a Perkin Elmer Lambda 12 spectrophotometer. IR spectra were obtained using a Perkin Elmer 727B spectrophotometer; only diagnostic peaks are reported. ^{1}H and ^{13}C NMR spectra were recorded on a Varian XL 300GS spectrometer working at 300 and 75.4 MHz, respectively, and chemical shifts are reported in ppm downfield from TMS. Multiplicities are indicated by one or more of the following: s (singlet), d (doublet), t (triplet), q (quartet), h (heptet), m (multiplet), br (broad); the list of coupling constants (*J*) corresponds to the order of the multiplicity assignment. NOE measurements were made with difference spectra (10). Analytical TLC was performed on silica gel 60 F_{254} coated aluminum sheets and visualized with UV light (254 nm). Electron impact mass spectra (EIMS) were recorded on a Hewlett Packard 5989A spectrometer. High-resolution (HR) and fast atom bombardment mass spectra (FABMS) were measured on a Jeol JMS-SX 102A spectrometer. Microanalytical determinations were performed by the MHW Laboratories, Phoenix, Ariz.

cis-(±)-Methyl 2,3,3a,8a-tetrahydro-3-cyano-3a-methyl-2-oxo-8*H*-furo[2,3-*b*]indole-8-carboxylate (3*a*)

To a solution of **2***a* (150 mg, 0.49 mol) in DMSO (1.5 mL) and H_2O (0.2 mL) was added NaCN (6 mg, 25 mol%). The resulting mixture was stirred at 100°C for 0.5 h and then concentrated in vacuo to a syrup. The residue was dissolved in EtOAc (40 mL), washed with brine, dried over anhydrous Na_2SO_4, and concentrated in vacuo. The crude product was purified by crystallization from EtOAc–*n*-hexane to afford **3***a* (94 mg, 70%) as white crystals: mp 211–212°C; IR (KBr) ν_{max}: 2253 (CN), 1794 (C=O γ- lactone), 1741 (C=O carbamate) cm^{-1}; **3***a anti* (from 4:1 *anti/syn* mixture) ^{1}H NMR (DMSO-d_6) δ: 7.75 (1H, br s, H7), 7.59 (1H, d, *J* = 7.4 Hz, H4), 7.43 (1H, td, *J* = 7.4, 1.0 Hz, H6), 7.23 (1H, td, *J* = 7.4, 1.0 Hz, H5), 6.44 (1H, s, H8a), 5.21 (1H, s, H3, D_2O exchangeable), 3.87 (3H, s, OCH_3), 1.57 (3H, s, CH_3);^{13}C NMR (DMSO-d_6) δ: 166.8 (s, CO), 152.0 (s, NCO), 139.2 (s, C7a), 130.3 (s, C3b), 130.1 (d, C6), 125.0 (d, C4), 124.1 (d, C5), 114.9 (d, C7), 114.0 (s, CN), 96.1 (d, C8a), 53.5 (q, OCH_3), 50.3 (s, C3a), 42.8 (d, C3), 23.1 (q, CH_3); **3***a syn* (from 4:1 *anti/syn* mixture) ^{1}H NMR (DMSO-d_6) δ: 7.75 (1H, br s, H7), 7.52 (1H, d, *J* = 7.4 Hz, H4), 7.37 (1H, td, *J* = 7.4, 1.0 Hz, H6), 7.17 (1H, td, *J* = 7.4, 1.0 Hz, H5), 6.54 (1H, s, H8a), 5.07 (1H, s, H3, D_2O exchangeable), 3.87 (3H, s, OCH_3), 1.63 (3H, s, CH_3); ^{13}C NMR (DMSO-d_6) δ: 166.8 (s, CO), 152.0 (s, NCO), 139.5 (s, C7a), 130.3 (s, C3b), 129.0 (d, C6), 125.0 (d, C4), 124.3 (d, C5), 115.5 (d, C7), 114.0 (s, CN), 96.8 (d, C8a), 53.4 (q, OCH_3), 49.3 (s, C3a), 42.3 (d, C3), 23.8 (q, CH_3); EIMS *m/z* (relative intensity): 272 (M^+, 68), 169 (100). HRMS (FAB) calcd. for $C_{14}H_{12}N_2O_4$ (M^+): 272.0797; found: 272.0807. Anal. calcd. for $C_{14}H_{12}N_2O_4$: C 61.76, H 4.44, N 10.29; found: C 61.55, H 4.23, N 10.24.

© 1997 NRC Canada

Can. J. Chem. Downloaded from www.nrcresearchpress.com by 88.146.161.215 on 09/08/12
For personal use only.

General procedure for the preparation of *cis*-(±)-dimethyl 3a,8a-dihydro-3a-alkyl-2-amino-8*H*-furo[2,3-*b*]indole-3,8-dicarboxylates (5*a–c*)

Method A

To a solution of 0.03 mmol of **2***a–c* in 3 mL of anhydrous methanol was added two drops of 0.5% sodium methoxide. The reaction mixture was refluxed until TLC analysis (4% EtOAc in CH_2Cl_2) showed complete loss of starting material (see Table 1 entries 4, 6, and 8). The solvent was evaporated in vacuo. The residue was dissolved in EtOAc (30 mL), washed with brine, dried over anhydrous Na_2SO_4, and concentrated in vacuo. The solid residue was purified by crystallization from $CHCl_3$–*n*-hexane to afford **5***a–c* in excellent yields.

Method B

To a solution of 0.35 mmol of **3***a–c* in 5 mL of anhydrous methanol was added two drops of 0.5% sodium methoxide. The reaction mixture was refluxed until TLC analysis (4% EtOAc in CH_2Cl_2) showed complete loss of starting material (see Table 2, entries 1–3). The solvent was evaporated in vacuo. After general work-up, the residue was purified by crystallization from $CHCl_3$–*n*-hexane to afford **5***a–c* in good yields.

cis-*(±)-Dimethyl 3a,8a-dihydro-2-amino-3a-methyl-8*H-*furo[2,3-*b*]indole-3,8-dicarboxylate (5*a*)*

Compound **5***a* was obtained as a white solid in 95% yield using method A and in 90% yield using method B; mp 202–203°C; R_f 0.30 (CH_2Cl_2/EtOAc 96:4); UV (MeOH) λ (log ε): 201 (4.52), 231 (4.12), 269 (4.02); IR ($CHCl_3$) ν_{max}: 3550 and 3358 (NH_2), 1720 (C=O carbamate), 1680 (C=O ester) cm^{-1}; ^1H NMR (DMSO-d_6) δ: 7.62 (1H, br s, H7), 7.52 (1H, d, J = 7.5 Hz, H4), 7.18 (1H, td, J = 7.5, 1.4 Hz, H6), 7.10 (2H, br s, NH_2, D_2O exchangeable), 7.00 (1H, td, J = 7.5, 1.0 Hz, H5), 6.22 (1H, s, H8a), 3.80 (3H, s, OCH_3 carbamate), 3.60 (3H, s, OCH_3 ester), 1.58 (3H, s, CH_3); ^{13}C NMR (DMSO-d_6) δ: 166.2, 152.9, 139.2, 138.0, 127.8, 124.1, 123.8, 114.2, 99.7, 79.5, 53.3, 53.0, 49.9, 24.2; EIMS *m/z* (relative intensity): 304 (M^+, 31), 255 (100); HRMS (FAB) calcd. for $C_{15}H_{16}N_2O_5$ (M^+): 304.1059; found: 304.1069. Anal. calcd. for $C_{15}H_{16}N_2O_5$: C 59.21, H 5.30, N 9.21; found: C 58.98, H 5.36, N 9.11.

cis-*(±)-Dimethyl 3a,8a-dihydro-2-amino-3a-ethyl-8*H-*furo[2,3-*b*]indole-3,8-dicarboxylate (5*b*)*

Compound **5***b* was obtained as a white solid in 93% yield using method A and in 90% yield using method B; mp 121–123°C; R_f 0.34 (CH_2Cl_2/EtOAc 96:4); UV (MeOH) λ (log ε): 200 (4.72), 234 (4.38), 270 (4.28); IR ($CHCl_3$) ν_{max}: 3500 and 3380 (NH_2), 1720 (C=O carbamate), 1680 (C=O ester) cm^{-1}; ^1H NMR (DMSO-d_6) δ: 7.65 (1H, br s, H7), 7.51 (1H, d, J = 7.4 Hz, H4), 7.20 (1H, t, J = 7.4 Hz, H6), 7.14 (2H, br s, NH_2, D_2O exchangeable), 7.01 (1H, t, J = 7.4 Hz, H5), 6.27 (1H, s, H8a), 3.82 (3H, s, OCH_3 carbamate), 3.61 (3H, s, OCH_3 ester), 2.13 and 1.87 (2H, ABX_3, 2m, CH_2), 0.71 (3H, ABX_3, t, CH_3); ^{13}C NMR (DMSO-d_6) δ: 166.5, 165.8, 152.5, 139.5, 136.9, 127.5, 123.9, 123.5, 113.9, 96.9, 76.9, 57.4, 53.0, 49.5, 27.8, 8.8; EIMS *m/z*: 318 (M^+, 35), 269 (100); HRMS (FAB) calcd. for $C_{16}H_{18}N_2O_5$ (M^+): 318.1216; found: 318.1231.

cis-*(±)-Dimethyl 3a,8a-dihydro-2-amino-3a-iso-propyl-8*H-*furo[2,3-*b*]indole-3,8-dicarboxylate (5*c*)*

Compound **5***c* was obtained as a white solid in 95% yield using both methods A and B; mp 95–97°C; R_f 0.34 (CH_2Cl_2/EtOAc 96:4); UV (MeOH) λ (log ε): 200 (4.66), 234 (4.29), 270 (4.19); IR ($CHCl_3$) ν_{max}: 3510 and 3380 (NH_2), 1730 (C=O carbamate), 1680 (C=O ester) cm^{-1}; ^1H NMR (DMSO-d_6) δ: 7.63 (1H, br s, H7), 7.51 (1H, d, J = 7.5 Hz, H4), 7.20 (1H, td, J = 7.5, 1.2 Hz, H6), 7.15 (2H, br s, NH_2, D_2O exchangeable), 7.01 (1H, td, J = 7.5, 0.9 Hz, H5), 6.27 (1H, s, H8a), 3.83 (3H, s, OCH_3 carbamate), 3.60 (3H, s, OCH_3 ester), 2.80 (1H, h, CH i-Pr), 0.91 and 0.50 (6H, 2d, J = 7.0 Hz, $2CH_3$ i-Pr); ^{13}C NMR (DMSO-d_6) δ: 166.2, 165.7, 152.4, 139.5, 136.7, 127.6, 123.6, 123.5, 113.8, 93.8, 77.4, 61.4, 53.1, 49.6, 30.1, 17.5, 16.4; EIMS *m/z* (relative intensity): 332 (M^+, 33), 283 (100); HRMS (FAB) calcd. for $C_{17}H_{20}N_2O_5$ (M^+): 332.1372; found: 332.1381. Anal. calcd. for $C_{17}H_{20}N_2O_5$: C 61.44, H 6.07, N 8.43; found: C 61.19, H 6.59, N 8.49.

***cis*-(±)-Dimethyl 3a,8a-dihydro-2-amino-3a-*tert*-butyl-8*H*-furo[2,3-*b*]indole-3,8-dicarboxylate (5*d*)**

To a solution of **3***d* (100 mg, 0.32 mmol) in 5 mL of anhydrous methanol was added two drops of 0.5% sodium methoxide in methanol. The reaction mixture was refluxed for 17 days and then concentrated in vacuo to a syrup. ^1H NMR analysis of the crude residue showed a 3:1 mixture of **3***d* and **5***d*. After general work-up, compounds **3***d* and **5***d* were separated on a silica gel column, 230–400 mesh, eluted with ether/*n*-hexane 3:2 to give 72 mg (71%) of unreacted **3***d* and 28 mg (25%) of **5***d* as a white solid; mp 194–196°C; R_f 0.42 (CH_2Cl_2/EtOAc 96:4); UV (MeOH) λ (log ε): 202 (4.74), 238 (4.42), 270 (4.28); IR ($CHCl_3$) ν_{max}: 3510 and 3380 (NH_2), 1730 (C=O carbamate), 1680 (C=O ester) cm^{-1}; ^1H NMR (DMSO-d_6) δ: 7.77 (1H, d, J = 7.7 Hz, H4), 7.67 (1H, br d, J = 7.7 Hz, H7), 7.23 (2H, br s, NH_2, D_2O exchangeable), 7.20 (1H, td, J = 7.7, 1.2 Hz, H6), 7.00 (1H, td, J = 7.7, 1.1 Hz, H5), 6.27 (1H, s, H8a), 3.83 (3H, s, OCH_3 carbamate), 3.55 (3H, s, OCH_3 ester), 0.96 (9H, s, $3CH_3$ *t*-Bu); ^{13}C NMR (DMSO-d_6) δ: 167.4, 166.1, 152.4, 140.2, 133.6, 127.4, 126.9, 122.6, 113.8, 96.1, 77.2, 63.9, 53.2, 49.4, 36.8, 26.4; EIMS *m/z* (relative intensity): 346 (M^+, 22), 273 (100); HRMS (FAB) calcd. for $C_{18}H_{22}N_2O_5$ (M^+): 346.1529; found: 346.1544. Anal. calcd. for $C_{18}H_{22}N_2O_5$: C 62.42, H 6.40, N 8.09; found: C 62.31, H 6.27, N 8.23.

Acknowledgments

This work was supported in part by CONACYT México. We thank I.Q. Luis Velasco Ibarra (Instituto de Química, UNAM) for recording the HRMS.

References

1. F.C. Schaefer and G.A. Peters. J. Org. Chem. **26**, 412 (1961).
2. (*a*) A.S. Alvarez-Insúa, M. Lora-Tamayo, and J.L. Soto. J. Heterocycl. Chem. **7**, 1305 (1970); (*b*) M.C. Chacón, M.C. Pardo, J.L. Soto, A. Lorente, and L. Fuentes. J. Heterocycl. Chem. **19**, 421 (1982); (*c*) A. Lorente, J.L. Alvarez-Barbas, J.L. Soto, P. Gómez-Sal, and A. Manzanero. Heterocycles, **43**, 33 (1996).
3. (*a*) H. Wamhoff and F. Korte. Synthesis, 151 (1972); (*b*) H. Wamhoff. Adv. Heterocycl. Chem. **38**, 300 (1985); (*c*) W.D.

© 1997 NRC Canada

Lubell, M. Kitamura, and R. Noyori. Tetrahedron: Asymmetry, **2**, 543 (1991); (*d*) C. Cimarelli, G. Palmieri, and G. Bartoli. Tetrahedron: Asymmetry, **5**, 1455 (1994).

4. (*a*) M.S. Morales-Ríos, C. García-Martínez, M.A. Bucio, and P. Joseph-Nathan. Monatsh. Chem. **127**, 691 (1996); (*b*) M.S. Morales-Ríos, M.A. Bucio, and P. Joseph-Nathan. Tetrahedron, **52**, 5339 (1996).
5. (*a*) B. Robinson. *In* The alkaloids. Vol. X. *Edited by* R.H.F. Manske. Academic Press, New York. 1968. Chap. 5; (*b*) *In* The alkaloids. Vol. XIII. *Edited by* R.H.F. Manske. Academic Press, New York. 1971. Chap. 4; (*c*) A.H. Salway. J. Chem Soc. **99**, 2148 (1911); (*d*) Q.-S. Yu, C. Liu, M. Brzostowska, L. Chrisey, A. Brossi, N.H. Greig, J.R. Atack, T.T. Soncrant, S.I. Rapoport, and H.-E. Radunz. Helv. Chim. Acta, **74**, 761 (1991); (*e*) M. Brzostowska, X. He, N.H. Greig, S.I. Stanley, and A. Brossi. Med. Chem. Res. **2**, 238 (1992); (*f*) A. Kawashima, H. Seto, M. Kato, A. Yasuda, K. Uchida, and N. Otake. J. Antibiot. **39**, 1495 (1986).
6. (*a*) C.W. Rees and C.R. Sabet. J. Chem. Soc. 870 (1965); (*b*) O. Buchardt, P.L. Kumler, and C. Lohse. Acta Chem. Scand. **23**, 1155 (1969); (*c*) D.M. Harrison. Tetrahedron Lett. **25**, 6063 (1984).
7. (*a*) A.P. Krapcho. Synthesis, 805 (1982); 893 (1982); (*b*) F. Hibbert and D.P.N. Satchell. J. Chem. Soc. (B), 565 (1968).
8. (*a*) G. Westöö. Acta Chem. Scand. **13**, 692 (1959); (*b*) S.A. Glickman and A.C. Cope. J. Am. Chem. Soc. **67**, 1012 (1945).
9. P.L. Pacini and R.G. Ghirardelli. J. Org. Chem. **31**, 4133 (1966).
10. J.K.M. Sanders and J.D. Mersh. Prog. Nucl. Magn. Reson. Spectrosc. **15**, 353 (1982).

Can. J. Chem. Downloaded from www.nrcresearchpress.com by 88.146.161.215 on 09/08/12
For personal use only.

© 1997 NRC Canada

Formation of quaternary centres via iron allyl cations. Rapid entry into spirocyclic ring systems

M. Anne Charlton and James R. Green

Abstract: Ester-substituted allyltetracarbonyliron cations react with cycloalkylidene-type silyl enol ethers, silyl ketene acetals, and β-keto-esters to give 1,6-dicarbonyl compounds containing a newly formed quaternary centre. Selected condensation products are converted by enolate chemistry into spirocyclic [4.4], [4.5], and [4.6] systems. Acyloin and other reductive cyclization reactions are employed to convert the condensation products into spirocyclic [4.5], [5.5], and [5.6] systems.

Key words: allyliron complexes, umpolung synthesis, 1,6-dicarbonyls, spirocycle synthesis.

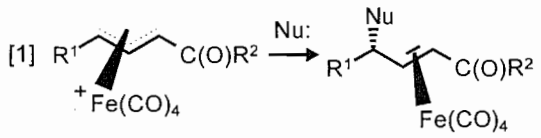
Résumé : Les cations allyltétracarbonylfer substitués par des fonctions esters réagissent avec des éthers énoliques silylés, des acétals de silylcétènes et des β-céto-esters de type cycloalkylidène; ils conduisent à des composés 1,6-dicarbonylés contenant un centre quaternaire nouvellement formé. Des produits de condensation choisis peuvent être transformés, par le biais de la chimie des énolates, en systèmes spirocycliques [4.4], [4.5] et [4.6]. On a fait appel à des réactions aux acyloïnes et à d'autres types de réactions de cyclisation réductrice pour transformer les produits de condensation en systèmes spirocycliques [4.5], [5.5] et [5.6].

Mots clés : complexes d'allylfer, réactions par inversion de polarité, 1,6-dicarbonyles, synthèse de spirocycles.

[Traduit par la rédaction].

Introduction

Homologous (1,5)-Michael reactions, or γ-carbonyl cation equivalents, are forms of umpolung synthesis that have received increased recent attention (1–6). We are actively engaged in the development of transition metal mediated versions of these homologous (1,5)-Michael reactions (2). In particular, we (3) and others (4) have found that ester- and ketone-substituted tetracarbonyliron allyl cations are effective as these umpolung synthons, as their electrophilic reactions occur exclusively at the allyl terminus remote from the carbonyl function (eq. [1]). Iron allyl cations substituted by phenyl sulphones (4) and lactams (5) behave in a closely analogous fashion. In addition, a reliable retention of configuration has been demonstrated for the formation and attack of these cations in enantiomerically enriched acyclic substrates (4). For cyclic substrates, electrophilic attack occurs on the face opposite the iron tetracarbonyl unit (5), regardless of the relative orientation of the leaving group. A wide variety of nucleophilic species react successfully with these cations, including silyl enol ethers, silyl ketene acetals, *N*-stannyl enamines, allylsilanes and stannanes, electron-rich arenes, amines, β-dicarbonyl compounds, and zinc cyanocuprates. γ-Carbonyl-*N*-acyliminium cation complexes have been shown to react with an even wider range of nucleophiles (6).



We are interested in applying these carbonyl-substituted iron allyl cations to the synthesis of spirocyclic compounds (7).[2] This requires the reaction of the γ-carbonyl cation complexes with nucleophiles of type **1**; few examples of the formation of quaternary carbon centres (and none for cycloalkylidene-type nucleophiles) have been demonstrated with iron allyl cations (4). If these nucleophiles can be readily introduced, then the condensation products (**2**) would be well set up for a general synthesis of spirocyclic [4.*n*] or [5.*n*] systems. As the centre α to the carbonyl of the original nucleophile is tetrasubstituted, enolization at that site is not possible, so that enolate chemistry of the 1,6-dicarbonyls is expected to give [4.*n*] systems in a predictable fashion by Dieckmann or aldol reactions. Alternatively, the disposition of ester functions suggests that acyloin or other reductive coupling reactions will give access to [5.*n*] spirocycles. This report describes our efforts to this end.

Received November 13, 1996.

M.A. Charlton and J.R. Green.[1] Department of Chemistry and Biochemistry, University of Windsor, Windsor, ON N9B 3P4, Canada.

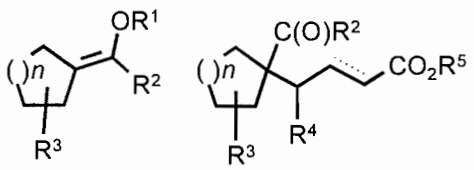
[1] Author to whom correspondence may be addressed. Telephone: (519) 253-4232, ext. 3545. Fax: (519) 973-7098. E-mail: jgreen@uwindsor.ca

[2] Among the other available γ-carbonyl cation equivalents reported, an alkoxycarbonylcyclopropylphosphonium salt has been shown to react with cyclic β-ketoaldehydes to give [4.*n*] spirocylic alkenoates (7).

© 1997 NRC Canada

Can. J. Chem. Downloaded from www.nrcresearchpress.com by 88.146.161.215 on 09/08/12
For personal use only.

Can. J. Chem. Downloaded from www.nrcresearchpress.com by 88.146.161.215 on 09/08/12
For personal use only.



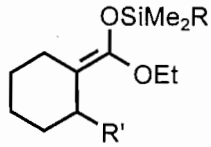
1 2

Results and discussion

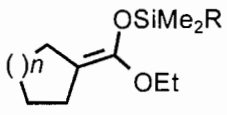
Formation of quaternary centres

Nucleophiles (**3–9**), containing five-, six-, and seven-membered cycloalkylidene groups, were chosen for reaction with the iron allyl cations, based on ready availability of the precursor carbonyl compounds. Silyl ketene acetals were prepared by standard deprotonation of the appropriate ester with lithium diisopropyl amide (LDA) and subsequent silylation with *tert*-butyldimethylsilyl chloride (TBDMSCl) (**3–6**) (8) or Me_3SiCl (**4a**, **6a**). Silyl ketene acetal **6** was more hydrolytically unstable than **3–5**, as the crude reaction products revealed a significant amount of ester stemming from hydrolysis of **6** during work-up. As a consequence, **6** was used in this impure form. β-Keto-ester **8** was expected to have a sufficient concentration of enol in solution such that activation as a silyl enol ether would be unnecessary (3). Finally, the trimethylsilyl enol ethers were prepared from the corresponding ketone or aldehyde either by Me_3SiI generated in the presence of Et_3N (**7**) (9) or by straightforward deprotonation (LDA) and silylation (**9**).

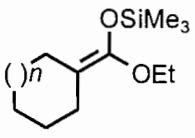
The γ-acetoxy enoates chosen as precursors to the iron allyl complexes in the condensation reactions were **10** (10) and **11**. These substrates readily form η^2-complexes **12** and **13** by stirring with $Fe_2(CO)_9$ in Et_2O. Subsequent ionization of the acetoxy function with Lewis acids, most successfully BF_3-etherate, is known to give solutions containing tetracarbonyliron allyl cations **14** and **15** (2). The cations were generated in the presence of nucleophiles **3–9**, and the CH_2Cl_2 solutions gradually warmed from −78°C to room temperature. The final isolated products (**16–26**) were obtained by treating the crude reaction product mixtures with Me_3NO, in order to liberate the alkenoate product from the $Fe(CO)_4$ unit.

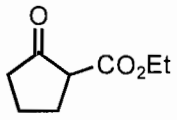


3,R' = H, R = Bu-*t*
4,R' = Me, R = Bu-*t*
4a, R = R' = Me



5, *n* = 1, R = Bu-*t*
6, *n* = 3, R = Bu-*t*
6a, *n* = 2, R = Me





7, *n* = 1, R = H
9, *n* = 0, R = Ph

8

Analysis of the product mixtures demonstrated that **3–8** and **14** and **15** did undergo addition reactions (Table 1). In all cases, the sole product of reaction was that of condensation of **14** or **15** at the position γ with respect to the ester function, to give 1,6-dicarbonyl compounds **16–26**. The regiochemistry of attack was clear from the spectroscopic characteristics of the addition products. Compound **16**, for example, gave an ^1H NMR spectrum displaying resonances for the vinyl hydrogens at δ 5.76 (d, J = 15.5 Hz) and δ 6.84 (dt), and a ^{13}C NMR spectrum containing vinyl carbon resonances at δ 124.0 and δ 144.1. These are indicative of an (*E*)-α,β-unsaturated ester with substitution at the γ-position. Recovered γ-acetoxyenoate was also observed in several of the cases, at the expense of condensation product. This stems from BF_3 induced decomplexation of η^2-complexes **12** and **13** and (or) desilyation of the silyl enol ether or silyl ketene acetal occurring at a rate competitive with the condensation.

Table 1. Nucleophilic attack on iron allyl cations.

Substrate	Nucleophile	Product	Yield[a]
10	**3**	**16**	72
11	**3**	**17**	66
10	**5**	**18**	66
11	**5**	**19**	62
10	**4**	**20**	46[b] (39)
10	**4a**	**20**	52[c] (23)
10	**6**	**21**	37 (44)
10	**6a**	**21**	42 (40)
10	**7**	**22**	74
11	**7**	**23**	68
10	**8**	**24**	43 (41)
11	**8**	**25**	41[d] (35)
10	**9**	**26**	59 (35)

[a]Numbers in parenthese refer to yield of recovered starting **10** or **11** based on integration of the ^1H NMR spectra of the crude reaction products.
[b]Diastereomer ratio, 80:20.
[c]Diastereomer ratio, 70:30.
[d]Diastereomer ratio, 67:33.

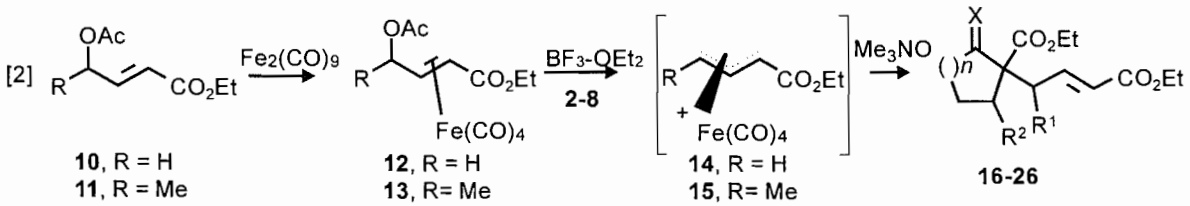
Products **20** and **25** were isolated as diastereomeric mixtures of products. Whereas there was very modest selectivity in the formation of **25** (67:33), compound **20** was obtained as a 80:20 mixture of diastereomers. The major diastereomer was assigned as (*R*,R**)-**20** (*syn*-**20**), the product resulting from attack on the face of **3** opposite the methyl group. The assignment was based on the precedented alkylation of the enolate of methyl 2-methylcyclohexanecarboxylate (11), and the reported attack of an allyliron cation on a C-6 silylated cyclohexanone enolate (4), both of which occur on the enolate face opposite to the additional substituent.

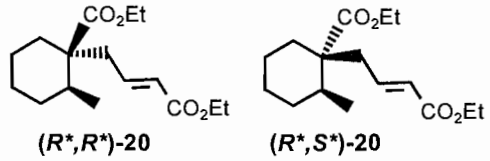
Yields were in general fair to good for the silyl ketene acetals, with the unactivated β-keto-esters giving condensation products in more modest yields. The yields of products **20** (46%) and **21** (37%) were anomalously low, and the corresponding reactions using trimethysilyl ketene acetals **4a** and **6a**, respectively, were investigated. In the event, silyl ketene acetal **4a** reacted with **12** to give **21** in slightly improved yields, at the expense of diastereoselection (52%, 70:30 *R*,R**:*R*,S**). The use of **6a** with **12** similarly gave a slight improvement in the yield of **21** (42%).

Spirocycle formation

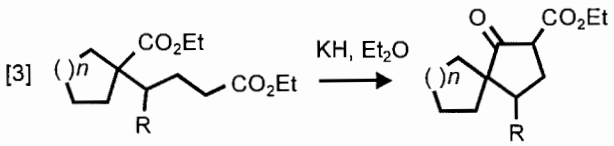
With the creation of the quaternary centres accomplished,

© 1997 NRC Canada





attention was turned to the manipulation of the 1,6-dicarbonyls into spirocyclic compounds. Dieckmann reactions were initially attempted on the condensation products (**16–26**) themselves. As the deprotonation of (*E*)-alkenoates and alkenamides has been shown to give (*Z*)-dienolate intermediates (12), it was expected that the dienolates derived from **16–26** would have a geometry suitable for cyclization. This proved not to be the case, as all attempts at Dieckmann cyclizations on **16** under a variety of conditions led only to complex mixtures of products. To circumvent this problem, the alkene functions of **16–18** and **21** were reduced by catalytic hydrogenation to give dicarbonyl compounds **16a–18a** and **21a**. Under such conditions, the ketone function of keto-ester **26** was reduced competitively with the alkene unit to give alcohol **26b**; this was simply reoxidized to keto-ester **26a** with PDC. Treatment of these dicarbonyl compounds with KH in Et_2O induced ready cyclization, to give [4.*n*] spirocycles **27–30** in fair to good yields (eq. [3], Table 2) (13).[3] Since **16a–18a** and **21a** contain five-, six-, and seven-membered ring systems, spirocyclic [4.4], [4.5], and [4.6] ring systems could be obtained in this manner. Under identical conditions, keto-ester **25a** underwent both intramolecular aldol condensation chemistry and saponification to give predominantly the acid **31**; higher yields on **31** were realized when the crude reaction product was subjected to complete saponification.



n	R	
2	H	**27**
2	Me	**28**
1	Me	**29**
3	H	**30**

The acyloin condensation chemistry of selected 1,6-dicarbonyl compounds was also explored. Like the Dieckmann cyclizations, reduction of the alkene unit of **16** (to **16a**) was necessary before tractable product mixtures were obtained. After experimentation with a variety of conditions, success was achieved on **16a** using a sodium–potassium alloy in conjunction with Me_3SiCl (13), giving bis(trimethylsilylated) enediol **32** in good yield. The analogous condensations on **18a**, **20a**, and **21a** similarly gave **33–35**, containing spirocyclic [4.5], [5.5], and [5.6] ring systems (eq. [4], Table 3). As desilylation of **32** gave regiochemical mixtures of α-hydroxyketones (15), characterization was performed on the silylated enediols themselves. These silylated enediols possessed moderate stability on silica gel, and significant material losses occurred if they were subjected to repeated chromatography. In the cyclization of **20a** to give **34**, the 70:30 ratio of diastereomers was preserved; this, in conjunction with the expected behaviour of the quaternary centre, leads us to assign (*R**,*R**)-**34** (*anti*-**34**) as the major diastereomer.

Due to an interest in the application of this methodology to synthesis of sesquiterpenes such as acorenone, we wished to investigate an alternative reductive coupling reaction that would afford a spirobicyclic-2-alkanone, and consequently we explored the feasibility of the preparation of **36** from aldehyde ester **22**. Although the coupling of aldehydes and esters by a variant of the McMurry reaction has been reported (16), we were unable to effect such a coupling on **22a**. As an alternative route, the aldehyde **22** was reduced to ester-alcohol **22b**, and subsequently converted to neopentyl iodide **37** (17). Treatment of this iodide with *t*-BuLi (18) afforded bicyclic ketone **36**, albeit in low yield (20%). Better results were obtained by using sodium metal in the presence of Me_3SiCl (19); this procedure gave **36** in 45% yield.

In summary, it has been demonstrated that the iron allyl cations derived from γ-acetoxyalkenonates react with

Table 2. Enolate-mediated cyclizations.

Substrate	Product	Yield (dr)
16a	**27**	84
18a	**29**	69
19a	**28**	53 (57:43)
21a	**30**	67
26a	**31**	75

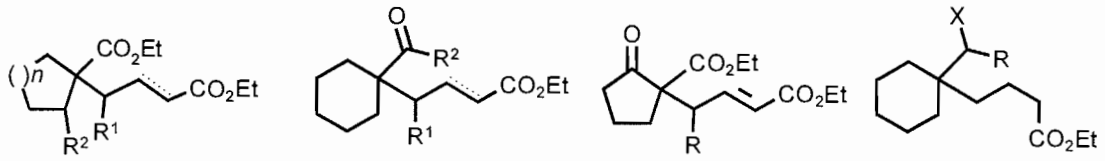
Table 3. Acyloin-type cyclizations.

Substrate	Product	Yield (dr)
16a	**32**	85
18a	**33**	67
20a	**34**	60 (70:30)
21a	**35**	70
37	**36**	45

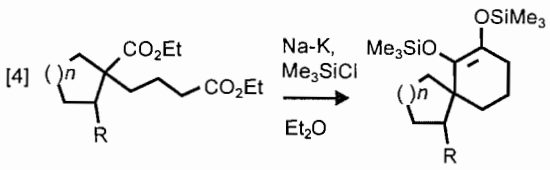
[3] The Dieckmann reaction of **16a** to give **27** with NaH was reported previously (13).

Can. J. Chem. Downloaded from www.nrcresearchpress.com by 88.146.161.215 on 09/08/12
For personal use only.

© 1997 NRC Canada

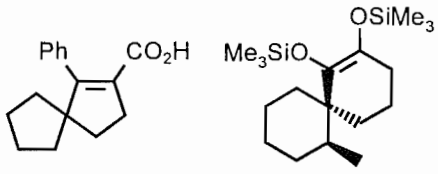


n	R^1	R^2	alkene	alkane	R^1	R^2	alkene	alkane	R		X	R	
2	H	H	**16**	**16a**	H	H	**22**	**22a**	H	**24**	OH	H	**22b**
2	Me	H	**17**		Me	H	**23**	**23a**	Me	**25**	OH	Ph	**26b**
2	H	Me	**20**	**20a**	H	Ph	**26**	**26a**			I	H	**37**
1	H	H	**18**	**18a**									
1	Me	H	**19**	**19a**									
3	H	H	**21**	**21a**									

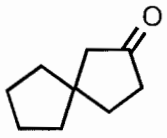


16a, 18a, 20a, 21a

n	R	
2	H	**32**
1	H	**33**
2	Me	**34**
3	H	**35**



31 **(R*,R*)-34**



36

cycloalkylidene-type silyl ketene acetal, silyl enol ethers, and β-keto-ester enols to form 1,6-dicarbonyl compounds containing quaternary centres in fair to good yields. The condensation products may be manipulated rapidly to give a variety of [4.*n*] and [5.*n*] spirocyclic ring systems (*n* = 4,5,6). The application of this methodology to synthesis will be reported in due course.

Experimental section

General data

Melting points are uncorrected. Boiling points refer to bulb-to-bulb distillation. ^{1}H NMR and ^{13}C NMR spectra were recorded in $CDCl_3$ at 300 and 75 MHz, respectively; coupling constants (*J*) are expressed in hertz (Hz). High-resolution mass spectra were recorded at the Department of Chemistry and Biochemistry Mass Spectrometry Facility, University of Windsor. Elemental analyses were performed by M-H-W Laboratories, Phoenix, Ariz.

BuLi was obtained from Aldrich Chemical Co., Ltd. The titre was determined using 2,5-dimethoxybenzyl alcohol as standard (20). Tetrahydrofuran (THF) was distilled from sodium benzophenone ketyl immediately prior to use. Dichloromethane was distilled from CaH_2 immediately prior to use. Column chromatography on silica gel (Merck, 0.04–0.063 mm) was performed according to the protocol of Still et al. (21).

General procedure for the preparation of silyl ketene acetals

*1-(*tert*-Butyldimethylsiloxy)-1-ethoxymethylenecyclohexane (3)*

To diisopropylamine (2.95 mL, 21.0 mmol) was added dry THF (15 mL) and the mixture was cooled to −78°C in a Dry Ice – acetone bath. *n*-BuLi (11 mL, 1.91 M, 21.0 mmol) was added and the mixture was allowed to stir for 5 min. The cooling bath was removed and the mixture was allowed to stir for an additional 5 min. The reaction was again immersed in a Dry Ice – acetone bath and ethyl cyclohexanecarboxylate (2.967 g, 19.0 mmol) was added. The mixture was allowed to warm to 0°C at which time HMPA (1.5 mL) was added and the mixture was allowed to stir for 15 min. A solution of *tert*-butyldimethylsilyl chloride (TBDMSCl, 3.165 g, 21.0 mmol) in THF (10 mL) was added and the mixture was allowed to warm to room temperature, at which time it was quenched with cold water and subjected to a conventional work-up to afford the crude product. The product was purified by bulb-to-bulb distillation to yield **3** (4.217 g, 84%): bp 80°C (0.50 Torr; 1 Torr = 133.3 Pa); IR (neat, KBr): 2929, 2856, 1697 cm^{-1}; ^{1}H NMR δ: 3.74 (q, 2H, *J* = 7.1), 2.10–1.65 (m, 10H), 1.19 (t, 3H, *J* = 7.1), 0.92 (s, 9H), 0.11 (s, 6H); ^{13}C NMR δ: 146.2, 100.6, 65.2, 27.8, 27.3, 27.2, 27.1, 26.9, 25.8, 18.2, 14.8, −4.6; MS *m/e*: 270 (M^+); HRMS calcd. for $C_{15}H_{30}O_2Si$ *m/e* (M^+): 270.2015; found: 270.2018.

*(*tert*-Butyldimethylsiloxy)ethoxymethylenecyclopentane (5)*

Subjecting ethyl cyclopentanecarboxylate (2.953 g, 23.1 mmol) to the general procedure, followed by bulb-to-bulb dis-

Can. J. Chem. Downloaded from www.nrcresearchpress.com by 88.146.161.215 on 09/08/12
For personal use only.

© 1997 NRC Canada

Can. J. Chem. Downloaded from www.nrcresearchpress.com by 88.146.161.215 on 09/08/12
For personal use only.

tillation, produced **5** (2.063 g, 79%): bp 95°C (3.0 Torr); IR (neat, KBr): 2955, 2859, 1711 cm^{-1}; ^1H NMR δ: 3.78 (q, 2H, J = 7.1), 1.21 (t, 3H, J = 7.1) 2.18–1.54 (m, 8H), 0.92 (s, 9H), 0.12 (s, 6H); ^{13}C NMR δ: 146.3, 102.3, 64.5, 28.4, 27.8, 27.1, 26.9, 25.7, 18.0, 15.1, −4.5; MS *m/e*: 256 (M^+); HRMS calcd. for $C_{14}H_{28}O_2Si$ *m/e* (M^+): 256.1859; found: 256.1864.

*2-Methyl-1-[(trimethylsiloxy)ethoxymethylene]cyclohexane (**4a**)*

To a −78°C solution of LDA (3.0 mmol) in THF (10 mL) was added a solution of ethyl 2-methylcyclohexane-1-carboxylate (0.4620 g, 2.71 mmol) in THF (5 mL). After stirring at −78°C for 1 h, Me_3SiCl (0.5 mL) was added, and the solution was allowed to warm to room temperature. The volatiles were removed under reduced pressure, and the resulting residue was distilled under reduced pressure to afford **3a** (0.5972 g, approx. 85%) which contained a small amount (approx. 6%) of the starting ester; bp 55–57°C (0.30 Torr); IR (neat, KBr): 2961, 2925, 2851, 1688 cm^{-1}; ^1H NMR δ: 3.70–3.85 (m, 2H), 2.74 (m, 1H), 2.40 (m, 1H), 1.85 (m, 1H), 1.72 (m, 1H), 1.35–1.60 (m, 5H), 1.21 (t, 3H, J = 7.1), 1.03 (d, 3H, J = 7.2), 0.21 (s, 9H); peaks from the minor isomer could be observed at 1.25 (t, 3H, J = 7.1), 1.05 (d, 3H, J = 7.1), 0.20 (s, 9H); ^{13}C NMR δ: 145.4, 104.1, 64.8, 33.0, 28.5, 28.2, 27.9, 22.7, 22.3, 21.0, 17.9, 14.7, 0.0; peaks from the minor isomer could be observed at 103.9, 64.2, 33.2, 28.3, 27.5, 22.7, 20.9, −0.1.

*1-(Trimethylsiloxy)ethoxymethylenecycloheptane (**6a**)*

To a −78°C solution of LDA (3.0 mmol) in THF (7 mL) was added a solution of ethyl 2-methylcyclohexane-1-carboxylate (0.2684 g, 1.58 mmol) in THF (3 mL). After stirring at −78°C for 1 h, Me_3SiCl (0.5 mL) was added, and the solution was allowed to warm to room temperature. The volatiles were removed under reduced pressure, and the resulting residue was distilled under reduced pressure to afford **6a** (0.3451 g, approx. 86%), which contained a small amount (ca. 5%) of the starting ester: bp 65–66°C (0.48 Torr); IR (neat, KBr): 2923, 2852, 1684 cm^{-1}; ^1H NMR δ: 3.77 (q, 2H, J = 7.1), 2.20 (m, 2H), 2.14 (m, 2H) 1.40–1.65 (m, 6H), 1.23 (t, 3H, J = 7.1), 0.22 (s, 9H); ^{13}C NMR δ: 148.1, 101.6, 64.5, 29.9, 29.7, 29.2, 28.9, 28.7, 28.0, 14.9, 0.1.

*(Trimethylsiloxy)methylenecyclohexane (**7**)*

Cyclohexanecarboxaldehyde (0.660 g, 6.00 mmol) and triethylamine (0.84 mL, 6.0 mmol) were added to a three-neck flask equipped with a reflux condenser and a pressure-equalizing addition funnel. Me_3SiCl (0.76 mL, 6.0 mmol) was added dropwise and, after completion, the reaction was heated to 35°C and allowed to stir for 10 min. NaI (0.90 g, 6.0 mmol) in CH_3CN (25 mL) was added through the addition funnel. The reaction was then heated to 70°C for 2 h and poured into cold water. A conventional work-up was performed, followed by bulb-to-bulb distillation to afford **7** (0.651 g, 60%), bp 39–41°C (0.4 Torr); IR (neat, KBr): 2957, 2926, 2853, 1679 cm^{-1}; ^1H NMR δ: 5.97 (s, 1H), 2.17 (m, 2H), 1.94 (m, 2H), 1.40–1.60 (m, 6H), 0.17 (s, 9H); ^{13}C NMR δ: 130.1, 122.5, 30.6, 28.4, 27.0, 25.3, −0.5; MS *m/e*: 184 (M^+); HRMS calcd. for $C_{10}H_{20}OSi$ *m/e* (M^+): 184.1283; found: 184.1287.

*Phenyl(trimethylsiloxy)methylenecyclopentane (**9**)*

To a −78°C solution of LDA (22.3 mmol) in THF (20 mL) was added cyclopentyl phenyl ketone (3.42 mL, 20.3 mmol). The solution was stirred for 1 h, and Me_3SiCl (2.83 mL, 22.3 mmol) was added. The cooling bath was removed and the solution was allowed to warm to room temperature. The reaction mixture was poured into ice-cold water. A conventional work-up gave a residue that was distilled under reduced pressure to afford **9** (4.633 g, 93%) as a colourless oil: bp 92–94°C (0.80 Torr); IR (KBr): 3057, 3026, 2956, 2869, 1682 cm^{-1}; ^1H NMR δ: 7.42 (m, 2H), 7.15–7.35 (m, 3H), 2.42 (m, 4H), 1.67 (m, 4H), 0.06 (s, 9H); ^{13}C NMR δ: 140.8, 139.5, 127.7, 127.6, 126.7, 125.9, 31.1, 30.3, 27.6, 25.8, 0.6; MS *m/e*: 246 (M^+); HRMS calcd. for $C_{15}H_{22}OSi$ *m/e* (M^+): 246.1440; found: 246.1433.

*Ethyl (*E*)-4-acetoxy-2-pentenoate (**11**)*

Ethyl (*E*)-4-hydroxy-pentenoate (22) (3.62 g, 25.2 mmol) and acetic anhydride (15 mL) were mixed in a two-neck flask and cooled in ice. Pyridine (2 mL) was added and the resultant mixture was allowed to stir overnight. A conventional work-up was performed and the crude product was purified by bulb-to-bulb distillation to yield ethyl (*E*)-4-acetoxy-2-pentenoate (3.20 g, 68%): bp 100°C (1.0 Torr); IR (neat, KBr): 1740, 1725, 1662 cm^{-1}; ^1H NMR δ: 6.84 (dd, 1H, J = 15.6, 5.0), 5.93 (d, 1H, J = 15.6), 5.46 (m, 1H), 4.18 (q, 2H, J = 7.1), 2.06 (s, 3H), 1.34 (d, 3H, J = 6.7), 1.27 (t, 3H, J = 7.1); ^{13}C NMR δ: 169.7, 165.8, 146.0, 120.8, 68.6, 60.3, 20.8, 19.4, 14.0; MS *m/e*: 127 ($M^+ - CH_3C(O)O$); HRMS calcd. for $C_9H_{14}O_4$ *m/e* ($M^+ - C_2H_3O_2$): 127.0754; found: 127.0759.

General procedure for the iron allyl cation addition reaction

*Ethyl (*E*)-4-(1-ethoxycarbonylcyclohexyl)-2-butenoate (**16**)*

A mixture of $Fe_2(CO)_9$ (1.94 g, 5.34 mmol) and ethyl 4-acetoxy-2-butenoate (**10**) (0.657 g, 3.82 mmol) in dry Et_2O (20 mL) was stirred under a CO atmosphere at room temperature for 5 h. The reaction product was then filtered through Celite® and concentrated under reduced pressure to yield a dark brown oil. The oil was redissolved in dry CH_2Cl_2 (20 mL) and the mixture was cooled to −78°C. Compound **3** (1.140 g, 4.20 mmol) was added, followed by BF_3-Et_2O (0.52 mL, 4.2 mmol). The reaction mixture was stirred for 12 h during which time it was allowed to warm to room temperature. The mixture was opened to the air and $NaHCO_3$ (10 drops) was added, followed by $Me_3NO{\cdot}2H_2O$ and acetone (20 mL). After stirring for 8 h, 3 M HCl was added and a conventional work-up was performed. The crude product was subjected to bulb-to-bulb distillation followed by flash chromatography (10:1 petroleum ether:Et_2O) to yield **16** (0.730 g, 72% yield): bp 93°C (0.70 Torr); IR (neat, KBr): 1723, 1657 cm^{-1}; ^1H NMR δ: 6.84 (dt, 1H, J = 15.5, 7.8), 5.76 (d, 1H, J = 15.5), 4.17 (q, 2H, J = 7.0), 4.14 (q, 2H, J = 7.0), 2.34 (d, 2H, J = 7.8), 2.06–1.52 (m, 10H), 1.27 (t, 3H, J = 7.0), 1.25 (t, 3H, J = 7.0); ^{13}C NMR δ: 175.6, 166.1, 144.0, 123.9, 60.3, 60.2, 47.0, 42.4, 33.8, 25.6, 22.9, 14.2; MS *m/e*: 268 (M^+); HRMS calcd. for $C_{15}H_{24}O_4$ *m/e* (M^+): 268.1675; found: 268.1663.

*Ethyl (*E*)-4-(1-ethoxycarbonylcyclohexyl)-4-methyl-2-butenoate (**17**)*

Ethyl 4-acetoxy-2-pentenoate (**11**) (0.511 g, 2.74 mmol) was subjected to the general procedure. The crude product was

© 1997 NRC Canada

Can. J. Chem. Downloaded from www.nrcresearchpress.com by 88.146.161.215 on 09/08/12
For personal use only.

subjected to bulb-to-bulb distillation, followed by flash chromatography (10:1 petroleum ether:Et_2O), to yield **17** (0.508 g, 66%): bp 88°C (0.60 Torr); IR (neat, KBr): 1721, 1652 cm^{-1}; ^1H NMR δ: 6.87 (dd, 1H, J = 15.6, 8.2), 5.76 (d, 1H, J = 15.6), 4.17 (q, 2H, J = 7.1), 4.15 (m, 2H), 2.38 (m, 1H), 2.08 (m, 2H), 1.45–1.70 (m, 3H), 1.27 (t, 3H, J = 7.1), 1.26 (t, 3H, J = 7.1), 1.00–1.40 (m, 5H), 0.98 (d, 3H, J = 8.2); ^{13}C NMR δ: 175.0, 166.5, 150.2, 122.0, 60.3, 50.3, 45.4, 32.6, 31.2, 25.8, 23.6, 23.4, 14.8, 14.4; MS *m/e*: 282 (M^+); HRMS calcd. for $C_{16}H_{26}O_4$ *m/e* (M^+): 282.1831; found: 282.1827.

Ethyl (E)*-4-(1-ethoxycarbonylcyclopentyl)-2-butenoate* (***18***)
Ethyl-4-acetoxy-2-butenoate (**10**) (0.653 g, 3.79 mmol) was subjected to the general procedure, using **5** (1.070 g, 4.172 mmol) in place of **3**. Bulb-to-bulb distillation of the crude reaction product, followed by flash chromatography (10:1, petroleum ether:Et_2O), provided **18** (0.632 g, 66%) as a colourless liquid: bp 90°C (0.35 Torr); IR (neat, KBr): 1723, 1651 cm^{-1}; ^1H NMR δ: 6.78 (dt, 1H, J = 7.7, J = 15.5), 5.75 (d, 1H, J = 15.5), 4.13 (q, 2H, J = 7.1), 4.08 (q, 2H, J = 7.1), 2.47 (d, 2H, J = 7.7), 2.10–1.23 (m, 8H), 1.20 (t, 3H, J = 7.1), 1.17 (t, 3H, J = 7.1); ^{13}C NMR δ: 176.7, 166.2, 145.1, 123.6, 60.5, 60.1, 53.0, 40.9, 35.9 (two resonances, incidental overlap), 25.0, 14.1; MS *m/e*: 254 (M^+); HRMS calcd. for $C_{14}H_{22}O_4$ *m/e* (M^+): 254.1518; found: 254.1512.

Ethyl (E)*-4-(1-ethoxycarbonylcyclopentyl)-4-methyl-2-butenoate* (***19***)
Ethyl 4-acetoxy-2-pentenoate (**11**) (0.581 g, 3.12 mmol) was subjected to the general procedure, using **5** (0.880 g, 3.44 mmol) in place of **3**. Bulb-to-bulb distillation, and subsequent flash chromatography (2:1 petroleum ether:Et_2O), gave **19** (0.519 g, 62%): bp 90°C (0.35 Torr); IR (neat, KBr): 1723, 1651 cm^{-1}; ^1H NMR δ: 6.95 (dd, 1H, J = 15.6, 8.6), 5.80 (d, 1H, J = 15.6), 4.19 (q, 2H, J = 7.1), 4.14 (m, 2H), 2.68 (m, 1H), 2.13 (m, 2H) 1.40–1.75 (m, 6H), 1.29 (t, 3H, J = 7.1), 1.26 (t, 3H, J = 7.1), 1.03 (d, 3H, J = 6.8); ^{13}C NMR δ: 176.4, 166.5, 150.6, 121.7, 60.5, 60.2, 57.6, 43.3, 34.5, 32.8, 25.1, 25.0, 15.9, 14.2; MS *m/e*: 268 (M^+); HRMS calcd. for $C_{15}H_{24}O_4$ *m/e* (M^+): 268.1675; found: 268.1665.

Ethyl (E)*-4-(1-ethoxycarbonyl-2-methylcyclohexyl)-2-butenoate* (***20***)
Compound **10** (0.1086 g, 0.631 mmol) was subjected to the general procedure, using **4a** (0.1910 g) in place of **3**. Purification of the crude reaction product by preparative TLC (10:1 petroleum ether:Et_2O) afforded **20** (0.0926 g, 52%) as a colourless liquid: bp 93°C (0.70 Torr); IR (neat, KBr): 1725, 1654 cm^{-1}; ^1H NMR δ, major diastereomer (*R**,*R**-**20**): 6.85 (dt, 1H, J = 15.5, 7.7), 5.83 (d, 1H, J = 15.5), 4.17 (q, 2H, J = 7.1), 4.15 (q, 2H, J = 7.1), 2.62 (dd, 1H, J = 14.1, 7.2), 2.51 (dd, 1H, J = 14.2, 8.3), 1.90–1.21 (m, 9H), 1.28 (t, 3H, J = 7.1), 1.26 (t, 3H, J = 7.1), 0.95 (d, 3H, J = 6.9); peaks from the minor diastereomer (*R**,*S**-**20**) could be observed at 6.93 (dd, 1H, J = 15.2, 6.9), 5.83 (d, 1H, J = 15.2), 2.30 (dd, 1H, J = 14.3, 8.8), 2.08 (m, 1H), 0.84 (d, 3H, J = 6.9); ^{13}C NMR δ: 175.2, 166.1, 144.7, 124.0, 60.1, 60.0, 49.3, 39.2, 37.3, 29.6, 29.5, 22.9, 21.9, 16.4, 14.2; peaks from the minor diastereomer could be observed at 176.1, 166.2, 145.8, 123.5, 60.3, 49.8, 36.0, 32.7, 30.8, 30.0, 23.8, 21.2, 16.0; MS *m/e*: 282 (M^+); HRMS calcd. for $C_{16}H_{26}O_4$ *m/e* (M^+): 282.1831; found: 282.1833.

Ethyl (E)*-4-(1-ethoxycarbonylcycloheptyl)-2-butenoate* (***21***)
Compound **10** (0.1182 g, 0.686 mmol) was subjected to the general procedure, using **6a** (0.2080 g) in place of **3**. Purification by preparative TLC (10:1 petroleum ether:Et_2O) afforded **21** (0.0780 g) as a colourless liquid: bp 100–105°C (0.50 Torr); IR (neat, KBr): 1724, 1654 cm^{-1}; ^1H NMR δ: 6.83 (dq, 1H, J = 15.4, 7.7), 5.80 (d, 1H, J = 15.4), 4.17 (q, 2H, J = 7.0), 4.15 (q, 2H, J = 7.0), 2.40 (d, 2H, J = 7.7), 1.95–2.20 (m, 2H), 1.4–1.65 (m, 10H), 1.28 (t, 3H, J = 7.0), 1.25 (t, 3H, J = 7.0); ^{13}C NMR δ: 176.7, 166.2, 144.7, 124.0, 60.5, 60.2, 49.7, 43.0, 36.2, 29.9, 23.5, 14.2 (2 resonances, incidental overlap); MS *m/e*: 282 (M^+); HRMS calcd. for $C_{16}H_{26}O_4$ *m/e* (M^+): 282.1831; found: 282.1830.

Ethyl (E)*-4-[1-(oxomethyl)cyclohexyl]-2-butenoate* (***22***)
Ethyl 4-acetoxy-2-butenoate (**3**) (0.193 g, 1.12 mmol) was subjected to the general procedure, using **7** (0.220 g, 1.23 mmol) in place of **3**. The crude product was purified by bulb-to-bulb distillation, followed by flash chromatography (2:1 petroleum ether:Et_2O), to afford **22** (0.186 g, 74%): bp 100°C (1.1 Torr); IR (neat, KBr): 1722, 1654 cm^{-1}; ^1H NMR δ: 9.48 (s, 1H), 6.80 (dt, 1H, J = 15.5, 7.8), 5.83 (d, 1H, J = 15.5), 4.18 (q, 2H, J = 7.2), 2.32 (d, 2H, J = 7.8), 1.88 (m, 2H), 1.20–1.80 (m, 8H), 1.28 (t, 3H, J = 7.2); ^{13}C NMR δ: 205.8, 165.9, 143.0, 124.7, 60.3, 49.7, 38.4, 30.7, 25.4, 22.2, 14.2; MS *m/e*: 224 (M^+); HRMS calcd. for $C_{13}H_{20}O_3$ *m/e* (M^+): 224.1412; found: 224.1405.

Ethyl (E)*-4-[1-(oxomethyl)cyclohexyl]-4-methyl-2-butenoate* (***23***)
Ethyl 4-acetoxy-2-pentenoate (**11**) (0.782 g, 4.20 mmol) was subjected to the general procedure using **7** (0.840 g, 4.62 mmol) in place of **3**. Purification by bulb-to-bulb distillation, followed by flash chromatography (2:1 petroleum ether:Et_2O), afforded **23** (0.620 g, 68%): bp 95°C (0.50 Torr); IR (neat, KBr): 1721, 1652 cm^{-1}; ^1H NMR δ: 9.49 (s, 1H), 6.86 (dd, 1H, J = 15.6, 9.4), 5.75 (d, 1H, J = 15.6), 4.18 (q, 2H, J = 7.1), 2.38 (m, 1H), 1.99 (m, 2H), 1.50–1.70 (m, 3H), 1.28 (t, 3H, J = 7.1), 1.05–1.40 (m, 5H), 0.99 (d, 3H, J = 6.6); ^{13}C NMR δ: 206.8, 166.2, 148.7, 122.7, 60.4, 52.2, 42.8, 30.0, 28.1, 25.5, 22.9, 22.6, 14.2, 14.1; MS *m/e*: 238 (M^+); HRMS calcd. for $C_{14}H_{22}O_3$ *m/e* (M^+): 238.1569; found: 238.1572.

Ethyl (E)*-4-(1-ethoxycarbonyl-2-oxocyclopentyl)-2-butenoate* (***24***)
Compound **3** (1.326 g, 7.70 mmol) was subjected to the general procedure, using **8** (1.330 g, 8.55 mmol) in place of compound **3**. Purification of the crude reaction product by bulb-to-bulb distillation, followed by flash chromatography (5:3 petroleum ether:ethyl acetate), gave **24** (0.893 g, 43%): bp 95°C (0.80 Torr); IR (neat, KBr): 1749, 1722, 1654 cm^{-1}; ^1H NMR δ: 6.78 (dt, 1H, J = 15.5, J = 7.6), 5.83 (d, 1H, J = 15.5), 4.12 (apparent q, J = 7.1, 4H), 2.82 (m, 1H), 1.85–2.70 (m, 7H), 1.25 (t, 3H, J = 7.1), 1.22 (t, 3H, J = 7.1); ^{13}C NMR δ: 213.9, 170.5, 166.0, 143.1, 125.2, 61.6, 60.5, 59.5, 37.9, 36.0, 32.5, 19.6, 14.3, 14.1; MS *m/e*: 268 (M^+); HRMS calcd. for $C_{14}H_{20}O_5$ *m/e* (M^+): 268.1311; found: 268.1302. Anal. calcd. for $C_{14}H_{20}O_5$: C 62.65, H 7.52; found: C 62.60, H 7.91.

Ethyl (E)*-4-(1-ethoxycarbonyl-2-oxocyclopentyl)-4-methyl-2-butenoate* (***25***)
Compound **11** (0.528 g, 2.84 mmol) was subjected to the

© 1997 NRC Canada

Can. J. Chem. Downloaded from www.nrcresearchpress.com by 88.146.161.215 on 09/08/12
For personal use only.

general procedure, using **8** (2.22 g, 14.2 mmol) in place of **3**. The crude reaction product was subjected to bulb-to-bulb distillation, followed by flash chromatography (5:3 petroleum ether:ethyl acetate), to provide compound **25** as a mixture of diastereomers (2:1) (0.330 g, 41%): bp 95°C (0.80 Torr); IR (neat, KBr): 1754, 1722, 1652 cm^{-1}; ^1H NMR δ, major diastereomer: 6.78 (dd, 1H, J = 15.5, 8.0), 5.80 (d, 1H, J = 15.5), 4.14 (q, 2H, J = 7.1), 4.10 (m, 2H), 3.23 (m, 1H), 2.30–2.50 (m, 2H), 1.70–2.35 (m, 4H), 1.24 (t, 3H, J = 7.1), 1.21 (t, 3H, J = 7.1), 0.97 (d, 3H, J = 6.6); peaks from the minor diastereomer could be observed at 6.72 (dd, 1H, J = 15.5, 7.8), 5.78 (d, 1H, J = 15.5), 1.04 (d, 3H, J = 6.6); ^{13}C NMR δ, major diastereomer: 213.6, 169.6, 166.3, 148.7, 122.6, 63.9, 61.9, 60.4, 39.9, 38.9, 28.6, 19.7, 14.8, 14.3, 14.1; peaks from the minor diastereomer could be observed at 213.4, 169.3, 166.3, 148.0, 123.4, 64.6, 39.8, 28.7, 15.0; MS *m/e*: 282 (M^+); HRMS calcd. for $C_{15}H_{22}O_5$ *m/e* (M^+): 282.1467; found: 282.1471. Anal. calcd. for $C_{15}H_{22}O_5$: C 63.79, H 7.86; found: C 63.43, H 7.83.

*Ethyl 4-(1-phenylcarbonylcyclopentyl)-2-butenoate (**26**)*
Ethyl 4-acetoxy-2-butenoate (**10**) (0.146 g, 0.848 mmol) was subjected to the general procedure using **9** (0.263 g, 1.06 mmol) in place of **3**. Purification by preparative TLC (10:1 petroleum ether:Et_2O), followed by bulb-to-bulb distillation, gave **26** as a colourless oil (0.144 g, 59%): bp 125–130°C (0.2 Torr); IR: 1717, 1655 cm^{-1}; ^1H NMR δ: 7.81 (d, 2H, J = 8.4), 7.49 (m, 1H), 7.41 (m, 2H), 6.71 (dt, 1H, J = 15.5, 7.6), 5.65 (dt, 1H, J = 15.5, 1.3), 4.13 (q, 2H, J = 7.1), 2.72 (dd, 2H, J = 7.6, 1.3), 2.36 (m, 2H), 1.60–1.85 (m, 6H), 1.24 (t, 3H, J = 7.1); ^{13}C NMR δ: 204.8, 166.0, 144.2, 136.6, 131.8, 128.6, 128.2, 124.0, 60.2, 58.3, 42.2, 36.0, 25.5, 14.4; MS *m/e*: 286 (M^+); HRMS calcd. for $C_{18}H_{22}O_3$ *m/e* (M^+): 286.1569; found: 286.1561.

General procedure for hydrogenations

*Ethyl (*E*)-4-(1-ethoxycarbonylcyclohexyl)butanoate (**16a**)*
Compound **16** (0.0858 g, 0.337 mmol) was added to ethanol (15 mL). Raney® nickel was added and the mixture was allowed to stir under a hydrogen atmosphere at room temperature for 8 h. The Raney® nickel was then removed by filtration through Celite® and the filtrate was concentrated under reduced pressure. The crude product was subjected to a bulb-to-bulb distillation to yield **16a** (0.0858 g, 99%): bp 95°C (0.90 Torr) (lit. (13) bp 135–36°C (1.3 Torr)); IR (neat, KBr): 1728 cm^{-1}; ^1H NMR δ: 4.14 (q, 2H, J = 7.1), 4.11 (q, 2H, J = 7.1), 2.23 (t, 2H, J = 6.6), 2.04 (m, 2H), 1.10–1.40 (m, 12H), 1.25 (t, 3H, J = 7.1), 1.24 (t, 3H, J = 7.1); ^{13}C NMR δ: 176.6, 173.4, 60.3, 60.1, 46.7, 39.8, 34.7, 34.1, 26.0, 23.2, 19.8, 14.4, 14.3; MS *m/e*: 270 (M^+).

*Ethyl 4-(1-ethoxycarbonylcyclohexyl)-4-methylbutanoate (**17a**)*
Subjecting compound **17** (0.0725 g, 0.257 mmol) to the general hydrogenation procedure afforded **17a** (0.0707 g, 97%) following bulb-to-bulb distillation: bp 97°C (0.50 Torr); IR (neat, KBr): 1735, 1725 cm^{-1}; ^1H NMR δ: 4.14 (q, 2H, J = 7.2), 4.10 (q, 2H, J = 7.1), 2.35 (m, 1H), 1.80–2.25 (m, 4H), 1.10–1.70 (m, 10H), 1.25 (t, 3H, J = 7.2), 1.23 (t, 3H, J = 7.1), 0.84 (d, 3H, J = 6.8); ^{13}C NMR δ: 175.8, 173.7, 60.3, 59.9, 50.7, 41.0, 33.1, 31.5, 31.2, 26.8, 25.9, 23.63, 23.57, 14.3, 14.2, 13.8; MS *m/e*: 284 (M^+).

*Ethyl (*E*)-4-(1-ethoxycarbonylcyclopentyl)butanoate (**18a**)*
Subjecting compound **18** (0.0949 g, 0.373 mmol) to the general hydrogenation procedure provided **18a** (0.0927 g, 97%) after bulb-to-bulb distillation: bp 95°C (0.80 Torr); IR (neat, KBr): 1738, 1726 cm^{-1}; ^1H NMR δ: 4.10 (q, 2H, J = 7.0), 4.09 (q, 2H, J = 7.2), 2.24 (t, 2H, J = 7.1), 2.09 (m, 2H), 1.70–1.40 (m, 10H), 1.19 (t, 6H, J = 7.1); ^{13}C NMR δ: 177.6, 173.4, 60.3, 60.3, 53.9, 38.6, 36.1, 34.7, 25.0, 21.5, 14.3; MS *m/e*: 256 (M^+).

*Ethyl 4-(1-ethoxycarbonyl-2-methylcyclohexyl)butanoate (**20a**)*
Subjecting compound **20** (0.0926 g, 0.328 mmol) to the general hydrogenation procedure afforded **20a** (0.0918 g, 98%) after bulb-to-bulb distillation; bp 85°C (0.3 Torr); IR (neat, KBr): 1735 cm^{-1}; ^1H NMR δ, major diastereomer: 4.10 (q, 2H, J = 7.1), 4.09 (q, 2H, J = 7.1), 2.24 (m, 2H), 1.30–1.90 (m, 10H), 1.23 (t, 3H, J = 7.1), 1.22 (t, 3H, J = 7.1), 0.92 (t, 6H, J = 6.6); peaks from the minor diastereomer could be observed at 0.81 (d, 3H, J = 7.1); ^{13}C NMR δ, major diastereomer: 176.7, 173.5, 60.3, 59.9, 49.2, 37.4, 35.7, 35.0, 34.8, 29.6, 27.9, 22.5, 22.1, 20.0, 16.5, 14.4; peaks from the minor diastereomer could be observed at 49.6, 30.4, 30.3, 29.8, 23.2, 22.2, 19.8, 15.6; MS *m/e*: 284 (M^+).

*Ethyl 4-(1-ethoxycarbonylcycloheptyl)butanoate (**21a**)*
Subjecting **21** (0.1063 g, 0.376 mmol) to the general hydrogenation procedure afforded **21a** (0.1023 g, 96%) after bulb-to-bulb distillation: bp 100–105°C (0.44 Torr); IR (neat, KBr): 1737, 1731 cm^{-1}; ^1H NMR δ: 4.12 (q, 2H, J = 7.1), 4.11 (q, 2H, J = 7.1), 2.24 (m, 2H), 2.07 (m, 2H), 1.4–1.6 (m, 14H), 1.24 (apparent t, 6H, J = 7.1); ^{13}C NMR δ: 177.6, 173.3, 60.2, 60.1, 49.4, 40.1, 36.1, 34.7, 29.9, 23.5, 20.3, 14.24, 14.21; MS *m/e*: 284 (M^+).

*Ethyl 4-[1-(hydroxymethyl)cyclohexyl]butanoate (**22b**)*
Subjecting **22** (0.1412 g, 0.330 mmol) to the general hydrogenation procedure afforded **22b** (0.1396 g, 97%) after bulb-to-bulb distillation: bp 100°C (1.0 Torr); IR (neat, KBr): 3447 (br), 1735 cm^{-1}; ^1H NMR δ: 4.13 (q, 2H, J = 7.1), 3.43 (s, 2H), 2.30 (t, 2H, 6.9), 2.10 (br, 1H), 1.20–1.60 (m, 14H), 1.26 (t, 3H, J = 7.1); ^{13}C NMR δ: 174.3, 68.4, 60.5, 37.2, 34.6, 33.8, 32.6, 26.5, 21.6, 18.2, 14.3; MS *m/e*: 228 (M^+).

*Ethyl 4-[(1-iodomethylcyclohexyl)butanoate (**37**)*
Compound **22b** (0.112 g, 0.491 mmol) was added to a flask containing triphenylphosphine (0.390 g, 1.49 mmol), imidazole (0.100 g, 1.49 mmol), and iodine (0.250 g, 0.99 mmol). Toluene (25 mL) was added and the mixture was allowed to reflux for 4 h. At this time the mixture was allowed to cool to room temperature, sodium bicarbonate was added, and stirring was allowed to continue for 5 min. Iodine was then added until the toluene layer remained orange. A saturated aqueous sodium thiosulphate was added to remove the excess iodine, at which time a conventional work-up was done, extracting with toluene. The crude product was purified by flash chromatography (20:1 petroleum ether:Et_2O) to afford **37** (0.145 g, 87%): bp 100°C (0.48 Torr); IR (neat, KBr): 2927, 2855, 1735

© 1997 NRC Canada

Can. J. Chem. Downloaded from www.nrcresearchpress.com by 88.146.161.215 on 09/08/12
For personal use only.

cm^{-1}; ^{1}H NMR δ: 4.14 (q, 2H, J = 7.1), 3.24 (s, 2H), 2.30 (t, 2H, J = 6.9), 1.30–1.55 (m, 14 H), 1.27 (t, 3H, J = 7.1); ^{13}C NMR δ: 173.6, 60.3, 37.2, 35.0, 34.9, 34.7, 26.0, 21.8, 18.2, 14.3; MS *m/e*: 338 (M$^+$); HRMS calcd. for $C_{13}H_{23}IO_2$ *m/e* (M$^+$): 338.0743; found: 338.0732.

*Ethyl 4-[1-(phenyloxomethyl)cyclopentyl]butanoate (**26a**)*
Compound **26** (0.0887 g, 0.310 mmol) was subjected to the general hydrogenation procedure. The crude reaction product (containing **26b**) was dissolved in CH_2Cl_2 (10 mL), and neutral alumina (ca. 0.5 g) and PDC (0.2 g) were added. After stirring for 4 h, an additional amount of PDC (0.2 g) was added. After stirring for a further 8 h, the reaction mixture was filtered through neutral alumina, and the filtrate was subject to a conventional work-up. Thin-layer chromatography (10:1 petroleum ether:Et_2O) afforded **26a** (0.0781 g, 88%) as a colourless oil: bp 125–130°C (0.2 Torr); IR (neat, KBr): 1735, 1671 cm^{-1}; ^{1}H NMR δ: 7.86 (dd, 2H, J = 8.5, 1.7), 7.47 (m, 1H), 7.39 (m, 2H), 4.01 (q, 2H, J = 7.1), 2.25–2.45 (m, 2H), 2.14 (t, 2H, J = 7.2), 1.80–1.95 (m, 2H), 1.50–1.77 (m, 6H), 1.35–1.50 (m, 2H), 1.16 (t, 3H, J = 7.1); ^{13}C NMR δ: 205.3, 173.0, 136.6, 131.7, 128.7, 128.1, 60.1, 58.9, 39.9, 36.2, 34.5, 25.5, 21.1, 14.1; MS *m/e*: 288 (M$^+$).

General procedure for Dieckmann condensations

*2-Ethoxycarbonyl-1-oxospiro[4.5]decane (**27**)*
KH (0.060 g, 1.6 mmol) was washed three times with dry Et_2O, with the supernatant Et_2O being removed by syringe each time. Dry Et_2O (20 mL) was added, followed by **16a** (0.355 g, 1.31 mmol). The mixture was allowed to stir overnight, at which time 3 M HCl was added. The mixture was stirred for an additional 5 min, after which an aqueous work-up was performed. The crude product was purified by bulb-to-bulb distillation to afford compound **27** (0.247 g, 84%); bp 85°C (0.20 Torr) (lit. (13) bp 100–101°C (0.1 Torr)); ^{1}H NMR δ: 4.17 (q, 2H, J = 7.1), 3.19 (t, 1H, J = 9.0), 2.21–1.49 (m, 14H), 1.26 (t, 3H, J = 7.1); ^{13}C NMR δ: 215.7, 169.7, 61.2, 57.1, 54.8, 50.3, 33.2, 32.2, 31.3, 25.5, 23.4, 22.1, 21.9, 14.1; MS *m/e*: 224 (M$^+$); HRMS calcd. for $C_{13}H_{20}O_3$ *m/e* (M$^+$): 224.1412; found: 224.1410.

*2-Ethoxycarbonyl-1-oxo-4-methylspiro[4.5]decane (**28**)*
Subjecting compound **19a** (0.048 g, 0.17 mmol) to the general procedure, followed by bulb-to-bulb distillation and preparative TLC (5:1 petroleum ether:ethyl acetate), afforded **28** (0.020 g, 53%): bp 90°C (0.68 Torr); IR (neat, KBr): 2931, 2857, 1748, 1723, 1654, 1450, 1254, 1177, 800 cm^{-1}; ^{1}H NMR δ, major diastereomer: 4.16 (q, 2H, J = 7.1), 3.26 (t, 1H, J = 9.2), 2.48 (m, 1H), 2.32 (m, 1H), 1.16–2.10 (m, 11H), 1.26 (t, 3H, J = 7.1), 0.93 (d, 3H, J = 7.1); peaks from the minor diastereomer could be observed at 4.18 (q, 2H, J = 7.3), 3.19 (t, 1H, J = 9.4), 2.23 (m, 1H), 1.02 (d, 3H, J = 6.8); ^{13}C NMR (diastereomeric mixture) δ: 215.1, 214.8, 169.9, 61.2, 53.8, 53.4, 52.2, 51.1, 39.6, 36.2, 32.1, 31.7, 30.8, 27.3, 25.8, 25.6, 25.3, 21.9, 21.6, 20.9, 15.9, 14.6, 14.1; MS *m/e*: 238 (M$^+$); HRMS calcd. for $C_{14}H_{22}O_3$ *m/e* (M$^+$): 238.1569; found: 238.1570. Resolution-enhanced ^{13}C NMR experiments resolved the 61.2 ppm resonance into 61.21 and 61.26 ppm resonances.

*2-Ethoxycarbonyl-1-oxospiro[4.4]nonane (**29**)*
Subjecting compound **18a** (0.178 g, 0.695 mmol) to the general procedure, followed by bulb-to-bulb distillation, produced compound **29** (0.101 g, 69%): bp 83°C (0.29 Torr); IR (neat, KBr): 1749, 1723 cm^{-1}; ^{1}H NMR δ: 4.16 (q, 2H, J = 7.1), 3.18 (t, 1H, J = 8.9), 2.20–1.44 (m, 12H), 1.25 (t, 3H, J = 7.1); ^{13}C NMR δ: 216.1, 169.8, 61.2, 56.9, 54.3, 37.1, 36.3, 36.1, 25.9, 25.7, 24.2, 14.1; MS *m/e*: 210 (M$^+$); HRMS calcd. for $C_{12}H_{18}O_3$ *m/e* (M$^+$): 210.1256; found: 210.1248.

*2-Ethoxycarbonyl-1-oxospiro[4.6]undecane (**30**)*
Subjecting **21a** (0.0481 g, 0.169 mmol) to the general procedure, followed by preparative TLC (5:1 petroleum ether:Et_2O), afforded **30** (0.0268 g, 67%): bp 85–90°C (1.2 Torr); IR (neat, KBr): 1749, 1724 cm^{-1}; ^{1}H NMR δ: 4.19 (m, 2H), 3.24 (apparent t, 1H, J = 9.0), 2.00–2.40 (m, 3H), 1.35–1.85 (m, 13H), 1.28 (apparent t, 3H, J = 7.1); ^{13}C NMR δ: 215.9, 169.8, 61.2, 54.3, 52.6, 36.1, 35.1, 34.5, 29.7, 23.8, 23.4, 23.2, 14.1; MS *m/e*: 238 (M$^+$); HRMS calcd. for $C_{14}H_{22}O_3$ *m/e* (M$^+$): 238.1569; found: 238.1564.

*1-Phenylspiro[4.4]non-1-ene-2-carboxylic acid (**31**)*
Subjecting **26a** (0.0691 g, 0.240 mmol) to the general reaction procedure afforded the crude product. This material was redissolved in 1:1 MeOH:H_2O (5 mL), and KOH (0.1 g) was added. After stirring 8 h, 10% NaOH (10 mL) was added, and the mixture extracted with Et_2O. The aqueous layer was acidified with 3 M HCl, and subsequently extracted three times with Et_2O. The combined Et_2O layers from the acidic solution extractions were dried over $MgSO_4$, filtered, and concentrated under reduced pressure. Preparative TLC (1:1 petroleum ether:Et_2O) afforded **31** (0.0435 g, 75%) as white crystals: mp 160–161°C (hexanes); IR (KBr): 3000 (v br), 1683, 1660 cm^{-1}; ^{1}H NMR δ: 7.20–7.40 (m, 3H), 7.03 (dd, 2H, J = 7.4, 1.3), 2.66 (apparent t, 2H, J = 7.2), 1.86 (apparent t, 2H, J = 7.2), 1.35–1.75 (m, 8H). The resonance of the carboxylic acid OH proton was insufficiently sharp to be detected; ^{13}C NMR δ: 170.1, 163.5, 136.3, 129.5, 128.0, 127.6, 127.1, 61.4, 37.4, 35.8, 30.6, 23.9; MS *m/e*: 242 (M$^+$); HRMS calcd. for $C_{16}H_{18}O_2$ *m/e* (M$^+$): 242.1307; found: 242.1312.

General procedure for acyloin condensation

*Bis(1,2-trimethylsiloxy)spiro[5.5]undec-1-ene (**32**)*
Sodium metal (0.010 g, 0.43 mmol) and potassium metal (0.030 g, 0.68 mmol) were placed in a two-neck flask under argon and washed three times with dry Et_2O. The metal alloy was formed by heating the flask with a heat gun under constant stirring. After formation, the alloy was allowed to cool and Et_2O (40 mL) was added. A solution of compound **16** (0.090 g, 0.33 mmol) and Me_3SiCl (0.150 g, 1.37 mmol) in Et_2O (1 mL) was added over 40 min using a syringe pump. The solution turned a purple colour during this time. The mixture was allowed to stir overnight, at which time it was filtered through Celite® under nitrogen. The solvent was removed under reduced pressure; flash chromatography on the residue (50:1 petroleum ether:Et_2O) gave **32** as a colourless liquid (0.092 g, 85%): IR (neat, KBr): 2929, 2860, 1676, 1292, 1250, 1207, 843, 758 cm^{-1}; ^{1}H NMR δ: 2.10 (m, 2H), 0.85–1.80 (m, 14H), 0.17 (s, 18H); ^{13}C NMR δ: 139.4, 131.8, 38.2, 33.7, 31.0, 30.2, 26.1, 21.8, 18.9, 1.4, 1.1; MS *m/e*: 326 (M$^+$); HRMS calcd. for $C_{17}H_{34}O_2Si_2$ *m/e* (M$^+$): 326.2097; found: 326.2109.

© 1997 NRC Canada

Can. J. Chem. Downloaded from www.nrcresearchpress.com by 88.146.161.215 on 09/08/12
For personal use only.

Bis(6,7-trimethylsiloxy)spiro[4.5]dec-6-ene (33)
Compound **18a** (0.0893 g, 0.348 mmol) was subjected to the general reaction procedure. Preparative TLC (100% petroleum ether) produced spirocycle **33** (0.0667 g, 67%): IR (neat, KBr): 2954, 2863, 1677, 1444, 1250, 842, 757 cm^{-1}; ^1H NMR δ: 2.11 (apparent t, 2H, J = 6.2), 1.80 (m, 2H), 1.20–1.65 (m, 10H), 0.17 (s, 9H), 0.15 (s, 9H); ^{13}C NMR δ: 137.4, 131.3, 46.6, 37.2, 36.8, 30.1, 25.6, 20.5, 1.5, 1.2; MS *m/e*: 312 (M^+); HRMS calcd. for $C_{16}H_{32}O_2Si_2$ *m/e* (M^+): 312.1941; found: 312.1941.

Bis(1,2-trimethylsiloxy)-7-methylspiro[5.5]undec-1-ene (34)
Compound **20a** (0.0918 g, 0.323 mmol) was subjected to the general reaction procedure. Flash chromatography (50:1 petroleum ether:Et_2O) afforded **34** as a mixture of diastereomers (70:30) (0.0660 g, 60%). The major diastereomer could be separated by preparative TLC (100% petroleum ether): IR (neat, KBr): 2955, 2930, 2862, 1668 cm^{-1}; ^1H NMR δ, major diastereomer (*R**, *R**-**34**): 2.13 (apparent t, 2H, J = 6.4), 0.80–2.05 (m, 13H), 0.98 (d, 3H, J = 6.7), 0.20 and 0.18 (2 s, 9H) 0.08 (s, 9H); peaks from the minor diastereomer could be observed at 2.49 (apparent dd, 2H, J = 7.6, 15.1), 0.80–2.20 (m, 13H), 0.74 (d, 3H, J = 6.7), 0.27 (s, 9H), 0.18 (s, 9H); ^{13}C NMR δ, major diastereomer: 139.8, 131.7, 40.4, 37.5, 35.2, 33.9, 30.3, 30.0, 22.3, 22.0, 18.5, 17.1, 1.72; peaks from the minor diastereomer could be observed at 138.4, 132.5, 42.0, 35.8, 33.7, 30.4, 30.0, 18.8, 17.3, 1.35; MS *m/e*: 340 (M^+); HRMS calcd. for $C_{18}H_{36}O_2Si_2$ *m/e* (M^+): 340.2254; found: 340.2261.

Bis(1,2-trimethylsiloxy)spiro[6.5]dodec-1-ene (35)
Compound **21a** (0.1023 g, 0.360 mmol) was subjected to the general reaction procedure. Flash chromatography (50:1 petroleum ether:Et_2O) of the crude product afforded spirocycle **35** (0.0857 g, 70%); IR (neat, KBr): 2923, 2851, 1674 cm^{-1}; ^1H NMR δ: 2.10 (apparent t, 2H, J = 6.2), 1.79 (dd, 2H, J = 14.1, 9.5) 1.23–1.70 (m, 14H), 0.20 (s, 9H), 0.19 (s, 9H); ^{13}C NMR δ: 141.2, 130.2, 40.7, 38.5, 35.5, 30.9, 30.3, 24.2, 19.1, 1.5, 1.2; MS *m/e*: 340 (M^+); HRMS calcd. for $C_{18}H_{36}O_2Si_2$ *m/e* (M^+): 340.2254; found: 340.2266.

Spiro[5.5]undecan-2-one (36)
Sodium metal (0.025 g) was heated in toluene at reflux (10 mL) with vigourous stirring. Stirring was continued as the solution was allowed to cool to room temperature. The toluene was removed by syringe, and the finely divided sodium suspended in Et_2O (20 mL). Me_3SiCl (0.5 mL) was added. Iodide **37** (0.0868 g, 0.257 mmol) was added as a solution in Et_2O over a period of 10 min. After stirring 12 h, the mixture was filtered through Celite®. Ethanol (95%, 10 mL) was added to the filtrate, and the solution stirred for 2 h. After concentration under reduced pressure, preparative TLC (5:1 petroleum ether:Et_2O) gave **36** (0.0190, 45%), whose spectral data were identical with the literature report (23).

Material on deposit

The ^{13}C NMR spectra of **11**, **16–23**, **26–35**, and **37** (20 pages) have been deposited as supplementary material.[4]

[4] Copies of material on deposit may be purchased from: The Depository of Unpublished Data, Document Delivery, CISTI, National Research Council Canada, Ottawa, Canada K1A 0S2.

Acknowledgments

We are grateful for the research support of the Natural Sciences and Engineering Research Council of Canada (NSERC) and the University of Windsor.

References

1. S. Danishefsky. Acc. Chem. Res. **12**, 66 (1979); H.N.C. Wong, H.-Y. Hon, C.-W. Tse, J. Tanko, and T. Hudlicky. Chem. Rev. **89**, 165 (1989); H.C. Brown and H. Nambu. J. Am. Chem. Soc. **92**, 1761 (1970); T. Ibuka and H. Minakata. Synth. Commun. **10**, 119 (1980); J. Tsuji, H. Ueno, Y. Kobayashi, and H. Okumoto. Tetrahedron Lett. **22**, 2573 (1981); A.J. Pearson. Chem. Ind. 742 (1982); P. Prempree, S. Radviroongit, and Y. Thebtaranonth. J. Org. Chem. **48**, 3553 (1983); F. Orsini and F. Pelizzoni. Synth. Commun. **13**, 523 (1983); B.M. Trost and C.-J. Li. J. Am. Chem. Soc. **116**, 3167 (1994).
2. J.R. Green and M.K. Carroll. Tetrahedron Lett. **32**, 141 (1991); T. Zhou and J.R. Green. Tetrahedron Lett. **34**, 4497 (1993); C.S. Vizniowski, J.R. Green, and T.L. Breen, and A.V. Dalacu. J. Org. Chem. **60**, 7496 (1995).
3. J.R. Green and W.A. Donaldson. *In* Encyclopedia of inorganic chemistry. Vol. 4. *Edited by* R.B. King. John Wiley and Sons, New York. 1994. pp. 1735–1784; A.J. Pearson. Iron compounds in organic synthesis. Academic Press, London. 1994. Chap. 3.
4. D. Enders and M. Finkam. Synlett, 401 (1993); Liebigs Ann. Chem. 551 (1993); D. Enders, B. Jandeleit, and G. Raabe. Angew. Chem. Int. Ed. Engl. **3**, 1949 (1994); D. Enders and B. Jandeleit. Synthesis, 1327 (1994); D. Enders, B. Jandeleit, and O.F. Prokopenko. Tetrahedron, **51**, 6273 (1995); D. Enders, S. von Berg, and B. Jandeleit. Synlett, 18 (1996); D. Enders, P. Fey, T. Schmitz, B.B. Lohray, and B. Jandeleit. J. Organomet. Chem. **514**, 227 (1996); D. Enders, U. Frank, P. Fey, B. Jandeleit, and B.B. Lohray. J. Organomet. Chem. **519**, 147 (1996).
5. W.J. Koot, H. Hiemstra, and W.N. Speckamp. J. Chem. Soc. Chem. Commun., 156 (1993); J.C.P. Hopman, H. Hiemstra, and W.N. Speckamp. J. Chem. Soc. Chem. Commun. 617 (1995).
6. J.C.P. Hopman. Ph.D. Dissertation. University of Amsterdam. 1996.
7. W.G. Dauben and D.J. Hart. J. Am. Chem. Soc. **99**, 7307 (1977).
8. Y. Kita, J. Segawa, J. Haruta, H. Yashuda, and Y. Tamura. J. Chem. Soc. Perkin Trans. 1, 1099 (1982).
9. N.D.A. Walshe, G.B.T. Goodwin, G.C. Smith, and F.E. Woodward. Org. Synth. **65**, 1 (1987).
10. N. Leonard and D. Felley. J. Am. Chem. Soc. **72**, 2537 (1950).
11. D.A. Evans. *In* Asymmetric synthesis. Vol. 3. *Edited by* J.D. Morrison. Academic Press, Orlando, Fla. 1984. Chap. 1; A.P. Krapcho and E.A. Dundulis. J. Org. Chem. **45**, 3236 (1980).
12. E.-P. Krebs. Helv. Chim. Acta, **64**, 1023 (1981); A.S. Kende and B.H. Toder. J. Org. Chem. 47, 167 (1982); J.R. Green. Ph.D. Thesis. University of Waterloo. 1987; P. Galatsis, J.J. Manwell, and S.D. Millan. Tetrahedron Lett. **37**, 5261 (1996).
13. R. Breiman and M. Avramoff. Isr. J. Chem. **9**, 57 (1971); J.F. Tinker. J. Org. Chem. **16**, 1417 (1951).
14. J.J. Bloomfield, D.C. Owsley, and J.M. Nelke. Org. React. **23**, 259 (1976).
15. T. Ibuka, K. Hayashi, H. Minakata, Y. Ito, and Y. Inubushi. Can. J. Chem. **57**, 1579 (1979).
16. J.E. McMurry and M.P. Fleming. J. Am. Chem. Soc. **105**, 1660 (1983); W. Li, Y. Li, and Y. Li. Chem. Lett. 741 (1994); Synthesis, 678 (1994).
17. P.J. Garegg and B. Samuelsson. J. Chem. Soc. Perkin Trans. 1, 2866 (1980).

© 1997 NRC Canada

18. M.P. Cooke, Jr. and I.N. Houpis. Tetrahedron Lett. **26**, 4987 (1985); T. van der Does, G.W. Klumpp, and M. Schakel. Tetrahedron Lett. **27**, 519 (1986); C.J. Flann and L.E. Overman. J. Am. Chem. Soc. **109**, 6115 (1987).
19. J. Salaün and J. Marguerite. Org. Synth. **63**, 147 (1984).
20. M.R. Winkle, J.M. Lasinger, and R.C. Ronald. J. Chem. Soc. Chem. Commun. 87 (1980).
21. W.C. Still, M. Kahn, and A. Mitra. J. Org. Chem. **43**, 2923 (1978).
22. A. Asheroft, D. Davies, and J. Sutherland. Tetrahedron, **40**, 4579 (1984).
23. P.A. Wender and A.W. White. J. Am. Chem. Soc. **110**, 2218 (1988).

Can. J. Chem. Downloaded from www.nrcresearchpress.com by 88.146.161.215 on 09/08/12
For personal use only.

© 1997 NRC Canada

Far-UV laser flash photolysis in solution. A time-resolved spectroscopic study of the chemistry of 1,1-dimethyl-1,3-(1-sila)-butadiene

Corinna Kerst, Martin Byloos, and William J. Leigh

Can. J. Chem. Downloaded from www.nrcresearchpress.com by 88.146.161.215 on 09/08/12
For personal use only.

Abstract: Laser flash photolysis (193 nm) of 1,1-dimethyl-(1-sila)cyclobut-2-ene in hexane solution leads to the formation of a transient species ($\tau \sim 1.5$ μs at 23°C) assigned to 1,1-dimethyl-1,3-(1-sila)butadiene on the basis of its UV absorption spectrum ($\lambda_{max} = 312$ nm), and reactivity toward methanol ($k_{MeOH} = (3.6 \pm 0.1) \times 10^9$ M^{-1} s^{-1}; $k_H/k_D = 1.3 \pm 0.1$), ethanol ($k_{EtOH} = (2.41 \pm 0.06) \times 10^9$ M^{-1} s^{-1}), *tert*-butanol ($k_{BuOH} = (1.8 \pm 0.1) \times 10^9$ M^{-1} s^{-1}; $k_H/k_D = 1.5 \pm 0.1$), and oxygen ($k_{O_2} = (3.0 \pm 0.9) \times 10^8$ M^{-1} s^{-1}). Experiments using isooctane and acetonitrile as solvent are also described. In acetonitrile, the lifetime of the silene is shortened considerably compared to hydrocarbon solvents, presumably due to quenching by adventitious water. In isooctane, under conditions of low excitation intensity, the siladiene decays with clean pseudo-first-order kinetics and a maximum lifetime of ~ 5 μs at 23°C. The decay rate constant varies only slightly with temperature over the 20–60°C range, leading to Arrhenius activation parameters of $E_a = 0.5 \pm 0.2$ kcal/mol and $\log A = 5.7 \pm 0.2$. While steady state irradiation experiments suggest that in the absence of silene traps the predominant fate of the silabutadiene is thermal ring closure to regenerate the precursor, it is concluded that the rate constants and activation parameters for decay of the siladiene measured by flash photolysis represent a composite of those due to thermal electrocyclic ring closure (with $E_a > \sim 3$ kcal/mol) and reaction with adventitious quenchers (probably water, with $E_a < 0$). The measured Arrhenius parameters for reaction of the siladiene with methanol in isooctane ($E_a = -2.6 \pm 0.3$ kcal/mol and $\log A = 7.6 \pm 0.3$) are consistent with this proposal. The potential and limitations of the use of 193-nm laser excitation for flash photolysis studies in solution are discussed.

Key words: far-UV, silene, flash photolysis, kinetics, electrocyclic.

Résumé : Une photolyse éclair à 193 nm du 1,1-diméthyl-(1-sila)cyclobut-2-ène en solution dans l'hexane conduit à la formation d'une espèce transitoire ($\tau \sim 1,5$ μs, à 23°C) qui serait du 1,1-diméthyl-1,3-(1-sila)butadiène si l'on se base sur son spectre d'absorption UV ($\lambda_{max} = 312$ nm) et sa réactivité vis-à-vis du méthanol ($k_{MeOH} = (3,6 \pm 0,1) \times 10^9$ M^{-1} s^{-1}; $k_H/k_D = 1,3 \pm 0,1$), de l'éthanol ($k_{EtOH} = (2,41 \pm 0,06) \times 10^9$ M^{-1} s^{-1}), du *tert*-butanol ($k_{BuOH} = (1,8 \pm 0,1) \times 10^9$ M^{-1} s^{-1}; $k_H/k_D = 1,5 \pm 0,1$) et de l'oxygène ($k_{O_2} = (3,0 \pm 0,9) \times 10^8$ M^{-1} s^{-1}). On décrit aussi des expériences impliquant de l'isooctane et de l'acétonitrile comme solvants. Dans l'acétonitrile, le temps de vie du silène est beaucoup plus court que dans les solvants hydrocarbonés, probablement à cause d'une désactivation par de l'eau qui s'y trouve par inadvertance. Dans l'isooctane, dans des conditions de faible intensité d'excitation, le siladiène se désagrège selon une cinétique propre de pseudo-premier ordre et un temps de vie maximal d'environ 5 μs, à 23°C. Dans la plage de température allant de 20 à 60°C, la constante de la vitesse de désactivation ne varie que faiblement avec la température; ce qui conduit aux paramètres d'activation d'Arrhenius $E_a = 0,5 \pm 0,2$ kcal/mol et $\log A = 5,7 \pm 0,2$. Même si des expériences d'irradiation en état stationnaire suggèrent que, en l'absence de pièges pour les silènes, le silabutadiène conduit principalement à une cyclisation thermique régénérant le précurseur, on conclut que les constantes de vitesse et les paramètres d'activation pour la décroissance du siladiène mesurés par la photolyse éclair correspondent à une situation mixte entre la cyclisation électrocyclique thermique (avec une E_a supérieure à environ 3 kcal/mol) et la réaction avec des molécules désactivantes présentes par inadvertance (probablement de l'eau, avec une $E_a < 0$). Les paramètres d'Arrhenius mesurés pour la réaction du siladiène avec le méthanol dans l'isooctane ($E_a = -2,6 \pm 0,3$ kcal/mol et $\log A = 7,6 \pm 0,3$) sont en accord avec cette hypothèse. On discute des possibilités et des limites de l'utilisation de l'excitation laser à 293 nm pour les études de photolyse éclair en solution.

Mots clés : UV lointain, silène, photolyse éclair, cinétique, électrocyclique.

[Traduit par la rédaction]

Received February 14, 1997.

This paper is dedicated to the memory of Sam Sugamori.

C. Kerst, M. Byloos, and W.J. Leigh.[1] Department of Chemistry, McMaster University, Hamilton, ON L8S 4M1, Canada.

[1] Author to whom correspondence may be addressed. Telephone: (905) 525-9140, ext. 23485/23715. Fax: (905) 522-2509. E-mail: leigh@mcmaster.ca

© 1997 NRC Canada

Can. J. Chem. Downloaded from www.nrcresearchpress.com by 88.146.161.215 on 09/08/12
For personal use only.

Introduction

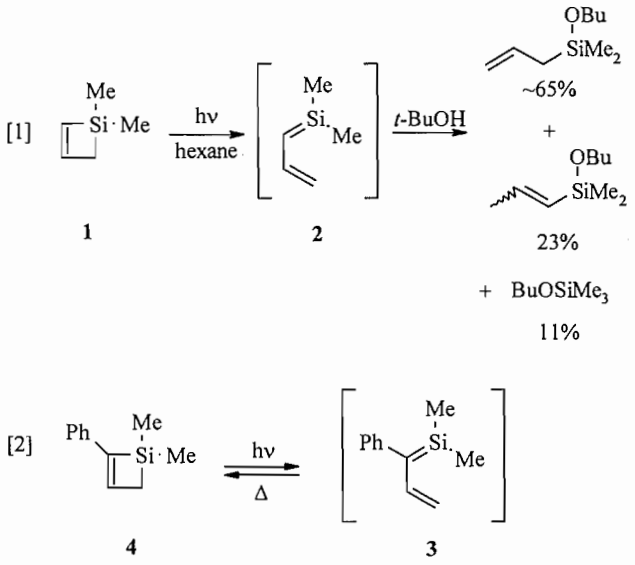
The chemistry of the silicon–carbon double bond has been an area of active interest over the past few decades. While a large number of stable (or at least, persistent) derivatives containing this functionality are known, *silenes* are more frequently encountered as reactive intermediates in various thermal and photochemical reactions of organosilicon compounds (1–4). Most commonly, their intermediacy is inferred from the results of trapping experiments, employing water, alcohols, or alkoxysilanes to trap the silene as the [1,2]-addition product. Numerous bimolecular pericyclic processes are also well known, such as ene-, [2+2]-, and [4+2]-cycloadditions with alkenes, dienes, and carbonyl compounds, and [2+2]-dimerization. Unimolecular pericyclic reactions have been much less extensively investigated.

Nanosecond laser flash photolysis techniques have proven to be extremely useful for the generation and direct detection of reactive silenes in solution (5–8) and, through determination of the effects of solvent, substituent, and temperature effects on absolute reaction rate constants, have allowed study of the mechanisms of several classic silene trapping reactions (9–15). To date, we have employed two general methodologies for the generation of transient silenes for these studies, photoinduced [1,3]-silyl migrations of aryl- (8, 11, 12, 15, 16), alkynyl- (17), and vinyldisilanes,[2] and photoinduced [2+2]-cycloreversion of arylsilacyclobutanes (10, 13, 14). The UV absorption spectra of these silene precursors extend to at least 260 nm in every case, which allows study of a wide variety of transient silenes using conventional pulsed UV lasers (KrF excimer (248 nm) or Nd/YAG (266 nm)) as excitation sources.

Time-resolved studies of silenes that are most conveniently derived from photolysis of precursors absorbing below ~240 nm have been largely confined to the gas phase, where 193 nm (ArF excimer) laser excitation can be employed (18, 19). In fact, this is true of *all* chemical reaction intermediates derived from precursors absorbing only in the far-UV. The principal reason for this is obvious — most organic solvents absorb significantly at such short wavelengths, either because of their intrinsic absorption characteristics or the presence of absorbing impurities in the commercially available materials. Water is the only solvent that might be identified as readily suitable for such studies and, indeed, the only reports of the use of the ArF laser for solution phase laser flash photolysis studies (to our knowledge) have been carried out in aqueous solution (20, 21). Furthermore, the selection of potential transient quenchers suitable for use with 193 nm excitation is rather limited, since accurate determination of bimolecular rate constants by flash photolysis can only be carried out when the quencher does not absorb significantly at the excitation wavelength (over the concentration range necessary to detect the reaction kinetically). These limitations notwithstanding, our experience with the use of far-UV excitation sources for solution phase *steady state* photochemical studies (22) suggested that, in fact, it might very well be possible — even practical — to employ the ArF laser as an excitation source for flash photolysis experiments in nonaqueous solvents.

[2] W.J. Leigh, C.J. Bradaric, G.W. Slugett, P.C. Venneri, R.T. Conlin, M.S.K. Dhurjati, and M.B. Ezhova. Unpublished results.

In this paper, we report the results of a nanosecond laser flash photolysis study of the chemistry of 1,1-dimethyl-1,3-(1-sila)butadiene (**2**) in hydrocarbon and acetonitrile solutions, using the 193 nm irradiation of 1,1-dimethyl-(1-sila)cyclobut-2-ene (**1**) to generate the silene under conditions where it can be detected directly. The photochemistry of **1** in solution has been reported previously (23), as has its gas phase thermolysis (24, 25). Under both sets of conditions, the formation of **2** as the major product has been demonstrated on the basis of chemical trapping experiments (e.g., eq. [1]). In this paper, we report absolute rate constants for the reaction of **2** with alcohols and oxygen in hexane and acetonitrile solution. An additional goal of this work was to determine rate constants and activation parameters for the thermal electrocyclic ring closure of **2** (which regenerates **1**) in solution at near ambient temperatures, to compare with previously reported data for the corresponding process in 1,1-dimethyl-2-phenyl-1,3-(1-sila)-butadiene (**3**; eq. [2]) (7).



Results and discussion

The laser flash photolysis experiments described below employed an ArF excimer laser (193 nm, ~15 ns, ~20 mJ, 1 Hz), a conventional front-face-excitation optical/detection system with nanosecond time resolution (26), and a 3 × 7 mm Suprasil quartz flow cell. Our system requires use of a single mirror to direct the excitation beam at the front face of the sample cell; for 193 nm experiments, the conventional Suprasil mirror that is used for longer wavelength excitation is replaced with a dichroic mirror manufactured specifically for 193 nm light. With a total travel distance of ~2 m through air, the intensity of the beam at the sample was reduced to about 50% of its value at the laser optic. The beam intensity was further reduced as required by use of stainless steel wire meshes as neutral density filters.

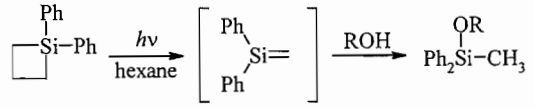
Various commercial solvents were examined for their potential suitability for 193-nm experiments. The main requirements are a low static absorbance at the laser wavelength (<0.1 through the path length of the sample cell is satisfactory), and the absence of absorbing transients in the 230–600 nm spectral range when the "pure" solvent is subjected to

© 1997 NRC Canada

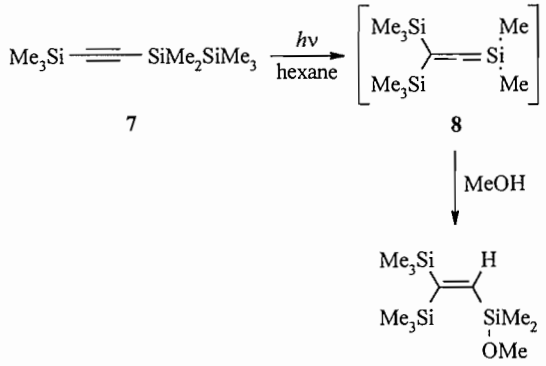
Can. J. Chem. Downloaded from www.nrcresearchpress.com by 88.146.161.215 on 09/08/12
For personal use only.

193-nm laser excitation. HPLC-grade hexane and isooctane ($A_{193}^{3\text{-mm}} \sim 0.1$ in both cases) both proved to yield satisfactory results after a single distillation. Acetonitrile was somewhat more problematic; 193-nm laser flash photolysis of an HPLC-grade sample ($A_{193}^{3\text{-mm}} \sim 0.2$) led to the formation of an unidentified transient species that absorbs more or less continuously over the 235–500 nm range and exhibits a lifetime of ~200 ns. Several distillations of the solvent from phosphorus pentoxide substantially reduced both the static absorbance at 193-nm ($A_{193}^{3\text{-mm}} \sim 0.06$) and the production of the transient absorption. The P_2O_5-distilled solvent contains small (ca. 10^{-2} M) amounts of water or other hydroxylic impurities (vide infra). However, further treatment of the solvent by passage through activated alumina (which reduces the water concentration to ca. 10^{-4} M (14)) reintroduced unacceptable levels of absorbing impurities.

A few initial experiments were carried out to establish the general reliability of far-UV laser flash photolysis data, by examining a couple of systems that were previously studied using a (248 nm) KrF excimer laser as the excitation source. For example, far-UV flash photolysis of a continuously deoxygenated hexane solution of 1,1-diphenylsilacyclobutane (**5**; 3.4×10^{-5} M) led to the formation of a transient whose decay characteristics, lifetime, and UV spectrum correspond very closely to those reported previously for 1,1-diphenylsilene (**6**; $\tau > 5$ μs; $\lambda_{max} = 325$ nm; see eq. [3]). The silene was quenched by methanol with a rate constant of $k_q = (2.8 \pm 0.1) \times 10^9$ M^{-1} s^{-1}, in excellent agreement with the value reported previously with 248 nm excitation and solutions of ~100-fold higher precursor concentrations (14). Similarly, a rate constant of $k_q = (1.3 \pm 0.5) \times 10^6$ M^{-1} s^{-1} was determined for methanol quenching of 1,1-dimethyl-3,3-bis(trimethylsilyl)-1-silaallene (**8**), produced by 193-nm excitation of a deoxygenated hexane solution of (trimethylsilylethynyl)pentamethyldisilane (**7**; 6.3×10^{-5} M; see eq. [4]). The transient absorption spectrum and quenching rate constant observed in this case are also in excellent agreement with those measured using 248-nm excitation (17).

[3] 

5 **6**

[4] 

7 **8**

Excitation of a deoxygenated hexane solution of **1** (8×10^{-4} M, $A_{193} \sim 0.6$) under similar conditions afforded readily detectable transient absorptions that decayed with mixed first- and second-order kinetics on the microsecond time scale ($\tau \sim 1.5$ μs). Reduction in the intensity of the excitation source with neutral density filters resulted in a change to clean pseudo-first-order decay kinetics and lengthening of the lifetime of the transient to a maximum of ca. 5 μs. The UV absorption spectrum of the transient, recorded in point-by-point fashion 0.23–0.55 μs after the pulse, is shown in Fig. 1 along with a typical decay trace. Similar results were obtained using distilled isooctane as the solvent.

The lifetime of the transient is shortened upon addition of methanol ($\varepsilon_{193} = (39 \pm 1)$ $M^{-1}cm^{-1}$), ethanol ($\varepsilon_{193} = (39 \pm 1)$ $M^{-1}cm^{-1}$), *tert*-butanol ($\varepsilon_{193} = (114 \pm 6)$, $M^{-1}cm^{-1}$) or oxygen[3] to the solution of **1**. Bimolecular rate constants for quenching of the transient by these compounds were obtained, as usual, from the slopes of plots of the rate constant for transient decay (k_{decay}) versus quencher concentration according to eq. [5]. These were linear in every case; Fig. 2 shows representative plots for quenching by methanol and methanol-*O*-*d*. Table 1 summarizes the results of these experiments. We assign the structure of the transient observed in these experiments to 1,1-dimethyl-1,3-(1-sila)butadiene (**2**), based on its reactivity toward alcohols and oxygen,[3] and comparison of its UV absorption spectrum ($\lambda_{max} = 312$ nm) to those of other transient silenes that have been reported — in particular, to that of 1,1-dimethyl-2-phenyl-1,3-(1-sila)butadiene (**3**) ($\lambda_{max} = 338$ nm in cyclohexane), which was reported by Conlin et al. (7). The spectrum of **2** consists of a single, rather sharp, absorption band, which may indicate that the conformational distribution of the molecule lies largely in favour of a single conformer, most likely the s-*trans* (23).

[5] $k_{decay} = k_d^0 + k_q[Q]$

A solution of **1** (0.001 M) and *tert*-butanol (0.005 M) in hexane was deoxygenated and irradiated with the ArF laser (5 Hz repetition rate) in a 10×10 mm Suprasil cuvette with vigorous stirring. GC–MS analysis of the solution after ~3% conversion of **1** verified the formation of the major product reported by Steinmetz et al., from experiments carried out with a Zn resonance lamp (214 nm) (23). This experiment indicates that the photolysis of **1** with the ArF laser proceeds in the same manner as that with the 214-nm lamp, and supports our assignment of the transient species observed in time-resolved experiments to silene **2**.

Far-UV flash photolysis of a deoxygenated 8×10^{-4} M solution of **1** in P_2O_5-treated acetonitrile afforded a transient with a similar absorption spectrum to that recorded for **2** in hexane solution, though it is considerably shorter-lived ($\tau = (120 \pm 8)$ ns). Judging from the magnitude of the rate constant for quenching of **2** by methanol in hexane, the short lifetime of the silene in P_2O_5-treated acetonitrile can most likely be attributed

[3] **Note added in proof:** Saturation of hydrocarbon solutions of **1** with oxygen results in only small reductions in the initial strength of the transient absorbance due to **2** at 312 nm. However, new transient absorptions centered at ~250 nm are also produced, probably through reaction of (directly) excited oxygen with the solvent (30). While the decay rate constant at 250 nm does not appear to depend on the presence of 1, it is clear that oxygen is not generally appropriate for use as a transient quencher in 193 nm experiments.

© 1997 NRC Canada

Fig. 1. Transient UV absorption spectrum from far-UV (193 nm) laser flash photolysis of 1,1-dimethylsilacyclobut-2-ene (**1**; 8×10^{-4} M) in deoxygenated hexane solution at 23°C. The spectrum was recorded in point-by-point fashion, 0.1–0.3 μs after the laser pulse. The insert shows a typical decay trace, recorded at a monitoring wavelength of 312 nm.

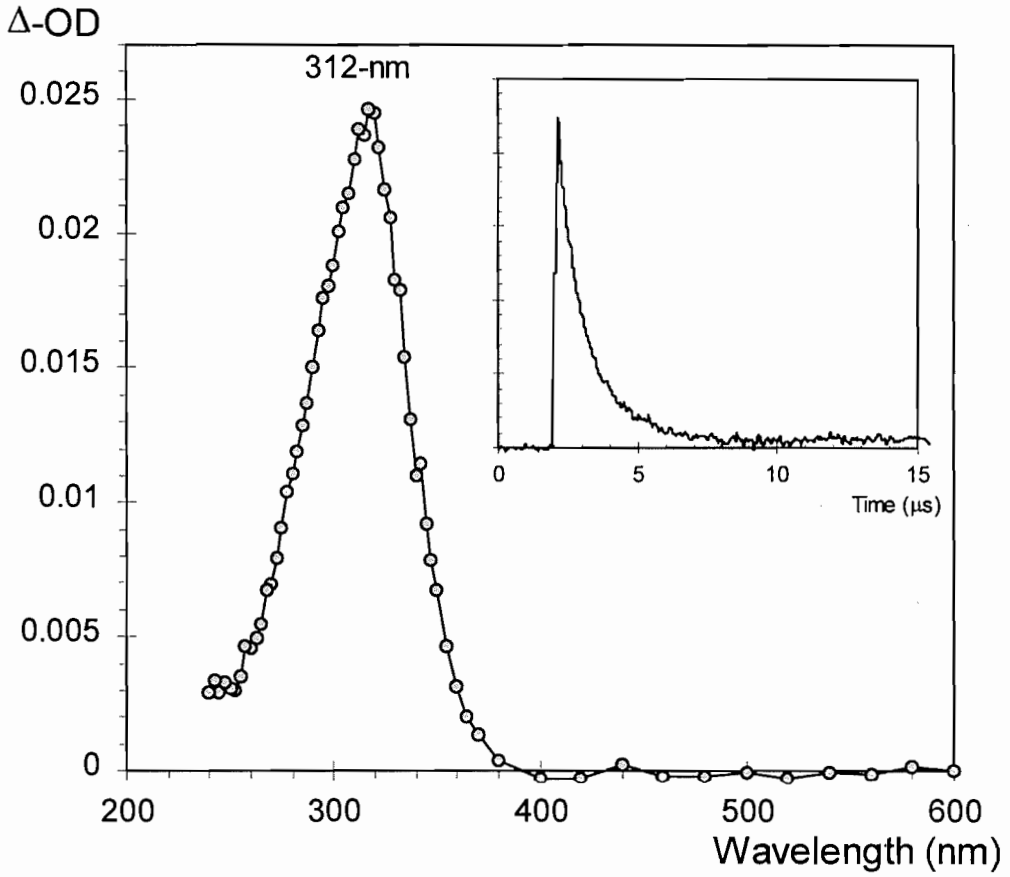


Table 1. Absolute rate constants for quenching of 1,1-dimethyl-1,3-(1-sila)butadiene (**2**) in deoxygenated hexane solution at 23.0 ± 0.2°C.[a]

Quencher	MeOH	MeOD	EtOH	*t*-BuOH	*t*-BuOD	O_2
$k_q/10^9$ M^{-1} s^{-1}	3.6 ± 0.1	2.8 ± 0.2	2.41 ± 0.06	1.8 ± 0.1	1.24 ± 0.04	0.30 ± 0.12

[a]From analysis of k_{decay} vs. concentration data according to eq. [5]. Errors are quoted as twice the standard deviation obtained from linear least-squares analysis of these data.

to the presence of small amounts of water or phosphoric acid (27). Because of the short lifetime of the silene in this solvent, determination of bimolecular quenching rate constants could not be carried out with the same level of precision as those determined for hexane solution. Nevertheless, values of k_q = (2.4 ± 0.4) × 10^9 and (2.8 ± 0.5) × 10^9 M^{-1} s^{-1} for methanol and *tert*-butanol, respectively, were estimated from data recorded over a limited range of alcohol concentrations.

A deoxygenated 0.05 M pentane solution of **1** was irradiated (214 nm) in a merry-go-round apparatus along with a similar solution containing 0.15 M *tert*-butanol, with periodic monitoring of the two solutions by gas chromatography. Over the time period necessary for ~20% consumption of **1** in the solution containing *tert*-butanol, there was no detectable destruction of **1** in the absence of the silene trap. This experiment indicates that the predominant fate of siladiene **2** in the absence of silene traps is thermal electrocyclic ring closure to regenerate the silacyclobutene (**1**).

Decay rate constants for **2** were measured as a function of temperature in deoxygenated isooctane solution, using neutral density filters to reduce the laser intensity sufficiently to produce clean pseudo-first-order transient decays, and a lifetime at 23°C of ~5 μs. Interestingly, the decay rate constant varies only slightly with temperature over the 20–60°C range. The Arrhenius plot for the data obtained in isooctane solution is shown in Fig. 3; least-squares analysis of the data affords activation parameters of E_a = 0.5 ± 0.2 kcal/mol and log A = 5.7 ± 0.2. These values are too small for a thermal electrocyclic ring closure of an acyclic diene system, assuming that the reaction proceeds from the s-*cis* conformer and that the s-*trans*

Can. J. Chem. Downloaded from www.nrcresearchpress.com by 88.146.161.215 on 09/08/12
For personal use only.

© 1997 NRC Canada

Can. J. Chem. Downloaded from www.nrcresearchpress.com by 88.146.161.215 on 09/08/12
For personal use only.

Fig. 2. Plots of k_{decay} versus alcohol concentration for quenching of 1,1-dimethyl-1,3-(1–sila)butadiene (**2**) by methanol (■) and methanol-*O*-*d* (●) in deoxygenated hexane solution at 23°C.

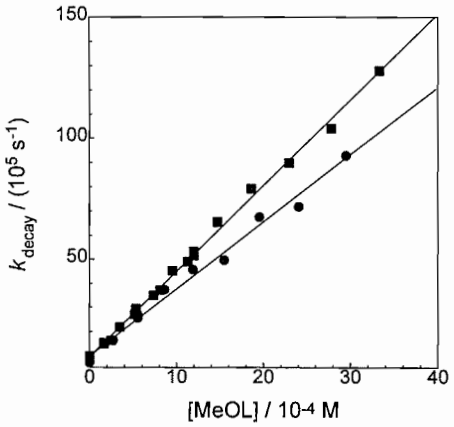
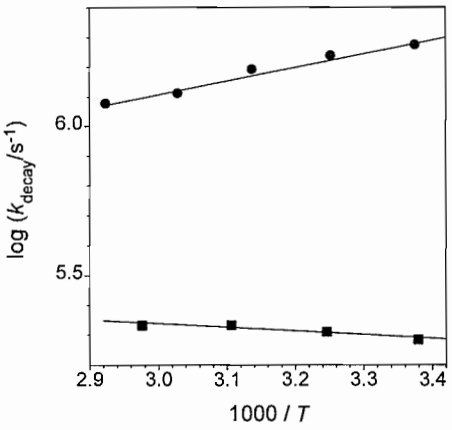


Fig. 3. Arrhenius plots for the pseudo-first-order decay of **2** in deoxygenated isooctane solution (■) and in deoxygenated isooctane containing 6×10^{-4} M methanol (●) over the 20–60°C temperature range, measured by far-UV laser flash photolysis.



conformer is the thermodynamically favoured one in solution; in such cases, the minimum obtainable value for the activation energy for ring closure will be the difference in enthalpy between the nonreactive s-*trans* and the reactive s-*cis* conformers. AM1 calculations on the individual conformers of **1** predict the s-*trans* conformer to be ~3 kcal/mol more stable than the s-*cis*, a result that is consistent with the results of ab initio calculations on the s-*cis* and s-*trans* conformers of 1,3-(1-sila)butadiene (23).

It is most likely that the pseudo-first-order rate constant for the decay of **2** in isooctane solution is at least partially controlled by impurity quenching, the most probable culprit being water. Assuming a quenching rate constant of $k_q \sim 2 \times 10^9$ M^{-1} s^{-1}, then a concentration of only 10^{-4} M water would be required to produce the observed lifetime of ~5 μs. It should be noted that the presence of such small concentrations of reactive impurities would *not* lead to appreciable consumption of **1** in steady state photolysis experiments, since the bulk concentration of **1** that was employed in these experiments was relatively high (0.05 M).

If this explanation is correct, then the unexpectedly low activation parameters for siladiene decay could result from the combination of a positive activation energy for ring closure with a *negative* activation energy for reaction with water. That the latter is reasonable can be inferred from the reported activation parameters for reaction of 1,1-diphenylsilene (**6**) with alcohols (13), which likely proceeds by an identical mechanism to that of the reaction with water (8). The negative E_a for alcohol addition to **6** has been explained in terms of a two-step mechanism involving reversible, exothermic formation of a silene–alcohol complex followed by rate-limiting proton transfer from oxygen to carbon (13).

This possible explanation was verified indirectly by measuring rate constants for decay of siladiene **2** in deoxygenated isooctane containing 6×10^{-4} M methanol as a function of temperature, the results of which are included in Fig. 3. Under these conditions, the concentration of the alcohol is such that at least 90% of the observed pseudo-first-order decay rate constant is due to bimolecular reaction. The activation energy for the reaction of **2** with methanol is indeed negative; an Arrhenius plot of the bimolecular quenching rate constants (calculated from the k_{decay} values) afford the activation parameters $E_a = -2.6 \pm 0.3$ kcal/mol and $\log A = 7.6 \pm 0.3$.

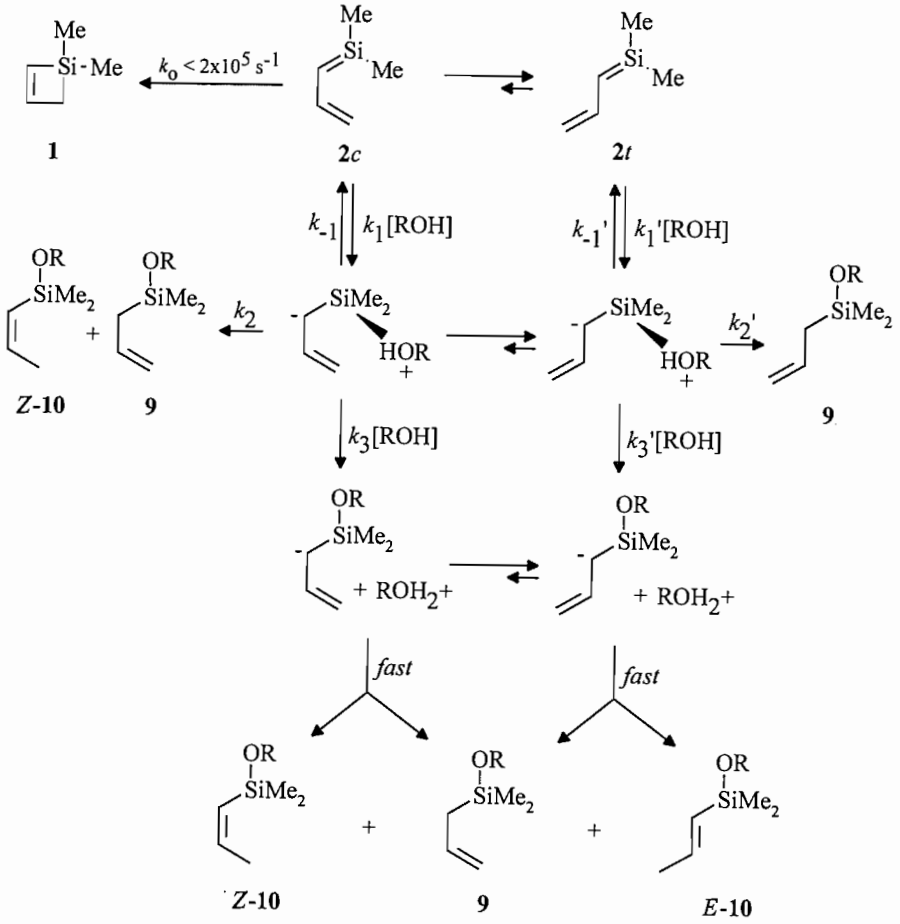
We conclude that the rapidity with which **2** reacts with trace amounts of hydroxylic impurities precludes a reliable determination of the rate constant for unimolecular reaction of the siladiene in solution, although our data indicate that it is significantly smaller than 2×10^5 s^{-1} at near-ambient temperatures. It is relevant to note that a similar rate constant was reported for the decay of the phenyl-substituted analogue (**3**; see eq. [2]) at ambient temperature and attributed to that of electrocyclic ring closure (7). Clearly, the reported Arrhenius parameters for ring closure of **3**, which were estimated from the single rate constant, are not likely to be meaningful.

The reaction of silenes with alcohols is thought to proceed by a mechanism initiated by reversible nucleophilic attack at silicon to yield a zwitterion (or σ-complex), which collapses to product by competing intra- and intermolecular proton transfer, the latter involving a second molecule of alcohol (8, 11, 13, 14, 28). Arrhenius data and kinetic isotope effect studies for the reaction of methanol and *tert*-butanol with 1,1-diphenylsilene indicate that the first step is exothermic and the intramolecular proton-transfer step, though slower than return of the zwitterion to starting materials, proceeds with a low enough activation enthalpy that the overall reaction exhibits a negative activation energy (13). The kinetic and Arrhenius data reported here for the reaction of siladiene **2** with methanol and *tert*-butanol are entirely consistent with this mechanism.

Intermolecular proton transfer from the zwitterion to a second molecule of alcohol competes with the intramolecular process at high alcohol concentrations, and can lead to concentration-dependent product distributions in appropriate cases (11, 14, 28). The intervention of this pathway in the reaction of **2** with *tert*-butanol was deduced by Steinmetz et al., from a careful study of the variation in product distribution with alcohol concentration (23). A detailed mechanism, illustrating the evolution of the various products of reaction of **2** with *tert*-butanol, is shown in Scheme 1. In terms of product

© 1997 NRC Canada

Scheme 1.



formation, the most important aspect of this mechanism is the fact that adduct *E*-**10** can *only* be formed by a pathway involving two or more molecules of alcohol. Indeed, the yield of *E*-**10** was found to increase quite significantly with increasing *tert*-butanol concentration (23). This result is also consistent with s-*trans* **2** being the favoured conformer in solution, as is suggested by theoretical calculations as well as the UV spectrum reported in the present work.

Conclusions

Despite the limited selection of solvents and quenchers that can be employed with 193-nm excitation, the far-UV nanosecond laser flash photolysis technique is clearly of considerable potential utility. It provides a method for studying the chemistry of a number of small, fundamentally important, reactive intermediates in solution, in cases where the most desirable precursor is devoid of absorption in the spectral range accessible with longer wavelength pulsed lasers, or where its absorption spectrum overlaps substantially with that of the reactive intermediate of interest. In the latter cases, the use of 193 nm excitation allows one to employ solutions of substantially lower concentration than are required for longer wavelength excitation, so that the 200–300 nm spectral range is not screened by the precursor, and transient decay pathways involving reaction with the precursor can be minimized. The ability to employ very low precursor concentrations is also advantageous in cases where it is difficult to obtain the compound in large enough quantities for study by conventional laser flash photolysis techniques. In cases where "kinetic identification" of a transient is required, it must exhibit substantial (i.e., $k_q \geq 10^8\ M^{-1}\ s^{-1}$) reactivity toward water, aliphatic alcohols, silanes, or other reagents that exhibit low absorptivity at the excitation wavelength. A number of reactive intermediates in organic and organosilicon chemistry satisfy this requirement, and are under investigation in our laboratory.

Experimental

^{1}H NMR spectra were recorded on a Bruker AC200 spectrometer in chloroform-*d* solution. Low-resolution mass spectra were recorded on a Hewlett–Packard 5890II gas chromatograph equipped with an HP-5971A mass selective detector and a DB5 fused silica capillary column (30 m × 0.25 mm; Chromatographic Specialties, Inc.). Ultraviolet absorption spectra were recorded on a Perkin Elmer Lambda 9 spectrometer interfaced to a Pentium™ microcomputer. Gas chromatographic (GC) analyses were carried out using a Hewlett–Packard 5890II+ gas chromatograph equipped with a conventional heated injector, a flame ionization detector, a Hewlett–Packard 3396A integrator, and a DB-1 megabore capillary column (15 m × 0.53 mm; Chromatographic Specialties, Inc).

© 1997 NRC Canada

Can. J. Chem. Downloaded from www.nrcresearchpress.com by 88.146.161.215 on 09/08/12
For personal use only.

Can. J. Chem. Downloaded from www.nrcresearchpress.com by 88.146.161.215 on 09/08/12
For personal use only.

Semi-preparative gas chromatographic separations were carried out using a Varian 3300 gas chromatograph equipped with a thermal conductivity detector and one of the following two columns (Supelco, Inc.): (a) 20% TCEP on 80/100 Chromosorb PNAW (10 ft × 4-mm i.d. glass); (b) 3.8% UCW982 on 80/100 Supelcoport (24 ft × 0.25 in. stainless steel).

Hexane (BDH Omnisolv) and 2,2,4-trimethylpentane (isooctane; BDH Omnisolv) exhibited absorbances of <0.2 at 193 nm in a 3-mm cell, and were distilled once before use. Acetonitrile (Aldrich HPLC) exhibited an absorbance at 193 nm of 0.2 in a 3-mm cell after a single distillation. Purification by reflux over phosphorus pentoxide for several hours followed by distillation (repeating the procedure six times, or until no discolouration of the solvent occurred during the initial reflux period) reduced the absorbance at 193 nm to 0.06 in a 3-mm cell. Methanol, methanol-*O-d*, ethanol, *tert*-butanol, and *tert*-butanol-*O-d* were of the highest purity available and were used as received from Aldrich Chemical Co.

1,1-Dimethyl-(1-sila)cyclobut-2-ene (**1**) was prepared by flash vacuum pyrolysis of dimethyldiallylsilane according to the published method (23, 29). The compound was isolated and obtained in >99% purity (as estimated by capillary GC analysis) after sequential semi-preparative gas chromatography on columns (a) and (b). The spectral and analytical data for the compound were in excellent agreement with those reported previously (23, 29).

Analytical-scale photolyses were carried out using a zinc resonance lamp (214 nm; Philips 93106E), with solutions contained in Suprasil quartz cuvettes (10 mm × 10 mm) and mounted in a merry-go-round apparatus, or the ArF laser (5 Hz repetition rate), with solutions contained in similar cuvettes and clamped ~2 m from the light source. In the latter case, the solutions were stirred during irradiation with a small magnetic stirrer. In all cases, the solutions were deoxygenated prior to photolysis with a stream of dry argon, and sealed with rubber septums. In each case, the course of the photolysis was monitored periodically by GC and (or) GC–MS analysis.

Nanosecond laser flash photolysis experiments employed the pulses (193 nm; ca. 15 ns; 20 mJ) from a Lumonics 510 excimer laser filled with F_2–Ar–He mixtures, and a microcomputer-controlled detection system (26). The laser beam was focussed on the front face of the sample compartment using a single 193-nm dichroic mirror and a Suprasil lens. The total travel distance of the excitation beam is ca. 2 m, which results in a loss of ~50% in power between the source and the sample compartment; the intensity of the beam was reduced to <2 mJ at the cell using a series of stainless steel wire meshes as neutral density filters. The system incorporates a brass sample holder whose temperature is controlled to within 0.1°C by a VWR 1166 constant temperature circulating bath. Solutions were prepared at concentrations such that the absorbance at the excitation wavelength (193 nm) was ca. 0.7 (~8×10^{-4} M), and were flowed continuously through a 3 × 7 mm Suprasil flow cell connected to a calibrated 100 mL reservoir. Nitrogen or nitrogen–oxygen mixtures were bubbled continuously through the reservoir throughout the experiments; the composition of the gas was controlled using a Matheson 7351–600 gas proportioner. Solution temperatures were measured with a Teflon-coated copper–constantan thermocouple that was inserted directly into the flow cell. Quenchers were added directly to the reservoir by microlitre syringe as aliquots of standard solutions. Rate constants were calculated by linear least-squares analysis of decay rate – concentration data (six or more points) which spanned at least one order of magnitude in the transient decay rate. Errors are quoted as twice the standard deviation obtained from the least-squares analysis in each case.

Acknowledgments

We wish to thank the Natural Sciences and Engineering Research Council of Canada for financial support, the Max-Planck-Gesellschaft zur Förderung der Wissenschaften and the Deutsche Forschungsgemeinschaft for fellowships to C.K, and the Reactive Intermediates Student Exchange (RISE) for a summer scholarship to M.B.

References

1. G. Raabe and J. Michl. Chem. Rev. **85**, 419 (1985).
2. A.G. Brook. *In* The chemistry of organic silicon compounds. *Edited by* S. Patai and Z. Rappoport. John Wiley & Sons, New York. 1989. p. 965.
3. M.G. Steinmetz. Chem. Rev. **95**, 1527 (1995).
4. A.G. Brook and M.A. Brook. Adv. Organomet. Chem. **39**, 71 (1996).
5. H. Shizuka, K. Okazaki, M. Tanaka, M. Ishikawa, M. Sumitani, and K. Yoshihara. Chem. Phys. Lett. **113**, 89 (1985).
6. P.P. Gaspar, D. Holten, S. Konieczny, and J.Y. Corey. Acc. Chem. Res. **20**, 329 (1987).
7. R.T. Conlin, S. Zhang, M. Namavari, K.L. Bobbitt, and M.J. Fink. Organometallics, **8**, 571 (1989).
8. G.W. Sluggett and W.J. Leigh. J. Am. Chem. Soc. **114**, 1195 (1992).
9. S. Zhang, R.T. Conlin, P.F. McGarry, and J.C. Scaiano. Organometallics, **11**, 2317 (1992).
10. W.J. Leigh, C.J. Bradaric, and G.W. Sluggett. J. Am. Chem. Soc. **115**, 5332 (1993).
11. W.J. Leigh and G.W. Sluggett. J. Am. Chem. Soc. **116**, 10468 (1994).
12. W.J. Leigh and G.W. Sluggett. Organometallics, **13**, 269 (1994).
13. C.J. Bradaric and W.J. Leigh. J. Am. Chem. Soc. **118**, 8971 (1996).
14. W.J. Leigh, C.J. Bradaric, C. Kerst, and J.H. Banisch. Organometallics, **15**, 2246 (1996).
15. N.P. Toltl and W.J. Leigh. Organometallics, **15**, 2554 (1996).
16. G.W. Sluggett and W.J. Leigh. Organometallics, **13**, 1005 (1994).
17. C. Kerst, C.W. Rogers, R. Ruffolo, and W.J. Leigh. J. Am. Chem. Soc. **119**, 466 (1997).
18. T. Brix, N.L. Arthur, and P. Potzinger. J. Phys. Chem. **93**, 8193 (1989).
19. J.M. Jasinski. Chem. Phys. Lett. **183**, 558 (1991).
20. U.K. Klaning, K. Sehested, and T. Wolff. J. Chem. Soc. Faraday Trans. 1, **80**, 2969 (1984).
21. U.K. Klaning, K. Sehested, and E.H. Appelman. Inorg. Chem. **30**, 3582 (1991).
22. W.J. Leigh. Chem. Rev. **93**, 487 (1993).
23. M.G. Steinmetz, B.S. Udayakumar, and M.S. Gordon. Organometallics, **8**, 530 (1989).
24. R.T. Conlin and M. Namavari. J. Am. Chem. Soc. **110**, 3689 (1988).
25. R.T. Conlin and M. Namavari. J. Organomet. Chem. **376**, 259 (1989).

© 1997 NRC Canada

26. W.J. Leigh, M.S. Workentin, and D. Andrew. J. Photochem. Photobiol. A: **57**, 97 (1991).
27. J.A. Riddick, W.B. Bunger, and T.K. Sakano. Organic solvents. Physical properties and methods of purification. 4th ed. John Wiley & Sons, New York. 1986. p. 1048.
28. M. Kira, T. Maruyama, and H. Sakurai. J. Am. Chem. Soc. **113**, 3986 (1991).
29. E. Block and L.K. Revelle. J. Am. Chem. Soc. **100**, 1630 (1978).
30. C. Kerst, R. Boukherroub, and W.J. Leigh. J. Photochem. Photobiol. A: In press.

Can. J. Chem. Downloaded from www.nrcresearchpress.com by 88.146.161.215 on 09/08/12
For personal use only.

© 1997 NRC Canada

A novel approach to carbohydrate clusters: the regioselective synthesis of non-glycosidically linked oligosaccharides[1]

Hassan Namazi and T. Bruce Grindley

Abstract: Dialkylstannylene acetals derived from a number of different carbohydrates having both *cis*- and *trans*-1,2-diols free were reacted with diacyl chlorides and disulfonyl chlorides in the presence of tertiary amines at room temperature to give symmetrical non-glycosidically linked disaccharides with excellent regioselectivity and in excellent yield. The regioselectivity obtained was the same as that previously found in acylation reactions of the same substrates. In one case, a symmetric non-glycosidically linked trisaccharide was also obtained in excellent yield. For methyl 4,6-*O*-benzylidene-α-D-glucopyranoside, a 16-membered ring macrocyclic tetralactone was obtained in 50% yield by altering the reaction stoichiometry and performing the reaction at 80°C.

Key words: carbohydrates, clusters, non-glycosidically linked oligosaccharides, disaccharides, trisaccharides.

Résumé : La réaction des acétals de dialkylstannylène, obtenus à partir de différents carbohydrates ayant à la fois des 1,2-diols *cis* et *trans* libres, avec le chlorure de sulfonyle en présence d'amines tertiaires à la température ambiante, donne, avec une excellente régiosélectivité et d'excellents rendements, des disaccharides symétriques dont la liaison n'est pas glycosidique. La régiosélectivité obtenue est la même que celle trouvée antérieurement lors des réactions d'acylation avec les mêmes substrats. On a, dans un cas avec un excellent rendement, obtenu un trisaccharide symétrique dont les liaisons ne sont pas glycosidiques. Avec le méthyl 4,6-*O*-benzylidène-α-D-glucopyranoside, on a obtenu une tétralactone macrocyclique à 16 chaînons avec un rendement de 50% en modifiant la stochiométrie de la réaction et en opérant à 80°C.

Mots clés : carbohydrates, aggrégats, oligosaccharides dont les liaisons ne sont pas glycosidiques, disaccharides, trisaccharides.

[Traduit par la rédaction]

Introduction

Although carbohydrate–protein binding plays an important role in biological recognition, the binding constants of proteins for individual carbohydrate molecules are small. Proteins achieve sufficient binding strength to carbohydrates on the surface of antibodies, viruses, bacteria, etc., by clustering the carbohydrate recognition domains of the proteins and also by recognizing clusters of carbohydrate molecules on the surfaces of these entities (2). To develop therapeutic agents that mimic this binding, it will be necessary either to prepare clusters of carbohydrates or to make compounds that attach to the carbohydrate recognition sites on the protein but bind more strongly. Previously described approaches to this problem include synthesis of small native carbohydrate clusters (3), preparation of carbohydrate dendrimers (4, 5), and preparation of carbohydrate mimics (6, 7). Here, we describe a versatile and efficient method for creating carbohydrate clusters. This method creates clusters without having to form glycosidic bonds, often the most difficult step in carbohydrate synthesis and one that is an integral part of the previous carbohydrate-based approaches.

Received October 17, 1996.

H. Namazi and T.B. Grindley.[2] Department of Chemistry, Dalhousie University, Halifax, NS B3H 4J3, Canada.

[1] A preliminary communication of part of this work has appeared (1).

[2] Author to whom correspondence may be addressed. Telephone: (902) 494-2041. Fax: (902) 494-1310. E-mail: Grindley@Chem1.Chem.Dal.Ca.

Results and discussion

Dialkylstannylene acetals serve as convenient intermediates for obtaining highly regioselective substitution of diols and polyols (8, 9). We demonstrate here that use of difunctional or trifunctional electrophiles can result in the efficient formation of non-glycosidically linked disaccharides or trisaccharides. For instance, reaction of the dibutylstannylene acetal of methyl 4,6-*O*-benzylidene-α-D-glucopyranoside (**1**) with a variety of diacyl chlorides in the presence of triethylamine (TEA) results in non-glycosidically linked disaccharides in a highly regioselective manner and in excellent yield as shown in Fig. 1. These reactions are essentially complete in 5 min at room temperature.

In theory, there are three possible products that contain two monosaccharide segments and one segment arising from a diacyl chloride molecule, namely, the 2,2′-, 2,3′-, and 3,3′-diesters. Methyl 4,6-*O*-benzylidene-2,3-*O*-dibutylstannylene-α-D-glucopyranoside is known to produce 2-*O*-acylated products with very good regioselectivity on reaction with one equivalent of acyl chloride (8, 9), leading to the expectation that the majority of products should have this regiochemistry. Confirmation of this expectation was obtained unambiguously

© 1997 NRC Canada

Can. J. Chem. Downloaded from www.nrcresearchpress.com by 88.146.161.215 on 09/08/12
For personal use only.

Fig. 1. The reaction of the dibutylstannylene acetal of methyl 4,6-*O*-benzylidene-α-D-glucopyranoside (**1**) with diacyl chlorides.

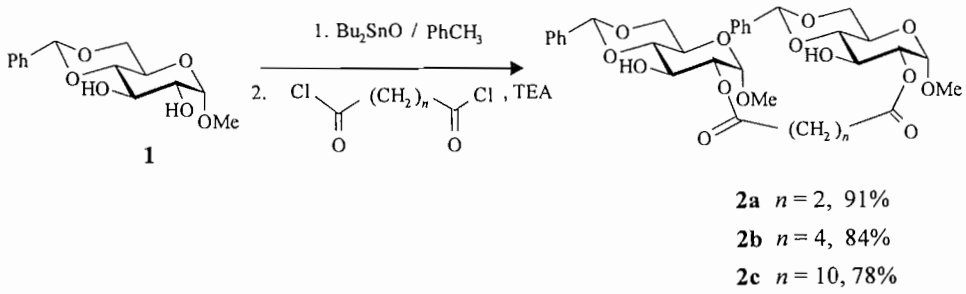
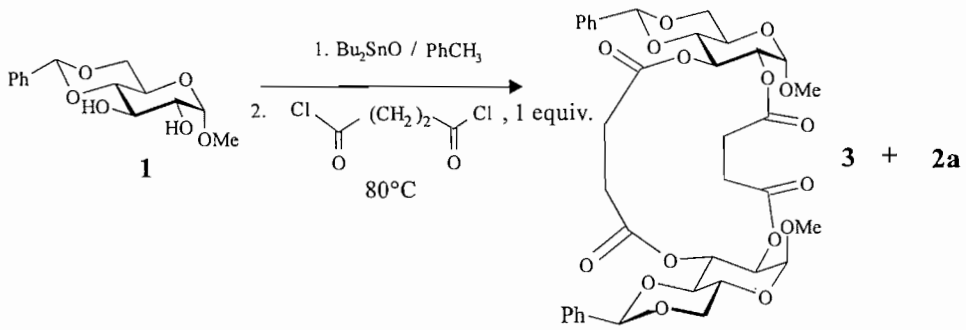
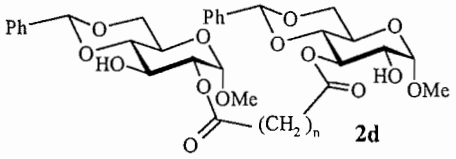


Fig. 2. The reaction of the dibutylstannylene acetal of methyl 4,6-*O*-benzylidene-α-D-glucopyranoside (**1**) with one equivalent of succinnyl chloride.



from the ^{1}H NMR spectra of the major products in each case. Those of the symmetric disaccharides contained signals assigned to carbohydrate and assigned to linker that integrated in the ratio of two to one. The signals of all carbohydrate protons were assigned by combinations of first-order analysis, and COSY and HETCOR experiments. It was immediately obvious that the spectra of the major products only contained one type of monosaccharide unit; thus, the products were symmetric, eliminating the 2,3′-diester structure. The location of the acyl linker was determined unambiguously from the identity of the secondary proton that was most deshielded by the presence of the attached acyl group. In addition, in the ^{1}H NMR spectra of carefully dried samples of **2a**, **2b**, and **2c** in dry chloroform-*d*, the signal of the hydroxyl proton appeared as a doublet, coupled to H-3. The fact that the single hydroxyl proton in these compounds is coupled to H-3 was established both by the size of the coupling constants and by COSY experiments. With the largest diacyl dichloride, a second product (**2d**) was obtained in 12% yield. This product was shown to be the 2,3′-diester by means of the lack of symmetry in its ^{1}H and ^{13}C NMR spectra.



These compounds are named here using the new IUPAC–IUBMB rules for carbohydrate nomenclature that redefine how carbohydrates are named as substituents (10*a*); thus, compound **2a** is bis(methyl 4,6-*O*-benzylidene-2-deoxy-α-D-glucopyranosid-2-yl) butanedioate.

Reactions of electrophiles with dialkylstannylene acetals performed in the absence of added nucleophiles often give different regiochemistry (11, 12) or, particularly with *trans*-diols, better regioselectivity than those performed in the presence of base (13), and initial experiments were performed under these conditions. Under these conditions, it was observed that the reactions required about 1 h to be complete at room temperature, much longer than in the presence of added triethylamine. More importantly, a second product (**3**) was obtained in yields of between 5 and 20%. The structure of this product, a cyclic diester dimer that is also a macrocyclic lactone, is shown in Fig. 2.

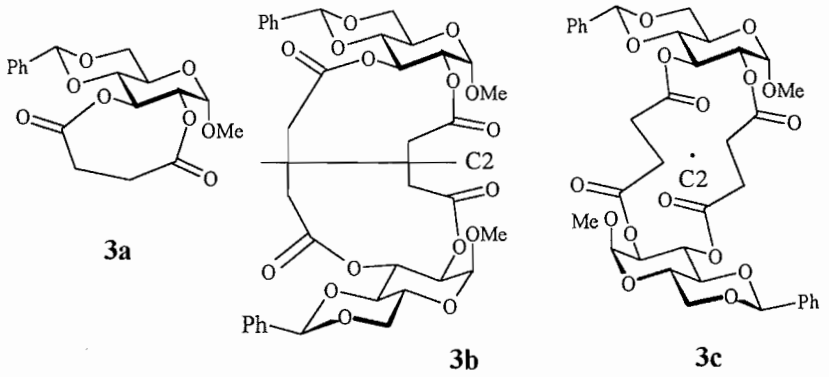
The structure of **3** was established from its molecular weight, and its NMR spectra. In the ^{1}H NMR spectrum, the signals of both H-2 and H-3 were deshielded by about 1 ppm with respect to their positions in the spectrum of the starting material, appearing at 4.80 and 5.50 ppm, respectively. This information indicated that both O-2 and O-3 were esterified. Integration of the ^{1}H NMR spectrum indicated that the ratio of succinyl units to monosaccharide units was 1:1. By changing the stoichiometry to 1:1, and by running the reaction at a higher temperature and under more dilute conditions, it was possible to raise the yield of this minor product (**3**) to 50%.

Monomeric and oligomeric structures were possible for **3** (see Fig. 3). No peaks at the monomer molecular weight (*m*/*z* 364) were present in the mass spectra of **3** recorded under a wide range of conditions (EI, electrospray, APCI) but a peak

Can. J. Chem. Downloaded from www.nrcresearchpress.com by 88.146.161.215 on 09/08/12
For personal use only.

© 1997 NRC Canada

Fig. 3. The structures of possible monomeric (**3a**) and dimeric (**3b** and **3c**) products containing methyl 4,6-*O*-benzylidene-α-D-glucopyranoside (**1**) and succinate in a 1:1 stoichiometry.



Can. J. Chem. Downloaded from www.nrcresearchpress.com by 88.146.161.215 on 09/08/12
For personal use only.

did occur at M^+ for the dimer (*m/z* 728) along with others between the dimer M^+ and 364 (*m/z* 411 and 368). This molecular ion peak had the correct exact mass. No peaks were observed at masses above *m/z* 730, confirming that the structure was not a higher oligomer. Two dimeric structures are possible, one in which the succinyl groups are linked through the same oxygen atoms on the two monosaccharides (O-2 to O-2′, and O-3 to O-3′) (**3b**), another, in which different oxygen atoms are linked (O-2 to O-3′, and O-3 to O-2′) (**3c**). Both potential dimers have C_2 symmetry, as indicated in Fig. 3. For **3b**, the C_2 axis relates the two CH_2 groups in each succinyl group but does not relate the two succinyl chains. For **3c**, the C_2 axis relates the two succinyl chains to each other but does not relate the CH_2 groups inside each succinyl chain. Since the two hydrogens in each CH_2 group are diastereotopic, the ^1H NMR spectrum of **3b** should contain two different AA′BB′ patterns, whereas that of **3c** should contain one ABCD pattern, which would also be observed for the monomer (**3a**). The complex region of the 400.14 MHz ^1H NMR spectrum of **3** assigned to the succinyl hydrogens was observed to contain two overlapping AA′BB′ patterns, and this was proven by simulation using the program LAME8 (14) (see Fig. 4). Thus, of the three possible structures considered for **3**, only dimeric structure **3b** fits the NMR data. Higher oligomers having both the correct symmetry and even numbers of glucose units would also give two AA′BB′ patterns but can be ruled out by the mass spectral data. The structure of the product suggests that **2a** or a mono- or di-chlorodibutyltin ether of **2a** is an intermediate in its formation, rather than a diesterified monosaccharide.

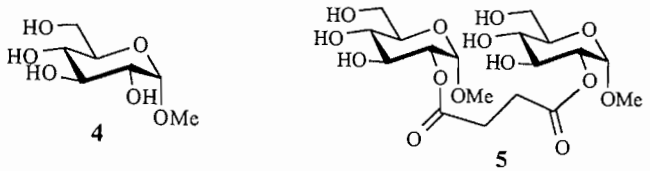
Compound **3b** was particularly difficult to name. The name used, (bis(methyl 4,6-*O*-benzylidene-2-deoxy-α-D-glucopyranosyl-2,3-diyl 2,2′:3,3′-butanedioate), contains modifiers of the principle functional group that are not included in the most recent rules (10*a*). However, these modifiers, which come from the previous rules (10*b*), are necessary to distinguish **3b** from **3a**.

Non-glycosidically linked disaccharides were also formed easily using aromatic acyl dichlorides. Compound **1** reacted with 0.43 equivalent of terephthaloyl chloride and phthaloyl dichloride in the presence of triethylamine to give the 2,2′ diester-linked disaccharides **2e** and **2f** in 95 and 81% yields, respectively (see Fig. 5 for structures) .

The ^1H and ^{13}C NMR spectra of **2e** displayed unusual concentration- and temperature-dependent features in chloroform-*d* (see Fig. 6). All non-aromatic signals in the 400.14 MHz ^1H NMR spectrum of a 0.016 M solution at room temperature were broadened. However, lowering the concentration to 0.008 M caused all signals to become sharp. This unusual effect must be caused by self-association and the precise nature of the association is currently under investigation. Effects like this were not observed for any of the other compounds studied.

In the same way, use of polyfunctional electrophiles leads to non-glycosidically linked oligosaccharides regioselectively in good yield. Reaction of **1** with 1,3,5-benzenetricarbonyl trichloride gave the corresponding non-glycosidically linked trisaccharide (**2g**) in excellent yield as shown in Fig. 7.

Formation of a non-glycosidically linked disaccharide from methyl α-D-glucopyranoside (**4**) had to be performed under conditions different than those above because of its lack of solubility in nonpolar solvents. Refluxing **4** with 1 equivalent of dibutyltin oxide in methanol gave a dibutylstannylene acetal derivative that was carefully dried, then reacted with succinyl chloride in dioxane to give a good yield (72%) of the symmetric 2,2′-linked disaccharide (**5**) plus a small amount (5%) of a syrupy product that was tentatively identified as a monomethyl ester, presumably arising from the residual methanol.



Another *trans*-diol was investigated, benzyl 4,6-*O*-benzylidene β-D-galactopyranoside (**6**). It also gave an excellent yield (78%) of a symmetric non-glycosidically linked disaccharide (**7**), joined through O-3, the site at which electrophiles are known to react with the dibutylstannylene acetal of **6**.

Similar reactions were conducted with the dibutylstannylene acetals derived from two *cis*-diols. Dibutylstannylene acetals derived from *cis*-diols on pyranose rings normally give highly regioselective reactions with electro-

© 1997 NRC Canada

Fig. 4. The region of the 400.14 MHz NMR spectrum of **3** (see Fig. 3 for possible structures) containing the signals of the two CH_2CH_2 groups: bottom, experimental spectrum; middle, LAME8 simulation of one AA′BB′ pattern; top, LAME8 simulation of the other AA′BB′ pattern. The iterative simulations were performed using the transitions from resolution-enhanced spectra. The simulations shown have a slightly narrower line width than the experimental spectrum to emphasize the extra peaks observed in the resolution-enhanced spectra.

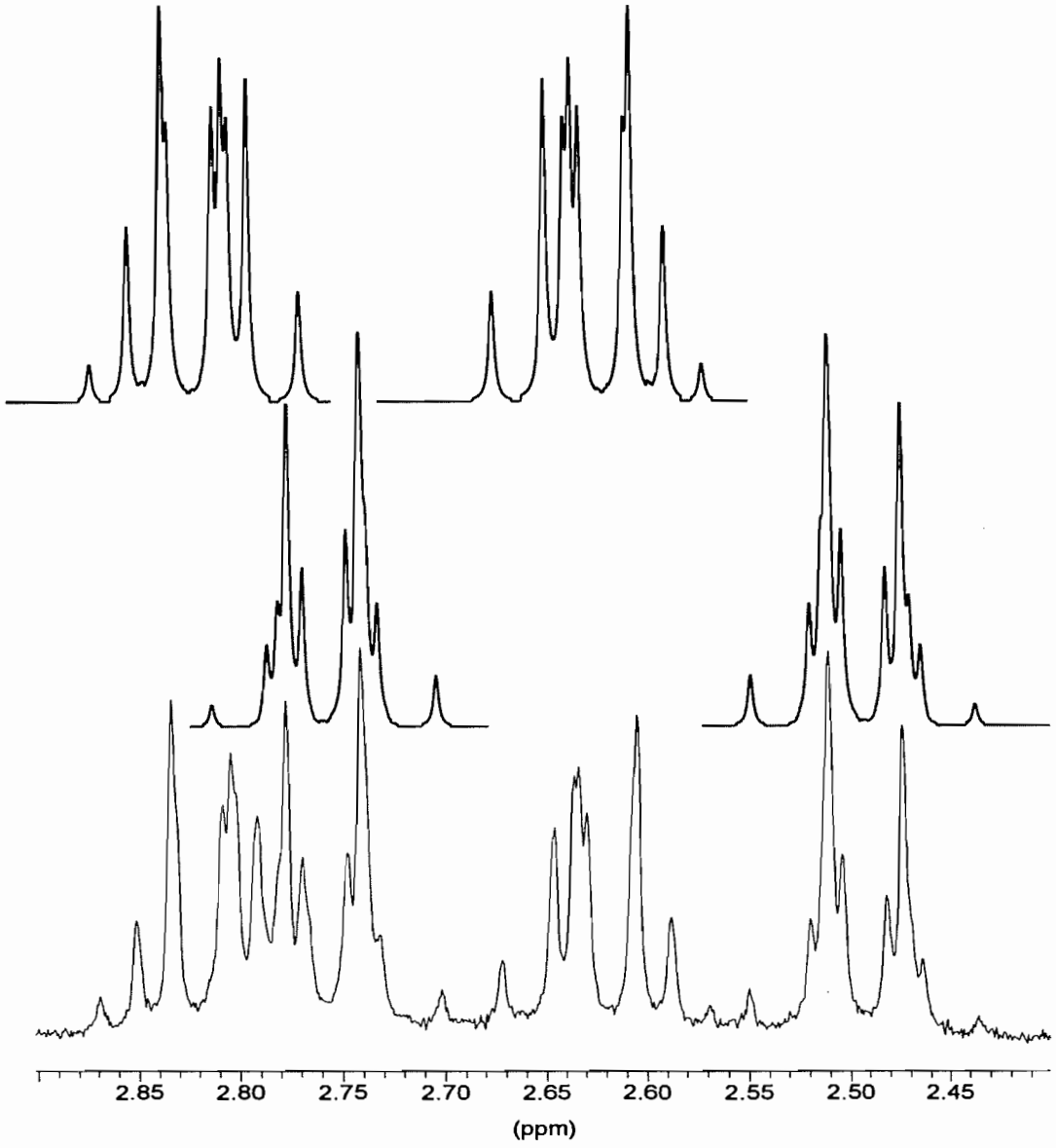
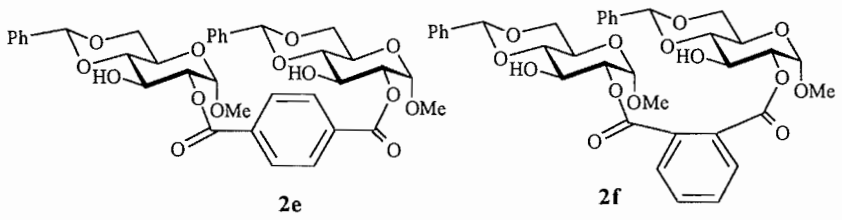


Fig. 5. Structures of products obtained from reactions of the dibutylstannylene acetal of methyl 4,6-*O*-benzylidene-α-D-glucopyranoside (**1**) with aromatic diacyl chlorides.



philes, favouring reaction on equatorial oxygen atoms over the axial oxygen atoms (8, 9) although exceptions have been observed, particularly with mannopyranose derivatives (11), and when the *cis*-diol is flanked by two axial substituents (15). These trends were followed here; methyl 4,6-*O*-benzylidene-α-D-allopyranoside (**8**) was converted to a symmetric non-glycosidically linked disaccharide (**9**) in a highly regioselective manner and in excellent yield (97%) but methyl 4,6-*O*-benzyl-

© 1997 NRC Canada

Can. J. Chem. Downloaded from www.nrcresearchpress.com by 88.146.161.215 on 09/08/12
For personal use only.

Can. J. Chem. Downloaded from www.nrcresearchpress.com by 88.146.161.215 on 09/08/12
For personal use only.

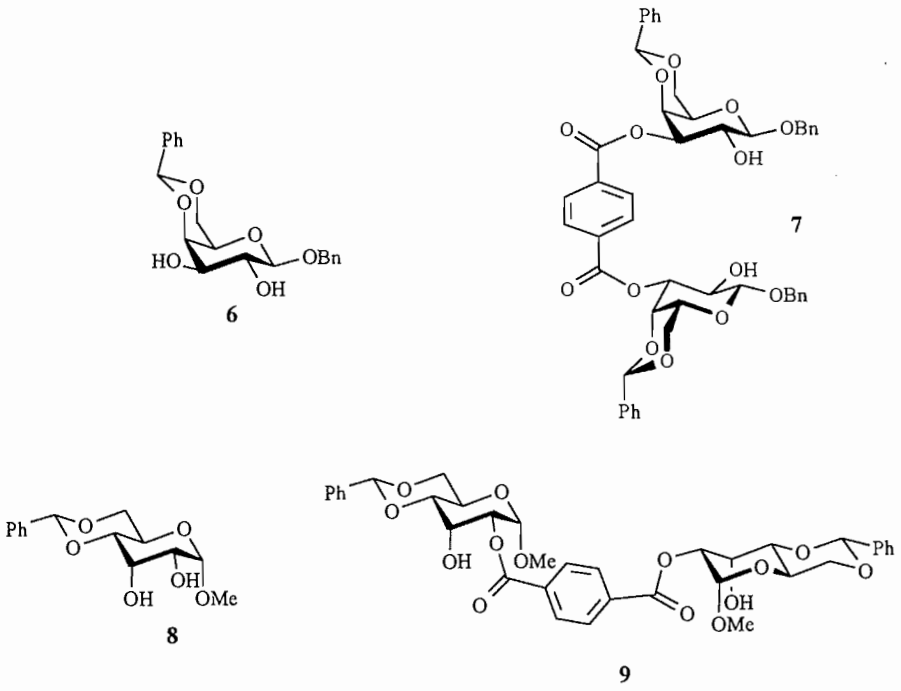
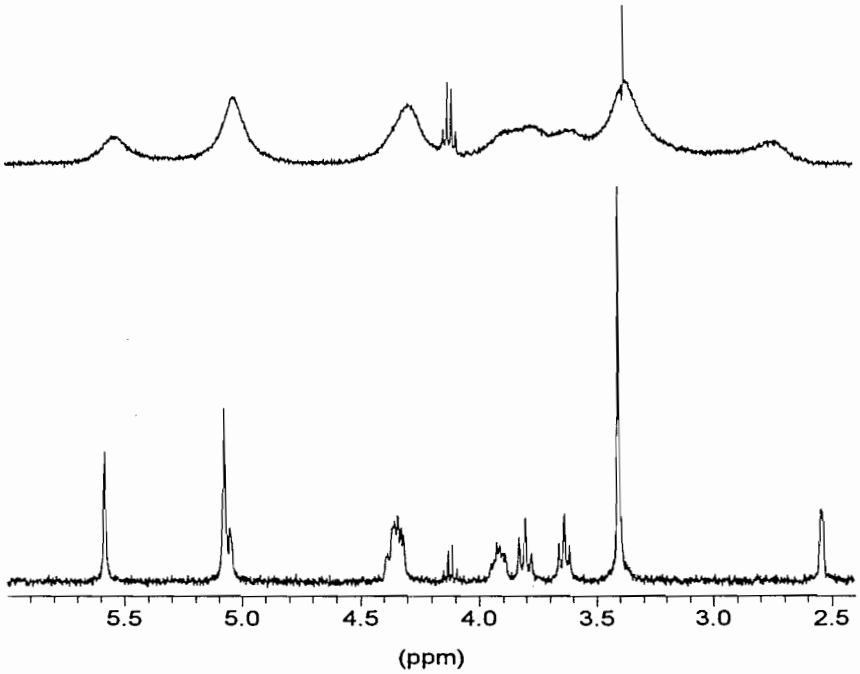


Fig. 6. The 400.14 MHz ^{1}H NMR spectra of bis(methyl 4,6-*O*-benzylidene-α-D-glucopyranoside) 2,2′-terephthalate (**2e**, see Fig. 5 for structure) in chloroform-*d* at two different concentrations: top, 0.016 M; bottom, 0.008 M. For assignments, see the experimental section.



idene-α-D-mannopyranoside (**10**) gave mixtures that varied with the reaction conditions as discussed below.

The reactions of the dibutylstannylene acetal of methyl 4,6-*O*-benzylidene-α-D-mannopyranoside (**10**) with adipoyl chloride under several different conditions are shown in Fig. 8. The structures of these products were established as above. In the reaction performed without added base, TLC evidence suggested that the initial product, the 2,2′-linked dimer (**11a**), rearranged as the reaction progressed. Similar rearrangements were observed in the benzoylation of the dialkylstannylene acetals of primary/secondary diols (16). Under these conditions, where acylation is slowest, the non-glycosidically linked disaccharides were obtained as a close to statistical distribution of 2,2′, 2,3′, and 3,3′ diesters. A monomer (**12**) was

© 1997 NRC Canada

Fig. 7. The reaction of the dibutylstannylene acetal of methyl 4,6-*O*-benzylidene-α-D-glucopyranoside (**1**) with 1,3,5-benzenetricarbonyl trichloride.

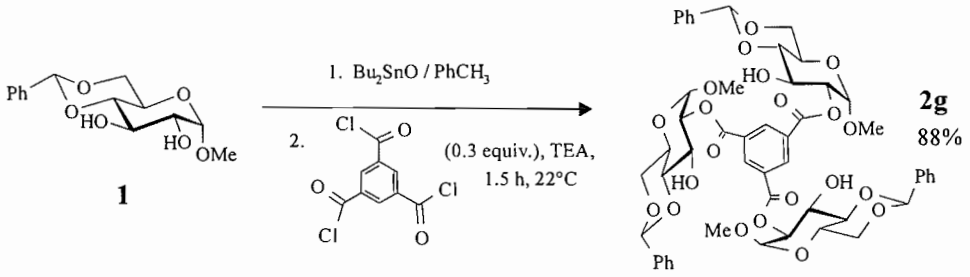
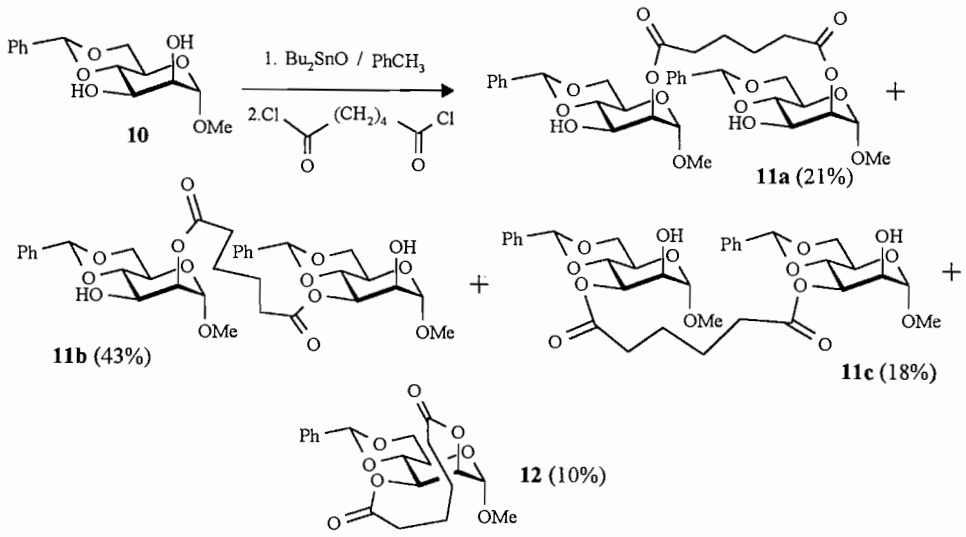
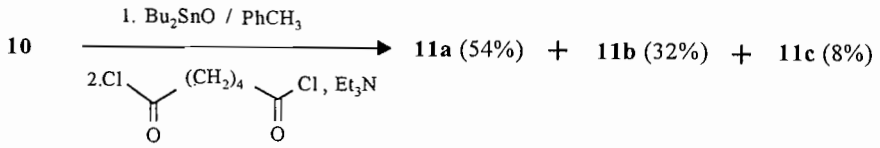
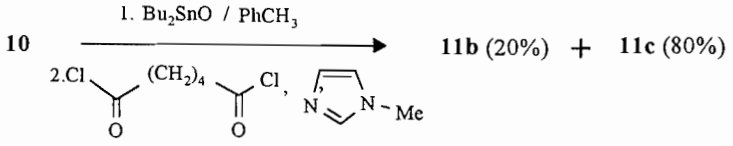


Fig. 8. The reactions of methyl 4,6-*O*-benzylidene-2,3-*O*-dibutylstannylene-α-D-mannopyranoside with adipoyl chloride under various conditions.







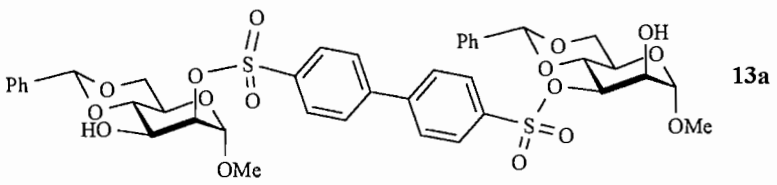
also obtained under these conditions in 10% yield. It was clearly demonstrated to be a monomer, rather than a doubly linked dimer with the same stoichiometry of adipoyl to sugar, by the presence of a M^+ peak (16%) in its EI mass spectrum. Apparently, the succinoyl linkage is too short to form an internal cyclic diester with the dibutylstannylene acetal derived from a *trans*-diol whereas an adipoyl linkage can assume the requisite geometry to give this type of diester with that from a *cis*-diol.

The best yield of a symmetrical non-glycosidically linked disaccharide, the 3,3′-linked compound (**11c**), was obtained from the *O*-dibutylstannylene acetal of **10** using *N*-methylimidazole as an added nucleophile, consistent with the observations of Holzapfel et al. on the benzoylation of the same compound (11). Interestingly, the best yield of the 2,2′-non-glycosidically linked disaccharide (**11a**) was obtained from **10** using triethylamine as an added nucleophile but conditions were never found that yielded a single product from this starting material.

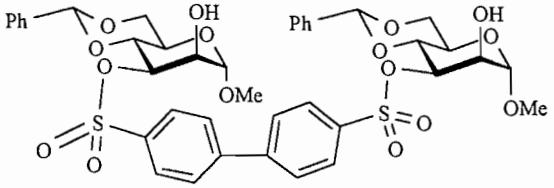
Reactions were also performed on the 2,3-*O*-dibutylstan-

© 1997 NRC Canada

Can. J. Chem. Downloaded from www.nrcresearchpress.com by 88.146.161.215 on 09/08/12
For personal use only.



13a



13b

Can. J. Chem. Downloaded from www.nrcresearchpress.com by 88.146.161.215 on 09/08/12
For personal use only.

nylene acetal of **10** with 4,4′-biphenyldisulfonyl dichloride. It had been found previously that sulfonates do not rearrange during reactions with dialkylstannylene acetals (16). The major product (93% yield) obtained in this reaction, performed in the presence of *N*-methylimidazole, was the 3,3′-non-glycosidically linked disaccharide (**13b**). Compound **13a** has the same regiochemistry as that of the major product obtained in the benzoylation of the dibutylstannylene acetal of **3** performed in the presence of added base (11). It should be noted that the structure of this compound was erroneously reported as the 2,2′-dimer in the preliminary communication (1). A small amount of the non-symmetrically substituted disaccharide (**13a**) was also obtained (5%).

Repetitive application of reactions of this type could result in the rapid formation of large clusters. Valverde et al. have recently shown that carbohydrates having single free hydroxyl groups can be reacted with anhydrides and the product acids converted to acid chlorides, which then can be reacted with stannylene acetals of other sugars to produce nonsymmetric non-glycosidically linked disaccharides with some of the same linkers as employed here (17). Hanessian et al. had earlier made an ester-linked pentaerythritol-centered cluster by first reacting benzyl 2,3,4-tri-*O*-benzyl-α-D-glucopyranoside with succinic anhydride, then esterifying 4 equivalents of the resulting carboxylic acid with pentaerythritol and DCC (18). Combination of the two-step nonselective method used by these two groups with our regioselective one-step approach will make a wide range of clusters available. The availability of a wide variety of possible linkers potentially allows adjustment of the distance between biologically active carbohydrate units to match that required for efficient binding. Investigations of some of these possibilities are in progress.

Conclusions

Symmetrical non-glycosidically linked disaccharides can be prepared with excellent regioselectivity and in excellent yield by reaction of dialkylstannylene acetals with diacyl chlorides and disulfonyl chlorides in the presence of tertiary amines at room temperature. The regioselectivity obtained is the same as previously observed for reaction of acyl chlorides with diols. Formation of diesters is a minor competing reaction that can be minimized by making the initial esterification as fast as possible through addition of added nucleophiles or bases and by controlling the stoichiometry by keeping the diacyl chloride concentration somewhat less than one-half that of the dialkylstannylene acetal. Diester formation is enhanced by using a 1:1 stoichiometry, raising the temperature, and conducting the reaction in the absence of added nucleophiles. Examples of diesters that are cyclic monomers and macrocyclic dimers were observed. Which is obtained depends on the structure of the carbohydrate (*cis*- or *trans*-diol) and on that of the diacyl chloride.

Experimental

General methods

Melting points were determined using a Fisher–Johns melting point apparatus and were uncorrected. Optical rotations were measured with a Perkin–Elmer 141 polarimeter. Thin-layer chromatography (TLC) was performed on Silica Gel aluminium sheets (60 PF-254, Merck, or Al Sil G/UV, Whatman) cut to be approximately 7 cm long, using solvent mixtures measured on a v/v basis. After chromatography was performed, components were located by examination under UV light and by spraying with 2% ceric sulfate in 12 M sulfuric acid and heating on a hot plate until colouration took place. Elemental analyses were performed by Canadian Microanalytical Service Ltd., Vancouver, B.C. Purification or separation of compounds was carried out with "dry column" flash chromatography on silica gel 60 (avg. particle size 2–5μm, Aldrich). Unless otherwise noted, ^{1}H and ^{13}C NMR spectra were recorded on a Bruker AC-250F spectrometer operating at 250.13 and 62.9 MHz, respectively, at ambient temperature on solutions in chloroform-*d*. One ^{1}H NMR spectrum was recorded with a Bruker AMX-400 NMR spectrometer at 400.14 MHz. Chemical shifts are expressed in ppm and referenced to internal Me_4Si (0.03%) or to the central line of the solvent: chloroform-*d* (δ_C = 77.0), dimethyl sulfoxide-d_6 (δ_H = 2.49 and δ_C = 39.7), benzene-d_6 (δ_H = 7.15 and δ_C = 128.0). Assignments and magnitudes of coupling constants were obtained for ^{1}H NMR spectra by first-order analyses and confirmed by COSY experiments. In some cases, HETCOR experiments also aided in assignment. The appearance of signals is indicated using the designations b, s, d, t, q, p, and m for broad, singlet, doublet, triplet, quartet, pentet, and multiplet, respectively. ^{13}C NMR spectral assignments were confirmed by JMD and HETCOR experiments. Accurate mass measure-

© 1997 NRC Canada

Can. J. Chem. Downloaded from www.nrcresearchpress.com by 88.146.161.215 on 09/08/12
For personal use only.

ments were made on Fisons VG ZAB-EQ (FAB) or Dupont-CEC 21-110 (EI) double focussing mass spectrometers at an accuracy of 3 ppm by voltage scanning using PEG Na and PFK reference ions, respectively. APCI or electrospray mass spectra were recorded on a Fisons VG Quattro mass spectrometer. All solvents used in experiments and also in column chromatography were dried and purified by standard methods and distilled before use. Methyl α-D-glucopyranoside, methyl α-D-mannopyranoside, and linker reagents were purchased from Aldrich.

General method for preparation of dibutylstannylene acetals

Unless otherwise stated, the specified monosaccharide 1,2-diol (1 mmol) and dibutyltin oxide (1.1 mmol) were refluxed for 12 h in toluene (20 mL) with continuous azeotropic removal of water. The reaction solution was concentrated to 12 mL and the residue was used directly without further purification for the synthesis of the oligosaccharide with the specified spacer reagent.

Standard work-up

Water (2 mL) was added to the reaction mixture in toluene and the mixture was stirred for 1 h at room temperature, then diluted with chloroform (15 mL). The organic layer was washed with a dilute solution of hydrochloric acid (0.1 M, 5 mL), with water (2 × 15 mL), and with a saturated solution of sodium bicarbonate (15 mL), unless otherwise mentioned, then dried over magnesium sulfate and concentrated.

*Bis(methyl 4,6-O-benzylidene-2-deoxy-α-D-glucopyranosid-2-yl) butanedioate (**2a**)*

Methyl 4,6-*O*-benzylidene-α-D-glucopyranoside (**1**) (19) (0.423 g, 1.5 mmol) was reacted with dibutyltin oxide (0.441g, 1.65 mmol) as in the general method to give the dibutylstannylene acetal. The stirred solution was cooled to room temperature and triethylamine (230 μL, 1.65 mmol) was added. After 0.5 h, a solution of freshly distilled succinyl chloride (72 μL, 0.652 mmol) in toluene (1 mL) was added slowly. The colour of the solution gradually changed to dark brown. Standard work-up after 30 min was followed by purification of the residue by dry column flash chromatography using a solvent gradient from cyclohexane to cyclohexane/ethyl acetate 1:5 as eluent. The product, a solid, was recrystallized from ethyl acetate and cyclohexane to give fine colourless needles of the title compound (**2a**); mp 117–118°C, R_F = 0.25 (ethyl acetate: hexane; 1:1), yield 0.383 g (91%); $[\alpha]_D^{24}$ +76.7 (*c* 1.25, chloroform); ^{1}H NMR δ: 2.72 (s, 4H, 2 × CH_2), 3.38 (s, 6H, 2 × OMe), 3.52 (t, 2H, $J_{4,5} = J_{3,4}$ = 8.9 Hz, 2 × H-4), 3.72 (t, 2H, $J_{5,6a} = J_{6a,6e}$ = 10.1 Hz, 2 × H-6_{ax}), 3.82 (td, 2H, $J_{5,6a} = J_{4,5}$ = 9.6 Hz, $J_{5,6e}$ = 4.2 Hz, 2 × H-5), 4.15 (t, 2H, $J_{2,3} = J_{3,4}$ = 9.2 Hz, 2 × H-3), 4.26 (X of ABX pattern, 2H, 2 × H-6_{eq}), 4.79 (dd, 2H, $J_{2,3}$ = 9.5 Hz, $J_{1,2}$ = 4.0 Hz, 2 × H-2), 4.90 (d, 2H, $J_{1,2}$ = 3.7 Hz, 2 × H-1), 5.51 (s, 2H, 2 × PhCH), 7.26–7.58 (m, 10H, 2 × ArH); ^{13}C NMR δ: 29.2 (2C, 2 × CH_2), 55.3 (2C, 2 × OMe), 62.0 (2C, 2 × C-5), 68.4 (2C, 2 × C-3), 68.7 (2C, 2 × C-6), 73.9 (2C, 2 × C-2), 81.1 (2C, 2 × C-4), 97.4 (2C, 2 × C-1), 101.9 (2C, 2 × PhCH), 126.2, 128.1, 129.2 (6C, 2 × Ar-C), 136.9 (2C, 2 × Ar-C_{ipso}), 172.0 (2C, 2 × COO). Anal. calcd. for $C_{32}H_{38}O_{14}$: C 59.44, H 5.92; found: C 59.12, H 5.95.

*Bis(methyl 4,6-O-benzylidene-2-deoxy-α-D-glucopyranosid-2-yl) hexanedioate (**2b**)*

Compound **1** (0.564 g, 2 mmol) was reacted with dibutyltin oxide (0.523 g, 2.1 mmol) as in the standard method. The solution was concentrated to 15 mL and triethylamine (297 μL, 2.1 mmol) was added to the stirred room temperature solution. After 30 min, the solution was cooled to 0°C and freshly distilled adipoyl chloride (98 μL, 0.67 mmol) was added dropwise. The cooling bath was removed 30 min later, then the reaction was stopped after a further 20 min and worked up in the standard fashion. Dry column flash chromatography (gradient from cyclohexane to ethyl acetate) gave the title compound (**2b**) as a solid: R_F = 0.23 (ethyl acetate/hexanes 1:1); yield 0.380 g (84%); mp 165–166°C; $[\alpha]_D^{22}$ +102 (*c* 1.08, chloroform); ^{1}H NMR δ: 1.71 (b m, 4H, 2 × $CH_2CH_2CH_2$), 2.43 (b m, 2 × CH_2CO), 2.94 (d, 2H, $J_{3,OH\text{-}3}$ = 3.1 Hz, 2 × OH-3), 3.37 (s, 6H, 2 × OMe), 3.53 (t, 2H, $J_{4,5} = J_{3,4}$ = 9.2 Hz, 2 × H-4), 3.74 (t, 2H, $J_{5,6ax} = J_{6eq,6ax}$ = 9.8 Hz, 2 × H-6_{ax}), 3.82 (td, 2H, $J_{5,6eq}$ = 4.3 Hz, $J_{4,5} = J_{5,6ax}$ = 9.8 Hz, 2 × H-5), 4.15 (dt, 2H, $J_{2,3} = J_{3,4}$ = 9.5 Hz, 2 × H-3), 4.27 (X of ABX pattern, 2H, 2 × H_{6eq}), 4.81 (dd, 2H, $J_{1,2}$ = 3.7 Hz, $J_{2,3}$ = 9.8 Hz, 2 × H-2), 4.93 (d, 2H, 2 × H-1), 5.53 (s, 2H, 2 × PhCH), 7.32–7.52 (m, 10H, 2 × Ar-H); ^{13}C NMR δ: 24.0 (2 × $CH_2CH_2CH_2$), 33.6 (2 × CH_2CO), 55.3 (2 × OMe), 62.0 (2 × C-5), 68.5 (2 × C-3), 68.8 (2 × C-6), 73.5 (2 × C-2), 81.3 (2 × C-4), 97.5 (2 × C-1), 101.9 (2 × PhCH), 126.3, 128.3, 129.2 (Ar-C), 136.9 (2 × Ar-C_{ipso}), 173.1 (2 × COO). Anal. calcd. for $C_{34}H_{42}O_{14}$: C 60.53, H 6.27; found: C 60.76, H 6.34.

*Bis(methyl 4,6-O-benzylidene-2-deoxy-α-D-glucopyranosid-2-yl) dodecanedioate (**2c**)*

Treatment of compound **1** (0.564 g, 2 mmol) with dibutyltin oxide (0.523 g, 2.1 mmol) as in the standard method gave the dibutylstannylene acetal. The reaction mixture was concentrated to 15 mL and triethylamine (297 μL, 2.1 mmol) was added. After 0.5 h, the solution was cooled to 0°C and freshly distilled dodecanedioyl chloride (175 μL, 0.7 mmol) was added dropwise to the magnetically stirred solution. The cooling bath was removed after 30 min and 1 h later the reaction was quenched by adding water. Standard work-up yielded a syrupy residue that was fractionated by means of dry column flash chromatography using ethyl acetate/cyclohexane 2:1 as eluent. The first fraction was the title compound (**10**), a solid, R_F = 0.76 (ethyl acetate/cyclohexane, 2:1); yield 0.415 g (78%); mp 123–124°C; $[\alpha]_D^{23}$ +256 (*c* 0.29, chloroform); ^{1}H NMR δ: 1.28 (b, 12H, 6 × CH_2), 1.65 (b p, *J* = 7 Hz, 4H, 2 × CH_2CH_2CO), 2.40 (t, 4H, *J* = 7.3 Hz, 2 × CH_2CO), 2.50 (d, 2H, $J_{3,OH\text{-}3}$ = 3.1 Hz, 2 × OH-3), 3.39 (s, 6H, 2 × OMe), 3.55 (t, 2H, $J_{3,4} = J_{4,5}$ = 9 Hz, 2 × H-4), 3.75 (t, 2H, $J_{5,6ax} = J_{6ax,6eq}$ = 9.8 Hz, 2 × H-6_{ax}), 3.84 (td, 2H, $J_{5,6e}$ = 4.2 Hz, $J_{4,5} = J_{5,6a}$ = 9.7 Hz, 2 × H-5), 4.17 (td, 2H, $J_{2,3} = J_{3,4}$ = 9.3 Hz, $J_{3,OH}$ = 2.8 Hz, 2 × H-3), 4.29 (dd, 2H, 2 × H-6_{eq}), 4.80 (dd, 2H, 2 × H-2), 4.97 (d, 2H, $J_{1,2}$ = 4.0 Hz, 2 × H-1), 5.54 (s, 2H, 2 × PhCH), 7.36–7.42 (m, 6H, Ar-H), 7.46–7.51 (m, 4H, Ar-H); ^{13}C NMR δ: 24.8 (2 × CH_2CH_2CO, 28.9, 29.1, 29.3 (6 × CH_2), 34.4 (2 × CH_2CO), 55.4 (2 × OMe), 61.9 (2 × C-5), 68.6 (2 × C-3), 65.8 (2 × C-6), 73.4 (2 × C-2), 81.3 (2 × C-4), 97.5 (2 × C-1), 102.0 (2 × PhCH), 126.3, 128.3, 129.3 (Ar-C), 136.9 (2 × Ar-C_{ipso}), 173.5 (2 × COO). Anal. calcd. for $C_{40}H_{54}O_{14}$: C 63.31, H 7.17; found: C 62.94, H 6.81.

Further elution gave (methyl 4,6-*O*-benzylidene-2-

© 1997 NRC Canada

Can. J. Chem. Downloaded from www.nrcresearchpress.com by 88.146.161.215 on 09/08/12
For personal use only.

deoxy-α-D-glucopyranosid-2-yl) (methyl 4,6-*O*-benzylidene-3-deoxy-α-D-glucopyranosid-3-yl) dodecanedioate (**2d**), a solid, recrystallized from ethyl acetate – cyclohexane, mp 134–135°C; R_F = 0.57 (ethyl acetate:cyclohexane, 2:1); yield 0.065 g (12%); $[\alpha]_D^{23}$ +171 (*c* 0.39, chloroform); ^{1}H NMR δ: 1.17–1.33 (m, 12H, 6 × CH_2), 1.56–1.70 (m, 5H, 2 × CH_2CH_2CO), 2.32(d, 1H, $J_{2',OH\text{-}2'}$ = 11.6 Hz, OH-2′), 2.36, 2.40 (2 t, 4H, *J* = 7.5 Hz, 2 × CH_2CO), 2.60 (br d, 1H, $J_{3,OH\text{-}3}$ = 2.2 Hz, OH-3), 3.39 (s, 3H, OMe), 3.45 (s, 3H, OMe′), 3.56 (t, 1H, $J_{3,4} = J_{4,5}$ = 9.3 Hz, H-4), 3.71 (t, 1H, $J_{3',4'} = J_{4',5'}$ = 9.5 Hz, H-4′), 3.65 (ddd, 1H, $J_{1',2'}$ = 3.8 Hz, $J_{2',3'}$ = 9.8 Hz, $J_{2',OH\text{-}2'}$ = 11.6 Hz, H-2′), 3.74 (t, 1H, $J_{5',6'ax} = J_{6'eq,6'ax}$ = 10.1 Hz, H-6′$_{ax}$), 3.76 (t, 1H, $J_{5,6ax} = J_{6eq,6ax}$ = 9.8 Hz, H-6$_{ax}$), 3.84, 3.86 (2 td, 2H, $J_{5,6e}$ = 3.4 Hz, $J_{4,5} = J_{5,6a}$ = 10.0 Hz, H-5 and H-5′), 4.17 (td, 1H, $J_{2,3} = J_{3,4}$ = 9.5 Hz, $J_{3,OH\text{-}3}$ = 2.2 Hz, H-3), 4.30 (dd, 2H, $J_{6eq,6ax} = J_{6'eq,6'ax}$ = 9.5 Hz, $J_{5,6eq} = J_{5',6'eq}$ = 4.0 Hz, H-6$_{eq}$ and H-6′$_{eq}$), 4.78 (d, 1H, $J_{1',2'}$ = 3.8 Hz, H-1′), 4.81 (dd, 1H, $J_{1,2}$ = 3.7 Hz, $J_{2,3}$ = 9.8 Hz, H-2), 4.95 (d, 1H, $J_{1,2}$ = 4.0 Hz, H-1), 5.33 (t, 1H, $J_{2',3'} = J_{3',4'}$ = 9.6 Hz, H-3′), 5.49 (s, 1H, PhCH′), 5.55 (s, 1H, PhCH), 7.33–7.52 (m, 10H, Ar-H and Ar′-H); ^{13}C NMR δ: 24.8, 25.0 (2 × CH_2CH_2CO), 28.8, 28.9, 29.1, 29.2, 29.3 (5 × CH_2), 34.0, 34.3 (2 × CH_2CO), 55.4, 55.5 (2 × OMe), 61.9 (C-5), 62.6 (C-5′), 68.6 (C-3), 68.8 (C-6 and C-6′), 71.8 (C-2′), 72.0 (C-3′), 73.3 (C-2), 78.6 (C-4′), 81.3 (C-4), 97.5 (C-1), 100.1 (C-1′), 101.4, 101.9 (2 × CHPh), 126.1, 126.3, 128.1, 128.3, 129.0, 129.2 (Ar-C), 136.91, 136.94 (Ar-C_{ipso}), 173.5, 173.9 (COO); Anal. calcd. for $C_{10}H_{54}O_{14}$: C 63.31, H 7.17; found: C 63.05, H 7.12.

*Bis(methyl 4,6-O-benzylidene-2-deoxy-α-D-glucopyranosid-2,3-diyl 2,2′:3,3′-butanedioate) (**3**)*

Compound **1** (0.423 g, 1.5 mmol) was reacted with dibutyltin oxide (0.373 g, 1.5 mmol) in toluene (20 mL) as in the general method. Toluene (350 mL) was added and the resulting solution was heated to 80°C. Succinyl chloride (1.5 mmol, 164 μL) in toluene (5 mL) was added dropwise to the solution stirred at that temperature. The reaction was stopped after 10 h and worked up as in the standard method. The solid residue were separated by means of dry column flash chromatography using a gradient from cyclohexane to ethyl acetate as eluent. The first fraction was present in very small amounts and was not identified. The second fraction was the title compound (**3**), a solid, which was recrystallized from ethyl acetate and cyclohexane; mp 209–210°C; yield 0.275 g (50%); R_F = 0.5 (ethyl acetate: hexane; 1:1); $[\alpha]_D^{23}$ +52.2 (*c* 0.465, chloroform); ^{1}H NMR (400.14 MHz) δ: 2.493, 2.757 (AA′XX′ pattern, 4H, $J_{AX} = J_{A'X'}$ = −17.3 Hz, $J_{AX'} = J_{A'X}$ = 2.4 Hz, $J_{AA'}$ = 10.6 Hz, $J_{XX=}$ = 8.1 Hz, one CH_2CH_2 unit, RMS error for LAME8 simulation 0.18 Hz), 2.620, 2.817 (AA′BB′ pattern, 4H, $J_{AB} = J_{A'B'}$ = −17.0 Hz, $J_{AB'} = J_{A'B}$ = 6.4 Hz, $J_{AA'} = J_{BB'}$ = 7.3 Hz, the 2nd CH_2CH_2 unit, RMS error for LAME8 simulation 0.14 Hz), 3.40 (s, 3H, OMe), 3.71 (t, 1H, $J_{3,4} = J_{4,5}$ = 9.6 Hz, H-4), 3.75 (t, 1H, $J_{5,6ax} = J_{6ax,6eq}$ = 10.1 Hz, H-6$_{ax}$), 3.91 (td, 1H, H-5), 4.30 (dd, 1H, $J_{6eq,6ax}$ = 9.8 Hz, $J_{5,6eq}$ = 4.3 Hz, H-6$_{eq}$), 4.80 (dd, 1H, $J_{2,3}$ = 9.8 Hz, $J_{1,2}$ = 3.7 Hz, H-2), 5.00 (d, 1H, H-1), 5.50 (t, 1H, $J_{2,3} = J_{3,4}$ = 9.6 Hz, H-3), 5.51 (s, 1H, PhCH), 7.24–7.55 (m, 5H, Ar-H); ^{13}C NMR δ: 28.9, 29.3 (2 CH_2), 55.4 (OMe), 62.2 (C-5), 68.8 (C-6), 69.9 (C-3), 72.8 (C-2), 78.6 (C-4), 97.5 (C-1), 101.7 (PhCH), 126.2, 128.2, 129.2 (Ar-C), 136.9 (Ar-C_{ipso}), 170.7, 171.5 (CO); mass spectrum (EI) (scan from *m/z* 800 to *m/z* 150) *m/z*: M^+ (11%), $M^+ - 1$ (2.7%), 579 (1.7%), 465 (2.9%), 410 (1.7%), 386 (4.2), 368 (2.5%), 247 (100%). HRMS (EI), calcd. for $C_{36}H_{40}O_{16}$: 728.2316; found: 728.2310. Anal. calcd. for $C_{36}H_{40}O_{16}\cdot H_2O$: C 58.56, H 5.58; found: C 58.68, H 5.60.

The third fraction was compound **2a**, yield 0.443 g (46%).

*Bis(methyl 4,6-O-benzylidene-2-deoxy-α-D-glucopyranosid-2-yl) terephthalate (**2e**)*

Compound **1** (0.282 g, 1 mmol) was reacted with dibutyltin oxide (0.2738 g, 1.1 mmol) as in the general method. To the dibutylstannylene acetal solution was added triethylamine (156 μL, 1.1 mmol) and the resulting solution was stirred for 0.5 h. Terephthaloyl chloride (79 mg, 0.43 mmol) was added slowly to the mixture and stirring was continued for 1 h, then standard work-up was performed. The residue was purified by flash dry column chromatography (cyclohexane – ethyl acetate, gradient elution), which gave the title compound (**2e**) as a solid, R_F = 0.54 (ethyl acetate/cyclohexane, 1:1), yield 0.283 g (95%), which was recrystallized from ethyl acetate and cyclohexane to give needle-like crystals: mp 139–140°C; $[\alpha]_D^{25}$ +129 (*c* 0.73, chloroform); ^{1}H NMR δ: 2.26 (d, 2H, $J_{3,3\text{-}OH}$ = 2.8 Hz, 2 × OH-3), 3.41 (s, 6H, 2 × OMe), 3.64 (t , 2H, $J_{3,4} = J_{4,5}$ = 9.2 Hz, 2 × H-4), 3.81 (t, 2H, $J_{5,6ax} = J_{6ax,6eq}$ = 10.1 Hz, 2 × H-6$_{ax}$), 3.92 (td, 2H, $J_{5,6eq}$ = 4.3 Hz, $J_{4,5} = J_{5,6ax}$ = 9.7 Hz, 2 × H-5), 4.34 (dd, 2H, $J_{5,6eq}$ = 4.3 Hz, $J_{6eq,6ax}$ = 9.8 Hz, H-6$_{eq}$), 4.37 (b dt, 2 × H-3), 5.04–5.09 (m, 4H, 2 × H-1 and 2 H-2), 5.59 (s, 2H, 2 × PhCH), 7.36–7.42 (m, 6H, 2 × Ar-H), 7.48–7.54 (m, 4H, 2 × Ar-H), 8.17 (s, 4H, Ar′-H); ^{13}C NMR ($CDCl_3$, 62.9 MHz), δ: 55.5 (2C, 2 × OMe), 62.0 (2C, 2 × C-5), 68.8 (2C, 2 × C-3), 68.9 (2C, 2 × C-6), 74.4 (2C, 2 × C-2), 81.5 (2C, 2 × C-4), 97.6 (2C, 2 × C-1), 102.1 (2C, 2 × PhCH), 126.3, 128.4, 129.0 (2 × Ar-C), 129.4 (2 × Ar′-C), 133.7 (2 × Ar′-C_{ipso}), 136.9 (2 × Ar-C_{ipso}), 165.3 (2C, 2 × COO).

*Bis(methyl 4,6-O-benzylidene-2-deoxy-α-D-glucopyranosid-2-yl) phthalate (**2f**)*

Compound **1** (0.564 g, 2 mmol) was reacted with dibutyltin oxide (0.523 g, 2.1 mmol) under standard conditions to give a solution of the dibutylstannylene acetal. The solution was concentrated to 15 mL and cooled to room temperature, triethylamine (297 μL, 2.1 mmol) was added, and the solution was stirred for 30 min. The solution was cooled to 0°C and freshly distilled phthaloyl dichloride (97 μL, 0.67 mmol) was added dropwise. The reaction mixture was stirred 30 min at 0°C, then another 30 min at room temperature. Work-up using the standard method gave a solid residue that was separated by dry column flash chromatography (hexane, ethyl acetate as gradient). The first fraction, yield (0.014 g, 4.4%) was not identified.

The second fraction was the title compound (**2f**), a solid: R_F = 0.51 (ethyl acetate/cyclohexane, 1:1); yield 0.378 g (81%). It was recrystallized from chloroform and hexane; mp 124–125°C, $[\alpha]_D^{22}$ +82.4 (*c* 0.418, chloroform); ^{1}H NMR δ: 3.32 (bd, 2H, $J_{3,OH\text{-}3}$ = 2.4 Hz, 2 × OH-3), 3.38 (s, 6H, 2 × OMe), 3.58 (t, 2H, $J_{4,5} = J_{3,4}$ = 9.2 Hz, 2 × H-4), 3.74 (t, 2H, $J_{5,6ax} = J_{6eq,6ax}$ = 9.8 Hz, 2 × H-6$_{ax}$), 3.84 (td, 2H, $J_{4,5} = J_{5,6ax}$ = 9.6 Hz, $J_{5,6eq}$ = 4.3 Hz, 2 × H-5), 4.23 (td, 2H, $J_{3,OH\text{-}3}$ = 1.8 Hz, $J_{2,3} = J_{3,4}$ = 9.2 Hz, 2 × H-3), 4.28 (dd, 2H, $J_{5,6eq}$ = 3.7 Hz, $J_{6eq,6ax}$ = 9.2 Hz, 2 × H-6$_{eq}$), 5.01 (m, 4H, 2 × H-2 and 2 × H-1), 5.52 (s, 2H, 2 × PhCH), 7.33–7.42 (m, 6H, Ar-H), 7.47–7.59 (m, 6H, ArH + 2 Phth ArH), 7.78–7.82 (m, 2H, F-Phth Ar-H); ^{13}C

© 1997 NRC Canada

Can. J. Chem. Downloaded from www.nrcresearchpress.com by 88.146.161.215 on 09/08/12
For personal use only.

NMR δ: 55.4 (2C, 2 × OMe), 62.0 (2C, 2 × C-5), 68.5 (2C, 2 × C-3), 68.7 (2C, 2 × C-6), 74.9 (2C, 2 × C-2), 81.1 (2C, 2 × C-4), 97.4 (2C, 2 × C-1), 101.9 (2C, 2 × PhCH), 126.3, 128.2, 129.1, 129.6 (Ar-C), 130.9 (Ar′-C_{ipso}), 131.6 (Ar-C), 136.9 (2 × Ar-C_{ipso}), 167.1 (2C, 2 × COO). HRMS (FAB) for M + H^+, $C_{36}H_{39}O_{14}$, calcd.: 695.2340; found: 695.2336; for M + H^+ − CH_3OH, $C_{35}H_{35}O_{13}$, calcd.: 663.2078; found: 663.2090.

*Tris(methyl 4,6-O-benzylidene-2-deoxy-α-D-glucopyranosid-2-yl) (1,3,5-benzenetricarboxylate)(**2g**)*

Compound **1** (0.564 g, 2 mmol) was treated with dibutyltin oxide (0.523 g, 2.1 mmol) in toluene (30 mL) as in the standard method. The resulting solution was concentrated to 15 mL, cooled to room temperature, and triethylamine (296 μL, 2.1 mmol) was added. The reaction mixture was stirred for 0.5 h, then cooled to 0°C. 1,3,5-Benzenetricarbonyl trichloride (0.159 g, 0.6 mmol) was added slowly to the cooled mixture. The cooling bath was removed after 30 min and the solution was stirred a further 1 h. Standard work-up gave a solid that was purified by means of dry flash column chromatography (cyclohexane, ethyl acetate) to give the title compound (**2g**), R_F = 0.8 (ethyl acetate: hexane, 3:2), as a colourless solid; mp 172–173°C; yield 0.531 g (88%); $[\alpha]_D^{24}$ + 123 (*c* 1.63, chloroform); ^{1}H NMR δ: 3.28 (s, 9H, 3 × OMe), 3.64 (t, 3H, $J_{3,4}$ = $J_{4,5}$ = 9.2 Hz, 3 × H-4), 3.75 (t, 3H, $J_{5,6ax}$ = $J_{6ax,6eq}$ = 9.6 Hz, 3 × H-6_{ax}), 3.86 (td, 3H, $J_{4,5}$ = $J_{5,6ax}$ = 9.6 Hz, $J_{5,6eq}$ = 4.2 Hz, 3 × H-5), 4.02 (b s, 3H, 3 × OH-3), 4.27 (X of ABX pattern, 3H, 3 × H-6_{eq}), 4.35 (t, 3H, $J_{2,3}$ = $J_{4,5}$ = 9.3 Hz, 3 × H-3), 4.99 (dd, 3H, $J_{1,2}$ = 3.7 Hz, $J_{2,3}$ = 9.2 Hz, 3 × H-2), 5.04 (d, 3H, $J_{1,2}$ = 4.0 Hz, 3 × H-1), 5.54 (s, 3H, 3 × PhCH), 7.28–7.35 (m, 9H, Ar-H), 7.46–7.52 (m, 6H, Ar-H), 8.74 (s, 3H, Ar′-H); ^{13}C NMR δ: 55.2 (3C, 3 × OMe), 62.0 (3C, 3 × C-5), 68.4 (3C, 3 × C-3), 68.7 (3C, 3 × C-6), 75.0 (3C, 3 × C-2), 81.2 (3C, 3 × C-4), 97.3 (3C, 3 × C-1), 102.0 (3C, 3 × PhCH), 126.3, 128.3, 129.2 (2 × Ar-C), 130.3 (3 × Ar′-C_{ipso}), 135.4 (2 × Ar-C_{ipso}), 137.0 (3 × Ar′-C), 164.4 (3C, 3 × COO). HRMS (ES) for M+H^+, $C_{51}H_{55}O_{21}$, calcd.: 1003.3236; found: 1003.3227.

*Bis(methyl 2-deoxy-α-D-glucopyranosid-2-yl) butanedioate (**5**)*

The milky solution resulting from refluxing methyl α-D-glucopyranoside (**4**) (0.583 g, 3 mmol) and dibutyltin oxide (0.747 g, 3 mmol) in freshly dried methanol (30 mL) became a clear homogenous solution after about 1 h and was refluxed for an additional 1.5 h. The solution was concentrated, then kept under vacuum (0.1 Torr; 1 Torr = 133.3 Pa) for an additional 1 h. This residue was dissolved in dry dioxane (15 mL), cooled to 0°C, and a solution of freshly distilled succinyl chloride (144 μL, 1.304 mmol) in dioxane (2 mL) was added dropwise. After 30 min, the cooling bath was removed, and the solution was stirred a further 8 h. The solution was concentrated and the syrupy residue was separated by dry column flash chromatography using a solvent gradient from ethyl acetate to ethanol. The first fraction was methyl (methyl 2-deoxy-α-D-glucopyranosid-2-yl) butanedioate as a syrup, R_F = 0.66 (ethyl acetate/methanol 1:2); yield 0.022 g (5.4%); $[\alpha]_D^{24}$ +131 (*c* 0.61, chloroform) ; ^{1}H NMR δ: 2.7 (m, 4H, 2 × CH_2), 3.38 (s, 3H, OMe), 3.55–3.75 (b m, 2H, H-4 and H-5), 3.70 (s, 3H, COO*Me*), 3.86 (b s, 2H, H-6 and H-6′), 3.96 (t, 1H, $J_{2,3}$ = $J_{3,4}$ = 8.9 Hz, H-3), 4.77 (dd, 1H, $J_{1,2}$ = 3.7 Hz, $J_{2,3}$ = 9.8 Hz, H-2), 4.86 (d, 1H, H-1); ^{13}C NMR δ: 29.0, 29.2 (2 CH_2), 52.1 (COO*Me*), 55.2 (glycoside OMe), 61.7 (C-6), 70.2 (C-5), 70.9 (C-4), 71.6 (C-3), 73.5 (C-2), 97.1 (C-1), 172.3, 173.3 (COO).

The second fraction was the title compound (**5**), R_F = 0.52 (ethyl acetate/ethanol, 2:7), a solid, mp 38–40°C; yield 0.441 g (72%); $[\alpha]_D^{23}$ + 105 (*c* 2.97, chloroform); ^{1}H NMR (D_2O) δ: 2.52 (s, 4H, 2 × CH_2), 3.13 (s, 6H, 2 × OMe), 3.24 (t, 2H, $J_{3,4}$ = $J_{4,5}$ = 9.5 Hz, 2 × H-4), 3.36–3.44 (m, 2H, 2 × H-5), 3.34–3.64 (m, 6H, 2 × H-3, 2 × H-6, and 2 × H-6′), 4.50 (dd, 2H, $J_{2,3}$ = 10.1 Hz, 2 × H-2), 4.68 (d, 2H, $J_{1,2}$ = 3.5 Hz, 2 × H-1); ^{13}C NMR (D_2O) δ: 31.3 (4C, 4 × CH_2), 57.5 (2C, 2 × OMe), 63.1 (2C, 2 × C-6), 72.1 (2C, 2 × C-4), 73.4 (2C, 2 × C-3), 74.2 (2C, 2 × C-5), 75.9 (2C, 2 × C-2), 99.1 (2C, 2 × C-1), 176.5 (2C, 2 × COO). Anal. calcd. for $C_{18}H_{30}O_{14}\cdot H_2O$: C 44.26, H 6.60; found: C 43.83, H 6.43.

*Bis(benzyl 4,6-O-benzylidene-3-deoxy-β-D-galactopyranosid-3-yl) terephthalate (**7**)*

The solution from the reaction of benzyl 4,6-*O*-benzylidene-β-D-galactopyranoside (**6**) (20) (0.197 g, 0.55 mmol) with dibutyltin oxide (0.192 g, 0.77 mmol) as in the standard method was concentrated to 10 mL, triethylamine (109 μL, 0.77 mmol) was added, and the resulting solution was stirred at room temperature for 0.5 h. Terephthaloyl chloride (65 mg, 0.32 mmol) was added and the mixture was was stirred until TLC (ethyl acetate:cyclohexane, 1:1) indicated that starting material was consumed (2 h). Standard work-up gave a syrupy residue that was purified using dry column flash chromatography with a solvent gradient from cyclohexane to ethyl acetate. The title compound (**7**), R_F = 0.41, a solid, was recrystallized from ethyl acetate – cyclohexane to give fine crystals: mp 223–224°C; yield 0.210 g (78%); $[\alpha]_D^{25}$ +69.9 (*c* 0.925, chloroform); ^{1}H NMR δ: 1.61 (s, 2H, H_2O), 2.52 (d, 2H, $J_{2,OH\text{-}2}$ = 1.8 Hz, 2 × OH-2), 3.56 (b s, 2H, H-5), 4.10 (dd, 2H, $J_{5,6ax}$ = 1.4 Hz, $J_{6ax,6eq}$ = 12.5 Hz, 2 × H-6_{ax}), 4.23 (ddd, 2H, $J_{1,2}$ = 7.9 Hz, $J_{2,3}$ = 10.4 Hz, 2 × H-2), 4.39 (b d, 2H, 2 × H-6_{eq}), 4.48 (b d, 2H, $J_{3,4}$ = 4.3 Hz, 2 × H-4), 4.51 (d, 2H, 2 × H-1), 4.65 (d, 2H, *J* = 11.6 Hz, $\frac{1}{2}$ $PhCH_2$), 5.01 (d, 2H, $\frac{1}{2}$ $PhCH_2$), 5.13 (dd, 2H, $J_{2,3}$ = 10.4 Hz, $J_{3,4}$ = 3.7 Hz, 2 × H-3), 5.51 (s, 2H, 2 × PhCH), 7.31–7.36 (m, 20H, Ar-H), 8.09 (s, 4H, tereph Ar-H); ^{13}C NMR δ: 66.6 (2 × C-5), 68.7 (2 × C-2), 69.0 (2 × C-6), 71.0 (2 × $PhCH_2$), 73.5 (2 × C-4), 74.4 (2 × C-3), 100.7 (2 × PhCH), 101.8 (2 × C-1), 126.1, 128.08, 128.11, 128.2, 128.5, 128.9, 129.9 (Ar-C), 133.7, 136.9, 137.5 (Ar-C_{ipso}), 165.5 (2 × COO). Anal. calcd. for $C_{48}H_{46}O_{14}.H_2O$: C 66.66, H 5.59; found: C 66.22, H 5.22.

*Bis(methyl 4,6-O-benzylidene-2-deoxy-α-D-allopyranosid-2-yl) terephthalate (**9**)*

Methyl 4,6-*O*-benzylidene-α-D-allopyranoside (**8**) (21) (0.113 g, 0.4 mmol) was reacted with dibutyltin oxide (0.110 g, 0.44 mmol) as in the standard method to give a solution that was concentrated to 6 mL and cooled to room temperature. Triethylamine (63 μL, 0.44 mmol) was added and the resulting solution was stirred at ambient temperature for 0.5 h. Then terephthaloyl chloride (41 mg, 0.2 mmol) was added and stirring was continued a further 20 min. Standard work-up gave a solid residue that was purified by means of dry column flash chromatography using cyclohexane – ethyl acetate gradient elution. The title compound (**9**) was obtained as a solid, then recrystallized from ethyl acetate and cyclohex-

© 1997 NRC Canada

Can. J. Chem. Downloaded from www.nrcresearchpress.com by 88.146.161.215 on 09/08/12
For personal use only.

ane to give fine crystals, mp 151–152°C; yield 0.135 g (97%); $[\alpha]_D^{29}$ +81.5 (*c* 5.97, chloroform); ^{1}H NMR δ: 3.23 (d, 2H, $J_{3,3\text{-OH}}$ = 7.6 Hz, 2 × OH-3), 3.48 (s, 6H, 2 × OMe), 3.68 (dd, 2H, $J_{3,4}$ = 2.4 Hz, $J_{4,5}$ = 9.8 Hz, 2 × H-4), 3.83 (t, 2H, $J_{5,6ax} = J_{6ax,6eq}$ = 10.2 Hz, 2 × H-6_{ax}), 4.25 (td, 2H, 2 × H-5), 4.41(dd, 2H, $J_{5,6eq}$ = 5.2 Hz, $J_{6ax,6eq}$ = 10.1 Hz, 2 × H-6_{eq}), 4.52 (b m, 2H, 2 × H-3), 5.05 (d, 2H, $J_{1,2}$ = 3.7 Hz, 2 × H-1), 5.10 (t, 2H, $J_{2,3}$ = 3.5 Hz, 2 × H-2), 5.63 (s, 2H, 2 × PhCH), 7.35–7.40 (m, 6H, ArH), 7.50–7.55 (m, 4H, ArH), 8.21 (s, 4H, tereph ArH); ^{13}C NMR δ: 56.2 (2 × OMe), 57.9 (2 × C-5), 68.1 (2 × C-3), 69.0 (2 × C-6), 70.2 (2 × C-2), 78.5 (2 × C-4), 98.5 (2 × C-1), 102.0 (2 × PhCH), 126.3, 128.3, 129.2, 130.1 (Ar-C), 133.5, 136.9 (Ar-C_{ipso}), 164.8 (2 × COO). Anal. calcd. for $C_{36}H_{38}O_{14}$: C 62.24, H 5.51; found: C 62.42, H 5.60.

Reaction of methyl 4,6-O-benzylidene-2-deoxy-α-D-mannopyranoside with adipoyl chloride

(a) Without added base: The stirred solution resulting from the reaction of methyl 4,6-*O*-benzylidene-α-D-mannopyranoside (**10**) (22) (0.282 g, 1 mmol) and dibutyltin oxide (0.274 g, 1.1 mmol) as in the general method was cooled to room temperature. A solution of freshly distilled adipoyl chloride (61 μL, 0.415 mmol) in toluene (2 mL) was added dropwise and stirring was continued for 45 min. Standard work-up gave a syrupy residue that was separated by means of dry column flash chromatography (eluent gradient: hexane to ethyl acetate). The first fraction from the column was methyl 4,6-*O*-benzylidene-2,3-deoxy-α-D-mannopyranosid-2,3-diyl hexanedioate (**12**), a solid; R_F = 0.8 (ethyl acetate: hexane, 2:1); yield 0.016 g (9.8%). It was recrystallized from ethyl acetate and hexane to give fine needles: mp 194–196°C; $[\alpha]_D^{23}$ −19.6 (*c* 0.32, chloroform); ^{1}H NMR δ: 1.90–1.98 (m, 2H, CH_2), 2.18–2.36 (m, 2H, CH_2), 2.37–2.52 (m, 4H, 2 × CH_2CO), 3.42 (s, 3H, OMe), 3.86 (t, 1H, $J_{5,6ax} = J_{6ax,6eq}$ = 9.8 Hz, H-6_{ax}), 3.98 (td, 2H, $J_{4,5} = J_{5,6ax}$ = 9.5 Hz, $J_{5,6eq}$ = 4.3 Hz, H-5), 4.08 (t, 2H, $J_{3,4} = J_{4,5}$ = 9.3 Hz, H-4), 4.33 (dd, 1H, $J_{5,6eq}$ = 4.6 Hz, $J_{6eq,6ax}$ = 9.6 Hz, H_{6eq}), 4.77 (d, 1H, $J_{1,2}$ = 1.2 Hz, H-1), 5.08 (dd, 1H, $J_{2,3}$ = 4.4 Hz, $J_{3,4}$ = 9.2 Hz, H-3), 5.56 (dd, 1H, $J_{1,2}$ = 1.2 Hz, $J_{2,3}$ = 4.3 Hz, H-2), 5.62 (s, 1H, PhCH), 7.35–7.46 (m, 5H, Ar-H), ^{13}C NMR δ: 26.5, 26.9 (CH_2), 35.1, 35.9 (CH_2CO), 55.1 (OMe), 62.1 (C-5), 68.9 (C-6), 69.8 (C-2), 70.1 (C-3), 76.5 (C-4), 99.7 (C-1), 102.2 (PhCH), 126.2, 128.3, 129.3 (Ar-C), 137.0 (Ar-C_{ipso}), 172.2, 173.8 (COO); EI MS for $C_{20}H_{24}O_8$: M^+ (16%), M − 30 (5%), 243 (34%), 55 (100%), no peaks at masses greater than 393. HRMS (EI), calcd. for $C_{20}H_{24}O_{14}$: 392.1471; found: 392.1460.

The second fraction was a solid, bis(methyl 4,6-*O*-benzylidene-2-deoxy-α-D-mannopyranosid-2-yl) hexanedioate (**11a**), mp 87–88°C; R_F = 0.65 (ethyl acetate: hexane, 2:1); yield 0.058 g (21%); $[\alpha]_D^{24}$ +11.2 (*c* 2.02, chloroform); ^{1}H NMR δ: 1.73–1.83 (m, 4H, 2 × CH_2), 2.45–2.51 (m, 4H, 2 × CH_2CO), 2.72 (b s, 2H, OH-3), 3.39 (s, 6H, 2 × OMe), 3.80–3.92 (m, 6H, 2 H-4, 2 × H-5 and 2 × H-6_{ax}), 4.15 (dd, 2H, $J_{2,3}$ = 3.7 Hz, $J_{3,4}$ = 9.5 Hz, 2 × H-3), 4.25–4.28 (m, 2H, 2 × H-6_{eq}), 4.67 (d, $J_{1,2}$ = 1.5 Hz, 2 × H-1), 5.21 (dd, 2H, $J_{1,2}$ = 1.5 Hz, $J_{2,3}$ = 3.7 Hz, 2 × H-2), 5.59 (s, 2H, 2 × PhCH), 7.33–7.51 (m, 10H, 2 × Ar-H); ^{13}C NMR δ: 24.1 (2 × CH_2), 33.8 (2 × CH_2CO), 55.2 (2 × OMe), 63.2 (2 × C-5), 67.1 (2 × C-3), 68.7 (2 × C-6), 71.8 (2 × C-2), 79.0 (2 × C-4), 99.6 (2 × C-1), 102.2 (2 × PhCH), 129.2, 128.3, 129.2 (Ar-C), 137.1 (2 × Ar-C_{ipso}), 172.9 (2 × COO). Anal. calcd. for $C_{34}H_{42}O_{14}$: C 60.53, H 6.27; found: C 59.94, H 5.94.

The third fraction, also a solid, was (methyl 4,6-*O*-benzylidene-2-deoxy-α-D-mannopyranosid-2-yl) (methyl 4,6-*O*-benzylidene-3-deoxy-α-D-mannopyranosid-3-yl) hexanedioate (**11b**), R_F = 0.38 (ethyl acetate/hexane 2:1); mp 87–88°C; yield 0.120 g (43%); $[\alpha]_D^{24}$ +19.7 (*c* 1.11, chloroform); ^{1}H NMR δ: 1.71–1.78 (m, 4H, 2 × CH_2), 2.40–2.48 (m, 4H, 2 × CH_2CO), 2.63 (d, 1H, $J_{3',OH\text{-}2'}$ = 4.3 Hz, OH-2′), 3.01 (d, 1H, $J_{2,OH\text{-}3}$ = 4.3 Hz, OH-3), 3.37, 3.38 (s, 2 × 3H, 2 OMe), 3.79–3.90 (m, 4H, H-5, H-5′, H-6_{ax}, and H-$6'_{ax}$), 4.05–4.15 (m, 4H, H-2′, H-3, H-4, and H-4′), 4.24–4.29 (m, 2H, H-6_{eq} and H-$6'_{eq}$), 4.66 (d, 1H, $J_{1,2}$ = 1.8 Hz, H-1), 4.71 (d, 1H, $J_{1',2'}$ = 1.2 Hz, H-1′), 5.22 (dd, 1H, $J_{1,2}$ = 1.8 Hz, $J_{2,3}$ = 3.7 Hz, H-2), 5.31 (dd, 1H, $J_{2',3'}$ = 3.7 Hz, $J_{3',4'}$ = 9.8 Hz, H-3′), 5.52, 5.60 (2s, 2H, 2 PhCH), 7.31–7.53 (m, 10H, PhCH and PhCH0); ^{13}C NMR δ: 23.7, 24.2 (2 CH_2), 33.5, 33.7 (2 CH_2CO), 55.0, 55.2 (OMe), 63.2, 63.8 (C-5 and C-5′), 67.1 (C-3), 68.7, 68.8 (C-6 and C-6′), 69.5 (C-2), 70.6 (C-3′), 71.9 (C-2), 76.0 (C-4′), 78.9 (C-4), 99.5 (C-1), 101.6 (C-1′), 101.8, 102.1 (PhCH), 126.16, 126.23, 128.2, 128.3, 129.0, 129.2 (Ar-C), 137.1, 137.2 (Ar-C_{ipso}), 172.2, 173.2 (COO). Anal. calcd. for $C_{34}H_{42}O_{14}$: C 60.53, H 6.27; found: C 60.16, H 6.36.

The fourth fraction was bis(methyl 4,6-*O*-benzylidene-3-deoxy-α-D-mannopyranosid-3-yl) hexanedioate (**11c**), a solid, mp 90–91°C; R_F = 0.16 (ethyl acetate/hexane, 2:1); yield 0.051 g (18%); $[\alpha]_D^{24}$ +32.0 (*c* 2.07, chloroform); ^{1}H NMR δ: 1.61–1.70 (b m, 4H, 2 × CH_2), 2.33–2.42 (b m, 4H, 2 × CH_2CO), 2.95 (d, $J_{2,OH\text{-}2}$ = 4.3 Hz, 2 × OH-2), 3.41 (s, 6H, 2 × OMe), 3.85 (t, 2H, $J_{5,6ax} = J_{6eq,6ax}$ = 10.4 Hz, 2 × H-6_{ax}), 3.93 (td, 2H, 4.11 (t, 2H, $J_{3,4} = J_{4,5}$ = 9.8 Hz, 2 × H-4), 4.14 (b m, 2H, 2 × H-2), 4.28 (dd, 2H, $J_{5,6ea}$ = 3.66 Hz, $J_{6eq,6ax}$ = 9.16 Hz, 2 × H-6_{eq}), 4.75 (d, 2H, $J_{1,2}$ = 1.8 Hz, 2 × H-1), 5.35 (dd, 2H, $J_{2,3}$ = 3.1 Hz, $J_{3,4}$ = 10.4 Hz, 2 × H-3), 5.52 (s, 2H, 2 × PhCH), 7.29–7.50 (m, 10H, 2 × Ar-H); ^{13}C NMR δ: 23.7 (2C, 2 × CH_2), 33.6 (2C, 2 × CH_2'), 55.0 (2C, 2 × OMe), 63.7 (2C, 2 × C-5), 68.8 (2C, 2 × C-6), 69.6 (2C, 2 × C-2), 70.8 (2C, 2 × C-3), 76.1 (2C, 2 × C-4), 101.6 (2C, 2 × C-1), 101.9 (2C, 2 × PhCH), 126.2, 128.2, 129.1 (Ar-C), 137.2 (2 × Ar-C_{ipso}), 172.7 (2C, 2 × COO). Despite repeated rechromatography, this compound was always obtained contaminated by a small amount of a dibutyltin-containing impurity, as apparent from small signals ascribed to a butyl group in its ^{1}H NMR spectra (not listed).

(b) In the presence of triethylamine: To the solution resulting from treatment of compound **10** (0.564 g, 2 mmol) with dibutyltin oxide (0.795 g, 2.2 mmol) in toluene (20 mL) as the general method was added triethylamine (0.307 mL, 2.2 mmol) and the product was stirred for 20 min at 25°C, then cooled to 0°C. A solution of adipoyl chloride (0121 mL, 0.83 mmol) in toluene (3 mL) was added dropwise. After 30 min, cooling was removed and the reaction mixture was stirred for 2 h. Standard work-up yielded a solid residue that was separated as previously to give compound **11a**, yield 0.305 g (54%); compound **11b**, yield 0.182 g (32%); and compound **11c**, yield 0.043 g (8%).

(c) In the presence of diisopropylethylamine (DIPEA): To the room temperature solution arising from the reaction of com-

© 1997 NRC Canada

Can. J. Chem. Downloaded from www.nrcresearchpress.com by 88.146.161.215 on 09/08/12
For personal use only.

pound **10** (0.141 g, 0.5 mmol) and dibutyltin oxide in toluene (15 mL) as in the general method was added freshly distilled diisopropylethylamine (0.96 mL, 0.55 mmol) and stirring was continued for 20 min. The reaction mixture was cooled to 0°C and a solution of adipoyl chloride (0.034 mL, 0.23 mmol) in toluene (2 mL) was added dropwise. The resulting solution was stirred at room temperature until TLC showed no further change in reaction (1.5 h). Standard work-up yielded a colourless solid residue that was analysed by ^{1}H NMR spectroscopy. Integration indicated that the products formed were compounds **11a** (20%), **11b** (42%), and **11c** (38%).

(d) In the presence of N-*methylimidazole (NMI)*: To the solution arising from treatment of compound **4** (1 mmol, 0.282 g) with dibutyltin oxide (0.274 g, 1.1 mmol) as in the general method was added *N*-methylimidazole (0.876 mL, 10 mmol) and stirring was continued for 20 min before the solution was cooled to 0°C. A solution of adipoyl chloride (61 μL, 0.415 mmol) in toluene (2 mL) was added dropwise to the cooled mixture, which was then stirred at room temperature for 1.5 h. Standard work-up gave a syrupy residue shown by TLC to contain only two products, **11b** and **11c**. ^{1}H NMR integration indicated that the ratio of compounds **11b** to **11c** was 1:4.

*Bis(methyl 4,6-O-benzylidene-3-deoxy-α-D-mannopyranosid-3-yl) (4,4′-biphenyldisulfonate) (**13b**)*

The solution resulting from treatment of compound **10** (0.564 g, 2 mmol) with dibutyltin oxide (0.523 g, 2.1 mmol) as in the general method was concentrated to 15 mL and cooled to the room temperature. *N*-Methylimidazole (796 μL, 10 mmol) was added and the solution was stirred for 20 min at room temperature, then cooled to 0°C. When a solution of 4,4′-biphenyldisulfonyl chloride (0.2985 g, 0.85 mmol) in toluene (2 mL) was added dropwise, the colour of the mixture turned yellowish immediately. The mixture was stirred at room temperature until TLC showed the starting material was consumed (14 h). Standard work-up yielded a solid residue that was separated by dry column flash chromatography using a gradient of hexane to ethyl acetate as eluent. The first fraction was (methyl 4,6-*O*-benzylidene-2-deoxy-α-D-mannopyranosid-2-yl) (methyl 4,6-*O*-benzylidene-3-deoxy-α-D-mannopyranosid-3-yl) (4,4′-biphenyldisulfonate) (**13a**), R_F = 0.72 (benzene/ethyl acetate, 1:1), a solid; mp 97–99°C; yield 0.034 g (5%); $[\alpha]_D^{23}$ +6.8 (*c* 2.26, chloroform); ^{1}H NMR δ: 2.42 (d, 1H, $J_{3,OH\text{-}3}$ = 4.6 Hz, OH-3), 3.04 (d, 1H, $J_{2',OH\text{-}2'}$ = 4.0 Hz, OH-2′), 3.38, 3.41 (2 s, 6H, 2 × OMe), 3.76–3.91 (m, 5H, H-5, H-5′, H-6$_{ax}$, H-6′$_{ax}$, and H-4), 4.08 (t,1H, $J_{3',4'} = J_{4',5'}$ = 9.3 Hz, H-4′), 4.15–4.32 (m, 3H, H-3, H-6$_{eq}$, H-6′$_{eq}$), 4.35 (m, 1H, H-2′), 4.76 (d, 1H, $J_{1',2'}$ = 1.5 Hz, H-1′), 4.82 (dd, 1H, $J_{2',3'}$ = 3.5, $J_{3',4'}$ = 10.1 Hz, H-3′), 4.84 (dd, 1H, $J_{1,2}$ = 1.5 Hz, $J_{2,3}$ = 3.7 Hz, H-2), 4.93 (d, 1H, $J_{1,2}$ = 1.5 Hz, H-1), 5.37 (s, 1H, PhCH′), 5.55 (s, 1H, PhCH), 7.13–7.19 (m, 5H, Ar-H), 7.33–7.37 (m, 5H, Ar-H), 7.43–7.47 (m, 2H, Ar), 7.59 (XX′ part of AA′XX′ pattern, 2H, ArH′ *meta* to SO_2), 7.89 (AA′ part of AA′XX′ pattern, 2H, J_o = 6.7 Hz, ArH *ortho* to SO_2), 8.08 (AA′ part of AA′XX′ pattern, 2H, J_o = 6.7 Hz, ArH′ *ortho* to SO_2); ^{13}C NMR δ: 55.1, 55.4 (OMe), 63.3, 63.7 (C-5, C-5′), 66.8 (C-3), 68.6, 69.3 (C-6, C-6′), 70.6 (C-2′), 75.5 (C-4′), 78.4 (C-4), 78.9 (C-2), 79.3 (C-3′), 99.6 (C-1), 101.4 (C-1′), 101.9 (PhCH′), 102.2 (PhCH), 126.1, 126.2, 127.6, 128.0, 128.3, 128.9, 129.0, 129.3 (Ar-C, Ar′-C, and Ar″-C), 135.8, 135.9, 136.8 (Ar-C_{ipso}), 140.0, 144.5 (Ar′-C_{ipso}).

The second fraction was the title compound **13b**, R_F = 0.55 (benzene/ethyl acetate, 1:1), a colourless solid; mp 141–143°C; yield 0.667 g (93%); $[\alpha]_D^{23}$ +23.3 (*c* 1.83, chloroform); ^{1}H NMR δ: 3.40 (s, 6H, 2 OMe), 3.48 (b s, 2H, 2 OH-2), 3.70–3.86 (m, 4H, H-5 and H-6$_{ax}$), 4.08–4.25 (m, 4H, H-4 and H-6$_{eq}$), 4.39 (bs, 2H, 2 × H-2), 4.81 (d, 2H, $J_{1,2}$ = 1.8 Hz, H-1), 4.84 (dd, $J_{2,3}$ = 3.1 Hz, $J_{3,4}$ = 10.1 Hz, H-3), 5.42 (s, 2H, PhCH), 7.08–7.27 (m, 14H, Ar-H and Ar-H′), 7.92 (d, 4H, $J_{ortho\text{-}Ar'\text{-}H}$ = 8.6 Hz, ArH *ortho* to SO_2); ^{13}C NMR δ: 55.1 (2 × OMe), 63.7 (2 × C-5), 68.5 (2 × C-6), 70.4 (2 × C-2), 75.4 (2 × C-3), 79.2 (2 × C-4), 101.5 (2 × C-1), 101.8 (2 × CHPh), 126.1, 127.2, 127.9, 128.7, 129.0 (Ar-C), 135.6 (2 × Ar′-C_{ipso}), 136.8 (2 × Ar-C_{ipso}), 143.8 (2 × Ar′-C_{ipso}). HRMS (ES) calcd. for M + H$^+$, $C_{40}H_{43}O_{16}S_2$: 843.1992; found: 843.2009.

Acknowledgements

T.B.G. thanks the Natural Sciences and Engineering Research Council of Canada for a research grant. H.N. thanks the Government of I. R. Iran for a graduate scholarship. We thank the Atlantic Region Magnetic Resonance Centre for NMR time and the Institute for Marine Biosciences for the use of their polarimeter. We also thank Dr. J. Curtis of IMB for recording three FAB HRMS spectra, Dr. J. Kim for recording some EI HRMS spectra, Glen D. Rockwell for help with LAME8 simulations, and Professor W.A. Szarek for discussions of nomenclature.

References

1. T.B. Grindley and H. Namazi. Tetrahedron Lett. **37**, 991 (1996).
2. Y.C. Lee and R.T. Lee. Acc. Chem. Res. **28**, 321 (1995); S.A. DeFrees, F.C.A. Gaeta, Y.-C. Lin, Y. Ichikawa, and C.-H. Wong. J. Am. Chem. Soc. **115**, 7549 (1993).
3. S.A. DeFrees, W. Kosch, W. Way, J.C. Paulson, S. Sabesan, R.L. Halcomb, D.-H. Huang, Y. Ichikawa, and C.-H. Wong. J. Am. Chem. Soc. **117**, 66 (1995).
4. R. Roy, D. Zanini, S.J. Meunier, and A. Romanowska. *In* Synthetic oligosaccharides: indispensible probes for the life sciences. *Edited by* P. Kováč. ACS, Washington. 1994. Chap. 7. p. 104.
5. T. Furuike, N. Nishi, S. Tokura, and S.-I. Nishimura. Chem. Lett. 823 (1995).
6. C.-C. Lin, M. Shimazaki, M.-P. Heck, S. Aoki, R. Wang, T. Kimura, H. Ritzèn, S. Takayama, S.-H. Wu, G. Weitz-Schmidt, and C.-H. Wong. J. Am. Chem. Soc. **118**, 6826 (1996).
7. Y. Suhara, J.E.K. Hildreth, and Y. Ichikawa. Tetrahedron Lett. **37**, 1575 (1996).
8. T.B. Grindley. *In* Synthetic oligosaccharides: indispensable probes for the life sciences. *Edited by* P. Kováč. ACS, Washington. 1994. Chap. 4. p. 51.
9. S. David and S. Hanessian. Tetrahedron, **41**, 643 (1985); M. Pereyre, J.P. Quintard, and A. Rahm. *In* Tin in organic synthesis. Butterworths, London. 1987. Chap. 11. p. 261.
10. (*a*) A.D. McNaught. Pure Appl. Chem. **68**, 1919 (1996); (*b*) British American Nomenclature Committee. J. Org. Chem. **28**, 281 (1963).
11. C.W. Holzapfel, J.M. Koekemoer, and C.F. Marais. S. Afr. J. Chem. **37**, 19 (1984).
12. S. David and A. ThiJffry. J. Chem. Soc. Perkin Trans. 1, 1568 (1979).
13. H. Qin and T.B. Grindley. J. Carbohydr. Chem. **13**, 475 (1994); H. Qin and T.B. Grindley. J. Carbohydr. Chem. **15**, 95 (1996).

© 1997 NRC Canada

14. C.W. Haigh. Annu. Rep. NMR Spectrosc. **4**, 311 (1971).
15. T.B. Grindley and R. Thangarasa. Can. J. Chem. **68**, 1007 (1990).
16. X. Kong and T.B. Grindley. Can. J. Chem. **72**, 2396 (1994).
17. S. Valverde, A.M. Gómez, A. Hernández, B. Herradón, and J.C. López. J. Chem. Soc. Chem. Commun. 2005 (1995).
18. S. Hanessian, C. Hoornaert, A.G. Pernet, and A.M. Nadzan. Carbohydr. Res. **137**, C14–C16 (1985).
19. M.H. David. Carbohydr. Res. **86**, 158 (1980).
20. J.R. Turvey and T.P. Williams. J. Chem. Soc. 2119 (1962).
21. B.R. Baker and D.H. Buss. J. Org. Chem. **30**, 2304 (1965); J.S. Brimacombe and A. Husain. Carbohydr. Res. **6**, 491 (1968).
22. J.J. Patroni, R.V. Stick, B.W. Skelton, and A.H. White. Aust. J. Chem. **41**, 91 (1988).

Can. J. Chem. Downloaded from www.nrcresearchpress.com by 88.146.161.215 on 09/08/12
For personal use only.

© 1997 NRC Canada

Theoretical study on the insertion reaction of CH($X^2\Pi$) with CH_4

Zhi-Xiang Wang, Ming-Bao Huang, and Ruo-Zhuang Liu

Abstract: The CH + CH_4 reaction has been studied by means of ab initio molecular orbital calculations incorporating electron correlation with Møller–Plesset perturbation theory up to second and fourth orders with the 6-31G(*d*,*p*) and 6-311++G(2*d*,*p*) basis sets. An energetically feasible insertion reaction path has been found in the potential energy surface that confirms the experimental proposal for the mechanism of the CH + CH_4 reaction. The feature of the mechanism for the CH + CH_4 insertion reaction is found to be different from the feature of the mechanisms for the CH + NH_3, CH + H_2O, and CH + HF insertion reactions, but somewhat similar to that for the CH_2 + CH_4 insertion reaction. Energetic results for the CH + CH_4 reactions are in agreement with experiment.

Key words: CH radical, methane, reaction mechanism.

Résumé : On a étudié la réaction CH + CH_4 en faisant appel aux calculs d'orbitales moléculaires ab initio incorporant une corrélation d'électrons, avec la théorie de la pertubation de Møller–Plesset, jusqu'à des ordres 2 et 4 avec les ensembles de base 6-31G(*d*,*p*) et 6-311++G(2*d*,*p*). On a trouvé une réaction d'insertion énergétiquement possible à la surface d'énergie potentielle, qui confirme le mécanisme expérimental proposé pour la réaction CH + CH_4. On a trouvé que le mécanisme de la réaction d'insertion CH + CH_4 est différent des mécanismes d'insertion de CH + NH_3, CH + H_2O et CH + HF, mais il est quelque peu similaire à celui de la réaction d'insertion CH_2 + CH_4. Les résultats énergétiques de la réaction CH + CH_4 sont en accord avec les valeurs expérimentales.

Mots clés : radical CH, méthane, mécanisme réactionnel.

[Traduit par la rédaction]

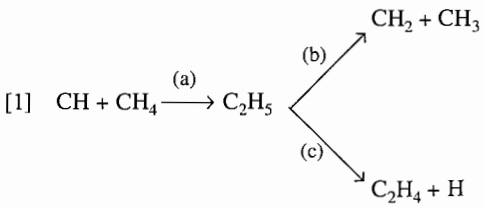
Can. J. Chem. Downloaded from www.nrcresearchpress.com by 88.146.161.215 on 09/08/12
For personal use only.

Introduction

Methylidyne, known to be one of the most reactive of all free radicals, is important in combustion and planetary atmospheric chemistry. The CH reactions with numerous small molecules have been studied by kinetic experiments (1). However, only a few theoretical studies (2–7) on the CH reactions have been reported, and those studies all show unexpected situations and complexities in the reaction paths.

We have been interested in the reactions of CH($X^2\Pi$) with the XH_n molecules (X = C, N, O, and F with n = 4, 3, 2, and 1, respectively). Experimental studies (8–10) have suggested that the insertion reaction path is the dominant channel for these CH reactions (no reported experimental study on the CH + HF reaction) because of the weak endothermicity of the abstraction reaction. The insertion mechanisms of the CH reactions with NH_3, H_2O, and HF were confirmed by our recent theoretical study (6). In the calculated reaction path of the energetically favorable insertion channel for each of the three reactions there exists an intermediate complex prior to the transition state that has a lower energy than the reactants. The MO interaction analyses imply that these intermediate complexes are stabilized due to the donation of the lone pair on the X-atom (X = N, O, and F) to the empty carbon p-orbital of the CH radical.

The CH reaction with CH_4, as a prototype of CH reactions with saturated hydrocarbons, is supposed to be more important than the above-mentioned three reactions. In 1983, Berman and Lin (8) carried out kinetic studies on the CH reaction with CH_4, and on the basis of their experimental results the following reaction mechanisms could be proposed:



where the reaction step (a) was proposed to proceed through CH inserting into a C—H bond of CH_4 to produce the ethyl radical, which contains 94.5 kcal/mol internal energy. In 1993, we investigated the mechanism of the CH + CH_4 reaction by ab initio calculations (4). Addition, insertion, and abstraction–addition reaction paths were examined by, in total, five meth-

Received February 3, 1997.

Z.-X. Wang and M.-B. Huang.[1] Graduate School at Beijing, University of Science and Technology of China, Academia Sinica, P.O. Box 3908, Beijing 100039, People's Republic of China.
R.-Z. Liu. Department of Chemistry, Beijing Normal University, Beijing 100875, People's Republic of China.

[1] Author to whom correspondence may be addressed.

© 1997 NRC Canada

Fig. 1. A schematic diagram of the potential energy curve of the CH($X^2\Pi$) reaction with CH_4. The values in parentheses are the UMP2/6-31G(*d,p*) relative energies in kcal/mol (see Table 1 for more sophisticated energetic results).

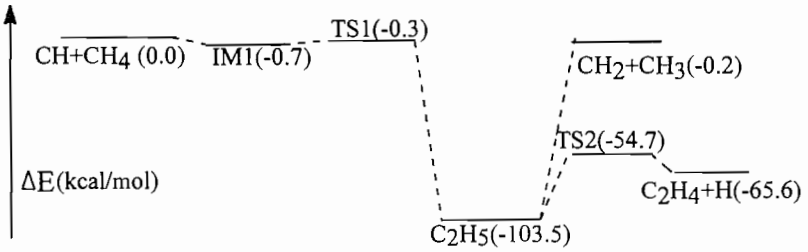


Table 1. Total energies (*E*, in a.u.), relative energies (R.E., in kcal/mol), and relative energies corrected for zero-point energies (R.E. + ZPE, in kcal/mol) for the reactants, intermediate complexes (IM1 and C_2H_5), transition states (TSn), and products of the CH reaction with CH_4.

	UMP2/6-31G(*d,p*)			UMP4/6-311++G(2*d,p*)//UMP2/6-31G(*d,p*)		
	E	R.E.	R.E. + ZPE[a]	*E*	R.E. + ZPE[a]	Exptl.
CH + CH_4	−78.720 94	0.0	0.0	−78.804 88	0.0	0.0
IM1	−78.722 00	−0.7	0.4	−78.811 96	−3.3	
TS1	−78.721 41	−0.3	3.7	−78.811 57	−0.2	
C_2H_5	−78.885 84	−103.5	−98.3	−78.952 12	−87.2	−94.5[b]
TS2	−78.80 804	−54.7	−53.6	−78.876 77	−44.0	
CH_2 + CH_3	−78.721 23	−0.2	−2.8	−78.801 11	−0.2	2.6[b]
C_2H_4 + H	−78.825 47	−65.6	−65.6	−78.900 01	−59.0	−59.0[b]

[a]The UMP2/6-31G(*d,p*) zero-point energies.
[b]Experimental values in kcal/mol for the heats of the CH + CH_4 reactions (refs. 1 and 8).

ods of approach. However, the reaction path calculations were performed at the HF level, and the results indicated that the assumed insertion path did not seem to exist and the most favorable channel was the abstraction–addition reaction path (with a considerable energy barrier), which was not in line with that proposed by experiment (1, 8).

We have reinvestigated the mechanism of the CH + CH_4 reaction by ab initio calculations at high levels, and this time we found the feasible insertion reaction path in the potential energy surface. In the present paper, we report our new theoretical results for the CH + CH_4 reaction and discuss the insertion mechanisms of the CH + CH_4 reaction and some related reactions.

Computational details

Ab initio molecular orbital calculations incorporating electron correlation with unrestricted Møller–Plesset perturbation theory (11) up to second order (UMP2) and up to fourth order (UMP4) were carried out with the Gaussian 92 (12) suite of programs, and the 6-31G(*d,p*) (13, 14) and 6-311++G(2*d,p*) (15, 16) basis sets were used. The reaction path calculations were carried out at the UMP2/6-31G(*d,p*) level, and these calculations include: (*i*) geometry optimization calculations for scanning all the stationary points along the paths; (*ii*) frequency analysis calculations for characterizing the stationary points as minima (intermediate complexes) or saddle points (transition states); and (*iii*) intrinsic reaction coordinate (IRC) (17) calculations from the transition states for tracing the reaction paths (minimum energy paths). No symmetry constraints were imposed on the reaction system. The UMP4/6-311++G(2*d,p*) single-point calculations were performed at the UMP2/6-31G(*d,p*) geometries of the intermediate complexes, transition states, reactants, and products.

Results and discussion

The potential energy curve shown in Fig. 1 represents the UMP2/6-31G(*d,p*) reaction paths of the CH reaction with CH_4. The part of the potential energy curve to the left of C_2H_5 represents the insertion reaction step (a) of eq. [1]. Along the path, the reaction system proceeds from the reactants, first via a very shallow energy minimum and then a very low energy barrier, to the insertion product C_2H_5. The intermediate complex corresponding to the minimum and the transition state corresponding to the barrier are denoted as IM1 and TS1, respectively.

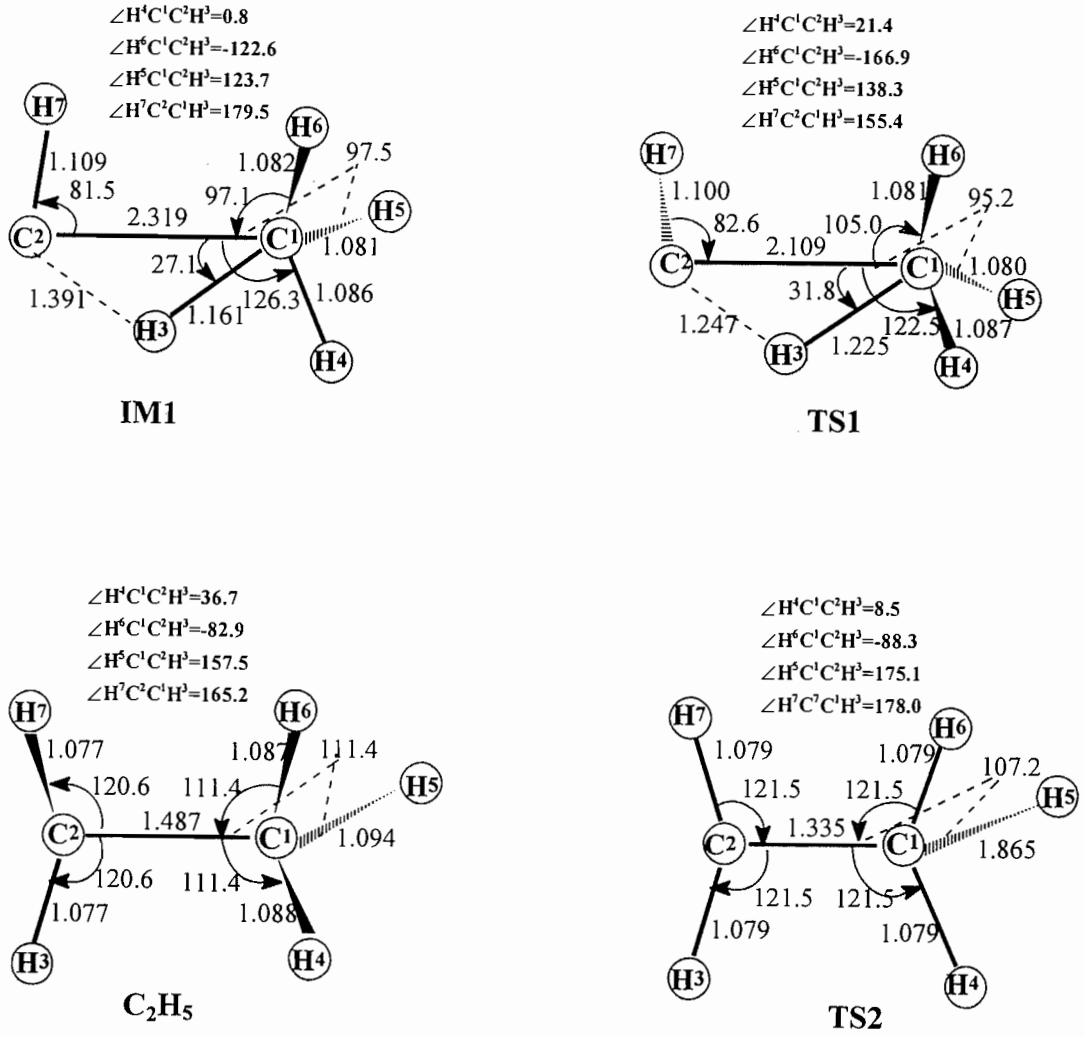
The two branches, starting at C_2H_5, of the potential energy curve shown in Fig. 1 describe the two subsequent (separate) reaction steps (b) and (c) in eq. [1], leading to the two sets of the final products, CH_2 (X^3B_1)+ CH_3 and C_2H_4 + H, respectively. In the calculated path for reaction step (c), there exists a transition state denoted as TS2.

In Fig. 1, the UMP2/6-31G(*d,p*) energies of IMn, TSn, and the products relative to the reactants are given. The energetic results for the CH + CH_4 reactions obtained in the present study are all collected in Table 1, and they include: (*i*) total energies, relative energies, and relative energies with zero-

Can. J. Chem. Downloaded from www.nrcresearchpress.com by 88.146.161.215 on 09/08/12
For personal use only.

© 1997 NRC Canada

Fig. 2. UMP2/6-31G(*d,p*) optimized structures of the intermediate complexes (IM1 and C_2H_5) and transition states (TS1 and TS2) for the $CH(X^2\Pi)$ reaction with CH_4. Bond lengths are given in Å and angles in degrees.



point energy corrections based on our UMP2/6-31G(*d,p*) calculations; and (*ii*) total energies and relative energies with (UMP2/6-31G(*d,p*)) zero-point energy corrections based on our UMP4/6-311++G(2*d,p*)//UMP2/6-31G(*d,p*) calculations. The UMP2/6-31G(*d,p*) optimized geometries for IM1, TS1, TS2, and C_2H_5 are given in Fig. 2. The spin contaminations in the wave functions calculated at all the stationary points, except TS2 (see below) in reaction step (c), along the potential energy curve shown in Fig. 1 are small ($\langle S^2\rangle < 0.77$).

1. Insertion reaction leading to the ethyl radical

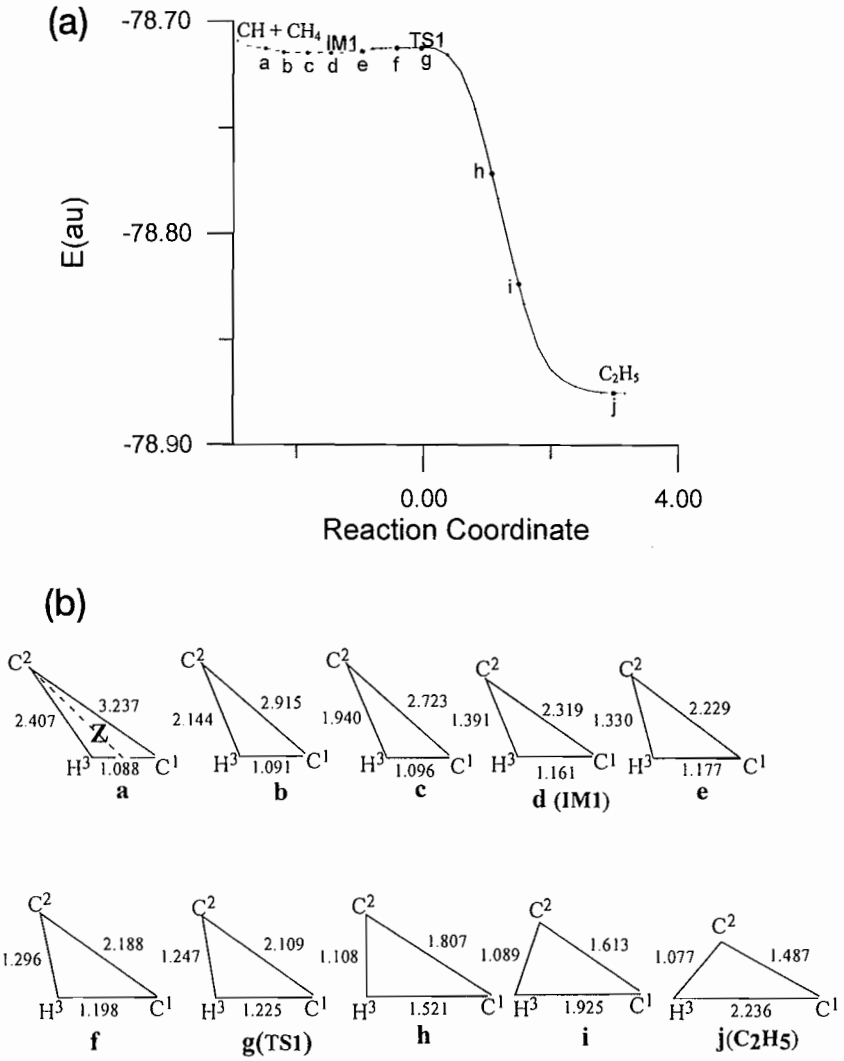
To confirm the fact that the part of the potential energy curve to the left of C_2H_5 shown in Fig. 1 describes the process of methylidyne insertion into CH_4, we examined the geometry evolution of the system. The UMP2/6-31G(*d,p*) IRC minimum energy path curve for reaction step (a) is given in Fig. 3(*a*) (the part to the left of IM1 was calculated by using the main reaction coordinate Z — the distance between the C-atom (denoted as C^2) of CH and the center of the attacked C—H (denoted as C^1—H^3) bond of CH_4. Ten geometries along this curve were examined and they are denoted in sequence as **a**, **b**, **c**, **d**(IM1), **e**, **f**, **g**(TS1), **h**, **i**, and **j**(C_2H_5), respectively. The main parts, the triangles $C^2H^3C^1$, of these geometries are given in sequence in Fig. 3(*b*). It is shown in Fig. 3(*b*) that, as the reaction proceeds (from **a** to **j**), the C^1—H^3 distance becomes longer and the C^2—C^1 and C^2—H^3 distances become shorter, finally leading to the breaking of the C^1—H^3 bond and simultaneous formation of the C^2—C^1 and C^2—H^3 bonds. The spin contaminations in the wave functions calculated at the 10 geometries are small ($\langle S^2\rangle < 0.77$). The geometry evolution definitely indicates that our calculated reaction path for step (*a*) of the CH + CH_4 reaction describes the insertion mechanism.

The energetic results for the CH + CH_4 → C_2H_5 insertion reaction are given in Table 1. The UMP2/6-31G(*d,p*) energies of IM1 and TS1 relative to the reactants are predicted to be −0.7 kcal/mol and −0.3 kcal/mol, respectively, and their relative energies corrected for zero-point energies (ZPEs) are small positive values. The UMP4/6-311++G(2*d,p*) //UMP2/6-31G(*d,p*) relative energies corrected for the UMP2/6-31G(*d,p*) ZPEs are considered to be the most sophisticated energetic results in the present study. At this level, the relative energies of IM1 and TS1 are predicted to be −3.3 kcal/mol

Can. J. Chem. Downloaded from www.nrcresearchpress.com by 88.146.161.215 on 09/08/12
For personal use only.

© 1997 NRC Canada

Fig. 3. (*a*) UMP2/6-31G(*d,p*) IRC minimum energy path curve for the CH + $CH_4 \rightarrow C_2H_5$ insertion reaction (the part left of IM1 was calculated by using the main reaction coordinate *Z* — the distance between the C-atom of CH and the center of the attacked C—H bond of CH_4). (*b*) Structures of $\Delta C^2H^3C^1$ abstracted from the 10 UMP2/6-31G(*d,p*) geometries (**a** – **j**) of the CH + CH_4 ($HC^2 + H^3C^1H_3$) system corresponding to the 10 points (**a–j**) along the UMP2/6-31G(*d,p*) path curve for the CH + CH_4 insertion reaction shown in (*a*). Distances are given in Å.



and −0.2 kcal/mol, respectively, which implies that the CH + $CH_4 \rightarrow C_2H_5$ insertion reaction is energetically feasible; the relative energy of C_2H_5 is predicted to be −87.2 kcal/mol, which is comparable with the available experimental value of −94.5 kcal/mol (1, 8) for the heat of the CH + $CH_4 \rightarrow C_2H_5$ reaction.

The UMP2/6-31G(*d,p*) optimized structures of IM1, TS1, and C_2H_5 are given in Fig. 2. The structure of IM1 seems to have a symmetry plane, but the structure of TS1 has no symmetry at all. The structure of C_2H_5 is actually identical with the UMP2/6-31G(*d,p*) geometry of the eclipsed conformer (the most stable conformer) of C_2H_5 reported by Suter and Ha (18), and our UMP2/6-31G(*d,p*) total energy value is also identical with theirs.

In our previous theoretical (UHFSCF) study (4) for the CH + CH_4 reaction, we examined the insertion path by taking the *Z*-parameter (see above) as the main reaction coordinate. We found that, when the *Z*-value decreased to 1.6 Å, the C—C distance and the attacked C—H bond distance suddenly became very long. The geometry evolution implied an abstraction process (CH + $CH_4 \rightarrow CH_2 + CH_3$), and we failed to find the insertion path. The main reason for the previous failure was probably that the reaction path calculations were carried out at only the HF level. Considering that the UMP2/6-31G(*d,p*) geometry of TS1 has no symmetry, we would suspect that another reason for the failure was the imposition of an artificial symmetry plane on the reaction system in the previous path calculations (4).

2. A comparison between different insertion mechanisms

As mentioned in the introduction, experimental studies (8–10) have already suggested insertion mechanisms for the CH + CH_4, CH + NH_3, and CH + H_2O reactions (no reported experimental study on the CH + HF reaction). In our previous theoretical study (6), the insertion reaction paths were found to be the favorable channels for the CH + NH_3, CH + H_2O, and

© 1997 NRC Canada

Can. J. Chem. Downloaded from www.nrcresearchpress.com by 88.146.161.215 on 09/08/12
For personal use only.

Can. J. Chem. Downloaded from www.nrcresearchpress.com by 88.146.161.215 on 09/08/12
For personal use only.

CH + HF reactions, and the skeletons of the potential energy curves describing the three insertion reactions indicate the same process: reactant → intermediate complex → transition state → insertion product. At the UMP2/6-31G(*d*,*p*) level, these intermediate complexes were predicted to be 31.4, 14.3, and 7.2 kcal/mol (the binding energies) more stable than their respective reactants. The skeleton of the potential energy curve for the CH + CH_4 insertion reaction (see Fig. 3(*a*) and Fig. 1) somehow seems to indicate the same process. However, the insertion mechanism for the CH + CH_4 reaction is considerd to have a completely different feature from those for the CH + NH_3, CH + H_2O, and CH + HF reactions, based on the analyses given below. The intermediate complexes, appearing in the insertion paths of the CH + NH_3, CH + H_2O, and CH + HF reactions, are donor–acceptor complexes stabilized because of the donation of the lone pair on the N, O, and F atoms to the empty carbon *p*-orbital of the CH radical (6). The decreasing order in binding energy for the three intermediate complexes is rationalized by the increasing order in electronegativity for the N, O, and F atoms (6). Since there is no lone pair on CH_4, no such donor–acceptor intermediate complex can be formed in the CH + CH_4 reaction. If IM1 were a donor–acceptor complex, its binding energy would be larger than that of the donor–acceptor complex for the CH + NH_3 insertion. The UMP2/6-31G(*d*,*p*) binding energy of IM1 toward CH + CH_4 is a very small value (0.7 kcal/mol). We would suppose that, at higher levels of calculation, IM1 and TS1 would disappear in the CH + CH_4 insertion path (we failed to find them in our preliminary UMP2/6-311G(*d*,*p*) optimization calculations).

The insertion reaction of CH_2 into CH_4 was theoretically studied by Gordon and Gano (19). The potential energy curve (see Fig. 2 of ref. 19) shows that at the early stage the energy of the system changes very slowly and it decreases rapidly after the transition state (the barrier disappears upon the introduction of correlation corrections). The geometry evolution of the CH_2 + CH_4 system (see Fig. 4 of ref. 19) shows that at the beginning of the insertion reaction the (H_2)C-H-C(H_3) angle is much larger than 90° (the "abstraction-like" initial approach) and it decreases monotonically. We note that the potential energy curve shown in Fig. 3(*a*), if the shallow minimum and low barrier are neglected, has the same general feature as that for the CH_2 + CH_4 insertion reaction and that the C^2-H^3-C^1 angle in the triangles shown in Fig. 3(*b*) varies, as the CH + CH_4 insertion reaction proceeds, in the same manner as the (H_2)C-H-C(H_3) angle of the CH_2 + CH_4 system. These facts imply that the mechanism for the CH + CH_4 insertion reaction has a feature similar to that for the CH_2 + CH_4 insertion reaction. It is also noted that, at the beginning of the CH + NH_3 insertion reaction, the C-H-N angle is very small while the C-N-H angle is very large (see Fig. 3 of ref. 6). For the insertion mechanism of the CH_2 + CH_4 reaction there has been a plausible MO interaction analysis that involves the empty *p*-orbital and lone pair on the methylene carbon (20, 21). It is realized that there are similar orbitals on the methylidyne carbon.

3. Subsequent reaction steps

Reaction steps (b) and (c) in eq. [1] are both dissociation processes of C_2H_5. In the UMP2/6-31G(*d*,*p*) calculations for the reaction paths of steps (b) and (c), the C^2—C^1 and C^1—H^5 distances (see the structure of C_2H_5 in Fig. 2) were taken as the main reaction coordinates, respectively.

The UMP2/6-31G(*d*,*p*) calculations for reaction step (b) indicate that the products ($CH_2(X^3B_1)$ + CH_3) are 103.3 kcal/mol higher in energy than the reactant (C_2H_5) and there is no transition state along the reaction path (see Fig. 1). At the UMP4/6-311++G(2*d*,*p*)//UMP2/6-31G(*d*,*p*) + ZPE(UMP2/6-31G(*d*,*p*)) level, the energy of the products relative to that of the original reactants (CH + CH_4) is predicted to be a very small value of −0.2 kcal/mol (see Table 1). The experimental value for the heat of the reaction CH + CH_4 → CH_2 + CH_3 is also a small value (2.6 kcal/mol) (1, 8).

The UMP2/6-31G(*d*,*p*) calculations for reaction step (c) indicate that the products (C_2H_4 + H) are 37.9 kcal/mol higher in energy than the reactant (C_2H_5) and the transition state TS2 is 48.8 and 10.9 kcal/mol higher in energy than C_2H_5 and C_2H_4 + H, respectively (see Fig. 1). At the UMP4/6-311++G(2*d*,*p*)//UMP2/6-31G(*d*,*p*) + ZPE(UMP2/6-31G(*d*,*p*) level, the energy of the products relative to that of the original reactants is predicted to be −59.0 kcal/mol (see Table 1), which is identical to the experimental value (1, 8) for the heat of the reaction CH + CH_4 → C_2H_4 + H. At the same level, the barrier in reaction step (c) is predicted to be 43.2 kcal/mol. The spin contaminations in the wave functions of TS2 are quite large ($\langle S^2\rangle \cong 0.95$), and the predicted barrier height for reaction step (c) may not be so accurate. Much higher levels of calculation are required for this reaction step (22).

Summary

For the CH($X^2\prod$) reaction with CH_4, an energetically feasible insertion reaction path has been found in the potential energy surface, which confirms the experimental proposal (1, 8) for the mechanism of this reaction. The feature of the mechanism for the CH + CH_4 insertion reaction is found to be different from the feature of the mechanisms for the CH + NH_3, CH + H_2O, and CH + HF insertion reactions, but similar to that for the CH_2 + CH_4 insertion reaction. Energetic results for the CH + CH_4 reactions (step (a), step (a) + step (b), and step (a) + step (c)) are in agreement with experiment.

Acknowledgment

We appreciate the financial support of this work that was provided by the National Natural Science Foundation Committee of China.

References

1. W.A. Sanders and M.C. Lin. *In* Chemical kinetics of small organic radicals. Vol. III. Reactions of special radicals. *Edited by* Z. Alfassi. CRC Press, Boca Raton, Fla. 1988.
2. (*a*) B.R. Brooks and H.F. Schaefer III. J. Chem. Phys. **67**, 5146 (1977); (*b*) T.H. Dunning, L.B. Harding, R.A. Baic, R.A. Eades, and R.L. Shepard. J. Phys. Chem. **90**, 344 (1986); (*c*) T.H. Dunning and L.B. Harding. *In* Theory of chemical reaction dynamics. Vol. I. *Edited by* M. Baer. CRC Press, Boca Raton, Fla. 1985.
3. R.K. Gosavi, I. Safarik, and O.P. Strausz. Can. J. Chem. **63**, 1689 (1985).
4. Z.-H. Yu , C. Chen, and M.-B. Huang. Can. J. Chem. **71**, 512 (1993).

© 1997 NRC Canada

5. (*a*) M.R. Manaa and D.R. Yarkony. J. Chem. Phys. **95**, 1808 (1991); (*b*) Chem. Phys. Lett. **188**, 352 (1992); (*c*) S.P. Walch. Chem. Phys. Lett. **208**, 214 (1993); (*d*) J.M.L. Martin and P.R. Taylor. Chem. Phys. Lett. **209**, 143 (1993).
6. Z.-X. Wang, R.-Z. Liu, M.-B. Huang, and Z.H. Yu. Can. J. Chem. **74**, 910 (1996).
7. S. Walch. J. Chem. Phys. **103**, 7064 (1995).
8. M.R. Berman and M.C. Lin. Chem. Phys. **82**, 435 (1983).
9. (*a*) J.E. Butler, J.W. Fleming, L.P. Goss, and M.C. Lin. Chem. Phys. **56**, 355 (1981); (*b*) S. Zabarnick, J.W. Fleming, and M.C. Lin. Chem. Phys. **132**, 407 (1989); (*c*) K.H. Becker, B. Engelhardt, H. Geiger, R. Kurtenbach, and P. Wissen. Chem. Phys. Lett. **210**, 135 (1993).
10. S. Zabarnick, J.W. Fleming, and M.C. Lin. Twenty-first Symp. (Int.) Combustion, 21st. The Combustion Institute, Pittsburgh, Pa. 1986. p. 713.
11. (*a*) C. Møller and M.S. Plesset. Phys. Rev. **46**, 618 (1934); (*b*) J.A. Pople, J.S. Binkley, and R. Seeger. Int. J. Quantum Chem. Symp. **10**, 1 (1976).
12. M.J. Frisch, G.W. Trucks, M. Head-Gordon, P.M.W. Gill, M.W. Wong, J.B. Foresman, B.G. Johnson, H.B. Schlegel, M.A. Robb, E.S. Replogle, R. Gomperts, J.L. Andres, K. Raghavachari, J.S. Binkley, C. Gonzalez, R.L. Martin, D.J. Fox, D.J. Defrees, J. Baker, J.J.P. Stewart, and J.A. Pople. Gaussian 92, Revision D.3. Gaussian, Inc., Pittsburgh, Pa. 1992.
13. P.C. Hariharan and J.A. Pople. Theor. Chim. Acta, **28**, 213 (1973).
14. M.J. Frisch, J.A. Pople, and J.S. Binkley. J. Chem. Phys. **80**, 3265 (1984).
15. R. Krishnan, J.S. Binkley, R. Seeger, and J.A. Pople. J. Chem. Phys. **72**, 650 (1980).
16. T. Clark, J. Chandraekhar, G.W. Spitznagel, and P.v.R. Schleger. J. Comput. Chem. **4**, 294 (1983)
17. C. Gonzalez and H.B. Schlegel. J. Phys. Chem. **90**, 2154 (1989).
18. H.U. Suter and T.-K. Ha. Chem. Phys. **154**, 227 (1991).
19. M.S. Gordon and D.R. Gano. J. Am. Chem. Soc. **106**, 5421 (1984).
20. H. Kollmar. J. Chem. Soc. **100**, 2660 (1978).
21. D. Jeziorek and B. Zurawski. Int. J. Quantum Chem. **16**, 277 (1979).
22. W.L. Hase, H.B. Schlegel, V. Balbyshev, and M. Page. J. Phys. Chem. **100**, 5354 (1996).

Can. J. Chem. Downloaded from www.nrcresearchpress.com by 88.146.161.215 on 09/08/12
For personal use only.

© 1997 NRC Canada

A ^{51}V NMR investigation of the interactions of aqueous vanadate with hydroxylamine

Sarah J. Angus-Dunne, Pradip C. Paul, and Alan S. Tracey

Can. J. Chem. Downloaded from www.nrcresearchpress.com by 88.146.161.215 on 09/08/12
For personal use only.

Abstract: The aqueous reactions of hydroxylamine and *N*-methylhydroxylamine with vanadate have been studied. Ligand, vanadium, and proton stoichiometries of the products have been obtained as have their formation constants. At lower ligand concentrations the predominant complex contains a single hydroxamido ligand and this has been assigned a five-coordinate, tetrahedral-like structure where the hydroxamido group is coordinated in a side-on fashion. Four bishydroxamido products were observed. These four complexes consisted of two distinct groups of two isomeric complexes each and have been assigned six-coordinate (tetrahedral-like) and seven-coordinate (trigonal bipyramidal-like) geometries. For the *N*-methylhydroxamido ligand, 10 bisligand products in 2 groups of 5 isomers each were observed. The additional products over the hydroxylamine situation arise from the relative orientations of the ligand methyl groups. For both ligands, the monoligand products carried a single negative charge and did not have a pK_a within the range of about 6–10. The bisligand products did not carry a charge under neutral conditions. The tetrahedral bisligand products could be protonated under acidic conditions ($pK_a \sim 6.6$) but could not be deprotonated. In contrast, the trigonal bipyramidal products were not protonated under acidic conditions but could give up a proton under basic conditions ($pK_a \sim 7.4$) to form anionic complexes. The relative orientations of the ligands and also the number of methyl groups and their relative orientations in the complex have a significant influence on the ^{51}V chemical shifts. One additional complex was observed to form and was assigned to an ester-like product formed by reaction at the hydroxyl group.

Key words: vanadate, complexes, hydroxylamine, methylhydroxylamine, peroxovanadate.

Résumé : On a étudié les réactions des solutions aqueuses d'hydroxylamine et de *N*-méthylhydroxylamine avec le vanadate. On a déterminé les stoechiométries ainsi que les constantes de formations du coordinat, du vanadium et du proton avec les produits. Aux concentrations faibles de coordinats, le complexe principal ne comprend qu'un seul coordinat hydroxamido et on lui a attribué une structure pentacoordinée, en forme de tétraèdre, dans laquelle le groupe hydroxamido est coordiné de façon à être sur le côté. On a observé quatre produits bishydroxamido. Ces quatre complexes comportent deux groupes distincts de deux complexes isomères chacun et on a leur a attribué des géométries hexacoordinées (de formes tétraédriques) et heptacoordinées (de formes bipyramides trigonales). Pour le coordinat *N*-méthylhydroxamido, on a observé 10 produits à biscoordination qui peuvent être divisés en 2 groupes comportant chacun 5 isomères. Les produits additionnels, par rapport à la situation avec l'hydroxylamine, proviennent des orientations relatives des groupes méthyles des coordinats. Pour les deux types de coordinats, les produits ne comportant qu'un coordinat portent une seule charge négative et présentent pas de pK_a dans la région de 6 à 10. Dans les conditions neutres, les produits à deux coordinats ne portent pas de charge. Les produits tétraédriques à deux coordinats peuvent être protonés dans des conditions acides (pK_a d'environ 6,6), mais il est impossible de les déprotoner. Par ailleurs, il est impossible de protoner les produits dicoordinés de forme bipyramide trigonale dans des conditions acides; toutefois, en milieu alcalin (pK_a d'environ 7,4), il est possible de leur enlever un proton pour former des complexes anioniques. Les orientations relatives des coordinats ainsi que le nombre et les orientations relatives des groupes méthyles influencent fortement les déplacements chimiques du ^{51}V. On a observé qu'il se forme un complexe additionnel et on lui a attribué une structure semblable à celle d'un ester qui se formerait par réaction du groupe hydroxyle.

Mots clés : vanadate, complexes, hydroxylamine, méthylhydroxylamine, peroxovanadate.

[Traduit par la rédaction]

Introduction

The past 10 years have seen a tremendous increase in our understanding of the aqueous chemistry of vanadium oxo-anions. This effort has focussed mainly on the V(IV) and V(V) oxidation states and, to a large extent, was driven by the desire to understand the biological and biochemical influences exerted by vanadium, particularly by its influence on the function of many phosphate-metabolizing enzymes (1–4), its function in vanadium-dependent haloperoxidases (5–8) and nitrogenases (9, 10), and by its insulin-mimetic properties (11–13).

The biochemical role of vanadate (V(V)) as an oxidant (14, 15) has been less well studied, while that of peroxovanadates has been largely restricted to its possible function in vanadium haloperoxidases (5, 8, 16–18). It is known, however, that oxovanadium(V) peroxides function as insulin-mimetic materials

Received December 3, 1996.

S.J. Angus-Dunne, P.C. Paul, and A.S. Tracey.[1] Department of Chemistry, Simon Fraser University, Burnaby, BC V5A 1S6, Canada.

[1] Author to whom correspondence may be addressed. Telephone: (604) 291 4464. Fax: (604)-291 3765. E-mail: tracey@sfu.ca

© 1997 NRC Canada

Can. J. Chem. Downloaded from www.nrcresearchpress.com by 88.146.161.215 on 09/08/12
For personal use only.

in live animals (11–13). In this case, it is by no means clear what the actual active material is.

Peroxovanadates have a strong influence on the function of numerous phosphatases and kinases (13, 19, 20). Although the mechanism of action is not known for most enzymes, recent work has provided evidence that the strong inhibition of protein tyrosine phosphatases occurs because of oxidation of the active site cysteines, certainly for the case of PTP-1B (21). A number of studies, over the past few years, have delineated peroxovanadate chemistry over the physiological pH range through studies of the complexation interactions with metabolic materials (22–24) and also of the oxidative reactions that peroxovanadate undergoes (6, 15, 22, 25, 26). These oxidative processes may well represent the underlying source of the insulin-mimetic properties of many peroxovanadium complexes.

Because of the importance of peroxovanadate in haloperoxidases, in influencing the function of phosphate-metabolizing enzymes, in potential insulin-mimetic applications, and because they are interesting compounds in their own right, we have extended our studies of peroxovanadates to include the closely related oxovanadium complexes with hydroxylamine. This ligand is isoelectronic with hydrogen peroxide but, because of the asymmetry resulting from replacement of OH by NH_2, it allows aspects of the chemistry of the vanadate complexes to be studied that would not otherwise be accessible. Furthermore, a naturally occurring hydroxylamine–vanadium(IV) complex, amavadin, which is readily oxidized to an amavadin V(V) complex, is known (27–29). The ligand in amavadin is highly substituted and multidentate. As a consequence, this study with a much simpler ligand is relevant to amavadin only to the extent that it provides information on possible modes of binding of hydroxamido ligands.

Initial studies of the interactions between vanadate and hydroxylamine were complicated by the instability of hydroxylamine, particularly at elevated pH. Consequently, our attention was directed towards the chemically less complicated *N*,*N*-dimethylhydroxylamine system. Using this ligand, it was possible to obtain details of the aqueous equilibria and to also obtain proton stoichiometry for the various reactions. A crystalline product was also obtained and its characterization by X-ray diffraction followed by NMR dissolution studies allowed structural assignments to the solution products to be made (30). Proton NMR studies also revealed a rapid internal isomerization of a type that, because of the higher symmetry, would not be observable with a similar hydrogen peroxide complex (30). With this information, together with that obtained from the studies of *N*-methylhydroxylamine–vanadate equilibria of this work, we have now been able to provide a detailed analysis of the aqueous hydroxylamine–vanadate system.

Experimental section

Materials

All reagents used in this study were reagent grade materials. Hydroxylamine hydrochloride and HEPES (*N*-(2-hydroxyethyl)piperazine-*N*′-2-ethanesulphonic acid) buffer were obtained from Sigma Chemical Co. Vanadium(V) oxide (99.99%) and methylhydroxylamine hydrochloride were obtained from Aldrich Chemical Co. All chemicals were used as supplied.

Solutions

A stock solution of sodium vanadate of strength 0.100 M was prepared by adding 0.5 mol equivalents of vanadium pentoxide to a 1.00 M solution of NaOH and stirring until the solution became colourless. This solution was diluted with distilled water to attain the desired concentration. Stock solutions of 1.0 M HEPES, 2.0 M KCl, 0.100 M hydroxylamine hydrochloride, and 0.100 M methylhydroxylamine hydrochloride were prepared by dissolving the requisite amount of the materials in distilled water. All solutions for NMR studies were kept at 1.0 M ionic strength by adding an appropriate volume of KCl solution. Solutions for the NMR studies were prepared by combining appropriate quantities of the stock solutions for the final desired concentration of vanadate, ligand, buffer, and KCl and diluting to near the final volume. The pH of the KCl solution was adjusted prior to use by NaOH or HCl, as required, so that the resultant pH of the solutions after mixing lies in the range 6.3–6.5. This procedure avoided the formation of decavanadate in solution. The pH levels of the solutions were finally adjusted to their desired value with dilute NaOH solution and the final volumes attained by the addition of distilled water. For ligand concentration studies the conditions of the experiments were maintained as follows: 3.00 mM vanadate, 1.0 M KCl, 20 mM HEPES, and 1–7 mM hydroxylamine or 1.5–5.5 mM methylhydroxylamine. The compositions of the solutions used for the pH variation studies, for both hydroxylamine and methylhydroxylamine, were 3.00 mM vanadate, 20 mM HEPES, 1.0 M KCl, and 5.00 mM hydroxylamine or 3.00 mM methylhydroxylamine ligand. Studies in the acidic pH range were carried out in the presence of excess ligand concentration and the conditions of the experiments were 3.00 mM vanadate, 20 mM hydroxylamine or methylhydroxylamine, 20 mM HEPES, and 1.0 M KCl.

All pH measurements were made with a pH-meter calibrated with freshly opened pH 4 and 7 standards.

An experiment was also conducted to check the stability of alkaline hydroxylamine in aqueous medium. A time-dependent pH measurement of aqueous hydroxylamine in alkaline medium showed a continuous change of pH with time.

Spectroscopy

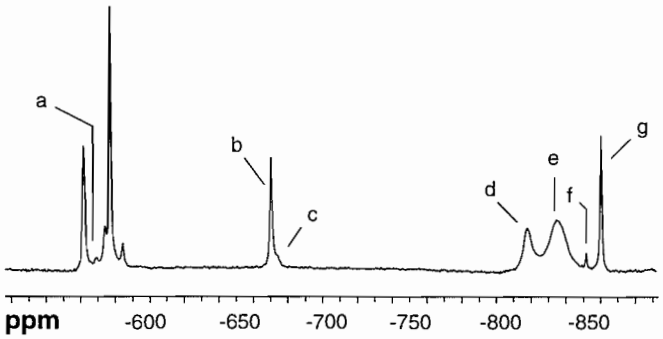
^{51}V spectra were recorded on a Bruker AMX-400 NMR spectrometer operating at 105.2 MHz at ambient temperature. Vanadium chemical shifts are relative to external reference $VOCl_3$ assigned to 0 ppm. A polynomial baseline correction was applied to all spectra before integrals were obtained. NMR spectral parameters were as follows: pulse widths, 60°; spectral widths, 80 kHz; acquisition times, 0.05 s; line broadening, 40 Hz; frequency domain size, 16 K data points.

Analysis

Time course studies were carried out to verify that decomposition of hydroxylamine during the course of the NMR experiments was negligible. For the equilibria analysis, the concentrations as provided from the NMR spectra were used. The process of data reduction and analysis, as outlined in the text, was followed. All errors in parameters are reported at the 95% (3σ) level.

© 1997 NRC Canada

Fig. 1. ^{51}V NMR spectrum showing the formation of various complexes of vanadate with hydroxylamine. The unlabelled signals derive from vanadate and its oligomers. Conditions of the experiment: 3.0 mM total vanadate; 5.3 mM total hydroxylamine; 1.0 M KCl; 20 mM HEPES buffer; pH 6.9.



Results

Hydroxylamine

To better understand the equilibria established in the presence of vanadate, a separate experiment was done to check the stability of aqueous hydroxylamine in basic medium. Continuous monitoring of the pH revealed that there was a change in pH as a function of time. This change was reasonably slow under neutral conditions but the rate of change increased with a more basic medium. This inconstancy of pH is probably due to the decomposition of hydroxylamine ligand in alkaline medium to form ammonia, nirogen, and water although other products such as hyponitrous acid can be formed (31). A consequence of this reaction was that equilibrium studies were reasonably easily carried out at neutral pH but pH-variation studies of the equilibria were more difficult.

In spite of these problems, it was possible to characterize the system and it is felt that reasonably good parameters were obtained from the pH studies. This work was aided substantially by concurrent equilibration studies of methylhydroxylamine and from studies of dimethylhydroxylamine with vanadate (30). These last two systems did not present the problems encountered with the hydroxylamine studies and provided confidence that the results were being correctly interpreted.

Hydroxylamine in the presence of vanadate gives rise to two main sets of ^{51}V NMR signals. As shown in Fig. 1, these signals occur near -670 and -820 ppm. These chemical shifts are within the range commonly encountered for peroxovanadium complexes (23, 32–34) and suggest a similar side-on coordination. Within the -820 ppm set of signals, there are two subsets, those giving rise to rather broad vanadium signals (signals d,e) and those giving comparatively sharp signals (signals f,g). A close examination of the -670 ppm region revealed the presence of a minor component (signal c) compared to the major product (signal b). An additional product signal (-571 ppm, signal a) was also observed.

The stoichiometries of the products were readily determined by vanadium and ligand concentration studies at neutral pH. Initial studies suggested that all products contained a single vanadium and one and two ligands, respectively, for the -670 and -820 ppm products. The equilibrium reactions can then be written as eqs. [1] through [3]

$$[1] \quad V + L \overset{K_{01}}{\rightleftharpoons} VL \qquad [V][L]K_{01} = [VL]$$

$$[2] \quad VL + L \overset{K_{12}}{\rightleftharpoons} VL_2 \qquad [VL][L]K_{12} = [VL_2]$$

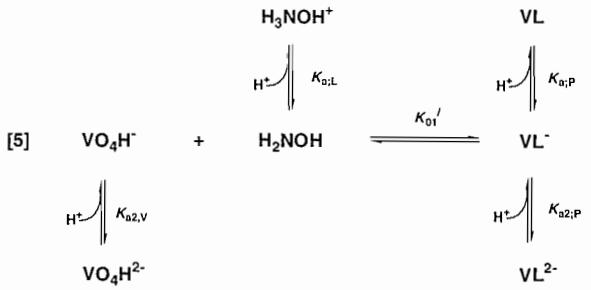
$$[3] \quad V + 2L \overset{K_{02}}{\rightleftharpoons} VL_2 \qquad [V][L]^2K_{02} = [VL_2]$$

where V refers to vanadate and L to hydroxylamine and VL and VL_2 to products. It was evident from the initial studies that product formation constants were so large that it was necessary to utilize the conservation equation, eq. [4], in order to specify the free ligand concentration as a function of the total amount of ligand (cL_t) and the product concentrations.

$$[4] \quad cL_t = [L] + [VL] + 2[VL_2]$$

Each of the graphs from the concentration studies for the -670 (eq. [1]) and -820 ppm (eq. [2]) products was linear. For the latter set of signals, the graph was broken into a plot for the broad, Fig. 2A, and sharp, Fig. 2B, signals although the product ratio is constant at fixed pH. The overall values, inclusive of minor and major products, obtained for the equilibrium constants of eqs. [1]–[3] were $K_{01} = (5.4 \pm 0.3) \times 10^2\ M^{-1}$) and $K_{02} = (9.1 \pm 0.7) \times 10^5\ M^{-2}$ ($K_{02} = K_{01}K_{12}$). The contribution of the individual products, within each group of products, to the overall formation constant is given simply by their relative concentrations, which are provided in Table 2.

Variation of the pH had a significant influence on the vanadium spectrum as shown in Fig. 3. Detailed analysis of the pH variation results requires consideration both of the pK_a's of the reactants and of the products. This is described by eq. [5] for the monoligand product.



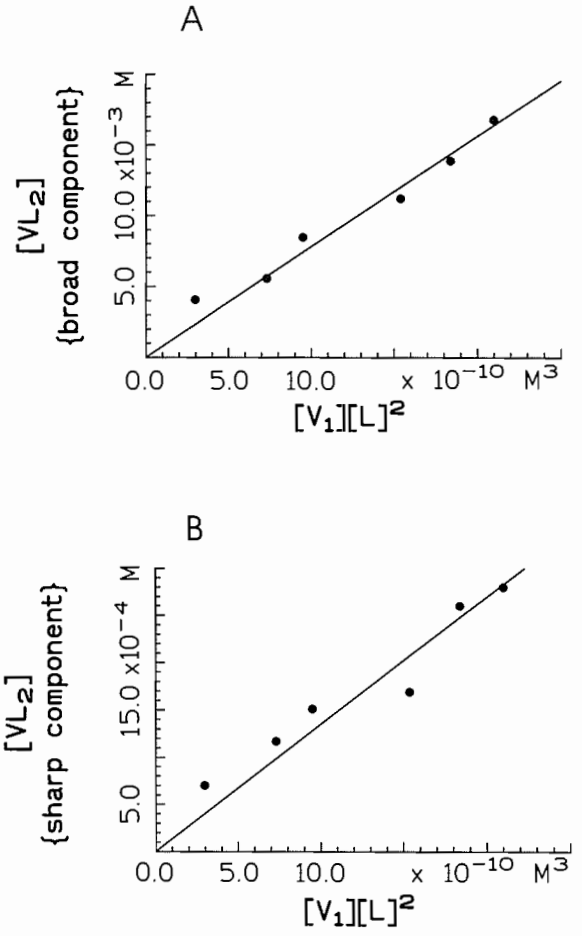
Since pH, $pK_{a2;V}$ (8.30) (35), $pK_{a;L}$ (6.02) (36), and the various concentrations are known, then, from the NMR spectra, all quantities required for the analysis of the results, according to eq. [5], are available. Figure 4 shows the result of plotting the equilibrium data according to the assumption that the monoligand product has no pK_a. The linear relationship obtained is in agreement with this assumption and a $K_{01}' = (8.1 \pm 0.8) \times 10^2\ M^{-1}$ was obtained. For this particular investigation, concentration studies were also carried out for various pH values and the individual sets of results analyzed according to eq. [1]. These pH-dependent formation constants, K_{01}, can then be written in terms of the pH-independent constants, K_{01}', of eq. [5] and the hydrogen ion concentrations. The relationship between K_{01} and K_{01}' is given by eq. [6], where it is assumed that the product can lose a proton. An analogous equation can readily be written for the alternative situation.

© 1997 NRC Canada

Can. J. Chem. Downloaded from www.nrcresearchpress.com by 88.146.161.215 on 09/08/12
For personal use only.

Can. J. Chem. Downloaded from www.nrcresearchpress.com by 88.146.161.215 on 09/08/12
For personal use only.

Fig. 2. Graphical display of the formation of vanadate/hydroxylamine products plotted according to eq. [2]. Good linear relationships were obtained. The graph establishes the VL_2 stoichiometry of the −860 ppm (A) and −820 ppm (B) products. Conditions of the experiments were: pH 7.05; 1.0 M KCl; 20 mM HEPES; 3.0 mM total vanadate; variable hydroxylamine total concentration, 1–7.0 mM.



$$[6] \quad (1 + K_{a2;V}/[H^+])\,(1 + [H^+]/K_{a;L}])K_{01} = K_{01}'(1 + K_{a;P}/[H^+])$$

When the term on the left of eq. [6] was plotted against $1/[H^+]$, a line with an intercept but no slope was obtained. The intercept gave a value for K_{01}' of $(7.5 \pm 0.6) \times 10^2$ M^{-1}, in good agreement with the above value for K_{01}'. The zero slope is expected if there is no change in protonation state throughout the pH range of the study (pH 6.7 through 8.8). With this value for K_{01}' and by neglecting the term in $K_{a;P}$, which has no measurable influence, eq. [6] can be used to calculate K_{01}, the pH-dependent formation constant, for any pH within the range of this study. It is possible that the monoligand product does have a pK_a outside the range of pH values that would influence this study.

The pH study made it possible to show that there is a fundamental chemical difference between the products giving rise to the broad and sharp NMR signals of the bisligand products. The influence that pH has on the relative populations of the two types of products is evident from Fig. 3. The products giving rise to the two broad signals (d and e, Fig. 1) were favoured by low pH while the products providing the two sharp signals (f and g, Fig. 1) were favoured by increasing pH. There was, however, no appreciable change in relative intensity of the NMR signals within the two groups. Furthermore, the broad signals showed a systematic change in chemical shift with change in pH while the sharp signals did not move. Since both sets of products contain one vanadium and two ligands, these observations are in keeping with different proton requirements for the two sets of products.

Since the two components of the bisligand products behave differently with the change in hydrogen ion concentration, they were treated separately in the detailed analysis of the pH variation study. To gather more information concerning the protonation states of the broad signal components, spectra were recorded from pH 8 to 3. A fivefold excess ligand concentration was maintained in order to attain a condition where no, or very little, decavanadate is formed in solution at low pH. The intensity of the sharp signal components of the bisligand product decreased with lower pH and finally was not observed below pH 5. In contrast to the sharp component, the intensity of the broad components increased with the rise in acidity and, also, the signals became progressively sharper and the chemical shifts changed. In addition, there was a relative change in chemical shifts of the two signals. This behavior clearly indicated that the chemical environment around the vanadium center of the complexes giving rise to the broad signals was being influenced. A plot of pH versus chemical shift of the products d and e (Fig. 1) was consistent with a change in protonation state of the complexes. In both plots an inflection point was observed. If the pH-dependent chemical shift derives from protonation/deprotonation of the products, then the chemical shift can be related to pK_a directly, according to eq. [7],

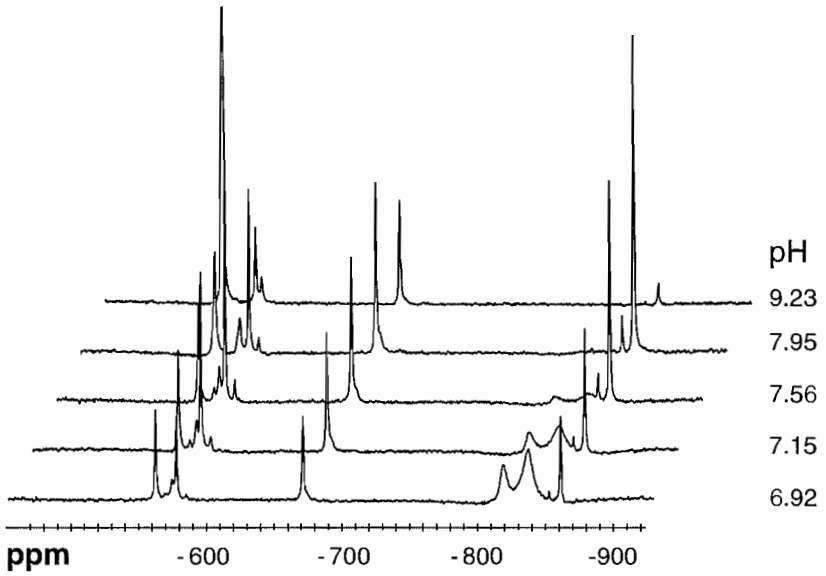
$$[7] \quad pH = pK_a + \log [(\delta_L - \delta_O)/(\delta_O - \delta_H)]$$

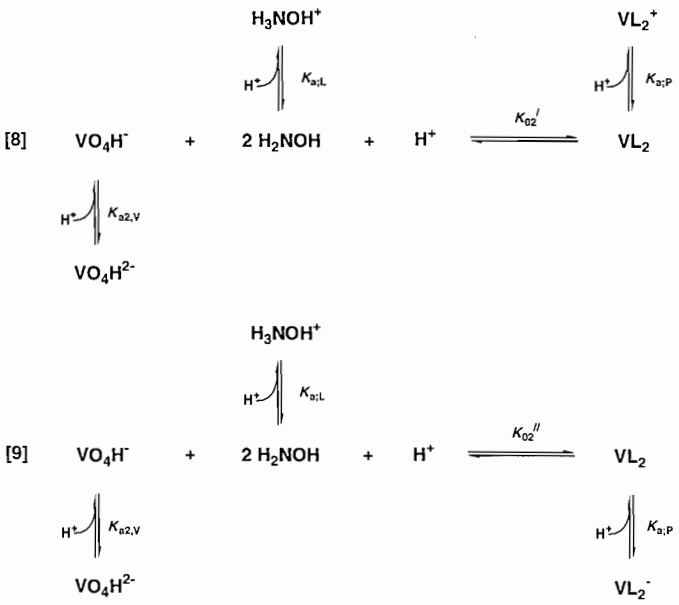
where δ_L is the limiting chemical shift at low pH, δ_H is the limiting chemical shift at high pH and δ_O is the observed chemical shift. A plot of pH versus the logarithm term gave a straight line having an intercept equal to the pK_a of the products in both cases. The pK_a values determined for the products d and e were 5.92 ± 0.12 and 6.60 ± 0.14, respectively. It is possible, but not very probable, that a change in coordination to a less hydrated product accompanies the protonation step but this cannot be determined from these studies. The ^{51}V chemical shifts corresponding to product d were −823 ppm for VL_2 and −801 ppm for VL_2^+. The corresponding shifts for product e were −848 and −815 ppm, respectively.

It is possible that the source of the chemical shift change is not a protonation/deprotonation of the complexes. It was necessary to confirm this from a detailed analysis of the pH dependence of product formation. This is also required in order to establish the proton stoichiometry and charge state of the products. Considering both protonation and deprotonation reactions, eqs. [8] and [9] can be derived. These equations anticipate the finding that the products do not carry a charge under neutral conditions.

© 1997 NRC Canada

Fig. 3. ^{51}V NMR spectra showing the change in relative intensities of the resonances of various vanadate hydroxylamine products as a function of pH. Conditions of the experiments: 3.0 mM total vanadate; 5.0 mM total hydroxylamine; 1.0 M KCl; 20 mM HEPES buffer; variable pH, pH 6.9–9.2.





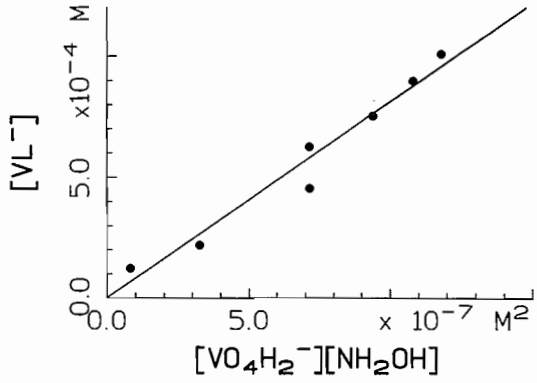
An intercept form of these equations, eqs. [10] and [11], can be derived from eqs. [8] and [9], respectively, where cVL_2, cV_1, and cL correspond to total concentrations of product (VL_2), of monomeric vanadate (V_1), and of free ligand (L).

$$[10]\quad K_{02}' + K_{02}'[H^+]/K_{a;P} = cVL_2/[H^+]\{cV_1/(1 + K_{a2;V}/[H^+])\}\{cL/(1 + [H^+]/K_{a;L})\}^2$$

$$[11]\quad K_{02}'' + K_{02}''K_{a;P}/[H^+] = cVL_2/[H^+]\{cV_1/(1 + K_{a2;V}/[H^+])\}\{cL/(1 + [H^+]/K_{a;L})\}^2$$

A plot of the term on the right-hand side of eq. [10] versus H^+ ion concentration yielded a linear relationship. The intercept of this line gave the pH-independent formation constant,

Fig. 4. Graphical representation of the formation of monoligand product as a function of pH. The graph is plotted according to eq. [5]. Experimental conditions: variable pH, pH 6.5–9.0; 3 mM total vanadate; 3.0 mM hydroxylamine; 1.0 M KCl; 20 mM HEPES buffer.



$K_{02}' = (9 \pm 3) \times 10^{12}\ M^{-3}$. The slope of the graph gave $K_{02}'K_{a;P}$, from which $K_{a;P} = (2.3 \pm 0.4) \times 10^{-7}$ was obtained, or $pK_{a;P} = 6.6$. This is an average value for the products giving rise to the two broad signals but is in good agreement with the values obtained from the variation of chemical shifts with change in pH. An average value was measured because the individual product signals were not well resolved over the entire pH range of the study. It is evident that neither of these products (d, e; Fig. 1) carry a charge under neutral conditions but are protonated and thus cationic under slightly acidic conditions. The equilibrium constants from this study are summarized in Table 1.

The overall pH-independent formation constant K_{02}'' for the sharp signal components of the bisligand products (f, g; Fig. 1) was obtained by plotting the appropriate parameters of eq. [11]. The value obtained for K_{02}'' was $(5 \pm 2) \times 10^{12}\ M^{-3}$. The $pK_{a;P}$ values for the two sharp components, within the

Can. J. Chem. Downloaded from www.nrcresearchpress.com by 88.146.161.215 on 09/08/12
For personal use only.

© 1997 NRC Canada

Can. J. Chem. Downloaded from www.nrcresearchpress.com by 88.146.161.215 on 09/08/12
For personal use only.

Table 1. Formation constants for hydroxamido and *N*-methylhydroxamido vanadate complexes.

Equilibrium equation	Hydroxylamine		*N*-Methylhydroxylamine	
	Chemical shift	Formation constant	Chemical shift	Formation constant
		pH-dependent equilibrium constants[a,b]		
$V + L \rightleftharpoons VL$	−569	$(7.0 \pm 0.4) \times 10\ M^{-1}$	−571	$(2.2 \pm 0.2) \times 10^2\ M^{-1}$
$V + L \rightleftharpoons VL$	−670	$(5.1 \pm 0.3) \times 10^2\ M^{-1}$	−651	$(1.2 \pm 0.2) \times 10^3\ M^{-1}$
$V + L \rightleftharpoons VL$	−674	$(3.0 \pm 0.2) \times 10\ M^{-1}$	−655	$(2.8 \pm 0.3) \times 10^2\ M^{-1}$
$VL + L \rightleftharpoons VL_2$	$-830_{2,br}$	$(1.5 \pm 0.2) \times 10^3\ M^{-1}$	$-760_{5,br}$	$(6.8 \pm 1.0) \times 10^2\ M^{-1}$
$VL + L \rightleftharpoons VL_2$	$-860_{2,sh}$	$(2.5 \pm 0.3) \times 10^2\ M^{-1}$	$-795_{5,sh}$	$(1.1 \pm 0.1) \times 10^3\ M^{-1}$
$V + 2L \rightleftharpoons VL_2$	$-830_{2,br}$	$(7.8 \pm 0.7) \times 10^5\ M^{-2}$	$-760_{5,br}$	$(1.0 \pm 0.2) \times 10^6\ M^{-2}$
$V + 2L \rightleftharpoons VL_2$	$-860_{2,sh}$	$(1.3 \pm 0.2) \times 10^5\ M^{-2}$	$-795_{5,sh}$	$(1.7 \pm 0.3) \times 10^6\ M^{-2}$
		pH independent equilibrium constants[a,b]		
$VO_4H_2^- + L \rightleftharpoons VL^-$	−670	$(8.1 \pm 0.8) \times 10^2\ M^{-1}$	−651	$(3.4 \pm 0.2) \times 10^3\ M^{-1}$
$VO_4H_2^- + 2L + H^+ \rightleftharpoons VL_2$	$-830_{2,br}$[c]	$(9 \pm 3) \times 10^{12}\ M^{-3}$	$-760_{5,br}$[c]	$(27 \pm 5) \times 10^{12}\ M^{-3}$
$VO_4H_2^- + 2L + H^+ \rightleftharpoons VL_2$	$-860_{2,sh}$	$(5 \pm 2) \times 10^{12}\ M^{-3}$	$-795_{5,sh}$	$(5 \pm 2) \times 10^{13}\ M^{-3}$
$VL_2^+ \rightleftharpoons VL_2 + H^+$	-801_{br}[c]	$(1.2 \pm 0.4) \times 10^{-6}$	$-769_{5,br}$[c]	$(8.2 \pm 2.0) \times 10^{-7}$
$VL_2^+ \rightleftharpoons VL_2 + H^+$	-815_{br}[c]	$(2.5 \pm 0.9) \times 10^{-7}$		
$VL_2 \rightleftharpoons VL_2^- + H^+$	$-860_{2,sh}$	$(4.0 \pm 0.6) \times 10^{-8}$	$-795_{5,sh}$	$(1.7 \pm 0.4) \times 10^{-8}$

[a]sh and br refer to broad and sharp NMR signal components, respectively.
[b]The pH-dependent equilibrium constants were determined at pH 7.05 and 7.50, respectively, for the hydroxamido and *N*-methylhydroxamido complexes and are overall values for the indicated number of products. For instance, *N*-methylhydroxylamine gives rise to five products with sharp signals near −795 ppm. The value quoted is for the sum. Errors in the equilibrium constants are reported at the 3σ level. See Table 2 for all signal positions and relative intensities.
[c]The position of these signals is pH dependent.

error of the experiments, were the same ($pK_{a;P}$ = 7.4). The results are summarized in Table 1. It is interesting to note that, although these products have a pK_a, their ^{51}V chemical shifts are not pH dependent.

The pH-independent formation constants, K_{02}' and K_{02}'', for the broad and sharp component can be related to the pH-dependent formation constant, K_{02}, for the individual products, according to the following equations:

$$[12] \quad (1 + K_{a2;V}/[H^+])(1 + [H^+]/K_{a;L})^2 K_{02} = K_{02}'[H^+](1 + [H^+]/K_{a;P})$$

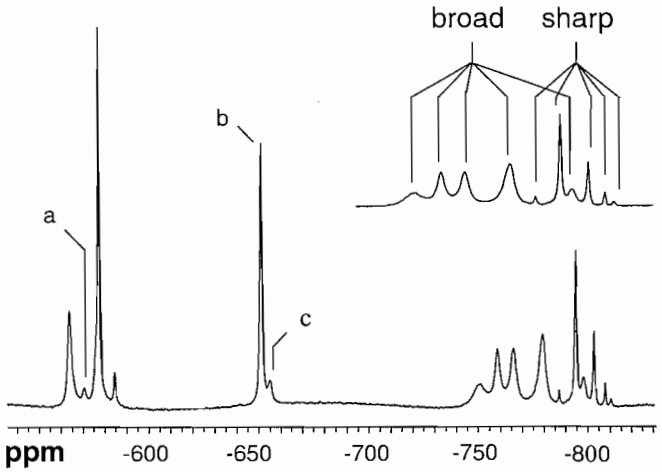
$$[13] \quad (1 + K_{a2;V}/[H^+])(1 + [H^+]/K_{a;L})^2 K_{02} = K_{02}''[H^+](1 + K_{a;P}/[H^+])$$

The calculated K_{02} values from eqs. [12] and [13] were consistent with the formation constants determined at specific pH values. With the appropriate juggling of pK_a values and relative intensities of the individual signals at pH 6.70 (Table 2), any concentration for any pH can be calculated using eqs. [12] and [13] together with eq. [3].

N-Methylhydroxylamine

The reactions of *N*-methylhydroxylamine with vanadate, not surprisingly, were very similar to the reactions with hydroxylamine. The complications arising from instability of the ligand at elevated pH were not encountered and, in this respect, it was easier to characterize the system. Complications did, however, arise because the ^{51}V NMR spectra were more complex. The complexity was a consequence of the occurrence of signals for each of the isomers formed as a result of the various relative orientations of the methyl groups of the ligand. A typical spectrum is displayed in Fig. 5.

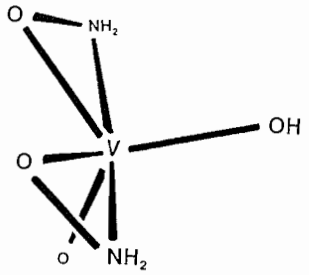
Fig. 5. ^{51}V NMR spectrum demonstrating the reaction of vanadate with methylhydroxylamine to yield various products. The inset spectrum shows the signals corresponding to the bisligand products. The experimental conditions were: 3.1 mM total vanadate; 4.1 mM total methylhydroxylamine; 1.0 M KCl; 20 mM HEPES buffer; pH 6.6.



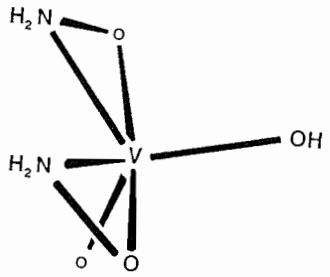
Analysis of the concentration and pH variation studies proceeded as for hydroxylamine and the various equilibrium constants are provided in Table 1. As for hydroxylamine, the monoligand product did not have pK_a while both types of bisligand products did. It was not possible to obtain pK_a values for all the broad signal products from the influence of pH on their chemical shifts. However, one signal was assignable over the pH range and a pK_a value of 5.7 ± 0.2 obtained. This agrees favourably with the value of 6.1 ± 0.2 obtained overall

© 1997 NRC Canada

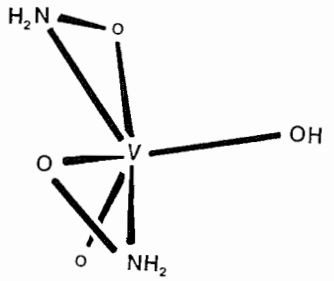
Scheme 1.



I



II



III

for the broad signal products from concentration studies under various pH conditions (Table 1), and compares with $pK_a = 7.8 \pm 0.1$ overall for the sharp signals. Here, as for the hydroxylamine system, there was little indication that there was significant variation of pK_a values within the set of products giving rise to the sharp signals.

Discussion

Both hydroxylamine and *N*-methylhydroxylamine undergo condensation reactions with vanadate to form four types of complexes. The least preferred products provide ^{51}V signals (−571 ppm) near those of vanadate and its oligomers. The formation constants for these materials are several orders of magnitude larger than those typically found for products formed from alkyl alcohols (37, 38) but comparable to those from phosphate (39). These products are formed equally well whether the ligand is $HONH_2$, $HONHCH_3$, or $HON(CH_3)_2$. This suggests that the reaction is not occurring at the nitrogen. As a consequence, it is proposed that these are ester-like compounds where monodentate complexation occurs at the hydroxyl group. Although similar peroxovanadium complexes have not been reported, it seems likely that corresponding complexes are formed. Such an "end-on" coordination may be important in the function of haloperoxidases.

Under moderate ligand concentrations, the predominant products are mono- and bisligand complexes. The two types of bisligand compounds are chemically quite distinct. Under neutral conditions, neither product carries a charge. However, the broad signal components can be protonated at lower pH to form cationic complexes. It cannot be ascertained from this work whether a change in coordination accompanies the protonation step but it is possible. Apparently these products do not release a proton at higher pH and, consequently, with increase in pH, they are rapidly lost from solution. The situation is opposite for the sharp signal components. They release a proton at higher pH but, because they do not accept protons, are lost from the solution as the acidity is increased. The NMR signals for these compounds occur within the same chemical shift range as those for peroxovanadates and this suggests that they are similarly coordinated. For the case of the broad signal component of the bisligand products of *N*,*N*-dimethylhydroxylamine, X-ray crystal structure analysis and NMR dissolution studies have been used to assign a six-coordinate (tetrahedral if the bonds to the hydroxylamine are formally considered to be unidentate) structure (30). Since the spectral patterns for the ligands of this study are similar to those for the dimethylhydroxylamine case and they have the same stoichiometry and a similar protonation pattern, a corresponding tetrahedral-like coordination is assigned to the products giving the broad signals (d, e; Fig. 1) of this study.

The chemical differences between the bisligand products giving rise to the sharp NMR signals (f, g; Fig. 1) and those giving rise to the broad signals clearly shows that these two products must have a different coordination. There is some evidence that the sharp signal components correspond to a pentagonal bipyramidal (trigonal bipyramidal for formal unidentate assumption) coordination. This coordination is found in the crystalline glycylglycine complex of bis(hydroxamido)vanadate (40, 41) and the NMR spectra of this complex provide a sharp signal that overlaps the chemical shift range of the sharp signals of the precursor bisligand complex (41). A somewhat similar structure is also found in a tris(hydroxylamine)–vanadate complex where the side-on coordination arises for only two of the three ligands, the third ligand being complexed only through the oxygen (42).

Scheme 1 shows the coordination proposed for the products giving rise to the broad signal products. A similar set of three

© 1997 NRC Canada

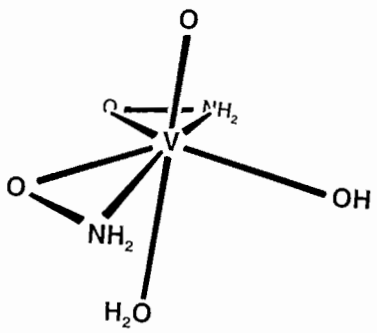
Can. J. Chem. Downloaded from www.nrcresearchpress.com by 88.146.161.215 on 09/08/12
For personal use only.

Table 2. ^{51}V chemical shifts of the complexes formed from the reaction of vanadate with hydroxylamine ligands, L (L = NH_2OH, CH_3NHOH, and $(CH_3)_2NOH$), at pH 6.7.

	Chemical shift[a]				Chemical shift[b]		
Product	NH_2OH	CH_3NHOH	$(CH_3)_2NOH$	Product	NH_2OH	CH_3NHOH	$(CH_3)_2NOH$
VL	−569	−571	−571				
VL	−670	−651	−630	VL	−674	−655	−635
VL[a,c]	−819 (1.0)	−751 (1.0)	−724 (1.0)	VL[b,c]	−852 (1.0)	−789 (1.0)	−750
	−839 (2.5)	−758 (1.3)	−740 (1.4)		−861 (8.5)	−794 (12.8)	
		−766 (1.4)				−803 (6.0)	
		−779 (1.8)				−808 (1.8)	
		−798 (0.6)				−810 (0.9)	

[a]Chemical shifts correspond to the broad signal components of the NMR spectrum.
[b]Chemical shifts correspond to the sharp signal components of the NMR spectrum.
[c]Values arranged vertically in parentheses correspond to the relative concentrations within each set of products.

Scheme 2.



rotational isomers is possible for the seven coordinate products, only one of which is displayed in Scheme 2. It is known for the dimethylhydroxylamine ligand that the isomers of the six-coordinate complex undergo a rapid exchange process (30). The arrangement in which the two oxygens are *cis* to each other is the predominant one observed in crystal structure studies. This suggests that this arrangement is the thermodynamically favoured one. For hydroxylamine and dimethylhydroxylamine, the ratio of products for the broad components is about 1:2 and is about 1:8 for the sharp components. A somewhat similar ratio (1:3) of glycylglycinato complexes is also found in the glycylglycine–hydroxylamine–vanadate system (41). On this basis, the *cis* arrangement in which the oxygens are close together is assigned to the major isomer (Scheme 1, I), the second *cis* arrangement in which the nitrogens are close together (Scheme 1, II) to the second isomer, and the *trans* arrangement (Scheme 1, III) to the least preferred isomer. It seems clear that a fundamental characteristic of both bisperoxo and bishydroxamido ligand complexes is that the liganding atoms of both ligands lie in a common plane. This arrangement and the isomer selectivity may be closely related and a consequence of an underlying physical property of this type of complex.

The information obtained from this study also allows a structural assignment to be made for the coordination of the monohydroxamido complexes. Two signals for monoligand products are observed for *N,N*-dimethylhydroxamido, *N*-methylhydroxamido, and hydroxamido complexes. They are found in an approximate 1:10 ratio for all three systems. For the monoligand situation, (except for methylhydroxylamine complexes) neither of the coordinations discussed for the bisligand compounds can give rise to more than one vanadium NMR signal. Therefore, the two signals observed correspond to distinct coordination geometries. Since, under neutral conditions, the major bisligand product is six-coordinate (tetrahedral-like if the hydroxylamine is formally considered unidentate), then it seems possible that the major monohydroxamido complex is five-coordinate and also tetrahedral-like. If the complex were trigonal bipyramidal, then, for the *N*-methylhydroxylamine ligand, two signals of roughly comparable intensities, corresponding to the two possible methyl group orientations similar to that observed for the bisligand complexes, would be expected and only one signal is observed (Fig. 5). Only one such signal is expected for a tetrahedral coordination. This suggests the coordination of the major monoligand product is tetrahedral but the possibility of rapid isomerization cannot be ruled out for this complex even though it is slow in the other complexes. Tetrahedral-like coordination would, however, explain why the monoligand complexes do not have a pK_a in the range 6–9. Products of such a structure would probably have a second pK_a somewhat closer to the third pK_a of the vanadate anion (about 12) as opposed to a much lower pK_a for a seven-coordinate structure. For instance, monoperoxovanadate, for which a trigonal bipyramidal coordination has been proposed on the basis of ^{17}O NMR studies (33), has a second pK_a of 6.2 (34). Furthermore, the complex giving rise to the sharp signal components of bis(hydroxamido)vanadate and the bisperoxovanadate complex have similar seven-coordinate geometries and similar pK_a's; pK_{a1} = 7.4 and pK_{a2} = 7.2, respectively.

The ^{51}V chemical shifts observed for the various bishydroxamido complexes are provided in Table 2. It is somewhat surprising that the vanadium chemical shifts are as sensitive to replacement of an NH by an NCH_3 as to a change in coordination from six to seven (tetrahedral to trigonal bipyramidal), ~30 ppm. Even the *cis*/*trans* isomerization can lead to about a 20 ppm change in chemical shifts. The average change in chemical shifts is about 50 ppm for replacement of NH by NCH_3 in the bisligand complexes but drops to about half this value for the monoligand products. This suggests that the

© 1997 NRC Canada

Can. J. Chem. Downloaded from www.nrcresearchpress.com by 88.146.161.215 on 09/08/12
For personal use only.

influence of the methyl groups is cumulative and corresponds to +20–+25 ppm per methyl group per ligand.

It is evident from this work that, despite the similarity of hydrogen peroxide and hydroxylamine, there are some significant differences in their complexation reactions with vanadate. The monoligand six-coordinate tetrahedral-like complexes have not been reported for peroxovanadium complexes although triperoxovanadate is known to have a tetrahedral coordination (43). Tetrahedral coordination in peroxovanadium complexes might well be more ubiquitous than presently anticipated. Since changes in coordination number have a rather small influence on chemical shifts compared to the influences attributable to side-on coordination, use of vanadium chemical shifts to characterize coordination geometry in these complexes could be highly misleading.

Acknowledgements

Thanks are extended to the Natural Sciences and Engineering Research Council of Canada for its support of this work in the form of an operating grant to A.S.T.

References

1. D.C. Crans. Comments Inorg. Chem. **16**, 35 (1994).
2. P.J. Stankiewicz and A.S. Tracey. Met. Ions Biolog. Syst. **31**, 259 (1995).
3. P.J. Stankiewicz, A.S. Tracey, and D.C. Crans. Met. Ions Biolog. Syst. **31**, 287 (1995).
4. M.J. Gresser and A.S. Tracey. *In* Vanadium in biological systems. *Edited by* N.D. Chasteen. Kluwer Academic Publishers, Dordrecht, Boston, London. 1990. pp. 63–79.
5. H. Vilter. Met. Ions Biolog. Syst. **31**, 325 (1995).
6. R. Wever and B.E. Krenn. *In* Vanadium in biological systems. *Edited by* N.D. Chasteen. Kluwer Academic Publishers, Dordrecht, Boston, London. 1990. pp. 81–97.
7. E.G.M. Vollenbroek, L.H. Simons, J.W.P.M. Schijndel, P. Barnett, M. Balzar, H. Dekker, C. van der Linden, and R. Wever. Biochem. Soc. Trans. **23**, 267 (1995).
8. R. Wever and K. Kustin. Adv. Inorg. Chem. **31**, 81 (1990).
9. R.E. Eady. Met. Ions Biolog. Syst. **31**, 363 (1995).
10. R.E. Eady. *In* Vanadium in biological systems. *Edited by* N.D. Chasteen. Kluwer Academic Publishers, Dordrecht, Boston, London. 1990. pp. 99–127.
11. C. Orvig, K.H. Thompson, M. Battell, and J.H. McNeill. Met. Ions Biolog. Syst. **31**, 575 (1995).
12. Y. Schechter, J. Meyerovitch, Z. Farfel, J. Sack, R. Bruck, S. Bar-meir, S. Amir, H. Degani, and S.J.D. Karlish. *In* Vanadium in biological systems. *Edited by* N.D. Chasteen. Kluwer Academic Publishers, Dordrecht, Boston, London. 1990. pp. 129–142.
13. B.I. Posner, R. Faure, J.W. Burgess, A.P. Bevan, D. Lachance, G. Zhang-Sun, I.G. Fantus, J.B. Ng, D.A. Hall, B. Soo Lum, and A. Shaver. J. Biol. Chem. **269**, 4596 (1994).
14. D.A. Wink, R.W. Nims, J.E. Saavedra, Jr., W.E. Utermahlen, and P.C. Ford. Proc. Natl. Acad. Sci. U.S.A. **91**, 6604 (1994).
15. M.J. Clague and A. Butler. J. Am. Chem. Soc. **117**, 3475 (1995).
16. A. Messershmidt and R. Wever. Proc. Natl. Acad. Sci. U.S.A. **93**, 392 (1996).
17. C.R. Cornman, J. Kampf, M.S. Lah, and V.L. Pecoraro. Inorg. Chem. **31**, 2035 (1992).
18. H.S. Soedjak and A. Butler. Biochim. Biophys. Acta, **1079**, 1 (1991).
19. V. Imbert, J.-F. Peyron, D. Farahi Far, B. Mari, P. Auberger, and B. Rossi. Biochem. J. **297**, 163 (1994).
20. M.J. Gresser, A.S. Tracey, and P.J. Stankiewicz. Adv. Protein Phosphatases, **4**, 35 (1987).
21. G. Huyer, S. Liu, J. Kelly, J. Moffat, P. Payette, B. Kennedy, G. Tsaprailis, M.J. Gresser, and C. Ramachandran. J. Biol. Chem. **272**. 843 (1997).
22. A. Butler, M.J. Clague, and G.E. Meister. Chem. Rev. **94**, 625 (1994).
23. A.S. Tracey and J.S. Jaswal. Inorg. Chem. **32**, 4235 (1993).
24. A.S. Tracey and J.S. Jaswal. J. Am. Chem. Soc. **114**, 3835 (1992).
25. A. Butler. *In* Vanadium in biological systems. *Edited by* N.D. Chasteen. Kluwer Academic Publishers, Dordrecht, Boston, London. 1990. pp. 25–49.
26. A.F. Ghiron and R.C. Thompson. Inorg. Chem. **29**, 4457 (1990).
27. E. Bayer, E. Koch, and G. Anderegg. Angew. Chem. Int. Ed. Engl. **26**, 545 (1987).
28. M.A. Nawi and T.L. Riechel. Inorg. Chim. Acta, **136**, 33 (1987).
29. E. Bayer. Met. Ions Biolog. Syst. **31**, 407 (1995).
30. P.C. Paul, S.J. Angus-Dunne, R.J. Batchelor, F.W.B. Einstein, and A.S. Tracey. Can. J. Chem. **75**, 429 (1997).
31. H. Remy. *In* Treatise on inorganic chemistry. Elsevier Publishing Company, Amsterdam, New York. 1956. p. 617.
32. O.W. Howarth. Prog. Nucl. Magn. Reson. Spectrosc. **22**, 453 (1990).
33. A.T. Harrison and O.W. Howarth. J. Chem. Soc. Dalton Trans. 1173 (1985).
34. J.S. Jaswal and A.S. Tracey. Inorg. Chem. **30**, 3718 (1991).
35. A.S. Tracey, J.S. Jaswal, and S.J. Angus-Dunne. Inorg. Chem. **34**, 5680 (1995).
36. T.C. Bissot, R.W. Parry, and D.H. Campbell. J. Am. Chem. Soc. **79**, 796 (1957).
37. A.S. Tracey and M.J. Gresser. Can. J. Chem. **66**, 2570 (1988).
38. A.S. Tracey, B. Galeffi, and S. Mahjour. Can. J. Chem. **66**, 2294 (1988).
39. M.J. Gresser, A.S. Tracey, and K.M. Parkinson. J. Am. Chem. Soc. **108**, 6229 (1986).
40. S.J. Angus-Dunne, P.C. Paul, and A.S. Tracey. 31st Int. Conf. Coord. Chem. Abstract 1P13 (1996).
41. P.C. Paul, S.J. Angus-Dunne, R.J. Batchelor, F.W.B. Einstein, and A.S. Tracey. Can. J. Chem. **75**, 183 (1997).
42. M. Shao, J. Leng, and Z. Pan. Wuji Huaxue Xuebao, **6**, 443 (1990).
43. R.E. Drew, F.W.B. Einstein, J.S. Field, and D. Begin. Angew. Chem. Int. Ed. Engl. **31A**, S135 (1975).

Can. J. Chem. Downloaded from www.nrcresearchpress.com by 88.146.161.215 on 09/08/12
For personal use only.

© 1997 NRC Canada

Diphenylmethane and diphenyl ether — experimental conformations and torsional surfaces calculated with AM1, MNDO, PM3, and density functional theory (Becke3LYP)

Thomas Straßner

Can. J. Chem. Downloaded from www.nrcresearchpress.com by 88.146.161.215 on 09/08/12
For personal use only.

Abstract: The complete energy surfaces of the torsion around the central C—O or C—CH_2 bonds in diphenyl ether (DPE) and diphenylmethane (DPM) are calculated with semiempirical methods (AM1, MNDO, PM3) and density functional theory (Becke3LYP/3-21G). Stationary points are optimized at the Becke3LYP/6-31G(d) level of theory. The geometry of a very recently published X-ray structure of 4,4′-bis[*N*-(2,4,6-trimethyl)benzenesulfonamide]diphenylmethane (**1**), as well as the solid state structures of many other diphenyl ethers and diphenylmethanes, is found in the low-energy regions of the AM1 surfaces of the parent compounds.

Key words: Conformational analysis, diphenyl ether, diphenylmethane, quantum chemistry (AM1, MNDO, PM3), density functional theory (Becke3LYP).

Résumé : On a calculé les surfaces complètes d'énergie pour la torsion autour des liaisons centrales C—O et C—CH_2 du diphényléther (DPE) et du diphénylméthane (DPM) en faisant appel à des méthodes semiempiriques (AM1, «MNDO», PM3) et à la théorie de la densité fonctionnelle (Becke3LYP-21G). On a optimisé les points stationnaires au niveau Becke3LYP/6-31G(d) de la théorie. On a trouvé que la géométrie du 4,4′-bis[*N*-(2,4,6-triméthyl)benzènesulfonamide]diphénylméthane (**1**), déterminée par diffraction des rayons X et rapportée très récemment, ainsi que les structures à l'état solide de plusieurs autres diphényléthers et diphénylméthanes se trouvent toutes dans des régions de faibles énergies de srufaces AM1 des composés fondamentaux.

Mots clés : analyse conformationnelle, diphényléther, diphénylméthane, chimie quantique (AM1, «MNDO», PM3), théorie de la densité fonctionnelle (Becke3LYP).

[Traduit par la rédaction]

Introduction

The geometry at the central atom of diphenylmethane and diphenyl ether has been under discussion for many years and several attempts have been made to explain and predict the torsional angles by calculational procedures. However, all these previous studies used assumptions o froze coordinates, due to the resources needed for the calculation of an energy surface without constraints. The present article is a complete study of the torsional energy hypersurfaces of diphenylmethane (DPM) and diphenyl ether (DPE). The results of semiempirical and density functional theory calculations are discussed and compared with experimental data.

Received February 19, 1997.

T. Straßner.[1,2] Institut für Organische Chemie, Technische Universität Dresden, Mommsenstraße 13, 01062 Dresden, Germany.

[1] Telephone: 0351-463-3211. Fax: 0351-463-7030. E-mail: strasner@organik.uni-erlangen.de

[2] Present address (until Nov. 30): Department of Chemistry and Biochemistry, University of California, Los Angeles, 405 Hilgard Avenue, CA 90095-1569, U.S.A. Telephone: (310) 825-0269. Fax: (310) 206-1843. E-mail: strasner@xenon.chem.ucla.edu

The geometries of compounds of the type aryl-X-aryl with different groups X (X = O, X = CH_2, X = SO_2, e.g., diphenyl ether (DPE) and diphenylmethane (DPM)) have been discussed now for several years (1–9). One of the reasons for this interest is the occurrence of the structural unit "aryl-X-aryl" in many important natural compounds like the thyroid hormone T_3 (10), in antibiotics like vancomycin (11) or bouvardin (12), as well as in aminopeptidase inhibitors like OF4949-III (13). Additionally, the aryl-X-aryl unit seems to account for the characteristics of polymeric materials with very special properties like PEK, PEEK, PES, and PEES,[3] where initial calculations of different conformations of such polymer chains have been published (2, 7).

Many authors have discussed the geometry of aryl-X-aryl structures on the basis of different calculational methods (EH (1), INDO (3), STO-3G (4), 3-21G (5), C-INDO (6), MNDO (7), MM2 (8), AM1 (9), and CNDO/2 (14)). However, all studies were either restricted to selected points on the torsional hypersurface or use symmetry constraints. The ab initio calculations (4, 5) are reported with small basis sets, assuming C_2 symmetry and (or) a frozen C-X-C angle. The C-INDO calcu-

[3] PEK = poly(aryl ether ketone); PEEK = poly(aryl ether ether ketone); PES = poly(ether sulfone); PEES = poly(ether ether sulfone).

© 1997 NRC Canada

Can. J. Chem. Downloaded from www.nrcresearchpress.com by 88.146.161.215 on 09/08/12
For personal use only.

lations (6) are based on assumptions about the hybridization of the central atom X. MNDO results were obtained with frozen bond lengths and bond angles. It seems to be questionable whether calculations with such restrictions will give valuable results. Very recently a paper was published using high-level ab initio methods (RHF/6-31G(d)) with full geometry optimization (15).

The most thorough way to check the torsional energy surface of diphenyl-X compounds is certainly ab initio calculations with high-level basis sets including electron correlation. On the other hand, the calculation of a whole ab initio surface requires a great deal of computational time and hardware. Is it necessary, for these systems, to spend a lot of computer time or are the semiempirical calculations sufficient? One of the advantages of density functional theory is the partial inclusion of correlation, also with smaller basis sets such as 3-21G; another is its more reasonable requirement of system resources. Furthermore, DFT has proven useful in cases where semiempirical calculations are known to fail (16). Therefore, the Becke3LYP/3-21G basis set was used to check the semiempirical calculations. Semiempirical methods are often used in industry due to their cost efficiency and because they have produced reliable results. For example, AM1 is capable of reproducing the ab initio results of the torsion in amides and ureas after introduction of a correction term (17). Therefore the surface was calculated using semiempirical methods and the Becke3LYP/3-21G level. The local minima and transition states were reoptimized at the Becke3LYP/6-31G(d) level. The results of the calculations have been compared to published experimental data and recently published ab initio calculations on the HF/6-31G(d) level (15).

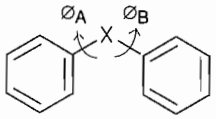
Methods

AM1, MNDO, and PM3 were used in the form of the computing package VAMP 4.50[4] (18) (running on a CONVEX C220 and an SGI-Indigo) using the EF-optimizer (19). All structures were calculated using the keyword PRECISE. The C-C-X-C torsions are calculated by reaction coordinates from 0° to 180° in 5° steps, optimizing all other coordinates. The density functional theory (DFT) (20) calculations were performed using the GAUSSIAN-94 set of codes (21). The surface is calculated by reaction coordinates from 0° to 180° in 15° steps. DFT takes into account electron correlation by a correlation functional (20). The introduction of gradient-corrected (non-local) functionals has significantly improved the theoretical predictions (22, 23). DFT includes dynamic and nondynamic electron correlation to some extent and appears to be the best choice for both efficiency and accuracy. The economy of DFT methods makes them a promising alternative approach to ab initio methods. The well-approved Hartree–Fock hybrid model Becke3LYP (23) implemented in Gaussian-94 was used throughout this study.

The split valence DZ basis sets 3-21G and 6-31G(d) were employed in the DFT calculations. The geometries and energies of stationary points were checked with force calculations to ensure that they were stationary points. Transition states can be distinguished from other stationary points by the fact that the Hessian matrix has a sole negative value for these states.

[4] The program package VAMP 4.50 (*V*ectorized *AMP*AC) by T. Clark is used for semiempirical calculations at the Universities Erlangen and Dresden, Germany.

Scheme 1. Definition of angles $\varnothing_A$, $\varnothing_B$.



Results

Structures and X-ray data

Structure **1** was recently published in Acta Crystallographica (24); important geometrical data are mentioned in Table 7. The angles $\varnothing_A$, $\varnothing_B$ are defined in Scheme 1.

The various conformations of aryl-X-aryl compounds are defined by the ring twist angles $\varnothing_A$, $\varnothing_B$, i.e., the dihedral angles between the angle C-X-C and the plane of the aromatic rings A and B, respectively (25*m*). The two torsional angles $\varnothing_A$ and $\varnothing_B$ lead to different conformational classes with C_s (**D**), C_2 (**E**), and, of course, C_1 (**F**) symmetry. Three additional conformations of high symmetry (**A**, **B**, and **C**), can be constructed where $\varnothing_A$ and (or) $\varnothing_B$ have values of 0° or 90°. The structures are shown in Scheme 2.

In agreement with previous publications, we will name the conformations shown in Scheme 2 as "all-planar" (**A**), as "perpendicular" (**B**), as "skewed" (**C**), and as "butterfly" forms (**D**, **E**, and **F**). Form **A** is expected to be very unstable due to the short H—H bond distance of the *ortho*-hydrogen atoms. Predictions cannot be made for the other structures. Of course, π-conjugation with the lone pair of the ether oxygen (DPE) and the steric demand of the CH_2 group (DPM) will influence the stability of the conformations.

Many X-ray structures of *para*-substituted aryl-X-aryl compounds are known from the Cambridge data base (25, 26). They have been useful for the evaluation of the calculated energy surfaces. The recently published X-ray structure of 4,4′-bis[*N*-(2,4,6-trimethyl)benzenesulfonamide]diphenylmethane shows angles of 54° and 57° degrees (**1**) relative to the central carbon atom, which is not unusual for this class of compounds (see Fig. 1). The geometry of **1** is comparable to some already published X-ray structures (25*m*) (see below).

Semiempirical energy surfaces of diphenylmethane and diphenyl ether

From comparison of the different diphenylmethane surfaces, it is obvious that the minimum of the AM1 surface is large and nearly flat. This is shown in Fig. 2, a three-dimensional plot of the AM1 surface of diphenylmethane.

The energy surfaces in $\varnothing_A$ and $\varnothing_B$, calculated with AM1, MNDO, and PM3 are given in Figs. 3–8. The distance between the lines of the energy contour maps in Figs. 3–8 is 0.1 kcal/mol. Marked points correspond to the data in Table 1 (diphenylmethane) and Table 2 (diphenyl ether).

The energy difference between points 1 and 2 in Fig. 3 is only 0.01 kcal/mol. The program used calculates that point 2 has no imaginary frequencies and is a local minimum. This might be a result of the numerical instabilities of the minimizer, which does not work properly for such very flat

© 1997 NRC Canada

Scheme 2. Possible conformations with different symmetry of aryl-X-aryl compounds.

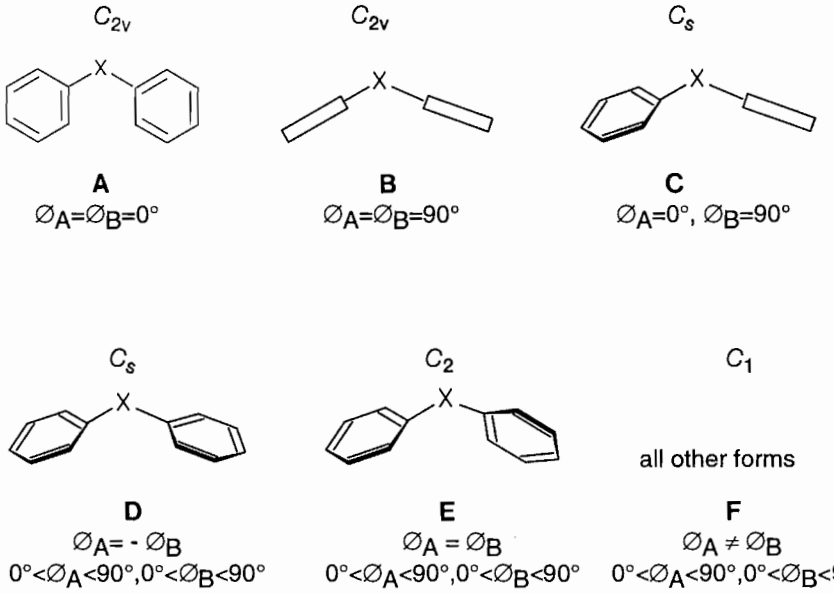
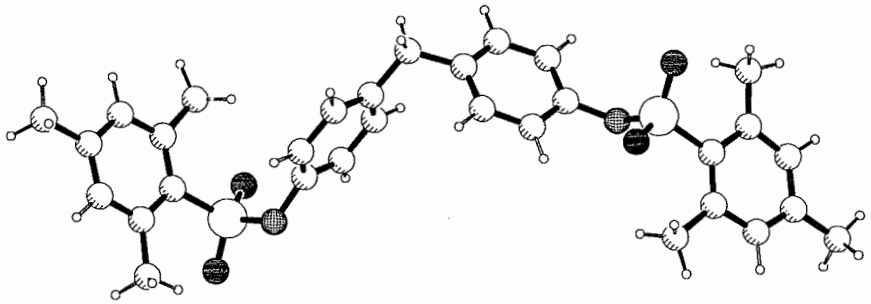


Fig. 1. 3D view of the X-ray structure of compound **1**.



1

$\varnothing_A=54°$, $\varnothing_B=57°$

surfaces (see Table 1). PM3 also calculates the C_{2v} structure to be a local minimum, but all other structures of type **B** (C_{2v} symmetry) are transition states (Tables 1 and 2). The diphenyl ether surfaces have minima at angles of about 36° ± 3°, the shape of the low-energy region obviously favouring C_2-symmetrical geometries.

Diphenylmethane

The different diphenylmethane surfaces are represented in Figs. 2–5, with results of frequency calculations for extrema in these surfaces given in Table 1.

Diphenyl ether

The results of all three Hamiltonians are similar for diphenylmethane. They differ in the degree of curvature of the minimum, but all three show a very large region of almost equal energy. The largest and flatest minimum region is calculated by AM1. In the case of diphenyl ether the results differ. While AM1 and PM3 calculate a minimum for $\varnothing_A/\varnothing_B$ of about 30°/30°, the MNDO minimum is about 50°/50°. All three Hamiltonians calculate the transition state at 90°/90°, between both minima, to be about 1 kcal/mol higher in energy. To decide which semiempirical method (AM1, MNDO, or PM3) better describes the conformation of diphenylmethane and diphenyl ether, the surfaces are compared with experimental and density functional theory data.

Energy surfaces of diphenylmethane and diphenyl ether calculated by density functional theory

The results of the DFT calculations agree very well with the semiempirical results. They, as well as published ab initio calculations (15), favour the C_2 conformation for the parent compounds.

The hypersurfaces shown in Figs. 9 and 10 are very similar

© 1997 NRC Canada

Can. J. Chem. Downloaded from www.nrcresearchpress.com by 88.146.161.215 on 09/08/12
For personal use only.

Fig. 2. Three-dimensional representation of the energy surface of diphenylmethane, calculated with AM1. The vertical axis is the heat of formation in kcal/mol. $\varnothing_A$, $\varnothing_B$ are given between 0° and 180° on the axis of the two-dimensional surface.

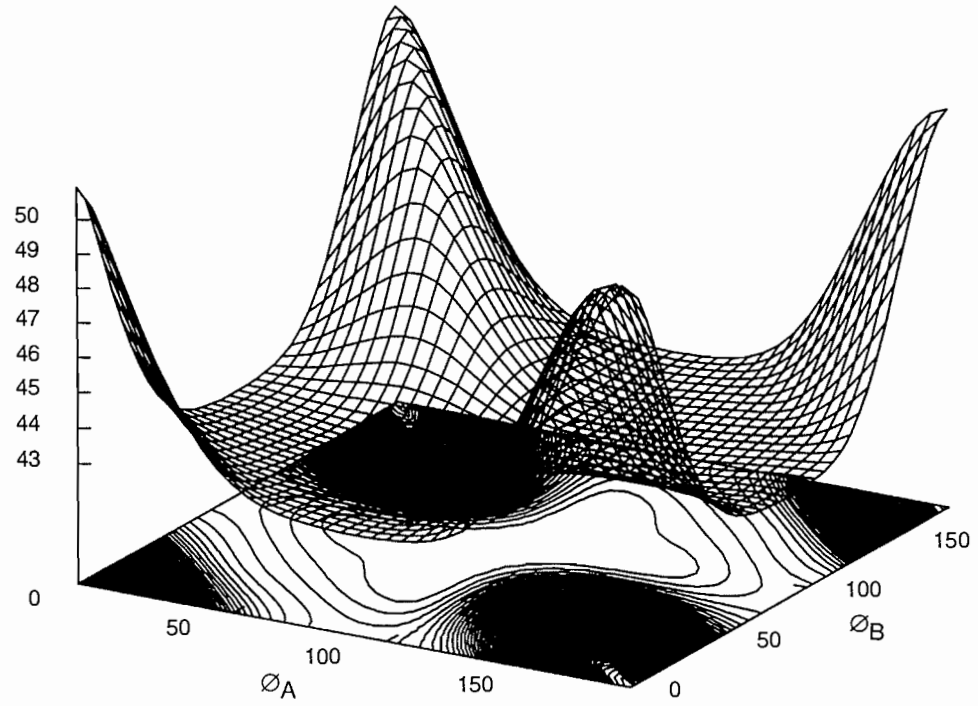


Fig. 3. Two-dimensional energy surface of diphenylmethane, calculated with AM1 from 0° to 180° (see Scheme 1 for the definition of $\varnothing_A$, $\varnothing_B$).

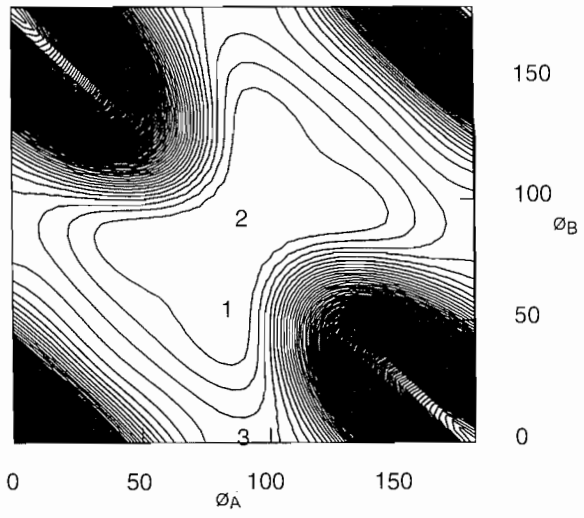
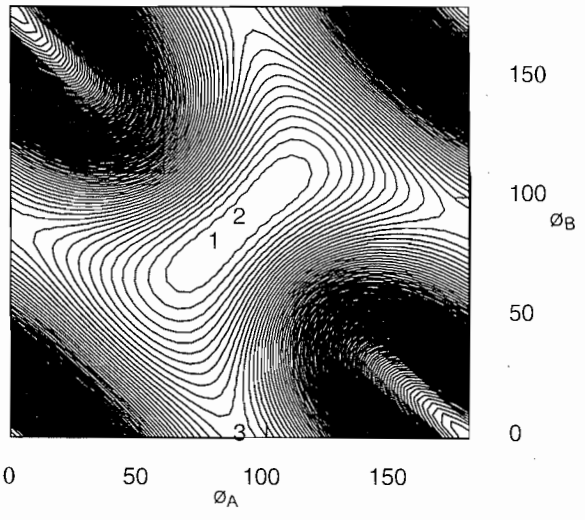


Fig. 4. Two-dimensional energy surface of diphenylmethane, calculated with MNDO from 0° to 180° (see Scheme 1 for the definition of $\varnothing_A$, $\varnothing_B$).



to the surfaces calculated by AM1, except for the lower smoothness of the density functional surfaces, which are calculated using a 15° grid. The energy difference between two lines is 0.25 kcal/mol, compared to 0.1 kcal/mol for the semiempirical surfaces. This does not influence the minimum, which is exactly the same when plotted with 0.1 kcal/mol, but, for the sake of simplicity, the higher energy difference was chosen.

In the case of diphenylmethane, the DFT and AM1 surfaces are almost identical. Both show a large, flat minimum between 30° and 95° degree with a C_2-symmetrical minimum structure at 57° (B3LYP/6-31G(d)). This is in perfect agreement with recent Hartree–Fock ab initio calculations (15), which calculate the minimum to be at 58.3° for RHF/6-31G(d) and at 58.5° for the MP2/6-31G(d) optimized geometry.

The minimum of the diphenyl ether surface is slightly narrower with AM1 than in the case of DFT. Becke3LYP calculates a minimum region for $\varnothing_A$ between 25° and 50°, while

© 1997 NRC Canada

Can. J. Chem. Downloaded from www.nrcresearchpress.com by 88.146.161.215 on 09/08/12
For personal use only.

Table 1. Results of frequency calculations for extrema marked in the diphenylmethane surfaces (Figs. 3–5).

Method	Point	$\varnothing_A$[a]	$\varnothing_B$[a]	ΔH_f (kcal/mol)	NIMAG	Symmetry	Type[b]
AM1	1	84.1	54.5	42.11	0	C_1	F
AM1	2	90.0	90.0	42.12	0	C_{2v}	B
AM1	3	90.0	0.0	42.44	1	C_s	C
MNDO	1	78.1	78.1	43.01	0	C_2	E
MNDO	2	90.0	90.0	43.02	1	C_{2v}	B
MNDO	3	90.0	0.0	44.39	1	C_s	C
PM3	1	90.0	0.0	43.68	1	C_s	C
PM3	2	90.0	90.0	42.79	0	C_{2v}	B

[a]See Scheme 1.
[b]See Scheme 2.

Fig. 5. Two-dimensional energy surface of diphenylmethane, calculated with PM3 from 0° to 180° (see Scheme 1 for the definition of $\varnothing_A$, $\varnothing_B$).

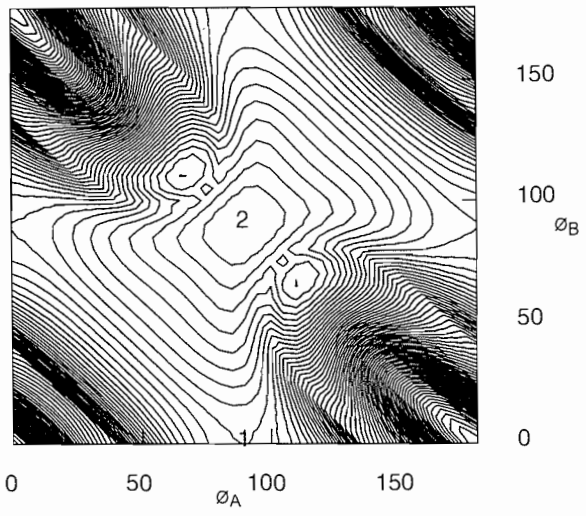


Fig. 6. Two-dimensional energy surface of diphenyl ether, calculated with AM1 from 0° to 180° (see Scheme 1 for the definition of $\varnothing_A$, $\varnothing_B$).

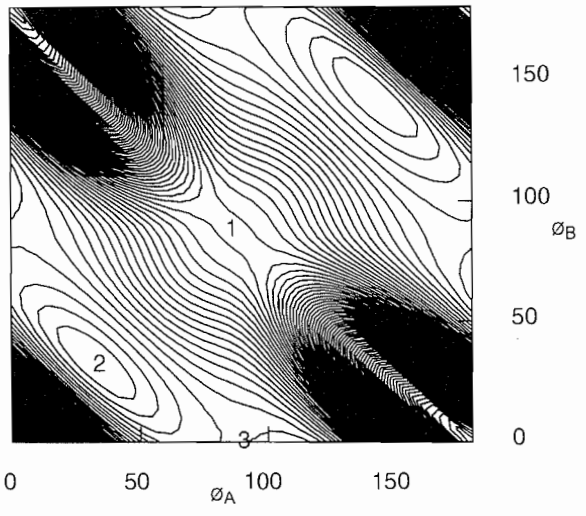


Fig. 7. Two-dimensional energy surface of diphenyl ether, calculated with MNDO from 0° to 180° (see Scheme 1 for the definition of $\varnothing_A$, $\varnothing_B$).

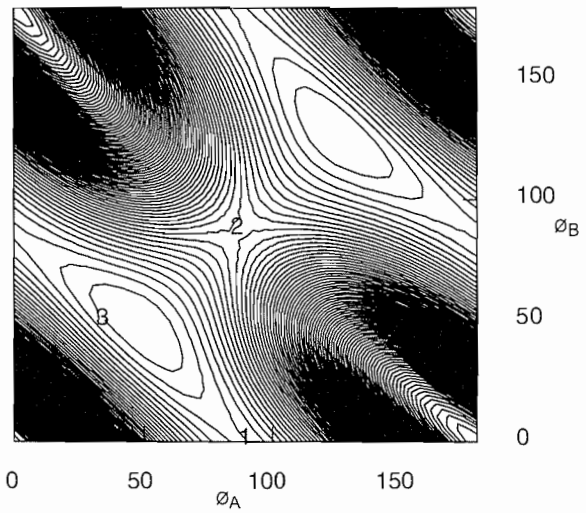
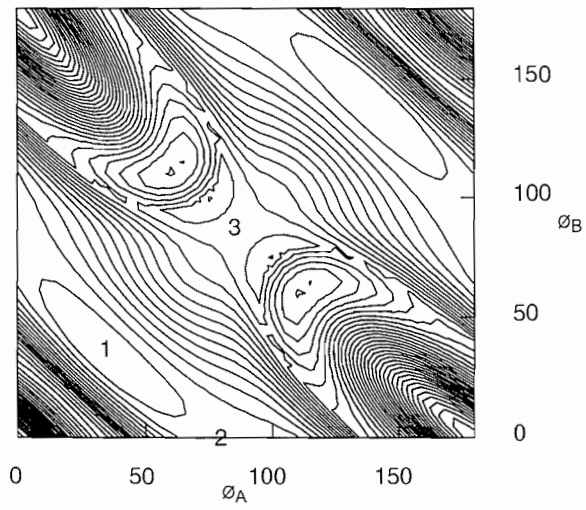


Fig. 8. Two-dimensional energy surface of diphenyl ether, calculated with PM3 from 0° to 180° (see Scheme 1 for the definition of $\varnothing_A$, $\varnothing_B$).



Can. J. Chem. Downloaded from www.nrcresearchpress.com by 88.146.161.215 on 09/08/12
For personal use only.

© 1997 NRC Canada

Can. J. Chem. Downloaded from www.nrcresearchpress.com by 88.146.161.215 on 09/08/12
For personal use only.

Fig. 9. Two-dimensional energy surface of diphenylmethane, calculated with Becke3LYP/3-21G from 0° to 180° (see Scheme 1 for the definition of of $\varnothing_A$, $\varnothing_B$). The energy difference between the lines is 0.25 kcal/mol.

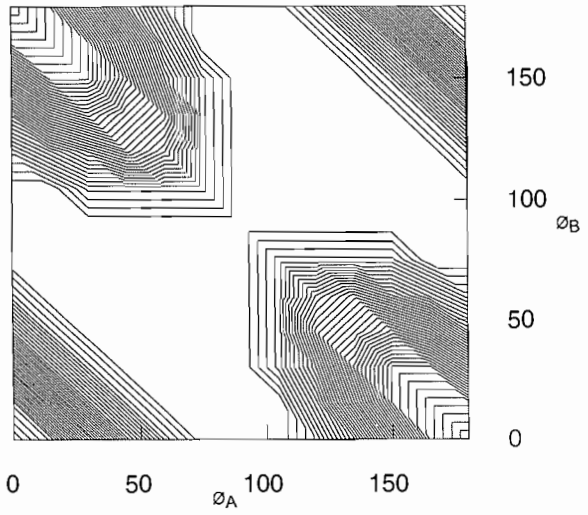
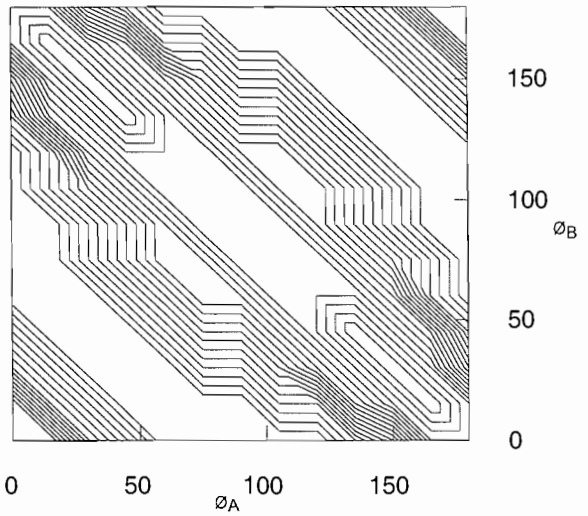


Fig. 10. Two-dimensional energy surface of diphenyl ether, calculated with Becke3LYP/3-21G from 0° to 180° (see Scheme 1 for the definition of of $\varnothing_A$, $\varnothing_B$). The energy difference between the lines is 0.25 kcal/mol.

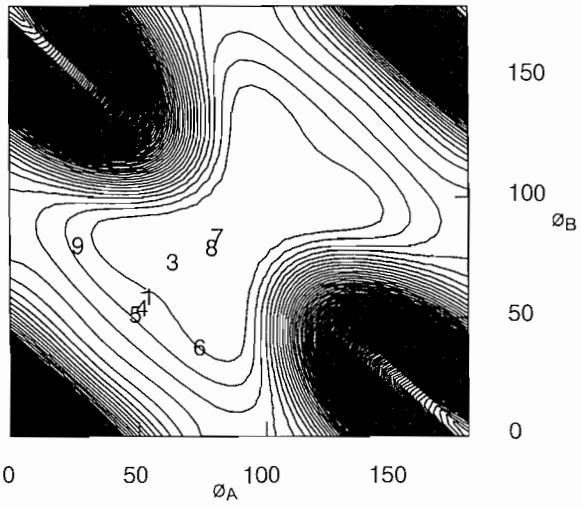


AM1 calculates it to be between 25° and 45°. The overall shape is again identical for the surfaces calculated by AM1 and Becke3LYP. The calculated minima at 35° (AM1) and 40° (B3LYP/6-31G(d)) are in agreement with RHF/6-31G(d) (44.1°) and MP2/6-31G(d) (39.4°) (15). But how do experimental results correlate with theory?

Comparison between experimental and theoretical data

As mentioned before (25, 26), there are many X-ray structures available for *para*-substituted aryl-X-aryl compounds. They fit very well, as can be seen from Tables 7 and 8. To include different substitution patterns, data for the molecules shown in Figs. 12 and 14 were used for the comparison of theory to experiment. Figs. 11 and 13 show the comparison between

Fig. 11. AM1 energy hypersurface of diphenylmethane; marked points represent the molecules shown in Fig. 12.



selected experimental (X-ray structures) and calculated data (AM1).

Molecules **2**–**8** shown in Fig. 12 are used to evaluate the energy surface of diphenylmethane. Their X-ray data have been published (25*m*).

Table 7 shows selected data of those compounds shown in Fig. 12. The dihedral angles are given in degrees (25*m*).

Diphenyl ether

As can be seen from Figs. 11 and 13, the experimental values from X-ray structures are in agreement with our theoretical calculations. All diphenylmethane X-ray structures are within 0.1 kcal/mol of the calculated minimum. In the case of diphenyl ether, the crosses are more widespread, but they still are within 0.7 kcal/mol of the calculated minimum.

Discussion of the energy surfaces

Structures of type **D** are on a line from the upper left corner of the surface down to the bottom right, which means from (0°/180°) to (180°/0°). Type **E**, in contrast, are on the line from (0°/0°) to (180°/180°). In general, structures with C_s symmetry (**D**) are higher in energy than those with C_2 symmetry (**E**). This is in agreement with high-level ab initio and density functional theory calculations. The C_s symmetrical structures (**C**) are transition states between the C_2-symmetrical minima and their mirror images.

The energy surfaces of DPE (Figs. 6–8), calculated with all three Hamiltonians, show a similar overall shape. The global minimum is a C_2 structure with approximately 35°/35°; the transition to its enantiomer is best achieved over the transition state marked as number 3 in Fig. 6, which has the type **C** structure (C_s symmetry) with very low activation barriers (AM1: 0.4 kcal/mol; MNDO: 0.29 kcal/mol; PM3: 0.13 kcal/mol). The second possible transition over the C_{2v}-symmetrical structure at 90°/90° requires slightly higher activation energies (AM1: 1.9 kcal/mol; MNDO: 1.1 kcal/mol; PM3: 1.2 kcal/mol). The energy barriers are not quite accurate compared to the density functional and ab initio calculations. The

© 1997 NRC Canada

Table 2. Results of frequency calculations for extrema marked in the diphenyl ether surfaces (Figs. 6–8).

Method	Point	$\varnothing_A$[a]	$\varnothing_B$[a]	ΔH_f (kcal/mol)	NIMAG	Symmetry	Type[b]
AM1	1	90.0	90.0	25.45	1	C_{2v}	B
AM1	2	34.4	34.4	23.55	0	C_2	E
AM1	3	90.0	0.0	23.95	1	C_s	C
MNDO	1	90.0	0.0	15.20	1	C_s	C
MNDO	2	90.0	90.0	15.99	1	C_{2v}	B
MNDO	3	39.4	39.4	14.91	0	C_2	E
PM3	1	36.6	36.6	20.35	0	C_2	E
PM3	2	90.0	0.0	20.48	1	C_s	C
PM3	3	90.0	90.0	21.54	1	C_{2v}	B

[a]See Scheme 1.
[b]See Scheme 2.

Table 3. Hartree–Fock energies (in hartrees) for diphenylmethane, calculated with Becke3LYP/3-21G. ΔE (kcal/mol) is given relative to the global minimum structure (HF = –499.85971).

$\varnothing_A$	$\varnothing_B$	HF (B3LYP/3-21G)	ΔE (kcal/mol)	$\varnothing_A$	$\varnothing_B$	HF (B3LYP/3-21G)	ΔE (kcal/mol)
0	0	–499.84301	10.48	0	15	–499.84514	9.14
0	30	–499.84992	6.14	0	45	–499.85460	3.21
0	60	–499.85754	1.36	0	75	–499.85881	0.56
0	90	–499.85917	0.34	15	15	–499.84938	6.49
15	30	–499.85394	3.62	15	45	–499.85710	1.64
15	60	–499.85867	0.65	15	75	–499.85922	0.31
15	90	–499.85915	0.35	15	105	–499.85819	0.95
15	120	–499.85575	2.49	15	135	–499.85152	5.14
15	150	–499.84669	8.17	30	30	–499.85699	1.70
30	45	–499.85868	0.65	30	60	–499.85938	0.21
30	75	–499.85942	0.18	30	90	–499.85891	0.50
30	105	–499.85725	1.55	30	120	–499.85390	3.65
30	135	–499.84958	6.36	30	150	–499.84646	8.31
45	45	–499.85943	0.17	45	60	–499.85959	0.07
45	75	–499.85939	0.20	45	90	–499.85851	0.76
45	105	–499.85647	2.03	45	120	–499.85319	4.09
45	135	–499.85022	5.95	60	60	–499.85960	0.07
60	75	–499.85923	0.30	60	90	–499.85841	0.82
60	105	–499.85663	1.93	60	120	–499.85440	3.33
75	75	–499.85904	0.42	75	90	–499.85857	0.72
75	105	–499.85756	1.35	90	90	–499.85865	0.66

barrier for the transition over the C_s-symmetrical structure is in the same range (0.65 kcal/mol for B3LYP/6-31G(d) and 0.30 kcal/mol for MP2/6-31G(d)) (15), but the transition via the C_{2v}-symmetrical structure is underestimated by about 2.5 kcal/mol compared to 4.22 kcal/mol for B3LYP/6-31G(d) and 3.59 kcal/mol for MP2/6-31G(d)) (15). However, the transition will follow the path of lower energy over the C_s-symmetrical structure, where the AM1 value is between the values calculated by ab initio and density functional theory.

Obviously, AM1 gives the highest barriers for this weakly conjugated system, a picture that is known from rotations at amide and urea bonds (16, 17). All available X-ray data are consistent with the calculations, as is obvious from Fig. 13, where the crosses are grouped together (up to a maximum deviation of 0.7 kcal/mol) close to the absolute minimum. This is surprising considering the large differences in structures **9**–**22**, but proves the usefulness of the semiempirical calculations for these compounds.

The shape of the diphenylmethane surfaces looks different at first sight when calculated with AM1, MNDO, and PM3.

Can. J. Chem. Downloaded from www.nrcresearchpress.com by 88.146.161.215 on 09/08/12
For personal use only.

© 1997 NRC Canada

Can. J. Chem. Downloaded from www.nrcresearchpress.com by 88.146.161.215 on 09/08/12
For personal use only.

Table 4. Hartree–Fock energies (in hartrees) for diphenyl ether, calculated with Becke3LYP/3-21G. ΔE (kcal/mol) is given relative to the global minimum structure (HF = –535.56019).

$\varnothing_A$	$\varnothing_B$	HF (B3LYP/3-21G)	ΔE (kcal/mol)	$\varnothing_A$	$\varnothing_B$	HF (B3LYP/3-21G)	ΔE (kcal/mol)
0	0	–535.55216	5.04	0	15	–535.55330	4.33
0	30	–535.55580	2.76	0	45	–535.55792	1.42
0	60	–535.55905	0.71	0	75	–535.55946	0.46
0	90	–535.55958	0.38	15	15	–535.55596	2.65
15	30	–535.55845	1.09	15	45	–535.55968	0.32
15	60	–535.55988	0.20	15	75	–535.55951	0.43
15	90	–535.55891	0.80	15	105	–535.55823	1.23
15	120	–535.55713	1.92	15	135	–535.55532	3.06
15	150	–535.55315	4.42	30	30	–535.55993	0.17
30	45	–535.56011	0.05	30	60	–535.55950	0.43
30	75	–535.55851	1.05	30	90	–535.55748	1.70
30	105	–535.55626	2.46	30	120	–535.55471	3.44
30	135	–535.55293	4.56	30	150	–535.55201	5.13
45	45	–535.55949	0.44	45	60	–535.55826	1.21
45	75	–535.55688	2.08	45	90	–535.55555	2.91
45	105	–535.55416	3.78	45	120	–535.55281	4.63
45	135	–535.55203	5.12	60	60	–535.55668	2.20
60	75	–535.55512	3.18	60	90	–535.55387	3.97
60	105	–535.55282	4.62	60	120	–535.55225	4.98
75	75	–535.55379	4.02	75	90	–535.55283	4.62
75	105	–535.55241	4.88	90	90	–535.55256	4.79

Table 5. Results of frequency calculations on optimized geometries for extrema of the diphenylmethane hypersurface calculated by density functional theory.

	HF (Becke3LYP/3-21G) NIMAG/[$\varnothing_A$, $\varnothing_B$]	ΔE (kcal/mol)	HF (Becke3LYP/6-31G(d)) NIMAG/[$\varnothing_A$, $\varnothing_B$]	ΔE (kcal/mol)
C_2	–499.85967 (0) [55/55]	0	–502.61539 (0) [57/57]	0
C_{2v}	–499.85919 (1) [90/90]	0.3	–502.61436 (1) [90/90]	0.65
C_s	–499.85866 (1) [90/00]	0.66	–502.61443 (1) [90/00]	0.6

Table 6. Results of frequency calculations on optimized geometries for extrema of the diphenyl ether hypersurface calculated by density functional theory.

	HF (Becke3LYP/3-21G) NIMAG / [$\varnothing_A$, $\varnothing_B$]	ΔE (kcal/mol)	HF (Becke3LYP/6-31G(d)) NIMAG / [$\varnothing_A$, $\varnothing_B$]	ΔE (kcal/mol)
C_2	–535.56019 (0) [37/37]	0	–538.51282 (0) [40/40]	0
C_{2v}	–535.55957 (1) [90/90]	0.39	–538.51223 (1) [90/90]	0.37
C_s	–535.55256 (1) [90/00]	4.79	–538.50609 (1) [90/00]	4.22

However, all three Hamiltonians yield only one minimum centered around the 90°/90° structure. The valley is more narrow with MNDO and PM3 than with AM1; only one transition state at 90°/0° is to be considered for all methods. The activation barriers (AM1: 0.3 kcal/mol; MNDO: 1.4 kcal/mol; PM3: 0.9 kcal/mol) are contrary to the diphenyl ether picture. The reason is that obvious sterical demands determine the transition state. Again, the experimental structures are embedded most comfortably in the AM1 surface (Fig. 11). They are within a deviation of 0.1 kcal/mol from the global minimum. For diphenylmethane the calculated energy difference compared to density functional theory and high-level ab initio

© 1997 NRC Canada

Table 7. Selected X-ray data of ring-substituted diphenylmethane structures.

Compound	$\varnothing_A$[a]	$\varnothing_B$[a]	Reference	Compound	$\varnothing_A$[a]	$\varnothing_B$[a]	Reference
1	54.35	56.70	24	**2**	63.9	71.1	25*m*
3	52.0	52.0	27	**4**	49.4	49.4	28
5	74.5	35.5	25*h*	**6**	81.6	81.3	29
7	79.3	77.0	30	**8**	27.0	78.1	31
ACPHDR	83.9	87.0	25*a*	BUBVEZ	49.7	49.7	25*b*
BUPHCB	74.3	74.3	25*c*	CEHCOH	20.2	68.1	25*d*
CEVFOY	41.9	73.1	25*e*	CISNIB	42.7	56.0	25*f*
CISNIB	52.2	86.9	25*f*	FISGOD	89.5	77.9	25*g*
FISGOD	87.0	77.9	25*g*	MEPHCB01	59.0	59.0	25*i*
VABDOR	47.5	47.5	25*k*	ZEXTEB	70.7	74.9	25*l*

[a]$\varnothing_A$, $\varnothing_B$ are defined in literature as the dihedral angles C_2-C_1-X-C_1'.

Table 8. Selected X-ray data of ring-substituted diphenyl ether structures.

Compound	$\varnothing_A$[a]	$\varnothing_B$[a]	Reference	Compound	$\varnothing_A$[a]	$\varnothing_B$[a]	Reference
9	73.2	73.2	32	**10**	34.8	34.8	33
11	64	21	34	**12**	72	33	35
13	88	5	36	**14**	90	11	37
15	87	21	38	**16**	75	34	39
17	6.6	70.1	40	**18**	90.3	4.6	41
19	94	2	42	**20**	80	5	43
21	79	8	44	**22**	84	26	45
CUCGOW	58.2	10.2	26*a*	CUMLUR	0.7	82.2	26*b*
CUXPUG	53.6	46.1	26*c*	DEPNOB	45.5	30.5	26*d*
DEPNOB	47.5	30.5	26*d*	DILDOR	84.7	23.1	26*e*
DILDOR	41.7	41.7	26*e*	GACXUD	40.9	43.0	26*f*
GACXUD01	54.1	34.5	26*g*	GACXUD01	41.3	43.8	26*g*
JAPNIX	2.8	81.1	26*h*	JAPNIX	0.6	79.0	26*h*
JEJWIE	4.6	89.1	26*i*	JEJWIE01	5.5	90.8	26*k*
KOWVEX	65.9	17.4	26*l*	NPHOPN	28.2	62.7	26*m*
NPHOPN	28.2	62.7	26*m*	SAFKEP	59.3	23.4	26*n*
SAFKEP	8.8	87.8	26*n*	SAFKIT	32.5	61.2	26*n*
SAFKIT	14.5	57.9	26*n*	SAPYAJ	19.8	54.6	26*o*
SUCVER	66.0	25.5	26*p*	SULFAG	68.8	16.3	26*q*
SULFAG	38.5	49.4	26*q*	SULFAG	78.4	2.0	26*q*
SULFAG	5.4	92.4	26*q*	THYRCM	67.8	37.6	26*r*
VELZAN	38.9	34.8	26*k*	VEXLAL	76.7	6.0	26*s*
VEXLAL	6.2	87.4	26*s*	YADDOW	88.8	1.4	26*t*
YUSKUS	70.8	30.1	26*u*	YUSKUS	1.35	88.7	26*u*
ZEXHUF	42.5	42.5	26*v*				

[a]$\varnothing_A$, $\varnothing_B$ are defined in literature as the dihedral angles C_2-C_1-X-C_1'.

calculations is not as large as in the diphenyl ether case (C_s symmetry: 0.6 kcal/mol for B3LYP/6-31G(d), 0.49 kcal/mol for MP2/6-31G(d)) (15); C_{2v} symmetry: 0.65 kcal/mol for B3LYP/6-31G(d), 0.51 kcal/mol for MP2/6-31G(d)) (15)).

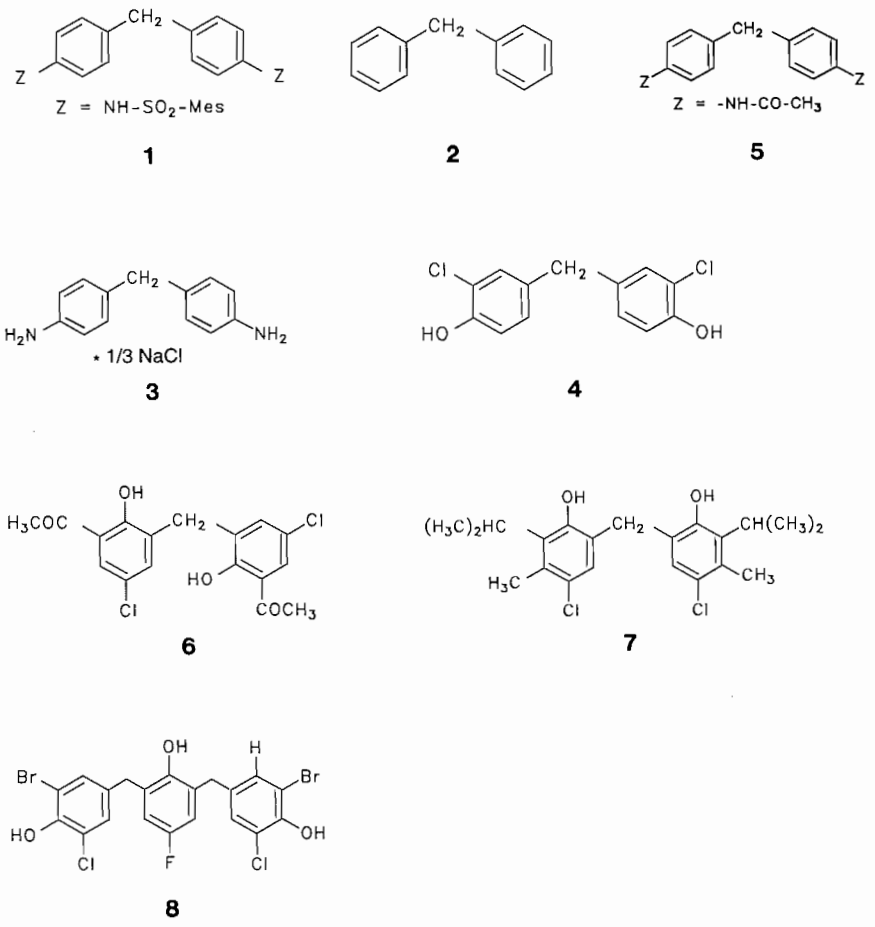
The symmetry of the surfaces reflects the symmetry of aryl-X-aryl compounds and is proof of the complete relaxation of all internal degrees of freedom except $\varnothing_A$ and $\varnothing_B$.

The differences between the results of semiempirical and density functional theory calculations are small. The minimizer problem of the C_{2v} structure of diphenylmethane, which was calculated to be a minimum by AM1 and PM3, is solved using DFT; it is a transition state with DFT as would be expected. Also, the influence of the basis set used is small. Tables 5 and 6 show the results of symmetry-imposed calculations with Becke3LYP/3-21G and Becke3LYP/6-31G(d). All extrema have the same number of imaginary frequencies

© 1997 NRC Canada

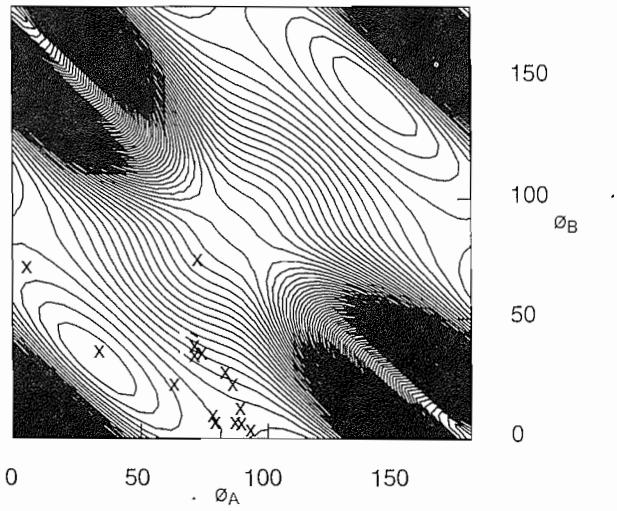
Can. J. Chem. Downloaded from www.nrcresearchpress.com by 88.146.161.215 on 09/08/12
For personal use only.

Fig. 12. Selected diphenylmethane derivatives with known solid state conformations (X-ray data).



Can. J. Chem. Downloaded from www.nrcresearchpress.com by 88.146.161.215 on 09/08/12
For personal use only.

Fig. 13. AM1 energy hypersurface of diphenyl ether; the crosses represent the compounds shown in Fig. 14. The exact values are shown in Table 8.

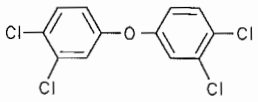


and differ only little in the calculated $\varnothing_A$ and $\varnothing_B$ values. Also, the energy differences between the different symmetries are small. The energy differences are compiled in Tables 5 and 6.

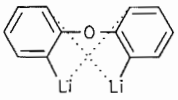
The shape of the surfaces is very similar and experimental data are reproduced very well by both methods. To evaluate properties of potential polymers it is absolutely necessary to get information about the molecular conformation of the monomers. But, as shown in this study, semiempirical methods also allow us to calculate oligomers with reasonable accuracy. In general, AM1 can calculate at least eight times as many atoms as density functional theory on the same computer and the results are qualitatively the same. Therefore semiempirical calculations seem to be very useful for all problems related to the phenyl rotation and especially AM1 is capable of calculating the molecular geometries of larger polymer units. Considering polymers in which conformational effects have a large influence on the potential usefulness of the blend, it might be necessary to calculate larger oligomers for a better prediction. This seems possible given the results of this study, which dealt with the main polymer structural units.

© 1997 NRC Canada

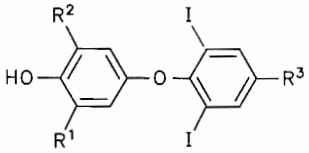
Fig. 14. Selected diphenyl ether derivatives with known solid state conformation (X-ray data).



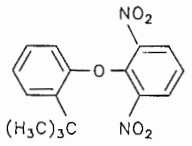
9



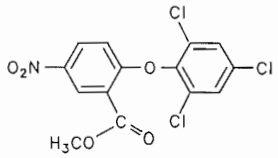
10



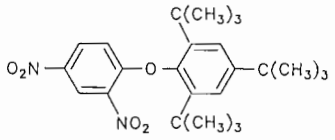
No.	R^1	R^2	R^3
11	H	I	$CH_2CH(NH_2)COOH$
12	H	I	$CH_2CH(NH_2)COOMe$
13	I	I	CH_2COO^- * $HN(CH_2CH_2OH)_2$
14	H	I	$CH_2CH(NH_2)COOH$ * HCl
15	H	H	$CH_2CH(NH_2)COOH$ * $H_3CNHCOCH_3$
16	I	I	$CH_2CH(NH_2)COOH$



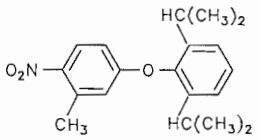
17



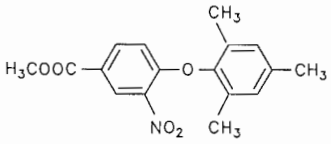
18



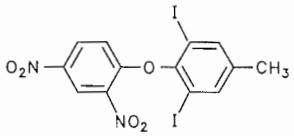
19



20



21



22

References

1. (*a*) R.J.W. Le Fèvre and J.D. Saxby. J. Chem. Soc. (B), 1064 (1966); (*b*) V. Galasso, G. DeAlti, and A. Bigotto. Tetrahedron **27**, 6151 (1971); (*c*) G. Montaudo, S. Caccamese, and P. Finocchiaro. J. Am. Chem. Soc. **93**, 4202 (1971); (*d*) G. Montaudo, P. Finocchiaro, and S. Caccamese. J. Org. Chem. **36**, 2860 (1971); (*e*) H.-B. Bürgi and J. Dunitz (*Editors*). Structure-correlation. Verlag Chemie, Weinheim. 1993.
2. H.A. Naik, I.W. Parsons, P.T. McGrail, and P.D. MacKenzie. Polymer, **32**, 140 (1991).
3. T. Schaefer, W. Niemczura, W. Danchura, and T.A. Wildman. Can. J. Chem. **57**, 1881 (1979).
4. (*a*) T. Schaefer, G.H. Peenner, C. Takeuchi, and P. Tseki. Can. J. Chem. **66**, 1647 (1988); (*b*) B. Uno, T. Kawakita, K. Kano, K. Ezumi, and T. Kubota. Bull. Chem. Soc. Jpn. **65**, 2697 (1992).
5. J. Kendrick. J. Chem. Soc. Faraday Trans. **86**, 3995 (1990).
6. I. Baraldi, E. Gallinella, and F. Momicchioli. J. Chim. Phys. **83**, 653 (1986).
7. (*a*) J. Hay and D.J. Kemmish. Polym. Commun. **30**, 77 (1989); (*b*) O. Herrmann-Schönherr, A. Schneller, A.M. Seifert, M. Soliman, and J.H. Wendorff. Makromol. Chem. **193**, 1955 (1992).
8. W. Weissensteiner. Monatsh. Chem. **123**, 1135 (1992).
9. (*a*) K.S. Pierce, A.K. Wisor, and M.R. Hoffmann, Theochem, **306**, 213 (1994); (*b*) T. Nevalainen and K. Rissanen. J. Chem. Soc. Perkin Trans. **2**, 271 (1994).
10. V. Cody. J. Am. Chem. Soc. **96**, 6720 (1974).
11. (*a*) G.M. Sheldrick, P.G. Jones, O. Kennard, D.H. Williams, and G.A. Smith. Nature, **271**, 223 (1978); (*b*) M.P. Williamson and D.H. Williams. J. Am. Chem. Soc. **103**, 6580 (1981); (*c*) C.M. Harris and T.M. Harris. J. Am. Chem. Soc. **104**, 4293 (1982); (*d*) D.H. Williams, M.P. Williamson, D.W. Butcher, and S.J. Hammond. J. Am. Chem. Soc. **105**, 1332 (1983); (*e*) M.J.

Can. J. Chem. Downloaded from www.nrcresearchpress.com by 88.146.161.215 on 09/08/12
For personal use only.

© 1997 NRC Canada

Can. J. Chem. Downloaded from www.nrcresearchpress.com by 88.146.161.215 on 09/08/12
For personal use only.

Mann, N. Pant, and A.D. Hamilton. J. Chem. Soc. Chem. Commun. 158 (1986); (*f*) D.A. Evans, C.J. Dinsmore, D.A. Evrard, and K.M. DeVries. J. Am. Chem. Soc. **115**, 6426 (1993).
12. (*a*) S.D. Jolad, J.J. Hoffmann, S.J. Torrance, R.M. Wiedhopf, R.J. Cole, S.K. Arora, R.B. Bates, R.L. Gargiulo, and G.R. Kriek. J. Am. Chem. Soc. **99**, 8040 (1977); (*b*) D.L. Boger and D. Yohannes. J. Org. Chem. **53**, 487 (1988).
13. (*a*) U. Schmidt, D. Weller, A. Holder, and A. Lieberknecht. Tetrahedron Lett. **29**, 3227 (1988); (*b*) S. Nishiyama, Y. Suzuki, and S. Yamamura. Tetrahedron Lett. **29**, 559 (1988).
14. S. Verot and P. Battesti. J. Can. Chem. **73**, 581 (1995).
15. M. Feigel. J. Mol. Struct. **366**, 83 (1996).
16. T. Strassner. J. Mol. Mod. (Electronic Publication), **2**, 217 (1996).
17. M. Feigel and T. Strassner. J. Mol. Struct. **283**, 33 (1993).
18. J.J.P. Stewart. AMPAC. QCPE Bull. **6**, 506 (1986).
19. J. Baker. J. Comput. Chem. **7**, 385 (1986).
20. J.M. Seminario and P. Politzer (*Editors*). Modern density functional theory. A tool for chemistry. Elsevier, Amsterdam. 1995.
21. M.J. Frisch, G.W. Trucks, H.B. Schlegel, P.M.W. Gill, B.G. Johnson, M.A. Robb, J.R. Cheeseman, T. Keith, G.A. Petersson, J.A. Montgomery, K. Raghavachari, M.A. Al-Laham, V.G. Zakrzewski, J.V. Ortiz, J.B. Foresman. J. Cioslowski, B.B. Stefanov, A. Nanayakkara, M. Challacombe, C.Y. Peng, P.Y. Ayala, W. Chen, M.W. Wong, J.L. Andres, E.S. Replogle, R. Gomperts, R.L. Martin, D.J. Fox, J.S. Binkley, D.J. Defrees, J. Baker, J.P. Stewart, M. Head-Gordon, C. Gonzalez, and J.A. Pople. Gaussian 94, Revision B.2. Gaussian, Inc., Pittsburgh, Pa. 1995.
22. (*a*) J. Andzelm and E. Wimmer. J. Chem. Phys. **96**, 1280 (1992); (*b*) B.G. Johnson, P.M.W. Gill, and J.A. Pople. J. Chem. Phys. **98**, 5612 (1993); (*c*) J. Baker, M. Muir, and J. Andzelm. J. Chem. Phys. **102**, 2063 (1995).
23. A.D. Becke. J. Chem. Phys. **98**, 1372 (1993); **98**, 5648 (1993).
24. M. Feigel, T. Strassner, J. Manero, and E. Weckert. Acta Crystallogr. Sect. C: Cryst. Struct. Commun. **C52**, 2303 (1996).
25. For **DPM**: (*a*) [ACPHDR] K. Odashima, A. Itai, Y.Iitaka, and K. Koga. J. Am. Chem. Soc. **102**, 2504 (1980); (*b*) [BUBVEZ] R.B. Wilson, Y.-S. Chen, I.C. Paul, and D.Y. Curtin. J. Am. Chem. Soc. **105**, 1672 (1983); (*c*) [BUPHCB] P.G. Forcier and J. Blackwell. Acta. Cryst. **37**, 286 (1981); (*d*) [CEHCOH] V.K. Bel'skii, V.K. Rotaru, and M.M. Kruchinin. Kristallografiya. **28**, 695, (1983); (*e*) [CEVFOY] L. Born. Z. Kristallogr. **165**, 309 (1983); (*f*) [CISNIB] L. Born. Z. Kristallogr. **167**, 145 (1984); (*g*) [FISGOD] J. Jazwinski, J.-M. Lehn, R. Meric, J.-P. Vigneron, M. Cesario, J. Guilhem, and C. Pascard. Tetrahedron, **28**, 3489 (1987); (*h*) [MEPHCB] K.H. Gardner and J. Blackwell; Acta Crystallogr. Sect. B: Struct. Crystallogr. Cryst. Chem. **B36**, 1972 (1980); (*i*) [MEPHCB01] L. Born, J. Hocker, H. Paulus, and E. Wolfel. Cryst. Struct. Commun. **10**, 187 (1981); (*k*) [VABDOR] H. Nakai, T. Saito, and M. Yamakawa. Acta Crystallogr. Sect. C: Cryst. Struct. Commun. **C44**, 2117 (1988); (*l*) [ZEXTEB] Rajnikant, D.J. Watkin, and G. Tranter. Acta Crystallogr. Sect. C: Cryst. Struct. Commun. **C51**, 2388 (1995); (*m*) [ZZZMKS01] J.C. Barnes, J.D. Paton, J.R. Damewood, Jr., and K. Mislow. J. Org. Chem. **46**, 4975 (1981).
26. For **DPE** (*a*) [CUCGOW] R.K. Chadha, J.E. Drake, and M.A. Khan. Can. J. Chem. **62**, 32 (1984); (*b*) [CUMLUR] S.P. Kolesnikov, I.V. Lyudkovskaya, O.M. Nefedov, D.S. Yufit, and Y.T. Struchkov. Izv. Akad. Nauk SSSR, Ser. Khim. 1131 (1984); (*c*) [CUXPUG] M. Cory, D.D. McKee, J. Kagan, D.W. Henry, and J.A. Miller. J. Am. Chem. Soc. **107**, 2528 (1985); (*d*) [DEPNOB] R.K. Chadha and J.E. Drake. J. Organomet. Chem. **293**, 37 (1985); (*e*) [DILDOR] S.V. Lindeman, Y.T. Struchkov, B.F. Malichenko, V.E. Shklover, and V.A.Vasnev. Makromol. Chem. **186**, 2087 (1985); (*f*) [GACXUD] R.K. Chadha and J.E. Drake. J. Cryst. Spectrosc. **16**, 907 (1986); (*g*) [GACXUD01] M. de Matheus, L. Torres, J.F. Piniella, J.L. Brianso, and C. Miravittles. Acta Crystallogr. Sect. C: Cryst. Struct. Commun. **C47**, 703 (1991); (*h*) [JAPNIX] G. Bocelli and A. Cantoni. Acta Crystallogr. Sect. C: Cryst. Struct. Commun. **C45**, 1660 (1989); (*i*) [JEJWIE] N.J. Clayden, D. Williams, and C.A. O'Mahoney. J. Chem. Soc. Perkin Trans. 2, 729 (1990); (*k*) [JEJWIE01], [VELZAN] L. Yuming, G. Fang, D. Cuichen, C. Zhendong, H. Shunian, and W.H. Xuebao. Acta Phys.-Chim. Sin. **5**, 141 (1989); (*l*) [KOWVEX] T.I. Savchenko, I.A. Zamaev, L.I. Kulezhova, V.E. Shklover, Y.T. Struchkov, N.M. Belomoina, E.S. Krongauz, and V.V. Korshak. Zh. Strukt. Khim. **32**, 60 (1991); (*m*) [NPHOPN] E. Subramanian, V. Lalitha, M.J. Nanjan, M. Balasubramaniam, and J. Bordner. Cryst. Struct. Commun. **9**, 873 (1980); (*n*) [SAFKEP], [SAFKIT] S.V. Lindeman, I.A. Khotina, M.M. Teplyakov, Y.T. Struchkov, and V.V. Korshak. Makromol. Chem. **189**, 471 (1988); (*o*) [SAPYAJ] J. Emsley, L.Y.Y. Ma, P.A. Bates, M. Motevalli, and M.B. Hursthouse. J. Chem. Soc. Perkin Trans. 2, 527 (1989); (*p*) [SUCVER] L.A. Chetkina, A.N. Sobolev, V.K. Bel'skii, L.E. Serdyuk, and I.E. Kardash. Kristallografiya, **36**, 902 (1991); (*q*) [SULFAG] R.K. Juneja, K.D. Robinson, C.P. Johnson, and J.L. Atwood. J. Am. Chem. Soc. **115**, 3818 (1993); (*r*) [THYRCM] A. Camerman and N. Camerman. Can. J. Chem. **52**, 3042 (1974); (*s*) [VEXLAL] G. Bocelli and C. Rizzoli. Acta Crystallogr. Sect. C: Cryst. Struct. Commun. **C46**, 2259 (1990); (*t*) [YADDOW] A.A. Freer, D.D. MacNicol, P.R. Mallinson, and I. Vallance. Tetrahedron Lett. **33**, 261 (1992); (*u*) [YUSKUS] G. Bandoli, M. Gleria, G.M. Lombardo, and G.C. Pappalardo. J. Chem. Soc. Dalton Trans. 1749 (1995); (*v*) [ZEXHUF] X.-Y. Huang, Q. Ye, Q.-J. Meng, and X.-Z. You. Acta Crystallogr. Sect. C: Cryst. Struct. Commun. **C51**, 2285 (1995).
27. E.J.W. Whittaker. Acta Crystallogr. **6**, 714 (1953).
28. J.W. Swardstrom, L.A. Duvall, and D.P. Miller. Acta Crystallogr. Sect. B: Struct. Crystallogr. Cryst. Chem. **B28**, 2510 (1972).
29. F. Nowshad and Mazhar-Ul-Haque. J. Chem. Soc. Perkin Trans. 2, 623 (1976).
30. S. Rantsordas and M. Perrin. Acta. Crystallogr. Sect. B: Struct. Crystallogr. Cryst. Chem. **B38**, 1871 (1982).
31. A.C. Sindt-Josem and M.F. Mackay. Aust. J. Chem. **34**, 81 (1981).
32. P. Singh and J.D. McKinsey. Acta Crystallogr. Sect. B: Struct. Crystallogr. Cryst. Chem. **B36**, 210 (1980).
33. M. Kranz, H. Dietrich, W. Mahdi, G. Müller, F. Hampel, T. Clark, R. Hacker, W. Neugebauer, A.J. Kos, and P.v.R. Schleyer. J. Am. Chem. Soc. **115**, 4698 (1993).
34. V. Cody. J. Am. Chem. Soc. **96**, 6720 (1974).
35. V. Cody. J. Med. Chem. **18**, 126 (1975).
36. V. Cody and W.L. Duax. Biochem. Biophys. Res. Commun. **52**, 430 (1973).
37. N. Cameraman and A. Cameraman. Science, **175**, 764 (1972).
38. V. Cody, W.L. Duax, and D.A. Norton, Acta Crystallogr. Sect. B: Struct. Crystallogr. Cryst. Chem. **B28**, 2244 (1972).
39. N. Cameraman and A. Cameraman. Proc. Natl. Acad. Sci. U.S.A. **69**, 2130 (1972).
40. K. Gurtu, W.D. Chandler, and B.E. Robertson. Can. J. Chem. **53**, 2093 (1975).
41. E.A.H. Griffith, W.D. Chandler, and B.E. Robertson. Can. J. Chem. **50**, 2979 (1972).
42. E.A.H. Griffith, W.D. Chandler, and B.E. Robertson. Can. J. Chem. **50**, 2972 (1972).
43. E.A.H. Griffith, W.D. Chandler, and B.E. Robertson. Can. J. Chem. **50**, 2963 (1972).
44. S.P.N. van der Heijden, E.A.H. Griffith, W.D. Chandler, and B.E. Robertson. Can. J. Chem. **53**, 2084 (1975).
45. P.A. Lehmann and E. Shefter. Rev. Latinoam. Quim. **3**, 91 (1972).

© 1997 NRC Canada

Electrochemical reduction of nickel(II) dithiocarboxylates at the mercury electrode

A. Safavi and L. Fotouhi

Abstract: The reduction mechanisms of a series of nickel(II) dithiocarboxylate complexes have been investigated in dimethyl sulphoxide at the mercury electrode. Various electrochemical techniques, including polarography, cyclic voltammetry, chronoamperometry, and controlled potential coulometry, were employed. The reduction of the complexes of the acid derivatives of 2-aminocyclopentene-1-dithiocarboxylate (ACD) proceeds initially by an ECE mechanism (electron transfer – chemical reaction – electron transfer) followed by a one-electron irreversible process. The nature of the complete electrode reaction suggests a metal-centered reduction. The nickel complexes of the ester derivatives of ACD underwent a one-electron reduction that was subject to a follow-up catalytic reaction (EC′ mechanism) and the original complex is regenerated through this regeneration reaction.

Key words: reduction, nickel(II) dithiocarboxylate, mercury electrode.

Résumé : On a étudié les mécanismes de la réduction d'une série de complexes de dithiocarboxylate de nickel(II) dans le diméthylsulfoxyde au niveau d'une électrode à mercure. On a utilisé divers techniques électrochimiques, incluant la polarographie, la voltampérométrie cyclique, la chronoampérométrie, et la coulométrie à potentiel contrôle. La réduction des complexes formés à partir des dérivés de l'acide 2-aminocyclopentène-1-dithiocarboxylate (ACD) se fait au début selon un mécanisme ECE (transfert d'électrons – réaction chimique – transfert d'électrons) suivi d'un processus irréversible à un électron. La nature de la réaction complète à l'électrode suggère une réduction centrée sur le métal. Les complexes de nickel des esters du composé ACD subissent une réduction à un électron suivie d'une réaction catalysée (mécanisme EC′) et le complexe original est regénéré par cette réaction de régénération.

Mots clés : réduction, dithiocarboxylate de nickel(II), électrode à mercure.

[Traduit par la rédaction]

Can. J. Chem. Downloaded from www.nrcresearchpress.com by 88.146.161.215 on 09/08/12
For personal use only.

Introduction

A number of articles and several reviews (1–3) deal with complexes of platinum metals with mono- and polyfunctional S-containing ligands. Dithiocarboxylic acids and their complexes are of interest because of their antifungal activity (4) and because they are used as models of sulfur–metal proteins (5–7). It has been reported that 2-aminocyclopentene-1-dithiocarboxylate (ACD) and some of its derivatives form intense coloured complexes with various bi- and trivalent metal ions (8–11). Complexes of Cu(II), Ni(II), and Zn(II) with methyl-2-amino-1-cyclopentene dithiocarboxylate (6) and *N*-alkyl methyl-2-aminocyclopentene dithiocarboxylate (7) have been prepared and characterized using NMR, ESR, electronic absorption, and electrochemical spectroscopy. To understand the role of metals in processes of vital importance and to evaluate the stability of the oxidation number of the central atom and the reactivity of ligands in these complexes, their redox properties must be known. Yet these are limited (12, 13) or practically lacking, as for Ni(II) complexes of dithiocarboxylic acids.

While the work on dithiocarboxylate complexes is very limited, many workers have pioneered the redox behaviour of their analogue, dithiocarbamates, and have found that dithiocarbamate complexes of the first-row transition metals on platinum electrodes (14–19) participate in simple, generally reversible, one-electron reduction reactions, where the orbitals involved in electron transfer are essentially ligand in character. However, it was shown later that at mercury electrodes, the electrochemistry of dithiocarbamate complexes is more complex than at platinum electrodes (14).

As part of a continuing study into the electrochemistry of the transition metal dithiocarboxylates, this paper describes a detailed electrochemical study on the reduction of nickel(II) complexes with 2-aminocyclopentene-1-dithiocarboxylate (ACD) and some of its acid and ester derivatives. Since the compounds were completely insoluble in water and most organic solvents, dimethyl sulphoxide (DMSO) was chosen as the solvent. The complexes are moderately soluble in this solvent. Previous investigations on free dithiocarboxylate anions showed an anodic wave at ~ -0.68 V relative to SCE (12), while a reduction wave at -1.65 V relative to the same electrode was obtained from dithiocarboxylic acids (13).

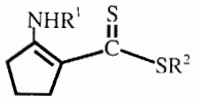
Received May 10, 1996.[1]

A. Safavi[2] and L. Fotouhi. Department of Chemistry, College of Sciences, Shiraz University, Shiraz, 71454, Iran.

[1] Revision received March 27, 1997.
[2] Author to whom correspondence may be addressed. Fax: 71-20027.

© 1997 NRC Canada

Scheme 1.



L_I, $R^1 = R^2 = H$ L_{IV}, $R^1 = n\text{-}C_4H_9$, $R^2 = H$

L_{II}, $R^1 = CH_3$, $R^2 = H$ L_V, $R^1 = H$, $R^2 = CH_3$

L_{III}, $R^1 = C_2H_5$, $R^2 = H$ L_{VI}, $R^1 = R^2 = CH_3$

Experimental

Instrumentation

Electrochemical measurements were performed in DMSO containing 0.5 M potassium perchlorate as supporting electrolyte using a Princeton Applied Research Corp. (PAR) electrochemical system, model 170. A three-electrode system was employed for all measurements. The working electrode was either a dropping mercury electrode (for polarographic measurements) or a hanging mercury drop electrode (H.M.D.E.). A platinum auxiliary electrode was used for all measurements while the reference electrode was a saturated calomel electrode (SCE).

Electrochemical measurements were made in solvent initially degassed with solvent-saturated argon.

Unless otherwise stated, all measurements were made under the following conditions: temperature, 25 ± 1°C; concentration of NiL_2, 2.0 mM; polarographic drop time, 1.0 s.

Cyclic voltammograms were recorded using a Metrohm hanging mercury drop electrode.

Controlled-potential electrolysis experiments were performed using a mercury pool electrode. The experiments were monitored both electrochemically and spectrophotometrically. Electronic spectra were recorded with a Philips 8750 ratio recording UV–visible spectrophotometer.

Materials

ACD and its derivatives were prepared according to the procedure described by Takeshima et al. (20) and Bordas et al. (21). Yellow crystalline powders of each compound were isolated and identified by comparison of their melting points and IR and NMR spectra with those of authentic samples.

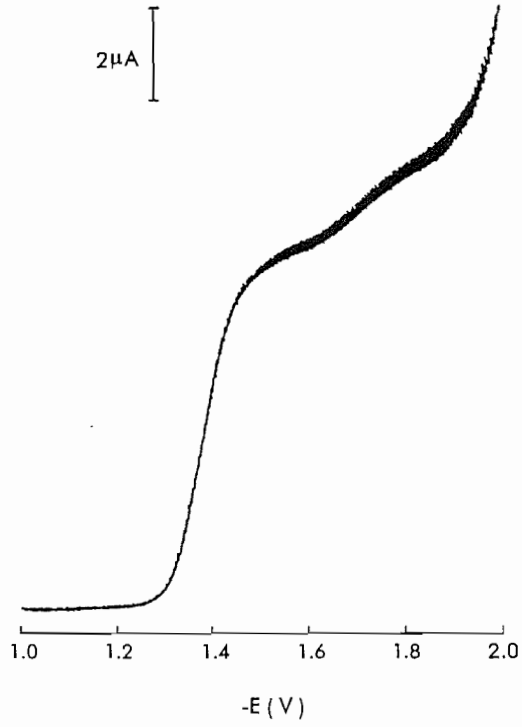
The Ni(II) complexes of ACD and its derivatives were prepared as described previously (9). Compound purity was established by elementary analysis.

Dimethyl sulphoxide (Fluka) was stored over type 4A molecular sieves. The potassium perchlorate used (Fluka) was recrystallized from triply distilled water and was oven-dried for several days.

Results and discussion

The ligands that were studied can be categorized into two groups: (*i*) the acid derivatives of ACD, which differ from each other by the substitution on nitrogen (L_I–L_{IV}), and (*ii*) the ester derivatives of ACD (L_V, L_{VI}), in which the hydrogen on the dithiocarboxylic acid group is substituted with an alkyl group. In this study, compounds L_I–L_{IV} are referred to as the acid derivatives of ACD, while L_V and L_{VI} are referred to as the ester derivatives (Scheme 1).

Fig. 1. The polarogram of $Ni(L_I)_2$ (3.3 mM) in 0.5 M $KClO_4$ in DMSO; drop time 5 s.



The electroanalytical behaviour of the nickel complexes of the acid derivatives is discussed first. When the acid derivatives are treated with Ni(II) solutions according to the procedure described previously (9), it has been claimed (9) that metal–ligand bond formation through the -SH site caused the -SH proton to be released from the molecule.

Nickel complexes of all the acid derivatives (L_I–L_{IV}) were prepared. However, complexes of L_{III} and L_{IV} were practically insoluble in aqueous and all the nonaqueous solvents tried, and thus it was not possible to investigate their electrochemical characteristics and the study was limited to complexes of L_I and L_{II}.

Nickel complexes of the ester derivatives (L_V, L_{VI}) were also prepared according to an established procedure (22). The complexes had limited solubility in DMSO, but their concentration was sufficient to investigate their electrochemistry.

Electrochemistry of the nickel complexes with the acid derivatives

Reduction at a dropping mercury electrode produced two dc polarographic reduction waves in the case of both acid derivatives (23). The second wave was not well defined and was later found to be a kinetic reduction (23) wave (Fig. 1, Table 1), the magnitude of which was governed by the rate of a chemical reaction (24). However, most of the interest lies in the first reduction wave, which will be considered in more detail.

The first wave, the less negative wave, was diffusion controlled in all cases. The diffusion current showed a linear dependence on the square root of the mercury column height and concentration within the range 0–3.5 mM, while the half-wave potentials were independent of concentration. Plots of

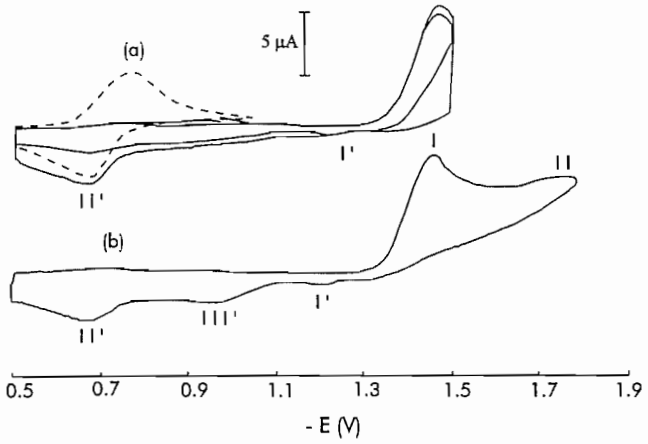
© 1997 NRC Canada

Can. J. Chem. Downloaded from www.nrcresearchpress.com by 88.146.161.215 on 09/08/12
For personal use only.

Table 1. Potentials ($E_{1/2}$) of the complexes (vs. SCE).

	Wave I		Wave II	
Compound	$E_{1/2}$ (V)	$E_{1/4} - E_{3/4}$ (mV)	$E_{1/2}$ (V)	$E_{1/4} - E_{3/4}$ (mV)
$Ni(L_I)_2$	−1.38	67	−1.72	80
$Ni(L_{II})_2$	−1.42	78	−1.80	85
$Ni(L_V)_2$	−1.65	65	—	—
$Ni(L_{VI})_2$	−1.35	60	—	—

Fig. 2. Cyclic voltammogram of $Ni(L_I)_2$ (3.0 mM) at H.M.D.E. (*a*) before and after holding for 15 s at −1.45 V (dotted line shows cyclic voltammogram of L_I^-); (*b*) from −0.5 to −1.8 V, 0.5 M $KClO_4$ in DMSO and scan rate 0.05 V s^{-1}.

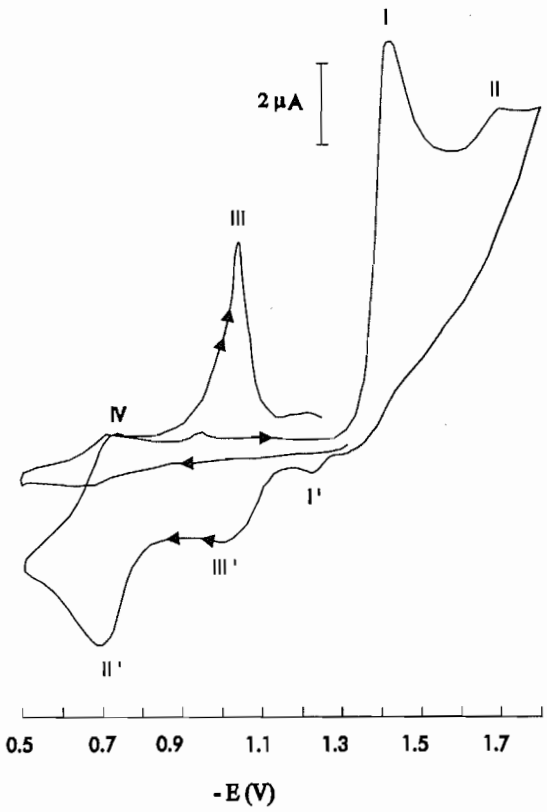


E vs. log $(i_d - i)/i$ were all linear ($r = 0.998$) with a slope of 67 and 80 mV for nickel complexes of L_I and L_{II}, respectively, indicative of a one-electron, quasi-reversible reduction in each case.

The second (more negative) wave for each of the complexes of acid derivatives is drawn out and arises from an irreversible one-electron reduction process. The associated $E_{1/4} - E_{3/4}$ values are large (Table 1). The height of the second wave is proportional to concentration in the range of 0–3.0 mM and is independent of mercury column height (h), thus showing a kinetic character. It is expected therefore that the magnitude of the current in this wave is governed by the kinetics of a chemical reaction (24).

Cyclic voltammetry was used to study the mechanism of reduction of the nickel complexes. Under cyclic voltammetric conditions, two reduction peaks and three anodic peaks were obtained with both complexes of nickel(II) with the acid derivatives. Taking $Ni(L_I)_2$ as an example, the following observations were made. When the switching potential was selected at −1.45 V, where only the first reduction peak was observed (Fig. 2*a*), only two anodic peaks, I′ and II′ (at −1.18 and −0.67 V, respectively) were observed. The height of the anodic peak II′ was increased after holding the potential at the switching potential for 15 s. When the current was recorded at −1.80 V (down to the second cathodic peak), another anodic

Fig. 3. The initial anodic scan of $Ni(L_I)_2$ (3.3 mM) from −1.3 V to −0.5 V (at H.M.D.E.) and reversing scan up to −1.8 V; scan rate 0.05 V s^{-1}.



peak III′ (−1.08 V) also appeared (Fig. 2*b*). As can be seen in Fig. 2*a* (dotted line, cyclic voltammogram of ammonium salt of the acid L_I, L_I^-), the anodic peak at −0.67 V (peak II′) is due to the mercury complex of L_I^- (12). L_I^- is supposed to be released via a coupled chemical reaction in the first cathodic peak. The initial anodic scan of $Ni(L_I)_2$ from −1.3 to −0.5 V and the reverse scan to −1.8 V are shown in Fig. 3. As can be seen, after reversing the scan at −1.8 V and the appearance of the two cathodic peaks ($E_{pc,I} = -1.4$ V and $E_{pc,II} = -1.75$ V), three anodic peaks appeared. These observations further prove that the three anodic peaks are related to the products of the two cathodic peaks at −1.4 and −1.75 V. Figure 3 also shows that multiscan cyclic voltammograms recorded in the absence of free ligand display waves in the anodic sweep and second cathodic sweep (peaks IV/II′) and the peak potentials correspond closely to those for the system (12):

[1] $Hg + L_I^- \rightleftharpoons Hg(L_I) + e^-$

The mercury(I) complex formed in this process later undergoes disproportionation to the mercury(II) complex (12).

The above observations indicate that the ligand should be released during the reduction step, presumably via a chemical reaction.

A cathodic peak (sharp peak) after the second scan reversal (peak III) was also observed. It is difficult to determine exactly to which process peak III/III′ is due, as this is obvi-

Can. J. Chem. Downloaded from www.nrcresearchpress.com by 88.146.161.215 on 09/08/12
For personal use only.

© 1997 NRC Canada

Can. J. Chem. Downloaded from www.nrcresearchpress.com by 88.146.161.215 on 09/08/12
For personal use only.

ously a very complicated reduction mechanism, with a number of processes occurring in solution after the reduction. It does appear to be formed as a consequence of the second reduction wave, peak II. The $E_{pc/2} - E_{pc}$ value for the first cathodic peak was changed from 55 to 60 mV by changing the scan rate from 0.02 to 0.2 mV s^{-1}. At slow scan rates, the cyclic voltammetric peak current function, represented by $i_{pc}/v^{1/2}$, is much higher than that expected for a reversible, one-electron, diffusion-controlled reduction. At high scan rates, the peak current function approaches the expected value of 0.446 and in fact is about 20% lower at 500 mV s^{-1}, probably as a result of the quasi-reversible nature of the electrode reaction. Although some of the above CV results, together with those derived from the analysis of dc wave (I), are consistent with a simple quasi-reversible electron transfer process, other results show that a more complex process prevails in this step and that, in fact, the assignment of an ECE mechanism to peak (I) is more appropriate. Analysis of the cyclic voltammetric parameters at various scan rates shows that at fast scan rates, where the influence of the coupled chemical reaction is slight, the CV half-wave peak widths ($E_{pc/2} - E_{pc}$) indicate a nearly reversible one-electron transfer process, while at slow scan rates deviation from this behaviour is observed. The calculated ratios of $i_{pa,II}/i_{pc,I}$ and $i_{pa,II}/v^{1/2}$ were decreased by increasing the scan rate (Fig. 4), which can be another reason for the presence of a coupled chemical reaction in the first cathodic peak.

For further elucidation of the mechanism, a chronoamperometric experiment was performed at an H.M.D.E., which demonstrated clearly that the reduction of $Ni(L_I)_2$ involves increasing departure from diffusion control with increasing electrolysis time. This result is illustrated by the variations in the main wave parameters shown in Fig. 5. At short electrolysis times, the slope of the chronoamperometric i against $t^{-1/2}$ plot is typical of a one-electron reduction for each complex, but approaches a slope representative of a two-electron reduction at longer electrolysis times.

Controlled potential coulometric analysis of the complexes, at a potential of -1.6 V, gave n values of 1.90 ± 0.2, with a change in colour from purple to orange (Fig. 6). The polarogram of the electrolysis product formed at this step showed an anodic wave due to the presence of free ligand (L^-_I), which appears because of the formation of a mercury complex (12).

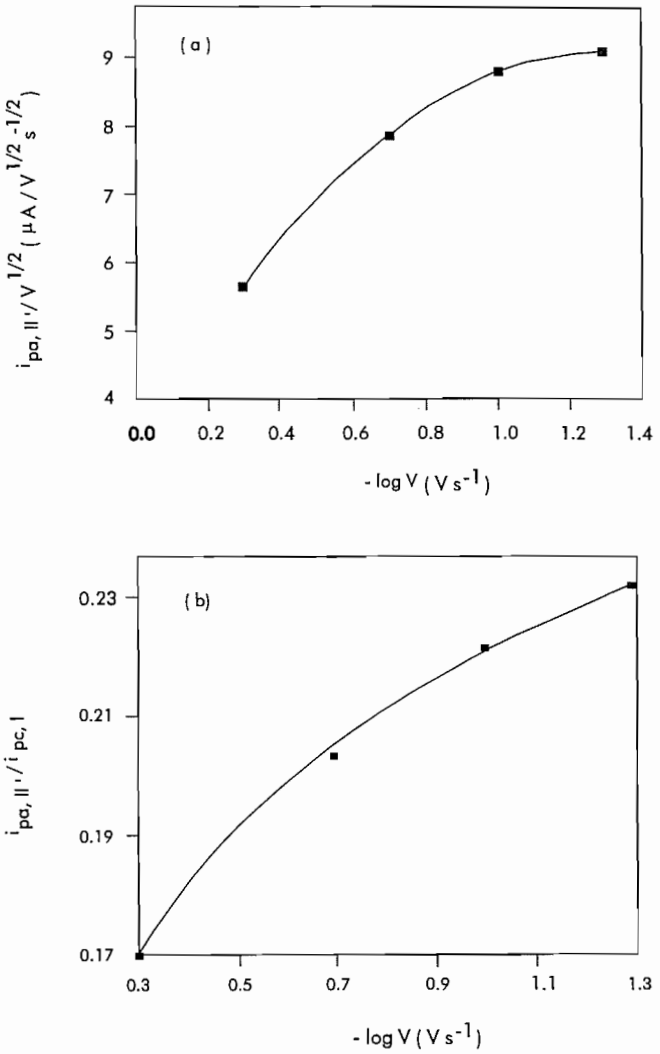
As mentioned previously, analysis of the dependence of E on $\log(i_d - i)/i$ showed a linear relationship (with $r = 0.996$) with a slope that is indicative of a one-electron process. If the assumption of a direct two-electron reduction step is accurate, the plot of E vs. $\log(i_d - i)/i$ should be linear with a slope of 29 mV. The experimentally determined slopes are much greater than this for the two nickel complexes, 67 and 80 mV for nickel complexes of L_I and L_{II}, respectively. Also, the $E_{1/4} - E_{3/4}$ values are close to the expected value for a one-electron process, while coulometry shows a two-electron transfer for this reduction step. Thus, all of the above observations are consistent with two one-electron processes with a chemical process interposed between them, as below.

[2] $A + n_1 e \longrightarrow B \qquad E_1^\circ$

[3] $B \xrightarrow{k} C$

[4] $C + n_2 e \longrightarrow D \qquad E_2^\circ$

Fig. 4. Variation of cyclic voltammetric parameters with voltage scan rate in the reduction of $Ni(L_I)_2$ in dimethyl sulphoxide: (*a*) cathodic peak current function, represented by $i_{p,c}/v^{1/2}$, against log v; (*b*) anodic to cathodic peak current ratio against log v.



where species C is more easily reduced than A, and $n_1 = n_2 = 1$ (24), where $E_2^\circ >> E_1^\circ$.

At long electrolysis times, or at sweep rates slow in comparison to the rate of the chemical reaction, the reduction current is the sum of $A + n_1e \rightarrow B$ and $C + n_2e \rightarrow D$. At high sweep rates or at short electrolysis times, only the simple diffusion-controlled reaction, $A + n_1e \rightarrow B$, is observed. At slow scan rates, B reacts chemically before it can be oxidized in the reverse anodic sweep and hence the anodic to cathodic peak current ratio decreases with decreasing scan rate.

Nicholson and Shain (25) introduced the theory of stationary electrode voltammetry for both single and cyclic triangular wave experiments to systems in which the preceding, following, or catalytic reactions are coupled with reversible or irreversible charge transfer processes. In the reduction wave of $Ni(L_I)_2$ at -1.4 V (ECE mechanism) and at high sweep rates, where the influence of the coupled chemical reaction is slight, the first charge transfer process seems to be reversible. Therefore, by recording the cyclic voltammogram of $Ni(L_I)_2$ at high

© 1997 NRC Canada

Can. J. Chem. Downloaded from www.nrcresearchpress.com by 88.146.161.215 on 09/08/12
For personal use only.

Fig. 5. The chronoamperometric data for $Ni(L_I)_2$ reduction at H.M.D.E. at −1.6 V, 0.5 M $KClO_4$ in DMSO.

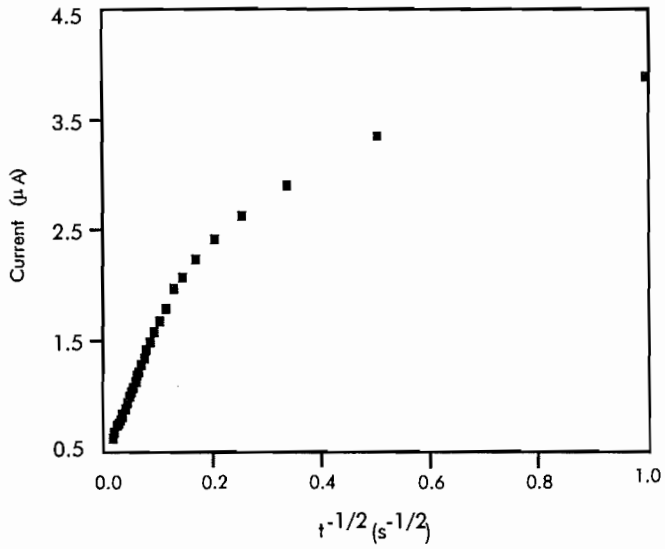
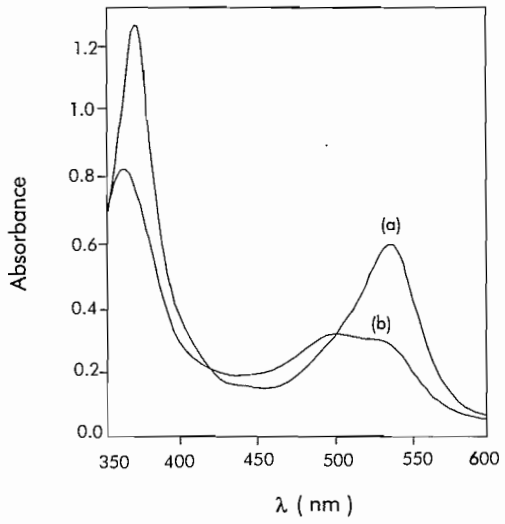


Fig. 6. The visible spectra of $Ni(L_1)_2$ (3.0 mM) (*a*) before electrolysis, (*b*) after electrolysis at −1.6 V at mercury pool electrode.



scan rates, such as 500 mV s^{-1}, the rate constant of the coupled chemical reaction (25) was calculated as 0.290 s^{-1}. The increase of the anodic peak due to the reaction of L^-_I with mercury upon holding the switching potential for 15 s can be good evidence that ligand loss is taking place through this coupled chemical reaction.

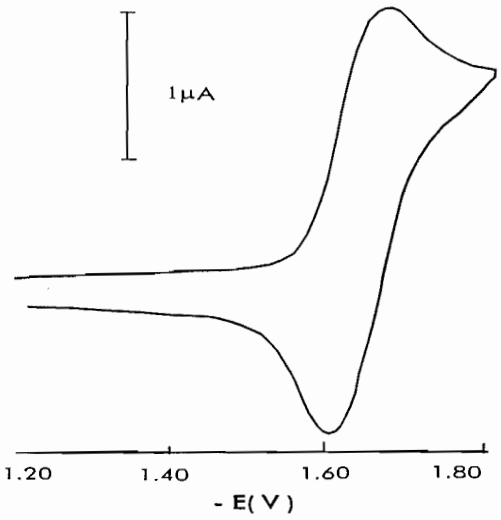
Thus, a possible mechanism for the first reduction wave of nickel complexes of the acid derivative ligands can be written as below:

[5] $Ni(L_I)_2 + e^- \longrightarrow [Ni(L_I)_2]^-$ (E)

[6] $[Ni(L_I)_2]^- \longrightarrow NiL_I + L_I^-$ (C)

[7] $NiL_I + e^- \longrightarrow [NiL_I]^-$ (E)

Fig. 7. Cyclic voltammogram of $Ni(L_v)_2$ (3.0 mM) at H.M.D.E.; scan rate 0.1 V s^{-1}; 0.5 M $KClO_4$ in DMSO.



For an ECE mechanism as above, where the second electron transfer is regarded as easier than the first one, the interference of the disproportionation reaction (24) in the overall kinetics must, however, be considered.

[8] $[Ni(L_I)_2]^- + NiL_I \longrightarrow [NiL_I]^- + Ni(L_I)_2$

This disproportionation step indeed favours the right-hand side since NiL_I is assumed to be more reducible than $Ni(L_I)_2$.

The analysis of the second wave at about −1.75 and −1.80 V, for $Ni(L_I)_2$ and $Ni(L_{II})_2$, respectively, showed that this wave has a drawn-out nature and a kinetic character, because its height was proportional to concentration in the range 0–3 mM and it was independent of mercury column height (*h*). The kinetic character of the wave suggests that the rate of electron transfer process in this step is controlled by the rate of a chemical reaction. The slopes of the plot of E vs. $\log(i_d - i)/i$ are 95 and 100 mV for Ni complexes of L_I and L_{II}, respectively, and the $E_{1/4} - E_{3/4}$ values (Table 1) show, together with the controlled potential coulometric data at −1.8 V ($n = 1.0 \pm 0.1$), that the process is an irreversible one-electron transfer process. The instability of the product formed in this step is emphasized by the irreversibility of its associated wave, which indicates that significant structural changes follow as a consequence.

Electrochemistry of the nickel complexes with the ester derivatives

The behaviour of the Ni(II) complexes with the ester derivative ligands (L_V and L_{VI}) differed from that of the nickel complexes of the acid derivatives. In these cases, only one reversible one-electron reduction wave was observed at −1.65 and −1.35 V for complexes of L_V and L_{VI}, respectively. Figure 7 shows the cyclic voltammogram of $Ni(L_v)_2$.

The polarographic slopes were consistent with a one-electron electrochemically reversible process, and CV measurements of peak separation (Table 2) confirmed this.

At CV scan rates between 0.02 and 0.20 V s^{-1}, the i_{pa}/i_{pc} ratio indicated a stable Ni(I) complex in the cyclic voltammet-

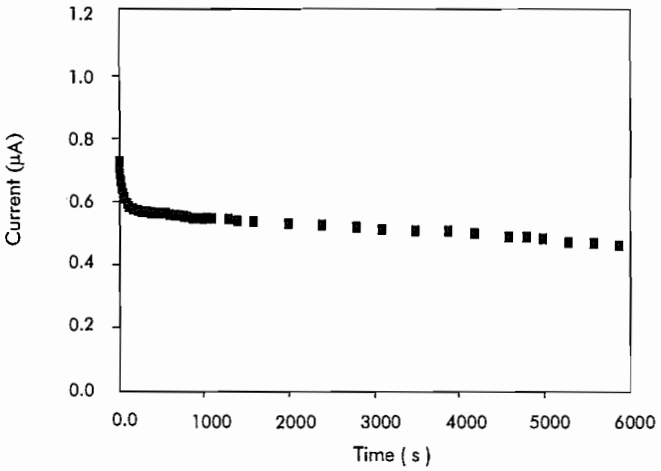
© 1997 NRC Canada

Can. J. Chem. Downloaded from www.nrcresearchpress.com by 88.146.161.215 on 09/08/12
For personal use only.

Table 2. Selected cyclic voltammetry data for the reduction of 2 mM $Ni(L_V)_2$ and $Ni(L_{VI})_2$ at a hanging mercury electrode.

v (mV/s)	i_{pa}/i_{pc}	$i_{pc}/v^{1/2}$ ($\mu A\ s^{1/2}/mV^{1/2}$)	$E_{pa} - E_{pc}$ (mV)	$E_{pc/2} - E_{pc}$ (mV)
		$Ni(L_V)_2$		
0.02	1.06	8.68	55	55
0.05	1.03	8.94	65	60
0.10	1.03	8.85	70	60
0.20	1.04	8.68	80	60
		$Ni(L_{VI})_2$		
0.02	1.09	21.4	55	55
0.05	1.07	20.4	65	60
0.10	1.00	22.1	75	60
0.20	1.04	21.2	80	60

Fig. 8. The plot of current vs. time for coulometry of $Ni(L_v)_2$, (3.0 mM) at mercury pool electrode; at −1.6 V; 0.5 M $KClO_4$ in DMSO.



ric time scale. The above observation suggests a simple one-electron reversible process. However, the reactions were more appropriately studied by long-term, large-scale electrolytic procedures. Inspection of the current–time curve for this electrolysis showed that, whereas the reduction of $Ni(L_I)_2$ and $Ni(L_{II})_2$ was 90% complete in about 1 h, a decrease of about 10% in electrolysis current required approximately 4 h for $Ni(L_V)_2$ and $Ni(L_{VI})_2$, electrolysis conditions being nominally identical (Fig. 8). Our coulometric measurements indicated that in this 4.0 h period, the equivalent of approximately 6 electrons per molecule was consumed. Polarograms obtained periodically throughout the electrolysis showed no waves except that due to the starting material (never was there an indication of an anodic current from the presence of the free ligand, as in the case of $Ni(L_I)_2$ and $Ni(L_{II})_2$, and the plateau currents for those waves remained practically constant as the electrolysis proceeded). This indicated that the steady-state concentration of the Ni(I) product was zero and that follow-up reaction(s) are coupled to the electron transfer step (a dark colour could be seen to develop at the electrode surface, but it rapidly dissipated in the bulk of solution). The electrolysis was also monitored spectrally in the uv–vis range with the in situ electrolysis cell. In several experiments during electrolysis, only spectroscopic characteristics of the Ni(II) complex starting material were observed.

Electrochemical and electronic absorption data on nickel complexes of L_V and L_{VI} were thus consistent with the following equation, in which the Ni(I) product is subject to the follow-up reaction, resulting in regeneration of the Ni(II) complex. This reaction occurs through reaction of the Ni(I)

$$[9]\quad Ni(L_V)_2 + e^- \longrightarrow [Ni(L_V)_2]^- \xrightarrow{[Z]}$$

species with some component of the electrolyte solution, likely the solvent itself, although the effect of undetected solvent impurities cannot be ruled out (24). It is likely that the oxidant, Z is present in excess of the nickel complex by several orders of magnitude and this is the reason for obtaining a high steady-state electrolysis current.

The above study clearly demonstrates the effect of ligand substitution and site of donation (6, 9, 22) on the electrochemical behaviour of the complex, even if the electron transfer process is metal based. Since the nature of the complete electrode reaction suggests a metal-centered reduction for both the acid and ester derivatives complexes, completely different mechanisms must prevail. For the Ni(II) complexes of the acid derivatives, where bonding occurs through amino nitrogen and deprotonated thiosulphur (9), the reduction proceeds via an ECE mechanism with $n = 1$ for each electron transfer process and the chemical reaction involves a dissociation to produce a nickel species more easily reduced than the Ni(II) ACD complex. However, for the Ni(II) complexes of the ester derivatives, where chelation occurs through thioketonate sulphur and amino nitrogen groups (6, 26), reduction occurs via an EC′ mechanism with $n = 1$ for the electron transfer step. Different reduction mechanisms are also suggested (14) for different Ni(II) dithiocarbamates based on the structural difference between their ligands. So, while some Ni(II) dithio-

© 1997 NRC Canada

carbamate complexes are reduced via an ECE mechanism, some others show an ECCE reduction mechanism of the type where the product of the first chemical reaction reacts further to produce a nickel species more difficult to reduce than Ni(II) dithiocarbamates.

In this work, the nature of the electrode reaction suggests a metal-centered reduction, in which the orbitals involved in the electron transfer process are essentially metallic in character. This is in agreement with the nature of the reduction process of nickel(II) dithiocarbamates at the mercury electrode (14).

Acknowledgments

The authors wish to express their gratitude to Shiraz University Research Council for support of this work. The technical assistance of Mr. N. Maleki and Miss Z. Ramezani is greatly appreciated.

References

1. A.M. Bond and R.L. Martin. Coord. Chem. Rev. **54**, 23 (1984).
2. W.E. Geiger, C.S. Allen, T.E. Mines, and F.C. Senftleber. Inorg. Chem. **16**, 2003 (1977).
3. J.G.M. Vander Linden and A.H. Dix. Inorg. Chim. Acta, **35**, 65 (1979).
4. G. Matolcsy, M. Hamran, and B. Bordas. Acta Phytopathol. **5**, 123 (1970).
5. D.M. Baird. J. Chem. Educ. **62**, 1694 (1969).
6. E.M. Martin and R.D. Bereman. Inorg. Chim. Acta, **188**, 221 (1991).
7. E.M. Martin and R.D. Bereman. Inorg. Chim. Acta, **188**, 233 (1991).
8. M. Yokoyama and T. Takeshima. Anal. Chem. **40**, 1344 (1968).
9. K. Nag and D.S. Joardar. Inorg. Chim. Acta, **14**, 133 (1975).
10. S.K. Mondal, D.S. Joardar, and K. Nag. Inorg. Chem. **17**, 191 (1978).
11. K. Nag and D.S. Joardar. Z. Naturforsch. B: Anorg. Chem. Org. Chem. **30B**, 107 (1975).
12. A. Safavi and M.B. Gholivand. Can. J. Chem. **74**, 95 (1996).
13. A. Safavi and L. Fotouhi. Electroanal. Chem. **339**, 229 (1995).
14. T.H. Randle, T.J. Cardwell, and R.J. Magee. Aust. J. Chem. **29**, 1191 (1976).
15. A.R. Hendrickson, R.L. Martin, and N.M. Rohde. Inorg. Chem. **14**, 2980 (1975).
16. A. Nieuwpoort, A.H. Dix, P.A.T.W. Porskamp, and J.G.M. Linden. Inorg. Chim. Acta, **35**, 221 (1979).
17. L.J. De Hayes, H.C. Faulkner, W.H. Doub, and D.T. Sawyer. Inorg. Chem. **14**, 2110 (1975).
18. A.M. Bond, R. Colton, M.L. Dillon, J.E. Moir, and D.R. Page. Inorg. Chem. **23**, 2883 (1984).
19. A.M. Bond, A.R. Hendrickson, R.L. Martin, J.E. Moir, and D.R. Page. Inorg. Chem. **22**, 3440 (1983).
20. T. Takeshima, M. Yokoyama, T. Imamoto, M. Akano, and H. Asaba. J. Org. Chem. **34**, 730 (1969).
21. B. Bordas, P. Sohar, G. Matolcsy, and P. Berencsi. J. Org. Chem. **37**, 1727 (1972).
22. D.S. Joardar, S.K. Mondal, and K. Nag. Bull. Chem. Soc. Jap. **50**, 1489 (1977).
23. L. Fotouhi. Ph.D. Thesis, Shiraz University, Shiraz, Iran. 1995.
24. A.J. Bard and L.R. Faulkner. Electrochemical methods, Wiley, New York. 1980.
25. R.S. Nicholson and I. Shain. Anal. Chem. **36**, 706 (1964).
26. E.M. Martin, R.D. Beremen, and J. Reibenspies. Inorg. Chim. Acta, **19**, 171 (1992).

Can. J. Chem. Downloaded from www.nrcresearchpress.com by 88.146.161.215 on 09/08/12
For personal use only.

© 1997 NRC Canada

cis-2,3-Di-*tert*-butylcyclopropanones

T.S. Sorensen and F. Sun

Abstract: The preparation of the strained *cis*-2,3-di-*tert*-butylcyclopropanone **2** from the acyclic compound, α,α′-dibromodineopentyl ketone **1**, using a previously reported methodology, is dramatic evidence of both the existence of oxyallyl intermediates in the mechanism of this reaction, and of the integrity with which oxyallyls ring-close to cyclopropanones by a disrotatory route. Because of the bulky *cis* substituents, cyclopropanone **2** exhibits a number of unusual spectroscopic features (as compared to the *trans* isomer **5**). With the aid of ab initio calculations on **2** and **5**, it can be shown that the C2—C3 bond in **2** interacts with the carbonyl π-orbitals, thus causing the carbonyl oxygen to bend 12° out of the plane; this interaction is absent in **5** and the latter has a planar carbonyl group. As with other cyclopropanones, **2** can be photochemically decarbonylated. This process itself appears to be stereospecific even though highly strained alkenes are produced. Cyclopropanone **2** is thermally rearranged to the *trans* isomer **5** and the kinetics for this are reported; our favoured mechanism involves oxyallyl intermediates. Other reactions of **2** also appear to proceed through these oxyallyl species; for example, alcohols initially add to **2** to give α-alkoxy enols, solutions of **2** enter into very facile diene cycloadditions, and the dimerization of neat **2** also appears to involve these oxyallyl species.

Key words: cyclopropanones, oxyallyl, stereomutation, stereospecific decarbonylation, nonplanar carbonyl.

Résumé : On a préparé la *cis*-2,3-di-*tert*-butylcyclopropanone (**2**) tendue à partir de l'α,α′-dibromodinéopentylcétone acyclique, **1**, en faisant appel à la méthodologie développée antérieurement. Cette synthèse est une preuve évidente à la fois de l'existence d'intermédiaires oxyallyles dans le mécanisme de cette réaction et de l'intégrité avec laquelle les oxyallyles se cyclisent en cyclopropanones par une voie disrotatoire. À cause de l'encombrement des substituants *cis*, la cyclopropanone **2** présente un certain nombre de caractéristiques spectroscopiques inhabituelles (par comparaison avec son isomère *trans*, **5**). En appliquant des calculs ab initio aux composés **2** et **5**, on peut montrer que la liaison C2—C3 du composé **2** interagit avec les orbitales π du carbonyle provoquant ainsi un déplacement de 12° de l'oxygène du carbonyle hors du plan; cette interaction est absente dans le composé **5** et ce dernier possède donc un groupe carbonyle planaire. Comme c'est le cas avec d'autres cyclopropanones, le composé **2** peut être décarbonylé photochimiquement. Ce processus semble être stéréospécifique, même s'il conduit à des alcènes fortement tendus. La cyclopropanone **2** se réarrange thermiquement en isomère *trans*, **5**, et on a mesuré la cinétique de cette réaction; le mécanisme que nous favorisons implique des intermédiaires oxyallyles. Il semble que d'autres réactions du composé **2** se produisent aussi par le biais de ces espèces oxyallyles; par exemple, les espèces oxyallyles semblent être aussi impliquées dans l'addition initiale des alcools à **2** pour donner des α-alkoxyénols, dans les réactions très faciles de cycloadditions diéniques des solutions de **2** ainsi que dans la dimérisation de **2** à l'état pur.

Mots clés : cyclopropanones, oxyallyle, stéréomutation, décarbonylation stéréospécific, carbonyle non planaire.

[Traduit par la rédaction]

Introduction

The reaction of the metallate salt, $PPN^+Cr(CO)_4NO^-$ with α,α′-dibromo ketones has recently been explored as a low-temperature route to cyclopropanones (1–3). The reaction is extremely rapid, even at −100°C, and is postulated to involve the intermediates **B** and **C** (eq. [1]).

The existence of the bromo enolate **B** can be shown by trapping experiments with $(CH_3)_3SiCl$ (1), and the oxyallyl species **C** is inferred from the similarity of this overall reaction to the early steps of the Favorski rearrangement, and by using a cyclopentyl ring system, whereby dimers of the oxyallyl can be characterized in this special case (4).

Received February 3, 1997.

T.S. Sorensen[1] and F. Sun. The Department of Chemistry, University of Calgary, Calgary, AB T2N 1N4, Canada.

[1] Author to whom correspondence may be addressed. Telephone: (403) 220-5361. Fax: (403) 289-9488. E-mail: sorensen@acs.ucalgary.ca

Another approach to clarifying the existence of **B** and **C** in eq. [1] is to use stereochemical markers, and we have recently communicated (2) the result that α,α′-dibromodineopentyl ketone **1** produces only *cis*-2,3-di-*tert*-butylcyclopropanone **2**, the thermodynamically much less stable of the two possible stereoisomeric cyclopropanones.

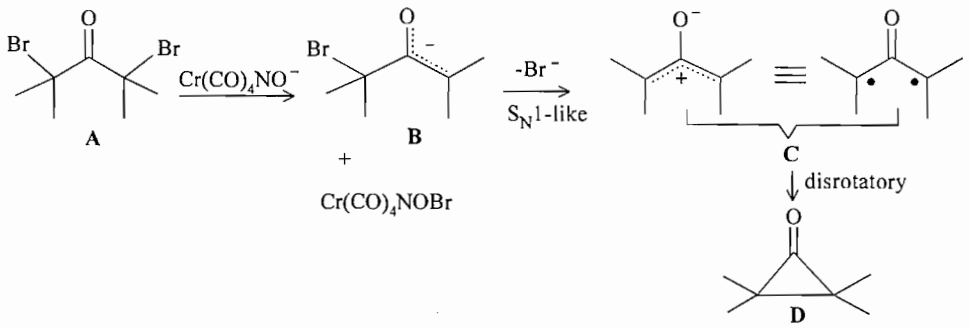
In this paper we expand on the earlier results and explore more fully the unusual chemical and physical properties of **2**.

Results and discussion

There are two possible diastereomers of **1**, the meso isomer **1a** and the racemic form **1b**. When dineopentyl ketone is brominated, only a single crystalline diastereomer is isolated in high yield (5). The CHBr ^1H NMR peak for this isomer is found at δ 4.40 (1.18 for the *t*Bu peak) and there is not much evidence for a second isomer in the small amount of mother liquor material. However, when **2** was brominated small additional peaks were observed in the crude reaction mixture, δ 4.50 and 1.20, approximately 5–8% of those for the major isomer. This minor isomer has a considerably shorter GLC retention time

© 1997 NRC Canada

Can. J. Chem. Downloaded from www.nrcresearchpress.com by 88.146.161.215 on 09/08/12
For personal use only.

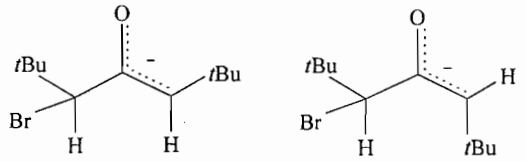
[1] 



than the major one and it could be isolated free of the latter by preparative GC.

Both dibromo diastereomers were separately reacted with $Cr(CO)_4NO^-$ at −78°C in CD_2Cl_2 solution to give **2** (NMR monitoring) in each case.

This single product result can be nicely rationalized from the eq. [1] mechanism. The bromo enolate formed from either **1a** or **1b** has two possible geometric forms, **B1** and **B2**, assuming a planar enol functionality. From MM2 or AM1 semiempirical calculations, the most stable conformers of **1a** and **1b** both have the C—Br bonds approximately perpendicular to



the plane of the carbonyl group, and the *t*Bu groups in both cases have a steric alignment that will lead to the bromo enolate **B1**, i.e., if "Br^+" loss takes place so that the newly forming enolate *p*-orbital is in conjugation with the carbonyl group. Semiempirical calculations (AM1) also predict that **B1** is about 4 kcal/mol more stable than **B2**.

The loss of Br^- in **B1** perpendicular to the enolate plane will lead to oxyallyl **C1** with both *t*Bu groups in the *syn* position relative to oxygen.

It is unlikely that either the C—Br reduction or the loss of Br^- is reversible, but the above analysis predicts that the kinetic products are also the thermodynamically stable ones up to, and including, the oxyallyl intermediate.

Finally, the ring closure of the oxyallyl **C1** is observed to be strongly pericyclic in nature and the least stable cyclopropanone is ultimately produced.

The above analysis also predicts that the diastereomers of **3** should form the cyclopropanone **4**, as is indeed the case.

cis-2,3-Di-*tert*-butylcyclopropanone **2** can be isolated using a sub-ambient temperature work-up, subliming as white crystals, mp ca. −22°C, onto a surface cooled by Dry Ice at about −10°C/0.01 Torr (1 Torr = 133.3 Pa). At room temperature this ketone is an unstable liquid (see later). In contrast, cyclopropanone **4** could only be examined as an in situ solution since it rapidly rearranges at −30°C, producing the α,β-unsaturated ketone **6**, a known compound (6).

As an aside, it is now known that cyclopropanone thermal stability is associated with having only tertiary alkyl substituents or hydrogen (2, 3), accounting for the stability of the previously reported *trans*-2,3-di-*tert*-butylcyclopropanone **5** (7), 2,2-di-*tert*-butylcyclopropanone (6), and trialkylsilyl-substituted cyclopropanones (8, 9), but not **4**.

The preparation of *cis*-2,3-di-*tert*-butyl-2,3-dimethylcyclopropanone by our procedure failed because the starting ketone could not be dibrominated.

Spectroscopic studies on 2, 4, and 5

As expected, the *cis* ketone **2** has only two ^1H NMR peaks, at δ 3.04 (2H) and 1.10 (18H) in $CDCl_3$. The spectra were also measured in several other solvents. The *trans* ketone **5** has a considerably higher field position for the CH hydrogens (7), δ 1.67. Cyclopropanone **4** has the CH peak at 2.66. The ^{13}C NMR spectrum of **2** ($CDCl_3$) shows the CH carbons at δ 47.1 (vs. 30.8 in **5**).

In **4**, the corresponding carbons are found at δ 50.5 (C_q) and 51.9 (CH). The ^{17}O NMR spectra of **2** and **5** were measured in this study because we expected (next section) to see a somewhat higher field shift in **2**, as was indeed the case, δ 487 in **2** vs. 530 in **5**.

The IR spectrum of **2** has a split C=O stretch at 1792 and 1819 cm^{-1}, with the former about twice the intensity of the latter. Coincidentally, the *trans* isomer **5** has (7) a single C=O stretch at 1819 cm^{-1}. This is a significant difference and in the next section we discuss in more detail a probable origin for this result. No IR data were measured for **4** because of its instability.

The $n\rightarrow\pi^*$ UV absorption for **2** is found at 329 nm, compared to a reported (7) 354 nm for **5**, both results for hydrocarbon solvents. This difference of 25 nm can also be rationalized from a detailed analysis of the computed structure for **2**.

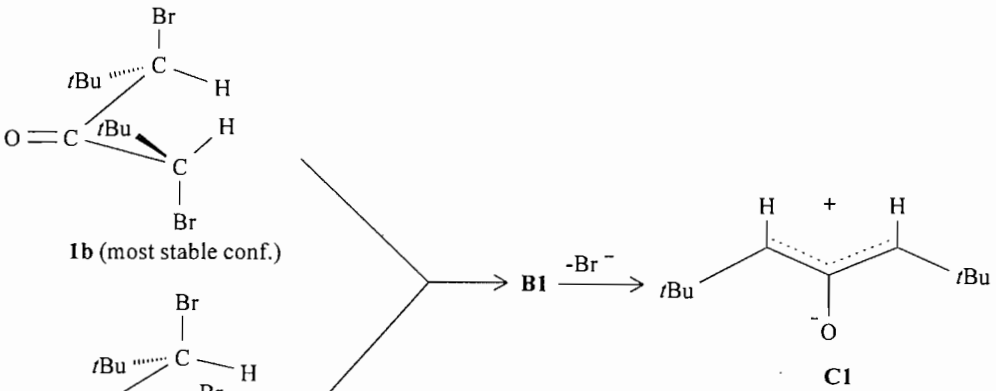
Ab initio calculations of 2 and 5. Onset in 2 of a unique delocalization of C2—C3 electron density into the C=O π* orbital. Correlation with spectroscopic data

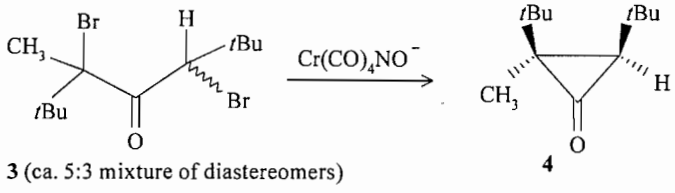
High-level ab initio calculations (B3LYP-6-31G**) were carried out on cyclopropanones **2** and **5**. Key bond lengths, angles, and dihedrals for the optimized structures are shown in Fig. 1. Although both isomers have severe bond angle distor-

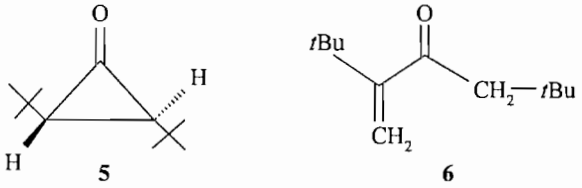
Can. J. Chem. Downloaded from www.nrcresearchpress.com by 88.146.161.215 on 09/08/12
For personal use only.

© 1997 NRC Canada

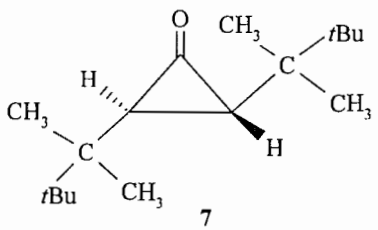
Can. J. Chem. Downloaded from www.nrcresearchpress.com by 88.146.161.215 on 09/08/12
For personal use only.







tions, the calculated bond distances are more normal in **5**, particularly the C2—C3 bond at 1.579 Å vs. 1.640 in the *cis* structure **2**. The calculated geometry of **5** is in good agreement with data from an X-ray structure of a closely related *trans*-dialkylcyclopropanone[2] (compound **7**, C2—C3 = 1.584 Å). No X-ray data have yet been obtained for *cis* dialkylcyclopropanones but there are several other benchmarks by which one can judge the quality of the calculations:



7

1. ^{1}H, ^{13}C, and ^{17}O NMR calculated shifts for **2** and **5** successfully mirror the experimental results (^{1}H, H2–H3 for **2** and **5**, respectively, calculated as δ 2.74 and 1.49; ^{13}C, C2–C3, δ 44.5 and 31.7; ^{17}O, 479 and 514).

2. Calculated C=O stretching frequencies for **2** and **5** are 1805.6 and 1826.2 cm^{-1}, successfully predicting a lower frequency value for **2**.

Besides the C2—C3 bond distance differences calculated for **2** and **5**, there is also a marked difference in the planarity of the >C=O group. In the calculated structure for **5**, and in the X-ray structure for **7**, the carbonyl group is essentially planar, whereas the *cis* isomer calculations give a markedly nonplanar >C=O, in which the oxygen atom is bent towards the *t*Bu face of the molecule (12° from the plane of the three carbons).

This distortion can be linked to an interaction between the C2—C3 bond and the π* orbital of the carbonyl. Because of the short C1—C2(C3) bonds in **2**, and the presence of a three-membered ring, the distance from the carbonyl carbon to the midpoint of the C2—C3 bond (calculated as the line of shortest distance) is only 1.18 Å. This short distance is normally of no great significance because the C2—C3 bond is orthogonal to the π* orbital in a planar cyclopropanone such as **5**, but in the isomer **2** the bulky tBu groups increase the *t*Bu-C2-C3 bond angle on one face compared to the H-C2-C3 angle of the other face (see Fig. 1), the computed angles being 135°–136° vs. 104°–105°. This imbalance has the effect of creating greater electron density on the *t*Bu "face" of the cyclopropanone so that the previously discussed orthogonality is no longer strictly in force and a favourable interaction with the empty π* orbital is possible. Only one lobe of the carbonyl carbon *p*-orbital interacts with this electron density, and a better orbital overlap can obviously be obtained if the carbonyl group tips toward this electron density. This slight C2—C3 bond asymmetry can be seen in an orbital plot of the HOMO-1 orbital (Fig. 2), which mainly comprises the C2—C3 σ bond. A small p_z orbital contribution on the carbonyl oxygen (seen in the Fig. 2 projection) shows that an interaction with the carbonyl π–π* orbitals is present.

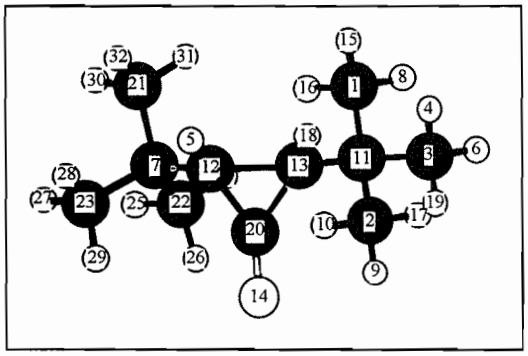
This electron delocalization from the C2—C3 bond into the π* orbital can be correlated with the following experimental and theoretical results:

1. a longer C2—C3 bond in **2** (vs. **5**) because of reduced electron density in the bond (clearly steric factors also apply).

[2] M. Parvez, T.S. Sorensen and F. Sun. Unpublished results.

© 1997 NRC Canada

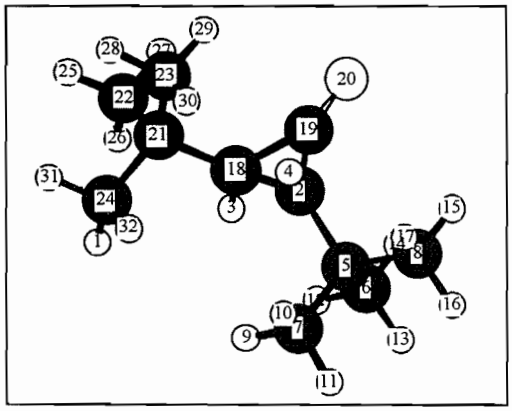
Fig. 1. Calculated geometry of cyclopropanones **2** and **5** (B3LYP/6-31G**) showing relevant bond distances and angles.



cis-di-*t*-butylcyclopropanone **2**

B3lyp/6-31G** Geometry

C12-C13	1.640	C11-C13-C12	135.300	C12-C13-C20-O14	159.118
C13-C20	1.468	C7-C12-C13	136.179		
C12-C20	1.464	H18-C13-C12	104.363		
C20-O14	1.211	H5-C12-C13	104.809		
C13-C18	1.090	C13-C20-C12	68.020		
C12-H5	1.091	C12-C13-C20	55.888		
C11-C13	1.544	C13-C12-C20	56.091		
C7-C12	1.538				



trans-di-*t*-butylcyclopropanone **5**

B3lyp/6-31G** Geometry

C2-C18	1.579	C5-C2-C18	124.333	C2-C18-C19-O20	-180.00
C2-C19	1.475	H4-C2-C18	113.625		
C19-O20	1.207	C2-C19-C18	64.738		
C2-H4	1.093	C2-C18-C19	57.644		
C2-C5	1.540				

2. in the "three-orbital interaction" picture (10), the "new" π* C═O orbital is somewhat raised in energy compared to the "no interaction" case. This can account for the smaller λ_{max} for the $n\rightarrow\pi^*$ UV absorption of **2** when compared to the *trans* isomer value (both values are unusually high wavelength, and we stress only the comparison here). It also accounts for the higher field shift in the ^{17}O NMR spectrum in **2**, since paramagnetic ^{17}O shifts are also related to the size of $n\rightarrow\pi^*$ transition energies.

3. electron donation into the π* carbonyl reduces the >C═O bond order and one predicts a lower stretching frequency in **2**, as is found.

We have no quantitative measure of how much energy stabilization is provided by the C2—C3 bond electron delocalization but we feel that the latter has more effect on spectroscopic properties than energies. An interesting comparison is the energy difference between **2** and **5**, compared to *cis*- and *trans*-1,2-di-*tert*-butylethene, 7.21 kcal/mol (calcd.) vs. 9.37 (expt.) (11). Given the quite different bond lengths in these sets, it does not appear that cyclopropanone **2** is appreciably stabilized.

Reactions of 2

Photochemistry

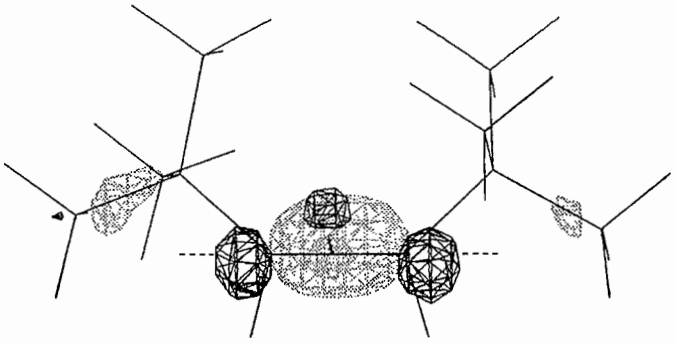
The photochemical decarbonylation of cyclopropanone itself (12, 13) and of several substituted derivatives has been reported, including the use of this procedure to create a strained alkene (14). As far as we are aware, *trans* cyclopropanone **5** is the only previous system where the alkene product could exhibit stereochemical differentiation and, in this case, only the *trans* alkene **8** is produced (7). Since this is the thermodynamic product as well, the observation in the present work that the *cis* cyclopropanone **2** produces the *cis* alkene **9**,

© 1997 NRC Canada

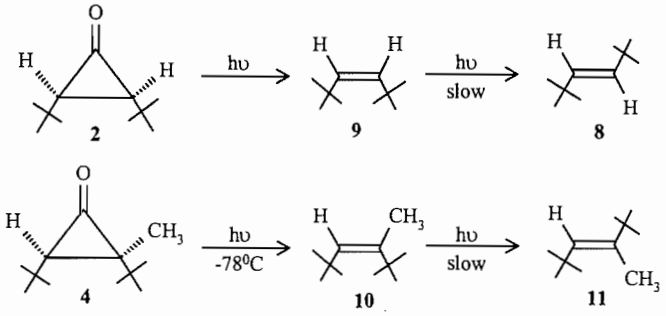
Can. J. Chem. Downloaded from www.nrcresearchpress.com by 88.146.161.215 on 09/08/12
For personal use only.

Can. J. Chem. Downloaded from www.nrcresearchpress.com by 88.146.161.215 on 09/08/12
For personal use only.

Fig. 2. Plot of the HOMO-1 orbital (the "non-bonding" combination) from the B3LYP/6-31G** calculation of cyclopropanone **2**. The view through the planar cyclopropane ring has the C2—C3 bond in front (C1 is hidden) and one can see that this orbital is not totally symmetrical with respect to a line connecting C2 and C3 (slightly larger on the *tert*-butyl side of **2**, and vice versa for the back lobes). The tipped carbonyl oxygen bond can be seen and the small out-of-phase *p*-orbital contribution of the oxygen to this HOMO-1 orbital can also be seen.

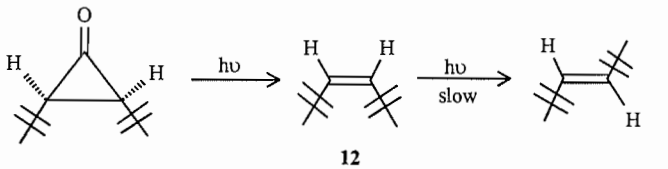


and that **4** produces the *cis* propene **10**, is a much more unambiguous demonstration that stereochemistry is retained in this decarbonylation.



In the actual results, a small amount of *trans* alkene (ca. 5% with both **2** and **4**) is present at the end of the photolysis of the cyclopropanones, but it can be shown that the *cis* alkene is itself photochemically labile (*cis* → *trans* alkene) under our conditions. If one compares the two photochemical rates with the ratio of *cis*:*trans* alkene present immediately after cyclopropanone disappearance, and extrapolates back to zero time, one sees a good correspondence, leading us to conclude that the cyclopropanone decarbonylation is stereospecific. Cyclopropanone **2** is obviously a stringent test of this stereospecificity since the *cis* alkene is 9.37 kcal/mol less stable than the *trans* isomer (11).

In unpublished work,[2] we also prepared the *cis* alkene **12** from the corresponding cyclopropanone, this alkene being even more strained than **9**. In this case the *cis* alkene → *trans* alkene photochemical reaction is relatively faster, leading to ca. 25% of the *trans* alkene at the end of the cyclopropanone photolysis, but the two alkenes can be easily separated by preparative GC.



The photochemical decarbonylation of **4** at −78°C illustrates the advantage of having a low-temperature preparation and work-up procedure since, as described earlier, this particular cyclopropanone rapidly rearranges to the α,β-unsaturated ketone **6** at −30°C.

This photochemical reaction is also useful as a structure proof tool. The stereochemistry assigned to **4** follows logically from the prior preparation of **2**, but we have no *trans* isomer of **4** for comparison purposes. However, the alkene produced from **4** clearly has the *cis*-di-*t*Bu structure **10** since the latter is photochemically isomerized to a more stable alkene that must then have the *t*Bu groups *trans*, i.e., **11**. Also, the H---CH_3 coupling of 1.2 Hz in **11** vs. unresolved coupling in **10** is consistent with this assignment.

cis- *to* trans-*2,3-Di*-tert-*butylcyclopropanone rearrangement* $2 \rightarrow 5$

Under the conditions of the in situ NMR tube reactions used initially to observe **2**, this compound was stable up to about 20°C. Starting at about 0°C, one of the reaction by-products, $Cr(CO)_4NOBr$, decarbonylates (remove NMR tube cap!). Although the resulting inorganic products are of unknown structure, it is possible that they have some Lewis acid properties that may be promoting the *cis*-**2** → *trans*-**5** conversion.

As evidence, when an alternative low-temperature work-up and isolation procedure is adopted, the resulting pure **2**, in various inert solvents at 20°C, only slowly rearranges over a period of days. Under GLC analysis it is possible to obtain a reasonable size peak for **2** (together with **5**) when on-column injection conditions are used, but with split-mode injections one sees mainly the peak for **5**. The shape of the *cis*-**2** peak indicates that no appreciable on-column rearrangement is occurring.

The rate of the thermal uncatalyzed rearrangement of **2** to **5** was measured at 80°C in toluene-d_8 solvent contained in a PTFE-lined 5 mm NMR tube, using ^{1}H NMR to monitor concentrations. Initially the analysis was based on the respective areas of the CH peak in the two isomers, assuming that the combined area was constant. However, the overall conversion is not totally clean and so the rate of the *trans*-**2** formation (first order) was measured directly using the residual ^{1}H peak of the toluene methyl group as a standard area, $k = (1.5 \pm 0.3) \times 10^{-4}$ s^{-1}, $\Delta G^{\ddagger} = 27.1 \pm 0.1$ kcal/mol.

There are several possible mechanisms for the $2 \rightarrow 5$ rearrangement. Cleavage of the C1—C2 bond and reclosure after bond rotation is one possibility. The *trans*-**5** can be thermally decarbonylated at 150°C (7), and this process presumably involves an initial C1—C2 bond cleavage. In the more strained **2**, such a bond cleavage could conceivably be even more favorable, but there is no evidence for any appreciable decarbonylation of **2** along with rearrangement into **5**. This possible mechanism is related to the more general case of stereomutation in cyclopropanes, the subject of much study (15).

Another possible mechanism involves bond rotation in the oxyallyl valence bond partner of **2**. From NMR line-broadening studies on the closely related *cis*-di-*tert*-amylcyclopropanone (2), we have estimated that the oxyallyl **C1** is about 11.3 kcal/mol higher free energy than the cyclopropanone. It is also known from the work of Greene and co-workers (16) that the *trans*-**5** − oxyallyl **C2** free energy difference is about 28 kcal/mol (in both cases we assume that $\Delta G \sim \Delta G^{\ddagger}$ (2, 17)).

© 1997 NRC Canada

Can. J. Chem. Downloaded from www.nrcresearchpress.com by 88.146.161.215 on 09/08/12
For personal use only.

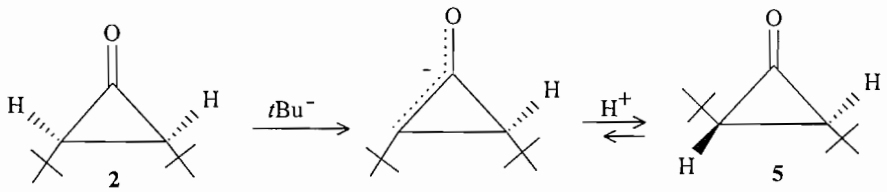
From our theoretical results discussed earlier, we calculate ΔG = 8.96 kcal/mol for the free energy difference between **2** and **5**. Putting these numbers together leads to the free energy diagram shown in Fig. 3. By difference, the two oxyallyls **C1** and **C2** are predicted to differ in energy by 7.7 kcal/mol, very similar to an AM1 semiempirical calculated difference (this work) of 7.6 kcal/mol. The origin of this energy difference is mainly steric so the AM1 method used here should give a reasonable estimate of this. If the *cis*-**2** → *trans*-**5** isomerization followed the route **2** ⇄ **C1** ⇄ **C2** ⇄ **5**, our observed free energy of activation would be above the **C2** oxyallyl free energy value, so this could clearly be a feasible route on energetic grounds. This route predicts a bond rotation barrier in **C1** of ca. 16 kcal/mol. There is almost nothing reported in the literature about rotation barriers in oxyallyls.

Finally, a conrotatory opening of **2** to directly give **C2** is also a possible rearrangement mechanism. If this mechanism were operative, there would be a 27 kcal/mol vs. 11.3 kcal/mol difference in conrotatory vs. disrotatory ring opening (almost a trillionfold rate difference at 25°C). If this mechanism is not operative, the inferred integrity of the disrotatory opening is even larger.

One cannot a priori rule out any of these mechanisms, but the absence of appreciable thermal decarbonylation in **2** leads one to favor the latter two postulates. These are, in any case, only subtly different.

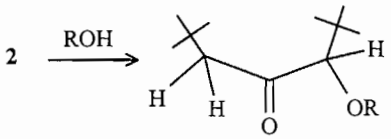
Although clearly not a possible reaction mechanism under our toluene-d_8 solvent conditions, a base-catalyzed enolate mechanism for the rearrangement of **2** to **5** is suggested from the literature results of Greene and co-workers (7). These authors prepared the *trans*-**5** by reacting α-bromodineopentyl ketone with *t*BuO⁻–*t*BuOH (Favorski reaction conditions). The question is, why was the *trans* isomer formed in this reaction? An oxyallyl mechanism cannot directly apply since we have just shown that this mechanism leads to the *cis* isomer **2**. An internal S_N2 displacement[3] (still shown this way in a well-known text (18)) is problematic from a steric viewpoint (19), and would also not explain why this internal displacement did not happen in our work.

The most appealing explanation is that the route used by Greene does initially yield the *cis* cyclopropanone **2**. Although it is expected to be very reactive at the C2—C3 bond under these alcohol–alkoxide conditions, a deprotonation to the enolate could be competitive with these other reactions, and reprotonation to the *trans*-**5** would of course be overwhelmingly preferred. Greene and co-workers were able to indirectly show that H–D exchange can take place with **5** in *t*BuO⁻–*t*BuOD; recovered **5** was not obtained but the Favorski product from **5** had extra deuterium atom substitution. Based on our calculated $\Delta\Delta G$ difference between **2** and **5** of 8.96 kcal/mol, and the fact that the enolate is common to both ketones, one can calculate that **2** is 6.5 pK_a units more acidic than **5**. The hydrogens in **2** are also more sterically accessible than those in **5** and so it would not be surprising if **2** formed the enolate several million times faster than **5**, and that this reaction could therefore be quite competitive with other possible reactions of **2**.



Reaction with alcohols and water

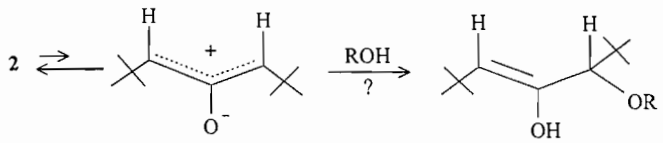
When **2** is reacted with methanol, 2-propanol, or benzyl alcohol (sub-ambient to ambient temperatures), the α-alkoxy ketones **13** are produced on work-up. In contrast, the *trans* isomer **5** is reported (7) to give cyclopropanone hemi-ketals under these conditions but, on heating these, the same α-alkoxy ketones are formed.



13 (R=CH_3, iPr or Bz)

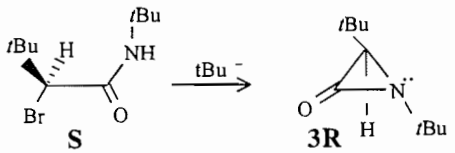
However, when **2** was treated with methanol or 2-propanol and the solution was examined by ^{1}H NMR, all starting ketone had reacted but only a small amount of α-alkoxy ketone **13** was present. The major product had two diagnostic low-field signals (at δ 4.76 and 4.11 in the methanol case, mutually coupled with $J \sim 1.5$ Hz). These peaks can be assigned to the enol of the α-methoxy ketone, structure **14**. Not surprisingly, this enol readily converts to the corresponding ketone on work-up. 2-Propanol likewise forms the enol under these same conditions.

The initial formation of an enol opens the possibility that the reactive species in this reaction may be the oxyallyl **C1**, although other mechanisms are also feasible.



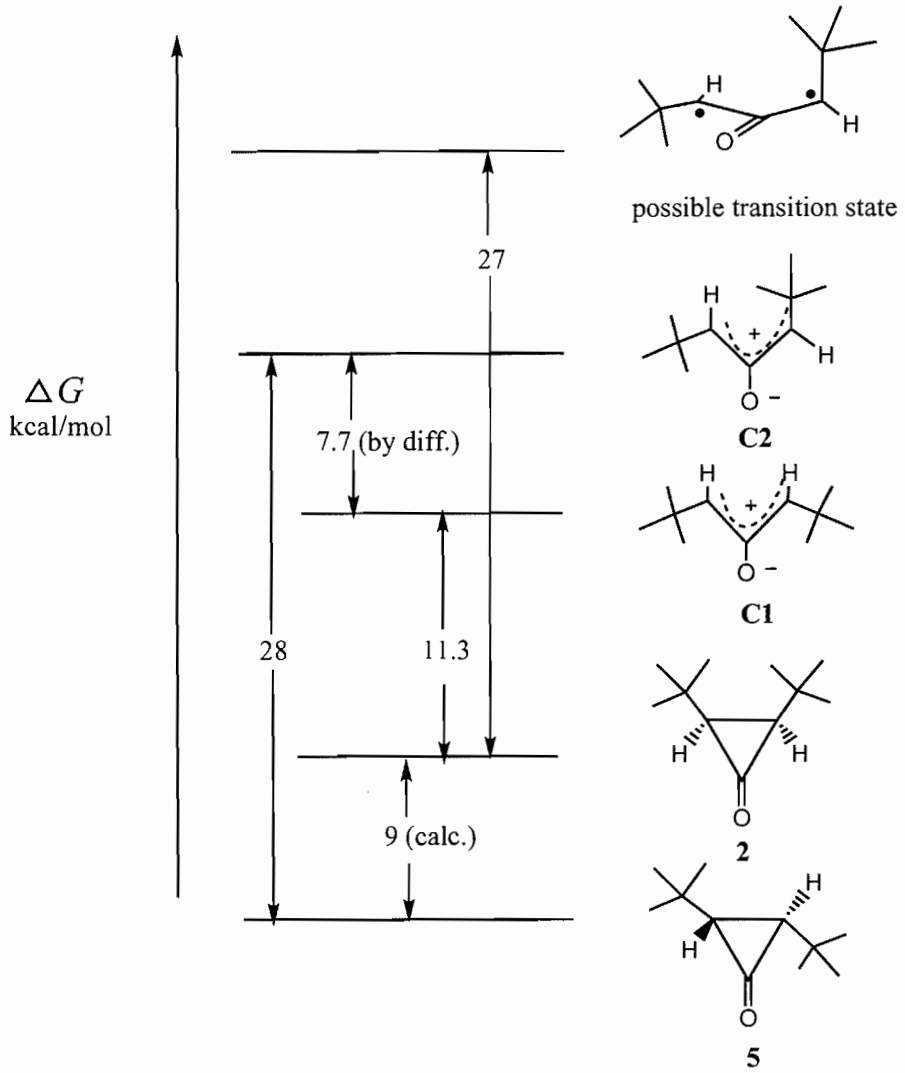
C1 **14** (R=CH_3, iPr)

[3] An internal S_N2-type mechanism is presumably operative in the preparation of 3-*R*-aziridinone (20) from the *S*-amide in the presence of *t*BuO⁻, but nitrogen has two lone pairs in the amide salt intermediate, one of which is in a suitable position to carry out the internal displacement.



© 1997 NRC Canada

Fig. 3. Relative free energies of cyclopropanones **2** and **5**, and their corresponding oxyallyl valence-bond partners **C1** and **C2**. These data are derived from a combination of experimental and computational data.



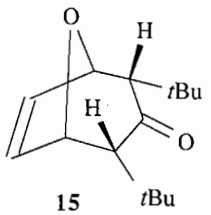
Water readily reacts with **2** to give the α-hydroxy ketone **13** (R = H).

Cycloaddition reactions

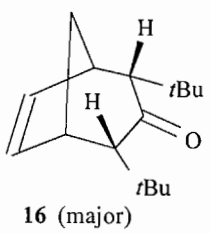
A sizeable literature, beginning with the early work of the Turro group (21), exists on 3+4 cycloaddition reactions involving characterized cyclopropanones. There is a much larger body of work involving in situ generated "oxyallyl" species for use in these same cycloaddition reactions; in most cases these can be better described as oxyallyl cations because of complexation of the oxygen (22, 23). In our work we find that **2**, despite the bulky *t*Bu groups, is very reactive with some dienes. Furan, cyclopentadiene, and 2,3-dimethyl-1,3-butadiene form adducts with **2** at (or below) room temperature.

This reactivity can be attributed to the oxyallyl **C1**, which is in equilibrium with **2** (see previous discussion). In contrast, the *trans* isomer **5** is in equilibrium (Fig. 3) with miniscule amounts of the **C2** oxyallyl, and this latter species is also sterically hindered. Not surprisingly, there have been no reports of cycloadditions involving **5**.

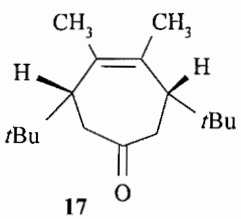
As expected from the oxyallyl **C1** structure, the *t*Bu groups have a *cis* orientation in the adducts **15**-**17**.



15



16 (major)
(4:1 mixture of)
stereoisomers



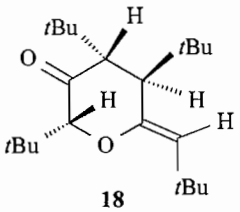
17

Can. J. Chem. Downloaded from www.nrcresearchpress.com by 88.146.161.215 on 09/08/12
For personal use only.

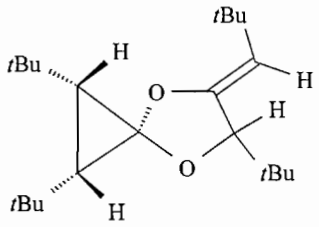
© 1997 NRC Canada

Can. J. Chem. Downloaded from www.nrcresearchpress.com by 88.146.161.215 on 09/08/12
For personal use only.

Cyclopropanone **2** is not stable in the condensed phase at 20°C (or even at −20°C on storage). Two major dimers are formed, and the structure of one of these differs from that of previously isolated cyclopropanone dimers. Based on the NMR spectrum, including a number of 2D techniques, the structure **18** was assigned. This compound is structurally related to dimers previously obtained from a cyclopentyl ring oxyallyl dimerization, but in the present case it may be more reasonable to postulate an addition of the oxyallyl **C1** to the C2—C3 bond of **2**. The other dimer may have structure **19**, which would arise from oxyallyl **C1** addition to the cyclopropanone carbonyl, a mode previously seen in the dimerization of 2,2-dimethylcyclopropanone (24).



18



19

Concluding discussion

The formation of *cis*-di-*tert*-butylcyclopropanone **2** from the acyclic precursor **1** provides a complete verification of the predicted mechanism shown in eq. [1]. Föhlisch et al. (25) previously used a related analysis to rationalize the formation of *cis*-2,3-dimethylcyclopropanone hemiacetal from the reaction of 2-chloro-3-pentanone in methoxide–methanol (Favorski conditions).

A detailed comparison of the bonding and spectroscopic properties in the *cis* and *trans* isomers **2** and **5** reveals the onset of a new type of σ-bond delocalization in the *cis*-**2**, e.g., a nonplanar carbonyl group is computed. This delocalization can potentially be found in any facially asymmetric cyclopropanone and further experiments are ongoing.

Cyclopropanone **2** is also shown to undergo stereospecific photochemical decarbonylation, a stringent test for this specificity given the steric strain in the *cis* alkene product. The overall sequence starting from dineopentyl ketone to give *cis*-1,2-di-*tert*-butylethene **9** can be made nearly stereospecific in a preparative sense, marred only by a competing photochemical isomerization of the *cis* to the *trans* alkene (ca. 5%).

Finally, **2** reacts with alcohols and in cycloaddition reactions as if the valence bond oxyallyl isomer **C1** were the reactive species. In the case of the reaction of alcohols with **2**, the initial adduct is an enol.

Experimental

Mass spectral and capillary GC measurements were carried out on a Hewlett–Packard model 5890 gas chromatograph equipped with a 5971 mass selective detector. Both split and direct on-column injections were used employing a 12 m × 0.2 mm i.d. OV-101 column. Preparative GC was done on an HP 5890A chromatograph employing a thermal conductivity detector and an 8 ft. × 4 mm i.d. column (3% OV-1, WHP-80/100). High-resolution mass spectra were obtained on a Kratos MS-80. NMR spectroscopy ($CDCl_3$ solution) was carried out on Bruker ACE-200, AMX-300, and AM-400 instruments (J in Hz, d = doublet, t = triplet). For $^{13}C\{^1H\}$ NMR, multiplicities were determined from DEPT 90 and 135 spectra. Two-dimensional spectra employed standard pulse sequences. For ^{17}O studies, the labelled dibromo ketone **1** was prepared by adding 15 μL of 20% $H_2{}^{17}O$ and excess Br_2 to a CCl_4 solution of the starting ketone (110 mg) and the closed mixture sonicated. External $H_2{}^{17}O$ was used as a reference for the ^{17}O NMR studies and the isolated dibromide **1** had δ 564. Infrared spectra were determined on a Mattson model 4030 interferometer.

Computational methods

The hybrid density functional (26) level B3LYP/6-31G** was used to calculate the optimized structures for **2** and **5**, employing the Gaussian 94 system of programs (27). NMR calculations employed the GIAO method, and the vibrational frequencies were scaled by a 0.95 factor. Energies and free energies were corrected for ZPVE contributions. Orbital plots were obtained by first importing the raw data into the Spartan program.[4] This latter program was also used for the AM1 and MM2 calculations.

Dibromo ketones

The solid diastereomer of **1** was prepared as described (5). The second diastereomer of **1** was obtained as a minor product (ca. 5–8%) of the direct bromination of **2**. A small sample (ca. 100 μg) was isolated by preparative GC and is apparently a liquid, ^1H NMR (400 MHz): 4.50 (2H), 1.20 (18H). The GC–MS pattern for this isomer is virtually identical to that of the major isomer.

3,5-Dibromo-2,2,3,6,6-pentamethylheptan-4-one ***3***

2,2,6,6-Tetramethylheptan-4-one, 1.24 g, 7.3 mmol, was added to LDA in THF (1.1 equiv.) at −78°C, warmed to −20°C, cooled to −78°C, followed by CH_3I (1.5 equiv.) addition and gradual warming to 20°C. After work-up the crude ketone (28) was directly brominated (sealed tube, excess Br_2 in CCl_4, 80°C, 24 h). Distillation of the residue gave two fractions: first, bp up to 52°C/10 Torr and second, >52°C/10 Torr. The second fraction was a nearly pure mixture of two diastereomers of the title compound (ca. 3:5 ratio of short retention: long retention isomers by GC analysis). ^1H NMR (400 MHz): 5.22 (major) and 4.91 (minor), 2.12 (minor) and 1.88 (major), 1.21–1.25 (overlapping *t*Bu peaks). Partial ^{13}C NMR (100 MHz): 83.3 (major) and 80.6 (minor), 59.7 (major) and 58.4 (minor).

cis-*2,3-Di*-tert-*butylcyclopropanone* ***2***

Dibromo ketone **1** (0.17 g, 0.52 mmol) in 1 mL of dry methylene chloride was added dropwise by syringe into a stirred solution of $PPN^+Cr(CO)_4NO^-$ (0.40 g, 0.54 mmol) (29) in 1 mL of dry methylene chloride. The latter solution was contained in a small Schlenk tube protected with a septum, was prepared under an N_2 atmosphere and was cooled to −78°C. After 20 min, 15 mL of dry, but not deoxygenated, pentane was slowly added by syringe, keeping the resulting mixture at −78°C. This mixture was stirred for a further 10 min, let stand for 30 min, and the supernatant transferred by double-ended

[4] Spartan. Wavefunciton Inc., Irvine, Calif.

© 1997 NRC Canada

Can. J. Chem. Downloaded from www.nrcresearchpress.com by 88.146.161.215 on 09/08/12
For personal use only.

needle to a clean Schlenk tube also equipped with a septum. The solvent was evaporated at ca. −40 to −50°C under vacuum (ca. 0.01 Torr) to leave a waxy solid. This residue was redissolved in 5 mL of pentane (at ca. −50°C), the solution let stand for 10 min and then filtered by quickly drawing the cold solution into a syringe, replacing the needle with one fitted with a Spartan 3 filter, and then reintroducing the filtered solution into a clean Schlenk tube. The solvent was evaporated as above to leave a solid residue. The septum was removed and a fitted sublimation cold finger was attached, a vacuum of 0.01 Torr was applied, Dry Ice – acetone was added to the cold finger, and the cooling bath temperature was slowly raised to about −20°C and then quickly to 0°C where the material sublimed onto the cold finger surface as white needles. The solid was washed off the cold finger with 3 mL of cold pentane and the solvent removed as above to yield 0.090 g (ca. quantitative) of the title ketone. The ^{1}H NMR spectrum indicates that the material is very nearly pure. ^{1}H NMR (400 MHz): 3.04 (2H), 1.01 (18 H). ^{13}C NMR (100 MHz, −40°C): 212.3 (C═O), 47.1 (CH), 31.2 (C), 29.9 (CH_3). ^{17}O NMR (40.7 MHz) 487. IR: 1818.5 and 1791.5 cm^{-1}, the latter about twice the intensity of the former. An IR spectrum is particularly useful for detecting the presence of $Cr(CO)_4NOBr$, which has a very strong band at 2067 cm^{-1}. The IR spectrum of **2** isolated by the above procedure is essentially free of this peak.

cis-*2,3-Di*-tert-*butyl-2-methylcyclopropanone* ***4***

This compound was not isolated in pure form because solutions of this ketone rearrange to **6** at −30°C. It was possible to conduct a partial purification of **4** by following the procedure described for isolating **2**. After decanting a pentane–CD_2Cl_2 solution of **4** from residual solid, the solvent was removed by vacuum distillation at < −50°C and the residue then taken up in fresh solvent. ^{1}H NMR experiments showed that the material still consisted mainly of **4**. ^{1}H NMR (400 MHz, CD_2Cl_2, −80°C): 2.66 (1H), 1.49 (3H), 0.97 (9H), 0.92 (9H). ^{13}C NMR (100 MHz, CD_2Cl_2, −80°C): 217.0 (C═O), 51.9 (CH, this value in $(CD_3)_2CO$ since it is obscured by solvent peaks in CD_2Cl_2), 50.5 (C), 32.2 (C), 31.3 (C), 29.9 (CH_3 of *t*Bu), 27.7 (CH_3 of *t*Bu), 23.0 (CH_3).

Photolysis experiments

A Westinghouse 275-W Sunlamp was used as a light source. To monitor the reaction progress, the photolysis of **2** was carried out in deuterated solvents in 5 mm NMR tubes. Acetone-d_6 and $CDCl_3$ were both used. Normally the NMR tube was photolyzed while immersed in ice water. Both quartz and Pyrex NMR tubes were used and gave similar results. Low-wavelength filtering was also tried, aqueous $SnCl_2$–HCl at 0°C and acetone – Dry Ice at −78°C. The latter conditions gave a *cis/trans* alkene ratio of better than 95:5 at the point where **2** had just been consumed. The photolysis kinetics were determined by NMR monitoring vs. time, using a rigid positioning of the NMR tube and light source. Cyclopropanone **4** is unstable above −30°C and was photolyzed at −78°C in acetone-d_6. The alkene products were isolated by preparative GC; **8** (11), **9** (11), **10** (30), and **11** (30) have all been reported previously.

Kinetics of the 2 → 5 rearrangement

Initial studies in $CDCl_3$ (^{1}H NMR detection) showed measurable rearrangement rates at 50°C and these were also quite clean reactions. However, we decided to use toluene-d_8 (degassed by N_2 purging) as solvent in order to be assured that no acid catalysis was possible. These rates were slower and could be conveniently carried out at 80°C ($t_{1/2}$ ca. 1.5 h); however, the reaction was not quantitative, and in addition to the product **5** peak, there were small peaks at 0.74, 0.87, and 0.94 ppm, combined area ca. 15%, presumably due to *t*Bu groups in by-products. The fact that these by-products were not produced in the lower temperature $CDCl_3$ solution reaction suggests that other minor thermal pathways are present and that these are more important at higher temperatures, or that toluene is partly reactive. Kinetic experiments were performed in 5 mm NMR tubes. Experiments with a PTFE insert did not change the results (no surface catalysis by the glass). Since competing reactions were diverting some of the **2** concentration, it was not possible to use the **2** + **5** ^{1}H NMR areas as a constant, and we therefore used the residual ^{1}H methyl signal of the toluene as a convenient integration standard to measure the increase per time in the concentration of **5**. The NMR tube was kept at 80.0 ± 0.1°C for a series of time intervals (about 10), the tube solution being quenched each time in cold water and the ^{1}H NMR spectrum quickly measured at ambient temperature. The rate of increase of the *trans*-**5** CH peak was used in the first-order kinetic plot. Experiments were also conducted with widely varying concentrations of initial **2** to confirm the first-order kinetics.

Alcohol and water adducts 13 and 14

When a large excess of methanol was added to a $CDCl_3$ solution of **2**, a new compound immediately formed, as shown by ^{1}H NMR. ^{1}H NMR (200 MHz): 4.77 (d, 1.5, 1H), 4.12 (d, 1.5, 1H), 3.27 (3H), 1.12 (9H), 0.88 (9H). These peaks can be assigned to the enol **14** (R = CH_3). On standing, or by evaporating the solvents and redissolving the residue in $CDCl_3$, these peaks are replaced by ones at 3.35 (3H), 3.11 (1H), 2.48 and 2.37 (AB doublets, 17.5, 1H each), 1.04 (9H), 0.95 (9H). ^{13}C NMR (50 MHz): 95.8, 59.4, 52.0, 35.0, 30.5, 29.7, 26.5. These peaks are assignable to **13** (R = CH_3), previously reported by Greene and co-workers (7). There are minor **13** (R = CH_3) peaks in the initial spectra of **14** (R = CH_3).

Similar results were seen using 2-propanol. Addition of the latter (excess) to a $CDCl_3$ solution of **2** at −10°C led to a new set of NMR peaks; ^{1}H NMR (200 MHz): 5.00 (d, 1.3, 1H), 3.56 (heptet, 6.5, 1H), 0.88 (9H), and 1.12 (9H). One peak is presumed to be buried under the 2-propanol methine heptet and the isopropyl methyl peaks are obscured by the 2-propanol methyl peaks. These peaks remain constant over 4 h at −10°C and can be assigned to the enol **14** (R = iPr). After evaporating the solvents and redissolving the residue in $CDCl_3$, a new set of peaks are observed. ^{1}H NMR (200 MHz): 3.44 (heptet, 6, 1H), 3.26 (1H), 2.52 and 2.44 (AB doublets, 18.7, 1H each), 1.18 (d, 6, 3H), 1.15 (d, 6, 3H), 1.04 (9H), 0.94 (9H). ^{13}C NMR (100 MHz): 214.5, 91.2, 72.1, 51.7, 34.7, 30.3, 29.7, 26.7, 23.0, 21.3. These peaks can be assigned to **13** (R = iPr).

When benzyl alcohol was added to a $CDCl_3$ solution of **2** and left for 3 days at −10°C, a spectrum assignable to **13** (R = benzyl) was obtained. ^{1}H NMR (400 MHz): 7.3–7.4 (complex), 4.575 and 4.380 (both d, 11.5, 1H each), 3.35 (1H), 2.52 and 2.40 (AB doublets, 18.5, 1H each), 1.035 (9H), 0.98 (9H).

© 1997 NRC Canada

^{13}C NMR (100 MHz): 213, 138.9 (C), 128.4 (CH), 127.7 (CH), 93.2 (CH), 73.4 (CH_2), 52.2 (CH_2), 35.1 (C), 30.5 (C), 29.7 (CH_3), 26.7 (CH_3). GC–MS: 177 (15), 99 (15), 91 (100), 57 (50).

Cyclopropanone **2** solutions react rapidly with water to give a compound with an NMR spectrum very similar to **13** (R = CH_3, iPr, or benzyl), ^{1}H NMR (400 MHz): 3.85 (d, 7.5, 1H), 3.16 (d, 7.5, 1H), 2.53 (d, 14.5, 1H), 2.31 (d, 14.5, 1H), 1.04 (9H), 0.98 (9H). ^{13}C NMR (100 MHz): 200.1, 84.4, 54.5, 35.8, 32.0, 29.7, 26.4. These spectral data can be assigned to compound **13** (R = H), with the peak at 3.85 being the hydroxyl hydrogen.

Diene adducts 15, 16, and 17

A large excess of the diene was added to a solution of **2** (0.05–0.5 mmol scale). Two methods were used: (1) pure **2** in $CDCl_3$ solvent, and (2) the diene was added to the initial CH_2Cl_2 (or CD_2Cl_2) solution of **2** (see preparation of **2**) at −78°C, the pentane diluent was added, and, after decanting, the solution was stored at −10°C overnight. Evaporation of the solvent and excess diene gave good yields of the residual adducts (**15** and **16** are solids), which were characterized by NMR and GC–MS methods.

endo-*2,4-Di*-tert-*butyl-8-oxabicyclo[3.2.1]oct-6-en-3-one* ***15***: ^{1}H NMR (200 MHz): 6.28 (2H), 5.07 (d, 4, 2H), 2.60 (d, 4, 2H), 1.05 (18H). ^{13}C NMR (50 MHz): 205.8 (CO), 132.9 (CH), 80.7 (CH), 66.6 (CH), 31.2 (C), 29.0 (CH_3). GC–MS: 236 (M^+), 180 (35), 179 (45), 123 (30), 95 (35), 83 (100). HRMS, calcd. for $C_{15}H_{24}O_2$: 236.1776; found: 236.1770.

endo-*2,4-Di*-tert-*butylbicyclo[3.2.1]oct-6-en-3-one* ***16***: ^{1}H NMR (400 MHz): 6.00 (2H), 3.04 (d, 5, 2H), 2.31 (d, 1, 2H), 2.14 (pent, 5, 10, 1H), 1.82 (d, 10, 1H), 1.01 (18H). ^{13}C NMR (100 MHz): 135.0 (CH), 66.8 (CH), 49.2 (CH_2), 43.6 (CH), 32.8 (C), 28.9 (CH_3). GC–MS: 234 (40, M^+), 219 (50), 163 (45), 91 (60), 83 (65), 75 (90), 77 (100).

Minor *exo* isomer, partial ^{1}H NMR (400 MHz): 6.14 (2H), 2.81 (d, 5, 2H), 1.03 (9H). Partial ^{13}C NMR (100 MHz): 138.7 (CH), 64.5 (CH), 40.5 (CH), 28.2 (CH_3). The GC–MS fragmentation was nearly identical to that of **16**.

cis-*2,7-Di*-tert-*butyl-4,5-dimethylcyclohept-4-enone* ***17***: ^{1}H NMR (400 MHz): 1.9–2.15 (ABC × 2, 6H), 1.78 (d, 0.6, 6H), 1.00 (18H). ^{13}C NMR (100 MHz): 217.5 (CO), 131.2 (C), 64.2 (CH), 35.8 (CH_2), 33.0 (C), 27.6 (CH_3), 20.8 (CH_3). GC–MS: 250 (M^+), 193 (20), 99 (40), 57 (100), 41 (50). HRMS; calcd. for $C_{17}H_{30}O$: 250.2289; found: 250.2297.

Cyclopropanone **2** on storage at ca. −20°C for several weeks is gradually destroyed. Two prominent GC–MS peaks, which correspond to dimers of **2**, are observed from the residual material, although many minor peaks are also present and considerable insoluble material is formed. These dimers can be separated by TLC or preparative GC.

Short-retention dimer ***19***: ^{1}H NMR (400 MHz): 4.40 (1H), 4.08 (1H), 1.16 (9H), 1.10 (9H), 1.07 (9H), 0.965 (9H), 0.96 (2H). Partial ^{13}C NMR (100 MHz): 147.7 (C), 110.1 (CH), 100.1 (C), 87.0 (CH), 39.7, 35.3, 31.6, 30.6, 31.5 (CH_3 × 6), 30.7 (CH_3 × 3), 25.5 (CH_3 × 3). GC–MS, *m/z*: 336 (M^+), 280, 279 (80), 151 (75), 111 (100).

Long-retention dimer ***18***: ^{1}H NMR (400 MHz), 4.39 (1H), 3.90 (1H), 2.55 (1H), 2.28 (1H), 1.16 (9H), 1.145 (9H), 1.04 (9H), 0.94 (9H). COSYDFQ: small coupling between 2.55 and 2.28 peaks, NOESY: interactions between 1.16–4.40, 1.145–3.90, 1.04–2.55 and 2.28, 0.94–2.55 and 2.28, 4.39–2.55. GC–MS, *m/z*: 336 (M^+), 321, 265, 223, 195, 167 (95), 57 (100). HRMS, calcd. for $C_{22}H_{40}O_2$: 336.302830; found: 336.3009.

Acknowledgement

We thank the Natural Sciences and Engineering Research Council of Canada for financial support.

References

1. C. Black, P. Lario, A.P. Masters, and F. Sun. Can. J. Chem. **71**, 1910 (1993).
2. T.S. Sorensen and F. Sun. J. Am. Chem. Soc. **117**, 5592 (1995).
3. T.S. Sorensen and F. Sun. Can. J. Chem. **74**, 79 (1996).
4. A.P. Masters, M. Parvez, T.S. Sorensen, and F. Sun. J. Am. Chem. Soc. **116**, 2804 (1994).
5. J. Ciabattoni and E.C. Nathan III. J. Am. Chem. Soc. **91**, 4766 (1969).
6. J.K. Crandall, W.W. Conover, J.B. Komin, and W.H. Machleder. J. Org. Chem. **39**, 1723 (1974).
7. J.F. Pazos, J.G. Pacifici, G.O. Pierson, D.B. Sclove, and F.D. Greene. J. Org. Chem. **39**, 1990 (1994).
8. G.S. Zaitseva, I.F. Lutsenko, A.V. Kisin, Yu. I. Baukov, and J. Lorberth. J. Organomet. Chem. **345**, 253 (1988).
9. G.S. Zaitzeva, A.V. Kisin, E.N. Fedorenko, V.M. Nosova, L.I. Livantsova, and Yu. I. Baukov. Zh. Obshch. Khim. **57**, 2049 (1987).
10. A. Rauk. Orbital interaction theory of organic chemistry. John Wiley and Sons, Toronto. 1994.
11. R.B. Turner, D.E. Nettleton, and M. Perelman. J. Am. Chem. Soc. **80**, 1430 (1958).
12. H.J. Rodriguez, J.-C. Chang, and T.F. Thomas. J. Am. Chem. Soc. **98**, 2027 (1976).
13. S. Yamabe, T. Minato, and Y. Osamura. J. Am. Chem. Soc. **101**, 4525 (1979).
14. N.M. Weinshenker and F.D. Greene. J. Am. Chem. Soc. **90**, 506 (1968).
15. S. J. Cianciosi, N. Ragunathan, T.B. Freedman, L.A. Nafie, and J.E. Baldwin. J. Am. Chem. Soc. **112**, 8204 (1990), and references therein.
16. D.B. Sclove, J.F. Pazos, R.L. Camp, and F.D. Greene. J. Am. Chem. Soc. **92**, 7488 (1970).
17. D. Lim, D.A. Hrovat, W.T. Borden, and W.L. Jorgensen. J. Am. Chem. Soc. **116**, 3494 (1994).
18. J. March. Advanced organic chemistry. 4th ed. John Wiley and Sons, Toronto. 1992. p. 1082.
19. J.G. Burr, Jr. and M.J.S. Dewar. Can. J. Chem. **32**, 1201 (1954).
20. G.V. Shustov, A.V. Kachanov, I.I. Chervin, R.G. Kostyanovsky, and A. Rauk. Can. J. Chem. **72**, 279 (1994).
21. N.J. Turro. Acc. Chem. Res. **2**, 25 (1969), and refs. contained in this review.
22. N. Shimizu, M. Tanaka, and Y. Tsuno. J. Am. Chem. Soc. **104**, 1330 (1982).
23. H.M.R. Hoffmann. Angew. Chem. Int. Ed. Engl. **23**, 1 (1984).
24. N.J. Turro, S.S. Edelson, J.R. Williams, T.R. Darling, and W.B. Hammond. J. Am. Chem. Soc. **91**, 2283 (1969).
25. B. Föhlisch, E. Gehrlach, J.J. Stezowski, P. Kollat, E. Martin, and W. Gottstein. Chem. Ber. **119**, 1661 (1986).
26. A.D. Becke. J. Chem. Phys. **98**, 5648 (1993).

© 1997 NRC Canada

Can. J. Chem. Downloaded from www.nrcresearchpress.com by 88.146.161.215 on 09/08/12
For personal use only.

27. M.J. Frisch, G.W. Trucks, H.B. Schlegel, P.M.W. Gill, B.G. Johnson, M.A. Robb, J.R. Cheeseman, T.A. Keith, G.A. Petersson, J.A. Montgomery, K. Rachavachari, M.A. Al-Laham, V.G. Zackrewski, J.V. Ortiz, J.B. Foresman, J. Cioslowski, B.B. Stefanov, A. Nanayakkara, M. Challacombe, C.Y. Peng, P.Y. Ayala, W. Chen, M.W. Wong, J.L. Andres, E.S. Replogle, R. Gomperts, R.L. Martin, D.J. Fox, J.S. Binkley, D.J. Defrees, J. Baker, J.P. Steward, M. Head-Gordon, C. Gonzales, and J.A. Pople. Gaussian 94 (Revision A.1). Gaussian Inc., Pittsburgh, Pa. 1995.
28. C. Lion and J.-E. Dubois. Tetrahedron, **31**, 1223 (1975).
29. D.R. Mantell and W.L. Gladfelter. J. Organomet. Chem. **347**, 333 (1988).
30. W.v.E. Doering, W.R. Roth, F. Bauer, R. Breuckmann, T. Ebbrecht, M. Herbold, R. Schmidt, H.-W. Lennartz, D. Lenoir, and R. Boese. Chem. Ber. **122**, 1263 (1989).

Can. J. Chem. Downloaded from www.nrcresearchpress.com by 88.146.161.215 on 09/08/12
For personal use only.

© 1997 NRC Canada

Theoretical study on naphthylphenylacetylenes for second-order nonlinear optical applications

B.V.V.S.N. Prabhakara Rao, S.C. Mathur, D.C. Dube, D.P. Tewari, and M. Banerjee

Abstract: The ground state dipole moments (μ_g), excited state dipole moments (μ_e), linear polarizabilities (α), first hyperpolarizabilities (β), and absorption maxima ($\hbar\omega_{eg}$) of a new series of 6,4′-disubstituted 2-naphthylphenylacetylenes have been calculated using the finite field – MNDO (Modified Neglect of Diatomic Overlap) technique and studied for second-order nonlinear optical (NLO) applications. Among all the molecules studied here, the strongest and the weakest electron donor/acceptor pairs [$N(CH_3)_2/NO_2$] and [CH_3/CN] exhibit the largest and the smallest β_μ (projection of β on the axis of the μ) of 46.3×10^{-30} esu and 10.2×10^{-30} esu, respectively. The coefficients of the power law that describes the dependence of α and β on the number of conjugated bonds (n) were calculated for $[NH_2/NO_2]_{n=1-5}$ and $[NH_2/CN]_{n=1-5}$ molecules. For β, exponents of 0.36 and 0.31 were obtained for $[NH_2/NO_2]_{n=1-5}$ and $[NH_2/CN]_{n=1-5}$ molecules, respectively, and for α, an exponent of 0.37 was obtained for both series of molecules. A comparison is made between naphthylphenylacetylenes and diphenylacetylenes on the basis of their hyperpolarizabilities.

Key words: nonlinear optics, organic molecules, hyperpolarizabilities.

Résumé : Utilisant une technique modifiée de négligence du recouvrement diatomique («MNDO») finie en fonction du champ, on a calculé les moments dipolaires de l'état fondamental (μ_g) et de l'état excité (μ_e) ainsi que les polarisabilités linéaires (α), les premières hyperpolarisabilités (β) et les maxima d'absorption ($\hbar\omega_{eg}$) d'une nouvelle série de 2-naphthylphénylacétylènes disubstitués en 6,4′ et on les a étudiés pour des applications optiques non linéaires (ONL) du deuxième ordre. Parmi les molécules examinées dans cette étude, les paires de donneur/accepteur d'électron les plus fortes et les plus faibles [$N(CH_3)_2/NO_2$] et [CH_3/CN] présentent respectivement les plus fortes et les plus faibles valeurs de β_μ (projection de β sur l'axe de μ), soit $46{,}3 \times 10^{-30}$ et $10{,}2 \times 10^{-30}$ esu. Utilisant les molécules $[NH_2/NO_2]_{n=1-5}$ et $[NH_2/CN]_{n=1-5}$, on a calculé les coefficients de la loi de puissance qui décrivent la relation de α et β avec le nombre de liaisons conjuguées (n). Pour β, on a obtenu des exposants de 0,36 et de 0,31 respectivement pour les molécules $[NH_2/NO_2]_{n=1-5}$ et $[NH_2/CN]_{n=1-5}$ alors que, pour α, on a obtenu un coefficient de 0,37 pour chacune de ces séries de molécules. En se basant sur leurs hyperpolarisabilités, on a effectué une comparaison entre les naphtylphényacétylènes et les diphénylacétylènes.

Mots clés : optique non linéaire, molécules organiques, hyperpolarisabilités.

[Traduit par la rédaction]

Introduction

Designing novel organic materials for second-order NLO applications such as frequency conversion and optical signal processing has generated immense interest due to their fast and high nonlinearities, high damage thresholds, and unlimited flexibility in chemical modifications (1–3). The macroscopic properties (frequency doubling or second harmonic generation) of the organic materials can be estimated from the microscopic properties (second-order polarizability) of individual molecules, with noncentrosymmetry as a prerequisite condition. Molecular design (4–8) has proven to be a very useful tool in determining the microscopic properties, in reproducing the experimental trends, and in understanding the NLO properties of new materials.

The most promising candidates for first hyperpolarizabilities (β) are molecules with strong electron donors/acceptors ([D/A]) on opposite ends that exhibit intramolecular charge transfer (ICT) interactions in the extended conjugated framework (9–14). Derivatives of 4-nitroaniline and *N,N*-dimethyl-4-nitroaniline are typical examples.

Adequate experimental and theoretical data are available on diphenylacetylenes (15–19) (Fig. 1*a*), which has led to good understanding of their NLO properties, whereas the available literature on naphthylphenylacetylenes (Fig. 1*b*) is very limited. Wong and Nicoud have recently reported (20) two new

Received January 6, 1997.

B.V.S.N. Prabhakara Rao, D.C. Dube,[1] and D.P. Tewari. Department of Physics, Indian Institute of Technology, New Delhi-110 016, India.
S.C. Mathur. Research Centre for Optical Physics, Department of Physics, University of Hampton, Hampton, Virginia, VA 23668, U.S.A.
M. Banerjee. Department of Chemistry, University of Burdwan, Burdwan-713 104, India.

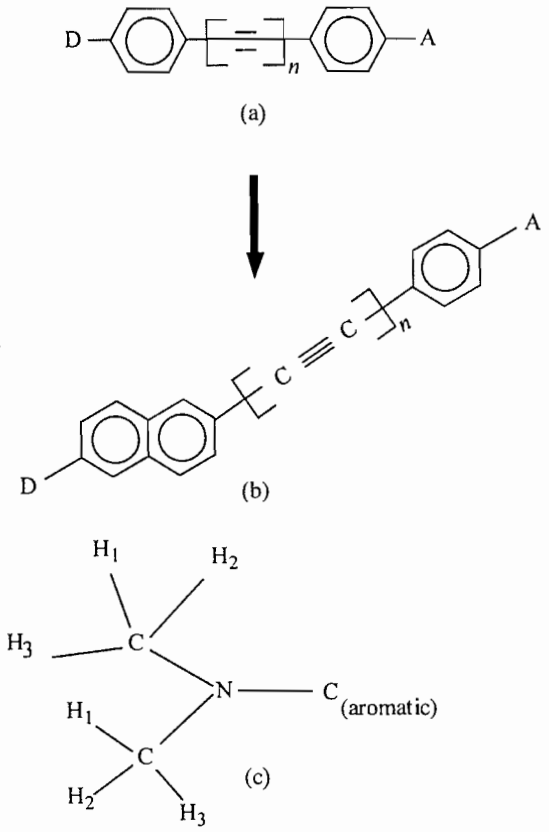
[1] Author to whom correspondence may be addressed. Telephone: 666-979, ext. 7322. Fax: 91-11-686-2037. E-mail: dcdube@physics.iitd.ernet.in

© 1997 NRC Canada

Can. J. Chem. Downloaded from www.nrcresearchpress.com by 88.146.161.215 on 09/08/12
For personal use only.

Can. J. Chem. Downloaded from www.nrcresearchpress.com by 88.146.161.215 on 09/08/12
For personal use only.

Fig. 1. (*a*) Molecular structure of the diphenylacetylenes; (*b*) molecular structure of the 6,4′ disubstituted 2-naphthylphenylacetylenes. **D**: electron donors; **A**: electron acceptors; and (*c*) orientation of the dimethylamino donor group ($N(CH_3)_2$).



classes of organic molecules (6,4′-disubstituted-2-naphthylphenylacetylenes and racemic 6,6′-bis(phenylethynyl)-1,1′-binaphthyls) for NLO applications.

That the main interest turns on naphthylphenylacetylenes is due to the following: (*i*) The limited experimental results (20) on these molecules showed a red shift in their absorption maxima when compared to diphenylacetylenes. This shows that there is an effective conjugation between the naphthalene moiety and the rest of the unsaturated system. Hence, one can anticipate a good charge transfer from donor to the acceptor through the conjugated bridge. (*ii*) There is an increase in conjugation length in these molecules when compared to diphenylacetylenes. These two factors will result in increasing β in naphthylphenylacetylenes. Moreover, the preliminary theoretical (AM1/FF) results (20) showed that β_μ for 6-methoxy-4′-nitronaphthylphenylacetylene is 29×10^{-30} esu, which is substantially greater than that of 4-methoxy-4′-nitrodiphenylacetylene ($\beta_\mu = 15 \times 10^{-30}$ esu).

Hence, in the present work, 6,4′-disubstituted 2-naphthylphenylacetylenes (Fig. 1*b*) have been studied for NLO applications by selective addition of different donor/acceptor groups. The electron [D/A] groups considered for the present studies are the following:

Donors(D) : $N(CH_3)_2$, NH_2, OCH_3, OH, CH_3
Acceptors(A) : NO_2, COOH, CHO, CN

Further, the studies have been extended to observe the effect of an increase in conjugation length (*n*) on μ, α, and β. The calculated hyperpolarizabilities of naphthylphenylacetylenes and diphenylacetylenes have been compared and the results discussed.

Method of calculations

The calculations of μ, α, β, and $\hbar\omega_{eg}$ were made with the MOPAC 5.0 (21) program using the MNDO (Modified Neglect of Diatomic Overlap) Hamiltonian and a finite-field approach (21–23). In this finite-field approach, the dipole moment, μ, of a molecule in the presence of a homogeneous electric field, E_i, can be expanded in a Taylor series in terms of the electric field

$$[1] \quad \mu_i = \mu_{i0} + \Sigma\, \alpha_{ij} E_j + 1/2\, \Sigma\, \beta_{ijk}\, E_j\, E_k + \ldots\ldots$$

where μ_{i0} is the *i*th component of the permanent dipole moment μ_0, and the tensors α_{ij} and β_{ijk} stand for the polarizability and first hyperpolarizability. The tensors α_{ij} and β_{ijk} are obtained by numerical differentiation of the dipole moment with respect to the electric field components in the limit of zero field (23).

The reliability of the model can be justified since it has been applied to a variety of molecules (19, 23–27) and the results are reasonably accurate. A number of authors have applied the finite field – MNDO technique to calculating linear polarizabilities and hyperpolarizabilities of small molecules (25), substituted benzenes (23), π-electron polycyclic hydrocarbons (24, 26), substituted stilbenes (27), and diphenylacetylenes (19). The details of the justification of model reliability are described elsewhere (28).

However, concerning the accuracy of the theoretical values, the ultimate verification of results will be given by experiment only. The aim of this work is to compare a series of related molecules and to establish reliable trends rather than attempting to predict their absolute hyperpolarizabilities; hence the approach adopted here remains meaningful.

The key words used in the MOPAC package (21) for calculating excited state dipole moment (μ_e) and absorption maxima ($\hbar\omega_{eg}$) are MNDO 1SCF MECI SINGLET ROOT = 2 C.I. = 4. Configuration interaction calculations are performed using the 36 lowest configurations derived from all excitations from the 4 highest occupied orbitals to the 4 lowest unoccupied orbitals. The absorption maxima are evaluated from the difference in energies between ground state (S_o) and first excited singlet state (S_1).

Since β is sensitive to the geometrical structure (24, 29) of the molecules, the geometry optimization has been done for all the molecules by keeping planar conformations. The present calculations were carried out at the field strength of 10^8 V/m for achieving self-consistency in the calculations.

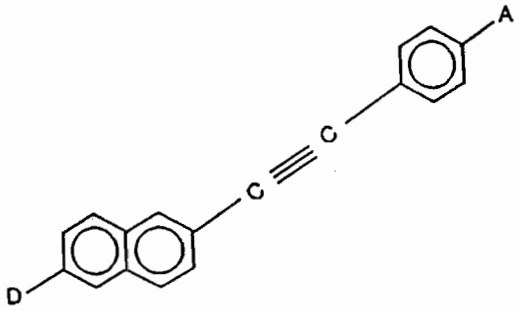
Throughout this paper, the dipole moments (μ_g and μ_e) are expressed in debye (D) units and absorption maxima ($\hbar\omega_{eg}$) are expressed in eV. The average linear polarizabilities are expressed in cubic angstroms ($Å^3$) and can be defined by the expression:

$$[2] \quad \langle\alpha\rangle = \frac{1}{3}(\alpha_{xx} + \alpha_{yy} + \alpha_{zz})$$

© 1997 NRC Canada

Can. J. Chem. Downloaded from www.nrcresearchpress.com by 88.146.161.215 on 09/08/12
For personal use only.

Table 1. Computed electronic properties of naphthylphenylacetylenes.[a]



D	A	μ_g	$\Delta\mu$	$\hbar\omega_{eg}$	<α>	β_μ
$N(CH_3)_2$	NO_2	8.9	8.1	3.28	38.3	46.3
NH_2	NO_2	9.0	7.6	3.28	35.0	39.2
OCH_3	NO_2	7.2	6.6	3.42	35.7	30.0
				(3.40)[b]		
OH	NO_2	6.8	6.3	3.43	33.6	27.2
				(3.36)[b]		
CH_3	NO_2	6.8	6.0	3.51	34.0	21.0
$N(CH_3)_2$	COOH	4.9	5.0	3.41	37.8	32.7
NH_2	COOH	5.2	4.5	3.41	34.4	30.0
OH	COOH	3.6	3.0	3.54	33.1	12.8
CH_3	COOH	2.9	3.4	3.61	33.6	11.0
$N(CH_3)_2$	CHO	5.4	4.8	3.42	37.3	31.2
NH_2	CHO	5.6	4.4	3.42	34.0	28.2
OCH_3	CHO	4.4	3.2	3.54	34.8	15.2
OH	CHO	4.1	2.8	3.55	32.6	12.3
CH_3	CHO	3.4	3.2	3.60	33.2	10.2
$N(CH_3)_2$	CN	6.1	5.0	3.41	37.8	32.4
NH_2	CN	6.2	4.8	3.41	34.3	29.0
OH	CN	4.1	3.3	3.53	33.2	16.0
				(3.59)[b]		
CH_3	CN	4.0	3.4	3.59	33.6	10.2

[a] μ_g and $\Delta\mu$ values are in D, the $\hbar\omega_{eg}$ (absorption maxima) values are in eV, the α values are in Å^3, and the β_μ values are in 10^{-30} esu.
[b] The experimental values were taken from ref. 20.

The first hyerpolarizabilities β_μ can be expressed as[2]

$$[3] \quad \beta_\mu = \frac{\beta.\mu}{\|\mu\|} = \frac{3/5\sum \beta_i\mu_i}{(\sum\mu_i^2)^{1/2}}$$

where component β_i is given by

$$[4] \quad \beta_i = \beta_{iii}\ 1/3 \sum (\beta_{jii} + 2\beta_{ij})$$

(with one atomic unit of $\beta = 8.63879 \times 10^{-33}$ esu)

Results and discussion

It is well known that the first hyperpolarizability (β) of organic molecules can be enhanced by increasing both [D/A] strengths and conjugation path length (30). The present series of molecules are obtained by replacing one of the benzene rings in diphenylacetylenes with naphthalene (Fig. 1*a*) and the position of the donor and acceptor are as shown in Fig. 1*b*.

The calculated ground state dipole moments (μ_g), differences between the excited state and ground state dipole moments ($\Delta\mu$), absorption maxima ($\hbar\omega_{eg}$), average linear polarizabilities (<α>), and first hyperpolarizabilities β_μ (calculated from eq. [3]) are presented in Table 1.

Dipole moment and linear polarizabilities

The substitution of different [D/A] pairs in the parent molecule [H/H] has shown a significant increase in the calculated μ. The [NH_2/NO_2] molecule possesses the largest dipole moment of 9.0 D and the molecule [CH_3/COOH] has shown the smallest dipole moment of 2.9 D. The μ values for the strongest donor, $N(CH_3)_2$, are slightly lower than those for the donor NH_2 for all acceptor (NO_2, COOH, CHO, and CN) combinations. This error obtained in the μ calculations may be interpreted as follows. All the molecules considered for the present studies were planar constrained, but in case of mole-

[2] In the EFISH experiment, the β component is measured along μ_g (the ground state dipole moment) of the molecule. Hence it is necessary to calculate the projection of β_{Vec} ($\sqrt{\beta_x^2+\beta_y^2+\beta_z^2}$) onto the axis of the μ_g, i.e., β_μ.

© 1997 NRC Canada

Can. J. Chem. Downloaded from www.nrcresearchpress.com by 88.146.161.215 on 09/08/12
For personal use only.

cules with the $N(CH_3)_2$ donor group, the torsional angles for H_1-C-N-$C_{aromatic}$, H_2-C-N-$C_{aromatic}$, and H_3-C-N-$C_{aromatic}$ (Fig. 1*c*) were fixed with −60°, +60°, and 180°, and these angles were obtained from AM1 optimized geometries. This orientation at the MNDO level of approximation might have resulted in an error in the μ values.

As the acceptor strength decreases from COOH to CN, the calculated μ increases for almost all the donors. This indicates that the intramolecular charge transfer (ICT), which influences the μ, in the ground state is stronger for the CN group than for CHO and COOH acceptor groups. A similar observation for disubstituted benzenes and styrenes has been reported for the MNDO-PM3 parametrization (15) and for experimental results (16, 17).

In the case of <α> (average polarizabilities), the values vary from 28.5 to 38.3 Å^3. The [D/A] pair [$N(CH_3)_2/NO_2$] exhibits the largest <α> of 38.3 Å^3. As expected, there is no appreciable variation in the calculated values of <α> with changing [D/A] strengths. This suggests that the linear polarizability (α) is purely a function of electron density and does not depend on polarity or charge transfer (31, 32).

First hyperpolarizabilities

Based on the present theoretical calculations of β, the following observations may be noted:

(*i*) The substitution of different [D/A] groups, which drastically enhanced the value of β_μ (0.12×10^{-30} esu) of the parent molecule ([H/H]).

(*ii*) The hyperpolarizabilities increase with increasing [D/A] strength and the molecule [$N(CH_3)_2/NO_2$] exhibits the largest β_μ (46.3×10^{-30} esu) followed by [NH_2/NO_2] with $\beta_\mu = 39.2 \times 10^{-30}$ esu, and the molecule [CH_3/CN] exhibiting the smallest β_μ (10.2×10^{-30} esu). A possible reason for exhibiting high β_μ values in $N(CH_3)_2$ and NH_2 donor combination molecules as compared to other donor combination molecules may be explained as follows. The connecting atom in all the donors except dimethylamino and amino is sp^3 hybridized and the tetrahedral geometry does not allow efficient overlap between the lone pair containing donor orbitals and the π-orbitals of the naphthalene ring. This causes maximum intramolecular charge transfer from donor to acceptor in $N(CH_3)_2$ and NH_2 donor molecules (33).

(*iii*) The present series of molecules possess nearly equal average linear polarizabilities, whereas β_μ varies by almost a factor of 5 from [$N(CH_3)_2/NO_2$] to [CH_3/CN].

From the present β calculations, the following ranking of efficiency of donor groups of the naphthylphenylacetylene series can be established:

$N(CH_3)_2 > NH_2 > OCH_3 > OH > CH_3$

This order is comparable to the ranking in strength of the same donor groups for *para*-disubstituted benzene derivatives, push–pull nitrotolans, nitrostilbenes, and hydrazone derivatives (19, 29, 34). In the case of acceptor groups, the nitro group is an effective acceptor due to its proper hybridization having an effective overlap with the *p*-orbitals of the benzene ring. A weak acceptor like the CN group is found to be comparable to the other COOH and CHO acceptor groups and a similar trend has also been observed in the case of carotenoids (35). Among the acceptor groups, the following ranking of efficiency can be established:

$NO_2 > COOH > CHO \geq CN$

Moreover, the hyperpolarizabilities of naphthylphenylacetylenes obtained from the present calculations are superior to two well known classic donor–acceptor systems, e.g., 4-nitroaniline and *N,N*-dimethyl-4-nitroaniline (36), even in the case of a weak donor (CH_3) group. This suggests a strong interaction between donor and acceptor groups in the present series of molecules. Further, the present β_μ values follow the hypsochromic experimental trends when electron attracting cyano group is inserted at nitro group as in [OCH_3/NO_2], [OCH_3/CN] and [OH/NO_2], [OH/CN] (shown in Table 1).

Relationship between electronic properties and first hyperpolarizability

According to the quantum mechanical two-level model (37, 38), the expression for second-order polarizability (β) is given by

$$[5] \quad \beta = \frac{3}{2} \frac{(\mu_{eg})^2 \Delta\mu}{(\hbar\omega_{eg})^2}$$

where μ_{eg} is the transition dipole moment. From the above expression, β can be enhanced by increasing $\Delta\mu$ and μ_{eg} and by decreasing $\hbar\omega_{eg}$. The above requirements can be achieved by changing [D/A] strengths and by increasing conjugation length.

The calculated $\Delta\mu$ and $\hbar\omega_{eg}$ values are presented in Table 1 and a relationship is established between β_μ, $\Delta\mu$, and $\hbar\omega_{eg}$. Indeed, understanding these relationships is very useful for the design of appropriate materials for nonlinear optics.

A good degree of linear relationship is obtained between β_μ and $\Delta\mu$ with a reasonable correlation coefficient ($r = 0.87$). The correlation factor obtained between β_μ and $(1/\hbar\omega_{eg})^2$ is 0.97. The correlation ($r = 0.86$) obtained between β_μ and $\Delta\mu/(\hbar\omega_{eg})^2$ strongly confirms that only $\hbar\omega_{eg}$ dominates the magnitude of β_μ in these molecules.

Effect of conjugation length

In principle, an increase in conjugation length (*n*) between an electronic donor and electronic acceptor causes an enhancement in second-order nonlinear response. A logarithmic relationship between *n* and β is usually assumed in both experimental (39, 40) and theoretical (41) studies, where the power law expression (eq. [6]) defines the exponential factor *k* and *C* is a constant:

$$[6] \quad \beta_\mu = Cn^k$$

The exponential factor (*k*) represents the efficiency of an increase in β with an increase in size of the molecule. Further, as the conjugation path length increases, there is a red shift in the absorption maxima ($\hbar\omega_{eg}$) and from the two-level model (eq. [5]) one can infer an increase in β.

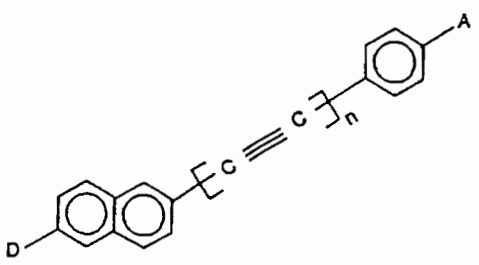
The present calculations have been carried out to explore the effect of increasing the conjugation length from $n = 1$ to $n = 5$ (triple bonds) on μ, <α>, and β for [NH_2/NO_2] and [NH_2/CN] molecules. The results are presented in Table 2.

In both molecules ([NH_2/NO_2] and [NH_2/CN]), the same trend is observed between conjugation length (*n*) and the calculated μ, α, and β. As can be noted from Table 2, there is no appreciable change in the calculated μ in passing from $n = 1$ to 5 triple bonds. However, α and β increase moderately with *n*.

© 1997 NRC Canada

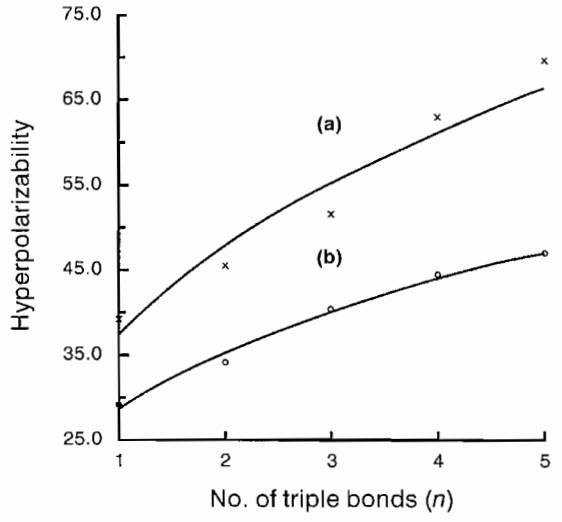
Can. J. Chem. Downloaded from www.nrcresearchpress.com by 88.146.161.215 on 09/08/12
For personal use only.

Table 2. Effect of conjugation length on the calculated μ (D), <α> (Å^3), and β_μ (10^{-30} esu) values for the [NH_2/NO_2] and [NH_2/CN] molecules.



	D	A	μ	<α>	β_μ
1	NH_2	NO_2	9.0	35.0	39.2
2	NH_2	NO_2	9.3	41.5	45.4
3	NH_2	NO_2	9.5	48.6	51.5
4	NH_2	NO_2	9.8	56.6	62.9
5	NH_2	NO_2	9.9	64.6	69.6
1	NH_2	CN	6.2	34.3	29.0
2	NH_2	CN	6.5	40.9	34.1
3	NH_2	CN	6.6	47.9	40.3
4	NH_2	CN	6.7	55.7	44.5
5	NH_2	CN	6.8	63.8	47.0

Fig. 2. Plot of hyperpolarizability versus the number of triple bonds (*n*) for (*a*) [NH_2/NO_2] and (*b*) [NH_2/CN] molecules.



The *n* dependence of the calculated β (Fig. 2) is $k = 0.36$ and 0.31 for $[NH_2/NO_2]_{n=1-5}$ and $[NH_2/CN]_{n=1-5}$ molecules, respectively. The β dependence on *n* is small and suggests that charge transfer via the conjugated system is ineffective for increasing β. In case of α, the power coefficient (*k*) is 0.37 for both series ($[NH_2/NO_2]_n$ and $[NH_2/CN]_n$) of molecules and suggests that α is independent of the strength of the donor or acceptor groups.

Table 3. Comparison between naphthylphenylacetylenes and diphenylacetylenes.[a]

[D/A]	μ_g (D)	$\Delta\mu$ (D)	$\hbar\omega_{eg}$ (eV)	<α> (Å^3)	β_μ (10^{-30} esu)
[NH_2/NO_2]	9.0 (9.0)	21.7 (23.8)	3.53 (3.86)	35.0 (27.6)	39.2 (35.4)
[NH_2/CN]	6.2 (6.3)	16.0 (18.5)	3.60 (3.98)	34.3 (26.9)	29.0 (24.8)
[OH/NO_2]	6.8 (6.7)	20.9 (19.1)	3.67 (3.65)	33.6 (26.1)	27.2 (21.6)
[OH/CN]	4.1 (4.1)	11.9 (11.5)	3.79 (3.76)	33.2 (25.7)	16.0 (13.3)
[CH_3/NO_2]	6.8 (6.6)	22.2 (15.7)	3.72 (4.10)	34.0 (26.5)	21.0 (15.1)
[CH_3/CN]	4.0 (3.9)	13.0 (8.3)	3.83 (3.84)	33.6 (26.1)	10.2 (7.8)

[a]The values for diphenylacetylenes are given in parentheses.

Comparison between diphenylacetylenes and naphthylphenylacetylenes

The results obtained from the present calculations for diphenylacetylenes and naphthylphenylacetylenes have been compared. It can be seen from Table 3 that the calculated β_μ values of naphthylphenylacetylenes are larger than those for diphenylacetylenes in all [D/A] molecules; however, the increment may not be appreciable. The reason for this small increment may be interpreted as follows. Although there is an increase in the effective conjugation path length between the donor and acceptor of the present series of molecules as compared to diphenylacetylenes, as far as charge transfer is concerned, the naphthalene ring may not be as efficient as the phenyl ring (42).

The present results on naphthylphenylacetylene clearly show a red shift in the absorption maxima as compared to their diphenylacetylene analogues. These trends are consistent with the experimental results (20). In general, a red shift indicates a better charge asymmetry in the π-conjugated systems and leads to higher second-order polarizabilities. A simple electron-in-a-box model also indicates that the excitations of naphthalene are more red shifted than those of benzene. Hence from the two-level model one can expect that the naphthalene would indeed exhibit more nonlinearity than benzene.

The introduction of a naphthalene moiety in the backbone of a classical [D/A] diphenylacetylene molecule leads to a nonlinear shape of the molecule. Hence this may enhance the probability of forming a noncentrosymmetric structure in the case of naphthylphenylacetylenes, an essential condition for achieving second-order nonlinearity (43, 44).

Conclusions

We have calculated the dipole moments and hyper (linear) polarizabilities of a new series of naphthylphenylacetylene molecules. The results obtained clearly indicate that the hyperpolarizability is a function of [D/A] strengths,

© 1997 NRC Canada

effectiveness, and path length of conjugation in these molecules.

We obtained the coefficients of the power law (k) for β as follows: 0.36 and 0.31 for [NH_2/NO_2] and [NH_2/CN] molecules, respectively, and for α, 0.37 for both series of molecules. The result confirms that the efficiency of enhancing β (or α) with n is rather low. The present calculations show that replacement of a benzene by a naphthalene ring in diphenylacetylenes has a small effect in enhancing the hyperpolarizabilities of naphthylphenylacetylenes.

Acknowledgments

We express our gratitude to Professor Mark A. Ratner, Department of Chemistry, Northwestern University, Illinois, U.S.A. and Dr. Isabelle Ledoux, CNET, Bagneux, France, for their many useful suggestions. Fruitful discussions with Professor A.S.N. Murthy, Department of Chemistry, IIT, Delhi, are gratefully acknowledged. We also thank the Computer Services Center, IIT, Delhi, for providing facilities.

References

1. D.S. Chemla and J. Zyss (*Editors*). Nonlinear optical properties of organic molecules and crystals. Vols. 1 and 2. Academic Press, New York. 1987.
2. S.R. Marder, J.E. Sohn, and G.D. Stucky (*Editors*). Materials for nonlinear optics, chemical perspectives, ACS Symp. Ser. **455**, 1991.
3. J. Meisser, F. Kajzar, and P.N. Prasad. Organic molecules for nonlinear optics and photonics. Kluwer Academic Publishers, Dordecht. 1991.
4. D.R. Kanis, M.A. Ratner, and T.J. Marks. Chem. Rev. **94**, 195 (1994).
5. Y. Itoh, K. Oono, I. Isogai, and A. Kakuta. Mol. Cryst. Liq. Cryst. **170**, 259 (1989).
6. P.C. Leung, J. Stevens, R.E. Harlestead, M. Spiering, D.J. Gerbi, C.V. Francis, J.E. Trend, G.V. Tiers, G.T. Boyd, D.A. Ender, and R.C. Williams. Proc. SPIE-Int. Soc. Opt. Eng. **1147**, 48 (1989).
7. R. Sen, D. Majumdar, and S.P. Bhattacharyya. J. Phys. Chem. **97**, 7491 (1993).
8. H.S. Nalwa, T. Watanabe, and S. Miyata. Opt. Mater. (Amsterdam), **2**, 73 (1993).
9. D.J. Williams. Angew. Chem. Int. Ed. Engl. **23**, 690 (1984).
10. B.F. Levine. Chem. Phys. Lett. **37**, 516 (1976).
11. S.D. Bella, I.L. Fragala, M.A. Ratner, and T.J. Marks. J. Am. Chem. Soc. **115**, 682 (1993).
12. D. Pugh and J.O. Morley. *In* Nonlinear optical properties of organic molecules and crystals. Vols. 1 and 2. *Edited by* D.S. Chemla and J. Zyss. Academic Press, New York. 1987. p. 193.
13. J.O. Morley. Int. J. Quantum Chem. **46**, 19 (1993).
14. J.O. Morley. J. Chem. Soc. Faraday Trans. **87**, 3015 (1991).
15. N. Matsuzawa and D.A. Dixon. J. Phys. Chem. **96**, 6232 (1992).
16. E.M. Graham, V.M. Miskowski, J.W. Perry, D.R. Coulter, A.E. Stiegman, W.P. Schaefer, and R.E. Marsh. J. Am. Chem. Soc. **111**, 8771 (1989).
17. A.E Stiegman, E. Graham, K.J. Perry, L.R. Khundkar, L.T. Cheng, and J.W. Perry. J. Am. Chem. Soc. **113**, 7658 (1991).
18. C. Dehu, F. Meyers, and J.L. Bredas. J. Am. Chem. Soc. **115**, 6198 (1993).
19. M. Barzoukas, A. Fort, G. Klein, A. Boeglin, C. Serbutoviez, L. Oswald, and J.F. Nicoud. Chem. Phys. **153**, 457 (1991).
20. M.S. Wong and J.F. Nicoud. J. Chem. Soc. Chem. Commun. 249 (1994).
21. H.A. Kurtz, J.J.P. Stewart, and K.M. Dieter. J. Comput. Chem. **11**, 82 (1990).
22. M.J.S. Dewar and W. Thiel. J. Am. Chem. Soc. **99**, 4899 (1977).
23. G.R.J. Williams. J. Mol. Struct.(Theochem), **151**, 215 (1987).
24. M.M. Bader, T. Hameda, and A. Kakuta. J. Am. Chem. Soc. **114**, 6475 (1992).
25. A.K. Chandra and M. Banerjee. J. Mol. Struct. (Theochem), **83**, 261 (1991).
26. Y.J. Lu and S.L. Lee. Int. J. Quantum Chem. **44**, 773 (1992).
27. M. Barzoukas, A. Fort, G. Klein, C. Serutoviez, L. Oswald, and J.F. Nicoud. Chem. Phys. **164**, 395 (1992).
28. B.V.V.S.N. Prabhakara Rao, S.C. Mathur, D.C. Dube, D.P. Tewari, and M. Banerjee. Can. J. Chem. Submitted.
29. F. Meyers, C. Adant, and J.L. Bredas. J. Am. Chem. Soc. **113**, 3715 (1991).
30. K.Y. Wong, A.K.-Y. Jen, V.P. Rao, and K.J. Drost. Appl. Phys. B: Photophys. Laser Chem. **B61**, 191 (1995).
31. D. Li, T.J. Marks, and M.A. Ratner. J. Phys. Chem. **96**, 4325 (1992).
32. B.H. Cardelino, C.E. Moore, and R.E. Stickel. J. Phys. Chem. **95**, 8645 (1991).
33. L.-T. Cheng, W. Tam, G.R. Meredith, G.L.J.A. Rikken, and E.W. Meijer. Proc. SPIE-Int. Soc. Opt. Eng. **1147**, 61 (1989).
34. C. Serbutoviez, C. Bosshard, G. Knopfle, P. Wyss, P. Pretre, P. Gunter, K. Schenk, E. Solari, and G. Chapuis. Chem. Mater. **7**, 1198 (1995).
35. A. Salma-Schwok, M. Blanchard-Desce, and J.-M. Lehn. J. Phys. Chem. **94**, 3894 (1990).
36. A. Ulman, C.S. Willard, W. Kohler, D.R. Robello, D.J. Williams, and L. Handley. J. Am. Chem. Soc. **112**, 7083 (1990).
37. J.L. Oudar and D.S. Chemla. J. Chem. Phys. **66**, 2664 (1977).
38. J.L. Oudar. J. Chem. Phys. **67**, 446 (1977).
39. M. Barzoukas, M. Blanchard-Desce, D. Josse, J.-M. Lehn, and J. Zyss. Chem. Phys. **133**, 323 (1989).
40. R.A. Huijts and G.L.J. Hesselink. Chem. Phys. Lett. **156**, 209 (1989).
41. N. Matsuzawa and D.A. Dixon. Int. J. Quantum Chem. **44**, 497 (1992).
42. I.D.L. Albert, J.O. Morley, and D. Pugh. J. Phys. Chem. **99**, 8024 (1995).
43. G.R. Desiraju and T.S.R. Krishna. J. Chem. Soc. Chem. Commun. 192 (1988).
44. T. Kurihara, H. Tabei, and T. Kaino. J. Chem. Soc. Chem. Commun. 959 (1987).

Can. J. Chem. Downloaded from www.nrcresearchpress.com by 88.146.161.215 on 09/08/12
For personal use only.

© 1997 NRC Canada

Lanthanide catalysts for the hetero Diels–Alder reaction: effect of ligand structure and acidity

Claude Spino, Laurel L. Clouston, and David J. Berg

Abstract: A series of yttrium, ytterbium, and lanthanum hexa- or heptacoordinate complexes were prepared and their catalytic activities tested in the hetero Diels–Alder reaction between crotonaldehyde and ethyl vinyl ether. It was found that a pK_a below 7 of the ligand was necessary but not sufficient for catalytic activity. It was determined that the ligand should possess a perfluoromethyl-β-diketonate functionality. Other factors such as bite angle and hinging motion may also play a determining role.

Key words: lanthanide, catalyst, hetero Diels–Alder, yttrium, ytterbium, lanthanum.

Résumé : L'activité catalytique d'une série de complexes d'yttrium, d'ytterbium et de lanthanum fait à partir de ligands hexa ou heptadentates a été mesurée pour la réaction d'hétéro Diels–Alder entre la crotonaldéhyde et l'éthyl vinyl éther. Nous en avons conclus qu'un pK_a inférieur à 7 du ligand est nécessaire mais pas suffisant pour engendré une activité catalytique. Nous avons déterminé que le ligand doit posséder la fonctionalité perfluorométhyl β-dicétone. D'autres facteurs tel que l'angle de mordage et une action de type charnière des ligands peuvent aussi jouer un rôle déterminant.

Mots clés : lanthanide, catalyseur, Diels–Alder hétéro, yttrium, ytterbium, lanthanum.

Can. J. Chem. Downloaded from www.nrcresearchpress.com by 88.146.161.215 on 09/08/12
For personal use only.

The hetero Diels–Alder cycloaddition has proven extremely useful in the synthesis of a multitude of heterocycles (1). The cycloaddition of α,β-unsaturated aldehydes with electron-rich dienes such as vinyl ethers is in the forefront of hetero Diels–Alder reactions due to the importance and prevalence of the dihydropyran and tetrahydropyran (2) substructures contained in such natural compounds as sugars and polyether antibiotics (3, 4). Lanthanide(III) complexes have demonstrated clear effectiveness and mildness in catalyzing this and other reactions (1, 5). The prototypical case of crotonaldehyde reacting with ethyl vinyl ether under $Yb(fod)_3$ catalysis serves to demonstrate this point with an isolated yield greater than 95% of a single *endo* cycloadduct at room temperature (6). In comparison, the thermal reaction of crotonaldehyde and ethyl vinyl ether proceeds at 175°C in sealed tube conditions to give 87% of cycloadducts (7) whereas under high pressure conditions (15 kbar (1 bar = 100 kPa), 75°C, 24 h) one obtains 89% of the *endo* product (8). Also, stronger Lewis acids give reduced yields of product, presumably because of product decomposition (vide infra). We have ourselves observed the high tolerance of lanthanide catalysts for sensitive functional groups such as acetals, silyl ethers, and esters (9).

So far, though, the asymmetric catalysis of the hetero [4+2]-cycloaddition has met with only limited success (10), especially in the case of lanthanide catalysts (1, 10, 6*b*, 11). In the latter case, the lability of the chiral ligands may be partly to blame. As part of a project directed at the preparation of efficient chiral lanthanide catalysts, we initiated a study of the ligand effect on the catalytic activity of ytterbium, lanthanum, and yttrium complexes. The focus of the study was to determine if ligands other than perfluoro-β-diketones could confer catalytic activity on the lanthanide complexes so as to ease the preparation of effective chiral ligands. Also, to address the ligand lability issue, complexes with multidentate ligand systems were investigated. The study not only provided helpful and incisive information on necessary structural features of the ligand for catalytic activity, it also provided novel, air-stable, and effective yttrium and ytterbium catalysts for the hetero Diels–Alder reaction (12). The well-defined and characterized tripodal structures of these catalysts will provide a solid model from which to design and develop highly effective chiral catalysts. Their stability in air is a good indication of low ligand lability.

Figure 1 provides a list of the structural formula of the different ligands prepared or purchased. Compounds **1a–d**, **3a,b**, **7b**, and **7c** were purchased (available from Aldrich). Compound **2** is commercially available but was purchased as its ytterbium complex (Aldrich). Ligand **1e** was prepared as per Morris and Koob (13). Ligands **4a** (14), **4b**, and **5** (14) were prepared by refluxing tris(aminoethyl)amine and **1a**, **1b**, or **3b**, respectively, in benzene with azeotropic removal of water.

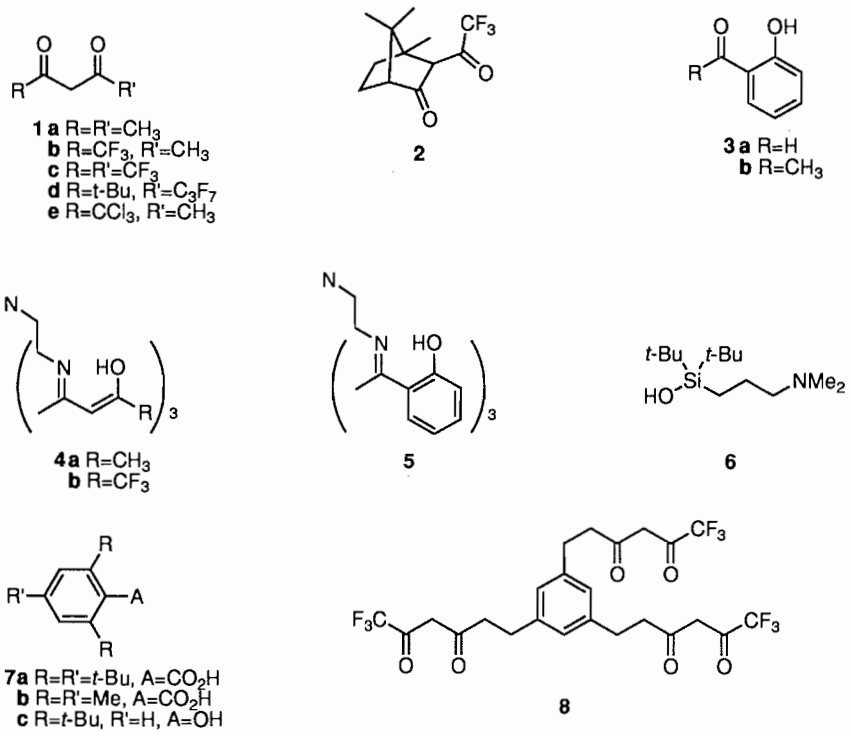
Received January 27, 1997.

C. Spino.[1] Département de chimie, Université de Sherbrooke, Sherbrooke, QC J1K 2R1, Canada.
L.L. Clouston and D.J. Berg.[1] Chemistry Department, University of Victoria, P.O. Box 3055, Victoria, BC V8W 3P6, Canada.

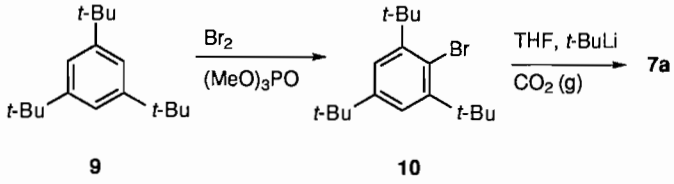
[1] Authors to whom correspondence may be addressed.
C.S.: Telephone: (819) 821-7087. Fax: (819) 821-8017.
Internet: jacs@structure.chimie.usherb.ca;
D.B.: Telephone: (604) 721-7161. Fax: (604) 721-7147.
Internet: dberg@uvic.ca

© 1997 NRC Canada

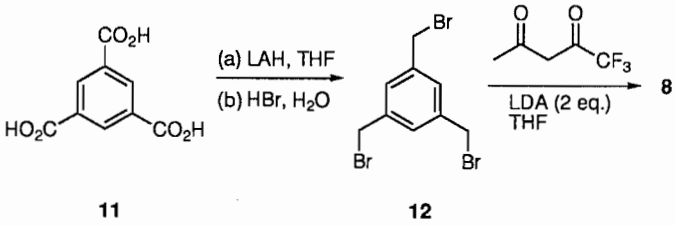
Fig. 1. Ligands tested as their lanthanide complexes.



Scheme 1.



Scheme 2.



Their purification was done by sublimation under reduced pressure. Compound **6** was prepared in four steps as described in the literature (15). Ligand **7a** was prepared by monobromination of 1,3,5-tri-*tert*-butylbenzene (16) followed by lithium–halogen exchange with *tert*-butyllithium in THF and quenching with gaseous carbon dioxide (Scheme 1) (17). Finally, ligand **8** was prepared by the reaction sequence shown in Scheme 2. Starting from 1,3,5-benzenetricarboxylic acid **11** using a one-pot procedure where the aluminium salts resulting from the reduction with LAH are directly treated with aqueous hydrobromic acid, we obtained an 80% yield of **12** (18). The dianion of 1,1,1-trifluoroacetylacetone was generated using slight modifications of a standard procedure (19). Though its reactivity was lower than that of non-fluorinated β-diketones, effective alkylation in THF at room temperature with tribromomesitylene **12** could be achieved. The tripodal ligand **8** was thus obtained in 40% yield after recrystallization and sublimation at 140°C / 10^{-2} Torr (1 Torr = 133.3 Pa).

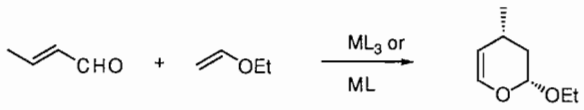
Except for the ytterbium complex of **2**, which was purchased (Aldrich), all other complexes were made by adding the ligand to a toluene solution of the lanthanide tris(bis(trimethylsilyl)amide) at 0°C (20). The complexes precipitated out from solution and were collected and sublimed whenever possible. When the reaction was carried out in THF or other coordinating solvents, the solution was first concentrated under reduced pressure to remove the solvent. Ytterbium complexes of **4a** (21), **5** (21), **6** (15) and the yttrium complex of **4b** were monomeric and characterized by single-crystal X-ray analysis.[2] The yttrium complexes **17a**, **17b**, and **19**·THF were shown to be monomeric by proton NMR spectroscopy. All other complexes were characterized by NMR (in the case of yttrium) and (or) by mass spectrometry and could be

[2] X-ray crystal data and tables of atomic coordinates, isotropic thermal equivalents, bond lengths and angles, torsion angles, and anisotropic displacement factors have been deposited and can be purchased from: The Depository of Unpublished Data, Document Delivery, CISTI, National Research Council Canada, Ottawa, Canada K1A 0S2. With the exception of the torsion angles and anisotropic displacement factors, this material has also been deposited with the Cambridge Crystallographic Data Centre, and can be obtained on request from The Director, Cambridge Crystallographic Data Centre, University Chemical Laboratory, 12 Union Road, Cambridge, CB2 1EZ, U.K.

© 1997 NRC Canada

Can. J. Chem. Downloaded from www.nrcresearchpress.com by 88.146.161.215 on 09/08/12
For personal use only.

Table 1. Reaction of crotonaldehyde with ethyl vinyl ether catalysed by the different lanthanide complexes.



13 14 15

Entry	L	pK_a of L	Ref.	M	Yield (%)[a]
1	**1a**	9	21*a*	Y, Yb	19
2	**1b**	6.3	21*a*	Y, Yb	86
3	**1c**	4.5	21*b*	Y, Yb	86
4	**1d**	5.1	21*c*	Yb	90
5	**1e**	8.5[b]		Y	17
6	**2**	6[c]		Yb	88
7	**3a**	8.2	21*a*	Yb	21
8	**3b**	10	21*a*	Yb	6
9	**4a**	12[c]		Y, Yb	9
10	**4b**	9[c]		Y, La	8
11	**5**	11	21*d*	Yb	0
12	**6**	13.6	21*e*	Y	0
13	**7a**	6.25	21*f*	Y, Yb	0
14	**7b**	5.25	21*g*	Y, Yb	0
15	**7c**	>11	21*h*	Y	0
16	**8**	6[c]		Y, Yb	96

[a]As measured by G.C.
[b]Measured in 40% dioxane/H_2O.
[c]Estimated.

oligomeric. β-Diketonate complexes of a variety of metals, including the lanthanides, are well known and mentioned throughout the literature (22–25). However, few β-diketonate lanthanide complexes have been rigorously characterized. The ytterbium complexes of **1d** (6), **4a** (21), **5** (21), and **6** (15) are known, while those of the remaining ligands are new. The yttrium complexes of all ligands except **1a** are new.

Starting from the observation that lanthanide complexes derived from β-diketone-type ligands are effective catalysts for the hetero Diels–Alder reaction, we initially believed that ligands such as **4a** and **5** would be well suited for our purpose, because they are heptadentate in nature, easily prepared (14), and easily altered for the eventuality of chiral design. Such tripodal ligands form stable complexes with lanthanides (21). In fact, the rationale for using these heptadentate ligands was to confer extra stability to the complex, in effect "locking" the ligand in place. Monomeric, tripodal structures would provide a solid base from which to design and develop highly effective chiral catalysts with well-defined coordination sites.

Catalytic activities were tested on the hetero Diels–Alder cycloaddition of crotonaldehyde **13** and ethyl vinyl ether **14**, the latter serving as solvent, with 2 mol% of catalyst (Table 1). Each reaction was monitored by GC at specific time intervals. As expected, the product isolated was regiochemically and diastereomerically pure (racemic) and was derived from the *endo* approach of the dienophile as verified by proton NMR (6). We were surprised to find that neither the yttrium nor the ytterbium complexes of **4a** and **5** displayed significant catalytic behaviour toward the cycloaddition reaction of crotonaldehyde and ethyl vinyl ether (Table 1, entries 9 and 11). Careful examination of the literature revealed that in fact only perfluoro-β-diketone-type ligands are known to be involved in the successful catalysis of the hetero Diels–Alder reaction by lanthanide complexes. We thus reasoned that lanthanide complexes of ligand **4b**, the 1,1,1-trifluoro analog of **4a**, should indeed catalyse the desired reaction. To our surprise, the yield of cycloadduct obtained with the yttrium and lanthanum complexes remained negligible even after several days (entry 10). Several factors could be responsible for this lack of activity and we suspected that either the imine nitrogens or the coordinating amine nitrogen could electronically saturate the metal thereby lowering its Lewis acidity.

The degree of Lewis acidity at the metal had to be established and therefore we began studying the effect of pK_a of the ligand on the catalytic activity of the resulting lanthanide complex. Although a direct correlation between the pK_a of the ligand and the Lewis acidity of the corresponding complex is only speculative, it is likely that a rough correlation exists among ligands of similar structure. We attempted to determine the Lewis acidity of some complexes by the method of Childs et al. using crotonaldehyde as the complexing agent (26). However, the low solubility of the catalysts in non-coordinating solvents precluded meaningful results.

$Yb(fod)_3$ is known to be a mild and effective catalyst for the hetero Diels–Alder reaction and it provided a reference point against which all other reactions were compared (6). The complexes having acac-type ligands with pK_a's lower than approximately 6.3 were effective as catalysts (Table 1, entries 2–4, and 6) (27). Other ligands with higher pK_a were less effective or ineffective in the time period studied (entries 1, 5, 7–15). Interestingly, there was no difference between the yttrium, ytterbium, and lanthanum complexes (entries 9–11, 13, 14, and 16). Yttrium and ytterbium have similar van der Waals radii and Lewis acidity but lanthanum is substantially larger and is a weaker Lewis acid. The high catalytic activity of the ytterbium complex of **2** suggests that steric bulk around the metal is not an important factor (entry 6). Complexes of ligands **3** gave modest catalytic activity in line with pK_a values (entries 7 and 8) and the complex of silanol **6** gave no activity at all (entry 12). A catalytic run was also performed with the yttrium complex of ligand **1a** in trifluoroethanol as solvent with no success. It therefore seems unlikely that the fluorines are playing a role other than simply lowering the pK_a of the diketone ligand.

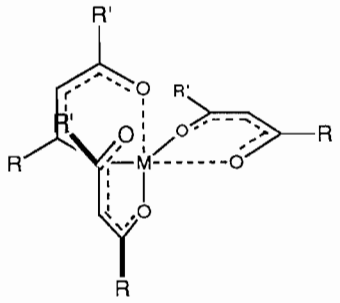
Confident that the Lewis acidity of the metal could be tuned by adjusting the pK_a of the ligand, we surmised that complexes of carboxylic acids would be efficient catalysts because of their low pK_a. We had in mind to eventually use linked amino acids to make chiral tripodal complexes of ytterbium and yttrium, thereby obtaining easy access to chiral catalysts. Before embarking on the synthesis of an elaborate ligand we decided to test the catalytic activity of the lanthanide complexes of acids **7**. The results were unequivocal: no catalysis whatsoever was observed (entries 13 and 14). All of the acids **7** have a pK_a below that of trifluoroacac **1b**. The Yb and Y complexes **17b** (Fig. 2) were tested to verify that the bulky *tert*-butyl groups in **17a** were not sterically blocking the active site; they were also inactive. Not surprisingly, the Y complex made with phenol **7c** did not lead to a better result (entry 15). Finally, the commercially available yttrium tris(hexanoate) was also screened and found to be inactive.

These results are reminders that the mechanism of catalysis

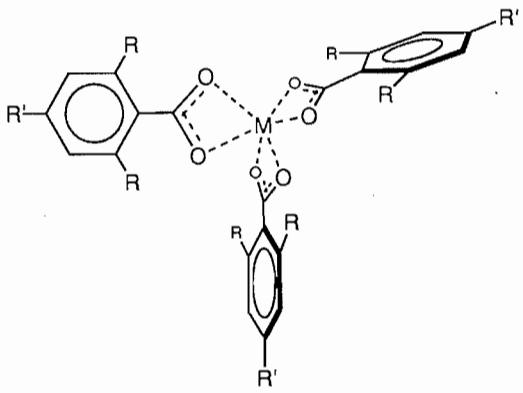
Can. J. Chem. Downloaded from www.nrcresearchpress.com by 88.146.161.215 on 09/08/12
For personal use only.

© 1997 NRC Canada

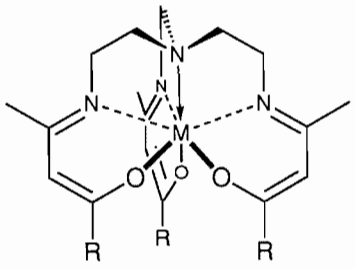
Fig. 2. Lanthanide complexes. No definite geometry intended for **17** and **19**.



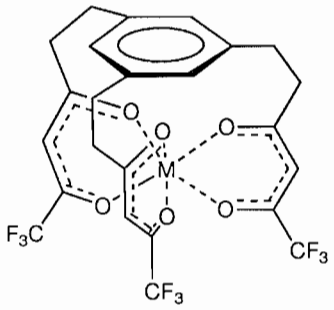
16 a R=R'=CH_3
b R=CF_3, R'=CH_3
c R=R'=CF_3
d R=*t*-Bu, R'=C_3F_7
e R=CCl_3, R'=CH_3



17 a R=R'=*t*-Bu, A=CO_2H
b R=R'=Me, A=CO_2H
c R=*t*-Bu, R'=H, A=OH



18 a R=CH_3
b R=CF_3



19

may involve more than just a simple chelation of the Lewis acid to the aldehyde with concurrent lowering of the oxadiene LUMO (28). We considered solubility as a possible explanation for the lack of activity of complexes **17**. However, they are more soluble than many active catalysts in ethereal solvents. The geometry, bulk, and bite angle of the ligand may of course affect the effective Lewis acidity of the metal independently of its pK_a. As stated earlier, a direct measurement of the Lewis acidity of the metal is possible by the method of Childs et al. (26), though Laszlo and Teston pointed out that NMR measurements of Lewis acidities of metals fail to accurately predict the chemical activity of Lewis acids as catalysts (28*a*). In any case, the generally low solubility of these complexes in non-coordinating solvents prevented meaningful measurements by the NMR method. Unfortunately the semiempirical MNDO calculations by the method of Laszlo could not be carried out on lanthanides because the parameters do not yet exist (28*a*). Nevertheless, the difference of catalytic activity between complexes **17** and **16** could not be due to ligand pK_a, steric bulk, or solubility. We considered three alternative explanations, namely, that the catalytic activity may be due to trace impurities emanating from the experimental preparation of the catalysts, or that the effective Lewis acidity of complexes **17** may be lower than that of complexes **16b–d** because of ligand geometry or oligomer formation, or last, that the displacement or, possibly, hinging of one of the ligands may be necessary to free a coordination site for catalysis (hinging specifically refers to partial dissociation of one arm, i.e., bidentate to monodentate for that arm). A hinging motion would be more favorable, from a geometric standpoint, in β-diketone-type ligands than in carboxylic acids.

Whatever the explanation, we concluded that an effective catalyst should possess the unaltered perfluoromethyl-β-diketone functionality on the ligand. Such units could be linked by the end methyl group via a number of linkers, thereby leaving the γ-perfluoro-β-diketone unit intact. 1,3,5-Tribromomesitylene **12** caught our attention as being a useful linker because of its relative ease of preparation and high reactivity toward alkylation. The yttrium and ytterbium complexes of **8** were prepared by mixing the ligand with a solution of yttrium or ytterbium tris(bis(trimethylsilyl)amide) in toluene as described earlier. In each case, an instantaneous reaction occurred with concomitant precipitation of the complex, which was washed several times with toluene. Unfortunately, we could not grow crystals of adequate quality to perform a single-crystal X-ray crystallographic analysis on either of the complexes and neither were soluble in non-coordinating solvents. To secure the structure of the yttrium complex **19**

© 1997 NRC Canada

Can. J. Chem. Downloaded from www.nrcresearchpress.com by 88.146.161.215 on 09/08/12
For personal use only.

Table 2. Compared efficiency of catalysts **19** on the hetero Diels–Alder reaction of **13** and **14**.

Entry	Catalyst	M	Conditions[a]	Time (h)	Conversion[b]	Yield (%)[c]
1	**19**	Y	A	72	98	95
2	**19**	Yb	A	96	80	80
3	$Yb(fod)_3$		A	96	98	90
4	$ZnCl_2$		A	48	98	46
5	$BF_3{\cdot}Et_2O$		A	48	98	12
6	**19**	Y	B	96	69	69
7	$Yb(fod)_3$		B	96	69	65
8	**19**	Y	C	96	89	89
9	**19**	Yb	C	96	89	89
10	$Yb(fod)_3$		C	96	0	0

[a]Method A = ethyl vinyl ether as solvent, 2 mol% catalyst, 25°C; Method B = method A + dioxane (0.5 equiv.) (similar results if **19** is prepared in a coordinating solvent); Method C = method A + deliberately exposed to air for 7 days.
[b]Disappearance of starting materials analysed by gas chromatography.
[c]Isolated yield after distillation.

(Fig. 2, M = Y), we prepared it in THF and isolated the powdery material by reduced pressure evaporation of the solvent. Although no X-ray quality crystals could be grown, the proton NMR analysis of the complex in benzene-d_6 was unequivocal and established the coordination of a molecule of THF (12). Mass spectral data and exact mass measurement on this compound were satisfactory. The structure of the ytterbium complex **19** (M = Yb) was inferred only from mass spectral data and by analogy to its yttrium analogue.

Catalytic activities of these new ligands were tested on the hetero Diels–Alder cycloaddition of crotonaldehyde and ethyl vinyl ether as described earlier (Table 2). In each example involving ytterbium or yttrium catalysts the isolated yields of the respective dihydropyran product **15** were excellent, testimony to their mildness (entries 1–3). In contrast, zinc chloride and BF_3-etherate gave 46% and 12% isolated yield, respectively, of **15** (entries 4 and 5). The yttrium catalyst **19** was superior to all others, including the commonly used $Yb(fod)_3$ (6), having the fastest conversion rate and giving a good isolated yield of **15** (entry 1). If dioxane was utilized as an internal standard for quantitative work, the reaction rate between **13** and **14** dropped (entries 6 and 7), indicating a competition for the active site between the coordinating solvent and crotonaldehyde. We found that when the complexes **19** were prepared in, or came in contact with, coordinating solvents, the reaction rate also dropped, presumably due to the incorporation of a coordinating solvent molecule. This coordinating solvent molecule may compete with crotonaldehyde for the active site or simply reduce the Lewis acidity of the complex. This outcome convinced us that in the case of complexes of **4** and **5** the coordinating amine nitrogen is playing the same role, only more efficiently, and no or very low conversion rates are observed. More importantly though, both catalysts **19** remained active even after several days of exposure to the ambient air (entries 8 and 9), even though the complexes may have picked up water molecules from exposure to air. Moreover, a 3-month-old sample of yttrium complex **19** stored in an opened vial still retained complete catalytic activity and the complex can be stirred in water (it is insoluble in water), extracted with THF, recovered, and used as a catalyst. The activity of the complex, even after exposure to air, is probably due to significantly reduced ligand lability. Multidentate ligands are known to exhibit this phenomenon. In contrast, all other catalysts including $Yb(fod)_3$ had to be kept in a rigorously dry atmosphere to remain active (entry 10).

In conclusion, we have prepared the first lanthanide complexes possessing a hexadentate ligand that are active catalysts. Their high stability, even in air, is not only desirable in terms of handling but is also very promising as a base from which to develop chiral catalysts showing high asymmetric induction. Our results clearly demonstrate that the ligand around the lanthanide should possess the unaltered perfluoromethyl-β-diketone functionality. It would seem that the role of the fluorines is to bring the pK_a of the β-diketone below a minimal level for catalysis and that, possibly, their hinging motion allows access to the catalytic site.

Experimental section

All solvents were distilled from sodium–benzophenone with the exception of di- and tetrachloromethane and dimethyl sulfoxide, which were distilled from calcium hydride. All reactions were performed under an atmosphere of argon unless otherwise stated. Flash column chromatography was done using Merck 60 silica gel. NMR spectra were taken in $CDCl_3$ at 250 or 360 MHz, and IR spectra were recorded in $CHCl_3$. ^{13}C NMR signal multiplicities were determined by DEPT experiments. Gas chromatography was performed on a DB-1 capillary column with FID detector. 2,4-Pentanedione (**1a**), 1,1,1-trifluoroacetylacetone (**1b**), and 1,1,1,5,5,5-hexafluoroacetylacetone (**1c**), were purchased and subsequently purified by distillation. Salicylaldehyde (**3a**), hydroxyacetophenone (**3b**), 2,4,6-trimethylbenzoic acid (**7a**), and 2,6-di-*tert*-butylphenol (**7c**) were purchased and purified by sublimation under vacuum. 1,1,1-Trichloroacetylacetone (**1e**) was synthesized as outlined in ref. 13. Tris(3-aza-4-methyl-6-oxohept-3-

Can. J. Chem. Downloaded from www.nrcresearchpress.com by 88.146.161.215 on 09/08/12
For personal use only.

© 1997 NRC Canada

Can. J. Chem. Downloaded from www.nrcresearchpress.com by 88.146.161.215 on 09/08/12
For personal use only.

en-1-yl)amine (**4a**), tris(3-aza-4-(2-hydroxyphenyl)-3-penten-1-yl)amine (**5**), and each of their respective yttrium and ytterbium complexes were synthesized and purified as outlined by Orvig and co-workers (14, 21). (*N,N*-Dimethyl-3-aminoprop-1-yl)di-*tert*-butylsilanol (**6**) and its tris-yttrium salt were prepared and isolated as outlined in Shao et al. (15). The yttrium complex of **7c** was prepared and isolated as outlined in Lappert et al. (29). The ytterbium complexes of **1d** and **2** were purchased from Aldrich.

Tris(3-aza-4-methyl-6-oxo-7,7,7-trifluorohept-3-en-1-yl)amine (4b)

In a 25 mL round-bottom flask equipped with a stirbar and a Dean Stark trap, 0.1 g (0.68 mmol) of tris(aminoethyl)amine was dissolved in 10 mL of dry benzene. Then 4.0 mL (5.1 g, 33.0 mmol) of 1,1,1-trifluoroacetylacetone was added via syringe and the reaction mixture was refluxed for 16 h. The resulting solution was concentrated under reduced pressure to obtain a sticky, golden powder. Purification by repeated triturations with Et_2O gave an isolated yield of 0.38 g (85%) of the desired tripodal ligand. ^{1}H NMR (300 MHz, C_6D_6) δ: 11.11 (br s, 3H), 5.24 (s, 3H), 3.48 (q, 6H, J = 7 Hz), 2.84 (t, 6H, J = 7 Hz), 2.06 (s, 3H). ^{13}C NMR (90 MHz, C_6D_6) δ: 175.45 (q, 2C, J_{CF} = 31 Hz), 170.02 (q), 117.63 (q, J_{CF} = 281 Hz), 89.73 (d), 54.36 (t), 42.41 (t), 19.38 (q). ^{19}F NMR (338 MHz, $CDCl_3$) δ: −76.84 (s). HRMS, calcd. for $C_{21}H_{27}F_9N_4O_3$: 152.1201; found: 152.1205.

2,4,6-Tri-*tert*-butylbenzoic acid (7a)

An oven-dried Schlenk tube was charged with 1.4 g (6.3 mmol) of 1-bromo-2,4,6-tri-*tert*-butylbenzene (16) in 125 mL of dry hexanes. Then 3.7 mL (6.3 mmol) of 1.7 M *t*-BuLi in pentanes was added and the resulting mixture was left to stir at −78°C for 1 h. Then, carbon dioxide was bubbled through the solution for 4 h. The mixture was quenched with 3 N aqueous HCl until the water layer was approximately at pH 1. The two phases were separated and the aqueous phase was extracted with ether. The combined organic portions were dried over $MgSO_4$, filtered, and concentrated under reduced pressure. Washing the product repeatedly with hexanes yielded 0.4 g (35%) of the desired product (16). ^{1}H NMR (250 MHz, $CDCl_3$) δ: 7.40 (s, 2H), 1.57 (s, 18H), 1.34 (s, 9H). ^{13}C NMR (63 MHz, $CDCl_3$) δ: 179.24 (s), 150.69 (s), 146.39 (s), 127.46 (s), 122.16 (d), 35.06 (s), 32.22 (s), 31.56 (q), 31.26 (q).

1,3,5-Tribromomesitylene (12)

In an oven-dried 1 L round-bottom flask equipped with a stirbar, was added 2.0 g (74 mmol) of lithium aluminum hydride in 200 mL of dry THF. Then, 5.0 g (23.8 mmol) of 1,3,5-benzenetricarboxylic acid in 200 mL of dry THF was added dropwise into the stirring slurry over 2 h under an atmosphere of N_2 while cooling with an ice bath. The resulting slurry was heated to reflux for 16 h using a condenser equipped with a drying tube. Enough water was then added to destroy excess reagent and the resulting salts were dried under high vacuum. To this vessel was added 150 mL of a 48% HBr solution and 250 mL of benzene. The mixture was heated to reflux for 16 h. The organic layer was separated and the aqueous portion was extracted with Et_2O; the organic layers were combined, dried over $MgSO_4$, and concentrated under reduced pressure. Recrystallization from hot cyclohexanes yielded 6.9 g (80%) of the desired product (18). ^{1}H NMR (360 MHz, $CDCl_3$) δ: 7.33 (s, 3H), 4.43 (s, 6H). ^{13}C NMR (90 MHz, $CDCl_3$) δ: 139.03 (s), 129.56 (d), 32.18 (t).

1,3,5-Tris(3,5-dioxo-6,6,6-trifluorohexan-1-yl)benzene (8)

A solution of 2.0 mL (2.6 g, 16.8 mmol) of 1,1,1-trifluoroacetylacetone in 20 mL of dry THF in an oven-dried Schlenk tube equipped with a stirbar was cooled to −78°C. In a separate oven-dried Schlenk tube was prepared an LDA solution in 10 mL of dry THF using 2.6 mL (2.0 g, 20.2 mmol) of dry diisopropylamine and 12.6 mL (20.2 mmol) of 1.6 M *n*-butyllithium in hexanes. After cooling to −78°C the trifluoroacetylacetone solution was transferred by cannula to the LDA solution while maintaining the temperature at −78°C. In a third oven-dried Schlenk tube was prepared a second LDA solution in 20 mL of dry THF using 2.0 mL (1.5 g, 15.2 mmol) of dry diisopropylamine and 9.5 mL (15.2 mmol) of 1.6 M *n*-butyllithium in hexanes. After cooling to −78°C this LDA solution was transferred into the previous one, while maintaining the temperature at −78°C. The mixture was stirred for 20 min and a solution of 1 g (2.8 mmol) of 1,3,5-tribromomesitylene in 20 mL of dry THF was added via cannula into the the dianion solution at −78°C. The reaction was stirred for 4 h while slowly warming to room temperature. The work-up consisted in adding a 3 M aqueous HCl solution, separating the layers, and, after ensuring that the water layer was acidic, extracting exhaustively with dichloromethane. The combined organic fractions were dried over magnesium sulfate, filtered, and concentrated under reduced pressure. Recrystallizing the resulting golden oil using a dry THF–hexanes mixed solvent system gave pale yellow crystals that could be further purified by sublimation at 140°C/10^{-2} Torr, yielding 0.63 g (40%) of the desired benzene-capped tripodal ligand **8**. ^{1}H NMR (250 MHz, C_6D_6) δ: 6.86 (s, 3H), 5.85 (s, 3H), 3.45 (t, 6H, J = 7 Hz), 2.87 (t, 6H, J = 7 Hz). ^{13}C NMR (63 MHz, C_6D_6) δ: 196.24 (q), 174.69 (q, $^2J_{CF}$ = 36 Hz), 140.57 (q), 126.51 (d), 117.01 (q, $^1J_{CF}$ = 282 Hz), 96.18 (d), 40.17 (t), 31.00 (t). ^{19}F NMR (338 MHz, C_6D_6) δ: −76.76 (s). HRMS, calcd. for $C_{24}H_{21}F_9O_6$: 576.1194; found: 576.1194.

Metal complexes

General procedure for the preparation of Y and Yb complexes of all ligands

Preparation was carried out in a similar manner for all complexes. β-Diketonates have been extensively investigated (22–25) and were previously prepared in high yields using this anhydrous method (23*a*). Hence various metal derivatives of **1a** (23), **1b** (23, 24), **1c** (23, 25), and **1e** (23) had been previously prepared and were used for comparison. In a Schlenk tube equipped with a stirbar, under an inert atmosphere, the ligand was dissolved in dry THF. In a separate oven-dried Schlenk tube equipped with a stirbar, under an inert atmosphere, $Y(N(SiMe_3)_2)_3$ (20) was dissolved in dry THF and transferred via cannula into the ligand solution while stirring. Stirring was continued for 20 min before removing the solvents and the resulting $Y(N(SiMe_3)_2)_3$ under reduced pressure, thereby isolating the desired product as a powder. The insoluble powders were repeatedly washed with toluene and hexanes to give free-flowing powders. The same procedure was used

© 1997 NRC Canada

Can. J. Chem. Downloaded from www.nrcresearchpress.com by 88.146.161.215 on 09/08/12
For personal use only.

with $Yb(N(SiMe_3)_2)_3$ and $La(N(SiMe_3)_2)_3$ for those complexes.

*Yttrium and ytterbium tris(acetylacetone) (**16a**)*: Prepared using the general procedure above. The reaction of 1.38 g (2.1 mmol) $Yb(N(SiMe_3)_2)_3$ with 0.65 mL (6.3 mmol) of dry acetylacetone yielded 0.51 g (52%) of the desired material. LRMS: 471 (M^+) with the expected isotopic pattern for ytterbium. Similar quantities, yields, and characterization for the yttrium complex.

*Yttrium and ytterbium tris(1,1,1-trifluoroacetylacetone) (**16b**)*: Prepared using the general procedure above. The reaction of 1.38 g (2.1 mmol) $Yb(N(SiMe_3)_2)_3$ with 0.77 mL (6.3 mmol) of dry trifluoroacetylacetone yielded 0.65 g (50%) of the desired material, purified by sublimation at 90°C at 10^{-4} Torr. LRMS: 633 (M^+) with the expected isotopic pattern for ytterbium. Similar quantities, yields, and characterization for the yttrium complex.

*Ytterbium tris(1,1,1,5,5,5-hexafluoroacetylacetone) (**16c**)*: Prepared using the general procedure above. The reaction of 1.38 g (2.1 mmol) $Yb(N(SiMe_3)_2)_3$ with 0.90 mL (6.3 mmol) hexafluoroacetylacetone yielded 0.83 g (50%) of the desired material, purified by sublimation at 120°C at 10^{-2} Torr. LRMS: 795 (M^+) with the expected isotopic pattern for ytterbium.

*Yttrium tris(1,1,1-trichloroacetylacetone) (**16e**)*: Prepared using the general procedure above. The reaction of 0.71 g (1.3 mmol) of $Y(N(SiMe_3)_2)_3$ with 0.76 g (3.9 mmol) of dry trichloroacetylacetone yielded 0.42 g (49%) of orange powder.

*Ytterbium tris(salicylaldehyde) (Yb of **3b**)*: Prepared using the general procedure above. The reaction of 1.38 g (2.1 mmol) $Yb(N(SiMe_3)_2)_3$ with 0.76 g (6.3 mmol) of dry salicylaldehyde yielded 0.58 g (51%) of pale yellow powder.

*Ytterbium tris(hydroxyacetophenone) (Yb of **3b**)*: Prepared using the general procedure above. The reaction of 1.38 g (2.1 mmol) $Yb(N(SiMe_3)_2)_3$ with 0.75 mL (6.3 mmol) of dry 2-hydroxyacetophenone yielded 0.58 g (48%) of yellow powder.

*Yttrium tris(2,4,6-tri-*tert*-butylbenzoate) (**17a**)*: Prepared as described in the general procedure above using 600 mg (2.1 mmol) of ligand **7a** in 5 mL of dry THF and 0.39 g (0.69 mmol) of $Y(N(SiMe_3)_2)_3$ in 5 mL of dry THF. A white soluble powder was isolated in 75% yield and purified by washing repeatedly with hexanes, giving a 73% overall yield. ^{1}H NMR (360 MHz, C_6D_6) δ: 7.42 (s, 6H), 1.46 (s, 54H), 1.31. (s, 27H). ^{13}C NMR (90 MHz, C_6D_6) δ: 179.94 (s), 150.68 (s), 146.33 (s), 127.53 (d), 122.16 (s), 37.63 (s), 35.05 (s), 32.22 (q), 31.26 (q).

*Yttrium and ytterbium tris(2,4,6-trimethylbenzoate) (**17b**)*: Prepared as described in the general procedure above using 0.38 g (0.67 mmol) $Y(N(SiMe_3)_2)_3$ with 0.33 g (2.0 mmol) of ligand **7b**. A white powder was isolated in 54% yield after repeated washing with hexanes. ^{1}H NMR (360 MHz, C_6D_6) δ: 7.23 (s, 6H), 2.43 (s, 18H), 2.24 (s, 9H). ^{13}C NMR (90 MHz, C_6D_6) δ: 177.74 (s), 149.32 (s), 144.42 (s), 126.92 (d), 121.20 (s), 35.55 (q), 33.43 (q). Similar quantities and yields for the ytterbium complex.

*Yttrium tris(3-aza-4-methyl-6-oxo-7,7,7-trifluorohept-3-en-1-yl)amine (**18b**)*: Prepared following the procedure for Y–**4a** complex described by Berg, Rettig, and Orvig (21) using 0.2 g (0.35 mmol) of $Y(N(SiMe_3)_2)_3$ with 0.195 g (0.35 mmol) of ligand **4b** in 20 mL of dry THF, affording a quantitative yield (0.22 g) of creamy white powder. This could be recrystallized from warm toluene upon standing, yielding colourless brick-like crystals in modest quantities. X-ray (see footnote 2), ^{1}H NMR (360 MHz, C_6D_6) δ: 5.46 (s, 3H), 2.68 (br m, 6H), 1.32 (br m, 6H), 1.29 (s, 9H). ^{13}C NMR (90 MHz, C_6D_6) δ: 173.47 (s), 161.89 (q, $^2J_{CF}$ = 29 Hz), 120.92 (q, $^1J_{CF}$ = 269 Hz), 98.77 (d), 52.68 (t), 46.72 (t), 21.96 (q). ^{19}F NMR (338 MHz, C_6D_6) δ: −74.76.

*Yttrium and ytterbium 1,3,5-tris(3,5-dioxo-6,6,6-trifluorohexan-1-yl)benzene (**19**)*: Prepared as described in the general procedure above using 76 mg (0.13 mmol) of ligand **8** in 5 mL of dry THF and 75 mg (0.13 mmol) of $Y(N(SiMe_3)_2)_3$ in 5 mL of dry THF to afford a pale yellow powder in quantitative yield. ^{1}H NMR (250 MHz, C_6D_6) δ: 6.41 (s, 3H), 5.83 (s, 3H), 3.75 (br t, THF), 2.43 (t, 6H, J = 7 Hz), 2.06 (t, 6H, J = 7 Hz), 1.27 (m, THF). ^{13}C NMR (63 MHz, C_6D_6) δ: 201.14 (s), 169.95 (q, $^2J_{CF}$ = 32 Hz), 138.55 (s), 128.02 (q), 127.87 (d), 97.35 (d), 69.17 (t, THF), 42.21 (t), 33.20 (t), 25.42 (t, THF). ^{19}F NMR (338 MHz, C_6D_6) δ: −75.66 (s). HRMS, calcd. for $C_{24}H_{18}F_9O_6Y$: 662.0018; found: 662.0000. Similar quantities and yields for the ytterbium complex.

Catalytic test run

Into an oven-dried Schlenk tube equipped with a stirbar was loaded 30.5 mg (2 mol%) of the catalyst metal complex. Then 5.0 mL of freshly distilled ethyl vinyl ether was added via syringe into the tightly capped vessel. The reaction mixture was stirred while adding 0.2 mL of distilled *trans*-crotonaldehyde via a syringe. Every 4 h an aliquot of solution was acquired, diluted in 0.5 mL of diethyl ether, and injected (0.5 μL) into a Fisons E980 gas chromotagraph to detect product formation. A 100 μL (1.2 mmol) dioxane standard can be used in the reaction mixture to better quantify results. However, dioxane slows the reaction rate somewhat as stated above. Upon reaction completion the mixture was quenched with 1 N aquous HCl and stirred for 30 min. Extraction of the organic layer with ether and removal of solvent from the combined organic fractions under reduced pressure gave a crude product that can be further purified (8*a*) by column chromatography using a 4:1 pentanes:ether eluant or by distillation (if crotonaldehyde is no longer present in crude product). NMR spectral data of the adduct were in accord with literature values (6).

Acknowledgments

We thank the Natural Sciences and Engineering Research Council of Canada and the University of Victoria for financial support. We thank Marc Drouin (Université de Sherbrooke) for carrying out the X-ray single crystal analysis of the Y complex **18b**.

© 1997 NRC Canada

References

1. (*a*) D.L. Bogerand S. Weinreb. *In* Hetero Diels–Alder methodology in organic synthesis. Academic Press, San Diego, Calif. 1987; (*b*) W. Carruthers. *In* Cycloaddition reactions in organic synthesis. Pergamon Press, Exeter, U.K. 1990.
2. T.L.B. Boivin. Tetrahedron, **43**, 3309 (1987), and refs. therein.
3. S. Danishefsky, N. Kato, D. Askin, and J.F. Kerwin, Jr. J. Am. Chem. Soc. **104**, 360 (1982); S. Danishefsky and J.F. Kerwin, Jr. J. Am. Chem. Soc. **104**, 3183 (1982), and refs. therein.
4. J.W. Westley. *In* Polyether antibiotics: naturally occurring acid ionophores. Vols. I and II. *Edited by* J.W. Westley. Marcel Dekker, Inc., New York. 1982.
5. (*a*) H.B. Kagan and J.L. Namy. Tetrahedron, **42**, 6573 (1986); (*b*) G.A. Molander. Chem. Rev. **92**, 29 (1992); (*c*) T. Imamoto. *In* Lanthanides in organic synthesis. Academic Press, San Diego, Calif. 1994.
6. (*a*) S. Danishefsky and M. Bednarski. Tetrahedron Lett. **25**, 721 (1984); (*b*) M. Bednarski and S. Danishefsky. J. Am. Chem. Soc. **105**, 6968 (1983).
7. R.I. Longley, Jr. and W.S. Emerson. J. Am. Chem. Soc. **72**, 3079 (1950).
8. (*a*) W.G. Dauben and H.D. Krabbenhoft. J. Org. Chem. **42**, 282 (1977); (*b*) B.B. Snider and G.B. Phillips. J. Org. Chem. **48**, 2790 (1983).
9. C. Spino, G. Liu, N. Tu, and S. Girard. J. Org. Chem. **59**, 5596 (1994).
10. T. Oh and M. Reilly. Org. Prep. Proced. Int. **26**, 129 (1994), and refs. cited therein.
11. (*a*) M. Bednarski, C. Maring, and S. Danishefsky. Tetrahedron Lett. **24**, 3451 (1983); (*b*) M. Bednarski and S. Danishefsky. J. Am. Chem. Soc. **108**, 7060 (1986).
12. C. Spino, L. Clouston, and D. Berg. Can. J. Chem. **74**, 1762 (1996).
13. M.L. Morris and R.D. Koob. Org. Mass Spectrom. **17**, 503 (1982).
14. A. Smith, S.J. Rettig, and C. Orvig. Inorg. Chem. **27**, 3929 (1988).
15. P. Shao, D.J. Berg, and G.W. Bushnell. Inorg. Chem. **33**, 3452 (1994).
16. A.H. Cowley, N.C. Norman, and M. Pakulski. Inorg. Synth. **27**, 235 (1990).
17. S.R. Ditto, R.J. Card, P.D. Davis, and D.C. Neckers. J. Org. Chem. **44**, 394 (1979).
18. F. Vögtle, M. Zuber, and R.G. Lictenthaler. Chem. Ber. **106**, 717 (1973).
19. S.N. Huckin and L. Weiler. J. Am. Chem. Soc. **96**, 1082 (1974).
20. D.C. Bradley, J.S. Ghotra, and F.A. Hart. J. Chem. Soc. Dalton Trans. 1021 (1973).
21. D.J. Berg, S.J. Rettig, and C. Orvig. J. Am. Chem. Soc. **113**, 2528 (1991).
22. R.C. Mehrotra, R. Bohra, and D.P. Gaur. *In* Metal β-diketonates and allied derivatives. Academic Press, New York. 1978.
23. (*a*) E.H. Barash, P.S. Coadn, E.B. Lobkovsky, W.E. Streib, and K.G. Caulton. Inorg. Chem. **32**, 497 (1993).
24. (*a*) M. Nakamura, R. Nakamura, K. Nagai, M. Shimoi, S. Tomoda, Y. Takeuchi, and A. Ouchi. Bull. Chem. Soc. Jpn. **59**, 332 (1986); (*b*) A.T. McPhail, P.S.W. Tschang, and P.M. Gross, J. Chem. Soc. Dalton Trans. 1165 (1974); (*c*) R.A. Lalancette, M. Cefola, W.C. Hamilton, and S.J. La Placa. Inorg. Chem. **6**, 2127 (1967); (*d*) J.G. Leipoldt, L.D.C. Bok, S.S. Basson, A.E. Laubscher, and J.S. van Vollenhoven. J. Inorg. Nucl. Chem. **39**, 301 (1977).
25. M.J. Bennett, F.A. Cotton, P. Legzdins, and S.J. Lippard. Inorg. Chem. **7**, 1770 (1968).
26. R.F. Childs, D.L. Mullholland, and A. Nixon. Can. J. Chem. **60**, 801 (1982).
27. (*a*) E.P. Serjeant and B. Dempsey. *In* IUPAC: Ionisation constants of organic acids in aqueous solution. Pergamon Press, Toronto. 1979; (*b*) R.L. Lintvedt and H.F. Hotzclow. Inorg. Chem. **5**, 239 (1966); (*c*) B.B. Martin and D.F.J. Martin. Inorg. Nucl. Chem. **41**, 1503 (1979); (*d*) R.W. Green and E.L. LeMesurier. Aust. J. Chem. **19**, 229 (1966); (*e*) J. Betts and J. Barclay. Can. J. Chem. **33**, 1768 (1955); (*f*) P.D. Maria, A. Fontana, D. Spinelli, C. Dell'Erba, and M. Novi. J. Chem. Soc. Perkin Trans. 2, **4**, 649 (1993).
28. (*a*) P. Laszlo and M. Teston. J. Am. Chem. Soc. **112**, 8750 (1990); (*b*) P.V. Bonnesen, G.L. Puckett, R.V. Honeychuck, and W.H. Hersh. J. Am. Chem. Soc. **111**, 6070 (1989).
29. M.F. Lappert, A. Singh, and R.G. Smith. Inorg. Synth. **27**, 164 (1990).

Can. J. Chem. Downloaded from www.nrcresearchpress.com by 88.146.161.215 on 09/08/12
For personal use only.

© 1997 NRC Canada

Photochemical nucleophile–olefin combination, aromatic substitution (photo-NOCAS) reaction, Part 13. The scope and limitations of the reaction with cyanide anion as the nucleophile[1]

Donald R. Arnold, Kimberly A. McManus, and Mary S.W. Chan

Can. J. Chem. Downloaded from www.nrcresearchpress.com by 88.146.161.215 on 09/08/12
For personal use only.

Abstract: The scope of the photochemical nucleophile–olefin combination, aromatic substitution (photo-NOCAS) reaction has been extended to include cyanide anion as the nucleophile. Highest yields of adducts were obtained when the alkene or diene has an oxidation potential less than ca. 1.5 V (SCE). No adducts were obtained from 2-methylpropene (**9**), oxidation potential 2.6 V. Oxidation of cyanide anion, by the radical cation of the alkene or diene, can compete with the combination. With the alkenes, 2,3-dimethyl-2-butene (**2**) and 2-methyl-2-butene (**10**), both nitriles and isonitriles were obtained; isonitriles were not detected from the reactions involving the dienes, 2-methyl-1,3-butadiene (**11**), 2,3-dimethyl-1,3-butadiene (**12**), 4-methyl-1,3-pentadiene (**13**), 2,4-dimethyl-1,3-pentadiene (**14**), and 2,5-dimethyl-2,4-hexadiene (**6**). The specificity, nitrile versus isonitrile, is explained in terms of the Hard-Soft-Acid-Base (HSAB) principle. The photo-NOCAS reaction also occurs with the allene, 2,4-dimethyl-2,3-pentadiene (**15**), cyanide combining at the central carbon. Factors influencing the regiochemistry of the combination step, Markovnikov versus *anti*-Markovnikov, have been defined. Cyanide anion adds preferentially to the less alkyl-substituted, less sterically hindered, end of an unsymmetric alkene or conjugated diene radical cation, forming the more heavily alkyl-substituted radical intermediate. High-level *ab initio* molecular orbital calculations (MP2/6-31G*//HF/6-31G*) have been used to determine the effect of alkyl substitution on the stability of the intermediates, β-cyano and β-isocyano alkyl radicals, and products, alkyl cyanides and isocyanides. The more heavily alkyl-substituted radical is not necessarily the more stable. The product ratio (Markovnikov versus *anti*-Markovnikov) must be kinetically controlled.

Key words: photochemistry, radical ions, electron transfer, nitriles, isonitriles.

Résumé : On a élargi le domaine d'application de la réaction photochimique de combinaison nucléophile–oléfine avec substitution aromatique («photo-NOCAS») de façon à inclure l'ion cyanure comme nucléophile. Les meilleurs rendements d'adduits sont obtenus lorsque le potentiel d'oxydation de l'alcène ou du diène est inférieur à environ 1,5 V («SCE»). On n'a pas obtenu d'adduits avec les 2-méthylpropène (**9**) dont le potentiel d'oxydation est de 2,6 V. L'oxydation de l'anion cyanure, par le cation radical de l'alcène ou du diène, est en compétition avec la combinaison. Avec les alcènes, 2,3-diméthylbut-2-ène (**2**) et 2-méthylbut-2-ène (**10**), on a obtenu les nitriles ainsi que les isonitriles; on n'a toutefois pas détecté d'isonitriles lors des réactions impliquant les diènes, 2-méthylpenta-1,3-diène (**11**), 2,3-diméthylbuta-1,3-diène (**12**), 4-méthylpenta-1,3-diène (**13**), 2,4-diméthylpenta-1,3-diène (**14**) et 2,5-diméthylhexa-2,4-diène (**6**). On explique la spécificité, nitrile versus isonitrile, en fonction du principe des acides et des bases durs et mous («HSAB»). La réaction de «photo-NOCAS» se produit aussi avec l'allène et le 2,4-diméthylpenta-2,3-diène (**15**); le cyanure s'attache au carbone central. On a défini que les facteurs qui influencent la régiochimie de l'étape de combinaison sont Markovnikov versus *anti*-Markovnikov. L'anion cyanure s'additionne préférentiellement à l'extrémité d'un ion radical d'alcène non symétrique ou de diène conjugué qui est la moins substituée, la moins stériquement encombrée, par des groupes alkyles; cette addition conduit à la formation du radical intermédiaire le plus substitué par des groupes alkyles. On a fait appel à des calculs d'orbitales moléculaires ab initio à niveau élevé (MP2/6-31G*// HF/6-31G*) pour déterminer l'effet de la substitution par des groupes alkyles sur la stabilité des intermédiaires, les radicaux β-cyanoalkyles et les β-isocyanoalkyles, et des produits, les cyanures et les isocyanures. Les radicaux les plus substitués ne sont pas nécessairement les plus stables. Le rapport des produits (Markovnikov versus *anti*-Markovnikov) doit donc être sous contrôle cinétique.

Mots clés : photochimie, ions radicaux, transfert d'électron, nitriles, isonitriles.

[Traduit par la rédaction]

Received March 7, 1997.

D.R. Arnold,[2] K.A. McManus, and M.S.W. Chan. Department of Chemistry, Dalhousie University, Halifax, NS B3H 4J3, Canada.

[1] This is also Part 42 of the series Radical Ions in Photochemistry. See refs. 1 and 2 for preceding parts of these series.

[2] Author to whom correspondence may be addressed. Telephone: (902) 494-3714. Fax: (902) 494-1310. E-mail: arnold@ac.dal.ca

© 1997 NRC Canada

Can. J. Chem. Downloaded from www.nrcresearchpress.com by 88.146.161.215 on 09/08/12
For personal use only.

Introduction

The scope and limitations of the photochemically induced nucleophile–olefin combination, aromatic substitution (photo-NOCAS) reaction, which combines a nucleophile and an alkene or diene radical cation, substituting on an aromatic radical anion, have been defined when an alcohol (methanol) serves as nucleophile (1). A main objective of this study was to extend the scope of this reaction with cyanide anion as the nucleophile (Scheme 1).

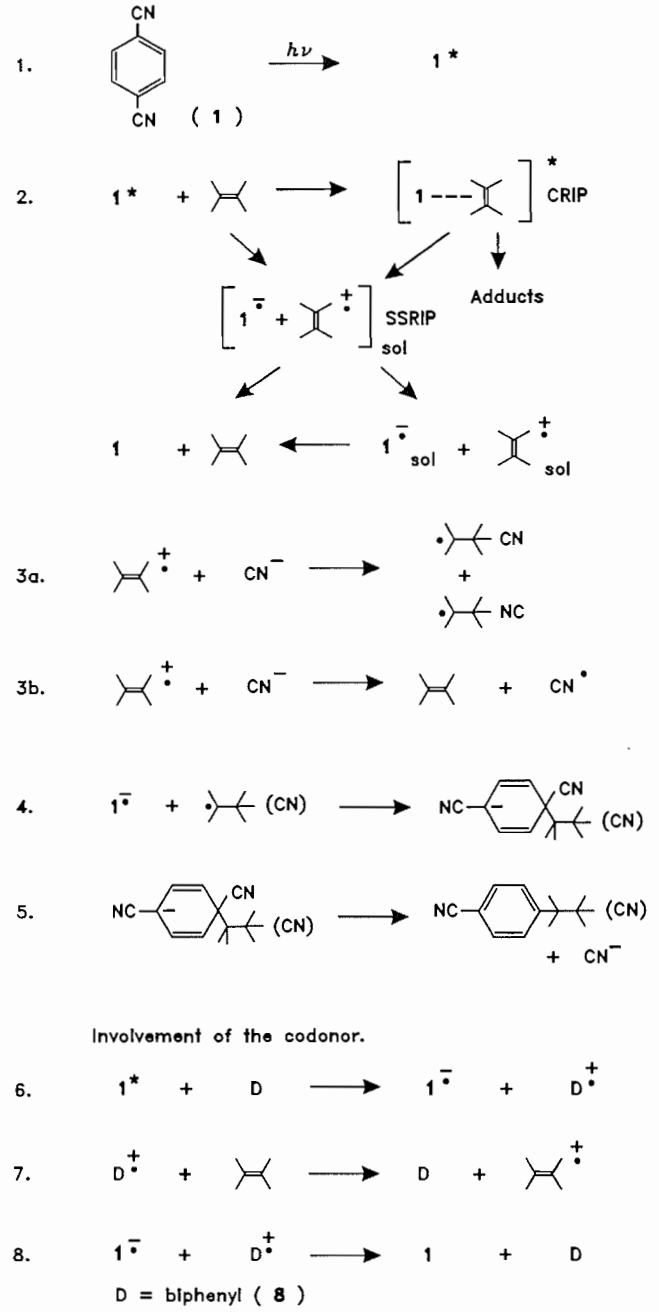
Some previous results were encouraging (1*a*–*c*). Irradiation of an acetonitrile solution (no methanol) of 1,4-dicyanobenzene (**1**) and 2,3-dimethyl-2-butene (**2**) gave primarily the expected 1:1 substitution products, 2,3-dimethyl-3-(4-cyanophenyl)-1-butene (**4**) and 2,3-dimethyl-1-(4-cyanophenyl)-2-butene (**5**), resulting from deprotonation of the alkene radical cation ($\mathbf{2}^{+\cdot}$) followed by coupling of the resulting allylic radical with the radical anion of 1,4-dicyanobenzene ($\mathbf{1}^{-\cdot}$). A minor product from this reaction was the photo-NOCAS adduct, 3-(4-cyanophenyl)-2,3-dimethylbutanenitrile (**3**), formed in "trace" amounts, which had incorporated cyanide anion (reaction [1]) (1*a*). The only source of cyanide anion in this reaction mixture was that generated during the aromatic substitution–rearomatization step (Scheme 1, step 5). This was the only previous report of incorporation of cyanide anion during a photo-NOCAS reaction involving an alkyl-substituted alkene.

One example of the photo-NOCAS reaction, involving cyanide anion combining with the radical cation of a conjugated diene has been reported (1*b*). Competitive formation of the nitrile was initially observed during the photo-NOCAS reaction of 2,5-dimethyl-2,4-hexadiene (**6**) and 1,4-dicyanobenzene (**1**) in acetonitrile–methanol (3:1). Subsequent irradiation of an acetonitrile solution of 2,5-dimethyl-2,4-hexadiene (**6**) and potassium cyanide, with 1,4-dicyanobenzene (**1**) serving as the electron acceptor, gave a good yield (80%) of the photo-NOCAS adduct, (*E*)-5-(4-cyanophenyl)-2,2,5-trimethyl-3-hexenenitrile (**7**) (reaction [2] (1*b*)).

With aryl-substituted alkenes, the products of addition of hydrogen cyanide were obtained (1*c*). For example, irradiation of an acetonitrile – 2,2,2-trifluoroethanol solution of 1,1-diphenylethylene and potassium cyanide, with 1-cyanonaphthalene or methyl 4-cyanobenzoate serving as the electron acceptor, gave the cyanation product, 3,3-diphenylpropanenitrile (reaction [3] (1*c*)). Cyanide anion serves as the nucleophile, adding to the 1,1-diphenylethylene radical cation. In this case, as with other aryl-substituted alkenes, the resulting benzylic radical intermediate is reduced to the carbanion by the radical anion of the initial electron acceptor, followed by protonation.

There is direct physical evidence for the reaction of cyanide anion with the radical cation of aryl alkenes and conjugated dienes. Flash photolysis studies have shown cyanide anion reacts (adds?) with the radical cation of aryl-substituted alkenes and conjugated dienes with rate constants approaching the diffusion-controlled limit (3). The relative rates of the reaction of substituted styrene radical cations with methanol and with cyanide anion reflect the well-established difference in nucleophilicity of these nucleophiles; the nucleophilicity, n (CH_3I), value for cyanide anion is 6.7 (methanol, $n = 0.0$ by definition (4)).

Scheme 1.



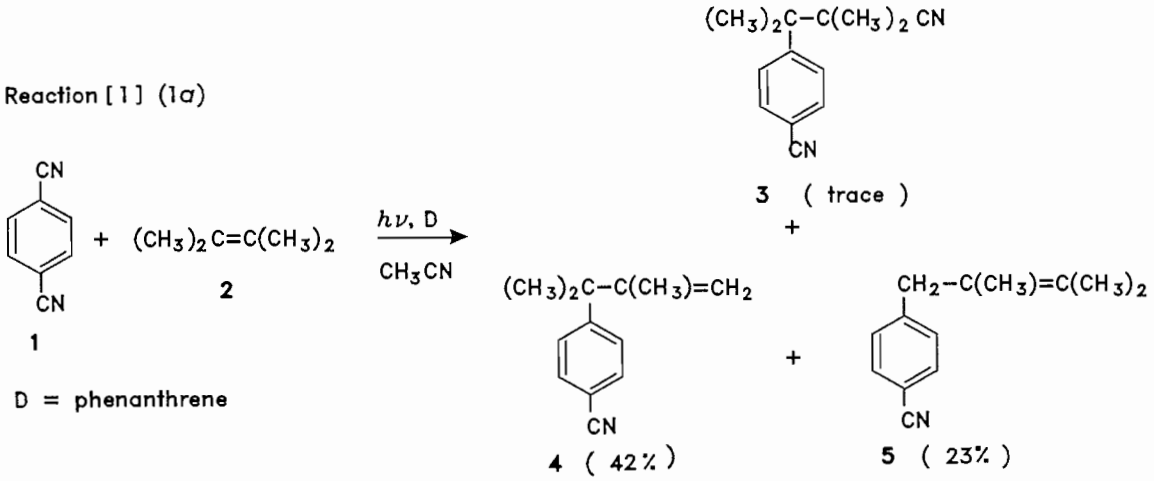
We report here results from the irradiation of acetonitrile, potassium cyanide, and solutions of several alkenes and dienes, using 1,4-dicyanobenzene (**1**) as the electron acceptor and with biphenyl (**8**) serving as a codonor. The alkenes and dienes chosen for study include: 2-methylpropene (**9**), 2-methyl-2-butene (**10**), 2,3-dimethyl-2-butene (**2**), 2,5-dimethyl-2,4-hexadiene (**6**), 2-methyl-1,3-butadiene (**11**), 2,3-dimethyl-1,3-butadiene (**12**), 4-methyl-1,3-pentadiene (**13**), 2,4-dimethyl-1,3-pentadiene (**14**), and the allene, 2,4-dimethyl-2,3-pentadiene (**15**).

Another objective of this study involved the identification of the factor(s) that influence the regiochemistry of the bonding of the nucleophile to the alkene or diene radical cation.

© 1997 NRC Canada

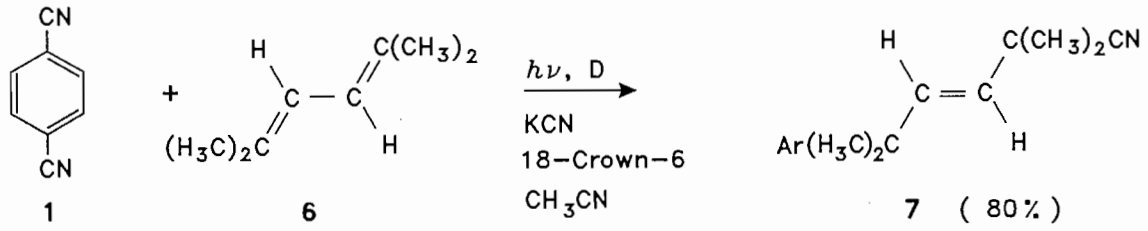
Can. J. Chem. Downloaded from www.nrcresearchpress.com by 88.146.161.215 on 09/08/12
For personal use only.

Reaction [1] (1*a*)



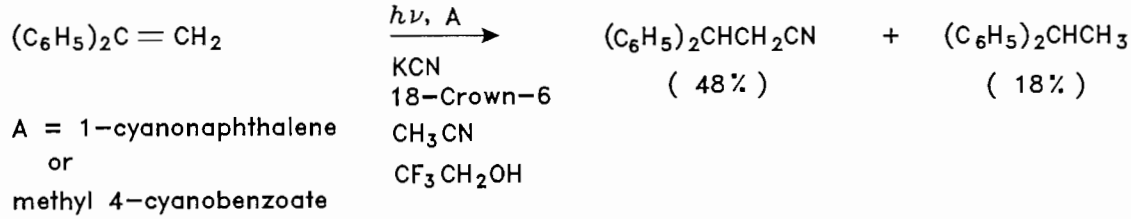
D = phenanthrene

Reaction [2] (1*b*)



D = biphenyl (8)
Ar = 4–cyanophenyl

Reaction [3] (1*c*)



A = 1–cyanonaphthalene
or
methyl 4–cyanobenzoate

Previous work, with methanol serving as the nucleophile, has led to the following hypothesis: the nucleophile (methanol) adds to that end of the alkene or diene radical cation which leads ultimately to formation of the more stable radical intermediate — the more stable radical intermediate is not necessarily that with the most heavily alkyl substituted radical moiety. The initial intermediate, formed upon addition of methanol, is the distonic radical cation, capable of bridging and equilibration. Of course, there is no distonic radical cation intermediate formed upon addition of a negatively charged nucleophile. High-level ab initio molecular orbital calculations (MP2/6-31G*//HF/6-31G* (5, 6)) have been used to determine the relative stability of the alternative radical intermediates formed upon addition of cyanide anion to the alkene or diene radical cation. These results will be compared with those for the analogous intermediates formed upon addition of methanol (1*i*).

Results

The reaction conditions used for the addition of cyanide anion are similar to those reported for the reactions involving methanol as the nucleophile (1). Acetonitrile solutions of the alkene or diene, 1,4-dicyanobenzene (**1**), biphenyl (**8**) serving as a

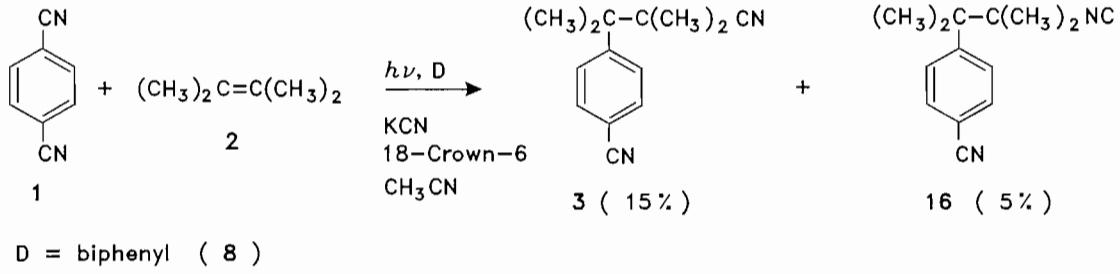
© 1997 NRC Canada

codonor, and potassium cyanide, were irradiated with a medium-pressure mercury vapour lamp through Pyrex. The solubility of the potassium cyanide in the acetonitrile was increased by the addition of 18-crown-6 ether (1,4,7,10,13,16-hexaoxacyclooctadecane). Progress of the reaction was followed by capillary column gas chromatography with a flame ionization detector (gc/fid). The first indication of the structure of the product(s) was gleaned from the mass spectrum obtained from a gas chromatograph equipped with a mass selective detector (gc/ms). The ratios of products were determined by integration of the peak areas in the gc/fid. The relative yields of isolated products were generally in agreement with these ratios. The yields were based upon the amount of 1,4-dicyanobenzene (**1**) consumed; the alkene or diene was generally present in excess.

Previous results had shown the photo-NOCAS adduct, **3**, was a minor product, formed along with the 1:1 adducts, **4** and **5**, upon irradiation of an acetonitrile solution of 1,4-dicyanobenzene (**1**) and 2,3-dimethyl-2-butene (**2**) (reaction [1] (1*a*)). When an acetonitrile solution of **1**, **2**, biphenyl (**8**), and potassium cyanide was irradiated, **3** became a major product (15%). The isonitrile (**16**) was also formed (5%), along with the 1:1 adducts (**4** and **5**) (reaction [4]).

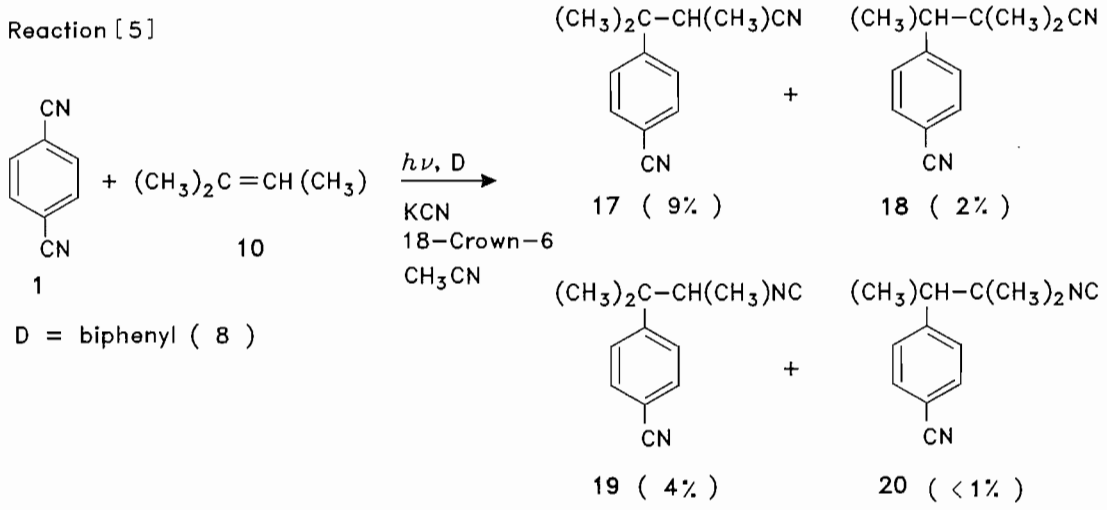
In marked contrast, no 1:1:1 adduct was detected (gc/ms) when 2-methylpropene (**9**) was subjected to these reaction conditions. However, irradiation of an acetonitrile solution of 2-methyl-2-butene (**10**), **1**, **8**, and potassium cyanide, did give the photo-NOCAS adducts, nitriles (**17**, **18**) and isonitriles (**19**, **20**), albeit in low yield (reaction [5]). The ratio of the isonitriles, **19** (*anti*-Markovnikov) : **20** (Markovnikov), determined from the integrated peak areas (gc/fid), was large (> 30:1).

Reaction [4]



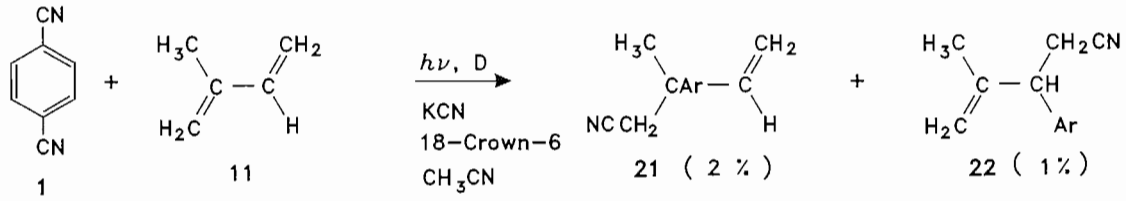
D = biphenyl (**8**)

Reaction [5]



D = biphenyl (**8**)

Reaction [6]



D = biphenyl (**8**)
Ar = 4–cyanophenyl

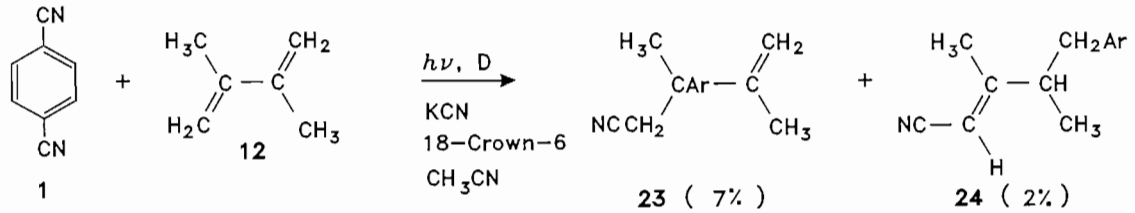
Can. J. Chem. Downloaded from www.nrcresearchpress.com by 88.146.161.215 on 09/08/12
For personal use only.

© 1997 NRC Canada

An acetonitrile solution of 2-methyl-1,3-butadiene (**11**), 1,4-dicyanobenzene (**1**), biphenyl (**8**), and potassium cyanide was irradiated; 3-(4-cyanophenyl)-3-methyl-4-pentenenitrile (**21**, 2%) and 3-(4-cyanophenyl)-4-methyl-4-pentenenitrile (**22**, 1%) were isolated in low yield (reaction [6]). Both of these adducts result from 1,2-addition to the diene; no 1,4-addition product was detected.

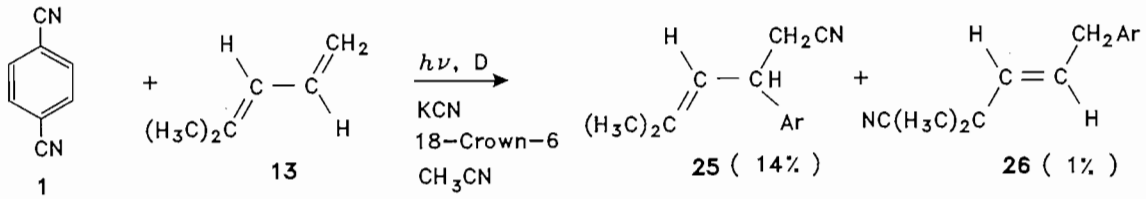
When an acetonitrile solution of 2,3-dimethyl-1,3-butadiene (**12**), **1**, **8**, and potassium cyanide was irradiated, 3-(4-cyanophenyl)-3,4-dimethyl-4-pentenenitrile (**23**, 7%) and (*E*)-5-(4-cyanophenyl)-3,4-dimethyl-2-pentenenitrile (**24**, 2%) were obtained (reaction [7]). Adduct **23** is a 1,2-addition product. No 1,4-addition product (i.e., neither (*E*)- nor (*Z*)-5-(4-cyanophenyl)-3,4-dimethyl-3-pentenenitrile) was detected; however, **24** may result from isomerization (tautomerization) of this 1,4-adduct.

Reaction [7]



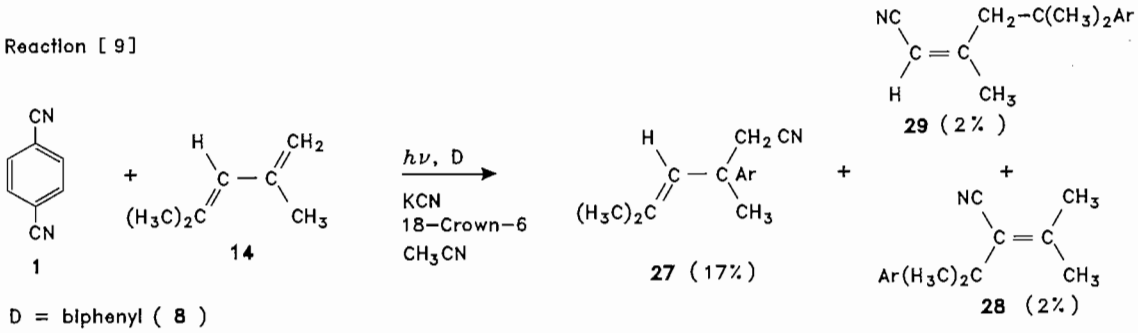
D = biphenyl (**8**)
Ar = 4–cyanophenyl

Reaction [8]



D = biphenyl (**8**)
Ar = 4–cyanophenyl

Reaction [9]



D = biphenyl (**8**)
Ar = 4–cyanophenyl

Two photo-NOCAS adducts were formed upon irradiation of a solution of 4-methyl-1,3-pentadiene (**13**), **1**, **8**, and potassium cyanide in acetonitrile (reaction [8]). The major adduct, 3-(4-cyanophenyl)-5-methyl-4-hexenenitrile (**25**, 14%), was the 1,2-addition product resulting from initial attack of the cyanide anion at the less substituted terminal end of the diene radical cation. A 1,4-addition product, (*E*)-5-(4-cyanophenyl)-2,2-dimethyl-3-pentenenitrile (**26**, 1%), resulting from initial attack of the cyanide anion at the more substituted terminal end of the diene radical cation, was the minor adduct.

When an acetonitrile solution of 2,4-dimethyl-1,3-pentadiene (**14**), **1**, **8**, and potassium cyanide was irradiated, three isomeric 1:1:1 adducts were formed: 3-(4-cyanophenyl)-3,5-dimethyl-4-hexenenitrile (**27**, 17%), 4-(4-cyanophenyl)-2,4-dimethyl-2-pentene-3-nitrile (**28**, 2%), and (*Z*)-5-(4-cyanophenyl)-3,5-dimethyl-2-hexenenitrile (**29**, 2%) (reac-

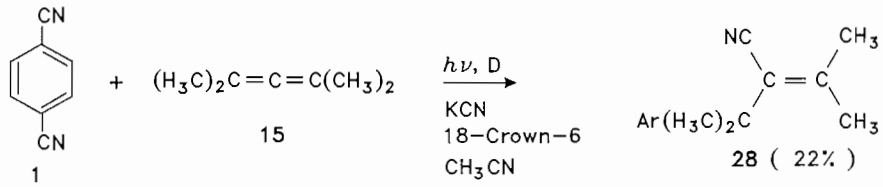
Can. J. Chem. Downloaded from www.nrcresearchpress.com by 88.146.161.215 on 09/08/12
For personal use only.

© 1997 NRC Canada

tion [9]). The major product, **27**, is the expected photo-NOCAS adduct resulting from 1,2-addition to the less substituted terminal end of the diene radical cation. Compound **29**, like compound **24**, may result from isomerization (tautomerization) of initially formed 1,4-addition product(s).

The other minor product, **28**, may result from a photo-NOCAS reaction involving the tautomeric diene, the allene 2,4-dimethyl-2,3-pentadiene (**15**), present as an impurity in the starting diene. To test this possibility a similar solution, starting with **15**, was irradiated under identical conditions; the photo-NOCAS adduct, **28**, was obtained in reasonable yield (22%) (reaction [10]).

Reaction [10]



D = biphenyl (8)
Ar = 4–cyanophenyl

Structural assignments

Structural assignments of the products were based primarily upon detailed analysis of ^1H and ^{13}C nmr, mass, and infrared spectra. For two of the products, 4-(4-cyanophenyl)-2,4-dimethyl-2-pentene-3-nitrile (**28**) and (*Z*)-5-(4-cyanophenyl)-3,5-dimethyl-2-hexenenitrile (**29**), structures were firmly established by X-ray crystallography on a single crystal.[3]

Irradiation of an acetonitrile solution of 1,4-dicyanobenzene (**1**), 2,3-dimethyl-2-butene (**2**), biphenyl (**8**), and potassium cyanide gave the nitrile, 3-(4-cyanophenyl)-2,3-dimethylbutanenitrile (**3**), and the isonitrile, 3-(4-cyanophenyl)-2,3-dimethyl-2-isocyanobutane (**16**) (reaction [4]).

The structure of **3** has been established previously (*1a*). The ^1H and ^{13}C nmr, and the infrared spectra provide convincing evidence for the structure of the isonitrile, **16**. The infrared spectrum shows peaks at both the aromatic nitrile (2229 cm^{-1}) and the aliphatic isonitrile (2131 cm^{-1}) carbon–nitrogen triple-bond stretching frequencies. The ^1H and ^{13}C nmr spectra show the expected patterns; particularly informative is coupling of the signal, in the ^1H nmr spectrum, assigned to the hydrogens vicinal to the isonitrile (1.34 ppm), due to the ^{14}N nuclear spin. In the ^{13}C nmr spectrum, signals due to the isonitrile carbon (155.95 ppm) and the carbon directly bonded to the isonitrile (63.78 ppm) also show distinctive coupling due to the ^{14}N nucleus.

Major photo-NOCAS adducts resulting from the irradiation of an acetonitrile solution of 2-methyl-2-butene (**10**), 1,4-dicyanobenzene (**1**), biphenyl (**8**), and potassium cyanide were the nitriles **17** and **18** (reaction [5]). The first indication of the regiochemistry of these isomers was from the mass spectrum (gc/ms), which showed a dominant fragment of 144 *m/z* ($C_{10}H_{10}N$) for **17**, due to the arylpropyl fragment, and of 130 *m/z* (C_9H_8N) for **18**, due to the arylethyl fragment. The aliphatic region of the ^1H nmr spectrum of **17** shows a doublet (1.10 ppm) corresponding to a methyl group adjacent to a methine group. The proton of the methine group bonded to the nitrile produces a quartet at lower field (2.97 ppm). The typical AA′XX′ pattern in the aromatic region of the ^1H nmr is indicative of the 4-cyanophenyl group. In the ^{13}C nmr spectrum, the cyano-substituted methine group shows up as a doublet (37.61 ppm) and the aryl-substituted carbon appears as a singlet (40.27 ppm).

The ^1H and ^{13}C nmr spectra for compound **18** show characteristic patterns similar to those of **17**. In the aliphatic region of the ^1H nmr spectrum a doublet (1.50 ppm) corresponds to the methyl group adjacent to a methine group. The proton of the methine group, bonded to the aryl group, produces a quartet at lower field (2.77 ppm). In the ^{13}C nmr spectrum, the cyano-substituted carbon appears as a singlet (37.06 ppm) and the benzylic carbon as a doublet (48.15 ppm). The major adduct (**17**:**18**, 4.5:1) results from initial bonding of the cyanide anion to the radical cation, $\mathbf{10}^{+\cdot}$, at the less substituted alkene carbon, giving the more heavily alkyl-substituted radical intermediate, i.e., *anti*-Markovnikov addition.

The isonitriles, **19** and **20**, are minor products from reaction [5]. The ^1H and ^{13}C nmr and the infrared spectra provide convincing evidence for the structures of **19** and **20**. The first indication for the structure of these isonitriles, **19** and **20**, came from the infrared spectra, which again show peaks at both the aromatic nitrile and aliphatic isonitrile carbon–nitrogen triple-bond stretching frequencies. The ^1H and ^{13}C nmr spectra show the expected patterns, including significant coupling of the geminal and vicinal hydrogens, due to the ^{14}N nuclear spin, in the ^1H nmr of **19** and to the vicinal hydrogens in the ^1H nmr of **20**. In the ^{13}C nmr spectrum, the isonitrile carbon, as well the carbon directly bonded to the isonitrile, shows distinctive coupling to the ^{14}N nucleus.

The products resulting from irradiation of an acetonitrile solution of 2-methyl-1,3-butadiene (**11**), **1**, **8**, and potassium cyanide, were 3-(4-cyanophenyl)-3-methyl-4-pentenenitrile

[3] Crystallographic data for **28** and **29** may be purchased from: The Depository of Unpublished Data, Document Delivery, CISTI, National Research Council Canada, Ottawa, Canada K1A 0S2. Details of data collection, structural analysis and refinement, and tables of interatomic distances and bond angles have also been deposited with the Cambridge Crystallographic Data Centre and may be obtained on request from the Director, Cambridge Crystallographic Data Centre, University Chemical Laboratory, 12 Union Road, Cambridge, CB2 1EZ, U.K.

© 1997 NRC Canada

Can. J. Chem. Downloaded from www.nrcresearchpress.com by 88.146.161.215 on 09/08/12
For personal use only.

Can. J. Chem. Downloaded from www.nrcresearchpress.com by 88.146.161.215 on 09/08/12
For personal use only.

(**21**) and 3-(4-cyanophenyl)-4-methyl-4-pentenenitrile (**22**) (reaction [6]). The ^{1}H and ^{13}C nmr spectra provide good evidence for the structures of **21** and **22** as photo-NOCAS 1,2-adducts. Compound **21** results from attack of cyanide anion at the more heavily substituted end of the diene radical cation (C-1), generating the more heavily substituted allylic radical. Coupling of this allylic radical at the more heavily substituted carbon, with the anion radical, $\mathbf{1}^{-\bullet}$, at the *ipso* position, generates the terminal alkene. Evidence for this regiochemistry is the two doublets and a multiplet (5.19, 5.34, and 6.02 ppm) in the vinyl proton region of the ^{1}H nmr spectrum. This spectrum also exhibits a singlet (1.61 ppm) due to the methyl group and a lower-field singlet (2.77 ppm) for the cyanomethylene group.

In the ^{13}C nmr spectrum of compound **21**, there is a triplet (29.82 ppm) indicative of a methylene carbon substituted by a cyano group. There is a lower-field singlet (43.58 ppm) that is consistent with an aryl-substituted quaternary carbon. There are also two low-field singlets (117.18 and 118.44 ppm) consistent with two distinctive cyano groups. The ^{13}C nmr spectrum also exhibits a triplet (115.34 ppm) for the terminal vinyl methylene and a doublet for the vinyl methine (141.93 ppm), additional evidence for the mono-substituted alkene.

Compound **22** was identified as 3-(4-cyanophenyl)-4-methyl-4-pentenenitrile, which would result from initial attack of cyanide anion at the less substituted end of the diene radical cation. The presence of the disubstituted alkene is supported by two apparent singlets in the vinyl proton region (4.99 and 5.11 ppm) assigned to the geminal protons. The ^{1}H nmr spectrum also exhibits a singlet (1.61 ppm) indicative of the methyl group and an ABX pattern (2.72, 2.85, and 3.66 ppm) for the protons of the methylene group, next to a cyano group, and of the benzylic, allylic methine group.

The ^{13}C nmr spectrum of compound **22** exhibits a triplet (22.43 ppm) that is indicative of the methylene group substituted by the cyano group. There is a lower-field doublet (48.55 ppm) that is consistent with an aryl-substituted methine group. And there are two singlets (117.83 and 118.95 ppm) supporting two cyano groups. The ^{13}C nmr spectrum also exhibits a triplet (113.21 ppm) for the terminal vinyl methylene and a singlet (143.18 or 145.06 ppm) due to the quaternary vinyl carbon, further supporting the existence of the disubstituted alkene.

When an acetonitrile solution of 2,3-dimethyl-1,3-butadiene (**12**), **1**, **8**, and potassium cyanide was irradiated, 1:1:1 adducts **23** and **24** were produced (reaction [7]). Compound **23** was identified as 3-(4-cyanophenyl)-3,4-dimethyl-4-pentenenitrile, a 1,2-addition product. The ^{1}H and ^{13}C nmr spectra were similar to those of **21**; however, there are only two singlets in the vinyl region of the ^{1}H nmr spectrum (5.07 and 5.15 ppm), indicative of a terminal, disubstituted alkene. In the ^{13}C nmr spectrum, there are signals due to a vinyl quaternary carbon (147.00 or 148.84 ppm) and a vinyl methylene (113.06 ppm).

Compound **24** was identified as (*E*)-5-(4-cyanophenyl)-3,4-dimethyl-2-pentenenitrile, which may result from isomerization (tautomerization) of the initially formed 1,4-adduct, 5-(4-cyanophenyl)-3,4-dimethyl-3-pentenenitrile. The ^{1}H and ^{13}C nmr spectra of **24** both support the assigned structure. The ^{1}H nmr spectrum shows a doublet (1.08 ppm) that represents a methyl group bonded to a methine group, a singlet (2.06 ppm) due to the methyl group bonded to a vinyl carbon, and multiplets of an ABC second-order pattern (2.62, 2.69, and 2.82 ppm) for the protons of the benzylic methylene group and the allylic methine group. One olefinic proton appears as a singlet (5.05 ppm) and the typical AA′XX′ pattern in the aromatic region of the ^{1}H nmr spectrum is indicative of the 4-cyanophenyl group.

The *E*-configuration was assigned on the basis of the observed nuclear Overhauser effect (nOe). When the signal due to the allylic methyl group was irradiated a small nOe was observed in the signal of the methine and methylene hydrogens (ABC second-order pattern) and of the *ortho*-aryl H's. Irradiation of the signal due to the vinyl hydrogen caused a large nOe on the signals due to the methine and methylene hydrogens (ABC second-order pattern) and the *ortho*- and *meta*-aryl hydrogens.

In the ^{13}C nmr spectrum, there are distinctive carbon shifts, further supporting the structure proposed for compound **24**. The signal at 95.89 ppm is distinctive for an alkene methine group, cyano substituted (7). The quaternary alkene carbon β to the cyano group absorbs at 167.39 ppm. There are also two low-field singlets (116.84 and 118.74 ppm) supporting two different cyano groups. These chemical shifts were reproduced using the Advanced Chemical Development's ^{13}C nmr spectra simulation program; the calculated values are in good agreement with the observed chemical shifts.[4]

When an acetonitrile solution of 4-methyl-1,3-pentadiene (**13**), **1**, **8**, and potassium cyanide was irradiated, two photo-NOCAS adducts, **25** and **26**, were obtained (reaction [8]). Compound **25** was identified as the *anti*-Markovnikov 1,2-addition product, 3-(4-cyanophenyl)-5-methyl-4-hexenenitrile. This regioisomer is the result of initial bonding of cyanide anion at the less substituted end of the diene radical cation, $\mathbf{13}^{+\bullet}$, generating the more heavily alkyl-substituted allylic radical intermediate. The presence of the trisubstituted alkene is supported by a doublet (5.35 ppm, J = 9.3 Hz) in the vinyl proton region of the ^{1}H nmr spectrum, which represents coupling to the allylic methine proton. The ^{1}H nmr spectrum also exhibits two singlets (1.69 and 1.77 ppm), indicative of the two nonequivalent methyl groups bonded to the alkene, and an ABX multiplet (2.66, 2.70, and 3.97 ppm) for the protons of the methylene group next to a cyano group and that of the benzylic, allylic methine group.

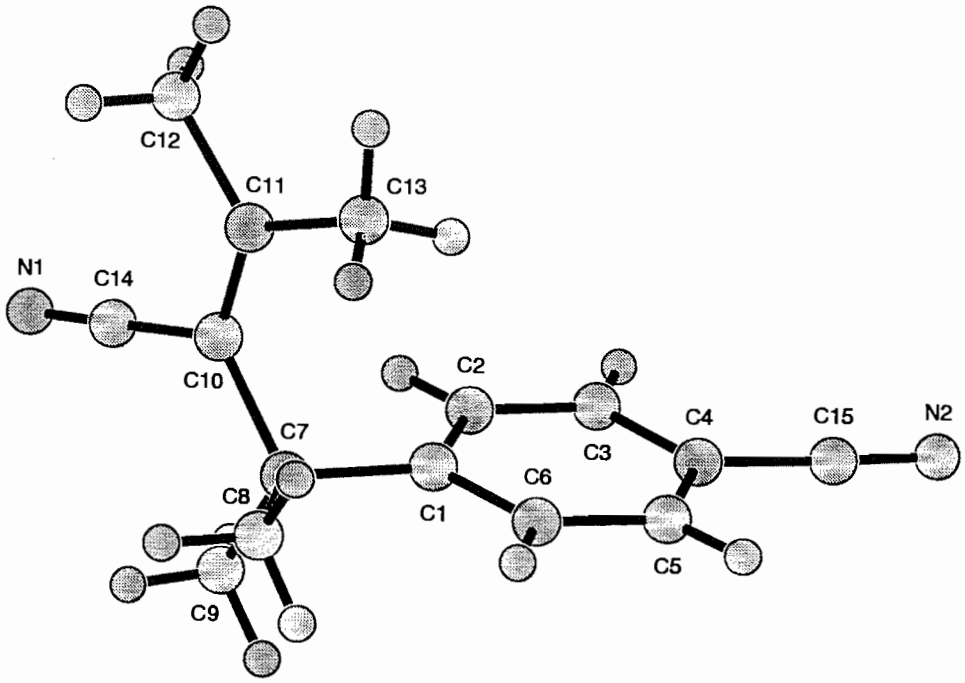
The ^{13}C nmr spectrum of compound **25** exhibits a triplet (24.90 ppm) indicative of the methylene group substituted by the cyano group. There is a lower-field doublet (40.56 ppm) that is consistent with an aryl-substituted methine carbon. There are two low-field singlets (117.92 and 118.64 ppm) consistent with two cyano groups. The ^{13}C nmr spectrum also exhibits a doublet (123.08 ppm), for the vinyl methine group, and a singlet (136.94 ppm), for the quaternary vinyl carbon, further supporting the presence of the trisubstituted alkene.

Compound **26** was identified as the 1,4-addition product, (*E*)-5-(4-cyanophenyl)-2,2-dimethyl-3-pentenenitrile, resulting from attack of the cyanide anion at the more heavily substituted terminal end of the diene. The first indication of the

[4] Software available from: Advanced Chemical Development, Inc., 141 Adelaide Street, West, Suite 1501, Toronto, ON M5H 3L5, Canada.

© 1997 NRC Canada

Fig. 1. X-ray crystal structure of 4-(4-cyanophenyl)-2,4-dimethyl-2-pentene-3-nitrile (**28**).



Can. J. Chem. Downloaded from www.nrcresearchpress.com by 88.146.161.215 on 09/08/12
For personal use only.

regiochemistry of this isomer was obtained from the mass spectrum (gc/ms), which shows a dominant fragment of 142 *m/z* ($C_{10}H_8N$) due to loss of the cyanopropyl fragment. There is a singlet (1.41 ppm) in the aliphatic region of the ^{1}H nmr spectrum, representing the two chemically equivalent methyl groups, a lower-field doublet (2.47 ppm) indicating the presence of an aryl-substituted allylic methylene group, and an AA′XX′ pattern in the aromatic region indicative of the 4-cyanophenyl group. A doublet of triplets and a doublet (6.40 and 6.55 ppm, respectively) appear in the vinyl region, each with a coupling constant (15.9 Hz) typical of a *trans* configuration. The infrared spectrum shows a peak at the C-H bending frequency (973 cm^{-1}) further supporting the *trans* configuration for this alkene. In the ^{13}C nmr spectrum of **26**, there is a singlet (32.65 ppm) due to the quaternary carbon substituted by a cyano group and a triplet (44.32 ppm) for the methylene carbon substituted by the aryl group.

Irradiation of an acetonitrile solution of 2,4-dimethyl-1,3-pentadiene (**14**), **1**, **8**, and potassium cyanide gave three 1:1:1 adducts: **27**, **28**, and **29** (reaction [9]). Compound **27** was identified as the *anti*-Markovnikov 1,2-addition product, 3-(4-cyanophenyl)-3,5-dimethyl-4-hexenenitrile. Initial attack of cyanide anion at the less substituted end of the diene radical cation, $\mathbf{14}^{+\bullet}$, gives the more heavily alkyl-substituted allylic radical intermediate. The presence of the trisubstituted alkene is supported by a broad singlet in the vinyl proton region (5.54 ppm) of the ^{1}H nmr spectrum. The ^{1}H nmr spectrum also exhibits three singlets (1.14, 1.64, and 1.76 ppm) indicative of the two nonequivalent methyl groups bonded to the alkene and the allylic methyl group. Also in the ^{1}H nmr spectrum, an AB apparent singlet was observed (2.68 ppm) for the diastereotopic protons of the methylene group bearing the cyano group.

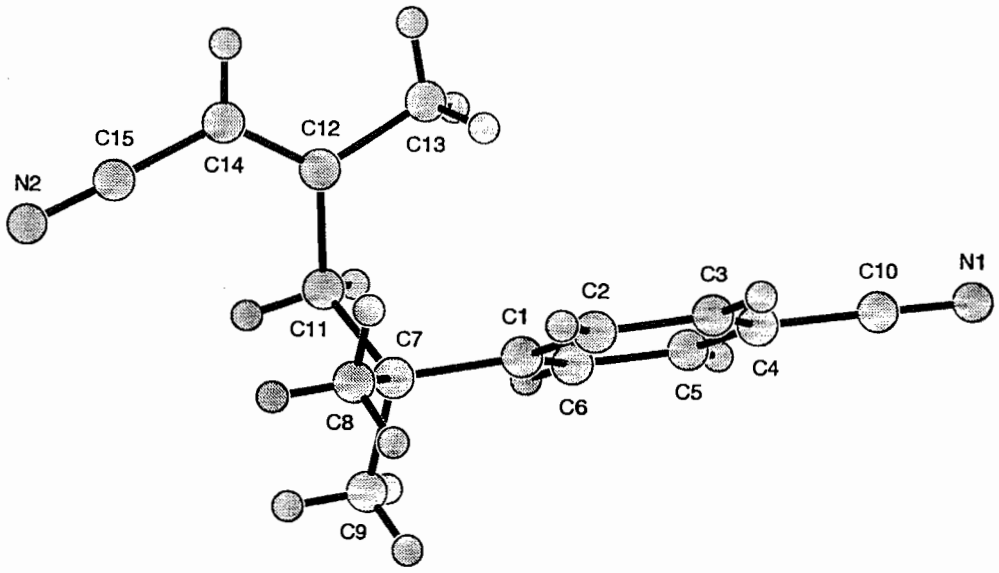
The ^{13}C nmr spectrum of compound **27** exhibits a triplet (33.44 ppm) indicative of the methylene group substituted by the cyano group. There is a lower-field singlet (41.90 ppm) that is consistent with an aryl-substituted quaternary carbon. There are also two singlets (117.63 and 118.71 ppm) supporting two cyano groups. The ^{13}C nmr spectrum also exhibits a doublet (129.15 ppm) for the vinyl methine group and the quaternary vinyl carbon shows up as a singlet (137.27 ppm), further indicating the trisubstituted alkene.

Compound **28**, 4-(4-cyanophenyl)-2,4-dimethyl-2-pentene-3-nitrile, was identified as a possible product of the allene, 2,4-dimethyl-2,3-pentadiene (**15**), which could be an impurity in the starting diene. The ^{1}H nmr spectrum exhibits three singlets (1.31, 1.58, and 2.11 ppm), indicative of the four methyl groups; the singlet at 1.58 ppm represents the pair of magnetically equivalent methyl groups. The ^{13}C nmr spectrum of compound **28** exhibits a singlet (41.08 ppm) that indicates a quaternary carbon substituted by the 4-cyanophenyl group. There are also three singlets (118.26, 118.32, and 118.71 ppm) supporting two types of cyano groups and the quaternary vinyl carbon, cyano substituted. The ^{13}C nmr spectrum also exhibits a singlet (154.57 or 155.69 ppm) representing a quaternary vinyl carbon, alkyl substituted. The overall structure of **28** was firmly established by X-ray analysis of a single crystal (Fig. 1).[3]

Compound **29** was identified as (**Z**)-5-(4-cyanophenyl)-3,5-dimethyl-2-hexenenitrile, which, we believe, results from the tautomerization of the initially formed 1,4-addition product, 5-(4-cyanophenyl)-3,5-dimethyl-3-hexenenitrile. The ^{1}H and ^{13}C nmr spectra are consistent with this structure for compound **29**. The ^{1}H nmr spectrum shows two high-field singlets (1.39 and 1.46 ppm) indicative of the three methyl groups; the singlet at 1.46 ppm is due to the two magnetically equivalent methyl groups. There is a low-field singlet (2.79 ppm) due to the allylic methylene group and a singlet (5.17 ppm) for the vinyl proton. In the ^{13}C nmr spectrum, a doublet (99.24 ppm) is distinctive for the alkene methine group, cyano substituted

© 1997 NRC Canada

Fig. 2. X-ray crystal structure of (*Z*)-5-(4-cyanophenyl)-3,5-dimethyl-2-hexenenitrile (**29**).



(7). The alkene carbon β to the cyano group shows up at low field (162.15 ppm). There are two singlets (117.21 and 118.79 ppm) supporting two types of cyano groups. The *Z*-configuration, as well as the overall structure of **29**, was firmly established by X-ray analysis on a single crystal (Fig. 2).[3]

Discussion

There is a dramatic increase in yield of the photo-NOCAS adduct(s), incorporating cyanide anion, through the series of alkenes: 2-methylpropene (**9**) (0%) < 2-methyl-2-butene (**10**) < 2,3-dimethyl-2-butene (**2**) (20%), and through the series of conjugated dienes: 2-methyl-1,3-butadiene (**11**) (3%) < 2,3-dimethyl-1,3-butadiene (**12**) < 4-methyl-1,3-pentadiene (**13**) < 2,4-dimethyl-1,3-pentadiene (**14**) < 2,5-dimethyl-2,4-hexadiene (**6**) (80%!). Increasing alkyl substitution on the alkene or diene correlates with increased yields of photo-NOCAS adduct(s) incorporating cyanide anion. This trend was not evident in the analogous reactions involving alcohol (methanol) as the nucleophile. The observed dependence in yield of photo-NOCAS adduct(s), through these series, can be attributed to the concomitant decrease in the oxidation potential of the alkene and diene associated with increasing alkyl substitution (Table 1).

The determination of the oxidation potential of cyanide anion, by electrochemical methods, is complicated by ion-pair formation, solvent interaction, adsorption on the electrode, etc. (9, 10). Under some conditions, oxidation begins at an electrode potential as low as +0.6 V (SCE) (9); however, the best estimate of the half-wave potential ($E_{½}^{ox}$, $CN^{-}/CN^{\cdot}$) is +1.65 V (SCE, DMF) (9*d*). Therefore, nucleophilic attack of cyanide anion on the radical cation of an alkene or diene that has an oxidation potential greater than ca. +1.5 V will be accompanied by electron transfer; oxidation of the cyanide anion to the cyano radical by the alkene or diene radical cation will compete with the combination. Similar results have been reported for the anodic cyanation of aromatic compounds where the highest yields of mono-cyanation products were obtained on aromatic substrates with oxidation potentials less than +1.3 V (SCE) (9*a*,*b* and 10*a*,*b*).

Table 1. Oxidation potentials of alkenes and dienes.

Alkene/diene	$E_{1/2}^{Ox}$ (V,SCE)	Reference
2-Methylpropene (**9**)	2.64	1*d*
2-Methyl-2-butene (**10**)	2.03	1*e*
2,3-Dimethyl-2-butene (**2**)	1.62	1*d*
2-Methyl-1,3-butadiene (**11**)	2.25	1*b*
2,3-Dimethyl-1,3-butadiene (**12**)	2.16	1*b*
4-Methyl-1,3-pentadiene (**13**)	1.51	This work[a]
2,4-Dimethyl-1,3-pentadiene (**14**)	1.52	This work[a]
2,5-Dimethyl-2,4-hexadiene (**6**)	1.24	1*b*
2,4-Dimethyl-2,3-pentadiene (**15**)	1.93	This work[a]
1,1-Diphenylethylene	1.82	2*a*

[a]The anodic wave was irreversible; the half-wave potential was taken as 0.028 V before the peak potential (8).

The ultimate fate of the cyano radical is not known. Certainly the cyano radical is very reactive; it reacts at essentially the diffusion-controlled rate with alkanes and alkenes, with itself, with cyanide anion, and with acetonitrile (11).

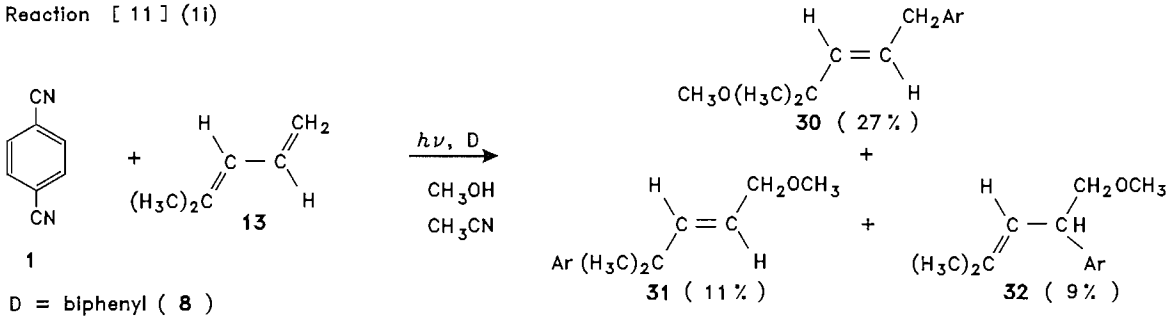
Since the first examples of the photo-NOCAS reaction, the regiochemistry of the initial bonding step has been termed *anti*-Markovnikov; that is, the nucleophile (methanol) adds to that end of the radical cation which is less heavily substituted, less sterically hindered, to give the more heavily substituted (more stable?) radical intermediate (1). The (superficial) analogy with the mechanism for free-radical addition to alkenes and dienes is obvious (12).

Usually the more heavily alkyl-substituted radical is also the more stable; however, there are exceptions. Compare the product ratios, Markovnikov *vs.* *anti*-Markovnikov, for the cyanide and methanol addition to the radical cation of 4-

© 1997 NRC Canada

Can. J. Chem. Downloaded from www.nrcresearchpress.com by 88.146.161.215 on 09/08/12
For personal use only.

Reaction [11] (1i)



D = biphenyl (**8**)
Ar = 4-cyanophenyl

methyl-1,3-pentadiene ($\mathbf{13}^{+\cdot}$) (reactions [8] and [11] (1*i*)). The major photo-NOCAS adduct isolated from reaction [8] is **25** (14%), the *anti*-Markovnikov adduct; the Markovnikov adduct, **26**, is a minor (1%) product. Relevant isodesmic reactions, [8*a*] and [8*b*], are in agreement; both high-level ab initio molecular orbital calculations (MP2/6-31G*//HF/6-31G*) and heats of formation based upon the empirically derived Benson's rules indicate that the more heavily substituted allylic radical, $\mathbf{25a}^{\cdot}$, is the more stable. The cyanide anion bonds preferentially to the less substituted, less sterically hindered, end of the radical cation, $\mathbf{13}^{+\cdot}$ which yields the more stable radical intermediate.

The major photo-NOCAS adduct from reaction [11] is **30**, the Markovnikov adduct. The product ratio, **30** (Markovnikov):**31** + **32** (*anti*-Markovnikov), is 1.4:1. Both ab initio molecular orbital calculations and empirically derived heats of

[8*a*] $NC-C(CH_3)_2-\dot{C}H-CH-CH_2 \rightleftharpoons (CH_3)_2\dot{C}-CH-CH-CH_2CN$

26a$^{\cdot}$ **25a**$^{\cdot}$

ΔH (kJ mol^{-1}) −4.7 (calcd.)[a]

[8*b*] $NC-C(CH_3)_3 + H_3C-\dot{C}H-CH-CH_2 \rightleftharpoons H_3C-CH_2CN + (CH_3)_2\dot{C}-CH-CH-CH_3$

ΔH (kJ mol^{-1}) −3.3 (calcd.)[a] −16.0 (calcd.)[b]

[11*a*] $H_3C-O-C(CH_3)_2-\dot{C}H-CH-CH_2 \rightleftharpoons (CH_3)_2\dot{C}-CH-CH-CH_2-O-CH_3$

30a$^{\cdot}$ **31a**$^{\cdot}$

ΔH (kJ mol^{-1}) +5.1 (calcd.)[a] +5.8 (calcd.)[b]

[11*b*] $H_3C-O-C(CH_3)_3 + H_3C-\dot{C}H-CH-CH_2 \rightleftharpoons H_3C-CH_2-O-CH_3 + (CH_3)_2\dot{C}-CH-CH-CH_3$

ΔH (kJ mol^{-1}) +2.0 (calcd.)[a] +0.8 (calcd.)[b]

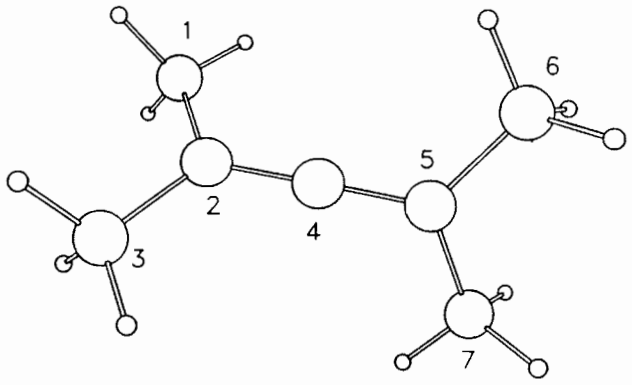
[a] MP2/6-31G*//HF/6-31G*
[b] Benson's rules.

Can. J. Chem. Downloaded from www.nrcresearchpress.com by 88.146.161.215 on 09/08/12
For personal use only.

© 1997 NRC Canada

Can. J. Chem. Downloaded from www.nrcresearchpress.com by 88.146.161.215 on 09/08/12
For personal use only.

Table 2. Calculated (MP2/6-31G*//HF/6-31G*) Mulliken charge (charge on hydrogens summed in with bound carbon) and spin density for the radical cation of 2,4-dimethyl-2,3-pentadiene (**15**$^{+\cdot}$).



Atom	Charge	Spin	Structure
1	0.186	−0.029	∠ 2,4,5 180°
2	0.059	0.361	Dihedral ∠ 1,2,3,4 180°
3	0.186	−0.029	Dihedral ∠ 1,2,5,6 55.2°
4	0.138	0.267	
5	0.059	0.361	Total energy (Hartree)
6	0.186	−0.029	−272.625 62 au
7	0.186	−0.029	

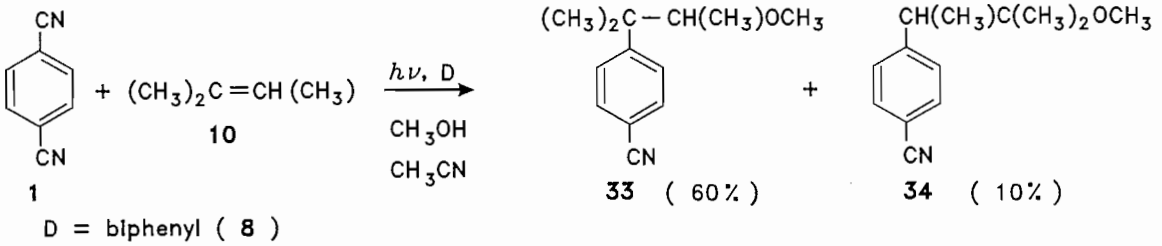
formation indicate that, in this case, the more heavily substituted allylic radical, **31a**$^{\cdot}$, is **not** the more stable (isodesmic reactions [11*a*] and [11*b*] (1*i*)). The effect of alkyl substitution on the carbon bearing the ether-oxygen obviously has a greater influence on the stability of this intermediate than does alkyl substitution on the allylic radical moiety. Of course, the total structure of the intermediate must be considered, not just the radical moiety. Upon addition of this neutral nucleophile, methanol, the initially formed distonic radical cation allows equilibration of the intermediates; steric factors, which generally influence the rate of addition, are less important.

There are previous reports of nucleophilic addition to the radical cation of an allene (13). Formation of 4-(4-cyanophenyl)-2,4-dimethyl-2-pentene-3-nitrile (**28**) indicates cyanide anion addition to the central carbon of the radical cation of 2,4-dimethyl-2,3-pentadiene (**15**$^{+\cdot}$) (reaction [10]). Nucleophilic attack at the central carbon of this radical cation is as expected; the molecular orbital calculations (MP2/6-31G*//HF/6-31G*) indicate the positive charge density is greater at the central carbon than at the terminal carbons (Table 2). In marked contrast, the spin density is greater at the termini than at the central carbon. Nucleophilic attack at the less sterically hindered central carbon also yields (ultimately) the stabilized allylic radical. The lack of isonitrile from this reaction is indicative that this allene radical cation is reacting as a "soft" electrophile; this is consistent with the delocalized charge. The calculated structure for the radical cation, **15**$^{+\cdot}$, is in good agreement with the experimentally determined structure and with lower level molecular orbital calculations (14).

The two photo-NOCAS reactions involving 2-methyl-2-butene (**10**), reactions [5] and [12] (1*b*), allow the comparison of the regiochemistry of the combination with cyanide anion, yielding both nitriles, **17** and **18**, and isonitriles, **19** and **20**, and, with methanol, yielding the ethers, **33** and **34**. The ratios of isomeric adducts (*anti*-Markovnikov:Markovnikov) are, for the nitriles, 4:1, for the isonitriles, >30:1, and, for the ethers, 6:1 (1*e*)). Relevant isodesmic reactions are summarized in Table 3.

For the nitriles, the two possible intermediates are directly compared in reaction [a]. The difference in total energy calculated by the ab initio molecular orbital method (MP2/6-31G*// HF/6-31G*) is still in agreement with the observed product

Reaction [12] (1e)



© 1997 NRC Canada

Table 3. Isodesmic reactions.

		ΔH (kJ mol^{-1})		
	R	MP2/6–31G*//HF/6–31G*[a]	Benson's rules[b]	Experimental[c]
[a]		R—$(CH_3)_2$C—$\dot{C}$H(CH_3)	⇌	$(CH_3)_2\dot{C}$—CH(CH_3)—R
	-CN	−5.6		
	-NC	+0.9		
	-OCH_3	−6.4	−2.1	
[b]		R—$(CH_3)_2$C—CH_3 + H_3C—$\dot{C}$H(CH_3)	⇌	H_3C—CH(CH_3)—R + $(CH_3)_2\dot{C}$—CH_3
	-CN	−3.5	−10.6	
	-NC	+2.0		
	-OCH_3	−4.1	−1.9	−6.7
[c]		R—$(CH_3)_2$C—CH_2CH_3	⇌	$(CH_3)_2$CH—CH(CH_3)—R
	-CN	+3.5	−2.5	
	-NC	+9.5		
	-OCH_3	+5.0	+6.3	
[d]		$CH_3)_2$CH—$\dot{C}$H(CH_3)	⇌	$(CH_3)_2\dot{C}$—CH_2CH_3
		−9.8	−8.1	
[e]		R—$(CH_3)_2$C—CH_2CH_3 + $(CH_3)_2$CH—$\dot{C}$H(CH_3)	⇌	$(CH_3)_2$CH—CH(CH_3)—R + $(CH_3)_2\dot{C}$—CH_2CH_3
	-CN	−6.3	−10.6	
	-NC	−0.3		
	-OCH_3	−4.8	−1.8	
[f]		R—$C(CH_3)_3$	⇌	$(CH_3)_2CCH_2$—R
	-CN	+8.4		
	-NC	+21.6		
	-OCH_3	+15.3	+21.3	

[a]Ab initio molecular orbital calculations (MP2/6-31G*//HF/6-31G*) (*5*, *6*).
[b]Empirically derived heats of formation, Benson's empirical rules (*15*).
[c]Experimentally determined heats of formation (*16*).

ratio; the *tertiary*-alkyl radical is more stable than the *secondary*-alkyl radical. The isodesmic reactions [b] and [e] are consistent. The ab initio calculations indicate that the nitrile with greater alkyl substitution on the carbon bearing the cyano group is slightly more stable (reaction [c]); as a result, the difference in stability between the *tertiary*- and *secondary*-alkyl radicals (reaction [d]) dominates.

For the isonitriles, the small difference in total energy of the two possible intermediates calculated by the ab initio molecular orbital method is now inconsistent with the observed product ratio (**19**:**20**, >30:1). In fact, in this case, the isodesmic reactions [a] and [b] indicate a preference for formation of the Markovnikov addition product (**20**). The isodesmic reaction [e] shows only a slight preference for the *tertiary*-alkyl radical. The isodesmic reaction [c] provides the explanation; increased alkyl substitution on the carbon bearing the isonitrile group is now significantly stabilizing, comparable to the effect of increased alkyl substitution on the alkyl radical.

For the ethers, the difference in total energy of the two possible β-alkoxyalkyl radicals (isodesmic reactions [a], [b], and [e]), calculated by the ab initio molecular orbital method is in good agreement with the observed product ratio; the *tertiary*-β-alkoxyalkyl radical is more stable than the *secondary*-β-alkoxyalkyl radical. The *tertiary* ether, methyl 2-methyl-2-butyl ether, is more stable than the *secondary* ether, methyl 3-methyl-2-butyl ether (isodesmic reaction [c]); however, the difference in stability between the *tertiary* and *secondary* alkyl radicals is even greater (isodesmic reaction [d]). Consequentially, the combined isodesmic reaction [e] is exothermic, consistent with the observed product ratio (1*e*,*i*).

These differences in the effect of alkyl substitution on the stability of the β-cyano, β-isocyano, and β-methoxy, alkyl radicals must be due to the difference in electron demand (the inductive effect) of the cyano, isocyano, and methoxy groups. The calculated (MP2/6-31G*//HF/6-31G*) charge and spin density distributions from Mulliken and natural population

© 1997 NRC Canada

Can. J. Chem. Downloaded from www.nrcresearchpress.com by 88.146.161.215 on 09/08/12
For personal use only.

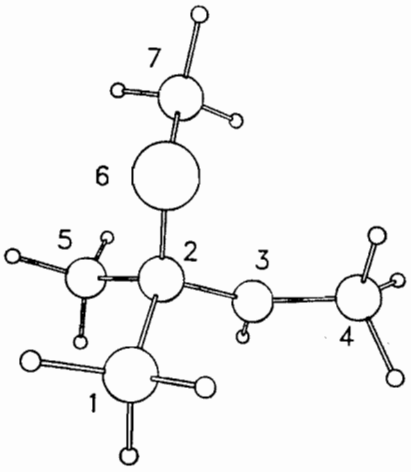
Can. J. Chem. Downloaded from www.nrcresearchpress.com by 88.146.161.215 on 09/08/12
For personal use only.

Table 4. Calculated (MP2/6-31G*//HF/6-31G*) Mulliken charge (charge on hydrogens summed in with bound carbon) and spin density.[a]

2-Methyl-2-butene – methanol radical (C-2 bonded) **34a**·

Atom	Charge	Spin
1	0.00 (0.00)	0.01 (0.01)
2	0.31 (0.27)	–0.13 (–0.07)
3	0.00 (0.07)	1.23 (1.02)
4	0.01 (–0.03)	–0.16 (–0.01)
5	0.03 (0.02)	0.03 (0.04)
6 (O)	–0.64 (–0.67)	0.01 (0.01)
7	0.30 (0.32)	0.01 (0.00)

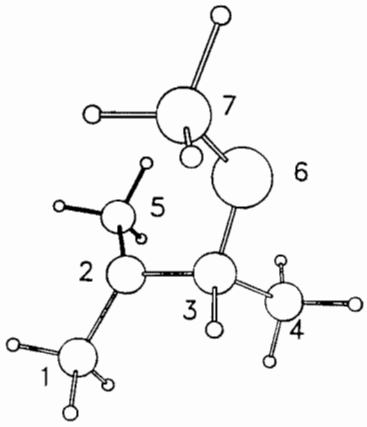
Structure
Length 3–6 2.4 Å
Dihedral ∠ 2,3,4,H 159.6°
Dihedral ∠ 6,2,3,4 48.4°
Total energy (Hartree)
–310.526 14 au



2-Methyl-2-butene – methanol radical (C-3 bonded) **33a**·

Atom	Charge	Spin
1	–0.01 (–0.02)	–0.16 (–0.01)
2	0.01 (0.07)	1.20 (1.03)
3	0.30 (0.30)	–0.13 (–0.06)
4	0.02 (0.01)	0.04 (0.04)
5	–0.01 (–0.03)	–0.16 (0.01)
6 (O)	–0.62 (–0.66)	0.01 (0.01)
7	0.30 (0.33)	0.01 (0.00)

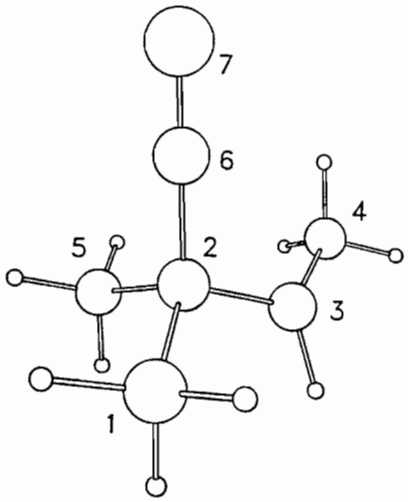
Structure
Length 2–6 2.4 Å
Dihedral ∠ 1,2,3,5 155.6°
Dihedral ∠ 6,3,2,1 156.5°
Total energy (Hartree)
–310.528 57 au



2-Methyl-2-butene – nitrile radical (C-2 bonded) **18a**·

Atom	Charge	Spin
1	0.08 (0.07)	0.04 (0.04)
2	–0.10 (–0.20)	–0.14 (–0.08)
3	0.05 (0.12)	1.23 (1.08)
4	0.03 (–0.02)	–0.16 (–0.09)
5	0.08 (0.07)	0.01 (0.01)
6	0.32 (0.33)	0.04 (0.04)
7 (N)	–0.47 (–0.38)	–0.03 (–0.03)

Structure
∠ 2,6,7 179.4°
Length 3–6 2.45 Å
Dihedral ∠ 2,3,4,H 158.1°
Dighedral ∠ 6,2,3,4 49.2°
Total energy (Hartree)
–288.347 30 au



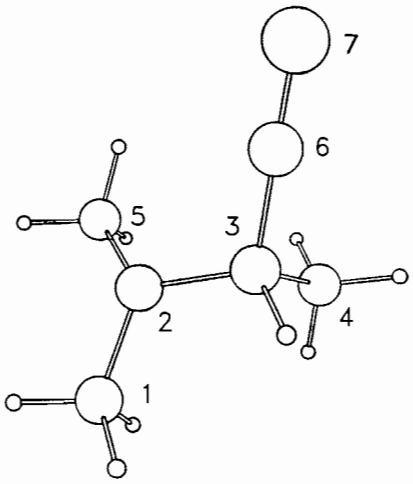
© 1997 NRC Canada

Table 4 (*continued*).

2-Methyl-2-butene – nitrile radical (C-3 bonded) **17a**·

Atom	Charge	Spin
1	0.01 (–0.02)	–0.16 (–0.09)
2	0.06 (0.12)	1.20 (1.04)
3	–0.01 (–0.11)	–0.15 (–0.08)
4	0.08 (0.06)	0.05 (0.05)
5	0.02 (–0.01)	–0.16 (–0.09)
6	0.31 (0.33)	0.05 (0.04)
7 (N)	–0.47 (–0.38)	–0.04 (–0.03)

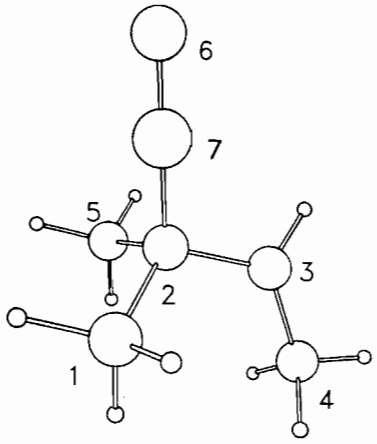
Structure
∠ 3,6,7 179.4°
Length 2–6 2.47 Å
Dihedral ∠ 1,2,3,5 155°
Dihedral ∠ 1,2,3,6 54.0°
Total energy (Hartree)
–288.349 44 au



2-Methyl-2-butene – isonitrile radical (C-2 bonded) **20a**·

Atom	Charge	Spin
1	0.08 (0.06)	0.04 (0.04)
2	0.13 (0.09)	–0.13 (–0.07)
3	0.05 (0.11)	1.23 (1.08)
4	0.02 (–0.02)	–0.16 (–0.09)
5	0.08 (0.05)	0.01 (0.01)
6	0.03 (0.35)	–0.02 (–0.02)
7 (N)	–0.38 (–0.65)	0.02 (0.02)

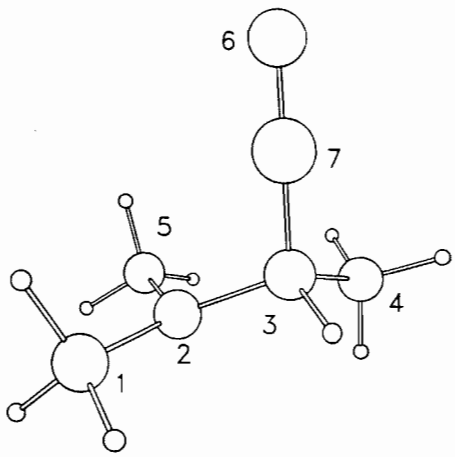
Structure
∠ 2,7,6 179.4°
Length 3–7 2.41 Å
Dihedral ∠ 2,3,4,H 156.7°
Dihedral ∠ 7,2,3,4 46.4°
Total energy (Hartree)
–288.311 70 au



2-Methyl-2-butene – isonitrile radical (C-3 bonded) **19a**·

Atom	Charge	Spin
1	0.01 (–0.02)	–0.16 (–0.09)
2	0.05 (0.12)	1.19 (1.03)
3	0.21 (0.17)	–0.11 (–0.06)
4	0.07 (0.05)	0.01 (0.01)
5	0.02 (–0.02)	–0.15 (–0.08)
6	0.03 (0.35)	0.00 (0.00)
7 (N)	–0.39 (–0.65)	0.03 (0.04)

Structure
∠ 3,7,6 178.6°
Length 2–7 2.4 Å
Dihedral ∠ 1,2,3,5 151.8°
Dihedral ∠ 7,3,2,1 73.8°
Total energy (Hartree)
–288.311 37 au



Can. J. Chem. Downloaded from www.nrcresearchpress.com by 88.146.161.215 on 09/08/12
For personal use only.

© 1997 NRC Canada

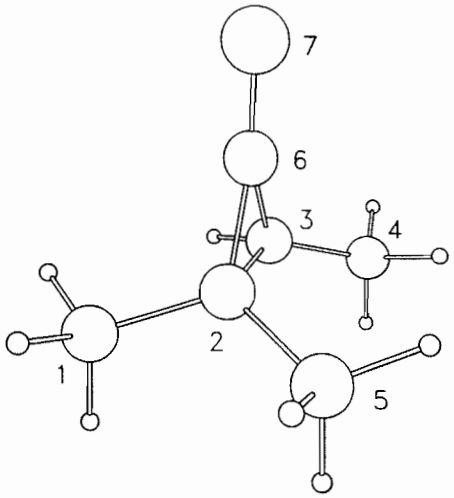
Can. J. Chem. Downloaded from www.nrcresearchpress.com by 88.146.161.215 on 09/08/12
For personal use only.

Table 4 (*concluded*).

2-Methyl-2-butene – nitrile radical (bridged)

Atom	Charge	Spin
1	0.05 (0.05)	−0.02 (−0.01)
2	−0.03 (−0.07)	0.23 (0.17)
3	0.00 (−0.01)	0.21 (0.16)
4	0.05 (0.04)	−0.02 (−0.01)
5	0.05 (0.05)	0.01 (−0.01)
6	0.24 (0.15)	−0.77 (−0.60)
7 (N)	−0.38 (−0.20)	1.37 (1.29)

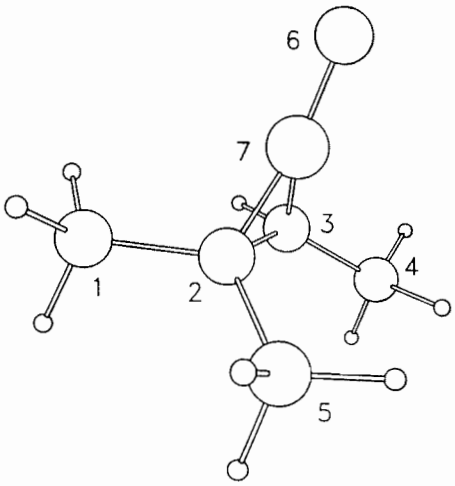
Structure
∠ 2,6,7 149.2°
∠ 3,6,7 148.9°
Length 2–6 1.50 Å
Length 3–6 1.49 Å
Length 2–3 1.53 Å
Length 6–7 1.23 Å
Dihedral ∠ 2,3,6,7 176.7°
Total energy (Hartree)
−288.313 00 au



2-Methyl-2-butene – isonitrile radical (bridged)

Atom	Charge	Spin
1	0.06 (0.04)	−0.01 (0.00)
2	0.15 (0.16)	0.13 (0.11)
3	0.19 (0.21)	0.12 (0.11)
4	0.05 (0.03)	−0.01 (0.00)
5	0.05 (0.04)	−0.01 (0.00)
6	−0.04 (0.18)	1.05 (0.99)
7 (N)	−0.45 (−0.66)	−0.27 (−0.20)

Structure
∠ 2,7,6 148.6°
∠ 3,7,6 148.3°
Length 2–7 1.44 Å
Length 3–7 1.44 Å
Length 2–3 1.51 Å
Length 6–7 1.28 Å
Dihedral ∠ 2,3,7,6 179.2°
Total energy (Hartree)
−288.247 17 au



[a]Values in parentheses are from natural charge and spin population analysis (*6d*).

analysis, for the radical intermediates involved in reactions [5], [8], and [12] are shown in Table 4. Summing the total charge on the substituent indicates the isocyano and methoxy groups are significantly more negative than the cyano group. This order is also evident from the charge on the β-carbon atoms. The carbon atoms directly bonded to the nitrogen of the isocyano group and to the ether oxygen are significantly more positively charged than the corresponding carbon bonded to the carbon of the cyano group. β-Substitution by a cyano, isocyano, or methoxy group has little effect on the spin density distribution of these radicals.

The calculations give an indication of the importance of bridging of the radical with these β-substituents (17). Starting with initially bridged β-cyano and β-isocyano radical structures, the calculations converge to relatively high-energy bridged radicals. Frequency calculations confirm that these bridged radicals are indeed minima. These bridged structures are significantly less stable than conformers that are not bridged, for the nitrile, 96 kJ mol^{-1}, and for the isonitrile 169 kJ mol^{-1}, above the global minimum. Starting with an initially bridged β-methoxy radical, constrained to equal carbon–oxygen bond lengths, the calculations did not converge. The calculations converge to the unbridged structure (**33a**$^{\bullet}$) upon removing the structural constraint.

These calculations also provide a direct comparison of the effect of alkyl substitution on the relative stability of the nitriles, the isonitriles, and the ethers, illustrated with the isodesmic reactions summarized in Table 3 [c] and [f]. The

© 1997 NRC Canada

Table 5. Isodesmic reactions indicating the difference in stability of nitriles and isonitriles.

$NC\text{-}C(CH_3)_3$ ⇌	$CN\text{-}C(CH_3)_3$
ΔH (kJ mol^{-1}) +92.1 (calcd.)[a]	
$H_3C\text{-}CH(CH_3)CN$ ⇌	$H_3C\text{-}CH(CH_3)NC$
ΔH (kJ mol^{-1}) +97.6 (calcd.)[a]	
$(CH_3)_2CH\text{-}CH_2CN$ ⇌	$(CH_3)_2CH\text{-}CH_2NC$
ΔH (kJ mol^{-1}) +105.3 (calcd.)[a]	

stabilizing effect of alkyl substitution on the carbon bearing the cyano group is relatively small; 2,2-dimethylpropanenitrile is 8.4 kJ mol^{-1} more stable than 3-methylbutanenitrile (*tertiary* vs. *primary*, reaction [f]) while 2,2-dimethylbutanenitrile is only 3.5 kJ mol^{-1} more stable than 2,3-dimethylbutanenitrile (*tertiary* vs. *secondary*, reaction [c]). The influence of alkyl substitution is greatest on the isonitrile; 2-isocyano-2-methylpropane is 21.6 kJ mol^{-1} more stable than 1-isocyano-2-methylpropane (*tertiary* vs. *primary*, reaction [f]) while 2-isocyano-2-methylbutane is 9.5 kJ mol^{-1} more stable than 2-isocyano-3-methylbutane (*tertiary* vs. *secondary*, reaction [c]). *tert*-Butyl methyl ether is also significantly (15.3 kJ mol^{-1}) more stable than isobutyl methyl ether (*tertiary* vs. *primary*, reaction [f]) and methyl 2-(2-methylbutyl) ether is more stable (5.0 kJ mol^{-1}) than methyl 2-(3-methylbutyl) ether (*tertiary* vs. *secondary*, reaction [c]) (1*i*).

It is also reassuring to note (Table 5) that there is good agreement between the differences in the calculated (ab initio) total energy and previously reported experimentally determined heats of isomerization for the alkyl isonitriles to nitriles (18).

Summary and conclusions

Cyanide anion can be an effective nucleophile in the photo-NOCAS reaction; yields of the nitrile can be high. Highest yields are obtained when the alkene or diene has an oxidation potential less than 1.5 V (SCE). When the oxidation potential of the alkene or diene is greater than 1.5 V, electron transfer from the cyanide anion to the alkene or diene radical cation competes with the combination.

With alkenes, both nitriles and isonitriles are obtained. Isonitriles were not observed from the dienes. The explanation is based upon the Hard-Soft-Acid-Base (HSAB) principle. The harder alkene radical cation adds to both the hard nitrogen and the soft carbon ends of the ambident cyanide anion. The relatively soft diene radical cation adds preferentially to the soft carbon end of this nucleophile.

The regiochemistry of the adduct, Markovnikov versus *anti*-Markovnikov, is determined during the initial bonding of the cyanide anion with the alkene or diene radical cation. Cyanide anion adds preferentially to the less sterically hindered end of the radical cation, which, on the way to nitrile, yields the more stable β-cyano alkyl radical intermediates. However, bonding of the cyanide anion at the nitrogen, on the way to isonitrile, gives the less stable β-isocyano alkyl radical intermediate.

The difference in regiochemistry of the photo-NOCAS reactions involving methanol and cyanide anion reflects the fact that the initially formed intermediate, upon the addition of methanol to the alkene or diene radical cation, is a distonic radical cation with the possibility of bridging and concomitant equilibration. The addition of cyanide anion to an alkene or diene radical cation leads directly to the β-cyano- or isocyanoalkyl radical, which are not bridged, and with no possibility for equilibration. Therefore, the addition of cyanide anion must be kinetically controlled, the reaction is significantly exothermic, the transition state is early; as with radical addition to alkenes and dienes, steric effects dominate.

The radical cation of allenes can also combine with cyanide anion in the photo-NOCAS reaction. The radical cation **15**$^{+\cdot}$ couples with the cyanide anion at the central carbon of the allene and only at the carbon of this ambident anion, as a soft-electrophile.

Experimental

General information

The ^{1}H and ^{13}C nmr spectra were obtained from a Bruker 250 MSL or a Bruker 400 MSL spectrometer. Spectra were recorded in parts per million (ppm) and frequencies are relative to tetramethylsilane. Infrared spectra (ir) were recorded on a Nicolet 205 or 510 FTIR and are reported in wave numbers (cm^{-1}). Elemental analyses were performed by the Canadian Microanalytical Service Ltd., B.C. Exact Mass determinations were obtained using a CEC 21-110 mass spectrometer. Melting points were determined using a Cybron Corporation Thermolyne apparatus with a digital thermocouple and are corrected. Product yields and progress of the reactions were determined using a Hewlett–Packard (HP) 5890 gas chromatograph with a DB-1701 fused silica WCOT column (30 m × 0.25 mm, 0.25-μm film thickness) and a calibrated flame ionization detector (gc/fid) and are based upon 1,4-dicyanobenzene (**1**) as the limiting reagent. An HP 3392A integrator was interfaced with the gc/fid to obtain peak areas. An HP 5890 gas chromatograph with a 5% phenyl methyl silicone fused silica WCOT column (25 m × 0.20 mm, 0.33-μm film thickness) interfaced with an HP 5970 mass selective detector (gc/ms) was also used for product analyses. Mass spectra are reported as *m/z* (relative intensity). Separation of product mixtures was generally carried out using preparative medium-pressure liquid chromatography (mplc) (1*d*). The mplc consists of a 2.5 cm × 1 m column packed with thin-layer chromatography (tlc) grade silica gel (without binder) (Rose Scientific Ltd., Cat. 81632) at a pressure of 19 psi using helium (1 psi = 6.9 kPa). Connected to the mplc was a uv spectrophotometer – fraction collector that collects ca. 10-mL fractions. Dry column flash chromatography (dc/fc) was also used (19). The column was packed with thin-layer chromatography grade silica gel (without binder) (Rose Scientific Ltd., Cat. 81632). Fraction sizes were ca. 5 mL.

Materials

Acetonitrile (Fisher ACS grade) was distilled twice, first from sodium hydride and then from phosphorus pentoxide. It was then passed through a column of basic alumina, refluxed over calcium hydride for 24 h (under a nitrogen atmosphere), fractionally distilled (under nitrogen), and stored over molecular sieves (3 Å) (20). Methanol was distilled and then stored over

© 1997 NRC Canada

Can. J. Chem. Downloaded from www.nrcresearchpress.com by 88.146.161.215 on 09/08/12
For personal use only.

Can. J. Chem. Downloaded from www.nrcresearchpress.com by 88.146.161.215 on 09/08/12
For personal use only.

molecular sieves (4 Å). 1,4-Dicyanobenzene (**1**) (Aldrich) was purified by treatment with Norite in methylene chloride, followed by recrystallization from 95% ethanol. Tetraethylammonium perchlorate (TEAP) (Aldrich) was recrystallized three times from water and then dried in a vacuum oven for 15 h, 70°C, 0.25 Torr (1 Torr = 133.3 Pa). 2,3-Dimethyl-2-butene, 98% (**2**), 2-methyl-2-butene, 99+% (**10**), 2-methyl-1,3-butadiene, 99% (**11**), 2,3-dimethyl-1,3-butadiene, 98% (**12**), 2,4-dimethyl-1,3-pentadiene, 98+% (**14**), 2,4-dimethyl-2,3-pentadiene, 97% (**15**), and 18-crown-6, 99% were obtained from the Aldrich Chemical Co. 2-Methylpropene (**9**) was obtained from Matheson and was of a minimum 99.0% purity. 4-Methyl-1,3-pentadiene, ≥98% (**13**) was obtained from Fluka Chemika-BioChemika. Biphenyl (**8**) (Eastman Kodak Co.) was recrystallized from methanol. Potassium cyanide was obtained from BDH, Inc.

Irradiations

Irradiations were generally carried out on acetonitrile solutions of the alkene or diene, 1,4-dicyanobenzene (**1**), biphenyl (**8**), potassium cyanide, and 18-crown-6 ether. Solutions were irradiated in either 2 cm i.d. Pyrex tubes or 5 mm Pyrex nmr tubes, which were degassed by nitrogen ebullition. These samples were irradiated at 10°C using a CGE 1-kW medium-pressure mercury vapour lamp contained in a water-cooled Pyrex immersion well.

Cyclic voltammetric measurements

Cyclic voltammetry was used to obtain the oxidation potential of the alkenes/ dienes. The apparatus has been described (21). The working electrode was a platinum sphere (1 mm diameter) and the counter electrode was a platinum wire. The reference electrode was a saturated calomel electrode (SCE), which was connected to the solution (TEAP 0.1 M, acetonitrile) through a Luggin capillary. The alkene/ diene concentration was ca. 0.005 M in acetonitrile. Since the anodic wave was irreversible, the half-wave potential was taken as 0.028 V before the anodic peak potential (8).

Formation of the cyanide anion, 2,3-dimethyl-2-butene (2), 1,4-dicyanobenzene (1) photo-NOCAS adducts 3 and 16: reaction [4]

A solution of 2,3-dimethyl-2-butene (**2**) (0.9 mL, 0.6 g, 0.0076 mol), 1,4-dicyanobenzene (**1**) (0.6 g, 0.0047 mol), biphenyl (**8**) (0.4 g, 0.0026 mol), potassium cyanide (0.3 g, 0.0046 mol), and 18-crown-6 (0.3 g, 0.0011 mol) in acetonitrile (40 mL) was degassed by nitrogen ebullition and irradiated for 43 h using a 1-kW lamp at 10°C. The solvent was removed to yield a crude photolysate. The crude photolysate was partially separated by repetitive chromatography (mplc) using a linear solvent gradient (hexanes – 10% diethyl ether, 90% hexanes). Two 1:1:1 adducts were detected (gc/ms) and were eluted (mplc) in the order **16** followed by **3**. Purification of **16** required preparative thin-layer chromatography on silica gel, eluting repeatedly with 5% diethyl ether, 95% hexanes.

*3-(4-Cyanophenyl)-2,3-dimethylbutanenitrile (**3**)*

The yield of **3** was 15%. The gc/ms of this compound was identical to that reported (1*a*).

*3-(4-Cyanophenyl)-2,3-dimethyl-2-isocyanobutane (**16**)*

The yield of **16** was 5%; infrared (Nicolet 205) ν: 2989(s), 2951(m), 2923(s), 2852(m), 2229(s), 2131(s), 1682(m), 1607(m), 1507(m), 1461(m), 1404(m), 1384(m), 1150(m), 1093(m), 1019(m), 843(m); ^{1}H nmr (250.13 MHz, $CDCl_3$) δ_{TMS}: 1.34 (st, 6H, $^3J_{1-N}$ = 1.8 Hz, 2 CH_3's (1-H)), 1.52 (s, 6H, 2 CH_3's), 7.58 (d, 2H, $^3J_{2'-3'}$ = 8.5 Hz, $^3J_{5'-6'}$ = 8.5 Hz, H's adjacent to alkyl-substituted aryl carbon (2′-H, 6′-H)), 7.64 (d, 2H, $^3J_{2'-3'}$ = 8.5 Hz, $^3J_{5'-6'}$ = 8.5 Hz, H's adjacent to cyano-substituted aryl carbon (3′-H, 5′-H)); ^{13}C nmr (62.90 MHz, $CDCl_3$) δ: 24.07 (q), 26.14 (q), 43.92 (s, quaternary carbon, aryl-substituted), 63.78 (st, quaternary carbon, isocyano substituted), 111.10 (s, quaternary aryl carbon, cyano substituted), 118.87 (s, CN), 129.13 (d, aromatic CH adjacent to alkyl-substituted aryl carbon), 131.67 (d, aromatic CH adjacent to cyano-substituted carbon), 149.40 (s, quaternary aryl carbon, alkyl substituted), 155.95 (st, R-N≡C); ms *m/z*: 51(7), 69(69), 76(5), 77(8), 89(10), 101(6), 102(6), 103(5), 104(17), 116(88), 117(10), 128(8), 130(7), 142(5), 144(100), 145(12), 170(6), 212(4). Exact Mass calcd. for $C_{14}H_{16}N_2$: 212.1313; found: 212.1326.

Irradiation of an acetonitrile solution of potassium cyanide, 2-methylpropene (9), 1,4-dicyanobenzene (1), and biphenyl (8)

A solution of 2-methylpropene (**9**) (0.054 g, 9.6×10^{-4} mol), 1,4-dicyanobenzene (**1**) (0.062 g, 4.8×10^{-4} mol), biphenyl (**8**) (0.040 g, 2.6×10^{-4} mol), potassium cyanide (0.030 g, 4.6×10^{-4} mol), and 18-crown-6 (0.025 g, 9.5×10^{-5} mol) in acetonitrile (4 mL) was degassed by nitrogen ebullition and irradiated for 16 h using a 1-kW lamp at 10°C. No photo-NOCAS products were detected (gc/ms, selective ion monitoring).

Formation of the cyanide anion, 2-methyl-2-butene (10), 1,4-dicyanobenzene (1) photo-NOCAS adducts 17, 18, 19, and 20: reaction [5]

A solution of 2-methyl-2-butene (**10**) (4.1 mL, 2.7 g, 0.038 mol), 1,4-dicyanobenzene (**1**) (2.5 g, 0.020 mol), biphenyl (**8**) (1.6 g, 0.010 mol), potassium cyanide (1.2 g, 0.018 mol), and 18-crown-6 (1.1 g, 0.0042 mol) in acetonitrile (160 mL) was degassed by nitrogen ebullition and irradiated for 24 h using a 1-kW lamp at 10°C. The solvent was removed to yield a crude photolysate. The crude photolysate was separated by repetitive chromatography (mplc) using a linear solvent gradient (hexanes – 10% diethyl ether, 90% hexanes). Four 1:1:1 adducts were detected (gc/ms) and these products were eluted (mplc) in the order **20**, **19**, **18** followed by **17**. Purification of **20** required preparative thin-layer chromatography on silica gel, eluting repeatedly with 5% diethyl ether, 95% hexanes.

*3-(4-Cyanophenyl)-2,3-dimethylbutanenitrile (**17**)*

The yield of **17** was 9%: the melting point was 70–71°C; infrared (Nicolet 205) ν: 2979(s), 2947(m), 2885(w), 2228(s), 1608(m), 1507(m), 1468(m), 1459(m), 1454(m), 1406(m), 1383(m), 1087(m), 1018(w), 915(m), 840(s), 734(s); ^{1}H nmr (250.13 MHz, $CDCl_3$) δ_{TMS}: 1.10 (d, 3H, $^3J_{1-2}$ = 7.3 Hz, CH_3 (1-H)), 1.52 (s, 6H, 2 CH_3's), 2.97 (q, 1H, $^3J_{1-2}$ = 7.3 Hz, H of methine group (2-H)), 7.52 (d, 2H, $^3J_{2'-3'}$ = 8.9 Hz, $^3J_{5'-6'}$ = 8.9 Hz, H's adjacent to alkyl-substituted aryl carbon (2′-H, 6′-H)), 7.66 (d, 2H, $^3J_{2'-3'}$ = 8.9 Hz, $^3J_{5'-6'}$ = 8.9 Hz, H's adjacent to cyano-substituted aryl carbon (3′-H, 5′-H)); ^{13}C nmr (62.90 MHz, $CDCl_3$) δ: 13.69 (q), 23.78 (q), 27.29 (q), 37.61 (d, CH, cyano substituted), 40.27 (s, quaternary carbon, aryl substi-

© 1997 NRC Canada

Can. J. Chem. Downloaded from www.nrcresearchpress.com by 88.146.161.215 on 09/08/12
For personal use only.

tuted), 110.75 (s, quaternary aryl carbon, cyano substituted), 118.62 (s, CN), 121.38 (s, CN), 127.07 (d, aromatic CH adjacent to alkyl-substituted aryl carbon), 132.31 (d, aromatic CH adjacent to cyano-substituted carbon), 150.46 (s, quaternary aryl carbon, alkyl substituted); ms *m/z*: 51(7), 75(6), 77(7), 89(8), 101(5), 102(5), 104(13), 116(70), 117(7), 128(6), 144(100), 145(11). Anal. calcd. for $C_{13}H_{14}N_2$: C 78.75, H 7.12, N 14.13; found: C 78.77, H 7.06, N 14.01.

*3-(4-Cyanophenyl)-2,2-dimethylbutanenitrile (**18**)*
The yield of **18** was 2%; infrared (Nicolet 205) ν: 2980(s), 2928(m), 2894(w), 2879(w), 2230(s), 1607(m), 1505(m), 1461(s), 1417(m), 1383(m), 1053(w), 841(s) ; ^{1}H nmr (250.13 MHz, $CDCl_3$) δ_{TMS}: 1.18 (s, 3H, CH_3), 1.44 (s, 3H, CH_3), 1.50 (d, 3H, $^3J_{3\text{-}4}$ = 7.3 Hz, CH_3 (4-H)), 2.77 (q, 1H, $^3J_{3\text{-}4}$ = 7.3 Hz, H of methine group (3-H)), 7.43 (d, 2H, $^3J_{2'\text{-}3'}$ = 8.5 Hz, $^3J_{5'\text{-}6'}$ = 8.5 Hz, H's adjacent to alkyl-substituted aryl carbon (2′-H, 6′-H)), 7.64 (d, 2H, $^3J_{2'\text{-}3'}$ = 8.5 Hz, $^3J_{5'\text{-}6'}$ = 8.5 Hz, H's adjacent to cyano substituted aryl carbon (3′-H, 5′-H)); ^{13}C nmr (62.90 MHz, $CDCl_3$) δ: 16.89 (q), 25.55 (q), 26.08 (q), 37.06 (s, quaternary carbon, cyano substituted), 48.15 (d, CH, aryl-substituted), 111.42 (s, quaternary aryl carbon, cyano-substituted), 118.64 (s, CN), 123.69 (s, CN), 129.23 (d, aromatic CH adjacent to alkyl-substituted aryl carbon), 132.25 (d, aromatic CH adjacent to cyano-substituted carbon), 147.05 (s, quaternary aryl carbon, alkyl substituted); ms *m/z*: 51(7), 69(8), 77(12), 103(21), 104(8), 130(100), 131(11). Exact Mass calcd. for $C_{13}H_{14}N_2$: 198.1157; found: 198.1167.

*3-(4-Cyanophenyl)-3-methyl-2-isocyanobutane (**19**)*
The yield of **19** was 4%; infrared (Nicolet 205) ν: 2981(s), 2943(m), 2229(s), 2138(s), 1608(m), 1508 (m), 1473(m), 1467(m), 1453(m), 1405(m), 1380(m), 1112(w), 1094(m), 1064(w), 1031(w), 1018(w), 840(s); ^{1}H nmr (250.13 MHz, $CDCl_3$) δ_{TMS}: 1.17 (dt, 3H, $^3J_{1\text{-}2}$ = 6.7 Hz, $^3J_{1\text{-}N}$ = 2.4 Hz, CH_3 (1-H)), 1.45 (s, 3H, CH_3), 1.47 (s, 3H, CH_3), 3.84 (qt, 1H, $^3J_{1\text{-}2}$ = 6.7 Hz, $^2J_{2\text{-}N}$ = 1.8 Hz, H of methine group (2-H)), 7.48 (d, 2H, $^3J_{2'\text{-}3'}$ = 9.2 Hz, $^3J_{5'\text{-}6'}$ = 9.2 Hz, H's adjacent to alkyl-substituted aryl carbon (2′-H, 6′-H)), 7.66 (d, 2H, $^3J_{2'\text{-}3'}$ = 9.2 Hz, $^3J_{5'\text{-}6'}$ = 9.2 Hz, H's adjacent to cyano-substituted aryl carbon (3′-H, 5′-H)); ^{13}C nmr (62.90 MHz, $CDCl_3$) δ: 17.06 (q), 22.65 (q), 25.38 (q), 41.46 (s, quaternary carbon, aryl substituted), 59.65 (dt, CH, isocyano substituted), 110.84 (s, quaternary aryl carbon, cyano substituted), 118.59 (s, CN), 127.20 (d, aromatic CH adjacent to alkyl-substituted aryl carbon), 132.23 (d, aromatic CH adjacent to cyano-substituted carbon), 150.00 (s, quaternary aryl carbon, alkyl substituted), 156.48 (st, R-N≡C); ms *m/z*: 51(9), 52(4), 54(4), 55(18), 63(5), 75(6), 76(5), 77(8), 89(9), 101(5), 102(5), 103(4), 104(15), 116(77), 117(8), 128(6), 144(100), 145(11), 198(4). Exact Mass calcd. for $C_{13}H_{14}N_2$: 198.1157; found: 198.1152.

*3-(4-Cyanophenyl)-2-methyl-2-isocyanobutane (**20**)*
The yield of **20** was < 1%; infrared (Nicolet 205) ν: 2981(s), 2927(s), 2229(s), 2131(s), 1608(m), 1505(m), 1461(s), 1416(m), 1208(m), 1185(w), 1162(m), 1091(m), 1075(m), 1055(m), 1020(w), 856(w), 839(s); ^{1}H nmr (250.13 MHz, $CDCl_3$) δ_{TMS}: 1.27 (t, 3H, $^3J_{1\text{-}N}$ = 1.8 Hz, CH_3 (1-H)), 1.46 (d, 3H, $^3J_{3\text{-}4}$ = 6.7 Hz, CH_3 (4-H)), 1.47 (t, 3H, $^3J_{1\text{-}N}$ = 1.8 Hz, CH_3 (1-H)), 2.84 (qt, 1H, $^3J_{3\text{-}4}$ = 6.7 Hz, $^3J_{3\text{-}N}$ = 2.4 Hz, H of methine group (3-H)), 7.41 (d, 2H, $^3J_{2'\text{-}3'}$ = 8.2 Hz, $^3J_{5'\text{-}6'}$ = 8.2 Hz, H's adjacent to alkyl-substituted aryl carbon (2′-H, 6′-H)), 7.64 (d, 2H, $^3J_{2'\text{-}3'}$ = 8.2 Hz, $^3J_{5'\text{-}6'}$ = 8.2 Hz, H's adjacent to cyano-substituted aryl carbon (3′-H, 5′-H)); ^{13}C nmr (62.90 MHz, $CDCl_3$) δ: 15.97 (q), 28.19 (q), 28.45 (q), 48.90 (d, CH, aryl substituted), 60.49 (st, quaternary carbon, isocyano substituted), 111.64 (s, quaternary aryl carbon, cyano substituted), 118.85 (s, CN), 129.75 (d, aromatic CH adjacent to alkyl-substituted aryl carbon), 132.29 (d, aromatic CH adjacent to cyano-substituted carbon), 146.85 (s, quaternary aryl carbon, alkyl substituted); ms *m/z*: 51(10), 69(35), 77(19), 103(31), 104(12), 130(100), 131(16), 142(13), 183(13), 198(11). Exact Mass calcd. for $C_{13}H_{14}N_2$: 198.1157; found: 198.1155.

Formation of the cyanide anion, 2-methyl-1,3-butadiene (11), 1,4-dicyanobenzene (1) photo-NOCAS adducts 21 and 22: reaction [6]

A solution of 2-methyl-1,3-butadiene (**11**) (5.0 mL, 3.4 g, 0.050 mol), 1,4-dicyanobenzene (**1**) (3.1 g, 0.024 mol), biphenyl (**8**) (2.0 g, 0.013 mol), potassium cyanide (1.5 g, 0.023 mol), and 18-crown-6 (1.2 g, 0.0047 mol) in acetonitrile (200 mL) was degassed by nitrogen ebullition and irradiated for 7 days using a 1-kW lamp at 10°C. The solvent was removed to yield a crude photolysate. The crude photolysate was separated by repetitive chromatography (mplc) using a linear solvent gradient (hexanes – 10% diethyl ether, 90% hexanes). Two 1:1:1 adducts were detected (gc/ms) and were eluted (mplc) in the order **21** followed by **22**.

*3-(4-Cyanophenyl)-3-methyl-4-pentenenitrile (**21**)*
The yield of **21** was 2%; infrared (Nicolet 205) ν: 3089(w), 2977(s), 2939(m), 2229(s), 1638(m), 1607(s), 1505(s), 1459(m), 1415(s), 1379(m), 1075(m), 1018(m), 1000(m), 929(s), 838(s); ^{1}H nmr (250.13 MHz, $CDCl_3$) δ_{TMS}: 1.61 (s, 3H, CH_3), 2.77 (s, 2H, CH_2CN), 5.19 (d, 1H, $^3J_{4\text{-}5trans}$ = 17.4 Hz, vinyl H (5*trans*-H)), 5.34 (d, 1H, $^3J_{4\text{-}5cis}$ = 10.7 Hz, vinyl H (5*cis*-H)), 6.02 (dd, 1H, $^3J_{4\text{-}5trans}$ = 17.4 Hz, $^3J_{4\text{-}5cis}$ = 10.7 Hz, vinyl H (4-H)), 7.46 (d, 2H, $^3J_{2'\text{-}3'}$ = 8.6 Hz, $^3J_{5'\text{-}6'}$ = 8.6 Hz, H's adjacent to alkyl-substituted aryl carbon (2′-H, 6′-H)), 7.66 (d, 2H, $^3J_{2'\text{-}3'}$ = 8.6 Hz, $^3J_{5'\text{-}6'}$ = 8.6 Hz, H's adjacent to cyano-substituted aryl carbon (3′-H, 5′-H)); ^{13}C nmr (62.90 MHz, $CDCl_3$) δ: 25.45 (q), 29.82 (t, CH_2, cyano substituted), 43.58 (s, quaternary carbon, aryl substituted), 111.04 (s, quaternary aryl carbon, cyano substituted), 115.34 (t, alkene CH_2), 117.18 (s, CN), 118.44 (s, CN), 127.20 (d, aromatic CH adjacent to alkyl-substituted aryl carbon), 132.52 (d, aromatic CH adjacent to cyano-substituted carbon), 141.93 (d, alkene CH), 148.94 (s, quaternary aryl carbon, alkyl substituted); ms *m/z*: 51(13), 52(4), 53(5), 62(3), 63(8), 64(4), 65(2), 74(3), 75(8), 76(8), 77(8), 78(2), 87(2), 88(2), 89(7), 90(2), 100(2), 101(6), 102(5), 103(3), 113(4), 114(4), 115(7), 116(25), 127(14), 128(14), 129(32), 130(4), 140(13), 141(7), 153(3), 154(12), 156(100), 157(11), 196(2). Exact Mass calcd. for $C_{13}H_{12}N_2$: 196.1000; found: 196.1023.

*3-(4-Cyanophenyl)-4-methyl-4-pentenenitrile (**22**)*
The yield of **23** was 1%; infrared (Nicolet 205) ν: 3088(w), 2971(s), 2925(s), 2855(w), 2229(s), 1720(m), 1650(m), 1608(s), 1505(s), 1430(m), 1414(s), 1378(m), 1291(w), 1279(w), 905(s), 835(s); ^{1}H nmr (250.13 MHz, $CDCl_3$) δ_{TMS}: 1.61 (s, 3H, CH_3), 2.72 (dd, 1H, $^2J_{2\text{-}2'}$ = 16.7 Hz, $^3J_{2\text{-}3}$ = 7.0

© 1997 NRC Canada

Can. J. Chem. Downloaded from www.nrcresearchpress.com by 88.146.161.215 on 09/08/12
For personal use only.

Hz, H of methylene group (2-H)), 2.85 (dd, 1H, $^2J_{2-2'}$ = 16.7 Hz, $^3J_{2'-3}$ = 7.0 Hz, H of methylene group (2′-H)), 3.66 (dd, 1H, $^3J_{2-3}$ = 7.0 Hz, $^3J_{2'-3}$ = 8.2 Hz, H of methine group (3-H)), 4.99 (s, 1H, terminal vinyl H), 5.11 (s, 1H, terminal vinyl H), 7.36 (d, 2H, $^3J_{2'-3'}$ = 7.0 Hz, $^3J_{5'-6'}$ = 8.2 Hz, H's adjacent to alkyl-substituted aryl carbon (2′-H, 6′-H)), 7.65 (d, 2H, $^3J_{2'-3'}$ = 8.2 Hz, $^3J_{5'-6'}$ = 8.2 Hz, H's adjacent to cyano-substituted aryl carbon (3′-H, 5′-H)); ^{13}C nmr (62.90 MHz, $CDCl_3$) δ: 21.59 (q), 22.43 (t, CH_2, cyano substituted), 48.55 (d, CH, aryl substituted), 112.10 (s, quaternary aryl carbon, cyano substituted), 113.21 (t, alkene CH_2), 117.83 (s, CN), 118.95 (s, CN), 128.49 (d, aromatic CH adjacent to alkyl-substituted aryl carbon), 132.76 (d, aromatic CH adjacent to cyano-substituted carbon), 143.18 (s), 145.06 (s); ms *m/z*: 51(16), 52(7), 53(7), 62(6), 63(15), 64(7), 74(5), 75(14), 76(12), 77(12), 88(4), 89(12), 101(12), 102(12), 103(6), 113(6), 114(7), 115(7), 116(31), 127(18), 128(26), 129(60), 130(8), 140(16), 141(12), 153(8), 154(23), 155(29), 156(100), 157(12), 169(8), 179(8), 196(4). Exact Mass calcd. for $C_{13}H_{12}N_2$: 196.1000; found: 196.0998.

Formation of the cyanide anion, 2,3-dimethyl-1,3-butadiene (12), 1,4-dicyanobenzene (1) photo-NOCAS adducts 23 and 24: reaction [7]

A solution of 2,3-dimethyl-1,3-butadiene (**12**) (6.0 mL, 4.4 g, 0.053 mol), 1,4-dicyanobenzene (**1**) (3.1 g, 0.024 mol), biphenyl (**8**) (2.0 g, 0.013 mol), potassium cyanide (2.0 g, 0.031 mol), and 18-crown-6 (1.2 g, 0.0047 mol) in acetonitrile (200 mL) was degassed by nitrogen ebullition and irradiated for 7 days using a 1-kW lamp at 10°C. The solvent was removed to yield a crude photolysate. The crude photolysate was separated by repetitive chromatography (mplc) using a linear solvent gradient (hexanes – 10% diethyl ether, 90% hexanes). Two 1:1:1 adducts were detected (gc/ms) and these products eluted (mplc) in the order **23** followed by **24**.

3-(4-Cyanophenyl)-3,4-dimethyl-4-pentenenitrile (23)

The yield of **23** was 7%; infrared (Nicolet 205) ν: 3092(w), 2976(s), 2952(m), 2926(m), 2887(w), 2229(s), 1642(m), 1607(s), 1505(s), 1451(m), 1431(m), 1406(m), 1382(m), 1072(w), 1019(w), 909(s), 842(s), 734(s); ^{1}H nmr (250.13 MHz, $CDCl_3$) δ_{TMS}: 1.55 (s, 3H, CH_3), 1.66 (s, 3H, CH_3), 2.84 (AB apparent singlet, 2H, CH_2CN), 5.07 (s, 1H, terminal vinyl H), 5.15 (s, 1H, terminal vinyl H), 7.43 (d, 2H, $^3J_{2'-3'}$ = 8.5 Hz, $^3J_{5'-6'}$ = 8.5 Hz, H's adjacent to alkyl-substituted aryl carbon (2′-H, 6′-H)), 7.66 (d, 2H, $^3J_{2'-3'}$ = 8.5 Hz, $^3J_{5'-6'}$ = 8.5 Hz, H's adjacent to cyano-substituted aryl carbon (3′-H, 5′-H)); ^{13}C nmr (62.90 MHz, $CDCl_3$) δ: 19.98 (q), 24.79 (q), 29.83 (t, CH_2, cyano substituted), 46.35 (s, quaternary carbon, aryl substituted), 111.25 (s, quaternary aryl carbon, cyano substituted), 113.06 (t, alkene CH_2), 117.49 (s, CN), 118.52 (s, CN), 127.11 (d, aromatic CH adjacent to alkyl-substituted aryl carbon), 132.54 (d, aromatic CH adjacent to cyano-substituted carbon), 147.00 (s), 148.84 (s); ms *m/z*: 51(24), 75(18), 77(19), 115(26), 116(39), 127(22), 128(29), 140(23), 142(71), 143(35), 153(24), 154(35), 155(21), 167(21), 168(33), 169(69), 170(100). Exact Mass calcd. for $C_{14}H_{14}N_2$: 210.1157; found: 210.1155.

(E)-5-(4-Cyanophenyl)-3,4-dimethyl-2-pentenenitrile (24)

The yield of **24** was 2%; infrared (Nicolet 205) ν: 2971(m), 2933(m), 2876(w), 2253(w), 2228(s), 2219(s), 1627(m), 1608(m), 1505(m), 1459(m), 1440(m), 1415(m), 1380(m), 913(s), 846(m), 822(m), 734(s); ^{1}H nmr (250.13 MHz, $CDCl_3$) δ_{TMS}: 1.08 (d, 3H, $^3J_{4-7}$ = 6.7 Hz, CH_3 (7-H)), 2.06 (s, 3H, CH_3), 2.62 (m, 1H, $^3J_{4-7}$ = 6.7 Hz, $^3J_{4-5}$ = 6.1 Hz, $^3J_{4-5'}$ = 6.1 Hz, H of methine group (4-H)), 2.69 (m, 1H, $^2J_{5-5'}$ = 12.9 Hz, $^3J_{4-5}$ = 6.1 Hz, H of methylene group, aryl substituted (5-H)), 2.82 (m, 1H, $^2J_{5-5'}$ = 12.9 Hz, $^3J_{4-5'}$ = 6.1 Hz, H of methylene group, aryl substituted (5′-H)), 5.05 (s, 1H, vinyl H), 7.22 (d, 2H, $^3J_{2'-3'}$ = 8.6 Hz, $^3J_{5'-6'}$ = 8.6 Hz, H's adjacent to alkyl-substituted aryl carbon (2′-H, 6′-H)), 7.60 (d, 2H, $^3J_{2'-3'}$ = 8.6 Hz, $^3J_{5'-6'}$ = 8.6 Hz, H's adjacent to cyano-substituted aryl carbon (3′-H, 5′-H)). The nOe experiment (400 MHz): the methyl group bonded to the alkene was irradiated; a small enhancement was observed for the methine and methylene H's (ABC splitting pattern) and the *ortho*-aryl H's were enhanced. The irradiation of the vinyl H showed a large methine and methylene H (ABC splitting pattern) enhancement and the *ortho*- and *meta*-aryl H's were enhanced; ^{13}C nmr (62.90 MHz, $CDCl_3$) δ: 18.34 (q), 18.47 (q), 41.21 (t, CH_2, aryl substituted), 43.67 (d), 95.89 (d, alkene CH), 110.58 (s, quaternary aryl carbon, cyano substituted), 116.84 (s, CN), 118.74 (s, CN), 129.61 (d, aromatic CH adjacent to alkyl-substituted aryl carbon), 132.34 (d, aromatic CH adjacent to cyano-substituted carbon), 144.71 (s, quaternary aryl carbon, alkyl substituted), 167.39 (s, alkene quaternary carbon); ms *m/z*: 51(5), 63(8), 65(5), 67(11), 89(22), 90(7), 94(13), 116(100), 117(36), 210(10). Exact Mass calcd. for $C_{14}H_{14}N_2$: 210.1157; found: 210.1150.

Formation of the cyanide anion, 4-methyl-1,3-pentadiene (13), 1,4-dicyanobenzene (1) photo-NOCAS adducts 25 and 26: reaction [8]

A solution of 4-methyl-1,3-pentadiene (**13**) (1.1 mL, 0.79 g, 0.0096 mol), 1,4-dicyanobenzene (**1**) (1.2 g, 0.0094 mol), biphenyl (**8**) (0.8 g, 0.0052 mol), potassium cyanide (0.6 g, 0.0092 mol), and 18-crown-6 (0.5 g, 0.0019 mol) in acetonitrile (80 mL) was degassed by nitrogen ebullition and irradiated for 21 h using a 1-kW lamp at 10°C. The solvent was removed to yield a crude photolysate. The crude photolysate was separated by repetitive chromatography (mplc) using a linear solvent gradient (hexanes – 20% diethyl ether, 80% hexanes). Two 1:1:1 adducts were detected (gc/ms) and these products eluted (mplc) in the order **25** followed by **26**.

3-(4-Cyanophenyl)-5-methyl-4-hexenenitrile (25)

The yield of **25** was 14%; infrared (Nicolet 510) ν: 2974(s), 2926(s), 2863(m), 2230(s), 1676(m), 1614(s), 1504(s), 1451(m), 1428(s), 1380(m), 840(s), 734(m); ^{1}H nmr (250.13 MHz, $CDCl_3$) δ_{TMS}: 1.69 (s, 3H, CH_3), 1.77 (s, 3H, CH_3), 2.66 (dd, 1H, $^2J_{2-2'}$ = 16.7 Hz, $^3J_{2-3}$ = 7.1 Hz, H of methylene group, cyano substituted (2-H)), 2.70 (dd, 1H, $^2J_{2-2'}$ = 16.7 Hz, $^3J_{2'-3}$ = 6.9 Hz, H of methylene group, cyano substituted (2′-H)), 3.97 (m, 1H, $^3J_{3-4}$ = 9.3 Hz, $^3J_{2-3}$ = 7.1 Hz, $^3J_{2'-3}$ = 6.9 Hz, H of methine group, aryl substituted (3-H)), 5.35 (d, 1H, $^3J_{3-4}$ = 9.3 Hz, vinyl H (4-H)), 7.38 (d, 2H, $^3J_{2'-3'}$ = 8.3 Hz, $^3J_{5'-6'}$ = 8.3 Hz, H's adjacent to alkyl-substituted aryl carbon (2′-H, 6′-H)), 7.63 (d, 2H, $^3J_{2'-3'}$ = 8.3 Hz, $^3J_{5'-6'}$ = 8.3 Hz, H's adjacent to cyano-substituted aryl carbon (3′-H, 5′-H)); ^{13}C nmr (62.90 MHz, $CDCl_3$) δ: 18.36 (q), 24.90 (t, CH_2, cyano substituted), 25.82 (q), 40.56 (d, CH, aryl substituted), 111.10 (s, quaternary aryl carbon, cyano substituted), 117.92 (s, CN),

© 1997 NRC Canada

Can. J. Chem. Downloaded from www.nrcresearchpress.com by 88.146.161.215 on 09/08/12
For personal use only.

118.64 (s, CN), 123.08 (d, alkene CH), 128.00 (d, aromatic CH adjacent to alkyl-substituted aryl carbon), 132.72 (d, aromatic CH adjacent to cyano-substituted carbon), 136.94 (s, alkene quaternary carbon), 147.40 (s, aromatic quaternary carbon); ms *m/z*: 51(9), 63(5), 75(5), 76(4), 77(5), 89(6), 101(5), 102(4), 115(9), 116(17), 127(11), 128(11), 129(5), 130(5), 140(9), 141(4), 142(36), 143(11), 153(11), 154(11), 155(9), 168(9), 170(100), 171(14). Anal. calcd. for $C_{14}H_{14}N_2$: C 79.96, H 6.71, N 13.32; found: C 80.23, H 6.83, N 13.17.

*(E)-5-(4-Cyanophenyl)-2,2-dimethyl-3-pentenenitrile (**26**)*
The yield of **26** was 1%; infrared (Nicolet 205) ν: 2978(m), 2919(s), 2850(m), 2227(s), 1605(s), 1504(m), 1467(m), 1413(m), 1392(m), 1371(m), 1177(m), 973(s), 856(m), 808(m); ^{1}H nmr (250.13 MHz, $CDCl_3$) δ_{TMS}: 1.41 (s, 6H, 2 CH_3's), 2.47 (d, 2H, $^3J_{4-5}$ = 6.7 Hz, CH_2, aryl substituted (5-H)), 6.40 (dt, 1H, $^3J_{3-4}$ = 15.9 Hz, $^3J_{4-5}$ = 6.7 Hz, vinyl H (4-H)), 6.55 (d, 1H, $^3J_{3-4}$ = 15.9 Hz, vinyl H (3-H)), 7.47 (d, 2H, $^3J_{2'-3'}$ = 8.5 Hz, $^3J_{5'-6'}$ = 8.5 Hz, H's adjacent to alkyl-substituted aryl carbon (2′-H, 6′-H)), 7.61 (d, 2H, $^3J_{2'-3'}$ = 8.5 Hz, $^3J_{5'-6'}$ = 8.5 Hz, H's adjacent to cyano-substituted aryl carbon (3′-H, 5′-H)); ^{13}C nmr (62.90 MHz, $CDCl_3$) δ: 26.46 (q, 2 CH_3's), 32.65 (s, quaternary carbon, cyano-substituted), 44.32 (t, CH_2, aryl substituted), 111.00 (s, quaternary aryl carbon, cyano substituted), 118.91 (s, CN), 124.44 (s, CN), 126.87 (d, aromatic CH adjacent to alkyl-substituted aryl carbon), 127.87 (d, alkene CH), 132.48 (d, aromatic CH adjacent to cyano-substituted carbon), 133.31 (d, alkene CH), 141.04 (s, aromatic quaternary carbon); ms *m/z*: 51(4), 52(3), 63(5), 75(3), 76(3), 89(8), 113(3), 114(4), 115(31), 116(18), 140(15), 142(100), 143(11), 210(5). Exact Mass calcd. for $C_{14}H_{14}N_2$: 210.1157; found: 210.1153.

Formation of the cyanide anion, 2,4-dimethyl-1,3-pentadiene (14), 1,4-dicyanobenzene (1) photo-NOCAS adducts 27, 28, and 29: reaction [9]
A solution of 2,4-dimethyl-1,3-pentadiene (**14**) (3.0 mL, 2.2 g, 0.023 mol), 1,4-dicyanobenzene (**1**) (1.9 g, 0.015 mol), biphenyl (**8**) (1.2 g, 0.0078 mol), potassium cyanide (0.9 g, 0.014 mol), and 18-crown-6 (0.8 g, 0.0030 mol) in acetonitrile (120 mL) was degassed by nitrogen ebullition and irradiated for 55 h using a 1-kW lamp at 10°C. The solvent was removed to yield a crude photolysate. The crude photolysate was separated by repetitive chromatography (mplc) using a linear solvent gradient (hexanes – 10% diethyl ether, 90% hexanes). Three 1:1:1 adducts were detected (gc/ms) and these products eluted (mplc) in the order **28**, **29**, then **27**.

*3-(4-Cyanophenyl)-3,5-dimethyl-4-hexenenitrile (**27**)*
The yield of **27** was 17%; infrared (Nicolet 205) ν: 2972(s), 2934(m), 2917(m), 2880(m), 2228(s), 1607(m), 1503(m), 1449(m), 1424(m), 1409(m), 1385(m), 1067(m), 839(s), 813(m), 737(m); ^{1}H nmr (250.13 MHz, $CDCl_3$) δ_{TMS}: 1.14 (s, 3H, CH_3), 1.64 (s, 3H, CH_3), 1.76 (s, 3H, CH_3), 2.68 (AB apparent singlet, 2H, CH_2CN), 5.54 (br s, 1H, vinyl H), 7.52 (d, 2H, $^3J_{2'-3'}$ = 8.6 Hz, $^3J_{5'-6'}$ = 8.6 Hz, H's adjacent to alkyl-substituted aryl carbon (2′-H, 6′-H)), 7.64 (d, 2H, $^3J_{2'-3'}$ = 8.6 Hz, $^3J_{5'-6'}$ = 8.6 Hz, H's adjacent to cyano-substituted aryl carbon (3′-H, 5′-H)); ^{13}C nmr (62.90 MHz, $CDCl_3$) δ: 19.62 (q), 26.79 (q), 27.08 (q), 33.44 (t, CH_2, cyano substituted), 41.90 (s, quaternary carbon, aryl substituted), 110.60 (s, quaternary aryl carbon, cyano substituted), 117.63 (s, CN), 118.71 (s, CN), 127.31 (d, aromatic CH adjacent to alkyl-substituted aryl carbon), 129.15 (d, alkene CH), 132.42 (d, aromatic CH adjacent to cyano-substituted carbon), 137.27 (s, alkene quaternary carbon), 151.53 (s, aromatic quaternary carbon); ms *m/z*: 51(7), 77(7), 115(8), 116(11), 127(8), 130(9), 140(9), 142(100), 143(12), 153(7), 154(10), 156(8), 168(11), 184(57), 185(8). Exact Mass calcd. for $C_{15}H_{16}N_2$: 224.1313; found: 224.1308.

*4-(4-Cyanophenyl)-2,4-dimethyl-2-pentene-3-nitrile (**28**)*
The yield of **28** was 2%; infrared (Nicolet 205) ν: 2975(s), 2934(m), 2929(m), 2922(m), 2229(s), 2206(s), 1608(s), 1504(s), 1467(m), 1444(m), 1405(m), 1381(m), 1375(m), 1100(m), 1058(m), 1019(m), 840(s); ^{1}H nmr (250.13 MHz, $CDCl_3$) δ_{TMS}: 1.31 (s, 3H, CH_3), 1.58 (s, 6H, 2 CH_3's), 2.11 (s, 3H, CH_3), 7.41 (d, 2H, $^3J_{2'-3'}$ = 8.5 Hz, $^3J_{5'-6'}$ = 8.5 Hz, H's adjacent to alkyl-substituted aryl carbon (2′-H, 6′-H)), 7.61 (d, 2H, $^3J_{2'-3'}$ = 8.5 Hz, $^3J_{5'-6'}$ = 8.5 Hz, H's adjacent to cyano-substituted aryl carbon (3′-H, 5′-H)); ^{13}C nmr (62.90 MHz, $CDCl_3$) δ: 22.26 (q), 26.40 (q), 30.66 (q, 2 CH_3's), 41.08 (s, quaternary carbon, aryl substituted), 110.14 (s, quaternary aryl carbon, cyano substituted), 118.26 (s), 118.32 (s), 118.71 (s), 126.43 (d, aromatic CH adjacent to alkyl-substituted aryl carbon), 132.55 (d, aromatic CH adjacent to cyano-substituted carbon), 154.57 (s), 155.69 (s); ms *m/z*: 51(15), 53(12), 77(15), 89(10), 104(10), 116(51), 140(14), 144(61), 154(15), 166(10), 167(15), 168(19), 169(12), 182(43), 183(11), 194(11), 209(100), 210(15), 223(11), 224(21). X-ray data: see footnote 3.

*(Z)-5-(4-Cyanophenyl)-3,5-dimethyl-2-hexenenitrile (**29**)*
The yield of **29** was 2%; melting point 105–106°C; infrared (Nicolet 205) ν: 3045(w), 2973(s), 2942(m), 2881(m), 2223(s), 2212(s), 1618(s), 1502(s), 1470(m), 1440(s), 1404(m), 1372(m), 1316(m), 1230(m), 1184(m), 1096(m), 1016(m), 835(s), 815(m); ^{1}H nmr (250.13 MHz, $CDCl_3$) δ_{TMS}: 1.39 (s, 3H, CH_3), 1.46 (s, 6H, 2 CH_3's), 2.79 (s, 2H, CH_2), 5.17 (br s, 1H, vinyl H), 7.52 (d, 2H, $^3J_{2'-3'}$ = 8.5 Hz, $^3J_{5'-6'}$ = 8.5 Hz, H's adjacent to alkyl-substituted aryl carbon (2′-H, 6′-H)), 7.64 (d, 2H, $^3J_{2'-3'}$ = 8.5 Hz, $^3J_{5'-6'}$ = 8.5 Hz, H's adjacent to cyano-substituted aryl carbon (3′-H, 5′-H)); ^{13}C nmr (62.90 MHz, $CDCl_3$) δ: 24.76 (q), 28.88 (q, 2 CH_3's), 39.48 (s, quaternary carbon, aryl substituted), 50.19 (t), 99.24 (d, alkene CH), 110.18 (s, quaternary aryl carbon, cyano substituted), 117.21 (s, CN), 118.79 (s, CN), 126.81 (d, aromatic CH adjacent to alkyl-substituted aryl carbon), 132.20 (d, aromatic CH adjacent to cyano-substituted carbon), 153.76 (s, quaternary aryl carbon, alkyl substituted), 162.15 (s, alkene quaternary carbon); ms *m/z*: 51(6), 52(3), 53(9), 63(3), 75(4), 76(4), 77(7), 81(3), 89(7), 101(4), 102(4), 104(13), 116(66), 117(7), 128(4), 144(100), 145(11). X-ray data: see footnote 3.

Formation of the cyanide anion, 2,4-dimethyl-2,3-pentadiene (15), 1,4-dicyanobenzene (1) photo-NOCAS adduct 28: reaction [10]
A solution of 2,4-dimethyl-2,3-pentadiene (**15**) (1.0 mL, 0.7 g, 0.0073 mol), 1,4-dicyanobenzene (**1**) (0.6 g, 0.0048 mol), biphenyl (**8**) (0.4 g, 0.0026 mol), potassium cyanide (0.3 g, 0.0046 mol), and 18-crown-6 (0.3 g, 0.0011 mol) in acetonitrile (40 mL) was degassed by nitrogen ebullition and irradi-

© 1997 NRC Canada

ated for 48 h using a 1-kW lamp at 10°C. The solvent was removed to yield a crude photolysate. The crude photolysate was separated by repetitive chromatography (dc/fc) using a linear solvent gradient (hexanes – 20% diethyl ether, 80% hexanes). One 1:1:1 adduct, 4-(4-cyanophenyl)-2,4-dimethyl-2-pentene-3-nitrile (**28**), was detected (gc/ms); the yield was 22%. The retention time and gc/ms of this compound were identical to the product obtained from **14** (reaction [9]).

Acknowledgements

This work was supported financially by the Natural Sciences and Engineering Research Council of Canada. We are grateful to Dr. T.S. Cameron at Dalhousie for the X-ray analysis of **28** and **29**. We thank Drs. D.L. Hooper and M.D. Lumsden at the Atlantic Regional Magnetic Resonance Centre at Dalhousie University for the high-field nmr spectra. We also thank Dr. Hooper for assistance with the preparation of the manuscript.

References

1. (*a*) R.M. Borg, D.R. Arnold, and T.S. Cameron. Can. J. Chem. **62**, 1785 (1984); (*b*) K.A. McManus and D.R. Arnold. Can. J. Chem. **72**, 2291 (1994); (*c*) A.J. Maroulis, Y. Shigemitsu, and D.R. Arnold. J. Am. Chem. Soc. **100**, 535 (1978); (*d*) D.R. Arnold and M.S. Snow. Can. J. Chem. **66**, 3012 (1988); (*e*) K.A. McManus and D.R. Arnold. Can. J. Chem. **73**, 2158 (1995); (*f*) D.R. Arnold, X. Du, and H.J.P. de Lijser. Can. J. Chem. **73**, 522 (1995); (*g*) D.A. Connor, D.R. Arnold, P.K. Bakshi, and T.S. Cameron. Can. J. Chem. **73**, 762 (1995); (*h*) D.R. Arnold, D.A. Connor, K.A. McManus, P.K. Bakshi, and T.S. Cameron. Can. J. Chem. **74**, 602 (1996); (*i*) D.R. Arnold, M.S.W. Chan, and K.A. McManus. Can. J. Chem. **74**, 2143 (1996); (*j*) D.R. Arnold, P.C. Wong, A.J. Maroulis, and T.S. Cameron. Pure Appl. Chem. **52**, 2609 (1980).
2. (*a*) D.R. Arnold and A.J. Maroulis. J. Am. Chem. Soc. **98**, 5931 (1976); (*b*) A.L. Perrott and D.R. Arnold. Can. J. Chem. **70**, 272 (1992); (*c*) D.R. Arnold, X. Du, and J. Chen. Can. J. Chem. **73**, 307 (1995); (*d*) H.J.P. de Lijser and D.R. Arnold. J. Phys. Chem. **100**, 3996 (1996).
3. (*a*) L.J. Johnston and N.P. Schepp. J. Am. Chem. Soc. **115**, 6564 (1993); (*b*) Pure Appl. Chem. **67**, 71 (1995).
4. (*a*) R.G. Pearson and J. Songstad. J. Am. Chem. Soc. **89**, 1827 (1967); (*b*) R.G. Pearson, H. Sobel, and J. Songstad. J. Am. Chem. Soc. **90**, 319 (1968); (*c*) P.L. Bock and G.M. Whitesides. J. Am. Chem. Soc. **96**, 2826 (1974); (*d*) T.-L. Ho. Chem. Rev. **75**, 1 (1975).
5. M.J. Frisch, G.W. Trucks, H.B. Schlegel, P.M.W. Gill, B.G. Johnson, M.W. Wong, J.B. Foresman, M.A. Robb, M. Head-Gordon, E.S. Replogle, R. Gomperts, J.L. Andres, K. Raghavachari, J.S. Binkley, C. Gonzales, R.L. Martin, D.J. Fox, D.J. Defrees, J. Baker, J.J.P. Stewart, and J.A. Pople. Gaussian 92/DFT, Revision F.2. Gaussian, Inc., Pittsburgh, Pa. 1993.
6. (*a*) C. Møller and M.S. Plesset. Phys. Rev. **46**, 618 (1934); (*b*) W.J. Hehre, L. Radom, P.v.R. Schelyer, and J.A. Pople. *Ab initio* molecular orbital theory. Wiley–Interscience, New York, 1987; (*c*) R.S. Mulliken. J. Chem. Phys. **23**, 1983 (1955); (*d*) A.E. Reed, R.B. Weinstock, and F. Weinhold. J. Chem. Phys. **83**, 735 (1985).
7. R.M. Silverstein, G.C. Bassler, and T.C. Morrill. Spectrometric identification of organic compounds. 5th ed. John Wiley & Sons, Inc., Toronto. 1991.
8. (*a*) R.S. Nicholson and I. Shain. Anal. Chem. **36**, 706 (1964); (*b*) Anal. Chem. **37**, 178 (1965).
9. (*a*) S. Andreades and E.W. Zahnow. J. Am. Chem. Soc. **91**, 4181 (1969); (*b*) J.F. Evans and H.N. Blount. J. Am. Chem. Soc. **100**, 4191 (1978); (*c*) R.G. Pearson. J. Am. Chem. Soc. **108**, 6109 (1986); (*d*) J.-M. Savéant. J. Phys. Chem. **98**, 3716 (1994).
10. (*a*) K. Yoshida and T. Fueno. J. Org. Chem. **36**, 1523 (1971); (*b*) K. Yoshida. J. Am. Chem. Soc. **101**, 2116 (1979); (*c*) K. Yoshida, T. Kanbe, and T. Fueno. J. Org. Chem. **42**, 2313 (1977); (*d*) K. Yoshida and S. Nagase. J. Am. Chem. Soc. **101**, 4268 (1979); (*e*) K. Koyama, T. Susuki, and S. Tsutsumi. Tetrahedron, **23**, 2675 (1967); (*f*) V.D. Parker and B.E. Burgert. Tetrahedron Lett. 4065 (1965).
11. (*a*) L. Herbert, I.W.M. Smith, and R.D. Spencer-Smith. Int. J. Chem. Kinet. **24**, 791 (1992); (*b*) D.L. Yang, T. Yu, N.S. Wang, and M.C. Lin. Chem. Phys. **160**, 317 (1992); (*c*) G.E. Bullock and R. Cooper. Trans. Faraday Soc. **67**, 3258 (1971).
12. (*a*) J.M. Tedder. Angew. Chem. Int. Ed. Engl. **21**, 401 (1982); (*b*) B. Giese. Angew. Chem. Int. Ed. Engl. **22**, 753 (1983); (*c*) K.N. Houk, M.N. Paddon-Row, D.C. Spellmeyer, N.G. Rondan, and S. Nagase. J. Org. Chem. **51**, 2874 (1986).
13. (*a*) M.W. Klett and R.P. Johnson. Tetrahedron Lett. 1107 (1983); (*b*) K. Somekawa, K. Haddaway, P.S. Mariano, and J.A. Tossell. J. Am. Chem. Soc. **106**, 3060 (1984).
14. (*a*) X.-Z. Qin and A.D. Trifunac. J. Phys. Chem. **95**, 6466 (1991); (*b*) Y. Kubozono, H. Ujita, M. Okada, M. Ata, Y. Matsuda, and Y. Gondo. Bull. Chem. Soc. Jpn. **65**, 2442 (1992).
15. (*a*) S.W. Benson. Thermochemical kinetics. 2nd ed. Wiley-Interscience, New York 1976; (*b*) H.E. O'Neal and S.W. Benson. Thermochemistry of free radicals. *In* Free radicals. Vol. II. *Edited by* J.K. Kochi. Wiley–Interscience, New York. 1973. Chap.17; (*c*) N. Cohen and S.W. Benson. Chem. Rev. **93**, 2419 (1993); (*d*) T. Ni, R.A. Caldwell, and L.A. Melton. J. Am. Chem. Soc. **111**, 457 (1989).
16. D.R. Lide (*Editor*). Handbook of chemistry and physics. 76th ed. (1995–1996). CRC Press, Inc., New York. 1995.
17. (*a*) D.D. Tanner, H. Yabuuchi, and E.V. Blackburn. J. Am. Chem. Soc. **93**, 4802 (1971); (*b*) P.S. Skell and K.J. Shea. *In* Free radicals. Vol. II. *Edited by* J.K. Kochi. Wiley–Interscience, New York. 1973. Chap. 26; (*c*) H.L. Goering, P.I. Abell, and B.F. Aycock. J. Am. Chem. Soc. **74**, 3588 (1952); (*d*) P.J. Krusic and J.K. Kochi. J. Am. Chem. Soc. **93**, 846 (1971); (*e*) D.A. Lindsay, J. Lusztyk, and K.U. Ingold. J. Am. Chem. Soc. **106**, 7087 (1984); (*f*) J.J. Russell, H.S. Rzepa, and D.A. Widdowson. J. Chem. Soc. Chem Commun. 625 (1983).
18. M. Meier, B. Dogan, H.-D. Beckhaus, and C. Rüchardt. New J. Chem. **11**, 1 (1987).
19. L.M. Harwood. Aldrichimica Acta, **18**, 25 (1985).
20. A. Okamoto, M.S. Snow, and D.R. Arnold. Tetrahedron, **42**, 6175 (1986).
21. D.R. Arnold and D.D.M. Wayner. Can. J. Chem. **64**, 100 (1986).

Can. J. Chem. Downloaded from www.nrcresearchpress.com by 88.146.161.215 on 09/08/12
For personal use only.

© 1997 NRC Canada

Asymmetric synthesis of lignans using oxazolidinones as chiral auxiliaries

James L. Charlton and Gaik-Lean Chee

Abstract: A simple procedure for the asymmetric synthesis of lignans via chiral β-benzyl-γ-butyrolactones has been developed. The key benzylbutyrolactone intermediates were efficiently synthesized using a six-step procedure, starting from 3,4-(methylenedioxy)cinnamic acid. The key step in this sequence was a highly diastereoselective alkylation of an *N*-acyloxazolidinone enolate. The resulting β-benzyl-γ-butyrolactones were subsequently transformed into the benzylidene lignans gossypifan and savinin (hibalactone) via aldol condensation–dehydration reactions, and into the dibenzylbutyrolactone lignan 4′-demethylyatein, through alkylation. Oxidation of 4′-demethylyatein with 2,3-dichloro-5,6-dicyano-1,4-benzoquinone (DDQ) afforded *cis*- and *trans*-benzylidenebenzylbutyrolactones, whereas oxidation with DDQ/TFA gave 4′-demethyldeoxyisopodophyllotoxin.

Key words: lignans, synthesis, asymmetric, biosynthesis, oxidation, benzylbutyrolactones.

Résumé : On a mis au point une méthode de synthèse simple des lignanes impliquant des β-benzyl-γ-butyrolactones chirales. On a synthétisé les intermédiaires benzylbutyrolactones clés d'une façon efficace en faisant appel à une procédure en six étapes, à partir de l'acide 3,4-(méthylènedioxy)cinnamique. L'étape clé de cette séquence est une alkylation hautement diastéréosélective d'un énolate *N*-acyloxazolidinone. Les β-benzyl-γ-butyrolactones qui en découlent sont ultérieurement transformées en benzylidènes des lignanes gossypifane et savinine (hibalactone) par le biais de réactions de condensation aldolique et de déshydratation et en lignane dibenzylbutyrolactone 4′-déméthylyatéine par alkylation. L'oxydation de la 4′-déméthylyatéine par la 2,3-dichloro-5,6-dicyano-1,4-benzoquinone (DDQ) conduit aux benzylidènebenzylbutyrolactones *cis* et *trans* alors que l'oxydation à l'aide de DDQ/TFA fournit de la 4′-démethyldéoxyisopodophyllotoxyine.

Mots clés : synthèse de lignanes, asymétrique, biosynthèse, oxydation, benzylbutyrolactones.

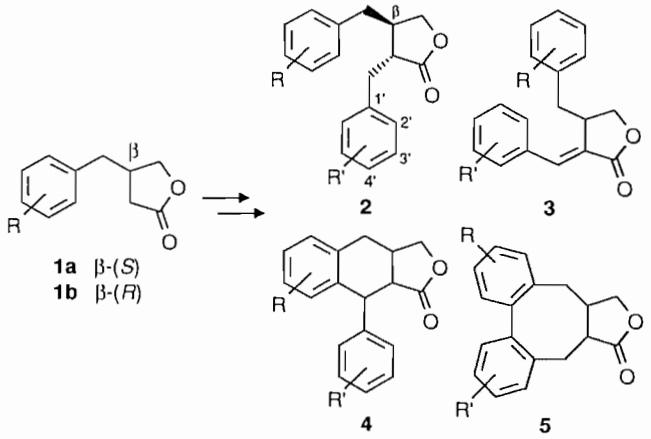
[Traduit par la rédaction]

Introduction

Many lignan natural products have interesting biological properties (1) and developing synthetic methods for this large class of compounds has been a challenge to synthetic chemists.[2] Many of the methods for the asymmetric synthesis of chiral lignans have involved the intermediacy of enantiomerically pure β-benzyl-γ-butyrolactones **1**. These have been used in the synthesis of dibenzylbutyrolactones **2**, benzylidenebenzylbutyrolactones **3**, aryltetralins **4**, and dibenzocyclooctadienes **5** (Scheme 1). In comparison to other general methods for lignan synthesis, using butyrolactones **1** as intermediates offers more structural variability than can be achieved otherwise.

Several synthetic approaches for the preparation of optically active butyrolactones having general structure **1** have been published. The first asymmetric synthesis of a butyrolactone of type **1b** (R = 3,4-methylenedioxy) was reported by Tomioka and Koga (3). In a lengthy procedure they diastereoselectively alkylated a chiral γ-substituted γ-butyrolactone followed by removal of the γ group. Posner et al. synthesized chiral benzylbutyrolactones by diastereoselective conjugate addition to an enantiomerically pure α-sulfinyl-γ-butenolide (4). Similar to the first example, the procedure is lengthy and the overall yield is relatively low. Yoda et al. carried out a conjugate addition on a chiral unsaturated lactam in the preparation of a butyrolactone of type **1b** (R = 3,4-methylenedioxy) (5). Once again, the yields for most steps were only moderate. An elegant catalytic asymmetric hydrogenation reaction was

Scheme 1.



Received February 19, 1997.

J.L. Charlton[1] **and G.-L. Chee.** Department of Chemistry, University of Manitoba, Winnipeg, MB R3T 2N2, Canada.

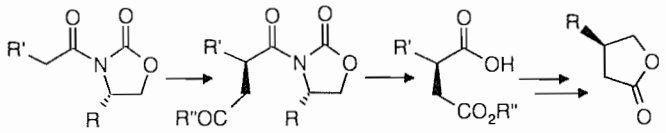
[1] Author to whom correspondence may be addressed. Telephone: (204) 474-9267. Fax: (204) 474-7608. E-mail: charltn@cc.umanitoba.ca

[2] Reviews on asymmetric synthesis of lignans: refs. 2*a*, 2*b*; Reviews on synthesis of lignans: refs. 2*c*–2*k*.

© 1997 NRC Canada

Can. J. Chem. Downloaded from www.nrcresearchpress.com by 88.146.161.215 on 09/08/12
For personal use only.

Scheme 2.



employed by Morimoto et al. to prepare **1a** and **1b** (R = 3,4-methylenedioxy and 3,4-dimethoxy) (6). Unfortunately, the chiral hydrogenation catalyst used by these authors is relatively unavailable. More recently, Honda et al. employed enantioselective deprotonation of a 3-benzylcyclobutanone in the synthesis of a lactone of type **1b** (R = 3,4-methylenedioxy) (7). Although only a few steps were involved in the synthesis, the enantioselectivity of the key reaction was moderate, affording **1b** in only 80% optical purity. Doyle et al. reported a novel and efficient synthesis of lactones **1a** and **1b** (R = H, 3-methoxy and 3,4-methylenedioxy) via an enantioselective intramolecular C-H insertion reaction of an alkyl diazoacetate (8). Chiral oxoimidazolidine carboxylate dirhodium catalysts were applied in the key reaction to afford a chiral benzylbutyrolactone in up to 94% ee, but neither the catalyst nor the chiral ligand that was used is commercially available. Two recent asymmetric syntheses of optically pure β-benzyl-γ-butyrolactones of structure **1a** (R = 3,4-dimethoxy and 4-methoxy) utilized an enzymatic transesterification of a prochiral diol (9). Although the process was highly enantioselective, relatively large amounts of the enzyme (lipase PS from *Pseudomonas fluorescens*) were needed.

Although the above reported methods have provided elegant routes to the preparation of lignan intermediates **1a** and **1b**, many problems still exist. These include laborious methods, poor overall yields, unsatisfactory enantiomeric purity, and (or) expensive reagents. A simple and efficient approach for the asymmetric synthesis of butyrolactones **1** is still required.

Substituted oxazolidinone heterocycles[3] are effective chiral auxiliaries giving excellent asymmetric induction in reactions such as alkylations, hydrogenations, and Diels–Alder reactions. Enolates derived from *N*-acyloxazolidinones can be alkylated with α-bromoacetate to afford diastereomerically pure substituted succinate derivatives (11). After the removal of the oxazolidinone chiral auxiliary, the chiral half acid can be reduced and lactonized to afford the β-substituted butyrolactone in high optical purity (Scheme 2) (11*a*).

We have adopted this simple and versatile method for the asymmetric synthesis of β-benzyl-γ-butyrolactones **11a** and **11b** (see Scheme 3). These were subsequently transformed into the lignans gossypifan (**14a**), savinin (hibalactone) (**14b**), and 4′-demethylyatein (**16**) (these are the first reported syntheses for gossypifan and 4′-demethylyatein) (Schemes 4 and 5).

4′-Demethylyatein (**16**) is considered to be a biosynthetic precursor to aryltetralin lignans having the podophyllotoxin pattern of substitution (see **23** in Scheme 7) (12). It has been proposed that oxidation to a quinone methide **20** is followed by cyclization to 4′-demethyldeoxypodophyllotoxin (the 1,2-*cis* isomer of **23**). Kende et al. were able to mimic the biosynthetic pathway and oxidatively cyclize a similar diarylbutane (13); however, attempts to cyclize 4′-demethylyatein itself have been unsuccessful (14*a*).[4] We have restudied the oxidation of this biologically important precursor using DDQ as oxidant. An aryltetralin lignan was successfully prepared and a better understanding of the biosynthesis of lignans was achieved.

Results and discussion

The enantiomerically pure (*S*)- and (*R*)-β-3,4-(methylenedioxy)benzyl-γ-butyrolactones (**11a** and **11b**) were efficiently synthesized in six steps from 3,4-(methylenedioxy)cinnamic acid, as shown in Scheme 3, in an overall yield of >45%. Dihydrocinnamic acid **6** was obtained in excellent yield from hydrogenation of commercially available 3,4-(methylenedioxy)cinnamic acid. Using a modified literature procedure (11), commercially available (4*R*)-benzyl and (4*S*)-isopropyl-2-oxazolidinone were *N*-acylated with dihydrocinnamic acid **6** to give N-acyloxazolidinones **7** and **8** in 88% and 84% yield, respectively. The *N*-acyloxazolidinones **7** and **8** were diastereoselectively alkylated with *tert*-butyl bromoacetate to afford one major diastereomer in each case (**9** and **10**, ca. 80% yield), having >95% diastereomeric excess as shown by the ^{1}H NMR spectrum. Although the absolute configuration could not be determined at this stage it was expected to be that shown in Scheme 3. The oxazolidinone chiral auxiliary was removed with LiOH–H_2O_2 without affecting the *tert*-butyl ester. The crude acid was reduced to an alcohol using BH_3·THF, then lactonized with TFA to afford the benzylbutyrolactone **11** in about 70% yield from the *N*-acyloxazolidinone. The benzylbutyrolactones **11a** and **11b** have optical activities and other spectroscopic characteristics consistent with the previously reported values (15). Based on their optical activity, the enantiomeric excesses of these lactones were >95%. The chiral auxiliaries, (4*S*)-isopropyl- and (4*R*)-benzyl-2-oxazolidinone, were readily recovered from the lactonized product by chromatography. Compared to previously reported methods, the present approach to the synthesis of β-benzyl-γ-butyrolactones is more efficient. It is simple, gives high asymmetric induction, and uses commercially available reagents.

Having obtained the enantiomerically pure butyrolactones **11a** and **11b**, their conversion to optically pure lignans was undertaken. The benzylidene lignans gossypifan (**14a**) and savinin (hibalactone) (**14b**) were synthesized from **11a** and **11b** following a modified literature procedure (16) as illustrated in Scheme 4. The β-benzyl-γ-butyrolactones **11a** and **11b** were each deprotonated with *N*-sodiohexamethyldisilazane (NaHMDS), and then treated with 3,4-dimethoxybenzaldehyde (for **11a**) and 3,4-(methylenedioxy)benzaldehyde (for **11b**) to afford aldol products **12a** and **12b**, which were acetylated in situ by adding a mixture of Ac_2O–DMAP–Et_3N to the reaction mixtures. The crude acetylated products **13a** and **13b** were then treated with DBU in refluxing toluene to produce the *trans*-benzylidene lignans gossypifan (**14a**) and savinin (**14b**) respectively, in >90% overall yield (from **11**). Gossypifan (**14a**) is a naturally occurring lignan recently isolated from a plant (*Jatropha gossypifolia*) and possesses medicinal and

[3] The use of oxazolidinones as chiral auxiliaries was recently reviewed in textbooks (refs. 10*a*–10*c*) and by Evans et al. (10*d*).

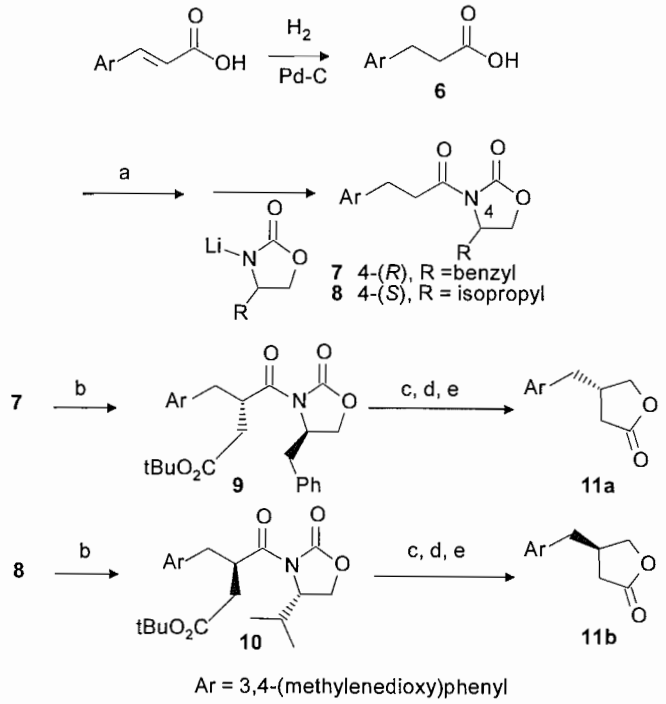
[4] The cyclization of yatein itself to aryltetralin and arylnaphthalene lignans has been more successful: see refs. 14*b*–14*d*.

© 1997 NRC Canada

Can. J. Chem. Downloaded from www.nrcresearchpress.com by 88.146.161.215 on 09/08/12
For personal use only.

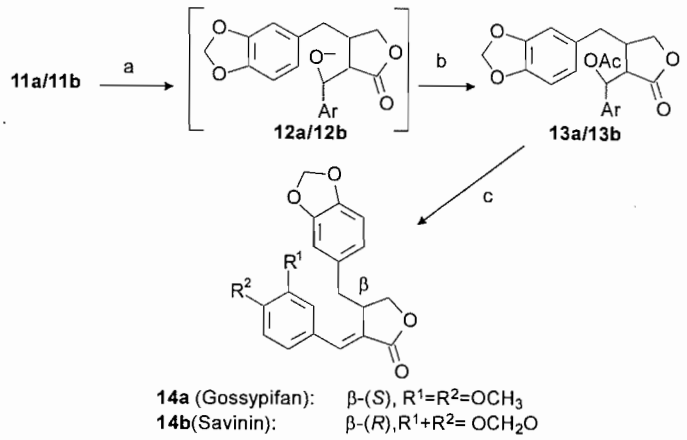
Can. J. Chem. Downloaded from www.nrcresearchpress.com by 88.146.161.215 on 09/08/12
For personal use only.

Scheme 3.



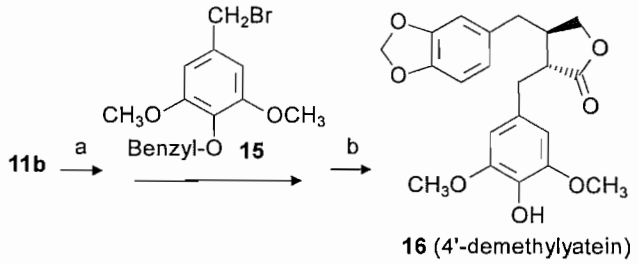
Key: (a) NEt_3, pivaloyl chloride; (b) NaHMDS, *tert*-butyl bromoacetate; (c) LiOH, H_2O_2, THF, H_2O; (d) BH3·THF; (e) TFA, CH_2CL_2.

Scheme 4.



Key: (a) NaHMDS, ArCHO; (b) Ac_2O, NEt_3, DMAP; (c) DBU

Scheme 5.



Key: (a) NaHMDS; (b) H_2, Pd-C.

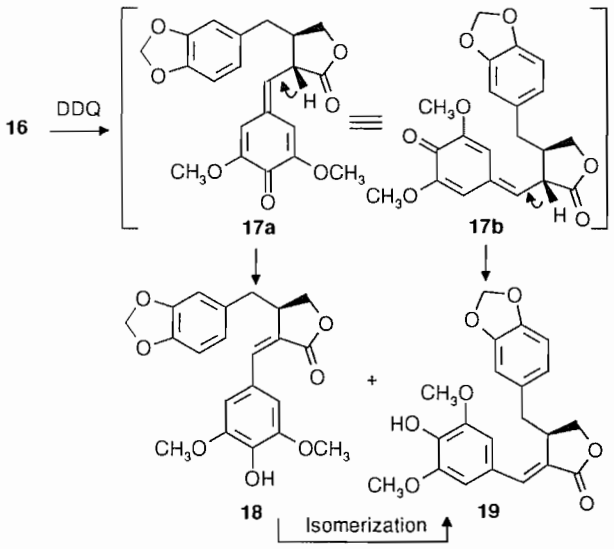
pesticidal properties (17). The synthetic material, **14a**, had both rotation and other spectroscopic properties consistent with those reported for the natural product (17). This is the first reported synthesis of this compound. Savinin (also known as hibalactone (18*a*)) (**14b**), which is an insecticide synergist, also had properties consistent with those previously reported (18*b*, 18*c*). It should be noted that savinin has been previously prepared from **11b** by Honda et al. in four steps and 37% yield (7). The method of Tanaka et al. (16) that was used in the current work has the advantage that it is a one-pot procedure that gives savinin in 90% yield.

In addition to savinin, butyrolactone **11b** was also converted to 4′-demethylyatein (**16**), a naturally occurring dibenzylbutyrolactone lignan that has been regarded as a biosynthetic precursor to 4′-demethylpodophyllotoxin derivatives (12). The anion of butyrolactone **11b** was reacted with benzyl bromide **15**, which was, in turn, prepared from syringic acid by benzylation, reduction, and bromination (19). Careful control of the reaction temperature during benzylation of **11b** was necessary to prevent formation of the dibenzylated product. HMPA, often used for this type of benzylation, was not required for this reaction. The resulting crude 4′-benzylated yatein was hydrogenated to afford 4′-demethylyatein in an overall yield of 62% from **11b** (see Scheme 5). The synthetic 4′-demethylyatein had spectroscopic properties identical to those reported previously (20).

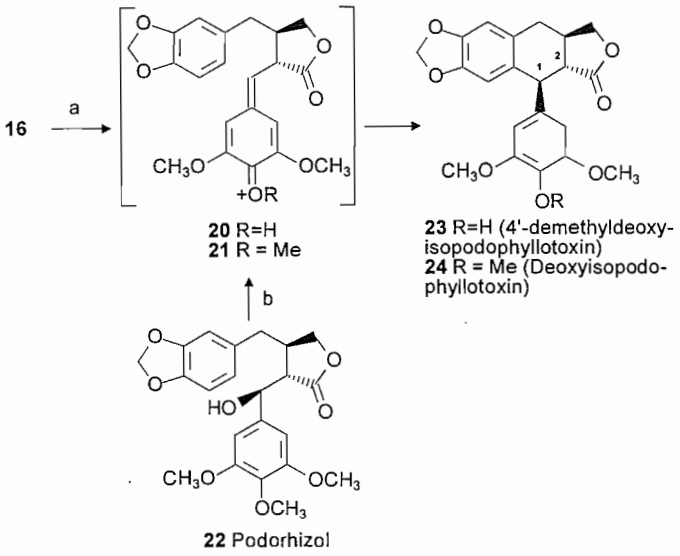
Previous attempts to oxidize racemic 4′-demethylyatein using metallic oxidants such as vanadium oxytrifluoride and thallium trifluoroacetate in order to induce cyclization to an aryltetralin lignan were totally unsuccessful (14*a*). On the other hand, Pelter et al. have reported a successful oxidative cyclization of a monophenolic lignan, which is structurally related to 4′-demethylyatein, using phenyliodonium bis(trifluoroacetate) (PIFA) as oxidant (21). The reaction afforded a mixture of dibenzocyclooctadiene diastereomers in good yield. In view of their success with the nonmetallic oxidant PIFA we decided to study the oxidation reaction of 4′-demethylyatein using DDQ. Oxidation of 4′-demethylyatein with DDQ in THF at room temperature resulted in the formation of a mixture of two compounds, *cis*- and *trans*-benzylidenelactones, **18** and **19**, in 95% total yield. The ratio of the *cis* to the *trans* isomer was about 1.3:1, as determined by ^{1}H NMR spectroscopy. The proposed elimination mechanism is shown in Scheme 6. Quinone methide **17** is considered to be the reactive intermediate. Elimination of a proton from **17** (from conformations **17a** and **17b**) could lead to **18** and **19**. It has previously been proposed that benzylidene lignans such as **18** and **19** (general structure **3**) may be formed biosynthetically via oxidation of dibenzylbutyrolactones **2** (12*a*). The oxidation result obtained for 4′-demethylyatein appears to confirm this possibility. After standing exposed to the air at room temperature for 2 weeks, *cis*-benzylidenelactone **18** isomerized completely to the *trans* isomer **19**. The isomerization process could also be achieved in 2 h by refluxing the *cis* and *trans* isomeric mixture with iodine in benzene, with UV irradiation. The isomerization process indicates the instability

© 1997 NRC Canada

Scheme 6.



Scheme 7.



Key: (a) DDQ, TFA.; (b) TFA.

of the *cis* isomer and may explain the lack of reports of isolation of *cis*-benzylidenelactone lignans from plants.

If quinone methide **17** were formed during oxidation of **16**, addition of acid might alter the course of the subsequent reactions of the quinone methide. Treating 4′-demethylyatein (**16**) with DDQ in the presence of TFA (see Scheme 7) resulted in the formation of 4′-demethyldeoxyisopodophyllotoxin (**23**), a naturally occurring all-*trans* aryltetralin lignan, in about 65% yield after preparative TLC and recrystallization. The concentration and the ratio of substrate to reagent were found to be very critical to the cyclization process. Protonated quinone methide **20** is proposed as the intermediate in the cyclization reaction. Friedel–Crafts substitution on the other aryl group leads to compound **23**. Notably, **23** has an all-*trans* geometry, in contrast to the podophyllotoxin type of stereochemistry (1,2-*cis*) often found in aryltetralin lignans formed biosynthetically.

An all-*trans* stereochemistry is also found in the product (see **24** in Scheme 7) obtained from the acid-catalysed cyclization of podorhizol (**22**) and structural analogues (12*a*). These reactions presumably involve the intermediate delocalized benzylic cation **21**, which is similar to **20** (Scheme 7).

To the best of our knowledge, the oxidative conversion of a monophenolic dibenzylbutyrolactone lignan to either an aryltetralin lignan or benzylidenebenzylbutyrolactone is unprecedented. Despite the fact that these reactions have been proposed biosynthetically they have not previously been demonstrated in the laboratory. Combining our current results with the earlier observations of Pelter et al. (21), it now seems reasonable to conclude that benzylidenebenzylbutyrolactone, aryltetralin, and dibenzocyclooctadiene lignans with 4′-hydroxyl groups (**3**, **4**, and **5** in Scheme 1) could all arise biosynthetically from a common 4′-hydroxydibenzylbutyrolactone precursor. The successful cyclization reaction of 4′-demethylyatein with DDQ–TFA has also provided a new method for the synthesis of aryltetralin lignans. Further investigations of structurally related compounds with other oxidants are in progress and will be reported in the near future.

Conclusion

A versatile asymmetric synthesis of β-benzyl-γ-butyrolactones, key intermediates in the synthesis of lignans, has been achieved using a six-step procedure, in an overall yield of >45% from 3,4-(methylenedioxy)cinnamic acid. The method afforded the β-benzyl-γ-butyrolactones in >95% optical purity. These intermediates were used in the synthesis of the benzylidene lignans gossypifan and savinin, and the dibenzylbutyrolactone lignan 4′-demethylyatein, in good to excellent yield. The DDQ oxidation of the latter product provides an alternative route for the preparation of aryltetralin lignans, and affords further substantiation of the proposed mechanism for the biosynthesis of lignans.

Experimental

General methods

The general experimental procedures and instrumentation have been described in a previous publication (22).

3,4-(Methylenedioxy)dihydrocinnamic acid (6)

3,4-(Methylenedioxy)cinnamic acid (1.86 g, 9.69 mmol) was dissolved in DMF (ca. 25 mL) and stirred with Pd–C (0.2 g) under H_2 (1 atm; 101.3 kPa) for 24 h. The suspension was filtered through Celite®, rinsing with water and EtOAc. The organic solution was separated, and the aqueous solution extracted with EtOAc (3 × 15 mL). The organic solutions were combined, washed with water (5 × 20 mL) to remove residual DMF, dried ($MgSO_4$), and concentrated under vacuum to afford a colorless crystalline solid (1.88 g, 100%): mp 82–84°C; IR (CH_2Cl_2): 3085 (COOH), 1711 (C=O) cm^{-1}; ^1H NMR ($CDCl_3$) δ: 2.64 (2H, t, J = 7.5), 2.88 (2H, t, J = 7.5), 5.92 (2H, s), 6.63–6.74 (3H, m); ^{13}C NMR ($CDCl_3$) δ: 30.3 (CH_2), 35.9 (CH_2), 100.8 (CH_2), 108.3 (CH), 108.7 (CH), 121.1 (CH), 133.9 (C), 146.0 (C), 147.6 (C), 179.1 (C); mass

© 1997 NRC Canada

Can. J. Chem. Downloaded from www.nrcresearchpress.com by 88.146.161.215 on 09/08/12
For personal use only.

Can. J. Chem. Downloaded from www.nrcresearchpress.com by 88.146.161.215 on 09/08/12
For personal use only.

spectrum *m/z* (relative intensity): 194 (M^+, 32), 176 (3), 149 (7), 135 (100); HRMS calcd. for $C_{10}H_{10}O_4$: 194.0579; found: 194.0570.

General procedure for the preparation of *N*-acyloxazolidinones 7 and 8

A modified literature procedure was used (11*b*). To a solution of 3,4-(methylenedioxy)dihydrocinnamic acid (**6**, 0.50 g, 2.53 mmol) in THF (6 mL) under N_2 at −70°C was successively added, dropwise, Et_3N (0.41 mL, 2.9 mmol) and pivaloyl chloride (0.32 mL, 2.6 mmol). The mixture was gradually warmed to 0°C, stirred for an hour, and then recooled to −70°C. *n*-BuLi (1.1 mL, 2.45 M in hexane, 2.6 mmol) was added dropwise to a solution of the (4*R*)-benzyl or (4*S*)-isopropyl-2-oxazolidinone (2.53 mmol) in THF (15 mL) under N_2 at −70°C. The resulting lithium salt was added dropwise to the above dihydrocinnamic acid mixture via a double-tipped needle at −70°C over a period of 15 min. The resulting mixture was stirred for an hour, and then warmed gradually to 0°C. After stirring at 0°C for 35 min, saturated aqueous NH_4Cl (2 mL) was added. The solution was concentrated under vacuum to remove most of the THF. Water (10 mL) was added and the solution was extracted with EtOAc (4 × 10 mL), dried ($MgSO_4$), and evaporated.

N-Acyloxazolidinone 7

Reacting dihydrocinnamic acid **6** and (4*R*)-benzyl-2-oxazolidinone as described above gave an oil (0.89 g) that slowly crystallized. Recrystallization from EtOAc–hexanes gave colorless crystals (0.78 g, 88%): mp 68–70°C; $[\alpha]_D^{20}$ −48 (*c* 0.30, $CHCl_3$): IR (CH_2Cl_2): 1783 and 1702 (C═O) cm^{-1}; ^1H NMR ($CDCl_3$) δ: 2.76 (1H, dd, *J* = 9.5, 13.4), 2.91–2.96 (2H, m), 3.13–3.32 (3H, m), 4.15–4.19 (2H, m), 4.66 (1H, m), 5.91 (2H, s), 6.71–6.76 (3H, m), 7.17 (2H, dd, *J* = 8.0, 1.67), 7.25–7.32 (3H, m); ^{13}C NMR ($CDCl_3$) δ: 30.0 (CH_2), 37.4 (CH_2), 37.8 (CH_2), 55.1 (CH), 66.2 (CH_2), 100.8 (CH_2), 108.2 (CH), 109.0 (CH), 121.3 (CH), 127.3 (CH), 128.9 (2 × CH), 129.4 (2 × CH), 134.2 (C), 135.2 (C), 145.9 (C), 147.6 (C), 153.4 (C), 172.3 (C); mass spectrum *m/z* (relative intensity): 353 (M^+, 40.5), 309 (4), 219 (5), 176 (34), 148 (82), 135 (100); HRMS calcd. for $C_{20}H_{19}O_5N$: 353.1263; found: 353.1263.

N-Acyloxazolidinone 8

Reacting dihydrocinnamic acid **6** and (4*S*)-isopropyl-2-oxazolidinone as described above gave an oil. This was chromatographed with 20% EtOAc–hexanes to afford a light yellow oil (0.65 g, 84%): $[\alpha]_D^{20}$ +61 (*c* 0.98, $CHCl_3$); IR (CH_2Cl_2): 1786 and 1708 (C═O) cm^{-1}; ^1H NMR ($CDCl_3$) δ: 0.84 (3H, d, *J* = 7.0), 0.90 (3H, d, *J* = 7.0), 2.35 (1H, dseptet, *J* = 3.9, 7.0), 2.90 (2H, m), 3.10–3.33 (2H, m), 4.22 (2H, m), 4.42 (1H, m), 5.91 (2H, s), 6.68–6.74 (3H, m); ^{13}C NMR ($CDCl_3$) δ: 14.6 (CH_3), 17.9 (CH_3), 28.4 (CH), 30.2 (CH_2), 37.4 (CH_2), 58.4 (CH), 63.4 (CH_2), 100.8 (CH_2), 108.2 (CH), 109.0 (CH), 121.3 (CH), 134.2 (C), 145.9 (C), 147.6 (C), 154.0 (C), 172.3 (C); mass spectrum *m/z* (relative intensity): 305 (M^+, 9), 180 (13), 179 (25), 178 (17), 176 (13), 149 (13), 148 (29), 135 (27); HRMS calcd. for $C_{16}H_{19}O_5N$: 305.1263; found: 305.1269.

General procedure for alkylation of *N*-acyloxazolidinones 7 and 8 with *tert*-butyl bromoacetate

This procedure is a modification of one found in the literature (11*b*). NaHMDS (2.10 mL, 1.0 M in THF, 2.10 mmol) was added dropwise to a solution of the *N*-acyloxazolidinone (2.0 mmol) in THF (15 mL) under N_2 at −73°C, over a period of 10 min. After stirring at −73°C for an hour, *tert*-butyl bromoacetate (0.92 mL, 6.30 mmol) was added dropwise. The mixture was stirred for 2 h before being quenched with saturated aqueous NH_4Cl (4 mL). It was concentrated under vacuum to remove most of the THF, and then diluted with EtOAc (15 mL) and water (10 mL). The organic layer was separated and the aqueous layer extracted with EtOAc (3 × 10 mL). The organic solutions were combined, washed with saturated aqueous NH_4Cl (15 mL), 5% aqueous $NaHCO_3$ (15 mL), and brine (15 mL), dried ($MgSO_4$), and concentrated to afford a liquid that crystallized when triturated with hexane. The hexane washings were concentrated and chromatographed using hexanes–2-propanol (15:1) to give more product. The colorless solid was combined and recrystallized (see below).

Alkylated product 9

N-Acyloxazolidinone **7** (0.706 g, 2.0 mmol) was alkylated as above to give a colorless solid that was further recrystallized from MeOH (0.72 g, 77%): mp 138–139°C; $[\alpha]_D^{20}$ −98.5 (*c* 0.135, $CHCl_3$); IR (CH_2Cl_2): 1782, 1722, 1700 (C═O) cm^{-1}; ^1H NMR ($CDCl_3$) δ: 1.40 (9H, s), 2.36 (1H, dd, *J* = 4.1, 16.9), 2.51 (1H, dd, *J* = 9.3, 13.2), 2.75 (1H, dd, *J* = 9.9, 13.4), 2.80 (1H, dd, *J* = 10.9, 17.0), 2.97 (1H, dd, *J* = 5.7, 13.2), 3.32 (1H, dd, *J* = 3.2, 13.6), 4.03–4.15 (2H, m), 4.39 (1H, m), 4.60 (1H, m), 5.91 (2H, s), 6.67–6.79 (3H, m), 7.25–7.36 (5H, m); ^{13}C NMR ($CDCl_3$) δ: 28.1 (3 × CH_3), 36.5 (CH_2), 37.6 (CH_2), 37.8 (CH_2), 41.6 (CH), 55.5 (CH), 66.0 (CH_2), 80.8 (C), 100.9 (CH_2), 108.1 (CH), 109.6 (CH), 122.2 (CH), 127.2 (CH), 128.9 (2 × CH), 129.5 (2 × CH), 131.7 (C), 135.6 (C), 146.3 (C), 147.6 (C), 153.0 (C), 171.2 (C), 175.2 (C); mass spectrum *m/z* (relative intensity): 467 (M^+, 1), 411 (5), 234 (25), 192 (16), 135 (100), 92 (90); HRMS calcd. for $C_{26}H_{29}O_7N$: 467.1944; found: 467.1924.

Alkylated product 10

N-Acyloxazolidinone **8** (0.610 g, 2.0 mmol) was alkylated as above to give a colorless solid that was further recrystallized from EtOAc–hexanes (0.67 g, 80%): mp 123–124°C; $[\alpha]_D^{20}$ +92 (*c* 0.37, $CHCl_3$); IR (CH_2Cl_2): 1779 and 1723 (C═O) cm^{-1}; ^1H NMR ($CDCl_3$) δ: 0.90 (3H, d, *J* = 6.8), 0.93 (3H, d, *J* = 6.8), 1.39 (9H, s), 2.32 (1H, dd, *J* = 4.3, 16.8), 2.34 (1H, m), 2.47 (1H, dd, *J* = 9.3, 13.2), 2.74 (1H, dd, *J* = 10.5, 16.8), 2.94 (1H, dd, *J* = 5.8, 13.2), 4.15 (2H, m), 4.36 (2H, m), 5.96 (2H, s), 6.67 (1H, dd, *J* = 1.5, 7.9), 6.72 (1H, d, *J* = 7.9), 6.78 (1H, d, *J* = 1.5); ^{13}C NMR ($CDCl_3$) δ: 14.7 (CH_3), 18.0 (CH_3), 28.0 (3 × CH_3), 28.3 (CH), 36.6 (CH_2), 37.6 (CH_2), 41.5 (CH), 58.8 (CH), 63.2 (CH_2), 80.6 (C), 100.8 (CH_2), 108.1 (CH), 109.6 (CH), 122.2 (CH), 131.9 (C), 146.2 (C), 147.6 (C), 153.5 (C), 171.1 (C), 175.1 (C); mass spectrum *m/z* (relative intensity): 419 (M^+, 3), 363 (36), 346 (9), 304 (8), 303 (6), 234 (17), 206 (19), 175 (20), 149 (14), 135 (100); HRMS calcd. for $C_{22}H_{29}O_7N$: 419.1944; found: 419.1951.

General procedure for the preparation of benzylbutyrolactones 11a and 11b

A modification of a literature procedure was used (11*a*). The alkylated product (**9** or **10**, 1.40 mmol) was dissolved in THF (20 mL), and water was added (7.0 mL). The solution was

© 1997 NRC Canada

Can. J. Chem. Downloaded from www.nrcresearchpress.com by 88.146.161.215 on 09/08/12
For personal use only.

cooled to ice temperature, followed by addition of H_2O_2 (0.66 mL, 30% in H_2O, 5.8 mmol) and $LiOH \cdot H_2O$ powder (0.12 g, 2.8 mmol). The resulting mixture was stirred at 0–5°C for 1.5 h, then at room temperature (rt) for 3 h. After recooling to 0°C, saturated aqueous $NaHSO_3$ (2 mL), cold water (50 mL), and 2% HCl (2 mL) were added. The solution was carefully kept at 0°C during the additions to prevent hydrolysis of the *tert*-butyl ester. The resulting mixture was extracted with EtOAc (4 × 25 mL). The organic solutions were combined, washed with water (20 mL) and brine (20 mL), dried ($MgSO_4$), and evaporated to give a liquid that was used in the following reaction without further purification. The crude liquid was redissolved in THF (25 mL) and cooled to 0°C. $BH_3 \cdot THF$ (1.68 mL, 1.0 M in THF, 1.68 mmol) was added dropwise to the acid solution over a period of 10 min. The resulting mixture was stirred at 0°C for 1 h, then at rt for 4 h. It was recooled to 0°C, MeOH (0.5 mL) added dropwise to destroy excess $BH_3 \cdot THF$, followed by cold water (10 mL) and 2% HCl (5 mL). The mixture was concentrated under vacuum to remove most of the THF. The remaining solution was extracted with EtOAc (3 × 15 mL). The combined EtOAc solution was washed with water (20 mL) and brine (20 mL), dried ($MgSO_4$), and concentrated to afford a light brown liquid. The crude product was redissolved in CH_2Cl_2 (4 mL), cooled to 0°C, and TFA (4 mL) was added dropwise. The mixture was stirred for 1 h at ice temperature and for 3 h at rt, followed by concentration under vacuum with several coevaporations with benzene to remove all of the TFA. The resulting brown liquid was chromatographed with 20–33% EtOAc–hexanes.

(*S*)-(−)-Benzylbutyrolactone 11a

Alkylated product **9** (0.65 g, 1.4 mmol) was hydrolysed, reduced, and lactonized as described in the above general procedure to give, after chromatography, a light yellow liquid (0.215 g, 70% from **9**): $[\alpha]_D^{20}$ −4.8 (*c* 0.50, $CHCl_3$) (lit. (15) $[\alpha]_D^{20}$ −4.78 (*c* 1.14, $CHCl_3$)); NMR spectral data were consistent with those published previously (15).

(*R*)-(+)-Benzylbutyrolactone 11b

Alkylated product **10** (0.586 g, 1.4 mmol) was treated as above to afford a light yellow liquid (0.202 g, 66% from **10**): $[\alpha]_D^{20}$ +4.8 (*c* 0.665, $CHCl_3$) (lit. (15) $[\alpha]_D^{20}$ +4.87 (*c* 0.87, $CHCl_3$)); spectroscopic data were identical to those obtained from **11a**.

General procedure for preparation of benzylidenebenzylbutyrolactones 14a and 14b

A modified literature procedure was employed (16). To a solution of benzylbutyrolactone **11a** or **11b** (61 mg, 0.28 mmol) in THF (1 mL) under N_2 at −70°C was added NaHMDS (0.33 mL, 1.0 M in THF, 0.33 mmol) over a period of 5 min. The solution was stirred at −70°C for 15 min, then at −20°C (CCl_4 – Dry Ice) for 15 min to ensure complete deprotonation. The color of the solution changed from light yellow to intense bright yellow. The mixture was recooled to −70°C and a solution of a benzaldehyde (3,4-dimethoxybenzaldehyde for **11a**; 3,4-(methylenedioxy)benzaldehyde for **11b**) (0.28 mmol) in THF (1 mL) was added dropwise. After stirring at −70°C for 1.3 h, a mixture of Ac_2O (78 μL, 0.83 mmol), Et_3N (0.16 mL, 1.14 mmol), and DMAP (6 mg, 0.049 mmol) in THF (1 mL) was added dropwise to the reaction mixture. The resulting thick mixture was warmed to rt and stirred for 1.5 h before water (1 mL) was added. The solution was concentrated to remove most of the THF, diluted with water (5 mL) and 2% HCl (2 mL), and then extracted with CH_2Cl_2 (3 × 10 mL). The combined CH_2Cl_2 phases were washed with 2% HCl (3 × 5 mL), 5% aqueous $NaHCO_3$ (2 × 5 mL), and brine (10 mL), dried ($MgSO_4$), and concentrated under vacuum to give a foamy residue. The crude product was redissolved in toluene (3 mL), DBU (90 μL, 0.61 mmol) was added, and the solution was heated to 80°C. After 1.5 h the mixture was diluted with EtOAc (10 mL), washed successively with 2% HCl (2 × 5 mL), water (2 × 10 mL), and brine (15 mL), dried ($MgSO_4$), and evaporated to afford a yellow residue that crystallized on standing under vacuum.

Gossypifan (14a)

(*S*)-(−)-benzylbutyrolactone **11a** (0.61 g, 0.28 mmol) was hydroxyalkylated with 3,4-dimethoxybenzaldehyde (46 mg, 0.28 mmol), acetylated, and treated with DBU as described above. The crude product was chromatographed with EtOAc–hexanes (1:2) to afford a light yellow solid (95 mg, 92%): mp 143–146°C (lit. (17) mp 145–146°C); $[\alpha]_D^{20}$ 79.1 (*c* 0.110, $CHCl_3$) (lit. (17) $[\alpha]_D^{20}$ 82.4 (*c* 0.875, $CHCl_3$)). NMR spectral data were consistent with those published previously (17).

Savinin (14b)

(*R*)-(+)-Benzylbutyrolactone **11b** (0.61 g, 0.28 mmol) was hydroxyalkylated with 3,4-(methylenedioxy)benzaldehyde (42 mg, 0.28 mmol), acetylated, and treated with DBU as described above. The yellow residue crystallized upon standing under vacuum and was recrystallized from ethanol–chloroform to afford colorless crystals (89 mg, 90%): mp 139–142°C (lit. (18*b*), from benzene and ethanol, mp 146.4–148.4°C); $[\alpha]_D^{20}$ −82.9 (*c* 0.135, $CHCl_3$) (lit. (18*c*) $[\alpha]_D^{20}$ −82 (*c* 2.5, $CHCl_3$); lit. (18d) $[\alpha]_D^{20}$ −88 (*c* 1.0, $CHCl_3$)). NMR spectral data were consistent with those published previously (7).

Benzyl ester of *p*-*O*-benzyl syringic acid

A mixture of syringic acid (3.12 g, 15.7 mmol), benzyl bromide (5.6 mL, 47 mmol), and dry K_2CO_3 (11 g, 78 mmol) in acetone (80 mL) was refluxed under N_2 for 24 h. The resulting suspension was cooled to rt, concentrated under vacuum, diluted with water (100 mL), and extracted with CH_2Cl_2 (4 × 20 mL). The organic solution was dried ($MgSO_4$), concentrated, and chromatographed with hexanes and 6% EtOAc–hexanes to remove benzyl bromide. The product was eluted with EtOAc and concentrated to leave a colorless solid (5.70 g, 95%): mp 64–65°C; IR (CH_2Cl_2): 1714 (C═O) cm^{-1}; ^1H NMR ($CDCl_3$) δ: 3.85 (6H, s), 5.08 (2H, s), 5.35 (2H, s), 7.27–7.48 (12H, m); ^{13}C NMR ($CDCl_3$) δ: 56.2 (2 × CH_3), 66.8 (CH_2), 74.9 (CH_2), 107.0 (2 × CH), 125.2 (C), 127.9 (CH), 128.1$_3$ (2 × CH), 128.1$_6$ (2 × CH), 128.2 (CH), 128.4 (2 × CH), 128.6 (2 × CH) 136.1 (C), 137.3 (C), 141.1 (C), 153.2 (2 × C), 166.1 (C); mass spectrum *m/z* (relative intensity): 378 (M^+, 4), 287 (6), 181 (6), 149 (7), 105 (11), 91 (100); HRMS calcd. for $C_{23}H_{22}O_5$: 378.1467; found: 378.1463.

p-*O*-Benzyl syringyl bromide (15)

To a solution of the benzyl ester of *p*-*O*-benzyl syringic acid (0.919 g, 2.43 mmol) in THF (10 mL) under N_2 at ice temperature was carefully added $LiEt_3BH$ (7.0 mL, 0.8 M in THF,

© 1997 NRC Canada

Can. J. Chem. Downloaded from www.nrcresearchpress.com by 88.146.161.215 on 09/08/12
For personal use only.

5.6 mmol). The resulting mixture was stirred for 2 h and then 10% HCl (15 mL) was slowly added. The solution was concentrated under vacuum, diluted with water (10 mL), and extracted with CH_2Cl_2 (3 × 20 mL). The organic layer was washed successively with 5% HCl (3 × 20 mL), 5% aqueous $NaHCO_3$ (2 × 20 mL), and brine (20 mL). It was then dried ($MgSO_4$) and concentrated to afford an oil. The crude product (0.893 g) was redissolved in anhydrous ether (10 mL), followed by addition of pyridine (0.6 mL) and PBr_3 (0.55 mL, 5.79 mmol). The resulting colorless suspension was stirred for 2.5 h before filtering through Celite®. The filtrate was diluted with CH_2Cl_2 (10 mL), washed with 3% HCl (3 × 20 mL), water (2 × 20 mL), and brine (25 mL), then dried ($MgSO_4$), concentrated, and chromatographed (6–15% EtOAc–hexanes) to give a colorless liquid (0.53 g, 65%) that slowly solidified on standing: mp 53–55°C (lit. (19*b*) mp 40–42°C); IR (CH_2Cl_2): 1593, 1503, 1461, 1336, 1130 (vs) cm^{-1}; ^1H NMR ($CDCl_3$) δ: 3.82 (6H, s), 4.45 (2H, s), 4.99 (2H, s), 6.60 (2H, s), 7.25–7.35 (3H, m), 7.48 (2H, dd, J = 8.1, 1.7); ^{13}C NMR ($CDCl_3$) δ: 34.3 (CH_2), 56.1 (2 × CH_3), 75.0 (CH_2), 106.2 (2 × CH), 127.8 (CH), 128.1 (2 × CH), 128.4 (2 × CH), 133.2 (C), 137.1 (C), 137.7 (C), 153.5 (2 × C); mass spectrum *m/z* (relative intensity): 338 ($M^+(^{81}Br)$, 0.1), 336 ($M^+(^{79}Br)$, 0.1), 148 (22), 136 (12), 91 (100); HRMS calcd. for $C_{16}H_{17}O_3{}^{79}Br$: 336.0361; found: 336.0333.

4′-Demethylyatein (16)

(*R*)-(+)-Benzylbutyrolactone **11b** (86 mg, 0.39 mmol) in THF (1.5 mL) under N_2 was cooled to −72°C. NaHMDS (0.45 mL, 1.0 M in THF, 0.45 mmol) was then added dropwise over a period of 10 min. The mixture was stirred at that temperature for 15 min, then at −20°C (CCl_4 – Dry Ice) for 25 min. It was recooled to −72°C and a solution of syringyl bromide **15** (0.135 g, 0.40 mmol) in THF (2 mL) was added. After stirring at −72°C for 5 h, the reaction mixture was quenched with 5% aqueous NH_4Cl (1 mL). The mixture was concentrated, diluted with 2% HCl (10 mL), and extracted with CH_2Cl_2 (3 × 7 mL). The organic fractions were combined, washed with water (10 mL) and brine (10 mL), dried ($MgSO_4$), and concentrated to afford an oil (0.20 g). The crude product was redissolved in EtOAc and stirred with Pd–C (40 mg) under H_2 overnight. The suspension was filtered through Celite® and the filtrate was concentrated and chromatographed (50% EtOAc–hexanes) to afford an oil (93 mg, 62%): $[\alpha]_D^{20}$ −25.8 (*c* 0.225, CH_2Cl_2): (lit. (20) $[\alpha]_D^{20}$ −25 (*c* 0.32, CH_2Cl_2)). NMR spectral data were consistent with those published previously (20).

***trans*-Benzylidene, 19**

To 4′-demethylyatein (**16**, 20 mg, 0.052 mmol) in THF (1 mL) was added dropwise a solution of DDQ (14 mg, 0.062 mmol) in THF under N_2. A temporary blue color appeared after each addition of the DDQ solution. The resulting mixture was stirred for 12 h and worked up by adding saturated aqueous $NaHSO_3$ (1 mL) and 2% HCl (2 mL), and extracting with EtOAc (3 × 5 mL). The organic solutions were combined, washed with 5% aqueous $NaHCO_3$ (5 × 5 mL), water (10 mL), and brine (10 mL), dried ($MgSO_4$), and concentrated to afford a light yellow oil (22 mg). The crude product contained two compounds, the *cis*- and *trans*-benzylidenes **18** and **19**, respectively, in a 1.3:1 ratio as determined by ^1H NMR spectroscopy. After standing exposed to the air at rt for about 2 weeks, the crude product was found to contain only the *trans* isomer **19**, as indicated by the ^1H NMR spectrum. This product resisted crystallization. It was purified by chromatography (EtOAc–hexanes 1:2 ratio) to afford an oil that slowly solidified (18 mg, total 95% from 4′-demethylyatein). The isomerization process observed above was also achieved by refluxing a crude product mixture of **18** and **19** (2 mg) in benzene (1.5 mL) in the presence of I_2 (1 mg), for 1.5 h, with UV irradiation for the first 10 min of reflux. The light pink solution was worked up by adding saturated aqueous $NaHSO_3$ (0.5 mL) and extracting with EtOAc (3 × 5 mL). The extract was dried ($MgSO_4$) and evaporated to give a light yellow residue (1.7 mg, 85%) that contained only *trans* isomer **19**, as shown by the ^1H NMR spectrum: mp 130–132°C; $[\alpha]_D^{20}$ −54 (*c* 0.31, $CHCl_3$); IR (CH_2Cl_2): 3529 (OH), 1748 (C=O) cm^{-1}; ^1H NMR ($CDCl_3$) δ: 2.65 (1H, dd, J = 10.0, 14.5), 3.04 (1H, dd, J = 4.6, 14.5), 3.84 (1H, m), 3.92 (6H, s), 4.23–4.32 (2H, m), 5.92 (2H, AB, Δδ = 2.4, J = 1.4), 6.61 (2H, m), 6.71 (1H, d, J = 7.9), 6.81 (2H, s), 7.50 (1H, d, J = 1.8); ^{13}C NMR ($CDCl_3$) δ: 37.6 (CH_2), 39.6 (CH), 56.4 (2 × CH_3), 69.6 (CH_2), 101.1 (CH_2), 107.2 (2 × CH), 108.4 (CH), 109.0 (CH), 121.8 (CH), 125.4 (C), 125.5 (C), 131.3 (C), 136.9 (C), 137.9 (CH), 146.6 (C), 147.2 (2 × C), 148.0 (C), 172.5 (C); mass spectrum *m/z* (relative intensity): 384 (M^+, 11), 249 (90), 189 (14), 135 (100); HRMS calcd. for $C_{21}H_{20}O_7$: 384.1209; found: 384.1222.

4′-Demethyldeoxyisopodophyllotoxin (23)

To 4′-demethylyatein (**16**, 35 mg, 0.091 mmol) in THF (3 mL) at 4°C was added TFA (24 μL, 0.31 mmol), followed by a solution of DDQ (42 mg, 0.185 mmol) in THF (1 mL). The solution became green for more than 1.5 h. It was stirred at ice temperature for 1.5 h, then at rt overnight. The color of the solution became deep red after stirring overnight. The reaction mixture was diluted with saturated aqueous $NaHSO_3$ (1 mL), concentrated to remove most of the THF, and diluted again with 5% aqueous $NaHCO_3$ (5 mL). The resulting bright yellow solution was extracted with CH_2Cl_2 (4 × 5 mL). The combined CH_2Cl_2 extracts were washed with 5% aqueous $NaHCO_3$ (5 × 5 mL) and water (10 mL), dried ($MgSO_4$), and concentrated to afford a light yellow solid (35 mg) that was sparingly soluble in EtOAc, Et_2O, and MeOH, but more soluble in CH_2Cl_2 and $CHCl_3$. Recrystallization of the crude solid from CH_2Cl_2 gave fine colorless needles (25 mg, 71%). The recrystallized product, analysed by ^1H NMR, was shown to be contaminated with an unknown component (ca. 5%) that could not be eliminated even after multiple recrystallizations from CH_2Cl_2. This by-product was removed by preparative TLC using a solvent mixture of $CHCl_3$–MeOH–AcOH (25:1:1) to yield a colorless solid (22 mg, 65% from 4′-demethylyatein); mp 282–285°C (lit. (15*a*) mp 285–287°C); $[\alpha]_D^{20}$ −77 (*c* 0.26, $CHCl_3$) (lit. (15*a*) $[\alpha]_D^{20}$ −81)). NMR spectral data were consistent with those published previously (15*a*).

Copies of ^1H and ^{13}C NMR spectra of all compounds have been deposited as supplementary material.[5]

[5] This material may be purchased from: The Depository of Unpublished Data, Document Delivery, CISTI, National Research Council Canada, Ottawa, Canada K1A 0S2.

© 1997 NRC Canada

Can. J. Chem. Downloaded from www.nrcresearchpress.com by 88.146.161.215 on 09/08/12
For personal use only.

Acknowledgments

We would like to acknowledge the financial assistance of the Natural Sciences and Engineering Research Council of Canada. We also acknowledge the technical assistance of Tad Foniok and Wayne Buchannon.

References

1. (*a*) L. Bohlin and B. Rosén. Drug Discovery Today, **1**, 343 (1996); (*b*) W.D. MacRae and G.H.N. Towers. Phytochemistry, **23**, 1207 (1984); (*c*) D.C. Ayres and J.D. Loike. *In* Lignans: chemical, biological and clinical properties. Cambridge University Press, Cambridge. 1990. pp. 85–132.
2. (*a*) T. Morimoto, M. Chiba, and K. Achiwa. Heterocycles, **33**, 435 (1992); (*b*) R.S. Ward. Tetrahedron, **46**, 5029 (1990); (*c*) Nat. Prod. Rep. **12**, 183 (1995); (*d*) Nat. Prod. Rep. **10**, 1 (1993); (*e*) Synthesis, 719 (1992); (*f*) D.C. Ayres and J.D. Loike. *In* Lignans: chemical, biological and clinical properties. Cambridge University Press, Cambridge. 1990. pp. 303–384; (*g*) D.C. Whiting. Nat. Prod. Rep. **7**, 349 (1990); (*h*) Nat. Prod. Rep. **4**, 499 (1987); (*i*) A. Pelter. Recent Adv. Phytochem. **20**, 201 (1986); (*j*) D.C. Whiting. Nat. Prod. Rep. **2**, 191 (1985); (*k*) R.S. Ward. Chem. Soc. Rev. **11**, 75 (1982).
3. (*a*) K. Tomioka and K. Koga. Tetrahedron Lett. **20**, 3315 (1979); (*b*) Heterocycles, **12**, 1523 (1979).
4. G.H. Posner, T.P. Kogan, S.R. Haines, and L.L. Frye. Tetrahedron Lett. **25**, 2627 (1984).
5. H. Yoda, H. Kitayama, T. Katagiri, and K. Takabe. Tetrahedron, **48**, 3313 (1992).
6. T. Morimoto, M. Chiba, and K. Achiwa. Tetrahedron, **49**, 1793 (1993).
7. T. Honda, N. Kimura, S. Sato, D. Kato, and H. Tominaga. J. Chem. Soc. Perkin Trans. 1, 1043 (1994).
8. M.P. Doyle, M.N. Protopopova, Q.L. Zhou, J.W. Bode, S.H. Simonsen, and V. Lynch. J. Org. Chem. **60**, 6654 (1995).
9. (*a*) L.M. Yang, S.J. Lin, T.H. Yang, and K.H. Lee. Bioorg. Med. Chem. Lett. **6**, 941 (1996); (*b*) S. Shiotani, H. Okada, T. Yamamoto, K. Nakamata, J. Adachi, and H. Nakamoto. Heterocycles, **43**, 113 (1996).
10. (*a*) D.J. Ager and M.B. East. *In* Asymmetric synthetic methodology. CRC Press, Florida. 1996; (*b*) J. Seyden-Penne. *In* Chiral auxiliaries and ligands in asymmetric synthesis. John Wiley & Sons, Inc., New York. 1995; (*c*) D.A. Evans. *In* Asymmetric synthesis. Vol. 3. *Edited by* J.D. Morrison. Academic Press, New York. 1984. p. 1; (*d*) D.A. Evans, J.M. Takacs, L.R. McGee, M.D. Ennis, D.J. Mathre, and J. Bartroli. J. Pure Appl. Chem. **53**, 1109 (1981).
11. (*a*) R.P. Beckett, M.J. Crimmin, M.H. Davis, and Z. Spavold. Synlett, **137** (1993); (*b*) J.J. Plattner, P.A. Marcotte, H.D. Kleinert, H.H. Stein, J. Greer, G. Bolis, A.K.L. Fung, B.A. Bopp, J.R. Luly, H.L. Sham, D.J. Kempf, S.H. Rosenberg, J.F. Dellaria, B. De, I. Merits, and T.J. Perun. J. Med. Chem. **31**, 2277 (1988); (*c*) A. Fadel and J. Salaün. Tetrahedron Lett. **29**, 6257 (1988); (*d*) C.P. Decicco, D.J. Nelson, R.L. Corbett, and J.C. Dreabit. J. Org. Chem. **60**, 4782 (1995).
12. (*a*) W.M. Kamil and P.M. Dewick. Phytochemistry, **25**, 2093 (1986); (*b*) A.J. Broomhead, M.M.A. Rahman, P.M. Dewick, D.E. Jackson, and J.A. Lucas. Phytochemistry, **30**, 1489 (1991).
13. (*a*) A.S. Kende, L.S. Liebeskind, J.E. Mills, P.S. Rutledge, and D.P. Curran. J. Am. Chem. Soc. **99**, 7082 (1977); (*b*) A.S. Kende and P.S. Rutledge. Synth. Commun. **8**, 245 (1978).
14. (*a*) J.K. Burden, R.C. Cambie, P.A. Craw, P.S. Rutledge, and P.D. Woodgate. Aust. J. Chem. **41**, 919 (1988); (*b*) A.S. Feliciano, M. Medarde, R.P.L. de Clairac, J.L. Lopez, P. Puebla, D.G. Gravalos, P.R. Lázaro, and T.G. de Quesada. Arch. Pharm. (Weinheim), **326**, 421 (1993); (*c*) R.C. Cambie, P.A. Craw, P.S. Rutledge, and P.D. Woodgate. Aust. J. Chem. **41**, 897 (1988); (*d*) R.E. Damon, R.H. Schlessinger, and J.F. Blount. J. Org. Chem. **41**, 3772 (1976).
15. (*a*) E. Brown and A. Daugan. Tetrahedron, **45**, 141 (1989); (*b*) Tetrahedron Lett. **26**, 3997 (1985).
16. (*a*) M. Tanaka, H. Mitsuhashi, M. Maruno, and T. Wakamatsu. Heterocycles, **42**, 359 (1996); (*b*) M. Tanaka, C. Mukaiyama, H. Mitsuhashi, M. Maruno, and T. Wakamatsu. J. Org. Chem. **60**, 4339 (1995).
17. B. Das and R. Das. Phytochemistry, **40**, 931 (1995).
18. (*a*) M. Masumura and F.S. Okumura. J. Am. Chem. Soc. **77**, 1906 (1956); (*b*) J.L. Hartwell, J.M. Johnson, D.B. Fitzgerald, and M. Belkin. J. Am. Chem. Soc. **75**, 235 (1953); (*c*) J.E. Batterbee, R.S. Burden, L. Crombie, and D.A. Whiting. J. Chem. Soc. Chem. Commun. 2470 (1969); (*d*) A.W. Schrecker and J.L. Hartwell. J. Am. Chem. Soc. **76**, 4896 (1954).
19. (*a*) J.P. Robin and Y. Landais. Tetrahedron, **48**, 819 (1992); (*b*) E. Brown and A. Daugan. Heterocycles, **26**, 1169 (1987).
20. S. Kawai, T. Hasegawa, M. Gotoh, and H. Ohashi. Phytochemistry, **37**, 1699 (1994).
21. A. Pelter, P. Satchwell, R.S. Ward, and K. Blake. J. Chem. Soc. Perkin Trans. 1, 2201 (1995).
22. S.P. Maddaford and J.L. Charlton. J. Org. Chem. **58**, 4132 (1993).

© 1997 NRC Canada

Speciation of trimethyltin(IV): hydrolysis, complexation equilibria, and structures of trimethyltin(IV) ion in aqueous solution

Akio Takahashi, Takayuki Natsume, Nobuyoshi Koshino, Shigenobu Funahashi, Yasuhiro Inada, and Hideo D. Takagi

Abstract: The hydrolysis constants of trimethyl- and triethyltin(IV) ions and the stability constants for the complexation of trimethyltin(IV) with trimethylamine, *N*-substituted glycines (*N,N*-dimethylglycine and *N,N,N*-trimethylglycine), and aminopolycarboxylate ions (*N*-methyliminodiacetate, nitrilotriacetate, and ethylenediamine-*N,N'*-diacetate) were determined by the potentiometric method at 25°C and $I = 0.1$ mol dm^{-3} ((H, Na)ClO_4 and (H, Na)NO_3). The structural parameters of $Me_3Sn(OH_2)_2$, $Et_3Sn(OH_2)_2$, and $Me_3Sn(OH_2)(OH)$ in solution were determined by the EXAFS method. The coordination structures of trimethyltin(IV) complexes with *N*-substituted glycines, trimethylamine, and aminopolycarboxylate ions are discussed on the basis of the electronic interaction between the donor atom and Sn(IV).

Key words: organotin(IV), EXAFS, structure, potentiometry.

Résumé : Utilisant la méthode potentiométrique à 25°C et $I = 0,1$ mol dm^3 ((H, NA)ClO_4 et (H, Na)NO_3), on a déterminé les constantes d'hydrolyse des ions triéthyl- et triéthylétain(IV) et les constantes de stabilité pour la complexation du triméthylétain(IV) avec la triméthylamine, les glycines *N*-substituées (*N,N*-diméthylglycine et *N,N,N*-triméthylglycine) et avec les ions aminopolycarboxylates (*N*-méthyliminodiacétate, nitrilotriacétate et éthylènediamine-*N,N'*-diacétate). Les paramètres structuraux des composés $Me_3Sn(OH_2)_2$, $Et_3Sn(OH_2)_2$, et $Me_3Sn(OH_2)(OH)$ ont été déterminés en solution par la méthode EXAFS. On discute des structures de coordination des complexes de triméthylétain(IV) avec les glycines *N*-substituées, la triméthylamine et les ions aminopolycarboxylates, en terme d'une interaction électronique entre l'atome donneur et Sn(IV).

Mots clés : organoétain(IV), EXAFS, structure, potentiométrie.

[Traduit par la rédaction]

Introduction

In recent years, interest in organotin chemistry has increased dramatically as a result of the wide range of industrial applications of organotin compounds (1). Various organotin(IV) compounds are widely used in the environment as antifoulants, agrochemicals, etc. Organotin compounds have the advantage of being very selective, and it had been believed that neither they nor their degradation products were particularly toxic to the higher animals, including humans. However, recent analysis has revealed that organotin compounds are toxic, even for the higher animals, due to their ability to bind to certain proteins such as haemoglobin, cysteine, and histidine residues (2–4). The toxicity of alkyltin(IV) compounds decreases in the order of $R_3SnX > R_4Sn \sim R_2SnX_2 > RSnX_3$ (R = alkyl group and X = halide ion). From the environmental point of view, the speciation of organotin(IV) compounds in water is important for a better understanding of their reactivities and recovery.

There are several studies concerning the stability constants and structures of dialkyl- and trialkyltin(IV) with various organic and inorganic ligands (5–10). However, most of the structural information reported has been for organotin compounds examined in the solid state, and no structural parameters for trimethyltin(IV) complexes with relatively weak donors in solution have been obtained, as such species cannot be successfully isolated as crystals (7, 10).

The main objective of this study is to analyze the coordination structures of the trimethyltin(IV) species in solution, by combining the EXAFS method (Extended X-ray Absorption Fine Structure) and the orthodox potentiometric method. The EXAFS method was utilized for the analyses of the structures of hydrolyzed species in solution. The coordination structures of various trimethyltin(IV) complexes with organic ligands were determined from the stability constants and the pK_a values of the complexes. For this purpose, trimethylamine and *N,N,N*-trimethylglycine were chosen as ligands to distinguish the stability and hydrolysis constants for the two structurally different trimethyltin(IV) complexes: the nitrogen-coordinated trimethylamine complex and the oxygen-coordinated *N,N,N*-trimethylglycinatotrimethyltin(IV) complex. The hydrolysis of trimethyl- and triethyltin(IV) ions and the complex formation reactions of trimethyltin(IV) with trimethyl-

Received March 19, 1997.

A. Takahashi, T. Natsume, N. Koshino, S. Funahashi, Y. Inada, and H.D. Takagi.[1] Inorganic and Analytical Chemistry Division, Research Department of Chemistry and Physics, Graduate School of Sciences, Nagoya University, Furo-cho, Chikusa, Nagoya, 464-01 Japan.

[1] Author to whom correspondence may be addressed. Telephone: +81-52-789-5473. Fax: +81-52-931-6670. E-mail: htakagi@chem4.chem.nagoya-u.ac.jp

© 1997 NRC Canada

Can. J. Chem. Downloaded from www.nrcresearchpress.com by 88.146.161.215 on 09/08/12
For personal use only.

Can. J. Chem. Downloaded from www.nrcresearchpress.com by 88.146.161.215 on 09/08/12
For personal use only.

Table 1A. Experimental conditions for the potentiometric measurements at 25.0°C and I = 0.10 mol dm^{-3} [(H, Na)ClO_4].

C_{Sn}^0/mmol dm^{-3}[a]	C_{H^+}/mmol dm^{-3}	C_{Ligand}/mmol dm^{-3}	C_{NaOH}^0/mol dm^{-3}	Measured range of –log([H$^+$]/mol dm^{-3})
Hydrolysis				
2.505	10.18		0.1158	2–10
4.850	10.18		0.1158	2–10
7.395	10.18		0.1158	2–10
Trimethylglycine				
	10.14	2.487	0.1146	2–5
	10.14	4.974	0.1146	2–5
	10.14	9.949	0.1146	2–5
1.720	10.14	4.974	0.1139	2–10
2.450	10.14	4.974	0.1139	2–10
4.884	10.14	4.974	0.1139	2–10
5.066	10.14	2.487	0.1139	2–10
Dimethylglycine				
	10.14	4.942	0.1139	2–10
	10.14	9.884	0.1139	2–10
3.341	10.14	9.869	0.1139	2–10
5.000	10.14	9.800	0.1139	2–10
4.978	10.14	4.906	0.1139	2–10
5.061	10.14	2.451	0.1139	2–10
Trimethylamine				
	10.14	3.278	0.1146	2–10
	10.14	6.572	0.1146	2–10
2.068	10.14	3.278	0.1158	2–10
3.141	10.14	3.278	0.1158	2–10

[a] C_{Sn}^0 denotes the initial concentration of trimethyltin(IV).

amine, *N,N,N*-trimethylglycine, *N,N*-dimethylglycine, *N*-methyliminodiacetate, nitrilotriacetate, and ethylenediamine-*N,N'*-diacetate ligands were examined potentiometrically in aqueous perchlorate and nitrate media. The coordination geometry of these species is discussed on the basis of the electronic interaction between the donor atom and Sn(IV).

Experimental

Reagents

Trimethyltin(IV) chloride and triethyltin(IV) chloride obtained from Strem were purified by a method similar to that described elsewhere (9, 10). Several trimethyl- and triethyltin(IV) complexes were prepared for the purpose of the EXAFS measurements. Trimethyl- and triethyltin(IV) hydroxide were synthesized by the reaction of trimethyl- or triethyltin(IV) chloride (Strem 98%) with 7 mol dm^{-3} sodium hydroxide. The white powder was filtered and dried in a vacuum. The crude compounds were then purified by sublimation. Bis(2,4-pentanedionato)dimethyltin(IV) was synthesized by the literature method (11) (calcd. for $C_{12}H_{22}SnO_2$: C 41.54, H 5.81%; found: C 40.67, H 5.58%). The sample was sufficiently pure for the EXAFS measurements (>97%).

Doubly distilled water was used throughout the experiment. Nitrilotriacetic acid, *N*-methyliminodiacetic acid, and ethylenediamine-*N,N'*-diacetic acid were obtained from Dojindo Co. Ltd. The glycine derivatives (*N,N*-dimethylglycine and *N,N,N*-trimethylglycine) were obtained from Nakarai Tesque Co. Ltd. Trimethylamine was obtained from Wako Pure Chemicals Inc., and the concentration of the stock solution was determined by titration. All the ligands, other than trimethylamine, used for the potentiometric measurements were recrystallized from doubly distilled water and dried in a vacuum prior to use. The concentrations of the stock solutions of sodium nitrate and sodium perchlorate were determined gravimetrically.

Electromotive force measurements

The potentiometric measurements were carried out using a Metrohm E 654 pH meter with a hand-piston burette, a glass electrode, and a calomel electrode. The electrolyte, KCl, in the original electrode was replaced by NaCl for use in the perchlorate media. The electrode couple was standardized by titrating either a standard perchloric acid or a nitric acid solution with a standard sodium hydroxide solution. Determination of the equivalence point by Gran's method allowed us to determine the standard potential $E°$ and the ionic product of water (12–15). The temperature of the sample solutions was maintained at 25.0 ± 0.1°C by circulating thermostatically controlled water through the jacket of the titration vessel. The ionic strength, I, was adjusted to 0.10 mol dm^{-3} with either sodium perchlorate or sodium nitrate. All potentiometric measurements were carried out for several different total concentrations of trimethyl- or triethyltin(IV) ion under nitrogen atmosphere. The experimental conditions used for the potentiometric titrations are listed in Tables 1*A*–1*C*. Each

© 1997 NRC Canada

Can. J. Chem. Downloaded from www.nrcresearchpress.com by 88.146.161.215 on 09/08/12
For personal use only.

Table 1*B*. Experimental conditions for the potentiometric measurements at 25.0°C and I = 0.10 mol dm^{-3} [(H, Na)NO_3].

C_{Sn}^0/mmol dm^{-3}[a]	C_{H^+}/mmol dm^{-3}	C_{Ligand}/mmol dm^{-3}	C_{NaOH}^0/mol dm^{-3}	Measured range of –log([H$^+$]/mol dm^{-3})
Hydrolysis				
1.039	5.036		0.1041	2–10
2.511	5.036		0.1041	2–10
1.039	5.036		0.1041	2–10
5.017	5.036		0.1041	2–10
10.04	5.036		0.1041	2–10
30.03	5.036		0.1041	2–10
Nitrilotriacetate				
1.003	3.014	1.043	0.1085	2–10
1.013	3.014	2.036	0.1085	2–10
2.013	3.014	3.010	0.1085	2–10
6.006	3.014	6.000	0.1085	2–10
3.052	3.014	6.000	0.1085	2–10
2.008	3.014	6.011	0.1085	2–10
Ethylenediamine-*N,N'*-diacetate				
1.037	5.036	1.011	0.1085	2–10
1.024	3.014	2.043	0.1085	2–10
2.010	3.014	3.014	0.1085	2–10
5.995	3.014	6.015	0.1085	2–10
1.037	3.014	6.023	0.1085	2–10
1.037	3.014	6.034	0.1085	2–10
***N*-Methyliminodiacetate**				
1.039	3.014	1.030	0.1041	2–10
1.015	3.014	2.027	0.1041	2–10
2.025	3.014	3.053	0.1041	2–10
6.093	3.014	6.048	0.1041	2–10
3.020	3.014	6.032	0.1041	2–10
2.028	3.014	6.170	0.1041	2–10

[a] C_{Sn}^0 denotes the initial concentration of trimethyltin(IV).

Table 1*C*. Experimental conditions for the potentiometric measurements at 25.0°C and I = 0.10 mol dm^{-3} [(H, Na)ClO_4].

C_{Sn}^0/mmol dm^{-3}[a]	C_{H^+}/mmol dm^{-3}	C_{Ligand}/mmol dm^{-3}	C_{NaOH}^0/mol dm^{-3}	Measured range of –log([H$^+$]/mol dm^{-3})
Hydrolysis				
0.9556	6.589		0.1146	2–10
2.202	5.597		0.1146	2–10
5.123	7.843		0.1146	2–10
10.13	7.801		0.1146	2–10

[a] C_{Sn}^0 denotes the initial concentration of triethyltin(IV).

experiment was repeated at least twice to confirm reproducibility.

EXAFS measurements and analyses

EXAFS spectra were measured around the Sn K-edge (E_0) at the BL6B station of the Photon Factory of the National Laboratory for High Energy Physics. The monochromatized X-ray was obtained by a Si(111) double crystal. The intensity of the incident X-ray was measured by an ionization chamber filled with nitrogen gas, while the intensity of the transmitted X-ray was measured by an ionization chamber filled with a nitrogen/argon (85:15) mixture.

The outline of the EXAFS analysis is as follows. The background absorption was estimated by fitting the Victoreen formula to the data in the pre-edge region (16), and the smooth K-shell absorption (μ_0) was approximated by the cubic spine function. The values of the extracted absorbance were normalized by μ_0 and then converted to the EXAFS oscillation, $\chi(k)$. The photoelectron wave vector, k, is equal to $[8m(E - E_0 - \Delta E_0)]^{1/2}\pi/h$, where E, E_0, ΔE_0, and m denote the energy of the incident X-ray, the threshold energy of the K-shell electron, shift of the energy for the individual sample, and the mass of the electron, respectively. The Fourier filtered $k^3\chi(k)$ values were analyzed by the least-squares method over the range of

© 1997 NRC Canada

Can. J. Chem. Downloaded from www.nrcresearchpress.com by 88.146.161.215 on 09/08/12
For personal use only.

Table 2. Experimental conditions used for the EXAFS measurements of trimethyl- and triethyltin(IV) species.[a]

Species	Concentration/mol dm^{-3}
$Me_2Sn(acac)_2$	Powder
$Me_2Sn(H_2O)_2^+$	0.3
$Et_3Sn(H_2O)_2^+$	0.3
$Me_3Sn(H_2O)(OH)$	0.3

[a]acac = acetylacetonate.

$2 < k/10^{-2}\ pm^{-1} < 12$, on the basis of the following model function for the EXAFS oscillation (17–22).

$$[1]\quad \chi_{calcd}(k) = \sum(n_j k R_j^2)\exp(-2\sigma_j^2 k^2 - 2R_j/\lambda)F_j(\pi,k) \times \sin[2kR_j - \alpha_j(k)]$$

where $F_j(\pi,k)$ is the backscattering amplitude from each scatterer j at a distance R_j from the X-ray absorbing atom, and $\alpha_j(k)$ is the total scattering phase shift experienced by the photoelectron. Reported values were used for the backscattering amplitude and the total scattering phase shift (23). In Table 2 are listed the experimental conditions of the tin(IV) samples used for the EXAFS measurements.

Results

Hydrolysis of trimethyl- and triethyltin(IV) and complex formation of trimethyltin(IV)

Trialkyltin(IV) ion hydrolyzes to form a series of hydroxo species. The hydrolysis of trimethyl- and triethyltin(IV) ions in aqueous solution can be expressed by the following equation.

$$[2]\quad pR_3Sn^+ + qH_2O \overset{\beta pq}{\rightleftharpoons} (R_3Sn)_p(OH)_q^{(p-q)+} + qH^+$$

where βpq is the overall stability constant defined as $[(R_3Sn)_p(OH)_q^{(p-q)+}][H^+]^q/[R_3Sn^+]^p$ (R = Me or Et). The stability constants were evaluated using the computer program SUPERQUAD (24). By using the data measured under the experimetal conditions in Tables 1*A*–1*C*, the calculations were carried out for various values of p and q. The stability constants for the (p, q) = (1, 1), (1, 2), and (2, 1) species are listed in Table 3, and the species distribution diagrams are shown in Figs. 1(*A*) and (*B*). The (2, 1) species may be a dimeric species bridged by the hydroxide ion. Other species corresponding to $p, q > 2$ were rejected by the SUPERQUAD criteria.

The protonation constants for the free ligands were determined by the SUPERQUAD program based on the experimental results obtained by the potentiometric titration. The experimental conditions for the potentiometric measurements are also listed in Table 1*A*, and the protonation constants defined by the following equation are listed in Table 4.

$$[3]\quad qH^+ + rL^{n-} \overset{\beta qr}{\rightleftharpoons} H_qL^{(q-rn)+}$$

where βqr is defined as $[H_qL^{(q-rn)+}]/[H^+]^q[L^{n-}]^r$, and n is the ionic charge of the free ligand, L. The protonation constants for the aminopolycarboxylate ligands were reported in a previous article (25).

Table 3. Stability constants of hydrolyzed trimethyl- and triethyltin(IV) species at 25°C.[a]

(p, q)	log β_{pq}	Conditions[b]	Reported values
Trimethyltin(IV)			
(1,1)	−6.35(2)	a	−6.26 (0.30 mol dm^{-3} $NaClO_4$)[c]
(1,2)	−17.90(12)	a	
(2,1)	−4.59(14)	a	
(1,1)	−6.26(1)	b	
(1,2)	−17.63(3)	b	
(2,1)	−4.84(5)	b	−5.40 (2 mol dm^{-3} KCl)[d]
Triethyltin(IV)			
(1,1)	−6.42(1)	a	−6.81(3 mol dm^{-3} $NaClO_4$)[e]
(1,2)	−17.70(5)	a	
(2,1)	−4.73(7)	a	

[a]Errors are shown in parentheses.
[b]a: I = 0.10 mol dm^{-3} (Na, H)ClO_4. b: I = 0.10 mol dm^{-3} (Na, H)NO_3.
[c]Reference 10.
[d]Reference 11.
[e]Reference 28.

Table 4. Protonation constants for the ligands used in this study.[a]

Ligand	(q, r)	log β_{qr}	Conditions[b]
tma	(1, 1)	9.70(3)	a
tmg	(1, 1)	1.92(1)	a
dmg	(1, 1)	9.71(3)	a
	(2, 1)	11.96(5)	a
nta	(1, 1)	9.26(3)	a
	(1, 1)	9.29(1)	b
	(2, 1)	11.94(1)	b
	(3, 1)	13.68(7)	b
edda	(1, 1)	9.56(1)	b
	(2, 1)	16.07(1)	b
mida	(1, 1)	9.54(3)	b
	(2, 1)	12.00(2)	b

[a]Errors are shown in parentheses.
[b]a: 0.1 mol dm^{-3} (Na, H)ClO_4. b: 0.1 mol dm^{-3} (Na, H)NO_3.

The stability constants corresponding to the following reaction were estimated for various ligands L in the aqueous (Na, H)ClO_4 and (Na, H)NO_3 media.

$$[4]\quad pMe_3Sn^+ + qH^+ + rL^{n-} \overset{\beta pqr}{\rightleftharpoons} (RMe_3Sn)_pH_qL_r^{(p+q-rn)+}$$

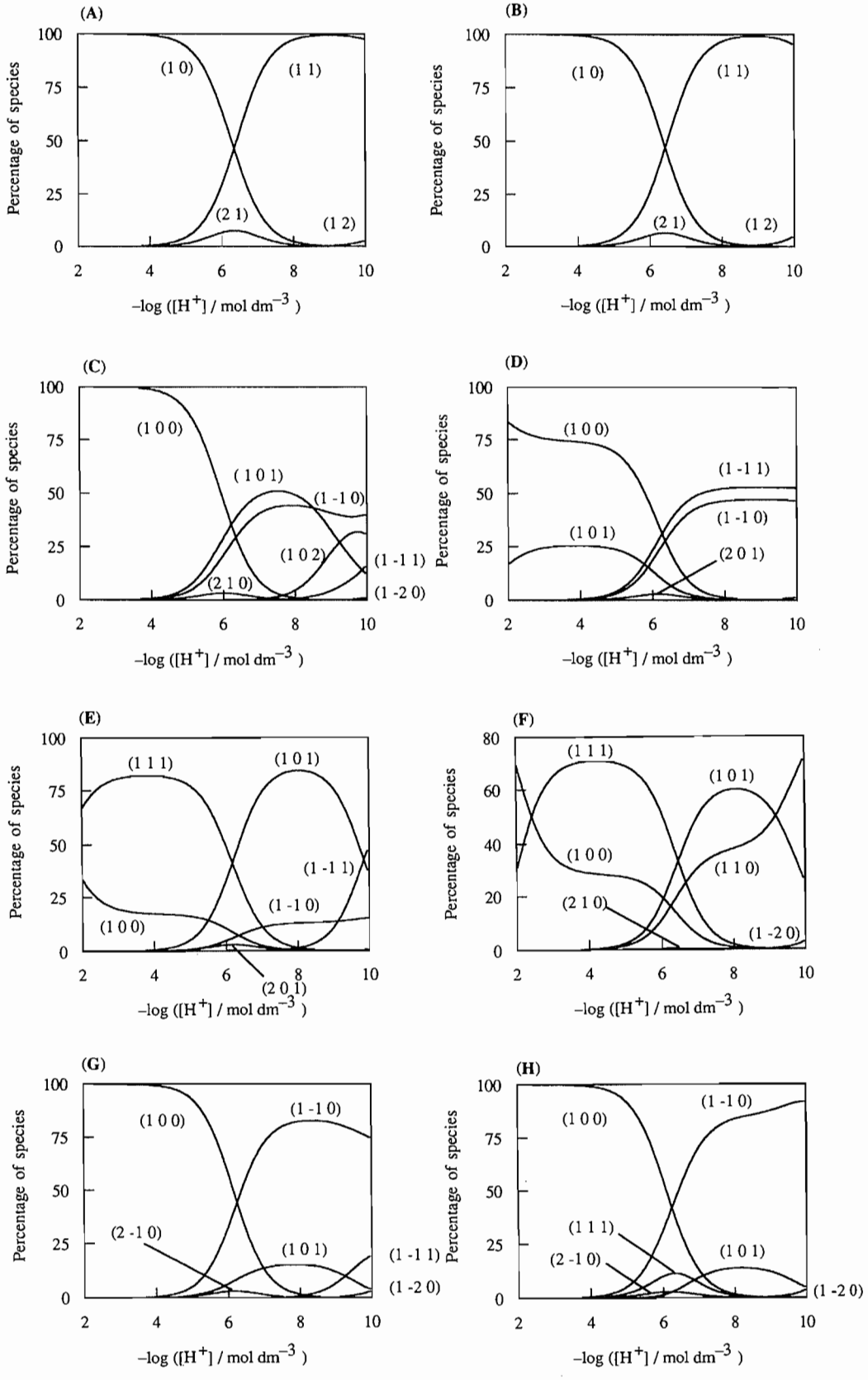
where $\beta pqr = [(R_3Sn)_pH_qL_r^{(p+q-rn)+}]/[R_3Sn^+]^p[H^+]^q[L^{n-}]^r$. The experimental conditions for the electrochemical measurements are listed in Tables 1*A*–1*B* and the stability constants for reaction [4] are listed in Table 5. The species distribution diagrams are shown in Figs. 1(*C*)–(*H*).

EXAFS analyses

The observed EXAFS oscillations of $\chi_{obsd}(k)$ weighted by k^3, the Fourier transforms of $k^3\chi_{obsd}(k)$, and the Fourier filtered

© 1997 NRC Canada

Fig. 1. Species distribution diagrams for the hydrolysis of trimethyltin(IV) (*A*) and triethyltin(IV) (*B*), and for the complexation of trimethyltin(IV) with trimethylamine (*C*), *N,N,N*-trimethylglycine (*D*), *N,N*-dimethylglycine (*E*), nitrilotriacetate (*F*), *N*-methyliminodiacetate (*G*), and ethylenediamine-*N,N'*-diacetate (*H*). For all diagrams, $C_{Sn(IV)} = 3.00 \times 10^{-3}$ mol dm^{-3} and $C_L = 6.00 \times 10^{-3}$ mol dm^{-3}. The species percentage is referred to the total tin(IV) concentration. The species (p,q) corresponds to $[(R_3Sn)_p(OH)_q]^{(p-q)+}$ (R = Me or Et), while the species $(p,q,r) = (Me_3Sn)_pH_qL_r$ (L = ligand).



Can. J. Chem. Downloaded from www.nrcresearchpress.com by 88.146.161.215 on 09/08/12
For personal use only.

© 1997 NRC Canada

Fig. 2. The observed EXAFS oscillations of $\chi_{obsd}(k)$ weighted by k^3 (*A*), the Fourier transforms of $k^3\chi_{obsd}(k)$ (*B*), and the Fourier filtered EXAFS oscillations $k^3(k)$ (*C*) for the species examined in this study. (a): $Me_2Sn(acac)_2$, (b): $Me_3Sn(OH_2)_2^+$, (c): $Et_3Sn(OH_2)_2^+$, (d): $Me_3Sn(OH)(OH_2)$.

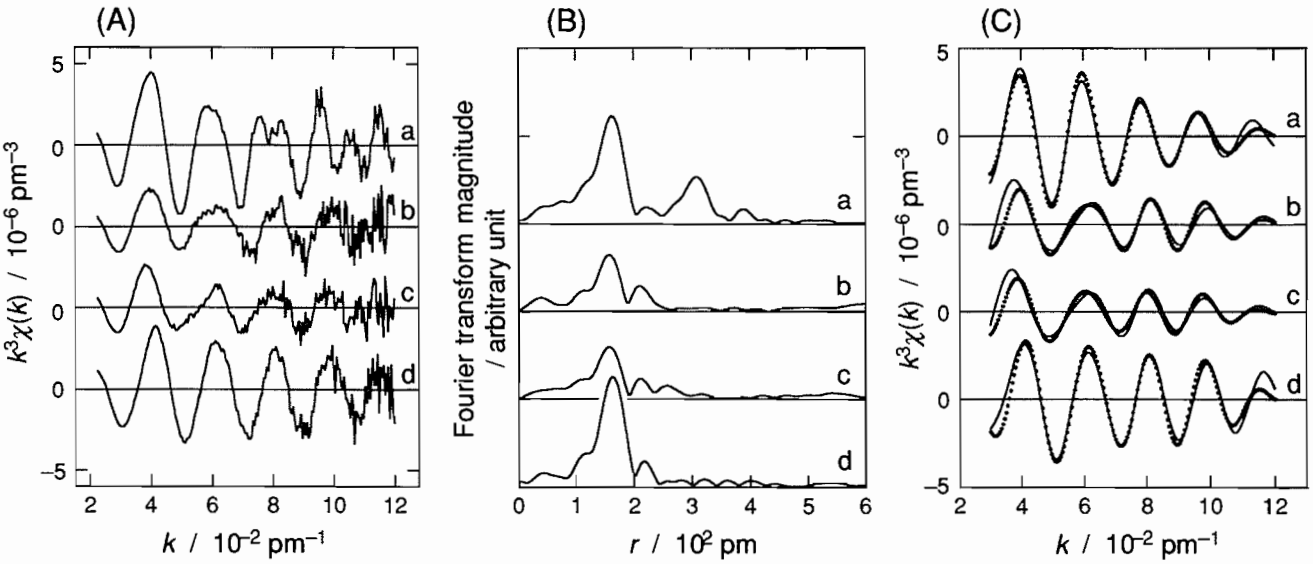


Table 5. Stability constants of the trimethyltin(IV) species with various ligands at 25°C.[a]

Ligand	(*p*, *q*, *r*)	log β_{pqr}	Conditions[b]
tmg			
	(1, 0, 1)	1.82(14)	a
	(1, −1, 1)	−3.94(6)	a
dmg			
	(1, 1, 1)	12.84(9)	a
	(1, 0, 1)	6.65(8)	a
	(1, −1, 1)	−3.19(9)	a
	(2, 0, 1)	8.79(14)	a
tma			
	(1, 0, 1)	5.78(2)	a
	(1, −1, 1)	−4.08(14)	a
	(1, 0, 2)	8.84(6)	a
nta			
	(1, 1, 1)	12.11(2)	b
	(1, 0, 1)	5.63(3)	b
edda			
	(1, 1, 1)	11.65(5)	b
	(1, 0, 1)	4.78(6)	b
mida			
	(1, 0, 1)	4.81(2)	b
	(1, −1, 1)	−4.44(3)	b

[a]Errors are shown in parentheses.
[b]a: 0.1 mol dm^{-3} (Na, H)ClO_4. b: 0.1 mol dm^{-3} (Na, H)NO_3.

EXAFS oscillations $k^3(k)$ for the species examined in this study are shown in Fig. 2. The X-ray energy at half-height of the absorption edge of the spectrum was used as E_0. Values of ΔE_0 and the mean free path of a photoelectron, λ, were evaluated by using the EXAFS data for bis(2,4-pentanedionato)dimethyltin(IV) by fixing the scatterer number n as 6 (equivalent to 4 positions in the equatorial plane and the 2 axial positions) on the basis of the crystal structure of this compound (11). The values of ΔE_0 and λ obtained for the bis(2,4-pentandionato)dimethyltin(IV) complex were used for the structural analyses of the other trimethyl- and triethyltin(IV) species. In Table 6 are listed the interatomic distance R, the Debye–Waller factor σ, and the scatterer numbers n for the trimethyl- and triethyltin(IV) species estimated by the EXAFS analyses.

Discussion

Earlier structural studies by means of X-ray, neutron, and electron diffraction studies (7*b*) and Mossbauer spectroscopy (7*c*) revealed that the five-coordinate tin structure is trigonal bipyramidal, and many polymeric compounds of trigonal bipyramidal structure have been found. It has been suggested that strong donors, which can make σ-bonding comparable to the alkyl group, bring about a distribution of the *s* character of the preexisting Sn—C bonds (10, 26). Crystallographic analysis revealed that the five-coordinate triphenyltin(IV) compound has slightly distorted trigonal bipyramidal structure, with the three phenyl groups in the equatorial plane (27). As the oxygen and nitrogen donor atoms of the substituted glycines and aminopolycaboxylate ligands analyzed in this study are moderate donors, it is plausible that the trimethyltin(IV) skeleton is kept triangular in the equatorial plane even by the coordination of these ligands. However, the coordination of OH^- (hydrolyzed species) may cause a significant deformation of the $Me_3Sn(IV)$ skeleton because of the relatively strong σ-donicity of this ligand.

According to the results of the EXAFS analyses (Table 6), the Sn—OH bond length is very short (207 pm) for $Me_3Sn(OH)(OH_2)$, while the Sn—OH_2 bond length is significantly elongated (280 pm) compared with the original bond length of Sn(IV)—OH_2 in the $Me_3Sn(OH_2)_2^+$ ion (243 pm). It has been suggested that OH^- forms a strong σ-bond with

© 1997 NRC Canada

Can. J. Chem. Downloaded from www.nrcresearchpress.com by 88.146.161.215 on 09/08/12
For personal use only.

Can. J. Chem. Downloaded from www.nrcresearchpress.com by 88.146.161.215 on 09/08/12
For personal use only.

Table 6. Structural parameters for various alkyltin(IV) species.[a]

Compound	Interaction	Scatterer number (n)	r/pm	σ/pm
$Me_2Sn(acac)$	Sn—C(Me)	2[b]	214[b]	5.2(3)
	Sn—O(acac)	4[b]	218[b]	10.2
$Me_3Sn(OH_2)_2^+$	Sn—C(Me)	3[b]	209(2)	7.6(3)
	Sn—O(H_2O)	2[b]	243(3)	10.2[b]
$Et_3Sn(OH_2)_2^+$	Sn—C(Et)	3[b]	211(2)	8.2(3)
	Sn—O(H_2O)	3[b]	245(3)	10.2[b]
$Me_3Sn(OH_2)(OH)$	Sn—C(Me)	3[b]	210(2)	4.3(6)
	Sn—O(H_2O)	1[b]	280(8)	10.2[b]
	Sn—O(OH^-)	1[b]	207(3)	7.2(7)

[a]Errors are shown in parentheses.
[b]Fixed value.

Sn(IV) (10, 26). Therefore, it is expected that the formation of Sn—OH bond distributes the *s* character of three Sn—C bonds towards the Sn—OH bond (10, 26), and the resulting sp^3 hybridization causes the deformation of the original trigonal bipyramidal structure to the pseudo-tetrahedral structure as shown in Fig. 3(*A*)-(1,1). As a result, the Sn—OH bond strength may be largely enhanced by the release of a proton from one of the coordinated water molecules. As the water molecule is attracted to the tin(IV) center by the ion–dipole interaction (26), the bond length between Sn(IV) and H_2O at the *trans* position of OH^- should be largely elongated because of the significant increase of the electron density on the central Sn(IV) atom. However, the elongation of the Sn(IV)—OH_2 bond caused by the coordination of trimethylamine, *N*-substituted glycines, and aminopolycarboxylate ligands may not be so large as that caused by the coordination of OH^-.

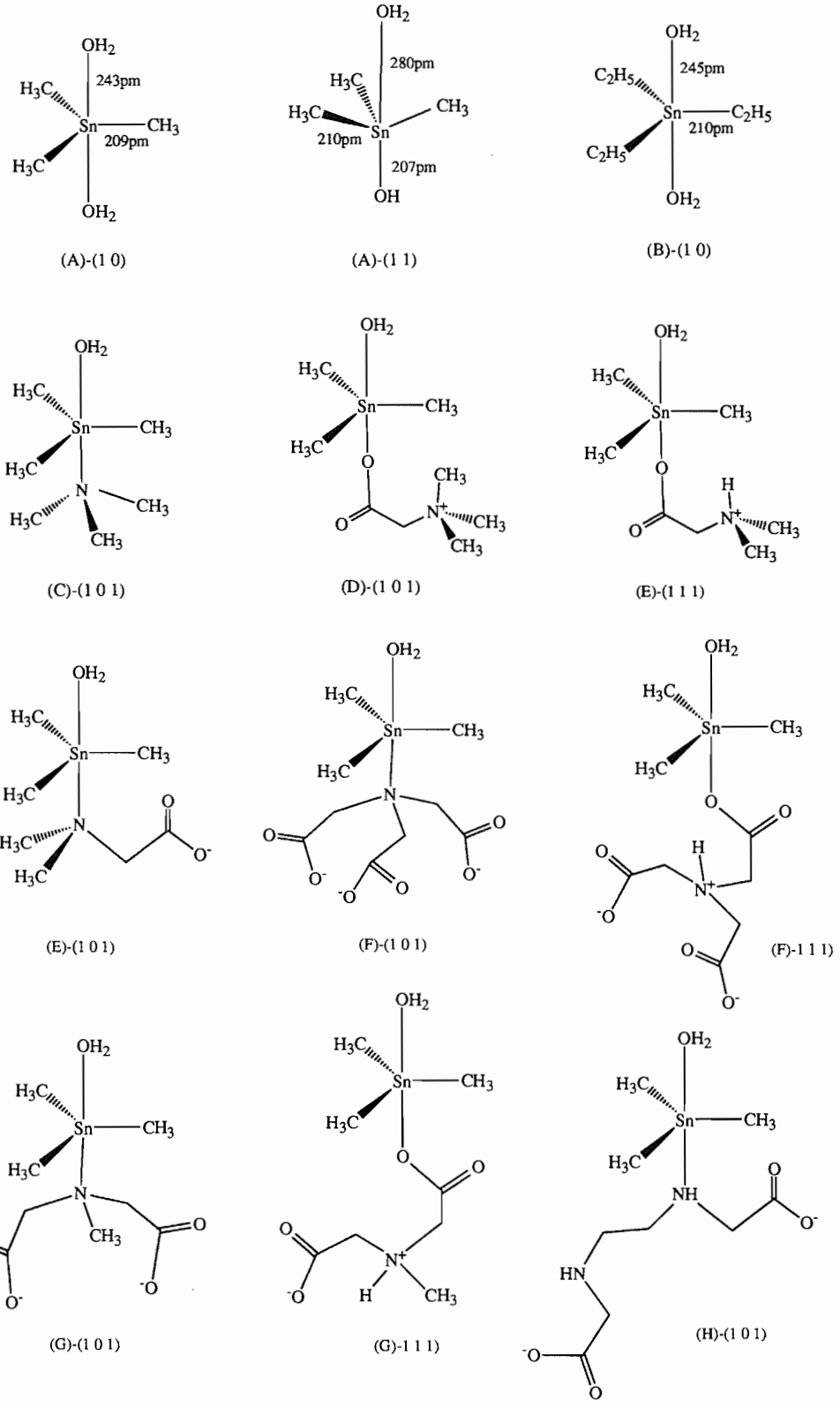
The previously reported values of the hydrolysis constants for trimethyl- and triethyltin(IV) ions were determined under different conditions from those used in this study ($\beta_{11} = -6.26$ at $I = 0.30$ mol dm^{-3} in perchlorate media) (10, 28). However, it is possible to compare the hydrolysis constants of trimethyl- and triethyltin(IV) species obtained in this study. The hydrolysis constants, β_{11}, of trimethyltin(IV) ion in perchlorate and nitrate solutions are slightly different, which suggests a difference in the medium effect between these two solutions. The difference between the hydrolysis constants for the triethyltin(IV) ion ($\log \beta_{11} = -6.42$) and the trimethyltin(IV) ion ($\log \beta_{11} = -6.35$) in perchlorate medium reflects the smaller electron density of the $Me_3Sn(IV)$ center caused by the less inductive effect of the methyl group in the equatorial plane, compared with the corresponding $Et_3Sn(IV)$ center.

The protonation constant for trimethylglycine was previouly measured by the NMR method (29). Considering the difference in the experimental conditions, the agreement is fair ($\log \beta_{11} = 1.87$ by the NMR method). The β_{11} value for *N,N*-dimethylglycine was consistent with the literature value (30).

As the β_{11} value for trimethylamine is identical to that of *N,N*-dimethylglycine, similar values of the stability constants are expected for the formation of the (1,0,1) species with trimethylamine and *N,N*-dimethylglycine in case the coordination of *N,N*-dimethylglycine to trimethyltin(IV) takes place through the nitrogen donor atom. The value of $\log \beta_{101}$ for the formation of *N,N,N*-trimethylglycinatotrimethyltin(IV) was 1.82, which is comparable to the reported $\log \beta_{101}$ value for the formation of the acetato complex (10) in which the coordination of acetate ion takes place through the carboxyl oxygen atom. The value of $\log \beta_{101}$ for the formation of *N,N*-dimethylglycinatotrimethyltin(IV) was 6.65, which is very different from the value obtained for the formation of the *N,N,N*-trimethylglycinatotrimethyltin(IV) species. This difference in the $\log \beta_{101}$ values indicates that the coordination of *N,N*-dimethylglycine to trimethyltin(IV) takes place through the nitrogen donor atom rather than the oxygen atom. The pK_a value for the hydrolysis of the *N,N,N*-trimethylglycinatotrimethyltin(IV) complex was calculated as 5.76 ($pK_a = \log \beta_{101} - \log \beta_{1-11}$). The corresponding pK_a values for the hydrolysis of the *N,N*-dimethylglycinato and trimethylamine complexes of trimethyltin(IV) were calculated as 9.84 and 9.86, respectively. The similarity of the pK_a values for hydrolysis of the trimethylamine complex and the *N,N*-dimethylglycinato complex also indicates that the coordination of *N,N*-dimethylglycine to the trimethyltin(IV) center occurs through the nitrogen atom, as the electron densities of the central tin(IV) should be similar for these two complexes. Rather high pK_a values for the hydrolysis of the *N,N*-dimethylglycinato and trimethylamine complexes reflect the stronger interaction between Sn(IV) and the coordinated nitrogen atom compared with the interaction between Sn(IV) and the carboxyl oxygen

© 1997 NRC Canada

Fig. 3. The structures of trimethyl- and triethyltin(IV) and the hydrolyzed species (A and B) in aqueous solution as determined by the EXAFS method. The structures of the trimethyltin(IV) complexes with trimethylamine, *N,N,N*-trimethylglycine, *N,N*-dimethylglycine, nitrilotriacetate, *N*-methyliminodiacetate, and ethylenediamine-*N,N'*-diacetate (C–H) in solution were estimated from the log β_{pqr} and pK_a values (see text).



Can. J. Chem. Downloaded from www.nrcresearchpress.com by 88.146.161.215 on 09/08/12
For personal use only.

© 1997 NRC Canada

donor atom. The pK_a value of the hydroxotrimethyltin(IV) was calculated as 11.55 ($pK_a = \log \beta_{11} - \log \beta_{12}$), which reflects the strong σ-interaction between the OH^- and Me_3Sn(IV) (10, 26): the strong σ-interaction between Sn(IV) and OH^- induces more symmetrical sp^3 hybidization at the tin(IV) center and the interaction between tin(IV) and the water molecule at the *trans* position of OH^- became significantly weak.

The (2,0,1) species in the reaction of trimethyltin(IV) and *N,N*-dimethylglycine is considered to be the dimeric trimethyltin(IV) species bridged by *N,N*-dimethylglycine through both of the N and O donor atoms. It has been reported that the pK_a values are 3.33 and 2.12 for protonation of the carboxyl oxygen of ethylenediamine-*N,N'*-diacetate and pyridine-2,6-dicarboxylate coordinated to dimethyltin(IV), re-spectively (25). Therefore, the (1,1,1) species found for the reaction of trimethyltin(IV) and *N,N*-dimethylglycine is probably the *N*-protonated *N,N*-dimethylglycine complex in which the coordination of *N,N*-dimethylglycine takes place through the oxygen atom, by considering the relatively large pK_a value ($\log \beta_{111} - \log \beta_{101} = 6.19$) for the formation of the (1,1,1) species.

The aminopolycarboxylate ions examined in this study are, therefore, supposed to coordinate to trimethyltin(IV) ion primarily through the nitrogen donor atom. The $\log \beta_{101}$ values for the formation of aminopolycarboxylatotrimethyltin(IV) are 4.81, 4.78, and 5.63 for the *N*-methyliminodiacetate, ethylenediamine-*N,N'*-diacetate, and nitrilotriacetate ligands, respectively. These values indicate that the coordination of these ligands to trimethyltin(IV) takes place through the nitrogen donor atom rather than through the carboxyl oxygen atom, from the analogy of the $\log \beta_{101}$ values for the formation of *N,N*-dimethylglycinato and trimethylamine complexes. The pK_a value ($pK_a = \log \beta_{101} - \log \beta_{1-11}$) for the hydrolysis of the trimethyltin(IV) complex with *N*-methyliminodiacetate is calculated as 9.25, which is also similar to the value obtained for the hydrolysis of the trimethylamine complex. In the (1,1,1) species found for the complex formation of trimethyltin(IV) with nitrilotriacetate and ethylenediamine-*N,N'*-diacetate, it is considered that the coordination takes place through the carboxyl oxygen atom of the *N*-protonated species, from the similarity of the pK_a values ($pK_a = \log \beta_{111} - \log \beta_{101}$) for the *N,N*-dimethylglycine complex (pK_a = 6.19, 6.48, and 6.92 for the *N,N*-dimethylglycine, nitrilotriacetato, and ethylenediamine-*N,N'*-diacetato complexes, respectively). Such structural changes from the (1,0,1) to (1,1,1) species are possible, considering the relatively weak ion–dipole interactions between these ligands and Me_3Sn(IV) (10, 26).

In conclusion, the trimethyltin(IV) ion primarily prefers coordination with strong σ-donors to achieve sp^3 hybridization. As for moderate donors such as *N*-substituted glycines and aminopolycarboxylate ions, Sn(IV) tends to form coordination bonds through the nitrogen rather than the oxygen atom. However, at lower pH, where the protonation of amine nitrogen is favorable, coordination through the carboxyl oxygen atom takes place. The $\log \beta_{qr}$ values for glycine are 2.34 and 11.94 at 25.0°C (I = 0.1 mol dm^{-3} KCl) for (q, r) = (1, 1) and (2, 1) species, respectively (30). Hynes and O'Dowd reported that they could not observe any complexation of trimethyltin(IV) with glycine at I = 0.3 mol dm^{-3} ($NaClO_4$) (10). As the $\log \beta_{21}$ value for *N,N*-dimethylglycine (11.96) is comparable to that for glycine, it is probable that the existence of (1, 0, 1) species was rejected in their study by the SUPERQUAD criteria, as the titration range was too narrow (pH < 6.5). Plausible structures of the species discussed above are summarized in Fig. 3(*C*)–(*H*). These results may provide basic knowledge for the application of these ligand systems against environmental pollution with organotin(IV) compounds.

Acknowledgement

This research was supported by the Grants-in-Aid for Scientific Research (Nos. 07454199, 07504003, and 07554061) from the Ministry of Education, Science, and Culture of Japan.

References

1. I. Ohmae. Organotin chemistry. Elsevier, Amsterdam. 1989. pp. 1–9.
2. A.G. Davis and P.J. Smith. Adv. Inorg. Chem. Radiochem. **23**, 1 (1980).
3. B.M. Elliot, W.N. Aldridge, and J.W. Bridges. Biochem. J. **177**, 461 (1979).
4. F. Taketa, K. Siebenlist, J. Kaster-Jolyy, and N. Palossari. Arch. Biochem. Biophys. **204**, 466 (1980).
5. R.S. Tobias, I. Ogrins, and B.A. Nevett. Inorg. Chem. **1**, 638 (1962).
6. M. Yasuda and R.S. Tobias. Inorg. Chem. **2**, 207 (1963).
7. (*a*) R.S. Tobias and M. Yasuda. Can. J. Chem. **42**, 781 (1964); (*b*) Y.K. Ho and J.J.J. Zuckerman. Organomet. Chem. **49**, 1 (1973); (*c*) G.M. Bancroft, V.G.K. Das, T.K. Sham, and M.G. Clark. J. Chem. Soc. Dalton Trans. 643 (1976).
8. G. Arena, R. Purrello, E. Rizzarelli, A. Gianguzza, L. Pellerito, and S. Musumeci. J. Chem. Soc. Dalton Trans. 773 (1989).
9. T. Natsume, S. Aizawa, K. Hatano, and S. Funahashi. J. Chem. Soc. Dalton Trans. 2749 (1994).
10. M.J. Hynes and J. O'Dowd. J. Chem. Soc. Dalton Trans. 563 (1987).
11. G.A. Miller and E.O. Schlemper. Inorg. Chem. **12**, 677 (1973).
12. G. Gran. Analyst (London), **77**, 661 (1952).
13. F.J.A. Rossotti and H. Rossotti. J. Chem. Educ. **42**, 375 (1965).
14. J.A.J. Boiani. Chem. Educ. **63**, 724 (1986).
15. H.S. Dunsmore and D. Midgley. Anal. Chim. Acta, **61**, 115 (1972).
16. International tables for X-ray crystallography. Vol. III. Kynoch Press, Birmingham, U.K. 1962.
17. D.E. Sayers, E.A. Stern, and F.W. Lytle. Phys. Rev. Lett. **27**, 1204 (1971).
18. E.A. Stern. Phys. Rev. B: Solid State, **10**, 3027 (1974).
19. F.W. Lytle, D.E. Sayers, and E.A. Stern. Phys. Rev. B: Solid State, **11**, 4825 (1975).
20. E.A. Stern, D.E. Sayers, and F.W. Lytle. Phys. Rev. B: Solid State, **11**, 4836 (1975).
21. B. Lengeler and P. Eisenberger. Phys. Rev. B: Condens. Matter, **21**, 4507 (1980).
22. P.A. Lee, P.H. Citrin, P. Eisenberger, and B.M. Kincaid. Rev. Mod. Phys. **53**, 769 (1981).
23. B.K. Teo and P.A. Lee. J. Am. Chem. Soc. **101**, 2815 (1979).
24. P. Gans, A. Sabatini, and A. Vacca. J. Chem. Soc. Dalton Trans. 1195 (1985).
25. S. Aizawa, T. Natsume, K. Hatano, and S. Funahashi. Inorg. Chim. Acta, **248**, 215 (1996).
26. M.M. McGrady and R.S. Tobias. Inorg. Chem. **2**, 1157 (1964).
27. P. Ganis, D. Furlani, D. Marton, G. Tagliavini, and G. Valle. J. Organomet. Chem. **293**, 207 (1985).
28. R.S. Tobias. Organomet. Chem. Rev. **1**, 93 (1966).
29. S. Libich and D.L. Rabenstein. Anal. Chem. **45**, 118 (1973).
30. R.M. Smith and A.E. Martell. Critical stability constants. Vol. 6. Plenum Press, New York. 1989.

© 1997 NRC Canada

Can. J. Chem. Downloaded from www.nrcresearchpress.com by 88.146.161.215 on 09/08/12
For personal use only.

The mechanism of the hydrolysis of acylimidazoles in aqueous mineral acids. The excess acidity method for reactions that are not acid catalyzed[1]

Robin A. Cox

Can. J. Chem. Downloaded from www.nrcresearchpress.com by 88.146.161.215 on 09/08/12
For personal use only.

Abstract: The mechanism of the hydrolysis of acetylimidazole in aqueous perchloric, sulfuric, and hydrochloric acid mixtures has been determined. Benzoylimidazole was also studied in the latter two acids. The method of analyzing the available data, pseudo-first-order reaction rate constants as a function of acid concentration and, in one case, temperature, is the excess acidity method, here applied to the same reaction in the three different acid media, allowing their comparison. The reaction is not acid catalyzed; the rates decrease with increasing acidity. The substrate reacts in the form that is monoprotonated on the imidazole ring; it is 100% protonated at acidities much lower than those used here. Acetylimidazole is shown to become diprotonated at high acidity ($pK_{SH_2^{2+}} = -6.7$), protonating on the carbonyl oxygen, but the diprotonated form is not reactive. The hydrolysis involves the reversible addition of one water molecule to the substrate to give a tetrahedral intermediate; at low acidities the decomposition of this hydrate is the rate-determining step, but as the acidity increases and the water activity decreases its formation becomes rate limiting. Hydroxide catalysis was also observed in dilute perchloric acid, but this is swamped by nucleophilic catalysis by the acid anion in HCl and H_2SO_4.

Key words: acylimidazoles, excess acidity, hydrolysis, protonation, tetrahedral intermediate.

Résumé : On a déterminé le mécanisme d'hydrolyse de l'acétylimidazole dans l'acide perchlorique aqueux, l'acide sulfurique aqueux et l'acide chlorhydrique aqueux. On a utilisé la méthode d'excès d'acidité pour analyser les données disponibles, les constantes de vitesse de la réaction de pseudo-premier ordre en fonction de la concentration d'acide et, dans un cas, la température; dans ce travail, on a appliqué la méthode à la même réaction dans trois milieux acides différents et ceci permet de les comparer. La réaction n'est pas catalysée par les acides; les vitesses diminuent avec une augmentation de l'acidité. Le substrat réagit sous la forme monoprotonée du noyau imidazole; il est 100% protoné à des acidités beaucoup plus faible que celles utilisées dans ce travail. À acidités élevées, on a montré que l'acétylimidazole devient diprotoné ($pK_{SH_2^{2+}} = -6,7$), par protonation sur l'oxygène du carbonyle; toutefois, la forme diprotonée n'est pas réactive. L'hydrolyse implique l'addition réversible d'une molécule d'eau sur le substrat conduisant à un intermédiaire tétraédrique. Aux acidités faibles, l'étape cinétiquement limitante est la décomposition de cet hydrate; toutefois, lorsque l'acidité augmente et que l'activité de l'eau diminue, sa formation devient cinétiquement limitante. Dans l'acide perchlorique dilué, on a aussi observé une catalyse par l'hydroxyde; toutefois, dans les acides chlorhydrique et sulfurique, elle est submergée par la catalyse nucléophile de l'anion acide.

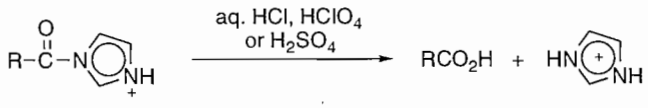
Mots clés : acylimidazoles, acidité en excès, hydrolyse, protonation, intermédiaire tétraédrique.

[Traduit par la rédaction]

Introduction

The hydrolysis of acylimidazoles in aqueous buffer media is fairly well understood (1), but the mechanism of the reaction in aqueous mineral acid (2, 3) and other nonideal solutions (2) has never been adequately described. Benzoylimidazole was originally used as a model for *N*-protonated benzamide in a study of the mechanism of amide hydrolysis (3), and it is true that the rate–acidity profiles for the hydrolyses of benzamide and benzoylimidazole are quite different. In this paper the excess acidity method (4, 5) will be used to analyze reaction rate data obtained as a function of medium composition for acetylimidazole and benzoylimidazole.

Substrates



R = CH_3, Ph

The excess acidity method has been widely used to determine the mechanisms of reactions in aqueous sulfuric acid, among the more recent studies being hydrations of fluoroalkyl-substituted vinyl ethers (6), cyclizations of substituted imidazolines (7), methyl azophenyl ether cleavages (8), and

Received February 1, 1997.

R.A. Cox.[2] Department of Chemistry, University of Toronto, 80 St. George St., Toronto, ON M5S 3H6, Canada.

[1] Mechanistic studies in strong acids, part 22; part 21 is ref. 18. Presented in part at the 78th Canadian Society for Chemistry Conference, Guelph, Ont., May 1995, no. 988.

[2] Telephone: (416) 978-4581. Fax: (416) 978-8775. E-mail: rcox@alchemy.chem.utoronto.ca

© 1997 NRC Canada

Can. J. Chem. Downloaded from www.nrcresearchpress.com by 88.146.161.215 on 09/08/12
For personal use only.

aromatic hydrogen exchange processes (9). It has also been used extensively for delineating the mechanisms of reactions in aqueous perchloric acid media, among them being alkene (10), alkyne (11), and ketene (12) hydrations, vinyl ether hydrolyses (13), thioacetal hydrolyses (14), and the hydrolyses of isothiocyanates (15), acid anhydrides (16), and acyl fluorides (17). Most recently it has been used to study the various decomposition mechanisms of several *N*-nitro amides and sulfonamides in aqueous sulfuric acid (18), to show that the mechanism of decomposition of aliphatic *N*-nitroamines in H_2SO_4 is an S_N2 displacement by water or bisulfate ion at the alkyl group (19), and to show that the parent molecule, nitramide (NH_2NO_2), decomposes in an acid-catalyzed process in relatively strong acid media, but that the decomposition mechanism involves neutral water molecules without acid catalysis in more dilute acid (20).

In two of these studies (18, 20), reactions that were not acid catalyzed were involved, and in one of them hydroxide catalysis was visible in dilute H_2SO_4 (18). One of the reasons for undertaking the work in this paper was to further study processes of this type. Also, although reactions in aqueous H_2SO_4 and $HClO_4$ have received a lot of attention, reactions in aqueous HCl have not. Since data for the hydrolysis of acetylimidazole were available in all three acid media (2), and data for the hydrolysis of benzoylimidazole in two of them (2, 3), a comparison of the same reaction in different acid solutions could be performed, to see whether the excess acidity analysis gives the same answers in different media. Values of pK_{BH^+} determined using the equilibrium version of the excess acidity analysis (21) are similar but not identical in different acid systems (21, 22).

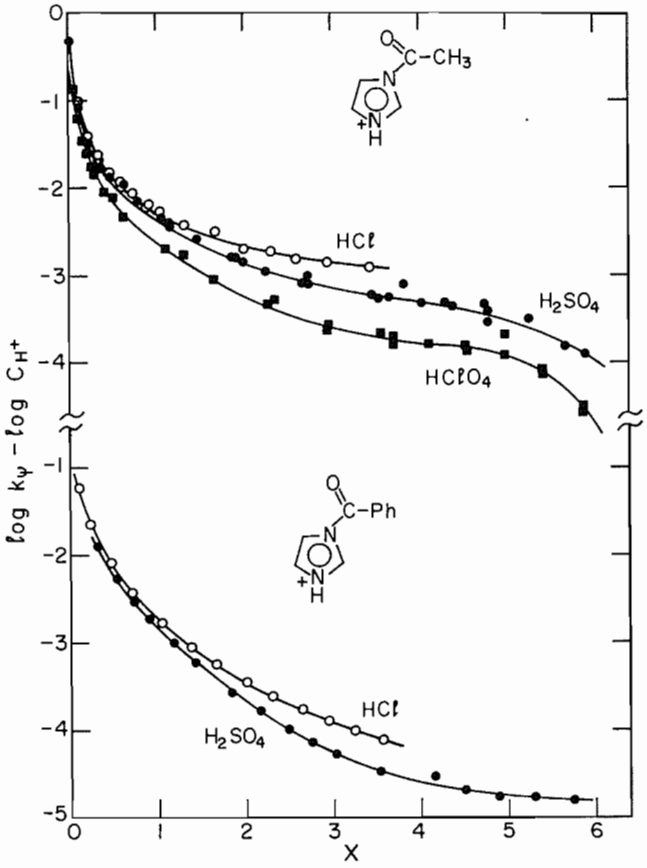
Results

Marburg and Jencks studied the hydrolyses of acetyl- and benzoyl-imidazole in many different aqueous media (2). Rate constants are not given in the paper, but fortunately the original concentration vs. time data are still available,[3] and these were curve-fitted to an exponential first-order rate equation (23) to obtain pseudo-first-order rate constants k_ψ as a function of acid concentration. Rate constants for the hydrolysis of benzoylimidazole as a function of sulfuric acid concentration and temperature are given by Smith and Yates (3). Excess acidities X, which are activity coefficient ratios of the form $\log(f_{B^*}f_{H^+}/f_{B^*H^+})$ for a standard base B* (21), were obtained from published sources (21, 22), which also give $\log C_{H^+}$ values for H_2SO_4; for HCl and $HClO_4$ these are simply the log acid molarities. These were adjusted to the reaction temperature as before if it was not 25°C (24). Water activities in H_2SO_4 at any temperature, a_{H_2O}, were calculated from available thermodynamic data (25), and 25°C values for HCl (26) and $HClO_4$ (27) were interpolated from published values.

The excess acidity kinetic method works by examining plots of $\log k_\psi - \log C_{H^+}$ against X, the excess acidity (21); for acid-catalyzed processes these are linear with positive slopes for A1 and A-S_E2 mechanisms, and curve downwards for A2 reactions (4, 5). Such plots for the experimental data used in this work are given in Fig. 1. It is at once apparent that these are not acid-catalyzed reactions, the rate constants decreasing

[3] W.P. Jencks. Personal communication.

Fig. 1. Conventional excess acidity plot, $\log k_\psi - \log C_{H^+}$ vs. the excess acidity X, for the hydrolyses of the acylimidazoles in different aqueous acid systems at 25°C.



continuously with acidity. By trial and error, it was found that in most cases the data could be fitted as two successive straight lines in plots of $\log k_\psi - \log a_{H_2O}$ against X. Plots of the 25°C data on this basis are given in Fig. 2 for acetylimidazole and in Fig. 3 for benzoylimidazole; to obtain the fitted lines a computer program, which fits experimental data to any equation(s) supplied, was used (23). The associated slopes, intercepts, statistical data, etc. from the computer fit for Figs. 2 and 3 are given in Tables 1 and 2 for the two substrates. For acetylimidazole in perchloric acid a hydroxide-catalyzed process was also apparent in dilute acid; the $X = 0$ intercept of this was -4.30 ± 0.11. For acetylimidazole in H_2SO_4 and $HClO_4$ the downturn at high acidity could be used to calculate $pK_{SH_2^{2+}}$ values, and these are given in Table 1.

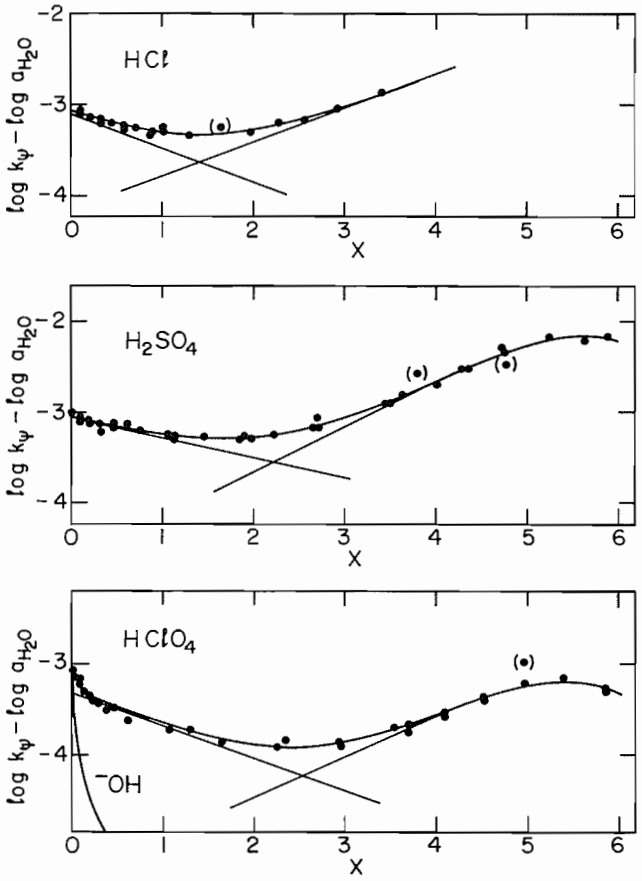
Discussion

The mechanism that applies to these reactions is given in Scheme 1, based on the original suggestion of Marburg and Jencks (2). The imidazole substrates are fully protonated at acidities much lower than those involved in this work, pK_a = 3.6 (28), and so at all acidities the substrate is the ring-protonated imidazolium species SH^+. This is assumed to add water reversibly to the hydrate or tetrahedral intermediate SHy^+ (K_{Hy}); thinking of the imidazolium ring as a strongly electron-withdrawing substituent on a carbonyl compound leads to the conclusion that hydration should be facile, much

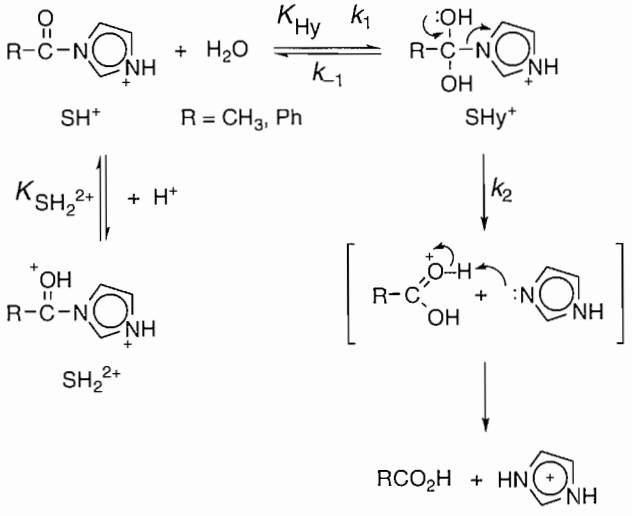
© 1997 NRC Canada

Can. J. Chem. Downloaded from www.nrcresearchpress.com by 88.146.161.215 on 09/08/12
For personal use only.

Fig. 2. Plots of log k_ψ − log a_{H_2O} vs. the excess acidity X for acetylimidazole in different aqueous acid systems at 25°C, showing the contributions of the different rate-determining steps at different acidities.

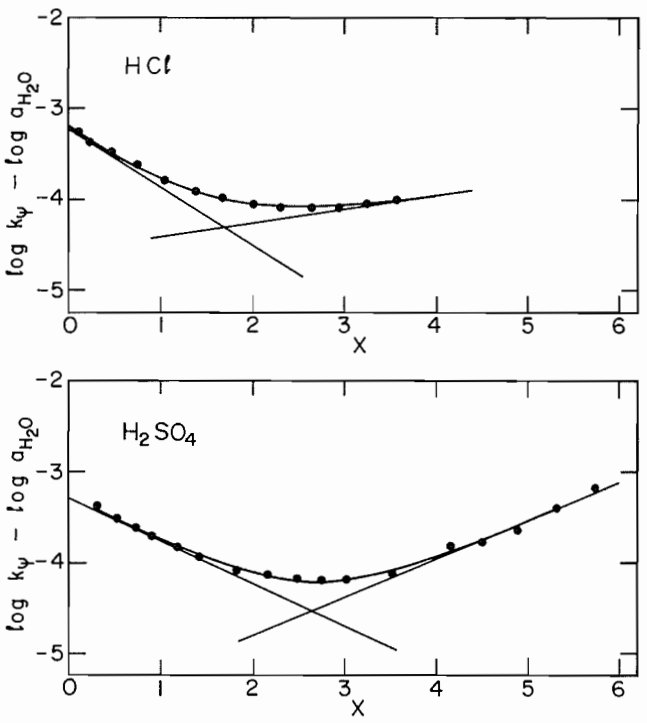


Scheme 1.



as is chloral hydrate formation from CCl_3CHO (29). (Unfortunately it is not possible to estimate K_{Hy} from the correlation line for other carbonyl compounds (30) because a σ* value for the protonated imidazole substituent, needed for the correlation (30), does not appear to be known.) Either the formation

Fig. 3. Plots of log k_ψ − log a_{H_2O} vs. the excess acidity X for benzoylimidazole in aqueous sulfuric and hydrochloric acids at 25°C, showing the contributions of the different rate-determining steps at different acidities.



of this hydrate (k_1) or its cleavage (k_2) can be rate determining; the former should be the case at high acidity (low water activity) and the latter at low acidity. Imidazolium cation and carboxylic acid product formation as shown should render the reaction essentially irreversible. At high acidities the substrate SH^+ may protonate again on the carbonyl group to give diprotonated SH_2^{2+}.

Deriving excess acidity rate equations based on this scheme is not particularly difficult. At low acidity, where the k_2 step is rate determining, absolute rate theory requires

[1] $k_\psi C_{SH^+} = k_2 a_{SHy^+}/f_\ddagger$

Using the definitions $K_{Hy} = k_1/k_{-1} = a_{SHy^+}/a_{SH^+}a_{H_2O}$ and $a_{SH^+} = C_{SH^+}f_{SH^+}$, eq. [1] becomes eq. [2]:

[2] $k_\psi C_{SH^+} = (k_1k_2/k_{-1})a_{H_2O}C_{SH^+}(f_{SH^+}/f_\ddagger)$

which on taking logs and rearranging gives eq. [3]:

[3] $\log k_\psi - \log a_{H_2O} = \log(k_1k_2/k_{-1}) + m_2X$

if we assume linearity in X: $\log(f_{SH^+}/f_\ddagger) = m_2X$. (Linearity for equations like this has been found previously, for instance in amide and lactam hydrolyses (31).)

At high acidity, where the k_1 step is rate determining, we can write eq. [4]:

[4] $k_\psi(C_{SH^+} + C_{SH_2^{2+}}) = k_1 a_{SH^+}a_{H_2O}/f_\ddagger = k_1 C_{SH^+}a_{H_2O}(f_{SH^+}/f_\ddagger)$

Now the substrate concentration has to be written as the sum

© 1997 NRC Canada

Can. J. Chem. Downloaded from www.nrcresearchpress.com by 88.146.161.215 on 09/08/12
For personal use only.

Table 1. Rate constants, slopes, and other parameters calculated for the hydrolysis of acetylimidazole in aqueous mineral acid media.

Parameter	H_2SO_4	HCl	$HClO_4$
Log (k_1k_2/k_{-1})	−3.082 ± 0.016	−3.111 ± 0.014	−3.337 ± 0.034
Slope m_2	−0.215 ± 0.032	−0.373 ± 0.046	−0.373 ± 0.042
Log k_1	−4.68 ± 0.14	−4.17 ± 0.12	−5.41 ± 0.23
Slope m_1	0.498 ± 0.034	0.373 ± 0.038	0.453 ± 0.056
$pK_{SH_2^{2+}}$	−6.77 ± 0.12	—[a]	−6.55 ± 0.17
r.m.s. error[b]	± 0.040	± 0.023	± 0.055
No. of points[c]	35 (2)	21 (1)	33 (1)
Log (k_2/k_{-1})	1.59	1.06	2.06

[a]Insufficient data to calculate.
[b]Root-mean-square deviation between the experimental points and the fitted lines in Fig. 2; in log k units.
[c]Any rejected by the curve-fitting program used as not being part of the same data set as the rest, to 95% confidence, are in parentheses here and in Fig. 2.

Table 2. Rate constants, slopes, and other parameters calculated for the hydrolysis of benzoylimidazole in aqueous sulfuric and hydrochloric acids.

Parameter	H_2SO_4	HCl
Log (k_1k_2/k_{-1})	−3.296 ± 0.029[a]	−3.236 ± 0.013
Slope m_2	−0.467 ± 0.027	−0.634 ± 0.032
Log k_1	−5.637 ± 0.096[b]	−4.565 ± 0.094
Slope m_1	0.419 ± 0.020	0.151 ± 0.028
r.m.s. error[c]	± 0.037	± 0.017
No. of points	24	13
Log (k_2/k_{-1})	2.34	1.33

[a]$\Delta H^{\ddagger}$ = 11.52 ± 0.72 kcal mol^{-1}; $\Delta S^{\ddagger}$ = −35.0 ± 2.4 cal mol^{-1} K^{-1}.
[b]$\Delta H^{\ddagger}$ = 16.98 ± 0.57 kcal mol^{-1}; $\Delta S^{\ddagger}$ = −27.4 ± 1.9 cal mol^{-1} K^{-1}.
[c]Root-mean-square deviation between the experimental points and the fitted lines in Fig. 3; in log k units.

of SH^+ and SH_2^{2+}, because at high acidity we would expect the protonation of the carbonyl group to become important. Rearranging and taking logs gives eq. [5], if we assume that $\log(f_{SH^+}/f_{\ddagger}) = m_1X$.

$$[5] \quad \log k_{\psi} - \log(C_{SH^+}/(C_{SH^+} + C_{SH_2^{2+}})) - \log a_{H_2O} = \log k_1 + m_1X$$

The protonation correction term can be obtained by dividing by C_{SH^+}, which enables it to be expressed in terms of the ionization ratio $I = C_{SH_2^{2+}}/C_{SH^+}$ as in eq. [6]:

$$[6] \quad (C_{SH^+}/(C_{SH^+} + C_{SH_2^{2+}})) = 1/(1 + I)$$

and this can be obtained from the excess acidity equilibrium equation, $\log I = pK_{SH_2^{2+}} + 0.6X + \log C_{H^+}$ (21). (It is known that the m^* value of 0.6 applies to carbonyl group protonations (21).)

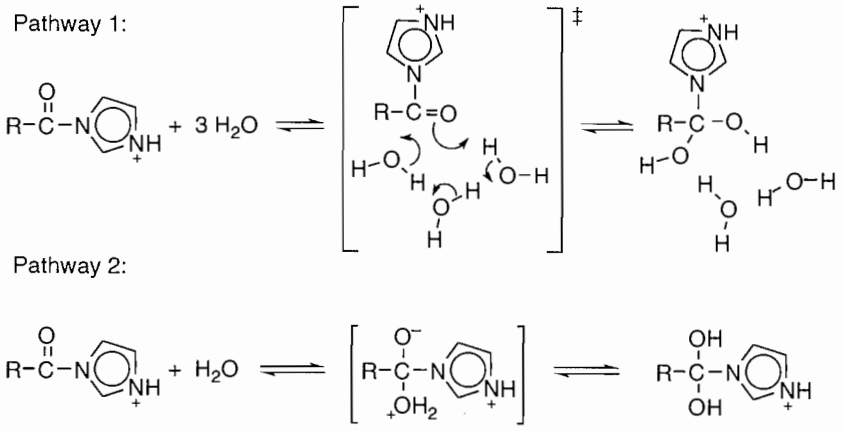
Equations [3] and [5] are the ones that give the lines in Figs. 2 and 3. In the topmost part of Fig. 2 (HCl) the theoretical curve is calculated with four coefficients, two slopes and two intercepts; for clarity the lines for the individual rate-determining steps are given in addition to the overall fitted curve. The middle curve (H_2SO_4) is calculated on the basis of five coefficients, the additional one being $pK_{SH_2^{2+}}$, calculated as above. The bottom plot ($HClO_4$) is also based on these five coefficients, with an additional one for the hydroxide mechanism, discussed below. In Fig. 3 the HCl plot is based on four coefficients, but the H_2SO_4 plot is based on six, with the data at additional temperatures being used to obtain $\Delta H^{\ddagger}$ and $\Delta S^{\ddagger}$ from the intercepts as before (18).

As can be seen from Figs. 2 and 3, the linearity assumption used in deriving eqs. [3] and [5] works very well. The slope values obtained are in Tables 1 and 2; there is not much that can be said about them as there are few studies to which they can be compared. The m_1 slopes for the k_1 processes compare favorably with the 0.56 ± 0.02 found for nitramide reacting in a similar way (20), and with the 0.3–0.7 found for some water additions to *N*-nitrobenzamides (18), which implies that the mechanisms of these processes are similar. The m_2 slopes for the tetrahedral intermediate breakup are all negative, but what this means, if anything, will have to wait until similar parameters for other substrates and reactions are obtained.

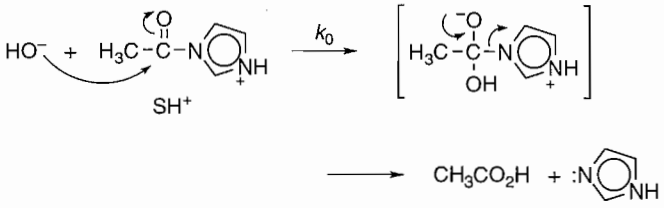
Two pathways can be visualized for the addition of water to SH^+, both of which result in rate equations involving one water molecule. Pathway 1 in Scheme 2 involves three water molecules in a proton switch, as proposed before for acid-catalyzed amide hydrolysis (31), and for the neutral hydrolyses of nitramide (20) and some *N*-nitro amides (18) in dilute acid. Pathway 2 is the conventional mechanism given in most textbooks (e.g., ref. 29). Both pathways will constrain several water molecules; the involvement of more than one in pathway 2 has been proposed before, based on a proton inventory analysis (32). Both are compatible with the entropy of activa-

© 1997 NRC Canada

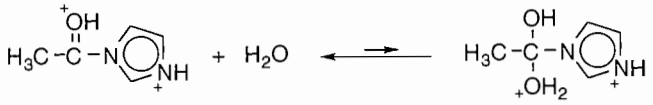
Scheme 2.



Scheme 3.



Scheme 4.



tion for the k_1 step in Table 2; however, pathway 1 involves no charge transfer at all, and is preferred on that basis.

The magnitudes of the intercept rate constants in Tables 1 and 2 seem reasonable; the breakup of the intermediate is slower than its formation in the standard state (water). The intercepts for the two rate-determining steps can be used to compare the rates of decomposition of the intermediate; values of $\log(k_2/k_{-1})$ given in the tables show that it goes on to product 10–100 times faster than it reverts to starting material. This implies that the hydrate should accumulate in solution in pure water; apparently this has never been tested experimentally.

The $pK_{SH_2^{2+}}$ values found for the second protonation at the carbonyl group of acetylimidazole are given in Table 1; they average to −6.7. This is much less basic than the values found for normal aliphatic (≈ −0.5) and aromatic (≈ −1.5) amides (33), which is only to be expected because of the positive charge already present in the molecule. Presumably the second protonation of benzoylimidazole is at least one pK unit more difficult, as there is no evidence of curvature at the higher acidities in Fig. 3. The technique used here shows that it is quite possible to obtain these values from kinetic data with a fair degree of accuracy, if they cannot be obtained directly.

Hydroxide addition to SH^+ would be highly favorable (Scheme 3); imidazole is a much better leaving group from the tetrahedral intermediate than is HO^-. An excess acidity rate equation for this can be based on eq. [7]:

$$[7] \quad k_\psi C_{SH^+} = k_0 a_{SH^+} a_{HO^-}/f_\ddagger$$

We have the definition $K_w = a_{H^+}a_{HO^-}/a_{H_2O}$ (one water molecule because the solvent is conventionally omitted from definitions of K_a and K_{BH^+}, so for consistency it is omitted from K_w also); substituting this, $a_{H^+} = C_{H^+}f_{H^+}$, and $a_{SH^+} = C_{SH^+}f_{SH^+}$ into eq. [7] gives eq. [8]:

$$[8] \quad k_\psi C_{SH^+} = (k_0 K_w) C_{SH^+}(a_{H_2O}/C_{H^+})(f_{SH^+}/f_\ddagger f_{H^+})$$

Rearranging, taking logs, and ignoring the activity coefficient ratio term gives eq. [9]:

$$[9] \quad \log k_\psi - \log a_{H_2O} + \log C_{H^+} = \log(k_0 K_w)$$

This is the equation that gives the HO^- curve in the lower part of Fig. 2. The activity coefficient term is omitted because the acidity region to which the equation refers is very close to ideality; actual testing in the one other case in which this behavior has been found (18) gave a slope value against X of zero. The intercept of this curve is −4.3, which means that k_0 is $10^{9.7}$, corresponding to diffusion control, which seems exactly what would be expected.

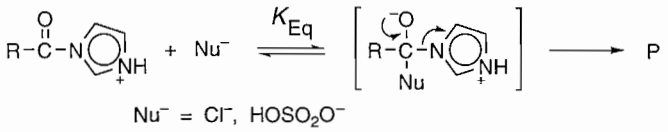
It was found that the diprotonated form is unreactive, hydrolysis only from the monoprotonated substrate being observed. This might seem surprising, but an examination of the tetrahedral intermediate formed when water adds, Scheme 4, reveals why this should be. There are two possible leaving groups here, neutral water and neutral imidazole, and of the two neutral water is far better. Thus the intermediate reverts to starting material very quickly, or more likely never forms in the first place as the $\Delta G^\ddagger$ is too unfavorable; SH_2^{2+} is resonance stabilized (to the carbonyl carbon), whereas the hydrate is not, ensuring an unfavorable equilibrium constant for its formation. Thus, when diprotonation starts to occur, the substrate SH^+ is simply being stored in an unreactive form, and this causes the reaction to slow down abruptly at high acidity (see Fig. 1).

The agreement between the results obtained in the three different aqueous mineral acid media can probably be best categorized as good but not great. However, it is apparent that the

© 1997 NRC Canada

Can. J. Chem. Downloaded from www.nrcresearchpress.com by 88.146.161.215 on 09/08/12
For personal use only.

Scheme 5.



excess acidity method *does* give the same answer in different acids. The further from the standard state, the worse the agreement; thus the log (k_1k_2/k_{-1}) values in the tables are much closer to one another than are the log k_1 values. In view of what is known of the agreement between pK_{BH^+} values measured in different acid media (21, 22), this is about what would have been expected. The $pK_{SH_2^{2+}}$ values agree quite well, and the slopes m_1 and m_2 fairly well, with the exception of the k_1 process for benzoylimidazole; perhaps this is due to the lack of rate constants at higher acidity for the reaction in HCl.

The really interesting observation in Fig. 2 is the difference between aqueous $HClO_4$ and the other two acids. In the former the log (k_1k_2/k_{-1}) process is slow enough that the hydroxide-catalyzed reaction is revealed, but this is swamped (presumably) by the faster log (k_1k_2/k_{-1}) process in aqueous HCl and aqueous H_2SO_4. The best guess as to what is going on here is that Cl^- and HSO_4^- can add to SH^+, as in Scheme 5, but ClO_4^- cannot, being non-nucleophilic. The resulting acid chloride and mixed anhydride will hydrolyze to the same carboxylic acid and protonated imidazole reaction products as given by the reaction with water in Scheme 1. Presumably this addition will be highly reversible; however, the mere existence of this extra reaction pathway is enough to accelerate the reaction in HCl and H_2SO_4. Perhaps this could be called nucleophilic catalysis by the acid anion.[4]

Marburg and Jencks (2) studied acetylimidazole hydrolysis in many aqueous salt solutions, as well as in the acid media discussed here, and the rate – salt concentration profiles for these solutions resemble the rate–acidity profiles. This means that derivation of an activity coefficient ratio term like X for salt or salt–acid media could prove useful in determining the mechanisms of reactions taking place in them. An equilibrium process that has large changes in K_{eq} with salt concentration, preferably over a wide concentration range, should enable a quantity like the excess acidity to be defined for salt solutions.

[4] One of the referees has commented that if this mechanism were important the reaction rate should increase as the acid concentration increases. It is not quite that simple, however; increasing C_{Nu^-} will certainly drive the Scheme 5 equilibrium further to the right, but the hydrolyses of the resulting acid chloride and anhydride products are not acid catalyzed in this acidity region, the observed rates actually decreasing with acidity according to Satchell's latest results (16, 17), and their actual hydrolysis rate constants may well be lower than those found in this work, as well (16, 17). Thus a decreasing rate constant with increasing acidity is in fact consistent with the contribution of the Scheme 5 pathway. It should be possible to separate out the rate constants due to the different processes, on the assumption that the same mechanism has the same rate parameters in the different acid media, but this is not thought to be justified experimentally at this time.

Acknowledgments

I would like to thank Professor W.P. Jencks for sending me the unpublished concentration vs. time data used here. Valuable discussions with Professor A.J. Kresge and his group are acknowledged, and I would like to thank Professor Kresge for reading the manuscript.

References

1. T.H. Fife. Acc. Chem. Res. **26**, 325 (1993).
2. S. Marburg and W.P. Jencks. J. Am. Chem. Soc. **84**, 232 (1962).
3. C.R. Smith and K. Yates. J. Am. Chem. Soc. **94**, 8811 (1972).
4. R.A. Cox. Acc. Chem. Res. **20**, 27 (1987).
5. R.A. Cox and K. Yates. Can. J. Chem. **57**, 2944 (1979).
6. J.-P. Bégué, F. Benayoud, D. Bonnet-Delpon, A.D. Allen, R.A. Cox, and T.T. Tidwell. Gazz. Chim. Ital. **125**, 399 (1995).
7. R.A. Cox, D.B. Moore, and R.S. McDonald. Can. J. Chem. **72**, 1910 (1994).
8. R.A. Cox, I. Onyido, and E. Buncel. J. Am. Chem. Soc. **114**, 1358 (1992).
9. R.A. Cox. J. Phys. Org. Chem. **4**, 233 (1991).
10. Y. Chiang, A.J. Kresge, P.A. Obraztsov, and J.B. Tobin. Croat. Chem. Acta, **65**, 615 (1992); Y. Chiang and A. J. Kresge. J. Am. Chem. Soc. **107**, 6363 (1985).
11. N. Banait, M. Hojatti, P. Findlay, and A.J. Kresge. Can. J. Chem. **65**, 441 (1987).
12. J. Andraos, A.J. Kresge, and N.P. Schepp. Can. J. Chem. **73**, 539 (1995).
13. A.J. Kresge and D. Ubysz. J. Phys. Org. Chem. **7**, 316 (1994); A.J. Kresge and M. Leibovitch. J. Org. Chem. **55**, 5234 (1990).
14. M. Ali and D.P.N. Satchell. J. Chem. Soc. Perkin Trans. 2, 167 (1995); 1825 (1993).
15. V.B. Joseph, D.P.N. Satchell, R.S. Satchell, and W.N. Wassef. J. Chem. Soc. Perkin Trans. 2, 339 (1992).
16. D.P.N. Satchell, W.N. Wassef, and Z.A. Bhatti. J. Chem. Soc. Perkin Trans. 2, 2373 (1993).
17. R.E. Moti, D.P.N. Satchell, and W.N. Wassef. J. Chem. Soc. Perkin Trans. 2, 1087 (1993).
18. R.A. Cox. J. Chem. Soc. Perkin Trans. 2. In press.
19. R.A. Cox. Can. J. Chem. **74**, 1774 (1996).
20. R.A. Cox. Can. J. Chem. **74**, 1779 (1996).
21. R.A. Cox and K. Yates. J. Am. Chem. Soc. **100**, 3861 (1978).
22. R.A. Cox and K. Yates. Can. J. Chem. **59**, 2116 (1981).
23. P.R. Bevington. Data reduction and error analysis for the physical sciences. McGraw–Hill, New York. 1969. pp. 232–245.
24. R.A. Cox and K. Yates. Can. J. Chem. **62**, 2155 (1984).
25. W.F. Giauque, E.W. Hornung, J.E. Kunzler, and T.R. Rubin. J. Am. Chem. Soc. **82**, 62 (1960).
26. M. Randall and L.E. Young. J. Am. Chem. Soc. **50**, 989 (1928).
27. H. Wai and K. Yates. Can. J. Chem. **47**, 2326 (1969); R.A. Robinson and O.J. Baker. Trans. R. Soc. N.Z. **76**, 250 (1946); J.N. Pearce and A.F. Nelson. J. Am. Chem. Soc. **55**, 3075 (1933).
28. W.P. Jencks and J. Carriuolo. J. Biol. Chem. **234**, 1272 (1959); **234**, 1280 (1959).
29. T.W.G. Solomons. Organic chemistry. 6th ed. Wiley, New York. 1996; J. March. Advanced organic chemistry. 4th ed. Wiley, New York. 1992.
30. P. Greenzaid, Z. Luz, and D. Samuel. J. Am. Chem. Soc. **89**, 749 (1967).
31. R.A. Cox and K. Yates. Can. J. Chem. **59**, 2853 (1981).
32. J.L. Hogg, M.K. Phillips, and D.E. Jergens. J. Org. Chem. **42**, 2459 (1977).
33. R.A. Cox, L.M. Druet, A.E. Klausner, T.A. Modro, P. Wan, and K. Yates. Can. J. Chem. **59**, 1568 (1981).

© 1997 NRC Canada

Can. J. Chem. Downloaded from www.nrcresearchpress.com by 88.146.161.215 on 09/08/12
For personal use only.

Near-infrared spectra of $Ba(NO_2)_2 \cdot X_2O$ (X = H,D) at 10 K. A local-mode approach

Ian M. Walker and Paul J. McCarthy

Abstract: The fundamental and overtone vibrational spectra of $Ba(NO_2)_2 \cdot X_2O$ (X = H,D) have been interpreted using the local-mode model. The calculated parameters are consistent with the structure, which has one strong hydrogen bond and one weak bifurcated hydrogen bond. Evidence for Fermi resonance between stretch and bend features having similar energies is discussed. Evidence for the breakdown of the simple Morse oscillator model, which was quite successful for O—H···Cl hydrogen bonds, is also presented.

Key words: overtone, spectra, near-infrared, hydrates, local-mode model.

Résumé : Faisant appel au modèle du mode local, on a interprété les spectres vibrationnels fondamentaux et harmoniques du $Ba(NO_2)_2 \cdot X_2O$ (X = H,D). Les paramètres calculés sont en accord avec la structure impliquant une liaison hydrogène forte et une faible liaison hydrogène bifurquée. On discute des données suggérant l'existence d'une résonance de Fermi entre les caractéristiques d'élongation et de déformation d'énergies semblables. On présente aussi des résultats suggérant que le modèle d'oscillateur simple de Morse, qui a été très utile pour les liaisons hydrogènes O—H···Cl, ne s'applique pas ici.

Mots clés : harmonique, spectre, proche infrarouge, hydrates, modèle du mode local.

[Traduit par la rédaction]

Can. J. Chem. Downloaded from www.nrcresearchpress.com by 88.146.161.215 on 09/08/12
For personal use only.

Introduction

We have, in a series of papers, used local-mode theory to analyze the vibrational overtone and combination bands of water (1–5) and of the NH_2 group in the guanidinium ion (6) in crystals. The purpose of these studies is to try to correlate the local-mode parameters with the length and strength of the hydrogen bonds formed by O—H and N—H bonds. For such studies barium nitrite monohydrate, $Ba(NO_2)_2 \cdot H_2O$, is a suitable material. It can be recrystallized to yield large, well-formed crystals, and polarized crystal spectra in the near-infrared (NIR) region can readily be recorded.

Crystal structure

The X-ray crystal structure of $Ba(NO_2)_2 \cdot H_2O$ at 298 K has been reported (7, 8). In addition, an extensive neutron diffraction study at 298, 102, and 20 K has appeared (9). These studies show that the material has a hexagonal unit cell, which at 20 K has the parameters a = 7.0524 Å, c = 17.6372 Å, Z = 6, and that the crystal belongs either to space group $P6_5$ (C_6^3, no. 170) or to the enantiomorphous $P6_1$ (C_6^2, no. 169). Since $Ba(NO_2)_2 \cdot H_2O$ is expected to crystallize in a statistical mixture of enantiomorphs, the experimental results might be reported for either space group. Thomas and Gomes (10) have shown that the crystal they studied is optically dextrorotatory in the visible region of the spectrum and so belongs to the latter space group. The structures in the neutron diffraction study were, however, refined on the basis of the former space group. For our study the difference is immaterial.

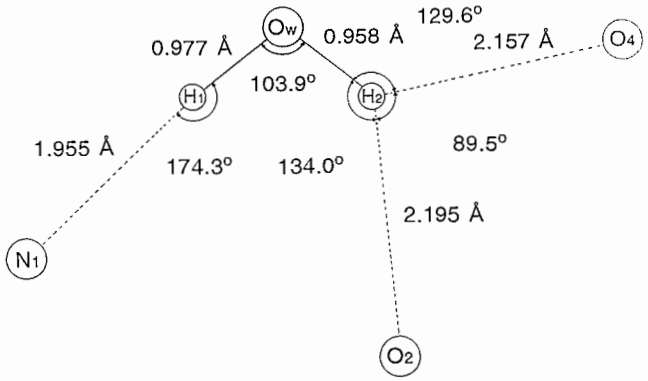


Fig. 1. The water molecule in $Ba(NO_2)_2 \cdot H_2O$ showing the hydrogen bonds to atoms on three nearby nitrite ions. The angles around H(2) do not sum to 360°, since H(2), O(w), O(2), and O(4) do not lie exactly in a plane. Atom designations are from ref. 9.

All the waters in the crystal are equivalent, and they form two different hydrogen bonds (see Fig. 1). The nearly linear O—H(1)···N(1) forms the stronger hydrogen bond, while O—H(2) forms a weaker bifurcated hydrogen bond to oxygens on two different nitrite groups. Kvick et al. (9) have noted that the HOH angle (103.9°) and the shorter O—H distance (0.958 Å) agree well with the values reported for gaseous water, 104.52° and 0.9572 Å (11). The other O—H bond is substantially longer, and this indicates a weakening of the

Received February 17, 1997.

I.M. Walker.[1] Department of Chemistry, York University, Downsview, ON M3J 1P3, Canada.
P.J. McCarthy. Department of Chemistry, Canisius College, Buffalo, NY 14208, U.S.A.

[1] Author to whom correspondence may be addressed. Telephone: (416) 736-2100, ext. 77726. Fax: (416) 736-5936. E-mail: iwalker@yorku.ca

© 1997 NRC Canada

Can. J. Chem. Downloaded from www.nrcresearchpress.com by 88.146.161.215 on 09/08/12
For personal use only.

O—H bond due to strong hydrogen-bond formation with N(1). The nitrite ions in the crystal are of two independent types, and the Ba^{2+} ion is coordinated with one nitrogen and nine oxygen atoms at an average distance of 2.881 Å at 20 K (9).

Spectra

The fundamental vibrational spectrum of this substance has been studied in considerable detail (12–17). Eriksson et al. (17) noted that as the crystal is cooled from 298 to 102 and then to 20 K the energy of most IR absorptions increases. (In the following, ν, δ, and ρ are stretching, bending, and librational vibrations, respectively.) As for the two ν(OH) or ν(OD) bands, the higher energy band increases a small amount in energy, while the band at lower energy decreases in energy to a greater extent. This was also noted earlier by Brink and Falk (13). The O—H···N hydrogen bond presumably gets stronger as the temperature is lowered. This is not unexpected, since molecular motion decreases with lowered temperature.

The large asymmetry of the water molecule in this compound was noted in the IR spectrum before it was confirmed by diffraction studies. It was early pointed out by Schiffer (18) that the two ν(OH) correspond to the stretches of the individual OH bonds rather than to symmetric and unsymmetric combinations of the two stretches. Brink and Falk (13) note that this is confirmed by the fact that the stretching fundamentals of H_2O and D_2O have values almost the same as those found in HOD. Eriksson et al. (17) noted that this is a "well-known consequence of an asymmetric bonding situation in the water molecule." This means that the local-mode model should apply very well in this case.

Brink and Falk (13) further noted that in this compound the separation of the two ν(OH) or ν(OD) in the two forms of HOD decreases with increasing temperature. This they ascribe to increased molecular motion, especially librational motion, in the crystals, which would tend to equalize the weak and strong hydrogen bonds.

The IR spectra of HOD in $Ba(NO_2)_2 \cdot 2HOD$ show two δ(HOD) bands. Since stronger hydrogen bonding augments the energy of the bending vibration, the band at 1481 cm^{-1} is assigned to δ(N···H-O-D···O), while that at 1442 cm^{-1} has H and D reversed; the data are for 102 K (17).

The polarized crystal spectra of $Ba(NO_2)_2 \cdot H_2O$ in the 1300–2700 nm region were recorded at room temperature by Wood (19). Our low-temperature study has revealed additional features; this enables us to make a more complete treatment of this system from a local-mode point of view.

Local-mode theory

The local-mode theory for water on general sites has been outlined elsewhere (2, 3). Its application here is very similar to the case of $CsMnCl_3 \cdot 2H_2O$, in which all waters are identical but form two different hydrogen bonds to adjacent chlorines (4). The vibrational basis functions for the O—H bonds are written as products of Morse oscillator eigenfunctions, each of which is described by a local-mode quantum number, v_i. The basis ket for a water molecule is accordingly written as $|v_1 v_2>$. After subtracting the energy of the ground $|00>$ state, the diagonal elements of the secular determinant can be calculated from the relation:

$$[1] \quad <v_i v_j|H|v_i v_j> = \omega_1 v_1 + \omega_2 v_2 + X_1 v_1(v_1 + 1) + X_2 v_2(v_2 + 1)$$

Here ω_1 and ω_2 are the harmonic frequencies and X_1 and X_2 the anharmonicity parameters of the O—H (O—D) bonds. Coupling between stretching modes in H_2O and D_2O is taken into account by the inclusion of off-diagonal elements of the form:

$$[2] \quad <v_i + 1, v_j - 1|H|v_i, v_j> = \lambda[(v_i + 1)v_j]^{1/2}$$

λ represents the coupling between the two O—H or O—D oscillators. From eq. [2] it is clear that only coupling between states with the same value of $(v_1 + v_2)$ need be considered. An initial parameter set is chosen and the vibrational energies are calculated by diagonalization of the appropriate matrices (2). An iterative process changes all parameters simultaneously so as to minimize the sum of the squares of the differences between calculated and observed energies. The procedure stops when successive iterations differ by less than a preset amount. The standard deviations were estimated by the method outlined by Cowan (20).

Experimental

Well-formed hexagonal prisms were obtained by slow evaporation of $Ba(NO_2)_2 \cdot H_2O$ from aqueous solution. Crystals with various H/D ratios were prepared by evaporating solutions of barium nitrite in mixtures of H_2O and D_2O in a desiccator over concentrated H_2SO_4. Spectra were recorded at 10 K on a Varian 2300 spectrophotometer with the sample cooled in a Displex cryogenic refrigerator. A pair of Glan–Thompson prisms provided polarized light. Spectra were recorded with the electric vector (E) of the light parallel and perpendicular to the crystal c axis.

Results and discussion

The spectra of crystals with various H/D ratios are shown together for easier comparison. Figure 2 presents the 4700–5300 cm^{-1} region, while Fig. 3 shows the 5900–7100 cm^{-1} region. Figure 4 contains the spectra of the 3ν region of the protiated crystal only, since we were not able to observe any distinctive bands in the appropriate region in deuterated crystals. Other spectral regions are not shown, but will be commented on briefly.

For some band energies there may be a difference of a few wave numbers between polarizations or within a single polarization as the D/H ratio changes. The precision of our measurements is also of this order of magnitude. Therefore, unless there is an unambiguous difference between polarizations or between spectra with various D/H ratios, we have used the average values for the band energies. In fact, for the most part, absorption energies in the two polarizations appear to be identical within experimental error.

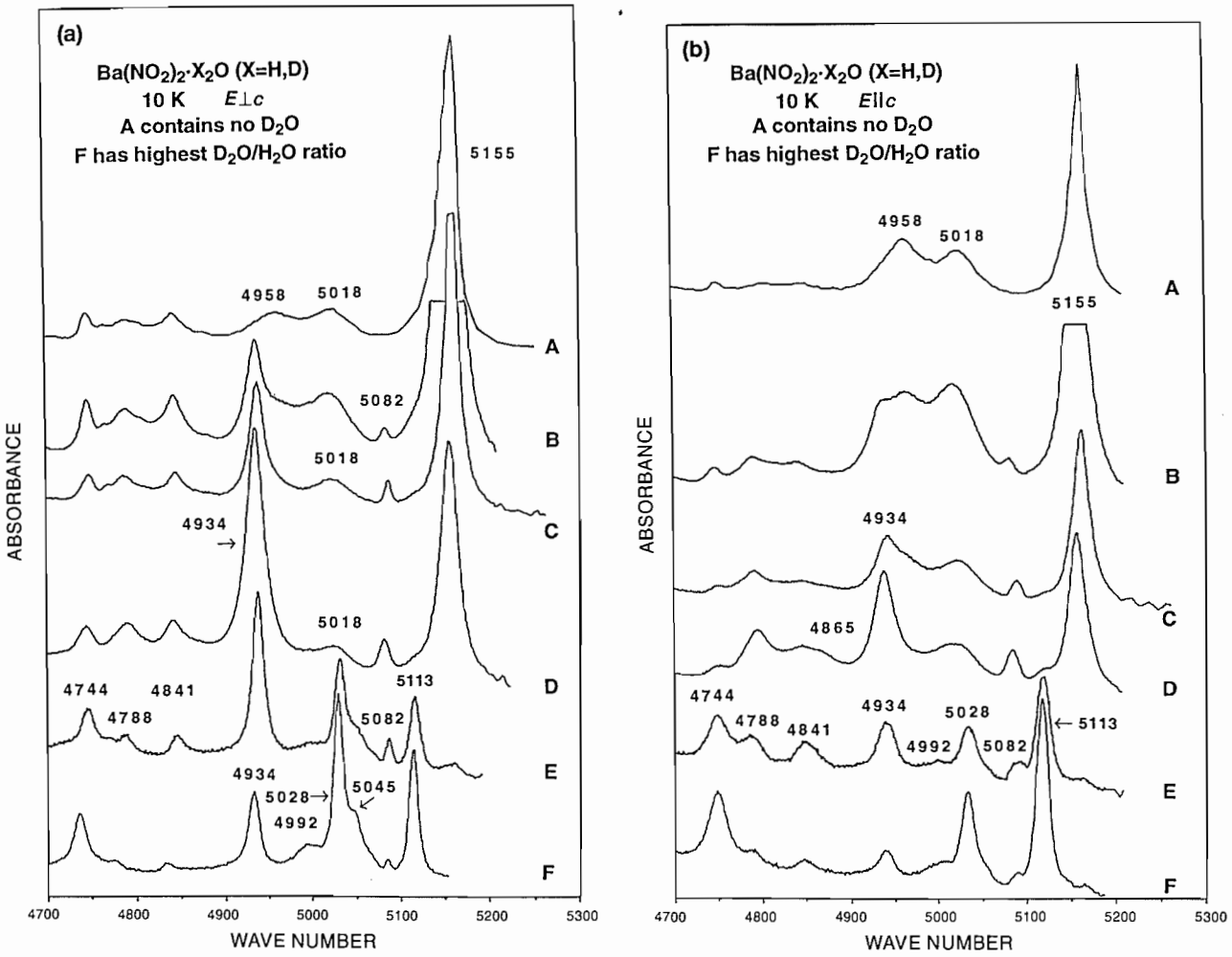
The observed vibrational energies of $Ba(NO_2)_2 \cdot H_2O$ and its deutero analogs are listed in Table 1 together with the band assignments. Along with these are the calculated energies and the parameters that yielded this best fit.

Spectra of $Ba(NO_2)_2 \cdot H_2O$

Our room-temperature spectra of $Ba(NO_2)_2 \cdot H_2O$ match those reported by Wood (19). When the crystal is cooled to 10 K, however, a great deal of detail is seen in all of the bands. The sums of fundamentals allow one to assign a group of band components of comparable intensity to a generic combination

© 1997 NRC Canada

Fig. 2. Spectra of $Ba(NO_2)_2 \cdot X_2O$ (X = H,D) at 10 K in the range 4700–5300 cm^{-1}; (*a*) $E \perp c$, (*b*) $E \parallel c$.



of the fundamentals. For example, the rather strong features between 3900 and 4150 cm^{-1} are due to $\nu + \rho$ of water in the crystal (19). The series of weak bands in the 4500–4900 cm^{-1} region are due to coupling of the stretches of water with those of the nitrite groups. The $\nu+2\rho$ bands of H_2O are calculated also to appear between 4350 and 4860 cm^{-1}. Finally, a group of very weak bands between 7200 and 7500 cm^{-1} are probably due to $2\nu + \rho$ of water.

For most of the bands such a generic assignment is all that is feasible, since no model is available that would allow the calculation of the energies of the individual band components. For some regions, however, such as those of the stretch overtones and the stretch–bend combinations of water, assignments of individual bands can be made with reasonable certitude, and we will concentrate on these.

In Figure 2 (trace A) the bands at 5018 and 5155 cm^{-1} are the $\nu + \delta$ combinations of H_2O. In the spectra of a thick crystal, weak bands lie 470, 587, and 746 cm^{-1} above the 5018 cm^{-1} band. Since the average values at 102 K for the three librations of water are 471, 579, and 724 cm^{-1} (17), these three bands can be assigned to $\nu + \delta + \rho$ combinations. It is interesting to note that the observed progressions in the librational modes are associated principally with $\nu + \delta$ of the **stronger** hydrogen bond. The other moderately strong band at 4958 cm^{-1} might be the 3δ band of H_2O, which is calculated to appear in this region. It seems inordinately strong for a ternary combination; the origin of its intensity will be discussed below.

Figure 3 (trace A) shows the stretch overtone region of water. The band at 6842 cm^{-1}, assigned to the |11> state of H_2O, is noticeably polarized $\perp c$. (See the discussion of the HOD spectrum below.) The strong band at 6820 cm^{-1} is |02> of the weakly hydrogen-bonded OH; it persists in the most highly deuterated samples. The |20> of the strongly hydrogen-bonded OH appears at considerably lower energy, 6287 cm^{-1}. The $\nu + 2\delta$ bands of water are also calculated to appear at about 6661 and 6830 cm^{-1} (17). Although the latter are ternary bands, they could gain intensity by Fermi resonance with the 2ν bands (see below). Accordingly, the strong band at 6787 cm^{-1} is assigned as one of these $\nu + 2\delta$ bands. The other is not clearly observed, but may be one of the weak bands between 6600 and 6700 cm^{-1}. This assignment is strengthened by the fact that in both polarizations the spectrum of this region is repeated at higher energy. Bands are found at 7924, 8434, and 8465 cm^{-1}. They are about 3% as intense as the 2ν features and they lie about 1624 cm^{-1} above the 2ν bands. Since δ = 1662 cm^{-1} at 102 K (17), the bands at higher energy can be assigned

© 1997 NRC Canada

Can. J. Chem. Downloaded from www.nrcresearchpress.com by 88.146.161.215 on 09/08/12
For personal use only.

Can. J. Chem. Downloaded from www.nrcresearchpress.com by 88.146.161.215 on 09/08/12
For personal use only.

Table 1. (*a*) Calculated and observed energies for $Ba(NO_2)_2 \cdot X_2O$ (X = H,D).

Band	Energy, cm^{-1} Obsd[a]	Calcd.	Assignment[b]
1	2461	2458	|10>(DOD)
2	2462	2464	|10>(DOH)
3	2591	2589	|01>(HOD)
4	2599	2596	|01>(DOD)
5	3327	3331	|10>(HOD)
6	3336	3331	|10>(HOH)
7	3502	3506	|01>(HOH)
8	3505	3506	|01>(DOH)
9	4744	4744	|20>(DOD)
10		4750	|20>(DOH)
11	5028	5028	0.79|11> + 0.60|02>(DOD)
12	5082	5082	|02>(HOD)
13	5113	5113	0.80|02> − 0.60|11>(DOD)
14	5915	5920	|11>(HOD)
15	5969	5970	|11>(DOH)
16	6287	6287	|20>(HOH)
17		6287	|20>(HOD)
18	6820	6817	0.93|02> + 0.36|11>(HOH)
19	6820	6820	|02>(DOH)
20	6842	6840	0.93|11> − 0.36|02>(HOH)
21		8868	|30>(HOH)
22		9793	|21>(HOH)
23	9940	9941	|03>(HOH)
24	10153	10152	|12>(HOH)

Root–mean–square deviation = 2.57 cm^{-1}

(*b*) Parameters used in best fit.[c]

Parameter	O—H	O—D	Ratio(O—D)/(O—H)[d]
ω_1	3706 (3)	2643 (6)	0.713
ω_2	3698 (3)	2686 (6)	0.726
X_1	−187 (1)	−89 (2)	0.477
X_2	−96 (1)	−48 (2)	0.502
λ	−5 (2)	−29 (2)	

[a]IR fundamentals (102 K) from ref. 17.

[b]The first letter refers to the isotope on site 1 and the third letter refers to that on site 2 (see Fig. 1). When different isotopes are present, the two isotopomers are written HOD and DOH. The parent states are listed for all eigenvector coefficients >0.3.

[c]Standard deviations in parentheses; all data in cm^{-1}.

[d]Theoretical ratios are 0.728 and 0.529.

to $2\nu + \delta$ of water. A band at 6787 + 1624 cm^{-1} is notably missing from this group. It would be the quaternary band, $\nu + 3\delta$, and is accordingly too weak to be observed.

Of particular interest is the complex feature on the high-energy side of the 6287 cm^{-1} band, the first overtone of O—H in the O—H···N hydrogen bond. It represents simultaneous excitation of H-bond acceptor vibrations with the |20> mode. The band contains broad maxima that appear to be short progressions in 50–60 and 100 cm^{-1}. They could represent the H-bond wag and stretch modes. Sandorfy made such an assignment in his study of the HCl – dimethyl ether system (21). The |02> and |11> bands should show similar structure. And in fact the overall |02> plus |11> band group is slightly broadened on its high-energy side and shows several weak, resolved features. The lowest band in the $2\nu + \delta$ complex (7924 cm^{-1}) also has associated structure in both polarizations. This band is stronger in the $E \| c$ spectrum, just as is the 6287 cm^{-1} band. We have also noted similar diffuse structure on the high-energy side of bands in the spectra of $CsMnCl_3 \cdot 2H_2O$ (4), $Cs_2MnCl_4 \cdot 2H_2O$ (5), and guanidinium salts (6).

Figure 4 shows the spectra of the 3ν region of the protiated crystal. The crystal was the thickest we could grow (1.7 mm) and the strongest band is about 2% as strong as the strongest band in the 2ν region. The |30> state was not included in the fitting routine described above, since no band was found near the expected value, 8868 cm^{-1} (Table 1). The band at 9065 cm^{-1} can, however, most likely be assigned to this strongly hydrogen-bonded |30> state, even though it lies so high in energy. It is possible to evaluate deviations from the simple model used in this paper due to the formation of such strong hydrogen bonds. The problem has been treated in depth by Foldes and Sandorfy (22), who showed that additional terms are needed in the Hamiltonian in order to account for the position of the second overtone in hydrogen-bonded alcohols. If the two terms

$$Y_i [v_i^3 + (3/2)\, v_i^2 + (3/4)\, v_i] \qquad (i = 1, 2)$$

are added to eq. [1], then it can be shown that

$$[3] \quad 2Y_1 = E(|10>) + E(|30>)/3 - E(|20>)$$

with a similar expression for Y_2. Using the data for oscillator 1 (Table 1), we estimate that $Y_1 = 35$ cm^{-1}, which is comparable to the value calculated for isopropanol (22). It is of interest that the signs of X and Y are opposite in this crystal, just as they are in associated alcohols. In contrast, for oscillator 2, $Y_2 = -2$ cm^{-1}. This indicates that this weakly hydrogen-bonded oscillator is very similar to a gas-phase Morse OH oscillator.

Spectra of $Ba(NO_2)_2 \cdot HOD$

The most interesting feature of the spectra of this species is the pair of bands at 5915 and 5969 cm^{-1} (see Fig. 3). They are assigned to combinations ν(OH) + ν(OD) in the two HOD molecules. Their energies match nicely the sums of the fundamentals at 102 K, namely, 5918 and 5967 cm^{-1} (17). The appearance of two bands in this region is consistent with the difference in hydrogen-bond strength for the two OH(OD) oscillators. Both components are almost completely polarized $\perp c$. The bisector of the HOD angle lies almost in the plane $\perp c$. If the resultant of the OH and OD vectors is taken to lie along this bisector, then the dipole strength of this resultant is calculated to be 97% polarized $\perp c$.

It is noteworthy that the two stretch combination bands differ in intensity. The band at lower energy (5915 cm^{-1}) has about half the area of the other band (5969 cm^{-1}). The 5915 cm^{-1} band contains the strong O—H···N(1) hydrogen bond and weak O—D bifurcated hydrogen bond, while the 5969 cm^{-1} band contains the opposite configuration. Barium chloride dihydrate contains two crystallographically distinct water

© 1997 NRC Canada

Fig. 3. Spectra of $Ba(NO_2)_2 \cdot X_2O$ (X = H,D) at 10 K in the range 5900–7100 cm^{-1}; (*a*) $E \perp c$, (*b*) $E \parallel c$. The bands marked P are due to the polarizers.

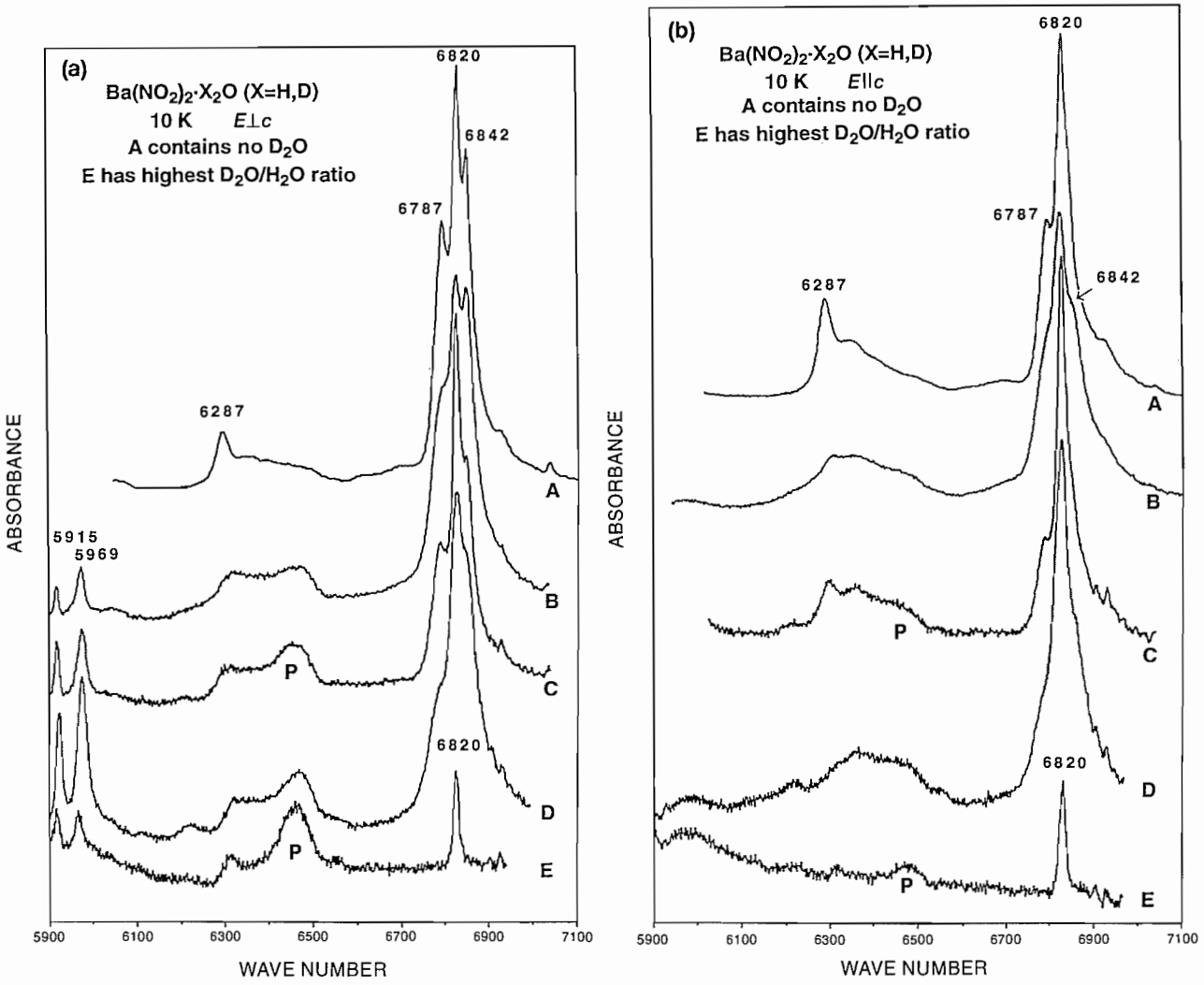
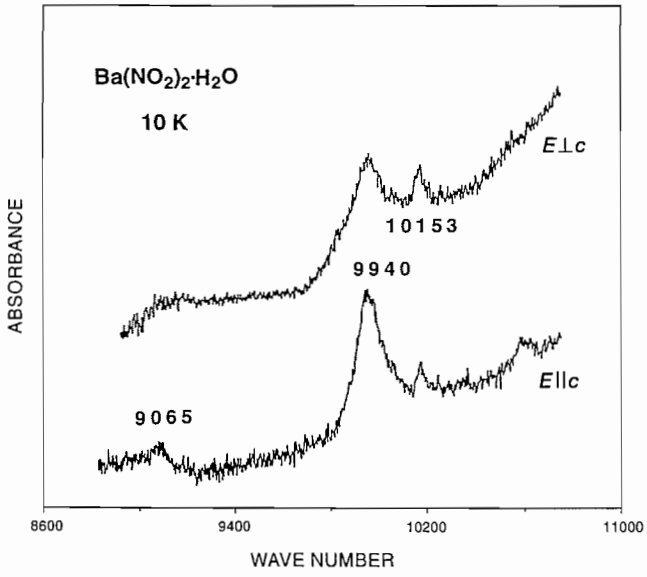


Fig. 4. Spectra of $Ba(NO_2)_2 \cdot H_2O$ at 10 K in the range 8600 – 11 000 cm^{-1}.



molecules, and the spectra of $BaCl_2 \cdot 2HOD$ show four $\nu(OH) + \nu(OD)$ combination bands (2, 3). In this case the band at highest energy is considerably less intense than the other three. This weakest band is due to the sum of a strong O—H hydrogen bond and a weak O—D bifurcated hydrogen bond in the water on site 2. It is interesting that the same trend is found in both crystals. We have no explanation of this at present. In the other compounds for which we have done deuterated studies, either the bands are roughly the same in area ($Cs_2MnCl_4 \cdot 2H_2O$ (5)) or only a single band is observed ($CsMnCl_3 \cdot 2H_2O$ (4)).

The $\nu(OD) + \delta(HOD)$ bands are calculated to appear at 3904 and 4072 cm^{-1}. Bands that intensify and then weaken on addition of H_2O are found at 3900 and 4062 cm^{-1} (not shown) and can therefore be assigned to these combinations. The pair of bands at 4788 and 4934 cm^{-1} behave similarly (see Fig. 2), and so are assigned to $\nu(OH) + \delta(HOD)$. They are calculated to be at 4808 and 4947 cm^{-1}. This confirms the assignment of the $\delta(HOD)$ features. Because of its behavior on the addition of H_2O, the band at 5082 cm^{-1} can be assigned as an absorption of HOD. It is likely the overtone of the weakly bonded OD oscillator.

Can. J. Chem. Downloaded from www.nrcresearchpress.com by 88.146.161.215 on 09/08/12
For personal use only.

© 1997 NRC Canada

Can. J. Chem. Downloaded from www.nrcresearchpress.com by 88.146.161.215 on 09/08/12
For personal use only.

Spectra of $Ba(NO_2)_2 \cdot D_2O$

In the spectra of a highly deuterated crystal a very strong band lies at 3795 cm^{-1} ($E \perp c$) (not shown). It is probably one of the $\nu + \delta$ bands of D_2O, which are calculated to appear at 3669 and 3805 cm^{-1}. The same spectra (see Fig. 2) show a weak band at 4992 cm^{-1} that can be assigned to one of the $\nu + 2\delta$ combinations of D_2O; the sums of the fundamentals at 102 K are 4875 and 5011 cm^{-1} (17). The bands at 4744, 5028, and 5113 cm^{-1} lose intensity rapidly on the addition of H_2O, and so have been assigned as the 2ν bands of D_2O. The band at 4744 cm^{-1} appears also to contain an absorption of H_2O. A few other band positions are noted in the figures, but at present we have no assignment for these bands.

Fermi resonance

To explore some of the fine details of the H_2O spectra, we have analyzed a more complete data set that includes the bend and bend–stretch combination features. The Hamiltonian of eqs. [1] and [2] was augmented by inclusion of Fermi resonance matrix elements (23) between stretch states and bend overtones and stretch–bend combinations of like energies. Inclusion of Fermi resonance can explain certain anomalies in the spectra without materially affecting the best-fit values of the local-mode parameters of Table 1.

First, in the IR spectrum the energy of the OH stretch of the strong hydrogen bond ($|10\rangle$) is anomalously high. If Fermi resonance were not present, this band should lie near 3327 cm^{-1}, as it does in the HOD spectrum. This suggests that the $|10\rangle$ state interacts with 2δ in H_2O, calculated to be at 3322 cm^{-1}. The interaction raises the value of the former state to 3336 cm^{-1}, while the energy of the latter is lowered to 3295 cm^{-1}. The other stretch is affected much less. Setting the Fermi resonance parameter to about 25 cm^{-1} accounts for this anomaly.

Second, the enhanced intensity of the $|01\rangle + 2\delta$ band at 6787 cm^{-1} can also be explained by Fermi resonance. Our calculations show that the same small parameter (about 25 cm^{-1}) causes strong mixing of this $\nu + 2\delta$ state with the adjacent $|02\rangle$ state of H_2O. The $|10\rangle + 2\delta$ band is very weak and is not observed. Calculations show that there is almost no mixing of this combination with the $|20\rangle$ state. This can be attributed to the rather large difference in their energies.

Finally, the 3δ band is abnormally strong. This can be ascribed to strong mixing of the 3δ state with the combination state $|10\rangle + \delta$, which lies nearby. This is confirmed by our calculations.

Conclusions

Our analysis of the data in Table 1 permits us to draw the following conclusions.

1. Although the two hydrogen bonds differ considerably in strength, this is not mirrored in the magnitude of ω. The two values differ only slightly and are about 5% lower than ω for gaseous H_2O (3876.2 cm^{-1}) (24) or D_2O (2818.8 cm^{-1}) (25). This was also found for several other systems that we have studied. Accordingly, the magnitude of ω is **not** a good indicator of the strength of the hydrogen bond formed by an O—H or O—D bond.

2. The values of X for the weaker hydrogen bond (−96 cm^{-1} (OH), −48 cm^{-1}(OD)) are somewhat more negative than the values for the corresponding oscillators in gaseous H_2O (−84.4 cm^{-1}) (24) or D_2O (−45.4 cm^{-1}) (25), while those for the stronger hydrogen bond (−187 cm^{-1}(OH), −89 cm^{-1}(OD)) are about twice as large as those for gaseous H_2O and D_2O. Therefore, in this study as well as earlier reports, we find that the value of X is a considerably better indicator of hydrogen-bond strength. While the data we have been able to amass do not provide a highly correlated relationship between X and hydrogen-bond length, the general trend is that the shorter (and therefore stronger) the hydrogen bond formed, the more negative the value of X. This matches what is reported in the literature for water in condensed phases and for numerous hydrogen-bonded alcohol multimers (22, 26). Berglund et al. (16) calculated the values of X(OH) for $Ba(NO_2)_2 \cdot H_2O$ by a simple method that uses the four stretch fundamentals of HOD and DOH. The values they obtained, −220 and −223 cm^{-1}, are quite unrealistic, however, given the extreme difference in hydrogen-bond environment of the two O—H bonds.

3. On hydrogen-bond formation, the value of λ in H_2O is considerably reduced from the value in gas-phase water. This is in accord with our earlier studies on $CsMnCl_3 \cdot 2H_2O$ (4) and $M_2MnCl_4 \cdot 2H_2O$ (M = Rb, Cs) (5). The value of λ is larger for D_2O than for H_2O, but it too is reduced upon hydrogen-bond formation. The reduction is not so marked, however, as in the case of H_2O. This is also consistent with our earlier studies.

4. The ratios ω(OD)/ω(OH) and X(OD)/X(OH) are 0.713 and 0.477 for the strong OH···N hydrogen bond and 0.726 and 0.502 for the weak bifurcated OH···O hydrogen bond. The second set is closer to the theoretical ratios (0.728 and 0.529) because such an oscillator most closely resembles a Morse oscillator. In the more strongly hydrogen bonded-case, the presence of the Y-term, which depends on the third power of the vibrational quantum number, is expected to cause substantial deviations from Morse behaviour (22).

Acknowledgements

I.M.W. thanks the Natural Sciences and Engineering Research Council of Canada for financial assistance. P.J.M. thanks the Research Corporation for a grant to purchase the cryogenic refrigerator. The authors thank Professor Richard Stanton for his help in developing the minimization program.

References

1. I.M. Walker and P.J. McCarthy. J. Phys. Chem. **93**, 2230 (1989).
2. P.J. McCarthy and I. M. Walker. Inorg. Chem. **29**, 820 (1990).
3. P.J. McCarthy and I.M. Walker. Inorg. Chem. **30**, 2772 (1991).
4. I.M. Walker and P.J. McCarthy. Can. J. Chem. **72**, 1211 (1994).
5. I.M. Walker and P.J. McCarthy. Can. J. Chem. **74**, 246 (1996).
6. I.M. Walker and P.J. McCarthy. Inorg. Chem. **31**, 4122 (1992).
7. G. Schaefer and K.F. Fischer. Z. Kristallogr. **155**, 75 (1981).
8. S.C. Abrahams, J.L. Bernstein, and R. Liminga. J. Chem. Phys. **72**, 5857 (1980).
9. Å. Kvick, R. Liminga, and S.C. Abrahams. J. Chem. Phys. **76**, 5508 (1982).
10. P.A. Thomas and E. Gomes. Acta Crystallogr. Sect. B: Struct. Sci. **B45**, 348 (1989).
11. K. Kuchitsu and Y. Morino. Bull. Chem. Soc. Jpn. **38**, 814 (1965).
12. A. Tramer and J.P. Mathieu. C. R. Hebd. Seances Acad. Sci. **249**, 392 (1959).

© 1997 NRC Canada

13. G. Brink and M. Falk. Spectrochim. Acta, **27A**, 1811 (1971).
14. O.P. Lamba and H.D. Bist. J. Phys. Chem. Solids. **44**, 445 (1983).
15. O.P. Lamba, H.D. Bist, and Y.S. Jain. Can. J. Chem. **61**, 608 (1983).
16. B. Berglund, J. Lindgren, and J. Tegenfeldt. J. Mol. Struct. **43**, 169 (1978).
17. A. Eriksson, J. De Villepin, and F. Romain. J. Mol. Struct. **140**, 19 (1986).
18. J. Schiffer. Ph.D. thesis, Princeton University, N.J. 1963.
19. D.L. Wood. J. Chem. Phys. **75**, 4809 (1981).
20. R.D. Cowan. The theory of atomic structure and spectra. University of California Press, Berkeley, Calif. 1981. pp. 468–473.
21. C. Sandorfy. *In* Top. Curr. Chem. Vol. 120. Springer-Verlag, Berlin. 1984. pp. 41–84.
22. A. Foldes and C. Sandorfy. J. Mol. Spectrosc. **20**, 262, (1966).
23. H.G. Kjaergaard, B.R. Henry, H. Wei, S. Lefebvre, T. Carrington, Jr., O.S. Mortensen, and M.L. Sage. J. Chem. Phys. **100**, 6228 (1994).
24. M.S. Child and L. Halonen. Adv. Chem. Phys. **57**, 1 (1984).
25. W.S. Benedict, N. Gailar, and E.K. Plyler. J. Chem. Phys. **24**, 1139 (1956).
26. M.G. Sceats and S.A. Rice. J. Chem. Phys. **71**, 973 (1979).

Can. J. Chem. Downloaded from www.nrcresearchpress.com by 88.146.161.215 on 09/08/12
For personal use only.

© 1997 NRC Canada

Synthesis of 2-methyl-2-[1-(3-benzoyl-4-phenyl-1,4-dihydropyridyl)]acetic acid methyl ester, acetic acid, and acetamide analogs as potential antiarthritic agents

Sammy A. Agudoawu, Sai-hay Yiu, and Edward E. Knaus

Can. J. Chem. Downloaded from www.nrcresearchpress.com by 88.146.161.215 on 09/08/12
For personal use only.

Abstract: The cuprous iodide catalyzed reaction of 2-methyl-2-[1-(3-benzoyl-4-phenylpyridinium)]acetic acid methyl ester bromide (**5**), prepared by reaction of 3-benzoylpyridine (**4**) with racemic methyl 2-bromopropionate, with phenylmagnesium chloride at −23°C afforded the 2-methyl-2-[1-(3-benzoyl-4-phenyl-1,4-dihydropyridyl)acetic acid methyl ester (**6**, 74%), which was a mixture of four diastereomers. Recrystallization of this diastereomeric mixture from diethyl ether afforded a solid product (**6a-solid**, 30%, 4*R**,2*R** and 4*S**,2*S**) and an oil product (**6b-oil**, 39%, 4*R**,2*S** and 4*S**,2*R**), each consisting of a mixture of two diastereomers that differ in relative configuration (*R** or *S**) at the 1,4-dihydropyridine C-4 position and the -*CH*(Me)CO_2Me moiety. Addition of the Grignard reagent from either of the two diastereotopically different faces of the planar pyridinium salt (**5**) gives rise to two diastereomeric products **6a-solid** and **6b-oil** in which the C-4 phenyl substituent is pseudo-axial to the boat-shaped 1,4-dihydropyridine ring. Alkaline hydrolysis, or ammonolysis, of the acetic acid methyl ester (**6**) afforded the respective acetic acid (**7**), or acetamide (**8**), derivative.

Key words: 1,4-dihydropyridines, diastereomers.

Résumé : On a préparé l'ester bromométhylique de l'acide 2-méthyl-2-[1-(3-benzoyl-4-phénylpyridinium)]acétique (**5**), en faisant réagir la 3-benzoylpyridine (**4**) avec le 2-bromopropionate de méthyle racémique. Le composé (**5**) en présence de iodure cuivreux comme catalyseur réagit avec le chlorure de phénylmagnésium à −23°C pour donner l'ester méthylique de l'acide 2-méthyl-2-[1-(3-benzoyl-4-phényl-1,4-dihydropyridyl)acétique (**6**, 74%) qui est un mélange de quatre diastéréoisomères. La recristallisation de ce mélange de diastéréoisomères dans l'éther donne un produit solide (**6a-solide**, 30%, 4*R**,2*R** et 4*S**,2*S**) et un produit huileux (**6b-huile**, 39%, 4*R**,2*S** et 4*S**,2*R**), ces deux produits étant un mélange de deux diastéréoisomères, qui diffèrent par la configuration relative (*R** ou *S**) au niveau du carbone en position 4 de la 1,4-dihydropyridine et au niveau de l'unité -*CH*(Me)CO_2Me. L'addition du réactif de Grignard sur l'une ou l'autre des faces, diastéréotypiquement différentes, du sel de pyridinium plan (**5**) donne deux produits diastéréoisomères **6a-solide** et **6b-huile** dans lesquels le substituant phényle en C-4 est pseudo-axial par rapport à la forme bateau du cycle 1,4-dihydropyridine. L'hydrolyse alcaline, ou l'ammonolyse, de l'acétate de méthyle (**6**) donne l'acide acétique (**7**) ou le dérivé acétamide (**8**) correspondant.

Mots clés : 1,4-dihydropyridines, diastéréoisomères.

[Traduit par la rédaction]

Introduction

A number of benzoylaryl or heteroaryl acetic acids (nonsteroidal anti-inflammatory drugs, NSAIDs) such as ketoprofen (**1**), tolmetin (**2**), and indomethacin (**3**) exhibit useful analgesic and anti-inflammatory activity (1). Unfortunately, NSAIDs that block arachidonate metabolism by acting as cyclooxygenase (COX) inhibitors are limited by toxicity and only provide temporary relief of pain and inflammation symptoms without any effect on the underlying disease process. New classes of anti-arthritic drugs, that act by novel mechanisms, are required to separate the potent anti-inflammatory effects from adverse effects associated with NSAID use, and to treat the disease process rather than simply relieving the symptoms associated with inflammation.

The 1,4-dihydropyridyl ring system in 2-methyl-2-[1-(3-benzoyl-4-phenyl-1,4-dihydropyridyl)]acetic acid analogs (**6–8**) has conformational and steric characteristics that are distinctly different from those present in the traditional benzoylaryl or heteroaryl acetic acids (NSAIDs, **1–3**). The 1,4-dihydropyridyl ring system is more puckered than the planar aryl(heteroaryl) ring system due to distortion at the 1,4-dihydropyridyl N-1 and C-4 positions. It has been reported, based on ab initio STO-3G calculations for 4-phenyl-3,5-dicarboxy-1,4-dihydropyridine, that a boat conformation is favored over a planar conformation, that ring distortion is greater at C-4 than at N-1, and that a pseudo-axial orientation

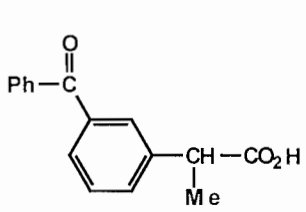
Received March 6, 1997.

S.A. Agudoawu, S.-H. Yiu,[1] and E.E. Knaus.[2] Faculty of Pharmacy and Pharmaceutical Sciences, University of Alberta, Edmonton, AB T6G 2N8, Canada.

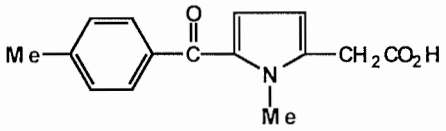
[1] Current address: Isotechnika Inc., 17208-108 Avenue, Edmonton, AB T5S 1E8.

[2] Author to whom correspondence may be addressed. Telephone: (403) 492-5993. Fax: (403) 492-1217. E-mail: eknaus@pharmacy.ualberta.ca

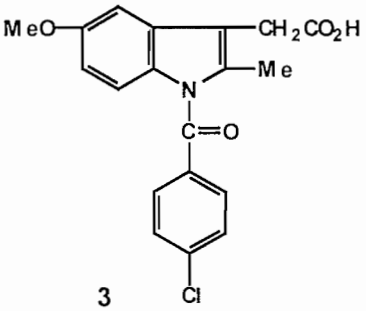
© 1997 NRC Canada



1



2



3

of the C-4 phenyl substituent is unequivocally favored (2, 3). Similar theoretical calculations also showed that 1,4-dihydronicotinamide (4) and Hantzsch 1,4-dihydropyridine calcium channel antagonists (5) exist in a boat conformation. These conformational differences, together with steric and physicochemical effects due to 1,4-dihydropyridyl N-1, C-3, and C-4 substituents, are expected to change the global size of the molecule, tissue biodistribution, and potential mechanism of action. We now report the synthesis and some structural features for a small group of 2-methyl-2-[1-(3-benzoyl-4-phenyl-1,4-dihydropyridyl)]acetic acid analogs (**6**–**8**).

Chemistry

Reaction of 3-benzoylpyridine (**4**) with racemic methyl 2-bromopropionate at reflux in acetone afforded the 2-methyl-2-[1-(3-benzoyl-4-phenylpyridinium)]acetic acid methyl ester bromide (**5**, 73%). The regiospecific copper-catalyzed reaction (6) of phenylmagnesium chloride with the pyridinium salt (**5**) yielded the 2-methyl-2-[1-(3-benzoyl-4-phenyl-1,4-dihydropyridyl)]acetic acid methyl ester (**6**, 74%) as a mixture of four diastereomers. No product resulting from reaction of the benzoyl substituent of the pyridinium salt (**5**) with the Grignard reagent was observed. This is consistent with a report that pyridinium salts are so reactive toward Grignard reagents in the presence of cuprous iodide that addition at C-4 of the pyridinium ring occurs selectively even in the presence of other reactive substituents, such as ketones, at C-3 (7). The position of other reactive groups is not important since they would not compete even at positions other than C-3. The 1,4-dihydropyridyl compound **6** is very stable to aromatization due to the electron-withdrawing effect of the 3-benzoyl group, which is conjugated with the enamine moiety (8).

2-Methyl-2-[1-(3-benzoyl-4-phenyl-1,4-dihydropyridyl)]-acetic acid methyl ester (**6**), which contains two asymmetric carbons at the dihydropyridine C-4 and α-methylacetate methine positions, could have four possible diastereomers (*SS*, *SR*, *RS*, *RR*). The ^{1}H NMR spectrum for **6** exhibited dual resonances for the 1,4-dihydropyridyl ring and ester O*Me* protons, whereas the ^{13}C NMR spectrum showed dual resonances for the dihydropyridine C-2, C-3, C-5, C-6, and ester -CH*Me* carbons. A variable-temperature ^{1}H NMR study, using DMSO as solvent, showed that no coalescence of dual resonances occurred up to a temperature of 333 K. Recrystallization of product **6** from diethyl ether afforded a solid product (**6a-solid**, 30%), and an oil product (**6b-oil**, 39%) that remained in the mother liquor. The ^{1}H NMR and ^{13}C NMR spectra for **6a-solid** and **6b-oil** did not exhibit dual resonances. The ^{1}H NMR coupling constants ($J_{4,5}$ = 4.8, $J_{5,6}$ = 7.8 Hz) were identical for **6a-solid** and **6b-oil**. ^{1}H NMR nuclear Overhauser enhancement (nOe) studies indicated that the magnitudes of the nOe effect between the 1,4-dihydropyridyl (DHP) H-4 and its neighboring protons were very similar for **6a-solid** and **6b-oil**, which suggests that the conformation of the DHP ring is similar in both compounds. Addition of the chiral shift reagent (+)-Eu(hfc)$_3$ to **6a-solid** or **6b-oil** separated the *Me*CH doublet into two doublets, and the *Me*O singlet into two singlets, respectively (see data in experimental section). This latter study suggests that **6a-solid** (4*R**,2*R** and 4*S**,2*S**) and **6b-oil** (4*R**,2*S** and 4*S**,2*R**) each consist of a mixture of two diastereomers, which differ in relative configuration (*R** or *S**) at the DHP C-4 position and the methine carbon of the -*CH*(Me)CO$_2$Me moiety. Addition of the Grignard reagent from either of the two diastereotopically different faces of the planar pyridinium salt **5** would give rise to the two diastereomeric products **6a-solid** and **6b-oil** in which the C-4 phenyl substituent is pseudo-axial to the boat-shaped 1,4-dihydropyridine ring.

Hydrolysis of the methyl ester (**6**, mixture of four diastereomers) with aqueous sodium hydroxide at 25°C for 1 h afforded the sodium acetate analog **7** (mixture of four diastereomers) in 95% yield. Ammonolysis of the methyl acetate ester (**6**, mixture of four diastereomers) yielded the acetamide derivative (**8**, mixture of four diastereomers) in 67% yield.

The pharmacological evaluation of compounds **6**–**8** as analgesic and anti-inflammatory agents is in progress and will the subject of a future report.

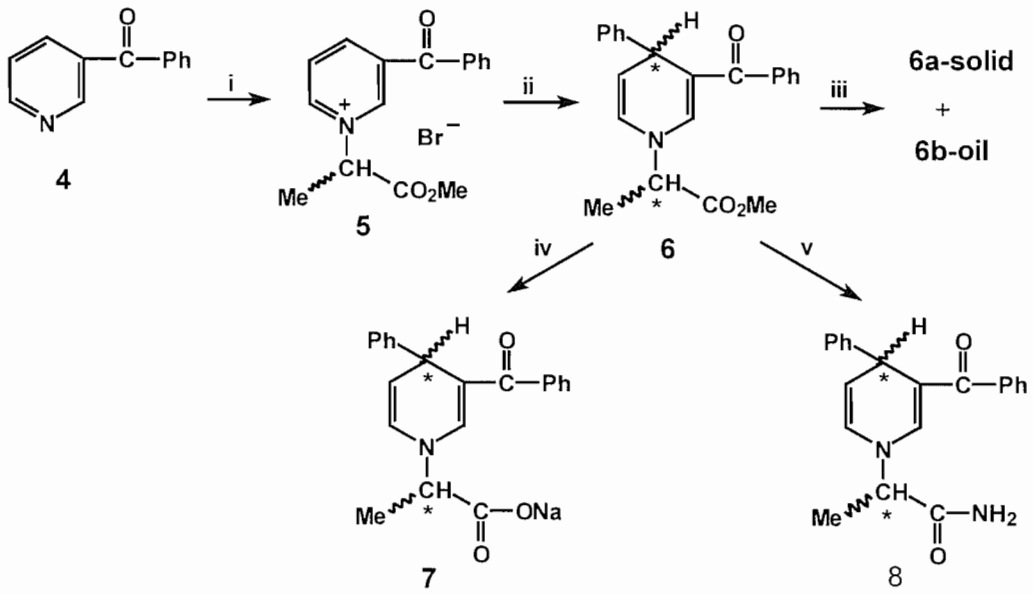
Experimental

Melting points were determined using a Thomas–Hoover capilliary apparatus and are uncorrected. Nuclear magnetic resonance spectra (^{1}H NMR, ^{13}C NMR) were recorded on a Bruker AM-300 spectrometer. The assignment of ^{1}H NMR exchangeable protons (O*H*, N*H*) was confirmed by the addition of D_2O. ^{13}C NMR spectra were acquired using the *J* modulated spin echo technique where methyl and methine carbon resonances appear as positive peaks, and methylene and quaternary carbon resonances appear as negative peaks. Infrared (IR) spectra were acquired using a Nicolet 5DX-FT spectrometer. Exact Mass measurements (HRMS) were obtained using an AEI MS-50 mass spectrometer (electron impact). Column chromatography was performed using Merck 7734 (100–200 mesh) silica gel. Preparative thin-layer chromatography (PTLC) was carried out using Camag Kieselgel DF-5 plates, 1 mm in thickness, activated at 120°C overnight prior to use.

Can. J. Chem. Downloaded from www.nrcresearchpress.com by 88.146.161.215 on 09/08/12
For personal use only.

© 1997 NRC Canada

Scheme 1.



Reagents and conditions: (i) racemic $BrCH(Me)CO_2Me$, acetone, reflux, 8 h; (ii) 0.1 equiv. CuI, THF, PhMgCl, −23°C; (iii) recrystallization from Et_2O; (iv) aqueous NaOH, EtOH-H_2O, 25°C, 1 h; (v) NH_3, MeOH, 25°C, 48 h.

Can. J. Chem. Downloaded from www.nrcresearchpress.com by 88.146.161.215 on 09/08/12
For personal use only.

Tetrahydrofuran (THF) was dried over sodium benzophenone and distilled just prior to use. Phenylmagnesium chloride and tris[3-heptafluoropropylhydroxymethylene)-(+)-camphorato]-europium(III) [(+)-Eu(hfc)$_3$] were purchased from the Aldrich Chemical Co.

2-Methyl-2-[1-(3-benzoyl-4-phenyl-1,4-dihydropyridyl)]acetic acid methyl ester diastereomers (6)

A solution of 3-benzoylpyridine (**4**, 2.0 g, 10.9 mmol) and racemic methyl 2-bromopropionate (2.6 g, 16.4 mmol) in anhydrous acetone (20 mL) was heated at reflux for 8 h. After cooling to 25°C, the solid was filtered and dried to give the pyridinium bromide salt (**5**, 2.8 g, 73%), which was used immediately in the subsequent reaction. A mixture of **5** (1.64 g, 4.7 mmol) and cuprous iodide (89 mg, 0.47 mmol) in dry THF (25 mL) was stirred under a nitrogen atmosphere for 5 min at −23°C (Dry Ice – CCl_4 bath), a solution of PhMgCl (6.1 mmol) in THF (3.1 mL of a 2 M solution) was added dropwise, and the reaction mixture was maintained at −23°C for 30 min prior to warming to 25°C. The reaction mixture was stirred for a further 1.5 h before quenching by addition of saturated aqueous NH_4Cl (5 mL). Removal of the solvent in vacuo gave a residue that was extracted with EtOAc (25 mL), and the EtOAc extract was washed successively with solutions of 30% NH_4OH:saturated NH_4Cl (3:1, v/v; 3 × 15 mL) and then water (3 × 15 mL). The organic phase was dried ($MgSO_4$), and the solvent was removed in vacuo to yield a brown oil that was purified by elution from a silica gel column using EtOAc–hexane (1:2, v/v) as eluent to afford a mixture of four diastereomers of **6** (1.21 g, 74%) as a yellow oil. Recrystallization of this mixture of diastereomers **6** (1.11 g) from diethyl ether afforded a white solid (**6a-solid**, 0.45 g), mp 134–135°C. Removal of the solvent from the mother liquor yielded a pale yellow oil (**6b-oil**, 0.58 g).

6a-solid: Yield, 30.1%; IR (KBr) ν: 1745 (CO_2), 1671 (CO) cm^{-1}; ^1H NMR ($CDCl_3$) δ: 7.15–7.50 (m, 10H, phenyl hydrogens), 6.95 (d, $J_{2,6}$ = 1.5 Hz, 1H, H-2), 6.02 (dd, $J_{5,6}$ = 7.8, $J_{2,6}$ = 1.5 Hz, 1H, H-6), 5.14 (dd, $J_{5,6}$ = 7.8, $J_{4,5}$ = 4.8 Hz, 1H, H-5), 4.87 (d, $J_{4,5}$ = 4.8 Hz, 1H, H-4), 4.00 (q, $J_{CH,Me}$ = 7.2 Hz, 1H, C*H*Me), 3.80 (s, 3H, O*Me*), 1.52 (d, $J_{CH,Me}$ = 7.2 Hz, 3H, CH*Me*); ^{13}C NMR ($CDCl_3$) δ: 194.55 (Ph*C*O), 171.28 (*C*O_2), 147.19 (phenyl C-1), 143.26 (C-2), 139.93 (benzoyl C-1), 130.20 (benzoyl C-4), 137.92–128.41 (other phenyl and benzoyl carbons), 126.16 (phenyl C-4), 124.49 (C-6), 113.99 (C-3), 110.53 (C-5), 60.42 (*C*HMe), 52.60 (O*C*H_3), 38.06 (C-4), 16.39 (CH*C*H_3). Anal. calcd. for $C_{22}H_{21}NO_3$: C 76.06, H 6.09, N 4.03; found: C 76.21, H 6.24, N 3.78.

6b-oil: Yield, 39%; IR (neat) ν: 1745 (CO_2), 1671 (CO) cm^{-1}; ^1H NMR ($CDCl_3$) δ: 7.14–7.52 (m, 10H, phenyl hydrogens), 6.96 (d, $J_{2,6}$ = 1.5 Hz, 1H, H-2), 5.99 (dd, $J_{5,6}$ = 7.8, $J_{2,6}$ = 1.5 Hz, 1H, H-6), 5.14 (dd, $J_{5,6}$ = 7.8, $J_{4,5}$ = 4.8 Hz, 1H, H-5), 4.88 (d, $J_{4,5}$ = 4.8 Hz, 1H, H-4), 4.00 (d, $J_{CH,Me}$ = 7.2 Hz, 1H, C*H*Me), 3.79 (s, 3H, OMe), 1.52 (d, $J_{CH,Me}$ = 7.2 Hz, 1H, CH*Me*); ^{13}C NMR ($CDCl_3$) δ: 196.66 (Ph*C*O), 171.32 (*C*O_2), 147.19 (phenyl C-1), 143.26 (C-2), 139.91 (benzoyl C-1), 130.26 (benzoyl C-4), 127.87–128.47 (other phenyl and benzoyl carbons), 126.21 (phenyl C-4), 124.71 (C-6), 113.91 (C-3), 110.65 (C-5), 60.42 (*C*HMe), 52.65 (O*C*H_3), 38.09 (C-4), 16.38 (CH*C*H_3). Exact Mass calcd. for $C_{22}H_{21}NO_3$: 347.1521; found (HRMS): 347.1521.

The interaction of products **6a-solid** and **6b-oil** (5 mg in 0.5 mL $CDCl_3$) with the chiral shift reagent [(+)-Eu(hfc)$_3$] (100 mg in 1 mL $CDCl_3$) was determined by ^1H NMR spectrome-

© 1997 NRC Canada

try. Addition of (+)-Eu(hfc)$_3$ (40 μL) to **6a-solid** separated the *Me*CH doublet at δ 1.52 into two doublets at δ 1.74 and 1.78, and the *Me*O singlet at δ 3.80 into two singlets at δ 3.97 and 4.0, respectively. A similar addition of (+)-Eu(hfc)$_3$ (40 μL) to **6b-oil** separated the *Me*CH doublet at δ 1.52 into two doublets at δ:1.74 and 1.76, and the *Me*O singlet at δ 3.79 into two singlets at δ 3.96 and 3.98, respectively.

2-Methyl-2-[1-(3-benzoyl-4-phenyl-1,4-dihydropyridyl)]acetic acid sodium diastereomers (7)

A solution of aqueous sodium hydroxide (4.2 mL of 0.56 N, 2.49 mmol) was added slowly with stirring to a solution of **6** (mixture of four diastereomers, 0.91 g, 2.62 mmol) in 95% EtOH:water (26:4, v/v) (30 mL) and the reaction was allowed to proceed at 25°C for 1 h. Removal of the solvent in vacuo gave a solid residue that was washed with dry diethyl ether (3 × 25 mL), and the pale yellow solid **7** (mixture of four diastereomers) was dried in vacuo at 25°C (0.85 g, 95%); mp 95–147°C; ^{1}H NMR (DMSO-d_6) δ: 7.09–7.46 (m, 11H, phenyl hydrogens, H-2), 6.11 (dd, $J_{5,6}$ = 7.6, $J_{4,5}$ = 3.2 Hz, 1H, H-6), 4.88–4.95 (m, 1H, H-5), 4.63–4.68 (m, 1H, H-4), 3.64–3.72 (m, 1H, C*H*Me), 1.22–1.27 (m, 3H, CH*Me*). The product **7** was characterized as the methyl ester **6**, which was prepared using the following procedure: An aliquot of product **7** (3 mg) was dissolved in methanol (2 mL), the pH of the solution was adjusted to 3 using HCl gas, and a solution of excess diazomethane in methanol was added at 25°C with stirring. When the evolution of nitrogen gas had ceased, the solvent was removed in vacuo to afford the methyl ester product **6**, in near quantitative yield, that was identical (^{1}H NMR) to the original product **6** described previously.

2-Methyl-2-[1-(3-benzoyl-4-phenyl-1,4-dihydropyridyl)]acetamide diastereomers (8)

A saturated solution of ammonia in MeOH (10 mL) was added to a solution of **6** (mixture of four diastereomers, 2.7 mmol) in MeOH (20 mL), the reaction flask was sealed with a rubber septum, and the reaction was allowed to proceed at 25°C for 48 h with stirring. Removal of the solvent in vacuo yielded a solid that was purified by preparative TLC using EtOAc–hexane (3:1, v/v) as development solvent. Extraction of the product band using EtOAc and removal of the solvent in vacuo gave **8** (mixture of four diastereomers) in 67% yield: mp 105–107°C; IR (KBr) ν: 3361 and 3301 (NH_2), 1730 (CONH), 1676 (CO) cm^{-1}; ^{1}H NMR ($CDCl_3$) δ: 7.22–7.40 (m, 10H, phenyl hydrogens), 7.02 and 7.04 (two d, $J_{2,6}$ = 1.5 Hz, 1H total, H-2), 6.14 and 5.75 (two s, 1H each, NH_2), 6.02 (dd, $J_{5,6}$ = 7.8, $J_{2,6}$ = 1.5 Hz, 1H, H-6), 5.18 (dd, $J_{5,6}$ = 7.8, $J_{4,5}$ = 4.8 Hz, 1H, H-6), 4.90 (d, $J_{4,5}$ = 4.8 Hz, 1H, H-4), 3.90 (q, J = 7.2 Hz, 1H, C*H*Me), 1.42 and 1.46 (two d, $J_{CH,Me}$ = 7.2 Hz, 3H total, CH*Me*). Exact Mass calcd. for $C_{21}H_{20}N_2O_2$: 332.1525; found (HRMS): 322.1526.

Acknowledgment

We are grateful to the Medical Research Council of Canada (Grant No. MA-13262) for financial support of this research.

References

1. R.F. Borne. *In* Principles of medicinal chemistry. 4th ed. *Edited by* W.O. Foye, T.L. Lemke, and D.A. Williams. Lea & Febiger Publishing Co., Philadelphia. 1995. pp. 535–580.
2. H.J. Hofmann and R. Cimiraglia. FEBS Lett. **241**, 38 (1988).
3. H.J. Hofmann and R. Cimiraglia. J. Mol. Struct. (Theochem), **205**, 1 (1990).
4. Y.-D. Wu and K.N. Houk. J. Org. Chem. **58**, 2043 (1993).
5. P.P. Mager, R.A. Coburn, A.J. Solo, D.J. Triggle, and H. Rothe. Drug Des. Discovery, **8**, 273 (1992).
6. D.L. Comins and A.H. Abdullah. J. Org. Chem. **47**, 4315 (1982).
7. D.L. Comins, E.D. Stroud, and J.J. Herrick. Heterocycles, **22**, 151 (1984).
8. U. Eisner and J. Kuthan. Chem. Rev. **42**, 1 (1972).

Can. J. Chem. Downloaded from www.nrcresearchpress.com by 88.146.161.215 on 09/08/12
For personal use only.

© 1997 NRC Canada

Calorimetric investigations of $Al^{3+}(aq)$, $Al(OH)_4^-(aq)$, and aluminum–citrate complexes at 298.15 K

Ching-hsien Wu, Celina Dobrogowska, Xin Zhang, and Loren G. Hepler

Abstract: We have combined results of earlier measurements leading to equilibrium constants for formation and reaction of aluminum–citrate complexes in aqueous solution at 298.15 K with results of our calorimetric measurements at this same temperature to obtain ΔH values for reactions of $Al^{3+}(aq)$ with citrate ions. Results of some of these calorimetric measurements also lead to a value of ΔH for the reaction $Al^{3+}(aq) + 4\ OH^-(aq) = Al(OH)_4^-(aq)$.

Key words: aluminum hydroxide, $Al(OH)_4^-(aq)$, thermodynamics; aluminum–citrate complexes, thermodynamics; citrate–aluminum complexes, thermodynamics; aluminum (3+, aq), thermodynamics.

Résumé : On a combiné les résultats de mesures effectuées antérieurement, conduisant à des constantes d'équilibre pour la formation et la réaction de complexes de citrate–aluminium en solutions aqueuses à 298,15 K, avec les résultats de nos mesures calorimétriques à la même température afin d'en déduire les valeurs de ΔH pour les réactions du $Al^{3+}(aq)$ avec les ions citrates. Les résultats de quelques-unes de ces mesures calorimétriques conduisent aussi à une valeur de ΔH pour la réaction : $Al^{3+}(aq) + 4\ OH^-(aq) = Al(OH)_4^-(aq)$.

Mots clés : thermodynamique, hydroxyde d'aluminium, $Al(OH)_4^-(aq)$, complexes de citrate–aluminium, aluminium(3+, aq).

[Traduit par la rédaction]

Introduction

Martin (1–4) has reviewed the biochemistry of aluminum, including some emphasis on the complexing of $Al^{3+}(aq)$ by citrate ions, which is important in the chemistry of blood and in the transport of aluminum through membranes. One of the purposes of this research has been to investigate the stoichiometry of reaction of one of the proposed aluminum–citrate complexes and also to obtain a ΔH value that can be used to calculate a corresponding ΔS° value.

There have been several equilibrium and calorimetric investigations intended to lead to the thermodynamic properties of $Al^{3+}(aq)$ and $Al(OH)_4^-(aq)$, which are of fundamental importance in the aqueous chemistry and geochemistry of aluminum. As reviewed by Hemingway and Robie (5), there are substantial differences between their recommended "best" values and those that have been reported elsewhere, such as in the useful tabulations from the US Bureau of Standards (6, 7). Another purpose of this research has been to obtain a value of ΔH for the reaction

[1] $Al^{3+}(aq) + 4\ OH^-(aq) = Al(OH)_4^-(aq)$

that can be used as part of a longer term effort to establish more reliable thermodynamic properties of $Al^{3+}(aq)$ and $Al(OH)_4^-(aq)$.

Received May 14, 1996.[1]

C.-h. Wu.[2] Science Department, LaGuardia College, City University of New York, 31-10 Thomson Avenue, Long Island City, NY 11101, U.S.A.

C. Dobrogowska, X. Zhang, and L.G. Hepler.[3] Department of Chemistry and Department of Chemical Engineering, University of Alberta, Edmonton, AB T6G 2G2, Canada.

[1] Revision received June 5, 1997.

[2] Author to whom correspondence may be addressed. Telephone: (718) 482-5763. E-mail: wuclg@cunyvm.cuny.edu

[3] Deceased June 8, 1996.

Experimental

Our calorimeter consisted of a glass Dewar vessel (360 cm^3) suspended in a brass can that was immersed in a constant temperature bath maintained at (25.00 ± 0.02)°C and held constant to ±0.001°C during each measurement. A small glass ampoule containing a solid or solution to be added to the solution in the calorimeter could be attached to the end of the stirrer and broken at an appropriate time to initiate the calorimetric reaction. The calorimeter was also fitted with a small-bore injection tube attached to a Metrohm automatic buret so that we could do titration calorimetry as in the research described here. Temperature changes in the calorimeter were measured with a thermistor (YSI 44005) combined with a resistance bridge (Guildline 9975). The calorimeter was calibrated electrically for each measurement. We have checked the accuracy of this calorimeter by way of test measurements of the enthalpy of solution of KCl, the enthalpy of solution of 4-aminopyridine in excess perchloric acid, the enthalpy of solution of THAM(cr) in excess hydrochloric acid, and the enthalpy of neutralization of THAM(aq) by hydrochloric acid. Results of all of these test measurements were in good agreement with the 'best' results from the literature (7–13).

Measurements of pH were carried out with an Accumet pH meter from Fisher Scientific and a combination glass-

© 1997 NRC Canada

Can. J. Chem. Downloaded from www.nrcresearchpress.com by 88.146.161.215 on 09/08/12
For personal use only.

Can. J. Chem. Downloaded from www.nrcresearchpress.com by 88.146.161.215 on 09/08/12
For personal use only.

reference electrode from Orion. Standard buffer solutions from Fisher were used for calibration.

Preparations and standardizations of solutions described below were all done by mass, which leads to compositions of solutions being described in terms of molalities, m (moles solute/kg of water).

Aluminum chloride hexahydrate, $AlCl_3 \cdot 6H_2O$, an ACS-certified reagent, was from Fisher Scientific. Two reagent grade (99% minimum assay) samples of sodium citrate dihydrate, $Na_3C_6H_5O_7 \cdot 2H_2O$, were from Matheson Coleman and Bell Manufacturing.

Carbonate-free sodium hydroxide solution was standardized by titration against potassium acid phthalate. Hydrochloric acid solution was then standardized by titration against the previously standardized sodium hydroxide solution.

A stock solution of aluminum chloride was prepared by dissolving aluminum chloride hexahydrate in dilute hydrochloric acid and was then standardized gravimetrically (14).

Our first calorimetric measurements were carried out to test earlier suggestions about stoichiometry of certain reactions and to establish conditions (amounts of NaOH needed) for subsequent measurements. The aluminum–citrate solutions placed in the calorimeter had initial pH = 7.00 and the stoichiometric compositions were Σ[Al] = 0.04303 m and Σ[citrate] = 0.1604 m. The experimental procedure involved relatively small incremental additions of NaOH solution to the aluminum–citrate solution in the calorimeter, with the enthalpy change associated with each addition being measured. This procedure of incremental addition of NaOH solution was continued for two additions after no more enthalpy of reaction was detectable.

To prepare solutions for our principal calorimetric measurements, we added known amounts of standardized hydrochloric acid to two aluminum–citrate solutions (prepared as described above) to obtain solutions having measured pH = 2.36. Stoichiometric compositions of these solutions were Σ[Al] = 7.769×10^{-3} m and Σ[citrate] = 7.985×10^{-3} m. Calorimetric measurements (duplicate runs) involved measuring the enthalpy change associated with adding an increment of standardized NaOH solution to the aluminum–citrate solution (pH = 2.36) in the calorimeter to obtain a solution having pH = 6.83. Next, without taking the calorimeter apart, we measured the enthalpy change associated with adding another increment of NaOH solution, leading to a final solution with pH = 11.8. The amounts of NaOH solution needed to achieve these changes in pH were established before doing the calorimetry by way of earlier titrations outside the calorimeter.

It should be noted that after each addition of NaOH (whether in small incremental additions or in bulk) to the aluminum–citrate solution in the calorimetric measurements, there appeared a slow drift of temperature and small pH changes after an instant, major change of temperature and pH of the solution. This observation is consistent with Ohman's finding (15) that in addition to the major aluminum–citrate species in the solution, there are other time-dependent, metastable species reaching a state of equilibrium. Since the equilibria of metastable species are much slower processes, this part of heats has been considered as a part of the temperature-drift correction in the treatment of data.

Table 1. Equilibrium constants and ΔH^0 values for ionization of aqueous citric acid and water at 298.15 K.

Reaction equation	pK^a	ΔH^0/kJ mol^{-1}
$H_3Ci(aq) = H^+(aq) + H_2Ci^-(aq)$	3.128[b]	4.17[b]
$H_2Ci^-(aq) = H^+(aq) + HCi^{2-}(aq)$	4.761[b]	2.44[b]
$HCi^{2-}(aq) = H^+(aq) + Ci^{3-}(aq)$	6.396[b]	−3.36[b]
$H_2O(liq) = H^+(aq) + OH^-(aq)$	13.999[c]	55.82[c]

[a] pK = −log K.
[b] Reference 16.
[c] Reference 17.

Results and calculations

Analysis of the results of our calorimetric results requires auxiliary information as follows.

Bates and Pinching (16) have reported pK values for all three ionizations of aqueous citric acid at 5° intervals over the range 0–50°C. Although there are good reasons for assigning large uncertainties to many ΔH^0 values derived from the temperature dependence of equilibrium constants, the pK values from Bates and Pinching are sufficiently accurate that their derived ΔH^0 values are also quite accurate. We have used results from Bates and Pinching, as summarized in Table 1.

Analysis of results of our calorimetric measurements has also required use of the accurately known (17) enthalpy of ionization of water, as given in Table 1.

Martin (2) has reviewed reported equilibria and corresponding equilibrium constants for the aluminum–citrate system, with his choices of most probable equilibria and equilibrium constants being largely based on the results that have been reported by Motekaitis and Martell (18). The conclusions based on Martin's analysis that are important for us are the following, where we follow usual practice in representing citric acid by H_3L. The principal aluminum species in our solutions at pH = 2.4 is $Al^{3+}(aq)$, the principal species at pH = 6.8 is traditionally represented by $(AlLH_{-1})^-(aq)$, and the principal species at pH > 9 is $Al(OH)_4^-(aq)$. We return later to explanation of what is meant by $(AlLH_{-1})^-$. Equations to represent the equilibria and corresponding equilibrium constants (from Martin) that are important for our solutions having pH = 6.8 are the following:

[2] $Al^{3+}(aq) + L^{3-}(aq) = AlL(aq)$ $\quad K_2 = 1.0 \times 10^8$

[3] $AlL(aq) = (AlLH_{-1})^-(aq) + H^+(aq)$ $\quad K_3 = 4.0 \times 10^{-4}$

Because the species represented by $(AlLH_{-1})^-$ is the principal aluminum–containing species at pH = 6.8, we combine eqs. [2] and [3] to obtain

[4] $Al^{3+}(aq) + L^{3-}(aq) = (AlLH_{-1})^-(aq) + H^+(aq)$ $\quad K_4 = 4.0 \times 10^4$

Before going on to use our calorimetric results for evaluation of ΔH_4, we consider the composition of the species represented by $(AlLH_{-1})^-$. The experimental results obtained by Motekaitis and Martell (18) showed that an important species is obtained by removal of H^+ from the electrically neutral species that is represented by AlL, but their results could not

© 1997 NRC Canada

provide structural information about AlL nor specify which hydrogen atom was lost as H^+. It was therefore reasonable to avoid this uncertainty by representing the negatively charged species as above, where H_{-1} indicates that one hydrogen has been removed. More recently, Martin (2) summarized evidence leading to the suggestion that the structure of the electrically neutral complex represented by AlL involves an Al^{3+} ion bound to the two end COO^- groups and the middle CO^- derived from citric acid. According to this picture, it might be best to represent citric acid by H_3LOH, which leads us to rewrite eq. [4] as follows:

[4*] $Al^{3+}(aq) + HOL^{3-}(aq) = AlLO^-(aq) + H^+(aq)$ $\quad K_4 = K_{4*}$

Although Martin (2) has summarized reasonable evidence (not proof) for the representation summarized above, there is another possible representation. It is well known that the aqueous aluminum ion "hydrolyzes" as often represented by

[5] $Al^{3+}(aq) + H_2O = AlOH^{2+}(aq) + H^+(aq)$

or, more realistically, by

[6] $Al^{3+}(H_2O)_n = [Al(OH)(H_2O)_{n-1}]^{2+} + H^+(aq)$

It is known that $\log K_5 = \log K_6 \approx -5$. We do not know of any report of a value of pK_4 for citric acid, but our electrochemical measurements (pH titration at high pH) show that pK_4 is at least as large as 14. It is therefore possible that the species represented by AlL involves bonding of Al^{3+} to three COO^- groups (in accord with the "ordinary" ionization of citric acid) and that the loss of H^+ from AlL is from a molecule of water bound to the aluminum ion. This picture leads to writing eq. [4] as

[4#] $Al(H_2O)^{3+}(aq) + L^{3-}(aq) = Al(OH)L^-(aq) + H^+(aq)$

in which we have included only one of the unknown number of molecules of water that are associated with aluminum in solution.

The equilibrium constant and the ΔH for the reaction being discussed do not depend on whether we choose to represent the reaction by eq. [4], [4*], or [4#]. This kind of choice cannot be made on the basis of thermodynamics. On the other hand, as will be shown, our calorimetric results do support the evidence from Motekaitis and Martell (18) that there is an aluminum–citrate species of the charge type specified in eq. [4], [4*], or [4#].

Two separate calorimetric measurements were made to obtain the enthalpy change associated with adding a known amount of sodium hydroxide solution to a known amount of solution of aluminum chloride, sodium citrate, and hydrochloric acid having pH = 2.36 to obtain a final solution having pH = 6.83. 'Correction' of the measured enthalpy change for reaction of $OH^-(aq)$ with $H^+(aq)$ and citric acid (using information in Table 1) and division by the number of moles of aluminum led to $\Delta H_4 = 42.6$ and 40.5 kJ mol^{-1} and thence to an average $\Delta H_4 = 41.6$ kJ mol^{-1}.

We combine this $\Delta H_4 = 41.6$ kJ mol^{-1} (ignoring the difference between ΔH and ΔH^o) with $\Delta G_4{}^0 = -26.3$ kJ mol^{-1} (calculated as $\Delta G^0 = -RT \ln K$) to obtain $\Delta S_4{}^0 = 228$ J K^{-1} mol^{-1}. Useful tests of the reality of chemical representation are often provided by comparing a ΔS^0 value obtained as above with whatever estimate of $\Delta S_4{}^0$ can be made on the basis of reliably known ΔS^0 values for more or less similar reactions. In this case, all that we can predict reliably is that the $\Delta S_4{}^0$ value is expected to be large and positive because the reaction represented by eq. [4] involves two highly charged species (+3 and −3) reacting to yield two less highly charged species (+1 and −1). This qualitative prediction of a large positive value is in accord with our $\Delta S_4{}^0 = 228$ J K^{-1} mol^{-1}.

As explained in the experimental section, our calorimetric procedure involved adding enough NaOH solution to the aluminum–citrate solution in the calorimeter to obtain a solution with pH = 6.83. The results of two separate calorimetric measurements of this kind have led to the $\Delta H_4 = 41.6$ kJ mol^{-1} cited above. Next, without taking the calorimeter apart or removing any solution, we added more NaOH solution to each of these solutions with pH = 6.83 to obtain final solutions with pH = 11.8. Equations to represent this latter reaction in the calorimeter are the following:

[5] $(AlLH_{-1})^-(aq) + 3\ OH^-(aq) + H_2O = Al(OH)_4{}^-(aq) + L^{3-}(aq)$

[5*] $AlLO^-(aq) + 3\ OH^-(aq) + H_2O = Al(OH)_4{}^-(aq) + HOL^{3-}(aq)$

[5#] $Al(OH)L^-(aq) + 3\ OH^-(aq) = Al(OH)_4{}^-(aq) + L^{3-}(aq)$

Because each of these equations is merely a different way of representing the same reaction, we have only one enthalpy of reaction, which we label ΔH_5. Our two independent measurements led to $\Delta H_5 = -28.8$ and -29.5 kJ mol^{-1}. We use the average $\Delta H_5 = -29.2$ kJ mol^{-1} for further calculations.

Reaction equations [5], [5*], and [5#] all indicate that only three $OH^-(aq)$ are required to form $Al(OH)_4{}^-(aq)$ from the aluminum–citrate complex that has charge −1. This (possibly surprising) indication that is based on appropriate balancing of reaction equations has been confirmed directly by the calorimetric measurements (small incremental titrations, as described in the seventh paragraph of the Experimental section), which showed clearly that the reaction to form $Al(OH)_4{}^-(aq)$ was complete after only three moles of hydroxide had been added for every mole of aluminum in the solution. The calorimetric results therefore provide support for the conclusion of Motekaitis and Martell (18) that the principal species at pH = 6.8 is the aluminum–citrate complex that was originally represented by $(AlLH_{-1})^-$, which can also be represented by $AlLO^-$ or by $Al(OH)L^-$.

The sum of the reactions represented by eqs. [4] and [5] with $H^+(aq) + OH^-(aq) = H_2O$ gives the reaction of $Al^{3+}(aq)$ with 4 $OH^-(aq)$ to form $Al(OH)_4{}^-(aq)$ as in eq. [1]. Similarly, we may add eq. {[4*] + [5*]} or {[4#] + [5#]} with $H^+(aq) + OH^-(aq) = H_2O$ to obtain eq. [1] for formation of $Al(OH)_4{}^-(aq)$ from $Al^{3+}(aq)$. It follows that

[7] $\Delta H_1 = \Delta H_4 + \Delta H_5 - \Delta H_w$

in which ΔH_w represents the enthalpy of ionization of water (Table 1). In this fashion we obtain $\Delta H_1 = 41.6 - 29.2 - 55.8 = -43.4$ kJ mol^{-1}.

In Table 2 we list some standard enthalpies of formation ($\Delta_f H^0$) of $Al^{3+}(aq)$ and $Al(OH)_4{}^-(aq)$ as taken from several

© 1997 NRC Canada

Can. J. Chem. Downloaded from www.nrcresearchpress.com by 88.146.161.215 on 09/08/12
For personal use only.

Table 2. Standard enthalpies of formation ($\Delta_f H^0$) of $Al^{3+}(aq)$ and $Al(OH)_4^-(aq)$ at 298.15 K.

$\Delta_f H^0$ of $Al^{3+}(aq)$/kJ mol^{-1}	$\Delta_f H^0$ of $Al(OH)_4^-(aq)$/kJ mol^{-1}
−524.7[a]	−1486.3[b]
−531[c]	−1502.6[d]
−538.25[e]	−1496.1[f]
	−1502.8[g]
	−1503.65[h]

[a]Reference 6.
[b]Reference 6 lists $\Delta_f H^0$ = −218.6 kcal mol^{-1} for $AlO_2^-(aq)$, which is equivalent to −1486.3 kJ mol^{-1} for $Al(OH)_4^-(aq)$.
[c]Reference 7.
[d]Reference 7 lists $\Delta_f H^0$ = −930.9 kJ mol^{-1} for $AlO_2^-(aq)$, which is equivalent to −1502.6 kJ mol^{-1} for $Al(OH)_4^-(aq)$.
[e]Reference 21.
[f]From Apps, cited in ref. 19.
[g]Reference 20.
[h]Reference 22.

sources. Combination of these values with $\Delta_f H^0 = -229.994$ kJ mol^{-1} for $OH^-(aq)$ from ref. 7 leads to calculated values of ΔH_1 that range from −35 to −58 kJ mol^{-1}, whereas we have found $\Delta H_1 = -43.4$ kJ mol^{-1}, with uncertainty that we estimate (considering enthalpies of dilution that we have ignored and the probable uncertainties in our calorimetric results) to be ±2 kJ mol^{-1}. If we use the recent values reported by Chen that $\Delta_f H^0 = -538.25$ kJ mol^{-1} for $Al^{3+}(aq)$ (21) and $\Delta_f H^0 = -1503.65$ kJ mol^{-1} for $Al(OH)_4^-(aq)$ (22), and combine them with $\Delta_f H^0 = -229.994$ kJ mol^{-1} for $OH^-(aq)$ from ref. 7, ΔH_1 would be −45.4 kJ mol^{-1}. This value is in good agreement with our $\Delta H_1 = -43.4$ kJ mol^{-1}, given the uncertainty inherent to our indirect and unconventional method. Pinning down the "best" $\Delta_f H^0$ values for $Al^{3+}(aq)$ and $Al(OH)_4^-(aq)$ requires complicated considerations of our value for ΔH_1 along with the thermodynamic properties of $Al(OH)_3$(gibbsite) and several other compounds of aluminum, which must be a subject for further research.

Acknowledgment

We thank the Natural Sciences and Engineering Research Council of Canada for support of this research.

A special note

Many of us in this field of chemistry have experienced a deep sense of sorrow since Dr. Loren G. Hepler passed away on June 8, 1996.

References

1. R.B. Martin. Clin. Chem. (Washington, D.C.), **32**, 1797 (1986).
2. R.B Martin. J. Inorg. Biochem. **28**, 181 (1986).
3. T.L. MacDonald and R.B. Martin. Trends Biochem. Sci. **13**, 12 (1988).
4. R.B. Martin. *In* Bioinorganic chemistry of aluminum. Vol. 24. *Edited by* H. Sigel. Marcel Dekker, Inc., New York. 1988. Chap. 1.
5. B.S. Hemingway and R.A. Robie. Geochim. Cosmochim. Acta, **42**, 1533 (1978).
6. F.D. Rossini, D.D. Wagman, W.H. Evans, S. Levine, and I. Jaffe. U.S. Natl. Bur. Stand. Circ. 500 (1952).
7. D.D. Wagman, W.H. Evans, V.B. Parker, R.H. Schumm, I. Halow, S.M. Bailey, K.L. Churney, and R.L. Nuttall. J. Phys. Chem. Ref. Data, Suppl. **11**, No. 2, 1 (1982).
8. T.E. Burchfield and L.G. Hepler. J. Chem. Thermodyn. **13**, 513 (1981).
9. M.J. Akello, M.I. Paz-Andrade, and G. Pilcher. J. Chem. Thermodyn. **15**, 949 (1983).
10. J.O. Hill, G. Ojelund, and I. Wadso. J. Chem. Thermodyn. **1**, 111 (1969).
11. L.D. Hansen and E.A. Lewis. J. Chem. Thermodyn. **3**, 35 (1971).
12. A.P. Brunetti, E.J. Prosen, and R.N. Goldberg. J. Res. Natl. Bur. Stand. Sect. A. **77A**, 599 (1973).
13. R.B. Ahmad, J.O. Hill, and R.J. Magee. Thermochim. Acta, **71**, 25 (1983).
14. A. Vogel. Textbook of quantitative inorganic analysis. 4th ed. *Revised by* J. Bassett, R.C. Denny, G.H. Jeffrey, and J. Mendham. Longman, New York. 1978.
15. L.-O. Ohman. Inorg. Chem. **27**, 2565 (1988).
16. R.G. Bates and G.D. Pinching. J. Am. Chem. Soc. **71**, 1274 (1949).
17. G. Olofsson and L.G. Hepler. J. Solution Chem. **4**, 127 (1975).
18. R.J. Motekaitis and A.E. Martell. Inorg. Chem. **23**, 18 (1984).
19. J.K. Hovey, L.G. Hepler, and P.R. Tremaine. J. Phys. Chem. **92**, 1323 (1988).
20. Q. Chen, Y. Xu, and L.G. Hepler. Can. J. Chem. **69**, 1685 (1991).
21. Q. Chen and W. Zeng. J. Cent. South Univ. Technol. (Engl. Ed.), **2**, 7 (1995).
22. Q. Chen and W. Zeng. J. Cent. South Univ. Technol. (Engl. Ed.), **1**, 7 (1994).

Can. J. Chem. Downloaded from www.nrcresearchpress.com by 88.146.161.215 on 09/08/12
For personal use only.

© 1997 NRC Canada

Rate constants for the reaction of the hydrogen atom with aliphatic ketones in water[1]

Stephen P. Mezyk, Annett Lossack, and David M. Bartels

Abstract: Arrhenius parameters for the reaction of hydrogen atoms with 3-methyl-2-butanone, 3-pentanone, cyclopentanone, 4-methyl-2-pentanone, and 2-butanone in aqueous solution have been directly calculated from electron paramagnetic resonance free induction decay (FID) attenuation measurements. For these compounds, absolute scavenging rate constants at 25.0°C of $(8.84 \pm 0.26) \times 10^7$, $(4.20 \pm 0.15) \times 10^7$, $(4.91 \pm 0.28) \times 10^7$, $(3.25 \pm 0.27) \times 10^7$, and $(2.20 \pm 0.32) \times 10^7$ dm^3 mol^{-1} s^{-1}, with corresponding activation energies of 17.43 ± 0.29, 20.69 ± 0.31, 18.73 ± 0.36, 22.24 ± 0.80, and 22.30 ± 1.04 kJ mol^{-1} were determined, respectively. Competition kinetic measurements based on total H_2 yields have established that for all of these ketones the dominant hydrogen atom reaction path is by $^{\cdot}$H atom abstraction. The new activation energy for 2-butanone is much lower than the previously reported value of 40.1 ± 0.7 kJ mol^{-1} with this difference attributed to interfering reactions from the added bromide previously used as a hydroxyl radical scavenger.

Key words: Arrhenius, kinetics, hydrogen atom, aqueous, ketones.

Résumé : En se basant sur des mesures d'atténuation de la décroissance de l'induction libre («FID») en résonance paramagnétique électronique, on a calculé directement les paramètres d'Arrhenius pour les réactions des atomes d'hydrogène avec les 3-méthylbutan-2-one, pentan-3-one, 4-méthylpentan-2-one et butan-2-one en solution aqueuse. Pour ces composés, on a déterminé que les constantes absolues de vitesse de piégeage, à 25°C, sont respectivement : $(8{,}84 \pm 0{,}26) \times 10^7$, $(4{,}20 \pm 0{,}15) \times 10^7$, $(4{,}91 \pm 0{,}28) \times 10^7$, $(3{,}25 \pm 0{,}27) \times 10^7$ et $(2{,}20 \pm 0{,}32) \times 10^7$ dm^3 mol^{-1} s^{-1}; ceci correspond à des énergies d'activation de 17,43 ± 0,29, 20,69 ± 0,31, 18,73 ± 0,36, 22,24 ± 0,80 et 22,30 ± 1,04 kJ mol^{-1} respectivement. Des mesures cinétiques en compétition basées sur les rendements globaux de H_2 ont permis d'établir que, pour chacune de ces cétones, la voie principale de réaction de l'atome d'hydrogène implique un enlèvement d'atome d'hydrogène. La nouvelle énergie d'activation pour la butan-2-one est beaucoup plus faible que la valeur de 40,1 ± 0,7 kJ mol^{-1} mesurée antérieurement; on attribue cette différence à des réactions d'interférence de la part du brome ajouté comme piège à radical dans le travail antérieur.

Mots clés : Arrhenius, cinétique, atome d'hydrogène, aqueux, cétones.

[Traduit par la rédaction]

Introduction

In a recent study (1), Arrhenius parameters for hydrogen atom reaction with acetone and 2-butanone in aqueous solution were determined. This work was part of a continuing investigation into the mechanisms of volatile iodine-species formation following a severe loss-of-coolant nuclear accident, a scenario of major concern to the nuclear reactor industry because radioactive iodine is one of the most hazardous fission products that could be released to the environment (2). Although the initial release of radioactive iodine into a containment building should be in the nonvolatile iodide form (3, 4), the presence of high radiation fields and elevated temperatures enhances the formation of volatile species such as low molecular weight iodoalkanes (5).

It has been demonstrated that one of the major sources of organics within containment arises from the leaching of paint solvents from the walls inside the building (6). This can give aqueous organic concentrations in the millimolar range. To understand iodoalkane formation under such conditions, a systematic program (7) utilizing steady-state radiolysis of the prototypical organic paint solvent 2-butanone in aqueous solution was undertaken. This and other related work (8) has shown that a large number of product species are produced, and a complete understanding of the process can only be obtained by detailed computer modeling. Such modeling is dependent on having rate constant data for the aqueous radiolysis species reaction with 2-butanone and its subsequent degradation products.

As few hydrogen atom rate constants for these reactions were available in the literature (9, 10), rates were determined for $^{\cdot}$H atom reaction with 2-butanone, propanal, acetone, and

Received March 24, 1997.

S.P. Mezyk.[2] Research Chemistry Branch, Atomic Energy of Canada Ltd. (AECL) – Whiteshell Laboratories, Pinawa, MB R0E 1L0, Canada.
A. Lossack[3] **and D.M. Bartels.** Chemistry Division, Argonne National Laboratory, Argonne, IL 60439, U.S.A.

[1] Work at Argonne performed under the auspices of the Office of Basic Energy Sciences, Division of Chemical Science, US-DOE, under contract W-31-109-ENG-38.
[2] Author to whom correspondence may be addressed. Telephone: (204) 753-2311, ext. 2340. Fax: (204) 753-2455. E-mail: MezykS@aecl.ca
[3] Permanent address: Institute for Physical Chemistry, University of Stuttgart, Stuttgart, Germany.

© 1997 NRC Canada

Can. J. Chem. Downloaded from www.nrcresearchpress.com by 91.121.58.235 on 09/08/12
For personal use only.

Can. J. Chem. Downloaded from www.nrcresearchpress.com by 91.121.58.235 on 09/08/12
For personal use only.

butyraldehyde as a function of temperature (1). The reactions with the ketones 2-butanone and acetone were characterized by activation energies of 40.1 and 30.7 kJ mol^{-1}, respectively. From previous direct measurements of the H_2 yield produced in the steady-state irradiation of acidic acetone solutions (11), it was shown that the hydrogen atom reaction pathways

[1] $^{\cdot}H + CH_3COCH_3 \rightarrow H_2 + {}^{\cdot}CH_2COCH_3$

[2] $^{\cdot}H + CH_3COCH_3 \rightarrow CH_3CO{}^{\cdot}HCH_3$

have a branching ratio of 2.0:1. For 2-butanone it was shown that the hydrogen atom reaction is almost quantitative abstraction (1).

The higher activation energy for hydrogen atom reaction with 2-butanone was very surprising, especially since the reaction is also much faster than with acetone. Hydrogen atom abstraction from 2-butanone is expected to occur at the methylene group, and based on the order of the gas phase activation energies for $^{\cdot}H$ atom abstraction from these two compounds (12), and on the fact that the methylene group C—H bond is weaker and the secondary carbon radical has greater stability (13), one expects a lower activation energy than for acetone.

To explain this experimental result, the higher activation energy for 2-butanone was attributed to a specific effect of solvation that provided a large degree of entropic compensation for the higher energy abstraction process. Two possible concerted reactions were postulated: either that abstraction at the methylene group stimulated the hydration of the carbonyl bond, which has been shown to give a positive entropy change for reaction with substituted acetones (14), or that reaction with 2-butanone occurred by abstraction from the terminal methyl group that was aided by a simultaneous keto–enol conversion involving a water molecule within the solvation shell to transform the terminal methyl groups into allylic positions, with much weaker C—H bonds (12, 15). Subsequent to publication of ref. 1, direct time-resolved EPR observation of the product showed it to be the expected radical at the methylene carbon.[4]

To obtain further insight into this reaction, and to establish whether 2-butanone can be used as a prototypical ketone for applied modeling studies, further hydrogen atom reaction experiments have been performed using the ketones 3-methyl-2-butanone (methyl isopropyl ketone), 3-pentanone (diethyl ketone), cyclopentanone, and 4-methyl-2-pentanone (methyl isobutyl ketone) in aqueous solution. These compounds were chosen to characterize the influence of position and number of methylene groups on the activation energy. Because of its great specificity, direct EPR detection of the decay of the $^{\cdot}H$ atom following electron pulse radiolysis was again used in this study (16, 17); the pulsed EPR-based free induction decay (FID) attenuation method (18–23) is particularly advantageous for these measurements because of the simple pseudo-first-order kinetics obtained.

Experimental

The experimental procedure for determining $^{\cdot}H$ atom reaction rate constants using this technique has been described in detail in several previous publications (18–21), and thus only a short description will be given here. Hydrogen atoms were generated in aqueous solution using 3 MeV electrons from a Van de Graaff accelerator. A microwave probe pulse was applied to the sample immediately after irradiation, and the resulting free induction decay of the $^{\cdot}H$ atom low-field EPR transition was recorded on a digital oscilloscope. Typically, 500–2000 pulses were averaged to measure each FID trace, at a repetition rate of 120 Hz.

All measurements were performed in acidic solution, to increase the initial yield of hydrogen atoms. Stock acid solutions (pH 1.0 and 2.0) were prepared by addition of $HClO_4$ (Mallinkrodt, A. R. Grade, 69.05%) to Millipore filtered water. Actual acid concentrations were determined by standardization of the concentrated acid against 1.029 N HCl (Aldrich, Volumetric Standard). A total aqueous sample of ~190 mL was recirculated through a flat cell within an EPR cavity, at a rate sufficient to ensure that each cell volume was replaced between pulses (the actual volume irradiated in each pulse was less than 0.1 mL).

Scavenging experiments were performed by the successive injection of known volumes of the ketone to the initial known volume of solution that had been fully deoxygenated by bubbling with argon. All of the ketones used in this study were from Aldrich, of the highest purity available, and used as received. Accuracy of the concentrations is estimated at better than 3%.

In the previous ketone experiments using this technique (1), it was observed that the measured scavenging rate constants were slightly dependent on the radiation dose used. This phenomenon was also found in the present study, as shown in Fig. 1*a* for hydrogen atom reaction with 3-methyl-2-butanone at 24.0°C. The general expression of the effective damping rate of the FID in these experiments is given by (18–21)

$$[3] \quad \frac{1}{T_2(\text{eff})} = \frac{1}{T_2^0} + k_s[S] + \Sigma k_{ex}^i[R_i]$$

where $k_s[S]$ is the $^{\cdot}H$ atom scavenging rate and $\Sigma k_{ex}^i[R_i]$ represents the spin-dephasing contribution of the second-order spin exchange and recombination reactions between $^{\cdot}H$ atoms and other free radicals. The latter term in eq. [3] is responsible for the shift in the intercept seen in Fig. 1*a*, as the total free radical concentration $\Sigma[R_i]$ increases. The scavenging reaction converts the hydrogen atoms into other free radicals, and the corresponding change in k_{ex}^i during the 5 μs experimental time period is responsible for the small change in the slopes. The systematic error due to this second-order chemistry can be avoided either by working with a very small $^{\cdot}H$ atom concentration, or by extrapolation to a "zero dose" limit.

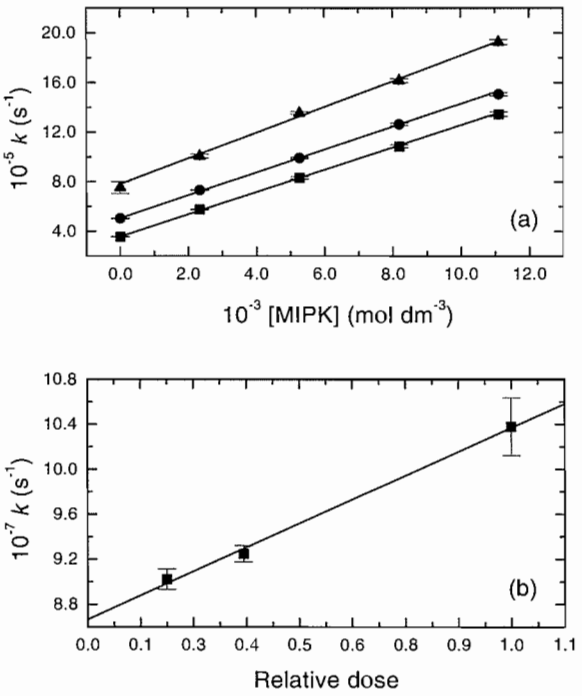
The technique used in this study was extrapolation to zero dose. The actual rate constants for hydrogen atom reaction with 3-methyl-2-butanone at this temperature, obtained from the second-order slopes of the data shown in Fig. 1*a*, were $(9.02 \pm 0.09) \times 10^7$, $(9.25 \pm 0.07) \times 10^7$, and $(1.04 \pm 0.03) \times 10^8$ dm^3 mol^{-1} s^{-1} for the 12, 25, and 55 ns pulse widths, respectively. These pulses corresponded to relative doses of 3.0, 5.9, and 16.0, where an absolute dose of approximately 3.0 krad/pulse was estimated for the 25 ns width. The relative values were simply the measurements of the average beam current on a shutter positioned before the irradiation cell, and

[4] D.M. Bartels, unpublished data.

© 1997 NRC Canada

Can. J. Chem. Downloaded from www.nrcresearchpress.com by 91.121.58.235 on 09/08/12
For personal use only.

Fig. 1. (*a*) Dose dependence of the hydrogen atom scavenging rate constants for methyl isopropyl ketone (MIPK) at pH 2.0 and 24.0°C. Solid lines correspond to fitted values of $(9.02 \pm 0.09) \times 10^7$ (■), $(9.25 \pm 0.07) \times 10^7$ (●), and $(1.04 \pm 0.03) \times 10^8$ (▲) dm^3 mol^{-1} s^{-1} for Van de Graaff pulse widths of 12, 25, and 55 ns, respectively. (*b*) Rate constant extrapolation to "zero dose" for methyl isopropyl ketone at pH 2.0 and 24.0°C, to give a limiting value of $k = (8.67 \pm 0.06) \times 10^7$ dm^3 mol^{-1} s^{-1}. Error bars correspond to one standard deviation obtained from weighted linear fit to scavenging plots.



were assumed to be proportional to the actual dose given to the sample. The beam current was monitored frequently to allow for any slight drift.

The extrapolation of these dose-dependent rate constants to zero dose is shown in Fig. 1*b*. A very good linear relationship is obtained, with a limiting, zero-dose, rate constant of $(8.67 \pm 0.06) \times 10^7$ dm^3 mol^{-1} s^{-1}. This behavior was consistent for all of the systems of this study.

For some of the highest temperatures investigated, where ketone concentrations were smallest, scavenging rate constants were obtained only using the 25 ns pulse. Values measured using the 12 ns pulse width under these conditions were extremely noisy and not reproducible, while those measured using the 55 ns pulse showed effects attributable to substrate depletion. For these single dose points the measured value with the 25 ns pulse was "corrected" to zero dose by multiplying by the average ratio of the extrapolated and 25 ns measured rate constants determined at lower temperatures. Larger error bars were included on these points, to allow for the inherent lack of precision in this extrapolation method.

Total hydrogen yield measurements were also performed for these ketones to determine the fractions of addition and abstraction for hydrogen atom reaction with these compounds. Stock solutions of 0.10 mol dm^{-3} $HClO_4$ containing 0.10 mol dm^{-3} methanol were saturated with argon before injecting sufficient ketone to allow equal reaction between the two organics calculated from their relative rate constants of hydrogen atom reaction at 28°C (see later). These samples were irradiated using a 10 MeV e-beam from an I-10/1 electron accelerator, with dosimetry performed using Far West Technologies radiochromic dye film.[5] The H_2 gas analyses were performed using a VG Instruments MM 8-80 magnetic sector mass spectrometer.

Results and discussion

Reaction with methyl isopropyl ketone

To obtain further insight into the possible mechanisms for hydrogen atom reaction with methyl ethyl ketone it was decided to investigate reactions with geometrically similar compounds. One of the simplest analogues of methyl ethyl ketone is methyl isopropyl ketone. The hydrogen atom reaction with this compound is expected to be abstraction of the tertiary hydrogen

[4] $^{\cdot}H + CH_3COCH(CH_3)_2 \rightarrow H_2 + CH_3COC^{\cdot}(CH_3)_2$

producing a carbon-centered radical adjacent to the carbonyl group.

From the kinetic data shown in Fig. 1, the extrapolated reaction rate constant for methyl isopropyl ketone at 24.0°C is $k_4 = (8.67 \pm 0.06) \times 10^7$ dm^3 mol^{-1} s^{-1}, about a factor of two higher than the hydrogen atom reaction with methyl ethyl ketone, $k = (3.82 \pm 0.32) \times 10^7$ dm^3 mol^{-1} s^{-1} at 25.0°C (1). Over the temperature range 8.1–80.4°C the rate constant was found to be well described by the equation

[5] $\log_{10} k_4 = (11.00 \pm 0.05) - [(17\,430 \pm 290)/2.303\,RT]$

(units of dm^3 mol^{-1} s^{-1} and K for k_4 and T, respectively), which corresponds to an activation energy of 17.43 ± 0.29 kJ mol^{-1}. This number is over a factor of two smaller than originally measured for methyl ethyl ketone (40.1 ± 0.7 kJ mol^{-1}), a difference much greater than can be attributed to the additional stability of the tertiary carbon radical product for the larger ketone. The pre-exponential factor of 1.00×10^{11} dm^3 mol^{-1} s^{-1} is also much lower than originally obtained for methyl ethyl ketone (4.4×10^{14} dm^3 mol^{-1} s^{-1}). All of the individual rate constants measured for methyl isopropyl ketone are listed in Table 1, and shown in comparison to the measured data for acetone and methyl ethyl ketone in Fig. 2.

Reaction with diethyl ketone

As the reaction of aqueous hydrogen atoms with methyl isopropyl ketone gave very different Arrhenius parameters from methyl ethyl ketone, it was decided to investigate the hydrogen atom reaction with a ketone containing intact methylene groups, using the compound diethyl ketone. The reaction anticipated here should be analogous to the methyl ethyl ketone reaction,

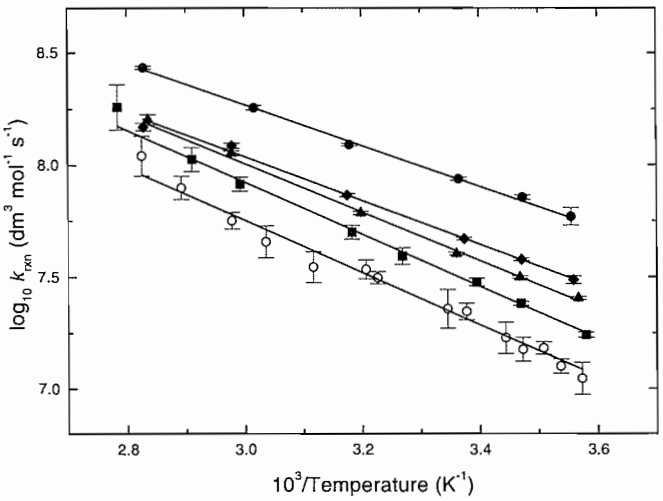
[6] $^{\cdot}H + CH_3CH_2COCH_2CH_3 \rightarrow H_2 + CH_3CH_2CO^{\cdot}CHCH_3$

[5] Far West Technology, Inc., Goleta, CA 93117, U.S.A.

© 1997 NRC Canada

Can. J. Chem. Downloaded from www.nrcresearchpress.com by 91.121.58.235 on 09/08/12
For personal use only.

Fig. 2. Arrhenius plot for methyl isopropyl ketone (●), diethyl ketone (▲), cyclopentanone (◆), and methyl isobutyl ketone (■) in comparison to the revised values for methyl ethyl ketone (○). Solid lines are fitted values of equations as given in text.



with symmetry, as well as gas phase reaction data (12), suggesting that similar Arrhenius parameters should be obtained. The EPR measurements for this compound at 24.4°C gave an extrapolated rate constant of $k_6 = (4.01 \pm 0.05) \times 10^7$ dm^3 mol^{-1} s^{-1}, which is almost identical to our original value for methyl ethyl ketone at this temperature. However, when these measurements were repeated over the range 7.1–79.4°C the overall temperature dependence was found to be well described by the equation

[7] $\log_{10} k_6 = (11.24 \pm 0.06) - [(20\,690 \pm 310)/2.303\,RT]$

(the rate constants are given in Table 1 and shown in Fig. 2). The activation energy of 20.69 ± 0.31 kJ mol^{-1} is much lower than previously obtained for methyl ethyl ketone.

Reaction with cyclopentanone

Analogous hydrogen atom reaction measurements were also undertaken with cyclopentanone

[8] $^{\cdot}H + c\text{-}(CH_2)_4CO \rightarrow H_2 + c(CH_2)_3{}^{\cdot}CHCO$

which only has methylene groups adjacent to the carbonyl bond. The extrapolated rate constant at 23.2°C was determined as $k_8 = (4.68 \pm 0.07) \times 10^7$ dm^3 mol^{-1} s^{-1} and, over the range 7.8–80.5°C, the temperature-dependent rate constants were found to be well predicted by the equation

[9] $\log_{10} k_8 = (10.97 \pm 0.06) - [(18\,730 \pm 360)/2.303\,RT]$

with individual rate constants again given in Table 1 and shown in Fig. 2. Both the activation energy of 18.73 ± 0.36 kJ mol^{-1} and the pre-exponential factor are in very good agreement with the values obtained for methyl isopropyl ketone, similar to those for diethyl ketone, and again much lower than the values originally measured for methyl ethyl ketone.

Table 1. Summary of zero-dose-extrapolated, temperature-dependent rate constants for hydrogen atom reaction with methyl isopropyl ketone, diethyl ketone, cyclopentanone, methyl isobutyl ketone, and methyl ethyl ketone in aqueous solution.

Ketone	Temperature (°C)	k_{rxn} (dm^3 mol^{-1} s^{-1})
Methyl isopropyl	8.1	$(5.88 \pm 0.55) \times 10^7$
	14.8	$(7.17 \pm 0.15) \times 10^7$
	24.0	$(8.67 \pm 0.06) \times 10^7$
	41.4	$(1.23 \pm 0.02) \times 10^8$
	58.4	$(1.80 \pm 0.04) \times 10^8$
	80.4	$(2.71 \pm 0.04) \times 10^8$
Diethyl	7.1	$(2.54 \pm 0.03) \times 10^7$
	15.2	$(3.16 \pm 0.05) \times 10^7$
	24.4	$(4.01 \pm 0.05) \times 10^7$
	39.5	$(6.10 \pm 0.10) \times 10^7$
	62.8	$(1.13 \pm 0.03) \times 10^8$
	79.4	$(1.60 \pm 0.08) \times 10^8$
Cyclopentanone	7.8	$(3.07 \pm 0.13) \times 10^7$
	14.9	$(3.79 \pm 0.05) \times 10^7$
	23.2	$(4.68 \pm 0.07) \times 10^7$
	41.8	$(7.40 \pm 0.13) \times 10^7$
	62.6	$(1.27 \pm 0.04) \times 10^8$
	80.5	$(1.48 \pm 0.06) \times 10^8$
Methyl isobutyl	6.2	$(1.74 \pm 0.05) \times 10^7$
	15.0	$(2.41 \pm 0.05) \times 10^7$
	21.4	$(3.00 \pm 0.12) \times 10^7$
	32.8	$(3.91 \pm 0.35) \times 10^7$
	41.0	$(5.00 \pm 0.37) \times 10^7$
	61.1	$(8.20 \pm 0.64) \times 10^7$
Methyl ethyl	6.7	$(1.11 \pm 0.20) \times 10^7$
	9.6	$(1.26 \pm 0.10) \times 10^7$
	11.9	$(1.52 \pm 0.10) \times 10^7$
	14.8	$(1.50 \pm 0.20) \times 10^7$
	17.2	$(1.69 \pm 0.30) \times 10^7$
	22.9	$(2.22 \pm 0.20) \times 10^7$
	25.7	$(2.28 \pm 0.50) \times 10^7$
	36.7	$(3.13 \pm 0.20) \times 10^7$
	38.7	$(3.41 \pm 0.35) \times 10^7$
	47.7	$(3.49 \pm 0.60) \times 10^7$
	56.2	$(4.53 \pm 0.80) \times 10^7$
	62.7	$(5.63 \pm 0.50) \times 10^7$
	72.6	$(7.90 \pm 1.00) \times 10^7$
	80.8	$(1.10 \pm 0.25) \times 10^8$

Reaction with methyl isobutyl ketone

The smaller Arrhenius parameter values obtained for the first three ketones in this study suggested that the presence of the α-methyl group in methyl ethyl ketone has an important role in the overall reaction mechanism. The fourth ketone investigated in this study was methyl isobutyl ketone, which incorporates the full geometry of methyl ethyl ketone,

[10] $^{\cdot}H + CH_3COCH_2CH(CH_3)_2 \rightarrow$ products

For this ketone hydrogen abstraction could occur both at the secondary and tertiary carbon hydrogens, the former pathway

© 1997 NRC Canada

Can. J. Chem. Downloaded from www.nrcresearchpress.com by 91.121.58.235 on 09/08/12
For personal use only.

being identical to the reaction with methyl ethyl ketone. Measurements performed over the temperature range 6.2–86.0°C were again found to have excellent Arrhenius behavior, and to be fitted by the equation

[11] $\log_{10} k_{10} = (11.41 \pm 0.14) - [(22\,240 \pm 800)/2.303\,RT]$

(see individual rate constant data in Fig. 2 and Table 1). This corresponds to a room temperature (22°C) value of $k_{10} = (2.98 \pm 0.25) \times 10^7$ dm^3 mol^{-1} s^{-1}, again similar to the value measured for methyl ethyl ketone. The activation energy of 22.24 ± 0.80 kJ mol^{-1} is again much lower than originally found for methyl ethyl ketone, but consistent with the other ketone measurements of this study.

Yield measurements

The ·H atom reaction with all four of the ketones measured in this study showed essentially the same Arrhenius parameters, with minor differences attributable to the slight variations in stability in the different carbon-centered radicals formed. None of these systems gave Arrhenius values close to those originally measured for methyl ethyl ketone, suggesting that the ·H atom reaction mechanism with this latter ketone is very different. One can also eliminate differences due to the direct reaction with the enol form of all of these ketones, as they all have extremely small (ca. 10^{-8}) enol fractions in aqueous solution (24). Likewise, reaction with an impurity can also be rejected.

To confirm the hydrogen atom abstraction mechanism, total H_2 gas yield measurements were also performed for these compounds. The technique used for these measurements was e-beam irradiation and mass spectrometry analysis. Preliminary tests showed that the temperature of the irradiated 100 mL aqueous samples was raised to 28°C by passage through the e-beam. Ketones were added to the methanol–acid solutions in sufficient concentration to allow the ·H atoms produced, both directly and by the reaction of the hydrated electrons with H^+, to react with the methanol and ketone in a 1.0:1.0 ratio at this temperature (1, 25). Acetone and methyl ethyl ketone were also included in these experiments to ensure the validity of the technique.

The H_2 yield from only the methanol–acid blank was found to be $G = 4.01 \pm 0.09$ (no. of molecules/100 eV). This yield corresponds to quantitative abstraction; subtracting the fundamental molecular yield of H_2 ($G = 0.41$ (26)) from this value gives $G(\cdot H) = 3.60 \pm 0.09$, which represents the yield of ·H atoms directly produced ($G \sim 0.6$) from the direct radiolysis of water and the initial yield of hydrated electrons in the presence of a high concentration of intra-spur scavenger such as 0.10 mol dm^{-3} methanol (27).

Quantitative H_2 yields for all the ketone systems were calculated relative to this methanol–acid value. Acetone was found to have $G(H_2) = 3.02 \pm 0.11$, which corresponds to an abstraction efficiency of 67.8 ± 3.7%, in excellent agreement with previous determinations of 67% (11, 28). *All* of the other ketones showed quantitative H_2 production.

Reaction with methyl ethyl ketone

As no convincing argument could be found to explain a higher activation energy for methyl ethyl ketone relative to the other ketones of this study it was decided to repeat this compound in this work. These experiments were performed as for all of the other ketones investigated in this study. For the expected reaction

[12] $\cdot H + CH_3COCH_2CH_3 \rightarrow H_2 + CH_3CO\cdot CHCH_3$

the initial measurement at 22.9°C gave a zero-dose-extrapolated value of $k_{12} = (2.22 \pm 0.20) \times 10^7$ dm^3 mol^{-1} s^{-1}, about 40% slower than previously measured at this temperature, $k = (3.82 \pm 0.32) \times 10^7$ dm^3 mol^{-1} s^{-1}. By repeating these measurements over the temperature range 6.7–80.8°C, the individual rate constants given in Table 1 and shown in Fig. 2 were obtained, and were found to be well described by the equation

[13] $\log k_{12} = (11.25 \pm 0.18) - [(22\,300 \pm 1000)/2.303\,RT]$

The activation energy, 22.3 ± 1.0 kJ mol^{-1}, and pre-exponential factor are in very good agreement with the values measured for the other ketones of this study, and much lower than previously determined.

While the newfound agreement between methyl ethyl ketone and the other ketones is gratifying, an explanation for our previous, high, Arrhenius parameters is also necessary. Given that the same bottle of methyl ethyl ketone was used in both experiments, this was not the source of the discrepancy. A close examination of original data books showed that the only difference between the two experiments was in the hydroxyl radical scavenger used; for the current experiments 0.02 mol dm^{-3} methanol was added to the system whereas previously the same concentration of bromide ion was used (9).

The reason for the original high activation energy has not been confirmed, but is believed to be due to the chemistry of bromide in an irradiation field. While the added bromide was an efficient and nonvolatile hydroxyl radical scavenger, its subsequent chemistry might produce Br_2 in solution, via reactions such as

[14] $\cdot OH + Br^- \rightarrow BrOH^{\cdot -}$

[15] $BrOH^{\cdot -} \rightarrow Br\cdot + OH^-$

[16] $Br\cdot + Br^- \rightleftharpoons Br_2^{\cdot -}$

[17] $2\,Br_2^{\cdot -} \rightleftharpoons Br_3^- + Br^-$

[18] $Br_3^- \rightleftharpoons Br^- + Br_2$

The presence of Br_2 and methyl ethyl ketone in acidic solution could allow an acid-catalyzed thermal bromination reaction to occur in the solution reservoir (13),

[19] $Br_2 + CH_3COCH_2CH_3 \xrightarrow{H^+} CH_3COCHBrCH_3 + HBr$

Reaction of the ·H atom with this brominated compound

[20] $\cdot H + CH_3COCHBrCH_3 \rightarrow HBr + CH_3CO\cdot CHCH_3$

would give an artificial increase in the scavenging rate constants measured previously. In fact, because hydrogen atom reaction with brominated compounds is nearly diffusion

© 1997 NRC Canada

Can. J. Chem. Downloaded from www.nrcresearchpress.com by 91.121.58.235 on 09/08/12
For personal use only.

controlled (9), essentially *all* subsequent ·H atom reaction might occur by reaction with this compound, not with methyl ethyl ketone. The activation energy of 40 kJ mol^{-1} previously measured would therefore correspond to the thermal reaction producing this species in the reservoir between the successive injections of the ketone. Given the routine nature of this experiment the time between injections was nearly constant and this background chemistry was missed.

A search of the literature failed to discover any experimental measurements for the thermal activation energy of the bromination process for 2-butanone under acidic conditions. One previous study (29), which looked at thermal iodonation of 2-butanone at 25.0 and 33.4°C (the 25°C rate constant for iodonation and bromination being very similar (29) in neutral solution) reported a 40% increase in the measured rate over this (admittedly small) temperature range. Assuming that solvent differences are not important (the higher temperature measurement was performed in D_2O, the lower in H_2O) then this difference corresponds to an activation energy of ca. 40 kJ mol^{-1}, consistent with our original determination.

In our previous study (1) bromide was only used in the methyl ethyl ketone and butyraldehyde measurements, and so the Arrhenius parameters reported for acetone and propanal are considered correct. The measured activation energy for butyraldehyde is very similar to that determined for propanal, and therefore it is believed that the bromide interference observed for methyl ethyl ketone is not important in the butyraldehyde experiments.

Conclusion

The temperature-dependent FID rate constant measurements of hydrogen atom reactions with methyl isopropyl ketone, diethyl ketone, cyclopentanone, and methyl isobutyl ketone in aqueous solution were found to be given by the equations

[5] $\log_{10} k_4 = (11.00 \pm 0.05) - [(17\,430 \pm 290)/2.303\,RT]$

[7] $\log_{10} k_6 = (11.24 \pm 0.06) - [(20\,690 \pm 310)/2.303\,RT]$

[9] $\log_{10} k_8 = (10.97 \pm 0.06) - [(18\,730 \pm 360)/2.303\,RT]$

[11] $\log_{10} k_{10} = (11.41 \pm 0.14) - [(22\,240 \pm 800)/2.303\,RT]$

respectively. The similarity of the activation energies and pre-exponential factors of these four ketones suggests that the model of hydrogen atom reaction is the same for all four compounds and, based on the results of H_2 yield measurements, is attributed to essentially quantitative ·H atom abstraction from these compounds. Further corroboration of this mechanism is given by the magnitude of the pre-exponential factors ($\log A$ = 11.0–11.4), these values being in the range expected for simple hydrogen atom abstraction. Upon remeasurement of the Arrhenius parameters for methyl ethyl ketone, a consistent temperature behavior described by

[13] $\log k_{12} = (11.25 \pm 0.18) - [(22\,300 \pm 1000)/2.303\,RT]$

was obtained. The original higher values are attributed to interfering background chemistry resulting from the added bromide used as a hydroxyl radical scavenger in ref. 1.

Acknowledgments

The authors would like to thank Dr. David Werst for his assistance in operating and maintaining the Van de Graaff accelerator. We would also like to thank Mr. R. MacFarlane and Mr. H.G. Delaney for performing the H_2 yield measurements and Drs. D.C. Walker and E. Roduner for helpful discussions throughout the course of this study.

References

1. S.P. Mezyk and D.M. Bartels. Can. J. Chem. **72**, 2516 (1994).
2. T.J. Thompson and J.G. Beckerley (*Editors*). The technology of nuclear reactor safety. MIT Press, Cambridge, Mass. 1973.
3. D.O. Campbell, A.P. Malinauskas, and W.R. Stratton. Nucl. Technol. **53**, 111 (1981).
4. D. Cubicciotti and B.R. Sehgal. Nucl. Technol. **65**, 266 (1984).
5. J. Paquette and B.L. Ford. Radiat. Phys. Chem. **36**, 353 (1990).
6. J.C. Wren, J.M. Ball, and C.A. Chuaqui. The chemistry of iodine in containment. CANDU Owners Group Report 94-116. In press.
7. C.A. Chuaqui and J.M. Ball. 4th Meeting, European Severe Accident Chemistry Group ENEL/CRTN, Milan, Italy, December 1992.
8. S.M.S. Akhtar, R.J. Woods, and J.A.E Bardwell. Int. J. Radiat. Phys. Chem. **7**, 603 (1975).
9. G.V. Buxton, C.L. Greenstock, W.P. Helman, and A.B. Ross. J. Phys. Chem. Ref. Data, **17**, 513 (1988).
10. M. Anbar, Farataziz, and A.B. Ross. Selected specific rates of reactions of transients from water in aqueous solution. II. Hydrogen atom. NSRDS-NBS 51, National Bureau of Standards, U.S. Department of Commerce, U.S. Government Printing Office, Washington, D.C. 1975.
11. R.A. Witter and P. Neta. J. Org. Chem. **38**, 484 (1973).
12. J.A. Kerr and M.J. Parsonage. Evaluated kinetic data on gas phase hydrogen transfer reactions of methyl radicals. Butterworths, London. 1976.
13. J. March. Advanced organic chemistry. 3rd ed. Wiley, New York. 1985.
14. R.P. Bell and A.O. McDougall. Trans. Faraday Soc. **56**, 1281 (1960).
15. J.A. Kerr. Chem. Rev. **66**, 465 (1966).
16. R.W. Fessenden and N.C. Varma. Faraday Discuss. Chem. Soc. **63**, 104 (1977).
17. D.M. Bartels, M.T. Craw, P. Han, and A.D. Trifunac. J. Phys. Chem. **93**, 2412 (1989).
18. P. Han and D.M. Bartels. Chem. Phys. Lett. **159**, 538 (1989).
19. P. Han and D.M. Bartels. J. Phys. Chem. **94**, 7294 (1990).
20. P. Han and D.M. Bartels. J. Phys. Chem. **96**, 4899 (1992).
21. E. Roduner and D.M. Bartels. Ber. Bunsen-Ges. Phys. Chem. **96**, 1037 (1992).
22. D.M. Bartels and S.P. Mezyk. J. Phys. Chem. **97**, 4101 (1993).
23. S.P. Mezyk, R.M. MacFarlane, and D.M. Bartels. J. Phys. Chem. **98**, 12594 (1994).
24. J.R. Keefe, A.J. Kresge, and N.P. Schepp. J. Am. Chem. Soc. **112**, 4862 (1990).
25. S.P. Mezyk and D.M. Bartels. J. Phys. Chem. **98**, 10578 (1994).
26. A.O. Allen. The radiation chemistry of water and aqueous solutions. Van Nostrand, Princeton, N.J. 1961.
27. J.A. LaVerne and S.M. Pimblott. J. Phys. Chem. **95**, 3196 (1991).
28. P. Neta, G.R. Holdren, and R.H. Schuler. J. Phys. Chem. **75**, 449 (1971).
29. A.C. Knipe and B.G. Cox. J. Chem. Soc. Perkin Trans. 2, 1391 (1973).

© 1997 NRC Canada

Peptide models XX. Aromatic side-chain – backbone interaction in phenylalanine-containing diamide model system. A systematic search for the identification of all the ab initio conformers of *N*-formyl-L-phenylalanine-amide

András Perczel, Ödön Farkas, Attila G. Császar, and Imre G. Csizmadia

Can. J. Chem. Downloaded from www.nrcresearchpress.com by 88.146.161.215 on 09/08/12
For personal use only.

Abstract: Phenylalanine is the simplest among the four natural amino acid residues that have aromatic side chains. The ab initio conformational analysis performed at the RHF/3-21G level on a phenylalanine-containing diamide model system (*N*-Formyl-L-Phe-NH_2) revealed 19 different structures. Single-point energy calculations were performed using RHF/6-31+G* and DFT(B3LYP)/6-311++G** levels for all conformers. The inverse (γ_L) and the normal (γ_D) gamma turn, the extended (β_L), the left-handed helical (α_D [$\phi \approx +60°$, $\psi \approx +60°$]), and the inverse polyproline II (ε_D [$\phi \approx 60°$, $\psi \approx 180°$]) backbone conformers each have three (g^+, *a*, and g^-) side-chain (χ_1) rotamers. The δ_L [$\phi \approx 240°$, $\psi \approx 60°$] and the δ_D [$\phi \approx 180°$, $\psi \approx -60°$] type main-chain conformers have only two side-chain orientations, respectively. No minima have been found for the conformational building unit of the right-handed helical (α_L [$\phi \approx -60°$, $\psi \approx -60°$]) and for the polyproline II (ε_L [$\phi \approx -60°$, $\psi \approx 180°$]) structures. The present ab initio conformational analysis for For-L-Phe-NH_2 is a unique example in which a systematic and complete conformational set was established for a diamide system with an aromatic side chain. Analytic vibrational frequency calculations were established for all stationary points found as minima on the potential energy surface. These data may be used in the future as reference conformers in more detailed vibrational and (or) chemical shielding calculations or during the structural analysis of peptides and proteins by X-ray or NMR techniques.

Key words: ab initio peptide conformers, all RHF/3-21G structures of For-L-Phe-NH_2, backbone – side-chain interaction in phenylalanine-containing peptide models.

Résumé : La phénylalanine est le plus simple des quatre acides aminés naturels comportant un noyau aromatique dans la chaîne latérale. Des calculs d'analyse conformationnelle effectués au niveau RHF/3-21G sur une phénylalanine comportant le système modèle diamide (*N*-formyl-L-Phe-NH_2) ont révélé l'existence de 19 structures différentes. On a effectué des calculs d'énergie en un seul point, aux niveaux RHF/6-31G+G* et DFT(B3LYP)/6-311++G**, pour chacun des conformères. Les squelettes des conformères à hélice gamme normale (γ_D) et inverse (γ_L), étendus (β_L), l'hélice *gauche* (α_D [$\phi \approx +60°$, $\psi \approx +60°$]) et la polyproline II (ε_D [$\phi \approx +60°$, $\psi \approx +180°$]) comportent tous les trois (g^+, *a* et g^-) rotamères dans la chaîne latérale (χ_1). Les conformères dont la chaîne principale est du type δ_L [$\phi \approx 240°$, $\psi \approx 60°$]) et δ_D [$\phi \approx 180°$, $\psi \approx -60°$]) ne comportent respectivement que deux orientations de la chaîne latérale. On n'a pas observé de minima pour les structures des unités conformationnelles de l'hélice droite (α_L [$\phi \approx -60°$, $\psi \approx -60°$]) et de la polyproline II (ε_L [$\phi \approx -60°$, $\psi \approx 180°$]). L'analyse conformationnelle ab initio de la For-L-Phe-NH_2 rapportée ici est un exemple unique dans laquelle on a déterminé un ensemble conformationnel systématique et complet d'un système diamide portant une chaîne latérale aromatique. On a effectué des calculs analytiques de fréquence de vibration pour tous les points stationnaires trouvés comme minima sur la surface d'énergie potentielle. Il sera possible d'utiliser ces données dans le futur comme conformères de référence dans des calculs plus détaillés de

Received February 23, 1996.[1]

A. Perczel.[2] Department of Organic Chemistry, Eötvös University, H-1518 Budapest 112, P.O.B. 32, Hungary.
Ö. Farkas and I.G. Csizmadia.[3] Department of Organic Chemistry, Eötvös University, H-1518 Budapest 112, P.O.B. 32, Hungary, and Department of Chemistry, University of Toronto, Toronto, ON M5S 1A1, Canada.
A.G. Császar. Department of Theoretical Chemistry, Eötvös University, H-1518 Budapest 112, P.O.B. 32, Hungary.

[1] Revision received April 21, 1997.
[2] Present address: Department of Biochemistry, Oxford University, South Parks Road, Oxford, OX1 3QU, England.
[3] Author to whom correspondence may be addressed (in Toronto). Telephone: (416) 978-3598. Fax: (416) 978-8775. E-mail: icsizmad@alchemy.chem.utoronto.ca

© 1997 NRC Canada

vibration et (ou) de blindage chimique ou dans des analyses de structures de peptides et de protéines par les techniques de rayons X ou de RMN.

Mots clés : conformères ab initio de peptides, toutes les structures RHF/3-21G de la For-L-Phe-NH_2, interactions entre le squelette et la chaîne latérale des modèles de peptide contenant de la phénylalanine.

[Traduit par la rédaction]

Can. J. Chem. Downloaded from www.nrcresearchpress.com by 88.146.161.215 on 09/08/12
For personal use only.

Introduction

General considerations

Ab initio investigation of aromatic–aromatic and polar–aromatic interactions (1) has recently emerged as an important tool in biochemical, pharmaceutical, and medical research. In the core region of proteins, interresidual interaction between amino acids containing an aromatic side chain (Phe, Tyr, Trp) is common (2–4). Formation of hydrophobic contacts in amphipatical helical networks (5) and the binding of aromatic substrates into receptors (6) or to the binding pocket of enzymes (7) are well known. Numerous examples can be found in the literature where the crucial role of a phenylalanine residue has been observed. Some well-known problems, such as that of cholecystokinin (CCK) (8*a*), have been around for almost 30 years, while other more recent ones, such as the binding site of the CD4 receptor for human immunodeficiency virus gp120 (8*b*, *c*) focus attention on the importance of aromatic–amide or aromatic–aromatic interaction. CD4 is a fascinating structural example, where the aromatic side chain is not buried inside the molecule but is exposed on the surface of the protein. According to Burley and Petsko (9) the aromatic–aromatic interaction between aromatic side chains may be effective from 4.5 to 7 Å. However, analysis of the most probable side-chain distances between Phe-Phe residues has quoted values in the range 3.5–4.2 Å (10).

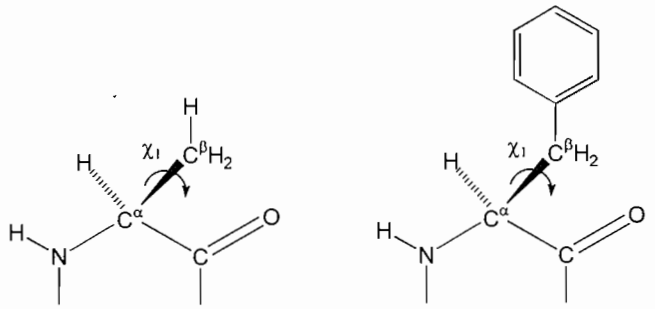
Based on the chemical nature of the side chains, L-amino acids may be classified as forming apolar and polar residues. Based on the pK_a values of the side chain, polar side chains may further be divided into acidic and bases subclasses. On the other hand, at least one representative element of each of these side-chain groups has aromatic character. Histidine is a weak base ($pK_a \approx 6$), tyrosine is a weak acid ($pK_a \approx 10$), while tryptophane and phenylalanine are apolar; however, all have a side chain with aromatic character.

Side-chain conformations

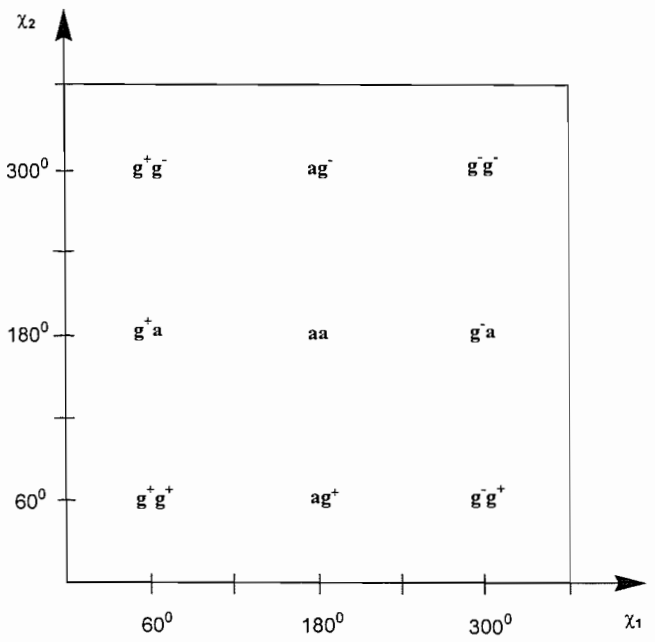
The purpose of the present paper is to explore the side-chain and backbone conformational subspaces of the conformational energy hyperspace, spanned by four torsional angles. Such an exploration will determine not only the location and relative stabilities of all conformers but it will also reveal the coupling between side-chain orientation and backbone structures.

Phenylalanine is the simplest side chain among the aromatic amino acid residues that can constitutionally be derived from alanine with the formal replacement of a β proton (H^{β}) with a phenyl (Phe = C_6H_5) group. While in alanine all three β protons (H^{β}_A, H^{β}_B, and H^{β}_C) can be considered as equivalent (and therefore energetically degenerate), in phenylalanine the β carbon is a prochiral center. Thus, an unambiguous description requires the inclusion of the two independent side-chain torsional angle variables: χ_1 and χ_2 (Scheme 1).

Scheme 1.



Scheme 2.



For amino acid residues that have both carbon atoms C^{β} and C^{γ} with an sp^3 character, a maximum of nine different side-chain conformers are expected (Scheme 2).

It has been demonstrated recently by using ab initio computations (11), that for selected amino acid residues having an sp^3 type C^{β} and an sp^3 type X^{γ} atom (e.g., X^{γ} = oxygen (ser, Thr) and X^{γ} = sulphur (Cys)) the expected nine minima can indeed be found. In contrast, in amino acid residues that have aromatic side chains the C^{γ} atom is of an sp^2 rather than an sp^3 type. In the latter constitution χ_2 may have fewer, or more than, three orientations and therefore such a molecule will not

© 1997 NRC Canada

Can. J. Chem. Downloaded from www.nrcresearchpress.com by 88.146.161.215 on 09/08/12
For personal use only.

Scheme 3.

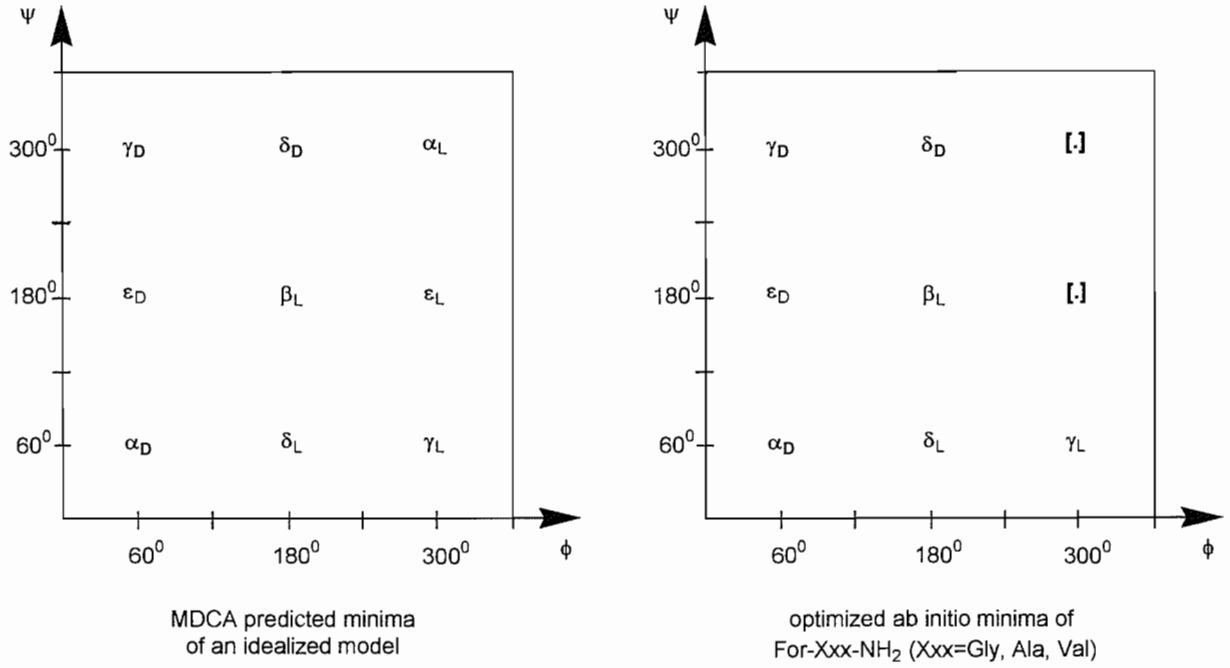
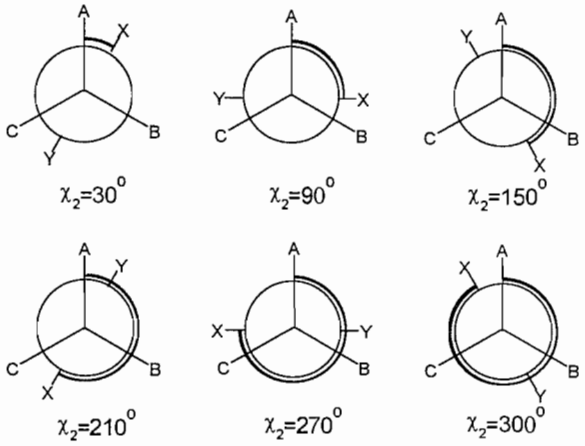


Fig. 1. Rotation about a C(sp^2)—C(sp^3) covalent bond with all six distinguishable minima [30°, 90°, 150°, 210°, 270°, and 330°]. If X = Y then the torsional potential shows sixfold degeneracy. (It is convenient to take A = C^{α} and B = C = H in the case of For-L-Phe-NH_2.)



show a side-chain conformation pattern similar to that of Scheme 2. Since in this case the two substituents attached to the sp^2 type C^{γ} atoms are constitutionally distinguishable (X ≠ Y), therefore, along χ_2 we may have as many as six different minima: [30°, 90°, 150°, 210°, 270°, and 330°] (Fig. 1). If the two substituents attached to the sp^2 C^{γ} atom are indistinguishable (X = Y) then three conformers remain. Thus, if X = Y, then $\chi_2[30°] = \chi_2[210°]$, $\chi_2[90°] = \chi_2[270°]$, and $\chi_2[150°] = \chi_2[330°]$ (Fig. 1). The latter situation is expected to occur in aspartate and in phenylalanine. For aspartate (Asp^-) both X and Y stand for oxygen, while in phenylalanine both X and Y are methyne (-CH-) groups. However, in any system that behaves as non-ideal, certain minima may be annihilated.

Backbone conformations

Multidimensional Conformational Analysis (12) (MDCA) predicts the existence of nine (13) legitimate backbone conformations denoted as α_L, α_D, β_L, γ_L, γ_D, δ_L, δ_D, ε_L, and ε_D, on the 2D-Ramachandran (14) map, $E = E(\phi, \psi)$, of a single amino acid diamide (HCONH-CHR-$CONH_2$) (Scheme 3).

Schäfer et al. (15) first noted that no minimum exists for CH_3CO-L-Ala-$NHCH_3$ in the neighborhood of the [$\phi \approx 300°$, $\psi \approx 300°$] conformational region, where the conformational building unit of the right-handed helix-like structure is expected. This region of the $E = E(\phi, \psi)$ potential energy surface is also called α_L (11, 13, 16, 17). Recent attempts confirmed that for diamide systems composed of apolar side chains (Ala, Val) no α_L-type minimum is present (11, 13, 15–17). Moreover, an additional minimum, the so-called ε_L [$\phi \approx 300°$, $\psi \approx 180°$] structure, which is the conformational building unit of the polyproline II structure, has so far not been observed during ab initio calculations of simple amino acid diamides (11, 13, 16, 17).

Backbone–backbone (18) and side-chain–backbone (19) interactions may stabilize the α_L conformation, as well as a special hydration effect (20), which exists in an intermolecular hydrogen-bonded complex. However, it is still a major challenge to understand the intrinsic relationship between the side-chain constitution and the expected ε_L backbone conformation. The ab initio conformers of For-L-Phe-NH_2 reported here could be used as reference conformers in further vibrational and (or) chemical shielding calculations, in structural analysis of peptides and proteins by X-ray or NMR techniques, as well as in understanding the fundamental problem of protein structure prediction based on primary sequence (21).

Computational details

Conformers of For-L-Phe-NH_2 were located at the restricted Hartree–Fock (RHF) level of theory (22) employing the stan-

© 1997 NRC Canada

Table 1. Optimized ab initio structures of (*A*) For-L-Phe-NH_2 and (*B*) For-L-Ala-NH_2.

A.

Backbone conformation type	Torsional angles[a] ω_0	ϕ	ψ	ω_1	χ_1	χ_2	ΔE^b	ΔE^c	ΔE^d
For-L-Phe-NH_2									
$\alpha_D[g^+]$	168.8	43.1	50.3	−178.4	44.6	78.1	11.16	8.59	9.21
$\alpha_D[a]$	174.7	60.6	41.1	179.7	−144.6	101.9	8.39	6.31	7.31
$\alpha_D[g^-]$	173.5	68.6	28.2	179.5	−56.7	98.9	6.75	2.70	4.48
$\beta_L[g^+]$	179.3	−175.9	174.7	−179.2	53.4	84.4	3.90	1.14	2.43
$\beta_L[a]$	177.9	−166.6	173.9	179.2	−146.6	68.5	1.54	−0.83	0.24
$\beta_L[g^-]$	176.6	−130.3	160.9	176.8	−61.8	91.5	7.11	0.84	2.48
$\gamma_L[g^+]$	−174.1	−83.0	59.8	179.5	40.7	76.3	0.00	0.00	0.00
$\gamma_L[a]$	−175.7	−85.6	72.5	−177.8	−162.0	94.5	1.51	−0.18	0.62
$\gamma_L[g^-]$	−172.4	−84.4	66.8	−178.9	−55.1	111.5	2.59	−0.87	—
$\gamma_D[g^+]$	170.1	34.9	−8.6	179.7	68.7	84.8	10.72	8.50	7.16
$\gamma_D[a]$	176.4	74.5	−65.2	179.0	−172.6	88.9	5.87	3.06	—
$\gamma_D[g^-]$	174.3	76.3	−57.6	−178.5	−57.2	100.3	3.66	0.90	1.62
$\delta_L[g^+]$	−173.0	−123.1	25.6	176.3	52.4	83.1	2.98	0.17	1.48
$\delta_L[g^-]$	−170.6	−119.6	23.2	176.2	−60.0	102.3	6.66	1.23	2.71
$\delta_D[g^+]$	173.4	173.9	−31.1	−176.7	58.0	89.7	8.54	5.39	6.87
$\delta_D[a]$	175.1	−169.9	−49.6	−177.6	−149.5	76.2	10.96	7.09	8.25
$\varepsilon_D[g^+]$	−172.0	34.0	−134.3	−177.8	71.6	175.7	17.61	13.20	—
$\varepsilon_D[a]$	−167.6	67.6	−177.6	−178.9	−158.3	64.6	9.89	5.58	6.68
$\varepsilon_D[g^-]$	−169.1	71.6	174.4	179.1	−58.4	97.7	9.46	6.37	7.73

[a]Torsion angles (ω_0, ϕ, ψ, ω_1, χ_1, and χ_2) in degrees according to IUPAC–IUB convention.
[b]RHF/3-21G energy differences (ΔE) are in kcal/mol (relative to the $E(\gamma_L[g^+]$ = −640.745 238).
[c]RHF/6-31+G*//RHF/3-21G energy differences (ΔE) are in kcal/mol (relative to the $E(\gamma_L[g^+]$ = −644.346 283).
[d]B3LYP/6-311++G**//RHF/3-21G energy differences (ΔE) are in kcal/mol (relative to the $E(\gamma_L[g^+]$ = −648.462 172).

B.

Backbone conformation type	Torsional angles[a] ω_0	ϕ	ψ	ω_1	χ_1	χ_2	Total energy[b]	ΔE^c
For-L-Ala-NH_2[d]								
α_D	−173.0	63.8	32.7	175.9	60.6	—	−412.465 294	5.95
β_L	−179.0	−168.3	170.5	177.8	59.0	—	−412.472 783	1.25
γ_L	−175.7	−84.5	67.3	178.2	64.2	—	−412.474 780	0.00
γ_D	175.4	74.0	−57.4	−179.9	60.4	—	−412.470 750	2.53
δ_L	173.2	−128.1	29.8	−179.4	58.5	—	−412.468 680	3.83
δ_D	−169.3	−178.6	−44.1	171.4	58.6	—	−412.463 135	7.31
ε_D	171.2	67.2	−171.9	−178.6	65.6	—	−412.461 774	8.16

[a]Torsion angles (ω_0, ϕ, ψ, ω_1, χ_1, and χ_2) in degrees according to IUPAC–IUB convention.
[b]Total energy (E) in hartrees.
[c]Energy differences (ΔE) in kcal/mol relative to the $E(\gamma_L[g^+]$ or $C_7^{eq}[g^+])$.
[d]All data taken from ref. 16.

dard 3-21G basis set (23). Minimization of all structures was performed by using a modified GDIIS (24) optimization algorithm with natural internal coordinates (25). RHF energies and gradients were calculated by the program package TX90.[4] Vibrational frequencies were obtained with the program TURBOMOLE taking advantage of its analytic second-derivatives facility. The maximum residual forces at the end of the geometry optimizations were always less than 10^{-6} au. The computed total energy values are summarized in Table 1, together with additional selected geometrical parameters. The relative energies of the fully optimized conformers are taken with respect to the global minimum; $E(\gamma_L[g^+])$ = −640.745 238 hartree. Single-point energies of the 19 conformers were also computed at the Hartree–Fock (RHF/6-31+G*) and density functional (B3LYP/6311++G**) levels of theory (Table 1*A*). The latter level of theory has been employed as in recent studies (26, 27). This level proved to yield accurate relative energies for several conformers of glycine (26) and alanine (27).

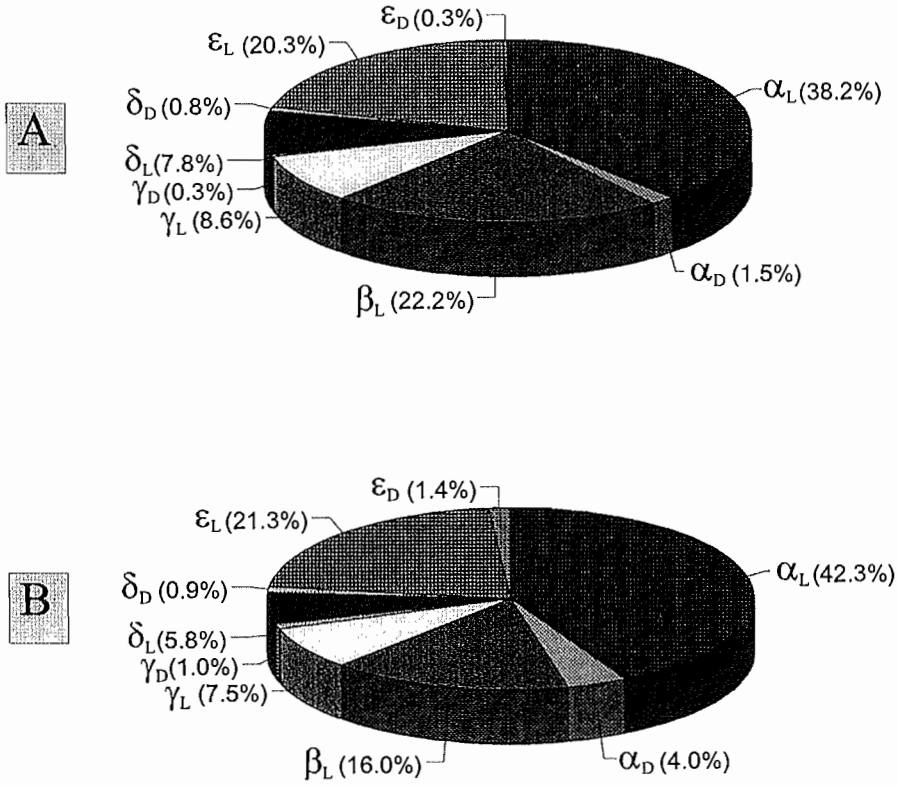
To limit the number of possible structures, preliminary

[4] P. Pulay and Associates. TX90. Fayetteville, Ariz. 1990.

© 1997 NRC Canada

Can. J. Chem. Downloaded from www.nrcresearchpress.com by 88.146.161.215 on 09/08/12
For personal use only.

Fig. 2. (*A*) The relative frequencies of the backbone conformers of the 2229 Phe residues in 267 proteins. (*B*) Same as *A* but all 20 natural amino acids (including a total of 54 269 amino acid residues) were incorporated in the analysis. Selection of the nonhomologous proteins[a] was made according to Hobom and Sander (29) using the January (1994) issue of PDB (30). The nine conformation centers on the Ramachandran-type surface were $\alpha_L[-62.4, -25.2]$, $\alpha_D[61.8, 31.9]$, $\beta_L[-167.6, 169.9]$, $\gamma_L[-84.5, 68.7]$, $\gamma_D[74.3, -59.5]$, $\delta_L[-126.2, 26.5]$, $\delta_D[-179.6, -43.7]$, $\varepsilon_L[-74.7, 167.8]$, $\varepsilon_D[64.7, -178.6]$.



[a] 8I1B, 8CATA, 1L92, 1LAP, 1LE4, 1LGAA, 1LTSA, 1MAMH, 1MDAA, 1MHU, 1MRRA, 1MS2A, 1MUP, 1NIPB, 1NXB, 1OFV, 1OMF, 1OMP, 1OSA, 1OVB, 1PAFA, 1PAZ, 1PDA, 1PDC, 1PFKA, 1PHH, 1POA, 1POC, 1PPFE, 1PPN, 1PRCC, 1PYP, 1RO94, 1R1A2, 1RBP, 1RCB, 1RHD, 1RND, 1RPRA, 1RRO, 1RVEA, 1SO1, 1SBP, 1SGT, 1SHAA, 1SHFA, 1SMRA, 1SNC, 1TABI, 1TEN, 1TFG, 1TFI, 1TGSI, 1THO, 1TIE, 1TLK, 1TNFA, 1TRB, 1TREA, 1TROA, 1TTBA, 1ULA, 1UTG, 1VAAB, 1VSGA, 1WSYA, 1XIMA, 1YCC, 2LALA, 2LIV, 2MADL, 2MEV1, 1AAF, 2MHR, 1AAK, 2MHU, 2MNR, 2MSBA, 2PF2, 1AAPA, 2PIA, 2PLV1, 2PMGA, 2POR, 2RN2, 2SAS, 1ABA, 2SCPA, 2SGA, 2SN3, 2SNV, 2STV, 1ABK, 1ABMA, 2TMD, 2TMVP, 2ZTAA, 3MONA, 1ACE, 3PGK, 3PGM, 3RUBS, 3SC2A, 3SGBI, 3SICI, 4RCRH, 4SBVA, 4SGBI, 4TGF, 1ADS, 4TMS, 4TS1A, 5NN9, 5P21, 7ZNF, 8RXNA, 9LDTA, 9RNT, 9RUBB, 9WGAA, 1MINA, 1GLAG, 1GPB, 1GPS, 1BBT2, 1CAUB, 1CPCL, 1CSEI, 1AOZA, 1FC2C, 1GLAF, 1LTSC, 1LTSD, 1MDAH, 1MINB, 1PRCM, 1WSYB, 1APS, 2ACHB, 2BPA2, 2BPA3, 2LALB, 1ARB, 2MEV4, 2PLV3, 3SC2B, 2GLSA, 1ATNA, 1ATX, 1AVHA, 1AYH, 1BAA, 1BABB, 1BARB, 1BBA, 1BBHA, 1BBL, 1BBO, 1BBPA, 1BBT1, 1BGC, 1BOVA, 1BRD, 1BTC, 1BW4, 1C2RA, 1C5A, 1CAJ, 1CAUA, 1CBN, 1CD8, 1CDTA, 1CID, 1CIS, 1CMBA, 1COBA, 1CPCA, 1CTAA, 1D66A, 1DFNA, 1DHR, 1DNKA, 1DRI, 1EAF, 1ECO, 1EGF, 1END, 1ERP, 1EZM, 1FAS, 1FBAA, 1FC1A, 1FCS, 1FDD, 1FHA, 1FIAB, 1FNR, 1FXIA, 1GKY, 1GLT, 1GMFA, 1GMPA, 1GOX, 1GRCA, 1GSSA, 1HC1, 1HCC, 1HDDC, 1HGEB, 1HILA, 1HIVA, 1HLEB, 1HSBA, 1ISUA, 1IXA, 256BA, 2AAA, 2AAIB, 2ACHA, 2ATCB, 2AVIA, 2AZAA, 2BDS, 2BOP, 2BPA1, 2CBH, 2CCYA, 2CDV, 2CPL, 2CRD, 2CRO, 2CTC, 2CTS, 2CYP, 2DPV, 2ECH, 2ER7E, 2GB1, 2HAD, 2HIPA, 2HPDA, 2IHL, 3ADK, 3B5C, 3CD4, 3CHY, 3CLA, 3COX, 3GAPA, 3GBP, 3GRS, 3IL8, 4BLMA, 4CPAI, 4ENL, 4FXN, 4GPD1, 4HTCI, 4ICD, 4INSB, 5FBPA, 7AATA, 7APIB, 8ABP, 8ACN, 8ADH, 8ATCA.

force field calculations investigated the space requirement of the phenyl group at different $[\chi_1, \chi_2]$ orientations. Setting χ_2 equal to 30°, 90°, and 150° and χ_1 to the most probable 60°, 180°, and 300° values, we analyzed the interatomic distances between the *ortho* hydrogens and the backbone atoms (H^α, N^α, and carbonyl C). Comprehensive analysis of these side-chain structures revealed that one or more of the above interatomic distances turned out to be shorter than 1.9 Å, which should be

© 1997 NRC Canada

Can. J. Chem. Downloaded from www.nrcresearchpress.com by 88.146.161.215 on 09/08/12
For personal use only.

Can. J. Chem. Downloaded from www.nrcresearchpress.com by 88.146.161.215 on 09/08/12
For personal use only.

Fig. 3. Location of the 19 RHF/3-21G relaxed structures For-L-Phe-NH_2 on a "ϕ, ψ" map. Backbone conformations (γ_D, β_L, etc.) are labelled according to the appropriate catchment region (α_L, α_D, β_L, etc.) plus their χ_1 conformers (g^+, a, or g^-). For the clarity of the catchment regions, both ϕ and ψ values are plotted using a 0°–360° scale. Note that for γ_D, ε_D, α_D, β_L, and γ_L backbone conformers three, and for δ_D and δ_L only two, χ_1 rotamers were found.

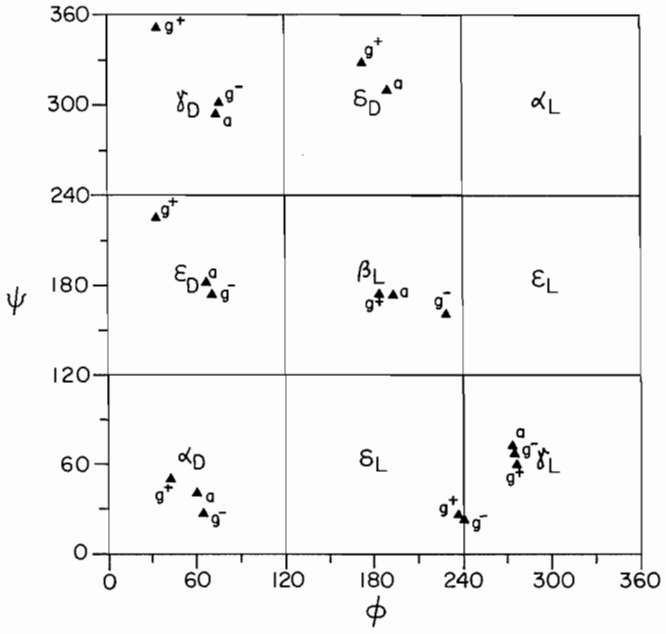
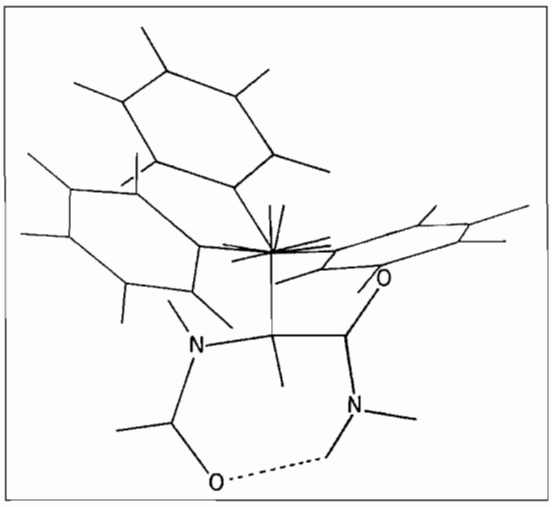
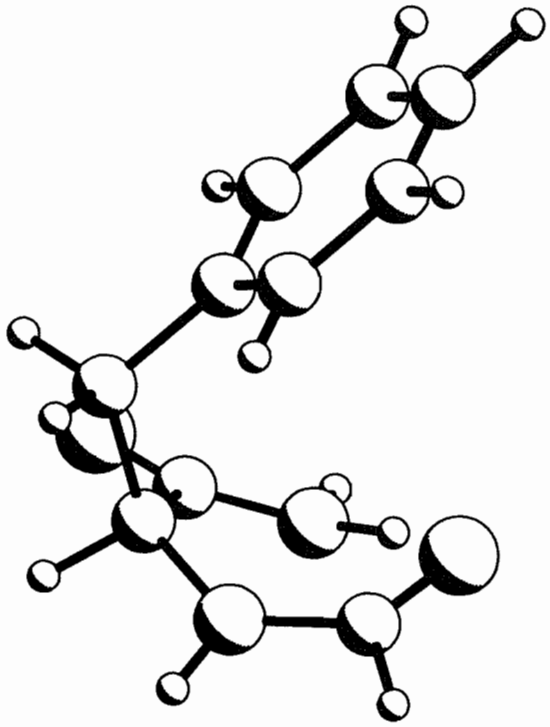


Fig. 4. Superimposed conformers of the three (g^+, a, and g^-) inverse gamma turn (γ_L) structures of For-L-Phe-NH_2.



considered unnatural. Therefore, two out of the three possible χ_2 orientations, $\chi_2 = 30°$ and $\chi_2 = 150°$, can be ignored. Keeping only the single minimum of $\chi_2 = 90°$, the conformational analysis of For-Phe-NH_2 would incorporate three different side-chain orientations, $\chi_1 \approx 60°$ [$\chi_2 \approx 90°$], $\chi_1 \approx 180°$ [$\chi_2 \approx 90°$], and $\chi_1 \approx 300°$ [$\chi_2 \approx 90°$], for each of the different backbone conformers. In three of these conformers the plane of the phenyl group is nearly perpendicular to the projection of the

Fig. 5. The $\gamma_D(g^+)$ structure of For-L-Phe-NH_2 (HF/DZP) ($\phi = 53.26°$, $\psi = -14.85°$, $\chi_1 = 68.87°$, $\chi_2 = 82.38°$; $E_{total} = -644.283\,6515$ hartree).



C^α—C^β bond. This is in agreement with the results of a conformational study carried out on ethyl benzene (Ph-CH_2-CH_3), where the carbon atom of the terminal -CH_3 group corresponds to the α carbon of the amino acid residue (28) (the benzyl group [Ph-CH_2-] is the actual side chain of the phenylalanine residue (28)). In the case of ethyl benzene the rotation of the Ph group has its global minimum at $\chi_2 = 90°$ and there is a very shallow local minimum, $\Delta E = 1.83$ kcal/mol higher on the energy scale, corresponding to $\chi_1 = 0°$.

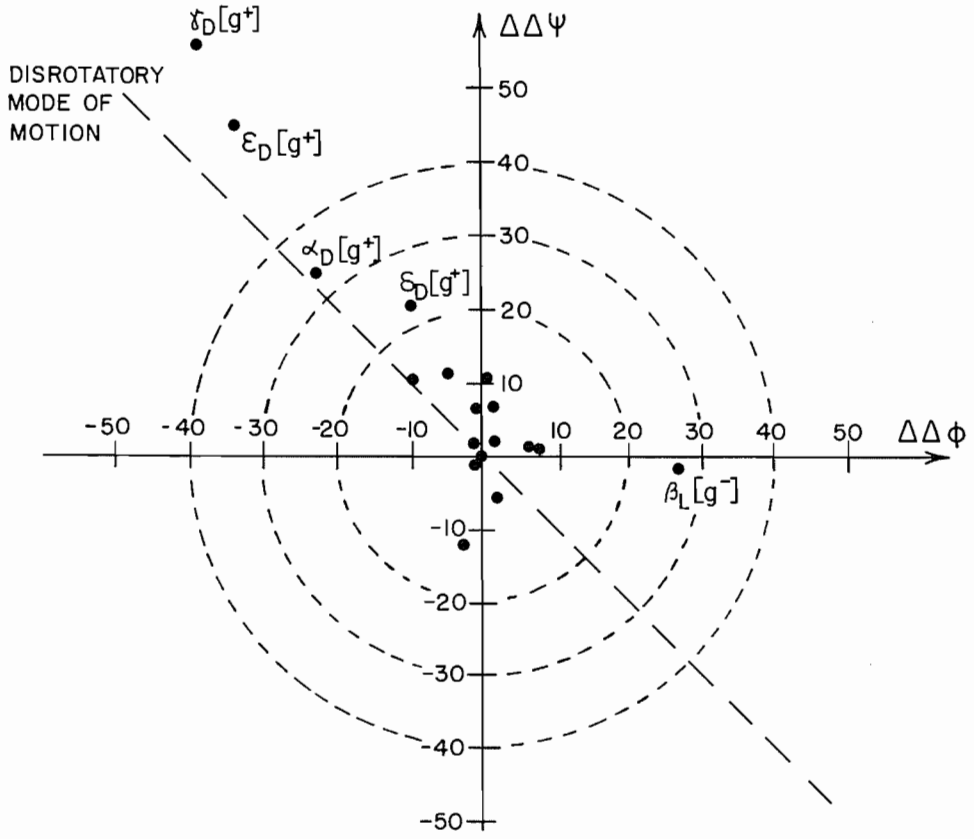
Results and discussion

Data-base analysis

In selected non-homologous proteins (29), we compared the relative frequencies of the nine different backbone conformers (α_L, α_D, β_L, ε_L, γ_L, γ_D, δ_L, δ_D, and ε_D) associated with a phenylalanine residue and with all 20 naturally occurring amino acid residues. All proteins included in this study had a a high-resolution X-ray structure taken from the January 1994 issue of the Protein Data Bank (PDB) (30, 31). From a total of 54 824 residues in 267 proteins, 2229 phenylalanine residues were counted. In all these, we compared the relative [ϕ, ψ] distribution of Phe with all 20 natural amino acid residues around the nine conformation clusters. The observed differences in relative frequencies slightly exceeded 7% for the β_L- and five percentage for the α_L-type backbone conformations (Fig. 2 *A*, *B*). The 7% increase in β_L is in favor of the Phe residues, while for the same amino acid residue there is a 5% drop in the α_L conformer. The frequency fluctuation of the other seven (α_D, ε_L, γ_L, γ_D, δ_L, δ_D, and ε_D) backbone conformations remains under 2.5%. Since phenylalanine shows an "average" conforma-

© 1997 NRC Canada

Fig. 6. Distribution of the computed For-L-Phe-NH_2 conformations on a double difference ($\Delta\Delta\phi$ and $\Delta\Delta\psi$) Ramachandran map.



tional character, which may be typical for aromatic amino acid, the present conformational results may be extrapolated with confidence for tyrosine and phenylalanine.

Conformational analysis

During the ab initio calculations, For-L-Phe-NH_2 has shown conformational features similar to those observed in glycine- (13, 16), alanine- (13, 16, 32, 33), and valine- (16, 17) containing diamide model compounds. All these diamide model systems (with the exception of Gly) have an apolar side chain. One striking conformational feature of all the above model compounds is that they do not have a minimum energy structure similar to the conformational building unit of the right-handed helical structure [$\phi \approx 300° \pm 30°$, $\psi \approx 330° \pm 30°$] (designated α_L) or to that of the polyproline II structure [$\phi \approx 300° \pm 30°$, $\psi \approx +220° \pm 30°$] (labelled as ε_L). The other seven (α_D, β_L, γ_L, γ_D, δ_L, δ_D, and ε_D) MDCA predicted backbone structures (13) were found within the quantum chemical calculations employed (Table 1). The location of the 19 ab initio For-L-Phe-NH_2 relaxed structures shows a clear separation on a "ϕ, ψ" map around seven distinguishable cluster centers. The γ_D, ε_D, α_D, β_L, and γ_L backbone conformers have three, while the δ_D and δ_L have two, different χ_1 rotamers (18 out of the 19 different structures have χ_2 around 90° in the range of 64.6° and 111.5°; thus $\chi_2 \approx 90 \pm 25°$. Note that the $\varepsilon_D(g^+)$ is an exception where χ_2 is shifted into the vicinity of 180° (Table 1).)

The inverse gamma turn (γ_L) is the only backbone conformer where all three χ_1 rotamers (g^+, *a*, and g^-) have rather similar [ϕ, ψ] values (Fig. 3). This indicates the lack of specific backbone–side-chain feedback. The intrinsic seven-membered intramolecular hydrogen bond between backbone NH and C=O units (Fig. 4) may explain this rigidity. Consequently, in the [$\phi = -84.3 \pm 1.3°$, $\psi = 66.5 \pm 6.7°$] region of the Ramachandran plot, where this hydrogen bond pattern is possible, it seems to be strong enough to "lock" the backbone conformation in all three (g^+, *a*, and g^-) side-chain conformers. Therefore, the γ_L backbone conformation is particularly useful to establish the magnitude of stabilization of the CH_2-C_6H_5 group on the backbone (34).

The "normal" gamma turn (γ_D) structure, the backbone conformational mirror image of the γ_L conformer, has a similar intramolecular hydrogen bond pattern. However, one out of the three γ_D type structures of For-L-Phe-NH_2, the $\gamma_D(g^+)$, shows a clear backbone conformational shift (Fig. 3). Due to the *gauche*$^+$ side-chain orientation, the [ϕ, ψ] values have shifted [$\Delta\psi \approx -40°$, $\Delta\psi \approx +60°$] from the expected region although the seven-membered hydrogen bond is preserved. Fearing the limitations of the RHF/3-21G basis set, this conformer was recalculated and geometry optimized using RHF/DZP level of theory. Although the more elaborate calculation resulted in ϕ, ψ torsional angles closer to the expected values [$\phi = 53.3°$, $\psi = 345.1°$] (Fig. 5) the moderate ϕ [$\Delta\phi \approx -25°$] and the large ψ [$\Delta\psi \approx +55°$] shift would need some explanation. One of these could be an aromatic–amide type interaction due to the spatial closeness of these two groups in the present conformers, which was quoted for cyclic peptide models in the literature (35–37).

Can. J. Chem. Downloaded from www.nrcresearchpress.com by 88.146.161.215 on 09/08/12
For personal use only.

© 1997 NRC Canada

Can. J. Chem. Downloaded from www.nrcresearchpress.com by 88.146.161.215 on 09/08/12
For personal use only.

Table 2. Ab initio backbone conformation and relative energy shifts of For-L-Phe-NH_2 with respect to For-L-Ala-NH_2.[a]

For-L-Phe-NH_2 conformers	Conformation shift[b]		Relative conformation shift[c]		Relative energy shift[d]
	$\Delta\phi$	$\Delta\psi$	$\Delta\Delta\phi$	$\Delta\Delta\psi$	$\Delta\Delta E$
$\alpha_D[g^+]$	−20.7	17.6	−22.2	25.1	5.21
$\alpha_D[a]$	−3.2	8.4	−4.7	15.9	2.44
$\alpha_D[g^-]$	4.8	−4.5	3.3	3.0	−2.05
$\beta_L[g^+]$	−7.6	4.1	−9.1	11.6	2.65
$\beta_L[a]$	1.7	3.4	0.2	10.9	0.29
$\beta_L[g^-]$	27.6	−9.6	26.1	−2.1	5.86
$\gamma_L[g^+]$	1.5	−7.5	0.0	0.0	0.00
$\gamma_L[a]$	−1.1	5.2	−2.6	12.7	1.51
$\gamma_L[g^-]$	0.1	−0.2	−1.4	7.3	2.59
$\gamma_D[g^+]$	−39.2	48.8	−40.7	56.3	8.19
$\gamma_D[a]$	0.5	−7.8	−1.0	−0.3	3.34
$\gamma_D[g^-]$	2.2	−0.2	0.7	7.3	1.13
$\delta_L[g^+]$	5.0	−4.1	3.5	3.4	−0.85
$\delta_L[g^-]$	8.5	−6.6	7.0	0.9	2.83
$\delta_D[g^+]$	−8.4	13.0	−9.9	20.5	1.23
$\delta_D[a]$	8.7	−5.5	7.2	2.0	3.65
$\varepsilon_D[g^+]$	−33.2	37.6	−34.7	45.1	9.45
$\varepsilon_D[a]$	0.4	−5.7	−1.1	1.8	1.73
$\varepsilon_D[g^-]$	4.4	−13.7	2.9	−5.2	1.30

[a]Shifts presented in this table are based on the data of Table 1.
[b]Torsional angle shifts (ϕ, ψ) are relative to those of For-L-Ala-NH_2.
[c]Relative to the $\Delta\phi$ and $\Delta\psi$ values of the $\gamma_L[g^+]$ conformer of For-L-Phe-NH_2.
[d]$\Delta\Delta E$ = ΔE(For-L-Phe-NH_2) − ΔE(For-L-Ala-NH_2). Values are in kcal/mol.

Similarly to the γ_D conformer, the g^+ side-chain orientation also has a remarkable impact in the ε_D and α_D backbone orientations. (Note that in all these conformers the ϕ has g^+ orientation.) In the $\varepsilon_D(g^+)$ and $\alpha_D(g^+)$ structures the [ϕ, ψ] values deviate once again from the other two ε_D and α_D backbone conformers (Fig. 6). Comparison of the energies (ΔE) of all three conformers (α_D, ε_D, and γ_D) at all three basis set types (3-21G, 631+G*, and 6311++G**) (Table 1*B*) reveals their high energy, relative to all the others.

While the *anti* and the *gauche*$^+$ side-chain conformers of the "extended" backbone structures, β_L(s), have very similar [ϕ, ψ] values, the *gauche*$^-$ orientation induces a significant backbone structural shift. It appears obvious that in the above four backbone conformers (γ_D, ε_D, α_D, and β_L) one among the three side-chain orientations (g^+ or g^-) has important backbone-structure-modifying effects. In these cases the aromatic group induces a considerable side-chain–backbone effect that shifts the [ϕ, ψ] values to the edge of the "catchment" region. In two additional backbone conformers, δ_D and δ_L, the side-chain-induced backbone-modifying effect is increased to such an extent that one of the three possible χ_1 orientations (g^+, a, g^-), namely the $\delta_D(g^-)$ for the δ_D(s) and $\delta_L(a)$ for the δ_L(s), are missing. In summary, due to the aromatic ring – backbone amide interactin in the $\gamma_D(g^+)$, $\varepsilon_D(g^+)$, $\alpha_D(g^+)$, and $\beta_L(g^-)$ structures, the [ϕ, ψ] values are strongly modified (Fig. 6), while in $\delta_L(a)$ and $\delta_D(g^-)$ the backbone conformation is transferred into one of the neighboring conformers. It should be emphasized again that when the backbone conformation of the input structure was of an α_L or ε_L type at any χ_1 value ($\alpha_L(g^+)$, $\alpha_L(a)$, and $\alpha_L(g^-)$ or $\varepsilon_L(g^+)$, $\varepsilon_L(a)$, and $\varepsilon_L(g^-)$), the ab initio computation resulted in a conformer that falls into another backbone conformation cluster.

The conformational shifts ($\Delta\phi$, $\Delta\psi$) of For-L-Phe-NH_2 with respect to For-L-Ala-NH_2 are summarized in Table 2. The relative conformational shifts ($\Delta\Delta\phi$, $\Delta\Delta\psi$) with respect to the $\Delta\phi$, $\Delta\psi$ values of the $\gamma_L[g^+]$ conformer of For-L-Phe-NH_2 are also collected in Table 2. The last column of this table summarizes the shift in relative energies.

When calculating these quantities the following equations were used:

$$\Delta\phi_x = \phi_x(\text{For-L-Phe-NH}_2) - \phi_x(\text{For-L-Ala-NH}_2)$$

$$\Delta\psi_x = \psi_x(\text{For-L-Phe-NH}_2) - \psi_x(\text{For-L-Ala-NH}_2)$$

$$\Delta\Delta\phi_x = \Delta\phi_x - \Delta\phi_{\gamma L(g^+)}$$

$$\Delta\Delta\psi_x = \Delta\psi_x - \Delta\psi_{\gamma L(g^+)}$$

$$\Delta E_x(\text{For-L-Phe-NH}_2) = E_x - E_{\gamma L(g^+)}$$

$$\Delta E_x(\text{For-L-Ala-NH}_2) = E_x - E_{\gamma L}$$

$$\Delta\Delta E_x = \Delta E_x(\text{For-L-Phe-NH}_2) - \Delta E_x(\text{For-L-Ala-NH}_2)$$

A number of interesting facts should be emphasized.

1. The $\Delta\Delta E$ values are all positive, with two exceptions:

© 1997 NRC Canada

Table 3. Ab initio backbone conformations of For-L-Phe-NH_2 and For-L-Ala-NH_2.

Backbone conformation type	For-L-Phe-NH_2[a]		For-L-Ala-NH_2		Average backbone conformational shift[b]	
	ϕ	ψ	ϕ	ψ	$\Delta\phi$	$\Delta\psi$
α_D	57.4	39.9	63.8	32.7	−11.9	13.0
β_L	−157.6	169.8	−168.3	170.5	10.6	−0.7
γ_L	−84.3	66.4	−84.5	67.3	0.2	−0.8
γ_D	61.9	−43.8	74.0	−57.4	−12.2	13.6
δ_L	−121.4	24.5	−128.1	29.8	6.7	−5.4
δ_D	−178.5	−40.4	−178.6	−44.1	0.1	3.7
ε_D	57.7	−165.8	67.2	−171.9	−9.5	6.1

[a]Averaged for all stable side-chain conformations.
[b]The conformational shift calculated between the appropriate backbone conformers of For-L-Phe-NH_2 and For-L-Ala-NH_2 molecules.

Table 4. Vibrational characteristics of For-Phe-NH_2.

Conformation	HB[a]	Vibrational total energy distribution: Unscaled $C^2{=}O^1$ (stretching)	Unscaled N^7H_2 (scissoring)	Unscaled $C^5{=}O^6$ (stretching)	Unscaled υ^b (cm^{-1})	Unscaled Relative intensity	Scaled υ^c (cm^{-1})
	Yes	22.97%	61.54%	—	1819.74	120.92	1633.88
$\gamma_L[a]$	Yes	45.66%	33.54%	—	1852.73	19.55	1674.58
	No	—	—	74.46%	1882.35	122.43	1710.62
	Yes	32.67%	45.38%	—	1813.42	143.79	1631.13
$\gamma_L[g^+]$	Yes	33.33%	48.74%	—	1854.04	25.43	1672.49
	No	—	—	74.48%	1874.06	127.66	1703.11
	Yes	32.43%	42.20%	—	1815.50	126.18	1633.39
$\gamma_L[g^-]$	Yes	28.99%	51.94%	—	1856.27	16.16	1673.35
	No	—	—	75.53%	1898.73	153.33	1725.11
$\beta_L[g^-]$	No	62.73%	—	13.57%	1877.42	146.55	1706.19
	No	12.21%	—	61.85%	1901.88	53.32	1729.59
$\alpha_D[g^+]$	No	—	—	67.34%	1893.64	90.04	1719.98
	No	68.80%	—	—	1901.16	92.92	1726.37
	Yes	15.16%	19.75%	41.42%	1828.62	109.12	1650.33
$\gamma_D[g^+]$	Yes	12.88%	32.65%	30.61%	1861.50	153.60	1685.62
	No	37.02%	41.18%	—	1896.29	19.94	1711.83
$\varepsilon_D[g^+]$	No	66.45%	—	—	1868.79	107.12	1694.33
	No	—	—	71.61%	1905.30	139.99	1730.62

[a]Indicates whether the C═O oxygen is involved in hydrogen bond (HB).
[b]Unscaled frequencies obtained at the RHF/3-21G level of theory.
[c]Scale factors chosen in the spirit of SQM methodology (36, 37) for the C═O stretching and NH_2 scissoring vibrations.

$\Delta\Delta E(\delta_L[g^+]) = -0.85$ kcal/mol and $\Delta\Delta E(\alpha_D[g^-]) = -2.05$ kcal/mol. This implies that in the $\delta_L(g^+)$ and $\alpha_D(g^-)$ conformers the Ph group of R = -CH_2-Ph, *indeed* acts as a stabilizing substituent with respect to the -H of the R = -CH_2-H of alanine. In all the other 17 cases the $\Delta\Delta E$ values are positive.

2. The trend in $\Delta\Delta\phi$ and $\Delta\Delta\psi$ values (Table 2, Fig. 6) is such that it may be classified as conrotatory (i.e., the signs of $\Delta\Delta\phi$ and $\Delta\Delta\psi$ are usually opposite to one another).

3. The five "ghost" conformers, $\gamma_D(g^+)$, $\varepsilon_D(g^+)$, $\alpha_D(g^+)$, $\delta_D(g^+)$, and $\beta_L(g^-)$, noticed in Fig. 3, occupy extended positions in Fig. 6. Perhaps these two extreme sites represent a different type of interaction. In the $\gamma_D(g^+)$, $\alpha_D(g^+)$, $\delta_D(g^+)$, and $\beta_L(g^-)$ conformers the Ph group has $\chi_2 \approx 90°$ but in the $\varepsilon_D[g^+]$ conformer the Ph group is twisted ($\chi_2 \approx 180°$).

4. One may speculate that the $\Delta\Delta E$ values associated with these five conformers

$\Delta\Delta E\ \{\gamma([g^+)\} = 8.19$ kcal/mol

$\Delta\Delta E\ \{\varepsilon_D(g^+)\} = 9.45$ kcal/mol

© 1997 NRC Canada

Can. J. Chem. Downloaded from www.nrcresearchpress.com by 88.146.161.215 on 09/08/12
For personal use only.

$\Delta\Delta E$ {$\alpha_D(g^+)$} = 5.21 kcal/mol

$\Delta\Delta E$ {$\delta_D(g^+)$} = 8.54 kcal/mol

$\Delta\Delta E$ {$\beta_L(g^-)$} = 5.86 kcal/mol

would be higher without a stabilizing interaction. The fact that their $|\Delta\Delta\phi|$ and $|\Delta\Delta\psi|$ values are significant indicates that there should be a stabilizing (e.g., charge transfer) interaction.

It is clear, when one compares the average deviations presented in Table 3 with the individual deviations, Table 2, that some of the differences have been averaged out.

Vibrational analysis of selected conformers

Table 4 summarizes computed fundamental vibrational frequencies, infrared intensities, and vibrational total energy distributions of the C═O stretching region of selected conformers. As shown by data compiled in Table 4, there are three normal modes expected in the C═O stretching region of the spectrum. As expected, the C═O stretching not involved in hydrogen bonds usually comes at the highest wave number. In conformers where the other C═O bond is involved in an intramolecular H-bond, the respective normal modes show strong mixing between the C═O stretching and the NH_2 scissoring motions.

Conclusions

Based on a preliminary force field study indicating that the phenyl ring is typically perpendicular to the C^α—C^β bond, MDCA predicted 27 different structures for the phenylalanine-containing diamide system (For-L-Phe-NH_2). Among these, 19 fully optimized structures were determined at the RHF/3-21G level of theory, while the other 8 relaxed to one of the 19 structures. Except for the inverse gamma turn (γ_L) conformers of this model system, a serious side-chain–backbone effect is operative in all other conformers. Such side-chain–backbone interactions markedly shift the [ϕ, ψ] values of the γ_D-, ε_D-, α_D-, and β_L-type structures in one out of the three side-chain conformations. The same effect is thought to be responsible for the "elimination" of the $\delta_L(a)$ and $\delta_D(g^-)$ structures. The aromatic side chain may have such an impact on some of the backbone structures that none of the three α_L nor any of the ε_L conformers have been found computationally. As observed previously for the hydroxymethyl-type side chain in the For-L-Ser-NH_2 molecule, the side-chain–backbone interaction may have a serious impact on the possible orientation of the two amide bonds influencing the ϕ and ψ values. The conformational analyses of For-L-Phe-NH_2 provide a unique example in which it was possible to monitor an apolar aromatic side-chain-induced backbone-modifying effect at the ab initio level of theory.

Acknowledgements

This research was supported by grants from the Hungarian Scientific Research Foundation (OTKA F013799, T017192, and T017604). Thanks are also due to FEFA (CFA/III-254) for providing computational facilities. The continuous financial support of the Natural Sciences and Engineering Research Council of Canada is gratefully acknowledged.

References

1. A.-M. Sapse, B.S. Schweitzer, A.P. Dicker, J.R. Bertino, and V. Frecer. Int. J. Pept. Protein Res. **39**, 18 (1992).
2. P.K. Warne and R.S. Morgan. J. Mol. Biol. **118**, 273 (1978).
3. J. Finer-Moore, J.F. Bazan, J. Rubin, and R.M. Stroud. *In* Prediction of protein structure and the principles of protein conformation. *Edited by* G.D. Fasman. Plenum Press, New York and London. 1989.
4. J. Singh and J.M. Thornton. FEBS Lett. **191**, 1 (1985).
5. P.C. Moews and R.H. Kretsinger. J. Mol. Biol. **91**, 201 (1975).
6. D.G. Hamgauer, A.F. Monzigo, and B.W. Mathews. Biochemistry, **23**, 5730 (1984).
7. D.M. Blow. Acc. Chem. Res. **9**, 145 (1976).
8. (*a*) N. Goudreau, J.H. Weng, and B.P. Roques. Biopolymers, **34**, 155, (1994); P. Fulcrand, M. Rodrigez, M.C. Galas, M.F. Lignon, J. Laur, A. Aumelas, and J. Martinez. Int. J. of Pept. Protein Res. **32**, 384 (1988); M.R. Pincus, R.P. Carty, J. Chen, J. Lubowsky, M. Avitable, D. Shah, H.A. Scheraga, and Murphy. Proc. Natl. Acad. Sci. U.S.A. **84**, 4821 (1987); (*b*) U. Moebius, L.K. Clayton, S. Abraham, S.C. Harrison, and E.L. Reinherz. J. Exp. Med. **176**, 507 (1992); (*c*) Z. Székely. J. Mol. Struct: THEOCHEM. **334**, 93 (1995).
9. S.K. Burley and G.A. Petsko. Science, **229**, 23 (1985).
10. J. Singh and J.M. Thornton. *In* Atlas of protein side-chain interactions. IRL Press, Oxford. 1992.
11. A. Perczel and I.G. Csizmadia. Int. Rev. Phys. Chem. **14**, 127 (1995).
12. (*a*) I.G. Csizmadia. *In* The chemistry of the thiol group (part of the series The chemistry of functional groups. *Edited by* S. Patai. John Wiley and Sons, New York. 1974. p. 1 (cf. particularly pp. 36–41 including Figs. 23, 24 and Table 20); (*b*) M.R. Peterson and I.G. Csizmadia. Prog. Theor. Org. Chem. **3**, 190 (1982); (*c*) I.G. Csizmadia. *In* New theoretical concept for understanding organic reactions. *Edited by* J.D. Bertran. Reidel Publishing Co. 1989. pp. 1–31.
13. A. Perczel, J.G. Ángyán, M. Kajtár, W. Viviani, J.-L. Rivail, J.F. Marcoccia, and I.G. Csizmadia. J. Am. Chem. Soc. **113**, 6256 (1991).
14. G.N. Ramachandran, C. Ramakrishnan, and V. Sasisekharan. J. Mol. Biol. **7**, 95 (1963).
15. L. Schäfer, V.J. Klimkowski, F.A. Momany, H. Chuman, and C. Van Alsenoy. Biopolymers, **23**, 2335 (1984).
16. M.A. McAllister, A. Perczel, P. Császár, W. Viviani, J.-L. Rivail, and I.G. Csizmadia. J. Mol. Struct. (THEOCHEM), **288**, 161 (1993).
17. W. Vladia, J.L. Rivail, A. Perczel, and I.G. Csizmadia. J. Am. Chem. Soc. **115**, 8321 (1993).
18. (*a*) A. Perczel, M.A. Mcallister, P. Császár, and I.G. Csizmadia. J. Am. Chem. Soc. **115**, 4849 (1993); (*b*) A. Perczel, G. Endredi, M.A. McAllister, O. Farkas, J. Ladik, and I.G. Csizmadia. J. Mol. Struct. (THEOCHEM), **331**, 5 (1995).
19. (*a*) O. Farkas, A. Perczel, J.-F. Marcoccia, M. Hollósi, and I.G. Csizmadia. I. Mol. Struct. (THEOCHEM), **331**, 27 (1995); (*b*) A. Perczel, O. Farkas, and I.G. Csizmadia. J. Comput. Chem. **17**, 821 (1996); (*c*) A. Perczel, O. Farkas, J.F. Marcoccia, and I.G. Csizmadia. Int. J. Quantum Chem. **61**, 797 (1997).
20. A. Perczel, O. Farkas, and I.G. Csizmadia. J. Am. Chem. Soc. **117**, 1653 (1995).
21. G.D. Fasman (*Editor*). Prediction of protein structure and the principles of protein conformation. Plenum Press, New York and London. 1989.
22. P. Pulay, G. Fogarasi, F. Pang, and J.E. Boggs. J. Am. Chem. Soc. **101**, 2550 (1979).
23. J.S. Binkley, J.A. Pople, and W.J. Hehre. J. Am. Chem. Soc. **102**, 939 (1980).

© 1997 NRC Canada

Can. J. Chem. Downloaded from www.nrcresearchpress.com by 88.146.161.215 on 09/08/12
For personal use only.

24. (*a*) P. Császár and P. Pulay. J. Mol. Struct. **114**, 31 (1984); (*b*) J. Baker. J. Comput. Chem. **7**, 385 (1986).
25. G. Fogarasi, X. Zhou, P.W. Taylor, and P. Pulay. J. Am. Chem. Soc. **114**, 8191 (1992).
26. A.G. Csaszar. J. Am. Chem. Soc. **114**, 9568 (1992).
27. A.G. Csaszar. J. Phys. Chem. **100**, 3541 (1996).
28. O. Farkas, S.J. Salpietro, P. Csaszar, and I.G. Csizmadia. J. Mol. Struct. (THEOCHEM), **367**, 25 (1996).
29. U. Hobohm and C. Sandre. Protein Sci. **3**, 522 (1994).
30. F.C. Bernstein, T.F. Koetzle, G.J.B. Williams, E.F. Meyer, M.D. Brice, Jr., J.R. Rodgers, O. Kennard, T. Shimanouchi, and M. Tasumi. J. Mol. Biol. **112**, 535 (1977).
31. E.E. Abola, F.G. Bernstein, S.H. Bryant, I.F. Koetzle, and J. Weng. Crystallographic database — Information content, software system, scientific applications. *In* Data Commission of the Int. Union Crystallogr. *Edited by* F.H. Allen, G. Bergerhoff, and R. Sievers. Bonn/Cambridge/Chester. 1987. p. 107.
32. T. Head-Gordon, M. Head-Gordon, M.J. Frisch, C. Brooks II, and J.A. Pople. Int. J. Quantum Chem. Quantum Biol. Symp. **16**, 311 (1989).
33. T. Head-Gordon, M. Head-Gordon, M.J. Frisch, C. Brooks II, and J.A. Pople. J. Am. Chem. Soc. **113**, 5989 (1991).
34. O. Farkas, M.A. McAllister, J.H. Ma, A. Perczel, M. Hollosi, and I.G. Csizmadia. J. Mol. Struct. (THEOCHEM), **369**, 105, (1996).
35. Z. Kopple and K.D. Kopple. J. Org. Chem. **35**, 253 (1970).
36. K.D. Kopple and D.H. Marr. J. Am. Chem. Soc. **89**, 6193, (1967).
37. D.R. Robinson and W.P. Jencks. J. Am. Chem. Soc. **87**, 2470, (1965).

Can. J. Chem. Downloaded from www.nrcresearchpress.com by 88.146.161.215 on 09/08/12
For personal use only.

© 1997 NRC Canada

3-Phosphorylated 1,5-hexadienes as precursors for vinylic or 3-silanylvinylic phosphonates

Michael F. Probst, Agnes M. Modro, and Tomasz A. Modro

Abstract: 3-(Diethylphosphono) substituted 1,5-hexadienes are prepared by the α-regioselective allylation of allylic phosphonates. The products can be converted into vinylic phosphonates via two types of reactions. The first involves Cope rearrangement yielding the terminal vinylphosphonates of the 1,5-hexadiene system. The second involves γ-silanylation leading to the formation of the 1-silanyl-3-phosphono derivatives of the 2,5-hexadiene skeleton.

Key words: allylic and vinylic phosphonates, nucleophilicity of allylphosphonate carbanions, electrophilic silanylation, Cope rearrangement of alkenylphosphonates.

Résumé : On a préparé les 3-(diéthylphosphono)-1,5-hexadiènes par allylation α-régiosélective des phosphonates allyliques. Les produits peuvent être transformés en phosphonates vinyliques en utilisant deux types de réactions. Le premier type implique une transposition de Cope conduisant aux phosphonates vinyliques avec le vinyle en position terminale du système 1,5-hexadiène. Le second type implique une γ-silanylation conduisant à la formation de dérivés 1-silanyl-3-phosphono du squelette 2,5-hexadiène.

Mots clés : phosphonates allyliques et vinyliques, nucléophilicité des carbanions allylphosphonate, silanylation électophile, transposition de Cope des alcénylphosphonates.

[Traduit par la rédaction]

Introduction

Synthetic usefulness of allylphosphonates (1) and allylsilanes (2) is well recognised. Although the corresponding vinyl silanes also found wide application in synthesis (ref. 2, chap. 3), relatively little is known about the synthetic use of vinylphosphonates. It has been shown recently that the latter systems can be used as substrates for the preparation of a variety of chain-substituted allylphosphonates (also valuable synthetic reagents) via the conjugate addition of organocuprates, followed by electrophilic quenching (3). Introduction of two heteroatom-containing functionalities, PO_3Et_2 and SiR_3, into the 1,3-positions of the propenyl backbone opens a possibility of a combination of the abovementioned reactive systems within a single molecular framework, and should offer new synthetic options. In the first paper of this series (4) we showed that 3-silanylprop-1-enylphosphonates **1** can be easily prepared by silylation of the corresponding allylphosphonates, and that **1** could be converted to the isomeric 3-silanylallylic phosphonates **2** via the 1,3-sigmatropic shift (eq. [1]). In this paper we report some chemistry of the 3-phosphorylated 1,5-hexadiene system leading to the formation of new vinylic and 3-silanylvinylic phosphonates.

Received February 17, 1997.

M.F. Probst, A.M. Modro, and T.A. Modro.[1] Centre for Heteroatom Chemistry, Department of Chemistry, University of Pretoria, Pretoria 0002, South Africa.

[1] Author to whom correspondence may be addressed. Telephone: 012-420-2512. Fax: 12-432-863. E-mail: tamodro@scientia.up.ac.za

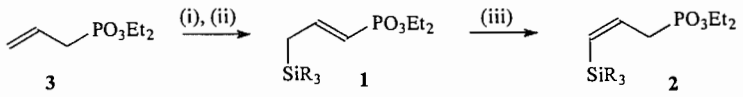
Results and discussion

The regioselectivity of the silylation of lithiated allylic phosphonates depends on the substitution of the propenyl skeleton. While diethyl prop-2-enylphosphonate **3a** undergoes silylation exclusively at the γ-carbon (5), its 3-methyl derivative **3b** was reported to give exclusively the α-silylated product **4a** (6). We have now found that the isomeric 2-methylallylphosphonate **3c** retains the exclusive γ-selectivity, yielding the corresponding 3-silanylprop-1-enylphosphonate **1b** (eq. [2]). As in the case of the unsubstituted substrate (4), only the *E* stereoisomer of **1c** was formed. Among many factors that contribute to the α vs. γ selectivity in nucleophilic reactivity of carbanions derived from the 1-heteroatom-substituted propenyl system, steric effects of the carbanion and of the electrophile are frequently suggested as playing an important role (7). The results given in eq. [2] do not confirm that conclusion; it would be difficult to accept that the difference in the steric hindrance for the substitution and C_α and C_γ in **3b** justifies the rigorous selectivity leading to the exclusive formation of **4a**. We believe that the regioselectivity of the silylation is determined rather by the combination of the effect of the substituents R, R′ on the charge distribution within the allylic carbanion, by the *stability* of the product, as measured by the number of the carbon atoms attached to the olefinic bond, and by the number of the allylic hydrogens available for the hyperconjugative stabilization of that bond (8). In all cases given in eq. [2] the formation of the observed isomer results in the increase of carbon substitution and of the number of allylic hydrogens, while the location of the phosphoryl group with respect to the olefinic bond seems to be of lesser importance. A weak (if any) stabilizing effect of the PO_3Et_2 substituent on

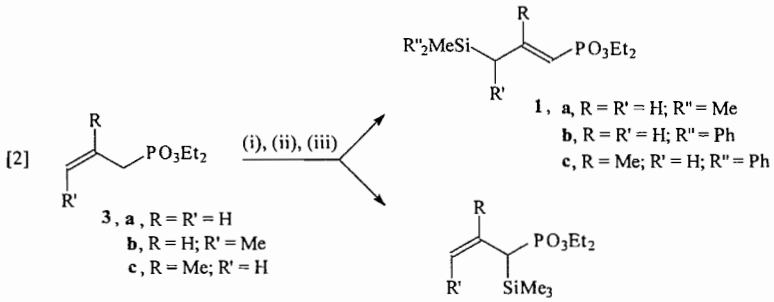
© 1997 NRC Canada

Can. J. Chem. Downloaded from www.nrcresearchpress.com by 88.146.161.215 on 09/08/12
For personal use only.

Can. J. Chem. Downloaded from www.nrcresearchpress.com by 88.146.161.215 on 09/08/12
For personal use only.

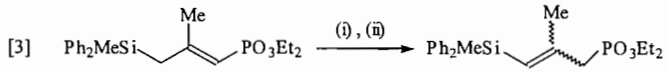
[1] 

(i) BuLi, THF
(ii) R_3SiCl
heat

[2] 

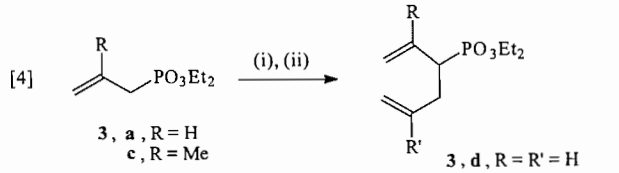
(i) BuLi, THF
(ii) $R''_2MeSiCl$
(iii) aq NH_4Cl

an adjacent olefinic bond has been demonstrated before (5) and in the present work by the thermal isomerization **1** → **2** (eq. [1], second step). We have now found that the isomerization can also be achieved via prototropic equilibrium (eq. [3]) leading to the silicon-substituted, rather than the phosphonyl-substituted alkene.

[3] 

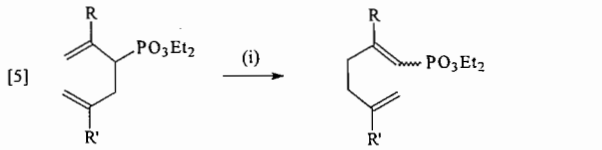
(i) BuLi or tBuLi or LDA
(ii) aq NH_4Cl

In electrophilic alkylation, as opposed to the silylation, allylic phosphonates **3a** and **3c** behaved as exclusive α-carbon nucleophiles; allylation of those substrates led to new allylphosphonates of the 1,5-hexadiene series (eq. [4]). Formation of the α-allylated products **3d–f** violates the rule of

[4] 

(i) BuLi
(ii) $CH_2=C(R')CH_2Br$

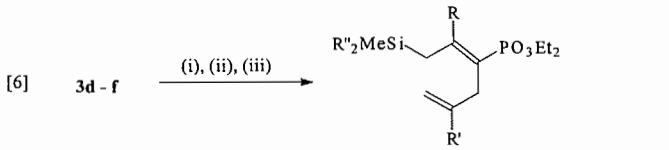
"carbon substitution and hyperconjugative hydrogens" (8), suggesting that **3d–f** represent the kinetic products of the alkylation, and not necessarily the more stable isomers. Indeed, when phosphonates **3d–f** were heated as neat liquids at 210°C, they underwent complete isomerisation via the Cope rearrangement to the corresponding vinylphosphonates **5** (eq. [5]). In each case, in addition to the location of one olefinic bond in

[5] 

(i) 210°C

the α,β-position with respect to the PO_3Et_2 group, the total number of the allylic hydrogens available for hyperconjugation with the olefinic bonds of the diene increased by one.

In addition to their conversion into the terminal vinylic phosphonates **5**, allylic phosphonates **3d–f** were also used as precursors of the vinylic phosphonates branched at the α-carbon and substituted at the terminal carbon with the silanyl group (eq. [6]). The silylation occurs exclusively at the γ-position, and the large (ca. 19 ppm) value of the $^3J_{CP}$ coupling

[6] 

(i) BuLi
(ii) $R''_2MeSiCl$
(iii) aq NH_4Cl

constant across the olefinic bond between carbon-1 and phosphorus indicates the *trans* geometry of the products (9). The synthetic potential of the resulting 3-silanyl derivatives of the

© 1997 NRC Canada

Can. J. Chem. Downloaded from www.nrcresearchpress.com by 88.146.161.215 on 09/08/12
For personal use only.

vinylphosphonates of the 1,4-hexadiene series is currently studied in our laboratory.

Experimental section

Solvents and commercially available substrates were purified by conventional methods immediately before use. All reactions were carried out in an atmosphere of dry nitrogen. NMR spectra were recorded as solutions in $CDCl_3$ on a Bruker AC 300 spectrometer. Chemical shifts are given in ppm relative to $SiMe_4$ (^1H, ^{13}C) as an internal standard, and 85% H_3PO_4 (^{31}P) as an external standard. Proton-coupled ^{13}C NMR spectra are given. Mass spectra were recorded on a Varian MAT-212 double-focusing direct-inlet spectrometer and a GC-coupled spectrometer at an ionization potential of 70 eV. For column chromatography, Merck Kieselgel 60 (0.063–0.200 mm) was used. Chlorotrimethylsilane and chlorodiphenylmethylsilane were purchased from Aldrich and were redistilled before use.

Diethyl prop-2-enylphosphonate **3a** was prepared as described before (4). Diethyl 2-methylprop-2-enylphosphonate **3c** was prepared from triethyl phosphite and 3-bromo-2-methylpropene (79%): bp 62°C at 0.1 Torr (1 Torr = 133.3 Pa); δ_P: 27.7 (lit. (10) δ_P: 26.5); δ_H: 1.26 (6H, t, J_{HH} 7.08), 1.83 (3H, dd, J_{HH} 1.08, 1.09), 2.53 (2H, d, J_{HP} 22.38), 4.05 (4H, quint, J_{HH}, J_{HP} 7.17), 4.85 (2H, m); δ_C: 15.8 (dq, J_{CP} 6.1, J_{CH} 127.0), 22.9 (dq, J_{CP} 11.7, J_{CH} 126.0), 34.8 (dt, J_{CP} 137.4, J_{CH} 131.0), 61.2 (dt, J_{CP} 6.6, J_{CH} 147.2), 115.4 (dt, J_{CP} 12.5, J_{CH} 131.0), 135.6 (d, J_{CP} 10.9); MS, *m/z*: 192 (M^+, 47%), 177 (21), 163 (10), 137 (100), 108 (33), 92 (24), 55 (80).

Silanylation of allylic phosphonates. General procedure

n-Butyllithium (1.6 M solution in hexane, 1.2 mol-equiv.) or *tert*-butyllithium (1.7 M solution in pentane, 1.1 mol-equiv.) or lithium diisopropylamide (10% suspension in pentane, 1.3 mol-equiv.) was cooled to −78°C. A solution of allylphosphonate (ca. 10 mmol, 1.0 mol-equiv.) in THF was added dropwise at −78°C and the solution was stirred at that temperature for 90 min. The silanylating reagent (1.2 mol-equiv.) was added slowly to the solution, the mixture was stirred at −78°C for an additional 45 min, allowed to warm up to room temperature, and stirred for 16 h. After quenching with 10% aqueous NH_4Cl, the product was extracted with ether, the ether solution was dried ($MgSO_4$), evaporated under reduced pressure, and the crude product was purified by distillation or bulb-to-bulb distillation.

(E) *Diethyl 3-(diphenylmethylsilanyl)prop-1-enylphosphonate* ***1b*** *(84%)*: oven temp. 138°C at 0.01 Torr; δ_P: 19.3; δ_H: 0.58 (3H, s), 1.20 (6H, t, J_{HH} 7.07), 2.28 (2H, d, J_{HH} 8.48), 3.84 (4H, quint, J_{HP}, J_{HH} 7.01), 5.38 (1H, dd, J_{HP} 20.94, J_{HH} 16.92), 6.79 (1H, m), 7.31 (10H, m); δ_C: −4.6 (q, J_{CH} 120.7), 16.3 (dt, J_{CP} 6.5, J_{CH} 126.9), 24.6 (dt, J_{CP} 22.2, J_{CH} 123.3), 61.3 (dt, J_{CP} 5.3, J_{CH} 146.5), 115.8 (dd, J_{CP} 188.3, J_{CH} 155.8), 128.0 (d, J_{CH} 160.3), 129.5 (d, J_{CH} 167.2), 134.4 (d, J_{CH} 158.9), 150.6 (dd, J_{CP} 5.9, J_{CH} 155.8); MS, *m/z*: 374 (M^+, 5%), 359 (4), 343 (4), 297 (13), 216 (10), 197 (9), 182 (6), 177 (25), 162 (17), 137 (11), 117 (100), 103 (34). Anal. calcd. for $C_{20}H_{27}O_3PSi$: C 63.47, H 7.19; found: C 63.11, H 7.05.

(E) *Diethyl 3-(diphenylmethylsilanyl)-2-methylprop-1-enylphosphonate* ***1c*** *(72%)*: oven temp. 151°C at 0.07 Torr; δ_P: 19.3; δ_H: 0.61 (3H, s), 1.24 (6H, t, J_{HH} 7.13), 1.90 (3H, d, J_{HP} 3.03), 2.29 (2H, s), 3.89 (4H, m), 5.11 (1H, d, J_{HP} 18.3), 7.42 (10H, m); δ_C: −4.3 (q, J_{CH} 120.7), 16.3 (dq, J_{CP} 6.8, J_{CH} 127.1), 22.6 (dq, J_{CP} 6.7, J_{CH} 124.9), 31.6 (dt, J_{CP} 23.0, J_{CH} 117.7), 60.9 (dt, J_{CP} 5.3, J_{CH} 146.6), 110.1 (dd, J_{CP} 190.0, J_{CH} 152.9), 127.9 (d, J_{CH} 160.4), 129.6 (d, J_{CH} 159.9), 134.4 (d, J_{CH} 157.3), 135.5 (s), 161.4 (d, J_{CP} 5.2); MS, *m/z*: 388 (M^+, 5%), 373 (4), 311 (15), 197 (100), 191 (99), 181 (13), 137 (13), 105 (19). Anal. calcd. for $C_{21}H_{29}O_3PSi$: C 64.26, H 7.45; found: C 64.07, H 7.40.

(E) *Diethyl 1-(prop-2-enyl)-3-(diphenylmethysilanyl)prop-1-enylphosphonate* ***1d*** *(82%)*: oven temp. 150°C at 0.06 Torr; δ_P: 22.4; δ_H: 0.58 (3H, s), 1.21 (6H, t, J_{HH} 7.03), 2.24 (2H, dd, J_{HP} 2.73, J_{HH} 8.82), 2.76 (2H, dd, J_{HP} 17.85, J_{HH} 6.31), 3.87 (4H, m), 4.95 (2H, two dd, $J_{HH\,trans}$ 15.42, $J_{HH\,cis}$ 10.71, $J_{HH\,gem}$ 1.64), 5.58 (1H, m), 6.75 (1H, dt, J_{HP} 8.84, J_{HH}, 8.82), 7.31 (10H, m); δ_C: −4.33 (q, J_{CH} 120.6), 16.2 (dq, J_{CP} 6.7, J_{CH} 127.2), 19.3 (dt, J_{CP} 19.2, J_{CH} 125.6), 31.1 (dt, J_{CP} 11.2, J_{CH} 126.8), 61.3 (dt, J_{CP} 5.1, J_{CH} 146.8), 115.5 (t, J_{CH} 153.9), 124.4 (d, J_{CH} 178.5), 128.0 (d, J_{CH} 159.5), 129.6 (d, J_{CH} 159.9), 133.9 (s), 134.4 (d, J_{CH} 158.5), 134.7 (dd, J_{CP} 10.4, J_{CH} 154.0), 145.0 (dd, J_{CP} 12.2, J_{CH} 157.6); MS, *m/z*: 414 (M^+, 19%), 399 (28), 331 (9), 309 (17), 294 (14), 217 (9), 197 (100), 137 (37), 105 (18), 79 (11). Anal. calcd. for $C_{23}H_{31}O_3PSi$: C 66.01, H 7.47; found: C 65.66, H 7.30.

(E) *Diethyl 1-(2-methylprop-2-enyl)-3-(diphenylmethylsilanyl)prop-1-enylphosphonate* ***1e*** *(90%)*: oven temp. 165°C at 0.05 Torr; δ_P: 22.34; δ_H: 0.58 (3H, s), 1.19 (6H, t, J_{HH} 7.10), 1.65 (3H, s), 2.22 (2H, dd, J_{HP} 3.05, J_{HH} 8.80), 2.67 (2H, d, J_{HP} 17.57), 3.85 (4H, m), 4.68 (2H, two d, $J_{HH\,gem}$ 2.14), 6.80 (1H, dt, J_{HP} 8.74, J_{HH} 8.71), 7.37 (10H, m); δ_C: −4.44 (q, J_{CH} 120.5), 16.2 (dq, J_{CP} 6.6, J_{CH} 126.9), 19.5 (dt, J_{CP} 19.2, J_{CH} 122.0), 22.6 (q, J_{CH} 119.3), 34.4 (dt, J_{CP} 11.2, J_{CH} 126.9), 61.2 (dt, J_{CP} 5.4, J_{CH} 146.9), 111.1 (t, J_{CH} 155.5), 124.7 (d, J_{CP} 180.5), 127.7 (d, J_{CH} 165.7), 129.5 (d, J_{CH} 159.8), 134.3 (d, J_{CH} 158.3), 135.4 (s), 141.5 (d, J_{CP} 2.3), 145.5 (dd, J_{CP} 11.9, J_{CH} 156.9); MS, *m/z*: 428 (M^+, 26%), 413 (39), 372 (5), 323 (14), 308 (16), 231 (18), 197 (100), 137 (15), 105 (13), 79 (12). Anal. calcd. for $C_{24}H_{33}O_3PSi$: C 67.26, H 7.76; found: C 66.89, H 7.90.

(E) *Diethyl 1-(2-methylprop-2-enyl)-2-methyl-3-(diphenylmethylsilanyl)prop-1-enylphosphonate* ***1f*** *(85%)*: oven temp. 175°C at 0.05 Torr; δ_P: 22.3; δ_H: 0.59 (3H, s), 1.23 (6H, t, J_{HH} 7.00), 1.65 (3H, s), 1.98 (3H, d, J_{HP} 3.21), 2.27 (2H, d, J_{HP} 1.48), 2.67 (2H, d, J_{HP} 17.40), 3.90 (4H, m), 4.69 (2H, two d, $J_{HH\,gem}$ 21.82), 7.42 (10H, m); δ_C: −3.68 (q, J_{CH} 120.6), 16.3 (dq, J_{CP} 6.9, J_{CH} 126.9), 23.2 (q, J_{CH} 125.7), 24.3 (dq, J_{CP} 7.6, J_{CH} 127.1), 27.1 (dt, J_{CP} 19.3, J_{CH} 121.3), 37.9 (dt, J_{CP} 12.2, J_{CH} 126.3), 61.0 (dt, J_{CP} 5.5, J_{CH} 146.8), 110.2 (t, J_{CH} 150.3), 118.9 (d, J_{CP} 180.9), 127.9 (d, J_{CH} 159.2), 129.5 (d, J_{CH} 159.8), 134.4 (d, J_{CH} 158.3), 136.3 (s), 142.5 (s), 142.7 (s); MS, *m/z*: 442 (M^+, 30%), 427 (72), 387 (5), 365 (8), 322 (22), 307 (11), 292 (21), 230 (16),197 (100), 181 (17), 137.25), 105 (19). Anal. calcd. for $C_{25}H_{35}O_3PSi$: C 67.84, H 7.97; found: C 68.43, H 8.08.

(E) *Diethyl 1-(2-methylprop-2-enyl)-2-methyl-3-(trimethylsilyl)prop-1-enylphosphonate* ***1g*** *(81%)*: bp 93–94°C at 0.03 Torr; δ_P: 22.7; δ_H: 0.03 (9H, s), 1.24 (6H, t, J_{HH} 7.06), 1.71

© 1997 NRC Canada

Can. J. Chem. Downloaded from www.nrcresearchpress.com by 88.146.161.215 on 09/08/12
For personal use only.

(3H, s), 1.73 (2H, d, J_{HP} 1.53), 2.08 (3H, d, J_{HP} 3.28), 2.85 (2H, d, J_{HP} 17.32), 3.97 (4H, m), 4.69 (2H, two d, $J_{HH\ gem}$ 20.77); δ_C: −0.52 (q, J_{CH} 118.8), 16.3 (dq, J_{CP} 6.6, J_{CH} 128.5), 23.2 (q, J_{CH} 130.0), 24.2 (dq, J_{CP} 7.9, J_{CH} 127.2), 29.3 (dt, J_{CP} 18.6, J_{CH} 121.2), 38.0 (dt, J_{CP} 12.3, J_{CH} 127.2), 61.0 (dt, J_{CP} 5.5, J_{CH} 146.6), 110.3 (t, J_{CH} 153.3), 117.3 (d, J_{CP} 180.7), 142.7 (s), 156.2 (d, J_{CP} 12.2). Anal. calcd. for $C_{15}H_{31}O_3PSi$: C 56.57, H 9.81; found: C 56.16, H 9.75.

Allylation of allylic phosphonates. General procedure

The procedure used was the same as for the silanylation reactions. 1.2 Mol-equivalents of BuLi and of 3-bromoprop-1-ene (or 2-methyl-3-bromoprop-1-ene) were used per 1.0 mol-equiv. of the substrate (ca. 10 mmol).

Diethyl 1-vinylbut-3-enylphosphonate ***3d*** *(74%)*: bp 72–73°C at 0.1 Torr; δ_P: 28.9; δ_H: 1.26 (6H, t, J_{HH} 7.07), 2.51 (1H, m), 2.94 (2H, m), 4.06 (4H, quint, J_{HP}, J_{HH} 7.13), 4.98 (2H, two dd, $J_{HH\ trans}$ 15.27, $J_{HH\ cis}$ 6.74, $J_{HH\ gem}$ 1.36), 5.17 (2H, two dd, $J_{HH\ trans}$ 14.59, $J_{HH\ cis}$ 9.04, $J_{HH\ gem}$ 1.29), 5.70 (2H, m); δ_C: 16.4 (dq, J_{CP} 66.2, J_{CH} 126.4), 32.6 (dt, J_{CP} 4.4, J_{CH} 130.9), 42.7 (dd, J_{CP} 138.3, J_{CH} 131.5), 61.7 (dt, J_{CP} 6.7, J_{CH} 147.8), 62.1 (dt, J_{CP} 6.8, J_{CH} 147.7), 116.6 (t, J_{CH} 154.0), 119.1 (dt, J_{CP} 13.5, J_{CH} 150.3), 132.6 (dd, J_{CP} 9.7, J_{CH} 148.2),135.6 (dd, J_{CP} 15.8, J_{CH}150.3); MS, *m/z*: 218 (M^+, 5%), 190 (8), 177 (40), 175 (9), 162 (11), 139 (100), 121 (48), 109 (40), 81 (74), 80 (99). Anal. calcd. for $C_{10}H_{19}O_3P$: C 55.04, H 8.76; found: C 54.90, H 8.84.

Diethyl 1-vinyl-3-methylbut-3-enylphosphonate ***3e*** *(76%)*: bp 73°C at 0.07 Torr; δ_P: 29.5; δ_H: 1.27 (3H, t, J_{HH} 7.11), 1.28 (3H, t, J_{HH} 7.00), 1.64 (3H, s), 2.51 (2H, two d, J_{HH} 10.07), 2.70 (1H, m), 4.07 (4H, quint, J_{HP}, J_{HH} 7.26), 4.71 (2H, two d, $J_{HH\ gem}$ 19.63), 5.12 (2H, m), 5.60 (1H, m); δ_C: 16.4 (dq, J_{CP} 5.8, J_{CH} 124.2), 21.8 (q, J_{CH} 127.8), 36.3 (dt, J_{CP} 4.2, J_{CH} 124.8), 41.0 (dd, J_{CP} 138.3, J_{CH} 132.7), 61.9 (dt, J_{CP} 6.9, J_{CH} 147.5), 62.2 (dt, J_{CP} 6.9, J_{CH} 149.8), 112.6 (t, J_{CH} 155.2), 118.9 (dt, J_{CP} 13.2, J_{CH} 155.6), 132.7 (dd, J_{CP} 9.9, J_{CH} 162.6), 142.0 (d, J_{CP} 16.9); MS, *m/z*: 232 (M^+, 5%), 177 (11), 139 (22), 111 (64), 94 (100), 93 (51), 79 (99). Anal. calcd. for $C_{11}H_{21}O_3P$: C 56.89, H 9.11; found: C 57.01, H 9.00.

Diethyl 1-(1-methylvinyl)-3-methylbut-3-enylphosphonate ***3f*** *(81%)*: bp 76°C at 0.06 Torr; δ_P: 29.7; δ_H: 1.28 (3H, t, J_{HH} 7.11), 1.29 (3H, t, J_{HH} 7.15), 1.67 (3H, s), 1.81 (3H, s), 2.47 (2H, d, J_{HH} 10.68), 2.76 (1H, ddd, J_{HP} 23.68, J_{HH} 10.68, 4.70), 4.08 (4H, quint, J_{HP}, J_{HH} 7.09), 4.71 (2H, two d, $J_{HH\ gem}$ 20.2), 4.92 (2H, two dd, J_{HP} 9.04, 4.52, $J_{HH\ gem}$ 33.0); δ_C: 16.3 (dq, J_{CP} 5.7, J_{CH} 126.9), 21.2 (dq, J_{CP} 2.4, J_{CH} 123.8), 21.6 (q, J_{CH} 125.8), 35.3 (dt, J_{CP} 3.7, J_{CH} 128.2), 43.7 (dd, J_{CP} 139.9, J_{CH} 131.7), 61.6 (dt, J_{CP} 7.1, J_{CH} 150.0), 62.1 (dt, J_{CP} 7.1, J_{CH} 149.8), 112.2 (t, J_{CH} 155.2), 115.5 (dt, J_{CP} 12.1, J_{CH} 156.1), 139.6 (d, J_{CP} 9.1), 142.2 (d, J_{CP} 17.4); MS, *m/z*: 246 (M^+, 10%), 231 (5), 203 (4), 191 (19), 176 (6), 139 (36), 108 (36), 93 (100). Anal. calcd. for $C_{12}H_{23}O_3P$: C 58.45, H 9.40; found: C 58.35, H 9.30.

Isomerization of 3-silanylprop-1-enylphosphonates. General procedure

A. Thermal

A sample of the vinylic phosphonate (ca. 10 mmol) was sealed in a glass tube and the tube was heated in an oil bath at 140°C for 6 h. The tube was opened and the product was purified by bulb-to-bulb distillation.

E/Z *Mixture of diethyl 3-(diphenylmethylsilanyl)prop-2-enylphosphonate* ***2a*** *(from* ***1b****) (89%)*: oven temp. 130°C at 0.2 Torr; E-*isomer* (55%), δ_P: 26.8; δ_H: 0.56 (3H, s), 1.26 (6H, t, J_{HH} 7.10), 2.56 (2H, dd, J_{HP} 22.09, J_{HH} 6.61), 4.06 (4H, quint, J_{HP}, J_{HH} 7.20), 6.08 (1H,m), 6.18 (1H, dd, J_{HP} 4.00, $J_{HH\ trans}$ 18.49), 7.50 (10H, m); δ_C: −3.95 (q, J_{CH} 120.4), 16.4 (dq, J_{CP} 7.6, J_{CH} 126.8), 35.0 (dt, J_{CP} 136.1, J_{CH} 128.0), 61.9 (dt, J_{CP} 6.4, J_{CH} 146.7), 127.7 (d, J_{CH} 160.1), 129.3 (d, J_{CH} 159.5), 132.6 (dd, J_{CP} 11.8, J_{CH} 159.2), 134.8 (d, J_{CH} 151.0), 135.4 (s), 138.7 (dd, J_{CP} 11.0, J_{CH} 161.7); MS, *m/z*: 374 (M^+, 11%), 359 (13), 343 (10), 297 (56), 225 (100), 197 (30), 163 (59),137 (19), 105 (38). Z-*isomer* (34%): δ_P: 27.7; δ_H: 0.63 (3H, s), 1.28 (6H, t, J_{HH} 7.09), 2.76 (2H, dd, J_{HP} 22.0, J_{HH} 7.30), 4.06 (4H, quint, J_{HP}, J_{HH} 6.98), 5.18 (1H, m), 5.76 (1H, m), 7.43 (10H, m); δ_C: −0.70 (q, J_{CH} 119.6), 16.3 (dq, J_{CP} 5.8, J_{CH} 123.1), 31.7 (dt, J_{CP} 154.3, J_{CH} 139.8), 61.9 (dt, J_{CP} 6.6, J_{CH} 147.1), 119.8 (dd, J_{CP} 14.3, J_{CH} 147.5), 127.6 (d, J_{CH} 160.3), 129.5 (d, J_{CH} 159.5), 133.9 (d, J_{CH} 152.2), 134.6 (dd, J_{CP} 7.5, J_{CH} 151.3), 134.7 (s). Anal. calcd. for $C_{20}H_{27}O_3PSi$: C 63.47, H 7.19; found: C 62.95, H 7.10.

B. Prototropic

E/Z *Mixture of diethyl 3-(diphenylmethylsilanyl)-2-methylprop-2-enylphosphonate* ***2b***

1c (10 mmol) was dissolved in THF (10 mL), the solution was cooled to −78°C, and buthyllithium (1.6 M solution in hexane, 12 mmol) was added. After stirring at −78°C for 3 h, the reaction mixture was quenched with aqueous NH_4Cl and the product was separated in the usual way. **2b** (90%): oven temp. 130°C at 0.2 Torr; E-*isomer* (32%): δ_P: 27.1; δ_H: 0.49 (3H, s), 1.25 (6H, t, J_{HH} 7.08), 2.21 (3H, d, J_{HH} 1.30), 2.56 (2H, d, J_{HP} 22.98), 4.09 (4H, quint, J_{HP}, J_{HH} 7.28), 5.74 (1H, m), 7.38 (10H, m); δ_C: −2.56 (q, J_{CH} 120.9), 16.0 (dq, J_{CP} 6.7, J_{CH} 126.9), 25.1 (dq, J_{CP} 5.8, J_{CH} 127.0), 39.9 (dt, J_{CP} 134.1, J_{CH} 138.0), 61.1 (dt, J_{CP} 6.7, J_{CH} 147.2), 125.4 (dd, J_{CP} 11.0, J_{CH} 159.0), 128.7 (d, J_{CH} 159.8), 128.8 (d, J_{CH} 159.2), 134.2 (d, J_{CH} 160.4),136.5 (s), 152.1 (d, J_{CP} 8.5); MS, *m/z*: 388 (M^+, 6%), 373 (4), 311 (13), 197 (100), 191 (12) 181 (27) 137 (13), 105 (19). Z-*isomer* (58%): δ_P: 27.8; δ_H: 0.58 (3H, s), 1.25 (6H, t, J_{HH} 7.11), 2.33 (3H, d, J_{HH} 1.80), 2.79 (2H, d, J_{HP} 22.74), 4.00 (4H, quint, J_{HP}, J_{HH} 7.33), 4.75 (1H, d, J_{HH} 5.08), 7.38 (10H, m); δ_C: −4.97 (q, J_{CH} 120.4), 16.0 (dq, J_{CP} 6.7, J_{CH} 128.9), 24.5 (dq, J_{CP} 2.3, J_{CH} 127.4), 35.2 (dt, J_{CP} 136.5, J_{CH} 131.7), 61.3 (dt, J_{CP} 6.7, J_{CH} 147.2), 113.7 (dd, J_{CP} 12.1, J_{CH} 156.5), 127.6 (d, J_{CH} 159.0), 129.0 (d, J_{CH} 159.7), 134.0 (d, J_{CH} 159.2), 136.3 (s), 148.0 (d, J_{CP} 10.2). Anal. calcd. for $C_{21}H_{29}O_3PSi$: C 64.26, H 7.45; found: C 63.95, H 7.55.

Cope rearrangement

A sample of **3d–f** (ca. 10 mmol) was placed in a glass tube, and the tube was evacuated to a pressure of 10^{-3} Torr, sealed, and heated in an oil bath at 210°C for 6 h. After the tube was opened, the product was purified by bulb-to-bulb distillation.

Diethyl hexa-1,5-dienylphosphonate ***5a*** *(from* ***3d****) (84%)*: oven temp. 130°C at 0.1 Torr; δ_P: 18.6; δ_H: 1.25 (6H, t, J_{HH} 7.09), 2.18 (2H, m), 4.01 (4H, m), 5.00 (2H, m), 5.59 (1H, m),

© 1997 NRC Canada

6.62–6.81 (2H, m); δ_C: 15.5 (dq, J_{CP} 6.4, J_{CH} 126.9), 31.1 (t, J_{CH} 122.5), 32.4 (dt, J_{CP} 22.3, J_{CH} 124.5), 60.6 (dt, J_{CP} 5.5, J_{CH} 137.5), 114.6 (t, J_{CH} 153.2), 116.7 (dd, J_{CP} 188.2, J_{CH} 162.1), 136.0 (d, J_{CH} 152.2), 151.6 (dd, J_{CP} 4.2, J_{CH} 156.1); MS, *m/z*: 218 (M^+, 3%), 203 (2), 190 (10), 177 (8), 162 (13), 139 (32), 121 (53), 111 (45), 80 (100). Anal. calcd. for $C_{10}H_{19}O_3P$: C 55.04, H 8.76; found: C 54.81, H 8.90.

Diethyl 5-methylhexa-1,5-dienylphosphonate ***5b*** *(from* ***3e****) (87%)*: oven temp. 130–140°C at 0.1 Torr; δ_P: 19.0; δ_H: 1.27 (6H, t, J_{HH} 7.05), 1.67 (3H, s), 2.12 (2H, t, J_{HH} 7.48), 2.32 (2H, m), 4.04 (4H, quint, J_{HP}, J_{HH} 7.29), 4.67 (2H, d, $J_{HH\,gem}$ 17.37), 5.59 (1H, dd, J_{HP} 21.17), $J_{HH\,trans}$ 16.87), 6.72 (1H, qdd, J_{HP} 22.04, $J_{HH\,trans}$ 17.07, J_{HH} 16.10); δ_C: 16.0 (dq, J_{CP} 6.2, J_{CH} 124.5), 21.9 (q, J_{CH} 125.1), 31.7 (dt, J_{CP} 22.1, J_{CH} 126.2), 35.4 (t, J_{CH} 135.9), 61.2 (dt, J_{CP} 5.2, J_{CH} 147.1), 110.5 (t, J_{CH} 149.8), 116.8 (dd, J_{CP} 187.7, J_{CH} 156.2), 144.0 (s), 153.0 (dd, J_{CP} 4.5, J_{CH} 156.1); MS, *m/z*: 232 (M^+, 4%), 217 (3), 177 (11), 139 (22), 111 (64), 94 (100), 93 (51), 79 (99). Anal. calcd. for $C_{11}H_{21}O_3P$: C 56.89, H 9.11; found: C 56.50, H 9.40.

E/Z *Diethyl 2,5-dimethylhexa-1,5-dienylphosphonate* ***5c*** *(from* ***3f****) (96%)*: oven temp. 130–140°C at 0.1 Torr; E-*isomer* (34%): δ_P: 19.5; δ_H: 1.22 (6H, t, J_{HH} 7.02), 1.68 (3H, s), 1.84 (3H, d, J_{HH} 1.01), 2.09 (2H, m), 2.57 (2H, m), 3.97 (4H, quint, J_{HP}, J_{HH} 7.60), 4.62 (2H, d, $J_{HH\,gem}$ 13.36), 5.32 (1H, d, J_{HP} 18.32); δ_C: 16.0 (dq, J_{CP} 6.5, J_{CH} 125.7), 22.0 (q, J_{CH} 12.2), 25.3 (dq, J_{CP} 7.1, J_{CH} 128.8), 33.1 (dt, J_{CP} 24.5, J_{CH} 142.2), 36.0 (t, J_{CH} 131.5), 60.8 (dt, J_{CP} 5.5, J_{CH} 147.2), 110.0 (t, J_{CH} 158.8), 112.5 (dd, J_{CP} 189.4, J_{CH} 152.9),144.7 (s), 162.6 (d, J_{CP} 6.1); MS, *m/z*: 246 (M^+, 8%), 231 (5), 191 (4), 176 (9), 139 (27), 108 (100), 93 (55). Z-*isomer* (62%): δ_P: 18.8; δ_H: 1.22 (6H, t, J_{HH} 7.02), 1.63 (3H, s), 2.00 (3H, dd, J_{HH} 0.81, 3.13), 2.09 (2H, m), 2.13 (2H, m), 3.96 (4H, quint, J_{HP}, J_{HH} 7.32), 4.61 (2H, d, $J_{HH\,gem}$ 13.4), 5.30 (1H, d, J_{HP} 18.3); δ_C: 16.0 (dq, J_{CP} 6.5, J_{CH} 125.6), 19.7 (dq, J_{CP} 7.1, J_{CH} 128.8), 22.0 (q, J_{CH} 126.2), 35.09 (t, J_{CH} 126.0), 39.2 (dt, J_{CP} 22.9, J_{CH} 127.7), 60.8 (dt, J_{CP} 5.5, J_{CH} 147.2), 110.4 (t, J_{CH} 154.9), 111.4 (dd, J_{CP} 188.9, J_{CH} 153.8), 144.0 (s), 154.9 (d, J_{CP} 6.1). Anal. calcd. for $C_{12}H_{23}O_3P$: C 58.45, H 9.40; found: C 57.99, H 9.38.

Acknowledgment

Financial support from the University of Pretoria and the Foundation for Research Development is gratefully acknowledged.

References

1. J.I.G. Cadogan. Organophosphorus reagents in organic synthesis. Academic Press, London. 1978. Chap. 3.
2. E.W. Colvin. Silicon reagents in organic synthesis. Academic Press, London. 1988. Chap. 5.
3. I.C. Baldwin, R.P. Beckett, and J.M.J. Williams. Synthesis, 34 (1996).
4. M.F. Probst and T.A. Modro. Heteroat. Chem. **6**, 579 (1995).
5. A.M.M. Phillips and T.A. Modro. Phosphorus, Sulfur, Silicon, **55**, 41 (1991).
6. H. Al-Badri, E. About-Jaudet, and N. Collignon. Tetrahedron Lett. **36**, 393 (1995).
7. E.J. Corey and D.E. Cane. J. Org. Chem. **34**, 3053 (1969); H. Al-Badri, E. About-Jaudet, and N. Collignon. J. Chem. Soc. Perkin Trans. 2, 931 (1996); S.E. Denmark and J.-H. Kim. J. Org. Chem. **60**, 7535 (1995); K. Tanaka, Y. Ohta, and K. Fuji. J. Org. Chem. **60**, 8036 (1995); L.-H. Li, D. Wang, and T.H. Chan. Tetrahedron Lett. **32**, 2879 (1991); C. Yuan, J. Yao, and S. Li. Phosphorus, Sulfur, Silicon, **55**, 125 (1991); O.I. Kolodyazhnyi and S.N. Yastenko. J. Gen. Chem. USSR (Engl. Transl.), **60**, 610 (1996).
8. J.P. Gerber, T.A. Modro, C.C.P. Wagener, and A. Zwierzak. Heteroat. Chem. **2**, 643 (1991).
9. S. Berger, S. Braun, and H.-O. Kalinowski. NMR-Spektroskopie von Nichtmetallen. Band 3. G. Thieme Verlag, Stuttgart. 1993. p. 143.
10. L. Maier. Phosphorus, **5**, 223 (1975).

Can. J. Chem. Downloaded from www.nrcresearchpress.com by 88.146.161.215 on 09/08/12
For personal use only.

© 1997 NRC Canada

The chemistry of thujone. XX.[1] New enantioselective syntheses of Ambrox and *epi*-Ambrox

James P. Kutney and Carles Cirera

Abstract: The development of a new synthetic approach to (−)-Ambrox® (**37**) and *epi*-Ambrox® (**29**) using thujone (**1**) as a chiral synthon, is presented. Thujone (**1**), a readily available starting material obtained from Western red cedar, can be efficiently converted to β-cyperone (**2**) and the latter is then chemically elaborated to the key intermediate, the enone **6**. A carbonyl transposition of **6** to enone **9** also allows a formal synthesis of (−)-Polywood® (**18**).

Key words: thujone, β-cyperone, (−)-Ambrox®, *epi*-Ambrox®, synthesis.

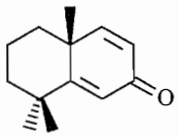
Résumé : On présente une nouvelle approche à la synthèse du (−)-Ambrox® (**37**) et de l'*epi*-Ambrox® (**29**) utilisant la thujone (**1**) comme synthon chiral. La thujone (**1**), un produit facilement disponible à partir des cèdres rouges de l'ouest, peut être transformé d'une façon efficace en β-cypérone (**2**) qui peut, par la suite, être converti en énone **6**, un intermédiaire clé. Une transposition du carbonyle de l'énone **6** en énone **9** permet de réaliser aussi une synthèse formelle du (−)-Polywood® (**18**).

Mots clés : thujone, β-cypérone, (−)-Ambrox®, *épi*-Ambrox®, synthèse.

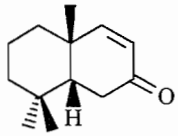
[Traduit par la rédaction]

The ambergris fragrances are well established as an important family of perfumes. Extensive reviews, which detail studies correlating their structure with smell, synthetic efforts, etc., are available (2–4). In particular, the classic members, (−)-Ambrox® (**37**) and (+)-iso-Ambrox® (**38**), form the basis of commercial products, for example, Fixateur 404 (trade name of Firmenich), which has been marketed in the perfumery industry for more than 30 years. In a previous study (5), we presented one of our synthetic approaches to these compounds from the readily available chiral synthon thujone (**1**). We now wish to detail our most recent studies, which afford alternative and novel enantioselective syntheses to (−)-Ambrox® (**37**) and (−)-*epi*-Ambrox® (**29**) from thujone.

In developing a possible route to the above, our consideration turned to the conjugated enone **6** (Scheme 1) available from β-cyperone (**2**), via a previously published procedure (6–8). To functionalize decalone **6** in a manner that would allow eventual synthesis of Ambrox® (**37**), it was evident that a two-carbon unit had to be attached at position C9. Based on unsuccessful attempts to achieve 1,4-addition products with **7** and only very moderate yields with the *cis*-decalone **8**, an alternative ketone transposition process (**6** → **9**, Scheme 2) appeared as an attractive alternative route. Based on the relatively inefficient published procedures (9–11), the route summarized in Scheme 2 was selected.



7



8

For this purpose, it was important to maintain the double bond functionality during the transposition steps, in order to ensure the regioselective alkylation at position C9, since competing alkylation is expected at C7 when both C7 and C9 positions are accessible for alkylation (12–14). As noted in the conversion of **6** to **10**, an oxidation at C8 is essential. For this purpose, the reaction involving α-hydroxylation of α,β-unsaturated ketones, by means of manganese(III) acetate originally described by Williams and Hunter (15), and subsequently improved by Watt and coworkers (16–18), was selected. When the reported conditions were applied to **6**, only low to moderate yields (35–60%) of the acetoxylated product were obtained even though special care was taken in drying the manganese(III) acetate. Since manganese(III) acetate is commercially available in its hydrated form, the reported drying method (phosphorus pentoxide and high vacuum for several days) proved to be insufficient for our purpose. Indeed, when azeotropic removal of water was carried out, the lower yields obtained by Watt (16, 17), could be improved and a mixture of the desired acetoxyketones **10/11** (R = Ac) were consistently obtained in 86% yield (Scheme 3). The mechanism proposed is consistent with that presented earlier (18).

α-Acetoxylation of enone **6** resulted in an inseparable mixture of isomers **10/11** in a 4:1 ratio. Assignment of the structures was done from the analysis of the C8 proton signal in the ^{1}H NMR spectrum. The proton at position C8 of the major

Received August 19, 1996.[2]

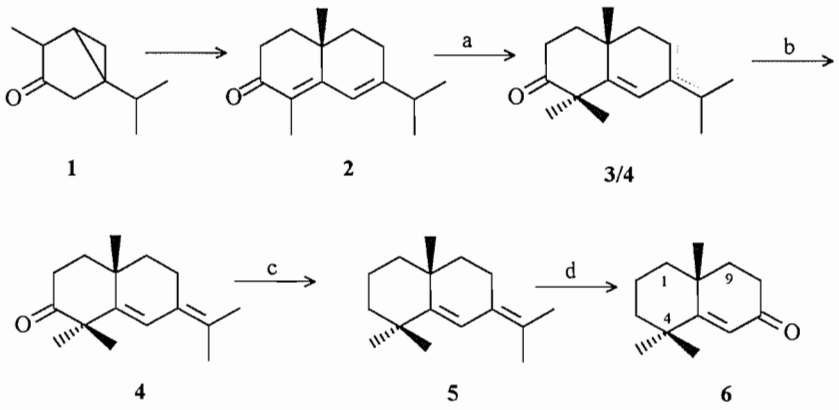
J.P. Kutney[3] and C. Cirera. Department of Chemistry, University of British Columbia, 2036 Main Mall, Vancouver, BC V6T 1Z1, Canada.

[1] For Part XIX, see ref. 1.
[2] Revision received May 21, 1997.
[3] Author to whom correspondence may be addressed: Telephone and Fax: (604) 822-2710. E-mail: Kutney@unixg.ubc.ca

© 1997 NRC Canada

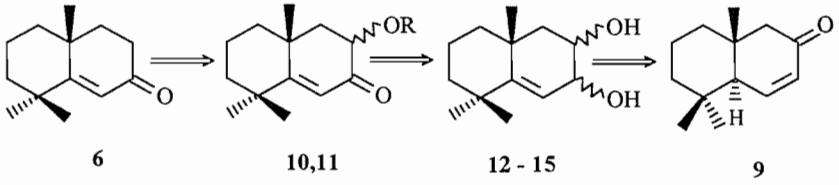
Can. J. Chem. Downloaded from www.nrcresearchpress.com by 88.146.161.215 on 09/08/12
For personal use only.

Scheme 1. Synthesis of enone **6** from thujone (**1**).



(a) NaOMe, DMSO; MeI; (b) I_2, hexane, reflux; (c) $H_2N–NH_2$, KOH, DEG; (d) O_3, MeOH–CH_2Cl_2, −78°C.

Scheme 2. A proposed ketone transposition sequence from enone **6** to enone **9**.



Scheme 3. Proposed mechanism for α-acetoxylation of enone **6**.

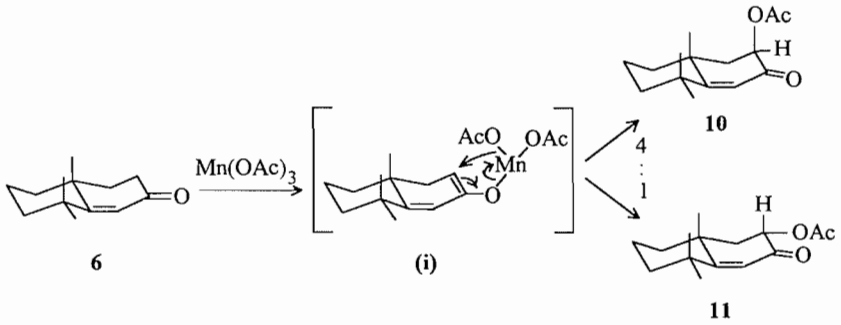
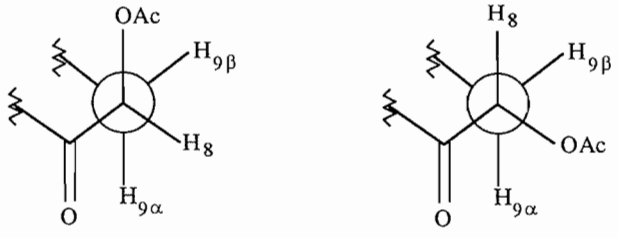


Fig. 1. The spatial relationship of the C8 and C9 protons in isomers **10/11**.



isomer displayed a triplet at δ 5.25 ppm (J = 4 Hz), which is in accordance with an equatorial position at C8 since it resides at an equal distance from the C9-αH and C9-βH (Fig. 1). On the other hand, the minor isomer, with its acetoxyl group in the α orientation, displayed a doublet of doublets at δ 5.60 ppm (J = 12, 4 Hz) for the axial C8 proton, being anti-periplanar to the C9-αH, and displaying therefore a large coupling constant (J = 12 Hz) when coupled with this hydrogen, and a small coupling constant (J = 4 Hz) when coupled with C9-βH, which corresponds to an angle of 60°.

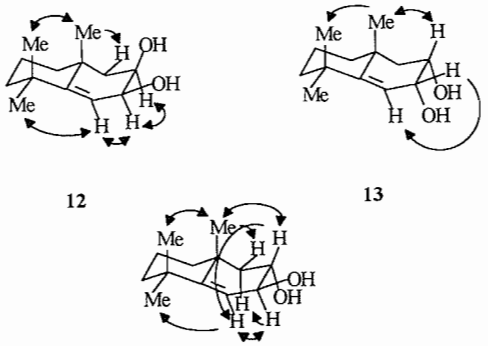
The mixture of isomers **10/11** was reduced with LAH, yielding a mixture of four isomeric diols **12/13/14/15** in a ratio of 50:1:3:18, as observed after isolation of the pure diols. The diols **12–15** were separated by column chromatography for characterization purposes. Assignment of the different configurations for diols **12–14** was done by ^{1}H NMR and NOE difference experiments (Fig. 2). It was expected that the two major isomers should possess the hydroxyl group at position C7 in the β orientation, since the reducing agent was expected to approach the carbonyl function predominantly from the less hindered side (α face). The remaining diol **15** was then assigned as the 7α,8β isomer.

The following dehydration step was experimentally rather "delicate." A selective dehydration of the hydroxyl at position C7 was required in order to furnish the desired ketone **9**. The expected different reactivity of the two hydroxyl groups was a key factor for the success of the sequence. Discrimination of

© 1997 NRC Canada

Can. J. Chem. Downloaded from www.nrcresearchpress.com by 88.146.161.215 on 09/08/12
For personal use only.

Fig. 2. A summary of proton interactions as determined from NOE difference experiments with alcohols **12**, **13**, and **14**.



12 **13**

14

the hydroxyl groups under acidic conditions was indeed achieved and the hydroxyl at C7 underwent selective dehydration and conversion to the desired product **9** (Scheme 4). The elimination of the hydroxyl group at C8 would simply regenerate the initial enone **6** but this was not observed. The final step, in which the migration of the double bond occurs, was expected to take place easily under acidic conditions, fortunately towards the desired *trans*-decalone system.

By using 1.2 equivalents of *p*-toluenesulfonic acid and 0.1 M concentration of diols **12–15** in anhydrous THF, 64% of the *trans*-enone **9**, 25% of the nonconjugated enone (**16**), and less than 2% of the *cis*-enone (**17**) were isolated. These results suggested that the transformation of **12–15** to the mixture of **9**, **16**, **17** is kinetically controlled since published studies (ref. 19, footnote 9) have determined that the proportions at thermodynamic equilibrium are **9** (26%), **16** (6%), and **17** (69%). In a separate experiment, when enone **16** was submitted to the same conditions, a 65% yield of the *trans*-decalone (**9**), and 31% of the nonconjugated enone (**16**) was obtained, while no *cis*-decalone was isolated.

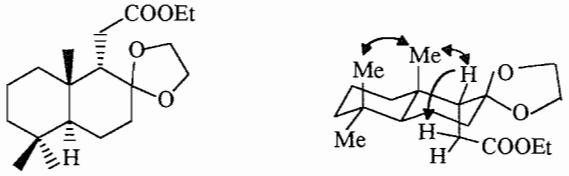
The overall yield in the three steps for the conversion, **12–15** to **9**, was 64% when the isolated nonconjugated enone (**16**) was recycled. A notable advantage of this novel sequence is that these three operations can be done without isolation of the intermediates, so that an effective route to **9** was now available. For preparative purposes, the sequence, **6** → **10/11** → **12–15** → **9**, can be conducted *without* isolation of the pure components in the various stages and in an overall yield of 64%.

Compound **9** displayed a peak at *m/z* 192 in the mass spectrum, corresponding to the molecular ion. Its ^{1}H and ^{13}C NMR spectra agreed with the published data (20), although an authentic sample was unavailable for direct comparison. Similarly, the data for the *cis*-decalone (**17**) and the nonconjugated enone (**16**) were also in agreement with the published data (20).

Enone **9** as well as **16** have been prepared as racemic intermediates, by a completely different route, by Snowden et al. (19) in their synthesis of (±)-Polywood® (**18**) and its unsaturated analogs. On this basis, a formal synthesis of (−)-Polywood® (**18**) and its chiral unsaturated analogs has been completed starting from thujone (**1**) (Scheme 5).

With the desired enone **9** on hand, introduction of a two-carbon unit at C9 was considered. Generation of the enolate by reacting **9** with lithium diisopropylamide at −78°C and subsequent reaction with ethyl iodoacetate afforded the desired intermediate **19** in 73% yield. The α orientation of the side chain in **19** was established from an analysis of the NMR data (see Experimental). It should be noted that a minor by-product (8% yield) was isolated and, on the basis of spectroscopic data (see Experimental), was assigned the structure **27**.

Fig. 3. A summary of proton interactions as determined from a NOE difference experiment with ketal **21**.



21

Catalytic hydrogenation of the double bond in **19** was achieved in quantitative yield by using catalytic amounts of 10% palladium on charcoal in ethanol at 40 psi of hydrogen (1 psi = 6.9 kPa). Under these conditions, the double bond in compound **19** was selectively hydrogenated in 20 min without reducing the carbonyl group.

Elaboration of the ester side chain in **20** to the required primary alcohol **22** (Scheme 6) via classical LAH reduction required prior protection of the ketone function. Preliminary experiments under acid-catalyzed ketalization conditions suggested a facile epimerization of the α-oriented side chain in **19** to the thermodynamic β-oriented position (see **28**, Scheme 6). On this basis, a series of reactions, under carefully controlled conditions and utilizing triflic acid (20) and TMS-triflate (21, 22) as catalysts, were undertaken. With the former catalyst, ketal **21** could be obtained in reasonable yield (67%) when the ketone **20** (1.0 mmol in anhydrous THF) was reacted with triflic acid (0.2 mmol) and 1,2-bis(TMSO)–ethane (1.9 mmol) at 0°C (14 h). Similar results were obtained with TMS-triflate and further details are provided in the experimental section. Detailed NOE experiments (Fig. 3 and Experimental) established that no epimerization of the axially oriented side chain had occurred during the ketalization reaction. The isomeric ketal **28** was obtained as a minor product (8%).

Having found a suitable protection method for the ketone functionality, we turned our attention to the synthetic steps required to obtain diol **26**. Reduction of the ester in **21**, protection of the alcohol, deprotection of the ketone, Grignard reaction, and finally deprotection of the primary alcohol, were the synthetic steps envisaged in order to obtain diol **26**.

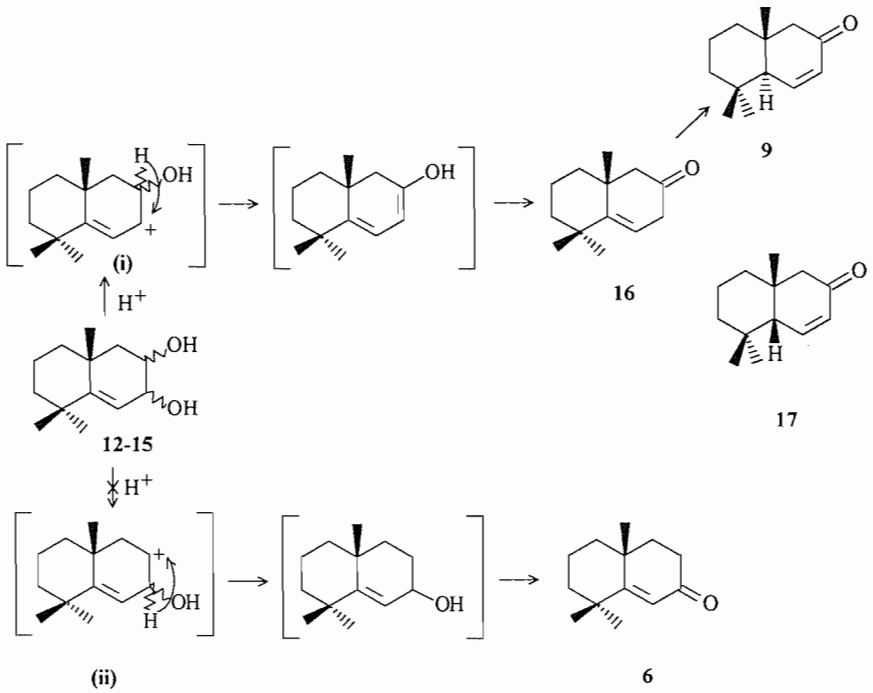
Ketal ester **21** was reduced with an excess of LAH in diethyl ether in 10 min at room temperature, affording the alcohol **22** in essentially quantitative yield.

Protection of the primary alcohol was required before further transformation could be done since removal of the ketal function under mild acidic conditions afforded only low recovery of the desired keto alcohol, indicating that decomposition took place to a considerable extent. In addition, attempted purification of the expected keto alcohol showed that this compound was unstable and a complex mixture of compounds was obtained. For this purpose, the benzyl group appeared ideal since it is expected to be stable under acidic conditions and could be subsequently removed by catalytic hydrogenolysis. Reaction of **22** with benzyl chloride in

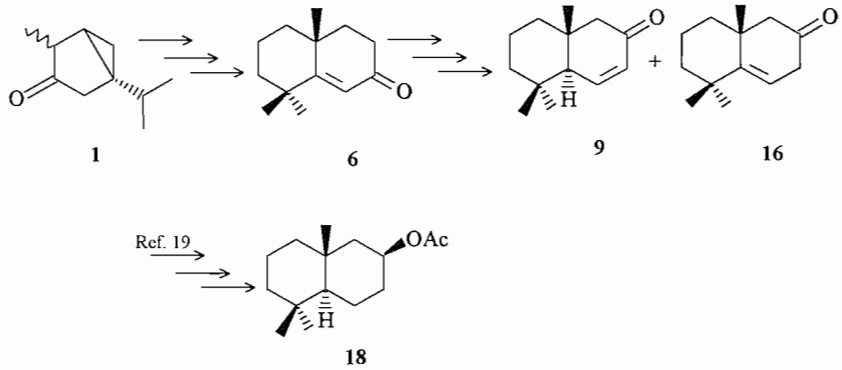
Can. J. Chem. Downloaded from www.nrcresearchpress.com by 88.146.161.215 on 09/08/12
For personal use only.

© 1997 NRC Canada

Scheme 4. Proposed mechanism for the dehydration of diols **12–15**.



Scheme 5. Formal synthesis of (−)-Polywood® (**18**) from thujone (**1**).



ethanol heated at reflux for 12 h in the presence of sodium hydride, potassium carbonate, and catalytic amounts of sodium iodide furnished the desired product in 68% yield (87% based on starting material recovered). A method reported by Provelenghiou and co-workers (23), used in the protection of hydroxyl groups in carbohydrates and claimed to be simple, rapid, and quantitative, was also evaluated. Removal of the weakly acidic alcoholic proton in compound **22** was done with sodium hydride, followed by addition of excess of benzyl bromide and 0.1 equivalent of tetrabutylammonium iodide followed by reflux, afforded an essentially quantitative yield of **23** (R = $CH_2C_6H_5$).

Regeneration of the carbonyl function to afford **24** (R = $CH_2C_6H_5$) was readily achieved (1 M HCl at room temperature). In summary, for preparative purposes, the three-step conversion, **21** → → **24**, could be achieved in a "one-pot" operation and in an overall yield of 87%.

With the ketone **24** (R = $CH_2C_6H_5$) available, the conversion to the tertiary alcohol **25** was now considered. Conventional Grignard reaction conditions (methylmagnesium iodide in refluxing ether) afforded **25** (R = $CH_2C_6H_5$) in low yield (20%). However, reaction of **24** (R = $CH_2C_6H_5$) with the methyl cerium(III) reagent, generated by reaction of methyllithium with anhydrous cerium(III) chloride (24–26), afforded **25** in essentially quantitative yield.

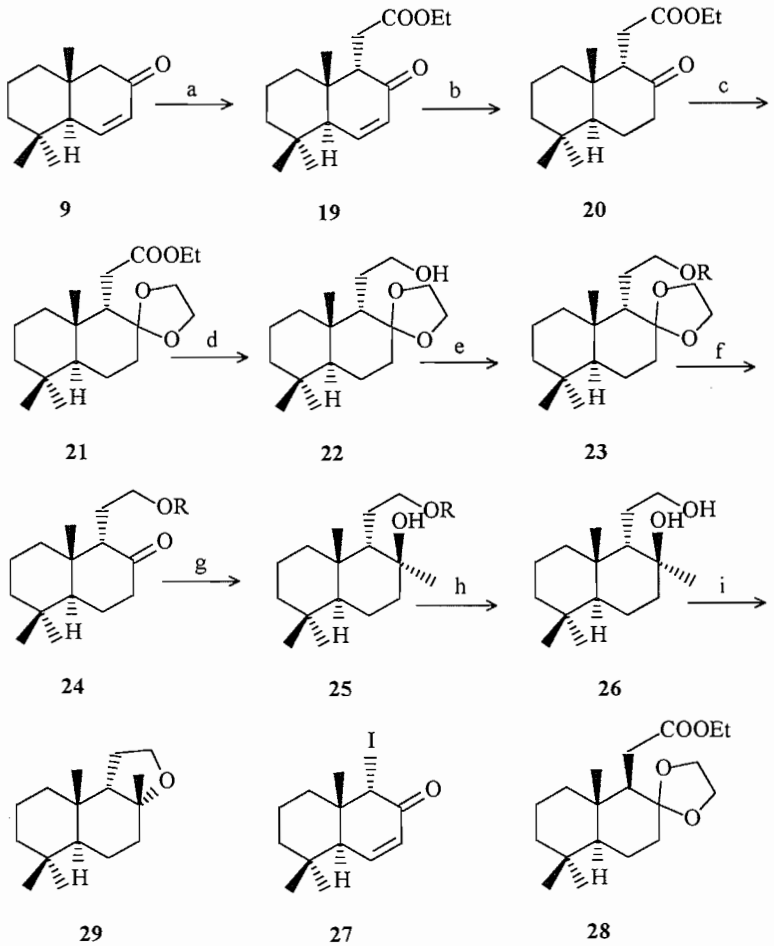
Removal of the benzyl group was achieved by catalytic hydrogenolysis (palladium in charcoal) to provide **26** in excellent yield (97%).

The final step in the synthetic route involved acid-catalyzed cyclization of **26** to (−)-*epi*-Ambrox® (**29**). Of the various approaches available from the literature (27–31), the method chosen involved *p*-toluenesulfonic acid as catalyst. When a nitromethane solution of **26** was treated with this catalyst at 80°C, the desired natural product **29** (32, 33) was obtained in 83% yield. For preparative purposes, (−)-*epi*-Ambrox® (**29**) has been prepared from the ketone **24** (R = $CH_2C_6H_5$) in 80%

© 1997 NRC Canada

Can. J. Chem. Downloaded from www.nrcresearchpress.com by 88.146.161.215 on 09/08/12
For personal use only.

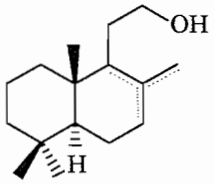
Scheme 6. Synthesis of (−)-*epi*-Ambrox® (**29**) from enone **9**.



(a) LDA; ICH_2CO_2Et; (b) H_2/Pd–C; (c) 1,2-bis(TMSO)ethane; TMS triflate; (d) LAH; (e) $PhCH_2Br$, *n*-Bu_4NI; (f) HCl, acetone; (g) MeLi, $CeCl_3$; (h) H_2/Pd–C; (i) *p*-TsOH, CH_3NO_2

overall yield without isolation of intermediates (see Method B, experimental section).

In addition to **29**, in the cyclization of **26**, a mixture of olefinic alcohols, tentatively assigned the general structure **30**, was also obtained (11%). This mixture could not be purified further by column chromatography and studies to clarify this mixture were not pursued.



30

In conclusion, the above five-step synthetic route from enone **6** (previously prepared from thujone) to **29** allows synthesis of the latter in 33% overall yield.

A similar sequence to the one reported for (−)-*epi*-Ambrox® (**29**) has been followed for the synthesis of (−)-Ambrox® (**37**). In this case, the secondary product **31** from the ketalization reaction under protic conditions (and the main product when thermodynamic equilibration conditions were applied), was used to develop a parallel sequence towards (−)-Ambrox® (**37**) (Scheme 7). The starting material **31** contains the desired equatorial side chain required for Ambrox® (**37**). Reduction of ketal **31** with LAH afforded alcohol **32** in 92% yield.

Benzylation of the hydroxyl group was performed as for compound **22**, yielding compound **33** in 92% yield.

Removal of the ketal group in **33** was performed as indicated for compound **23** although in this case longer reaction times were required when the same conditions were employed.

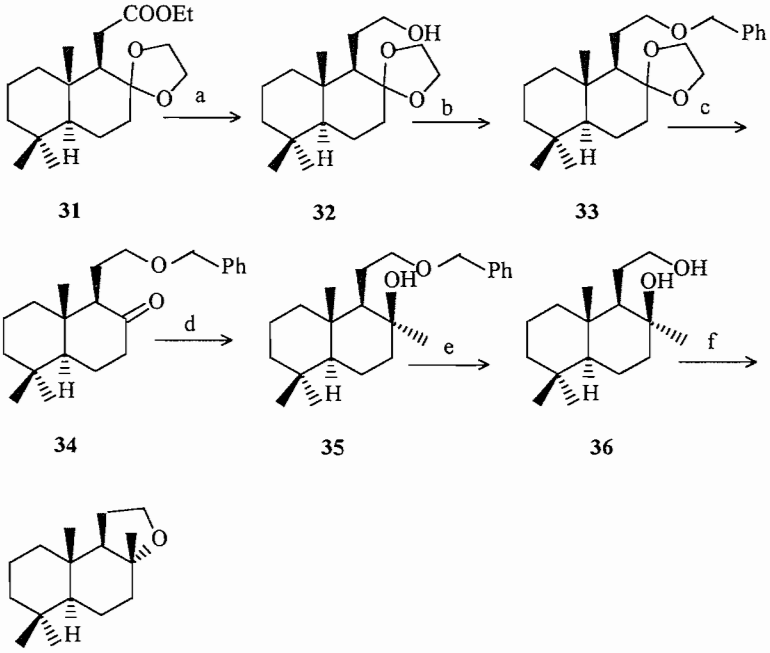
Ketone **34** was also obtained by isomerization of the axial side chain in compound **24** (R = $CH_2C_6H_5$) under equilibrating conditions (sodium methoxide in THF–MeOH, 22 h reflux). Under these conditions, an equilibrium mixture containing a 9:1 ration of **34**:**24** (R = $CH_2C_6H_5$), respectively, was observed.

Methylation of the carbonyl function in **34** was performed

© 1997 NRC Canada

Can. J. Chem. Downloaded from www.nrcresearchpress.com by 88.146.161.215 on 09/08/12
For personal use only.

Scheme 7. Synthesis of (−)-Ambrox® (**37**) from ketone **31**.



(a) $LiAlH_4$; (b) $PhCH_2Br$, n-Bu_4NI; (c) HCl; (d) MeLi, $CeCl_3$; (e) H_2, Pd–C; (f) p-TsOH, CH_3NO_2.

as for compound **24** (R = $CH_2C_6H_5$) using the organocerium reagent chemistry described earlier. Although in this case, having the side chain in an equatorial position may well facilitate the attack by a classical (and less reactive) Grignard reagent, as utilized by Buchi and Wuest (30), to achieve the desired stereochemistry at C8.

Hydrogenolysis of the benzyl group using palladium on charcoal, afforded diol **36**.

The cyclization of **36** was performed as for compound **26**. It was recognized that in this case the cyclization step, under acidic conditions, could generate the thermodynamically more stable *cis*-fused tetrahydrofuran ring, giving iso-Ambrox® (**38**) instead. It has been established that Ambrox® (**37**), with a *trans*-fused tetrahydrofuran ring, isomerizes to iso-Ambrox® (**38**) when treated with acid (34), demonstrating that the latter is the thermodynamically preferred isomer (35).

Equatorial approach to the tertiary carbocation at C8 should be preferred over the axial approach due to steric hindrance from the angular methyl group (30, 31). Therefore, Ambrox® (**37**) is preferentially produced through a lower energy transition state. However, iso-Ambrox® (**38**), resulting from the β-face attack, becomes the major product under prolonged reaction times under the same conditions. Investigation of the optimum conditions to effect such a cyclization by Buchi and Wuest (30) showed that treatment of diol **36** with a catalytic amount of *p*-toluenesulfonic acid in nitromethane at 80°C minimizes the formation of **38** in favour of Ambrox® (**37**).

In our case, under the same conditions, no formation of **38** was observed. The melting point and specific rotation $[\alpha]_D^{25}$ of the (−)-Ambrox® (**37**) obtained were measured to be 76–77°C and −24.1 (c = 1.00, $CHCl_3$), respectively. They agree well with the reported values (mp 77–77.5°C and −24.7 (c = 1.00, $CHCl_3$) (36). As in the previous study, a mixture of alcohols, tentatively assigned the general structure **30**, was also isolated (21% yield).

In summary, a novel route to (−)-Ambrox® (**37**) and (−)-*epi*-Ambrox® (**29**) has been developed from the thujone-derived enone **6**. Since a number of conversions can be achieved without isolation of intermediates, the overall yield from **6** to **29** is 33% while the synthetic route to **37** is 27%.

It should be noted that a very recent report by Tanimoto and Oritani (37) provides a completely different route to enantiomerically pure Ambrox from farnesyl acetate. The key reaction in this study involves a lipase-catalyzed kinetic resolution of (±)-drimane-8,11-diol. An extensive list of previous syntheses of Ambrox is also provided in this publication (37).

Experimental

General

Solvents used for chromatographic separations were glass-distilled prior to use. The term "petroleum ether" refers to a commercially available hydrocarbon mixture boiling in the 35–60°C range. All anhydrous solvents were prepared according to standard procedures. *n*-Butyllithium and methyllithium solutions were standardized by titration against diphenylacetic acid in anhydrous THF. Thujone was distilled from Western red cedar leaf oil generously donated by Intrinsic Research and Development Incorporated. All reactions were performed under a positive pressure of argon.

Reactions were monitored by analytical TLC and (or) gas chromatography. Analytical TLC was performed using Merck precoated silica gel 60 F_{254} aluminum-backed TLC plates. Visualization of the samples was realized with UV light and

© 1997 NRC Canada

Can. J. Chem. Downloaded from www.nrcresearchpress.com by 88.146.161.215 on 09/08/12
For personal use only.

Can. J. Chem. Downloaded from www.nrcresearchpress.com by 88.146.161.215 on 09/08/12
For personal use only.

(or) by spraying with a 10% solution of ammonium molybdate in 10% sulfuric acid followed by heating at 180°C until blue spots developed. Gas chromatography analyses were performed on a Hewlett–Packard 5890A gas chromatograph fitted with a fused silica capillary column coated with cyanopropylphenyl silicone gum (DB 1701) (J & W Scientific: 15 m × 0.262 mm) connected to a Hewlett–Packard 3388A integrator and flame ionization detector (carrier gas: helium; injection temperature: 250°C).

Ozone was generated in a Welsbach model T-23 laboratory ozonator.

Purification of all reaction products was carried out, unless otherwise stated, by flash chromatography using silica gel (Sigma, 10–40 μm), with nitrogen gas pressure to obtain a suitable flow.

Bulb-to-bulb distillation was performed using a Kugelrohr distillation apparatus (the air bath temperature at which distillation occurred is given in parentheses).

All melting points were recorded on a Reichert melting point apparatus and are uncorrected. Optical rotations were recorded on a Perkin–Elmer 141 automatic polarimeter using quartz cells of 10 cm path length, in chloroform solution unless otherwise stated. The concentration (g/100 mL) is given in parentheses.

UV spectra were recorded on a Perkin–Elmer Lambda 4B UV/VIS spectrophotometer using quartz cells of 1 cm path length. IR spectra were recorded on a Perkin–Elmer 710B infrared spectrophotometer. Fourier transform IR spectra were recorded on either Perkin–Elmer 1710 or Bomen Michelson 100 Fourier transform infrared spectrophotometers.

^{1}H NMR spectra were recorded in $CDCl_3$ at 400 MHz on a Bruker WH 400 spectrometer, unless otherwise noted. Chemical shifts were recorded in ppm relative to TMS (internal standard). ^{13}C NMR spectra were recorded on a Bruker AE-200 spectrometer and chemical shifts are reported in ppm relative to TMS.

Low-resolution mass spectra were recorded on Kratos MS 50 and MS 80 mass spectrometers. High-resolution mass spectra were recorded on a Kratos MS 50 mass spectrometer. Chemical ionization mass spectra were recorded on a Delsi–Nermag R10–10C mass spectrometer using ammonia as carrier gas.

Elemental analyses were carried out by Mr. P. Borda of the Microanalytical Laboratory, University of British Columbia, Vancouver.

All compounds are named in accordance with Chemical Abstracts Rules. The skeletal numbering system employed in the Discussion section, as well as proton and carbon designations to interpret the NMR spectra, follows the normal conventions of terpenoid and steroid literature. This allows an easier comparison between the compounds under discussion with related natural products.

4,4a,5,6,7,8-Hexahydro-3-acetyloxy-4aβ,8,8-trimethylnaphthalen-2(3*H*)-one (10/11)

To a solution of enone **6** (5.10 g, 26 mmol) in anhydrous benzene (280 mL), manganese triacetate dihydrate (20.40 g, 76 mmol) was added. The brown suspension was heated at reflux for 1 h with azeotropic removal of water. After cooling to room temperature, additional manganese triacetate dihydrate (20.40 g, 76 mmol) was added and the mixture was heated at reflux for 20 h. The reaction was then cooled to room temperature, diluted with ethyl acetate (500 mL), and washed with 1 M HCl (200 mL), saturated sodium bicarbonate solution (200 mL), and brine (200 mL). The organic fraction was dried, filtered, and concentrated in vacuo to yield 9.03 g of a yellow oil. Chromatographic purification of the oil using diethyl ether/hexanes 3:7 as eluent gave 5.71 g (86%) of a white solid. GC analysis (200°C) of this product showed a 4:1 mixture of isomers (**10/11**, R = Ac). Recrystallization from ethyl acetate gave colourless needles with the same isomeric ratio, mp 114–115°C; IR ($CHCl_3$) of the mixture ν_{max}: 3051, 2917, 1718, 1660, 1596 cm^{-1}; UV (methanol) λ_{max} (log ε): 240 (3.99); ^{1}H NMR of the mixture, signals corresponding to the major isomer, β acetate) δ: 1.18 (3H, s), 1.25 (3H, s), 1.40 (3H, s), 2.12 (3H, s), 5.25 (1H, t, J = 4 Hz, C8-H), 6.07 (1H, s, C6-H); (signals corresponding to the minor isomer, α acetate) δ: 1.17 (3H, s), 1.24 (3H, s), 1.39 (3H, s), 2.11 (3H, s), 5.60 (1H, t, J = 12, 4 Hz, C8-H), 5.98 (1H, s, C6-H); ^{13}C NMR (signals corresponding to the minor isomer) δ: 17.79, 20.92, 25.83, 29.28 (×2), 36.93, 38.01, 40.22, 40.83, 46.74, 71.00, 121.99, 170.31, 177.68, 194.85; MS *m/z*: 250 (M$^+$, 2.9), 208 (4.1), 193 (1.6), 164 (100); HRMS calcd. for $C_{15}H_{22}O_3$: 250.1570; found: 250.1568. Anal. calcd. for $C_{15}H_{22}O_3$: C 7.98, H 8.85; found: C 72.19, H 8.82.

2,3,4,4a,5,6,7,8-Octahydro-2β,3β-dihydroxy-4aβ,8,8-trimethylnaphthalene (12), 2,3,4,4a,5,6,7,8-octahydro-2α,3α-dihydroxy-4aβ,8,8-trimethylnaphthalene (13), 2,3,4,4a,5,6,7,8-octahydro-2α,3β-dihydroxy-4aβ,8,8-trimethylnaphthalene (15), and 2,3,4,4a,5,6,7,8-octahydro-2β,3α-dihydroxy-4aβ,8,8-trimethylnaphthalene (14)

To a solution of **10/11** (1.44 g, 5.76 mmol) (4:1 isomeric mixture) in anhydrous THF (80 mL) was added lithium aluminum hydride (LAH) (726 mg, 19.1 mmol). After stirring at room temperature for 10 min, the reaction was quenched by adding 1 M HCl (100 mL) slowly to the suspension and then extracted with diethyl ether (400 mL). The combined organic layers were washed with water (100 mL), dried over anhydrous Na_2SO_4, filtered, and concentrated in vacuo, to yield 1.45 g of the crude products **12–15**. Chromatographic purification using EtOAc/petroleum ether (3:2) as eluent afforded 7β,8β diol **12** (770.8 mg, 63.7%) as well as 7α,8α diol **13** (15.4 mg, 1.3%). Further elution afforded 7α,8β diol **15** (46.2 mg, 3.8%) and 7β,8α diol **14** (277.5 mg, 23%).

*7β,8β-Diol **12***: mp 103–104°C (EtOAc); $[\alpha]_D^{25}$ +41.8 (c = 1.00); IR (KBr) ν_{max}: 3349, 3012, 2927, 1627 cm^{-1}; ^{1}H NMR δ: 1.09 (3H, s, C4-αCH_3), 1.16 (3H, s, C4-βCH_3), 1.35 (3H, s, C10-CH_3), 1.10–1.60 (5H, m), 1.51 (1H, dd, J = 14, 3 Hz, C9-H), 1.85 (2H, dd, J = 13, 8 Hz), 2.08 (2H, br s, O-H), 3.93 (1H, ddd, J = 7, 4, 3 Hz, C8-H), 4.21 (1H, dd, J = 4, 4 Hz, C7-H), 5.45 (1H, d, J = 4 Hz, C6-H); ^{13}C NMR δ: 18.59, 28.28, 29.22, 32.67, 35.51, 36.57, 42.09, 42.16, 45.30, 67.08, 68.58, 118.85, 154.15; MS *m/z*: 210 (M$^+$, 21.2), 192 (33.6), 177 (21.1), 166 (17.5), 151 (36.1), 135 (100); HRMS calcd. for $C_{13}H_{22}O_2$: 210.1620; found: 210.1615. Anal. calcd. for $C_{13}H_{22}O_2$: C 74.25, H 10.53; found: C 74.36, H 10.60.

^{1}H NMR decoupling experiment: irradiation of the signal resonating at δ 3.93 ppm simplified the doublet of doublets resonating at δ 4.21 ppm to a doublet with a coupling constant

© 1997 NRC Canada

Can. J. Chem. Downloaded from www.nrcresearchpress.com by 88.146.161.215 on 09/08/12
For personal use only.

of 4 Hz, and the doublet of doublets resonating at δ 1.51 ppm to a doublet with coupling constant of 14 Hz. Irradiation of the signal resonating at δ 4.21 ppm collapsed the doublet resonating at δ 5.45 ppm to a singlet, and the doublet of doublet of doublets resonating at δ 3.93 ppm was simplified to a doublet of doublets with coupling constants of 3 and 7 Hz.

^{1}H NMR NOE difference experiment: irradiation of the singlet resonating at δ 1.09 ppm led to enhancement of the signal resonating at δ 5.45 ppm; irradiation of the singlet resonating at δ 1.16 ppm led to enhancement of the signal resonating at δ 1.35 ppm; irradiation of the singlet resonating at δ 1.35 ppm led to enhancement of the signals resonating at δ 1.16 and 1.51 ppm; irradiation of the signal resonating at δ 3.93 ppm led to enhancement of the signal resonating at δ 4.21 ppm; irradiation of the doublet of doublets resonating at δ 4.21 ppm led to enhancement of the signals resonating at δ 3.93 and 5.45 ppm; irradiation of the doublet resonating at δ 5.45 ppm led to the enhancement of the signals resonating at δ 1.09 and 4.21 ppm.

7α,8α-Diol ***13***: mp 139–140°C (EtOAc); IR (KBr) ν_{max}: 3456, 3295, 3002, 2921, 1631 cm^{-1}; ^{1}H NMR δ: 1.10 (3H, s, C4-βCH$_3$). 1.11 (3H, s, C4-αCH$_3$), 1.24 (3H, s, C10-CH$_3$), 1.10–1.90 (9H, m), 2.34 (1H, br s, O-H), 3.95 (1H, m, C8-H), 4.10 (1H, dd, *J* = 5, 5 Hz, C7-H), 5.66 (1H, d, *J* = 5 Hz, C6-H); ^{13}C NMR δ: 18.17, 27.08, 29.35, 32.19, 35.81, 37.69, 41.18, 41.49, 45.47, 66.40, 66.73, 118.86, 156.66; MS *m/z*: 210 (M$^+$, 13.1), 192 (39.8), 177 (7.2), 166 (100); HRMS calcd. for $C_{13}H_{22}O_2$: 210.1620; found: 210.1612. Anal. calcd. for $C_{13}H_{22}O_2$: C 74.25, H 10.53; found: C 74.10, H 10.63.

^{1}H NMR decoupling experiment: irradiation of the multiplet resonating at δ 3.95 ppm collapsed the doublet of doublets resonating at δ 4.10 ppm to a doublet of coupling constant value of 5 Hz; irradiation of the doublet of doublets resonating at δ 4.10 ppm collapsed the doublet resonating at δ 5.66 ppm to a singlet and altered the multiplet resonating at δ 3.95 ppm.

^{1}H NMR NOE difference experiment: irradiation of the singlet at δ 1.24 ppm led to enhancement of the signals resonating at δ 1.10 and 3.95 ppm; irradiation of the signal resonating at δ 3.95 ppm led to enhancement of the singlet resonating at δ 1.24 ppm; irradiation of the signal resonating at δ 4.10 ppm led to enhancement of the doublet resonating at δ 5.66 ppm.

7α,8β-Diol ***15***: mp 73–74°C (EtOAC); IR (KBr) ν_{max}: 3337, 3011, 2926, 1638 cm^{-1}; ^{1}H NMR δ: 1.10 (3H, s), 1.16 (3H, s), 1.22 (3H, s), 1.10–1.60 (6H, m), 1.67 (1H, dd, *J* = 13, 4 Hz, C9-H), 1.80 (1H, m), 2.17 (2H, br s, O-H), 3.51 (1H, ddd, *J* = 11, 7, 4 Hz, C8-H), 4.00 (1H, dd, *J* = 7, 2 Hz, C7-H), 5.35 (1H, d, *J* = 2 Hz, C6-H); ^{13}C NMR δ: 19.35, 28.12, 29.86, 32.92, 36.75, 38.23, 41.04, 41.71, 46.18, 71.49, 74.24, 121.18, 152.07; MS *m/z*: 210 (M$^+$, 45.7), 192 (7.4), 177 (5.5), 166 (100); HRMS calcd. for $C_{13}H_{22}O_2$: 210.1620; found: 210.1614. Anal. calcd. for $C_{13}H_{22}O_2$: C 74.25, H 10.53; found: C 74.36, H 10.57.

^{1}H NMR decoupling experiment: irradiation of the signal resonating at δ 3.51 ppm collapsed the doublet of doublets resonating at δ 4.00 ppm to a doublet of coupling constant value of 2 Hz; irradiation of the doublet resonating at δ 4.00 ppm simplified the doublet of doublet of doublets resonating at δ 3.51 ppm to a doublet of doublets with coupling constant values of 4 and 11 Hz, and the doublet resonating at δ 5.35 ppm collapsed to a singlet.

7β,8α-Diol ***14***: mp 92–93°C (EtOAc); $[\alpha]_D^{25}$ −28.80° (*c* = 1.00); IR (KBr) ν_{max}: 3329, 3005, 2925, 1640 cm^{-1}; ^{1}H NMR δ: 1.08 (3H, s, C4-αCH$_3$), 1.11 (3H, s, C4-βCH$_3$), 1.28 (3H, s, C10-CH$_3$), 1.20–1.70 (7H, m), 1.80 (1H, m, C2-βH), 3.75 (2H, br s, O-H), 3.85 (1H, ddd, *J* = 12, 8, 4 Hz, C8-H), 4.08 (1H, dd, *J* = 8, 2.5 Hz, C7-H), 5.35 (1H, d, *J* = 2.5 Hz, C6-H); ^{13}C NMR δ: 18.35, 27.80, 29.03, 32.36, 35.54, 37.37, 41.62, 41.94, 48.95, 70.67, 75.58, 120.44, 152.45; MS *m/z*: 210 (M$^+$, 8.3), 192 (52.0), 177 (23.0), 135 (100); HRMS calcd. for $C_{13}H_{22}O_2$: 210.1620; found: 210.1625. Anal. calcd. for $C_{13}H_{22}O_2$: C 74.25, H 10.53; found: C 74.10, H 10.47.

^{1}H NMR decoupling experiment: irradiation of the signal at δ 3.85 ppm collapsed the doublet of doublets at δ 4.08 ppm to a doublet with a coupling constant value of 2.5 Hz and simplified the multiplet resonating at δ 1.50 ppm. Irradiation of the doublet of doublets resonating at δ 4.08 ppm collapsed the signal resonating at δ 5.35 ppm to a singlet, and simplified the signal at δ 3.85 ppm to a doublet of doublets with coupling constant values of 4 and 12 Hz.

^{1}H NMR NOE difference experiment: irradiation of the singlet resonating at δ 1.28 ppm led to enhancement of the signals resonating at δ 1.11, 1.50, 1.80, and 3.85 ppm; irradiation of the signal resonating at δ 1.80 ppm led to enhancement of the singlets resonating at δ 1.11 and 1.28 ppm; irradiation of the signal resonating at δ 3.85 ppm led to enhancement of the signals resonating at δ 1.28 and 5.35 ppm; irradiation of the doublet of doublets resonating at δ 4.08 ppm led to enhancement of the signals resonating at δ 1.50 and 5.35 ppm; irradiation of the doublet resonating at δ 5.35 ppm. led to enhancement of the signals resonating at δ 1.08 and 4.08 ppm.

4aα,5,6,7,8,8a-Hexahydro-5,5,8aβ-trimethylnaphthalen-2(1*H*)-one (9), 3,5,6,7,8,8a-hexahydro-5,5,8aβ-trimethylnaphthalen-2(1*H*)-one (16), and 4aβ,5,6,7,8,8a-hexahydro-5,5,8aβ-trimethylnaphthalen-2(1*H*)-one (17)

Method A

To a solution of isomeric diols **12–15** (1.35 g, 6.4 mmol) in glacial acetic acid (80 mL), concentrated sulfuric acid (395 μL) was added. The reaction mixture was heated at reflux for 2 h, cooled to room temperature, and diluted with water (300 mL). The aqueous layer was extracted with diethyl ether (400 mL). The combined organic layers were washed with saturated sodium bicarbonate solution (200 mL), water (200 mL), dried, filtered, and concentrated in vacuo. Chromatographic purification of the residue, using EtOAc/petroleum ether 5:95 as eluent, gave ketone **16** (60.9 mg, 5%) as a colourless oil, enone **17** (50.5 mg, 4%) as a light yellow oil, and enone **9** (72.5 mg, 6%) as a colourless oil that solidified upon standing. The spectroscopic data are in agreement with published values (19).

Method B

A mixture of 7β,8β-diol **12** (1.09 g, 5.2 mmol) and *p*-toluenesulfonic acid (1.19 g, 6.2 mmol) in anhydrous THF (50 mL) was heated at reflux for 24 h. After cooling to room temperature, the solvent was removed in vacuo and the residue was

© 1997 NRC Canada

Can. J. Chem. Downloaded from www.nrcresearchpress.com by 88.146.161.215 on 09/08/12
For personal use only.

chromatographed on silica gel using EtOAc/cyclohexane 1:9 as eluent, affording ketone **16** (250.5 mg, 25%) as a colourless oil. Further elution afforded enone **17** (18.0 mg, 2%) as a light yellow oil and enone **9** (643.0 mg, 64%) as a colourless oil that solidified on standing.

Method C

To a solution of 7β,8α-diol **14** (25.0 mg, 0.12 mmol) in anhydrous THF (5 mL), *p*-toluenesulfonic acid (27.0 mg, 0.14 mmol) was added. The mixture was heated at reflux for 24 h. After cooling the reaction to room temperature, the solvent was removed in vacuo and the residue was purified by column chromatography on silica gel using EtOAc/cyclohexane 1:9 as eluent, affording ketone **16** (3.0 mg, 13%) and enone **9** (15 mg, 66%).

Method D

To a solution of enone **6** (2.30 g, 12.0 mmol) in anhydrous benzene (130 mL) was added manganese triacetate dihydrate (9.00 g, 33.5 mmol). The brown suspension was heated at reflux for 1 h with azeotropic removal of water. After cooling to room temperature, additional manganese triacetate dihydrate (9.00 g, 33.5 mmol) was added and the mixture was heated at reflux for a further 20 h. The reaction was cooled to room temperature, diluted with ethyl acetate (200 mL), and sequentially washed with 1 M HCl (75 mL), saturated sodium bicarbonate solution (75 mL), and brine (75 mL). The organic layer was dried, filtered, and concentrated in vacuo. The residue was dissolved in anhydrous THF (160 mL) and LAH (1.60 g, 42 mmol) was added. After stirring for 10 min at room temperature, the suspension was slowly poured into 1 M HCl (200 mL) and extracted with diethyl ether (600 mL). The combined organic layers were washed with water (100 mL), dried over anhydrous Na_2SO_4, filtered, and concentrated in vacuo to yield a crude mixture of isomeric diols **12–15** (3.12 g) as a white solid. This solid was dissolved in anhydrous THF (115 mL). *p*-Toluenesulfonic acid (2.70 g, 14.2 mmol) was added and the mixture was heated at reflux for 24 h. After cooling to room temperature, the reaction was diluted with diethyl ether (500 mL), washed with saturated sodium bicarbonate solution (200 mL) and with water (200 mL), then dried, filtered, and concentrated in vacuo to yield 2.35 g of residue. Chromatographic purification of the crude using EtOAc/cyclohexane 1:9 as eluent gave ketone **16** (342 mg, 15%), enone **17** (40.5 mg, 2%), and enone **9** (1.12 g, 49%).

Method E

A solution of ketone **16** (230.7 mg, 1.2 mmol) and *p*-toluenesulfonic acid (286.8 mg, 1.5 mmol) in anhydrous THF (18 mL) was heated at reflux for 24 h. After cooling the reaction mixture to room temperature, the solution was concentrated in vacuo, and the residue was chromatographed on silica gel using EtOAc/cyclohexane 1:9 as eluent, yielding unreacted ketone **16** (72.0 mg, 31%), enone **17** (3.0 mg, 1%), and enone **9** (149.3 mg, 65%).

4aα,5,6,7,8,8a-Hexahydro-5,5,8aβ-trimethyl-2,oxo-lα-naphthalene acetic acid ethyl ester (19), and 4aα,5,6,7,8,8a-hexahydro-1α-iodo-5,5,8aβ-trimethylnaphthalen-2(1*H*)-one (27)

A solution of diisopropylamine (1.47 mL, 10.5 mmol) in anhydrous THF (12 mL) was cooled to −78°C and *n*-butyllithium (7.33 mL, 9.17 mmol) was added. The solution was allowed to warm up to −15°C for 30 min, then cooled to −78°C, and a solution of enone **9** (1.26 g, 6.56 mmol) in anhydrous THF (50 mL) was added dropwise. The reaction was warmed to 0°C for 30 min, then cooled to −78°C, and freshly distilled ethyl iodoacetate (2.32 mL, 19.65 mmol) was added. The reaction mixture was stirred at −78°C for 1 h and then warmed to 0°C for another hour, poured into a saturated ammonium chloride solution (200 mL), and extracted with diethyl ether (400 mL). The organic extracts were washed with water (200 mL), dried, filtered, and concentrated in vacuo to yield 2.12 g of residue as a yellow oil. Chromatographic purification of the residue, using EtOAc/hexanes 1:9 as eluent, gave unreacted starting material **9** (230 mg, 18%), enone **27** (185 mg, 9%) as a white solid, and enone **19** (1.33 g, 73%) as a yellowish oil.

Enone 27: mp 109–110°C (EtOAc); $[\alpha]_D^{25}$ −164.6 (c = 1.00); IR (KBr) ν_{max}: 3006, 2927, 1675, 1610 cm^{-1}; UV (methanol) ν_{max} (log ε): 245 (3.6); ^1H NMR δ: 0.95 (3H, s, C4-βCH$_3$), 1.11 (3H, s, C4-αCH$_3$), 1.16 (3H, s, C10-CH$_3$), 1.19–1.70 (6H, m), 2.16 (1H, dd, J = 3, 2 Hz, C5-H), 4.26 (1H, d, J = 1.4 Hz, C9-H), 6.12 (1H, ddd, J = 10, 3, 1.4 Hz, C7-H), 6.89 (1H, dd, J = 10, 2 Hz, C6-H); ^{13}C NMR δ: 15.34, 18.54, 22.40, 32.22, 32.45, 39.14, 40.74, 41.68, 50.79, 51.59, 127.23, 149.94, 193.08; MS *m/z*: 318 (M^+, 1.1), 191 (66.7), 147 (39.9), 135 (37.3), 121 (100); HRMS calcd. for $C_{13}H_{19}OI$: 318.0479; found: 318.0481. Anal. calcd. for $C_{13}H_{19}OI$: C 49.07, H 6.01, I 39.88; found: C 49.00, H 6.00, I 39.73.

^1H NMR NOE difference experiment: irradiation of the singlet resonating at δ 0.95 ppm led to enhancement of the signals resonating at δ 1.16 and 6.89 ppm; irradiation of the singlet resonating at δ 1.11 ppm led to enhancement of the signals resonating at δ 2.16 and 6.89 ppm; irradiation of the singlet resonating at δ 1.16 ppm led to enhancement of the signals resonating at δ 0.95 and 4.26 ppm; irradiation of the signal resonating at δ 2.16 ppm led to enhancement of the signals resonating at δ 1.11 and 6.89 ppm; irradiation of the doublet resonating at δ 4.26 ppm led to enhancement of the signal resonating at δ 1.16 ppm; irradiation of the signal resonating at δ 6.89 ppm led to enhancement of the signals resonating at δ 0.95, 1.11, 2.16, and 6.12 ppm.

Enone 19: $[\alpha]_D^{25}$ −126.80 (c = 1.00); IR (neat) ν_{max}: 3051, 2936, 1737, 1679, 1612 cm^{-1}; UV (methanol) ν_{max} (log ε): 236 (3.6); ^1H NMR δ: 0.92 (3H, s, C4-βCH$_3$), 1.06 (3H, s, C4-αCH$_3$), 1.08 (3H, s, C10-CH$_3$), 1.25 (3H, t, J = 8 Hz, *CH$_3$*-CH$_2$), 1.28–1.80 (6H, m), 2.14 (1H, dd, J = 3, 2 Hz, C5-H), 2.22 (1H, dd, J = 15, 8 Hz, C11-H$_A$), 2.50 (1H, dd, J = 8, 8 Hz, C9-H), 2.64 (1H, dd, J = 15, 8 Hz, C11-H$_B$), 4.15 (2H, q, J = 8 Hz, CH$_3$-*CH$_2$*), 6.00 (1H, ddd, J = 10, 3, 1 Hz, C7-H), 6.85 (1H, dd, J = 10, 2 Hz, C6-H); ^{13}C NMR δ: 14.13, 18.16, 21.38, 22.80, 31.81, 32.62, 32.69, 35.16, 40.87, 41.16, 48.40, 57.61, 60.87, 128.62, 149.25, 171.94, 201.33; MS *m/z*: 278 (M^+, 36.5), 263 (31.9), 232 (79.2), 217 (100); HRMS calcd. for $C_{17}H_{26}O_3$: 278.1883; found: 278.1884. Anal. calcd. for $C_{17}H_{26}O_3$: C 73.36, H 9.41; found: C 73.29, H 9.42.

^1H NMR NOE experiment: irradiation of the singlet resonating at δ 0.92 ppm led to enhancement of the signals resonating at δ 1.06, 1.08, and 6.85 ppm, irradiation of the singlet resonating at δ 1.06 ppm led to enhancement of the signals

© 1997 NRC Canada

resonating at δ 0.92, 2.14, and 6.85 ppm; irradiation of the singlet resonating at δ 1.08 ppm led to enhancement of the signals resonating at δ 0.92 and 2.50 ppm; irradiation of the signal resonating at δ 2.14 ppm led to enhancement of the signals resonating at δ 1.06 and 2.64 ppm, irradiation of the signal resonating at δ 2.22 ppm led to enhancement of the signals resonating at δ 2.50 and 2.64 ppm; irradiation of the signal resonating at δ 2.50 ppm led to enhancement of the signals resonating at δ 1.08 and 2.22 ppm; irradiation of the signal resonating at δ 2.64 ppm led to enhancement of the signals resonating at δ 2.14 and 2.22 ppm.

3,4,4aα,5,6,7,8,8a-Octahydro-5,5,8aβ-trimethyl-2-oxo-1α-naphthalene acetic acid ethyl ester (20)

A hydrogenation vessel containing a suspension of enone **19** (2.106 g, 7.6 mmol) and 10% palladium on charcoal (210 mg) in EtOAc (100 mL) was purged three times with hydrogen at a pressure of 15 psi. The vessel was then pressurized to 40 psi with hydrogen and shaken for 20 min at room temperature. A sample taken for analytical TLC (EtOAc/hexanes 1:4) indicated the reaction was complete. The mixture was filtered through Celite 545, and the flask and Celite were washed with EtOAc (175 mL). The solution was concentrated in vacuo to yield 2.50 g of crude product. Chromatographic purification using EtOAc/hexanes 1:4 as eluent gave keto ester **20** (2.11 g, 100 %) as a colourless oil. $[\alpha]_D^{25}$ −34.8 (c = 1.00); IR (neat) ν_{max}: 2943, 1732 cm^{-1}; ^1H NMR δ: 0.87 (3H, s), 0.98 (3H, s), 0.99 (3H, s), 1.24 (3H, t, J = 8 Hz, CH_3-CH_2), 1.10–1.70 (8H, m), 1.95 (1H, m), 2.30–2.75 (5H, m), 4.11 (2H, q, J = 8 Hz, CH_3-CH_2) ; ^{13}C NMR δ: 14.08, 18.52, 21.55, 22.01, 23.33, 33.30 (×2), 33.44, 36.37, 38.54, 40.08, 42.15, 44.94, 60.38, 60.86, 171.72, 213.04; MS *m/z*: 280 (M^+, 1.4), 262 (3.6), 247 (6.3), 232 (30.1), 109 (100); HRMS calcd. for $C_{17}H_{28}O_3$: 280.2038; found: 280.2044. Anal. calcd. for $C_{17}H_{28}O_3$: C 72.83, H 10.06; found: C 72.68, H 9.99.

1,2,3,4,4aα,5,6,7,8,8a-Decahydro-5,5,8aβ-trimethyl-2,2-ethylenediozy-1α-naphthalene acetic acid ethyl ester (21), and 1,2,3,4,4aα,5,6,7,8,8a-decahydro-5,5,8aβ-trimethyl-2,2-ethylenedioxy-1β-naphthalene acetic acid ethyl ester (28)

Method A

A solution of keto ester **20** (133.2 mg, 0.5 mmol), *p*-toluenesulfonic acid (3.8 mg, 2×10^{-2} mmol), and ethylene glycol (0.159 mL, 2.8 mmol) in anhydrous benzene (7 mL) was heated at reflux with azeotropic removal of water. The reaction was monitored by GC and showed 90% conversion after 6 h. The reaction mixture was then cooled to room temperature, diluted with benzene (20 mL), washed with saturated sodium bicarbonate solution (10 mL) and with water (10 mL), then dried, filtered, and concentrated in vacuo. The resulting oil was purified by column chromatography using EtOAc/hexanes 1:4 as eluent. The silica gel was treated with a mixture of EtOAc/hexanes/Et_3N in a ratio of 1: 4: 4×10^{-2}, prior to use. Purification yielded ketal **21** (71.4 mg, 46%) as a colourless oil that solidified upon standing, ketal **28** (46.3 mg, 29%) as a colourless oil, and starting keto ester **20** (13 mg, 10%).

A longer reflux (19 h) proved to increase the ratio of ketal **28** (61% by GC), lowering the ratio of ketal **21** to 11% (by GC).

*Ketal **21***: mp 42°C; $[\alpha]_D^{25}$ −7.7 (c = 1.00); IR ($CHCl_3$) ν_{max}: 2946, 1735 cm^{-1}; ^1H NMR δ: 0.82 (3H, s, C4-βCH$_3$), 0.87 (3H, s, C4-αCH$_3$), 0.90–1.18 (2H, m), 1.19 (3H, s, C10-CH$_3$), 1.27 (3H, t, J = 7 Hz, CH_3-CH_2), 1.30–1.40 (2H, m), 1.50–1.70 (7H, m), 2.08 (1H, ddd, J = 5, 5, 2 Hz, C9-H), 2.47 (2H, dd, J = 5, 3.6 Hz, C11-2H), 3.80 (2H, dt, J = 6.5, 3 Hz), 3.98 (2H, m), 4.14 (2H, dq, J = 7, 1 Hz, CH_3-CH_2); ^{13}C NMR δ: 14.20, 18.51, 20.13, 21.74, 22.23, 32.69, 33.03, 33.42, 33.59, 37.01, 38.08, 42.22, 46.59, 50.30, 60.25, 63.34, 64.46, 111.04, 174.21; MS *m/z*: 324 (M^+, 29), 309 (6.4), 279 (18.8), 99 (100); HRMS calcd. for $C_{19}H_{32}O_4$: 324.2302; found: 324.2293. Anal. calcd. for $C_{19}H_{32}O_4$: C 70.35, H 9.93; found: C 70.50, H 10.04.

^1H NMR NOE difference experiment: irradiation of the singlet resonating at δ 0.82 ppm led to enhancement of the signal resonating at δ 1.19 ppm; irradiation of the singlet resonating at δ 0.87 ppm affected the multiplet resonating at δ 1.60 ppm; irradiation of the singlet resonating at δ 1.19 ppm led to enhancement of the signals resonating at δ 0.82 and 2.08 ppm; irradiation of the signal resonating at δ 2.08 ppm led to enhancement of the signals resonating at δ 1.19 and 2.47 ppm.

*Ketal **28***: $[\alpha]_D^{25}$ +8.3 (c = 1.00); IR (neat) ν_{max}: 2946, 1736 cm^{-1}; ^1H NMR δ: 0.83 (3H, s), 0.87 (3H, s), 0.89 (3H, s), 1.25 (3H, t, J = 7.5 Hz, CH_3-CH_2), 1.00–1.21 (2H, m), 1.30–1.50 (5H, m), 1.55–1.65 (3H, m), 1.91 (1H, dd, J = 3, 9 Hz), 2.15 (2H, rn), 2.29 (1H, dd, J = 17, 9 Hz), 3.73–3.88 (2H, m), 3.92–4.16 (4H, m); ^{13}C NMR δ: 14.25, 14.73, 18.56, 19.69, 21.68, 28.83, 33.24, 33.60, 35.76, 38.47, 39.26, 41.80, 53.99, 54.92, 60.07, 63.24, 65.00, 110.50, 174.69; MS *m/z*: 324 (M^+, 19.3), 309 (3.4), 279 (9.2), 99 (100); HRMS calcd. for $C_{19}H_{32}O_4$: 324.2302; found: 324.2308. Anal. calcd. for $C_{19}H_{32}O_4$: C 70.35, H 9.93; found: C 70.43, H 9.87.

Method B

To a solution of trimethylsilyl triflate (30 μL, 0.15 mmol) in anhydrous methylene chloride (1 mL) at −78°C was added 1,2-bis(trimethylsilyloxy)ethane (0.42 mL, 1.7 mmol). A solution of keto ester **20** (434.6 mg, 1.55 mmol) in anhydrous methylene chloride (5 mL) was added to the reaction and the mixture was warmed to 0°C and stirred for 2 h; the reaction was monitored by GC. (Strict anhydrous conditions were required; traces of moisture were found to lower the yield of ketal **21** to 44%, increasing the presence of ketal **28** up to 30%.) The reaction was quenched with dry pyridine (0.35 mL), poured into saturated sodium bicarbonate solution (10 mL), and extracted with diethyl ether (50 mL). The combined organic layers were washed with 10% copper sulfate solution (30 mL) and water, dried, filtered, and concentrated in vacuo. Bulb-to-bulb distillation of the crude product gave 482 mg of a colourless oil (bp 118°C at 9 Torr (1 Torr = 133.3 Pa)). GC analysis of the oil showed a 93:5:2 mixture of products, the minor compounds being ketal **28** and starting keto ester **20**, respectively, and the major one being ketal **21**. The mixture was not further purified.

Method C

A solution of triflic acid (17.4 μL, 0.2 mmol) in anhydrous THF (2.4 mL) was cooled to −78°C, and 1,2-bis(trimethylsilyloxy)ethane (0.48 mL, 1.9 mmol) was added to the solution with temperature maintained at −78°C. A solution of

Can. J. Chem. Downloaded from www.nrcresearchpress.com by 88.146.161.215 on 09/08/12
For personal use only.

© 1997 NRC Canada

keto ester **20** (276.1 mg, 1.0 mmol) in anhydrous THF (12.2 mL) was added and the reaction mixture was stirred at 0°C. After 14 h, GC analysis showed a mixture of **21**, **28**, and **20** in an 8:1:1 ratio. The reaction was quenched with dry pyridine (150 μL), poured into saturated sodium bicarbonate solution (10 mL), and extracted with diethyl ether (50 mL). The combined organic layers were washed with 10% copper sulfate solution (20 mL) and with water (20 mL), then dried, filtered, and concentrated in vacuo. The residue was purified by chromatography on silica gel treated with EtOAc/hexanes/Et_3N in a 1:4:4 × 10^{-2} ratio prior to use, and eluted with EtOAc/hexanes 1:4, affording ketal **21** (214.4 mg, 67%), ketal **28** (27.1 mg, 8%), and starting keto ester **20** (27.0 mg, 10%).

1,2,3,4,4aα,5,6,7,8,8α-Decahydro-2,2-ethylenedioxy-1α-(2′-hydroxyethylen)-5,5,8aβ-trimethylnaphthalene (22)

To a solution of ketal **21** (621.9 mg, 1.9 mmol) in anhydrous diethyl ether (50 mL) was added LAH (218 mg, 5.7 mmol). The suspension was stirred at room temperature. After 10 min, analytical TLC (EtOAc/hexanes 1:1) showed reaction completion. Water (10 mL) was slowly added to the reaction mixture and stirred for 5 min, then 15% sodium hydroxide solution (10 mL) was added and stirred for 5 min more. The mixture was then filtered and the filtrate was washed with diethyl ether (50 mL). The aqueous layer was extracted with diethyl ether (60 mL). The combined organic layers were washed with water (60 mL), dried over anhydrous Na_2SO_4, filtered, and concentrated in vacuo. The residue was chromatographed on silica gel, treated with EtOAc/hexanes/Et_3N in a 1:1:2 × 10^{-2} ratio prior to use, and eluted with EtOAc/hexanes 1:1, affording hydroxy ketal **22** (537.8 mg, 100%) as a colourless oil. $[\alpha]_D^{25}$ −7.5 (c = 1.00); IR (neat) $-\nu_{max}$: 3300, 2947 cm^{-1}; ^1H NMR δ: 0.83 (3H, s), 0.88 (3H, s), 1.00–1.15 (2H, m), 1.17 (3H, s), 1.25 (1H, m), 1.35–1.71 (10H, m), 1.82 (1H, m, C11-H_A), 2.02 (1H, m, C11-H_B), 3.49 (1H, m, C12-H_A), 3.68 (1H, m, C12-H_B), 3.85 (2H, m), 3.98 (2H, m); ^{13}C NMR δ: 16.46, 20.13, 21.52, 22.71, 30.95, 32.88, 32.96, 33.36, 36.09, 38.90, 42.31, 46.29, 52.72, 63.09, 64.46, 64.63, 112.32; MS *m/z*: 282 ($M^{+\cdot}$ 2.4), 267 (03), 252 (0.2), 99 (100); HRMS calcd. for $C_{17}H_{30}O_3$: 282.2195; found: 282.2195. Anal. calcd. for $C_{17}H_{30}O_3$: C 72.31, H 10.70; found: C 72.41, H 10.75.

^1H NMR decoupling experiment: irradiation of the signal resonating at δ 3.49 ppm affected the multiplets resonating at δ 1.82, 2.02, and 3.68 ppm; irradiation of the signal resonating at δ 3.68 ppm affected the multiplets resonating at δ 1.82, 2.02, and 3.49 ppm.

1,2,3,4,4aα,5,6,7,8,8a-Decahydro-2,2-ethylenedioxy-1α-(2′-*O*-benzyl ethyl)-5,5,8aβ-trimethylnaphthalene (23)

Method A

Sodium hydride, 60% dispersion in paraffin oil (9.2 mg, 0.23 mmol), was weighed and then washed three times with anhydrous THF (9 mL), under argon atmosphere. Anhydrous THF (3 mL) was added. A solution of hydroxy ketal **22** (58.7 mg, 0.21 mmol) in anhydrous THF (10 mL) was added dropwise with good stirring. Sodium iodide (3.3 mg, 0.02 mmol) and potassium carbonate (55 mg, 0.40 mmol) were added to the suspension, then benzyl chloride (25.3 μL, 0.22 mmol) was added. The reaction mixture was heated at reflux for 12 h. After cooling the reaction to room temperature, water (5 mL) was added slowly. The aqueous layer was extracted with diethyl ether (15 mL). The combined organic layers were washed with water (5 mL), dried, filtered, and concentrated in vacuo. The residue was chromatographed on silica gel treated with EtOAc/hexanes/Et_3N 1:9:1 × 10^{-2} ratio prior to use, and eluted with EtOAc/hexanes 1:9, affording hydroxybenzyl ketal **23** (52.8 mg, 68%) as a colourless oil and starting hydroxy ketal **22** (12.8 mg).

*Hydroxybenzyl ketal **23***: $[\alpha]_D^{25}$ +0.95 (c = 1.00); IR (neat) ν_{max}: 2946 cm^{-1}; ^1H NMR δ: 0.82 (3H, s), 0.87 (3H, s), 1.06 (3H, m), 1.15 (3H, s), 1.35–1.80 (11H, m), 3.44 (2H, m), 3.80 (2H, m), 3.92 (2H, m), 4.52 (2H, d, J = 3 Hz, CH_2-Ph), 7.25 (1H, m), 7.32 (4H, m); ^{13}C NMR δ: 16.46, 20.13, 21.53, 22.67, 27.94, 32.87, 33.23, 33.36, 36.38, 38.66, 42.21, 46.19, 51.11, 63.25, 64.36, 71.98, 72.59, 112.15, 127.37, 127.59 (×2), 128.26 (×2), 138.75; MS *m/z*: 372 (M^+, 25.7), 357 (2.1), 281 (42.1), 99 (100); HRMS calcd. for $C_{24}H_{36}O_3$: 372.2666; found: 372.2665. Anal. calcd. for $C_{24}H_{36}O_3$: C 77.39, H 9.73; found: C 77.32, H 9.67.

Method B

Sodium hydride, 80% dispersion in paraffin oil (169 mg, 5.63 mmol), was weighed, and then washed three times with anhydrous THF (15 mL), under argon atmosphere. Anhydrous THF (24 mL) was added. A solution of hydroxy ketal **22** (529.5 mg, 1.88 mmol) in anhydrous THF (35 mL) was added dropwise with good stirring. Benzyl bromide (0.67 mL, 5.63 mmol) and tetrabutylammonium iodide (67.6 mg, 0.18 mmol) were added to the suspension. The reaction mixture was refluxed for 22 h, and monitored by analytical TLC (EtOAc/hexanes 1:4). After reaction completion, the mixture was cooled to room temperature and water (10 mL) was added slowly. The aqueous layer was extracted with diethyl ether (30 mL). The combined organic layers were washed with water (30 mL), dried, filtered, and concentrated in vacuo. The residue was chromatographed on silica gel treated with EtOAc/hexanes/Et_3N 1:9:1 × 10^{-2} ratio prior to use, and eluted with EtOAc/hexanes 1:9, affording hydroxybenzyl ketal **23** (684.7 mg, 98%) as a colourless oil.

3,4,4aα,5,6,7,8,8a-Octahydro-1α(2′-*O*-benzyl ethyl)-5,5,8aβ-trimethylnaphthalen-2(1*H*)-one (24)

Method A

To a solution of hydroxybenzyl ketal **23** (683 mg, 1.83 mmol) in acetone (20 mL), 1 M HCl (5.5 mL) was added. The reaction mixture was stirred at room temperature. After 1 h, analytical TLC (EtOAc/hexanes 1:4) showed reaction completion. Saturated sodium bicarbonate solution (20 mL) was added and the solution was extracted with diethyl ether (80 mL). The combined organic layers were washed with water (30 mL), dried, filtered, and concentrated in vacuo. Chromatographic purification of the crude product using EtOAc/hexanes 1:4 as eluent gave hydroxybenzyl ketone **24** (584 mg, 97%) as a colourless oil. $[\alpha]_D^{25}$ −27.6 (c = 1.00); IR (neat) ν_{max}: 2947, 1708 cm^{-1}; ^1H NMR δ: 0.86 (3H, s), 0.94 (3H, s), 0.95 (3H, s), 1.05–1.25 (2H, m), 1.40–1.70 (6H, m), 1.80–1.95 (3H, m), 2.02 (1H, m), 2.27 (1H, m), 2.54 (1H, m), 3.30 (1H, m), 3.42 (1H, m), 4.42 (2H, s), 7.32 (5H, m). ^{13}C NMR δ: 18.61, 21.78, 22.07, 23.48, 27.73, 33.29, 33.46,

© 1997 NRC Canada

Can. J. Chem. Downloaded from www.nrcresearchpress.com by 88.146.161.215 on 09/08/12
For personal use only.

Can. J. Chem. Downloaded from www.nrcresearchpress.com by 88.146.161.215 on 09/08/12
For personal use only.

36.93, 38.50, 40.02, 42.34, 44.80, 62.22, 68.85, 73.26, 127.57, 127.78 (×2), 128.33 (×2), 138.20, 215.00; MS *m/z*: 328 (M^+, 1.6), 313 (2.1), 269 (8.3), 221 (11.4), 206 (10.7), 91 (100); HRMS calcd. for $C_{22}H_{32}O_2$: 328.2402; found: 328.2396. Anal. calcd. for $C_{22}H_{32}O_2$: C 80.45, H 9.81; found: C 80.40, H 9.79.

Method B

To a solution of ketal **21** (3.95 g, 12.2 mmol) in anhydrous diethyl ether (120 mL), LAH (1.39 g, 36.6 mmol) was added and the solution was stirred at room temperature for 10 min. Water (50 mL) was added slowly and stirred for 5 min, then 15% sodium hydroxide solution (30 mL) was added and stirred for 5 min more. The mixture was filtered and the filtrate was washed with diethyl ether (150 mL). The aqueous layer was extracted with diethyl ether (200 mL). The combined organic layers were washed with water (150 mL), dried over anhydrous Na_2SO_4, filtered, and concentrated in vacuo to yield 3.60 g of crude hydroxy ketal **22**. This was dissolved in anhydrous THF (100 mL) and added to a solution of sodium hydride (80% dispersion in paraffin oil) (1.10 g, 36.6 mmol) in anhydrous THF (22 mL). Benzyl bromide (4.35 mL, 36.6 mmol) and tetrabutylammonium iodide (439 mg, 1.2 mmol) were added to the suspension. The reaction mixture was heated at reflux for 22 h. After cooling to room temperature, water (70 mL) was added slowly. The aqueous layer was extracted with diethyl ether (250 mL). The combined organic layers were washed with water (100 mL), dried, filtered, and concentrated in vacuo. The residue was dissolved in acetone (122 mL) and 1 M HCl (37 mL) was added. The reaction was stirred at room temperature for 1 h. Saturated sodium bicarbonate solution (130 mL) was added and the solution was extracted with diethyl ether (500 mL). The combined organic layers were washed with water (200 mL), dried, filtered, and concentrated in vacuo. Chromatographic purification of the residue using EtOAc/hexanes 1:4 as eluent afforded hydroxybenzyl ketone **24** (3.50 g, 87% from **21** over three steps) as a colourless oil.

1,2,3,4,4aα,5,6,7,8,8a-Decahydro-1α-(2′-*O*-benzyl ethyl)-2α,5,5,8aβ-tetramethylnaphthalen-2β-ol (25)

Method A

To a solution of hydroxybenzyl ketone **24** (44.5 mg, 0.13 mmol) in anhydrous diethyl ether (10 mL) was added methylmagnesium iodide (70 μL, 0.21 mmol). The mixture was refluxed for 5 h, then cooled to room temperature and saturated ammonium chloride solution (6 mL) added. The aqueous layer was extracted with diethyl ether (30 mL). The combined organic layers were washed with water (20 mL), dried, filtered, and concentrated in vacuo. Chromatographic purification of the residue, eluting with EtOAc/hexanes 1:6, afforded starting ketone **24** (32.0 mg, 72%) as well as alcohol **25** (6.9 mg, 15%) as a white solid; mp 85–86°C (EtOAc); $[\alpha]_D^{25}$ −12.1 (c = 1.00); IR (KBr) ν_{max}: 3397, 2946 cm^{-1}; ^1H NMR δ: 0.83 (3H, s), 0.86 (3H, s), 1.02 (2H, m), 1.14 (2H, m), 1.25 (3H, s), 1.27 (3H, s), 1.35–1.60 (9H, m), 1.70 (1H, m), 1.87 (1H, m, C11-H), 3.40 (2H, dd, J = 8, 8 Hz, C12-2H), 4.52 (2H, s, CH_2-Ph), 7.26 (1H, m), 7.36 (4H, m); ^{13}C NMR δ: 18.33, 18.76, 21.38, 24.65, 29.44, 31.15, 32.89, 33.30, 36.18, 36.97, 38.71, 42.20, 46.63, 55.38, 72.12, 72.96, 75.08, 127.54, 127.58 (×2), 128.37 (×2), 138.50; MS *m/z*: 344 (M^+, 0.5), 329 (0.7), 253 (2.3), 91 (100); HRMS calcd. for $C_{23}H_{36}O_2$: 344.2715; found: 344.2706. Anal. calcd. for $C_{23}H_{36}O_2$: C 80.19, H 10.52; found: C 80.00, H 10.45.

^1H NMR decoupling experiment: irradiation of the doublet of doublets resonating at δ 3.40 ppm affected the signals resonating at δ 1.40 and 1.86 ppm.

Method B

Cerium chloride heptahydrate (652.0 mg, 1.75 mmol) was dried at 140°C for 2 h under high vacuum, then cooled to room temperature. Anhydrous THF (11 mL) was added and the suspension was stirred for 1 h at room temperature, then cooled to −78°C; methyllithium (1.25 mol, 1.75 mmol) was added and stirred for 1 h (at −78°C). Hydroxybenzyl ketone **24** (441.4 mg, 1.34 mmol) in anhydrous THF (14 mL) was added to the suspension. After the addition was completed, the syringe was rinsed into the reaction with anhydrous THF (2 mL). Analytical TLC (EtOAc/hexanes 1:6) showed reaction completion after 10 min. The reaction was quenched with saturated ammonium chloride solution (20 mL) at −78°C. The mixture was allowed to warm to room temperature, and the aqueous layer was extracted with EtOAc (100 mL). The combined organic layers were dried, filtered, and concentrated in vacuo. Chromatographic purification of the crude product, eluting with EtOAc/hexanes 1:6, gave alcohol **25** (458.5 mg, 100%) as a white solid.

1,2,3,4,4aα,5,6,7,8,8a-Decahydro-1α-(2′-hydroxyethyl)-2α,5,5,8aβ-tetramethylnaphthalen-2β-ol (26)

A suspension of alcohol **25** (114.4 mg, 0.33 mmol) and 10% palladium on charcoal (117.2 mg) in absolute EtOH (20 mL), was purged three times with hydrogen at a pressure of 15 psi in a hydrogenation vessel. The pressure was increased to 20 psi of hydrogen and the vessel was shaken for 10 min at room temperature. A sample taken for analytical TLC (EtOAc/hexanes 1:1) showed reaction completion. The suspension was filtered through Celite 545. The flask and Celite were washed with EtOH (60 mL). Concentration in vacuo afforded diol **26** (95.5 mg) as a white solid; mp 145.5–146°C (EtOAc); $[\alpha]_D^{25}$ −22.7 (c = 1.00). IR (KBr) ν_{max}: 3315, 2947 cm^{-1}; ^1H NMR δ: 0.84 (3H, s), 0.85 (1H, m, C9-H), 0.88 (3H, s), 0.98–1.20 (4H, m), 1.27 (3H, s), 1.29 (3H, s), 1.30–1.75 (10H, m), 1.84 (1H, m, C11-H), 3.57 (2H, dd, J = 8, 8 Hz, C12-2H); ^{13}C NMR δ: 18.31, 18.72, 21.35, 24.65, 31.15, 32.48, 32.88, 33.28, 36.28, 36.97, 38.65, 42.22, 46.71, 55.15, 64.50, 75.03; MS *m/z*: 254 (M^+, 4.9), 239 (27.1), 236 (50.9), 221 (100); HRMS calcd. for $C_{16}H_{30}O_2$: 254.2246; found: 254.2242. Anal. calcd. for $C_{16}H_{30}O_2$: C 75.55, H 11.88; found: C 75.50, H 11.79.

^1H NMR decoupling experiment: irradiation of the signal resonating at δ 3.57 ppm simplified the multiplet resonating at δ 1.34 ppm to a doublet of doublets with coupling constant values of 3 and 13 Hz, and simplified the multiplet resonating at δ 1.84 ppm to a doublet of doublets with coupling constant values of 4 and 13 Hz.

1,2,3β,3a,4,5,5aα,6,7,8,9,9a-Dodecahydro-3aβ,6,6,9aβ-tetramethylnaphtho[2,1-*b*]furan, (−)-*epi*-Ambrox® (29)

Method A

p-Toluenesulfonic acid (33 mg, 0.17 mmol) was added to a suspension of diol **26** (337 mg, 1.33 mmol) in nitromethane

© 1997 NRC Canada

Can. J. Chem. Downloaded from www.nrcresearchpress.com by 88.146.161.215 on 09/08/12
For personal use only.

(30 mL). The reaction mixture was heated to 80°C (oil bath temperature) for 30 min; after cooling to room temperature, it was diluted with diethyl ether (50 mL) and washed with saturated sodium bicarbonate solution (25 mL). The organic layer was dried, filtered, and concentrated in vacuo. Chromatographic purification of the crude product, eluting with EtOAc/hexanes 1:4 mixture, yielded (−)-*epi*-Ambrox® (**29**) (261 mg, 83%) as a colourless oil that solidified upon standing. The spectroscopic and other data were in agreement with the published data (36). The primary alcohol **30** was also obtained (33.8 mg, 11%).

Method B

Cerium chloride heptahydrate (1.45 g, 3.90 mmol) was dried at 140°C for 2 h under high vacuum, then cooled to room temperature. Anhydrous THF (16 mL) was added and the suspension was stirred for 1 h at room temperature, then cooled to −78°C. Methyllithium (2.9 mL, 3.90 mmol) was added and stirred for 1 h at −78°C. Hydroxybenzyl ketone **24** (640 mg, 1.95 mmol) in anhydrous THF (20 mL) was added dropwise to the suspension. After 10 min, analytical TLC (EtOAc/hexanes 1:6) showed reaction completion. Saturated ammonium chloride solution (30 mL) was added. The mixture was allowed to warm to room temperature, and the aqueous layer was extracted with EtOAc (150 mL). The combined organic layers were dried, filtered, and concentrated in vacuo. The residue was dissolved in absolute ethanol (20 mL) in a hydrogenation vessel. 10% Palladium on charcoal (670 mg) was added and the vessel was purged 3 times with hydrogen at 15 psi, then shaken for 10 min at hydrogen pressure of 20 psi, at room temperature. The suspension was filtered through Celite 545 using a water aspirator. The flask and Celite were washed with ethanol (60 mL). Concentration in vacuo yielded 565 mg of an oil. Nitromethane (44 mL) was added to the crude product, then *p*-toluenesulfonic acid (49 mg, 0.26 mmol) was added, and the mixture was heated to 80°C (oil bath temperature) for 30 min. After cooling to room temperature, the reaction mixture was diluted with diethyl ether (100 mL). The organic layer was washed with saturated sodium bicarbonate solution (50 mL), dried, filtered, and concentrated in vacuo. Chromatographic purification of the residue, eluting with EtOAc/hexanes: 1:4, yielded (−)-*epi*-Ambrox® (**29**) (371 mg, 80% from **24**, three steps) as a colourless oil that solidified in vacuo, and 50 mg (11%) mixture of primary alcohols (**30**).

1,2,3,4,4aα,5,6,7,8,8a-Decahydro-2,2-ethylenedioxy-1β-(2′-hydroxyethylen)-5,5,8aβ-trimethylnaphthalene (32)

To a solution of ketal **31** (428 mg, 1.32 mmol) in anhydrous diethyl ether (40 mL), LAH (150 mg, 3.95 mmol) was added. The suspension was stirred at room temperature. After 10 min, analytical TLC (EtOAc/hexanes 1:1) showed reaction completion. Water (5 mL) was added and stirrred for 5 min, then 15% sodium hydroxide solution (5 mL) was added and stirred for 5 min more. The mixture was filtered and the filtrate was washed with diethyl ether (50 mL). The aqueous layer was extracted with diethyl ether (50 mL). The combined organic layers were washed with water (50 mL), dried over anhydrous Na_2SO_4, filtered, and concentrated in vacuo. The remaining oil was chromatographed on silica gel treated with EtOAc/hexanes/Et_3N in a $1:1:2 \times 10^{-2}$ ratio, prior to use, and eluted with EtOAc/hexanes 1:1 to yield hydroxy ketal **32** (342.7 mg, 92%) as a white solid, mp 69–70°C (EtOAc); $[\alpha]_D^{25}$ +9.3 (c = 1.00, EtOH); IR (KBr) ν_{max}: 3228, 2916 cm^{-1}; ^1H NMR (acetone-d_6) δ: 0.84 (3H, s), 0.90 (6H, s), 0.90–1.00 (4H, m), 1.15–1.65 (8H, m), 1.73 (1H, m), 1.94 (1H, ddd, J = 12, 4, 4 Hz), 2.82 (1H, br s, O-H), 3.50 (2H, m), 3.80 (1H, dd, J = 8, 8 Hz), 3.90 (1H, m), 4.00 (2H, m); ^{13}C NMR (acetone-d_6) δ: 15.02, 19.17, 20.56, 22.04, 28.04, 33.81, 33.91, 36.60, 39.74, 39.82, 42.73, 55.02, 55.98, 63.94, 64.40, 65.73, 111.68; MS *m/z*: 282 (M^+, 0.1), 264 (0.5), 249 (1.1), 220 (15.6), 205 (100); HRMS calcd. for $C_{17}H_{30}O_3$: 282.2195; found: 282.2189. Anal. calcd. for $C_{17}H_{30}O_3$: C 72.31, H 10.70; found: C 72.52, H 10.85.

1,2,3,4,4aα,5,6,7,8,8a-Decahydro-2,2-ethylenedioxy-1β(2′-*O*-benzyl ethyl)-5,5,8aβ-trimethylnaphthalene (33)

Sodium hydride, 80% dispersion in paraffin oil (108.8 mg, 3.62 mmol) was weighed and washed three times with anhydrous THF (15 mL), under argon atmosphere. Anhydrous THF (15 mL) was added. A solution of hydroxy ketal **32** (340 mg, 1.20 mmol) in anhydrous THF (23 mL) was added dropwise with good stirring. Benzyl bromide (0.43 mL, 3.62 mmol) and tetrabutylammonium iodide (43.5 mg, 0.12 mmol) were added to the suspension. The reaction mixture was heated at reflux. After 22 h, TLC (EtOAc/hexanes 1:4) showed reaction completion. The reaction was cooled to room temperature and water (7 mL) was added slowly. The aqueous layer was extracted with diethyl ether (25 mL). The combined organic layers were washed with water (25 mL), dried over anhydrous Na_2SO_4, filtered, and concentrated in vacuo. The residue was chromatographed on silica gel treated with EtOAc/hexanes/Et_3N $1:9:1 \times 10^{-2}$, prior to use, and eluted with EtOAc/hexanes 1:9, affording hydroxy benzyl ketal **33** (412.2 mg, 92%) as a white solid, mp 85–86°C (EtOAc); $[\alpha]_D^{25}$ +22.9 (c = 1.00); IR (KBr) ν_{max}: 2910 cm^{-1}; ^1H NMR δ: 0.82 (3H, s), 0.88 (3H, s), 0.90 (3H, s), 0.90–0.96 (2H, m), 1.15 (1H, ddd, J = 13, 13, 5 Hz), 1.25–1.80 (10H, m), 1.90 (1H, ddd, J = 10, 3, 3 Hz), 3.40 (1H, m, C12-H_A), 3.60 (1H, m, C12-H_B), 3.75 (1H, dd, J = 4, 4 Hz), 3.86 (1H, ddd, J = 7, 7, 5 Hz), 3.96 (1H, ddd, J = 7, 7, 7 Hz), 4.03 (1H, m), 4.50 (2H, d, J = 3 Hz, CH_2-Ph), 7.27 (1H, m), 7.34 (4H, m); ^{13}C NMR δ: 14.43, 18.50, 19.80, 21.68, 24.01, 33.22, 33.58, 36.09, 39.02, 39.17, 41.98, 53.84, 55.23, 63.28, 65.09, 72.39, 72.62, 111.35, 127.31, 127.54 (×2), 128.24 (×2), 138.90; MS *m/z*: 372 (M^+, 1.2), 357 (0.3), 281 (5.3), 205 (13.9), 99 (100); HRMS calcd. for $C_{24}H_{36}O_3$: 372.2664; found: 372.2656. Anal. calcd. for $C_{24}H_{36}O_3$: C 77.39, H 9.73; found: C 77.47, H 9.68.

3,4,4aα,5,6,7,8,8a-Octahydro-1β(2′-*O*-benzyl ethyl)-5,5,8aβ-trimethyl-1-naphthalene (34)

Method A

To a solution of hydroxybenzyl ketal **33** (411 mg, 1.1 mmol) in acetone (40 mL) was added 1 M HCl (3.3 mL). The reaction mixture was stirred at room temperature for 4 h. Saturated sodium bicarbonate solution (20 mL) was added slowly, and the solution was extracted with diethyl ether (200 mL). The combined organic layers were washed with water (100 mL), dried, and concentrated in vacuo. Chromatographic purification of the residue, eluting with EtOAc/hexanes 1:4, afforded hydroxybenzyl ketone **34** (346.7 mg, 96%) as a colourless oil. $[\alpha]_D^{25}$ −19.6 (c = 1.00); IR (neat) ν_{max}: 2947, 1709 cm^{-1}; ^1H NMR δ: 0.73 (3H, s), 0.86 (3H, s), 0.97 (3H, s), 1.15–1.30

© 1997 NRC Canada

Can. J. Chem. Downloaded from www.nrcresearchpress.com by 88.146.161.215 on 09/08/12
For personal use only.

(3H, m), 1.40–1.90 (6H, m), 2.04 (2H, m), 2.28 (2H, m), 2.41 (1H, ddd, J = 12, 5, 2 Hz), 3.29 (1H, ddd, J = 10, 9, 6 Hz, C12-H_A), 3.53 (1H, m, C12-H_B), 4.42 (1H, d, J = 12 Hz, CH_A-Ph), 4.49 (1H, d, J = 12 Hz, CH_B-Ph), 7.32 (5H, m); ^{13}C NMR δ: 14.67, 18.96, 21.63, 22.00, 23.93, 33.46, 33.65, 39.11, 41.88, 42.30, 42.41, 54.13, 60.06, 69.51, 72.60, 127.39, 127.54 (×2), 128.27 (×2), 138.68, 212.03; MS *m/z*: 328 (M^+, 2.7), 313 (2.5), 269 (10.3), 237 (62.6), 221 (8.9), 179 (88.9), 91 (100); HRMS calcd. for $C_{22}H_{32}O_2$: 328.2402; found: 328.2398. Anal. calcd. for $C_{22}H_{32}O_2$: C 80.45, H 9.81; found: C 80.54, H 9.81.

Method B

To a solution of hydroxybenzyl ketone **24** (546.0 mg, 1.66 mmol) in THF/MeOH 1:1 (20 mL) was added sodium methoxide (270.0 mg, 5.0 mmol) and the solution was heated at reflux for 22 h. After cooling to room temperature, saturated ammonium chloride solution (15 mL) was added and the mixture was extracted with diethyl ether (150 mL). The combined organic layers were washed with water (75 mL), dried, filtered, and concentrated in vacuo. Chromatographic purification of the residue, eluting with EtOAc/hexanes 1:4, afforded hydroxybenzyl ketone **34** (487.6 mg, 89%) as a colourless oil and starting ketone **24** (52.3 mg, 10%).

1,2,3,4,4aα,5,6,7,8,8a-Decahydro-1β-(2′-*O*-benzyl ethyl)-2α,5,5,8aβ-tetramethylnaphthalen-2β-ol (35)

Cerium chloride heptahydrate (720.0 mg, 1.93 mmol) was dried at 140°C under high vacuum for a period of 2 h, then cooled to room temperature. Anhydrous THF (12 mL) was added, and the suspension was stirred at room temperature for 1 h, then cooled to −78°C, and methyllithium (1.38 mL, 1.93 mmol) was added. The mixture was stirred at −78°C for 1 h. A solution of hydroxybenzyl ketone **34** (487.6 mg, 1.49 mmol) in anhydrous THF (15 mL) was added dropwise to the suspension, with maintenance of the temperature. After 10 min, a sample taken for analytical TLC (EtOAc/hexanes 1:4) showed reaction completion. Saturated ammonium chloride solution (15 mL) was added to the reaction mixture, and the temperature was allowed to rise to 25°C. The aqueous layer was extracted with EtOAc (80 mL). The combined organic layers were washed with water (40 mL), dried, filtered, and concentrated in vacuo. Chromatographic purification of the residue with EtOAc/hexanes 1:4 afforded hydroxybenzyl alcohol **35** (502.8 mg, 98%) as a white solid, mp 88.5–89°C (EtOAc/hexane); $[\alpha]_D^{25}$ +10.8 (c = 1.00); IR (KBr) ν_{max}: 3479, 2910 cm^{-1}; ^{1}H NMR δ: 0.83 (3H, s), 0.86 (3H, s), 0.70–0.90 (2H, m), 0.97 (3H, s), 1.10 (3H, s), 1.20–1.80 (13H, m), 3.44 (2H, m), 4.50 (2H, s), 7.27 (1H, m), 7.33 (4H, m); ^{13}C NMR δ: 15.07, 18.13, 18.30, 21.64, 25.28, 30.68, 33.25, 33.42, 38.63, 39.22, 41.98, 42.18, 54.91, 55.89, 72.42, 72.73, 72.89, 127.43, 127.48 (×2), 128.31 (×2), 138.63; CI MS *m/z*: 345 (M^+, +1), 326 (0.2), 311 (0.2), 267 (0.2), 235 (10.3), 218 (34.2), 91 (100). Anal. calcd. for $C_{23}H_{36}O_2$: C 80.19, H 10.52; found: C 80.40, H 10.58.

1,2,3,4,4aα,5,6,7,8,8a-Decahydro-1β-(2′-hydroxyethyl)-2α,5,5,8aβ-tetramethylnaphthalen-2β-ol (36)

A suspension of hydroxybenzyl alcohol **35** (502.8 mg, 1.46 mmol) and 10% palladium on charcoal (500.6 mg) in absolute ethanol (15 mL) was purged three times with hydrogen at 15 psi. The hydrogen pressure was then increased to 20 psi and the vessel was shaken for 10 min. A sample taken for analytical TLC (EtOAc/hexanes 1:1) showed reaction completion. The suspension was then filtered through Celite 545. The vessel and the Celite were washed with ethanol (50 mL). Concentration in vacuo and chromatographic purification of the residue, using diethyl ether/hexanes 5:1 as eluent, afforded diol **36** (370.0 gm, 100%) as a white solid, mp 168–170°C (EtOAc); $[\alpha]_D^{25}$ +15.7 (c = 1.00, ethanol); IR (KBr) $\nu_{max:}$ 3358, 3322, 2925 cm^{-1}; ^{1}H NMR δ: 0.83 (3H, s), 0.87 (3H, s), 0.80–0.90 (2H, m), 0.98 (3H, s), 1.14 (3H, s), 1.30–1.80 (14H, m), 3.56–3.68 (2H, m, C12-2H); ^{13}C NMR δ: 15.13, 18.13, 18.30, 21.64, 28.66, 30.68, 33.27, 33.42, 38.52, 39.33, 41.96, 42.25, 54.65, 55.88, 64.94, 72.91; MS *m/z*: 254 (M^+, 1.2), 236 (6.7), 221 (11.2), 43 (100); HRMS calcd. for $C_{16}H_{30}O_2$: 254.2247; found: 254.2254. Anal. calcd. for $C_{16}H_{30}O_2$: C 75.55, H 11.88; found: C 75.58, H 11.80.

1,2,3β,3a,4,5,5aα,6,7,8,9,9a-Dodecahydro-3aβ,6,6,9aβ-tetramethylnaphtho[2,1-*b*]furan, (−)-Ambrox® (37)

To a suspension of diol **36** (370 mg, 1.46 mmol) in nitromethane (29 mL) was added *p*-toluenesulfonic acid (11.6 mg, 6×10^{-2} mmol). The reaction mixture was heated to 80°C (oil bath temperature) for 30 min with good stirring. It was then cooled to room temperature and diluted with diethyl ether (60 mL). The organic layer was washed with saturated sodium bicarbonate solution (40 mL), dried, and concentrated in vacuo. Chromatographic purification of the residue, eluting with EtOAc/hexanes 1:4, gave pure (−)-Ambrox® (**37**) (261.4 mg, 76%). The spectroscopic and other data were in agreement with the published data (36).

Acknowledgements

We would like to express our gratitude to the Natural Sciences and Engineering Research Council of Canada for financial support, and to Intrinsic Research and Development Inc. for generous samples of Western red cedar leaf oil.

References

1. J.P. Kutney, Y.H. Chen, and S.J. Rettig. Can. J. Chem. **74**, 1753 (1996).
2. G. Ohloff. *In* Fragrance chemistry. The science of the sense and smell. *Edited by* E.T. Theimer. Academic Press, New York. 1982. p. 535, and refs. cited therein.
3. G. Frater and D. Lamparsky. *In* Perfumes, art, science and technology. *Edited by* P.M. Muller and D. Lamparsky. Elsevier Applied Science, New York. 1991. p. 289, and refs. cited therein.
4. G. Ohloff, B. Winter, and C. Fehr. *In* Perfumes, art, science and technology. *Edited by* P.M. Muller and D. Lamparsky. Elsevier Applied Science, New York. 1991. p. 289, and references cited therein.
5. J.P. Kutney and Y.H. Chen. Can. J. Chem. **72**, 1570 (1994).
6. J.P. Kutney, K. Piotrowska, Y.H. Chen, K.P.N. Cheng, Z. Gao, and S.J. Rettig. Can. J. Chem. **68**, 1687 (1990).
7. B. Jansen, J. Kreuzer, and A. de Groot. Tetrahedron, **45**, 1447 (1989).
8. Y.H. Chen. Ph.D. Thesis, University of British Columbia, 1992.
9. T. Mimura and T. Nakai. Chem. Lett. 1099 (1980).
10. C.H. Heathcock, E.G. Delmar, and L.A. Paquette. J. Am. Chem. Soc. **104**, 1907 (1982).
11. W.E. Fristad, T.R. Bailey, and L.A. Paquette. J. Org. Chem. **45**, 3028 (1980).

© 1997 NRC Canada

12. B.R. Davis, S.R. Gupta, and T.G. Halsall. J. Chem. Soc. 4211 (1961).
13. S.K. Mukhopadhyay and P.C. Dutta. J. Chem. Soc. C, 1876 (1967).
14. H.J. Swarts, A.A. Haaksma, B.J.M. Jansen, and A. de Groot. Tetrahedron, **48**, 5497 (1992).
15. G.J. Williams and N.R. Hunter. Can. J. Chem. **54**, 3830 (1976).
16. A.S. Demir, R.S. Gross, N.K. Dunlap, A.B. Hashemi, and D.W. Watt. Tetrahedron Lett. **27**, 5567 (1986).
17. A. Jeganathan, S.K. Richardson, and D.S. Watt. Synth. Commun. **19**, 1091 (1989).
18. A.S. Demir, H. Akgun, C. Tanyeli, T. Sayrac, and D.S. Watt. Synthesis, 719 (1991).
19. R.L. Snowden, S.M. Linder, and M. Wust. Helv. Chim. Acta, **72**, 892 (1989).
20. T. Harada, Y. Kagamihara, S. Tanaka, K. Sakamoto, and A. Oku. J. Org. Chem. **57**, 1637 (1992).
21. D. Herlem, J. Kervagoret, and F. Khuong-Huu. Tetrahedron Lett. **30**, 553 (1989).
22. T. Tsunoda, M. Suzuki, and R. Noyori. Tetrahedron Lett. **21**, 1357 (1980).
23. S. Czernecki, C. Georgoulis, and C. Provelenghiou. Tetrahedron Lett. **39**, 3535 (1976).
24. T. Imamoto, Y. Sugiura, and N. Takiyama. Tetrahedron Lett. **25**, 4233 (1984).
25. T. Imamoto, T. Kusumoto, Y. Tawarayama, Y. Sugiura, T. Mita, Y. Hatanaka, and M. Yokoyama. J. Org. Chem. **49**, 3904 (1984).
26. T. Imamoto, N. Takiyama, K. Nakamura, T. Hatajima, and Y. Kamiya. J. Am. Chem. Soc. **111**, 4392 (1989).
27. M. Hinder and M. Stoll. Helv. Chim. Acta, **33**, 1308 (1950).
28. R.C. Cambie, K.N. Joblin, and A.F. Preston. Aust. J. Chem. **24**, 583 (1971).
29. I.C. Coste-Manier, J.P. Zahra, and B. Waegell. Tetrahedron Lett. **29**, 1017 (1988).
30. G. Buchi and H. Wuest. Helv. Chim. Acta, **72**, 996 (1989).
31. R.L. Snowden, J.C. Eichenberger, S.M. Linder, P. Sonnay, C. Vial, and K.H. Schulte-Elte. J. Org. Chem. **57**, 955 (1992).
32. P.F. Vlad, M.N. Koltsa, I.P. Dragalin, L.A. Zadorozhnaya, V.E. Sibirseva, and L.M. Sitnova. Russ. Chem. Rev. **58**, 2037 (1988).
33. G. Ohloff, W. Giersch, W. Pickenhagen, A. Furrer, and B. Frei. Helv. Chim. Acta, **68**, 2022 (1985).
34. L.A. Paquette and R.E. Maleczka. J. Org. Chem. **56**, 6538 (1991).
35. M. Stoll and M. Hinder. Helv. Chim. Acta, **33**, 1251 (1950).
36. G. Ohloff, C. Vial, E. Demole, P. Enggist, and W. Giersch. Helv. Chim. Acta, **69**, 163 (1986).
37. H. Tanimoto and T. Oritani. Tetrahedron: Asymmetry, **7**, 1695 (1996).

Can. J. Chem. Downloaded from www.nrcresearchpress.com by 88.146.161.215 on 09/08/12
For personal use only.

© 1997 NRC Canada

β-Cyclodextrin effects on photo-Claisen rearrangement of allyl phenyl ether

Ana M. Sanchez, Alicia V. Veglia, and Rita H. de Rossi

Abstract: The photo rearrangement of allyl phenyl ether (**1**) in water and in solutions containing β-cyclodextrin (β-CD) leads to the *para* (**2**) and *ortho* (**3**) allyl phenols and phenol (**4**) as principal products. The substrate associates with β-CD forming a **1**:CD complex with a $K_{1\text{-CD}} = (4.6 \pm 0.6) \times 10^2\ M^{-1}$. When the photolysis is carried out in presence of oxygen there is a decrease in the total yields of products, but the inhibition is less marked in the presence of β-CD. The product quantum yields (Φ) for the complexed substrate are different for the free substrate, being higher for the *ortho* product, almost the same for the *para* product, and lower for phenol. The *ortho* selectivity was confirmed in the photolysis of the solid complex; these results are in agreement with those reported by this laboratory for the photo-Fries rearrangement of acetanilide and phenyl acetate.

Key words: cyclodextrin, photo-Claisen rearrangement, selectivity.

Résumé : Le photoréarrangement de l'oxyde d'allyle et de phényle (**1**), dans l'eau et dans des solutions contenant de la β-cyclodextrine (β-CD), conduit à la formation de *para* (**2**) et d'*ortho* (**3**) allylphénol et de phénol (**4**) comme produits principaux. Le substrat s'associe avec la β-CD conduisant à la formation d'un complexe **1** : CD avec un $K_{1\text{-CD}} = (4{,}6 \pm 0{,}6) \times 10^2\ M^{-1}$. Lorsqu'on effectue la photolyse en présence d'oxygène, les rendements globaux en produits augmentent, mais l'inhibition est moins marquée en présence de β-CD. Les rendements quantiques en produit (Φ) pour le substrat complexé sont différents de ceux du substrat libre; Φ est plus élevé pour le produit *ortho*, pratiquement le même pour le produit *para* et plus faible pour le phénol. La sélectivité pour le produit *ortho* a été confirmée lors de la photolyse du complexe solide; ces résultats sont en accord avec ceux rapportés par ce laboratoire pour le réarrangement de photo-Fries de l'acétanilide et l'acétate de phényle.

Mots clés : cyclodextrine, réarrangement de photo-Claisen, sélectivité.

[Traduit par la rédaction]

Introduction

During the last 10 years we have been concerned with the study of several aspects of the chemistry of cyclodextrins (CD), which are doughnut-shaped molecules formed by six, seven, or eight glucose units (α, β, and γ) and are able to form inclusion complexes with a great variety of compounds (1). This property of CD is responsible for certain changes in the reactivity and selectivity of organic reactions, of which we have reported some examples (2, 3).

Results from this laboratory concerning the selectivity induced by CD in organic reactions indicated *ortho* selectivity in the case of the photo-Fries rearrangement of acetanilide (4) and phenyl acetate (5), this effect being produced by sterically blocking certain potential sites of reaction in the complexed substrate. In the reactions of phenyl alkyl esters with different alkyl chain length (6), the *ortho* selectivity depends on the hydrophobicity of the alkyl chain competing with the aromatic group for the apolar cavity of CD.

Received March 26, 1997.

A.M. Sanchez, A.V. Veglia, and R.H. de Rossi.[1] Instituto de Investigaciones en Físico Química de Córdoba (INFIQC), Departamento de Química Orgánica, Facultad de Ciencias Químicas, Universidad Nacional de Córdoba, Agencia Postal 4, Casilla 61, 5000 Córdoba, Argentina.

[1] Author to whom correspondence may be addressed. Telephone: 54-51-334170/54-51-334173. Fax: 54-51-334174. E-mail: ritah@dqo.uncor.edu.

We have undertaken the study of the photo-Claisen rearrangement of allyl phenyl ether (**1**) in water solutions in the presence of β-cyclodextrin (β-CD) in order to determine the effect of inclusion complex formation on the quantum yields for the *ortho* and *para* rearrangement products and phenol.

Results

Inclusion complex formation

The addition of β-CD to a water solution of the substrate **1** (0.76 mM) produced a bathochromic shift (2 nm) in the absorption maximum of **1** centered at 268.8 nm and an increase of absorbance, indicating the formation of a complex. The change in absorbance (ΔA) of the difference spectrum between the solution without β-CD and the solution with the higher concentration of β-CD employed was measured in order to choose the wavelength showing maximum ΔA value (λ = 277.9 nm). From the absorbance values measured at this wavelength at various β-CD concentrations (0–15 mM), Fig. 1, we obtained the equilibrium constant for the 1:1 association, $K_{1\text{-CD}} = (4.6 \pm 0.6) \times 10^2\ M^{-1}$, by nonlinear regression analysis of eq. [1] (7). This value is similar to those obtained for phenyl alkanoates (5, 6). Rearrangement of eq. [1] yields eq. [2].

$$[1] \quad A = A_0 + \{(\Delta A_{max} K_{1\text{-CD}}[\beta\text{-CD}])/(1 + K_{1\text{-CD}}[\beta\text{-CD}])\}$$

$$[2] \quad ([\mathbf{1}] \times [\beta\text{-CD}]_0)/\Delta A = (1/K_{1\text{-CD}}\Delta\varepsilon) + ([\beta\text{-CD}]_0/\Delta\varepsilon)$$

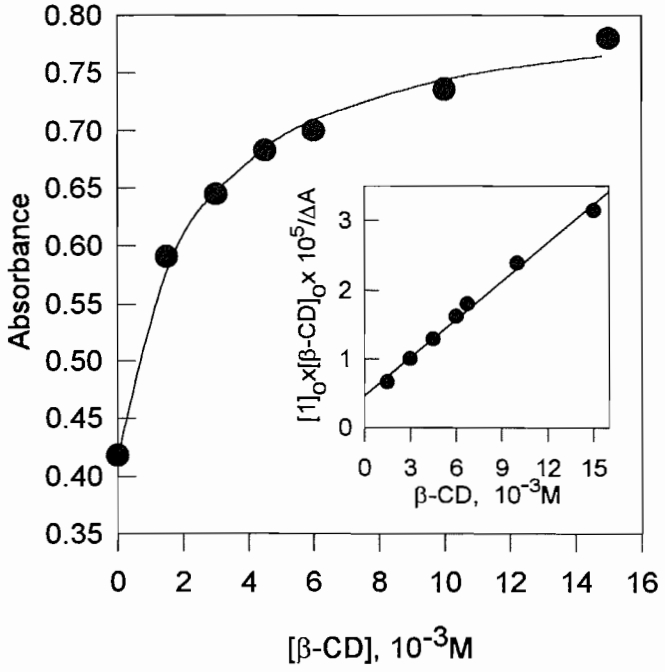
A plot of the left-hand side of eq. [2] vs. [β-CD] (7, 8) is

© 1997 NRC Canada

Can. J. Chem. Downloaded from www.nrcresearchpress.com by 88.146.161.215 on 09/08/12
For personal use only.

Can. J. Chem. Downloaded from www.nrcresearchpress.com by 88.146.161.215 on 09/08/12
For personal use only.

Fig. 1. Absorbance of solutions of **1** (0.76 mM) at different concentrations of β-CD. The curve is the fit using eq. [1]. *Inset:* Plot of the data and regression line according to eq. [2].



linear (correlation coefficient = 0.993) (Fig. 1, inset) and from the ratio of the slope and the intercept a value of $K_{1\text{-CD}} = (4.0 \pm 0.7) \times 10^2\ M^{-1}$ is calculated, in good agreement with the value obtained by nonlinear regression. Linearity of the plot according to eq. [2] confirms the stoichiometric ratio 1:1 (9).

The lack of an isosbestic point in the spectrum may indicate that complexes of higher stoichiometry are formed or that the spectra of the species are dependent on the reaction medium (7). Since similar results were obtained with other substrates (3, 5, 6), we think that the major complexes have 1:1 stoichiometry.

Photolysis

The photolysis of **1** in water solution and in solution containing β-CD leads to *p*-allylphenol (**2**), *o*-allylphenol (**3**), and phenol (**4**) as major products (eq. [3]). The formation of some minor quantities of *m*-allylphenol and cyclic products in protic solvents have been reported (10). Since compounds **2** and **3** decompose under these conditions, it is difficult to determine the contribution of the minor products to the total products yield; however, as can be seen in Table 2, we have a good material balance, which indicates that the formation of other products besides **2**–**4** must be very small.

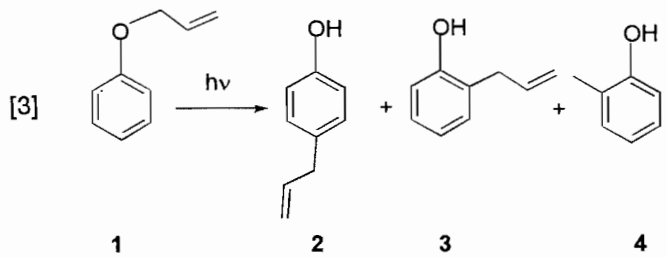


Table 1. UV–visible characteristics of substrate and products[a]

Compound	λ_{max}, nm	ε, $cm^{-1}\ M^{-1}$
Allylphenyl ether[b]	268.8	1036
o-Allyl phenol[c]	271.4	1796
p-Allyl phenol[d]	273.0	1429
Phenol[e]	269.6	1427

[a] T = 25°C; water as solvent. The error in ε is less than 3%.
[b] [Allylphenyl ether] = $(4.5–17.8) \times 10^{-5}$ M.
[c] [*o*-Allylphenol] = $(8.7–34.5) \times 10^{-5}$ M.
[d] [*p*-Allylphenol] = $(3.7–16.5) \times 10^{-5}$ M
[e] [Phenol] = (4-10) x 10^{-5} M.

Table 2. Effect of oxygen and β-cyclodextrin on the photolysis of allyphenyl ether in aqueous solution.[a]

	Yield,[b] %				
Condition	**1**[b,c]	**2**[d]	**3**[d]	**4**[c]	[3]/[2]
N_2	63.1	15.6	22.1	2.3	1.4 ± 0.1
N_2/β-CD	38.7	21.9	40.2	2.1	1.8 ± 0.1
O_2	88.7	6.56	3.99	0.90	1.6 ± 0.1
O_2/β-CD	82.0	11.5	7.33	0.70	1.6 ± 0.1

[a] T = 25°C; water as solvent; $[1]_0$ = 1.5 mM. Irradiation time = 4 h.
[b] Absolute yields based on the initial substrate concentration.
[c] The error in the determinations is less than 3%.
[d] Values corrected by the decomposition percentage determined at the same reaction conditions. The error in **2** and **3** is estimated as less than 5 and 3%, respectively.

We determined the product distribution by high-pressure liquid chromatography (HPLC) (see details in experimental section) because the UV–visible (UV) spectra of substrates and products are very similar (Table 1) making quantification by spectrophotometry impossible.

The results of the photolysis experiments are summarized in Table 2, where it can be seen that the yield of products decreases when oxygen is present (aerated solutions), from 37% in nitrogen to 11% in oxygen without β-CD and from 61% in nitrogen to 18% in oxygen in the presence of β-CD.[2] The **3**/**2** ratio is the same in both cases within the experimental error. It should be noticed that the overall yield increases in the presence of β-CD.

Quantum yield determinations

The addition of β-CD results in an increase in the quantum yield (Φ) of **3** (≈36%), but the change in the quantum yield of

[2] The value of the total yield of products calculated from the difference between the initial and the remaining substrate is considered to be more accurate than that calculated from the sum of the concentrations of **2** + **3** + **4** because this involves the accumulation of errors due to the measurements of three concentrations.

© 1997 NRC Canada

Can. J. Chem. Downloaded from www.nrcresearchpress.com by 88.146.161.215 on 09/08/12
For personal use only.

Table 3. Quantum yields of the products formed in the photolysis of allylphenyl ether in aqueous solution.[a]

	$\Phi^b \times 10^3$			
Condition	**3**	**2**	**4**	[**3**]/[**2**]
Water	3.30[c]	1.50[c]	0.14[c]	2.2 ± 0.1
Water/β-CD[d]	4.48[c]	1.40[c]	0.04[c]	3.2 ± 0.2
β-CD[e]	3.88	1.15	0.02	3.4 ± 0.2

[a]T = 25°C; water as solvent; $[\mathbf{1}]_0$ = 1.5 mM. Irradiation time 30 min.
[b]Quantum yields for the formation of the product indicated below.
[c]The error is less than 3%.
[d]$[CD]_0$ = 15 mM.
[e]Calculated from eq. [4], see text.

2 is barely outside the experimental error. In these experiments we observed an important decrease in the quantum yield of **4**. These results are summarized in Table 3. The **3/2** ratio increases with β-CD from 2.2 to 3.2.

Cyclodextrin complex photolysis

The solid **1**-CD complex, prepared as in previous papers (5, 6, 11), was irradiated during 4 h with a continuous flow of nitrogen. About 80.5% of substrate was recovered and the only product formed was **3** (18.2%). This result is similar to those obtained upon irradiation of solid complexes of *meta*-alkoxyphenylallyl ethers with α- and β-cyclodextrin (12) and indicates a more restricted environment for the substrate inside the cavity.

Discussion

The photo-Claisen rearrangement has received very scant attention, due mainly to the extensive polymerization products observed upon photolysis. The photochemical rearrangement of **1** has been studied in protic and nonprotic solvents (10, 13) but there have not been detailed studies in aqueous solutions. Some results about the reaction of *meta*-alkoxyphenylallyl ethers complexed with α- and β-CD have been published (12).

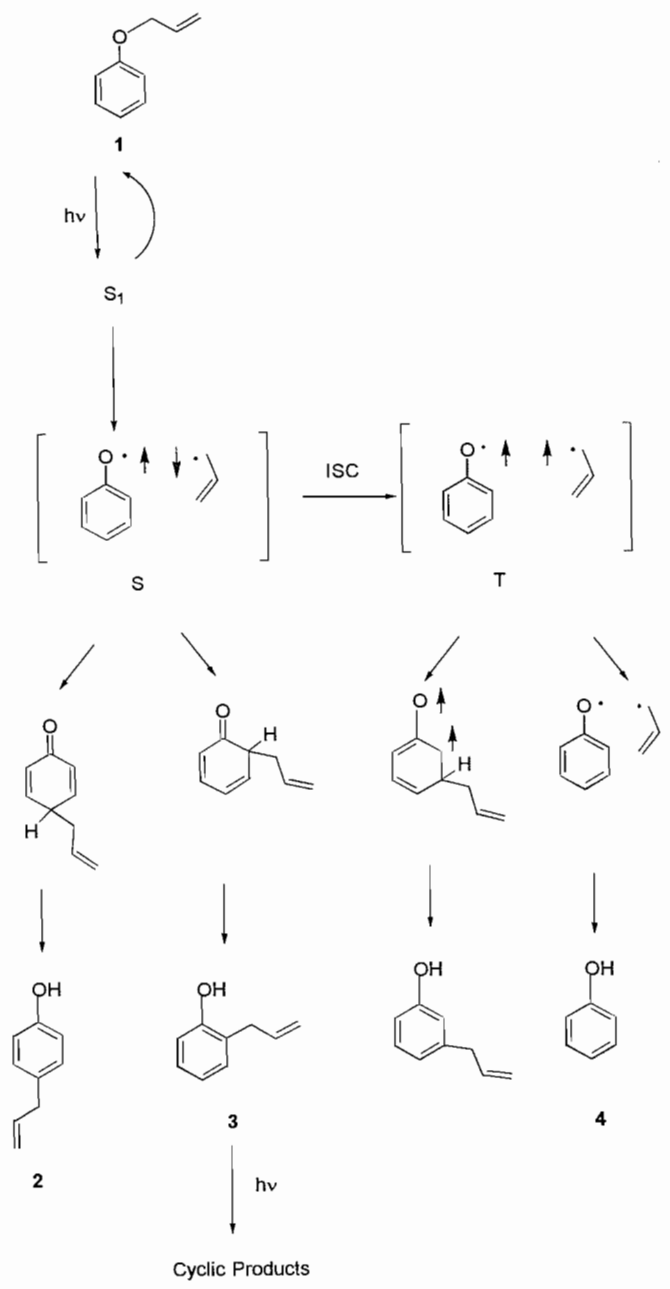
The composition of the photo products depends largely on the nature of the solvent (10). In protic solvents the principal products are 2- and 4-allylphenol and 3-allylphenol is formed in very small amounts (0.02%) (10). However, in aromatic hydrocarbons or cyclohexane, 3-allylphenol, as well as cyclic products, is obtained in significant amount (10).

The general mechanism proposed for the reaction is shown in Scheme 1 (10, 14).

The primary photochemical process produces a pair of radicals from the singlet excited state by homolytic rupture in the solvent cage. This radical pair leads to the *ortho* and *para* rearrangement products or, by intersystem crossing, it produces the triplet radical pair. The triplet radical pair leads to the *meta*-substituted compound and to phenol by escape of the radicals from the solvent cage (10). Cyclic products arise from photocyclization of *ortho* allylphenol, mainly in hydrocarbon solvents (10, 15).

In the presence of cyclodextrin at the maximum concentration used, 87% of the substrate is complexed; therefore the photochemical reaction must be taking place in both environments.[3] The kinetic scheme can be represented as in Scheme 2, where Φ_w^i and Φ_{CD}^i are the quantum yield for each product (i = **2**–**4**) in water and in β-CD, respectively.

Scheme 1.

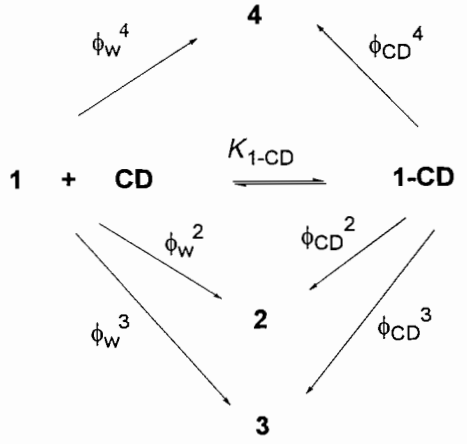


The observed quantum yield for each product, Φ_{exp}, may be described by eq. [4],

[3] We assume that the photochemical and photophysical primary processes are not appreciably altered by association with CD. We think that the possibility of diffusion outside the cyclodextrin cavity is unlikely because singlet-state lifetimes are in the order of 10^{-9} s, whereas the diffusion rate of organic species outside the cavity of CD is in the range of 10^4–10^6 s^{-1} (see, for instance, ref. 16). On the other hand, escape of the radical pair from the cyclodextrin cavity and recombination in the bulk solution should lead to the same product ratio as in the absence of β-CD.

© 1997 NRC Canada

Scheme 2.



[4] $\Phi_{exp}^{\ i} = \Phi_w^{\ i}(1 - f) + \Phi_{CD}^{\ i}(\varepsilon_{CD}/\varepsilon_W)f$

where $f = K_{1\text{-}CD}[\beta\text{-CD}]/(1 + K_{1\text{-}CD}[\beta\text{-CD}])$ is the fraction of complexed substrate (**1–CD**) and $(\varepsilon_{CD}/\varepsilon_W)$ is a correction factor for the differences in light absorption by **1–CD** and **1.** The value of $\varepsilon_{CD}/\varepsilon_W = 1.2$ was determined from the absorbance at 254.0 nm of solutions with known initial concentration of **1** and β-CD, using the equilibrium concentration determined from $K_{1\text{-}CD}$. The $\Phi_{CD}^{\ i}$ values (Table 3) were calculated from eq. [4] using the measured value of $\Phi_w^{\ i}$ and the value of $K_{1\text{-}CD}$ (see above) determined independently.

The *ortho* selectivity in the presence of β-CD is consistent with the results for the Fries rearrangements of acetanilide (4) and phenyl acetate (5) that involve a similar mechanism, namely, a homolytic radical rupture and posterior recombination in the solvent cage. The change in the quantum yield for the *para* product is also similar. The decrease in phenol found in this work contrasts with the increase observed for this product in the Fries rearrangement of phenyl alkanoates (5, 6). This difference may be attributed to the distinct mechanism of formation of phenol, which in the case of the Fries rearrangement comes from the escape of radicals from the singlet radical pair whereas in the Claisen rearrangement it comes from the triplet radical pair. The results may indicate that in the complexed substrate the transformation of singlet to triplet radical pair is inhibited. Another possibility is that the rate of singlet–triplet interconversion is the same but the rate of recombination of the singlet radical pair increases.

The overall quantum yield for formation of **2** + **3** increases in the presence of β-CD despite the fact that it is known that the photo rearrangement of allyl phenyl ether is favored by polar solvents (10). Since the cavity of β-CD is less polar than water, the increase in quantum yield may indicate that the inclusion in the cavity protects the reactive excited state from quenching (17). The increase in *ortho* reactivity may be due to the geometry of the complex, which may place the migrating group in the appropriate position for reaction. The penetration of **1** into the β-CD cavity probably occurs, as usual, through the wider side (18); in this case the *ortho* position is relatively exposed to water and with little steric constraint.

Experimental section

Reagents

Water was obtained from a Millipore apparatus. Compounds **1** and **3** (Aldrich) and **4** (Merck, analytical grade) were commercial reagents and were used as received. Compound **2** was synthesized as indicated in the literature (19) from phenol (Carlo Erba); other compounds used were allyl chloride (BDH), ZnCl (Merck), and chloroform (Eclaire). The purity of compounds **1–4** was checked by HPLC. β-Cyclodextrin (Roquette)[4] was used as received. Its purity was controlled by UV spectrophotometry. Methanol was HPLC grade (Sintorgan).

Apparatus

The spectrophotometric determinations were carried out in a Shimadzu UV 260. A Varian Vista 5500 liquid chromatograph equipped with a Varian 2550 UV–vis detector and a Varian 4290 integrator was used for the HPLC analysis. The analytic column was a Micro Pack 15 cm × 4 mm MCH-5-n-cap.

Photolysis method

The reactions were carried out in a quartz reactor for 4 h. Solutions of **1** (1.5 mM) with or without CD were irradiated at 254 nm with an immersion-type low-pressure mercury lamp of 6 W with either bubbling nitrogen or nothing. The solid complex **1–CD** was irradiated in the same reactor but in a horizontal position at the same height of the filament lamp. In all cases the reactor was covered with aluminum foil. To check the photostability of the products, solutions containing **2** or **3** (0.2 mM) in water and in water with β-CD were irradiated under the same experimental conditions for the same period of time, taking the UV spectrum of samples every 30 min. The decrease in absorption was undetectable in 30 min but it amounted to ~40% for **2** and ~10% for **3** after 4 h irradiation. The values reported are the corrected ones. The correction was done by increasing the amount of the measured compound by the percentage of the observed decomposition product in a sample of the product irradiated during the same period of time.

Quantum yield determinations

Aqueous solutions of allyl phenyl ether (1.5 mM) with or without 15 mM of β-CD contained in square quartz cuvettes were placed in a merry-go-around apparatus. They were irradiated with a low-pressure mercury lamp (254 nm, 6 W); the lamp was covered every 10 min to stop irradiation and the yield of products was determined as indicated below. The irradiation was stopped at 30 min (3% conversion). The concentrations of **2–4** were plotted vs. time, and the slopes were used to calculate the quantum yields. These values and those of [**3**]/[**2**] ratios are reported in Table 3. The quantum yields were determined by using a solution of acetanilide in water as actinometer as previously reported (4, 5). Control experiments using **2** and **3** instead of the substrate showed that the products are stable under these conditions.

[4] β-Cyclodextrin was a gift from the Pharmaceutical Company Ferromet S.A., Buenos Aires, Argentina.

© 1997 NRC Canada

Can. J. Chem. Downloaded from www.nrcresearchpress.com by 88.146.161.215 on 09/08/12
For personal use only.

Analytical methods

Attempts to quantify the photolysis products by UV spectrophotometry were unsuccessful because of the similarity of the spectra of compounds **1**–**4**. Analysis of the products by HPLC was carried out at room temperature, using methanol/water/acetic acid (70/30/1) as solvent, with a flux program from 0.3 mL/min (time = 0) up 1 mL/min (time = 12 min); 4-hydroxypropiophenone (st) was used as internal standard. The UV detector was fixed at 269 nm. The quantification factors (qf) are defined as $Area_i \times mg_{st}/mg_i \times Area_{st}$. $Area_i$ and $Area_{st}$ are the areas of the compound analyzed and the standard, respectively, and mg_i and mg_{st} are the corresponding milligrams. The qf and retention times (rt, min) are: (qf, rt) 0.016, 22.05 for **1**; 0.010, 18.42 for **2**, 0.032, 12.97 for **3**; 0.126, 7.17 for **4**; and the rt is 15.77 for st. The concentrations reported are averages of at least three determinations; the differences between them are 2–3%.

Acknowledgement

This research was supported in part by the Consejo Nacional de Investigaciones Científicas y Técnicas (CONICET), Argentina, the Consejo Provincial de Investigaciones Científicas y Tecnológicas (CONICOR) Córdoba, Argentina, and the Secretaría de Ciencia y Tecnologia de la Universidad Nacional de Córdoba (SECyT-UNC).

References

1. M.L. Bender and M. Komiyama. Cyclodextrin chemistry. Springer-Verlag, Berlin. 1978; P. Bartolus, G. Kohler, and S. Monti. Coord. Chem. Rev. **125**, 261 (1993); D.F. Eaton. Tetrahedron, **43**, 1551 (1987).
2. R.H. de Rossi, M. Barra, and E.B. de Vargas. J. Org. Chem. **51**, 2157 (1986).
3. A.V. Veglia, and R.H. de Rossi. J. Org. Chem. **53**, 5281 (1988).
4. M. Nassetta, R.H. de Rossi, and J.J. Cosa. Can. J. Chem. **66**, 2794 (1988).
5. A.V. Veglia, A.M. Sanchez, and R.H. de Rossi. J. Org.Chem. **55**, 4083 (1990).
6. A.V. Veglia and R.H de Rossi. J. Org. Chem. **58**, 4941 (1993).
7. K.A. Connors. Binding constants. John Wiley & Sons, New York. 1987.
8. F. Cramer, W. Saenger, and H. Spatz. J. Am. Chem. Soc. **89**, 1 (1967).
9. A. Muñoz de la Peña, F. Salinas, I. Durán-Merás, and M.D. Moreno. Anal. Chem. **27**, 1893 (1994).
10. H.R. Waespe, H. Heimgartner, H. Schmid, H.J. Hansen, H. Paul, and H. Fischer. Helv. Chim. Acta, **61**, 401 (1978).
11. B. Nageshwer Rao, M.S. Symala, N.J. Turro, and V. Ramamurthy. J. Org. Chem. **52**, 5517 (1987).
12. M.S. Symala and V. Ramamurthy. Tetrahedron, **44**, 7223 (1988).
13. J.J. Houser, M. Chen, and S. Wang. J. Org. Chem. **39**, 1388 (1974).
14. W. Adam, H. Fischer, H.J. Hansen, H. Heimgartner, H. Schmid, and H.R. Waespe. Angew. Chem. Int. Ed. Engl. **12**, 662 (1973).
15. M.A. Miranda and R. Tormos. J. Org. Chem. **58**, 3304 (1993).
16. R.L. Schiller, S.F. Lincoln, and J.H. Coates. J. Chem. Soc. Faraday Trans. 1, **82**, 2123 (1986); M. Barra, C. Bohne, and J.C. Scaiano. J. Am. Chem. Soc. **112**, 8075 (1990); J. Liao, J. Frank, J.F. Holzwarth, and C. Bohne. J. Chem. Soc. Chem. Commun. 199 (1995).
17. C.N. Sanramé, R.H. de Rossi, and G.A. Argüello. J. Phys. Chem. **100**, 8151 (1996).
18. Y. Wang and D.F. Eaton. Chem. Phys. Lett. **120**, 441 (1985).
19. D.S. Tarbell. Org. React. **2**, 2 (1944).

Can. J. Chem. Downloaded from www.nrcresearchpress.com by 88.146.161.215 on 09/08/12
For personal use only.

© 1997 NRC Canada

Orientational order of 1,3-dichloro-2-ethenylbenzene in liquid-crystal solvents

J.C.T. Rendell, D.S. Zimmerman, A.J. van der Est, and E.E. Burnell

Abstract: The order parameter matrices of a molecule that has no symmetry, 1,3-dichloro-2-ethenylbenzene, dissolved in two different nematic liquid-crystal solvents are analyzed in terms of various models for the intermolecular mean-field potential. In a mixture of liquid crystals for which the interaction between the molecular quadrupole moment tensor and the average electric field gradient of the nematic solvent has been minimized, the orientational order is best described by models for the short-range anisotropic potential. The most successful potentials are written in terms of anisotropic interactions between the solute surface and the liquid-crystal mean field. This represents a strong test of such models because they simultaneously fit the five independent orientational parameters obtained from the same solute, thus removing the problems associated with comparing results among different solutes in either the same or a different sample tube.

Key words: liquid crystals, intermolecular forces, order parameters, anisotropic.

Résumé : Les matrices des paramètres d'ordre d'une molécule qui ne possède pas de symétrie, le 1,3-dichloro-2-éthénylbenzène, dissous dans deux solvants de cristaux liquides nématiques différents, sont analysées en termes de divers modèles pour le potentiel de champ moyen intermoléculaire. Dans un mélange de cristaux liquides pour lequel l'interaction entre le tenseur du moment quadripolaire moléculaire et le gradient moyen du champ électrique du solvant nématique ont été minimisés, la meilleure façon de décrire l'ordre d'orientation implique des modèles pour le potentiel anisotropique à courte distance. Les potentiels les meilleurs sont décrits en termes d'interactions anisotropiques entre la surface du soluté et le champ moyen du cristal liquide. Ceci représente un bon test pour de tels modèles parce qu'ils permettent d'ajuster simultanément les cinq paramètres d'orientation indépendants obtenus pour un même soluté, éliminant ainsi les problèmes associés à une comparaison de résultats de divers solutés dans un même ou dans différents tubes à échantillonage.

Mots clés : cristaux liquides, forces intermoléculaires, paramètres d'ordre, anisotropique.

[Traduit par la rédaction]

1. Introduction

A detailed understanding of the mechanisms responsible for orientational ordering in liquid crystalline systems is crucial to the comprehension of this important class of compounds. In recent years we have shown that a considerable contribution comes from the interaction between the average electric field gradient (efg) present in liquid-crystal systems and the anisotropy in the molecular quadrupole moment of an individual molecule (1–7). The molecule can be either a small solute or a liquid-crystal molecule itself. Since the anisotropies in the electric field gradients can be of opposite sign in different nematic liquid crystals, we have been able to produce mixtures where the average electric field gradient as measured at the deuteron in the solute dideuterium is zero (6, 8–10). In such zero efg mixtures the anisotropic interactions involving the molecular quadrupole moment mechanism are assumed to be unimportant. These zero efg mixtures provide an excellent medium for the study of the remaining anisotropic interactions in these nematic phases (2, 11–15).

Most studies in zero efg mixtures have involved solutes with sufficiently high symmetry that three or fewer independent elements of the order parameter matrix are needed to describe the average solute orientation. An exception is provided by the single and multiple quantum NMR spectra of the solute 1,3-dichloro-2-ethenylbenzene (DCEB, Fig. 1), which have been analyzed to obtain the five independent elements of the order parameter matrix of this molecule dissolved in the zero efg mixture 55 wt.% 1132–EBBA[6] (16). A further problem that was treated in this analysis involves the averaging of the dipolar couplings over the internal rotation of the vinyl group. It was shown that for this molecule the NMR data are consistent with a deep minimum in the potential

Received September 4, 1996.[1]

J.C.T. Rendell,[2] D.S. Zimmerman,[3] A.J. van der Est,[4] and E.E. Burnell.[5] Department of Chemistry, 2036 Main Mall, The University of British Columbia, Vancouver, BC V6T 1Z1, Canada.

[1] Revision received April 11, 1997.

[2] Present address: Institute for Biodiagnostics, National Research Council Canada, 435 Ellice Ave., Winnipeg, MB R3B 1Y6, Canada.

[3] Present address: SEA++ INC, 301 6055 Balsam Street, Vancouver, BC V6M 4C2, Canada.

[4] Present address: Fachbereich Physik, Freie Universität Berlin, Arnimallee 14, D-14195 Berlin, Germany.

[5] Author to whom correspondence may be addressed. Telephone: (604) 822-2603. E-mail: bur@nematic.chem.ubc.ca

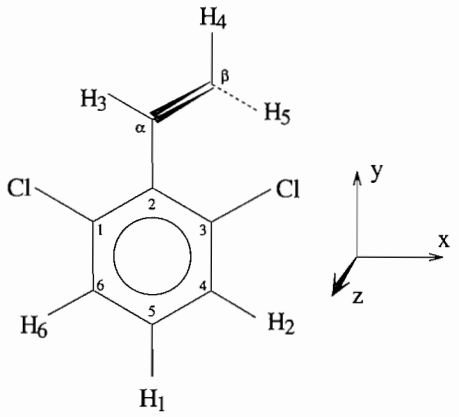
[6] See Table 1 (caption) for definition of liquid crystal solvents.

© 1997 NRC Canada

Can. J. Chem. Downloaded from www.nrcresearchpress.com by 88.146.161.215 on 09/08/12
For personal use only.

Can. J. Chem. Downloaded from www.nrcresearchpress.com by 88.146.161.215 on 09/08/12
For personal use only.

Fig. 1. The molecule – fixed axis system used for 1,3-dichloro-2-ethenylbenzene, DCEB.



surface for the four symmetry-related structures described by $\phi_{min} = 45.4°$. However, there is a correlation among ϕ_{min}, S_{xz}, and the depth of the potential surface. For realistic values of the potential, all order parameters (except S_{xz}) are equal within 5% to those for a simple model involving rapid interconversion among four rigid symmetry-related sites. A 5% uncertainty is less than that associated with the mean-field models that are used for comparisons with NMR data of average orientations of solutes in nematic solvents. Hence, for the purposes of the present study it is sufficient to use order parameters under the rigid molecule assumption. The results of analysis of the NMR spectra, assuming rapid interconversion among the four rigid symmetry-related sites, are summarized in Table 1, and the experimental details are given in ref. 16.

In this paper we shall examine the experimental order parameters of Table 1 in terms of various models that have been proposed to describe orientational ordering. Because in this case there are five independent parameters associated with a single molecule, the data in Table 1 provide an excellent opportunity to test models; all five parameters must arise from precisely the same intermolecular interaction, and thus an acceptable model will be one that can predict all five numbers with a minimum of adjustable parameters. We shall examine models that attempt to account for short-range intermolecular interactions in terms of molecular size and shape anisotropy. We shall not attempt to include in our analysis models that are based on the potential of mean torque. Such models have been successfully applied to the analysis of liquid crystals and of flexible hydrocarbons as solutes in liquid crystals (17–20). We feel that to include properly the double bond and chlorine atoms would introduce too many adjustable parameters.

2. A comparison of shape-ordering models

If we know the potential energy of the molecule as a function of orientation, the order matrix of the solute is found classically (21) to be

$$[1] \qquad S_{ab} = \frac{\int(3\cos\theta_a\cos\theta_b - \delta_{ab})\exp(-U(\Omega)/kT)\mathrm{d}\Omega}{2\int\exp(-U(\Omega)/kT)\mathrm{d}\Omega}$$

The difficulty lies in determining U. As has already been mentioned, for small molecules U may encompass several contributions. One is an interaction between the molecular quadrupole moment and the anisotropy in a mean electric field gradient in the liquid-crystal solvent. In the mixture 55 wt.% 1132–EBBA used in this paper this interaction is negligible, as demonstrated by experiments using molecular hydrogen (6, 8) and methane (22). We shall assume that the dominant interaction in this mixture involves short-range anisotropic forces. The test of this assumption will be the quality of the fits obtained using models for these short-range interactions.

2.1. Estimate of shape anisotropy from inertial properties of the solute

Years ago Anderson noted that the order parameters and the principal moments of inertia for a series of 27 substituted benzenes showed a reasonable correlation (23) and these findings have been corroborated by other workers (24). Samulski followed up on these ideas and proposed two methods for the prediction of the order matrix from the inertia tensor of the solute (25, 26). These methods have been employed with success in explaining the ordering of flexible solutes such as *n*-octane in nematic solvents. To do this Samulski used the principal moments of inertia to define the semiaxes of the inertia ellipsoid (27) in the manner

$$[2] \qquad A_\alpha = \left[(I_{\beta\beta} + I_{\gamma\gamma} - I_{\alpha\alpha})\frac{5}{2m}\right]^{1/2}$$

The first method, which is purely phenomenological, defines order parameters that are proportional to the dimensions of this ellipsoid as

$$[3] \qquad S_{zz} \propto 1 - \frac{(A_x + A_y)}{2A_z}$$

$$[4] \qquad S_{xx} \propto -\frac{1}{2} + \frac{A_x}{2A_z}$$

$$[5] \qquad S_{yy} \propto -\frac{1}{2} + \frac{A_y}{2A_z}$$

where the semiaxes are chosen such that $A_x \leq A_y \leq A_z$. Definitions [3]–[5] imply one positive (S_{zz}) and two negative order parameters. This is at odds with the experimental results for DCEB (and other prolate solutes) where one principal value of the order matrix is negative and two are positive. Simply reversing the signs of [3]–[5] would rectify the problem, and would in fact lead to an excellent fit for the order parameters of DCEB obtained in the EBBA sample (28). However, there is no physical justification for such a sign reversal. In addition, EBBA is known to have a non-zero mean electric field gradient, and the interaction between this gradient and the quadrupole moment of DCEB should contribute toward the orientational order. Thus the excellent fit for EBBA, obtained with the arbitrary sign reversal, would appear to be accidental. While it is possible to generate different models that are based on the inertial ellipsoid, this is not likely a useful pursuit. The values of the semiaxes of this ellipsoid (which are in the ratio 1.0 : 0.75 : 0.11) are all rather

© 1997 NRC Canada

Table 1. Experimental order parameters from ref. 16 along with those recalculated from best-fit model parameters. The molecular structure used for calculations in this paper is taken from ref. 16. The k_i from ref. 15 are those from the fit to 46 solutes in 55 wt.% 1132–EBBA at 301.4 K. The k_i refer to the parameters k, k_s, k, k, and k_z for the C, I, CI, CZ, and AR models. For CI, CZ, and AR the second parameter ($k_j/k_i = k_s/k$, ξ, or k_{xy}/k_z) is fixed to the value from ref. 15. Least-squares error estimates are given in parentheses. The liquid crystal solvents are *N*-(4-ethoxybenzylidene)-4′-*n*-butylaniline (EBBA) and the commercial mixture Merck ZLI 1132 (1132).

	Experiment	fitted				
	(16)	C	I	CI	CZ	AR
2 mol% DCEB in 55 wt.% 1132/EBBA						
S_{xx}	0.1284	0.1132	0.1253	0.1218	0.1016	0.1156
S_{yy}	0.1161	0.1289	0.1189	0.1231	0.1444	0.1325
S_{zz}	−0.2445	−0.2421	−0.2443	−0.2449	−0.2460	−0.2480
S_{xy}	0.0100	0.0322	0.0058	0.0128	0.0259	0.0133
S_{xz}	−0.0030	−0.0097	−0.0130	−0.0120	−0.0074	−0.0114
S_{yz}	−0.0215	−0.0412	−0.0324	−0.0352	−0.0400	−0.0326
k_i/dyne cm^{-1}		7.2(6)	66(4)	2.04(13)	5.0(5)	6.1(4)
k_j/k_i				23.59	3.91	3.04
rms		0.015	0.007	0.008	0.019	0.010
15 mol% DCEB in 55 wt.% 1132/EBBA						
S_{xx}	0.1031	0.0894	0.0981	0.0957	0.0842	0.0919
S_{yy}	0.0872	0.1019	0.0933	0.0963	0.1092	0.1020
S_{zz}	−0.1903	−0.1913	−0.1915	−0.1921	−0.1934	−0.1938
S_{xy}	0.0065	0.0212	0.0035	0.0081	0.0175	0.0091
S_{xz}	−0.0016	−0.0071	−0.0099	−0.0091	−0.0058	−0.0093
S_{yz}	−0.0180	−0.0322	−0.0255	−0.0275	−0.0313	−0.0259
k_i/dyne cm^{-1}		5.3(5)	46(3)	1.43(10)	3.5(4)	4.3(3)
k_j/k_i				23.59	3.91	3.04
rms		0.012	0.006	0.007	0.014	0.009
20 mol% DCEB in 55 wt.% 1132/EBBA						
S_{xx}	0.0952	0.0823	0.0902	0.0881	0.0784	0.0848
S_{yy}	0.0796	0.0939	0.0859	0.0886	0.0996	0.0934
S_{zz}	−0.1748	−0.1762	−0.1761	−0.1767	−0.1780	−0.1782
S_{xy}	0.0057	0.0186	0.0030	0.0070	0.0155	0.0081
S_{xz}	−0.0013	−0.0064	−0.0091	−0.0083	−0.0053	−0.0086
S_{yz}	−0.0167	−0.0295	−0.0235	−0.0252	−0.0288	−0.0239
k_i/dyne cm^{-1}		4.7(5)	41(3)	1.28(10)	3.1(4)	3.9(3)
k_j/k_i				23.59	3.91	3.04
rms		0.011	0.005	0.007	0.013	0.008
20 mol% DCEB in EBBA						
S_{xx}	0.1127	0.0761	0.0835	0.0815	0.0724	0.0782
S_{yy}	0.0362	0.0867	0.0796	0.0819	0.0904	0.0857
S_{zz}	−0.1489	−0.1627	−0.1631	−0.1633	−0.1629	−0.1639
S_{xy}	0.0054	0.0164	0.0027	0.0062	0.0136	0.0072
S_{xz}	0.0061	−0.0059	−0.0083	−0.0076	−0.0049	−0.0080
S_{yz}	−0.0210	−0.0272	−0.0218	−0.0233	−0.0263	−0.0221
k_i/dyne cm^{-1}		4.3(4)	37(3)	1.16(9)	2.8(3)	3.5(3)
k_j/k_i				23.59	3.91	3.04
rms		0.027	0.023	0.024	0.029	0.026
Fit to 46 solutes in ref. 15						
k_i/dyne cm^{-1}		5.44	76.7	2.04	4.00	6.6
k_j/k_i				23.59	3.91	3.04

Can. J. Chem. Downloaded from www.nrcresearchpress.com by 88.146.161.215 on 09/08/12
For personal use only.

© 1997 NRC Canada

Can. J. Chem. Downloaded from www.nrcresearchpress.com by 88.146.161.215 on 09/08/12
For personal use only.

dissimilar because they are dominated by the heavy chlorine atoms. A theory involving these values will invariably yield principal order parameters that are all considerably different. In contrast, the experimental results obtained for DCEB in the zero efg mixture (Table 1) show that the two positive order parameters are almost equal. Therefore, we conclude that models based on the inertial moments are not capable of explaining these results. In cases where inertial properties are successful in describing orientational order, it is because they are providing a reasonable estimate of molecular size and shape.

The second and later method employed by Samulski is based on an excluded volume model, introduced by Straley (29), in which the molecules are approximated by parallelepipeds; the linear dimensions of length, breadth, and width are estimated from the three semiaxes of the inertia ellipsoid defined by eq. [2] (30). There are problems associated with application of this model to solutes in nematic solvents. First, the model is developed in terms of the volume excluded by two identical particles, and the equations do not apply for the volume excluded by dissimilar particles such as two different liquid crystals of a mixture or of a solute and a liquid crystal. If we follow the prescription in the literature (20, 30–32), we predict positive order parameters for the symmetry axes of both prolate and oblate objects. This is consistent with a collection of oblates forming a discotic phase but is not consistent with the negative order parameter anticipated, and observed, for such oblate objects as solutes in a nematic phase. In addition, the second-rank part of the interaction tensor defined in ref. 29 is not traceless; this leads to incorrect Boltzmann factors for the molecular orientational distribution, and hence to incorrect estimates of orientational order parameters. Thus we shall not use this particular excluded volume model for comparison purposes in this paper. Instead, a more reasonable possibility is that the orientation is related to solute size and shape, and that it has little to do with inertial properties. In the next section, we shall discuss models that attempt to account for the size and shape (and therefore the volume) of solutes in a more precise fashion.

2.2. Ordering due to solute size and shape

For molecules much larger than dihydrogen and methane, repulsive interactions dependent upon the size and shape of the solute molecule can be expected to play a dominant role in the orientation mechanism. The effect of molecular size and shape on the interaction potential U has been modeled in several different ways. A simple approach assumes that the interaction along a molecular axis is proportional to the van der Waals dimensions along that axis; this model has been applied with success to a series of aromatic molecules (13). In the case of DCEB it predicts that S_{xx} is of order $0.7 \times S_{yy}$, whereas the experimental numbers in Table 1 have $S_{xx} > S_{yy}$. However, the values predicted with this simple model are closer to the experimental values for the zero electric field gradient mixture 55 wt.% 1132–EBBA than are those for the PMI models discussed above.

In ref. 15 five models that take molecular size and shape into account in a more detailed way are reviewed and fitted to order parameters of 46 solutes of varying symmetry measured in the zero electric field gradient mixture 55 wt.% 1132–EBBA. One model considers the liquid crystal to be an elastic tube surrounding the solute. The Z axis of the tube is coincident with the director of the liquid crystal. The walls of the tube are rigid, so the circumference of the tube surrounding the solute may be found by looking down the axis of the tube at the projection of the solute in the XY plane. As the solute reorients it will, depending on its size, shape, and orientation, deform the walls of the tube. This model considers the tube to resist deformation with a Hooke's Law force,

$$[6] \qquad F(\Omega) = -kC(\Omega)$$

i.e., the restoring force is directly proportional to the circumferential displacement of the walls of the tube. Here, k is the Hooke's Law force constant and $C(\Omega)$ is the circumference of the XY projection of the molecule held in some orientation Ω. The potential energy of the molecule in this orientation is then

$$[7] \qquad U(\Omega) = \frac{1}{2}\, kC^2(\Omega)$$

This potential, which will be referred to as model C (for circumference), is used in numerical integration of eq. [1] over all possible orientations to predict the values of the various elements of the order matrix.

Another one-parameter model assumes that the solute experiences an anisotropic surface potential. The magnitude of this potential varies with $\sin\theta$, where θ is the angle between the solute surface normal and the director Z direction, and is given by

$$[8] \qquad U(\Omega) = -\frac{1}{2}\, k_s \int_{Z_{min}}^{Z_{max}} C_Z(\Omega)\mathrm{d}Z$$

$C_Z(\Omega)$ is the molecular circumference at position Z. This potential will be referred to as model I (for integral).

Three two-parameter models were also considered. The first one developed adds to eq. [7] a term that depends on the length of the solute projected onto the Z axis:

$$[9] \qquad U(\Omega) = \frac{1}{2}\, k[1 - \xi Z_P(\Omega)/C(\Omega)]C^2(\Omega)$$

Equation [9], which will be referred to as the CZ model, involves terms that vary as C^2 and $C \times Z$. If we think of the solute as occupying a cylindrical cavity, these terms are the area of the top, bottom, and sides of the cavity. In fact it was the success of this "anisotropic surface potential" that led to the evolution of two models that attempt to account for anisotropic surface interactions more precisely. One is eq. [8], and the other is that proposed by Ferrarini et al. (14). An additional attempt to account for surface interactions led to the AR (for area) model, eq. [10], where the molecule is assumed to fit tightly into a cavity with top and bottom area $A_{xy}(\Omega)$ and side area $D(\Omega)Z_P(\Omega)$:

$$[10] \qquad U(\Omega) = 2k_{xy}A_{xy}(\Omega) - k_z D(\Omega)Z_P(\Omega)$$

The most successful two-parameter model, referred to as CI, attempts to account for the physical ideas expressed in both

© 1997 NRC Canada

Can. J. Chem. Downloaded from www.nrcresearchpress.com by 88.146.161.215 on 09/08/12
For personal use only.

eqs. [7] and [8] by combining them:

$$[11] \qquad U(\Omega) = \frac{1}{2} kC^2(\Omega) - \frac{1}{2} k_s \int_{Z_{min}}^{Z_{max}} C_Z(\Omega) dZ$$

It evolved from the simpler CZ model.

The five potentials of eqs. [7]–[11] have proved useful in explaining the orientation of a variety of symmetrical solutes in several liquid crystals (10, 15, 33, 34). In fits to the order parameters of 46 solutes, the I model is the most successful one-parameter model, and the CI the most successful two-parameter model. However, the AR model is also a very successful two-parameter model.

For the solution of 20 mol% DCEB in 55 wt.% 1132–EBBA, where the electric field gradient – molecular quadrupole moment orientation mechanism is removed, a prediction using the C model of the five independent elements of the order matrix based upon an estimated geometry of the molecule yielded a starting point for the analysis of the NMR spectrum that was startlingly close to the final solution (16, 28). From these predictions using the C model one is already tempted to judge it a qualified success for even such unsymmetrical solutes such as DCEB.

For each of the models, one of the constants k_i has been adjusted in a least-squares fit to the experimental values of $S_{\alpha\beta}$. For the CI, CZ, and AR models the ratios k_s/k, ξ, and k_{xy}/k_z have been fixed to the values obtained in the fit to 46 solutes in the 55 wt.% 1132–EBBA mixture (15). For all of the models used, the geometry of DCEB was kept fixed to the rigid structure established in ref. 16. Values predicted by the fits to eqs. [7]–[11] for the order matrices of DCEB in the 55 wt.% 1132–EBBA mixtures and in EBBA are reported in Table 1, where the quality of the fits is indicated by the rms difference between predicted and experimental order parameters.

The fits to the order parameters obtained from the spectrum in EBBA are poor for all models. In all cases the asymmetry $(S_{xx} - S_{yy})/S_{zz}$ is poorly predicted. The results do not improve much if both parameters of the two-parameter models are allowed to vary. The poor fits for EBBA are expected because no attempt has been made to account for the mean electric field gradient – molecular quadrupole moment interaction that is anticipated to be important in this liquid crystal.

For the three zero-efg 55 wt.% 1132–EBBA samples, the best results are obtained with the same models that provided the best fits to the 46 solutes in the same mixture (15). The one-parameter I model gives particularly impressive results, and only the I model predicts the correct sign of the asymmetry $(S_{xx} - S_{yy})/S_{zz}$. The CI model also gives excellent fits. All models predict the correct signs of the off-diagonal $S_{\alpha\beta}$ observed in the mixture.

All the models considered in Table 1 give better fits than do the simpler approaches, which assume either that the order parameter matrix is related to the inertial tensor (see previous section), or that the interaction along a molecular axis is proportional to the van der Waals dimensions along that axis (13). We note that the best models are those that take the particulars of the molecular size and shape into account in the most detailed fashion. For example, the I model and the anisotropic surface model of Ferrarini et al. (14) both account for the three-dimensional shape of the solute at each orientation, whereas the projections involved in the C, CZ, and AR models offer a less precise description of the actual molecular shape. As long as precisely the same method is used to define the solute surface, quite similar predictions are obtained with both the I and Ferrarini models.[7]

Also included in Table 1 are the k_i parameters obtained in the fits to 46 solutes (15). Because these values are for results obtained using dilute solutions, they should be compared to the numbers obtained for the dilute 2 mol% DCEB in 55 wt.% 1132–EBBA mixture. In ref. 15 the C and I models were found to require k_i values that varied depending on solute size. The variation tended to be in opposite directions, and this same trend is noted in Table 1. The opposing effects of the C and I calculations are compensated for by adding the two contributions to generate the CI potential. For the CI model, the number obtained for the 2 mol% DCEB in 55 wt.% 1132–EBBA solution is in exact agreement with the number obtained for the 46 solutes in ref. 15. The success of this model is consistent with ref. 15 where CI was found to be the most successful potential in fitting a series of solutes, and with ref. 35 where CI provided the best "fit" to Monte Carlo simulations that employ only hard-body interactions between solute and solvent hard ellipsoids.

3. Conclusion

In this paper we have studied a molecule that has no symmetry, and thus requires five independent second-rank orientational parameters to specify its partial orientation in a nematic phase. Results from liquid crystals in which the average electric field gradient is zero are best rationalized by models for anisotropic short-range interactions, and especially those that involve an anisotropic surface potential. This represents a strong test of such models because they simultaneously fit the five independent orientational parameters obtained from the same solute, thus removing the problems associated with comparing results among different solutes in either the same or a different sample tube.

The results presented in Table 1 demonstrate that the models described above, and especially the one-parameter I and the two-parameter CI models, provide an excellent description of the short-range anisotropic interactions. These are the models that take the particulars of the molecular size and shape into account in the most detailed fashion. All of the models considered in Table 1 give better fits than do the simpler approaches, which assume that the order parameter matrix is related either to the inertial tensor or to van der Waals lengths along molecular axes (13).

The success of the CI model in predicting order parameters *both* of solutes in zero efg mixtures *and* of Monte Carlo simulations that involve only hard-body interactions is important from two points of view. First, it demonstrates that short-range interactions that depend on molecular size and shape are dominant in the zero efg mixtures. Secondly, the CI model provides an excellent way of modeling these interactions. While one can think of this model as being purely phenomenological, there is an interesting physical interpretation to its two contributions. The first term of eq. [11] is associated with an elastic distortion of the liquid crystal, and

[7] A. Ferrarini. Private communication.

© 1997 NRC Canada

the second with an anisotropic interaction between the solute surface and the liquid-crystal mean field.

While it may be risky to base general conclusions upon the analysis of only one system with no symmetry, the success of the models, and especially the one-parameter anisotropic surface potential I model of eq. [8], and of the two-parameter CI model of eq. [11], for orientation based upon the size and shape of a molecule such as 1,3-dichloro-2-ethenylbenzene is quite remarkable.

4. Acknowledgments

We wish to thank C.A. de Lange and R.T. Syvitski for useful discussions. Acknowledgment is made to the Natural Sciences and Engineering Research Council of Canada (NSERC) and to The Petroleum Research Fund, administered by the American Chemical Society, for support of this research. J.C.T.R. and A.J. vdE. thank NSERC for the award of Graduate Scholarships.

References

1. G.N. Patey, E.E. Burnell, J.G. Snijders, and C.A. de Lange. Chem. Phys. Lett. **99**, 271 (1983).
2. A.J. van der Est, M.Y. Kok, and E.E. Burnell. Mol. Phys. **60**, 397 (1987).
3. A. Weaver, A.J. van der Est, J.C.T. Rendell, G.L. Hoatson, G.S. Bates, and E.E. Burnell. Liq. Cryst. **2**, 633 (1987).
4. M.Y. Kok. A.J. van der Est, and E.E. Burnell. Liq. Cryst. **3**, 485 (1988).
5. G.L. Hoatson, A.L. Bailey, A.J. van der Est, G.S. Bates, and E.E. Burnell. Liq. Cryst. **3**, 683 (1988).
6. A.J. van der Est, E.E. Burnell, and J. Lounila. J. Chem. Soc. Faraday Trans. 2, **84**, 1095 (1988).
7. A.L. Bailey, G.S. Bates, E.E. Burnell, and G.L. Hoatson. Liq. Cryst. **5**, 941 (1989).
8. P.B. Barker, A.J. van der Est, E.E. Burnell, G.N. Patey, C.A. de Lange, and J.G. Snijders. Chem. Phys. Lett. **107**, 426 (1984).
9. E.E. Burnell, A.J. van der Est, G.N. Patey, C.A. de Lange, and J.G. Snijders. Bull. Magn. Reson. **9**, 4 (1987).
10. J.B.S. Barnhoorn, C.A. de Lange, and E.E. Burnell. Liq. Cryst. **13**, 319 (1993).
11. D.S. Zimmerman and E.E. Burnell. Mol. Phys. **69**, 1059 (1990).
12. D.S. Zimmerman, K.Y. Li, and E.E. Burnell. Mol. Cryst Liq. Cryst. **203**, 61 (1991).
13. C.T. Yim and D.F.R. Gilson. J. Phys. Chem. **95**, 980 (1991).
14. A. Ferrarini, G.J. Moro, P.L. Nordio, and G.R. Luckhurst. Mol. Phys. **77**, 1 (1992).
15. D.S. Zimmerman and E.E. Burnell. Mol. Phys. **78**, 687 (1993).
16. J.C.T. Rendell and E.E. Burnell. Mol. Phys. **90**, 541 (1997).
17. J.W. Emsley, G.R. Luckhurst, and C.P. Stockley. Proc. R. Soc. London Ser. A, **381**, 117 (1982).
18. D.J. Photinos, E.T. Samulski, and H. Toriumi. J. Phys. Chem. **94**, 4688 (1990).
19. D.J. Photinos, E.T. Samulski, and H. Toriumi. J. Chem. Phys. **94**, 2758 (1991).
20. M.E. Rosen, S.P. Rucker, C. Schmidt, and A. Pines. J. Phys. Chem. **97**, 3858 (1993).
21. P. Diehl and C.L. Khetrapal. NMR: Basic Princ. Prog. **1**, 1 (1969); J.W. Emsley and J.C. Lindon. NMR spectroscopy using liquid crystal solvents. Pergamon, Oxford. 1975; J. Lounila and J. Jokisaari. Prog. NMR Spectrosc. **15**, 249 (1982); C.L. Khetrapal and A.C. Kunwar. Adv. Liq. Cryst. **6**, 173 (1983).
22. A.J. van der Est, P.B. Barker, E.E. Burnell, C.A. de Lange, and J.G. Snijders. Mol. Phys. **56**, 161 (1985).
23. J.M. Anderson. J. Magn. Reson. **4**, 231 (1971).
24. T.C. Wong and E.E. Burnell. J. Magn. Reson. **22**, 227 (1976).
25. E.T. Samulski. Ferroelectrics, **30**, 83 (1980).
26. E.T. Samulski and H. Toriumi. J. Chem. Phys. **79**, 5194 (1982).
27. K.R. Symon. Mechanics. 3rd ed. Addison-Wesley, Reading, Mass. 1971.
28. J.C.T. Rendell. Ph.D. thesis, University of British Columbia. 1987.
29. J.P. Straley. Phys. Rev. A: Gen. Phys. **10**, 1881 (1974).
30. B. Janik, E.T. Samulski, and H. Toriumi. J. Phys. Chem. **91**, 1842 (1987).
31. M. Gochin, A. Pines, M.E. Rosen, S.P. Rucker, and C. Schmidt. Mol. Phys. **69**, 671 (1990).
32. J.M. Polson and E.E. Burnell. J. Chem. Phys. **103**, 6891 (1995).
33. L.C. ter Beek, D.S. Zimmerman, and E.E. Burnell. Mol. Phys. **80**, 177 (1993).
34. T. Chandrakumar. Ph. D. thesis, University of British Columbia. 1994.
35. J.M. Polson and E.E. Burnell. Mol. Phys. **88**, 767 (1996).

Can. J. Chem. Downloaded from www.nrcresearchpress.com by 88.146.161.215 on 09/08/12
For personal use only.

© 1997 NRC Canada

1996 Merck Frosst Award Lecture Synthetic adventures along a Rocky Mountain road[1]

Brian A. Keay, Shawn P. Maddaford, Walter A. Cristofoli, Neil G. Andersen, Marco S. Passafaro, Noel S. Wilson, and James A. Nieman

Abstract: This paper describes the chemistry presented during the Merck Frosst Centre for Therapeutic Research Lecture Award given at the 79th Chemistry in Canada Conference held in St. John's, Newfoundland in June 1996. The first section describes the synthesis of (+)-xestoquinone using an asymmetric palladium-catalyzed polyene cyclization as the key step that creates the C and D rings and the stereogenic centre (68% ee) in one step. Extensions of the work involving an in situ Suzuki reaction are presented. The synthesis of C_2-symmetric biaryls and the synthesis of a recently isolated binaphthyl natural product is described using this new method. A new one-pot desilylation–oxidation procedure of silyl ethers is described in detail for the preparation of aldehydes and ketones directly without the need for the isolation of the alcohol intermediate. Finally, a highly diastereoselective (>97%) Diels–Alder reaction is presented using (+)-*cis,cis*-spiro[4.4]nonane-1,6-diol as a new chiral auxiliary. One of the alcohols is attached to a pivalate, the other to an acrylate, and the Diels–Alder reaction with cyclopentadiene provides only one adduct (by ^{1}H NMR and HPLC) with the *endo* stereochemistry.

Key words: (+)-xestoquinone, asymmetric palladium-catalyzed polyene cyclization, in situ Suzuki reaction, desilylation–oxidation reaction, spirodiols, chiral auxiliaries.

Résumé : Cette publication décrit la chimie présentée lors de la remise du prix du Centre Merck–Frosst pour la recherche thérapeutique, lors de la 79ème Conférence de chimie au Canada, tenue à St-Jean, Terreneuve, en juin 1996. La première section décrit la synthèse de la (+)-xestiquinone impliquant, comme étape clé, une cyclisation de polyène catalysée par du palladium asymétrique conduisant, en une étape, à la création des cycles C et D et du centre stéréogène (68% ee). On présente des extensions de ce travail impliquant une réaction de Suzuki in situ. Faisant appel à cette méthode, on a réalisé la synthèse de biaryles de symétrie C_2 et d'un produit naturel de la série des binaphtyles qui a été isolé récemment. On décrit en détail une procédure unipot de désilylation–oxydation des éthers silylés permettant de préparer directement des aldéhydes et des cétones sans avoir à isoler l'alcool intermédiaire. Enfin, on présente une réaction de Diels–Alder fortement diastéréosélective (>97%) faisant appel au (+)-*cis,cis*-spiro[4,4]nonane-1,6-diol comme nouvel auxiliaire chiral. On a attaché l'un des groupes hydroxyles à un pivalate et l'autre à un acrylate, et la réaction de Diels–Alder avec le cyclopentadiène ne fournit qu'un seul adduit (RMN du ^{1}H et CLHP) dont la stéréochimie est *endo*.

Mots clés : (+)-xestoquinone, cyclisation de polyène catalysée par du palladium asymétrique, réaction de Suzuki in situ, réaction de désilylation–oxydation, spirodiols, auxiliaires chiraux.

[Traduit par la rédaction]

Introduction

The title of the talk was chosen for two reasons. First, it was important to incorporate the fact that most of the work in this presentation was performed in Calgary. This was done by incorporating "Rocky Mountain" into the title since Calgary is very close (~90 km) to the Rocky Mountains. Second, if one word is removed from the title, its context changes dramatically. Removing the word "Mountain" provides the title, "Synthetic Adventures Along a Rocky Road." This title is a reminder that ideas, and what are believed to be the best thought-out plans, do not always proceed[3] in a smooth and orderly manner. Many unforeseen obstacles are encountered during the course of academic research. It is the perseverance, hard work, and dedication of excellent graduate students and post-doctoral Fellows that result in solutions to unforeseen problems and oftentimes lead to new discoveries. It is to past[4]

Received January 15, 1997.

B.A. Keay,[2] S.P. Maddaford, W.A. Cristofoli, N.G. Andersen, M.S. Passafaro, N.S. Wilson, and J.A. Nieman. Department of Chemistry, University of Calgary, Calgary, AB T2N 1N4, Canada

[1] This paper is an invited review article based on the Merck Frosst Centre for Therapeutic Research Award Lecture presented by Professor Keay at the 79th Annual Conference of the Canadian Society for Chemistry, St. John's, Newfoundland, June 1996.

[2] Author to whom correspondence may be addressed. Telephone: (403) 220-5354. Fax: (403) 284-1372. E-mail: keay@chem.ucalgary.ca

[3] It has been my experience that most of the ideas proposed to date have developed problems at some point along the way. Investigations almost *never* proceed as planned. Many new discoveries and some very interesting chemistry have been found as a result of these obstacles, and some of the chemistry that has developed from these pitfalls is presented in this paper.

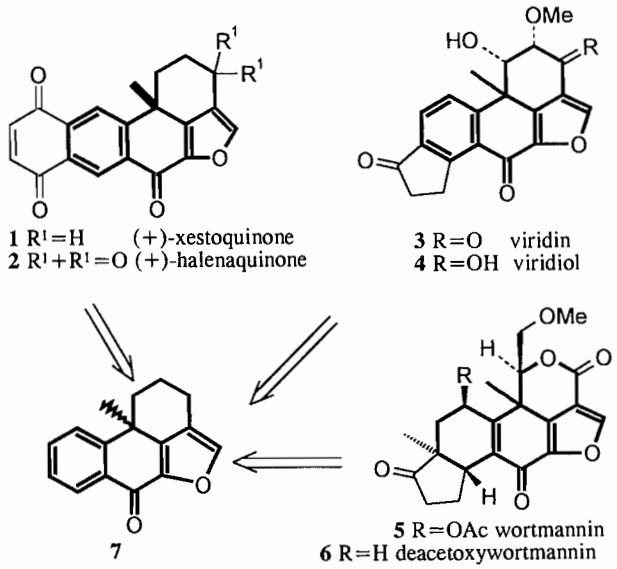
[4] I did not present work done by the following past members of my group: Ted J. Bures, Patrick G. Spinazzé, Jean-Louis J. Bontront, Giovanna Beese, Dr. Christine Rogers, Dr. Simon Woo, and Dr. Shuyuan Yu.

© 1997 NRC Canada

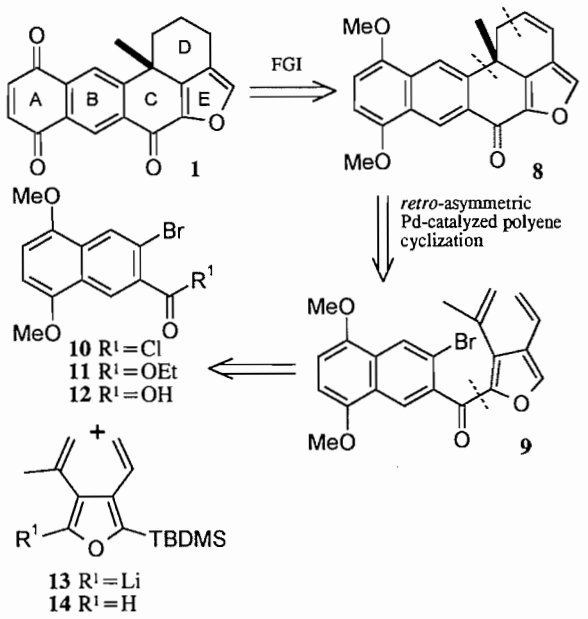
Can. J. Chem. Downloaded from www.nrcresearchpress.com by 91.121.58.235 on 09/08/12
For personal use only.

Can. J. Chem. Downloaded from www.nrcresearchpress.com by 91.121.58.235 on 09/08/12
For personal use only.

Scheme 1.



Scheme 2.



and present members[5] of my group that I dedicate this talk, since I would not be presenting this work if not for the excellent chemistry discovered and performed by these people. For this I thank them.

The paper will be divided into four parts. First, the synthesis of (+)-xestoquinone will be discussed, in which an asymmetric palladium-catalyzed polyene cyclization was used to create rings C and D and the stereogenic centre in one step. Second, extensions of our modified in situ Suzuki reaction in which the Shapiro and Suzuki reactions are combined into a one-pot procedure will be illustrated and a new method for the preparation of C_2-symmetric biaryls is described along with the synthesis of a C_2-symmetric binaphthalene natural product. Third, a new one-pot procedure that combines a desilylation–oxidation sequence using catalytic quantities of $PdCl_2$ will be presented in detail. Finally, the use of (+)- and (−)-*cis,cis*-spiro[4.4]nonane-1,6-diol as new chiral auxiliaries for the Diels–Alder reaction, in which one of the alcohols is substituted with a pivalate and the other with an acrylate, will be described.

Synthesis of (+)-xestoquinone

Xestoquinone **1** (1) and halenaquinone **2** (2) were isolated from Pacific sponges and shown to possess a unique pentacyclic carbon framework (Scheme 1). Both **1** and **2** (especially **2**) are irreversible inhibitors of oncogenic protein tyrosine kinase $pp60^{v\text{-}src}$ and the human epidermal growth factor kinase (EGF) (3). Xestoquinone also has a positive inotropic effect on cardiac muscle that leads to it being a potent cardiotonic agent (4). Four of the rings common to both **1** and **2** are found in the Viridin class of natural products **3**-**6** (5) as illustrated in Scheme 1. We envisioned that if a short asymmetric route to tetracycle **7** could be developed, then the approach could be applicable towards the preparation of natural products **1**-**6**. We also chose (+)-xestoquinone as our initial target as it contained the least number of functional groups and had not been synthesized asymmetrically, although Harada reported the diastereoselective synthesis of **1** starting with optically pure Wieland–Miescher ketone (6).[6]

Space limitations do not permit the description of the many unsuccessful approaches towards the synthesis of **1** (11). The retrosynthesis that was finally successful is illustrated in Scheme 2 (12). Functional group interconversion of **1** provides **8**, which after a retro-palladium-catalyzed polyene cyclization gives **9**. Disconnection between the furan ring and ketone in **9** provides tetrasubstituted naphthoyl chloride **10** and lithio-furan **13**. The advantages of this approach are (*i*) that rings C and D are introduced in a single step with concurrent formation of the single stereogenic centre; (*ii*) that the polyene cyclization can be performed in the presence of a chiral ligand such as (+)-BINAP so that the synthesis is asymmetric; and (*iii*) that the synthesis is convergent, requiring the preparation and coupling of naphthalene **10** and furan **13**. Other asymmetric polyene cyclizations sequences (13) and Heck reactions (14) have been reported; however, the former has not been applied to the enantioselective synthesis of a natural product (12).

Naphthoyl chloride **10** was prepared from the known ester **11** (15) in two steps by hydrolysis of ester **11** (K_2CO_3, refluxing methanol, 95%) followed by treatment of acid **12** with oxalyl chloride in methylene chloride containing a drop of DMF (>99%) (Scheme 2).

Furan **14** was prepared using some chemistry we discovered in 1988 (16). Furan rings tend to lithiate at the C-2 position and (or) at the C-5 position if the C-2 position is substituted. Thus, the preparation of 3,4-disubstituted furan rings is difficult. We reported that 2-silylated-3-hydroxymethylfuran

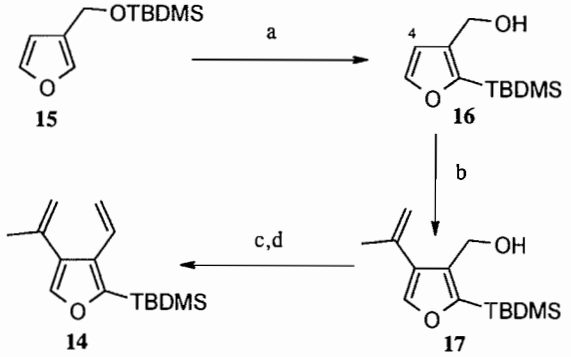
[5] I did not present work done by the following current members of my group: Dr. Ian R. Hunt and Bryon E. Carpenter.

[6] Kanematstu et al. have reported a formal synthesis of (±)-**1** (7). Harada et al. (8), Shibasaki and co-workers (9) have reported syntheses of **2** and Rodrigo and co-workers (10) have reported the synthesis of **1** and **2**.

© 1997 NRC Canada

Can. J. Chem. Downloaded from www.nrcresearchpress.com by 91.121.58.235 on 09/08/12
For personal use only.

Scheme 3.



Reagents: (a) *n*-BuLi, THF, HMPA, 0°C–rt, 12 h (87%); (b) 2.2 equiv. *n*-BuLi, DME, 0°C; then $B(O^iPr)_3$, 1 h, 0°C; then $Pd(PPh_3)_4$, Na_2CO_3, 2-bromop[ene, reflux, 13 h (95%); (c) PDC, CH_2Cl_2, rt (85%); (d) Ph_3PCH_2, THF, 1 h, reflux (95%).

when treated with 2.2 equiv. of *n*-BuLi results in exclusive lithiation at the C-4 position (16). We used this chemistry to prepare furan **14** (Scheme 3). Treatment of **15** with 1.1 equiv. of *n*-BuLi in THF containing 1 equiv. of HMPA resulted in the formation of furan **16** (87%) via an intramolecular 1,4 O → C silyl migration (17).

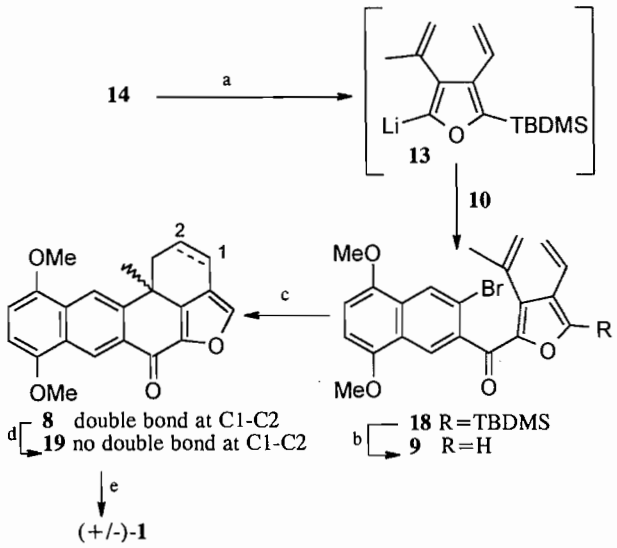
We investigated using the Stille (18) and Suzuki (19) reactions to introduce the 2-propenyl group through a palladium coupling with the corresponding C-4 stannane and boronic acid, respectively; however, the Stille coupling gave very poor yields (20) and the C-4 boronic acid species of **16** could not be isolated by quenching the C-4 anion with trimethylborate (21). An in situ variant of the Suzuki reaction was developed (12, 21, 22) in which the C-4 anion of **16** was quenched with triisopropylborate and, after 1 h, immediately treated with $Pd(PPh_3)_4$ (3 mol%), 2 M Na_2CO_3, and 2-bromopropene at reflux for 13 h. Furan **17** was obtained in 95% yield. The required trisubstituted furan **14** was prepared by PDC oxidation of **17** (85%) followed by a standard Wittig reaction (95%).

Furan **14** was lithiated at C-5 by treatment with 1.5 equiv. of *n*-BuLi in the presence of 1.2 equiv. HMPA (THF, −78°C) to form **13**, which was immediately reacted with freshly distilled naphthoyl chloride **10**. Furan **18** was isolated in 79% yield (Scheme 4). Compound **18** is the precursor for a palladium-catalyzed polyene cyclization. Although we attempted to perform the cyclization reaction on **18**, a mixture of products was always obtained. Removal of the silyl group prior to attempting the polyene cyclization alleviated the formation of complex mixtures (vide infra) (12, 13*a*). The silyl group in **18** was removed with *n*-Bu_4NF (THF, 0°C), providing **9** in 95% yield.

We initially decided to prepare (±)-xestoquinone **1** in order to demonstrate the viability of the synthetic strategy. Refluxing a mixture of **9** with $Pd(PPh_3)_4$ or $Pd_2(dba)_3$ (10 mol%) in NMP containing Et_3N provided pentacycle **8** in 82% yield. Compound **8** was converted into (±)-xestoquinone **1** by catalytic hydrogenation (H_2, Pd/C, 1 atm (101.3 kPa), 4 h, 99%) to form **19** followed by a ceric ammonium nitrate oxidation (CH_3CN/H_2O, 0°C, 5 min) according to the procedure reported by Harada et al. (6) (Scheme 4).

With a successful route towards (±)-xestoquinone in hand, we turned our attention to attempting an asymmetric

Scheme 4.



Reagents: (a) *n*-BuLi (1.5 equiv.), HMPA (1.5 equiv.), THF, 0°C; then add **10** (79%); (b) *n*-Bu_4NF, THF, 0°C (95%); (c) $Pd(PPh_3)_4$, NMP, Et_3N, (82%); (d) H_2 (1 atm), 5% Pd/C, EtOH, rt (99%); (e) CAN, CH_3CN, H_2O, 5 min.

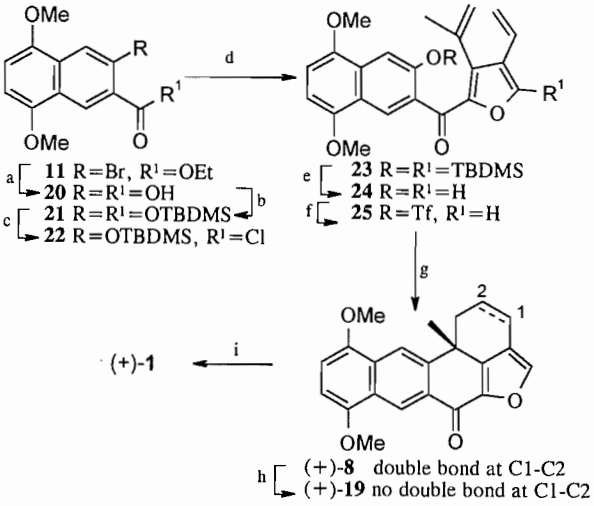
palladium-catalyzed polyene cyclization. Treatment of **9** with a variety of chiral palladium catalysts provided **8** with very poor enantiomeric excesses (ee's) ($Pd((R)\text{-BINAP})_2/Et_3N$ (5% ee), $Pd((R)\text{-BINAP})_2$/PMP (13% ee), or $Pd((2R,3R)\text{-chiraphos})_2$/PMP (7% ee)) that could not be improved by the addition of silver salts (23). In hopes of increasing the %ee of the polyene cyclization we investigated the use of a triflate instead of a bromine atom in **9**, since it has been reported that triflates provide much higher ee's than bromides or iodides in the Heck reaction due to the increased liability of the Pd—OTf bond when compared to Pd—Br and Pd—I bonds (14*b*).

The bromine atom in **11** (Scheme 5) was changed into a hydroxy group and subsequently converted into a naphthyl triflate prior to the polyene cyclization. Halogen–metal exchange of the bromine atom in **11** with *n*-BuLi (−95°C, THF) followed by the immediate addition of trimethylborate and a basic H_2O_2 work-up provided acid **20** (87%). Bis-silylation of **20** with TBDMSOTf (2 equiv.) gave **21** (79%), which was converted into naphthoyl chloride **22** by treatment with oxalyl chloride in refluxing hexanes containing a drop of DMF (99%). Acid chloride **22** was added slowly to a solution of anion **13**, which was generated by treatment of **14** with *s*-BuLi (THF, −78°C) to provide ketone **23** after work-up (42% from **20**). Removal of both silyl groups with *n*-Bu_4NF (THF, 0°C) provided **24**, which when treated with NaH in DMF followed by the addition of $PhNTf_2$ gave triflate **25**.

Triflate **25** was used immediately in the asymmetric polyene cyclization, since it was found to be very sensitive to air and moisture. Treatment of **25** using $Pd((S)\text{-BINAP})_2$ gave pentacycle (+)-**8** with 68% ee (82% from **24**). Compound (+)-**8** was also shown to have the correct absolute stereochemistry required for the preparation of (+)-**1** (12). Finally, (+)-xestoquinone (**1**) (68% ee) was synthesized by catalytic hydrogenation of (+)-**8** to provide (+)-**19** (100%) followed by a ceric

© 1997 NRC Canada

Scheme 5.



Reagents: (a) *n*-BuLi, THF, −95°C; then $(MeO)_3B$; then add H_2O_2, NaOH; then 10% HCl (87%); (b) TBDMSOTf, Et_3N (79%); (c) oxalyl chloride, 1 drop of DMF, hexanes (99%); (d) **13** generated from *s*-BuLi/THF (42% from **20**); (e) *n*-Bu_4NF, THF, 0°C (95%); (f) NaH, DMF, rt, $PhNTf_2$ and used immediately; (g) $Pd_2(dba)_3$(2.5 mol%), *S*-BINAP (10 mol%), PMP, toluene, reflux, 22 h (82% from **24**; 68% ee); (h) H_2 (1 atm), 5% Pd/C, EtOH, rt (95%); (i) CAN, CH_3CN, H_2O, 5 min.

ammonium nitrate oxidation (Scheme 5). The ^1H NMR and CD spectra of synthetic (+)-xestoquinone were identical with those provided to us by Prof. Harada (6).

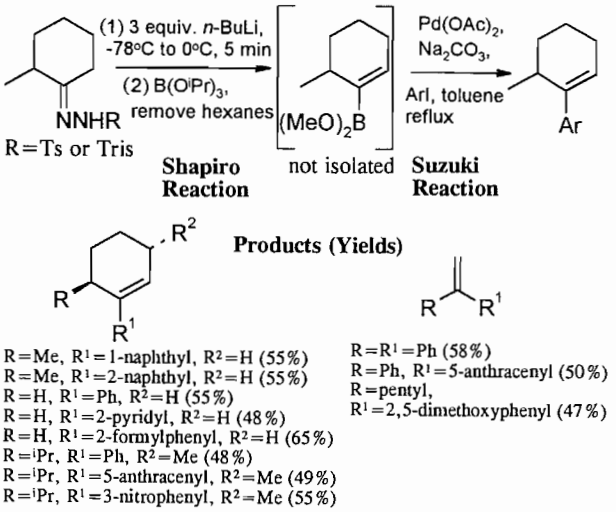
Thus, we have developed a short convergent asymmetric route to (+)-xestoquinone, which represents the first synthesis of a natural product incorporating an asymmetric palladium-catalyzed polyene cyclization. Work is continuing on: (*i*) improving the %ee of the polyene cyclization, (*ii*) developing a rationale to explain the observed absolute stereochemistry of the cyclization; and (*iii*) applying this reaction towards the synthesis of other natural products (i.e., **2**-**6**, Scheme 1).

Further extensions of the in situ Suzuki reaction

As mentioned above, compound **17** was prepared by developing an in situ variation of the Suzuki reaction (21, 22). We have recently expanded the scope and limitations of this reaction by showing that: (*i*) the Shapiro (24) and Suzuki (19) reactions can be combined into a one-pot reaction sequence (25); and (*ii*) C_2-symmetric biaryls can be prepared in one step starting with a haloarene (26). These new applications are summarized below.

It is well known that when tosyl- or trisylhydrazones are treated with excess *n*-BuLi (>3 equiv.), a vinyl anion develops that can be trapped with a variety of electrophiles (Scheme 6) (24). We investigated whether the anion could be trapped with trimethylborate and subsequently used in a Suzuki reaction without the need for isolation of the vinyl boronic acid. Although we were successful in combining the reactions in one pot, unfortunately a change of solvent was required for the Suzuki reaction. The Shapiro reaction was performed in a mixture of hexanes and TMEDA but the Suzuki reaction would not proceed unless the hexanes were removed and replaced with toluene. Similarly, the Shapiro reaction did not proceed in

Scheme 6.



toluene. Nevertheless, the reaction can be performed in one pot and appears to be quite general. Thus, the anion that forms from the Shapiro reaction is quenched with $B(OMe)_3$, and after 1 h the hexanes are removed in vacuo. The addition of toluene, Na_2CO_3, $Pd(OAc)_2$ (5 mol%), PPh_3 (10 mol%), the aryl or vinyl iodide (or bromide), and reflux of the resulting mixture affords the desired products in yields ranging from 47 to 65% (Scheme 6) (25). It was determined that the yields are limited by the Shapiro reaction since isolation of the vinyl boronic acids and subsequent treatment under Suzuki conditions provided the coupled products in excellent yield. We are currently applying this combined reaction sequence towards the preparation of monoterpenylmagnolol (27).

The second extension of the in situ Suzuki reaction involves the formation of C_2-symmetric biaryls starting only from the arylhalide. In 1994, we reported on the scope and limitations of the in situ Suzuki reaction (22) and showed that iodobenzene could be completely halogen–metal exchanged with *t*-BuLi and the resulting anion quenched with $B(OMe)_3$. A second aryl- or vinylhalide was added along with a palladium catalyst, which after refluxing afforded the coupled product in good to excellent yields. In this procedure, the two aryl components could be different. However, if a C_2-symmetric biaryl was required, we reasoned that the above procedure could be modified slightly so that the second equivalent of arylhalide would not have to be added to the solution after the $B(OMe)_3$ was added (26). The modification was to initially add only 0.5 equiv. of *n*-BuLi so that only 50% of the arylhalide would undergo a halogen–metal exchange. The addition of $(MeO)_3B$ would quench the resulting anion and leave a 50/50 mixture of arylboronate and arylhalide (Scheme 7, **26** and **27**), that should undergo a Suzuki coupling if a palladium catalyst is introduced into the flask. This modification was realized when bromobenzene **26**, when treated as above, provided biphenyl **28** in 85% yield when toluene, $Pd(PPh_3)_4$, and $Ba(OH)_2$ were added to the solution and subsequently refluxed (Scheme 7) (26). The procedure is quite general and a variety of C_2-symmetric biaryl compounds have been prepared in moderate to good yields (Scheme 7).

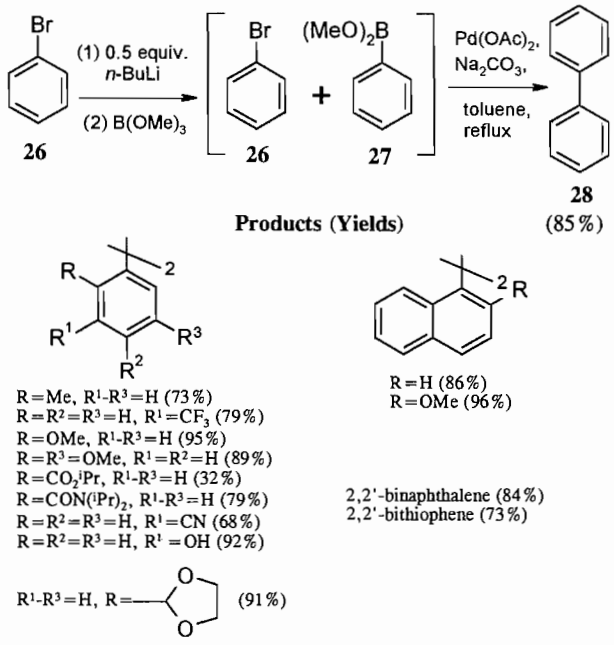
This method has also been used to prepare 4,4′-

Can. J. Chem. Downloaded from www.nrcresearchpress.com by 91.121.58.235 on 09/08/12
For personal use only.

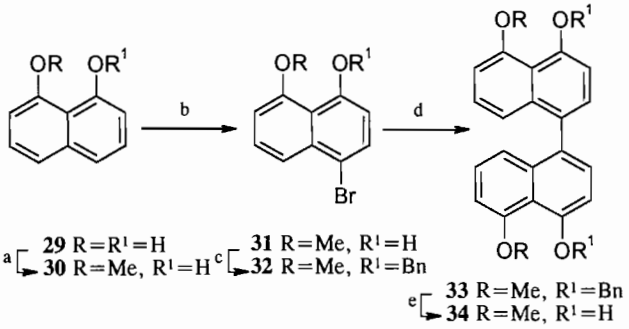
© 1997 NRC Canada

Can. J. Chem. Downloaded from www.nrcresearchpress.com by 91.121.58.235 on 09/08/12
For personal use only.

Scheme 7.



Scheme 8.

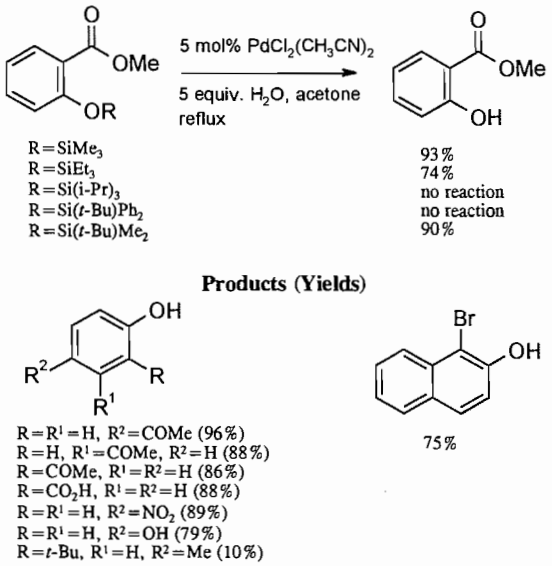


Reagents: (a) 1 equiv. NaH, DMF, 5 equiv. MeI (95%); (b) NaH, CCl_4, 1 equiv. Br_2 (60%); (c) NaH, DMF, BnBr (100%); (d) 0.5 equiv. *n*-BuLi, THF, −78°C; then $B(OMe)_3$, rt, 12 h; then toluene, EtOH, H_2O, Na_2CO_3, $Pd(PPh_3)_4$, reflux, 12 h (72%); (e) H_2, Pd/C, $EtOH/CH_2Cl_2$ (100%).

dihydroxy-5,5′-dimethoxy-1,1′-binaphthalene **34**, which has been isolated from the fungus (Ascomycetes) *Daldinia concentrica* (28). Our synthesis began with 1,8-naphthalenediol **29**, which was prepared from 1,8-naphthosultone (29). Diol **29** was converted into **34** in five steps with an overall yield of 41% (Scheme 8). Monomethylation of **29** produced **30**, which underwent a regioselective bromination *para* to the hydroxyl group, giving **31**. Unfortunately, the synthesis was extended by two steps because the hydroxy group in **31** had to be protected. Halogen–metal exchange of **31** by treatment with *n*-butyllithium provided an excellent yield of 8-methoxy-1-naphthol (30). Protection of the free hydroxyl group with a benzyl group alleviated this problem. Binaphthalene **34** was prepared by an in situ palladium coupling of **32** (to give **33**) followed by removal of the benzyl protecting groups by hydrogenolysis.

We have shown that the in situ variant of the Suzuki reaction is a general viable process for the preparation of a variety of compounds. It was used in the preparation of furan **14**, which was a key intermediate in the syntheses of (+)-xestoquinone **1** and binaphthalene **34**. Further extensions of this reaction are currently underway.

Scheme 9.



Development of a one-pot desilylation-oxidation of silyl ethers using catalytic amounts of $PdCl_2$

During some work on the palladium-catalyzed polyene cyclization towards xestoquinone, we noticed that a phenol protected as its *tert*-butyldimethylsilyl ether was cleaved in the presence of $Pd(OAc)_2$. Since we could not find any reports on the removal of phenolic silyl ethers with palladium catalysts, we investigated this reaction further (31–35).

A variety of phenolic *tert*-butyldimethylsilyl ethers were cleaved to their respective phenols by treatment with 1–5 mol% $PdCl_2(CH_3CN)_2$ in refluxing reagent grade acetone containing 5 equiv. of water (Scheme 9) (36).[7] Products were formed in yields ranging from 10 to 96%. Both the water and palladium catalyst were necessary for a successful reaction. Hindered silyl ethers were removed very slowly (see the last example) and a variety of functional groups were tolerated during this reaction (halides, esters, nitriles, nitro, aldehydes, and ketones). The reaction was not limited to the *tert*-butyldimethylsilyl ether; trimethyl- and triethylsilyl ethers were desilylated, while triisopropyl- and *tert*-butyldiphenylsilyl ethers were inert under these reaction conditions. Since phenolic silyl ethers were removed with catalytic amounts of $PdCl_2$ we looked at whether aliphatic silyl ethers could be desilylated under similar reaction conditions.

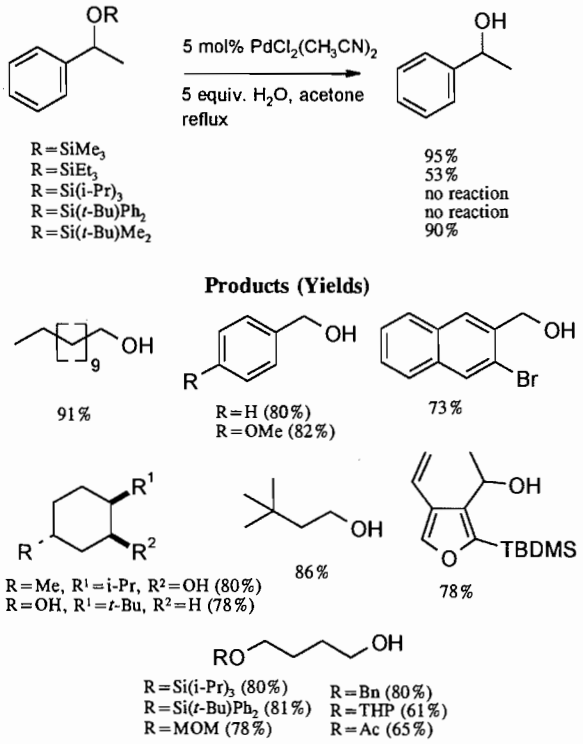
Treatment of a variety of aliphatic *tert*-butyldimethylsilyl ethers with 5 mol% $PdCl_2(CH_3CN)_2$ in acetone containing

[7] We have recently shown that trimethyl-, triethyl-, *tert*-butyldimethyl-, triisopropyl-, and *tert*-butyldiphenyl-silyl phenolic ethers can be removed by refluxing the silyl ether in ethanol containing 1.1 equiv. of K_2CO_3. Aliphatic silyl ethers were not removed under these reaction conditions. See ref. 37 for further details.

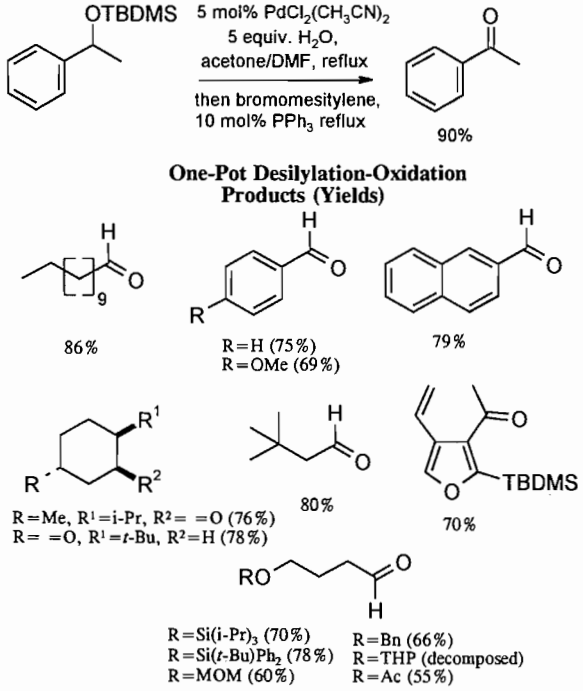
© 1997 NRC Canada

Can. J. Chem. Downloaded from www.nrcresearchpress.com by 91.121.58.235 on 09/08/12
For personal use only.

Scheme 10.



Scheme 11.



5 equiv. of water provided desilylated materials in yields ranging from 73 to 91% (Scheme 10) (38).[8] The reaction conditions also desilylated trimethylsilyl ethers; however, triisopropyl- and *tert*-butyldiphenyl-silyl ethers did not react under these conditions. Triethylsilyl ethers were somewhat capricious and approximately 50% desilylation was all that could be obtained under the best of conditions. The *tert*-butyldimethylsilyl group could also be removed selectively in the presence of triisopropylsilyl, *tert*-butyldiphenylsilyl, methoxymethyl, benzyl, tetrahydropyranyl, and acetate protecting groups (Scheme 10). The reaction is quite general and a number of functional groups were tolerated. In addition, a Si—O bond could be selectively cleaved in the presence of a Si—C bond (see the furan example).

Tamaru et al. reported in 1979 that alcohols could be oxidized to aldehydes and ketones with catalytic amounts of palladium acetate and a stoichiometric amount of 2-bromomesitylene in dry DMF (40). Since desilylations are possible using $PdCl_2(CH_3CN)_2$, we investigated whether the desilylation and oxidation reactions could be combined into a one-pot sequence using catalytic amounts of a palladium catalyst (38). We have successfully combined the two reactions into a one-pot sequence using a 1:1 mixture of acetone:DMF as the solvent with 5 mol% $PdCl_2(CH_3CN)_2$. The mixed solvent system is essential for the success of the combined reactions since the desilylation reaction would not proceed in wet (or dry) DMF and the oxidation would not proceed in wet (or dry) acetone. At this time we do not understand why the mixed solvent system works while the individual solvents do not work on opposite reactions, but we are still investigating this intriguing observation.

The reaction is performed by mixing the silyl ether with the palladium catalyst in an acetone–DMF mixture containing 5 equivalents of water. The mixture is heated to reflux and, once TLC or GC indicates the silyl group has been removed, 2-bromomesitylene (oxidizing agent), PPh_3 (10 mol%), and K_2CO_3 are added and refluxed until the reaction is complete. Aldehydes and ketones are formed in yields ranging from 69 to 90% depending on the substrate (Scheme 11). Aldehydes are not overoxidized to the carboxylic acid, and even benzaldehyde was isolated in 75% yield. The reaction is not general and we have found three limitations so far: (*i*) aryl bromides and iodides are dehalogenated during the procedure. Thus, 3-bromo-2-(*tert*-butyldimethylsilyl)oxymethyl-naphthalene provided a 79% yield of 2-naphthaldehyde; (*ii*) *O*-(*tert*-butyldimethylsilyl)cinnaminol provided cinnamaldehyde in only 10% yield. Allylic alcohols appear to require stoichiometric amounts of the palladium species; finally (*iii*) a THP and acetate protecting group were not tolerated very well during this one-pot sequence (Scheme 11). Nevertheless, many examples provided aldehydes and ketones in good to excellent yield and we highly recommend this procedure over the two-step process that is normally used.

cis,cis-Spiro[4.4]nonane-1,6-diol: new chiral auxiliaries for the Diels–Alder reaction

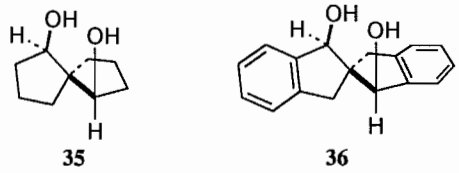
For the past 4 years we have been investigating the synthesis and use of C_2-symmetric spirodiols as auxiliaries in various organic transformations (41–44). To date, we have concentrated our efforts on the preparation of *cis,cis*-spiro-[4.4]nonane-1,6-diol **35** and *cis,cis*-2,2′-spirobiindane-1,1′-diol **36** (Scheme 12). At the time we started our investigation,

[8] Lipshutz et al. reported the desilylation of a *tert*-butyldimethylsilyl ether as a side reaction when an acetal was being cleaved using $PdCl_2$. See ref. 39.

© 1997 NRC Canada

Can. J. Chem. Downloaded from www.nrcresearchpress.com by 91.121.58.235 on 09/08/12
For personal use only.

Scheme 12.



there were no reports on the use of **35** and **36** as chiral auxiliaries; however, in 1992 Kumar and co-workers reported that **36** could be used with lithium aluminium hydride for the asymmetric reduction of aromatic ketones (45). Attempts to repeat these results by us, and later by Seebach's group (46), failed to reproduce the results reported by Kumar. We therefore carried on with our investigation. The synthesis and resolution of (±)-**35** (41) and (±)-**36** (43) and the confirmation of the absolute stereochemistry of **35** using a combination of an X-ray crystal structure, VCD spectra, and ab initio calculations have been reported (42) and will not be presented in this article. Instead, the application of (+)- and (−)-**35** as chiral auxiliaries in the Diels–Alder reaction will be discussed in detail. While other diols have been used as chiral auxiliaries in the Diels–Alder reaction (47), to our knowledge this is the first time **35** has been used as such (48).

Although we have used (+)-**35** as a Lewis acid bound chiral auxiliary in the Diels–Alder reaction (Ti) (49), cyclopropanation reaction (Zn) (50), Grignard addition to aryl ketones (Mg) (51), and hydrocyanation reaction (Ti) (52), the enantiomeric excesses (ee's) of the products were never any better than those reported with other diols (48). We then looked at using **35** as a substrate-bound chiral auxiliary. When **35** was used as the alcohol component to prepare acetals and ketals from aldehydes and ketones and used in a variety of diastereotopic reactions (i.e., *ortho*-lithiation of arylacetals and condensation of the anion with aldehydes (53), diastereoselective Ullmann (54) and Suzuki couplings (19, 22) with *ortho*-bromoarylacetals, and cyclopropanation of unsaturated acetals (55)), the diastereomeric excesses (de's) were similar to those reported with other diols (48). The best result obtained with **35** was in the Diels–Alder reaction when a dienophile was attached to one alcohol and a blocking group to the other.

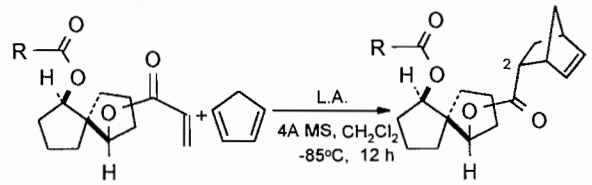
Initially we focused our attention on determining which Lewis acid would provide the highest yield and greatest amount of *endo* isomer in the Diels–Alder reaction between an acrylate and cyclopentadiene. The blocking group chosen was the 2-naphthoate group as Maitra and Mathivanan have reported success with this group when attached to a steroidal backbone (47*d* and *e*). Some selected results are illustrated in Table 1 (entries 1–6). The best result was when **37** (R = 2-Np) was treated at −85°C with 2 equiv. of boron trichloride containing freshly distilled cyclopentadiene. Adduct **38** (R = 2-Np) was formed in 100% yield with 96% *endo* stereochemistry and had a de of 75%.

A variety of blocking groups were used to replace the 2-naphthyl group and the Diels–Alder reaction was attempted using BCl_3. Changing the blocking group to a 1-naphthyl group did not noticeably change the results, but an increase in the de from 75% to 88% was observed when a phenyl group was used in **37**. Replacing the phenyl group with an electron-deficient (R = *p*-NO_2Ph) and electron-rich (R = MeOPh) aromatic ring did not noticeably change the %de, indicating stereoelectronic factors were not really important in this reaction. The steric size of the blocking group was increased by adding a diphenylbenzoate group to **37**, which resulted in a slight increase in the de to 90%. Following along the lines of increasing the steric bulk, a pivalate was attached to **37**. When the cyclopentadiene was precooled to −85°C prior to its addition to a mixture of **37** (R = CMe_3) and BCl_3, only one *endo* isomer was detected by HPLC and ^{1}H NMR spectroscopy.

This result is remarkable when one considers all the possible conformations that **37** can adopt prior to the Diels–Alder reaction. Either one conformation is preferentially formed with **37** (R = CMe_3) in the presence of 2 equiv. of BCl_3, thereby exposing only one face of the dienophile, or more than one conformation exists; but within each, the same face of the dienophile is exposed so that only one *endo* isomer is formed. Whatever the case, the result indicates that the spirononane **35** is a useful auxiliary in the Diels–Alder reaction.

The absolute stereochemistry of the bicyclo component of **38** was determined by treatment of **38** with I_2–KI in CH_2Cl_2 to form tricyclolactone **40** and alcohol **39**. Comparison of the sign of optical rotation of synthetic **40** with that reported in the literature (47*e*, 56) showed that when (+)-**35** was used to form

Table 1. Results for the Diels–Alder reaction of **37**.



R	Equiv. of Lewis acid	Lewis acid	*endo*[a,b] (%)	%de[b] (%ee)	**38**[b] (%)
2-Np	—	—	84	7	100[c]
2-Np	1.1	$TiCl_4$	97	54	6
2-Np	1.1	$SnCl_4$	95	80	15
2-Np	2.1	$SbCl_5$	94	53	74
2-Np	3	$AlMeCl_2$	97	59	100
2-Np	2	BCl_3	96	75	100
(*R*)-1-Np[d]	2	BCl_3	98	75[e]	100
Ph	2	BCl_3	99	88[e]	100
p-NO_2Ph	2	BCl_3	98	84[e]	100
p-MeOPh	2	BCl_3	98	88[e]	100
(*R*)-Ph[d]	2	BCl_3	99	88[e](89)	100
Ph_2CH	2	BCl_3	97[f]	90[f]	100[f]
(*S*)-Me_3C[d]	2	BCl_3	99	>97[e](97)	100

[a]The remainder was the *exo* isomer.

[b]*endo* Diastereomers, determined by HPLC using an ODS column with MeOH/H_2O (90:10), unless otherwise indicated.

[c]Cyclopentadiene was added to the reaction mixture at 8°C until the reaction was complete.

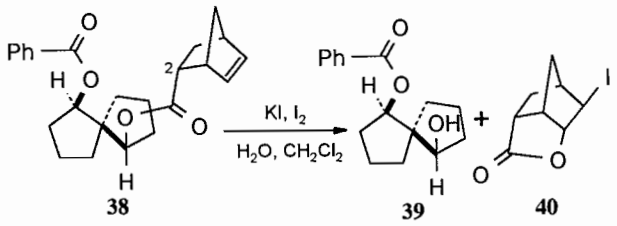
[d]The letter in parentheses refers to the absolute configuration of the *cis*,*cis*-diol used (i.e., *R* = 1*R*,5*R*,6*R*).

[e]Cyclopentadiene was precooled to −85°C in CH_2Cl_2 and transferred to the reaction by cannula addition.

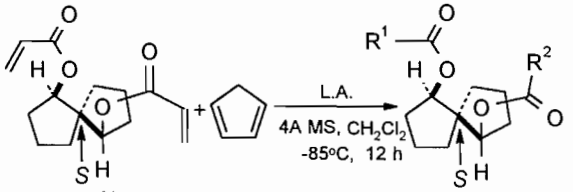
[f]Determined by ^{1}H NMR spectroscopy.

© 1997 NRC Canada

Scheme 13.



Scheme 14.



37 (and subsequently **38**), lactone (−)-**40** was obtained (Scheme 13). This indicated that the absolute stereochemistry at C-2 in the bicyclo[2.2.1]system of **38** (Table 1) was *R* when 1*R*,5*R*,6*R*-(+)-**35** was used as the chiral auxiliary.

A drawback of using **37** (R=CMe_3) is that both components are attached to spirodiol **35** through an ester functional group. This makes it somewhat difficult to remove the bicyclo adduct without cleaving the pivalate group as well. Although an iodolactonization provides lactone **40** and alcohol **39**, which can be recycled, lactone **40** must be treated further to regenerate the bicyclo acid. To alleviate this problem we investigated whether placing two acrylate groups on diol **35** would lead to a high de of the required bicyclo adduct. Hopefully, each acrylate would be bulky enough and adopt a conformation that would preferentially block the same face on the other acrylate. This would lead to the Diels–Alder reaction at each acrylate giving the same bicyclo adduct. Treatment of **41** with cyclopentadiene in the presence of BCl_3 at −85°C provided only two (**42b** and **42c**) of three possible diastereomers (Scheme 14) with a de of 76%. This was initially disappointing until we removed the bicyclo adducts from **42b** and **42c** by iodolactonization and found the %ee of the resulting mixture of was actually 89% (measured by optical rotation). The %ee was higher than the %de since three bicyclo *endo* isomers with the *S* configuration (at C-2) were formed per bicyclo *R* isomer (at C-2) in **42b** and **42c**, thereby providing **40** with an 89% ee [(88 + 88 + 12 − 12)/(88 + 88 + 12 + 12)] after iodolactonization of the mixture of diastereomers (Scheme 14).

This is as far as we have taken this project to date. Work is continuing to: (*i*) improve the diastereoselectivity of this latter reaction; (*ii*) understand better reasons for the observed absolute stereochemistry; and (*iii*) to increase the scope of the Diels–Alder reaction with **35** by using a variety of dienophiles, dienes, and blocking groups.

Can. J. Chem. Downloaded from www.nrcresearchpress.com by 91.121.58.235 on 09/08/12
For personal use only.

Acknowledgements

I thank the Natural Sciences and Engineering Research Council of Canada (NSERC), the Merck Frosst Centre of Therapeutic Research (Canada), and The University of Calgary for financial support. In addition, I thank NSERC and the Killam Foundation for postgraduate scholarships (to N.G.A.), the Alberta Heritage Scholarship Fund for a PDF scholarship (to S.P.M.), and the Department of Chemistry for a scholarship (to J.A.N.). I would also like to thank the Department of Chemistry and Biochemistry at the University of Windsor for their support (both financial and moral) during the beginning of my career as an Assistant Professor (1985–1989). Finally, I thank all the members (support staff and faculty, both past and present) of the Department of Chemistry at The University of Calgary for their support and guidance over the last 7 years.

References

1. H. Nakamura, J. Kobayashi, M. Kobayashi, Y. Ohizumi, and Y. Hirata. Chem. Lett. 713 (1985).
2. D.M. Roll, P.J. Scheuer, G.K. Matsumoto, and J. Clardy. J. Am. Chem. Soc. **105**, 6177 (1983).
3. R.H. Lee, P.L. Slate, R. Moretti, K.A. Alvi, and P. Crews. Biochem. Biophys. Res. Commun. **184**, 765 (1992).
4. (*a*) M. Kobayashi, H. Nakamura, J. Kobayasi, and J. Ohizumi. J. Pharmacol. Exp. Ther. **257**, 90 (1991); (*b*) H. Sakamoto, K. Furukawa, K. Matsunaga, H. Nakamura, and Y. Ohizumi. Biochemistry, **34**, 12 570 (1995).
5. J.R. Hanson. Nat. Prod. Rep. 381 (1995).
6. N. Harada, T. Sugioka, H. Uda, and T. Kuriki. J. Org. Chem. **55**, 3158 (1990).
7. K. Kanematsu, S. Soejima, and G. Wang. Tetrahedron Lett. **32**, 4761 (1991).
8. N. Harada, T. Sugioka, Y. Ando, H. Uda, and T. Kuriki. J. Am. Chem. Soc. **110**, 8483 (1988).
9. A. Kajima, T. Takemoto, M. Sodeoka, and M. Shibasaki. J. Org. Chem. **61**, 4876 (1996).
10. (*a*) R. Carlini, K. Higgs, C. Older, S. Randhawa, and R. Rodrigo. J. Org. Chem. **62**, 2330 (1997); (*b*) P.A. Burns, N.J. Taylor, and R. Rodrigo. Can. J. Chem. **72**, 42 (1994).
11. (*a*) W.A. Cristofoli. Ph.D. dissertation, The University of Calgary, 1995; (*b*) J.-L.J. Bontront. M.Sc. thesis, University of Windsor, 1988.
12. S.P. Maddaford, N.G. Andersen, W.A. Cristofoli, and B.A. Keay. J. Am. Chem. Soc. **118**, 10766 (1996).
13. (*a*) W.A. Cristofoli and B.A. Keay. Synlett, **8**, 625 (1994); (*b*) L.E. Overman, D.J. Ricca, and V.D. Tran. J. Am. Chem. Soc. **115**, 2042 (1993); (*c*) J.M. Takacs and S.V. Chandramouli. J. Org. Chem. **58**, 7315 (1993); (*d*) F.E. Meyer, H. Henniges, and A. de Meijere. Tetrahedron Lett. **33**, 8039 (1992); (*e*) F.E. Meyer, J. Brandenburg, P.J. Parson, and A. de Meijere. J. Chem. Soc. Chem. Commun. 390 (1992); (*f*) E.-i. Negishi. Pure Appl. Chem. **64**, 323 (1992); (*g*) F.E. Meyer, P.J. Parsons, and A. de Meijere. J. Org. Chem. **56**, 6487 (1991); (*h*) W. Oppolzer and R.J. DeVita. J. Org. Chem. **56**, 6256 (1991); (*i*) R. Grigg, M.J. Dorrity, J.F. Malone, S. Visuvanathar, and S. Sukirthalingam. Tetrahedron Lett. **31**, 1343 (1990); (*j*) Y. Zhang, G.-z. Wu, G. Agnel, and E.-i. Negishi. J. Am. Chem. Soc. **112**, 8590 (1990); (*k*) M.M. Abelman and L.E. Overman. J. Am. Chem. Soc. **110**, 2328 (1988).
14. (*a*) A. de Meijere and F.E. Meyer. Angew. Chem. Int. Ed. Engl. **33**, 2379 (1994); (*b*) W. Cabri and I. Candiani. Acc. Chem. Res. **28**, 2 (1995); (*c*) K. Kondo, M. Sodeoka, and M. Shibasaki. Tetrahedron Asymmetry, **6**, 2453 (1995); (*d*) K. Kondo, M. Sodeoka, and M. Shibasaki. J. Org. Chem. **60**, 4322 (1995), and references therein.

© 1997 NRC Canada

Can. J. Chem. Downloaded from www.nrcresearchpress.com by 91.121.58.235 on 09/08/12
For personal use only.

15. N.G. Andersen, S.P. Maddaford, and B.A. Keay. J. Org. Chem. **61**, 2885 (1996).
16. E.J. Bures and B.A. Keay. Tetrahedron Lett. **29**, 1247 (1988).
17. E.J. Bures and B.A. Keay. Tetrahedron Lett. **28**, 5965 (1987).
18. D.R. McKean, G. Parrinello, A.F. Renaldo, and J.K. Stille. J. Org. Chem. **52**, 422 (1987).
19. (*a*) A. Suzuki and N. Miyaura. Chem. Rev. Washington, D.C. **95**, 2457 (1995); (*b*) N. Miyaura, T. Yanagi, and A. Suzuki. Synth. Commun. **11**, 513 (1981); (*c*) Y. Hoshino, N. Miyaura, and A. Suzuki. Bull. Chem. Soc. Jpn. **61**, 3008 (1988); (*d*) M. Satoh, N. Miyaura, and A. Suzuki. Chem. Lett. 1405 (1989); (*e*) A. Suzuki. Pure Appl. Chem. **63**, 419 (1991).
20. B.A. Keay and J.-L.J. Bontront. Can. J. Chem. **69**, 1326 (1991).
21. W.A. Cristofoli and B.A. Keay. Tetrahedron Lett. **32**, 5881 (1991).
22. S.P. Maddaford and B.A. Keay. J. Org. Chem. **59**, 6501 (1994).
23. (*a*) Y. Sato, M. Sodeoka, and M. Shibasaki. Chem. Lett. 1953 (1990); (*b*) Y. Sato, S. Watanabe, and M. Shibasaki. Tetrahedron Lett. **33**, 2589 (1992); (*c*) Y. Sato, S. Nukui, M. Sodeoka, and M. Shibasaki. Tetrahedron, **50**, 371 (1994).
24. (*a*) R.H. Shapiro and M.J. Heath. J. Am. Chem. Soc. **89**, 5734 (1967); (*b*) R.H. Shapiro. Org. React. N.Y. **23**, 405 (1976); (*c*) R.M. Adlington and A.G.M. Barrett. Acc. Chem. Res. **16**, 55 (1983); (*d*) A.R. Chamberlin and S.H. Bloom. Org. React. N.Y. **39**, 1 (1990).
25. M.S. Passafaro and B.A. Keay. Tetrahedron Lett. **37**, 429 (1996).
26. N.G. Andersen, S.P. Maddaford, and B.A. Keay. J. Org. Chem. **61**, 9556 (1996).
27. (*a*) T. Konoshima, M. Kozuka, H. Tokuda, H. Nishino, A. Iwashima, M. Haruna, and K. Ito. J. Nat. Prod. **54**, 816 (1991); (*b*) K. Ito, T. Iida, K. Ichino, T. Masao, and T. Namba. Chem. Pharm. Bull. **30**, 3347 (1982); (*c*) M.R. Agharahimi and N.A. LeBel. J. Org. Chem. **60**, 1856 (1995).
28. T. Hashimoto, S. Tahara, S. Takaoka, M. Tori, and Y. Askawa. Chem. Pharm. Bull. **42**, 1528 (1994).
29. (*a*) A.P. Lurie, G.H. Brown, J.R. Thirtle, and A. Weissberger. J. Am. Chem. Soc. **83**, 5015 (1961); (*b*) F. Hibbert and K. Spiers. J. Chem. Soc. Perkin Trans. 2, 571 (1988).
30. P. Beak, T.J. Musick, and C.-w. Chen. J. Am. Chem. Soc. **110**, 3538 (1988).
31. T.W. Greene and P.G.W. Wuts. *In* Protective groups in organic synthesis. 2nd ed. John Wiley and Sons, Inc., New York. 1991.
32. P.M. Kendall and J.V. Johnson. J. Org. Chem. **44**, 1421 (1979).
33. (*a*) A.K. Sinhababu, M. Kawase, and R.T. Borchardt. Synthesis, 710 (1988); (*b*) A.K. Sinhababu, M. Kawase, and R.T. Borchardt. Tetrahedron Lett. **28**, 4139 (1987).
34. E.A. Schmittling and J.S. Sawyer. Tetrahedron Lett. **32**, 7207 (1991).
35. R.S. Varma, J.B. Lamture, and M. Varma. Tetrahedron Lett. **34**, 3029 (1993).
36. N.S. Wilson and B.A. Keay. Tetrahedron Lett. **37**, 153 (1996).
37. N.S. Wilson and B.A. Keay. Tetrahedron Lett. **38**, 187 (1997).
38. N.S. Wilson and B.A. Keay. J. Org. Chem. **61**, 2918 (1996).
39. B.H. Lipshutz, D. Pollart, J. Monforte, and H. Kotsuki. Tetrahedron Lett. **26**, 705 (1985).
40. (*a*) Y. Tamaru, Y. Yamada, K. Inoue, Y. Yamamoto, and Z.-I. Yoshida. J. Org. Chem. **48**, 1286 (1983); (*b*) Y. Tamaru, K. Inoue, Y. Yamada, and Z.-I. Yoshida. Tetrahedron Lett. **22**, 1801 (1981); (*c*) Y. Tamaru, Y. Yamamoto, Y. Yamada, and Z.-I. Yoshida. Tetrahedron Lett. **20**, 1401 (1979); (*d*) B.M. Choudary, N.P. Reddy, M.L. Kantam, and Z. Jamil. Tetrahedron Lett. **26**, 6257 (1985).
41. J.A. Nieman, M.Parvez, and B.A. Keay. Tetrahedron Asymmetry, **4**, 1973 (1993).
42. J.A. Nieman, B.A. Keay, M. Kubicki, D. Yang, A. Rauk, D. Tsankov, and H. Wieser. J. Org. Chem. **60**, 1918 (1995).
43. J.A. Nieman and B.A. Keay. Tetrahedron: Asymmetry, **6**, 1575 (1995).
44. J.A. Nieman and B.A. Keay. Tetrahedron: Asymmetry, **7**, 3521 (1996).
45. N. Srivastava, A. Mital, and A. Kumar. J. Chem. Soc. Chem. Commun. 493 (1992).
46. D. Seebach, A.K. Beck, R. Dahinden, M. Hoffmann, and F.N.M. Kuhnle. Croat. Chem. Acta, **69**, 459 (1996).
47. (*a*) W. Oppolzer. Angew. Chem. Int. Ed. Engl. **23**, 876 (1984). (*b*) D.A. Evans, K.T. Chapman, and J. Bisaha. J. Am. Chem. Soc. **110**, 1238 (1988). (*c*) J.-L. Gras, and H. Pellissier. Tetrahedron Lett. **35**, 7451 (1994). (*d*) U. Maitra and P. Mathivanan. J. Chem. Soc., Chem. Commun. 1469 (1993). (*e*) P. Mathivanan and U. Maitra. J. Org. Chem. **60**, 364 (1995).
48. J.A. Nieman. Ph.D. dissertation, University of Calgary, Calgary, Alberta, 1996.
49. M.T. Reetz, S.-K. Kyung, C. Bolm, and T. Zurke. Chem. Ind. Dig. 824 (1986).
50. (*a*) Y. Ukaji, M. Nishimura, and T. Fujisawa. Chem. Lett. 61 (1992); (*b*) Y. Ukaji, K. Sada, and K. Inomata. Chem. Lett. 1227 (1993).
51. (*a*) B. Weeber and D. Seebach. Angew. Chem. Int. Ed. Engl. **31**, 84 (1992); (*b*) B. Weeber and D. Seebach. Tetrahedron, **50**, 6117 (1994).
52. (*a*) K. Narasaka, T. Yamada, and H. Minamikawa. Chem. Lett. 2073 (1987); (*b*) H. Minawikawa, S. Hayakawa, T. Yamada, N. Iwasawa, and K. Narasaka. Bull. Chem. Soc. Jpn. **61**, 4379 (1988).
53. M. Commercon, P. Mangeney, T. Tejero, and A. Alexakis. Tetrahedron: Asymmetry, **1**, 287 (1990).
54. (*a*) P.E. Fanta. Synthesis, 9 (1974); (*b*) M. Sainsbury. Tetrahedron, **36**, 3327 (1980); (*c*) B.H. Lipshutz, K. Siegmann, E. Garcia, and F. Kayser. J. Am. Chem. Soc. **115**, 9276 (1993).
55. (*a*) A. Mori, I. Arai, and H. Yamamoto. Tetrahedron, **42**, 6447 (1986); (*b*) A. Mori, I. Arai, and H. Yamamoto. J. Am. Chem. Soc. **107**, 8254 (1985).
56. H. Waldmann. Liebigs Ann. Chem. 671 (1990).

© 1997 NRC Canada

Synthesis of thaxtomin C

Russell R. King

Abstract: *N*-Methyl-L-4-nitrotryptophan methyl ester (**2**) and *t*-Boc-L-phenylalanine (**3**) were condensed to form the dipeptide **4**, which was then cyclized to give 12-*N*-methylcyclo-(L-4-nitrotryptophyl-L-phenylalanyl) (**1**), a.k.a. thaxtomin C, the principle phytotoxin associated with *Streptomyces ipomoeae*.

Key words: *Streptomyces ipomoeae*, phytotoxin, thaxtomin C.

Résumé : On a condensé l'ester méthylique du *N*-méthyl-L-4-nitrotryptophan (**2**) et la *t*-Boc-L-phénylalanine (**3**) pour conduire au dipeptide **4** qui a alors été cyclisé pour donner le 12-*N*-méthylcyclo-(L-4-nitrotryptophényl-L-phénylalanyl) (**1**), aussi connu sous le nom de thaxtomine C, la principale phytotoxine associée au *Streptomyces ipomoeae*.

Mots clés : *Streptomyces ipomoeae*, phytotoxine, thaxtomine C.

[Traduit par la rédaction]

Introduction

The bacterium *Streptomyces ipomoeae* (Person and Martin) Waksman and Henrici is the causal agent of an economically important disease of sweet potato, *Ipomoeae batatas* (L.) ham. Infection is characterized by substantial yield reductions and disfigured lesions on the fleshy storage roots (1). Our recent investigations examining the host–parasite relationship of pathogenic *S. ipomoeae* isolates have identified the presence of a phytotoxin, 12-*N*-methylcyclo-(L-4-nitrotryptophyl-L-phenylalanine) a.k.a. thaxtomin C (**1**), which is associated with infection (2). As *S. ipomoeae* isolates could not be enticed to generate the phytotoxin when grown on any of the usual culture media, synthesis to provide convenient access to reasonable quantities for further host-interaction studies was required. Herein we describe a synthesis of the phytotoxin in acceptable yields utilizing standard procedures for the diketopiperazine ring-formation step.

Results and discussion

Thaxtomin C can be envisaged as being derived biosynthetically from the combination (diketopiperazine ring formation) of two amino acids: tryptophan and phenylalanine, with the required nitration and *N*-methylation steps occurring at some point along the way. In line with this approach a synthetically prepared sample of *N*-methyl-L-4-nitrotryptophan methyl ester (**2**) (3) was condensed with *t*-Boc-L-phenylalanine (**3**) (Scheme 1) to give the dipeptide methyl ester (**4**), the formate salt of which was cyclized by standard procedures (4). This gave 12-*N*-methylcyclo-(L-4-nitrotryptophyl-L-phenylalanyl) (**1**), a.k.a. thaxtomin C, in moderate yield (36%) after purification by precipitation. Since no diastereoisomers were detected (TLC, NMR), it was presumed that no racemization had occurred during the process. Unequivocal evidence for confirmation of the integrity of the synthetic sample was then obtained by comparing it with an authentic sample of thaxtomin C (UV, IR, MS, NMR, TLC, and biological activity (2)).

We have previously demonstrated (5) that the minimum structural criterion necessary for induction of scab by the thaxtomins is the presence of the 4-nitroindol-3-yl and phenylalanine groups linked in an L,L configured cyclodipeptide; i.e., elimination of the nitro group, replacement of the phenyl side chain, movement of the 4-nitro group to the 5, 6, or 7 positions, or conversion to a D,L configuration resulted in a complete loss of bioactivity.

Experimental section

Melting points were determined on a Kofler hot-stage microscope and are uncorrected. IR spectra were determined by using a Perkin–Elmer 467 grating infrared spectrophotometer. UV spectra were recorded in absolute ethanol using a Varian Cary 219 spectrophotometer. NMR spectra were recorded for solutions in deuterated chloroform on a Varian Unity 400 operating at 400 MHz for ^{1}H and at 100 MHz for ^{13}C. Chemical shifts were measured downfield from the signal of internal tetramethylsilane. MS were obtained on a Finnigan MAT 312 mass spectrometer. TLC was performed on 0.25 mm Merck silica gel 60 F_{254} plates and 0.2 mm Whatman $KC_{18}F$ plates.

Preparation of 12-*N*-methylcyclo-(L-4-nitrotryptophyl-L-phenylalanyl) (1)

t-Boc-L-Phenylalanine (**3**, 80 mg, 0.3 mmol) was dissolved in methylene chloride (20 mL) at 0°C and *N*-methyl-L-4-nitrotryptophan methyl ester (**2**, 83 mg, 0.3 mmol) was added. After addition of *N*-ethyl-*N'*-(3-dimethylaminopropyl) carbodiimide hydrochloride (58 mg, 0.3 mmol), the solution was stirred at 0°C overnight. The reaction mixture was then washed with water, citric acid (1 N), and sodium bicarbonate, and the solution was evaporated to dryness. The *t*-Boc-dipeptide (**4**, 86 mg) was eluted from a silica gel column ($CHCl_3$:MeOH, 9:1), dissolved in formic acid (10 mL, 98%),

Received February 26, 1997.

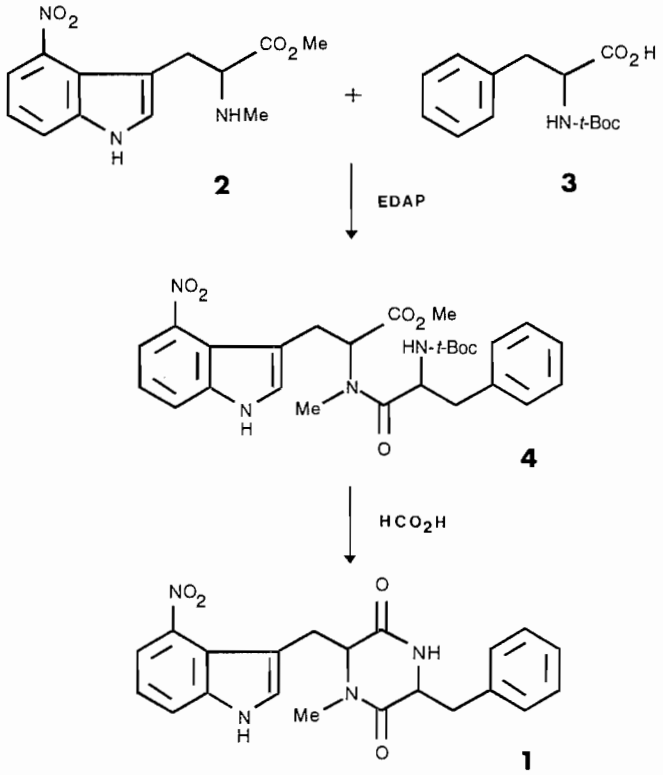
R.R. King.[1] Agriculture and Agri–Food Canada, Research Branch, Fredericton Research Centre, P.O. Box 20280, Fredericton, NB E3B 4Z7, Canada.

[1] Telephone: (506) 452-3260. Fax: (506) 452-3316.

© 1997 NRC Canada

Can. J. Chem. Downloaded from www.nrcresearchpress.com by 91.121.58.235 on 09/08/12
For personal use only.

Scheme 1.



and the solution was kept at room temperature for 2 h. After removal of the excess formic acid in vaccuo at 25°C, the residue containing the dipeptide ester formate was dissolved in 2-butanol (15 mL) and toluene (5 mL). The solution was boiled for 30 min and the solvents removed in vacuo at 25°C. The residue precipitated from methanol to yield 12-*N*-methylcyclo-(L-4-NO_2-tryptophyl-L-phenylalanyl) (**1**, 42 mg, 0.107 mmol) as yellow plates, mp >225°C (dec.); IR (Nujol), ν_{max}: 1670, 1650, 1600, and 1510 cm^{-1}; λ_{max} (EtOH): 395 (ε, 4050) nm. ^1H NMR δ: 1.88 (dd, 1H, J = 13.3, 9.9 Hz, H-17a), 2.93 (dd, 1H, J = 14.5, 7.0 Hz, H-10a), 3.09 (dd, 1H, J = 13.5, 3.8 Hz, H-17b), 3.09 (s, 3H, N-CH_3), 3.61 (dd, 1H, J = 14.6, 4.6 Hz, H-10b), 4.03 (dd, 1H, J = 9.7, 3.2 Hz, H-14), 4.12 (dd, 1H, J = 7.0, 4.5 Hz, H-11), 6.84 (m, 2H, H-19 and H-23), 7.17–7.31 (m, 3H, H-20, H-21, and H-22), 7.21 (s, 1H, H-2), 7.26 (m, 1H, H-6), 7.65 (dd, 1H, J = 8.1, 1.0 Hz, H-7), 7.95 (dd, 1H, J = 7.9, 1.0 Hz, H-5). ^{13}C NMR δ: 29.70 (q, N-CH_3), 32.59 (t, C-10), 38.99 (t, C-17), 55.95 (d, C-14), 62.75 (d, C-11), 108.40 (s, C-3), 115.05 (d, C-7), 117.17 (d, C-5), 118.32 (s, C-8), 119.84 (d, C-6), 126.52 (d, C-21), 128.22 (d, C-20), 128.22 (d, C-22), 129.61 (d, C-19), 129.61 (d, C-23), 130.70 (d, C-2), 136.62 (s, C-18), 138.89 (s, C-9), 142.18 (s, C-4), 165.26 (s, C-13 or C-16), 165.54 (s, C-13 or C-16). Mass spectrum M^+: 392.1475 for $C_{21}H_{20}N_4O_4$.

Acknowledgments

We thank Peter Penner (Department of Chemistry, University of New Brunswick, Fredericton) for recording the NMR spectra.

References

1. L.H. Person and W.J. Martin. Phytopathology, **30**, 913 (1940).
2. R.R. King, C.H. Lawrence, L.A. Calhoun and J.B. Ristaino. J. Agric. Food Chem. **42**, 1791 (1994).
3. R.R. King and C.H. Lawrence. Phytochemistry, **40**, 41 (1995).
4. D.E. Nitecki, B. Halpern, and J.W. Westley. J. Org. Chem. **33**, 964 (1968).
5. R.R. King, C.H. Lawrence, and L.A. Calhoun. J. Agric. Food Chem. **40**, 834 (1992).

Can. J. Chem. Downloaded from www.nrcresearchpress.com by 91.121.58.235 on 09/08/12
For personal use only.

© 1997 NRC Canada

Benzenoid hydrocarbon aromaticity in terms of charge density descriptors

S.T. Howard and T.M. Krygowski

Abstract: Hartree–Fock/6-31G** calculations on the benzenoid hydrocarbons benzene, naphthalene, phenanthrene, anthracene, pyrene, tetracene, triphenylene, chrysene, perylene, and coronene are used to investigate the link between aromaticity and the electron distribution. Topological charge density analysis is used, concentrating on the electron distribution ρ (and its Hessian) at bond and ring critical points. With regard to the bond critical point data, it is shown that ρ_c, $\nabla^2\rho_c$, and the bond "ellipticity" ε are closely correlated with the bond lengths so, as aromaticity indicators, they have little to add over and above existing indices based on structure. However, the same properties evaluated at the ring critical points in the total density, and also at the equivalent stationary points in the π and σ densities, correlate closely with two different aromaticity indices (one based on structure, the other on magnetic properties), the curvature of ρ perpendicular to the ring plane giving (marginally) the best results. Hence a ring critical point (RCP) index is proposed as a way of quantifying aromaticity, based directly on the electron distribution.

Key words: quantum chemistry, electron density, aromaticity, aromaticity index, HOMA, NICS.

Résumé : On a utilisé des calculs Hartree–Fock/6-31G** sur les hydrocarbures benzénoïdes benzène, naphtalène, phénanthrène, anthracène, pyréne, tétracène, triphénylène, chrysène, péryléne et coronène pour étudier la corrélation entre l'aromaticité et la distribution électronique. On utilise une analyse topologique de la densité de charge qui se concentre sur la distribution électronique ρ (et son hessoise) à des points critiques des liaisons et des cycles. En ce qui a trait aux données relatives aux points critiques des liaisons, on a démontré que ρ_c, $\nabla^2\rho_c$ et l'« ellipticité » ε des liaisons sont intrinsèquement liés aux longueurs des liaisons; comme indicateurs de l'aromaticité, ils n'ont pas beaucoup de chose à ajouter aux indices existants basés sur la structure. Toutefois, les mêmes propriétés évaluées aux points critiques des noyaux dans la densité totale ainsi que les points stationnaires équivalents dans les densités π et σ présentent une excellente corrélation avec deux indices différents d'aromaticité (l'un basé sur la structure et l'autre sur les propriétés magnétiques) alors que la courbure de ρ perpendiculaire au plan du noyau conduit à des résultats marginalement meilleurs. Pour quantifier l'aromaticité, on propose donc un indice de point critique du noyau qui est basé directement sur la distribution électronique.

Mots clés : chimie quantique, densité électronique, aromaticité, indice d'aromaticité, «HOMA», «NICS».

[Traduit par la rédaction]

Introduction

The definition of aromaticity has long been a topic of vivid discussion. Since the term was first coined, it has been defined in a dichotomic way, e.g., structural (1) or behaviouristic (2). The Hückel $4n + 2$ rule (3) has served to associate these two ways of defining "aromatic character," by linking the π-electron structure and ring shape with an increase in energetic stability. Most chemists have subsequently abided by the definition summarized by Jackman and Elvidge (4). In brief, this defines aromaticity as a consequence of π-electron delocalization in cyclic systems, which may be characterized by: (*i*) averaging of bond lengths; (*ii*) increased stability (by an amount of energy called the resonance energy); and (*iii*) the presence of certain magnetic properties (shown inter alias by proton NMR spectra). Thus, more generally, aromaticity is "the set of properties associated with cyclic conjugation" (5).

The most extensively studied property has been stabilization energy; hence various definitions of resonance energy have been developed using calorimetric measurements (6) or theoretical ideas (7–10). However, there have been a multitude of other approaches, including: graph-topological (11–13); geometrical structure (bond lengths, bond length/order alternation) (14–21); magnetic properties (diamagnetic susceptibilities, chemical shifts) (22–26); and HOMO–LUMO gap criteria (27, 28). Recently it has been shown that these various measures of aromaticity need not be unequivocally the same (26, 29).

Central to all these ideas about aromaticity is the concept of a conjugated π-electron framework, that is to say, aromatic systems should have a characteristic distribution of electrons. It is therefore a little surprising that not much attention has been paid to the relationship between the topological characteristics of the charge distribution and aromatic character. Instead, theoretical chemists have historically concentrated on Molecular Orbital (MO)-based descriptions of aromaticity — this is implicit when we talk about σ- and π-electron frame-

Received February 10, 1997.

S.T. Howard.[1] Department of Chemistry, University of Wales, Cardiff, Cardiff CF1 3TB, U.K.
T.M. Krygowski. Department of Chemistry, University Of Warsaw, ul. Pasteura 1, 02-093 Warszawa, Poland.

[1] Author to whom correspondence may be addressed. Telephone: +44 (01222) 874950. Fax: +44 (01222) 874029. E-mail: howardst@cardiff.ac.uk

© 1997 NRC Canada

Can. J. Chem. Downloaded from www.nrcresearchpress.com by 91.121.58.235 on 09/08/12
For personal use only.

Table 1. HF/6-31G** energetic data.

	HOMO–LUMO gap (eV)	Total energy (au)
Benzene	13.1	–230.713 86
Naphthalene	10.6	–383.369 37
Phenanthrene	10.4	–536.016 69
Anthracene	8.9	–536.027 65
Pyrene	9.1	–611.785 87
Tetracene	7.8	–688.660 07
Triphenylene	10.4	–668.681 69
Chrysene	9.7	–668.682 39
Perylene	8.1	–764.427 90
Coronene	9.0	–915.974 08

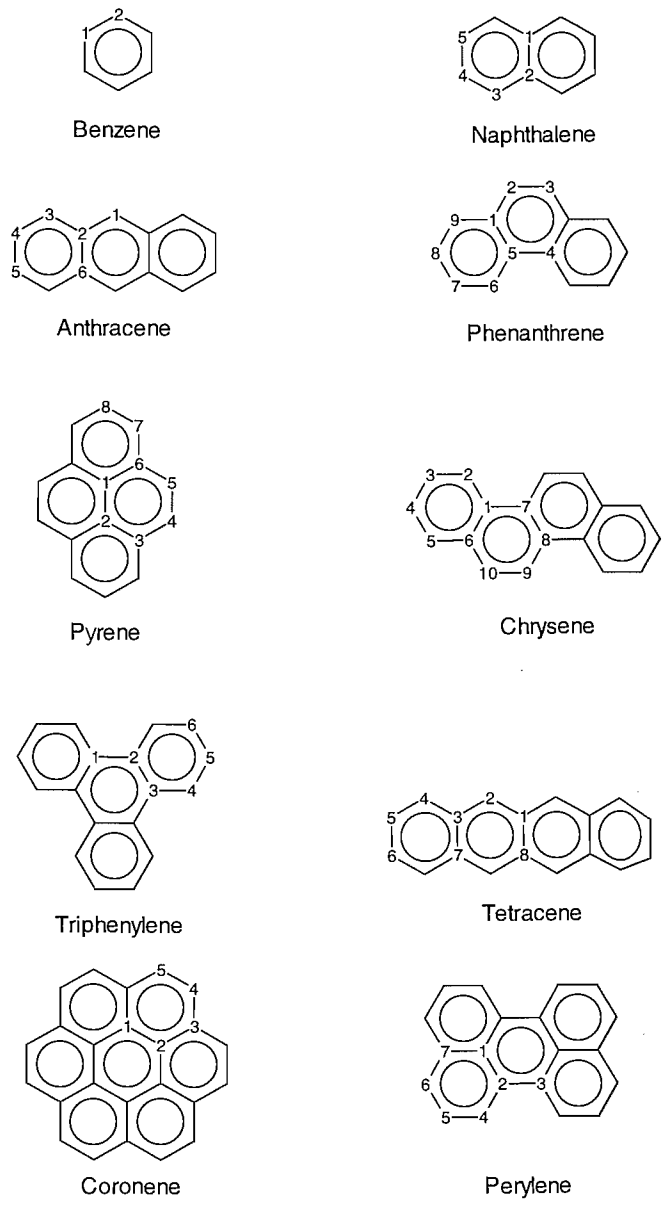
works. Alternative descriptions based on physical, observable properties are surely preferable. This approach is epitomized by the work of Bader and co-workers over the last 25 years or so (30), and it has illuminated many aspects of chemistry.

In this topological approach, the charge distribution ρ is characterized by its stationary points or "critical points" (CPs) in the scalar fields ρ and $\nabla^2\rho$. We shall be concerned with two of the four CP types that occur in ρ: so-called bond CPs (BCPs) and ring CPs (RCPs). BCPs are located at the minumum along the line of maximal charge density between nuclei: in benzenoid C—C bonds this is always close to the geometric bond centre. (In heteronuclear bonds the position of the critical point is linked to the relative electronegativities of the atoms (31, 32).) RCPs occur close to the geometric centroid in benzenoid hydrocarbon rings, at the position of minimal charge density in the ring plane.

The Hessian of ρ (matrix of partial second derivatives with respect to $\{x, y, z\}$) fully specifies its curvature. The trace of the Hessian, $\nabla^2\rho$, measures the charge concentration or depletion at a point (negative values of $\nabla^2\rho$ mean that charge is locally concentrated, positive values correspond to charge depletion). The ratio of the two negative eigenvalues of the Hessian matrix at a BCP may be used to quantify double bond character (33). More precisely, the ellipticity ϵ is defined as $\varepsilon = \lambda_1/\lambda_2 - 1$, where the λ's are the two Hessian eigenvalues corresponding to directions perpendicular to the bond, and $|\lambda_1| > |\lambda_2|$. At RCPs, two eigenvalues of the Hessian are positive and (in benzenoid hydrocarbons) approximately equal, while the remaining (negative) eigenvalue (λ_3) measures the curvature of ρ perpendicular to the ring plane.

In benzenoid hydrocarbons, each molecular orbital may be classified as σ or π without any ambiguity, unlike the partitioning of the total energy into σ and π contributions, which remains a subject of dispute (34–37). Consequently, the total electron density ρ may be subdivided into corresponding contributions: $\rho = \rho_\sigma + \rho_\pi$. The topological analysis presented above can equally well be applied to these separated ρ_σ and ρ_π densities, and we will present results for the σ, π, and total electron densities. The RCPs and BCPs in the total density ρ occur in the ring plane or nodal plane of the π-electron structure, so at these points $\rho = \rho_\sigma$ and $\rho_\pi = 0$. However, the *curvature* of the electron distribution in this

Fig. 1. The 10 benzenoid hydrocarbons considered in this work, together with the atom labelling scheme.



nodal plane is strongly dependent on both σ and π electrons. We will be concerned especially with the curvature perpendicular to the ring plane (λ_3), which has a positive contribution from π electrons (since these are concentrated above and below the plane) and a negative contribution from σ electrons (concentrated in the plane). The remaining two perpendicular curvatures lie in the ring plane, and therefore again only have non-zero contributions from σ electrons (i.e., $\nabla^2\rho_\pi = \lambda_{3,\pi}$ in this plane).

In this work, we determine the topological properties ρ, $\nabla^2\rho$, and the eigenvalues of the Hessian of ρ at both bond and ring critical points in 10 benzenoid hydrocarbons. To establish whether these quantities may be used as indices of aromatic character, we must somehow correlate these data with an established index of aromatic character, preferably one that can be derived from the same data. We have chosen to concen-

Can. J. Chem. Downloaded from www.nrcresearchpress.com by 91.121.58.235 on 09/08/12
For personal use only.

© 1997 NRC Canada

Can. J. Chem. Downloaded from www.nrcresearchpress.com by 91.121.58.235 on 09/08/12
For personal use only.

Fig. 2. Relationship between bond length and ρ_c at the 58 bond critical points (correlation coefficient $r = -0.998$).

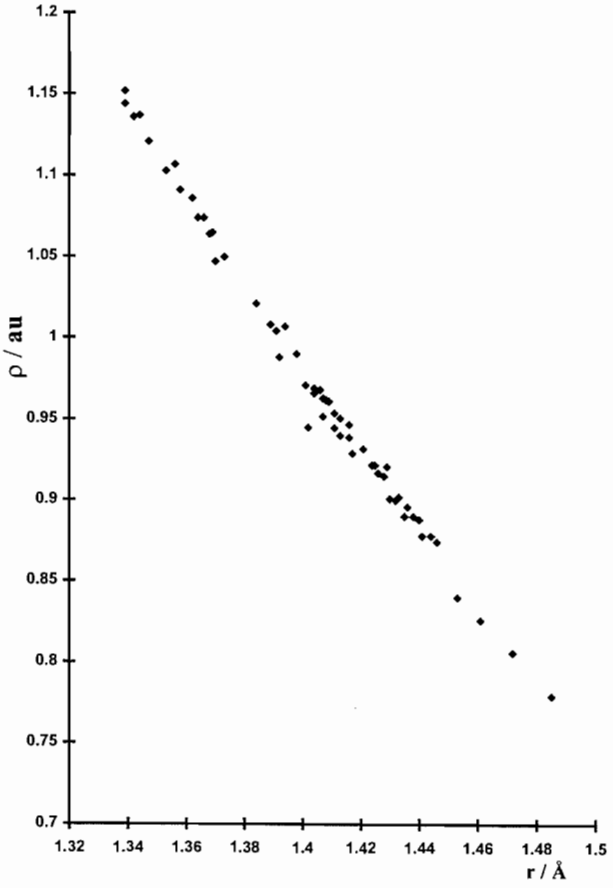
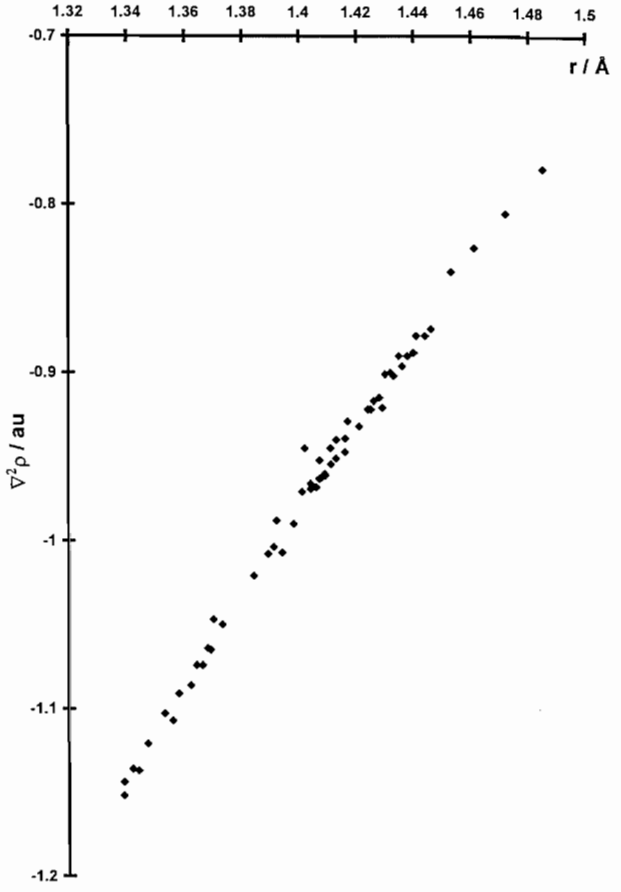


Fig. 3. Relationship between bond length and $\nabla^2\rho_c$ at the 58 bond critical points (correlation coefficient $r = +0.997$).



trate on the so-called HOMA index (harmonic oscillator model of aromaticity) (15), since it is simple to compute (it needs only the bond lengths in a ring $\{r_i\}$) and has found wide application (as reviewed in ref. 16). We will also demonstrate a relationship between this index and an established independent index NICS (based on magnetic susceptibility).

In the case of benzenoid hydrocarbons, the HOMA index for a particular ring is found from a simple sum over the six bonds making up the ring

$$[1] \quad \text{HOMA} = 1 - \left[\sum_{i=1}^{6} 257.7\,(r_i - 1.388)^2\right]/6$$

The constant 257.7 is chosen on the basis of C—C bond lengths and bond stretching force constants, i.e., in general HOMA can take into account heteroatoms by choosing appropriate values of constant for each bond. In this way, the energy to distort the structure from some idealized set of bond lengths is taken into account — it is an energy-weighted sum. The value of 1.388 Å is an optimized C—C bond length for compressing single/expanding double bonds assuming a harmonic potential with a single-bond force constant equal to half the double-bond force constant. The HF/6-31G** optimized value of the C—C bond length in benzene is very close to this (1.386 Å), so benzene gives a HOMA value that is very close to unity (0.999). Thus the index defined in eq. [1], using the set of bond lengths $\{r_i\}$ derived from ab initio optimization, effectively measures the mean deviation of the ring structure from that of benzene.

Computational details

The Hartree–Fock calculations were carried out with GAMESS (38) running on DEC Alpha RISC workstations. The topological analysis of ρ utilized the program SADDLE (39). The 6-31G** basis set (40) was used in geometry optimizations, and the charge distributions were computed and analyzed at the same level. All molecules were constrained to be planar and, furthermore, were optimized within the following point group symmetries: phenanthrene (C_{2v}); chrysene (C_{2h}); naphthalene, anthracene, tetracene, pyrene, perylene (D_{2h}); benzene, coronene (D_{6h}); triphenylene (C_{3h}).

Results and discussion

Table 1 summarizes some energetic data for the 10 hydrocarbons, optimized at the HF/6-31G** level. Anthracene is found to be more stable by $\approx$29 kJ mol^{-1} than its isomorphous partner phenanthrene, and similarly chrysene is marginally more stable than its isomers tetracene and triphenylene. We also report the HOMO–LUMO gaps for the canonical orbitals,

© 1997 NRC Canada

Can. J. Chem. Downloaded from www.nrcresearchpress.com by 91.121.58.235 on 09/08/12
For personal use only.

Fig. 4. Relationship between bond length and ε at the 58 bond critical points (correlation coefficient $r = -0.978$).

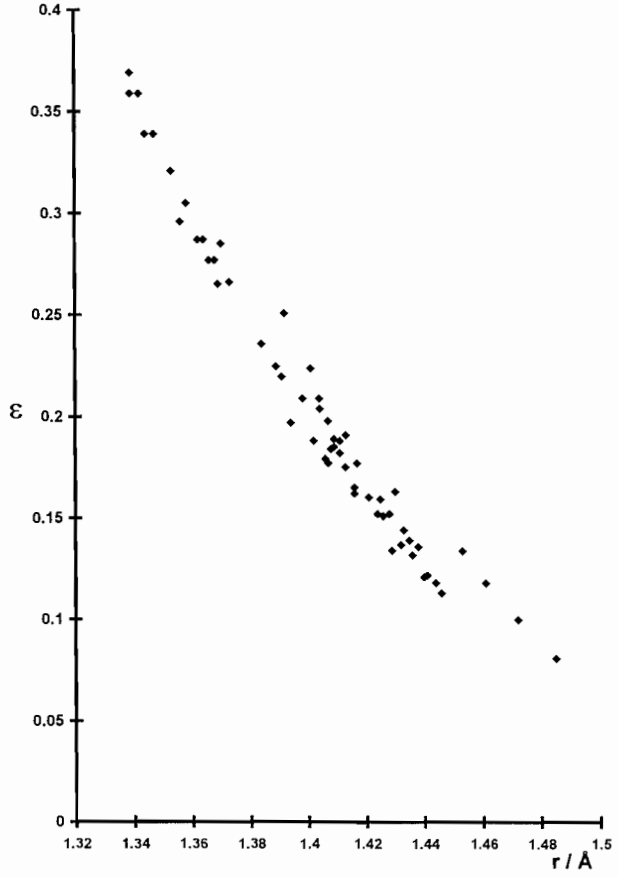


Table 2. (*a*) HF/6-31G** data[a] evaluated at the σ-framework RCP.

	ρ_σ	$\nabla^2\rho_\sigma$	$\lambda_{\sigma,3}$	$\nabla^2\rho_\pi = \lambda_{\pi,3}$
Benzene	0.0205	0.1599	−0.0269	0.0125
Naphthalene	0.0198	0.1519	−0.0255	0.0115
Anthracene (I)[b]	0.0194	0.1474	−0.0247	0.0110
(II)	0.0195	0.1489	−0.0251	0.0112
Phenanthrene (I)	0.0201	0.1545	−0.0261	0.0120
(II)	0.0186	0.1402	−0.0234	0.0102
Pyrene (I)	0.0200	0.1527	−0.0258	0.0117
(II)	0.0188	0.1408	−0.0235	0.0103
Tetracene (I)	0.0191	0.1444	−0.0241	0.0106
(II)	0.0194	0.1465	−0.0246	0.0109
Triphenylene (I)	0.0203	0.1557	−0.0264	0.0122
(II)	0.0173	0.1269	−0.0210	0.0088
Chrysene (I)	0.0201	0.1540	−0.0260	0.0118
(II)	0.0190	0.1431	−0.0240	0.0107
Perylene (I)	0.0198	0.1504	−0.0254	0.0115
(II)	0.0167	0.1210	−0.0199	0.0081
Coronene (I)	0.0194	0.1470	−0.0248	0.0110
(II)	0.0181	0.1340	−0.0223	0.0093
r(HOMA)[c]	0.918	0.451	−0.919	0.902
r(NICS)[d]	−0.876	−0.516	0.876	−0.854

[a]Units are e Bohr^{-3} for ρ, e Bohr^{-5} for $\nabla^2\rho$ and λ_3.
[b](I) = outer ring; (II) = central ring.
[c]Correlation coefficient with the aromaticity index HOMA.
[d]Correlation coefficient with the aromaticity index NICS.

since these may be considered as one measure of (overall) aromaticity (27, 28). For example, benzene has the largest HOMO–LUMO gap and is predicted to be the most aromatic compound, in agreement with all indices of aromaticity. These data are some of the most comprehensive so far reported for benzenoid hydrocarbons, at a consistent ab initio level of theory.

The 10 compounds studied provide a total of 58 unique C—C bonds and 18 unique six-membered rings (tables of bond lengths and critical point analyses are available as supplementary data).[2] The molecules are illustrated, together with the atom labelling scheme, in Fig. 1.

First, we explore whether useful analogous aromaticity indices like HOMA could be constructed on the basis of charge density descriptors like $\{\rho_c, \nabla^2\rho_c, \varepsilon\}$ at the bond CPs. The rationale for this is simple. Indices such as HOMA and (to give another example) the so-called bond-alternation coefficient (BAC) (20):

$$[2] \quad \mathrm{BAC} = 1 - 3.46\left[\sum_{i=1,3}(d_i - d_{i+1})^2\right]$$

[2] These tables can be purchased from: The Depository of Unpublished Data, Document Delivery, CISTI, National Research Council Canada, Ottawa, Canada K1A 0S2.

have already proved to be very useful measures of aromatic character. Yet definitions of aromaticity are invariably linked to the cyclic delocalization of *electrons*. Although the nuclear framework responds to changes in the electron distribution, some subtle changes in ρ may hardly affect the structure. So indices based directly on the charge distribution could potentially provide more sensitive measures of aromaticity.

With this aim in mind, we consider the interrelationships between parameters from the ab initio optimizations alone, particularly the relationships between bond length and $\{\rho_c, \nabla^2\rho_c, \varepsilon\}$ at bond CPs. These are illustrated in Figs. 2–4. Clearly there are extremely strong linear relationships between all three electron density descriptors and the ring bond lengths. Even ε, which shows the most scatter, correlates with *r* at the level of 0.978. This makes it clear that the bond length can be considered as a controlling parameter (especially for ρ) in benzenoid hydrocarbons, in that it is completely representative of the charge density at the bond CPs. This simple observation has a far-reaching consequence: so far as benzenoid hydrocarbons are concerned, bond charge density descriptors provide very little extra information beyond that in the (Born–Oppenheimer) equilibrium structure. It also explains the past successes of indices based only on structure such as HOMA and BAC, in describing aromatic character.

Table 2*a* reports the ring topological descriptors for both σ and π electrons, evaluated for the σ-density framework (these

© 1997 NRC Canada

Table 2. (*b*) HF/6-31G** data[a] evaluated at the π-framework RCP.

	d^c (Å)	$\nabla^2\rho_\sigma$	$\lambda_{\sigma,3}$	ρ_π	$\nabla^2\rho_\pi$	$\lambda_{\pi,3}$
Benzene	0.7851	0.0415	0.0101	0.0045	0.0223	–0.0066
Naphthalene	0.7913	0.0391	0.0091	0.0042	0.0199	–0.0061
Anthracene (I)[b]	0.7948	0.0380	0.0083	0.0040	0.0182	–0.0058
(II)	0.7937	0.0381	0.0094	0.0041	0.0192	–0.0060
Phenanthrene (I)	0.7891	0.0399	0.0097	0.0043	0.0209	–0.0063
(II)	0.8008	0.0357	0.0082	0.0038	0.0163	–0.0055
Pyrene (I)	0.7907	0.0393	0.0094	0.0043	0.0202	–0.0062
(II)	0.8004	0.0358	0.0083	0.0039	0.0159	–0.0055
Tetracene (I)	0.7968	0.0373	0.0076	0.0039	0.0171	–0.0056
(II)	0.7955	0.0374	0.0090	0.0040	0.0184	–0.0058
Triphenylene (I)	0.7879	0.0403	0.0099	0.0044	0.0215	–0.0064
(II)	0.8114	0.0032	0.0077	0.0034	0.0133	–0.0048
Chrysene (I)	0.7897	0.0040	0.0095	0.0043	0.0206	–0.0063
(II)	0.7981	0.0365	0.0086	0.0040	0.0176	–0.0057
Perylene (I)	0.7923	0.0387	0.0092	0.0042	0.0196	–0.0061
(II)	0.8166	0.0303	0.0073	0.0032	0.0110	–0.0045
Coronene (I)	0.7953	0.0376	0.0090	0.0041	0.0182	–0.0059
(II)	0.8067	0.0336	0.0083	0.0036	0.0136	–0.0051
r(HOMA)[d]	–0.902	0.376	0.949	0.919	0.897	–0.919
r(NICS)[d]	0.870	–0.301	–0.795	–0.857	–0.860	0.860

[a,b]As in Table 2(*a*).
[c]Perpendicular distance from the molecular plane to the CP in the π electron density.
[d]Correlation coefficients, described in the legend of Table 2(*a*).

occur at the same points as the RCPs in total density ρ). Sample correlation coefficients for each parameter with the HOMA and NICS indices (taken from ref. 41 in the latter case) are also reported. Table 2*b* contains the same information, but evaluated at a set of stationary points in ρ_π. These points lie above the ring centres at perpendicular distances $d \approx 0.8$ Å (exact values for d are given in Table 2*b* for each ring), unlike the RCPs that lie in the ring planes. Lastly, Table 3 summarizes the HOMA indices derived from our HF/6-31G** optimized structures and the NICS values for the same species computed by Schleyer et al. (41).

However, we first consider the relationship between the HOMA index and RCP indicators $\{\rho_c, \nabla^2\rho_c, \varepsilon\}$, based on the *total* electron density (Figs. 5–7). Evidently, good linear correlations exist between HOMA and all three total electron density descriptors. The correlation found between the indices HOMA and NICS (−0.896, see Fig. 8) demonstrates that these total density descriptors must also correlate with the latter index.

Now we turn to how the HOMA index correlates separately with the σ and π electron density descriptors. Looking at the sample correlation coefficients reported in Tables 2*a* and *b* it is evident that, whether these properties are measured in the ring plane (σ-electron framework) or above the plane (π-electron framework), the correlations of the various descriptors with HOMA and NICS rival those found with the total density. The one exception uncorrelated with HOMA is the value of $\nabla^2\rho_\sigma$, i.e., the concentration of σ-charge density evaluated either at the (in-plane) RCP or at the stationary point in ρ_{pi}. In fact we can be more specific than this, since $\nabla^2\rho_\sigma = \lambda_{\sigma,1} + \lambda_{\sigma,2} + \lambda_{\sigma,3}$, and a good correlation exists between HOMA and $\lambda_{\sigma,3}$ (the curvature perpendicular to the ring plane); evidently it is the sum $\lambda_{\sigma,1} + \lambda_{\sigma,2}$ (the in-plane curvatures) that is independent of aromatic character. This seems to be an important point — both σ and π electrons contribute to aromatic character, in the sense that their values at stationary points in these distributions correlate with two independent aromaticity indices. But the contribution of σ electrons to aromatic character is anisotropic: only the component of σ orbitals in the direction of the π system makes a contribution. In the case of the scalar parameter ρ_σ, the correlations with HOMA and NICS are clearly significant.

The fact that both σ and π electron density measures correlate with aromaticity indices can be rationalized simply: the total charge density consists of only these two symmetry components, so changes in one of them directly affects the other (i.e., $\{\lambda_\sigma, \lambda_\pi\}$ and $\{\rho_\sigma, \rho_\pi\}$ must be mutually correlated). So all things considered, it seems not to be important whether the total, σ, or π density is examined, or which set of points is chosen: the density and (or) its various curvatures correlate very well with two *independent* measures of aromatic character.

Conclusions

Three important conclusions arise from this study. Firstly, it appears that all three of the charge density descriptors ρ_c, $\nabla^2\rho_c$, and ε at the bond critical points in benzenoid hydrocarbons are

© 1997 NRC Canada

Can. J. Chem. Downloaded from www.nrcresearchpress.com by 91.121.58.235 on 09/08/12
For personal use only.

Can. J. Chem. Downloaded from www.nrcresearchpress.com by 91.121.58.235 on 09/08/12
For personal use only.

Fig. 5. Relationship between HOMA and ρ_c at the 18 unique ring critical points (correlation coefficient $r = +0.918$).

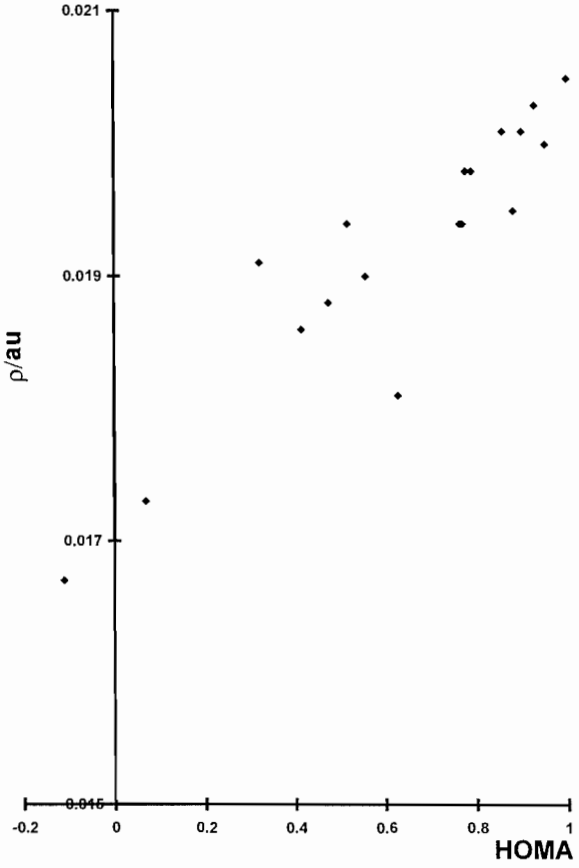


Fig. 6. Relationship between HOMA and $\nabla^2\rho_c$ at the 18 unique ring critical points (correlation coefficient $r = +0.911$).

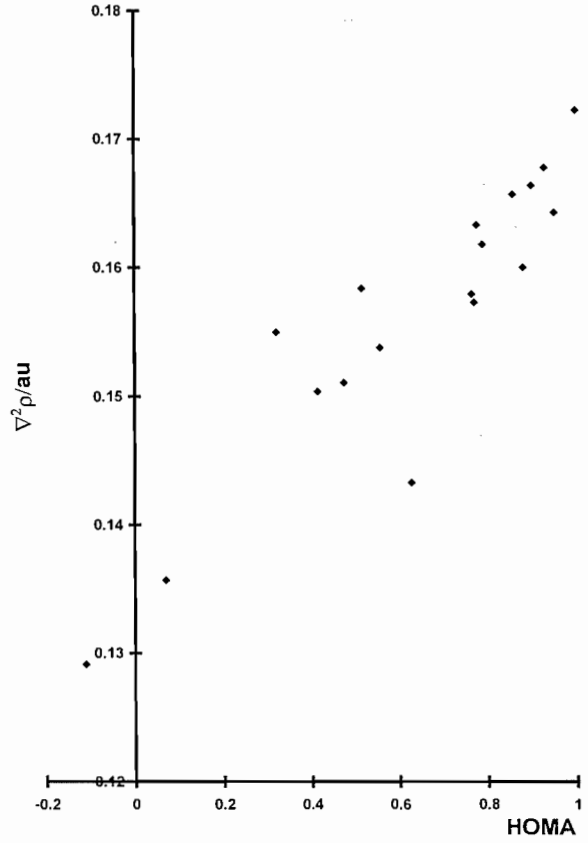


Table 3. HF/6-31G** HOMA values and associated NICS values.[a]

	HOMA	NICS
Benzene	0.999	−11.5
Naphthalene	0.777	−11.4
Anthracene (I)[b]	0.516	−9.6
(II)	0.882	−14.3
Phenanthrene (I)	0.901	−11.7
(II)	0.414	−7.4
Pyrene (I)	0.952	−14.5
(II)	0.475	−5.6
Tetracene (I)	0.321	−6.7
(II)	0.770	−13.1
Triphenylene (I)	0.929	−10.8
(II)	0.069	−3.0
Chrysene (I)	0.858	−11.5
(II)	0.557	−8.7
Perylene (I)	0.790	−9.4
(II)	−0.111	+6.8
Coronene (I)	0.765	−12.1
(II)	0.628	−5.4

[a]NICS values at the HF/6-31G*//B3LYP/6–31G* level, taken from ref. 41.

[b](I) = outer ring; (II) = central ring.

linearly related to the bond length. The best relationship occurs for the charge density ρ_c. It is therefore unlikely that indices of aromatic character could be constructed as functions of bond critical point density properties, which would give new information not derivable from the ground state (Born–Oppenheimer) equilibrium structures.

Secondly, the same charge density descriptors evaluated at the ring critical points are linearly related to the HOMA aromaticity index. We cannot explain this correlation in any trivial way. For example: on a simple level, it could be suspected that these electron density descriptors would correlate with the mean area of the ring. But the HOMA index is more sophisticated than this, since it takes account of the *difference* in size of a given ring from that of a reference structure (benzene in this case), i.e., HOMA (ring) $\approx |$area (ring) − area (benzene)$|$. So these results provide further evidence (were it needed) that aromaticity is more than just a concept, and it may be quantified by a number of schemes that should broadly agree, at least in families of structurally related systems. The HOMA index applied here is one of a family of indices based on geometrical structure that has been applied extensively in the analysis of the benzene ring in various chemical and topological environments (16). These results suggest a new set of "RCP" (Ring Critical Point) indices of aromaticity, based directly on the electron distribution. For benzenoid hydrocarbons at least, it seems that the most appropriate RCP charge density descriptor for describing aromaticity is the (negative) Hessian eigen-

© 1997 NRC Canada

Fig. 7. Relationship between HOMA and λ_3 at the 18 unique ring critical points (correlation coefficient $r = -0.936$).

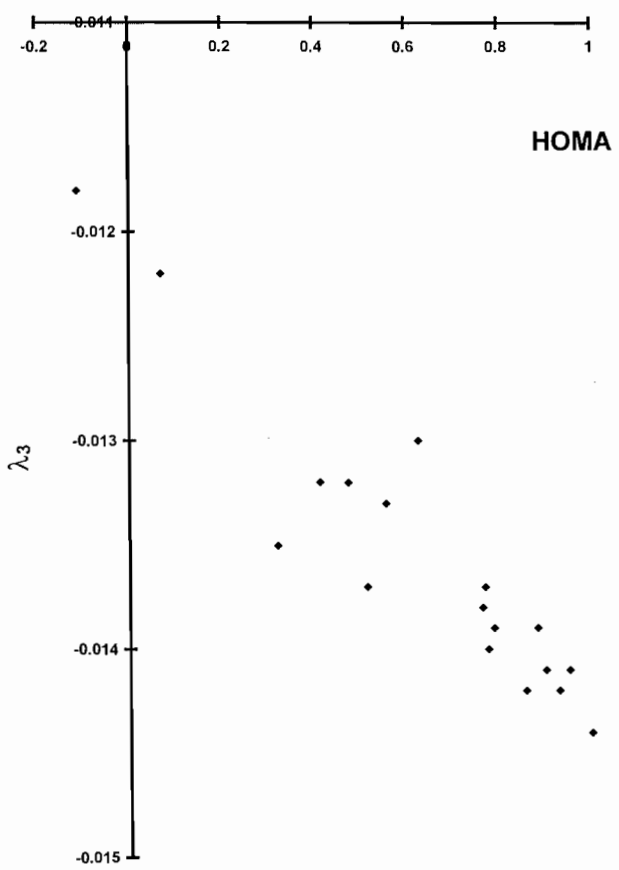
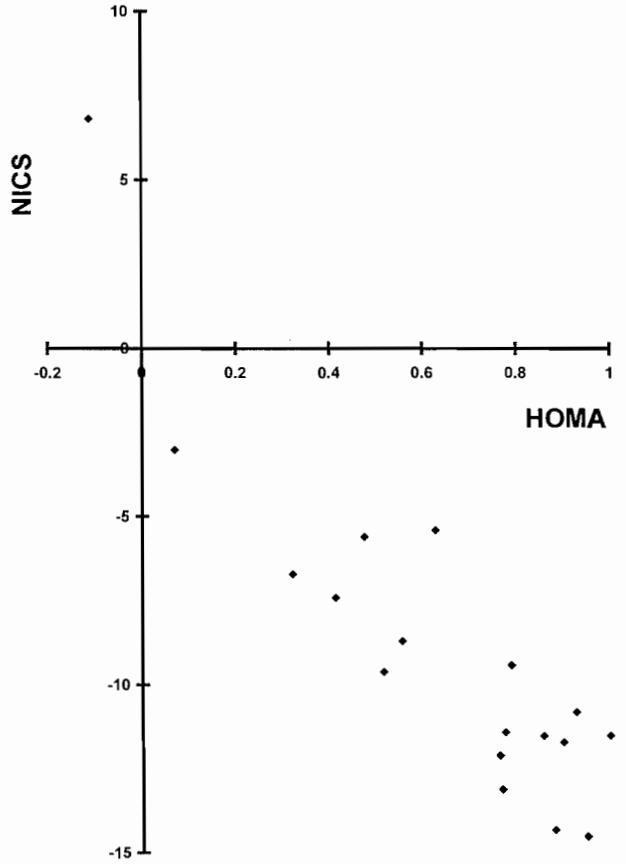


Fig. 8. Relationship between HOMA and NICS for the 18 unique rings (correlation coefficient $r = -0.896$).



value λ_3. The HF/6-31G** values calculated for the 18 unique rings in this work may be used to calibrate an RCP scale of aromaticity, provided that the same technique and basis set is always applied.

Thirdly, it appears that the σ and π density topological descriptors correlate almost equally well with two fundamentally different and independent aromaticity indices. The same descriptors based on the *total* electron density actually correlate slightly better. Choosing another set of points for evaluating the electron density descriptors, such as a set of equivalent stationary points in the π-electron framework, does not change this conclusion.

Given the intense interest in defining aromatic character, this is hardly likely to be the last word on this topic nor the last (or "best") proposed indicator of it. However, it appears to offer some new insight into the phenomenon — in particular, it is not necessary to invoke either unphysical "σ/π" separations of the charge distribution or total energy or hypothetical Kekule-type reference structures in order to arrive at useful working definitions of aromaticity. We feel there is much more to be gained from definitions of benzenoid aromaticity based on observables, e.g., bond length equalization, sizeable ring currents, and *the presence of a characteristic distribution of electrons, conveniently summarized at the ring critical point.*

Indices that can assign individual aromaticities to each ring in a large molecule are perhaps more useful than an overall index for a whole compound (such as the HOMO–LUMO gap criterion of Zhou and Parr). It seems reasonable to suppose that the RCP index (like the HOMA index) can be extended to describe the aromatic character of non-six-membered rings or rings containing heteroatoms, although this remains to be demonstrated.

Acknowledgements

We are grateful to the Royal Society and the Polish Academy of Sciences for travel grants that have supported this cooperative work. S.T.H. acknowledges the award of an Advanced Fellowship by the U.K. Engineering and Physical Sciences Research Council. Thanks to Joel P. Foreman and David E. Hibbs for their help in preparing the figures.

References

1. A. Kekule. Bull. Soc. Chim. Fr. **3**, 98 (1865).
2. E. Erlenmayer. Ann. Chem. Pharm. **137**, 327 (1866).
3. (*a*) E. Hückel. Z. Phys. **70**, 204 (1931); (*b*) Grundzüge der Theorie Ungesättiger und Aromatischer Verbindungen Chemie. Berlin. 1938.
4. L.M. Jackman and J.A. Elvidge. J. Chem. Soc. 859 (1961).
5. F. Sondheimer. Pure Appl. Chem., **7**, 363 (1964).
6. G. Wheland. Resonance in organic chemistry. Wiley, New York. 1955.
7. A. Streitwieser, Jr. Molecular orbital theory for organic chemists. Wiley, New York. 1961.

© 1997 NRC Canada

Can. J. Chem. Downloaded from www.nrcresearchpress.com by 91.121.58.235 on 09/08/12
For personal use only.

8. M.J.S. Dewar and C. de Llano. J. Am. Chem. Soc. **91**, 789 (1969).
9. B.A. Hess, Jr. and L.J. Schaad. J. Am. Chem. Soc. **93**, 305 (1971).
10. B.A. Hess, Jr., L.J. Schaad, and C.W. Holyoke. Tetrahedron, **28**, 3657 (1972).
11. M. Randić. Chem. Phys. Lett. **38**, 68 (1976).
12. I. Gutman and S.J. Cyvin. Introduction to the theory of benzenoid hydrocarbons. Springer Verlag, Berlin. 1989.
13. D.J. Klein. Pure Appl. Chem. **61**, 2107 (1989).
14. A. Julg and P.H. Francois. Theor. Chim. Acta, **7**, 249 (1967).
15. J. Kruszewski and T.M. Krygowski. Tetrahedron Lett. 3842 (1972).
16. T.M. Krygowski. J. Chem. Inf. Comput. Sci. **33**, 70 (1993).
17. C.W. Bird. Tetrahedron, **41**, 1409 (1985).
18. C.W. Bird. Tetrahedron, **42**, 89 (1986).
19. G. Binsch and I. Tamir. J. Am. Chem. Soc. **91**, 450 (1969).
20. A. Ciesielski, T.M. Krygowski, C.W. Bird, and A. Kotschy. J. Chem. Inf. Comput. Sci. **35**, 203 (1995).
21. A.F. Pohzarsky. Chem. Heterocycl. Comp. **21**, 717 (1985).
22. M.H. Palmer, R.H. Findley, and W.J. Moyes. J. Chem. Soc. Perkin Trans. 2, 841 (1975).
23. P. von R. Schleyer, P.K. Freeman, H. Jiao, and B. Goldfuss. Angew. Chem. Int. Ed. Engl. **34**, 337 (1995).
24. R.F.W. Bader and T.A. Keith. J. Chem. Phys. **99**, 3683 (1993).
25. C.P. Slichter. Principles of magnetic resonance. 2nd ed. Springer Verlag, Berlin. 1978. pp. 71–76.
26. K. Jug and A. Koester. J. Phys. Org. Chem. **4**, 163 (1991).
27. Z.X. Zhou, R.G. Parr, and J.F. Garst. Tetrahedron Lett. **29**, 4843 (1988).
28. Z.X. Zhou and R.G. Parr. J. Am. Chem. Soc. **111**, 7371 (1989).
29. A.R. Katritzky, P. Barczynski, G. Musumurra, D. Pisano, and M. Szafran. J. Am. Chem. Soc. **111**, 7 (1989).
30. R.F.W. Bader. Atoms in molecules: a quantum theory. Oxford University Press, Oxford. 1990.
31. R.J. Boyd and K.E. Edgecombe. J. Comput. Chem. **8**, 489 (1987).
32. R.J. Boyd and K.E. Edgecombe. J. Am. Chem. Soc. **110**, 4182 (1988).
33. V.I. Minkin, M.N. Glukhovtsev, and B.Y. Simkin. Aromaticity and antiaromaticity, electronic and structural aspects. John Wiley & Sons, New York. 1994. pp. 84–87.
34. S.S. Shaik, P.C. Hiberty, J.M. Lefour, and G. Ohanessian. J. Am. Chem. Soc. **109**, 363 (1987).
35. K. Jug and A. Koester. J. Am. Chem. Soc. **112**, 6772 (1990).
36. E.D. Glendening, R. Faust, A. Streitwieser, K.P.C. Vollhardt, and F. Weinhold. J. Am. Chem. Soc. **115**, 10952 (1993).
37. I. Gutman, S. Markovic, and G.G. Hall. Chem. Phys. Lett. **234**, 21 (1995).
38. M.W. Schmidt, K.K. Baldridge, J.A. Boatz, S.T. Elbert, M.S. Gordon, J.H. Jensen, S. Koseki, N. Matsunaga, K.A. Nguyen, S.J. Su, T.L. Windus, M. Dupuis, and J.A. Montgomery. J. Comput. Chem. **14**, 1347 (1993).
39. F.W. Biegler–Konig, R.F.W. Bader, and T.H. Tang. J. Comput. Chem. **13**, 317 (1992).
40. P.C. Hariharan and J.A. Pople. Theor. Chim. Acta, **28**, 213 (1973).
41. P. von R. Schleyer, C. Maerker, A. Dransfeld, H. Jaio, and N.J.R.V. Hommes. J. Am. Chem. Soc. **118**, 6317 (1996).

Can. J. Chem. Downloaded from www.nrcresearchpress.com by 91.121.58.235 on 09/08/12
For personal use only.

© 1997 NRC Canada

Electrochemical reduction of the unsaturated cyclic trinuclear $Pd_3(dppm)_3CO^{2+}$ cluster (dppm = $((C_6H_5)_2P)_2CH_2$)

Isabelle Gauthron, Yves Mugnier, Karine Hierso, and Pierre D. Harvey

Abstract: $Pd_3(dppm)_3CO^{2+}$ exhibits a two-electron reduction process at ~−0.5 V vs. SCE in 0.2 M Bu_4NPF_6 solutions of organic solvents such as dry acetonitrile, *N,N*-dimethylformamide (DMF), tetrahydrofuran (THF), and dichloromethane to reversibly produce the zero valent $Pd_3(dppm)_3CO$, which exhibits a ν(CO) band in the 1761–1766 cm^{-1} range in the IR spectra. The mechanistic aspects of this multistep two-electron process are discussed experimentally on the basis of r.d.e. (rotating disk electrode) voltammetry, cyclic voltammetry, and electrolysis results. Geometry optimizations using DFT (Density Functional Theory) predict that the Pd—Pd and C═O bond lengths are 3.008 and 1.182 Å, respectively, which compare favorably with the experimental data for other zero valent polynuclear complexes.

Key words: palladium, cluster, reduction, electrochemistry, density functional theory.

Résumé : En solution dans des solvants organiques, tels que l'acétonitrile, le *N,N*-diméthylformamide (DMF), le tétrahydrofurane et le dichlorométhane secs, contenant 0,2 M de Bu_4NPF_6, le $Pd_3(dppm)_3CO^{2+}$ donne lieu à un processus de réduction à deux électrons à ~0,5 V vs. SCE conduisant à la formation réversible de $Pd_3(dppm)_3CO$ zérovalent dont le spectre IR présente une bande ν(CO) autour de 1761 à 1766 cm^{-1}. On discute des aspects mécanistiques de ce processus à deux électrons en plusieurs étapes en se basant sur des données expérimentales de voltampérométrie à électrode à disque tournant, de voltampérométrie cyclique et d'électrolyse. Des optimisations sur la base de la théorie de densité fonctionnelle permettent de prédire des longueurs de 3,008 et 1,182 Å respectivement pour les liaisons Pd—Pd et C═O; ces prédictions se comparent favorablement avec les données expérimentales obtenues avec d'autres complexes zérovalents polynucléaires.

Mots clés : palladium, agrégats, réduction, électrochimie, théorie de la densité fonctionnelle.

[Traduit par la rédaction]

Introduction

The $Pd_3(dppm)_3CO^{2+}$ cluster (dppm = $((C_6H_5)_2P)_2CH_2$) was reported by Puddephatt and co-workers over 10 years ago (1, 2). The preparation consists of a reaction between $Pd(O_2CF_3)_2$, dppm, and CO in an acetone–CF_3CO_2H–H_2O mixture. Recently, the formation mechanism of this cluster has been studied in detail (1, 3, 4). Although this cluster and the $Pt_3(dppm)_3CO^{2+}$ analogue exhibit a particularly rich addition and oxidative addition reactivity towards small molecules (4), the chemical reduction has never been successful (2). We now wish to report the electrochemical behaviour of $Pd_3(dppm)_3CO^{2+}$ in aprotic media. It will be shown that for the first time the zero valent neutral $Pd_3(dppm)_3CO$ cluster can be prepared under electrolysis conditions. Only a few electrochemical studies of mono- and binuclear palladium complexes containing chelating diphosphine ligands have been reported in the literature (5–7). Density functional theory has been used to predict the structures of one intermediate and the final product.

Received January 24, 1997.

I. Gauthron and Y. Mugnier.[1] Laboratoire de synthèse et d'électrosynthèse organométalliques associé au Centre national de la recherche scientifique (UMR 5632), Faculté des sciences, Université de Bourgogne, 6 Boulevard Gabriel, 21000 Dijon, France.

K. Hierso and P.D. Harvey.[1] Département de chimie, Université de Sherbrooke, Sherbrooke, QC J1K 2R1, Canada.

[1] Authors to whom correspondence may be addressed. Telephone: (819) 821-7092. Fax: (819) 821-8017. E-mail: pharvey@structure.chimie.usherb.ca

Experimental

Materials

The $Pd_3(dppm)_3CO^{2+}$ cluster as $CF_3CO_2^-$ (**1**) and PF_6^- (**1′**) salts has been prepared according to literature procedures (1, 2).

IR measurements

All IR measurements were performed on a Nicolet 205 spectrophotometer. The electrolysis solutions were transferred into an airtight IR cell via canular techniques. No attempt to isolate the palladium species was made.

Electrochemistry

All manipulations were performed by using standard Schlenk techniques in an atmosphere of dry oxygen, free nitrogen, or argon. Tetrahydrofuran was distilled under argon from sodium and benzophenone. CH_2Cl_2 and acetonitrile (ACN) were purified by simply passing the solvent through a column packed with alumina previously dried at 120°C; it was deoxygenated by argon bubbling immediately before use. These salts were dried and degassed before use. In cyclic voltammetry experi-

© 1997 NRC Canada

Can. J. Chem. Downloaded from www.nrcresearchpress.com by 91.121.58.235 on 09/08/12
For personal use only.

Can. J. Chem. Downloaded from www.nrcresearchpress.com by 91.121.58.235 on 09/08/12
For personal use only.

ments the concentration of $Pd_3(dppm)_3CO^{2+}$ was nearly 10^{-3} M. Voltammetry analysis was carried out in a standard three-electrode cell with a Tacussel UAP4 unit cell. The reference electrode was a saturated calomel electrode separated from the solution by a sintered glass disk. The auxiliary electrode was a platinum wire. For all voltammetric measurements the working electrode was a vitreous carbon electrode. The controlled potential electrolysis was performed with an Amel 552 potentiostat coupled to an Amel 721 electronic integrator. High-scale electrolysis was performed in a cell with three compartments being separated with fritted glasses of medium porosity. A carbon gauze was used as the cathode, a platinum plate was used as the anode, and a saturated calomel electrode was used as the reference electrode. The electrolyte was either tetrahydrofuran or methylene chloride 0.2 M in tetrabutylammonium hexafluorophosphate. For thin-layer cyclic voltammetry, the vitreous carbon electrode was lowered until it came into contact with the flat floor of the electrolytic cell so that only a thin layer of solution existed between them.

Computational details

The reported density functional calculations were all carried out utilizing the program called Amsterdam Density Functional, which was developed by Baerends et al. (8, 9) and vectorized by Raveneck (10). The numerical integration procedure applied for the calculations was developed by te Velde and co-workers (11). The geometry optimization procedure was based on the method developed by Versluis and Ziegler (12). The electronic configurations of the molecular systems were described by an uncontracted double-ζ basis set (13) on palladium for 4*s*, 4*p*, and 5*s*, and triple-ζ for 5*d*. Double-ζ STO basis sets (14) were used for phosphorus (3*s*, 3*p*), oxygen (2*s*, 2*p*), carbon (2*s*, 2*p*), nitrogen (2*s*, 2*p*), and hydrogen (1*s*), augmented with a single 4*d* polarization function for P, a single 3*d* function for O and C, and a 2*p* function for H. No polarization function was used for palladium. The $1s^2\ 2s^2\ 2p^6\ 3s^2\ 3d^{10}$ configuration on palladium, the $1s^2\ 2s^2$ configuration on phosphorus, and the $1s^2$ configurations on oxygen and carbon were treated by the frozen-core approximation (9). A set of auxiliary (15) *s*, *p*, *d*, *f*, and *g* STO functions, centered on all nuclei, was used in order to fit the molecular density and present Coulomb and exchange potentials accurately in each SCF cycle. Energy differences were calculated by including the local exchange–correlation potential by Vosko et al. (16). No nonlocal exchange and correlation corrections were made for the geometry optimizations.

Results and discussion

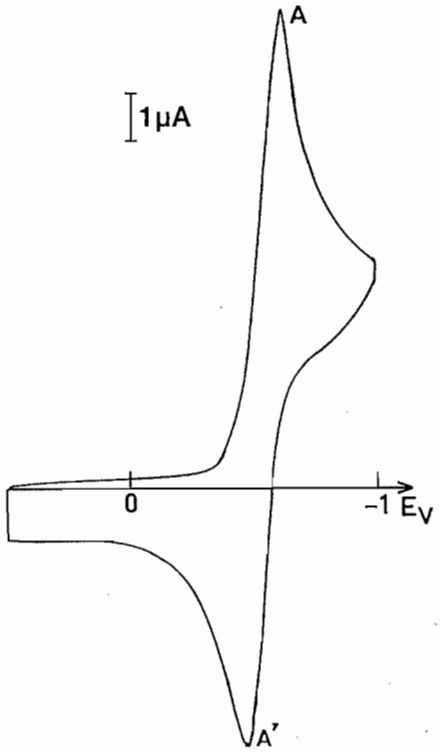
1. Electrochemistry

We have studied the electrochemical reduction of dicationic cluster $Pd_3(dppm)_3CO^{2+}$ in such different solvents as THF, ACN, DMF, and CH_2Cl_2.

1. (a) Electrochemical behaviour of $Pd_3(dppm)_3CO^{2+}$ in THF

An electrochemical process *A*/*A*′ (*A* = −0.62 V, *A*′ = −0.46 V vs. SCE) is observed in the cyclic voltammogram using THF containing 0.2 M Bu_4NPF_6 for $[Pd_3(dppm)_3CO](CF_3CO_2)_2$ **1** (Fig. 1). Upon bulk electrolysis performed at −0.80 V vs. SCE, coulometric measurements indicate that two electrons (n_{exp} = 2.01 F mol^{-1}) are consumed until the current drops to zero. The resulting solution exhibits the same *A*/*A*′ peaks system. These results are consistent with a mechanism described by eq. [1]:

Fig. 1. Cyclic voltammogram of $[Pd_3(dppm)_3CO](CF_3CO_2)_2$ **1** in THF containing 0.2 M Bu_4NPF_6: starting potential = +0.5 V, sweep rate = 0.02 V s^{-1}.



[1] $Pd_3(dppm)_3CO^{2+} + 2e^- \leftrightarrows Pd_3(dppm)_3CO$
1 **2**

The oxidation–reduction electrolysis is quantitative without any evidence of loss of the starting $Pd_3(dppm)_3CO^{2+}$ material, since the two-electron oxidation of **2** gives quantitatively the starting complex. According to the morphology of the cyclic voltammograms exhibiting only a single *A*/*A*′ peaks system, we suggest that the intermediate monocationic $Pd_3(dppm)_3CO^+$ must be reduced at a lower negative potential than $Pd_3(dppm)_3CO^{2+}$ itself. Recently Pierce and Geiger showed that increases in cyclic voltammetry sweep rates change the redox couple for a dicationic ruthenium complex (17). In this case, a single wave associated with a two-electron process could be changed into two waves each associated with a one-electron transfer simply by changing the sweep rates (17). For $Pd_3(dppm)_3CO^{2+}$, no change is observed with sweep rates of 0.01 V s^{-1} to 0.5 V s^{-1}.

The cyclic voltammogram of $[Pd_3(dppm)_3CO](PF_6)_2$ **1′** in the same experimental conditions (THF – 0.2 M Bu_4NPF_6) exhibits two systems A_1/A'_1 and A_2/A'_2 (A_1 = −0.38 V, A'_1 = −0.20 V, A_2 = −0.65 V, A'_2 = −0.46 V vs. SCE at 0.2 V s^{-1}) (Fig. 2). After a two-electron reduction (n_{exp} = 1.88 F mol^{-1}), the rotating disk electrode (r.d.e.) voltammogram shows two waves A'_1 and A'_2 that correspond to the oxidation of $Pd_3(dppm)_3CO$. The mechanism is described by reactions [2] and [3]:

© 1997 NRC Canada

Can. J. Chem. Downloaded from www.nrcresearchpress.com by 91.121.58.235 on 09/08/12
For personal use only.

Fig. 2. Cyclic voltammogram of $[Pd_3(dppm)_3CO](PF_6)_2$ **1** in THF containing 0.2 M Bu_4NPF_6: starting potential = 9 V, sweep rate = 0.2 V s^{-1}.

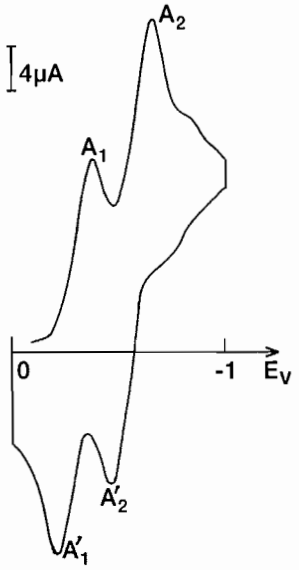
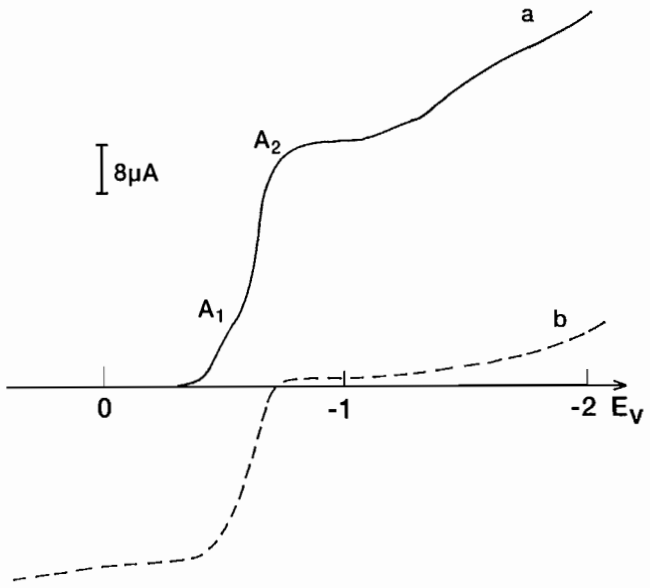


Fig. 3. The r.d.e. voltammograms of $[Pd_3(dppm)_3CO](CF_3CO_2)_2$ **1** in acetonitrile containing 0.2 M Bu_4NPF_6: (*a*) before electrolysis; (*b*) after a two-electron reduction at −1.2 V vs. SCE.



[2] $Pd_3(dppm)_3CO^{2+} + e^- \leftrightarrows Pd_3(dppm)_3CO^+$ (system A_1/A'_1)

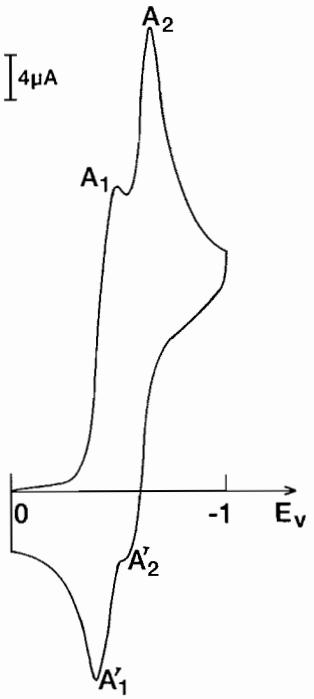
[3] $Pd_3(dppm)_3CO^+ + e^- \leftrightarrows Pd_3(dppm)_3CO$ (system A_2/A'_2)

Under these conditions, even by using Schlenk techniques, this neutral cluster proved to be too unstable for IR spectroscopy studies (a ν(CO) band at 1686 cm^{-1} appears that corresponds to the decomposition product).

1.(b) Electrochemical behaviour of $Pd_3(dppm)_3CO^{2+}$ in ACN

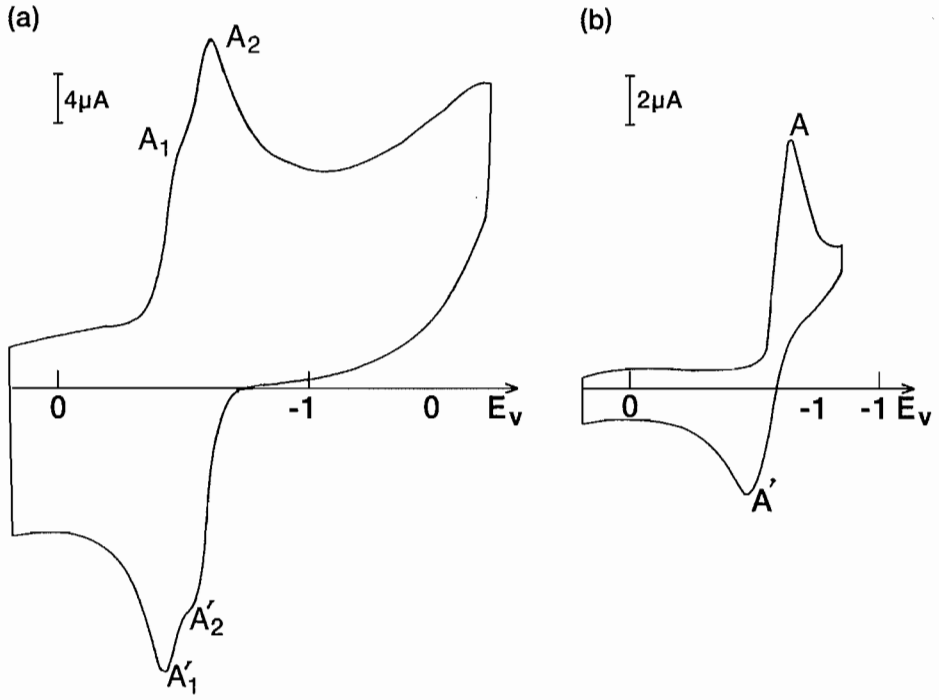
The r.d.e. voltammogram of $[Pd_3(dppm)_3CO](CF_3CO_2)_2$ **1** in 0.2 M Bu_4NPF_6 – acetonitrile solution exhibits two reduction electrochemical processes at −0.50 and −0.65 V vs. SCE and are marked by A_1 and A_2, respectively (Fig. 3*a*). By cyclic voltammetry using a vitreous carbon disk electrode, the corresponding peaks A_1 and A_2 are indeed observed. The anodic sweep at a starting potential of −1.50 V vs. SCE exhibits two return peaks (−0.40 V A'_1 and −0.55 V A'_2) (Fig. 4). The electrolysis at −1.2 V on a carbon gauze electrode at room temperature leads to a complete drop of current after a two-electron consumption per mole of cluster (n_{exp} = 2.05 F mol^{-1}). During this electrolysis, the red solution turns brown, and the r.d.e. voltammogram of the resulting solution exhibits two well-defined oxidation waves (A'_1, A'_2) (Fig. 3*b*). Similarly the cyclic voltammogram exhibits the same A_1/A'_1 and A_2/A'_2 peaks systems. These results indicate that the overall electrochemical processes follow reaction [1]. The monitoring of this electrolysis by IR spectroscopy indicates a large decrease in the ν(CO) band intensity located at 1835 cm^{-1}. In this experiment no new IR band is observed and the strong 1695 cm^{-1} ν(CO) band (CF_3CO^{2-}) remains unchanged. No evidence for free CO is found. We believe that ν(CO) of the new species is hidden under the strong 1695 cm^{-1} band (see below). The reduced species appears to be partially soluble in acetonitrile and, even stored under Ar(g), the product exhibits an evolution during which a decrease in intensity of the A'_1 and A'_2 oxidation peaks system is observed. At room temperature, the species produced exhibits limited stability, and no NMR spectroscopic study has been possible. To determine the ν(CO) band in IR spectroscopy, we have examined the electrochemical behaviour of $[Pd_3(dppm)_3CO](PF_6)_2$ **1′**. After a two-electron reduction (n_{exp} = 2.05 F mol^{-1}), the IR spectroscopy of the electrolyzed solution exhibits a ν(CO) band at

Fig. 4. Cyclic voltammogram of $[Pd_3(dppm)_3CO](CF_3CO_2)_2$ **1** in acetonitrile containing 0.2 M Bu_4NPF_6: starting potential = +0.5 V, sweep rate = 0.2 V s^{-1}.



© 1997 NRC Canada

Fig. 5. Cyclic voltammograms of $[Pd_3(dppm)_3CO](CF_3CO_2)_2$ **1** in (*a*) dimethylformamide containing 0.2 M Bu_4NPF_6: starting potential = +0.2 V, sweep rate = 0.2 V s^{-1} , and (*b*) dimethylformamide containing 0.2 M LiCl: starting potential = +0.2 V, sweep rate = 0.02 V s^{-1}.



1761 cm^{-1} that is readily attributed to the formation of $Pd_3(dppm)_3CO$.

[4] $Pd_3(dppm)_3CO^{2+} + 2e^- \leftrightarrows Pd_3(dppm)_3CO$
(ν_{CO} = 1835 cm^{-1}) (ν_{CO} = 1761 cm^{-1})

1.(c) Electrochemical behaviour of $Pd_3(dppm)_3CO^{2+}$ in CH_2Cl_2

Using CH_2Cl_2 as a solvent, the $Pd_3(dppm)_3CO^{2+}$ electrochemical behaviour is similar to that described for acetonitrile where two systems A_1/A'_1 and A_2/A'_2 are observed by cyclic voltammetry (sweep rate (v) range = 0.01–0.5 V s^{-1}). The constant ratio $i_p/v^{1/2}$ (i_p = peak current) indicates that the electrochemical processes are diffusion controlled. A reduction electrolysis performed at −0.9 V vs. SCE consumes two electrons (n_{exp} = 1.98 F mol^{-1}), and the anodic sweep in the cyclic voltammograms exhibits the typical A'_1 and A_2' oxidation peaks associated with the formation of the neutral $Pd_3(dppm)_3CO$. The mechanism is described by reactions [2] and [3].

The monitoring of the bulk electrolysis of $[Pd_3(dppm)_3CO](PF_6)_2$ **1′** (in CH_2Cl_2) by IR spectroscopy indicates that the 1835 cm^{-1} band disappears while a band located at 1766 cm^{-1} appears that is also assigned to the formation of $Pd_3(dppm)_3CO$.

[5] $Pd_3(dppm)_3CO^{2+} + 2e^- \leftrightarrows Pd_3(dppm)_3CO$
(ν_{CO} = 1835 cm^{-1}) (ν_{CO} = 1766 cm^{-1})

The comparison between 1835 and 1766 cm^{-1} (dication vs. neutral) indicates a decrease in C═O bond strength and, therefore, a C═O lengthening (assuming that both species are triply bridged μ^3-CO). The diatomic approximation (ν = $(2\pi c)^{-1}(F/\mu)^{1/2}$; c = speed of light, F = force constant, μ = reduced mass) predicts that F(CO) are 13.63 and 12.62 m dyn $Å^{-1}$ for the dicationic and neutral clusters, respectively. Morrison and Turner have recently reported an empirical equation relating the force constant of a complexed CO group (F(CO)) and the CO distance (r(CO)) (18):

[6] $r(CO) = 1.674 - 0.184 \ln F(CO)$

that allows the estimation of r(CO) calculated with a standard deviation of ±0.005 Å. For the dicationic and neutral species, eq. [6] predicts that the calculated r(CO) values are 1.193 and 1.208 Å, respectively. r(CO) evaluated crystallographically is ~1.165 Å for $Pd_3(dppm)_3CO^{2+}$ (19). Taking into account that the Pd_3 center is ignored in the F(CO) estimation, this comparison is reasonable. The calculated bond length increase is 0.015 Å and is associated with an increase in back donation going from Pd_3^{2+} to Pd_3^0. Interestingly the average r(CO) value for the zero valent related $Pd_6(\mu^2\text{-CO})_6(dppm)_3$ cluster is ~1.20 Å (20) according to X-ray results. The favorable comparison between this 1.208 Å for the neutral $Pd_3(dppm)_3CO$ complex further supports the IR assignment.

1.(d) Electrochemical behaviour of $Pd_3(dppm)_3CO^{2+}$ in DMF

Using dimethylformamide as a solvent, the electrochemical behaviour depends upon the nature of the electrolytic salts. While the A_1/A_1' and A_2/A_2' peaks systems are present with Bu_4NPF_6, only an A/A' peaks system is observed with LiCl (also with a 0.2 M concentration; figs. 5*a* and *b*, respectively). In the presence of 0.2 M LiCl, $Pd_3(dppm)_3CO^{2+}$ is reduced at higher negative potential than in DMF–LiCl-free solutions.

Can. J. Chem. Downloaded from www.nrcresearchpress.com by 91.121.58.235 on 09/08/12
For personal use only.

© 1997 NRC Canada

Can. J. Chem. Downloaded from www.nrcresearchpress.com by 91.121.58.235 on 09/08/12
For personal use only.

Table 1. Peak potentials of **1** and **1′** at 0.05 V s^{-1}.

Solvent	Compound	Supporting electrolyte	A_1	A'_1	E^0_1	A_2	A'_2	E^0_2
ACN	**1**	Bu_4NPF_6	−0.50	−0.40	−0.45	−0.65	−0.55	−0.60
DMF	**1**	Bu_4NPF_6	−0.50	−0.42	−0.46	−0.61	−0.53	−0.57
CH_2Cl_2	**1**	Bu_4NPF_6	−0.38	−0.28	−0.33	−0.54	−0.46	−0.50
THF[b]	**1**	Bu_4NPF_6				−0.62	−0.46	−0.54
DMF[a,b]	**1**	LiCl				−0.69	−0.48	−0.58
DMF:1/ACN:4[b]	**1**	LiCl				−0.60	−0.53	−0.56
DMF:1/H_2O:1[b]	**1**	LiCl	−0.40	−0.32	−0.36			
ACN	**1′**	Bu_4NPF_6	−0.43	−0.37	−0.40	−0.64	−0.58	−0.61
CH_2Cl_2	**1′**	Bu_4NPF_6	−0.41	−0.32	−0.37	−0.75	−0.65	−0.70
THF[a]	**1′**	Bu_4NPF_6	−0.38	−0.20	−0.29	−0.65	−0.46	−0.55

[a]At 0.2 V s^{-1}.
[b]These are *A*/*A′* systems.

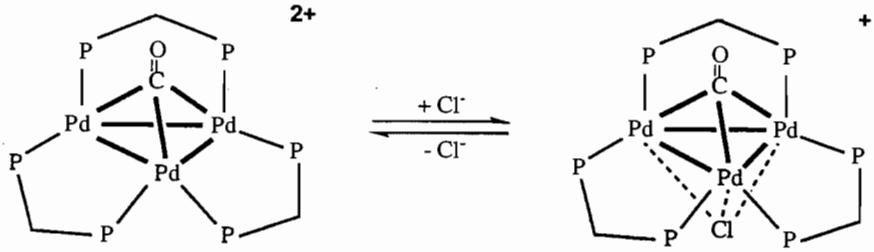
Table 2. Selected bond distances for the geometry optimization calculations.

	$Pd_3(dppm)_3CO^{2+}$ [a] X-ray	$Pd_3(PH_3)_6CO^{2+}$ [a]	$Pd_3(PH_3)_6CO^{+}$	$Pd_3(PH_3)_6CO$
r(Pd—Pd)	2.604(30)	2.592	2.734	3.008
r(Pd—P)	2.318(30)	2.317	2.342	2.342
r(Pd—C)	2.105(17)	2.080	2.067	2.062
r(C—O)	1.165(5)	1.170	1.170	1.182

[a]From ref. 25. The values in parentheses are the difference between the average value tabulated here and the maximum and minimum values experimentally observed.

This shift is due to the formation of the monocationic species $Pd_3(dppm)_3(CO)(Cl)^+$ as demonstrated by Puddephatt and co-workers (21):

Scheme 1.



The electrolysis performed at −1.1 V vs. SCE using DMF–Bu_4NPF_6 also consumes two electrons (n_{exp} = 2.04 F mol^{-1}), where a quasi-complete disappearance of the 1833 cm^{-1} IR peak band is observed as expected. Upon a two-electron reoxidation (n_{exp} = 1.7 F mol^{-1}) at 0 V vs. SCE, the dicationic cluster is regenerated quantitatively.

1.(e) Concluding remarks

In all cases, the two-electron reduction of $Pd_3(dppm)_3CO^{2+}$ gives the neutral cluster $Pd_3(dppm)_3CO$ characterized by IR spectroscopy (ν(CO) = 1761 cm^{-1} in ACN, 1766 cm^{-1} in CH_2Cl_2) and by its electrochemical behaviour. In some cases, a single two-electron reversible system *A*/*A′* is observed, while two one-electron systems A_1/A'_1 and A_2/A'_2 appear in other cases (see Table 1 for details). Further $Pd_3(dppm)_3CO^{2+}$ is more easily reduced in CH_2Cl_2 than in DMF. We propose that host–guest interaction (22, 23) be at the origin of this phenomenon (host = cluster; guest = solvent molecule). Indeed, one of us recently demonstrated evidence for the host–guest chemistry in the $Pd_3(dppm)_3CO^{2+}$ ground (18) and lowest energy triplet excited states ($^3A_2$) (24) with various neutral substrates. Since we could not isolate the neutral product in the pure state for structural characterization, the geometry was optimized by the theoretical calculations below.

2. Theoretical calculations

Based upon recent EHMO computations that indicate that the

© 1997 NRC Canada

Can. J. Chem. Downloaded from www.nrcresearchpress.com by 91.121.58.235 on 09/08/12
For personal use only.

LUMO in $Pd_3(PH_3)_6CO^{2+}$ (model compound for $Pd_3(dppm)_3CO^{2+}$) (25) is formally Pd···Pd antibonding, Pd—Pd bond cleavages are anticipated upon the two-electron reduction of $Pd_3(dppm)_3CO^{2+}$. This proposal is supported by the zero valent $Pd_2(dppm)_3$ X-ray structure where no formal Pd—Pd bond is observed ($r(Pd_2)$ = 2.956 Å) (26). Furthermore, the two-electron reduction of $Pd_3(dppm)_3CO^{2+}$ in the presence of an excess of dppm does not lead to the formation of other zero valent Pd complexes.

The structural features of the model compounds $Pd_3(PH_3)_6CO^n$ where $n = 0, +1, +2$ are addressed theoretically using DFT via geometry optimizations. In a recent study, the geometry of the model compound $Pd_3(PH_3)_6CO^{2+}$ has already been optimized by one of us (27) and compared to that of $Pd_3(dppm)_3CO^{2+}$. These data are reported in Table 2. In the $Pd_3(PH_3)_6CO^n$ cases ($n = 0, +1, +2$), the computations were performed using both the C_{3v} symmetry and the "no symmetry" restrictions. Both sets of calculations always gave the same results. The comparison between the experimental data reported for $Pd_3(dppm)_3CO^{2+}$ (X-ray crystallography) and the computed values for $Pd_3(PH_3)_6CO^{2+}$ is excellent with much less than 1% difference.

Upon a one-electron reduction of the dicationic cluster, the computed Pd—Pd (+0.24 Å) and Pd—P (+0.025 Å) bond lengths exhibit the largest increases, which are associated with the antibonding nature of the LUMO and also with the weak anti-bonding behaviour of the Pd—P bonds (25). An $r(Pd_2)$ value of 2.73 Å is one of the longest Pd—Pd bonds (here calculated) for polynuclear complexes (28) and is consistent with a lower bond order (BO) description: $0 < BO < 1$. Upon a second one-electron reduction the Pd—Pd bond length increases dramatically up to ~3 Å, which indicates complete homolytic Pd—Pd bond cleavages. The $r(Pd_2)$ value (3.088 Å) is close to that of $Pd_2(dppm)_3$ ($r(Pd_2)$ = 2.956 Å) (26). Further, the computed C═O bond length has indeed increased as experimentally observed (up to 1.182 Å from 1.170 Å in the dication). The back-donation effect responsible for this bond lengthening is also observed from the slight decrease in computed Pd—C bond lengths (2.080 → 2.062 Å, for $n = +2, +1$, and 0, respectively). The computed C═O bond length change (+0.012 Å) is practically the same as that estimated from IR findings described above (+0.015 Å). The computed r(CO) value for the neutral species (1.182 Å) also compares favorably to that of the zero valent $Pd_6(\mu^2\text{-}CO)_6(dppm)_3$ cluster (1.20 Å) (20).

Final remarks

The two-electron reduction of $Pd_3(dppm)_3CO^{2+}$ leads to $Pd_3(dppm)_3CO$, which has been characterized by IR spectroscopy. This neutral cluster is relatively stable within hours under electrolysis condition but not sufficiently for ^{31}P NMR characterization.

Acknowledgments

This research was supported by the Natural Sciences and Engineering Research Council of Canada (NSERC), le Fonds pour la formation de chercheurs et l'aide à la recherche (FCAR, Québec), and Électricité de France (E.D.F. – Club d'électrochimie organique).

References

1. B.R. Lloyd and R.J. Puddephatt. Inorg. Chim. Acta, **90**, L77 (1984).
2. L. Manojlovic–Muir, K.W. Muir, B.R. Lloyd, and R.J. Puddephatt. J. Chem. Soc. Chem. Commun. 1336 (1983).
3. B.R. Lloyd, L. Manojlovic–Muir, K.W. Muir, and R.J. Puddephatt. Organometallics, **12**, 1231 (1993).
4. R.J. Puddephatt, L. Manojlovic–Muir, and K.W. Muir. Polyhedron, **9**, 2767 (1990).
5. M. Matelli, G. Pilloni, G. Zotti, and S. Dalio. Inorg. Chim. Acta, **11**, 155 (1974).
6. G. Nemra, P. Lemoine, P. Braunstein, C. de Meric de Bellefon, and M. Ries. J. Organomet. Chem. **304**, 245 (1986).
7. T. Tanase, K. Kawahara, H. Ukaji, K. Kobayaski, H. Yamazaki, and Y. Yamamoto. Inorg. Chem. **32**, 3682 (1993), and refs. therein.
8. E.J. Baerends, D.E. Ellis, and P. Ros. Chem. Phys. **2**, 41 (1973).
9. R.J. Baerends. Ph.D. thesis, Vrije Universiteit, Amsterdam. 1975.
10. W. Raveneck. Algorithms and applications on vector and parallel computers. *Edited by* H.J.J. Rigie, Th. J. Dekkor, and H.A. van de Vorst. Elsevier, Amsterdam. 1987.
11. P.M. Boerrigter, G. te Velde, and E.J. Baerends. Int. J. Quantum Chem. **33**, 87 (1988).
12. L. Versluis and T. Ziegler. J. Chem. Phys. **88**, 322 (1988).
13. (*a*) G.J. Snijders, E.J. Baerends, and P. Vernooÿs. At. Data Nucl. Data Tables, **26**, 483 (1982); (*b*) P. Vernooÿs, G.J. Snijders, and E. Baerends. Slater type basis functions for the whole periodic system. Internal Report. Free University of Amsterdam, Amsterdam. 1981.
14. (*a*) L. Noodleman and J.G. Norman. J. Chem. Phys. **70**, 4903 (1979); (*b*) L. Noodleman. J. Chem. Phys. **74**, 5737 (1981); (*c*) L. Noodleman and E.J. Baerends. J. Am. Chem. Soc. **106**, 2316 (1984).
15. J. Krijn and E.J. Baerends. *In* Fit function in the HFS-method. Internal Report (in Dutch). Free University of Amsterdam, Amsterdam. 1984.
16. S.D. Vosko, L. Wilk, and M. Nusair. Can. J. Phys. **58**, 1200 (1980).
17. D.T. Pierce and W.E. Geiger. J. Am. Chem. Soc. **114**, 6063 (1992).
18. S.L. Morrison and J.J. Turner. J. Mol. Struct. **317**, 39 (1994).
19. R. Provencher, D.T. Aye, M. Drouin, J. Gagnon, N. Boudreault, and P.D. Harvey. Inorg. Chem. **33**, 3689 (1994).
20. D.G. Holah, A.N. Hughes, E. Krysa, and V.R. Magnuson. Organometallics, **12**, 4721 (1993).
21. L. Manojlovic–Muir, K.W. Muir, B.R. Lloyd, and R.J. Puddephatt. J. Chem. Soc. Chem. Commun. 536 (1985).
22. T. Zhang, M. Douin, and P.D. Harvey. Chem. Commun. 877 (1996).
23. K.A. Connors. Binding constants: the measurements of molecular complex stability. Wiley, New York. 1987.
24. P.D. Harvey, S.M. Hubig, and T. Ziegler. Inorg. Chem. **33**, 3700 (1994).
25. P.D. Harvey and R. Provencher. Inorg. Chem. **32**, 61 (1993).
26. R.V. Kirss and R. Eisenberg. Inorg. Chem. **28** (1989).
27. R. Provencher and P.D. Harvey. Inorg. Chem. **35**, 2113 (1996).
28. P.D. Harvey and Z. Murtaza. Inorg. Chem. **32**, 4721 (1993).

© 1997 NRC Canada

Intramolecular redox cyclization upon oxidation of a sulfur(II)-containing diazene: X-ray structures of $PhS(O)NC(Ar)NNC(Ar)=NSO_2Ph$ (Ar = 4-$CH_3C_6H_4$) and $MeSO_2N(4\text{-}CH_3C_6H_4)CN=NC(C_6H_4CH_3\text{-}4)NSO_2Me$

Vadapalli Chandrasekhar, Tristram Chivers, Laura Ellis, Ian Krouse, Masood Parvez, and Ignacio Vargas-Baca

Abstract: The reaction of *Z,E,Z*-PhSN=C(Ar)N=NC(Ar)=NSPh (Ar = 4-$CH_3C_6H_4$) (**1a**) with MCPBA results in ring closure via an intramolecular redox process to give the 1,2,3,5-thiatriazole $PhS(O)NC(Ar)NNC(Ar)=NSO_2Ph$ (**4**). An X-ray structural determination revealed that **4** contains a planar five-membered CNS(VI)NN ring with *d*(N—N) = 1.402(6) Å. The reaction of $ArCN_2(SiMe_3)_3$ (Ar = 4-$CH_3C_6H_4$) with one equivalent of $MeSO_2Cl$, followed by two equivalents of PhSeCl, produces the sulfonyl-containing diazene $MeSO_2N=C(Ar)N=N(Ar)C=NSO_2Me$ (**11**), which was shown by X-ray crystallography to adopt a *Z,E,Z* geometry. By contrast, the reaction of $ArCN_2(SiMe_3)_3$ with one equivalent of ArS(O)Cl, followed by two equivalents of PhSeCl, yielded the sulfur(II)-containing diazene *Z,E,Z*-ArSN=C(Ar)N=NC(Ar)=NSAr (Ar = 4-$CH_3C_6H_4$) (**1b**).

Key words: thiatriazoles, sulfonyl diazenes, intramolecular redox cyclization.

Résumé : La réaction du *Z,E,Z*-PhSN=C(Ar)N=NC(Ar)=NSPh (Ar = 4-$CH_3C_6H_4$) (**1a**) avec l'acide *m*-chloroperbenzoïque (AMCPB) conduit à une fermeture de cycle par le biais d'un processus rédox intramoléculaire qui conduit au 1,2,3,5-thiatriazole, $PhS(O)NC(Ar)NNC(Ar)=NSO_2Ph$ (**4**). Une détermination de structure par diffraction des rayons X révèle que le composé **4** comporte un noyau CNS(VI)NN planaire à cinq chaînons dans lequel *d*(N—N) = 1,402(6) Å. La réaction de $ArCN_2(SiMe_3)_3$ (Ar = 4-$CH_3C_6H_4$) avec un équivalent de $MeSO_2Cl$, suivie par deux équivalents de PhSeCl, conduit à un diazène contenant des sulfonyles, $MeSO_2N=C(Ar)N=N(Ar)C=NSO_2Me$ (**11**), qui, d'après la diffraction des rayons X, adopte une géométrie *Z,E,Z*. Par opposition, la réaction du $ArCN_2(SiMe_3)_3$ avec un équivalent de ArS(O)Cl, suivie par deux équivalents de PhSeCl, conduit à un diazène contenant du soufre(II), le *Z,E,Z*-ArSN=C(Ar)N=NC(Ar)=NSAr (Ar = 4-$CH_3C_6H_4$) (**1b**).

Mots clés : thiatriazoles, diazènes de sulfonyle, cyclisation rédox intramoléculaire.

[Traduit par la rédaction]

Introduction

Intramolecular interactions can have a profound influence on the structure and properties of chalcogen–nitrogen compounds. For example, diazenes of the type **1** (1, 2) and the bicyclic imine **2** (3) are deep purple compounds with planar structures imposed by S···N interactions of ca. 2.7 Å. In the sulfur(II)-containing diazenes **1** this interaction stabilizes *Z,E,Z* relative to *E,E,E* isomers (2). It involves donation from a chalcogen lone pair into the π^*(N=N) orbital and the intense visible absorption band at 535–550 nm can be attributed to the π-HOMO $\rightarrow$ π-LUMO transition (2). The interannular interaction in **2** also has a remarkable effect on the relative reactivities of the sulfur(II) centres. Treatment of **2** with an excess of MCPBA produces the trioxide **3** in which the S(II) centre involved in that interaction is unaffected by the oxidation process (3*c*).

To determine the influence of oxidizing the two sulfur(II) centres on the S···N interaction in **1**, we have investigated the synthesis of the sulfinyl (S(IV)) and sulfonyl (S(VI)) analogues of **1** by two different routes. The first method was the oxidation of **1a** with MCPBA. The second approach involved the treatment of sulfinyl- or sulfonyl-substituted benzamidinates 4-$CH_3C_6H_4CN[S(O)_nR][N(SiMe_3)_2]$ (R = 4-$CH_3C_6H_4$, *n* = 1; R = Me, *n* = 2) with two equivalents of PhSeCl.

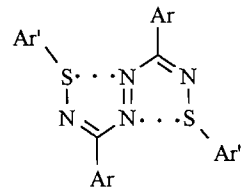
Received March 27, 1997.

V. Chandrasekhar, T. Chivers,[1] L. Ellis, I. Krouse, M. Parvez, and I. Vargas-Baca. Department of Chemistry, The University of Calgary, Calgary, AB T2N 1N4, Canada.

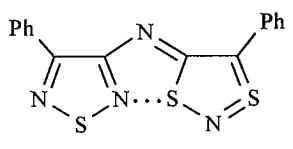
[1] Author to whom correspondence may be addressed. Telephone: (403) 220-5741. Fax: (403) 289-9488. E-mail: chivers@acs.ucalgary.ca

© 1997 NRC Canada

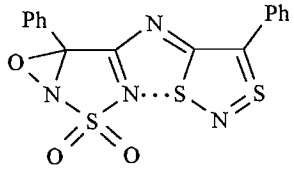
Can. J. Chem. Downloaded from www.nrcresearchpress.com by 91.121.58.235 on 09/08/12
For personal use only.



1a (Ar = 4-$CH_3C_6H_4$, Ar' = Ph)
1b (Ar = Ar' = 4-$CH_3C_6H_4$)



2



3

Experimental section

Reagents and general procedures

All reactions and the manipulation of reagents and products were carried out under an atmosphere of dry nitrogen gas. The reagents *p*-tolunitrile, *p*-tolyl disulfide, PhSeCl, and $ClSiMe_3$ (all from Aldrich) were used as received. Celite 545 and sea sand (Fisher) were oven-dried (110°C) before use. $LiN(SiMe_3)_2$ (Aldrich) was dissolved in hexanes and 1.1 equiv. of diethyl ether was added to give a precipitate of $LiN(SiMe_3)_2 \cdot OEt_2$, which was washed twice with hexanes. Sulfuryl chloride (SO_2Cl_2) and $MeSO_2Cl$ (Aldrich) were distilled at ca. 0.01 Torr (1 Torr = 133.3 Pa) over predried molecular sieves (300°C for 3 h) prior to use. A commercial sample of *m*-chloroperbenzoic acid (MCPBA) was purified by the literature procedure (4). The reagents 4-$CH_3C_6H_4CN_2(SiMe_3)_3$ (5), *p*-toluenesulfinyl chloride (6), and PhSNC(Ar)N=N(Ar)-CNSPh (Ar = 4-$CH_3C_6H_4$) (**1a**) (2) were prepared by the published methods. All solvents were dried and distilled immediately prior to use: toluene, tetrahydrofuran, hexane, diethyl ether (Na-benzophenone); dichloromethane, acetonitrile (P_4O_{10} followed by CaH_2); and carbon tetrachloride (P_4O_{10}).

Instrumentation

Infrared spectra (4000–400 cm^{-1}) were recorded as Nujol mulls (KBr windows) on a Mattson Instruments 4030 FT-IR spectrophotometer. UV-visible spectra were obtained by using a Cary 219 spectrophotometer. ^1H and ^{13}C NMR spectra were measured on a Bruker ACE 200 spectrometer, or a Bruker AM 400 spectrometer in the case of variable-temperature experiments. Chemical shifts are reported in ppm relative to Me_4Si (0 ppm) in $CDCl_3$. Mass spectra were obtained by using a Kratos MS80RFA instrument (EI/70 eV). Elemental analyses were provided by the Analytical Services Division, Department of Chemistry, The University of Calgary.

Preparation of PhS(O)NC(Ar)NNC(Ar)=NSO_2Ph (Ar = 4-$CH_3C_6H_4$) (4)[2]

A solution of MCPBA (0.445 g, 2.58 mmol) in diethyl ether (25 mL) was added with stirring to a purple solution of PhSN(4-$CH_3C_6H_4$)CN=NC(4-$CH_3C_6H_4$)NSPh (**1a**) (0.413 g, 0.859 mmol) in diethyl ether (25 mL) at 23°C. After 2 h the deep purple colour of the solution had faded with the formation of a pale yellow precipitate, that, after recrystallization from CH_2Cl_2–diethyl ether, was separated by filtration and identified as **4** (0.345 g, 0.652 mmol, 76%); mp 141–143°C (dec.). ^1H NMR spectrum in $CDCl_3$, δ: 2.40 (s, 3H, $CH_3C_6H_4$), 2.45 (s, 3H, $CH_3C_6H_4$), 7.2–7.9 (m, 18H, C_6H_5 and C_6H_4). ^{13}C {^1H} NMR spectrum in $CDCl_3$, δ: 21.8 ($CH_3C_6H_4$), 22.0 ($CH_3C_6H_4$), 126.3, 126.7, 127.3, 127.7, 128.7, 128.8, 129.3, 129.9, 130.2, 130.5, 132.6, 134.9, 135.2, 141.7, 141.9, 143.2 (C_6H_4 and C_6H_5), 157.6 ($CH_3C_6H_4C$), 161.2 ($CH_3C_6H_4C$). Anal. calcd. for $C_{28}H_{24}N_4O_3S_2$: C 63.62, H 4.58, N 10.61; found: C 63.69, H 4.64, N 10.60.

Preparation of bis(*C*-*p*-tolyl, *N*-methanesulfonyl-formidinyl)-*trans*-diazene $MeSO_2N(4\text{-}CH_3C_6H_4)CN{=}NC(C_6H_4CH_3\text{-}4)NSO_2Me$ (11)

A solution of benzeneselenenyl chloride (0.65 g, 3.34 mmol) in CH_2Cl_2 (30 mL) was added to a CH_2Cl_2 solution of 4-$CH_3C_6H_4C(NSO_2Me)[N(SiMe_3)_2]$ (**12**) at 23°C, prepared in situ from equimolar amounts (1.71 mmol) of $MeSO_2Cl$ and 4-$CH_3C_6H_4CN_2(SiMe_3)_3$ in CH_2Cl_2. After 2 h the solvent and volatile products were removed from the orange solution to give a dark red residue, which was extracted with hexanes (2 × 30 mL) to give Ph_2Se_2 (0.49 g, 92%). The orange product was recrystallized from diethyl ether to give **11** (0.214 g, 60%), mp 170–171°C. ^1H NMR (δ, $CDCl_3$): 7.94 and 7.32 (m, 4H, $CH_3C_6H_4$), 3.29 (s, 3H, CH_3SO_2), 2.45 (s, 3H, $CH_3C_6H_4$). ^{13}C NMR (δ, $CDCl_3$): 198.2 (*C*N=), 146.3, 131.0, 129.6, 125.4 ($CH_3C_6H_4$), 43.2 (CH_3SO_2), 21.9 ($CH_3C_6H_4$). Anal. calcd. for $C_{18}H_{20}N_4O_4S_2$: C 51.41, H 4.79, N 13.32; found: C 50.78, H 5.54, N 12.20.

In a separate experiment ^1H and ^{13}C NMR spectra were obtained for **12**. ^1H NMR (in $CDCl_3$), δ: 0.11 (s, 18H, $Si(CH_3)_3$), 1.97 (s, 3H, $CH_3C_6H_4$), 2.66 (s, 3H, CH_3SO_2), 7.67–6.86 (AB quartet, 4H, C_6H_4). ^{13}C {^1H} NMR (in $CDCl_3$), δ: 3.1 ($Si(CH_3)_3$), 21.7 ($CH_3C_6H_4$), 43.5 (CH_3SO_2), 129.2 and 130.9 (C_6H_4).

Preparation of N,N-bis(trimethylsilyl), *N'*-(*p*-toluenesulfinyl)-*p*-toluamidine 4-$CH_3C_6H_4C[NS(O)C_6H_4CH_3\text{-}4][N(SiMe_3)_2]$ (13)

A solution of 4-$CH_3C_6H_4S(O)Cl$ (0.60 g, 3.43 mmol) in CH_2Cl_2 (25 mL) was added to 4-$CH_3C_6H_4CN_2(SiMe_3)_3$ (1.20 g, 3.42 mmol) in CH_2Cl_2 (25 mL) at −78°C. After 1 h at 23°C, solvent and volatile products were removed under vacuum to give **13** (1.22 g, 2.93 mmol, 86%) as extremely moisture-sensitive colourless crystals, mp 90–95°C. The ^1H NMR spectrum suggested that **13** is a mixture of isomers (see Results and discussion).

Preparation of 4-$CH_3C_6H_4C[(NHS(O)C_6H_4CH_3\text{-}4)](NH)$ (14)

A solution of *p*-toluenesulfinyl chloride (0.667 g, 3.82 mmol) in dichloromethane (25 mL) was added to a solution of 4-$CH_3C_6H_4C(NSiMe_3)[N(SiMe_3)_2]$ (1.34 g, 3.82 mmol) in dichloromethane (25 mL). After 15 min a mixture of water (0.07 mL) and methanol (5 mL) was added by

[2] 2-Hydro-1-phenyl-2-(*C*-*p*-tolyl,*N*-phenylsulfonyl-formidinyl)-4-*p*-tolyl-1,2,3,5-thiatriazole-1-oxide.

Can. J. Chem. Downloaded from www.nrcresearchpress.com by 91.121.58.235 on 09/08/12
For personal use only.

© 1997 NRC Canada

Can. J. Chem. Downloaded from www.nrcresearchpress.com by 91.121.58.235 on 09/08/12
For personal use only.

Table 1. Crystallographic data for **4** and **11**.

	4	**11**
Formula	$C_{28}H_{24}N_4O_3S_2$	$C_{18}H_{20}N_4O_4S_2$
fw	528.64	420.50
Crystal size, mm^3	0.46 × 0.29 × 0.11	0.45 × 0.12 × 0.08
Space group	$P2_1/a$ (No. 14)	$P2_1/c$ (No. 14)
a, Å	14.035 (3)	10.483 (1)
b, Å	12.686 (2)	5.128 (2)
c, Å	14.799 (2)	18.180 (2)
β, deg	97.56 (1)	101.81 (1)
V, $Å^3$	2612.0 (7)	956.6 (3)
Z	4	2
T, K	200	170
λ, Å	0.71069	0.71069
ρ_{calcd}, g cm^{-3}	1.344	1.460
$F(000)$	1104	440
μ, cm^{-1}	2.41	3.12
2θ range, deg	4.0–50.0	4.0–50.0
Scan speed, deg/min	8.0	4.0
No. of unique data	4858	1916
No. of obsd data	1806	808
No. of parms refined	334	128
R[a]	0.046	0.064
R_w[b]	0.042	0.063
Goodness of fit	1.67	2.26
Max (min) resid. dens., e $Å^{-3}$	0.25, (–0.25)	0.42, (–0.39)

[a] $R = \Sigma||F_o| - |F_c||/\Sigma|F_o|$.
[b] $R_w = (\Sigma w(|F_o| - |F_c|)^2 / \Sigma w|F_o|^2)^{1/2}$.

syringe. Solvent was removed under vacuum to give 4-$CH_3C_6H_4C[(NHS(O)C_6H_4CH_3$-4)](NH) as a beige solid (0.95 g, 91%). A pure sample was obtained by recrystallization from methanol. IR, ν(SO): 1068 cm^{-1}. EI-MS, *m/z*: 272 (M^+). Anal. calcd. for $C_{15}H_{16}N_2OS$: C 66.15, H 5.92, N 10.29; found: C 65.79, H 5.92, N 10.21.

Reaction of 4-$CH_3C_6H_4CN_2[S(O)C_6H_4CH_3$-4](SiMe$_3$)$_2$ (13) with PhSeCl

A solution of benzeneselenenyl chloride (1.43 g, 7.47 mmol) in CH_2Cl_2 (25 mL) was added dropwise (10 min) to a CH_2Cl_2 solution of **13** (3.74 mmol) at −78°C prepared in situ as described above. After 1 h at 23°C the solvent and volatile products were removed under vacuum to give a purple solid, which was extracted with hexanes (2 × 30 mL) to give Ph_2Se_2 (1.07 g, 3.43 mmol). The residual purple product was identified as ArSN(Ar)CN=NC(Ar)NSAr (Ar = 4-$CH_3C_6H_4$) (**1b**) (0.89 g, 1.75 mmol, 94%) by comparison of the UV and ^{1}H NMR spectra with those of an authentic sample (2).

X-ray analysis

A colourless plate of **4** was obtained by recrystallization from a dichloromethane – diethyl ether solution. Yellow needles of **11** were produced by the slow evaporation of a dichloromethane solution. X-ray structures were determined by using a Rigaku AFC6S diffractometer. Experimental details are summarized in Table 1.[3] The structure of **4** was solved by direct methods (7) and expanded using Fourier techniques (8). The structure of **11** was solved by the heavy-atom method (9). In both cases the non-hydrogen atoms were refined anisotropically. Hydrogen atoms were included at geometrically idealized positions but not refined. Scattering factors were those of Cromer and Waber (10), and allowance was made for anomalous dispersion (11). All calculations were performed using *teXsan* (12).

Results and discussion

Preparation and X-ray structure of PhS(O)NC(Ar)NNC(Ar)=NSO$_2$Ph (4)

The reaction of **1a** with an excess of MCPBA in diethyl ether unexpectedly produces **4** as a slightly moisture-sensitive pale yellow precipitate in 76% yield after ca. 2 h at 23°C. The reac-

[3] Tables of atomic coordinates and displacement parameters, complete bond lengths and angles, and other refinement data may be purchased from: The Depository of Unpublished Data, Document Delivery, CISTI, National Research Council Canada, Ottawa, Canada K1A 0S2. This supplementary material has also been deposited with the Cambridge Crystallographic Data Centre, and can be obtained on request from The Director, Cambridge Crystallographic Data Centre, University Chemical Laboratory, 12 Union Road, Cambridge, CB2 1EZ, U.K.

© 1997 NRC Canada

Can. J. Chem. Downloaded from www.nrcresearchpress.com by 91.121.58.235 on 09/08/12
For personal use only.

Fig. 1. Molecular structure of PhS(O)NNC(Ar)NC(Ar)=NSO_2Ph (Ar = 4-$CH_3C_6H_4$) (**4**) with atomic numberings.

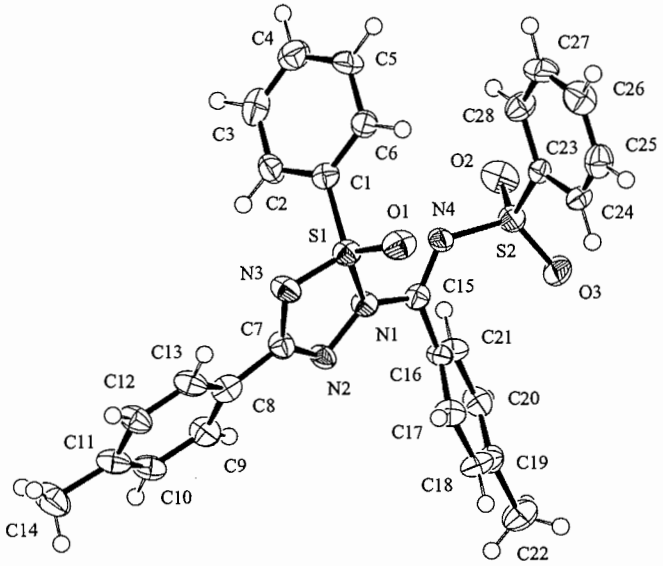
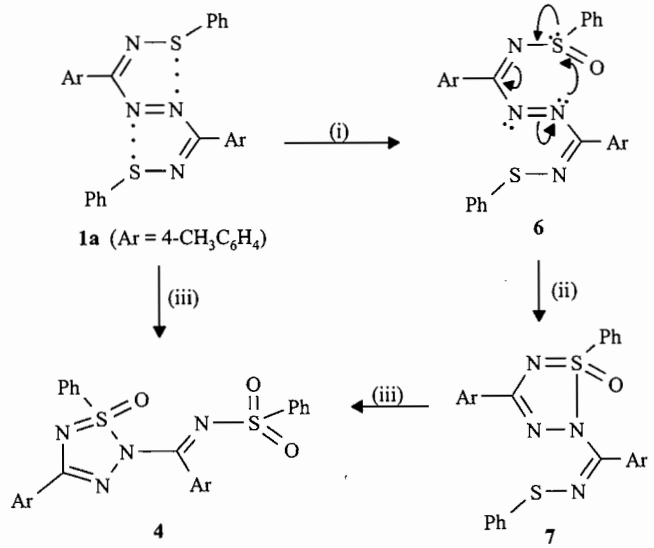


Table 2. Selected bond lengths (Å) and bond angles (deg) for **4**.

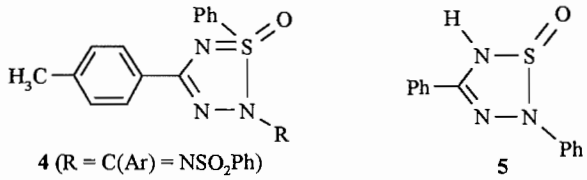
Bond	Length (Å)	Bond	Angle (deg)
S(1)—O(1)	1.440 (4)	N(1)-S(1)-N(3)	94.3 (3)
S(1)—N(1)	1.712 (5)	S(1)-N(1)-N(2)	110.3 (4)
S(1)—N(3)	1.545 (5)	S(1)-N(1)-C(15)	123.5 (4)
S(2)—O(2)	1.444 (4)	N(2)-N(1)-C(15)	125.9 (4)
S(2)—O(3)	1.437 (4)	N(1)-N(2)-C(7)	106.5 (5)
S(2)—N(4)	1.647 (5)	N(2)-N(7)-N(3)	119.9 (6)
N(1)—N(2)	1.402 (6)	S(1)-N(3)-C(7)	108.5 (4)
N(1)—C(15)	1.368 (7)	N(1)-C(15)-N(4)	114.1 (6)
N(2)—C(7)	1.289 (7)	S(2)-N(4)-C(15)	126.2 (5)
N(3)—C(7)	1.402 (7)		
N(4)—C(15)	1.280 (7)		

tion is instantaneous at 50°C. Both the ^1H and ^{13}C NMR spectra of **4** show two equally intense resonances for the 4-$CH_3C_6H_4$ groups. In addition, the ^{13}C NMR spectrum exhibits resonances at δ 157.6 and 161.2 for the carbon atoms attached to *p*-tolyl groups, suggesting that the product contains inequivalent sulfur centres. The formation of a product with the sulfur atoms in different oxidation states, e.g., sulfinyl and sulfonyl, is consistent with the NMR data. However, an X-ray structural determination (see Fig. 1) revealed that **4** consists of a five-membered CNSNN (thiatriazole) ring in which the sulfur atom S(1) has been oxidized to S(VI) and the -N=N- double bond of the diazene **1a** has been reduced to an =N—N= single bond (1.402(6) Å, cf. 1.29(1) Å in **1b**). The second sulfur atom S(2) has also been oxidized to S(VI). Pertinent bond lengths and bond angles are summarized in Table 2. The SN (1.545(5) and 1.712(5) Å) and CN (1.289(7) and 1.402(7) Å) bond distances are consistent with localized single and double bonds in the heterocyclic ring of **4**, but the geometry at the three-coordinate nitrogen atom N(1) is essentially planar (Σ 359.7°). In contrast to the related S(IV) system, 2,5-dihydro-2,4-

Scheme 1. Proposed mechanism for the formation of the thiatriazole **4** by the oxidation of the diazene **1a** by MCPBA. (*i*) MCPBA, Et_2O, −78°C, (*ii*) cyclization, (*iii*) excess MCPBA, Et_2O, 23°C.



diphenyl-1,2,3,5-thiatriazole 1-oxide (**5**), in which the sulfur atom is displaced by 0.49 Å from the NCNN least-squares plane (13), the five-membered ring in **4** is essentially planar with maximum deviations from the least-squares planes through all five atoms of 0.043(5) and 0.050(5) Å for N(3) and N(1), respectively.



As indicated in Scheme 1, the formation of **4** probably occurs via the oxidation of **1a** to the sulfoxide **6**, followed immediately by ring closure to give **7**, and then sequential oxidation of the second S(II) centre to a sulfone. Steps (ii) and (iii) apparently occur very rapidly, since only **4** and unreacted **1a** were isolated when the oxidation of **1a** with MCPBA was carried out in 1:1 or 1:2 molar ratios.

The reactivity of **1a** upon oxidation with MCPBA provides an interesting contrast to the inertness of the sulfur(II) centre involved in the interannular S···N contact in **2** (3*c*). We also note that the related sulfur(II)-containing diazene PhSN=C(Ph)N=NPh (**8**) yields the corresponding sulfoxide **9** upon oxidation with H_2O_2 (14). Neither **8**, or **9** were structurally characterized. The intense colour of **8**, which forms "almost black" crystals (14), suggests a structural resemblance to diazenes of the type **1**, i.e., an intramolecular S···N interaction. In the light of the present work, the cyclic structure **10** should also be considered for **9**.

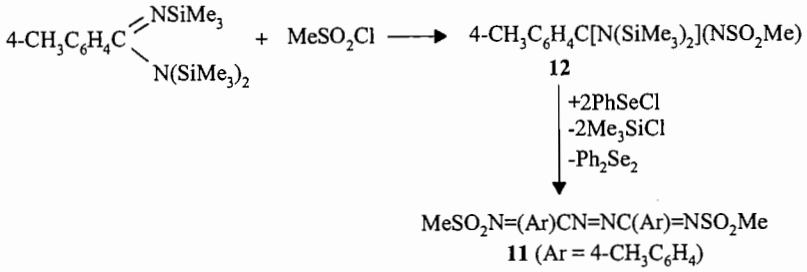
Preparation and X-ray structure of $MeSO_2N(4\text{-}CH_3C_6H_4)CN{=}NC(C_6H_4CH_3\text{-}4)NSO_2Me$ (11)

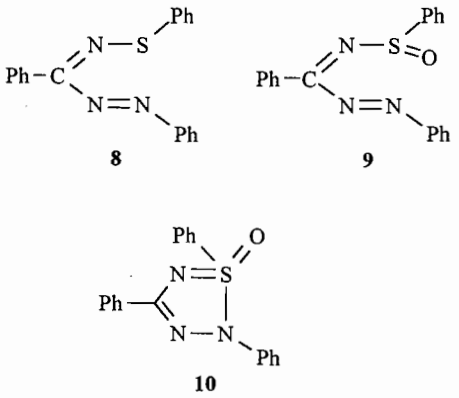
Since the direct oxidation of the sulfur(II)-containing diazene **1a** did not produce the desired sulfonyl or sulfinyl analogues,

© 1997 NRC Canada

Can. J. Chem. Downloaded from www.nrcresearchpress.com by 91.121.58.235 on 09/08/12
For personal use only.

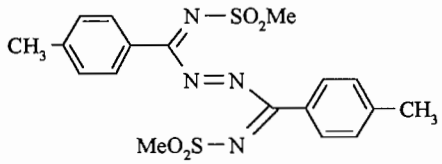
Scheme 2. Synthetic route to sulfonyl-containing diazenes.





an alternative approach that has been applied successfully to the synthesis of diazenes of the type **1** (2) was investigated. As indicated in Scheme 2, this involved the preparation of the sulfonyl-substituted benzamidinate **12**, followed by treatment with two equivalents of PhSeCl.

The reaction of $4\text{-}CH_3C_6H_4CN_2(SiMe_3)_3$ with methanesulfonyl chloride produces the monosubstituted product, $4\text{-}CH_3C_6H_4C(NSO_2Me)[N(SiMe_3)_2]$, as an extremely moisture-sensitive pale yellow oil, which was characterized by ^1H and ^{13}C NMR spectra. For the synthesis of **11**, the reagent **12** was generated in situ prior to the addition of two equivalents of PhSeCl. The sulfonyl-containing diazene **11** was obtained as orange needles in ca. 60% yield, after extraction of the by-product Ph_2Se_2. The ^1H and ^{13}C NMR spectra of **11** show resonances for equivalent $MeSO_2$ and $4\text{-}CH_3C_6H_4$ groups with the appropriate relative intensities (see Experimental section). The IR spectrum of **11** exhibits strong bands at 1377 and 1307 cm^{-1} attributed to $\nu_{asym}(SO_2)$ and $\nu_{sym}(SO_2)$, respectively (cf. R_2SO_2) (15).



11

In view of the three double bonds (C=N, N=N, and N=C) in **11**, several geometric isomers are possible. Density functional theory calculations for the corresponding sulfur(II)-containing diazenes indicate that *Z,E,Z* isomers are stabilized by intramolecular S···N interactions (2). However, an *E,E,E* isomer is obtained when the aryl substituent attached to carbon has an *ortho* substituent (Br or CF_3) (2). Interestingly, an X-ray structural determination of **11** revealed a *Z,E,Z* geometry (see Fig. 2), although there is no significant intramolecular interaction between the sulfonyl (SO_2) group and the diazene (N=N) functionality. Pertinent bond lengths and bond angles are summarized in Table 3. In contrast to the essentially planar geometry of diazenes of the

Fig. 2. Molecular structure of $MeSO_2N{=}C(4\text{-}CH_3C_6H_4)N{=}N(4\text{-}CH_3C_6H_4)C{=}NSO_2Me$ (**11**) with atomic numberings. Asterisks indicate symmetry-related atoms.

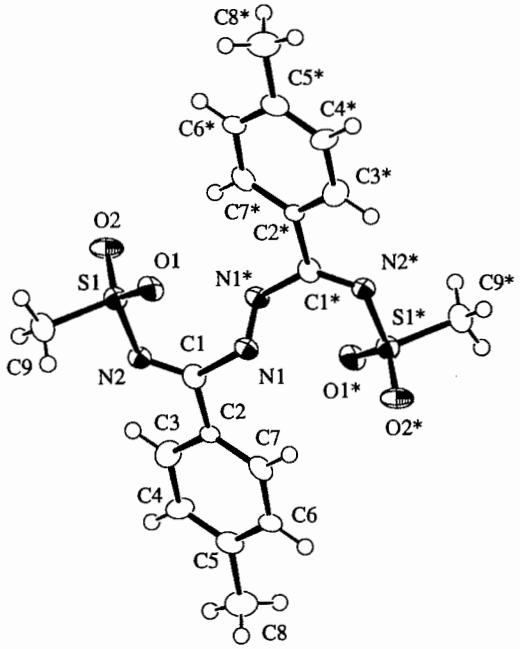


Table 3. Selected bond lengths (Å) and bond angles (deg) for **11**.

Bond	Length (Å)	Bond	Angle (deg)
S(1)—O(1)	1.429 (5)	O(1)-S(1)-O(2)	117.9 (4)
S(1)—O(2)	1.426 (6)	O(1)-S(1)-N(2)	112.7 (4)
S(1)—N(2)	1.652 (2)	O(1)-S(1)-C(9)	108.7 (4)
N(2)—C(1)	1.260 (9)	O(2)-S(1)-N(2)	108.9 (4)
C(1)—N(1)	1.466 (9)	O(2)-S(1)-C(9)	108.6 (5)
N(1)—N(1)*	1.20 (1)	N(2)-S(1)-C(9)	98.2 (4)
S(1)—C(9)	1.766 (8)	N(1)*-N(1)-C(1)	113.2 (9)
		S(1)-N(2)-C(1)	125.7 (6)
		N(1)-C(1)-N(2)	125.6 (7)
		N(1)-C(1)-C(2)	113.4 (7)
		N(2)-C(1)-C(2)	120.8 (7)

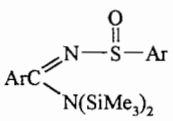
© 1997 NRC Canada

Can. J. Chem. Downloaded from www.nrcresearchpress.com by 91.121.58.235 on 09/08/12
For personal use only.

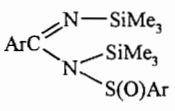
type **1** (2), the backbone of **11** is markedly twisted. The torsion angle N(1)*-N(1)-C(1)-N(2) is 63(1)°, so that the S(1)—N(1)* distance is 3.08 Å, only slightly less than the sum of the van der Waals radii for S and N (3.35 Å) (16). Although the sequence of atoms S(1)-N(2)-C(1)-N(1) is perfectly planar, the S(1)—N(1) separation is 3.16 Å. The lack of a significant intramolecular S···N interaction is also borne out by the relatively short N(1)—N(1)* distance of 1.20(1) Å. By contrast, the N—N distances in S(II)- or Se(II)-containing diazenes fall within the range 1.26–1.29 Å, as a result of donation from a chalcogen lone pair into the N=N (π^*) orbital (1, 2). In the case of **11** there is no lone pair available on sulfur for this interaction. The C—N distances of 1.260(9) and 1.466(9) Å in **11** indicate essentially localized π-bonding within the diazene chain. The S—N bond length of 1.652(6) Å is comparable to the value of 1.647(5) Å found for the corresponding S—N bond in **4**. The mean S(VI)—N single bond distance for comparable compounds is 1.642 Å (17).

Preparation of 4-$CH_3C_6H_4C[NS(O)C_6H_4CH_3$-4][$N(SiMe_3)_2$]

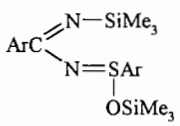
An attempt to extend the approach depicted in Scheme 2 to the synthesis of a sulfinyl-containing diazene produced an unexpected result. The reaction of 4-$CH_3C_6H_4CN_2(SiMe_3)_3$ with *p*-toluene sulfinyl chloride in CH_2Cl_2 proceeds in a straightforward manner to give 4-$CH_3C_6H_4C[NS(O)C_6H_4CH_3$-4]-[$N(SiMe_3)_2$] (**13**) as extremely moisture-sensitive colorless crystals in 86% yield. The EI-MS of **13** displays a parent ion at m/z = 416 amu ($C_{21}H_{32}N_2OSSi_2^+$). The IR spectrum exhibits a strong band at 1045 cm^{-1}, attributable to ν (SO) (15). However, the broad melting point range (90–95°C) suggests that **13** is not a single compound. Consistently, the ^{1}H NMR spectra of **13** indicate that this product consists of a mixture of structural isomers (Ar = 4-$CH_3C_6H_4$), e.g., **13a–c**. At 0°C three sets of resonances are observed at δ 7.2–7.9 (C_6H_4), 2.40–2.46 (CH_3), and 0.17–0.40 [$Si(CH_3)_3$], with the appropriate relative intensities (4:3:9). Each of these resonances consists of several components, which are still apparent when the spectrum is recorded at −78°C. The ^{1}H NMR spectrum could not be assigned to the individual isomers **13a**, **13b**, and **13c** (Ar = $C_6H_4CH_3$-4), owing to the overlap of several resonances. Further evidence for the composition of **13** was obtained by conversion to the hydrolysis product 4-$CH_3C_6H_4C(NH)[(NHS(O)C_6H_4CH_3$-4)] (**14**).



13a



13b



13c

The sulfinyl derivative **13** was generated in situ for the reaction with two equivalents of PhSeCl. Surprisingly, this reaction produces the known sulfenyl-containing diazene **1b** in 94% yield, in addition to Ph_2Se_2 and Me_3SiCl. The fate of the sulfinyl oxygen atom in the reagent **13** is puzzling. The formation of $(Me_3Si)_2O$ in the reactions of trisilylated benzamidines with oxygen-containing reagents such as FeOCl (18) has been suggested. However, the formation of the diazene **1b** at different temperatures was monitored by ^{1}H NMR spectroscopy, and only one trimethylsilyl-containing product, i.e., Me_3SiCl, was detected. An oxygen transfer from sulfur to selenium could also account for the formation of **1b**, but Ph_2Se_2 was isolated in 92% yield. No $(PhSe)_2O$ was detected.

Conclusions

The oxidation of a sulfenyl-containing diazene with MCPBA resulted in a novel intramolecular redox cyclization to give a thiatriazole rather than the corresponding sulfinyl- or sulfonyl-containing diazene. A sulfonyl-containing diazene was obtained from a trisilylated benzamidine via a two-step (substitution–elimination) process, but in the case of the sulfinyl derivative this approach resulted in reduction to give the corresponding sulfenyl-containing diazene.

Acknowledgements

We thank the Natural Sciences and Engineering Research Council of Canada (NSERC) for financial support, and the Direccíon General de Asuntos del Personal Académico – Universidad Nàcional Autónoma de Mexico (DGAPA-UNAM) for a postgraduate scholarship (Ignacio Vargas-Baca).

References

1. V. Chandrasekhar, T. Chivers, T.F. Fait, and S.S. Kumaravel. J. Am. Chem. Soc. **112**, 5373 (1990); V. Chandrasekhar, T. Chivers, S.S. Kumaravel, M. Parvez, and M.N.S. Rao. Inorg. Chem. **30**, 4125 (1991).
2. T. Chivers, I. Krouse, I. Vargas-Baca, T. Ziegler, and P. Zoricak. Inorg. Chem. **35**, 5836 (1996).
3. (*a*) S.T.A.K. Daley and C.W. Rees. J. Chem. Soc. Perkin Trans. 1, 207 (1987); (*b*) S.T.A.K. Daley, C.W. Rees, and D.J. Williams. J. Chem. Soc. Chem. Commun. 57 (1984); (*c*) P.J. Dunn, C.W. Rees, A.M.Z. Slawin, and D.J. Williams. J. Chem. Soc. Chem. Commun. 1134 (1989).
4. T.G. Traylor, W.A. Lee, and D.V. Stynes. J. Am. Chem. Soc. **106**, 755 (1984).
5. R.T. Boeré, R.T. Oakley, and R.W. Reed. J. Organomet. Chem. **331**, 161 (1987).
6. J.-H. Youn and R. Herrmann. Tetrahedron Lett. **27**, 1493 (1986).
7. *SAPI91, Fan Hai-Fun*: Structure Analysis Programs with Intelligent Control. Rigaku Corporation. Tokyo, Japan. 1991.
8. P.T. Beurskens, G. Admiraal, G. Beurskens, W.P. Bosman, S. Garcia-Granada, R.O. Gould, J.M.M. Smits, and C. Smykalla. DIRDIF92, The DIRDIF program system. Technical Report of the Crystallography Laboratory, University of Nijmegen, The Netherlands. 1992.
9. P.T. Beurskens, G. Admiraal, G. Beurskens, W.P. Bosman, S. Garcia-Granada, R.O. Gould, J.M.M. Smits, and C. Smykalla. PATTY: The DIRDIF program system. Technical Report of the Crystallography Laboratory, University of Nijmegen, The Netherlands. 1992.
10. D.T. Cromer and J.T. Waber. International tables for X-ray crystallography. Vol. IV. The Kynoch Press, Birmingham, England. 1974.
11. D.C. Creagh and W.J. McAuley. *In* International tables for crystallography. Vol. C. *Edited by* A.J.C. Wilson. Kluwer Academic Publishers, Boston. Table 4.2.6.8. 1992. pp. 219–222.
12. *teXsan*: Crystal Structure Analysis Package. Molecular Structure Corporation. The Woodlands, Tex. 1985 and 1992.
13. F.A. Neugebauer, H. Fischer, R. Crocket, and C. Krieger. J. Chem. Soc. Perkin Trans. 2, 1619 (1990).

© 1997 NRC Canada

14. J. Almog, D.H.R. Barton, P.D. Magnus, and R.K. Norris. J. Chem. Soc. Perkin Trans. 1, 853 (1974).
15. L.J. Bellamy. The infrared spectra of complex molecules. Methuen & Co. Ltd., London, U.K. 1960. pp. 357–363.
16. L. Pauling. The nature of the chemical bond. 3rd ed. Cornell University Press, Ithaca, N.Y. 1960. p. 260.
17. F.H. Allen, O. Kennard, D.G. Watson, L. Brammer, A.G. Orpen, and R. Taylor. J. Chem. Soc. Perkin Trans. (1), S1 (1987).
18. A. Zinn, H. von Arnim, W. Massa, M. Schäfer, J. Pebler, and K. Dehnicke. Z. Naturforsch. B: Chem. Sci. **46**, 1300 (1991).

Can. J. Chem. Downloaded from www.nrcresearchpress.com by 91.121.58.235 on 09/08/12
For personal use only.

© 1997 NRC Canada

Characterization of low-barrier hydrogen bonds. 3. Hydrogen maleate. An ab initio and DFT investigation

Michael A. McAllister

Abstract: High-level ab initio molecular orbital and density functional theory calculations predict the existence of a very short-strong hydrogen bond in the monoanion of maleic acid (hydrogen maleate). At all levels of theory (HF, MP2, BLYP, and B3LYP) except B3PW91 the potential energy surface is predicted to contain two minima, and hence resembles a double well. The barrier to proton transfer via a symmetrical transition state is calculated to be very small at all levels of theory. In all cases the calculated zero point vibrational energy available to the system is larger than the calculated barrier for proton transfer, thus the resulting hydrogen bond formed in hydrogen maleate is predicted to be symmetrical. Using the B3PW91 functional and the 6-31+G(d,p) basis set results in a single-well potential and a symmetrically positioned hydrogen. All correlated methods predict the gas phase hydrogen bond energy to be approximately 27 kcal/mol. Effects due to solvents were estimated using solvent cavity methods. Approximating the solvent as a dielectric continuum reduces the calculated hydrogen bond energy by roughly 6 kcal/mol at all levels of theory.

Key words: low-barrier hydrogen bonds, short-strong hydrogen bonds, hydrogen maleate, ab initio, density functional theory.

Résumé : Des calculs théoriques, ab initio à niveau élevé, d'orbitales moléculaires et de la théorie de la densité fonctionnelle permettent de prédire l'existence d'une liaison hydrogène très courte et forte dans la monoanion de l'acide maléique (maléate d'hydrogène). À tous les niveaux de la théorie (HF, MP2, BLYP et B3LYP), excepté B3PW91, on prédit que la surface d'énergie potentielle comporte deux minima et que, en conséquence, elle ressemble à un double puits. À tous les niveaux de la théorie, on a évalué que la barrière au transfert de proton par la biais d'un état de transition symétrique est très faible. Dans tous les cas, il a été calculé que l'énergie vibrationnelle pour le point zéro disponible pour le système est plus importante que la barrière calculée pour le transfert de proton; on prédit donc que la liaison hydrogène qui se forme dans le maléate d'hydrogène est symétrique. Des calculs utilisant la fonction B3PPW91 ou l'ensemble de base 6-31+G(d,p) conduisent à un potentiel à un seul puits et à un hydrogène en position symétrique. Toutes les méthodes soumises à la corrélation permettent de prédire que l'énergie de la liaison hydrogène en phase gazeuse est d'environ 27 kcal/mol. On a évalué les effets dus aux solvants en utilisant les méthodes de la cavité de solvant. Si l'on fait l'hypothèse que le solvant provoque un effet diélectrique continue, la valeur calculée de l'énergie de la liaison hydrogène est réduite par environ 6 kcal/mol, à tous les niveaux de la théorie.

Mots clés : liaisons hydrogènes à faible barrière, liaisons hydrogènes courtes et fortes, maléate d'hydrogène, ab initio, théorie de la densité fonctionnelle.

[Traduit par la rédaction]

Introduction

There has been a great deal of interest in "short-strong" or "low-barrier" hydrogen bonds (LBHBs) in recent years (1–16). Most of this interest has stemmed from the suggestion by Cleland, Kreevoy, Gerlt, and Gassman that the formation of a single short-strong, or low-barrier, hydrogen bond during an enzyme catalytic event can provide enough stabilization energy to account for the resulting rate enhancements typically seen in enzymatic reactions (4–6). Briefly, their proposal involves a mechanism whereby an enzyme-bound intermediate, or transition state, is stabilized by the formation of a single LBHB. They hypothesize that such a bond, if formed, could provide 15–20 kcal/mol of stabilization energy to the enzyme complex. This would then be enough to rationalize the rate accelerations observed during most enzyme-catalyzed reactions. This hypothesis has certainly not been without criticism. The most ardent opponents of the low-barrier hydrogen bond facilitated enzyme mechanism have been Guthrie and Kluger (7), Warshel et al. (8), Scheiner (9), and Perrin and Thoburn (10), although there have certainly been others (2, 3, 12).

Experimental evidence for the formation of LBHBs in the gas and solid phases is considerable. Excellent reviews by Hibbert and Emsley (13) detail the conditions necessary for the formation of such bonds, and a recent paper by Gilli et al. (14) extends these studies to the solid state. All of the available experimental and theoretical evidence to date suggests that the formation of LBHBs is dependent on several conditions being

Received April 15, 1997.

M.A. McAllister.[1] Department of Chemistry, University of North Texas, P.O. Box 5068, Denton, TX 76203, U.S.A.

[1] Telephone: (940) 565-4584. Fax: (940) 565-4318. E-mail: McAllister@unt.edu

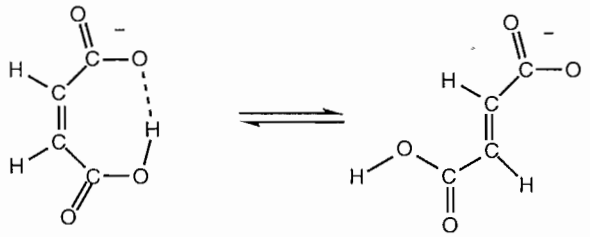
© 1997 NRC Canada

Can. J. Chem. Downloaded from www.nrcresearchpress.com by 91.121.58.235 on 09/08/12
For personal use only.

Can. J. Chem. Downloaded from www.nrcresearchpress.com by 91.121.58.235 on 09/08/12
For personal use only.

met: (*i*) the proton donor and proton acceptor must have identical, or nearly identical, pK_a values; (*ii*) the proton donor must be a fairly strong acid; (*iii*) almost all LBHBs are charged systems; (*iv*) absence of a hydrogen bonding, or polar, solvent. Most opponents of the LBHB facilitated enzyme mechanism use this last criterion to sermonize their point. That is, if a LBHB cannot exist in solution, surely it cannot exist in an enzyme active site. Of course, that argument assumes that bulk solution and enzyme active sites are similar. That may or may not be true.

Recent solution phase studies by Schwartz and Drueckhammer (3) have shown quite convincingly that LBHBs do not form to an appreciable extent in polar or protic solvents. They studied the maleic acid monoanion (hydrogen maleate) system **1** in considerable detail. By measuring the necessary equilibria they were able to determine that the difference in energy between the *cis* **1a** and *trans* **1b** forms of hydrogen maleate was of the order of 0–5.5 kcal/mol, depending on the actual solvent employed. Clearly, this is nowhere near the 15–20 kcal/mol necessary for the LBHB facilitated enzyme mechanism.



1a **1b**

However, those measurements must be biased towards isomer **1b**, since the *trans* double bond orientation is necessarily more stable than the *cis* linkage. Thus, in an equilibrium like the one above, there are two competing effects; one is the stabilizing effect of the formation of a strong hydrogen bond in **1a**, but the other is the destabilizing effect of forming a *cis* double bond. Thus, the measured "hydrogen bond strength" of 5.5 kcal/mol must be a *lower* limit for this system.

Another intriguing aspect of this particular system is whether or not the hydrogen bond formed is symmetric. Perrin has published the results of some very interesting studies in this area (10). His studies all suggest that the hydrogen bond, once formed, is quite asymmetric. He concludes that, for the most part, it is the inherent asymmetry of the solvent systems that actually cause the hydrogen bond to become asymmetrically placed, and that, in the absence of a solvent, these systems should form symmetrical hydrogen bonds.

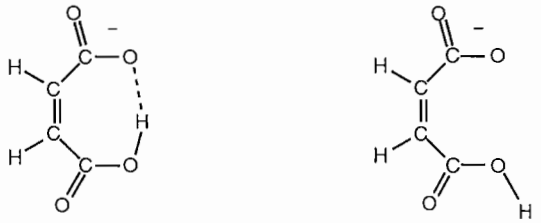
We recently became very interested in theoretical studies of LBHBs. Through high-level calculations we hope to be able to study systems like hydrogen maleate in sufficient detail to understand its behaviour in both the gas phase and in solution. In this study we present the results of high-level ab initio and density functional calculations toward this end.

Methodology

Ab initio and density functional calculations were carried out using the Gaussian 94 suite of programs (17). Calculations were carried out at several levels of theory (18), specifically: Hartree–Fock (HF), Moller–Plesset many-body perturbation truncated at the second order (MP2), and using density functionals (DFT) (19). The density functionals that were chosen for this study were BLYP, B3LYP, and B3PW91. BLYP is a gradient-corrected nonlocal functional incorporating the 1988 Becke exchange functional (20) and the correlation functional of Lee, Yang, and Parr (LYP) (21). B3LYP is a hybrid functional made up of Becke's exchange functional, the LYP correlation functional, and a Hartree–Fock exchange term (22). The B3PW91 functional is similar to the B3LYP functional but uses the 1991 correlation functional of Perdew and Wang (23) instead of the LYP functional. The standard 6-31+G(d,p) basis set was used for all calculations.

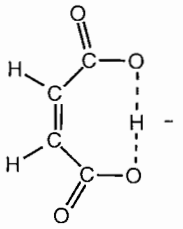
All structures were fully optimized. The most stable conformations of structures **1** and **3** were those with C_s symmetry, necessary due to the planarity of these systems. Full analytical second derivatives of the energy with respect to nuclear displacements were performed to determine vibrational frequencies and to ascertain the nature of each stationary point.

The hydrogen bond energy in hydrogen maleate was estimated as the difference in energy between isomers **1** and **2**:



1 **2**

To determine the barrier for proton transfer in this system it was necessary to consider structure **3**, where the proton is symmetrically situated between both carboxyl groups:



3

Solvent effects were investigated via use of the self-consistent isodensity polarizable continuum method (SCI–PCM) as developed by Tomasi and co-workers (24) and implemented in Gaussian 94. In this method the solute "cavity" is defined as an isosurface of the total electron density. The surface potential is then calculated via numerical differentiation, and its interaction with the solvent potential, defined by the dielectric constant chosen, is determined self-consistently. This method has been shown to give fairly reliable relative solvation free energies for a wide variety of organic solutes (25, 26).

© 1997 NRC Canada

Can. J. Chem. Downloaded from www.nrcresearchpress.com by 91.121.58.235 on 09/08/12
For personal use only.

Table 1. Calculated relative energies (kcal/mol) using 6-31+G(d,p) basis set.

Theory	1	2	3
HF	0.00	23.15	1.88
HF + ZPVE	0.00	22.87	-0.61
MP2	0.00	26.76	0.03
MP2 + ZPVE	0.00	27.42	-0.32
BLYP	0.00	26.17	0.00
BLYP + ZPVE	0.00	27.61	-0.02
B3LYP	0.00	26.70	0.02
B3LYP + ZPVE	0.00	27.82	-0.81
B3PW91	—	27.91	0.00
B3PW91 + ZPVE	—	29.28	0.00

Results and discussion

Energetics

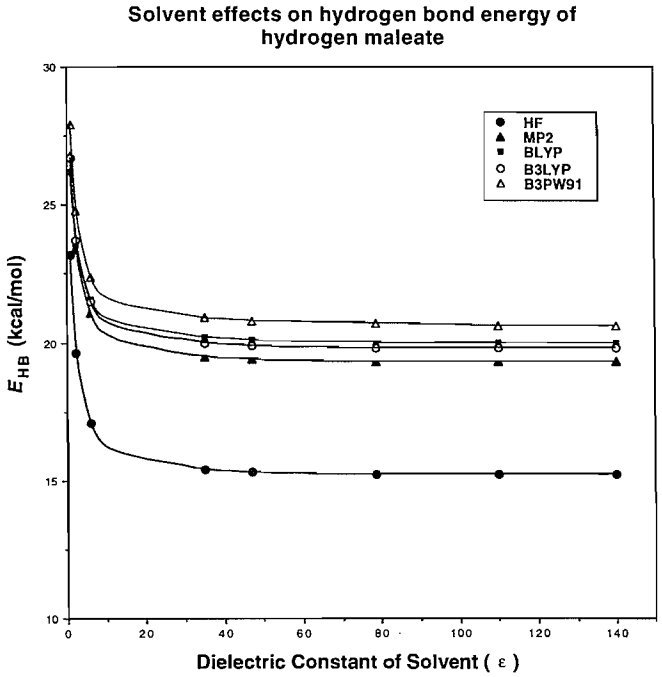
Table 1 shows the calculated hydrogen bond strength (E_{HB}) in hydrogen maleate. At the HF level E_{HB} is 23.2 kcal/mol. When electron correlated levels of theory are used E_{HB} increases to approximately 27 kcal/mol, depending on the exact method used. At the HF, MP2, BLYP, and B3LYP levels of theory structures **1** and **3** are both legitimate critical points on the calculated potential energy surface. At the B3PW91 level of DFT theory only structure **3** exists.

The very large interaction (E_{HB}) energies predicted for the hydrogen maleate system in the gas phase are consistent with the results of studies on other strongly hydrogen-bonded complexes (16). It is clear that in the gas phase such strong interactions can exist.

The calculated barrier for proton transfer is extremely small at all levels of theory studied. In fact, at the correlated levels it is so small as to be insignificant to one decimal place in kcal/mol. Accounting for the effects of zero point vibrational energy in these systems results in negative barriers of activation for proton transfer in all cases. Thus, on the true adiabatic potential energy surface the proton is predicted to be free to travel along the proton transfer coordinate without barrier. Presumably this would result in the observation of a symmetrically hydrogen-bonded hydrogen maleate in any experiment where the environment is also symmetric, such as is possible in crystal lattices and apolar aprotic solutions (10). This is also in agreement with a recent quantum dynamics study (27) of the low-barrier hydrogen bond formed between water and hydroxide ion, which concluded that the proton in such a system is most likely to be centrosymmetrically located, due to a combination of classical and quantum effects.

Table 2 contains results of our extensive solvent study using the SCIPCM solvent cavity reaction field approximation. Each optimized geometry for **1**, **2**, and **3** from a specific level of theory (HF, MP2, BLYP, B3LYP, B3PW91) was used to recalculate the total SCRF energy, incorporating the given dielectric constant of the medium (ε). This led to a new set of relative energies, as shown in Table 2. The difference in energy between the calculated energies of **1** and **2** corresponds to the hydrogen bond energy. Table 2 clearly shows that as the

Fig. 1. Calculated hydrogen bond energy (E_{HB}) (kcal/mol) in hydrogen maleate as a function of the dielectric constant of the medium (ε) for HF, MP2, BLYP, B3LYP, and B3PW91 levels of theory with the 6-31+G(d,p) basis set.



dielectric constant of the medium is increased the calculated hydrogen bond energy decreases very rapidly and then levels off. Figure 1 shows this relationship graphically for all five levels of theory employed here.

Table 2 and Fig. 1 reveal the importance of solvent, or cavity, polarity on the calculated hydrogen bond strength in hydrogen maleate. In each case there is a very rapid decrease in E_{HB} as one goes from the gas phase (ε = 1.0) to even very nonpolar solvents like benzene (ε = 2.3) and chloroform (ε = 6.0). Once the dielectric constant hits values approximating methanol (ε = 35.0), DMSO (ε = 47.0), and water (ε = 78.5), there is a significant leveling-off effect. That is, making the solvent cavity more polar than methanol has very little, if any, effect on the calculated hydrogen bond energy. Calculations on "super-polar" media were performed using ε values of 110.0 and 140.0 to ascertain what effect a hyperpolarized environment might have on a low-barrier hydrogen bond. The observed leveling-off trend continued throughout this region so that the calculated E_{HB} at ε = 140.0 was within 0.3 kcal/mol of the value calculated at ε = 35.0. This would suggest that solvent polarity effects hit a maximum corresponding to the dielectric constant of methanol. Of course, this does not suggest that all solvent effects are predicted to be the same in methanol as in water. It merely predicts that *polarity*-induced effects should be about the same in those two solvents — at least as applied to the study of low-barrier hydrogen bonds. The major shortcoming behind self-consistent reaction field (i.e., SCIPCM) calculations is that they do not, in any way, account for specific or explicit interactions of the solvent with the solute. All observed effects are strictly based on solvent–solute polarity differences. Nonetheless, SCRF calculations

© 1997 NRC Canada

Can. J. Chem. Downloaded from www.nrcresearchpress.com by 91.121.58.235 on 09/08/12
For personal use only.

Table 2. Calculated relative SCRF energies (kcal/mol) using 6-31+G(d,p) basis set.

	ε							
	1.0	2.3	6.0	35.0	47.0	78.5	110.0	140.0
HF								
1	0.0	0.0	0.0	0.0	0.0	0.0	0.0	0.0
2	23.2	19.6	17.1	15.4	15.3	15.2	15.2	15.2
3	1.9	1.9	2.0	2.0	2.0	2.0	2.0	2.0
MP2[a]								
1	0.0	0.0	0.0	0.0	0.0	0.0	0.0	0.0
2	26.1	22.7	20.3	18.7	18.6	18.5	18.5	18.5
3	−1.1	−1.0	−1.0	−1.0	−1.0	−1.0	−1.0	−1.0
MP2[b]								
1	0.0	0.0	0.0	0.0	0.0	0.0	0.0	0.0
2	26.8	23.4	21.1	19.5	19.4	19.3	19.3	19.3
3	0.0	0.0	0.0	0.0	0.0	0.0	0.0	0.0
BLYP								
1	0.0	0.0	0.0	0.0	0.0	0.0	0.0	0.0
2	26.2	23.6	21.6	20.2	20.1	20.0	20.0	20.0
3	0.0	0.0	0.0	0.0	0.0	0.0	0.0	0.0
B3LYP								
1	0.0	0.0	0.0	0.0	0.0	0.0	0.0	0.0
2	26.7	23.7	21.5	20.0	19.9	19.8	19.8	19.8
3	0.0	0.0	0.0	0.0	0.0	0.0	0.0	0.0
B3PW91								
1	—	—	—	—	—	—	—	—
2	27.9	24.8	22.4	20.9	20.8	20.7	20.6	20.6
3	0.0	0.0	0.0	0.0	0.0	0.0	0.0	0.0

[a]MP2/6-31+G(d,p)//HF/6-31+G(d,p).
[b]MP2/6-31+G(d,p)//MP2/6-31+G(d,p).

do provide invaluable information about the relative effects of solvents with differing polarities on calculated hydrogen bond energies.

As Table 2 and Fig. 1 clearly show, the calculated E_{HB} for hydrogen maleate decreases by approximately 6 kcal/mol (depending on the exact level of theory chosen) on going from the gas phase to reasonably polar solvents, like methanol and water. Still, the remaining hydrogen bond is calculated to be worth approximately 20 kcal/mol! This is certainly much higher than the experimental value of 2.0 kcal/mol observed in methanol (3). This would suggest that specific interactions between solvent and hydrogen maleate must play a very important role in decreasing the strength of E_{HB} in solvents like methanol and water. This has significant implications for the purported importance of low-barrier hydrogen bonds in enzyme catalysis. These calculations would suggest that a polar environment alone is not enough to disrupt a LBHB. We are currently undertaking related studies of this system to better understand the specific role of solvent molecules in determining the hydrogen bond strength in hydrogen maleate. As one of the referees pointed out, if there are very strong (LBHB?) specific interactions of a solvent molecule with both conformers of hydrogen maleate (**1a**, **1b**) then one might expect only a very small preference for **1a** versus **1b**.

Geometries

Table 3 shows calculated hydrogen bond distances (O—H) and heteroatom–heteroatom (O—O) distances for the atoms involved in the LBHB of hydrogen maleate. Results for all five levels of theory using the 6-31+G(d,p) basis set are presented there. These results clearly show the effects of electron correlation. At the HF level of theory the hydrogen bond distance is 1.49 Å; whereas at the correlated levels of theory that distance shrinks to approximately 1.29 Å. The correlated methods all predict a very nearly delocalized proton in the hydrogen bond. Even though the surface is still technically a double well, with two distinct minima corresponding to when the proton is closer to oxygen 1 versus when it is closer to oxygen 2, it is a very shallow potential. This is certainly reflected in the calculated hydrogen-bonding distances.

The potential energy surface calculated by the B3PW91 functional, on the other hand, is single welled. That is, the only stable minima on this surface is that due to the symmetrically H-bonded structure **3**.

Full geometries for structures **1**, **2**, and **3** are provided in Tables 4–6 for the five levels of theory employed. It is very encouraging that the fully optimized structures from MP2, BLYP, and B3LYP are so similar. This suggests that BLYP and B3LYP may be viable alternatives to MP2 calculations on the larger LBHB containing systems we wish to study in

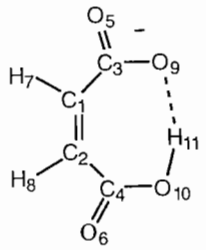
© 1997 NRC Canada

Can. J. Chem. Downloaded from www.nrcresearchpress.com by 91.121.58.235 on 09/08/12
For personal use only.

Table 3. Calculated hydrogen bonding distances (Å) and angles (°) using 6-31+G(d,p).

	HF	MP2	BLYP	B3LYP	B3PW91
1					
O_1—H_1	1.491	1.287	1.230	1.290	—
O_2—H_1	1.001	1.123	1.204	1.127	—
O_1—O_2	2.485	2.410	2.433	2.416	—
O_1—H_1—O_2	172.1	178.2	177.7	176.9	—
2					
O_2—H_1	0.946	0.973	0.984	0.972	0.970
O_1—O_2	2.804	2.769	2.832	2.802	2.802
3					
O_1—H_1	1.179	1.199	1.216	1.200	1.198
O_1—O_2	2.356	2.396	2.433	2.402	2.394
O_1—H_1—O_2	175.5	178.5	177.8	177.2	177.6

Table 4. Optimized geometries for **1** using 6-31+G(d,p) basis set.

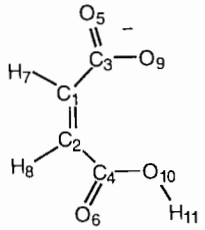


	HF	MP2	BLYP	B3LYP	B3PW91
Bond length					
C_1—C_2	1.331	1.354	1.361	1.348	—
C_1—C_3	1.530	1.512	1.522	1.519	—
C_2—C_4	1.503	1.503	1.520	1.509	—
O_5—C_3	1.221	1.252	1.255	1.243	—
O_6—C_4	1.204	1.244	1.254	1.236	—
H_7—C_1	1.077	1.085	1.096	1.089	—
H_8—C_2	1.076	1.085	1.096	1.088	—
O_9—C_3	1.251	1.297	1.315	1.291	—
O_{10}—C_4	1.297	1.313	1.318	1.307	—
H_{11}—O_{10}	1.001	1.123	1.204	1.127	—
Bond angle					
C_1—C_2—C_4	131.7	131.0	131.0	131.0	—
C_2—C_1—C_3	131.5	130.9	131.0	130.9	—
C_1—C_3—O_9	117.6	118.2	118.4	118.1	—
O_5—C_3—O_9	128.1	125.9	124.5	125.7	—
C_3—C_1—H_7	112.0	112.2	111.5	111.7	—
C_1—C_2—H_8	117.9	117.4	117.5	117.8	—
C_2—C_4—O_{10}	119.7	118.7	118.5	118.7	—
O_6—C_4-O_{10}	122.2	123.8	124.2	123.7	—
C_4—O_{10}—H_{11}	112.5	111.0	111.6	111.7	—

the future. Specifically, the study of enzyme active sites will likely never be possible with MP2 methods; however, recent advances in DFT methodology suggest that very large-scale calculations of this type may be possible in the near future. Before this study, there were no investigations of how DFT methods perform on systems involving short-strong hydrogen bonds. This study suggests that the BLYP and B3LYP functionals give results in excellent agreement with MP2 cal-

© 1997 NRC Canada

Table 5. Optimized geometries for **2** using 6-31+G(d,p) basis set.



	HF	MP2	BLYP	B3LYP	B3PW91
Bond length					
C_1—C_2	1.335	1.358	1.367	1.362	1.352
C_1—C_3	1.554	1.538	1.557	1.549	1.545
C_2—C_4	1.480	1.474	1.481	1.475	1.472
O_5—C_3	1.237	1.276	1.283	1.266	1.263
O_6—C_4	1.206	1.240	1.249	1.234	1.232
H_7—C_1	1.078	1.088	1.099	1.091	1.092
H_8—C_2	1.076	1.085	1.096	1.089	1.089
O_9—C_3	1.223	1.260	1.265	1.250	1.247
O_{10}—C_4	1.315	1.349	1.367	1.345	1.340
H_{11}—O_{10}	0.946	0.973	0.984	0.972	0.970
Bond angle					
C_1—C_2—C_4	134.2	134.3	134.8	134.5	134.4
C_2—C_1—C_3	136.4	135.8	136.4	136.2	136.3
C_1—C_3—O_9	119.0	119.2	119.5	119.3	119.4
O_5—C_3—O_9	130.4	129.9	129.6	129.8	129.9
C_3—C_1—H_7	110.0	110.8	110.1	110.1	110.0
C_1—C_2—H_8	117.1	116.7	116.7	116.9	117.0
C_2—C_4—O_{10}	119.0	118.5	118.5	118.6	118.7
O_6—C_4-O_{10}	120.6	120.7	120.2	120.7	120.3
C_4—O_{10}—H_{11}	107.2	103.8	103.9	104.9	104.5

culations, while the B3PW91 functional gives slightly different results. Obviously, from only one study it would be too harsh to conclude that the B3PW91 functional is inappropriate for further use. However, the present study reveals that MP2, BLYP, and B3LYP all give very similar results, both energetically (quantitatively) and geometrically (qualitatively), while the B3PW91 functional gives qualitatively different results. The conclusion would thus be that further studies of similar systems, with comparison to known experimental results wherever possible, are needed before a final determination can be made as to the usefulness of B3PW91 functionals for the study of short, strong, or low-barrier hydrogen bonds.

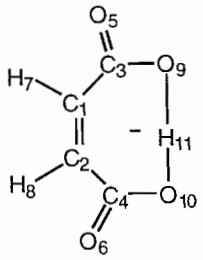
Conclusions

High-level ab initio molecular orbital and density functional theory calculations predict the existence of a very short-strong hydrogen bond in the monoanion of maleic acid (hydrogen maleate). At all levels of theory (HF, MP2, BLYP, and B3LYP) except B3PW91 the potential energy surface is predicted to contain two minima, and hence to resemble a double well. The barrier to proton transfer via a symmetrical transition state is calculated to be very small at all levels of theory. In all cases the calculated zero point vibrational energy available to the system is larger than the calculated barrier for proton transfer, thus the resulting hydrogen bond formed in hydrogen maleate is predicted to be symmetrical. All correlated methods predict the gas phase hydrogen bond energy to be approximately 27 kcal/mol. This is clearly an upper limit to the true hydrogen bond energy of this system, since we have not taken into account the *cis/trans* isomerization of the hydrogen maleate system. The gas phase hydrogen bond distance in hydrogen maleate is very short, in accordance with the observed strong hydrogen bond. Solvent effects, approximated using self-consistent reaction field theory with the SCIPCM procedure, were found to weaken the calculated hydrogen bond in hydrogen maleate by roughly 6 kcal/mol. This suggests that, even in a highly polar, possibly charged, environment (perhaps like an enzyme active site), low-barrier hydrogen bonds could still exist, even though they may not exist in solutions due to specific solvent–solute interactions. The density functionals BLYP and B3LYP were found to give results in excellent agreement with MP2 calculations. B3PW91 gave quantitatively very similar, but qualitatively different results. It is thus concluded that the BLYP and B3LYP functionals are excellent candidates for

Can. J. Chem. Downloaded from www.nrcresearchpress.com by 91.121.58.235 on 09/08/12
For personal use only.

© 1997 NRC Canada

Table 6. Optimized geometries for **3** using 6-31+G(d,p) basis set.



	HF	MP2	BLYP	B3LYP	B3PW91
Bond length					
C_1—C_2	1.330	1.354	1.361	1.348	1.346
C_1—C_3	1.515	1.507	1.521	1.513	1.510
O_5—C_3	1.212	1.248	1.255	1.240	1.237
H_7—C_1	1.077	1.085	1.096	1.090	1.089
O_9—C_3	1.272	1.305	1.316	1.299	1.295
H_{11}—O_9	1.179	1.199	1.216	1.200	1.198
Bond angle					
C_2—C_1—C_3	130.4	130.8	131.0	130.8	130.8
C_1—C_3—O_9	118.0	118.4	118.4	118.4	118.3
O_5—C_3—O_9	125.5	124.8	124.7	124.4	124.8
C_3—C_1—H_7	111.8	112.0	111.5	111.5	111.6
C_1—C_2—H_8	117.8	117.2	117.5	117.7	117.7
C_3—O_9—H_{11}	113.9	111.6	111.6	112.3	112.1

the study of much larger low-barrier hydrogen bonded systems, such as those possibly found in enzyme active sites (4–6).

Supplementary material

Tables 7–13 are available as supplementary material. They contain the calculated total energies of compounds **1–3** in the gas phase, and using the SCIPCM SCRF solvent cavity method with various dielectric constants.[2]

Acknowledgments

Financial support from the Texas Advanced Research Program (no. 41508), as administered by the Texas Higher Education Coordinating Board, is gratefully acknowledged.

References

1. (*a*) M. Garcia-Viloca, A. Gonzalez-Lafont, and J.M. Lluch. J. Am. Chem. Soc. **119**, 1081 (1997); (*b*) K.E. Laidig and J.A. Platts. J. Phys. Chem. **100**, 13455 (1996); (*c*) S. Scheiner and M. Yi. J. Phys. Chem. **100**, 9235 (1996); (*d*) T. Wesolowski, R.P. Muller, and A. Warshel. J. Phys. Chem. **100**, 15444 (1996).
2. (*a*) S. Shan and D. Herschlag. J. Am. Chem. Soc. **118**, 5515 (1996); (*b*) S. Shan, S. Loh, and D. Herschlag. Science (Washington, D.C.), **272**, 97 (1996); (*c*) S. Shan and D. Herschlag. Proc. Natl. Acad. Sci. U.S.A. **93**, 14474 (1996).
3. B. Schwartz and D.G. Drueckhammer. J. Am. Chem. Soc. **117**, 11902 (1995).
4. W.W. Cleland and M.M. Kreevoy. Science (Washington, D.C.), **264**, 1927 (1994).
5. W.W. Cleland. Biochemistry, **31**, 317 (1992).
6. (*a*) J.A. Gerlt, and P.G. Gassman. J. Am. Chem. Soc. **115**, 11552 (1993); (*b*) Biochemistry **32**, 11943 (1993); (*c*) J. Am. Chem. Soc. **114**, 5928 (1992).
7. (*a*) J.P. Guthrie and R. Kluger. J. Am. Chem. Soc. **115**, 11569 (1993); (*b*) J.P. Guthrie. Chem. Biol. **3**, 163 (1996).
8. A. Warshel, A. Papazyan, and P.A. Kollman. Science (Washington, D.C.), **269**, 102 (1995).
9. S. Scheiner and T. Kar. J. Am. Chem. Soc. **117**, 6970 (1995).
10. (*a*) C.L. Perrin. Science (Washington, D.C.), **266**, 1665 (1994); (*b*) C.L. Perrin and J.D. Thoburn. J. Am. Chem. Soc. **114**, 8559 (1992).
11. (*a*) P.A. Frey, J.B. Tobin, and S.A. Whitt. Science (Washington, D.C.), **264**, 1887 (1994); (*b*) P.A. Frey. Science (Washington, D.C.), **269**, 104 (1995).
12. Y. Kato, L.M. Toledo, and J. Rebek, Jr. J. Am. Chem. Soc. **118**, 8575 (1996).
13. (*a*) F. Hibbert and J. Emsley. Adv. Phys. Org. Chem. **26**, 255 (1990); (*b*) J. Emsley. Chem. Soc. Rev. **9**, 91 (1980).
14. P. Gilli, V. Bertolasi, V. Ferretti, and G. Gilli. J. Am. Chem. Soc. **116**, 909 (1994).
15. G.A. Jeffrey. An introduction to hydrogen bonding. Oxford University Press, New York. 1997.
16. P. Wenthold and R. Squires. J. Phys. Chem. **99**, 2002 (1995).
17. M.J. Frisch, G.W. Trucks, H.B. Schlegel, P.M.W. Gill, B.G. Johnson, M.A. Robb, J.R. Cheeseman, T.A. Keith, G.A. Petersson, J.A. Montgomery, K. Raghavachari, M.A. Al-Laham, V.G. Zakrzewski, J.V. Ortiz, J.B. Foresman, J. Cioslowski, B.B. Stefanov, A. Nanayakkara, M. Challacombe, C.Y. Peng, P.Y. Ayala, W. Chen, M.W. Wong, J.L. Andres, E.S. Replogle, R.

[2] These tables can be purchased from: The Depository of Unpublished Data, Document Delivery, CISTI, National Research Council of Canada, Ottawa, Canada K1A 0S2.

Can. J. Chem. Downloaded from www.nrcresearchpress.com by 91.121.58.235 on 09/08/12
For personal use only.

© 1997 NRC Canada

Gomperts, R.L. Martin, D.J. Fox, J.S. Binkley, D.J. Defrees, J. Baker, J.P. Stewart, M. Head-Gordon, C. Gonzalez, and J.A. Pople. Gaussian 94, Revision D.3. Gaussian, Inc., Pittsburgh Pa. 1996.
18. W.J. Hehre, L. Radom, P.v.R. Schleyer, and J.A. Pople. Ab Initio molecular orbital theory. Wiley–Interscience, New York. 1986, and refs. therein.
19. (*a*) W. Kohn, A.D. Becke, and R.G. Parr. J. Phys. Chem. **100**, 12974 (1996); (*b*) R.G. Parr and W.Yang. Density functional theory of atoms and molecules. Oxford University Press, New York. 1989; (*c*) R.M. Dreizler and E.K.V. Gross. Density functional theory. Springer, Berlin. 1990.
20. A.D. Becke. Phys. Rev. A: At. Mol. Opt. Phys. **38**, 3098 (1988).
21. C. Lee, W. Yang, and R.G. Parr. Phys. Rev. B: Condens. Matter, **37**, 785 (1988).
22. (*a*) A.D. Becke. J. Chem. Phys. **98**, 5648 (1993); (*b*) A.D. Becke. J. Chem. Phys. **104**, 1040 (1996); (*c*) A.D. Becke. *In* Modern electronic structure theory. *Edited by* D.R. Yarkony. World Scientific, Singapore. 1995.
23. J.P. Perdew. *In* Electronic structure of solids. *Edited by* P. Ziesche and H. Eschrig. Akademie Verlag, Berlin. 1991.
24. (*a*) S. Miertus, E. Scrocco, and J. Tomasi. Chem. Phys. **55**, 117 (1981); (*b*) J. Tomasi, R. Bonaccorsi, R. Cammi, and F.J.O. Valle. J. Mol. Struct. (Theochem), **234**, 401 (1991); (*c*) J. Tomasi and R. Bonaccorsi. Croat. Chem. Acta, **65**, 29 (1992).
25. J.B. Foresman, T.A. Keith, K.B. Wiberg, J. Snoonian, and M.J. Frisch. J. Phys. Chem. **100**, 16098 (1996).
26. (*a*) K.B. Wiberg, T.A. Keith, M.J. Frisch, and M. Murcko. J. Phys. Chem. **99**, 9072 (1995); (*b*) K.B. Wiber, P.R. Rablen, D.J. Rush, and T.A. Keith. J. Am. Chem. Soc. **117**, 4261 (1995).
27. M.E. Tuckerman, D. Marx, M.L. Klein, and M. Parrinello. Science (Washington, D.C.), **275**, 817 (1997).

Can. J. Chem. Downloaded from www.nrcresearchpress.com by 91.121.58.235 on 09/08/12
For personal use only.

© 1997 NRC Canada

Novel boron chelate complexes from the reaction of salicylaldehydes, tertiary amines, and diphenylborinic or phenylboronic acid. Crystal and molecular structures of two new types of chelated organoborate salts[1]

Wolfgang Kliegel, Jörg Metge, Steven J. Rettig, and James Trotter

Can. J. Chem. Downloaded from www.nrcresearchpress.com by 91.121.58.235 on 09/08/12
For personal use only.

Abstract: The one-pot reaction of equimolar amounts of salicylaldehyde, diphenylborinic acid anhydride, and a tertiary amine in the presence of an alkanol (R′OH) led to the addition of R′OH to the aldehyde group and the formation of an *O,O*-acetal moiety within the chelate anion with the charge balanced by an ammonium cation arising from the tertiary amine. Exchanging the diphenylborinic acid in the three-component reaction system for phenylboronic acid did not give the analogous adduct or chelate but one additional mole equivalent of phenylboronic acid (anhydride) was incorporated, leading to a polycyclic anion containing pyroboronate and acetal boronate functions with an associated ammonium cation. Crystals of 1-methylpiperidinium 4-ethoxy-2,2-diphenyl-1,3-dioxa-2-borata-1,2,3,4-tetrahydronaphthalenate, **6***d*, are monoclinic, a = 9.522(1), b = 17.703(1), c = 14.974(1) Å, β = 98.275(10)°, Z = 4, space group $P2_1/n$, and those of 1-methylpiperidinium 6,10-epoxy-4-methoxy-6,8-diphenyl-5,7,9-trioxa-8-bora-6-borata-5,6,7,8,9,10-hexahydrobenzocyclooctenate, **10***e*, are monoclinic, a = 7.968(1), b = 19.3707(4), c = 15.9400(5) Å, β = 100.186(5)°, Z = 4, space group $P2_1/n$. The structures were solved by direct methods and refined by full-matrix least-squares procedures to R = 0.050 and 0.033 (R_w = 0.040 and 0.032) for 2815 and 3529 reflections with $I \geq 3\sigma(F^2)$, respectively. Compounds **6***d* and **10***e* are both representative of new classes of organoboron chelates.

Key words: salicylaldehyde semiacetal diphenylboron chelate, salicylaldehyde bisboronate, organoboron compound, crystal structure.

Résumé : La réaction unipot de quantités équimolaires de salicylaldéhyde, d'anhydride de l'acide diphénylborinique et d'une amine tertiaire en présence d'un alcanol (R′OH) conduit à une addition du R′OH sur le groupe aldéhydique et à la formation d'une portion *O,O*-acétal dans un anion chélate dont la charge est compensée par un cation ammonium dérivé de l'amine tertiaire. Remplaçant l'acide diphénylborinique du système réactionnel à trois composants par de l'acide phénylboronique ne conduit pas à la formation de l'adduit/chélate analogue, mais l'équivalent d'une mole additionnelle d'acide phénylboronique (anhydride) est incorporée et conduit à un anion polycyclique contenant les fonctions pyroboronate et acétalboronate avec un cation ammonium associé. Les cristaux du 4-éthoxy-2,2-diphényl-1,3-dioxa-2-borata-1,2,3,4-tétrahydronaphtalénate de 1-méthylpipéridinium, **6***d*, sont monocliniques, groupe d'espace $P2_1/n$, a = 9,522(1), b = 17,703(1) et c = 14,974(1) Å, β = 98,275(10)° et Z = 4 alors que ceux du 6,10-époxy-4-méthoxy-6,8-diphényl-5,7,9-trioxa-8-bora-6-borata-5,6,7,8,9,10-hexahydrobenzocycloocténate de 1-méthylpipéridinium, **10***e*, sont monocliniques, groupe d'espace $P2_1/n$, a = 7,968(1), b = 19,3707(4) et c = 15,9400(5) Å, β = 100,186(5)° et Z = 4. Les structures ont été résolues par les méthodes directes et affinées par les méthodes des moindres carrés (matrice complète) jusqu'à des valeurs de R = 0,050 et 0,033 (R_w = 0,040 et 0,032) pour 2815 et 3529 réflexions $I \geq 3\sigma(F^2)$ respectivement.

Mots clés : chélate du diphénylbore et du semiacétal du salicylaldéhyde, bisboronate du salicylaldéhyde, composé organoboré, structure cristalline.

[Traduit par la rédaction]

Received March 9, 1997.

W. Kliegel and J. Metge. Institut für Pharmazeutische Chemie der Technischen Universität Braunschweig, Beethovenstrasse 55, 38106 Braunschweig, Germany.
S.J. Rettig and J. Trotter.[2] Department of Chemistry, University of British Columbia, 2036 Main Mall, Vancouver, BC V6T 1Z1, Canada.

[1] Structural studies of organoboron compounds LXV. Previous paper in this series: ref. 22.
[2] Author to whom correspondence may be addressed. Telephone: (604) 822-4865. Fax: (604) 822-2847. E-mail: jtrt@xray4.chem.ubc.ca

© 1997 NRC Canada

Can. J. Chem. Downloaded from www.nrcresearchpress.com by 91.121.58.235 on 09/08/12
For personal use only.

Introduction

The interaction of salicylaldehyde, amines, and chelate-forming boron compounds is of considerable interest in the study of intermediate steps in catalytic reactions or as enzyme models (1, 2). Considering the partial structural relationships to pyridoxal, pyridoxal-dependent enzyme reactions (3–5) are of particular relevance. In the course of our investigations of boron chelate compounds we synthesized and structurally characterized the zwitterionic diphenylboron chelate **3** (R_3N = quinuclidine) that could be generally obtained from the reaction of salicylaldehyde (**1**, X = H), the tertiary amine, and diphenylborinic acid (anhydride) in water-free aprotic solvents, or from the preformed boron chelate **2** by addition of the amine (6) (Scheme 1). However, carrying out the reaction in ethanol or other alcohols (R′OH) results in crystalline compounds whose elemental analyses show the incorporation of an additional molecule of R′OH into **3**, regardless of the applied tertiary amine. By simple infrared and ^{1}H nmr spectroscopic means it was not possible to distinguish between a ring-opened addition product like **4**, a solvent-type adduct like **5** (retaining the *B,N*-betaine structure of the chelate **3**), or the trialkylammonium salt **6** with an *O,O*-acetal moiety within the chelate anion. For an unambiguous determination of molecular structure by X-ray crystallographic analysis, we synthesized various compounds for the selection of an example providing suitable crystals.

The study was later extended by using phenylboronic acid instead of diphenylborinic acid in the same three-component system. This could possibly lead to similar complexes such as **7**, possessing a B(OH)Ph instead of the BPh_2 moiety in **3**, or perhaps to the corresponding R′OH adducts or condensates when alkanols are used as solvents. Surprisingly, the resulting crystalline compounds did not have the expected compositions. Elemental analyses as well as ^{1}H and ^{11}B nmr spectra instead indicated a condensation of **7** with a second molecule of phenylboronic acid. The distinction between the alternative molecular structures **8**–**10** was again not possible by simple spectroscopic methods. A series of compounds derived from variously substituted salicylaldehydes was synthesized in order to produce a representative example yielding crystals suitable for X-ray structure analysis.

Experimental

Quinuclidinium 4-ethoxy-2,2-diphenyl-1,3-dioxa-2-borata-1,2,3,4-tetrahydronaphthalenate, 6*a*

2 (0.29 g, 1.0 mmol) (7) and quinuclidine (0.11 g, 1.0 mmol) are refluxed in 10 mL of ethanol for 5 min. Upon cooling, crystallization yields 0.39 g (88%) of the colorless compound; mp 116–117°C. Infrared (KBr): 1604 (C═C) cm^{-1}; ^{1}H nmr (90 MHz, DMSO-d_6–TMS), δ (ppm): 1.06 (t, J = 7 Hz, CH_3), 1.53–1.83, and 2.96–3.30 (m and m, $N(C_2H_4)_3CH$), 3.43 (q, J = 7 Hz, OCH_2), 5.50 (s, O-CH-O), 6.80–7.73 (m, 14 aromatic H); ^{1}H nmr (90 MHz, $CDCl_3$–TMS), δ (ppm): 1.10–3.06 (m, CH_3, $N(C_2H_4)_3CH$), 3.53–4.23 (m, OCH_2), 5.36 (s, 80% of 1H, O-CH-O), 6.16 (s, broad, exchangeable, NH), 6.50–7.90 (m, 14 aromatic H), 9.83 (s, 20% of 1H, CH═O). Anal. calcd. for $C_{28}H_{34}BNO_3$: C 75.85, H 7.73, B 2.44, N 3.16; found: C 75.93, H 7.86, B 2.55, N 2.99. The product gives a blue-colored solution upon addition of diphenylcarbazone in ethanol, indicating the presence of the chelated diphenylborenium (Ph_2B^+) ion (8).

An identical product is obtained by the three-component one-pot reaction of salicylaldehyde (**1**, X = H), oxybis(diphenylborane) (0.5 mol equivalent), and quinuclidine in ethanol, and also by recrystallization of **3** (R_3N = quinuclidine) (6) from ethanol.

1,4-Diazabicyclo[2.2.2]octanium 4-ethoxy-2,2-diphenyl-1,3-dioxa-2-borata-1,2,3,4-tetrahydronaphthalenate, 6*b*

2 (0.29 g, 1.0 mmol) and 1,4-diazabicyclo[2.2.2]octane (0.11 g, 1.0 mmol) are reacted as described for **6***a*. Yield: 0.39 g (88%) of the colorless compound; mp 128°C (EtOH). Infrared (KBr): 1605 (C═C) cm^{-1}; ^{1}H nmr (90 MHz, DMSO-d_6–TMS), δ (ppm): 1.06 (t, J = 7 Hz, CH_3), 2.90 (s, $N(C_2H_4)_3N$), 3.45 (q, J = 7 Hz, OCH_2), 5.85 (s, O-CH-O), 6.73–7.76 (m, 14 aromatic H); ^{1}H nmr (90 MHz, $CDCl_3$–TMS), δ (ppm): 1.26 (t, J = 7 Hz, CH_3), 2.75 (s, $N(C_2H_4)_3N$), 3.90 (q, J = 7 Hz, OCH_2), 6.86–7.80 (m, 14 aromatic H), 9.86 (s, 90% of 1H, CH═O); ^{11}B nmr (64 MHz, DMSO-d_6–Et_2OBF_3), δ (ppm): 2.9 ($W_{1/2} \approx$ 200 Hz); ^{11}B nmr (64 MHz, $CDCl_3$–Et_2OBF_3), δ (ppm): 4.0 ($W_{1/2}$ = 340 Hz) and 45.1 ($W_{1/2}$ = 340 Hz), ratio of peak areas: 1:1. Anal. calcd. for $C_{27}H_{33}BN_2O_3$: C 72.98, H 7.49, B 2.43, N 6.30; found: C 73.00, H 7.68, B 2.46, N 6.15. **6***b* gives a blue-colored solution upon addition of diphenylcarbazone as described for **6***a*.

1-Methylpyrrolidinium 4-ethoxy-2,2-diphenyl-1,3-dioxa-2-borata-1,2,3,4-tetrahydronaphthalenate, 6*c*

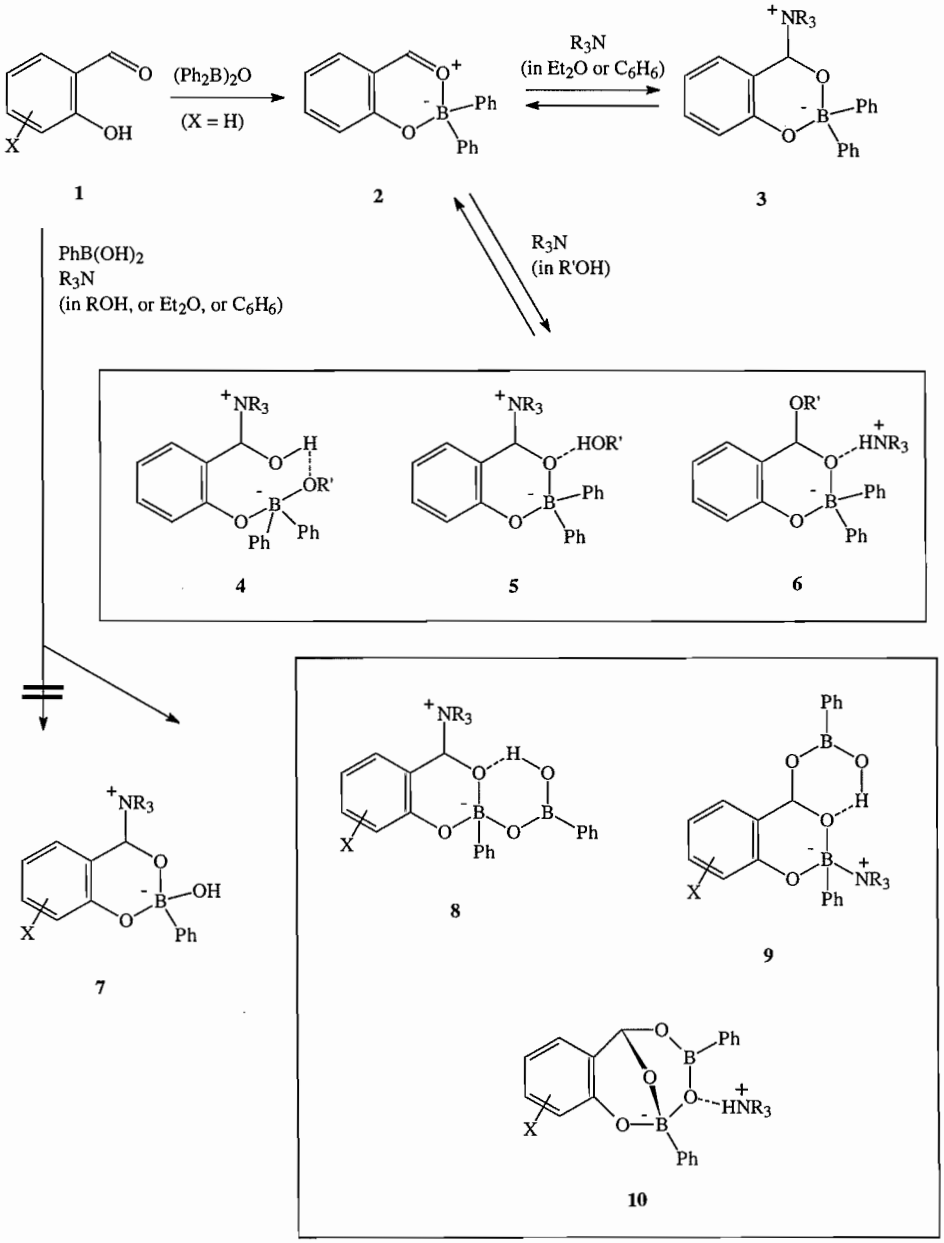
2 (0.29 g, 1.0 mmol) and 1-methylpyrrolidine (0.09 g, 1.0 mmol) are reacted as described for **6***a*. Yield: 0.32 g (77%) of slightly yellow crystals; mp 188°C (EtOH). Infrared (KBr): 1602 (C═C) cm^{-1}; ^{1}H nmr (90 MHz, DMSO-d_6–TMS), δ (ppm): 1.06 and 1.17 (t and t, J = 7 Hz, ratio of peak areas: 8:2, C-CH_3), 1.46–1.83 (m, $C(CH_2)_2C$), 2.48 (s, N-CH_3), 2.66–3.06 (m, CH_2NCH_2), 3.45 and 3.90 (q and q, J = 7 Hz, ratio of peak areas: 8:2, OCH_2), 5.52 (s, 80% of 1H, O-CH-O), 6.26 (s, broad, exchangeable, NH), 6.40–7.76 (m, 14 aromatic H), 10.30 (s, 20% of 1H, CH═O), 11.03 (s, partially exchangeable, 20% of 1H, phenolic OH); ^{1}H nmr (90 MHz, $CDCl_3$–TMS), δ (ppm): 1.28 (t, J = 7 Hz, C-CH_3), 1.20–1.66 (m, $C(CH_2)_2C$), 2.12 (s, N-CH_3), 2.16–2.50 (m, CH_2NCH_2), 3.63–4.13 (m, OCH_2), 5.60 (s, 50% of 1H, O-CH-O), 6.40–7.83 (m, 14 aromatic H), 8.30 (s, broad, exchangeable, NH), 9.82 (s, 50% of 1H, CH═O); ^{11}B nmr (64 MHz, $CDCl_3$–Et_2OBF_3), δ (ppm): 3.7 ($W_{1/2}$ = 170 Hz) and 44.9 ($W_{1/2}$ = 260 Hz), ratio of peak areas: 3:2. Anal. calcd. for $C_{26}H_{32}BNO_3$: C 74.82, H 7.73, B 2.59, N 3.36; found: C 74.78, H 8.18, B 2.68, N 3.23. **6***c* gives a blue-colored solution upon addition of diphenylcarbazone as described for **6***a*.

1-Methylpiperidinium 4-ethoxy-2,2-diphenyl-1,3-dioxa-2-borata-1,2,3,4-tetrahydronaphthalenate, 6*d*

2 (0.29 g, 1.0 mmol) and 1-methylpiperidine (0.10 g, 1.0 mmol) are reacted as described for **6***a*. Yield: 0.34 g (79%) of yellowish crystals; mp 102–103°C (EtOH). Infrared (KBr): 1605 (C═C) cm^{-1}; ^{1}H nmr (90 MHz, DMSO-d_6–TMS), δ (ppm): 0.96–1.23 (m, C-CH_3), 1.30–1.73 (m, $C(CH_2)_3C$), 2.48 (s, N-CH_3), 2.60–2.86 (m, CH_2NCH_2), 3.33–3.96 (m, OCH_2), 5.43 (s, broad, exchangeable, NH), 5.50 (s, 80% of 1H, O-CH-O), 6.33–7.76 (m, 14 aromatic H), 10.25 (s, 20% of 1H,

© 1997 NRC Canada

Scheme 1.



	R_3N	R′	X
6*a*	Quinuclidine	C_2H_5	
6*b*	1,4-Diazabicyclo[2.2.2]nonane	C_2H_5	
6*c*	1-Methylpyrrolidine	C_2H_5	
6*d*	1-Methylpiperidine	C_2H_5	
6*e*	1-Methylpiperidine	CH_3	
6*f*	1-Methylpiperidine	n-C_3H_7	
6*g*	1-Methylpiperidine	i-C_3H_7	
10*a*	Quinuclidine		H
10*b*	1,4-Diazabicyclo[2.2.2]nonane		H
10*c*	1-Methylpiperidine		H
10*d*	Triethylamine		H
10*e*	1-Methylpiperidine		4-CH_3O
10*f*	1-Methylpiperidine		2-Cl
10*g*	1-Methylpiperidine		2-NO_2

Can. J. Chem. Downloaded from www.nrcresearchpress.com by 91.121.58.235 on 09/08/12
For personal use only.

© 1997 NRC Canada

Can. J. Chem. Downloaded from www.nrcresearchpress.com by 91.121.58.235 on 09/08/12
For personal use only.

CH═O), 11.00 (s, 20% of 1H, OH ?); ^{1}H nmr (90 MHz, $CDCl_3$–TMS), δ (ppm): 1.06–1.56 (m, CH_3, $C(CH_2)_3C$), 1.93–2.26 (m, CH_2NCH_2), 2.05 (s, N-CH_3), 3.76–4.16 (m, OCH_2), 5.62 (s, 50% of 1H, O-CH-O), 6.40–8.20 (m, 14 aromatic H), 8.78 (s, broad, exchangeable, NH), 9.82 (s, 50% of 1H, CH═O); ^{11}B nmr (64 MHz, DMSO-d_6–Et_2OBF_3), δ (ppm): 4.5 ($W_{1/2}$ = 385 Hz); ^{11}B nmr (64 MHz, $CDCl_3$–Et_2OBF_3), δ (ppm): 4.3 ($W_{1/2}$ = 215 Hz) and 45.3 ($W_{1/2}$ = 300 Hz), ratio of peak areas: 3:2. Anal. calcd. for $C_{27}H_{34}BNO_3$: C 75.17, H 7.94, B 2.51, N 3.25; found: C 75.19, H 7.94, B 2.81, N 3.16. **6***d* gives a blue-colored solution upon addition of diphenylcarbazone as described for **6***a*. Crystals suitable for X-ray analysis were obtained by very slow crystallization from ethanol.

1-Methylpiperidinium 4-methoxy-2,2-diphenyl-1,3-dioxa-2-borata-1,2,3,4-tetrahydronaphthalenate, 6*e*

2 (0.29 g, 1.0 mmol) and 1-methylpiperidine (0.10 g, 1.0 mmol) are reacted in 10 mL of methanol in a procedure similar to that described for **6***a*. Yield: 0.30 g (72%) of colorless crystals; mp 98°C (MeOH). Infrared (KBr): 1608 (C═C) cm^{-1}; ^{1}H nmr (90 MHz, DMSO-d_6–TMS), δ (ppm): 1.23–1.73 (m, $C(CH_2)_3C$), 2.50 (s, N-CH_3), 2.63–2.90 (m, CH_2NCH_2), 3.20 (s, 60% of 3H, OCH_3), 3.40 (s, 40% of 3H, OCH_3), 5.26 (s, broad, exchangeable, NH), 5.46 (s, 60% of 1H, O-CH-O), 6.30–7.78 (m, 14 aromatic H), 10.30 (s, 40% of 1H, CH═O), 11.03 (s, partially exchangeable, 40% of 1H, phenolic OH); ^{1}H nmr (90 MHz, $CDCl_3$–TMS), δ (ppm): 1.13–1.80 (m, $C(CH_2)_3C$), 1.96–2.26 (m, CH_2NCH_2), 2.10 (s, N-CH_3), 3.70 (s, broad, OCH_3), 5.56 (s, 50% of 1H, O-CH-O), 6.46–7.90 (m, 14 aromatic H), 8.95 (s, broad, exchangeable, NH), 9.83 (s, 50% of 1H, CH═O); ^{11}B nmr (64 MHz, DMSO-d_6–Et_2OBF_3), δ (ppm): 4.4 ($W_{1/2}$ = 385 Hz); ^{11}B nmr (64 MHz, $CDCl_3$–Et_2OBF_3), δ (ppm): 3.9 ($W_{1/2}$ = 255 Hz) and 45.5 ($W_{1/2}$ = 300 Hz), ratio of peak areas: 3:2. Anal. calcd. for $C_{26}H_{32}BNO_3$: C 74.82, H 7.73, B 2.59, N 3.36; found: C 74.78, H 7.72, B 2.62, N 3.26. **6***e* gives a blue color reaction with diphenylcarbazone as described for **6***a*.

1-Methylpiperidinium 2,2-diphenyl-4-propoxy-1,3-dioxa-2-borata-1,2,3,4-tetrahydronaphthalenate, 6*f*

2 (0.29 g, 1.0 mmol) and 1-methylpiperidine (0.10 g, 1.0 mmol) are reacted in 10 mL of propanol in a procedure similar to that described for **6***a*. Yield: 0.32 g (72%) of yellowish crystals; mp 92°C (PrOH). Infrared (KBr): 1604 (C═C) cm^{-1}; ^{1}H nmr (90 MHz, DMSO-d_6–TMS), δ (ppm): 0.76–1.06 (m, C-CH_3), 1.20–1.73 (m, $OCCH_2$, $C(CH_2)_3C$), 2.46 (s, N-CH_3), 2.60–2.86 (m, CH_2NCH_2), 3.30–3.96 (m, OCH_2C), 5.50 (s, 70% of 1H, O-CH-O), 6.30–7.76 (m, 14 aromatic H), 11.03 (s, 30% of 1H, CH═O); ^{1}H nmr (90 MHz, $CDCl_3$–TMS), δ (ppm): 0.96 (t, J = 7 Hz, C-CH_3), 1.16–1.83 (m, $OCCH_2$, $C(CH_2)_3C$), 1.96–2.33 (m, CH_2NCH_2), 2.13 (s, N-CH_3), 3.90 (t, J = 7 Hz, OCH_2C), 5.36 (s, 50% of 1H, O-CH-O), 6.46–7.93 (m, 14 aromatic H), 8.96 (s, broad, exchangeable, NH), 9.80 (s, 50% of 1H, CH═O); ^{11}B nmr (64 MHz, DMSO-d_6–Et_2OBF_3), δ (ppm): 4.2 ($W_{1/2}$ = 342 Hz); ^{11}B nmr (64 MHz, $CDCl_3$–Et_2OBF_3), δ (ppm): 4.1 ($W_{1/2}$ = 300 Hz) and 45.3 ($W_{1/2}$ = 342 Hz), ratio of peak areas: 3:2. Anal. calcd. for $C_{28}H_{36}BNO_3$: C 75.51, H 8.15, B 2.43, N 3.14; found: C 75.05, H 8.20, B 2.92, N 3.00. **6***f* gives a blue color reaction with diphenylcarbazone as described for **6***a*.

1-Methylpiperidinium 4-isopropoxy-2,2-diphenyl-1,3-dioxa-2-borata-1,2,3,4-tetrahydronaphthalenate, 6*g*

2 (0.29 g, 1.0 mmol) and 1-methylpiperidine (0.10 g, 1.0 mmol) are reacted in 10 mL of 2-propanol in a procedure similar to that described for **6***a*. Yield: 0.38 g (85%) of yellowish crystals; mp 95°C (2-PrOH). Infrared (KBr): 1604 (C═C) cm^{-1}; ^{1}H nmr (90 MHz, DMSO-d_6–TMS), δ (ppm): 1.06 (d, J = 6 Hz, $(CH_3)_2C$), 1.33–1.73 (m, $C(CH_2)_3C$), 2.52 (s, N-CH_3), 2.63–2.90 (m, CH_2NCH_2), 3.66–4.26 (m, O-$CH(C)_2$), 5.56 (s, 60% of 1H, O-CH-O), 6.30–7.80 (m, 14 aromatic H and 1H, exchangeable, NH), 11.03 (s, 40% of 1H, CH═O); ^{1}H nmr (90 MHz, $CDCl_3$–TMS), δ (ppm): 1.23 (d, J = 6 Hz, $(CH_3)_2C$), 1.30–1.73 (m, $C(CH_2)_3C$), 2.20 (s, N-CH_3), 2.23–2.40 (m, CH_2NCH_2), 4.06–4.50 (m, O-$CH(C)_2$), 5.70 (s, 20% of 1H, O-CH-O), 6.83–7.90 (m, 14 aromatic H and 1H, exchangeable, NH), 9.83 (s, 80% of 1H, CH═O); ^{11}B nmr (64 MHz, DMSO-d_6–Et_2OBF_3), δ (ppm): 4.6 ($W_{1/2}$ = 385 Hz); ^{11}B nmr (64 MHz, $CDCl_3$–Et_2OBF_3), δ (ppm): 4.2 ($W_{1/2}$ = 300 Hz) and 45.1 ($W_{1/2}$ = 300 Hz), ratio of peak areas: 2:1. **6***g* gives a blue color reaction with diphenylcarbazone as described for **6***a*.

Quinuclidinium 6,10-epoxy-6,8-diphenyl-5,7,9-trioxa-8-bora-6-borata-5,6,7,8,9,10-hexahydrobenzocyclooctenate, 10*a*

Salicylaldehyde (0.61 g, 5.0 mmol) and phenylboronic acid (1.22 g, 10.0 mmol) are dissolved in 20 mL of ethanol. After the addition of quinuclidine (0.56 g, 5.0 mmol) to the stirred solution crystallization starts spontaneously after a few seconds or is provoked by refluxing for a short time. The colorless substance is recrystallized from absolute ethanol. Yield: 1.82 g (83%); mp 145°C (EtOH). Infrared (KBr): 1604 (C═C) cm^{-1}; ^{1}H nmr (90 MHz, DMSO-d_6–TMS), δ (ppm): 1.50–1.83 (m, $C(CH_2)_3C$), 1.93 (sept, J = 3 Hz, $HC(C)_3$), 2.90–3.23 (m, $N(CH_2)_3$), 5.96 (s, 80% of 1H, O-CH-O), 6.63 (s, broad, exchangeable, NH), 6.43–7.83 (m, 14 aromatic H), 10.22 (s, 20% of 1H, CH═O); ^{1}H nmr (90 MHz, $CDCl_3$–TMS), δ (ppm): 1.43–1.73 (m, $C(CH_2)_3C$), 1.85 (sept, J = 3 Hz, $HC(C)_3$), 2.86–3.16 (m, $N(CH_2)_3$), 6.50 (s, 10% of 1H, O-CH-O), 6.83–7.10 (m, 2 aromatic H), 7.20–7.60 (m, 8 aromatic H), 7.90–8.13 (m, 4 aromatic H), 8.96 (s, broad, exchangeable, NH), 9.86 (s, 90% of 1H, CH═O); ^{11}B nmr (64 MHz, DMSO-d_6–Et_2OBF_3), δ (ppm): 2.9 ($W_{1/2}$ = 342 Hz) and 28.3 ($W_{1/2} \approx$ 600 Hz), ratio of peak areas: 1:1. Anal. calcd. for $C_{26}H_{29}B_2NO_4$: C 70.79, H 6.63, B 4.90, N 3.18; found: C 70.59, H 6.72, B 4.83, N 2.99.

The identical compound is obtained by using only 5.0 mmol of phenylboronic acid (in an equimolar three-component reaction) in proportionate yields (40–45%). Using solvents such as methanol, benzene, or diethyl ether in place of ethanol has no effect on the result of the reaction.

1,4-Diazabicyclo[2.2.2]octanium 6,10-epoxy-6,8-diphenyl-5,7,9-trioxa-8-bora-6-borata-5,6,7,8,9,10-hexahydrobenzocyclooctenate, 10*b*

Salicylaldehyde (0.61 g, 5.0 mmol), phenylboronic acid (1.22 g, 10.0 mmol), and 1,4-diazabicyclo[2.2.2]octane (0.56 g, 5.0 mmol) are reacted as described for **10***a*. Yield: 1.70 g (77%) of colorless crystals; mp 110°C (EtOH). Infrared (KBr): 1605 (C═C) cm^{-1}; ^{1}H nmr (90 MHz, DMSO-d_6–TMS), δ (ppm): 2.90 (s, $N(C_2H_4)_3$), 5.86 (s, exchangeable,

© 1997 NRC Canada

Can. J. Chem. Downloaded from www.nrcresearchpress.com by 91.121.58.235 on 09/08/12
For personal use only.

NH), 6.06 (s, 70% of 1H, O-CH-O), 6.60–8.10 (m, 14 aromatic H), 10.40 (s, 30% of 1H, CH═O); ^{1}H nmr (90 MHz, $CDCl_3$–TMS), δ (ppm): 2.90 (s, $N(C_2H_4)_3$), 6.83–8.13 (m, 14 aromatic H), 9.83 (s, CH═O); ^{11}B nmr (64 MHz, DMSO-d_6–Et_2OBF_3), δ (ppm): 2.9 ($W_{1/2}$ = 342 Hz) and 28.3 ($W_{1/2} \approx$ 500 Hz), ratio of peak areas: 1:1. Anal. calcd. for $C_{25}H_{28}B_2N_2O_4$: C 67.92, H 6.38, B 4.89, N 6.34; found: C 67.88, H 6.47, B 4.80, N 6.34.

1-Methylpiperidinium 6,10-epoxy-6,8-diphenyl-5,7,9-trioxa-8-bora-6-borata-5,6,7,8,9,10-hexahydrobenzocyclooctenate, 10*c*

Salicylaldehyde (0.61 g, 5.0 mmol), phenylboronic acid (1.22 g, 10.0 mmol), and 1-methylpiperidine (0.50 g, 5.0 mmol) are reacted as described for **10***a*. Yield: 1.80 g (84%) of colorless crystals; mp 128°C (EtOH). Infrared (KBr): 1607 (C═C) cm^{-1}; ^{1}H nmr (90 MHz, DMSO-d_6–TMS), δ (ppm): 1.26–1.76 (m, $C(CH_2)_3C$), 2.53 (s, CH_3), 2.66–2.93 (m, CH_2NCH_2), 5.80 (s, broad, exchangeable, NH), 5.98 (s, 80% of 1H, O-CH-O), 6.46–7.90 (m, 14 aromatic H), 10.26 (s, 20% of 1H, CH═O); ^{1}H nmr (90 MHz, $CDCl_3$–TMS), δ (ppm): 1.20–1.76 (m, $C(CH_2)_3C$), 2.40 (s, CH_3), 2.53–2.83 (m, CH_2NCH_2), 6.10 (s, 10% of 1H, O-CH-O), 6.83–8.16 (m, 14 aromatic H), 9.60 (s, exchangeable, NH), 9.88 (s, 90% of 1H, CH═O); ^{11}B nmr (64 MHz, $CDCl_3$–Et_2OBF_3), δ (ppm): 3.1 ($W_{1/2}$ = 342 Hz) and 21.8 ($W_{1/2}$ = 600 Hz), ratio of peak areas: 1:10. Anal. calcd. for $C_{25}H_{29}B_2NO_4$: C 69.97, H 6.81, B 5.04, N 3.26; found: C 69.89, H 6.96, B 5.16, N 3.22.

Triethylammonium 6,10-epoxy-6,8-diphenyl-5,7,9-trioxa-8-bora-6-borata-5,6,7,8,9,10-hexahydrobenzocyclooctenate, 10*d*

Salicylaldehyde (0.61 g, 5.0 mmol), phenylboronic acid (1.22 g, 10.0 mmol), and triethylamine (0.51 g, 5.0 mmol) are reacted as described for **10***a*. Yield: 1.50 g (70%) of colorless crystals; mp 125°C (EtOH). Infrared (KBr): 1609 (C═C) cm^{-1}; ^{1}H nmr (90 MHz, DMSO-d_6–TMS), δ (ppm): 1.10 (t, J = 8 Hz, 3 CH_3), 2.92 (q, J = 8 Hz, $N(CH_2)_3$), 5.06 (s, broad, exchangeable, NH), 5.96 (s, 80% of 1H, O-CH-O), 6.43–7.86 (m, 14 aromatic H), 10.25 (s, 20% of 1H, CH═O); ^{1}H nmr (90 MHz, $CDCl_3$–TMS), δ (ppm): 0.90 (t, J = 8 Hz, 3 CH_3), 2.46 (t, J = 8 Hz, $N(CH_2)_3$), 6.03 (s, 50% of 1H, O-CH-O), 6.63–8.03 (m, 14 aromatic H), 8.85 (s, broad, exchangeable, NH), 9.90 (s, 50% of 1H, CH═O); ^{11}B nmr (64 MHz, $CDCl_3$–Et_2OBF_3), δ (ppm): 3.4 ($W_{1/2}$ = 428 Hz) and 28.7 ($W_{1/2} \approx$ 700 Hz), ratio of peak areas: 1:1. Anal. calcd. for $C_{25}H_{31}B_2NO_4$: C 69.65, H 7.25, B 5.01, N 3.25; found: C 69.65, H 7.46, B 5.12, N 3.18.

1-Methylpiperidinium 6,10-epoxy-4-methoxy-6,8-diphenyl-5,7,9-trioxa-8-bora-6-borata-5,6,7,8,9,10-hexahydrobenzocyclooctenate, 10*e*

2-Hydroxy-3-methoxybenzaldehyde (0.76 g, 5.0 mmol), phenylboronic acid (1.22 g, 10.0 mmol), and 1-methylpiperidine (0.50 g, 5.0 mmol) are reacted as described for **10***a*. Yield: 1.90 g (83%) of pale yellow crystals; mp 146°C (EtOH). Infrared (KBr): 1601 (C═C) cm^{-1}; ^{1}H nmr (90 MHz, DMSO-d_6–TMS), δ (ppm): 1.23–1.80 (m, $C(CH_2)_3C$), 2.62 (s, NCH_3), 2.83–3.06 (m, CH_2NCH_2), 3.70 (s, 80% of 3H, OCH_3), 3.83 (s, 20% of 3H, OCH_3), 6.00 (s, 80% of 1H, O-CH-O), 6.43–7.93 (m, 13 aromatic H and 1 NH, exchangeable), 10.32 (s, 20% of 1H, CH═O); ^{1}H nmr (90 MHz, $CDCl_3$–TMS), δ (ppm): 1.20–1.73 (m, $C(CH_2)_3C$), 2.40 (s, NCH_3), 2.46–2.80 (m, CH_2NCH_2), 3.73 (s, 25% of 3H, OCH_3), 3.90 (s, 75% of 3H, OCH_3), 6.13 (s, 25% of 1H, O-CH-O), 6.73–8.16 (m, 13 aromatic H), 8.70 (s, exchangeable, NH), 9.93 (s, 75% of 1H, CH═O); ^{1}H nmr (90 MHz, pyridine-d_5–TMS), δ (ppm): 1.26–1.70 (m, $C(CH_2)_3C$), 2.18 (s, NCH_3), 2.20–2.36 (m, CH_2NCH_2), 6.76–7.70 (m, 9 aromatic H), 8.16–8.46 (m, 4 aromatic H), 10.30 (s, broad, exchangeable, NH), 10.70 (s, CH═O); ^{11}B nmr (64 MHz, DMSO-d_6–Et_2OBF_3), δ (ppm): 2.9 ($W_{1/2}$ = 342 Hz) and 28.5 ($W_{1/2} \approx$ 700 Hz), ratio of peak areas: 1:1; ^{11}B nmr (64 MHz, $CDCl_3$–Et_2OBF_3), δ (ppm): 3.0 ($W_{1/2} \approx$ 700 Hz) and 21.2 ($W_{1/2} \approx$ 600 Hz). Anal. calcd. for $C_{26}H_{31}B_2NO_5$: C 68.01, H 6.81, B 4.71, N 3.05; found: C 67.91, H 6.96, B 4.36, N 3.04.

Crystals suitable for X-ray analysis were obtained by very slow cooling of an ethyl acetate solution of **10***e*.

1-Methylpiperidinium 2-chloro-6,10-epoxy-6,8-diphenyl-5,7,9-trioxa-8-bora-6-borata-5,6,7,8,9,10-hexahydrobenzocyclooctenate, 10*f*

5-Chloro-3-methoxybenzaldehyde (0.78 g, 5.0 mmol), phenylboronic acid (1.22 g, 10.0 mmol), and 1-methylpiperidine (0.50 g, 5.0 mmol) are reacted as described for **10***a*. Yield: 1.52 g (66%) of pale yellow crystals; mp 146°C (EtOH). Infrared (KBr): 1601 (C═C) cm^{-1}; ^{1}H nmr (90 MHz, DMSO-d_6–TMS), δ (ppm): 1.26–1.80 (m, $C(CH_2)_3C$), 2.60 (s, CH_3), 2.80–3.03 (m, CH_2NCH_2), 5.60 (s, broad, exchangeable, NH), 5.99 (s, 90% of 1H, O-CH-O), 6.62 (d, 1 aromatic H), 6.69–7.86 (m, 12 aromatic H), 10.25 (s, 10% of 1H, CH═O); ^{11}B nmr (64 MHz, DMSO-d_6–Et_2OBF_3), δ (ppm): 3.1 ($W_{1/2}$ = 300 Hz) and 30.3 ($W_{1/2}$ = 640 Hz), ratio of peak areas: 5:1. Anal. calcd. for $C_{25}H_{28}B_2ClNO_4$: C 64.77, H 6.09, B 4.66, Cl 7.65, N 3.02; found: C 64.36, H 6.08, B 4.77, Cl 7.67, N 2.90.

1-Methylpiperidinium 6,10-epoxy-2-nitro-6,8-diphenyl-5,7,9-trioxa-8-bora-6-borata-5,6,7,8,9,10-hexahydrobenzocyclooctenate, 10*g*

2-Hydroxy-5-nitrobenzaldehyde (0.84 g, 5.0 mmol), phenylboronic acid (1.22 g, 10.0 mmol), and 1-methylpiperidine (0.50 g, 5.0 mmol) are reacted as described for **10***a*. Yield: 1.40 g (59%) of pale yellow crystals; mp 170°C (EtOH). Infrared (KBr): 1608 (C═C) cm^{-1}; ^{1}H nmr (90 MHz, DMSO-d_6–TMS), δ (ppm): 1.30–1.83 (m, $C(CH_2)_3C$), 2.70 (s, CH_3), 4.76 (s, broad, partially exchangeable, NH), 6.21 (s, 90% of 1H, O-CH-O), 6.80 (d, 1 aromatic H), 7.10–8.20 (m, 12 aromatic H), 10.23 (s, 10% of 1H, CH═O); ^{11}B nmr (64 MHz, DMSO-d_6–Et_2OBF_3), δ (ppm): 3.5 ($W_{1/2}$ = 428 Hz) and 27.9 ($W_{1/2} \approx$ 700 Hz), ratio of peak areas: 5:1. Anal. calcd. for $C_{25}H_{28}B_2N_2O_6$: C 63.33, H 5.95, B 4.56, N 5.91; found: C 63.29, H 6.04, B 4.58, N 5.82.

X-ray crystallographic analyses of 6*d* and 10*e*

Crystallographic data appear in Table 1. The final unit-cell parameters were obtained by least-squares on the setting angles for 25 reflections with 2θ = 82.7–93.1° for **6***d* and 88.2–95.9° for **10***e*. The intensities of three standard reflections, measured every 200 reflections throughout the data collections, decayed linearly by 3.7% for **6***d* and showed only small

© 1997 NRC Canada

Can. J. Chem. Downloaded from www.nrcresearchpress.com by 91.121.58.235 on 09/08/12
For personal use only.

Table 1. Crystallographic data.[a]

Compound	**6***d*	**10***e*
Formula	$C_{27}H_{34}BNO_3$	$C_{26}H_{31}B_2NO_5$
fw	431.38	459.15
Crystal system	Monoclinic	Monoclinic
Space group	$P2_1/n$	$P2_1/n$
a, Å	9.522(1)	7.968(1)
b, Å	17.703(1)	19.3707(4)
c, Å	14.974(1)	15.9400(5)
β, °	98.275(10)	100.186(5)
V, Å^3	2497.8(4)	2421.6(2)
Z	4	4
ρ_{calc}, g/cm^3	1.147	1.259
F(000)	928	976
μ(Cu K_α), cm^{-1}	5.41	6.84
Crystal size, mm	0.35 × 0.45 × 0.50	0.25 × 0.25 × 0.30
Transmission factors	0.87–1.00	0.98–1.00
Scan type	ω–2θ	ω–2θ
Scan range, deg in ω	1.21 + 0.20 tan θ	0.94 + 0.20 tan θ
Scan speed, deg/min	32 (up to 9 scans)	16 (up to 9 scans)
Data collected	$+h, +k, \pm l$	$+h, +k, \pm l$
$2\theta_{max}$, deg	155	155
Crystal decay, %	3.7	Negligible
Total reflections	5658	5340
Total unique reflections	5330	4960
R_{merge}	0.027	0.016
Reflections with $I \geq 3\sigma(F^2)$	2815	3529
No. of variables	294	432
R	0.050	0.033
R_w	0.040	0.032
gof	1.02	2.63
Max Δ/σ (final cycle)	0.001	0.003
Residual density e/Å^3	−0.16 to 0.19	−0.12 to 0.16

[a]Temperature 294 K, Rigaku AFC6S diffractometer, Cu K_α radiation (λ = 1.54178 Å), graphite monochromator, takeoff angle 6.0°, aperture 6.0 × 6.0 mm at a distance of 285 mm from the crystal, stationary background counts at each end of the scan (scan:background time ratio 2:1), $\sigma^2(F^2) = [S^2(C + 4B)]/Lp^2$ (S = scan rate, C = scan count, B = normalized background count), function minimized $\Sigma w(|F_o| - |F_c|)^2$ where $w = 1$ for **6***d* and $w = 4F_o^2/\sigma^2(F_o^2)$ for **10***e*, $R = \Sigma||F_o| - |F_c||/\Sigma|F_o|$, $R_w = (\Sigma w(|F_o| - |F_c|)^2/\Sigma w|F_o|^2)^{1/2}$, and gof = $[\Sigma w(|F_o| - |F_c|)^2/(m-n)]^{1/2}$. Values given for *R*, R_w, and gof are based on those reflections with $I \geq 3\sigma(F^2)$.

random fluctuations for **10***e*. The data were processed,[3] corrected for Lorentz and polarization effects, decay (**6***d*), and absorption (based on azimuthal scans).

The structures were both solved by direct methods, the coordinates of the non-hydrogen atoms being determined from *E*-maps or from subsequent difference Fourier syntheses. For **6***d* the N-H hydrogen atom was refined with an isotropic thermal parameter and the carbon-bound hydrogen atoms were fixed in calculated positions with C—H = 0.98 Å and B_H = 1.2 $B_{bonded\ atom}$, and for **10***e* all hydrogen atoms were refined with isotropic thermal parameters. Corrections for secondary extinction were applied (Zachariasen type, isotropic, Gaussian), the final values of the extinction coefficients being $6.66(13) \times 10^{-6}$ for **6***d* and $2.26(5) \times 10^{-6}$ for **10***e*. Neutral atom scattering factors for all atoms and anomalous dispersion corrections for the non-hydrogen atoms were taken from the *International Tables for X-Ray Crystallography* (9). Final atomic coordinates and equivalent isotropic thermal parameters, bond lengths, bond angles, and intra-annular torsion angles appear in Tables 2–5, respectively. Hydrogen atom parameters, anisotropic thermal parameters, and torsion angles, intermolecular contacts, and least-squares planes are included as supplementary material.[4]

[3] *teXsan: Crystal structure analysis package*. Unix version 1.7. Molecular Structure Corporation. The Woodlands, Tex, U.S.A. 1995.

[4] Copies of material on deposit may be purchased from the Depository of Unpublished Data, Document Delivery, CISTI, National Research Council Canada, Ottawa, Canada K1A 0S2. Tables of hydrogen atom coordinates and bond lengths and angles involving hydrogen atoms have also been deposited with the Cambridge Crystallographic Data Centre and can be obtained on request from The Director, Cambridge Crystallographic Data Centre, University Chemical Laboratory, 12 Union Road, Cambridge CB2 1EZ, UK.

© 1997 NRC Canada

Can. J. Chem. Downloaded from www.nrcresearchpress.com by 91.121.58.235 on 09/08/12
For personal use only.

Table 2. Final atomic coordinates (fractional) and B_{eq} (10^3 Å^2).[a]

Atom	x	y	z	B_{eq}
		6*d*		
O(1)	0.1584(2)	0.34686(9)	0.1150(1)	6.39(5)
O(2)	0.0400(2)	0.26274(8)	0.2098(1)	4.83(4)
O(3)	−0.0164(2)	0.14154(9)	0.1641(1)	6.66(5)
N(1)	0.2424(3)	0.1909(1)	0.3365(2)	6.43(7)
C(1)	0.1745(3)	0.2865(1)	0.0630(2)	5.15(6)
C(2)	0.0986(3)	0.2195(1)	0.0686(2)	4.79(6)
C(3)	0.1214(3)	0.1593(1)	0.0130(2)	6.06(7)
C(4)	0.2164(4)	0.1649(2)	−0.0478(2)	7.66(10)
C(5)	0.2907(4)	0.2313(2)	−0.0532(2)	7.82(10)
C(6)	0.2699(3)	0.2914(2)	0.0010(2)	6.66(8)
C(7)	−0.0052(3)	0.2159(1)	0.1345(2)	5.23(7)
C(8)	−0.1449(4)	0.1283(2)	0.1999(3)	10.7(1)
C(9)	−0.1860(5)	0.0542(2)	0.2012(3)	11.8(1)
C(10)	−0.0917(3)	0.3824(1)	0.1440(2)	5.52(7)
C(11)	−0.0975(4)	0.4445(2)	0.0868(2)	7.56(9)
C(12)	−0.2242(6)	0.4822(2)	0.0569(3)	10.5(1)
C(13)	−0.3467(6)	0.4579(3)	0.0842(3)	11.3(2)
C(14)	−0.3467(4)	0.3966(2)	0.1401(3)	8.9(1)
C(15)	−0.2207(3)	0.3599(2)	0.1687(2)	6.67(8)
C(16)	0.1307(3)	0.3877(1)	0.2727(2)	5.31(7)
C(17)	0.0625(3)	0.3928(2)	0.3483(2)	6.45(8)
C(18)	0.1232(4)	0.4271(2)	0.4275(2)	8.3(1)
C(19)	0.2562(5)	0.4587(2)	0.4328(3)	9.2(1)
C(20)	0.3248(4)	0.4567(2)	0.3594(3)	8.4(1)
C(21)	0.2650(3)	0.4213(2)	0.2813(2)	6.71(8)
C(22)	0.3681(4)	0.2407(2)	0.3594(3)	8.4(1)
C(23)	0.4475(4)	0.2469(2)	0.2809(3)	9.7(1)
C(24)	0.4982(4)	0.1697(3)	0.2544(3)	10.3(1)
C(25)	0.3731(4)	0.1173(2)	0.2342(3)	8.5(1)
C(26)	0.2867(4)	0.1139(2)	0.3100(3)	8.02(10)
C(27)	0.1587(5)	0.1869(2)	0.4117(2)	10.2(1)
B(1)	0.0588(3)	0.3440(2)	0.1838(2)	5.17(7)
		10*e*		
O(1)	0.2922(1)	0.22259(5)	0.36873(6)	3.57(2)
O(2)	0.1606(1)	0.20601(5)	0.49132(7)	3.74(2)
O(3)	0.3382(1)	0.11100(5)	0.54496(6)	3.99(3)
O(4)	0.4664(1)	0.21310(5)	0.51041(6)	3.54(2)
O(5)	0.2456(2)	0.18386(5)	0.20693(6)	4.28(3)
N(1)	−0.1014(2)	0.22808(8)	0.3342(1)	4.91(4)
C(1)	0.3412(2)	0.14061(7)	0.26449(9)	3.32(3)
C(2)	0.3600(2)	0.16134(7)	0.35029(9)	3.05(3)
C(3)	0.4496(2)	0.11884(7)	0.41301(9)	3.13(3)
C(4)	0.5235(2)	0.05786(8)	0.3909(1)	3.80(4)
C(5)	0.5083(2)	0.03895(8)	0.3069(1)	4.18(4)
C(6)	0.4152(2)	0.07982(8)	0.2437(1)	3.90(4)
C(7)	0.4700(2)	0.14127(8)	0.50435(10)	3.58(3)
C(8)	0.2167(3)	0.1634(1)	0.1197(1)	5.07(5)
C(9)	0.2952(2)	0.32249(8)	0.47302(9)	3.34(3)
C(10)	0.3453(2)	0.36948(9)	0.4169(1)	4.23(4)
C(11)	0.3348(3)	0.4402(1)	0.4281(1)	5.79(5)
C(12)	0.2737(3)	0.4657(1)	0.4972(2)	6.54(6)
C(13)	0.2242(3)	0.4208(1)	0.5548(1)	6.19(6)
C(14)	0.2347(2)	0.35038(9)	0.5428(1)	4.64(4)
C(15)	0.0515(2)	0.12079(8)	0.58899(10)	3.60(3)
C(16)	−0.0512(2)	0.16814(9)	0.6216(1)	4.00(4)
C(17)	−0.1641(2)	0.14814(10)	0.6734(1)	4.38(4)
C(18)	−0.1821(2)	0.07946(10)	0.6911(1)	4.67(4)
C(19)	−0.0858(3)	0.03117(10)	0.6582(1)	5.49(5)
C(20)	0.0319(3)	0.05139(9)	0.6086(1)	4.84(4)
C(21)	−0.1086(3)	0.2682(1)	0.2534(1)	5.00(5)
C(22)	−0.0782(3)	0.3433(1)	0.2714(1)	5.20(5)
C(23)	−0.2029(3)	0.3727(1)	0.3229(1)	5.44(5)
C(24)	−0.1974(3)	0.3320(1)	0.4030(1)	5.97(6)
C(25)	−0.2271(3)	0.2568(1)	0.3860(1)	6.19(6)
C(26)	−0.1248(4)	0.1532(1)	0.3176(3)	8.24(9)
B(1)	0.3076(2)	0.24037(9)	0.4616(1)	3.26(4)
B(2)	0.1885(2)	0.14726(9)	0.5375(1)	3.58(4)

[a] $B_{eq} = (8/3)\pi^2\Sigma\Sigma(U_{ij}a_i{\cdot}a_j{\cdot}(\mathbf{a}_i\,\mathbf{a}_j))$.

Results and discussion

Compound 6

The reaction of **2** with a tertiary amine, or the one-pot reaction of equimolar amounts of salicylaldehyde, diphenylborinic acid anhydride, and a tertiary amine in the presence of an alkanol (R′OH), led to compounds with elemental analyses of "**3**+R′OH." The spectroscopic data cannot distinguish between the alternative structures **4**–**6** but the intermolecular salt structure **6** is established by the X-ray analysis of **6***d*, verifying the addition of R′OH to the aldehyde group and the formation of an *O*,*O*-acetal moiety within the chelate anion (at least in the solid state). The tertiary amine appears as a trialkylammonium cation hydrogen bonded to the organoborate anion in the crystal lattice.

In the ^{1}H nmr spectra of **6***a*–*g* partial solvolysis can be observed to different extents in the two chosen solvents, DMSO-d_6 and $CDCl_3$. In DMSO-d_6 between 60 and 100% of the acetalic O-CH-O grouping is retained, whereas in $CDCl_3$ an average of 50% of the acetal structure remains. Only compound **6***a* shows mostly (80%) acetal structure in $CDCl_3$, presumably due to the somewhat higher basicity of the incorporated quinuclidine relative to the other tertiary amines used (10). The partial elimination of R′OH from **6** leads to the free aldehyde group, similar to the observed elimination of the tertiary amine from **3** (6). Correspondingly, the ^{11}B nmr spectra of **6** in DMSO-d_6 mainly display a 100% signal for tetracoordinated (sp^3) boron between δ(Et_2OBF_3) values of 2.9 and 4.6 ppm, whereas in $CDCl_3$ only about 60% of the signal is found between 3.7 and 4.3 ppm (corresponding to tetracoordinated boron) while the remaining 40% appears between 44.9 and 45.5 ppm (trivalent (sp^2) boron) indicating esterified or free diphenylborinic acid (Ph_2B-O-R) (11). Considering the portion of intact acetal function in the ^{1}H nmr spectra of **6***d*–*g*, prepared with different alkanols, it seems that the isopropanol

© 1997 NRC Canada

Can. J. Chem. Downloaded from www.nrcresearchpress.com by 91.121.58.235 on 09/08/12
For personal use only.

Table 3. Bond lengths (Å) with estimated standard deviations in parentheses.

Bond	Length	Bond	Length
	6d		
O(1)—C(1)	1.343(3)	O(1)—B(1)	1.498(3)
O(2)—C(7)	1.415(3)	O(2)—B(1)	1.508(3)
O(3)—C(7)	1.398(3)	O(3)—C(8)	1.425(4)
N(1)—C(22)	1.487(4)	N(1)—C(26)	1.496(4)
N(1)—C(27)	1.472(4)	C(1)—C(2)	1.398(3)
C(1)—C(6)	1.392(4)	C(2)—C(3)	1.389(3)
C(2)—C(7)	1.495(3)	C(3)—C(4)	1.376(4)
C(4)—C(5)	1.379(4)	C(5)—C(6)	1.370(4)
C(8)—C(9)	1.368(4)	C(10)—C(11)	1.390(4)
C(10)—C(15)	1.391(4)	C(10)—B(1)	1.620(4)
C(11)—C(12)	1.395(5)	C(12)—C(13)	1.361(6)
C(13)—C(14)	1.370(6)	C(14)—C(15)	1.378(4)
C(16)—C(17)	1.387(4)	C(16)—C(21)	1.399(4)
C(16)—B(1)	1.605(4)	C(17)—C(18)	1.382(4)
C(18)—C(19)	1.376(5)	C(19)—C(20)	1.357(5)
C(20)—C(21)	1.376(4)	C(22)—C(23)	1.490(5)
C(23)—C(24)	1.522(5)	C(24)—C(25)	1.505(5)
C(25)—C(26)	1.497(5)		
	10e		
O(1)—C(2)	1.357(2)	O(1)—B(1)	1.504(2)
O(2)—B(1)	1.495(2)	O(2)—B(2)	1.352(2)
O(3)—C(7)	1.451(2)	O(3)—B(2)	1.371(2)
O(4)—C(7)	1.395(2)	O(4)—B(1)	1.462(2)
O(5)—C(1)	1.370(2)	O(5)—C(8)	1.424(2)
N(1)—C(21)	1.497(2)	N(1)—C(25)	1.512(3)
N(1)—C(26)	1.481(3)	C(1)—C(2)	1.408(2)
C(1)—C(6)	1.384(2)	C(2)—C(3)	1.391(2)
C(3)—C(4)	1.393(2)	C(3)—C(7)	1.500(2)
C(4)—C(5)	1.373(2)	C(5)—C(6)	1.388(2)
C(9)—C(10)	1.384(2)	C(9)—C(14)	1.396(2)
C(9)—B(1)	1.606(2)	C(10)—C(11)	1.387(2)
C(11)—C(12)	1.372(3)	C(12)—C(13)	1.373(3)
C(13)—C(14)	1.382(3)	C(15)—C(16)	1.390(2)
C(15)—C(20)	1.395(2)	C(15)—B(2)	1.564(2)
C(16)—C(17)	1.380(2)	C(17)—C(18)	1.373(2)
C(18)—C(19)	1.372(3)	C(19)—C(20)	1.387(3)
C(21)—C(22)	1.493(3)	C(22)—C(23)	1.509(3)
C(23)—C(24)	1.495(3)	C(24)—C(25)	1.495(3)

derivative (**6***g*) is the most responsive to solvolysis,[5] probably due to the sterically facilitated elimination of the bulkier alkanol group.

As expected, the solid state infrared spectra (KBr pellets) of **6** do not display any C═O stretching absorption in the region

[5] The degree of solvolysis is solvent dependent and does not seem to proceed uniformly in the different solvents. The behavior also varies for different derivatives of **6**. In most cases a signal for the methine CH═O proton of the restored aromatic aldehyde is found in the ^{1}H nmr spectra. In DMSO-d_6 solution this signal is sometimes accompanied by a signal arising from an associated OH proton, possibly from the released phenol group of the salicylaldehyde. The presence of free diphenylborinic acid (Ph_2BOH), however, cannot be ruled out.

Table 4. Bond angles (deg) with estimated standard deviations in parentheses.

Bonds	Angle (deg)	Bonds	Angle (deg)
	6d		
C(1)-O(1)-B(1)	120.5(2)	C(7)-O(2)-B(1)	112.8(2)
C(7)-O(3)-C(8)	112.5(2)	C(22)-N(1)-C(26)	110.7(3)
C(22)-N(1)-C(27)	111.0(3)	C(26)-N(1)-C(27)	111.3(3)
O(1)-C(1)-C(2)	122.5(2)	O(1)-C(1)-C(6)	118.5(2)
C(2)-C(1)-C(6)	119.0(2)	C(1)-C(2)-C(3)	119.2(2)
C(1)-C(2)-C(7)	118.1(2)	C(3)-C(2)-C(7)	122.6(2)
C(2)-C(3)-C(4)	121.0(3)	C(3)-C(4)-C(5)	119.5(3)
C(4)-C(5)-C(6)	120.6(3)	C(1)-C(6)-C(5)	120.6(3)
O(2)-C(7)-O(3)	109.2(2)	O(2)-C(7)-C(2)	110.3(2)
O(3)-C(7)-C(2)	109.6(2)	O(3)-C(8)-C(9)	115.2(3)
C(11)-C(10)-C(15)	115.6(3)	C(11)-C(10)-B(1)	120.8(3)
C(15)-C(10)-B(1)	123.4(2)	C(10)-C(11)-C(12)	122.1(4)
C(11)-C(12)-C(13)	119.4(4)	C(12)-C(13)-C(14)	120.7(4)
C(13)-C(14)-C(15)	119.1(4)	C(10)-C(15)-C(14)	123.0(3)
C(17)-C(16)-C(21)	115.2(3)	C(17)-C(16)-B(1)	120.9(2)
C(21)-C(16)-B(1)	123.8(3)	C(16)-C(17)-C(18)	122.8(3)
C(17)-C(18)-C(19)	119.7(3)	C(18)-C(19)-C(20)	119.3(3)
C(19)-C(20)-C(21)	120.8(3)	C(16)-C(21)-C(20)	122.2(3)
N(1)-C(22)-C(23)	110.1(3)	C(22)-C(23)-C(24)	110.8(4)
C(23)-C(24)-C(25)	109.5(3)	C(24)-C(25)-C(26)	112.2(3)
N(1)-C(26)-C(25)	111.7(3)	O(1)-B(1)-O(2)	108.6(2)
O(1)-B(1)-C(10)	110.3(2)	O(1)-B(1)-C(16)	108.5(2)
O(2)-B(1)-C(10)	111.3(2)	O(2)-B(1)-C(16)	107.3(2)
C(10)-B(1)-C(16)	110.6(2)		
	10e		
C(2)-O(1)-B(1)	116.6(1)	B(1)-O(2)-B(2)	119.0(1)
C(7)-O(3)-B(2)	116.2(1)	C(7)-O(4)-B(1)	110.5(1)
C(1)-O(5)-C(8)	117.2(1)	C(21)-N(1)-C(25)	110.5(2)
C(21)-N(1)-C(26)	111.7(2)	C(25)-N(1)-C(26)	112.6(2)
O(5)-C(1)-C(2)	115.3(1)	O(5)-C(1)-C(6)	124.7(1)
C(2)-C(1)-C(6)	120.0(1)	O(1)-C(2)-C(1)	118.8(1)
O(1)-C(2)-C(3)	122.4(1)	C(1)-C(2)-C(3)	118.8(1)
C(2)-C(3)-C(4)	120.4(1)	C(2)-C(3)-C(7)	118.7(1)
C(4)-C(3)-C(7)	120.9(1)	C(3)-C(4)-C(5)	120.3(2)
C(4)-C(5)-C(6)	119.9(2)	C(1)-C(6)-C(5)	120.5(2)
O(3)-C(7)-O(4)	110.3(1)	O(3)-C(7)-C(3)	110.7(1)
O(4)-C(7)-C(3)	110.9(1)	C(10)-C(9)-C(14)	116.1(2)
C(10)-C(9)-B(1)	123.2(1)	C(14)-C(9)-B(1)	120.7(1)
C(9)-C(10)-C(11)	122.4(2)	C(10)-C(11)-C(12)	119.8(2)
C(11)-C(12)-C(13)	119.6(2)	C(12)-C(13)-C(14)	120.0(2)
C(9)-C(14)-C(13)	122.0(2)	C(16)-C(15)-C(20)	117.1(2)
C(16)-C(15)-B(2)	119.5(1)	C(20)-C(15)-B(2)	123.3(1)
C(15)-C(16)-C(17)	121.9(2)	C(16)-C(17)-C(18)	119.9(2)
C(17)-C(18)-C(19)	119.8(2)	C(18)-C(19)-C(20)	120.4(2)
C(15)-C(20)-C(19)	120.9(2)	N(1)-C(21)-C(22)	111.1(2)
C(21)-C(22)-C(23)	111.9(2)	C(22)-C(23)-C(24)	110.0(2)
C(23)-C(24)-C(25)	112.3(2)	N(1)-C(25)-C(24)	111.0(2)
O(1)-B(1)-O(2)	106.1(1)	O(1)-B(1)-O(4)	110.7(1)
O(1)-B(1)-C(9)	110.0(1)	O(2)-B(1)-O(4)	108.9(1)
O(2)-B(1)-C(9)	109.8(1)	O(4)-B(1)-C(9)	111.2(1)
O(2)-B(2)-O(3)	122.4(2)	O(2)-B(2)-C(15)	119.9(1)
O(3)-B(2)-C(15)	117.6(1)		

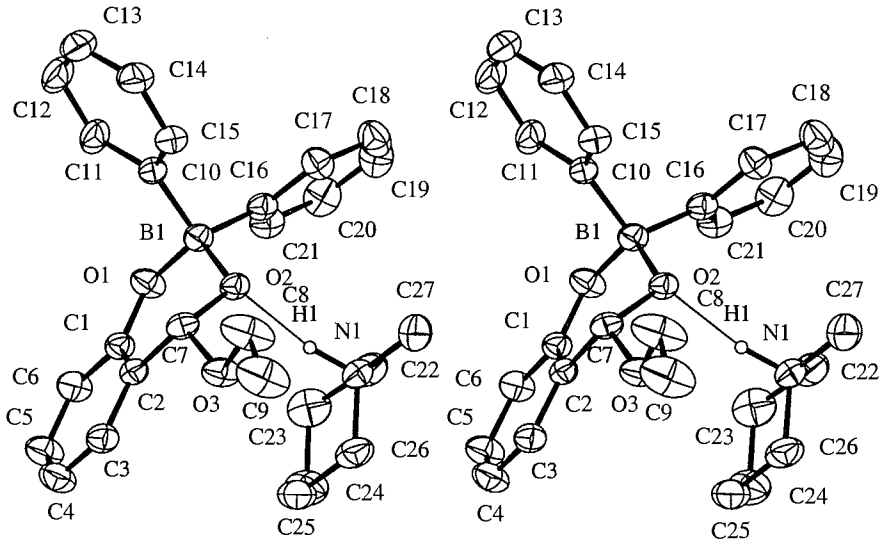
© 1997 NRC Canada

Can. J. Chem. Downloaded from www.nrcresearchpress.com by 91.121.58.235 on 09/08/12
For personal use only.

Table 5. Intra-annular torsion angles (deg) with standard deviations in parentheses.

Atoms	Value (deg)	Atoms	Value (deg)
		6d	
O(1)-C(1)-C(2)-C(7)	0.7(4)	N(1)-C(22)-C(23)-C(24)	−59.8(4)
C(1)-C(2)-C(7)-O(2)	−30.4(3)	C(22)-C(32)-C(24)-C(25)	56.8(4)
C(2)-C(7)-O(2)-B(1)	57.9(3)	C(23)-C(24)-C(25)-C(26)	−53.7(5)
C(7)-O(2)-B(1)-O(1)	−54.9(3)	C(24)-C(25)-C(26)-N(1)	53.7(4)
O(2)-B(1)-O(1)-C(1)	24.2(3)	C(25)-C(26)-N(1)-C(22)	−55.5(4)
B(1)-O(1)-C(1)-C(2)	1.4(4)	C(26)-N(1)-C(22)-C(23)	58.6(4)
		10e	
O(1)-C(2)-C(3)-C(7)	0.8(2)	O(2)-B(2)-O(3)-C(7)	3.3(2)
C(2)-C(3)-C(7)-O(4)	−27.8(2)	B(2)-O(3)-C(7)-O(4)	35.4(2)
C(3)-C(7)-O(4)-B(1)	57.5(2)	O(3)-C(7)-O(4)-B(1)	−65.5(1)
C(7)-O(4)-B(1)-O(1)	−61.3(2)	C(7)-O(4)-B(1)-O(2)	55.0(1)
O(4)-B(1)-O(1)-C(2)	33.4(2)	O(4)-B(1)-O(2)-B(2)	−16.4(2)
B(1)-O(1)-C(2)-C(3)	−4.3(2)	B(1)-O(2)-B(2)-O(3)	−12.3(2)
N(1)-C(21)-C(22)-C(23)	−56.5(2)	C(23)-C(24)-C(25)-N(1)	55.7(3)
C(21)-C(22)-C(23)-C(24)	55.2(3)	C(24)-C(25)-N(1)-C(21)	−55.4(2)
C(22)-C(23)-C(24)-C(25)	−54.9(3)	C(25)-N(1)-C(21)-C(22)	56.0(2)

Fig. 1. Stereoview of ***6d***; 20% probability thermal ellipsoids are shown for the non-hydrogen atoms.

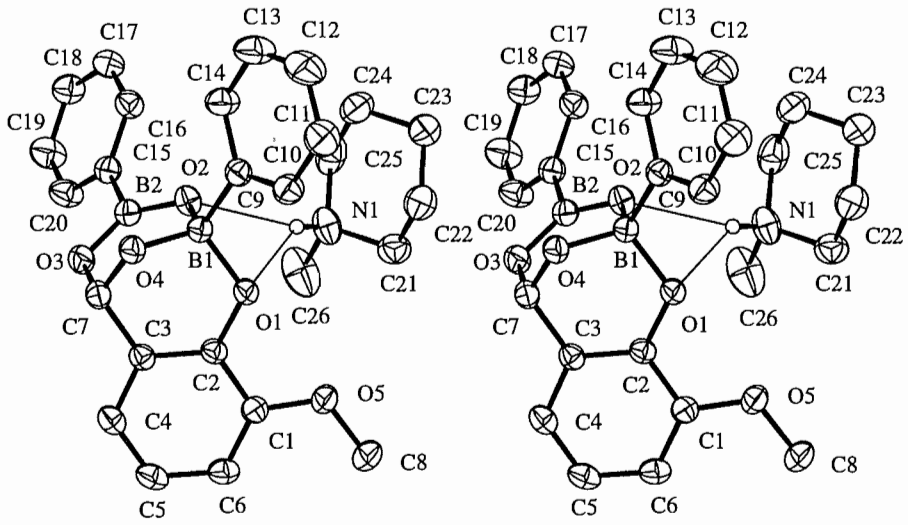


of aldehyde carbonyl vibrations, indicative of the conversion of the aldehyde group in **1** or **2** into the *O,O*-acetal function of **6**. This also provides additional proof that the chelate anion of **6** is stable in the crystalline state.

To the best of our knowledge, ***6d*** is the first structurally characterized diphenylboron chelate of a salicylaldehyde semiacetal. The structure of ***6d*** consists of cation–anion pairs (Fig. 1), associated by a N—H···O hydrogen bond (N(1)—H(1) = 1.01(3) Å, H(1)···O(2) = 1.81(3) Å, N(1)···O(2) = 2.808(3) Å, N(1)-H(1)···O(2) = 170(3)°). The slightly bent geometry of the N(1)—H(1)···O(2) hydrogen bond may be the result of a weak N—H···π(phenyl) interaction. Atom H(1) is displaced 2.48 Å from the mean plane of the C(1–6) phenyl ring and the H(1)···C(2) distance is 3.23(3) Å. The ion pairs are separated from one another by normal van der Waals distances. The general geometry of the chelate ring is reminiscent of the ring system in compound **3** (6). The carbonyl C=O double bond of the salicylaldehyde diphenylboron chelate **2**, which has a C—O bond distance of 1.261(4) Å (12), is lengthened by 0.15 Å in the ethanol adduct ***6d*** to 1.415(3) Å. The lengthening in this case is even greater than that observed for the quinuclidine adduct **3** (R_3N = quinuclidine) (6), which retains some of the double bond character of its C—O bond (1.362(4) Å) with an estimated π-bond order of 0.3 (from plots of bond lengths vs. π-bond order (13)). Compound ***6d*** shows a nearly complete loss of the double bond character of

© 1997 NRC Canada

Fig. 2. Stereoview of **10***e*; 33% probability thermal ellipsoids are shown for the non-hydrogen atoms. Carbon-bound hydrogen atoms are omitted for clarity.



the C(7)—O(2) bond. An additional factor in the lengthening of the C(7)—O(2) bond in **6***d* may be the involvement of one oxygen electron pair in the O(2)···H(1)—N(1) hydrogen bond to the tertiary amine.

The six-membered boron chelate ring in **6***d* displays a distorted "O(2)-envelope" conformation (see Table 5), the fused benzene ring being coplanar with the approximately planar B(1)-O(1)-C(1)-C(2)-C(7) ring segment. In contrast to the quinuclidine adduct **3**, with a (pseudo-) axial orientation of the added tertiary amine (6), the ethoxy group in **6***d* is in a (pseudo-) equatorial position. As in **2** (12) and in **3** (6) the (pseudo-) axial *B*-phenyl group in the molecule **6***d* has a somewhat longer B—C(phenyl) bond distance than the equatorial *B*-phenyl substituent (**2**: 1.610(5) Å (ax), 1.603(5) Å (eq); **3**: 1.623(5) Å (ax), 1.613(5) Å (eq); **6***d*: 1.620(4) Å (ax), 1.605(4) Å (eq)). This is a general trend in complexes of this type (ref. 6, and refs. therein).

The tetrahedral arrangement about the boron atom includes a nearly strain-free O-B-O angle of 108.6(2)°, similar to the corresponding angle of 108.0(3)° in **3** (R_3N = quinuclidine) (6). There is a chiral centre at C(7), the *R* enantiomer being depicted in Fig. 1. The centrosymmetric crystal structure contains equal numbers of *R* and *S* enantiomers. The hydrogen-bonded *N*-methpiperidinium cation has a normal chair conformation (see Table 5) with the methyl group in an equatorial position and the hydrogen atom in an axial position.

The relatively short C—C distance between the carbonyl C atom and the aryl carbon atom in **2** (1.413(5) Å) (12) is lengthened in **6***d* to 1.495(3) Å between C(2) and C(7) because of the loss of resonance between the benzene ring and the carbonyl double bond. Similar lengthening of the C(carbonyl)—C(aryl) bond can be seen in the molecule of **3** (R_3N = quinuclidine, C—C = 1.504(5) Å) (6), and also in another salicylaldehyde derivative **11** (1.494(2) Å) that represents an intramolecular adduct of a nitrogen base to a salicylaldehyde boron chelate (14). The ammonium salt structure of the ethanol adduct **6***d* corroborates structural postulations made for the diphenylphosphine oxide adducts **12** (15).

Compound 10

The exchange of diphenylborinic acid for phenylboronic acid in the three-component reaction system did not lead to an adduct or chelate **7** by analogy to compound **3** (6) nor to the postulated structure **7** (R_3N = H_2N-CH(C_4H_9)COOH) of an amino acid adduct to the phenylboronate complex (2). Instead the analytical data suggested a composition "**7** + PhBO." This means the incorporation of one additional mole equivalent of phenylboronic acid (anhydride), and could be the result of pyroboronate formation to give **8** as a direct derivative from **7**. A similar hydrogen bond-stabilized anhydride structure **13** has been formulated for the boronates of 1,3-diketones (16). However, an isomeric amine adduct **9** with incorporation of the second boronic acid molecule at the acetal function could not be overlooked. The structure **10**, combining the pyroboronate and the acetal boronate functions in a polycyclic anion with an associated ammonium cation, also had to be considered. Indeed, the latter molecular structure **10** is established by an X-ray analysis of **10***e* (Fig. 2), which gave the most suitable single crystals.

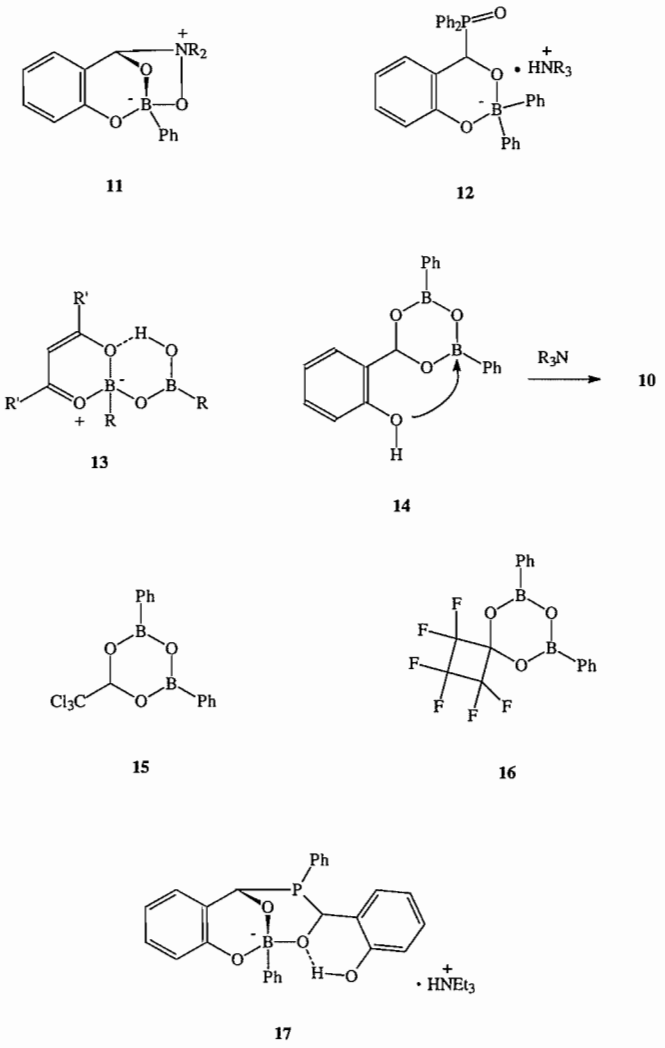
The acetal pyroboronate partial structure in **10** can be thought of as stabilized by ring-closing intramolecular complex formation of the monocyclic salicylaldehyde derivative **14** in the presence of a proton-accepting amine (Scheme 2). Stable six-membered condensates of a carbonyl compound and two molecules of phenylboronic acid were otherwise obtained only from aldehydes or ketones with strong electron-withdrawing substituents, as reported for **15** (17) or **16** (18). The compounds **10** are obtained in approximately the same yields, no matter whether one or two mole equivalents of phenylboronic acid are applied in the reaction. It seems that the formation of the bridged anion of **10** is favored and the relatively poor solubility of the salts **10** leads to spontaneous crystallization, withdrawing the product from an equilibrium reaction. In the solutions prepared for nmr spectra, a solvent-dependent instability is obvious. In DMSO-d_6 the ratio of the intact acetalic group to the solvolytic free-set aldehyde group ranges from 9:1 to 2:1, based on integration of the O-CH-O

Can. J. Chem. Downloaded from www.nrcresearchpress.com by 91.121.58.235 on 09/08/12
For personal use only.

© 1997 NRC Canada

Can. J. Chem. Downloaded from www.nrcresearchpress.com by 91.121.58.235 on 09/08/12
For personal use only.

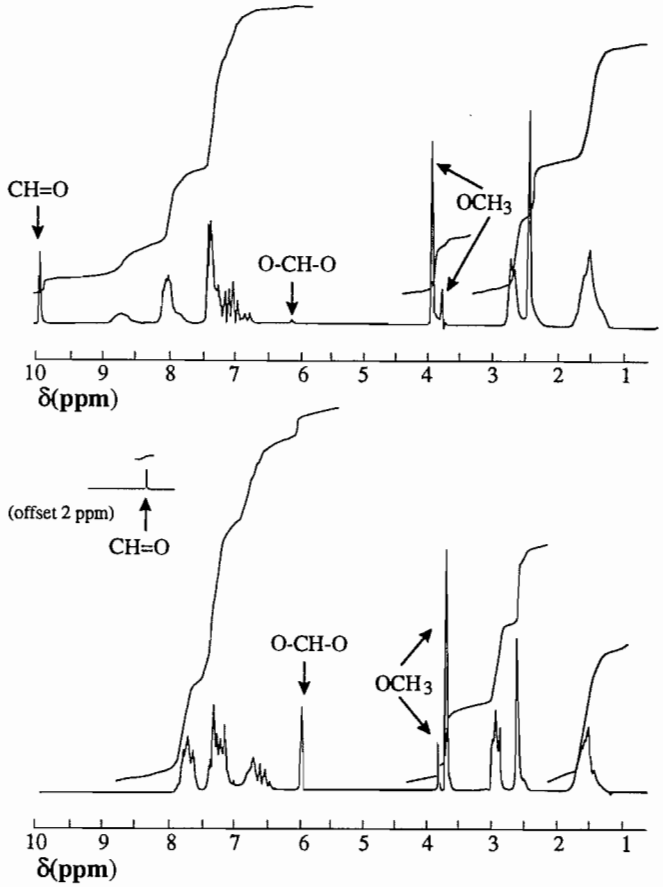
Scheme 2.



and CH═O signals in the ^{1}H nmr spectra. The ^{11}B nmr spectra in DMSO-d_6 show an expected 1:1 ratio of tetracoordinate (sp^3) boron to trivalent (sp^2) boron nuclei or, in some instances, a predominant tetracoordinate boron species. In the $CDCl_3$ solutions of **10** the proportions are essentially reversed, in the ^{1}H as well as in the ^{11}B nmr spectra. This is clearly demonstrated by the ^{1}H nmr spectra of **10***e* (characterized by X-ray analysis) in DMSO-d_6 and $CDCl_3$ shown in Fig. 3. The correspondence of the ratios of the aldehyde or acetal methine proton signals with those of the *ortho*-methoxy group of the aldehyde or acetal moiety is striking. The nature and structures of the various possible solvolysis products and the pathways of interaction with the solvents, however, is not clear at this point.

The overall geometry of **10***e* is characterized by two main (folded-leaf) planes, defined by the atoms [O(2), O(3), C(15)] and [O(1), C(2), C(3), C(7)] with a dihedral angle of 64.9°, parted by an oxygen bridge O(4) into two six-membered rings with O(4)-envelope ("sofa") conformations (see Table 5). The bond angle at the oxygen bridge (110.5(1)°) shows a lesser degree of strain than observed for the oxygen-bridged compound **11** (B-O-C = 102.1(1)°) where the oxygen bridge produces six- and five-membered heterocycles (14).

Fig. 3. The ^{1}H nmr spectra of **10***e* in $CDCl_3$ (top) and in DMSO-d_6 (bottom).



The planar boronate function at B(2) involves two short O—B bonds (1.371(2) and 1.352(2) Å), demonstrating the partial π-bond character that results from the *pp*(π) back donation from the two oxygen atoms to the boron atom. The O(2)—B(2) distance is shorter by 0.02 Å because of the more distinct double bond character typical for bonds within B(sp^3)-O-B(sp^2) anhydridic systems. The involvement of O(2) in the hydrogen bond to N(1) does not significantly decrease the partial double bond character of the O(2)—B(1) bond. The B(2)—C(15) bond length of 1.564(2) Å is similar to those observed for other phenylboronates with trigonal (sp^2) boron atoms. The B(1)—C(9) distance of 1.606(2) Å, similarly, corresponds to a normal B(sp^3)—C(phenyl) bond. The slightly distorted tetrahedron about B(1) is completed by longer O—B bonds in the range 1.462(2)–1.504(2) Å. Despite a supposed interaction between the trigonal planar boron atom B(2) and the aromatic system of the *B*-phenyl ring, the 32.6° angle between normals to the mean planes of the *B*-phenyl ring and the planar O-B-O boronate ring segment of the BOBOCO heterocycle represents a considerable deviation from coplanarity.

The difference between the two acetalic C—O bond lengths corresponds to different adjacent boron connections: the longer C(7)—O(3) bond (1.451(2) Å) involves the boronic ester group and resembles the C—O distances in acylals (19), whereas the shorter C(7)—O(4) bond (1.395(2) Å) is part of the anionic tetrahedral boronate moiety and is like the C—O bonds in acetal systems (19). Correspondingly, the O(3)—

© 1997 NRC Canada

B(2) bond is shorter than the O(4)—B(1) bond. The sum of bond lengths for the two C(7)-O-B ring segments, however, remains fairly consistent (C(7)-O(3)-B(2): 2.822 Å, C(7)-O(4)-B(1): 2.857 Å).

The structure of **10***e* consists of cation–anion pairs (Fig. 2), associated by a weak three-centre ("bifurcated") N-H(···O)$_2$ hydrogen bond system involving O(1) and O(2). The hydrogen bond geometry is as follows: N(1)—H(18) = 0.88(2) Å, H(18)···O(2) = 2.24(2) Å, N(1)···O(2) = 2.994(2) Å, N(1)-H(18)···O(2) = 144(2)°, H(18)···O(1) = 2.32(2) Å, N(1)···O(1) = 3.089(2) Å, N(1)-H(18)···O(1) = 146(2)°. Both N···O distances in this system are at the long end of the reported range of N—H···O distances (20). The acute O(1)···H(18)···O(2) angle of 63(2)° is a consequence of the fact that O(1) and O(2) are separated by only one atom (both are bonded to B(1)). Another factor contributing to the overall weakness of this bifurcated hydrogen-bonding system is a nonideal angle of approach by the N-H vector to both oxygen atoms. In the case of sp^3-hybridized O(1) the C(2)-O(1)···H(18) and B(1)-O(1)···H(18) angles (ideally 109.5°) are 120(2)° and 85(2)°, respectively, and for sp^2-hybridized O(2) the B(1)-O(2)···H(18) and B(2)-O(2)···H(18) angles (ideally 120°) are 88(2)° and 134(2)°, respectively. Furthermore, H(18) is displaced 1.42 Å from the B(1)O(2)B(2) plane suggesting that the interaction with O(2) has a significant π-component. The associated ion-pair units are linked by weak C—H···O interactions: C(8)—H(5)···O(4)($-1/2 + x$, $1/2 - y$, $-1/2 + z$), C(8)—H(5) = 0.96(2) Å, H(5)···O(4) = 2.44(2) Å, C(8)···O(4) = 3.393(2) Å, C(8)-H(5)···O(4) = 175(2)°. The anion of **10***e* possesses two chiral centres at B(1) and C(7), the *R,R* enantiomer being depicted in Fig. 2. The crystal lattice contains equal numbers of *R,R* and *S,S* enantiomers.

Compound **10***e*, to the best of our knowledge, is the first example of a salicylaldehyde bisboronate to be structurally characterized. In contrast to the intramolecular compensation of charge in the *N,B*-betainic hydroxylamine derivative **11** (14), the incorporation of phenylboronic acid into the salicylaldehyde–boronate complex leads to the benzocyclooctene ring system and results in the overall negative charge. Another heterocyclic benzocyclooctene compound **17**, derived from salicylaldehyde, phenylboronic acid, and a phosphorus component, has been crystallized as a tertiary ammonium salt and structurally characterized (21).

Acknowledgments

We thank the Natural Sciences and Engineering Research Council of Canada and the Fonds der Chemischen Industrie, Frankfurt am Main, for financial support. We are grateful to the Chemische Institute der Technishen Universität Braunschweig for running the ^{11}B nmr spectra.

References

1. W.P. Jencks. Catalysis in chemistry and enzymology. McGraw–Hill, New York. 1969.
2. G. Rao and M. Philipp. J. Org. Chem. **56**, 1505 (1991), and refs. therein.
3. R.H. Holm. *In* Inorganic biochemistry. *Edited by* G.L. Eichhorn. Elsevier, Amsterdam. 1975. pp. 1137–1190.
4. P.R. Andrews, J.M. Gulbis, M.N. Iskander, and M.F. Mackay. Aust. J. Chem. **40**, 1073 (1987).
5. W. Kliegel. Bor in Biologie, Medizin und Pharmazie. Springer, Berlin. 1980.
6. W. Kliegel, K. Drückler, S.J. Rettig, and J. Trotter. Can. J. Chem. **71**, 919 (1993).
7. (*a*) F. Umland and C. Schleyerbach. Angew. Chem. **77**, 426 (1965); (*b*) I. Bally, A. Arsene, M. Bacescu–Roman, and A.T. Balaban. Tetrahedron Lett. 3929 (1965).
8. (*a*) R. Neu. Z. Anal. Chem. **176**, 334 (1960); (*b*) B. Friese and F. Umland. Anal. Chim. Acta, **96**, 303 (1978).
9. (*a*) International tables for X-Ray crystallography. Vol. IV. Kynoch Press, Birmingham, U.K. (present distributor Kluwer Academic Publishers, Boston, Mass., U.S.A.). 1974. pp. 99–102; (*b*) International tables for crystallography. Vol. C. Kluwer Academic Publishers, Boston, Mass., U.S.A. 1992. pp. 200–206.
10. D.D. Perrin. Dissociation constants of organic bases in aqueous solution. Butterworths, London. 1965.
11. (*a*) H. Nöth and B. Wrackmeyer. Nuclear magnetic resonance spectroscopy of boron compounds. Springer, Berlin. 1978; (*b*) R. Köster. Organoborverbindungen III. Vol. XIII/3c. *Edited by* Houben-Weyl. Thieme, Stuttgart. 1984.
12. S.J. Rettig and J. Trotter. Can. J. Chem. **54**, 1168 (1976).
13. G. Häfelinger. Chem. Ber. **103**, 2922 (1970).
14. W. Kliegel, H.-W. Motzkus, K. Drückler, S.J. Rettig, and J. Trotter. Can. J. Chem. **68**, 64 (1990).
15. A.S. Balueva, S.R. Prokhorova, and G.N. Nikonov. Izv. Akad. Nauk SSSR Ser. Khim. 196 (1992); Bull. Russ. Acad. Sci. Div. Chem. Sci. 162 (1992).
16. R. Köster, K. Angermund, A. Sporzynski, and J. Serwatowski. Chem. Ber. **119**, 1931 (1986).
17. R.L. Letsinger and S.B. Hamilton. J. Org. Chem. **25**, 592 (1960).
18. G.W. Parshall. Inorg. Chem. **4**, 52 (1965).
19. A.G. Orpen, L. Brammer, F.H. Allen, O. Kennard, D.G. Watson, and R. Taylor. *In* Structure correlation. Vol. 2. *Edited by* H.-B. Bürgi and J.D. Dunitz. VCH, Weinheim. 1994. p. 751.
20. (*a*) F. Hibbert and J. Emsley. Adv. Phys. Org. Chem. **26**, 255 (1990); (*b*) J. Bernstein, M.C. Etter, and L. Leiserowitz. *In* Structure correlation. Vol. 2. *Edited by* H.-B. Bürgi and J.D. Dunitz. VCH, Weinheim. 1994. p. 431.
21. I.A. Litvinov. Zh. Strukt. Khim. **31**, 194 (1990); J. Struct. Chem. **31**, 359 (1990).
22. W. Kliegel, U. Schumacher, S.J. Rettig, and J. Trotter. Can. J. Chem. **74**, 445 (1996).

Can. J. Chem. Downloaded from www.nrcresearchpress.com by 91.121.58.235 on 09/08/12
For personal use only.

© 1997 NRC Canada

Ring A building blocks for taxoids and taxamycins

Michael W. Tjepkema, Peter D. Wilson, Hélène Audrain, and Alex G. Fallis

Abstract: The syntheses of a series of oxygenated cyclohexene ring A synthons **20**, **22–27**, **34**, **36**, and **37** that possess suitable functionality for further elaboration for taxoid synthesis are described. These compounds have been prepared from β-ionone by a series of oxidative and addition reactions or alternatively by Lewis acid catalyzed Diels–Alder cycloadditions with the oxygen-containing trimethyl substituted dienes **31** and **33**.

Key words: taxoid, paclitaxel, dienes, Diels–Alder, β-ionone.

Résumé : On décrit les synthèses d'une série de synthons (**20**, **22–27**, **34**, **36** et **37**) du cycle A, à cyclohexène oxygéné, qui possèdent des fonctions appropriées pour des élaborations ultérieurs dans la synthèse de taxoïdes. On a préparé ces produits à partir de la β-ionone par une série de réactions d'oxydation et d'addition ou, d'une façon alternative, par des cycloadditions de Diels–Alder catalysées par les acides de Lewis avec les dienes triméthylés **31** et **33** contenant de l'oxygène.

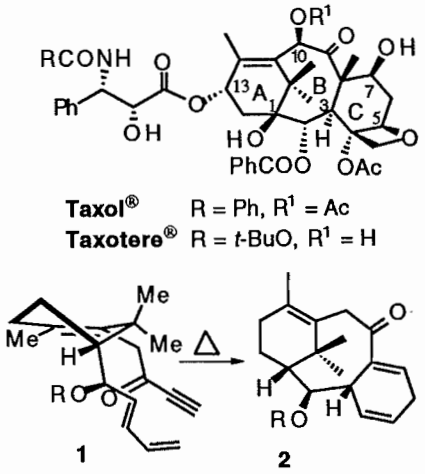
Mots clés : taxoïde, paclitaxel, dienes, Diels–Alder, β-ionone.

[Traduit par la rédaction]

Introduction

The proven clinical utility of the potent antitumor agents paclitaxel (Taxol®) (1) and docetaxel (Taxotere®) for the treatment of ovarian and breast cancer has established the taxoids as an important new class of chemotherapeutic agents. These compounds belong to a new group of antitumor drugs that interfere with the normal microtubule–tubulin cascade prior to cell division (2). This novel mode of action, plus the significant synthetic challenge presented by the sterically congested multicyclic structure has stimulated worldwide interest in these molecules (3). Recently, three groups have reported total syntheses of Taxol® (4–6). In spite of this success, many factors remain to be investigated and over the next decade it is likely that simpler analogues with a better therapeutic profile will be synthesized and become useful pharmaceutical products. They will thus follow the path from natural products to medicine established earlier for penicillins, tetracyclines, etc. This path depends upon an improved knowledge of structure–activity relationships, the further development of efficient synthetic and (or) semi-synthetic routes to the functionalized tricyclo[9.3.1.$0^{3,8}$]pentadecene nucleus, and the development and synthesis of medicinally interesting analogues that possess a better therapeutic profile than paclitaxel itself. The semi-synthetic analogue docetaxel has established that this is possible (7).

Scheme 1. Previous studies.



We have been developing an intramolecular Diels–Alder strategy that proceeds in the left to right direction (ring A to ABC) (8). Ring A cyclohexene building blocks are used as anchors to facilitate an intramolecular Diels–Alder reaction to construct the B and C rings simultaneously. Model studies using this convergent approach led to the functionalized tricyclo[9.3.1.$0^{3,8}$]pentadecene skeleton. The C_2 epimer controls the adduct stereochemistry in accord with other studies concerning the π-facial selectivity of related cycloadditions (9). This is represented by the successful preparation of the adduct **2** from **1** (Scheme 1).

Synthetic strategy

As our research has progressed the field has advanced rapidly and a better understanding of the factors that must be considered in any synthetic approach to the taxoids has emerged. In

Received February 26, 1997.

This paper is dedicated to Professor W.A. Ayer on the occasion of his 65th birthday. Presented with respect and gratitude for his contributions to chemical education and organic chemistry.

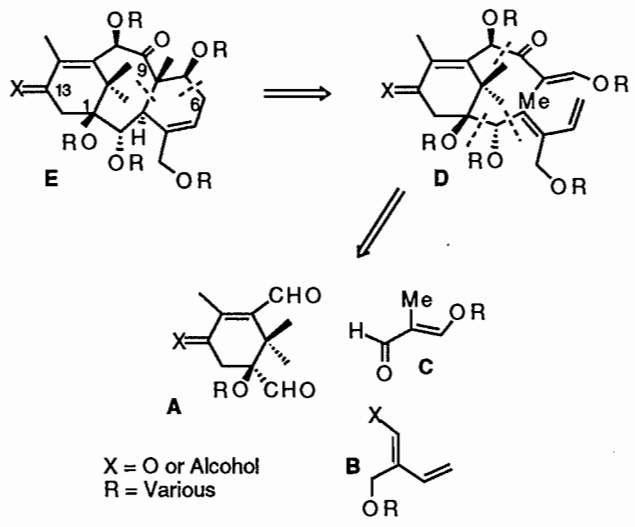
M.W. Tjepkema, P.D. Wilson, H. Audrain, and A.G. Fallis.[1] Department of Chemistry, University of Ottawa, 10 Marie Curie Street, Ottawa, ON K1N 6N5, Canada.

[1] Author to whom correspondence may be addressed. Telephone: (613) 562-5732. Fax: (613) 562-5170. E-mail: afallis@oreo.uottawa.ca

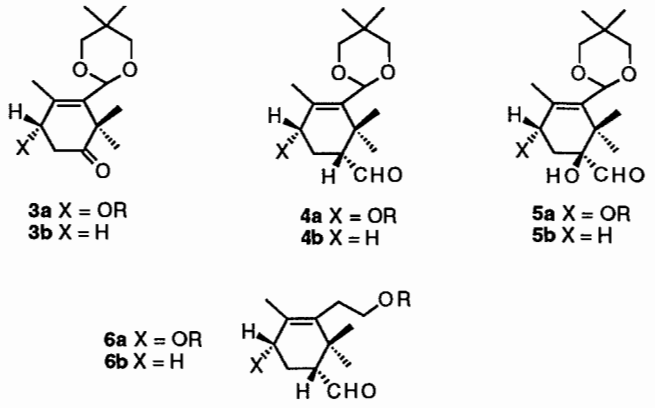
© 1997 NRC Canada

Can. J. Chem. Downloaded from www.nrcresearchpress.com by 91.121.58.235 on 09/08/12
For personal use only.

Scheme 2. Convergent A to ABC intramolecular Diels–Alder approach.



Scheme 3. Ring A building blocks.



particular, it has proven difficult to manipulate many of the required oxygen-containing centres in the intact nucleus. Consequently, it is preferable to carry several of the required functional groups from an early stage. In a retrosynthetic sense, removal of the ring D oxetane followed by a double disconnection between C_6—C_7 and C_3—C_8 in ring C (retro-Diels–Alder) in an intermediate such as **E** suggests a precursor related to the tetraene **D** (Scheme 2). In principle this intermediate could contain the majority of the paclitaxel (Taxol®) oxygen substituents, although in practice the use of less substituted systems may be more prudent. Construction of **D** may be envisaged in a direct manner from further disconnections between C_2—C_3 or C_3—C_4 and C_9—C_{10}. In total this leads to a highly convergent approach to the taxane nucleus from a suitably functionalized ring A building block in the form of a masked dialdehyde synthon related to **A** followed by attachment of the lower diene and upper dienophile units **B** and **C**, respectively. An intramolecular Diels–Alder cycloaddition should then afford the carbocyclic nucleus. Based on the success of our model system we wish to report the extension of these ideas through the synthesis of more highly functionalized ring A building blocks by more efficient routes than our original sequence (10). Suitable substituted cyclohexene ring A synthons are represented by the structures **3**–**6** (Scheme 3). These arise retrosynthetically from cleavage of the C_1—C_2 and C_9—C_{10} bonds or, alternatively, the C_2—C_3 and C_9—C_{10} bonds. These structures may be compared with the idealized compound **A**. The interconversions and cycloadditions described afford direct routes to a diverse family of ring A building blocks. These have formed the basis of our initial studies for the synthesis of taxoids and the related bicyclic taxoid-enediyne mimics the taxamycins (11).

Results and discussion

β-Ionone functionalization

Initially, an attractive target for further functionalization was the enol ether β-diketone represented by **15** (Scheme 4). This planar ketone lacks chirality but direct conversion into the desired optically active compounds may be envisaged via the asymmetric addition of a silyl cyanide in the presence of a titanium catalyst as a hydroxy aldehyde equivalent (12). To investigate this possibility the side-chain double bond of β-ionone (**8**) was cleaved selectively with ozone (13) followed by dimethyl sulfide work-up. (Scheme 4) The resulting aldehyde was treated directly with oxalic acid and ethylene glycol to afford the acetal **9** in 45% yield. Various allylic oxidation reagents failed to provide ketone **11**, and the acetal displayed a tendency to hydrolyze readily. Thus a bromination, solvolysis, oxidation protocol was developed. The reaction of **9** with *N*-bromosuccinimide (NBS) in the presence of the radical initiator 2,2′-azobis(isobutyronitrile) (AIBN) afforded the allylic bromide. Direct treatment with potassium carbonate – water – dimethyl sulfoxide afforded the alcohol, which was oxidized under Swern conditions to provide the desired enone **11** (94%). The triisopropylsilyl enol ether **12** was prepared by exposure to potassium hexamethyldisilazide and quenching with triisopropylsilyl chloride (TIPSCl) (86%). Unfortunately, conditions could not be found to effect allylic oxidation and generate the masked β-diketone **15** directly. The fragility of the ethylidene acetal, plus the multistep oxidation sequence required, prompted a change in our approach.

The ozonolysis of **8** was repeated and the intermediate aldehyde was treated with 2,2-dimethyl-1,3-propanediol in refluxing benzene to afford the acetal **7** (64%). Allylic oxidation was accomplished efficiently by a two-step, one-pot sequence. Initial treatment of **7** under buffered conditions with selenium dioxide in refluxing toluene afforded a keto-alcohol mixture that was oxidized directly with pyridinium dichromate (PDC) in dichloromethane containing magnesium sulfate to provide the unsaturated ketone **10** (62%) Direct introduction of the double bond to provide the dienone **13** (85%) with 2,3-dichloro-5,6-dicyano-1,4-benzoquinone (DDQ) failed. Thus the dienone was prepared by selenoxide elimination. Treatment of the ketone **10** with lithium diisopropylamide (LDA) and phenylselenylbromide gave the selenide, which was oxidized with Oxone® in methanol to provide the diene **13** (65%). Of several oxidants examined, Oxone® was the only one that afforded reasonable yields of the diene.

Various nucleophiles (MeS^-, CN^-) could be added in a conjugate manner to the dienone **13** but the size of the nucleophile plus the balance between its nucleophilicity and leaving group ability was critical. For example, lithium thiophenoxide was

© 1997 NRC Canada

Can. J. Chem. Downloaded from www.nrcresearchpress.com by 91.121.58.235 on 09/08/12
For personal use only.

Reaction conditions:
(*a*) O_3, CH_2Cl_2, −78°C; Me_2S; oxalic acid, $HOCH_2CH_2OH$, C_6H_6, 80°C, 45%; (*b*) NBS, AIBN, CCl_4, 78%; KOH, DMSO, H_2O, 50°C, 29%; $(COCl_2)_2$, DMSO, CH_2Cl_2, Et_3N, −78 to 21°C, 94%; (*c*) $KN(TMS)_2$, THF, −78°C; TIPSCI, HMPA, 86%; (*d*) O_3, CH_2Cl_2, −78°C; Me_2S; oxalic acid, $HOCH_2CMe_2CH_2OH$, C_6H_6, 80°C, 64%; (*e*) SeO_2, KH_2PO_4, toluene, 110°C; PDC, $MgSO_4$, CH_2Cl_2, 62%; (*f*) LDA, THF, −78°C, PhSeBr; Oxone,® $NaHCO_3$, MeOH, 56%; (*g*) LiSMe, MeOH, 0°C, 87%; (*h*) THF, CH_2=CHMgBr, CuI, TMSCI, −78°C, 69%; (*i*) NCS, CCl_4, 78°C, 97%; (*j*) TlPSOTf, CH_2Cl_2, collidine, 21°C, 95%; (*k*) $NaBH_4$, MeOH, $CeCl_3 \cdot 7H_2O$, 0°C, 96%; (*l*) O_3, CH_2Cl_2, −78°C, Me_2S, 56%; (*m*) TBSTf, collidine, CH_2Cl_2, 21°C, 72%; (*n*) TPSCl, imidazole, DMAP, CH_2Cl_2, 21°C, 96%; (*o*) O_3, CH_2Cl_2, −78°C, Me_2S, 99%; (*p*) O_3, CH_2Cl_2, −78°C, Me_2S, 97%; (*q*) TBSOTf, collidine, CH_2Cl_2, 21°C; O_3, CH_2Cl_2, −78°C; Me_2S, 17%; (*r*) TMSCN, KCN, 18-crown-6, 21°C, 94%.

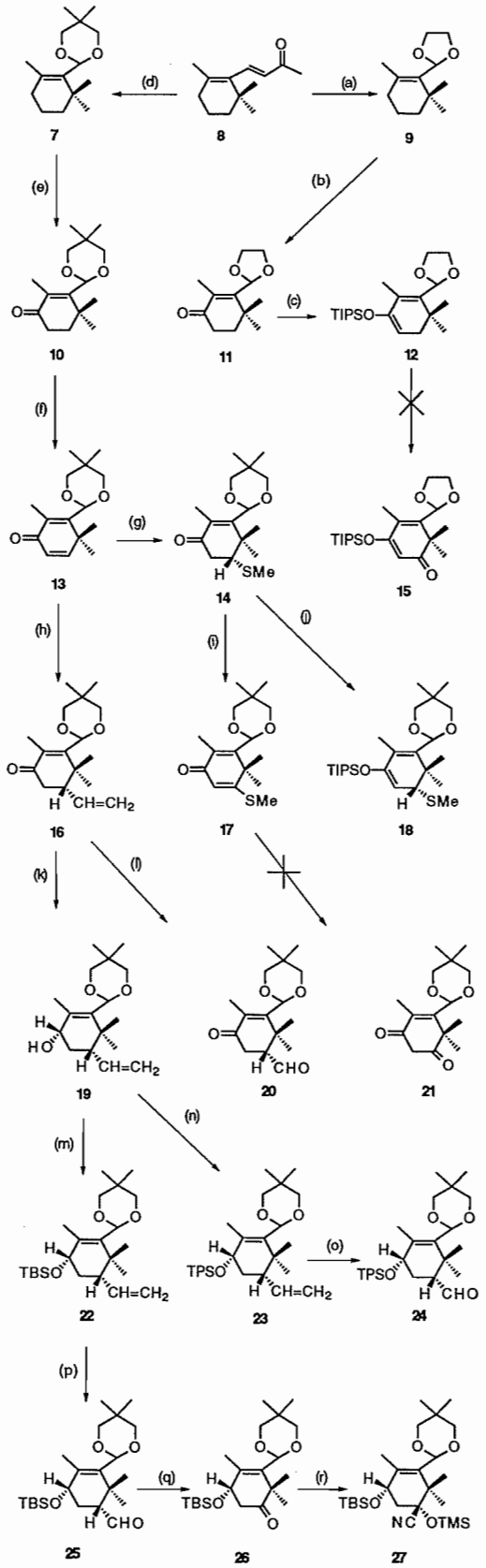
Fig. 1. Preferential direction of nucleophilic attack.



inert while lithium thiomethoxide afforded an 87% yield of ketone **14**. Treatment of this keto-sulfide with *N*-chlorosuccinimide (NCS) in refluxing carbon tetrachloride afforded the thio-enol ether **17** in 97% yield. Thus the reaction did not stop after the initial chlorination, but elimination occurred rapidly to give the unsaturated material. In principle it should be straightforward to convert this compound to the diketone **21.** However, exposure to mercuric chloride in the presence of calcium carbonate in aqueous acetonitrile at temperatures from 21 to 100°C failed to generate any of the diketone. A final attempt was made to prepare a compound related to **21** by conversion of ketone **14** to the enol ether **18** by exposure to collidine and triisopropylsilyl trifluoromethanesulfonate (95%). In this case also, attempted oxidation to the sulfoxide with dimethyldioxirane at 0°C followed by Pummerer rearrangement failed to provide the acetal enol-ether ketone related to structure **15**, and instead gave the dienone **13**, which presumably arose from sulfoxide elimination instead.

The desired oxygenated cyclohexenes have therefore been synthesized by the following route. The addition of the cuprate derived from vinyl magnesium bromide, cuprous iodide, and trimethylsilyl chloride (TMSCl) to the dienone **13** proceeded smoothly to afford the vinyl ketone **16** in 69% yield. Carbonyl reduction with sodium borohydride in the presence of cerium trichloride generated the C_{13} alcohol **19** as a single diastereomer in which attack occurred preferentially *anti* to the vinyl substituent (Fig. 1, **28**). Protection of the hydroxyl function in **19** as a silyl ether with collidine and *tert*-butyldimethylsilyl trifluoromethanesulfonate (TBSTf) afforded ether **22**. Alternatively treatment of **19** with 4–dimethylaminopyridine, triethylamine, and *tert*-butyldiphenylchlorosilane (TPSCl) afforded the vinyl ether **23** (96%). Selective ozonolysis of the vinyl group in ketone **16** provided direct access to the keto-aldehyde **20** (56%). In a parallel manner ozonolysis of **22** gave the aldehyde **25** in 96% yield. Similarly ozonolysis of **23**

Scheme 4. Ring A functionalization.



Can. J. Chem. Downloaded from www.nrcresearchpress.com by 91.121.58.235 on 09/08/12
For personal use only.

© 1997 NRC Canada

afforded **24**. These aldehydes correspond to the building block **4a**. The aldehyde group in **25** was converted to its *tert*-butyldimethylsilyl enol ether and treated directly with ozone to provide the ketone **26** containing a C_1 carbonyl (Taxol® numbering) corresponding to the building block **3a**. Subsequent addition of trimethylsilylcyanide (TMSCN) to **26** afforded the bis-silyl ether nitrile **27** in which the two ether substituents possessed a *syn* relationship. This stereochemistry is a consequence of the addition *anti* to the C_{13} ether as illustrated in **29** (Fig. 1). This compound is a masked form of the compound **5a** in which the oxygen substituents have the opposite relative orientation to the C_{13} and C_2 oxygens in paclitaxel (Taxol®). However, for our Diels–Alder approach to the tricyclic nucleus, this relative stereochemistry appeared to be required to avoid a 1,3 interaction between this C_{13} group and the diene side chain (8). While this research was in progress Stork and co-workers (14) have developed a different preparation of epimeric C_{13} ring A alcohol intermediates, and Kuwajima and co-workers (15) utilized a related silyl enol ether from an aldehyde related to **25** to prepare chiral C_1 hydroxyaldehyde systems. Many other routes to ring A synthons have also been reported (16) including some that employ an intramolecular Diels–Alder reaction to construct the required cyclohexene ring (17).

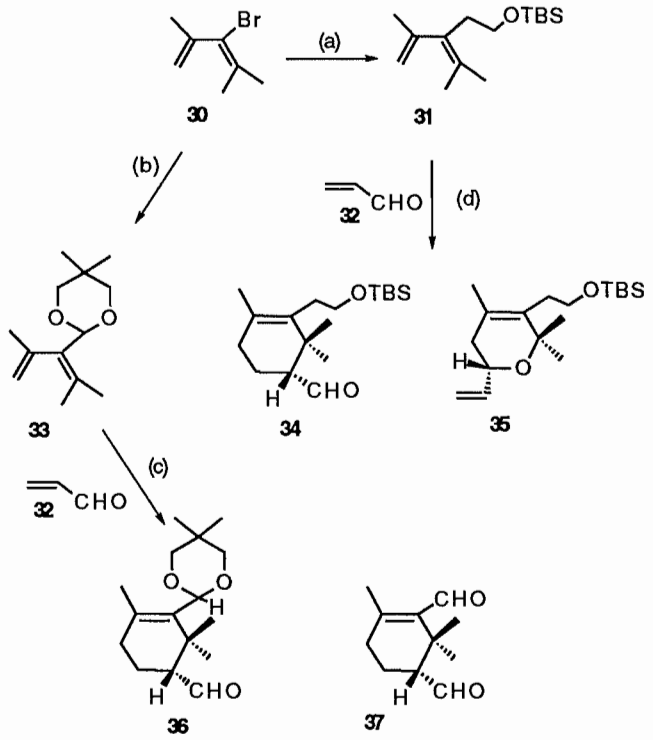
Cycloaddition route

Our earlier studies (8) and the results above demonstrated that the C_{13} oxygen could be introduced by allylic oxidation. Consequently for certain investigations it was desirable to have ring A synthons available that lacked this oxygenation pattern and could be synthesized rapidly. A cycloaddition approach was thus very attractive. The desired trimethyldienes **31** and **33** (Scheme 5) were synthesized from the bromodiene **30**. This compound was prepared in 90% yield in two steps from 2,3-dimethylbutene via rapid pyrolysis of the corresponding 1,1-dibromo-2,2,3,3-tetramethylcyclopropane (18). Treatment of **30** with *tert*-butyllithium to effect halogen metal exchange, followed by nucleophilic addition of the organolithium reagent to ethylene oxide, afforded the primary alcohol, which was protected directly as the *tert*-butyldimethylsilyl ether **31**. Alternatively, condensation of the organolithium reagent derived from **30** with dimethylformamide (DMF) provided the anticipated vinyl aldehyde, which upon treatment with 2,2-dimethyl-1,3-propanediol and oxalic acid afforded the diene acetal **33** in 84% overall yield.

Cycloaddition in various combinations generated the requisite ring A synthons. Diels–Alder cycloaddition of diene **33** with acrolein (**32**) at −78°C in the presence of boron trifluoride etherate ($BF_3{\cdot}Et_2O$) provided the adduct **36** in 60% yield accompanied by 15% of the dialdehyde **37**. In a similar fashion, cyclization of diene **31** also proceeded smoothly with acrolein at −78°C to afford the adduct **34** (67%, i.e., **6**, Scheme 3). In this instance the hetero Diels–Alder adduct **35** was also formed (27%). This product, although not unexpected, does not appear to have been observed by others in these systems.

In conclusion, commencing with β-ionone, sequential modification of the cyclohexene nucleus has provided access to several highly functionalized ring A building blocks. Alternatively, less oxygenated synthons may be constructed rapidly by appropriate [4 + 2] cycloadditions. These building blocks have been utilized for the synthesis of more advanced intermediates for taxoids and for the preparation of diverse taxamycin systems of various ring sizes.[2]

Scheme 5. Cycloaddition route to ring A.



Reaction conditions:
(*a*) *t*-BuLi, ethylene oxide, −78 to 21°C, 78%; TBSCl, imidazole, CH_2Cl_2, 62%; (*b*) *t*-BuLi, DMF, −78 to 21°C, $HOCH_2CMe_2CH_2OH$, oxalic acid, C_6H_6, 80°C, 84%; (*c*) $BF_3{\cdot}Et_2O$, CH_2Cl_2, −78°C, 60%; (*d*) $BF_3{\cdot}Et_2O$, CH_2Cl_2, −78°C, 67%.

Experimental

For general methods see ref. 8.

2,6,6-Trimethylcyclohexene-1-carboxaldehyde neopentylidene acetal (7)

Ozone was passed through a stirred solution of β-ionone **8** (20.0 g, 104 mmol) in dichloromethane (250 mL) at −78°C until the starting material was consumed (TLC). Dimethyl sulfide (7 mL) was then added and the reaction mixture was allowed to warm slowly to ambient temperature (21°C) over 12 h. The reaction mixture was then concentrated to afford the crude enal. 2,2-Dimethyl-1,3-propanediol (44 g, 0.42 mol) and oxalic acid dihydrate (0.5 g) were added to a stirred solution of the crude enal in benzene (150 mL) and the resultant mixture was heated at reflux in a Dean–Stark water separator for 10 h. The reaction mixture was then cooled to ambient temperature and treated with a saturated aqueous solution

[2] S. Py and A.G. Fallis, unpublished results; C.W. Harwig, Ph.D thesis, University of Ottawa, January 1997; B. Comanita, Ph.D thesis, University of Ottawa, January 1997.

© 1997 NRC Canada

Can. J. Chem. Downloaded from www.nrcresearchpress.com by 91.121.58.235 on 09/08/12
For personal use only.

Can. J. Chem. Downloaded from www.nrcresearchpress.com by 91.121.58.235 on 09/08/12
For personal use only.

of sodium bicarbonate (100 mL) and diluted with ether (500 mL). The organic phase was separated, washed with water (5 × 50 mL), brine (2 × 25 mL), dried, and concentrated. Chromatography (hexanes) afforded the acetal **7** (15.8 g, 64%) as a light yellow oil that was crystallized from hexane to afford a white solid; mp 38–40.5°C; IR ($CHCl_3$): 3011, 2935, 1658, 1464, 1220, 1090 cm^{-1}; ^1H NMR (200 MHz, $CDCl_3$) δ: 0.73 (s, 3H), 1.03 (s, 6H), 1.27 (s, 3H), 1.38–1.43 (m, 2H), 1.51–1.58 (m, 2H), 1.94–2.00 (m, 2H), 1.96 (s, 3H), 3.47–3.69 (m, 4H), 4.86 (s, 1H); ^{13}C NMR (50 MHz, $CDCl_3$) δ: 19.1, 20.7, 22.0, 23.9, 28.1, 30.0, 33.6, 39.5, 78.3, 101.8, 134.3, 135.2; HRMS (EI) calcd. for $C_{15}H_{26}O_2$: 238.1934; found: 238.1918.

2,6,6-Trimethylcyclohexene-1-carboxaldehyde ethylidene acetal (9)

Ozone was passed through a stirred solution of β-ionone **8** (10.0 mL, 49.1 mmol) in dichloromethane (125 mL) at −78°C until the starting material was consumed (TLC). Dimethyl sulfide (20 mL) was then added and the reaction mixture was allowed to warm slowly to ambient temperature over 12 h. The reaction mixture was then concentrated to afford the crude enal. Ethylene glycol (30 mL) and oxalic acid dihydrate (100 mg) were added to a stirred solution of the crude enal in benzene (150 mL) and the resultant mixture was heated at reflux in a Dean–Stark water separator for 22 h. The reaction mixture was then cooled to ambient temperature, treated with a saturated aqueous solution of sodium bicarbonate (20 mL), and diluted with ether (100 mL). The organic phase was separated, washed with a saturated aqueous solution of sodium bicarbonate (25 mL), then with brine (2 × 50 mL), dried, and concentrated. The residual oil was distilled (Kugelrohr, oven temperature ~130°C, 20 Torr (1 Torr = 133.3 Pa) to afford the acetal **9** (4.3 g, 45%) as a pale yellow oil; IR ($CHCl_3$): 2940, 1450, 1230, 1035 cm^{-1}; ^1H NMR (200 MHz, $CDCl_3$) δ: 1.06 (s, 6H), 1.37–1.49 (m, 2H), 1.52–1.55 (m, 2H), 1.74 (s, 3H), 1.93–2.02 (m, 2H), 3.82–4.06 (m, 4H), 5.31 (s, 1H); ^{13}C NMR (50 MHz, $CDCl_3$) δ:19.1, 23.9, 28.2, 34.1, 35.1, 40.1, 64.4, 102.3, 132.2, 137.3; HRMS (EI) calcd. for $C_{12}H_{20}O_2$: 196.1464; found: 196.1462.

3-Oxo-2,6,6-trimethylcyclohexene-1-carboxaldehyde neopentylidene acetal (10)

Potassium dihydrogen phosphate (8.59 g, 63.1 mmol) and selenium dioxide (4.95 g, 47.0 mmol) were added to a stirred solution of the acetal **7** (4.80 g, 20.0 mmol) in toluene (280 mL). The resultant mixture was heated at reflux until the starting material was consumed (~2 h, TLC and GC) and then cooled to ambient temperature. The reaction mixture was then treated with a saturated aqueous solution of sodium bicarbonate (100 mL) and diluted with ether (250 mL). The organic phase was separated, washed with a saturated aqueous solution of sodium bicarbonate (50 mL), then with brine (50 mL), dried, and concentrated to afford a mixture of the ketone **10** and the corresponding allylic alcohol as a viscous black oil. Magnesium sulfate (1.75 g, 14.6 mmol) and pyridinium dichromate (7.52 g, 20.0 mmol) were added sequentially to a solution of the above mixture of products in dichloromethane (50 mL). The resultant mixture was stirred at ambient temperature for 3.5 h and then filtered through a pad of Florisil® with ether. The filtrate was concentrated and then chromatographed (10% ethyl acetate in hexanes) to afford the ketone **10** (3.1 g, 62%) as a pale yellow oil that crystallized on standing; mp 67.5–69.5°C; IR ($CHCl_3$): 2946, 1673, 1466, 1086, 1017 cm^{-1}; ^1H NMR (200 MHz, $CDCl_3$) δ: 0.75 (s, 3H), 1.23 (s, 9H), 1.28 (s, 3H), 1.79 (apparent t, 2H), 2.45 (apparent t, 2H), 3.50 (apparent d, J = 11.1 Hz, 2H), 3.72 (apparent d, J = 11.1 Hz, 2H), 5.07 (s, 1H); ^{13}C NMR (50 MHz, $CDCl_3$) δ: 11.9, 22.0, 23.8, 26.4, 30.2, 34.0, 35.0, 37.8, 78.1, 101.5, 133.8, 155.3, 199.8; HRMS (EI) calcd. for $C_{15}H_{24}O_3$: 252.1726; found: 252.1742.

3-Oxo-2,6,6-trimethylcyclohexene-1-carboxaldehyde ethylidene acetal (11)

Anhydrous potassium carbonate (2.0 g), *N*-bromosuccinimide (5.5 g, 31 mmol), and 2,2′-azobis(isobutyronitrile) (AIBN) (100 mg, 0.6 mmol) were added sequentially to a stirred solution of the acetal **9** (5.5 g, 28 mmol) in carbon tetrachloride (50 mL) and the resultant mixture was heated at reflux. During the first 30 min additional AIBN (4 × 50 mg, 1.2 mmol) was added at intervals of 5–10 min. Heating was continued for a total of 2 h. The reaction mixture was then cooled to ambient temperature and potassium carbonate (2.0 g) was added. The resultant mixture was filtered through a small plug of magnesium sulfate onto potassium carbonate (2.0 g). The filtrate was concentrated and the residue dissolved in water (5 mL) and dimethyl sulfoxide (20 mL). This mixture was heated at 50°C for 48 h and then cooled to ambient temperature. Ether (300 mL) was added, the organic phase separated, and the aqueous phase was extracted further with ether (5 × 100 mL). The combined organic extracts were washed with water (5 × 40 mL), then with brine (2 × 40 mL), dried, and concentrated to afford the corresponding crude allylic alcohol as an oil. This crude product was used in subsequent experiments. Chromatography (30% ethyl acetate in hexanes containing 0.3% v/v triethylamine) of the crude product (300 mg) afforded an analytically pure sample of the allylic alcohol (92 mg, 29%) as a colourless oil. IR (neat): 3409, 2920, 1449, 1226, 1050 cm^{-1}; ^1H NMR (200 MHz, $CDCl_3$) δ: 1.40 (s, 3H), 1.10 (s, 3H), 1.30–1.40 (m, 1H), 1.48–1.95 (m, 3H), 1.86 (s, 3H), 3.82–3.97 (m, 3H), 4.02–4.10 (m, 2H), 5.30 (s, 1H); ^{13}C NMR (50 MHz, $CDCl_3$) δ: 16.6, 27.0, 27.9, 28.3, 34.2, 35.4, 64.5, 64.6, 70.6, 102.0, 136.0, 137.7; HRMS (EI) calcd. for $C_{12}H_{20}O_3$: 212.1413; found: 212.1389. Oxalyl chloride (1.90 mL, 22 mmol) was added to a stirred solution of dimethyl sulfoxide (1.70 mL, 24 mmol) in dichloromethane (200 mL) at −78°C. The resultant mixture was stirred at −78°C for 15 min and then a solution of the above crude allylic alcohol (4.2 g, ~6 mmol) in dichloromethane (25 mL) was added. After an additional 15 min triethylamine (13 mL, 93 mmol) was added. After a further 30 min the reaction mixture was allowed to warm to ambient temperature and then a saturated aqueous solution of sodium bicarbonate (50 mL) and ether (400 mL) were added. The organic phase was separated, washed with a saturated aqueous solution of sodium bicarbonate (50 mL), then with brine (2 × 50 mL), dried, and concentrated. Chromatography (15% ethyl acetate in petroleum ether containing 0.3% v/v triethylamine) afforded the ketone **11** (1.1 g, 87%) as a colourless oil. IR ($CHCl_3$): 2940, 1673, 1460, 1228, 1027 cm^{-1}; ^1H NMR (200 MHz, $CDCl_3$) δ: 1.22 (s, 6H), 1.29 (apparent t, 2H), 1.32 (s, 3H), 2.46 (apparent t, 2H), 3.86–4.12 (m, 4H), 5.45 (s, 1H); ^{13}C NMR (75 MHz, $CDCl_3$) δ: 11.2,

© 1997 NRC Canada

Can. J. Chem. Downloaded from www.nrcresearchpress.com by 91.121.58.235 on 09/08/12
For personal use only.

26.4, 34.1, 38.2, 64.8, 101.8, 135.3, 154.7, 199.6; HRMS (EI) calcd. for $C_{12}H_{18}O_3$: 210.1256; found: 210.1256.

3-Triisopropylsilyloxy-2,6,6-trimethyl-1,3-cyclohexadiene-1-carboxaldehyde ethylidene acetal (12)

Potassium hexamethyldisilazide (3.3 mL, 0.5 M in toluene, 1.7 mmol) and HMPA (200 μL, 1.15 mmol) were added sequentially to a stirred solution of the ketone **11** (273 mg, 1.29 mmol) in THF (80 mL) at −78°C. The resultant mixture was stirred for 15 minutes and then triisopropylsilylchloride (357 μL, 1.67 mmol) was added and the reaction was allowed to warm to 0°C. A saturated aqueous solution of sodium bicarbonate (20 mL) was then added and the THF was removed in vacuo. The resultant aqueous residue was extracted with ether (200 mL) and the extract was washed with a saturated aqueous solution of sodium bicarbonate (25 mL), then with brine (2 × 25 mL), dried, and concentrated. Chromatography (5% ethyl acetate in hexanes) afforded the silyl enolether **12** (407 mg, 86%) as a colourless oil. IR (neat): 2947, 2867, 1655, 1465, 1221, 1069 cm^{-1}; ^1H NMR (200 MHz, $CDCl_3$) δ: 1.02–1.22 (m, 28H), 1.85 (s, 3H), 2.00 (apparent d, J = 4.7 Hz, 1H), 3.82–4.08 (m, 4H), 4.81 (apparent t, J = 4.7 Hz, 1H), 5.59 (s, 1H); ^{13}C NMR (75 MHz, $CDCl_3$) δ: 12.7, 13.0, 18.1, 26.2, 33.4, 39.4, 69.4, 100.7, 102.8, 134.1, 134.3, 149.0; HRMS (EI) calcd. for $C_{21}H_{38}O_3Si$: 366.2592; found: 366.2590.

3-Oxo-2,6,6-trimethyl-1,4-cyclohexadiene-1-carboxaldehyde neopentylidene acetal (13)

n-Butyllithium (19.5 mL, 2.5 M in hexanes, 49 mmol) was added to a stirred solution of *N,N*-diisopropylamine (7.0 mL, 50 mmol) in THF (100 mL) at 0°C. The resultant mixture was stirred at 0°C for 30 min. and then cooled to −78°C. A solution of the ketone **10** (10.1 g, 40.0 mmol) in THF (50 mL) was then added and, after a further 15 min, a solution of phenylselenyl bromide (11.3 g, 47.9 mmol) in THF (50 mL) was added. The resultant mixture was allowed to warm to ambient temperature and a saturated aqueous solution of sodium bicarbonate (150 mL) was added. The THF was removed in vacuo and the aqueous residue was then dissolved in methanol (300 mL) and stirred at 0°C. Oxone® (61.5 g, 100 mmol) was added and the resultant mixture was stirred at ambient temperature for 12 h. The methanol was then removed in vacuo and the resultant aqueous residue was diluted with water (100 mL) and extracted with ether (3 × 300 mL). The combined organic extracts were dried and concentrated. Chromatography (3:1 to 1:2, petroleum ether/ether) afforded the ketone **10** (3.42 g, 34%) and the dienone **13** (5.64 g, 56%, 85% based on recovered starting material) as a white solid; mp 84–86°C; IR ($CHCl_3$): 2950, 1662, 1633, 1169, 1088 cm^{-1}; ^1H NMR (200 MHz, $CDCl_3$) δ: 0.76 (s, 3H), 1.30 (s, 9H), 2.13 (s, 3H), 3.49–3.77 (m, 4H), 5.17 (s, 1H), 6.14 (d, J = 9.9 Hz, 1H), 6.67 (d, J = 9.9 Hz, 1H); ^{13}C NMR (75 MHz, $CDCl_3$) δ: 11.8, 22.1, 23.9, 25.3, 30.3, 39.2, 78.3, 101.5, 125.1, 135.0, 153.0, 157.5, 187.2; HRMS (EI) calcd. for $C_{15}H_{22}O_3$: 250.1570; found: 250.1564. Anal. calcd. for $C_{15}H_{22}O_3$: C 71.97, H 8.86; found: C 71.79, H 8.78.

(5*R)-Methylthio-3-oxo-2,6,6-trimethylcyclohexene-1-carboxaldehyde neopentylidene acetal (14)**

A solution of lithium methylthiolate (~24 mmol) (prepared by adding methyllithium (17.2 mL, 1.4 M in ether, 24.1 mmol) to a stirred solution of methyl disulfide (6.00 mL, 66.6 mmol) in THF (100 mL) at 0°C) was added to a stirred solution of the dienone **13** (400 mg, 1.60 mmol) and 12-crown-4 (48 μL, 0.30 mmol) in THF (20 mL) at 0°C . Methanol (1.0 mL, 25 mmol) was then added and the resultant mixture was stirred at ambient temperature for 12 h. A saturated aqueous solution of ammonium chloride (50 mL) was then added and the THF was removed in vacuo. The resultant aqueous residue was extracted with ether (200 mL) and the organic extract was washed with brine (2 × 25 mL), dried, and concentrated. Chromatography (10% ethyl acetate in hexanes) afforded the thioether **14** (414 mg, 87%) as a colourless oil that solidified on standing; mp 76.5–78.5°C; IR ($CHCl_3$): 3019, 1672, 1469, 1321, 1217, 1082 cm^{-1}; ^1H NMR (200 MHz, $CDCl_3$) δ: 0.73 (s, 3H), 1.20 (s, 3H), 1.25 (s, 3H), 1.41 (s, 3H), 2.00 (s, 3H), 2.07 (s, 3H), 2.59–2.83 (m, 3H), 3.44–3.50 (m, 2H), 3.67–3.73 (m, 2H), 5.07 (s, 1H); ^{13}C NMR (75 MHz, $CDCl_3$) δ: 11.9, 15.5, 20.9, 22.1, 23.9, 25.4, 30.3, 40.4, 40.7, 54.0, 78.2, 101.6, 134.0, 155.0, 198.2; HRMS (EI) calcd. for $C_{16}H_{26}O_3S$: 298.1610; found: 298.1605. Anal. calcd. for $C_{16}H_{26}O_3S$: C 64.39, H 8.78; found: C 64.25, H 8.47.

3-Oxo-(5*S)-vinyl-2,6,6-trimethylcyclohexene-1-carboxaldehyde neopentylidene acetal (16)**

Vinylmagnesium bromide (69.0 mL, 1 M in THF, 69.0 mmol) was added to a stirred suspension of copper(I) iodide (6.50 g, 34.1 mmol) in THF (200 ml) at −20°C. The resultant mixture was stirred for 10 min and then cooled to −78°C. A solution of the dienone **13** (5.71 g, 22.8 mmol) and trimethylsilylchloride (11.5 mL, 90.6 mmol) in THF (50 mL) was then added via a cannula. The reaction mixture was then allowed to warm to ambient temperature over 1 h and was recooled to 0°C. A saturated aqueous solution of ammonium chloride (100 mL) was then added, the resultant mixture was filtered through a pad of Celite, and the filter cake was washed with ether (200 mL). The aqueous phase of the filtrate was extracted further with ether (3 × 100 mL) and the combined organic extracts were dried and concentrated. Chromatography (4:1 to 3:1, petroleum ether/ether) afforded the vinyl ketone **16** (4.37 g, 69%) as a white solid; mp 85.5–87°C; IR ($CHCl_3$): 3018, 2964, 1671, 1468, 1218, 1085 cm^{-1}; ^1H NMR (200 MHz, $CDCl_3$) δ: 0.75 (s, 3H), 1.09 (s, 3H), 1.23 (s, 3H), 1.28 (s, 3H), 2.04 (s, 3H), 2.45 (m, 2H), 2.46 (m, 1H), 3.47–3.75 (m, 4H), 4.99–5.34 (m, 2H), 5.10 (s, 1H), 5.68–5.86 (m, 1H); ^{13}C NMR (75 MHz, $CDCl_3$) δ: 11.9, 20.5, 22.1, 23.9, 25.4, 30.3, 38.1, 39.4, 49.2, 101.6, 117.2, 133.8, 137.3, 155.3, 199.3; HRMS (EI) calcd. for $C_{17}H_{26}O_3$: 278.1882; found: 278.1870. Anal. calcd. for $C_{17}H_{26}O_3$: C 73.35, H 9.41; found: C 73.34, H 9.26.

5-Methylthio-3-oxo-2,6,6-trimethyl-1,4-cyclohexadiene-1-carboxaldehyde neopentylidene acetal (17)

N-Chlorosuccinimide (129 mg, 0.97 mmol) was added to a stirred solution of the thioether **14** (204 mg, 0.685 mmol) in carbon tetrachloride (50 mL) at ambient temperature. The resultant mixture was heated at reflux for 3.5 h and then cooled to ambient temperature. The reaction mixture was then filtered through a small pad of magnesium sulfate and concentrated. Chromatography (60% ether in hexanes) afforded the thio enolether **17** (196 mg, 97%) as a colourless oil that solidified on standing; mp 89–91.5°C; IR ($CHCl_3$): 3016, 2961, 1647, 1620, 1348, 1216, 1170 cm^{-1}; ^1H NMR (200 MHz,

© 1997 NRC Canada

Can. J. Chem. Downloaded from www.nrcresearchpress.com by 91.121.58.235 on 09/08/12
For personal use only.

$CDCl_3$) δ: 0.77 (s, 3H), 1.31 (s, 3H), 1.41 (s, 6H), 2.20 (s, 3H), 2.32 (s, 3H), 3.50–3.79 (m, 4H), 5.15 (s, 1H), 6.06 (s, 1H); ^{13}C NMR (75 MHz, $CDCl_3$) δ: 11.9, 14.3, 22.1, 24.0, 27.0, 30.3, 42.9, 78.5, 101.6, 118.2, 134.3, 153.3, 171.7, 183.6; HRMS (EI) calcd. for $C_{16}H_{24}O_3S$: 296.1447; found: 296.1442.

(5*R**)-Methylthio-3-triisopropylsilyloxy-2,6,6-trimethyl-1,3-cyclohexadiene-1-carboxaldehyde neopentylidene acetal (18)

Collidine (67 μL, 0.51 mmol) and triisopropylsilyltrifluoromethanesulfonate (90 μL, 0.33 mmol) were added sequentially to a stirred solution of the thioether **14** (50 mg, 0.17 mmol) in dichloromethane (5 mL) at 0°C. After 5 min a saturated aqueous solution of sodium bicarbonate (5 mL) and ether (50 mL) were added and the phases were separated. The organic phase was washed with a saturated aqueous solution of sodium bicarbonate (5 mL), brine (2 × 10 mL), dried, and concentrated. Chromatography (10% ethyl acetate in hexanes) afforded the silyl enolether **18** (72 mg, 95%) as a colourless oil. IR (neat): 2947, 2867, 1649, 1596, 1465, 1238, 1090 cm^{-1}; ^1H NMR (200 MHz, $CDCl_3$) δ: 0.72 (s, 3H), 1.05–1.15 (m, 21H), 1.20 (s, 3H), 1.25 (s, 3H), 1.43 (s, 3H), 1.93 (s, 3H), 1.94 (s, 3H), 3.00 (d, J = 6.4 Hz, 1H), 3.41–3.72 (m, 4H), 4.89 (d, J = 6.4 Hz, 1H), 5.17 (s, 1H); ^{13}C NMR (75 MHz, $CDCl_3$) δ: 12.7, 12.8, 13.4, 18.1, 22.2, 23.9, 24.4, 28.2, 30.2, 38.1, 54.9, 78.3, 100.9, 102.2, 131.3, 135.8, 150.0; HRMS (EI) calcd. for $C_{24}H_{43}O_3Si$ ($M^+ - CH_3S$): 407.2983; found: 407.2949.

(3*S**)-Hydroxy-(5*S**)-vinyl-2,6,6-trimethylcyclohexene-1-carboxaldehyde neopentylidene acetal (19)

Cerium trichloride heptahydrate (353 mg, 0.95 mmol) was added to a stirred solution of the ketone **16** (252 mg, 0.91 mmol) in methanol (10 mL) at ambient temperature. After 10 min the reaction mixture was cooled to 0°C and sodium borohydride (76 mg, 2.0 mmol) was then added in one portion. The reaction was monitored (TLC) and, once complete, a saturated aqueous solution of ammonium chloride (2 mL) was added. The methanol was removed in vacuo and the resultant aqueous residue was extracted with ether (4 × 25 mL). The combined organic extracts were dried and concentrated to afford, as a single diastereomer, the alcohol **19** (245 mg, 96%) as a white solid; mp 42–44°C; IR ($CHCl_3$): 3402, 2955, 1639, 1464, 1387, 1089 cm^{-1}; ^1H NMR (200 MHz, $CDCl_3$) δ: 0.73 (s, 3H), 0.93 (s, 3H), 1.05 (s, 3H), 1.28 (s, 3H), 1.41–1.63 (m, 1H), 1.89–2.14 (m, 2H), 2.09 (s, 3H), 3.45–3.73 (m, 4H), 4.04–4.12 (apparent br t, 2H), 4.86 (s, 1H), 4.96–5.07 (m, 2H), 5.69–5.87 (m, 1H); ^{13}C NMR (50 MHz, $CDCl_3$) δ: 15.7, 21.5, 22.0, 23.9, 25.7, 30.0, 34.2, 37.4, 47.7, 71.1, 78.3, 115.8, 137.1, 137.3, 139.0; HRMS (HI) calcd. for $C_{17}H_{28}O_3$: 280.2039; found: 280.2038.

(3*S**)-*tert*-Butyldimethylsilyloxy-(5*S**)-vinyl-2,6,6-trimethylcyclohexene-1-carboxaldehyde neopentylidene acetal (22)

Collidine (2.0 mL, 15 mmol) and *tert*-butyldimethylsilyltrifluoromethanesulfonate (2.2 mL, 9.6 mmol) were added sequentially to a stirred solution of the alcohol **19** (2.25 g, 8.04 mmol) in dichloromethane (50 mL) at 0°C. The resultant mixture was stirred for 5 min and then a saturated aqueous solution of sodium bicarbonate (100 mL) and ether (350 mL) were added. The organic phase was separated and washed with a saturated aqueous solution of sodium bicarbonate (50 mL), brine (50 mL), dried, and concentrated. Chromatography (5% ethyl acetate in hexanes) afforded the alcohol **19** (0.57 g, 25%) and the silylether **22** (2.29 g, 72%) as a white solid; mp 100–101°C; IR ($CHCl_3$): 2952, 2857, 1639, 1468, 1215, 1083 cm^{-1}; ^1H NMR (200 MHz, $CDCl_3$) δ: 0.03 (s, 3H), 0.05 (s, 3H), 0.73 (s, 3H), 0.87 (s, 9H), 0.92 (s, 3H), 1.04 (s, 3H), 1.27 (s, 3H), 1.56–1.72 (m, 3H), 2.01 (s, 3H), 3.49–3.73 (m, 4H), 4.06–4.15 (m, 1H), 4.85 (s, 1H), 4.94–5.05 (m, 2H), 5.68–5.86 (m, 1H); ^{13}C NMR (75 MHz, $CDCl_3$) δ: −4.9, −4.1, 16.4, 18.1, 21.7, 22.1, 24.1, 25.9, 30.1, 34.7, 37.4, 48.1, 71.9, 78.4, 78.5, 102.2, 115.6, 136.2, 138.4, 139.5; HRMS (EI) calcd. for $C_{23}H_{42}O_3Si$: 394.2905; found: 394.2887. Anal. calcd. for $C_{23}H_{42}O_3Si$: C 70.00, H 10.73, found: C 70.04, H 10.73.

(3*S**)-*tert*-Butyldiphenylsilyloxy-(5*S**)-vinyl-2,6,6-trimethylcyclohexene-1-carboxaldehyde neopentylidene acetal (23)

Imidazole (1.60 g, 23.5 mmol), *tert*-butyldiphenylsilylchloride (4.20 g, 15.3 mmol), and *N,N*-dimethyl-4-aminopyridine (0.93 g, 7.6 mmol) were added sequentially to a stirred solution of the alcohol **19** (2.13 g, 7.59 mmol) in dichloromethane (20 mL) at 0°C. The reaction mixture was stirred for 16 h at ambient temperature and then a saturated aqueous solution of ammonium chloride (50 mL) was added. The aqueous phase was separated and extracted further with dichloromethane (3 × 50 mL). The combined organic extracts were dried and concentrated. Chromatography (9:1, petroleum ether/ether) afforded the silylether **23** (3.98 g, 100%) as a white solid; mp 119–122°C; IR ($CHCl_3$): 3017, 2954, 2859, 1639, 1426, 1216 cm^{-1}; ^1H NMR (200 MHz, $CDCl_3$) δ: 0.74 (s, 3H), 0.92 (s, 3H), 0.98 (s, 3H), 1.05 (s, 9H), 1.26 (s, 3H), 1.57–1.85 (m, 3H), 2.07 (s, 3H), 3.44–3.78 (m, 4H), 4.11–4.19 (m, 1H), 4.73–4.96 (m, 2H), 4.85 (s, 1H), 5.59–5.77 (m, 1H), 7.30–7.46 (m, 6H), 7.51–7.76 (m, 4H); ^{13}C NMR (75 MHz, $CDCl_3$) δ: 16.6, 19.2, 21.6, 21.9, 23.8, 25.4, 26.9, 29.9, 33.9, 37.0, 47.4, 72.9, 78.1, 78.3, 101.9, 115.2, 127.0, 127.3, 129.1, 129.3, 133.3, 134.4, 135.9, 136.0, 138.2, 138.9; HRMS (EI) calcd. for $C_{33}H_{46}O_3Si$: 518.3218; found: 518.3199. Anal. calcd. for $C_{33}H_{46}O_3Si$: C 76.40, H 8.94; found: C 76.44, H 8.88.

(5*R**)-Carboxaldehyde-3-oxo-2,6,6-trimethylcyclohexene-1-carboxaldehyde neopentylidene acetal (20)

Ozone was passed through a stirred solution of the vinyl ketone **16** (107 mg, 0.39 mmol) in dichloromethane (10 mL) at −78°C until the starting material was consumed (TLC). Dimethyl sulfide (2 mL) was then added and the reaction mixture was allowed to warm to ambient temperature over 12 h. The reaction mixture was maintained at this temperature for a further 40 h and then concentrated. Chromatography (15% ethyl acetate in petroleum ether) afforded the ketoaldehyde **20** (60 mg, 56%) as a pale yellow solid; mp 67–69°C; IR ($CHCl_3$): 2958, 2720, 1720, 1676, 1223, 1086 cm^{-1}; ^1H NMR (200 MHz, $CDCl_3$) δ: 0.76 (s, 3H), 1.27 (s, 3H), 1.34 (s, 3H), 1.51 (s, 3H), 1.99 (s, 3H), 2.53–2.78 (m, 3H), 3.46–3.75 (m, 4H), 5.12 (s, 1H), 9.87 (d, J = 1.6 Hz, 1H); ^{13}C NMR (75 MHz, $CDCl_3$) δ: 11.8, 21.9, 22.1, 23.9, 26.5, 30.3, 33.7, 37.6, 56.5, 78.2, 101.3, 134.4, 153.4, 197.4, 202.2; HRMS (EI) calcd. for $C_{16}H_{24}O_4$: 280.1675; found: 280.1672.

© 1997 NRC Canada

Can. J. Chem. Downloaded from www.nrcresearchpress.com by 91.121.58.235 on 09/08/12
For personal use only.

(3*S)-*tert*-Butyldimethylsilyloxy-(5*R**)-carboxaldehyde-2,6,6-trimethylcyclohexene-1-carboxaldehyde neopentylidene acetal (25)**

Ozone was passed through a stirred solution of the alkene **22** (2.28 g, 5.79 mmol) in dichloromethane (100 mL) at −78°C until the starting material was consumed (TLC). Dimethyl sulfide (10 mL) was then added and the reaction mixture was allowed to warm to ambient temperature over 12 h. The reaction mixture was then heated (~40°C) for 24 h and then concentrated to afford the aldehyde **25** (2.22 g, 97%) as a light yellow viscous oil. IR ($CHCl_3$): 2957, 2858, 1709, 1467, 1216, 1086 cm^{-1}; ^1H NMR (200 MHz, $CDCl_3$) δ: 0.07 (s, 3H), 0.10 (s, 3H), 0.74 (s, 3H), 0.88 (s, 9H), 1.15 (s, 3H), 1.70–1.80 (m, 1H), 2.02 (s, 3H), 2.08–2.13 (m, 1H), 2.20–2.29 (m, 1H) 2.28 (s, 3H), 2.29 (s, 3H), 3.47–3.77 (m, 4H), 4.07 (apparent t, 1H), 4.91 (s, 1H), 9.83 (d, J = 3.1 Hz, 1H); ^{13}C NMR (75 MHz, $CDCl_3$) δ: 205.0 (CO); HRMS (EI) calcd. for $C_{22}H_{40}O_4Si$: 396.2697; found: 396.2705.

(3*S)-*tert*-Butyldiphenylsilyloxy-(5*R**)-carboxaldehyde-2,6,6-trimethylcyclohexene-1-carboxaldehyde neopentylidene acetal (24)**

Ozone was passed through a stirred solution of the alkene **23** (3.91 g, 7.49 mmol) in dichloromethane (150 mL) at −78°C until the starting material was consumed (TLC). Dimethyl sulfide (5 mL) was then added and the reaction mixture was allowed to warm to ambient temperature over 16 h. The resultant mixture was concentrated to afford the crude aldehyde **24** (4.1 g, 99%) as a colourless oil that was used directly in subsequent experiments. IR ($CHCl_3$): 3018, 2955, 2858, 2754, 1718, 1675, 1216 cm^{-1}; ^1H NMR (200 MHz, $CDCl_3$) δ: 0.75 (s, 3H), 1.05 (s, 9H), 1.14 (s, 3H), 1.19 (s, 3H), 1.27 (s, 3H), 1.80–1.98 (m, 3H), 1.98 (s, 3H), 3.44–3.77 (m, 4H), 4.07 (apparent t, 1H), 4.87 (s, 1H), 7.31–7.46 (m, 6H), 7.64–7.74 (m, 4H), 9.63 (d, J = 3.1 Hz, 1H); ^{13}C NMR (75 MHz, $CDCl_3$) δ: 17.1, 19.4, 22.1, 23.0, 24.0, 26.7, 27.0, 29.3, 30.1, 36.3, 55.7, 71.9, 78.4, 78.5, 101.5, 127.4, 127.5, 127.6, 127.8, 129.6, 129.7, 133.2, 136.0, 136.1, 138.5, 204.4; HRMS (EI) calcd. for $C_{32}H_{44}O_4Si$: 520.3010; found: 520.3028.

(3*S)-*tert*-Butyldimethylsilyloxy-5-oxo-2,6,6-trimethyl-cyclohexene-1-carboxaldehyde neopentylidene acetal (26)**

Collidine (580 μL, 4.39 mmol) and *tert*-butyldimethylsilyltrifluoromethanesulfonate (500 μL, 2.18 mmol) were added sequentially to a stirred solution of the aldehyde **25** (206 mg, 0.52 mmol) in dichloromethane (5 mL) at ambient temperature. The resultant mixture was stirred for 8 h and then a saturated aqueous solution of sodium bicarbonate (5 mL) and ether (100 mL) were added. The organic phase was separated, washed with a saturated aqueous solution of sodium bicarbonate (10 mL), then with brine (2 × 10 mL), dried, and concentrated to afford the corresponding silyl enolether. ^1H NMR (200 MHz, $CDCl_3$) δ: 0.05 (s, 6H), 0.71 (s, 3H), 0.84 (s, 9H), 1.10 (s, 3H), 1.15 (s, 3H), 1.24 (s, 3H), 1.82–1.90 (m, 2H), 2.02 (s, 3H), 3.38–3.72 (m, 4H), 4.07 (d, J = 5 Hz), 4.74 (s, 1H), 5.40 (s, 1H). Ozone was passed through a stirred solution of the above silyl enolether in dichloromethane (10 mL) at −78°C until the starting material was consumed (TLC). Dimethyl sulfide (2 mL) was then added and the reaction mixture was allowed to warm to ambient temperature over 12 h. On concentration of the reaction mixture, chromatography (5% to 20% ethyl acetate in petroleum ether) afforded the ketone **26** (33 mg, 17%) as a white solid; mp 88–90.5°C; IR ($CHCl_3$): 2958, 1718, 1468, 1216, 1083 cm^{-1}; ^1H NMR (200 MHz, $CDCl_3$) δ: 0.048 (s, 6H), 0.74 (s, 3H), 0.84 (s, 9H), 1.20 (s, 3H), 1.24 (s, 3H), 1.28 (s, 3H), 2.10 (s, 3H), 2.57 (dd, J = 13.4, 6.0 Hz, 1H), 2.74 (dd, J = 13.4, 4.6 Hz, 1H), 3.45–3.74 (m, 4H), 4.25 (apparent t, 1H), 4.90 (s, 1H); ^{13}C NMR (75 MHz, $CDCl_3$) δ: −4.8, −4.6, 17.7, 17.9, 22.2, 23.8, 24.0, 24.6, 25.7, 30.2, 45.7, 47.1, 72.1, 78.5, 101.7, 134.7, 137.4, 212.2; HRMS (EI) calcd. for $C_{17}H_{29}O_4Si$ (M^+ − *t*-Bu): 325.1836; found: 325.1806. Anal. calcd. for $C_{21}H_{38}O_4Si$: C 65.92, H 10.01; found: C 66.09, H 9.87.

3(*S)-*tert*-Butyldimethylsilyloxy-(5*S**)-cyano-5-trimethylsilyloxy-2,6,6-trimethylcyclohexene-1-carboxaldehyde neopentylidene acetal (27)**

Trimethylsilyl cyanide (500 μL, 3.75 mmol) was added to a stirred mixture of the ketone **26** (23 mg, 0.06 mmol), 18-crown-6 (5 mg, 0.02 mmol), and potassium cyanide (1 mg, 0.02 mmol) at ambient temperature. The resultant mixture was stirred for 3 h and then the excess trimethylsilylcyanide was removed in vacuo. A saturated aqueous solution of sodium bicarbonate (5 mL) and ether (100 mL) were then added. The organic phase was separated, washed with a saturated aqueous solution of sodium bicarbonate (5 mL), then with brine (2 × 10 mL), dried, and concentrated to afford the cyanohydrin **27** (27 mg, 94%) as a colourless oil. ^1H NMR (200 MHz, $CDCl_3$) δ: 0.22 (s, 6H), 0.72 (s, 3H), 0.87 (s, 9H), 1.08 (s, 3H), 1.25 (s, 3H), 1.33 (s, 3H), 1.95 (s, 3H), 1.95–2.00 (m, 1H), 2.18–2.29 (m, 1H), 3.38–3.72 (m, 4H), 4.30–4.40 (m, 1H), 4.90 (s, 1H); HRMS (EI) calcd. for $C_{25}H_{47}O_4NSi$: 481.3046; found: 481.3030.

3-(2-*tert*-Butyldimethylsilyloxyethyl)-2,4-dimethyl-1,3-pentadiene (31)

A solution of *tert*-butyllithium (46 mL, 1.58 M in pentane, 73 mmol) was added to a stirred solution of 3-bromo-2,4-dimethyl-1,3-pentadiene **30** (18) (5.77 g, 33.0 mmol) in THF (100 mL) at −78°C. After 15 min ethylene oxide (13 mL, 0.3 mol) was added via a cannula. The reaction mixture was then stirred for 1 h at −78°C, for 1 h at 0°C, and then for 30 min at ambient temperature. Water (100 mL) was then added and the aqueous phase was extracted with ether (3 × 100 mL). The combined organic extracts were washed with brine (2 × 100 mL), dried, and concentrated. Chromatography (25% ether in petroleum ether) afforded the corresponding alcohol (3.60 g, 78%) as a colourless liquid. IR (neat): 3330, 2920, 1632, 1444, 1039 cm^{-1}; ^1H NMR (500 MHz, C_6D_6) δ: 1.68 (m, 9H), 1.80 (br m, 1H), 2.33 (t, J = 7.0 Hz, 2H), 2.33 (t, J = 7.0 Hz, 2H), 3.56 (t, J = 7.1 Hz, 2H), 4.60 (m, 1H), 4.91 (m, 1H); ^{13}C NMR (125 MHz, C_6D_6) δ: 19.8, 21.8, 22.6, 34.7, 61.2, 113.5, 128.3, 133.4, 146.8; HRMS (EI) calcd. for $C_9H_{16}O$: 140.1202; found: 140.1199. Anal. calcd. for $C_9H_{16}O$: C 77.09, H 11.50; found: C 76.98, H 11.72.

Imidazole (3.24 g, 47.6 mmol) and *tert*-butyldimethylsilylchloride (5.50 g, 36.5 mmol) were added sequentially to a stirred solution of the above alcohol (3.60 g, 25.7 mmol) in dichloromethane (100 mL) at ambient temperature. The resultant mixture was stirred for 20 min and then a saturated aqueous solution of sodium bicarbonate (30 mL) was added.

© 1997 NRC Canada

Can. J. Chem. Downloaded from www.nrcresearchpress.com by 91.121.58.235 on 09/08/12
For personal use only.

The phases were separated and the aqueous phase was extracted further with dichloromethane (3 × 30 mL). The combined organic extracts were washed with brine (30 mL), dried, and concentrated. Chromatography (petroleum ether) afforded the diene **31** (5.20 g, 80%, 62% overall) as a colourless liquid. IR (neat): 2918, 1631, 1457, 1253, 1096, 841 cm^{-1}; ^1H NMR (200 MHz, $CDCl_3$) δ: 0.03 (s, 6H), 0.87 (s, 9H), 1.64 (s, 3H), 1.67 (s, 3H), 1.74 (s, 3H), 2.32 (t, J = 8.1 Hz, 2H), 3.54 (dd, J = 8.1 Hz, 2H), 4.51 (br d, J = 2.7 Hz, 1H), 4.89 (m, 1H); ^{13}C NMR (50 MHz, $CDCl_3$) δ: −5.2, 18.3, 19.8, 21.7, 22.6, 26.0, 34.8, 61.8, 113.1, 127.2, 132.8, 146.6; HRMS (EI) calcd. for $C_{11}H_{21}OSi$ (M^+ − *t*-Bu): 197.1363; found: 197.1347.

2,4-Dimethyl-1,3-pentadiene-3-carboxaldehyde neopentylidene acetal (33)

A solution of *tert*-butyllithium (49 mL, 1.7 M in pentane, 83 mmol) was added to a stirred solution of 3-bromo-2,4-dimethyl-1,3-pentadiene **30** (6.60 g, 37.7 mmol) in THF (100 mL) at −78°C. The resultant mixture was stirred for 30 min and then *N,N*-dimethylformamide (8.7 mL, 113 mmol) was added. The reaction mixture was allowed to warm to ambient temperature over a period of 1 h and then a saturated aqueous solution of ammonium chloride (40 mL) and ether (200 mL) were added. The organic phase was separated and washed with a saturated aqueous solution of ammonium chloride (2 × 40 mL), dried, and concentrated. 2,2-Dimethyl-1,3-propanediol (12.0 g, 115 mmol) and oxalic acid dihydrate (1.0 g) were added to a stirred solution of the above crude aldehyde in benzene (100 mL) and the resultant mixture was heated at reflux in a Dean–Stark water separator for 16 h. The reaction mixture was then cooled to ambient temperature and was treated with a saturated aqueous solution of sodium bicarbonate (40 mL) and diluted with ether (100 mL). The organic phase was separated, washed with a saturated aqueous solution of sodium bicarbonate (2 × 40 mL), dried, and concentrated. The residual oil was distilled (Kugelrohr, oven temperature ~125°C, 1 Torr) to afford the diene **33** (6.62 g, 84%) as a colourless oil. IR (neat): 2908, 1635, 1457, 1098, 924 cm^{-1}; ^1H NMR (500 MHz, $CDCl_3$) δ: 0.70 (s, 3H), 1.19 (s, 3H), 1.71 (s, 3H), 1.77 (s, 3H), 1.88 (dd, J = 1.4, 1.0 Hz, 3H), 3.46 (m, 2H), 3.65 (m, 2H), 4.64 (m, 1H), 5.04 (m, 1H), 5.15 (s, 1H); ^{13}C NMR (125 MHz, $CDCl_3$) δ: 19.8, 21.9, 22.2, 23.3, 23.9, 30.1, 77.7, 100.9, 114.8, 132.9, 134.8, 143.6; HRMS (EI) calcd. for $C_{13}H_{22}O_2$: 210.1621; found: 210.1632.

1-(2-*tert*-Butyldimethylsilyloxyethyl)-(5*R**)-carboxaldehyde-2,6,6-trimethylcyclohexene (34) and 3-(2-*tert*-butyldimethylsilyloxyethyl)-2,2,4-trimethyl-(6*S**)-vinyl-5,6-dihydro-2*H*-pyran (35)

Boron trifluoride diethyl etherate (1.70 mL, 13.8 mmol) was added to a stirred solution of the diene **31** (3.20 g, 12.6 mmol) and acrolein **32** (5.0 mL, 75 mmol) in dichloromethane (50 mL) at −78°C. The resultant mixture was stirred for 1 h and then a saturated aqueous solution of sodium bicarbonate (50 mL) was added and the reaction mixture was allowed to warm to ambient temperature. Ether (200 mL) was then added and the organic phase separated, washed with a saturated aqueous solution of sodium bicarbonate (2 × 50 mL), dried, and concentrated. Chromatography (10:1, petroleum ether/ether) afforded the aldehyde **34** (2.63 g, 67%) as a colourless oil and the dihydropyran **35** (1.0 g, 27%) as a colourless oil. Aldehyde **34**: IR (neat): 2944, 2858, 2726, 2353, 1722, 1467, 1253, 1089, 842 cm^{-1}; ^1H NMR (200 MHz, $CDCl_3$) δ: 0.05 (s, 6H), 0.88 (s, 9H), 1.03 (s, 3H), 1.18 (s, 3H), 1.64 (s, 3H), 1.82–1.69 (m, 2H), 1.99–1.96 (m, 2H), 2.14 (dt, J = 10.0, 3.4 Hz, 1H), 2.30 (br t, J = 8.0 Hz, 2H), 3.55 (t, J = 8.0 Hz, 2H), 9.81 (d, J = 3.1 Hz, 1H); ^{13}C NMR (50 MHz, $CDCl_3$) δ: −5.2, 18.4, 19.7, 20.2, 23.5, 26.0, 27.7, 30.6, 32.1, 36.9, 57.6, 62.8, 129.4, 132.7, 206.4; HRMS (EI) calcd. for $C_{14}H_{25}O_2Si$ (M^+ − *t*-Bu): 253.1625; found: 253.1604. Anal. calcd. for $C_{18}H_{34}O_2Si$: C 69.62, H 11.04; found: C 69.01, H 11.22. Dihydropyran **35**: IR (neat): 2920, 1467, 1361, 1255, 1092, 841 cm^{-1}; ^1H NMR (500 MHz, $CDCl_3$) δ: 0.05 (s, 6H), 0.88 (s, 9H), 1.27 (s, 6H), 1.66 (s, 3H), 1.78 (dd, J = 16.6, 3.2 Hz, 1H), 2.08 (ddd, J = 16.6, 10.9, 1.1 Hz, 1H), 2.23 (t, J = 8.5 Hz, 2H), 3.55 (m, 2H), 4.09 (m, 1H), 5.09 (dt, J = 10.4, 1.4 Hz, 1H), 5.22 (dt, J = 17.4, 1.4 Hz, 1H), 5.86 (ddd, J = 17.4, 10.4, 5.6 Hz, 1H); ^{13}C NMR (50 MHz, $CDCl_3$) δ: −5.2, 18.4, 19.6, 25.0, 26.0, 28.5, 32.9, 37.2, 62.4, 68.9, 76.0, 115.1, 126.5, 132.2, 139.4; HRMS (EI) calcd. for $C_{17}H_{31}O_2Si$ (M^+ − Me): 295.2095; found: 295.2073.

(5*R**)-Carboxaldehyde-2,6,6-trimethylcyclohexene-1-carboxaldehyde neopentylidene acetal (36) and 2,6,6-trimethylcyclohexene-1,5(*RS*)-dicarboxaldehyde (37)

Boron trifluoride diethyl etherate (3.60 mL, 29.3 mmol) was added to a stirred solution of the diene **33** (5.60 g, 26.6 mmol) and acrolein **32** (9.0 mL, 135 mmol) in dichloromethane (100 mL) at −78°C. After 20 min a saturated aqueous solution of sodium bicarbonate (150 mL) was added and the resultant mixture was allowed to warm to ambient temperature. Ether (200 mL) was then added and the organic phase was separated, washed with a saturated aqueous solution of sodium bicarbonate (2 × 25 mL), dried, and concentrated. Chromatography (5:1 to 1:1, petroleum ether/ether) afforded the aldehyde **36** (4.23 g, 60%) as white crystalline solid and the dialdehyde **37** (0.711 g, 25%) as a colourless oil. Aldehyde **36**: mp 63–66°C; IR (neat): 2914, 2868, 2833, 1719, 1465, 1090, 981 cm^{-1}; ^1H NMR (200 MHz, $CDCl_3$) δ: 0.73 (s, 3H), 1.10 (s, 3H), 1.26 (s, 3H), 1.27 (s, 3H), 1.58–1.78 (m, 2H), 1.97 (s, 3H), 2.03–2.20 (m, 3H), 3.47 (d, J = 11.2 Hz, 2H), 3.70 (d, J = 11.2 Hz, 2H), 4.88 (s, 1H), 9.83 (d, J = 2.9 Hz, 1H); ^{13}C NMR (50 MHz, $CDCl_3$) δ: 19.4, 20.7, 22.1, 23.4, 24.0, 27.2, 30.2, 31.7, 36.1, 57.5, 78.5, 78.6, 101.4, 134.0, 135.6, 205.9; HRMS calcd. for $C_{16}H_{26}O_3$ (EI): 266.1883; found: 266.1874. Dialdehyde **37**: IR (neat): 2916, 2759, 1720, 1671, 1612, 1458, 1374, 1288, 1118 cm^{-1}; ^1H NMR (200 MHz, $CDCl_3$) δ: 1.23 (s, 3H), 1.43 (s, 3H), 1.62–1.91 (m, 3H), 2.08 (s, 3H), 2.12–2.31 (m, 2H), 9.85 (d, J = 2.2 Hz, 1H), 10.08 (s, 1H); ^{13}C NMR (50 MHz, $CDCl_3$) δ: 18.4, 19.2, 22.7, 27.1, 33.6, 35.5, 57.7, 139.5, 155.9, 191.5, 204.9; HRMS calcd. for $C_{11}H_{16}O_2$ (EI): 180.1150; found: 180.1142.

Acknowledgment

We are grateful to the Natural Sciences and Engineering Research Council of Canada, Rhône–Poulenc Rorer, the Canadian Breast Cancer Research Initiative of the National Cancer Institute of Canada, and the Saunders–Matthey Foundation for Breast Cancer Research for financial support of this research, and to the Association pour la Recherche sur le Cancer (France) for a fellowship to H. Audrain.

© 1997 NRC Canada

References

1. M.C. Wani, H.L. Taylor, M.E. Wall, P. Coggan, and A.T. McPhail. J. Am. Chem. Soc. **93**, 2325 (1971).
2. (*a*) G.I. Georg, T.T. Chen, I. Ojima, and D.M. Vyas. (*Editors*). ACS Symp. Ser. **583** (1994); (*b*) M.L. Rothenberg. Curr. Opin. Invest. Drugs **2**, 1269 (1993); (*c*) J.J. Manfredi and S.B. Horwitz. Pharmacol. Ther. **25**, 83 (1984).
3. (*a*) A.N. Boa, P.R. Jenkins, and N.J. Lawerence. Contemp. Org. Synth. **1**, 47 (1994); (*b*) K.C. Nicolaou, W.-M. Dai, and R.K. Guy. Angew. Chem. Int. Ed. Engl. **33**, 15 (1994).
4. (*a*) R.A. Holton, C. Somoza, H.-B. Kim, F. Liang, R.J. Biediger, P.D. Boatman, M. Shindo, C. C. Smith, S. Kim, H. Nadizadeh, Y. Suzuki, C. Tao, P. Vu, S. Tang, P. Zhang, K. K. Murthi, L. N. Gentile, and J.-H. Liu. J. Am. Chem. Soc. **116**, 1597 (1994); (*b*) R.A. Holton, H.-B. Kim, C. Somoza, F. Liang, R.J. Biediger, P.D. Boatman, M. Shindo, C.C. Smith, S. Kim, H. Nadizadeh, Y. Suzuki, C. Tao, P. Vu, S. Tang, P. Zhang, K.K. Murthi, L.N. Gentile, and J.-H. Liu. J. Am. Chem. Soc. **116**, 1599 (1994).
5. (*a*) K.C. Nicolaou, Z. Yang, J.J. Liu, H. Ueno, P.G. Nantermet, R.K. Guy, C.F. Claiborne, J. Renaud, E.A. Couladouros, K. Paulvannan, and E.A. Sorensen. Nature (London), **367**, 630 (1994); (*b*) K.C. Nicolaou, P.G. Nantermet, H. Ueno, R.K. Guy, E.A. Couladouros, and E.J. Sorensen. J. Am. Chem. Soc. **117**, 624 (1995); (*c*) K.C. Nicolaou, J.-J. Liu, Z. Yang, H. Ueno, E.J. Sorensen, C.F. Claiborne, R.K. Guy, C.K. Hwang, M. Nakada, and P.G. Nantermet. J. Am. Chem. Soc. **117**, 634 (1995); (*d*) K.C. Nicolaou, Z. Yang, J.J. Liu, P.G. Nantermet, C.F. Claiborne, J. Renaud, R.K. Guy, and K. Shibayama. J. Am. Chem. Soc. **117**, 645 (1995); (*e*) K.C. Nicolaou, H. Ueno, J.J. Liu, P.G. Nantermet, Z. Yang, J. Renaud, K. Paulvannan, and R. Chadha. J. Am. Chem. Soc. **117**, 653 (1995).
6. (*a*) J.J. Masters, J.T. Link, L.B. Snyder, W.B. Young, and S.J. Danishefsky. Angew. Chem., Int. Ed. Engl. **34**, 1723 (1995); (*b*) S.J. Danishefsky, J.J. Masters, W.B. Young, J.T. Link, L.B. Snyder, T.V. Magee, D.K. Jung, R.C.A. Isaacs, W.G. Bornmann, C.A. Alaimo, C.A. Coburn, and M.J. Di Grandi. J. Am. Chem. Soc. **118**, 2843 (1996).
7. F. Lavelle, F. Guéritte-Voegelin, and D. Guénard. Bull. Cancer, **80**, 326 (1993).
8. (*a*) Y.-F. Lu and A.G. Fallis. Tetrahedron Lett. **34**, 3367 (1993); (*b*) Y.-F. Lu and A.G. Fallis. Can. J. Chem. **73**, 2239 (1995).
9. A.G. Fallis and Y.-F. Lu. *In* Advances in cycloadditions. Vol. 3. *Edited by* D.P. Curran. JAI Press, Greenwich, Conn. 1993. pp. 1–66.
10. M.W. Tjepkema, P.D. Wilson, T. Wong, M.A. Romero, H. Audrain, and A.G. Fallis. Tetrahedron Lett. **36**, 6039 (1995).
11. (*a*) Y.-F. Lu, C.W. Harwig, and A.G. Fallis. J. Org. Chem. **58**, 4202 (1993); (*b*) Y.-F. Lu, C.W. Harwig, and A.G. Fallis. Can. J. Chem. **73**, 2253 (1995).
12. M. Hayashi, T. Matsuda, and N. Oguni. J. Chem. Soc. Chem. Commun. 1364 (1990).
13. Y. Ohtsuka and T. Oishi. Chem. Pharm. Bull. **36**, 4722 (1988).
14. T. Doi, J. Robertson, G. Stork, and A. Yamashita. Tetrahedron Lett. **35**, 1481 (1994).
15. T. Nakamura, N. Waizumi, Y. Horiguchi, and I. Kuwajima. Tetrahedron Lett. **35**, 7813 (1994).
16. (*a*) A.S. Kende, S. Johnson, P. Sanfilippo, J.C. Hodges, and L.N. Jungheim. J. Am. Chem. Soc. **108**, 3513 (1986); (*b*) Y. Queneau, W.J. Krol, W.G. Bornmann, and S.J. Danishefsky. J. Org. Chem. **57**, 4043 (1992); (*c*) M. Polla and T. Frejd. Tetrahedron **49**, 2701 (1993); (*d*) M. Golinski, S. Vasudevan, R. Floresca, C.P. Brock, and D.S. Watt. Tetrahedron Lett. **34**, 55 (1993); (*e*) S. Arseniyadis, D.V. Yashunsky, R. Pereira de Feitas, M. Munoz Dorado, E. Toromanoff, and P. Potier. Tetrahedron Lett. **34**, 1137 (1993); (*f*) D. Crich and J.Z. Crich. Tetrahedron Lett. **35**, 2469 (1994); (*g*) M.J. Di Grandi, D.K. Jung, W.J. Krol, and S.J. Danishefsky. J. Org. Chem. **58**, 4989 (1993); (*h*) M.H. Kress, R. Ruel, W.H. Miller, and Y. Kishi. Tetrahedron Lett. **34**, 5999 (1993); (*i*) J.D. Winkler, S. K. Bhattacharya, F. Liotta, R.A. Batey, G.D. Heffernan, D.E. Cladingboel, and R.C. Kelly. Tetrahedron Lett. **36**, 2211 (1995); (*j*) M.S. Ermolenko, T. Shekharam, G. Lukacs, and P. Potier. Tetrahedron Lett. **36**, 2461 (1995); (*k*) L. Alcaraz, J.J. Harnett, C. Mioskowski, T.L. Gall, D.-S. Shin, and J.R. Falck. J. Org. Chem. **60**, 7209 (1995); (*l*) P.A. Wender, L.A. Wessjohann, B. Peschke, and D.B. Rawlins. Tetrahedron Lett. **36**, 7181 (1995); (*m*) D. Crich and S. Natarajan. J. Chem. Soc., Chem. Commun. 85 (1995); (*n*) D.F. Taber, A. Sahli, H. Yu, and R.P. Meagley. J. Org. Chem. **60**, 6571 (1995); (*o*) Y. Kishi and M.H. Kress. Tetrahedron Lett. **36**, 4583 (1995); (*p*) F. Delaloge, J. Prunet, A. Pancrazi, and J-Y. Lallemand. Tetrahedron Lett. **38**, 237 (1997).
17. (*a*) K.C. Nicolaou, C.-K. Hwang, E.J. Sorensen, and C.F. Clairborne. J. Chem. Soc. Chem. Commun. 1117 (1992); (*b*) S.A. Hitchcock and G. Pattenden. Tetrahedron Lett. **33**, 4843 (1992); (*c*) R.L. Funk and K.J. Yost, III. J. Org. Chem. **61**, 2598 (1996).
18. (*a*) P.S. Skell and A.Y. Garner. J. Am. Chem. Soc. **78**, 5430 (1956); (*b*) W. von E. Doering and W.A. Henderson, Jr. J. Am. Chem. Soc. **80**, 5274 (1958).

Can. J. Chem. Downloaded from www.nrcresearchpress.com by 91.121.58.235 on 09/08/12
For personal use only.

© 1997 NRC Canada

Calculation of barriers to rotation in PEEK and some of its substituted derivatives[1]

S. Brownstein and J. Roovers

Abstract: Barriers to rotation have been calculated by molecular mechanics, using the force field MM+, for a fragment of PEEK and its methyl, ethyl, isopropyl, *tert*-butyl and di-*tert*-butyl, substituted derivatives. The barrier for the nearer C—O bond increases from 2.0 kcal/mol in KEEK to 16 kcal/mol in dibutyl substituted KEEK as the bulkiness of the substituent increases. The rotation barrier of the further C—O bond is not affected by the substituent.

Key words: rotation barriers, PEEK, molecular mechanics.

Résumé : Faisant appel à la mécanique moléculaire et au champ de forces MM+, on a calculé les barriéres à la rotation d'un fragment de «PEEK» et de ses dérivés méthyle, éthyle, isopropyle, *tert*-butyle et di-*tert*-butyle. Lorsque l'encombrement stérique du substituant augmente, la barrière de la liaison C—O la plus proche passe de 2,0 kcal/mol dans le «KEEK» à 16,0 kcal/mol dans le «KEEK» portant deux substituants butyles. La barrière à la rotation de la liaison C—O la plus éloignée n'est pas affectée par le substituant.

Mots clés : barriéres à la rotation, «PEEK», méchanique moléculaire.

[Traduit par la rédaction]

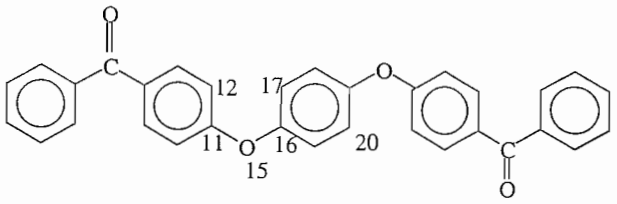
Can. J. Chem. Downloaded from www.nrcresearchpress.com by 91.121.58.235 on 09/08/12
For personal use only.

Introduction

The effect of substituents on the performance of glassy polymeric membranes in gas permeation and gas separation is under intense study (1, 2). We mention the systematic studies of Paul and Koros and co-workers on the effects of substituents in polysulfones (3), polycarbonates (4), and polyphenylene oxide (5). Poly(aryl ether ketones), PEEK, are potential materials for high-temperature gas separation membranes because of their high thermal, chemical, and radiation stability (6). However, to optimize the gas permeation properties, substituents may have to be introduced into the parent polymers (7). The gas diffusion process is thought to be promoted by small local sub-T_g motions of the polymer chain and its substituents. These motions occur within a polymeric matrix with a disordered packing, which itself depends on the type of the polymer chain and of the substituents. For these reasons sub-T_g dynamic mechanical properties and the free volume of the polymer and its modified analogues are related to experimental gas permeation results (8).

In addition, one can simulate the energetics of simple motions of polymer chain fragments. There have been several studies of the barriers to rotation about the ether and carbonyl bonds in molecules relevant to small sections of poly(phenyl ether ether ketone) (PEEK) (9–11). Although fairly sophisticated calculations, e.g., 3-21G (9), CNDO/2 (11), and STO-3G (12), have been used in these studies, they have not considered the effect of substituents on the phenyl rings of the polymer. There have also been X-ray studies on PEEK and some model compounds to determine bond lengths, bond angles, and torsion angles (13–15). It seems worthwhile to calculate, by relatively simple methods, barriers to rotation about the ether bonds in longer fragment chains to compare with the calculations already reported with more elaborate methods and also to perform similar calculations with substituted phenyl rings. Since only a fragment of the polymer is being modeled, the name KEEK, or a variation thereof, is used for the various fragments.

Fig. 1. The connectivity and atom numbering of the polymer fragment used in the calculations.



Geometrical considerations and calculation procedures

The fragment of the PEEK chain used for the calculations is shown in Fig. 1 along with the numbering employed. Hydrogen atoms are not included in the figure for purposes of clarity but their presence was included in the calculations. The calculations were done using the force field MM+ in the computational package of HYPERCHEM 4.0.[3] The force field MM+ is a

Received January 14, 1997.

S. Brownstein[2] and J. Roovers. Institute for Chemical, Process, and Environmental Technology, National Research Council of Canada, Ottawa, ON K1A 0R9, Canada.

[1] Issued as NRCC No. 37630.

[2] Author to whom correspondence may be addressed. Telephone: (613) 993-2785. Fax: (613) 991-2384. E-mail: sydney.brownstein@nrc.ca

[3] HYPERCHEM 4.0 is a product of Hypercube Inc., Waterloo, Ont.

© 1997 NRC Canada

Can. J. Chem. Downloaded from www.nrcresearchpress.com by 91.121.58.235 on 09/08/12
For personal use only.

Fig. 2. Minimum energy, kcal/mol, as a function of torsional angle about the 11–15 bond in KEEK.

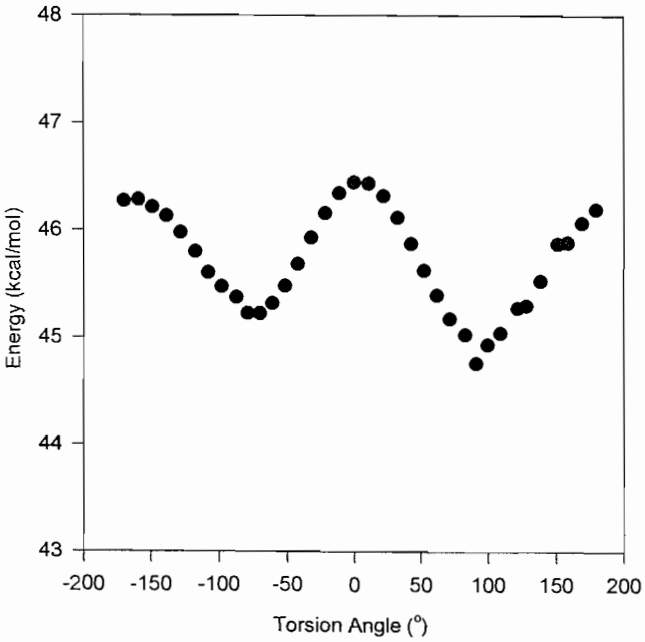


Fig. 3. Minimum energy, kcal/mol, as a function of torsional angle about the 15–16 bond in DBKEEK.

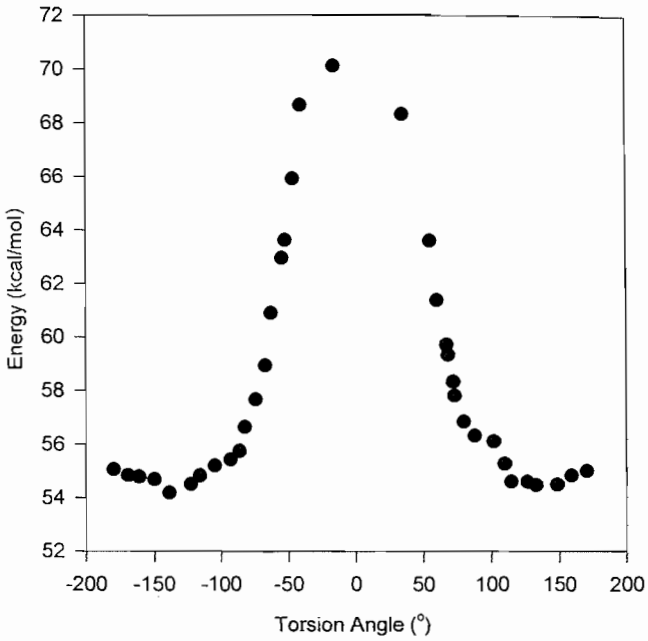
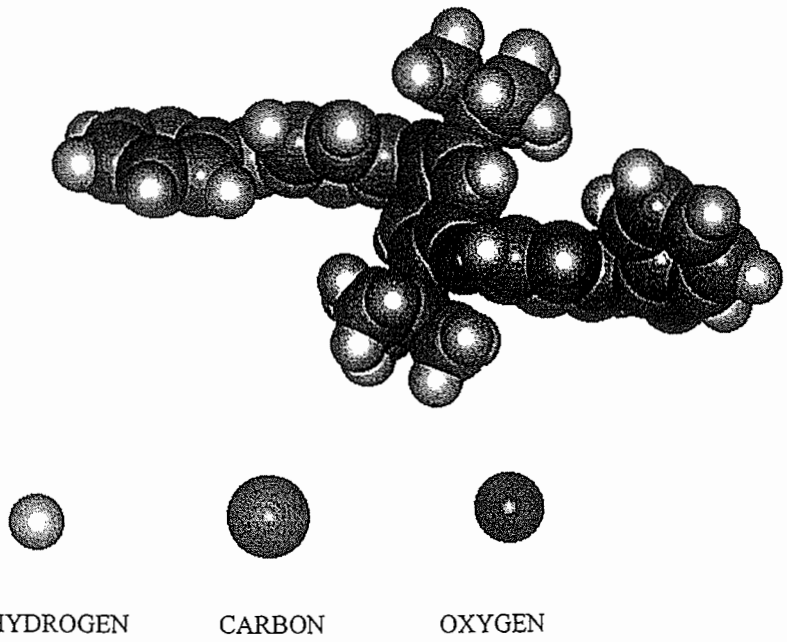


Fig. 4. The minimum conformational energy structure for DBKEEK.



variation of MM2 (16). Calculations were performed on a 486 personal computer operating at 33 MHz. Bond lengths and bond angles obtained in this study are compared with the values reported in other references and all are listed in Table 1.

Energies were calculated for the most stable conformations with the only restraint being the torsion angle about either the 15–16 or 11–15 carbon–oxygen bonds, since these are considered to be the most affected by substituents on carbon 17. It is found that if these calculations are performed while uniformly increasing or decreasing the restrained torsion angle, a true minimum energy conformation might be missed. Therefore the restrained angles are chosen in a somewhat arbitrary order to insure that energies for the real minima are always found. The barriers to rotation are taken as the difference in energy between the highest and lowest calculated minimum energies. The actual barriers will be somewhat higher than those

© 1997 NRC Canada

Can. J. Chem. Downloaded from www.nrcresearchpress.com by 91.121.58.235 on 09/08/12
For personal use only.

Table 1. Lengths and angles of significant bonds used in the energy calculations.

Bond	Length(Å)	Angle (°)	Compound	Conformation	Reference
C-O-C	1.380–1.403	132.3–120	$C_6H_5OC_6H_5$	Variable	9
	1.390	123.3	$C_6H_5OC_6H_5$	Optimum	9
	1.374		$C_6H_5OC_6H_5$	Optimum	10
	1.407	115.6	$C_6H_5OC_6H_5$	Optimum	12
	1.28–1.43	123	$C_6H_5OC_6H_5$		7
	1.42	126	$C_6H_5OC_6H_5$		17
	1.40	117	$C_6H_5OC_6H_5$		11
	1.387	121.2	$C_6H_5OC_6H_5$		15
	1.362	121.3	KEEK[a]	Optimum	[b]
	1.359	123.3	PEEK	Optimum	13
	1.366		PEEK	Optimum	14
	1.362	121.2	MKEEK[c]	Optimum	(b)
	1.361	121.5	ETKEEK[d]	Optimum	(b)
	1.363	120.9	IPKEEK[e]	Optimum	(b)
	1.362	122.2	BKEEK[f]	Optimum	(b)
	1.363	123.2	DBKEEK[g]	Optimum	(b)
C-C-C	1.39	120	$C_6H_5OC_6H_5$	N\A	11
Aromatic	1.394	119.9	$C_6H_5OC_6H_5$	N\A	12
	1.384		$C_6H_5OC_6H_5$		15
	1.397	117.1	KEEK	Optimum	[b]
	1.408		PEEK	Optimum	13
	1.389		PEEK	Optimum	14
	1.402	117.9	MKEEK	Optimum	[b]
	1.401	117.9	ETKEEK	Optimum	[b]
	1.404	118.1	IPKEEK	Optimum	[b]
	1.408	118.9	BKEEK	Optimum	[b]
	1.404	118.8	DBKEEK	Optimum	[b]
C—H	1.08		$C_6H_5OC_6H_5$	N\A	11
Aromatic	1.082		$C_6H_5OC_6H_5$	Optimum	12
	1.10		KEEK	Optimum	[b]
	1.103		MKEEK	Optimum	[b]
	1.103		ETKEEK	Optimum	[b]
	1.103		IPKEEK	Optimum	[b]
	1.103		BKEEK	Optimum	[b]
	1.099		DBKEEK	Optimum	[b]

[a]KEEK is the unsubstituted compound of Fig. 1.
[b]This work.
[c]MKEEK is the 17-methyl substituted compound of Fig. 1.
[d]ETKEEK is the 17-ethyl substituted compound of Fig. 1.
[e]IPKEEK is the 17-isopropyl substituted compound of Fig. 1.
[f]BKEEK is the 17-*tert*-butyl substituted compound of Fig. 1.
[g]DBKEEK is the 17,20-di-*tert*-butyl substituted compound of Fig. 1.

Table 2. Calculated energy barriers to bond rotation (kcal/mol).

Compound	Bond 11–15	Bond 15–16	Reference
$C_6H_5OC_6H_5$	3.4, 2.5		9–12
KEEK	1.6	2.0	[a]
MKEEK	2.1	4.4	[a]
ETKEEK	1.9	5.0	[a]
IPKEEK	1.9	6.5	[a]
BKEEK	4.0	16	[a]
DBKEEK	1.1	16	[a]

[a]This work.

© 1997 NRC Canada

reported since the program did not permit restraining the torsion angles to the values that would correspond exactly to the highest energies.

Sample results for the 11–15 bond of KEEK and the 15–16 bond of DBKEEK are shown in Figs. 2 and 3. The value of 0° represents the two end bonds in the same plane adopting a *cis* position, and 180° is when they adopt the *trans* position.

Results and conclusions

The energy barriers to rotation about the carbon–oxygen bond on the ether linkage side of the polymer chain (O_{15}—C_{16}) and on the carbonyl side of the chain (C_{11}—O_{15}) are listed in Table 2, along with pertinent data from previous calculations. It can be seen that the results of the present calculations using a larger fragment and a simpler force field agree satisfactorily with previous results on diphenyl ether where more elaborate calculation methods were employed and smaller fragments were used in the calculations. Therefore we may conclude that satisfactory results can be obtained for polymer fragments of reasonable size using the simpler method and a less powerful computer, as in this study, to calculate conformations and energetics. It is also apparent that, within the limits of accuracy of the calculations, lengthening the fragment upon which calculations are made does not have any effect upon the barriers calculated for the central bonds. Of course it must be remembered that these calculations are for isolated fragments and do not include any interactions between individual chains in the bulk polymer.

It is also evident that a substituent in position 17 primarily affects the rotation barrier about the 15–16 bond with negligible disturbance of the 11–15 bond. This is in agreement with chemical intuition, which suggests that distant effects will be negligible. The addition of a bulky substituent in the 20 position does not appear to alter the barrier about the 15–16 bond, showing that there is no buttressing effect, as expected, since it is on the opposite side of the benzene ring. This is reasonable given the structure of the lowest energy conformation of DBKEEK, which is shown in Fig. 4. It should be noted that there is departure from strict planarity for this molecule because of the large steric effects of the two *tert*-butyl groups. Minor changes are not further discussed since they may be within the accuracy limits of the calculations.

In addition, these calculations suggest that the *tert*-butyl groups in DBKEEK encourage the polymer to adopt a particular extended chain conformation. Adjacent molecules could pack with the *tert*-butyl groups offset to give the high crystallinity that is observed (17)[4] in the di-*tert*-butyl PEEK homopolymer.

References

1. S.A. Stern. J. Membr. Sci. **94**, 1 (1994).
2. K. Ghosal and B.D. Freeman. Polym. Adv. Technol. **5**, 673 (1994).
3. J.S. McHattie, W.J. Koros, and D.R. Paul. Polymer, **32**, 840 (1991); **33**, 1701 (1992).
4. N. Muruganandam and D.R. Paul. J. Membr. Sci. **34**, 185 (1987); S.M. Jordan, G.K. Fleming, and W.J. Koros. J. Polym. Sci. Part B: Polym. Phys. **28**, 2305 (1990).
5. M. Aguilar-Vega and D.R. Paul. J. Polym. Sci. Part B: Polym. Phys. **31**, 1577 (1993).
6. T.E. Attwood, P.C. Dawson, J.L. Freeman, L.R.J. Hoy, J.B. Rose, and P.A. Staneland. Polymer, **22**, 1096 (1981).
7. P. Moulinie, Z.Y. Wang, J. Roovers, and P. Handa. North American Membrane Society, Ottawa, May 1996. p. 75.
8. C.L. Aitken, J.S. McHattie, and D.R. Paul. Macromolecules, **25**, 2910 (1992).
9. J. Kendrick. J. Chem. Soc. Faraday Trans. **86**, 3995 (1990).
10. J. Kendrick, E. Robson, and M. Weaver. J. Chem. Soc. Faraday Trans. **91**, 2609 (1995).
11. S. Verot and P. Battesti. Can. J. Chem. **73**, 581 (1995).
12. B.C. Laskowski, R.L. Jaffe, and A. Komornicki. Int. J. Quantum Chem. **29**, 563 (1986).
13. P. Iannelli. Macromolecules, **26**, 2309 (1993).
14. A.V. Fratini, E.M. Cross, R.B. Whitaker, and W.W. Adams. Polymer, **27**, 861 (1987).
15. H.M. Colquhoun, C.A. O'Mahoney, and D.J. Williams. Polymer, **34**, 218 (1993).
16. N.L. Allinger. J. Am. Chem. Soc. **99**, 8127 (1977).
17. C.L. Chen, J.L. Chang, and A.C. Su. Macromolecules, **25**, 1941 (1992).

[4] J. Roovers, P. Handa, and Z. Zhang. Unpublished work.

© 1997 NRC Canada

Can. J. Chem. Downloaded from www.nrcresearchpress.com by 91.121.58.235 on 09/08/12
For personal use only.

Isotope effects on the reaction of proton transfer to benzene anions in ethanol

Ricard Gelabert, Miquel Moreno, and José M. Lluch

Abstract: A theoretical study on the reaction of proton transfer from ethanol to benzene anions was performed at the ab initio level. It was found that in the gas phase the reaction proceeds without potential energy barrier with respect to reactants held at infinite distance, even though a potential energy barrier exists when measured from the prebarrier complex formed by the reactant molecules. When restrictions on orientation of the reactant molecules in the solid phase are taken into account, the potential energy barrier found exceeds 40 kcal/mol. A theoretical estimate of the kinetic isotope effect due to the tunneling effect, κ_H/κ_D, of 9.0×10^3 is found, in good agreement with available experimental data.

Key words: isotope effects, proton transfer, tunneling.

Résumé : Opérant au niveau ab initio, on a effectué une étude théorique de la réaction de transfert de proton de l'éthanol à des anions du benzène. On a trouvé que, en phase gazeuse, la réaction se produit sans barrière d'énergie potentielle par rapport aux réactifs à distance infinie, même s'il existe une barrière d'énergie potentielle lorsqu'on la mesure à partir du complexe précédant la barrière. Lorsqu'on tient compte des restrictions sur l'orientation des molécules de réactif à l'état solide, on observe que la barrière d'énergie potentielle est supérieure à 40 kcal/mol. L'évaluation théorique de l'effet isotopique cinétique dû à l'effet tunnel, κ_H/κ_D, conduit à une valeur de $9{,}0 \times 10^3$ en bon accord avec les données expérimentales disponibles.

Mots clés : effets isotopiques, transfert de proton, effet tunnel.

[Traduit par la rédaction]

Can. J. Chem. Downloaded from www.nrcresearchpress.com by 91.121.58.235 on 09/08/12
For personal use only.

1. Introduction

Quantum mechanical phenomena, such as tunneling, are important in molecules and chemical reactions that involve significant motion of light atoms (1). Proton transfer reactions in particular are among the processes that exhibit a large tunneling effect (2–6). Chemical processes involving tunneling can be identified by several telltale factors such as surprisingly small activation energies due to the flattening of Arrhenius plots in the low-temperature end, and very large kinetic isotope effects (KIEs) when substituting transferring hydrogen atoms with deuterium (k_H/k_D) (1). These pieces of evidence become more obvious at lower temperatures.

When temperature is very low, reaction via tunneling is likely to become much more important than reaction through classical means, due to the fact that the chemical system under study is unlikely to have sufficient energy to cross over the potential energy barrier. In addition, at very low temperatures most reactant systems are found in condensed phases, either solid or liquid. These phase changes will have foreseeable effects on the rate constant of such processes, mostly due to the constraints enforced on the motion of the reactant molecules of the system, preventing these from adopting the optimal conformation for the reaction. Under such conditions, the contribution of tunneling to the overall rate constant is likely to become much more important, to the point that at certain temperatures the whole process could take place via a pure tunneling mechanism.

Miyazaki et al. studied the reaction of proton transfer from ethanol to a benzene anion produced by electron pulse radiolysis of an ethanol–benzene (5% mol) mixture at 77 K (7):

[1] $C_6H_6^- + CH_3CH_2OH \longrightarrow C_6H_7^{\cdot} + CH_3CH_2O^-$

This reaction has some points of interest. To begin with, reactions between neutral species and ions are known to generally occur with little or no activation energy in the gas phase (8). However, given that this reaction was studied at 77 K, it seemed likely that this could change, once in the solid phase. Additionally, tunneling could have an important role to play in this reaction at very low temperatures.

Experiments were carried out at 77 K and lower temperatures. It was seen that at temperatures around 20 K only benzene anions were formed after electron capture. When the experiment was carried out at 77 K it was discovered that reaction [1] had an activation energy of only 0.2 kcal/mol. Furthermore, it was found that when C_2H_5OH was used, reaction [1] took place in less than 1 μs, whereas it took between 100 μs and 30 min when C_2D_5OD was used instead. Accordingly, the kinetic isotope effect involved was estimated to be greater than 100 (7).

Both the magnitude of the kinetic isotope effect and the small value of the activation energy seem to indicate that an

Received April 15, 1997.

R. Gelabert, M. Moreno, and J.M. Lluch.[1] Departament de Química, Universitat Autònoma de Barcelona, 08193 Bellaterra, Barcelona, Spain.

[1] Author to whom correspondence may be addressed. Telephone: +34-3-5812138. Fax: 34-3-5812920. E-mail: lluch@klingon.uab.es

© 1997 NRC Canada

important tunneling effect is involved in this reaction at 77 K. Miyazaki et al. tried to estimate theoretically the height of the potential energy barrier by means of the following equation for the rate constant at a given temperature (7):

$$[2] \quad k = \frac{A}{RT} \int_0^\infty G(\omega)\, e^{-\frac{\omega}{RT}}\, d\omega$$

where $G(\omega)$ is the permeability of the potential energy barrier for a particle of energy ω, and A is the frequency factor. When the dimensionality of the problem is reduced to just 1 dimension and the shape of the potential energy barrier is assumed to be parabolic or Eckart-type, analytic expressions exist for $G(\omega)$. Even though the local structure around a benzene molecule in an ethanol–benzene mixture at 77 K is not known, Miyazaki et al. estimated the jump distance of the proton from ethanol to benzene anion to be approximately 0.85 Å (7), assuming that the structure would be similar to that of crystalline ethanol. In this way the width of the energy barrier could be estimated.

By using eq. [2] it can be seen that, in order to theoretically reproduce a primary kinetic isotope effect of 100, a potential energy barrier of at least 4.5 kcal/mol should exist when an Eckart energy profile is used, and probably greater than that, given that 100 is just the lower limit for the KIE in this reaction at 77 K.

Our purpose in this paper has been to perform ab initio calculations in order to theoretically analyze the kinetics of reaction [1] in the gas phase. In a second stage, steps will be taken to estimate and justify the barrier height of the proton transfer in the solid phase, which should be large enough to account for the large KIE found experimentally.

2. Calculational details

Ab initio calculations were carried out with the GAUSSIAN 94 series of programs (9). The system under study has an odd number of electrons and hence the unrestricted Hartree–Fock formalism (UHF) was used throughout the calculations. The basis set chosen for these calculations had to be flexible enough to describe anionic species, and therefore diffuse functions had to be considered. Geometry optimizations were carried out with the 3-21+G split valence basis set (10), and the energies obtained in this way were recalculated with the higher 6-31+G basis set (10*b*, 11). Both basis sets include diffuse functions on heavy atoms in order to provide ampler space allowance for the additional electron in the system. Overall, the number of basis functions for the complete system was 141. No symmetry constraints, either local or global, were enforced at any point of the calculations. Due to severe convergence problems in the electronic wave function, the quadratic convergence algorithm, as implemented in GAUSSIAN 94, had to be used by default (12).

Schlegel's gradient optimization algorithm was used to perform geometry optimizations (13). When necessary, analytical second derivatives of the electronic energy were evaluated to characterize stationary points of the potential energy surface.

An important part of this chemical problem had much to do with the fact that the system was at 77 K, that is, in the solid phase. Steps were taken in order to simulate this fact in the calculations. The main difference when comparing solid and gas phases is that in the solid state the molecules are held fixed in a rigid crystalline matrix, and consequently they are not able to freely adopt the most favorable orientation for reacting. In other words, both reactants are initially neutral, but upon electron capture by benzene they are able to reach the best conformation in the gas phase to produce the reaction. Conversely, in the solid state the system is also initially neutral but, after electron capture, being part of the crystalline structure, it cannot achieve the optimal structure for ethanol + benzene anions. Hence, in order to take this particularity into account, calculations referring to the solid state were carried out fixing the relative distance and orientation of the ethanol molecule and the benzene anion to the optimum values of the ethanol molecule + benzene molecule in the gas phase (both taken as neutral species). After that, to simulate the proton transfer process once the electron has been captured by the benzene molecule, all geometry optimizations were carried out allowing internal relaxation of the internal structures of both molecules *but* holding them fixed in their previous relative positions, so that they cannot approach, rotate, or in any other way modify their relative situation in space. Additional information will be provided in the discussion section of this paper.

3. Results and discussion

The first point to be addressed is, logically, to determine the potential energy barrier height and geometries of reactants and transition state structures for reaction [1] in the gas phase. It was found that the reactants formed a stable "prebarrier complex," stabilized by 10.1 kcal/mol with respect to reactants separated at infinite distance at the 6-31+G//3-21+G level of calculation. From now on all energies will be given as corresponding to this same level of calculation. The transition state structure for the proton transfer was also sought. Both stationary points are depicted in Figs. 1*a* and *b*.

The transition state structure in Fig. 1*b* involved an intrinsic potential energy barrier of 9.6 kcal/mol. However, this structure is still 0.47 kcal/mol below the potential energy of the reactants held at infinite distance. Even though these values lack thermodynamical corrections, it can be seen that, as was expected for ion–molecule reactions in gas phase (8), the reaction will proceed with no potential energy barrier relative to reactants held at infinite distance. In any case, it is expected that the overall process may still have a positive free energy barrier due to entropic effects, according to Variational Transition State Theory (14).

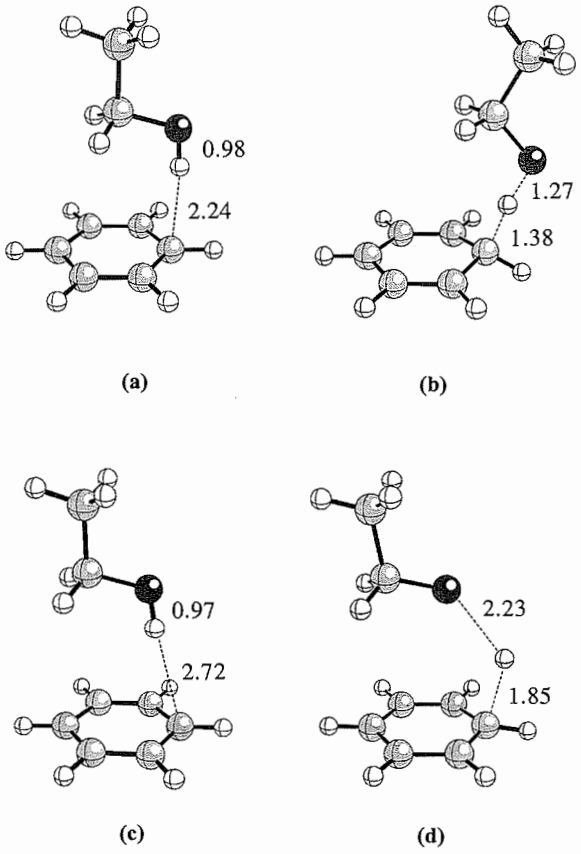
Potential energy barriers are caused by the deformations that reactants must undergo to turn into products. There are semiquantitative methods that allow separation of the factors that contribute to a given energy barrier. In this paper we have used a partitive method based on a scheme first proposed by Morokuma and co-workers to quantify how much of the potential energy barrier is due to geometrical distortion (15, 16). Within this procedure, the contribution to the energy barrier coming from geometrical distortions of the reactants is evaluated as the difference in potential energy between the reactant molecule in its equilibrium conformation and the same molecule in the transition state structure geometry. This last energy is obtained in a calculation of the transition state structure in which all atoms not belonging to the reactant molecule under study have their nuclear charges changed to

© 1997 NRC Canada

Can. J. Chem. Downloaded from www.nrcresearchpress.com by 91.121.58.235 on 09/08/12
For personal use only.

Can. J. Chem. Downloaded from www.nrcresearchpress.com by 91.121.58.235 on 09/08/12
For personal use only.

Fig. 1. Reaction [1] in the gas phase: (*a*) prebarrier complex; (*b*) transition state structure. Simulation of reaction [1] in the solid phase, in which the relative position of both reactant molecules has been fixed to the optimum values of the ethanol molecule + benzene molecule in the gas phase (both taken as neutral species); (*c*) reactants; (*d*) transition state structure. Distances are given in Å.



zero, and their corresponding electrons have been eliminated from the system. In this way the energies of distortion of a given reactant molecule can be determined.

The reactant molecule that is most distorted upon reaching the transition state structure is the ethanol molecule, which experiences geometrical distortions amounting to 34.3 kcal/mol of the whole destabilization, this being 39.4 kcal/mol. This fact can be better understood if the nature of the geometrical distortions involved on going from reactants to transition state structure is considered. Concretely, the main geometrical distortion experienced by the system is the elongation of the oxygen–hydrogen distance. This geometrical parameter has a value of 0.98 Å in the free ethanol molecule at this level of calculation, whereas in the transition state structure the same distance measures 1.27 Å, which yields a total elongation of 0.29 Å. On the other hand, the benzene anion fragment, which a priori should undergo a severe geometrical distortion (one of the C—H bonds must go out of plane to make enough room for the incoming proton), only provokes an increase in energy of 5.1 kcal/mol. The stabilization energy can be obtained as the difference between the energy barrier and the sum of distortion energies:

$$[3] \quad \Delta V_{\text{stabilization}} = \Delta V_{\text{barrier}} - \sum \Delta V_{\text{distortion}}$$

Obviously, $\Delta V_{\text{stabilization}}$ is negative in sign. In this case, the energy of stabilization is −39.8 kcal/mol.

One of the goals of this paper has been to quantify the differences between solid phase and gas phase for the model reaction. To this end, some effort must be devoted to reproducing the experimental settings in the calculations. The procedure outlined in Sect. 2 has been adopted. Experiments begin with a crystal of frozen ethanol–benzene mixture at 77 K. After electron capture, and depending on temperature and isotopic substitutions carried out, the rate of reaction [1] becomes faster or slower. However, at 77 K the system is in the solid phase and in these conditions the reactant molecules can be considered fixed in a given relative orientation, while frozen in the positions they occupy in the crystal. What we have done to somehow reproduce this situation was to maintain the relative orientation and distances of the reactant system at the minimum values of these parameters found in the gas phase when both reactants are neutral, that is, before benzene anions are formed. It was assumed, then, that the crystal's structure does not significantly differ locally from the one found in the gas phase. This same assumption was adopted by Miyazaki et al. in the original paper, because the structure of a crystal corresponding to an ethanol–benzene mixture is not known experimentally (7). In all that follows, these restrictions on relative distances and orientation have been enforced, allowing the structures to relax internally. In this way, the "constrained" minimum and transition state were obtained, as is depicted in Figs. 1*c* and *d*.

Foreseeably, the potential energy barrier that will be obtained upon lengthening the O—H bond, while forcing the general orientation of the reactant molecules to remain as it was in the equilibrium situation of the neutral system, will be larger than the one found in the gas phase, relative to the prebarrier complex. Concretely, the potential energy barrier found was 39.2 kcal/mol, taking as origin of energies the structure of the neutral minimum in which an additional electron has been added to the system but without allowing the structure of the minimum to relax, or 44.3 kcal/mol above the structure of the anion if only internal relaxation was allowed. The barrier, in either case, is both *very* high and broad, and much higher than the 4.5 kcal/mol estimated by Miyazaki et al. as a lower minimum.

In addition, a different set of calculations was performed here, taking into account that Miyazaki et al. estimated the total distance moved by the proton being transferred as approximately 0.85 Å, based on the crystallographic data of pure ethanol. In our case, the rough distance the proton moved was substantially greater (about twice that value). To check the effects that a smaller distance between the ethanol molecule and the benzene anion would have on the barrier, we performed a different set of calculations in which the distance that the proton should move during the transference was about 1.0 Å. We observed that if both reactant molecules were forced to remain that close, then the proton transfer would occur without barrier.

Interesting information can be learned by analyzing the spin densities along the points of this constrained reaction coordinate and comparing them with those for the reaction in the gas phase. In the gas phase transition state structure, the spin density on the transferring atom has a value of 0.06 au, which would correspond to a proton (a hydrogen atom

© 1997 NRC Canada

deprived of electrons). In the transition state of the solid phase reaction, however, this spin density has a value of 0.84 au, much closer to the value one should expect for a free hydrogen atom (that is, 1.0 au). This difference in the nature of the transition state of both reactions, however, was not unexpected. Examining the O—H and H—C distances in both transition state structures, it can be seen that the solid phase distances ($R_{O—H}$ = 2.23 Å, $R_{C—H}$ = 1.85 Å) are much longer than those for the gas phase ($R_{O—H}$ = 1.27 Å, $R_{C—H}$ = 1.38 Å).

What effects would such a barrier have on the kinetic isotope effect for reaction [1] in the solid phase? To answer this, an expression for the value of the KIE is needed. Within transition state theory (TST), the KIE for the substitution of hydrogen by deuterium can be evaluated in the following way (14):

$$[4]\quad \mathrm{KIE} = \frac{\kappa_H(T)}{\kappa_D(T)} \times \frac{k_H(T)}{k_D(T)}$$

where $k_H(T)(k_D(T))$ is the kinetic rate constant within TST with classical motion along the reaction coordinate, and $\kappa_H(T)(\kappa_D(T))$ is the semiclassical transmission coefficient, which is the ratio of the thermally averaged quantum transmission probability through the potential energy barrier to the thermally averaged classical transmission probability across the same barrier (14):

$$[5]\quad \kappa_i(T) = \frac{\int_0^\infty P_i(E)\, e^{-\frac{E}{k_B T}}\, dE}{\int_{V^\ddagger}^\infty e^{-\frac{E}{k_B T}}\, dE}$$

$$= \frac{1}{k_B T}\, e^{\frac{V^\ddagger}{k_B T}} \int_0^\infty P_i(E)\, e^{-\frac{E}{k_B T}}\, dE$$

In eq. [5], $V^\ddagger$ is the height of the potential energy barrier for the reaction under study, and $P_i(E)$ is the quantum transmission probability of the potential energy barrier for the reactant system that transfers isotope i with total energy E. Bearing in mind that $V^\ddagger$ does not depend on the isotopic substitutions made on the system, eq. [4] becomes:

$$[6]\quad \mathrm{KIE} = \frac{\int_0^\infty P_H(E)\, e^{-\frac{E}{k_B T}}\, dE}{\int_0^\infty P_D(E)\, e^{-\frac{E}{k_B T}}\, dE} \times \frac{k_H(T)}{k_D(T)}$$

The ratio $k_H(T)/k_D(T)$ accounts for the thermodynamic and zero-point energy differences between the system that transfers hydrogen and the one that transfers deuterium, in the transition state and in the minimum. Even though differences exist at this level, these are due mainly to differences in zero-point vibrational energy, which are not likely to produce a KIE as great as the one reported experimentally (greater than 100) (1). However, the first term of eq. [6] is the ratio between the quantum permeabilities of the barrier for two identical reactions that differ only in the nature of the hydrogen isotope being transferred (14). This is the part that accounts for tunneling in the reaction under study. Within the WKB formalism, $P_i(E)$ can be expressed as (14, 17):

$$[7]\quad P_i(E) = \begin{cases} 0 & E < V_0 \\ \dfrac{1}{1 + e^{2\theta(E)}} & V_0 \le E \le V^\ddagger \\ 1 - P_i(2V^\ddagger - E) & V^\ddagger \le E \le 2V^\ddagger - V_0 \\ 1 & 2V^\ddagger - V_0 \le E \end{cases}$$

where V_0 is the highest of the energies of either reactants and products, and $\theta(E)$ is given by:

$$[8]\quad \theta(E) = \frac{1}{\hbar} \int_s \sqrt{2[V(s) - E]}\, ds$$

where s, in mass-weighted Cartesian coordinates, denotes the path along which tunneling is assumed to occur. As can be seen, $P_i(E)$ depends on both the height and the width of the barrier, becoming exponentially lower when the barrier increases its height or width. Even though the height of the potential energy barrier is invariant with the isotopic substitution, the width is not, for it is evaluated in mass-weighted Cartesian coordinates. In this way it can be seen that the same potential energy profile becomes much longer when deuterium is the transferring atom.

Finally, we have tried to estimate the ratio $\kappa_H(T)/\kappa_D(T)$. To calculate it, a tunneling path must be assumed. In our case, we have assumed a tunneling path consisting of a linear interpolation in mass-weighted Cartesian coordinates from the internally relaxed structure of the reactants to the transition state structure of the solid phase, followed by another linear interpolation in mass-weighted Cartesian coordinates from the transition state structure in the solid phase to the structure of the products, also internally relaxed. These interpolations were made in such a way that neither linear nor angular momenta were generated (18). Once this was done, the estimated value of $\kappa_H(T)/\kappa_D(T)$ at 77 K was found to be 9.0×10^3, very high and in good accord with experimental reports of KIEs for this reaction in the solid phase.

4. Conclusions

In this paper we have analyzed, from a theoretical point of view, the reaction of ethanol with benzene anions in the gas phase and in the solid phase.

In the gas phase no potential energy barrier with respect to reactants held at infinite distance has been found for the proton transfer reaction under study. However, we found that the reactants form a stable prebarrier complex stabilized by 10.1 kcal/mol with respect to reactants held at infinite distance. With respect to this prebarrier complex, an intrinsic barrier of 9.6 kcal/mol exists.

When the solid phase was simulated by forcing the relative orientation of both reactants to remain as we found them to be in the neutral, gas phase complex, a very high and broad potential energy barrier was found. This is partly due to the fact that the structure is not allowed to relax, and partly due to the fact that in this case the starting point (reactant's mini-

Can. J. Chem. Downloaded from www.nrcresearchpress.com by 91.121.58.235 on 09/08/12
For personal use only.

© 1997 NRC Canada

mum) for the reaction does not correspond to that of the reactants held at infinite distance. Be this as it may, in this case the transferring atom is forced to jump a much longer distance. In effect, it seems that in the solid phase the reaction under study changes and what is being transferred at the transition state is a hydrogen atom instead of a proton.

Given the potential energy barrier height in the solid phase calculations, reaction [1] should proceed through a tunneling mechanism at low temperatures. This being the case, one should expect huge values of the kinetic isotope effect (KIE) when substituting hydrogen with deuterium. In our calculations, an estimate of this KIE was obtained by using the semiclassical expression of the transmission coefficient, yielding a final value of 9.0×10^3 at 77 K. This value only applies to KIEs due to tunneling, so that it would be even greater once thermodynamic and zero-point energy differences were included. This value is in good accord with the range of experimental KIEs reported by Miyazaki et al. (7) for this reaction in the solid phase at 77 K.

Even though the values we have found are not quantitatively valid, they manage to explain the experimentally reported facts and justify qualitatively the differences between the reaction in the gas phase and in the solid phase.

Acknowledgments

Financial support from the Dirección General de Enseñanza Superior (DGES) through project PB95-0637 and the use of the computational facilities of the "Centre de Computació i de Comunicacions de Catalunya" are gratefully acknowledged.

References

1. R.P. Bell. The tunnel effect in chemistry. Chapman & Hall, London. 1980.
2. M.M. Szczęśniak and S. Scheiner. J. Phys. Chem. **89**, 1835 (1985).
3. D. Borgis, S. Lee, and J.T. Hynes. Chem. Phys. Lett. **162**, 19 (1989).
4. D. Borgis and J.T. Hynes. *In* The enzyme catalysis process. *Edited by* A. Cooper, J. Houben, and L. Chien. Plenum, New York. 1989. p. 293.
5. N. Shida, P.F. Barbara, and J.E. Almlöf. J. Chem. Phys. **91**, 4061 (1989).
6. E. Bosch, M. Moreno, and J.M. Lluch. J. Am. Chem. Soc. **114**, 2072 (1992).
7. T. Miyazaki, T. Shiba, K. Fueki, and Y. Kamiya. J. Phys. Chem. **95**, 9115 (1991).
8. M. Meot-Ner. Gas phase ion chemistry. Academic Press, New York. 1979.
9. M.J. Frisch, G.W. Trucks, H.B. Schlegel, P.M.W. Gill, B.G. Johnson, M.A. Robb, J.R. Cheeseman, T.A. Keith, G.A. Petersson, J.A. Montgomery, K. Raghavachari, M.A. Al-Laham, V.G. Zakrzewski, J.V. Ortiz, J.B. Foresman, J. Cioslowski, B.B. Stefanov, A. Nanayakkara, M. Challacombe, C.Y. Peng, P.Y. Ayala, W. Chen, M.W. Wong, J.L. Andres, E.S. Replogle, R. Gomperts, R.L. Martin, D.J. Fox, J.S. Binkley, D.J. Defrees, J. Baker, J.P. Stewart, M. Head-Gordon, C. Gonzalez, and J.A. Pople, Gaussian 94. Gaussian Inc., Pittsburgh Pa., 1995.
10. (*a*) G.W. Spitznagel, T. Clark, J. Chandrasekhar, and P. von R. Schleyer. J. Comput. Chem. **3**, 363 (1982). (*b*) T. Clark, J. Chandrasekhar, G.W. Spitznagel, and P. von R. Scheyer. J. Comput. Chem. **4**, 294 (1983).
11. R. Ditchfield, W.J. Hehre, and J.A. Pople. J. Chem. Phys. **54**, 724 (1971).
12. G.B. Bacskay. Chem. Phys. **61**, 385 (1981).
13. H.B. Schlegel. *In* Ab Initio Methods in Quantum Chemistry. Vol. I. *Edited by* K.P. Lawley. John Wiley & Sons Ltd., Chichester. 1987. p. 249.
14. D.G. Truhlar, A.D. Isaacson, and B.C. Garrett. *In* Theory of chemical reaction dynamics. Vol. IV. *Edited by* M. Baer. CRC Press, Boca Raton, Fla. 1985. p. 65.
15. K. Kitaura and K. Morokuma. Int. J. Quantum Chem. **10**, 325 (1976).
16. S. Nagase and K. Morokuma. J. Am. Chem. Soc. **100**, 1666 (1978).
17. E. Merzbacher. Quantum mechanics. John Wiley & Sons, New York. 1970.
18. W.H. Miller, B.A. Ruf, and Y. Chang. J. Chem. Phys. **89**, 6298 (1988).

Can. J. Chem. Downloaded from www.nrcresearchpress.com by 91.121.58.235 on 09/08/12
For personal use only.

© 1997 NRC Canada

Stereoselective hydrogenation of lignin degradation model compounds

Thomas Q. Hu, Brian R. James, Steven J. Rettig, and Chung-Li Lee

Abstract: Di-μ-chloro-bis(η^4-1,5-hexadiene)dirhodium(I) in a two-phase hexane–aqueous medium catalyzes the diastereoselective H_2-hydrogenation of lignin degradation model compounds 4-propylphenol, 2-methoxy-4-propylphenol, and 2,6-dimethoxy-4-propylphenol. The all-*cis* diastereomer is obtained selectively when the phenolic hydroxy group is protected as a methyl ether or when a model compound possessing two methoxy substituents adjacent to the phenolic hydroxy group is used. The relative stereochemistries of the hydrogenated products are established by X-ray crystal structure analysis and (or) ^{1}H NMR.

Key words: catalytic hydrogenation, diastereomer, lignin degradation model compounds, stereoselective, X-ray crystal structure.

Résumé : Dans un milieu aqueux à deux phases avec de l'hexane, le di-μ-chlorobis(η^4-hexa-1,5-diène)dirhodium(I) catalyse l'hydrogénation diastéréosélective des composés modèles de la dégradation de la lignine, 4-propylphénol, 2-méthoxy-4-propylphénol et 2,6-diméthoxy 4-propylphénol. On obtient sélectivement le diastéréomère complètement *cis* lorsque le groupe hydroxyle phénolique est protégé sous la forme d'éther méthylique ou lorsqu'on utilise un composé modèle possédant deux substituants méthoxy dans les positions adjacentes du groupe hydroxyle phénolique. On a déterminé les stéréochimies relatives des produits d'hydrogénation par le biais de la diffraction des rayons X et (ou) de la RMN du ^{1}H.

Mots clés : hydrogénation, diastéréomère, composés modèles de dégradation de la lignine, stéréosélective, structure cristalline par diffraction des rayons X.

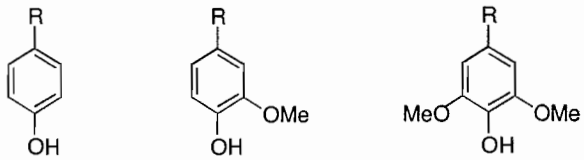
[Traduit par la rédaction]

Introduction

Lignin, a plant constituent, is the second most abundant biopolymer on earth. The biosphere is estimated to contain 3×10^{11} metric tons of lignin with an annual biosynthesis rate of approximately 2×10^{10} tons (1, 2). Every year more than 50 million tons of lignin are produced as the by-products from the chemical pulping of wood at pulp mills worldwide (3). The lignin so obtained has been used mainly as a low-grade fuel for the pulping process (4). Despite extensive research on the conversion of lignin into valuable fine chemicals over the past 20 years or so, only a few systems have been successfully developed and commercialized. One of these commercialized fine chemicals is vanillin, a common flavoring additive in foods and drinks (5).

The major impediments to the exploitation of lignin as a source of fine chemicals are the difficulties involved in separating a mixture of lignin degradation products and the low commercial values of the isolated products. Degradation of lignin obtained from the chemical pulping of wood via neutral or alkaline hydrogenolysis gives 4-substituted-phenols (**1**), 2-methoxy-4-substituted-phenols (**2**) and 2,6-dimethoxy-4-substituted-phenols (**3**) (Scheme 1) in various yields (6–9).

Scheme 1. Products from the degradation of lignin via hydrogenolysis (R = $CH_2CH_2CH_3$, $CH_2CH_2CH_2OH$, CH_2CH_2COOH, CH_2CH_3, CH_2CH_2OH, CH_2COOH, CH_3, COOH, H) (6).



1 **2** **3**

Since the late 1960s sporadic attempts have been made to convert these aromatic compounds into cyclohexanol derivatives via catalytic hydrogenation (10–12). Typically, the reaction was carried out either at high temperature (>200°C) under high pressure (>1000 psi H_2 (1 psi = 6.9 kPa)) (10) or in the presence of strong acid or base (11, 12). Under such reaction conditions, the hydrogenation of the aromatic rings was accompanied by hydrogenolysis of the substituent side chains, giving a multitude of products (10–12). In addition, the hydrogenation was not stereoselective, further complicating the problems of product isolation and development.

In this paper we present the ^{1}H NMR spectroscopic and X-ray crystallographic evidence for the stereoselective hydrogenation of a number of lignin degradation model compounds catalyzed by di-μ-chloro-bis(η^4-1,5-hexadiene)dirhodium(I), $[(1,5\text{-}C_6H_{10})RhCl]_2$. This catalyst was previously used by others for the hydrogenation of carbonyl and simple aromatic

Received December 20, 1996.

T.Q. Hu[1] and C.-L. Lee. Pulp and Paper Research Institute of Canada, Vancouver Laboratory, 3800 Wesbrook Mall, Vancouver, BC V6S 2L9, Canada.
B.R. James[1] and S.J. Rettig. Department of Chemistry, University of British Columbia, Vancouver, BC V6T 1Z1, Canada.

[1] Authors to whom correspondence may be addressed. TQH: Telephone: (604) 222-3200. Fax: (604) 222-3207. E-mail: Hu_Thomas@Vanlab.Paprican.Ca and BRJ: Telephone: (604) 822-6645. Fax: (604) 822-2847. E-mail: brj@chem.ubc.ca

© 1997 NRC Canada

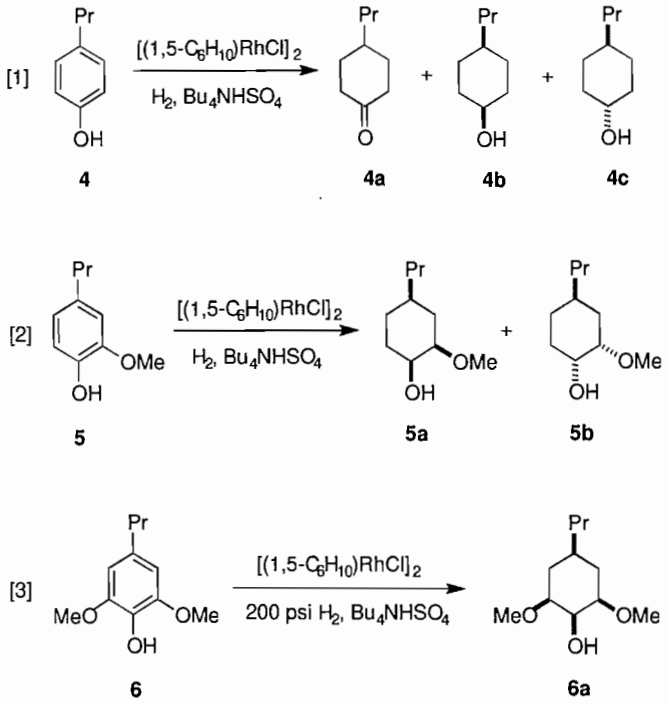
Can. J. Chem. Downloaded from www.nrcresearchpress.com by 91.121.58.235 on 09/08/12
For personal use only.

Can. J. Chem. Downloaded from www.nrcresearchpress.com by 91.121.58.235 on 09/08/12
For personal use only.

compounds in a two-phase hexane–aqueous medium at room temperature under 1 atm H_2 (101.3 kPa) (13, 14). The extremely mild reaction conditions prompted us to evaluate its potential in the stereoselective (*cis* vs. *trans* diastereomer) hydrogenation of lignin degradation model compounds. We have reported preliminary work on the catalytic hydrogenation of such model compounds using this Rh system; the aim of this work was to inhibit light-induced yellowing of lignin-rich mechanical wood pulp and paper (15).

Results and discussion

Propylphenol (**4**), 2-methoxy-4-propylphenol (**5**), and 2,6-dimethoxy-4-propylphenol (**6**) were selected as the model substrates (16). The catalytic hydrogenation reactions of these three model compounds are summarized in eqs. [1]–[3] (Pr = *n*-propyl).



Hydrogenation of **4** (50 h at ambient conditions in a two-phase medium with Bu_4NHSO_4 as a phase-transfer agent) afforded 4-propylcyclohexanone (**4a**), *cis*-4-propylcyclohexanol (**4b**), and *trans*-4-propylcyclohexanol (**4c**) in a 1:6:2 ratio with an 89% isolated yield. With a longer reaction time, **4a** was further hydrogenated to **4b** and **4c**. The diastereoselectivity of the hydrogenation was 3:1 in favor of **4b** (Table 1). The presence of a methoxy substituent adjacent to the phenolic hydroxyl group increases the diastereoselectivity of the reaction: hydrogenation of **5** afforded predominantly *cis*-2-methoxy-*cis*-4-propylcyclohexanol (**5a**) and *cis*-2-methoxy-*trans*-4-propylcyclohexanol (**5b**) in a 6:1 ratio, while the hydrogenation of **6** gave exclusively the all-*cis* diastereomer (**6a**) (100% diastereoselectivity) (Table 1). Hydrogenation of **6** was carried out under 200 psi H_2 because the reaction was extremely slow under 1 atm H_2.

The relative stereochemistries of **4b** and **4c** were established by ^{1}H NMR. **4b** has a multiplet signal (m) centered at δ 3.94 ascribable to the equatorial methine proton adjacent to the OH group in the *cis* diastereomer, while **4c** has a signal centered at

Table 1. Diastereoselectivity of the hydrogenation of lignin degradation model compounds.

Model compound	Major diastereomer (%)
4	**4b** (75)
5	**5a** (86)
6	**6a** (~100)

Fig. 1. ^{1}H NMR assignment of the relative stereochemistries of **4b** and **4c**.

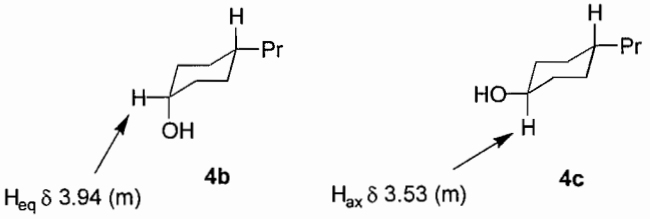
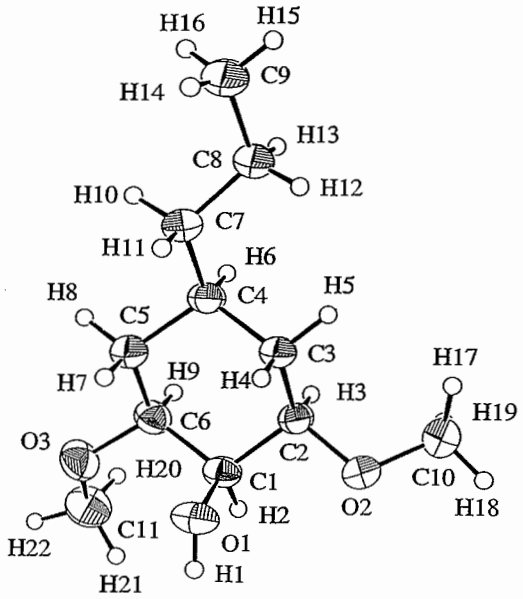


Fig. 2. ORTEP diagram of **6a**, showing 33% probability thermal ellipsoids.

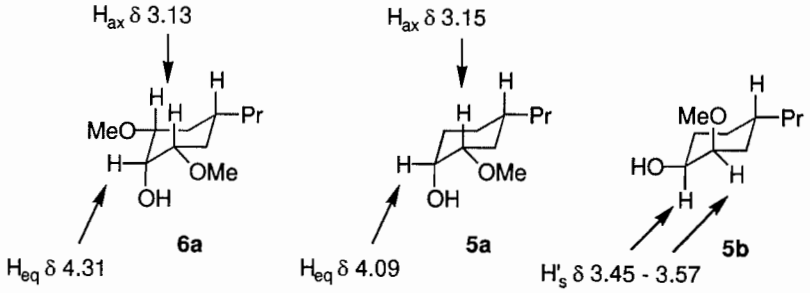


δ 3.53 (m) ascribable to the axial methine proton adjacent to the OH group in the *trans* diastereomer (Fig. 1) (17).

The relative stereochemistry of **6a** was established by X-ray crystal structure analysis, the ORTEP diagram being given in Figure 2. The atomic coordinates and equivalent isotropic thermal parameters for the C and O atoms are given in Table 2. The two OMe substituents are both *cis* to the OH group, with the torsion angles involving the OMe and the OH oxygens (O(1)-C(1)-C(2)-O(2) and O(1)-C(1)-C(6)-O(3)) being close to *gauche* (61.0° and −57.1°, respectively), while the torsion angles involving the hydrogens at the OMe carbon atoms and the OH oxygen (O(1)-C(1)-C(2)-H(3) and O(1)-C(1)-C(6)-H(9)) are close to *trans* (175° and −176°, respectively). The Pr substituent is *cis* to both OMe groups and thus *cis* to the OH group; H(6) and H(3) are mutually *cis*, and are both *trans* to

© 1997 NRC Canada

Fig. 3. ^{1}H NMR assignment of the relative stereochemistries of **5a** and **5b**.



Scheme 2. Enol–keto tautomerization in the formation of *trans*-4-propylcyclohexanol (**4c**).

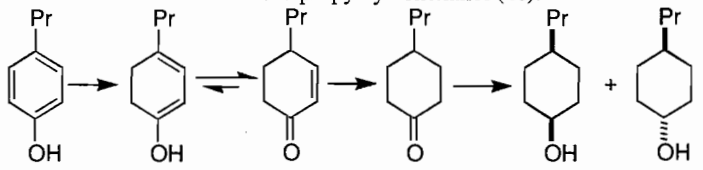


Table 2. Oxygen and carbon atomic coordinates and B_{eq} with estimated standard deviations in parentheses.

Atom	*x*	*y*	*z*	B_{eq}
O(1)	0.05506(5)	−0.1784(3)	0.06829(9)	4.99(3)
O(2)	0.04632(4)	0.2087(3)	−0.04806(7)	4.75(3)
O(3)	0.10087(5)	−0.0139(3)	0.23677(8)	5.89(4)
C(1)	0.07017(6)	0.0925(4)	0.0910(1)	4.12(4)
C(2)	0.08871(6)	0.2159(4)	0.0339(1)	3.97(4)
C(3)	0.13617(6)	0.0735(4)	0.0399(1)	4.11(4)
C(4)	0.18023(6)	0.0840(4)	0.1283(1)	4.06(4)
C(5)	0.16179(7)	−0.0324(5)	0.1868(1)	4.44(5)
C(6)	0.11401(7)	0.1066(4)	0.1788(1)	4.33(4)
C(7)	0.22941(7)	−0.0525(5)	0.1384(1)	4.67(5)
C(8)	0.25327(8)	0.0669(6)	0.0887(2)	5.48(6)
C(9)	0.30576(10)	−0.0456(9)	0.1095(2)	7.10(8)
C(10)	0.04989(9)	0.4084(6)	−0.1002(1)	5.85(6)
C(11)	0.0646(1)	0.1343(8)	0.2506(2)	7.12(9)

the CH_2 hydrogen H(4) (the torsion angles H(4)-C(3)-C(4)-H(6) and H(3)-C(2)-C(3)-H(4) are 176° and −179°, respectively). The bond lengths and angles are in the usual ranges.

The ^{1}H NMR data of **6a** were then used to establish the relative stereochemistries of **5a** and **5b**. The equatorial methine proton in **6a** has an ^{1}H NMR signal at δ 4.31 while the two axial methine protons adjacent to the OMe groups have signals (m) centered at δ 3.13 (Fig. 3). Based on these assignments for **6a**, the major diastereomer **5a** is thus drawn as shown in Fig. 3, with its assigned ^{1}H NMR signals; the slightly lower δ 4.09 value for the equatorial proton in **5a** compared to that of **6a** (δ 4.31) is due to the presence of only one OMe group β to the proton. A similar effect is also seen in **4b** where there is no OMe group and the equatorial methine proton adjacent to the OH group is seen at δ ~3.94. The minor diastereomer **5b** has two one-proton signals at δ 3.45–3.57 and at δ 3.49–3.56. This is possible only when the methine protons adjacent to the OH and the OMe groups are in the axial and equatorial position, respectively (Fig. 3).

The formation of a predominant or an exclusive *cis* diastereomer must be due to a "continuous" substrate coordination mechanism involved in the hydrogenation, similar to the situation found by others using Co(I)–phosphite complexes for the catalytic hydrogenation of arenes (18) (i.e., the arene substrate remains coordinated throughout successive hydrogen transfer from the metal to give addition of hydrogen on one side of the substrate via η^6-, η^4-, η^3-, and η^2-hydrocarbon moieties). The formation of a small amount of *trans* diastereomer in the hydrogenation of **4** and **5** likely arises from the enol–keto tautomerization of the hydrogenation intermediates. Hydrogenation of the first C=C double bond of the aromatic ring of **4** at the less sterically hindered position will give enol **4d**, which can either hydrogenate directly to the *cis* diastereomer **4b** via the "continuous" substrate coordination mechanism or tautomerize to **4e** and then hydrogenate to **4b** and **4c** through **4a** (Scheme 2). The isolation of **4a** and its further hydrogenation to **4b** and **4c** are consistent with such an enol–keto tautomerization.

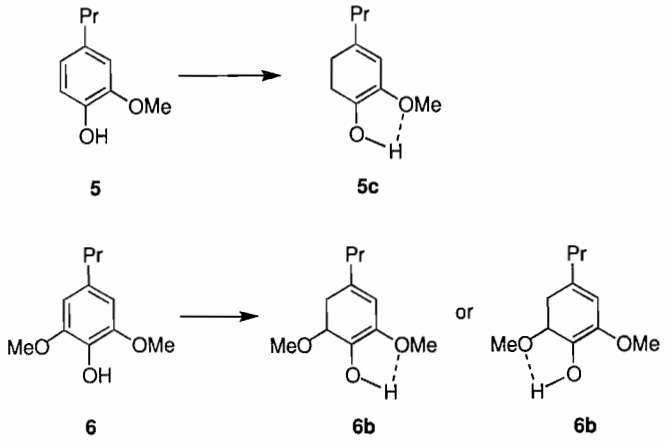
Hydrogenation of the first C=C double bond of the aromatic ring of **5** at the least sterically hindered position will give enol **5c**, which is likely stabilized by the OMe substituent via the formation of an intramolecular H-bond (Scheme 3). The opportunities for H-bonding are increased and, hence, the enol is more likely stabilized when a second OMe substituent is present adjacent to the OH group, as in the hydrogenation of **6** (Scheme 3). This increasing enol stabilization could account for the increasing *cis* diastereoselectivity for the hydrogenation of substrates **4**, **5**, and **6**, respectively.

Additional evidence for the contribution of such an enol–keto tautomerization to the formation of the *trans* diastereomer was obtained when we carried out the hydrogenation of 1,2-dimethoxy-4-propylbenzene (**7**). Only *cis,cis*-1,2-dimethoxy-*cis*-4-propylcyclohexane (**7a**) was isolated (eq. [4]). The relative stereochemistry of **7a** was established in a way similar to that used to define the stereochemistries of **5a**

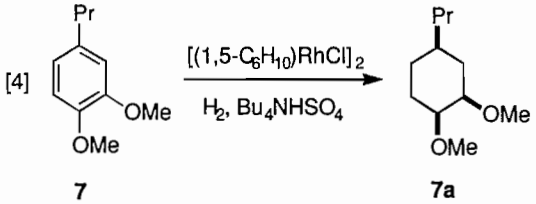
© 1997 NRC Canada

Can. J. Chem. Downloaded from www.nrcresearchpress.com by 91.121.58.235 on 09/08/12
For personal use only.

Scheme 3. Stabilization of enols **5c** and **6b** via the formation of intramolecular H-bonds.



and **5b**. The stereoselective hydrogenation of a similar but simpler compound, *p*-methylanisole, to *cis*-4-methylcyclohexyl methyl ether has been reported by others (14).



The active Rh catalyst is probably present in a colloidal form: as the hydrogenation proceeds, metal particles accumulate and these are not active for subsequent hydrogenation reactions. The presence of the aqueous buffer and Bu_4NHSO_4 (a phase-transfer reagent) (14) is essential for effective catalysis.

Experimental section

General procedures

All the hydrogenation reactions were monitored by TLC and (or) GC. Analytical TLC was performed on aluminum-backed, precoated silica gel plates (E. Merck, type 5554), which were "visualized" by UV fluorescence or by heating after spraying with a mixture of MeOH, HOAc, H_2SO_4, and anisaldehyde (90:10:5:1 by volume). GC analysis was carried out on a Hewlett Packard model 5890 GC with an FID detector and a Carbowax column. Flash column chromatography (19) was performed using Silica Gel 60, 230–400 mesh ASTM (E. Merck). Infrared spectra were recorded on a Bomem Michelson 100 FT-IR spectrophotometer using internal calibration; liquid samples were placed between two 3-mm NaCl plates, and solid samples were dissolved in $CHCl_3$. ^1H NMR spectra were recorded on Bruker WH-400 or Varian XL-300 spectrometers; chemical shifts (δ) were measured in $CDCl_3$ using TMS as the internal standard. LRMS and HRMS spectra were determined on a Kratos-AEI model MS 50 spectrometer operating at 70 eV.

Materials

Propylphenol (**4**) was obtained from Aldrich and purified by vacuum distillation (20). 2-Methoxy-4-propylphenol (**5**), 2,6-dimethoxy-4-propylphenol (**6**), and 1,2-dimethoxy-4-propylbenzene (**7**) were prepared as described below. $RhCl_3 \cdot 3H_2O$ was obtained from Johnson Matthey Ltd; $[(1,5\text{-}C_6H_{10})RhCl]_2$ was prepared by treatment of $RhCl_3 \cdot 3H_2O$ with 1,5-hexadiene in aqueous EtOH according to the literature (21). All other reagents and solvents were obtained from Aldrich and used without further purification.

Preparation of 2-methoxy-4-propylphenol (5) (ref. 22)

To 2.07 g (12.6 mmol) of eugenol (4-allyl-2-methoxyphenol) in 40 mL of EtOH was added 268 mg of 5% Pd on charcoal (0.126 mmol in Pd). The solution was deaerated using the freeze–pump–thaw technique. H_2 at 1 atm was bubbled through the stirred solution overnight at room temperature. The Pd catalyst was filtered off and EtOH was removed under reduced pressure. Et_2O (40 mL) was introduced to the residue and the solution was washed with saturated NaCl (2 × 20 mL), and dried over $MgSO_4$ for 30 min. Removal of the drying agent by filtration and removal of the solvent under reduced pressure gave the crude products, which were then purified by vacuum distillation to give 2.08 g (94%) of 2-methoxy-4-propylphenol (**5**): IR ν_{max}: 3476, 2958, 2930, 2867, 1608, 1514, 1459, 1430, 1367, 1268, 1234, 1151, 1123, 1034, 931, 846, 816, 795, 777, 736; ^1H NMR (300 MHz) δ: 0.93 (t, 3H), 1.53–1.70 (m, 2H), 2.51 (t, 2H), 3.89 (s, 3H), 5.44 (s, 1H), 6.63–6.89 (m, 3H); mass spectrum (EI), *m/z*: 166 (M^+: 30.7); HRMS calcd.: 166.0994; found: 166.0994.

Preparation of 2,6-dimethoxy-4-propylphenol (6)

The procedure was as described for **5**. 4-Allyl-2,6-dimethoxyphenol (9.50 g, 48.9 mmol) was hydrogenated with 1.03 g of 5% Pd/C in 100 mL of EtOH to give 8.53 g (89%) of **6**: IR ν_{max}: 3477, 2944, 2869, 2841, 1610, 1514, 1458, 1427, 1344, 1321, 1279, 1239, 1214, 1150, 1111, 1035, 967, 915, 824, 801, 770, 738; ^1H NMR (300 MHz) δ: 0.94 (t, 3H), 1.56–1.70 (m, 2H), 2.51 (t, 2H), 3.88 (s, 6H), 5.37 (s, 1H), 6.40 (s, 2H); mass spectrum (EI), *m/z*: 196 (M^+: 30.1); HRMS calcd.: 196.1099; found: 196.1096.

Preparation of 1,2-dimethoxy-4-propylbenzene (7)

The procedure was as described for **5**. 4-Allyl-1,2-dimethoxybenzene (8.99 g, 50.5 mmol) was hydrogenated with 1.07 g of 5% Pd/C in 100 mL of EtOH to give 9.01 g (99%) of **7**: IR ν_{max}: 2996, 2956, 2932, 2868, 2834, 1606, 1589, 1513, 1458, 1415, 1377, 1333, 1262, 1236, 1188, 1156, 1140, 1030, 938, 846, 806, 762; ^1H NMR (300 MHz) δ: 0.93 (t, 3H), 1.58–1.69 (m, 2H), 2.53 (t, 2H), 3.88 (s, 3H), 3.89 (s, 3H), 6.68–6.87 (m, 3H); mass spectrum (EI), *m/z*: 180 (M^+: 24.7); HRMS calcd.: 180.1150; found: 180.1145.

Catalytic hydrogenation of 4-propylphenol (4) (ref. 14)

To 28 mg (0.063 mmol) of $[(1,5\text{-}C_6H_{10})RhCl]_2$ in 10 mL of hexane were added **4** (857 mg, 6.30 mmol) dissolved in 5 mL of hexane, Bu_4NHSO_4 (135 mg, 0.40 mmol), and 5 mL of an aqueous buffer of pH 7.5 (boric acid, citric acid, and sodium phosphate) (23). The solution was deaerated using the freeze–pump–thaw technique. H_2 was then bubbled through the stirred solution at room temperature under atmospheric pressure. Upon the completion of the reaction (~50 h), the metal particles that accumulated as the reaction proceeded were removed by suction filtration. The filtrate was diluted with

© 1997 NRC Canada

Can. J. Chem. Downloaded from www.nrcresearchpress.com by 91.121.58.235 on 09/08/12
For personal use only.

Can. J. Chem. Downloaded from www.nrcresearchpress.com by 91.121.58.235 on 09/08/12
For personal use only.

25 mL of Et_2O. The organic layer was separated, washed twice with saturated NaCl (2 × 20 mL), and dried over $MgSO_4$ for 30 min. Removal of the drying agent by filtration and removal of the solvent under reduced pressure gave the crude products, which were then separated by flash column chromatography (silica gel) using a mixture of hexanes and ethyl acetate (9:1 by volume) as the eluent to give 88 mg (10%) of 4-propylcyclohexanone (**4a**): IR ν_{max}: 2940, 2865, 1716, 1454, 1377, 1329, 1241, 1172, 1123, 1071, 943, 882, 816, 743; ^{1}H NMR (300 MHz) δ: 0.72–1.02 (m, 3H), 1.15–1.52 (m, 5H), 1.53–1.80 (m, 2H), 1.96–2.12 (m, 2H), 2.25–2.42 (m, 4H); mass spectrum (EI), *m/z*: 140 (M^+: 38.3); HRMS calcd.: 140.1201; found: 140.1197; 528 mg (59%) of *cis*-4-propylcyclohexanol (**4b**): IR ν_{max}: 3360, 2931, 2864, 1453, 1371, 1334, 1253, 1209, 1141, 1064, 1049, 1033, 1021, 961, 927, 908, 885, 865, 819, 734; ^{1}H NMR (400 MHz) δ: 0.87 (t, 3H), 1.14–1.42 (m, 7H), 1.43–1.62 (m, 5H), 1.63–1.72 (m, 2H), 3.90–3.98 (m, 1H); mass spectrum (EI), *m/z*: 142 (M^+: 2.7); HRMS calcd.: 142.1358; found: 142.1350; and 179 mg (20%) of *trans*-4-propylcyclohexanol (**4c**): IR ν_{max}: 3343, 2933, 2860, 1456, 1370, 1246, 1204, 1146, 1096, 1054, 1010, 951, 906, 836, 734; ^{1}H NMR (400 MHz) δ: 0.86 (t, 3H), 1.10–1.33 (m, 9H), 1.47 (s, br, 1H), 1.70–1.78 (m, 2H), 1.90–2.00 (m, 2H), 3.48–3.57 (m, 1H); mass spectrum (EI), *m/z*: 142 (M^+: 0.5); HRMS calcd.: 142.1358; found: 142.1366.

Catalytic hydrogenation of 2-methoxy-4-propylphenol (5)

The hydrogenation procedure was as described for **4**. **5** (1.046 g, 6.30 mmol) was hydrogenated to give 748 mg (69%) of *cis*-2-methoxy-*cis*-4-propylcyclohexanol (**5a**): IR ν_{max}: 3468, 2933, 2867, 1459, 1440, 1378, 1328, 1267, 1225, 1194, 1158, 1137, 1110, 1089, 1020, 981, 942, 884, 868, 824, 784, 739; ^{1}H NMR (400 MHz) δ: 0.88 (t, 3H), 1.18–1.45 (m, 9H), 1.70–1.80 (m, 1H), 1.85 (s, br, 1H), 1.94–2.12 (m, 1H), 3.11–3.19 (m, 1H), 3.39 (s, 3H), 4.09 (m, 1H); mass spectrum (EI), *m/z*: 172 (M^+: 13.6); HRMS calcd.: 172.1464; found: 172.1464; and 119 mg (11%) of *cis*-2-methoxy-*trans*-4-propylcyclohexanol (**5b**): IR ν_{max}: 3425, 2956, 2928, 2870, 1459, 1374, 1260, 1211, 1180, 1097, 1058, 969, 806; ^{1}H NMR (400 MHz) δ: 0.89 (t, 3H), 1.12–1.38 (m, 6H), 1.42–1.62 (m, 2H), 1.68–1.77 (m, 2H), 1.80 (s, br, 1H), 2.02–2.12 (m, 1H), 3.38 (s, 3H), 3.45–3.57 (m, 1H), 3.49–3.56 (m, 1H); mass spectrum (EI), *m/z*: 172 (M^+: 8.0); HRMS calcd.: 172.1464; found: 172.1459.

Catalytic hydrogenation of 2,6-dimethoxy-4-propylphenol (6)

To 28 mg (0.063 mmol) of $[(1,5\text{-}C_6H_{10})RhCl]_2$ in 10 mL of hexane in a 25-mL glass liner were added **6** (1.235 g, 6.30 mmol) dissolved in 5 mL of hexane, Bu_4NHSO_4 (135 mg, 0.40 mmol), and 5 mL of the aqueous, pH 7.5 buffer. The solution was deaerated. The glass liner was inserted into a 60-mL laboratory stainless steel autoclave that had been flushed with N_2. The autoclave was sealed and pressurized with H_2 to 200 psi, and the reaction was allowed to proceed at room temperature under magnetic stirring. After 6 h, excess H_2 was carefully released. The metal particles were removed by suction filtration, and the filtrate was diluted with 25 mL of Et_2O. The organic layer was separated, washed twice with saturated NaCl (2 × 20 mL), and dried over $MgSO_4$ for 30 min. Removal of the drying agent by filtration and removal of the solvent under reduced pressure gave the crude product, which was purified by flash column chromatography (silica gel) using a mixture of hexanes and ethyl acetate (12:1 by volume) as the eluent and by recrystallization from EtOH to give 1.044 g (82%) of *cis,cis*-2,6-dimethoxy-4-cis-propylcyclohexanol (**6a**) as colorless crystals: IR ν_{max}: 3580, 3472, 2990, 2933, 2860, 2827, 1459, 1379, 1300, 1099, 994, 956, 900, 861; ^{1}H NMR (400 MHz) δ: 0.90 (t, 3H), 1.25–1.40 (m, 6H), 1.70–1.78 (m, 4H), 3.09–3.17 (m, 2H), 3.40 (s, 6H), 4.31 (s, br, 1H); mass spectrum (EI), *m/z*: 202 (M^+: 0.3); HRMS calcd.: 202.1569; found: 202.1560.

X-ray crystallographic analysis of 6a

A colorless plate crystal of **6a** having approximately dimensions of 0.15 × 0.30 × 0.35 mm was mounted in a glass capillary. Unit-cell parameters were refined by least-squares on 2 sin θ/λ values for 25 reflections (75.10° < 2θ < 91.09°) measured on a Rigaku AFC6S diffractometer with graphite monochromated Cu-Kα radiation (λ(CuKα) = 1.54178 Å). Crystal data at 21°C are: $C_{11}H_{22}O_3$; FW = 202.29; a = 29.277(1) Å; b = 4.982(1) Å; c = 18.403(1) Å; β = 117.776(4)°; V = 2375.0(4) Å^3; Z = 8, ρ_{calc} = 1.131 g/cm^3; $F(000)$ = 896; μ (MoKα) = 6.47 cm^{-1}. Absent reflection: hkl ($h + k \neq 2n$), $h0l$ ($l \neq 2n$), space group = $C2/c$ (no. 15).

The data were collected at a temperature of 21 ± 1°C using the ω–2θ scan technique to a maximum 2θ value of 155.0°. Omega scans of several intense reflections, made prior to data collection, had an average width at half-height of 0.25° with a take-off angle of 6.0°. Scans of (1.00 + 0.20 tan θ)° were made at a speed of 16.0°/min (in ω). The weak reflections (I < 40.0σ(I)) were rescanned (maximum of 8 rescans) and the counts were accumulated to ensure good counting statistics. Stationary background counts were recorded on each side of the reflection. The ratio of peak counting time to background counting time was 2:1. The diameter of the incident beam collimator was 0.5 mm and the crystal to detector distance was 285 mm. Of the 2781 reflections that were collected, 2725 were unique (R_{int} = 0.028); equivalent reflections were merged. The intensities of three representative reflections were measured after every 200 reflections. No decay correction was applied. The linear absorption coefficient, μ, for Cu-Kα radiation is 6.5 cm^{-1}. An empirical absorption correction based on azimuthal scans of several reflections was applied, which resulted in transmission factors ranging from 0.73 to 1.00. The data were corrected for Lorentz and polarization effects. A correction for secondary extinction was applied (coefficient = 9.1(3) × 10^{-6}).

The structure was solved by direct methods (24) and expanded using Fourier techniques (25). The non-hydrogen atoms were refined anisotropically. Hydrogen atoms were refined isotropically. The final cycle of full-matrix least-squares refinement was based on 1537 observed reflections (I > 3.00 σ(I)) and 216 variable parameters and converged (largest parameter shift was 0.005 times its esd) with unweighted and weighted agreement factors of $R = \Sigma||F_o| - |F_c||/\Sigma|F_o| = 0.036$, $R_w = (\Sigma w(|F_o| - |F_c|)^2/\Sigma w|F_o|^2)^{1/2} = 0.041$. The standard deviation of an observation of unit weight was 2.55. The weighting scheme was based on counting statistics. Plots of $\Sigma w(|F_o| - |F_c|)^2$ versus $|F_o|$, reflection order in data collection, sin θ/λ, and various classes of indices showed no unusual trends. The maximum and minimum peaks on the

© 1997 NRC Canada

final difference Fourier map corresponded to 0.13 and −0.11 e/Å^3, respectively. Neutral atom scattering factors were taken from Cromer and Waber (26). Anomalous dispersion effects were included in F_{calc} (27); the values for $\Delta f'$ and $\Delta f''$ and the mass attenuation coefficients were taken from the literature (28, 29). All calculations were performed using the *teXsan* crystallographic software package of Molecular Structure Co.[2] A listing of bond lengths, bond angles, hydrogen atom parameters, anisotropic thermal parameters, torsion angles, and intermolecular contacts are included as supplementary materials (Tables S1–S6).[3] Measured and calculated structure factor amplitudes are available from the authors.

Catalytic hydrogenation of 1,2-dimethoxy-4-propylbenzene (7)

The hydrogenation procedure was as given for **4**. **7** (1.135 g, 6.30 mmol) was hydrogenated to give 927 mg (79%) of *cis,cis,cis*-1,2-dimethoxy-4-propylcyclohexane (**7a**): IR ν_{max}: 2930, 2871, 2825, 1456, 1377, 1307, 1192, 1163, 1114, 1096, 983, 946, 851, 786, 739; ^{1}H NMR (400 MHz) δ: 0.89 (t, 3H), 1.11–1.44 (m, 9H), 1.72–1.81 (m, 1H), 2.01–2.10 (m, 1H), 3.10–3.18 (m, 1H), 3.37 (s, br, 6H), 3.63 (s, br, 1H); mass spectrum (EI), *m/z*: 186 (M^+: 9.7); HRMS calcd.: 186.1620; found: 186.1614.

Acknowledgements

We thank the Natural Sciences and Engineering Research Council of Canada for providing an Industrial Postdoctoral Fellowship (T.Q.H.), and Johnson Matthey Ltd for a loan of $RhCl_3 \cdot 3H_2O$.

References

1. R.H. Whittaker and G.E. Likens. *In* Primary production of the biosphere. *Edited by* H. Lieth and R.H. Whitaker. Springer-Verlag, Berlin. 1975. pp. 305–328.
2. H. Sandermann, D. Scheel, and T. Trenck. Appl. Polym. Symp. **37**, 407 (1983).
3. W.G. Glasser and S.S. Kelley. *In* Encyclopedia of polymer science and engineering. Vol. 8. *Edited by* J.I. Kroschwitz. John Wiley and Sons, New York. 1987. pp. 795–852.
4. S.L. Buchwalter. Tappi J. **68**, 116 (1985).
5. P.J. Chenier. *In* Survey of industrial chemistry. John Wiley and Sons, New York. 1986. pp. 348–349.
6. B.F. Hrutfiord. *In* Lignins — occurrence, formation, structure and reactions. *Edited by* K.V. Sarkanen and C.H. Ludwig. Wiley–Interscience, New York. 1971. pp. 487–509.
7. B.F. Hrutfiord and J.L. McCarthy. Adv. Chem. Ser. **59**, 226 (1966).
8. J.M. Pepper, W.F. Steck, R. Swoboda, and J.C. Karapally. Adv. Chem. Ser. **59**, 238 (1966).
9. J.G. Miller and C. Schuerch. Tappi J. **51**, 273 (1968).
10. S.W. Eachus and C.W. Dence. Holzforschung, **29**, 41 (1975).
11. V.W. Schweers. Holzforschung, **23**, 120 (1969).
12. V.W. Schweers and O. Beinhoff. Holzforschung, **28**, 20 (1974).
13. B., Heil, S. Toros, S. Vastag, and L. Marko. J. Organomet. Chem. **94**, C47 (1975).
14. K.R. Januszkiewicz and H. Alper. Organometallics, **2**, 1055 (1983).
15. T.Q. Hu, B.R. James, and C.-L. Lee. J. Pulp Paper Sci. **23**, J153 (1997).
16. T.J. Fullerton. J. Wood Chem. Technol. **7**, 441 (1987).
17. R.M. Silverstein, G.C. Bassler, and T.C. Morrill. *In* Spectrometric identification of organic compounds. John Wiley and Sons, New York. 1981. pp. 189–190.
18. J.R. Bleeke and E.L. Muetterties. J. Am. Chem. Soc. **103**, 556 (1981).
19. W.C. Still, M. Kahn, and A. Mitra. J. Org. Chem. **43**, 2923 (1978).
20. D.D. Perrin, W.L.F. Armarego, and D.R. Perrin. *In* Purification of laboratory chemicals. Pergamon Press, Oxford. 1966.
21. G. Winkhaus and H. Singer. Chem. Ber. **99**, 3602 (1966).
22. A. Castellan, A. Nourmamode, P. Fornier de Violet, N. Colombo, and C. Jeager. J. Wood Chem. Technol. **12**, 1 (1992).
23. W.R. Carmody. J. Chem. Educ. **38**, 559 (1961).
24. G.M. Sheldrick. *In* Crystallogrphic computing 3; SHELX586. *Edited by* G.M. Sheldrick, C. Kruger, and R. Goddard. Oxford Univ. Press, Oxford. 1985. pp. 175–189.
25. P.T. Beurskens, G. Admiraal, G. Beurskens, W.P. Bosman, S. Garcia-Granda, R.O. Gould, J.M.M. Smits, and C. Smykalla. The DIRDIF program system. Technical report of the crystallography laboratory, University of Nijmegen, The Netherlands. 1992.
26. D.T. Cromer and J.T. Waber. *In* International table for X-ray crystallography. Vol. 4. The Kynoch Press, Birmingham, England. 1974. Table 2.2A.
27. J.A. Ibers and W.C. Hamilton. Acta Crystallogr. **17**, 781 (1964).
28. D.C. Creagh and W.J. McAuley. *In* International tables for crystallography. Vol. C. *Edited by* A.J.C. Wilson. Kluwer Academic Publishers, Boston. 1992. Table 4.2.6.8. pp. 219–222.
29. D.C. Creagh and J.H. Hubbell. *In* International tables for crystallography. Vol. C. *Edited by* A.J.C. Wilson. Kluwer Academic Publishers, Boston. 1992. Table 4.2.4.3. pp. 200–206.

[2] TEXSAN/TEXRAY structure analysis package (Version 5.1), Molecular Structure Corp., The Woodlands, Tex. 1985.

[3] Supplementary materials mentioned in the text may be purchased from: The Depository of Unpublished Data, Document Delivery, CISTI, National Research Council Canada, Ottawa, Canada K1A 0S2. The tables of bond lengths, bond angles, and hydrogen atom parameters have also been deposited with the Cambridge Crystallographic Data Centre, and can be obtained on request from The Director, Cambridge Crystallographic Data Centre, University Chemical Laboratory, 12 Union Road, Cambridge, CB2 1EZ, U.K.

Can. J. Chem. Downloaded from www.nrcresearchpress.com by 91.121.58.235 on 09/08/12
For personal use only.

© 1997 NRC Canada

Évaluation de l'effet électroattracteur du motif 4-nitrobenzofurazanyle : ionisation de 7-anilino 4-nitrobenzofurazanes

Jean-Claude Hallé, Malika Mokhtari, Pascale Soulié et Marie-José Pouet

Résumé : L'acidité NH/N⁻ d'une série de 7-(4′-X anilino) 4-nitrobenzofurazanes (**4H**) (X = NO_2, CN, CO_2Me, F, H, Me, OMe) a été déterminée par spectrophotométrie UV–visible dans un milieu H_2O–Me_2SO de fraction molaire N_{Me_2SO} = 0,509. Les pK_a mesurés s'inscrivent dans un domaine assez restreint : 6,40 (X = NO_2)/7,98 (X = OMe), et montrent que **4H** est environ 3 fois plus acide que la 2,4,6-trinitrodiphénylamine identiquement substituée. Ces résultats, complétés par l'analyse des effets du substituant X sur les δ_{H_i} et δ_{C_i}, et l'examen des paramètres de déprotonation $\Delta\delta$ (particulièrement importants pour H_6, C_4, C_6 et C_7) atteste d'un très fort pouvoir électroattracteur du motif 4-nitrobenzofurazanyle. En outre, la mise en évidence d'excellentes corrélations entre les déplacements chimiques ($\delta_{^1H}$ et $\delta_{^{13}C}$) de **4H** et **4**⁻ et les pK_a, a permis de contrôler, et même de préciser, certaines attributions (δ_{C7} et δ_{C9}).

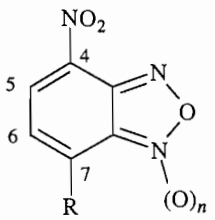
Mots clés : 7-anilino 4-nitrobenzofurazanes, acidités, paramètres de déprotonation (RMN ^1H et ^{13}C, milieux eau–diméthylsulfoxyde.

Abstract: The ionization of a series of 7-(4′-X anilino) 4-nitrobenzofurazans (**4H**) (X = NO_2, CN, CO_2Me, F, H, Me, OMe) to give the conjugate amide anions **4**⁻ has been studied by ^1H and ^{13}C NMR in Me_2SO-d_6. Concomitantly, their acidity (pK_a) has been measured spectrophotometrically in a H_2O–Me_2SO mixture with a molar fraction N_{Me_2SO} = 0,509. Although the measured pK_a values for the whole series of compounds **4H** lie in a relatively narrow range (6.40, X = NO_2 / 7.98, X = OMe), they reveal that each derivative is about 3 times more acidic than the similarly X-substituted 2,4,6-trinitrodiphenylamines. These results, together with an analysis of substituent effects on the proton and carbon chemical shifts (δ_{H_i} et δ_{C_i}) and the related deprotonation parameters ($\Delta\delta$), which are specially significant for H_6, C_4, C_6, and C_7, emphasize the very strong electron-withdrawing character of the 4-nitrobenzofurazanyl moiety. In addition, the observation of nice linear correlations of the type $\delta_{H_i(C_i)} = f(pK_{ai})$ has enabled us to control and sometimes to firmly assign the various chemical shifts.

Key words: 7-anilino 4-nitrobenzofurazans, acidities, ^1H and ^{13}C NMR deprotonation shifts, water – dimethyl sulfoxide mixtures.

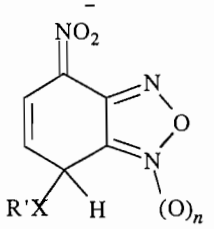
Introduction

L'intérêt porté au 4-nitrobenzo-2-oxa-1,3-diazole **1***a* (R = H, *n* = 0), plus communément nommé 4-nitrobenzofurazane, et à ses dérivés N-oxydés, notamment **1***b* (R = H, *n* = 1, 4-nitrobenzofuroxane), remonte à 1968, lorsque Ghosh et Whitehouse ont découvert les activités antileucémiques potentielles de ces hétérocycles, inhibiteurs de la synthèse des acides nucléiques dans les lymphocytes (1–5). C'est le caractère électrophile très important de **1***a* et de **1***b* qui, en bloquant les fonctions thiol et amine des protéines par formation des adduits σ **2**, a été rendu responsable de cette intéressante inhibition (1, 4, 5).



1

a *n* = 0, R = H
b *n* = 1, R = H
c *n* = 0, R = NHR_1 OU NR_1R_2
d *n* = 0, R = Cl
e *n* = 0, R = F



2

X = S
X = NH

Au cours de l'exploration des potentialités biologiques et médicales variées inhérentes à ces hétérocycles (compilées dans une excellente revue (5)), Ghosh et Whitehouse ont également mis en évidence les propriétés fortement fluorescentes des dérivés 7-alkylaminés du 4-nitrobenzofurazane (**1***c*).

Ce comportement a conduit à l'utilisation du 7-chloro

Reçu le 6 mars 1997.

J.-C. Hallé,[1] **P. Soulié et M.-J. Pouet.** Université de Versailles-Saint Quentin en Yvelines, Synthèse, interactions et réactivité en chimie organique et bioorganique, EP 102 du Centre national de la recherche scientifique, Bâtiment Lavoisier, 45 avenue des États-Unis, 78035 Versailles Cedex, France.
M. Mokhtari. Laboratoire de chimie hétérocyclique, Institut de chimie, Université de Tlemcen, BP 119, 13000 Tlemcen, Algérie.

1. Auteur auquel la correspondance doit être adressée. Téléphone : 39254455. Télécopie : 39254452.

© 1997 NRC Canada

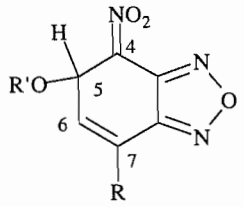
Can. J. Chem. Downloaded from www.nrcresearchpress.com by 91.121.58.235 on 09/08/12
For personal use only.

Can. J. Chem. Downloaded from www.nrcresearchpress.com by 91.121.58.235 on 09/08/12
For personal use only.

4-nitrobenzofurazane **1***d*, et de son homologue fluoré **1***e*, pour l'analyse fluorimétrique des amines primaires (aminoacides notamment) et secondaires, ainsi que pour leur détection chromatographique (5–14). Ces deux composés sont maintenant très utilisés, notamment le dérivé chloré (noté NBD-Cl) (6).

Dans la mesure où la fluorescence de ces dérivés est étroitement liée à la conjugaison entre le substituant 4-nitro et le groupement fixé en position 7, et que cette émission lumineuse (comme d'ailleurs l'absorption) est très sensible à la nature du milieu et à son pH (5, 14, 15), il est surprenant qu'aucune étude systématique n'ait été entreprise pour chiffrer le caractère électroattracteur du motif NBD. Les seules données actuellement disponibles concernent les déterminations de l'acidité du 4-hydroxy 7-nitrobenzofurazane (NBD-OH) dans l'eau ($pK_a \leq 1{,}8$) (16) et divers solvants organiques (17) : MeOH ($pK_a = 5{,}5$), DMF ($pK_a = 3{,}2$) et Me_2SO ($pK_a = 2{,}6$). Quelques pK_a de dérivés monoalkylés du NBD (**1***c*) ont également été rapportés : $pK_a \approx 10$ (18).

Par ailleurs, le marquage de nombreux lipides au NBD a permis, par l'examen de la fluorescence (très sensible au pH) des modèles obtenus, une meilleure connaissance de l'organisation des membranes biologiques (14, 19). Bien qu'un pK_a d'environ 11,5 ait été avancé pour la sonde NBD des phospholipides ainsi marqués, les auteurs n'ont malheureusement pu conclure si l'équilibre réversible associé correspond à la simple déprotonation de la fonction 7-aminée, ou plutôt à la formation de l'adduit σ-hydroxylé **3***a* (14, 19). La formation de



3

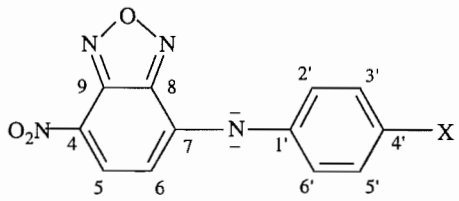
a (R' = H, R = NHR")

b (R' = Me, R = F, Cl ou Br)

tels adduits σ de type **3**, étudiée en détail dans l'eau et dans le méthanol (20), complique l'étude de la déprotonation de toute fonction acide située sur la position-7 du motif NBD (14, 20, 21). En fait la formation de complexes de type **3** est à l'origine du peu d'informations quantitatives concernant le caractère électrophile du motif NBD.

Le travail présenté a pour but de chiffrer l'aptitude électroattractrice du motif NBD et de la comparer à celle du groupement picryle (2,4,6-trinitrophényle) qui reste une référence en la matière (20, 22). Pour atteindre cet objectif nous avons examiné une série de 7-anilino 4-nitrobenzofurazanes **4H**, diversement substitués en *para* du cycle phényle. Ces composés présentent l'avantage d'être facilement accessibles par simple réaction de substitution nucléophile aromatique (S_NAr) entre le NBD-Cl commercial **1***d* et l'aniline substituée correspondante (23) (eq. [1]).

Après avoir analysé l'influence du substituant X sur l'acidité (NH/N$^-$) de **4H** dans un milieu eau–diméthylsulfoxyde de composition convenable, nous démontrons par analyse RMN ^1H et ^{13}C des molécules **4H** et de leurs anions **4**$^-$ la très grande aptitude du motif 4-nitrobenzofurazanyle (NBD) à délocaliser les électrons.



4 $^-$

Résultats

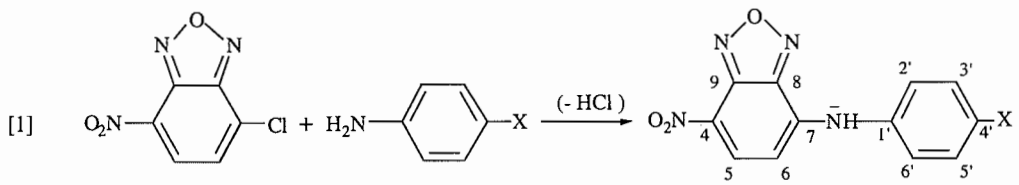
I. Détermination des constantes d'acidité de 4H

En raison d'une très faible solubilité des molécules **4H** en solution aqueuse, les constantes d'acidité K_a^{4H} afférentes à leur ionisation selon l'équation [2] ont été mesurées spectrophotométriquement dans un milieu H_2O–Me_2SO 20/80 (v/v),(0,491/0,509 en fraction molaire), noté S. Pour un couple **4H/4**$^-$ donné, la conversion de la forme acide en forme basique a été étudiée dans divers tampons de pH appropriés

$$[2]\quad \mathbf{4H} + S \underset{}{\overset{K_a^{4H}}{\rightleftharpoons}} \mathbf{4}^- + HS^+$$

$$[3]\quad pK_a^{4H} = pH - \log\frac{\varepsilon - \varepsilon_{4H}}{\varepsilon_{4^-} - \varepsilon} - \log f_{4^-}$$

(figure 1), et le pK_a correspondant calculé selon l'équation [3] où ε_{4H}, ε_{4^-} et ε représentent respectivement les coefficients d'absorption molaire de la molécule pure, de l'anion pur et du mélange des deux formes à l'équilibre au pH de mesure. Pour tous les systèmes étudiés, les niveaux de basicité atteints dans divers tampons CAPS se sont avérés suffisants pour déterminer ε_{4^-}. Ceci a permis d'éviter le recours à des solutions de soude diluées où la formation compétitive des adduits σ de type **3** aurait compliqué les déterminations. L'obtention de faisceaux isosbestiques (cf. figure 1) conforte l'existence d'un seul processus d'ionisation. La réversibilité de la déprotonation de **4H** en **4**$^-$ a d'ailleurs été vérifiée, non seulement par spectroscopie UV–visible dans le mélange eau–Me_2SO

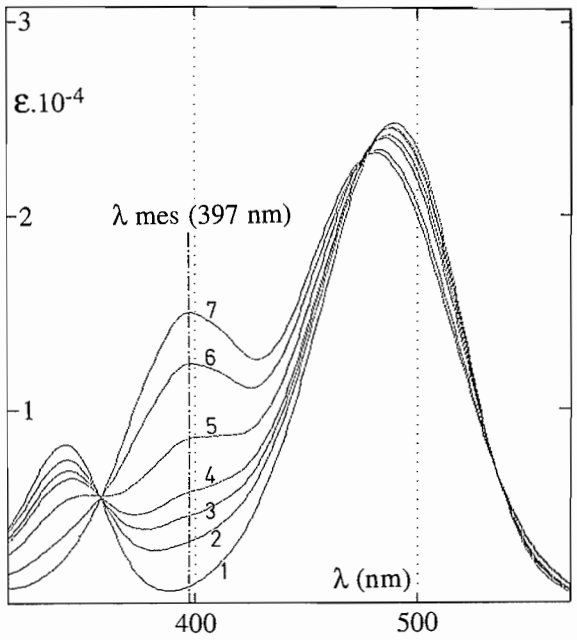


1*d* **4H**

X=NO_2,CN,CO_2Me,F,H,Me,OMe.

© 1997 NRC Canada

Figure 1. Ionisation du 7-anilino 4-nitrobenzofurazane (**4H**, X = H) dans le milieu H_2O–Me_2SO contenant 50,9% de Me_2SO en fraction molaire; t = 25°C; Points isosbestiques : λ = 358 nm (ε = 5440), λ = 477 nm (ε = 22 900); λ_{mesure} = 397 nm. (1) pH = 3,02 (HCl), ε_{4H}^{397} = 840; (2) pH = 6,90, ε^{397} = 3175; (3) pH = 7,15, ε^{397} = 4520; (4) pH = 7,38, ε^{397} = 5730; (5) pH = 7,72, ε^{397} = 8460; (6) pH = 8,17, ε^{397} = 12 120; (7) pH = 10,53, ε_4^{397} = 14 910.



(20/80) utilisé, mais aussi par RMN dans le Me_2SO-d_6. Dans les deux cas la reprotonation de $\mathbf{4}^-$ par un acide fort ($MeSO_3H$) se traduit par la régénération des paramètres spectroscopiques de **4H**. Les structures de **4H** et $\mathbf{4}^-$ ont été confirmées par RMN (vide infra).

Toutes les solutions tamponnées ont été préparées de telle sorte que la force ionique I soit égale à 0,01 mol L^{-1}. Ceci a permis le calcul du coefficient d'activité de $\mathbf{4}^-$ par l'expression simplifiée de Debye–Hückel (24) : $\log f_{4^-} = -A\sqrt{I}$ avec A = 0,5 pour le mélange H_2O–Me_2SO (20/80) retenu (25).

Il convient de noter que les six tampons utilisés pour couvrir la gamme de pH (5,7–10,5), nécessaire au suivi de l'ionisation de l'ensemble des composés **4H** étudiés, sont des tampons biologiques dont les pK_a n'étaient connus qu'à 20°C dans ce milieu (26). Ces tampons ont donc été recalibrés à 25°C suivant une méthode potentiométrique décrite dans la partie expérimentale.

Le tableau 1 rassemble les pK_a de **4H** ainsi déterminés.

II. Études RMN ^{1}H et ^{13}C des 7-anilino 4-nitrobenzofurazanes 4H et de leurs anions 4^-

La numérotation retenue pour **4H** et $\mathbf{4}^-$ est indiquée dans l'équation [1].

II. 1. Analyse des spectres ^{1}H

Pour les molécules **4H**, chaque spectre ^{1}H présente un système AX assorti d'un système AA′XX′ (NO_2, CO_2Me, OMe) qui dégénère en système AA′BB′ pour les substituants CN, F et Me. L'analyse de ces systèmes a été faite au premier ordre et les attributions tiennent compte des intégrations relatives et des effets connus (blindage ou déblindage) des différents substituants (28). Par addition progressive de base, on aboutit aux paramètres de l'anion $\mathbf{4}^-$ dont les protons sont tous blindés par rapport à ceux de **4H**. Le tableau 2 regroupe les paramètres spectroscopiques ^{1}H de **4H** et $\mathbf{4}^-$.

II. 2. Analyse des spectres ^{13}C

Les molécules **4H** et leurs anions $\mathbf{4}^-$ comportent six carbones quaternaires dont l'un d'eux, C_4, va nous servir de sonde puisque, de par sa conjugaison avec le site ionisable, les variations de ses déplacements chimiques dues, d'une part, à la nature du substituant X et, d'autre part, à la déprotonation de la fonction NH, doivent être le reflet des densités de charge et de leurs variations au cours de l'ionisation.

L'identification des carbones a été réalisée en utilisant les méthodes classiques (mesure des constantes de couplage et irradiations sélectives des H à faible puissance) mais aussi par des corrélations ^{1}H/^{13}C optimisées pour les couplages ^1J et ^3J. Le tableau 3 (documentation complémentaire)[2] donne un exemple des paramètres δ^{13}C et $J_{^{13}CH}$ relevés sur les spectres non découplés du 7-(paraméthoxy anilino) 4-nitrobenzofurazane et de son anion et la figure 2 (documentation complémentaire)[2] illustre la corrélation ^{1}H/^{13}C obtenue pour ce même substrat. Dans la mesure où les couplages $^3J_{^{13}CH}$ sont supérieurs aux couplages $^2J_{^{13}CH}$ dans les cycles aromatiques (29), les attributions ne soulèvent aucune ambiguïté à l'exception de celles des deux carbones quaternaires C_7 et C_9 qui sont tous deux uniquement couplés avec H_5 (tableau 3 et figure 2). Dans ce cas les attributions ont été faites sur la base des corrélations $\delta_{^{13}C}/pK_a^{4H}$ (cft. Disussion). Le tableau 4 rassemble les $\delta_{^{13}C}$ relatifs aux molécules **4H** et de leurs anions $\mathbf{4}^-$.

Discussion

I. Mesures d'acidité

Il ressort du tableau 1 que les valeurs de $pK_a^{4H,X}$ mesurées varient de 6,40 pour le composé le plus acide (X = NO_2) à 7,98 pour le composé le moins acide (X = OMe). Ces pK_a correspondent à des acidités relativement importantes pour des équilibres de type NH/N^-. En effet, si l'on se réfère à l'acidité de la *p*-nitroaniline ($ArNH_2/ArNH^-$) dont le pK_a est voisin de 19 dans le milieu étudié (30), c'est par un facteur 4×10^{12} que le motif 4-nitrobenzofurazanyle exalte la déprotonation de la fonction amine. On constate également que l'acidité du 7-anilino 4-nitrobenzofurazane (X = H, pK_a = 7,68) est, dans ce milieu, 3,3 fois plus grande que celle de la 2,4,6-trinitrodiphénylamine (pK_a = 8,20) (30). Ainsi, vis-à-vis de notre modèle ($ArNH/ArN^-$), le *pouvoir électroattracteur du groupement NBD s'avère supérieur à celui du groupement picryle.*

La forte délocalisation des électrons vers le motif NBD de ces molécules a nécessairement lieu au détriment du cycle phényle *para*-substitué. Cette idée est confirmée par un traitement selon Hammett (équation [4]) des pK_a^{4H} obtenus :

$$[4] \quad pK_a^{4H,H} - pK_a^{4H,X} = \rho^S \cdot \sigma_X$$

2. Cette documentation complémentaire (tableau 3 et figure 2) peut être achetée de : Dépot des données non publiées, Service de fourniture de documents, ICIST, Conseil national de recherches Canada, Ottawa, Canada K1A 0S2.

© 1997 NRC Canada

Can. J. Chem. Downloaded from www.nrcresearchpress.com by 91.121.58.235 on 09/08/12
For personal use only.

Tableau 1. Influence de la *para* X-substitution sur l'acidité des 7-anilino 4-nitrobenzofurazanes **4H**; milieu eau–Me_2SO contenant 50,9% de Me_2SO en fraction molaire; t = 25°C; corrélation avec les σ de Hammett.

X	NO_2	CN	CO_2Me	F	H	Me	OMe
$pK_a^{4H,X}$	6,40	6,75	7,05	7,61	7,68	7,87	7,98
σ_X[a]	1,27[b]	1,00[b]	0,64[b]	0,06[c]	0	−0,17[c]	−0,27[c]

$pK_a^{4H,X} = -0,9947\sigma_X + 7,6938$ $\quad r = 0,9989$

[a]Réference 27, [b]σ_{p^-}, [c]σ_p.

Tableau 2. Paramètres spectroscopiques ^1H des molécules **4H** et de leurs anions **4**$^-$ ($c \leq 0,05$ M, Me_2SO-d_6).

X		δ_{H_5}[a]	δ_{H_6}[a]	$\delta_{H_{2'6'}}$[a,b]	$\delta_{H_{3'5'}}$[a,b]	δ_{NH}	δ_X	$^3J_{56}$	$^3J_{2'3}$
NO_2	**4H**	8,61	7,18	7,72	8,32	11,27		8,7	9,2
	4$^-$	7,87	5,73	7,11	8,21			10,0	8,9
CN	**4H**	8,58	7,07	7,67	7,93	11,16		8,7	8,6
	4$^-$	7,82	5,67	7,06	7,77			10,0	8,2
COOMe	**4H**	8,57	7,01	7,63	8,05	11,16	3,87	8,8	8,7
	4$^-$	7,80	5,69	7,00	7,94		3,84	9,9	8,2
F[c]	**4H**	8,45	6,58	7,50	7,34	11,01	48,11[d]	8,8	9,1
	4$^-$	7,76	5,75	6,93	7,17		44,59	10,0	8,9
H	**4H**	8,54	6,73	7,52	7,50	11,08	7,34[b]	8,9	
	4$^-$	7,71	5,70	6,89	7,34		7,04	10,1	
Me	**4H**	8,50	6,63	7,36	7,32	11,03	2,36	8,9	8,6
	4$^-$	7,70	5,77	6,79	7,14		2,28	10,2	8,0
OMe	**4H**	8,51	6,54	7,40	7,08	11,01	3,81	8,9	8,9
	4$^-$	7,68	5,81	6,86	6,92		3,75	10,2	9,1

δ en ppm/Me_4Si, J en Hz.
[a]La numérotation est celle de l'équation [1].
[b]Analyse au premier ordre.
[c]**4H** : $^3J_{F,3'} = 8,5$, $^4J_{F,2'} = 5,0$; **4**$^-$: $^3J_{F,3'} = 8,9$, $^4J_{F,2'} = 5,1$.
[d]δ_F/hexafluorobenzène.

Tableau 4. Déplacements chimiques des ^{13}C des molécules **4H** et de leurs anions **4**$^-$ ($c \approx 0,08$ M, Me_2SO-d_6).

X		C_4	C_5	C_6	C_7	C_8	C_9	$C_{1'}$	$C_{2'6'}$	$C_{3'5'}$	$C_{4'}$	X
NO_2	**4H**	125,9	136,9	105,7	140,0	145,8	144,3	145,4	122,1	125,5	143,5	
	4$^-$	112,1	134,7	103,8	151,1	149,1	147,1	159,0	122,0	125,8	142,7	
CN	**4H**	125,7	137,4	104,9	140,4	145,8	144,4	143,2	123,0	134,1	107,3	119,1
	4$^-$	111,5	134,0	103,0	150,6	148,8	146,8	156,4	121,9	133,5	104,5	119,6
COOMe	**4H**	124,8	137,2	103,7	140,6	145,4	144,1	142,8	122,3	130,8	126,2	165,6
	4$^-$	111,2	133,8	103,5	150,6	149,0	146,9	156,6	121,0	130,8	123,9	166,3
F	**4H**	123,0	137,5	101,4	142,5	144,7	144,0	134,0	126,2	116,4	160,1	
	4$^-$	112,6	133,6	103,0	149,5	148,3	146,3	145,4	122,8	115,7	158,6	
H	**4H**	123,3	137,9	101,9	142,6	145,2	144,4	138,0	124,2	129,9	126,8	
	4$^-$	111,2	133,3	104,4	150,8	149,4	147,2	151,3	121,1	129,6	123,6	
Me	**4H**	122,7	137,6	101,3	142,6	144,9	144,2	135,1	123,9	130,1	136,1	20,7
	4$^-$	110,5	132,6	103,8	150,7	149,0	147,1	149,5	120,7	129,7	131,9	20,7
OMe	**4H**	122,2	137,6	100,9	143,1	144,7	144,2	130,3	125,8	114,8	157,8	55,4
	4$^-$	110,4	132,4	104,0	150,6	149,6	147,0	144,4	122,0	114,5	155,6	55,3

δ en ppm/Me_4Si, J en Hz. La numérotation est celle de l'équation [1].

© 1997 NRC Canada

Can. J. Chem. Downloaded from www.nrcresearchpress.com by 91.121.58.235 on 09/08/12
For personal use only.

Can. J. Chem. Downloaded from www.nrcresearchpress.com by 91.121.58.235 on 09/08/12
For personal use only.

Figure 3. Corrélation entre δ_{1H} des molécules **4H** et de leurs anions **4**$^-$ (Me_2SO-d_6) avec les pK_a (H_2O–Me_2SO contenant 50,9% de Me_2SO en fraction molaire).

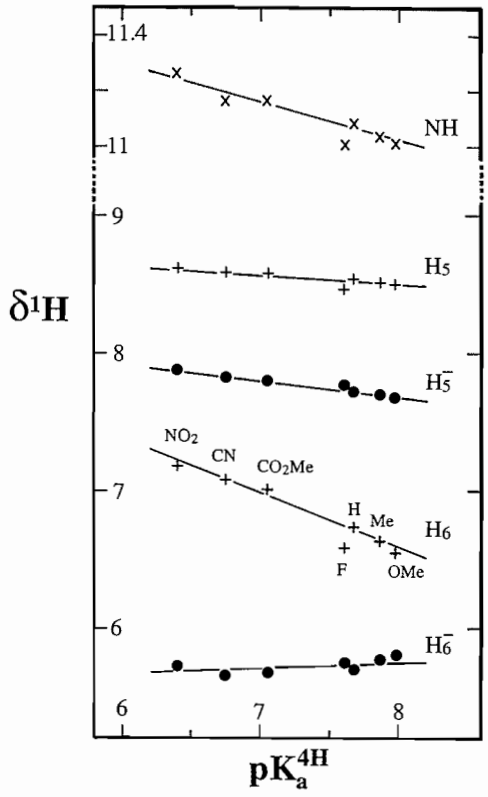
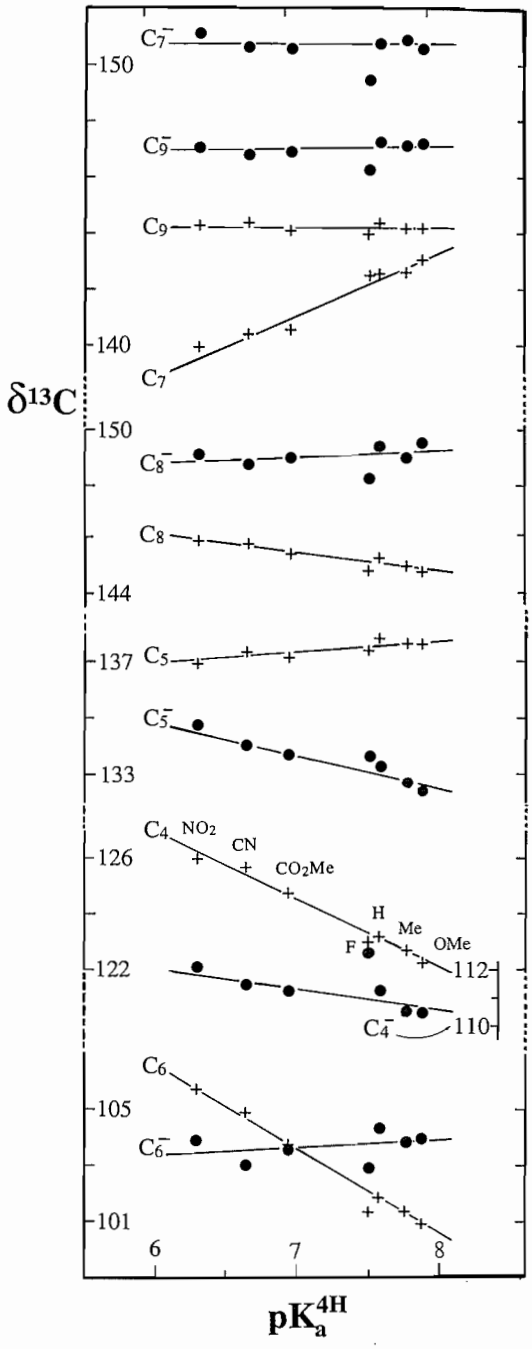


Figure 4. Corrélation entre δ_{13C} des molécules **4H** et de leurs anions **4**$^-$ (Me_2SO-d_6) avec les pK_a (H_2O–Me_2SO contenant 50,9% de Me_2SO en fraction molaire).



La constante de réaction ρ^S déduite de l'excellente corrélation linéaire observée, en utilisant les constantes σ_{p-} pour les substituants à effet mésomère attracteur, est en effet très faible (ρ^S = 1,0; cf. tableau 1), ce qui implique bien l'existence d'une faible conjugaison entre le groupe NH ionisable et le substituant X. Cette constante de réaction est 3,5 fois plus petite que celle afférente à l'ionisation des phénols où les effets de conjugaison entre le site ionisable et le substituant *para* sont très importants (ρ^S = 3,52 dans ce même milieu S eau–Me_2SO) (31, 32). Elle est aussi très inférieure à celle qui gouverne la déprotonation des acides benzoïques *para*-substitués dans ce même milieu (ρ^S = 1,85) (32). La faible valeur de ρ^S pour l'équilibre **4H**/**4**$^-$ témoigne donc bien du *peu d'influence du substituant X sur l'aptitude des composés 4H* à se déprotoner.

L'analyse des δ_{1H} et δ_{13C} des molécules **4H** et des anions **4**$^-$ va nous conduire à la même conclusion.

II. Analyse des δ^1H et δ^{13}C des molécules 4H et des anions 4$^-$

II. 1. Influence du substituant X

Comme le montrent les figures 3 et 4, d'excellentes corrélations linéaires régissent l'influence du substituant X sur les déplacements chimiques des divers protons et carbones du motif NBD des molécules **4H** et des anions conjugués **4**$^-$. Seules les valeurs de δ_H et δ_C afférentes au dérivé fluoré, s'éloignent parfois sensiblement des corrélations. À cet égard, il est connu que la constante σ_p de F, atome très accepteur de liaison hydrogène, est très sensible à la nature du solvant (33). Il se peut donc que le passage du Me_2SO utilisé pour les mesures RMN, au milieu H_2O–Me_2SO (20/80) utilisé pour les mesures d'acidité, soit à l'origine des écarts observés.

L'existence de corrélations linéaires δ vs. pK_a est intéressante à plusieurs titres. En premier lieu, elles constituent un contrôle a posteriori des attributions proposées pour les δ_{1H} et δ_{13C} dans les tableaux 2 et 4. En particulier, ces corrélations lèvent toute ambiguïté concernant les attributions des déplacements chimiques des carbones 7 et 9 de **4H** et **4**$^-$ (vide supra). En effet, outre le regroupement des δ relatifs à C_7 et des δ rela-

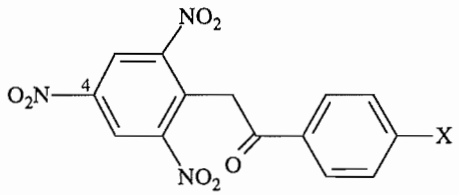
© 1997 NRC Canada

Can. J. Chem. Downloaded from www.nrcresearchpress.com by 91.121.58.235 on 09/08/12
For personal use only.

tifs à C_9 que ces corrélations permettent, il est logique d'attribuer à C_7 la droite de corrélation sensible à la *para* X-substitution (δ variant de 140 (X = NO_2) à 143 (X = OMe)) et à C_9 celle de pente nulle (δ ≈ 144 ppm).

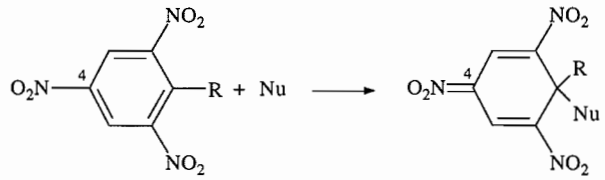
Il est connu que la déprotonation du phénol s'accompagne d'un déblindage très important (13 ppm) du carbone hydroxylé (réf. 29, p. 257). Par analogie, nous avons attribué au carbone 7 des anions **4**$^-$ (C_7^-, fig. 4) la droite de corrélation située à 150,7 ppm, ce qui correspond à un déblindage variant de 10,7 ppm (X = NO_2) à 7,7 ppm (X = OMe), pour le carbone 7 du motif NBD de **4H**. Quant au carbone 9, le déblindage observé est moins important et peu sensible au substituant X ($\delta_{C_7^-} - \delta_{C_7} = 2{,}6 \pm 0{,}3$ ppm). Il convient également de noter que ces attributions conduisent à des constantes de couplage $^3J_{^{13}C_7H_5}$ homogènes entre elles (≈ 9,2/**4H**; ≈ 10/**4**$^-$) et supérieures aux constantes de couplage $^3J_{^{13}C_9H_5}$ (≈ 8/**4H**; ≈ 7,4/**4**$^-$).

En ce qui concerne l'influence de la déprotonation sur les autres carbones du motif benzofurazanyle, on remarque le fort blindage subi par le carbone **4** : $\Delta\delta_{C_4} \approx -13$. Ce résultat est à rapprocher du blindage observé pour le carbone 4 du motif picryle, que ce soit lors de la déprotonation en position benzylique de picryl-acétophénones **5** : $\Delta\delta_{C_4} = -18$ (34), ou bien au cours de la formation des nombreux σ-adduits **6** (eq. [5]) (35–42) par exemple : $\Delta\delta_{C_4} = -24$, R = Nu = OMe (37).



5

[5]



6

Ce déplacement vers les champs forts est en faveur d'une forte délocalisation de la charge négative, générée par la déprotonation de **4H**, par le motif 4-nitrobenzofurazanyle. Notons également que dans les anions **4**$^-$ l'influence du substituant X sur les déplacements chimiques des six carbones du motif NBD reste toujours très faible puisqu'elle ne dépasse jamais 2 ppm (C_4^- et C_5^-) et est le plus souvent nulle (cf. fig. 4). Ceci atteste de la conjugaison quasiment inexistante entre les deux cycles de **4**$^-$.

En ce qui concerne la résonance du proton aminé des molécules **4H**, on constate qu'elle est située à champs très faibles comparée à celle du NH_2 des anilines identiquement substituées (43) et que, contrairement à ces anilines où δ_{NH_2} varie de 2,13 ppm (Me_2SO-d_6) quand on passe du substituant *para* méthoxy (δ_{NH_2} = 4,5) au substituant *para* nitro (δ_{NH_2} = 6,63) (43), elle est ici peu sensible à l'influence du substituant : $11{,}01 < \delta_{NH} < 11{,}27$; cf. tableau 2. D'autre part, le fait que le NH du 7-anilino 4-nitrobenzofurazane (δ_{NH} = 11,08, Me_2SO-d_6) résonne à champ plus faible que le NH de la 2,4,6-trinitrodiphénylamine (δ_{NH} = 10,24, Me_2SO-d_6) (44) est une preuve supplémentaire que le motif NBD est plus électroattracteur que le groupement picryle.

II. 2. Influence de la para-*X anilino substitution*

Si l'on se réfère au 4-nitrobenzofurazane **1***a* dont les déplacements chimiques dans Me_2SO-d_6 sont les suivants : 8,70 (H_5), 7,88 (H_6), 8,60 (H_7), 136,4 (C_4), 131,9 (C_5), 131,5 (C_6), 124,5 (C_7) (45),[3] on constate que l'introduction du groupement *para*-X anilino en position-7 n'engendre qu'un très faible blindage du proton H_5 (0,1 à 0,25 ppm, cf. tableau 2). En revanche, le blindage produit sur H_6 est beaucoup plus conséquent et varie notablement avec X puisque de 1,34 ppm dans le cas de la *para*-méthoxy anilino substitution (X = OMe), il passe à 0,70 ppm, minimum observé dans le cas de la *para*-nitro anilino substitution (X = NO_2). Ce résultat, qui atteste de l'apport électronique important des groupements anilino introduits, s'explique par la contribution plus (X = OMe) ou moins (X = NO_2) importante de la forme mésomère c des molécules **4H** : cf. schéma 1.

Ces observations se trouvent confirmées par l'examen des δ ^{13}C. En effet, la *para*-X anilino substitution blinde notablement le carbone 4 et encore plus le carbone 6 ($\Delta\delta_{C4} = -13{,}1$, $\Delta\delta_{C6} = -29{,}6$ pour X = H) ce qui confirme, non seulement l'importante contribution de la forme mésomère **4H** (c) mais aussi celle de la forme mésomère **4H** (b) du schéma 1.[4]

Partie expérimentale

Préparation des 7-anilino 4-nitrobenzofurazanes 4H

La condensation des anilines *para*-substituées (produits Aldrich) sur le NBD-Cl (Fluka) a été réalisée en utilisant le protocole décrit par Ghosh (23). Si pour les anilines les plus nucléophiles (X = OMe, Me, H), la condensation se fait dans l'éthanol (23), le recours à un solvant dipolaire aprotique, tel que le diméthylsulfoxyde, connu pour faciliter les réactions S_NAr (22), a été nécessaire pour condenser les autres anilines. La moins basique notamment (X = NO_2, pK_a = 1,00) (31) exige un long chauffage à reflux dans Me_2SO pour réaliser la substitution du chlore de NBD-Cl avec un rendement convenable. Le tableau 5 regroupe les conditions utilisées ainsi que les caractéristiques physiques des composés **4H** préparés.

Préparation et standardisation des solutions tampons

La préparation des solutions tampons (produits Aldrich, Janssen ou Sigma, recristallisés dans des mélanges eau–éthanol) ainsi que la purification du Me_2SO (Chimiphar) a déjà été décrite (26). Pour chacun des six composés retenus (cft. tableau 6), dont la forme acide est zwittérionique ($TH^{\pm}$), nous avons standardisé trois solutions tampons présentant les rapports d'ionisation $C_{T^-}/C_{TH^{\pm}}$ égaux à 1/3, 1 et 3 en mesurant leur pH à partir de la chaîne électrolytique déjà décrite

3. J.-C. Hallé et M.-J. Pouet, résultats non publiés.
4. Comme l'a suggéré un référé, on notera toutefois qu'il ne peut être exclu que le blindage observé ne soit pas en partie lié à des effets stériques. Dans ce cas, la conjugaison entre les deux cycles pourrait être légèrement réduite par une rotation du cycle X-substitué autour de la liaison N-$C_{1'}$.

© 1997 NRC Canada

Can. J. Chem. Downloaded from www.nrcresearchpress.com by 91.121.58.235 on 09/08/12
For personal use only.

Schéma 1.

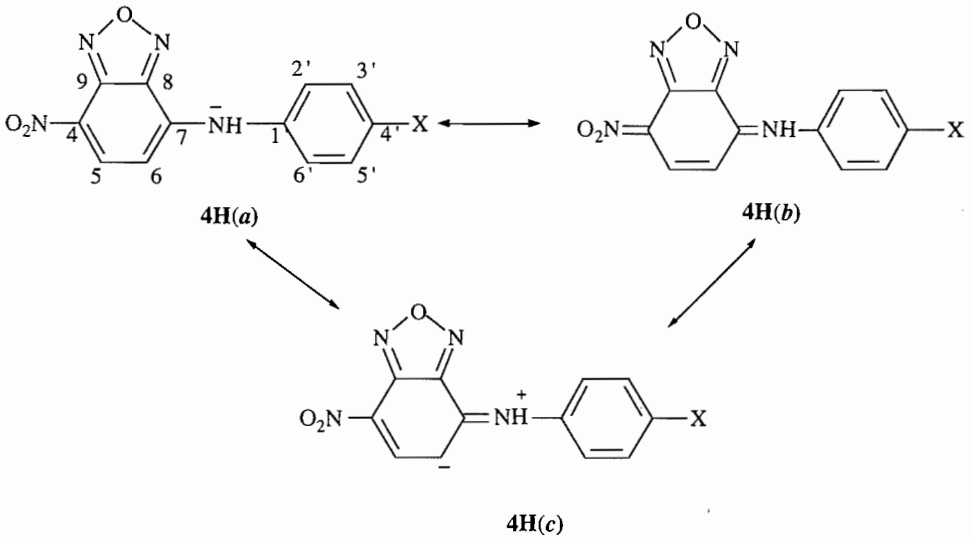


Tableau 5. Conditions de préparation et caractéristiques des 7-anilino 4-nitrobenzofurazanes X substituées **4H**.

X	Solvant	Température	Durée	*F* (°C) (litt.) (EtOH)	Rdt (%)	Trouvé (%) C	Trouvé (%) H	Trouvé (%) N	Calculé (%) C	Calculé (%) H	Calculé (%) N
OMe	EtOH	Ambiante	8 h	228	93						
				223–224 (23)							
Me	EtOH	Ambiante	8 h	192	70	57,87	3,52	20,70	57,78	3,73	20,73
H	EtOH	Reflux	2 h	152	69						
				150–151 (23)							
F	Me_2SO	Ambiante	2 h	194	71	52,65	2,18	20,12	52,56	2,57	20,43
CO_2Me	Me_2SO	Ambiante	8 h	238	66	53,80	3,31	17,58	53,51	3,21	17,83
CN	Me_2SO	Ambiante	8 h	290	85	55,75	2,29	24,89	55,52	2,51	24,90
NO_2	Me_2SO	Reflux	3 j	243	67	47,88	2,21	23,05	47,85	2,34	23,25

(25, 26), où l'électrode à hydrogène est indicatrice de l'activité du proton solvaté (25, 26, 46) : $a_{HS^+} = 10^{-pH}$. Le tableau 6 rassemble les valeurs de pH obtenues. Elles conduisent à des valeurs de $pK_a^{TH^\pm}$ (= pH − log ($C_{T^-}/C_{TH^\pm}$) + 0,05) sensiblement inférieures à celles préalablement mesurées dans des conditions légèrement différentes (26) (cf. tableau 6).

Mesures spectroscopiques

L'ionisation des molécules **4H** a été suivie sur un spectrophotomètre UVIKON 930. Les enregistrements RMN ont été réalisés sur des spectromètres Bruker AM 250 ou AC 300. Malgré le solvant utilisé, Me_2SO-d_6, la solubilité de certains substrats est restée faible (≈ 0,08 M) ce qui en RMN ^{13}C a impliqué de longues accumulations. Les anions $\mathbf{4}^-$ ont été préparés dans le tube RMN par ajout à **4H** d'un équivalent ou plus de triéthylamine (pK_a = 9,0 dans Me_2SO) (47) et leur formation quantitative contrôlée en vérifiant qu'un ajout supplémentaire de Et_3N ou d'un peu de base forte (*t*BuOK par exemple) est sans incidence sur les δ.

Tableau 6. Valeurs des pH obtenus pour les solutions tamponnées $TH^\pm/T^-$ et des $pK_a^{TH^\pm}$ correspondants : milieu eau–Me_2SO contenant 50,9% de Me_2SO en fraction molaire; *t* = 25°C.

		MES[d]	MOPS[d]	BES[d]	HEPES[d]	TES[d]	CAPS[d]
pH	[a]	5,72	6,27	6,76	6,90	8,17	9,57
	[b]	6,20	6,75	7,27	7,38	8,65	10,05
	[c]	6,68	7,15	7,72	7,86	9,13	10,53
$pK_a^{TH^\pm}$		6,25	6,77	7,30	7,43	8,70	10,10
$pK_a^{TH^\pm}$	[e]	6,30	6,89	7,36	7,56	8,79	10,29

[a,b,c]Rapports d'ionisation $C_{T^-}/C_{TH^\pm}$ respectivement égaux à 1/3[a], 1[b] et 3[c] avec $C_{T^-} = C_{Na^+}$ = 0,01 M.

[d]MES : acide 2-(*N*-morpholino) éthane sulfonique; MOPS : acide 3-(*N*-morpholino) propane sulfonique; BES : acide *N*,*N*-bis(2-hydroxyéthyl) 2-amino éthane sulfonique; HEPES : acide *N*-(2-hydroxyéthyl) pipérazine *N*′-éthane sulfonique; TES : acide *N*-(tris(hydroxyméthyl)méthyl) 2-amino éthane sulfonique; CAPS : acide 3-cyclohexylamino propane sulfonique.

[e]Milieu eau–Me_2SO contenant 48,7% de Me_2SO en fraction molaire, *t* = 20°C; réf. 26.

© 1997 NRC Canada

Bibliographie

1. P.B. Ghosh et M.W. Whitehouse. J. Med. Chem. **11**, 305 (1968).
2. M.W. Whitehouse et P.B. Ghosh. Biochem. Pharmacol. **17**, 158 (1968).
3. P.B. Ghosh et M.W. Whitehouse. J. Med. Chem. **12**, 505 (1969).
4. P.B. Ghosh, B. Ternai et M.W. Whitehouse. J. Med. Chem. **15**, 255 (1972).
5. P.B. Ghosh, B. Ternai et M.W. Whitehouse. Med. Res. Rev. **1**, 159 (1981).
6. P.B. Ghosh et M.W. Whitehouse. Biochem. J. **108**, 155 (1968).
7. (*a*) K. Imai et Y. Watanabe. Anal. Chim. Acta, **130**, 377 (1981); (*b*) H. Miyano, T. Toyo'oka et K. Imai. Anal. Chim. Acta, **170**, 81 (1985).
8. R.S. Fager, C.B. Kutina et E.W. Abrahamson. Anal. Biochem. **53**, 290 (1973).
9. D.E. Draper et L. Gold. Biochemistry, **19**, 1774 (1980).
10. M. Ahnoff, I. Grundevik, A. Arfwidsson, J. Fonselius et B-A. Persson. Anal. Chem. **53**, 485 (1981).
11. (*a*) Y. Watanabe et K. Imai. Anal. Biochem. **116**, 471 (1981); (*b*) J. Chromatogr. **234**, 723 (1982); (*c*) J. Chromatogr. **309**, 279 (1984).
12. P. Moree-Testa, Y. Saint-Jalm et A. Testa. J. Chromatogr. **290**, 263 (1984).
13. M. Hauck et H. Köhler. Z. Lebensm.-Unters.-Forsch. **191**, 322 (1990).
14. A. Chattopadhyay. Chem. Phys. Lipids, **53**, 1 (1990) et références citées.
15. (*a*) S. Fery-Forgues, J-P. Fayet et A. Lopez. J. Photochem. Photobiol. A : **70**, 229 (1993); (*b*) S. Fery-Forgues, C. Vidal et D. Lavabre. J. Chem. Soc. Perkin Trans. 2, **1**, 73 (1996); (*c*) S. Fery-Forgues, D. Lavabre et J. Lozar. New. J. Chem. **19**, 1177 (1995).
16. H. Heberer et H. Matschiner. J. Prakt. Chem. **326**, 385 (1984).
17. V.M. Tsentovskii, M.I. Evgen'ev, I.V. Shulaeva et I.I. Evgen'eva. Zh. Obshch. Khim. **59**, 2711 (1989).
18. A.A. Aboderin, R.E.K. Semakula, E. Boedefeld et R.A. Kenner. FEBS. Lett. **34**, 90 (1973).
19. A. Chattopadhyay et E. London. Biochim. Biophys. Acta, **938**, 24 (1988); Biophys. J. **51**, 531a (1987).
20. F. Terrier. Chem. Rev. **82**, 77 (1982) et références citées.
21. H-W. Meyers, R. Jurss, H.R. Brenner, G. Fels, H. Prinz, H. Watzke et A. Maelieke. Eur. J. Biochem. **137**, 399 (1983).
22. F. Terrier. *Dans* Nucleophilic aromatic displacement: the influence of the nitro group. Organic Nitrochemistry Series. *Édité par* H. Feuer. VCH Publishers, New-York. 1991. Chaps. 1 and 2.
23. P.B. Ghosh. J. Chem. Soc. (B), 334 (1968).
24. R.A. Robinson et R.H. Stockes. *Dans* Electrolyte solutions. (2e éd. revisée). Butterworth, 1965. p. 230.
25. J-C. Hallé, R. Gaboriaud et R. Schaal. Bull. Soc. Chim. Fr. 1851 (1969); 2047 (1970).
26. C.A. Vega et J-C. Hallé. Bull. Soc. Chim. Fr. I, 124 (1979).
27. C. Hansch, A. Leo et R.W. Taft. Chem. Rev. **91**, 165 (1991).
28. J.W. Emsley. J. Feeney et L.H. Sutcliffe. High resolution spectroscopy. Pergamon Press, 1968.
29. E. Breitmaier et W. Voelter. Carbon-13 NMR spectroscopy, high resolution methods and applications in organic chemistry and biochemistry. 3e éd. VCH Publishers, New-York. 1987. p. 145.
30. J-C. Hallé, F. Terrier et R. Schaal. Bull. Soc. Chim. Fr. **1225** (1973).
31. A.I. Biggs et R.A. Robinson. J. Chem. Soc. 338 (1961).
32. J-C. Hallé et R. Schaal. Anal. Chim. Acta, **60**, 197 (1972).
33. R. Benhaddou, S. Czernecki, G. Ville et A. Zegar. Organometallics, **7**, 2435 (1988) et références citées.
34. G. Moutiers, B. El Fahid, R. Goumont, A-P. Chatrousse et F. Terrier. J. Org. Chem. **61**, 1978 (1996).
35. K.A. Kovar et E. Breitmaier. Chem. Ber. **111**, 1646 (1978).
36. G.A. Olah et H. Mayr. J. Org. Chem. **41**, 3448 (1976).
37. M-P. Simonnin, M-J. Pouet et F. Terrier. J. Org. Chem. **43**, 855 (1978).
38. R.A. Renfrow, M.J. Strauss et F. Terrier. J. Org. Chem. **45**, 471 (1980).
39. J.A. Chudek, R. Foster et A. Marr. J. Chem. Soc. Perkin Trans. 2, 1341 (1987).
40. V. Machacek, V. Sterba, A. Lycka et D. Snobl. J. Chem. Soc., Perkin Trans. 2, 355 (1982).
41. H. Wennerström et O. Wennerström. Acta Chem. Scand. **26**, 2883 (1972).
42. P. Caveng, P.B. Fischer, E. Heilbronner, A.L. Miller et H. Zollinger. Helv. Chem. Acta, **50**, 848 (1967).
43. (*a*) B. M. Lynch, B.C. MacDonald et J.G.K. Webb. Tetrahedron, **24**, 3595 (1968); (*b*) B.M. Lynch. Tetrahedron Lett. **17**, 1357 (1969).
44. J-C. Hallé, M-L. Filleux-Blanchard, F. Terrier, R. Schaal et G-J. Martin. C.R. Acad. Sci. Paris, **269**, 705 (1969).
45. F. Terrier, F. Millot, A-P. Chatrousse, M-J. Pouet et M-P. Simonnin. Org. Magn. Reson. **8**, 56 (1976).
46. J-C. Hallé, R. Harivel et R. Gaboriaud. Can. J. Chem. **52**, 1774 (1974).
47. I.M. Kolthoff, M.K. Chantooni, Jr. et S. Bhowmik. J. Am. Chem. Soc. **90**, 23 (1968).

Can. J. Chem. Downloaded from www.nrcresearchpress.com by 91.121.58.235 on 09/08/12
For personal use only.

© 1997 NRC Canada

Sedimentation of fine colloidal particles adsorbed onto a long polymer chain

Waldemar Nowicki and Grażyna Nowicka

Abstract: A system containing aggregates composed of several fine colloidal particles attached to a single very long polymer molecule is considered. It is shown that the sedimentation equilibrium of the system depends on the extent of restriction over the Brownian motions of particles. On the basis of analysis of sedimentation equilibrium, a simple stability model for such systems is developed. The model elucidates the deterioration of the ability of ultralarge polymers to flocculate fine suspensions.

Key words: high polymers, fine colloidal particles, sedimentation, diffusion, flocculation, stabilization of suspensions.

Résumé : On a examiné un système contenant des agrégats formés de plusieurs particules colloïdales fines attachées à une seule molécule de polymère très longue. On démontre que l'équilibre de sédimentation du système dépend du degré de restriction sur les mouvements browniens des particules. En se basant sur l'analyse de l'équilibre de sédimentation, on a développé un modèle de stabilité simple pour de tels systèmes. Le modèle permet d'élucider la détérioration de l'habilité des polymères extrêmement longs à faire floculer des suspensions fines.

Mots clés : hauts polymères, particules colloïdales fines, sédimentation, diffusion, floculation, stabilisation de suspensions.

[Traduit par la rédaction]

1. Introduction

It has been observed experimentally that when the size of polymer coils exceeds that of particles, aggregates composed of many particles attached to a single macromolecule are formed (1–6). One can expect that the formation of aggregates should affect the stability of the suspension. However, when the sedimentation of aggregates is insignificant, then no effect of polymer addition on the suspension stability is macroscopically observed. Therefore, discussion of the stability of the system of aggregates composed of colloidal particles attached to a long-chain macromolecule seems to be more suitable in terms of sedimentation behavior than aggregation kinetics.

The sedimentation can be described by two parameters: the sedimentation velocity and a factor describing sedimentation equilibrium. These parameters are determined by the density and size of colloidal particles and can be affected by an aggregation process as well as by interparticle interaction and the excluded volume effect (7). In the case of complex random aggregates, their elastic and plastic properties may also affect the sedimentation phenomenon (8). Thus, the intra-aggregate movements of particles attached to a macromolecule should also be taken into account in analysis of the sedimentation behavior of the system.

The stability of suspensions containing particles and their aggregates whose formation does not involve polymers was discussed on the basis of a population balance model for aggregates of different types, their diffusion, and settling behavior (9). The stability of suspensions of fine particles after introduction of supersized linear nonionic polymers undergoing adsorption onto particles was also studied in terms of sedimentation phenomena (10, 11). A number of models describing the flocculation and adsorption phenomena in such systems have been developed. Analysis of the system at equilibrium showed that the degree of polymer-induced flocculation is determined by the size of polymer coils in the solution, the particle radius, and the maximum number of particles that can be bound to a single macromolecule (10). Distribution of particles among molecules was studied by a direct simulation of diffusion and binding of particles to polymer molecules (11), the modelling of reversible and irreversible adsorption of macromolecules onto particles (12), and on the basis of dynamic analysis in which the transient behavior of particle adsorption to a polymer molecule and the particle–particle interactions are taken into account (13). In the above models, destabilization of the colloidal system was assumed to occur when aggregates reached a critical number n_f of particles per macromolecule (10, 11). However, in these models a refined analysis of the sedimentation rate and (or) the sedimentation equilibrium in systems containing polymer molecules carrying different numbers of attached particles was not performed.

In this work we replace the study of the influence of an arbitrarily chosen parameter n_f on the colloid stability by a more accurate analysis of the sedimentation process. We performed a two-stage analysis of the influence of aggregate properties on the colloidal system stability. At first, we defined the parameters describing the colloid stability in terms of sedimentation and examined the dependence between the structure of aggregates and the values of these parameters. Then, we discussed the random Brownian motions of fine colloidal particles attached to a very long polymer chain and studied the influence of such polymer–particle aggregate properties on the stability criteria.

Received February 6, 1997.

W. Nowicki[1] **and G. Nowicka.** Department of Physical Chemistry, Faculty of Chemistry, A. Mickiewicz University, Grunwaldzka 6, 60-780 Poznań, Poland.

[1] Author to whom correspondence may be addressed. Telephone: 48-61-699-181, ext. 457. Fax: 48-61-658-008. E-mail: gwnow@chem.amu.edu.pl

© 1997 NRC Canada

Can. J. Chem. Downloaded from www.nrcresearchpress.com by 91.121.58.235 on 09/08/12
For personal use only.

Can. J. Chem. Downloaded from www.nrcresearchpress.com by 91.121.58.235 on 09/08/12
For personal use only.

2. Model

The model is designed for a system containing identical fine colloidal particles and identical very long polymer chains in a good solvent. In the system, the aggregation process takes place due to adsorption of the polymer segments onto the surface of the particles. We assumed that the process of aggregate formation was complete. The colloidal suspension was assumed to be dilute, so that the aggregates could be considered as separate species.

2.1. Sedimentation velocity and sedimentation equilibrium

In the gravitational field, a colloidal suspension is a heterogeneous fluid characterized by a dependence of the number of particles $n(z)$ on the altitude z. In a monodisperse and sufficiently dilute colloidal system, where interactions among particles can be neglected, $n(z)$ is proportional to the Boltzmann factor, i.e., it is given by the barometric law (14):

$$[1] \quad n(z) = n_0 \exp\left(-\frac{z}{\xi}\right)$$

where n_0 is the number of particles at the zero altitude and ζ is the gravitational length:

$$[2] \quad \xi = \frac{RT}{Mg} = \frac{k_B T}{m_{eff}\, g} = \frac{k_B T}{V(\rho_p - \rho_s)g}$$

M, m_{eff} are the macromolecular mass and the effective colloidal particle mass (corrected by Archimedes law), R, k_B are gas and Boltzmann constants, ρ_p, ρ_s are densities of particles and dispersion medium (for $\rho_p > \rho_s$ one can observe the sedimentation process, otherwise the creaming process), respectively, V is the particle volume, T is the temperature, and g denotes acceleration due to gravity.

Let us assume that the velocity of a colloidal particle falling down in the gravitational field has reached a stable value. In this case:

$$[3] \quad m_{eff}\, g = f\frac{z_g}{t}$$

where z_g is the distance that the particle covers during time t due to gravity, and f is the friction factor. The mean-square displacement covered by the particle in its random Brownian walk in the vertical direction $\langle z^2 \rangle$ is given by the Einstein equation (15):

$$[4] \quad \langle z^2 \rangle = 2Dt$$

where D is the diffusion coefficient of the colloidal particle or the aggregate.

Combining eqs. [2]–[4] (and taking into account that $Df = k_B T$) we find:

$$[5] \quad \xi = \frac{\langle z^2 \rangle}{2z_g} = \frac{Df}{m_{eff}\, g}$$

The probability p that n particles can be found at the level z is given on the basis of eq. [1] by

$$[6] \quad p(z,z+dz) = \frac{n(z,z+dz)}{n_T} = \frac{n_0}{n_T}\exp\left(-\frac{z}{\xi}\right)dz$$

where n_T denotes the total number of particles in the system.

Since the sum of the numbers of particles on all levels of the vessel of height z_H should be equal to n_T, we have

$$[7] \quad n_0 \int_{z=0}^{z=z_H} \exp\left(-\frac{z}{\xi}\right)dz = n_T$$

Finally, we obtain the probability distribution:

$$[8] \quad p = \frac{1/\xi}{1 - \exp(-z_H/\xi)}\exp\left(-\frac{z}{\xi}\right)$$

For the sedimentation equilibrium attained in the centrifugal field, parameter g in eq. [2] is replaced by $\omega^2 z$, where ω is an angular velocity. Equation [8] then takes the form:

$$[9] \quad p = \frac{1}{\sum_{k=0}^{\infty} \frac{1}{(\xi^c)^k} \frac{z_B^{2k+1} - (z_B - z_H)^{2k+1}}{(2k+1)k!}} \exp\left(\frac{(z_B - z)^2}{\xi^c}\right)$$

where k is an integer, z_B denotes the radial position of the bottom of the centrifugal vessel, and

$$[10] \quad \xi^c = \frac{2g}{\omega^2}\xi$$

It is noteworthy that the distributions defined by eqs. [8] and [9] depend on only one parameter. This parameter, the gravitational length ζ (or ξ^c), determines behavior of particles and (or) aggregates of different types, which are suspended in liquid in either the gravitational or centrifugal field. This parameter can be influenced by various aggregate properties; unfortunately, the parameter cannot provide information about any of these properties separately.

The gravitational length ξ characterizes the colloidal system at the sedimentation equilibrium. Thereafter, the value of this parameter is considered a criterion of the suspension stability. However, a full description of the sedimentation process should also include the rate of the equilibrium attainment. The rate is determined by the sedimentation coefficient s, defined by eq. [11]:

$$[11] \quad s \equiv \frac{v}{a}$$

where v is sedimentation velocity and a is acceleration due to the force causing the sedimentation. Below, we consider the values of ξ and s parameters of colloidal systems in which aggregation occurred, taking into account different types of aggregates that could be formed.

1. A suspension composed of particle–polymer aggregates, consisting of one colloidal particle of radius r covered by an adsorbed polymer layer of a thickness δ and of density ρ_l.

© 1997 NRC Canada

Can. J. Chem. Downloaded from www.nrcresearchpress.com by 91.121.58.235 on 09/08/12
For personal use only.

The gravitational length ξ_{agg} for the suspension composed of such aggregates can be described as

$$[12] \quad \xi_{agg} = \frac{k_B T}{m_{eff}\, g} = \frac{k_B T}{\frac{4}{3}\pi g \left(r^3(\rho_p - \rho_s) + ((r+\delta)^3 - r^3)(\rho_l - \rho_s)\right)}$$

Taking into account that usually $\rho_l \cong \rho_s$ (16) it is found that

$$[13] \quad \xi_{agg} = \xi$$

which means that the same sedimentation equilibrium is attained for the suspension of polymer-covered particles and for the suspension of bare particles.

On the other hand, the sedimentation coefficient of the suspension of polymer-covered particles depends, as has recently been shown by Siffert and Li (16), on the thickness of the polymer layer. If one assumes $\rho_l \cong \rho_s$ and the absence of free, nonadsorbed polymer in the dispersion medium, the sedimentation coefficient of the suspension of polymer-covered particles, s_{agg}, is equal to

$$[14] \quad s_{agg} = \frac{r}{r+\delta} s$$

2. A suspension consisting of compact aggregates built of N primary particles.

Such aggregates can be formed in the process of coagulation. If one assumes, for the sake of simplicity, that the aggregation of particles leads to coalescence, the gravitational length and sedimentation coefficient of the suspension are given by

$$[15] \quad \xi_{agg} = \frac{\xi}{N}$$

and

$$[16] \quad s_{agg} = s\sqrt[3]{N^2}$$

3. A suspension of rigid, spherical aggregates built of a very large polymer molecule (or molecules) and of N primary particles.

According to eq. [5], the gravitational length is equal to

$$[17] \quad \xi_{agg} = \frac{k_B T}{\frac{4}{3}\pi g(r^3 N(\rho_p - \rho_l) + r_{agg}^3(\rho_l - \rho_s))}$$

where r_{agg} denotes the aggregate radius. Taking into account that $\rho_l \cong \rho_s$, one can easily find that

$$[18] \quad \xi_{agg} = \frac{\xi}{N}$$

and that the sedimentation equilibrium is independent of the aggregate radius.

In this case the sedimentation coefficient is given by

$$[19] \quad s_{agg} = \frac{r}{r_{agg}} Ns$$

4. A suspension consisting of aggregates composed of N primary particles attached to a flexible linear very large polymer molecule.

For the suspension under consideration (according to eq. [5]) we have

$$[20] \quad \xi_{agg} = \frac{\langle z_{agg}^2 \rangle}{2\, z_{g_{agg}}} = \frac{D_{agg}\, f_{agg}}{m_{agg}\, g}$$

where parameters with subscript "agg" refer to polymer-bound particles.

A colloidal particle, which belongs to a suspended aggregate, covers a distance that is a superposition of two displacements: a downward movement due to gravity and a random Brownian walk. The downward movements of all particles attached to a macromolecule are mutually independent. On the contrary, the particle displacement due to the Brownian walk, $(\langle z_{agg}^2 \rangle)^{1/2}$, is restricted by the length of the polymer chain and the displacements of other particles. However, if one assumes that the aggregate is built of an infinitely long expanded polymer molecule, particle motions are mutually independent ($\langle z_{agg}^2 \rangle = \langle z^2 \rangle$), and the sedimentation equilibrium of the system composed of such aggregates is the same as for the system of primary particles, provided that the diffusion coefficient and the friction factor of a particle in an infinite aggregate do not differ from those of the primary particles.

In the case of an aggregate formed by a finite but very long chain, in which particles are far away from each other and their friction factors are the same as for primary particles, one can assume that the only parameter determining the particle motion is the space available for the random walk. The shortening of a polymer chain results in a depression of self-diffusion of colloidal particles and hence in a decrease of the diffusion coefficient of the particle attached to the chain, D_{ap}. Thus, eq. [20] can be simplified to

$$[21] \quad \xi_{agg} = \frac{\langle z_{agg}^2 \rangle}{2 z_g} = \frac{D_{ap} f}{m_{eff}\, g}$$

Because for an infinitely long polymer chain the sedimentation velocity v takes the same value for the suspension of primary particles and that of aggregates, the sedimentation coefficient reads

$$[22] \quad s_{agg} = s$$

provided that the intra-aggregate viscosity is the same as the viscosity of the dispersion medium.

2.2. Diffusion of attached particles

Let us assume that the aggregate consists of identical colloidal

© 1997 NRC Canada

Can. J. Chem. Downloaded from www.nrcresearchpress.com by 91.121.58.235 on 09/08/12
For personal use only.

particles connected by a weightless thread instead of a physical polymer chain. Individual motions of particles in such an aggregate are mutually independent, unless the distance between two neighbouring particles exceeds the length of the thread fragment between them. For the sake of simplicity, let us assume that no particle can be placed any further from the mass centre of the aggregate than r_{agg} (considered here as the aggregate radius). Moreover, the model is simplified by considering a one-dimensional description in which the only spatial coordinate z, parallel to the vessel axis, is taken into account. The Brownian motion of a particle in the aggregate can be evaluated in the way described below.

The single-body probability density for the particle position z at time t_S is given by the Gaussian distribution with the expected value equal to 0 (15):

$$[23] \quad \varphi(z) = \frac{1}{\sigma_{fp}\sqrt{2\pi}} \exp\left(-\frac{1}{2}\left(\frac{z}{\sigma_{fp}}\right)^2\right)$$

The deviation of the particle position from the mean value at time t is analogous to the *root-mean-square* (rms) displacement of a single colloidal particle given by the Einstein equation (eq. [4]) (15). Choosing the standard time t_S at which the deviation of the distribution is equal to the standard deviation σ_{fp} of the normal distribution of free colloidal particles, and according to the Einstein equation [4], the probability density (eq. [23]) can be expressed:

$$[24] \quad \varphi(z) = \frac{1}{\sqrt{4\pi D_{fp} t_S}} \exp\left(-\frac{z^2}{4D_{fp}t_S}\right)$$

where D_{fp} denotes the diffusion coefficient of primary particle.

The position of a particle attached to a macromolecule is restricted to the space occupied by the whole aggregate. Let us assume that the probability distribution of the position of the particle can be expressed by a normal distribution [24] truncated to the interval $(-r_{agg}, r_{agg})$ (the particle volume was assumed to be negligible):

$$[25] \quad \varphi(z)dz = \begin{cases} \dfrac{1}{\sigma_{fp}\sqrt{2\pi}} Y \exp\left(-\dfrac{z^2}{2\sigma_{fp}^2}\right) dz & \text{for } -r_{agg} < z < r_{agg} \\ 0 & \text{for } z \le -r_{agg} \text{ or } z \ge r_{agg} \end{cases}$$

where Y is the normalization constant.

The calculation of the normalization constant leads to:

$$[26] \quad \varphi(z) = \begin{cases} \dfrac{1}{\sigma_{fp}\sqrt{2\pi}} \dfrac{1}{\operatorname{erf}\left(\dfrac{r_{agg}}{\sqrt{2}\sigma_{fp}}\right)} \exp\left(-\dfrac{z^2}{2\sigma_{fp}^2}\right) & \text{for } -r_{agg} < z < r_{agg} \\ 0 & \text{for } z \le -r_{agg} \text{ or } z \ge r_{agg} \end{cases}$$

The standard deviation σ_{rap} of the distribution [26] is given by eq. [27] (17):

$$[27] \quad \frac{\sigma_{rap}}{\sigma_{fp}} = \left(\frac{\left[\operatorname{erf}\left(\dfrac{r_{agg}}{\sqrt{2}\sigma_{fp}}\right) - \sqrt{\dfrac{2}{\pi}} \exp\left(-\left(\dfrac{r_{agg}}{\sqrt{2}\sigma_{fp}}\right)^2\right)\dfrac{r_{agg}}{\sigma_{fp}}\right]}{\operatorname{erf}\left(\dfrac{r_{agg}}{\sqrt{2}\sigma_{fp}}\right)}\right)^{1/2}$$

The dependence of the relative standard deviation σ_{rap}/σ_{fp} of the position of a particle attached to a chain on the relative aggregate radius R_{agg} ($R_{agg} = r_{agg}/\sigma_{fp}$) is shown in Fig. 1. The standard deviation σ_{rap} takes the maximum value (equal to the standard deviation of free particle) when r_{agg} tends to infinity. Assuming the same standard time t_S (at which the deviation is equal to the standard deviation), the diffusion coefficient of a particle attached to a chain in the coordinate system with the beginning at the aggregate centre, D_{rap}, can be evaluated as follows:

$$[28] \quad \frac{D_{rap}}{D_{fp}} = \frac{\left[\operatorname{erf}\left(\dfrac{R_{agg}}{\sqrt{2}}\right) - \sqrt{\dfrac{2}{\pi}} \exp\left(-\left(\dfrac{R_{agg}}{\sqrt{2}}\right)^2\right) R_{agg}\right]}{\operatorname{erf}\left(\dfrac{R_{agg}}{\sqrt{2}}\right)}$$

It is worth noticing that R_{agg} is a function of the Brownian displacement of the particle at time t_S, so this parameter depends also on temperature. The aggregate radius r_{agg} also depends on temperature since the temperature influences the expansion factor of polymer coil.

The total diffusion coefficient of a particle attached to a polymer molecule, D_{ap}, can be treated as a superposition of two components: the diffusion coefficient of single particle, D_{rap}, and the diffusion coefficient of mass centre of all other particles attached to the chain, D_{mc}. Since the mean-square sum of displacements of a single particle z_{rap} and of the centre of mass z_{mc}, $\langle(z_{rap} + z_{mc})^2\rangle$, is equal to $\langle z_{rap}^2\rangle + \langle z_{mc}^2\rangle$ (as the value of $z_{rap}z_{mc}$ is zero), the total diffusion coefficient D_{ap} is the sum of D_{rap} and D_{mc}. In estimating the D_{mc} component for a very large aggregate, it can be assumed that the diffusion coefficient of the aggregate mass centre is equal to the mean diffusion coefficient of an attached particle divided by N (as the standard deviation of the mean value is equal to the mean standard deviation divided by $\sqrt{N}$ (17)). Assuming the mean diffusion coefficient as equal to D_{fp}, we obtain the approximation of D_{ap} given by eq. [29]:

$$[29] \quad D_{ap} = D_{rap} + \frac{D_{fp} - D_{rap}}{N}$$

Another approximation of D_{ap} can be obtained if the D_{mc} value is calculated as the diffusion coefficient of the sphere that is formed by the coalescence of primary particles of a

© 1997 NRC Canada

Can. J. Chem. Downloaded from www.nrcresearchpress.com by 91.121.58.235 on 09/08/12
For personal use only.

Fig. 1. Dependence of the relative standard deviation of the position of a particle attached to polymer chain, σ_{rap}/σ_{fp}, on the relative aggregate radius R_{agg}.

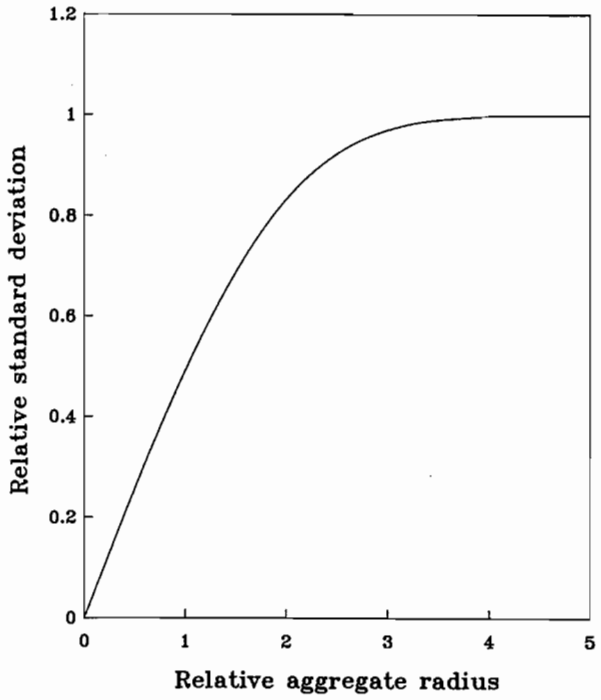
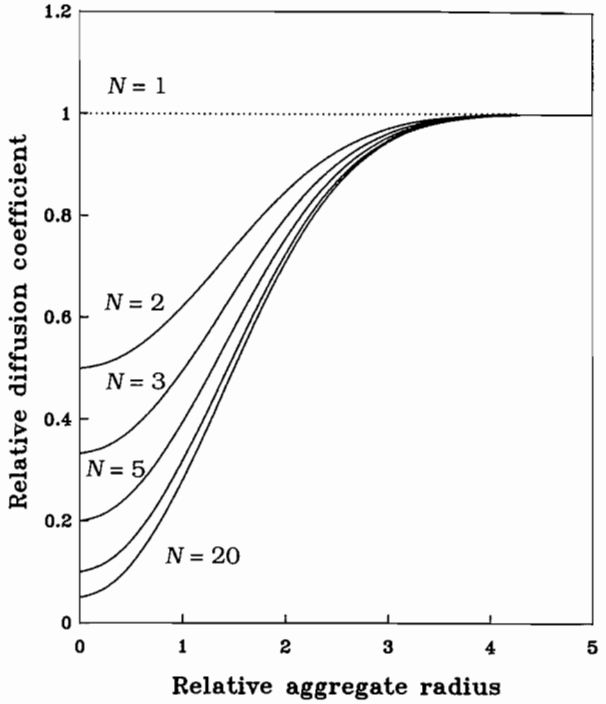


Fig. 2. D_{ap}/D_{fp} versus R_{agg} plots calculated for different N values.



relative radius R ($R = r/\sigma_{fp}$, $R_{agg} = R\sqrt[3]{N}$, $f_{agg} = f\sqrt[3]{N}$, and the diffusion coefficient of the aggregate centre for all attached particles is equal to $D_{fp}/\sqrt[3]{N}$):

$$[30] \quad D_{ap} = D_{rap} + \frac{D_{fp} - D_{rap}}{\sqrt[3]{N}}$$

Thus, eq. [29] is a better estimation of the dependence of D_{ap} on R_{agg} in the case of large and loose aggregates whereas approximation [30] is better in the case of rigid and compact aggregates.

The dependence of the relative diffusion coefficient on a single particle attached to a macromolecule D_{ap}/D_{fp} and the relative aggregate radius is shown in Fig. 2. The diffusion coefficient takes the maximum value (equal to the diffusion coefficient of free primary particles) when R_{agg} tends to infinity. When R_{agg} tends to zero, the diffusion coefficient takes a value characteristic of a rigid aggregate.

One can expect the intra-aggregate viscosity η_{agg} to be greater than the viscosity of the dispersion medium η_0. If the intra-aggregate viscosity is taken into account, the total diffusion coefficient of an attached particle takes the form:

$$[31] \quad D_{ap}(\eta) = D_{rap}(\eta_0/\eta_{agg}) + \frac{D_{fp} - D_{rap}(\eta_0/\eta_{agg})}{N}$$

The intra-aggregate viscosity η_{agg} can be estimated experimentally according to the Taylor equation (18):

$$[32] \quad \eta_{agg} = \frac{(\Phi_2 + 1)\eta_0 - \eta}{-\left(\frac{5}{2}\Phi_2 + 1\right)\eta_0 + \eta}\eta_0$$

where η is the viscosity of the system and Φ_2 is the volume fraction occupied by polymer chains.

The size of polymer coils in the solution is mainly determined by the polymer molecular weight (MW) and the quality of the solvent. In view of a comparison between systems containing a polymer of the same MW but of different coil size, we assumed a simple linear dependence of the viscosity on the polymer segment concentration. The intra-aggregate viscosity can be approximated now by eq. [33]:

$$[33] \quad \eta_{agg} = \frac{\eta_{intr}}{R_{agg}^3} + \eta_0$$

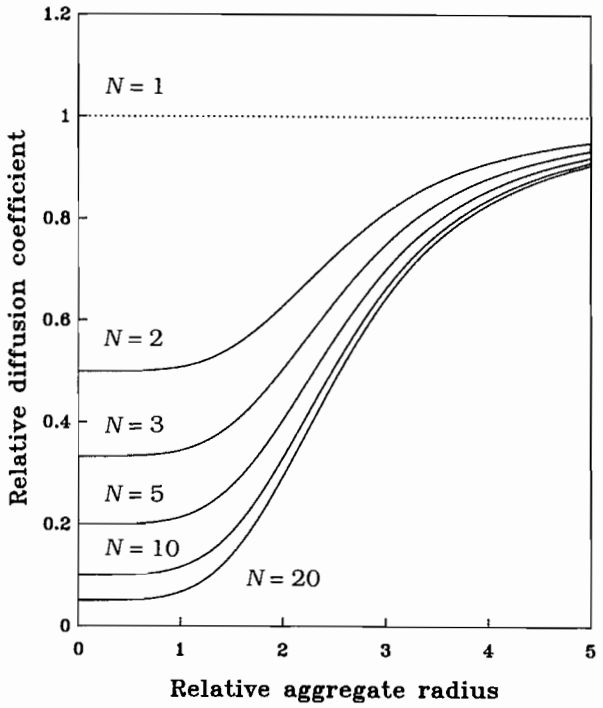
where η_{intr} is the parameter characteristic of the polymer.

Figure 3 illustrates relations between ratio $D_{ap}(\eta)/D_{fp}$ and the parameter R_{agg} for different N values. The dependencies were calculated assuming that intra-aggregate viscosity can be evaluated from eq. [33]. From a comparison of Figs. 2 and 3 one can state that the higher the intra-aggregate viscosity, the smaller the increase in the diffusion coefficient of an attached particle that accompanies the increase in R_{agg}.

© 1997 NRC Canada

Can. J. Chem. Downloaded from www.nrcresearchpress.com by 91.121.58.235 on 09/08/12
For personal use only.

Fig. 3. $D_{ap}(\eta)/D_{fp}$ versus R_{agg} dependencies calculated for different N values ($\eta_{intr} = 10$ assumed).



3.3. A relation between the colloid stability and the diffusion of particles attached to polymer chains

As we have shown above, the stability of the colloidal system can be described by the gravitational length ξ which can be calculated from eqs. [21], [28], and [31]. However, it is difficult to measure ξ directly. Therefore, let us introduce a new parameter, the stability coefficient S, which can be easily obtained from experiment:

$$[34] \quad S = \frac{n}{n_T}$$

where n_T denotes the number of particles in a unit volume of a colloidal system of uniform particle distribution and n is the mean number of particles in the unit volume of the upper half of the vessel after the completion of the sedimentation process and after the particles have achieved a uniform distribution. The definition of S is based on the typical experimental procedure.

With the equilibrium of the system in the gravitational field and for n calculated from eq. [8], the dependence between S and ξ, represented by eq. [35], is obtained:

$$[35] \quad S = \frac{n}{n_T} = \int_{z=z_H/2}^{z=z_H} \frac{2/\xi}{1 - \exp\left(-\frac{h}{\xi}\right)} \exp\left(-\frac{z}{\xi}\right) dz$$

The profiles of distribution of colloidal particles versus the distance from the bottom of the vessel, as well as the values of stability coefficients for different ξ are shown in Fig. 4. Large ξ values indicate that the distribution of particles at the sedimentation equilibrium does not differ significantly from the uniform particle distribution, and hence they correspond to relatively stable suspensions. Small ξ values correspond to unstable suspensions in which particles gather at the bottom of the vessel.

According to eqs. [21], [28], [31], and [35], the stability coefficient S is a function of N and R_{agg} parameters. Figure 5 shows S versus R_{agg} dependencies calculated for suspensions of aggregates of different N. In these calculations we assumed that the suspensions are monodisperse, i.e., composed of identical aggregates. As can be seen in Fig. 5, the smaller the number of particles attached to a polymer molecule and the greater the relative aggregate radius, the more stable is the suspension. The model parameter R_{agg} (eq. [28]) is a measure of the extent of restriction of Brownian motions of particles. Physically, this restriction depends on the relative sizes of polymer coils and particles. In other words, the model predicts that very large polymers in a good solvent are not effective flocculants for fine suspensions.

The process of polymeric flocculation of suspensions is very complex. It consists of many steps such as formation of primary aggregates, rearrangement of their structure, formation of macroscopic "flocs," sedimentation, formation of the sediment structure, et cetera. An outcome depends on a number of factors that can influence the equilibrium and (or) kinetics of the steps. These factors can interfere, which makes the description of the process very difficult. Therefore, the model presented does not pretend to explain all details of flocculation of fine suspensions by very large polymers. It emphasizes only the effect of quasi-free Brownian motions of particles attached to a very long polymer chain on the sedimentation equilibrium. In systems where this effect plays an important role in the whole flocculation process, the model can be used in a discussion of the stability of the colloidal suspension.

Experiments on the effect of chain polymers of different MW on the stability of fine suspensions are reported in the literature and their results seem to confirm the predictions of the model. Otsubo and Watanabe (19) studied the flocculation of suspension of 10 nm silica particles with the aid of polyacrylamides of different MW, and they observed that with increasing MW the ability of polymer to flocculate the suspension first increased, then reached a maximum, and finally decreased at MW over $(2–5) \times 10^6$. Also, Furusawa et al. (20), studying the flocculation of the tungstic acid sol by polyacrylamide, found an optimum polymer MW ($(3–6) \times 10^6$) for the flocculation efficiency. We believe that whereas the increase in the flocculation efficiency with increasing polymer MW can be explained using the classical theory of bridging flocculation (21), the deterioration of the flocculation ability at MW over a few millions can result from increased quasi-free Brownian motions of particles when they are attached to a very long polymer chain.

Also, results of our studies on the effect of very high MW polyacrylamides on the stability of silver iodide hydrosol at various electrolyte concentrations (22) seem to agree, although somewhat indirectly, with the model predictions. We found that the polymer-induced destabilization efficiency (defined as $F = 1 - n/n_T = 1 - S$, provided that the coagulation due to an electrolyte can be neglected) increased with the ionic strength of the medium. In the system examined, in which the adsorption of few particles onto a single macromolecule could

© 1997 NRC Canada

Fig. 4. A relationship between the macroscopic stability of the colloidal system and the gravitational length ξ; (*a*) particle concentration *c* versus *z*, calculated for different ξ; (*b*) *S* versus ξ.

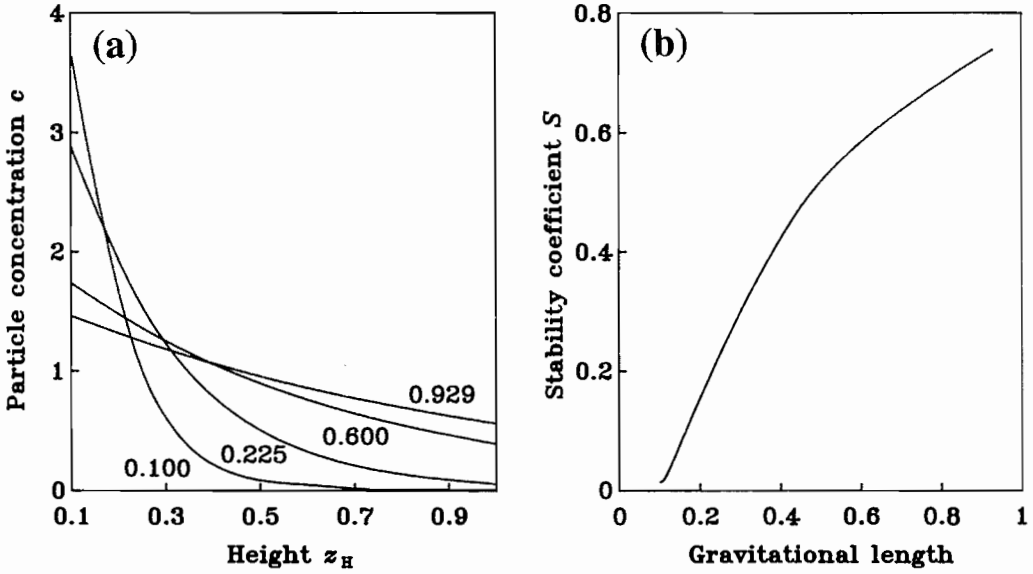
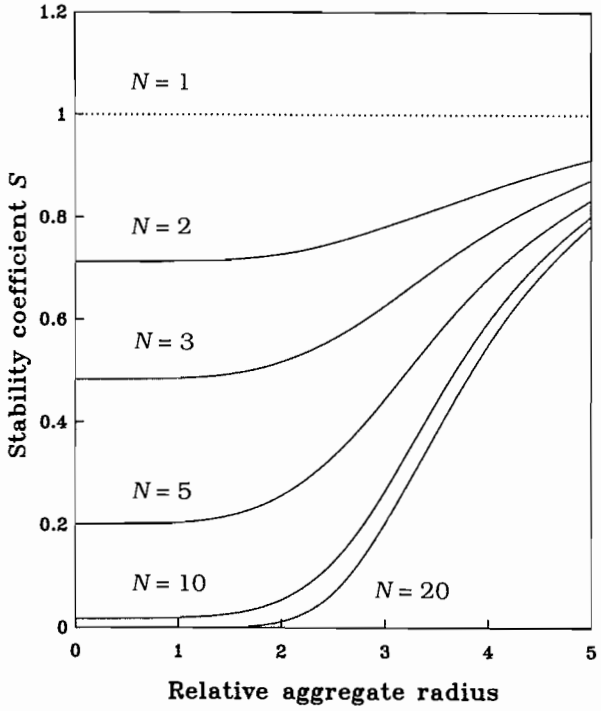


Fig. 5. *S* versus R_{agg} relationships calculated for different *N* values (the monodisperse aggregate system assumed).



be assumed (12), the increase in the ionic strength simultaneously caused two effects facilitating destabilization. It brought about a decrease in the polymer coil dimension as a result of the deterioration of solvent quality and, at the same time, a reduction of the distance of closest approach between particles (12). However, we found that the increase in electrolyte concentration had a much stronger effect on the dimensions of the polyacrylamide coil than on the effective radius of the AgI particles (obtained by adding the distances of effective interparticle repulsion, calculated from DLVO theory, to the mean AgI particle radius determined electron microscopically) (12, 23). Thus, one can conclude that the restriction of the space available for quasi-free motions of AgI particles attached to a polyacrylamide molecule was an important factor, if not the main one, that promoted the destabilization process.

5. Concluding remarks

A simple model describing the stability of a colloidal system containing aggregates composed of ultralarge polymer chains and fine colloidal particles is presented. The model describes monodisperse and diluted colloidal systems. The model is based on the following ideas: (*i*) a single polymer molecule may bind a number of colloidal particles; (*ii*) the Brownian mobility of an attached particle is restricted by the polymer chain length and by the number of particles attached to a polymer molecule; (*iii*) a change in the Brownian mobility of particles attached to the polymer chain influences the sedimentation equilibrium of the colloidal system. The model predicts that (*a*) the longer the polymer chain (i.e., the larger the MW), the lower the flocculation effectiveness of the polymer, and (*b*) the more particles that are attached to a single polymer molecule, the less stable the colloidal system. The former effect is contrary to the commonly known influence of polymer MW on flocculation efficiency. Therefore we wish to emphasize that the model presented deals only with systems containing macromolecules and particles of considerably different sizes. Thus, the model results can be employed to elucidate the deterioration of the ability of ultralarge polymers to flocculate fine suspensions. They do not allow, however, a generalization of the relationship obtained between the stability coefficient and the macromolecule size for the whole range of polymer MW.

Can. J. Chem. Downloaded from www.nrcresearchpress.com by 91.121.58.235 on 09/08/12
For personal use only.

© 1997 NRC Canada

References

1. A. Takahashi. Polym. J. (Tokyo), **23**, 715 (1991).
2. K. Wong, P. Lixon, F. Lafuma, P. Lindner, and O. Augerre Charriol. J. Colloid Interface Sci. **153**, 55 (1992).
3. K. Furusawa, Z. Shou, and N. Nagahashi. Colloid Polym. Sci. **270**, 212 (1992).
4. Y. Otsubo. J. Colloid Interface Sci. **153**, 584 (1992).
5. O. Spalla and B. Cabane. Colloid Polym. Sci. **271**, 357 (1993).
6. Y. Otsubo. J. Rheol. (N.Y.) **37**, 799 (1993).
7. G.C. Barker and M.J. Grimson. Colloid Surf. **43**, 55 (1990).
8. R. Buscal and J.R. White. J. Chem. Soc. Faraday Trans. 1, **83**, 873 (1987).
9. J.S. Abel, G.C. Stangle, C.H. Schilling, and I.A. Aksay. J. Mater. Res. **9**, 451 (1994).
10. A. Molski and W. Nowicki. Colloid Polym. Sci. **267**, 506 (1989).
11. W. Nowicki and G. Nowicka. Colloid Polym. Sci. **273**, 298 (1995).
12. W. Nowicki and G. Nowicka. Colloid Polym. Sci. **273**, 473 (1995).
13. J-P. Hsu and D-P. Lin. Colloid Polym. Sci. **274**, 172 (1996).
14. T. Biben and J.P. Hansen. J. Phys.: Condens. Matter, **6**, A345 (1994).
15. P.C. Hiemenz. Principles of colloid and surface chemistry. Marcel Dekker, Inc., New York, Basel. 1986.
16. B. Siffert and J.F. Li. Colloid Surf. **62**, 307 (1992).
17. J. Czermiński, A. Iwasiewicz, Z. Paszek, and A. Sikorski. *In* Statistical methods in applied chemistry. Elsevier, Amsterdam. 1990. p. 39.
18. H. Morawetz. *In* Macromolecules in solution. Interscience Publ., New York. 1965. p. 300.
19. Y. Otsubo and K. Watanabe. J. Colloid Interface Sci. **122**, 346 (1988).
20. K. Furusawa, Y. Tezuka, and K. Watanabe. J. Colloid Interface Sci. **73**, 21 (1980).
21. Y. Adachi. Adv. Colloid Interface Sci. **56**, 1 (1995).
22. W. Nowicki, G. Nowicka, and A. Molski. Pol. J. Chem. **58**, 553 (1984).
23. W. Nowicki and G. Nowicka. Pol. J. Chem. **65**, 103 (1991).

Can. J. Chem. Downloaded from www.nrcresearchpress.com by 91.121.58.235 on 09/08/12
For personal use only.

© 1997 NRC Canada

Reactions of alkoxyaryloxycarbenes with tethered triple bonds: a new synthesis of substituted benzofurans

Karim Kassam, Paul C. Venneri, and John Warkentin

Abstract: Cyclic 3-alkoxy-3-aryloxyvinylcarbenes can be generated by a highly *exo*-selective intramolecular cyclization of a dioxycarbene onto a tethered triple bond. Like their dialkoxy counterparts, the 3-alkoxy-3-aryloxyvinylcarbene intermediates are capable of interesting reactions. In contrast to 3,3-dialkoxyvinylcarbenes, which undergo a formal [3+2] cycloaddition with highly electron-deficient olefins such as benzylidenemalononitrile, 3-alkoxy-3-aryloxyvinylcarbenes undergo a highly diastereoselective [1+2] cycloaddition with benzylidenemalononitrile to give cyclopropylketene acetals. At high temperatures, those cyclopropylketene acetals undergo a clean vinylcyclopropane rearrangement in which the stereochemical integrity of the cyclopropane is retained.

Key words: carbene, alkoxyaryloxy, [1+2] cycloaddition, ketene acetal, vinylcyclopropane rearrangement, oxadiazoline.

Résumé : Il est possible de générer des 3-alkoxy-3-aryloxyvinylcarbènes cycliques par le biais d'une cyclisation intramoléculaire *exo*-sélective d'un dioxycarbène sur une triple liaison fixée. À l'instar de leurs analogues dialkoxy, les intermédiaires 3-alkoxy-3-aryloxyvinylcarbènes peuvent donner lieu à des réactions intéressantes. Par opposition aux 3,3-dialkoxyvinylcarbènes, qui subissent une cycloaddition formelle [3+2] avec les oléfines hautement déficientes en électrons tel que le benzylidènemalononitrile, les 3-alkoxy-3-aryloxyvinylcarbènes réagissent avec le benzylidènemalononitrile pour donner une cycloaddition [1+2] hautement diastéréosélective conduisant à ces acétals de cyclopropylcétènes. À températures élevées, ces acétals de cyclopropylcétènes subissent un réarrangement propre de vinylcyclopropane dans lequel l'intégrité stéréochimique du cyclopropane est maintenue.

Mots clés : alkoxyaryloxycarbène, cycloaddition [1+2], acétal de cétène, réarrangement de vinylcyclopropane, oxadiazoline.

[Traduit par la rédaction]

Introduction

Ring-forming reactions through reactive intermediates such as anions, cations, radicals, carbenes, and ylides have long held a prominent place in organic synthesis. In an extensive study, Boger et al. demonstrated that 3,3-dialkoxyvinylcarbenes such as **1**, which are reversibly generated by the thermal (≈80°C) ring opening of the corresponding cyclopropenone acetals (**2**), are interesting and synthetically useful reactive intermediates (1). These vinylcarbenes undergo a variety of reactions that depend highly upon the nature of the reacting partner. In one reaction pathway, the vinylcarbenes can react with olefins in a [1+2] cycloaddition (1*c*), a process that is also common to other carbenes. For example, thermal generation of **1** from **2** in the presence of an olefin such as methylacrylate or acrylonitrile, with one electron-withdrawing substituent, leads to the participation of the vinylcarbene (**1**) in a [1+2] cycloaddition reaction with the olefin to give the corresponding cyclopropylketene acetal (**3**) (Scheme 1). This reaction proceeds with a pronounced *endo* effect to give primarily the *cis* cycloadduct (1*h*). Due to the labile nature of the ketene acetal moiety, **3** were intentionally hydrolyzed (1*h*) with aqueous acid prior to chromatography to give the corresponding *cis*-cyclopropane esters (**4**).

In contrast to the above reaction, generation of 3,3-dialkoxyvinylcarbenes such as **1** in the presence of a highly electron-deficient olefin such as benzylidenemalononitrile or dimethyl benzylidenemalonate, each possessing two geminal electron-withdrawing groups (EWG), leads to overall [3+2] cycloaddition between the vinylcarbene and the olefin (Scheme 1) (1*b*, *g*). In this case, the vinylcarbene (**1**) behaves as a 1,3-dipole to give a substituted cyclopentenone acetal (**5**). This reaction, which is unique to this particular class of vinylcarbenes (2), represents one of a few all-carbon, overall [3+2] cycloadditions (3) and may provide a valuable complement to the Diels–Alder reaction.[2] The mechanism for the *Boger cycloaddition* is believed to involve a single electron transfer

Received April 23, 1997.

K. Kassam, P.C. Venneri, and J. Warkentin.[1] Department of Chemistry, McMaster University, Hamilton, ON L8S 4M1, Canada.

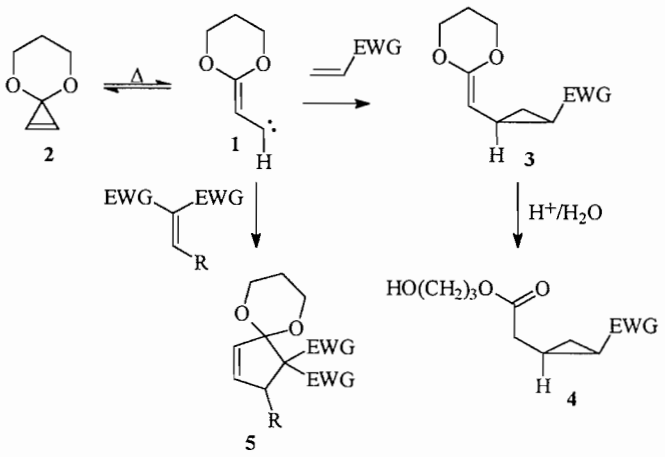
[1] Author to whom correspondence may be addressed. Telephone: (905) 525-9140. Fax: (905) 522-2509. E-mail: warkent@mcmaster.ca

[2] Such vinylcarbenes are not 4π systems (not vinyl anions) and cannot undergo concerted [$_{\pi}4_{s}$ + $_{\pi}2_{s}$] cycloadditions with 2π systems (1*a*). For that reason we use the words "formal" or "overall" to denote the [3+2] outcome of the reaction rather than the mechanism.

© 1997 NRC Canada

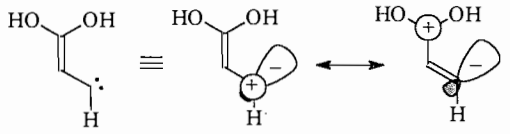
Can. J. Chem. Downloaded from www.nrcresearchpress.com by 84.22.46.98 on 09/08/12
For personal use only.

Scheme 1.



from the electron-rich vinylcarbene to the electron-deficient olefin, followed by subsequent radical-cation – radical-anion collapse (1*a*). This proposed mechanism nicely accounts for the fact that only highly electron-deficient olefins, which are good electron acceptors, undergo the overall [3+2] cycloaddition with 3,3-dioxyvinylcarbenes, whereas mildly electron-deficient olefins react via the [1+2] cycloaddition pathway.

Ab initio calculations with electron correlation (at the MP2/6-31^{++}G(d)//6G-31^{++}G(d) level) on 3,3-dihydroxyvinylmethylene revealed that the *anti* π-delocalized closed-shell singlet (**6**) is the most stable state of this vinylcarbene (1*a*). This result is consistent with the observed dual reactivity of 3,3-dialkoxyvinylcarbenes as three carbon 1,1- and 1,3-dipole equivalents.



6

Following the investigation by Boger and Brotherton, Nakamura and co-workers reported the preparation and subsequent thermal reactions of a variety of substituted cyclopropenone acetals (4). In this study a number of substituents, of different electronic character, were investigated. It was found that anion-stabilizing substituents (such as ester or phenylthio) dramatically control the regioselectivity of the cyclopropenone acetal ring opening to give exclusively the more stable vinylcarbene **8**. Like their unsubstituted counterparts, the substituted vinylcarbenes (**8**) also effectively participate in overall [3+2] cycloadditions with highly electron-deficient olefins (Scheme 2). Moreover, ester- or phenylthio-substituted cyclopropenone acetals undergo thermal ring opening at temperatures well below 25°C. With careful preparation of the substituted cyclopropenone acetals (**7**), followed by immediate addition of a suitable electron-deficient olefin, a mild and regioselective construction of highly substituted cyclopentenone acetals (**9**) is available. The low temperature sufficient for the thermal ring opening of these cyclopropenone acetals (**7**) is also a disadvantage because, in contrast to **2**, the cyclopropenone acetals cannot be stored for future application.

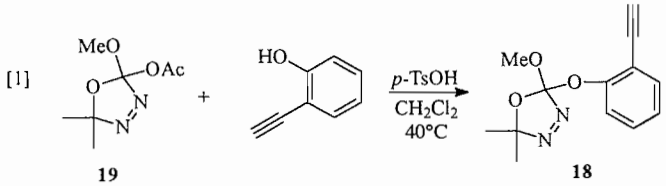
Recently, we have demonstrated that cyclic 3,3-dialkoxyvinylcarbenes (**10** or **11**) can be generated efficiently by the intramolecular cyclization of dialkoxycarbene **12** onto a tethered alkyne moiety (Scheme 3) (5). This reaction could proceed either via a cyclopropenone acetal intermediate (**13**) or via direct intramolecular attack of the dialkoxycarbene onto one of the two alkyne carbon atoms. It was found that the nature of the alkynyl substituent (R) controls the regioselectivity of the vinylcarbene formation. For example, when R = H or CH_3 and n = 1, an endocyclic 3,3-dialkoxyvinylcarbene (**10**) is generated, as inferred from trapping of the intermediate vinylcarbene with an alcohol to give ketene acetal **14**. Conversely, when R = E (ester) and n = 1 or n = 2, an exocyclic vinylcarbene (**11**) is generated exclusively. Vinylcarbene **11** can be trapped by an alcohol to give the corresponding ketene acetal (**15**), or it can participate in a formal [3+2] cycloaddition with benzylidenemalononitrile. The latter reaction has significant synthetic potential as it leads to the rapid and selective construction of a highly functionalized bicyclic ring system (**16**).

The requisite dialkoxycarbenes possessing a tethered triple bond (**12**) can be generated conveniently by the thermal decomposition of the corresponding oxadiazolines (**17**) (5, 6). Such oxadiazolines can undergo thermal decomposition (110°C) by the loss of N_2 and acetone to generate dialkoxycarbenes cleanly. The fact that oxadiazolines are easily prepared (7) and are stable at room temperature makes them convenient dioxycarbene precursors for synthetic applications.

Herein we report a study of aryloxymethoxy analogues of **17**. These systems are strikingly different from those studied previously, in terms of the regioselectivity of the vinylcarbene formation as well as the reactions of the vinylcarbene intermediate.

Results and discussion

Aryloxymethoxy-substituted oxadiazoline **18** was of interest in order to investigate whether the carbene resulting from thermolysis would undergo an intramolecular cyclization onto the tethered alkyne moiety and, if so, whether the resulting vinylcarbene would be formed regioselectively as observed for **12** with R = H or CH_3. It could be prepared by an acid-catalyzed exchange reaction between the acetoxymethoxy oxadiazoline **19** (7) and *ortho*-hydroxyphenylacetylene (8) in CH_2Cl_2 (eq. [1]). The geometry of the initially formed aryloxymethoxycarbene **20**, Scheme 4, is considerably different from that of **12** (R = H), Scheme 3, in that the tether now consists of five atoms (from oxygen to the terminal alkyne carbon atom) that are coplanar. In addition, the electronic properties of both the carbene and the alkyne are presumably different from those of **12** (R = H) due to the aromatic ring.



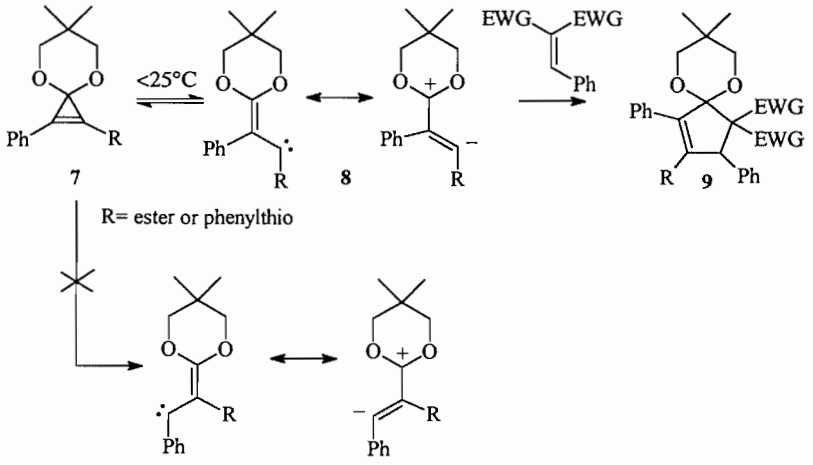
19 **18**

Thermolysis (refluxing toluene) of oxadiazoline **18** in the presence of *tert*-butyl alcohol at a low concentration (to minimize capture of the first-formed carbene) gave one major product with the mass of the carbene plus the alcohol. This composition was inferred from the GC–MS trace of the crude

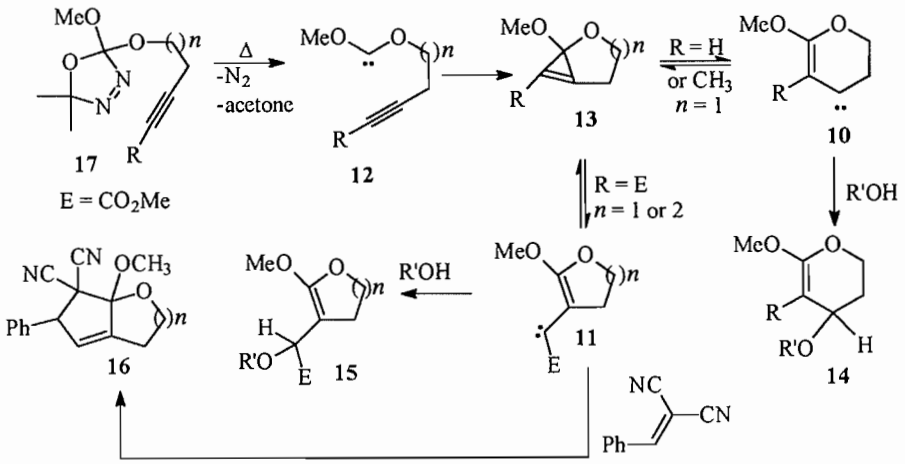
© 1997 NRC Canada

Can. J. Chem. Downloaded from www.nrcresearchpress.com by 84.22.46.98 on 09/08/12
For personal use only.

Scheme 2.



Scheme 3.



thermolysis product. Attempted purification of this product by chromatography or by distillation led to decomposition. This sensitivity was not surprising given that the expected product is a ketene acetal, a class of compounds that are prone to hydrolysis or polymerization (9). Consequently, the crude thermolysis product was intentionally hydrolyzed (*p*-TsOH–H_2O) to give a stable compound that could easily be purified by chromatography. The major product obtained from hydrolysis was isolated in 40% yield and was shown to have structure **21** on the basis of spectral data. Formation of **21** is attributed to hydrolysis of **22**, which is derived from an O-H insertion reaction of the exocyclic vinylcarbene **23** with the alcohol. The presence of **22** was confirmed from the spectroscopic data of the crude thermolysis mixture. Therefore, in contrast to **12** (R = H), which cyclizes to give an endocyclic vinylcarbene (**10**) exclusively, the cyclization of **20** seems to give primarily the exocyclic vinylcarbene (**23**). Analysis of the ^{1}H NMR spectra and GC–MS trace of the crude hydrolysis mixture also showed evidence for the formation of coumarin (**24**), which is likely obtained from hydrolysis of **25**. The formation of **25** can be attributed to trapping of the endocyclic vinylcarbene **26** with *tert*-butyl alcohol. The ratio, **21**:**24**, was estimated to be approximately 5:1 by ^{1}H NMR spectroscopy, indicating a moderately high preference for the formation of **23**.

The preferential formation of an exocyclic vinylcarbene (**23**) upon thermolysis of oxadiazoline **18** raised the possibility of capturing **23** in a formal [3+2] cycloaddition with a highly electron-deficient olefin such as benzylidenemalononitrile. This cycloaddition would lead to a novel functionalized tricyclic benzofuran ring system **27** (Scheme 5).

Thermolysis of oxadiazoline **18** in the presence of benzylidenemalononitrile in low concentration led to the formation of one major product in 67% yield. This product had the mass (by EI mass spectrometry) expected for **27**. Surprisingly, only a single diastereomer was obtained. The ^{1}H NMR and ^{13}C NMR spectra of this product, on the other hand, were not consistent with structure **27**. Most significantly, in the ^{1}H NMR spectrum, two doublets corresponding to two methine protons were too far upfield to be consistent with structure **27** and, in addition, the ^{13}C NMR spectrum included a signal at high field (δ: 14.4 ppm), which could not be assigned to a carbon of **27**. The product was eventually shown to have structure **28**, based on comparison of its ^{1}H and ^{13}C NMR spectra with those of a close analogue (**30**, vide infra), the structure of which was secured by single crystal X-ray diffraction.

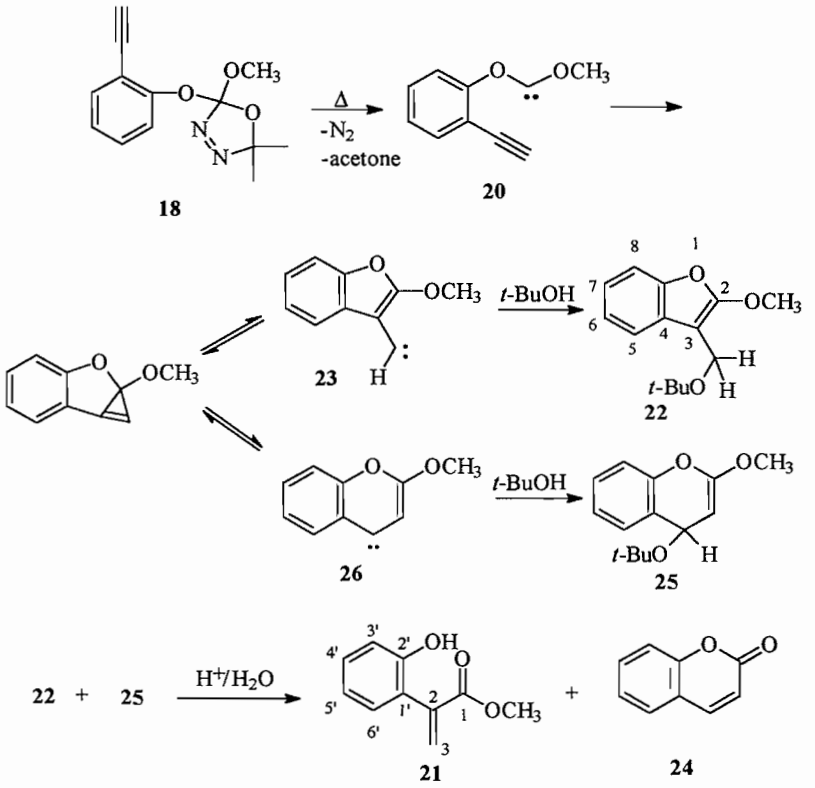
The formation of **28** is highly unusual, given that reactions of a 3,3-dioxyvinylcarbene with benzylidenemalononitrile, or related olefins, have been shown to give cyclopentene

© 1997 NRC Canada

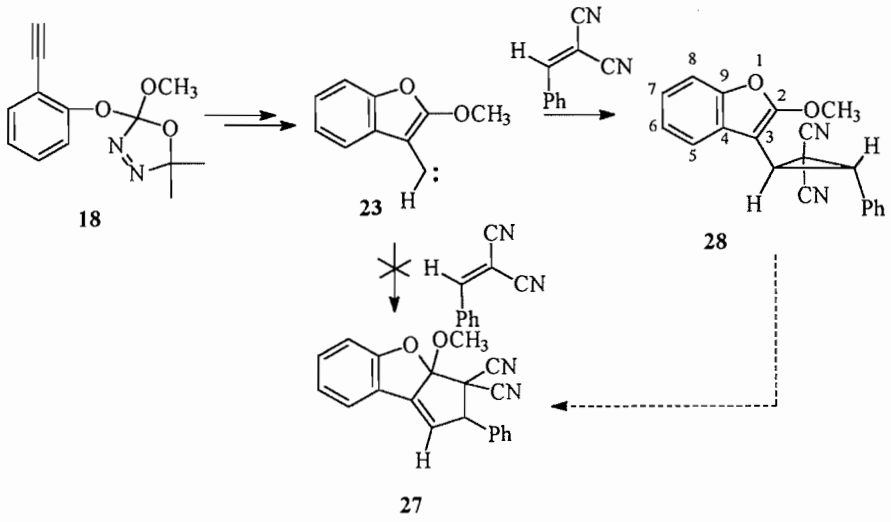
Can. J. Chem. Downloaded from www.nrcresearchpress.com by 84.22.46.98 on 09/08/12
For personal use only.

Can. J. Chem. Downloaded from www.nrcresearchpress.com by 84.22.46.98 on 09/08/12
For personal use only.

Scheme 4.



Scheme 5.



products in every previous case studied (1, 4, 5). There has not been any evidence in support of formation of a [1+2] cycloadduct. Of additional interest is the fact that **28** was formed with *trans* stereoselectivity on the cyclopropane ring.

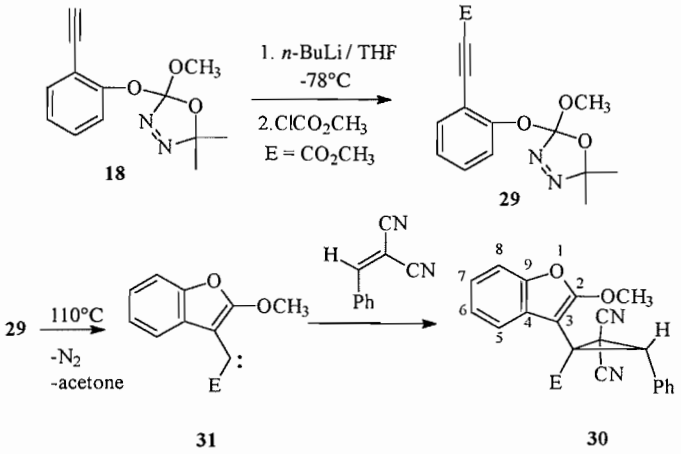
An ester-substituted analog of **18** was prepared in order to investigate whether the ester group may have played a role in facilitating the overall [3+2] cycloaddition of **12** (R = E) with benzylidenemalononitrile. Oxadiazoline **29** was prepared from **18** by deprotonation of the alkyne moiety with *n*-butyllithium, to form the corresponding acetylide, followed by treatment of the acetylide with methyl chloroformate (Scheme 6).

Thermolysis of **29** in the presence of benzylidenemalononitrile in low concentration led to the formation of one major product (**30**) with NMR spectra closely resembling those of **28** (Scheme 6). This product was isolated in 37% yield and its structure was determined by single crystal X-ray diffraction.[3]

[3] A manuscript containing details of the molecular and crystal structures will be submitted to Acta Crystallogr. Sect. C.

© 1997 NRC Canada

Scheme 6.



The formation of **30** can be attributed to a [1+2] cycloaddition of the intermediate 3,3-dioxyvinylcarbene (**31**) and, as in the case of **27**, only one stereoisomer, with the benzofuran and the phenyl groups *trans*, was obtained.

The stereochemistry observed for both **28** and **30** can be rationalized simply on the basis of steric effects. The transition state for the [1+2] cycloaddition, which has the benzofuran moiety of the vinylcarbene *syn* with respect to the phenyl group of the olefin, suffers greater steric hindrance than that in which the two groups are *anti*.

The surprising [1+2] cycloaddition of both vinylcarbenes **23** and **31**, in the face of precedents for exclusive overall [3+2] cycloadditions by analogues (Introduction), can also be rationalized. Presumably both **23** and **31** have less 1,3-dipole character[4] than dialkoxy counterparts and are therefore more likely to behave as typical localized carbenes. The reduced 1,3-dipole character could stem from two possible sources. First, π-donation into the formally vacant carbene *p*-orbital is reduced because of the inherently poorer electron-donating ability of an aryloxy substituent than of an alkoxy substituent. Second, benzofuran is a 10 π-electron aromatic ring system, and both **23** and **31** presumably have reduced contributions from 1,3-dipolar contributors in order to maintain most of the aromaticity (Scheme 7).

As a result of the poorer π-electron delocalization of carbenes **23** and **31**, a single electron transfer from the carbene to the olefin, which, according to Boger and Brotherton-Pleiss, is required for an overall [3+2] cycloaddition (1*a*), would result in a radical cation that is less stabilized than the corresponding radical cation from systems such as **11** (Scheme 7). Consequently, the reason why **23** and **31** undergo a [1+2] cycloaddition, instead of a formal [3+2] cycloaddition, with benzylidenemalononitrile probably lies in the higher oxidation potentials of these carbenes. Nevertheless, the fact that vinylcarbenes **23** and **31** undergo facile reaction with the highly electron-deficient olefin implies that these carbenes still have nucleophilic character.

Thermolysis of **18** or **29** in the presence of dimethyl acetylenedicarboxylate (DMAD) at a low concentration produced a complex mixture of products that were not identified. This clearly indicates the dramatically different nature of vinylcarbenes **23** and **31** in comparison to vinylcarbenes **11** (n = 1 or 2), which undergo a relatively clean, formal [3+2] cycloaddition with DMAD (5*a*).

Vinylcyclopropane rearrangement of adducts 28 and 30

The vinylcyclopropane rearrangement in simple unsubstituted systems has been studied extensively (10). This transformation has also been exploited in a number of synthetic applications for the construction of substituted cyclopentenes (11).

In theory, cycloadducts **28** and **30** can undergo a vinylcyclopropane rearrangement, to afford the ring system that was initially expected from overall [3+2] cycloaddition of vinylcarbenes **23** or **31** to benzylidenemalononitrile. However, Boger and Brotherton-Pleiss had shown that cyclopropyl ketene acetals such as **3** (Introduction), which are closely related to **28** and **30**, do not undergo vinylcyclopropane rearrangement even at temperatures as high as 200°C (1*a*). Nevertheless, adducts **28** and **30** might be more likely than **3** to undergo the vinylcyclopropane rearrangement because of the presence of the two geminal electron-withdrawing cyano groups on the cyclopropane ring, which would be expected to stabilize a possible zwitterionic or biradical intermediate. Added interest in the rearrangement was derived from the potential for diastereoselectivity, **28** and **30** being diastereomerically pure.

Heating a degassed[5] sample in toluene indeed converted **30** to the expected product (**32**) of a vinylcyclopropane rearrangement, as inferred from the spectroscopic data and later confirmed by single crystal X-ray diffraction.[3] The reaction proceeded cleanly but very slowly; even after 4 days at 150°C, the conversion was only about 50%.

Of particular interest was the fact that a single diastereomer was obtained, indicating that the vinylcyclopropane rearrangement proceeded with very high diastereoselectivity. Specifically, the closure of a possible dipolar or diradical intermediate in this rearrangement proceeds with π-facial selectivity (Scheme 8) or, alternatively, the rearrangement is concerted, as in the case reported recently by Gajewski et al. (12). In favour of a diradical process, either as the mechanism of formation of **32** or as a minor side reaction, was the observation that bibenzyl (from toluene solvent) could be detected by GC–MS. In any case, this two-step approach involving an initial [1+2] cycloaddition to give a cyclopropylketene acetal, followed by a vinylcyclopropane rearrangement, results in the diastereoselective formation of an interesting ring system (**32**).

Cyclopropylketene acetal **28** was also shown to undergo a vinylcyclopropane rearrangement, albeit more slowly, under similar conditions. After four days at 150°C, the conversion was about 33% complete. The rearrangement in this case also proceeded diastereoselectively to provide **27**. A minor coproduct, detectable by GC–MS, was bibenzyl, presumably from

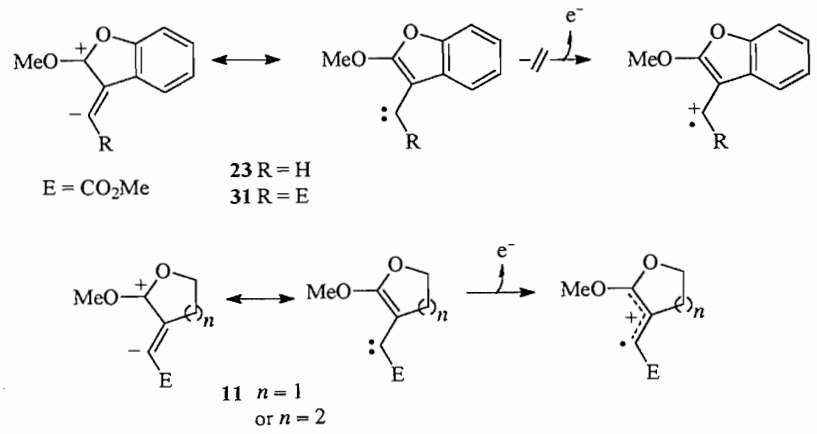
[4] Alternatively, one can write "are less easily oxidized," to emphasize the proposed radical cation mechanism (1*a*).

[5] An undegassed sample afforded a product containing an extra atom of oxygen (HRMS). Although it was a solid, attempts to grow a crystal satisfactory for single crystal X-ray diffraction failed. The NMR spectroscopic data were inconclusive and further work on that potentially interesting product is required.

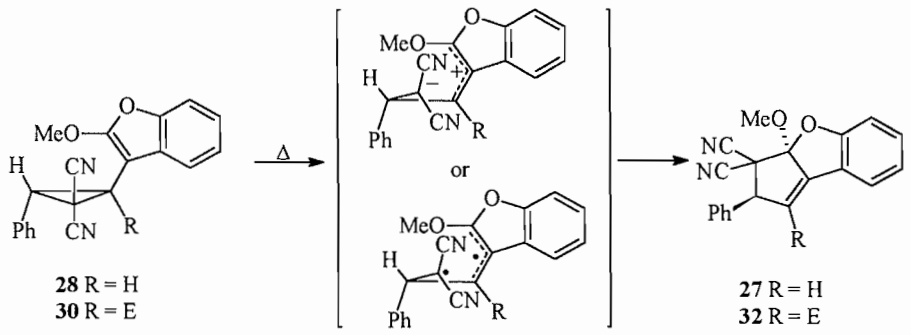
Can. J. Chem. Downloaded from www.nrcresearchpress.com by 84.22.46.98 on 09/08/12
For personal use only.

© 1997 NRC Canada

Scheme 7.



Scheme 8.



coupling of solvent-derived benzyl radicals. It is not clear whether this product indicates a biradical mechanism or a minor side reaction unrelated to the formation of **27**.

Experimental

General methods

NMR spectra were obtained with a Bruker AM-500, AC-300, or AC-200 spectrometer. Chemical shifts for ^{1}H NMR spectra are referenced to TMS (δ = 0), C_6H_6 (δ = 7.15) , or $CHCl_3$ (δ = 7.24), while ^{13}C NMR spectra are referenced to the chloroform-*d* triplet (δ = 77.0) or the benzene-d_6 triplet (δ = 128.0). Mass spectra were obtained with a ZAB-E double-focusing mass spectrometer or a Hewlett Packard MSD GC–MS. FTIR spectra were obtained with a Bio-Rad, FTS-40 instrument. Benzene, toluene, and THF were distilled from sodium benzophenone ketyl and dichloromethane was distilled from calcium hydride. Chromatography solvents (EtOAc, hexanes) were distilled before use. Unless otherwise indicated, all reactions were carried out under an atmosphere of nitrogen.

Preparation of *ortho*-hydroxy phenyl acetylene (8)

A suspension of 2,3-benzofuran (5.89 g, 49.9 mmol) and finely cut sodium (3.30 g, 143.5 mmol) in pyridine (50 g) was refluxed under a blanket of nitrogen for 4 h. After cooling to room temperature, pyridine (20 mL) and water (30 mL) were slowly added to the "tar-like" mixture. The excess 2,3-benzofuran was extracted with ether (30 mL) from the aqueous pyridine solution, which was then acidified to pH = 2 with dilute HCl. The free phenol was then extracted (3 × 20 mL) with ether and the combined organic extracts were washed once with dilute HCl (20 mL) and once with water (20 mL). Upon drying the organic layer with Na_2SO_4 and concentrating in vacuo, the title compound (3.54 g, 30.0 mmol) of high purity was obtained in 61% yield. ^{1}H NMR (200 MHz, $CDCl_3$) δ: 3.43 (s, 1H, C≡CH), 4.75 (br, OH), 6.90 (m, 1H, $^3J_{5,4}$ = 7.4 Hz, $^3J_{5,6}$ = 7.7 Hz, $^4J_{5,3}$ = 1.2 Hz, H-5), 6.93 (dd, 1H, $^3J_{4,3}$ = 8.3 Hz, $^4J_{3,5}$ = 1.2 Hz, H-3), 7.25 (m, 1H, $^3J_{4,3}$ = 8.3 Hz, $^3J_{5,4}$ = 7.4 Hz, $^4J_{4,6}$ = 1.7 Hz, H-4), 7.37 (dd, 1H, $^3J_{6,5}$ = 7.7 Hz, $^4J_{4,6}$ = 1.7 Hz, H-6); ^{13}C NMR (50 MHz, $CDCl_3$) δ: 78.4 (C≡*C*H), 84.0 (*C*≡CH), 108.3 (C-1), 114.8 (C-4), 120.2 (C-3), 130.8 (C-5), 132.2 (C-6), 157.4 (C-2); MS (GC–MS, EI) *m/z* (rel. intensity): 118 ($M^{+\bullet}$, 80), 90 (90), 89 (100), 75 (2), 74 (4).

Preparation of 2-(2-ethynylphenoxy)-2-methoxy-5,5-dimethyl-Δ^3-1,3,4-oxadiazoline (18)

A solution of 2-acetoxy-2-methoxy-5,5-dimethyl-Δ^3-1,3,4-oxadiazoline (70% pure) (7) (1.60 g, 5.96 mmol of oxadiazoline), *o*-hydroxy phenyl acetylene (0.70 g, 5.93 mmol), and *p*-toluene sulfonic acid (0.10 g) in CH_2Cl_2 (50 mL) was refluxed for 48 h before dilute KOH (5%, 10 mL) was added. The mixture was stirred for 1 h followed by extraction (3 × 20 mL) with CH_2Cl_2. After drying the combined organic extracts with Na_2SO_4 and concentrating in vacuo, **18** was obtained as a yellow oil upon chromatography (Chromatotron, 4 mm plate, 10% EtOAc – hexanes) in 37% yield. ^{1}H NMR (200 MHz, $CDCl_3$) δ: 1.29 (s, 3H, CH_3), 1.54 (s, 3H, CH_3), 3.22 (s, 1H,

Can. J. Chem. Downloaded from www.nrcresearchpress.com by 84.22.46.98 on 09/08/12
For personal use only.

© 1997 NRC Canada

C≡CH), 3.64 (s, 3H, OCH_3), 7.01–7.47 (m, 5H, Ar); ^{13}C NMR (50 MHz, $CDCl_3$) δ: 23.4 (CH_3) , 24.1 (CH_3), 52.6 (CH_3O), 79.5 (C≡*C*H), 81.5 (*C*≡CH), 116.0 (aryl), 120.8 (C-5), 121.2 (aryl), 124.1 (aryl), 129.6 (aryl), 133.7 (aryl), 136.7 (C-2), 153.0 (aryl); MS (GC–MS, EI) *m/z* (rel. intensity): 218 ($M^+ - N_2$, 1), 215 ($M^+ - CH_3O$, 1), 203 (4), 160 ($M^+ - C_3H_6O - N_2$, 15), MS (CI, NH_3) *m/z*: 264 $(M + NH_4)^+$, 247 $(M + H)^+$.

Thermolysis of 18 in the presence of *tert*-butyl alcohol

A solution of 2-(2-ethynylphenoxy)-2-methoxy-2,2-dimethyl-Δ^3-1,3,4-oxadiazoline (0.235 g, 0.957 mmol) and *tert*-butyl alcohol (0.26 g, 3.5 mmol) in dry toluene (100 mL) was refluxed for 24 h. Analysis of the crude thermolysis mixture (0.1985 g) by ^1H NMR spectroscopy indicated that it consisted mainly of 3-(*tert*-butoxymethyl)-2-methoxy-2,3-benzofuran (**22**). This compound is sensitive to moisture, and attempts to isolate a pure sample failed. The spectral data below are those of the crude thermolysis product that was primarily **22** (>80% by ^1H NMR). ^1H NMR (300 MHz, $CDCl_3$) δ: 1.31 (s, 9H, Me_3), 4.04 (s, 3H, MeO), 4.43 (s, 2H, CH_2O), 7.09 (m, $^3J_{6,7}$ = 7.5 Hz, $^3J_{7,8}$ = 7.4 Hz, $^4J_{5,7}$ = 1.6 Hz, 1H, H-7), 7.16 (m, $^3J_{5,6}$ = 7.5 Hz, $^3J_{6,7}$ = 7.5, $^4J_{6,8}$ = 1.4 Hz, 1H, H-6), 7.25 (dd, $^3J_{7,8}$ = 7.4 Hz, $^4J_{6,8}$ = 1.8 Hz, 1H, H-8), 7.25 (dd, $^3J_{5,6}$ = 7.5 Hz, $^4J_{5,7}$ = 1.6 Hz, 1H, H-5); ^{13}C NMR (75 MHz, $CDCl_3$) δ: 27.6 (Me_3), 53.2 (OMe), 58.6 (OCH_2), 73.1 (*C*Me_3), 82.5 (C-3), 91.2 (C-2), 110.0 (C-8), 118.7 (C-6), 121.8 (C-4), 122.9 (C-5), 129.9 (C-7), 159.1 (C-9).

Methyl 2-(2-hydroxyphenyl)propenoate (21)

To the crude thermolysis product (0.058 g) consisting of mainly **22** was added *para*-toluene sulfonic acid (0.010 g) in water (0.10 mL). The solution was stirred for 1.5 h at room temperature before it was extracted with CH_2Cl_2 (3 × 5 mL). The combined extracts were then dried over Na_2SO_4 and concentrated in vacuo. Chromatography (1 mm plate, 10% EtOAc – hexanes) yielded **21** (0.0152 g) in 40% yield. ^1H NMR analysis of the crude hydrolysis mixture revealed that **24** was also formed. The ratio **21**:**24** was estimated to be approximately 5:1 by ^1H NMR spectroscopy. ^1H NMR of **21** (200 MHz, $CDCl_3$) δ: 3.85 (s, 3H, OMe), 5.89 (d, 1H, ^2J = 1.3, H-3), 6.42 (d, 1H, ^2J = 1.3, H-3), 6.89 (m, 1H, $^3J_{5',6'}$ = 7.9 Hz, $^3J_{4',5'}$ = 7.3 Hz, $^4J_{3',5'}$ = 1.2 Hz, H-5′), 6.92 (dd, 1H, $^3J_{3',4'}$ = 7.1 Hz, $^4J_{3',5'}$ = 1.2 Hz, H-3′), 7.12 (dd, 1H, $^3J_{5',6'}$ = 7.9 Hz, $^4J_{4',6'}$ = 1.8 Hz, H-6′), 7.25 (m, 1H, $^3J_{4',5'}$ = 7.3 Hz, $^3J_{3',4'}$ = 7.1 Hz, $^4J_{4',6'}$ = 1.8 Hz, H-4′), 7.50 (s, br, 1H, OH); ^{13}C NMR (50 MHz, $CDCl_3$) δ: 53.0 (MeO), 117.8 (C-3), 120.7 (C-2), 124.7 (C-1′), 130.3, 130.4, 130.7 (C-6′, C-5, C-4′), 139.4 (C-3′), 153.6 (C-2′), 169.7 (C=O).

Thermolysis of 18 in the presence of benzylidenemalononitrile

From a solution of 2-(2-ethynylphenoxy)-2-methoxy-2,2-dimethyl-Δ^3-1,3,4-oxadiazoline (**18**) (36 mg, 0.15 mmol) and benzylidinemalononitrile (25 mg, 0.16 mmol) in 150 mL of dry toluene, 20 mL of solvent was distilled off at atmospheric pressure to remove adventitious water by azeotropic distillation. Following heating at reflux for 20 h and concentration in vacuo, the crude thermolysis product that remained was purified by chromatography (Chromatotron, 1 mm plate, 5–15% EtOAc – hexanes) to give **28** in 67% yield. Slow crystallization at room temperature from hexanes – ethyl acetate gave fine crystals, mp 141–142°C . ^1H NMR (200 MHz, $CDCl_3$) δ: 3.42 (d, ^3J = 8.7 Hz, 1H, allylic CH), 3.89 (d, ^3J = 8.7 Hz, 1H, benzylic CH), 4.14 (s, 3H, MeO), 7.16–7.91 (m, 9H); ^{13}C NMR (50 MHz, $CDCl_3$) δ: 14.4 (*C*$(CN)_2$), 29.8 (allylic C), 38.7 (benzylic C), 58.4 (OCH_3), 83.2 (C-3), 110.7 (C-8), 112.5 (CN), 113.6 (CN), 117.3 (C-6), 122.6 (C-5), 123.8 (C-7), 128.4 (C-4), 129.1, 129.4, 130.6, 134.5 (4 Ar), 147.9 (C-2), 159.9 (C-9); MS (EI), *m/z* (rel. intensity): 314 ($M^{+\cdot}$, 13), 237 ($M^{+\cdot} - Ph$, 5), 154 (100), 127 (50), 103 (55), 91 (80); MS (HR) *m/z*, calcd. for $C_{20}H_{14}O_2N_2$ ($M^{+\cdot}$): 314.1055; found: 314.1057.

Preparation of 2-[2-(methylpropiolato)]-phenoxy-2-methoxy-5,5-dimethyl-Δ^3-1,3,4-oxadiazoline (29)

A stirred solution of 2-(2-ethynylphenoxy)-2-methoxy-5,5-dimethyl-Δ^3-1,3,4-oxadiazoline **18** (500 mg, 2.0 mmol) in dry THF (30 mL) was cooled at −78°C for 1 h under nitrogen. A solution of *n*-butyllithium (2.4 M) in hexanes (0.85 mL, 2.0 mmol) was then added dropwise. This solution was stirred at −78°C for 1 h before addition of methylchloroformate (0.5 mL, 6 mmol). The reaction mixture was allowed to reach room temperature slowly overnight with the cooling bath left in place. Water (15 mL) was then added cautiously and the THF was removed in vacuo by rotary evaporation. The aqueous residue was extracted with CH_2Cl_2 (3 × 20 mL), and the combined extracts were dried over anhydrous Na_2SO_4 before they were concentrated in vacuo. Chromatography (Chromatotron, 4 mm plate, 10–15% EtOAc – hexanes) gave **29** as an oil in 40% yield. FTIR (NaCl, neat) cm^{-1}: 2991, 2954, 2916 (C-H), 2227 (C≡C), 1714 (C=O); ^1H NMR (200 MHz, $CDCl_3$) δ: 1.28 (s, 3H, Me), 1.54 (s, 3H, Me), 3.66 (s, 3H, OMe), 3.80 (s, 3H, OMe), 7.06–7.54 (m, 4H); ^{13}C NMR (50 MHz, $CDCl_3$) δ: 23.3 (Me), 24.1 (Me), 52.7 (2 × MeO), 82.6 (alkyne), 84.1 (alkyne), 113.8 (C-5), 121.1, 121.6, 124.4, 131.6, 134.4 (5 Ar), 136.6 (C-2), 153.9 (Ar), 154.3 (C=O); MS (EI) *m/z* (rel. intensity): 273 ($M^{+\cdot}$ − MeO, 6), 235 (5), 217 (18), 203 (20), 185 (20), 173 (30), 159 (18), 145 (16), 129 ($M^{+\cdot} - C_{10}H_7O_2$, 100), MS (CI, NH_3) *m/z*: 322 $(M + NH_4)^{+\cdot}$.

Thermolysis of 2-[2-(methylpropiolato)]-phenoxy-2-methoxy-5,5-dimethyl-Δ^3-1,3,4-oxadiazoline (29) in the presence of benzylidenemalononitrile

At atmospheric pressure, 20 mL of toluene was distilled from a solution of 2-[2-(methylpropiolato)]-phenoxy-2-methoxy-5,5-dimethyl-Δ^3-1,3,4-oxadiazoline (154 mg, 0.63 mmol) and benzylidinemalononitrile (100 mg, 0.65 mmol) in 150 mL of dry toluene. The solution was refluxed for 20 h and concentrated in vacuo to afford a crude thermolysis product that was purified by chromatography (Chromatotron, 1 mm plate, 5–15% EtOAc – hexanes) to give a single major product (**30**, 99.7 mg, 0.41 mmol, 37%) as a solid, mp 188–190°C. This product was recrystallized from hexanes–EtOAc. Slow crystallization at room temperature gave crystals suitable for X-ray diffraction (10). ^1H NMR (200 MHz, $CDCl_3$) δ: 3.60 (s, 3H, MeO), 3.89 (s, 1H, benzylic CH), 4.20 (s, 3H, MeO), 7.16–7.50 (m, 9H); ^{13}C NMR (50 MHz, $CDCl_3$) δ: 18.5 (*C*$(CN)_2$), 40.0 (allylic C), 42.5 (benzylic C), 58.4 (OMe), 58.4 (OMe), 85.2 (C-3), 110.9 (C-8), 111.1 (CN), 113.5 (CN), 117.4 (C-6), 122.8 (C-5), 124.1 (C-7), 127.8 (C-4), 128.6, 129.1, 129.3 (3 Ar), 147.9 (C-2), 160.7 (C-9), 164.8 (C=O).

© 1997 NRC Canada

Can. J. Chem. Downloaded from www.nrcresearchpress.com by 84.22.46.98 on 09/08/12
For personal use only.

Can. J. Chem. Downloaded from www.nrcresearchpress.com by 84.22.46.98 on 09/08/12
For personal use only.

Vinylcyclopropane rearrangement of 30

A solution of vinylcyclopropane **30** (18.7 mg, 0.049 mmol) in toluene (20 mL) was prepared. At atmospheric pressure, 10 mL of the toluene was then distilled from the solution to remove adventitious water by azeotropic distillation. The remaining solution was transferred to a 50 mL glass tube and degassed by three freeze–pump–thaw cycles, before the tube was sealed and heated for 4 days in an oil bath at 150 ± 0.1°C. The sample was cooled and concentrated in vacuo to afford a crude product that consisted of **30** and **32** in ca 1:1 ratio by ^{1}H NMR spectroscopy. Chromatography (Chromatotron, 4 mm plate, 10–15% EtOAc – hexanes) gave **32** as a white powder in approximately 40% yield and the unreacted **30** was recovered. Very slow crystallization of **32** from EtOAc–hexanes at room temperature yielded crystals suitable for X-ray diffraction (10); white solid, *trans* configuration, mp 217–218°C. ^{1}H NMR (200 MHz, $CDCl_3$) δ: 3.31 (s, 3H, MeO), 3.68 (s, 3H, MeO), 5.30 (s, 1H, benzylic CH), 7.11–7.55 (m, 8H), 8.07 (m, 1H); ^{13}C NMR (125 MHz, $CDCl_3$) δ: 51.9 (OMe), 53.4 (OMe), 62.9 (benzylic C), 110.4, 110.8, 111.5, 112.2, 114.8, 118.9, 122.5, 127.2, 128.6, 128.8, 128.9, 129.2, 129.4, 133.8, 135.1, 163.2, 165.5 (C=O); MS (EI), *m/z* (rel. intensity): 372 ($M^{+\cdot}$, 8), 313 ($M^{+\cdot} - CO_2Me$, 28), 141 (29) , 84 (30); MS (HR) *m/z*, calcd. for $C_{22}H_{16}N_2O_4$ ($M^{+\cdot}$): 372.1110; found: 372.1112.

Vinylcyclopropane rearrangement of 28

Toluene (10 mL) was distilled at atmospheric pressure from a solution of vinylcyclopropane **28** (15.0 mg, 0.048 mmol) in toluene (30 mL). The remaining solution was transferred to a 50 mL glass tube, degassed by three freeze–pump–thaw cycles, and then sealed before it was heated for 4 days in an oil bath operating at 150 ± 0.1°C. Following thermolysis, the sample was cooled and then concentrated in vacuo. Compound **27** was isolated by chromatrography (Chromatotron, 1 mm plate, 10–15% EtOAc – hexanes) as a yellow oil in 33% yield and unreacted **28** (8 mg, 0.025 mmol) was recovered. Attempted crystallization of the yellow oil was not successful. ^{1}H NMR (200 MHz, $CDCl_3$) δ: 3.33 (s, 3H, MeO), 5.21 (d, ^3J = 1.9 Hz, 1H, alkene CH), 6.35 (d, ^3J = 1.9 Hz, 1H, benzylic CH), 7.06–7.51 (m, 9H); ^{13}C NMR (125 MHz, $CDCl_3$) δ: 53.3 (OMe), 62.4 (benzylic), 97.0, 110.9, 111.5 (C_6H_4), 119.7 (C_6H_4), 122.6 (C_6H_4), 123.1 (=CH), 125.4 (C_6H_4), 128.6 (C_6H_5), 128.8, 129.2 (C_6H_5), 129.6 (C_6H_5), 130.9, 132.4 (C_6H_4), 134.2, 143.2 (C_6H_5), 167.7 (C_6H_4); MS (EI), *m/z*: (rel. intensity): 314 ($M^{+\cdot}$, 45), 299 ($M^{+\cdot} - CH_3$, 36), 207 (30), 149 (20), 85 (24), 71 (47), 57 (100), 43 (69); MS (HR) *m/z*, calcd. for $C_{20}H_{14}N_2O_2$ ($M^{+\cdot}$): 314.1055; found: 314.1051. The *trans* structure was assigned, there being no reasonable basis to assume that the *trans* precursor could afford the *cis* product cleanly when the analogous rearrangement of **30** to **32** went with retention.

Acknowledgements

The authors gratefully acknowledge financial support from the Natural Sciences and Engineering Research Council of Canada (NSERC) and the assistance of Drs. Richard Smith and Don Hughes with mass spectrometry and NMR spectroscopy, respectively. For the molecular and crystal structures of **30** and **32**, we thank Dr. Jim Britten.

References

1. (*a*) D.L. Boger and C.E. Brotherton-Pleiss. *In* Advances in cycloaddition. Vol. 2. *Edited by* D.P. Curran. JAI Press, Greenwich, Conn. 1990. p. 147; (*b*) D.L. Boger and R.J. Wysocki, Jr. J. Org. Chem. **53**, 3408 (1988); (*c*) D.L. Boger and C.E. Brotherton. J. Am. Chem. Soc. **108**, 6695 (1986); (*d*) J. Am. Chem. Soc. **108**, 6713 (1986); (*e*) Tetrahedron, **42**, 2777 (1986); (*f*) J. Org. Chem. **50**, 3425 (1985); (*g*) J. Am. Chem. Soc. **106**, 805 (1984); (*h*) Tetrahedron Lett. **25**, 5611 (1984); (*i*) D.L. Boger, C.E. Brotherton, and G.I. Georg. Tetrahedron Lett. **25**, 5615 (1984).
2. (*a*) M.S. Baird. Top. Curr. Chem. **144**, 137 (1988); (*b*) E.J. York, W. Dittmar, J.R. Stevenson, and R.G. Bergman. J. Am. Chem. Soc. **95**, 5680 (1973); (*c*) J.A. Pincock, R. Morchat, and D.R. Arnold. J. Am. Chem. Soc. **95**, 7536 (1973); (*d*) J.A. Pincock and R.J. Boyd. Can. J. Chem. **55**, 2482 (1977); (*e*) M.G. Steinmetz, R. Srinivasan, and W.J. Leigh. Rev. Chem. Intermed. **5**, 57 (1984).
3. (*a*) R. Huisgen. *In* 1,3-Dipolar cycloaddition chemistry. *Edited by* A. Padwa. Wiley-Interscience, New York. 1984; (*b*) J.A. Berson, D.M. McDaniel, L.R. Corwin, and J.H. Davis. J. Am. Chem. Soc. **94**, 5509 (1972); (*c*) S. Yamago and E. Nakamura. J. Am. Chem. Soc. **111**, 7285 (1989); (*d*) J. Org. Chem. **55**, 5553 (1990).
4. H. Tokuyama, M. Isaka, and E. Nakamura. J. Am. Chem. Soc. **114**, 5523 (1992).
5. (*a*) K. Kassam and J. Warkentin. Can. J. Chem. **75**, 120 (1977); (*b*) J. Org. Chem. **59**, 5071 (1994).
6. (*a*) M. El-Saidi, K. Kassam, D.L. Pole, T. Tadey, and J. Warkentin. J. Am. Chem. Soc. **114**, 8751(1992); (*b*) W.W. Win, M. Kao, M. Eiermann, J.J. McNamara, F.Wudl, D.L. Pole, K. Kassam, and J. Warkentin. J. Org. Chem. **59**, 5871 (1994); (*c*) D.L. Pole and J. Warkentin. Liebigs Ann. Chem. 1907 (1995).
7. K. Kassam, D.L. Pole, M. El-Saidi, and J. Warkentin. J. Am. Chem. Soc. **116**, 1161 (1994).
8. V. Prey and G. Pieh. Monatsh. Chem. **80**, 790 (1949).
9. (*a*) H.W. Scheeren. Recl. Trav. Chim. Pays-Bas, **105**, 71 (1986); (*b*) H.W. Scheeren, A.J.R. van Rossum, and R.J.F. Nivard. Tetrahedron, **39**, 1345 (1983).
10. J.E. Baldwin, K.A. Villarica, D.I. Freedberg, and F.A.L. Anet. J. Am. Chem. Soc. **116**, 10845 (1994), and refs. therein.
11. (*a*) E.J. Corey and X.-M. Cheng. The logic of chemical synthesis. Wiley, New York. 1989. pp. 88–89; (*b*) T. Hudlicky, F. Rulin, T.C. Lovelace, and J.W. Reed. Stud. Nat. Prod. Chem. (Stereosel. Synth. Part B), **3**, 3 (1989); (*c*) T. Hudlicky, and J.W. Reed. *In* Comprehensive organic synthesis. Vol. 5. *Edited by* L.A. Paquette. Pergamon Press, Oxford. 1991. Chap. 8.1.
12. J.J. Gajewski, L.P. Olson, and M.R. Willcott III. J. Am. Chem. Soc. **118**, 299 (1996).

© 1997 NRC Canada

Spiro-fused 2-alkoxy-2-amino-Δ^3-1,3,4-oxadiazolines. Synthesis and thermolysis to corresponding aminooxycarbenes

Philippe Couture and John Warkentin

Abstract: Δ^3-1,3,4-Oxadiazolines spiro-fused at C2 to C2 to oxazolidines (**12**) or to C2 of tetrahydro-1,3-oxazines (**13**) were synthesized. The oxadiazolines undergo thermolysis in benzene at 90°C with first-order rate constants of $(1.6–50) \times 10^{-5}$ s^{-1}. The dependence of these rate constants on the nature of the substituents present on the oxadiazoline ring is consistent with a mechanism involving a carbonyl ylide intermediate. Substituents on N of the oxazolidine or tetrahydro-1,3-oxazine moieties play a major role in determining the fragmentation pathways. Oxadiazolines with N-carbonyl groups (**12***c–j*, **13***d,e*) afford essentially quantitative yields of the corresponding aminooxycarbenes, while other fragmentation reactions compete with carbene generation in the case of oxadiazolines with N-methyl (**12***b*, **13***c*) or N-sulfonyl (**12***k*) groups.

Key words: nucleophilic carbene, aminooxycarbene, oxadiazoline, oxazolidin-2-ylidene, carbonyl ylide.

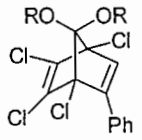
Résumé : On a synthétisé des Δ^3-1,3,4-oxadiazolines spirocondensées en C2 à la position C2 d'oxazolidines (**12**) ou en C2 de tétrahydro-1,3-oxazines (**13**). Les oxadiazolines subissent une thermolyse dans le benzène à 90°C; les constantes de vitesse du premier ordre de la réaction varient de 1,6 à 50×10^{-5} s^{-1}. La relation entre ces constantes de vitesse et la nature des substituants présents sur le noyau oxadiazoline est en accord avec un mécanisme impliquant un ylure de carbonyle comme intermédiaire. Les substituants présents sur l'azote des portions oxazolidine ou tétrahydro-1,3-oxazine jouent un rôle important dans la détermination des voies de fractionnement. Les oxadiazolines portants de groupes N-carbonyles (**12***c–j*, **13***d,e*) fournissent des rendements pratiquement quantitatifs des aminooxycarbènes correspondants alors que, dans les cas des oxadiazolines portant des groupes N-méthyles (**12***b*, **13***c*) ou N-sulfonyles (**12***k*), d'autres réactions de fragmentation sont en compétition avec la génération de carbène.

Mots clés : carbène nucléophile, aminooxycarbène, oxadiazoline, oxazolidin-2-ylidène, ylure de carbonyle.

[Traduit par la rédaction]

Introduction

In recent years, there has been a renewed interest in the chemistry of nucleophilic carbenes, from both mechanistic (1) and synthetic (2) points of view. Classically, the most useful methods of generation of nucleophilic carbenes are based on the formal extrusion of the carbene by cycloreversion from rings made up of an odd number of atoms. These processes are generally driven by the formation of thermodynamically stable products such as N_2 or aromatic compounds. Thermolysis of 7,7-dialkoxynorbornadienone ketals (**1**) at temperatures of 85–200°C, for instance, afforded the first dioxycarbenes (3). Diazirines (**2**) are now well-established alternative thermal and photochemical sources of carbenes that have been used for the generation of some dioxycarbenes (1*d,f,l,o*).



1



2

The thermolysis of Δ-1,3,4-oxadiazolines constitutes a relatively new method for the generation of nucleophilic carbenes (eq. [1]) (1*j,k,q–t*, 2*f–l*, 4). 2,2-Dioxy-Δ^3-1,3,4-oxadiazolines (**3**) are conveniently prepared in a two-step process involving the oxidative cyclization of an (oxycarbonyl)hydrazone of acetone (**4**) with $Pb(OAc)_4$, followed by exchange of the acetoxy substituent in **5** with alcohols or phenols (eq. [2]) (4). Variations of this method have also provided access to oxythio- (1*s*) and dithiocarbenes.[2]

In this report, we describe the synthesis of Δ^3-1,3,4-oxadiazolines, substituted at C2 with one O and one N, as precursors of aminooxycarbenes. The mechanisms involved in their thermolysis are also examined. A preliminary account of some of this work has been published (5).

Received March 31, 1997.

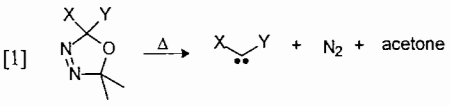
P. Couture and J. Warkentin.[1] Department of Chemistry, McMaster University, Hamilton, ON L8S 4M1, Canada.

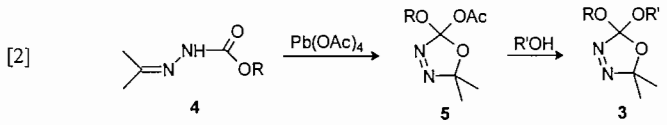
[1] Author to whom correspondence may be addressed. Telephone: (905) 525-9140. Fax: (905) 522-2509. E-mail: Warkent@McMaster.ca

[2] H.-T. Er and J. Warkentin. Unpublished results.

© 1997 NRC Canada

Can. J. Chem. Downloaded from www.nrcresearchpress.com by 91.121.58.235 on 09/08/12
For personal use only.

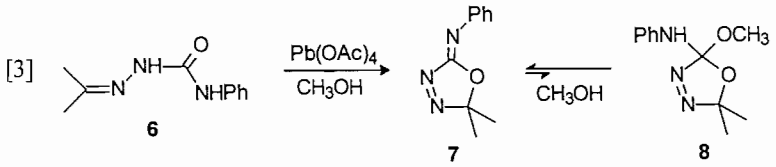




Methods, results, and discussion

Syntheses of 12 and 13

Investigations on the application of the "acetoxy exchange" method described above to the synthesis of 2-alkoxy-2-amino-Δ^3-1,3,4-oxadiazolines were disappointing, affording little or none of the desired products in complex mixtures. An alternative approach involving the addition of an alcohol to a 2-imino oxadiazoline was considered. The oxidation of semicarbazone **6** with $Pb(OAc)_4$ in methanol was previously found to produce a mixture of **7** and **8**, but the instability of the latter did not allow its separation from **7** (eq. [3]) (6). The intramolecular analogue of this reaction, however, involving quaternization of C2 of the oxadiazoline by the addition of a tethered hydroxyl group, was successful.



A series of substituted semicarbazones **9** was prepared, in 59–81% yields, by refluxing the semicarbazone of acetone (**10**, R^1 = Me) or of cyclohexanone (**10**, $R^1R^1 = (CH_2)_5$) with an appropriate amino alcohol **11** in toluene (7) for 7–15 h (Scheme 1). Although $Pb(OAc)_4$ oxidation of **9** (n = 2, R^1 = Me, R^2 = H) produced **12***a* in reasonable yield, it repeatedly failed in the case of the oxidation of **9** (n = 2, $R^1 = R^2$ = Me) to **12***b*. Instead, $PhI(OAc)_2$, which has been utilized in the synthesis of 2-alkoxy-Δ^3-1,3,4-oxadiazolines (8), was found to be the reagent of choice. Thus, semicarbazones **9** were oxidized with $PhI(OAc)_2$ in dichloromethane or, in one case, in methanol, to afford oxadiazolines **12***a,b* and **13***a–c* in 35–66% yields.[3]

N-Carbonyl oxadiazolines **12***d–i* and **13***d,e* were prepared by acylation of **12***a* and **13***a,b*, respectively, using standard methods, in yields ranging from ca. 10% to 33% (from **9**). The reaction between **12***a* and 4-nitrophenyl formate (9) gave oxadiazoline **12***c*. The preparation of carbamate derivative **12***j* was most conveniently carried out by stirring **12***a* with 4 equivalents of methyl chloroformate and 6 equivalents of K_2CO_3 in acetone at room temperature for 2 days (10). Sulfonamide derivative **12***k* was prepared by treating **12***a* with benzenesulfonyl chloride in the presence of pyridine.

^{13}C NMR spectroscopy was the most useful tool in the identification of these spiro oxadiazolines, with two characteristic signals generally found at 116–123 ppm (C2) and 128–139 ppm (C5). The ^1H NMR spectra of **12***a–k*, in which the oxadiazoline ring is fused to an oxazolidine, exhibit complex splitting of the four methylene protons; the coupling constants for the ABMX spin system of **12***b*, determined by spectral simulation, are listed in the experimental section. In addition, the ^1H spectra of N-carbonyl derivatives **12***c–j* are complicated by slow *cis–trans* isomerism, on the NMR time scale, of the amide bond. This generally results in broad signals for spectra recorded at room temperature.[4] The fragility of these oxadiazolines dictated the application of special techniques for the acquisition of mass spectra, as described in the experimental section.[5]

Thermolysis rate constants

Oxadiazolines **12***a–k* and **13***c–e* were thermolysed in benzene-d_6, at 90°C, in sealed NMR tubes. Disappearance of starting material was monitored by means of integration of appropriate signals in the 300 MHz ^1H NMR spectra. The choice of the ^1H signal(s) for integration was sometimes limited by the complexity of the spectrum and, in several cases, resonances were broad due to restricted rotation about the amide bond, as mentioned above. Nevertheless, good fits to the first-order rate equation were obtained for five to ten experimental points generally covering the range 0–60% (or more) of completion.

The rate data, collected in Table 1, show a relatively low sensitivity to structure. There is some risk of overinterpretation of the data because the observed values span only a 30-fold rate change. Moreover, there is not a unique decomposition pathway for all oxadiazolines and, in some cases, at least two competing initial steps may be involved in a thermolysis. Nonetheless, some trends in the rate constants are evident and understandable.

Both steric and electronic factors are expected to influence the rate of decomposition of oxadiazolines **12** and **13**. The initial thermolysis step is generally a cycloreversion affording molecular nitrogen and a carbonyl ylide (vide infra). At the

[3] It is noteworthy that oxidation of **9** (n = 2, R^1 = Me, R^2 = Ph) with either $Pb(OAc)_4$ or $PhI(OAc)_2$ failed to produce the corresponding **12** in useful quantity (R^1 = Me, R^2 = Ph).

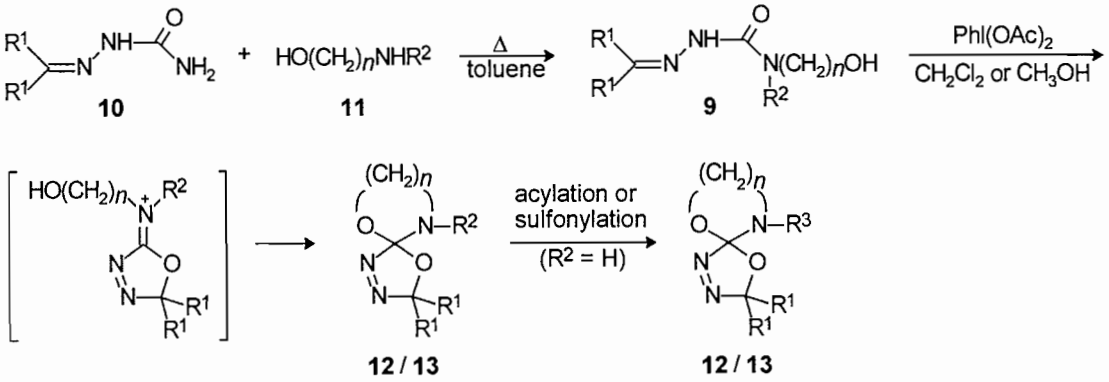
[4] A study aimed at determining the relationship between structure and the activation parameters for rotation is currently in progress, in collaboration with Professor A.D. Bain and Mr. P. Hazendonk.

[5] A detailed mass spectral study involving **12***b*, in collaboration with Professor J.K. Terlouw and Mr. D. Lavorato, is in progress.

© 1997 NRC Canada

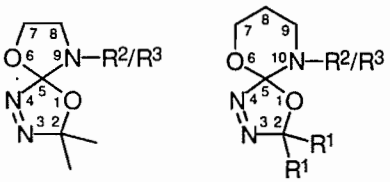
Can. J. Chem. Downloaded from www.nrcresearchpress.com by 91.121.58.235 on 09/08/12
For personal use only.

Scheme 1.



12 (n = 2, R^1 = Me), *a*: R^2 = H; *b*: R^2 = Me; *c*: R^3 = C(O)H; *d*: R^3 = C(O)Me; *e*: R^3 = C(O)C(Me) = CH_2; *f*: R^3 = C(O)Ph; *g*: R^3 = C(O)C_6H_4(2-OMe); *h*: R^3 = C(O)C_6H_4(4-OMe); *i*: R^3 = C(O)C_6H_4(4-NO_2); *j*: R^3 = C(O)Me; *k*: R^3 = SO_2Ph.
13 (n = 3), *a*: R^1 = Me, R^2 = H; *b*: R^1R^1 = $(CH_2)_5$, R^2 = H; *c*: R^1R^1 = $(CH_2)_5$, R^2 = Me; *d*: R^1 = Me, R^3 = C(O)Ph; *e*: R^1R^1 = $(CH_2)_5$, R^3 = C(O)Ph.

Table 1. First-order rate constants for the thermolysis of oxadiazolines **12** and **13** at 90°C in benzene-d_6.

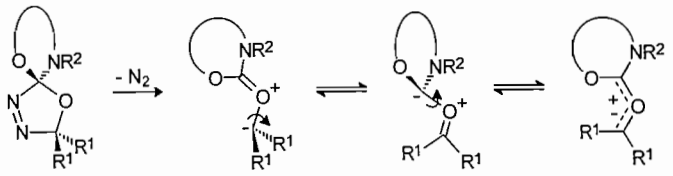


	R^1	R^2/R^3	k, s^{-1} ($\times 10^5$)[a]	k_{rel}
12*a*		H	1.61 ± 0.16	1.00
12*b*		Me	4.78 ± 0.21	2.97
12*c*		C(O)H	4.66 ± 0.14	2.89
12*d*		C(O)Me	14.0 ± 0.3	8.70
12*e*		C(O)C(Me)=CH_2	5.62 ± 0.23	3.49
12*f*		C(O)Ph	7.14 ± 0.50	4.43
12*g*		C(O)C_6H_4(2-OMe)	5.76 ± 0.36	3.58
12*h*		C(O)C_6H_4(4-OMe)	5.60 ± 0.32	3.48
12*i*		C(O)C_6H_4(4-NO_2)	8.74 ± 0.29	5.43
12*j*		C(O)OMe	(>12 h)[b]	<1
12*k*		SO_2Ph	3.28 ± 0.02	2.04
13*c*	R^1R^1 = $(CH_2)_5$	Me	9.02 ± 0.29	5.60
13*d*	Me	C(O)Ph	48.2 ± 5.5	29.9
13*e*	R^1R^1 = $(CH_2)_5$	C(O)Ph	16.2 ± 0.6	10.1

[a]Based on error limits of slope at 95% confidence level.
[b]Could not be determined precisely due to wide, unresolved resonances.

transition state, the 1,3-interactions between groups R^1 at C2 and the substituents at C5 will be relieved because of bond rotations, as shown in Scheme 2, which depicts oxygen and R^1 as moving into *endo* positions of the ylide. Thus, relief of strain from nonbonded interactions (two in the oxadiazoline; one in the ylide) should be a factor. In addition, as ylide character develops, negative charge accumulates at C2 and C5 of the oxadiazoline, and electron-withdrawing groups in proximity to the sites of charge development should cause some rate

Scheme 2.



enhancement from inductive effects. Such thermolysis rate enhancements caused by inductive effects of electron-withdrawing groups were previously observed in spiro-fused β-lactam oxadiazolines (11).

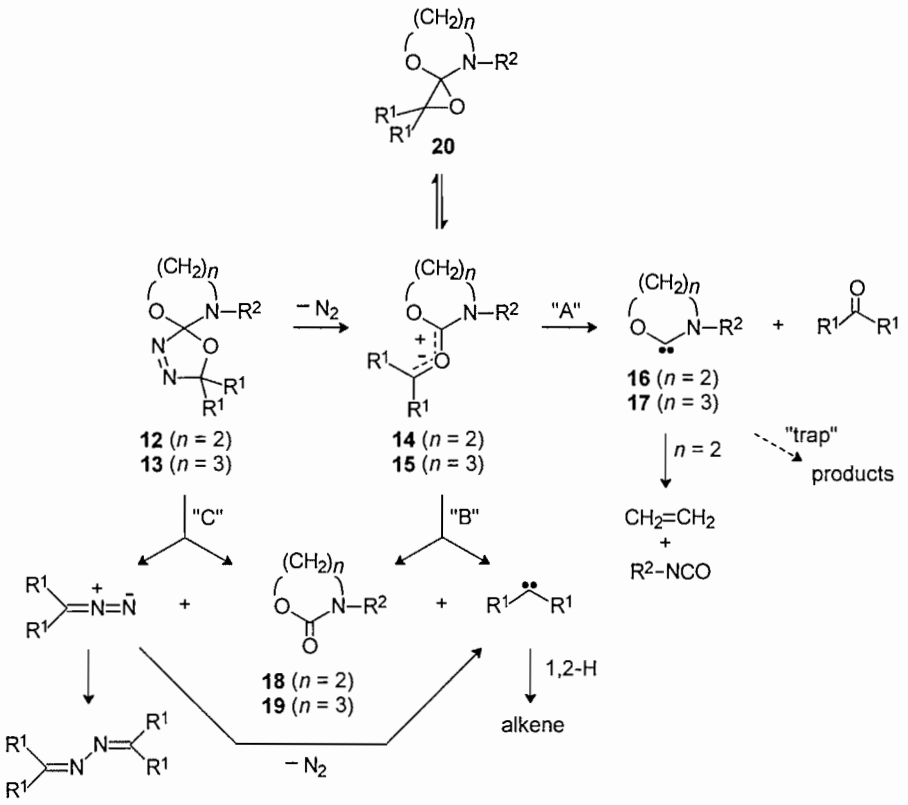
Experimentally, it was found that compounds in which the oxadiazoline moiety is fused to a six-membered ring have larger thermolysis rate constants than analogous compounds in which the oxadiazoline ring is fused to a five-membered ring: k_{13d}, $k_{13e} > k_{12f}$, and $k_{13c} > k_{12b}$. This effect may be due in part to a small increase in 1,3-interactions in going from a five-membered to a six-membered ring fused at C5, and to easier increase, in the larger ring system, of the OCN bond angle as the relevant carbons rehybridize from sp^3 in the oxadiazoline to roughly sp^2 in the ylide. The origin of the 3-fold increase in rate constant from **13***e* to **13***d* could be ascribed to the same feature, **13***e* having a bond angle constraint at both C2 and C5.

The nature of the substituent (R^2) at N also affects the rate of thermolysis. For instance, in the series **12***a*, **12***b*, **12***f*, and **12***k*, there is an observable effect on the rate constant in changing R^2 from hydrogen (k_{rel} = 1.00) to methyl (2.97), benzoyl (4.43), or phenylsulfonyl (2.04), more or less consistent with the expected destabilization of the ground state by steric factors and stabilization of the transition state by electron-withdrawing groups. Within the N-carbonyl series, the following trend in relative rate constants was found (k_{rel}): k_{12j} (OCH_3, <1) < k_{12c} (H, 2.89) < k_{12e} (vinyl, 3.49) < k_{12f} (Ph, 4.43) < k_{12d} (CH_3, 8.70). Thus, substituents that reduce the electron-withdrawing effect of the N-carbonyl group (e.g., methoxy in **12***j*) tend to decrease the rate of decomposition of the oxadiazoline,

Can. J. Chem. Downloaded from www.nrcresearchpress.com by 91.121.58.235 on 09/08/12
For personal use only.

© 1997 NRC Canada

Scheme 3.



but the reason for the relatively large rate constant of **12***d* is not understood. Comparison of the analogous N-benzoyl derivatives also shows a slight rise in the rate constants[6] caused by increasingly electron-withdrawing substituents, although the spread of k values is small: k_{12g} (2-OMe, 3.58) ≈ k_{12h} (4-OMe, 3.48) < k_{12f} (unsubstituted, 4.43) < k_{12i} (4-NO_2, 5.43).

The observed trends in thermolysis rate constants support the intermediacy of carbonyl ylides in the thermolysis of these spiro-fused oxadiazolines rather than the fully concerted mechanism proposed recently by Smith (12). If carbenes were the initial species formed, then electron-donating groups, which stabilize the carbenes, would be expected to stabilize the corresponding transition states also, and therefore to increase the rate of thermolysis. Clearly, the opposite effect is observed.

General thermolytic scheme

Thermolysis experiments for product studies on **12** and **13** were carried out in sealed NMR tubes, as described above, with initial oxadiazoline concentrations of ca. 0.25 M. Larger scale thermolyses were also conducted with each substrate, at ca. 0.05 M oxadiazoline in benzene in resealable tubes.

The mechanism of thermolysis of oxadiazolines, resulting in the extrusion of carbenes, has been described in terms of successive fragmentations, rather than as a single-step process (1*k*,*s*, 2*h*, 13). In the case of 2-alkyl-2-oxy oxadiazolines, products apparently derived from carbonyl ylides have been identified, thus providing strong support for their intermediacy (13*a*,*c*, 14). However, for 2,2-dioxy oxadiazolines, the postulate of a stepwise mechanism had rested mostly on the analogy to the monoalkoxy system until ketene acetals, thought to be formed from carbonyl ylides, were recently observed as thermolysis products of 2-aryloxy-2-aryloxy-2-methoxy oxadiazolines (1*t*).

Scheme 3 illustrates the thermolytic pathways common to most oxadiazolines **12** and **13**. The major route appears to be an orbital-symmetry-allowed 1,3-dipolar cycloreversion that liberates N_2 and produces carbonyl ylide **14/15**. Fragmentation of this transient species may then occur through pathway A, to generate aminooxycarbene **16/17** and a ketone, or via pathway B, which yields carbonyl compound **18/19** and a dialkyl carbene. The latter undergoes a fast 1,2-H migration to the alkene. Electrocyclic ring closure of **14/15**, as observed with some dioxy analogues (1*t*), is possible although no definitive evidence for the generation of spiro-fused oxiranes **20** could be obtained. Thermal decomposition of **12/13** may also take place through a different 1,3-dipolar cycloreversion to form a diazoalkane and, again, **18/19** (pathway C). Under our thermolytic conditions, most of the diazoalkane undergoes self-condensation to make an azine, while only a small fraction of it generates a dialkyl carbene from loss of molecular nitrogen.

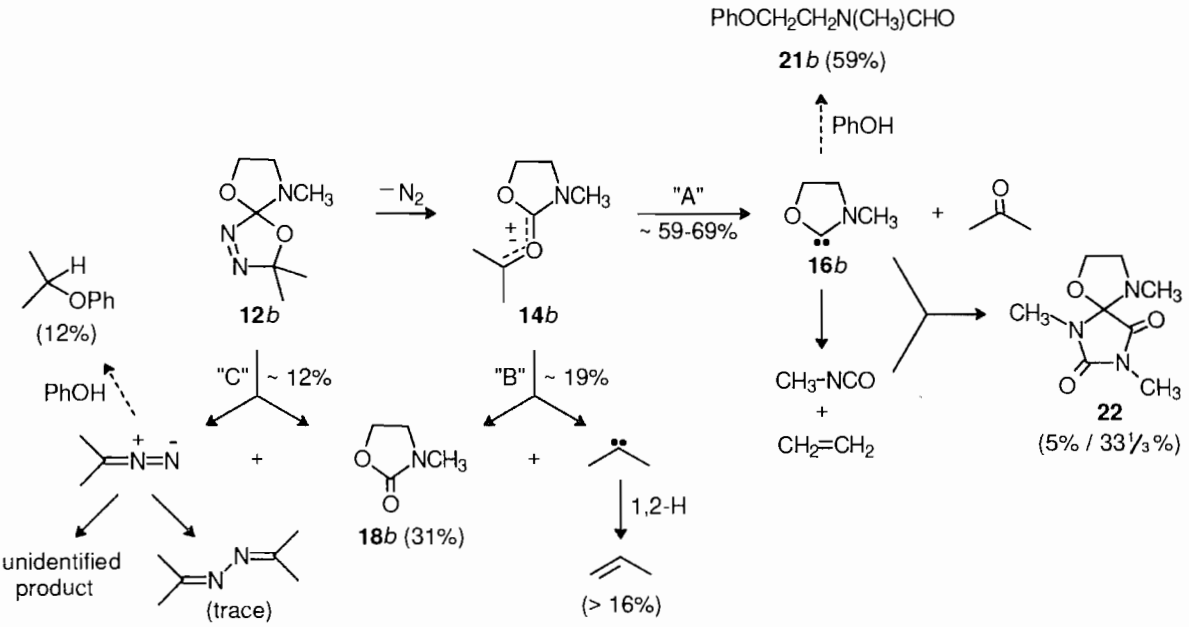
Five-membered aminooxycarbenes **16**, when produced at elevated temperatures, sometimes fragment to ethylene and an isocyanate in a lifetime-limiting reaction similar to that for the dioxa (15) and dithia (15*e*, 16) analogues where CO_2 and CS_2, respectively, are the coproducts of ethylene. The isocyanates

[6] For consistency, rate constants for **12***f*, **12***h*, and **12***i* were all measured from an analogous OCH_2 multiplet, but that multiplet could not be used in the case of **12***g*.

Can. J. Chem. Downloaded from www.nrcresearchpress.com by 91.121.58.235 on 09/08/12
For personal use only.

© 1997 NRC Canada

Scheme 4.



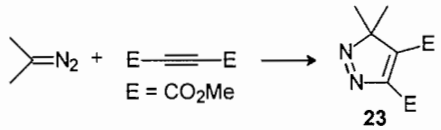
thus produced may then participate in subsequent reactions, in particular with carbenes **16**, as discussed below.

Thermolysis of 12*b*

For oxadiazoline **12***b*, the intermediate carbonyl ylide **14***b* fragments predominantly via pathway A to form 3-methyl-oxazolidin-2-ylidene, **16***b*, and acetone (Scheme 4). Trapping of **16***b* with phenol, in an NMR tube, gave product **21***b* in 59% yield.[7] In the absence of an added trap, carbene **16***b* does not dimerize, but rather fragments to ethylene and methyl isocyanate. The latter then acts as a trap for newly formed **16***b*, and a 1:2 (carbene:isocyanate) adduct, spiro hydantoin **22**, is found as a final product in about 15% yield; this product is analogous to those formed in the reactions of dimethoxycarbene (17) and (dimethylamino)-methoxy-carbene (18) with aryl isocyanates. Formation of **22** was confirmed by comparison of the NMR and GC–MS data of the thermolysate with an authentic sample prepared by thermolysing **12***b* in the presence of an excess of methyl isocyanate.

Other products resulting from the thermal decomposition of **12***b* include 3-methyl-2-oxazolidinone (**18***b*) and propene, as well as traces of acetone azine. Their formation suggests that both pathways B and C compete with pathway A. Although diazo compounds are known thermal sources of carbenes, under our experimental conditions 2-diazopropane produced almost exclusively acetone azine, and very little 2-propylidene. This was confirmed with two independent experiments. In the first one, 2-methoxy-5,5-dimethyl-2-phenoxy-Δ^3-1,3,4-oxadiazoline, a compound known to decompose partially via a pathway analogous to C (1*t*), was thermolysed under our experimental conditions and found to produce a significant amount of acetone azine, but only traces of propene, a result which is opposite to that from **12***b*. The second experiment, described in more detail in the experimental section, involved thermolysis of 2-diazopropane in benzene-d_6, in a sealed NMR tube, at 90°C. Product analysis by ^{1}H NMR spectroscopy revealed acetone azine in 86% yield, with only traces of propene present.

The apparent discrepancy between the yield of **18***b* (31%), a product common to pathways B and C, and those of propene (>16%) and acetone azine (traces), may be accounted for by the diversion of 2-diazopropane from its usual azine-forming reaction. In fact, the formation of an unidentified product, apparently derived from 2-diazopropane, was quenched with phenol, and 2-phenoxypropane was formed in its place in 12% yield. In the light of these results, it appears that pathway C in Scheme 4 contributes to approximately 12% of the decomposition of **12***b*, while pathway B must account for the remaining 19% of the **18***b* produced. This therefore provides an upper limit of about 69% for the yield of carbene **16***b*.

[4] 

23

The formation of both ethylene and propene from **12***b*, observed by ^{1}H NMR spectroscopy, was confirmed by their conversion to 1,2-dibromoethane and 1,2-dibromopropane, respectively, followed by GC–MS detection. Formation of 2-diazopropane was also confirmed by the identification of pyrazole **23**, when **12***b* was thermolysed in the presence of dimethyl acetylenedicarboxylate (eq. [4]) (19).

Thermolysis of 13*c*

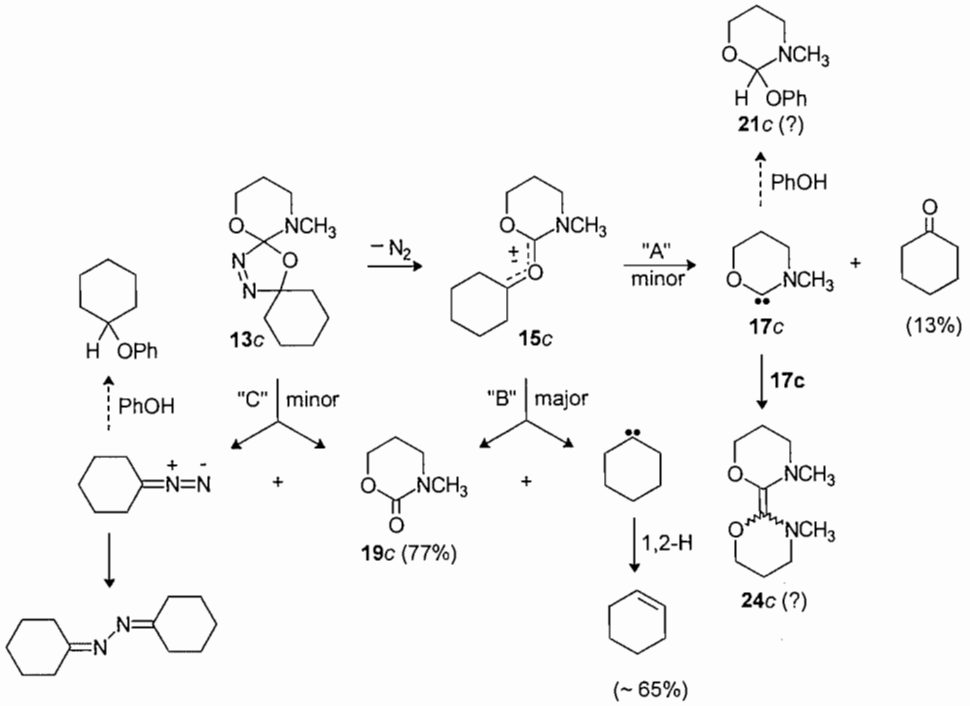
Oxadiazoline **13***c* was synthesized as a possible precursor to the six-membered aminooxycarbene **17***c*. In contrast to the five-membered analogue (**16***b*), fragmentation of **17***c* should

[7] Other aminooxycarbene + phenol trapping experiments are in the following paper.

© 1997 NRC Canada

Can. J. Chem. Downloaded from www.nrcresearchpress.com by 91.121.58.235 on 09/08/12
For personal use only.

Scheme 5.



not occur to limit its lifetime. Results from the product studies on the thermolysis of **13***c*, however, were disappointing. With this oxadiazoline, competition between pathways A and B for the decomposition of carbonyl ylide **15***c* was found to favour pathway B (Scheme 5). Thus, the observed yields (by NMR) were 77% for carbonyl compound **19***c* and ca. 65% for cyclohexene, compared to only 13% for cyclohexanone, the coproduct in the formation of carbene **17***c*. A small amount of the azine of cyclohexanone was also observed, indicating the occurrence of pathway C; this accounts, at least in part, for the discrepancy between the yields found for **19***c* and cyclohexene. Carbene dimers (**24***c*) could not be unambiguously identified in the thermolysates, perhaps because of their lability towards hydrolysis. In addition, no evidence was found for the formation of **21***c* following the thermolysis of **13***c* in the presence of phenol, phenoxycyclohexane being the only recognizable phenol-derived product.

Thermolysis of 12*f*

The results presented above showed that oxadiazolines **12***b* and **13***c* (both N-methyl) do generate aminooxycarbenes upon thermolysis, although the yields of these reactive intermediates are not quantitative because of competing decomposition reactions. Speculation that fragmentation of the carbonyl ylide in the desired sense might be optimized by destabilizing the unwanted fragmentation product led to replacement of the N-substituent with an electron-withdrawing group.

Experimentally, *N*-carbonyl oxadiazolines such as **12***f* proved to be very efficient sources of cyclic aminooxycarbenes. Extrusion of N_2 from **12***f* results in carbonyl ylide **14***f*, which fragments essentially unidirectionally via pathway A to oxazolidin-2-ylidene **16***f* and acetone (Scheme 6). Thermolysis of **12***f* in the presence of phenol in an NMR tube gave phenol insertion product **21***f* in 94% yield. In comparison, the yield of 3-benzoyl-2-oxazolidinone (**18***f*), formed by either routes B or C, was too low to be measured by integration of its ^{1}H NMR signals; however, **18***f* was isolated from larger scale thermolyses in ca. 2% yield. Also observed were ethylene and traces of its coproduct, benzoyl isocyanate, as well as benzamide and *N*-[2-(formyloxy)ethyl]benzamide (**25**). Benzamide is attributed to decarboxylation of the *N*-benzoyl-carbamic acid formed from hydrolysis of benzoyl isocyanate by traces of water present during or after thermolysis.[8] Compound **25** is most likely a hydrolysis product derived from the aminooxycarbene, **16***f*. Thermolysis of **12***f* in the presence of a few drops of water yielded **25** as the main product (ca. 56%), along with benzamide (ca. 20%). In accordance with the proposed scheme neither propene nor acetone azine were produced in detectable quantities.

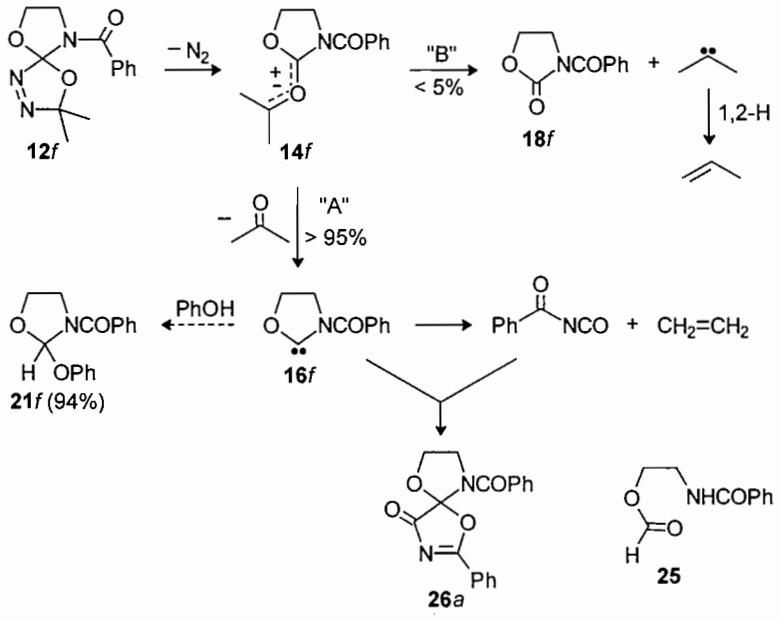
The instability of the major nonvolatile product formed from **12***f* complicated the elucidation of its structure. For example, its purification by radial chromatography was impossible, and it did not survive GC. However, a reasonably pure, white solid could be obtained by dissolving the crude product in diethyl ether and reevaporating most of the solvent in vacuo. The ^{1}H NMR spectrum of these crystals was very similar to that of the crude thermolysate, thus demonstrating a nearly quantitative yield. Eventually, this major product was identified as spiro 4(5*H*)-oxazolone **26***a*. The proposed structure is consistent with NMR, IR, and MS data. Characteristic ^{13}C resonances included ($CDCl_3$, in ppm): 47.14 (NCH_2), 68.43 (OCH_2), 108.38 (spiro C), 167.73 (PhC(O)), as well as

[8] A sample of benzoyl isocyanate stored on the shelf was gradually converted to benzamide and *N,N'*-dibenzoylurea, the latter presumably arising from the reaction of benzamide with benzoyl isocyanate.

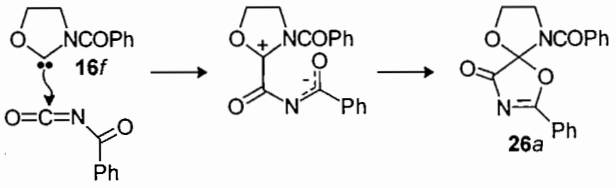
Can. J. Chem. Downloaded from www.nrcresearchpress.com by 91.121.58.235 on 09/08/12
For personal use only.

© 1997 NRC Canada

Scheme 6.



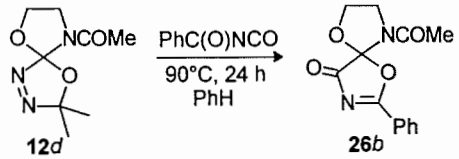
Scheme 7.

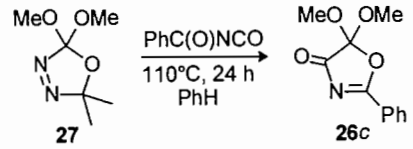


181.80 and 184.13, which were assigned to carbons 2 and 4 of the oxazolone ring. Its EI-MS spectrum showed a low-intensity molecular ion (*m/z* 322, too weak to obtain high-resolution data), while CI-MS with NH_3 showed a signal corresponding to $(M + H)^+$. IR spectra of 4(5*H*)-oxazolones show characteristic bands in the ranges 1786–1754 cm^{-1} for C=O stretching and 1575–1499 cm^{-1} for C=N stretching (20). Consistent with expectation, intense bands appeared at 1783 and 1558 cm^{-1} in the IR spectrum of **26***a*.

The novel spiro oxazolone **26***a*, with two heteroatom substituents at C5, presumably arises from nucleophilic attack of carbene **16***f* on the isocyanate carbonyl group of benzoyl isocyanate, followed by cyclization of the dipolar intermediate (Scheme 7).

To obtain independent support for structure **26***a*, as well as to probe for the generality of the reaction between benzoyl isocyanate and nucleophilic carbenes, aminooxycarbene **16***d* and dimethoxycarbene, generated from **12***d* and **27**, respectively, were separately reacted with benzoyl isocyanate. In both cases, spectroscopic data obtained from crude thermolysates paralleled those from **26***a*, indicating formation of oxazolones **26***b* and **26***c* as major products (eqs. [5], [6]).[9] Analogous [1 + 4] cycloadditions between 3-methyloxazolidin-2-ylidene (**16**b) or dimethoxycarbene and vinyl isocyanates have recently been reported by Rigby et al. (*2l*). These cycloadditions contrast with the usual hydantoin-forming reactions of nucleophilic carbenes with alkyl or aryl isocyanates (cf. compound **22**).

[5] 

[6] 

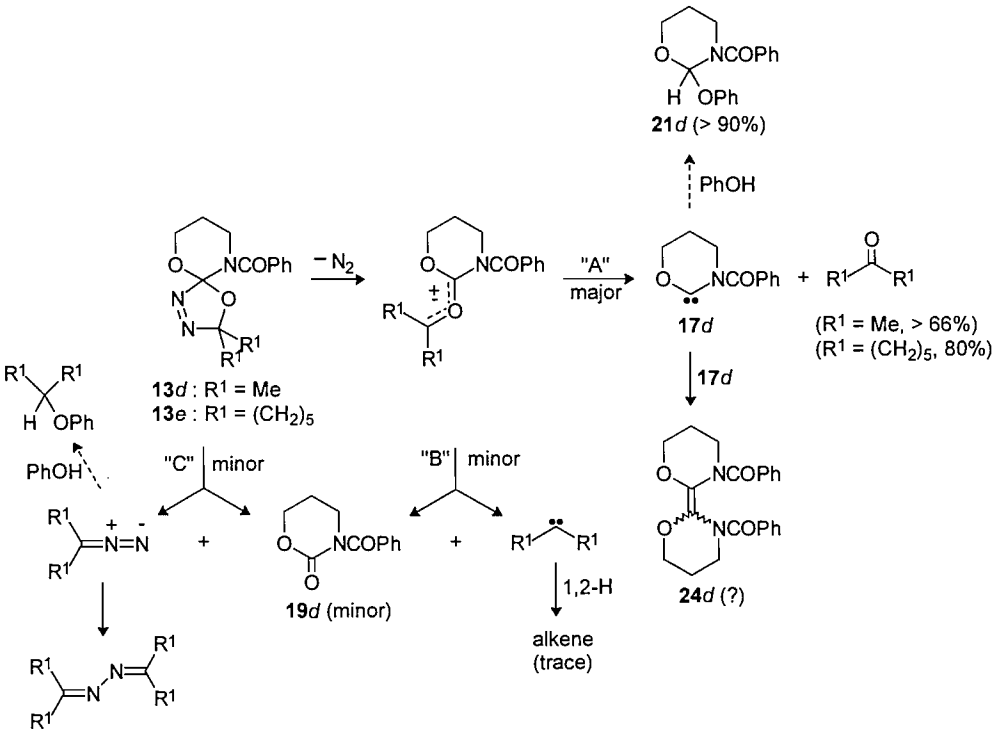
Oxazolone **26***a* was deliberately hydrolysed by adding a few drops of water to the thermolysate from **12***f* (eq. [7]). As with its precursor oxazolone, attempted purification of the product by chromatography resulted in its complete decomposition. A reasonably pure solid was obtained, however, by precipitation from a benzene solution. Spectroscopic data (^1H and ^{13}C NMR, IR, MS) are consistent with oxalic acid derivative **28**. Hydrolysis of a 4(5*H*)-oxazolone fused at C5 to C2 of an oxazolidine thus results in cleavage of the C(5)—O bond of the oxazolone; this contrasts with hydrolyses reported for other 4(5*H*)-oxazolones, in which cleavage occurs at the carbon–nitrogen double bond (21).

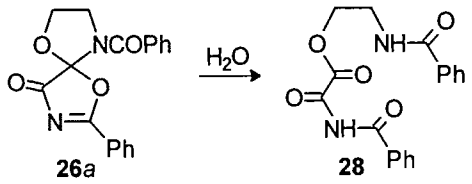
[9] A control experiment in which a slightly decomposed sample of benzoyl isocyanate was submitted to our thermolysis conditions, without any oxadiazoline present, gave benzamide and *N,N'*-dibenzoylurea as major products.

Can. J. Chem. Downloaded from www.nrcresearchpress.com by 91.121.58.235 on 09/08/12
For personal use only.

© 1997 NRC Canada

Scheme 8.



[7] 

Thermolysis of other *N*-carbonyl oxadiazolines 12

A number of the *N*-carbonyl oxadiazolines **12** shown in Table 1 were synthesized mainly for the purpose of investigating the rotational barriers of their amide bonds,[4] and their thermolysis chemistry was therefore not investigated in detail. However, **12***d* (*N*-acetyl) and **12***e* (*N*-methacryloyl) have been used extensively as thermal sources of carbenes, which they produce, like **12***f* (*N*-benzoyl), in essentially quantitative yields (5).

Thermolysis of 13*d*,*e*

Initial attempts to generate carbene **17***d* involved dispiro oxadiazoline **13***e*. Thermolyses of this compound in NMR tubes resulted in the production of cyclohexanone, the coproduct of **17***d*, in about 80% yield (Scheme 8). In addition to traces of cyclohexene, a small amount of carbonyl compound **19***d* was produced. Thermolysis of **13***e* in the presence of phenol resulted in the formation of **21***d* in high yield, together with a minor amount of phenoxycyclohexane presumably produced from the reaction of diazocyclohexane with phenol. The formation of these products suggests that both pathways B and C are involved in the decomposition of this oxadiazoline, although pathway A, leading to the desired tetrahydro-1,3-oxazin-2-ylidene (**17***d*) is, by far, the most important route. Similarly, thermolysis of the related oxadiazoline **13***d* resulted in the production of carbene **17***d*, which was trapped by phenol to give adduct **21***d* in over 90% yield.

The fate of carbene **17***d*, generated in solution in the absence of a trap, is uncertain. It is likely that this carbene dimerizes to *E* and *Z* alkenes (**24***d*). However, these products could not be clearly identified. The NMR spectra were very complex, as expected for the geometric isomers of **24***d* because of slow rotation about the amide CN bond, and separation of **24***d* from coproducts and from each other was not possible because of their sensitivity towards moisture. Interestingly, ions with *m/z* 378, corresponding to the molecular ions of carbene dimers (**24***d*), were found in MS experiments carried out with the aim of confirming the identity of oxadiazoline **13***e*; these species were generated in the gas phase, inside the spectrometer, by the unavoidable partial thermolysis of the fragile oxadiazoline.

Thermolysis of 12*k*

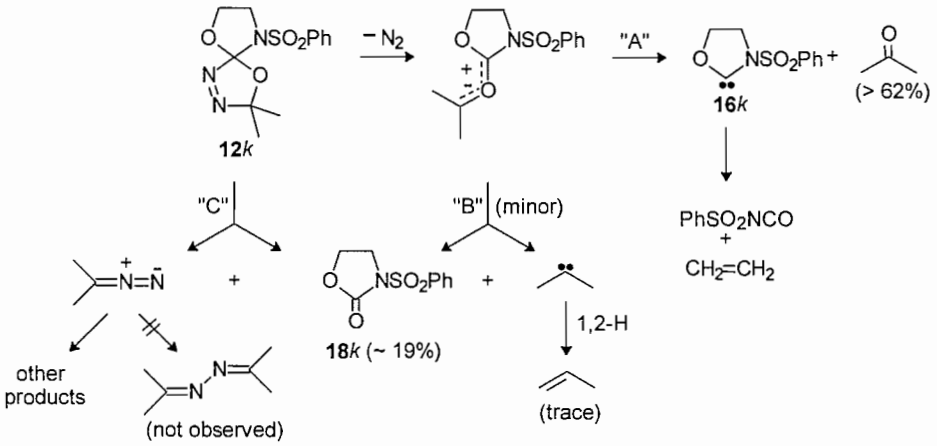
As for *N*-methyl oxadiazoline **12***b*, compound **12***k* did not generate the aminooxycarbene quantitatively under our thermolysis conditions although acetone, the coproduct of carbene **16***k*, was formed in >62% yield (by ^{1}H NMR spectroscopy), Scheme 9. Formation of the latter was supported by the detection of ethylene, presumably formed in its thermal fragmentation. 3-(Phenylsulfonyl)-2-oxazolidinone, **18***k*, was produced in ca. 19% yield. The fact that only traces of propene were detected suggests that **18***k* is generated mostly via pathway C rather than through pathway B. However, acetone azine, which usually results from the self-reaction of 2-diazopropane, was not observed. Any 2-diazopropane formed may have reacted with another species present in the thermolysis solution to form unidentified products, as in the case of **12***b*.

A compound assigned structure **29**, on the basis of its spec-

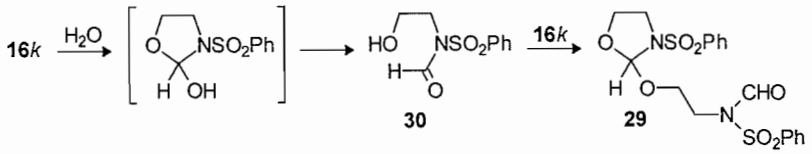
© 1997 NRC Canada

Can. J. Chem. Downloaded from www.nrcresearchpress.com by 91.121.58.235 on 09/08/12
For personal use only.

Scheme 9.



Scheme 10.



tral data (^{1}H and ^{13}C NMR, IR, and MS), was isolated from a thermolysis experiment in which wet **12***k* was used. One possible route for its formation is shown in Scheme 10.[10] The isolation of **29** thus provides additional, although indirect, evidence for the generation of carbene **16***k*.

Experimental

General methods

NMR spectra were recorded on a Bruker AC-200 or AC-300 NMR spectrometer. Some compounds show complex NMR spectra due to the slow interconversion, on the NMR time scale, between two isomers.[4] In some cases, this results in two distinct sets of resonances, while some spectra show broad, unresolved multiplets labelled below as "um". Infrared spectra were recorded with a Biorad FTS-40 spectrophotometer, with the sample either in CCl_4 or in KBr as a pellet. The IR bands are labelled qualitatively with the symbols br for broad, app for apparent, and s, m, and w for strong, medium, and weak intensities, respectively. Bands from C–H stretching vibrations between 2850 and 3100 cm^{-1} are omitted, as are very weak bands. Melting points were recorded on a Thomas Hoover capillary melting point apparatus, and are reported uncorrected. Elemental analyses were performed by Guelph Chemical Laboratories, Ltd. (Guelph, Ont.).

Synthesis of ketone semicarbazones 10

Ketone semicarbazones were prepared by the method described by Vogel (22), and were recrystallized from 50% aqueous ethanol.

*Acetone semicarbazone (**10**, R^1 = Me)*: White solid (78% yield), mp 185–186°C (lit. (23) mp 190–191°C); ^{1}H NMR (200 MHz, $CDCl_3$) δ: 1.83 (s, 3H), 1.99 (s, 3H), 7.4 (br s, 1H) (the NH_2 signal was not visible).

*Cyclohexanone semicarbazone (**10**, R^1R^1 = $(CH_2)_5$)*: White solid (75% yield), mp 165–166°C (lit. (23) mp 166–167°C); ^{1}H NMR (200 MHz, $CDCl_3$) δ: 1.50–1.90 (m, 6H), 2.15–2.45 (m, 4H), 5.6 (br s, 2H), 8.53 (s, 1H).

Synthesis of 4-substituted ketone semicarbazones 9

The procedure for the preparation of compounds **9** is based on that of Iwao (7). Typically, a solution of the appropriate ketone semicarbazone (0.30 mol) and aminoalcohol (0.32 mol) (all commercially available, except for 3-(methylamino)-1-propanol, which was prepared as described by Michejda and co-workers (24)) was refluxed in toluene (100 mL), under dry nitrogen, for 7–15 h, until evolution of ammonia had subsided. The solution was allowed to cool to room temperature, and precipitation of the product usually occurred within a few hours. In some cases, crystallization was induced by addition of diethyl ether. The product was then collected by filtration and triturated with diethyl ether. When appropriate recrystallization solvents could not be found, the semicarbazones were used without further purification; recrystallization solvents for the others are listed below. Several semicarbazones did not give useful mass spectra under routine conditions.

*Acetone 4-(2-hydroxyethyl)semicarbazone (**9**, n = 2, R^1 = Me, R^2 = H)*: Pale yellow solid (81% yield), mp 89–94°C (lit. (7) mp 94–96°C); IR (KBr) cm^{-1}: 3379br, 3317br, 3210br, 3070br, 1652s (C=O), 1554s (C=N), 1458w, 1427m, 1365m, 1337m, 1281w, 1254m, 1212m, 1157w, 1132m, 1088w, 1068m, 980w, 884w, 836w, 773m, 722m; ^{1}H NMR (200 MHz, $CDCl_3$) δ: 1.84 (s, 3H), 1.97 (s, 3H), 3.39–3.53 (m,

[10] Sulfonamide **30** has also been isolated from thermolysis of **12***k*.

© 1997 NRC Canada

Can. J. Chem. Downloaded from www.nrcresearchpress.com by 91.121.58.235 on 09/08/12
For personal use only.

Can. J. Chem. Downloaded from www.nrcresearchpress.com by 91.121.58.235 on 09/08/12
For personal use only.

2H), 3.69–3.82 (m, 2H), 6.56 (br s, 1H), 8.02 (br s, 1H); ^{13}C NMR (50 MHz, $CDCl_3$) δ: 16.36 (CH_3), 25.20 (CH_3), 42.85 (NCH_2), 63.35 (OCH_2), 147.85 (C═N), 157.88 (C═O); mass spectrum not useful.

*Acetone 4-(2-hydroxyethyl)-4-methylsemicarbazone (**9**, n = 2, $R^1 = R^2 = Me$)*: White solid (60% yield) after recrystallization from ethanol – diethyl ether, mp 132–134°C; IR (KBr) cm^{-1}: 3223br, 1644s (C═O), 1557s (C═N), 1471m, 1424w, 1394m, 1359w, 1276m, 1223m, 1187m, 1115w, 1080w, 1041m, 965w, 871w, 757w; ^{1}H NMR (200 MHz, $CDCl_3$) δ: 1.83 (s, 3H), 2.00 (s, 3H), 2.95 (s, 3H), 3.39 (t, ^3J = 4.6 Hz, 2H), 3.84 (t, ^3J = 4.6 Hz, 2H), 4.92 (br s, 1H), 8.79 (br s, 1H); ^{13}C NMR (50 MHz, $CDCl_3$) δ: 16.89 (═C-*C*H$_3$), 25.19 (═C-*C*H$_3$), 35.02 (NCH_3), 52.45 (NCH_2), 61.05 (OCH_2), 150.33 (C═N), 157.83 (C═O); mass spectrum not useful. Anal. calcd. for $C_7H_{15}N_3O_2$: C 48.54, H 8.73; found: C 48.83, H 8.79.

*Acetone 4-(2-hydroxyethyl)-4-phenylsemicarbazone (**9**, n = 2, R^1 = Me, R^2 = Ph)*: White solid after recrystallization first from ethanol – diethyl ether, then from benzene; mp 125–126°C; IR (KBr) cm^{-1}: 3414br, 3385br, 3233br, 1726s (C═O), 1652w, 1603m, 1509s, 1457w, 1434w, 1374w, 1315w, 1278m, 1242m, 1221s, 1133w, 1061w, 1036m, 935w, 886w, 755m; ^{1}H NMR (200 MHz, $CDCl_3$) δ: 1.84 (s, 3H), 2.06 (s, 3H), 3.45 (t, ^3J = 5.4 Hz, 2H), 4.45 (t, ^3J = 5.4 Hz, 2H), 6.61–6.78 (m, 3H), 7.13–7.25 (m, 2H), 7.57 (br s, 1H); ^{13}C NMR (50 MHz, $CDCl_3$) δ: 16.06 (═C-*C*H$_3$), 25.26 (═C-*C*H$_3$), 43.22 (NCH_2), 64.21 (OCH_2), 112.79 (Ar C2, C6), 117.65 (Ar C4), 129.19 (Ar C3, C5), 147.63 (Ar C1), 151.39 (C═N), 154.00 (C═O); MS (EI) *m/z*: 235 (M^+, 6), 119 (75), 106 (100), 91 (17), 77 (63), 65 (22), 56 (13), 51 (16); MS (CI, NH_3) *m/z*: 236 $(M + H)^+$; HRMS *m/z*, calcd. for $C_{12}H_{17}N_3O_2$ (M^+): 235.1321; found: 235.1337.

*Acetone 4-(3-hydroxypropyl)semicarbazone (**9**, n = 3, R^1 = Me, R^2 = H)*: White solid (60% yield), mp 107–109°C; IR (KBr) cm^{-1}: 3396br, 3303br, 3206br, 1643s (C═O), 1552s (C═N), 1439w, 1423w, 1380w, 1330w, 1254w, 1223w, 1116w, 1071w, 986w; ^{1}H NMR (200 MHz, $CDCl_3$) δ: 1.62–1.78 (m, 2H), 1.84 (s, 3H), 1.97 (s, 3H), 3.40–3.53 (m, 2H), 3.60–3.80 (m, 3H), 6.36 (m, 1H), 8.01 (br s, 1H); ^{13}C NMR (50 MHz, $CDCl_3$) δ: 16.33 (CH_3), 25.19 (CH_3), 33.14 (NCH_2), 35.43 (C*C*H$_2$C), 58.47 (OCH_2), 147.68 (C═N), 157.85 (C═O); mass spectrum not useful.

*Cyclohexanone 4-(3-hydroxypropyl)semicarbazone (**9**, n = 3, $R^1R^1 = (CH_2)_5$, R^2 = H)*: White solid (79% yield) after recrystallization from ethanol – diethyl ether, mp 124–126°C; IR (KBr) cm^{-1}: 3363br, 3299br, 3200br, 1639s (C═O), 1558s (C═N), 1470w, 1440m, 1378w, 1350w, 1318m, 1273w, 1254w, 1225w, 1197w, 1138w, 1111w, 1071m, 1019w, 988m, 907w, 831w, 810w, 702m; ^{1}H NMR (300 MHz, $CDCl_3$) δ: 1.56–1.75 (m) and 1.93 (br s) and 2.22–2.35 (m) (12H), 3.46 (app q, ^3J = 6.3 Hz, 2H), 3.65 (app q, ^3J = 6.0 Hz, 2H), 3.85 (app t, ^3J = 6.8 Hz, 1H), 6.38 (ut, 1H), 8.46 (br s, 1H); ^{13}C NMR (75 MHz, $CDCl_3$) δ: 25.54, 25.72, 26.40, 27.00, 33.22 (NCH_2), 35.41 (C*C*H$_2$C of propyl chain and another CH_2 signal overlapped), 58.43 (OCH_2), 154.04 (C═N), 158.43 (C═O); mass spectrum not useful.

*Cyclohexanone 4-(3-hydroxypropyl)-4-methylsemicarbazone (**9**, n = 3, $R^1R^1 = (CH_2)_5$, R^2 = Me)*: Pale yellow solid (60% yield) after recrystallization from ethyl acetate, mp 94–96°C; IR (KBr) cm^{-1}: 3222br, 1661s (C═O), 1547s (C═N), 1473m, 1446w, 1416w, 1389m, 1343w, 1289w, 1216m, 1196m, 1139m, 1077m, 1018w, 989w, 952w, 910w, 756w; ^{1}H NMR (300 MHz, $CDCl_3$) δ: 1.52–1.77 (m, 8H), 2.17–2.40 (m, 4H), 2.90 (s, 3H), 3.43 (t, ^3J = 5.7 Hz, 2H) 3.58 (t, ^3J = 5.7 Hz, 2H), 4.27 (br s, 1H), 8.20 (br s, 1H); ^{13}C NMR (75 MHz, $CDCl_3$) δ: 25.50, 25.64, 26.61, 26.72, 29.31, 33.87, 35.18 (CH_3), 44.72 (NCH_2), 57.39 (OCH_2), 157.36 (C═N or C═O), 157.70 (C═N or C═O); mass spectrum not useful.

Synthesis of oxadiazolines 12 and 13

Typical procedures for the preparations of **12***a–k* and **13***a–e* are given below. Under routine conditions, these compounds do not give useful mass spectra. To confirm their identity, MS experiments involving LRP and HRP electron impact (EI), collisional activation (CA) spectrometry,[11] and chemical ionization (CI) with ammonia were performed on **12***b,d,f* and **13***c,d*. In agreement with earlier work on **12***a* and related compounds (1*j,r*), the EI spectra do not show molecular ions (CI yields $[M + H]^+$ and $[M + H + NH_3]^+$ ions) but rather $[M - N_2]^{\bullet+}$ ions, which (as established by CA spectrometry) form the precursor of most of the fragment ions. Principal peaks (*m/z*; elemental compositions in parentheses were experimentally determined; rel. intensity) in the 70 eV EI mass spectra are as indicated below. For most solid oxadiazolines, the reported melting points are approximate because these compounds generally start to decompose on heating above ca. 80°C.

*3,4,9-Triaza-2,2-dimethyl-1,6-dioxaspiro[4.4]non-3-ene (**12**a) (1j)*

Under dry nitrogen, $PhI(OAc)_2$ (7.47 g, 0.023 mol), dissolved in CH_2Cl_2 (150 mL), was added dropwise, over 1–2 h, to a stirred solution of semicarbazone **9** (n = 2, R^1 = Me, R^2 = H) (3.50 g, 0.022 mol) in CH_2Cl_2 (200 mL) at 0°C. After addition was complete, the solution was kept in the ice bath for another 2 h before it was allowed to warm to room temperature overnight. After ca. half of the solvent had been evaporated in vacuo, the solution was washed with 4 × 30 mL of aqueous $NaHCO_3$ (5%), followed by 30 mL of brine. Drying ($MgSO_4$), filtration by gravity, and evaporation of the solvent afforded an oil (ca. 6 g) containing a mixture of **12***a* and PhI, which were separated by radial chromatography on silica, starting with 10% ethyl acetate in hexane and gradually increasing solvent polarity to 60% ethyl acetate in hexane. This typically gave slightly impure **12***a* in 47% yield. It could be further purified by bulb-to-bulb distillation (ca. 30–40°C, 2 Torr (1 Torr = 133.3 Pa)) to obtain pure **12***a* as a clear, colourless oil. IR (CCl_4) cm^{-1}: 3397br (NH), 1794s, 1711s, 1574w (N═N), 1481w, 1459w, 1417w, 1384m, 1362w, 1309m, 1229m, 1207m, 1138w, 1105w, 1057w, 1038w, 987w, 957w, 915w;

[11] See Terlouw and co-workers (1*j*). The experiments were performed on a VG Analytical ZAB-R mass spectrometer of BEE geometry. Compounds were introduced using a direct insertion probe kept at room temperature at a source temperature of 100–120°C. Under these conditions the degree of thermolysis is negligible.

© 1997 NRC Canada

^{1}H NMR (300 MHz, $CDCl_3$) δ: 1.48 (s, 3H, CH_3), 1.53 (s, 3H, CH_3), 2.87 (br s, 1H, NH), 3.44–3.54 (m, 2H, NCH_2), 4.14–4.33 (m, 2H, OCH_2); ^{13}C NMR (75 MHz, C_6D_6) δ: 24.45 (CH_3), 24.64 (CH_3), 44.71 (NCH_2), 67.87 (OCH_2), 117.68 (C2), 139.18 (C5).

*3,4,9-Triaza-2,2,9-trimethyl-1,6-dioxaspiro[4.4]non-3-ene (**12**b)*

Oxidation of semicarbazone **9** (n = 2, R^1 = R^2 = Me) by the procedure for preparation of **12***a* gave **12***b*, which was purified by radial chromatography with 5–40% ethyl acetate in hexane. Pale yellow oil typically obtained in 66% yield; IR (neat) cm^{-1}: 1757m, 1576w (N=N), 1459s, 1363s, 1295s, 1238s, 1209s, 1132s, 1079s, 1041m, 988m, 953w, 902s, 846m, 762w, 714w; ^{1}H NMR (300 MHz, $CDCl_3$) δ: 1.45 (s, 3H, CCH_3), 1.59 (s, 3H, CCH_3), 2.37 (s, 3H, NCH_3), 3.31 (m, 1H, NCH_2-H_X), 3.46 (m, 1H, NCH_2-H_M), 4.22 (m, 2H, OCH_2-H_B), 4.22 (m, 2H, OCH_2-H_A), J_{AB} = −7.50 Hz, J_{MX} = −8.13 Hz, J_{AM} = 7.03 Hz, J_{AX} = 4.46 Hz, J_{BM} = 7.35 Hz, J_{BX} = 6.30 Hz;[12] ^{13}C NMR (50 MHz, $CDCl_3$) δ: 24.07 (CCH_3), 24.93 (CCH_3), 32.36 (NCH_3), 51.38 (NCH_2), 65.66 (OCH_2), 116.46 (C2), 139.17 (C5); MS: 143 ([M − N_2]$^{\bullet+}$ ($C_7H_{13}NO_2$), 15), 102 ([M − N_2 − $C_3H_5^{\bullet}$]$^+$, 90), 101 ([M − N_2 − C_3H_6]$^{\bullet+}$, 95), 86 (23), 85 ([M − N_2 − C_3H_6O]$^{\bullet+}$, 68), 58 (81), 57 (68), 56 (39), 43 (100), 42 (75), 28 (90).

*3,4,9-Triaza-9-formyl-2,2-dimethyl-1,6-dioxaspiro[4.4]non-3-ene (**12**c)*

Oxadiazoline **12***a* (0.85 g, 5.4 mmol) was stirred at room temperature in CH_2Cl_2 (10 mL) with 4-nitrophenyl formate (0.99 g, 5.9 mmol) (9). After 3 days, the yellow solution was diluted with CH_2Cl_2 (40 mL), washed successively with aqueous $NaHCO_3$ (5%) and brine, and dried ($MgSO_4$). Separation of **12***c* by chromatography, with either 10–40% ethyl acetate in hexane or 1% methanol in chloroform, was repeated several times to obtain a pure sample of **12***c* as a pale orange oil (41% yield, one trial); IR (CCl_4) cm^{-1}: 1702s (C=O), 1573w (N=N), 1474w, 1459w, 1412w, 1377m, 1340w, 1271m, 1234m, 1208w, 1179m, 1115m, 1060w, 1031w, 1008w, 980w, 911w; ^{1}H NMR (200 MHz, $CDCl_3$) δ: 1.50 (s, 3H, CH_3), 1.64 (s, 3H, CH_3), 3.80–4.05 (m, 2H, NCH_2), 4.22–4.45 (m, 2H, NCH_2), 7.90 (s, 1H, C(O)H); ^{13}C NMR (50 MHz, $CDCl_3$) δ: 23.96 (CH_3), 24.70 (CH_3), 42.00 (NCH_2), 65.67 (OCH_2), 120.26 (C2), 133.13 (C5), 158.65 (C=O); routine mass spectrum not useful.

*3,4,9-Triaza-9-acetyl-2,2-dimethyl-1,6-dioxaspiro[4.4]non-3-ene (**12**d)*

The method described below for **12***f* was used, with acetic anhydride for the acetylation. White solid (33% yield, from **9**) after recrystallization from methanol – diethyl ether, mp 87–88°C; IR (CCl_4) cm^{-1}: 1690s (C=O), 1580w (N=N), 1392s, 1350m, 1277m, 1234m, 1208m, 1138w, 1109s, 1046w, 1019w, 982w, 908w; ^{1}H NMR (300 MHz, $CDCl_3$; slow exchange) δ: 1.49 (s, 3H, C(2)CH_3), 1.73 (s, 3H, C(2)CH_3), 1.77 (s) and 2.14 (s) (3H, C(O)CH_3), 3.85–4.08 (m, 2H, NCH_2), 4.13–4.45 (m, 2H, OCH_2); ^{13}C NMR (75 MHz, $CDCl_3$; slow exchange, resonances obviously from the major isomer are underlined) δ: 21.64, 22.02, 22.20, 23.94, 25.20, 25.45, 45.36 and 46.15 (NCH_2), 64.65 and 65.22 (OCH_2), 118.77 and 120.72 (C2), 131.86 and 133.15 (C5), 167.96 (C=O); MS: 171 ([M − N_2]$^{\bullet+}$ ($C_8H_{13}NO_3$), 0.7%), 130 ([M − N_2 − $C_3H_5^{\bullet}$]$^+$, 6), 129 ([M − N_2 − C_3H_6]$^{\bullet+}$, 6), 113 ([M − N_2 − C_3H_6O]$^{\bullet+}$, 23), 88 (50), 85 (4), 72 (6), 69 (24), 59 (14), 43 ([CH_3CO^+], 100). Anal. calcd. for $C_8H_{13}N_3O_3$: C 48.23, H 6.58; found: C 48.50, H 6.70.

*3,4,9-Triaza-9-methacryloyl-2,2-dimethyl-1,6-dioxaspiro[4.4]non-3-ene (**12**e)*

The method described for **12***f*, with methacryloyl chloride in the acylation step, gave **12***e* as a white solid (19% yield, from **9**), mp ca. 45–47°C (dec.) after repeated recrystallizations from ethyl acetate – hexane; IR (CCl_4) cm^{-1}: 1676s (C=O), 1636m, 1578w (N=N), 1454w, 1415w, 1386s, 1366s, 1344w, 1277m, 1233s, 1180s, 1120m, 1096m, 1048w, 1018w, 982w, 920m, 861w, 834w; ^{1}H NMR (300 MHz, $CDCl_3$) δ: 1.48 (s, 3H, C(2)CH_3), 1.69 (s, 3H, C(2)CH_3), 1.93 (s, 3H, =C-CH_3), 3.90–4.08 (m, 2H, NCH_2), 4.22–4.40 (m, 2H, OCH_2), 5.21 and 5.23 (overlapped s, 2H, $=CH_2$); ^{13}C NMR (75 MHz, $CDCl_3$) δ: 19.67 (=C-CH_3), 21.44 C(2)CH_3), 25.24 (C(2)CH_3), 46.48 (NCH_2), 65.15 (OCH_2), 118.16 ($=CH_2$), 120.14 (C2), 132.95 (C5), 140.11 ($=CR_2$), 169.80 (C=O); MS (EI) *m/z*: 156 (4), 139 (9), 124 (7), 110 (50), 100 (15), 95 (22), 84 (46), 69 (90), 49 (34), 41 (100).

*3,4,9-Triaza-9-benzoyl-2,2-dimethyl-1,6-dioxaspiro[4.4]non-3-ene (**12**f)*[13]

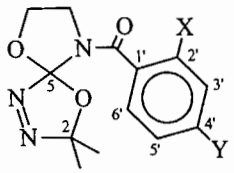
The crude mixture containing **12***a* and PhI (starting with 22 mmol of **9**) was dissolved in CH_2Cl_2 (25mL), and pyridine (1.10 g, 13.9 mmol) was added. Benzoyl chloride (1.86 g, 13.2 mmol) was added dropwise to this stirred solution over ca. 10 min. After stirring at room temperature for another 30 min, the solution was diluted with CH_2Cl_2 and washed successively with water, aqueous $NaHCO_3$ (5%), and brine. The organic phase was dried over $MgSO_4$, the solvent was evaporated, and hexane was added to the crude product to induce crystallization. Recrystallization from methanol – diethyl ether yielded 1.41 g (25%, from **9**) of **12***f* as a white solid, mp ca. 108–110°C (dec.); IR (KBr) cm^{-1}: 1655s (C=O), 1578w (N=N), 1453w, 1389s, 1272m, 1222m, 1162m, 1115m, 1081w, 1046w, 1011w, 973w, 921m, 856w, 817w, 798w, 722m; ^{1}H NMR (300 MHz, $CDCl_3$, slow exchange) δ: 1.47 (s) and 1.62 (s) and 1.20–1.80 (br) (6H, CH_3), 3.85–4.00 (um, 1H, NCH_2), 4.05–4.20 (um, 1H, NCH_2), 4.25–4.45 (m, 2H, OCH_2), 7.35–7.60 (m, 5H, Ar); ^{13}C NMR (75 MHz, $CDCl_3$) δ: 21.40 (CH_3), 25.19 (CH_3), 47.35 (NCH_2), 65.40 (OCH_2), 120.41 (C2), 127.26 (Ar C2, C6), 128.36 (Ar C3, C5), 130.94 (Ar C4), 133.22 (C5), 135.40 (Ar C1), 169.00 (C=O); MS: 233 ([M − N_2]$^{\bullet+}$, 0.9), 192 ([M − N_2 − $C_3H_5^{\bullet}$]$^+$, 5), 175 ([M − N_2 − C_3H_6O]$^{\bullet+}$ ($C_{10}H_9NO_2$), 27), 174 (30), 147 (15), 146 (10), 145 (12), 131 (43), 117 (20), 105 ([$C_6H_5CO^+$], 100), 103 (21), 88 (25), 77 ([$C_6H_5^+$], 35), 51 (21).

[12] Determined by spectral simulation using PANIC (Bruker).

[13] X-ray crystallography data will be submitted for publication elsewhere.

Can. J. Chem. Downloaded from www.nrcresearchpress.com by 91.121.58.235 on 09/08/12
For personal use only.

© 1997 NRC Canada



12*g-i*

*3,4,9-Triaza-9-(2-methoxybenzoyl)-2,2-dimethyl-1,6-dioxaspiro[4.4]non-3-ene (**12**g)*

Prepared as described for **12*f***, using o-anisoyl chloride as the acylating agent. White solid (26% yield, from **9**) after recrystallization from ethyl acetate – hexane, mp ca. 143–144°C (dec.); IR (KBr) cm^{-1}: 1656s (C═O), 1603m, 1581w (N═N), 1493m, 1462m, 1438m, 1399s, 1364m, 1272m, 1250m, 1224m, 1162m, 1123s, 1079m, 1037w, 1017m, 973w, 922m, 899w, 858w, 830w, 763m, 725w; ^1H NMR (300 MHz, $CDCl_3$, slow exchange) δ: 0.50 (br s) and 1.30 (br s) and 1.54 (br s) and 1.81 (br s) (6H, $C(CH_3)_2$), 3.60–4.45 (br. m's, 7H, NCH_2, OCH_2, OCH_3), 6.75–7.50 (br m's, 4H, Ar); ^{13}C NMR (75 MHz, $CDCl_3$, slow exchange, resonances due to major isomer are underlined) δ: 20.93 and 21.66 (CCH_3), 24.79 and 25.38 (CCH_3), 45.55 and 46.01 (NCH_2), 55.72 (OCH_3), 64.24 and 65.57 (OCH_2), 111.23 (Ar), 118.45 (C2), 119.69 and 120.91 (Ar), 124.80 and 125.70 (Ar), 127.55 and 128.26 (Ar), 130.93 and 131.45 (Ar), 133.31 (C5), 155.34 and 156.49 (Ar C2′), 166.63 (C═O); MS (EI) *m/z*: 248 (3), 204 (4), 174 (6), 148 (4), 135 (100), 118 (28), 92 (11), 77 (22); MS (CI, NH_3) *m/z*: 309 $(M + NH_4)^+$, 292 $(M + H)^+$.

*3,4,9-Triaza-9-(4-methoxybenzoyl)-2,2-dimethyl-1,6-dioxaspiro[4.4]non-3-ene (**12**h)*

Prepared as described for **12*f***, with purified **12*a*** for the acylation with *p*-anisoyl chloride. White solid (63% yield) after recrystallizations from ethyl acetate – hexane and methanol – diethyl ether, mp ca. 110°C (dec.); IR (CCl_4) cm^{-1}: 1671s (C═O), 1609m, 1579w (N═N), 1513m, 1462w, 1418w, 1374s, 1306w, 1255s, 1228s, 1173s, 1119m, 1037m, 982w, 921m, 861w, 841w; ^1H NMR (200 MHz, $CDCl_3$, slow exchange) δ: 1.48 (br s, 6H, $C(CH_3)_2$), 3.82 (s, 3H, OCH_3), ca. 3.80–3.98 (overlapped m, 1H, NCH_2), 4.03–4.21 (m, 1H, NCH_2), 4.22–4.44 (m, 2H, OCH_2), 6.88 (d, ^3J = 8.8 Hz, 2H, CH (3′, 5′)), 7.50 (d, ^3J = 8.8 Hz, 2H, CH (2′, 6′)); ^{13}C NMR (50 MHz, $CDCl_3$, slow exchange) δ: 21.32 and 21.62 (CCH_3), 24.98 and 25.28 (CCH_3), 47.54 (NCH_2), 55.20 and 55.47 (OCH_3), 65.46 (OCH_2), 113.42 and 113.57 (C3′, C5′), 120.25 (C2), 127.48 (C1′), 129.26 and 129.58 (C2′, C6′), 133.45 (C5), 161.72 (Ar C4′), 168.56 (C═O); MS (EI) *m/z*: 205 (M − N_2 − acetone, 11), 177 (7), 135 ($ArCO^+$, 100), 92 (10), 77 (12); MS (CI, NH_3) *m/z*: 309 $(M + NH_4)^+$, 292 $(M + H)^+$.

*3,4,9-Triaza-9-(4-nitrobenzoyl)-2,2-dimethyl-1,6-dioxaspiro[4.4]non-3-ene (**12**i)*

Prepared as described for **12*f***, using purified **12*a*** for the acylation with 4-nitrobenzoyl chloride. Pale yellow solid (50% yield) after recrystallization from ethyl acetate – hexane, mp ca. 135°C (dec.); IR (KBr) cm^{-1}: 1665s (C═O), 1604w, 1524s (NO_2), 1415m, 1392m, 1346s (NO_2), 1266w, 1224m, 1158m, 1119m, 1081w, 1040w, 1012w, 980w, 922m, 870w, 849m, 817w, 725m; ^1H NMR (300 MHz, $CDCl_3$, slow exchange) δ: 1.47 (s, on top of a broad resonance, 6H, $C(CH_3)_2$), 3.81–4.18 (um, 2H, NCH_2), 4.26–4.46 (m, 2H, OCH_2), 7.67 (br. d, app, ^3J = 7.7 Hz, 2H, (CH (2′, 6′)), 8.26 (d, ^3J = 8.5 Hz, CH (3′, 5′)); ^{13}C NMR (75 MHz, $CDCl_3$, slow exchange) δ: 21.40 (CH_3), 25.07 (CH_3), 47.07 (NCH_2), 65.27 (OCH_2), 120.73 (br, C2), 123.65 (C2′, C6′), 128.33 (C3′, C5′), ca. 133 (br, C5), 141.00 (C1′), 148.98 (C4′), 166.51 (C═O); MS (EI) *m/z*: 237 (8), 219 (20), 176 (46), 150 ($ArCO^+$, 100), 104 (38), 76 (26); MS (CI, NH_3) *m/z*: 324 $(M + NH_4)^+$, 307 $(M + H)^+$.

*3,4,9-Triaza-9-methoxycarbonyl-2,2-dimethyl-1,6-dioxaspiro[4.4]non-3-ene (**12**j)*

This compound was prepared from **12*a***, based on the method of Corey et al. (10). To a vigorously stirred mixture of **12*a*** (2.41 g, 15.3mmol) and K_2CO_3 (12.72 g, 92.0 mmol) in acetone (35 mL) was added methyl chloroformate (5.80 g, 61.4 mmol). After 2 days at room temperature, the solution was filtered and the solvent was evaporated. Radial chromatography, using 10–60% ethyl acetate in hexane, followed by drying over $MgSO_4$, afforded **12*j*** as a colourless oil (50% yield); IR (CCl_4) cm^{-1}: 1742s (C═O), 1578w (N═N), 1448m, 1380s, 1280m, 1232m, 1211s, 1159w, 1117m, 1063m, 1040m, 985w, 935w, 911w, 845w; ^1H NMR (200 MHz, $CDCl_3$, slow exchange) δ: 1.47 (s, 3H, CCH_3), 1.70 (br s, 3H, CCH_3), 3.67 (br s, 3H, OCH_3), 3.75–4.05 (um, 2H, NCH_2), 4.18–4.42 (m, 2H, OCH_2); ^{13}C NMR (50 MHz, $CDCl_3$, some peaks are broad due to slow exchange) δ: 22.15 (CCH_3), 25.24 (CCH_3), 45.14 (NCH_2), 52.62 (OCH_3), 65.34 (OCH_2), 120.16 (C2), 132.86 (C5), 152.27 (C═O); routine mass spectrum not useful.

*3,4,9-Triaza-2,2-dimethyl-1,6-dioxa-9-phenylsulfonyl-spiro[4.4]non-3-ene (**12**k)*

Oxadiazoline **12*a*** (1.50 g, 9.54 mmol) in CH_2Cl_2 (25 mL) was stirred at room temperature for 13 days with benzenesulfonyl chloride (2.00 g, 11.3 mmol) in the presence of pyridine (0.94 g, 12 mmol). Aqueous $NaHCO_3$ (5%, ca. 25 mL) was then added, and the mixture was stirred vigorously for 20 min. The organic layer was separated, and the aqueous layer was extracted with 4 portions of CH_2Cl_2. After drying the combined organic layers ($MgSO_4$) and evaporating the solvent, the crude product was dissolved in diethyl ether – methanol and decanted, to leave most of the undissolved pyridine behind. White crystals of **12*k*** that precipitated from the ether–methanol solution after several days in the refrigerator were collected, washed well with ether and cold methanol, and kept in a desiccator (46% yield); IR (KBr) cm^{-1}: 1576w (N═N), 1481w, 1448m, 1359s (NSO_2), 1270m, 1227m, 1211m, 1169s (NSO_2), 1125s, 1053m, 1022m, 976w, 914m, 836m, 760w, 728m, 687m, 614m, 573m; ^1H NMR (200 MHz, $CDCl_3$) δ: 1.46 (s, 3H, CH_3), 1.81 (s, 3H, CH_3), 3.60–3.87 (m, 2H, NCH_2), 4.14–4.35 (m, 2H, OCH_2), 7.50–7.64 (m, 3H, Ar-*m,p*), 7.89–7.96 (m, 2H, Ar-*o*); ^{13}C NMR (75 MHz, $CDCl_3$) δ: 22.36 (CH_3), 25.14 (CH_3), 46.47 (NCH_2), 65.23 (OCH_2), 120.46 (C2), 127.96 (Ar C2, C6), 129.02 (Ar C3, C5), 133.30 (Ar C4 and oxadiazoline C5, overlapped), 138.57 (Ar C1); MS (EI) *m/z*: 281 (2), 228 (15), 210 (31), 183 (4), 141 ($PhSO_2^+$, 37), 117 (26), 88 (50), 77 (100), 51 (26); MS (CI, NH_3) *m/z*: 315 $(M+NH_4)^+$.

Can. J. Chem. Downloaded from www.nrcresearchpress.com by 91.121.58.235 on 09/08/12
For personal use only.

© 1997 NRC Canada

Can. J. Chem. Downloaded from www.nrcresearchpress.com by 91.121.58.235 on 09/08/12
For personal use only.

*5,14,15-Triaza-5-methyl-1,7-dioxadispiro[5.1.5.2]pentadec-14-ene (**13**c)*

Prepared essentially as for **12***a*, from 2.36 g (10.4 mmol) of **9** (n = 3, R^1R^1 = $(CH_2)_5$, R^2 = Me) and 3.51 g (10.9 mmol) of $PhI(OAc)_2$, in a total of 300 mL of CH_2Cl_2. Purification of the resulting oil by column chromatography on silica (20% ethyl acetate in hexane) resulted in slightly impure **13***c*, which was further purified by radial chromatography, using the same solvent mixture, to give 0.82 g (35%) of **13***c* as a pale yellow oil; IR (CCl_4) cm^{-1}: 1715w, 1572w (N=N), 1478m, 1450m, 1377m, 1346w, 1306m, 1282m, 1241s, 1218m, 1157m, 1142m, 1103s, 1061m, 1023w, 997m, 953w, 908m, 880m, 842w; ^1H NMR (300 MHz, $CDCl_3$) δ: 1.40–2.10 (m), 2.30–2.36 (m) (12H, CCH_2C), 2.14 (s, 3H, CH_3), 2.90–3.05 (m, 1H, NCH_2), 3.23–3.34 (m, 1H, NCH_2), 3.93–4.05 (m, 1H, OCH_2), 4.14–4.27 (m, 1H, OCH_2); ^{13}C NMR (75 MHz, $CDCl_3$) δ: 22.53, 22.93, 24.48, 24.75, 32.69, 34.54, 37.11, 49.61 (NCH_2), 64.22 (OCH_2), 120.27 (C2), 132.94 (C5); MS: 197 ($[M - N_2]^{\bullet+}$ ($C_{11}H_{19}NO_2$), 8), 116 ($[M - N_2 - C_6H_9^{\bullet}]^+$, 25), 115 ($[M - N_2 - C_6H_{10}]^{\bullet+}$, 40), 114 (17), 99 ($[M - N_2 - C_6H_{10}O]^{\bullet+}$ (C_5H_9NO), 48), 98 ((C_5H_8NO), 100), 88 (25), 44 ((C_2H_6N), 57), 42 (59), 28 (25).

*3,4,10-Triaza-10-benzoyl-2,2-dimethyl-1,6-dioxaspiro[4,5]-dec-3-ene (**13**d)*

$PhI(OAc)_2$ (6.14g, 19.1 mmol), dissolved in 75 mL of methanol, was added dropwise to an ice-cold solution of **9** (n = 3, R^1 = CH_3, R^2 = H) (3.00 g, 17.3 mmol) in 75 mL of methanol, under nitrogen. After completion of the addition (1.5 h), the solution was stirred at room temperature for 24 h. Evaporation of the solvent gave an oil, which was redissolved in CH_2Cl_2 and washed successively with aqueous $NaHCO_3$ (5%) and water. The crude product containing **13***a*, obtained after drying ($MgSO_4$) the solution and evaporating the solvent, was redissolved in 20 mL of CH_2Cl_2, together with pyridine (1.44 g, 18.2 mmol), and benzoyl chloride (2.46 g, 17.5 mmol) was added dropwise. After 1.5 h at room temperature, the usual work-up was performed (see **12***f*). Separation of the crude mixture by column chromatography, using first 5% and then 10% ethyl acetate in hexane, gave an oil (ca. 15%) that proved to be a mixture of **13***d* and, possibly, an isomer that could not be identified. Pure **13***d* crystallized out of a methanol – diethyl ether solution kept at ca. −10°C. White solid, mp ca. 94°C (dec.); IR (CCl_4) cm^{-1}: 1678s (C=O), 1601w, 1581w (N=N), 1492w, 1448w, 1380s, 1279m, 1213s, 1156m, 1096s, 984w, 949w, 912m, 849w, 700m; ^1H NMR (200 MHz, $CDCl_3$) δ: 1.53 (s, 3H, CH_3), 1.70 (s, 3H, CH_3), 1.95–2.31 (m, 2H, CCH_2C), 3.59–3.93 (m, 2H, NCH_2), 3.98–4.30 (m, 2H, OCH_2), 7.30–7.64 (m, 5H, Ar); ^{13}C NMR (50 MHz, $CDCl_3$) δ: 21.87 (CH_3), 23.59 (CCH_2C), 25.20 (CH_3), 43.02 (NCH_2), 60.79 (OCH_2), 121.22 (C2), 127.40 (Ar C2, C6), 128.38 (Ar C3, C5), 129.01 (C5), 130.64 (Ar C4), 135.29 (Ar C1), 170.92 (C=O); MS: 247 ($[M - N_2]^{\bullet+}$, 0.4), 206 ($[M - N_2 - C_3H_5^{\bullet}]^+$, 1), 189 ($[M - N_2 - C_3H_6O]^{\bullet+}$ ($C_{11}H_{11}NO_2$), 17), 188 (($C_{11}H_{10}NO_2$), 50), 161 (10), 160 (29), 145 (40), 119 (10), 117 (17), 105 ($[C_6H_5CO^+]$, 100), 102 (15), 77 ($[C_6H_5^+]$, 35).

*5,14,15-Triaza-5-benzoyl-1,7-dioxadispiro[5.1.5.2]pentadec-14-ene (**13**e)*

After oxidation of **9** (n = 3, R^1R^1 = $(CH_2)_5$, R^2 = H) (2.50 g, 11.7 mmol) with $PhI(OAc)_2$ (4.09 g, 12.7 mmol), carried out as for **12***a*, the resulting mixture containing **13***b* was treated with benzoyl chloride (1.58 g, 11.2 mmol) in 22 mL of benzene, in the presence of pyridine (1.16 g, 14.7 mmol), as described for **12***f*. As crystallization of **13***e* from the crude could not be induced, it was purified by repeated chromatography and obtained, in ca. 8% yield (from **9**), as a gummy mass that only partially crystallized in the refrigerator over several weeks; IR (CCl_4) cm^{-1}: 1678s (C=O), 1602w, 1580w (N=N), 1493w, 1448m, 1378s, 1263m, 1218m, 1157m, 1087s, 976w, 948w, 895m, 847w, 700m; ^1H NMR (300 MHz, $CDCl_3$) δ: 1.40–1.75 (m, 5H), 1.75–2.00 (m, 4H), 2.00–2.27 (m, 3H), 3.70–3.80 (m, 1H, NCH_2), 3.80–3.90 (m, 1H, NCH_2), 4.00–4.14 (m, 1H, OCH_2), 4.14–4.28 (m, 1H, OCH_2), 7.36–7.60 (m, 5H, Ar); ^{13}C NMR (75 MHz, $CDCl_3$) δ: 22.73, 23.22, 23.65, 24.86, 30.93, 34.72, 43.06 (NCH_2), 60.85 (OCH_2), 123.16 (C2), 127.49 (Ar C2, C6), 128.00 (C5), 128.35 (Ar C3, C5), 130.61 (Ar C4), 135.46 (Ar C1), 170.96 (C=O); MS (EI) *m/z*: 206 (3), 188 (30), 160 (13), 145 (15), 105 ($PhCO^+$, 100), 84 (18), 77 (32), 67 (38); MS (CI, NH_3) *m/z*: 316 $(M + H)^+$.

General methods for thermolyses

All thermolyses were carried out by immersing the sealed tubes containing the samples in a constant-temperature oil bath at 90.0 ± 0.2°C for 24 h (or until complete decomposition of the oxadiazolines; see Table 1). Spectroscopic data of products isolated from large-scale experiments (or of authentic compounds from other sources) were used for peak assignments in the spectra of thermolysates from NMR-scale experiments.

Thermolysis rate constants

The rates of decomposition of the oxadiazolines were monitored by ^1H NMR spectroscopy at 300 MHz. Samples typically containing 1.25×10^{-4} mol of an oxadiazoline and 7 mg of *p*-xylene, used as an internal standard for integration, in 0.5 mL of C_6D_6 were degassed and sealed into medium-walled NMR tubes. At appropriate time intervals during thermolysis, the tubes were removed from the thermolysis bath and quickly chilled to room temperature to record ^1H NMR spectra. Linear regression analyses were performed for the plots of $\ln(I/I_0)$ vs. time, where I and I_0 are the normalized integrals of a given resonance at time t and at time zero, respectively. The first-order decomposition rate constants were obtained from the slopes of the calculated best lines forced to pass through the origin. The thermolysis data and regression analysis results are available as supplementary material.[14]

Determination of product yields

For small-scale thermolysis experiments done in sealed NMR tubes, product yields were determined by comparison of the integrals of appropriate ^1H NMR resonances, after completion of thermolysis, to the integrals of the oxadiazoline peaks at t = 0, using internal *p*-xylene for normalization. Yields from thermolyses in the presence of phenol were determined in a similar way from samples containing 1.0×10^{-4} mol of oxadiazoline and 1.25 equivalents of phenol in ca. 0.5 mL of

[14] These supplementary data can be purchased from: The Depository of Unpublished Data, Document Delivery, CISTI, National Research Council Canada, Ottawa, Canada K1A 0S2.

© 1997 NRC Canada

Can. J. Chem. Downloaded from www.nrcresearchpress.com by 91.121.58.235 on 09/08/12
For personal use only.

C_6D_6; experimental details of the isolation of these carbene + phenol adducts, and some related compounds, are in the following paper. Typically, for larger scale thermolyses, a benzene solution (10 mL) of the oxadiazoline (0.5 mmol) was placed in a resealable thermolysis tube that was evacuated before thermolysis.

Thermolysis of 12*b*

Acetone azine: ^{1}H NMR (200 MHz, C_6D_6) δ: 1.86 (s, 6H), 1.89 (s, 6H); MS (EI) *m/z*: 112 (M^+, 25), 97 (79), 70 (17), 56 (100), 39 (58), 28 (17).

*3-Methyl-2-oxazolidinone (**18**b) (ref. 25)*: ^{1}H NMR (200 MHz, $CDCl_3$) δ: 2.89 (s, 3H), 3.51–3.63 (m, 2H), 4.26–4.38 (m, 2H); ^{13}C NMR (50 MHz, $CDCl_3$) δ: 31.14 (CH_3), 46.85 (NCH_2), 61.45 (OCH_2), 158.76 (C=O); MS (EI) *m/z*: 101 (M^+, 17), 72 (2), 56 (25), 42 (100), 28 (33).

2-Phenoxypropane (ref. 26): MS (EI) *m/z*: 136 (M^+, 15), 121 (4), 107 (2), 94 (100), 77 (15), 66 (62), 51 (16), 39 (59), 27 (17).

Bromination of ethylene and propene
After thermolysis of 98 mg (0.57 mmol) of **12*b*** in 10 mL of benzene, the thermolysis tube was immersed in liquid nitrogen for several minutes. About 1 mL of bromine solution (0.5 M, in CCl_4) was then added, the tube was sealed again, and the contents were allowed to thaw. After mixing the solution at room temperature, the tube was reopened and the solution was washed with two portions of aqueous $NaHCO_3$ (5%) and one of water. Analysis of the resulting solution by GC–MS demonstrated the presence of both 1,2-dibromoethane and 1,2-dibromopropane, their spectra matching those from authentic samples.

Thermolysis of 2-diazopropane
Two medium-walled NMR tubes, each containing ca. 22 mg (0.14 mmol) of 2,2-dimethoxy-5,5-dimethyl-Δ^3-1,3,4-oxadiazoline (4) and ca. 0.5 mL benzene-d_6, were sealed after three freeze–pump–thaw cycles. Both tubes were irradiated with 300 nm light in a Rayonet apparatus for 50 min. One of the tubes was then immersed in an oil bath at 90°C for 20 h, while the other tube was kept at room temperature in the dark. Within experimental error, the final product ratios in the two samples were identical. Integration of the resonances of acetone azine (1.86 and 1.89 ppm), relative to that of dimethylcarbonate (3.38 ppm), indicated that 86% of the 2-diazopropane had produced acetone azine, assuming equimolar amounts of dimethylcarbonate and 2-diazopropane were generated in the photolysis of the oxadiazoline (27). An unidentified product giving rise to two singlets (1.64 and 1.68 ppm) accounted for most of the difference, while propene was observed only in trace quantities.

*Spiro-fused hydantoin **22***
Oxadiazoline **12*b*** (102 mg, 0.60 mmol) was thermolysed with MeNCO (85 mg, 1.5 mmol) in 10 mL of benzene. The major product, **22**, was purified by radial chromatography, using 30–40% ethyl acetate in hexane (44% yield). White solid, mp 71–73°C; IR (CCl_4) cm^{-1}: 1785m (C=O), 1729s (C=O), 1461s, 1419m, 1392m, 1299m, 1267w, 1231w, 1184w, 1144w, 1079s, 1015w, 993w, 973w, 949w; ^{1}H NMR (200 MHz, C_6D_6) δ: 1.97 (s, 3H, oxazolidine NCH_3), 2.65 (s, 3H, CH_3), 2.73 (s, 3H, CH_3), ca. 2.52–2.77 (overlapped m, 1H, NCH_2), 3.10–3.27 (m, 1H, NCH_2), 3.57–3.72 (m, 1H, OCH_2), 3.77–3.90 (m, 1H, OCH_2); ^{13}C NMR (75 MHz, C_6D_6) δ: 23.06 (CH_3), 23.43 (CH_3), 32.69 (CH_3), 51.18 (NCH_2), 65.17 (OCH_2), 101.67 (spiro C), 155.33 (N*C*(O)N), 170.24 (NC(O)C); MS (EI) *m/z*: 199 (M^+, 1), 171 (M − CO, 4), 154 (16), 141 (4), 127 (9), 113 (92), 99 (2), 86 (21), 70 (36), 57 (100), 42 (71), 28 (36); MS (CI, NH_3) *m/z*: 200 (M + H)$^+$. Anal. calcd. for $C_8H_{13}N_3O$: C 48.23, H 6.58, N 21.09; found: C 48.03, H 6.81, N 21.00.

*Dimethyl 3,3-dimethyl-3*H*-pyrazole-4,5-dicarboxylate (**23**) (ref. 19)*
Oxadiazoline **12*b*** (98 mg, 0.58 mmol) was thermolysed with dimethyl acetylenedicarboxylate (254 mg, 1.79 mmol) in 10 mL of benzene. A complex of mixture of products was obtained, from which **23** could be separated by radial chromatography. IR (CCl_4) cm^{-1}: 1732s (C=O), 1647w, 1438w, 1334w, 1264s, 1198w, 1167w, 1114w, 1033w, 909m; ^{1}H NMR (200 MHz, $CDCl_3$) δ: 1.58 (s, 6H), 3.92 (s, 3H), 4.00 (s, 3H); ^{13}C NMR (50 MHz, $CDCl_3$) δ: 20.86 (C(CH_3)$_2$), 52.98 (2 × OCH_3, coincident), 97.46 (C3), 144.68 (C4), 153.56 (C5), 160.81 (C=O), 162.97 (C=O); MS (EI) *m/z*: 183 (3), 169 (3), 152 (33), 141 (50), 125 (36), 109 (34), 93 (55), 79 (65), 67 (100), 59 (43), 53 (31), 39 (50), 29 (18).

Thermolysis of 13*c*

Cyclohexanone azine: MS (EI) *m/z*: 192 (M^+, 60), 163 (57), 149 (100), 136 (59), 124 (26), 110 (69), 96 (43), 81 (24), 67 (45), 55 (57), 41 (93), 27 (27).

*3-Methyltetrahydro-2*H*-1,3-oxazin-2-one (**19**c) (ref. 28)*: ^{1}H NMR (300 MHz, C_6D_6) δ: 1.10–1.20 (m, 2H), 2.40 (t, ^3J = 6.3 Hz, 2H), 2.68 (s, 3H), 3.58 (t, ^3J = 5.3 Hz, 2H); MS (EI) *m/z*: 115 (M^+, 21), 87 (13), 70 (13), 56 (27), 42 (100), 28 (27).

Phenoxycyclohexane (ref. 29): MS (EI) *m/z*: 176 (M^+, 10), 94 (100), 77 (10), 65 (15), 55 (14), 51 (7), 41 (14), 39 (22), 27 (5).

Thermolysis of 12*f*
Oxadiazoline **12*f*** was thermolysed several times in order to obtain the data that follow. The major product, **26*a***, was formed in almost quantitative yield. Attempted purification by chromatography resulted in its complete decomposition. Small amounts of essentially pure crystals could be obtained by dissolving the crude product mixture in diethyl ether, followed by removal of most of the solvent on a rotary evaporator. Similarly, its sole hydrolysis product, **28**, which was obtained by leaving the crude product in contact with a few drops of water over several days, did not survive chromatography. However, pure **28** precipitated from a benzene solution left at or below room temperature over a few weeks. Of the minor nonvolatile products resulting from thermolysis of **12*f***, benzoyl isocyanate was detected by GC–MS (and matched an authentic sample); **18*f*** was repeatedly isolated by radial chromatography from various samples of thermolysed **12*f***; benzamide and **25**, detected by GC–MS when **12*f*** was thermolysed

© 1997 NRC Canada

Can. J. Chem. Downloaded from www.nrcresearchpress.com by 91.121.58.235 on 09/08/12
For personal use only.

without added trap, were both isolated by chromatography from the thermolysis of **12***f* in the presence of water.

Thermolysis of ***12****f in the presence of water*
Oxadiazoline **12***f* (224 mg, 0.86 mmol) was thermolysed in 100 mL benzene, with about 15 drops of water. Repeated separation by radial chromatography, using ethyl acetate – hexane in various proportions, afforded about 21 mg (20%) of benzamide and 92 mg (56%) of **25**.

Thermolysis of ***12****f with benzoyl isocyanate*
Oxadiazoline **12***f* (118 mg, 0.45 mmol) was thermolysed with benzoyl isocyanate (110 mg, 0.75 mmol), prepared as described by Speziale and Smith (30), in 10 mL of benzene. Spectroscopic data (GC–MS, ^{1}H and ^{13}C NMR in both C_6D_6 and $CDCl_3$) for the crude thermolysate were similar to those obtained from thermolyses of **12***f* without added trap, indicating formation of **26***a* as the major product.

*3-Benzoyl-2-oxazolidinone (****18****f) (ref. 31)*: ^{1}H NMR (300 MHz, $CDCl_3$) δ: 4.19 (t, ^3J = 7.8 Hz, 2H), 4.51 (t, ^3J = 7.8 Hz, 2H), 7.40–7.50 (m, 2H), 7.51–7.60 (m, 1H), 7.62–7.70 (m, 2H); ^{13}C NMR (75 MHz, $CDCl_3$) δ: 43.71 (NCH_2), 62.22 (OCH_2), 127.87 (Ar C2, C6), 129.10 (Ar C3, C5), 132.43 (Ar C4) (Ar C1 and C=O peaks not observed due to low S/N); MS (EI) *m/z*: 191 (M^+, 15), 163 (3), 147 (3), 121 (1), 105 ($PhCO^+$, 100), 91 (1), 77 (82), 63 (2), 51 (35), 42 (5), 28(6).

*Spiro-fused 4(5*H*)-oxazolone* ***26****a*: IR (crude product, CCl_4) cm^{-1}: 1783s (oxazolone C=O), 1736w, 1677s (PhC=O), 1605m, 1558s (C=N), 1492w, 1451m, 1384s, 1274w, 1196m, 1170m, 1141m, 1100w, 1055w, 854w; ^{1}H NMR (300 MHz, $CDCl_3$) δ: 4.00–4.12 (m, 2H, NCH_2), 4.47–4.59 (m, 2H, OCH_2), 7.25–7.80 (m, 8H, Ar), 8.21–8.31 (m, 2H, PhCO-*o*); ^{13}C NMR (75 MHz, $CDCl_3$) δ: 47.14 (NCH_2), 68.43 (OCH_2), 108.38 (spiro C), 125.35 (Ar), 127.18 (Ar), (127.59?, Ar), 128.32 (Ar), 128.70 (Ar), 130.21 (Ar), 131.25 (Ar), 135.60 (Ar), 167.73 (PhC=O), 181.80 and 184.13 (oxazolone C2 and C4); MS (EI) *m/z*: 322 (M^+, 1), 175 (20), 147 (9), 131 (12), 105 ($PhCO^+$, 100), 83 (53), 78 (57), 49 (100); MS (CI, NH_3) *m/z*: 323 $(M + H)^+$.

Oxalic acid derivative ***28***: White solid, mp ca. 170°C; IR (KBr) cm^{-1}: 3453m (NH), 3306br (NH), 1753s, 1721m, 1682m, 1641s, 1602w, 1578w, 1536s, 1464m, 1427w, 1399m, 1365m, 1318m, 1250m, 1208m, 1182s, 1121w, 1021m, 972w, 909w, 799w, 773w, 741w, 700s; ^{1}H NMR (300 MHz, $CDCl_3$) δ: 3.87–3.97 (m, 2H, NCH_2), 4.59 (t, ^3J = 4.9 Hz, 2H, OCH_2), 7.05 (br s, 1H, NH), 7.30–7.60 (m, 5H, Ar), 7.63–7.73 (m, 1H, Ar), 7.75–7.83 (m, 2H, PhCO-*o*), 7.86–7.94 (m, 2H, PhCO-*o*), 9.64 (br s, 1H, NH); ^{13}C NMR (50 MHz, CD_3OD, slow exchange) δ: 39.68 (NCH_2), 65.95 and 66.20 (OCH_2), 128.31 (Ar C2, C6), 128.64 (Ar C2, C6), 129.51 (2 × Ar C3, C5), 132.76 (Ar C4), 132.91 (2 × Ar C4), 134.96 (Ar C1), 135.43 (Ar C1), 158.81 (oxalyl C=O), 159.48 (oxalyl C=O), 170.61 (PhC=O), 172.41 (PhC=O); MS (EI) *m/z*: 164 (17), 147 (42), 117 (32), 105 ($PhCO^+$, 100), 77 (43), 51 (22), 44 (11); MS (CI, NH_3) *m/z*: 341 $(M + H)^+$; a satisfactory elemental analysis could not be obtained.

N-*[2-(Formyloxy)ethyl]benzamide (****25****) (ref. 32)*: White solid, mp 59–60°C (slightly impure sample); IR (CCl_4) cm^{-1}: 3465br (NH), 1735s (OC=O), 1677s (NC=O), 1517m, 1486w, 1302m, 1174s, 909w; ^{1}H NMR (200 MHz, $CDCl_3$) δ: 3.77 (q, ^3J = 5.4 Hz, 2H, NCH_2), 4.39 (t, ^3J = 5.2 Hz, 2H, OCH_2), 6.55 (br s, 1H, NH), 7.35–7.60 (m, 3H, Ar-*m,p*), 7.72–7.84 (m, 2H, Ar-*o*), 8.11 (s, 1H, C(O)H); ^{13}C NMR (75 MHz, $CDCl_3$) δ: 38.94 (NCH_2), 62.58 (OCH_2), 126.88 (Ar C2, C6), 128.41 (Ar C3, C5), 131.50 (Ar C4), 133.98 (Ar C1), 160.89 (O-C=O), 167.79 (N-C=O); MS (EI) *m/z*: 193 (M^+, 5), 164 (3), 147 (19), 134 (5), 105 ($PhCO^+$, 100), 77 (58), 51 (22), 31 (8); MS (CI, NH_3) *m/z*: 211 $(M + NH_3)^+$, 194 $(M + H)^+$.

*Spiro-fused 4(5*H*)-oxazolone* ***26****b*
Oxadiazoline **12***d* (90 mg, 0.45 mmol) was thermolysed with benzoyl isocyanate (124 mg, 0.84 mmol) in 10 mL of benzene. GC–MS, as well as ^{1}H and ^{13}C spectra of the crude thermolysate, indicated that **26***b* was the major product. IR (CCl_4, major bands only) cm^{-1}: 1782 (oxazolone C=O), 1603, 1557 (C=N); ^{1}H NMR (200 MHz, $CDCl_3$, possible slow exchange) δ: 2.13 (s, ~3H, CH_3), 3.90–4.07 (m, 2H, NCH_2), 4.40–4.64 (m, 2H, OCH_2), ca. 7.34–7.76 (m, 3H, Ar-*m,p*), 8.13–8.27 (m, 2H, Ar-*o*); ^{13}C NMR (50 MHz, $CDCl_3$) δ: 22.42 (CH_3), 45.76 (NCH_2), 68.30 (OCH_2), 108.02 (spiro C), 125.51 (Ar C2, C6), 128.77 (Ar C3, C5), 130.31 (Ar C4), 135.63 (Ar C1), 168.18 (PhC=O), 181.67 and 184.11 (oxazolone C2 and C4).

*5,5-Dimethoxy-2-phenyl-4(5*H*)-oxazolone (****26****c)*
2,2-Dimethoxy-5,5-dimethyl-Δ^3-1,3,4-oxadiazoline (4), **27**, (85 mg, 0.53 mmol) was thermolysed at 110°C for 24 h with benzoyl isocyanate (143 mg, 0.97 mmol) in 10 mL of benzene. GC–MS, as well as ^{1}H and ^{13}C spectra of the thermolysate, indicated that **26***c* was the major product. IR (CCl_4, major bands only) cm^{-1}: 1778 (C=O), 1734, 1600, 1553 (C=N); ^{1}H NMR (200 MHz, $CDCl_3$) δ: 3.60 (s, 6H, OCH_3), ca. 7.33–7.80 (m, 3H, Ar-*m,p*), 8.21–8.35 (m, 2H, Ar-*o*); ^{13}C NMR (50 MHz, $CDCl_3$) δ: 52.22 (OCH_3), 114.02 (C5 oxazolone), 125.15 (Ar), 128.96 (Ar), 130.27 (Ar), 136.02 (Ar), 181.45 and 184.62 (oxazolone C2 and C4); MS (EI) *m/z*: 221 (M^+, 2), 193 (1), 190 (1), 162 (5), 147 (2), 131 (8), 118 (9), 103 (100), 91 (3), 77 (37), 59 (35), 51 (13), 39 (2), 29 (4).

Control "thermolysis" of benzoyl isocyanate
Slightly impure benzoyl isocyanate (110 mg, 0.75 mmol) was dissolved in 10 mL of dry benzene and subjected to the usual thermolysis conditions. GC–MS, as well as ^{1}H and ^{13}C spectra of the crude, sparingly soluble, product mixture indicated that very little benzoyl isocyanate remained (detected only by GC–MS, not by ^{13}C NMR). Inspection of the ^{13}C spectrum demonstrated the presence of benzamide and of *N,N′*-dibenzoylurea. The latter was identified by comparison with a pure sample obtained by recrystallization (ethyl acetate) of a completely decomposed sample of benzoyl isocyanate.

N,N′-*Dibenzoylurea*: White solid, mp 213–217°C (lit. (33) mp 212–216°C); IR (KBr) cm^{-1}: 3431br (NH), 1757s (C=O), 1670m (C=O), 1475s, 1262m, 1197m, 775w; ^{1}H NMR (200 MHz, $CDCl_3$) δ: 7.50–7.75 (m, 6H, Ar-*m,p*), 7.97–8.12 (m, 4H, Ar-*o*) (the NH signals were not visible); ^{13}C NMR (50 MHz, $CDCl_3$) δ: 128.09 (Ar C2, C6), 128.93 (Ar C3, C5), 131.90 (Ar C4), 133.53 (Ar C1), 150.42 (NC(O)N), 167.16 (PhCO).

© 1997 NRC Canada

Can. J. Chem. Downloaded from www.nrcresearchpress.com by 91.121.58.235 on 09/08/12
For personal use only.

Thermolysis of 13*d,e*

*3-Benzoyltetrahydro-2*H*-1,3-oxazin-2-one (**19**d) (ref. 31)*: MS (EI) *m/z*: 205 (M^+, 15), 177 (28), 105 ($PhCO^+$, 100), 77 (60), 51 (22), 28 (8).

Thermolysis of 12*k*

*Oxazolidine **29***

The hygroscopic oxadiazoline **12***k* was thermolysed in a benzene solution that visibly contained some water. Separation of the products by radial chromatography, using 10–40% ethyl acetate in hexane, gave **18***k* (see below) and **29**: IR (CCl_4) cm^{-1}: 1730s, 1476w, 1449w, 1412w, 1366s (NSO_2), 1270w, 1175s (NSO_2), 1092w, 999w, 937w, 909w; ^1H NMR (300 MHz, $CDCl_3$) δ: 3.29–3.39 (m, 2H, NCH_2), 3.40–3.54 (m, 1H, OCH_2), 3.55–3.75 (m, 2H, NCH_2), 4.01–4.12 (m, 1H, OCH_2), 4.21–4.40 (m, 2H, OCH_2), 6.60 (s, 1H, oxazolidine C(2)H), 7.48–7.78 (m, ca. 6H, Ar-*m,p*), 7.90–8.02 (m, ca. 5H, Ar-*o*, C(O)H); ^{13}C NMR (50 MHz, $CDCl_3$) δ: 40.47 (NCH_2), 46.61 (NCH_2), 62.08 (OCH_2), 65.72 (OCH_2), 96.33 (oxazolidine C2), 127.83 (Ar C2, C6), 127.97 (Ar C2, C6), 129.00 (Ar C3, C5), 129.57 (Ar C3, C5), 133.16 (Ar C4), 133.80 (Ar C4), 136.61 (Ar C1), 139.19 (Ar C1), 160.61 (C═O); MS (EI) *m/z*: 212 (34), 141 ($PhSO_2^+$, 30), 77 (100); MS (CI, NH_3) *m/z*: 459 $(M + NH_4)^+$, 442 $(M + H)^+$.

*3-(Phenylsulfonyl)-2-oxazolidinone (**18**k) (ref. 31)*: IR (CCl_4) cm^{-1}: 1801s, 1480w, 1450w, 1382m (NSO_2), 1264w, 1180s (NSO_2), 1147s, 1094w, 1050w, 909w; ^1H NMR (200 MHz, $CDCl_3$) δ: 4.00–4.15 (m, 2H), 4.32–4.46 (m, 2H), 7.50–7.80 (m, 3H), 8.02–8.13 (m, 2H); ^{13}C NMR (50 MHz, $CDCl_3$) δ: 44.61 (NCH_2), 62.28 (OCH_2), 128.26 (Ar C2, C6), 129.30 (Ar C3, C5), 134.55 (Ar C4), 136.81 (Ar C1), 151.91 (C═O); MS (EI) *m/z*: 163 (30), 141 ($PhSO_2^+$, 12), 118 (8), 104 (53), 91 (6), 77 (100), 56 (6), 51 (28), 28 (2); MS (CI, NH_3) *m/z*: 245 $(M + NH_4)^+$.

N-*Formyl*-N-*(2-hydroxyethyl)benzenesulfonamide (**30**)*: IR (CCl_4) cm^{-1}: 3425–3000 (OH), 1736s (C═O), 1449w, 1417w, 1345m (NSO_2), 1264m, 1165s (NSO_2), 1097m, 1027w, 950w, 909w, 858w; ^1H NMR (200 MHz, $CDCl_3$, slow exchange) δ: 3.20-3.36 (m, 2H, NCH_2), 4.04–4.26 (m, 2H, OCH_2), 5.03 (br s, 1H, OH), 7.44–7.93 (m, ca. 6H, Ar and C(O)H); ^{13}C NMR (50 MHz, $CDCl_3$, only peaks from major conformer are given) δ: 41.99 (NCH_2), 62.41 (OCH_2), 126.99 (Ar C2, C6), 129.24 (Ar C3, C5), 132.91 (Ar C4), 139.83 (Ar C1), 160.42 (C═O); MS (EI) *m/z*: 183 (16), 170 (43), 141 ($PhSO_2^+$, 57), 119 (6), 92 (4), 77 (100), 51 (22), 31 (5); MS (CI, NH_3) *m/z*: 247 $(M + NH_4)^+$, 230 $(M + H)^+$.

Acknowledgements

This work was supported by the Natural Sciences and Engineering Research Council (NSERC) of Canada. P.C. was the recipient of an Ontario Graduate Scholarship. We thank Prof. J.K. Terlouw for special mass spectrometric experiments on some oxadiazolines. We also gratefully acknowledge the assistance of Drs. Donald Hughes and Richard Smith and of Mssrs. Brian Sayer and Fajar Ramelan for some aspects of the NMR spectroscopy and the mass spectrometry. We also thank Mr. Chris Barr for the spectral simulation on **12***b*.

References

1. (*a*) R.A. Moss and J.K. Huselton. J. Chem. Soc. Chem. Commun. 950 (1976); (*b*) N.G. Rondan, K.N. Houk, and R.A. Moss. J. Am. Chem. Soc. **102**, 1770 (1980); (*c*) R.A. Moss, H. Fan, L.M. Hadel, S. Shen, J. Włostowska, M. Włostowski, and K. Krogh-Jespersen. Tetrahedron Lett. **28**, 4779 (1987); (*d*) R.A. Moss, M. Włostowski, J. Terpinski, G. Kmiecik-Lawrynowicz, and K. Krogh-Jespersen. J. Am. Chem. Soc. **109**, 3811 (1987); (*e*) R.S. Sheridan, R.A. Moss, B.K. Wilk, S. Shen, M. Włostowski, M.A. Kesselmayer, R. Subramanian, G. Kmiecik-Lawrynowicz, and K. Krogh-Jespersen. J. Am. Chem. Soc. **110**, 7563 (1988); (*f*) R.A. Moss, M. Włostowski, S. Shen, K. Krogh-Jespersen, and A. Matro. J. Am. Chem. Soc. **110**, 4443 (1988); (*g*) R.A. Moss, S. Shen, and M. Włostowski. Tetrahedron Lett. **29**, 6417 (1988); (*h*) R.A. Moss. Acc. Chem. Res. **22**, 15 (1989); (*i*) X.-M. Du, H. Fan, J.L. Goodman, M.A. Kesselmayer, K. Krogh-Jespersen, J.A. LaVilla, R.A. Moss, S. Shen, and R.S. Sheridan. J. Am. Chem. Soc. **112**, 1920 (1990); (*j*) T. Wong, J. Warkentin, and J.K. Terlouw. Int. J. Mass Spectrom. Ion Processes, **115**, 33 (1992); (*k*) M. El-Saidi, K. Kassam, D.L. Pole, T. Tadey, and J. Warkentin. J. Am. Chem. Soc. **114**, 8751 (1992); (*l*) C.-S. Ge, E.A. Jefferson, and R.A. Moss. Tetrahedron Lett. **34**, 7549 (1993); (*m*) G.A. McGibbon, C.A. Kingsmill, and J.K. Terlouw. Chem. Phys. Lett. **222**, 129 (1994); (*n*) P.C. Burgers, G.A. McGibbon, and J.K. Terlouw. Chem. Phys. Lett. **224**, 539 (1994); (*o*) R.A. Moss and C.-S. Ge. J. Fluorine Chem. **73**, 101 (1995); (*p*) A.J. Arduengo III, J.R. Goerlich, and W.J. Marshall. J. Am. Chem. Soc. **117**, 11027 (1995); (*q*) D.L. Pole and J. Warkentin. Liebigs Ann. 1907 (1995); (*r*) D. Suh, D.L. Pole, J. Warkentin, and J.K. Terlouw. Can. J. Chem. **74**, 544 (1996); (*s*) H.-T. Er, D.L. Pole, and J. Warkentin. Can. J. Chem. **74**, 1480 (1996); (*t*) P. Couture, M. El-Saidi, and J. Warkentin. Can. J. Chem. **75**, 326 (1997).
2. (*a*) J.E. Baldwin and J.A. Walker. J. Chem. Soc. Chem. Commun. 354 (1972); (*b*) G. Büchi, M. Cushman, and H. Wüest. J. Am. Chem. Soc. **96**, 5563 (1974); (*c*) J.E. Baldwin and J.A. Walker. J. Am. Chem. Soc. **96**, 596 (1974); (*d*) K.-K. Chan and G. Saucy. J. Org. Chem. **42**, 3828 (1977); (*e*) T. Nakai and K. Mikami. Chem. Lett. 1081 (1979); (*f*) L. Isaacs and F. Diederich. Helv. Chim. Acta, **76**, 2454 (1993); (*g*) W.W. Win, M. Kao, M. Eiermann, J.J. McNamara, F. Wudl, D.L. Pole, K. Kassam, and J. Warkentin. J. Org. Chem. **59**, 5871 (1994); (*h*) K. Kassam and J. Warkentin. J. Org. Chem. **59**, 5071 (1994); (*i*) D.L. Pole, P.K. Sharma, and J. Warkentin. Can. J. Chem. **74**, 1335 (1996); (*j*) A. de Meijere, S.I. Kozhushkov, D.S. Yufit, R. Boese, T. Haumann, D.L. Pole, P.K. Sharma, and J. Warkentin. Liebigs Ann. 601 (1996); (*k*) R. González, F. Wudl, D.L. Pole, P.K. Sharma, and J. Warkentin. J. Org. Chem. **61**, 5837 (1996); (*l*) J.H. Rigby, A. Cavezza, and G. Ahmed. J. Am. Chem. Soc. **118**, 12848 (1996); (*m*) K. Kassam, P.C. Venneri, and J. Warkentin. Can. J. Chem. **75**, 120 (1997).
3. (*a*) R.W. Hoffmann and H. Häuser. Tetrahedron Lett. 197 (1964); (*b*) D.M. Lemal, E.P. Gosselink, and A. Ault. Tetrahedron Lett. 579 (1964).
4. K. Kassam, D.L. Pole, M. El-Saidi, and J. Warkentin. J. Am. Chem. Soc. **116**, 1161 (1994).
5. P. Couture, J.K. Terlouw, and J. Warkentin. J. Am. Chem. Soc. **118**, 4214 (1996).
6. M. Zoghbi. Ph.D. Thesis, McMaster University, Hamilton, Ontario. 1991.
7. J.-i. Iwao. Pharm. Bull. **4**, 247 (1956).
8. R.-Y. Yang and L.-X. Dai. J. Org. Chem. **58**, 3381 (1993).
9. J. Martinez and J. Laur. Synthesis, 979 (1982).
10. E.J. Corey, M.G. Bock, A.P. Kozikowski, A.V.R. Rao, D. Floyd, and B. Lipshutz. Tetrahedron Lett. 1051 (1978).
11. M. Zoghbi and J. Warkentin. Can. J. Chem. **71**, 907 (1993).

© 1997 NRC Canada

12. W.B. Smith. J. Org. Chem. **60**, 7456 (1995).
13. (*a*) M. Békhazi and J. Warkentin. J. Am. Chem. Soc. **103**, 2473 (1981); (*b*) A.P. Hitchcock, S. Sweep, T. Steel, M. Békhazi, and J. Warkentin. Can. J. Chem. **60**, 2914 (1982); (*c*) M. Békhazi and J. Warkentin. Can. J. Chem. **61**, 619 (1983); (*d*) J. Am. Chem. Soc. **105**, 1289 (1983); (*e*) D. Keus, M. Kaminski, and J. Warkentin. J. Org. Chem. **49**, 343 (1984); (*f*) M. Békhazi, P.J. Smith, and J. Warkentin. Can. J. Chem. **62**, 1646 (1984); (*g*) M.W. Majchrzak and J. Warkentin. Can. J. Chem. **67**, 1753 (1989).
14. P.K. Sharma and J. Warkentin. Tetrahedron Lett. **36**, 7591 (1995).
15. (*a*) E.J. Corey and R.A.E. Winter. J. Am. Chem. Soc. **85**, 2677 (1963); (*b*) E.J. Corey, F.A. Carey, and R.A.E. Winter. J. Am. Chem. Soc. **87**, 934 (1965); (*c*) D.M. Lemal, R.A. Lovald, and R.W. Harrington. Tetrahedron Lett. 2779 (1965); (*d*) R.R. Sauers. Tetrahedron Lett. **35**, 7213 (1994); (*e*) Tetrahedron Lett. **37**, 149 (1996).
16. (*a*) D.M. Lemal and E.H. Banitt. Tetrahedron Lett. 245 (1964); (*b*) D.L. Coffen. Tetrahedron Lett. 2633 (1970).
17. R.W. Hoffmann, K. Steinbach, and B. Dittrich. Chem. Ber. **106**, 2174 (1973).
18. M. Reiffen and R.W. Hoffmann. Chem. Ber. **110**, 37 (1977).
19. M. Franck-Neumann and M. Miesch. Tetrahedron, **39**, 1247 (1983).
20. R.M. Rodehorst and T.H. Koch. J. Am. Chem. Soc. **97**, 7298 (1975).
21. (*a*) J.C. Sheehan and P.T. Izzo. J. Am. Chem. Soc. **71**, 4059 (1949); (*b*) Y.S. Rao and R. Filler. *In* Oxazoles. *Edited by* I.J. Turchi. John Wiley and Sons, New York. 1986. pp. 361–729.
22. A.I. Vogel. *In* Elementary practical organic chemistry. Part II. Qualitative organic analysis. Longmans, Green, and Co., Ltd., London. 1957.
23. J. Buckingham and S.M. Donaghy (*Editors*). Dictionary of organic compounds. 6th ed. Chapman and Hall, New York. 1996.
24. S.R. Koepke, R. Kupper, and C.J. Michejda. J. Org. Chem. **44**, 2718 (1979).
25. N. Sonoda, G. Yamamoto, K. Natsukawa, K. Kondo, and S. Murai. Tetrahedron Lett. 1969 (1975).
26. M. Fujita, M. Nagai, and T. Inoue. Chem. Pharm. Bull. **30**, 1151 (1982).
27. J.P. Pezacki, B.D. Wagner, C.S.Q. Lew, J. Warkentin, and J. Lusztyk. J. Am. Chem. Soc. **119**, 1789 (1997).
28. M. Fujiwara, A. Baba, and H. Matsuda. J. Heterocycl. Chem. **26**, 1659 (1989).
29. G.S. Chandler and W.H.F. Sasse. Aust. J. Chem. **16**, 20 (1963).
30. A.J. Speziale and L.R. Smith. J. Org. Chem. **28**, 1805 (1963).
31. I. Shibata, K. Nakamura, A. Baba, and H. Matsuda. Bull. Chem. Soc. Jpn. **62**, 853 (1989).
32. S. Kobayashi, M. Isobe, and T. Saegusa. Bull. Chem. Soc. Jpn. **55**, 1921 (1982).
33. C.-H. Kwon and H.T. Nagasawa. J. Org. Chem. **55**, 3403 (1990).

Can. J. Chem. Downloaded from www.nrcresearchpress.com by 91.121.58.235 on 09/08/12
For personal use only.

© 1997 NRC Canada

Chemistry of cyclic aminooxycarbenes

Philippe Couture and John Warkentin

Abstract: A series of oxazolidin-2-ylidenes and one tetrahydro-1,3-oxazin-2-ylidene, generated by thermolysis of Δ^3-1,3,4-oxadiazolines in benzene at 90°C, were intercepted by insertion into the OH bond of phenols. In two cases the initial products rearranged to *N*-(2-aryloxyethyl)-*N*-methylformamides. The activation energy for rotation about the amide CN bond of those ultimate products was measured as 20.4 kcal/mol. The aminooxycarbenes reacted with two equivalents of methyl or phenyl isocyanate to give spiro-fused hydantoins. Major products from the reactions of the *N*-carbonyl carbenes with dimethyl acetylenedicarboxylate or with methyl propiolate were 2-oxazolines resulting from apparent acyl transfers from N to C in the proposed dipolar intermediates; minor products of 1:2 (carbene:trap) stoichiometry were also observed.

Key words: nucleophilic carbene, aminooxycarbene, oxadiazoline, amide rotation, oxazolidine.

Résumé : Une série d'oxazolidin-2-ylidènes et un tétrahydro-1,3-oxazin-2-ylidène, générés par thermolyse de Δ^3-1,3,4-oxadiazolines dans le benzène à 90°C, ont pu être interceptés par insertion dans la liaison OH de phénols. Dans deux cas, les produits initiaux se transposent en *N*-(2-aryloxyéthyl)-*N*-méthylformamides. On a établi que l'énergie autour de la liaison C—N de l'amide des produits ultimes est égale à 20,4 kcal/mol. Les aminooxycarbènes réagissent avec deux équivalents d'isocyanate de méthyle ou de phényle pour donner des hydantoïnes à jonction spiro. Les produits principaux des réactions des *N*-carbonylcarbènes avec l'acétylènedicarboxylate de diméthyle ou avec le propiolate de méthyle sont des 2-oxazolines provenant de transferts apparents d'acyle du N au C dans les intermédiaires dipolaires suggérés; on a aussi observé la présence de produits mineurs de stoechiométrie 1 : 2 (carbène : piège).

Mots clés : carbène nucléophile, aminooxycarbène, oxadiazoline, rotation d'amide, oxazolidine.

[Traduit par la rédaction]

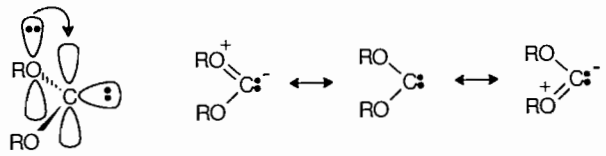
Can. J. Chem. Downloaded from www.nrcresearchpress.com by 91.121.58.235 on 09/08/12
For personal use only.

Introduction

The driving force behind carbene reactions, in general, is the completion of the octet of electrons at the electron-deficient carbon. It is therefore expected that carbenes should behave as electrophiles, and react more rapidly with electron-rich substrates than with electron-deficient ones. Indeed, relative reactivity measurements carried out by Skell and Garner (1) and Doering and Henderson (2) in the late 1950s demonstrated such electrophilic natures for both CBr_2 and CCl_2. Since then, however, the selection of carbenes available has grown tremendously, and "philicity" in singlet carbenes now extends from the traditional electrophiles to the more unconventional ambiphiles and nucleophiles (3).

The intrinsic need to acquire a completed valence shell is not as strong in carbenes bearing one or two π-donor substituents on the carbene centre. Conjugative donation to the formally vacant carbenic *p*-orbital by heteroatoms such as N and O stabilizes the singlet state substantially and gives the carbene dipolar character (Fig. 1). Such carbenes react as nucleophiles or ambiphiles (3*b*). Dimethoxycarbene, the archetypal nucleophilic carbene, is generally unreactive towards electron-rich alkenes, but it adds readily to chloroacrylonitrile (4) and other electron-deficient alkenes (5).

Fig. 1.



Carbene reactivity thus spans an enormous range. For instance, whereas simple alkylcarbenes are notoriously difficult to study because of rapid intramolecular reactions (6), methoxymethylcarbene undergoes intermolecular cycloaddition reactions with a variety of alkenes (7). Dialkoxycarbenes do not react with toluene or benzene by either cyclopropanation or by C—H insertion, but dimerize in such solvents (8). This stabilization of singlet carbenes by substituents reaches an extreme in the case of the stable diaminocarbenes first isolated by Arduengo et al. (9).

Carbenes in which the two substituents are aza, oxa, or thia groups, or any permutations of such groups, are carbonyl group equivalents and, as such, they have considerable synthetic potential. One strategy for optimizing their utility involves the tuning of their reactivity by using different combinations of OR, NRR′, and SR as carbene substituents. The aza substituent is the most versatile because of the two variable moieties R and R′. In this paper, we present some results on the intermolecular reactivity of carbenes possessing the combination of OR and NRR′ substituents.[2] Aminooxycarbenes have only rarely been reported (10), and little is there-

Received May 1, 1997.

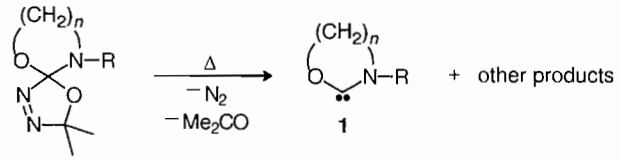
P. Couture and J. Warkentin.[1] Department of Chemistry, McMaster University, Hamilton, ON L8S 4M1, Canada.

[1] Author to whom correspondence may be addressed. Telephone: (905) 525-9140. Fax: (905) 522-2509. E-mail: Warkent@McMaster.ca

[2] A preliminary report on some of this work has been published (10*q*).

© 1997 NRC Canada

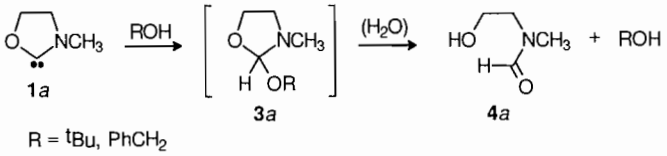
Scheme 1.



2 (n = 1, 2)

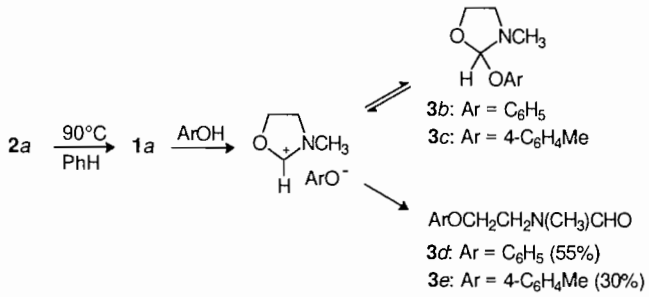
a: n = 2, R = Me; *b*: n = 2, R = C(O)H; *c*: n = 2, R = C(O)Me; *d*: n = 2, R = C(O)C(Me)=CH_2; *e*: n = 2, R = C(O)Ph; *f*: n = 2, R = C(O)OMe; *g*: n = 2, R = SO_2Ph; *h*: n = 3, R = C(O)Ph.

Scheme 2.



R = ^{t}Bu, $PhCH_2$

Scheme 3.



fore known about their properties. In particular, we demonstrate herein that fragmentation of 5-membered aminooxycarbenes **1** (n = 2) to ethylene and an isocyanate (11) is sufficiently slow to allow the carbenes to participate in bimolecular reactions with a variety of substrates, in contrast to the dioxy (10*d*, 12) and dithio (13) analogues.

Methods, results, and discussion

Aminooxycarbenes **1** were generated by thermolysis of Δ^3-1,3,4-oxadiazolines (**2**) in benzene solutions at 90°C (Scheme 1). Details of the syntheses and thermolyses of the oxadiazolines **2** have been described in the preceding paper (11) and **2***a* was also reported recently by Rigby's group (10*p*).

Insertions into OH bonds

The reaction of nucleophilic carbenes with hydroxyl compounds results in the net insertion of the carbene into the O—H bond (14). In fact, the formation of such adducts is often regarded as evidence for the intermediacy of carbenes. Trapping of carbene **1***a* was first attempted by thermolysing the precursor oxadiazoline, **2***a*, in the presence of *tert*-butyl alcohol. Instead of the expected product (**3***a*), ^{1}H NMR and GC–MS analyses of the thermolysate revealed *N*-(2-hydroxyethyl)-*N*-methylformamide (**4***a*) to be the major alcohol-derived product.[3] The same product was obtained in the thermolysis of **2***a* in the presence of benzyl alcohol.[4] These results may be explained in terms of the facile hydrolysis of the 2-oxy oxazolidines **3***a* upon exposure to the atmosphere (Scheme 2).

Table 1. Selected NMR data[a] for *N*-(2-aryloxyethyl)-*N*-methylformamides **3***d*, *e*.

		3*d* (~53:47)	**3***e* (~54:46)
^{1}H NMR	NCH_3	**2.96** (s), 3.12 (s)	**2.95** (s), 3.10 (s)
	NCH_2	**3.62** (t), 3.73 (t)	**3.60** (t), 3.71 (t)
	OCH_2	**4.07** (t), 4.14 (t)	**4.03** (t), 4.10 (t)
	CHO	8.08 (s), **8.14** (s)	8.07 (s), **8.13** (s)
^{13}C NMR	NCH_3	30.24, **36.42**	30.18, **36.35**
	NCH_2	44.29, **49.04**	44.28, **49.04**
	OCH_2	**64.90**, 66.17	**65.11**, 66.34
	CHO	162.86, **163.25**	162.82, **163.23**

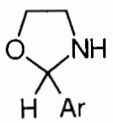
[a]Reported in ppm, in $CDCl_3$. Resonances from major conformers, assigned from the relative intensities of signals, are in bold, with the relative populations indicated in parentheses in the heading.

Like **3***a*, 2-aryloxyoxazolidines **3***b* and **3***c*, expected from the trapping of **1***a* with phenol and *p*-cresol, respectively, were not stable enough to survive the reaction conditions. The actual products, **3***e* and **3***d*, were again those of ring opening, presumably by reversible ion pair formation and eventual substitution by phenoxide at the OCH_2 group (Scheme 3).[5]

To confirm that the isolated products were formamides and not the novel oxazolidines **3***b* and **3***c*, NMR spectra were acquired at different temperatures to estimate the barrier, either to pyramidal inversion at nitrogen for the cases of **3***b*, *c* or to amide rotation for the cases of **3***d*, *e*. At room temperature, two sets of well-resolved signals of almost equal intensity, each one corresponding to one conformer, were observed in both the ^{1}H and ^{13}C spectra; selected NMR data are shown in Table 1.[6]

The nearly equal conformer populations allowed us to estimate the magnitude of the barrier by means of the coalescence method (15). Figure 2 shows the ^{1}H spectrum of **3***e* as a function of temperature, where coalescence of the N-methyl singlets was observed at ca. 135°C. Within experimental error, identical barriers of 20.4 kcal/mol were found for **3***d* and **3***e*.

Although high inversion barriers are common in small N-heterocycles such as aziridines (16), to our knowledge only



5

[3] The identity of **4***a* was confirmed by comparison with an authentic sample.

[4] A small amount of benzyl formate was also observed, suggesting the occurrence of a competing hydrolysis mechanism.

[5] The lower yield of **3***d* is attributed to some loss of material during purification.

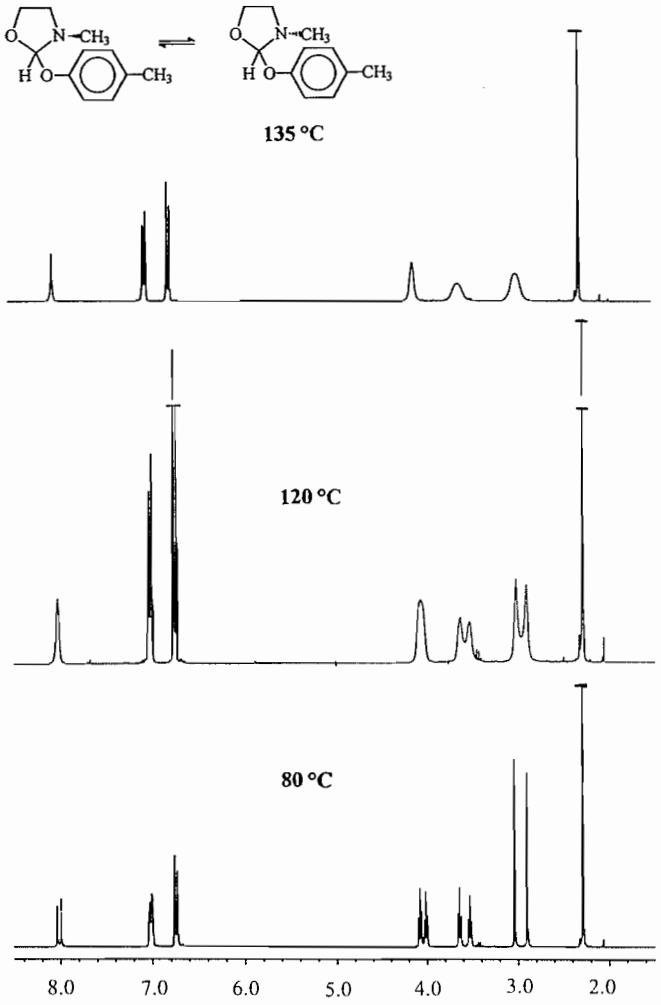
[6] Peak assignments were confirmed by means of double-irradiation experiments; for instance, the OCH_2 triplet at 4.07 ppm in **3***d* is coupled to the NCH_2 triplet at 3.62 ppm.

© 1997 NRC Canada

Can. J. Chem. Downloaded from www.nrcresearchpress.com by 91.121.58.235 on 09/08/12
For personal use only.

Can. J. Chem. Downloaded from www.nrcresearchpress.com by 91.121.58.235 on 09/08/12
For personal use only.

Fig. 2. 300 MHz ^{1}H spectrum of **3***c*, in hexachloro-1,3-butadiene, as a function of temperature. Spectra at 110, 130, and 140°C were also taken.



one report of such high barriers involving oxazolidines appears in the literature. Yang et al. (17) reported $\Delta G^{\ddagger}$ values of 20.7–22.3 kcal/mol for N-inversion in a series of 2-aryloxazolidines **5** unsubstituted at N. The much lower barriers in other known oxazolidines,[7] and the fact that amide rotation is associated with a barrier of ca. 20 kcal/mol, suggested that our products were amides. The ^{1}H and ^{13}C spectra (Table 1) are in agreement with the formamide assignments, **3***d*, *e*. In particular, the signal at 163 ppm would have to be assigned to C2, and that at 8.1 ppm to the proton at C2 of **3***b*, *c* if those structures were applicable. Oxazolidines with a heteroatom substituent at C2 are relatively rare, and they usually bear an electron-withdrawing group on N. In these compounds, the C2 signal typically appears near 112 ppm (ca. 50 ppm to higher field), as shown in Fig. 3 for two 2-alkoxyoxazolidines and some related compounds (18–20). Similarly, the C2 signal of 2-aryloxyoxazolidines bearing a carbonyl group on N appears near 105 ppm, and the C2-H is observed at 6.0–6.7 ppm (see **3***f–m* below). If oxazolidines **3***b*, *c* were applicable structures, they would have to exist as ion pairs in chloroform solution in order to match observed spectral characteristics. Models for both an undissociated oxazolidine (**6**) and the corresponding cation resulting from the loss of MeO^- (Fig. 4) were reported by Scholastico and co-workers (21).

N-Carbonyl oxadiazolines **2***b–f*, *h* fragmented to the corresponding aminooxycarbenes **1***b–f*, *h* (11) in high yields, as indicated by the results of trapping with phenols (Scheme 4, Table 2). *N*-Carbonyl adducts **3***f–m* were sensitive to hydrolysis and they could not be purified by chromatography. Compound **3***j* crystallized by addition of a mixture of ethyl acetate and hexane to the crude oil. Unfortunately, this procedure failed to produce crystals in most other cases. However, essentially pure products could be obtained in high yields by simply base-washing the thermolysates in order to remove the excess phenol; the benzene solutions were then dried over $MgSO_4$, and the solvent and volatile products were evaporated in vacuo to afford products **3**.

The ^{1}H and ^{13}C NMR spectra of compounds **3***f–m*, which were briefly discussed above, usually showed broad resonances and (or) more than one set of peaks due to restricted rotation about the amide CN bond. Low-intensity molecular ions in the mass spectra were generally observed, in addition to the characteristic M − OAr cations.

Hydrolysis of a sample of **3***j* kept in $CDCl_3$ cleanly produced *N*-[2-(formyloxy)ethyl]benzamide (**7***a*) and phenol over the course of a few weeks, as shown in Scheme 5.[8] Tetrahydro-1,3-oxazine **3***m* was more labile and partial hydrolysis was observable immediately after dissolving it in $CDCl_3$. In this solvent, **7***b* and phenol were the only products (Scheme 5). In contrast, the major fraction collected during an attempt to purify **3***m* by chromatography on silica consisted of a mixture of two related products, **7***b* and a material tentatively identified as **4***b*. Periodic recording of the ^{1}H NMR spectrum of this mixture, kept in $CDCl_3$, showed the gradual conversion of **4***b* into **7***b*, which was complete within 1 month (Scheme 5).

Thermolysis of **2***g* in the presence of phenol led to the formation of several products (11), but the anticipated carbene insertion product, **3***n*, could not be unambiguously identified. However, formamide **4***c*, probably derived from hydrolysis of **3***n*, was isolated (Scheme 6).

Reactions with isocyanates

Nucleophilic carbenes have been reported to react with alkyl or aryl isocyanates to give hydantoins (**8**) as final products (8, 10*k*, 22). Their formation was explained in terms of an initial attack of the carbene on the carbonyl carbon of the isocyanate, followed by 1,3-dipolar cycloaddition of the intermediate across the C=N bond of a second molecule of isocyanate (Scheme 7).[9] As anticipated, the generation of aminooxycarbenes **1** in the presence of methyl or phenyl isocyanate led to the isolation of the corresponding spiro-fused hydantoins **8***a–f* (Scheme 8, Table 3).

[7] For examples of related oxazolidines, see ref. (18).

[8] Sample was kept in the refrigerator for about 2 months and it was not examined regularly.

[9] These reactions contrast with the [1 + 4] cycloadditions between nucleophilic carbenes and benzoyl isocyanate, which yield 4(5*H*)-oxazolones (11).

© 1997 NRC Canada

Fig. 3. Selected NMR data for some models for **3***b, c*.

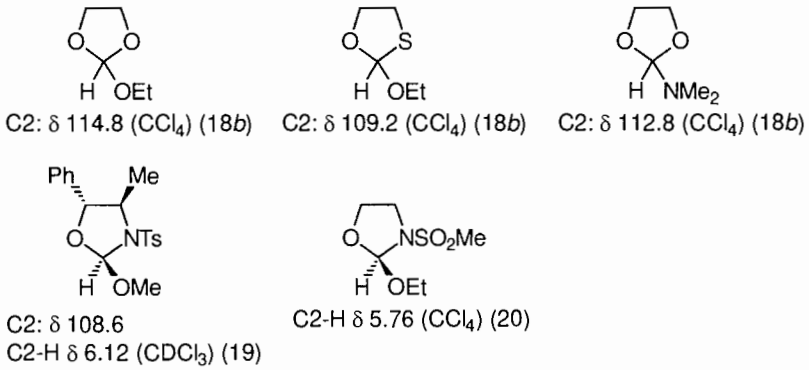
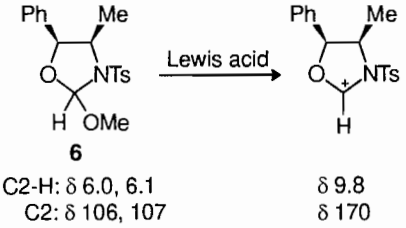
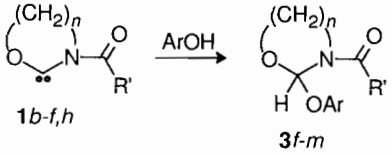


Fig. 4. Selected NMR data for **6** and the corresponding oxazolidinium cation (21).



Scheme 4.



Reactions with alkynes

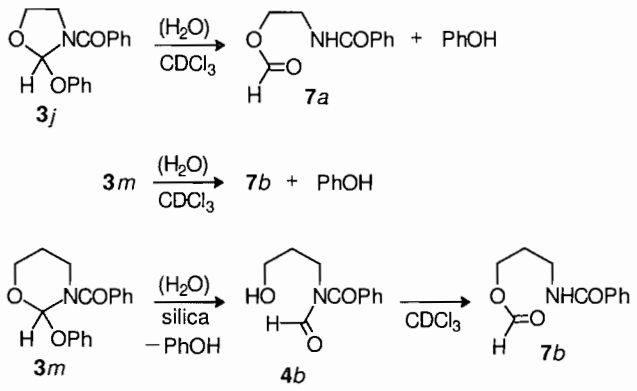
The reactivity of aminooxycarbenes **1** towards activated alkynes was also examined. Thermolysis of oxadiazoline **2***e* with 2.1 equivalents of dimethyl acetylenedicarboxylate (DMAD) gave three products, derived from reactions of carbene **1***e* with DMAD, that were isolated by chromatography, Scheme 9. The major product, oxazoline **9***a*, obtained in 73% yield, was apparently formed via benzoyl group transfer from N to C in the presumed 1,3-dipolar intermediate **10** (10*q*). That rearrangement is analogous to an aryl group transfer reported by Scherowsky's group (23). One of the minor products was assigned structure **11***a* (one of two possible diastereomers), by comparison of its spectral data with those of analogous dihydrofurans formed in the reaction of DMAD with other nucleophilic carbenes (5, 24). Its formation is rationalized in terms of the mechanism proposed by Hoffmann et al. (5) for the reaction of dimethoxycarbene with DMAD, where the dipolar intermediate (**10**, in the present case), formed by attack of the carbene at a triple-bonded carbon, adds across the carbonyl group of a second molecule of the alkyne (Scheme 9). For the third product, all spectral data were consistent with a 1:2 stoichiometry (carbene:DMAD), but its structure could not be elucidated.[10]

[10] Not the diastereo isomer of **11***a*.

Table 2. *N*-Carbonyl carbene–phenol adducts (**3**) isolated.

	n	R′	Ar	Yield (%)
3*f*	2	H	Ph	75
3*g*	2	Me	Ph	89
3*h*	2	C(Me)=CH_2	Ph	97
3*i*	2	C(Me)=CH_2	4-C_6H_4CN	84
3*j*	2	Ph	Ph	76
3*k*	2	Ph	4-C_6H_4CN	90
3*l*	2	OMe	Ph	>90
3*m*	3	Ph	Ph	97

Scheme 5.



2-Oxazolines bearing a substituent at C2 can be cleaved by hydrolysis or alcoholysis to the corresponding carboxylic acids or esters, respectively (25). As shown in Scheme 10, treatment of **9***a* with acetic acid in methanol gave a mixture of two inseparable compounds, namely, the expected triester **12** and an isomer tentatively assigned structure **13***a* (isomer **13***b* was ruled out (26)). Dihydrofuran derivative **13***a* likely results from the acid-catalyzed rearrangement of **12**.

In view of the reaction of **1***e* with DMAD, it was of interest to see if the same carbene would react with the less electrophilic methyl propiolate. From ^{1}H NMR analysis of the crude product after thermolysis, oxazoline **14** was clearly the major product (Scheme 11). However, substantial decomposition occurred during two successive separations by chromatography, and **14** was isolated in only 4% yield.

© 1997 NRC Canada

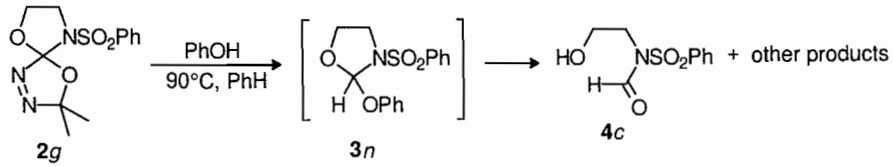
Can. J. Chem. Downloaded from www.nrcresearchpress.com by 91.121.58.235 on 09/08/12
For personal use only.

Can. J. Chem. Downloaded from www.nrcresearchpress.com by 91.121.58.235 on 09/08/12
For personal use only.

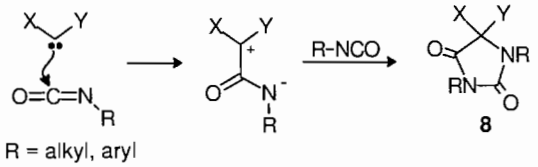
Table 3. Hydantoins **8** isolated from reactions of **1** with methyl or phenyl isocyanate.

	n	R	R′	Yield (%)
8*a*	2	Me	Me	44
8*b*	2	Me	Ph	27
8*c*	2	C(O)Me	Ph	87
8*d*	2	C(O)C(Me)=CH_2	Ph	72
8*e*	2	C(O)Ph	Ph	76
8*f*	3	C(O)Ph	Me	78

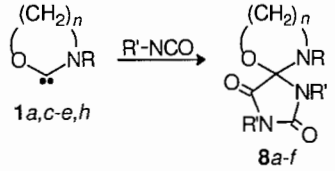
Scheme 6.



Scheme 7.



Scheme 8.



Reactions of aminooxycarbenes **1***c* (*N*-acetyl) and **1***d* (*N*-methacryloyl) with DMAD were also investigated and, in both cases, carbonyl group transfers were observed. Thus, thermolysis of oxadiazoline **2***d* with an excess of the alkyne afforded oxazoline **9***b*, isolated in 54% yield, as the major product (Scheme 12).

Thermolysis of **2***c* under similar conditions produced at least five different 1:2 adducts (carbene:DMAD), in addition to oxazoline **9***c*, as shown in Scheme 13. The latter, which appeared to be a major product from analysis of the crude thermolysate, decomposed completely during attempted separation by chromatography. This procedure, however, was successful in separating the 1:2 adducts from one another. Two of them were identified as the pair of diastereomers **11***b* and **11***c*, the latter (see experimental) being the analogue of **11***a*. Of the remaining three low-yield adducts, one was the analogue of the unidentified product reported above in the reaction of **1***e* with DMAD (Scheme 9).

Thermolysis of *N*-sulfonyl oxadiazoline **2***g* in the presence of DMAD also led to the isolation of several products, Scheme 14. Among them was oxazolidinone **15**, produced in a thermolytic fragmentation that competes with carbene generation (11). 2-Diazopropane, the coproduct of **15**, reacted with DMAD to give pyrazole **16** (11, 27). The only carbene + DMAD adduct that could be unambiguously identified was spiro-fused cyclopentadiene **17**, which apparently results from the unusual addition of the dipolar intermediate (the analogue of **10**) across the triple bond of a second molecule of DMAD.[11] Finally, compound **18** was also isolated in low yield; its origin is not known at present.

Experimental

General methods

Radial chromatography was performed with a Chromatotron apparatus, model 7924T (Harrison Research Inc.), with silica-coated plates of 1 mm, 2 mm, or 4 mm thickness. NMR spectra were recorded on a Bruker AC-200 or AC-300 spectrometer; signals labelled "um" appear as broad unresolved multiplets because of slow exchange. Infrared spectra were recorded with a Biorad FTS-40 spectrophotometer, with the sample either in CCl_4 or in KBr as a pellet. The IR bands are labelled qualitatively with the symbols br for broad, app for apparent, and s, m, and w for strong, medium, and weak intensities, respectively. Bands from C–H stretching vibrations between 2850 and 3100 cm^{-1} are omitted, as are very weak bands. Mass spectra were obtained on a VG Analytical ZAB-E double focusing mass spectrometer or on a HP-5890 Series II gas chromatograph with a 5971A mass selective detector. Melting points were recorded on a Thomas Hoover capillary melting point apparatus, and are reported uncorrected. Elemental analyses were performed by Guelph Chemical Laboratories, Ltd. (Guelph, Ontario).

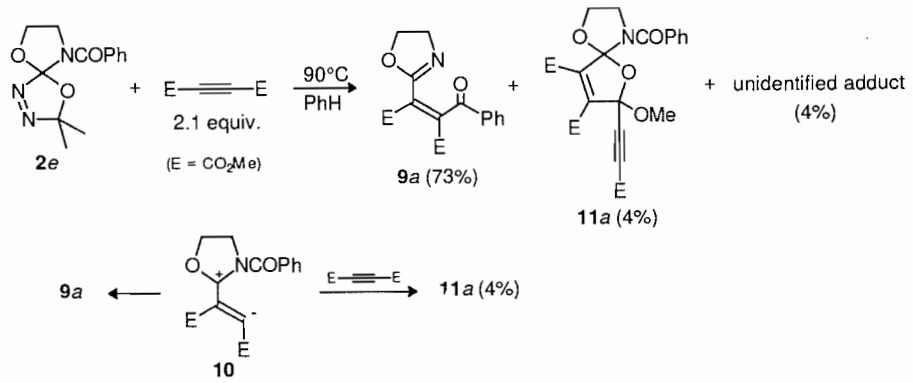
General methods for thermolyses

Benzene used as a thermolysis solvent was distilled from sodium benzophenone, and stored over molecular sieves.

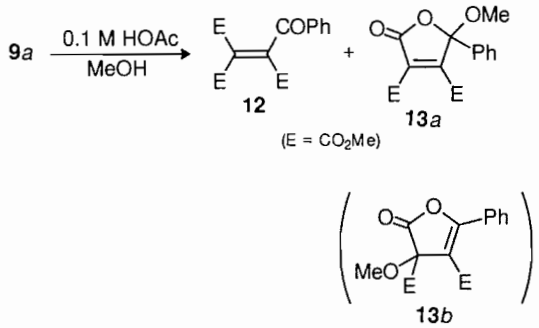
[11] The more commonly observed adducts of type **11** were probably formed but they could not be identified with certainty, due to difficulties in the separation. In addition, a 1:3 adduct (carbene:DMAD) was isolated, but its low yield (ca. 1%) prevented a definite structural assignment.

© 1997 NRC Canada

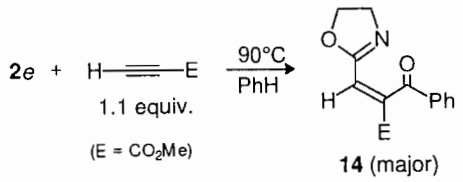
Scheme 9.



Scheme 10.



Scheme 11.



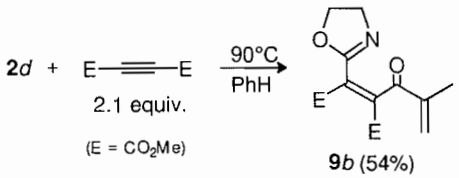
Typically, a benzene solution (10 mL) of the oxadiazoline[12] (0.5 mmol, 50 mM) and a specified amount of compound used as carbene trap were transferred to a sealable thermolysis tube. In some cases, this was preceded by distilling, under a dry nitrogen atmosphere, approximately 20 mL of the solution to be thermolysed down to 10 mL, in order to azeotrope out any water. The tube was then evacuated, sealed, and immersed in a constant temperature oil bath at 90°C ± 0.2°C for 24 h unless otherwise stated. The solvent and volatile products were removed with a rotary evaporator prior to analysis of the crude thermolysate by NMR and, in some cases, GC–MS. Thermolysis products were then separated and purified as described below.

Reactions with alcohols

Thermolysis of **2**a *with* tert*-butyl alcohol*

Oxadiazoline **2***a* (15 mg, 0.085 mmol) was heated with *tert*-butyl alcohol (40 μL, 0.42 mmol, dried by refluxing over calcium hydride followed by distillation) in a sealed NMR tube in ca. 0.5 mL of benzene-d_6. Analysis of the crude thermolysate by ^{1}H NMR and GC–MS revealed the presence of **4***a*.

Scheme 12.



N-*(2-Hydroxyethyl)*-N-*methylformamide (***4**a*)*: An authentic sample was prepared from the reaction of 2-(methylamino)-1-ethanol with ethyl formate, as described by Shibanuma et al. (28). Colourless oil; ^{1}H NMR (300 MHz, $CDCl_3$, slow exchange, signals due to major isomer are underlined, A:B ≈ 60:40) δ: 2.87 (s) and 3.02 (s) (3H, NCH_3), 3.24–3.85 (m) and 4.25–4.35 (m) (5H, CH_2CH_2, OH), 8.00 (s) and 8.05 (s) (1H, C(O)H); ^{13}C NMR (50 MHz, $CDCl_3$) δ: 29.78 and 35.81 (NCH_3), 47.54 and 52.13 (NCH_2), 58.62 and 60.11 (OCH_2), 163.56 and 163.78 (C=O); MS (EI) *m/z*: 103 (M^+, 2), 85 (5), 72 (19), 60 (11), 56 (8), 44 (100), 29 (45).

Thermolysis of **2**a *with benzyl alcohol*

Oxadiazoline **2***a* (103 mg, 0.60 mmol) was heated with benzyl alcohol (99 mg, 0.91 mmol) in 10 mL of benzene. Formamide **4***a* (above) was the major aminooxycarbene-derived product (by ^{1}H NMR and GC–MS); a small amount of benzyl formate was also observed.

Benzyl formate (ref. 29): MS (EI) *m/z*: 136 (M^+, 27), 108 (37), 91 (100), 77 (75), 65 (37), 51 (43), 39 (26), 29 (49).

Reactions of carbene 1*a* with phenols

N-*Methyl*-N-*(2-phenoxyethyl)fomamide (***3**d*)

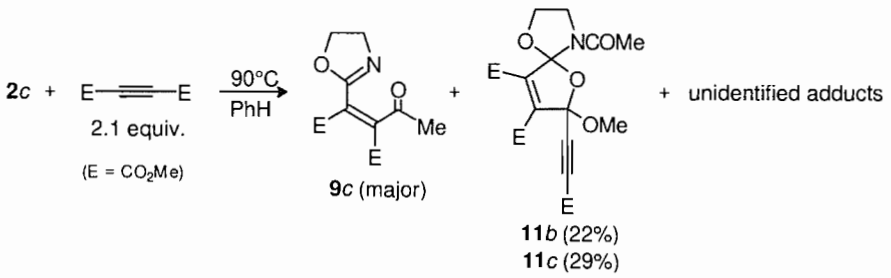
Oxadiazoline **2***a* (84 mg, 0.49 mmol) was heated with phenol (58 mg, 0.62 mmol) in 10 mL of benzene. Purification by radial chromatography, with 10–60% ethyl acetate in hexane, gave **3***d* in 55% yield. Colourless oil; IR (CCl_4) cm^{-1}: 1771m, 1684s, 1600m, 1497s, 1382m, 1301w, 1242s, 1173w, 1081m,

[12] Details of the syntheses of oxadiazolines **2** have been described (11).

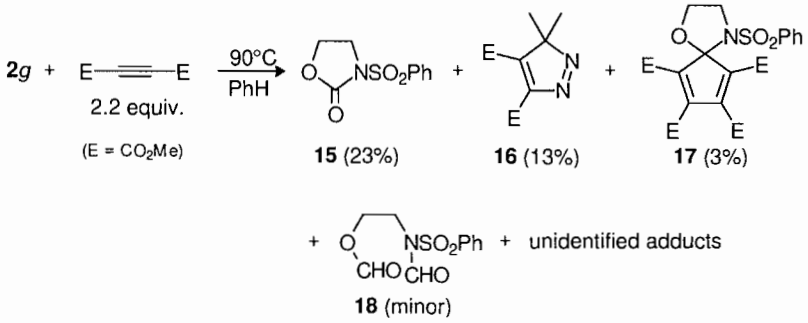
Can. J. Chem. Downloaded from www.nrcresearchpress.com by 91.121.58.235 on 09/08/12
For personal use only.

© 1997 NRC Canada

Scheme 13.



Scheme 14.



1056m, 908w; ^{1}H NMR (300 MHz, $CDCl_3$, slow rotation, signals from the major rotamer are underlined, A:B ≈ 53:47) δ: 2.96 (s) and 3.12 (s) (3H, NCH_3), 3.62 (t, ^3J = 5.2 Hz) and 3.73 (t, ^3J = 5.2 Hz) (2H, NCH_2), 4.07 (t, ^3J = 5.2 Hz) & 4.14 (t, ^3J = 5.2 Hz) (2H, OCH_2), 6.84–7.02 (m, 3H, Ar-*o,p*), 7.23–7.33 (m, 2H, Ar-*m*), 8.08 (s) and 8.14 (s) (1H, CHO); ^{13}C NMR (75 MHz, $CDCl_3$) δ: 30.24 and 36.42 (NCH_3), 44.29 and 49.04 (NCH_2), 64.90 and 66.17 (OCH_2), 114.42 and 114.56 (OPh C2, C6), 121.14 and 121.46 (OPh C4), 129.59 (OPh C3, C5), 158.13 and 158.41 (OPh C1), 162.86 and 163.25 (CHO); MS (EI) *m/z*: 179 (M^+, 1), 149 (1), 120 (14), 107 (6), 91 (19), 86 (M-OPh, 100), 77 (81), 72 (21), 65 (42), 58 (84), 51 (45), 44 (81), 39 (47), 28 (36); MS (CI, NH_3) *m/z*: 197 $(M + NH_4)^+$, 180 $(M + H)^+$.

N-*Methyl*-N-*(2-(4-methylphenoxy)ethyl)formamide (3*e)
Oxadiazoline **2***a* (90 mg, 0.52 mmol) was heated with *p*-cresol (93 mg, 0.86 mmol) in 10 mL of benzene. Purification by radial chromatography, with 20–40% ethyl acetate in hexane, gave **3***e* in 30% yield. Colourless oil; ^{1}H NMR (200 MHz, $CDCl_3$, slow rotation, signals from the major rotamer are underlined, A : B ≈ 54 : 46) δ: 2.28 (s, 3H, Ar-CH_3), 2.95 (s) and 3.10 (s) (3H, NCH_3), 3.60 (t, ^3J = 5.2 Hz) and 3.71 (t, ^3J = 5.2 Hz) (2H, NCH_2), 4.03 (t, ^3J = 5.2 Hz) and 4.10 (t, ^3J = 5.2 Hz) (2H, OCH_2), 6.77 (app d, ^3J = 8.6 Hz, 2H, Ar C(2,6)H), 7.08 (app d, ^3J = 8.6 Hz, 2H, Ar C(3,5), 8.07 (s) and 8.13 (s) (1H, CHO); ^{13}C NMR (50 MHz, $CDCl_3$) δ: 20.46 (Ar-CH_3), 30.18 and 36.35 (NCH_3), 44.28 and 49.04 (NCH_2), 65.11 and 66.34 (OCH_2), 114.29 and 114.45 (OAr C2, C6), 130.00 (OAr C3, C5), 130.34 and 130.72 (OAr C4), 156.06 and 156.31 (OAr C1), 162.82 and 163.23 (CHO); MS (EI) *m/z*: 193 (M^+, 1), 149 (1), 134 (5), 119 (7), 107 (15), 91 (40), 86 (M − OPh, 100), 77 (37), 65 (28), 58 (73), 51 (16), 44 (42), 28 (19).

Reactions of carbenes 1*b–g* with phenols
Compounds **3***f–n* are very easily hydrolysed and they could not be purified by chromatography. Products of reasonable purity were generally obtained after the following work-up: the excess phenol was removed by washing the thermolysate, diluted to 25 mL with fresh benzene, with 4 × 5 mL of aqueous NaOH (5%), followed by 5 mL of water or brine; this was followed by extraction of the combined aqueous layers with one portion of benzene, and drying of the organic phase over $MgSO_4$.

*3-Formyl-2-phenoxyoxazolidine (3*f)
Oxadiazoline **2***b* (49 mg, 0.26 mmol) was heated with phenol (39 mg, 0.41 mmol) in 10 mL of benzene. Work-up as indicated above gave **3**f as a colourless oil in 75% yield. IR (CCl_4) cm^{-1}: 1699s (C═O), 1591m, 1494m, 1415m, 1385m, 1356m, 1297w, 1205s, 1117w, 1083m, 1030w, 1010m, 991m, 953w, 876w; ^{1}H NMR (200 MHz, C_6D_6, slow exchange) δ: ca. 2.4–3.9 (um's, 4H, OCH_2CH_2N), 6.03 (s) and 6.07 (s) (1H, C(2)H), 6.85–7.40 (m, 5H, Ar), 7.90 (br s) and 8.27 (br s) (1H, C(O)H); ^{13}C NMR (50 MHz, C_6D_6, slow exchange, signals from major isomer are underlined) δ: 41.12 and 42.09 (NCH_2), 64.61 (OCH_2), 102.91 and 104.34 (C2), 117.96 and 118.52 (OPh C2, C6), 123.18 (OPh C4), 129.79 (OPh C3, C5), 155.47 (OPh C1), 158.87 and 159.27 (C═O); MS (EI) *m/z*: 193 (M^+, 1), 134 (2), 107 (1), 100 (M − OPh, 100), 94 (27), 78 (8), 72 (68), 65 (28), 51 (7), 44 (72), 39 (31), 29 (15); MS (CI, NH_3) did not give useful information.

*3-Acetyl-2-phenoxyoxazolidine (3*g)
Oxadiazoline **2***c* (96 mg, 0.48 mmol) was heated with phenol (59 mg, 0.63 mmol) in 10 mL of benzene. The usual work-up gave **3***g* as an oil in 89% yield; all attempts to crystallize the oil failed. IR (CCl_4) cm^{-1}: 1735w, 1683s (C═O), 1594m, 1494m, 1406m, 1357m, 1210s, 1099w, 1061w, 1007m, 980m, 946m; ^{1}H NMR (200 MHz, $CDCl_3$, slow exchange) δ: 1.85 (s) and 2.15 (s) (3H, CH_3), 3.58–3.92 (m, 2H, NCH_2), 4.20–4.52 (m,

© 1997 NRC Canada

Can. J. Chem. Downloaded from www.nrcresearchpress.com by 91.121.58.235 on 09/08/12
For personal use only.

Can. J. Chem. Downloaded from www.nrcresearchpress.com by 91.121.58.235 on 09/08/12
For personal use only.

2H, OCH_2), 6.39 (s) and 6.66 (s) (1H, C(2)H), 7.06–7.17 (m, 3H, Ar-*o,p*), 7.25–7.40 (m, 2H, Ar-*m*); ^{13}C NMR (50 MHz, $CDCl_3$, slow exchange, signals from major isomer are underlined) δ: 22.41 and 22.79 (CH_3), 43.27 and 44.65 (NCH_2), 64.83 and 65.31 (OCH_2), 103.84 and 104.34 (C2), 117.52 and 118.21 (OPh C2, C6), 122.96 and 123.24 (OPh C4), 129.41 and 129.68 (OPh C3, C5), 154.93 and 155.45 (OPh C1), 168.12 and 168.43 (C=O); MS (EI) *m/z*: 207 (M^+, 2), 135 (3), 114 (M − OPh, 65), 94 (29), 84 (13), 72 (100), 65 (18), 49 (20), 44 (39); MS (CI, NH_3) *m/z*: 208 $(M + H)^+$.

*3-Methacryloyl-2-phenoxyoxazolidine (**3**h)*

Thermolysis of oxadiazoline **2***d* (71 mg, 0.32 mmol) in the presence of phenol (44 mg, 0.68 mmol) in 10 mL of benzene gave, after the usual work-up, **3***h* as a viscous, colourless oil in 97% yield. IR (CCl_4) cm^{-1}: 1734w, 1667s (C=O), 1632m, 1591w, 1496m, 1454w, 1396m, 1370m, 1200s, 1118w, 1084w, 1007m, 982s, 948m, 891; ^1H NMR (200 MHz, $CDCl_3$, slow exchange, some peaks are broad) δ: 2.00 (app t, ^4J = 1.3 Hz, 3H, CH_3), 3.75–3.87 (m, 2H, NCH_2), 4.20–4.44 (m, 2H, OCH_2), 5.31 (br s, 1H, $=CH_2$), 5.42 (app t, ^4J = 0.9 Hz, 1H, $=CH_2$), 6.51 (br s, 1H, C(2)H), 7.00–7.13 (m, 3H, Ar-*o,p*), 7.25–7.39 (m, 2H, Ar-*m*); ^{13}C NMR (50 MHz, $CDCl_3$) δ: 19.98 (CH_3), 43.31 (NCH_2), 64.52 (OCH_2), 105.23 (C2), 117.62 and 117.82 (OPh C2, C6, and $=CH_2$), 123.02 (OPh C4), 129.85 (OPh C3, C5), 141.66 ($=CR_2$), 155.69 (OPh C1), 169.09 (C=O); MS (EI) did not give useful information; MS (CI, NH_3) *m/z*: 234 $(M + H)^+$.

*2-(4-Cyanophenoxy)-3-methacryloyloxazolidine (**3**i)*

Thermolysis of oxadiazoline **2***d* (100 mg, 0.44 mmol) in the presence of 4-cyanophenol (62 mg, 0.52 mmol) in 10 mL of benzene gave a partially crystalline oil (84% yield) after the usual work-up. ^1H NMR (200 MHz, C_6D_6, slow exchange) δ: 1.81 (s, 3H, CH_3), ca. 3.0–4.0 (um, 4H, NCH_2, OCH_2), 4.89 (br s, 1H, $=CH_2$), 5.11 (br s, 1H, CH_2), 6.14 (br s) and 6.38 (br s) (1H, C(2)H), 6.55–7.20 (um, 4H, Ar); ^{13}C NMR (50 MHz, C_6D_6) δ: 19.84 (CH_3), 43.47 (br, NCH_2), 65.11 (OCH_2), 104.69 (OAr C4), 106.62 (C2), 117.53 (OAr C2, C6), 118.12 ($=CH_2$), 122.66 (C≡N), 134.00 (OAr C3, C5), 141.31 ($=CR_2$), 158.35 (OAr C1), 169.06 (C=O); MS (EI) *m/z*: 140 (M − OAr, 35), 119 (6), 84 (5), 69 (methacryloyl cation, 100), 64 (4), 49 (10), 41 (72); MS (CI, NH_3) *m/z*: 276 $(M + NH_4)^+$, 259 $(M + H)^+$.

*3-Benzoyl-2-phenoxyoxazolidine (**3**j)*

Oxadiazoline **2***e* (105 mg, 0.40 mmol) was heated with phenol (72 mg, 0.77 mmol) in 10 mL of benzene. After removal of the solvent and volatile products on the rotary evaporator, **3***j* solidified upon addition of 20% ethyl acetate in hexane. Recrystallization from the same solvent mixture yielded a white solid, mp 89–91°C (76% yield). IR (KBr) cm^{-1}: 1660s (C=O), 1591s, 1493w, 1448w, 1399s, 1201m, 1168w, 1115w, 1084m, 951m, 933m, 887m, 791w, 770w, 725w; ^1H NMR (200 MHz, $CDCl_3$, slow exchange) δ: 3.70–4.10 (um, 2H, NCH_2), 4.10–4.45 (um, 2H, OCH_2), 6.21 (br s, 1H, C(2)H), 6.70–7.10 (um, 3H, Ar), 7.10–7.45 (um, 5H, Ar), 7.55–7.65 (m, 2H, Ar); ^{13}C NMR (50 MHz, $CDCl_3$) δ: 43.48 (NCH_2), 64.60 (OCH_2), 105.19 (C2), 117.79 (OPh C2, C6), 123.12 (OPh C4), 127.58 (benzoyl C2, C6), 128.42 (benzoyl C3, C5), 129.52 (OPh C3, C5), 130.92 (benzoyl C4), 135.45 (benzoyl C1), 154.67 (OPh C1), 169.00 (C=O); MS (EI) *m/z*: 269 (M^+, 2), 198 (2), 176 (M − OPh, 14), 147 (18), 117 (20), 105 ($PhCO^+$, 100), 94 (21), 84 (42), 77 (42), 49 (54); MS (CI, NH_3) *m/z*: 270 $(M+H)^+$; HRMS calcd. for $C_{10}H_{10}NO_2$ (M − OPh): *m/z* 176.0712, found: *m/z* 176.0705.

*2-(4-Cyanophenoxy)-3-benzoyloxazolidine (**3**k)*

Oxadiazoline **2***e* (107 mg, 0.41 mmol) was thermolysed with 4-cyanophenol (59 mg, 0.49 mmol) in 10 mL of benzene. The usual work-up gave **3***k* as a white solid in 90% yield. IR (CCl_4) cm^{-1}: 2230m (C≡N), 1751s, 1672s (C=O), 1605s, 1507m, 1451w, 1384s, 1257m, 1210s, 1172m, 1080m, 1056m, 1022w, 962s, 889w, 836w; ^1H NMR (200 MHz, $CDCl_3$, slow exchange) δ: ca. 3–4 (um, 4H, NCH_2, OCH_2), ca. 5.8–8.3 (um, 10H, C(2)H, Ar); ^{13}C NMR (50 MHz, C_6D_6) δ: 44.06 (br, NCH_2), 65.10 (OCH_2), 104.96 (OAr C4), 106.74 (C2), 117.57 (OAr C2, C6), 122.74 (C≡N), ca. 128 (overlapped with solvent triplet, aroyl C2, C6 and C3, C5), 131.04 (aroyl C4), 135.83 (aroyl C1), 133.88 (OAr C3, C5), 158.19 (OAr C1), 168.6 (C=O); MS (EI) *m/z*: 176 (M − OAr, 38), 105 ($PhCO^+$, 100), 90 (6), 77 (32), 51 (10); MS (CI, NH_3) *m/z*: 295 $(M+H)^+$.

*3-Methoxycarbonyl-2-phenoxyoxazolidine (**3**l)*

Oxadiazoline **2***f* (55 mg, 0.26 mmol) was heated with phenol (30 mg, 0.32 mmol) in 10 mL of benzene. The usual work-up gave **3***l* as a colourless oil in quantitative yield. IR (CCl_4) cm^{-1}: 1728s (C=O), 1593m, 1494m, 1451s, 1391s, 1301w, 1212s, 1137w, 1076m, 987s, 692; ^1H NMR (200 MHz, C_6D_6, slow exchange) δ: ca. 2.9–4.1 (um's, 7H, OCH_2CH_2N, CH_3), 6.46 (br s) and 6.74 (br s) (1H, C(2)H), ca. 6.8–7.4 (um, 5H, Ar); ^{13}C NMR (50 MHz, C_6D_6, slow exchange) δ: 43.83 (NCH_2), 52.42 (CH_3), 64.73 and 65.14 (OCH_2), 104.52 and 105.52 (C2), 118.18 (OPh C2, C6), 122.97 (OPh C4), 129.79 (OPh C3, C5), 153.38 and 156.35 (OPh C1 and C=O); MS (EI) *m/z*: 223 (M^+, <1), 192 (2), 130 (M − OPh, 100), 94 (8), 78 (5), 70 (5), 65 (17), 58 (35), 39 (16), 30 (8); MS (CI, NH_3) did not give useful information.

*3-Benzoyl-2-phenoxytetrahydro-2H-1,3-oxazine (**3**m)*

Oxadiazoline **2***h* (100 mg, 0.36 mmol) was heated with phenol (52 mg, 0.55 mmol) in 10 mL of benzene. The usual work-up gave essentially pure **3***m* (97% yield), which crystallized upon addition of 10% ethyl acetate in hexane. White solid, mp ca. 83–92°C; IR (CCl_4) cm^{-1}: 1732w, 1663s (C=O), 1597m, 1496m, 1448w, 1416m, 1381m, 1356w, 1333w, 1287m, 1218m, 1196m, 1173m, 1090m, 1017m, 977s, 930m, 903w, 853w; ^1H NMR (300 MHz, C_6D_6, slow exchange) δ: 0.86–1.12 (um, 1H, CCH_2C), 1.63–1.85 (um, 1H, CCH_2C), 3.34–3.53 (um, 2H, NCH_2), 3.81–4.00 (um, 1H, OCH_2), 4.16–4.35 (um, 1H, OCH_2),[13] 6.80–7.25 (um, 9H) and 7.40–7.65 (um, 2H) (Ar and C(2)H); ^{13}C NMR (75 MHz, C_6D_6, slow exchange) δ: 24.28 (CCH_2C), 37.97 (NCH_2),[14] 59.49 (OCH_2), 99.66 (C2),[15] 117.26 (OPh C2, C6), 122.74 (OPh C4), ca. 127.5 (benzoyl C2, C6, under solvent triplet), 128.57 (benzoyl

[13] One of the OCH_2 proton signals disappears at room temperature; at 90%C, it appears at 4.16–4.35 (um).

[14] At room temperature, the NCH_2 signal appears as a very wide resonance in the range 35–40 ppm; at 77°C, it is a slightly broadened singlet at 37.97 ppm.

[15] Taken at 77°C; at room temperature, the signal is broad, in the range 97–102 ppm.

© 1997 NRC Canada

Can. J. Chem. Downloaded from www.nrcresearchpress.com by 91.121.58.235 on 09/08/12
For personal use only.

C3, C5), 129.85 (OPh C3, C5), 130.21 (benzoyl C4), 135.68 (benzoyl C1), 155.58 (OPh C1), 169.36 (C=O); MS (EI) *m/z*: 266 (2), 190 (M − OPh, 66), 172 (4), 105 ($PhCO^+$, 100), 94 (6), 84 (8), 77 (23), 65 (5), 49 (12); MS (CI, NH_3) *m/z*: 284 $(M + H)^+$.

N-*[2-(Formyloxy)ethyl]benzamide (***7**a*)*

White solid, mp 59-60°C (slightly impure sample, previously reported to be a liquid (30)); IR (CCl_4) cm^{-1}: 3465br (NH), 1735s (OC=O), 1677s (NC=O), 1517m, 1486w, 1302m, 1174s, 909w; ^1H NMR (200 MHz, $CDCl_3$) δ: 3.77 (q, ^3J = 5.4 Hz, 2H, NCH_2), 4.39 (t, ^3J = 5.2 Hz, 2H, OCH_2), 6.55 (br s, 1H, NH), 7.35–7.60 (m, 3H, Ar-*m,p*), 7.72–7.84 (m, 2H, Ar-*o*), 8.11 (s, 1H, C(O)H); ^{13}C NMR (75 MHz, $CDCl_3$) δ: 38.94 (NCH_2), 62.58 (OCH_2), 126.88 (Ar C2, C6), 128.41 (Ar C3, C5), 131.50 (Ar C4), 133.98 (Ar C1), 160.89 (OC=O), 167.79 (NC=O); MS (EI) *m/z*: 193 (M^+, 5), 164 (3), 147 (19), 134 (5), 105 ($PhCO^+$, 100), 77 (58), 51 (22), 31 (8); MS (CI, NH_3) *m/z*: 211 $(M + NH_3)^+$, 194 $(M + H)^+$.

N-*[3-(Formyloxy)propyl]-benzamide (***7**b*) (30)*

The major band collected in an attempt to purify a sample of **3***m* by radial chromatography (20–60% ethyl acetate in hexane) was found to consist, initially, of a mixture of **7***b* and an isomer tentatively identified as **4***b*. The latter was completely converted to **7***b* when the mixture was left in $CDCl_3$ over 1 month, at or below room temperature. **7***b*: colourless oil; IR (CCl_4) cm^{-1}: 3454m (NH), 1728s (OC=O), 1674s (NC=O), 1605w, 1580w, 1519s, 1487m, 1304w, 1278m, 1176s, 913w, 711m; ^1H NMR (300 MHz, $CDCl_3$) δ: 1.90–2.08 (m, 2H, CCH_2C), 3.53 (app q, ^3J = 6.4 Hz, 2H, NCH_2), 4.30 (t, ^3J = 6.1 Hz, 2H, OCH_2), 6.66 (br s, 1H, NH), 7.30–7.65 (m, 3H, Ar-*m,p*), 7.70–7.85 (m, 2H, Ar-*o*), 8.10 (s, 1H, C(O)H); ^{13}C NMR (75 MHz, $CDCl_3$) δ: 28.61 (CCH_2C), 36.58 (NCH_2), 61.48 (OCH_2), 126.82 (Ar C2, C6), 128.55 (Ar C3, C5), 131.47 (Ar C4), 134.36 (Ar C1), 161.21 (HC=O), 167.61 (PhC=O); MS (EI) *m/z*: 207 (M^+, 3), 162 (14), 134 (8), 105 ($PhCO^+$, 100), 77 (53), 51 (18); MS (CI, NH_3) *m/z*: 225 $(M + NH_4)^+$, 208 $(M + H)^+$.

N-*[3-(Hydroxy)propyl]*-N-*formylbenzamide (***4**b*)*

Obtained as a mixture with **7***b*. ^1H NMR (200 MHz, $CDCl_3$) δ: 1.85–ca. 2.0 (m, 2H, CCH_2C), 3.64 (t, ^3J = 5.7 Hz, 2H, NCH_2), 4.04 (t, ^3J = 6.4 Hz, 2H, OCH_2), ca. 7.30–7.85 (Ar), 8.96 (s, 1H, C(O)H); ^{13}C NMR (50 MHz, $CDCl_3$, partial spectrum) δ: 30.70 (CCH_2C), 37.36 (NCH_2), 59.22 (OCH_2), 128.85 (Ar), 129.00 (Ar), 132.35 (Ar), 164.75 (HC=O), 172.90 (PhC=O).

N-*Formyl*-N-*(2-hydroxyethyl)benzenesulfonamide (***4**c*)*

Oxadiazoline **2***g* (143 mg, 0.48 mmol) was heated at 90°C for 48 h in the presence of phenol (69 mg, 0.74 mmol) in 10 mL of benzene. The usual base wash was performed. Compound **4***c* was isolated from the thermolysate by radial chromatography (10–30% ethyl acetate in hexane). IR (CCl_4) cm^{-1}: 3425–3000 (OH), 1736s (C=O), 1449w, 1417w, 1345m (NSO_2), 1264m, 1165s (NSO_2), 1097m, 1027w, 950w, 909w, 858w; ^1H NMR (200 MHz, $CDCl_3$, slow exchange) δ: 3.20–3.36 (m, 2H, NCH_2), 4.04–4.26 (m, 2H, OCH_2), 5.03 (br s, 1H, OH), 7.44–7.93 (m, ca. 6H, Ar and C(O)H); ^{13}C NMR (50 MHz, $CDCl_3$, only peaks from major conformer are given) δ: 41.99 (NCH_2), 62.41 (OCH_2), 126.99 (Ar C2, C6), 129.24 (Ar C3, C5), 132.91 (Ar C4), 139.83 (Ar C1), 160.42 (C=O); MS (EI) *m/z*: 183 (16), 170 (43), 141 ($PhSO_2^+$, 57), 119 (6), 92 (4), 77 (100), 51 (22), 31 (5); MS (CI, NH_3) *m/z*: 247 $(M + NH_4)^+$, 230 $(M + H)^+$.

Reactions with isocyanates

*Hydantoin **8**a*

Oxadiazoline **2***a* (102 mg, 0.60 mmol) was thermolysed in the presence of MeNCO (85 mg, 1.5 mmol) in 10 mL of benzene. Purification by radial chromatography, with 30–40% ethyl acetate in hexane, gave **8***a* in 44% yield. White solid, mp 71–73°C; IR (CCl_4) cm^{-1}: 1785m (C=O), 1729s (C=O), 1461s, 1419m, 1392m, 1299m, 1267w, 1231w, 1184w, 1144w, 1079s, 1015w, 993w, 973w, 949w; ^1H NMR (200 MHz, C_6D_6) δ: 1.97 (s, 3H, oxazolidine NCH_3), 2.65 (s, 3H, CH_3), 2.73 (s, 3H, CH_3), ca. 2.52–2.77 (overlapped m, 1H, NCH_2), 3.10–3.27 (m, 1H, NCH_2), 3.57–3.72 (m, 1H, OCH_2), 3.77–3.90 (m, 1H, OCH_2); ^{13}C NMR (75 MHz, C_6D_6) δ: 23.06 (CH_3), 23.43 (CH_3), 32.69 (CH_3), 51.18 (NCH_2), 65.17 (OCH_2), 101.67 (spiro C), 155.33 (NC(O)N), 170.24 (N*C*(O)C); MS (EI) *m/z*: 199 (M^+, 1), 171 (M − CO, 4), 154 (16), 141 (4), 127 (9), 113 (92), 99 (2), 86 (21), 70 (36), 57 (100), 42 (71), 28 (36); MS (CI, NH_3) *m/z*: 200 $(M + H)^+$. Anal. calcd. for $C_8H_{13}N_3O$: C 48.23, H 6.58, N 21.09; found: C 48.03, H 6.81, N 21.00.

*Hydantoin **8**b*

Oxadiazoline **2***a* (101 mg, 0.59 mmol) was heated with PhNCO (168 mg, 1.4 mmol) in 10 mL of benzene to give a product that precipitated from the crude thermolysate by addition of 30% ethyl acetate in hexane. After various unsuccessful attempts at recrystallizing the precipitate, it was triturated with the same solvent mixture (27% yield). White solid, mp 156–158°C; IR (KBr) cm^{-1}: 1786w (C=O), 1730s (C=O), 1647w, 1596w, 1494m, 1405m, 1372w, 1278w, 1188w, 1163w, 1069w, 941w, 760w; ^1H NMR (200 MHz, C_6D_6) δ: 2.20 (s, 3H, CH_3), 2.47–2.58 (m, 1H, NCH_2), 3.10–3.28 (m, 1H, NCH_2), 3.50–3.68 (m, 1H, OCH_2), 3.71–3.86 (m, 1H, OCH_2), 6.93–ca. 7.35 (m, 6H, Ar-*m,p*, overlapped with solvent), 7.46–7.58 (m, 2H, Ar-*o*), 7.58–7.70 (m, 2H, Ar-*o*); ^{13}C NMR (50 MHz, acetone-d_6) δ: 33.28 (CH_3), 52.02 (NCH_2), 66.09 (OCH_2), 103.42 (spiro C), 119.37, 122.80, 127.54, 129.55, 129.67, 132.53, 135.11, 153.72 (NC(O)N), 172.14 (N*C*(O)C) (two Ar peaks are coincident); MS (EI) *m/z*: 323 (M^+, 3), 292 (1), 212 (3), 203 (6), 176 (30), 162 (7), 127 (100), 119 ($PhNCO^+$, 18), 105 (6), 93 (22), 85 (18), 77 (11), 57 (16); MS (CI, NH_3) *m/z*: 324 $(M + H)^+$; HRMS calcd. for $C_{18}H_{17}N_3O_3$ (M^+): *m/z* 323.1270; found: *m/z* 323.1262.

*Hydantoin **8**c*

Oxadiazoline **2***c* (101 mg, 0.51 mmol) was heated with PhNCO (137 mg, 1.2 mmol) in 10 mL of benzene. The product could not be purified by chromatography due to its low solubility in most common solvents. The crude oil crystallized from a solvent consisting of 20% ethyl acetate in hexane to give **8***c*, as a slightly impure solid, in 87% yield; mp (selected crystals) 132–133°C; IR (KBr) cm^{-1}: 1735s (C=O), 1664m, 1598m, 1557m, 1500m, 1440m, 1411m, 1322m, 1266w, 1201w, 1169w, 1138w, 1111m, 1018w, 980w, 845w, 755m;

© 1997 NRC Canada

^{1}H NMR (200 MHz, $CDCl_3$) δ: 3.62 (s, 3H, CH_3), 3.52–3.70 (m, 1H, NCH_2), 4.03–4.18 (m, 1H, NCH_2), 4.23–4.54 (m, 2H, OCH_2), 7.08–7.55 (m, 10H, Ar); ^{13}C NMR (50 MHz, C_6D_6) δ: 24.00 (CH_3), 43.76 (NCH_2), 68.69 (OCH_2), 109.88 (spiro C), 119–139 (Ar, overlapped with solvent), 157.14 (NC(O)N), 164.80 (N*C*(O)C), 167.64 (N*C*(O)CH_3); MS (EI) *m/z*: 248 (2), 220 (52), 217 (3), 178 (1), 146 (2), 133 (1), 119 ($PhNCO^+$, 100), 101 (24), 91 (22), 77 (3), 71 (18), 64 (11), 56 (23), 51 (4), 42 (13), 28 (4); MS (CI, NH_3) did not give useful information.

Hydantoin ***8***d

Oxadiazoline **2***d* (115 mg, 0.51 mmol) was heated in the presence of PhNCO (136 mg, 1.1 mmol) in 10 mL of benzene. The product was obtained as a pale yellow solid in 72% yield after washing with ethyl acetate – hexane. Crystals obtained from recrystallization in the same solvent mixture melted at 240–241°C. IR (CCl_4) cm^{-1}: 1805w (hydantoin C═O), 1747s (hydantoin C═O), 1679m (methacryloyl C═O), 1624w, 1598w, 1502w, 1438w, 1400m, 1322m, 1246w, 1167m, 1138w, 1107w, 1080m, 1050m, 911w, 853w; ^{1}H NMR (300 MHz, $CDCl_3$) δ: 1.63 (s, 3H, CH_3), 3.48–3.63 (m, 1H, NCH_2), 4.02–4.13 (m, 1H, NCH_2), 4.25–4.38 (m, 1H, OCH_2), 4.43–4.54 (m, 1H, OCH_2), 5.22 (s, 1H, ═CH_2), 5.29 (s, 1H, ═CH_2), 6.64 (d, ^3J = 7.5 Hz, 2H, Ar), 6.85–7.60 (m, 8H, Ar); ^{13}C NMR (75 MHz, $CDCl_3$) δ: 20.20 (CH_3), 43.82 (NCH_2), 69.75 (OCH_2), 109.00 (spiro C), 119–130 (overlapping signals), 131.05, 134.08, 145.83 (═CR_2), 156.17 (NC(O)N), 157.32 (methacryloyl C═O), 163.57 (N*C*(O)C); MS (EI) *m/z*: 377 (M^+, 3), 258 (5), 230 (32), 217 (26), 202 (6), 173 (22), 146 (10), 139 (12), 119 ($PhNCO^+$, 100), 112 (15), 98 (11), 91 (40), 77 (12), 69 (86), 64 (16), 42 (62); MS (CI, NH_3) *m/z*: 378 (M + H)$^+$; HRMS calcd. for $C_{14}H_{14}N_2O_3$ (M − PhNCO): *m/z* 258.1004; found: *m/z* 258.1010.

Hydantoin ***8***e

Oxadiazoline **2***e* (90 mg, 0.35 mmol) was heated with PhNCO (132 mg, 1.1 mmol) in 10 mL of benzene. The sparingly soluble oily product crystallized after addition of ethyl acetate, and it was then recrystallized from the same solvent (76% yield). White solid, mp 151–152°C; IR (KBr) cm^{-1}: 1796w (hydantoin C═O), 1741s (hydantoin C═O), 1667m (PhC═O), 1594w, 1501w, 1451w, 1398m, 1326w, 1292w, 1240w, 1168w, 1141w, 1111w, 1079m, 1043m, 911w, 852w, 768w, 748w; ^{1}H NMR (300 MHz, acetone-d_6) δ: 3.72–3.86 (m, 1H, NCH_2), 4.13–4.28 (m, 1H, NCH_2), 4.47–4.60 (m, 1H, OCH_2), 4.60–4.73 (m, 1H, OCH_2), 6.62–6.74 (m, 2H, Ar), 6.95–7.06 (m, 1H, Ar), 7.13–7.50 (m, 12H, Ar); ^{13}C NMR (75 MHz, acetone-d_6) δ: 44.73 (NCH_2), 70.88 (OCH_2), 110.53 (spiro C), 121.80, 124.45, 127.43, 128.79, 129.13, 129.18, 129.63, 129.94, 130.23, 131.85, 132.74, 147.28, 156.31 (NC(O)N), 157.79 (PhC(O)N), 164.41 (N*C*(O)C); MS (EI) *m/z*: 216 (34), 189 (8), 146 (8), 119 ($PhNCO^+$, 100), 105 ($PhCO^+$, 57), 98 (13), 91 (28), 86 (37), 84 (56), 77 (38), 70 (37). Anal. calcd. for $C_{24}H_{19}N_3O_4$: C 69.72, H 4.63; found: C 69.33, H 4.86.

Hydantoin ***8***f

Oxadiazoline **2***h* (100 mg, 0.36 mmol) was heated with MeNCO (54 mg, 0.95 mmol) in 10 mL of benzene. The product, crystallized from the crude oil upon addition of ethyl acetate – hexane, was washed with 10% ethyl acetate in hexane (78% yield). White solid, mp 87–89°C; IR (CCl_4) cm^{-1}: 1794w (hydantoin C═O), 1734s (hydantoin C═O), 1673m (PhC═O), 1465m, 1396w, 1334w, 1298w, 1273w, 1231w, 1169w, 1140w, 1081w, 1056m, 962w, 924w; ^{1}H NMR (300 MHz, $CDCl_3$) δ: 1.57–1.72 (m, 1H, CCH_2C), 1.90–2.13 (m, 1H, CCH_2C), 3.12 (s, 3H, CH_3), 3.25 (s, 3H, CH_3), ca. 2.98–3.32 (overlapped m, 1H, NCH_2), 4.02–4.22 (m, 3H, NCH_2, OCH_2), 7.37–7.62 (m, 5H, Ar); ^{13}C NMR (75 MHz, $CDCl_3$) δ: 23.89 (CH_3), 24.74 (CH_3), 35.22 and 35.36 (CCH_2C and NCH_2), 63.62 (OCH_2), 126.80, 128.16, 128.52, 131.48, 135.23, 154.90 (NC(O)N), 169.05 (PhC(O)N), 174.48 (N*C*(O)C) (some aromatic Cs overlap); MS (EI) *m/z*: 303 (M^+, 1), 198 (2), 190 (4), 169 (100), 141 (9), 118 (6), 113 (5), 105 ($PhCO^+$, 13), 84 (14), 77 (15), 56 (15); MS (CI, NH_3) *m/z*: 304 (M + H)$^+$. Anal. calcd. for $C_{15}H_{17}N_3O_4$: C 59.40, H 5.65; found: C 59.20, H 6.00.

Reactions with alkynes

Thermolysis of ***2***e *with DMAD*

Oxadiazoline **2***e* (187 mg, 0.72 mmol) was heated with DMAD (217 mg, 1.5 mmol) in 14 mL of benzene. The products were separated by chromatography, with ethyl acetate – hexane as elution solvent.

Oxazoline ***9***a: White solid isolated in 73% yield, mp 109–111°C. IR (CCl_4) cm^{-1}: 1745s (OC═O's), 1688s (PhC═O), 1645m (C═N), 1611m (C═C), 1507w, 1443m, 1381w, 1242s, 1115m, 1028s, 976w, 910m, 879w, 843w; ^{1}H NMR (300 MHz, $CDCl_3$) δ: 3.73 (s, 3H, OCH_3), 3.96 (s, 3H, OCH_3), 3.86 (app dt, $J \sim 1$ Hz, ^3J = 6.5 Hz, 2H, NCH_2), 4.04 (app dt, $J \sim 1$Hz, ^3J = 6.5 Hz, 2H, OCH_2), 7.44–7.56 (m, 2H, Ar-*m*), 7.57–7.65 (m, 1H, Ar-*p*), 7.86–7.94 (m, 2H, Ar-*o*); ^{13}C NMR (75 MHz, $CDCl_3$) δ: 53.26 (2 × OCH_3, coincident signals), 55.13 (NCH_2), 68.42 (OCH_2), 128.71 and 128.76 (Ar C2, C6 and Ar C3, C5), 132.60 (Ar C4), 133.76 and 135.73 and 137.02 (Ar C1 and C═C), 159.87 and 163.02 and 164.55 (2 × OC═O and oxazoline C2), 190.02 (PhC═O); MS (EI) *m/z*: 317 (M^+, 20), 302 (M − CH_3, 10), 288 (63), 257 (16), 230 (38), 199 (17), 171 (24), 105 ($PhCO^+$, 100), 77 (87); MS (CI, NH_3) *m/z*: 318 (M + H)$^+$; HRMS calcd. for $C_{16}H_{15}NO_6$ (M^+): *m/z* 317.0899; found: *m/z* 317.0901.

Dihydrofuran ***11***a: Isolated in 4% yield. IR (CCl_4) cm^{-1}: 2257w (C≡C), 1741s (OC═O's), 1637m (NC═O), 1577w, 1494w, 1437m, 1361m, 1254s, 1210m, 1119m, 1067w, 1020m, 995m, 909m; ^{1}H NMR (300 MHz, $CDCl_3$) δ: 3.35–3.45 (m, 1H, NCH_2), ca. 3.60–3.75 (overlapped m, 1H, NCH_2), 3.62 (s, 3H, OCH_3), 3.77 (s, 3H, OCH_3), 3.83 (s, 3H, OCH_3), 3.85 (s, 3H, OCH_3), 4.22–4.42 (m, 2H, OCH_2), 7.35–7.50 (m, 3H, Ar-*m,p*), 7.76–7.84 (m, 2H, Ar-*o*); ^{13}C NMR (75 MHz, $CDCl_3$) δ: 48.34 (NCH_2), 51.21 (OCH_3), 52.21 (OCH_3), 52.83 (OCH_3), 53.11 (OCH_3), 69.42 (≡C), 69.64 (OCH_2), 104.09 (≡C), 120.76 (*C*(C)(C)(O)(O)), 127–131 (overlapping peaks, Ar and ═C), 142.86 (═C), 161.02 and 163.69 and 163.80 and 165.32 and 166.81 (3 × OC═O, PhC═O, and spiro C); MS (EI) *m/z*: 400 (M − CO_2Me, 16), 354 (M − C(O)Ph, 100), 344 (8), 105 ($PhCO^+$, 54), 77 (20); MS (CI, NH_3) *m/z*: 460 (M + H)$^+$.

*Unidentified 1:2 adduct (***1***e:DMAD)*: Isolated in 4% yield. IR (CCl_4) cm^{-1}: 1776m (C═O), 1737s (C═O), 1697m (C═O),

© 1997 NRC Canada

Can. J. Chem. Downloaded from www.nrcresearchpress.com by 91.121.58.235 on 09/08/12
For personal use only.

Can. J. Chem. Downloaded from www.nrcresearchpress.com by 91.121.58.235 on 09/08/12
For personal use only.

1582w, 1506m, 1441m, 1338w, 1232s, 1122m, 1012w, 949w, 910w; ^{1}H NMR (300 MHz, $CDCl_3$) δ: 3.53 (s, 3H, OCH_3), 3.72 (s, 3H, OCH_3), 3.74 (s, 3H, OCH_3), 3.82 (s, 3H, OCH_3), 4.49 (t, ^3J = 8.1 Hz, 2H, NCH_2), 4.98 (t, ^3J = 8.1 Hz, 2H, OCH_2), 7.32–7.47 (m, 5H, Ar); ^{13}C NMR (75 MHz, $CDCl_3$) δ: 45.90 (OCH_3), 51.67 (OCH_3), 51.86 (OCH_3), 55.28 (OCH_3), 75.06 (NCH_2), 92.26 (OCH_2), 111.43, 114.58, 124.23, 127.98, 128.07, 129.00, 129.53, 131.18, 134.81, 151.61, (152.48), 152.65, 160.20, 164.12, 167.23; MS (EI) *m/z*: 459 (M^+, 35), 428 (M − OCH_3, 6), 415 (6), 400 (M − CO_2CH_3, 12), 384 (23), 372 (20), 369 (6), 356 (4), 344 (30), 340 (3), 326 (6), 310 (5), 298 (6), 282 (7), 268 (6), 252 (11), 236 (6), 151 (12), 105 ($PhCO^+$, 100), 84 (39), 77 (56), 61 (18), 49 (39); MS (CI, NH_3) did not give useful information; HRMS calcd. for $C_{22}H_{21}NO_{10}$ (M^+): *m/z* 459.1165; found: *m/z* 459.1159.

Alcoholysis of ***9***a
Compound ***9a*** (1.12 g, 3.5 mmol) was stirred in 10 mL of 0.1 M acetic acid in methanol for 13 days at room temperature. After evaporation of the solvent, the oil was redissolved in 20 mL of CH_2Cl_2, and washed successively with $NaHCO_3$ (5%, 4 × 10 mL) and water, and the combined organic layers were dried over $MgSO_4$. Separation by radial chromatography, using 10–50% ethyl acetate in hexane, gave a mixture of two inseparable products, **12** and an isomer tentatively identified as **13**, in a ratio of ca. 70:30. The spectral data shown below are those of the mixture.

*(Z)-3-Oxo-3-phenyl-1-propene-1,1,2-tricarboxylic acid, trimethyl ester (**12**)* Lit. (27): mp 66–68°C; ^{1}H NMR (200 MHz, $CDCl_3$) δ: 3.65 (s, 3H, OCH_3), 3.75 (s, 3H, OCH_3), 3.94 (s, 3H, OCH_3), ca. 7.35–7.70 (m, 3H, Ar-*m,p*), ca. 7.84–7.98 (m, 2H, Ar-*o*); ^{13}C NMR (50 MHz, $CDCl_3$) δ: 52.4–53.6 (overlapped OCH_3's), 128.67 and 128.91 (Ar C2, C6 and Ar C3, C5), 134.09 (Ar C4), 135.19 (Ar C1), 142.44 (=C; other alkene C not observed due to low S/N), 161.94 (OC=O), 162.63 (OC=O), 163.94 (OC=O), 190.00 (PhC=O); MS (EI) *m/z*: 306 (M^+, 16), 275 (M − OCH_3, 12), 247 (M − CO_2CH_3, 3), 229 (1), 215 (1), 198 (1), 157 (1), 129 (3), 105 ($PhCO^+$, 100), 77 (41), 59 (5), 51 (8), 44 (3), 29 (1).

*4,5-Dihydro-4-methoxy-5-oxo-2-phenyl-3,4-furandicarboxylic acid, dimethyl ester (**13**a)*: ^{1}H NMR (200 MHz, $CDCl_3$) δ: 3.50 (s, 3H, OCH_3), 3.79 (s, 3H, OCH_3), 3.92 (s, 3H, OCH_3), ca. 7.35–7.70 (m, 5H, Ar); ^{13}C NMR (50 MHz, $CDCl_3$) δ: 52.4–53.6 (overlapped OCH_3's), 107.50, 126.22, 126.93, 129.28, 130.21, 133.16, 135.06, (157.05), 159.71 (OC=O), 160.44 (OC=O), 164.17 (OC=O); MS (EI) *m/z*: 306 (M^+, 8), 275 (M − OCH_3, 39), 247 (M − CO_2CH_3, 38), 230 (91), 215 (70), 203 (34), 187 (15), 175 (8), 157 (13), 151 (5), 144 (10), 140 (10), 129 (15), 111 (19), 105 ($PhCO^+$, 100), 102 (11), 91 (5), 82 (5), 77 (62), 59 (19), 51 (15), 39 (12), 29 (4).

Thermolysis of **2**e *with methyl propiolate*
Oxadiazoline ***2e*** (187 mg, 0.72 mmol) was heated with methyl propiolate (67 mg, 0.80 mmol) in 14 mL of benzene. By ^{1}H NMR, the product mixture was found to consist mainly of **14**. Substantial decomposition of the product occurred during the two successive separations (radial chromatography, ethyl acetate – hexane). Consequently, **14** was obtained in only 4% yield.

*Oxazoline **14***: ^{1}H NMR (200 MHz, $CDCl_3$) δ: 3.76 (s, 3H, OCH_3), 3.87 (app t, ^3J = 8.9 Hz, 2H, NCH_2), 4.06 (app t, ^3J = 8.9 Hz, 2H, OCH_2), 7.37 (s, 1H, =C-H), ca. 7.35–7.65 (overlapped m, 3H, Ar-*m,p*), 7.81–7.95 (m, 2H, Ar-*o*); ^{13}C NMR (50 MHz, $CDCl_3$) δ: 53.05 (OCH_3), 55.17 (NCH_2), 68.21 (OCH_2), 127.66 (=C-H), 128.66 and 128.89 (Ar C2, C6 and Ar C3, C5), 133.63 (Ar C4), 136.07 and 139.90 (Ar C1 and $=CR_2$), 162.20 (oxazoline C2), 164.18 (OC=O), 192.27 (PhC=O); MS (EI) *m/z*: 259 (M^+, 22), 230 (100), 216 (45), 172 (27), 128 (9), 105 ($PhCO^+$, 63), 84 (24), 77 (55), 49 (16); MS (CI, NH_3) *m/z*: 260 (M + H)$^+$; HRMS calcd. for $C_{14}H_{13}NO_4$ (M^+): *m/z* 259.0845; found: *m/z* 259.0857.

Thermolysis of **2**d *with DMAD*
Thermolysis of oxadiazoline ***2d*** (112 mg, 0.50 mmol) in the presence of DMAD (146 mg, 1.0 mmol) in 10 mL of benzene gave a thermolysate that was found (by ^{1}H NMR) to consist almost entirely of ***9b***, in addition to the excess DMAD. Repeated separations by radial chromatography (ethyl acetate – hexane) gave pure ***9b*** in 54% yield.

*Oxazoline **9***b: IR (CCl_4) cm^{-1}: 1745s (OC=O's), 1682s (NC=O's), 1644m, 1611m, 1435m, 1379m, 1321m, 1285m, 1251s, 1152m, 1055m, 1026m, 976w, 909m, 877w, 845w; ^{1}H NMR (200 MHz, $CDCl_3$) δ: 1.95 (s, 3H, CCH_3), 3.76 (s, 3H, OCH_3), 3.90 (s, 3H, OCH_3), 3.95 (app dt, $J \sim 1$ Hz, ^3J = 9.4 Hz, NCH_2), 4.25 (app dt, $J \sim 1$ Hz, ^3J = 9.4 Hz, OCH_2), 5.82 (app d, ^4J = 0.7 Hz, 1H, $=CH_2$), 5.92 (app d, ^4J = 1.4 Hz, 1H, $=CH_2$); ^{13}C NMR (50 MHz, $CDCl_3$) δ: 16.66 (CCH_3), 53.23 (2 × OCH_3, coincident signals), 55.22 (NCH_2), 68.50 (OCH_2), 128.30 ($=CH_2$), 132.20 and 137.44 (tetrasubstituted alkene C's), 144.36 ($H_2C=CR_2$), 160.00 (oxazoline C2), 163.09 (OC=O), 164.57 (OC=O), 191.69 (ketone C=O); MS (EI) *m/z*: 282 (M + H^+, 8), 266 (M − CH_3, 8), 252 (100), 241 (19), 239 (18), 222 (30), 208 (23), 194 (30), 190 (18), 181 (6), 163 (25), 154 (7), 135 (31), 124 (9), 111 (22), 96 (8), 84 (36), 71 (34), 59 (26), 49 (28), 45 (37), 41 (70); MS (CI, NH_3) *m/z*: 282 (M + H)$^+$; HRMS calcd. for $C_{13}H_{16}NO_6$ (M + H^+): *m/z* 282.0978; found: 282.0966.

Thermolysis of **2**c *with DMAD*
Oxadiazoline ***2c*** (99 mg, 0.50 mmol) was heated with DMAD (158 mg, 1.1 mmol) in 12 mL of benzene. ^{1}H NMR analysis of the crude thermolysate revealed ***9c*** to be the major product. Repeated separations by radial chromatography, with mixtures of ethyl acetate and hexane as elution solvent, gave the five 1:2 (carbene:DMAD) adducts described below. The major product could not be recovered, presumably due to its decomposition on the silica plate.

*Oxazoline **9***c: Not isolated, data from crude thermolysate; ^{1}H NMR (200 MHz, $CDCl_3$) δ: 2.45 (s, 3H, $C(O)CH_3$), 3.82 (s, 3H, OCH_3), 3.91 (s, 3H, OCH_3), 4.03 (app dt, $J \sim 1$ Hz, ^3J = 9.4 Hz, 2H, NCH_2), 4.37 (app dt, $J \sim 1$ Hz, ^3J = 9.4 Hz, 2H, OCH_2); MS (EI) *m/z*: 255 (M^+, 7), 240 (M − CH_3, 100), 224 (M − OCH_3, 27), 208 (55), 196 (19), 182 (20), 168 (20), 154 (32), 140 (8), 125 (37), 111 (62), 97 (34), 80 (17), 66 (26), 59 (28), 53 (18), 43 (64), 39 (20), 29 (11).

*Dihydrofuran **11***b: Pale yellow oil, isolated in 22% yield. IR (CCl_4) cm^{-1}: 1740s (C=O's), 1643m, 1559m, 1437m, 1386w,

© 1997 NRC Canada

Can. J. Chem. Downloaded from www.nrcresearchpress.com by 91.121.58.235 on 09/08/12
For personal use only.

1322m, 1288s, 1254s, 1223s, 1164m, 1126w, 1082m, 1045m; ^{1}H NMR (200 MHz, $CDCl_3$) δ: 1.83 (s, 3H, $C(O)CH_3$), 3.68 (s, 3H, OCH_3), 3.77 (s, 3H, OCH_3), 3.80 (s, 3H, OCH_3), 3.86 (s, 3H, OCH_3), ca. 3.60–3.90 (overlapped m, 2H, NCH_2), 4.27–4.57 (m, 2H, OCH_2); ^{13}C NMR (50 MHz, $CDCl_3$) δ: 19.07 ($C(O)CH_3$), 45.34 (NCH_2), 51.60 (OCH_3), 52.32 (OCH_3), 52.57 (OCH_3), 53.01 (OCH_3), 67.65 (OCH_2), 81.97 (alkyne), 104.08 (alkyne), 114.03 (*C*(C)(C)(O)(O)), 125.22 (alkene), 140.89 and 144.04 (alkene and spiro C), 161.49 (C═O), 162.43 (C═O), 163.73 (C═O), 164.47 (C═O); MS (EI) *m/z*: 366 (M − OCH_3, 6), 354 (M − $C(O)CH_3$, 100), 338 (M − CO_2CH_3, 7), 237 (6), 179 (10), 84 (35), 59 (12), 49 (21); MS (CI, NH_3) *m/z*: 415 (M + NH_4)$^+$, 398 (M + H)$^+$.

Dihydrofuran ***11****c*: Isolated as a partially solidified oil in 29% yield. IR (CCl_4) cm^{-1}: 1740s (C═O's), 1655m, 1624w, 1438m, 1382w, 1358w, 1332w, 1253s, 1204m, 1139m, 1111w, 1053w, 995m, 934w, 906w, 882w; ^{1}H NMR (200 MHz, $CDCl_3$) δ: 2.28 (s, 3H, $C(O)CH_3$), 3.23–3.38 (m, 1H, NCH_2), ca. 3.56–3.70 (overlapped m, 1H, NCH_2), 3.64 (s, 3H, OCH_3), 3.73 (s, 3H, OCH_3), 3.78 (s, 3H, OCH_3), 3.81 (s, 3H, OCH_3), 4.14–4.37 (m, 2H, OCH_2); ^{13}C NMR (50 MHz, $CDCl_3$) δ: 14.18 ($C(O)CH_3$), 48.37 (NCH_2), 51.03 (OCH_3), 52.15 (OCH_3), 52.75 (OCH_3), 53.01 (OCH_3), 68.10 (alkyne), 69.52 (OCH_2), 104.48 (alkyne), 121.35 (*C*(C)(C)(O)(O)), 130.60 (alkene C), 142.26 (alkene C), 160.90 and 163.76 and 164.13 and 166.67 and 168.77 (4 × C═O, spiro C); MS (EI) *m/z*: 397 (M$^+$, 2), 366 (M − OCH_3, 4), 354 (M − $C(O)CH_3$, 100), 338 (M − CO_2CH_3, 7), 322 (3), 310 (6), 278 (3), 264 (3), 250 (14), 236 (3), 218 (14), 204 (2), 192 (3), 176 (3), 165 (2), 150 (2), 135 (3), 118 (2), 106 (2), 91 (2), 77 (2), 59 (12), 43 (9); MS (CI, NH_3) *m/z*: 398 (M + H)$^+$; HRMS calcd. for $C_{16}H_{16}NO_9$ (M − OCH_3): *m/z* 366.0825; found: *m/z* 366.0816.

*Unidentified 1:2 adduct (****1****c:DMAD)*: Isolated as a solid in 4% yield. IR (CCl_4) cm^{-1}: 1743s (C═O's), 1601w, 1521w, 1436m, 1397w, 1332m, 1293m, 1244m, 1209s, 1133m, 1072w, 910w; ^{1}H NMR (200 MHz, $CDCl_3$) δ: 2.31 (s, 3H, $C(O)CH_3$), ca. 3.6–4.0 (overlapped m, 1H?, NCH_2),[16] 4.05–4.25 (m, 1H, NCH_2), 4.50–4.65 (m, 2H, OCH_2), 3.72 (s, 3H, OCH_3), 3.76 (s, 3H, OCH_3), 3.79 (s, 3H, OCH_3), 3.95 (s, 3H, OCH_3); ^{13}C NMR (50 MHz, $CDCl_3$) δ: 17.51 ($C(O)CH_3$), 44.11 (NCH_2), 51.77 (OCH_3), 52.09 (OCH_3), 53.57 (OCH_3), 54.10 (OCH_3), 67.23 (OCH_2), 68.04, 107.67, 111.61, 139.51, 145.05, 163.30, 163.73, 165.35, 166.19, 168.62; MS (EI) *m/z*: 397 (M$^+$, 1), 366 (M − OCH_3, 10), 353 (1), 338 (M − CO_2CH_3, 100), 306 (5), 235 (6), 221 (6), 163 (10), 84 (9), 61 (4), 49 (7); MS (CI, NH_3) *m/z*: 415 (M + NH_4)$^+$, 398 (M + H)$^+$; HRMS calcd. for $C_{16}H_{16}NO_9$ (M − OCH_3): *m/z* 366.0825, found: *m/z* 366.0809.

*Unidentified 1:2 adduct (****1****c:DMAD)*: Isolated as a solid in ca. 1% yield. IR (CCl_4) cm^{-1}: 1769s (C═O), 1730s (C═O), 1695s (NC═O), 1651w, 1592w, 1505m, 1445m, 1378w, 1335m, 1246s, 1211m, 1158m, 1123m, 1065w, 1007w; ^{1}H NMR (200 MHz, $CDCl_3$) δ: 2.49 (s, 3H, $C(O)CH_3$), 3.69 (s, 3H, OCH_3), 3.77 (s, 3H, OCH_3), 3.81 (s, 3H, OCH_3), 3.82 (s, 3H, OCH_3), 4.47 (app t, ^3J = 8.0 Hz, 2H, NCH_2), 4.95 (app t, ^3J = 8.0 Hz, 2H, OCH_2); MS (EI) *m/z*: 354 (M − $C(O)CH_3$, 18), 84 (100); MS (CI, NH_3) *m/z*: 415 (M + NH_4)$^+$, 398 (M + H)$^+$.

*Unidentified 1:2 adduct (****1****c:DMAD)*: Isolated as an oil in 6% yield. IR (CCl_4) cm^{-1}: 1748s (C═O), 1719s (C═O), 1597m, 1477w, 1437m, 1421m, 1353w, 1298m, 1236s, 1196m, 1144m, 1057w; ^{1}H NMR (200 MHz, $CDCl_3$) δ: 2.42 (s, 3H, $C(O)CH_3$), 3.71 (s, 3H, OCH_3), 3.73 (s, 3H, OCH_3), 3.76 (s, 3H, OCH_3), 3.90 (s, 3H, OCH_3), ca. 3.55–3.90 (overlapped m, ~2H, NCH_2). 4.62 (app t, ^3J = 7.8 Hz, 2H, OCH_2); ^{13}C NMR (50 MHz, $CDCl_3$) δ: 27.71 ($C(O)CH_3$), 44.82 (NCH_2), 51.49 (OCH_3), 52.30 (OCH_3), 52.81 (OCH_3), 53.39 (OCH_3), 62.39, 68.34 (OCH_2), 80.97, 102.44, 107.49, 110.04, 137.52, 156.35, 163.21, 165.44, 166.22, 171.60, 203.94; MS (EI) *m/z*: 366 (M − OCH_3, 6), 354 (M − $C(O)CH_3$, 100), 338 (M − CO_2CH_3, 6), 237 (6), 179 (8), 121 (6), 84 (6), 59 (5), 49 (4); MS (CI, NH_3) *m/z*: 415 (M + NH_4)$^+$, 398 (M + H)$^+$.

Thermolysis of ***2****g with DMAD*

Oxadiazoline ***2****g* (297 mg, 1.00 mmol) was heated with DMAD (310 mg, 2.18 mmol) in 16 mL of benzene. The products were separated by radial chromatography (ethyl acetate – hexane).

*3-(Phenylsulfonyl)-2-oxazolidinone (****15****) (ref. 31)*: Isolated in 23% yield, mp 136–138°C; IR (CCl_4) cm^{-1}: 1801s, 1480w, 1450w, 1382m (NSO_2), 1264w, 1180s (NSO_2), 1147s, 1094w, 1050w, 909w; ^{1}H NMR (200 MHz, $CDCl_3$) δ: 4.00–4.15 (m, 2H, NCH_2), 4.32–4.46 (m, 2H, OCH_2), 7.50–7.80 (m, 3H, Ar-*m,p*), 8.02–8.13 (m, 2H, Ar-*o*); ^{13}C NMR (50 MHz, $CDCl_3$) δ: 44.61 (NCH_2), 62.28 (OCH_2), 128.26 (Ar C2, C6), 129.30 (Ar C3, C5), 134.55 (Ar C4), 136.81 (Ar C1), 151.91 (C═O); MS (EI) *m/z*: 163 (30), 141 ($PhSO_2^+$, 12), 118 (8), 104 (53), 91 (6), 77 (100), 56 (6), 51 (28), 28 (2); MS (CI, NH_3) *m/z*: 245 (M + NH_4)$^+$.

*Dimethyl 3,3-dimethyl-3*H*-pyrazole-4,5-dicarboxylate (****16****) (ref. 26)*: Isolated in 13% yield. IR (CCl_4) cm^{-1}: 1732s (C═O), 1647w, 1438w, 1334w, 1264s, 1198w, 1167w, 1114w, 1033w, 909m; ^{1}H NMR (200 MHz, $CDCl_3$) δ: 1.58 (s, 6H, $C(CH_3)_2$), 3.92 (s, 3H, OCH_3), 4.00 (s, 3H, OCH_3); ^{13}C NMR (50 MHz, $CDCl_3$) δ: 20.86 ($C(CH_3)_2$), 52.98 (2 × OCH_3, coincident), 97.46 (C3), 144.68 (C4), 153.56 (C5), 160.81 (C═O), 162.97 (C═O); MS (EI) *m/z*: 183 (3), 169 (3), 152 (33), 141 (50), 125 (36), 109 (34), 93 (55), 79 (65), 67 (100), 59 (43), 53 (31), 39 (50), 29 (18).

Cyclopentadiene ***17***: Obtained as a pale yellow oil in 3% yield. IR (CCl_4) cm^{-1}: 1730s (C═O), 1649w, 1437m, 1368m (NSO_2), 1342m, 1262s, 1203m, 1169m (NSO_2), 1096w, 1015w, 995w, 909s; ^{1}H NMR (200 MHz, $CDCl_3$) δ: 3.58 (s, 6H, OCH_3), 3.89 (s, 6H, OCH_3), 3.97 (t, ^3J = 6.5 Hz, 2H, NCH_2), 4.39 (t, ^3J = 6.5 Hz, 2H, OCH_2), 7.42–7.65 (m, 3H, Ar-*m,p*), 7.80–7.88 (m, 2H, Ar-*o*); ^{13}C NMR (50 MHz, $CDCl_3$) δ: 47.66 (NCH_2), 52.08 (OCH_3), 52.85 (OCH_3), 67.44 (OCH_2), 101.18 (spiro C), 127.78 (Ar C2, C6), 128.97 (Ar C3, C5), 132.80 (Ar C4), 138.29 (probably Ar C1), 139.00 (probably ═*C*-C-*C*═), 140.32 (probably ═C-C═), 160.45

[16] The following resonances were also observed, which could account for one of the NCH_2 protons: δ 3.56 (app t, J = 2.3 Hz, ~0.5H) and 3.62 (app t, J = 2.3 Hz, ~0.5H) (slow exchange is expected in these compounds); alternatively, these could be due to impurities.

© 1997 NRC Canada

(C═O), 162.60 (C═O); MS (EI) *m/z*: 495 (M^+, 2), 464 (M − OCH_3, 5), 431 (3), 354 (M − SO_2Ph, 30), 322 (28), 310 (49), 290 (14), 264 (30), 182 (12), 141 ($PhSO_2^+$, 15), 84 (26), 77 (100), 59 (27); MS (CI, NH_3) *m/z*: 513 $(M + NH_4)^+$; HRMS calcd. for $C_{21}H_{21}NO_{11}S$ (M^+): *m/z* 495.0835, found: *m/z* 495.0835.

N-*Formyl*-N-*[2-(formyloxy)ethyl]benzenesulfonamide* ***18***: IR (CCl_4) cm^{-1}: 1737s (C═O), 1710s (C═O), 1449w, 1401w, 1371m (NSO_2), 1311w, 1286w, 1232w, 1172s (NSO_2), 1091w, 1013w, 975w, 944w; ^1H NMR (200 MHz, $CDCl_3$) δ: 3.79 (t, ^3J = 5.7 Hz, 2H, NCH_2), 4.28 (t, ^3J = 5.7 Hz, 2H, OCH_2), 7.50–7.80 (m, 3H, Ar-*m,p*), 7.81–8.00 (m, 3H, Ar-*o* and NC(O)H), 9.15 (s, 1H, OC(O)H); ^{13}C NMR (50 MHz, $CDCl_3$) δ: 41.00 (NCH_2), 60.21 (OCH_2), 127.45 (Ar C2, C6), 129.80 (Ar C3, C5), 134.47 (Ar C4), 137.80 (Ar C1), 160.26 (C═O), 161.28 (C═O); MS (EI) *m/z*: 230 (2), 186 (4), 170 (10), 141 ($PhSO_2^+$, 36), 94 (58), 84 (42), 77 (100), 49 (37); MS (CI, NH_3) *m/z*: 275 $(M + NH_4)^+$.

*Unidentified 1:3 adduct (**1**g:DMAD)*: Isolated in ca. 1% yield. IR (CCl_4) cm^{-1}: 1748s (C═O), 1607m, 1500m, 1469w, 1435m, 1362w (NSO_2), 1343w, 1259s, 1164m (NSO_2), 1108w, 1025m; ^1H NMR (300 MHz, $CDCl_3$) δ: 3.31 (s, 3H, OCH_3), 3.70 (s, 3H, OCH_3), 3.73 (s, 3H, OCH_3), 3.82 (s, 3H, OCH_3), 3.83 (s, 3H, OCH_3), 3.94 (s, 3H, OCH_3), (NCH_2 overlapped with OCH_3's), 4.72–4.84 (m, 2H, OCH_2), 7.52–7.72 (m, 3H, Ar-*m,p*), 7.99–8.05 (m, 2H, Ar-*o*); ^{13}C NMR (50 MHz, $CDCl_3$, partial spectrum) δ: 46.21 (NCH_2), 51.38 (OCH_3), 51.56 (OCH_3), 52.46 (OCH_3), 53.49 (OCH_3), 54.06 (OCH_3), 54.25 (OCH_3), 69.43 (NCH_2), 128.82 and 128.88 (Ar C2, C6 and Ar C3, C5), 134.40 (probably Ar C4), 139.56, 145.33, 161–168 (several overlapping peaks); MS (EI) *m/z*: 606 (M − OCH_3, 5), 578 (M − CO_2CH_3, 100), 438 (5), 394 (6), 378 (11), 364 (6), 354 (18), 320 (7), 141 ($PhSO_2^+$, 8), 77 (35), 59 (18); MS (CI, NH_3) *m/z*: 638 $(M + H)^+$.

Acknowledgments

The authors thank Dr. Richard Smith and Mr. Fajar Ramelan for most of the mass spectra. Support of this research by the Natural Sciences and Engineering Research Council (NSERC) of Canada, and by the Ministry of Education and Training of Ontario in the form of a Scholarship to P.C., is gratefully acknowledged.

References

1. P.S. Skell and A.Y. Garner. J. Am. Chem. Soc. **78**, 5430 (1956).
2. W.E. Doering and W.A. Henderson, Jr. J. Am. Chem. Soc. **80**, 5274 (1958).
3. (*a*) R.A. Moss. Acc. Chem. Res. **13**, 58 (1980); (*b*) Acc. Chem. Res. **22**, 15 (1989).
4. R.A. Moss, M. Wlostowski, S. Shen, K. Krogh-Jespersen, and A. Matro. J. Am. Chem. Soc. **110**, 4443 (1988).
5. R.W. Hoffmann, W. Lilienblum, and B. Dittrich. Chem. Ber. **107**, 3395 (1974).
6. R.A. Moss. *In* Advances in carbene chemistry. *Edited by* U.H. Brinker. JAI Press, Greenwich, Conn. 1997. pp. 59–88.
7. R.S. Sheridan, R.A. Moss, B.K. Wilk, S. Shen, M. Włostowski, M.A. Kesselmayer, R. Subramanian, G. Kmiecik-Lawrynowicz, and K. Krogh-Jespersen. J. Am. Chem. Soc. **110**, 7563 (1988).
8. M. El-Saidi, K. Kassam, D.L. Pole, T. Tadey, and J. Warkentin. J. Am. Chem. Soc. **114**, 8751 (1992).
9. A.J. Arduengo III, J.R. Goerlich, and W.J. Marshall. J. Am. Chem. Soc. **117**, 11027 (1995), and refs. cited therein.
10. (*a*) T. Wong, J. Warkentin, and J.K. Terlouw. Int. J. Mass Spectrom. Ion Processes, **115**, 33 (1992); (*b*) P.J.A. Ruttink, P.C. Burgers, and J.K. Terlouw. Int. J. Mass Spectrom. Ion Processes, **145**, 35 (1995); (*c*) P. Haake, L.P. Bausher, and W.B. Miller. J. Am. Chem. Soc. **91**, 1113 (1969); (*d*) R.R. Sauers. Tetrahedron Lett. **37**, 149 (1996); (*e*) N.G. Rondan, K.N. Houk, and R.A. Moss. J. Am. Chem. Soc. **102**, 1770 (1980); (*f*) T. Nakai and K. Mikami. Chem. Lett. 1081 (1979); (*g*) K.-K. Chan and G. Saucy. J. Org. Chem. **42**, 3828 (1977); (*h*) G. Büchi, M. Cushman, and H. Wüest. J. Am. Chem. Soc. **96**, 5563 (1974); (*i*) A. Kümmell and G. Seitz. Tetrahedron Lett. **32**, 2743 (1991); (*j*) C. Gerninghaus, A. Kümmell, and G. Seitz. Chem. Ber. **126**, 733 (1993); (*k*) M. Reiffen and R.W. Hoffmann. Chem. Ber. **110**, 37 (1977); (*l*) H.-W. Wanzlick and H. Steinmaus. Chem. Ber. **101**, 244 (1968); (*m*) J.M. Brown and B.D. Place. J. Chem. Soc. Chem. Commun. 533 (1971); (*n*) P. Jutzi and F.-W. Schröder. Angew. Chem. Int. Ed. Engl. **10**, 339 (1971); (*o*) P. Couture, D.L. Pole, and J. Warkentin. J. Chem. Soc. Perkin Trans. 2, 1565 (1977); (*p*) J.H. Rigby, A. Cavezza, and G. Ahmed. J. Am. Chem. Soc. **118**, 12848 (1996); (*q*) P. Couture, J.K. Terlouw, and J. Warkentin. J. Am. Chem. Soc. **118**, 4214 (1996).
11. P. Couture and J. Warkentin. Can. J. Chem. **75**, 1264 (1997).
12. (*a*) E.J. Corey and R.A.E. Winter. J. Am. Chem. Soc. **85**, 2677 (1963); (*b*) D.M. Lemal, R.A. Lovald, and R.W. Harrington. Tetrahedron Lett. 2779 (1965); (*c*) R.R. Sauers. Tetrahedron Lett. **35**, 7213 (1994).
13. D.M. Lemal and E.H. Banitt. Tetrahedron Lett. 245 (1964).
14. W. Kirmse. *In* Advances in carbene chemistry. *Edited by* U.H. Brinker. JAI Press, Greenwich, Conn. 1997. pp. 1–57.
15. R.J. Abraham, J. Fisher, and P. Loftus. Introduction to NMR spectroscopy. John Wiley & Sons, New York. 1988.
16. (*a*) T. Drakenberg and J.M. Lehn. J. Chem. Soc., Perkin Trans. 2, 532 (1972); (*b*) J.B. Lambert, W.L. Oliver, Jr., and B.S. Packard. J. Am. Chem. Soc. **93**, 933 (1971).
17. L. Yang, K. Gao, S.-L. Kong, and Y.-Z. Chen. Chin. J. Chem. 430 (1990).
18. (*a*) F.A. Alimerzoev, A.A. Lapshova, V.V. Zorin, A.U. Stepanyants, V.P. Lezina, F.N. Lapytova, S.S. Zlotskii, and D.L. Rakhmankulov. J. Appl. Chem. **53**, 718 (1980); (*b*) V.I. Dostovalova, S.S. Zlotsky, D.L. Rakhmankulov, and A.B. Terent'ev. Magn. Reson. Chem. **25**, 1 (1987); (*c*) T. Harder, T. Löhl, M. Bolte, K. Wagner, and D. Hoppe. Tetrahedron Lett. **35**, 7365 (1994); (*d*) K. Higashiyama, H. Fujikura, and H. Takahashi. Chem. Pharm. Bull. **43**, 722 (1995); (*e*) K. Higashiyama, K. Nakagawa, and H. Takahashi. Heterocycles, **41**, 2007 (1995).
19. K. Conde-Frieboes and D. Hoppe. Tetrahedron, **48**, 6011 (1992).
20. G. Crank and F.W. Eastwood. Aust. J. Chem. **18**, 1967 (1996).
21. A. Bernardi, S. Cardani, G. Poli, D. Potenza, and C. Scolastico. Tetrahedron Lett. **48**, 1343 (1992).
22. (*a*) J. Hocker and R. Merten. Liebigs Ann. Chem. **751**, 145 (1971); (*b*) R.W. Hoffmann, K. Steinbach, and B. Dittrich. Chem. Ber. **106**, 2174 (1973); (*c*) R.W. Hoffmann and M. Reiffen. Chem. Ber. **109**, 2565 (1976); (*d*) H. Giesecke and J. Hocker. Synthesis, 806 (1977); (*e*) E. Haug, W. Kantlehner, H. Hagen, P. Speh, and H.-J. Bräuner. Liebigs Ann. Chem. 605 (1988).
23. G. Scherowsky, K. Dünnbier, and G. Höfle. Tetrahedron Lett. 2095 (1977).
24. (*a*) D.L. Pole, P.K. Sharma, and J. Warkentin. Can. J. Chem. **74**, 1335 (1996); (*b*) H.-T. Er, D.L. Pole, and J. Warkentin. Can. J. Chem. **74**, 1480 (1996).

Can. J. Chem. Downloaded from www.nrcresearchpress.com by 91.121.58.235 on 09/08/12
For personal use only.

© 1997 NRC Canada

25. (*a*) H.L. Wehrmeister. J. Org. Chem. **27**, 4418 (1962); (*b*) A.I. Meyers, D.L. Temple, R.L. Nolen, and E.D. Mihelich. J. Org. Chem. **39**, 2778 (1974).
26. M.L. Graziano, M.R. Iesce, G. Cimminiello, and R. Scarpati. J. Chem. Soc. Perkin Trans. 1, 241 (1989).
27. M. Franck-Neumann and M. Miesch. Tetrahedron, **39**, 1247 (1983).
28. T. Shibanuma, M. Iwanami, M. Fujimoto, T. Takenaka, and M. Murakami. Chem. Pharm. Bull. **28**, 2609 (1980).
29. Y. Yonekawa, Y. Kuwahara, and T. Suzuki. Agric. Biol. Chem. **51**, 3387 (1987).
30. S. Kobayashi, M. Isobe, and T. Saegusa. Bull. Chem. Soc. Jpn. **55**, 1921 (1982).
31. I. Shibata, K. Nakamura, A. Baba, and H. Matsuda. Bull. Chem. Soc. Jpn. **62**, 853 (1989).

Can. J. Chem. Downloaded from www.nrcresearchpress.com by 91.121.58.235 on 09/08/12
For personal use only.

© 1997 NRC Canada

1997 Noranda Award Lecture
Chemical applications of electron–matter interactions: from probing low-temperature industrial plasmas and atmospheric chemistry of "environment-safe" Freon substitutes to enhancing novel surface reactions on metals and semiconductors[1]

K.T. Leung

Can. J. Chem. Downloaded from www.nrcresearchpress.com by 91.121.58.235 on 09/08/12
For personal use only.

Abstract: Since the discovery of the electron by Sir Joseph John Thomson a century ago, the limitless applications of the electron in chemistry have been both profound and fun. We present recent results from two of our experiments that involve such applications of the electron beam in the study of new aspects of gas-phase chemical physics and of surface chemistry. In particular, our precise measurements of momentum-transfer-resolved "absolute" excitation transition probabilities of the low-lying transitions in "environment-safe" Freon substitutes using a high-energy electron beam are finding applications in the modelling of low-temperature industrial plasma and atmospheric processes. The use of low-energy electrons as a powerful in situ means to activate and to probe "novel" surface reactions, including oxide and carbide formation and CO oxidation, has been demonstrated on Cu(100) and Si(111) surfaces. These experiments further illustrate the value and the enormous potential of technological payoffs of electron-based fundamental research.

Key words: electron scattering and interactions, surface chemistry.

Résumé : Depuis la découverte de l'électron par Sir John Thomson il y de cela un siècle, les applications illimitées de l'électron en chimie furent à la fois plaisantes et profondes. Nous présentons les récents résultats de deux de nos expériences qui impliquent l'application d'un faisceau d'électrons dans l'étude des nouveaux aspects de la chimie physique en phase gazeuse et de la chimie de surface. En particulier, nos mesures précises de résolution du transfert du moment des probabilités de transition d'excitation «absolue» des transitions de basse énergie dans des substituts du Fréon situés dans un «environnement propre», en utilisant un faisceau d'électrons à haute énergie, ont trouvé des applications dans la modélisation des plasmas industriels à basse température et dans les processus atmosphériques. On a utilisé des surfaces de Cu(100) et de Si(111) pour illustrer le fait que des électrons de faible énergie constituent un puissant moyen in situ pour activer et sonder de «nouvelles» réactions de surface, incluant la formation d'oxyde et de carbure et l'oxydation du CO. Ces expéreinces illustrent de plus la valeur et l'énorme potentiel rentabilité technologique de la recherche fondamentale basée sur l'électron.

Mots clés : diffraction d'électrons et interactions, chimie de surface.

[Traduit par la rédaction]

1. The centennial of the electron discovery

The word "electron," coined by G. Johnstone Stoney in 1891, had been used to denote the unit of charge found in experiments involving passing electric current through chemicals. It was Joseph John Thomson, who on April 30, 1897, announced that the cathode rays were negatively charged particles that he called "corpuscles," and later in 1897 recognised that these corpuscles (electrons) represented "matter being the substance from which the chemical elements are built up" (1). Since then, the electron has become possibly the most popular fundamental particle with extraordinary physical properties and chemical and technological power. Indeed, most of today's computation, communications, entertainment, etc. that defines modern civilization depends on technical knowledge of the electron and its properties. As we celebrate the Centennial Year of the discovery of the electron in 1997, it seems appro-

Received June 23, 1997.

K.T. Leung.[2] Department of Chemistry, The University of Waterloo, Waterloo, ON N2L 3G1, Canada.

[1] This is an invited review article based on the 1997 Noranda Award Lecture presented by Professor Leung at the 80th Annual Conference of the Canadian Society for Chemistry, held in Windsor, Ontario, in June 1997.

[2] Telephone: (519) 888-4567, ext. 5826. Fax: (519) 746-0435. E-mail: tong@uwaterloo.ca.

© 1997 NRC Canada

Can. J. Chem. Downloaded from www.nrcresearchpress.com by 91.121.58.235 on 09/08/12
For personal use only.

priate to examine from a chemist's perspective some of the notable applications of the electron in experimental chemical physics and modern surface chemistry. In particular, we shall, in the rest of this article, focus on two modest applications of the electron beam itself. These experiments are part of our gas-phase chemical physics and surface science programs developed over the past decade at The University of Waterloo. These results illustrate the enormous importance of creative use of the electron not only as a unique probe for "dark" transitions in matters of technological and environmental relevance but also as an initiator for "novel" surface reactions.

2. Electrons as a unique probe for the electronic structure and interactions: non-optical excited-state spectroscopy of Freon substitutes

The ground-state electronic structures of simple polyatomic molecules have been the subject of intense research both spectroscopically and theoretically. Although significant progress in the description of the ground-state structure has been made using new and improved quantum computational methods, knowledge about the electronic structures of the excited states is less complete (2). In principle, it is possible to probe the electronic structure of an excited state by measuring excited-state-related properties, such as the transition energy and oscillator strength of a particular electronic transition, if the ground-state electronic structure is well understood. Angle-resolved electron energy loss spectroscopy (EELS) has proven to be an effective tool for investigating non-dipole phenomena (3). In particular, dipole-forbidden transitions, which are difficult to detect in single-photon optical experiments, have been observed using angle-resolved EELS in the valence shell (4) and inner shells (5).

Briefly, a typical angle-resolved EELS experiment involves a simple inelastic electron–molecule scattering process:

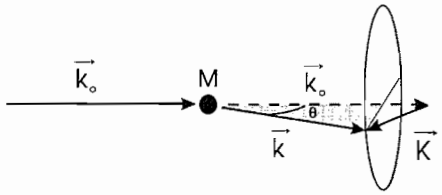
$$[1]\quad \underset{(k_0,E_0)}{M + e^-} \longrightarrow \underset{(k,E_1)}{e^- + M^*}$$

in which the target molecule M is promoted to some excited state M* by a fast incident electron (typically with a kinetic energy of 2.5 keV), which undergoes energy loss $E\,(=E_0-E_1)$ and momentum transfer $\boldsymbol{K}\,(=\boldsymbol{k}_0-\boldsymbol{k})$. Figure 1 shows a schematic diagram of the scattering kinematics. The magnitude of the momentum transfer K is related to the scattering angle (i.e., $K^2 = k_0^2 + k^2 - 2k_0k\cos\theta$). The intensity of the scattered electrons (with momentum $\boldsymbol{k}$ and scattering angle θ) that suffer an energy loss E is proportional to the double differential cross section $d^2\sigma/d\Omega dE$. In the first Born approximation, the differential generalized oscillator strength (GOS), $df\,(K,E)/dE$, is related to the cross section by the Bethe–Born formula (6):

$$[2]\quad \frac{df(K,E)}{dE} = \frac{k_0}{k}K^2\frac{E}{4}\frac{d^2\sigma}{d\Omega dE}$$

where $d\Omega$ corresponds to the acceptance solid angle of the scattered electrons. The GOS $f(K,E)$ is also defined in Rydberg atomic units as:

Fig. 1. Schematic diagram of scattering kinematics in a typical electron energy loss process involving non-zero momentum transfer $\boldsymbol{K}$ to a molecular target M.



$$[3]\quad f(K,E) = \frac{E}{K^2}\left|\left\langle \Psi_n\left|\sum_{j=1}^{N}\exp(i\boldsymbol{K}\cdot\boldsymbol{r}_j)\right|\Psi_0\right\rangle\right|^2$$

where Ψ_0 and Ψ_n are the (N-electron) electronic wave functions of the initial (ground) and final states respectively, and $\boldsymbol{r}_j$ is the position of the jth electron with respect to the centre-of-mass of the target. At small momentum transfer, the GOS can be expanded into a power series (7):

$$[4]\quad f(K,E) = E[\varepsilon_1^2 + (\varepsilon_2^2 - 2\varepsilon_1\varepsilon_3)|\boldsymbol{K}|^2 + (\varepsilon_3^2 - 2\varepsilon_2\varepsilon_4 + 2\varepsilon_1\varepsilon_5)|\boldsymbol{K}|^4 + \cdots]$$
$$= f_0 + f_1|\boldsymbol{K}|^2 + f_2|\boldsymbol{K}|^4 + \cdots$$

where the multipole transition moment is given by

$$\varepsilon_m = \frac{1}{m!}\left\langle \Psi_n\left|\sum_{j=1}^{N}\left(\frac{\boldsymbol{K}}{|\boldsymbol{K}|}\cdot\boldsymbol{r}_j\right)^m\right|\Psi_0\right\rangle$$

The GOS therefore converges to the dipole oscillator strength (DOS), f_0, as the momentum transfer approaches zero (8). The term f_1 is related to the difference of the square of the quadrupole matrix element and the product of the dipole and octupole matrix elements (9). It may therefore be possible to qualitatively infer whether a particular excitation is dominated by dipole or non-dipole (quadrupole, octupole, etc.) interactions by comparing the relative magnitudes and signs of the f_n values. Furthermore, the GOS in the valence shell can be made absolute by single-point normalization to the corresponding photoabsorption data at $K = 0$ or by using the Bethe sum rule at any selected constant value of K, i.e.,

$$[5]\quad \int \frac{df(K,E)}{dE}\,dE = N$$

where N is the total number of electrons in the valence shell of the target. With the appropriate fitting procedure that takes into account the background function and the contribution from the inner shells (10), the sum-rule normalization procedure provides a convenient means of obtaining absolute cross section without performing an "absolute" experiment. Since the relative normalization among all the spectra has been maintained automatically by collecting the EELS spectra at different θ's sequentially in repetitive scans, it is only necessary to perform the sum-rule normalization at a single K value (the smallest K value in this case) to put the entire GOS data on an absolute scale. Angle-resolved EELS therefore offers a powerful technique for "complete" determination of all the existing excited states, including both the dipole-allowed and

© 1997 NRC Canada

Can. J. Chem. Downloaded from www.nrcresearchpress.com by 91.121.58.235 on 09/08/12
For personal use only.

the optically inaccessible non-dipole or "dark" transitions. Furthermore, the GOSs measured at different momentum-transfer values are related to the corresponding Fourier transform components of the overlap function between the initial-state and final-state wave functions (eq. [3]). In effect, GOS measurement can provide a detailed "mapping" of the overlap function in momentum space, which can in turn be used as effective feedback for theoretical modelling of excited-state wave functions.

2.1 Non-dipole HOMO → LUMO excitations in Freons

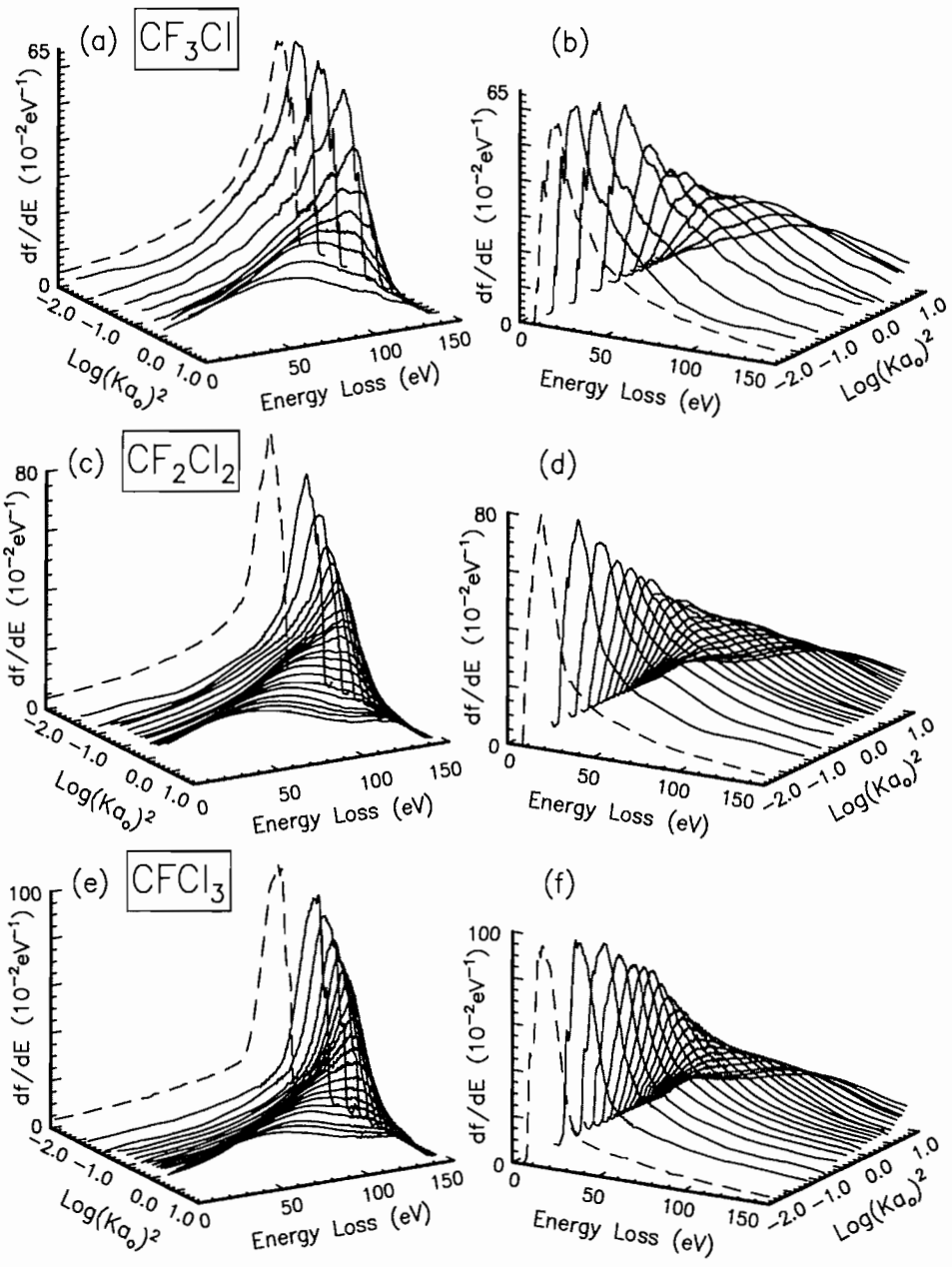
The importance of studying the electronic structures of Freons is attested to not only by their influential roles in atmospheric science (11), but also by their wide-ranging industrial applications as common aerosol and refrigerant materials and as important plasma etchants in semiconductor processing (12). Using a home-built electron scattering spectrometer (13), we conducted a series of comprehensive studies on the electron-impact excitation of a series of chlorofluorocarbons (CFCs) (14–16) and their common hydrogen-substituted chlorofluorocarbons (HCFCs) (17–19) in the valence-shell (5–150 eV) region. As an example, we show in Fig. 2 the variation of the GOS of valence-shell energy loss features over an extended momentum-transfer range in the form of a Bethe surface plot for CF_3Cl (Freon 13), CF_2Cl_2 (Freon 12), and $CFCl_3$ (Freon 11) (15). The Bethe surface gives a comprehensive description of the electron–molecule inelastic scattering process, and is particularly useful for analyzing such quantities as stopping power, total inelastic scattering cross section, and polarizability (6). In particular, Figs. 2*a*, 2*c*, and 2*e* emphasize the impact-scattering domain of large momentum transfer and energy loss, which corresponds to the kinematical region for "close" collisions. In this domain, a broad ridge is seen to disperse to a higher energy loss with increasing momentum transfer. This ridge is the result of momentum conservation in the inelastic electron–molecule collision and becomes the well-known Bethe ridge in the Born approximation (6). Figures 2*b*, 2*d*, and 2*f*, on the other hand, emphasize the dipole-scattering domain of small momentum transfer and energy loss, which involves "distant" collisions and where sharp "optical" features of the valence shell are more apparent. Although the overall appearance of the Bethe surfaces of the three molecules appears to be similar (Fig. 2), the GOS evidently becomes more concentrated in the dipole-scattering region with increasing Cl content in the CF_3Cl, CF_2Cl_2, and $CFCl_3$ series (15). This trend can be qualitatively understood by considering the differences in the spatial distributions of the valence-shell electron densities of these molecules. In general, the electron-binding energy is inversely related to the size of an orbital (as approximated, e.g., by the average Bohr radius). In the series CF_3Cl, CF_2Cl_2, and $CFCl_3$ (15), the valence orbitals become more diffuse with successive chlorination, which therefore gives rise to increasingly lower ionization potentials (IPs) of the valence shell and hence a higher concentration of the GOS in the low energy loss region, as observed in Figs. 2*b*, 2*d*, and 2*f*. Moreover, a larger size of the valence shell (as the result of an increased Cl content) also gives rise to a lower average charge density, hence favouring "distant" collisions (i.e., with a small momentum-transfer). Consequently, the Bethe surface of $CFCl_3$ appears to be the most strongly peaked in the lower momentum-transfer region among the three molecules, giving rise to a more rapid drop-off along the K direction (Fig. 2).

To demonstrate the K-dependence of the spectral features observed in the valence shell of CF_3Cl, we show in Fig. 3 a selected number of K-resolved (angle-resolved) electron energy loss spectra collected at a series of scattering angles (14). Our small-angle spectrum (Fig. 3*a*) is found to be consistent with the earlier dipole EELS (20) and photoabsorption data (21), and the observed features may be assigned to appropriate dipole-allowed Rydberg transitions. In particular, features 2–7 have been assigned to $5e \rightarrow 4s$ (9.5 eV), $5e \rightarrow 5s$ and (or) $5e \rightarrow 3d$ (11.5 eV), $4e \rightarrow 4s$ and (or) $1a_2 \rightarrow 4p$ (13.5 eV), $4a_1 \rightarrow 4s$ (16.5 eV), $4a_1 \rightarrow 5s$ and (or) $2e \rightarrow 4p$ (18.5 eV), and $2a_1 \rightarrow 3s$ (22.3 eV) transitions, respectively. In addition to these "optical" features, our K-resolved spectra (at larger angles) clearly indicate the presence of a weak broad feature at 40.5 eV (feature 8), which has also been reported previously (20). The broad 40.5 eV feature likely contains the ionization edges of both inner-valence $(1e)^{-1}$ and $(1a_1)^{-1}$ states, which are at 40.0 and 42.5 eV, respectively. This broad peak (located at 37–42 eV) appears to be a common feature among other members of the Freon series (including CF_2Cl_2 and $CFCl_3$ (15)). The strong correlation between the intensity of this broad peak and the number of F atom(s) in the Freon molecules further suggests that these broad features are related to transitions near the ionization onsets of the inner-valence F 2*s* orbitals (20). Finally, the spectra clearly reveal the presence of a "new" state at 7.7 eV (14), i.e., at an energy that is 1.7 eV below the onset of the (dipole) Rydberg states observed in the $\theta = 1°$ spectrum (Fig. 3*a*).

To investigate in more detail the K-dependence of the newly observed non-dipole feature at 7.7 eV, we have estimated its peak intensity with a Gaussian profile, after removing an appropriate contribution from the nearby discrete dipole transition(s), in each of the K-resolved spectra. Figure 4 shows the resulting GOS profile (14), which clearly contains a relative maximum (at $K^2 \sim 1.0$ a.u.) characteristic of a non-dipole transition. Only a limited number of non-dipole electronic transitions in the valence shell have been previously characterized by means of GOS measurements. In particular, the GOS of the well-known Lyman–Birge–Hopfield (LBH) band in N_2 at 9.3 eV was found to have a maximum at $K^2 \sim 0.8$ a.u. and has been identified as a quadrupole-allowed $a^1\Pi_g \leftarrow X^1\Sigma_g^+$ transition (13, 22). In addition, a second quadrupole transition at 31.4 eV in N_2 has also been observed with the GOS maximum at $K^2 \sim 1.1$ a.u. and could be attributed to the $2\sigma_g \rightarrow 1\pi_g$ single excitation and discrete double excitations (23). Other non-dipole transitions have also been found in C_2H_2 (24), benzene (25), and *p*-difluorobenzene (26). These studies generally demonstrate that dipole-allowed non-Rydberg transitions have maximum GOSs at $K = 0$ while non-dipole transitions (quadrupole or octupole) usually have maximum GOSs at non-zero K values (e.g., ~ 1 a.u. for most non-dipole valence-shell transitions observed to date). Figure 4 therefore gives direct evidence for a non-dipole non-Rydberg transition lying below all previously reported dipole transitions in CF_3Cl (14). Moreover, we can also derive the absolute DOS by fitting the measured GOS profile using a power series expansion (the so-called Lassettre series (27)) shown in eq. [4], the coefficients derived from which are consistent with those of a predominantly quadrupole transition.

© 1997 NRC Canada

Fig. 2. Bethe surfaces of the valence shells of CF_3Cl (*a*), (*b*), CF_2Cl_2 (*c*), (*d*), and $CFCl_3$ (*e*), (*f*) determined at 2.5 keV impact energy. EELS spectra are collected in steps of 1.0° from 1.0° to 9.0° for CF_3Cl, and in steps of 0.5° from 1.0° to 9.5° for CF_2Cl_2 and $CFCl_3$. The spectra collected above 4° have been smoothed for clarity. The dipole EELS spectra of CF_3Cl, CF_2Cl_2, and $CFCl_3$ obtained from the literature (15) are shown as broken lines and have been placed at an approximate momentum transfer (*K*) position (0.1 a.u.), that corresponds to the lower limit of our scale. The impact-scattering (large momentum transfer) domain is emphasized in (*a*), (*c*), and (*e*), while the dipole-scattering domain is depicted in (*b*), (*d*), and (*f*).



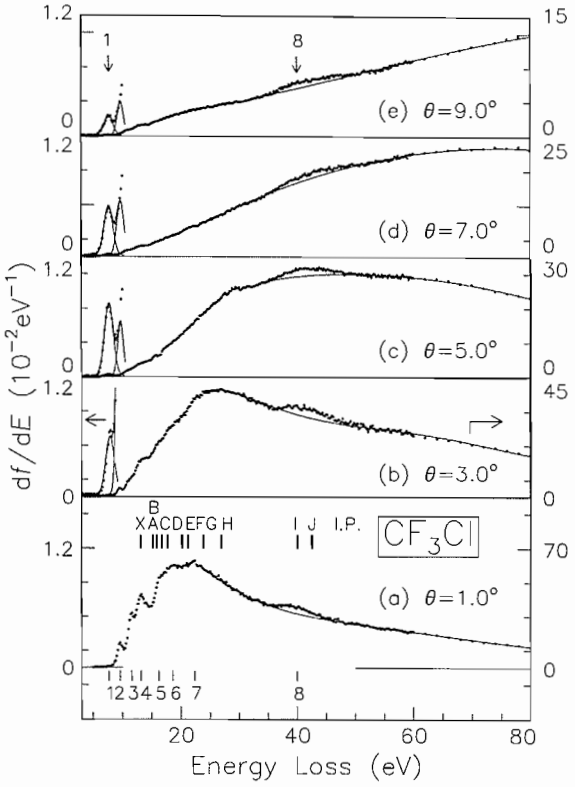
Also shown in Fig. 4 are the results of ab initio GOS calculations for the $(7e \rightarrow 11a_1)\ ^1E \leftarrow\ ^1A_1$ excitation (14). The calculations employed an improved virtual orbital (IVO) representation (28) of the ^1E state and a Hartree–Fock ground state. Evidently, reasonably good agreement is obtained between theory and experiment for the shape, although the calculated GOS is somewhat larger, with the minima of both the theoretical and experimental GOS curves at zero momentum transfer and maxima near $K^2 = 1$ a.u. The finite DOS value is consistent with the small value of the computed optical (dipole) oscillator strength. In addition, using a separate single-excitation configuration interaction (CI) excited-state calculation with a 6-31G (6-31^{++}G**) basis set and an internally optimized geometry for CF_3Cl (14), we also found the transition energy of the $^1E \leftarrow\ ^1A_1$ transition to be 8.59 eV (9.01 eV) with a small dipole transition moment of 0.0024 (0.0064). The

© 1997 NRC Canada

Can. J. Chem. Downloaded from www.nrcresearchpress.com by 91.121.58.235 on 09/08/12
For personal use only.

Can. J. Chem. Downloaded from www.nrcresearchpress.com by 91.121.58.235 on 09/08/12
For personal use only.

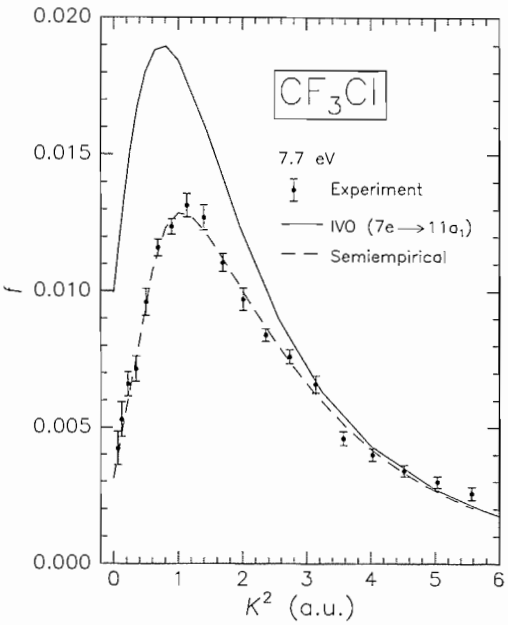
Fig. 3. Angle-resolved electron energy loss spectra of the valence shell of CF_3Cl at 2.5 keV impact energy and θ = (*a*) 1.0°, (*b*) 3.0°, (*c*) 5.0°, (*d*) 7.0°, and (*e*) 9.0°. The intensity variation of the weak peak at 7.7 eV (feature 1) is shown using an expanded scale (left axis) while the rest of the spectrum corresponds to the right vertical scale. Two Gaussian profiles are used to estimate the intensities of feature 1 and its neighbour, respectively, by a curve-fitting procedure, as illustrated in (*b*)–(*e*). The vertical ionization potentials (IPs) of the X–J states (vertical bars) are obtained experimentally (15).



reasonably good agreement of the experimental transition energy (7.7 eV) and the DOS value (0.003) with the calculations provides further support for the proposed assignment. These calculations therefore strongly support the assignment of the 7.7 eV transition as the $^1E \leftarrow {}^1A_1$ excitation.

This lowest-energy singlet transition involves excitation of an electron from the 7*e* HOMO, with Cl 3*p* lone-pair character ($n_{Cl\ 3p}$), into the $11a_1$ LUMO, with C—Cl σ* character ($\sigma^*_{C—Cl}$). Figure 5 compares the contour maps of the wave function density functions of the initial-state and final-state orbitals involved in this type of $n_{Cl\ 3p} \rightarrow \sigma^*_{C—Cl}$ transitions for CF_3Cl (and CHF_2Cl) (17). The contour maps were generated from ab initio self-consistent field (SCF) wave functions obtained by GAUSSIAN 90 (29) with a 6-31G basis set and internally optimized geometries. The Cl 3*p* lone-pair nature of the doubly degenerate orbitals, labeled as 7*e* and 7*e*′, in CF_3Cl is clearly illustrated in Figs. 5*e* and 5*f*, respectively, while the $11a_1$ orbital shown in Fig. 5*d* is seen to consist of antibonding overlap between the C(2*s*, 2p_x) and Cl 3p_x atomic orbitals, with its characteristic nodal plane bisecting the C—Cl bond. In the case of the $n_{Cl\ 3p} \rightarrow \sigma^*_{C—Cl}$ ($7e \rightarrow 11a_1$) transition in CF_3Cl,

Fig. 4. Absolute generalized oscillator strength as a function of momentum transfer (*K*) squared for the 7.7 eV transition in CF_3Cl. The broken curve corresponds to a semiempirical polynomial fit based upon the Lassettre series expansion. The solid line represents the result of an Improved Virtual Orbital (IVO) calculation (14).



overlap between the initial-state and final-state orbital wave function occurs mostly at the Cl site. The transition moment of this $n_{Cl\ 3p} \rightarrow \sigma^*_{C—Cl}$ electronic transition is therefore expected to resemble that of a *p*-to-*p* transition in a Cl atom, which readily explains the observed quadrupole nature of this transition.

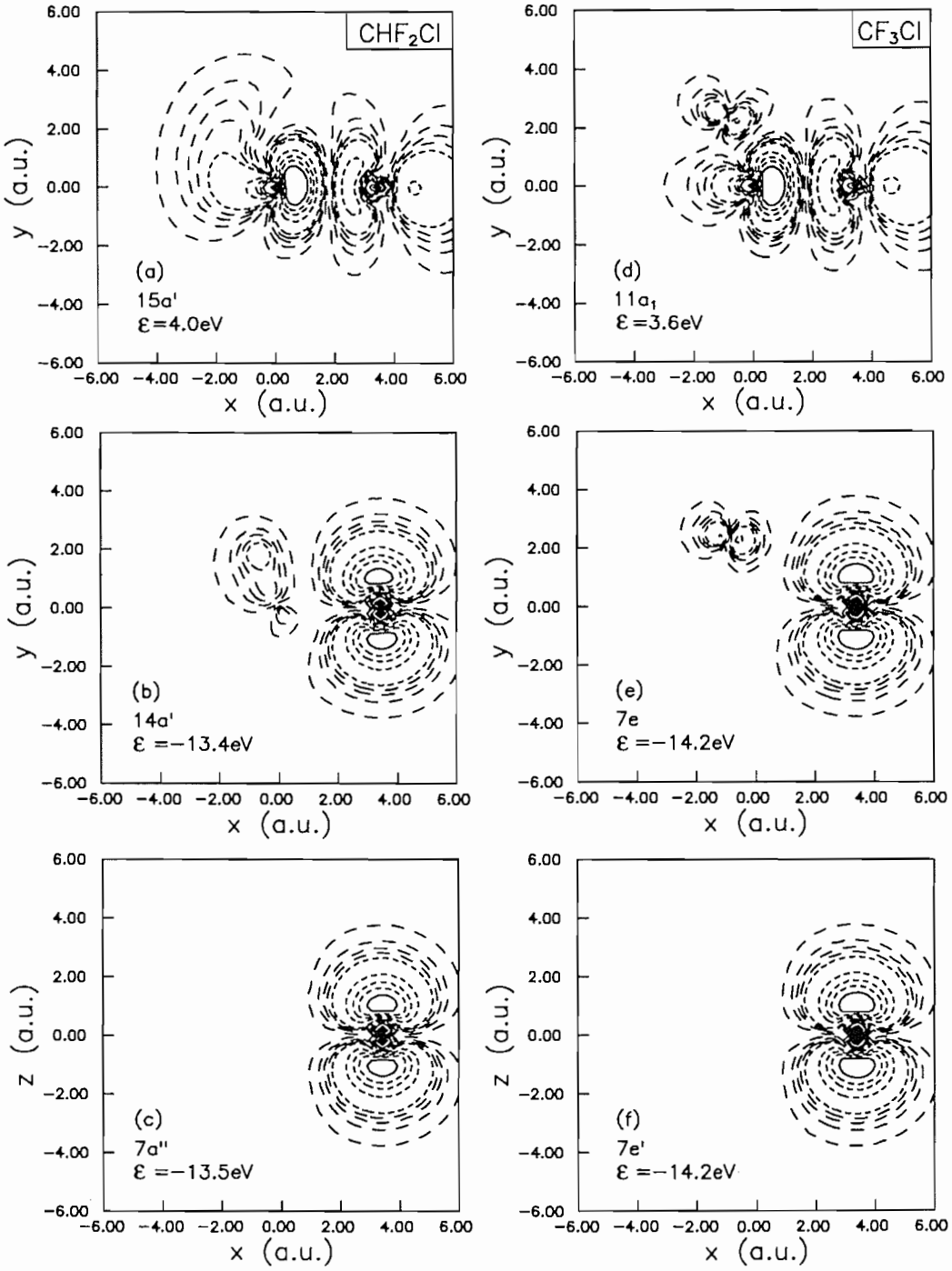
In Fig. 6, we show the potential energy curves of the $^1A_1$ and ^1E states along the C—Cl bond direction, generated by using the 6-31G and 6-31^{++}G** basis sets (14). Clearly, other than the apparent shift of the potential energy curves to a lower energy for the 6-31^{++}G** basis set, there is no obvious change in the general shapes of the potential energy curves between these two basis sets. Since the direct product table for the symmetry group C_{3v} indicates that the $^1E \leftarrow {}^1A_1$ transition is both dipole allowed and quadrupole allowed, the small transition dipole moment observed earlier therefore suggests that this transition can be attributed predominantly to quadrupole interactions, which are consistent with the dominant molecular orbital coefficients. Of particular interest, shown in the simple potential energy diagram, is that a vertical transition originating from the ground vibrational level of the $^1A_1$ state terminates at the repulsive part of the potential energy curve of the ^1E state above its dissociation limit. Figure 6 therefore provides qualitative support for the predissociative nature of the "metastable" ^1E state and that transition to this state would lead to breakage of the C—Cl bond.

2.2 Analogous non-dipole transitions in "environment-safe" Freon substitutes

The large-scale consumption of chlorofluorocarbons or Freons (as refrigerants, aerosol propellants, and semiconductor

© 1997 NRC Canada

Fig. 5. Two-dimensional wave function density contour maps for (*a*) the 15*a*′, (*b*) 14*a*′, and (*c*) 7*a*″ orbitals of CHF_2Cl, and for (*d*) the 11a_1, (*e*) 7*e*, and (*f*) 7*e*′ orbitals of CF_3Cl. The molecules are oriented with the carbon atoms located at the origin. The H-C-Cl group in CHF_2Cl and an F-C-Cl group in CF_3Cl have been positioned on the *xy* plane with the C—Cl bond oriented along the *x* axis. The contour values are 0.1, 0.3, 0.5, 0.7 (broken lines), 1, 3, 5, 7 (dotted lines), 10, 30, 50, 70, and 90% (solid lines) of the maximum density. The contour maps are calculated using ab initio SCF wave functions of 6-31G quality generated with internally optimized geometries (29). The molecular orbital symbols and calculated SCF orbital energies (ε) are also shown in the plots (note that a positive value for the orbital energy indicates a virtual orbital).

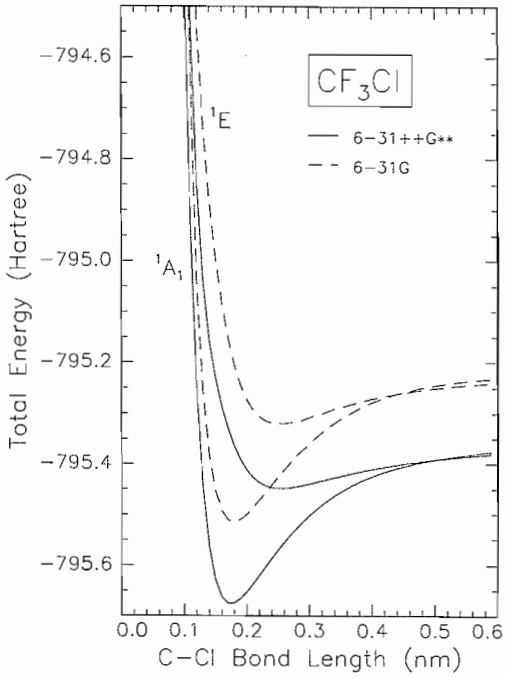


etchants, etc.) in many industrial applications (11, 12) has become a major environmental concern because of their destructive effect on ozone in the stratosphere. Many of the popular CFCs, including CF_3Cl (discussed above), CF_2Cl_2, $CFCl_3$ (15), and CCl_4 (16), are being replaced with "temporary" substitutes, which usually consist of the more "environment-safe" HCFCs, including CHF_2Cl (17), $CHFCl_2$ (18), and $CHCl_3$ (19) as well as their derivatives. Unlike the simple CFCs, however, the electronic structure and photochemistry of HCFC molecules are less well understood. For instance,

© 1997 NRC Canada

Can. J. Chem. Downloaded from www.nrcresearchpress.com by 91.121.58.235 on 09/08/12
For personal use only.

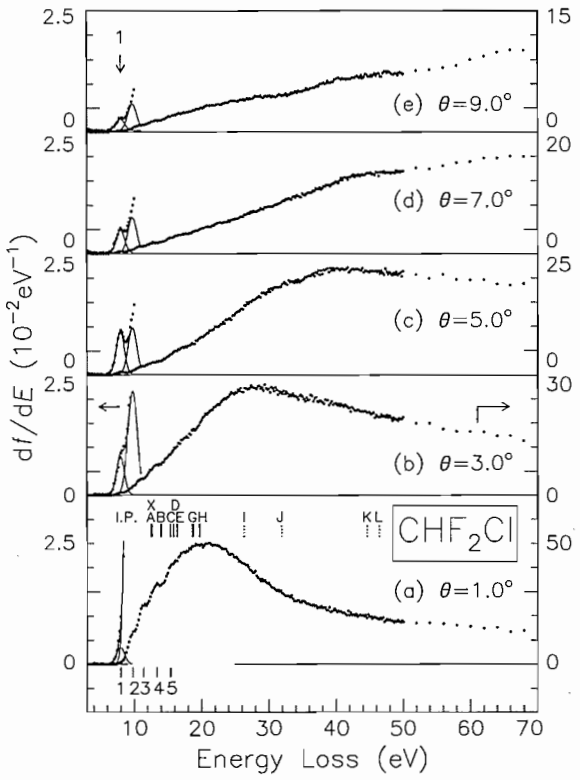
Fig. 6. Potential energy diagram along the C—Cl bond direction for the $^1A_1$ and ^1E states of CF_3Cl. The potential energy curves of the two states are obtained using single-excitation configuration interaction calculations with 6-31G (broken lines) and 6-31^{++}G** (solid lines) basis sets (29). Except for the C—Cl bond length, all other structural parameters obtained in an internally optimized geometry are held constant in the potential energy curve calculations.



there is no information on the important excitation cross sections of low-lying or any other electronic transitions, which, like their counterparts in CFCs, may play a key role in the relevant atmospheric and industrial processes. A few of these $n \rightarrow \sigma^*$ transitions in the 6–9 eV region for some of the more common CFC and HCFC molecules have been reported as "weak" features in the early vacuum ultraviolet photoabsorption (30) and small-angle high-resolution EELS studies (20). We have conducted a series of comparative studies involving HCFCs (17–19) with the goal of elucidating the effects of halogen content and symmetry change from, for example, C_{3v} (CF_3Cl) to C_s (CHF_2Cl) on the GOS profiles and the nature of this type of $n \rightarrow \sigma^*$ and other relevant low-lying electronic excitations.

The angle-resolved EELS spectra of CHF_2Cl (Freon 22) in Fig. 7 (17) reveal electronic structure similar to that of its CFC counterpart (CF_3Cl, Fig. 3). Except for the weak feature at 8.0 eV, most of the observed features below the ionization edge could again be attributed to Rydberg transitions. The GOS profile of this feature in CHF_2Cl is compared with that in CF_3Cl in Fig. 8 (17). The two GOS profiles appear to be very similar both in shape and magnitude. The maximum at $K^2 \sim 1$ a.u. in the GOS profile of the 8.0 eV feature in CHF_2Cl (like that of the 7.7 eV feature in CF_3Cl) is therefore characteristic of and provides evidence for the non-dipole nature of the transitions involved. We can again perform a single-excitation CI excited-state calculation using a 6-31G basis set and an inter-

Fig. 7. Angle-resolved electron energy loss spectra of the valence shell of CHF_2Cl at 2.5 keV impact energy and θ = (*a*) 1.0°, (*b*) 3.0°, (*c*) 5.0°, (*d*) 7.0°, and (*e*) 9.0°. The intensity variation of the weak peak at 8.0 eV (feature 1) is shown using an expanded scale (left axis) while the rest of the spectrum corresponds to the right vertical scale. Three Gaussian profiles are used to estimate the intensities of feature 1 (8.0 eV) and two neighbouring discrete states (at 9.8 and 11.4 eV) in a curve-fitting procedure (note that the fitting results of the third Gaussian peak are not shown). The vertical ionization potentials (IPs) of the X–H states (vertical bars) are obtained experimentally (21). State F is not labelled because of its ambiguity. The I.P.'s for states I–L (dotted vertical bars) are obtained from an ab initio SCF calculation with a 6-31G basis set (29).



nally optimized geometry for CHF_2Cl (29) to identify the nature of the transitions involved (17). Only singlet-to-singlet electronic transitions are calculated here because the contribution to the low-lying 8.0 eV feature from the spin-forbidden singlet-to-triplet transitions is negligible at the high impact energy (2.5 keV) employed in the present experiment. The calculation (17) shows that the feature at 8.0 eV can be adequately assigned as two predominant transitions to the $^1A'$ ($14a' \rightarrow 15a'$) and $^1A''$ ($7a'' \rightarrow 15a'$) excited states, which correspond, respectively, to electronic transitions from two essentially Cl 3*p* lone-pair orbitals (the HOMO $14a'$ and next HOMO $7a''$) to a $\sigma^*_{C—Cl}$ antibonding orbital (the LUMO $15a'$). The corresponding calculated transition energies from the ground state to the two excited states, $^1A'$ and $^1A''$, are 8.62 and 8.68 eV, respectively, which are in good accord with the experimental excitation energy of 8.0 eV. The total calculated DOS of 0.0052 for the two excited states (0.0039 for the $^1A'$ state and 0.0013 for the $^1A''$ state) is also in good agreement with the small experimentally derived f_0 value of 0.0043. The

© 1997 NRC Canada

Can. J. Chem. Downloaded from www.nrcresearchpress.com by 91.121.58.235 on 09/08/12
For personal use only.

Can. J. Chem. Downloaded from www.nrcresearchpress.com by 91.121.58.235 on 09/08/12
For personal use only.

Fig. 8. Absolute generalized oscillator strength f as a function of momentum transfer K squared for (*a*) the 8.0 eV feature in CHF_2Cl and (*b*) the 7.7 eV feature in CF_3Cl. The broken curves correspond to semiempirical polynomial fits based upon the Lassettre series expansion. Projected dipole oscillator strengths are indicated by crosses (x).

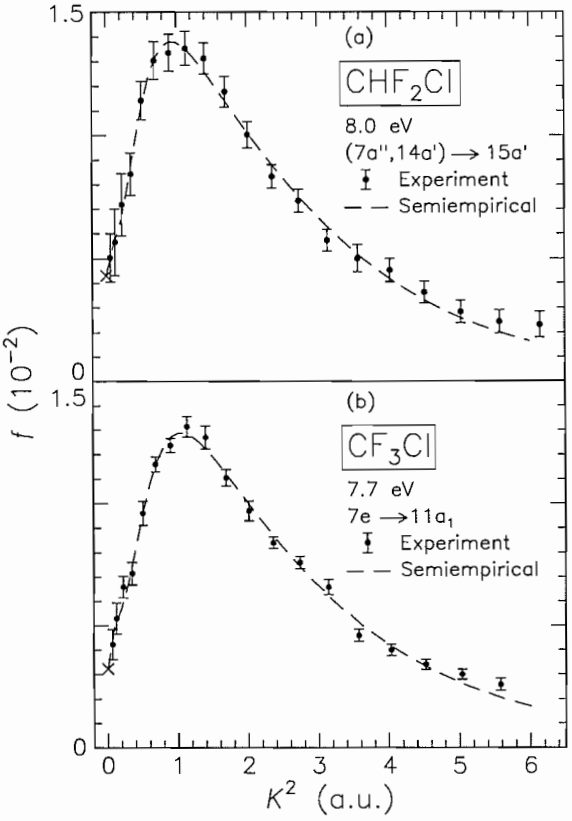
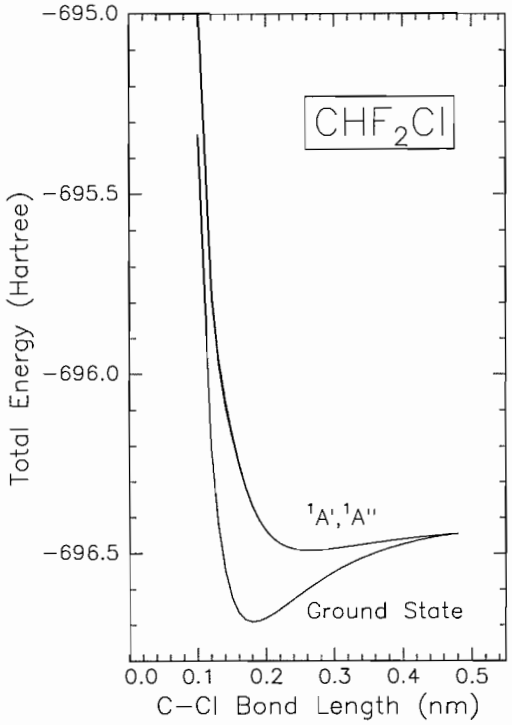


Fig. 9. Potential energy diagram along the C—Cl bond direction for the ground state and the two lowest-lying excited states ($^1A'$ and $^1A''$) of CHF_2Cl. The potential energy curves are obtained using single-excitation configuration interaction calculations with a 6-31G basis set (29). Except for the C—Cl bond length, all other structural parameters obtained from an internal geometry optimization are held constant in the potential energy curve calculations.



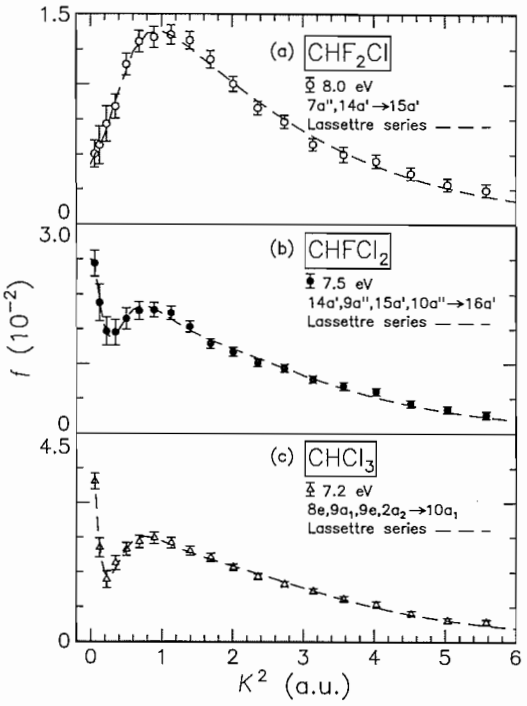
agreements obtained in the excitation energy and in the DOS between the calculation and experiment therefore provide strong evidence for the assignment of the $14a' \rightarrow 15a'$ and $7a'' \rightarrow 15a'$ electronic transitions to the observed low-lying feature at 8.0 eV in CHF_2Cl.

We can also understand the similarities in the GOS profiles between these HOMO → LUMO transitions in CHF_2Cl and CF_3Cl by examining the electron densities of the orbitals involved in the two molecules. Figure 5*a* shows the antibonding σ* character of the $15a'$ orbital, while Figs. 5*b* and 5*c* clearly illustrate the lone-pair nature of the $14a'$ and $7a''$ orbitals (17), which consist mainly of the in-plane Cl $3p_y$ and out-of-plane Cl $3p_z$ orbitals, respectively. The contour maps of the $\sigma^*_{C—Cl}$ antibonding ($15a'$) and $n_{Cl\ 3p}$ lone-pair ($14a'$ and $7a''$) orbitals in CHF_2Cl (Figs. 5*a*–5*c*) depict striking similarities to those of the corresponding orbitals in CF_3Cl (Figs. 5*d*–5*f*). Essentially the same descriptions for the antibonding and lone-pair orbitals and for the quadrupole nature of the *p*-to-*p* type transitions between these orbitals in CF_3Cl can also be applied to those in CHF_2Cl. Given these similarities, it is therefore not surprising to find that the potential energy curves along the C—Cl bond direction calculated using the single-excitation CI approach for these $n_{Cl\ 3p} \rightarrow \sigma^*_{C—Cl}$ transitions in CHF_2Cl (17), shown in Fig. 9, would also be similar to those for CF_3Cl (Fig. 6). It is also obvious from this potential energy diagram (Fig. 9) that the electronic transitions, $14a' \rightarrow 15a'$ and $7a'' \rightarrow 15a'$, may both lead to the dissociation of the C—Cl bond. The results of these potential energy curve calculations strongly suggest that dissociation of the C—Cl bond is a common consequence of the $n_{Cl\ 3p} \rightarrow \sigma^*_{C—Cl}$ transitions in CHF_2Cl and CF_3Cl.

Our studies on the GOS profiles of the $n_{Cl\ 3p} \rightarrow \sigma^*_{C—Cl}$ transitions in the common CFC (CF_3Cl, CF_2Cl_2, and $CFCl_3$) series (15) and their "environment-safe" HCFC substitutes (CHF_2Cl (17), $CHFCl_2$ (18), and $CHCl_3$ (19)) have revealed two interesting empirical trends: (*i*) the relative maximum intensity of the GOS profile within the aforementioned CFC and HCFC series increases nearly proportionally with increasing Cl content, and (*ii*) the relative amount of dipole (peak at $K = 0$) to non-dipole (peak at $K^2 \sim 1$ a.u.) component also increases with increasing chlorination. Figure 10 illustrates these general trends in the GOS profiles of the HOMO → LUMO transitions for the CHF_2Cl, $CHFCl_2$, and $CHCl_3$ series (18). In particular, the maxima for the respective GOS profiles approximately follow the 1:2:3 ratio, in concert with increasing chlorination. The relative contribution from the dipole component also increases with increasing Cl content, with the strongest dipole peak (at $K = 0$) in $CHCl_3$, which is also consistent with the relative ratio of the calculated (experimental) DOS values, 1:3.8:8.8 (1:5.8:13.4), for

© 1997 NRC Canada

Fig. 10. Absolute generalized oscillator strength f as a function of momentum transfer K squared for (*a*) the 8.0 eV feature in CHF_2Cl, (*b*) the 7.5 eV feature in $CHFCl_2$, and (*c*) the 7.2 eV feature in $CHCl_3$. The broken curves correspond to semiempirical polynomial fits based upon the Lassettre series expansion.



CHF_2Cl:$CHFCl_2$:$CHCl_3$. Although there are close correspondences in the GOS profiles of the HOMO → LUMO transitions between CHF_2Cl and CF_3Cl and between $CHCl_3$ and $CFCl_3$, the similarities between $CHFCl_2$ and CF_2Cl_2 are less striking, with a considerably sharper GOS secondary maximum in $CHFCl_2$ (Fig. 10*b*) relative to the broad peak in CF_2Cl_2 (15). The trend observed for the relative "dipole-to-non-dipole" contributions for these transitions suggests that molecular symmetry plays a key role in defining the contributions from different types of transitions to the GOS profile. In particular, the excited states of a more cage-like molecule such as $CHCl_3$ may be more susceptible to distortion due to Jahn–Teller effects, which in turn give rise to the more intense $K = 0$ (dipole) peak in the corresponding GOS profile. Finally, a noteworthy trend obtained in our recent angle-resolved EELS studies is that most of the $n_{Cl\,3p} \rightarrow \sigma^*_{C—Cl}$ transitions in the aforementioned CFC and HCFC molecules contain non-dipole interactions that lead to dissociation of the C—Cl bond. In particular, simple potential energy curve calculations suggest that the following $n_{Cl\,3p} \rightarrow \sigma^*_{C—Cl}$ transitions are predissociative: the $7e \rightarrow 11a_1$ transition at 7.7 eV in CF_3Cl (Fig. 6), $(3a_2, 8b_2) \rightarrow 13a_1$ transitions at 6.9 eV in CF_2Cl_2 (15), $10e \rightarrow 12a_1$ transition at 6.8 eV in $CFCl_3$ (15), and $2t_1 \rightarrow 7a_1$ transition at 7.2 eV in CCl_4 (16), as well as the $(7a'', 14a') \rightarrow 15a'$ transitions at 8.0 eV in CHF_2Cl (Fig. 9), $(10a'', 9a'') \rightarrow 16a'$ transitions at 7.5 eV in $CHFCl_2$ (18), and $9e \rightarrow 10a_1$ transition at 7.2 eV in $CHCl_3$ (19). The predissociative nature of the HOMO → LUMO transitions in these molecules is apparently quite common and clearly of interest to the understanding of the photochemical and electron-induced processes in the upper atmosphere and in plasma-related industrial applications.

3. Electrons as a powerful initiator for "novel" surface reactions

The use of low-energy electron or ion beam has become an increasingly powerful tool for the development of new materials (31). In particular, electron irradiation has been used to produce reactive ions and free radicals on surfaces (e.g., by means of an ion sputtering gun) and the resulting direct electron interactions and (or) ion interactions with the surface provide other important mechanisms and synthetic pathways not available in traditional thermal chemistry. In addition to electron-induced dissociation, electron/ion irradiation could, depending on the impact energy (IE) of the charged particle beam, also introduce other effects such as reaction activation, adsorbate removal (as in electron-stimulated desorption and ion sputtering), and creation of surface defect sites (which might affect the subsequent reaction processes and adsorption properties). In the case of ion irradiation, ion implantation and bulk atomic displacement (i.e., creation of bulk defects) could also occur. As in many applications in materials processing that involve film growth and surface modification by charged particle beam bombardment (32), these processes occur concurrently with the reaction activation process, making the study of an isolated chemical reaction difficult. Most studies have thus far been focussing on parameter optimization in the engineering of various new materials involving the use of these charged particle beams. Since many important reactions induced by low-energy electrons or ions remain unknown, it would therefore be of practical interest to investigate the fundamental mechanisms that control the initial adsorption and subsequent surface reactions induced by low-energy electron/ion irradiation.

Below we shall focus our discussion on two typical applications of the electron beam in experimental surface chemistry: (*i*) the use of electrons as a direct means of reaction activation by dissociation of adsorbates on surfaces; and (*ii*) the use of electrons as a means to produce free ions that are then used for reaction activation and ion–surface interactions. Several standard surface analytical techniques including low-energy electron diffraction (LEED), thermal desorption spectrometry (TDS), and high-resolution EELS are used for these experiments. Details of the experiments and our apparati, including our home-built angle-resolved high-resolution electron energy loss spectrometer (based on a novel design), have been described elsewhere (33, 34). Unless stated otherwise, electron irradiation was accomplished by bombarding the sample with electrons from the LEED gun or with electrons thermionically emitted from a heated tungsten filament, positioned 40 mm from the sample, at an electron flux of 2–3 $\mu A/mm^2$. Ion irradiation was performed by operating the ion sputtering gun at an ambient gas pressure of 1×10^{-6} Torr (1 Torr = 133.3 Pa) with an ion flux of ~10 nA/mm^2. The IE of the electron or ion beam could be controlled by adjusting the floating voltage applied to the sample with respect to a preselected beam voltage of the electron or ion sputtering gun.

Can. J. Chem. Downloaded from www.nrcresearchpress.com by 91.121.58.235 on 09/08/12
For personal use only.

© 1997 NRC Canada

Can. J. Chem. Downloaded from www.nrcresearchpress.com by 91.121.58.235 on 09/08/12
For personal use only.

3.1 Electron-induced chemistry of pyridine and aromatic compounds on Si(111)7 × 7

Although the TDS studies for both pyridine (35) and benzene (36) reported two desorption peaks with similar desorption maxima, we found that the adsorption and reactivity of pyridine on Si(111)7 × 7 are significantly different from its homocyclic analog, benzene. In particular, the molecular desorption of pyridine (35) is found to be considerably less intense than that of benzene (36) for a similar exposure, which suggests that the adsorption of pyridine on Si(111)7 × 7 is significantly less than that of benzene (because their ionization cross sections are expected to be similar to each other). Furthermore, unlike benzene, pyridine is found to be considerably more sensitive to low-energy electron irradiation on the 7 × 7 surface. Figure 11 shows the LEED pattern of 100 L (1 Langmuir = 1×10^{-6} Torr-second) of pyridine at room temperature (RT) (35). The relatively strong intensities of the (±3/7, ±3/7) and (±4/7, ±4/7) fractional-order spots in the observed "modified" 7 × 7 LEED pattern indicate that the adsorption of pyridine on the Si surface is not truly random and that preferential adsorption of pyridine may occur at specific types of dangling-bond sites of the 7 × 7 unit cell (37). The "modified" 7 × 7 pattern is found to convert rapidly to a 1 × 1 pattern by the low-energy (~50–100 eV) electron irradiation.

The effects of electron irradiation have also been examined by thermal desorption and are demonstrated in Fig. 12 (35). In particular, the reduction in the mass 84 (molecular) desorption of d_5-pyridine adsorbed on the 7 × 7 surface at RT and the large increase in the mass 4 (D_2) desorption due to electron irradiation provide further evidence that a significant portion of the adsorbed pyridine undergoes electron-induced dissociation. Whether pyridine dissociates completely to C, N, and H atoms or to smaller fragments that in turn undergo further dissociation during thermal desorption is, however, unclear. Of all the aromatic compounds on Si(111)7 × 7 studied by us (36, 38, 39), pyridine appears to be the only compound that is found to have significant interaction with electron irradiation. Despite the similarities in the TDS profiles (and electronic structures), thiophene and furan (unlike pyridine) adsorbed on the 7 × 7 surface were not affected by the exposure to low-energy electrons during the LEED experiment (39). Furthermore, the diffuse 7 × 7 LEED pattern observed for the adsorption of benzene (36) or toluene (38) on Si(111)7 × 7 was also not found to have degraded noticeably during the LEED analysis. Evidently, these aromatic compounds are not significantly affected by low-energy electron irradiation. The factors responsible for the high sensitivity to electron irradiation of pyridine adsorbed on Si(111)7 × 7 remain unknown, which demonstrates that the surface chemistry of a series of homologous molecules can be very complex and different from one another.

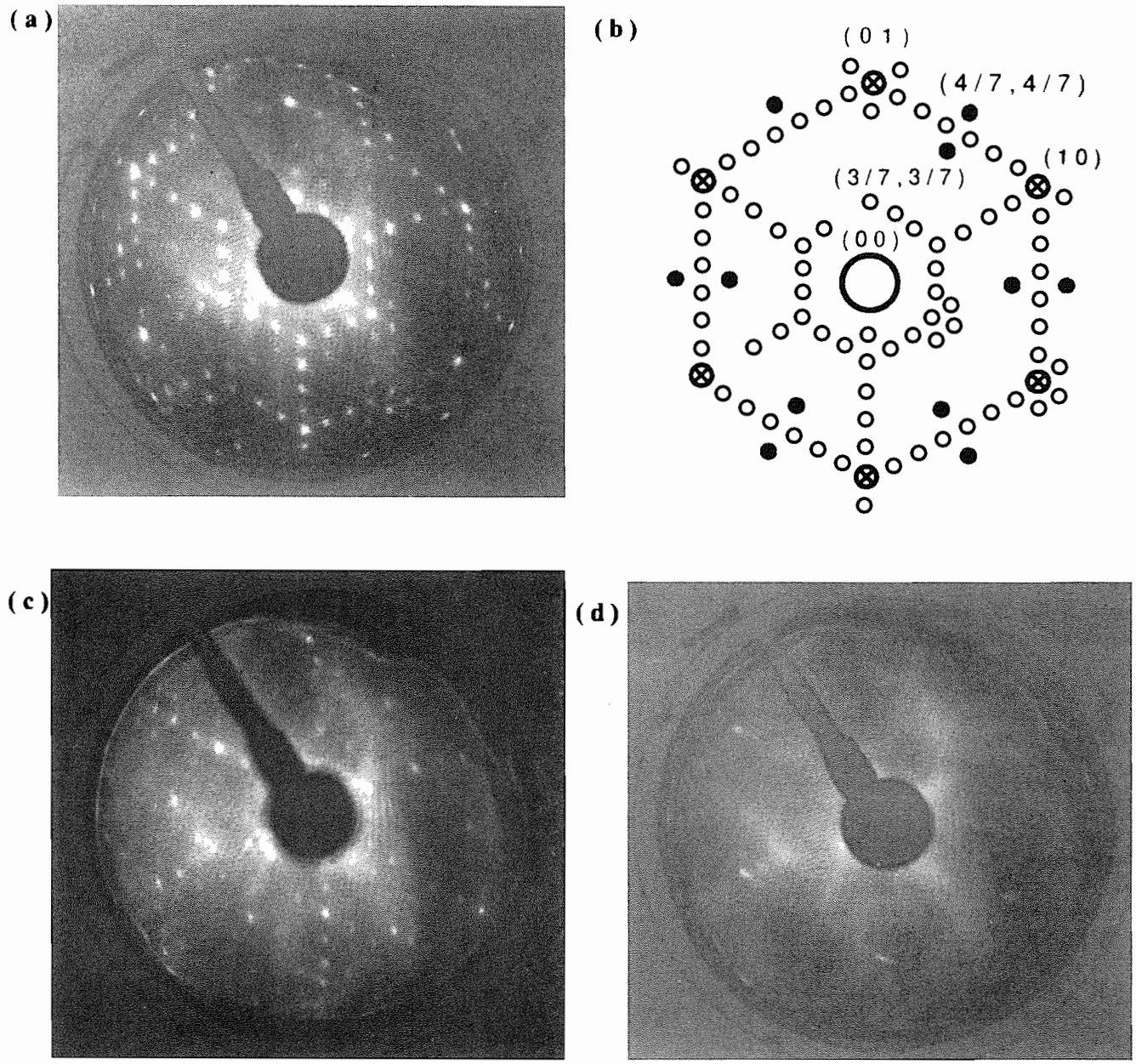
3.2 "Novel" surface reactions involving CO on Cu(100) induced by low-energy electrons and ions

One of the fundamental questions about the relevance of basic research in surface science to industrial applications is the effect of "dirt" on the observed surface phenomena or processes. In particular, common surface atomic contaminants (coadsorbates) such as O, N, and C present in the forms of oxides, nitrides, and graphitic or carbidic carbons have all been found to have a major effect on chemisorption and surface reactions. For example, unlike typical reaction poisons such as S and P, the presence of O (created by techniques involving electron or ion irradiation) has been found to have a stabilizing effect on the adsorption of CO on Cu(100), a chemisorption system that could only be observed below 200 K (40–43). In Fig. 13, we show the effects of low-energy electron irradiation on this "classic" chemisorption system, CO/Cu(100) (34). In particular, a typical vibrational (high-resolution) EELS spectrum for 100 L of CO on Cu(100) at 120 K is shown in Fig. 13*a*. The characteristic peaks for the Cu–CO stretch, ν(Cu–CO), at 338 cm^{-1} and the C–O stretch, ν(C–O), at 2084 cm^{-1} were found to be in good accord with the previously published data (40–42). The c(2 × 2)CO/Cu(100) sample was then irradiated with electrons (thermionically emitted from a heated tungsten filament positioned 40 mm away at a typical flux of 2.7 $\mu A/mm^2$) at 100 eV IE for 10 min, which gave rise to a less sharp c(2 × 2) LEED pattern. The ν(C–O) peak for the electron-irradiated sample remained at the same energy-loss position (Fig. 13*b*) but with a reduction in intensity, which was likely the result of electron-induced desorption and dissociation. On the other hand, the corresponding ν(Cu–CO) peak at 338 cm^{-1} became a broad shoulder, which could be attributed to additional contribution from the well-known Cu–O stretch at 305 cm^{-1} as previously observed for c(2 × 2)O/Cu(100) (44). When the sample temperature was slowly increased from 120 K, the peak at 2084 cm^{-1} was found to gradually diminish (Fig. 13*c*) and disappear at 200 K (Fig. 13*d*), revealing the peak at 2011 cm^{-1}. At this point, the LEED pattern became a diffused 1 × 1. The observed intensity reduction with increasing temperature of the ν(C–O) peak at 2084 cm^{-1} was consistent with the previous work (40). The new feature at 2011 cm^{-1} was clearly the result of low-energy electron irradiation and could be tentatively attributed to a "perturbed" C–O stretch (i.e., a red-shifted ν(C–O)). After the electron-irradiated sample was annealed to 160 K, the broad shoulder at ~338 cm^{-1} became a single peak at 310 cm^{-1}, which could be assigned to the Cu–O stretch (44), indicating the presence of atomic oxygen on the surface. The intensity of the peak at 2011 cm^{-1} remained essentially unchanged upon annealing to 370 K (Fig. 13*e*) and then almost completely diminished upon further annealing to 420 K (Fig. 13*f*). In contrast, the peak at 310 cm^{-1} decreased in intensity gradually upon annealing from 160 K (Fig. 13*c*) to 420 K (Fig. 13*f*).

Additional experiments to further elucidate the nature of this red-shifted ν(C–O) peak gave the following results (34): (*i*) Reducing the electron IE from 100 to 40 eV appeared to have no significant effect on the corresponding EELS spectra, which indicates that an electron IE of 40 eV was sufficient to activate the surface reactions that generated the "stabilized" CO. (*ii*) Exposing a high dose (1200 L) of CO to an amorphous Cu surface (obtained by sputtering Cu(100) in 2×10^{-5} Torr of Ar for 20 min at 500 eV IE) at 120 K and then annealing it to RT without electron irradiation did not produce the red-shifted CO peak (at 2011 cm^{-1}). Since Ar^+ sputtering is believed to introduce defect sites on Cu(100), this observation indicates that the presence of "stabilized" CO was not due to adsorption on defect sites. (*iii*) Exposing CO to an oxygen-covered Cu(100) surface (which was prepared by exposing a clean Cu(100) surface at RT with different dosages of O_2 ranging from 0.5 to 300 L) at 120 K without electron irradiation and then annealing the resulting sample to RT did not generate the

© 1997 NRC Canada

Fig. 11. The LEED pattern (*a*) and the corresponding schematic diagram (*b*) of the LEED spots shown in (*a*) for a clean Si(111)7 × 7 surface, and the LEED patterns for Si(111)7 × 7 exposed with 100 L of pyridine at room temperature at the beginning of the LEED experiment (*c*) and after 60 s of electron irradiation at ~80 eV and 10 μA (*d*). The integer-order spots are shown as circles with crosses and the (1 0) and (0 1) directions are chosen arbitrarily. Fractional-order spots connecting the integer-order spots are represented by smaller open circles, and the off-axis (±3/7, ±3/7) and (±4/7, ±4/7) fractional-order spots are shown as solid circles. The small distortion in the upper right corner of the LEED pattern is due to electron back-scattering from the nearby mass spectrometer chamber.



Can. J. Chem. Downloaded from www.nrcresearchpress.com by 91.121.58.235 on 09/08/12
For personal use only.

red-shifted CO peak. This result indicates that without electron irradiation CO could neither adsorb on an "oxidized" Cu(100) surface nor coadsorb with surface oxygen atoms to produce the "stabilized" CO. Finally, (*iv*) exposing CO to a carbon-covered Cu(100) surface (obtained by sputtering Cu(100) in C_2H_4 at RT and then annealing to 600 K) at 120 K without electron irradiation followed by annealing the resulting sample to RT also did not produce the red-shifted CO peak. This observation suggests that the red-shifted CO peak was not caused by coadsorption of CO with the surface carbon. All these experiments suggest that the observed red-shifted peak at RT was due to "stabilized" CO species that were generated in situ during CO exposure by electron irradiation.

From the results of other additional experiments involving ion irradiation, we conclude that the formation of "stabilized" CO may be considered as a two-step process (34): (*i*) Formation of reactants on the surface: C by electron/ion irradiation in CO or C_2H_4, and O by electron/ion irradiation in CO or by

© 1997 NRC Canada

Can. J. Chem. Downloaded from www.nrcresearchpress.com by 91.121.58.235 on 09/08/12
For personal use only.

Fig. 12. Comparison of the mass 84 (molecular) and mass 4 (D_2) desorption profiles for a 50 L room-temperature exposure of d_5-pyridine to Si(111)7 × 7 with electron irradiation at 0.2 mA and 80 eV for 30 min (– –) to that without electron irradiation (——).

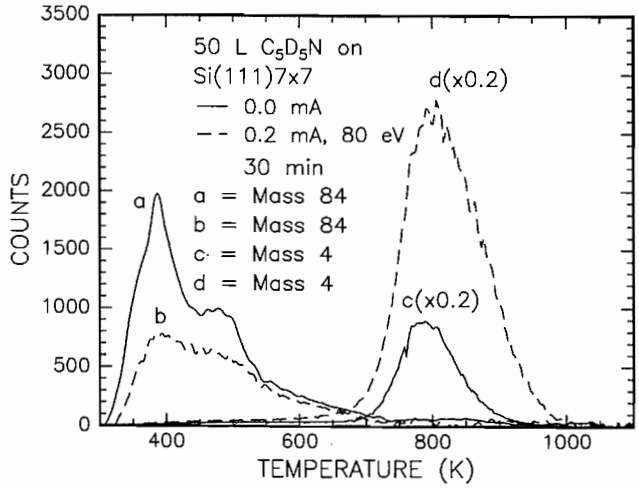
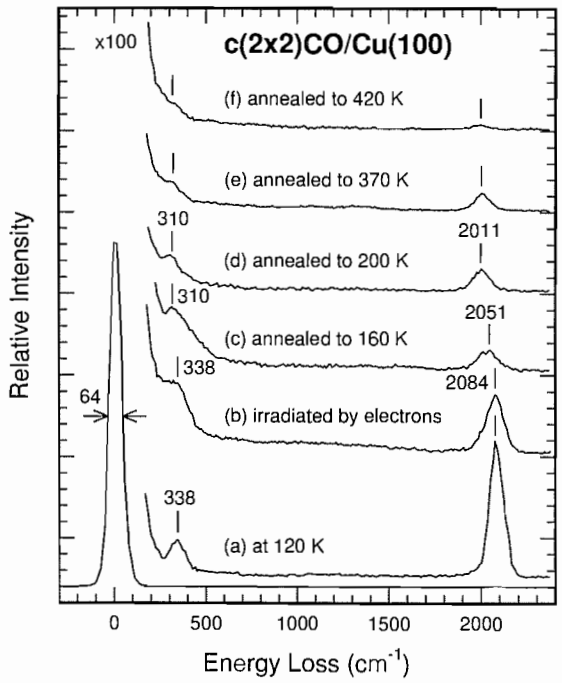


Fig. 13. Vibrational electron energy loss spectra for (*a*) 100 L of CO adsorbed on Cu(100) at 120 K, and (*b*) sample (*a*) irradiated with electrons at 100 eV and 2.7 μA/mm^2 for 10 min at 120 K, followed by annealing to (*c*) 160 K, (*d*) 200 K, (*e*) 370 K, and (*f*) 420 K.



directly exposing O_2 to the sample at RT; and (*ii*) In situ surface reaction between the surface C and O reactants following the equation: C (ad.) + O (ad.) → CO (ad.) during electron/ion irradiation or by thermal annealing to 370 *K*. In particular, by ion irradiation with a relatively low dose (600 L) of C_2H_4 at 50 eV IE, we show in Fig. 14 that surface carbon was generated to react with atomic oxygen predeposited on the Cu(100) surface

Fig. 14. Vibrational electron energy loss spectra for (*a*) Cu(100) exposed with 500 L of O_2 at 300 K, and (*b*) sample (*a*) sputtered in 1×10^{-6} Torr of ethylene at 50 eV and 10 nA/mm^2 for 10 min, following by annealing to (*c*) 370 K, and (*d*) 430 *K*.

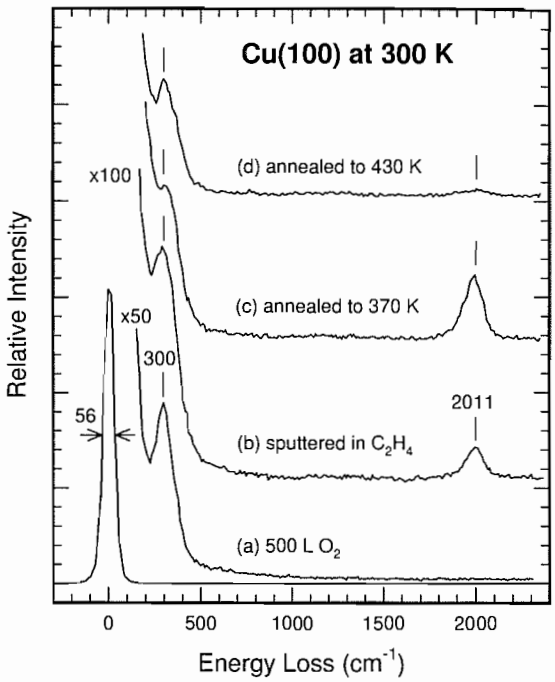
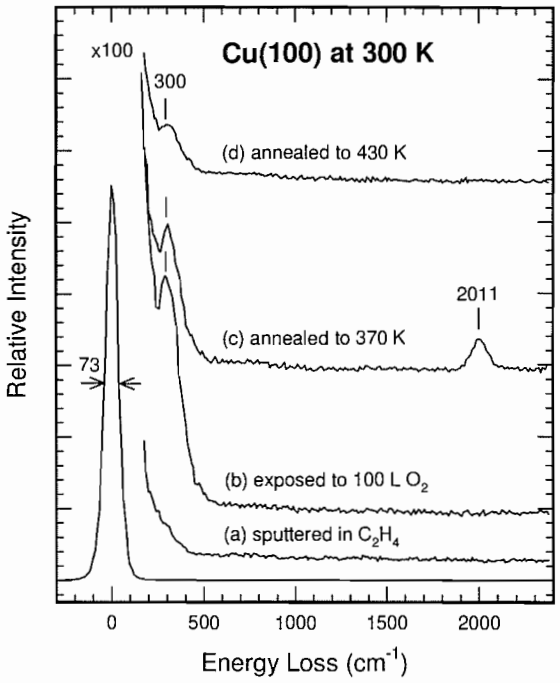


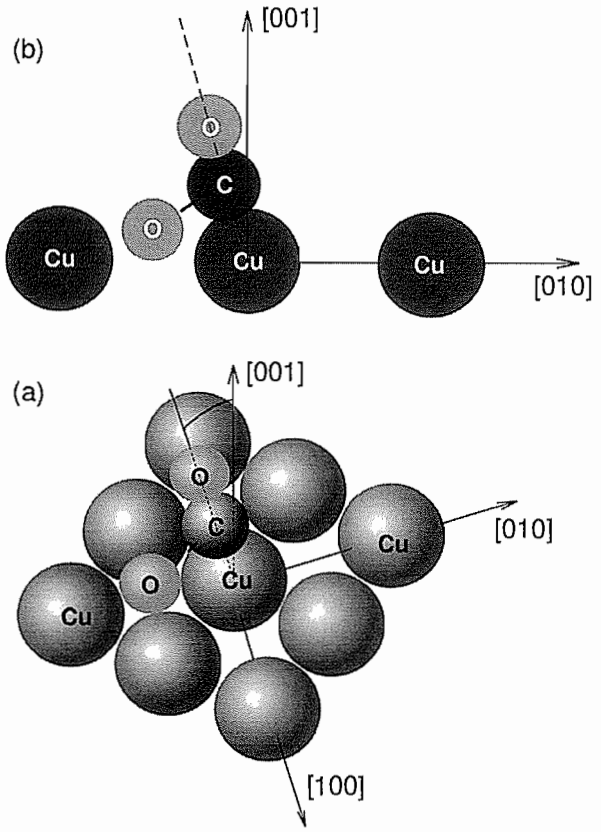
Fig. 15. Vibrational electron energy loss spectra for (*a*) Cu(100) sputtered in 1×10^{-6} Torr of ethylene at 50 eV and 10 nA/mm^2 for 10 min at 300 K, and (*b*) sample (*a*) exposed with 100 L of O_2, followed by annealing to (*c*) 370 K, and (*d*) 430 K.



© 1997 NRC Canada

Can. J. Chem. Downloaded from www.nrcresearchpress.com by 91.121.58.235 on 09/08/12
For personal use only.

Fig. 16. Perspective (*a*) and side-view (*b*) diagrams of a proposed bonding structure for as-formed CO adsorbed in the presence of predeposited O on Cu(100).



(34). It should be noted that an oxygen-covered Cu(100) surface can be readily obtained by directly dosing O_2 to Cu(100) at RT (44), as identified by the characteristic ν(Cu–O) peak near 300 cm^{-1} (Fig. 14*a*) and a c(2 × 2) LEED pattern. Evidently, the energy loss peak at 2011 cm^{-1}, characteristic of the previously observed "stabilized" CO adsorption, could again be obtained by ion irradiation of the oxidized sample in C_2H_4 at RT (Fig. 14*b*). This peak became more intense as the sample was annealed from RT to 370 *K* (Fig. 14*c*) and then almost completely diminished upon further annealing to 430 *K* (Fig. 14*d*).

The presence of the red-shifted CO peak did not appear to depend on the order of dosing O_2 and ion irradiation in C_2H_4 (Fig. 15), i.e., by reacting O with a Cu(100) surface predeposited with carbon-containing species (34). Although C_2H_4 (like CO) was found to adsorb on Cu(100) only at low temperature (45), we could increase the concentration of surface C (and (or) C-containing species) by ion irradiation of a clean Cu(100) surface at 50 eV IE in 600 L of C_2H_4 at RT. Despite the lack of any discernible feature in the EELS spectrum (Fig. 15*a*), the increase in surface C concentration was verified by Auger electron spectroscopy. After 100 L of O_2 was subsequently exposed to the surface (Fig. 15*b*), a prominent ν(Cu–O) peak at 300 cm^{-1} was observed. When the sample was annealed to 370 K (Fig. 15*c*), the CO peak at 2011 cm^{-1} reappeared and could again be removed by annealing to 430 K. In

Fig. 17. Vibrational electron energy loss spectra for (*a*) Cu(100) sputtered with 9 kL (1 kL = 1000 L) of ethylene at 200 eV and 10 nA/mm^2 at 300 K, and for sample (*a*) annealed to (*b*) 370 K, (*c*) 470 K, (*d*) 570 K, and (*e*) 670 K.

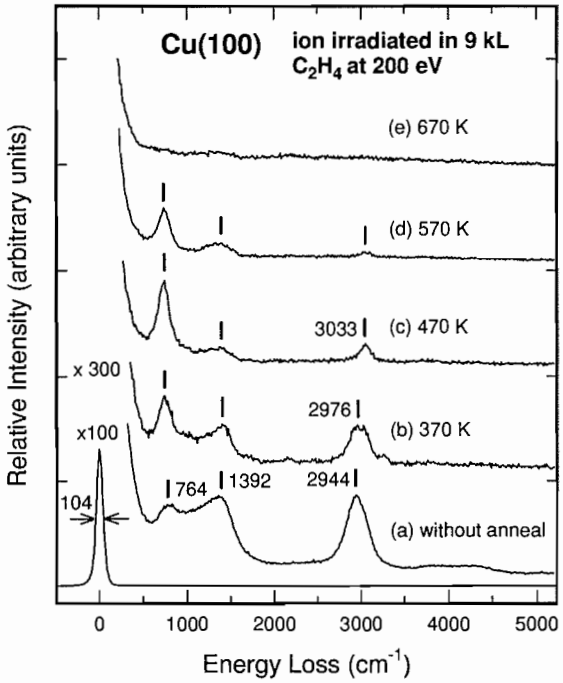
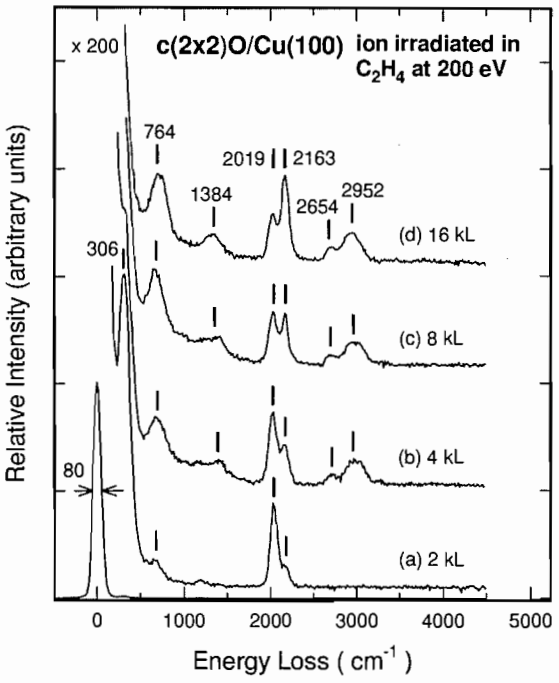


Fig. 18. Vibrational electron energy loss spectra for an oxygen-precovered Cu(100) surface ion-irradiated at 200 eV impact energy in (*a*) 2 kL, (*b*) 4 kL, (*c*) 8 kL, and (*d*) 16 kL of ethylene.



© 1997 NRC Canada

keeping with the EELS results shown in Figs. 14 and 15, the corresponding TDS data revealed that maximum desorption of both CO and CO_2 from the surface occurred near 400 K (34). CO_2 could be produced in situ by recombinative desorption of the adsorbed O and CO, i.e., O (ad.) + CO (ad.) $\rightarrow$ CO_2 (g). Evidently, the peak at 2011 cm^{-1} in Figs. 14 and 15 could be attributed to the same "stabilized" CO adsorption obtained earlier by electron irradiation (Fig. 13). On the other hand, if the C-covered surface (Fig. 15*a*) was first annealed to 500 K and then followed by O_2 exposure at RT, no red-shifted CO peak was observed even upon annealing the sample to 370 K. This indicates that the presence of surface atomic carbon and (or) C-containing species, produced by ion irradiation in C_2H_4, was essential to the formation of the red-shifted CO peak. As the C-covered sample was annealed to 500 K, the carbon atoms either combined with one another to form graphite or diffused into the bulk, preventing the formation of the "stabilized" CO species on Cu(100). From considerations of the available mechanisms that have been proposed to explain the observed red shift and stabilization effects (46), we favour a direct-interaction bonding model involving an O–CO quasi-complex, shown in Fig. 16 (34). In particular, the unusual stabilization of CO adsorption found in our experiments can be explained by a partial bond between a CO molecule adsorbed on an atop site and a preadsorbed O atom.

If the dosage of ethylene ions to Cu(100) was increased significantly by, for example, ion sputtering with 9 kL (1 kL = 1000 L) at a higher impact energy of 200 eV, the corresponding EELS spectra (over a set of annealing temperatures) shown in Fig. 17 revealed broad vibrational features at 764, 1392, and 2944 cm^{-1} attributable to C–H rock, C=C stretch and C–H stretch, respectively. These features could be identified by examining the corresponding EELS spectra for the sample prepared with C_2D_4 instead of C_2H_4 (isotopic substitution experiments). With the exception of the band at 764 cm^{-1}, the other two bands diminished in intensity more rapidly after successive annealing to a higher temperature (Figs. 17*b–d*). There was also a small shift to a higher energy for the 2944 cm^{-1} band. In Fig. 18, we show the effects of increasing the ion dosage of C_2H_4 on the Cu(100) sample predeposited with O (discussed earlier in Fig. 14*a*). In addition to the ethylene related peaks found in Fig. 17, two additional C–O stretch features at 2019 and 2163 cm^{-1} are particularly interesting. The peak at 2019 cm^{-1} corresponds to the red-shifted ν(C–O) of the O–CO quasi-complex in Fig. 15. Using arguments involving the intensity variation of the ion dosage, the new feature at 2163 cm^{-1} can be tentatively attributed to a "blue-shifted" ν(C–O) of a CO molecule stabilized by direct interaction with a nearby C-containing species. The temperature dependence of the red-shifted and blue-shifted ν(C–O) features provide further evidence that the adsorption of CO molecule could be stabilized by direct interaction with either a neighbouring O atom or a C-containing species.

The present work therefore not only provides direct support for in situ CO production at RT by electron- and ion-induced surface reactions on an "unreactive" surface such as Cu(100), but also illustrates the importance of common surface contaminants ("dirt") such as O and (or) C-containing species on the adsorption and surface reactions. It also demonstrates the enormous potential of activating surface reactions by means of low-energy electron or ion irradiation.

4. Concluding remarks

As we celebrate the centennial birthday of the electron, we as chemists have come a long way in the creative use of the electron not just as a unique tool for spectroscopic studies of technological materials such as Freons and their substitutes, but also as a powerful energy carrier for initiating new surface reactions directly or via radicals and ions generated by electron dissociation. We are optimistic that the development and applications of novel electron-based techniques for studying fundamental aspects of both gas-phase and surface chemistry will continue into the 21st century.

Acknowledgement

The financial support for the above work has been provided by the Natural Sciences and Engineering Research Council of Canada (NSERC) and in part by the J.P. Bickell Foundation, the Ontario Centre for Materials Research (OCMR), the Network of Centres of Excellence in Molecular and Interfacial Dynamics (CEMAID), NATO, and the Petroleum Research Fund (PRF). The above work would not have been possible without the ingenuity and dedication of four of my former and present graduate students: De-Qing Hu, Charles MacPherson, Ji-Feng Ying, and Hui Yu. I am indebted to Mr. Jacek Szubra and the current and early-retired staff of the Science Shops for their skillful workmanship in the development of all of our machines in our laboratory in the past decade.

References

1. J.J. Thomson. Philos. Mag. **44**, 295 (1897).
2. J.B. Foresman, M. Head-Gordon, J.A. Pople, and M.J. Frisch. J. Phys. Chem. **96**, 135 (1992).
3. R.A. Bonham, J.S. Lee, R. Kennerly, and W. St. John. Adv. Quantum Chem. **2**, 1 (1978); R.A. Bonham. *In* Electron spectroscopy: theory, techniques and applications. Vol. 3. *Edited by* C.R. Brundle and A.D. Baker. Academic, New York. 1979. p. 127.
4. J.F. Ying and K.T. Leung. Phys. Rev. A: At. Mol. Opt. Phys. **53**, 1476 (1996), and refs. therein.
5. J.F. Ying, C.P. Mathers, and K.T. Leung. Phys. Rev. A: At. Mol. Opt. Phys. **47**, R5 (1993).
6. M. Inokuti. Rev. Mod. Phys. **43**, 297 (1971).
7. E.N. Lassettre and A. Skerbele. *In* Methods of experimental physics. Vol. 3 (Part B). *Edited by* D. Williams. Academic Press, New York. 1974. Chap. 7.2. p. 868.
8. E.N. Lassettre. J. Chem. Phys. **43**, 4479 (1965); M.A. Dillon and E.N. Lassettre. J. Chem. Phys. **62**, 2373 (1975).
9. W.M. Huo. J. Chem. Phys. **71**, 1593 (1979).
10. R.S. Barbieri and R.A. Bonham. Phys. Rev. A: **44**, 7361 (1991).
11. R.D. Hudson (*Editor*) Chlorofluoromethanes and the stratosphere. NASA Ref. Publ. 1010, NASA Scientific and Technical Information Office. 1977.
12. Plasma reactions and their applications. *Japan Materials Report*. Japan Technical Information Services, ASM International. 1988.
13. J.F. Ying, T.A. Daniels, C.P. Mathers, H. Zhu, and K.T. Leung. J. Chem. Phys. **99**, 3390 (1993).
14. J.F. Ying, C.P. Mathers, K.T. Leung, H.P. Pritchard, C. Winstead, and V. McKoy. Chem. Phys. Lett. **212**, 289 (1993).
15. J.F. Ying and K.T. Leung. J. Chem. Phys. **101**, 8333 (1994), and refs. therein.
16. J.F. Ying and K.T. Leung. J. Chem. Phys. **100**, 7120 (1994).

© 1997 NRC Canada

Can. J. Chem. Downloaded from www.nrcresearchpress.com by 91.121.58.235 on 09/08/12
For personal use only.

17. J.F. Ying and K.T. Leung. J. Chem. Phys. **100**, 1011 (1994).
18. J.F. Ying and K.T. Leung. J. Chem. Phys. **105**, 2188 (1996).
19. J.F. Ying and K.T. Leung. Phys. Rev. A: At. Mol. Opt. Phys. **53**, 1476 (1996).
20. G.C. King and J.W. McConkey. J. Phys. B: Condens. Matter, **11**, 1861 (1978); W. Zhang, G. Cooper, T. Ibuki, and C.E. Brion. Chem. Phys. **151**, 343 (1991), and refs. therein.
21. R. Gilbert, P. Sauvageau, and C. Sandorfy. J. Chem. Phys. **60**, 4820 (1974); L.C. Lee, E. Phillips, and D.L. Judge. J. Chem. Phys. **67**, 1237 (1977).
22. R.S. Barbieri and R.A. Bonham. Phys. Rev. A: At. Mol. Opt. Phys. **63**, 7929 (1992), and refs. therein.
23. G.G.B. de Souza, C.E. Bielschowsky, C.A. Lucas, and A.C.A. Souza. Phys. Rev. A: At. Mol. Opt. Phys. **42**, 1363 (1990), and refs. therein.
24. D.G. Wilson, J. Comer, and S. Taylor. J. Phys. B: Condens. Matter, **13**, 2849 (1980); A.C.A. Souza and G.G.B. de Souza. Phys. Rev. A: **38**, 4488 (1988).
25. K.N. Klump and E.N. Lassettre. Chem. Phys. Lett. **51**, 99 (1977).
26. K.N. Klump and E.N. Lassettre. J. Chem. Phys. **68**, 3511 (1978).
27. E.N. Lassettre. J. Chem. Phys. **43**, 4479 (1965); M.A. Dillon and E.N. Lassettre. J. Chem. Phys. **62**, 2373 (1975).
28. W.A. Goddard III and W.J. Hunt. Chem. Phys. Lett. **3**, 414 (1969).
29. M.J. Frisch, M. Head-Gordon, G.W. Trucks, J.B. Foresman, H.B. Schlegel, K. Raghavachari, M. Robb, J.S. Binkley, C. Gonzalez, D.J. Defrees, D.J. Fox, R.A. Whiteside, R. Seeger, C.F. Melius, J. Baker, R.L. Martin, L.R. Kahn, J.J.P. Stewart, S. Topiol, and J.A. Pople. GAUSSIAN 90. Revision F. Gaussian Inc., Pittsburgh, Pa. 1990.
30. R. Gilbert, P. Sauvageau, and C. Sandorfy. J. Chem. Phys. **60**, 4820 (1974); J. Doucet, P. Sauvageau, and C. Sandorfy. J. Chem. Phys. **58**, 3708 (1973).
31. D. L. Smith. Thin film deposition principles and practice. McGraw–Hill, New York. 1995.
32. J.J. Cuomo, S.M. Rossnagel, and H.R. Kaufman (*Editors*). Handbook of ion beam processing technology. Noyes Publications, Park Ridge, N.J. 1989.
33. D.Q. Hu. Ph.D. Thesis. The University of Waterloo. 1993.
34. H. Yu, D.Q. Hu, and K.T. Leung. J. Vac. Sci. Technol. A: **15**, 2653 (1997).
35. C.D. MacPherson and K.T. Leung. Surf. Sci. **324**, 202 (1995).
36. C.D. MacPherson, D.Q. Hu, and K.T. Leung. Solid State Commun. **80**, 217 (1991); D.Q. Hu, C.D. MacPherson, and K.T. Leung. Surf. Sci. **273**, 21 (1992).
37. K. Takayanagi, Y. Tanishiro, M. Takahashi, and S. Takahashi. J. Vac. Sci. Technol. A: **3**, 1502 (1985).
38. C.D. MacPherson and K.T. Leung. Surf. Sci. **326**, 141 (1995).
39. C.D. MacPherson, D.Q. Hu, and K.T. Leung. Surf. Sci. **276**, 156 (1992).
40. S. Andersson. Surf. Sci. **89**, 477 (1979).
41. S. Andersson and B.N.J. Persson. Phys. Rev. Lett. **45**, 1421 (1980); Phys. Rev. B: Condens. Matter, **24**, 3659 (1981).
42. B.A. Sexton. Chem. Phys. Lett. **63**, 451 (1979).
43. S. Andersson and J.B. Pendry. Phys. Rev. Lett. **43**, 363 (1979).
44. M. Wuttig, R. Franchy, and H. Ibach. J. Electron Spectrosc. Relat. Phenom. **44**, 317 (1987), and refs. therein.
45. C. Nyberg, C.G. Tengstal, and S. Andersson. Chem. Phys. Lett. **87**, 87 (1982).
46. G. Pacchioni and P.S. Bagus. Chem. Phys. **177**, 373 (1993).

Can. J. Chem. Downloaded from www.nrcresearchpress.com by 91.121.58.235 on 09/08/12
For personal use only.

© 1997 NRC Canada

Correlation between the electron solvation time and the solvent dielectric relaxation times τ_2 and τ_{L1} in liquid alcohols and water: towards a universal concept of electron solvation?

Jean-Paul Jay-Gerin

Abstract: A simple model of electron solvation in polar liquids is presented, in which we attempt to link the electron solvation time τ_s to τ_2, the time for reorientation of monomeric molecules, and to τ_{L1}, the longitudinal dielectric relaxation time of the solvent. It is shown that this model, which is suggested by the so-called hybrid model of electron solvation previously described for methanol, can satisfactorily account for electron solvation in all polar liquids, including linear alcohols (methanol to decanol), 1,2-ethanediol, H_2O, and D_2O, for which data are available from the literature. A close similarity is indeed obtained between our calculated values of τ_s and those measured experimentally. The observation of such a correlation supports a universal concept of electron solvation.

Key words: polar liquids, electron solvation time, solvent dielectric relaxation times, universal concept of electron solvation.

Résumé : Nous présentons un modèle simple de la solvatation de l'électron dans les liquides polaires, sur la base duquel nous tentons de relier le temps de solvatation de l'électron τ_s à τ_2, le temps de réorientation des molécules monomères, et à τ_{L1}, le temps de relaxation diélectrique longitudinal du solvant. Nous montrons que ce modèle, suggéré par celui dit «hybride» décrit précédemment pour la solvatation de l'électron dans le méthanol, peut rendre compte de façon satisfaisante de la solvatation de l'électron dans tous les liquides polaires, incluant les alcools linéaires (méthanol au décanol), l'éthanediol-1,2, H_2O et D_2O, pour lesquels des données sont disponibles dans la littérature. Une proche similarité est effectivement obtenue entre nos valeurs de τ_s calculées et celles mesurées expérimentalement. L'observation d'une telle corrélation plaide en faveur d'un concept d'universalité de la solvatation de l'électron.

Mots clés : liquides polaires, temps de solvatation de l'électron, temps de relaxation diélectrique du solvant, concept d'universalité de la solvatation de l'électron.

Solvated excess electrons (e^-_s) in polar solvents have been a subject of considerable experimental and theoretical interest since their discovery and identification in liquid water in the 1960s (for a recent review, see ref. 1). Time-resolved dynamical studies of electron solvation were first conducted in low- and room-temperature liquid alcohols, and a number of experimental data have been obtained over the last 25 years (2–14). In an attempt to identify which solvent motions may be responsible for the solvation, the measured electron solvation times (τ_s) were compared with the alcohol Debye dielectric relaxation times τ_1, τ_2, and τ_3 (15–18) associated with the cooperative hydrogen-bond dynamics in the liquid, the rotation of non-hydrogen-bonded monomeric molecules, and the reorientation of the OH group around the C—O bond, respectively. A correlation was observed between τ_s and τ_2 in a series of linear alcohols (methanol to decanol) (5, 9).

Recently, ultrafast spectroscopic measurements on electron solvation in liquid alcohols at room temperature have been reported (19–23), and have led to the determination of new precise data for τ_s in those liquids. In particular, the femtosecond laser experiments of Pépin et al. (20, 21) in methanol provided evidence that the solvation of electrons in this liquid may well be described with a model called "hybrid," which involves, among other things, two electronic states (one weakly bound e^-_{wb} and one strongly bound e^-_{sb}), both of them relaxing via a continuous blue shift and between which there is, concurrently, a stepwise transfer mechanism. Essentially similar results were obtained by Hirata and Mataga (13) and by Shi et al. (23), at least for the continuous evolution of the relatively stable form of the electron, e^-_{sb}, towards e^-_s. Most recently, this same hybrid model was also found capable of describing the spectral manifestations of electron solvation in deuterated water (24), as well as in H_2O and in various small-chain alcohols (25).

In this paper, we present a simple model of the electron solvation process, in which we attempt to link τ_s to the solvent dielectric relaxation times τ_2 and τ_{L1}, where $\tau_{L1} = (\varepsilon_\infty/\varepsilon_0)\tau_1$ is

Received April 11, 1997.

J.-P. Jay-Gerin.[1] Département de médecine nucléaire et de radiobiologie, Faculté de médecine, Université de Sherbrooke, Sherbrooke, QC J1H 5N4, Canada.

[1] Telephone: (819) 346-1110, ext. 14682. Fax: (819) 564-5442. E-mail: jaygerin@courrier.usherb.ca

© 1997 NRC Canada

Can. J. Chem. Downloaded from www.nrcresearchpress.com by 91.121.58.235 on 09/08/12
For personal use only.

Can. J. Chem. Downloaded from www.nrcresearchpress.com by 91.121.58.235 on 09/08/12
For personal use only.

the well-known longitudinal relaxation time.[2] We show that this model, which is in essence suggested by the hybrid model of Pépin et al. (20, 21, 24, 25), can satisfactorily account for electron solvation in all polar liquids, including linear alcohols (methanol to decanol), 1,2-ethanediol, H_2O, and D_2O, for which data are available from the literature, a result, in turn, in favor of a universal concept of electron solvation.

As already proposed (13, 20, 21, 24, 25), we interpret, in the model presented here, the continuous blue shift of e^-_{wb}, as well as that of e^-_{sb}, as due to the long-range relaxation of the solvent whose characteristic time is given by τ_{L1} (26). In the light of the known correlation between τ_s and τ_2 in liquid alcohols (5, 9), we also assume that the stepwise transfer process from e^-_{wb} to e^-_{sb} or e^-_s is controlled by rotational motions of solvent monomers whose characteristic time is given by τ_2.

In the context of these hypotheses, we consider that there are *three* different relaxation processes of e^-_{wb}, which operate *in parallel*: the first one includes the formation of e^-_s through a direct stepwise transition with characteristic time τ_2; the second one proceeds via a stepwise transfer to e^-_{sb} with time constant τ_2, followed by a continuous blue shift of e^-_{sb} with time constant τ_{L1}; and the third process is similar to both preceding ones, except that it begins with a continuous blue shift of e^-_{wb} with time constant τ_{L1}. For simplicity, we neglect in this model the trapping time of a quasifree thermalized electron (e^-_{qf}) into the e^-_{wb} state, as well as the direct deep trapping of e^-_{qf} into the e^-_{sb} or e^-_s state without transit through e^-_{wb} (these processes are assumed to be practically instantaneous).

Figure 1 presents a schematic picture of our proposed model of the electron solvation process, which may simply be viewed as an (infinite) series of elementary steps (n = 1,2,...) with corresponding characteristic times $\tau_{s(1)}$, $\tau_{s(2)}$,... According to this scheme, the time $\tau_{s(1)}$ involved in the relaxation process of e^-_{wb} for the first-order step (n = 1) considered, is given by

$$[1]\quad \frac{1}{\tau_{s(1)}} = \frac{1}{\tau_2} + \frac{1}{\tau_2 + \tau_{L1}} + \frac{1}{\tau_{L1}}$$

while for the second-order step (n = 2), we have

$$[2]\quad \frac{1}{\tau_{s(2)}} = \frac{1}{\tau'_2} + \frac{1}{\tau_{L1} + \tau_{s(1)}}$$

where

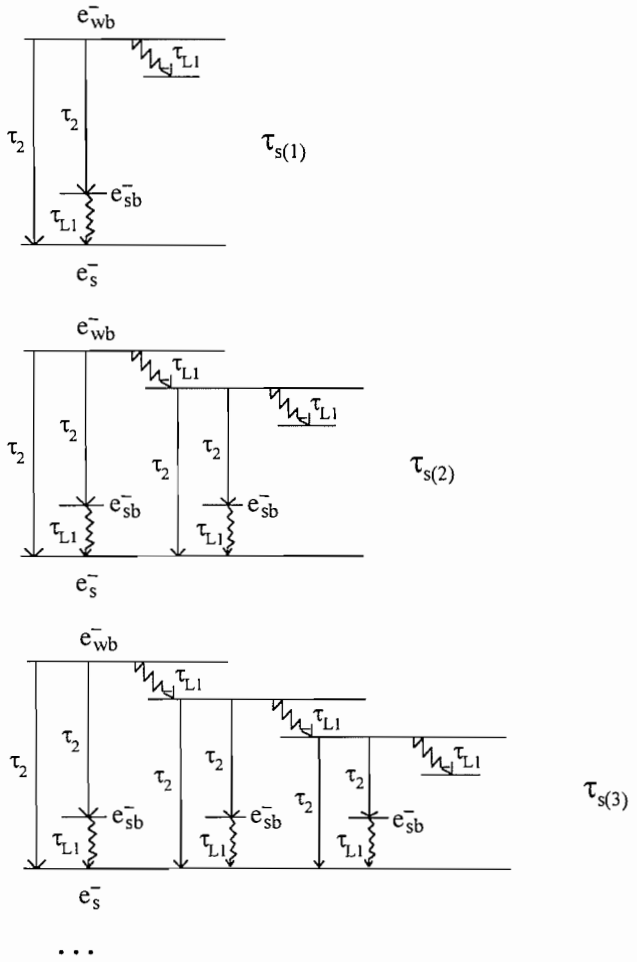
$$[3]\quad \frac{1}{\tau'_2} = \frac{1}{\tau_2} + \frac{1}{\tau_2 + \tau_{L1}}$$

This result may readily be extended to the nth-order step, for which we get

$$[4]\quad \frac{1}{\tau_{s(n)}} = \frac{1}{\tau'_2} + \frac{1}{\tau_{L1} + \tau_{s(n-1)}}$$

[2] Note that in the relation $\tau_{L1} = (\varepsilon_\infty/\varepsilon_0)\tau_1$, τ_1 is the dielectric relaxation time associated with the long-range, cooperative hydrogen-bond dynamics in the solvent, and ε_∞ and ε_0 are the "infinite" and zero-frequency solvent dielectric constants, respectively. For a discussion of the physical meaning of τ_{L1}, see, for example, ref. 26.

Fig. 1. Schematic picture of our proposed model of electron solvation. There are *three* different relaxation processes of the weakly bound electron (e^-_{wb}) to the fully relaxed solvated electron (e^-_s), which operate *in parallel*: the first one corresponds to a direct stepwise transition to the e^-_s state with characteristic time τ_2; the second one includes a stepwise transfer to the intermediate strongly bound (e^-_{sb}) state with time constant τ_2, in series with a continuous blue shift of e^-_{sb} with time constant τ_{L1}; and the third process is similar to both of the two preceding ones, except that it is initiated by a gradual blue shift of e^-_{wb} with time constant τ_{L1}. The overall solvation process of the excess electron may be viewed as an (infinite) series of elementary steps (n) with corresponding characteristic times $\tau_{s(1)}$, $\tau_{s(2)}$,..., $\tau_{s(n)}$. In this model, the electron solvation time τ_s is simply given by $\tau_{s(n)}$ as $n \to \infty$ (see text).



Upon using the recurrence relation [4] for the limiting case where $n \to \infty$, we easily obtain the following formula for the overall electron solvation time τ_s:

$$[5]\quad \tau_s = \frac{\tau_{L1}}{2}\left[\left(1 + \frac{4\,\tau'_2}{\tau_{L1}}\right)^{1/2} - 1\right]$$

or, equivalently, if we introduce the (dimensionless) parameter $x = 4\,\tau'_2/\tau_{L1}$,

$$[6]\quad \frac{\tau_s}{\tau'_2} = \frac{2}{x}\left[(1 + x)^{1/2} - 1\right]$$

© 1997 NRC Canada

Can. J. Chem. Downloaded from www.nrcresearchpress.com by 91.121.58.235 on 09/08/12
For personal use only.

Table 1. Comparison of the electron solvation time τ_s with the solvent dielectric relaxation times τ_2 (corresponding to single-molecule reorientation processes) and τ_{L1} (reflecting the time scale of the cooperative hydrogen-bond dynamics in the bulk solvent).[a] The solvents are listed in order of increasing τ_{L1}. Reference numbers are in parentheses.

Solvent	τ_s (ps)[b]	τ_2 (ps)	τ_{L1} (ps)	x[c]	τ_s (ps)[d]
H_2O	<0.3 (27), 0.24 ± 0.04 (28), 0.54 ± 0.05 (29), 0.62 ± 0.06 (30), 0.55 ± 0.17 (31), 0.31 ± 0.08 (32), 0.50 ± 0.15 (33), 0.54 ± 0.08 (34)	1.02 (18, 35), 1–2(35)	0.659 (18), 0.549 (36)	3.9	0.40
D_2O	0.41 ± 0.02 (24), 0.25 (37), ~30% slower than in H_2O (38)	~1.4 (18, 35)[e]	0.636 (36)	5.2	0.47
Methanol	10 ± 1 (5), 11 ± 1 (9), 17 ± 3 (10), <10 (12), 9.5 ± 2 (19), 6.1 ± 0.6 (20), 5.5 ± 0.4 (21), 7.1 ± 0.3 (23)	7.09 (18)	8.44 (17), 9.37 (18), 8.2 (39), 9.2 (40)	2.1	3.6
$(CH_2OH)_2$	5 ± 3 (5), <5 (9), <10 (12), ~5 (19)	10 (41)[f]	22.2 (41)[f]	1.4	6.0
Ethanol	21 ± 2 (5, 7), 18 ± 2 (9, 12), 26 ± 5 (10), 11 (13), ~21 (19), 15.2 ± 1 (23)	8.97 (18)	31.5 (17), 30.1 (18)	0.97	6.1
1-Propanol	31 ± 3 (5, 7), 25 ± 3 (9), ~20 (11), 22 ± 2 (12), 21 (13), ~36[g]	20.9 (15), 15.3 (16), 19.1 (17), 15.1 (18)	74.4 (17), 60.2 (18)	0.84	10.7
2-Propanol	24 ± 2 (9), 23 ± 2 (12), 22 (13), ~36[g]	14.5 (18)	79.9 (17), 64.2 (18)	0.76	10.5
1-Butanol	34 ± 5 (5, 7), 30 ± 3 (9), ~30 (11), 21 ± 4 (12), 26 (13), 45 ± 15 (19), 33 ± 3 (23)	25.7 (15)	104 (17) 120 (40), 127 (42)	0.73	18.9
1-Pentanol	34 ± 3 (9), 22 ± 6 (12), 41 ± 10 (19)	26.3 (15), 25.8 (16)	176 (15), 163 (16, 18)	0.57	20.5
1-Hexanol	~52 (19)	29.2 (15)	242 (15)	0.44	24.0
1-Octanol	45 ± 5 (9), ~45 (19)	36.3 (15)	418 (15), 406 (42)	0.33	31.2
1-Decanol	51 ± 5 (9), ~50 (11)	43.9 (15), 76.2 (16)	565 (42), 539 (16, 43)	0.30	38.1

[a]Data are for room temperature, assumed to be ~298 K. Preferred values are underlined.
[b]Measured.
[c]$x = 4\,\tau'_2/\tau_{L1}$, with τ'_2 calculated from eq. [3].
[d]Calculated from eqs. [3] and [5] or [6].
[e]Estimated assuming an isotope effect of $\sqrt{2}$, equal to the square root of the D/H mass ratio, for rotational motion (see refs. 18 and 35).
[f]Interpolated.
[g]Estimated from the data shown in Fig. 5 of ref. 14.

Interestingly, for all the solvents considered in this study, only a limited number of steps (typically, $n = 3$ or 4) suffices in practice to achieve very good convergence for τ_s.

Two limiting cases of eq. [6] are worth mentioning. In the case where $x << 1$, eq. [6] reduces to the asymptotic form:

$$[7] \quad \frac{\tau_s}{\tau'_2} \approx 1 - \frac{x}{4} + \ldots$$

which shows that $\tau_s \rightarrow \tau'_2$ (or τ_2 in this limit) as $x \rightarrow 0$. In the other limit where x is sufficiently large, eq. [6] shows that τ_s/τ'_2 decreases monotonically as a function of x and approaches zero as $2\sqrt{x}$ when $x \rightarrow \infty$.

To examine the validity of the correlation between τ_s and τ_2 and τ_{L1}, expressed by eqs. [3] and [5] or [6], we have gathered in Table 1 all the presently available experimental data for these parameters for 12 polar liquids at room temperature, including linear alcohols (methanol to decanol), 1,2-ethanediol, H_2O, and D_2O. Also listed in Table 1 are the corresponding values of x and τ_s that we calculated using eqs. [3] and [5] or [6]. As can be seen, in spite of the (rather large) experimental uncertainties and dispersion in the values of the observed solvation times, a close similarity between our calculated τ_s values[3] and the measured ones clearly holds for all the solvents considered. In particular, our calculated values of τ_s reproduce well the trend of the experimental data over the range of x values studied (from 0.3 for 1-decanol to 5.2 for D_2O), even though they may appear, in certain cases, slightly too low (especially, for 1-propanol, 2-propanol, and 1-hexanol). In view of these results, we are thus inclined to conclude that the present model offers a satisfactory description of the electron solvation process, at least for the liquids

[3] Note that the present model contains no adjustable parameter.

© 1997 NRC Canada

Can. J. Chem. Downloaded from www.nrcresearchpress.com by 91.121.58.235 on 09/08/12
For personal use only.

considered here, and to suggest that, in turn, a universal concept of electron solvation is, indeed, plausible.

As can be seen in Table 1, we note that, for the series of alcohols considered, our model also reproduces well the previously observed (5, 9) correlation between τ_s and τ_2. This is especially true for longer chain alcohols, where τ_2 (or τ'_2) is much shorter than τ_{L1} (see eq. [7]). Electron solvation in that case proceeds on the time scale of τ_2 and can thus be interpreted as primarily due to single-molecule rotational motions that accompany the short-range conformational changes of the medium in the strong electric field of the localized excess electron (44). In fact, the alcohol molecules that are involved in these reorientational motions can be considered as belonging to the first solvation shells, as they are considerably less associated than in the bulk.

When the length of the carbon chain decreases, however, τ_2 and τ_{L1} both decrease, τ_{L1} decreasing much faster than τ_2 (or τ'_2) so that x increases. Under these conditions, the asymptotic form of eq. [7] becomes less and less valid and eq. [6] must clearly be used instead. Such a situation is most evident for liquid methanol, where τ_2 and τ_{L1} are practically identical and where x reaches a value of 2.1 (see Table 1). In this case, electron solvation is not only controlled by the short-range, single-molecule reorientation of the medium in the vicinity of the electron, but equally reflects the long-range, collective reorganization of the solvent hydrogen-bond structure (through the longitudinal relaxation time τ_{L1}).

For H_2O and D_2O, the situation is exactly opposite to that encountered for the alcohols, as τ_{L1} now dominates over τ_2. In other words, for these two liquids, the long-range solvent relaxation driven by the excess electron takes over from the short-range molecular reorientations and then plays a dominant role in the electron solvation process. As we see from Table 1, our model predicts values of τ_s close to τ_{L1} for both these solvents, in good agreement with experiment.

Most interestingly, one should note here that the above results are at variance with the mechanism of electron solvation in liquid water put forward by molecular simulations of the process (45–47) that assigns the weakly bound electron e^-_{wb} to an "excited" state of the fully hydrated electron (e^-_{aq}). This question concerning the nature of the e^-_{wb} state in relation to its view as an excited state of e^-_{aq} has received a great deal of attention over the last decade. It has been addressed in some detail in three recent papers by our group (1, 24, 25) and will thus not be developed any further here.

In conclusion, we have formulated in this paper a simple model of electron solvation in polar liquids, which favors a microscopic picture of the electron solvation process relying on both short- and long-range structural rearrangement and molecular motions of the solvent. This model suggests, in accord with the available experimental data, a correlation between the electron solvation time τ_s and the solvent dielectric relaxation times τ_2 and τ_{L1} (see eqs. [3] and [5] or [6]). The fact that this correlation successfully holds for all the solvents considered, including liquid alcohols, 1,2-ethanediol, H_2O, and D_2O, supports a universal concept of electron solvation. Nevertheless, it would be most important to further test the hypotheses of the model and thus the validity of the suggested correlation. To this aim, femtosecond or picosecond laser experiments would be of considerable interest, especially in long-chain alcohols (for example, pentanol to dodecanol, including primary, secondary, and tertiary alcohols) and in other associated solvents (for example, diols, such as 1,2-ethanediol and 1,2-propanediol, and triols, such as 1,2,3-propanetriol or glycerol) where electron solvation has not yet been explored by means of these techniques. Simultaneously, measurements of the dielectric relaxation parameters (and especially τ_2 and τ_{L1}) of the selected solvents would also be in order. Finally, experiments in unassociated polar liquids would also be of unique help in increasing our overall understanding of electron solvation dynamics and in further examining the concept of universality of electron solvation.

Acknowledgments

Financial assistance from the Medical Research Council of Canada is gratefully acknowledged.

References

1. A. Bernas, C. Ferradini, and J.-P. Jay-Gerin. Can. J. Chem. **74**, 1 (1996), and refs. therein.
2. J.H. Baxendale and P. Wardman. Nature (London), **230**, 449 (1971); J. Chem. Soc. Faraday Trans. 1, **69**, 584 (1973).
3. G. Beck and J.K. Thomas. J. Phys. Chem. **76**, 3856 (1972).
4. L. Gilles, J.E. Aldrich, and J.W. Hunt. Nature (London), Phys. Sci. **243**, 70 (1973).
5. W.J. Chase and J.W. Hunt. J. Phys. Chem. **79**, 2835 (1975); W.J. Chase. M.Sc. Thesis, University of Toronto (1976); J.W. Hunt. Adv. Radiat. Chem. **5**, 185 (1976); J.W. Hunt and W.J. Chase. Can. J. Chem. **55**, 2080 (1977).
6. R.S. Dixon, V.J. Lopata, and C.R. Roy. Int. J. Radiat. Phys. Chem. **8**, 707 (1976).
7. L. Gilles, M.R. Bono, and M. Schmidt. Can. J. Chem. **55**, 2003 (1977).
8. K. Okazaki and G.R. Freeman. Can. J. Chem. **56**, 2305 (1978); **56**, 2313 (1978).
9. G.A. Kenney-Wallace and C.D. Jonah. Chem. Phys. Lett. **39**, 596 (1976); **47**, 362 (1977); J. Phys. Chem. **86**, 2572 (1982); G.A. Kenney-Wallace. Can. J. Chem. **55**, 2009 (1977); Adv. Chem. Phys. **47**, 535 (1981).
10. Y. Wang, M.K. Crawford, M.J. McAuliffe, and K.B. Eisenthal. Chem. Phys. Lett. **74**, 160 (1980).
11. D. Huppert, G.A. Kenney-Wallace, and P.M. Rentzepis. J. Chem. Phys. **75**, 2265 (1981).
12. H. Miyasaka, H. Masuhara, and N. Mataga. Laser Chem. **7**, 119 (1987).
13. Y. Hirata and N. Mataga. J. Phys. Chem. **94**, 8503 (1990); **95**, 9067 (1991); Prog. React. Kinet. **18**, 273 (1993).
14. X. Zhang and C.D. Jonah. Chem. Phys. Lett. **262**, 649 (1996).
15. S.K. Garg and C.P. Smyth. J. Phys. Chem. **69**, 1294 (1965); L. Glasser, J. Crossley, and C.P. Smyth. J. Chem. Phys. **57**, 3977 (1972).
16. Y. Dutuit, J.L. Salefran, A.M. Bottreau, R. Chahine, and T.K. Bose. Adv. Mol. Relax. Interact. Processes, **23**, 75, 97 (1982).
17. E.W. Castner, Jr., B. Bagchi, M. Maroncelli, S.P. Webb, A.J. Ruggiero, and G.R. Fleming. Ber. Bunsen-Ges. Phys. Chem. **92**, 363 (1988).
18. J. Barthel, K. Bachhuber, R. Buchner, and H. Hetzenauer. Chem. Phys. Lett. **165**, 369 (1990); J. Barthel and R. Buchner. Pure Appl. Chem. **63**, 1473 (1991); R. Buchner and J. Barthel. J. Mol. Liq. **63**, 55 (1995); J. Barthel. Personal communication.
19. M. Sander. Dissertation, Universität Göttingen (1992); M. Sander, U. Brummund, K. Luther, and J. Troe. Ber. Bunsen-Ges. Phys. Chem. **96**, 1486 (1992); M.U. Sander, K. Luther, and J. Troe. J. Phys. Chem. **97**, 11489 (1993).

© 1997 NRC Canada

20. C. Pépin, T. Goulet, D. Houde, and J.-P. Jay-Gerin. J. Phys. Chem. **98**, 7009 (1994).
21. C. Pépin, T. Goulet, D. Houde, and J.-P. Jay-Gerin. J. Chim. Phys. **93**, 182 (1996).
22. P.K. Walhout, J.C. Alfano, Y. Kimura, C. Silva, P.J. Reid, and P.F. Barbara. Chem. Phys. Lett. **232**, 135 (1995).
23. X. Shi, F.H. Long, H. Lu, and K.B. Eisenthal. J. Phys. Chem. **99**, 6917 (1995).
24. C. Pépin, T. Goulet, D. Houde, and J.-P. Jay-Gerin. J. Phys. Chem. A, **101**, 4351 (1997).
25. T. Goulet, C. Pépin, D. Houde, and J.-P. Jay-Gerin. Radiat. Phys. Chem. Submitted.
26. D. Kivelson and H. Friedman. J. Phys. Chem. **93**, 7026 (1989); A.J. Benigno, E. Ahmed, and M. Berg. J. Chem. Phys. **104**, 7382 (1996).
27. J.M. Wiesenfeld and E.P. Ippen. Chem. Phys. Lett. **73**, 47 (1980).
28. Y. Gauduel, J.L. Martin, A. Migus, N. Yamada, and A. Antonetti. *In* Ultrafast phenomena V. *Edited by* G.R. Fleming and A.E. Siegman. Springer-Verlag, Berlin. 1986. p. 308; A. Migus, Y. Gauduel, J.L. Martin, and A. Antonetti. Phys. Rev. Lett. **58**, 1559 (1987).
29. F.H. Long, H. Lu, and K.B. Eisenthal. Phys. Rev. Lett. **64**, 1469 (1990); X. Shi, F.H. Long, H. Lu, and K.B. Eisenthal. J. Phys. Chem. **100**, 11903 (1996).
30. D. Houde, C. Pépin, T. Goulet, and J.-P. Jay-Gerin. *In* Mode-locked and solid state lasers, amplifiers, and applications. Proc. SPIE—Soc. Photo-Opt. Instrum. Eng. Vol. 2041. *Edited by* M. Piché and P.W. Pace. Bellingham, Wash. 1993. p. 139.
31. J.C. Alfano, P.K. Walhout, Y. Kimura, and P.F. Barbara. J. Chem. Phys. **98**, 5996 (1993).
32. Y. Kimura, J.C. Alfano, P.K. Walhout, and P.F. Barbara. J. Phys. Chem. **98**, 3450 (1994).
33. J.L. McGowen, H.M. Ajo, J.Z. Zhang, and B.J. Schwartz. Chem. Phys. Lett. **231**, 504 (1994).
34. A. Reuther, A. Laubereau, and D.N. Nikogosyan. J. Phys. Chem. **100**, 16794 (1996), and personal communication.
35. N. Agmon. J. Phys. Chem. **100**, 1072 (1996), and refs. therein.
36. U. Kaatze. J. Chem. Eng. Data, **34**, 371 (1989); Chem. Phys. Lett. **203**, 1 (1993).
37. Y. Gauduel, S. Pommeret, A. Migus, and A. Antonetti. J. Phys. Chem. **95**, 533 (1991).
38. F.H. Long, H. Lu, and K.B. Eisenthal. Chem. Phys. Lett. **160**, 464 (1989); H. Lu, F.H. Long, and K.B. Eisenthal. J. Opt. Soc. Am. B: **7**, 1511 (1990).
39. G.H. Barbenza. J. Chim. Phys. **65**, 906 (1968).
40. E.W. Castner, Jr., M. Maroncelli, and G.R. Fleming. J. Chem. Phys. **86**, 1090 (1987).
41. B.P. Jordan, R.J. Sheppard, and S. Szwarnowski. J. Phys. D: Appl. Phys. **11**, 695 (1978).
42. Y. Lin and C.D. Jonah. J. Phys. Chem. **97**, 295 (1993).
43. M. Maroncelli. J. Mol. Liq. **57**, 1 (1993).
44. I. Rips, J. Klafter, and J. Jortner. J. Chem. Phys. **88**, 3246 (1988), and refs. therein.
45. P.J. Rossky and J. Schnitker. J. Phys. Chem. **92**, 4277 (1988); J. Schnitker, K. Motakabbir, P.J. Rossky, and R.A. Friesner. Phys. Rev. Lett. **60**, 456 (1988).
46. R.N. Barnett, U. Landman, and A. Nitzan. J. Chem. Phys. **90**, 4413 (1989).
47. P.J. Rossky and J.D. Simon. Nature, **370**, 263 (1994).

Can. J. Chem. Downloaded from www.nrcresearchpress.com by 91.121.58.235 on 09/08/12
For personal use only.

© 1997 NRC Canada

Stabilized haloylides: synthesis and reactivity

Margaret M. Kayser, Jun Zhu, and Donald L. Hooper

Abstract: This paper describes simple and successful methods for the preparation of stabilized halogenated phosphoylides and discusses their stability, reactivity, and utility in organic synthesis. Preparations of several halogenated compounds including pharmaceutically interesting enol lactones are reported.

Key words: halogenated stabilized ylides, preparation, structure, stability, reactivity, applications; vinylic halides, halo enol lactones.

Résumé : Dans ce travail, on décrit des méthodes simples et réalisables de préparer des phosphoylures halogénés stabilisés et on discute de leur stabilité, de leur réactivité et de leur utilité en synthèse organique. On rapporte les préparations de plusieurs composés halogénés, y compris des lactones énoliques intéressantes d'un point de vue pharmaceutique.

Mots clés : ylures halogénés stabilisés, préparation, structure, stabilité, réactivité, applications; halogénures vinyliques, lactones énoliques halogénées.

[Traduit par la rédaction]

Can. J. Chem. Downloaded from www.nrcresearchpress.com by 91.121.58.235 on 09/08/12
For personal use only.

Introduction

Stabilized phosphoylides are reagents for the synthesis of vinylic halides, an important family of compounds that includes inhibitors of serine proteases (1) and diverse starting materials that can be further transformed into a multitude of strategically halogenated molecules. The formation of haloylides by direct halogenation of the carbomethoxymethylenetriphenylphosphorane **1** was investigated by several groups in the early sixties and the ylides were isolated and characterized (2–5). Our NMR investigation of the direct bromination of several stabilized ylides of the type $Ph_3P{=}CHCOOR$ showed that direct halogenations are accompanied by side reactions and are not suitable for preparative applications.

In an effort to obtain consistently high yields of pure haloylides that can be generated and used in situ without isolation and purification we set out to investigate alternative approaches and in due course developed successful protocols leading to the formation of chloro-, bromo-, iodo-, and fluoroylides. In this paper we report on the synthesis of these ylides and the subsequent study of their reactivities with aldehydes and cyclic anhydrides.

Results and discussion

In situ formation of chloro-, bromo-, and iodoylides

In a series of preliminary experiments all intermediates and products formed during the reaction of ylide **1** (R = CH_3) with bromine were identified.[3] The equilibria involved are illustrated in Scheme 1. These experiments show that a buildup of the conjugate acids **1a** and **2a** interferes with the accumulation of bromoylide in the reaction mixture. This suggested that replacing Br_2 with N-bromosuccinimide (NBS) may produce more satisfactory results since the succinimide anion formed should deprotonate the conjugate acids. In practice, NMR experiments in which a solution of ylide **1** was mixed with an equimolar quantity of NBS in $CDCl_3$ at −40°C gave bromoylide in better than 90% yield. Similar reactions of **1** with *N*-chlorosuccinimide (NCS) and *N*-iodosuccinimide (NIS) produced chloro- and iodoylides in 85 and 97% yields, respectively. The spectroscopic data for all halogenated ylides are assembled in Table 1.

The above protocol for generating haloylides in situ gave the purest product in the case of iodoylide **4**, which was contaminated only with a trace amount of its conjugate acid **4a**. Under identical reaction conditions, bromoylide **2** contained a slightly higher proportion of its conjugate acid **2a**. Moreover, during several runs with NBS, a small quantity of ylide **1** in equilibrium with its conjugate acid **1a** was also detected as a broad **1/1a** signal. The reaction of **1** with NCS, on the other hand, consistently produced mixtures containing **1/1a** in addition to the chloroylide **3** and its conjugate acid **3a**. Variations in temperature had no effect on product composition. An increase in the proportion of NCS (1.8:1) caused the disappearance of the broad **1/1a** signal, but at the same time most of **3** was converted into its conjugate acid **3a** and the dichlorophosphorane salt **3b**. These observations suggested that the relative basicity of haloylides increases from iodo- to bromo- to chloroylide. Thus chloroylide, the most basic of the three haloylides and comparable in reactivity to ylide **1**, is involved in proton exchange with all acidic species present in the reaction mixture including **1a** and traces of water.

Received October 11, 1996.[1]

M.M. Kayser[2] and J. Zhu. Department of Physical Sciences, University of New Brunswick, P.O. Box 5050, Saint John, NB E2L 4L5, Canada.
D.L. Hooper. Department of Chemistry, Dalhousie University, Halifax, NS B3H 4J3, Canada.

[1] Revision received July 7, 1997.
[2] Author to whom correspondence may be addressed. Telephone: (506) 648-5576. Fax: (506) 648-5650. E-mail: KAYSER@UNBSJ.CA

[3] M.M. Kayser and D.L. Hooper. Unpublished results. Copies of these and other NMR spectral data may be purchased from: The Depository of Unpublished Data, Document Delivery, CISTI, National Research Council Canada, Ottawa, Canada K1A 0S2.

© 1997 NRC Canada

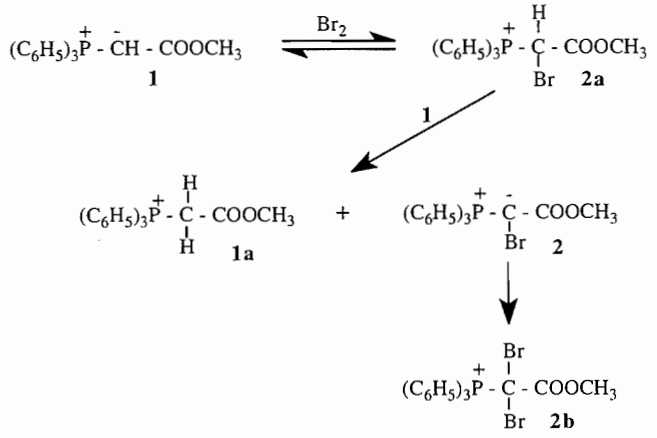
Can. J. Chem. Downloaded from www.nrcresearchpress.com by 91.121.58.235 on 09/08/12
For personal use only.

Table 1. NMR data for halogenated ylides.

Ylide		^{31}P (ppm)	^{13}C (ppm)	^{1}H (ppm)	Ref.
$Ph_3P{=}CBrCOOCH_3$	At rt	23 (br)	29.6	3.50	3, 4, 5
2	At −40°C	22.97, 22.86	52.1		
		ratio, 1:3	178.5		
$Ph_3P{=}CClCOOCH_3$	At rt	22.93	29.6	3.50	3, 4, 5
3	At −40°C	22.87, 22.40	51.0		
		ratio, 1:3	178.0		
$Ph_3P{=}CICOOCH_3$	At rt	24.2	29.0	3.55	3, 4, 5
4	At −40°C	23.90, 22.76	53.8		
		ratio, 1:2	178.0		
$Ph_3P{=}CFCOOEt$[a]	At rt	13.9	13.6	1.0 t,	6
5	At −40°C	13.65 d, 13.93 d	63.7	4.1 q	
		ratio, 1:3	163.5 d		

[a] ^{19}F NMR: chemical shifts −239.2 (d, 56.2 Hz) and −239.6 (d, 42.6 Hz) are identical with those reported in the literature (6).

Scheme 1.



$Ph_3P{=}CClCOOR$ **3** $Ph_3P^+CCl_2COOR$ **3b** $(PhSO_2)_2NF$ **6**

$Ph_3P{=}CICOOR$ **4** $Ph_3P^+CI_2COOR$ **4b**

$Ph_3P{=}CFCOOR$ **5** $Ph_3P^+CF_2COOR$ **5b**

In situ formation of fluoroylide

Attempts to use a similar procedure to generate fluoroylide **5** (R = Et) were not encouraging. Direct fluorination of ylide **1** (R = Et) with *N*-fluorodiphenylsulfonamide **6** in the presence of K_2CO_3 led to formation of the conjugate acid of fluoroylide **5a**, difluorophosphorane **5b**, and **1a**. There was no detectable accumulation of **5**. Changes in the ratio of reactants with variations in temperature between −40 and +25°C did not alter the composition of the product.[4]

Although the reaction of **1** with **6** failed to produce a signal for ylide **5**, trace quantities must have been present in the reaction mixture. This was demonstrated by the following experiment. Freshly distilled benzaldehyde was added to the mixture of **5a** and **1a**, generated as outlined above, and the reaction was monitored by ^{31}P NMR for several days. After 3 days, **5a** had disappeared and only a Ph_3PO signal remained in the ^{31}P spectrum. The proton and fluorine NMR spectra of the product showed that it was composed of *trans* and *cis* cinnamates in a 9:1 ratio (65%), and *Z* and *E* fluorocinnamates in a 3:1 ratio (35%). In a parallel experiment with phthalic anhydride, the reaction was also slow; nonetheless, after 3 days a mixture of *Z* and *E* (4:1) fluoro enol lactones was formed in 20–30% yield. No change could be detected when this reaction was allowed to proceed for an additional 3 days. When the latter reaction was repeated with **1** (R = *t*-Bu) the yield of fluorinated products was similar, but the ratio of the two enol lactones was shifted and, after 6 days, the *E* isomer was the major product.

Preparative-scale reactions of haloylides with aldehydes and cyclic anhydrides

Wittig reactions employing haloylides are complicated by the very nature of these reagents. Haloylides react easily with traces of acids, including their own and other conjugate acids. They decompose upon exposure to moisture and also when treated with more BuLi than the minimum quantity required to remove acidic impurities.[5] These problems prompted our efforts to devise one-pot procedures that would allow high-yield condensation reactions with aldehydes and cyclic anhydrides without isolation and purification of haloylides.

[4] Ylide **5** did form, as witnessed by the emergence of a doublet centred at 13.9 ppm in the ^{31}P NMR spectrum[3] after a drop of a dilute solution of BuLi in hexane was added to the reaction mixture.

[5] The addition of BuLi to the solution of an ylide in equilibrium with its conjugate acid converts the acid to ylide and removes traces of other acidic impurities and water (9, 10). It should be remembered that, when added in excess, BuLi decomposes stabilized ylides. On the other hand, we did not observe, under the reaction conditions described, any reaction with the two solvents used in these reactions, neither chloroform nor dichloromethane.

© 1997 NRC Canada

Scheme 2.

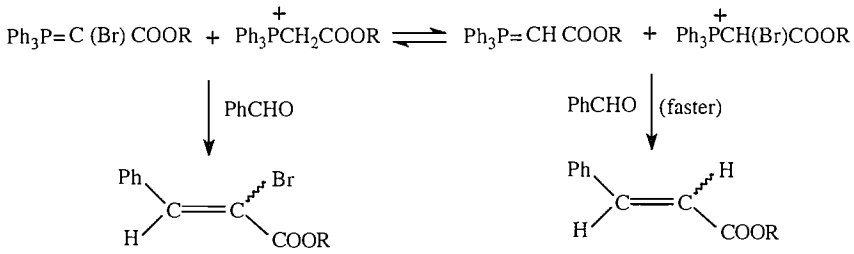
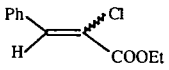
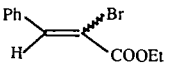
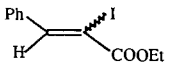
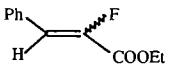
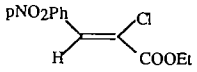
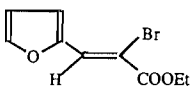


Table 2. Condensations of $Ph_3P{=}CXCOOR$ with aldehydes.

Ylide	Aldehyde	Products	No.	*Z*:*E*	Yield (%)	Ref.
$Ph_3P{=}CClCOOEt$	PhCHO		**9**	80:20	83	11, 12
$Ph_3P{=}CBrCOOEt$	PhCHO		**10**	83:17	85	12
$Ph_3P{=}CICOOEt$	PhCHO		**11**	85:15	87	
$Ph_3P{=}CFCOOEt$	PhCHO		**12**	70:30	36	13
$Ph_3P{=}CClCOOEt$	pNO_2PhCHO		**13**	100:—	59	5
$Ph_3P{=}CBrCOOEt$	Furfural		**14**	100:—	95	

Although in the course of our NMR studies we developed successful methods for the in situ generation of chloro-, bromo-, and iodoylides, we soon discovered that the same protocols were not suitable for preparative-scale Wittig reactions. The disappointing yields obtained in these reactions were caused by unfavourable equilibria. Haloylides generated in situ, according to the method described above, are in equilibrium with ylide **1**, which competes efficiently for an aldehyde or anhydride. During the condensation with a carbonyl group, ylide **1** is depleted and the shift in equilibrium brings about the conversion of haloylide to its conjugate acid (Scheme 2).

To minimize problems associated with equilibria and to increase yields of methyl bromocinnamate, the procedure was modified to include another base in addition to succinimide ion. Anhydrous K_2CO_3 turned out to be particularly suitable for this reaction. According to the new protocol, ylide **1** dissolved in methylene chloride was treated with 1.1 equivalent of NBS followed by 2.5 equivalents of anhydrous K_2CO_3. After a few minutes, freshly distilled benzaldehyde in dichloromethane was added to the mixture and stirred under a N_2 atmosphere for 24 h at room temperature. Under these conditions, the yield of methyl bromocinnamate was excellent, and the procedure was extended to the preparation of chloro, iodo, and fluoro derivatives. The results of these experiments are shown in Tables 2 and 3. The same procedure was used in the reactions of haloylides with cyclic anhydrides. Here, an excess of anhydrous K_2CO_3 was even more critical in securing good yields of the halogenated products. In the absence of a suitable base, yields were low since the addition of ylide **1** to a cyclic anhydride produces an acyclic keto phosphorane harbouring an acid that participates in proton exchange (Scheme 3). This causes further shifts in the already complex equilibria and ultimately a conversion of large proportions of ylides into conjugate acids.

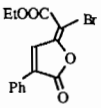
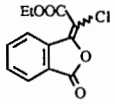
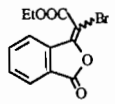
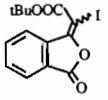
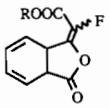
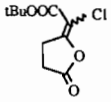
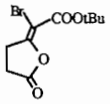
When an excess of anhydrous K_2CO_3 was added, the Wittig condensations produced satisfactory results with the more reactive phthalic and maleic anhydrides but ran into difficulties with the less reactive succinic and glutaric anhydrides. For example, chloroylide **3** (R = *t*-Bu) and succinic anhydride gave a mixture of **21-*Z*** and **21-*E*** (32:68) in 85% yield with the

Can. J. Chem. Downloaded from www.nrcresearchpress.com by 91.121.58.235 on 09/08/12
For personal use only.

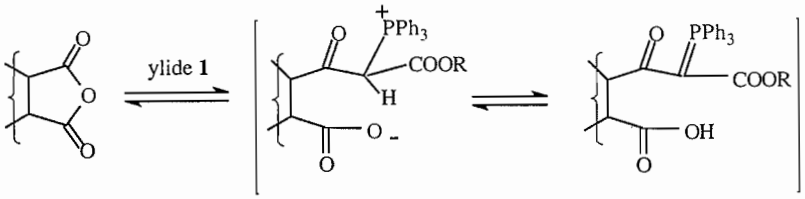
© 1997 NRC Canada

Can. J. Chem. Downloaded from www.nrcresearchpress.com by 91.121.58.235 on 09/08/12
For personal use only.

Table 3. Condensation of $Ph_3P{=}CXCOOR$ with cyclic anhydrides.

Ylide	Aldehyde	Products	No.	*Z*:*E*	Yield (%)
$Ph_3P{=}CBrCOOEt$	Phenyl maleic		**15**	100:—	40
$Ph_3P{=}CClCOOEt$	Phthalic		**16**	92:8	78
$Ph_3P{=}CBrCOOEt$	Phthalic		**17**	90:10	87
$Ph_3P{=}CICOOtBu$	Phthalic		**18**	55:45	93
$Ph_3P{=}CFCOOEt$	Phthalic	 R=Et	**19**	83:17	43
$Ph_3P{=}CFCOO$*t*Bu	Phthalic	R=tBu	**20**	35:65	52
$Ph_3P{=}CClCOO$*t*Bu	Succinic		**21**	32:68	80
$Ph_3P{=}CBrCOO$*t*Bu	Succinic		**22**	—:100	30

Scheme 3.



nonchlorinated enol lactone making up the remaining 15% of the product. The reaction with bromoylide **2** produced pure **22-Z**, but in a low 30% yield and highly contaminated with the conjugated acid **1a** (R = *t*-Bu). Longer reaction times did not improve the yield of bromo enol lactone. Iodoylide **4** did not react with succinic anhydride, and none of the halogenated ylides reacted with glutaric anhydrides and with ketones under the reaction conditions described above. Reactions with fluoroylide **5** gave consistently low yields even in condensations with aldehydes, and the procedure for the synthesis of fluorinated compounds required modifications. An improved protocol was reported recently (7). On the other hand, an entirely different strategy was needed to cope with the problems of the less reactive succinic and glutaric anhydrides. Synthetic efforts to prepare halo enol lactones from the latter compounds are described in another communication (8).

Comparison of the reactivity of haloylides towards benzaldehyde

To better understand the behaviour of haloylides, we compared the reactivity of in situ generated haloylides towards benzaldehyde. In a series of experiments, reactions of ylide **1** (R = Me, *t*-Bu) with NXS (1:1.2) in $CDCl_3$ were followed by ^{31}P NMR at room temperature until the maximum accumulation of haloylide was reached. At that point, an excess (2:1) of freshly distilled benzaldehyde was added to the reaction mixture. The ^{31}P spectra were recorded 5–6 min after mixing. The results show that chloroylide reacts faster than bromoylide, which in turn is significantly faster than iodoylide. The identical pattern of reactivity emerged in condensations with *p*-nitrobenzaldehyde. Here, the order of reactivity of haloylides towards aldehydes parallels their behaviour as bases.

In another series of experiments, chloro-, bromo-, and

© 1997 NRC Canada

Can. J. Chem. Downloaded from www.nrcresearchpress.com by 91.121.58.235 on 09/08/12
For personal use only.

iodoylides, prepared as above and cooled to −40°C, were pretreated with BuLi. The quantity of BuLi used was just adequate to convert all of the conjugate acids into ylides. The temperature was raised to 0°C, 1 equivalent of benzaldehyde was added, and the ensuing reaction was monitored by NMR. This procedure was not suitable for the reactions with fluoroylide. After several unsuccessful attempts to make uncontaminated **5** in situ via direct fluorination, a different protocol was adopted. Treatment of conjugate acid **5a**[6] with an equivalent of BuLi (dilute solution in hexane) at −40°C gave **5**, which was shown by ^{31}P and ^{19}F NMR spectra to be uncontaminated. It was the latter ylide that was used in the reactivity studies.

The reactivity trend was confirmed, placing fluoroylide as the most reactive of the four haloylides with the other ylides being significantly slower. To illustrate the time frame: at 0°C, fluoroylide **5** was completely consumed within the 3–6 min it takes to run an NMR spectrum after mixing, the reactions with chloro- and bromoylides were finished in 30–50 min at 20°C, while the condensations with iodoylide took several hours at room temperature. These results are in agreement with our initial deductions that reactivity and basicity of the four ylides decrease from fluoro- to iodoylide, with the nonhalogenated ylide **1** falling somewhere between the fluoro- and chloroylides.

Experimental

Melting points were determined on a Fisher–Johns melting point apparatus and were uncorrected. Gas chromatography analyses were carried out with a Shimadzu GC 9A chromatograph. Infrared spectra were obtained on a Perkin–Elmer 297 infrared spectrophotometer. Nuclear magnetic resonance spectra were recorded on Varian T-60 or Varian XL-200 spectrometers at UNB or on Nicolet 360 NB, Bruker AC 250, and Bruker AMX 400 spectrometers at the Atlantic Regional Magnetic Resonance Centre. All spectra were recorded in $CDCl_3$ solutions unless otherwise specified, with TMS as an internal reference for ^1H and ^{13}C and with $CDCl_3$ as secondary reference for ^{13}C; 85% H_3PO_4 was external reference for ^{31}P and $CFCl_3$ the external reference for ^{19}F. In all NMR spectral data *J* values are in Hz. Mass spectra were obtained on a Kratos MS 550 TC mass spectrometer.

General procedure for the condensation of haloylides with aldehydes and cyclic anhydrides

A 50 mL three-necked flask equipped with a septum port, a glass stopper, a magnetic stirbar, and a reflux water condenser was topped with a nitrogen tee tube leading to a source of nitrogen, and a mineral oil bubbler was charged sequentially with 20 mL of dry THF or methylene chloride and 5.0 mmol of a phosphorane. The contents of the flask were cooled to −20°C. To the cooled solution, 1.1 equivalent of *N*-halosuccinimide or *N*-fluorodiphenylsulfonamide was added via counter flow. The solution was stirred for 20 min at −20°C, and then 2.5 equivalents of potassium carbonate followed by 5.0 mmol of aromatic aldehyde or cyclic anhydride were added. The mixture was stirred at room temperature for 12–72 h. After filtration and washing with 30 mL methylene chloride, the solvents were evaporated under reduced pressure and 10 mL ether was added to precipitate most of the triphenylphosphine oxide. Chromatography was carried out on a silica gel column using petroleum ether/acetone (3:1) as the elutant.

Ethyl 3-phenyl-2-chloro-2-propenoate ***9*** *(refs. 11, 12)*
Carboethoxymethylenetriphenylphosphorane **1**, R = Et (1.74 g, 5.0 mmol), potassium carbonate (2.5 equiv.), and *N*-chlorosuccinimide (734 mg, 1.1 equiv.) reacted with benzaldehyde (530 mg, 5.0 mmol) in methylene chloride for 24 h according to the general procedure to give **9** (0.87 g, 83%) as a mixture of *Z*:*E* = 80:20. ^1H NMR ($CDCl_3$, δ ppm): 1.13 (t, *E* isomer), 1.32 (t, *Z* isomer) integrating together for 3H, 4.1–4.4 (2H, overlapping q), 5.94 (s, *E*), 7.9 (s, *Z*) integrating together for 1H, 7.1–7.8 (5H, m, overlapping *E* and *Z*). Repeated chromatography provided a sample of **9-*Z*:** MS (EI) : 210 (M, 49.1%), 176 (39.9%), 165 (17.1%), 131 (100%), 103 (41.2%), 102 (40.8%), 77 (19.4%).

Ethyl 3-phenyl-2-bromo-2-propenoate ***10*** *(ref. 12)*
Carboethoxymethylenetriphenylphosphorane **1**, R = Et (1.74 g, 5.0 mmol), potassium carbonate (2.5 equiv.), and *N*-bromosuccinimide (980 mg, 1.1 equiv.) reacted with benzaldehyde (530 mg, 5.0 mmol) in methylene chloride for 24 h according to the general procedure to give **10** (1.09 g, 85%) as a mixture of *Z*:*E* = 83:17. ^1H NMR ($CDCl_3$, δ ppm): 1.18 (t, *E* isomer), 1.39 (t, *Z* isomer) integrating together for 3H, 4.22 (*E* isomer), 4.35 (*Z* isomer) (2H, overlapping q), 5.81 (*E*), 8.2 (*Z*) (both s, 1H), 7.2–7.8 (5H, overlapping aromatic m); ^{13}C NMR ($CDCl_3$, δ ppm): 13.81 (CH_3, *E* isomer), 14.2 (CH_3, *Z* isomer), other distinct signals: 62.8, 113.17, 128.43, 130.29, 133.77, 139.62, 140.80, 163.38. Repeated chromatography provided a sample of **10-*Z*:** MS (EI): 256 (M, 37.0%), 254 (M, 37.7%), 175 (86%), 147 (100%), 129 (19.4%), 102 (57.6%), 77 (8.4%).

Ethyl 3-phenyl-2-iodo-2-propenoate ***11***
Carboethoxymethylenetriphenylphosphorane **1**, R = Et (1.74 g, 5.0 mmol), potassium carbonate (2.5 equiv.), and *N*-iodosuccinimide (1.24 g, 1.1 equiv.) reacted with benzaldehyde (530 mg, 5.0 mmol) in methylene chloride for 24 h according to the general procedure to give **11** (1.31 g, 87%) as a mixture of *Z*:*E* = 85:15. Extensive chromatography provided a sample of pure **11-*Z*** isomer. ^1H NMR ($CDCl_3$, δ ppm): 1.37 (3H, t), 4.33 (2H, q), 8.25 (1H, s), 7.2–7.9 (5H, aromatic); ^{13}C NMR ($CDCl_3$, δ ppm): 14.20 (CH_3) 62.99, 91.16, 128.83, 129.41, 129.68,129.97, 130.18, 134.40, 47.86, 163.70; MS (EI):302 (M, 100%), 257 (27.5%), 175 (50.9%), 147 (83.4%), 131 (27.0%), 103 (26.9%), 102 (63.3%), 77 (13.6%).

Ethyl 3-phenyl-2-fluoro-2-propenoate ***12*** *(ref. 13)*
Carboethoxymethylenetriphenylphosphorane **1**, R = Et (1.74 g, 5.0 mmol), potassium carbonate (2.5 equiv.), and *N*-fluorodiphenylsulfonamide (1.74 g, 1.1 equiv.) reacted with benzaldehyde (5.0 mmol, 530 mg) in methylene chloride for 72 h according to the general procedure to give **12** (349 mg 36%) as a mixture of *Z*:*E* = 70:30. ^1H NMR ($CDCl_3$, δ ppm): 0.95 (3H, overlapping t), 4.0 (2H, overlapping q), 7.2–8.0 (6H,

[6] Prepared by condensation of triphenylphosphine with 2-bromo-2-fluoroethylacetate.

© 1997 NRC Canada

Can. J. Chem. Downloaded from www.nrcresearchpress.com by 91.121.58.235 on 09/08/12
For personal use only.

complex m); ^{19}F NMR ($CDCl_3$, δ ppm): −117.01 (*E* isomer J_{HF} = 22), −125.15 (*Z* isomer J_{HF} = 39).

(Z) *Ethyl* p-*nitrophenyl-2-chloro-2-propenoate* ***13*** *(ref. 5)*
Carboethoxymethylenetriphenylphosphorane **1**, R = Et (3.48 g, 10.0 mmol), potassium carbonate (2.5 equiv.), and *N*-chlorosuccinimide (1.47 g, 1.1 equiv.) reacted with *p*-nitrobenzaldehyde (1.51 g, 10.0 mmol) in methylene chloride for 24 h according to the general procedure to give **13-*Z*** (1.5 g, 59%); mp 111–112°C; ^{1}H NMR ($CDCl_3$, δ ppm): 1.36 (3H, t), 4.30 (2H, q), 7.5–8.3 (4H, m), 8.95 (1H, s); ^{13}C NMR ($CDCl_3$, δ ppm): 14.29, 61.06, 122.59, 123.71, 124.20, 128.64, 131.13, 134.28, 141.65, 148, 166.08.

(Z) *Ethyl 3-furfural-2-bromo-2-propenoate* ***14***
Carboethoxymethylenetriphenylphosphorane **1**, R = Et (1.74 g, 5.0 mmol), potassium carbonate (2.5 equiv.), and *N*-bromosuccinimide (980 mg, 1.1 equiv.) reacted with furfural (540 mg, 5.0 mmol) in methylene chloride for 12 h according to the general procedure to give **14-*Z*** (1.16, 95%) as the only product. ^{1}H NMR ($CDCl_3$, δ ppm): 1.35 (3H, t), 4.4 (2H, q), 6.5–7.6 (3H, m), 8.1 (s). Since compound **14** decomposed rapidly on handling, further purification was not attempted.

(Z) *Ethyl 3-bromo-5-ethoxycarbonylmethylidene-3-phenylfuran-2-one* ***15***
Carboethoxymethylenetriphenylphosphorane **1**, R = Et (1.74 g, 5.0 mmol), potassium carbonate (2.5 equiv.), and *N*-bromosuccinimide (980 mg, 1.1 equiv.) reacted with phenylmaleic anhydride (870 mg, 5.0 mmol) in THF for 12 h according to the general procedure to give **15-*Z*** (646 mg, 40%). ^{1}H NMR ($CDCl_3$, δ ppm): 1.35 (3H, t), 4.35 (2H, q), 7.4–7.9 (5H, m), 8.30 (1H, s). This compound was contaminated with nonhalogenated enol lactones and several attempts to obtain a pure sample by chromatography were not successful.

Ethyl chloro(3-oxo-1,3-dihydroisobenzofuran-1-ylidene)acetate ***16*** *(ref. 14)*
Carboethoxymethylenetriphenylphosphorane **1**, R = Et (1.74 g, 5.0 mmol), potassium carbonate (2.5 equiv.), and *N*-chlorosuccinimide (734 mg, 1.1 equiv.) reacted with phthalic anhydride (740 mg, 5.0 mmol) in THF for 14 h according to the general procedure to give **16** (985 mg, 78%) as a mixture of *Z*:*E* = 92:8. IR ($CHCl_3$) ν_{max} cm^{-1}: 2980, 1850, 1710, 1645; ^{1}H NMR ($CDCl_3$, δ ppm): 1.40 (t, *E*), 1.45 (t, *Z*) integrating together for 3H, 4.42 (*E*) and 4.45 (*Z*) (2H, overlapping q), 7.75 (1H, td), 7.85 (1H, td), 8.05 (1H, dt), 8.50 (1H, dt); ^{13}C NMR (*Z* isomer) 14.10, 62.07, 101.88, 125.34, 125.89, 128.16 132.50, 135.24, 149.10, 158.00, 165.55. Note: The vinylic carbon atom signal at 96.60 ppm is characteristic for the *E* isomer.

Ethyl bromo(3-oxo-1,3-dihydroisobenzofuran-1-ylidene)acetate ***17*** *(ref. 14)*
Carboethoxymethylenetriphenylphosphorane **1**, R = Et (1.74 g, 5.0 mmol), potassium carbonate (2.5 equiv.), and *N*-bromosuccinimide (980 mg, 1.1 equiv.) reacted with phthalic anhydride (740 mg, 5.0 mmol) in THF for 12 h according to the general procedure to give **17** (1.29 g, 87%) as a mixture of *Z*:*E* = 90:10. IR ($CHCl_3$) ν_{max} cm^{-1}: 2980, 1850, 1700, 1655; ^{1}H NMR ($CDCl_3$, δ ppm): 1.45 (t, *E*) and 1.50 (t, *Z*) integrating together for 3H, 4.40 (*E* and *Z*) (2H, overlapping q), 7.70 (1H, td), 7.80 (1H, td), 8.00 (1H, dt), 8.45 (1H, dt); ^{13}C NMR (*Z* isomer): 14.19, 62.97, 102.10, 125.63, 125.88, 126.06, 126.83, 132.10, 135.40, 154.67, 162.67, 164.37.

tert-Butyl iodo(3-oxo-1,3-dihydroisobenzofuran-1-ylidene)acetate ***18***
Carboethoxymethylenetriphenylphosphorane **1**, R = *t*-Bu (1.79 g, 5.0 mmol), potassium carbonate (2.5 equiv.), and *N*-iodosuccinimide (1.24 g, 1.1 equiv.) reacted with phthalic anhydride (740 mg, 5.0 mmol) in THF for 15 h according to the general procedure to give **18** (93% yield) as a mixture of *Z*:*E* = 55:45. IR ($CHCl_3$) ν_{max} cm^{-1}: 2980, 1840, 1715, 1650; ^{1}H NMR ($CDCl_3$, δ ppm): 1.58 (*t*-Bu, s, *Z* isomer), 1.62 (*t*-Bu, *E* isomer), 7.6–8.0 (3H, m), 8.20 (d, *E* isomer), 8.82 (d, *Z* isomer). Several attempts to separate **18-*E*** and **18-*Z*** were not successful.

(Z) *Ethyl fluoro(3-oxo-1,3-dihydroisobenzofuran-1-ylidene)acetate* ***19***
Carboethoxymethylenetriphenylphosphorane **1**, R = Et (1.74 g, 5.0 mmol), potassium carbonate (2.5 equiv.), and *N*-fluorodiphenylsulfonamide (1.1 equiv.) reacted with phthalic anhydride (740 mg, 5.0 mmol) in THF for 72 h at 50°C according to the general procedure to give **19** (542 mg, 43%) as a mixture of *Z*:*E* = 83:17. Separation by chromatography provided a sample of **19-*Z***; mp 78–82°C; IR ($CHCl_3$) ν_{max} cm^{-1}: 1840, 1765, 1700, 1645; ^{1}H NMR ($CDCl_3$) δ: 1.45 (3H, t), 4.40 (2H, q), 7.60-8.10 (m), 8.90 (1H, d); ^{13}C NMR (50.32 Hz, $CDCl_3$) δ: 14.15, 62.37, 125.32, 126.08, 127.03, 131.91, 135.22, 135.41, 136.95, 143.23, 160.96, 165.16; ^{19}F NMR δ: −132.57 (*Z* isomer); MS (EI), *m/z*: 236 (M, 29%), 164 (51.1%), 148 (40.1%), 104 (100%), 76 (88%); ms (HR), *m/z*; calcd. for $C_{12}H_9O_4F$: 236.0485; found: 236.0477. Note: ^{19}F signal for the *E* isomer: δ: −152.9.

tert-Butyl fluoro(3-oxo-1,3-dihydroisobenzofuran-1-ylidene)acetate ***20***
Carboethoxymethylenetriphenylphosphorane **1**, R = *t*-Bu (1.79 g, 5.0 mmol), potassium carbonate (2.5 equiv.), and *N*-fluorodiphenylsulfonamide (1.1 equiv.) were reacted with phthalic anhydride (740 mg, 5.0 mmol) in THF for 72 h at 50°C according to the general procedure to give **20** (792 mg, 52%) as a mixture of *Z*:*E* = 35:65. ^{1}H NMR ($CDCl_3$) δ: 1.10 (9H, s), 7.6–8.2(4H, m); ^{19}F NMR δ: −128.05 (*Z* isomer); −151.73 (*E* isomer).

(E) *tert-Butyl chloro(5-oxotetrahydrofuran-2-ylidene)acetate* ***21***
Carboethoxymethylenetriphenylphosphorane **1**, R = *t*-Bu (1.79 g, 5.0 mmol), potassium carbonate (2.5 equiv.), and *N*-chlorosuccinimide (734 mg, 1.1 equiv.) reacted with succinic anhydride (500 mg, 5.0 mmol) in THF for 24 h according to the general procedure to give **21** (928 mg, 80%) as a mixture of *Z*:*E* = 32:68. IR ($CHCl_3$) ν_{max}cm^{-1}: 2980, 1850, 1700, 1655; ^{1}H NMR ($CDCl_3$, δ ppm): 1.54 (9H, overlapping s), 2.76 (*Z* isomer, m, 2H), 2.82 (*E* isomer, m, 2H), 3.10 (*Z* isomer, m, 2H), 3.25 (*E* isomer, m, 2H). Separation by chromatography provided a pure sample of **21-*E***: mp 120–121°C; ^{13}C NMR ($CDCl_3$, δ ppm): 25.60, 27.14, 28.09, 83.27, 95.46,157.24, 163.02, 173.33; MS (EI), *m/z*: 234 (M, 1.6%), 232 (M, 0.8%), 176 (47.2%), 159 (92.6%), 123 (67.4%), 57 (100%); MS

© 1997 NRC Canada

(HR), *m/z*: calcd. for $C_{10}H_{13}O_4{}^{35}Cl$:232.0502; found: 232.0508. Note: **21-*Z*:** ^{13}C NMR ($CDCl_3$, δ ppm): 14.14, 25.58, 27.15, 33.01, 104.39, 158.44, 161.02, 176.10.

(E) *tert-Butyl bromo(5-oxotetrahydrofuran-2-ylidene)acetate* ***22***

Carboethoxymethylenetriphenylphosphorane **1**, R = *t*-Bu, (1.74 g, 5.0 mmol), potassium carbonate (2.5 equiv.), and *N*-bromosuccinimide (980 mg, 1.1 equiv.) reacted with succinic anhydride (500 mg, 5.0 mmol) in THF for 24 h according to the general procedure to give **22-*E*** (414 mg, 30% yield); mp 113–115°C; IR ($CHCl_3$) ν cm^{-1}: 2980, 1830, 1715, 1640; ^1H NMR ($CDCl_3$, δ ppm): 1.55 (9H, s), 2.75 (2H, m), 3.08 (2H, m); ^{13}C NMR ($CDCl_3$, δ ppm): 26.20, 28.01, 29.10, 83.29, 96.04, 157.86, 173.57, 177.90; MS (EI), *m/z*: 278 (M, 2.7%), 232 (M, 3.0), 123 (48.1%), 57 (100%); MS (HR), *m/z*, calcd. for $C_{10}H_{13}O_4{}^{79}Br$: 275.9997; found: 275.9997; calcd. for $C_{10}H_{13}O_4{}^{81}Br$: 277.9997; found: 277.9982.

Acknowledgements

We thank the Natural Sciences and Engineering Research Council of Canada for financial support and Dr. Carl K. Tompkins for reading the entire manuscript.

References

1. W. Dai and J.A. Katzenellenbogen. J. Org. Chem. **56**, 6893 (1991); S.B. Daniels and J.A. Katzenellenbogen. Biochemistry, **25**, 1436 (1986), and refs. therein.
2. H.J. Bestmann and R. Zimmerman. *In* Comprehensive organic synthesis. Vol. 6. *Edited by* B.M. Trost and I. Fleming. Pergamon Press, Oxford. 1991. pp. 171–198.
3. G. Markl. Chem. Ber. **64**, 2996 (1961).
4. D.B. Denney and K.W. Ross. J. Org. Chem. **27**, 998 (1962).
5. A.J. Speziale and K.W. Ratts. J. Org. Chem. **28**, 465 (1963); A.J. Speziale and K.W. Ratts. J. Am. Chem. Soc. **85**, 2790 (1963).
6. A. Thenappan. PhD Thesis. The University of Iowa, 1989. U.M.I. Dissertation Information Service.
7. J. Zhu and M.M. Kayser. Synth. Commun. **24**, 1179 (1994).
8. M.M. Kayser, J. Zhu, and D.L. Hooper. Can J. Chem. **75**, 1322 (1997).
9. M.M. Kayser and D.L. Hooper. Can. J. Chem. **68**, 2123 (1990).
10. D.L. Hooper, S. Garagan, and M.M. Kayser. J. Org. Chem. **59**, 1126 (1994).
11 D.J. Burton and J. Greenwald. Tetrahedron Lett. 1535 (1967).
12. H. Gault. Ann. Chem. **6**, 220 (1951).
13. A. Thenappan and D.J. Burton. J. Org. Chem. 55, 4639 (1990).
14. A.D. Abell, D.A. Hoult, K.M. Morris, J.M. Taylor, and J.O. Trent. J. Org. Chem. **58**, 1531 (1993).

Can. J. Chem. Downloaded from www.nrcresearchpress.com by 91.121.58.235 on 09/08/12
For personal use only.

© 1997 NRC Canada

On the synthesis and the mechanism of formation of halogenated enol lactones

Margaret M. Kayser, Jun Zhu, and Donald L. Hooper

Abstract: The synthesis of halo enol lactones from cyclic anhydrides via lactonization of the corresponding keto phosphoranes provides a direct route to these interesting compounds, which possess important biological properties and are useful intermediates in organic synthesis. In this paper we outline the syntheses of several halo enol lactones and discuss mechanistic consequences of these reactions on the understanding of Wittig reactions with cyclic anhydrides.

Key words: halolactonization, cyclic anhydrides, halo enol lactones, Wittig reaction mechanism.

Résumé : La synthèse de lactones énoliques halogénées à partir d'anhydrides cycliques, par le biais d'une lactonisation des cétophosphoranes correspondants, fournit une route directe vers ces composés intéressants qui possèdent des propriétés biologiques importantes et qui sont utiles comme intermédiaires en synthèse organiques. Dans ce travail, on décrit les synthèses de plusieurs lactones énoliques halogénées et on discute des conséquences mécanistiques de ces réactions sur la compréhension des réactions de Wittig avec les anhydrides cycliques.

Mots clés : halolactonisation, anhydrides cycliques, lactones énoliques halogénées, mécanisme de la réaction de Wittig.

[Traduit par la rédaction]

Can. J. Chem. Downloaded from www.nrcresearchpress.com by 91.121.58.235 on 09/08/12
For personal use only.

Introduction

Halo enol lactones can be transformed into a variety of highly functionalized compounds and, as such, are useful intermediates in organic synthesis. Furthermore, since certain classes of halogenated enol lactones have been established as effective serine protease inhibitors (1), it is not surprising that these versatile compounds have attracted significant attention in recent years (2). In previous communications we reported the preparation of halo enol lactones by Wittig condensation reactions between cyclic anhydrides and in situ generated halo ylides (3, 4). In the course of these experiments we discovered that, although condensations with "reactive" phthalic and maleic anhydrides gave consistently excellent yields, problems were encountered with "less reactive" succinic and glutaric anhydrides.[3] Thus, while succinic anhydride reacted successfully with chloroylide, the condensation with bromoylide gave only 30% yield of bromo enol lactone and no significant reaction was observed with the iodoylide. None of the above ylides reacted with glutaric anhydride. In this paper we recount how the above problems were circumvented by using an alternate synthetic approach involving halide-induced lactonization of keto phosphoranes. This methodology, apart from giving access to the desired products, also provides insight into the mechanism of Wittig reactions with cyclic anhydrides.

Received October 11, 1996.[1]

M.M. Kayser[2] and J. Zhu. Department of Physical Sciences, University of New Brunswick, P.O. Box 5050, Saint John, NB E2L 4L5, Canada.
D.L. Hooper. Department of Chemistry, Dalhousie University, Halifax, NS B3H 4J3, Canada.

[1] Revision received July 7, 1997.
[2] Author to whom correspondence may be addressed. Telephone: (506) 648-5576. Fax: (506) 648-5650. e-mail: KAYSER@UNBSJ.CA

Results and discussion

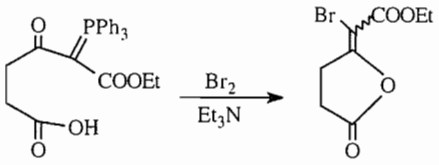
The reactivity of halo ylides towards aldehydes and cyclic anhydrides decreases from the fluoro- to the iodoylide. While fluoroylide **2** reacts more rapidly than the non-halogenated carbomethoxymethylenetriphenylphosphorane **1**, chloroylide **3** appears to be comparable in reactivity to **1**, whereas bromoylide **4** and particularly iodoylide **5** are considerably slower (4). As a result, Wittig condensations between ylides **4** and **5** and the less reactive succinic and glutaric anhydrides are very slow or fail entirely (4).

$Ph_3P{=}CHCOOR$ **1** $Ph_3P{=}CFCOOR$ **2** $Ph_3P{=}CClCOOR$ **3**
$Ph_3P{=}CBrCOOR$ **4** $Ph_3P{=}ClCOOR$ **5** $Ph_3P{=}C(CH_3)COOR$ **6**

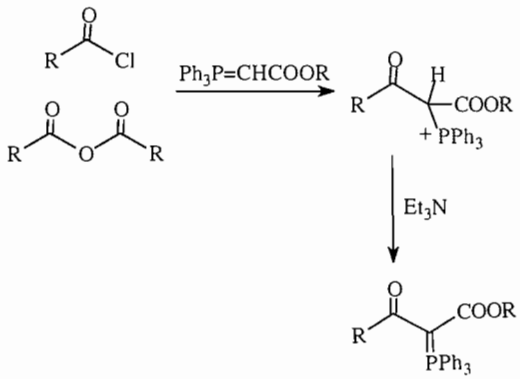
[3] We have observed (^1H and ^{31}P NMR) that all stabilized ylides and their conjugate acids studied decompose slowly to Ph_3PO at room temperature unless special care is taken to maintain moisture-free conditions. This is quite evident during slow condensation reactions with succinic and glutaric anhydrides. Stabilized ylides also decompose to give Ph_3PO when treated with BuLi in an attempt to convert traces of their conjugate acids to ylides. This presents problems, particularly with the more basic fluoro- and chloroylides, which are frequently contaminated with their conjugate acids. The corresponding dihalo salts are decomposed to Ph_3PO even more rapidly than their parent ylides. The useful conclusion derived from the above observation is that, in order to obtain ylides free from acidic contaminants, including traces of moisture, a dilute solution of BuLi should be used and any excess should be carefully minimized.

© 1997 NRC Canada

Scheme 1.



Scheme 2.

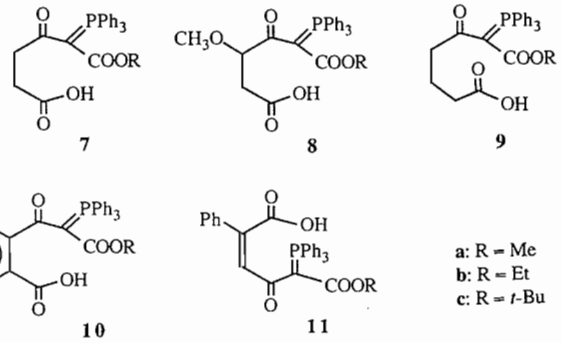


Halo enol lactones used in inhibition studies of serine proteases were typically prepared by bromine-induced lactonization of the acetylenic acids (2*c*). Recently, Abell and Trent (5) reported that acyl phosphoranes, such as **7b**, treated with bromine in the presence of triethylamine gave bromo enol lactones, as shown in Scheme 1. Based on these results, we expected that the halolactonization of keto phosphoranes would provide a general route to halo enol lactones from cyclic anhydrides, particularly from succinic and glutaric anhydrides that failed to give acceptable yields through direct condensations with haloylides (4).

Keto phosphoranes can be prepared by reactions of certain stabilized ylides such as **1** with acid chlorides or anhydrides, as shown in Scheme 2 (6–8). The reactions with cyclic anhydrides lead to the formation of acyclic adducts (**7–11**). The additions of ylide **1** to phthalic, maleic, and succinic anhydrides have been shown to be reversible (9). However, while acyclic adducts from succinic or glutaric anhydrides are stable compounds, those from phthalic and maleic anhydrides tend to be considerably less stable and generally can be observed by NMR or trapped only at low temperatures (9). Ylides that do not possess an ylidic hydrogen atom, such as methyl ylide **6**, do not give unambiguously identifiable acyclic adducts. For example, at −40°C the ^{31}P signal for methyl ylide **6** appears at 23.3 ppm. Upon addition of phthalic anhydride a new broad peak appears at 27.6 ppm and, as the temperature is raised to −20°C, the two peaks coalesce to give a very broad signal at 24.5 ppm. At that temperature enol lactone is starting to form. As the temperature is raised further the formation of the product can be followed by observing the increase in the Ph_3PO peak at 31 ppm, while the broad signal at 24.5 is diminished as it shifts slowly to 27.9 ppm. It appears, therefore, that although addition of this ylide to phthalic anhydride is taking place, the resulting acyclic adduct is not stable enough to be observed as a discrete NMR signal but rather exists in rapid equilibrium with the parent ylide **6**. When the same reaction was carried out at room temperature the signal at 27.9 ppm was not detected, and in the parallel reaction, monitored by ^1H NMR, only the disappearance of ylide **6** and the formation of the corresponding enol lactone could be observed. On the other hand, not even a transient signal could be detected during the low-temperature (−40°C) reactions of bromo- and fluoroylides with phthalic anhydride. These experiments do not entirely eliminate the possibility of acyclic compound formation, but they do suggest that, if such an addition actually occurs, the resulting acyclic intermediates are in rapid equilibrium with the starting materials and that the rapid collapse to enol lactones occurs as the temperature is raised. In any case, these adducts are not observable by NMR as discrete signals. Certain of these NMR spectra have been deposited as supplementary material.[4]

Syntheses of halo enol lactones via halolactonization of keto phosphoranes

Keto phosphoranes from glutaric, succinic, phthalic, and phenylmaleic anhydrides, illustrated below, were prepared by the reaction of ylide **1** with the appropriate anhydrides at –20°C. The adducts **7** and **9** made from succinic and glutaric anhydrides were stable and could be isolated at room temperature and stored indefinitely, while the more reactive compounds **8**, **10**, and **11** were generated in situ and used immediately in halolactonization reactions (Scheme 3).



During preliminary experiments, keto phosphoranes **7** and **10** treated with Br_2 according to the procedure described in the literature (5) gave disappointingly low yields of the corresponding bromo enol lactones. When the reaction of keto phosphorane **7** with Br_2 was followed by NMR it became apparent that large quantities of the conjugate acids $Ph_3P^+CH_2COOR\ Br^-$ and $Ph_3P^+CHBrCOOR\ Br^-$ of ylides **1** and **4** were formed as by-products.

An effective proton scavenger was needed to remove the "mobile" protons formed in the process of ring opening. Switching to halosuccinimides (NXS: X = Cl, Br, I) as halogenating agents, with *N*-fluorodiphenyl sulphonamide (NFS) serving as a fluorinating agent, provided sufficiently basic succinimide (or phenyl sulphonamide) anions to prevent the formation of conjugate acids and to promote cyclization to halo enol lactones. Under the modified conditions succinic and phthalic anhydrides were converted to halo enol lactones, generally in good to excellent yields. The results for all anhydrides studied are listed in Table 1.

[4] Copies of material on deposit may be purchased from: The Depository of Unpublished Data, Document Delivery, CISTI, National Research Council Canada, Ottawa, Canada K1A 0S2.

© 1997 NRC Canada

Can. J. Chem. Downloaded from www.nrcresearchpress.com by 91.121.58.235 on 09/08/12
For personal use only.

Scheme 3.

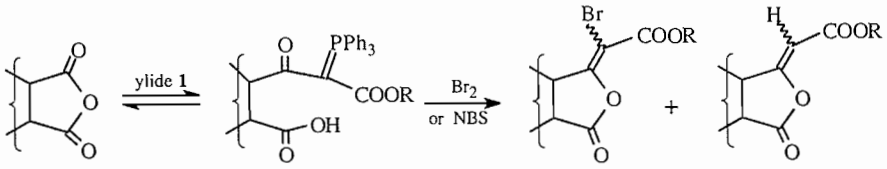
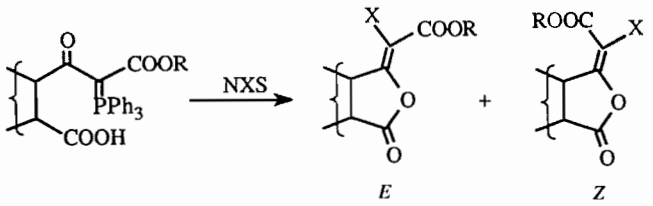
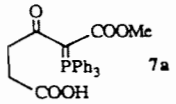
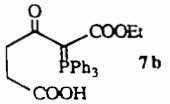
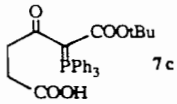
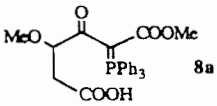
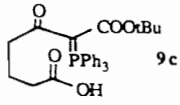
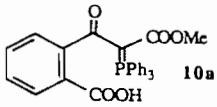
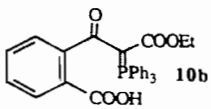
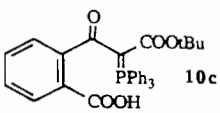
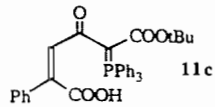


Table 1. Halolactonization of acyclic phosphoranes.

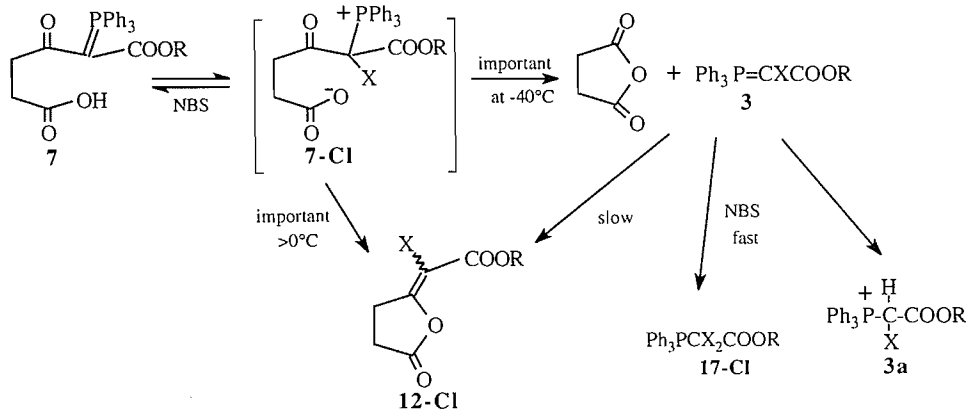


Phosphorane	NXS	Conditions T (°C), h	Yield (%)	E:Z (%)	Product no.
 **7a**	Cl	0, 2	93	74:26	**12a-Cl**
	Br	0, 4	81	67:33	**12a-Br**
	I	0, 5	87	68:32	**12a-I**
 **7b**	Cl	0, 2	83	72:28	**12b-Cl**
	Br	0, 2	88	72:28	**12b-Br**
	I	0, 5	64	48:52	**12b-I**
	F	20, 12	67	15:85	**12b-F**
 **7c**	Cl	0, 2	95	100:—	**12c-Cl**
	Br	0, 4	90	100:—	**12c-Br**
	I	0, 5	88	95:5	**12c-I**
	F	20, 12	83	—:100	**12c-F**
 **8a**	Br	−10, 2	45	25:75	**13a-Br**
 **9c**	Cl	0, 6	57	98:2	**14c-Cl**
	Br	0, 6	55	90:10	**14c-Br**
 **10a**	Cl	−20, 2	57	40:60	**15a-Cl**
	Br	−20, 2	92	45:55	**15a-Br**
 **10b**	Cl	−20→+20, 2	55	90:10	**15b-Cl**
	F	−20, 2	50	5:95	**15b-F**
 **10c**	I	−20, 2	81	50:50	**15c-I**
	F	−10, 4	75	75:25	**15c-F**
 **11c**	Br	−10, 2	50	—:100	**16c-Br**

Can. J. Chem. Downloaded from www.nrcresearchpress.com by 91.121.58.235 on 09/08/12
For personal use only.

© 1997 NRC Canada

Scheme 4.



The highest yields of halo lactones were obtained from succinic anhydride, which is converted completely to a stable acyclic adduct. Keto phosphoranes derived from the more reactive methoxysuccinic **8**, phthalic **10**, and phenylmaleic **11** anhydrides, generated in situ at −20°C, reacted with NXS or NFS to give lower yields of the corresponding halo enol lactones. In the course of these reactions, 10–20% of nonhalogenated enol lactones were always formed and extensive chromatography was required to remove these by-products. From a synthetic point of view, it was desirable to modify the reaction conditions in such a way as to minimize their formation. Variation in the NXS to keto phosphorane ratios and in reaction temperatures did not, however, significantly improve the situation. It appears that in all cases the spontaneous recyclization competes effectively with halolactonization.

Halolactonizations carried out with keto phosphorane **9c** generated from glutaric anhydride gave lower yields for the opposite reason. Here, the spontaneous recyclization of **9c** is known to be difficult even at high temperatures and, hence, halolactonization is also sluggish. As a result, yields of halogenated products were lower, but the products formed were not contaminated with nonhalogenated enol lactones and could be purified readily by rapid chromatography on a short silica gel column.

The configuration of halo enol lactones was established from the ^{1}H NMR spectra and isomerization experiments as described elsewhere (3, 10, 11). The stereoselectivity observed in halolactonization of keto phosphoranes was not significantly different from that observed in the direct Wittig condensation reactions (3). In general, the *E* configuration was predominant in derivatives from succinic and glutaric anhydrides, particularly with *tert*-butyl esters. The notable exception was observed with fluorinated products that were tentatively identified as *Z* isomers on the basis of their NMR spectra (Table 1). Reactions with phthalic and maleic anhydrides, carried out at lower temperatures, gave mixtures of products. These results indicate that the *E* configuration is thermodynamically preferred, except when the halo substituent is an iodine atom. When the reaction can be performed successfully at lower temperatures, as is the case with the more reactive anhydrides, the kinetic product (*Z* isomer), can constitute an important component of the mixture (entries **10a**, **10b**, **10c**, and **11c**, Table 1). For example, the reaction of phthalic anhydride with NCS at −20°C (2 h) gave a 50:50 mixture of *E* and *Z* isomers. When the same reaction was carried out at −20 to +20°C for 2 h, the *E* isomer was the main product (*E*:*Z* = 90:10).

NMR study of halolactonization reactions

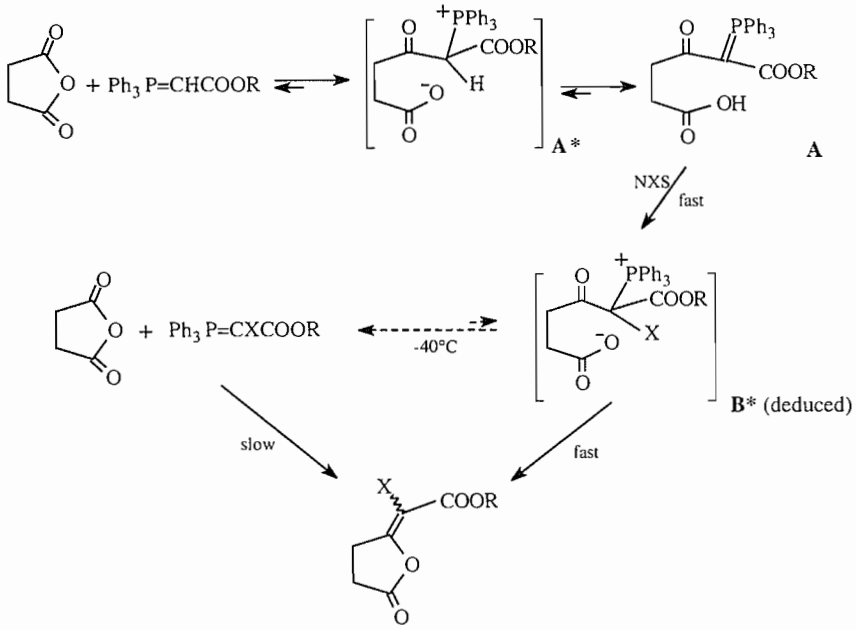
NMR monitored reactions show that chloro and bromolactonizations of **7** occur rapidly at −20°C. Upon addition of NCS or NBS, **7** is converted to lactones **12-Cl** and **12-Br** and to Ph_3PO within 5 min after mixing. The iodolactonization is slow at −20°C, but rapid reaction takes place when the mixture is warmed to +20°C. Treatment of keto phosphorane **7** with NXS (X = Cl, Br, I) gives pure bromo and iodo enol lactones, but chloro enol lactone is always contaminated with dichloro phosphorane **17-Cl**. This indicates that the unstable (not detected by NMR) initial adduct **7-Cl** (Scheme 4) has two possible competing pathways: (*a*) lactonization to give **12-Cl**, (*b*) recycling to succinic anhydride with concomitant expelling of chloroylide **3**. The latter compound can be chlorinated to **17-Cl**, it can pick up a proton to become conjugate acid **3a**, or it can add back to the anhydride. At temperatures between −40°C and −20°C the formation of **17-Cl** is an important side reaction. It can be minimized when chlorolactonizations are carried out at 0°C, thus giving higher yields of chloro enol lactone. The formation of dihalophosphoranes is generally less of a problem in the reactions with NBS and NIS and, in general, can be avoided by performing the reactions at higher temperatures under the optimum conditions described in Table 1. When keto phosphoranes **8** and **10** were treated with NBS or NIS at −40°C, the halogenated ylides **4** and **5** (in equilibrium with their conjugate acids) were formed as major products. Only traces of the desired enol lactones were detected in the proton and phosphorus spectra. The outcome of the corresponding reaction with NCS was similar except that the major product was the conjugate acid **3a**. These results show that, as in the case of **7-Br** and **7-I**, the chlorinated equivalents can revert to the anhydride and chloro ylide **3**. However, **3**, being more basic than either **4** or **5**, is rapidly protonated to its conjugate acid **3a**.

An interesting and general observation was made in the course of the chlorolactonizations monitored by ^{31}P NMR. As the dichloro phosphorane **17-Cl** was forming, the chemical shift of the other product, Ph_3PO, was slowly shifted down field. At the end of the reaction, when all of the keto phospho-

Can. J. Chem. Downloaded from www.nrcresearchpress.com by 91.121.58.235 on 09/08/12
For personal use only.

© 1997 NRC Canada

Scheme 5.



rane was consumed, the signal for Ph_3PO appeared at 32.5 ppm, more than 2 ppm lower than its usual position at 30 ppm. Upon standing, the signal for **17-Cl** slowly decreased until it almost disappeared completely and the signal for Ph_3PO drifted back towards its usual position. We soon discovered that the disappearance of **17-Cl** from the spectrum was caused by its precipitation from the $CDCl_3$ solution. Our interpretation of these data is as follows: when the concentration of dichloro phosphorane **17-Cl** rises, it forms a complex with the oxygen atom of Ph_3PO, thus deshielding the phosphorus atom and causing its downfield shift. As the salt precipitates from the solution, Ph_3PO is liberated and the phosphorus signal returns to its normal chemical shift.

In summary, the halolactonization route is the method of choice, sometimes the only successful method, for the preparation of halo enol lactones from the relatively less reactive succinic and glutaric anhydrides. Halolactonization can be used also with phthalic and substituted maleic anhydrides; with the latter compounds, however, direct condensations with in situ generated halo ylides are simpler and frequently give superior results. It should be stressed, however, that in order to obtain consistently high yields of halo enol lactones the acyclic adducts should be prepared from freshly purified anhydrides and ylides uncontaminated by their conjugate acids. The quality of *N*-halosuccinimides is also important, and the best results are obtained when these reagents are crystallized and stored in a darkened desiccator.

Mechanism of halo lactonization of acyclic adducts

The above study brings us back to consideration of the mechanism of Wittig reactions between stabilized ylides and cyclic anhydrides. It was pointed out in the introduction that, at low temperatures, ylide **1** reacts with succinic anhydride to give an acyclic addition product that immediately equilibrates to give a stable keto phosphorane. The formation of Wittig product, an enol lactone, can be observed only when the temperature of the reaction is raised significantly. These reactions can be conveniently monitored by NMR and the only species observable are starting materials, keto phosphoranes, and enol lactones. Although keto phosphoranes have been referred to as "intermediates," it is not clear if and how they are transformed into enol lactones. Low-temperature NMR studies and crossover experiments have shown unambiguously that the formation of keto phosphoranes is a reversible process and that the corresponding Wittig products often show regioselectivity different from that of the "intermediate" keto phosphoranes. It appears, therefore, that two distinct reactions may be involved: one, reversible, via a betaine-like, low-energy transition state leading to the formation of acyclic adducts; the other, a higher energy process, leading directly to enol lactones via an oxaphosphetane-like transition state (8, 12, 13). Stabilized ylides without an ylidic proton do not give stable, unambiguously identifiable keto phosphoranes. Thus, when such ylides react with cyclic anhydrides the only reaction pathway leading to observable products, enol lactones, would be via the oxaphosphetane route (14, 15).

The most recent series of experiments described in this paper does not fit the simple two-reaction picture described above. This is most apparent in the case of succinic anhydride. Succinic anhydride reacts with ylide **1** to give a stable keto phosphorane **7**, which has to be refluxed in THF or methylene chloride before it cyclizes to the corresponding enol lactone **12** in good yield. When chloroylide **3** is added to succinic anhydride the formation of chloro enol lactone **12-Cl** occurs slowly at room temperature (4). On the other hand, chlorolactonization of **7** occurs rapidly at 0°C. Careful monitoring of the last two reactions by ^{31}P and ^{1}H NMR at various temperatures did not reveal the existence of any intermediates corresponding to either acyl phosphorane **B*** or 4-member oxaphosphetane (13). In view of the above observations the previously suggested mechanism requires a modification that can accommodate a lower energy pathway to Wittig products through halolactonization. The possible sequence of events is shown in Scheme 5.

© 1997 NRC Canada

Can. J. Chem. Downloaded from www.nrcresearchpress.com by 91.121.58.235 on 09/08/12
For personal use only.

Can. J. Chem. Downloaded from www.nrcresearchpress.com by 91.121.58.235 on 09/08/12
For personal use only.

In conclusion, we have shown that ylides react with cyclic anhydrides to give acyclic adducts that are observable by NMR when an initial addition product (**A***) can be deprotonated to give relatively stable (at least at low temperatures) keto phosphoranes (**A**). When an ylide does not possess an ylidic proton, nucleophilic addition results in an unstable species (**B***), which may be observed as a transient signal (reactions with ylide **6**) or may not be detected by NMR (reactions with haloylides, Scheme 5).

Reactions of haloylides with succinic and glutaric anhydrides are very slow or inefficient or fail entirely depending on the ylide. Halolactonizations, on the other hand, are comparatively rapid even at −20 to −10°C for all (except NIS) reactions. This indicates that pathways, alternative to the direct 2+2 addition, exist for reactions of cyclic anhydrides with stabilized ylides. The actual pathway each individual reaction takes varies with the reactivity of the anhydride, the nature of the ylide, and the stabilities of the initially formed acyclic adducts.

Experimental section

All starting materials were supplied by Aldrich Chemical Company or Caledon Laboratories Ltd. Solvents were dried over sodium or molecule sieves and distilled. Melting points were determined on a Fisher–Johns melting point apparatus and were uncorrected. Infrared spectra were obtained on a Perkin–Elmer 297 infrared spectrometer. Nuclear magnetic resonance spectra were recorded on a Varian XL-200 spectrometer at the University of New Brunswick or Bruker AC 250 and Bruker AMX 400 spectrometers at the Atlantic Regional Magnetic Resonance Center. All spectra were recorded in $CDCl_3$ solutions with TMS as an internal reference for ^1H and ^{13}C and $CDCl_3$ as a secondary reference; 85% H_3PO_4 was the external reference for ^{31}P, and $CFCl_3$ the external reference for ^{19}F. In all NMR spectral data J values are in Hz. Mass spectra were obtained on a Kratos MS 550 TC mass spectrometer.

General procedure for the preparation of keto phosphoranes (refs. 7, 8)

A phosphoylide (14.4 mmol) dissolved in dry THF or $CHCl_3$ (40 mL) and cooled to 0°C was added to the cooled solution of a cyclic anhydride (14.4 mmol). The resultant (usually highly coloured) solution was stirred for 1–10 h at −20 to 0°C under a nitrogen atmosphere until all the cyclic anhydride had reacted as shown by TLC. Evaporation of the solvent under reduced pressure at 30°C gave the crude keto phosphorane, which was purified by crystallization from petroleum ether – acetone.

*Methyl 5-carboxy-3-oxo-2-triphenylphosphoranediylpentanoate, **7a***: Carbomethoxymethylene triphenylphosphorane **1**, R = Me (4.80 g), in $CHCl_3$ reacted with succinic anhydride (1.44 g) at −5°C for 30 min and then at 0°C for 8 h to give **7a** (5.17 g, 83%). ^1H NMR ($CDCl_3$, δ ppm): 2.5 (2H, t), 3.3 (2H, t), 3.8 (3H, s), 7.2–7.8 (15H, m), 12.0 (1H).

*Ethyl 5-carboxy-3-oxo-2-triphenylphosphoranediylpentanoate, **7b***: Carboethoxymethylene triphenylphosphorane **1**, R = Et (5.0 g), in THF reacted with succinic anhydride (1.44 g) at −5°C for 30 min then at 0°C for 5 h, to give compound **7b** (6.24 g, 97%). ^1H NMR ($CDCl_3$, δ ppm): 0.65 (3H, t, J = 7.1 Hz), 2.55 (2H, t, J = 5.8 Hz), 3.35 (2H, t, J = 5.8 Hz), 3.70 (2H, q, J = 7.1 Hz), 7.60 (15H, m), 12.2 (1H, s); ^{13}C NMR ($CDCl_3$, δ ppm): 13.64, 31.51, 34.22 (d, J = 4.5 Hz), 59.03, 126–134 (aromatic), 167.00, 175.80, 196.84. MS (EI): 347, 303, 277, 262, 201, 183, 152, 108, 77, 51.

tert-*Butyl 5-carboxy-3-oxo-2-triphenylphosphoranediylpentanoate, **7c***: Carbo-*tert*-butoxymethylene triphenylphosphorane **1**, R = *t*-Bu (5.4 g), in THF reacted with succinic anhydride (1.44 g) at −5°C for 30 min, and then at 0°C for 2 h, to give **7c** (6.49 g, 95%). ^1H NMR ($CDCl_3$, δ ppm): 1.05 (9H, s), 2.55 (2H, t), 3.32 (2H, t), 7.40–7.80 (15H, m).

tert-*Butyl 6-carboxy-3-oxo-2-triphenylphosphoranediylhexanoate, **9c***: Carbo-*tert*-butoxymethylene triphenylphosphorane **1**, R = *t*-Bu (5.40 g), in THF reacted with glutaric anhydride (1.64 g) at 0°C for 12 h to give **9c** (4.08 g, 58%). ^1H NMR ($CDCl_3$, δ ppm): 0.85 (9H, s), 1.70 (2H, m), 2.45 (2H, m), 2.85 (2H, m), 7.60–7.90 (15H, m).

tert-*Butyl 3-oxo-3-(2-carboxy)phenyl-3-triphenylphosphoranediylpentanoate, **10c***: Carbo-*tert*-butoxymethylenetriphenylphosphorane **1**, R = *t*-Bu (5.40 g), in THF reacted with phthalic anhydride (2.13 g) at −20°C for 2 h to give **10c** (6.40 g, 85%). The product was stored at −15–−20°C. ^1H NMR ($CDCl_3$, δ ppm): 0.80 (9H, s), 7.30–8.10 (19H, m).

General procedure for the preparation of halo enol lactones

A solution of ketophosphorane (4.1 mmol) in dry THF (20 mL) was cooled to 0°C and added to a cooled solution of halosuccinimide (1.1 equiv.). The mixture was stirred at 0°C for 2–4 h under N_2 atmosphere. The solvent was evaporated under vacuum. Ether (10 mL) was added to precipitate most of triphenylphosphine oxide. After filtration and washing with 15 mL of ether, the residue was chromatographed on a silica gel column to remove the remaining triphenylphosphine oxide.

(E,Z) *Methyl chloro(5-oxotetrahydrofuran-2-ylidene)acetate, **12a-Cl***: Methyl 5-carboxy-3-oxo-2-triphenylphosphoranediylpentanoate **7a**, 955 mg (2.2 mmol), reacted with 323 mg (1.1 equiv.) of chlorosuccinimide at 0°C for 2 h to give **12a-Cl** (389 mg 93%) as a mixture of isomers E:Z = 74:26. IR ($CHCl_3$) ν_{max} cm^{-1}: 2950, 1835, 1720, 1645; ^1H NMR ($CDCl_3$, δ ppm): 2.80 (2H, m overlap E and Z), 3.15 (2H, m, E), 3.40 (2H, m, Z), 3.84 (3H, s, Z), 3.86 (3H, s, E). Chromatography on silica gel gave a sample of **12a-Cl** E isomer: ^{13}C NMR ($CDCl_3$, δ ppm): 25.65, 27.19, 63.03, 104.0, 158.50, 161.40, 172.90; MS (EI), m/z: 190 (M, 20.8%), 164 (23.6%), 159 (37.6%), 135 (22.0%), 130 (33.0%), 101 (100%), 55 (40.70%); MS (HR), m/z, calcd. for $C_7H_7O_4$ ^{35}Cl: 190.0033; found: 190.0002.

(E,Z) *Methyl bromo(5-oxotetrahydrofuran-2-ylidene)acetate, **12a-Br***: **7a**, 955 mg (2.2 mmol), reacted with 431 mg (1.1 equiv.) of bromosuccinimide at 0°C for 4 h to give **12a-Br** (419 mg, 81%) as a mixture of isomers E:Z = 67:33. IR ($CHCl_3$) ν_{max} cm^{-1}: 2980, 1850, 1700, 1645. Chromatography with ethyl acetate – petroleum ether gave oily samples of both

© 1997 NRC Canada

Can. J. Chem. Downloaded from www.nrcresearchpress.com by 91.121.58.235 on 09/08/12
For personal use only.

isomers. ^{1}H NMR ($CDCl_3$, δ ppm) *E*: 2.80 (2H, m), 3.86 (3H, s), 3.12 (2H, m); *Z*: 3.83 (3H, s), 2.9 (2H, m), 3.45 (2H, m); MS (EI) for *E*, *m/z*: 236 (M, 22.7%), 234 (M, 25.5%), 208 (78.9%), 179 (23.5%), 149 (27.0%), 123 (100%), 59 (25.8%), 55 (50.9%); MS (HR), *m/z*, calcd. for $C_7H_7O_4{}^{79}Br$: 233.9528; found: 233.9518; calcd. for $C_7H_7O_4{}^{81}Br$: 235.9507; found: 235.9507.

(E,Z) *Methyl iodo(5-oxotetrahydrofuran-2-ylidene)acetate,* ***12a-I***: **7a**, 955 mg (2.2 mmol), reacted with 545 mg (1.1 equiv.) of iodosuccinimide at 0°C for 5 h to give **12a-I** (539 mg, 87%) as an inseparable mixture of isomers *E*:*Z* = 68:22. IR ($CHCl_3$) ν_{max} cm^{-1}: 2985, 1850, 1700, 1645, 1290, 1250, 1100; ^{1}H NMR ($CDCl_3$, δ ppm) data obtained from the mixture, *E*: 2.80 (2H, m), 3.83 (3H, s), 3.08 (2H, m); *Z*: 3.81 (3H, s), 2.90 (2H, m), 3.45 (2H, m).

(E,Z) *Ethyl chloro(5-oxotetrahydrofuran-2-ylidene)acetate,* ***12b-Cl*** (ref. 16): Ethyl 5-carboxy-3-oxo-2-triphenylphosphoranediylpentanoate **7b**, 1.84 g (4.1 mmol), reacted with 602 mg (1.1 equiv.) of chlorosuccinimide at 0°C for 2 h to give **12b-Cl** (694 mg, 83%) as an inseparable mixture of isomers *E*:*Z* = 72:28. IR ($CHCl_3$) ν_{max} cm^{-1}: 2985, 1850, 1720, 1645, 1280, 1250, 1100; ^{1}H NMR ($CDCl_3$, δ ppm): 1.30 (3H, m, overlapping *E* and *Z*), 4.30 (2H, m, overlapping *E* and *Z*), 2.95 (2H, m, *E*), 3.40 (2H, m, *Z*); ^{13}C NMR ($CDCl_3$, δ ppm), *E* isomer: 26.59, 27.39, 28.38, 62.15, 104.40, 158.44, 161.02, 173.33; MS (EI), *m/z*: 206 (M, 10.3%), 204 (M, 31.3%), 178 (28.5%), 176 (88.7), 159 (60.0%), 123 (100%), 121 (52.7%) 55 (52.2%).

(E,Z) *Ethyl bromo(5-oxotetrahydrofuran-2-ylidene)acetate,* ***12b-Br*** (ref. 16): **7b**, 1.84 g (4.1 mmol), reacted with 803 mg (1.1 equiv.) of bromosuccinimide at 0°C for 4 h to give **12b-Br** (898 mg, 88%) as a mixture of isomers *E*:*Z* = 75:25. ^{1}H NMR ($CDCl_3$, δ ppm): 1.40 (3H, m, overlapping *E* and *Z*), 4.30 (2H, m, overlapping *E* and *Z*), *E*: 2.70 (2H, m), 3.10 (2H, m); *Z*: 2.80 (2H, m,), 3.40 (2H, m); ^{13}C NMR ($CDCl_3$, δ ppm), *E* isomer: 13.87, 27.13, 33.67, 63.35, 94.0, 159.07, 165.04, 177.9; MS (EI), *m/z*: 250 (M, 41.5%), 248 (M, 42.9%), 222 (83.9%), 220 (84.5%), 176 (29.7%), 174 (26.9%), 167 (30.8%), 165 (30.8%), 123 (100%).

(E,Z) *Ethyl iodo(5-oxotetrahydrofuran-2-ylidene)acetate,* ***12b-I***: **7b**, 1.84 g (4.1 mmol), reacted with 1.01 g (1.1 equiv.) of iodosuccinimide at 0°C for 5 h to give **12b-I** (775 mg, 64%) as a mixture of isomers *E*:*Z* = 48:52. Several attempts to separate the two isomers by chromatography were not successful. IR ($CHCl_3$) ν_{max} cm^{-1}: 2980, 1835, 1710, 1640, 1620, 1290, 1100; ^{1}H NMR ($CDCl_3$, δ ppm): 1.30 (3H, m, *E* and *Z*), 4.25 (2H, m, *E* and *Z*), 2.80 (2H, m, *E* and *Z*), 3.15 (2H, m, *E*), 3.40 (2H, m, *Z*); MS (EI), *m/z*: 55 (20.8%), 73 (14.3%), 94 (13.8), 101 (100%), 129 (33.4%), 254 (22%).

(E) tert-*Butyl chloro(5-oxotetrahydrofuran-2-ylidene)acetate,* ***12c-Cl***: *tert*-Butyl 5-carboxy-3-oxo-2-triphenylphosphoranediylpentanoate **7c**, 1.95 g (4.1 mmol), reacted with 602 mg (1.1 equiv.) of chlorosuccinimide at 0°C for 2 h to give only **12c-Cl** (907 mg, 95%) as pure *E* isomer; mp 120–121°C; IR ($CHCl_3$) ν_{max} cm^{-1}: 2980, 1835, 1720, 1645; ^{1}H NMR ($CDCl_3$, δ ppm): 1.54 (9H, s), 2.76 (2H, m), 3.12 (2H, m); ^{13}C NMR ($CDCl_3$, δ ppm): 25.70, 27.14, 28.09, 83.27, 95.46, 157.24, 163.0, 173.3; MS (EI), *m/z*: 234 (M, 0.8%), 232 (M, 1.6%), 176 (47.2%), 159 (92.6%), 123 (67.4%), 57 (100%); MS (HR), *m/z*, calcd. for $C_{10}H_{13}O_4{}^{35}Cl$: 232.0502; found: 232.0508.

(E) tert-*Butyl bromo(5-oxotetrahydrofuran-2-ylidene)acetate,* ***12c-Br***: **7c**, 1.95 g (4.1 mmol), reacted with 803 mg (1.1 equiv.) of bromosuccinimide at 0°C for 4 h to give **12c-Br** (1.02 g, 90%) as pure *E* isomer; mp 113–115°C; IR ($CHCl_3$) ν_{max} cm^{-1}: 2980, 1850, 1710, 1655, 1645, 1280, 1100, 1050; ^{1}H NMR ($CDCl_3$, δ ppm): 1.55 (9H, s), 2.75 (2H, m), 3.08 (2H, m); ^{13}C NMR ($CDCl_3$, δ ppm): 26.24, 28.06, 29.15, 83.29, 96.80, 157.85, 166.0, 173.57; MS (EI), *m/z*: 278 (M, 2.7%), 276 (M, 3.0), 222 (28.5%), 220 (27.8%), 194 (29.8%), 192 (31%), 123 (48.1%), 57 (100%); MS (HR), *m/z*, calcd. for $C_{10}H_{13}O_4{}^{79}Br$: 275.9997; found: 275.9997; calcd. for $C_{10}H_{13}O_4{}^{81}Br$: 277.9997; found: 277.9982.

(E,Z) tert-*Butyl iodo(5-oxotetrahydrofuran-2-ylidene)acetate,* ***12c-I***: **7c**, 1.95 g (4.1 mmol), reacted with 1.01 g (1.1 equiv.) of iodosuccinimide at 0°C for 5 h to give **12c-I** (1.17 g, 88%) as a mixture of isomers *E*:*Z* = 95:5. Chromatography on silica gel gave a sample of pure **12c-I**, *E* isomer; mp 98–101°C; ^{1}H NMR ($CDCl_3$, δ ppm): 1.50 (9H, s), 2.74 (2H, m), 3.06 (2H, m); ^{13}C NMR ($CDCl_3$, δ ppm): 27.21, 27.97, 32.43, 70.05, 83.29, 159.36, 167.0, 174.07; MS (EI), *m/z*: 316 (20.8%), 299 (33.3%), 272 (75.9%), 149 (60.8%), 104 (48.5%), 57 (57.5%). MS (HR), *m/z*, calcd. for base peak $[C_6H_5O_4I]^+$: 267.9231; found: 267.9230. Note: ^{1}H NMR signals for *Z* isomer: 2.87 (m), 3.40 (m).

(E,Z) *Methyl bromo(3-methoxy-5-oxotetrahydrofuran-2-ylidene)acetate,* ***13a-Br***: Methoxysuccinic anhydride reacted with 1 equivalent of ylide **1** (R = Me) at room temperature for 30 min to give the corresponding keto phosphorane: ^{1}H NMR: 2.92 (2H AB quartet), 3.18 (3H, s), 3.39 (3H, s), 5.28 (1H, m): ^{13}C NMR ($CDCl_3$, δ ppm) distinguishable signals: 38.43, 50.18, 57.68, 120–135 (aromatic), 167.48, 172.7, 193.63; ^{31}P ($CDCl_3$, δ ppm): 18.71. The reaction mixture was cooled to −10°C and 1.1 equiv. of NBS was added to give **13a-Br** (50% yield) as a mixture of isomers *E*:*Z* = 25:75 and the corresponding non-halogenated enol lactone (45%). ^{1}H NMR, *E* isomer: (2.90, m), 3.44 (3H, s), 3.63 (3H, s), 4.85 (1H, m); *Z* isomer: 2.90 (m), 3.42 (3H, s), 3.87 (3H, s), 5.32 (1H, m); ^{1}H NMR, the non-halogenated enol lactone, *E* isomer only: 2.78 (2H, m), 3.45 (3H, s), 3.74 (3H, s), 5.28 (1H, m), 5.86 (1H, s).

(E) tert-*Butyl chloro(6-oxotetrahydropyran-2-ylidene)acetate,* ***14c-Cl*** (ref. 16): *tert*-Butyl 6-carboxy-3-oxo-2-triphenylphosphoranediylhexanoate **9c**, 1.08 g (2.2 mmol), reacted with 323 mg (1.1 equiv.) of chlorosuccinimide at 0°C for 6 h to give **14c-Cl** (309 mg, 57%) *E* isomer as an oil. ^{1}H NMR ($CDCl_3$, δ ppm): 1.49 (9H, s), 1.96 (2H, m), 2.43 (2H, m), 2.79 (2H, m); a trace of the *Z* isomer was present as witnessed by a signal at 1.44 (s); ^{13}C NMR ($CDCl_3$, δ ppm): 18.36, 27.76, 32.49, 37.54, 38.83, 61.78, 84.75, 163.83, 178.70.

(E,Z) tert-*Butyl bromo(6-oxotetrahydropyran-2-ylidene)acetate,* ***14c-Br*** (ref. 16): **9c** 1.08 g (2.2 mmol), reacted with 431 mg (1.1 equiv.) of bromosuccinimide at 0°C for 6 h to give

© 1997 NRC Canada

Can. J. Chem. Downloaded from www.nrcresearchpress.com by 91.121.58.235 on 09/08/12
For personal use only.

14c-Br (352 mg, 55%) as a mixture of isomers *E*:*Z* = 90:10. IR ($CHCl_3$) ν_{max} cm^{-1}: 2980, 1850, 1700, 1655, 1645, 1290, 1250, 1100, 1050, 900; ^1H NMR ($CDCl_3$, δ ppm), *E* isomer: 1.52 (9H, s), 1.95 (2H, m), 2.43 (2H, m), 2.82 (2H, m); *Z* isomer: 2.62 (m), 2.78 (m).

(E,Z) *Methyl chloro(3-oxo-1,3-dihydroisobenzofuran-1-ylidene)acetate,* ***15a-Cl***: Methyl 3-oxo-3-(2-carboxy)phenyl-3-triphenylphosphoranediylpentanoate **10a**, 2.41 g (5.0 mmol), reacted with 734 mg (1.1 equiv.) of chlorosuccinimide at −20°C for 2 h to give **15a-Cl** (681 mg, 57%) as an inseparable mixture of isomers *E*:*Z* = 40:60. ^1H NMR ($CDCl_3$, δ ppm), *E*: 3.85 (3H, s), 8.74 (1H, d); *Z*: 3.98 (3H, s), 8.50 (1H, d), and 7.60–8.15 (3H, m) overlapping aromatic protons for *E* and *Z* isomers. ^{13}C NMR ($CDCl_3$, δ ppm): 53.35, 104.0, 125.89, 126.19, 127.25, 132.11, 135.41, 158.00, 136.10, 158.0, 163.0, 164.0 (assigned as signals for *Z* isomer).

(E,Z) *Methyl bromo(3-oxo-1,3-dihydroisobenzofuran-1-ylidene)acetate,* ***15a-Br***: **10a**, 2.41 g (5.0 mmol), reacted with 797 mg (1.1 equiv.) of bromosuccinimide at −20°C for 2 h to give **15a-Br** (1.30 g, 92%) as a mixture of isomers *E*:*Z* = 45:55. ^1H NMR ($CDCl_3$, δ ppm), *E*: 3.96 (3H, s), 8.61 (1H, d); *Z*: 3.98 (3H, s), 8.68 (1H, d), and overlapping aromatic protons for *E* and *Z* isomers 7.70–8.10 (3H, m); ^{13}C NMR ($CDCl_3$, δ ppm): 53.66, 96.47, 126.42, 126.53, 134.99, 135.97, 137.62, 149.81, 154.06, 162.34 164.56.

(E,Z) *Ethyl chloro(3-oxo-1,3-dihydroisobenzofuran-1-ylidene)acetate,* ***15b-Cl*** (ref. 16): Ethyl 3-oxo-3-(2-carboxy)phenyl-3-triphenylphosphoranediylpentanoate **10b**, 2.48 g (5.0 mmol), reacted with 734 mg (1.1 equiv.) of chlorosuccinimide at −20 to +20°C for 2 h to give **15b-Cl** (696 mg, 55%) as a mixture of isomers *E*:*Z* = 90:10. ^1H NMR ($CDCl_3$, δ ppm), *E*: 1.40 (3H, t), 4.42 (2H, q), 8.50 (1H, d); *Z*: 1.38 (3H, t), 4.15 (2H, q), 8.70 (1H, d), and overlapping aromatic protons 7.72–8.10 (3H, m).

(E,Z) tert-*Butyl iodo(3-oxo-1,3-dihydroisobenzofuran-1-ylidene)acetate,* ***15c-I***: *tert*-Butyl 3-oxo-3-(2-carboxy)phenyl-3-triphenylphosphoranediylpentanoate **10c**, 2.62 g (5.0 mmol), reacted with 1.24 g (1.1 equiv.) of iodosuccinimide at −20°C for 2 h to give **15c-I** (1.50 g, 81%) as a mixture of isomers *E*:*Z* = 50:50. IR ($CHCl_3$) ν_{max} cm^{-1}: 2980, 1835, 1710, 1645; ^1H NMR ($CDCl_3$, δ ppm): 1.64 (9H, s, overlapping *E* and *Z*), 7.6–8.10 (3H, m, overlapping *E* and *Z*), 8.25 (1H, d, *E*), 8.8 (1H, d, *Z*); ^{13}C NMR ($CDCl_3$, δ ppm): 27.97, 125.50, 125.87, 126.19, 131.67, 134.54, 135.22, 163.72, 164.91; MS (EI), *m*/*z*: 372 (M, 19.9%), 316 (68.7%), 299 (14.2%), 226 (33.1%), 173 (45.7%), 149 (95.1%), 104 (47.7%), 57 (100%); MS (HR), *m*/*z*, calcd. for $C_{14}H_{13}O_4I$: 371.9859; found: 371.9856.

(Z) *3-Bromo-5-t-butoxcarbonlymethlidene-3-phenylfuran-2-one,* ***16c-Br***: Phenylmaleic anhydride reacted in an NMR tube with 1 equiv. of ylide **1** (R = *t*-butyl) at −10°C to give the corresponding keto phosphorane, to which 1.1 equiv. of NBS was added in situ to give (*Z*) **16c-Br** as the *Z*-isomer in 50% yield. ^1H NMR: 1.55 (9H, s), 7.30–7.90 (5H, m), 8.40 (1H, s).

General procedure for the preparation of fluoro enol lactones

A three-neck flask equipped with a dropping funnel, stir bar, gas inlet and outlet, and a bubbler was cooled under a steady stream of nitrogen. *tert*-Butyl 5-carboxy-3-oxo-2-triphenylphosphoranediylpentanoate, 2.38 g (5.0 mmol), in 50 mL dry THF was added and cooled to −20°C. *N*-Fluorodiphenyl sulfonamide, 1.79 g (5.5 mmol), in 15 mL THF was added dropwise to the solution over a period of 30 min and the reaction mixture was stirred for 4–12 h at room temperature. The solvent was evaporated under a vacuum and 10 mL ether was added to precipitate triphenylphosphine oxide. After filtration and washing with 15 mL of ether, the residue was chromatographed on a short column to give fluoro enol lactones.

(E,Z) *Ethyl fluoro(5-oxotetrahydrofuran-2-ylidene)acetate* ***12b-F*** Ethyl 5-carboxy-3-oxo-2-triphenylphosphoranediylpentanoate **7b**, 2.24 g (5.0 mmol), reacted with *N*-fluorodiphenyl sulfonamide, 1.79 g (5.5 mmol), for 12 h to give **12b-F** (630 mg, 67%) as an inseparable mixture of *E*:*Z* = 15:85. ^1H NMR ($CDCl_3$, δ ppm): 1.33 (3H, t), 2.75 (2H, m), 3.30 (2H, m), 4.30 (2H, q); signals at 1.25 (t), 2.65 (m), 2.85 (m), 4.10 (q) were assumed to belong to the *E* isomer; ^{13}C NMR ($CDCl_3$, δ ppm): 14.22, 24.26, 25.87, 60.92, 89.79, 130.23, 134.23, 147.73 (d, J_{CP} = 12 Hz), 161.30 (d, J_{CP} = 27 Hz), 172.29; ^{19}F ($CDCl_3$, δ ppm): −149.99 (*Z* isomer); a small signal at −163.43 was interpreted as belonging to the *E* isomer.

(Z) tert-*Butyl fluoro(5-oxotetrahydrofuran-2-ylidene)acetate* ***12c-F***: **7c**, 2.38 g (5.0 mmol), reacted with *N*-fluorodiphenyl sulfonamide, 1.79 g (5.5 mmol), for 12 h to give **12c-F** as a *Z* isomer (898 mg, 83%). Chromatography on silica gel failed to remove unidentified fluorinated impurities. ^1H NMR ($CDCl_3$, δ ppm): 1.55 (9H, s), 2.78 (2H, m), 3.25 (2H, m); ^{13}C NMR ($CDCl_3$, δ ppm): 24.27, 25.84, 27.85, 83.20, 130.35, 134.73, 147.72 (d, J_{CP} = 14 Hz), 160.31 (d, J_{CP} = 27 Hz), 72. 155; ^{19}F ($CDCl_3$, δ ppm): −146.56.

(Z) *Ethyl fluoro(3-oxo-1,3-dihydroisobenzofuran-1-ylidene)acetate* ***15b-F***: All spectral data are identical to those reported in ref. 3.

(Z) tert-*Butyl fluoro(3-oxo-1,3-dihydroisobenzofuran-1-ylidene)acetate* ***15c-F***: **10c**, 2.62 g (5.0 mmol), reacted with *N*-fluorodiphenyl sulfonamide, 1.79 g (5.5 mmol), at −10°C for 4 h to give **15c-F** (952 mg, 75%) as a mixture of *E*:*Z* = 75:25. IR ($CHCl_3$) ν_{max} cm^{-1}: 2950, 1820, 1785, 1710, 1655, 1100, 895: ^1H NMR ($CDCl_3$, δ ppm), *E* isomer: 1.56 (s); *Z* isomer: 1.63 (s), integrating together for 9H, *E* and *Z* overlapping aromatic protons 7.58–8.05, (3H, m), 9.0 (1H, d) (*Z* isomer); ^{13}C NMR ($CDCl_3$, δ ppm): 28.18, 104.61, 125.76, 128.22, 129.52, 129.88, 131.35, 136.10, 168.0. ^{19}F ($CDCl_3$, δ ppm): −128.83 (*Z* isomer); −152.51 (*E* isomer).

Acknowledgements

We wish to thank the Natural Sciences and Engineering Research Council of Canada for financial support.

© 1997 NRC Canada

References

1. R.R. Rando. Science, **185**, 320 (1974); M.J. Sofia, P.K. Chakravarty, and J.A. Katzenellenbogen. J. Org. Chem. **48**, 3318 (1983); S.B. Daniels and J.A. Katzenellenbogen. Biochemistry, **25**, 1436 (1986).
2. (*a*) R.W. Spencer, T.F. Tam, E. Thomas, V.J. Robinson, and A.J. Kranz. J. Am. Chem. Soc. **108**, 5589 (1986); (*b*) D.J. Beak, S.B. Daniels, P.E. Reed, and J.A. Katzenellenbogen. J. Org. Chem. **54**, 3963 (1989); (*c*) W. Dei and J.A. Katzenellenbogen. J. Org. Chem. **56**, 6893 (1991); S. Ma and X. Lu. J. Org. Chem. **58**, 1245 (1992).
3. J. Zhu and M.M. Kayser. Synth. Commun. **24**, 1179 (1994).
4. M.M. Kayser, J. Zhu, and D.L. Hooper. Can. J. Chem. **75**, 1315 (1997).
5. A.D. Abell and J.O. Trent. J. Chem. Soc. Chem. Commun. 409 (1989).
6. M.P. Cook and R. Goswami. J. Am. Chem. Soc. **99**, 642 (1977).
7. A.D. Abell, J.O. Trent, and B.I. Whittington. J. Org. Chem. **54**, 2762 (1989).
8. A.D. Abell and R.M. Massey-Westropp. Aust. J. Chem. **35**, 2077 (1982); A.D. Abell, I.R. Doyle, and R.M. Massey-Westropp. Aust. J. Chem. **35**, 2277 (1982); R.W. Lang and H.J. Hansen. Helv. Chim. Acta, **63**, 438 (1980).
9. M.M. Kayser, K.L. Hatt, and D.L. Hooper. Can. J. Chem. **70**, 1985 (1992).
10. D.W. Knight and G. Pattenden. J. Chem. Soc. Perkin Trans. 1, 62, (1979).
11. L. Breau. M.Sc. Thesis. Mount Allison University, Sackville, N.B. 1986.
12. M.M. Kayser, K.L. Hatt, H. Yu, and D.L. Hooper. Can. J. Chem. **71**, 1010 (1993).
13. E. Vedejs and C.F. Marth. J. Am. Chem. Soc. **112**, 3905 (1990); E. Vedejs and T.J. Fleck. J. Am. Chem. Soc. **111**, 5861 (1989); E. Vedejs, T.J. Fleck, and S. Hara. J. Org. Chem. **52**, 4637 (1987).
14. M.M. Kayser and D.L. Hooper. Can. J. Chem. **68**, 2123 (1990).
15. M.M. Kayser, K.L. Hatt, and D.L. Hooper. Can. J. Chem. **69**, 1929 (1991).
16. A.D. Abell, D.A. Hoult, K.M. Morris, J.M. Taylor, and J.O. Trent. J. Org. Chem. **58**, 1531 (1993).

Can. J. Chem. Downloaded from www.nrcresearchpress.com by 91.121.58.235 on 09/08/12
For personal use only.

© 1997 NRC Canada

Nucleophilic aromatic substitution with dialkoxycarbenes

Joseph P. Ross, Philippe Couture, and John Warkentin

Abstract: Dimethoxycarbene, generated at 110°C by thermolysis of 2,2-dimethoxy-5,5-dimethyl-Δ^3-1,3,4-oxadiazoline, displaces fluoride from aromatic rings that are activated with electron-withdrawing groups. Intermolecular substitution on Sanger's reagent and on hexafluorobenzene are reported, together with intramolecular substitution by a dioxycarbene with a tethered aryl group.

Key words: aromatic substitution, aryl(dimethoxy)fluoromethanes, aryl fluoride, dialkoxycarbene, nucleophilic substitution.

Résumé : La diméthoxycarbène, obtenu par thermolyse du 2,2-diméthoxy-5,5-diméthyl-$\Delta^3$1,3,4-oxadiazoline, déplace le fluor des noyaux aromatiques activés par des groupes électroattracteurs. On rapporte les réactions de substitutions intermoléculaires sur le réactif de Sanger et sur l'hexafluorobenzène ainsi que la substitution intramoléculaire d'un dioxycarbène fixé sur un groupe aryle.

Mots clés : substitution aromatique, aryl(diméthoxy)fluorométhanes, fluorure d'aryle, dialkoxycarbène, substitution nucléophile.

[Traduit par la rédaction]

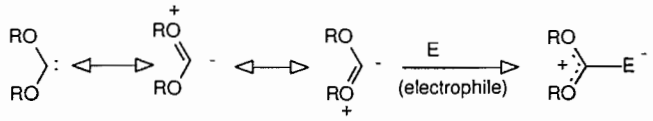
Can. J. Chem. Downloaded from www.nrcresearchpress.com by 91.121.58.235 on 09/08/12
For personal use only.

Introduction

The fact that donor substituents, such as alkoxy or amino, at a carbene center have a strong influence on a carbene's properties is now well established. Diaminocarbenes (1–6) and dialkoxycarbenes (7) have large singlet/triplet energy gaps attributed to conjugative stabilization of the singlet. Such carbenes have nucleophilic properties (8–10), rather than the more commonplace electrophilic properties associated with carbenes as a class. Their nucleophilicity is presumably a consequence of delocalization in the carbene itself and, probably to a greater extent, of the conjugative delocalization in the transition state for attack by the carbene on an electrophilic substrate (Scheme 1). Nucleophilic properties of dialkoxycarbenes have been demonstrated in terms of their preference for reaction with Michael acceptors instead of electron-rich alkenes such as tetramethylethylene (11, 12), with examples of reactions with isocyanates and isothiocyanates (12, 13), with tetrazines (14–16), and with the carbonyl groups of maleic and other anhydrides (17), for example (Scheme 2).

Nucleophilic aromatic substitution by carbenes has, apparently, not been observed. Arduengo et al. (18) reported that a stable diaminocarbene reacts with iodopentafluorobenzene to afford an ylide, by attack of the carbene at iodine. Although some pentafluorobenzene was obtained as the solution of the ylide aged, that product was not from displacement by a carbene carbon moiety.

Scheme 1.



We now report that dimethoxycarbene attacks 2,4-dinitrofluorobenzene (Sanger's reagent) and hexafluorobenzene, in each case with overall displacement of fluoride by the carbene carbon, to afford unstable "acetals" of aroyl fluorides. A similar reaction occurs intramolecularly, with a dialkoxycarbene tethered *ortho* to an aryl fluorine substituent.

Results and discussion

Dimethoxycarbene (**1**) was generated by thermolysis of 2,2-dimethoxy-5,5-dimethyl-Δ^3-1,3,4-oxadiazoline (**2**) (19–23) and carbene **5** was generated from oxadiazoline **4**, prepared by the exchange method (24–26) from 2-acetoxy-2-methoxy-5,5-dimethyl-Δ^3-1,3,4-oxadiazoline (**3**) (Scheme 3). Thermolysis of **2** at 110°C, in benzene containing 2,4-dinitrofluorobenzene (**6**) at 0.2 M initial concentration, afforded **7** (Scheme 4). Although it was quite sensitive to moisture and could not be isolated, its structure was secured by means of ^{19}F NMR spectroscopy, mass spectrometry, and hydrolysis to methyl 2,4-dinitrobenzoate (**8**) (Scheme 4). In the ^{19}F NMR spectrum of the crude, taken immediately after opening of the thermolysis tube, there was a strong doublet (J = 2.3 Hz) at δ = −82 (external ref. $CFCl_3$). The position of that signal and the long-range coupling to one H is consistent with structure **7**.[3] In the mass

Received April 21, 1997.

J.P. Ross,[1] P. Couture, and J. Warkentin.[2] Department of Chemistry, McMaster University, Hamilton, ON L8S 4M1, Canada.

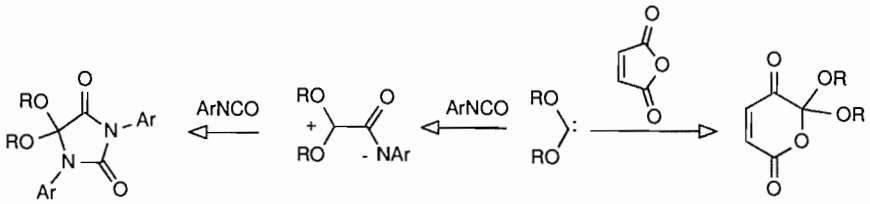
[1] Summer research assistant, 1995 and 1996, sponsored in part by Human Resources Canada.

[2] Author to whom correspondence may be addressed. Telephone: (905) 525-9140. Fax: (905) 522-2509. E-mail: Warkent@McMaster.ca

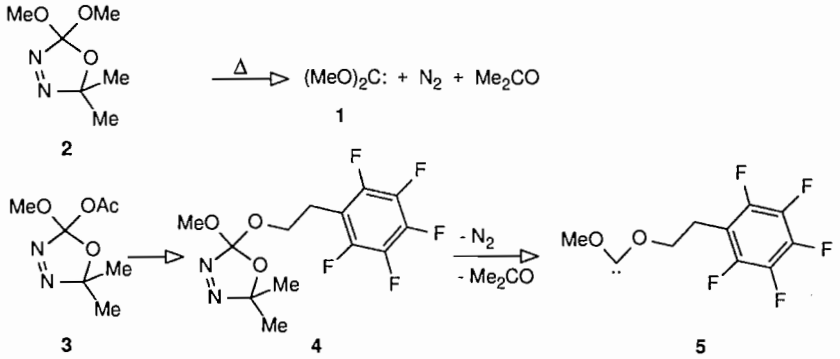
[3] In the ^{19}F NMR spectrum of trifluoromethylbenzene there is also long-range coupling of the fluorines to the *ortho* hydrogens of the aromatic ring ($^4J_{HF}$ = ca. 0.7 Hz) (27).

© 1997 NRC Canada

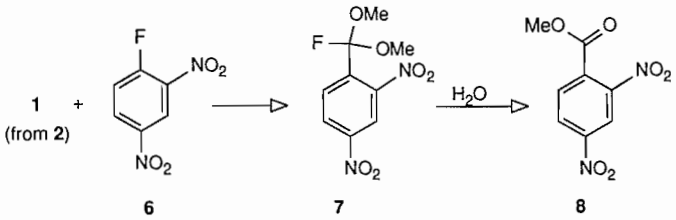
Scheme 2.



Scheme 3.



Scheme 4.



spectrum (GC–MS) the highest mass:charge ratio was m/z = 241, corresponding to $[M - F]^+$, as expected for **7**. The fact that aging the sample, in a capped NMR tube, led to fading of the ^{19}F NMR signal is also in keeping with structure **7**, which is the "acetal" of 2,4-dinitrobenzoyl fluoride. Hydrolysis of the crude thermolysis product with aqueous methanol containing acetic acid afforded methyl ester **8**, (Scheme 4).

Thermolysis of **1** in hexafluorobenzene, in a sealed tube at 110°C, gave pentafluorobenzoyl fluoride dimethyl acetal (**9**) (Scheme 5) and tetramethoxyethylene as major products, in ca. 40:60 ratio by GC–MS. Product **9** was also very sensitive to moisture, and it could not be isolated. In the ^{19}F NMR spectrum of the crude thermolysate, there was a triplet at $\delta = -82$ (external ref. $CFCl_3$), $^4J_{FF}$ = 22 Hz, consistent with benzylic fluorine coupled to equivalent *ortho* fluorines. For example, the analogous coupling constant in pentafluoro(trifluoromethyl)benzene is 22.7 Hz (28). The mass spectrum (GC–MS) again failed to show a molecular ion at m/z = 260, but both $[M - F]^+$ at m/z = 241 and $[M - OMe]^+$ at m/z = 229 were present. Attempted hydrolysis with aqueous methanol acidified with acetic acid led to disappearance of **9** but **11** was not obtained. Instead one product appeared to be the *ortho* ester **10** on the basis of its longer retention time (relative to that of **9**) in a GC column and its mass spectrum; m/z = 241 $(M - OMe)^+$, by GC–MS. Apparently the *ortho* ester **10** (and presumably the corresponding hemi *ortho* ester too) is not easily converted to the corresponding ester, undoubtedly because of the destabilizing effect of five fluorine atoms on the carbonyl group. Acidification of the crude product containing **10** in CH_2Cl_2 with concentrated sulfuric acid gave the known methyl pentafluorobenzoate (**11**) (29).

An intramolecular analogue of the substitutions in Schemes 4 and 5 was observed upon thermolysis of **4**, which afforded **12** as an unstable intermediate that was hydrolyzed to lactone **13** (Scheme 6). Carbene dimers (**14**), indicated by GC–MS, were formed in approximately 40% combined yield.

These reactions are readily explained in terms of nucleophilic aromatic substitution, through an intermediate (**15**) that resembles the classical Meisenheimer intermediate (30) except in that **15** is a dipole rather than an ion, as illustrated in Scheme 7 for the case of Sanger's reagent. Dipole **15** presumably rearranges quickly by 1,2 F-migration to afford **7** (Scheme 7). Intermolecular attack on the aromatic ring to afford **15** (or an analogue) must be slow, at least for the case of hexafluorobenzene, as indicated by the coformation of carbene dimer (Scheme 5). Similarly, in the case of **5**, where five fluorines activate the ring for nucleophilic aromatic substitution, the intramolecular reaction is difficult also, and carbene dimers are formed in competition (Scheme 6).

In summary, dialkoxycarbenes are nucleophiles capable of aromatic substitution on activated aryl fluorides. Although the method is not currently of interest for synthetic purposes because of the low yields, it could find application in highly specialized pursuits such as those involved in the preparation of labelled compounds.

Experimental

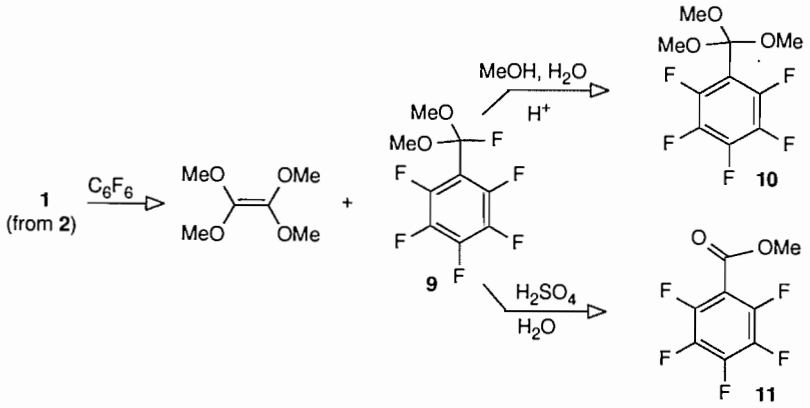
Oxadiazolines 2 and 4

2,2-Dimethoxy-5,5-dimethyl-Δ^3-1,3,4-oxadiazoline (**2**) was prepared as described in the literature (19). 2-Methoxy-5,

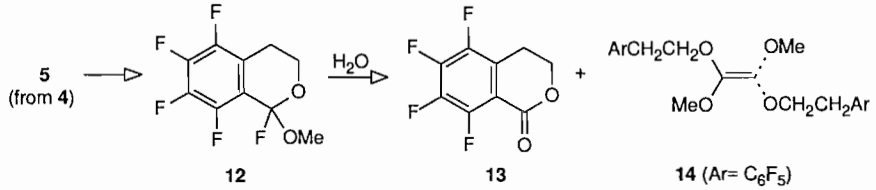
© 1997 NRC Canada

Can. J. Chem. Downloaded from www.nrcresearchpress.com by 91.121.58.235 on 09/08/12
For personal use only.

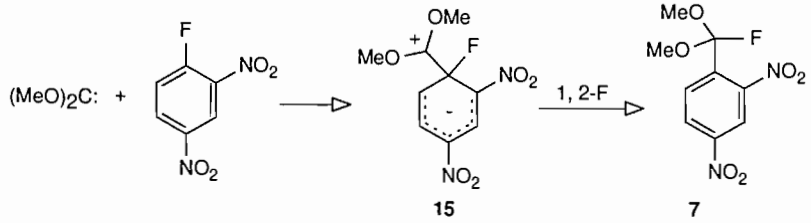
Scheme 5.



Scheme 6.



Scheme 7.



5-dimethyl-2-(2-pentafluorophenylethoxy)-Δ^3-1,3,4-oxadiazoline (**4**) was prepared from 2-acetoxy-2-methoxy-5,5-dimethyl-Δ^3-1,3,4-oxadiazoline (**3**) by the exchange method (24). A solution of 2-pentafluorophenylethanol (1.38 g, 6.51 mmol), **3** (1.23 g, 6.52 mmol), and acetic acid (1 mL) in dichloromethane (15 mL) was left for 7 days at room temperature. Extraction with aqueous bicarbonate, drying, and removal of the solvent with a rotary evaporator left a residue that was chromatographed (Chromatotron apparatus, 4 mm plate, 5% ethyl acetate in hexanes) to afford **4** as a clear oil in 78% yield. Its structure followed from the method of preparation and from its NMR spectra, particularly the ^{13}C signals characteristic of C2 and C5 of the oxadiazoline ring (25). IR(cm^{-1}): 2992–2847 (CH), 1657, 1522, 1460, 1383; ^1H NMR (200 MHz, $CDCl_3$) δ: 1.47 (s, 3H), 1.52 (s, 3H), 3.01 (m, 2H), 3.37 (s, 3H), 3.94 (m, 2H); ^{13}C NMR (50 MHz, $CDCl_3$) (multiplets that are components of doublets with $^1J_{CF}$ = 244–250 Hz are listed as discrete signals) δ: 23.07, 23.81 (2C), 51.21, 62.65, 111.52 (t, $^2J_{CF}$ = 18.4 Hz, CH_2C_{Ar}), 119.27 (C5), 134.85 (m), 136.72 (C2), 137.4 (m), 139.9 (m), 142.4 (overlapping m), 147.8 (m); MS (EI) *m/z* (rel. intensity): 254 ($(M - N_2 - Me_2CO)^+$, 10), 195 (40).

Thermolysis of 2 in presence of 2,4-dinitrofluorobenzene

A solution of **2** (0.25 g, 1.6 mmol) and 2,4-dinitrofluorobenzene (0.50 g, 2.7 mmol) in benzene (15 mL) was sealed into a glass tube of 30 mL volume after three sequences of freeze–pump–thaw degassing at 0.1 Torr (1 Torr = 133.3 Pa). The tube was then kept in an oil bath at 110°C for 24 h before it was cooled and opened. The solvent was evaporated with a rotary evaporator and the residue was examined immediately with spectroscopic methods. Although signals from Sanger's reagent dominated the ^1H NMR spectrum, those from 2,4-dinitrobenzoylfluoride dimethyl acetal (**7**), formed in ca. 10% yield, could be identified. ^1H NMR (500 MHz, C_6D_6) δ: 3.14 (s, 6H), 7.36 (d, ^3J = 8.6 Hz, 1H), 7.71 (dd, ^3J = 8.6 Hz, ^4J ca. 2 Hz, not completely resolved from Sanger's reagent signal), 7.86 (br s, $^4J < 2$ Hz, 1H); ^{13}C NMR (125 MHz, C_6D_6) δ: 51.3 (d, $^3J_{CF}$ = 3.8 Hz, CH_3), 118.91 (s), 119.21 (d, $^1J_{CF}$ = 244.5 Hz), 125.03, 130.38 (d, $^3J_{CF}$ = 8.4 Hz), 133.50 (d, $^2J_{CF}$ = 42.0 Hz),[4] 148.62, 149.40; ^{19}F NMR (470 MHz, C_6D_6, external ref.

[4] In trifluoromethylbenzene $^2J_{CF}$= 42.2 Hz (29).

Can. J. Chem. Downloaded from www.nrcresearchpress.com by 91.121.58.235 on 09/08/12
For personal use only.

© 1997 NRC Canada

Can. J. Chem. Downloaded from www.nrcresearchpress.com by 91.121.58.235 on 09/08/12
For personal use only.

$CFCl_3$) δ: −82.84; MS (GC–MS, EI) *m/z* (rel. intensity): 241 ($(M - F)^+$, 100), 210 ($(M - F - OMe)^+$, 11).

Chromatography of the crude reaction mixture (Chromatotron apparatus, 1 mm silica plate, 5% ethyl acetate in hexanes) afforded methyl 2,4-dinitrobenzoate (**8**) as a yellow solid, mp 82°C (lit. (31) mp 82°C); IR (cm^{-1}): 3088–2950, 1610, 1539; ^1H NMR (200 MHz, C_6D_6) δ: 3.11 (s, 3H), 6.06 (d, ^3J = 9.3 Hz, 1H), 7.77 (d of d, ^3J = 9.3 Hz, ^4J = 2.8 Hz, 1H), 8.26 (d, ^4J = 2.8 Hz); ^{13}C NMR (50 MHz, C_6D_6) δ: 56.68, 113.35, 121.37, 128.48, 138.89, 140.04, 156.84, 204.91; GC–MS (EI) *m/z* (rel. intensity): 226 (M^+, 10), 195 ($(M - OMe)^+$, 100).

Thermolysis of 2 in hexafluorobenzene

A solution of **2** (97 mg, 0.60 mmol) in hexafluorobenzene (2.0 mL) was sealed into a glass tube after three cycles of freeze–pump–thaw degassing. The tube was left in an oil bath at 110°C for 24 h before it was cooled and opened. GC analysis (not corrected for differential response from the FID detector) showed two major products, tetramethoxyethylene and pentafluorobenzoylfluoride dimethyl acetal (**9**) in ca. 60:40 ratio. NMR data were obtained from a crude thermolysate generated in a sealed NMR tube. ^1H NMR (500 MHz, C_6D_6) δ: 2.93 (s); ^{19}F NMR (470 MHz, C_6D_6, external ref. $CFCl_3$) δ: −80.21 (t, $^4J_{FF(\alpha\text{-}ortho)}$ = 38.1 Hz, 1F), −141.13 (m, 2F), −152.70 (m, 1F), −162.31 (m, 2F); MS (GC–MS, EI) *m/z* (rel. intensity): 260 (M^+, 9), 241 ($(M - F)^+$, 15), 229 ($(M - OMe)^+$, 90), 195 (100), 167 (15).

Hydrolysis of 9

Addition of aqueous methanol and acetic acid led to the disappearance of **9**, but the expected ester **11** was not obtained. Instead the hydrolysis led to a material that was probably *ortho* ester **10**, as indicated by the increased GC retention time and a signal consistent with $C_6F_5C(OMe)_2^+$ (*m/z* = 241, 93%) in the GC–MS. The parent ion signal for **10** was not present and the base peak was at *m/z* = 195, as it was in the MS of **11**. Sulfuric acid, added to a solution of **10** in CH_2Cl_2 gave, after work-up and purification by radial chromatography, methyl pentafluorobenzoate **11** in ca. 2% yield, from **2**. IR ($CDCl_3$, cm^{-1}): 2958, 1742, 1524, 1500, 1333, 1242, 1010, 980; ^1H NMR (500 MHz, $CDCl_3$) δ: 3.96 (s), both in excellent agreement with published data for **11** (29); ^{19}F NMR ($CDCl_3$, external ref. $CFCl_3$) δ: −160.58 (m, 2F), correlated to ^{13}C at 169.4, −148.75 (m, 1F), correlated to ^{13}C at 175.0, −138.36 (m, 2F), correlated to ^{13}C at 177.2; ^{13}C shifts obtained by means of a $^{19}F/^{13}C$ correlation experiment. MS (GC–MS, EI) *m/z*: 226 (M^+, 24), 207 ($(M - F)^+$, 5), 195 ($(M - OMe)^+$, 100), 167 (39), 117 (28).

Thermolysis of oxadiazoline 4

A solution of 2-methoxy-5,5-dimethyl-2-(2-pentafluorophenylethoxy)-Δ^3-1,3,4-oxadiazoline (0.100 g, 0.294 mmol) in benzene (20 mL) was sealed into a glass tube of 30 mL volume after degassing as described above. The tube was kept in an oil bath at 110°C for 24 h before it was cooled and opened. The solvent was removed with a rotary evaporator and the crude residue was examined immediately by means of NMR spectroscopy. The crude product consisted of **12** (ca. 13%, by ^1H NMR spectroscopy), and of compounds tentatively identified by ^1H NMR and GC–MS as the dimers (**14**) of methoxy(2-pentafluorophenylethoxy)carbene, each in ca. 20% yield. Spectra of **12** had to be gleaned from the composite spectrum of the crude, **12** being too sensitive to moisture to survive attempts at separation. The presumed carbene dimers were not separable by chromatography.

^1H NMR of **12** (500 MHz, C_6D_6) δ: 2.46 (t of d, ^2J = 1.6 Hz, ^3J = 6.4 Hz, 2H), 3.39 (s, 3H), 3.92 (t, ^3J = 6.4 Hz, 2H); ^{19}F NMR (470 MHz, C_6D_6, external ref. $CFCl_3$ δ: −71.75 (d, $^4J_{FF}$ = 5.2 Hz), −139.51 (m), −145.58 (m), −155.46 (m), −163.42 (m); MS (GC–MS, EI) *m/z* (rel. intensity): 234 ($(M-HF)^+$ 88), 223 ($(M - OMe)^+$, 33), 203 ($(M - F - MeOH)^+$, 100), 191 (77), 175 (96). MS (GC–MS, EI) *m/z* (rel. intensity): 235 ($(M - F)^+$, 100), 221 (12), 203 (75), 191 (42), 175 (32), 162 (34).

Hydrolysis of the crude with aqueous methanol (4% water by vol.) containing acetic acid (4% by vol.) gave, after extraction with dichloromethane, washing with dilute base, drying, and evaporation of the solvent, a residue that was examined by GC–MS, which suggested the presence of lactone **13**. Chromatography (Chromatotron, 1 mm plate, 5% ethyl acetate in hexanes) of the residue afforded lactone **13** as a yellowish oil in 5% yield. IR (cm^{-1}): 2300–2902, 1757, 1520; ^1H NMR (500 MHz, C_6D_6) δ: 1.77 (t, ^3J = 5.8 Hz, 2H), 3.34 (t, ^3J = 5.9 Hz, 2H); ^{13}C NMR (125 MHz, C_6D_6, ^{19}F decoupled) δ: 20.29 (correlated with ^1H triplet at 1.77), 65.45 (correlated with ^1H triplet at δ = 3.34), 123.4, 140.2, 142.7, 142.8, 143.3, 149.0, 178.6; ^{19}F NMR (470 MHz, C_6D_6, external ref. $CFCl_3$ δ: −134.3 (m, correlated to C at δ = 149.0), −144.7 (m, correlated to C at δ = 142.7), −148.5 (m, correlated to C at δ = 143.3), −156.9 (m, correlated to C at δ = 140.2); MS (EI) *m/z* (rel. intensity): 220 (M^+, 12), 190 (20), 162 (20).

Dimers **14**, E/Z mixture in ca. 1:1 ratio. ^1H NMR (200 MHz, C_6D_6) δ: 2.62 (br t, $J \cong 6.6$ Hz, $ArCH_2$, overlapping signals from both isomers), 3.21 (s, OMe), 3.28 (s, OMe), 3.68 (t, J = 6.7 Hz, OCH_2) overlapping 3.70 (t, J = 6.6 Hz, OCH_2); MS (GC–MS) *m/z*: 255 ($(M + H)^+$, 18), 195 (100).

Acknowledgements

Financial support for this work, in the form of an operating grant from The Natural Sciences and Engineering Research Council of Canada, is gratefully acknowledged. P.C. held an Ontario Graduate Scholarship and J.P.R. was the recipient of two support awards, from Human Resources Canada, for work as a summer assistant. The authors are indebted to Dr. Donald Hughes for his expert ^{13}C and ^{19}F NMR correlations on small samples of ester **11** and lactone **13**.

References

1. A.J. Arduengo III, H.V.R. Dias, R.L. Harlow, and M. Kline. J. Am. Chem. Soc. **114**, 5530 (1992).
2. C. Heinemann and W. Thiel. Chem. Phys. Lett. **217**, 11 (1994).
3. A.J. Arduengo III, J.R. Goerlich, and W.J. Marshall. J. Am. Chem. Soc. **117**, 11027 (1995).
4. D. Enders, K. Breuer, G. Raabe, J. Runsink, J.H. Teles, J.-P. Melder, K. Ebel, and S. Brode. Angew. Chem. Int. Ed. Engl. 1021 (1995).
5. C. Heinemann, T. Mueller, Y. Apeloig, and H. Schwarz. J. Am. Chem. Soc. **118**, 2023 (1996).
6. G. Raabe, K. Breuer, D. Enders, and J.H. Teles. Z. Naturforsch. A: Phys. Sci. **51a**, 95 (1996).
7. R.A. Moss, M. Wlostowski, S. Shen, K. Krogh-Jespersen, and A. Matro. J. Am. Chem. Soc. **110**, 4443 (1988).

© 1997 NRC Canada

8. R.A. Moss, C.M. Young, L.A. Perez, and K. Krogh-Jespersen. J. Am. Chem. Soc. **103**, 2413 (1981).
9. R.W. Hoffmann, W. Lilienblum, and B. Dittrich. Chem. Ber. **107**, 3395 (1974).
10. J.H. Teles, J.-P. Melder, K. Ebel, R. Schneider, E. Gehrer, W. Harder, S. Brode, D. Enders, K. Breuer, and G. Raabe. Helv. Chim. Acta, **79**, 61 (1996).
11. R.A. Moss. Acc. Chem. Res. **13**, 58 (1980).
12. D. Enders, K. Breuer, J. Runsink, and J.H. Teles. Liebigs Ann. Chem. 2019 (1996).
13. R.W. Hoffmann, K. Steinbach, and B. Dittrich. Chem. Ber. **106**, 2174 (1973).
14. A. Kümmell and G. Seitz. Tetrahedron Lett. **32**, 2743 (1991).
15. C. Gerninghaus, A. Kümmell, and G. Seitz. Chem. Ber. **126**, 733 (1993).
16. G. Frenzen, A. Kümmell, C. Meyer-Dulheuer, and G. Seitz. Chem. Ber. **127**, 1803 (1994).
17. D.L. Pole and J. Warkentin. Liebigs Ann. Chem. 1907 (1995).
18. A.J. Arduengo III, M. Kline, J.C. Calabrese, and F. Davidson. J. Am. Chem. Soc. **113**, 9704 (1991).
19. M. El-Saidi, K. Kassam, D.L. Pole, T. Tadey, and J. Warkentin. J. Am. Chem. Soc. **114**, 8751 (1992).
20. L. Isaacs and F. Diederich. Helv. Chim. Acta, **76**, 2454 (1993).
21. W.W. Win, M. Kao, M. Eiermann, J.J. McNamara, F. Wudl, D.L. Pole, K. Kassam, and J. Warkentin. J. Org. Chem. **59**, 5871 (1994).
22. A. de Meijere, S.I. Kozhushkov, D.S. Yufit, R. Boese, T. Haumann, D.L. Pole, P. K. Sharma, and J. Warkentin. Liebigs Ann. Chem. 601 (1996).
23. J.D. Colomvakos, I. Egle, J. Ma, D.L. Pole, T.T. Tidwell, and J. Warkentin. J. Org. Chem. **61**, 9522 (1996).
24. K. Kassam, D.L. Pole, M. El-Saidi, and J. Warkentin. J. Am. Chem. Soc. **116**, 1161 (1994).
25. K. Kassam and J. Warkentin. J. Org. Chem. **59**, 5071 (1994).
26. D.L. Pole, P.K. Sharma, and J. Warkentin. Can. J. Chem. **74**, 1335 (1996).
27. R.J. Kostelnik, M.P. Williamson, D.E. Wisnowsky, and S.M. Castellano. Can. J. Chem. **47**, 3313 (1969).
28. C.W. Haigh, J. Hilton, L.J. Sutcliffe, and J.T. Tiddy. J. Magn. Reson. **18**, 241 (1975).
29. J.F.W. Keana and S.X.J. Cai. J. Org. Chem. **55**, 3640 (1990).
30. (*a*) E. Buncel, M.R. Crampton, M.J. Strauss, and F. Terrier. Studies in organic chemistry. Vol. 14. Electron deficient aromatic– and heteroaromatic–base interactions: the chemistry of anionic sigma complexes. Elsevier, Amsterdam. p. 14; 1984; (*b*) E. Buncel, J.M. Dust, and F. Terrier. Chem Rev. (Washington, D.C.) **95**, 2261 (1995).
31. J.W. Barton, A.J. Bolton, P.M. Collins, R.S. Edmundson, F.D. Gunstone, P.C.B. Paige, and S.B. Walker. (*Editors*). Dictionary of organic compounds. Vol. 3. 6th ed. Chapman and Hall, London. 1996. p. 2770.

Can. J. Chem. Downloaded from www.nrcresearchpress.com by 91.121.58.235 on 09/08/12
For personal use only.

© 1997 NRC Canada

Preparation of symmetric dibromides of 1,10-phenanthroline

Yutaka Saitoh, Take-aki Koizumi, Kohtaro Osakada, and Takakazu Yamamoto

Abstract: Bromation of 1,10-phenanthroline with Br_2 proceeds smoothly in the presence of S_2Cl_2 and pyridine to give 3,8-dibromo-1,10-phenanthroline in good yield. Bromation of 2,9-dibutoxy-1,10-phenanthroline with Br_2 in an aqueous medium gives 5,6-dibromo-2,9-dibutoxy-1,10-phenanthroline selectively. Similar bromination of 4,7-dibutoxy-1,10-phenanthroline with Br_2 gives 3,8-dibromo-4,7-dibutoxy-1,10-phenanthroline, which forms a 1:1 adduct with $Cu(NO_3)_2$. Molecular structure of the 1: 1 adduct has been determined by X-ray crystallography.

Key words : bromination, 1,10-phenanthroline, 3,8-dibromo-1,10-phenanthroline.

Résumé : La bromation de la 1,10-phénanthroline par le Br_2 se produit facilement en présence de S_2Cl_2 et de pyridine et elle conduit à la 3,8-dibromo-1,10-phénanthroline avec un bon rendement. La bromation de la 2,9-dibutoxy-1,10-phénanthroline par le Br_2 en milieu aqueux conduit sélectivement à la 5,6-dibromo-2,9-dibutoxy-1,10-phénanthroline. Une bromation semblable de la 4,7-dibutoxy-1,10-phénanthroline avec du Br_2 donne de la 3,8-dibromo-4,7-dibutoxy-1,10-phénanthroline qui forme un adduit 1 : 1 avec le $Cu(NO_3)_2$. La structure moléculaire de l'adduit 1 : 1 a été déterminée par diffraction des rayons X.

Mots clés : bromation, 1,10-phénanthroline, 3,8-dibromo-1,10-phénanthroline.

[Traduit par la rédaction]

1. Introduction

Aryl halides are important starting materials, and numerous methods have been developed for direct halogenation of aromatic compounds with halogen X_2. However, among the aromatic compounds, those containing electron-withdrawing imine nitrogen (C═N-) have a π-deficient nature (1), and their electrophilic substitution with X_2 usually requires very severe reaction conditions. For example, effective bromination of pyridine with Br_2 was achieved in fuming sulfuric acid (1, 2).

1,10-Phenanthroline (Phen) is a typical π-deficient aromatic compound, and its direct and selective halogenation has not been explored. Dénes and Chira (3) reported direct bromination of Phen in thionyl chloride; however, selectivity of the bromination as well as yields of the products was low. Recently, Tor, Siegel and co-workers (4) reported direct bromination of Phen by modifying its reactivity by forming an HCl salt and carrying out the reaction in heated nitrobenzene; however, the selectivity and yields of two products, 33% for 3-bromo-1,10-phenanthroline and 17% for 3,8-dibromo-1,10-phenanthroline, were low. Although Yamada et al. (5) reported chlorination of Phen by PCl_5 through unique methods, they have not reported its direct bromination. On this basis, we have investigated conditions for the direct bromination of Phen and its derivatives, and herein report the results.

Received January 7, 1997.

Y. Saitoh, T.-a. Koizumi, K. Osakada, and T. Yamamoto.[1]
Research Laboratory of Resources Utilization, Tokyo Institute of Technology, 4259 Nagatsuta, Midori-ku, Yokohama 226, Japan.

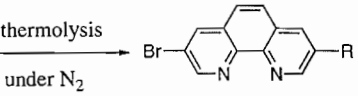
[1] Author to whom correspondence may be addressed. Fax: 011-81-45-924-5276. E-mail: tyamamot@res.titech.ac.jp

New applications for Phen and its derivatives, including their transition metal coordination compounds, have recently been developed (*i*) to form supramolecules (6), (*ii*) to make photochemically and electrochemically active molecules (7, 8), and (*iii*) to selectively cleave DNA (9). In these new areas symmetrically substituted Phens have mainly been used, and consequently symmetrically dibrominated Phens are considered to be particularly important. On this basis, the present research is focussed on the preparation of symmetrically dibrominated Phens.

2. Results and discussion

Bromination of Phen

We initially tried bromination of Phen with Br_2 in $CHCl_3$ without additives, and found that the reaction gave (55%) a yellow precipitate with the approximate composition of Phen·Br_2. Eisch (10) reported that a reaction of quinoline and Br_2 gave a similar 1:1 adduct and its thermolysis gave 3-bromoquinoline; however, thermolysis of Phen·Br_2 at 190°C and 260°C gave no signs of C-bromination. Thermolysis of the adduct in the presence of excess Br_2 gave 3-bromo-1,10-phenanthroline (**1a**) and 3,8-dibromo-1,10-phenanthroline (**1b**) in 15 and 5% yields, respectively, as estimated from an NMR spectrum of the crude product.

[1] [Phen • Br_2] + Br_2 —(thermolysis; under N_2)→ 

1a (R = H; 15%)
1b (R = Br; 5%)

In contrast to the poor yield of **1b** in the simple bromination system, addition of sulfur chloride S_2Cl_2 (11) and pyridine to

© 1997 NRC Canada

Can. J. Chem. Downloaded from www.nrcresearchpress.com by 91.121.58.235 on 09/08/12
For personal use only.

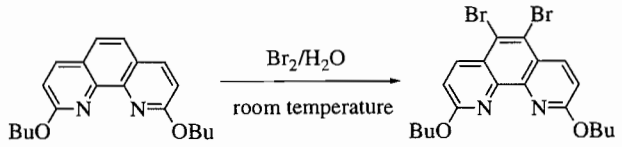
the reaction mixture leads to increased yields (crude = 63%, isolated = 34%) of **1b**.

[2] $\text{Phen} + Br_2 \xrightarrow[\text{1-chlorobutane,reflux}]{S_2Cl_2 + \text{pyridine}} \text{1b}$

The reaction proceeds smoothly in various chlorinated hydrocarbons such as $CHCl_3$, $CHCl_2CHCl_2$, and 1-chlorobutane. Without addition of pyridine, the yield of **1b** was negligible (3%). Garcia et al. (12) reported bromination of pyridine and quinoline under similar reaction conditions and proposed a pyridinium salt-type intermediate. Since Phen also forms pyridinium-type salts with alkyl halides (13), intermediacy of a similar Phen salt-type compound[2] in the present bromination is conceivable. **1b** thus prepared can be isolated by recrystallization from $CHCl_2CHCl_2$ or by complex formation with Br_2 (cf. Experimental). Although **1b** is considered to be an important starting material for liquid crystalline compounds, macrocyles, and π-conjugated polymers, its preparation in good yield was difficult.

Bromination of dibutoxy-1,10-phenanthroline

When Phen has an electron-donating O-substituent, electrophilic substitution with Br_2 takes place without addition of special reagents such as S_2Cl_2. Similar activation of pyridine by an electron-donating amino group has been reported in halogenation (14). Thus, the direct bromination of 2,9-dibutoxy-1,10-phenanthroline, **2a**, proceeds at room temperature.

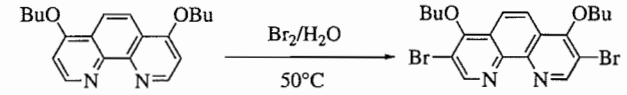
[3] 

2a **3a** 89%

However, direct bromination requires the use of a mixture of Br_2 and H_2O, and attempts to carry out similar bromination in organic solvents (benzene, THF, and $CHCl_3$) were unsuccessful. Although the direct bromination of **2a** proceeds without addition of H_2O, the yield of **3a** is considerably lower. H_2O will trap evolved HBr, which may cleave the C—OBu bonds in **2a** and the product, and this may be the rationale for the necessity of added H_2O. An AMI Hamiltonian calculation (15) indicates that the 3,8-carbon atoms of **2a** have the highest, and those in the 5,6 positions have a somewhat lower, electron population. Steric repulsion from the butoxy group and the relatively small difference in the electron population between the 3,8 and 5,6 positions seem to lead to the preferential bromination of the latter.

Similar direct bromination of 4,7-dibutoxy-1.10-phenanthroline, **2b**, is also possible; however, it requires somewhat higher temperature, and yield of the product is moderate.

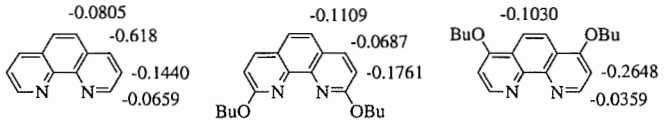
[2] Formation of salt-type compounds is considered to be enhanced by the added pyridine (12).

[4] 

2b **3b** 20%

The bromination positions agree with the results of the AMI Hamiltonian calculation (Chart 1).

Chart 1. Electron population of Phen and its dibutoxy derivatives calculated by an AMI Hamiltonian calculation. Effective charge is shown.



Phen **2a** **2b**

Cu(II) complex of 3b

Assignment of the brominated position of **3a** and **3b** is mainly based on NMR data of the products. To confirm the bromination position, we tried to obtain a crystal suited to X-ray crystallography; however, the attempts were not successful. On the other hand, reaction of **3b** with $Cu(NO_3)_2$ gives a crystal suitable for X-ray crystallography, and Fig. 1 depicts the molecular structure of the 1:1 adduct of **3b** and $Cu(NO_3)_2$.

[5] $3b + Cu(NO_3)_2 \xrightarrow{C_2H_5OH} \underset{4}{\text{1:1 adduct}}$

Table 1 summarizes selected bond distances and angles of complex **4**. As shown in Fig. 1 and Table 1, complex **4** has a square planar coordination mode around the central Cu(II), and its molecular structure confirms the structure of **3b**; thus, unequivocal assignments of the ^1H NMR signals of **3b** and **2b** become possible.

3. Experimental

Materials

Phen, S_2Cl_2, and Br_2 were purchased from Tokyo Chemical Industry Co., Ltd. **2a** and **2b** were prepared according to the literature (16).

Preparation of 1b

A stirred 1-chlorobutane solution (200 cm^3) containing Phen (5 g, 27.8 mmol), S_2Cl_2 (12.3 g, 91.1) mmol), pyridine (7.10 g, 89.8 mmol), and Br_2 (14 g, 87.6 mmol) was refluxed for 12 h. After cooling to 25°C, the solid formed was separated, and an aqueous solution of NaOH (excess) and $CHCl_3$ (ca. 100 cm^3) was added to the solid. The $CHCl_3$ solution was separated and chromatographed through a short SiO_2 column and then dried to obtain crude **1b** (5.9 g, 63% yield). The IR spectrum of crude **1b** is almost identical to that of pure **1b**. Recrystallization from $CHCl_2CHCl_2$ (25 cm^3) gave analytically pure **1b** (yield 34%). Anal. calcd. for $C_{12}H_6N_2Br_2$: C 42.6, H 1.8, N 8.3, Br 47.3%; found: C 42.7, H 1.8, N 8.4, Br 47.0%. IR(KBr, cm^{-1}): 3024, 1583, 1475, 1411, 1204, 1101, 906, 892, 776,

© 1997 NRC Canada

Can. J. Chem. Downloaded from www.nrcresearchpress.com by 91.121.58.235 on 09/08/12
For personal use only.

Can. J. Chem. Downloaded from www.nrcresearchpress.com by 91.121.58.235 on 09/08/12
For personal use only.

Fig. 1. ORTEP drawing of complex **4** at 50% ellipsoidal level.

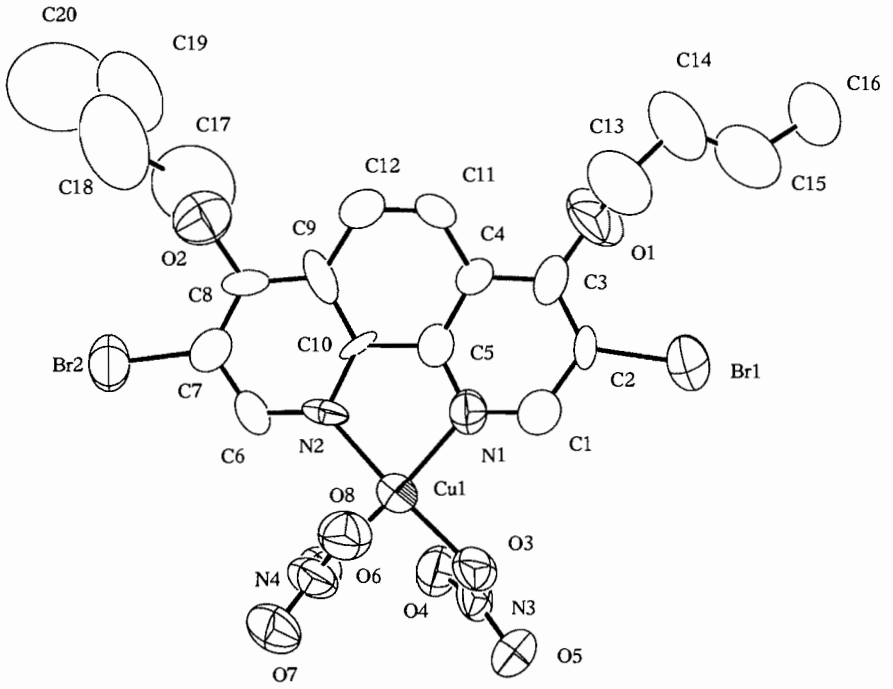


Table 1. Selected bond distances (Å) and angles (deg) of complex **4**.

Bond	Distance	Bonds	Angle
Cul—N1	1.97 (1)	N1-Cul-N2	83.0 (7)
Cul—N2	1.98 (1)	O3-Cul-O6	91.1 (5)
Cul—O3	1.98 (1)	O3-Cul-N1	92.8 (7)
Cul—O6	1.97 (1)	O6-Cul-N2	93.4 (6)
N1—C1	1.30 (2)	O6-Cul-N1	173.5 (7)
N2—C6	1.34 (2)	O3-Cul-N2	174.6 (6)
C2—Br1	1.87 (2)	Cu1-N1-C5	112 (1)
C7—Br2	1.87 (2)	Cu1-N2-C10	115 (1)
C11—C12	1.35 (2)	Cu1-N1-C1	130 (1)
C3—O1	1.41 (3)	Cu1-N2-C6	131 (1)
C8—O2	1.42 (2)	C1-C2-Br1	116 (1)
		C6-C7-Br2	116 (1)

Table 2. Crystal data and data collection conditions of complex **4**.

Formula	$C_{20}H_{22}Br_2CuN_4O_8$
mw	669.77
Crystal size (mm^3)	0.045
Crystal system	Triclinic
Space group	*P*1 (no. 2)
a (Å)	13.655 (6)
b (Å)	16.508 (8)
c (Å)	12.342 (4)
α (deg)	96.71 (4)
β (deg)	102.69 (4)
γ (deg)	67.12 (4)
V ($Å^3$)	2498
Z	
λ (Å)	0.710 69
d_{calcd} ($g\ cm^{-1}$)	1.78
μ (cm^{-1})	41.3
F (000)	1332
R	0.045
R_w[a]	0.032
No. of variables	631
No. of measured reflections	4816
No. of reflections used ($I > 3\sigma(I)$)	1915

[a] $w = [\sigma(F_o)]^{-2}$.

720; ^{1}H NMR ($CDCl_3$) δ: 7.73 (s, 2H), 8.39 (d, J = 2.2 Hz, 2H) 9.17 (d, J = 2.2 Hz, 2H).

Addition of Br_2 (3.0 g, 19 mmol) to the above $CHCl_3$ (60 cm^3) solution after elution through the short SiO_2 column led to formation of an orange precipitate, which was collected by filtration. The solid was treated with aqueous NaOH (ca. 50 mmol) solution, and extracted with $CHCl_3$ (ca. 50 cm^3). The extracted solution was condensed and eluted through an SiO_2 column (eluent, $CHCl_3$). The $CHCl_3$ solution was evaporated and recrystallized from benzene to yield **1b** (yield 23%).

Preparation of 3a

2a (1.0 g, 3.1 mmol) was added to a mixture of 5 cm^3 of Br_2 and 10 cm^3 of H_2O. The reaction mixture was vigorously stirred at 25°C for 10 h. After addition of an aqueous solution of $Na_2S_2O_4$ (excess), the product was extracted with $CHCl_3$ (ca. 10 cm^3), and the $CHCl_3$ extract was washed with H_2O and dried. The solid was recrystallized from EtOH twice. Yield 89% (1.36 g, 2.8 mmol); mp 109–110°C. ^{1}H NMR ($CDCl_3$) δ: 8.53 (d, J = 9.0 Hz, 2H), 7.08 (d, J = 9.0 Hz, 2H), 4.70 (t, J = 6.6 Hz, 4H), 1.4–2.0 (m, 8H), 1.02 (t, 6H). Anal. calcd. for

© 1997 NRC Canada

$C_{20}H_{22}Br_2N_2O_2$: C 49.8, H 4.6, N 5.8, Br 33.1; found: C 49.5, H 4.5, N 5.9, Br 32.8.

Preparation of 3b

To a mixture of 12 cm^3 of Br_2 and 100 cm^3 of H_2O was added **2b** (2.0 g, 6.2 mmol). The reaction mixture was vigorously stirred at 50°C for 10 h. After cooling to 25°C, an aqueous solution of NaOH (excess) and $Na_2S_2O_4$ (excess) was added. The product was extracted with $CHCl_3$ (ca. 30 cm^3), and the $CHCl_3$ extract was washed with H_2O and dried. The solid was dissolved in toluene–dioxane (in a 4:1 v/v ratio), and the solution was passed through an Al_2O_3 column, dried, and after concentration in vacuo the residue was recrystallized from MeOH. Yield 20.2%; mp 110–112°C. ^1H NMR ($CDCl_3$) δ: 9.14 (s, 2H, 2,9-phen H), 8.13 (s, 2H, 5,6-phen H), 4.30 (t, J = 6.7 Hz, 4H, -OCH_2-), 2.2–1.4 (m, 8H, CH_2), 1.30 (t, 6H, CH_3). Anal. calcd. for $C_{20}H_{22}Br_2N_2O_2$: C 49.8, H 4.6, N 5.8, Br 33.1; found: C 49.6, H 4.4, N 5.8, Br 33.2.

Preparation of complex 4 for X-ray crystallography

A hot ethanol (1.0 cm^3) solution of **3b** (10 mg, 2.1×10^{-5} mol) and a hot ethanol (1.0 cm^3) solution of $Cu(NO_3)_2 \cdot 6H_2O$ (5 mg, 1.7×10^{-5} mol) were combined and allowed to stand at 25°C. Blue-green plates of **4** were obtained in 95% yield.

Measurements

IR spectra were measured on a JASCO 810 spectrophotometer. ^1H NMR spectra were recorded on JEOL FX-100 and EX-400 spectrometers. Elemental analyses were carried out by a Yanagimoto type MT-2 CHN autocorder.

Crystal structure determination of complex 4

Crystallographic data and the results of structure refinement are summarized in Table 2. The unit-cell parameters were obtained by least-squares refinement of 2θ values of 25 reflections with $25° \leq 2\theta \leq 35°$. Intensities were collected on a Rigaku AFC-5R automated four-circle diffractometer by using Mo Kα radiation (γ = 0.710 69 Å) and the ω–2θ method. Calculations were carried out by using the program package TEXSAN on a DEC Micro VAXII computer.

Of the 5145 collected reflections for complex **4**, 4816 were unique (R_{int} = 0.055). No decay correction was applied. An empirical absorption correction based on azimuthal scans of several reflections was applied, which resulted in transmission factors ranging from 0.59 to 1.00. The data were corrected for Lorentz and polarization effects. The structure was solved by heavy-atom Patterson methods and expanded using Fourier techniques.

Tables of atomic coordinates, anisotropic displacement parameters, and bond lengths and angles are available as supplementary material.[3]

[3] The complete set of tables can be purchased from: The Depository of Unpublished Data, Document Delivery, CISTI, National Research Council Canada, Ottawa, Canada K1A 0S2. The tables of atomic coordinates and of bond lengths and angles have also been deposited with the Cambridge Crystallographic Data Centre, and can be obtained on request from The Director, Cambridge Crystallographic Data Centre, University Chemical Laboratory, 12 Union Road, Cambridge, CB2 1EZ, U.K.

Acknowledgement

We are grateful to Mr. Imase of our university for his assistance in the AMl Hamiltonian calculation. This work has been partly supported by CREST (Core Research for Evolution Science and Technology) of the Japan Science and Technology Corporation (JST).

References

1. G.R. Newkome and W.W. Paudler. Contemporary heterocyclic chemistry. John Wiley, New York. 1982.
2. (*a*) R.T. Brown. Comprehensive organic chemistry. Vol. 4. *Edited by* D. Barton and W.D. Ollis. Pergamon, Oxford. 1979; (*b*) H.J. den Hertog, L. van der Does, and C.A. Landhere. Recl. Trav. Chim. Pays-Bas, **81**, 864 (1962).
3. V. Dénes and R. Chira. J. Prakt. Chem. **320**, 172 (1978).
4. D. Tzalis, Y. Tor, S. Failla, and J.S. Siegel. Tetrahedron Lett. **36**, 3489 (1995).
5. (*a*) M. Yamada, Y. Nakamura, S. Kuroda, and I. Shimao. Bull. Chem. Soc. Jpn. **63**, 2710 (1990); (*b*) M. Yamada, Y. Nakamura, T. Hasegawa, A. Itoh, S. Kuroda, and I. Shimao. Bull. Chem. Soc. Jpn. **65**, 2007 (1992).
6. (*a*) A. Livoreil. C.O. Dietrich-Buchecker, and J.-P. Sauvage. J. Am. Chem. Soc. **116**, 9399 (1994); (*b*) O.B. Amabiliano, C.O. Dietrich-Buckecker, A. Livoreil, L. Pérez-Garci, J.-P. Sauvage, and F. Stoddart. J. Am. Chem. Soc. **118**, 3905 (1996); (*c*) S.-S. Chern, G.-H. Lee, and S.-M. Peng. J. Chem. Soc. Chem. Commun. 1645 (1994).
7. (*a*) E. Kimura, W. Bu, M. Shionoya, S. Wada, and S. Maruyama. J. Am. Chem. Soc. **31**, 4542 (1992); (*b*) X. Xu, K. Shreder, B.L. Iverson, and A.J. Bard. J. Am. Chem. Soc. **118**, 3656 (1996); (*c*) S.D. Cumming and R. Eisenberg. J. Am. Chem. Soc. **118**, 1949 (1996); (*d*) H. Sugihara, J.-P. Collin, and K. Hiratani. Chem. Lett. 397 (1994); (*e*) T. Tsutsui, N. Takada, S. Saito, and E. Ogino. Appl. Phys. Lett. **65**, 1868 (1994); (*f*) Y. Lei and F.C. Anson. Inorg. Chem. **33**, 5003 (1994); (*g*) D. Tzalis and Y. Tor. Tetrahedron Lett. **36**, 6017 (1995).
8. (*a*) Y. Saitoh and T. Yamamoto. Chem. Lett. 785 (1995); (*b*) T. Yamamoto. J. Synth. Org. Chem. Jpn. **53**, 999 (1995); (*c*) H. Inaba, K. Kawase, M. Kitagawa, and N. Oyama. Denki Kagaku, **62**, 476 (1994).
9. (*a*) G. Pratviel, J. Bernadou, and B. Meunier. Angew. Chem. Int. Ed. Engl. **34**, 746 (1995); (*b*) L.E. Marshall, D.R. Graham, K.A. Riech, and D.S. Sigman. Biochemistry, **20**, 244 (1981).
10. J.J. Eisch. J. Org. Chem. **27**, 1318 (1962).
11. (*a*) B. Beagley, G.H. Eckersley, D.P. Brown, and D. Tomlinson. Trans. Farady Soc. **65**, 2300 (1969); (*b*) R. Knip, L. Korte, and d. Mootz. Z. Naturforsch. B: Anorg. Chem. Org. Chem. **38B**, 1 (1983); (*c*) G. Lewandowicz, and A. Zuk. Chem. Stosow. **31**, 319 (1987).
12. E.E. Garcia, C.V. Greco, and I.M. Hunsberger. J. Am. Chem. Soc. **82**, 4430 (1960).
13. K. Jackson, J.H. Ridd, and M.L. Tobe. J. Chem. Soc. Perkin Trans. 2, 607 (1979).
14. O.V. Schickh, A. Binz, and A. Schulz. Chem. Ber. **69B**, 2593 (1936).
15. M.J.S. Dewer, E.G. Zoebisch, E.F. Healy, and J.J.P. Stewart. J. Am. Chem. Soc. **107**, 3902 (1985).
16. S. Ogawa and M. Iwamoto. Jpn. Kokai Tokkyo Koho JP 04-01, 194 [02-01, 194] (1992).

Can. J. Chem. Downloaded from www.nrcresearchpress.com by 91.121.58.235 on 09/08/12
For personal use only.

© 1997 NRC Canada

Naphthalene-based poly(aryl ether)s. I. Synthesis and characterization of poly(ether sulfone)s and poly(ether ketone)s containing one 1,4-naphthylene moiety in the repeat unit

Judy E. Douglas and Zhi Yuan Wang

Can. J. Chem. Downloaded from www.nrcresearchpress.com by 91.121.58.235 on 09/08/12
For personal use only.

Abstract: The effect of insertion of one 1,4-naphthylene unit into several PEEK-like and Udel®-like commercial polymers is examined. Two series of poly(ether ketone)s and poly(ether sulfone)s were made from the polycondensations of 1-chloro-4-(4-fluorobenzoyl)naphthalene and 1-chloro-4-(4-fluorobenzenesulfonyl)naphthalene with phenolphthalein (PP), 2,2′,6,6′-tetramethyl-4,4′-biphenol (TMBP), and 4,4′-biphenol (BP). Each polymer was soluble in chloroform, from which dense films could be cast. Glass transition temperatures increased 14-19°C with TMBP, 30–43°C with BP, and 39–60°C in the case of PP. The 1,4-naphthylene insertion reduced the crystallinity of the biphenol-based polymers. The onset temperatures for 5% weight loss ranged from 390 to 536°C in nitrogen, as assessed by thermogravimetry. Young's moduli varied from 0.54 to 2.1 GPa. In the case of the poly(ether ketone) containing TMBP, incorporation of the 1,4-naphthylene moiety increased gas permselectivity at the cost of decreased permeability, whereas there seemed only to be a decrease in permeability with its poly(ether ketone) counterpart.

Key words: naphthalene, poly(ether sulfone)s, poly(ether ketone)s, glass transition temperature, gas permeability.

Résumé : On étudie l'effet de l'insertion d'une unité 1,4-naphtylène dans plusieurs polymères commerciaux tels le PEEK et le Udel. On a préparé deux séries de poly(éther cétone) et poly(éther sulfone) par polycondensation du 1-chloro-4-(4-fluorobenzoyl)naphtalène et du 1-chloro-4-(4-fluorobenzènesulfonyl)naphtalène avec la phénolphtaléine (PP), avec le 2,2′,6,6′-tétraméthyl-4,4′-biphénol (TMBP) et avec le 4,4′-biphénol (BP). Chaque polymère solubilisé dans le chloroforme permet d'obtenir des films denses que l'on peut mouler. Les températures de transition du verre augmentent de 14 à 19°C avec le TMBP, de 30 à 43°C avec le BP et de 39 à 60°C dans le cas du PP. L'insertion du 1,4-naphtylène réduit la cristallinité des polymères à base de biphénol. Faisant appel à la thermogravimétrie on a déterminé que les températures, à partir desquelles on observe un perte de 5% en poids, varient de 390 à 536°C dans l'azote. Le module de Young varie de 0,54 à 2,1 GPa. Dans le cas du poly(éther cétone) contenant du TMBP, l'insertion d'une unité 1,4-naphtylène augmente la perméation sélectivite des gaz au détriment de la perméabilité, tandis que dans le cas de son homologue poly(éther cétone) on ne semble observer qu'une diminution de la perméabilité.

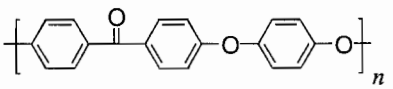
Mots clés : naphtalène, poly(éther sulfone), poly(éther cétone), température de transition du verre, perméabilité gazeuse.

[Traduit par la rédaction]

Introduction

Poly(aryl ether ketone)s (PAEK) and poly(aryl ether sulfone)s (PAES) represent two classes of engineering thermoplastics that exhibit superior mechanical and thermal properties (1, 2). Both display excellent electrical insulating properties, good flame, hydrolytic, and solvent resistance, and can be found in a variety of forms such as molded parts, films, fibers, and coatings (3). Applications of these two plastics include (*i*) coatings for high-performance wiring in aeronautics, (*ii*) advanced structural composites, (*iii*) household molded products, (*iv*) car engine parts, and (*v*) sterilizable medical equipment (3, 4). ICI's PEEK (Fig. 1) has received much commercial success due to its high operating temperature and superior strength (1). PEEK has a glass transition temperature (T_g) of 143°C and a melting point (T_m) of 334°C. The 4,4′-biphenol-based poly(ether ketone) (**3c**, Fig. 2) is crystalline (T_g = 167°C, T_m = 416°C) and solvent resistant, and the 'sulfone analogue (**1c**, Union Carbide's Radel®, Fig. 2) is also quite solvent resistant (3).

Fig. 1. Poly(ether ether ketone) (PEEK).



PEEK

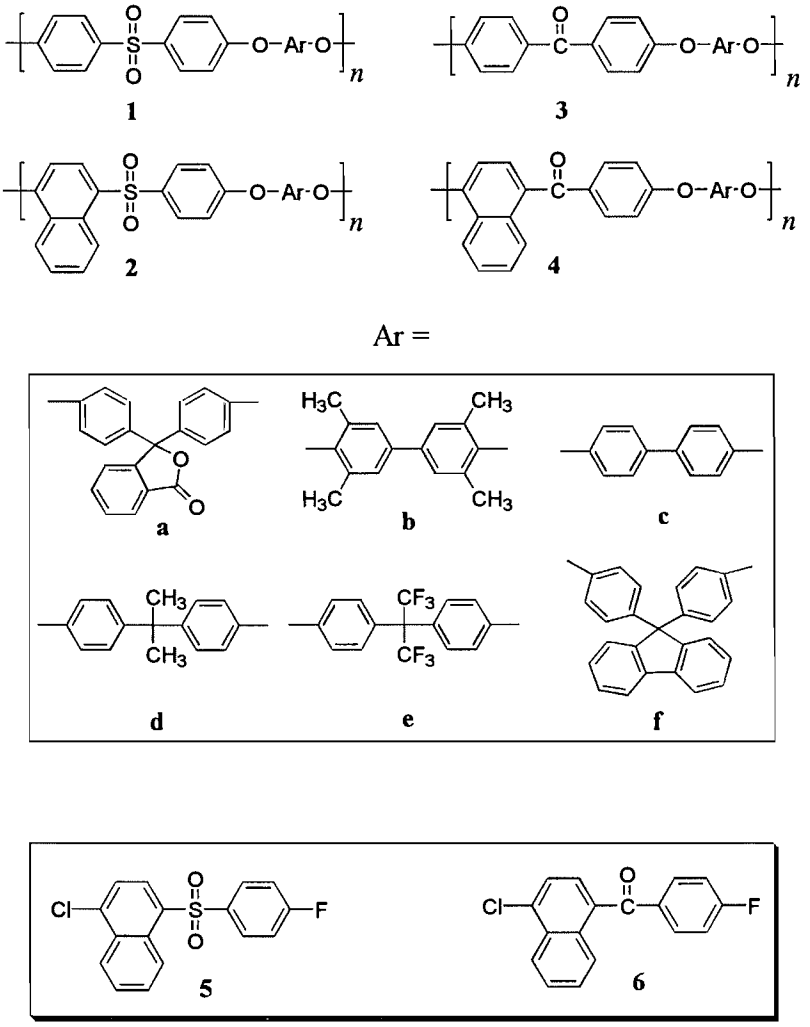
Received April 23, 1997.

J.E. Douglas and Z.Y. Wang.[1] Ottawa–Carleton Chemistry Institute, Department of Chemistry, Carleton University, 1125 Colonel By Drive, Ottawa, ON K1S 5B6, Canada.

[1] Author to whom correspondence may be addressed. Telephone: (613) 520-2600, ext. 2713. Fax (613) 520-3749. E-mail: wangw@ccs.carleton.ca

© 1997 NRC Canada

Fig. 2. Phenylene- and naphthylene-containing poly(ether sulfone)s (**1**, **2**) and poly(ether ketone)s (**3**, **4**) and dihalo monomers (**5**, **6**).



Can. J. Chem. Downloaded from www.nrcresearchpress.com by 91.121.58.235 on 09/08/12
For personal use only.

More recently, there has been much effort in studying structure–property relationships of poly(aryl ether)s for the use of gas separation (5, 6). Polysulfones generally exhibit higher gas permeabilities than their ketone equivalents. Union Carbide's Udel® (**1d**, Fig. 2), a polysulfone that contains bisphenol A (BPA) in the repeat unit, has been successfully commercialized as a gas membrane (6). For a polymer to be successful as a gas membrane, it must combine both high permeability and high selectivity (7). Generally speaking, the structural changes that lead to increased gas permeability also cause loss in selectivity. Thus, a compromise between the two must be achieved in order to be successful. A common strategy to improve gas transport properties is to increase chain rigidity and decrease chain packing. Often this can be done by the addition of a pendant group.

There is a growing demand for new materials to meet increased performance requirements in many areas such as the one just described. Thus there has been considerable research effort made toward the modification of known poly(aryl ether)s (8) as well as the design of polymers with novel structures (9). To date, most modifications have been made to the bisphenol part, due in large part to the ease with which it can be changed.

Earlier work of ours demonstrated that the replacement of one 1,4-phenylene with one 1,4-naphthylene moiety in the repeat unit of semi-crystalline PEEK significantly reduced the crystallinity of the resulting polymer and increased the T_g by 45°C (10). Likewise, 1,4-naphthylene insertion into several poly(ether sulfone)s also increased the polymer's T_g (11). The dense membrane of the naphthylene-containing poly(ether sulfone) derived from BPA was found to improve permselectivities at the cost of lowering its permeabilities towards oxygen, nitrogen, carbon dioxide, and methane gases (11). From a polymer design standpoint, the 1,4-naphthylene insertion serves to modify the structure of poly(aryl ether) by addition of a benzo moiety perpendicular to the main chain. Therefore, it seemed worthwhile to pursue the investigation of the effects of naphthylene insertion on other poly(aryl ether)s. Two series of polymers **2a–c** and **4a–c** (Fig. 2) were synthesized in order to incorporate the 1,4-naphthalene unit into PAES and PAEK derived from bulky bisphenols for study of the gas transport property, and to see if it could

© 1997 NRC Canada

Can. J. Chem. Downloaded from www.nrcresearchpress.com by 91.121.58.235 on 09/08/12
For personal use only.

further increase the T_g and reduce the crystallinity for the biphenol-based polymers.

Results and discussion

Polymer synthesis

Polymers **2a–c** and **4a–c** were made by the polycondensation reactions of 1-chloro-4-(4-fluorobenzenesulfonyl)naphthalene, **5** (11), and 1-chloro-4-(4-fluorobenzoyl)naphthalene, **6** (10), (Fig. 2), respectively, with phenolphthalein (PP), 2,2′,6,6′-tetramethyl-4,4′-biphenol (TMBP), and 4,4′-biphenol (BP). Polymerizations were all done in $TMSO_2$ at 200°C with chlorobenzene as an azeotroping agent, using stoichiometric amounts of the dihalide and bisphenol monomer in the presence of potassium carbonate (1.8 molar equiv.). Typically, the reaction was heated from room temperature to 140–150°C within 0.5 to 1 h and the water formed during the reaction was removed as an azeotropic mixture with chlorobenzene. The polymerization temperature was then increased to 200°C and the reaction proceeded for 3 h before GPC monitoring showed a lack of increase in molecular weight, at which point the reaction was stopped. The resulting polymers were coagulated in an excess of methanol with a few drops of HCl, followed by reverse precipitation to remove any remaining oligomers.

Polymer characterization

Under these polymerization conditions, polymers **2a–c** and **4a–c** were obtained as off-white, fibrous solids. All the polymers were soluble at room temperature in chloroform, 1,1,2,2–tetrachloroethane (TCE), CH_2Cl_2, and *N*-methylpyrrolidinone (NMP), with the exception of **4b**, which was only partially soluble in CH_2Cl_2. In addition, the polymers **2a** and **4a** derived from PP were also soluble in dimethylacetamide (DMAc), tetrahydrofuran (THF), and dimethylformamide (DMF) due to the presence of the cardo group. The TMBP-based polymers **2b** and **4b** were also quite soluble in all the above mentioned solvents with the exception of DMF. The BP-based polymers **2c** and **4c** were the least soluble. The poly(ether ketone) **4c** was only partially soluble in DMAc, CH_2Cl_2, and DMF. The sulfone polymer **2c** had difficulty dissolving in THF and DMF. It is known that the biphenyl moiety promotes chain packing, as polymer **3c** is semicrystalline with a T_m of 416°C. Due to the tetrahedral sulfone unit, polymer **2c** showed higher solubility than the ketone analogue **4c**.

Gel permeation chromatography (GPC) showed moderate to high molecular weights relative to polystyrene in all cases (Table 1). The highest molecular weights were achieved using PP as a bisphenol (254 000 for **2a** and 229 000 for **4a**). The inherent viscosities supported the GPC results, with values ranging from 0.42 to 1.09 dL/g.

The structures of the polymers synthesized (**2a–c** and **4a–c**) were confirmed by spectroscopic means (NMR, IR). Evidence was found by NMR that showed the unsymmetric nature of the polymer's repeat unit due to the unsymmetry of the starting dihaloaryl monomer. Previously, the presence of three singlets was seen in the ^1H NMR spectra of BPA-based poly(ether ketone) **4d** (10*b*) and poly(ether sulfone) **2d** (11) at 1.6 and 1.8 ppm, respectively. This was attributed to the methyl groups of the bisphenol unit in three slightly different magnetic environments due to the presence of three possible diads. In the TMBP series (**2b** and **4b**), four singlets exist at ~2.1 and 2.2 ppm, respectively, in the ^1H NMR spectra (Fig. 3) and four aliphatic carbon peaks at about 16 ppm in the ^{13}C NMR spectra. This is indicative of the four different magnetic environments to which the methyl groups are exposed in the head-to-head, tail-to-tail, and head-to-tail diads (Fig. 4). In the head-to-head and tail-to-tail formations, all four methyl groups are either closer to a naphthalene or a benzene ring and are therefore in two different magnetic environments corresponding to two of the four singlets. In the head-to-tail diad, two of the methyl groups are closer to a naphthalene ring, whereas the other two are closer to a benzene ring, thereby giving rise to the presence of the remaining two proton peaks. The intensities of the two outer peaks appear the same, likewise with the smaller two inner peaks. COSY and HETCOR experiments were done and supported the peak assignments in Fig. 3.

Infrared (IR) spectra showed the conjugated ketone stretching for the ketone polymers **4a**, **4b**, and **4c** at 1654, 1652, and 1654 cm^{-1}, respectively. Polymer **4a** showed a second C=O peak at 1772 cm^{-1} due to the lactone of phenolphthalein. The IR spectra of the sulfone polymers were a little less diagnostic but generally showed S=O asymmetric and symmetric stretching at ca. 1240 cm^{-1} and 1146 cm^{-1}.

Differential scanning calorimetry (DSC) indicated that all the polymers were amorphous, thus substitution of a 1,4-phenylene unit with a 1,4-naphthylene moiety reduced the crystallinity of the biphenol-based polymer (**2c** and **4c**). Table 2 shows that in every case of 1,4-naphthylene insertion, T_g was

Table 1. Characterization of polymers **2a–c** and **4a–c**.

Polymer	M_w[a] ($\times 10^{-4}$)	M_w/M_n	η_{inh}[b] (dL/g)	T_d[c] (°C)	E'[d] (GPa)
2a	25.4	1.81	0.71	446	0.54
2b	15.6	2.02	1.09	390	0.73
2c	8.33	2.00	0.70	470	0.64
4a	22.9	1.99	0.70	481	1.20
4b	5.02	2.42	0.42	440	0.76
4c	15.4	1.82	0.56	536	2.10

[a]Molecular weights taken by GPC relative to polystyrene standards.
[b]Inherent viscosity taken of a 0.5% chloroform solution at 25°C.
[c]Onset temperature taken at 5% weight loss in nitrogen.
[d]Young's moduli taken at room temperature in static air.

Table 2. Comparison of T_g values of polymers **1–4**.

Polymer	T_g(°C) **1**	T_g(°C) **2**	ΔT_g(°C)	T_g(°C) **3**	T_g(°C) **4**	ΔT_g(°C)
a	244[a]	280	36	214[b]	253	39
b	262[c]	307	45	266[d]	280	14
c	220[e]	250	30	167[f]	210	43

[a]Data taken from ref. 3*b*, p. 5940.
[b]Data taken from ref. 2, p. 143.
[c]Data taken from ref. 5*d*.
[d]Data taken from ref. 12*a*.
[e]Data taken from ref. 3*a*.
[f]T_m = 416°C, data taken from ref. 13.

© 1997 NRC Canada

Fig. 3. ^{1}H NMR spectra of polymers **2b** and **4b**.

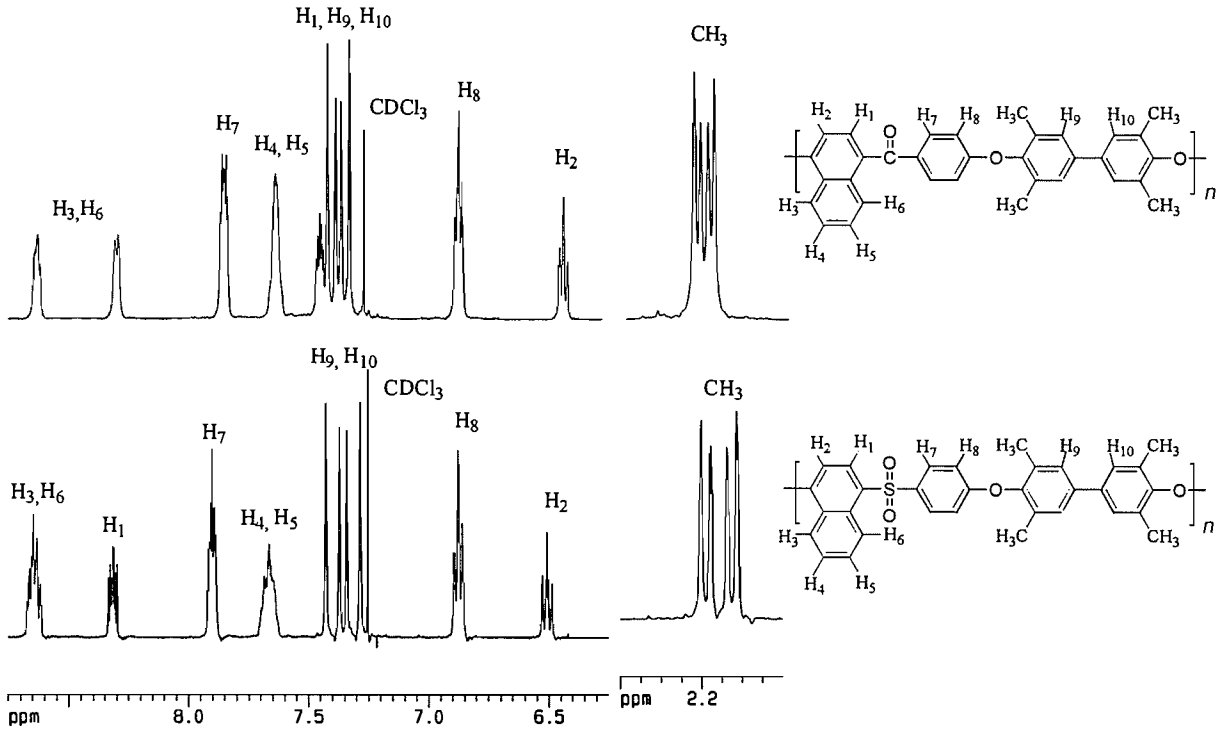


Fig. 4. Three possible diads of TMBP-based polymers.

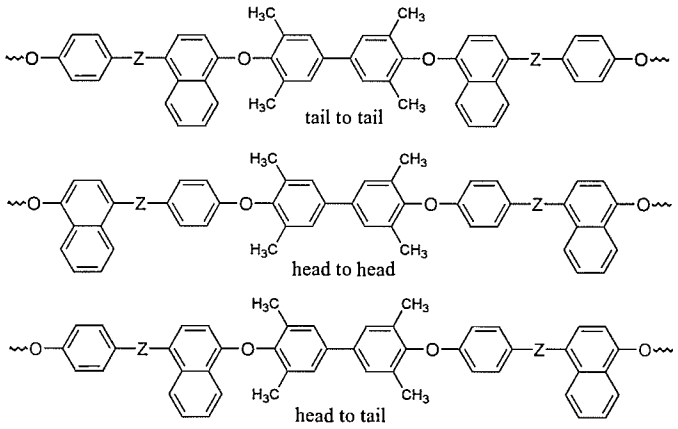


Table 3. Gas transport properties of some phenylene- and naphthylene-based polymers.

Polymer	P_{O_2} Barrer	P_{N_2} Barrer	α (O_2/N_2)	P_{CO_2} Barrer	P_{CH_4} Barrer	α (CO_2/CH_4)
1b[b]	5.80	1.21	4.8	31.8	1.27	25
2b	5.90	1.09	5.4	27.0	0.97	28
3b[c]	5.98	1.12	5.3	23.6	0.98	24
4b	4.20	0.84	5.0	19.0	0.79	24
2d[d]	1.20	0.15	8.0	4.70	0.08	59
4e[e]	1.88	0.34	5.5	7.30	0.22	33
4f[e]	1.46	0.27	5.4	6.40	0.20	32

[a]Data taken at room temperature at 10 atm (1 atm = 101.3 kPa).
[b]Data from ref. 5*d*.
[c]Data from ref. 13.
[d]Data from ref. 9.
[e]Data from ref. 12.

increased compared to its 1,4-phenylene-based equivalent. The increase in T_g was highest for **2a** and **4a** containing bulky phenolphthalein (36 and 39°C) and lowest for **2b** and **4b** with TMBP (14 and 19°C). The 4,4′-biphenol-based polymers, **2c** and **4c,** also showed significant increases in T_g (30 and 43°C). These results follow the trend found in our earlier work with other bisphenols (10, 11). The decomposition, as assessed by the onset temperature (T_d), of 5% weight loss by T_g occurred in the range of 390–536°C in nitrogen. The T_d values of the ketone series (**4a–c**) were greater than those of the sulfone counterparts (**2a–c**).

Thin rectangular strips of polymer films cast from chloroform solution were used to measure Young's modulus in the tensile stress–strain mode. The moduli varied from 0.54 to 2.1 GPa (Table 1). The Young's moduli of the ketone series were larger than their sulfone equivalents, demonstrating the superior mechanical strength of the poly(ether ketone)s.

Gas transport property

Table 3 shows the gas permeability and selectivity coefficients of the ketone and sulfone polymers (**2b**, **4b**) derived from TMBP, including the 1,4-naphthylene-based poly(ether ketone)s **4e** and **4f** and the poly(ether sulfone) **2d** for comparison. The gas permeabilities of the TMBP series (**1b**, **2b**, **3b**, **4b**) are two to five times larger than those of the polymers derived from other bisphenols (**2d**, **4e**, **4f**). This trend has been

© 1997 NRC Canada

Can. J. Chem. Downloaded from www.nrcresearchpress.com by 91.121.58.235 on 09/08/12
For personal use only.

noted elsewhere in the literature (*5d*). But an increase of permeability due to the presence of TMBP comes as the trade-off of reducing the selectivity coefficients of **2b** (5.4 for O_2/N_2 and 28 for CO_2/CH_4) and **4b** (5.0 for O_2/N_2 and 24 for CO_2/CH_4). Within the TMBP series (**1b**, **2b**, **3b**, **4b**), it was found that 1,4-naphthylene insertion marginally improves O_2/N_2 and CO_2/CH_4 selectivity coefficients, while lowering the permeabilities for most of the gases when comparing poly(ether sulfone) **1b** with **2b**. In contrast, when poly(ether ketone) **3b** is compared with **4b**, insertion of the 1,4-naphthylene moiety lowered permeabilities with no significant change to permselectivities. Thus, 1,4-naphthylene insertion in both the ketone and sulfone polymers always lowers the permeability, with the benefit of increasing permselectivity within the poly(ether sulfone) series but with little effect in the poly(ether ketone) family. The use of TMBP, compared to the other bisphenols, has enhanced gas permeability.

Conclusion

Two new series of poly(ether sulfone)s and poly(ether ketone)s containing unsymmetric benzonaphthone and phenylnaphthylsulfone moieties have been synthesized. 1,4-Naphthylene insertion into the backbones of the ketone and sulfone poly(aryl ether)s serves to reduce crystallinity and increase T_g. Addition of the 1,4-naphthylene moiety to the poly(ether sulfone) containing TMBP increases its gas permselectivity but appears to have no immediate advantage with the TMBP-based poly(ether ketone).

Experimental section

General

The ^1H and ^{13}C NMR spectra were recorded on the Bruker-400 instrument using tetramethylsilane as the internal reference. Infrared measurements were performed on a Perkin–Elmer Series 1600 FTIR instrument. Molecular weights were determined on a Perkin–Elmer LC-250 GPC instrument relative to polystyrene standards using chloroform as an eluent at a flow rate of 1.0 mL/min; a UV detector was set at 254 nm wavelength. Inherent viscosities were measured in a 0.5 g/dL chloroform solution at 25°C using an Ubbelohde dilution viscometer. The glass transition temperatures were determined by differential scanning calorimetry (DSC) on a Seiko DSC 220 at a heating rate of 10°C/min under nitrogen (50 mL/min) and taken as the midpoint in the change in slope of the baseline. Thermogravimetric analysis (TGA) was performed on a Seiko TG/DTA 220 at a heating rate of 10°C/min in nitrogen (200 mL/min). Thin films were cast from chloroform solution, dried from room temperature to 140°C in 4 days under vacuum (1 Torr (= 133.3 Pa)), and cut into rectangular strips (length = 10 mm, width = 2 mm, thickness ~0.1 mm). Young's moduli (E') were recorded using a Seiko TMA/SS 120C at 25°C in static air with the following parameters: offset = 10–30 g, load = 5–15 g, amplitude = 5–10 g, and cycling frequency = 0.05–0.2 Hz. Young's moduli were obtained from the average of the tangential slopes of the elliptical stress–strain plots.

Materials

Anhydrous potassium carbonate, phenolphthalein, 4,4′-biphenol, and chlorobenzene were purchased from Aldrich Chemical Co. and used as received. Reagent grade tetramethylene sulfone ($TMSO_2$) from Aldrich was fractionally distilled under vacuum (120°C/3 Torr). 2,2′,6,6′-Tetramethyl-4,4′-biphenol was recrystallized from methanol. The two dihalo monomers, 1–chloro-4-(4-fluorobenzenesulfonyl)-naphthalene, **5**, and 1–chloro-4-(4-fluorobenzoyl)naphthalene, **6**, were prepared as previously reported (11, 10).

Polymer synthesis

All polymerizations were carried out in a flame-dried, 50 mL, three-neck round-bottomed flask equipped with a stirring bar, a Dean–Stark trap fitted with a condenser, and a nitrogen purge inlet. The flask was charged with a bisphenol and a dihalo monomer (3.00 mmol each) and crushed anhydrous K_2CO_3 (5.4 mmol). Tetramethylene sulfone (adjusted to final concentration of 40% w/v) and an equal volume of chlorobenzene were then added. The reaction mixture was heated under nitrogen from room temperature to 200°C in 30 min. The water formed and the chlorobenzene were codistilled off. The polymerization was monitored by GPC and stopped when the molecular weight failed to increase. If the reaction mixture became too viscous to stir, it was diluted with tetramethylene sulfone (1–2 mL). The polymer was isolated by precipitation in methanol. All polymers were purified by dissolving in a large quantity of "good" solvent (~100 mL $CHCl_3$) chloroform and filtering through a pad of Celite to remove salts. Reverse precipitation was done on all the polymers to remove low molecular weight fractions. This involved adding methanol, a "bad" solvent, (~25–50 mL) to the polymer solution to give a gummy ball. After decanting the low molecular weight fractions, the gummy ball was dissolved again in a minimal amount of "good" solvent (20 mL $CHCl_3$), then reprecipitated into a large amount of methanol to give a white fibrous polymer. Molecular weights of the reprecipitated polymers were taken and are listed in Table 1.

Polymer **2a**: IR (film, cm^{-1}): 1771 (C═O), 1243 (S═O), 1146 (S═O); ^1H NMR (400 MHz, $CDCl_3$) δ: 8.59–8.67 (d, 1H), 8.30–8.40 (m, 2H), 7.90–8.10 (m, 1H), 7.85–7.90 (d, 2H), 7.67–7.79 (m, 1H), 7.50–7.67 (m, 4H), 7.28–7.98 (m, 4H), 7.05–7.15 (t, 2H), 6.90–7.03 (m, 4H), 6.78–6.85 (m, 1H); ^{13}C NMR (100 MHz, $CDCl_3$) δ: 169.3, 161.0, 158.7, 155.7, 155.5, 151.6, 137.4, 137.1, 136.2, 134.5, 131.0, 130.2, 130.1, 129.8, 129.7, 129.2, 129.1, 129.0, 126.9, 126.6, 126.3, 125.5, 124.4, 124.0, 122.9, 120.3, 120.0, 118.1.

Polymer **2b**: IR (film, cm^{-1}): 1235 (S═O), 1146 (S═O); ^1H NMR (400 MHz, $CDCl_3$) δ: 8.60–8.70 (m, 2H); 8.28–8.35 (m, 1H), 7.85–7.95 (m, 2H), 7.60–7.72 (m, 2H), 7.25–7.45 (d of d, 4H), 6.82–6.91 (t, 2H), 6.48–6.55 (t, 1H), 2.10–2.22 (4s, 12) ; ^{13}C NMR (100 MHz, $CDCl_3$) δ: 161.4, 158.3, 150.0, 150.1, 149.9, 149.8, 138.2, 138.0, 135.0, 131.4, 131.3, 130.3, 129.8, 128.9, 128.1, 128.0, 127.9, 129.8, 126.7, 125.5, 124.6, 123.0, 115.2, 104.7, 16.47, 16.45, 16.32, 16.30.

Polymer **4a**: IR (film, cm^{-1}): 1772 (C═O), 1654 (C═O), 1240 (C—O); ^1H NMR (400 MHz, $CDCl_3$) δ: 8.25–8.31 (m, 1H), 8.15–8.19 (m, 1H), 7.94–7.98 (d, 1H), 7.80–7.85 (d, 2H), 7.68–7.75 (t, 1H), 7.50–7.60 (m, 4H), 7.45–7.49 (d, 1H), 7.32–7.40 (t, 4H), 6.95– 7.10 (m, 6H), 6.84–6.68 (d, 1H); ^{13}C NMR (100 MHz, $CDCl_3$) δ: 195.8, 169.5, 169.4, 161.3, 157.1, 160.0,

© 1997 NRC Canada

Can. J. Chem. Downloaded from www.nrcresearchpress.com by 91.121.58.235 on 09/08/12
For personal use only.

155.4, 151.9, 151.8, 151.7, 136.9, 136.8, 136.4, 136.3, 134.4, 133.6, 132.8, 132.7, 131.7, 129.6, 129.0, 128.7, 128.1, 126.8, 126.7, 126.3, 125.9, 125.6, 124.0, 122.3, 119.8, 119.2, 117.7, 110.9, 91.0, 90.9.

Polymer **4b**: IR (film, cm^{-1}): 1652 (C=O), 1228 (C-O); ^1H NMR (400 MHz, $CDCl_3$) δ: 8.61–8.69 (m, 1H) 8.28–8.35 (m, 1H), 7.81–7.89 (m, 2H), 7.60–7.69 (m, 2H), 7.41–7.49 (m, 1H), 7.30–7.41 (q, 4H), 6.82–6.90 (m, 2H), 6.40–6.48 (m, 1H), 2.14–2.30 (4s, 12H); ^{13}C NMR (100 MHz, $CDCl_3$) δ: 195.0, 161.7, 155.8, 150.5, 150.1, 138.0, 137.9, 133.0, 132.6, 131.6, 131.4, 129.7, 129.6, 128.0, 127.8, 126.4, 126.2, 125.2, 124.4, 114.4, 122.3, 104.5, 16.55, 16.47, 16.35, 16.25.

Polymer **4c**: IR (film, cm^{-1}): 1654(C=O),1237 (C-O); ^1H NMR (400 MHz, $CDCl_3$) δ: 8.38–8.42 (m, 1H), 8.19–8.25 (m, 1H), 7.85–7.91 (d, 2H), 7.55–7.64 (m, 6H), 7.49–7.54 (d, 1H), 7.17–7.23 (d, 2H), 7.12–7.17 (d, 2H), 7.03–7.09 (d, 2H), 6.88–6.93 (d, 1H); ^{13}C NMR (100 MHz, $CDCl_3$) δ: 195.9, 161.9, 156.1, 154.9, 136.9, 136.8, 136.5, 136.4, 133.3, 132.9, 132.8, 131.3, 128.9, 128.5, 128.1, 126.7, 126.5, 125.9, 122.4, 120.5, 120.0, 117.3.

Dense membrane preparation

The polymer film was cast from a 2% (w/w) chloroform solution to form a 100 μm thick circular membrane. Chloroform was allowed to evaporate slowly (1–2 days) in air atmosphere until the film was tack free. Then while under vacuum (1 Torr), the membrane was heated slowly from room temperature to 140°C over 4 days. TGA was used to ensure the absence of solvent.

Gas permeation measurements

Gas permeation measurements were carried out using a constant volume system. The polymer film was tightly sealed in a permeation cell. The downstream face of the cell was connected to a 100 Torr pressure transducer and vacuum. Nitrogen, oxygen, methane, and carbon dioxide (all in ultra high purity, supplied by Canox) were used on the upstream side as the penetrating gases at 150 psi (1 psi = 6.9 kPa). Downstream pressure versus time data were collected until a steady state was achieved and the slope of their plot from 3θ to 6θ (θ = time lag) could be calculated. From this slope, the volumetric flux can be obtained and, finally, the permeability.

Acknowledgment

We thank the Natural Sciences and Engineering Research Council (NSERC) of Canada for support of our research program.

References

1. R. May. *In* High performance polymers and composites. *Edited by* J.I. Kroschwitz. John Wiley & Sons, New York. 1991. p. 769.
2. R.J. Cotter. Engineering plastics: Handbook of polyaryl ethers. Gordon and Breach Publishers, Basel. 1995.
3. (*a*) J.E. Harris and R.N. Johnson. *In* Encyclopedia of polymer science and engineering. Vol. 13. 2nd ed. *Edited by* H.F. Mark, N.M. Bikales, C.G. Overberger, and G. Menges. John Wiley & Sons, New York. 1988. pp. 196–211; (*b*) A. Tickton and K. Elbel-Weiser. *In* Polymeric materials encyclopedia. Vol. 8. *Edited by* J.C. Salamone. CRC Press, New York. 1996. pp. 5936–5943.
4. C. Eckert. Chem. Ind. (London), **14**, 556 (1995).
5. (*a*) C.L. Aitken, W.J. Koros, and D.R. Paul. Macromolecules, **25**, 3651 (1992); (*b*) Macromolecules, **25**, 3424 (1992); (*c*) J.S. McHattie, W.J. Koros, and D.R. Paul. Polymer, **33**, 1702 (1992); (*d*) M.R. Pixton and D.R. Paul. Polymer, **36**, 3165 (1995); (*e*) C.L. Aitken and D.R. Paul. J. Polym. Sci. Part B: Polym. Phys. **31**, 1061 (1993); (*f*) C.L. Aitken, D.R. Paul, and D.K. Mohanty. J. Polym. Sci. Part B: Polym. Phys. **31**, 983 (1993).
6. R.E. Kesting and A.L. Fritzche. Polymeric gas separation membranes. John Wiley and Sons, Toronto. 1993. pp. 63–77 and pp. 115–135.
7. (*a*) T. Matsuura. Synthetic membranes and membrane separation processes. CRC Press, Boca Raton, Fla. 1994; (*b*) R.E. Kesting. Synthetic polymeric membranes: a structural perspective. 2nd ed. John Wiley & Sons, Toronto. 1985; (*c*) L.M. Robeson, W.F. Burgoyne, M. Langsam, A.C. Savoca, and C.F. Tien. Polymer, **35**, 4970 (1994).
8. (*a*) S.K. Brownstein and M.D. Guiver. Macromolecules, **25**, 5181 (1992); (*b*) M.D. Guiver, O. Kutowy, and J.W. ApSimon. Polymer, **30**, 1137 (1989); (*c*) M.D. Guiver, S. Croteau, J.D. Hazlett, and O. Kutowy. Br. Polym. J. **23**, 29 (1990); (*d*) M. D. Guiver and G.P. Robertson. Macromolecules, **28**, 294 (1995); (*e*) M.D. Guiver, G.P. Robertson, and S. Foley. Macromolecules, **28**, 7612 (1995); (*f*) M. Beasy, F. Wang, and J. Roovers. Polym. Bull. **32**, 281 (1994); (*g*) F. Wang and J. Roovers. Macromolecules, **26**, 5296 (1993); (*i*) F. Wang, J. Roovers, and P.M. Toporowski. **26**, 3826 (1995).
9. (*a*) Z.Y. Wang and X. Zhang. Polym. Prep. **33**, 352 (1992); (*b*) W.G. Kim and A.S. Hay. Polym. Prep. **32**, 389 (1991); (*c*) F.W. Mercer, M.M. Fone, and M.T. McKenzie. J. Polym. Sci. Part A: Polym. Chem. **35**, 251 (1997); (*d*) F.A. Bottino, G. DiPasquale, N. Leonardi, and A. Pollicino. J. Polym. Sci. Part A: Polym. Chem. **33**, 843 (1995); (*e*) M. Ohno, T. Takata, and T. Endo. J. Polym. Sci. Part A: Polym. Chem. **33**, 2647 (1995).
10. (*a*) J.E. Douglas and Z.Y. Wang. Macromolecules, **28**, 5970 (1995); (*b*) ACS Symp. Ser. **624**, 226 (1996).
11. J.E. Douglas and Z.Y. Wang. Macromol. Rapid. Commun. **17**, 795 (1996).
12. (*a*) P.R. Moulinié, Z.Y. Wang, P. Handa, and J. Roovers. Polym. Mater. Sci. Eng. **75**, 422 (1996); (*b*) P.R. Moulinie. PhD. dissertation. Carleton University, Ottawa. 1996.
13. T.E. Attwood, P.C. Dawson, J.L. Freeman, L.R.J. Hoy, J.B. Rose, and P.A. Staniland. Polymer, **22**, 1096 (1981).

Can. J. Chem. Downloaded from www.nrcresearchpress.com by 91.121.58.235 on 09/08/12
For personal use only.

© 1997 NRC Canada

Naphthalene-based poly(aryl ether)s. II. Synthesis and characterization of poly(ether ketone)s containing two 1,4-naphthylene moieties in the repeat unit

Zhi Yuan Wang and Peter W. Broughton

Can. J. Chem. Downloaded from www.nrcresearchpress.com by 91.121.58.235 on 09/08/12
For personal use only.

Abstract: Two new monomers, 4-chloro-1-(4′-fluoro-1-naphthoyl)naphthalene and 1,4-bis(4′-fluoro-1′-naphthoyl)benzene, have been synthesized and polymerized with four different bisphenols to give two series of the naphthalene-based poly(ether ketone)s that are analogous to commercial PEEK and PEEKK. The effect of the introduction of one or two 1,4-naphthylene moieties, in the backbone of the repeat unit, on the glass transition temperatures has been studied. The glass transition temperatures usually increased by 20–45°C upon replacing one 1,4-phenylene with one 1,4-naphthylene moiety. All new poly(ether ketone)s prepared in tetramethylene sulfone were amorphous, with the glass transition temperatures in a range of 212–273°C. The polymer produced from 1,4-bis(4′-fluoro-1′-naphthoyl)benzene and 1,4-hydroquinone in phenyl sulfone as a solvent at 300°C showed semicrystalline properties with a melting temperature of 310°C.

Key words: naphthalene, poly(ether ketone)s, synthesis, characterization, glass transition temperature.

Résumé : On a synthétisé deux nouveaux monomères, le 4-chloro-1-(4′-fluoro-1′-naphtoyl)naphtalène et le 1,4-bis(4′-fluoro-1′-naphtoyl)benzène, et on les a polymérisés avec quatre différents biphénols pour obtenir une série de poly(éther cétone), contenant du naphtalène, qui sont analogues aux polymères commerciaux PEEK et PEEKK. On a étudié l'influence de l'insertion d'une ou deux unités, 1,4-naphtylène, dans le squelette du monomère, sur les températures de transition du verre. Les températures de transition du verre augmentent habituellement par 20–45°C lorsqu'on remplace une unité 1,4-phénylène par une unité 1,4-naphtylène. Tous les nouveaux poly(éther cétone) préparés dans le tétraméthylène sulfone sont amorphes et les températures de transition du verre sont de l'ordre de 212–273°C. Le polymère obtenu par polymérisation du 1,4-bis(4′-fluoro-1′-naphtoyl)benzène avec la 1,4-hydroquinone dans le phényl sulfone comme solvant montre à 300°C des propriétés semi-cristallines avec une température de fusion de 310°C.

Mots clés : naphtalène, poly (éther cétone), synthèse, caractérisation, température de transition du verre.

[Traduit par la rédaction]

Introduction

Aromatic poly(ether ketone)s (1) make up one of the major polymer families that are known for their superior performance characteristics in an unsurpassed number of application areas. Poly(ether ketone)s **1a** (2, 3) and **4a** (3) (Fig. 1) are typical examples, commercially available under the trade names of Victrex PEEK and Hostatec PEEKK, respectively. Key properties of these two poly(ether ketone)s, such as excellent thermal and oxidative stability, superior chemical resistance, high mechanical strength and stiffness, and excellent wear and abrasion resistance, allow them to be used as bearings, seals, wear rings, wire and cable coatings, composite matrices, and compressor parts. It has long been recognized that the fundamental basis for their performance resides in the phenylene–ether–ketone linkages that are present in their polymeric structures. The semicrystalline nature of **1a** and **4a**, as characterized by a melting point (T_m) of 344°C for **1a** and 358°C for **4a** (4), can be attributed to the regular phenylene–ether–ketone structure in their backbones. However, due to the same structural features, amorphous **1a** and **4a** exhibit relatively low glass transition temperatures (T_g) of 143°C and 154°C, respectively.

Earlier work of ours showed that the replacement of one 1,4-phenylene with one 1,4-naphthylene moiety in the repeat unit of poly(ether ketone) **1a** significantly reduced the crystallinity and increased the T_g of the resulting polymer **2a** to 188°C (up by 45°C) (5). Insertion of the 1,4-naphthylene moiety is equivalent to the addition of a benzo moiety perpendicular to the 1,4-phenylene unit in the main chain of poly(ether ketone)s. Thus, incorporation of two 1,4-naphthylene units into poly(ether ketone)s seemed worthwhile as it could further increase the T_g and reduce their crystallinity. In this paper, we report the synthesis and characterization of two series of poly(ether ketone)s (**3** and **5**) containing two naphthalene

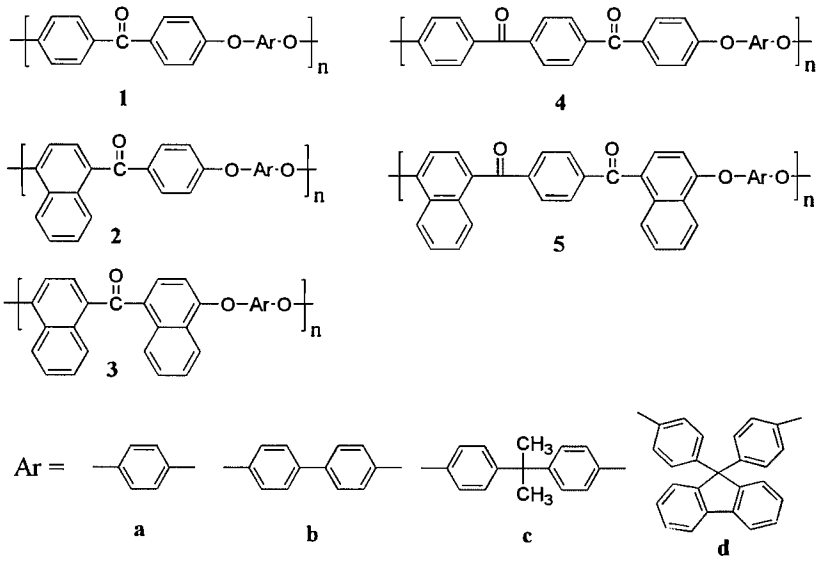
Received April 23, 1997.

Z.Y. Wang[1] and P.W. Broughton. Ottawa–Carleton Chemistry Institute, Department of Chemistry, Carleton University, 1125 Colonel By Drive, Ottawa, ON K1S 5B6, Canada.

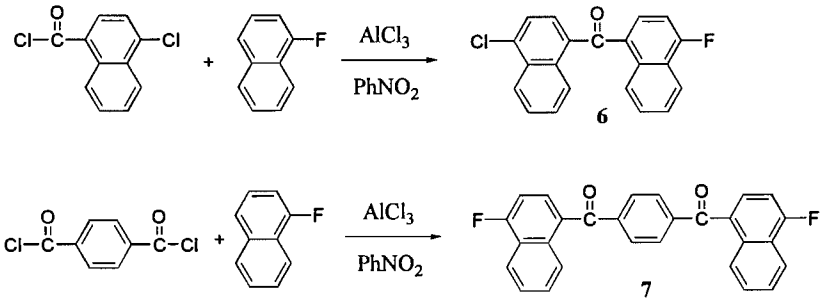
[1] Author to whom correspondence may be addressed. Telephone: (613) 520-2600, ext. 2713. Fax: (613) 520-3749. E-mail: wangw@ccs.carleton.ca

© 1997 NRC Canada

Fig. 1. Phenylene- and naphthylene-containing poly(ether ketone)s **1**–**5**.



Scheme 1. Synthesis of naphthalene-based monomers **6** and **7**.



rings in the repeat unit (Fig. 1). This study is part of an ongoing effort by our group to investigate structure–property relationships of poly(ether ketone)s and to design and identify potential new high-performance thermoplastics.

Results and discussion

Monomer synthesis

Incorporation of the 1,4-naphthylene unit in poly(ether ketone)s was accomplished through the syntheses and polycondensations of two new dihalide monomers, 4-chloro-1-(4′-fluoro-1-naphthoyl)naphthalene (**6**) and 1,4-bis(4′-fluoro-1-naphthoyl)benzene (**7**). The Friedel–Crafts acylation route was used, based on 1-fluoronaphthalene, 4-chloro-1-naphthaloyl chloride, and terephthaloyl chloride as starting materials (Scheme 1). 4-Chloro-1-naphthoic acid was obtained by hypochlorite oxidation of 4-chloro-1-acetonaphthone, which was prepared by acylation of 1-chloronaphthalene with acetyl chloride (6). The transformation of 4-chloro-1-naphthoic acid to the acid chloride was done using an excess of thionyl chloride in high yield. The subsequent Friedel–Crafts reaction was carried out at 70–80°C with a 3:1 molar ratio of 1-fluoronaphthalene to the acid chloride in nitrobenzene. Monomer **6** was obtained in good yield as yellow crystals with a melting point of 111–112°C after purification, twice by vacuum distillation, followed by recrystallization from xylenes. It was soluble in the solvents suitable for polymerization such as *N*-methyl-2-pyrrolidinone (NMP), *N*,*N*-dimethylacetamide (DMAc), dimethyl sulfoxide (DMSO), and tetramethylene sulfone ($TMSO_2$).

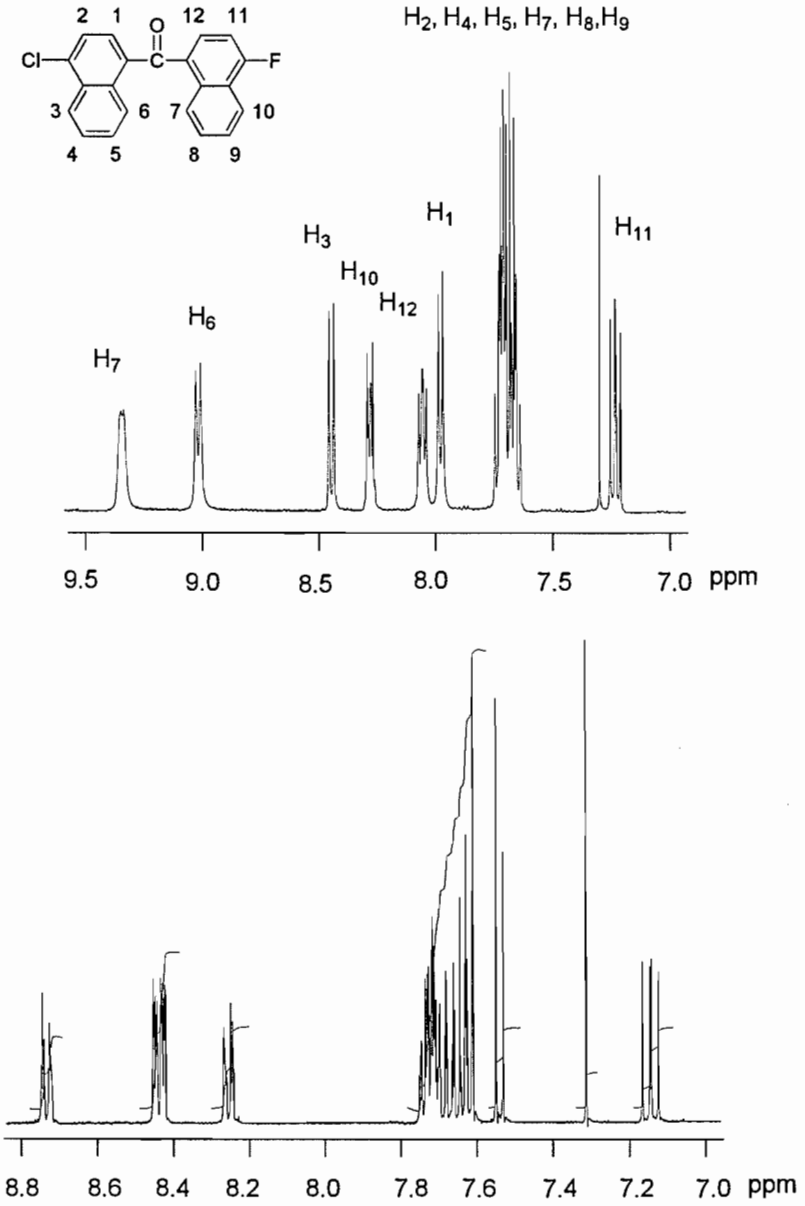
Monomer **6** was fully characterized by spectroscopic means. The presence of two magnetically nonequivalent 1,4-naphthylene moieties and the long-range F–H couplings made its ^{1}H NMR spectrum very complicated (bottom of Fig. 2). However, the use of the $Eu(fod)_3$ lanthanide shift reagent, coupled with COSY and HETCOR experiments, allowed us to obtain the well-resolved ^{1}H NMR spectrum of **6** and a complete assignment (top of Fig. 2). The ^{19}F NMR spectrum displayed only one peak at -114.15 ppm relative to CCl_3F. The IR spectrum of **6** showed a peak at 1645 cm^{-1}, attributed to the conjugated ketone. MS gave the parent molecular ion at *m*/*z* 334 and the base peak at *m*/*z* 173, corresponding to the loss of the fluoronaphthoyl radical. The rest of the fragmentation patterns were indicative of the structure. Moreover, HRMS indicated the correct molecular formula.

The synthesis of the monomer **7** was achieved in good yield by the Friedel–Crafts acylation of 1-fluoronaphthalene using a 2.6:1 molar ratio of aluminum chloride to terephthaloyl dichloride in nitrobenzene (Scheme 1). Recrystallization three times from DMF afforded **7** in high purity as a yellow crystal-

Can. J. Chem. Downloaded from www.nrcresearchpress.com by 91.121.58.235 on 09/08/12
For personal use only.

© 1997 NRC Canada

Fig. 2. ^{1}H NMR (400 MHz, $CDCl_3$) spectra of monomer **6** (2.5 mg); top: containing 11 mg of $Eu(fod)_3$; bottom: without $Eu(fod)_3$.



line solid with a melting point of 230–231°C. Its structure was consistent with the ^{1}H and ^{13}C NMR data supported by COSY and HETCOR experiments. The ^{19}F NMR spectrum of **7** displayed a peak at −114.81 ppm relative to CCl_3F. The IR spectrum showed a strong peak at 1651 cm^{-1}, indicating the conjugated carbonyl moiety. MS gave the parent molecular ion at *m/z* 422, as expected, and the base peak at *m/z* 173 corresponding to the fragment ion due to the loss of fluoronaphthoyl radical. HRMS indicated the correct molecular formula.

Polymer synthesis

The following common solvents for nucleophilic substitution polycondensations were tested in the syntheses of polymers **3** and **5**: NMP, DMAc, and $TMSO_2$. In NMP, it was found that the cleavage of the ether linkage of the resulting poly(ether ketone)s occurred at elevated temperatures as reported before (7). DMAc was also not a suitable solvent, since the resulting polymers **3** and **5** exhibited very limited solubility. Polymerizations were then best carried out at 210°C in $TMSO_2$ with chlorobenzene as an azeotroping agent using a stoichiometric mixture of a dihalide and a bisphenol in the presence of potassium carbonate (2 mol-equiv.). The water formed during the reaction was removed as an azeotrope with chlorobenzene at 140°C over a period of 1–2 h. The polymerization temperature was then gradually raised to 210°C. The polymerization was stopped when the molecular weight, as analyzed by gel permeation chromatography (GPC), began to decrease. The resulting polymers were coagulated in an excess of methanol, followed by reverse precipitation to remove any remaining oligomers.

Under these reaction conditions, polymers **3** and **5** were obtained as off-white to yellow fibrous solids in moderate to high molecular weights. However, polymers **3a, b** and **5a, b** still exhibited low solubility in $TMSO_2$ and precipitated out of

© 1997 NRC Canada

Can. J. Chem. Downloaded from www.nrcresearchpress.com by 91.121.58.235 on 09/08/12
For personal use only.

Table 1. Characterizations of polymers **3** and **5**.

Polymer	M_w ($\times 10^{-4}$)	M_n ($\times 10^{-4}$)	M_w/M_n	η_{inh}[a](dL/g)	T_d[b](N_2)	T_d[b](air)
3a	N/A	N/A	N/A	0.31[c]	510	524
3b	N/A	N/A	N/A	0.31[c]	488	466
3c	5.71	2.13	1.58	0.24	497	478
3d	3.80	2.13	1.78	0.23	525	453
5a	N/A	N/A	N/A	0.33[c]	493	489
5a[d]	N/A	N/A	N/A	0.23[c]	504	474
5b	N/A	N/A	N/A	0.34[c]	480	430
5c	5.71	2.74	2.08	0.34	492	436
5d	8.32	4.12	2.02	0.66	526	464

[a]In 0.5% chloroform at 25°C.
[b]Onset temperature for 5% weight loss by TGA.
[c]In 0.5% NMC at 25°C.
[d]Polymerized in phenyl sulfone; N/A = not available.

solution prematurely during polymerization. Although being soluble in high-boiling 1-cyclohexyl-2-pyrrolidinone (bp 280°C) and *N*-methylcaprolactam (NMC, bp 260°C), polymers **3a, b** and **5a, b** with higher molecular weights could not be obtained in these two solvents.

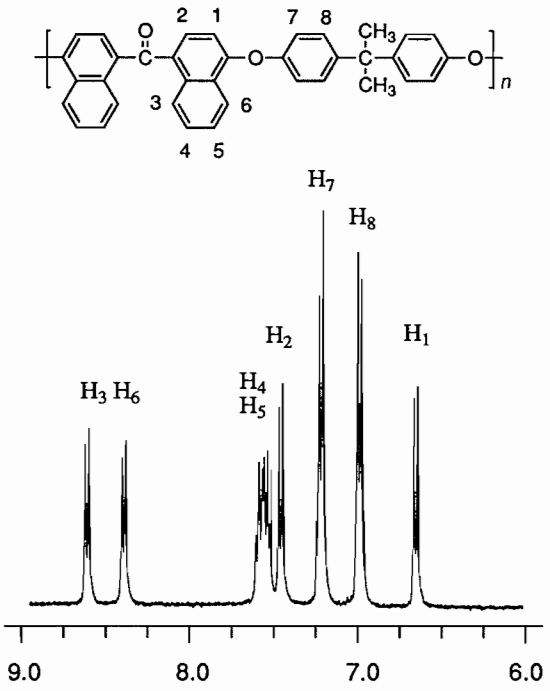
Phenyl sulfone (bp 379°C) is frequently used as a high-boiling solvent for the preparation of semicrystalline poly(aryl ether)s such as PEEK (2). Thus, the polymerization of **7** and 1,4-hydroquinone was performed in phenyl sulfone at 300°C. Although having a molecular weight similar to the sample prepared in $TMSO_2$, polymer **5a** produced in phenyl sulfone appeared to be semicrystalline and showed a T_m of 310°C by differential scanning calorimetry (DSC).

Polymer characterization

Polymers **3c, d** and **5c, d** containing the flexible isopropylidene and bulky spiro fluorene groups showed good solubility in chlorinated hydrocarbons, DMAc, and NMP. Polymers **3a, b** and **5a, b**, on the other hand, displayed much more solvent resistance than the others. Comparing three polymers **1a**, **2a**, and **3a** derived from 1,4-hydroquinone, PEEK (**1a**) is the most solvent resistant and polymer **2a** is the least solvent resistant. The former is only soluble in concentrated sulfuric acid at room temperature, while the latter is readily soluble in chloroform, 1,1,2,2-tetrachloroethane (TCE), DMAc, and NMP. However, the structurally related **3a**, having two naphthalene rings in the repeat unit, displayed much more solvent resistance than **2a**, being only soluble in NMP and *N*-methylcaprolactam (NMC). Thus, the good solubility of **2a** is attributed mainly to its microstructure, consisting of a random distribution of the head-to-tail, head-to-head, and tail-to-tail diads (5). A similar trend in solubility has been found for polymers **1b**, **2b**, and **3b**. Comparing polymers **4a,b** with polymers **5a,b**, the former two semicrystalline poly(ether ketone)s are insoluble in common organic solvents, and the latter two naphthalene-based analogues are soluble in NMP and NMC at ambient temperatures and can also be dissolved in hot TCE.

Polymers **3** gave much simpler NMR spectra than the spectrum of monomer **6**, due to the fact that two naphthylene units in the repeat unit of **3** are magnetically equivalent without the fluorine splitting. For example, the ^1H NMR spectrum of the aromatic region of polymer **3c** (Fig. 3) is simple and well

Fig. 3. ^1H NMR (400 MHz, $CDCl_3$) spectrum of the aromatic region of polymer **3c**.



resolved, yet still shows the characteristic pattern of the 1,4-naphthylene moiety. The methyl groups of the BPA unit in polymer **3c** appears as a singlet at 1.65 ppm but is not shown in Fig. 3. The peak assignments were supported by COSY and HETCOR experiments. The ^{13}C NMR spectrum of **3c** showed 17 distinguishable peaks for each of the magnetically non-equivalent carbon atoms. IR spectra indicated the carbonyl groups for polymers **3** and **5** in the region of 1648–1658 cm^{-1} and the ether linkages in the region of 1238–1243 cm^{-1}.

Polymers **3c** and **3d** had the same number-average molecular weight of 21 300, relative to polystyrene determined by GPC, and similar inherent viscosities of about 0.23 dL/g in chloroform (Table 1). In comparisons with **3c** and **3d**, polymers **5c** and **5d** had higher molecular weights (M_n = 27 400 and 41 200 for **5c** and **5d**, respectively) and higher inherent

Can. J. Chem. Downloaded from www.nrcresearchpress.com by 91.121.58.235 on 09/08/12
For personal use only.

© 1997 NRC Canada

Table 2. Comparison of T_g values of polymers **1**–**3**.

Polymer	T_g(°C) **1**[a]	T_g(°C) **2**[b]	T_g(°C) **3**	ΔT_g(°C) (**2** – **1**)	ΔT_g(°C) (**3** – **2**)	ΔT_g(°C) (**3** – **1**)
a	143	188	232	45	44	89
b	170	210	235	40	25	65
c	155	189	212	34	23	57
d	252	272	273	20	1	21

[a]Taken from ref. 4.
[b]Taken from ref. 5.

Table 3. Comparison of T_g values of polymers **4** and **5**.

Polymer	T_g(°C) **4**	T_g(°C) **5**	ΔT_g(°C) (**5** – **4**)
a	154[a]	217	63
b	168[b]	230	62
c	165[b]	204	39
d	243[b]	265	22

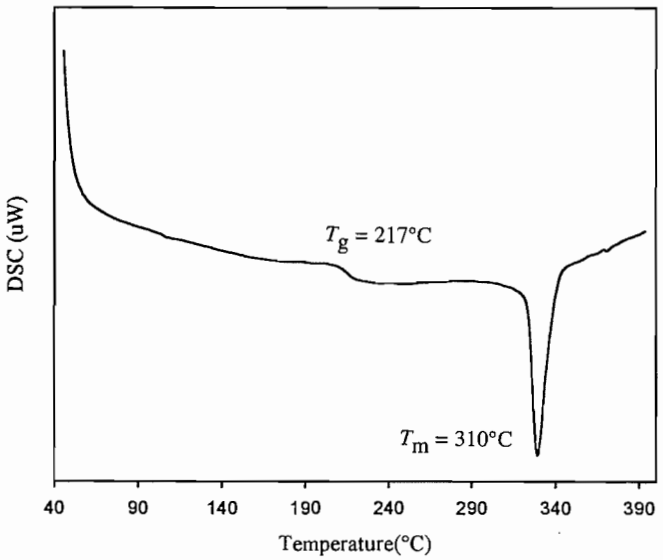
[a]Taken from ref. 3.
[b]Taken from ref. 4.

viscosities (0.34 and 0.66 dL/g). Less soluble polymers **3a, b** and **5a, b** had moderate molecular weights, as indicated by their inherent viscosities, above 0.30 dL/g in NMC (Table 1). Tough, flexible films were successfully prepared for polymers **3c, d** and **5c, d** but not for polymers **3a, b** and **5a, b**. Overall, polymers **3** were obtained in relatively lower molecular weights than polymers **5** under the same polymerization conditions.

The naphthalene-based poly(ether ketone)s **3** and **5** had high thermal and thermooxidative stabilities, comparable to the phenylene analogues **1** and **4**. The onset temperatures for 5% weight loss, as assessed by TGA, occurred above 480°C in nitrogen and 430°C in air (Table 1).

All polymers **3** and **5** produced in $TMSO_2$ showed no crystalline behavior as assessed by DSC. The T_g values for polymers **3** ranged from 212 to 273°C depending on the units derived from bisphenol monomers (Table 2). As expected, polymer **3c** had the lowest T_g (212°C), due to the presence of a flexible isopropylidene group, and polymer **3d** containing a bulky cardo group had the highest T_g of 273°C. By comparing with the T_g values of polymers **1** and **2**, the effect on the T_g of the insertion of the 1,4-naphthylene moiety in the backbone of the repeat unit can be seen clearly. On the basis of semicrystalline PEEK (**1a**), the T_g increases by 45°C upon the insertion of one naphthalene ring as in the case of **2a** (188°C) and further increases to 232°C (up by another 44°C) for polymer **3a** having two naphthalene rings in the repeat unit. Going from **1b** (8) and **1c** (1*a*, 9) to **2b** (10) and **2c** (5) the T_g values increase 35–40°C but only about 25°C from **2b** and **2c** to **3b** and **3c**. Similarly, there was a moderate increase of about 20°C in T_g from **1d** (9) to **2d** (5), but almost no difference in T_g between polymers **2d** and **3d**. For the diketone-containing polymers (**4** and **5**), the increase in T_g upon replacing 1,4-phenylene with 1,4-naphthylene in the repeat unit was also observed (Table 3). Polymers **5a** and **5b** had T_g values of 217 and 230°C, respectively, over 60°C higher than those of the phenylene analogues **4a** (3) (154°C) and **4b** (11) (168°C). A moderate increase (about 20°C and 40°C) was observed for the poly(ether ketone)s derived from 4,4′-isopropylidenediphenol and 9,9-bis(4-hydroxyphenyl)fluorene (**5c** and **5d**), in comparison with their analogues **4c** (1*a*) and **4d** (9).

Fig. 4. DSC trace of the polymer **5a** prepared in phenyl sulfone at 300°C.



Although amorphous when produced in $TMSO_2$, polymer **5a** appeared to be semicrystalline when it was prepared in phenyl sulfone at 300°C. The DSC trace showed a T_g of 217°C and a T_m of 310°C (Fig. 4). In comparison with its phenylene analogue **4a**, with a T_g of 154°C and a T_m of 358°C, the polymer **5a** prepared in phenyl sulfone had a much higher T_g and a slightly lower T_m. Accordingly, the semicrystalline **5a** has a higher T_g/T_m ratio (0.84) than that (0.68) of commercial PEEKK (**4a**), which is desirable when considering the melt-processing temperatures and the final-use temperatures of the polymer.

Thermomechanical measurements were performed on thin strips of flexible, tough films cast from chloroform solutions using a thermomechanical analyzer in the tensile stress–strain mode. Young's moduli of three polymers **3d**, **5c**, and **5d** were 1.20, 3.44, and 2.84 GPa, respectively, at 25°C. These values are comparable to those of the phenylene-based poly(ether ketone)s, indicative of the characteristics of high-performance thermoplastics.

Can. J. Chem. Downloaded from www.nrcresearchpress.com by 91.121.58.235 on 09/08/12
For personal use only.

© 1997 NRC Canada

Conclusion

Two series of the naphthalene-based poly(ether ketone)s analogous to commercial PEEK and PEEKK were prepared. It has been found that the increase in T_g upon replacing the 1,4-phenylene with the 1,4-naphthylene moieties in the repeat unit is much greater for the semicrystalline phenylene poly(ether ketone)s than for the amorphous analogues derived from 1,4-hydroquinone and 4,4-biphenol. Semicrystalline poly(ether ketone) **5a** shows potential as a new high-performance thermoplastic, owing to its high T_g and high T_g/T_m ratio.

Experimental section

General

Melting points were taken on a Fisher–Johns apparatus and are uncorrected. The ^1H and ^{13}C NMR spectra were recorded on either a Varian Gemini-200 or a Bruker-400 instrument using tetramethylsilane as the internal solvent. The ^{19}F NMR spectra were recorded on a Varian XL-300 using CCl_3F as a reference. Infrared measurements were performed on a Perkin–Elmer Series 1600 FTIR instrument. Molecular weights were determined on a Perkin–Elmer LC-250 GPC instrument relative to polystyrene standards using chloroform as an eluent at a flow rate of 1.0 mL/min; a UV detector was set at 254 nm wavelength. Inherent viscosities were measured in a 0.5 g/dL chloroform solution (or in *N*-methylcaprolactam where indicated) at 25°C using a Ubbelohde dilution viscometer. The glass transition temperatures were determined by differential scanning calorimetry (DSC) on a Seiko DSC 220 at a heating rate of 10°C/min under nitrogen (50 mL/min) and taken as the midpoint of the change in slope of the base line. Thermogravimetric analysis (TGA) was performed on a Seiko TG/DTA 220 at a heating rate of 10°C/min in nitrogen and air (200 mL/min). Thin films were cast from the chloroform solution, dried at 200–250°C under vacuum over 14 days, and cut out as a strip (length = 10 mm, width = 2 mm, thickness = 0.01–0.03 mm). Young's moduli of the thin films were obtained on a Seiko TMA/SS 120C TMA/SS analyzer. The films were tested by measuring the stress and strain while applying a linear load program. For Young's modulus at 25°C, the parameters were set as: offset load = 10–20 g, load amplitude = 5–10 g, and cycling frequency = 0.05 Hz. Young's moduli (E') were obtained from the slope of the linear portion of the stress–strain plots. After the data were collected, the same film was used, without changing the parameters to Young's modulus variation with temperature, by heating to 400°C at a ramp rate of 3°C/min in static air.

Materials

Aluminum chloride, potassium carbonate, sodium hypochlorite (NaOCl), 1-fluoronaphthalene, tetramethylene sulfone ($TMSO_2$), *N*-methyl-2-pyrrolidinone (NMP), *N*-methylcaprolactam (NMC), *N*,*N*-dimethylacetamide (DMAc), phenyl sulfone, acetyl chloride, thionyl chloride, and other common organic solvents were purchased from Aldrich Chemical Co. and used as received. 1-Chloronaphthalene was fractionally distilled under vacuum (using a water aspirator). 4,4′-Isopropylidenediphenol, 4,4′-biphenol, 9,9-bis(4-hydroxyphenyl)fluorene, and 1,4-hydroquinone were purchased from Aldrich Chemical Co. and purified by recrystallization.

Monomer synthesis

4-Chloro-1-naphthoic acid

A 1 L 3-neck, round-bottomed flask equipped with a solid addition funnel and a condenser was purged with nitrogen for 20 min prior to use, and flame dried. The flask was charged with 1-chloronaphthalene (100.0 g, 0.615 mol), acetyl chloride (24.1 g, 0.30 mol), and dichloromethane (650 mL), forming a clear, colorless solution. Aluminum chloride (53.3 g, 0.40 mol) was added slowly at 0–5°C (ice bath temperature), resulting in a deep red colored mixture. The reaction mixture was stirred at this temperature for 1 h and then the temperature was raised to ca. 40–60°C and maintained for 12 h. The reaction mixture was poured into an ice-cold 10% aqueous HCl solution (500 mL) and stirred for 30 min. The organic layer was partitioned and the dark colored aqueous phase was extracted with chloroform. The combined organic extracts were washed with 5% aqueous NaOH solution and water, and then dried over $MgSO_4$. Removal of solvent afforded an oily residue, which was distilled under vacuum (20 Torr (1 Torr = 133.3 Pa), water aspirator) yielding 53.5 g (86.8%) of 4-chloro-1-acetonaphthone. To a 3 L round-bottomed flask equipped with mechanical stirrer, 4-chloro-1-acetonaphthone (52.10 g, 0.255 mol), NaOCl (1.20 L, 1.63 mol), and methanol (120 mL) were added. The mixture was stirred at 40–60°C for 12 h. The aqueous solution of sodium bisulfite (60 g in 300 mL of water) was then added, turning the reaction mixture from brown to opaque white in color. Upon acidification with 100 mL of 4 M HCl(aq), slowly added, a fluffy white precipitate was formed. The precipitate was dissolved in 5% NaOH solution. The solution was filtered to remove any residual insoluble materials and the filtrate was acidified again with 4 M HCl(aq) to give the crude product. Recrystallization from ethanol gave 4-chloro-1-naphthoic acid: 27.9 g (53.0%); mp 221–222°C (lit. (6) mp 223–224°C).

*4-Chloro-1-(4′-fluoro-1-naphthoyl)naphthalene (**6**)*

A 1 L round-bottomed flask was charged with 4-chloro-1-naphthoic acid (27.8 g, 0.14 mol) and $SOCl_2$ (40 mL) and the mixture was stirred at 80°C for 12 h. The excess $SOCl_2$ was distilled off under reduced pressure (20 Torr, water aspirator), leaving a light-brown solid residue. The crude acid chloride was vacuum distilled (1 Torr), yielding 4-chloro-1-naphthoyl chloride: 28.3 g (93.5%); mp 222–223°C (lit. (6) mp 223–224°C).

A 100 mL 3-neck round-bottomed flask was flame dried, purged with nitrogen, and charged with 4-chloro-1-naphthoyl chloride (8.00 g, 35.5 mmol), 1-fluoronaphthalene (15.3 g), and nitrobenzene (30 mL). To the solution at 0–5°C (ice bath temperature) was added aluminum chloride (4.21 g, 31.6 mmol). The resulting deep-red solution was stirred at this temperature for 1 h and then at ca. 60–70°C for 8 h. The reaction mixture was poured into an ice-cold 10% HCl – water solution (500 mL) and stirred for 30 min. The resulting oily residue was washed with 3 aliquots of methanol to remove residual nitrobenzene and then once with water, leaving a solid residue. The crude product was filtered and recrystallized from ethanol to afford monomer **6**: 6.21 g (52.2%); mp 111–112°C; IR (KBr, cm^{-1}): 1645 (C=O), 1244 (C-F), 759 (C-Cl); ^1H NMR (400 MHz, $CDCl_3$, $Eu(fod)_3$) δ: 9.40 (d, 1H, J_{H-H} = 4.8 Hz), 9.06 (d, 1H, J_{H-H} = 8.6 Hz), 8.46 (d, d, 1H, J_{H-H} = 8.4 Hz, $^4J_{H-H}$ = 0.8 Hz), 8.29 (m, 1H), 8.01 (m, 1H), 7.85 (d, 1H,

Can. J. Chem. Downloaded from www.nrcresearchpress.com by 91.121.58.235 on 09/08/12
For personal use only.

© 1997 NRC Canada

Can. J. Chem. Downloaded from www.nrcresearchpress.com by 91.121.58.235 on 09/08/12
For personal use only.

J_{H-H} = 7.6 Hz), 7.68 (m, 5H), 7.19 (t, 1H, J_{H-H} = 8.4 Hz); ^{13}C NMR (100 MHz, $CDCl_3$) δ: 198.9, 163.0, 160.4, 137.6, 136.5, 133.2, 132.9, 131.3, 130.1, 129.4, 128.6, 127.8, 127.1, 126.8, 126.5, 125.1, 125.0, 124.3, 121.1; ^{19}F NMR (300 MHz, DMSO-d_6) δ: −114.15 (s); MS (EI) (*m/z*): 334 (M^+), 299 (M^+ − Cl), 189 (M^+ − Fnaph), 173 (M^+ − Clnaph), 161 (M^+ − COnaphF), 145 (M^+ − COnaphCl), 126 (M^+ − Cl − COnaphF); HRMS calcd. for $C_{21}H_{12}OFCl$: 334.0561; found: 334.0566.

1,4-Bis(4′-fluoro-1′-naphthoyl)benzene (7)

A 500 mL 3-neck, round-bottomed flask equipped with a solid addition funnel and a condenser was purged with nitrogen for 20 min before it was charged with terephthaloyl dichloride (12.6 g, 62.1 mmol), 1-fluoronaphthalene (22.8 g, 0.16 mol), and nitrobenzene (160 mL). Once solvation was complete, aluminum chloride (21.5 g; 0.16 mol) was added to the yellow solution in portions at 0–5°C (ice bath temperature). The resulting red solution was stirred while the reaction temperature was allowed to reach room temperature during 1 h. The reaction then continued at 60–80°C for 3 h. The reaction mixture was worked up as with monomer **6** and the crude product was recrystallized three times in DMF to afford monomer **7** as yellow crystals: 17.0 g (64.8%); mp 230–231°C; IR (KBr, cm^{-1}) 1651 (C═O), 1245 (C-F); ^1H NMR (400 MHz, $CDCl_3$) δ: 8.32 (m, 1H), 8.22 (m, 1H), 7.92 (s, 2H), 7.64 (m, 3H), 7.19 (t, 1H, J_{H-H} = 8.0 Hz); ^{13}C NMR (100 MHz, $CDCl_3$) δ: 195.9, 102.0, 159.4, 141.7, 131.2, 129.9, 129.7 (J_{C-F} = 10 Hz), 128.5, 126.8, 125.4 (J_{C-F} = 2.0 Hz), 120.7 (J_{C-F} = 6.0 Hz), 107.9 (J_{C-F} = 21.0 Hz), ^{19}F NMR (300 MHz, TCE-d_2) δ: −114.8 (s); MS (EI) (*m/z*): 422 (M^+), 277 (M^+ − Fnaph), 249 (M^+ − COnaphF), 173 (M^+ − PhCOnaphF), 145 (M^+ − Fnaph-COPhCO); HRMS calcd. for $C_{28}H_{16}O_2F_2$: 422.1118; found: 422.1110.

Polymer synthesis

Polymerizations were all carried out in 50 mL 3-neck round-bottomed flasks equipped with a stirring bar, a Dean–Stark trap fitted with a condenser, and a nitrogen purge inlet. A typical procedure is as follows: A flask was charged with 4-chloro-1-(4′-fluoro-1′-naphthoyl)naphthalene (1.00 g, 3.00 mmol), 1,4-hydroquinone (330 mg, 3.00 mmol), potassium carbonate (829 mg, 6.00 mmol), chlorobenzene (30 mL), and $TMSO_2$ (4.8 mL, 28% w/v). The reaction temperature was rapidly raised to 140–150°C and held for 1 h. During this time, the water formed was removed with toluene and fresh toluene was introduced to the system. The temperature was then raised to 210°C, and the polymerization continued for 2 h. The reaction mixture was then cooled to about 80°C and poured into methanol (200 mL) containing 2–3 drops of concentrated HCl. The spaghetti-like polymer was collected and dissolved in chloroform (50 mL). The chloroform solution was filtered through a thin pad of Celite, and then reverse precipitated with methanol, yielding yellow fibrous polymer **3a**.

Polymer **3c**: IR (film, cm^{-1}): 1648.7 (C═O), 1238.0 (C-O-C); ^1H NMR (400 MHz, $CDCl_3$) δ: 8.60 (d, 1H, J_{H-H} = 8.2 Hz), 8.38 (d, 1H, J_{H-H} = 8.1 Hz), 7.55 (m, 2H), 7.45 (d, 1H, J_{H-H} = 8.1 Hz), 7.21 (d, 1H, J_{H-H} = 8.6 Hz), 6.98 (d, 1H, J_{H-H} = 8.6 Hz), 6.65 (d, 1H, J_{H-H} = 8.0 Hz), 1.65 (s, 6H); ^{13}C NMR (100 MHz, $CDCl_3$) δ: 198.0, 157.2, 153.8, 146.7, 133.0, 131.7, 131.7, 128.5, 128.3, 126.4, 126.0, 122.3, 119.6, 109.0, 42.3, 30.9.

Polymer **3d**: IR (film, cm^{-1}): 1654.2 (C═O), 1239.9 (C-O-C); ^1H NMR (400 MHz, $CDCl_3$) δ: 8.61 (d, 1H, J_{H-H} = 8.4 Hz), 8.37 (d, 1H, J_{H-H} = 8.0 Hz), 7.74 (d, 1H, J_{H-H} = 7.4 Hz), 7.56 (m, 2H), 7.42 (d, 1H, J_{H-H} = 6.9 Hz), 7.39 (d, 1H, J_{H-H} = 7.5 Hz), 7.34 (t, 1H, J_{H-H} = 7.4 Hz), 7.25 (t, 1H, J_{H-H} = 7.6 Hz), 7.22 (d, 1H, J_{H-H} = 8.7 Hz), 6.95 (d, 1H, J_{H-H} = 8.6 Hz), 6.65 (d, 1H, J_{H-H} = 8.0 Hz); ^{13}C NMR (100 MHz, $CDCl_3$) δ: 197.9, 156.9, 154.9, 150.9, 141.8, 140.0, 133.0, 131.9, 131.6, 129.6, 128.5, 127.8, 127.7, 127.5, 126.4, 126.0, 126.0, 122.2, 120.3, 119.6, 109.4, 64.4.

Polymer **5c**: IR (film, cm^{-1}): 1654.4 (C═O), 1239.1 (C-O-C); ^1H NMR (400 MHz, $CDCl_3$) δ: 8.41 (m, 2H), 7.86 (s, 2H), 7.56 (m, 2H), 7.50 (d, 1H, J_{H-H} = 8.0 Hz), 7.28 (d, 1H, J_{H-H} = 8.6 Hz), 7.05 (d, 1H, J_{H-H} = 8.5 Hz), 6.76 (d, 1H, J_{H-H} = 8.0 Hz); ^{13}C NMR (100 MHz, $CDCl_3$) δ: 196.4, 157.5, 153.8, 149.9, 142.2, 132.9, 130.9, 130.1, 129.4, 128.5, 127.8, 126.5, 126.5, 125.8, 122.4, 119.7, 108.8, 42.4, 31.0.

Polymer **5d**: IR (film, cm^{-1}): 1654.5 (C═O), 1238.2 (C-O-C); ^1H NMR (400 MHz, $CDCl_3$) δ: 8.35 (d, 2H, J_{H-H} = 8.1 Hz), 7.82 (s, 2H), 7.74 (d, 1H, J_{H-H} = 7.6 Hz), 7.55 (m, 2H), 7.44 (d, 1H, J_{H-H} = 8.1 Hz), 7.41 (d, 1H, J_{H-H} = 7.5 Hz), 7.35 (t, 1H, J_{H-H} = 7.4 Hz), 7.25 (m, 2H), 6.98 (d, 1H, J_{H-H} = 8.8 Hz), 6.73 (d, 1H, J_{H-H} = 8.0 Hz); ^{13}C NMR (100 MHz, $CDCl_3$) δ: 196.3, 157.1, 154.8, 150.9, 142.2, 142.0, 140.0, 132.8, 130.8, 130.0, 129.7, 129.3, 128.5, 127.9, 127.7, 126.6, 126.5, 126.0, 125.7, 122.3, 120.4, 119.7, 109.1.

Semicrystalline polymer ***5a***

A flask was charged with monomer **7** (1.27 g, 3.00 mmol), 1,4-hydroquinone (330 mg, 3.00 mmol), potassium carbonate (289 mg, 6.00 mmol), chlorobenzene (10 mL), and phenyl sulfone (7.82 g). The water formed in the reaction was removed together with chlorobenzene at 100-140°C. The reaction temperature was raised to 300°C and maintained for 3 h. The hot reaction mixture was poured into stirring methanol (200 mL) containing 2–3 drops of concentrated HCl. The spaghetti-like polymer was crushed up and refluxed in acetone and chloroform, respectively, for 1 h. The polymer was collected by filtration and dried in a vacuum (5 Torr) oven at 100°C for 12 h.

Acknowledgment

We thank the Natural Sciences and Engineering Research Council (NSERC) of Canada for support of our research program.

References

1. (*a*) R.N. Johnson, A.G. Farnham, R.A. Clendinning, W.F. Hale, and C.N. Merriam. J. Polym. Sci. Polym. Chem. Ed. **5**, 2375 (1967); (*b*) W.F. Hale, A.G. Farnham, R.N. Johnson, and R.A. Clendinning. J. Polym. Sci. Polym. Chem. Ed. **5**, 2399 (1967).
2. (*a*) P.C. Dawson and D.J. Blundell. Polymer, **21**, 370 (1980); (*b*) T.C. Stening, C.P. Smith, and P.J. Kimber. Mod. Plast. **11/81**, 86 (1981).
3. T.E. Atwood, P.C. Dawson, J.L. Freeman, L.R.J. Hoy, J.B. Rose, and P.A. Staniland. Polymer, **22**, 1096 (1980).

© 1997 NRC Canada

4. R.J. Cotter. Engineering plastics: handbook of ethers. Gordon and Breach Publishers, Basel. 1995.
5. (*a*) J.E. Douglas and Z.Y. Wang. Macromolecules, **28**, 5970 (1995); (*b*) ACS Symp. Ser. **624**, 226 (1996).
6. T.L. Jacobs, S. Winstein, J.W. Ralls, and J.H. Robson. J. Org. Chem. **11**, 21 (1946).
7. V. Carlier, B. Jambe, J. Devaux, and P.S. McGrail. Polymer, **34**, 167 (1993).
8. T.E. Atwood, T. King, I.D. McKenzie, and J.B. Rose. Polymer, **18**, 365 (1977).
9. P.M. Hergenrother, B.J. Jensen, and S.J. Havens. Polymer, **29**, 358 (1988).
10. J.E. Douglas and Z.Y. Wang. Can. J. Chem. **75**, 1340 (1997).
11. F.N. Cogswell, D.C. Leach, P.T. McGrail, H.M. Colquhoun, P. MacKenzie, and R.M. Turner. SAMPE, **32**, 382 (1987).

Can. J. Chem. Downloaded from www.nrcresearchpress.com by 91.121.58.235 on 09/08/12
For personal use only.

© 1997 NRC Canada

Information on the noncrystalline phase of nascent iPP given by slow calorimetry

X. Zhang, H. Phuong-Nguyen, P. Bernazzani, I. Lapes, and G. Delmas

Abstract: Nascent isotactic polypropylene (iPP) has a lower crystallinity and a different X-ray pattern than recrystallized iPP. Heat flows during the melting of nascent highly stereoregular iPP samples are recorded with a Setaram C80 calorimeter over a wide T range (30–280°C). The rate of heating–cooling is 1–3 K/h, i.e., much lower than with conventional DSC. Melting is performed after annealing at $30 < T_{annealing} < 140$°C and with or without substrate. The main peak, that found by DSC, is associated with melting of monoclinic crystals and gives an enthalpy ΔH_{DSC}. Two other peaks, usually above and below the main peak, are observed. These are associated with a slower process of disordering a physical network, which was produced in the sample during polymerization. The sum of ΔH_{DSC} and $\Delta H_{network}$ equals ΔH_{total}. When melting is complete ΔH_{total} is equal to ΔH_0, the heat of fusion of perfect iPP crystals. This work presents new information on: (*i*) the noncrystalline phase of nascent iPP and the heat content of a semicrystalline polymer; (*ii*) the modifications of the melting process due to strain development, brought about by expansion in the material during the temperature ramp when a physical network is present; and (*iii*) the effect of a substrate on the polymer melting process.

Key words: nascent iPP, slow calorimetry, strain-melting, change of enthalpy, substrates.

Résumé : La cristallinité et le patron de diffraction des rayons X du polypropylène isotactique naissant (PPi) diffèrent des propriétés correspondantes du PPi recristallisé. Faisant appel à un calorimètre Setaram C80 et opérant sur une plage étendue de températures (de 30 à 280°C), on a enregistré les évolutions de chaleur au cours de la fusion des échantillons de PPi naissant hautement stéréorégulier. La vitesse de chauffage–refroidissement est de 1 à 3 K/h, un taux beaucoup plus faible qu'avec l'analyse calorimétrique différentielle (ACD) utilisée couramment. La fusion se produit après un recuit à $30 < T_{recuit} < 140$°C, avec ou sans substrat. Le pic principal, observé par ACD, est associé à la fusion des cristaux monocliniques et il fournit une enthalpie, ΔH_{ACD}. On observe aussi deux autres pics qui sont généralement au-dessus et au-dessous du pic principal. Ceux-ci sont associés à un processus plus lent conduisant à un désordre dans le réseau physique produit dans l'échantillon au cours de la polymérisation. La somme des ΔH_{ACD} et $\Delta H_{réseau}$ est égale à ΔH_{total}. Lorsque la fusion est complétée, le ΔH_{total} est égal à ΔH_0, la chaleur de fusion des cristaux parfaits de PPi. Dans ce travail, on présente de nouvelles informations sur : (*i*) la phase non-cristalline du PPi naissant et sur l'enthalpie d'un polymère semi-cristallin; (*ii*) les modifications du processus de fusion dues au développement de tensions provoquées par l'expansion du matériel au cours de l'augmentation de la température lorsqu'un réseau physique est présent; (*iii*) l'effet d'un substrat sur le processus de fusion du polymère.

Mots clés : PPi naissant, calorimétrie lente, fusion sous contrainte, changement d'enthalpie, substrats.

[Traduit par la rédaction]

Introduction

While melt-crystallized crystals have been extensively investigated (1–10) since the synthesis of isotactic polypropylene (iPP) as a highly stereoregular polyolefin forty years ago, nascent iPP has attracted little interest. The difference between nascent and recrystallized iPP is expected to be similar to that observed for polyethylene (PE).

The morphology and melting behaviour of nascent PE is similar to that of the sample obtained by crystallization under shear. Comparative studies of crystals grown from sheared and quiescent solutions have revealed their distinct morphology (11–14). Microscopy (15), fast DSC (15), ^{13}C NMR (16), and ^{1}H NMR (16) investigations of nascent PE reveal that it has a unique morphology that is lost by melting and recrystallization. A recent Raman investigation of PE samples (17) reveals the complex nature of the nascent polymer (where four phases are identified) compared to the melt-crystallized.

Perfect crystals like those made for PE under pressure have not been produced for iPP. Hence, the equilibrium values of the melting temperature T_0 and of the enthalpy of fusion ΔH_0, which rely on extrapolation procedures, are still somewhat uncertain (18). Analysis by different techniques of material from various sources leads to the estimation of T_0 at 187.5°C and of ΔH_0 at 208 J/g (1).

The origin of strain-melting and the profile of a typical trace in slow calorimetry

When a semicrystalline polymer is submitted to a fast T-ramp (i.e., 10 K/min or 600 K/h), its melting trace shows the well-known sharp peak, which is completed a few K above T_m, its

Received November 5, 1996.

X. Zhang. Institute of Chemistry, Academia Sinica, Beijing, China.
H. Phuong-Nguyen, P. Bernazzani, I. Lapes, and G. Delmas.[1] Université du Québec à Montréal, Département de chimie, C.P. 8888, Succ. Centre-Ville, Montréal, QC H3C 3P8, Canada.

[1] Author to whom correspondence may be addressed. Telephone: (514) 987-3000, ext. 8238. Fax: (514) 987-4054. E-mail: r25421@er.uqam.ca

© 1997 NRC Canada

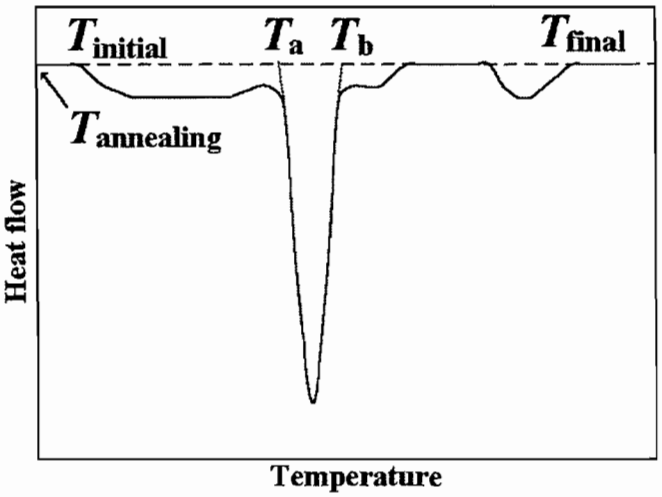
Can. J. Chem. Downloaded from www.nrcresearchpress.com by 91.121.58.235 on 09/08/12
For personal use only.

Table 1. Characteristics of iPP samples as received and after high-T treatment.

Sample	Characterization[a]		Fast DSC[b]			As received			After melting/crystallization[c]		
	$10^{-3}M_w$	M_w/M_n	T_m (°C)	ΔH_m (J/g)	d (g/cm^3)	$\alpha_c(d)$	Crystallinity α_c(X-ray)	$(\Delta H)^b$	(d)	Crystallinity α_c(X-ray)	$\alpha_c(\Delta H)^d$
F	300	3	163	87	0.8994	0.55	0.50	0.42	0.70	0.74	0.77
S, S[e]	140	3	164	85	0.8998	0.56	0.48	0.41	0.76	0.75	—
U	10^3	—	165	91	0.8996	0.55	0.52	0.44	0.72	0.75	—

[a]By turbidity at the LCST (24).
[b]v = 10 K/min.
[c]Crystallization at T_c = 156°C after $T_{equilibrium}$ = 280°C. Substrate Hg.
[d]Using ΔH_0 = 208 J/g and $\Delta H_{exp.} = \Delta H_{DSC} + 0.5\ \Delta H_{network}$.
[e]Samples S and S′ had similar characteristics but were of different lots.

Fig. 1. Schematic trace of melting a semicrystalline polymer by slow calorimetry (3 K/h). $T_{annealing}$ is the temperature of thermal equilibrium before the *T-ramp*. Integration for ΔH_{total} is done between $T_{initial}$ and T_{final}. ΔH_{DSC} is obtained by integration between T_a and T_b. $\Delta H_{network,\ low\ T}$ and $\Delta H_{network\ high\ T}$ are two other parts of ΔH_{total} at low and high T.



melting temperature. The melting trace starts at $T_{initial}$, which can be 50 K or more below T_m, but the main contribution to the enthalpy of melting comes from the part of the endotherm that is situated 15–20 K below T_m. For nascent iPP for instance, $T_{initial}$ = 50°C, T_m = 163–165°C, and ΔH = 85–91 J/g. The absence of high-T endotherms on the trace would justify the widely accepted assumption that there is no more meltable fraction in the semicrystalline polymers when the end of the melting endotherm is reached. Slow calorimetry, however, seems to indicate otherwise.

Figure 1 shows a schematic melting trace obtained through slow calorimetry (i.e., 0.05 K/min or 3 K/h). In Fig. 1, the flat endotherms occurring below and above the main peak lead to the idea of three fractions in the polymer. In the original work, the high-T endotherm was called fraction III; now it is termed the network. As presented in previous work (16, 19–23), the temperature ramp induces strain in chains linked by a physical network. For long-chain molecules, entanglements constitute the junctions in the network. The strain displaces the solid–liquid equilibrium towards high temperatures. The main characteristic of the flat endotherms is their high sensitivity to the history of the sample. The building up of strain in the network depends on nonequilibrium effects, which are narrowly dependant on the conditions of melting. The profile in Fig. 1 is the same as that found for cooling. An example for iPP is given in Fig. 6.

The original reasons for using a slow T-ramp are as follows. In the course of an investigation of gel formation in high molecular weight (MW) PE solution (20), heats of dissolution in dilute solution (0.5–1%) were obtained using a sensitive calorimeter equipped with a stirring device. It was found that complete dissolution of these high MW samples required long residence time in the calorimeter (i.e., a very slow T-ramp such as 1–3 K/h). The presence of a structure stable in solution even at high temperature has led to the understanding of physical gels (22) and of other intriguing properties of PE solutions (11–14).

The aim of the present paper is to investigate, with iPP, the meltability of the phases in which long-range order is absent. The technique used is slow calorimetry, which, by reducing the usual DSC rate by a large factor (two hundred or so), extends the range of accessible meltable order into the region not detectable by X-ray measurements. The concepts of strain-melting and the physical network have been developed (21) to interpret melting results on nascent polyethylene (19).

Experimental

Samples

The nascent samples consist of one very high molecular weight (MW) sample U (Himont, Willimington, Del., USA) and three medium MW samples F, S, and S′ = (Himont, Varennes, Qué., Canada) used in previous work (23, 24). The nascent samples F, S, S′ and U were received as fine powders. The characteristics of the samples, as received and after heat treatment and crystallization at T_c = 156°C, are given in Table 1. The values of the weight average (M_w) and the number average (M_n) molecular weights can be obtained from Table 1 (24). The solubility in xylene, an ASTM procedure to estimate the amorphous content, was 3% for F, S, and S′ and was not measured for U. After isothermal crystallization at T_c = 156°C, the crystallinity of the four samples was comparable (Table 1).

© 1997 NRC Canada

Can. J. Chem. Downloaded from www.nrcresearchpress.com by 91.121.58.235 on 09/08/12
For personal use only.

Can. J. Chem. Downloaded from www.nrcresearchpress.com by 91.121.58.235 on 09/08/12
For personal use only.

Calorimeters

The Setaram C80 calorimeter is a sensitive, differential calorimeter that accommodates large stainless steel cylindrical cells (o.d. = 16 mm, length = 95 mm) that hold the sealed glass tubes containing the sample and the reference. The reference cell is made as similar as possible to the sample cell. A heating rate v of 1–12 K/h, is used and the background noise is 5–10 μW. During the temperature ramp (from 30 to 290°C), the background signal is displaced by about 0.7 mW due to the imperfect radial balance of the calorimeter. In our recent work (23, 25–27), including the present one, the base line has been subtracted. The base line is constructed for each experiment by using the points at temperatures where there is no signal due to melting or crystallization. In traces with arrested melting there are three such regions, at low, medium, and high T. In other cases where the endotherms overlap there are only two regions, at low and high T.

The signal of the flat endotherms is considered significant when it is at least five times greater than the base line fluctuations. The large T range of integration introduces uncertainty in the integrated heats, which depends on the shape of the network endotherms, i.e., on the melting conditions. The uncertainty is at best 15 J/g and at worst 40 J/g. The reproducibility for the same set of conditions is usually very good. However, the effect of the different conditions on the range of melting of the network is clear and not affected by this uncertainty. Fast calorimetry is performed in a standard DuPont apparatus (DSC V40B).

Total enthalpy of fusion: ΔH_{solid}

The change of enthalpy in the material during the T-ramp is obtained by integrating the heat flow between $T_{initial}$ and T_{final}:

[1] $$\Delta H_{total} = \Delta H_{DSC} + \Delta H_{network}$$

where ΔH_{DSC} and $\Delta H_{network}$ are the enthalpies corresponding, respectively, to the sharp and the flat endotherms. ΔH_{DSC}, obtained by integrating the signal between T_a and T_b in Fig. 1, is equal to, or slightly smaller than, the enthalpy change obtained by fast DSC.

In the case of Fig. 1, the $\Delta H_{network}$ is divided into two contributions, and eq. [1] becomes

[2] $$\Delta H_{total} = \Delta H_{network,\ low\ T} + \Delta H_{DSC} + \Delta H_{network,\ high\ T}$$

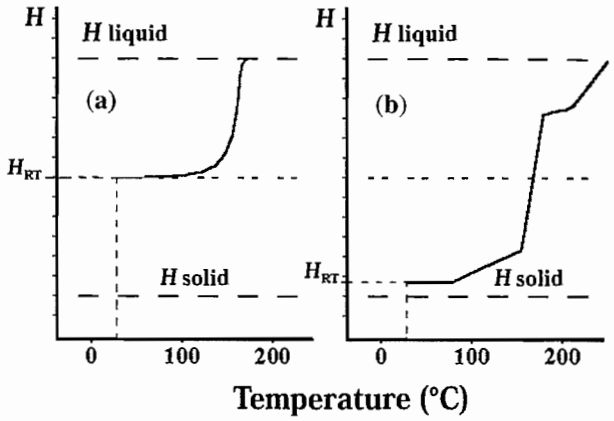
ΔH_{total} has been found to be much larger than that obtained by the fast T-ramp experiment for PE. It is usually near ΔH_0, the heat of fusion of perfect crystals.

Crystallinity

The value of α_c (X-rays) (the fraction of long-range order) is obtained by standard procedures from the diffractograms taken with a Wahrus camera and the Cu Kα radiation. α_c increases from 0.50 to 0.74 by melting and slow crystallization.

There is no unique way of decomposing the endotherms between ΔH_{DSC} and $\Delta H_{network}$. In the tables, ΔH_{DSC} is the value obtained by integrating the main peak using a temperature interval on the base line, which is almost constant (155–176°C) from one sample to another. This interval is found as shown in Fig. 1. With this method, the possibility that part of $\Delta H_{network}$ evolves at the same temperature as ΔH_{DSC} is ignored.

Fig. 2. The enthalpy of a semicrystalline polymer at room temperature and in a *T-ramp* as deduced from the usual DSC (Fig. 2(*a*)) and slow calorimetry (Fig. 2(*b*)). In Fig. 2(*a*) the enthalpy of a semicrystalline polymer H_{RT} is about halfway between H_{solid} and H_{liquid}, and H_{liquid} is reached in one rapid step. In Fig. 2(*b*), H_{RT} is near H_{solid} and reaches H_{liquid} through several steps, one of which is the rapid one seen in Fig. 2(*a*).



To obtain α_c (slow calorimetry) and compare it to α_c (X-ray), the fraction of long-range order in the sample, one has to take into account the contribution of small crystals that melt below 155°C and contribute to X-ray scattering and to α_c (X-ray). ΔH_{total} given by eq. [2] leads to $\alpha_c = 1$ because it includes short- and long-range order. The data of α_c (slow calorimetry), tabulated in Table 1, have been obtained using the relation:

[3] $$\alpha_c\ (\text{slow calorimetry}) = (208)^{-1}\ (\Delta H_{DSC} + 0.5\ \Delta H_{network})$$

The estimation of the contribution of $\Delta H_{network}$ to α_c (slow calorimetry), i.e., 0.5 $\Delta H_{network}$, is rather arbitrary but it gives values of α_c (slow calorimetry) comparable to α_c (*d*) and α_c (X-ray).

PP degrades easily in bulk in the presence of oxygen and even more so in solution (23, 24). Effective antioxidants, such as Irganox, limit the degradation during processing and characterization. In the conditions of the experiments, however, an antioxidant was not required in O_2-purged samples. After the high-T treatment, no change of colour of the sample was observed and its carbonyl content was not increased.

Results

State of the noncrystalline phase of nascent iPP

Our initial inquiry was to find the state of the noncrystalline phase at RT in nascent iPP by measuring the integrated heat between $T_{initial}$ and T_{final} for a sample equilibrated at $T_{annealing}$. A low value would have indicated that this phase was liquid and a high value that the sample had short-range order and melted in the conditions of the T-ramp. By analogy with PE, we expected to find that using the slow ramp would have led to a significant increase of ΔH_{total} from about 90 to about 200 J/g. Indeed, as shown in the tables, we found that ΔH_{total} was about equal to ΔH_0 (208 J/g).

This result leads to a reevaluation of the enthalpy change in a T-ramp. The schematics in Figs. 2(*a*) and (*b*) compare the information from the rapid and slow techniques for a sample

© 1997 NRC Canada

Table 2. Characteristics of the melting traces of the nascent iPP without substrate or on Hg after annealing at different temperatures.

$T_{annealing}$ (°C)	Sample	Substrate	m (mg)	v (K/h)	ΔH_{total} (J/g)	T_m[a] (°C)	Fig.	ΔH_{DSC} (J/g)	$\Delta H_{network,\ low\ T}$ (J/g)	$\Delta H_{network,\ high\ T}$ (J/g)	Number of runs
30	S′	Hg	12.6	3	**205**	170		95 (135–176)	40 (120–155)	70 (178–224)	1
—	S′–F	Hg	45.4–47.7	—	175	171	3(*a*)	85 (155–176)	55 (48–155)	35 (178–210)	3[b]
80	S′–S	Hg	15.4–22.8	—	150	171		87 (155–176)	20 (125–155)	43 (176–200)	2
	S′	none	68.3	—	135	171		85 (155–176)	15 (86–155)	35 (155–260)	1
100	U	Hg	64.5	—	115	174		75 (155–182)	15 (118–155)	25 (182–250)	1
130	F	Hg	12.8 — 12.9	—	150	165		−30 (144–156) 50 (160–172)	—	130 (172–240)	2

[a]Rounded figures.
[b]When the data in a row correspond to several traces, an average of the ΔH and the T interval is taken.

Table 3. Characteristics of the melting traces of the nascent iPP on Cu after annealing at 30°C and 120°C.

$T_{annealing}$ (°C)	Sample	Substrate	m (mg)	v (K/h)	ΔH_{total} (J/g)	T_m (°C)	ΔH_{DSC} (J/g)	$\Delta H_{network,\ low\ T}$ (J/g)	$\Delta H_{network,\ high\ T}$ (J/g)	r	Number of runs
30	S, F, U	Cu	37.2–42.4	3	170	171–173	80 (154–178)	80 (38–154)	10 (178–200)	0.04–0.10	3
120	S, F, U	—	14.6–16.1	—	**209**	171–174	95 (154–179)	12 (128–154)	102 (178–268)	0.04	3
—	U	—	53.7	—	154	174	86 (154–182)	20 (131–154)	48 (182–280)	0.12	2

having a DSC or X-ray crystallinity of, for instance 0.5. In the usual model (Fig. 2(*a*)), the noncrystalline part of the material is liquid, so its specific enthalpy at room temperature, H_{RT}, is midway between the enthalpy of the perfect crystals, H_{solid}, and the enthalpy of a totally disordered liquid, H_{liquid}. During the fast *T-ramp*, the enthalpy of the material reaches H_{liquid} at the end of the main endotherm. Figure 2(*b*) shows the change of enthalpy as recorded by the slow *T-ramp*. The enthalpy H_{RT} is now lower and closer to H_{solid} at RT, corresponding to a higher crystallinity. The three contributions of Fig. 1 and eq. [2] to ΔH_{total} are represented by two different slopes of $H(T)$, the slow slope for the disordering in the network and the fast slope for the destruction of long-range order.

The description of Fig. 2(*b*) indicates that, in spite of a low value of α_c, the properties of nascent iPP are more similar to those of a solid than of a liquid. This is consistent with cohesive and viscous properties of semicrystalline polymers.

A noncalorimetric analysis of nascent iPP (28), which supports the presence of a semiordered phase, comes from a recent advanced X-ray investigation. The authors show that the diffraction pattern is consistent with the superposition, in about equal amounts, of large crystals of the α form and of small and medium size crystallites of the γ form.

Conditions for obtaining a complete value of ΔH_{total}

As seen in the tables, ΔH_{total} is always higher than ΔH_{DSC} (90 J/g), but it does not always reach 200 J/g. This indicates that under some conditions only a part of the network organization is melted in the slow *T-ramp*. Two reasons can be advanced for an incomplete melting trace: the occurrence of partial melting during the residence time at $T_{annealing}$, and inadequate conditions for melting the strained fraction. For instance, the available time up to the calorimeter limit (290°C) may be insufficient when the sample mass m is too large or the *T-ramp* is too fast.

The best conditions for having the trace of Fig. 1 complete are then to avoid melting during annealing by using a low temperature (30–40°C), to melt a small quantity ($m < 20$ mg), and to use a slow *T-ramp* (v = 3 K/h). Then, the two parts of $\Delta H_{network}$ have about the same magnitude between 40 and 60 J/g.

In the early part of the present work, traces were obtained with $T_{annealing}$ equal to 100°C, a condition that seemed quite reasonable for a polymer with a T_m of 170°C. ΔH_{total} was found to be low because part of $\Delta H_{network,\ low\ T}$ had already occurred during the residence time at $T_{annealing}$.

© 1997 NRC Canada

Can. J. Chem. Downloaded from www.nrcresearchpress.com by 91.121.58.235 on 09/08/12
For personal use only.

Can. J. Chem. Downloaded from www.nrcresearchpress.com by 91.121.58.235 on 09/08/12
For personal use only.

Table 4. Characteristics of the melting traces of the nascent iPP on stainless steel after annealing at different temperatures.

$T_{annealing}$ (°C)	Sample	Substrate	m (mg)	v (K/h)	ΔH_{total} (J/g)	T_m (°C)	Fig.	ΔH_{DSC} (J/g)	$\Delta H_{network,\ low\ T}$ (J/g)	$\Delta H_{network,\ high\ T}$ (J/g)	r	Number of runs
30	S	stainless steel	14.4	3	**200**			85 (155–178)	40 (80–160)	75 (186–231)	<0.04	1
60	F	stainless steel	15.0	—	**211**	172		95 (155–177)	116 (111–157)			1
80	F, S	stainless steel	15.6–19.6	—	**205**	171		92 (155–179)	36 (120–155)	77 (180–244)		3
80	F	stainless steel	40.9	—	**217**	170		80 157–177	55 (116–157)	82 (177–270)		1
100	F, S, U	—	42.7–69.7	—	152	171 174		82	30 (108–153)	40 (181–230)	≈0.20[b]	5
	U	—	107.3	—	128	174		74 153–183	16 (112–153)	38 (183–254)	0.15	1
110	F	stainless steel	37.2	**1**	**222**	171	3(*b*)	67[a] (161–179)	150 (116–161)	5 (181–187)	<0.04	1

[a]The endotherms for ΔH_{DSC} and $\Delta H_{network,\ low\ T}$ are well separated.
[b]Note the effect of r on ΔH_{total}.

The recrystallization technique

The recrystallization of iPP quenched from the melt during the *T-ramp* below T_m has been reported in the literature. The recrystallized fraction melts in the fast DSC as long-range order. However, the present nascent samples do not recrystallize during fast melting in spite of their low crystallinity.

To clarify the present work with regard to the melting of substrates, we will explain the origin of its use. When ΔH_{total} was found to be incomplete using $T_{annealing}$ = 100°C, we did not think that the low-T fraction was melted, only that it was not distinct enough. Therefore, we were induced to increase m and to mix the nascent polymer with a fine powder of metals (stainless steel, Cu) to improve the mediocre heat transfer associated with a larger m. The effect was more than expected. The ΔH_{total} became complete or near complete. It turned out that this was not only an effect of increased m and thermal conductivity but a specific effect of the substrate. Thanks to the nucleating effect of the substrate, the network part of the nascent sample mixed with the substrate had recrystallized at $T_{annealing}$. Consequently, complete melting was possible in the *T-ramp*.

An unexpected finding of the work on substrates is that for large values of m, the amount of substrate is important in order to have ΔH_{total} complete. Equal amounts of polymer and substrate are insufficient for complete melting, while a large excess (for instance a factor of 20) is adequate. In the tables, the parameter $r = m$ (polymer)/m (substrate) is listed for the different traces. It is thought that two effects contribute to have ΔH_{total} incomplete when r is too large, namely, incomplete recrystallization at $T_{annealing}$ and incomplete melting of the strained fraction in the *T-ramp*.

The results are given separately for each substrate. Table 2 corresponds to melting with Hg or no substrate, Tables 3–5 with substrates Cu, stainless steel, and glass beads, respectively. The different columns give the conditions ($T_{annealing}$, sample, substrate, m), the melting characteristics (ΔH_{total}, T_m), and the decomposition according to eq. [2]. The data are arranged in order of increasing $T_{annealing}$ (30–130°C). The cases where ΔH_{total} is complete are printed in bold figures.

Melting on mercury and without substrate

Table 2 presents the results for different values of $T_{annealing}$ and m. To minimize the size of the tables, the results of ΔH_{total} and the different contributions have been averaged over different runs in Tables 2–5 for the traces corresponding to the same conditions. The last column gives the number of different runs in each row. With $T_{annealing}$ = 30°C, ΔH_{total} is complete with low values of m but incomplete when m increases (second row). The trace of Fig. 3(*a*) (ΔH_{total} = 185 J/g and m = 45.9 mg) corresponds to these conditions.

The next three rows with 80°C < $T_{annealing}$ < 100°C illustrate the effect of increased $T_{annealing}$ and increased m on ΔH_{total}, which drops to 115 J/g for $T_{annealing}$ = 100°C and m = 64.5 mg. Note that the fast DSC with m = 5 mg and v = 600 K/h gives a still lower value of ΔH_{total}, although the integration starts at 50°C. The last row corresponds to $T_{annealing}$ = 130°C. The traces show an exotherm followed by an endotherm of melting.

The partial melting that takes place at $T_{annealing}$ (not recorded) leads to recrystallization above $T_{annealing}$ followed by melting. During the time of annealing, an incomplete

© 1997 NRC Canada

Table 5. Characteristics of the melting traces of the nascent iPP on glass beads after annealing at 60 and 80°C.

$T_{annealing}$ (°C)	Sample	Substrate	m (mg)	v (K/h)	ΔH_{total} (J/g)	T_m (°C)	ΔH_{DSC} (J/g)	$\Delta H_{network,\ low\ T}$ (J/g)	$\Delta H_{network,\ high\ T}$ (J/g)	r	Number of runs
60, 80	U	glass beads	15.8–31	3	**220**	175	86 (153–181)	62 (111–153)	72[a] (180–275)	<0.04	4
80	U	glass beads	78.3	—	186	174	89 (153–183)	68 (110–183)	29 183–229	<0.04[b]	1
—	U	glass beads	92.9	—	121	175	79 (151–184)	27 (101–151)	15 (239–280)	0.4[b]	1

[a] T_{final} = 275°C corresponds to m = 31 mg.
[b] Note the effect of r on ΔH_{total}.

Can. J. Chem. Downloaded from www.nrcresearchpress.com by 91.121.58.235 on 09/08/12
For personal use only.

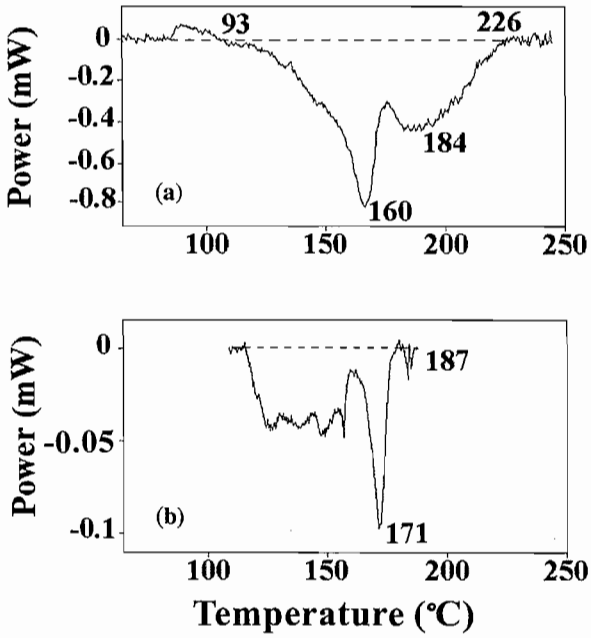


Fig. 3. (*a*) Melting trace of sample S′ at 3 K/h on Hg with ΔH_{total} incomplete, $T_{annealing}$ = 30°C (second row of Table 2), m = 45.9 mg. **Fig. 3.** (*b*) Trace in a very slow *T-ramp* (1 K/h), sample F (m = 37.2 mg) melted on stainless steel with $T_{annealing}$ = 110°C (last line of Table 4). Note that $\Delta H_{network}$ evolves entirely at low T and is well separated from ΔH_{DSC}.

transformation takes place in the nascent sample, which continues in the ramp and makes the analysis complex. The strained fraction is large (130 J/g) and melts over 70 K. The trace with $T_{annealing}$ = 140°C will be analyzed at the end.

Melting on substrates: Effect of $T_{annealing}$ on the range of melting of the strained fraction

Traces have been obtained by varying $T_{annealing}$ between 30 and 120°C. Conditions can be found to have ΔH_{total} complete over that range. The temperature of annealing/recrystallization has, however, a clear effect on the temperature of the high-T endotherm: the higher the $T_{annealing}$, the higher the high-T endotherm.

In Table 3 with Cu as substrate, two values of $T_{annealing}$ are given. The results for $T_{annealing}$ = 30°C are very similar to those on Hg as substrate, with an incomplete ΔH_{total} (170 J/g) for m = 40 mg and a range of r (0.04–0.10). The end of the high-T endotherm (T_{final}) is 200°C and its size is small (<10 J/g). When $T_{annealing}$ = 120°C, ΔH_{total} is complete and T_{final} is about 263°C. The efficiency of Cu powder for melting/recrystallization of nascent iPP is clear when these traces are compared to those in Table 2 on Hg with $T_{annealing}$ = 80–100°C (ΔH_{total} = 150–115 J/g). In the last row of Table 3, the effect of a smaller amount of substrate can be noted. ΔH_{total} is incomplete (154 J/g) for m = 53.7 mg and r = 0.12.

Effect of the ratio between the sample mass (m) and the substrate mass

With substrates other than Cu, it has again been found that a small value of r is important in order to have ΔH_{total} complete. The generality of the effect is seen in Fig. 4 where ΔH_{total} for each trace has been plotted against m in Fig. 4(*a*) and against r in Fig. 4(*b*). ΔH_{total} is seen to diminish when m and r increase. Figure 4(*b*) shows that if r is <0.04 (i.e., if there are 25 times more substrate than sample), ΔH_{total} is complete. The points with no substrate or with Hg as substrate have been omitted from Fig. 4(*b*). Speculations on the molecular reasons for this effect will be presented later.

In Table 4 with stainless steel as substrate, $T_{annealing}$ ranges between 30 and 110°C. ΔH_{total} is complete for the first four rows with $T_{annealing}$ = 30–80°C. For the next two rows ΔH_{total} is incomplete, but this is not due to the high value of $T_{annealing}$ (100°C) but to the insufficient amount of substrate (r = 0.15–0.20).

In Table 5 the substrate is glass beads and $T_{annealing}$ = 60 and 80°C. ΔH_{total} is complete for the conditions of the first row. The comparison of the last two rows illustrates dramatically the effect of r. With a large amount of glass beads (m = 78.6 and r = 0.02), ΔH_{total} is not too far from complete (186 J/g) and T_{final} is low (229°C), while in the last row for m, which is not much larger (m = 92.9), ΔH_{total} has dropped to 120 J/g due to a want of substrate (r = 0.4).

Efficient method to reduce strain: melting on a substrate in a very low *T-ramp*

The last row of Table 4 (m = 37.2 mg) corresponds to $T_{annealing}$ = 110°C and r = 0.04. The difference from the other traces is the small size of the high-T endotherm. ΔH_{total} is complete and T_{final} is 187°C, as can be seen in Fig. 3(*b*). This trace was made

© 1997 NRC Canada

Fig. 4. Influence of the ratio $r = m$ (polymer) $/m$ (substrate) on the completeness of ΔH_{total}. The abscissa of Figs. 4(*a*) and (*b*) are m (polymer) and r respectively.

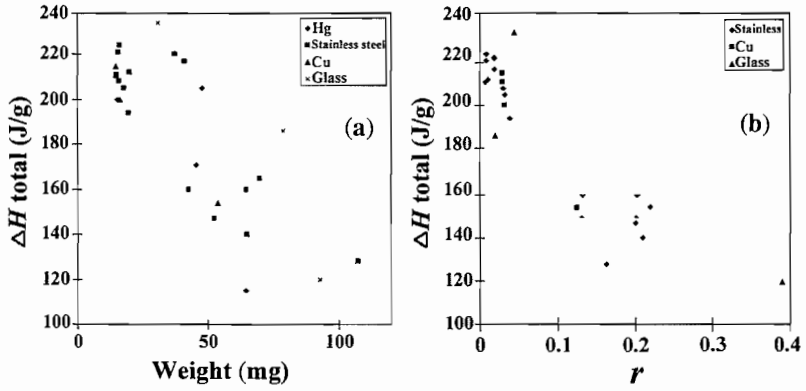


Table 6. Characteristics of the melting and recrystallized traces of the nascent iPP on Hg after annealing at 140°C.

$T_{annealing}$ (°C)	Sample	Substrate	m (mg)	v (K/h)	ΔH_{total} (J/g)	T_m/T_c (°C)	Fig.	ΔH_{DSC} (J/g)	$\Delta H_{network,\ low\ T}$ (J/g)	$\Delta H_{network,\ high\ T}$ (J/g)	Number of runs
140	S′	Hg	14.3	3	**237**	170.7	5(*a*)	135 (155–176)	15 (177–217)	80 (235–280)	1
	S′	—	14.3	—	**254**	141.3	5(*b*)	150 177–111	15 (111–71)	82 (240–177)	1

at $v = 1$ K/h instead of the usual 3 K/h. One sees that the melting of the network fraction is now well separated from that of the monoclinic crystals. A mechanism to explain this effect (also found on PE) will be presented below. The demonstration given by the trace of Fig. 3(*b*) that strain-building can be avoided in the *T-ramp* is worth the calorimeter time for that experiment (90 h instead of the usual 73 h for $v = 3$K/h).

Effect of annealing at 140°C

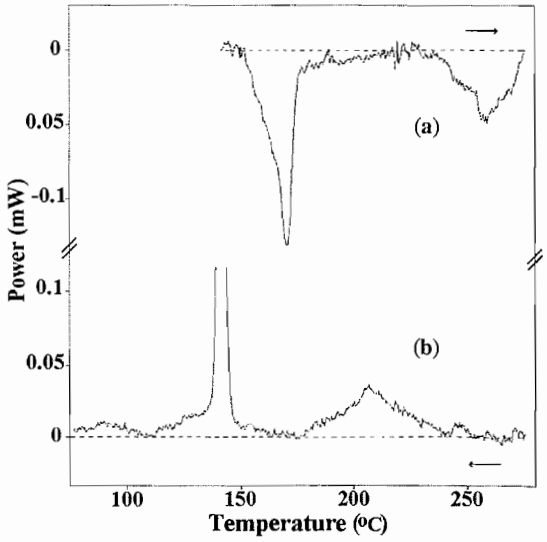
Highly crystalline samples are prepared by annealing a quenched sample between 140 and 160°C (8, 10). To ensure the complete growth of monoclinic crystals, the sample is left for several days at 140°C. The melting trace of a sample annealed at 140°C during the usual time (17 h) is given in Fig. 5(*a*). Its characteristics are given in Table 6 together with those of the crystallizing trace of the same run. One notes in Fig. 5(*a*) a large peak (135 J/g) at the melting temperature of the monoclinic crystals. In these conditions, the recrystallization that was observed at lower $T_{annealing}$ (Table 2) was completed and melting started at 152°C. The size of the peak indicates that the sample is no longer nascent but has a higher monoclinic content. Obviously, part of $\Delta H_{network,\ low\ T}$ overlaps with ΔH_{DSC} but, even if this is taken into account, ΔH_{DSC} is higher than in the nascent or the samples annealed at lower T. The high-T endotherm that occurs between 230 and 276°C is well separated from the first endotherm.

Reversibility of the phase change

The crystallization trace of the same sample is given in Fig. 5(*b*). The two main peaks of the melting and crystallizing traces match in magnitude, as can be seen in the figures or in Table 6. A small exotherm is seen on the crystallization trace at low-T. One should note the rapidity of the crystallization of the monoclinic crystals. In another work investigating the crystallization in a *T-ramp* (23), it was found that crystalliza-

Fig. 5. (*a*) Melting trace after $T_{annealing} = 140$°C on stainless steel. ΔH_{DSC} is now 150 J/g and $\Delta H_{network,\ high\ T}$ (87 J/g) is well detached from the main peak. The sample is no longer nascent after 17 h at $T_{annealing}$.

Fig. 5. (*b*) Crystallization trace of a portion of the same sample on stainless steel at 3 K/h (Table 6). Note the rapid crystallization of the monoclinic crystals and the symmetry of the two traces.

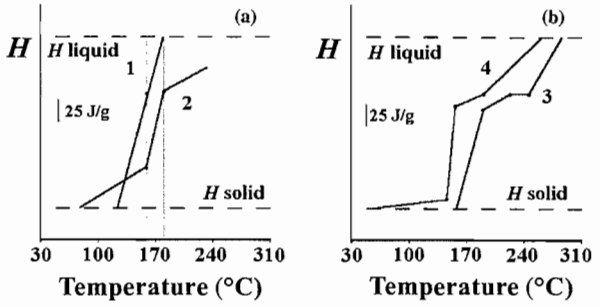


Can. J. Chem. Downloaded from www.nrcresearchpress.com by 91.121.58.235 on 09/08/12
For personal use only.

© 1997 NRC Canada

Can. J. Chem. Downloaded from www.nrcresearchpress.com by 91.121.58.235 on 09/08/12
For personal use only.

Fig. 6. Changes of enthalpy $H(T)$ for iPP as in Fig. 2. Curves 1 and 2 of Fig. 6(*a*) correspond to the traces of Fig. 4. Curves 3 and 4 of Fig. 6(*b*) correspond to the melting and crystallization traces of Fig. 5 after $T_{annealing}$ = 140°C. Explanations in the text.



tion was more rapid after a long treatment at high temperature. The molecular reason is likely to be the formation of larger domains where the network phase and the random-coil phase do not overlap. As a consequence the crystals are less impinged upon by the physical network than in the usual condition (9) and they grow faster. The reversibility of the melting and crystallization traces has also been reported on PE. Uncertainty in the base line is minimal for Figs. 6(*a*) and (*b*) so the cause of the large values of ΔH_{total} (237–254 J/g) is not known.

Change of enthalpy between H_{liquid} and H_{solid} for nascent iPP

The data in the tables show that the path going from H_{solid} to H_{liquid} for a nascent sample depends on the conditions of melting.

The variation of $H(T)$ for iPP can be followed as in Fig. 2. There are many possibilities that correspond to the data in the tables. Only the paths deduced from the traces in Figs. 3(*a*), (*b*), and 5 have been reported as examples in Figs. 6(*a*) and (*b*). In the two schematic curves of Fig. 6(*a*) with $T_{annealing}$ < 120°C, only the network phase change is modified by annealing and the slow ramp. Curve 1 corresponds to the very special case of the 1 K/h *T-ramp* (Fig. 3(*b*)) where the kinetics of the network phase change and the monoclinic phase change are not too different, so that H increases almost continuously between $T_{initial}$ and T_{final} (116–187°C). In curve 2, the change of enthalpy due to the network occurs in part before and in part above the main peak. The end of curve 2 does not quite reach H_{liquid} because melting is incomplete (Fig. 3(*a*)).

In Fig. 6(*b*), curve 3 corresponds to $H(T)$ for the sample annealed at 140°C (Fig. 5(*a*)). Annealing has increased the monoclinic crystal content. The change of enthalpy due to the network occurs completely in the melt, the largest part occurring above 230°C. In curve 4, which corresponds to the crystallization trace, the changes of $H(T)$ in the cooling ramp are similar to those during the melting except for the small part at low T. The crystallization of the monoclinic crystals gives a very sharp exotherm. The unusual result that the monoclinic crystals in the same *T-ramp* take more time, or a longer interval of temperature, to melt than to grow is to be noted.

Mechanism of action of the substrate

A conducting substrate increases the heat transfer between the glass tube and the polymer, and across the sample, and accelerates the phase changes. The rates of crystallization from the melt or recrystallization below T_m of iPP are known to be enhanced by nucleating agents. However, these are usually used in very small quantities. These mechanisms must occur in the case of the slow melting of nascent iPP and lead to a more complete ΔH_{total}. However, there must be another effect at work, particularly in view of the efficiency of a poorly conducting substrate such as glass beads. It may be related to the movement of the more mobile chains to be adsorbed on the substrate. The mobility of the chains well below their melting point has been established by different techniques (C_p, X-ray patterns and molecular simulation). In the temperature ramp, phase separation between the network chains and the free chains is enhanced by the interaction with the substrate. As a consequence, strain is reduced and the liquid phase in the melt is easier to reach. The effect of a very slow *T-ramp* (Fig. 3(*b*)) may also be to permit phase separation to occur before extensive expansion and melting take place.

Other possible models relevant to the present work

Earlier work in the literature (29) has provided in-depth analysis of the melting and crystallization process. Experimental evidence of superheating has been reported for a variety of materials whose melting traces were taken at different rates of heating. These are organic (sucrose or sugars, amines) or inorganic compounds (silicates, quartz, tin, and others). The studies have followed the displacement of the melting endotherm to a higher temperature with emphasis on the T_m value. The temperature shift in some systems was very large. Measurements were made in fast DSC, the lowest ramp being higher than those used in the present work. The variation of the enthalpy changes with the rate of heating has not been investigated systematically. The fact that part of the enthalpy of melting was missing at a high heating rate could have been found if accurate measurements had been possible.

It was found that the concept of strain-melting and the effect of the expansion of a physical network is useful in interpreting data from slow calorimetry. Other models may be equally successful, particularly if they are developed from molecules that are not chain molecules. A nonequilibrium melt is a sure way to raise T_m. The nonequilibrium would be the result of steric hindrance due either to large side groups or to strong intermolecular forces. The discrepancy between melting and dissolution characteristics of poly-4-methyl pentene has been explained in this way (27). Current work on the melting and dissolution of sugars seems to be explained in these terms. The effect of a substrate on melting has been associated with a phase separation between network chains and free chains, facilitated by the foreign solid surface. Parameters characteristic of the crystalline and melted phases, such as the irregularity of the crystal surface, may change the viscosity of the melt in the presence of a substrate. Without involving phase separation, these effects can modify the melting and crystallization rate of iPP as was found above.

Conclusion

This work provides new information on the phases and enthalpy content of nascent and semicrystalline iPP. It is comparable to that obtained on PE and is thought to be generalizable to other polymers.

© 1997 NRC Canada

Analysis of the melting trace of nascent iPP indicates that the noncrystalline phase is meltable with an enthalpy as large as that of the monoclinic crystals. Conditions have been found where the organization in the noncrystalline phase of the nascent sample melts below T_m as would be expected for short-range order. This short-range order occurs between chains linked by a physical network. The conditions for melting the network below T_m are not met in the usual fast melting, so that strain, which builds up in the temperature ramp and at T_m, does not allow the network fraction melt. The monoclinic crystals are rather insensitive to the history of the sample but the network phase is not. By modifying the conditions, one can follow the changes in the network phase of nascent iPP in a *T-ramp*. They cover a range between two extremes: the network phase melts without strain, or it is transformed into a mixture of monoclinic crystals and a highly strained fraction. To reach a better understanding of the phase difference between nascent and melt/recrystallized polymer, the crystallization traces and the melting traces of melt/crystallized samples have been investigated (30).

Acknowledgements

The support of the Natural Sciences and Engineering Research Council of Canada is acknowledged. We thank Dr. T. Bohossian who started the investigation and Dr. Kartoo and Dr. Dziemianovitch of Himont (Varennes, Qué., Canada and Wilmington, Del., USA) for the iPP samples.

References

1. H.S. Bu, S.Z.D. Cheng, and B. Wunderlich. Makromol. Chem. Rapid Commun. **9**, 75 (1988).
2. D.R. Gee and T.P. Melia. Makromol. Chem. **132**, 195 (1970).
3. B. Monasse and J.M. Haudin. Colloid Polym. Sci. **263**, 822 (1985).
4. F. De Candia, P. Iannelli, O. Staulo, and V. Vittoria. Colloid Polym. Sci. **266**, 608 (1988).
5. F.J. Balta Calleja, J. Martinez Salazar, and T.J. Asano. Mater. Sci. Lett. **7**, 165 (1988).
6. J.J. Janimak, S.Z.D. Cheng, A. Zhang, and E.T. Hsieh. Polymer, **33**, 728 (1992).
7. R.J.J. Samuels. J. Polym. Sci. Polym. Phys. Ed. **13**, 1417 (1975).
8. J. Varga, F. Schulek-Töt, and A. Ille. Colloid Polym. Sci. **269**, 655 (1991).
9. K. Mexghani, R.A. Campbell, and P.J. Philips. Macromolecules, **27**, 997 (1994).
10. R.Kitamaru, F. Horri, and K. Murayama. Macromolecules, **19**, 636 (1986).
11. A.M. Rijke and L. Mandelkern. J. Polym. Sci. Polym. Phys. Ed. **8**, 225 (1970).
12. A. Zwijnenburg and A.J. Pennings. Colloid Polym. Sci. **253**, 452 (1975).
13. K.A. Narh, P.J. Barham, and A. Keller. Macromolecules, **15**, 464 (1982).
14. (*a*) P. Smith, P.J. Lemstra, J.P.L. Pijpers, and A.M. Kiel. Colloid Polym. Sci. **259**, 1080 (1981); (*b*) P. Smith and P.J. Lemstra. Colloid Polym. Sci. **258**, 891 (1980).
15. H.D. Chanzy, E. Boujour, and R.H. Marchessault. Colloid Polym. Sci. **252**, 8 (1974).
16. F. Morin, G. Delmas, and D. Gilson. Macromolecules, **28**, 3248 (1995).
17. R. Matter, W. Stille, and G. Strobl. J. Polym. Sci. Part B: Polym. Phys. **31**, 99 (1993).
18. B. Wunderlich. Macromolecular physics. Academic Press, London. 1973. pp. 48, 72.
19. H. Phuong-Nguyen and G. Delmas. Macromolecules, **408**, 25 (1992).
20. H. Phuong-Nguyen and G. Delmas. Macromolecules, **414**, 25 (1992).
21. G. Delmas. J. Polym. Sci. Part B: Polym. Phys. **31**, 2011 (1993).
22. H. Phuong-Nguyen and G. Delmas. J. Mater. Sci. **29**, 3612 (1994).
23. H. Phuong-Nguyen and G. Delmas. Collect. Czech. Chem. Commun. **60**, 1905 (1995).
24. T. Bohossian and G. Delmas. J. Polym. Sci. Part B: Polym. Phys., **30**, 993 (1992).
25. H. Phuong-Nguyen and G. Delmas. Thermochim. Acta, **238**, 257 (1994).
26. H. Phuong-Nguyen and G. Delmas. J. Solution Chem. **23**, 249 (1994).
27. H. Phuong-Nguyen, G. Charlet, and G. Delmas. J. Therm. Anal. **46**, 809 (1996).
28. E. Ferracini, A. Ferrero, V. Malta, S. Martelli, and W. Vogel. Colloid Polym. Sci. **269**, 1241 (1991).
29. E. Hellmuth and B. Wunderlich. J. Appl. Phys. **36**, 3030 (1965), and refs. therein.
30. X. Zhang, I. Lapes, H. Phuong-Nguyen, and G. Delmas. To be published.

Can. J. Chem. Downloaded from www.nrcresearchpress.com by 91.121.58.235 on 09/08/12
For personal use only.

© 1997 NRC Canada

Structural studies and redox reactivity of platinum complexes of 14-membered tetraaza macrocyclic ligands

S. Chandrasekhar, W.L. Waltz, L. Prasad, and J.W. Quail

Can. J. Chem. Downloaded from www.nrcresearchpress.com by 91.121.58.235 on 09/08/12
For personal use only.

Abstract: Pt(II) monomeric complexes of N-containing macrocycles have been synthesized and characterized in solution by ^{1}H NMR, ^{13}C NMR, and electrospray mass spectroscopy (ESMS) and in the solid state by X-ray crystallography. Crystals of [Pt(cyclam)]$(ClO_4)_2$ (cyclam = 1,4,8,11-tetraazacyclotetradecane) are orthorhombic, space group $P2_1cn$, a = 9.596 (3), b = 14.595 (21), c = 24.8782 (20) Å, Z = 8. The structure was solved by direct methods and was refined by the full-matrix least-squares method to R = 0.073 and R_w = 0.093 for 2976 reflections with $I \geq 2.5\sigma(I)$. Crystals of [Pt(*N*-methylcyclam)]-$(ClO_4)_2 \cdot CH_3CN$ (N-methylcyclam = 1,4,8,11 tetramethyl-1,4,8,11-tetraazacyclotetradecane = NMe_4cyclam = tmc) are orthorhombic, space group *Pmcn*, a = 9.574 (8), b = 14.116 (5), c = 17.5456 (15) Å, Z = 4. The structure was solved by direct methods and was refined by the full-matrix least-squares method to R = 0.067 and R_w = 0.091 for 2216 reflections with $I \geq 2.5\sigma(I)$. Cyclic voltammetry and EPR spectroscopy have been used to study the redox reactivity of the Pt(II)and Pt(IV) complex ions. The solution chemistry of Pt(IV) complexes based on cyclam and *N*-methylcyclam was investigated by electrospray mass spectrometry. Electrospray mass spectral evidence has been obtained for the formation of [Pt(III)(cyclam)Cl_2]$^+$ and [Pt(III)(N-methylcyclam)Cl_2]$^+$ ions.

Key words: Pt macrocycles, crystallography, electrospray mass spectroscopy, cyclic voltammetry, Pt(III) complex ions, tetraaza macrocycles.

Résumé : On a préparé des complexes monomères du Pt(II) contenant des macrocycles azotés et on les a caractérisés en solution par la RMN du ^{1}H, du ^{13}C, par la spectroscopie de masse par électrovaporisation et par la cristallographie de rayons X dans l'état solide. Les cristaux de [Pt(cyclam)]$ClO_4)_2$ (cyclam = 1,4,8,11-tétraazacyclotétradécane) sont orthorombiques et appartiennent au groupe d'espace $P2_1cn$, avec a = 9,596 (3), b = 14,595 (21), c = 24,8782 (20) Å, Z = 8. On a résolu les structures par les méthodes directes et on les a affinées par la méthode des moindres carrés, matrice complète, jusqu'à des valeurs de R = 0,073 et de R_w = 0,093 pour 2976 réflexions avec $I \geq 2.5\sigma(I)$. Les cristaux de [Pt(*N*-méthylcyclam) $(ClO_4)_2 \cdot CH_3CN$ (*N*-méthylcyclam = 1,4,8,11-tétraméthyl-1,4,8,11-tétraazacyclotétradécane = NMe_4cyclam = tmc) sont orthorombiques et appartiennent au groupe d'espace *Pmcn*, avec a = 9,574 (8), b = 14,116 (5), c = 17,5456 (15) Å, Z = 4. On a résolu les structures par les méthodes directes et on les a affinées par la méthode des moindres carrés, matrice complète, jusqu'à des valeurs de R = 0,067 et de R_w = 0,091 pour 2216 réflexions avec $I \geq 2.5\sigma(I)$. On a fait appel à la voltampérométrie cyclique et à la spectroscopie de RPE pour étudier la réactivité redox des ions complexes de Pt(II) et de Pt(IV). On a étudié, par spectroscopie de masse et par électrovaporisation, la chimie de solution des ions complexes Pt(IV) formés à partir de cyclam et de *N*-méthylcyclam. La spectroscopie de masse par électrovaporisation a fourni des preuves spectrales de la formation des ions de [Pt(III)(cyclam)Cl_2]$^+$ et de [Pt(III) (*N*-méthylcyclam)Cl_2]$^+$.

Mots clés : macrocycles de Pt, cristallographie, spectroscopie de masse par électrovaporisation, voltampérométrie cyclique, ions complexes de Pt(III) tétraazamacrocycles.

[Traduit par la rédaction]

Received August 23, 1996.[1]

This paper is dedicated to Professor Henry Taube, on the occasion of the Taube Fest celebration at the University of Saskatchewan in October 1995.

S. Chandrasekhar.[2] Department of Chemistry, University of Prince Edward Island, 550 University Avenue, Charlottetown, PEI C1A 4P3, Canada.
W.L. Waltz[2] and J.W. Quail.[2] Department of Chemistry, 110 Science Place, University of Saskatchewan, Saskatoon, SK S7N 5C9, Canada.
L. Prasad. Department of Biochemistry, University of Saskatchewan, Saskatoon, SK S7N 5C9, Canada.

[1] Revision received August 15, 1997.
[2] Authors to whom correspondence may be addressed. University of Prince Edward Island: Telephone: (902) 566-0375. Fax: (902) 566-0632. E-mail: schandrasekh@upei.ca
University of Saskatchewan: Telephone: (306) 966-4708. Fax: (306) 966-4730. E-mail: waltz@sask.usask.ca

© 1997 NRC Canada

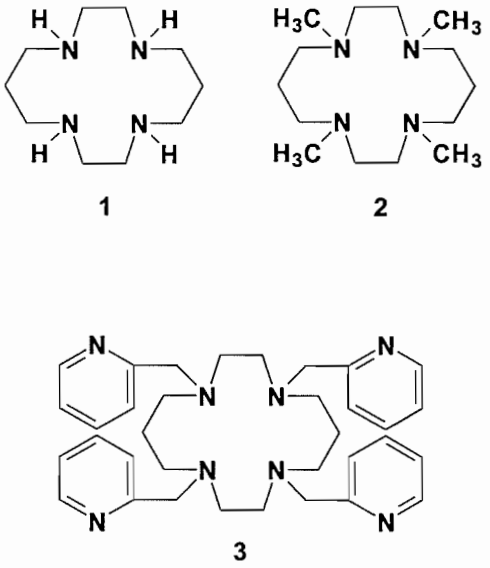
Can. J. Chem. Downloaded from www.nrcresearchpress.com by 91.121.58.235 on 09/08/12
For personal use only.

Introduction

The use of macrocyclic ligands such as 1,4,8,11-tetraazacyclotetradecane (cyclam or [14]-ane N_4, **1**, Scheme 1) complexed to transition metal ions has provided many new opportunities to form and stabilize systems where the metal center is in a less common oxidation state (1–4). In some instances, single crystal structures of monomeric Pd(III) complexes have been determined (5–7) in which the macrocyclic ligand has been used to stabilize the 3+ oxidation state. In contrast to the numerous redox studies on Ni(II) and Pd(II) complex ions, the redox reactivity of Pt(II) macrocyclic complexes has not been well understood. In many cases, di- or polymetallic species with metal–metal bonds have been obtained (8) and a monomeric Pt(III) complex is rarely observed. A case in isolation is the stabilization of a Pt(III) complex of a trithia macrocyclic ligand (9). Electrochemical oxidation of the distorted square-pyramid *bis*-Pt(II) complex of [9]-aneS_3 yielded the Pt(III) complex ion, as evidenced in the EPR spectrum. However, the Pt(II) complex of [18]-aneS_6 could not be oxidized chemically or electrochemically (10). Most of the Pt(III) complexes have been obtained as transients in pulse radiolysis (11, 12) or by X-ray or γ-irradiation of single crystals of Pt(II) complexes (13, 14). Recently, the redox reactivity of Pt(II)complexes based on cyclam and *N*-methylcyclam with free radicals formed by pulse radiolysis of aqueous media, in conjunction with UV–visible absorption and conductivity detection, was studied in our laboratory (15). One of the objectives of the present investigation is to obtain complementary views on the formation and detection of Pt(III) transient species using EPR spectroscopy, cyclic voltammetry, and electrospray mass spectroscopy (ESMS). Also, the Pt(I) monomeric species is rarely observed with aza ligands and usually dimerizes in solution. Recently, Ni(I), Cu(I), and Pd(I) monomeric species have been stabilized using macrocyclic ligands such as [14]-aneS_4 and *N*-methylcyclam and pendant arm macrocycles (5, 16–18). Low-valent metal macrocyclic complexes have been utilized in the catalytic and electrocatalytic reduction of small molecules such as CO_2 (19–22) and O_2 (23, 24). As a result of the stabilization of Ni(I) species with *N*-methylcyclam, this ligand has been used to model F_{430} (wherein the nickel cycles between Ni(II) and Ni(I) during catalysis (25)), and the Ni(I) complex, *RRSS*-Ni(tmc)](CF_3SO_3) has been crystallographically characterized (26).

In the present study, Pt(II) complexes of cyclam, **1**, and *N*-methylcyclam (NMe_4cyclam), **2** (Scheme 1), have been synthesized and the crystal structures have been determined in order to understand structure–reactivity relationships and stacking effects, if any. The ligand 2-pyridylmethyl-1,4,8,11-tetraazacyclotetradecane, **3** (tpmc, Scheme 1), and its Pt complex were also synthesized with a view to combining the properties of the relatively rigid and kinetically inert structural element of the macrocycle with those of the more flexible and kinetically labile open-chain ligands. The Cu(II) complex of tpmc is dinuclear with two copper atoms coordinated outside the macrocyclic cavity (27) while in the rhenium complex only three of the N atoms from the macrocyclic ring are coordinated (28). The Pd(II) complex of the pendant arm macrocycle 1,4,7-tris(2-pyridylmethyl)-1,4,7-triazacyclononane is a distorted square-base pyramidal environment of five coordinated nitrogen atoms, two of which are pyridyl nitrogen atoms in equatorial positions (29). Recent studies (30) on the Pd(II) complex of a related pendant arm macrocycle, 1-thia-4,7-bis(pyridylmethyl)diazacyclononane, revealed coordination of both the pyridyl nitogens to the Pd(II) ion along with two nitrogens from the macrocycle with strong axial interaction from the S atom of the macrocycle. Hence it was of interest to study the coordinating ability of tpmc with Pt(II) ion and to investigate axial coordination of the pendant arms of the macrocycle in going from square-planar Pt(II) to octahedral Pt(IV) geometry. The redox behavior of the Pt(II)cyclam-based complexes has been studied using EPR spectroscopy and cyclic voltammetry to elucidate various reaction pathways that involve either a metal-based species or ligand-based radicals. The relatively new technique of electrospray mass spectroscopy (31) has been used to characterize and investigate the solution chemistry of platinum complex ions. ESMS is also useful in the detection of transient species in solution because of its short time domain and minimal fragmentation.

Scheme 1.



Experimental

Materials and methods

The ligands 1,4,8,11-tetraazacyclotetradecane ([14]-aneN_4, cyclam) and 1,4,8,11-tetramethyl-1,4,8,11-tetraazacyclotetradecane (*N*-methylcyclam = tmc = NMe_4cyclam) were obtained from Aldrich and used as received. All solvents were of BDH (Analar) grade. Acetonitrile was distilled over CaH_2 prior to use. Water purified by a Millipore Super-Q system was used to prepare the aqueous solutions.

UV–visible spectra were recorded on a Cary 2315 spectrophotometer. Infrared spectra were recorded with a BIORAD FTS-40 FTIR and 3240-SPC data station. ^1H and ^{13}C NMR were obtained with a Bruker AM-300 FT NMR instrument using a broad probe at 75.47 MHz for ^{13}C nuclei. EPR spectra were recorded on a Bruker ESP 300 instrument. Diphenylpicrylhydrazyl radical was used as a field marker (g = 2.0037). Elemental analyses were obtained either from the microanalytical services, Department of Chemistry, University of Saskatchewan, or the Guelph Chemical laboratories Ltd., Guelph, Ontario, Canada. Electrochemical measurements

© 1997 NRC Canada

Can. J. Chem. Downloaded from www.nrcresearchpress.com by 91.121.58.235 on 09/08/12
For personal use only.

were made using MICROEL program microvoltammetry, version 5.0, developed and modified by Prof. A. Baranski[3] using PC-Labcard, model no. PCL-812PG. The electrochemical cell employed the standard three-electrode configuration with a Pt working microelectrode, a Pt auxiliary electrode, and the reference electrode. In aqueous solutions, an Ag/AgCl electrode linked to the cell via a bridge containing saturated KCl was used as the reference and 1 M NaCl was used as the supporting electrolyte. In nonaqueous solutions (acetonitrile), $Ag/AgNO_3$ (0.1 M) or a silver wire was used as the reference electrode. All potentials in nonaqueous solutions are reported vs. Fc^+/Fc couple. Electrospray mass spectral studies were conducted on a VG Quattro II (FISONS) triple-quadrupole electrospray mass spectrometer with 100% methanol as the mobile phase. The compounds were dissolved in methanol (2 mM) and diluted (1:10) with methanol. The diluted solution was injected directly into the spectrometer via a Rheodyne injector using a FISONS LC syringe pump to deliver the solution at a flow rate of 20 μL min^{-1}. Nitrogen was used both for nebulization and as a drying gas with flow rates of approximately 20 and 250 L h^{-1}, respectively.

Syntheses

*[Pt(cyclam)]$(ClO_4)_2$ and [Pt(*N*-methylcyclam)]$(ClO_4)_2$*

Pt(II)cyclam complexes, viz., [Pt(cyclam)]$(ClO_4)_2$, **4**, and [Pt(*N*-methylcyclam]$(ClO_4)_2$, were synthesized using published procedures (32) with suitable modifications. Both complexes gave satisfactory C, H, and N analyses. Crystals suitable for X-ray diffraction were obtained by diffusion of ether into acetonitrile solutions of the Pt(II) complexes. The Pt(II) complex based on *N*-methylcyclam crystallized with one molecule of acetonitrile as a solvent of crystallization ([Pt(*N*-methylcyclam)] $(ClO_4)_2 \cdot CH_3CN$), compound **5**.

*[Pt{N-methylcyclam)Cl_2]$(BF_4)_2$, **6***

An acetonitrile solution of [Pt(*N*-methylcyclam)]$(ClO_4)_2$ (100 mg, 0.17 mmoL) containing NBu_4Cl was oxidized with $NOBF_4$. Diffusion of ether into the acetonitrile solution yielded greenish yellow crystals that were dried under vacuum. Yield 100 mg; 90%. Anal. calcd. for $PtC_{14}H_{32}N_4Cl_2B_2F_8 \cdot 0.5\ CH_3CN$: C 25.11, H 4.71, N 8.79%; found: C 24.89, H 4.39, N 8.51%. A similar species was obtained using $Na_2S_2O_8$ as an oxidant in aqueous solutions of [Pt(cyclam)]$(ClO_4)_2$ containing NaCl.

*1,4,8,11-Tetrakis(2-pyridylmethyl)-1,4,8,11-tetraazacyclotetra-decane, **3** (tpmc)*

The ligand 1,4,8,11-tetrakis(2-pyridylmethyl)-1,4,8,11-tetraaza-cyclotetradecane, **3**, was synthesized by a modification of the literature method (27). An aqueous solution of cyclam (500 mg, 2.5 mmol) and sodium hydroxide (1.2 g, 30 mmol) was added dropwise to an aqueous solution of picolyl chloride hydrochloride (1.9 g, 15 mmol). The solution was stirred vigorously for 3 days, over which period the color changed from pink to golden-yellow, and a white solid was obtained. The solid was filtered and dried under suction. Upon cooling an ethanolic solution, colorless crystals of the ligand, **3**, were obtained. The crystals were filtered and dried under vacuum. Yield 925 mg; 66%. ^1H NMR, δ($CDCl_3$): 1.74 (q, 4H, -C-CH_2-C), 2.55 (t, 8H, *N*-CH_2-CH_2-CH_2-N), 2.65 (s, 8H, -N-CH_2-CH_2-N-CH_2), 3.59 (s, 8H, -N-CH_2-C_5H_4N), 7.03–8.43 (m, 16H, -C_5H_4N). ^{13}C NMR, δ($CDCl_3$): 23.7 (-C-CH_2-C), 50.9 (N-CH_2-CH_2-CH_2-N-), 51.8 (-N-CH_2-CH_2-N-), 61.4 (-N-CH_2-C_5H_4N), 122, 123, 136, 149, 160 (-C_5H_4N). Anal. calcd. for $C_{34}H_{44}N_8$: C 72.30, H 7.85, N 19.84%; found: C 72.20, H 7.90, N 19.70%.

[Pt(tpmc)]$(ClO_4)_2$, 7

K_2PtCl_4 (163 mg, 0.393 mmol) was dissolved in DMSO (7 mL) and heated to 50°C under helium or dinitrogen atmosphere for 1 h. This solution was added dropwise to a hot ethanolic solution of the ligand (244 mg; 0.432 mmoL; 30 mL). The mixture was heated to 100°C for 2 h. The solution was cooled to room temperature and diethyl ether (50 mL) was added to it. Upon cooling the mixture, a colorless solid was obtained that was filtered and dried under vacuum. Crude yield: 265 mg. Metathesis to the perchlorate salt was achieved by dissolving the chloride salt in a minimum amount of water and adding a saturated solution of sodium perchlorate. Yield: 175 mg. This was recrystallized from acetonitrile solution at 5°C and a colorless solid of [Pt(tpmc)]$(ClO_4)_2$ was obtained. Yield 41 mg; 11%. ^{13}C NMR, δ (d^6-DMSO): 23.0 (-C-CH_2-C), 58.4 (N-CH_2-CH_2-CH_2-N-), 59.8 (-N-CH_2-CH_2-N-), 59.8 (-N-CH_2-C_5H_4N), 124, 127, 137, 150, 151 (-C_5H_4N). Anal. calcd. for $PtC_{34}H_{44}N_8Cl_2O_8$: C 42.59, H 4.63, N 11.69%; found: C 42.39, H 4.44, N 11.72%.

Caution: The perchlorate salts prepared in this work are potentially explosive and must be handled with great care.

Structure solution and refinement

Single-crystal X-ray intensity measurements were carried out on an Enraf–Nonius CAD-4 automated diffractometer with MoK_α radiation (λ = 0.71073 Å) and graphite monochromator at 123 K using an ω–2θ scan mode. Crystallographic data for the Pt(II) complexes are shown in Table 1. The final unit-cell parameters for both compounds were obtained by least-squares analysis of setting angles of 25 carefully centered reflections (2θ = 20.1°–29.0° for compound **4** and 2θ = 30.2°–35.2° for compound **5**) chosen from diverse regions of reciprocal space. Orientation was checked with three test reflections after every 400 reflections for both compounds. Intensities of three standard reflections were measured every 2 h for compound **4** (3 h for compound **5**) with no significant decay being observed for either compound. The structure was solved by direct methods using NRCVAX (33) and was refined by the full-matrix least-squares method for both compounds. A total of 3389 reflections were obtained for [Pt(cyclam)]$(ClO_4)_2$, compound **4**, of which 2976 with $I > 2.5\ \sigma(I)$ were used. The coordinates of the Pt atoms were obtained by direct methods and those of the remaining non-hydrogen atoms from a Fourier map phased using the Pt positions. The Pt and Cl atoms were refined with anisotropic thermal parameters. All other atoms were refined isotropically. Hydrogen atoms were placed in calculated positions for both compounds with both N—H and C—H = 0.98 Å. Atomic scattering factors and anomalous dispersion corrections for the non-hydrogen atoms were taken from the *International tables for X-ray crystallography* (34) for both compounds. Fractional atomic

[3] Department of Chemistry, University of Saskatchewan.

© 1997 NRC Canada

Can. J. Chem. Downloaded from www.nrcresearchpress.com by 91.121.58.235 on 09/08/12
For personal use only.

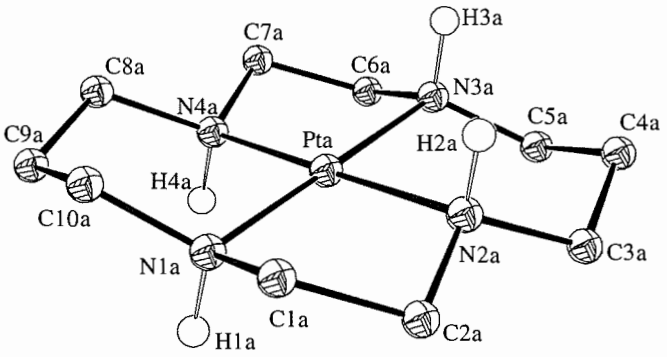
Table 1. Crystallographic parameters for [Pt(cyclam)]$(ClO_4)_2$ (compound **4**) and [Pt(*N*-methylcyclam)]$(ClO_4)_2 \cdot CH_3CN$ (compound **5**).

Parameter	**4**	**5**
Compound	$[(C_{10}H_{24}N_4)Pt](ClO_4)_2$	$[(C_{14}H_{32}N_4)Pt](ClO_4)_2$
Formula	$PtCl_2O_8N_4C_{10}H_{24}$	$PtCl_2O_8N_5C_{16}H_{35}$
M (g/mol)	594.31	691.45
Crystal system	Orthorhombic	Orthorhombic
Space group	$P2_1cn$ (No. 33, $Pna2_1$)	*Pmcn* (No. 62, *Pnma*)
a, Å	9.596 (3)	9.574 (8)
b, Å	14.595 (21)	14.116 (5)
c, Å	24.8782 (20)	17.5456 (15)
V, Å^3	3484 (5)	2371 (2)
Z	8	4
D_{calc} (Mg m^{-3})	2.266	1.928
T, K	123	123
Radiation	Mo	Mo
λ, Å	0.71073	0.71073
μ, (mm^{-1})	8.49	6.91
R (F_{obs})	0.073	0.067
R_w (F_{obs})	0.093	0.091
Scan type	ω – 2θ	ω – 2θ

coordinates and equivalent isotropic thermal parameters, and selected bond lengths and bond angles, are given in Tables 2 and 3, respectively. More detailed tables of crystallographic data, hydrogen atom parameters, bond lengths and bond angles, are available as supplementary material.[4] Final values of $R = 0.073$ and $R_w = 0.093$ were obtained. The ORTEP (35) plot of the $[Pt(cyclam)]^{2+}$ ion illustrating the geometry and labelling scheme is shown in Fig. 1.

For Pt(*N*-methylcyclam)]$(ClO_4)_2 \cdot CH_3CN$, compound **5**, with four molecules in the unit cell, only half the molecule had to be solved, since the molecule was in a special position ($x = 0.25$) with the mirror plane defined by the three atoms Pt, C5, and C6 (Fig. 2). A total of 2736 reflections were obtained for compound **5**, of which 1844 with $I > 2.5F(I)$ were used. All of the non-hydrogen atoms were found on the *E*-map and refined isotropically. Atoms C7, C9, and C2 were disordered and attempts were made to model the disorder for these atoms. Alternate positions for atoms C7 and C9 could be discerned in the difference map but the corresponding position for atom C2 was not clear and hence the disorder could not be modelled. Final values of $R = 0.067$ and $R_w = 0.091$ were obtained. Final atomic coordinates and equivalent isotropic thermal parameters, and selected bond lengths and bond angles, are given in Tables 4 and 5, respectively. The ORTEP (35) plot of the [Pt(*N*-methylcyclam)]$^{2+}$ ion with atomic numbering scheme is shown in Fig. 2. In both structures, the peaks found in the final difference maps were close to Pt and ClO_4^- positions.

Fig. 1. ORTEP diagram (31) of cation "a" of compound **4**, [Pt(cyclam)]$(ClO_4)_2$. Thermal spheres of arbitrary radius are used for all atoms. H atoms on C atoms are excluded for clarity. H atoms on N atoms were placed from the geometry of the non-H atoms.



Results and discussion

Syntheses

The Pt(II) and Pt(IV) complexes synthesized in the present study gave satisfactory elemental analyses. The IR spectra for

[4] Supplementary material available: A more detailed table of crystallographic data for both compounds (S1); tables of hydrogen atom fractional coordinates and isotropic thermal parameters, and of anisotropic thermal parameters for the non-hydrogen atoms for both compounds (S2–S5); tables of bond lengths and bond angles for compounds **4** and **5** (S6 and S7)have been deposited and may be purchased from: The Depository of Unpublished Data, Document Delivery, CISTI, National Research Council Canada, Ottawa, Canada K1A 0S2. Structure factor amplitudes are no longer being deposited and may be obtained directly from the authors. With the exception of the data for thermal parameters, these tables have also been deposited with the Cambridge Crystallographic Data Centre, and can be obtained on request from The Director, Cambridge Crystallographic Data Centre, University Chemical Laboratory, 12 Union Road, Cambridge, CB2 1EZ, U.K.

© 1997 NRC Canada

Can. J. Chem. Downloaded from www.nrcresearchpress.com by 91.121.58.235 on 09/08/12
For personal use only.

Table 2. Fractional atomic coordinates for [Pt(cyclam)]$(ClO_4)_2$ (compound **4**).[a]

	x	y	z	B_{iso}
Pta	0.62596	0.14261 (6)	0.14220 (4)	0.83 (4)
Nla	0.433 (3)	0.1231 (17)	0.1142 (10)	1.6 (4)
N2a	0.6817 (25)	0.0465 (16)	0.0854 (9)	1.7 (4)
N3a	0.8285 (24)	0.1628 (16)	0.1717 (9)	1.3 (4)
N4a	0.578 (3)	0.2381 (17)	0.1988 (9)	1.6 (4)
Cla	0.437 (3)	0.0390 (20)	0.0787 (12)	1.3 (5)
C2a	0.574 (3)	0.0427 (19)	0.0465 (11)	1.5 (5)
C3a	0.826 (3)	0.0634 (20)	0.0604 (12)	1.3 (5)
C4a	0.941 (3)	0.0725 (20)	0.1002 (12)	1.6 (5)
C5a	0.939 (3)	0.1634 (20)	0.1331 (11)	1.3 (5)
C6a	0.824 (3)	0.2499 (23)	0.2055 (13)	1.9 (5)
C7a	0.689 (3)	0.2493 (23)	0.2360 (11)	1.9 (6)
C8a	0.440 (3)	0.2166 (20)	0.2269 (11)	1.2 (5)
C9a	0.320 (3)	0.2006 (22)	0.1920 (12)	1.9 (5)
Cl0a	0.326 (3)	0.1172 (20)	0.1558 (11)	1.4 (5)
Ptb	1.14363 (17)	0.62045 (6)	0.11072 (4)	1.02 (4)
Nlb	1.298 (3)	0.5267 (25)	0.1215 (13)	2.2 (6)
N2b	1.310 (3)	0.7083 (22)	0.0942 (12)	2.3 (6)
N3b	0.9913 (23)	0.7156 (17)	0.1008 (9)	0.7 (4)
N4b	0.982 (3)	0.5287 (23)	0.1239 (12)	1.7 (5)
Clb	1.432 (4)	0.565 (3)	0.1013 (15)	2.0 (6)
C2b	1.434 (3)	0.6617 (22)	0.1163 (12)	1.4 (5)
C3b	1.290 (4)	0.8010 (25)	0.1181 (14)	2.1 (6)
C4b	1.151 (4)	0.8449 (20)	0.0978 (11)	2.4 (5)
C5b	1.032 (4)	0.810 (3)	0.1214 (15)	2.5 (7)
C6b	0.861 (4)	0.680 (3)	0.1270 (15)	2.7 (7)
C7b	0.851 (4)	0.579 (3)	0.1065 (16)	2.4 (7)
C8b	0.998 (4)	0.441 (3)	0.0962 (17)	2.3 (7)
C9b	1.131 (5)	0.3905 (20)	0.1167 (11)	2.8 (6)
C10b	1.266 (4)	0.436 (3)	0.0945 (17)	2.5 (8)
Cll	0.6389 (9)	0.3444 (4)	0.04097 (23)	1.6 (3)
O11	0.624 (3)	0.4298 (14)	0.0132 (8)	3.0 (4)
O21	0.642 (3)	0.3570 (12)	0.0984 (7)	2.3 (4)
O31	0.5265 (24)	0.2836 (17)	0.0248 (10)	2.3 (5)
O41	0.765 (3)	0.3029 (18)	0.0258 (10)	2.7 (5)
O12	0.6358 (11)	−0.0756 (4)	0.2211 (3)	2.2 (3)
O12	0.649 (3)	−0.1594 (15)	0.2504 (8)	3.0 (4)
O22	0.629 (3)	−0.0015 (14)	0.2596 (7)	2.7 (4)
O32	0.757 (3)	−0.0642 (24)	0.1884 (14)	3.9 (7)
O42	0.514 (3)	−0.0765 (24)	0.1880 (14)	3.9 (7)
C13	0.5783 (9)	0.5013 (5)	0.2389 (3)	2.0 (3)
O13	0.717 (3)	0.5258 (23)	0.2175 (13)	4.7 (7)
O23	0.5961 (23)	0.4640 (14)	0.2907 (8)	2.3 (4)
O33	0.509 (3)	0.4383 (18)	0.2055 (10)	3.3 (5)
O43	0.498 (3)	0.5844 (19)	0.2420 (10)	3.6 (5)
C14	0.6687 (8)	0.7882 (4)	0.0053 (3)	1.9 (3)
O14	0.531 (3)	0.8180 (18)	0.0166 (10)	2.9 (5)
O24	0.767 (3)	0.8356 (17)	0.0386 (10)	2.8 (5)
O34	0.6948 (23)	0.8073 (15)	−0.0500 (8)	2.4 (4)
O44	0.6855 (24)	0.6899 (15)	0.0152 (8)	2.5 (4)

[a]Estimated standard deviations are given in parentheses. B_{iso} is the mean of the principal axes of the thermal ellipsoid for platinum and chlorine atoms and the isotropic value for all other atoms.

© 1997 NRC Canada

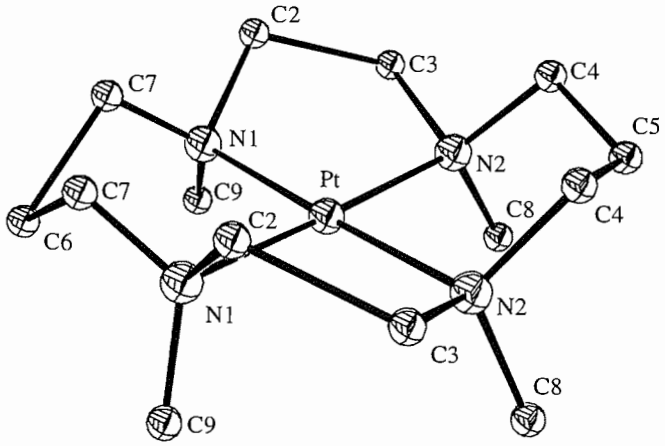
Can. J. Chem. Downloaded from www.nrcresearchpress.com by 91.121.58.235 on 09/08/12
For personal use only.

Table 3. Selected bond lengths (Å) and bond angles (°) for compound **4**.[a]

Molecule "a"			
Atoms	Distance	Atoms	Distance
Pta—N1a	2.00(3)	N2—C2a	1.42(4)
Pta—N2a	2.061(23)	N2a—C3a	1.53(4)
Pta—N3a	2.098(23)	N3a—C5a	1.43(4)
Pta—N4a	2.034(24)	N3a—C6a	1.53(4)
N1a—C1a	1.51(4)	N4a—C7a	1.42(4)
N1a—C10a	1.46(4)	N4a—C8a	1.52(4)
	Angle		Angle
N1a-Pta-N2a	84.5(10)	N2a-Pta-N3a	95.4(9)
N1a-Pta-N3a	179.9(12)	N2a-Pta-N4a	178.1(10)
N1a-Pta-N4a	97.4(10)	N3a-Pta-N4a	82.7(9)
Molecule "b"			
Atoms	Distance	Atoms	Distance
Ptb—N1b	2.04(3)	N2b—C2b	1.48(4)
Ptb—N2b	2.09(3)	N2b—C3b	1.49(5)
Ptb—N3b	2.031(24)	N3b—C5b	1.52(5)
Ptb—N4b	2.07(3)	N3bC6b	1.50(5)
N1b—C1b	1.49(5)	N4b—C7b	1.52(5)
N1b—C10b	1.52(6)	N4b—C8b	1.47(5)
	Angle		Angle
N1b-Ptb-N2b	83.2(13)	N2b-Ptb-N3b	96.1(11)
N1b-Ptb-N3b	179.0(12)	N2b-Ptb-N4b	176.9(12)
N1b-Ptb-N4b	95.1(13)	N3b-Ptb-N4b	85.6(11)

[a]Estimated standard deviations are given in parentheses.

Fig. 2. ORTEP diagram (31) of cation of **5**, [Pt(*N*-methylcyclam)]-$(ClO_4)_2 \cdot CH_3CN$. Thermal spheres of arbitrary radius are used for all atoms. H atoms on C atoms are excluded for clarity.



both Pt(II) and Pt(IV) complexes based on cyclam showed an -NH stretch at 3525 cm^{-1} and 3515 cm^{-1}, respectively whereas for the complexes based on *N*-methylcyclam and tpmc the -NH stretch was absent.

NMR spectra

The proton NMR spectrum of $[Pt(cyclam)](ClO_4)_2$, **4**, in D_2O is shown in Fig. 3*a*. The spectrum is similar to that obtained by Waknine et al. (32). However, in the present case the spectrum is better resolved and includes analysis. The protons attached to each carbon atom in the complex are rendered inequivalent due to chelation and can be differentiated into axial and equatorial protons with respect to the PtN_4 square plane. Coupling can occur between these sets of protons, giving rise to second-order effects and resulting in a more complicated spectrum. The spectrum can be analyzed as ABC_2D_2 and E_2F_2 subspectra (see inset in Fig. 3 for labels). The axial protons (2H) from the -C-CH_2-C- portion of the molecule are centred at δ 1.47 with the equatorial protons (2H) at δ 1.98. This is the AB part of the subspectrum. The *N*-CH_2-C-CH_2-N protons (8H in a molecule) can be divided into axial protons (4H) centred at δ 2.56 and equatorial protons centred at δ 2.94. This is the C_2D_2 part of the subspectrum (C_2 can be described as CC′ with H_c and $H_{c'}$ being equivalent). The simulated spectrum (obtained using the GNMR software, version 3.6) is shown in Fig. 3*b*, and the simulated parameters are provided in Table 6 (the spectrum has been simulated using standard iterative techniques). This spectrum matches well with the experimentally obtained spectrum and confirms the identity and presence of one symmetric isomer (*meso-RRSS*) for the complex in solution. The

© 1997 NRC Canada

Can. J. Chem. Downloaded from www.nrcresearchpress.com by 91.121.58.235 on 09/08/12
For personal use only.

Table 4. Fractional atomic coordinates for [Pt(*N*-methylcyclam)]$(ClO_4)_2 \cdot CH_3CN$ (compound **5**).[a]

	x	*y*	*z*	B_{iso}
Pt	3/4	0.19191 (5)	0.21666 (4)	1.61 (3)
CL1	1/4	0.9530 (3)	0.1242 (3)	2.81 (22)
O11	1/4	1.0522 (15)	0.1158 (12)	6.0 (5)
O12	1/4	0.9235 (14)	0.2021 (10)	4.7 (4)
O13	0.3682 (24)	0.9204 (15)	0.0879 (13)	11.5 (6)
CL2	3/4	0.6222 (4)	0.0186 (3)	3.02 (21)
O21	0.6250 (18)	0.5706 (12)	0.0150 (10)	7.8 (4)
O22	3/4	0.6897 (18)	0.0803 (17)	9.1 (7)
O23	3/4	0.6804 (20)	–0.0443 (18)	10.0 (8)
N1	0.5954 (15)	0.1494 (10)	0.2900 (7)	3.5 (6)
N2	0.5952 (15)	0.2409 (10)	0.1449 (7)	3.8 (6)
C2	0.50649	0.23067	0.28854	12.0 (11)
C3	0.456 (3)	0.2472 (21)	0.1924 (15)	7.4 (6)
C4	0.620 (3)	0.3423 (19)	0.1241 (15)	7.5 (6)
C5	3/4	0.343 (3)	0.0816 (22)	7.6 (9)
C6	3/4	0.077 (4)	0.376 (3)	11.6 (15)
C7	0.63575	0.16482	0.36129	13.2 (12)
C8	0.5616 (22)	0.1801 (13)	0.0788 (11)	4.9 (4)
C9	0.51721	0.07162	0.26626	9.0 (8)
C10	3/9	0.9226 (20)	0.0572 (16)	4.6 (5)
C11	3/4	0.9079 (19)	0.1372 (16)	4.5 (5)
N3	3/4	0.9004 (25)	0.2036 (16)	8.2 (19)

[a]Estimated standard deviations are given in parentheses. B_{iso} is the mean of the principal axes of the thermal ellipsoid for platinum and chlorine atoms and the isotropic value for all other atoms.

Table 5. Selected bond lengths (Å) and bond angles (°) for compound **5**.[a]

Atoms	Distance	Atoms	Distance
Pt—N1	2.051(12)	N1-C9	1.392(13)
Pt—N2	2.064(12)	N2—C3	1.57(3)
N1—C2	1.429(15)	N2—C4	1.50(3)
N1—C7	1.328(13)	N2—C8	1.478(23)
Atoms	Angle	Atoms	Angle
N1-Pt-N1a	92.4(6)	N1a-Pt-N2	177.4(5)
N1-Pt-N2	87.8(6)	N2-Pt-N2a	91.8(6)

[a]Estimated standard deviations are given in parentheses.

^{13}C NMR spectrum showed three peaks at δ 52.2, 49.0, 26.4 and in an inverse gate experiment these three peaks were found to have an integrated ratio of 2:2:1, respectively. Analyses of the ^1H and ^{13}C NMR spectra suggest that the molecule is rigid in solution and has the Bosnich Type III (36), *meso-RRSS*, configuration at the N atoms. This is consistent with the solid state structure (vide infra).

The ^1H NMR spectrum of [Pt(NMe_4cyclam)]$(ClO_4)_2$, **5**, in D_2O is complicated. Variable temperature ^1H NMR (20–150°C) in d^6-DMSO and −30–+20°C in CD_3CN did not show any changes in the spectrum. The ^{13}C NMR spectrum (18 lines) is characteristic of two isomers in solution: one an asymmetric isomer (14 lines) and another a symmetric isomer (4 lines). ^{13}C NMR with *J*-modulation shows five lines due to CH_3 groups, four of which (δ 47.68, 48.0, 50.1, and 53.2) belong to the asymmetric isomer (three methyl groups above the PtN_4 plane and one methyl group below the plane) and the remaining one (δ 51.0) to the symmetric isomer (<15%, all four methyl groups below the PtN_4 plane or two methyl groups above and two below the PtN_4 plane). Thirteen lines due to $-CH_2$ groups are also seen, of which ten belong to the asymmetric isomer (all carbon atoms inequivalent) and three to the symmetric isomer. Other complexes in the group, viz. $[Pd(NMe_4cyclam)]^{2+}$ ion, show the presence of one symmetric isomer in solution with all four methyl groups on the same side of the Pd(II) ion (*RSRS* configuration as determined from the crystal structure (18)) whereas the ^{13}C DEPT NMR spectrum for the $[RhCl_2(tmc)]^+$ ion showed the presence of both symmetric (*RRSS* or *RSRS)* and asymmetric (*RSRR*) isomers in solution in the ratio 1:1 (37).

The ^1H NMR spectrum of the [Pt(IV)(*N*-methylcyclam)Cl_2]]$(BF_4)_2$ in D_2O is complicated. The ^{13}C NMR spectrum with *J*-modulation of a freshly prepared solution of the Pt(IV) complex in D_2O shows four lines at δ 50.8, 51.4, 52.9, and 56.7 due to four $-CH_3$ groups of the tetramethylcyclam ligand. Ten lines are seen at δ 24.6, 25.8, 57.0, 57.7, 62.6, 65.0, 65.7, 66.6, 66.9, and 67.9 due to the ten $-CH_2$ groups in the ligand framework. In addition, three lines are seen at δ 53.8, 63.5, and 66.8 and are attributed to small quantities (<15%)of the Pt(IV) symmetric species in solution.

© 1997 NRC Canada

Fig. 3. Comparison of experimental (*a*, top) and simulated (*b*, bottom) ^{1}H NMR spectra for [Pt(cyclam)]$(ClO_4)_2$ in D_2O.

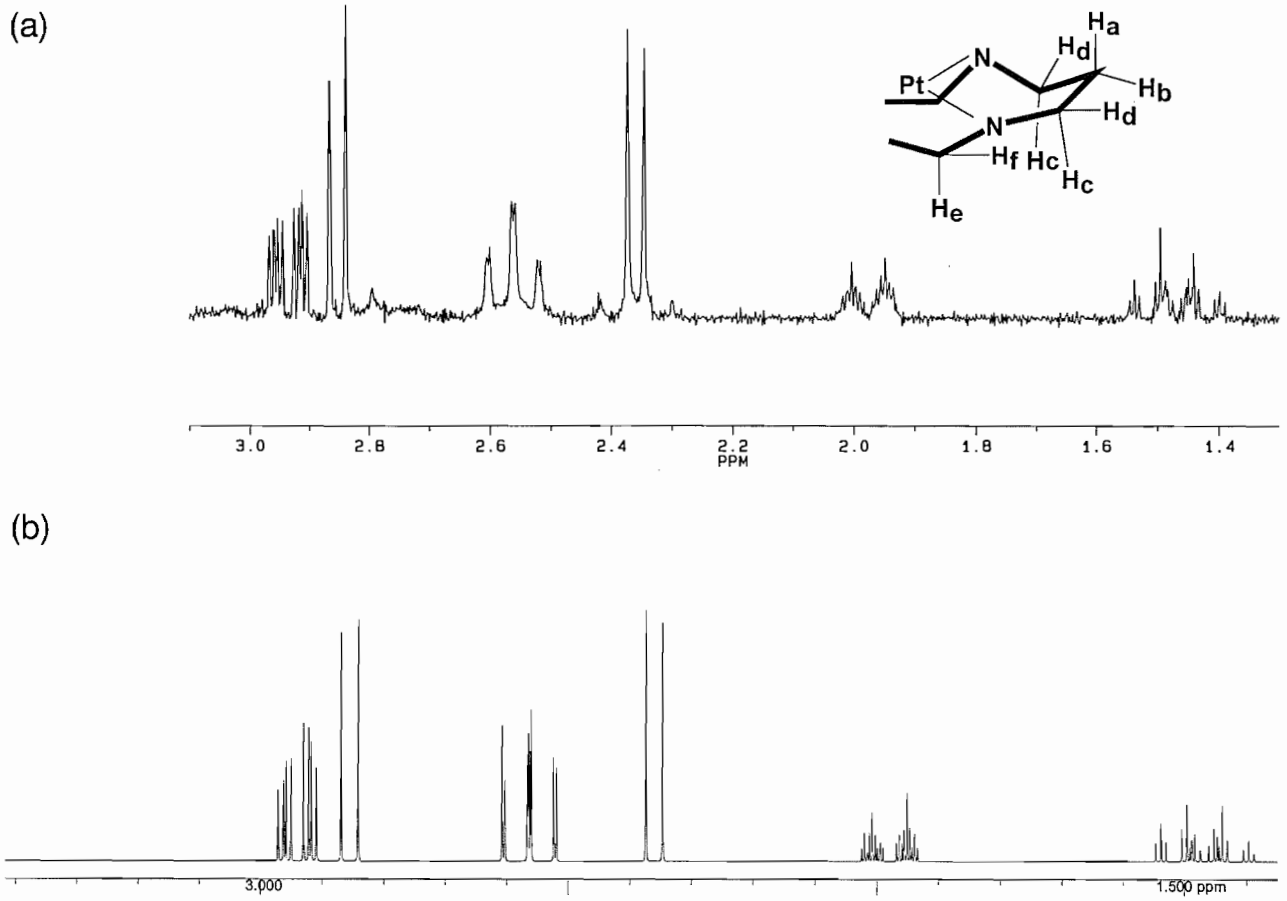


Table 6. Simulated ^{1}H NMR parameters (chemical shifts (ppm) and coupling constants (Hz)) for $[Pt(cyclam)]^{2+}$ ion (ABC_2D_2 and E_2F_2 subspectra).

$\delta_a = 1.47$	$\delta_b = 1.98$	$\delta_c = 2.56$	$\delta_d = 2.94$	$\delta_e = 2.36$	$\delta_f = 2.86$
$J_{ab} = 16.90$	$J_{bc} = 1.31$	$J_{cd} = 12.31$		$J_{ef} = 8.20$	
$J_{ac} = 12.96$	$J_{bd} = 3.80$				
$J_{ad} = 2.48$					

The free ligand, tpmc, **3**, was characterized by ^{1}H and ^{13}C NMR, elemental analyses, and by electrospray mass spectroscopy. The ^{13}C NMR spectra showed nine lines: one due to a pair of equivalent C atoms and each of the remaining eight lines due to four equivalent C atoms with a total of 34 C atoms in the molecule. The ^{1}H NMR spectrum is typical of tpmc, compound **3** (see experimental section). Of interest is the singlet at δ 3.59 due to the methylene protons attached to the pyridyl moiety in the pendant arms. At ambient temperatures, the molecule undergoes free rotation of the pendant arms, making the protons equivalent and thus giving rise to a singlet. If the pyridyl nitrogen atoms were coordinated to the metal ion, the equivalence of these methylene protons would be lost. In addition, the singlet at δ 2.65 due to the equivalent methylene protons of the ethylene bridge in the macrocycle is characteristic of rapid inversion of the nitrogen atoms at ambient temperatures. Upon coordination of the N atoms from the cyclam to the Pt(II)ion, the magnetic equivalence of the protons in the cyclam ring is lost, giving rise to a complex spectra. The ^{1}H NMR of $[Pt(tpmc)](ClO_4)_2$ is characteristic of the Pt(II) ion coordinated to the N atoms of the cyclam ring. The protons in the cyclam ring appear between δ 2.1 and 3.7. The singlet due to methylene protons (8H) attached to the pyridyl ring appears at δ 4.40. For a related complex ion, $[Pd(py_2[9]aneN_2\,S)]^{2+}$, the protons of the methylene group in the pendant arm are magnetically inequivalent (as evidenced in the ^{1}H NMR spectrum), indicating that the Pd(II) ion is coordinated to the N atoms of the pyridyl moiety (30). The aromatic protons (16H) appear at δ 7.4–8.8. The ^{13}C NMR shows nine lines and is characteristic of one symmetric isomer in solution. Both ^{1}H and ^{13}C NMR spectra are consistent with the Pt(II) metal ion being coordinated to the four nitrogen atoms from the cyclam ring forming a square-planar complex.

Can. J. Chem. Downloaded from www.nrcresearchpress.com by 91.121.58.235 on 09/08/12
For personal use only.

© 1997 NRC Canada

Can. J. Chem. Downloaded from www.nrcresearchpress.com by 91.121.58.235 on 09/08/12
For personal use only.

Table 7. Electrospray mass spectral data for Pt macrocyclic complexes.

Compound	Ions (ESMS) (*m/z*)[a]
$[Pt(cyclam)](ClO_4)_2$	$[Pt(II)cyclam](ClO_4)^+$ (495)
	$[Pt(II)cyclam]^{2+}$ (197)
$[Pt(IV)(cyclam)Cl_2](ClO_4)_2$	$[Pt(IV)(cyclam)Cl_2]^{2+}$ (233)
	$[Pt(III)(cyclam)Cl_2]^+$ (465)
	$[Pt(II)cyclam]^{2+}$ (197)
$[Pt(N\text{-methylcyclam})](ClO_4)_2$	$[Pt(II)(N\text{-methylcyclam})](ClO_4)^+$ (551)
	$[Pt(II)(N\text{-methylcyclam})]^{2+}$ (226)
$[Pt(N\text{-methylcyclam})Cl_2](BF_4)_2$	$[Pt(IV)(N\text{-methylcyclam})Cl_2]^{2+}$ (261)
	$[Pt(III)(N\text{-methylcyclam})Cl_2]^+$ (522)
	$[Pt(III)(N\text{-methylcyclam})Cl]^{2+}$ (242)
	$[Pt(II)(N\text{-methylcyclam})Cl]^+$ (487)
	$[Pt(II)(N\text{-methylcyclam})]^{2+}$ (226)
$[Pt(tpmc)](ClO_4)_2$	$[Pt(tpmc)](ClO_4)^+$ (858)
	$[Pt(tpmc)]^{2+}$ (380)

[a]Most intense peak of isotopic mass distribution.

Electronic spectra

The UV–visible absorption spectrum of $[Pt(cyclam)](ClO_4)_2$ in water shows peaks at 268 nm (ε = 47 M^{-1} cm^{-1}; assigned to a *d–d* transition) and 210 nm (ε = 7660 M^{-1} cm^{-1}; assigned to a charge transfer band) and a shoulder at 231 nm (494 M^{-1} cm^{-1}). The spectrum is similar to that obtained by Waknine et al. (32) for the corresponding chloride salt. The corresponding $[Pt(N\text{-methylcyclam})]^{2+}$ exhibits peaks at 296 nm (70 M^{-1} cm^{-1}; assigned to a *d–d* transition) and 225 nm (638 M^{-1} cm^{-1}). No absorptions were found in the visible region of the spectrum, indicating high ligand field strengths for both low-spin d^8 Pt(II) complexes.

Electrospray mass spectra

ESMS data for the various Pt(II) complexes are listed in Table 7. The electrospray mass spectrum of $[Pt(cyclam)](ClO_4)_2$ in methanol shows two peaks at *m/z* 495 and 197 due to the presence of intact ions $[Pt(cyclam)](ClO_4)^+$ and $[Pt(cyclam)]^{2+}$, respectively. ESMS of $[Pt(N\text{-methylcyclam})](ClO_4)_2$ shows the presence of intact ions at *m/z* 551 and 226 due to $[Pt(N\text{-methylcyclam})](ClO_4)^+$ and the dication $[Pt(N\text{-methylcyclam})]^{2+}$, respectively. However, ESMS of the Pt(IV) species based on cyclam and *N*-methylcyclam in methanol showed the presence of Pt(III) as well as Pt(IV) and Pt(II) complex ions (vide infra).

The electrospray mass spectrum of $[Pt(II)tpmc](ClO_4)_2$ in methanol (Table 7) shows two peaks at *m/z* 858 and *m/z* 380 due to the monocation $\{[Pt(tpmc)](ClO_4)\}^+$ and the dication $[Pt(tpmc)]^{2+}$, respectively. X-ray quality crystals of the Pt(II) complex could not be obtained and this prevented a crystal structure determination. However, elemental analysis together with electrospray mass spectral data confirmed the formation of the $[Pt(II)tpmc](ClO_4)_2$ complex.

Crystallography

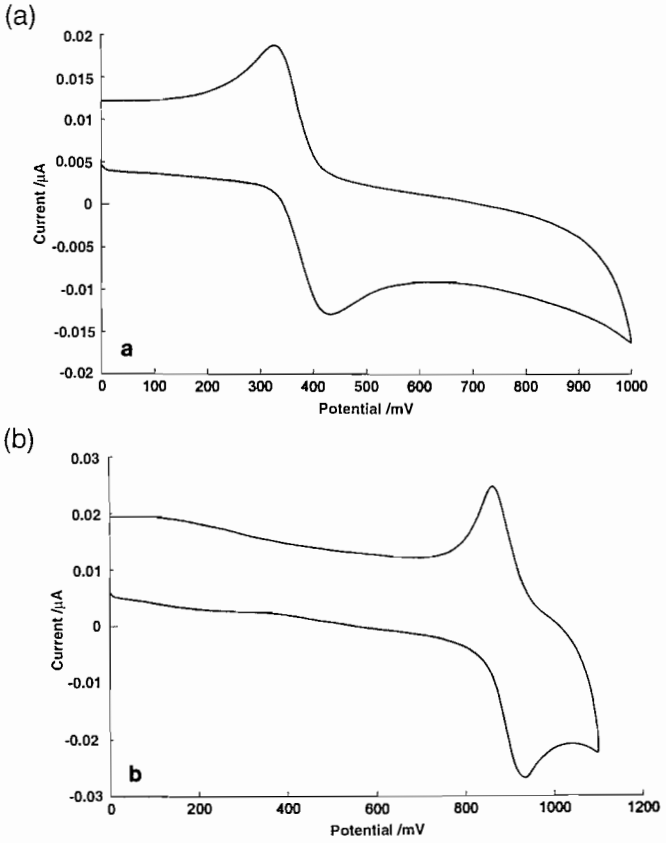
The crystal structure of $[Pt(cyclam)](ClO_4)_2$ is square planar with the Pt(II) ion in the center of the PtN_4 plane (Fig. 1). The average Pt—N bond length is 2.05(3) Å and is similar to that obtained for the corresponding Pt(IV) complex ion, $[Pt(cyclam)Cl_2]^{2+}$ (32). The configuration at the N atoms is *meso-RRSS*, Bosnich Type III (36), with two amine protons above and two below the PtN_4 plane. The five-membered rings are *gauche* with a bite angle of 83.6°(10) while the six-membered rings with a bite angle of 96.4°(10) assume the chair conformation. These values are similar to those obtained for the $[Pt(cyclam)Cl_2]^{2+}$ ion (32). Structural analysis shows that the -NH groups are involved in hydrogen bonding with the perchlorate oxygen atoms, linking the two molecules in the unit cell; however, this does not result in an infinite network.

The configuration at the N atoms in the transition metal complexes of cyclam is generally planar (*trans*) Bosnich Type III or a folded (*cis*) Bosnich Type V configuration (36). This is consistent with the observation of a planar (*trans*) Type III configuration at the N atoms in the $[Pt(II)(cyclam)]^{2+}$ ion. However, in the case of the corresponding *N*-methylated complex, viz. the $[Pt(II)(N\text{-methylcyclam})]^{2+}$ ion, the solid state structure is symmetric, Bosnich Type I (36), *RSRS*, with all four CH_3 groups on one side of the PtN_4 plane. This is in keeping with strain energy minimization calculations made on Ni(II) complexes of *N*-methylcyclam wherein it was shown that *RSRS* conformations are preferred by four-coordinate square-planar complexes of *N*-methylcyclam (38). The average Pt—N distance is 2.06(1) Å. Bite angles of the five-membered chelate rings are 87.8°(16) and those of the six-membered chelate rings are 92.4°(6). The ORTEP plot (Fig. 2) shows the presence of a crystallographic mirror plane through atoms C5, Pt, and C6. The five-membered chelate rings are *gauche* δδ forming an eclipsed conformation, in contrast to the five-membered chelate ring, which is *gauche* δλ (non-eclipsed conformation) in the case of the $[Pt(II)cyclam]^{2+}$ complex ion. The structure of the $[Pt(II)(N\text{-methylcyclam})]^{2+}$ ion is similar to that of the corresponding Ni(II) complex prepared in strongly coordinating solvents (4) and to that of the $Pt([14]\text{-aneS}_4)^{2+}$ ion (39) with all the C atoms of the ligand framework on one side of the PtN_4 plane. The present structure is also similar to that of the $[Pd(N\text{-methylcyclam})]^{2+}$ ion, although in that case the Pd(II) ion is displaced towards the *N*-bound methyl groups by 0.082 Å out of the plane of the four N atoms (11). In the case under study, the N_4 donor set is essentially planar and the Pt(II) is in the plane. This structure is

© 1997 NRC Canada

Can. J. Chem. Downloaded from www.nrcresearchpress.com by 91.121.58.235 on 09/08/12
For personal use only.

Fig. 4. Cyclic voltammograms of (*a*) [Pt(cyclam)]$(ClO_4)_2$ in 1 M NaCl; (*b*) [Pt(*N*-methylcyclam)]$(ClO_4)_2$ in 1 M NaCl.



consistent with the minor symmetric isomer in solution although the major isomer in solution is the chiral Type II, *RRSR*, configuration as evidenced in the NMR spectra (vide infra).

Although tiny crystals of [Pt(IV)(*N*-methylcyclam)Cl_2]-$(BF_4)_2 \cdot CH_3CN$ were obtained, they were extremely sensitive to solvent loss and lost crystallinity during data collection in X-ray diffraction studies. ^{13}C NMR and electrospray mass spectra confirm the presence of the Pt(IV) complex ion in solution. This suggests that the $(CH_2)_n$ backbones of both rings are likely to be relatively displaced to accommodate six-coordination. This is in keeping with the steric energy minimized geometries of the $[Pt([n]\text{-ane})S_4)Cl_2]^{2+}$ ion (n = 12–16) wherein MM2 simulations indicate that six-coordination with Cl^- tends to flatten S_4 rings although the structure is not centrosymmetric (39). Six-coordination in the $[RhCl_2(N\text{-methylcyclam})]^+$ has been achieved with two methyl groups above and two methyl groups below the RhN_4 coordination plane (*RRSS* configuration, Type III) (36). Steric interactions between the *N*-methyl groups and with the macrocyclic backbone determine the stability of the [Pt(IV)(*N*-methylcyclam)Cl_2]$^{2+}$ ion.

Redox reactivity

The cyclic voltammograms of [Pt(cyclam)]$(ClO_4)_2$ and [Pt(*N*-methylcyclam)]$(ClO_4)_2$ in aqueous solutions containing 1 M NaCl using a Pt microelectrode are shown in Figs. 4*a* and 4*b*, respectively. The redox potentials are dependent on the nature of the macrocyclic ligand. Both cyclic voltammograms are characteristic of the formation of quasi reversible $Pt^{4+/2+}$ couples, although the driving forces are largely different. For the $[Pt(cyclam)Cl_2]^{2+}/[Pt(cyclam)]^{2+}$ couple, the half-wave potential is quasi reversible and found to be 0.385 V vs. Ag/AgCl ($i_{pa}/i_{pc} \sim 1$). The peak-to-peak separation (ΔE_p) is dependent on the scan rate for both complexes and is more reversible at smaller scan rates (ΔE_p = 100 mV at 0.5 V s^{-1} and 380 mV at 5 V s^{-1}). The half-wave potential is consistent with that obtained by Endicott and co-workers (32). Cyclic voltammetry of solutions of [Pt(NMe_4cyclam)]$(ClO_4)_2$ in aqueous 1 M NaCl shows a redox wave at 0.90 V vs. Ag/AgCl ($i_{pa}/i_{pc} \sim 1$, Fig. 4*b*). The same value for the half-wave potential was obtained starting with the corresponding [Pt(IV)-(NMe_4cyclam)Cl_2]$(BF_4)_2$ complex. The $E_{1/2}$ value of 0.90 V vs. Ag/AgCl has been assigned to the $[Pt(NMe_4cyclam)Cl_2]^{2+}/[Pt(NMe_4cyclam)]^{2+}$ couple. The large difference in the $E_{1/2}$ values for the $Pt^{4+/2+}$ couples based on cyclam and *N*-methylcyclam is attributed to the steric hindrance imposed by the *N*-methylated groups and interligand repulsions. The $E_{1/2}$ value for the $[Pt(NMe_4cyclam)Cl_2]^{2+}/[Pt(NMe_4cyclam)]^{2+}$ couple is comparable to that for the $[Pt([14]\text{-ane}S_4)Cl_2]^{2+}/[Pt([14]\text{-ane}S_4)]^{2+}$ couple (32). In that case, the soft S donor atoms stabilize Pt(II) relative to the Pt(IV) ion and the "*exo*" conformation of the equatorial S ligands leads to interligand repulsions with the axial Cl^- ligands, thus making the Pt(IV) dichloride species less stable. In the complex based on *N*-methylcyclam, the poorer σ-donating ability of the tertiary N atoms together with steric hindrance from the methyl substituents lead to interligand repulsions with the axial Cl^- ligands, thus again making the Pt(IV) dichloride species less stable. However, in the case of [14]-aneN_4, the lesser interligand repulsions between the axial Cl^- ligands and the equatorial N atoms of the macrocycle make the Pt(IV) dichloride species more stable (approach of axial chloro ligand is favorable) relative to the complex based on *N*-methylcyclam. However, the cyclic voltammogram of solutions of Pd(cyclam)$(ClO_4)_2$ in 1 M NaCl shows a redox wave at $E_{1/2}$ = 0.91 V vs. Ag/AgCl ($i_{pa}/i_{pc} \sim 1$) and has been attributed to the $[Pd(cyclam)Cl_2]^{2+}/[Pd(cyclam)]^{2+}$ couple. Similar results were obtained starting from the Pd(IV) dichloro complex synthesized using previously reported procedures (40). The preference of the Pt(IV) ion to adopt a six-coordinate geometry relative to the less stable Pd(IV) octahedral species is clearly reflected in the redox potentials for the cyclam-based species. Steric hindrance from the *N*-methylated species and interligand repulsions seem to play a major role in determining the thermodynamic stability of solutions of [Pt(IV)*N*-methylcyclam)Cl_2]$^{2+}$ ions.

A cyclic voltammogram of [Pt(cyclam)]$(ClO_4)_2$ in CH_3CN containing 0.1 M NBu_4Br shows the presence of Pt(I) monomeric species in solution. An irreversible cathodic wave is seen at −1.35 V vs. Fc^+/Fc. For the N-methylated species, viz. [Pt(NMe_4cyclam)]$(ClO_4)_2$, under the same conditions a cathodic peak is seen at −0.540 V vs. Fc^+/Fc and an anodic peak is seen at −0.230 V vs. Fc^+/Fc. The cathodic peak has been assigned to the formation of the Pt(I) monomeric species in solution. The anodic peak may be due to a dimeric species or other species containing the bromide ion. The relative stability of [Pt(NMe_4cyclam)]$^+$ over [Pt(cyclam)]$^+$ is typical of the N-methylated ligand being able to stabilize low oxidation

© 1997 NRC Canada

states. Meyerstein and co-workers (4) have shown that N-methylation leads to the net stabilization of $Cu(tmc)^+$ and $Ni(tmc)^+$ ions. In 0.1 M NBu_4ClO_4 the cathodic peak due to $[Pt(NMe_4cyclam)]^+$ now occurs at -1.57 V vs. Fc^+/Fc and is similar to that obtained for the corresponding $Pd^{2+}/^+$ couple under the same conditions (18).

Chemical oxidation of $[Pt(cyclam)](ClO_4)_2$ in CH_3CN using $NOBF_4$ or Co^{3+} in aqueous solutions did not exhibit any EPR active species at room temperature or at 77 K. Similar results were obtained with [Pt(*N*-methylcyclam)]$(ClO_4)_2$. Consequently, neither cyclic voltammetry using microelectrodes nor chemical oxidation followed by EPR spectroscopy provided viable routes to detectable Pt(III) species. However, reduction of [Pt(*N*-methylcyclam)]$(ClO_4)_2$ in 90% ethanol containing $NaBH_4$ yielded a paramagnetic species and the EPR spectrum of the frozen glass exhibited an isotropic signal at $g = 2.008$, indicating the formation of a Pt(I) monomeric species. The isoelectronic $[Pd(I)(tmc)]^+$ shows an anisotropic EPR spectrum ($g_\parallel = 2.302$, $g_\perp = 2.076$) (18). This is characteristic of a Pt(I) monomeric species with the unpaired electron in the d_x2–d_y2 orbital (^2E ground state). In contrast, chemical reduction of $[Pt(II)cyclam]^{2+}$ did not yield an EPR active species. The relative stability of [Pt(*N*-methylcyclam)]$^+$ may be due to steric hindrance to dimerization.

Although the technique of ESMS is widely used in the study of biomolecules, its use in the characterization of complex ions in solution has been sparse. Electrospray mass spectrometry is unique in that it allows for transferring preexisting ions from solution to the gas phase with minimal fragmentation. Conventional mass spectrometry leads to extensive fragmentation and in most cases observation of the relatively nonvolatile inorganic compounds is difficult. Recently, ESMS has also been used to study rapidly exchanging labile systems and it provides an alternative to low-temperature NMR studies (41). It has also been used to detect Pt(III) transient species. The five-coordinate Pt(III) complex ion has been stabilized using sterically hindered ligands and $\{Pt(S_2CNEt_2)(P_2P')\}^{2+}$ (42) has been confirmed by ESMS techniques.

The ESMS spectra of solutions containing $[Pt(IV)(cyclam)Cl_2]^{2+}$ ions are very interesting because they show the presence of Pt(III) as well as Pt(II) and Pt(IV) complex ions (Table 7). The peaks at *m/z* 233, 465, and 197 are due to the presence of $[Pt(IV)(cyclam)Cl_2]^{2+}$, $[Pt(III)(cyclam)Cl_2]^+$, and the $[Pt(II)cyclam]^{2+}$ ions, respectively. The ESMS of the N-methylated complex [Pt(*N*-methylcyclam)Cl_2]$(BF_4)_2$ in methanol shows several peaks. Product complex ions that are formed as a result of the axial lability of the chloro ligands in the Pt(III) complex are observed in the mass spectrum. Five- and six-coordinate Pt(III) species are seen at *m/z* 242 and 522, respectively. Because the Pt(III) complex ion tends to disproportionate, its observation both by cyclic voltammetry (using microelectrodes) and EPR spectroscopy is difficult. The ESMS spectrum shows the formation of a Pt(III) five-coordinate species that is intermediate between the four-coordination of Pt(II) and the six-coordination of Pt(IV) complex ions. The formation of the six-coordinate $[Pt(III)(cyclam)Cl_2]^+$ and five-coordinate $[Pt(III)(cyclam)Cl]^{2+}$ ions as proposed in pulse radiolysis (15) is supported by ESMS results obtained in the present study.

Can. J. Chem. Downloaded from www.nrcresearchpress.com by 91.121.58.235 on 09/08/12
For personal use only.

Acknowledgements

We gratefully thank the Natural Sciences and Engineering Research Council of Canada for financial support. We also thank Prof. A Baranski and Mr. B. Wilson for allowing us to use the undergraduate electrochemical facility. The authors gratefully acknowledge the assistance of Dr. K. Brown, Mr. B. Chatson, and Mr. D.W. Strickland in recording and simulation of the NMR spectra and of Prof. G. McKay and Dr. Q. Li in recording the electrospray mass spectra for the Pt complexes. The authors also wish to thank Dr. K.S. Chandrasekhar for useful suggestions and discussion.

References

1. J.C. Brodovitch and A. McAuley. Inorg. Chem. **20**, 1667 (1981).
2. A. McAuley and T.W. Whitcombe. Inorg. Chem. **27**, 3090 (1988).
3. S. Chandrasekhar and A. McAuley. Inorg. Chem. **31**, 2663 (1992).
4. N. Jubran, G. Ginzberg, H. Cohen, and D. Meyerstein. J. Chem. Soc. Chem. Commun. 517 (1982); Inorg. Chem. **24**, 251 (1985).
5. A.J. Blake, A.J. Holder, T.I. Hyde, and M. Schroder. J. Chem. Soc. Chem. Commun. 987 (1987).
6. X. Chen, S.E. Rokita, and C.J. Burrows. J. Am. Chem. Soc. **113**, 5884 (1991).
7. J.F. Kinneary, J.S. Albert, and C.J. Burrows. J. Am. Chem. Soc. **110**, 6124 (1988).
8. J.D. Woolins and P.F. Kelly. Coord. Chem. Rev. **65**, 115 (1985).
9. A.J. Blake, R.O. Gould, A.J. Holder, T.I. Hyde, A.J. Lavery, M.O. Odulate, and M. Schroder. J. Chem. Soc. Chem. Commun. 118 (1987).
10. A.J. Blake, R.O. Gould, A.J. Lavery, and M. Schroder. Angew. Chem. **98**, 282 (1986); Angew. Chem. Int. Ed. Engl. **26**, 274 (1986).
11. W.L. Waltz and J. Lilie. Inorg. Chem. **19**, 3284 (1980).
12. D.K. Storer and W.L. Waltz. Int. J. Radiat. Phys. Chem. **7**, 693 (1975).
13. M. Geoffrey, G. Bernardinelli, P. Castan, H. Chermette, D. Deguenon, S. Nour, J. Weber, and M. Wermeille. Inorg. Chem. **312**, 5056 (1992).
14. H.A. Boucher, G.A. Lawrance, P.A. Lay, A.M. Sargeson, A.M. Bond, D.F. Sangster, and J.C. Sullivan. J. Am. Chem. Soc. **105**, 4652 (1983).
15. W.L. Waltz, J. Lilie, S. Chandrasekhar, D. Woo, and K. Brown. Inorg. Chem. **35**, 124 (1996).
16. M.N. Bell, A.J. Blake, R.O. Gould, A.J. Holder, T.I. Hyde, A.J. Lavery, J. Reid, and M. Schroder. J. Inclusion Phenom. **5**, 169 (1987).
17. A.J. Blake, R.O. Gould, T.I. Hyde, and M. Schroder. J. Chem. Soc. Chem. Commun. 1730 (1987).
18. A.J. Blake, R.O. Gould, T.I. Hyde, and M. Schroder. J. Chem. Soc. Chem. Commun. 431 (1987).
19. B. Fisher and R. Eisenberg. J. Am. Chem. Soc. **102**, 7361 (1980).
20. I. Taniguchi. Modern aspects of electrochemistry. Plenum Press, New York. 1989.
21. H. Fujihira, Y. Hirata, and K. Suga. J. Electroanal. Chem. **292**, 199 (1990).
22. F. Abba, G. de Santis, L. Fabbrizzi, M. Licchelli, A.M.M. Lanfredi, P. Pallavicini, A. Poggi, and F. Ugozzoli. Inorg. Chem. **33**, 1366 (1994).
23. J.P. Collman, P. Denisevich, M. Marrocco, C. Koval, and F.C. Anson. J. Electroanal. Chem. **101**, 117 (1979).

© 1997 NRC Canada

24. J.P. Collman, P. Denisevich, Y, Konai, M. Marrocco, C. Koval, and F.C. Anson. J. Am. Chem. Soc. **102**, 6027 (1980).
25. S.P.J. Albracht, D. Ankel-Fuchs, R. Bocher, J. Ellermann, J. Moll, J.W. van der Zwaan, and R.K. Thauer. Biochem. Biophys. Acta, **955**, 86 (1988).
26. M.S. Ram, C.G. Riordan, R. Ostrander, and A.L. Rheingold. Inorg. Chem. **34**, 5884 (1995).
27. N.W. Alcock, K.P. Balakrishnan, and P.J. Moore, J. Chem. Soc. Dalton Trans. 1743 (1986).
28. (*a*) Md.A. Masood and D.J. Hodgson. Inorg. Chem. **33**, 2488 (1994); (*b*) C.-M. Che, W.-T. Tang, and T.C.W. Mak. J. Chem. Soc. Dalton Trans. 2879 (1988).
29. K. Wieghardt, E. Schoffmann, B. Nuber, and J. Weiss. Inorg. Chem. **25**, 4877, (1986).
30. B. Chak, A. McAuley, and T.W. Whitcombe. Can. J. Chem. **72**, 1525 (1994).
31. A. van den Bergen, R. Colton, M. Percy, and B.O. West. Inorg. Chem. **32**, 3408 (1993).
32. D. Waknine, M.J. Heeg, J.F. Endicott, and L.A. Ochrymowycz. Inorg. Chem. **30**, 3691 (1991).
33. E.J. Gabe, Y. Le Page, J.-P. Charland, F.L. Lee, and P.S. White. J. Appl. Crystallogr. **22**, 384 (1989).
34. International tables for X-ray crystallography. Vol. IV. Kynoch Press, Birmingham, England. 1974.
35. C.K. Johnson. ORTEP — A Fortran thermal ellipsoid plot program. Technical Report ORNL-5138, Oak Ridge, Tenn. 1976.
36. B. Bosnich, C.K. Poon, and M.L. Tobe. Inorg. Chem. **4**, 1102 (1965).
37. A.J. Blake, G. Reid, and M. Schroder. J. Chem. Soc. Dalton Trans. 1561 (1988).
38. T.W. Hambley. J. Chem. Soc. Dalton Trans. 565 (1986).
39. M.A. Watzky, D. Waknine, M.J. Heeg, J.F. Endicott, and L.A. Ochrymowycz. Inorg. Chem. **32**, 4882 (1993).
40. M. Yamashita, H. Ito, K. Toriumi, and T. Ito. Inorg. Chem. **22**, 1566 (1983).
41. R. Colton, B.D. James, I.D. Potter, and J.C. Traeger. Inorg. Chem. **32**, 2626 (1993).
42. A. Bond, R. Colton, D.A. Fiedler, J.E. Kevekordes, V. Tedesco, and T.F. Mann. Inorg. Chem. **33**, 5761 (1994).

Can. J. Chem. Downloaded from www.nrcresearchpress.com by 91.121.58.235 on 09/08/12
For personal use only.

© 1997 NRC Canada

Difunctional derivatives of bis(*m*-phenylene)-32-crown-10

Harry W. Gibson and Devdatt S. Nagvekar

Abstract: Optimization studies of the condensation of methyl 3,5-dihydroxybenzoate (**1**) with tetra(ethylene glycol) dichloride (**3**) resulted in improvement of the yield of the 1+1 cyclization product, 5-carbomethoxy-*m*-phenylene-16-crown-5 (**5**), to 67% (HPLC), but no improvement in the yield (28%, HPLC) of the desired 2+2 product, bis(5-carbomethoxy-*m*-phenylene)-32-crown-10 (**4**). However, after optimization, a two-step procedure provided improved yields of **4** and this procedure was generalized to afford other difunctional monomers. Condensation of substituted resorcinols with **3** and subsequent transformations yielded substituted (R) 3,5-bis(11-chloro-3,6,9-trioxaundecyl-oxy)benzenes (**7**, **9**–**14**). Reaction of dihalides **7** (R = $COOCH_3$), **13** (R = CHO), and **12** (R = $CH_2OSi(Me)_2$-*t*-Bu) with methyl 3,5-dihydroxybenzoate (**1**) produced bis(5-carbomethoxy-*m*-phenylene)-32-crown-10 (**4**) (43%), 5-carbomethoxy-*m*-phenylene-5′-formyl-*m*′-phenylene-32-crown-10 (**15**) (32%), and the lactone (**16a**) (18%, derived from the initially formed 5-hydroxymethyl-*m*-phenylene-5′-carbomethoxy-*m*′-phenylene-32-crown-10 (**16**)), respectively. Subsequent reactions gave the corresponding diacid (**17**), bis(hydroxymethyl) (**19**), bis(bromomethyl) (**20**), diacetyl (**18**), diformyl (**21**), bis(*p*-nitrophenoxymethyl) (**22**), and di(acetoxymethyl) (**23**) derivatives.

Key words: cyclization, functionalized bis(*m*-phenylene) crown ethers.

Résumé : Des études d'optimisation de la condensation du 3,5-dihydroxybenzoate de méthyle (**1**) avec le dichlorure de tétra(éthylèneglycol) (**3**) ont conduit à une amélioration du rendement du produit de cyclisation 1+1, 5-carbométhoxy-*m*-phénylène-16-couronne-5 (**5**) (à 67% selon la CLHP), sans amélioration du rendement (28% selon la CLHP) du produit désiré 2+2, bis(5-carbométhoxy-*m*-phénylène)-32-couronne-10 (**4**). Toutefois, après optimisation, une méthode en deux étapes a permis d'obtenir de meilleurs rendements de **4**; on a généralisé cette méthode pour obtenir d'autres monomères difonctionnels. La condensation de résorcinols substitués avec le composé **3** et des transformations subséquentes ont conduit aux 3,5-bis(11-chloro-3,6,9-trioxaundécyloxy)benzènes substitués (R) (**7**, **9**–**14**). La réaction des dihalogénures **7** (R = $COOCH_3$), **13** (R = CHO) et **12** (R = $CH_2OSi(Me)_2$-*t*-Bu) avec le 3,5-dihydroxybenzoate de méthyle (**1**) fournissent respectivement du bis(5-carbométhoxy-*m*-phénylène)-32-couronne-10 (**4**) (43%), du 5-carbométhoxy-*m*-phénylène-5′-formyl-*m*′-phénylène-32-couronne-10 (**15**) (32%) et la lactone (**16a**) (18%, dérivée de la 5-hydroxyméthyl-*m*-phénylène-5′-carbométhoxy-*m*′-phénylène-32-couronne-10 (**16**) formée initialement). Des réactions subséquentes ont permis d'obtenir les dérivés diacide (**17**), bis(hydroxyméthyle) (**19**), bis(bromométhyle) (**20**), diacétyle (**18**), diformyle (**21**), bis(*p*-nitrophénoxyméthyle) (**22**) et di(acétoxyméthyle) (**23**) correspondants.

Mots clés : cyclisation, éthers couronnes bis(*m*-phénylène) fonctionnalisées.

[Traduit par la rédaction]

Introduction

The ability of crown ethers to complex with alkali and alkaline earth metal ions was recognized by Pedersen when he discovered crown ethers (1) and has subsequently been studied in detail (2). This area, the seminal point for host–guest or supramolecular chemistry (3), has fascinated a great number of chemists worldwide and has led to important discoveries in a number of areas.

Work in our laboratory has been directed to the synthesis of aliphatic crown ethers ranging from 21- to 60-membered rings (4). Threading of these and bisphenylene crown ethers by aliphatic and aromatic linear species has provided rotaxanes (5, 6), catenanes (5, 6*c*, 7), and polyrotaxanes (5, 8). We reported earlier that the one-pot reaction of methyl 3,5-dihydroxybenzoate (**1**) and tetra(ethylene glycol) dichloride (**3**) gave only a 9% yield of bis(5-carbomethoxy-*m*-phenylene)-32-crown-10 (**4**) along with a 15% yield of 5-(carbomethoxy-*m*-phenylene)-16-crown-5 (**5**) (Scheme 1) (9).

The present article reports the optimization of the synthesis of diester crown ether **4** and its generalization to produce a variety of functionally substituted derivatives of bis(*m*-phenylene)-32-crown-10. Coupled with standard functional group conversions, this approach provides acceptable yields of an array of useful crown ethers.

Received January 31, 1997.

H.W. Gibson[1] **and D.S. Nagvekar.** Department of Chemistry, Virginia Polytechnic Institute & State University, Blacksburg, VA 24061, U.S.A.

[1] Author to whom correspondence may be addressed. Telephone: (540) 231-5902. Fax: (540) 231-8517. E-mail: hwgibson@vt.edu

Results and discussion

A. Optimization of one-step approach

1. HPLC analysis

The first phase of this research involved the implementation of HPLC to detect and estimate the product distribution. Several

© 1997 NRC Canada

Can. J. Chem. Downloaded from www.nrcresearchpress.com by 91.121.58.235 on 09/08/12
For personal use only.

Table 1. Optimization of one-step synthesis of bis(5-carbomethoxy-*m*-phenylene)-32-crown-10 (**4**) by reaction of **1** and **3** in DMF.

Expt.	Final conc. (mM)	Base	Added salt (equiv.)	Temp. (°C)	Time (days)	HPLC products (%)			
						1	**5**	**6**	**4**
1	64.3	NaH[a]	—	85	3	3.2	37.2	13.9	0
2	32.1	NaH[a]	—	85	3	9.5	50.1		11.7
3	18.4	NaH[a]	—	85	3	30.6	57.6	0	3.0
4	18.5	NaH[a]	CsCl(3)	85	3	26.4	52.4	4.2	6.9
5	32.1	NaH[a]	CsCl(3)	85	3	27.5	40.0	5.1	4.5
6	32.1	NaH[a]	$(n\text{-Bu})_4$NI(2)	85	3	27.4	41.1	2.9	8.1
7	23.9	NaH[b]	—	85	3	0	51.1	20.9	11.7
8	46.9	NaH[b]	—	85	3	18.9	46.9	10.6	3.3
9	59.4	NaH[b]	—	85	3	0	52.9	4.4	24.0
10	79.8	NaH[b]	—	85	3	4.9	59.7	7.4	16.0
11	95.2	NaH[b]		85	3	0	61.4	12.8	13.7
12	103	NaH[b]	$(n\text{-Bu})_4$NI(1)	85	3	1.0	55.5	0	20.0
13	119	NaH[b]	—	85	3	0	53.9[c]	0	28.1[c]
14	120	NaH[b]	CsCl(3)	85	3	18.9	45.8	12.0	9.1
15	159	NaH[b]	—	85	3	4.0	60.7	7.5	17.5
16	119	NaH[b]	—	110	3	3.3	57.0	0	22.6
17	119	NaH[b]	—	130	3	11.8	56.8	0	21.1
18	119	NaH[b]	—	153	3	15.9	60.7	0	10.5
19	519	NaH[d]	—	110	4	0	53.3	0	25.0
20	519	K_2CO_3[d]	—	110	4	0	63.3	0	24.4
21	519	Cs_2CO_3	—	110	4	0	67.3	0.6	9.2

[a]Method A: Na salt of **1** (made with NaH at 25°C) added to 1 equiv. of **3**; 1/2 equiv. over 4 h, stirred 10 h, diluted 3×, add 1/2 equiv. quickly.
[b]Method B: **3** quickly added to 1 equiv. of Na salt of **1** (made with NaH at 85°C).
[c]Isolated yield of **4**: 7%; **5**: 15% (9).
[d]Method C: equivalent amounts of **1** and **3** and base mixed together in DMF.

solvent systems were examined; a combination of chloroform and isopropanol (94:6) was found to work the best. The small and the large macrocycles (**4** and **5**) were well resolved. Detection by UV absorption and integration of peak areas was found to give accurate percentage compositions of synthetic mixtures. The dichloro intermediate **7**, the monochloro intermediate **6**, and starting material **1** were also resolved. A peak of longer retention time was attributed to intermediate **8**. Other unidentified peaks were attributed to linear oligomers.

2. Summary

As a result of variation of concentration, temperature, the nature of the base, and order of addition (Table 1) the yield of desired macrocycle **4** was not improved relative to our earlier work (9) (expt. 13), although high yields (67%) of the smaller macrocycle **5** were obtained (expt. 21). We thus turned our attention to other routes to **4**.

B. Optimization of a two-step approach

1. Precursor synthesis: methyl 3,5-bis(11-chloro-3,6,9-trioxaundecycloxy)benzoate (7)

Production of bis(5-carbomethoxy-*m*-phenylene)-32-crown-10 (**4**) and 5-carbomethoxy-*m*-phenylene-16-crown-5 (**5**) depends on the intermediates methyl 3,5-bis(11-chloro-3,6,9-trioxaundecycloxy)benzoate (**7**) and methyl 3-(11-chloro-3,6,9-trioxaundecyloxy)-5-hydroxybenzoate (**6**), respectively (Scheme 1). The use of dichloride **7** as a starting material eliminates the possibility of forming **5** and should result in improved yields of **4**.

Tetra(ethylene glycol) was converted to its monochloride, using toluene as a diluent and slow thionyl chloride addition (67% yield, see Experimental). However, its reaction with **1** afforded only 29% of the desired diol, methyl 3,5-bis(11-hydroxy-3,6,9-trioxaundecycloxy) benzoate (see Experimental), so this approach was abandoned.

The synthesis of **7** from **1** was achieved using a 10 equiv. excess of tetra(ethylene glycol) dichloride (**3**) and by use of a variety of bases (Table 2, Scheme 2). In the best method the disodium salt solution of methyl 3,5-dihydroxybenzoate (**1**) was prepared at 110°C using sodium hydride as a base. The reaction after 2 h was cooled to room temperature and stirred with excess tetra(ethylene glycol) dichloride. Excess **3** was removed by vacuum distillation. The crude material was only partially soluble in cold or hot hydrocarbon solvents such as toluene, hexane, and petroleum ether (39–59°C), which was found to be the most selective solvent. Its use in continuous liquid–liquid extraction of the crude material gave methyl 3,5-bis(11-chloro-3,6,9-trioxaundecyloxy)benzoate (**7**) in 68% yield. Alternatively, column chromatography gave a 70% yield.

2. Cyclization

Cyclization is greatly dependent on the nature of the metal ion (3*b*, 10) and the ring size. In addition, by increasing the dilution the fraction of cyclic components can be increased at the

Can. J. Chem. Downloaded from www.nrcresearchpress.com by 91.121.58.235 on 09/08/12
For personal use only.

© 1997 NRC Canada

Scheme 1.

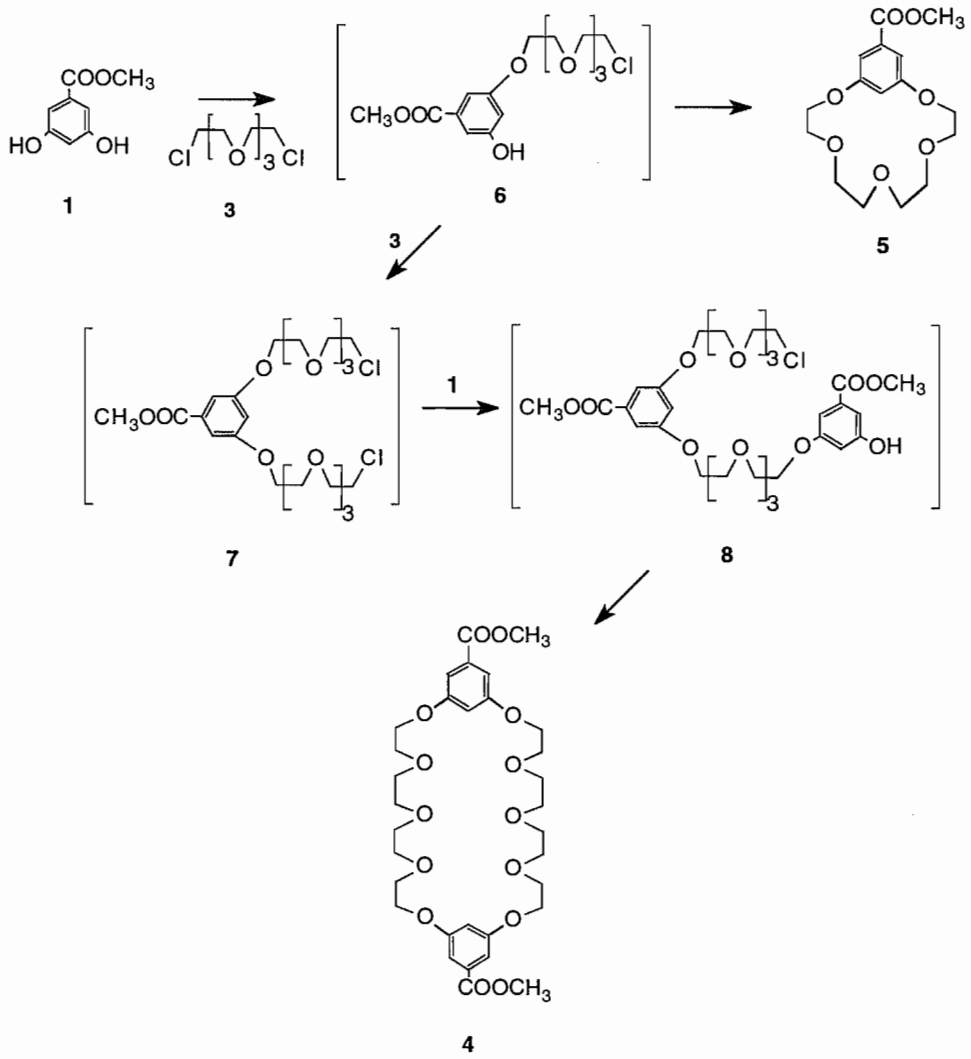


Table 2. Optimization of synthesis of methyl 3,5-bis(11-chloro-3,6,9-trioxaundecyloxy)benzoate (**7**).[a]

Expt.	Base	Temp. (°C)	Time (h)	Conc. (mM)	Product distribution via HPLC (%)		
					1	**6**	**7**
1	NaH	110	2	285	7.0	21.0	51.6
2	NaH	RT	18	285	0	11.5	81.5[b]
3	K_2CO_3	RT	96	238	51.1	31.7	10.6
4	K_2CO_3	110	24	284	0	28.5	71.5
5	Cs_2CO_3	110	30	227	10.8	28.2	57.6

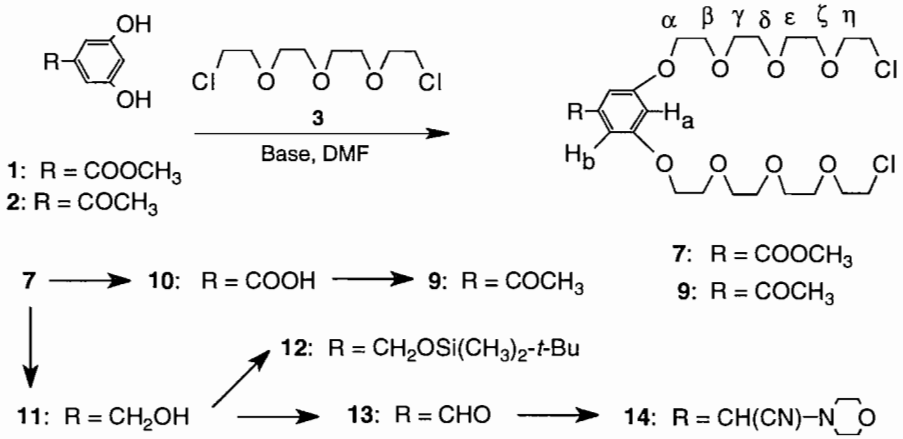
[a]By reaction of preformed anion of **1** with 10 equiv. of **3**.
[b]Isolated yield of compound **7**: 70%.

expense of linear oligomers; the maximum concentration that favors the intramolecular versus intermolecular reaction is generally of the order of 10^{-3} mol/L (3*b*, 11). Higher temperatures generally favor cyclization (3*b*, 12). Cesium-assisted cyclization reactions have been used quite successfully in recent years. Stoddart and co-workers (13) synthesized a 68-membered macrocycle in 62% yield by employing a combination of a high-dilution reaction in DMF at high temperature

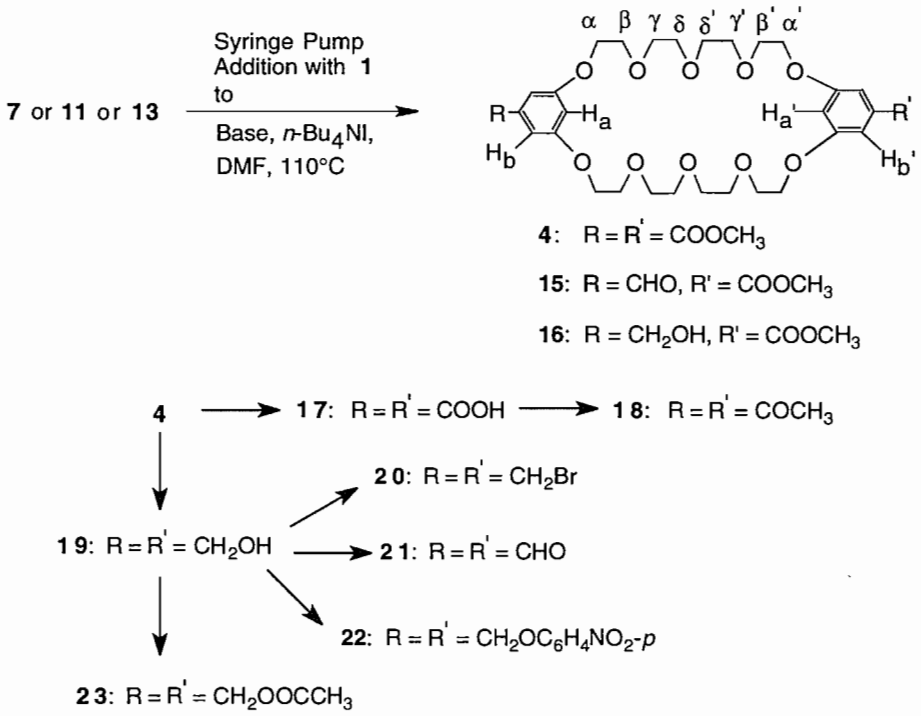
© 1997 NRC Canada

Can. J. Chem. Downloaded from www.nrcresearchpress.com by 91.121.58.235 on 09/08/12
For personal use only.

Scheme 2.



Scheme 3.



(110°C) with the cesium effect (14) and a phase transfer catalyst. Considering all of the above factors, we performed the cyclization by syringe pump addition of a solution of either (*i*) **7** or (*ii*) both **7** and **1** to a stirred mixture of base and *n*-Bu_4NI (TBAI, phase transfer agent) (and **1** in case (*i*)) in DMF (Scheme 3).

F^- is basic enough to cause deprotonation of weak acids in dipolar aprotic solvents (15); the driving force is believed to be the formation of the stable H—F bond (569 kJ/mol) (16). Use of the weaker bases and addition of both **1** and **7** gave better yields than with NaH by addition of **7** only to the preformed dianion of **1** (Table 3). CsF and K_2CO_3 provided nearly identical yields of **4** (42 and 43%) in spite of the difference in the sizes of the metal ions. The ionic radius of K^+ (1.33 Å), although much smaller than Cs^+ (1.65 Å), may be involved in multiple complexations with the oxyethylene side chain. Such multiple complexation behavior is indeed quite well known (*3b*, 17) and holds especially true for crown ethers greater than 27-membered. Furthermore, the yield of the macrocycle **4** is lower with Cs_2CO_3 than with CsF.

C. Synthesis of other derivatives using optimized procedures

1. Dichloro precursors

Several derivatives of **7** were synthesized by functional group conversions (Scheme 2). Acetophenone derivative **9** was synthesized directly in 53% yield utilizing excess tetra(ethylene glycol) dichloride (**3**) and 3,5-dihydroxyacetophenone (**2**), using NaH as base at 50°C.

Can. J. Chem. Downloaded from www.nrcresearchpress.com by 91.121.58.235 on 09/08/12
For personal use only.

© 1997 NRC Canada

Table 3. Synthesis of bis(5-carbomethoxy-*m*-phenylene)-32-crown-10 (**4**) from **1** and **7** at 110°C.

Base	% Yield
NaH	18[a]
K_2CO_3	43[b]
Cs_2CO_3	37[b]
CsF	42[b]

[a] **7** added to dianion of **1** by syringe pump.
[b] **1** and **7** added to base by syringe pump.

Hydrolysis of ester **7** with KOH in ethanol (EtOH) gave the acid **10** in 98% yield. Reduction of **7** with lithium aluminum hydride (LAH) gave 3,5-bis(11-chloro-3,6,9-trioxaundecyloxy)benzyl alcohol (**11**) in 94% yield. The alcohol **11** was converted to the silyl ether **12** (97%) by treatment with *tert*-butyldimethylsilyl chloride (*t*-BDMSCl). Oxidation of the alcohol **11** with pyridinium chlorochromate (PCC) in dichloromethane (DCM) gave, after column chromatography, an 86% yield of 3,5-bis(11-chloro-3,6,9-trioxaundecyloxy)benzaldehyde (**13**). Reaction of aldehyde **13** with morpholine and trimethylsilyl cyanide (TMSCN) in DCM produced a 92% yield of aminonitrile **14**. The use of methyllithium (MeLi) to convert carboxylic acids to methyl ketones is a well-known general method (18); the major side reaction, the formation of tertiary alcohol (18, 19), can be eliminated by the use of excess chlorotrimethylsilane (TMSCl) to quench the dilithiated intermediate (20). Thus sequential treatment of the acid **10** with MeLi in tetrahydrofuran (THF) at 0°C, followed by quenching with TMSCl, produced 3,5-bis(11-chloro-3,6,9-trioxaundecyloxy)acetophenone (**9**) in 66% yield.

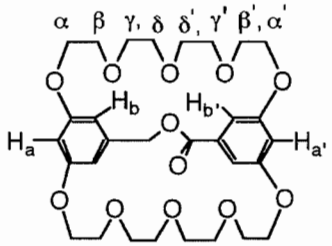
2. *Cyclization to other difunctional bis(*m*-phenylene)-32-crown-10 derivatives*

Reaction of dichloride **13** with **1** using CsF as the base afforded a 32% yield of 5-carbomethoxy-*m*-phenylene-5′-formyl-*m*′-phenylene-32-crown-10 (**15**) (Scheme 3).

Condensation of silyl ether **12** with **1** using Cs_2CO_3 was expected to produce the alcohol/ester **16** through hydrolysis of the intermediate silyl ether during work-up. However, the related lactone **16a** was isolated in 18% yield. Its structure is supported by the lack of a methoxy signal in its ^1H NMR spectrum (integration), the lack of the ^{13}C NMR signal at ca. 52 ppm as seen in methyl esters **4**, **7**, and **15**, and by the MS data, all of which fit the lactone structure well. Furthermore, there are significant downfield shifts of the α and α′ signals (4.0–4.4 ppm), $H_{b'}$ (7.29 ppm), and the benzylic methylene protons (5.29 ppm), relative to monocyclic analogs (α and α′ average: 4.09 ppm in **4**, **15**, **17**-**22**; H_b average: 7.15 in **4** and **15**; $ArCH_2$ 4.99 ppm in **23**); this is due to the change in conformation of the cryptand **16a** in comparison to the crown ethers. **16a** apparently forms by intramolecular transesterification of **16**, either during the reaction itself or in work-up and (or) purification.

3. *Difunctional derivatives by functional group conversions*

Several other derivatives of bis(*m*-phenylene)-32-crown-10 were synthesized via classical organic functional group conversions. The diacid **17** was synthesized in 93% yield by hydrolysis of the diester **4** in aqueous NaOH – EtOH. We also synthesized diacetyl macrocycle **18** from the diacid **17** in 45% yield by treatment with MeLi in THF, followed by quenching with TMSCl and aqueous work-up.



16a

Bis(5-hydroxymethyl-*m*-phenylene)-32-crown-10 (**19**) was synthesized in 95% yield via LAH reduction of the diester **4**. Treatment of **19** with PBr_3 gave bis(5-bromomethyl-*m*-phenylene)-32-crown-10 (**20**) in 88% yield. The oxidation of diol **19** with PCC afforded bis(5-formyl-*m*-phenylene)-32-crown-10 (**21**) in 85% yield. Treatment of diol **19** first with NaH and then with *p*-fluoronitrobenzene in THF provided a 100% yield of bis(*p*-nitrophenyl ether) **22**. The diacetate **23** was prepared in 98% yield by treatment of diol **19** with acetyl chloride in THF, with catalysis by pyridine.

Conclusions

A two-step strategy involving the synthesis of intermediates **7**, **9**–**14** in the first step followed by cyclization with methyl 3,5-dihydroxybenzoate (**1**) using a syringe pump to maintain pseudo-high-dilution conditions afforded bis(*m*-phenylene)-32-crown-10 derivatives **4** (43%), **15** (32%), and **16a** (18%). Thus, a significant yield improvement over our previously reported procedure (9%) (9) was realized for **4**. Several other new derivatives of bis(*m*-phenylene)-32-crown-10 were synthesized by functional group conversions; these include diketone **18**, diol **19**, dihalide **20**, dialdehyde **21**, bis(*p*-nitrophenyl ether) **22** (a diamine precursor), and diacetate **23**.

The use of these new difunctional crown ethers in the syntheses of polymers containing macrocycles in the backbones (i.e., poly(macrocycle)s) and supramolecular structures by self assembly is currently being explored. These studies will be reported in due course.

Experimental

Materials

Unless specified otherwise, reagent grade reactants and solvents were used as received from chemical suppliers. THF was distilled over sodium–benzophenone. Tetra(ethylene glycol) dichloride (**3**) (*1b*) and methyl 3,5-dihydroxybenzoate (**1**) (*9a*) were synthesized according to literature procedures.

Measurements

HPLC analyses were performed on an ISCO dual pump system comprising two model 2350 pumps and the V^4 variable wavelength UV/VIS detector set at 274 nm. $CHCl_3$:i-PrOH (94:6, v:v) was used for elution of products on a 4.6 × 250 mm

© 1997 NRC Canada

Can. J. Chem. Downloaded from www.nrcresearchpress.com by 91.121.58.235 on 09/08/12
For personal use only.

Can. J. Chem. Downloaded from www.nrcresearchpress.com by 91.121.58.235 on 09/08/12
For personal use only.

5 μm silica column at a flow rate of 1 mL/min. The system was interfaced with the ISCO ChemResearch chromatographic data management system, used for data analyses. A Harvard syringe infusion pump model 22 was used in the cyclization reactions. Melting points were taken in capillary tubes with a Haake–Buchler melting point apparatus and have been corrected. ^{1}H and ^{13}C NMR spectra were obtained at ambient temperature on Varian Unity 400 MHz and Bruker 270 MHz spectrometers using acetone-d_6 or $CDCl_3$ as solvents with tetramethylsilane (δ = 0) as internal standard. Infrared spectra (KBr pellets, unless otherwise noted) were recorded on a Nicolet MX-1 FTIR spectrometer. Mass spectra (MS) were measured at the Nebraska Center for Mass Spectrometry, Department of Chemistry, University of Nebraska, Lincoln, Nebr., and at the Center for Mass Spectrometry at Washington University, St. Louis, Mo.; fast atom bombardment (FAB) MS utilized 3-nitrobenzyl alcohol as the matrix; EI = electron impact; HR = high resolution. Elemental analyses were performed by Atlantic Microlab, Norcross, Ga.

HPLC analyses

A synthetic mixture comprising 40.5:59.5 (w:w) macrocycles **5**:**4** was subjected to quantitative analysis using integrated peak areas with the following results: 40.6% **5**, 59.4% **4** (avg. of 2 determinations). Elution times: **4** @ 6.0 min, **5** @ 3.4 min, methyl 3,5-dihydroxybenzoate (**1**) @ 5.0 min, **7** @ 3.5 min; from the synthesis of **7** using K_2CO_3 (Table 2) the kinetic evolution of the products indicated that the compound with elution time 4.0 min was monochloride **6**. The peak with elution time 8.0 min was attributed to precursor **8**, and higher oligomers eluted @ 9.5 min. All percentages are based on integrated peak areas.

Optimization of synthesis of 4 via one-step method

Method A

NaH (0.20 g, 8.3 mmol) was added to a stirred solution of methyl 3,5-dihydroxybenzoate (**1**, 0.54 g, 3.2 mmol) in DMF (25 mL). The mixture was stirred at room temperature for 2 h. The resulting brown solution was diluted with DMF (25 mL) and added slowly to neat tetra(ethylene glycol) dichloride (**3**, 1.49 g, 6.45 mmol) over a period of 0.5 h at 85°C. The resulting mixture was stirred for 10 h at 85°C, diluted with DMF (100 mL), and the second portion of the disodium salt of methyl 3,5-dihydroxybenzoate (**1**, 0.54 g (3.2 mmol) in DMF (50 mL)) was added quickly. The resulting mixture was stirred for 2 days at 85°C. The cooled reaction mixture was filtered and DMF was stripped to give a brown gummy product. The crude product (15–17 mg in 10 mL DCM) was subjected to HPLC analysis.

Method B

NaH (0.87 g, 36 mmol) was added to a stirred solution of methyl 3,5-dihydroxybenzoate (**1**, 2.39 g, 14.2 mmol) in DMF (57 mL). The resulting mixture was stirred for 2 h at 85°C. A solution of tetra(ethylene glycol) dichloride (**3**, 3.29 g, 14.2 mmol) in DMF (62.5 mL) was added quickly and the mixture was stirred vigorously at 85°C for 48 h under a blanket of nitrogen. The mixture was cooled, filtered, and the DMF was stripped to give a crude product. The crude product (15–17 mg in DCM (10 mL)) was subjected to HPLC analysis.

2-{2′-[2″-(2‴-Chloroethoxy)ethoxy]ethoxy}ethanol

$SOCl_2$ (11.5 mL, 0.158 mol) was added over a period of 5 h to a solution of tetra(ethylene glycol) (30.54 g, 157 mmol), toluene (250 mL), and pyridine (12.2 mL, 151 mmol). The reaction was exothermic. The solution was refluxed for 36 h, cooled, and evaporated. The crude product was dissolved in H_2O (75 mL) and tetra(ethylene glycol) dichloride (**7**) was removed by extraction with toluene (3 × 50 mL). The aqueous layer was evaporated. The mixture was diluted with saturated NaCl (75 mL) and extracted with Et_2O (3 × 100 mL). Pure product (22.5 g, 67.4%) was obtained via vacuum distillation, bp 132–133°C/1.25 Torr (1 Torr = 133.3 Pa) (lit. (21) bp 134.6–136°C/0.094 Torr); (22) bp 123–125°C/2.0 Torr). IR (neat): 3450 (OH), 2860 (CH), 1085 (COC) cm^{-1}. ^{1}H NMR ($CDCl_3$) δ (ppm): 2.72 (br s, 1H, OH), 3.57–3.67 (m, 4H, CH_2Cl and OCH_2), 3.68 (s, 8H, OCH_2), 3.69–3.79 (m, 4H, OCH_2).

Methyl 3,5-bis(11-hydroxy-3,6,9-trioxa-1-undecyloxy)-benzoate

A mixture of methyl 3,5-dihydroxybenzoate (**1**, 2.01 g, 12 mmol) and NaH (0.74 g, 31 mmol) in anhydrous DMF (25 mL) was heated for 2 h at 85°C. To the brown-colored mixture was added 2-{2′-[2″-(2‴-chloroethoxy)ethoxy]ethoxy}ethanol (5.11 g, 24.0 mmol) and the mixture was stirred vigorously for 2 days. The cooled solution was filtered and the DMF removed to give a crude product. Column chromatography with EtOH as eluent gave methyl 3,5-bis(11-hydroxy-3,6,9-trioxa-1-undecyloxy)benzoate (1.80 g, 29%), an oil. IR (neat): 3446 (OH), 2865 (-CH), 1716 (C═O), 1600 (C═C), and 1135 (C-O-C). ^{1}H NMR ($CDCl_3$) δ (ppm): 3.12 (br s, 2H, OH), 3.6–3.7 (m, 24H, γ-η-OCH_2), 3.82 (t, J = 4.7 Hz, 4H, β-CH_2), 3.86 (s, 3H, OCH_3), 4.12 (t, J = 4.7 Hz, 4H, α-CH_2), 6.68 (t, J = 2.3 Hz, 1H, H_a), and 7.16 (d, J = 2.3 Hz, 2H, H_b). MS (EI): 520 (M^+, 11%), 489 [$(M - OCH_3)^+$, 2%], 445 [$(M - OCH3 - CH_2CH_2O)^+$, 3%], 344 {$[M - (OCH_2CH_2)_4]^+$, 9%], 194 (31%), 163 (50%), 89 (100%).

Methyl 3,5-bis(11-chloro-3,6,9-trioxaundecyloxy)-benzoate (7)

NaH (9.37 g, 312 mmol, 80% in mineral oil, 2.1 equiv.) was added to a solution of methyl 3,5-dihydroxybenzoate (**1**, 25.0 g, 149 mmol) in DMF (150 mL). The mixture was stirred for 3 h at 110°C and cooled to room temperature (RT). The resulting suspension of dianion was added to a mixture containing tetra(ethylene glycol) dichloride (**3**, 343.6 g, 1.487 mol, 10 equiv.) in DMF (100 mL) over a period of 6 h and then the mixture was stirred for 5 days at 50°C. The mixture was filtered and DMF was removed on a rotary evaporator. Excess **3** (280 mL) was removed via vacuum distillation. A continuous liquid–liquid extraction with petroleum ether gave 47.2 g (68%) of **7**, an oil. Alternatively, silica gel column chromatography with EtOAc afforded a 70% yield. IR (neat): 3064 (C═C-H), 2877 (-CH), 1729 (C═O), 1596 (C═C), 1118 (C-O-C), and 733 (-CH_2Cl) cm^{-1}. ^{1}H NMR ($CDCl_3$) δ (ppm): 3.55–3.65 (m, 4H, CH_2Cl), 3.65–3.75 (m, 20H, γ-η-CH_2), 3.86 (t, J = 4.8 Hz, 4H, β-CH_2), 3.89 (s, 3H, CH_3), 4.15 (t, J = 4.8 Hz, 4H, α-CH_2), 6.70, (t, J = 2.3 Hz, 1H, H_a), and 7.19 (d, J = 2.3 Hz, 2H, H_b). ^{13}C NMR δ (ppm): 42.68, 52.19, 67.69, 69.54, 70.59, 70.61, 70.64, 70.80, 71.30, 106.84, 107.95, 131.83, 159.70, and 166.70 (14 peaks as required). MS (EI) *m/z* (rel. int.): 558 [$M(^{35}Cl_1{}^{37}Cl_1)]^+$ (3%),

© 1997 NRC Canada

Can. J. Chem. Downloaded from www.nrcresearchpress.com by 91.121.58.235 on 09/08/12
For personal use only.

556 $[M(^{35}Cl_2)]^+$ (5%), 527 $[M(^{35}Cl_1{}^{37}Cl_1) - OCH_3]^+$ (0.8%), 525 $[M(^{35}Cl_2 - OCH_3]^+$ (1%), and 63 $[C_2H_3Cl]$ (100%). HRFAB, calcd. for $C_{24}H_{38}{}^{35}Cl_2O_{10}$: $[M]^+$ *m/z* 556.1842; found: 556.1818 (error 3.0 ppm).

Optimization of synthesis of bis(5-carbomethoxy-*m*-phenylene)-32-crown-10 (4) by cyclization of 1 and 7 (see Table 3)

$CsCO_3$

A mixture of methyl 3,5-dihydroxybenzoate (**1**, 0.17 g, 1.0 mmol) and methyl 3,5-bis(11-chloro-3,6,9-trioxaundecyloxy)benzoate (**7**, 0.56 g, 1.0 mmol) in DMF (10 mL) was added using a syringe pump (1.67 mL/h) to a suspension containing Cs_2CO_3 (3.30 g, 1.0 mmol), CsCl (0.35 g, 2.0 mmol), and TBAI (10 mg) in DMF (40 mL) at 110°C. The mixture was stirred vigorously for 3 days at 110°C, cooled, and filtered. DMF was removed and the crude product was purified via column chromatography using EtOAc as solvent to afford pure **4** (0.24 g, 37%). The product was recrystallized from acetone, mp 107.8–108.5°C (lit. (*9a*) mp 106.5–107.5°C).

NaH

A solution of methyl 3,5-bis(11-chloro-3,6,9-trioxaundecyloxy)benzoate (**7**, 0.558 g, 1.0 mmol) in DMF (10 mL) was added via a syringe pump (1.67 mL/h) to a mixture initially containing methyl 3,5-dihydroxybenzoate (**1**, 0.17 g, 1.0 mmol), NaH (64.3 mg, 2.68 mmol), CsCl (0.87 g, 5.3 mmol), and TBAI (10 mg) in DMF (40 mL) at 110°C. The mixture was stirred vigorously for 3 days at 110°C, cooled, and filtered. DMF was removed and the crude product was purified via column chromatography using EtOAc as a solvent, which gave pure **4** (0.12 g, 18%). The product was recrystallized from acetone, mp 107.8–108°C (lit. (*9a*) mp 106.5–107.5°C).

K_2CO_3 (optimized method)

A mixture containing methyl 3,5-bis(11-chloro-3,6,9-trioxaundecyloxy)benzoate (**7**, 7.66 g, 13.7 mmol) and methyl 3,5-dihydroxybenzoate (**1**, 2.33 g, 13.9 mmol) in DMF (total volume 22 mL) was added via a syringe pump at 0.75 mL/h to a suspension containing K_2CO_3 (19.04 g, 137.7 mmol) and TBAI (20 mg) in DMF (670 mL) at 110°C. After complete addition, the mixture was stirred at 110°C for 5 days. The cooled reaction mixture was evaporated to remove DMF, treated with DCM, and filtered. Removal of DCM followed by flash column chromatography using Et_2O as eluent gave pure **4** (3.89 g, 43%), mp 107.2–108.7°C (lit. (*9a*) mp 106.5–107.5°C). IR: 1717 (C═O), 1600 (C═C), 1067–1137 (C-O-C) cm^{-1}. ^1H NMR ($CDCl_3$) δ (ppm): 3.65–3.75 (m, 16H, γ, δ-CH_2), 3.84 (t, *J* = 4.5 Hz, 8H, β-CH_2), 3.87 (s, 6H, CH_3), 4.10 (t, *J* = 4.6 Hz, 8H, α-CH_2), 6.67 (t, *J* = 2.0 Hz, 2H, H_a), and 7.15 (d, *J* = 2.0 Hz, 4H, H_b). ^{13}C NMR ($CDCl_3$) δ (ppm): 52.10, 67.76, 69.48, 70.77, 70.83, 106.73, 107.91, 131.73, 159.65, and 166.63 (10 peaks as required).

CsF

A mixture containing methyl 3,5-bis(11-chloro-3,6,9-trioxaundecyloxy)benzoate (**7**, 18.62 g, 3.34 mmol) and methyl 3,5-dihydroxybenzoate (**1**, 5.65 g, 3.36 mmol) in DMF (total volume 55 mL) was added via a syringe pump (0.75 mL/h) to a suspension containing CsF (50.86 g, 3.35 mmol) and TBAI (50 mg) in DMF (1650 mL) at 110°C. After complete addition, the mixture was stirred vigorously at 110°C for 5 days. The cooled reaction mixture was evaporated to remove DMF and filtered to remove all salts using DCM. Removal of DCM followed by flash column chromatography using Et_2O as eluent gave pure **4** (9.10 g, 41.8%), mp 107.3–108.6°C (lit. (*9a*) mp 106.5–107.5°C).

3,5-Bis(11-chloro-3,6,9-trioxaundecyloxy)acetophenone (9)

Method A

NaH (1.05 g, 35.0 mmol, 80% in mineral oil) was added to a solution of 3,5-dihydroxyacetophenone (**2**, 2.525 g, 16.6 mmol) in DMF (25 mL). The mixture was stirred for 3 h at 110°C and brought to 50°C before adding excess tetra(ethylene glycol) dichloride (**3**, 40.05 g, 173.3 mmol, 10 equiv.). The mixture was stirred for 5 days at 50°C and filtered. After removal of DMF, the excess **3** was removed via vacuum distillation. Silica gel column chromatography with Et_2O as eluent gave pure **9** (4.72 g, 53%), an oil. ^1H NMR ($CDCl_3$) δ (ppm): 2.56 (s, 3H, CH_3), 3.63 (t, *J* = 5.8 Hz, 4H, CH_2Cl), 3.65–3.75 (m, 20H, γ-η-CH_2), 3.87 (t, *J* = 4.8 Hz, 4H, β-CH_2), 4.15 (t, *J* = 4.8 Hz, 4H, α-CH_2,), 6.70 (t, *J* = 2.4 Hz, 1H, H_a), and 7.11 (d, *J* = 2.4 Hz, 2H, H_b). ^{13}C NMR ($CDCl_3$) δ (ppm): 42.68, 52.19, 67.69, 69.54, 70.59, 70.61, 70.64, 70.80, 71.30, 106.84, 107.95, 131.83, 159.70, and 166.70 (14 peaks as required). MS FAB *m/z* (rel. int.): 565.1 $[M(^{37}Cl_1{}^{35}Cl_1) + Na]^+$ (70%), 563.1 $[M(^{35}Cl_2) + Na]^+$ (100%); HRFAB, calcd. for $C_{24}H_{38}Cl_2O_9Na$: $[M + Na]^+$ 565.1761 ($^{37}Cl_1$ $^{35}Cl_1$) and 563.1791 ($^{35}Cl_2$); found: 565.1759 (error 0.3 ppm) and 563.1782 (error 1.5 ppm).

Method B

To a solution of 3,5-bis(11-chloro-3,6,9-trioxaundecyloxy)-benzoic acid (**10**, 3.76 g, 6.92 mmol) in dry THF (100 mL) at 0°C was added MeLi (20 mL, 1.4 M, 2.8 mmol). Stirring was continued at 0°C for 3.5 h; then TMSCl (18.0 mL, 141 mmol) was added and stirring was continued for 2 h. The solution was allowed to warm to RT and quenched with 25 mL 1 N HCl. The mixture was stirred for 12 h and extracted with Et_2O. The extract was washed with H_2O, dried (Na_2SO_4), and evaporated to afford 2.47 g (66%) of **9** as a slightly reddish oil with the same spectral characteristics as a sample made by Method A above. Anal. calcd. for $C_{24}H_{38}Cl_2O_9$: C 61.45, H 7.47; found: C 61.59, H 7.42.

3,5-Bis(11-chloro-3,6,9-trioxaundecyloxy)benzoic acid (10)

A solution of methyl 3,5-bis(11-chloro-3,6,9-trioxaundecyloxy)benzoate (**7**, 10.32 g, 18.5 mmol), 3.21 g (48.6 mmol) of KOH, 60 mL of EtOH, and 30 mL of H_2O was heated at reflux for 3 h, cooled, and neutralized with 2 N HCl. The solvents were removed in vacuo and the residue was extracted with DCM. The solution was dried (Na_2SO_4) and evaporated to give 10.06 g (98%) of **10**, which after purification by elution through silica gel with Et_2O remained an oil. ^1H NMR ($CDCl_3$) δ (ppm): 3.65–3.75 (m, 24H, γ-η-CH_2 + CH_2Cl), 3.87 (t, *J* = 4.6 Hz, 4H, β-CH_2,), 4.16 (t, *J* = 4.6Hz, 4H, α-CH_2), 6.73 (t, *J* = 2.0 Hz, 1H, H_a), and 7.25 (d, *J* = 2.0 Hz, 2H, H_b). ^{13}C NMR ($CDCl_3$) δ (ppm): 42.69, 67.73, 69.57, 70.60, 70.62, 70.66, 70.81, 71.32, 107.55, 108.47, 131.09, 159.75,

© 1997 NRC Canada

Can. J. Chem. Downloaded from www.nrcresearchpress.com by 91.121.58.235 on 09/08/12
For personal use only.

170.61 (13 peaks as required). MS (FAB) *m/z* (rel. int.): 567.1 [M($^{35}Cl_1{}^{37}Cl_1$) + Na]$^+$, 45%}, 565.1{[M($^{35}Cl_2$) + Na)$^+$, 100%]; HRFAB, calcd. for $C_{22}H_{36}Cl_2O_{10}$: [M + Na]$^+$ *m/z* 565.1583 ($^{35}Cl_2$) and 567.1554 ($^{35}Cl_1{}^{37}Cl_1$); found: 565.1581 (error 0.4 ppm) and 567.1548 (error 0.9 ppm) .

3,5-Bis(11-chloro-3,6,9-trioxaundecyloxy)benzyl alcohol (11)

A solution of LAH (15.0 mL, 15 mmol, 1.0 M) in THF was added to a solution of methyl 3,5-bis(11-chloro-3,6,9-trioxaundecyloxy)benzoate (**7**, 15.55 g, 27.9 mmol) in THF (300 mL) at RT. After the mixture had stirred for 15 h at RT, excess LAH was destroyed using EtOAc. The solution was diluted with H_2O and acidified with 2 N HCl. The product was extracted with Et_2O (3 × 75 mL). The combined organic layer was washed with H_2O and saturated NaCl. Evaporation of the solvent after drying (Na_2SO_4) gave **11** (13.84 g, 94%), an oil. ^{1}H NMR ($CDCl_3$) δ (ppm): 3.65–3.75 (m, 24H, γ-η-CH_2 + CH_2Cl), 3.83 (t, *J* = 4.8 Hz, 4H, β-CH_2), 4.10 (t, *J* = 4.8 Hz, 4H, α-CH_2), 4.59 (s, 2H, CH_2O), 6.40 (t, *J* = 2.0 Hz, 1H, H_a), and 6.53 (d, *J* = 2.0 Hz, 2H, H_b). ^{13}C NMR ($CDCl_3$) δ (ppm): 42.66, 65.04, 67.42, 69.64, 70.53, 70.57, 70.61, 70.72, 71.27, 100.77, 105.36, 143.44, and 159.98 (13 peaks as required). MS (FAB) *m/z* (rel. int.): 553.1 [M($^{35}Cl_1{}^{37}Cl_1$) + Na]$^+$ (9%), 551.0 [M($^{35}Cl_2$) + Na]$^+$ (13%), 530.0 [M($^{35}Cl_1{}^{37}Cl_1$)]$^+$ (15%), 528.1 [M($^{35}Cl_2$]$^+$ (21%), 154 (100%); HRFAB, calcd. for $C_{23}H_{38}Cl_2O_9$: [M($^{35}Cl_2$)]$^+$ *m/z* 528.1893; found: 528.1898 (error 0.9 ppm).

3,5-Bis(11-chloro-3,6,9-trioxaundecyloxy)benzyl *tert*-butyldimethylsilyl ether (12)

To a solution of **11** (7.54 g, 14.1 mmol), imidazole (1.05 g, 1.1 equiv.), and 70 mL of DMF was added 2.22 g (1.05 equiv.) of *t*-BDMSCl and the solution was stirred at RT for 12 h, then at 70°C for 6 h. H_2O was added and the resulting mixture was extracted with Et_2O. The extract was washed with H_2O and brine, dried (Na_2SO_4), and evaporated to afford 8.87 g (98%) of **12**. ^{1}H NMR ($CDCl_3$) δ (ppm): 0.08 (s, 6H, $SiCH_3$), 0.89 (s, 9H, C-CH_3), 3.65–3.75 (m, 24H, γ-η-CH_2 + CH_2Cl), 3.82 (t, *J* = 4.8 Hz, 4H, β-CH_2), 4.08 (t, *J* = 4.8 Hz, 4H, α-CH_2), 4.64 (s, 2H, CH_2O), 6.35 (t, *J* = 2.0 Hz, 1H, H_a), and 6.47 (d, *J* = 2.0 Hz, 2H, H_b). MS (FAB) *m/z* (rel. int.): 667.4 [M($^{35}Cl_1{}^{37}Cl_1$) + Na]$^+$ (3%), 665.4 [M($^{35}Cl_2$) + Na]$^+$ 4%), 644.4 [M($^{35}Cl_1{}^{37}Cl_1$)]$^+$ (4%), 642.4 [M($^{35}Cl_2$)]$^+$ (5%), 509.3; HRFAB, calcd. for $C_{29}H_{52}SiCl_2N_2O_9$: [M($^{35}Cl_2$)]$^+$ *m/z* 642.2757; found: 642.2730 (error 4.3 ppm).

3,5-Bis(11-chloro-3,6,9-trioxaundecyloxy)benzaldehyde (13)

PCC (5.16 g, 23.9 mmol) was added to a solution of 3,5-bis(11-chloro-3,6,9-trioxaundecyloxy)benzyl alcohol (**11**, 11.55 g, 21.8 mmol) in DCM (150 mL). After 15 h at RT, the mixture was filtered and the solid was washed with DCM. The solution after concentration was passed through a short silica gel column with Et_2O as eluent. The fractions were dried (Na_2SO_4) and evaporated to give pure **13** (9.89 g, 86%), an oil. ^{1}H NMR ($CDCl_3$) δ (ppm): 3.55–3.65 (m, 24H, γ-η-CH_2 + CH_2Cl), 3.87 (t, *J* = 4.8 Hz, 4H, β-CH_2), 4.17 (t, *J* = 4.8 Hz, 4H, α-CH_2), 6.76 (t, *J* = 2.2 Hz, 1H, H_a), 7.02 (d, *J* = 2.2 Hz, 2H, H_b), and 9.89 (s, 1H, CHO). ^{13}C NMR ($CDCl_3$) δ (ppm): 42.67, 67.81, 69.51, 69.76, 70.60, 70.62, 70.66, 70.82, 71.31, 107.94, 108.26, 138.27, 160.35, and 191.77 (14 peaks as required). MS (FAB) *m/z* (rel. int.): 551.1 [M($^{35}Cl_1{}^{37}Cl_1$) + Na]$^+$ (69%), 549.1 [M($^{35}Cl_2$) + Na]$^+$ (100%), 515.2 [M($^{35}Cl_2$) + Na − ^{35}Cl] (35%); HRFAB, calcd. for $C_{23}H_{36}Cl_2O_9Na$: [M($^{35}Cl_1{}^{37}Cl_1$) + Na]$^+$ *m/z* 551.1605 and [M($^{35}Cl_2$) + Na]$^+$ *m/z* 549.1634; found: 551.1595 (error 1.7 ppm) and 549.1629 (error 0.9 ppm).

α-Morpholino-3,5-bis(11-chloro-3,6,9-trioxaundecyloxy)-benzyl cyanide (14)

TMSCN (0.32 mL, 2.4 mmol) was added to a mixture of 3,5-bis(11-chloro-3,6,9-trioxaundecyloxy)benzaldehyde (**13**, 1.10 g, 2.09 mmol), $ZnCl_2$ (10 mg), and DCM (10 mL). The mixture was stirred at RT for 3 days, heated at reflux for 2 days, and poured into 50 mL of ice. The organic phase was washed with H_2O and evaporated to give 1.30 g (97%) of an oil. Silica gel chromatography using Et_2O afforded 1.2 g (92%) of **14**, an oil. ^{1}H NMR ($CDCl_3$) δ (ppm): 2.5–2.7 (m, morpholino), 3.65–3.75 (m, 24H, γ-η-CH_2 + CH_2Cl), 3.86 (t, *J* = 4.8 Hz, 4H, β-CH_2), 4.11 (t, *J* = 4.8 Hz, 4H, α-CH_2), 4.72 (s, 1H, CHCN), 6.49 (t, *J* = 2.0 Hz, 1H, H_a), and 6.71 (d, *J* = 2.0 Hz, 2H, H_b). ^{13}C NMR ($CDCl_3$) δ (ppm): 42.71, 49.96, 66.64, 67.62, 69.59, 69.78, 70.61, 70.64, 70.67, 70.82, 71.34, 101.86, 106.85, 115.06, 134.65, 160.21 (16 peaks as required). MS (FAB) *m/z* (rel. int.): 623.4 [M($^{35}Cl_1{}^{37}Cl_1$) − H]$^+$ (8%), 621.4 [M($^{35}Cl_2$) − H]$^+$ (9%), 598.4 [M($^{35}Cl_1{}^{37}Cl_1$) − CN] (37%), 596.4 [M($^{35}Cl_2$) − CN]$^+$ (57%), 564.5 [M($^{35}Cl_1{}^{37}Cl_1$) + H − CN − ^{35}Cl] (37%), 562.5 [M($^{35}Cl_2$) + H − CN − ^{35}Cl]$^+$ (100%), 528.5 (62%); HRFAB (3-NBA/GLY/TFA), calcd. for $C_{28}H_{43}{}^{35}Cl_2N_2O_9$: [M − H]$^+$ *m/z* 621.2346; found: 621.2340 (error 0.9 ppm).

5-Carbomethoxy-*m*-phenylene-5′-formyl-*m*′-phenylene-32-crown-10 (15)

A solution containing 3,5-bis(11-chloro-3,6,9-trioxaundecyloxy)benzaldehyde (**13**, 6.00 g, 11.4 mmol) and methyl 3,5-dihydroxybenzoate (**1**, 1.91 g, 11.4 mmol) in DMF (total volume 18 mL) was added via a syringe pump at 0.75 mL/h to a suspension containing CsF (18.11 g, 119.2 mmol) and TBAI (20 mg) in DMF (550 mL) at 110°C. After complete addition, the mixture was stirred at 110°C for 5 days. The cooled reaction mixture was evaporated, treated with DCM, and filtered. Removal of DCM followed by flash silica gel column chromatography using Et_2O as eluent gave pure **15** (2.26 g, 32%) as an oil that crystallized upon standing, mp 70.2–72.0°C. ^{1}H NMR ($CDCl_3$) δ (ppm): 3.65–3.75 (m, 16H, γ, γ′, δ, δ′-CH_2), 3.85–3.95 (m, 8H, β,β′-CH_2), 3.87 (s, 3H, CH_3), 4.05–4.15 (m, 8H, α,α′-CH_2), 6.67 (t, *J* = 2.4 Hz, 1H, $H_{a'}$), 6.73 (t, *J* = 2.4 Hz, 1H, H_a), 6.98 (d, *J* = 2.4 Hz, 2H, H_b), 7.14 (d, *J* = 2.4 Hz, 2H, $H_{b'}$), and 9.84 (s, 1H, CHO). ^{13}C NMR ($CDCl_3$) δ (ppm): 52.17, 67.77, 67.87, 69.49, 69.52, 70.77, 70.79, 70.84, 106.78, 107.93, 108.18, 131.77, 138.17, 159.67, 160.31, 166.68, and 191.86 (17 peaks; theory 18). MS (FAB) *m/z* (rel. int.): 623.2 [M + H]$^+$ (100%), 591.3 (M$^+$ − OCH_3) (44%); HRFAB, calcd. for $C_{31}H_{43}O_{13}$: [M + H]$^+$ *m/z* 623.2703; found: 623.2681 (error 3.5 ppm).

Lactone (16a) from 5-hydroxymethyl-*m*-phenylene-5′-carbomethoxy-*m*′-phenylene-32-crown-10 (16)

To a stirred suspension of Cs_2CO_3 (38.51 g, 118 mmol) and TBAI (20 mg) in DMF (560 mL) at 110°C was added a solu-

© 1997 NRC Canada

Can. J. Chem. Downloaded from www.nrcresearchpress.com by 91.121.58.235 on 09/08/12
For personal use only.

tion of 3,5-bis(11-chloro-3,6,9-trioxaundecyloxy)benzyl *tert*-butyldimethylsilyl ether (**12**) (7.56 g, 11.7 mmol) and methyl 3,5-dihydroxybenzoate (**1**) in DMF (20 mL) at a rate of 0.75 mL/h. The mixture was stirred for 4 days at 110°C, cooled, and filtered throught Celite, which was rinsed with DCM. The filtrate was rotary evaporated to yield a dark brown oil, 11 g, which was subjected to silica gel column chromatography with 7/1 EtOAc/EtOH to afford pure **16a**, an oil, 1.56 g (18%). ^{1}H NMR ($CDCl_3$) δ (ppm): 3.7–3.9 (m, 24H, β, γ, δ, β′, γ′, δ′-CH_2), 4.0–4.4 (m, 8H, α,α′-CH_2), 5.29 (s, 2H, CH_2), 6.41 (t, J = 2.0 Hz, 1H, H_a), 6.59 (t, J = 2.0 Hz, 1H, H_b), 6.73 (d, J = 2.0 Hz, 1H, $H_{a'}$), and 7.29 (d, J = 2.0 Hz, 1H $H_{b'}$). ^{13}C NMR ($CDCl_3$) δ (ppm): 66.62, 67.85, 67.98, 69.45, 69.83, 70.45, 70.55, 70.62, 70.86, 103.43, 108.05, 108.94, 109.29, 132.06, 138.38, 159.63, 159.65, 165.68 (18 peaks; 19 peaks theory). MS (FAB) *m/z* (rel. int.): 615.2 $[M + Na]^+$ (100%), 483.2 $[M + Na - (OCH_2CH_2)_3]^+$ (14%), 176.0 $[(OCH_2CH_2)_4]^+$ (44%); HRFAB, calcd. for $C_{30}H_{40}O_{12}Na$ (lactone, i.e., **16a** + Na^+): $[M]^+$ *m/z* 615.2417; found: 615.2425 (error 1.2 ppm).

Bis(5-carboxy-*m*-phenylene)-32-crown-10 (17)

Aqueous NaOH (27 mL, 4 M) was added to a solution of diester crown **4** (1.26 g, 1.93 mmol) in absolute EtOH (120 mL). The mixture was refluxed for 48 h, cooled to RT, acidified with 4 M HCl, diluted with H_2O, and extracted with DCM (3 × 50 mL). The organic extract was concentrated and the crude solid was purified by recrystallization from EtOH to give **17** (1.12 g, 93%), mp 171.1–171.5°C (lit. (9*a*) mp 169.5–170.5°C). IR: 3501 (-OH), 1696 (C=O), 1600 (C=C), 1129 (C-O-C) cm^{-1}. ^{1}H NMR (DMSO-d_6) δ (ppm): 3.55–3.65 (m, 16H, γ,δ-CH_2), 3.65–3.75 (m, 8H, β-CH_2), 4.09 (t, J = 4.4 Hz, 8H, α-CH_2), 6.75 (t, J = 2.2 Hz, 2H, H_a), and 7.02 (d, J = 2.2 Hz, 4H, H_b). ^{13}C NMR (DMSO-d_6) δ (ppm): 67.51, 68.83, 70.01, 70.02, 105.65, 107.51, 132.73, 159.54, and 166.90 (9 peaks; theory 9).

Bis(5-acetyl-*m*-phenylene)-32-crown-10 (18)

MeLi in Et_2O (28.0 mL, 1.4 M, 38.4 mmol, 15.9 equiv.) was added to an ice cold solution of bis(5-carboxy-*m*-phenylene)-32-crown-10 (**17**, 1.51 g, 2.42 mmol) in THF (100 mL). After 3 h at 0°C, TMSCl (25.6 mL, 202 mmol) was rapidly added while stirring continued. After 30 min at 0°C, the mixture was allowed to come to RT at which point 1 N HCl (25 mL) was added. The resulting two-phase system was stirred at RT for 2 h and the product was extracted with Et_2O (3 × 50 mL). The organic layer was washed with H_2O and dried (Na_2SO_4). The pure product **18** (0.67 g, 45%), mp 95.2–96.1°C, a white powder, was obtained via silica gel column chromatography with EtOAc as eluent. ^{1}H NMR ($CDCl_3$) δ (ppm): 2.53 (s, 6H, CH_3), 3.65–3.75 (m, 16H, γ,δ-CH_2), 3.85 (t, J = 4.6 Hz, 8H, β-CH_2), 4.10 (t, J = 4.6 Hz, 8H, α-CH_2), 6.67 (t, J = 2.2 Hz, 2H, H_a), and 7.07 (d, J = 2.2 Hz, 4H, H_b). ^{13}C NMR ($CDCl_3$) δ (ppm): 26.70, 67.80, 69.57, 70.85, 70.86, 106.34, 107.00, 138.83, 159.92, and 197.67 (10 peaks as required). MS (FAB) *m/z* (rel. int.): 621.5 $[M + H]^+$ (100%); HRFAB, calcd. for $C_{32}H_{44}O_{12}$: $[M + H]^+$ *m/z* 621.2911; found: 621.2915 (error 0.6 ppm).

Bis(5-hydroxymethyl-*m*-phenylene)-32-crown-10 (19)

LAH in THF (3.6 mL, 1.0 M, 3.6 mmol, 1.11 equiv.) was added to a solution of bis(5-carbomethoxy-*m*-phenylene)-32-crown-10 (**4**, 2.11 g, 3.23 mmol) in anhydrous THF (100 mL) at RT. The mixture was stirred for 12 h, excess LAH was destroyed with EtOAc, and the mixture was diluted with H_2O (30 mL). Upon neutalization with 2 N HCl the mixture was extracted with Et_2O (3 × 30 mL). The organic layer was dried (Na_2SO_4) and evaporated. Recrystallization from acetone gave pure **19** (1.82 g, 94%), mp 99.5–100.4°C. IR: 3435 (-OH), 2924 (-CH), 1602 (C=C), and 1122 (C-O-C) cm^{-1}. ^{1}H NMR (CD_3COCD_3) δ (ppm): 3.55–3.65 (m, 16H, γ,δ-CH_2), 3.79 (t, J = 4.6 Hz, 8H, β-CH_2), 4.06 (t, J = 4.6 Hz, 8H, α-CH_2), 4.16 (t, J = 6.0 Hz, 2H, OH), 4.54 (d, J = 6.0 Hz, 4H, CH_2), 6.37 (t, J = 2.2 Hz, 2H, H_a), and 6.52 (d, J = 2.2 Hz, 4H, H_b). ^{13}C NMR (CD_3COCD_3) δ (ppm): 64.59, 68.33, 70.32, 71.46, 71.44, 104.88, 105.76, 145.78, and 161.01 (9 peaks as required). MS (FAB) *m/z* (rel. int.): 596.3 $(M + H)^+$ (100%), 561.3 $(M^+ - 2OH)$ (32%), and 534.9 $(M^+ - 2CH_2OH)$ (12.5%); HRFAB, calcd. for $C_{30}H_{44}O_{12}$: $[M + H]^+$ *m/z* 596.2833; found: 596.2848 (error 2.5 ppm).

Bis(5-bromomethyl-*m*-phenylene)-32-crown-10 (20)

PBr_3 (1.60 mL, 16.9 mmol, 5.20 equiv.) was added to a solution of bis(5-hydroxymethyl-*m*-phenylene)-32-crown-10 (**19**, 1.92 g, 3.22 mmol) in a mixture of Et_2O (250 mL) and EtOAc (30 mL). The mixture was stirred for 36 h at RT. The resulting white solid was filtered and washed several times with Et_2O. Pure **20** (2.04 g, 88%), mp 108.5–110.1°C, was obtained by recrystallization from EtOAc. ^{1}H NMR ($CDCl_3$) δ (ppm): 3.65–3.75 (m, 16H, γ,δ-CH_2), 3.83 (t, J = 4.6 Hz, 8H, β-CH_2), 4.05 (t, J = 4.6 Hz, 8H, α-CH_2), 4.37 (s, 4H, CH_2), 6.40 (t, J = 2.2 Hz, 2H, H_a), and 6.53 (d, J = 2.2 Hz, 4H, H_b). ^{13}C NMR ($CDCl_3$) δ (ppm): 33.61, 67.60, 69.59, 70.81, 70.84, 101.59, 107.87, 139.55, and 159.96 (9 peaks as required). MS (FAB) *m/z* (rel. int.): 721.2 $[M + H]^+$ (100%); HRFAB, calcd. for $C_{30}H_{42}Br_2O_{10}$: $[M + H]^+$ *m/z* 721.1222; found: 721.1214 (error 1.1 ppm).

Bis(5-formyl-*m*-phenylene)-32-crown-10 (21)

PCC (1.16 g, 5.38 mmol, 2.21 equiv.) was added to a solution of bis(5-hydroxymethyl-*m*-phenylene)-32-crown-10 (**19**, 1.45 g, 2.43 mmol) in DCM (20 mL). After 2 h the mixture was filtered and the solid washed with DCM. The solution upon concentration was passed through a short silica gel column with EtOAc as eluent to give a white solid. Recrystallization from acetone gave pure **21** (1.22 g, 85%), mp 92.3–95.8°C. ^{1}H NMR ($CDCl_3$) δ (ppm): 3.65–3.75 (m, 16H, γ,δ-CH_2), 3.86 (t, J = 4.6 Hz, 8H, β-CH_2), 4.12 (t, J = 4.6 Hz, 8H, α-CH_2), 6.73 (t, J = 2.2 Hz, 2H, H_a), 6.98 (d, J = 2.2 Hz, 4H, H_b), and 9.85 (s, 2H, CHO). ^{13}C NMR ($CDCl_3$) δ (ppm): 67.90, 69.52, 70.81, 70.88, 107.95, 108.24, 138.22, 160.33, and 191.84 (9 peaks as required). MS (FAB) *m/z* (rel. int.): 593.6 $[M + H]^+$ (100%); HRFAB, calcd. for $C_{30}H_{40}O_{12}$: $[M + H]^+$ *m/z* 593.2598; found: 593.2577 (error 3.5 ppm).

Bis[5-(*p*-nitrophenoxymethyl)-*m*-phenylene]-32-crown-10 (22)

NaH (0.108 g, 60%, 2.70 mmol) was added to a solution of bis(5-hydroxymethyl-*m*-phenylene)-32-crown-10 (**19**, 0.718 g, 1.20 mmol) in dry THF (20 mL). The mixture was heated at reflux for 3 h, cooled, treated with *p*-fluoronitrobenzene (0.30 mL, 2.8 mmol), and stirred at RT for 24 h. After solvent removal the residue was extracted with $CHCl_3$, evaporation of which gave crude **22**, a yellow solid, 1.0 g (100%). After silica gel column chromatography, using first Et_2O and then EtOAc

© 1997 NRC Canada

followed by recrystallization from acetone, pure **22**, mp 133.1–134.0°C, was obtained. ^{1}H NMR ($CDCl_3$) δ (ppm): 3.65–3.75 (m, 16H, γ, δ-CH_2), 3.83 (t, J = 4.8 Hz, 8H, β-CH_2), 4.06 (t, J = 4.8 Hz, 8H, α-CH_2,), 5.04 (s, 4H, CH_2), 6.43 (t, J = 2.0 Hz, 2H, H_a), 6.54 (d, J = 2.0 Hz, 4H, H_b), 6.98 (d, J = 9.1 Hz, 4H, Ar), and 8.17 (d, J = 9.1Hz, 4H, Ar). ^{13}C NMR ($CDCl_3$) δ (ppm): 67.63, 69.61, 70.44, 70.85, 101.09, 106.03, 114.86, 125.89, 137.77, 141.65, 160.28, 163.53 (12 peaks, 13 peaks theory). Anal. calcd. for $C_{42}H_{50}N_2O_{16}$: C 60.14, H 6.01, N 3.34; found: C 59.87, H 6.03, N 3.26.

Bis(5-acetoxymethyl-*m*-phenylene)-32-crown-10 (23)

To a solution of bis(5-hydroxymethyl-*m*-phenylene)-32-crown-10 (**19**, 0.581 g, 0.974 mmol) and pyridine (0.17 mL) in dry THF (75 mL) was added acetyl chloride (0.080 mL, 1.1 mmol) and the mixture was stirred at RT for 30 h. After filtration the solvent was evaporated. The residue was taken up in Et_2O. The solution was washed with H_2O (2 × 50 mL), 2 N HCl (30 mL), and H_2O, dried (Na_2SO_4), and rotary evaporated to give **23**, 0.65 g (98%), an oil that subsequently crystallized, mp 68.9–70.1°C. ^{1}H NMR ($CDCl_3$) δ (ppm): 2.05 (s, 3H, CH_3), 3.58–3.68 (m, 16H, γ, δ-CH_2), 3.79 (t, J = 4.8 Hz, 8H, β-CH_2), 4.07 (t, J = 4.8 Hz, 8H, α-CH_2), 4.99 (s, 4H, CH_2O), 6.45 (t, J = 2.0 Hz, 2H, H_a), and 6.52 (d, J = 2.0 Hz, 4H, H_b). ^{13}C NMR ($CDCl_3$) δ (ppm): 29.77, 66.23, 68.46, 70.27, 71.44, 71.47, 101.39, 107.33, 139.58, 161.14, 170.78 (11 peaks as required). MS (FAB) *m/z* (rel. int.): 680.4 $[M]^+$ (13%); HRFAB, calcd. for $C_{34}H_{48}O_{14}$: $[M]^+$ *m/z* 680.3044; found: 680.3022 (error 3.2 ppm).

Acknowledgements

We acknowledge support from the National Science Foundation (CHE-95-21738) for this work. MS were provided by the Washington U. Mass Spectrometry Resource, a National Institutes of Health Research Resource (Grant No. P41RR0954), and the University of Nebraska.

References

1. (*a*) C.J. Pedersen. J. Am. Chem. Soc. **89**, 2495 (1967); (*b*) J. Am. Chem. Soc. **89**, 7017 (1967); (*c*) Angew. Chem. Int. Ed. Engl. **27**, 1021 (1988).
2. R.M. Izatt, K. Pawlak, T.S. Bradshaw, and R.L. Bruening. Chem. Rev. **91**, 1721 (1991).
3. (*a*) J.-M. Lehn. Supramolecular chemistry. VCH Publishers, Inc., New York. 1995; (*b*) D.J. Cram and J.M. Cram. Container molecules and their guests. Royal Society of Chemistry, Cambridge, U.K. 1994; (*c*) B. Dietrich, P. Viout, and J.-M. Lehn. Macrocyclic chemistry. VCH Publishers, Inc., New York. 1993; (*d*) F. Vögtle. Supramolecular chemistry. John Wiley and Sons, New York. 1991; (*e*) Frontiers in supramolecular organic chemistry and photochemistry. *Edited by* H.-J. Schneider and H. Durr. VCH Publishers, Inc., New York. 1991.
4. H.W. Gibson, M.C. Bheda, P.T. Engen, Y.X. Shen, J. Sze, H. Zhang, M.D. Gibson, Y. Delaviz, S. Lee, S. Liu, L. Wang, D.S. Nagvekar, J. Rancourt, and L.T. Taylor. J. Org. Chem. **59**, 2186 (1994); M. Bheda, J. Merola, W. Woodward, V. Vasudevan, and H.W. Gibson. J. Org. Chem. **59**, 1694 (1994).
5. H.W. Gibson. *In* Large ring molecules. *Edited by* J.A. Semlyen. John Wiley & Sons, New York. 1996. pp. 191–262; D.B. Amabilino and J.F. Stoddart. Chem. Rev. **95**, 2725 (1995); H.W. Gibson, M.C. Bheda, and P.T. Engen. Prog. Polym. Sci. **19**, 843 (1994).
6. (*a*) P.R. Ashton, A.N. Collins, M.C.T. Fyfe, S. Menzer, J.F. Stoddart, and D.J. Williams. Angew. Chem. Int. Ed. Engl. **36**, 735 (1997); (*b*) M. Asakawa, P.R. Ashton, R. Ballardini, V. Balzani, M. Belohradsky, M.T. Gandolfi, O. Kocian, L. Prodi, F.M. Raymo, J.F. Stoddart, and M. Venturi. J. Am. Chem. Soc. **119**, 302 (1997); (*c*) J.-C. Chambron, V. Heitz, and J.-P. Sauvage. Bull. Soc. Chim. Fr. **132**, 340 (1995); (*d*) C. Wu, P.R. Lecavalier, Y.X. Shen, and H.W. Gibson. Chem. Mater. **3**, 569 (1991), and refs. therein.
7. M. Asakawa, P.R. Ashton, S.E. Boyd, C.L. Brown, R.E. Gillard, O. Kocian, F.M. Raymo, J.F. Stoddart, M.S. Tolley, A.J.P. White, and D.J. Williams. J. Org. Chem. **62**, 26 (1997). J.-M. Kern, J.-P. Sauvage, G. Bidan, M. Billon, and B. Divisia-Blohorn. Adv. Mater. **8**, 580 (1996). D.B. Amabilino, C.O. Dietrich-Buchecker, A. Livoreil, L. Perez-Garcia, J.-P. Sauvage, and J.F. Stoddart. J. Am. Chem. Soc. **118**, 3905 (1996); R.F. Carina, C. Dietrich-Buchecker, and J.-P. Sauvage. J. Am. Chem. Soc. **118**, 9110 (1996), and refs. therein.
8. C. Gong and H.W. Gibson. J. Am. Chem. Soc. **119**, 8585 (1997); Angew. Chem. Int. Ed. Engl. In press; Macromolecules. In press; C. Gong, Q. Ji, T.E. Glass, and H.W. Gibson. Macromolecules. **30**, 4807 (1997); H.W. Gibson, D.S. Nagvekar, J. Powell, C. Gong, and W.S. Bryant. Tetrahedron, **53**, in press (1997); C. Gong and H.W. Gibson. J. Am. Chem. Soc. **119**, 5862 (1997); H.W. Gibson, S. Liu, C. Gong, and E. Joseph. Macromolecules, **30**, 3711 (1997); C. Gong and H.W. Gibson. Macromol. Chem. Phys. **198**, 2331 (1997); Macromolecules, **29**, 7029 (1996); E. Marand, Q. Hu, H.W. Gibson, and B. Veytsman. Macromolecules, **29**, 2555 (1996); H.W. Gibson and S. Liu. Macromol. Symp. **102**, 55 (1996); H.W. Gibson, S. Liu, P. Lecavalier, C. Wu, and Y.X. Shen. J. Am. Chem. Soc. **117**, 852 (1995); D. Loveday, G.L. Wilkes, M.C. Bheda, Y.X. Shen, and H.W. Gibson. J. Macromol. Sci. **A32**, 1 (1995); Y.X. Shen, D. Xie, and H.W. Gibson. J. Am. Chem. Soc. **116**, 537 (1994); Y.X. Shen, P.T. Engen, M.A.G. Berg, J.S. Merola, and H.W. Gibson. Macromolecules, **25**, 2786 (1992); C. Wu, C.M. Bheda, C. Lim, Y.X. Shen, J. Sze, and H.W. Gibson. Polym. Commun. **32**, 204 (1991).
9. (*a*) Y. Delaviz and H.W. Gibson. Macromolecules, **25**, 18 (1992); (*b*) Y. Delaviz, J.S. Merola, M.A.G. Berg, and H.W. Gibson. J. Org. Chem. **60**, 516 (1995).
10. G. Dijkstra, W.H. Kruizinga, and R.M. Kellogg. J. Org. Chem. **52**, 4230 (1987); T. Hiroshi. Talanta, **40**, 1313 (1993).
11. C. Galli and L. Mandolini. J. Chem. Soc. Chem. Commun. 251 (1982); W.L. Mattice and G.R. Newkome. J. Am. Chem. Soc. **104**, 5942 (1982); J. Chojnowski, S. Rubinsztajn, and L. Wilgzek. J. Chem. Soc. Chem. Commun. 69 (1983).
12. P.J. Hammond, P.D. Beer, and C.D. Hall. J. Chem. Soc. Chem. Commun. 1161 (1983).
13. P.R. Ashton, C.L. Brown, E.J.T. Chrystal, K.P. Parry, M. Pietraszkiewicz, N. Spencer, and J.F. Stoddart. Angew Chem. **30**, 1042 (1991).
14. A. Ostrowicki, E. Koepp, and F. Vögtle. Top. Curr. Chem. **161**, 37 (1992).
15. D.J. Burton and F.R. Herkes. Tetrahedron Lett. 4509 (1965); J.H. Clark and J.M. Miller. J. Am. Chem. Soc. **99**, 498 (1977); K. Seppelt. Angew. Chem. Int. Ed. Engl. **31**, 292 (1992).
16. J.H. Clark. Chem. Rev. **80**, 429 (1980).
17. C.A. Vitali and B. Masci. Tetrahedron, **45**, 2213 (1989).
18. M.J. Jorgenson. J. Org. React. (N.Y.), **18**, 1 (1970).
19. H.O. House and T.M. Bare. J. Org. Chem. **33**, 943 (1968).
20. G.M. Rubottom and C.-W. Kim. J. Org. Chem. **48**, 1550 (1983).
21. A.F. Gallaugher and H. Hibbert. J. Am. Chem. Soc. **58**, 813 (1936).
22. A. Abe and S. Watanabe. Kogyo Kagaku Zasshi, **66**, 471 (1967).

Can. J. Chem. Downloaded from www.nrcresearchpress.com by 91.121.58.235 on 09/08/12
For personal use only.

© 1997 NRC Canada

Monosaccharide permethylation products for gas chromatography – mass spectrometry: how reaction conditions can influence isomeric ratios

Daniel Derbie Asres and Hélène Perreault

Can. J. Chem. Downloaded from www.nrcresearchpress.com by 91.121.58.235 on 09/08/12
For personal use only.

Abstract: Methylation analysis has been widely used for determination of carbohydrate structures by mass spectrometry. Permethylation of monosaccharides yields mixtures of anomeric pyranosides and furanosides. This paper discusses the influence of some of the permethylation reaction parameters on the proportions of isomeric products obtained. The ratios of three five- and six-membered ring products obtained from two permethylated monosaccharides, D-galactose and L-fucose, have been determined as a function of reaction parameters. The method of Ciucanu and Kerek (1) (methyl iodide in dimethyl sulfoxide (DMSO) in the presence of sodium hydroxide (NaOH)) was used as a starting point. The "conventional" method consists of mixing all of the reagents with the substrate and allowing the reaction to proceed with stirring. Both D-galactose and L-fucose under these conditions produced two main permethylated isomers, a furanoside and a pyranoside, along with two other minor isomeric components. We have investigated the effect on the proportion of products obtained of mixing DMSO, substrate, and NaOH for various times prior to the addition of methyl iodide. Results for D-galactose showed that shorter times enhanced the formation of permethylated furanoside isomers, while reducing the proportion of pyranosides. In other sets of experiments, the time and temperature of reaction, following the addition of methyl iodide, were studied. The indication is that 15 min are sufficient to produce complete methylation, with longer reaction times yielding the same results. Again for D-galactose, low reaction temperatures (ca. 10°C) favored formation of furanoside products. Higher temperatures yielded higher pyranoside/furanoside ratios. Higher quantities of NaOH also favored formation of the main galactopyranoside product. As for L-fucose, the ratio of the main furanoside vs. pyranoside products obtained by permethylation varied in a way similar to permethylated galactoside. Thus, higher temperatures and longer reaction times favored the main fucopyranoside product. Gentler conditions (i.e., shorter reaction times and lower temperatures) significantly favored the formation of the main fucofuranoside product. These results are interesting as they show the possibility of controlling the relative abundance of permethylated isomers of fucose and galactose. They also constitute a warning to chemists who use methylation procedures in their analyses, to the effect that permethylation products may vary considerably if the reaction conditions are not carefully controlled.

Key words: glucose, galactose, fucose, TLC, GC–MS, permethylation, monosaccharides.

Résumé : On a fait appel à la méthode fréquemment utilisée d'analyse par méthylation pour déterminer les structures de carbohydrates par spectrométrie de masse. La perméthylation des monosaccharides fournit des mélanges de pyranosides et de furanosides anomères. Dans ce travail, on discute de l'influence de quelques paramètres de la réaction de perméthylation sur les proportions des produits isomères obtenus. On a déterminé les rapports des trois produits à cinq et à six chaînons obtenus à partir de deux monosaccharides perméthylés, D-galactose et L-fucose, en fonction des paramètres de réaction. Comme point de départ, on a utilisé la méthode de Ciucanu et Kerek (iodure de méthyle dans le diméthylsulfoxyde (DMSO) en présence d'hydroxyde de sodium (NaOH)). La méthode «conventionnelle» consiste à mélanger tous les réactifs avec le substrat et à laisser la réaction se produire sous agitation. Dans ces conditions, le D-galactose et le L-fucose conduisent tous les deux à deux isomères perméthylés principaux, un furanoside et un pyranoside, avec deux autres composants isomériques mineurs. On a examiné l'influence que peut avoir le mélange du DMSO, du substrat et du NaOH, pour des temps variables avant l'addition de l'iodure de méthyle, sur la proportion des produits obtenus. Les résultats avec le D-galactose ont montré que les temps les plus courts augmentent la formation des isomères furanosides perméthylés avec une réduction concomitante de la proportion des pyranosides. Dans d'autres ensembles d'expériences, on a étudié l'influence du temps et de la température de la réaction après l'addition de l'iodure de méthyle. Les résultats indiquent que 15 min sont suffisantes pour conduire à une méthylation complète; des temps de réaction plus longs conduisent aux même résultats. Encore une fois, avec le D-galactose, les températures de réaction plus basses (environ 10°C) favorisent la formation de produits furanosides. Les températures plus élevées conduisent

Received March 19, 1997.

D.D. Asres and H. Perreault.[1] Department of Chemistry, University of Manitoba, 144 Dysart Road, Winnipeg, MB R3T 2N2, Canada.

[1] Author to whom correspondence may be addressed. Telephone: (204) 474-7418. Fax: (204) 474-7608. E-mail: perreau@cc.umanitoba.ca

© 1997 NRC Canada

à des rapports pyranoside/furanoside plus élevés. Des quantités plus élevées de NaOH favorisent aussi la formation de galactopyranoside comme produit principal. Dans le cas du L-fucose, le rapport du furanoside principal et des produits pyranosides obtenus par perméthylation varient d'une façon semblable à celle observée avec les galactosides perméthylés. Ainsi, aux températures les plus élevées et aux temps de réaction plus longs, les produits fucopyranosides principaux sont favorisés. Des conditions plus douces (c'est-à-dire des temps de réaction plus courts et des températures plus basses) favorisent fortement la formation du fucofuranoside comme produit principal. Ces résultats sont intéressants parce qu'ils démontrent la possibilité de contrôler les quantités relatives d'isomères perméthylés du fucose et du galactose. Ils constituent aussi un avertissement pour les chimistes qui utilisent les méthodes de méthylation dans leurs analyses; en effet, la nature des produits de perméthylation peut varier d'une façon significative si les conditions réactionnelles ne sont pas bien contrôlées.

Mots clés : glucose, galactose, fucose, CCM, CG–SM, perméthylation, monosaccharides.

[Traduit par la rédaction]

Can. J. Chem. Downloaded from www.nrcresearchpress.com by 91.121.58.235 on 09/08/12
For personal use only.

Introduction

The analysis of carbohydrates by mass spectrometric techniques often requires derivatization of the samples in order to enhance sensitivity and improve the quantity and quality of information obtained. The Ciucanu and Kerek (1) permethylation method figures amongst the most popular derivatization methods and has been used in many laboratories for the analysis of carbohydrates and glycolipids. This method yields fully methylated sugars in remarkably short reaction times, on the order of 15 min, based on optimal proportions of powdered sodium hydroxide (NaOH), dimethyl sulfoxide (DMSO), methyl iodide (CH_3I), and substrate.

In a recent publication (2), we discussed the gas chromatographic – mass spectrometric (GC–MS) data for permethylated monosaccharides and observed the presence of two or more isomeric products. Similar results had been reported earlier (3, 4). We observed that permethylated D-glucose, D-galactose, and L-fucose each yielded two major GC–MS peaks. In the case of D-glucose, the two peaks corresponded to the α and β anomers of the permethylated glucopyranoside species, as reported by Ciucanu and Kerek (1). In the cases of D-galactose and L-fucose, the two peaks had been tentatively assigned to pyranoside and furanoside, or open-ring structures (2), although the products were not fully characterized. Pyranoside-type products yielded electron impact (EI) mass spectra that corresponded quite well to the spectra found in the NIST library (5), while the other type of products (furanoside or open ring) could not be readily identified in the collection of reference spectra, including those of furanosides.

We have recently compared a collection of mass spectra of permethylated monosaccharides obtained using our Finnigan MAT 800 ion trap GC–MS system to those from our HP 5988A GC–MS system. We observed from this comparison that the Finnigan MAT system in general produced less fragmentation than the HP instrument, although similar ionization conditions (EI, 70 eV) were used. The nature of the fragment ions was also different from one instrument to the other. These differences agree well with the fact that some EI-formed ions can undergo chemical ionization or cooling while in the trap, thus producing different extents and patterns of fragmentation relative to EI-formed ions travelling through a magnetic sector or quadrupole mass analyzer. The HP spectra matched the NIST library spectra (5) much better and more reliably than the Finnigan MAT spectra, which were discussed in our previous publication (2). In general, we found that the EI spectra obtained with the ion trap system were not always reliable for identification of unknowns, or for diverse classes of compounds. From the HP data obtained with a quadrupole analyzer, we have reassigned the permethylation products of D-galactose and L-fucose as pyranosides and furanosides, eliminating the possibility of open-ring structures. As an example, Fig. 1 shows comparative spectra for a furanoside product from permethylation of D-galactose, where (*a*) is the Finnigan MAT-acquired spectrum, (*b*) is the HP-acquired spectrum, and (*c*) shows the library spectrum that best matched the HP spectrum. Library data (5) allowed for preliminary assignments of permethylation products. Accordingly, the compound of interest in Fig. 1 was identified as methyl 2,3,5,6-tetra-*O*-methyl-α-D-galactofuranoside (compound **3**). The other permethylation products of D-galactose were identified as methyl 2,3,5,6-tetra-*O*-methyl-β-D-galactofuranoside (compound **1**) and methyl 2,3,4,6-tetra-*O*-methyl-β-D-galactopyranoside (compound **2**). The retention times of these compounds using the Finnigan MAT system were on average 20:42, 20:50, and 21:00 min for **1**, **2**, and **3**, respectively. These identity assignments were confirmed with the use of the corresponding permethylated galactoside standards. Perfect matches between retention times and mass spectra were obtained between standards and galactose permethylation products.

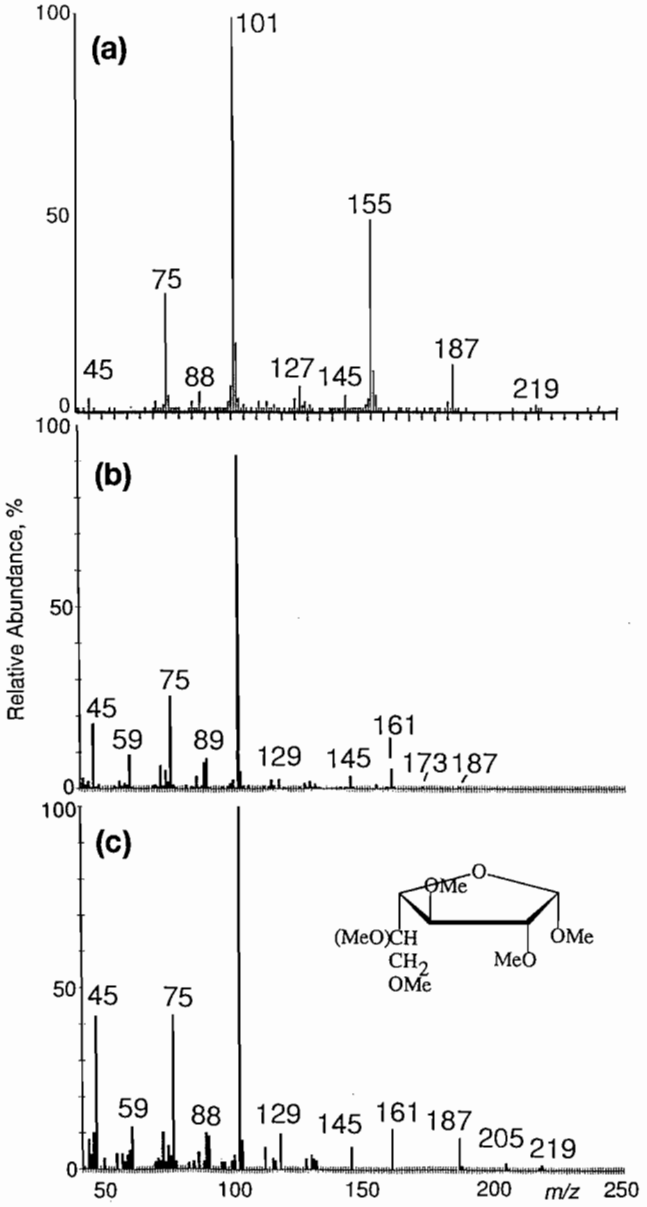
The present paper discusses the influence of some of the permethylation reaction parameters on the proportions of compounds **1**, **2**, and **3** found. The overall quantity of compound **1**, a minor product, did not vary significantly with any of the parameters. The other expected product, methyl 2,3,4,6-tetra-*O*-methyl-α-D-galactopyranoside, was found only in relative amounts lower than 1% and eluting simultaneously with compound **2**.

In the case of L-fucose (6-deoxy-L-galactose), no reference mass spectra were available for preliminary identification of permethylated fucofuranoside anomers. In our earlier publication (2), we showed that permethylation of fucose produced two major products, and according to the features of their mass spectra, they should correspond to fucopyranose (compounds **4** and **5**, retention times 19:15 and 19:20) and fucofuranose structures (compound **6**, 19:30 min). In this paper, the proportions of these three compounds (**4**, **5**, and **6**) were determined as a function of reaction parameters. Further GC–MS experiments were performed with permethylated fucoside standards in order to confirm the identity of the products. Compounds **4**, **5**, and **6** were identified as methyl 2,3,4-tri-

© 1997 NRC Canada

Can. J. Chem. Downloaded from www.nrcresearchpress.com by 91.121.58.235 on 09/08/12
For personal use only.

Fig. 1. Mass spectra of product **3**, tentatively identified as permethylated α-D-galactofuranoside; (*a*) obtained using the Finnigan MAT ion trap system; (*b*) obtained with the Hewlett Packard system; and (*c*) from the spectrum library (5).



O-methyl β-L-6-deoxygalactopyranoside, methyl 2,3,4-tri-*O*-methyl α-L-6-deoxygalactopyranoside, and methyl 2,3,5-tri-*O*-methyl α-L-6-deoxygalactofuranoside, respectively. A fourth compound, methyl 2,3,5-tri-*O*-methyl β-L-6-deoxygalactofuranoside, was not taken into account as its relative abundance never exceeded 3%. This compound eluted earlier than the other three.

Permethylation of the monosaccharides D-galactose and L-fucose was carried out using the Ciucanu and Kerek (1) method, and the effects of varying the following parameters were investigated: time of mixing (of DMSO, NaOH, and monosaccharide) prior to addition of CH_3I, time of reaction in the presence of CH_3I, temperature of reaction, quantity of NaOH, and quantity of DMSO and CH_3I.

When saccharides are dissolved in solution there is a slow equilibration between anomeric forms as well as an equilibrium between pyrano- (six-membered ring) and furano- (five-membered ring) forms. Our results suggest that the nature of permethylation products depends on the proportions of the four possible species (or their anions) in solution at the time the CH_3I is added. These proportions are dependent on the length of time the solution is stirred before CH_3I is added, on the alkalinity of the solution, and on the temperature of the solution.

Experimental

Chemicals

Monosaccharide standards D-galactose (99.9%) and L-fucose (99%) were purchased from Sigma Chemicals (St. Louis, Mo.) and used without further purification. Dimethyl sulfoxide (DMSO) was obtained from Pierce Chemicals (Rockford, Ill.) and methyl iodide from Fluka (Buchs, Switzerland). All solvents (acetonitrile, methanol, dichloromethane, and chloroform) were glass-distilled and obtained from Mallinckrodt (Paris, Ky.). Distilled, deionized nanopure water was utilized.

Standards

Methyl D-galactopyranoside (α and β) and methyl L-fucopyranoside (α and β) were obtained from Sigma. Methyl D-galactofuranoside (α and β) and methyl L-fucofuranoside (β only) were purchased from Color Your Enzyme (Bath, Ont.). All of these standards were permethylated using the Ciucano and Kerek (1) method as outlined below. No anomerization and epimerization were observed according to GC–MS analyses, as a single sharp peak was obtained for each permethylated standard.

Permethylation

This derivatization was conducted using the method of Larsson et al. (6), which itself was adapted from Ciucanu and Kerek's method (1). Briefly, galactose or fucose (ca. 5 mg) was dissolved in (450–1000) μL of DMSO, followed by addition of (32–82) mg of powdered NaOH. The mixture was sonicated at room temperature (0–60 min). Methyl iodide (100–200 uL) was then added and the mixture was sonicated for (15–180) min at 10–50°C. The underlined numbers represent parameters used in our typical permethylation procedure, at room temperature. The extent of variation of each parameter is indicated by the two hyphenated numbers. Permethylated monosaccharides were recovered by chloroform or dichloromethane extraction.

Gas chromatography – mass spectrometry

The main GC–MS system used in this study consisted of a Varian 3400 gas chromatograph (Varian Chromatographic Systems, Walnut Creek, Calif.) coupled to a Finnigan Mat 800 ion trap detector (Finnigan Corp., San Jose, Calif.) equipped with an ITD 4.10 applications data system. The second system used was a HP 5890 gas chromatograph (Hewlett Packard Canada, Calgary, Alta.) coupled to a HP 5988A single quadrupole mass analyzer. For both GC–MS instruments, repetitive 1 s scans were effected on a range of 50–650 Da. Each gas chromatograph was equipped with a 30 m × 0.25 mm i.d. DB-5 column (J & W Scientific Inc., Folsom, Calif.), with a

© 1997 NRC Canada

Table 1. Experimental conditions for permethylation of D-(+) galactose, based on the method of Ciucanu and Kerek (1); relative proportions[a] of the products.

Method no.	Galactose (mg)	DMSO (μL)	NaOH (mg)	1st sonic. (min)	CH_3I (μL)	React. time (min)	Temp. (°C)	Prod. **1**[b] (rel. conc., %)	Prod. **2**[c] (rel. conc., %)	Prod. **3**[d] (rel. conc., %)
1	4.7	450	35.7	60	100	180	20–50	12	67	22
2	4.9	450	35.6	45	100	85	20–50	7	61	32
3	4.7	450	35.5	20	100	85	20–50	7	45	48
4	5	500	31.8	0	100	85	20–50	9	20	71
5	5	500	31.8	0	100	15	20–25	10	23	68
6	5.3	500	82.4	0	100	15	20–25	5	32	63
7	8.2	1000	81.9	0	100	10	10–14	5	14	81

[a]Relative proportions: ±2%.
[b]Methyl 2,3,5,6-tetra-*O*-methyl β-D-galactofuranoside.
[c]Methyl 2,3,4,6-tetra-*O*-methyl β-D-galactopyranoside.
[d]Methyl 2,3,5,6-tetra-*O*-methyl α-D-galactofuranoside.

Can. J. Chem. Downloaded from www.nrcresearchpress.com by 91.121.58.235 on 09/08/12
For personal use only.

0.25 mm film thickness. The oven temperature program was as follows: the initial temperature of 80°C was held for 10 min, followed by a linear temperature ramp to 260°C at a rate of 10°C/min, and was then held constant at 260°C for 10 min.

Results and discussion

The GC–MS trace that we had previously obtained for permethylated D-glucose (2) is very similar to the chromatogram published earlier by Ciucanu and Kerek (1), for the same compound. The trace (not shown) features two major peaks, which, according to these authors (1), respectively correspond to β- and α-glucopyranoside, in a ratio of ca. 2 to 1. The mass spectra obtained at the apex of each peak with our HP GC–MS system matched the NIST library spectra and suggested permethylated β- and α-glucopyranoside products for the respective peaks.

Ciucanu and Kerek (1) had briefly discussed the effect of pH on the equilibrium between the different forms of D-glucose in solution, but no specific details were given by these authors regarding the initial equilibrium in a basic solution of D-glucose in DMSO. More recently, Angyal (7) reported the proportions of glucopyranosides and glucofuranosides observed when D-glucose is dissolved in DMSO, without a base. The relative amounts reported were 45% α-glucopyranose and 55% β-glucopyranose, with no mention of the two other possible isomers. Proportions close to the above were also found when D-glucose was dissolved in pyridine. In this solvent, the amount of β-glucopyranose was decreased by 2% and both glucofuranosides made up for that 2%. These proportions, although measured in a nonbasic environment, reflect the numbers reported by Ciucanu and Kerek (1) and our laboratory (2) for the permethylated derivatives.

Permethylation products of D(+)-galactose

Angyal (7) also reported the following proportions for the forms of D-galactose in pyridine: 31% α-galactopyranose, 46% β-galactopyranose, 5% α-galactofuranose, and 18% β-galactofuranose, in comparison to 30, 64, 2.5, and 3.5%, respectively, in water (8). Unfortunately, no such data were given for galactose in DMSO. According to Ferrier and Collins (9), aprotic solvents (e.g., *N,N*-dimethylformamide (DMF) and DMSO) do not solvate sugars as well as water does, and as a consequence they enhance the anomeric effect and yield a higher proportion of five-membered ring compounds. The figures given above for galactose in pyridine agree with this statement.

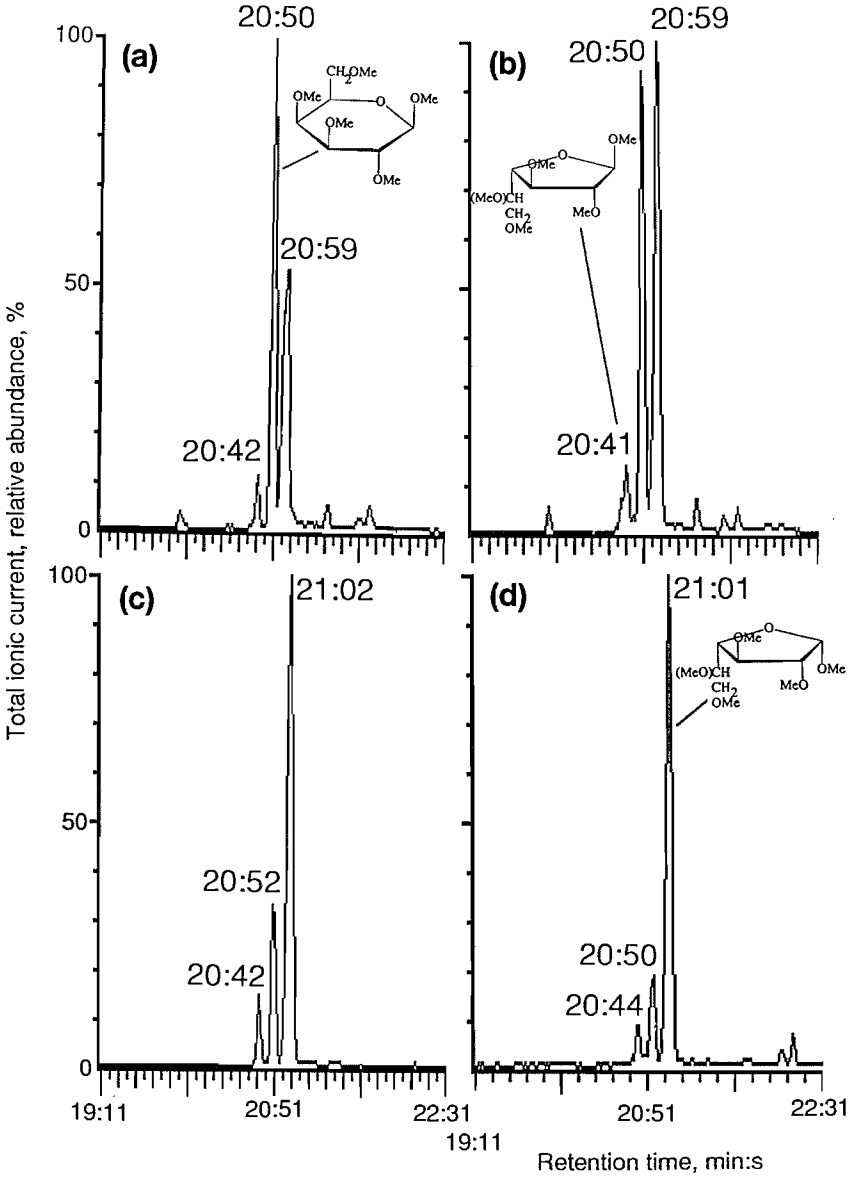
As for the effect of a basic environment on the proportions of hexose species, it has been suggested (8) that in aqueous solution it will influence the rate of mutarotation, and thus the rate of approach of the anomers in solution to an equilibrium mixture. It is difficult to evaluate the pH values of basic solutions in DMSO, but typically DMSO solutions of NaOH are much more basic than the corresponding aqueous solutions. In assuming that the permethylation method of Ciucanu and Kerek (1) is performed at an effective pH > 14, substrates such as D-glucose (pK_a = 12.28) and D-galactose (pK_a = 12.30) should be in their monoanionic forms (10), if not dianionic. The proportions of anomeric anionic species, as opposed to electrically neutral species, has not been discussed in detail in the literature. The ability of hydroxide ions vs. silver, barium, and strontium oxides to act as acid receptors has been discussed as a possible factor influencing the proportions of ionic–nonionic substrate molecules in methylation reactions (9). According to Walker et al. (11), D-galactose, permethylated using methyl iodide and silver oxide, yields the following products: 80% α-D galactofuranoside, 10% β-D-galactofuranoside, and 10% (α and β)-galactopyranosides.

Gee (4) performed thin-layer chromatography on permethylated galactosides and reported separation into three spots, corresponding to β-D-galactofuranoside, α-D-galactofuranoside overlapping with β-D-galactopyranoside, and α-D-galactopyranoside. The compounds were prepared using Kuhn's procedure (12) (DMF as the solvent), and no mention of the relative proportions was made.

In our hands (2), using our former routine permethylation method (method 2 in Table 1), D-(+) galactose yielded two major products and a third minor component. A composition of (7 ± 2)% of galactofuranoside (**1**), (61 ± 2)% of galactopyranoside (**2**), and (32 ± 2)% of galactofuranoside (**3**) was found. Figure 2(*a*) shows the GC–MS total ion current (TIC) obtained from permethylation method 2 (Table 1) as a bench-

© 1997 NRC Canada

Fig. 2. Total GC–MS ion chromatograms obtained for the permethylation products of D-galactose. Refers to Table 1, (*a*) method 2, (*b*) method 3, (*c*) method 5, and (*d*) method 7. The three time-labelled peaks on each chromatogram correspond to products **1**, **2**, and **3**.



mark for starting the present investigation. A similar trace was obtained from method 1, which involved longer sonication times than method 2, both before and after addition of methyl iodide.

The influence of sonication time of the (DMSO–galactose–NaOH) mixture was originally investigated as part as an attempt to shorten the overall reaction time. This step was thus aimed at making the (DMSO–galactose–NaOH) solution as homogeneous and base saturated as possible. Interestingly, a shorter sonication time (see method 3, Table 1) was found to have an important impact on the nature of the products (Fig. 2(*b*)).

While initially performing the experiments, not much thought was given to the kinetics of mutarotation and anomerization at the pH and temperature used. Previous reports, however, demonstrated the importance of such factors. Collins and Ferrier (9) reported that when galactose is heated under reflux in methanol containing 2% HCl, 12 h or more are necessary to reach an equilibrium between the different glycoside forms. It seems reasonable to assume a similar situation exists for anionic galactose in basic solution, in which case the first sonication time involved in methods 1–3 would be too short for an equilibrium to be reached. If the addition of CH_3I "interrupts" the progression toward equilibrium, a systematic variation in the proportions of permethylated galactosides should be observed, as appears to be the case, from method 3 to method 1. The proportions of products **1** and **2** increase, while product **3** becomes less abundant.

Smirnyagin and Bishop (13) studied the kinetics of glycosylation of D-galactose. Their results confirmed an earlier observation for D-xylose (14): when D-galactose is subjected to methanolysis in methanolic HCl, galactofuranosides are preferentially formed first, and their relative concentrations decay as they isomerize into galactopyranoses or anomerize.

Can. J. Chem. Downloaded from www.nrcresearchpress.com by 91.121.58.235 on 09/08/12
For personal use only.

© 1997 NRC Canada

Table 2. Experimental conditions for the permethylation of L(−) fucose, based on the method of Ciucanu and Kerek (1) and relative proportions[a] of the products obtained.[b]

Method no.	1st sonic. (min)	React. time (min)	Temp. (°C)	Prod. **4**[c] (rel. conc., %)	Prod. **5**[d] (rel. conc., %)	Prod. **6**[e] (rel. conc., %)
8	60	60	20–50	100	0	0
9	30	15	20–30	100	0	0
10	20	15	20–27	79	4	17
11	10	15	20–25	44	10	46
12	1	15	20–23	29	12	59
13	0	15	20–23	28	14	58
14	0	25	20–33	40	13	47
15	0	60	20–50	54	14	32
16	0	60	10–20	36	12	52

[a]Relative proportions: ±2%.
[b]Fucose: 4.5–4.8 mg; DMSO: 450 μL; NaOH: 50 mg; CH_3I: 100 μL.
[c]Methyl 2,3,4-tri-*O*-methyl β-L-6-deoxygalactopyranoside.
[d]Methyl 2,3,4-tri-*O*-methyl α-L-6-deoxygalactopyranoside.
[e]Methyl 2,3,5-tri-*O*-methyl α-L-6-deoxygalactofuranoside.

Can. J. Chem. Downloaded from www.nrcresearchpress.com by 91.121.58.235 on 09/08/12
For personal use only.

These authors also showed the effect of temperature on the relative concentrations of galactosides over more than 200 h.

It is clear that in a methanolic HCl solution, glycosides would be far from equilibrium after 45 min or 1 h of reflux, which corresponds more with our times used for the first sonication. Our experimental conditions are far different from those used by these authors (14). However, this rationalization helps in understanding that our starting material in alkaline DMSO is changing with time and temperature. Thus, method 3 yields different proportions of products relative to methods 2 and 1, which involve longer prereaction sonication times.

The sonication time was further reduced to zero with yet another increase in the proportion of α-galactofuranoside **3** to 71% of the total (see method 4, Table 1).

In the fifth experiment (see method 5, Table 1) the reaction time with CH_3I was reduced from 85 to 15 min. The results were very similar to those of method 4, indicating that the reaction was complete after 15 min. Figure 2(*c*) illustrates the results. Collins and Ferrier (8) indicated the possibility that permethylated hexosides may mutarotate in pyridine, but no mention was made of DMSO. The similarity in the proportion of products obtained with method 4 (85 min reaction time) and method 5 (15 min) suggests that no mutarotation took place once permethylation was complete.

When the amount of NaOH was increased (see method 6, Table 1), there was a small increase in the amount of β-galactopyranoside **2** (rt 20:50 min), at the expense of **1** and **3**. The effects of bases on hexoses in aqueous solutions are well documented (8). Epimerization, although it is the most common effect, did not seem to occur in our experiments. The permethylated hexosides obtained with methods 1–7 had GC retention times and mass spectra that characterized galactosides.

In aqueous solutions where the concentration of the base exceeds 1%, sugars may be converted into isomeric deoxyaldonic acids (saccharinic and isosaccharinic acids) (8). Also, prolonged treatment of hexoses with bases may yield 3-carbon fragments such as 2-hydroxypropionaldehyde, pyruvic acid, methyl glyoxal, and lactic acid (8). No such information could be found for solutions of sugars in DMSO. However, these facts may explain the presence of side products after long first sonication – reaction times. We made no further attempt to identify the side products, present at low levels relative to the galactosides (e.g., Fig. 2(*a*) and (*b*)).

The effect of altering the temperature of the methylation reaction was investigated next. In previous experiments (see methods 1–6, Table 1), the reactions were started at room temperature (ca. 22–25°C); however, the temperature of the sonication bath gradually increased, reaching 50°C after 1 h of reaction. Holding the temperature of this reaction constant at 50, 30, 20, 15, and 10°C showed that low temperatures (15 and 10°C) favored formation of the main galactofuranoside **3** and almost eliminated the six-membered ring species **2** (Fig. 2(*d*)). Temperatures above 15°C (20–50°C, methods 4 and 5) all yielded approximately the same proportions of products. Although the reaction appeared to be complete after 15 min at the lower temperatures, we felt that it was safer to allow 1 h for permethylation, as indicated in method 7, Table 1. We believe that a lower starting temperature will alter the initial proportions of galactosides, as observed by Smirnyagin and Bishop (13) for methyl galactosides at 25 and 44°C. Conducting permethylation at a low temperature, such as 10°C, is also likely to slow down by-product formation processes.

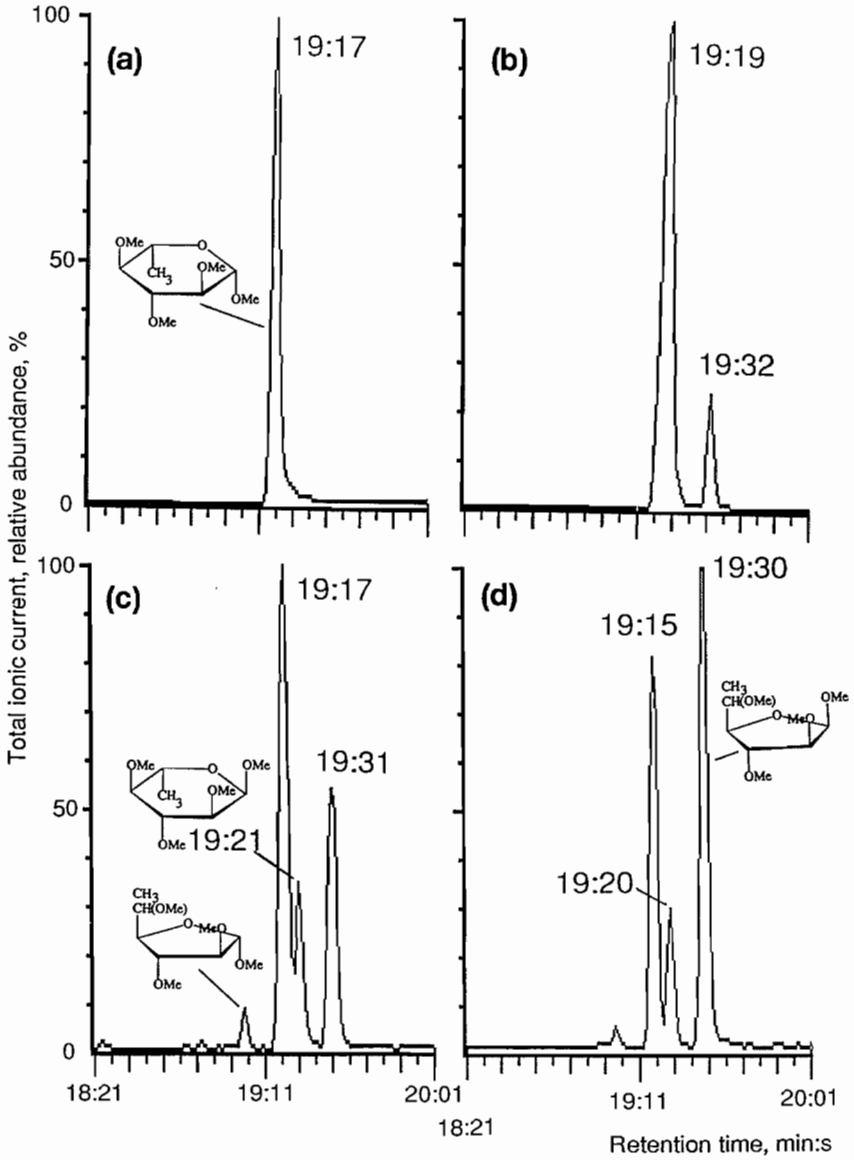
The effect of altering the amounts of DMSO and methyl iodide relative to the other reagents was also investigated. No significant changes in the nature or proportions of the products were observed.

Method 7 (Table 1) provided an 81% relative yield of galactopyranoside **3** (Fig. 2(*d*)), indicating that this method might be preparatively useful.

Vain attempts were made to prepare the galactopyranoside **2** *exclusively*. Large concentrations of NaOH and long sonication times before addition of methyl iodide were investigated, but the results were very similar to those of method 1, i.e., the relative yield of product **2** peaked at approximately 67%. The only effect associated with excess NaOH and long permethylation–sonication times was the appearance of small amounts of unidentified side products, possibly saccharic-type acids and smaller fragments as discussed above.

© 1997 NRC Canada

Fig. 3. Total GC–MS ion chromatograms obtained for the permethylation products of L-fucose. Refers to Table 2, (*a*) method 8, (*b*) method 10, (*c*) method 15, and (*d*) method 16. The time-labelled peaks on the chromatograms correspond to products **4**, **5**, and **6**.



Can. J. Chem. Downloaded from www.nrcresearchpress.com by 91.121.58.235 on 09/08/12
For personal use only.

Permethylation products of L(−)-fucose

Results from the GC–MS TIC trace previously obtained for the three major products of permethylated L(−)-fucose (2) are reported in Table 2, method 11. A minor peak appears first and corresponds to a permethylated fucofuranoside. This product has not been taken into account in the following discussion since it constitutes less than 3% of the total product mixture. With method 11, fucopyranosides **4** and **5** made up 54% of the three main products, with the remainder (46%) being the fucofuranoside anomer **6**. The permethylated fucopyranosides **4** and **5** were first tentatively identified by library comparison to the spectra obtained on the HP system (5), as methyl 2,3,4-tri-*O*-methyl-6-deoxy-β- and α-galactopyranosides. Although no library spectra were available for permethylated fucofuranosides, they were identified by the similarity of spectral features between the fucose and galactose-derived products: permethylated fuco- and galactofuranosides each yield a main peak at *m/z* 101. More systematic identification was carried out with the use of the corresponding standards.

Varying the reaction parameters for the permethylation of L(−)-fucose was accomplished based on the results obtained for D(+)-galactose. Hence, the relative amounts of DMSO, CH_3I, NaOH, and fucose used remained constant in all experiments. These quantities are indicated in Table 2. Parameters subjected to variation were: time of first sonication, reaction time, and temperature. Table 2 lists nine different methods, along with the corresponding proportions of products (**4**, **5**, and **6**) obtained. In methods 8–12, fucose, NaOH, and DMSO were sonicated prior to addition of CH_3I. The general trend shows increasing proportions of **5** and **6** relative to **4** with shorter prereaction sonication times. In methods 13–15, the first sonication step was omitted and the reaction time was incremented. Longer reaction times (25 min, method 14 and 60 min, method 15) had the effect of increasing the propor-

© 1997 NRC Canada

tions of **4** vs. **5** and **6**, i.e., the effect was similar to that of longer first sonication times. Lowering the reaction temperature (method 16) favored product **6**, and brought down the relative concentration of **4** from that observed using method 15. Interestingly, the relative proportion of product **5** was not significantly altered with methods 11–16.

The results obtained from methods 8 and 9 (e.g., Fig. 3(*a*)) suggest that longer mixing times of the (fucose–DMSO–NaOH) solution yield 100% of β-fucopyranoside, neutral or anionic, prior to the addition of CH_3I. Methods 8 and 9 are therefore advisable if preparation of β-fucopyranoside as a single isomer is desired.

Shorter mixing of the ternary solution, as in methods 10–13, showed a change in the proportions of fucosides, with a tendency towards α-fucopyranoside **5** and fucofuranoside **6** relative to the previously predominant β-fucopyranoside. Figure 3(*b*) illustrates this trend. Here compound **5** is a minor constituent and has not been resolved from **4**. The slight shoulder at the right base of the peak assigned to **4** led us to assign a proportion of 4% to compound **5**.

So far, these results are in agreement with the general trend observed for the galactose permethylation reactions. However, much less information is available about the chemistry of fucose in solution than about galactose and therefore interpretation of the results is more difficult.

In methods 8–13, we estimated that a 15 min reaction time was the minimum required to ensure complete permethylation of the sugar. We also assumed that no further isomerization took place once the products were formed. In methods 14 and 15, where the reaction time was deliberately pushed above 15 min, isomerization seemed to occur, either during permethylation itself, or once the reaction was completed. It could also be possible that one (or more) of the isomers is selectively being degraded. This would change the ratio of isomers and give the impression that equilibration between isomers was occurring. This process overall favored product **4**, to the detriment of **5** and **6** (Fig. 3(*c*)).

Lowering the reaction temperature as in method 16 seemed to slow down the process and the proportions were pushed in favor of product **6**. Figure 3(*d*) shows the corresponding chromatogram.

Conclusion

It has been shown that permethylation conditions, based on the method of Ciucanu and Kerek (1), have a profound influence on the composition of the products obtained from permethylation of D-galactose and L-fucose. For both of the monosaccharides, permethylation produced a mixture of four isomers: two pyranoside and two furanoside α and β anomers. In each case, three compounds out of the four were predominant and well separated on the GC–MS chromatograms. The fourth component in each case was very minor and its proportions did not appear to vary from one set of conditions to another. Changes in the relative proportions of the three main compounds were reported as different reaction parameters were varied. The most influential parameter appeared to be the time the DMSO solution of the sugar and NaOH was mixed by sonication before reaction with methyl iodide. The initial temperature of reaction also had an important effect. It is assumed that these two parameters influenced the initial proportion of the four possible isomers, or isomeric anions, of the monosaccharides in solution prior to permethylation.

In both cases (galactose and fucose), formation of the β-pyranoside product was noticeably favored when longer pre-reaction sonication times and higher temperatures were used. Opposite trends in the conditions favored formation of the α-furanoside product.

Above all, it has been shown that care has to be taken when performing permethylation of sugars as a routine operation. The reaction conditions must be very carefully controlled in order to obtain reproducible meaningful results.

Acknowledgments

The authors wish to acknowledge the technical assistance of Wayne Buchannon of the Chemistry Department, Mass Spectrometry Facility, University of Manitoba. Sincere thanks are also addressed to the Natural Sciences and Engineering Research Council of Canada (NSERC) for financial support.

References

1. I. Ciucanu and F. Kerek. Carbohydr. Res. **131**, 209 (1984).
2. D.D. Asres and H. Perreault. Can. J. Chem. **74**, 1512 (1996).
3. H.W. Kircher. Anal. Chem. **32**, 1103 (1960).
4. M. Gee. Anal. Chem. **35**, 350 (1963).
5. NIST Standard Reference Data Base, Series 1a, NIST/EPA/NIH Database Version 4.5, February 1994, US Department of Commerce.
6. G. Larsson, H. Karlsson, G.C. Hansson, and W. Pimlott. Carbohydr. Res. **161**, 281 (1987).
7. S.J. Angyal. Adv. Carbohydr. Chem. Biochem. **49**, 19 (1991).
8. P. Collins and R.J. Ferrier. Monosaccharides: their chemistry and their roles in natural products. Wiley, Chichester, U.K. 1995.
9. R.J. Ferrier and P.M. Collins. Monosaccharide chemistry. Penguin Books Ltd., London, U.K. 1972.
10. Technical Note No. 20. Dionex Corporation, Sunnyvale, Calif. 1993.
11. H.G. Walker, Jr., M. Gee, and R.M. McCready. J. Org. Chem. **27**, 2100 (1962).
12. R. Kuhn, H. Trishmann, and I. Low. Angew. Chem. **67**, 32 (1955).
13. V. Smirnyagin and C.T. Bishop. Can. J. Chem. **46**, 3085 (1968).
14. C.T. Bishop and F.P. Cooper. Can. J. Chem. **41**, 2743 (1963).

Can. J. Chem. Downloaded from www.nrcresearchpress.com by 91.121.58.235 on 09/08/12
For personal use only.

© 1997 NRC Canada

Substituent effects on the reactivity of the silicon–carbon double bond. Arrhenius parameters for the reaction of 1,1-diarylsilenes with alcohols and acetic acid

Christine J. Bradaric and William J. Leigh

Can. J. Chem. Downloaded from www.nrcresearchpress.com by 91.121.58.235 on 09/08/12
For personal use only.

Abstract: Absolute rate constants for the reaction of a series of ring-substituted 1,1-diphenylsilene derivatives with methanol, *tert*-butanol, and acetic acid in acetonitrile solution have been determined using nanosecond laser flash photolysis techniques. The three reactions exhibit small positive Hammett ρ-values at 23°C, consistent with a mechanism involving initial, reversible nucleophilic attack at silicon to form a σ-bonded complex that collapses to product via rate-limiting proton transfer. Deuterium kinetic isotope effects and Arrhenius parameters have been determined for the reactions of 1,1-di-(4-methylphenyl)silene and 1,1-di-(4-trifluoromethylphenyl)silene with methanol, and are compared to those for the parent compound. Proton transfer within the complex is dominated by entropic factors, resulting in negative activation energies for reaction. The trends in the data can be rationalized in terms of variations in the relative rate constants for reversion to reactants and proton transfer as a function of temperature and substituent. A comparison of the Arrhenius activation energies for reaction of acetic acid with 1,1-diphenylsilene (E_a = +1.9 ± 0.3 kcal/mol) and the more reactive di-trifluoromethyl analogue (E_a = +3.6 ± 0.5 kcal/mol) suggests that carboxylic acids also add by a stepwise mechanism, but with formation of the complex being rate determining.

Key words: silene, substituent effects, kinetics, Arrhenius, flash photolysis.

Résumé : Faisant appel aux techniques de photolyse éclair avec laser à la nanoseconde, on a déterminé les constantes de vitesse absolues pour les réactions d'une série de 1,1-diphénylsilènes substitués sur le cycle avec le méthanol, le *tert*-butanol et l'acide acétique en solutions dans l'acétonitrile. À 23°C, les trois réactions présentent des valeurs ρ de Hammett faiblement positives qui sont en accord avec un mécanisme impliquant une attaque initiale nucléophile réversible au niveau du silicium qui conduit à la formation d'un complexe à liaison σ qui se décompose en produit par le biais d'un transfert de proton qui est cinétiquement limitant. On a déterminé les effets isotopiques cinétiques du deutérium ainsi que les paramètres d'Arrhenius pour les réactions du 1,1-di-(4-méthylphényl)silène et du 1,1-(di-4-trifluorométhylphényl)silène avec le méthanol et on les a comparés avec les valeurs correspondantes du composé parent. Le transfert de proton dans le complexe est dominé par des facteurs entropiques; ceci conduit à des valeurs négatives pour les énergies d'activation de ces réactions. On peut rationaliser les tendances dans ces résultats en termes de variations dans les constantes de vitesse relatives pour la retransformation en réactifs et celle du transfert de proton en fonction de la température et du substituant. Une comparaison des énergies d'activation d'Arrhenius pour la réaction de l'acide acétique avec le 1,1-diphénylsilène (E_a = +1,9 ± 0,3 kcal/mol) et celle avec l'analogue plus réactif ditrifluorométhyle (E_a = +3,6 ± 0,5 kcal/mol) suggère que les acides carboxyliques s'additionnent aussi par un mécanisme par étapes; toutefois la formation du complexe serait toutefois l'étape cinétiquement limitante.

Mots clés : silène, effets de substituants, cinétique, Arrhenius, photolyse éclair.

[Traduit par la rédaction]

Introduction

The best-known reactions of silenes are [2+2]-dimerization and nucleophilic addition of alcohols (1–3). Since the very first experimental demonstrations that silenes are formed as reactive intermediates in the thermolysis (4) and (or) photolysis (5, 6) of silacyclobutanes and disilanes, the formation of 1,3- or 1,2-disilacyclobutanes from dimerization or alkoxysilanes from trapping with alcohols have come to be identified as classic indicators of silene involvement in the reactions of organosilicon compounds.

From a mechanistic standpoint, the reaction with alcohols has been more extensively studied (7–17). Wiberg published the first experimental evidence that alcohol nucleophilicity — and not acidity — is the main factor affecting the kinetics of the reaction, and suggested a mechanism involving complex-

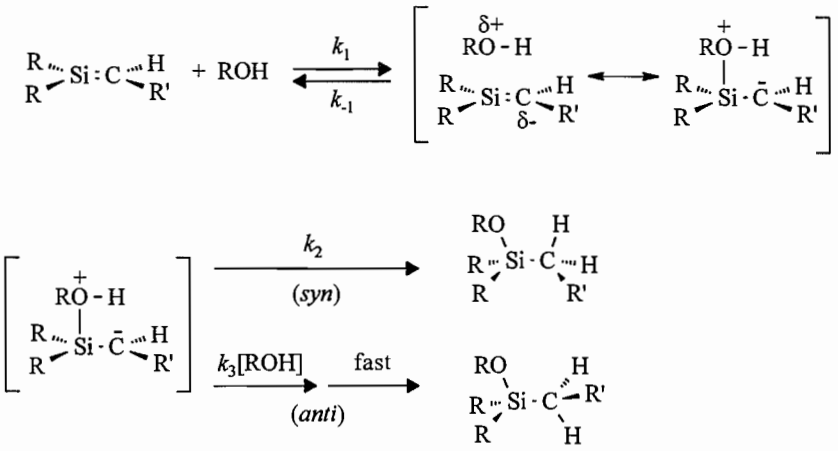
Received May 25, 1997.

C.J. Bradaric and W.J. Leigh.[1] Department of Chemistry, McMaster University, 1280 Main Street West, Hamilton, ON L8S 4M1, Canada.

[1] Author to whom correspondence may be addressed. Telephone: (905) 525-9140, ext. 23485/23715. Fax: (905) 522-2509. E-mail: leigh@mcmaster.ca

© 1997 NRC Canada

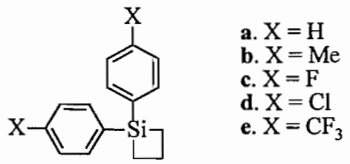
Scheme 1.



ation of the alcohol at silicon followed by proton transfer from oxygen to carbon (8). This was soon followed by reports of examples of both nonstereoselective (9) and stereoselective (11) alcohol additions, as well as an indication that in cases where more than one regio- or stereoisomeric product can be formed, the product distribution can vary with alcohol concentration (12). Sakurai and co-workers published the first comprehensive mechanism to explain these results (13), in a study of the effects of alcohol concentration on the ratio of *syn* and *anti* adducts obtained from reaction of various aliphatic alcohols with a cyclic, disilane-derived silene reactive intermediate. They proposed a refined version of Wiberg's mechanism, in which reaction is initiated with formation of a silene–alcohol complex, which proceeds to product by competing intracomplex (*syn*) and extracomplex (*anti*) proton-transfer pathways. The latter involves a second molecule of alcohol and hence increases in importance with increasing alcohol concentration. We have published kinetic and product studies for other transient silenes that support this mechanism (see Scheme 1), with the additional requirement that formation of the silene–alcohol complex be fully reversible (14–20). For each of the reactive silenes that we have studied, variations in solvent polarity and alcohol nucleophilicity, acidity, and isotopic substitution affect the kinetics and product distribution in ways that are fully compatible with this mechanism.

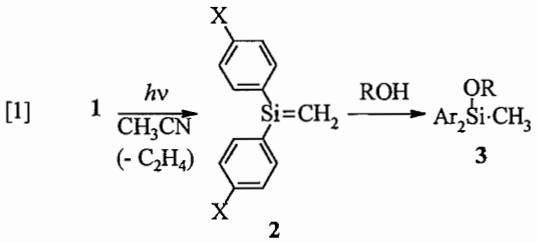
While theory suggests that substituents that reduce the natural polarity of the Si=C bond should lead to lower reactivity toward nucleophilic addition (10, 21), there has been little experimental effort directed toward developing a quantitative understanding of the effects of polar factors on silene reactivity. One relatively straightforward way of undertaking such a study would be through investigation of a series of ring-substituted 1,1-diphenylsilene derivatives (**2**), which might be generated by photolysis of the corresponding 1,1-diarylsilacyclobutanes (**1**) (6, 16, 17, 22–24). We have previously shown that the parent compound, 1,1-diphenylsilacyclobutane (**1a**), is a convenient source of 1,1-diphenylsilene (**2a**) for time-resolved spectroscopic studies, and have reported kinetic studies of the reactions of this silene with alcohols and acetic acid (16, 17).

In this paper, we report a study of the effects of ring substituents on the rate constants for addition of methanol, *tert*-butanol, and acetic acid to 1,1-diphenylsilene. We have employed the photocycloreversion of the series of 1,1-diarylsilacyclobutanes **1** to generate the corresponding silenes (**2**) in acetonitrile solution (eq. [1]), and have measured absolute rate constants, deuterium kinetic isotope effects, and Arrhenius parameters for reaction with these three reagents.



a. X = H
b. X = Me
c. X = F
d. X = Cl
e. X = CF_3

1



2 **3**

Results

Compounds **1b–e** were synthesized from 1,1-dichlorosilacyclobutane and the appropriate aryl magnesium bromide, using a method similar to that reported for the parent compound **1a** (17, 25). They were purified by column chromatography to >99% purity, and exhibited spectral and analytical data that are consistent with their assigned structures.

Direct irradiation of **1b–e** (0.007–0.013 M) in the presence of 0.05 M methanol results in the formation of the corresponding alkoxysilanes **3b–e** in high chemical yields.[2] No other products were observed in significant yield from the photoly-

[2] The 4,4′-dimethoxy analogue of **1** was also synthesized, but steady state photolysis of the compound under the same conditions yielded a number of products in minor yields. Furthermore, no evidence for the formation of the corresponding silene could be obtained by flash photolysis of the compound.

© 1997 NRC Canada

Can. J. Chem. Downloaded from www.nrcresearchpress.com by 91.121.58.235 on 09/08/12
For personal use only.

Can. J. Chem. Downloaded from www.nrcresearchpress.com by 91.121.58.235 on 09/08/12
For personal use only.

Table 1. Bimolecular rate constants, deuterium kinetic isotope effects, and Hammett ρ-values for reaction of 1,1-diarylsilenes (**2**) with MeOH, *t*-BuOH, and AcOH in deoxygenated acetonitrile solution at 23°C.[a]

2 (X)	k_{MeOH} (10^9 M^{-1} s^{-1})	$k_{t\text{-}BuOH}$ (10^9 M^{-1} s^{-1})	k_{AcOH} (10^9 M^{-1} s^{-1})
2b (X = Me)	1.12 ± 0.06	0.130 ± 0.006	1.41 ± 0.05
	(k_H/k_D = 1.9 ± 0.1)	(k_H/k_D = 1.9 ± 0.2)	(k_H/k_D = 1.2 ± 0.2)
2a (X = H)[b]	1.5 ± 0.1	0.22 ± 0.02	1.5 ± 0.2
	(k_H/k_D = 1.5 ± 0.1)	(k_H/k_D = 1.6 ± 0.1)	(k_H/k_D = 1.1 ± 0.1)
2c (X = F)	1.89 ± 0.08	0.33 ± 0.02	1.8 ± 0.2
2d (X = Cl)	2.13 ± 0.10	0.39 ± 0.02	2.0 ± 0.2
2e (X = CF_3)	2.99 ± 0.16	0.75 ± 0.04	2.3 ± 0.4
	(k_H/k_D = 1.0 ± 0.1)	(k_H/k_D = 1.7 ± 0.2)	(k_H/k_D = 1.1 ± 0.1)
ρ	+0.31 ± 0.05	+0.55 ± 0.08	+0.17 ± 0.02
	(r^2 = 0.980)	(r^2 = 0.985)	(r^2 = 0.987)

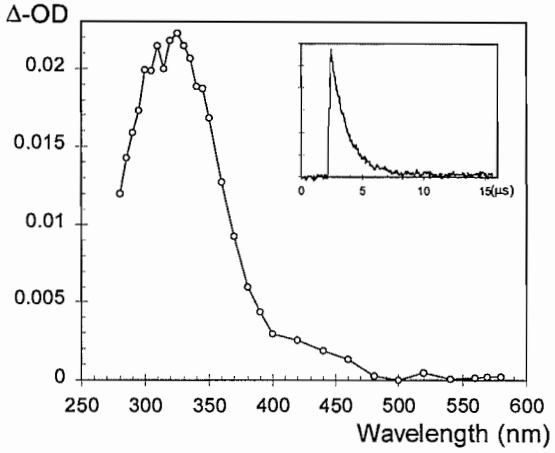
[a]Errors are listed as twice the standard deviation from least-squares analysis of k_{decay} – concentration data according to eq. [2].
[b]Data from ref. 17.

sis of any of the four compounds below ~40% conversion. The alkoxysilanes were isolated from the crude photolysis mixtures by semi-preparative GC, and identified on the basis of their NMR, IR, and mass spectra.

Nanosecond laser flash photolysis of continuously flowing, air-saturated solutions of **1b–e** (0.003–0.006 M) in acetonitrile affords weak, but readily detectable transient absorptions (λ_{max} ~ 325 nm) that decay with clean pseudo-first-order kinetics to within 10% of the pre-pulse level. The transients exhibit lifetimes in the 150–250 ns range in acetonitrile dried by distillation from calcium hydride, but these were extended to the 2–3 μs range using more scrupulously dried (i.e., $\leq 10^{-4}$ M water) samples of the solvent. The UV absorption spectra, lifetimes, and kinetic response of the transients to added silene quenchers (vide infra) are similar to those reported previously for 1,1-diphenylsilene, formed by photolysis of **1a** under similar conditions (17), and we thus assign them to the corresponding 1,1-diarylsilenes **2b–e**. For example, Fig. 1 shows the time-resolved UV absorption spectrum of **2e**, recorded 80–240 ns after the laser pulse for an air-saturated solution of **1e** in acetonitrile. As expected (17, 24), the lifetimes of the transients were not measurably shortened upon saturation of the solutions with oxygen.

Addition of methanol, *tert*-butanol, acetic acid, or water to the acetonitrile solutions of **1b–e** resulted in a reduction in the lifetimes of the 325-nm transient absorptions, consistent with their assignment to the silenes **2b–e**. Plots of the rate constant for decay (k_{decay}) versus concentration of added quencher (ROH) according to eq. [2] (where k_0 is the first-order rate constant for the decay of the transient in the absence of added quencher and k_{ROH} is the second-order quenching rate constant) were linear in all cases. Typical plots are shown in Fig. 2 for quenching of the four silenes by methanol. Similar experiments were carried out using MeOD, *t*-BuOD, and AcOD for **2b,e**. The absolute rate constants for reaction of silenes **2b–e** with MeOH, *t*-BuOH, and AcOH in acetonitrile are collected in Table 1, along with k_H/k_D values calculated from the data for the protiated and deuterated reagents. The corresponding data for **2a** (17) are included in the table for comparison.

Fig. 1. Time-resolved UV absorption spectrum recorded at 23 ± 1°C by nanosecond laser flash photolysis of an air-saturated acetonitrile solution of 1,1-di(4-trifluoromethylphenyl)silacyclobutane (**1e**, 0.0042 M). The spectrum was recorded over a time window of 80–240 ns after the laser pulse. The insert shows a typical decay trace, recorded at a monitoring wavelength of 325 nm.



[2] $k_{decay} = k_0 + k_{ROH}[ROH]$

Absolute rate constants for reaction of silenes **2b** and **2e** with MeOH in acetonitrile were determined at several temperatures between −20°C and 55°C. Similar experiments were carried out for reaction of **2a** with MeOD and **2e** with HOAc in acetonitrile. The Arrhenius plots for quenching by MeOH(D) are shown in Fig. 3, along with that reported previously for quenching of **2a** by MeOH (16). Figure 4 shows the Arrhenius plots for quenching of **2a** (16) and **2e** with HOAc. Linear least-squares analysis of these data afforded the Arrhenius parameters collected in Table 2. In the case of **2e**–MeOH, only the data for temperatures above 13°C were employed for calculation of the Arrhenius parameters listed in the table. The Arrhenius plot for diffusion in acetonitrile, calculated using the modified Debye equation ($k_{diff} = 8RT/3000\eta$) and values

© 1997 NRC Canada

Table 2. Arrhenius activation parameters for addition of methanol, methanol-O-*d*, and acetic acid (ROL, where L = H or D) to selected 1,1-diarylsilenes (**2a**, **2b**, and **2e**) in acetonitrile solution.[a]

2 (X)	ROL	k_{ROL}^{25C} (10^9 M^{-1} s^{-1})[b]	$(k_H/k_D)^{23C}$	E_a (kcal mol^{-1})	log *A*	r^2
2b (X = Me)	MeOH	0.9 ± 0.1	1.9 ± 0.2	−2.7 ± 0.2	6.9 ± 0.3	0.973
2a (X = H)[c]	MeOH	1.3 ± 0.1	1.9 ± 0.2	−2.5 ± 0.3	7.3 ± 0.2	0.983
	MeOD	0.7	—	−3.2 ± 0.3	6.5 ± 0.2	0.979
	HOAc	1.3 ± 0.3	1.1 ± 0.1	1.9 ± 0.3	10.5 ± 0.4	0.982
2e (X = CF_3)	MeOH	2.2 ± 0.3	1.0 ± 0.1	−1.9 ± 0.2[d]	7.9 ± 0.1[d]	0.996
	HOAc	2.2 ± 0.2	[e]	3.6 ± 0.5	12.0 ± 0.4	0.980

[a]Errors are listed as twice the standard deviation from least-squares analysis of k_{decay} – concentration data according to eq. [2].
[b]Interpolated from Arrhenius data.
[c]Data from ref. 16.
[d]High temperature limiting values, from analysis of kinetic data obtained at $T > 13$°C.
[e]Not determined.

Fig. 2. Plots of ($k_{decay} - k_0$) versus [MeOH] from laser flash photolysis of air-saturated acetonitrile solutions of **1b–e** in the presence of methanol (X = Me, ■; X = F, ◆; X = Cl, Δ; X = CF_3, ●).

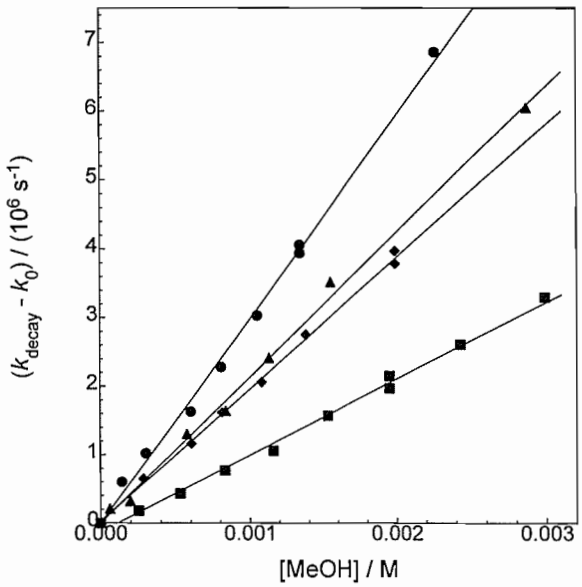
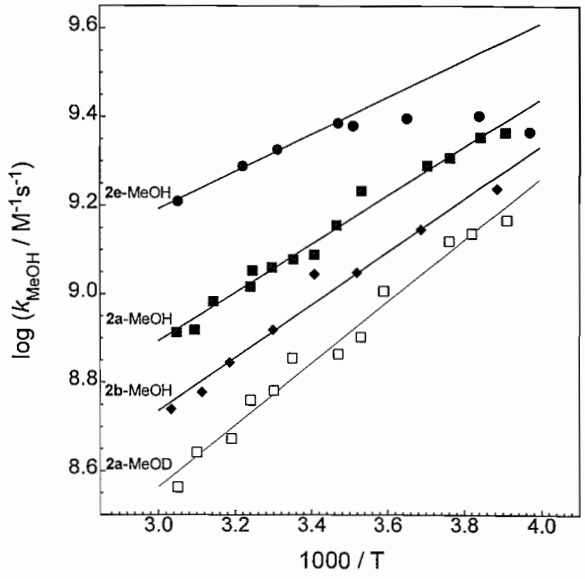


Fig. 3. Arrhenius plots for quenching of 1,1-diarylsilenes **2a** (X = H; ■), **2b** (X = Me; ◆), and **2e** (X = CF_3; ●) by methanol and **2a** by methanol-*O*-*d* (□) in acetonitrile solution. The **2a**-MeOH data are from ref. 16.



of η extrapolated from published temperature–viscosity data (26), is included in Fig. 4. Arrhenius parameters for addition of methanol to **2a** were also determined in hexane solution, from data recorded over a temperature range of −6–40°C. The values obtained are $E_a = -2.7 \pm 0.3$ kcal/mol and $\log A = 7.40 \pm 0.26$ ($r^2 = 0.996$). The rate constant for reaction at 23°C was found to be $(2.9 \pm 0.3) \times 10^9$ M^{-1} s^{-1}, in satisfactory agreement with our previously determined value (17).

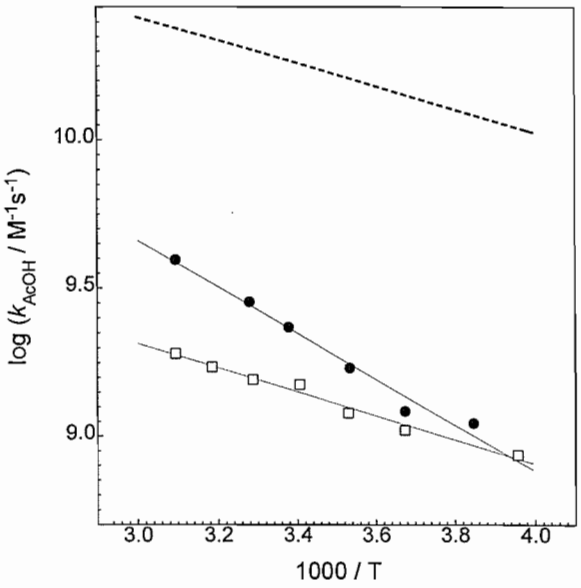
Addition of 0.5 M methanol to nitrogen-saturated acetonitrile or hexane solutions of **1a,d,e** — enough to reduce the lifetimes of the corresponding silene to $\tau < 10$ ns — allowed the detection of weak residual signals that decayed with pseudo-first-order kinetics and lifetimes of 0.5–2 μs. The intensity of this signal was greatest in the case of the *para*-chloro compound **1d**, and for all three compounds was greater in hexane than in acetonitrile. The time-resolved absorption spectra of these transients showed $\lambda_{max} \sim 360$ nm in all cases, and the lifetimes proved to be sensitive to the presence of oxygen or 1,3-octadiene. Plots of the observed transient decay rate constants versus diene concentration were linear, and afforded quenching rate constants in the range $(3–4) \times 10^9$ M^{-1} s^{-1} in hexane solution at 23°C. On the basis of these data, the transients observed under these conditions are assigned to the silacyclobutane triplet states. Addition of 0.01 M 1,3-octadiene to nitrogen-saturated solutions of **1a–e** in the absence of methanol resulted in no discernible change in either the lifetime or the initial absorbance of the transient signal assigned to the corresponding silene (at 325 nm), indicating that the formation of the silene does not involve the triplet state of the disilacyclobutane.

© 1997 NRC Canada

Can. J. Chem. Downloaded from www.nrcresearchpress.com by 91.121.58.235 on 09/08/12
For personal use only.

Can. J. Chem. Downloaded from www.nrcresearchpress.com by 91.121.58.235 on 09/08/12
For personal use only.

Fig. 4. Arrhenius plots for quenching of 1,1-diphenylsilene (**2a**; □) and 1,1-di-(4-trifluoromethylphenyl)silene (**2e**; ●) by acetic acid in acetonitrile solution. The data for **2a** are from ref. 16. The broken line corresponds to that for diffusion in acetonitrile, calculated using the modified Debye equation and published viscosity data (see text).



Discussion

The four substituted 1,1-diarylsilacyclobutanes studied in this work all exhibit analogous photochemical behaviour to that of the parent compound, 1,1-diphenylsilacyclobutane (**1a**). All five compounds yield the corresponding methoxydiarylmethylsilane (**3**) in high chemical yield upon direct irradiation in hexane or acetonitrile solution in the presence of methanol or other silene traps (27), consistent with the formation of the corresponding 1,1-diarylsilene (**2**). The rates of formation of the alkoxysilanes from photolysis of **1a–e** indicate that there is no appreciable variation throughout the series in the quantum yield for silene formation ($\Phi_2 = 0.24 \pm 0.03$ in the case of **1a** (17)). Intersystem crossing to yield the silacyclobutane triplet state also occurs, but this is relatively minor and is clearly unrelated to the formation of the silene by cycloreversion in the lowest excited singlet state.

The five silenes exhibit similar behaviour as well; they all exhibit long-wavelength absorption bands with $\lambda_{max} \sim 325$ nm, decay with pseudo-first-order kinetics in dried acetonitrile in the absence of (intentionally) added trapping reagents, and exhibit lifetimes in the 2–3 μs range. These lifetimes probably reflect limiting quenching by residual water in the solvent; since quenching of **2a** by water is as fast as by methanol (17), a concentration of only $\sim 10^{-4}$ M would result in a lifetime in the microsecond range. In agreement with this, the lifetimes vary slightly through the series, with that of **2b** being the longest and that of **2e** the shortest. The normal fate of **2a** in the absence of traps is dimerization (23, 25, 28), which should result in second-order decay kinetics. However, even in sodium-dried hexane, silene **2a** decays with mixed second- and pseudo-first-order kinetics. We conclude that dimerization of these silenes is relatively slow, probably due to steric factors.

The addition of alcohols to reactive silenes has received a great deal of attention over the past several years (7–17). As shown in Scheme 1, the mechanism is thought to involve initial nucleophilic attack at silicon followed by proton transfer from oxygen to carbon. A mechanism involving a silenium ion, formed by initial protonation at carbon, can be ruled out simply by the fact that the rate of reaction generally does *not* depend in a straightforward way on ROH acidity; the more important factor appears to be nucleophilicity (8, 14, 15, 17). The overall rate constant generally exhibits a small primary deuterium isotope effect, indicating that the initial intermediate (a zwitterionic silene–alcohol "complex") reverts to the free silene and alcohol at least as fast as it collapses to alkoxysilane by proton transfer (14, 15, 17). The involvement of this intermediate is further suggested by the fact that silenes characteristically form complexes with ethers (29). As well, several reactive silenes (including **2a**) have been found to exhibit negative activation energies in their reactions with methanol and (or) *tert*-butanol (16, 20, 30). While this is a common feature of fast reactions that proceed by mechanisms of this general type (31–40), it does not in itself rule out the possibility that the reaction proceeds by a concerted mechanism (32, 35, 37, 41–43).

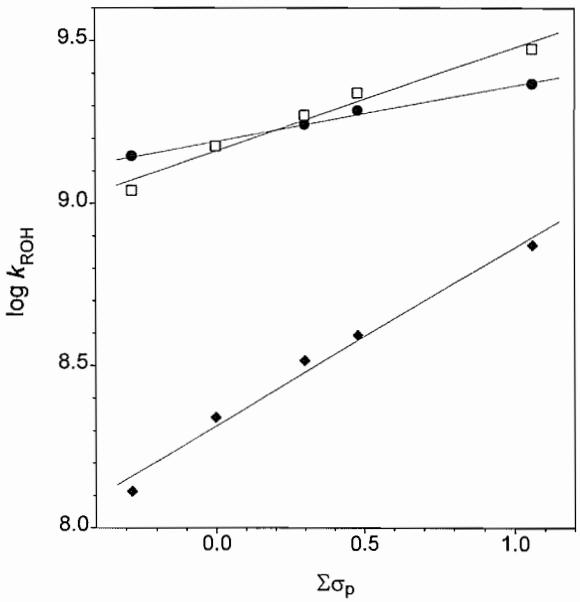
The best evidence for the intermediacy of the σ-bonded complex in alcohol additions to silenes is the fact that the product distribution quite commonly varies with bulk alcohol concentration (12, 13, 15, 17). There is good evidence to suggest that this is due to proton transfer proceeding by two competing pathways: a unimolecular pathway involving [1,3]-proton migration within the complex, and a bimolecular pathway involving a second molecule of alcohol. This aspect of the mechanism was originally proposed on the basis of a study of the addition of various aliphatic alcohols to a cyclic transient silene, where it was found that for methanol, the stereochemistry of addition depends on bulk alcohol concentration (13). *syn*-Addition predominates at low alcohol concentrations where the intracomplex (unimolecular) proton transfer pathway should be operative, while *anti*-addition predominates at high alcohol concentrations due to increased importance from the extracomplex proton transfer pathway. *tert*-Butanol was found to add with 100% *syn*-stereochemistry at all alcohol concentrations, indicating that it reacts only by the unimolecular pathway in this particular case. Other workers, including us, have reported analogous concentration dependences in the *regio*chemistry of addition of aliphatic alcohols to conjugated silenes (12, 15). In the case of **2a**, the competing proton transfer pathways manifest themselves in competition experiments with methanol and *tert*-butanol, where the yield of the methanol adduct (relative to the *tert*-butanol adduct) increases with increasing bulk alcohol concentration (17). Sakurai and co-workers originally proposed that the bimolecular pathway involves protonation at carbon followed by rapid deprotonation from oxygen (13), but solvent and deuterium isotope effect studies seem more compatible with a deprotonation–protonation sequence (15, 17).

Kinetic studies have also provided evidence for a mechanism involving mixed first- and second-order dependences on alcohol concentration (14, 15), in the form of a quadratic variation in the pseudo-first-order rate constant for silene consumption (k_{decay}) with [ROH]. The expression shown in eq. [3], derived using the steady state assumption for the complex, collapses to a simple quadratic expression in [ROH] under

© 1997 NRC Canada

Can. J. Chem. Downloaded from www.nrcresearchpress.com by 91.121.58.235 on 09/08/12
For personal use only.

Fig. 5. Hammett plots for quenching of 1,1-diarylsilenes by MeOH (□), *t*-BuOH (◆), and AcOH (●) in acetonitrile solution.



conditions where reversion of the complex to reactants is significantly faster than proton transfer (i.e., $k_{-1} > (k_2 + k_3[ROH])$) and uni- and bimolecular proton transfer proceed with comparable rate constants. Behaviour of this type has been reported for silenes in which conjugating substituents on the silenic carbon (14, 15) stabilize the complex toward intramolecular proton transfer. Simpler silenes such as **2a** (17) and others (16, 17, 20, 30)[3] exhibit higher overall reactivity toward alcohols, and show linear dependences of k_{decay} on [ROH] over the alcohol concentration ranges that can be studied using nanosecond time-resolved techniques.

$$[3] \quad k_{decay} = k_0 + \frac{k_1[ROH]}{(k_{-1} + k_2 + k_3[ROH])}(k_2 + k_3[ROH])$$

Not surprisingly, the latter behaviour is also observed for **2b–e** for quenching by both MeOH and *t*-BuOH (Fig. 2). It indicates that over the concentration ranges employed for our kinetic measurements (<0.01 M for MeOH; <0.05 M for *t*-BuOH), reaction occurs predominantly by the intracomplex proton transfer pathway for both alcohols. Under these conditions, the expression for k_{decay} simplifies to that in eq. [4].

$$[4] \quad k_{decay} = k_0 + \frac{k_1 k_2}{k_{-1} + k_2}[ROH]$$

The trends in the observed rate constants for reaction of **2a–e** with MeOH and *t*-BuOH indicate that electron-withdrawing substituents at silicon increase silenic reactivity toward alcohols, providing additional evidence for a mechanism in which nucleophilic attack at silicon precedes protonation at carbon. Hammett plots, shown in Fig. 5, afford ρ-values of +0.31 and +0.55 for reaction with MeOH and *t*-BuOH, respectively. The difference between the ρ-values for the two alcohols is small, presumably because the overall rate constants for both alcohols are so large. However, the effect is slightly greater for the less reactive alcohol, as would be expected.

To a first approximation, these reaction constants can be viewed as the sum of those of the individual complexation and proton transfer steps (see Scheme 1). The ρ-value for the complexation step would clearly be expected to be positive, while that for the proton transfer step should be small because the process involves charge neutralization within the zwitterionic complex. Thus, the positive overall reaction constants can be interpreted as reflecting mainly the effects of substituents on the initial reaction of the silene with the neutral nucleophile. This has obvious analogies to Michael addition reactions and, indeed, the addition of various nucleophiles such as amines (44), cyanide ion, and enolates (45) to substituted β-nitrostyrenes exhibit Hammett ρ-values in the range +0.2–1 depending on the nucleophile and the solvent.

The trend in the k_H/k_D values for reaction of methanol with **2a–e** (decreasing with increasing substituent electron-withdrawing power; see Table 1) can be explained in terms of variations in the relative magnitudes of the rate constants for reversion of the complex to reactants (k_{-1}) and collapse to product (k_2), since the isotope effect on k_1 should be a secondary one and indistinguishable from unity. The overall isotope effect is predicted to be a maximum in the limit of $k_{-1} >> k_2$ (i.e., fully reversible complex formation) and reduce in magnitude as k_{-1} decreases and (or) k_2 increases. Only a secondary isotope effect should be obtained in the limit of $k_2 >> k_{-1}$, where complex formation is fully rate determining. The data are consistent with an increase in the ratio k_2/k_{-1} with increasing substituent electron-withdrawing power, a trend which also manifests itself in the Arrhenius behaviour of the reactions of MeOH with **2a**, **2b**, and **2e**.

A reaction proceeding by a mechanism of the general type shown in Scheme 1 will exhibit a negative Arrhenius activation energy if the free energy of activation for the second step (in this case, proton transfer) is dominated by the entropic term, so that the enthalpy of the transition state is lower than that of the reactants. In addition, the first step must be reversible; i.e., reversion of the intermediate to reactants (k_{-1}) must be faster than its collapse to product (k_2) (31). If the opposite is true, then the first step is clearly the rate-determining step for reaction and the overall activation energy will be positive, of a value equal to or greater than that of diffusion (E_{diff}). The changeover from the situation where $k_{-1} >> k_2$ (E_a at the maximum negative value) to that where $k_{-1} << k$ (E_a at the maximum positive value) arises because the two reaction channels available to the intermediate have opposing entropic requirements (i.e., $\Delta S_{-1}^{\neq} > 0$ and $\Delta S_2^{\neq} < 0$) and the enthalpic barrier for product formation is small. Provided that a large enough temperature range can be spanned experimentally, the Arrhenius plot for a situation of this type should thus be bell shaped, with the region of the apex in the plot corresponding to the temperature range where k_{-1} is comparable to k_2 (34, 36). In the present case where the second step involves proton transfer, the primary isotope effect on k_{obs} would be predicted to decrease with decreasing temperature from its maximum value at the high-temperature limit (i.e., where $k_{-1} >> k_2$),

[3] Also, R. Boukherroub, C.J. Bradaric, C. Cserti, and W.J. Leigh. To be published.

© 1997 NRC Canada

Can. J. Chem. Downloaded from www.nrcresearchpress.com by 91.121.58.235 on 09/08/12
For personal use only.

reducing to a secondary effect as k_2 overtakes k_{-1} in magnitude.

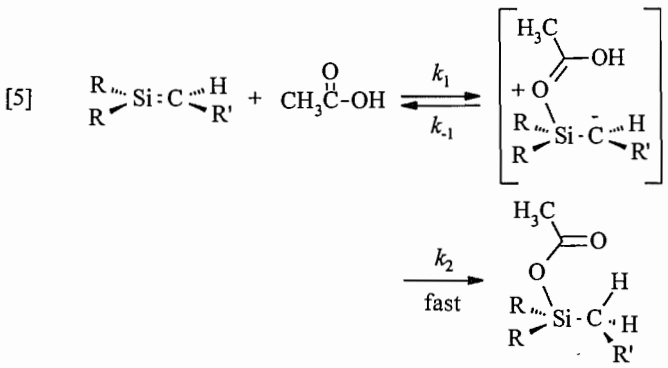
The Arrhenius plot for reaction of **2e** with methanol (Fig. 3) shows precisely this behaviour, exhibiting an apparent negative activation energy at temperatures above ~13°C and distinct curvature over the −20–13°C temperature range as the rate of product formation (k_2) approaches and then surpasses that of reversion of the complex to reactants. The less negative value of the high-temperature E_a observed for this compound compared to those for **2a,b** probably results from the fact that complex formation is not fully reversible over the limited "high-temperature" range examined. In the case of **2a**, and more so with **2b**, k_{-1} is proportionately larger than k_2 over our high-temperature range, resulting in larger negative values of the apparent activation energy. Silene **2e** exhibits no significant deuterium isotope effect at 23°C, because this temperature is within the range where the rate constant is starting to be dominated by that of complex formation. We have not measured k_H/k_D at higher temperatures for this derivative, but as Fig. 3 illustrates, the deuterium kinetic isotope effect on the reaction of the parent compound (**2a**) with methanol increases as predicted with increasing temperature. The difference in the slopes of these two lines is significant at the 95% confidence level.

The relative placement of the Arrhenius plots shown in Fig. 3 for **2e**, **2a**, and **2b** can also be explained simply in terms of a successive decrease in the magnitude of k_2/k_{-1} throughout the series **2e** > **2a** > **2b**, as the trend in the isotope effects suggests. One might also expect the rate constant for complex formation (k_1) to decrease in the same order, provided that it is not diffusion controlled; this would contribute to the relative placement of the Arrhenius plots in the same way as the proposed variation in k_2/k_{-1}. Unfortunately, determination of k_1 for these compounds would require rate constant measurements at temperatures that are considerably below the present capability of our system. Given the placement of the −20°C point in relation to the apex of the plot, the measured value of k_{obs} for **2e** at −20°C (~ 2.2×10^9 M^{-1} s^{-1}) is expected to be a factor of 2–3 lower than the actual value of k_1 for this compound at this temperature. This suggests that $k_1 \sim 5 \times 10^9$ M^{-1} s^{-1}, a value very close to the diffusional rate constant (k_{diff} ~ 1×10^{10} M^{-1} s^{-1}), calculated using the modified Debye equation ($k_{diff} = 8RT/3000\eta$) and a value of η extrapolated from published temperature–viscosity data (26). Given the assumptions inherent in the Debye treatment, we conclude that formation of the methanol complex of **2e** is subject to at most a small barrier in excess of that of diffusion. The fact that the low-temperature data for the three compounds are clearly not converging to a single line suggests that k_1 is somewhat sensitive to substituent, and provides a better indication that, in general, the rate constant for complex formation is lower than that of diffusion.

The observed rate constant for reaction of **2a** with MeOH is about a factor of two higher in hexane than in acetonitrile, which is somewhat surprising since the more polar solvent might be expected to enhance reactivity through stabilization of the complex relative to reactants. However, the fact that the apparent E_a is less negative in acetonitrile than in hexane suggests that the opposite is true, probably as a result of weak Lewis acid–base complexation between the nitrile solvent and the silene.

Acetic acid invariably reacts with silenes with clean overall second-order kinetics, and rate constants that are generally larger than those for reaction with methanol (14, 15, 19). However, the reaction does not exhibit an isotope effect distinguishable from unity and, with **2a**, it exhibits a small positive Arrhenius activation energy (16). In this case, the carbonyl oxygen is the likely site of bonding to silicon, in which case proton transfer would occur via a six-membered transition state. The data are compatible with a stepwise mechanism analogous to that for alcohol additions, but with complex formation being fully rate determining. Complex formation should be slower with HOAc than MeOH because of its lower nucleophilicity (as estimated from the pK_b's in acetonitrile (46)), while proton transfer would clearly be expected to be much faster. However, it is difficult to rule out a concerted mechanism in this case since little isotope effect would be expected for such a strongly exothermic reaction.

The Hammett ρ-value of +0.17 observed for the reactions of **2a–e** with HOAc at 23°C indicates the reaction to be relatively insensitive to polar factors, a result which seems more consistent with a concerted addition mechanism. However, the fact that the Arrhenius activation energy for addition to the most reactive compound (**2e**) is *higher* than that of **2a** indicates otherwise. As mentioned above, the full Arrhenius plot is expected to be bell shaped, with an extended temperature region where the mechanistic changeover occurs from rate-determining proton transfer (at high temperatures) to rate-determining complex formation (at low temperatures). The smaller apparent activation energy observed for **2a** may result

[5] 

simply from the fact that the temperature range monitored is within that over which reversion of the complex to reactants is still marginally competitive with collapse to product. With **2e**, a larger k_1 and larger k_2/k_{-1} ratio would result in a shift in the "peak" of the Arrhenius plot to higher temperatures (as is observed for MeOH addition). Thus, over the temperature range monitored for the two compounds, we are simply observing the region of steeper temperature dependence of k_{obs} in the case of **2e**, compared to the situation with **2a**. If this explanation is correct, then the measured Arrhenius parameters for **2e** ($E_a = 3.6 \pm 0.5$; log A = 12.0 ± 0.4; $\Delta S^{\neq}_{23C} = -6 \pm 2$ cal deg^{-1} mol^{-1}) more closely reflect those for formation of its complex with HOAc than do those for **2a** ($E_a = 1.9 \pm 0.2$; log $A = 10.5 \pm 0.2$; $\Delta S^{\neq}_{23C} = -12.5 \pm 0.9$ cal deg^{-1} mol^{-1}). The activation energy for reaction of **2e** is significantly higher than that for diffusion ($E_a = 1.8 \pm 0.4$; log $A = 11.6 \pm 0.5$), indicating the presence of a small enthalpic barrier for complex formation. The data of Fig. 4 indicate that the sensitivity

© 1997 NRC Canada

of the overall rate constant for HOAc addition to ring substituents increases at higher temperatures, where reversibility of complex formation is a more important contributor to the magnitude of k_{obs}.

Summary and conclusions

The effects of ring substituents on the rate constants, deuterium kinetic isotope effects, and Arrhenius parameters for addition of aliphatic alcohols to 1,1-diphenylsilene are most easily explained in terms of a mechanism involving fast, reversible formation of a zwitterionic silene–alcohol complex, followed by rate-limiting proton transfer from oxygen to carbon (Scheme 1). Because the Arrhenius activation energies for the reaction with methanol are consistently negative, little quantitative information on the enthalpies and entropies of activation for the individual steps in the sequence can be obtained. Nevertheless, the variation in Arrhenius behaviour and isotope effect as a function of substituent indicates that electron-withdrawing substituents at silicon increase both the rate at which the complex is formed and the relative rates of its collapse to alkoxysilane product and reversion to starting materials. In extreme cases, this results in a change in the identity of the slower step from proton transfer to complex formation over the temperature range studied (−20–50°C), allowing observation of the bell-shaped Arrhenius plot that is predicted for a mechanism of this type.

Addition of acetic acid, which yields the corresponding acetoxyaryldimethylsilane (17), proceeds with overall rate constants that are similar in magnitude to those for methanol addition but vary less with substituent ($\rho = +0.17 \pm 0.02$). These reactions exhibit isotope effects indistinguishable from unity and positive Arrhenius activation energies, consistent with complex formation being rate determining. The activation energy for reaction *increases* with increased silene reactivity, which is most easily explained in terms of the stepwise mechanism. Our results indicate there to be a small but significantly higher enthalpic barrier to complex formation than is the case for methanol addition.

Further studies of the effects of substituents on the reactivity of the Si=C bond are in progress in our laboratory.

Experimental

NMR spectra were recorded in deuteriochloroform and are referenced to tetramethylsilane. ^{1}H and ^{13}C NMR spectra were recorded on a Bruker AC200 spectrometer, while ^{29}Si NMR spectra were recorded on Bruker DRX500 or AC300 spectrometers in deuterated chloroform solution; all are referenced to tetramethylsilane. Ultraviolet absorption spectra were recorded on Hewlett–Packard HP8451 or Perkin Elmer Lambda 9 spectrometers. Low-resolution mass spectra were determined by GC–MS, using a Hewlett–Packard 5890II gas chromatograph equipped with a HP-5971A mass selective detector and DB-5 fused silica capillary column (30 m × 0.25 mm; Chromatographic Specialties, Inc). High-resolution desorption electron impact (DEI) mass spectra and Exact Masses were recorded on a VGH ZABE mass spectrometer. Exact Masses employed a mass of 12.000000 for carbon. Infrared spectra were recorded as thin films on a BioRad FTS-40 FTIR spectrometer and are reported in wave numbers (cm^{-1}).

Analytical gas chromatographic analyses were carried out using a Hewlett–Packard 5890 gas chromatograph equipped with conventional heated splitless injector, a flame ionization detector, a Hewlett–Packard 3396A integrator, and a DB1701 megabore capillary column (15 m × 0.53 mm; Chromatographic Specialties, Inc.). Semi-preparative gas chromatographic separations were carried out using a Varian 3300 gas chromatograph equipped with a thermal conductivity detector and a metal column (3% OV 101 on Chromosorb W, HP 80/100; 6 ft × 0.25 in; Chromatographic Specialties, Inc.).

Acetonitrile (BDH or Caledon Reagent) was refluxed over calcium hydride (Fisher) for several days, distilled under dry nitrogen, and then cycled three times through a 1 in. × 6 in. column of neutral alumina (Aldrich) that had been activated by heating under vacuum (ca. 0.05 Torr; 1 Torr = 133.3 Pa) at 320°C for 10 h with periodic shaking. Methanol (Sigma Aldrich HPLC; <0.05% H_2O) and *tert*-butyl alcohol (Sigma Aldrich HPLC; <0.05% H_2O) were stored over activated 4 Å molecular sieves. Hexane (EM Science Omnisolv), glacial acetic acid (Caledon Reagent), and deuterated reagents (Isotec, Inc.) were used as received from the suppliers.

The 1,1-diarylsilacyclobutanes **1b–1e** were prepared from 1,1-dichlorosilacyclobutane and the appropriate aryl magnesium bromide, according to the published method for **1a** (17, 25). The only significant variation in procedure was the reaction time, which decreased from 8 h for **1b** to 5 h for **1e**. The diarylsilacyclobutanes were obtained as colourless oils, in yields of 50–90% after purification by column chromatography on silica gel. Each contained <0.01% of the corresponding 1,1-biaryl derivative as determined by capillary gas chromatography. Spectral and analytical data for the diarylsilacyclobutanes are listed below.

*1,1-Di-(4-methylphenyl)silacyclobutane (**1b**)*: IR: 3067 (s), 3035 (s), 3013 (s), 2990 (s), 1603 (s), 1501 (s), 1394 (s), 1121 (s), 1081 (s), 854 (s), 716 (s), 634 (s); ^{1}H NMR, δ (ppm): 1.45 (t, 8.2 Hz, 4 H), 2.23 (p, 8.4 Hz, 2H), 2.36 (s, 6H), 7.20 (d, 7.8 Hz, 4H), 7.50 (d, 7.7 Hz, 8H); ^{13}C NMR, δ (ppm): 14.0, 18.3, 21.7, 128.8, 133.0, 134.6, 139.6; ^{29}Si NMR, δ (ppm): 6.51; MS, *m/e* (*I*): 252 (15), 226 (22), 224 (100), 211 (12), 209 (48), 160 (10) 119 (8). Exact Mass, calcd. for $C_{17}H_{20}Si$: 252.1334; found: 252.1346.

*1,1-Di-(4-fluorophenyl)silacyclobutane (**1c**)*: IR: 2971 (m), 2928 (s), 2875 (m), 1588 (s), 1500 (s), 1390 (m), 1236 (s), 1162 (s), 1123 (s), 1109 (s), 855 (s), 826 (s), 670 (s); ^{1}H NMR, δ (ppm): 1.46 (t, 8.3 Hz, 4H), 2.23 (p, 8.3 Hz, 2H), 7.08 (d, 8.7 Hz, 4H), 7.55 (d, 8.7 Hz, 4H); ^{13}C NMR, δ (ppm): 14.1, 18.1, 115.3, 131.7, 136.5, 164.2; ^{19}F NMR, δ (ppm): −110.1 (s); ^{29}Si NMR, δ (ppm): 6.60; MS, *m/e* (*I*): 260 (5), 233 (20), 232 (100), 231 (43), 219 (20), 217 (62), 183 (8), 165 (20), 164 (6), 152 (9), 151 (18), 150 (14), 123 (40), 75 (6). Exact Mass, calcd. for $C_{15}H_{14}SiF_2$: 260.0833; found: 260.0852.

*1,1-Di-(4-chlorophenyl)silacyclobutane (**1d**)*: IR: 2971 (m), 2927 (m), 1579 (s), 1483 (m), 1381 (m), 1121 (m), 1084 (s), 1015 (m), 853 (s), 713 (m), 677 (m); ^{1}H NMR, δ (ppm): 1.47 (t, 8.2 Hz, 4 H), 2.25 (p, 8.3 Hz, 2H), 7.37 (d, 8.2 Hz, 4H), 7.50 (d, 8.2 Hz, 8H); ^{13}C NMR, δ (ppm): 13.9, 18.2, 128.4, 134.2, 135.8, 136.3; ^{29}Si NMR, δ (ppm): 6.95; MS, *m/e* (*I*): 294 (8), 292 (10), 268 (15), 266 (70), 264 (100), 253 (18), 251 (45),

© 1997 NRC Canada

Can. J. Chem. Downloaded from www.nrcresearchpress.com by 91.121.58.235 on 09/08/12
For personal use only.

250 (40), 231 (10), 229 (25), 165 (20), 152 (10), 141 (15), 139 (45), 103 (8), 89 (8), 77 (8),65 (28), 63 (78). Exact Mass, calcd. for $C_{15}H_{14}SiCl_2$: 292.0242; found: 292.0239.

*1,1-Di-(4-trifluoromethylphenyl)silacyclobutane (**1e**)*: IR: 2974 (s), 2931 (s), 1392 (s), 1324 (s), 1166 (s), 1104 (s), 1060 (s), 1019 (s), 827 (s), 704 (s); ^{1}H NMR, δ (ppm): 1.56 (t, 8.3 Hz, 4 H), 2.31 (p, 8.3 Hz, 2H), 7.66 (d, 8.0 Hz, 4H), 7.72 (d, 8.0 Hz, 4H); ^{13}C NMR, δ (ppm): 13.6, 18.4, 124.1, 124.7, 132.0, 134.7, 140.4; ^{19}F NMR, δ (ppm): −62.7 (s); ^{29}Si NMR: δ (ppm): 7.73; MS, *m/e* (*I*): 360 (10), 341 (12), 333 (22), 332 (100), 319 (20), 317 (6), 263 (15), 251 (10), 173 (15), 140 (30). Exact Mass, calcd. for $C_{17}H_{14}SiF_6$: 360.0769; found: 360.0766.

Steady-state photolysis experiments were carried out using a Rayonet reactor containing five RPR2537 lamps. Quartz tubes (25 cm × 1.2 cm) containing hexane solutions (ca. 20 mL) of **1b–e** (0.007–0.013 M) and 0.05 M methanol were sealed with rubber septa and irradiated for 70–110 min, resulting in 40–75% conversion of **1** to a single detectable product in each case. The volatiles were stripped from the photolysates on the rotary evaporator, and the products were isolated by semipreparative GC. They were identified as **3b–e** on the basis of the following data.

*Di-(4-methylphenyl)methoxymethylsilane (**3b**)*: IR: 2959 (s), 2927 (s), 2860 (m), 1601 (m), 1550 (m), 1254 (m), 1112 (m), 1088 (m), 1006 (m), 979 (m); ^{1}H NMR, δ (ppm): 0.59 (s, 3H), 2.35 (s, 6H), 3.51 (s, 3H), 7.20 (d, 7.7 Hz, 4H), 7.49 (d, 7.8 Hz, 4H); ^{13}C NMR, δ (ppm): −3.4, 21.5, 46.2, 128.7, 133.3, 134.8, 139.8; ^{29}Si NMR, δ (ppm): −0.96; MS, *m/e* (*I*): 256 (6), 242 (21), 241 (100), 212 (5), 211 (23), 165 (11), 131 (11), 119 (13), 105 (8), 93 (6), 91 (7), 65 (5). Exact Mass, calcd. for $C_{16}H_{20}OSi$: 256.1283; found: 256.1287.

*Di-(4-fluorophenyl)methoxymethylsilane (**3c**)*: IR: 2962 (s), 2938 (s), 2835 (m), 1588 (s), 1499 (s), 1388 (s), 1110 (s), 878 (s), 824 (s), 756 (s); ^{1}H NMR, δ (ppm): 0.59 (s, 3H), 3.50 (s, 3H), 7.04 (d, 8.7 Hz, 4H), 7.50 (d, 8.8 Hz, 4H); ^{13}C NMR, δ (ppm): −3.6, 46.1, 115.0, 131.1,136.3, 164.1; ^{29}Si NMR, δ (ppm): −2.49; MS, *m/e* (*I*): 264 (10), 249 (100), 220 (8), 219 (42), 169 (8), 139 (16), 123 (11), 109 (6), 59 (12). Exact Mass, calcd. for $C_{14}H_{14}F_2OSi$: 264.0782; found: 264.0782.

*Di-(4-chlorophenyl)methoxymethylsilane (**3d**)*: IR: 2959 (s), 2928 (s), 2850 (m), 1602 (m), 1550 (m), 1260 (m), 1110 (m), 1088 (m), 1006 (m), 969 (m); ^{1}H NMR, δ (ppm): 0.62 (s, 3H), 3.52 (s, 3H), 7.38 (d, 8.3 Hz, 4H), 7.50 (d, 8.4Hz, 4H); ^{13}C NMR, δ (ppm): −3.6, 51.2, 128.3, 134.2, 135.7, 136.3; ^{29}Si NMR, δ (ppm): −2.67; MS, *m/e* (*I*): 298 (11), 296 (16), 285 (14), 284 (13), 283 (70), 282 (20), 281 (100), 253 (20), 251 (30), 185 (13), 157 (7), 155 (20), 152 (13), 139 (11), 125 (7), 91 (7), 75 (9), 65 (9), 63 (21), 59 (22). Exact Mass, calcd. for $C_{14}H_{14}Cl_2OSi$: 296.0191; found: 296.0185.

*Di-(4-trifluoromethylphenyl)methoxymethylsilane (**3e**)*: IR: 2959 (s), 2929 (s), 2841 (m), 1392 (m), 1325 (s), 1269 (m), 1168 (s), 1132 (s), 1088 (s), 1061 (s), 1019 (s), 909 (m), 813 (s), 760 (s), 735 (s), 703 (m); ^{1}H NMR, δ (ppm): 0.68 (s, 3H), 3.55 (s, 3H), 7.62 (d, 7.8 Hz, 4H), 7.66 (d, 7.7 Hz, 4H); ^{13}C NMR, δ (ppm): −3.9, 51.3, 124.6, 131.8, 132.1, 134.5, 139.8; ^{29}Si NMR, δ (ppm): −2.83; MS, *m/e* (*I*): 364 (5), 350 (21), 349 (100), 320 (7), 319 (34), 271 (7), 252 (11), 219 (19), 189 (22), 173 (8), 159 (6), 127 (12), 126 (27), 59 (15). Exact Mass, calcd. for $C_{16}H_{14}OSiF_6$: 364.0718; found: 364.0709.

Nanosecond laser flash photolysis experiments employed the pulses (248 nm; ca. 16 ns; 70–120 mJ) from a Lumonics 510 excimer laser, filled with F_2/Kr/He mixtures, and a microcomputer-controlled detection system (47). The system incorporates a brass sample holder whose temperature is controlled to within 0.1°C by a VWR 1166 constant-temperature circulating bath. Solutions were prepared at concentrations such that the absorbance at the excitation wavelength (248 nm) was ca. 0.7 (0.004 M) and were flowed continuously through a 3 × 7 mm Suprasil flow cell connected to a calibrated 100 mL reservoir. Solution temperatures were measured with a Teflon-coated copper–constantan thermocouple that was inserted directly into the flow cell. Quenchers were added directly to the reservoir by microlitre syringe as aliquots of standard solutions. Rate constants were calculated by linear least-squares analysis of decay rate – concentration data (6–10 points), which spanned at least a factor of 5 (usually more than 1 order of magnitude) in the transient decay rate. Errors are quoted as twice the standard deviation obtained from the least-squares analysis in each case.

Acknowledgments

We wish to thank the Natural Sciences and Engineering Research Council of Canada for financial support, and the McMaster Regional Centre for Mass Spectrometry for exact mass determinations.

References

1. G. Raabe and J. Michl. Chem. Rev. **85**, 419 (1985).
2. M.G. Steinmetz. Chem. Rev. **95**, 1527 (1995).
3. A.G. Brook and M.A. Brook. Adv. Organomet. Chem. **39**, 71 (1996).
4. L.E. Gusel'nikov and M.C. Flowers. J. Chem. Soc. Chem. Commun. 864 (1967).
5. P. Boudjouk, J.R. Roberts, C.M. Golino, and L.H. Sommer. J. Am. Chem. Soc. **94**, 7926 (1972).
6. P. Boudjouk and L.H. Sommer. J. Chem. Soc. Chem. Commun. 54 (1973).
7. S. Nagase and T. Kudo. J. Chem. Soc. Chem. Commun. 363 (1983).
8. N. Wiberg. J. Organomet. Chem. **273**, 141 (1984).
9. A.G. Brook, K.D. Safa, P.D. Lickiss, and K.M. Baines. J. Am. Chem. Soc. **107**, 4338 (1985).
10. S. Nagase, T. Kudo, and K. Ito. *In* Applied quantum chemistry. *Edited by* V.H.J. Smith, H.F. Schaefer, and K. Morokuma. D. Reidel, Dordrecht. 1986. p. 249.
11. P.R. Jones and T.F. Bates. J. Am. Chem. Soc. **109**, 913 (1987).
12. M.G. Steinmetz, B.S. Udayakumar, and M.S. Gordon. Organometallics, **8**, 530 (1989).
13. M. Kira, T. Maruyama, and H. Sakurai. J. Am. Chem. Soc. **113**, 3986 (1991).
14. G.W. Sluggett and W.J. Leigh. J. Am. Chem. Soc. **114**, 1195 (1992).
15. W.J. Leigh and G.W. Sluggett. J. Am. Chem. Soc. **116**, 10468 (1994).
16. C.J. Bradaric and W.J. Leigh. J. Am. Chem. Soc. **118**, 8971 (1996).

© 1997 NRC Canada

Can. J. Chem. Downloaded from www.nrcresearchpress.com by 91.121.58.235 on 09/08/12
For personal use only.

17. W.J. Leigh, C.J. Bradaric, C. Kerst, and J.H. Banisch. Organometallics, **15**, 2246 (1996).
18. C. Kerst, C.W. Rogers, R. Ruffolo, and W.J. Leigh. J. Am. Chem. Soc. **119**, 466 (1997).
19. C. Kerst, R. Ruffolo, and W.J. Leigh. Organometallics, In press.
20. C. Kerst, R. Boukherroub, and W.J. Leigh. J. Photochem. Photobiol. A. In press.
21. Y. Apeloig and M. Karni. J. Am. Chem. Soc. **106**, 6676 (1984).
22. M. Elsheikh, N.R. Pearson, and L.H. Sommer. J. Am. Chem. Soc. **101**, 2491 (1979).
23. P. Jutzi and P. Langer. J. Organomet. Chem. **202**, 401 (1980).
24. W.J. Leigh, C.J. Bradaric, and G.W. Sluggett. J. Am. Chem. Soc. **115**, 5332 (1993).
25. N. Auner and J. Grobe. J. Organomet. Chem. **188**, 25 (1980).
26. R.C. Weast (*Editor*). CRC handbook of chemistry and physics. 75th ed. CRC Press, Boca Raton, Fla. 1995. pp. 6–241.
27. A. Sekiguchi and W. Ando. Organometallics, **6**, 1857 (1987).
28. N. Auner and J. Grobe. J. Organomet. Chem. **197**, 147 (1980).
29. N. Wiberg, G. Wagner, G. Muller, and J. Riede. J. Organomet. Chem. **271**, 381 (1984).
30. C. Kerst, M. Byloos, and W.J. Leigh. Can. J. Chem. **75**, 975 (1997).
31. V.D. Kiselev and J.G. Miller. J. Am. Chem. Soc. **97**, 4036 (1975).
32. A.A. Gorman, G. Lovering, and M.A.J. Rodgers. J. Am. Chem. Soc. **101**, 3050 (1979).
33. N.J. Turro, G.F. Lehr, J.A. Butcher, R.A. Moss, and W. Guo. J. Am. Chem. Soc. **104**, 1754 (1982).
34. I.R. Gould, N.J. Turro, J. Butcher, Jr., C. Doubleday, Jr., N.P. Hacker, G.F. Lehr, R.A. Moss, D.P. Cox, W. Guo, R.C. Munjal, L.A. Perez, and M. Fedorynski. Tetrahedron. **41**, 1587 (1985).
35. K.N. Houk, N.G. Rondan, and J. Mareda. Tetrahedron, **41**, 1555 (1985).
36. R.A. Moss, W. Lawrynowicz, N.J. Turro, I.R. Gould, and Y. Cha. J. Am. Chem. Soc. **108**, 7028 (1986).
37. R.A. Moss. Acc. Chem. Res. **22**, 15 (1989).
38. J.E. Baggott, M.A. Blitz, H.M. Frey, and R. Walsh. J. Am. Chem. Soc. **112**, 8337 (1990).
39. M.A. Blitz, H.M. Frey, F.D. Tabbutt, and R. Walsh. J. Phys. Chem. **94**, 3294 (1990).
40. Y. Chen, A. Rauk, and E. Tschuikow-Roux. J. Phys. Chem. **95**, 9900 (1991).
41. J.E. Jackson, N. Soundararajan, M.S. Platz, M.P. Doyle, and M.T.H. Liu. Tetrahedron Lett. **30**, 1335 (1989).
42. H. Mayr, R. Schneider, and U. Grabis. J. Am. Chem. Soc. **112**, 4460 (1990).
43. M. Patz, H. Mayr, J. Bartl, and S. Steenken. Angew. Chem. Int. Ed. Engl. **34**, 490 (1995).
44. K.M. Baines and W.G. Stibbs. Adv. Organomet. Chem. **39**, 275 (1996).
45. J.W.F.L. Seetz, B.J.J. Van De Heisteeg, G. Schat, O.S. Akkerman, and F. Bickelhaupt. J. Org. Chem. **277**, 319 (1984).
46. K. Izutsu. Acid–base dissociation constants in dipolar aprotic solvents. IUPAC Chemical Data Series no. 35. Blackwell Scientific Publications, Oxford. 1990. p. 17.
47. W.J. Leigh, M.S. Workentin, and D. Andrew. J. Photochem. Photobiol. A: **57**, 97 (1991).

Can. J. Chem. Downloaded from www.nrcresearchpress.com by 91.121.58.235 on 09/08/12
For personal use only.

© 1997 NRC Canada

Solubility of anthracene in binary alcohol + alkoxyalcohol solvent mixtures. Comparison of observed versus predicted values based upon Mobile Order theory

Mary E.R. McHale, Karen S. Coym, Lindsay E. Roy, Carmen E. Hernández, and William E. Acree, Jr.

Can. J. Chem. Downloaded from www.nrcresearchpress.com by 91.121.58.235 on 09/08/12
For personal use only.

Abstract: Experimental solubilities are reported for anthracene dissolved in eight binary mixtures containing 2-isopropoxyethanol with 1-propanol, 2-propanol, 1-butanol, 2-butanol, 1-pentanol, 2-pentanol, 3-methyl-1-butanol, and 1-octanol at 25°C. Results of these measurements, along with previously published solubility data for anthracene in binary alcohol + alkoxyalcohol (2-methoxyethanol, 2-ethoxyethanol, 2-propoxyethanol, 2-butoxyethanol, 3-methoxy-1-butanol) solvent mixtures, are used to test the limitations and applications of expressions derived from Mobile Order theory. For the 50 different binary solvent systems considered, the derived expressions were found to provide reasonably accurate predictions for the observed anthracene solubility behavior, with the average absolute deviation between measured and predicted values being on the order of 3% or less. A single numerical value of K_{eq} = 5000 cm^3 mol^{-1} was assumed for all self-association and cross-association hydrogen-bond stability constants.

Key words: anthracene solubilities, alcohol solvents, solubility predictions, hydrogen-bonding, model.

Résumé : On a mesuré les solubilités expérimentales, à 25°C, de l'anthracène dans huit mélanges binaires formés de 2-isopropoxyéthanol + propan-1-ol, propan-2-ol, butan-1-ol, butan-2-ol, pentan-1-ol, pentan-2-ol, 3-méthylbutan-1-ol ou octan-1-ol. Utilisant les résultats de ces mesures, de concert avec les données de solubilité publiées antérieurement pour l'anthracène dans des mélanges binaires de solvants formés d'alcool + alkoxyalcool (2-méthoxyéthanol, 2-éthoxyéthanol, 2-propoxyéthanol, 2-butoxyéthanol, 3-méthoxybutan-1-ol), on évalue les limitations et les possibilités d'appliquer des expressions dérivées de la théorie de l'ordre mobile. Pour les 50 systèmes de solvants binaires considérés, on a trouvé que les expressions dérivées permettent de faire des prédictions assez correctes pour la solubilité de l'anthracène; la déviation absolue moyenne entre les valeurs mesurées et prédites sont de l'ordre de 3% ou moins. On a utilisé une seule valeur numérique, K_{eq} = 5000 cm^3 mol^{-1}, pour toutes les constantes de stabilité des liaisons hydrogènes auto-associées et à association croisée.

Mots clés : solubilités de l'anthracène, solvants alcooliques, prédictions des solubilités, liaison hydrogène, modèle.

[Traduit par la rédaction]

Introduction

Solid–liquid equilibrium data of organic nonelectrolyte systems are becoming increasingly important in the petroleum industry, particularly in light of present trends towards heavier feedstocks and known carcinogenicity/mutagenicity of many of the larger polycyclic aromatic compounds. Solubility data for a number of polycyclic aromatic hydrocarbons (i.e., anthracene and pyrene) and heteroatom polynuclear aromatics (i.e., carbazole, dibenzothiophene, and xanthene) have been published in the recent chemical literature (for listing of references see Acree (1–3)). Despite efforts by experimentalists and scientific organizations, both in terms of new experimental measurements and critically evaluated data compilations, there still exist numerous systems for which solubility data are not readily available.

To address this problem, researchers have turned to predictive methods as a means to generate desired quantities. Numerous equations have been suggested for predicting solute solubilities in binary solvent mixtures. For the most part, the predictive methods do provide fairly reasonable estimates for noncomplexing systems. There still remains, however, the need to develop better predictive expressions and mixing models to describe the more nonideal complexing systems believed to contain hydrogen-bonding solvent components. Hydrogen bonding that occurs in mixtures of alcohols is an example of specific interaction in that highly "preferential" contacts between proton-donor and proton-acceptor sites of neighboring alcohol molecules are established. The resulting H-bonds are labile. During their lifetime they confer a higher degree of "order" to the liquid solution. The order introduced in the liquid by the formation of H-bonds and the perpetual movement of the H-bonds constitute the basic foundations of Mobile Order theory (4–13).

Received March 14, 1997.

M.E.R. McHale, K.S. Coym, L.E. Roy, C.E. Hernández, and W.E. Acree, Jr.[1] Department of Chemistry, University of North Texas, Denton, TX 76203-5070, U.S.A.

[1] Author to whom correspondence should be addressed. Fax: (940) 565-4318. E-mail: acree@unt.edu

© 1997 NRC Canada

Can. J. Chem. Downloaded from www.nrcresearchpress.com by 91.121.58.235 on 09/08/12
For personal use only.

The thermodynamics of Mobile Order expresses the equilibrium condition in terms of time fractions for the time schedule of a given molecule, and not in terms of concentrations of various entities in the ensemble. Thus, in the case of alcohols and alkoxyalcohols one considers the time fraction $\gamma_{Ch:}$ and not the concentrations of the various *i*-mers in the ensemble (this does not mean that these *i*-mers do not exist, but their concentrations do not govern the thermodynamic probability). $\gamma_{Ch:}$ is the fraction of the time during which a given molecule of the ensemble is free from H-bonding. The given molecule does not possess the energy of the H-bond. But it is by no means the fraction of the time during which the molecule is free at both sides. A molecule bonded at one side is free from H-bonding only half of the time.

Ruelle et al. (6, 7, 14–17) have presented a very impressive set of comparisons between experimental and predicted solubilities for anthracene, naphthalene, pyrene (see also Powell et al. (18)), biphenyl, carbazole, benzil (see also Fletcher et al. (19)), *p*-benzoquinone, thianthrene (see also Fletcher et al. (20)), tricosane, octacosane, 10-nonadecanone, 11-heneicosanone, and 12-tricosanone in a wide range of both noncomplexing and complexing solvents to document the predictive ability of Mobile Order theory. More recently, Acree and co-workers successfully extended Mobile Order theory to binary alkane + alcohol (21), alcohol + alcohol (22–24) and alcohol + 2-alkoxyethanol (25) solvent mixtures. Derived expressions predicted anthracene solubilities in 35 binary alcohol + alcohol and 32 binary alcohol + 2-alkoxyethanol mixtures to within an overall average absolute deviation between predicted and observed mole fraction solubilities of about 1.6 and 3.0%, respectively. A single numerical value of $K_{Alcohol}$ = 5000 cm^3 mol^{-1} was assumed for the association constant of the nine monofunctional alcohols and of the four 2-alkoxyethanol cosolvents studied.

In the present communication, we expand the list of cosolvents studied to include branched alkoxyalcohols. Only linear 2–alkoxyalcohols were considered in the earlier comparison involving Mobile Order theory. Experimental solubilities are reported for anthracene dissolved in eight binary alcohol + 2-isopropoxyethanol solvent mixtures containing 1-propanol, 2–propanol, 1-butanol, 2-butanol, 1-pentanol, 2-pentanol, 3-methyl-1-butanol and 1-octanol at 25°C. Results of these measurements, combined with recently published anthracene solubility data for alcohol + 3-methoxy-1-butanol solvent mixtures (26), are used to further assess the limitations and applications of predictive expressions derived from Mobile Order theory.

Experimental methods

Anthracene (Acros, 99.9+%) was recrystallized several times from acetone. 2–Isopropoxyethanol (Aldrich, 99+%), 1-propanol (Aldrich, 99+%, anhydrous), 2-propanol (Aldrich, 99+%, anhydrous), 1-butanol (Aldrich, HPLC, 99.8%), 2-butanol (Aldrich, 99+%, anhydrous), 1-pentanol (Aldrich, 99+%), 2-pentanol (Acros, 99+%), 3–methyl-1-butanol (Aldrich, 99+%, anhydrous), and 1–octanol (Aldrich, 99+%, anhydrous) were stored over anhydrous sodium sulfate and molecular sieves before use. Gas chromatographic analysis showed solvent purities to be 99.5 mol% or better. Karl Fischer titrations gave water contents (mass/mass%) of <0.01% for the nine alcohols. Binary solvent mixtures were prepared by mass so that compositions could be calculated to ±0.0001 mole fraction.

Excess solute and solvent were placed in amber glass bottles and allowed to equilibrate in a constant temperature water bath at (25.0 ± 0.1)°C with periodic agitation for at least 3 days (often longer). Attainment of equilibrium was verified both by repetitive measurements after a minimum of 3 additional days and by approaching equilibrium from supersaturation by preequilibrating the solutions at a higher temperature. Aliquots of saturated anthracene solutions were transferred through a coarse filter into a tared volumetric flask to determine the amount of sample and were diluted quantitatively with methanol for spectrophotometric analysis at 356 nm on a Bausch and Lomb Spectronic 2000. Concentrations of the dilute solutions were determined from a Beer–Lambert law absorbance versus concentration working curve. Molar absorptivities of the nine standard solutions varied systematically with molar concentration, and ranged from about ε(L mol^{-1} cm^{-1}) = 7450 to ε(L mol^{-1} cm^{-1}) = 7150 for anthracene concentrations ranging from $C(M) = 6.75 \times 10^{-5}$ to $C(M) = 2.25 \times 10^{-4}$. Identical molar absorptivities were obtained for select anthracene standard solutions that contained up to 5 vol% of the neat alcohol cosolvents. Experimental molar concentrations were converted to (mass/mass) solubility fractions by multiplying by the molar mass of anthracene, volume(s) of volumetric flask(s) used, and any dilutions required to place the measured absorbances on the Beer–Lambert law absorbance versus concentration working curve, and then dividing by the mass of the saturated solution analyzed. Mole fraction solubilities were computed from (mass/mass) solubility fractions using the molar masses of the solute and solvent. Experimental anthracene solubilities in the eight binary solvent mixtures studied are listed in Table 1. Numerical values represent the average of between four and eight independent determinations, with the measured values being reproducible to within ±1.5%.

Results and discussion

In the case of an inert solute dissolved in a binary solvent mixture containing either two monofunctional self-associating alcoholic solvent components or containing a monofunctional self-associating alcohol + alkoxyalcohol, Mobile Order theory may take one of two different paths, depending upon how one models the hydrogen bonding. The simplest predictive treatment (22) expresses the volume fraction solubility of the solute ϕ_A^{sat}:

$$\begin{aligned}[1]\quad \ln \phi_A^{sat} = {} & \phi_B^\circ \ln (\phi_A^{sat})_B + \phi_C^\circ \ln (\phi_A^{sat})_C - 0.5\,[\ln (x_B^\circ V_B \\ & + x_C^\circ V_C) - \phi_B^\circ \ln V_B \\ & - \phi_C^\circ \ln V_C] + (V_A K_B \phi_B^\circ/V_B^2)(1 + K_B/V_B)^{-1} \\ & - [V_A K_B \phi_B^{\circ 2}/V_B^2](1 + \phi_B^\circ K_B/V_B)^{-1} \\ & + (V_A K_C \phi_C^\circ/V_C^2)(1 + K_C/V_C)^{-1} \\ & - [V_A K_C \phi_C^{\circ 2}/V_C^2](1 + \phi_C^\circ K_C/V_C)^{-1} \\ & + V_A \phi_B^\circ \phi_C^\circ (\delta_B' - \delta_C')^2 (RT)^{-1}\end{aligned}$$

in terms of the measured solubility data in both pure solvents,

© 1997 NRC Canada

Can. J. Chem. Downloaded from www.nrcresearchpress.com by 91.121.58.235 on 09/08/12
For personal use only.

Table 1. Experimental mole fraction solubilities of anthracene (x_A^{sat}) in binary alcohol (B) + 2-isopropoxyethanol (C) solvent mixtures at 25.0°C.

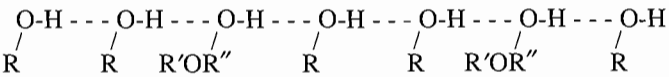
x_C°	x_A^{sat}
1-Propanol (B) + 2-isopropoxyethanol (C)	
0.0000	0.000591
0.0825	0.000739
0.1426	0.000856
0.3014	0.001190
0.3913	0.001401
0.5016	0.001684
0.7069	0.002229
0.8564	0.002595
1.0000	0.003093
2-Propanol (B) + 2-isopropoxyethanol (C)	
0.0000	0.000411
0.0720	0.000542
0.1441	0.000683
0.3008	0.001029
0.3990	0.001276
0.4866	0.001504
0.7178	0.002175
0.8512	0.002550
1.0000	0.003093
1-Butanol (B) + 2-isopropoxyethanol (C)	
0.0000	0.000801
0.0871	0.000985
0.1739	0.001147
0.3397	0.001498
0.4222	0.001687
0.5397	0.001964
0.7714	0.002580
0.8913	0.002878
1.0000	0.003093
2-Butanol (B) + 2-isopropoxyethanol (C)	
0.0000	0.000585
0.0903	0.000759
0.1634	0.000903
0.3412	0.001313
0.4474	0.001574
0.4873	0.001669
0.7570	0.002378
0.8622	0.002655
1.0000	0.003093
1-Pentanol (B) + 2-isopropoxyethanol (C)	
0.0000	0.001097
0.0991	0.001283
0.1956	0.001458
0.3904	0.001836
0.4832	0.002006
0.5774	0.002220
0.7838	0.002655
0.8851	0.002875
1.0000	0.003093
2-Pentanol (B) + 2-isopropoxyethanol (C)	
0.0000	0.000800
0.1088	0.001033
0.1839	0.001184
0.3794	0.001590
0.4744	0.001807

Table 1 (*concluded*).

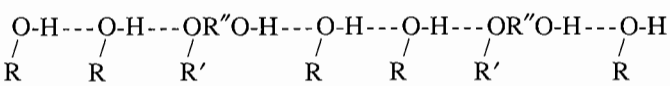
x_C°	x_A^{sat}
0.5883	0.002056
0.7790	0.002521
0.8806	0.002740
1.0000	0.003093
3-Methyl-1-butanol (B) + 2-isopropoxyethanol (C)	
0.0000	0.000727
0.1000	0.000911
0.1948	0.001094
0.3847	0.001480
0.4836	0.001703
0.5827	0.001953
0.7856	0.002442
0.8927	0.002753
1.0000	0.003093
1-Octanol (B) + 2-isopropoxyethanol (C)	
0.0000	0.002160
0.1495	0.002391
0.2593	0.002536
0.4700	0.002762
0.5790	0.002860
0.6758	0.002990
0.8584	0.003088
0.9123	0.003111
1.0000	0.003093

$(\phi_A^{sat})_B$ and $(\phi_A^{sat})_C$. (The various symbols used in eq. [1] and in subsequent expressions are defined in the Appendix.) The alcohol(s) and alkoxyalcohol(s) are permitted to retain their own individual chemical identity and are allowed to form homogeneous self-associated hydrogen bonds with surrounding solvent molecules of the same type. Formation of heterogeneous hydrogen bonds between two dissimilar solvent molecules is not allowed.

Monofunctional alcohols and alkoxyalcohols do form self-associated species, and there is no a priori experimental evidence or computational reason to preclude formation of heterogeneous B_iC_j complexes, particularly if we are using a single equilibrium constant to describe the self-association characteristics of every monofunctional alcohol and alkoxyalcohol. Such mixtures are characterized not only by the presence of long H-bonded chains of the type



wherein hydrogen bonding occurs through the hydroxyl group, but also by chains



involving hydrogen bonding through the ether linkage. From the point of view of Mobile Order theory, both scenarios lead

© 1997 NRC Canada

Can. J. Chem. Downloaded from www.nrcresearchpress.com by 91.121.58.235 on 09/08/12
For personal use only.

to extension of the H-bonded chain. The maximum possible number of hydrogen bonds formed in any given solution depends upon the chemical nature of the various compounds present. Monofunctional alcohols have one hydrogen "donor" site and the lone pairs on the oxygen atom provide two "acceptor" sites. Alkoxyalcohols have two additional donor sites provided by the lone electron pairs on the ether oxygen atom. Molar concentrations of the hydroxylic OH and ether O donor sites are equal in the case of alkoxyalcohols, and it is expected that hydrogen bonding should occur largely through the hydroxylic OH groups because of its much greater K_C stability constant. Calculated Mobile Order theory stability constants for hydrogen bond formation involving alcohols and ethers typically range between K_{eq} = 100 and 300 cm^3 mol^{-1} (12, 27). Close proximity of the OH and O functional groups may further encourage proton fixation at the OH "acceptor" site.

The fraction of time that the alcohol (B)

$$[2]\quad \gamma_{Bh:} = 1/[1 + K_B\,\phi_B/V_B + K_{BC}\,\phi_C/V_C + K_{OBC}\,\phi_C/V_C] = 1/[1 + K_B\,\phi_B/V_B + (K_{BC} + K_{OBC})\,\phi_C/V_C]$$

and 2-alkoxyethanol (C) molecules

$$[3]\quad \gamma_{Ch:} = 1/[1 + K_{CB}\,\phi_B/V_B + K_C\,\phi_C/V_C + K_{OC}\,\phi_C/V_C] = 1/[1 + K_{CB}\,\phi_B/V_B + (K_C + K_{OC})\,\phi_C/V_C]$$

are not involved in hydrogen-bond formation is given by eqs. [2] and [3], respectively. For convenience, two "pseudo" equilibrium/stability constants K^*_{BC} and K^*_C are now defined such that $K^*_{BC} = K_{BC} + K_{OBC}$ and $K^*_C = K_C + K_{OC}$. It can be readily shown that this set of conditions leads to the following expressions for the Gibbs energy

$$\begin{aligned}[4]\quad G = {} & n_A\,\mu^\circ_A + n_B\,\mu^\circ_B + n_C\,\mu^\circ_C + n_B\,RT\ln\gamma_{Bh:} \\ & + n_C\,RT\ln\gamma_{Ch:} + 0.5\,RT\,\{n_A\ln\phi_A + n_B\ln\phi_B \\ & + n_C\ln\phi_C + n_A\ln x_A + n_B\ln x_B + n_C\ln x_C\} \\ & + (n_AV_A + n_BV_B + n_CV_C)[\phi_A\,\phi_B\,(\delta'_A - \delta'_B)^2 \\ & + \phi_A\,\phi_C\,(\delta'_A - \delta'_C)^2 + \phi_B\,\phi_C\,(\delta'_B - \delta'_C)^2]\end{aligned}$$

and saturation solubility of a sparingly soluble solute

$$\begin{aligned}[5]\quad \ln\phi_A^{sat} = {} & \phi^\circ_B\ln(\phi_A^{sat})_B + \phi^\circ_C\ln(\phi_A^{sat})_C - 0.5\,[\ln(x^\circ_BV_B \\ & + x^\circ_CV_C) - \phi^\circ_B\ln V_B - \phi^\circ_C\ln V_C] \\ & - (V_A/V_B)\,\phi^\circ_B\,[\phi^\circ_B\,(K_B/V_B) + \phi^\circ_C\,(K^*_{BC}/V_C)]/[1 \\ & + \phi^\circ_B\,(K_B/V_B) + \phi^\circ_C\,(K^*_{BC}/V_C)] \\ & + (V_A\,K_B\,\phi^\circ_B/V^2_B)(1 + K_B/V_B)^{-1} \\ & - (V_A/V_C)\,\phi^\circ_C\,[\phi^\circ_B\,(K_{CB}/V_B) \\ & + \phi^\circ_C\,(K^*_C/V_C)]/[1 + \phi^\circ_B\,(K_{CB}/V_B) + \phi^\circ_C\,(K^*_C/V_C)] \\ & + (V_A\,K^*_C\,\phi^\circ_C/V^2_C)(1 + K^*_C/V_C)^{-1} \\ & + V_A\,\phi^\circ_B\,\phi^\circ_C\,(\delta'_B - \delta'_C)^2\,(RT)^{-1}\end{aligned}$$

dissolved in a binary alcohol + alkoxyalcohol solvent mixture.

Despite the complex appearance of eqs. [1] and [5], their application to solubilities in mixed solvents is relatively straightforward and is similar in concept to numerical examples presented previously (for example, see McCargar and Acree (28)). The quantities $(\phi_A^{sat})_B$ and $(\phi_A^{sat})_C$ are calculated from the measured mole fraction solubility of anthracene in the two neat solvents assuming that the excess molar volume (or, alternatively, the volume change upon mixing) is zero. These quantities, along with the molar volumes, modified solubility parameters, and assumed values for the self-association (K_B and K^*_C) and cross-association (K_{CB} and K^*_{BC}) hydrogen-bond stability constants are then used in eqs. [1] and (5) to calculate ϕ_A^{sat} at each different binary solvent composition.

Table 2 provides a summarized comparison between measured anthracene solubilities in 50 binary alcohol + alkoxyalcohol solvent systems and predicted values for both the self-association and cross-association treatments. Solubility data for the first 42 systems were taken from the published chemical literature (25, 26, 29–31). Solute and solvent properties used in these computations are tabulated in Table 3. Modified solubility parameters account for only nonspecific interactions and, in the case of the alcoholic and alkoxyalcohol cosolvents, the hydrogen bonding contributions have been removed. Numerical values of $\delta'_{solvent}$ for the monofunctional alcohols were obtained from published compilations (6–8), and were either estimated using known values for similar compounds or deduced by regressing solubility data of solid *n*-alkanes in organic solvents in accordance with the configurational entropic model of Huyskens and Haulait-Pirson (32). Any errors or uncertainties in the measured alkane data would naturally affect the calculated numerical values of $\delta'_{solvent}$, as would any shortcomings of the Huyskens and Haulait-Pirson model to back-calculate the observed mole fraction solubilities. Modified solubility parameters for the six alkoxyalcohols were estimated by the authors, and were calculated by adding an incremental ether-group contribution value to the known modified solubility parameters of alcohols of comparable molecular size. The numerical value of the ether-group contribution value to δ'_i was computed from differences between the known modified solubility parameters of dialkyl ethers and the corresponding *n*-alkane homomorph hydrocarbon, taking into account the length of the alkyl chain.

Careful examination of Table 2 reveals that Mobile Order theory provides reasonably accurate (though by no means perfect) predictions for the observed anthracene solubility behavior in all 50 binary alcohol + alkoxyalcohol solvent systems. Each system consists of anthracene solubility data measured at seven different solvent compositions spanning the entire mole fraction range, plus the experimental anthracene mole fraction solubilities in both neat solvents. Experimental solubility data were reproducible to within ±1.8% (or better), and cover up to a 9-fold range in anthracene mole fraction. Anthracene is considerably more soluble in 2-butoxyethanol (x_A^{sat} = 0.003 785 (31)) than in the smaller monofunctional alcohols (i.e., x_A^{sat} = 0.000 411 for 2-propanol and x_A^{sat} = 0.000 470 for 2-methyl-1-propanol (31)). Columns 2 and 3 of Table 2 correspond to the self-association (eq. [1]) and cross-association (eq. [5]) treatments, respectively. Both treatments provided reasonably accurate predictions; however, slightly lower deviations between observed and calculated values were obtained whenever the two cosolvents were assumed to form cross-associated hydrogen bonded chains. A single numerical value of K_{eq} = 5000 cm^3 mol^{-1} was assumed for all self-association and cross-association stability constants.

© 1997 NRC Canada

Can. J. Chem. Downloaded from www.nrcresearchpress.com by 91.121.58.235 on 09/08/12
For personal use only.

Table 2. Summarized comparison between experimental anthracene solubilities and predicted values based upon Mobile Order theory eqs. [1]) (with K_C*) and [5].

Solvent (B) + Solvent (C)	% Deviations[a] Eq. [1]	Eq. [5]
1-Propanol + 2-methoxyethanol	1.9	2.1
2-Propanol + 2-methoxyethanol	3.4	4.3
1-Butanol + 2-methoxyethanol	2.3	3.6
2-Butanol + 2-methoxyethanol	4.6	5.8
2-Methyl-1-propanol + 2-methoxyethanol	3.6	2.9
1-Pentanol + 2-methoxyethanol	2.3	3.4
3-Methyl-1-butanol + 2-methoxyethanol	+5.5	3.9
1-Octanol + 2-methoxyethanol	3.0	2.7
1-Propanol + 2-ethoxyethanol	1.7	−1.1
2-Propanol + 2-ethoxyethanol	1.1	−1.8
1-Butanol + 2-ethoxyethanol	1.7	1.5
2-Butanol + 2-ethoxyethanol	0.7	−3.1
2-Methyl-1-propanol + 2-ethoxyethanol	+2.6	1.6
1-Pentanol + 2-ethoxyethanol	+3.5	1.2
3-Methyl-1-butanol + 2-ethoxyethanol	+5.3	+2.6
1-Octanol + 2-ethoxyethanol	+3.4	2.4
1-Propanol + 2-propoxyethanol	+3.6	1.1
2-Propanol + 2-propoxyethanol	0.7	−2.2
1-Butanol + 2-propoxyethanol	+2.4	0.5
2-Butanol + 2-propoxyethanol	1.1	−2.5
2-Methyl-1-propanol + 2-propoxyethanol	+2.9	1.4
1-Pentanol + 2-propoxyethanol	+4.0	1.7
3-Methyl-1-butanol + 2-propoxyethanol	+6.3	+3.7
1-Octanol + 2-propoxyethanol	4.3	3.1
1-Propanol + 2-butoxyethanol	1.1	2.0
2-Propanol + 2-butoxyethanol	2.4	−4.7
1-Butanol + 2-butoxyethanol	+1.5	1.2
2-Butanol + 2-butoxyethanol	2.3	3.5
2-Methyl-1-propanol + 2-butoxyethanol	1.9	2.3
1-Pentanol + 2-butoxyethanol	+2.7	0.8
3-Methyl-1-butanol + 2-butoxyethanol	+5.1	2.7
1-Octanol + 2-butoxyethanol	+5.0	2.5
1-Propanol + 3-methoxy-1-butanol	+2.8	0.4
2-Propanol + 3-methoxy-1-butanol	2.6	−5.0
1-Butanol + 3-methoxy-1-butanol	+2.9	1.2
2-Butanol + 3-methoxy-1-butanol	+3.0	1.8
1-Pentanol + 3-methoxy-1-butanol	2.1	1.3
2-Pentanol + 3-methoxy-1-butanol	1.1	−1.6
3-Methyl-1-butanol + 3-methoxy-1-butanol	+5.9	3.3
4-Methyl-2-pentanol + 3-methoxy-1-butanol	+5.9	+3.2
1-Octanol + 3-methoxy-1-butanol	+5.2	2.9
2-Ethyl-1-hexanol + 3-methoxy-1-butanol	+2.3	0.5
1-Propanol + 2-isopropoxyethanol	+4.3	+1.6
2-Propanol + 2-isopropoxyethanol	1.4	2.4
1-Butanol + 2-isopropoxyethanol	0.4	−2.5
2-Butanol + 2-isopropoxyethanol	1.3	2.5
1-Pentanol + 2-isopropoxyethanol	+2.9	0.7
2-Pentanol + 2-isopropoxyethanol	2.3	2.5
3-Methyl-1-butanol + 2-isopropoxyethanol	+5.6	3.1
1-Octanol + 2-isopropoxyethanol	+3.9	1.5
Average absolute percent deviation	3.0	2.4

[a]% Deviation = $(100/N) \sum |\ln [(x_A^{sat})^{calc}/(x_A^{sat})^{exp}]|$. The algebraic sign indicates that all deviations were of the same sign.

Table 3. Solvent and solute properties used in Mobile Order predictions.

Component (*i*)	V_i (cm^3 mol^{-1})	δ_i' (MPa$^{1/2}$)[a]
1-Propanol	75.10	17.29
2-Propanol	76.90	16.80
1-Butanol	92.00	17.16
2-Butanol	92.4	16.60
2-Methyl-1-propanol	92.8	16.14
1-Pentanol	108.60	16.85
2-Pentanol	109.50	16.45
3-Methyl-1-butanol	109.8	16.00
4-Methyl-2-pentanol	127.25	15.85
1-Octanol	158.30	16.38
2-Ethyl-1-hexanol	157.09	16.60
2-Methoxyethanol	79.40	20.80
2-Ethoxyethanol	97.50	20.30
2-Propoxyethanol	114.92	19.80
2-Butoxyethanol	131.92	19.20
3-Methoxy-1-butanol	115.09	19.80
2-Isopropoxyethanol	116.2	19.30
Anthracene	150.0	

[a]Unless otherwise noted, tabulated δ_i' values are taken from a compilation given in Ruelle et al. (6–8) or are estimated using known values for similar alcohols. Modified solubility parameters for the six alkoxyalcohols were estimated by the authors, and were calculated by adding an incremental ether-group contribution value to the known modified solubility parameters of alcohols of comparable molecular size. The numerical value of the ether-group contribution value to δ_i' was computed from differences between the known modified solubility parameters of dialkyl ethers and the corresponding *n*-alkane homomorph hydrocarbon, taking into account the length of the alkyl chain.

In closing, we note that the expressions considered in this study assumed that the aromatic hydrocarbon solute, anthracene, did not form association complexes with either the monofunctional alcohol, alkoxyalcohol, or any of the presumed polymeric entities. Introduction of additional "curve-fit" association parameters for formation of anthracene–alcohol and anthracene–alkoxyalcohol molecular complexes would lead to reduced deviations between observed and calculated values. At this time, we do not feel that the slight reduction in percentage deviation necessarily warrants the increased calculational complexity whenever one realizes that it is possible to predict anthracene solubilities at all 350 binary solvent compositions (seven compositions for each of the 50 binary solvents) to within an overall average absolute deviation of less than 3% in the case of cross-association treatment.

Acknowledgements

Carmen Hernández thanks the University of North Texas and the U.S. Department of Education for support provided under the Ronald E. McNair Postbaccalaureate Achievement Program.

References

1. W.E. Acree, Jr. Polycyclic aromatic hydrocarbons in pure and binary solvents. IUPAC Solubility Data Ser. Vol. 54. Oxford University Press, Oxford, U.K. 1994.

© 1997 NRC Canada

2. W.E. Acree, Jr. Polycyclic aromatic hydrocarbons: binary nonaqueous systems: Part 1 (Solutes A–E). IUPAC Solubility Data Ser. Vol. 58. Oxford University Press, Oxford, U.K. 1995.
3. W.E. Acree, Jr. Polycyclic aromatic hydrocarbons: binary nonaqueous systems: Part 2 (Solutes F–Z). IUPAC Solubility Data Ser. Vol. 59. Oxford University Press, Oxford, U.K. 1995.
4. P.L. Huyskens and G.G. Siegel. Bull. Soc. Chem. Belg. **97**, 821 (1988).
5. G.G. Siegel, P.L. Huyskens, and G. Vanderheyden. Ber. Bunsen-Ges. Phys. Chem. **94**, 549 (1990).
6. P. Ruelle, C. Rey-Mermet, M. Buchmann, H. Nam-Tran, U.W. Kesselring, and P.L. Huyskens. Pharm. Res. **8**, 840 (1991).
7. P. Ruelle, M. Buchmann, H. Nam-Tran, and U.W. Kesselring. Int. J. Pharm. **87**, 47 (1992).
8. P. Ruelle, M. Buchmann, H. Nam-Tran, and U.W. Kesselring. Pharm. Res. **9**, 788 (1992).
9. P.L. Huyskens. J. Mol. Struct. **270**, 197 (1992).
10. K. Nelis, L. Van den Berge-Parmentier, and F. Huyskens. J. Mol. Liq. **67**, 157 (1995).
11. P.L. Huyskens, D.P. Huyskens, and G.G. Siegel. J. Mol. Liq. **64**, 283 (1995).
12. P.L. Huyskens and K. Seghers. J. Mol. Struct. **322**, 75 (1994).
13. P.L. Huyskens. J. Mol. Struct. **297**, 141 (1993).
14. P. Ruelle, M. Buchmann, and U.W. Kesselring. J. Pharm. Sci. **83**, 396 (1994).
15. P. Ruelle, E. Sarraf, and U.W. Kesselring. Int. J. Pharm. **104**, 125 (1994).
16. P. Ruelle, E. Sarraf, L. Van den Berge, K. Seghers, M. Buchmann, and U.W. Kesselring. Pharm. Acta Helv. **68**, 49 (1993).
17. P. Ruelle and U.W. Kesselring. J. Mol. Liq. **67**, 81 (1995).
18. J.R. Powell, D. Voisinet, A. Salazar, and W.E. Acree, Jr. Phys. Chem. Liq. **28**, 269 (1994).
19. K.A. Fletcher, S. Pandey, M.E.R. McHale, and W.E. Acree, Jr. Phys. Chem. Liq. **33**, 181 (1996).
20. K.A. Fletcher, M.E.R. McHale, J.R. Powell, K.S. Coym, and W.E. Acree, Jr. Phys. Chem. Liq. **34**, 41 (1997).
21. W.E. Acree, Jr., A.I. Zvaigzne, and S.A. Tucker. Fluid Phase Equilib. **92**, 223 (1994).
22. W.E. Acree, Jr. and A.I. Zvaigzne. Fluid Phase Equilib. **99**, 167 (1994).
23. A.I. Zvaigzne, J.R. Powell, W.E. Acree, Jr., and S.W. Campbell. Fluid Phase Equilib. **121**, 1 (1996).
24. J.R. Powell, M.E.R. McHale, A.-S.M. Kauppila, W.E. Acree, Jr., and S.W. Campbell. J. Solution Chem. **25**, 1001 (1996).
25. M.E.R. McHale, J.R. Powell, A.-S.M. Kauppila, W.E. Acree, Jr., and P.L. Huyskens. J. Solution Chem. **25**, 1089 (1996).
26. M.E.R. McHale, A.-S.M. Horton, S.A. Padilla, A.L. Trufant, N.U. De La Sancha, E. Vela, J.R. Powell, and W.E. Acree, Jr. J. Chem. Eng. Data, **42**, 54 (1997).
27. J.R. Powell, W.E. Acree, Jr., and P.L. Huyskens. Phys. Chem. Liq. In press.
28. J.W. McCargar and W.E. Acree, Jr. Phys. Chem. Liq. **17**, 123 (1987).
29. M.E.R. McHale, J.R. Powell, A.-S.M. Kauppila, and W.E. Acree, Jr. J. Chem. Eng. Data, **41**, 105 (1996).
30. M.E.R. McHale, J.R. Powell, A.-S.M. Kauppila, and W.E. Acree, Jr. J. Chem. Eng. Data, **41**, 272 (1996).
31. M.E.R. McHale, A.-S.M. Kauppila, J.R. Powell, and W.E. Acree, Jr. J. Chem. Thermodyn. **28**, 209 (1996).
32. P.L. Huyskens and M.C. Haulait-Pirson. J. Mol. Liq. **31**, 135 (1985).

Appendix: glossary of symbols

K_I Mobile Order stability (equilibrium) constant describing the homogeneous self-association of monofunctional alcohol I, where the concentration units are molarity.

K_{OC} Mobile Order stability (equilibrium) constant describing the hydrogen bonding of the hydroxylic proton on an alcohol (or 2-alkoxyethanol) solvent and of the ether O atom on an ether (or 2-alkoxyethanol) molecule.

K_{BC}, K_{CB} Mobile Order cross-association stability (equilibrium) constant describing the heterogeneous association of monofunctional alcohols B and C, where the concentration units are molarity.

V_i Molar volume of component *i*.

x_B°, x_C° Mole fraction compositions of the binary solvent mixture, calculated as if the solute were not present.

x_A^{sat} Mole fraction solubility of the solute.

Greek letters

$\gamma_{I:}$ Fraction of time that alcoholic solvent I is not involved in hydrogen bond formation.

δ_i' Modified solubility parameter of component *i*.

ϕ_B°, ϕ_C° Volume fraction compositions of the binary solvent mixture, calculated as if the solute were not present and assuming that the excess volume of mixing is zero.

ϕ_A^{sat} Volume fraction solubility of the solute, calculated assuming that the excess volume of mixing is zero.

ϕ_{solv} Volume fraction of solvent, calculated assuming that the excess volume is zero.

Can. J. Chem. Downloaded from www.nrcresearchpress.com by 91.121.58.235 on 09/08/12
For personal use only.

© 1997 NRC Canada

2-Trichloromethylimidazole. Condensation reactions with anions stabilized by carbonyl groups[1]

Jaime González, Arturo Pérez-Medrano, and Joseph M. Muchowski

Abstract: 2-Trichloromethylimidazole **2**, a stable but moisture-sensitive solid, is readily prepared by cyclization of the amidine **1** in trifluoroacetic acid (99+%). Compound **2** reacted with the enolates derived from 1,1-di- and monocarbonyl compounds to give the β-chlorovinyl carbonyl compounds **5** *a–c* and **6** *a*, *b*, respectively.

Key words: 2-trichloromethylimidazole, condensation reactions, mono- and dicarbonyl compounds.

Résumé : Le 2-trichlorométhylimidazole **2**, un solide stable mais sensible à l'humidité, est préparé facilement par cyclisation de l'amidine **1** dans l'acide trifluoroacétique (99+%). Le composé **2** réagit avec les énolates dérivés des composés 1,1-di- et mono-carbonyles pour donner les composés β-chlorovinylcarbonyles **5** *a–c* et **6** *a*, *b*, respectivement.

Mots clés : 2-trichlorométhylimidazole, réactions de condensation, composés mono- et dicarbonyles.

[Traduit par la rédaction]

Can. J. Chem. Downloaded from www.nrcresearchpress.com by 91.121.58.235 on 09/08/12
For personal use only.

We recently described improved, three-step syntheses of imidazole-2-carboxylic acid (**4***a*, Scheme 1) and its ethyl ester **4***b* by hydrolysis and ethanolysis, respectively, of 2-trichloromethylimidazole **2**, the trifluoroacetic acid induced cyclization product of the amidine **1** (1). Although **2** was not obtained pure, its transformation into **4***a* and **4***b*, as well as mass spectral data, left little doubt of its identity as the major cyclization product of **1**. We have now succeeded in isolating **2** in the pure state, have characterized it fully, and have studied some of its condensation reactions with anions stabilized by one or two carbonyl groups.

By the simple expedient of avoiding exposure to water during its formation and isolation (see Experimental), we were able to obtain substantial quantities of **2** (ca. 60% yield) as a white, crystalline solid that was indefinitely stable under anhydrous conditions. It is of interest that the base peak in the mass spectrum of **2** is *m/z* 148, which arises by loss of HCl from the molecular ion.[4] This ion most certainly corresponds to the diazafulvene **3**, a species that is likely to be an intermediate in the formation of **4***a* and **4***b* (2–4). The propensity of 6,6-dihalodiazafulvenes to react with a variety of nucleophiles by an addition–elimination sequence (2, 4) caused us to examine the reaction of **2** with diethyl sodiomalonate. As expected, the addition of a mixture of this anionic species (1 equiv.) and sodium hydride (2 equiv.) to a THF solution of **2** at room temperature gave the monochloromethylene malonate derivative **5***a* (65% yield). Compounds **5***b* and **5***c* were prepared in a similar manner from ethyl acetoacetate and acetylacetone, respectively. At low temperatures and in the presence of LDA (2 equiv.), **3** also reacted with the enolates of acetone and acetophenone to generate the β-chloroenones **6***a* and **6***b*.

An especially noteworthy feature of the nmr spectrum of **6***a* is that the olefinic proton appears at δ 7.50, ca. 1.3 ppm downfield from the corresponding proton in 4-chloro-3-buten-2-one (5). This dramatic deshielding must be caused by the imidazole nitrogen atoms, an effect that incidentally confirms the stereochemistry of **6***a* as depicted in Scheme 1. The olefinic proton of **6***b* is also found at considerably lower field (δ 8.20) than might have been predicted. Analogous, but even greater deshielding, has recently been observed for aliphatic hydrogens spatially close to the nitrogen atom of 1-azafulvenes (6).

Although the addition of various nucleophiles to C-6 of 1,3-diazafulvenes is known (4, 7), the use of stabilized carbanions in such reactions has not previously been reported. The products (**5**, **6**), which may well be of synthetic interest, would be quite challenging to prepare by other means.

Experimental

The melting points are not corrected. The ir spectra were recorded as solid dispersions in KBr unless otherwise indi-

Received April 29, 1997.

J. González[2] and A. Pérez-Medrano. Syntex S.A. de C.V., División de Investigación, Apartado Postal 272-CIVAC, 62500 Jiutepéc, Morelos, Mexico.
J.M. Muchowski.[3] Syntex Research, Institute of Organic Chemistry, 3401 Hillview Avenue, Palo Alto, CA 94304, U.S.A.

[1] Contribution no. 940 from the Syntex Institute of Organic Chemistry.

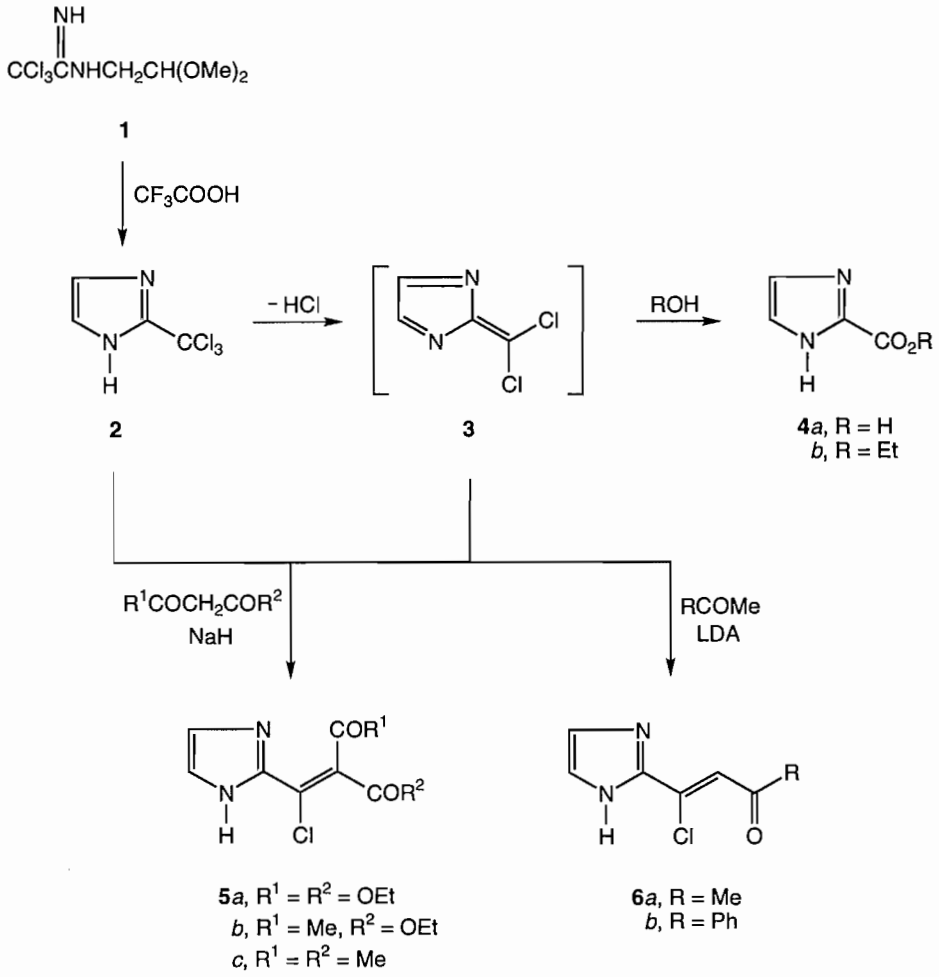
[2] This work was carried out by J.G. in partial fulfillment of the requirements for the degree of Licenciatura en Química at the Universidad Autónoma del Estado de México, Toluca.

[3] Author to whom correspondence may be addressed at Roche Bioscience, 3401 Hillview Avenue (R6E-151A), Palo Alto, CA 94304, U.S.A. Telephone: (415) 855-5200. Fax: (415) 354-2442. E-mail: joseph.muchowski@roche.com

[4] Isotopic ions at *m/z* 150 and 152 are also observed, as are three ions of lesser intensity at *m/z* 149, 151, and 153 stemming from the loss of ^{35}Cl and ^{37}Cl from the molecular ions (see Experimental).

© 1997 NRC Canada

Scheme 1.



cated. The ^{1}H nmr spectra were measured on a 200 MHz instrument as solutions in $CDCl_3$ unless otherwise indicated, and the chemical shifts are reported in ppm (δ) from internal tetramethylsilane. The low- and high-resolution mass spectra were obtained as previously described (6). The amidine **1** was synthesized as described in the previous publication (1).

2-Trichloromethylimidazole (2)

N-(2,2-Dimethoxy)ethyl-2,2,2-trichloroacetamidine (1, 5.0 g, 60 mmol) was added with stirring and cooling (−5°C) to trifluoroacetic acid (92 mL, 99+%) maintained in an argon atmosphere. The cooling bath was removed, stirring at room temperature was continued for 17 h, anhydrous toluene (100 mL) was added, and the solution was evaporated to dryness in vacuo. Toluene (100 mL) was added to the residue and the mixture was evaporated to dryness in vacuo. After an additional repetition of this process, a thick oil was obtained and taken up in anhydrous acetone at room temperature (argon atmosphere). Scratching the vessel walls with a spatula caused the crystallization of a white solid (6.3 g, 57% yield) that was indefinitely stable in the absence of moisture, mp 180°C (dec.); ^{1}H nmr (DMF-d_7) δ: 7.57 (s, 2H), 17.01 (br, 1H); ^{13}C nmr (DMF-d_7) δ: 119.14, 123.19 (2C), 134.05; MS (EI) *m/z*: 188, 186, 184 (2, 9, 8; M^+), 153 (6), 152 (11), 151 (35), 150 (64), 149 (54), 148 (100), 125 (8), 124 (6), 123 (53), 122 (9), 121 (85), 88 (20), 86 (61). Exact Mass calcd. for $C_4H_3{}^{35}Cl_3N_2$: 183.9362; found: 183.9357, 183.9365, 183.9359.

Ethyl 2-ethoxycarbonyl-3-chloro-3-(imidazol-2-yl)-2-propenoate (5*a*)

A solution of diethyl malonate (0.259 g, 1.62 mmol) in dry THF (5 mL) was added to a stirred suspension of sodium hydride (4.86 mmol, obtained by washing a suspension of 60% NaH in mineral oil with dry hexane) in anhydrous THF (7 mL) at 0°C. This mixture was cannulated into a stirred, room-temperature solution of **2** (0.300 g, 1.62 mmol) in anhydrous THF (15 mL) under argon. The mixture was stirred for 48 h and then partitioned between dichloromethane and water. The dried (Na_2SO_4) organic phase was evaporated in vacuo, and the residue was subjected to column chromatographic purification on silica gel using dichloromethane–methanol (95:5) to elute **5***a* as a solid (0.286 g, 65%), mp 99–101°C; ir ($CHCl_3$): 3184, 1732, 882 cm^{-1}; nmr δ: 1.34 (t, 6H, J = 7.1 Hz), 4.35 (q, 4H, J = 7.1 Hz), 7.26 (s, 2H), 12.90 (br, 1H). Anal. calcd. for $C_{11}H_{13}ClN_2O_4$: C 48.44, H 4.80, Cl 13.00, N 10.27; found: C 48.25, H 4.95, Cl 12.86, N, 10.18.

Ethyl 2-acetyl-3-chloro-3-(imidazol-2-yl)-2-propenoate (5*b*)

This compound was prepared in the same manner as described

© 1997 NRC Canada

Can. J. Chem. Downloaded from www.nrcresearchpress.com by 91.121.58.235 on 09/08/12
For personal use only.

for **5***a* except that the THF was removed in vacuo and the residue was purified by column chromatography to give a solid, mp 99–100°C; ir: 3142, 1712, 855 cm^{-1}; nmr δ: 1.38 (t, 3H, J = 7.2 Hz), 3.49 (s, 3H), 4.36 (q, 2H, J = 7.2 Hz), 7.26 (s, 2H), 12.01 (br, 1H). Exact Mass calcd. for $C_{10}H_{11}{}^{35}ClN_2O_3$: 242.0458; found: 242.0461. Anal. calcd. for $C_{10}H_{11}ClN_2O_3$: C 49.49, H 4.56, Cl 14.61, N 11.54; found: C 49.31, H 4.56, Cl 14.05, N 11.35.

3-Acetyl-4-chloro-4-(imidazol-2-yl)-3-buten-2-one (*5c*)
This compound was prepared by the method used for **5***b* except that the reaction was carried out at −35°C for 2 h and then at room temperature for 2 h. The solvent was removed in vacuo and the residue was purified by column chromatography as described for **5***a*. Compound **5***c* was obtained as a solid (64.5% yield), mp 81–82°C; ir: 3141, 1658, 882 cm^{-1}; nmr δ: 2.50 (s, 3H), 2.65 (s, 3H), 7.33 (s, 2H), 11.55 (br, 1H). Exact Mass calcd. for $C_9H_9{}^{35}ClN_2O_2$: 212.0353; found: 212.0353. Anal. calcd. for $C_9H_9ClN_2O_2$: C 50.83, H 4.26, Cl 16.67, N 13.17; found: C 50.89, H 4.24, Cl 15.36, N 12.85.

4-Chloro-*trans*-4-(imidazol-2-yl)-3-buten-2-one (*6a*)
Anhydrous acetone (0.12 mL, 0.095 g, 1.64 mmol) was added to a cooled (−23°C) solution of LDA (0.68 mL, 2.38 M in THF, 1.62 mmol) in anhydrous THF (5 mL). After 15 min, this solution was cannulated into a stirred solution of **2** (0.100 g, 0.54 mmol) in THF (5 mL) at −78°C (argon atmosphere). After 2 h at −78°C the solvent was removed in vacuo and the residue was purified by column chromatography as described for **5***a*. Compound **6***a* was obtained as a solid (0.021 g, 23%), mp 117–118°C; ir: 3152, 1650, 1595, 853 cm^{-1}; nmr δ: 2.41 (s, 3H), 7.19 (s, 2H). 7.50 (s, 1H). Exact Mass calcd. for $C_7H_7{}^{35}ClN_2O$: 170.0247; found: 170.0252. Anal. calcd. for $C_7H_7ClN_2O$: C 49.28, H 4.13, N 16.42; found: C 49.87, H 3.99, N 16.34.

Phenyl 2-chloro-*trans*-2-(imidazol-2-yl) vinyl ketone (*6b*)
This compound was prepared by the method described for **6***a*, except that the reaction temperature was −45°C. After purification by column chromatography **6***b* was obtained as a solid (52% yield), mp 161–162°C; ir: 3144, 1664, 1606, 840 cm^{-1}; nmr δ: 7.44–7.63 (m, 5H), 8.03–8.08 (m, 2H), 8.20 (s, 1H). Exact Mass calcd. for $C_{12}H_9{}^{35}ClN_2O$: 232.0403; found: 232.0403. Anal. calcd. for $C_{12}H_9ClN_2O$: C 61.94, H 3.89, Cl 15.23, N 12.04; found: C 61.90, H 3.71, Cl 15.82, N 11.87.

References

1. E. Galeazzi, A. Guzmán, J.L. Nava, Y. Liu, M.L. Maddox, and J.M. Muchowski. J. Org. Chem. **60**, 1090 (1995).
2. H. Kimoto, K.L. Kirk, and L.A. Cohen. J. Org. Chem. **43**, 4381 (1978); H. Kimoto and L.A. Cohen. J. Org. Chem. **44**, 2902 (1979).
3. K.H. Büchel and H. Erdmann. Chem. Ber. **109**, 1638 (1976).
4. G. Beck, F. Döring, H. Heitzer, and H. Holtschmidt. Ger. Offen. 2,545,326 (1976) (Chem. Abstr. **85**, 63071z (1976)); G. Beck, H. Heitzer, and K. Luerssen. Ger. Offen. 2,550,157 (1976); (Chem. Abstr. **87**, 85003x (1977)); G. Beck, K. Sasse, H. Heitzer, H. Eue, and R.R. Schmidt. Ger. Offen. 2,610,527 (1977) (Chem. Abstr. **88**, 6886g (1978)); G. Beck, K. Sasse, H. Heitzer, I. Hammann, and W. Brandes. Ger. Offen. 2,624,759 (1977) (Chem. Abstr. **88**, 10538m (1978)); G. Beck, K. Sasse, H. Heitzer, L. Eue, R.R. Schmidt, H. Scheinpflug, and W. Brandes. Ger. Offen. 2,634,053 (1978) (Chem. Abstr. **88**, 190831j (1978)); F. Seng, K. Sasse, G. Beck, and L. Eue. Ger. Offen. 2,646,142 (1978) (Chem. Abstr. **89**, 24310q (1978)); K. Sasse, G. Beck, L. Eue, and R.R. Schmidt. Ger. Offen. 2,646,143 (1978) (Chem. Abstr. **89**, 59887k (1978)); Ger. Offen. 2,646,144 (1978) (Chem. Abstr. 89, 109477z (1978)); G. Beck. Ger. Offen. 2,919,821 (1980) (Chem. Abstr. **94**, 156927j (1981)).
5. A.N. Nesmeyanov, K. Ahmed, L.V. Rybin, M.I. Rybinskaya, and Y.A. Ustynyuk. J. Organomet. Chem. **10**, 121 (1967).
6. S.L. Berthiaume, B.L. Bray, P. Hess, Y. Liu, M.L. Maddox, J.M. Muchowski, and M.E. Scheller. Can. J. Chem. **73**, 675 (1995).
7. W. Rohr, R. Swoboda, H.A. Staab. Chem. Ber. **101**, 3491 (1968).

Can. J. Chem. Downloaded from www.nrcresearchpress.com by 91.121.58.235 on 09/08/12
For personal use only.

© 1997 NRC Canada

Thermodynamics of mixtures containing the CO and OH groups. I. Estimation of the DISQUAC interchange coefficients for 1-alkanol + *n*-alkanone systems

Juan Antonio González

Can. J. Chem. Downloaded from www.nrcresearchpress.com by 91.121.58.235 on 09/08/12
For personal use only.

Abstract: 1-Alkanol + *n*-alkanone mixtures are treated in terms of the DISQUAC group contribution model, reporting the interaction parameters for hydroxyl–carbonyl contacts. The quasichemical interchange coefficients are independent of the compounds in the mixture; the dispersive interchange coefficients depend on the intramolecular environment of the hydroxyl and (or) carbonyl groups. Mixtures of a given 1-alkanol with isomeric ketones are characterized by the same first dispersive interaction parameter, which is constant from 2-pentanone. This type of system, when including an alcohol up to 1-pentanol, needs different dispersive enthalpic parameters depending on the symmetry of the ketone. In this case, such parameters are constant from 2-pentanone or 3-pentanone. A detailed comparison is presented between DISQUAC results and data available in the literature on vapor–liquid equilibria, VLE (including azeotropic data), molar Gibbs energies, G^E, molar excess enthalpies, H^E, solid–liquid equilibria, SLE, natural logarithms of activity coefficients, $\ln \gamma_i^\infty$, and partial molar excess enthalpies at infinite dilution, $H_i^{E,\infty}$. For 54 systems, the mean relative standard deviation in pressure is 0.018; for 61 systems, this magnitude in the case of the H^E is 0.059. It is noteworthy that the model yields good predictions over a very wide range of temperature for VLE and SLE. H^E is also reasonably well represented at different temperatures. Larger discrepancies are encountered, as usual, for partial molar quantities at infinite dilution.

Key words: liquids, mixtures, thermodynamic properties, group contributions.

Résumé : On a considéré les mélanges d'alcan-1-ols et de *n*-alcanones en termes du modèle DISQUAC de contribution de groupe et on rapporte les paramètres d'interaction pour les contacts hydroxyle–carbonyle. Les coefficients d'interchange quasichimique sont indépendants de la nature des composés présents dans le mélange; les coefficients d'interchange de dispersion dépendent de l'environnement intramoléculaire des groupes hydroxyle et (ou) carbonyle. Les mélanges d'un alcan-1-ol avec des cétones isomères sont caractérisés par le même paramètre initial d'interaction de dispersion qui est constant à partir de la pentan-2-one. Ces types de systèmes, jusqu'au pentan-1-ol, requièrent des paramètres enthalpiques de dispersion qui dépendent de la symétrie de la cétone. Dans ces cas, ces paramètres sont constants à partir des pentan-2-one ou pentan-3-one. On présente une comparaison détaillée des résultats DISQUAC et des données desponibles dans la littérature sur l'équilibre vapeur–liquide, EVL (y compris des données azéotropiques), les énergies molaires de Gibbs, G^E, les enthalpies molaires en excès, H^E, les équilibres solide–liquide, ESL, les logarithmes naturels des coefficients d'activité, $\ln \gamma_i^\infty$, et les enthalpies molaires partielles en excès à dilution infinie, $H_i^{E,\infty}$. Pour 54 systèmes, la déviation relative moyenne standard sur la pression est de 0,018; pour 61 systèmes, cette valeur pour H^E est de 0,059. Il est remarquable que pour un large éventail de températures le modèle conduise à de bonnes prédictions des EVL et ESL et que la valeur de H^E soit aussi bien représentée à diverses températures. Comme d'habitude, on observe de plus grandes différences avec les quantités molaires partielles à dilution infinie.

Mots clés : mélanges liquides, propriétés thermodynamiques, contributions de groupe.

[Traduit par la rédaction]

1. Introduction

In the framework of the DISQUAC (1, 2) group contribution model for representing thermodynamic properties, it has been shown that the hypothesis of considering structure-dependent interaction parameters is essential for practical purposes. As a matter of fact, it leads to improved predictions, mainly in the case of branched and cyclic molecules, and for the first members of homologous series.

Under this basic assumption, in recent years we have carried out detailed research on the ability of DISQUAC to represent a complete set of thermodynamic properties (vapor–liquid equilibria, VLE; liquid–liquid equilibria, LLE; solid–liquid equilibria; SLE; G^E, H^E, or heat capacities at constant pressure, as well as the related partial molar excess quantities at infinite dilution) of mixtures containing self-associated compounds. Thus, we have treated systems of alkanols: 1-alkanols (3–11), *sec*- (12) or *tert*-alkanols (13), cycloalkanols (14), or phenol (15), with organic solvents such as *n*-alkanes,

Received April 16, 1997.

J.A. González.[1] Departamento de Termodinámica y Física Aplicada, Universidad de Valladolid, 47071 Valladolid, Spain.

[1] Telephone: +34 83 42 31 37. Fax: +34 83 42 31 36 or +34 83 42 30 13. e-mail: jagl@wamba.cpd.uva.es

© 1997 NRC Canada

Table 1. Relative group increments for molecular volumes, $r_G = V_G/V_{CH_4}$, and areas, $q_G = A_G/A_{CH_4}$, calculated by Bondi's method (24) ($V_{CH_4} = 17.12 \times 10^{-6}$ m^3 mol^{-1}; $A_{CH_4} = 2.90 \times 10^{-5}$ m^2 mol^{-1}).

Group	r_G	q_G
CH_3-[a]	0.798 48	0.731 03
-CH_2-[a]	0.597 55	0.465 52
-OH[b]	0.469 63	0.503 45
-CO-[c]	0.683 44	0.551 74

[a]Reference 25.
[b]Reference 3.
[c]Reference 33.

cyclohexane, benzene, toluene, or CCl_4; that is, with inert, or non-associated but active, components (particularly, nonpolar but polarizable molecules).

In the same way, we have studied the problem of systems including two self-associated compounds, which together then also present a cross-association, showing that DISQUAC is indeed a reliable tool to represent such systems. Thus, we have focused our attention on binary mixtures containing two 1-alkanols (16), two linear monocarboxylic acids (17), or 1-alkanols and monocarboxylic acids (17). However, in this case, both dispersive (DIS) *and* quasichemical (QUAC) interchange coefficients are needed (17). In exchange, when the molecules in the mixture have the same functional group (OH or COOH), the dispersive approximation of DISQUAC is enough to represent the thermodynamic properties of the system under study (16, 17). It should be remarked here that binary mixtures containing two 1-alkanols have been successfully described in terms of Flory's theory (18).

On the other hand, VLE and H^E of ternary systems containing one or two 1-alkanols are usually well described on the basis of binary parameters only (16, 19).

As a continuation of these investigations, the aim of the present work is to report a complete DISQUAC treatment of alcoholic solutions including as second component a polar but non-associated compound, namely 1-alkanol + *n*-alkanone mixtures. In these systems the formation of O—H---O=C hydrogen-bonded complexes is vastly outweighed by the rupture of the alkanol–alkanol hydrogen bonds, ketone–ketone interactions, and by physical interactions between equal molecules (20–22), leading to H^Es that are positive over the entire composition range. Therefore, the complexes mentioned are much weaker than those created in 1-alkanol + linear monocarboxylic acid mixtures that are characterized, in many cases, by negative or s-shaped H^Es (17). Obviously, this means that the treatment of the actual systems should be more accessible in terms of a purely physical theory such as DISQUAC.

2. The DISQUAC model

2.1 Theory

In the framework of DISQUAC, mixtures of 1-alkanols with *n*-alkanones are regarded as possessing three types of surface: (*i*) type a, aliphatic (CH_3, CH_2 in ketones and alcohols); (*ii*) type h (OH in 1-alkanols); and (*iii*) type k (CO in *n*-alkanones).

The equations used to calculate G^E and H^E are the same as in other applications (3). The coordination number was chosen as reference value, that is, $z = 4$.

On the other hand, the solid–liquid equilibrium curve of a pure solid component 1 was calculated to the equation (23) according:

$$[1] \quad -\ln x_1 = (\Delta H_{m1}/R)[1/T - 1/T_{m1}] - (\Delta C_{pm1}/R)[\ln (T/T_{m1}) + (T_{m1}/T) - 1] + \ln \gamma_1$$

Table 2. Interchange energy coefficients, dispersive $C_{kh,l}^{DIS}$ and quasichemical $C_{kh,l}^{QUAC}$ values ($l = 1$, Gibbs energy; $l = 2$, enthalpy), for the contacts between ketone (type k, CO in *n*-alkanones [CH_3-$(CH_2)_{u-1}$-CO-$(CH_2)_{v-1}$ - CH_3]) and hydroxyl groups (type h, OH in 1-alkanols). The coordination number used for the QUAC part is $z = 4$. The QUAC parameters are independent of the 1-alkanol and *n*-alkanone present in the mixture considered.

	(u, v)			
	(1, 1)	(1, 2)	(1, ≥3) (asymmetric ketones)	(≥2; ≥2) (symmetric ketones)
	$C_{kh,1}^{QUAC} = 1.65$; $C_{kh,2}^{QUAC} = 5.00$			
	Methanol + CH_3-$(CH_2)_{u-1}$-CO-$(CH_2)_{v-1}$ - CH_3			
$C_{kh,1}^{DIS}$	0.20	1.05	2.75	2.75
$C_{kh,2}^{DIS}$	−2.80	−1.65	−1.65	−0.85
	Ethanol + CH_3-$(CH_2)_{u-1}$-CO-$(CH_2)_{v-1}$ - CH_3			
$C_{kh,1}^{DIS}$	1.25	1.60	3.50	3.50
$C_{kh,2}^{DIS}$	−0.20	1.25	1.80[a]	1.70
	1-Propanol + CH_3-$(CH_2)_{u-1}$-CO-$(CH_2)_{v-1}$ - CH_3			
$C_{kh,1}^{DIS}$	1.60	1.95	3.80[a]	3.80[a]
$C_{kh,2}^{DIS}$	0.90	2.20	4.60	3.90
	1-Butanol + CH_3-$(CH_2)_{u-1}$-CO-$(CH_2)_{v-1}$ - CH_3			
$C_{kh,1}^{DIS}$	2.20[a]	2.40	4.20[a]	4.20[a]
$C_{kh,2}^{DIS}$	1.35	3.00	5.00[a]	4.40[a]
	1-Pentanol + CH_3-$(CH_2)_{u-1}$-CO-$(CH_2)_{v-1}$ - CH_3			
$C_{kh,1}^{DIS}$	2.50[a]	2.70[a]	4.50[a]	4.50[a]
$C_{kh,2}^{DIS}$	1.90	3.40[a]	5.45	5.20[a]
	1-Hexanol + CH_3-$(CH_2)_{u-1}$-CO-$(CH_2)_{v-1}$ - CH_3			
$C_{kh,1}^{DIS}$	3.80	4.30	5.60[a]	5.60[a]
$C_{kh,2}^{DIS}$	2.10	3.80[a]	6.20	6.20
	1-Heptanol + CH_3-$(CH_2)_{u-1}$-CO-$(CH_2)_{v-1}$ - CH_3			
$C_{kh,1}^{DIS}$	8.50[a]	10.50[a]	12.00[a]	12.00[a]
$C_{kh,2}^{DIS}$	2.30[a]	4.20[a]	6.70	6.70
	1-Octanol + CH_3-$(CH_2)_{u-1}$-CO-$(CH_2)_{v-1}$ - CH_3			
$C_{kh,1}^{DIS}$	11.00[a]	13.50	15.00[a]	15.00[a]
$C_{kh,2}^{DIS}$	3.00[a]	4.70[a]	7.30	7.30
	1-Nonanol + CH_3-$(CH_2)_{u-1}$-CO-$(CH_2)_{v-1}$ - CH_3			
$C_{kh,1}^{DIS}$	12.00[a]	14.50[a]	16.00[a]	16.00[a]
$C_{kh,2}^{DIS}$	3.50[a]	5.60[a]	9.00	9.00
	1-Decanol + CH_3-$(CH_2)_{u-1}$-CO-$(CH_2)_{v-1}$ - CH_3			
$C_{kh,1}^{DIS}$	12.00[a]	14.50[a]	16.00[a]	16.00[a]
$C_{kh,2}^{DIS}$	4.00[a]	6.50[a]	10.55	10.55

[a]Estimated value.

Can. J. Chem. Downloaded from www.nrcresearchpress.com by 91.121.58.235 on 09/08/12
For personal use only.

© 1997 NRC Canada

Can. J. Chem. Downloaded from www.nrcresearchpress.com by 91.121.58.235 on 09/08/12
For personal use only.

Table 3. Molar excess Gibbs energies G^E (T; $x_1 = 0.5$) for 1-alkanol(1) + linear alkanone(2) systems at various temperatures T(K), and equimolar composition. Comparison of experimental results (exp.) with DISQUAC values calculated (calcd.) using the coefficients from Table 2. Also listed are the relative standard deviations in pressure, σ_r (P) (eq. [2]), given by DISQUAC (N is the number of data points for each system).

				G^E/J mol^{-1}		
Alkanone	T/K	N	σ_r (P)	Calcd.	Exp.	Reference
			Methanol + *n*-alkanones			
2-Propanone	288.15	10	0.041	446	370	34
	298.15	10	0.055	438	293	34
		12	0.004		446[a]	35
	313.15	12	0.004	425	433	36
	323.15	26	0.005	416	431	37
		16	0.004		423	36
	328.15	10	0.047	411	284	34
	372.7	12	0.006	359	379	38
	397.7	9	0.007	317	341	38
	422.6	10	0.012	261	306	38
2-Butanone	288.15	10	0.004	551	542	39
	298.15	10	0.001	546	540[a]	39
	313.15	10	0.001	537	529	39
	323.15	13	0.015	530	569	40
		10	0.003		517	39
2-Pentanone	343.15			706	730	41
3-Pentanone	345.15			707	633	42
2-Heptanone	298.15	16	0.020	741	746[a]	43
3-Heptanone	298.15	16	0.018	759	783	43
4-Heptanone	298.15	16	0.009	760	738	43
			Ethanol + *n*-alkanones			
2-Propanone	288.15	10	0.048	539	637	34
	298.15	10	0.010	519	507	34
	318.15	10	0.022	477	420	34
	323.15	13	0.007	466	473[a]	37
	328.15	10	0.031	455	382	34
	344.19	9	0.008	419	410	44
	353.18	9	0.006	399	397	44
	363.19	9	0.032	375	465	44
	372.7	9	0.003	352	345	45
	397.7	10	0.008	289	318	45
	422.6	11	0.008	226	256	45
2-Butanone	278.15	10	0.006	584	598	39
	288.15	10	0.006	568	578	39
	298.15	12	0.007	551	549	46
		10	0.005		561[a]	39
	313.15	10	0.006	524	532	39
	323.15	10	0.006	504	509	39
	328.15	14	0.028	494	568	40
2-Pentanone	353.15			627	675	47
			1-propanol + *n*-alkanones			
2-Propanone	343.15			381	377[a]	48
2-Butanone	278.15	10	0.014	584	580	49
	288.15	10	0.012	561	555	49
	298.15	10	0.015	536	512[a]	49
	313.15	10	0.010	499	488	49

© 1997 NRC Canada

Table 3 (*concluded*).

Alkanone	T/K	N	σ_r (P)	G^E/J mol^{-1} Calcd.	G^E/J mol^{-1} Exp.	Reference
	323.15	10	0.009	473	456	49
	357.15			377	364	50
			1-butanol + *n*-alkanones			
2-Propanone	343.15			374	449	51
2-Butanone	278.15	10	0.025	581	574	52
	288.15	10	0.021	552	542	52
	298.15	10	0.020	523	509[a]	52
	313.15	10	0.014	478	462	52
	323.15	10	0.009	447	441	52
		7	0.047		418	53
			1-pentanol + *n*-alkanones			
2-Butanone	363.45			266	196	54
			1-hexanol + *n*-alkanones			
2-Propanone	343.15			331	339[a]	55
2-Butanone	288.15	11	0.045	555	556	56
	298.15	11	0.037	520	525[a]	56
	313.15	11	0.035	466	477	56
	323.15	11	0.031	430	449	56
			1-octanol + *n*-alkanones			
2-Butanone	298.15	10	0.042	533	542[a]	56
	313.15	10	0.038	474	487	56
	323.15	10	0.036	435	457	56

[a]System used in the estimation of the interaction parameters.

Table 4. Comparison of experimental (exp.) coordinates of azeotropes: temperature (T^{az}); mole fraction (x_1^{az}) and pressure (P^{az}) for 1-alkanol(1) + *n*-alkanone(2) mixtures with DISQUAC results calculated (calcd.) using the coefficients from Table 2.

Alkanone	T^{az}/K	x_1^{az} Calcd.	x_1^{az} Exp.	P^{az}/kPa Calcd.	P^{az}/kPa Exp.	Reference
			Methanol + *n*-alkanones			
2-Propanone	298.15	0.0991	0.0946	31.041	30.949	35
	313.15	0.1508	0.1519	57.708	57.485	36
	323.15	0.1847	0.1990	84.179	84.099	37
			0.1972		83.891	36
	328.39	0.2032	0.225	101.376	101.325	60
	372.7	0.4598	0.460	402.3	405.8	38
	397.7	0.6290	0.582	774.8	782.6	38
	422.6	0.812	0.740	1388.2	1401.0	38
2-Butanone	288.15	0.6783	0.670	11.021	10.973	39
	298.15	0.7083	0.709	18.497	18.478	39
	313.15	0.7569	0.757	37.629	37.607	39
	323.15	0.7904	0.790	58.097	57.727	39
			Ethanol + *n*-alkanones			
2-Propanone	422.6	0.1702	0.190	112.84	113.62	45
2-Butanone	278.15	0.1766	0.185	4.457	4.452	39
	288.15	0.2111	0.221	7.731	7.737	39
	298.15	0.2538	0.259	12.974	12.907	39
			0.261		13.040	46
	313.15	0.3170	0.326	25.897	26.002	39
	323.15	0.3662	0.371	39.597	39.773	39

Can. J. Chem. Downloaded from www.nrcresearchpress.com by 91.121.58.235 on 09/08/12
For personal use only.

© 1997 NRC Canada

Can. J. Chem. Downloaded from www.nrcresearchpress.com by 91.121.58.235 on 09/08/12
For personal use only.

Fig. 1. VLE at different temperatures for the methanol(1) + 2-propanone(2) system. Points, experimental results: ● (35), ■ (37); solid lines, DISQUAC calculations (x_1 and y_1 are, respectively, the mole fractions in the liquid and vapor phases).

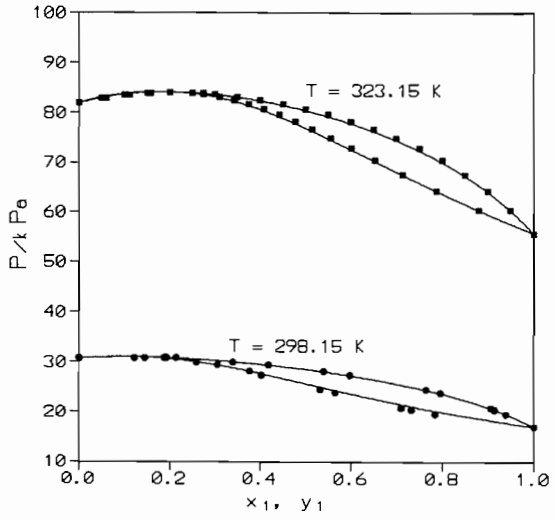


Fig. 2. VLE at different temperatures for the ethanol(1) + 2-propanone(2) system. Points, experimental results: ● (37), ■ (45); solid lines, DISQUAC calculations (x_1 and y_1 are, respectively, the mole fractions in the liquid and vapor phases).

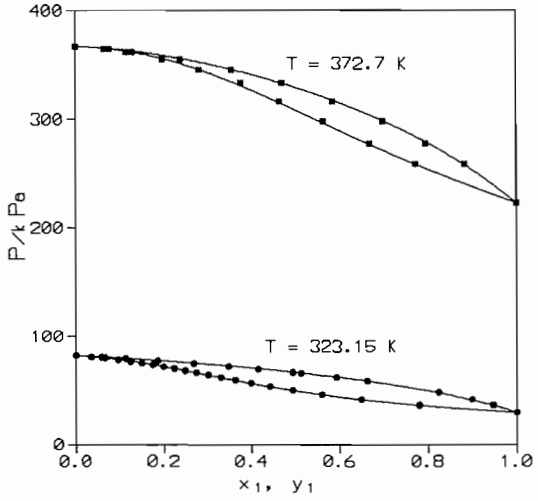


Fig. 3. VLE at 298.15 K for the ethanol(1) + 2-butanone(2) system. Points, experimental results: ● (46), ■ (39); solid lines, DISQUAC calculations (x_1 and y_1 are, respectively, the mole fractions in the liquid and vapor phases).

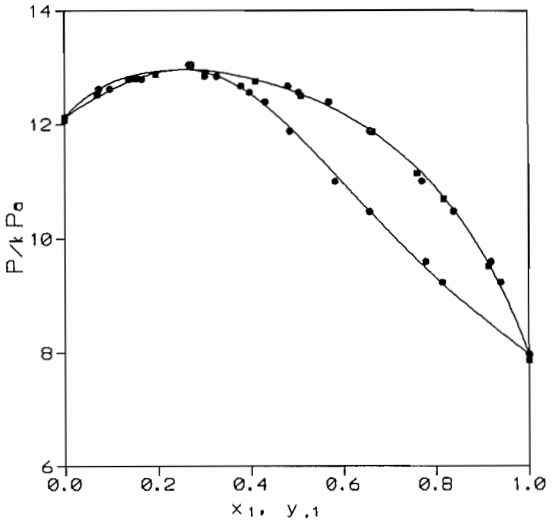
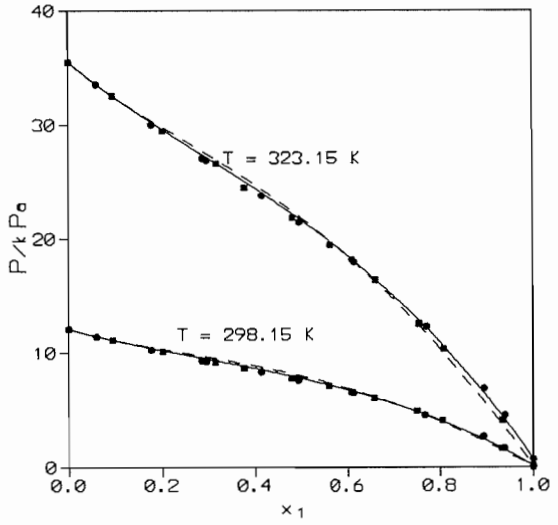


Fig. 4. VLE at different temperatures for 1-alkanol(1) + 2-butanone(2) mixtures. Points, experimental results (56): ● 1-hexanol; ■ 1-octanol; lines, DISQUAC calculations: (——), 1-hexanol, (---), 1-octanol.



where γ_1 is the activity coefficient of component 1 in the solvent mixture at temperature T, calculated using DISQUAC. ΔH_{m1}, T_{m1}, and ΔC_{pm1} stand for the molar enthalpy of fusion, the melting temperature, and the molar heat capacity change during the melting process of component 1. Equation [1] assumes (*i*) that there is no first-order transition in the solid phase; (*ii*) absence of miscibility in the solid phase; and (*iii*) that ΔC_{pm1} is independent of T.

The temperature dependence of the interaction parameters is expressed in terms of the dispersive (DIS) or quasichemical (QUAC) interchange coefficients $C_{st,l}^{DIS}$ and $C_{st,l}^{QUAC}$, where s, t = a, h, or k and $l = 1$ (Gibbs energy), $l = 2$ (enthalpy), and $l = 3$ (heat capacity).

2.2 Assessment of geometrical parameters

The relative molecular volumes, r_i, the surfaces, q_i, and the surface fractions, α_{si}, of all the molecular species have been calculated on the basis of the group volumes and surfaces recommended by Bondi (24), taking the volume and surface of methane arbitrarily as unity (25).

Table 1 lists the values of r_i and q_i of the groups referred to in this work.

2.3 Estimation of the interaction parameters

The three types of surface generate three pairs of contacts: (a,h), (a,k), and (h,k).

The alkane–alkanol (a,h) and alkane–ketone (a,k) interac-

© 1997 NRC Canada

Can. J. Chem. Downloaded from www.nrcresearchpress.com by 91.121.58.235 on 09/08/12
For personal use only.

Fig. 5. G^E at 298.15 K for 1-alkanol(1) + *n*-alkanone(2) mixtures. Points, experimental results: ●, methanol(1) + 2-propanone(2) (35); ▲, methanol(1) + 2-heptanone(2) (43); ■, 1-propanol(1) + 2-butanone(2) (49); ▼, 1-hexanol(1) + 2-butanone(2) (56); solid lines, DISQUAC calculations.

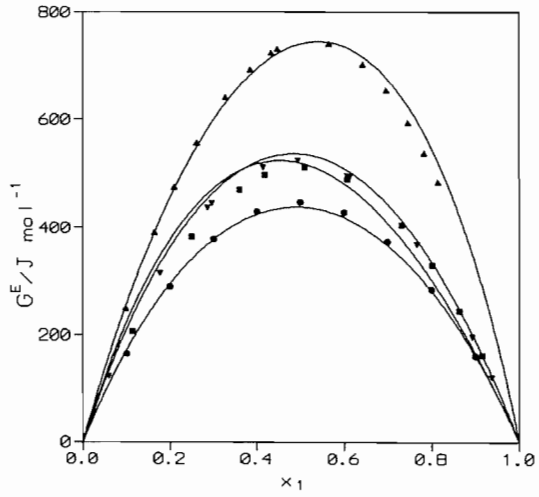


Fig. 6. H^E at 298.15 K for 1-alkanol(1) + 2-propanone(2) mixtures. Points, experimental results: ●, methanol (63); ■, ethanol (67); ▲, 1-propanol (70); ▼, 1-butanol (62); ◆, 1-hexanol (62); solid lines, DISQUAC calculations.

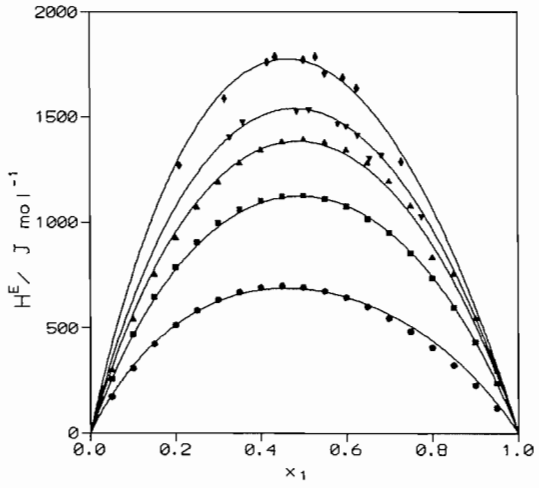


Fig. 7. H^E at 298.15 K for 1-alkanol(1) + 2-butanone(2) mixtures. Points, experimental results: ●, methanol (64); ■, ethanol (64); ▲, 1-propanol (71); ▼, 1-butanol (76); solid lines, DISQUAC calculations.

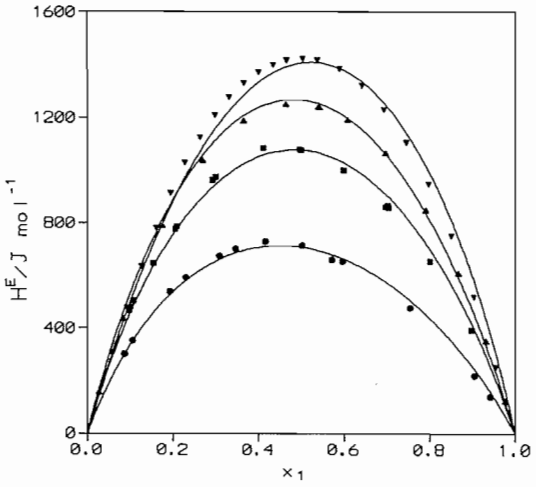
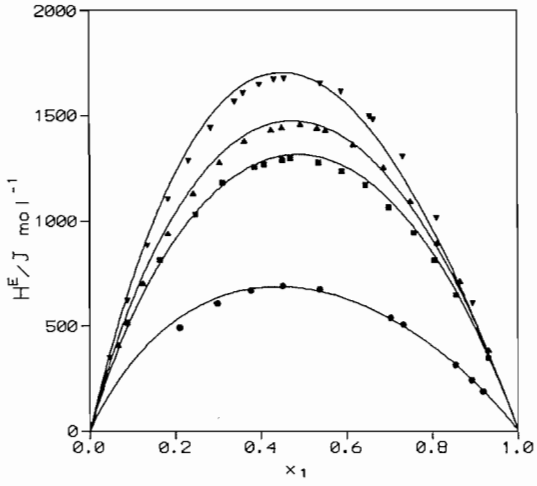


Fig. 8. H^E at 298.15 K for 1-alkanol(1) + 2-pentanone(2) mixtures. Points, experimental results: ●, methanol (28); ■, 1-propanol (20); ▲, 1-pentanol (20); ▼, 1-octanol (20); solid lines, DISQUAC calculations.



tions are described by DIS and QUAC coefficients reported previously (3, 7, 16, 26). Hence, because the (a,h) and (a,k) parameters are known, only the DIS and QUAC interchange coefficients for the (h,k) contacts need to be fitted.

The general procedure used in the fitting of any set of interchange coefficients has been described elsewhere (3, 16, 27). In our detailed study of alcoholic solutions, we have shown that the first QUAC interaction parameter can be kept constant along each series investigated (13). Similarly, here the same $C_{hk,1}^{QUAC}$ coefficient has been used for all the systems treated. In the absence of appropiate VLE data that can be used in the determination of the $C_{hk,1}^{DIS/QUAC}$ coefficients, this is important because the quasichemical contribution to H^E depends not only on $C_{hk,2}^{QUAC}$ but also on $C_{hk,1}^{QUAC}$ via the surface fractions and Boltzmann's factor (eqs. 40, 66 and 68 in ref. 25). Moreover, in order to keep a lower number of interaction parameters, the $C_{hk,2}^{QUAC}$ coefficients were also made independent of the compounds in the mixture. After several calculations developed to study the change in the symmetry of the G^E and H^E curves with the interaction parameters, we finally took $C_{hk,1}^{QUAC}$ = 1.65 and $C_{hk,2}^{QUAC}$ = 5.00 together with the corresponding $C_{hk,l}^{DIS}$ (l = 1, 2) coefficients (Table 2). Due to the lack of enough data for H^E at different temperatures, we took $C_{hk,3}^{DIS/QUAC}$ = 0.

© 1997 NRC Canada

Table 5. Molar excess enthalpies H^E (T; $x_1 = 0.5$) for 1-alkanol(1) + linear alkanone(2) systems at various temperatures T(K), and equimolar composition. Comparison of experimental results (exp.) with DISQUAC values calculated (calcd.) using the coefficients from Table 2. Also listed are the relative standard deviations for H^E, σ_r (H^E) (eq. [2]), given by DISQUAC (N is the number of data points for each system).

				H^E ($x_1 = 0.5$)		
Alkanone	T/K	N	σ_r (H^E)	Calcd.	Exp.	Reference
			Methanol + *n*-alkanones			
2-Propanone	298.15	22	0.11	686	683	61
		10	0.068		713	62
		19	0.066		694[a]	63
2-Butanone	298.15	13	0.056	708	708[a]	64
					679	39
	308.15	12	0.029	728	744	64
2-Pentanone	298.15	10	0.037	678	686[a]	28
3-Pentanone	298.15	11	0.017	719	725[a]	28
			Ethanol + *n*-alkanones			
2-Propanone	282.28			1097	1150	65
	283.15	19	0.11	1098	1046[b]	29
	298.15	10	0.042	1125	1133	62
		12	0.045		1111	66
		19	0.083		1105[b]	29
		19	0.011		1127[a]	67
	323.15	13	0.059	1166	1236	66
		17	0.078		1271[b]	29
	343.15	17	0.094	1203	1307	29
	363.15	19	0.16	1246	1222[b]	29
2-Butanone	298.15			1075	1190	68
		17	0.038		1071[a]	64
		13	0.065		1028	69
	308.15	11	0.017	1101	1121	64
		12	0.032		1077	69
2-Pentanone	298.15	10	0.170	1027	886	28
3-Pentanone	298.15	11	0.028	985	987[a]	28
			1-propanol + *n*-alkanones			
2-Propanone	298.15	10	0.038	1383	1369	62
		19	0.038		1390[a]	70
2-Butanone	298.15	14	0.033	1267	1251[a]	71
		13	0.049		1237	49
	308.15	11	0.044	1289	1317	64
2-Pentanone	298.15	16	0.023	1313	1286[a]	20
		11	0.120		1209	28
3-Pentanone	298.15	22	0.019	1222	1232[a]	72
		10	0.053		1160	28
2-Heptanone	298.15	14	0.065	1183	1259	22
			1-butanol + *n*-alkanones			
2-Propanone	298.15			1536	1372	73
					1370	74
		20	0.130		1770	75
		10	0.020		1537[a]	62
2-Butanone	298.15	11	0.120	1407	1324	69
		23	0.074		1421[a]	76
	308.15	10	0.059	1424	1383	69
		11	0.046		1473	64

Can. J. Chem. Downloaded from www.nrcresearchpress.com by 91.121.58.235 on 09/08/12
For personal use only.

© 1997 NRC Canada

Table 5 (*concluded*).

Alkanone	T/K	N	σ_r (H^E)	H^E (x_1 = 0.5) Calcd.	Exp.	Reference
1-pentanol + *n*-alkanones						
2-Propanone	298.15			1671	1661	77
		10	0.051		1667[a]	62
2-Pentanone	298.15	17	0.035	1469	1451[a]	20
2-Heptanone	298.15	15	0.046	1286	1339	22
1-hexanol + *n*-alkanones						
2-Propanone	298.15			1764	1691	77
		10	0.019		1773[a]	62
2-Butanone	298.15	10	0.080	1577	1512	69
	308.15	10	0.081	1586	1542	69
2-Pentanone	298.15	19	0.043	1545	1523	20
3-Pentanone	298.15	20	0.020	1472	1435[a]	30
2-Hexanone	298.15	18	0.051	1473	1431[a]	21
2-Heptanone	298.15	13	0.076	1338	1389	22
1-heptanol + *n*-alkanones						
2-Pentanone	298.15	17	0.047	1643	1603[a]	20
3-Pentanone	298.15	20	0.048	1578	1510[a]	30
2-Hexanone	298.15	19	0.057	1509	1479	21
2-Heptanone	298.15	12	0.047	1410	1427	22
1-octanol + *n*-alkanones						
2-Butanone	298.15	14	0.089	1735	1711	69
	308.15	12	0.086	1716	1709	69
2-Pentanone	298.15	18	0.046	1685	1676[a]	20
2-Hexanone	298.15	18	0.068	1544	1545	21
2-Heptanone	298.15	13	0.069	1440	1494	22
1-nonanol + *n*-alkanones						
2-Hexanone	298.15	18	0.057	1617	1611[a]	21
1-decanol + *n*-alkanones						
2-Butanone	298.15	15	0.100	1846	1844	69
	308.15	15	0.092	1826	1829	69
2-Hexanone	298.15	19	0.050	1676	1688[a]	21

[a]System used in the estimation of the interaction parameters.
[b]Data at 0.4 MPa.

Can. J. Chem. Downloaded from www.nrcresearchpress.com by 91.121.58.235 on 09/08/12
For personal use only.

In summary, we note the simple rules followed by the interchange coefficients:

1. $C_{hk,l}^{QUAC}$ (l = 1, 2) are independent of the class of compounds in the mixture.

2. The dispersive coefficients increase with the size of the alkanol for a given *n*-alkanone, or with the size of the alkanone for a given alcohol. It is noteworthy that $C_{hk,1}^{DIS}$ is the same for mixtures of the type 1-alkanol + isomeric ketones, being constant from 2-pentanone. However, such systems, when including an alcohol up 1-pentanol, need different $C_{hk,2}^{DIS}$ coefficients depending on the symmetry of the ketone. Then, $C_{hk,2}^{DIS}$ is constant from 2-pentanone (for asymmetric ketones), or from 3-pentanone (for symmetric ketones).

The increase in the dispersive interaction parameter with the size of the alkanol and (or) alkanone may be attributed to an inductive effect that has also been encountered in other alcoholic solutions, such as 1-alkanol + benzene, + toluene, or + CCl_4 mixtures (5, 6). In exchange, there is no steric effect on the quasichemical coefficients.

3. Comparison with experiment and discussion

A comparison between experimental data and DISQUAC results is collected in Tables 3–8. This comparison is presented in a graphical way in Figs. 1–10 for selected mixtures.

For the sake of major clarity, Tables 3, 5, 6 also list the relative standard deviations defined by:

$$[2] \quad \sigma(F) = \{1/N\sum [(F_{exp} - F_{calc})/F_{exp}]^2\}^{1/2}$$

where N is the number of data points for each mixture, and F = P, H^E, or T.

We note the good results obtained for VLE, G^E, and H^E

© 1997 NRC Canada

Table 6. Values of the relative standard deviations of the solid–liquid equilibrium temperatures, σ_r (T) eq. [2]), obtained using DISQUAC for ethanol(1) + isomeric heptanone(2) mixtures (78) (N is the number of data points for each system).

Alkanone	T^a_{m1}/K	T^a_{m2}/K	ΔH^b_{m1}/J mol^{-1}	ΔH^b_{m2}/J mol^{-1}	N	σ_r (T)
2-Heptanone(2)	158.65	237.65	5012.7	19 711.8	19	0.005
3-Heptanone(2)		235.94		17 531.6	19	0.005
4-Heptanone(2)		240.15		16 159.5	19	0.008

[a]Melting temperature of pure compound.
[b]Molar heat of fusion. Due to the lack of appropriate data, $\Delta C_{pm} = 0$ in eq. [1].

Fig. 9. H^E at 298.15 K for 1-alkanol(1) + 2-hexanone(2) mixtures. Points, experimental results (21): ●, 1-hexanol; ■, 1-octanol; ▲, 1-decanol; solid lines, DISQUAC calculations.

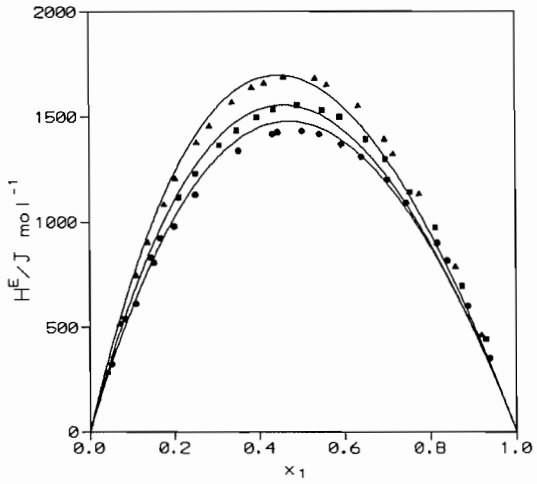
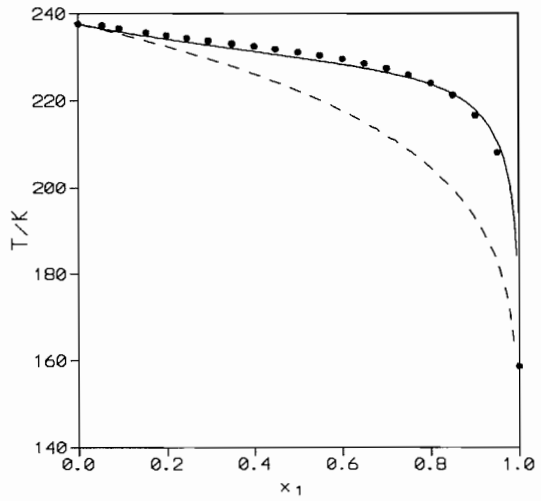


Fig. 10. SLE for the ethanol(1) + 2-heptanone(2) mixture. Points, experimental results (78); solid line, DISQUAC calculation; broken line, ideal solubility curve.



(Tables 3–5). Thus, for 54 systems, the mean relative standard deviation in pressure is 0.018; in the case of H^E this magnitude is 0.059 for 61 systems. It should be noted again that the G^E_s of 1-alkanol + isomeric n-alkanone mixtures are calculated using the same $C^{DIS}_{hk,1}$ coefficient. Unfortunately, different values of $C^{DIS}_{hk,2}$ are needed to evaluate H^E for such systems including the lower 1-alkanols (see above, Table 2).

The symmetry of the excess functions G^E and H^E is usually well reproduced (Figs. 5–9). In the same way, the entire VLE diagrams are well represented (Figs. 1–4). We note the good predictions given by the model regarding the coordinates of azeotropes (Table 4).

The larger discrepancies observed in some cases between experimental and calculated values can be attributed to experimental inaccuracies. For example, the H^E data from Letcher and Nevines (28) for the ethanol + 2-pentanone system seem to be too low when are compared with data for other 1-alkanol + 2-pentanone mixtures reported by different authors (Table 5). The data mentioned, as reported by Letcher and Nevines, for the ethanol + 2-pentanone system can be represented using $C^{DIS}_{hk,2} = 0.10$ ($\sigma_r = 0.060$). However, this value does not fit into the general scheme of the variation of the interaction parameters (Table 2), indicating that such data are not reliable.

On the other hand, it is noted that the model usually yields accurate predictions over a wide range of temperature. So, for example, the VLE of the ethanol + 2-propanone system is well characterized between 288.15 and 422.9 K (Table 3, Fig. 3). At very low temperatures (204–240 K), DISQUAC represents the SLE data of mixtures containing ethanol and isomeric heptanones (Table 6, Fig. 10) well. Regarding H^E, this magnitude is well described at temperatures close to 298.15 K (Table 5). Predictions at higher temperatures are still acceptable as shown by comparison of the data reported by Lietzmann et al. at 0.4 MPa (29) with results calculated for the ethanol + 2-propanone mixture (Table 5).

In the framework of DISQUAC, the temperature dependence is given via Boltzmann's factor and the third interchange coefficients. In the present mixtures, $C^{DIS/QUAC}_{ak,3} = C^{DIS/QUAC}_{hk,3} = 0$. So, Boltzmann's factor and the $C^{DIS/QUAC}_{ah,3}$ coefficients seem to be sufficient to evaluate the variation with temperature of the thermodynamic properties.

The poorer results are obtained when predicting partial molar quantities at infinite dilution (Tables 7 and 8). So, for the ethanol(1) + 2-propanone(2) system, the mean deviation is 19% for $H^{E,\infty}_1$, and 13% for $H^{E,\infty}_2$. Similar results are obtained when investigating other alcoholic solutions (3–6).

Finally, it should be mentioned that preliminary calculations show that it is possible to predict thermodynamic properties, VLE and H^E, of ternary systems including 1-alkanols, n-alkanones, and one organic solvent on the basis of binary

© 1997 NRC Canada

Can. J. Chem. Downloaded from www.nrcresearchpress.com by 91.121.58.235 on 09/08/12
For personal use only.

Can. J. Chem. Downloaded from www.nrcresearchpress.com by 91.121.58.235 on 09/08/12
For personal use only.

Table 7. Natural logarithms of activity coefficients at infinite dilution of compound *i*, $\ln \gamma_i^\infty$, in 1-alkanol(1) + *n*-alkanone(2) mixtures at various temperatures (*T*/K). Comparison of experimental results (exp.) with DISQUAC values calculated (calcd.) using the coefficients from Table 2.

		$\ln \gamma_1^\infty$		$\ln \gamma_2^\infty$		
Alkanone	*T*/K	Calcd.	Exp.	Calcd.	Exp.	Reference
		Methanol + *n*-alkanones				
2-Propanone	298.15	0.814	0.609	0.741	0.824	79[a]
	308.2	0.760	0.688	0.701	0.713	80[b]
	313.15	0.735	0.667	0.683	0.697	36[c]
	313.2	0.734	0.747	0.683	0.698	80[b]
	323.15	0.685	0.618	0.649	0.656	36[c]
			0.628		0.656	37[c]
2-Butanone	308.14	0.918	—	0.944	0.815	80[b]
	308.21	0.918	—	0.944	0.788	80[b]
	308.6	0.916	—	0.942	0.819	81[b]
	312.93	0.891	0.806	0.927	—	80[b]
	318.5	0.861	—	0.908	0.793	81[b]
	328.5	0.807	—	0.876	0.747	81[b]
	333.07	0.783	0.770	0.862	—	80[b]
	337.0	0.763	—	0.850	0.727	81[b]
2-Heptanone	298.15	1.199	1.136	1.673	1.388	43[c]
3-Heptanone	298.15	1.263	1.248	1.680	1.491	43[c]
4-Heptanone	298.15	1.268	0.960	1.676	1.556	43[c]
		Ethanol + *n*-alkanones				
2-Propanone	293.15	0.980	—	0.892	0.867	82[d]
	298.15	0.941	0.916	0.856	—	79[a]
	298.3	0.941	0.892	0.856	—	81[b]
	303.23	0.902	0.842	0.823	—	80[b]
	308.2	0.866	0.806	0.790	—	81[b]
	313.20	0.823	0.737	0.759	—	80[b]
	314.23	0.822	—	0.753	0.888	80[b]
	318.3	0.794	0.727	0.728	—	81[b]
	322.95	0.762	—	0.702	0.797	80[b]
	323.15	0.761	0.678	0.701	0.781	37[c]
	328.5	0.725	0.652	0.671	—	81[b]
2-Butanone	312.93	0.887	0.806	0.841	—	80[b]
	313.85	0.881	—	0.835	0.806	80[b]
	333.07	0.747	0.683	0.732	—	80[b]
		1-butanol + *n*-alkanones				
2-Propanone	293.15	1.082	—	0.830	0.875	82[d]
		1-octanol + *n*-alkanones				
2-Propanone	293.15	1.288	—	0.540	0.944	82[d]
2-Butanone	293.15	1.299	—	0.696	0.703	82[d]

[a]From gas stripping method.
[b]From differential ebulliometry.
[c]From *P*–*x* data extrapolated to $x_i = 0$.
[d]From gas–liquid chromatography.

parameters only, that is, by neglecting ternary interactions. For example, in the case of the 1-propanol + 3-pentanone + 1-hexanol system at 298.15 K, with 54 data points (30), $\sigma_r(H^E) = 0.033$. A more detailed study will be presented in the following article.

4. Discussion and conclusions

For a given alkanol, H^E decreases as the aliphatic chain length of the ketone increases. This may be due to the fact that although the dipole moments, μ, of the ketones are approxi-

© 1997 NRC Canada

Table 8. Partial molar excess enthalpies of 1-alkanol(1) + *n*-alkanone(2) mixtures at infinite dilution, $H_i^{E,\infty}$, and at various temperatures (*T*/K). Comparison of experimental results (exp.) with DISQUAC values calculated (calcd.) using the coefficients from Table 2.

		$H_1^{E,\infty}$		$H_2^{E,\infty}$	
System	*T*/K	Calcd.	Exp.	Calcd.	Exp.
Methanol + 2-butanone	323.15[a]	4646	—	2805	2800
Ethanol + 2-propanone	283.15[b]	5628	4910	5287	3940
	298.15[b]	5719	5120	5107	4640
	313.15[a]	5806	4750	4958	—
	323.15[b]	5864	5080	4879	5390
	343.15[b]	5980	4970	4781	5410
	363.15[b]	6072	4670	4774	4750

[a]Reference 83.
[b]Reference 84.

mately constant (2.78, 2.77 and 2.66 D for 2-propanone, 2-pentanone and 2-heptanone, respectively (31)), the effective dipole moments, $\bar{\mu}$ (defined by eqs. [3] and [4] in ref. 31), decrease as the size of the ketone increases: 0.75, 0.61, and 0.49 for the *n*-alkanones mentioned above (31). As a consequence, the ketoxy interactions in the condensed phase become weaker, and hence H^E decreases.

In a similar way, μ is also practically constant for 1-alkanols (1.7, 1.8, and 1.8 D (32) for methanol, 1-butanol, and 1-decanol, respectively), while $\bar{\mu}$ decreases with the length of the aliphatic chain of the alcohol (the respective values are 0.60, 0.41, and 0.18). However, for a given ketone, H^E increases with the size of the alcohol. This implies that the rupture of the alkanol–alkanol bonds predominates over the formation of O—H---O=C bonds. Nevertheless, because both effects decrease with increasing alkanol chain length, such a trend is probably due to the physical interactions between equal molecules then become very important.

This complex behaviour is well described by means of structure-dependent interchange coefficients that follow rather simple rules. So, the DIS interaction parameters show an inductive effect, while no steric effect is found for the QUAC parameters; that is, the latter do not depend on the class of components in the mixture. This may be considered the main conclusion in terms of the framework of DISQUAC.

References

1. H.V. Kehiaian. Fluid Phase Equilib. **13**, 243 (1983).
2. H.V. Kehiaian. Pure Appl. Chem. **57**, 15 (1985).
3. J.A. González, I. García de la Fuente, J.C. Cobos, and C. Casanova. Ber. Bunsen-Ges. Phys. Chem. **95**, 1658 (1991).
4. J.A. González, I. García de la Fuente, J.C. Cobos, and C. Casanova. J. Solution Chem. **23**, 399 (1994).
5. J.A. González, I. García de la Fuente, J.C. Cobos, and C. Casanova. Fluid Phase Equilib. **93**, 1 (1994).
6. J.A. González, I. García de la Fuente, J.C. Cobos, and C. Casanova. Thermochim. Acta, **237**, 261 (1994).
7. J.A. González, I. García de la Fuente, J.C. Cobos, C. Casanova, and U. Domańska. Ber. Bunsen-Ges. Phys. Chem. **98**, 955 (1994).
8. J.A. González. I. García de la Fuente, J.C. Cobos, C. Casanova, and U. Domańska. Fluid Phase Equilib. **94**, 167 (1994).
9. U. Domańska and J.A. González. Fluid Phase Equilib. **119**, 131 (1996).
10. U. Domańska and J.A. González. Fluid Phase Equilib. **123**, 167 (1996).
11. J.A. González, I. García de la Fuente, and J.C. Cobos. Ber. Bunsen-Ges. Phys. Chem. **101**, 219 (1997).
12. J.A. González, I. García de la Fuente, and J.C. Cobos. Fluid Phase Equilib. **123**, 39 (1996).
13. J.A. González, I. García de la Fuente, J.C. Cobos, and U. Domańska. Fluid Phase Equilib. **119**, 81 (1996).
14. J.A. González, I. García de la Fuente, and J.C. Cobos. Thermochim. Acta, **278**, 57 (1996).
15. J.A. González, I. García de la Fuente, and J.C. Cobos. Ber. Bunsen-Ges. Phys. Chem. **100**, 1746 (1996).
16. J.A. González, I. García de la Fuente, J.C. Cobos, and C. Casanova. Fluid Phase Equilib. **78**, 61 (1992).
17. J.A. González, I. García de la Fuente, and J.C. Cobos. Fluid Phase Equilib. **135**, 1 (1997).
18. G.C. Benson and H.D. Pflug. J. Chem. Eng. Data, **15**, 382 (1970).
19. J.A. González, I. García de la Fuente, J.C. Cobos, and C. Casanova. Ber. Bunsen-Ges. Phys. Chem. **98**, 106 (1994).
20. G. Prieto, P. Nogueira, R. Bravo, F. Sarmiento, and M.I. Paz Andrade. J. Chem. Thermodyn. **24**, 905 (1992).
21. J.L. Legido, R. Bravo, M.I. Paz Andrade, L. Romaní, F. Sarmiento, and J. Ortega. J. Chem. Thermodyn. **18**, 21 (1986).
22. P. Noguiera, G. Prieto, F. Sarmiento, R. Bravo, and M.I. Paz Andrade. Phys. Chem. Liq. **27**, 149 (1994).
23. J.M. Prausnitz. Molecular thermodynamics of fluid phase equilibria. Prentice-Hall, Englewood-Cliffs, N.J. 1969.
24. A. Bondi. Physical properties of molecular crystals, liquids and glasses. J. Wiley & Sons, New York. 1968.
25. H.V. Kehiaian, J.-P.E. Grolier, and G.C. Benson. J. Chim. Phys. **75**, 1031 (1978).
26. H.V. Kehiaian, S. Porcedda, B. Marongiu, L. Lepori, and E. Matteoli. Fluid Phase Equilib. **63**, 231 (1991).
27. J.A. González, I. García de la Fuente, J.C. Cobos, C. Casanova, and A. Ait-Kaci. Fluid Phase Equilib. **112**, 63 (1995).
28. T.M. Letcher and J.A. Nevines. J. Chem. Eng. Data, **40**, 995 (1995).
29. A. Lietzmann, B. Löwen, and S. Schulz. J. Chem. Eng. Data, **39**, 785 (1994).

Can. J. Chem. Downloaded from www.nrcresearchpress.com by 91.121.58.235 on 09/08/12
For personal use only.

© 1997 NRC Canada

30. M. López, J.L. Legido, L. Romaní, J. Peleteiro, and M.I. Paz Andrade. J. Chem. Eng. Data, **38**, 238 (1993).
31. J.A. González, J.M. Fernández Martínez, I. García de la Fuente, and J.C. Cobos. Can. J. Chem. **74**, 1815 (1996).
32. R.C. Reid, J.M. Prausnitz, and B.E. Poling. The properties of gases and liquids. 4th ed. McGraw–Hill, New York. 1987.
33. H.V. Kehiaian, J.-P.E. Grolier, M.R. Kechavarz, and G.C. Benson. Fluid Phase Equilib. **5**, 159 (1980).
34. J.N. Rhim and S.S. Park. Hwahak Konghak, **13**, 147 (1975) (cf. ref. 59).
35. A. Tamir, A. Appelblat, and M. Wagner. Fluid Phase Equilib. **6**, 113 (1981).
36. M. Goral, G. Kolasińska, P. Oracz, and S. Warycha. Int. DATA Ser. Sel. Data Mixtures, Ser. A: **3**, 203 (1985).
37. H.C. Van Ness and M.M. Abbott. Int. DATA Ser. Sel. Data Mixtures, Ser. A: **1**, 65 (1978).
38. R.A. Wilsak, S.W. Campbell, and G. Thodos. Fluid Phase Equilib. **28**, 13 (1986).
39. R. Garriga, F. Sánchez, P. Pérez, and M. Gracia. J. Chem. Thermodyn. **28**, 567 (1996).
40. I. Nagata, T. Ohta, and S. Nakagama. J. Chem. Eng. Jpn. **9**, 276 (1976) (cf. ref. 57).
41. W.D. Hill and M. Van Winkle. Ind. Eng. Chem. 44, 208 (1952) (cf. ref. 57).
42. M.I. Glukhareva, E.N. Taravkova, and A.M. Chashchin. Zh. Prikl. Khim. (S.-Peterburg), **49**, 660 (1976) (cf. ref. 59).
43. R.G. Rubio, J.A.R. Renuncio, and M. Díaz Peña. J. Chem. Thermodyn. **15**, 779 (1983).
44. M.-J. Lee and C.-H. Hu. Fluid Phase Equilib. **109**, 83 (1995).
45. S.W. Campbell, R.A. Wilsak, and G. Thodos. J. Chem. Eng. Data, **32**, 357 (1987).
46. T. Ohta, J. Koyabu, and I. Nagata. Fluid Phase Equilib. **7**, 65 (1981).
47. L.R. Hellwig and M. Van Winkle. Ind. Eng. Chem. **45**, 624, (1953).
48. N. Gültekin. J. Chem. Eng. Data, **34**, 168 (1989)
49. R. Garriga, F. Sánchez, P. Pérez, and M. Gracia. Fluid Phase Equilib. **124**, 123 (1996).
50. W.K. Park, B.Y. Chung, and H.S. Shim. Hwahak Konghak, **10**, 281 (1972) (cf. ref. 59).
51. H. Michalski, S. Michalowski, M. Serwinski, and C. Strumillo. Zesz. Nauk. Politech. Lodz. **10**, 73 (1961) (cf. ref. 58).
52. R. Garriga, F. Sánchez, P. Pérez, and M. Gracia. J. Chem. Eng. Data, **41**, 451 (1996).
53. V.Y. Aristovich, A.G. Morachevsky, and I.I. Sabylin. Zh. Prikl. Khim., (S.-Peterburg), **38**, 2694 (1965) (cf. ref. 58).
54. K.J. Miller and H.-Sh. Huang. J. Chem. Eng. Data, **17**, 77 (1972).
55. P. Ramanchandra Rao, C. Chiranjivi, and C.J. Dasarao. J. Appl. Chem. **17**, 118 (1967).
56. R. Garriga, F. Sánchez, P. Pérez, and M. Gracia, J. Chem. Eng. Data, **41**, 1091 (1996).
57. J. Gmehling and U. Onken. Vapor-liquid equilibrium data collection. Vol. I. Part 2a. DECHEMA. 1977.
58. J. Gmehling, U. Onken, and W. Arlt. Vapor-liquid equilibrium data collection. Vol. I. Part 2b. DECHEMA. 1990.
59. J. Gmehling, U. Onken, and W. Arlt. Vapor-liquid equilibrium data collection. Vol. I. Part 2c. DECHEMA. 1982.
60. T. Hiaki, K. Kurihara, and K. Kojima. J. Chem. Eng. Data, **39**, 714 (1994).
61. I. Nagata and K. Tamura. Fluid Phase Equilib. **15**, 67 (1983).
62. B.A. Coomber and Ch. J. Wormald. J. Chem. Thermodyn. **8**, 793 (1976).
63. I. Nagata. Thermochim. Acta, **236**, 23 (1994).
64. I. Nagata. Int. DATA Ser. Sel. Data Mixtures, Ser. A: **2**, 81 (1984).
65. T.V.J. Findlay. Aust. J. Chem. **14**, 520 (1961)
66. G.L. Nicolaides and C.A. Eckert. J. Chem. Eng. Data, **23**, 152 (1978).
67. I. Nagata and A. Ksiazczak. J. Chem. Thermodyn. **26**, 165 (1994).
68. M. Takami, S. Murakami, and R. Fujishiro. Bull. Chem. Soc. Jpn. **38**, 291 (1965).
69. J. Iñarrea, J. Valero, P. Pérez, M. Gracia, and C. Gutiérrez Losa. J. Chem. Thermodyn. **20**, 193 (1988).
70. I. Nagata and K. Takeuchi. Thermochim. Acta, **242**, 103 (1994).
71. K. Tamura and I. Nagata. J. Chem. Thermodyn. **23**, 359 (1991).
72. M. López, J.L. Legido, L. Romaní, E. Carballo, E. Pérez Martell, E. Jiménez, and M.I. Paz Andrade. J. Chem. Thermodyn. **24**, 205 (1992).
73. M.I. Paz Andrade and M.I. Casas. An. Quim. **66**, 709 (1970).
74. S. Murakami and R. Fujishiro. Bull. Chem. Soc. Jpn. **39**, 720 (1966).
75. I. Nagata, K. Tamura, H. Kataoka, and A. Ksiazczak. J. Chem. Eng. Data, **41**, 593 (1996).
76. J.P. Chao and M. Dai. J. Chem. Thermodyn. **23**, 117 (1991).
77. M.I. Paz Andrade, E. Jiménez, and D. López García. An. Quim. **69**, 283 (1973).
78. C. Fiege, R. Joh, J.M. Petri, and J. Gmehling. J. Chem. Eng. Data, **41**, 1431 (1996).
79. J.-B. Bao and Sh.J. Han. Fluid Phase Equilib. **112**, 307 (1995).
80. L. Dallinga, M. Shiller, and J. Gmehling. J. Chem. Eng. Data, **38**, 147 (1993).
81. D.M. Trampe and C.A. Eckert. J. Chem. Eng. Data, **35**, 156 (1990).
82. E.R. Thomas, B.A. Newman, Th.C. Long, D.A. Wood, and C.A. Eckert. J. Chem. Eng. Data, **27**, 399 (1982).
83. D.M. Trampe and C.A. Eckert. J. Chem. Eng. Data, **36**, 112 (1991).
84. Th. Pfeffer, B. Löwen, and S. Schultz. Fluid Phase Equilib. **106**, 139 (1995).

Can. J. Chem. Downloaded from www.nrcresearchpress.com by 91.121.58.235 on 09/08/12
For personal use only.

© 1997 NRC Canada

Thermodynamics of mixtures containing the CO and OH groups. II. DISQUAC predictions on VLE and H^E for ternary mixtures containing 1-alkanols, *n*-alkanones, and one organic solvent

Juan Antonio González, I. García de la Fuente, and J.C. Cobos

Abstract: Thermodynamic properties: vapor–liquid equilibria, VLE, or excess enthalpies, H^E, for a set of 21 ternary mixtures of the type 1-alkanol + *n*-alkanone + organic solvent are studied in the framework of the DISQUAC group contribution model. This treatment is extended to the binaries involved. The DISQUAC analysis is developed on the basis of binary interactions only, that is, ternary interactions are neglected. Most of the interchange coefficients needed are available in the literature. The average relative standard deviations are 0.026 for pressure in the VLE (12 systems) and 0.098 in the H^E (9 systems). The discrepancies observed are briefly discussed.

Key words: 1-alkanols, *n*-alkanones, group contribution, liquids, ternary systems, thermodyamics.

Résumé : Opérant dans le cadre du modèle DISQUAC de la contribution de groupe, on a étudié les propriétés thermodynamiques (équilibre vapeur–liquide, EVL, et enthalpies en excès, H^E) de 21 mélanges ternaires du type alcan-1-ol + *n*-alcanone + solvant organique. On a étendu ce traitement aux systèmes binaires impliqués. On a développé l'analyse DISQUAC en se basant uniquement sur les interactions binaires; les interactions ternaires sont donc négligées. La plupart des coefficients d'interéchange nécessaires sont disponibles dans la littérature. Les déviations relatives moyennes standards sont de 0,026 pour la pression dans les EVL (12 systèmes) et de 0,098 pour les H^E (9 systèmes). On discute brièvement des différences observées.

Mots clés : alcan-1-ols, *n*-alcanones, contribution de groupe, liquides, systèmes ternaires, thermodynamique.

[Traduit par la rédaction]

1. Introduction

In a previous work (1), binary mixtures containing 1-alkanols and *n*-alkanones were treated in terms of the DISQUAC group contribution model (2, 3). Interaction parameters for the hydroxyl–carbonyl contacts were reported, and it was shown that DISQUAC consistently described such mixtures over a wide range of temperatures, on the basis of structure-dependent interaction parameters. As a continuation, we now present a detailed study of the ability of the model to represent thermodynamic properties, VLE and H^E, for ternary mixtures including 1-alkanols, *n*-alkanones, and one organic solvent from binary parameters only, that is, neglecting ternary interactions. This is important because, although a large amount of data has been reported in the literature for binary systems, data for ternary and higher multicomponent mixtures is much scarcer due to the time and effort required to obtain a meaningful set of multicomponent data. One of the most essential tasks of thermodynamics is to predict thermodynamic properties of multicomponent systems using data obtained from more simple mixtures and, in the case of VLE, for pure substances. From this point of view, it should be emphasized that we have already shown that DISQUAC is a reliable tool to describe ternary systems containing only hydrocarbons (4) or one or two 1-alkanols and hydrocarbons (5–7).

Received May 14, 1997.

J.A. González,[1] I. García de la Fuente, and J.C. Cobos. Departamento de Termodinámica y Física Aplicada, Universidad de Valladolid, 47071 Valladolid, Spain.

[1] Author to whom correspondence may be addressed. Telephone: +34 83 42 31 37. Fax: +34 83 42 31 36 or -30 13. E-mail: jagl@wamba.cpd.uva.es

2. Ternary systems considered

Table 1 lists all the ternary systems considered in this work. Also indicated are the temperature, T (in K), the number of data points measured, N, the thermodynamic property studied for each mixture, VLE or H^E, the minimum (F^E_{min}) and the maximum (F^E_{max}) direct experimental values (in J mol^{-1}) of the excess function related to the thermodynamic property studied, when available, and the source of data.

In a similar way, Table 2 lists the binary mixtures and their related ternary systems. To develop a more complete study, we have considered, when possible, those binaries originally cited in papers regarding the ternary mixtures treated.

We note that, for the following systems, the excess functions are endothermic. Ternary system nos. 13–15 (Table 1) have ternary H^E data with maxima that are larger than those of the related binaries (Table 2). This is not the case for mixtures

© 1997 NRC Canada

Can. J. Chem. Downloaded from www.nrcresearchpress.com by 91.121.58.235 on 09/08/12
For personal use only.

Can. J. Chem. Downloaded from www.nrcresearchpress.com by 91.121.58.235 on 09/08/12
For personal use only.

Table 1. Ternary systems studied in this work. N is the number of measured data points and T is the temperature (K). F^{E}_{min} and F^{E}_{max} are, respectively, the direct minimum and maximum experimental values of the excess function related to the thermodynamic property treated for each system considered.

No.	Ternary system[a]	N	T/K	Property	F^{E}_{min}/J mol^{-1}	F^{E}_{max}/J mol^{-1}	Reference
1	MeOH + 1CO1 + n-C_5	36	372.7	VLE	—	—	8
2	MeOH + 1CO1 + n-C_6	54	313.15	VLE	—	—	9
3	EtOH + 1CO1 + n-C_5	36	372.7	VLE	—	—	10
4	EtOH + 1CO1 + n-C_6	21	328.15	VLE	—	—	11
5	MeOH + 1CO1 + C_6H_{12}	64	293.15	VLE	—	—	12
6		65	303.15	VLE	—	—	12
7		21	308.15	VLE	—	—	13
8		63	313.15	VLE	—	—	14
9		21	328.15	VLE	—	—	13
10	EtOH + 1CO1 + C_6H_6	24	318.15	VLE	524	1096	15
11	EtOH + 1CO2 + C_6H_6	33	298.15	VLE	252	1043	16
12		22	328.15	VLE	—	—	17
13	PrOH + 2CO2 + n-C_6	50	298.15	H^E	418	1558	18
14	PrOH + 2CO2 + n-C_7	58	298.15	H^E	548	1638	19
15	PrOH + 2CO2 + n-C_8	60	298.15	H^E	361	1702	19
16	PrOH + 2CO2 + HxOH	54	298.15	H^E	226	1364	20
17	PrOH + 2CO2 + HpOH	60	298.15	H^E	169	1424	20
18	MeOH + 1CO1 + C_6H_6	57	298.15	H^E	85	745	21
19	EtOH + 1CO1 + C_6H_6	57	298.15	H^E	118	1099	22
20	PrOH + 1CO1 + C_6H_6	57	298.15	H^E	157	1330	23
21	PrOH + 1CO2 + C_6H_6	54	298.15	H^E	105	1150	24

[a]The abbreviations used are MeOH, methanol; EtOH, ethanol; PrOH, 1-propanol; HxOH, 1-hexanol; HpOH, 1-heptanol; 1CO1, 2-propanone; 1CO2, 2-butanone.

Fig. 1. Calculated pressures, P_{calc}, vs. experimental values (8), P_{exp}, for the methanol(1) + 2-propanone(2) + n-C_5 (3) system at 372.7 K.

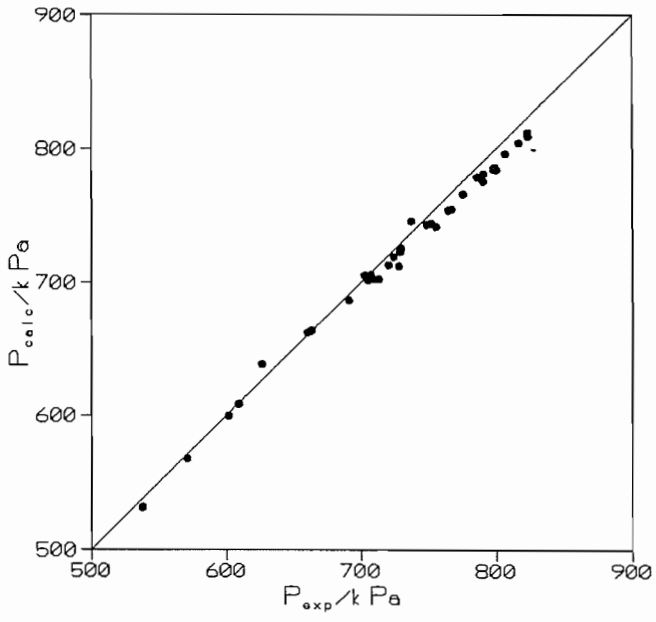
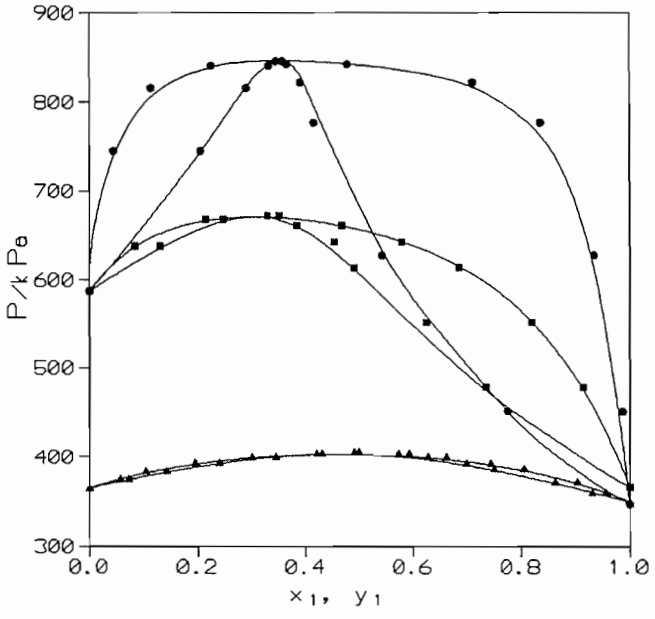


Fig. 2. VLE at 372.7 K for the binaries involved in the methanol(1) + 2-propanone(2) + n-C_5 (3) system at the same temperature. Lines, DISQUAC results; points, experimental values: ▲, methanol(1) + 2-propanone(2) (25); ●, methanol(1) + n-C_5 (2) (26); ■, 2-propanone(1) + n-C_5 (2) (27) (x_1 and y_1 are, respectively, the mole fractions in the liquid and vapor phases).



© 1997 NRC Canada

Table 2. Binary systems involved in the ternary mixtures studied in this work. N is the number of measured data points. F^{E}_{max} is the experimental value of the excess function at equimolar composition and at temperature T (K).

No.	Binary system	T/K	N	Property	F^{E}_{max}/J mol^{-1}	Related ternary system[e]	Reference
1	MeOH + 1CO1	372.8	12	VLE	383[b]	1	25
2	MeOH + n-C_5	372.7	9	VLE	1669[b]	1	26
3	1CO1 + n-C_5	372.7	8	VLE	917[b]	1,3	27
4	MeOH + 1CO1	313.15	12	VLE	433[b]	2,8	28
5	MeOH + n-C_6	313.15	53	VLE	1640[b]	2	9
6	1CO1 + n-C_6	318.15	14	VLE	1051[b]	2	29
7	EtOH + 1CO1	372.7	9	VLE	348[b]	3	30
8	EtOH + n-C_5	372.7	8	VLE	1415[b]	3	31
9	EtOH + 1CO1	328.15	8	VLE	415[b]	4	11
10	EtOH + n-C_6	328.15	17	VLE	1500[b]	4	32
11	1CO1 + n-C_6	328.15	9	VLE	1029[b]	4	33
12	MeOH + 1CO1	293.15	16	VLE	456[b]	5	12
13	MeOH + C_6H_{12}	293.15	23	VLE	854[b,c]	5	12
14	1CO1 + C_6H_{12}	293.15	25	VLE	1122[b]	5	12
15	MeOH + 1CO1	303.15	15	VLE	448[b]	6	12
16	MeOH + C_6H_{12}	303.15	69	VLE	867[b,c]	6	12
17	1CO1 + C_6H_{12}	303.15	41	VLE	1108[b]	6	12
18	MeOH + 1CO1	308.15	11	VLE	474[b]	7	34
19	MeOH + C_6H_{12}	313.15	34	VLE	885[b,c]	8	14
20	1CO1 + C_6H_{12}	313.15	30	VLE	1091[b]	8	35
21	MeOH + 1CO1	328.15	11	VLE	481[b]	9	34[f]
22	MeOH + C_6H_{12}	328.15	9	VLE	1690[b]	9	36[f]
23	1CO1 + C_6H_{12}	323.15	25	VLE	1047[b]	9	37
24	EtOH + 1CO1	323.15	13	VLE	473[b,d]	10	38
25	EtOH + C_6H_6	313.15	15	VLE	1128[b]	10,12	39
26	1CO1 + C_6H_6	318.15	11	VLE	282[b,d]	10	40
27	EtOH + 1CO2	298.15	12	VLE	549[b]	11	16
28	EtOH + C_6H_6	298.15	11	VLE	1100[b]	11	16
29	1CO2 + C_6H_6	298.15	10	VLE	138[b,d]	11	16
30	EtOH + 1CO2	328.15	14	VLE	568[b]	12	41
31			5	VLE	575[b]	12	17
32	EtOH + C_6H_6	328.15	6	VLE	1180[b]	12	17
33	1CO2 + C_6H_6	313.15	22	VLE	116[b]	12	42
34	PrOH + 2CO2	298.15	22	H^E	1232[a,d]	13,14,15,16,17	18
35	PrOH + n-C_6	298.15	21	H^E	561[a]	13	18
36	2CO2 + n-C_6	298.15	20	H^E	1024[a]	13	18
37	PrOH + n-C_7	298.15	18	H^E	617[a]	14	19
38	2CO2 + n-C_7	298.15	20	H^E	1105[a]	14	19
39	PrOH + n-C_8	298.15	18	H^E	673[a]	15	19
40	2CO2 + n-C_8	298.15	18	H^E	1165[a]	15	19
41	PrOH + HxOH	298.15	16	H^E	64[a]	16	20
42	HxOH + 2CO2	298.15	20	H^E	1435[a,d]	16	20
43	PrOH + HpOH	298.15	18	H^E	103[a]	17	20
44	HpOH + 2CO2	298.15	20	H^E	1510[a,d]	17	20
45	MeOH + 1CO1	298.15	19	H^E	694[a,d]	18	21
46	MeOH + C_6H_6	298.15	19	H^E	622[a,d]	18	43
47	1CO1 + C_6H_6	298.15	19	H^E	138[a,d]	18,19,20	44
48	EtOH + 1CO1	298.15	19	H^E	1124[a,d]	19	22
49	EtOH + C_6H_6	298.15	20	H^E	761[a,d]	19	43
50	PrOH + 1CO1	298.15	19	H^E	1390[a,d]	20	23

Can. J. Chem. Downloaded from www.nrcresearchpress.com by 91.121.58.235 on 09/08/12
For personal use only.

© 1997 NRC Canada

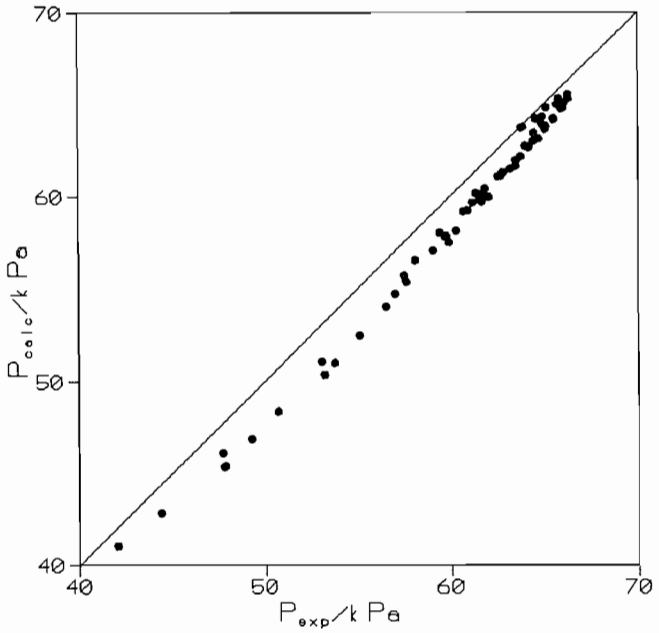
Table 2 (*concluded*).

No.	Binary system	*T*/K	*N*	Property	F^E_{max}/J mol^{-1}	Related ternary system[e]	Reference
51	PrOH + C_6H_6	298.15	25	H^E	950[a,d]	20,21	43
52	PrOH + 1CO2	298.15	14	H^E	1251[a,d]	21	24
53	1CO2 + C_6H_6	298.15	23	H^E	−50[a]	21	45

[a]$F^E = H^E$.
[b]$F^E = G^E$.
[c]System with miscibility gap, value at $x_1 = 0.125$.
[d]System previously used in the fitting of interchange coefficients. For abbreviations see Table 1.
[e]From Table 1.
[f]Some data attributed to refs. 34 and 36 have been taken from ref. 62.

Can. J. Chem. Downloaded from www.nrcresearchpress.com by 91.121.58.235 on 09/08/12
For personal use only.

Fig. 3. Calculated pressures, P_{calc}, vs. experimental values (14), P_{exp}, for the methanol(1) + 2-propanone(2) + C_6H_{12} (3) system at 313.15 K.



containing only hydrocarbons (4), or two 1-alkanols and an *n*-alkane or cyclohexane (6, 7). In this study, ternary system nos. 16–21 (Table 1) have maximum H^E values similar to the larger H^E values of the related binary systems (Table 2).

3. The DISQUAC model

3.1 Theory

The equations used to calculate thermodynamic properties in the framework of DISQUAC are given elsewhere (46). The temperature dependence of the interaction parameters is expressed in terms of the dispersive (DIS) and quasichemical (QUAC) interchange coefficients $C^{DIS}_{st,l}$ and $C^{QUAC}_{st,l}$, where s, t are different types of groups: (s, t = a, aliphatic in *n*-alkanes; b, aromatic in benzene; c, cyclic in cyclohexane; h, hydroxyl in 1-alkanols; k, carbonyl in linear ketones; and *l* is the order of interchange coefficient: *l* = 1, Gibbs energy; *l* = 2, enthalpy; *l* = 3, heat capacity. For the QUAC part, the coordination number is *z* = 4.

3.2 Assessment of geometrical parameters

The relative molecular volumes, r_i, the surfaces, q_i, and the surface fractions, α_{si}, of all the molecular species have been calculated on the basis of the group volumes and surfaces recommended by Bondi (47), taking the volume and the surface of methane arbitrarily as unity (48). The values of r_i and q_i of the groups referred to in this work are given elsewhere (46, 48, 49).

3.3 The interaction parameters

The ternary mixtures studied can be classified, based on the different groups present in the system being considered.

1. In ternary mixtures 1–4 and 13–15, there are three groups: hydroxyl, carbonyl, and aliphatic and, consequently, only three contacts:

hydroxyl–aliphatic	(7, 46, 50)
carbonyl–aliphatic	(51)
hydroxyl–carbonyl	(1)

2. In mixtures 5–12 and 18–21, the groups involved are hydroxyl, carbonyl, aliphatic, and cyclic or aromatic giving six interactions:

hydroxyl–aliphatic	(7, 46, 50)
carbonyl–aliphatic	(51)
hydroxyl–carbonyl	(1)
hydroxyl–cyclic or hydroxyl–aromatic	(52–55)
carbonyl–cyclic or carbonyl–aromatic	(51)
aliphatic–cyclic or aliphatic–aromatic	(56, 57)

3. Mixtures 16 and 17 contain two alcohols and, hence, two different hydroxyl groups, because in our approach the different self-association of each alcohol is characterized by its own set of interaction parameters (1, 7, 46, 52–55). Thus, in these mixtures there are also four groups: two hydroxyl, one carbonyl, and one aliphatic, and six interactions:

© 1997 NRC Canada

Table 3. Comparison of the direct maximum (F^E_{max}) and minimum (F^E_{min}) experimental results (exp.) of the excess function related to the thermodynamic property treated for each ternary system considered in this work with DISQUAC calculations (calcd.). This comparison is extended to the binaries involved (F^E_{max} is then the value at equimolar composition). σ_r is the relative standard deviation.

Ternary system	Binaries involved	F^E_{min}/J mol^{-1}		F^E_{max}/J mol^{-1}		σ_r
		Exp.	Calcd.	Exp.	Calcd.	
1		—	—	—	—	0.012
	1	383[a]	359			0.006
	2	1669[a]	1616			0.029
	3	917[a]	926			0.003
2		—	—	—	—	0.027
	4	433[a]	425			0.004
	5	1640[a]	1579			0.038
	6	1051[a]	1054			0.010
3		—	—	—	—	0.008
	7	348[a]	352			0.003
	8	1415[a]	1382			0.012
	3	917[a]	926			0.003
4		—	—	—	—	0.009
	9	415[a]	455			0.015
	10	1500[a]	1440			0.030
	11	1029[a]	1035			0.008
5		—	—	—	—	0.031
	12	456[a]	442			0.005
	13	854[a,b]	821			0.057
	14	1122[a]	1132			0.019
6		—	—	—	—	0.030
	15	448[a]	434			0.005
	16	867[a,b]	834			0.056
	17	1108[a]	1117			0.010
7		—	—	—	—	0.012
	18	474[a]	429			0.015
8		—	—	—	—	0.029
	4	433[a]	425			0.004
	19	885[a,b]	845			0.059
	20	1091[a]	1102			0.008
9		—	—	—	—	0.021
	21	481[a]	411			0.020
	22	1690[a]	1631			0.044
	23	1090[a]	1086			0.012
10		1096[a]	1101	524	549	0.050
	24	473[a]	466			0.007
	25	1128[a]	1130			0.006
	26	282[a]	263			0.006
11		1043[a]	1031	252	266	0.069
	27	549[a]	551			0.007
	28	1100[a]	1117			0.010
	29	141[a]	139			0.005
12		—	—	—	—	0.021
	30	568[a]	494			0.028
	31	575[a]				0.026
	32	1180[a]	1131			0.018
	25	1128[a]	1130			0.006
	33	116[a]	150			0.012
13		1558[c]	1372	418	318	0.120
	34	1232[c]	1222			0.019
	35	561[c]	547			0.049
	36	1024[c]	968			0.069

Can. J. Chem. Downloaded from www.nrcresearchpress.com by 91.121.58.235 on 09/08/12
For personal use only.

© 1997 NRC Canada

Can. J. Chem. Downloaded from www.nrcresearchpress.com by 91.121.58.235 on 09/08/12
For personal use only.

Table 3 (*concluded*).

Ternary system	Binaries involved	F^E_{min}/J mol^{-1} Exp.	F^E_{min}/J mol^{-1} Calcd.	F^E_{max}/J mol^{-1} Exp.	F^E_{max}/J mol^{-1} Calcd.	σ_r
14		1638[c]	1429	548	488	0.120
	34	1232[c]	1222			0.019
	37	617[c]	603			0.031
	38	1105[c]	1040			0.078
15		1702[c]	1482	361	314	0.120
	34	1232[c]	1222			0.019
	39	673[c]	657			0.037
	40	1165[c]	1106			0.080
16		1364[c]	1417	226	220	0.030
	34	1232[c]	1222			0.019
	41	64[c]	63			0.034
	42	1435[c]	1472			0.020
17		1424[c]	1456	169	151	0.120
	34	1232[c]	1222			0.019
	43	103[c]	105			0.059
	44	1510[c]	1578			0.048
18		745[c]	614	85	87	0.130
	45	694[c]	686			0.066
	46	622[c]	615			0.034
	47	138[c]	123			0.140
19		1099[c]	944	118	119	0.120
	48	1124[c]	1127			0.011
	49	761[c]	740			0.028
	47	138[c]	123			0.140
20		1330[c]	1191	157	159	0.089
	50	1390[c]	1383			0.038
	51	950[c]	932			0.061
	47	138[c]	123			0.140
21		1150[c]	1096	105	134	0.089
	52	1251[c]	1267			0.033
	51	950[c]	932			0.061
	53	−50[c]	−50			1.9

[a]Excess function, G^E; σ_r calculated for pressure.
[b]Nonmiscible system, value at $x_1 = 0.125$.
[c]Excess function, H^E; σ_r calculated for H^E.

hydroxyl–aliphatic (two)	(7, 46, 50)
hydroxyl–carbonyl (two)	(1)
carbonyl–aliphatic	(51)
hydroxyl–hydroxyl	(7)

As indicated above, most of the interaction parameters are available in the literature, and since ternary interactions are neglected, new interchange coefficients are not needed to develop the calculations.

Only the interchange coefficients for the carbonyl–aromatic contact need to be estimated. This was previously done for the 2-butanone + benzene mixture, assuming that the carbonyl–aromatic contact is represented by dispersive parameters only (58). Under this assumption, the interchange coefficients for the 2-propanone + benzene system were estimated to be $C^{DIS}_{bk,1} = 5.50$ and $C^{DIS}_{bk,2} = 5.30$, on the basis of the data given in refs. 40 and 44. For the 2-butanone + benzene mixture system, we used $C^{DIS}_{bk,1} = 5.50$ (slightly different than 5.40, previously reported (58)) and $C^{DIS}_{bk,2} = 5.50$. We note the large difference between experimental and calculated H^E at 298.15 K for this system (No. 53 Table 3: $\sigma_r = 1.9$). This is due to the low endothermic value of H^E (ca. 9 J mol^{-1}), even though the s-shape of H^E is well-represented by DISQUAC.

4. Results and discussion

A comparison between experimental and calculated values of the excess functions, G^E and H^E, maximum and minimum, at the same compositions for the ternary systems considered is given in Table 3. Also listed are the relative standard deviations σ_r defined as:

$$[1] \quad \sigma_r = [1/N \Sigma (M_{calc} - M_{exp})^2/M^2_{exp}]^{1/2}$$

© 1997 NRC Canada

Fig. 4. VLE at 313.15 K for the binaries involved in the methanol(1) + 2-propanone(2) + C_6H_{12} (3) system at the same temperature. Lines, DISQUAC results; points, experimental values: ▲, methanol(1) + 2-propanone(2) (28); ●, methanol(1) + C_6H_{12} (2) (14); ■, 2-propanone(1) + C_6H_{12} (2) (14) (x_1 and y_1 are, respectively, the mole fractions in the liquid and vapor phases).

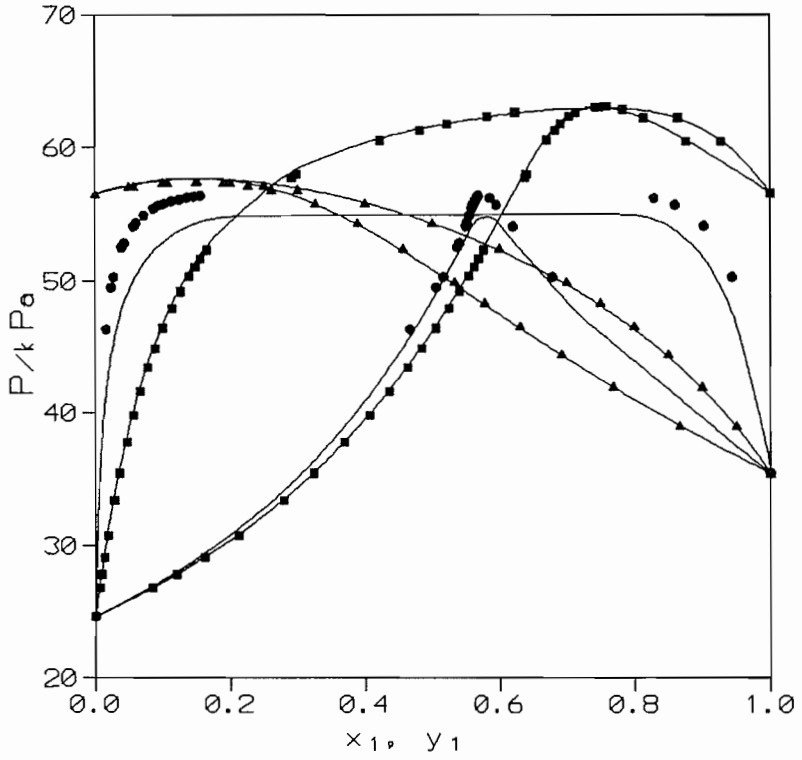


Fig. 5. H^E for 1-propanol(1) + 3-pentanone(2) + organic solvents(3) systems at 298.15 K and at different x_1/x_2 ratios. Lines, DISQUAC results;(—), 1-hexanol(3); (---), n-C_6(3); points, experimental values: for 1-hexanol(3), ●, $x_1/x_2 = 0.333$; ■, $x_1/x_2 = 1.000$; ▲, $x_1/x_2 = 3.008$ (20); for n-C_6 (3), ▼, $x_1/x_2 = 3.016$ (18).

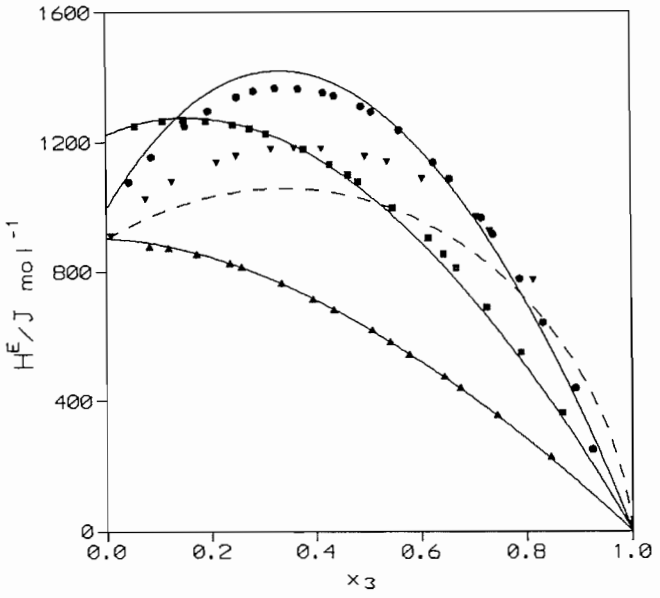
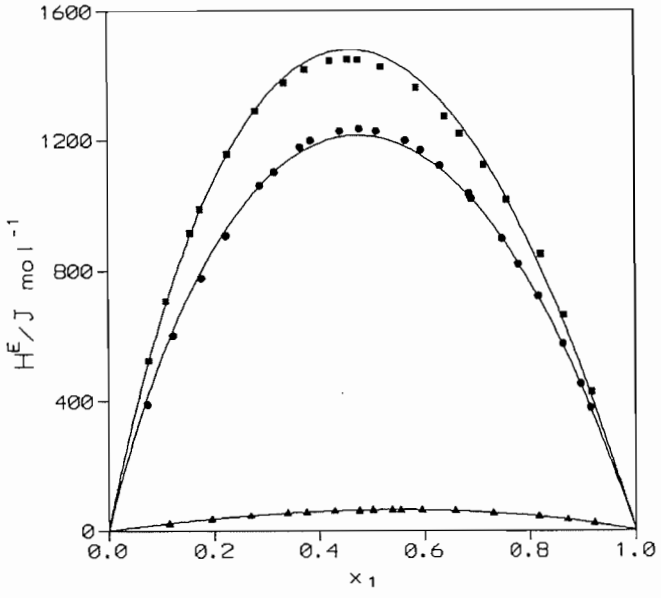


Fig. 6. H^E at 298.15 K for the binaries involved in the 1-propanol(1) + 3-pentanone(2) + 1-hexanol(3) system at the same temperature. Lines, DISQUAC results; points, experimental values: ●, 1-propanol(1) + 3-pentanone(2) (18); ▲, 1-propanol(1) + 1-hexanol(2) (20); ■, 1-hexanol(1) + 3-pentanone(2) (20).



Can. J. Chem. Downloaded from www.nrcresearchpress.com by 91.121.58.235 on 09/08/12
For personal use only.

© 1997 NRC Canada

Can. J. Chem. Downloaded from www.nrcresearchpress.com by 91.121.58.235 on 09/08/12
For personal use only.

Table 4. Comparison of experimental (exp.) coordinates of azeotropes: pressure (P^{az}), temperature (T^{az}), and mole fraction (x_1^{az}) for some of the mixtures involved in the ternary systems nos. 1–12 (property investigated: VLE) with DISQUAC values (calcd.).

		P^{az}/kPa		x_1^{az}		
Mixture[a]	T^{az}/K	Exp.	Calcd.	Exp.	Calcd.	Reference
1CO1 + *n*-C_5	238.15	4.274	4.317	0.2061	0.2004	29
	372.7	672.0	671.2	0.299	0.3055	27
1CO1 + *n*-C_6	253.15	4.047	4.084	0.6219	0.6110	29
	318.15	86.40	85.12	0.6420	0.6373	29
	328.15	120.3	120.6	0.6440	0.6497	60
1CO1 + C_6H_{12}	293.15	28.08	27.75	0.740	0.7101	12
	313.15	63.07	63.03	0.748	0.7458	14
	323.15	90.47	89.48	0.7677	0.7595	37
1CO2 + C_6H_6	298.15	13.39	13.34	0.271	0.2714	16
	313.15	25.26	25.68	0.3332	0.3145	61
MeOH + *n*-C_5	372.7	846.0	845.4	0.348	0.3476	26
MeOH + *n*-C_6	313.15	69.03	66.82	0.479	0.4867	9
EtOH + *n*-C_5	372.7	685.0	680.1	0.221	0.2149	31
EtOH + *n*-C_6	328.15	90.35	88.05	0.333	0.3322	32
EtOH + C_6H_6	298.15	16.89	16.82	0.307	0.3165	16
	313.15	33.42	33.35	0.356	0.3658	39
MeOH + 1CO1	313.15	57.48	57.71	0.1519	0.1508	28
	372.7	405.8	402.3	0.460	0.4598	25
EtOH + 1CO2	298.15	13.04	12.97	0.261	0.2538	16

[a]For abbreviations see Table 1.

Fig. 7. H^E at 298.15 K for the binaries involved in the 1-propanol(1) + 3-pentanone(2) + *n*-C_6 (3) system at the same temperature. Lines, DISQUAC results; points, experimental values (18): ●, 1-propanol(1) + 3-pentanone(2) (18); ■, 1-propanol(1) + *n*-C_6 (2); ▲, 3-pentanone(1) + *n*-C_6.

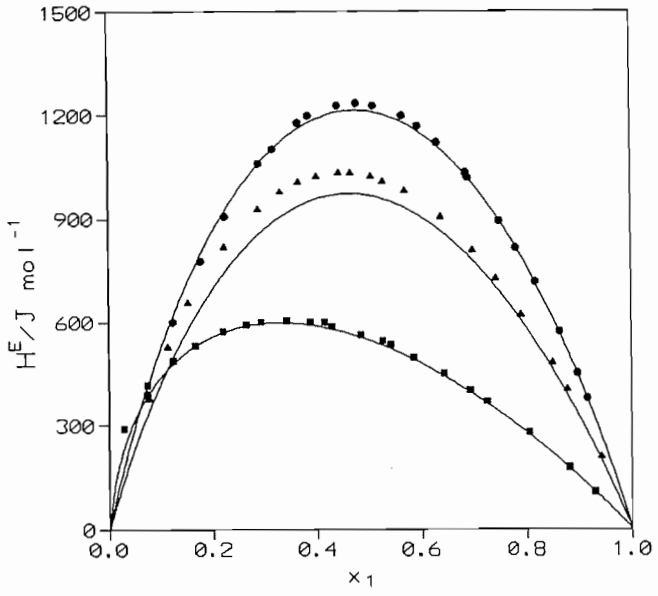
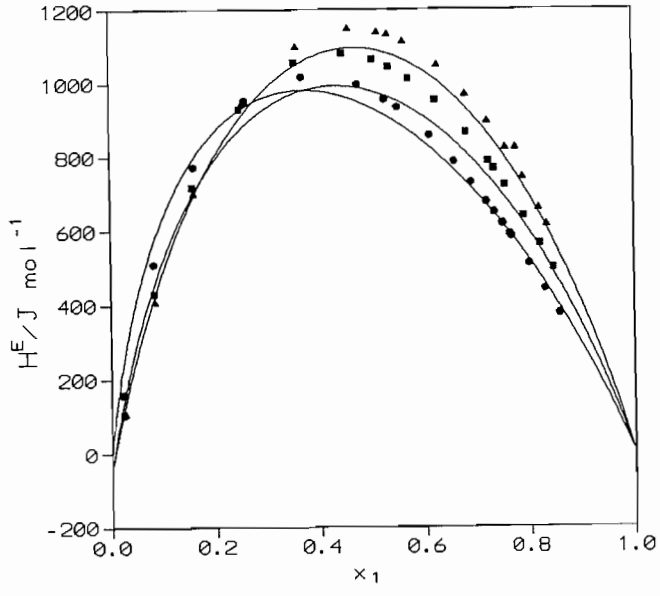
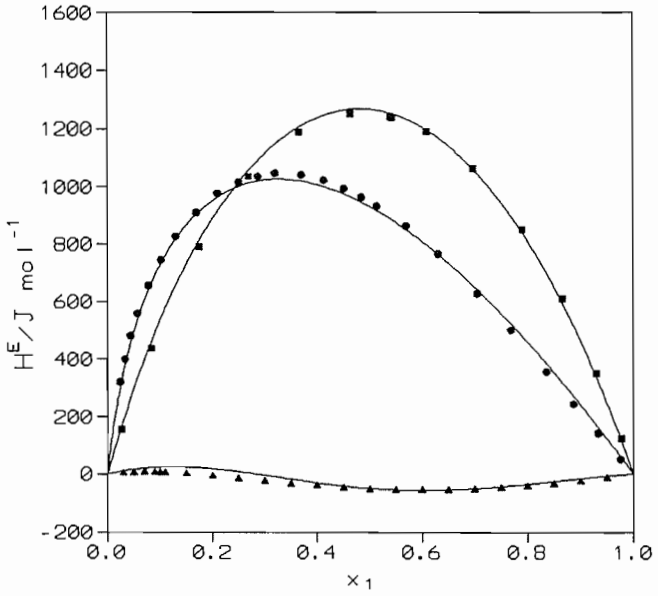


Fig. 8. H^E for 1-propanol(1) + 2-butanone(2) + C_6H_6 (3) system at 298.15 K and at different x_2/x_3 ratios. Lines, DISQUAC results; points, experimental values (24): ●, x_2/x_3 = 0.333; ■, x_2/x_3 = 1.000; ▲, x_2/x_3 = 3.000.



© 1997 NRC Canada

Fig. 9. H^E at 298.15 K for the binaries involved in the 1-propanol(1) + 2-butanone(2) + C_6H_6 (3) system at the same temperature. Lines, DISQUAC results; points, experimental values: ■, 1-propanol(1) + 2-butanone(2) (24); ●, 1-propanol(1) + C_6H_6 (2) (43); ▲, 2-butanone(1) + C_6H_6 (2) (45).



where M is the pressure or the H^E, and N is the number of experimental data points. In a similar way, we extend this comparison for the binaries involved in the ternary mixtures studied. A comparison between experimental and calculated values of some ternary and binary systems are presented graphically in Figs. 1–9.

As indicated in Table 3, DISQUAC yields a better representation of the ternary VLE than of H^E. Thus, the average relative standard deviation, calculated as $\Sigma\sigma_r$/(no. of systems), is 0.026 for the pressure (12 systems) and 0.098 for H^E (9 systems). Of course, this model, and any similar model, reproduces such a primary fluid phase equilibrium rather accurately. Nevertheless, it is noteworthy that good results are obtained for the prediction of VLE for these rather complex ternary mixtures at very high temperatures (systems 1, 3), or when some of the binaries involved present a miscibility gap (systems 5–8). It is also remarkable that DISQUAC yields good predictions close to the critical points (see ref. 59 and results for the methanol + *n*-hexane mixture at 313.15 K, Table 3). On the other hand, we note that σ_r (ternary) $\simeq$ σ_r (binary) for VLE, and that the experimental values are in excellent agreement with those calculated for the azeotrope coordinates of the binaries involved in ternary system nos. 1–12, even over a wide range of temperature (Table 4).

In the case of H^E, σ_r (ternary) > σ_r (binary), and DISQUAC results for the ternary systems considered here depend on the third compound added to the 1-alkanol + *n*-alkanone binary mixture, not on the number of the interactions present.

When an *n*-alkane is added, the H^E of the ternary system formed (characterized in terms of DISQUAC by three interactions, see above) is larger than the H^E of the binaries involved. This is probably due to the increase in the number of broken alkanol–alkanol hydrogen bonds, the rupture of the OH---O=C hydrogen bond complexes, and the increasing importance of the ketone–ketone interactions. Some of these effects are already taken into account by DISQUAC to rather accurately represent the thermodynamic properties of the binaries 1-alkanols + *n*-alkanones (1). However, now they become more marked and DISQUAC yields H^E s that are lower than the experimental values.

However, if a third active compound is added, e.g., benzene (the ternary system is then characterized by six interactions), the effects mentioned above are compensated by new interactions between dissimilar molecules, such as alkanol–benzene or ketone–benzene, lowering the H^E in comparison to that of a ternary system of the type 1-alkanol + *n*-alkanone + *n*-alkane. DISQUAC results are then improved (Table 3). On the other hand, we note that the H^E maxima of the 1-alkanol + *n*-alkanone + benzene systems are similar to those of the binary 1-alkanol + *n*-alkanone (Tables 1, 2).

Thus, better predictions are obtained when the ternary system (also characterized by six interactions) contains two alkanols because, in this case, the system is more similar to the binary 1-alkanol + *n*-alkanone.

5. Conclusions

DISQUAC rather accurately describes the VLE of the ternary systems studied, even when some of the binaries involved show a miscibility gap. However, predictions of H^E are poorer. They depend on a third compound added to the binary 1-alkanol + *n*-alkanone. The more active this component, the better the results.

References

1. J.A. González. Can. J. Chem. **75**, 1412 (1997).
2. H.V. Kehiaian. Fluid Phase Equilib. **13**, 243 (1983).
3. H.V. Kehiaian. Pure Appl. Chem. **57**, 15 (1985).
4. J.A. González, I. García, J.C. Cobos, and C. Casanova. Thermochim. Acta, **168**, 31 (1990).
5. J.A. González, J.C. Cobos, I. García, and C. Casanova. Thermochim. Acta, **171**, 153 (1990).
6. J.A. González, I. García de la Fuente, J.C. Cobos, and C. Casanova. Ber. Bunsen-Ges. Phys. Chem. **98**, 106 (1994).
7. J.A. González, I. García de la Fuente, J.C. Cobos, and C. Casanova. Fluid Phase Equilib. **78**, 61 (1992).
8. R.A. Wilsak, S.W. Campbell, and G. Thodos. Fluid Phase Equilib. **33**, 173 (1987).
9. P. Oracz and S. Warycha. Fluid Phase Equilib. **108**, 199 (1995).
10. S.W. Campbell, R.A. Wilsak, and G. Thodos. J. Chem. Eng. Data, **32**, 454 (1987).
11. I.G. Vinichenko and M.P. Susarev. Zh. Prikl. Khim. (S.-Peterburg), **39**, 1583 (1966) (cf. ref. 62).
12. P. Oracz, M. Goral, G. Wilczek-Vera, and S. Warycha. Fluid Phase Equilib. **126**, 71 (1996).
13. A.N. Marinichev and M.P. Susarev. Zh. Prikl. Khim. (S.-Peterburg), **38**, 1054 (1965) (cf. ref. 62).
14. P. Oracz, M. Goral, G. Wilczek-Vera, and S. Warycha. Fluid Phase Equilib. **112**, 291 (1995).
15. I. Nagata and K. Tamura. J. Chem. Eng. Data, 41, 870 (1996).
16. T. Ohta, J. Koyabu, and I. Nagata. Fluid Phase Equilib. **7**, 65 (1981).
17. V.T. Zharov and T.A. Buevich. Zh. Prikl. Khim. (S.-Peterburg), **41**, 2032 (1968) (cf. ref. 62).
18. M. López, J.L. Legido, L. Romaní, E. Carballo, E. Pérez Martell, E. Jiménez, and M.I. Paz Andrade. J. Chem. Thermodyn. **24**, 205 (1992).

Can. J. Chem. Downloaded from www.nrcresearchpress.com by 91.121.58.235 on 09/08/12
For personal use only.

© 1997 NRC Canada

19. M. López, J.L. Legido, E. Jiménez, L. Romaní, E. Carballo, and M.I. Paz Andrade. J. Chem. Thermodyn. **25**, 321 (1993).
20. M. López, J.L. Legido, L. Romaní, J. Peleteiro, and M.I. Paz Andrade. J. Chem. Eng. Data, **38**, 238 (1993).
21. I. Nagata. Thermochim. Acta, **236**, 23 (1994).
22. I. Nagata and A. Ksiazczak. J. Chem. Thermodyn. **26**, 165 (1994).
23. I. Nagata and K. Takeuchi. Thermochim. Acta, **242**, 103 (1994).
24. K. Tamura and I. Nagata. J. Chem. Thermodyn. **23**, 359 (1991).
25. R.A. Wilsak, S.W. Campbell, and G. Thodos. Fluid Phase Equilib. **28**, 13 (1986).
26. R.A. Wilsak, S.W. Campbell, and G. Thodos. Fluid Phase Equilib. **33**, 157 (1987).
27. S.W. Campbell, R.A. Wilsak, and G. Thodos. J. Chem. Eng. Data, **31**, 424 (1986).
28. M. Goral, G. Kolasińska, P. Oracz, and S. Warycha. Int. DATA Ser. Sel. Data Mixtures Ser. A, **3**, 203 (1985).
29. J.R. Loehe and H.C. Van Ness. Int. DATA Ser. Sel. Data Mixtures, Ser. A, **1**, 45 (1979).
30. S.W. Campbell, R.A. Wilsak, and G. Thodos. J. Chem. Eng. Data, **32**, 357 (1987).
31. S.W. Campbell, R.A. Wilsak, and G. Thodos. J. Chem. Thermodyn. **19**, 449 (1987).
32. K.S. Yuan, B.C.-Y. Lu, J.C.K. Ho, and A.K. Keshpande. J. Chem. Eng. Data, **8**, 549 (1963).
33. G.C. Benson. Int. DATA Ser. Sel. Data Mixtures Ser. A, **1**, 55 (1979).
34. A.N. Marinichev and M.P. Susarev. Zh. Prikl. Khim. (S-Peterburg), **38**, 378 (1965) (cf. ref. 62).
35. M. Goral, P. Oracz, and S. Warycha. Fluid Phase Equilib. **81**, 261 (1992).
36. A.N. Marinichev and M.P. Susarev. Zh. Prikl. Khim. (S.-Peterburg), **38**, 1619 (1965) (cf. ref. 62).
37. A. Crespo Colín, A. Compostizo, and M. Díaz Peña. J. Chem. Thermodyn. **16**, 497 (1984).
38. H.C. Van Ness and M.M. Abbott. Int. DATA Ser. Sel. Data Mixtures, Ser. A, **1**, 65 (1978).
39. J. Zielkiewicz, P. Oracz, and S. Warycha. Fluid Phase Equilib. **58**, 191 (1990).
40. I. Brown and F. Smith. Aust. J. Chem. **10**, 423 (1957).
41. I. Nagata, T. Ohta, and S. Nakagama. J. Chem. Eng. Jap. **9**, 276 (1976) (cf. ref. 62).
42. N. Van Nhu and F. Kohler. Int. DATA Ser. Sel. Data Mixtures Ser. A, **4**, 240 (1990).
43. H.C. Van Ness and M.M. Abbott. Int. DATA Ser. Sel. Data Mixtures Ser. A, **1**, 5 (1976).
44. Y. Akamatsu, H. Ogawa, and S. Murakami. Thermochim. Acta, **113**, 141 (1987).
45. O. Kiyohara, G.C. Benson, and J.-P.E. Grolier. J. Chem. Thermodyn. **9**, 315 (1977).
46. J.A. González, I. García de la Fuente, J.C. Cobos, and C. Casanova. Ber. Bunsen-Ges. Phys. Chem. **95**, 1658 (1991).
47. A. Bondi. Physical properties of molecular crystals, liquids and glasses. J. Wiley & Sons, New York. 1968.
48. H.V. Kehiaian, J.-P.E. Grolier, and G.C. Benson. J. Chim. Phys. Phys.-Chim. Biol. **75**, 1031 (1978).
49. H.V. Kehiaian, J.-P.E. Grolier, M.R. Kechavarz, and G.C. Benson. Fluid Phase Equilib. **5**, 159 (1980).
50. J.A. González, I. García de la Fuente, J.C. Cobos, C. Casanova, and U. Domańska. Ber. Bunsen-Ges. Phys. Chem. **98**, 955 (1994).
51. H.V. Kehiaian, S. Porcedda, B. Marongiu, L. Lepori, and E. Matteoli. Fluid Phase Equilib. **63**, 231 (1991).
52. J.A. González, I. García de la Fuente, J.C. Cobos, and C. Casanova. J. Solution Chem. **23**, 399 (1994).
53. U. Domańska and J. A. González. Fluid Phase Equilib. **123**, 167 (1996).
54. J.A. González, I. García de la Fuente, J.C. Cobos, and C. Casanova. Fluid Phase Equilib. **93**, 1 (1994).
55. U. Domańska and J.A. González. Fluid Phase Equilib. **119**, 131 (1996).
56. J.A. González, I. García de la Fuente, J.C. Cobos, C. Casanova, and A. Ait-Kaci. Fluid Phase Equilib. **112**, 63 (1995).
57. A. Ait-Kaci. Ph.D. thesis, University of Lyon, France. 1982.
58. A. Yahiaoui, J.A. González, A. Ait-Kaci, and H.V. Kehiaian. Fluid Phase Equilib. **98**, 179 (1994).
59. J.A. González, I. García de la Fuente, and J.C. Cobos. Ber. Bunsen-Ges. Phys. Chem. **101**, 219 (1996).
60. G.C. Benson. Int. DATA Ser. Sel. Data Mixtures Ser. A, **1**, 58 (1979).
61. H.C. Van Ness and F. Kohler. Int. DATA Ser. Sel. Data Mixtures Ser. A, **4**, 251 (1990).
62. J. Gmehling and U. Onken. Vapor–liquid equilibrium data collection. Vol. I. Part 2a. DECHEMA. 1977; J. Gmehling, U. Onken, and W. Arlt. Vapor–liquid equilibrium data collection. Vol. I. Part 2b. DECHEMA. 1980; J. Gmehling, U. Onken, and W. Arlt. Vapor–liquid equilibrium data collection. Vol. I. Part 2c. DECHEMA. 1982.

Can. J. Chem. Downloaded from www.nrcresearchpress.com by 91.121.58.235 on 09/08/12
For personal use only.

© 1997 NRC Canada

Transition state stabilization by micelles: the hydrolysis of *p*-nitrophenyl alkanoates in cetyltrimethylammonium bromide micelles

Oswald S. Tee and Alexei A. Fedortchenko

Abstract: The cleavage of *p*-nitrophenyl alkanoates (acetate to octanoate) at high pH is modestly catalyzed by micelles formed from cetyltrimethylammonium bromide (CTAB) in aqueous solution. Rate constants exhibit saturation behaviour with respect to [CTAB], consistent with substrate binding in the micelles. The strength of substrate binding and transition state binding to the micelles increases monotonically with the acyl chain length, and with exactly the same sensitivity. As a result, the extent of acceleration (or catalytic ratio) is independent of the ester chain. These and earlier results are consistent with the reaction centre being located in the Stern layer of the micelle, with the acyl chain of the ester being directed into the hydrophobic micellar interior. The chain length dependence of kinetic parameters found in this work is comparable to that found previously for ester cleavage by cyclodextrins and by various enzymes with hydrophobic binding sites, as well as to that observed for other phenomena involving hydrophobic effects.

Key words: catalysis, ester hydrolysis, micelles, transition state.

Résumé : Le clivage des *p*-nitrophényl alcanoates (allant de l'acétate à l'octanoate) à pH élevé est modérément catalysé par des micelles formées à partir du bromure de cétyltriméthylammonium (BCTA) en solution aqueuse. Les constantes de vitesse exhibent un comportement de saturation par rapport à [BCTA], ce qui est en accord avec un substrat lié dans les micelles. La force de la liaison du substrat et la liaison de l'état de transition aux micelles augmente de façon monotone avec la longueur de la chaîne acyle, et avec exactement la même sensibilité. Conséquemment, l'importance du taux d'accélération (ou rapport catalytique) est indépendante de la chaîne de l'ester. Ces résultats ainsi que des résultats antérieurs sont en accord avec le centre de réaction localisé dans la couche de Stern de la micelle, avec la chaîne de l'ester dirigée vers l'intérieur hydrophobe de la micelle. L'influence de la longueur de la chaîne sur les paramètres cinétiques, mise en évidence dans ce travail, est comparable à celle trouvée antérieurement lors du clivage des esters par la cyclodextrine et par divers enzymes ayant des sites hydrophobes de liaison, aussi bien que celle observée pour d'autres phénomènes impliquant des effets hydrophobes.

Mots clés : catalyse, hydrolyse d'ester, micelles, état de transition.

[Traduit par la rédaction]

Introduction

One of our current interests is the stabilization of transition states by catalysts (1). In this regard, we make use of an approach developed by Kurz for acid-catalyzed reactions (2), based on transition state theory. As detailed elsewhere (1–3), we define an apparent constant (K_{TS}) for dissociation of the transition state of the catalyzed reaction (TS.cat) into the transition state of the normal reaction (TS) and the catalyst (cat), as in eq. [1].

$$[1] \quad K_{TS} = \frac{[TS][cat]}{[TS.cat]} = \frac{k_u}{k_2} = \frac{k_u K_S}{k_c}$$

Received May 16, 1997.

O.S. Tee[1] and A.A. Fedortchenko. Department of Chemistry and Biochemistry, Concordia University, Montréal, QC H3G 1M8, Canada.

[1] Author to whom correspondence may be addressed. Telephone: (514) 848-3348. Fax: (514) 848-2868. E-mail: ostee@vax2.concordia.ca.

In eq. [1], k_u is the rate constant in the absence of catalysis, and k_2 is the second-order rate constant for reaction with the catalyst. If saturation kinetics are observed, with a dissociation constant K_S for the {substrate.catalyst} complex, and rate constant k_c for its reaction, then $k_2 = k_c/K_S$. Note that according to eq. [1], $k_c/k_u = K_S/K_{TS}$, which implies that catalytic acceleration is a consequence of transition state binding that is stronger than substrate binding.

We have applied eq. [1] to many reactions mediated by cyclodextrins (1, 3–6) but it is equally applicable to reactions catalyzed by enzymes, catalytic antibodies, metal ions, acids, bases, and micelles (1). In fact, the approach has been used by enzymologists for many years (7), and it has recently been adopted by Kirby (8) for reactions catalyzed by enzyme mimics. In the present paper we again apply eq. [1] to a reaction that is catalyzed by micelles.

The effects of micelles on organic reactions have been extensively studied (9). These effects may be catalytic, or inhibitory, depending on the structure of the reactants, the charge type of the reaction, and the type of surfactant (cationic, anionic, or neutral) forming the micelles. For the most part, catalytic effects can be understood in terms of the ability of micelles to provide a new reaction environment, and to con-

© 1997 NRC Canada

Can. J. Chem. Downloaded from www.nrcresearchpress.com by 91.121.58.235 on 09/08/12
For personal use only.

Can. J. Chem. Downloaded from www.nrcresearchpress.com by 91.121.58.235 on 09/08/12
For personal use only.

centrate reagents at the micelle–water interface, in the so-called Stern layer.

One of the classic papers in the field of micellar catalysis is that by Menger and Portnoy (10), who introduced a pseudophase model of catalysis. Among other things, they studied the basic hydrolysis of *p*-nitrophenyl acetate and *p*-nitrophenyl octanoate (pNPA and pNPO) in the presence of micelles formed from dodecyltrimethylammonium bromide. Previously, Cordes and co-workers (11) had looked at the effects of micelles on several reactions, including the hydrolysis of pNPA and *p*-nitrophenyl hexanoate (pNPH) in micelles formed from cetyltrimethylammonium bromide (CTAB). Shortly after, Romsted and Cordes (12) studied the effect of various *n*-alkyltrimethylammonium bromides on the cleavage of pNPH and *p*-nitrophenyl laurate (dodecanoate). The main conclusions of these early studies were that catalysis of the ester hydrolysis is greater for longer esters and longer surfactants, and that it is promoted by inclusion of the substrates in the micelles because hydroxide ions are concentrated in the Stern layer of cationic (but not anionic) micelles, near the reactive part of the ester.

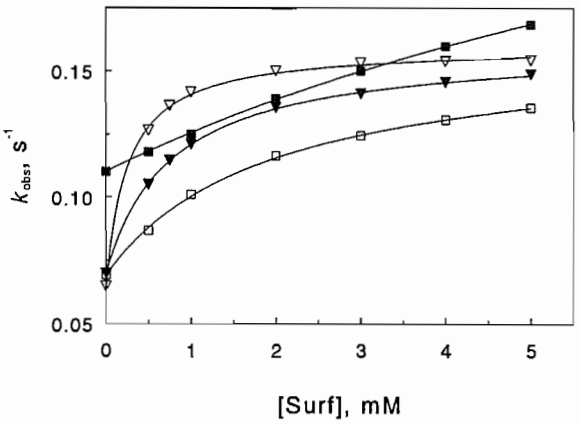
Later, Quina et al. (13) showed that the diminished rate of CTAB-catalyzed hydrolysis of pNPA and pNPO observed at high [CTAB] (>1 mM) can be explained by a preferential exchange of bromide ions for hydroxide ions in the Stern layer of the micelles. This and similar work on other micelle-catalyzed reactions gave rise to the pseudophase ionic exchange (PIE) model (14).

Much more recently, Al-Awadi and Williams (15) studied the hydrolysis of nine phenyl laurates (dodecanoates) in CTAB micelles. They found that the sensitivity of the micelle-catalyzed reaction to the leaving group ($\beta_{lg} = -0.51 \pm 0.06$) is virtually the same as that for hydrolysis in the basic aqueous medium ($\beta_{lg} = -0.56 \pm 0.05$). As we pointed out earlier (1), this situation arises because the binding of the esters and their transition states to the micelles is essentially independent of the substituent on the phenyl group. It also means that the transition state stabilization afforded by the CTAB micelles is the same regardless of the phenoxide leaving group, and it is consistent with the reaction centre being in a largely aqueous environment, while the acyl chain of the ester is directed into the hydrophobic interior of the micelle. It was suggested that this interpretation could be tested by studying a series of esters with different acyl chain lengths, to see if they show an appropriate sensitivity of transition state parameters to ester structure (1). The present paper describes just such a study.

Results

We have measured the kinetics of hydrolysis of a series of *p*-nitrophenyl alkanoates (acetate to octanoate) at high pH (11.6, phosphate buffer) as a function of the concentration of cetyltrimethylammonium bromide (CTAB), which forms cationic micelles. Reactions were carried out with constant bromide ion concentration (= 5 mM) to avoid the problem of ion exchange in the Stern layer of the micelles (13–15). As expected from previous studies, the reaction is modestly catalyzed, and it exhibits saturation behaviour with respect to [CTAB], as shown by the examples presented in Fig. 1. Experiments with dodecyltrimethylammonium bromide (DDTB) were also attempted but they were not as successful, because the catalytic effect is small. This probably arises because the micelles of DDTB are smaller and the critical micellar concentration (cmc) of DDTB is higher (16), so that inclusion of the alkanoate esters (and their transition states) in the micelles is less favorable.

Fig. 1. Effect of cetyltrimethylammonium bromide (CTAB) on the rate of hydrolysis of *p*-nitrophenyl alkanoates: acetate, ■; butanoate, □; pentanoate, ▼; hexanoate, ▽.



Analysis of the kinetic data was based on the pseudophase model introduced by Menger and Portnoy (10). In this model, it is assumed that the organic substrate is distributed between the aqueous phase and the micellar phase, in accord with an apparent dissociation constant, K_S (eq. [3]), and allowance is made for the hydrolysis of free ester (E) in the basic medium (eq. [2]) and of ester sequestered in the micellar pseudophase (E.Surf), eq. [3]. Together these two processes lead to a dependence of the overall rate constant for ester hydrolysis on concentration [Surf] as given in eq. [4].

$$[2] \quad \mathrm{E} \xrightarrow{k_u} \text{products}$$

$$[3] \quad \mathrm{E} + \mathrm{Surf} \underset{K_S}{\rightleftharpoons} \mathrm{E.Surf} \xrightarrow{k_c} \text{products}$$

$$[4] \quad k_{obs} = \frac{(k_u K_S + k_c[\mathrm{Surf}])}{(K_S + [\mathrm{Surf}])}$$

From experiments carried out over a range of [Surf] one can find values of k_c and K_S by nonlinear fitting of eq. [4], keeping k_u fixed at the measured value. Often, the correction [Surf] = ([Surf]$_0$ − cmc) is made (9), where [Surf]$_0$ is the stoichiometric concentration of the surfactant. However, since the critical micellar concentration (cmc) of CTAB is 9.2×10^{-4} M at zero ionic strength and much lower at high [salt] (16), we have followed Al-Awadi and Williams (15) and dispensed with the correction, in the interests of simplicity.[2] The measured values of k_u and fitted values of k_c and K_S are collected in Table 1, which also contains values of K_{TS}, calculated from eq. [1].

[2] In fact, we have determined that use of the correction makes no significant difference to the fitted values of k_c and K_S, or to the correlations of pK_S and pK_{TS} with chain length that are discussed below.

© 1997 NRC Canada

Table 1. Constants for the hydrolysis of *p*-nitrophenyl alkanoates in CTAB micelles, as a function of acyl chain length, *N*.[a]

N	k_u, s^{-1}	K_S, mM	k_c, s^{-1}	k_2, M^{-1} s^{-1}	K_{TS}, mM
2	0.110	11.4 ± 0.6	0.301 ± 0.008	26.4	4.17
3	0.107	5.29 ± 0.17	0.236 ± 0.003	44.6	2.39
4	0.0693	1.96 ± 0.10	0.161 ± 0.002	82.1	0.844
5	0.0697	0.769 ± 0.014	0.160 ± 0.001	208	0.335
6	0.0649	0.257 ± 0.013	0.160 ± 0.001	623	0.104
7	0.0630	0.0819 ± 0.0021	0.162 ± 0.001	1980	0.0319
8	0.0591	0.0423 ± 0.0031	0.147 ± 0.002	3480	0.0170

[a]At 25°C, in a 0.2 M aqueous phosphate buffer of pH 11.6 and with bromide ion concentration = [CTAB] + [NaBr] = 5.0 mM.

Discussion

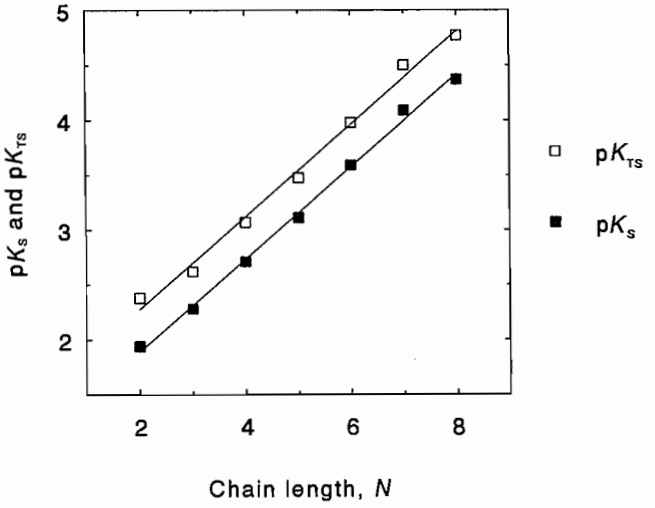
The constants in Table 1 can be used to probe the origins of the micellar catalysis of the hydrolysis of the esters. In particular, we can compare the sensitivities of substrate binding, reflected in pK_S (= $-\log K_S$), and transition state binding, through pK_{TS} (= $-\log K_{TS}$), to variations in the structure of the substrates (1).

From the data of Al-Awadi and Williams for phenyl laurate esters (15), both substrate and transition state binding parameters (pK_S and pK_{TS}) are independent of the phenoxide leaving group (1). For the present results for *p*-nitrophenyl alkanoates, the plot of pK_S against the ester chain length (*N*) is a straight line of slope 0.42 ± 0.01, and the plot of pK_{TS} against N is parallel, with a slope of 0.42 ± 0.02 (Fig. 2). Moreover, the plot of pK_{TS} against pK_S is a good straight line ($r = 0.999$), and has a slope of 1.00 ± 0.01, implying that the variations in substrate binding and transition state binding are governed by the same factors.

According to eq. [1], the limiting acceleration, or catalytic ratio, $k_c/k_u = K_S/K_{TS}$. As a consequence, the parallelism between pK_S and pK_{TS}, seen in Fig. 2, means that this ratio is essentially constant, at 2.4 ± 0.3, for acyl chain lengths from C_2 to C_8. So, contrary to what was surmised earlier from more limited data, the magnitude of the catalysis does not increase appreciably with the ester chain length, but the strength of substrate binding *and* transition binding does. Correspondingly, values of k_2 (= k_c/K_S) increase 130-fold, from 26 to 3480 M^{-1} s^{-1}, under the reaction conditions. For the catalytic ratio k_c/k_u to increase significantly with chain length would require the transition state binding (pK_{TS}) to be more sensitive to the acyl chain length than the initial state binding (pK_S).

The parallel dependence of pK_S and pK_{TS} on acyl chain length (Fig. 2) is consistent with incorporation of the substrates and their transition states in CTAB micelles being largely determined by hydrophobic effects. This assertion is based on the knowledge that many phenomena associated with hydrophobicity of *n*-alkyl derivatives vary linearly with chain length (16–21). For example, a plot of −log (cmc) against chain length (*N* = 10,12,14,16) for the micellization of *n*-alkyltrimethylammonium bromides is a straight line (r = 0.9998), with slope of 0.313 ± 0.004 (from data in Rosen (16)); other *n*-alkyl ionic surfactants show comparable behaviour (16, 17). Also, free energies of transfer (water → micelle, water → organic medium, and water → gas phase) for organic solutes vary linearly with solute chain length, and the solubility of organic solutes in micelles increases exponentially with surfactant chain length (16–19). In a similar way, the Hansch hydrophobicity parameters (π), which are based on partition coefficients, are also linear in *N* (20), as are microhydrophobicity parameters derived by Menger from kinetic measurements (21).

Fig. 2. Dependence of transition state binding (pK_{TS}, □) and substrate binding (pK_S, ■) to CTAB micelles on the acyl chain length (*N*) of *p*-nitrophenyl alkanoate esters. The slopes of both graphs are 0.42 ± 0.02. The corresponding plot of pK_{TS} against pK_S is linear (r = 0.999), and has a slope of 1.00 ± 0.01, suggesting that the same factors affect transition state binding and substrate binding.



In other work, we have shown that the strength of binding of many *n*-alkyl derivatives to cyclodextrins (22) is sensitive to chain length, with slopes of pK_S vs. *N* generally falling in the range 0.3–0.6 (23). Moreover, pK_{TS} values for the basic cleavage of *p*-nitrophenyl alkanoates by cyclodextrins vary linearly with *N*, with slopes of 0.2–0.3, except for short acyl chains (4*a*, 4*c*, 4*d*). These sensitivities to chain length are due, at least in part to hydrophobic effects (4*e*).

Another interesting comparison, derived from observations made by O'Connor and co-workers (24), is with the cleavage of esters, including *p*-nitrophenyl alkanoates, by various enzymes (lipases, chymotrypsin, trypsin, horse liver esterase),

Can. J. Chem. Downloaded from www.nrcresearchpress.com by 91.121.58.235 on 09/08/12
For personal use only.

© 1997 NRC Canada

which also shows distinct chain length dependences, with plots of log (k_{obs}) vs. N having slopes of 0.3–0.4. These values are consistent with the acyl binding site of the enzymes being quite hydrophobic. Similarly, values of log (k_{cat}/K_M), and hence pK_{TS}, for the cleavage of methyl esters of *N*-acetyl-L-α-amino acids by α-chymotrypsin correlate strongly with the Hansch hydrophobicity parameters of the α-substituents (1, 25).

It seems reasonable to conclude from all these observations that stabilization of the transition states in the various cases are partially or largely governed by similar hydrophobic effects.

Conclusions

In his recent discussions of the "molecular recognition of transition states," Kirby (8, 26) has emphasized two distinct components to transition state stabilization: *passive binding*, which arises from non-covalent interactions, comparable to those involved in equilibrium binding; *dynamic binding*, due to interactions at the reaction centre, particularly those associated with the making and breaking of covalent bonds. Seen in these terms, our conclusions for the hydrolysis of phenyl alkanoates in CTAB micelles are as follows: (*a*) the passive binding of the transition state involves hydrophobic binding of the acyl chain of the esters in the micelles, as does the substrate binding (Fig. 2); (*b*) the dynamic component is small and essentially constant, arising from the acyl transfer taking place in the largely aqueous environment of the Stern layer (1, 15).

Experimental

The esters were purchased from Sigma or were available from previous studies (4*a*, 4*c*, 4*d*, 4*e*). Cetyltrimethylammonium bromide (hexadecyltrimethylammonium bromide, CTAB) was obtained from ICN Biochemicals. All other chemicals were from the Aldrich Chemical Company, except for standard NaOH solutions, which were obtained from A & C Chemicals (Montreal).

The kinetics of the ester cleavage were followed by monitoring the first-order appearance of the *p*-nitrophenolate ion at 405 nm, using an Applied Photophysics SX17MV stopped-flow spectrophotometer, with the temperature of the cell kept at 25.0 ± 0.1°C. Usually, about 5–10 absorbance traces were computer averaged before estimation of k_{obsd} by nonlinear least-squares fitting of an exponential growth curve, using software supplied with the instrument.

Substrate concentrations were kept low with respect to [CTAB] so that the properties of the micelles were not significantly perturbed by the presence of the substrate (9, 10). Stock ester solutions (0.1 M in acetonitrile) were diluted in water to give twice the desired final concentrations. These were mixed 1:1 with a solution containing 0.4 M phosphate buffer + CTAB + NaBr whose pH had been adjusted to 11.6. Both reactant solutions were sonicated for 10–20 min to facilitate solubilization. The final reacting solutions contained 0.2 M phosphate buffer, CTAB (0–5 mM), NaBr (5 mM − [CTAB]), and ester concentrations as follows: acetate to pentanoate, 50 μM; hexanoate, 25 μM; heptanoate, 5 μM; octanoate, 2.5 μM.

Nonlinear fitting of eq. [4], and other such equations, was carried out with commercial (Prism) software.

Acknowledgement

We thank the Natural Sciences and Engineering Research Council of Canada for an operating grant and an equipment grant. Some exploratory studies were carried out a few years ago by Mr. T.A. Gadosy.

References

1. O.S. Tee. Adv. Phys. Org. Chem. **29**, 1, (1994).
2. J.L. Kurz. J. Am. Chem. Soc. **85**, 987 (1963); Acc. Chem. Res. **5**, 1 (1972).
3. O.S. Tee. Carbohydr. Res. **192**, 181 (1989).
4. (*a*) O.S. Tee, C. Mazza, and X.-X. Du. J. Org. Chem. **55**, 3603 (1990); (*b*) O.S. Tee and X.-X. Du. J. Am. Chem. Soc. **114**, 620 (1992); (*c*) T.A. Gadosy and O.S. Tee. J. Chem. Soc. Perkin Trans. 2, 715 (1994); 2609 (1994); (*d*) O.S. Tee and T.A. Gadosy. J. Chem. Soc. Perkin. Trans. 2, 2191 (1994); (*e*) O.S. Tee, C. Mazza, R. Lozano-Hemmer, and J.B. Giorgi. J. Org. Chem. **59**, 7602 (1994); (*f*) O.S. Tee and M.J. Boyd. J. Chem. Soc. Perkin Trans. 2, 1237 (1995); (*g*) O.S. Tee and R. Donga. J. Chem. Soc. Perkin. Trans. 2, 2763 (1996); (*h*) O.S. Tee and J.B. Giorgi. J. Chem. Soc. Perkin Trans. 2, 1013 (1997).
5. (*a*) O.S. Tee, M. Bozzi, J.J. Hoeven, and T.A. Gadosy. J. Am. Chem. Soc. **115**, 8990 (1993); (*b*) O.S. Tee, M. Bozzi, N. Clement, and T.A. Gadosy. J. Org. Chem. **60**, 3509 (1995); (*c*) J.B. Giorgi and O.S. Tee. J. Am. Chem. Soc. **117**, 3633 (1995); (*d*) T.A. Gadosy and O.S. Tee. Can. J. Chem. **74**, 745 (1996).
6. (*a*) O.S. Tee and T.A. Gadosy. J. Chem. Soc. Perkin Trans. 2, 2307 (1994); T.A. Gadosy and O.S. Tee. J. Chem. Soc. Perkin Trans. 2, 71 (1995); (*b*) O.S. Tee, T.A. Gadosy, and J.B. Giorgi. Can. J. Chem. **75**, 83 (1997).
7. (*a*) R. Wolfenden. Acc. Chem. Res. **5**, 10 (1972); (*b*) G.E. Leinhard. Science (Washington, D.C.), **180**, 149 (1973); (*c*) W.P. Jencks. Adv. Enzymol. **43**, 219 (1975); (*d*) R.L. Schowen. *In* Transition states in biochemical processes. *Edited by* R.D. Gandour and R.L. Schowen. Plenum, New York. 1978. Chap. 2. pp. 77–114; (*e*) J. Kraut. Science (Washington, D.C.), **242**, 533 (1988); (*f*) R. Wolfenden and W.M. Kati. Acc. Chem. Res. **24**, 209 (1991).
8. A.J. Kirby. Angew. Chem. Int. Ed. Engl. **35**, 707 (1996).
9. (*a*) I.V. Berezin, K. Martinek, and A.K. Yatsimirski. Russ. Chem. Rev. Eng. Trans. **42**, 787 (1973); (*b*) J.H. Fendler and E.J. Fendler. Catalysis in micellar and macromolecular systems. Academic Press, New York. 1975; (*c*) C.A. Bunton. *In* The chemistry of enzyme action. *Edited by* M.I. Page. Elsevier, Amsterdam. 1984. Chap. 13. pp. 461–500; (*d*) C.A. Bunton and G. Savielli. Adv. Phys. Org. Chem. **22**, 21 (1986).
10. F.M. Menger and C.E. Portnoy. J. Am. Chem. Soc. **89**, 4698 (1967).
11. M.T.A. Behme, J.G. Fullington, R. Noel, and E.H. Cordes. J. Am. Chem. Soc. **87**, 265 (1965).
12. L.R. Romsted and E.H. Cordes. J. Am. Chem. Soc. **90**, 4404 (1968).
13. F.H. Quina, M.J. Politi, I.M. Cuccovia, E. Baumgarten, S.M. Martins-Frachetti, and H. Chaimovich. J. Phys. Chem. **84**, 361 (1980).
14. C.A. Bunton, F. Nome, F.H. Quina, and L.S. Romsted. Acc. Chem. Res. **24**, 357 (1991).
15. N. Al-Awadi and A. Williams. J. Org. Chem. **55**, 2001 (1990).
16. M.J. Rosen. Surfactants and interfacial phenomena. 2nd ed. John Wiley and Sons, New York. 1989.
17. K.S. Birdi. *In* Micellization, solubilization and microemulsions. Vol. 1. *Edited by* K.L. Mittal. Plenum Press, New York. 1977. pp. 151–169.
18. (*a*) C. Tanford. The hydrophobic effect: formation of micelles and biological membranes. 2nd ed. John Wiley and Sons, New

Can. J. Chem. Downloaded from www.nrcresearchpress.com by 91.121.58.235 on 09/08/12
For personal use only.

© 1997 NRC Canada

York. 1980; (*b*) A. Ben-Naim. Hydrophobic interactions. Plenum, New York. 1980; (*c*) Solvation thermodynamics. Plenum, New York. 1987.
19. M.H. Abraham. J. Chem. Soc. Faraday Trans. 1, **80**, 153 (1984).
20. C. Hansch and A. Leo. Substituent constants for correlation analysis in chemistry and biology. John Wiley and Sons, New York. 1979.
21. F.M. Menger and U.V. Venkataram. J. Am. Chem. Soc. **108**, 2980 (1986).
22. (*a*) J. Szejtli. Cyclodextrins and their inclusion complexes. Akademiai Kiado, Budapest. 1982; (*b*) W. Saenger. Angew. Chem. Int. Ed. Engl. **19**, 344 (1980); (*c*) M. Bender and M. Komiyama. Cyclodextrin chemistry. Springer Verlag, New York. 1978.
23. (*a*) O.S. Tee, T.A. Gadosy, and J.B. Giorgi. Can. J. Chem. **74**, 736 (1996); (*b*) O.S. Tee, A.A. Fedortchenko, P.G. Loncke, and T.A. Gadosy. J. Chem. Soc. Perkin Trans. 2, 1243 (1996).
24. C.J. O'Connor, A.S.H. Mitha, and P. Walde. Aust. J. Chem. **39**, 249 (1986).
25. V.N. Dorovska, S.D. Varfolomeyev, N.F. Kazanskaya, A.A. Klyosov, and K. Martinek. FEBS Lett. **23**, 122 (1972).
26. A.J. Kirby. Philos. Trans. R. Soc. London, Ser. A: **345**, 67 (1993).

Can. J. Chem. Downloaded from www.nrcresearchpress.com by 91.121.58.235 on 09/08/12
For personal use only.

© 1997 NRC Canada

A study of the electrochemical synthesis of ZnO thin films

Z.H. Gu, T.Z. Fahidy, R. Hornsey, and A. Nathan

Abstract: The principal characteristics of the cathode deposition of zinc oxide from slightly acidified aqueous zinc nitrate solution at 65°C were studied via potentiodynamic electrolysis, potentiostatic electrolysis, and X-ray diffraction patterns. The results indicate the reliability of a low-temperature electrolytic path of synthesis, and avenues of further exploration.

Key words: zinc oxide, cathode deposition, XRD patterns, FBM theory.

Résumé : En se basant sur les résultats d'électrolyses potentiodynamique et potentiostatique ainsi que sur les patrons de diffraction des rayons X, on a étudié les principales caractéristiques du dépôt à la cathode d'oxyde de zinc à partir de solutions légèrement acidifiées de nitrate de zinc, à 65°C. Les résultats indiquent que la voie électrolytique à basse température est fiable pour la synthèse et qu'elle offre de nouvelles voies d'exploration.

Mots clés : oxyde zinc, dépôt à la cathode, patrons de diffraction des rayons X, théorie «FMB».

[Traduit par la rédaction]

Can. J. Chem. Downloaded from www.nrcresearchpress.com by 91.121.58.235 on 09/08/12
For personal use only.

Introduction

Zinc oxide (ZnO), in the bulk or thin film form, is an important material for a wide variety of applications. It is used as a vulcanizing activator for rubber (1, 2), a coloring agent in paints (3), a photoconducting material for copying machines (3), a highly transparent electrode material for solar cells (4), a phosphor material for converting radiation to visible light at low voltage (5), a piezoelectric material in mechanical transducers (6), and as a gas-detection material for microsensors (6).

Chemical preparation procedures in combination with various modern techniques have yielded ZnO films of high optical and electrical quality. The films have been synthesized by ion-assisted cyclic sputtering (7), radio-frequency sputtering (8), cold remote nitrogen plasma (9), zinc evaporation in mixed radio-frequency plasma (10), pulsed laser deposition (11), chemical beam deposition (12), chemical bath deposition (13), and spray pyrolysis (14, 15). A sol–gel technique has been used to prepare nanoparticles of ZnO (16), and an electrophorus-based technique has recently been developed to produce phosphor glasses (17). Among various techniques, low-temperature and relatively inexpensive electrochemical synthesis of thin films is highly attractive; in particular, specific film thickness and other properties can be achieved by controlling the electrode potential and chemical parameters of the electrolytes (18). An anode process (19) produces ZnO by first depositing zinc doped with nickel and cobalt onto a substrate in an acidic solution, and then oxidizing it in an alkaline solution. Ni and Co are homogeneously distributed within the anodically formed oxide layer, which shows *n*-type semiconductive properties. Most recently, a cathode process to produce various oxides was shown to be promising due to in situ doping capability (20), and initial applications of the cathode process for ZnO have also been reported (21–23).

The purpose of this paper is to describe an exploratory study of the cathode synthesis of zinc oxide films, and to outline the analysis of the experimental time-series data in terms of fractional Brownian motion (FBM) theory (24, 25). It is expected that this material will contribute to a deeper understanding of the cathode method of ZnO production, and of criteria for the optimal selection of the operating parameters.

Experimental apparatus and procedure

Figure 1 illustrates the overall apparatus. Electrolysis was carried out at 65°C in a $120 \times 90 \times 45$ mm^3 glass cell using a 60×10 mm^2 zinc anode. The cathodes, acting as substrates for the ZnO film deposits, were copper, platinum, and ITO (indium – tin oxide) coated glass plates with a 600 mm^2 active area, separated by a 30 mm distance from the anode. A saturated calomel electrode (SEC) with its Luggin capillary probe located 2 mm from the working electrode served as reference electrode. The electrolyte was an aqueous solution of 0.075 or 0.100 mol L^{-1} $Zn(NO_3)_2$ with its initial pH (pH_i) adjusted to 6.0 in order to avoid $Zn(OH)_2$ precipitation in the bulk solution. The effect of the initial pH was determined by setting pH_i = 4.1 and 6.8 in certain experiments. The deposition process was monitored via linear sweep voltammetry and potentiostatic electrolysis. A model AFRDE5 Pine potentiostat was

Received February 7, 1997.

This paper is dedicated to Professor Brian E. Conway on the occasion of his 70th birthday.

Z.H. Gu and T.Z. Fahidy.[1] Department of Chemical Engineering, University of Waterloo, Waterloo, ON N2L 3G1, Canada.

R. Hornsey and A. Nathan. Department of Electrical and Computer Engineering, University of Waterloo, Waterloo, ON N2L 3G1, Canada.

[1] Author to whom correspondence may be addressed. Telephone: (519) 888-4567, ext. 3310. Fax: (519) 746-4979. e-mail: tfahidy@dean.watstar.uwaterloo.ca

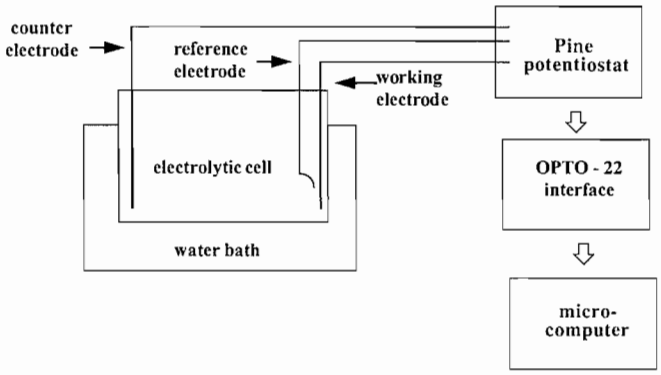
© 1997 NRC Canada

Table 1. Fundamental physicochemical properties of cathodic ZnO synthesis in an aqueous zinc nitrate solution of $[Zn(NO_3)_2]$ = 0.075 mol/L.

Cathode process, or chemical reaction	Equilibrium potential/constant at 65°C; potential unit: V (NHE scale)
(1) $2H_2O + 2e^- = H_2 + 2OH^-$	$E_1 = 0.0372 - 0.06692$ pH[a]
(2) $NO_3^- + 2H_2O + 2e^- = NO_2^- + 2OH^-$	$E_2 = 0.8902 - 0.06692$ pH[a]
(3) $Zn^{2+} + 2e^- = Zn$	$E_3 = -0.762$[a]
(4) $2H^+ + 2e^- = H_2$	$E_4 = 0.03484 - 0.06692$ pH[a]
(5) $Zn(OH)_2 + 2e^- = Zn + 2OH^-$	$E_5 = 0.03864 - 0.06692$ pH[a]
potential of SCE	$E_{sce} = 0.2119$[b]
$H_2O = H^+ + OH^-$	$\ln K_w = -29.72$[c]
$[Zn^{2+}]\,[OH^-]^2 = Zn(OH)_2$	$\ln K_{sp} = -36.11$[a]

[a]Computed from data in ref. 26.
[b]Computed from data in ref. 28.
[c]Computed from data in ref. 27.

Fig. 1. Sketch of the experimental setup.



used for potential control, and the electric current – time relationship was recorded by means of an OPTO-22 interface–microcomputer assembly.

Physicochemical properties at equilibrium conditions

Literature data assembled in Table 1 indicate that nitrate ion reduction is strongly favoured thermodynamically (at pH = 6, for example, E_2 = 0.475 V). It may appear at first glance that ZnO synthesis is essentially a three-stage process: in the first stage nitrate reduction liberates hydroxide ions, which react with zinc ions or metallic zinc to form zinc hydroxide in the second stage. In the final stage zinc hydroxide is converted to ZnO. Both overall reactions:

[1] $NO_3^- + Zn + H_2O = Zn(OH)_2 + NO_2^-$ $\quad \ln K = 87.7$

[2] $NO_3^- + Zn = ZnO + NO_2^-$ $\quad \ln K = 98.6$

possess a very high equilibrium constant at 65°C, guaranteeing the thermodynamic feasibility of ZnO synthesis at appropriate pH values and, in the absence of dilute mineral acids, in order to avoid the redissolution stage (29):

[3] $\varepsilon\text{-}Zn(OH)_2 + 2H^+ = Zn^{2+} + 2H_2O$ $\quad \ln K = 26.92$

Zinc is prone to form (mononuclear) hydroxide complexes (30, 31), whose equilibrium properties were investigated in detail by Hepler and co-workers (32). $Zn(OH)_2$ itself has six forms (α; β_1; β_2; χ; δ; ε) of which only ε-$Zn(OH)_2$ is stable in water below 39°C. Their solubility in water is widely different (31). In alkaline solutions the hydroxo species (e.g., $Zn(OH)^+$, $Zn(OH)_3^-$, and $Zn(OH)_4^{2-}$) are stable, with standard free energies of formation ranging from −300 to −900 kJ mol^{-1}. Spontaneous $Zn(OH)_2$ formation may be expected for pH > 6.35 (25°C) and pH > 5.63 (65°C) in the case of the 0.075 mol L^{-1} zinc nitrate solution, and for pH > 6.29 (25°C) and pH > 5.56 (65°C) when $[Zn(NO_3)_2]$ = 0.1 mol L^{-1}.

The standard free energy change of the

[4] $ZnO + H_2O = Zn(OH)_2$

process is computed from thermodynamic data and their temperature dependence (27, 33, 34) to be about 1884 J/mol (25°C) and 2031 J/mol (65°C). The experimental zinc nitrate concentrations have a negligible effect on the numerical value of free energy change, which indicates relative stability of the oxide species with respect to the hydroxide species under standard equilibrium conditions.

Nitrate-ion reduction in alkaline media may also occur in principle (35, 36) as a 2-, 3-, 5-, 6-, or 8-electron transfer process yielding nitrogen and ammonia as cathode products with standard potentials ranging from about −0.17 V to +0.41 V (NHE) at 25°C. To the authors' knowledge, the importance of these reactions in neutral or acidic media has not been demonstrated.

Electrolytic synthesis of ZnO in the experimental cell

1. Current–potential relationships

A typical current–potential curve, obtained at a sweep rate of 20 mV s^{-1}, is shown in Fig. 2. The magnitude of the cathode potential with respect to the saturated calomel electrode is

© 1997 NRC Canada

Can. J. Chem. Downloaded from www.nrcresearchpress.com by 91.121.58.235 on 09/08/12
For personal use only.

Can. J. Chem. Downloaded from www.nrcresearchpress.com by 91.121.58.235 on 09/08/12
For personal use only.

Fig. 2. Linear sweep voltammogram of the cathode process. Sweep rate: 20 mV s^{-1}; copper substrate.

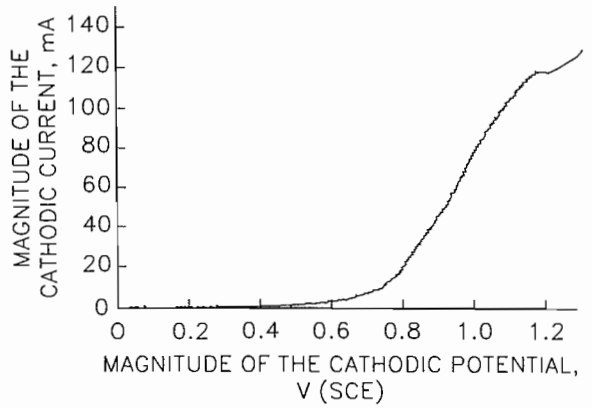
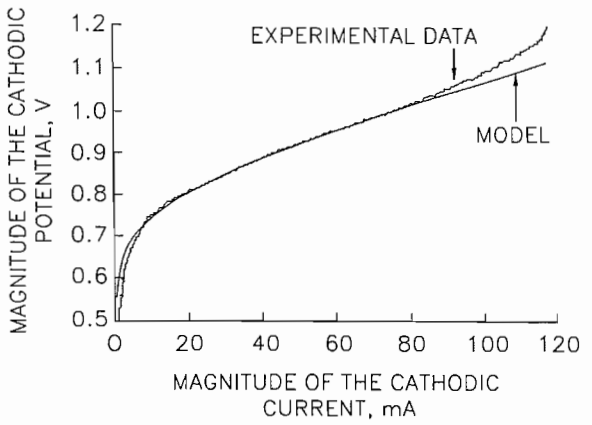


Fig. 3. Comparison of experimental observations with model-based prediction eq. [6].



defined as $V_c = |V_c\,(\text{NHE})| + 0.2412$ V, where V_c (NHE) is the cathode potential on the normal hydrogen electrode scale (e.g. the value of $V_c = 0.4$ V implies that $V_c = -0.1588$ V, since the measured cathode potential is -0.4 V). The cathode current is the sum of three components:

$$[5] \quad I = I_1 + I_2 + I_3$$

where the subscripts refer to the cathode processes of the same numbering in Table 1. The relative magnitude of the current components depends on the cathode potential. In the $\sim 0.4 < V_c < 0.71$ V range the cathode reaction is essentially nitrate reduction. In the $0.71 < V_c < 1.1$ V range, the current increases rapidly and proton discharge and hydrogen evolution, visibly discernible at the cathode, indicate H_2O decomposition. The short plateau appearing at about $V_c = 1.18$ V probably indicates a relatively narrow zone of mass transport control. At higher magnitudes of the cathode potential the appearance of gray particles on the cathode surface indicates the contribution of processes (3) and (5), shown in Table 1. Due to ZnO/$Zn(OH)_2$ formation on the cathode surface, it is tempting to consider that the overpotential in the intermediate range ($0.71 < V_c < 1.1$ V) depends not only on an "activation barrier," but

Fig. 4. The variation of the current-regression residual with cathode potential.

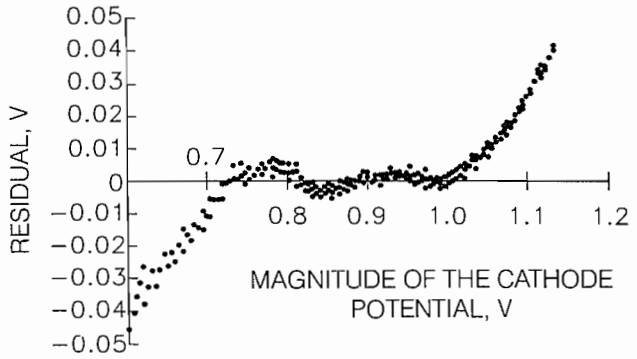
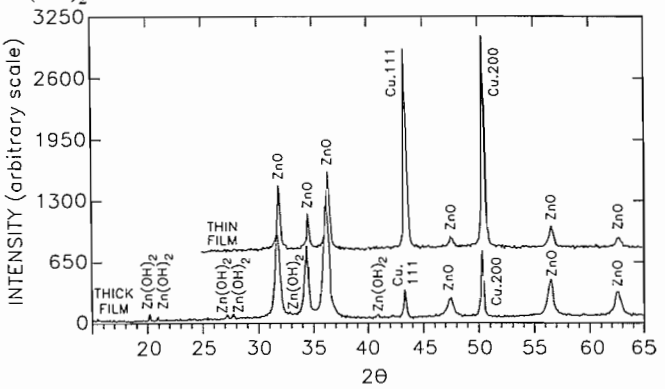


Fig. 5. X-ray diffraction patterns of oxide films deposited on copper substrates. The upper pattern for the thin film formed at $V_c = 0.75$ V (SCE) indicates only ZnO, whereas the lower pattern for the thick film formed at $V_c = 0.95$ V (SCE) indicates a mixture of ZnO and $Zn(OH)_2$.



also on the passivating ZnO/$Zn(OH)_2$ layer. If it is assumed (*i*) that charge transfer proceeds through a dual barrier made up of the passive film and the double layer (37), with an apparent resistance R^* caused mainly by the passivation layer, and (*ii*) that R^* may be taken as a constant over a sufficiently short time period, a modified Tafel equation:

$$[6] \quad V_c = a' + b' \log |I| + R^* |I|$$

may be postulated, whose parameters are obtained via a non-linear regression technique. Figure 3 demonstrates close agreement between experimental observations and eq. [6] with the numerical values of the regression parameters $a' = 0.5908$ V; $b' = 0.130$ V dec^{-1}; $R^* = 2.0$ ohm; and the coefficient of determination $r^2 = 0.99$ in the $0.71 < V_c < 1.0$ range. The residual plot shown in Fig. 4 has a narrow band of ± 7 mV in this domain and exhibits a slight wavy trend that is presumably due to perturbation caused by H_2 bubbles. At $V_c < 0.71$ V, the consistently negative residual values indicate incipient solid layer deposition with an apparent ohmic resistance below the regression-predicted value. By contrast, the consistently positive residual values at $V_c > 1.0$ V indicate an apparent resistance above the regression-predicted values, due to a considerable accumulation of the ZnO/$Zn(OH)_2$ layer on the cathode surface.

© 1997 NRC Canada

Table 2. Summary of data analysis based on FBM theory ($Zn(NO_3)_2$ = 0.075 mol/L; pH_i = 6.0).

Magnitude of Cathode potential V_c (SCE)	Cathodic substrate material	Pox diagram: Hurst exponent H	Pox diagram: Coefficient of determination r^2
0.70	Copper	0.92	0.96
0.80	Copper	0.80	0.86
0.95	Copper	0.64	0.99
0.80	Platinum	0.84	0.88
0.80	ITO-coated glass	0.88	0.98

Fig. 6. Variation of the cathode current with time at different cathode potentials. Copper substrate; $[Zn(NO_3)_2]$ = 0.075 mol L^{-1}, pH_i = 6.0.

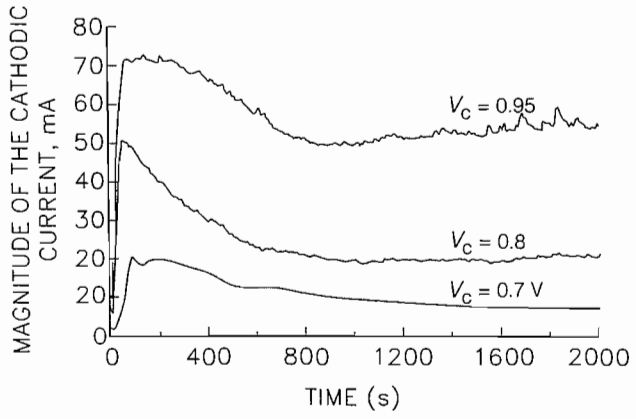


Fig. 7. Variation of the cathode current with time at different pH_i values. V_c = 0.75 V (SCE), platinum substrate.

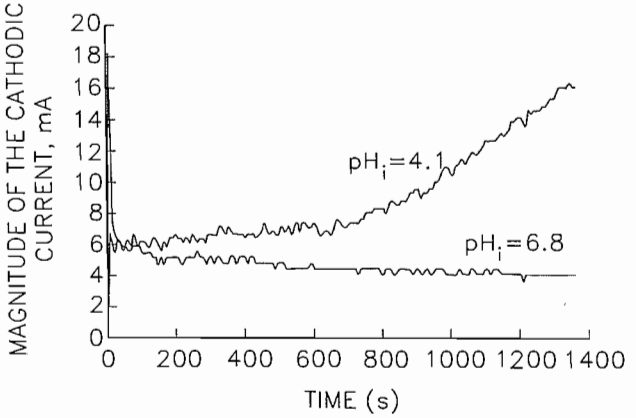


Fig. 8. Variation of the cathode current with time at different substrates. V_c = 0.80 V (SCE); $[Zn(NO_3)_2]$ = 0.100 mol L^{-1}, pH_i = 6.0.

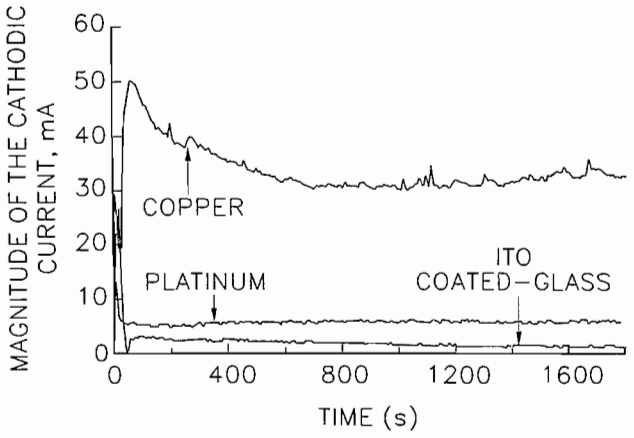
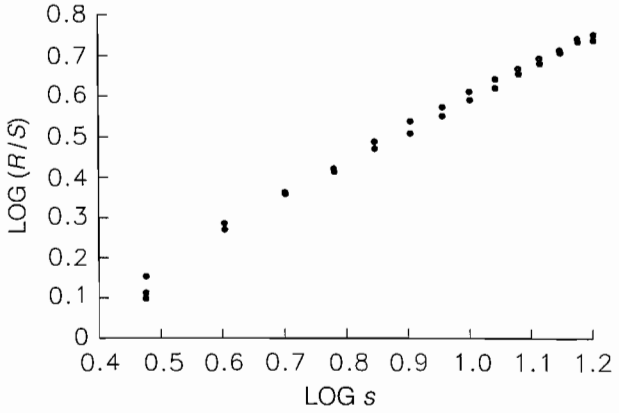


Fig. 9. A typical Pox diagram of the cathode process. Copper substrate; V_c = 0.80 V (SCE); $[Zn(NO_3)_2]$ = 0.075 mol L^{-1}, pH_i = 6.0. See Nomenclature for explanation of symbols.



Can. J. Chem. Downloaded from www.nrcresearchpress.com by 91.121.58.235 on 09/08/12
For personal use only.

© 1997 NRC Canada

Can. J. Chem. Downloaded from www.nrcresearchpress.com by 91.121.58.235 on 09/08/12
For personal use only.

The $V_c < 0.71$ V zone, where the passivation layer is not yet significantly developed, may be used for an *approximate* determination of the electrode–kinetic parameters of the nitrate reduction (first) step by neglecting the ohmic term in eq. [6] under low-V_c conditions. Regression analysis yields a = 0.6902 V and b = 0.242 V dec^{-1} with r^2 = 0.994 in the Tafel equation:

$$[7] \quad \eta = a + b \log |i|$$

where η is the activation overpotential and i is the cathode current density (A cm^{-2}). It follows that an approximate value of the exchange current density of the nitrate reduction process is $i_0 = 1.41 \times 10^{-6}$ A cm^{-2}.

2. The effect of the cathode potential

The cathode potential effect is demonstrated by the nature of the cathode deposit as well as the variation of the cathode current with time. No significant amount of ZnO can be detected at $V_c < 0.7$ V, while at $V_c > 1.1$ V gray particles can readily be seen embedded in the white film. At $V_c = 0.7$ V, the transparent film contains pure ZnO, whereas at $V_c = 0.95$ V the loose polycrystalline film contains a certain amount of $Zn(OH)_2$ as shown by XRD analysis (Fig. 5) of the deposit samples. The presence of hydroxide is due to a more rapid buildup of [OH^-] ion concentration at high cathode potentials, which promotes $Zn[OH]_2$ precipitation in the vicinity of the cathode followed by deposition onto the cathode surface. On a copper substrate, the current–time variation remains smooth up to about $V_c = 0.8$ V; at higher potentials high-frequency fluctuations become increasingly larger as the potential magnitude is increased, due to the progressively stronger effect of H_2 evolution. Within the $1000 < t < 2000$ s time interval, the mean value of the measured current is 8.03, 20.19, and 53.41 mA at corresponding potential magnitudes of V_c = 0.7, 0.8, and 0.95 V (Fig. 6).

3. The effect of the initial pH of the solution

Cathode current behavior is highly dependent on the initial pH of the electrolyte. As shown in Fig. 7, the mean current is essentially constant at $pH_i = 6.8$, but at $pH_i = 4.1$ the current is consistently higher and increases with time. The lower pH_i favours hydrogen evolution and accelerates the cathode process.

4. The effect of the cathode substrate

The effect of the substrate material is depicted in Fig. 8. At the same cathode potential, the current is the lowest on the ITO-coated glass since its electrical resistivity is much higher than in the case of metals. It is not understood at present why the current on a copper cathode is higher than on platinum (given that hydrogen overpotential on copper is appreciably higher than on platinum under otherwise identical conditions), and why its relaxation from a large initial peak value is much slower than in the case of platinum and coated glass.

Analysis of time-series data

The experimentally observed cathode currents under constant potential are fluctuating functions of time. FBM theory has been extensively applied to fluctuating phenomena (e.g., ref. 24) and its utility in analyzing anode processes has been well demonstrated (25, 38). The FBM technique generates, via Pox diagrams, a numerical measure of the degree of (long-term) correlation in an experimental time series and provides a yardstick of relative stability in terms of the slope H of the Pox diagram. The $0.5 < H < 1$ region is the domain of "persistence": the closer the H-value to 1, the larger the structural stability. H = 0.5 represents pure random Brownian motion, and $0 < H < 0.5$ is the domain of "antipersistence," with progressively decreasing structural stability as H approaches zero, the state of pure chaos. A typical Pox diagram is illustrated in Fig. 9, and Table 2 summarizes the results of FBM-based analysis of the experimental Pox diagrams. For a given cathode substrate material, the Hurst exponent expectedly decreases as V_c increases, indicating the enhancing effect of hydrogen gas evolution on the cathode current fluctuation. At a given cathode potential (e.g., 0.80 V), the progressively smaller numerical values of H indicate that current on ITO-coated glass exhibits the largest relative degree of stability, followed by platinum and copper; this finding is also in agreement with Fig. 8.

Conclusions

Experimental results hitherto obtained offer sufficient encouragement for a further systematic study of the best conditions for an electrolytic synthesis of zinc oxide, under optimal cathode-potential and solution-pH control for a given substrate material. An extended investigation including a morphological determination of layer quality and the exact composition of the cathode layer is now underway in our laboratory.

Acknowledgments

This work has been supported by the Natural Sciences and Engineering Research Council of Canada. The authors are grateful to Dr. S. Petrov of the Department of Chemistry, University of Toronto, for XRD analysis of cathode layer specimens.

References

1. C.H. Mathewson. Zinc – the metal, its alloys and compounds. Reinhold Publishing Corp, New York. 1959.
2. F. Porter. Zinc handbook – Properties, processing and use in design. Marcel Dekker Inc., New York. 1991. Sect. 29, II.
3. H.E. Brown. ZnO oxide, properties and applications. International Lead Zinc Research Organization, Inc., Research Triangle Park, N.C. 1976.
4. J.H. Morgan and D.E. Brodie. Can. J. Phys. **60**, 1387 (1982).
5. S.S. Chadha, D.W. Smith, A. Vecht, and C.S. Gibbons. SID Int. Digest, **25**, 51 (1994).
6. S.M. Size. (*Editor*) Semiconductor sensors. J. Wiley, New York. 1994.
7. I. Novotny, P. Sutta, F. Mika, and V. Tvarozek. *In* Proc. Int. Conf. Microelectron. IEEE, Piscataway, N.J. 1995. Vol. 1. p. 65.
8. F.S. Mahmood, R.D. Gould, A.K. Hassan, and H.M. Salih. Thin Solid Films, **270**, 376 (1995).
9. B. Mutel, A. B. Taleb, O. Deddaux, P. Goudmand, L. Gengembre, and J. Grimblot. Thin Solid Films, **266**, 119 (1995).
10. Y. Sato and S. Sato. Thin Solid Films, **281–282**, 445 (1996).
11. A.Suzuki, T. Matsushita, N. Wada, Y. Sakamoto, and M. Okuda. Jpn. J. Appl. Phys. Part I: **35**, L56 (1996).
12. H. Sato, T. Minami, S. Takata, T. Miyata, and M. Ishii. Thin Solid Films, **236**, 14 (1993).

© 1997 NRC Canada

13. T. Saeed and P. O'Brien. Thin Solid Films, **271**, 35 (1995).
14. J. D. Merchant and M. Cocivera. Chem. Mater. **7**, 1742 (1995).
15. M. Krunks and E. Mellikov. Thin Solid Films, **270**, 33 (1995).
16. B. Zou, G Tang, G. Zhang, and W. Chen. Wuli Xuebao, **44**, 164 (1995).
17. B.S. Jeon, J.S. Yoo, and T.D. Lee. J. Electrochem. Soc. **143**, 3923 (1996).
18. Z.H. Gu, T.Z. Fahidy, S. Damaskinos, and A.E. Dixon. J. Electrochem. Soc. **141**, L153 (1994).
19. J.R. Vilche, K. Juttner, W.J. Lorenz, W. Kautek, W. Paatsch, M.H. Dean, and U. Stimming. J. Electrochem. Soc. **136**, 3773 (1989).
20. J.A. Switzer, C.J. Hung, B.E. Breyfogle, M. G. Shumsky, R. V. Leeuwen, and T. D. Golden. Science, **264**, 1505 (1994).
21. M. Izaki and T. Omi. J. Electrochem. Soc. **143**, L53 (1996).
22. M. Izaki and T. Omi. Appl. Phys. Lett. **68**, 2439 (1996).
23. P. Sophie and L. Daniel. Adv. Mater. (Weinheim, Ger.), **8**, 166 (1996).
24. J. Feder. Fractals. Plenum Press, New York. 1988.
25. T.Z. Fahidy and Z.H. Gu. *In* Modern aspects of electrochemistry. No. 27. *Edited by* R.E. White, J.O'M. Bockris, and B.E. Conway. Plenum Press, New York. 1995. Chap. 5.
26. A.J. de Bethune and N.A. Swendewan Loud. Standard aqueous electrode potentials and temperature coefficients at 25°C. Clifford A. Hampel, Skokie, Ill. 1964.
27. J.A. Dean. Lange's handbook of chemistry. 13th ed. McGraw Hill, New York. 1985. Table 5-5.
28. L. Antropov. Theoretical electrochemistry. Mir, Moscow. 1972. Chap. 7.
29. Stability constants of metal–ion complexes. Spec. Publ. — Chem. Soc. n17 (1964).
30. J.N. Butler. Ionic equilibria, a mathematical approach. Addison–Wesley, Reading, Mass. 1964.
31. A.F. Trotman-Dickenson (*Editor*). Comprehensive inorganic chemistry. Vol. B. Pergamon, Oxford. 1973. Sect. 24.5.
32. R.A. Reichle, K.G. McCurdy, and L.G. Hepler. Can. J. Chem. **53**, 3841 (1975).
33. C.E. Wicks and F.E. Block. Thermodynamic properties of 65 elements, their oxides, halides and nitrides. Bulletin 605. Bureau of Mines, U.S. Department of the Interior, Washington, D.C. 1963.
34. NBS Circular 500, Parts 1 and 2: Selected values of chemical thermodynamic properties. U.S. Department of Commerce, Washington, D.C. 1961.
35. J.O'M. Bockris and J.Kim. J. Electrochem. Soc. **143**, 3801 (1996).
36. H.-L. Li, J.Q. Chambers, and D.T. Hobbs. J. Appl. Electrochem. **18**, 454 (1988).
37. M. Noel and K.I. Vasu. Cyclic voltammetry and the frontiers of electrochemistry. Aspect Publ. Ltd., London. 1990. Sect. 14.4.6.
38. Z.H. Gu, S.J. Xia, and T.Z. Fahidy. Electrochim. Acta, **41**, 2837 (1996).

Nomenclature

$a';b'$	Regression parameters in eq. [6]
$a;b$	Regression parameters in eq. [7]
E	(Equilibrium) electrode potential
F	Faraday's constant (96487 C mol^{-1})
I	Current
i	Current density
K	Equilibrium constant
R_g	Universal gas constant (8.314 J mol^{-1} K^{-1})
R^*	Apparent oxide/hydroxide layer resistance
R/S	Rescale range; ordinate-base in the Pox diagram
r^2	Coefficient of determination
s	Time lag; abscissa-base in the Pox diagram
T	Temperature (absolute scale)
V_c	Magnitude of the (imposed) cathode potential
η	Overpotential

Can. J. Chem. Downloaded from www.nrcresearchpress.com by 91.121.58.235 on 09/08/12
For personal use only.

© 1997 NRC Canada

Thermodynamics of micellization and solubilization in systems of water – sodium *n*-alkylcarboxylates – alkoxyethanols at 25°C

H. Huang and R.E. Verrall

Can. J. Chem. Downloaded from www.nrcresearchpress.com by 91.121.58.235 on 09/08/12
For personal use only.

Abstract: The apparent molar volumes and adiabatic compressibilities, $Y_{\phi,S}$, of carboxylate surfactants, C_nNa (n = 8, 10, 12), in aqueous solutions in the absence and presence of medium-chain-length alkoxyethanols, C_4EO_X (EO = ethylene oxide group, X = 0–4), and of alkoxyethanols, $Y_{\phi,A}$, in aqueous solutions in the absence and presence of surfactant, were determined at 25°C from density and sound velocity measurements as a function of both the surfactant and alcohol concentrations. The partial molar volumetric properties of C_nNa and the transfer functions of C_4EO_X from water to aqueous surfactant solutions were calculated from the apparent molar properties. Values of the thermodynamic parameters of micellization for C_nNa, i.e., the critical micelle concentration, the partial molar property of the monomer at infinite dilution, Y_S^0, and in the micellar state, Y_S^M, were obtained from simulations of the experimental data, $Y_{\phi,S}$, using a mass-action model. As expected, these properties are strongly dependent on the surfactant chain length. The distribution coefficient of C_4EO_X between the micelle and aqueous phases, K_D, and the change in the molar property of alcohols due to micellization, Y_A^M, extracted from fitting the transfer function data of C_4EO_X using a chemical equilibrium model, show that the solubilization of alkoxyethanols in carboxylate micelles is enhanced by increasing the surfactant chain length and the number of EO groups in the alcohol. The deeper penetration of C_4EO_X into the micelles of longer chain surfactants is associated with increasingly stronger interactions between surfactant head groups and EO segments of the alcohol on (or near) the micelle surface. Aggregation numbers of C_nNa–C_4EO_X mixed micelles show that addition of a small amount of C_4EO_X has little effect on the structure of the micelles formed from C_8Na and $C_{10}Na$, but leads to significant change in $C_{12}Na$ micelles.

Key words: sodium carboxylate salts, alkoxyethanols, partial molar volume and compressibility, transfer functions, distribution coefficient, mean aggregation number.

Résumé : En se basant sur des mesures, à 25°C, de densité et de vélocité du son en fonction des concentrations tant de l'agent de surface et de l'alcool, on a déterminé les volumes molaires apparents et les compressibilités adiabatiques, $Y_{\phi,S}$ et $Y_{\phi,A}$, respectivement d'agents de surface carboxylates, C_nNa (n = 8, 10, 12), en solutions aqueuses en présence et en l'absence d'alkoxyéthanols de longueur de chaîne moyenne, C_4EO_X (EO = groupe d'oxyde d'éthylène, X = 0–4) et d'alkoxyéthanols en solutions aqueuses en présence et en l'absence d'agent de surface. À partir des propriétés molaires apparentes, on a calculé les propriétés volumétriques molaires partielles de C_nNa et les fonctions de transfert de C_4EO_X de l'eau vers les solutions aqueuses d'agent de surface. Utilisant un modèle d'action de masse et des simulations des données expérimentales, $Y_{\phi,S}$, on a déterminé les valeurs des paramètres thermodynamiques de micellisation des C_nNa, c'est-à-dire la concentration micellaire critique, la propriété molaire partielle du monomère à dilution infinie, Y_S^0, et dans l'état micellaire, Y_S^M. Tel qu'on pouvait s'y attendre, ces propriétés dépendent fortement de la longueur de la chaîne de l'agent de surface. Le coefficient de distribution des C_4EO_X entre la micelle et les phases aqueuses, K_D, et le changement dans la propriété molaire des alcools dû à la micellisation, ΔY_A^M, qui ont été extrait en ajustant les données de fonction de transfert des C_4EO_X à l'aide d'un modèle d'équilibre chimique, montrent que la solubilisation des alkoxyéthanols dans des micelles de carboxylate est promue par une augmentation de la longueur de la chaîne de l'agent de surface ainsi que par le nombre de groupes EO dans l'alcool. La pénétration plus grande des C_4EO_X dans les micelles des agents de surface de chaînes plus longues est associée à des interactions de plus en plus fortes entre les groupes de tête de l'agent de surface et les segments d'EO de l'alcool sur (ou près de) la surface de la micelle. Les nombres d'agrégation des micelles mixtes C_nNa–C_4EO_X montre que l'addition d'une faible quantité de C_4EO_X n'a qu'un faible effet sur la structure des micelles formées à partir des C_8Na et $C_{10}Na$, mais qu'elle conduit à un changement important dans les micelles de $C_{12}Na$.

Mots clés : sels de sodium d'acides carboxyliques, alkoxyéthanols, volume molaire partiel, compressibilité molaire partielle, fonctions de transfert, coefficient de distribution, nombre d'agrégation moyen.

[Traduit par la rédaction]

Received March 7, 1997.

This paper is dedicated to Professor Brian E. Conway with best wishes on the occasion of his 70th birthday.

H. Huang and R.E. Verrall.[1] Department of Chemistry, University of Saskatchewan, 110 Science Place, Saskatoon, SK S7N 5C9, Canada.

[1] Author to whom correspondence may be addressed. Telephone: (306) 966-4669. Fax: (306) 966-4730. E-mail: verrallr@sask.usask.ca

© 1997 NRC Canada

Can. J. Chem. Downloaded from www.nrcresearchpress.com by 91.121.58.235 on 09/08/12
For personal use only.

Introduction

In many practical formulations of surfactants, the addition of a third component such as a medium-chain alcohol (cosurfactant) can help to control the stability of the system and improve the performance of the surfactants, well beyond the level achieved by the surfactants themselves (1). The synergistic effect of surfactant mixtures on the properties of the system (2) has led to theoretical interest in developing a quantitative understanding of the behaviour of mixed surfactant systems that can be exploited in new applications.

Micellar systems can be characterized by structural parameters such as the mean aggregation number, micelle size and shape, and also by thermodynamic parameters. In recent years, along with the development of a variety of methods for studying the structure and kinetic processes of surfactant systems (3), thermodynamic studies have led to a better molecular interpretation of thermodynamic properties of surfactant solutions through the use of various theoretical models of micellization (4–7). Modeling studies enable the extraction of estimates of important parameters of the micelle systems with a minimum of experimental data. The effect of additives on the properties of water–surfactant–additive ternary systems can be investigated through quantitative analysis of the partial molar properties of the additive and the transfer functions of the additive from water to aqueous surfactant solution, using appropriate models. At the present time there are two modeling methodologies (8–11) that are widely used to extract fundamental parameters. A model proposed by DeLisi et al. (8, 9) assumes a pseudo phase transition for the micellization process and a mass-action equilibrium for the additive distribution between the micelle and aqueous phases. This model is more applicable to long-chain hydrocarbon surfactants. Another model proposed by Desnoyers and co-workers (10, 11) combines a mass-action equilibrium for the micellization process with a pseudo phase transition for the distribution of additive between the micelles and the aqueous phases. It treats systems of short-chain surfactants somewhat better than those having a long chain.

While much of the work in recent years has focused on the interactions of *n*-alcohols (and some branched isomers) and hydrocarbons with ionic and nonionic micelles (12), there has been a growing interest in studying nonionic ethoxylated alcohols (alkoxyethanols) in surfactant systems (13–20). The aqueous bulk phase solubility of a typical nonionic alkoxyethanol is enhanced by increasing the number of ethylene oxide (EO) segments. On the other hand, an increase in the length of the hydrocarbon chain for a fixed number of EO segments is accompanied by a pronounced decrease in the critical micelle concentration (cmc). However, an increase in the number of EO segments for a fixed hydrocarbon chain length results in a less significant increase in the cmc (21). Previous studies have shown some interesting features of the EO group in systems of anionic surfactant. For example: the insertion of EO groups into the hydrocarbon chain of alkyl polyoxyethylene sulfates decreases the cmc and increases both the surface activity and the mean aggregation number of the micelles (20); the cmc value of the anionic surfactant sodium decanoate has been found to be lower in the presence of 2-butoxyethanol than in the presence of *n*-butanol, for a fixed alcohol concentration (17); the cmc values of both sodium decyl sulfate (14) and of sodium dodecyl sulfate (19) decrease with an increasing number of EO groups for an alcohol of a given chain length; and the solubility of oil-soluble azo-dyes in mixed micelles of sodium dodecyl sulfate – alkoxyethanols (13) is enhanced by increasing the number of EO segments in the alcohol.

Of particular interest is the observation that the distribution coefficient of ethoxylated alcohols between anionic micelles and the aqueous phase increases as a function of the number of EO groups in the alcohol (14, 15). The increasingly negative Gibbs energy of transfer, as the number of EO groups increases, implies that the role of the EO group is to enhance the interactions between the alkoxyethanol molecules and anionic micelles, analogous to the contribution of an EO group to increasing the hydrophobicity of the alkyl polyoxyethylene sulfate monomer (20). These results are contrary to the hydrophilic character of the ethylene oxide chain in nonionic surfactants (22) where they tend to decrease the driving force leading to the formation of nonionic micelles (23). This feature is also contrary to the results obtained for cationic surfactant systems where both the cmc of the surfactant and the distribution of alkoxyethanols between the two phases are virtually independent of the number of EO groups (14). The different behaviour exhibited by EO groups in an alcohol, when they interact with either anionic or cationic micelles in aqueous medium, is an intriguing result. Much of the previous work dealing with surfactant and alkoxyethanol mixed systems has focused on changes in the micellization properties of the surfactant and the degree of solubilization of the alcohol in the micelle (13–20). There has been a paucity of information concerning the effect of the alcohol on the structure of the micelle (24). To this time, no comprehensive study has been undertaken to obtain a satisfactory explanation of the specificity of interactions between EO groups and different types of ionic micelles. The present systematic study of mixed micelle systems comprising ionic surfactants of varying chain length and alkoxyethanols having a varying number of EO groups was initiated in order to obtain more information about the different characteristics of EO groups in anionic and cationic micelles.

We present the results of thermodynamic studies of mixed micelle systems of anionic carboxylates C_nNa (n = 8, 10, 12) and polyoxyethylene butyl ether compounds C_4EO_X (EO = ethylene oxide group, X = 0–4). Two thermodynamic properties, the apparent molar volume and the apparent molar adiabatic compressibility, have been determined for the sodium carboxylates as a function of their concentration in the absence and presence of polyoxyethylene butyl ether compounds of a given concentration and for the ethoxylated alcohols as a function of their concentration in binary aqueous surfactant systems of varying surfactant concentration. Values of the micellization parameters of the carboxylate surfactants were obtained by analyzing apparent molar volumetric properties of the binary surfactant–water systems using a mass-action model (6, 7). The transfer thermodynamic functions of the ethoxylated alcohols from water to surfactant solutions were obtained by comparing the apparent molar properties for the alcohols in aqueous surfactant solutions and in water at a given low concentration of alcohol. The transfer functions were analyzed using a chemical equilibrium model (10, 11) to obtain estimates of the solubilization parameters of C_4EO_X in C_nNa micelles.

© 1997 NRC Canada

Can. J. Chem. Downloaded from www.nrcresearchpress.com by 91.121.58.235 on 09/08/12
For personal use only.

Macroscopic thermodynamic properties give little direct information about changes in the structure of the mixed micelles (25). Information concerning changes in the mean aggregation number of the micelle as a function of changes in the chemical structure of the components forming the micelle is essential in order to obtain a comprehensive understanding of the aggregation phenomenon in surfactant solutions. Some results of a previous study[2] of the mean aggregation number of the three carboxylate surfactants in the absence and presence of the ethoxylated alcohols, and of the average number of alcohol molecules per micelle as a function of the number of EO groups in the alcohol, are also included in this paper to facilitate a discussion of the thermodynamic results.

Experimental

Materials

The surfactants sodium octanoate, C_8Na (Sigma, 99–100%), sodium decanoate, $C_{10}Na$ (Sigma, 99–100%), and sodium dodecanoate, $C_{12}Na$ (Sigma, 99–100%), were used as received. *n*-Butanol, C_4EO_0 (BDH, AR); diethylene glycol monobutyl ether, C_4EO_2 (Pfaltz & Bauer, AR); 2-butoxyethanol, C_4EO_1 (Fluka, AR); and triethylene glycol monobutyl ether, C_4EO_3 (Fluka, 80%), were purified by fractional distillation under reduced pressure. Tetraethylene glycol monobutyl ether, C_4EO_4, was obtained as a by-product from the original C_4EO_3 material. The purity of the recovered materials was checked by GC–MS analysis.

Measurements

The solution densities were measured using a vibrating-tube flow densimeter (model 02D, Sodev) with a reproducibility of $(\pm)2 \times 10^{-6}$ g cm^{-3}. Ultrasonic velocities were measured at a frequency of 4 MHz using a Nusonics (model 6080 Mapco) single transducer velocimeter. The effect of the hydrolysis of the carboxylate anion on the determination of the apparent molar properties of C_nNa was minimized by adjusting the pH of water and of the water–alcohol mixed solvent systems to above 9.5 with NaOH. The operation and calibration of the instruments were described previously (26). The temperature of the densimeter and velocimeter cells was kept at 25°C using a closed-loop temperature controller (model CT-L, Sodev). All solutions used for thermodynamic measurements were prepared on a weight basis using water obtained from a Millipore Super-Q system. The surfactants were readily dissolved in water and aqueous C_4EO_X solutions at the experimental temperature and in the concentration ranges studied.

Results

Apparent molar volumes, V_ϕ, and apparent molar adiabatic compressibilities, K_ϕ, of the solute in solution at a given concentration, m, were calculated from the densities of the solution, d, the solvent, d_0 (mixed solvent in the case of ternary systems), the adiabatic compressibility coefficients of the solution, β_S, and the solvent, β_0, and the molar mass, M, of the solute using the following relations:

$$[1] \quad V_\phi = \frac{M}{d} - \frac{10^3(d - d_0)}{mdd_0}$$

$$[2] \quad K_\phi = V_\phi\beta_S + \frac{10^3(\beta_S - \beta_0)}{md_0}$$

$$[3] \quad \beta_S = \frac{100}{u^2 d}$$

where u is the speed of sound in the solution.

The partial molar properties $\overline{V}_S$ and $\overline{K}_S$ of the surfactant were calculated from the apparent molar properties using (7)

$$[4] \quad \overline{Y} = \frac{\Delta(Y_\phi m)}{\Delta m}$$

Figures 1 and 2 illustrate typical features of the volume and compressibility properties of two surfactants, C_8Na and $C_{12}Na$, respectively, in the absence and presence of a given concentration of ethoxylated alcohol, C_4EO_X, (0.02 *m* for C_8Na and 0.05 *m* for $C_{12}Na$, respectively). Similar graphs for $C_{10}Na$ systems are not presented here for the sake of brevity. The solid lines represent the results of the theoretical simulation using relations derived from the mass-action model (6, 7)

$$[5] \quad V_{\phi,S} = \alpha_0[\overline{V}_S^0 + A_V\sqrt{\alpha_0 m_S} + B_V\alpha_0 m_S] + (1 - \alpha_0)[V_S^M + (1 - \alpha_0)C_V m_S]$$

$$[6] \quad K_{\phi,S} = \alpha_0[\overline{K}_S^0 + A_K\sqrt{\alpha_0 m_S} + B_K\alpha_0 m_S] + (1 - \alpha_0)[K_S^M + (1 - \alpha_0)C_K m_S] + \frac{\alpha_0(1 - \alpha_0)}{1 - \alpha_0 + \alpha_0/N_S}\frac{(\Delta V_S^M)^2}{RT}$$

where α_0 is the fraction of surfactant monomer in the aqueous phase, A_Y is the Debye–Hückel limiting slope, B_Y and C_Y are the pair interaction terms for the surfactant monomers and micelles, respectively, and N_S is the mean aggregation number of the micelles. The simulations were carried out by choosing a value of the mean aggregation number, N_S, so that quicker convergence could be achieved. For the systems $C_{10}Na$ and $C_{12}Na$, the value of the cmc was also fixed. Derived values of the thermodynamic parameters for the binary water–C_nNa systems, obtained from simulation at different mean aggregation numbers, are summarized in Table 1.

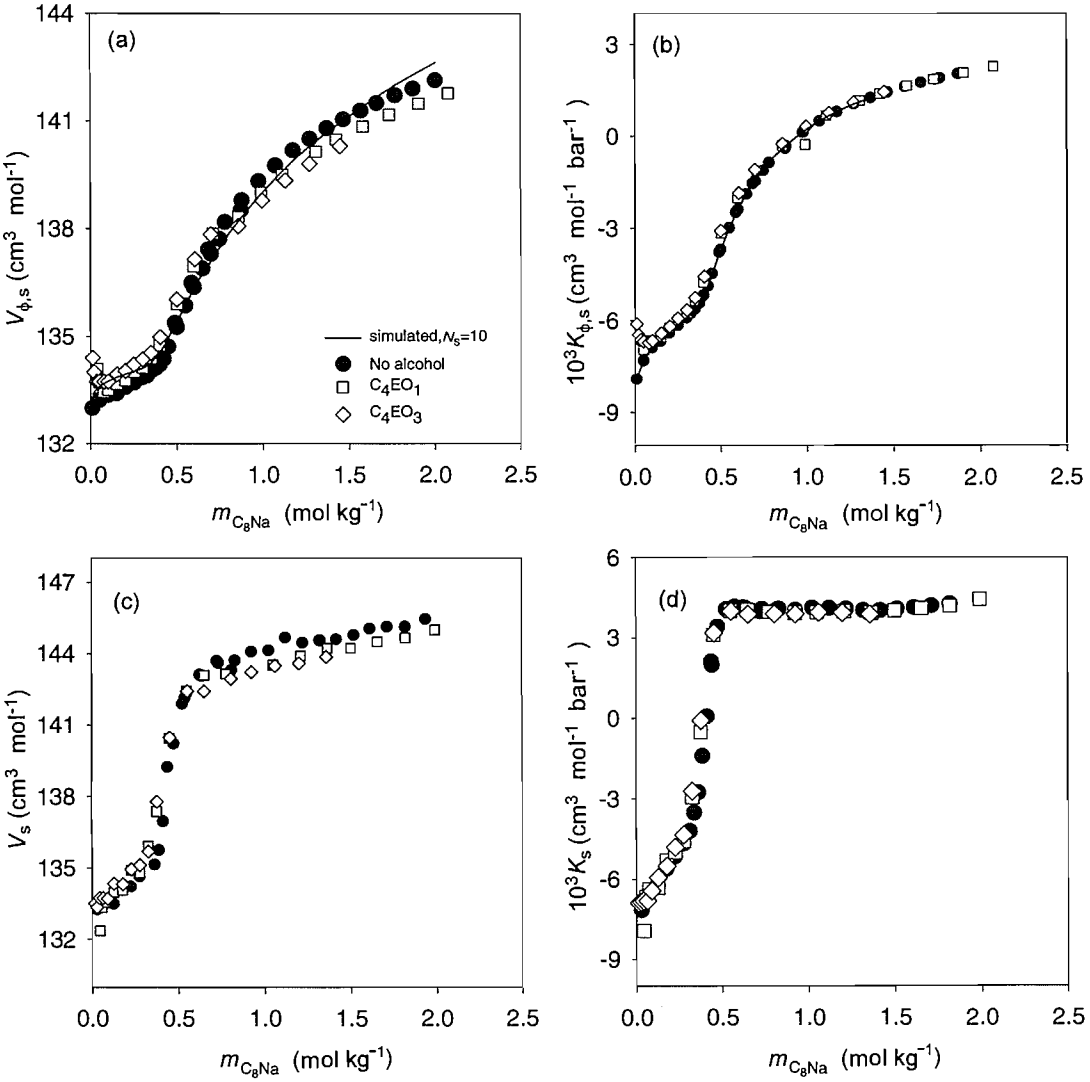
Figures 3 and 4 show the apparent molar volumes and adiabatic compressibilities of C_4EO_1 as a function of alcohol concentration in aqueous C_8Na and $C_{12}Na$ solutions of different concentration, respectively (results for C_4EO_1 in $C_{10}Na$ solutions are quite similar to those in C_8Na systems and are not shown). They are typical examples of the volumetric behaviour of the ethoxylated alcohols in water–C_nNa mixed solvents. The partial molar properties of the alcohol at infinite dilution (standard state) in the water–surfactant solutions, $\overline{V}_A^0$ and $\overline{K}_A^0$, were obtained by extrapolating the apparent molar property data to $m_A = 0$. The effect of the number of EO groups in the alcohol on $\overline{V}_A^0$ and $\overline{K}_A^0$ is illustrated (Fig. 5) by showing the results of $\overline{V}_A^0$ for the C_4EO_1–C_8Na systems. Figures 6 and 7 illustrate the effect of surfactant chain length on the $\overline{V}_A^0$ and $\overline{K}_A^0$ proper-

[2] Manuscript accepted, Langmuir.

© 1997 NRC Canada

Can. J. Chem. Downloaded from www.nrcresearchpress.com by 91.121.58.235 on 09/08/12
For personal use only.

Fig. 1. Apparent molar volumes (*a*), apparent molar adiabatic compressibilities (*b*), partial molar volumes (*c*), and partial molar adiabatic compressibilities (*d*) of C_8Na in the presence of 0.02 *m* C_4EO_X.



ties for C_4EO_1 as a function of C_nNa concentration in the mixed solvents.

The transfer functions of the alcohol from water to aqueous surfactant solutions were calculated from the apparent molar property data at low alcohol content (0.05 *m* in C_8Na and $C_{10}Na$, 0.02 *m* in $C_{12}Na$ systems) using the relation

$$[7] \quad \Delta Y_A(W \rightarrow W + S) = Y_A(W + S) - Y_A(W)$$

At sufficiently low concentration of m_A, $\Delta Y_A(W \rightarrow W + S)$ approaches the standard state transfer function, $\Delta Y_A^0(W \rightarrow W + S)$, and these data were simulated using relations derived from the chemical equilibrium model (10, 11)

$$[8] \quad \Delta V_A(W \rightarrow W + S) = 2\alpha\beta B_{V,SA} m_S + \frac{m_S}{m_A}(\alpha_0 - \alpha)\Delta V_S^M + (1 - \beta)\Delta V_A^M$$

$$[9] \quad \Delta K_A(W \rightarrow W + S) = 2\alpha\beta B_{K,SA} m_S + \frac{m_S}{m_A}(\alpha_0 - \alpha)\Delta K_S^M + (1 - \beta)\Delta K_A^M - \frac{m_S}{m_A}\left(\frac{\partial\alpha_0}{\partial P} - \frac{\partial\alpha}{\partial P}\right)\Delta V_S^M + \frac{\partial\beta}{\partial P}\Delta V_A^M$$

In the simulation, values of the equilibrium constant of micellization, K_M, the mean aggregation number, N_S, of the surfactant, and the thermodynamic micellization parameter for the surfactant, ΔY_S^M, which is calculated from

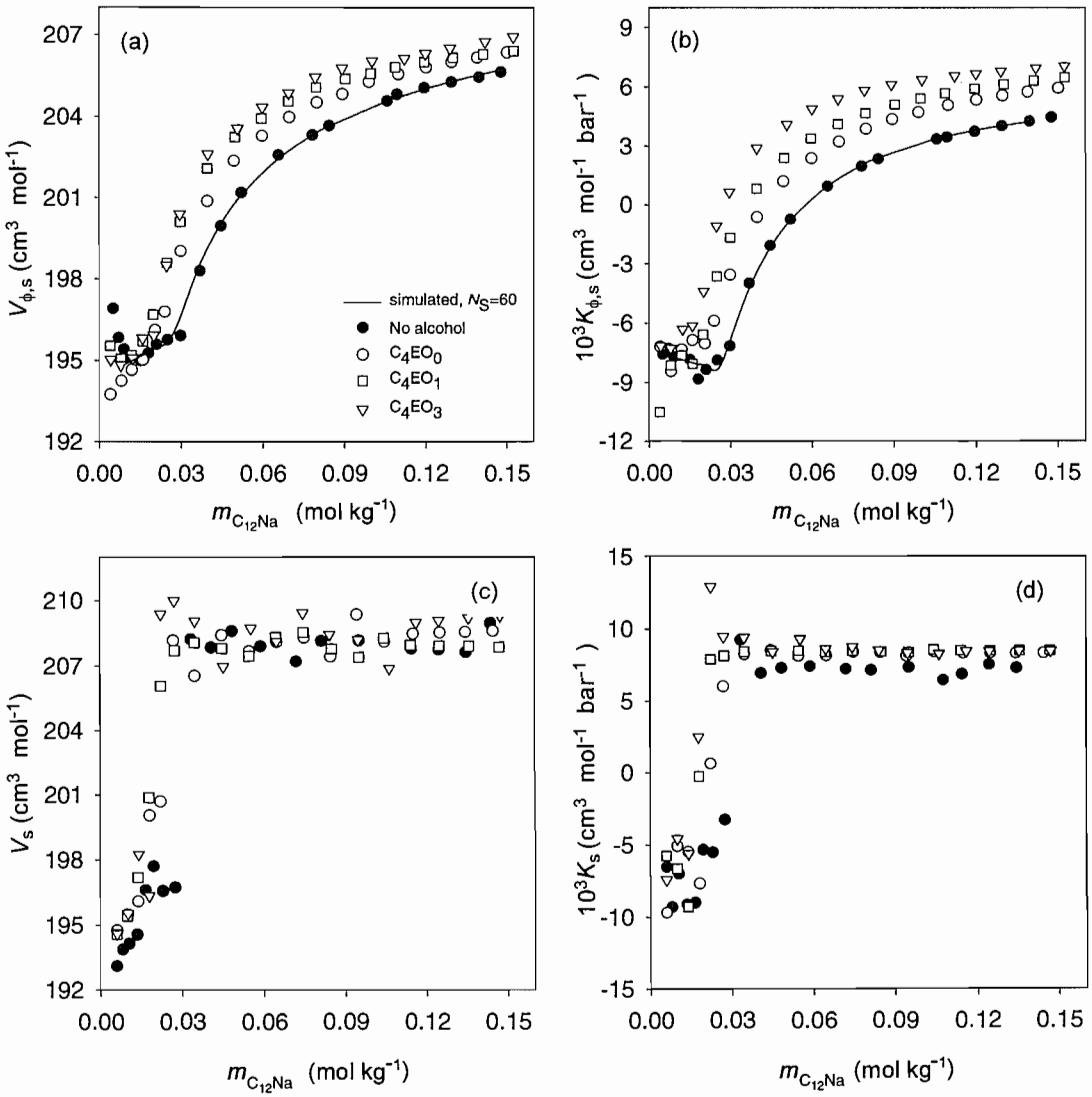
$$[10] \quad \Delta Y_S^M = Y_S^M - Y_S^0 - A_Y\sqrt{(\alpha_0 m_S)} - B_Y\alpha_0 m_S$$

were taken from the respective water–surfactant binary systems. The transfer functions were fitted by adjusting the pair interaction parameter, $B_{Y,SA}$, the distribution coefficient for the alcohol between the micellar and aqueous phases, K_D, and the micellization parameter for the alcohol, ΔY_A^M, to optimize the values of α (the fraction of surfactant monomer in the

© 1997 NRC Canada

Can. J. Chem. Downloaded from www.nrcresearchpress.com by 91.121.58.235 on 09/08/12
For personal use only.

Fig. 2. Apparent molar volumes (*a*), apparent molar adiabatic compressibilities (*b*), partial molar volumes (*c*), and partial molar adiabatic compressibilities (*d*) of $C_{12}Na$ in the presence of 0.05 *m* C_4EO_X.



aqueous phase in the presence of alcohol) and β (the fraction of alcohol in the aqueous phase) until the agreement between the simulated results and the experimental data was quantitatively acceptable. In the C_8Na system, the mean aggregation number used for the transfer volume simulation was 11 while a good fit for the transfer compressibility required a value of 15. In the $C_{10}Na$ and $C_{12}Na$ systems, the mean aggregation number was assumed to remain unchanged and values of 30 and 60, respectively, were used in the simulations. The general behaviour of the transfer functions for C_4EO_X in aqueous C_nNa solutions is illustrated by the comparisons between the simulated and the experimental results of transfer functions for C_4EO_{0-3} from water to $C_{10}Na$ solutions, as shown in Fig. 8. Values of the parameters of the ternary systems extracted from the simulation are presented in Table 2. The dependence of the parameters on the number of EO groups in the alcohol and the chain length of C_nNa is shown in Fig. 9.

Values of the mean aggregation number of C_nNa micelles at a given surfactant concentration, the aggregation number of surfactant in the mixed micelles in the presence of a given low concentration of ethoxylated alcohol (0.04–0.05 *m*), and the average number of alcohols per micelle are summarized in Table 3.

Discussion

Volumetric properties of C_nNa in water

The volumetric behaviour of C_nNa as a function of concentration in the presence and absence of the ethoxylated alcohols (Figs. 1 and 2) displays a number of trends. In the binary C_8Na–water system, the apparent molar volume, $V_{\phi,S}$ (Fig. 1*a*), increases gradually in the low-concentration region up to m_S = 0.39 *m* and then shows a sharp increase thereafter, corresponding to the change in the thermodynamic property of micellization (4–7). It continues to increase, though less rapidly, in the higher concentration region. As the surfactant chain length increases, the onset of micellization occurs at much lower concentrations, for

© 1997 NRC Canada

Can. J. Chem. Downloaded from www.nrcresearchpress.com by 91.121.58.235 on 09/08/12
For personal use only.

Table 1. Thermodynamic parameters for C_nNa at 25°C from simulation.[a]

Property	N_S	Y^0	B_Y[b]	Y^M	C_Y[c]	m_t[d]	ΔY^{M}[e]	Relaxation	σ
					C_8Na				
V_ϕ	5	132.65	−0.50	151.49	3.17	0.59	17.70		0.14
	10	133.10	−0.50	143.98	1.57	0.52	9.79		0.41
	15	133.68	−0.50	143.52	1.74	0.56	8.72		1.51
	20	133.73	−0.50	144.04	1.26	0.58	9.18		1.63
	25	133.80	−0.50	144.00	1.29	0.59	9.06		1.97
	30	133.85	−0.50	144.83	0.42	0.60	9.83		1.97
10^3K_ϕ	5	−7.59	3.95	−4.13	4.10	0.77	−0.07	9.47	1.0×10^{-3}
	10	−7.69	5.39	3.66	2.96	0.63	7.68	2.65	3.0×10^{-4}
	15	−7.71	5.64	4.32	4.97	0.58	8.49	1.58	3.0×10^{-4}
	20	−7.76	6.01	4.32	1.10	0.58	8.33	1.42	4.0×10^{-4}
	25	−7.68	5.78	2.63	1.13	0.59	6.63	2.14	1.0×10^{-3}
	30	−7.49	4.81	4.24	2.35	0.53	8.93	1.30	1.0×10^{-3}
					C_{10}Na				
V_ϕ	15	164.45	4.56	175.74	1.23	0.12	10.10		0.12
	20	164.50	4.45	175.52	1.43	0.12	9.84		0.12
	25	164.53	4.45	175.43	1.45	0.12	9.72		0.13
	30	164.55	4.45	175.36	1.51	0.12	9.63		0.13
	35	164.57	4.45	175.33	1.53	0.12	9.57		0.13
	40	164.58	4.45	175.31	1.53	0.12	9.55		0.14
	45	164.59	4.45	175.29	1.52	0.12	9.52		0.15
10^3K_ϕ	15	−7.70	5.52	7.09	1.55	0.12	14.01	−0.08	6.0×10^{-6}
	20	−7.75	6.87	6.63	1.04	0.12	13.44	0.05	7.2×10^{-6}
	25	−7.79	7.85	6.37	0.75	0.12	13.10	0.13	1.3×10^{-5}
	30	−7.82	8.72	6.21	0.58	0.12	12.86	0.16	1.9×10^{-5}
	35	−7.85	9.48	6.11	0.48	0.12	12.70	0.17	2.4×10^{-6}
	37	−7.87	9.98	6.06	0.42	0.12	12.61	0.17	2.8×10^{-6}
	40	−7.94	11.52	5.93	0.26	0.12	12.34	0.18	4.7×10^{-6}
					C_{12}Na				
V_ϕ	30	194.19	44.5	207.51	6.65	0.03	11.66		0.35
	45	194.23	44.5	207.45	6.40	0.03	11.56		0.27
	50	194.23	44.5	207.45	6.32	0.03	11.56		0.25
	55	194.24	44.5	207.46	6.07	0.03	11.56		0.24
	60	194.24	44.5	207.44	6.20	0.03	11.54		0.23
	65	194.25	44.5	207.44	6.15	0.03	11.53		0.22
10^3K_ϕ	30	−7.10	−0.06	8.77	9.35	0.03	15.81	0.58	2.4×10^{-6}
	45	−7.34	−0.05	8.46	7.94	0.03	15.74	0.48	2.5×10^{-6}
	50	−7.38	−0.04	8.40	7.63	0.03	15.72	0.48	2.5×10^{-6}
	55	−7.40	−0.04	8.34	7.33	0.03	15.68	0.51	2.5×10^{-6}
	60	−7.41	−0.04	8.29	7.04	0.03	15.64	0.54	2.5×10^{-6}
	65	−7.42	−0.04	8.24	6.76	0.03	15.60	0.57	2.5×10^{-6}

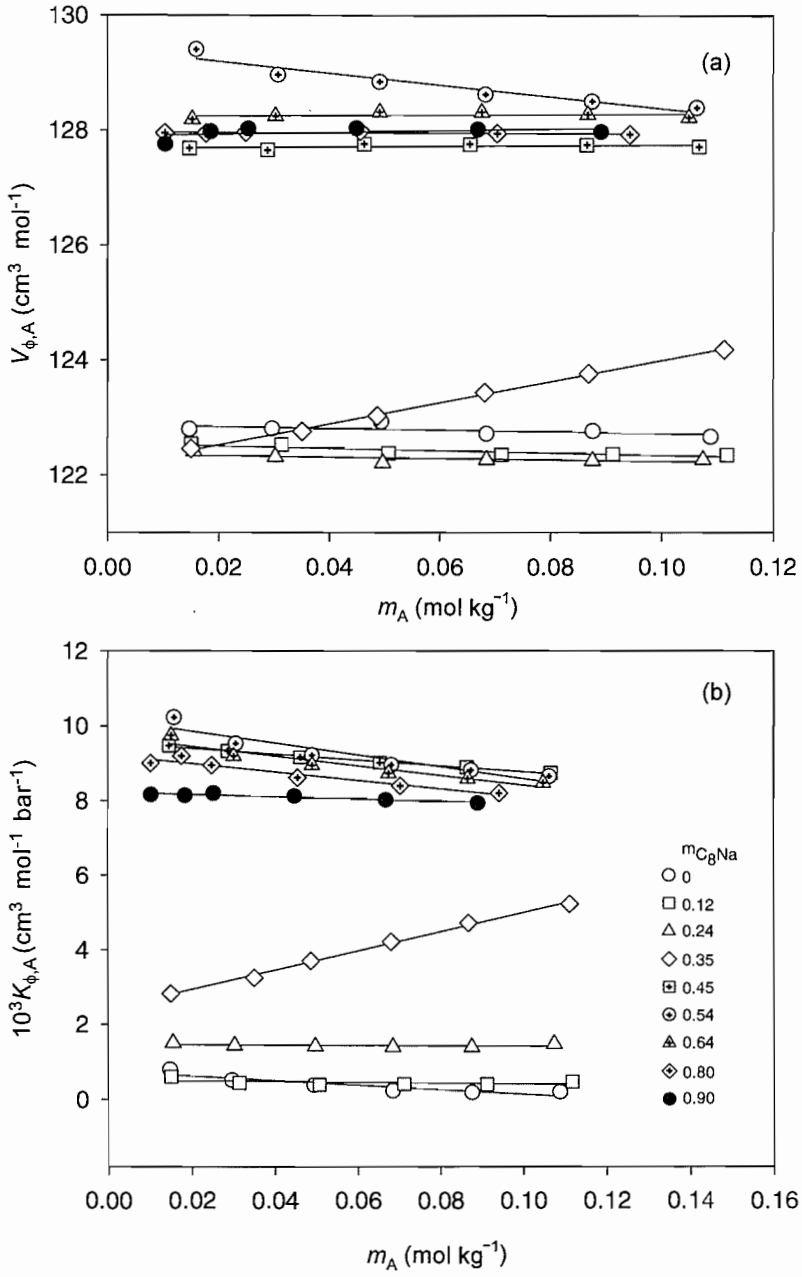
[a] V^0 and V^M in cm^3 mol^{-1}, K^0 and K^M in cm^3 mol^{-1} bar^{-1}.
[b] B_Y an interaction parameter between monomers.
[c] C_V in cm^3 kg mol^{-2} and C_K in 10^{-3} cm^3 kg mol^{-2} bar^{-1}.
[d] m_t the operating CMC value defined in refs. 6 and 7.
[e] ΔY^M the micellization function.

example, $m_S = 0.12\ m$ for C_{10}Na and $m_S = 0.03\ m$ for C_{12}Na (Fig. 2*a*), respectively. The values of the cmc determined from the break point in $V_{\phi,S}$ are in good agreement with previously reported values of 0.37–0.40 *m* for C_8Na (27, 28), 0.11 *m* for C_{10}Na (16, 18, 27), and 0.028 *m* for C_{12}Na (27, 28). When the apparent molar volume data of C_nNa in the concentration region below the cmc are plotted as $V_{\phi,S} - 1.86\sqrt{m_S}$ vs. m_S, i.e., applying the Debye–Hückel theory for the apparent molar property of a dilute solution of a strong 1:1 electrolyte (28),

$$[11] \quad Y_{\phi,S} = Y^0_{\phi,S} + 1.86\sqrt{m_S} + B_Y m_S$$

© 1997 NRC Canada

Fig. 3. Apparent molar volumes (*a*) and apparent molar adiabatic compressibilities (*b*) of C_4EO_1 in aqueous C_8Na solutions.



the slope, B_V, is estimated to be approximately zero for C_8Na. In the case of $C_{10}Na$ system, B_V is ca. zero at m_S <0.05 m, but it increases significantly thereafter. A similar change in B_V for $C_{12}Na$ is observed at $m_S \cong 0.01$ m. Since there is a large uncertainty in the value of $V_{\phi,S}$ due to the less accurate values of densities measured at very low concentrations, the significance of B_V for $C_{12}Na$ cannot be ascertained with any confidence. The near-zero value of the interaction parameter between the shorter chain C_8Na monomers seems to indicate that an increasing hydrophilicity in the carboxylate head group, -COO^-, has counterbalanced the hydrophobic attractions between C_8Na monomers. The latter effect has been observed in some shorter chain alkylammonium surfactant systems (29). The positive deviation in B_V as the hydrocarbon chain increases in length may reflect the effect of the formation of pre-micellar subaggregates on the thermodynamic volume.

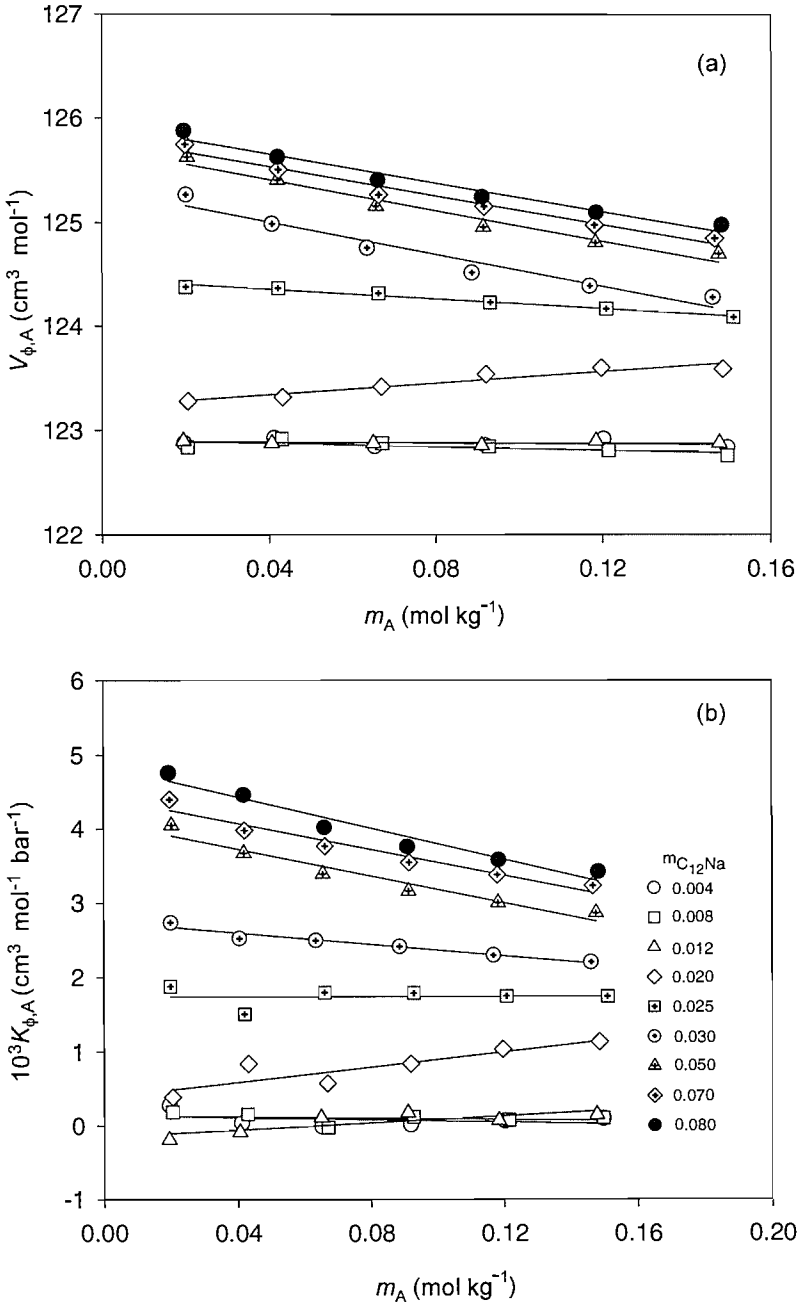
The apparent molar adiabatic compressibilities, $K_{\phi,S}$, for C_nNa in the absence of alcohol show nearly parallel behaviour to the apparent molar volumes except that the values of $K_{\phi,S}$ decrease initially, then increase, in the concentration region below the cmc for both $C_{10}Na$ and $C_{12}Na$. For surfactant monomers in the aqueous phase, it has been shown that the contribution of the hydrophobic part of the surfactant molecule to the compressibility is small (30), and it is the -COO^- group that makes $K_{\phi,S}$ for C_nNa negative (31). The increase in water structure due to elongation of the hydrocarbon chain length will make a positive contribution to the compressibility

© 1997 NRC Canada

Can. J. Chem. Downloaded from www.nrcresearchpress.com by 91.121.58.235 on 09/08/12
For personal use only.

Can. J. Chem. Downloaded from www.nrcresearchpress.com by 91.121.58.235 on 09/08/12
For personal use only.

Fig. 4. Apparent molar volumes (*a*) and apparent molar adiabatic compressibilities (*b*) of C_4EO_1 in aqueous $C_{12}Na$ solutions.

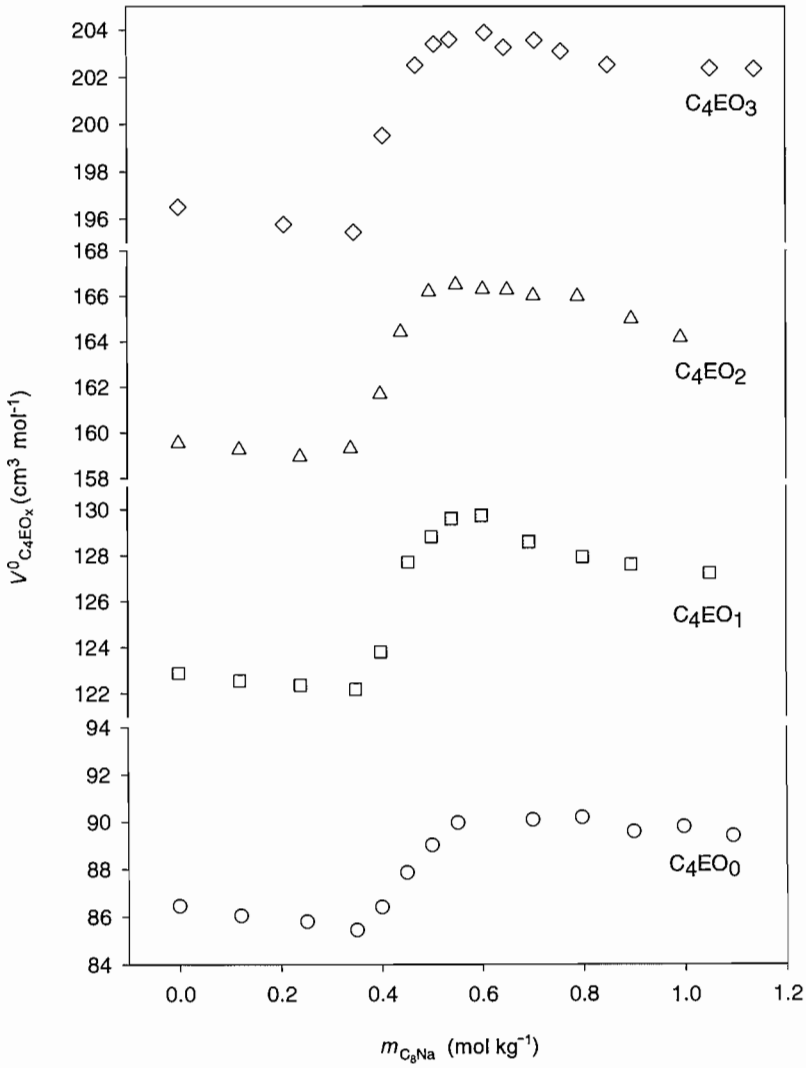


(32). Therefore, the compressibility behaviour of surfactant monomers in the pre-micellar region will be a compromise between the effects mentioned above; however, it is inappropriate to elaborate in detail about $K_{\phi,S}$ for $C_{10}Na$ and $C_{12}Na$ systems due to the relatively large uncertainty in the density measurements in this low-concentration region.

The values of the parameters derived from application of the mass-action model to $V_{\phi,S}$ and $K_{\phi,S}$ experimental data from binary solutions of C_nNa (Table 1) show that the agreement between the simulated and experimental results, when different mean aggregation numbers are chosen in the simulation, is not unique in the three systems. For the case of C_8Na, the theoretical simulation curve of the apparent molar volume data resembles, in general, the experimental data but deviates in both the low- and high-concentration regions (Fig. 1*a*). The infinite dilution, V_S^0, values of the volume obtained from simulation (except the one for a mean aggregation number of 5) are larger than the value of 132.8 cm^3 mol^{-1} obtained from extrapolating experimental $V_{\phi,S}$ values to $m_S = 0$. It increases from 133.1 to 133.8 cm^3 mol^{-1} as the mean aggregation number of the micelle varies from 10 to 25. These values are also higher than previously reported experimental values of 132.4 cm^3 mol^{-1} (27) and 132.7 cm^3 mol^{-1} (28). The value of the molar volume of C_8Na in the micellar form, V_S^M, also varies between 143.5 and 144.0 cm^3 mol^{-1} with variation of the mean aggregation number. A graphical comparison of the apparent

© 1997 NRC Canada

Fig. 5. Partial molar volumes of C_4EO_X in aqueous C_8Na solutions.



molar volumes of C_8Na obtained from simulations using different aggregation numbers was presented previously (15). The simulation of the apparent molar compressibility data of C_8Na gives results that agree well with the experimental data (Fig. 1*b*). The simulation values of K_S^0 ($(-7.7--7.5) \times 10^{-3}$ cm^3 mol^{-1} bar^{-1}) and K_S^M ($(3.7–4.3) \times 10^{-3}$ cm^3 mol^{-1} bar^{-1}) agree with $K_S^0 = -7.4 \times 10^{-3}$ cm^3 mol^{-1} bar^{-1} and $K_S^M = 3.9 \times 10^{-3}$ cm^3 mol^{-1} bar^{-1} values previously reported (27). These results generally show that K_S^0 and K_S^M are less sensitive to change in the mean aggregation number than is the volume property. Although the simulation predicts a value of V_S^0 (132.7 cm^3 mol^{-1}) and gives a good fit to the experimental data in the concentration region below the cmc when a low mean aggregation number of 5 is used, the unrealistically high value of V_S^M and the low value of K_S^M do not justify this as a reasonable value to use for the mean aggregation number of C_8Na micelles. Previous studies have shown the micellization of C_8Na takes place over a broad concentration range and that the micelle grows from an aggregation number of 11 around the cmc (0.4 M) to 26 at a concentration of 1.8 M (33). The values of the simulation parameters indicate that the mean aggregation number of C_8Na micelles is in the range of 10–20, which is not inconsistent with the value of 12 determined experimentally at a concentration of $m_S = 0.6$ *m* (Table 3).

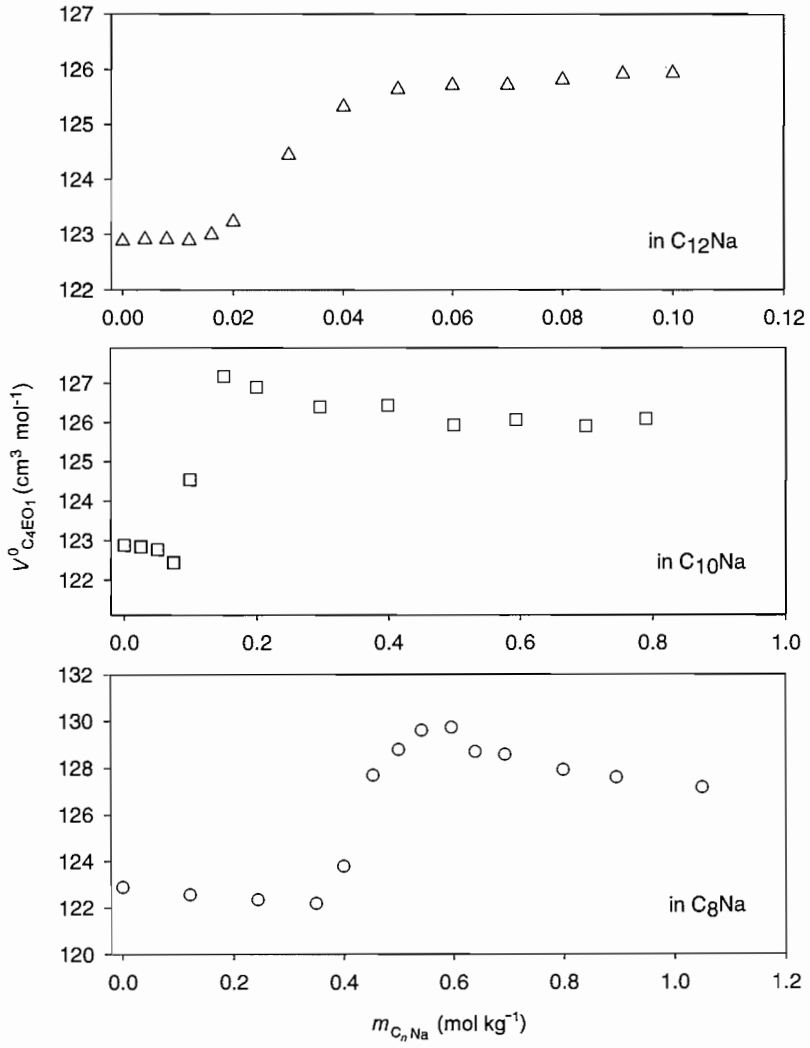
For $C_{10}Na$ there is little change in the values of the molar volume in water at infinite dilution, V_S^0 (164.5–164.6 cm^3 mol^{-1}), and in the micelles, V_S^M (175.7–175.4 cm^3 mol^{-1}), when the simulation is carried out using mean aggregation numbers ranging from 15 to 45. These values are slightly larger than the previously reported values of $V_S^0 = 164.0$ cm^3 mol^{-1} and $V_S^M = 175.2$ cm^3 mol^{-1} obtained from simulation using the same model (18), and $V_S^0 = 164.2$ cm^3 mol^{-1} and $V_S^M = 175.0$ cm^3 mol^{-1}, obtained experimentally (27). The range of values of the apparent molar adiabatic compressibility properties ($K_S^0 = (-7.7--7.8) \times 10^{-3}$ cm^3 mol^{-1} bar^{-1} and $K_S^M = (7.1–6.2) \times 10^{-3}$ cm^3 mol^{-1} bar^{-1}) obtained from simulation are comparable to the experimental results of $K_S^0 = -7.8 \times 10^{-3}$ cm^3 mol^{-1} bar^{-1} and $K_S^M = 6.0 \times 10^{-3}$ cm^3 mol^{-1} bar^{-1} (27). A negative relaxational contribution to compressibility (-0.08 cm^3 mol^{-1} bar^{-1}), obtained by using a mean aggregation number of 15 (Table 1) in the simulation of $K_{\phi,S}$, is theoretically incorrect: it should be positive because it is a function of $(\Delta V_S)^2$ in the mass-action model (6, 7). This anomaly probably reflects the fact that 15 is an unrealistically low mean aggre-

Can. J. Chem. Downloaded from www.nrcresearchpress.com by 91.121.58.235 on 09/08/12
For personal use only.

© 1997 NRC Canada

Can. J. Chem. Downloaded from www.nrcresearchpress.com by 91.121.58.235 on 09/08/12
For personal use only.

Fig. 6. Partial molar volumes of C_4EO_1 in aqueous C_nNa solutions.



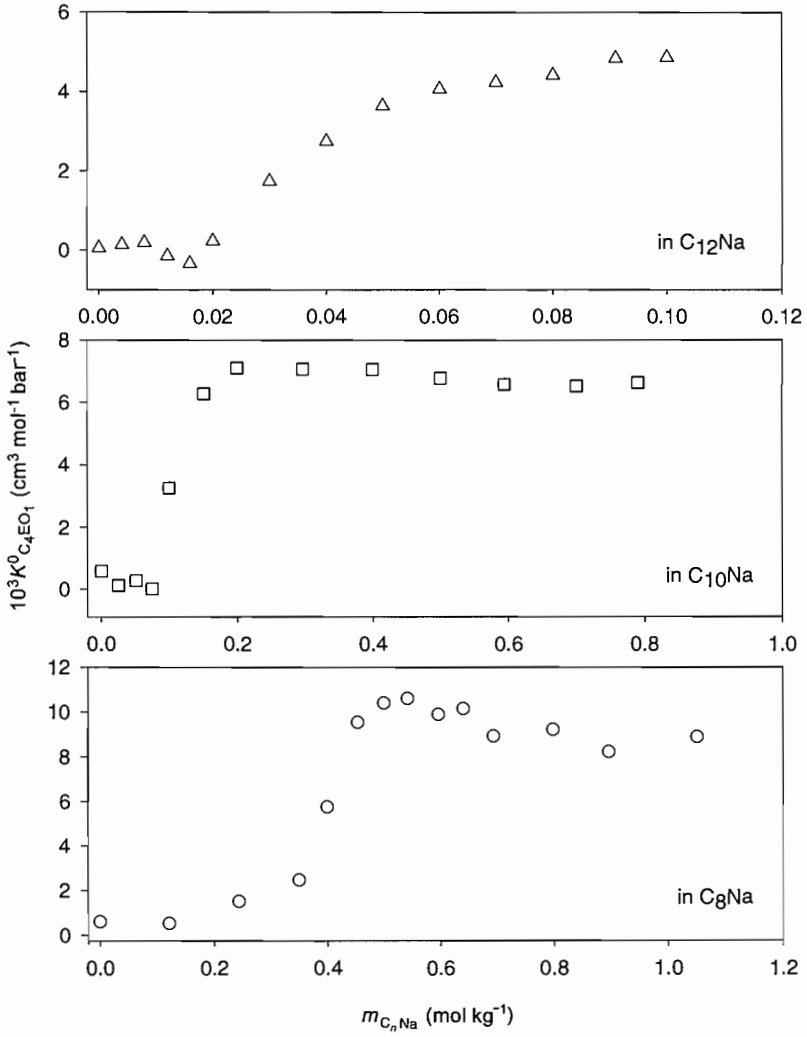
gation number for $C_{10}Na$ micelles as this mean aggregation number of $C_{10}Na$ micelles has been experimentally determined to be 34 at a concentration of $m_S = 0.3$ *m* (Table 3). The insensitivity of the aggregation number to the process of extracting the thermodynamic parameters for long-chain surfactants using the mass-action model has been previously addressed (7).

For $C_{12}Na$ the change in the simulated values of the Y^0_S and Y^M_S properties using different mean aggregation numbers is similar to that observed for $C_{10}Na$, i.e., varying the mean aggregation number from 30 to 65 has a minor effect on the simulated results. The value of V^0_S (194.2 cm^3 mol^{-1}) is 1.0 cm^3 mol^{-1} lower than the previously reported values of 195.0–195.5 cm^3 mol^{-1} (27, 28). Because the experimental uncertainty in $V_{\phi,S}$ increases substantially with decreasing concentration and the estimated error in $V_{\phi,S}$ could be as large as 0.8 cm^3 mol^{-1} for $C_{12}Na$ (28), our result is considered to be in good agreement with the literature values. The value of V^M_S (207.5 cm^3 mol^{-1}) agrees well with 207.3 cm^3 mol^{-1} estimated from the experimental data of $V_{\phi,S}$ in the post-micellar region (27). The values of both K^0_S ($(-7.1--7.4) \times 10^{-3}$ cm^3 mol^{-1} bar^{-1}) and K^M_S ($(8.8–8.4) \times 10^{-3}$ cm^3 mol^{-1} bar^{-1}) are higher by 1.0×10^{-3} cm^3 mol^{-1} bar^{-1} than values reported from previous work (27). A mean aggregation number of 59 for $C_{12}Na$ micelles has been experimentally determined at a concentration of $m_S = 0.12$ *m* (Table 3).

The values of ΔV^M_S (9.2 cm^3 mol^{-1} for C_8Na, 9.6 cm^3 mol^{-1} for $C_{10}Na$, and 11.6 cm^3 mol^{-1} for $C_{12}Na$) are in good agreement with those reported in the literature (27). The values of ΔK^M_S (8.4×10^{-3} cm^3 mol^{-1} bar^{-1} for C_8Na, 12.8×10^{-3} cm^3 mol^{-1} bar^{-1} for $C_{10}Na$, 15.7×10^{-3} cm^3 mol^{-1} bar^{-1} for $C_{12}Na$) are smaller by 1.0×10^{-3} cm^3 mol^{-1} bar^{-1} for C_8Na, but larger by 1.5×10^{-3} cm^3 mol^{-1} bar^{-1} for both $C_{10}Na$ and $C_{12}Na$, than previously reported values (27). The uneven increment in ΔY^M_S as the hydrocarbon chain length of the surfactant is increased by a $-CH_2CH_2-$ segment may be due to the change in the extent of hydration of the micelle. Using a value of 28.3 cm^3 mol^{-1} as the partial molar volume for the $-CH_2COO^-Na^+$ ion pair in aqueous micelle solution (34), the surface area per head group, S/N_S, in a spherical micelle of radius equal to the fully extended hydrocarbon chain, is calculated to be 134 Å^2 for C_8Na, 71 Å^2 for $C_{10}Na$, and 58 Å^2 for $C_{12}Na$. These values correspond to mean aggregation numbers of 12, 34, and 59, respectively. Obviously, there is more exposure of the micelle

© 1997 NRC Canada

Fig. 7. Partial molar compressibilities of C_4EO_1 in aqueous C_nNa solutions.



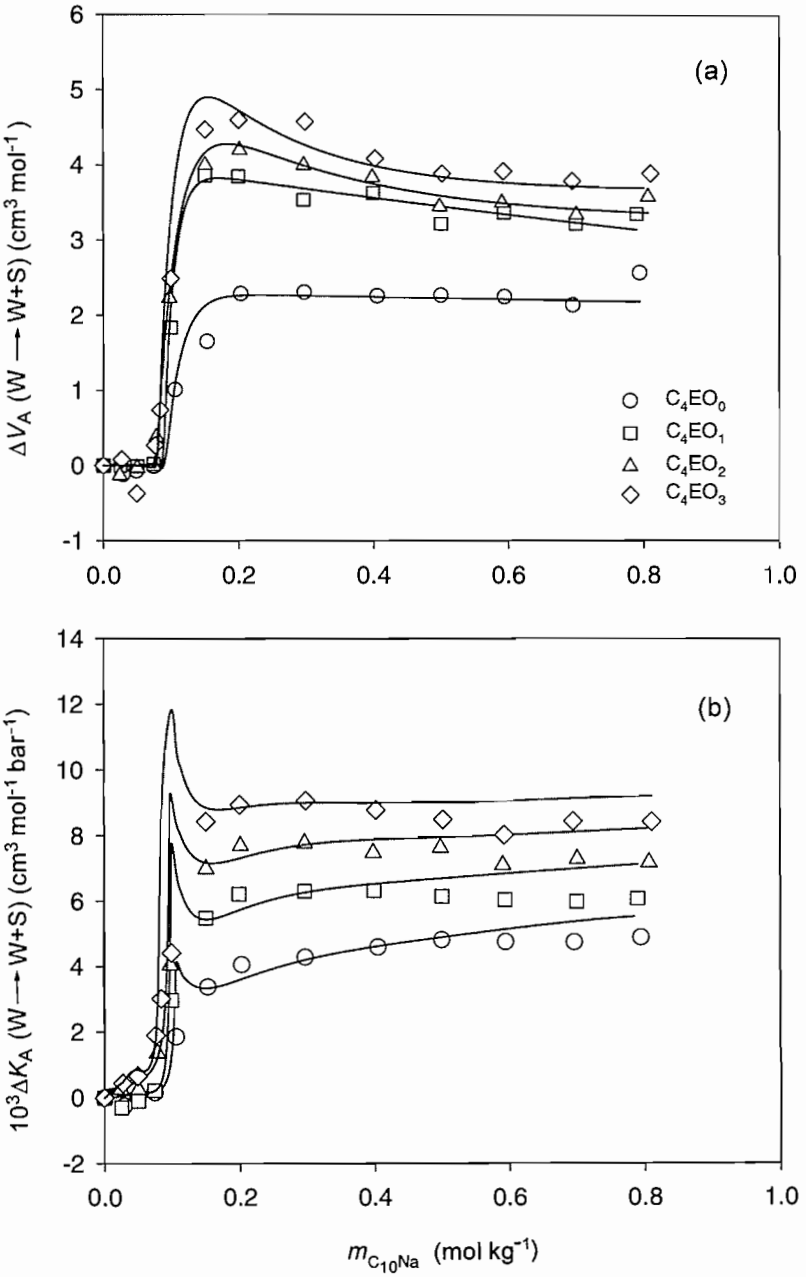
interior to the bulk phase in the case of smaller micelles compared to the larger ones and the micelles have undergone a significant change from a "looser" assembly in C_8Na to a better packed, larger aggregate in $C_{10}Na$ and $C_{12}Na$. Since the repulsion between head groups becomes less important when S/N_S is sufficiently large (35), the small increase in ΔV_S^M of $C_{10}Na$ (9.6 cm^3 mol^{-1}) compared to ΔV_S^M of C_8Na (9.2 cm^3 mol^{-1}) is attributed to a significant increase in the interactions between the -COO^- groups in $C_{10}Na$ micelles. For example, the distance between head groups, d_{h-h}, decreases significantly from 13.1 Å in C_8Na to 9.5 Å in $C_{10}Na$. On the other hand, the relatively large increase in ΔV_S^M of $C_{12}Na$ (11.5 cm^3 mol^{-1}) compared to that of $C_{10}Na$ is due to modification of the $C_{12}Na$ micelle interior, as only a moderate increase in the head group interactions should occur because of the relatively smaller decrease in d_{h-h}, (8.6 Å). Therefore, the change in the value of ΔV_S^M as a function of surfactant chain length reflects, simultaneously, the effects of the hydrocarbon chain and the head group on the change in volumetric properties of micelle formation. The dependence of ΔK_S^M on the surfactant chain length is different. The relatively large increase in ΔK_S^M between $C_{10}Na$ (12.8×10^{-3} cm^3 mol^{-1} bar^{-1}) and C_8Na (8.4×10^{-3} cm^3 mol^{-1} bar^{-1}), and the further moderate increase in ΔK_S^M for $C_{12}Na$ (15.7×10^{-3} cm^3 mol^{-1} bar^{-1}) suggests that this property is more sensitive to changes in the micelle interior than in the micelle surface region.

Comparisons of the partial molar volumes, $\overline{V}_S$, of C_nNa, in the absence of C_4EO_X, show that the values increase steadily for C_8Na in the post-micellar region in the concentration range studied (<2.0 *m*) while it levels off to a constant value of 176 cm^3 mol^{-1} for $C_{10}Na$ and 208 cm^3 mol^{-1} for $C_{12}Na$. On the other hand, the partial molar adiabatic compressibilities, $\overline{K}_S$, of C_nNa are independent of composition in the post-micellar region. The steady increase in $\overline{V}_S$ of C_8Na over a broad concentration range above the cmc may reflect a continuous modification in the micelle due to its growth, as discussed above. In the case of the longer hydrocarbon chain $C_{10}Na$ and $C_{12}Na$ surfactants, the relative independence of $\overline{V}_S$ as a function of surfactant concentration in the post-micellar region indicates that increasing the concentration of surfactant simply produces more micelles of relatively constant structure.

Can. J. Chem. Downloaded from www.nrcresearchpress.com by 91.121.58.235 on 09/08/12
For personal use only.

© 1997 NRC Canada

Fig. 8. Comparisons between the simulated (solid lines) and the experimental transfer volumes (*a*) and transfer compressibilities (*b*) of C_4EO_X from water to aqueous $C_{10}Na$ solutions.



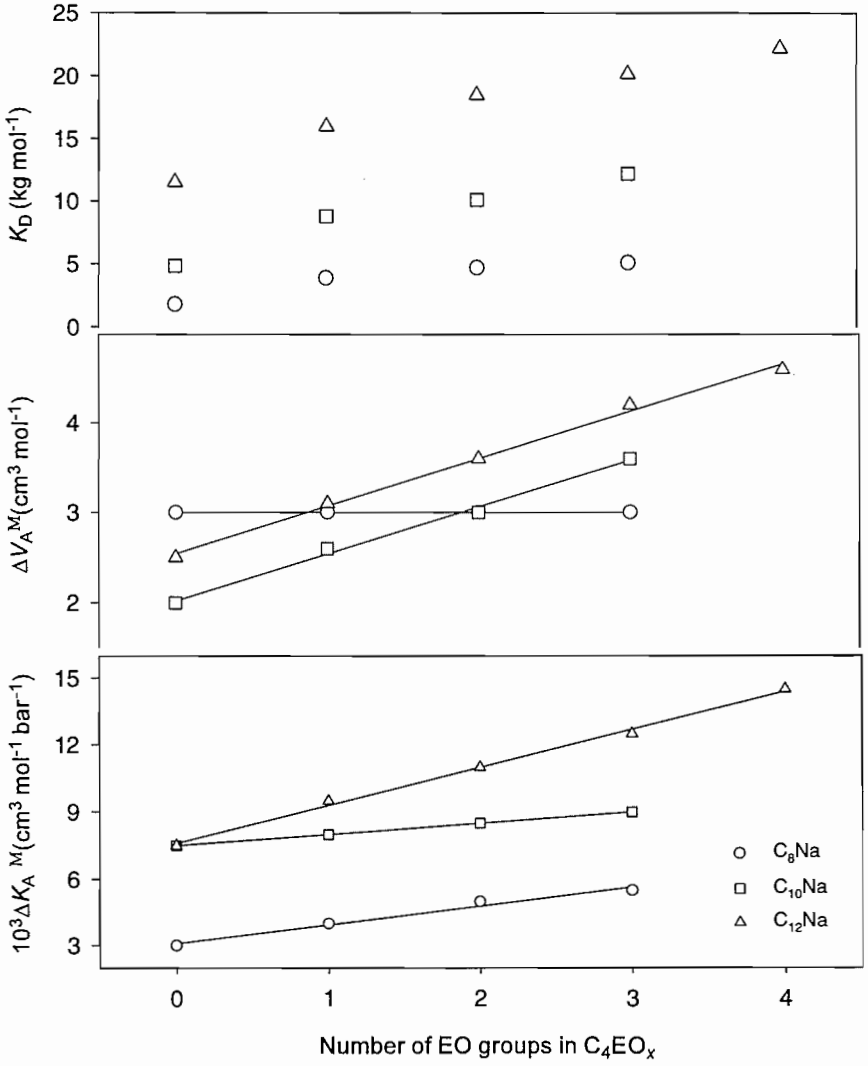
Effects of C_4EO_X on the volumetric properties of C_nNa in water

In the ternary aqueous solutions containing C_4EO_X, the addition of 0.02 *m* C_4EO_X has an insignificant effect on the molar volumetric properties of the short-chain C_8Na compared to the values in the binary system (Fig. 1). For a "loose" aggregate such as C_8Na, there is more exposure of the micelle interior to the bulk phase and the head groups of the surfactant are likely hydrated to the same extent as in the bulk solution. Therefore, the solubilization of a small fraction of C_4EO_X molecules, whose EO segments are highly hydrated, in the micelle should not induce a significant change in the environment around the octanoate species in the micelle. In contrast, the values of the apparent molar properties of $C_{10}Na$ in the presence of 0.055 *m* C_4EO_X are greater than in the binary aqueous systems over the concentration range investigated. Furthermore, the increase in $V_{\phi,s}$ is greater in the case of alcohols containing EO group(s) than in the case of butanol, especially in the transition region. A shift in the cmc to lower values is also observed with an increase in the number of EO groups in the alcohol. This behaviour corroborates previous reports that the cmc of $C_{10}Na$ in the ternary system containing C_4EO_1 is lower than that containing C_4EO_0 at the same concentration of alcohol (17), and that the cmc of aqueous SDS solutions containing alkoxyethanols of constant alkyl chain length is reduced by increasing the number of EO groups (19). In spite of the shift in the cmc,

© 1997 NRC Canada

Can. J. Chem. Downloaded from www.nrcresearchpress.com by 91.121.58.235 on 09/08/12
For personal use only.

Fig. 9. Dependence of solubilization parameters from simulations of the transfer function of C_4EO_X from water to aqueous C_nNa solutions on the number of EO groups in the alcohol.



values of the partial molar properties, $\overline{Y}_S$, for $C_{10}Na$ at concentrations above the cmc in the presence of 0.055 *m* C_4EO_X do not differ from $\overline{V}_S$ in water (16). This indicates that the addition of a small quantity of C_4EO_X has an insignificant effect on the micellization properties of $C_{10}Na$, $\Delta\overline{Y}_S^M$ (the change in the molar properties of the surfactant as the monomeric surfactant species associate into micelles). Therefore, there will be little change in the size and shape of $C_{10}Na$ micelles with the incorporation of some ethoxylated alcohol molecules. The nearly constant mean aggregation number of $C_{10}Na$ micelles (N_S = 33/34, Table 3) determined in the presence of 0.044 *m* C_4EO_X confirms this argument. The presence of EO groups in the alcohol at a concentration of 0.05 *m* has a more profound effect on the volumetric properties of $C_{12}Na$ than in the case of $C_{10}Na$ systems. The decrease in the cmc is approximately 30%, and there is a significant increase in the molar properties, especially the molar compressibility (Fig. 2). Although the behaviour of $\overline{V}_A^M$ gives no conclusive information, the appreciable increase in the partial molar adiabatic compressibility, $\overline{K}_A^M$, in the presence of C_4EO_X indicates that the $C_{12}Na$ micelle interior becomes more compressible, and changes in the micelle structure are likely to take place. Indeed, some of the $C_{12}Na$ species in the micelles are replaced by C_4EO_X molecules as shown by the results of the mean aggregation number measurements (Table 3). The relatively higher ratio of m_A/m_S (0.05 m_A/0–0.15 m_S) in the $C_{12}Na$ systems compared to the $C_{10}Na$ systems (0.055 m_A/0–0.8 m_S) is one possible reason for this change. These results are similar to those observed for other ionic surfactant and *n*-alcohol systems when the chain length of alcohol is increased (31, 36). It is believed that the presence of the EO moiety within the micelle contributes to the reduction of the electrostatic interactions between surfactant head groups in the mixed micelles of anionic surfactant – ethoxylated alcohol. These results provide additional evidence that increasing the number of EO groups in the alcohol enhances interactions between ethoxylated alcohols and anionic micelles (14–20).

Volumetric properties of C_4EO_X in C_nNa and water mixed solvents

The general behaviour of apparent molar properties, $V_{\phi,A}$ and $K_{\phi,A}$, for C_4EO_X alcohols in water–C_nNa mixed solvents is

Can. J. Chem. Downloaded from www.nrcresearchpress.com by 91.121.58.235 on 09/08/12
For personal use only.

© 1997 NRC Canada

Can. J. Chem. Downloaded from www.nrcresearchpress.com by 91.121.58.235 on 09/08/12
For personal use only.

Table 2. Parameters used for the adjusted simulation of the transfer properties of C_4EO_X from water to aqueous C_nNa solutions at 25°C.[a]

Alcohol	Property	$\Delta\overline{Y}_A^M$	K_D	$B_{Y,SA}$	CMC	p	p^b
		0.05 m_A in C_8Na (N_S = 10/15)					
C_4EO_0	ΔV	3.0	1.8	−1.43	0.30		
	ΔK	0.0030	1.9	0.0013	0.30		
C_4EO_1	ΔV	3.0	4.0	−1.11	0.30		
	ΔK	0.0040	3.9	0.0016	0.30		
C_4EO_2	ΔV	3.0	4.8	−1.19	0.28		
	ΔK	0.0050	4.7	0.0027	0.28		
C_4EO_3	ΔV	3.0	5.2	−1.55	0.27		
	ΔK	0.0055	5.0	0.0037	0.27		
		0.05 m_A in $C_{10}Na$ (N_S = 30)					
C_4EO_0	ΔV	2.0	4.7	−0.10	0.11	0.41	0.35 ± 0.05
	ΔK	0.0075	5.0	0.0010	0.11		
C_4EO_1	ΔV	2.6	8.7	−0.20	0.10	0.52	0.47 ± 0.05
	ΔK	0.0080	8.8	0.0015	0.10		
C_4EO_2	ΔV	3.0	10.0	−0.50	0.10	0.58	0.54 ± 0.05
	ΔK	0.0085	10.2	0.0075	0.10		
C_4EO_3	ΔV	3.6	12.0	−0.50	0.10	0.65	0.59 ± 0.05
	ΔK	0.0090	12.5	0.0013	0.10		
		0.02 m_A in $C_{12}Na$ (N_S = 60)					
C_4EO_0	ΔV	2.5	11.0	0	0.025		
	ΔK	0.0075	12.0	−0.010	0.025		
C_4EO_1	ΔV	3.1	16.0	5.0	0.024		
	ΔK	0.0095	15.5	−0.003	0.025		
C_4EO_2	ΔV	3.6	19.0	1.0	0.024		
	ΔK	0.0110	18.0	0.0075	0.025		
C_4EO_3	ΔV	4.2	20.5	3.50	0.024		
	ΔK	0.0125	20.0	0.0170	0.024		
C_4EO_4	ΔV	4.6	22.0	−6.01	0.024		
	ΔK	0.0145	22.5	0.0046	0.025		

[a] K_D in kg mol^{-1}, $B_{V,SA}$ in cm^3 kg mol^{-2}, $B_{K,SA}$ in cm^3 kg mol^{-2} bar^{-1}, CMC in mol kg^{-1}.
[b] At m_A = 0.05 and m_S = 0.463, p = 1 − β, the degree of solubilization of additive in micelle (ref. 14).

illustrated for the case of C_4EO_1 in aqueous C_nNa solutions of different concentrations (Figs. 3 and 4). The changes in $V_{\phi,A}$ and $K_{\phi,A}$ for C_4EO_{0-3} in water as a function of alcohol concentration ($m_A < 0.12\ m$) have been previously discussed (15). The values of the partial molar volume at infinite dilution, $\overline{V}_A^0$, obtained from extrapolating $\overline{V}_{\phi,A}$ to m_A = 0, 86.45 (C_4EO_0), 122.88 (C_4EO_1), 159.54 (C_4EO_2), and 196.49 (C_4EO_3) cm^3 mol^{-1} are in good agreement with those previously reported (37). More recently, we obtained a value of 233.56 cm^3 mol^{-1} for $\overline{V}_A^0$ of C_4EO_4. An average value of 36.78 cm^3 mol^{-1} per EO group in aqueous medium is in good agreement with the literature value of 36.96 cm^3 mol^{-1} (38). With the exception of C_4EO_4, the partial molar adiabatic compressibility, $\overline{K}_S^0$, in aqueous medium gradually decreases from a small positive value (0.72×10^{-3} cm^3 mol^{-1} bar^{-1} for C_4EO_0) to a small negative value (-0.35×10^{-3} cm^3 mol^{-1} bar^{-1} for C_4EO_3) as the number of EO groups in C_4EO_X increases. This behaviour is similar to that of aqueous solutions of normal alcohols of increasing hydrocarbon chain length (30).

The apparent molar volumetric properties of these alcohols in water–C_nNa mixed solvents show a number of features that are characteristic of the process of forming C_nNa–C_4EO_X mixed micelles. At a concentration of C_nNa significantly below the cmc (<0.12 m_S for C_8Na, <0.07 m_S for $C_{10}Na$, and <0.015 m_S for $C_{12}Na$, respectively), the apparent molar volumes of the C_4EO_X are invariant or decrease slightly (in most of the cases) with increasing concentration of alcohol, and the values of $V_{\phi,A}$ are close to those observed in water (Figs. 3 and 4). This indicates that the presence of monomer surfactant at low concentration has little effect on the dissolution of the alcohols into the aqueous media or that there is a small enhancement of hydrophobic interactions between the alcohol monomers in the surfactant solution, but without the formation of any aggregates. When the concentration of C_nNa in the sys-

© 1997 NRC Canada

Table 3. Values of the aggregation numbers of the components for mixed micelles of C_nNa/C_4EO_X from DFQ using 2,3-DMN/C_{12}PyCl (probe/quencher).

Alcohol	m_A (m)	α^a	β^a	N_S	N_A
		C_8Na (m_S = 0.597 m)			
No	0	0.747	0	12	0
C_4EO_0	0.040	0.708	0.874	12	0.4
C_4EO_1	0.040	0.707	0.761	12	0.7
C_4EO_2	0.041	0.705	0.717	13	0.9
C_4EO_3	0.041	0.704	0.693	13	1.0
C_4EO_4	0.041	0.703[b]	0.670[b]	14	1.1
		$C_{10}Na$ (m_S = 0.299 m)			
No	0	0.410	0	34	0
C_4EO_0	0.043	0.377	0.684	34	2.5
C_4EO_1	0.045	0.370	0.579	33	3.5
C_4EO_2	0.045	0.365	0.509	33	3.9
C_4EO_3	0.044	0.358	0.439	33	4.3
C_4EO_4	0.044	0.358[b]	0.393[b]	33	4.7
		$C_{12}Na$ (m_S = 0.129 m)			
No	0	0.240	0	56	0
C_4EO_0	0.050	0.228	0.710	50	7
C_4EO_1	0.049	0.214	0.633	47	8
C_4EO_2	0.051	0.214	0.550	45	10
C_4EO_3	0.051	0.213	0.477	41	11
C_4EO_4	0.050	0.212	0.440	41	11

[a]α and β are the fraction of surfactant and alcohol monomers in the aqueous phase, respectively, obtained at corresponding m_A and m_S values from the simulation of transfer thermodynamic properties.
[b]Obtained from extrapolating curves of α and β vs. number of EO units.

Can. J. Chem. Downloaded from www.nrcresearchpress.com by 91.121.58.235 on 09/08/12
For personal use only.

tems approaches levels just below the cmc (0.35 m_S for C_8Na, 0.075 m_S for $C_{10}Na$, and 0.015 m_S for $C_{12}Na$, respectively), there is a significant increase in $V_{\phi,A}$ as a function of m_A (Figs. 3 and 4). This is due to the formation of C_nNa–C_4EO_X mixed micelles, which is promoted by the addition of alcohol. The changes in $V_{\phi,A}$ at concentrations of C_nNa above the cmc are different in the systems containing C_8Na and $C_{10}Na$ than in those containing $C_{12}Na$. In the former systems, the variations of $V_{\phi,A}$ vs. m_A are less steep for C_4EO_0, but the limiting slopes become quite negative for those alcohols containing EO groups. As the concentration of surfactant continues to increase, the limiting slopes become positive. Correspondingly, the value of V_A^0 for alcohols containing EO groups shows a convex dependence on surfactant concentration (Fig. 5). Since the concentration of C_8Na and of $C_{10}Na$ in the micellar form, m_S^M, is relatively low at concentrations not too far above the cmc, the strong dependence of the apparent molar volumes of the alcohols containing an increasing number of EO groups on both the alcohol and surfactant concentrations illustrates that the mole ratio of alcohol to surfactant in the mixed micelles is an important factor affecting the properties of micelles containing a greater fraction of alcohol (9). As the concentration of C_8Na and $C_{10}Na$ increases further above the cmc, the less significant changes in $V_{\phi,A}$ indicate that the influence of alcohol on the mixed micelles diminishes, as the alcohols dissolve almost ideally into C_8Na and $C_{10}Na$ micelles. On the other hand, in systems of water–C_4EO_X–$C_{12}Na$ the negative limiting slope of $V_{\phi,A}$ vs. m_A becomes steeper with increasing number of EO groups in the alcohol. The maximum in V_A^0 for C_4EO_1 in C_8Na and $C_{10}Na$ systems no longer appears in the $C_{12}Na$ system (Fig. 6), indicating that the alcohols dissolve more readily into the mixed micelles of the longer chain surfactant.

As shown in Figs. 3*b*, 4*b*, and 7, both the apparent molar adiabatic compressibility and the partial molar compressibility properties for C_4EO_X in aqueous C_nNa solutions behave similarly to the apparent molar volume, except that the limiting slopes of $K_{\phi,A}$ vs. m_A are all negative at concentrations of surfactant above the cmc. Eventually, the magnitudes of both $V_{\phi,A}$ and $K_{\phi,A}$ become independent of surfactant concentration in C_8Na and $C_{10}Na$ systems, and in the $C_{12}Na$ system when the alcohol concentration is high. This result is similar to the dependence of the apparent molar heat capacity of hexanol on alcohol concentration in dodecyltrimethylammonium bromide aqueous solutions (39) and it was explained as being due to the formation of alcoholic microstructures that are stabilized by surfactant molecules. This occurs because the mixed micelles break down as the solution composition becomes richer in alcohol (39). The explanation seems to be reasonable for water–alcohol – long-chain surfactant systems when the surfactant concentration is not very high. But for systems containing shorter chain surfactants at high concentration, especially C_8Na, the addition of limited amounts of alcohol does not break down the micelles. Rather, the alcohol dissolves

© 1997 NRC Canada

Can. J. Chem. Downloaded from www.nrcresearchpress.com by 91.121.58.235 on 09/08/12
For personal use only.

almost ideally into the micelles, as mentioned above. This argument is supported by the fact that the mean aggregation number of decyltrimethylammonium bromide (C_{10}TAB) in mixed micelle systems containing 2-butoxyethanol (C_4EO_1) changes from ca. 30 to 28 at a fixed concentration of $m_S = 0.12$ *m* when the concentration of C_4EO_1 increases from 0.2 *m* to 0.56 *m* (40).

Solubilization of C_4EO_X in C_nNa micelles

The solubilization of C_4EO_X alcohols in C_nNa micelles can be rationalized based on the changes in the parameters $B_{Y,SA}$, K_D, and ΔY_A^M, which are extracted from quantitative analysis of the transfer functions, $\Delta Y_A(W \rightarrow W + S)$, of the alcohol from water to aqueous surfactant solutions. The fit of the transfer volumes and compressibilities of C_4EO_{1-3} from water to aqueous C_8Na, $\Delta V_A(W \rightarrow W + S)$ and $\Delta K_A(W \rightarrow W + S)$, at a given low alcohol concentration of 0.05 *m* is quantitatively acceptable. A nearly quantitative fit of the transfer volumes of C_4EO_{1-3} from water to aqueous C_{10}Na is obtained in the concentration range up to 0.8 *m* (Fig. 8*a*), while good agreement between the simulated and experimental results for the transfer compressibilities is obtained in the concentration range up to 0.5 *m*, but it becomes poorer at higher m_S (Fig. 8*b*). The simulated results for the transfer functions of C_4EO_{1-4} from water to aqueous C_{12}Na are in good agreement with the experimental data except for the transfer compressibility property in the pre-micelle region. The values of the various parameters extracted from the simulations of the transfer volume and compressibility data are consistent (Table 2).

The negative values of $B_{V,SA}$ for C_4EO_{1-3} alcohols in aqueous C_8Na indicate that attractive pair interactions occur between C_8Na and C_4EO_{1-3} monomers in water. The small negative values of $B_{V,SA}$ for these alcohols in aqueous C_{10}Na make it difficult to assess the extent of the interactions between monomers of C_{10}Na and C_4EO_{0-3} in the pre-micelle region, which ought to be hydrophobic in nature. The values of $B_{V,SA}$ for C_4EO_{1-4} alcohols in aqueous C_{12}Na are not reliable because the magnitude of the transfer volume is too small ($\sim$0.1 cm^3 mol^{-1}) to be discriminated from the error in the volume measurement.

The values of K_D for C_4EO_X in C_nNa micelles increase as a function of the number of EO groups in the alcohol and of the surfactant chain length (Table 2). It appears that they do not correlate linearly with the number of EO groups in the alcohol, as shown in Fig. 9. The value of K_D doubles when the first EO group is added to butanol, i.e., $K_D = 4.0$ kg mol^{-1} for C_4EO_1 compared to 1.8 kg mol^{-1} for C_4EO_0 in C_8Na micelle solutions, but further increase in the value of K_D is small as more EO groups are added. However, the difference between the K_D values for C_4EO_1 and C_4EO_0 becomes less significant and the increase in the value of K_D in the C_4EO_{2-4} series becomes more significant in the longer chain C_{10}Na and C_{12}Na micelles. In the systems containing 0.40 *m* C_{10}Na and 0.05 *m* C_4EO_X, values of the solubilization of C_4EO_X alcohols in C_{10}Na micelles determined in this study, expressed in terms of the degree of solubilization of the alcohol in the micelle, are slightly higher than those obtained from an NMR – paramagnetic relaxation study of the same systems at similar concentration conditions (14). Nevertheless, the trends are the same (Table 2). The marked increase in the solubilization of C_4EO_1 compared to C_4EO_0 in C_nNa micelles provides evidence that the inclusion of the first EO group into a medium-chain-length *n*-alcohol significantly enhances the hydrophobic interactions between the alcohol and surfactant species of the micelle. However, the relatively moderate increase in K_D for alcohols having more than one EO group indicates that further addition of EO groups increases the hydrophobic character of the alcohol to a lesser extent. The low values of K_D for C_4EO_X alcohols in C_8Na micelles is partly due to the fact that the short-chain C_8Na surfactant forms micelles of small size, which limits the penetration of alcohol molecules (15). The significant increase in the values of K_D for C_4EO_X alcohols in C_{10}Na and C_{12}Na micelle solutions, compared to that in C_8Na micelle solutions, is consistent with previous results in which the solubilization of *n*-pentanol was observed to increase linearly with surfactant chain length (41). The increased solubilization of C_4EO_X in C_{10}Na and C_{12}Na micelles confirms that mixed micelles formed from surfactants of longer chain length provide an environment that allows the alcohols to penetrate deeper into the micelles.

The values of ΔV_A^M for C_4EO_X alcohols in C_nNa solutions, obtained from the simulation, are quite small (Table 2) but clearly show characteristics that are indicative of interactions between ethoxylated alcohols and anionic micelles (Fig. 9). For example, $\Delta V_A^M = 3.0$ cm^3 mol^{-1} for C_4EO_0 in C_8Na micelles is smaller than the value $\Delta V_A^{Hc} = 5.4$ cm^3 mol^{-1}, which is the difference between the partial molar volume of C_4EO_0 in a pure hydrocarbon solvent and in water at infinite dilution (34). Similar behaviour has been observed for transfer of *n*-alcohols from water to a number of micelle systems, especially anionic surfactant solutions (8–11, 17, 41). Since the change in ΔV_A^M is a net result of the loss of hydrophobic hydration when the alcohol molecule penetrates into the micelle interior (a positive contribution to ΔV_A^M) and the electrostatic interactions between the anionic head groups and EO segments (a negative contribution to ΔV_A^M) (8, 41), the relatively low values of ΔV_A^M for the C_4EO_X alcohols suggest that strong electrostatic interactions occur between the carboxylate ions of C_nNa and the polar segments of C_4EO_X in the micelle palisade layer (8), and that a large part of the alcohol molecule resides in the micelle surface area. The small increase in ΔV_A^M for C_4EO_{2-3}, the virtually constant value of ΔV_A^M for C_4EO_1, and the slight decrease in ΔV_A^M for C_4EO_0 as a function of surfactant chain length (Table 2), provide additional evidence that the interactions between the surfactant head groups and EO segments of C_4EO_X are stronger in the palisade layer of the more compact micelles. The constant value of ΔV_A^M of C_4EO_{0-3} (3.0 cm^3 mol^{-1}) in the C_8Na micelles implies a relatively constant degree of alcohol penetration in these small aggregates. The gradual increase in the values of ΔV_A^M from C_4EO_0 to C_4EO_3 in the C_{10}Na and C_{12}Na micelle systems suggests that the alcohols may penetrate more deeply into the larger micelles as the number of EO groups increase in the alcohol, which is consistent with the results for K_D, as discussed above. The values of $\Delta V_A^M = 2.0$ cm^3 mol^{-1} and $K_D = 8.8$ kg mol^{-1} for C_4EO_1 in C_{10}Na micelles, assuming a mean aggregation number of $N_S = 30$, are lower than the previously reported values of 3.67 cm^3 mol^{-1} and 10.0 kg mol^{-1} using $N_S = 20$ (18). When $N_S = 20$ is used to fit our data, a value of $\Delta V_A^M = 3.6$ cm^3 mol^{-1} can be obtained with $K_D = 8.9$ kg mol^{-1}. It is seen that our results are not that different from those previously reported.

© 1997 NRC Canada

Can. J. Chem. Downloaded from www.nrcresearchpress.com by 91.121.58.235 on 09/08/12
For personal use only.

The correlation of ΔK_A^M with the number of EO groups in the alcohol and the surfactant chain length is generally similar to ΔV_A^M (Fig. 9). It is known that the partial molar compressibility of medium-chain-length *n*-alcohols in $C_{10}Na$ micelles becomes increasingly positive as a function of the chain length and, eventually, exceeds that in pure liquid hydrocarbons (34). The moderate increase of ΔK_A^M with increasing number of EO groups confirms that C_4EO_X alcohols solubilize themselves in $C_{10}Na$ and $C_{12}Na$ anionic micelles in a manner similar to *n*-alcohols. The significant increase in the magnitude of ΔK_A^M for C_4EO_X in the $C_{12}Na$ micelles is quite striking. The partial molar compressibility of $C_{12}Na$ becomes increasingly positive in the presence of longer chain *n*-alcohols due to a decrease in the mean aggregation number of the micelle upon addition of alcohol. This reduces the surface charge density of the micelles and, hence, the electrostriction of water molecules at the micelle surface (31). Under this condition, the compressibility of the alcohol in the micelle would be expected to be high. The relatively large values of ΔK_A^M for C_4EO_X in the $C_{12}Na$ micelles likely reflects this effect. This is supported by the mean aggregation number data (Table 3), which show that a decrease in N_S of $C_{12}Na$ in the mixed micelles is partially compensated by an increase in the number of C_4EO_X molecules. In contrast to this system, the mean aggregation number of surfactants in the smaller C_8Na and $C_{10}Na$ micelles remains unchanged while the number of C_4EO_X molecules increases steadily as more EO groups are added to the alcohol. The nearly constant value of the mean aggregation number for C_8Na and $C_{10}Na$ micelles in the presence of 0.04 *m* C_4EO_X alcohols indicates that the assumption made in the chemical equilibrium model, i.e., that a small amount of additive in the mixed micelle has a negligible effect on the mean aggregation number of the surfactant (10, 11), is valid for small- and medium-size micelles. For larger micelles, adjustment of the mean aggregation number in the simulation may be required to take into account the effect of the change in the mean aggregation number of surfactant induced by the alcohols.

Conclusion

Numerical values of the micellization parameters of sodium carboxylates, C_nNa (n = 8, 10, 12), in water have been obtained from quantitative analysis of the volumetric properties of aqueous solutions of these surfactants using a mass-action model (6, 7). The micelles of C_nNa vary from small, loose aggregates having a mean aggregation number of approximately 10–15 in the case of C_8Na, to well-defined regular micelles of mean aggregation number 60 in the case of $C_{12}Na$. The effect of small quantities of polyoxyethylene butyl ether compounds, C_4EO_X, on the volumetric properties of C_8Na is minor, but becomes increasingly significant for $C_{10}Na$ and $C_{12}Na$. The changes in the volumetric properties are also dependent on the number of EO groups in the alcohol. The behaviour of the molar volumetric properties of C_4EO_X in aqueous C_nNa solutions is characteristic of the formation of mixed micelles of C_nNa–C_4EO_X. The changes in the various solubilization parameters obtained from fitting the thermodynamic transfer functions of C_4EO_X from water to aqueous C_nNa solutions, using a chemical equilibrium model (10, 11), show that the solubilization of C_4EO_X alcohols in C_nNa micelles is enhanced by increasing the hydrophobicity of the surfactant and the number of EO groups in the alcohol. The latter suggests that the EO groups behave as though they make a hydrophobic contribution to interactions between the alcohol and C_nNa surfactants in the mixed micelles. In C_nNa–C_4EO_X mixed micelles, the aggregation numbers of C_8Na and $C_{10}Na$ remain unchanged in the presence of a small quantity of C_4EO_X, while a significant number of the long-chain $C_{12}Na$ surfactant ions are replaced by C_4EO_X molecules in the $C_{12}Na$ micelles.

Acknowledgments

We thank the Natural Sciences and Engineering Research Council of Canada for financial support, and Dr. Zhenglei Cao for assistance in writing the simulation programs.

References

1. P.M. Holland and D. Rubingh. ACS Symp. Ser. **501**, 2 (1992).
2. M.J. Rosen. Surfactant and interfacial phenomena. 2nd ed. John Wiley and Son, New York. 1989. pp. 393–419.
3. R. Zana. Surfactant solutions: new methods of investigation. Surfactant Sci. Ser. Vol. 22. Marcel Dekker, New York. 1987.
4. E.M. Woolley and T.E. Burchfield. J. Phys. Chem. **89**, 714 (1985).
5. T.S. Brun, H. Hoiland, and E. Vikingstad. J. Colloid Interface Sci. **63**, 89 (1978).
6. J.E. Desnoyers, G. Caron, R. DeLisi, D. Roberts, A. Roux, and G. Perron. J. Phys. Chem. **87**, 1397 (1983).
7. G. Caron, M. Lindheimer, G. Perron, and J.E. Desnoyers. J. Colloid Interface Sci. **106**, 324 (1985).
8. R. DeLisi, C. Genova, R. Testa, and V. Turco Liveri. J. Solution Chem. **13**, 121 (1984).
9. R. DeLisi, V. Turco Liveri, M. Castagnolo, and A. Inglese. J. Solution Chem. **15**, 23 (1986).
10. H. Roux, D. Hétu, G. Perron, and J.E. Desnoyers. J. Solution Chem. **13**, 1 (1984).
11. D. Hétu, H. Roux, and J.E. Desnoyers. J. Solution Chem. **16**, 529 (1987).
12. V. Degiorgio and M. Corti. Physics of amphiphiles, micelles, vesicles, and microemulsions. Elsevier, Amsterdam. 1985.
13. H. Uchiyama, M. Abe, and K. Ogino. J. Jpn. Oil Chem. Soc. **35**, 1031 (1986).
14. G. Marangoni and J.C.T. Kwak. Langmuir, **7**, 2083 (1991).
15. H. Huang and R.E. Verrall. J. Solution Chem. **23**, 925 (1994).
16. H. Huang and R.E. Verrall. J. Solution Chem. **26**, 135 (1997).
17. F. Yamashita, G. Perron, J.E. Desnoyers, and J.C.T. Kwak. J. Colloid Interface Sci. **114**, 548 (1986).
18. F. Yamashita, G. Perron, J.E. Desnoyers, and J.C.T. Kwak. ACS Symp. Ser. **311**, 79 (1986).
19. M. Manabe and M. Koda. Bull. Chem. Soc. Jpn. **51**, 1599 (1978).
20. M. Schwuger. ACS Symp. Ser. **253**, 3 (1984).
21. P. Becher. *In* Nonionic surfactants. Surfactant Sci. Ser. Vol. 1. *Edited by* M.J. Schick. Marcel Dekker, New York. 1967. pp. 478–515.
22. M.J. Rosen, A.W. Cohen, M. Dahanayake, and X. Hua. J. Phys. Chem. **86**, 541 (1982).
23. Y. Saito and T. Sato. J. Phys. Chem. **89**, 2110 (1985).
24. G. Marangoni, A. Rodenhiser, J. Thomas, and J.C.T. Kwak. ACS Symp. Ser. **501**, 194 (1992).
25. J.E. Desnoyers. J. Surf. Sci. Technol. **5**, 289 (1989).
26. M. Iqbal and R.E. Verrall. J. Phys. Chem. **91**, 967 (1987).
27. E. Vikingstad, A. Skauge and H. Hoiland. J. Colloid Interface Sci. **66**, 240 (1978).

© 1997 NRC Canada

28. J. Rosenholm, R. Grigg, and L. Hepler. J. Chem. Thermodyn. **18**, 1153 (1986).
29. P.A. Leduc, J.L. Fortier, and J.E. Desnoyers. J. Phys. Chem. **78**, 1217 (1973).
30. H. Hoiland and E. Vikingstad. Acta. Chem. Scand. **A30**, 692 (1976).
31. E. Vikingstad and O. Kvammen. J. Colloid Interface Sci. **74**, 16 (1980).
32. B.E. Conway and R.E. Verrall. J. Phys. Chem. **70**, 3952 (1966).
33. T. Zemb, M. Drifford, M. Hayoun, and A. Jehanno. J. Phys. Chem. **87**, 4524 (1983).
34. E. Vikingstad. *In* Aggregation process in solution. *Edited by* E. Wyn-Jones and J. Gormally. Elsevier, Amsterdam. 1983. pp. 100–117.
35. C. Tanford. J. Phys. Chem. **76**, 3020 (1972).
36. D.A. Doughty. J. Phys. Chem. **85**, 3545 (1981).
37. M.I. Davis. Chem. Soc. Rev. **23**, 127 (1993).
38. S. Harada, T. Nakajima, T. Kamatsu, and T. Nakagawa. J. Solution Chem. **7**, 463 (1978).
39. R. DeLisi, S. Milioto, and A. Inglese. J. Phys. Chem. **95**, 3322 (1991).
40. D.J. Jobe, R.E. Verrall, and B.D. Skalski. Langmuir, **9**, 2814 (1993).
41. D. Hétu, C. Camiré, G. Perron, and J.E. Desnoyers. Langmuir, **10**, 4039 (1994).

Can. J. Chem. Downloaded from www.nrcresearchpress.com by 91.121.58.235 on 09/08/12
For personal use only.

© 1997 NRC Canada

A note on the thermodynamics of intercalation

Roger Parsons

Abstract: The thermodynamics of an electrochemical cell with an intercalation electrode is discussed in the light of two recent analyses (Gerischer et al. J. Electrochem. Soc. **141**, 2297 (1994) and Li et al. J. Electrochem. Soc. **141**, 2310 (1994)). The assumptions necessary to obtain a simple result are emphasized.

Key words: thermodynamics, intercalation electrode.

Résumé : À la lumière de deux analyses récentes (Gerischer et al. J. Electrochem. Soc. **141**, 2297 (1994) et Li et al. J. Electrochem. Soc. **141**, 2310 (1994)), on discute de la thermodynamique d'une cellule électrochimique avec une électrode d'intercalation. On met en relief les hypothèses nécessaires pour obtenir un résultat simple.

Mots clés : thermodynamique, électrode d'intercalation.

[Traduit par la rédaction]

1. The electronic and ionic contributions to the intercalation energy

In a recent paper (1) Gerischer et al. discussed the thermodynamics of an intercalation cell in terms of an electronic and an ionic contribution to the emf of the cell. While their analysis is undoubtedly correct, it seems worthwhile to present an alternative and more direct way of treating this problem.

The cell considered may be represented:

$$\begin{array}{cccccc} \text{Cu} & \text{M} & \text{M}^{z+} + z\text{X}^- & \text{M-S} & \text{Cu} \\ \text{A} & \text{I} & \text{II} & \text{III} & \text{B} \end{array}$$

where Cu represents the terminals of the cell, M is a pure sample of the metal being intercalated, forming the left-hand electrode designated phase I. Phase II is an electrolytic solution containing the ions M^{z+} of the metal M and a monovalent anion X^-. Phase III is the intercalation compound of M in the host lattice S. Apart from the terminals, this notation is identical to that used in ref. 1.

The equilibrium potential (emf), E, of this cell may be written:

$$[1] \quad E = \phi^{\text{B}} - \phi^{\text{A}}$$

where ϕ^α is the inner potential of phase α. This can be rewritten:

$$[2] \quad E = (\phi^{\text{B}} - \phi^{\text{III}}) + (\phi^{\text{III}} - \phi^{\text{I}}) + (\phi^{\text{I}} - \phi^{\text{A}})$$

in terms of the Galvani potential differences at each phase boundary (although the phase boundaries I|III and II|III are taken together).

Since there is electronic equilibrium between phases I and A,

$$[3] \quad \tilde{\mu}_{\text{e}}^{\text{I}} = \mu_{\text{e}}^{\text{I}} - F\phi^{\text{I}} = \tilde{\mu}_{\text{e}}^{\text{A}} = \mu_{\text{e}}^{\text{A}} - F\phi^{\text{A}}$$

where $\tilde{\mu}_{\text{e}}^{\alpha}$ is the electrochemical potential of electrons in phase α, μ_{e}^{α} is their chemical potential, and F is Faraday's constant. Hence,

$$[4] \quad \phi^{\text{I}} - \phi^{\text{A}} = (\mu_{\text{e}}^{\text{I}} - \mu_{\text{e}}^{\text{A}})/F$$

and, as both phases A and I are pure metals, both chemical potentials on the right-hand side of eq. [4] are constant, so that eq. [2] may be written:

$$[5] \quad E = (\phi^{\text{B}} - \phi^{\text{III}}) + (\phi^{\text{III}} - \phi^{\text{I}}) + \text{const.}$$

Since there is also electronic equilibrium between phases III and B, the first term on the right-hand side of eq. [5] becomes

$$[6] \quad \phi^{\text{B}} - \phi^{\text{III}} = (\mu_{\text{e}}^{\text{B}} - \mu_{\text{e}}^{\text{III}})/F$$

Similarly, the ionic equilibrium of M^{z+} between phases I, II, and III leads to:

$$[7] \quad \phi^{\text{III}} - \phi^{\text{I}} = (\mu_{\text{M}}^{\text{I}} - \mu_{\text{M}}^{\text{III}})/zF$$

for the second term on the right-hand side of eq. [5], where μ_{M}^{α} is the chemical potential of M^{z+} in phase α.

When eqs. [6] and [7] are substituted into eq. [5], the following equation is obtained:

$$[8] \quad E = (\mu_{\text{e}}^{\text{B}} - \mu_{\text{e}}^{\text{III}})/F + (\mu_{\text{M}}^{\text{I}} - \mu_{\text{M}}^{\text{III}})/zF + \text{const.}$$

which, like eq. [3] of ref. 1, has two components relating to the intercalation process, i.e., $(\mu_{\text{e}}^{\text{B}} - \mu_{\text{e}}^{\text{III}})/F$ and $(\mu_{\text{M}}^{\text{I}} - \mu_{\text{M}}^{\text{III}})/zF$. They may be regarded as representing the electronic and chemical components of this process, respectively.

Received February 14, 1997.

This paper is dedicated to Professor Brian E. Conway on the occasion of his 70th birthday.

R. Parsons.[1] Department of Chemistry, University of Southampton, Southampton SO17 1BJ, U.K.

[1] Telephone: +44-1703-59 3371. Fax: +44-1703-67 6960. E-mail: rp3@soton.ac.uk

© 1997 NRC Canada

Can. J. Chem. Downloaded from www.nrcresearchpress.com by 91.121.58.235 on 09/08/12
For personal use only.

Can. J. Chem. Downloaded from www.nrcresearchpress.com by 91.121.58.235 on 09/08/12
For personal use only.

The nature of the electronic component may be seen by considering the work function ($-\alpha_e^{III}$) of the electron in phase III. α_i^β is known as the "real potential" of a charged species i in a phase β; when i is the electron, it is exactly equal to the electronic work function with the sign reversed. The real potential arises from the interaction of the charged species with the bulk of the phase (μ_i^β),together with the contribution of the surface potential (χ^β), due to the double layer at the free surface of phase β. (In a metal this arises because the electronic cloud at the surface spreads out beyond the positive charge of the atomic cores.) Thus:

$$[9] \quad \alpha_e^\beta = \mu_e^\beta - F\chi^\beta$$

From this, it follows that the first term on the right-hand side of eq. [8] can be written:

$$[10] \quad (\mu_e^B - \mu_e^{III}) = \mu_e^B - (\alpha_e^{III} - \chi^{III})$$

This shows that changes in the first term of eq. [8] during intercalation may be related to changes in the work function of electrons in phase III, provided that there is no change in the surface potential. (μ_e^B must remain constant at constant temperature as the composition of B does not change.) With this condition, changes in the first term of eq. [8] indicate changes of the Fermi level in phase III. Alternatively, μ_e^{III} may be considered as reflecting directly the energy of interaction of the electron with the bulk of phase III, i.e., the Fermi energy, which will depend on the band structure of phase III.

The second term on the right-hand side of eq. [8] may be expanded as:

$$[11] \quad (\mu_M^I - \mu_M^{III}) = \mu_M^I - (\mu_M^{III,o} + RT \ln (a_M / a_M^o)$$

where a_M is the activity of the intercalated ion in the host, and a_M^o is its activity in the standard state. In this form it can be seen that as intercalation proceeds at constant temperature, a_M is the only variable since μ_M^I represents the energy of M^{z+} in a sample of pure M (which is constant), and $\mu_M^{III,o}$ is the corresponding energy in the host phase III in the standard state. Thus changes in this second term lead to the changes in the energy of interaction of M^{z+} with the host.

2. Stability of an intercalation compound

The question of the stability of an intercalation compound was considered by Li et al. (2) in a paper nearly adjacent to ref. 1. This again is a correct analysis, but it may be more transparent if the usual electrochemical approach is used.

It is evident from eq. [11] that the emf of the above cell is independent of the concentration of MX_z in phase II. Since the cell reaction consists of the transfer of M^{z+} from phase I to phase M-S, the electrolyte (phase II) plays the role of a semipermeable membrane allowing the passage of M^{z+} only. This corresponds to the situation represented in Fig. 1 of ref. 2. However, if the initial dissolution from M-S into pure water is considered, the reaction at the right-hand electrode may be written:

$$[12] \quad M_{(S)}^{z+} + ze^- + zH_2O \rightarrow M_{(aq)}^{z+} + zOH^- + (z/2)H_2$$

If phase II is considered to be infinitely dilute and activity coefficients are ignored, the corresponding Nernst equation is

$$[13] \quad E = E^o - (RT/zF) \ln \{[M_{(aq)}^{z+}][OH^-]^z p_{H_2}^{z/2}/[M_{(S)}^{z+}]\}$$

where the square brackets indicate concentrations.

Dissolution in pure water leads to an equivalent concentration of M^{z+} and OH^-:

$$[14] \quad [M_{(aq)}^{z+}] = z[OH^-]$$

and if $p_{H_2} = 1$, eq. [13] may be written:

$$[15] \quad E = E^o + (RT/zF) \ln \{[M_{(S)}^{z+}]/[M_{(S)}^{z+}]_o\} - (RT/F) \ln [OH^-]$$

where E^o is the electrode potential in the standard state of M-S when the concentration of M^{z+} is $[M_{(S)}^{z+}]_o$. For the left-hand electrode the cell reaction and Nernst equation are formally the same, but the E^o is the standard potential of the pure metal M, and the second term on the right-hand side of eq. [15] vanishes. This corresponds to the situation described in Fig. 2 of ref. 2.

3. Generalization

It may be noted that this analysis does not depend on the detailed nature of the host S. Thus, it applies equally to such processes as intercalation, amalgamation, hydrogen insertion into a metal, and the insertion of ions into the film on a modified electrode. However, in the case of amalgamation it is well known (3) that the surface potential changes with addition of the guest metal, and this may occur with other systems. Although the simplest interpretation follows when S is an electronic conductor, it is possible to apply it to ionic conductors by defining the electrochemical potential of electrons in S in terms of a redox couple in that phase (see, for example, the discussion of the electrochemical potential of electrons in a redox electrolyte (4)). For either type of conductor it should be noted that this analysis depends on the assumption that there is no transfer of M^{z+} ions across the boundary between phase III and phase B. If, for example, metal M exists between these two phases, and there is ionic equilibrium between it and phase III, the emf of the above cell is zero, independent of the composition of phases II and III. It seems also that the electrolyte (phase II) performs the essential function of a semipermeable membrane, as mentioned above. If it were possible to intercalate M^{z+} directly from the metal (phase I), then it would be equally possible to de-intercalate it at the terminal B and the emf would consequently drop to zero.

References

1. H. Gerischer, F. Decker, and B. Scrosati. J. Electrochem. Soc. **141**, 2297 (1994).
2. W. Li, W.R. McKinnon, and J.R. Dahn. J. Electrochem. Soc. **141**, 2310 (1994).
3. A. Frumkin, B. Damaskin, N. Grigoryev, and I. Bagotskaya. Electrochim. Acta, **19**, 69 (1974).
4. R. Parsons. *In* Standard electrode potentials in aqueous solution. *Edited by* A.J. Bard, R. Parsons, and J. Jordan. Marcel Dekker Inc., New York. 1985. Chap. 2, esp. eq. (2.39).

© 1997 NRC Canada

Temperature-dependent oxygen electrochemistry on platinum low-index single crystal surfaces in acid solutions

B.N. Grgur, N.M. Marković, and P.N. Ross

Can. J. Chem. Downloaded from www.nrcresearchpress.com by 91.121.58.235 on 09/08/12
For personal use only.

Abstract: Using the rotating ring-disk technique ($RRD_{Pt(hkl)}E$), the oxygen-reduction reaction (ORR) was studied in sulfuric acid solution over the temperature range 298–333 K. At the same temperature, the exchange current density increased in the order, $i^0_{111} < i^0_{100} < i^0_{110}$ which gives the order of absolute kinetic activities of Pt(*hkl*) in 0.05 mol/L H_2SO_4: Pt(111) < Pt(100) < Pt(110). We found that at high current densities every crystal face has an ideally temperature-dependent Tafel slope, i.e., $-2 \times 2.3(RT/F)$. The activation energy for the ORR is independent of the surface geometry, $\Delta H^{\#}_{hkl} = 42$ kJ/mol. The insensitivity of the activation energy to surface structure implies that the reaction pathway for the ORR is the same on all three single-crystal faces. A "series" pathway for the ORR was proposed, with the first electron transfer being the rate-determining step. The structure sensitivity in the kinetics of the ORR on Pt(*hkl*) is attributed to the structure-sensitive adsorption of bisulfate and hydroxyl anions and a simple site-blocking effect of these adsorbed anions on the rate of the ORR.

Key words: platinum single crystals, oxygen reduction, peroxide reduction, temperature effects, activation energy.

Résumé : Faisant appel à la technique du disque tournant ($RRD_{Pt(hkl)}E$) on a étudié la réaction de réduction le l'oxygéne (RRO) en solution dans l'acide sulfurique, à des températures allant de 298 à 333 K. À température constante, la densité du courant d'échange augmente dans l'ordre $i^0_{111} < i^0_{100} < i^0_{110}$ qui permet de déduire l'ordre des activités cinétiques absolues du Pt(*hkl*) dans le H_2SO_4 0,05 mol/L : Pt(111) < Pt(100) < Pt(110). On a trouvé que, à des densités de courant élevées, chaque face du cristal présente une pente de Tafel qui dépend d'une façon idéale sur la température, c'est-à-dire que $-2 \times 2.3(RT/F)$. L'energie d'activation de la RRO est indépendante de la géométrie de la surface, $\Delta H^{\#}_{hkl} = 42$ kJ/mol. Le fait que l'énergie d'activation soit insensible à la structure de la surface implique que la voie réactionnelle de la RRO est la même sur les trois faces individuelles du cristal. On propose une « série » de voies réactionnelles pour la RRO dans lesquelles le premier transfert d'électron est l'étape cinétiquement déterminante. La sensibilité de la cinétique de la RRO sur le Pt(*hkl*) sur la structure est attribuée à une adsorption sensible à la structure des anions bisulfate et hydroxyle et à un effet simple de blocage de site de ces anions adsorbés sur la vitesse de la RRO.

Mots clés : cristaux uniques de platine, réduction de l'oxygéne, réduction du peroxyde, effets de la température, énergie d'activation.

[Traduit par la rédaction]

1. Introduction

The last decade has witnessed substantial advances in the understanding of the dependence of the oxygen reduction reaction (ORR) on the Pt surface structure. In earlier studies with platinum single crystals, the variations in the kinetics of the ORR with the crystallographic symmetry of the Pt surface were contradictory (1–4). Recently, by utilizing single crystals in a true rotating ring-disk electrode geometry, $RRD_{Pt(hkl)}E$, we were able to obtain more accurate corrections to the mass transport contribution to the polarization and, thus, obtain more accurate measurements of the kinetics. We found that the structure sensitivity arises primarily from the structure-sensitive adsorption of ions, e.g., bisulfate (5), hydroxyl (6, 7), and halides (8), that are not intermediates in the ORR and actually impede the ORR. However, a complete understanding of how these adsorbed anions impede the rate of the ORR, including a quantitative kinetic model, has not yet evolved (5–8).

All previous studies of the ORR on Pt(*hkl*) single crystals were conducted at a fixed, essentially ambient, temperature. In this paper, we present a study of the temperature dependence of the kinetics of the ORR on Pt(*hkl*) single crystals in 0.05 mol/L sulfuric acid solutions. From these measurements we were able to determine the effect of the surface geometry on the activation energy for the ORR on Pt(*hkl*), which, in turn, illuminated important new details related to the reaction pathway of the ORR, and to the role of bisulfate anion adsorption in the reaction.

2. Experimental

The pretreatment and assembling of the Pt(*hkl*) crystal in a $RRD_{Pt(hkl)}E$ configuration was fully described in our previous

Received March 14, 1997.

This paper is dedicated to Professor Brian E. Conway on the occasion of his 70th birthday.

B.N Grgur, N.M. Marković,[1] and P.N. Ross. Materials Sciences Division, Lawrence Berkeley National Laboratory, University of California, Berkeley, CA 94720, U.S.A.

[1] Author to whom correspondence may be addressed.

© 1997 NRC Canada

Can. J. Chem. Downloaded from www.nrcresearchpress.com by 91.121.58.235 on 09/08/12
For personal use only.

paper. Briefly summarizing, following flame annealing (9), the single crystal was mounted in the disk position of an insertable rotating ring-disk electrode assembly (Pine Instruments).[2] Subsequently, it was transferred into a standard electrochemical cell and immersed into 0.05 mol/L H_2SO_4 (ULTREX II, J.T. Baker Reagent) under potential control at ≈0.2 V. The reference electrode was a saturated calomel electrode separated by a bridge in order to prevent Cl^- contamination of solutions. However, all potentials are referenced to the reversible hydrogen electrode (RHE), calibrated and corrected to a "constant temperature" (thus, a potential scale that is vs. a RHE in the same solutions at the same temperature). This was done experimentally from the hydrogen oxidation/evolution polarization curve on the working electrode at 1 atm (101.3 kPa) hydrogen in the same solutions. All experimental measurements reported in this study were conducted in a standard three-compartment electrochemical cell equipped with a water jacket. A circulating constant temperature bath (Fisher Isotemp Circulator) maintained the temperatures of the solutions within ±0.5 K. All measurements were conducted *nonisothermally*, i.e., keeping the temperature of reference electrode constant (ca. 298 K) while that of the working electrode was varied over the temperature range 298–333 K. A Pine Instruments Bipotentiostat (model AFRDE 4; potential response 0.5 V/ms) was used for all the RRDE experiments. The measured collection efficiency, N, for our RRDE geometry is ≈0.22 (±5%). The geometrical surface area of the disk electrode was 0.283 cm^2. Ring and disk currents were recorded in real time simultaneously on a chart recorder and digitally on an IBM PC (486) computer using Labview for Windows.

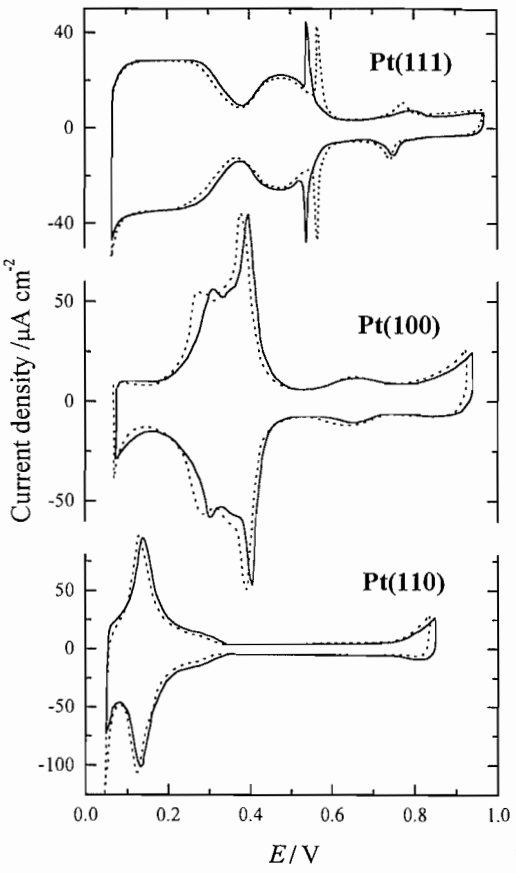
In this work, the fractional coverage for adspecies is based on the surface atomic density assuming one-electron transfer per surface atom. The surface atomic densities for Pt(111) and (100) were based on their unreconstructed (1 × 1) geometry, for the Pt(111) (1.5×10^{15} atoms/cm^2) and Pt(100) (1.3×10^{15} atoms/cm^2) (10). For the Pt(110)-(1 × 2), we have found that Pt(110), prepared by the flame-annealing – hydrogen cooling method, is reconstructed into a (1 × 2) structure, which has a surface density of 4.6×10^{14} atoms/cm^2. However, the theoretical charge for the formation of a monolayer of H_{upd} or OH_{ad} on a (1 × 2) surface is the same as for the (1 × 1) surface, since two H_{upd} and OH_{ad} adatoms can be adsorbed per unit cell of the reconstructed Pt(110)-(1 × 2) surface (11).

3. Results and discussion

3.1 Temperature effects on cyclic voltammetry of Pt(*hkl*)

A detailed examination of the temperature effects on the underpotential deposition of hydrogen on Pt(*hkl*) in sulfuric acid will be presented elsewhere (12). For our present purposes, only the cyclic voltammograms for Pt(*hkl*) recorded at two different temperatures will be shown and discussed briefly. Figure 1 shows that voltammetric features for all three single crystals, recorded over the range of temperature studied (298–333 K), are very similar to those observed at room temperature (ref. 12, refs. therein). The positive potential limits were chosen to be sufficient to characterize all important voltammetric features, yet to avoid irreversible "oxide" formation that would result in surface disordering. In the case of Pt(110), on the positive-going sweep, the desorption of hydrogen along the step sites is accompanied by bisulfate adsorption (0.075 < E < 0.2 V). At more positive potentials, the desorption of hydrogen from the terrace sites (0.2 < E < 0.3 V) is followed first by a double layer charging, and then by the adsorption of OH_{ad} species (E > 0.8 V). The absolute charge evaluated by integration of the current in the hydrogen adsorption–region varied little with temperature and equals ≈180 μC/cm^2. The difference between the experimental value and the theoretical charge, ca. 30 μC/cm^2, may be assigned to the charge from a concomitant bisulfate adsorption–desorption process in this potential region (12). The main voltammetric characteristics of well-ordered Pt(100) are sharp multiple peaks in the region of 0.25–0.45 V, and a broad peak centered at ca. 0.7 V. The former are assigned to the coupled adsorption–desorption of underpotential hydrogen (H_{upd}) and bisulfate anion, while the latter is attributed to the reversible adsorption of OH_{ad} produced by the dissociation of water, analogous to the adsorption from perchloric acid solution (13). At more positive potentials, the observed asymmetry between the positive and negative sweep directions represents the transition to an irreversible state of adsorption of OH_{ad}. On Pt(100) in the hydrogen adsorption region the absolute charge equals

Fig. 1. Cyclic voltammograms of Pt(*hkl*) in the $RD_{Pt(hkl)}E$ configuration in argon-purged 0.05 mol/L H_2SO_4 at (——) 298 K, (-----) 333 K. Rotation rate, 900 rpm. Sweep rate, 50 mV/s.

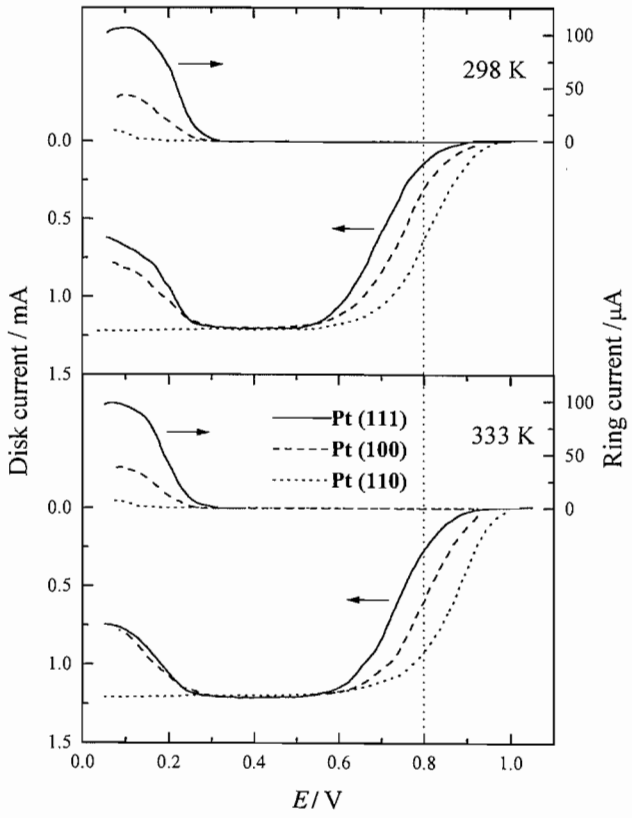


[2] Pine Instrument Company, 101 Industrial Drive, Grove City, Pennsylvania 16127, U.S.A.

© 1997 NRC Canada

Can. J. Chem. Downloaded from www.nrcresearchpress.com by 91.121.58.235 on 09/08/12
For personal use only.

Fig. 2. Disk and ring currents during oxygen reduction on Pt(*hkl*) in 0.05 mol/L H_2SO_4 at 298 K and 333 K. Rotation rate, 900 rpm. Sweep rate, 20 mV/s.



≈225 μC/cm^2, compared to the theoretical charge for one monolayer (1 ML) of H_{upd} on Pt(100) of 208 μC/cm^2. The difference between the experimental value and the theoretical charge, ca. 20 μC/cm^2, may be assigned to the charge from concomitant bisulfate adsorption–desorption in this potential region. The voltammetry curves of Pt(111) show a broad flat-topped hydrogen desorption–adsorption peak among values $\approx 0.05 < E < 0.375$ V, and the so-called "anomalous" feature at ≈0.4–0.6 V. This pseudocapacitance corresponds to the adsorption–desorption of bisulfate anions (see, for example, ref. 14). The integrated charge associated with the underpotential deposition of hydrogen on the Pt(111) surface at 298 K is ≈160 μC/cm^2, versus a theoretical charge assuming one hydrogen atom for each surface platinum atom of 240 μC/cm^2. In dramatic contrast to the other two surfaces, the maximum coverage of H_{upd} on Pt(111) is less than a monolayer, only ca. 0.67 ML. A close inspection of Fig. 1 reveals that there are two characteristics of the voltammetric curves for Pt(*hkl*) in 0.05 mol/L H_2SO_4 that represent the temperature effects. The first is that no new features are observed that would result from the temperature increase, and the second is that, on all single-crystal surfaces, hydrogen adsorption–desorption peaks are shifted negatively by increasing the temperature. These observations have been reported previously for both polycrystalline (15) and single crystal platinum electrodes (12, 16). Note that the "anomalous" peaks on Pt(111) are shifted positively by increasing the temperature. This is further confirmation that this pseudocapacitance is associated with the adsorption of bisulfate anions, and not with the underpotential deposition of hydrogen.

3.2 The effect of temperature on the polarization curves for the ORR

Our study of the ORR on Pt(*hkl*) in 0.05 mol/L H_2SO_4 at room temperature was reported previously (5). We summarize here some of those results for the purpose of comparison with new results for the ORR on Pt(*hkl*) at elevated temperatures. Figure 2 shows ring-disk measurements on Pt(*hkl*) in O_2 saturated solutions at room temperature. On all three single-crystal electrodes, below the potential region where there is mixed kinetic–diffusion control of the reaction, well-defined diffusion-limiting currents were recorded over a wide potential region. In both potential regions the ring currents on Pt(*hkl*) surfaces were a very small fraction of the disk current. Figure 2 also shows that, on both Pt(111) and Pt(100), peroxide was detected on the ring electrode in the hydrogen adsorption region, indicating a change in the pathway of the ORR on these surfaces in this potential region. It should be noted that on Pt(110) the ring currents for peroxide oxidation are negligible at all potentials. A simple comparison of the currents at 0.8 V clearly reveals that the ORR on Pt(*hkl*) is a structure-sensitive reaction, with activity increasing in the order Pt(111) < Pt(100) < Pt(110). At 333 K the polarization curves for the ORR are qualitatively similar to the curves recorded at room temperature, and the order of activity remains the same as at room temperature, i.e., Pt(111) < Pt(100) < Pt(110). As expected, the currents associated with the ORR on the disk electrode are higher at elevated temperatures in both the mixed diffusion–kinetic potential region and in the hydrogen adsorption potential region. Consequently, a smaller amount of peroxide was produced on the disk electrode in the hydrogen adsorption region. The higher currents for the ORR on Pt(*hkl*) recorded at elevated temperatures reflect the temperature dependence of the chemical rate constant, which is approximately proportional to $\exp(-\Delta H^{0\#}/kT)$; where $\Delta H^{0\#}$ is the apparent enthalpy of activation at reversible potential (hereafter simply termed the activation energy), k is the Boltzmann constant, and T is the absolute temperature.

3.3 Kinetic analysis

All kinetic analysis was done with the polarization curves recorded at positive-going sweep at 900 rpm, as in Fig. 2. Figures 3–5 show Tafel plots of mass-transport corrected currents (below the limiting current) for the ORR at Pt(*hkl*) surfaces in 0.05 mol/L H_2SO_4 at 298 K, 313 K, and at 333 K, (data were actually obtained at five different temperatures). Only data below ≈0.9 V were analyzed, to avoid the region of irreversible "oxide" formation. For Pt(111), we fitted the curves with one slope, $-2 \times 2.3(RT/F)$ mV/dec over almost the entire potential region, covering more than two decades of current (!). On Pt(100) and Pt(110), the ORR has two Tafel slopes; $\approx -2 \times 2.3(RT/F)$ mV/dec for $\approx 0.65 < E < 0.85$ V, with a possible transition to a lower Tafel slope of $-2.3RT/F$ mV/dec above ca. 0.85 V. The number of data points in this "double" Tafel region is, however, relatively small, and barely more than the minimum of three points to determine the slope. This is an experimental and not a fundamental problem, with the transition occurring at ≈0.85 V. The transition in the Tafel slopes on both Pt(110) and Pt(100) appears to be related to

© 1997 NRC Canada

Can. J. Chem. Downloaded from www.nrcresearchpress.com by 91.121.58.235 on 09/08/12
For personal use only.

Fig. 3. Tafel plots for the ORR on Pt(111) obtained from polarization curves recorded in 0.05 mol/L H_2SO_4 at 298 K, 313 K, and 333 K.

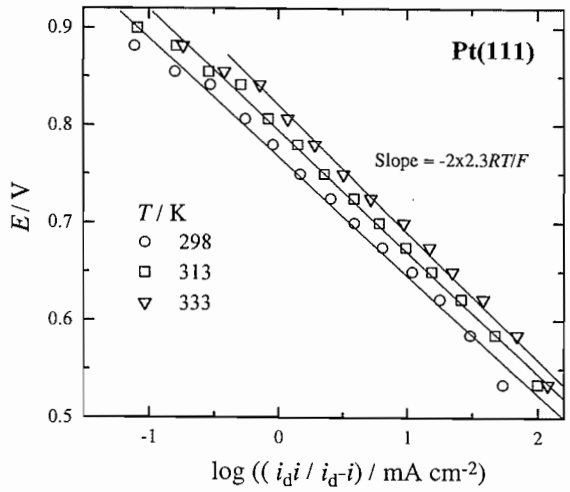
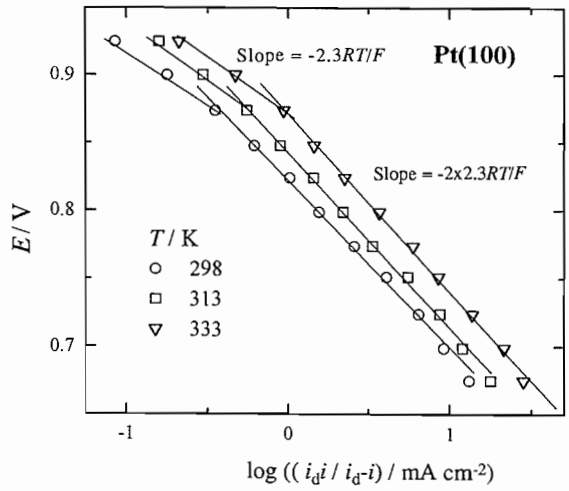


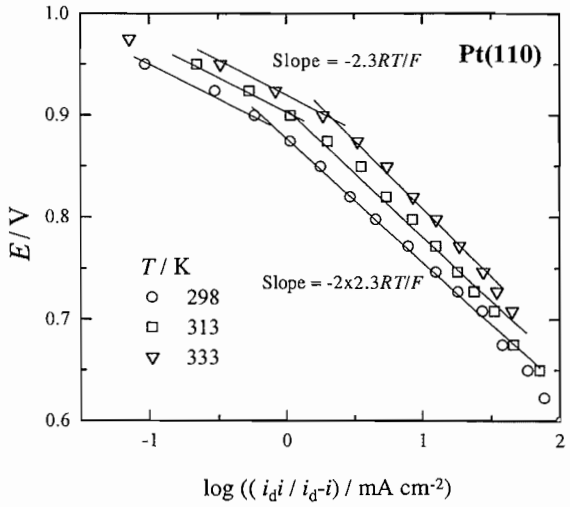
Fig. 4. Tafel plots for the ORR on Pt(100) obtained from polarization curves recorded in 0.05 mol/L H_2SO_4 at 298 K, 313 K, and 333 K.



changes in the nature of OH_{ad} with potential, a transition that strongly affects the ORR (6, 17). It is also important to note that the analysis of the polarization curves recorded for the ORR at elevated temperatures revealed that the Tafel slopes were directly proportional to the temperature, with the symmetry coefficient, β, for the oxygen reaction being *independent of temperature*.

In classical electrochemical kinetic theory, the Tafel slope is usually considered to be directly proportional to the temperature, with the transfer coefficient α (which is a function of the symmetry coefficient, β, and the stoichiometric number) a temperature-independent factor (18). The data on the temperature dependence of the Tafel slope for the ORR at the Pt electrode from different groups are not in good agreement; for example, both temperature-dependent (19, 22) and -independent (20, 21, 23) Tafel slopes have been reported. According to various authors, several different phenomena can be

Fig. 5. Tafel plots for the ORR on Pt(110) obtained from polarization curves recorded in 0.05 mol/L H_2SO_4 at 298 K, 313 K, and 333 K.



invoked to explain a temperature-dependent transfer coefficient; the temperature effect in proton and (or) electron tunneling, a shift in the rate-determining step with temperature, or changes in the symmetry of the potential energy barrier with temperature, but also artifacts such as impurity effects, can contribute to the temperature dependence of β. For example, Scharifker et al. (21) proposed that the temperature independence of the Tafel slope for the ORR for Pt in concentrated (85 wt.%) phosphoric acid is due to an impurity effect. Certainly, hot concentrated phosphoric acid is a challenging medium in which to conduct fundamental studies of electrode kinetics. Therefore, even without experimental difficulties, it is not clear how these results could be applicable to more conventional solutions. Our results for the ORR on the Pt(*hkl*) are consistent with the previous reports for polycrystalline Pt in dilute acid solution by Damjanovic and Sepa (23), i.e., a Tafel slope that is directly proportional to the temperature with the symmetry coefficient a temperature-independent factor.

The well-defined linear Tafel regions for the ORR on Pt(*hkl*) were used to extrapolate the current to the theoretical equilibrium potential to obtain the exchange current densities for the ORR on "oxide"-free Pt. At the same temperature, the exchange current density increases in the order $i_{0(111)} < i_{0(100)} < i_{0(110)}$, which gives the order of absolute kinetic activities of the three surfaces. The activation energies for the ORR on each Pt(*hkl*) face were obtained from the exchange current density at different temperatures using the Arrhenius plots (18).

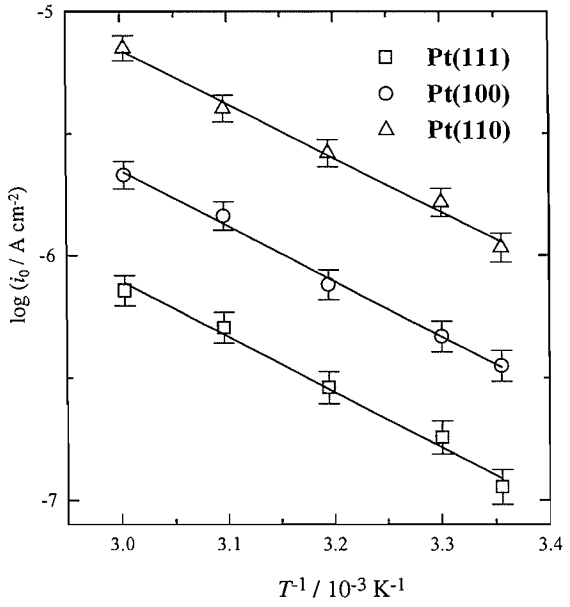
$$[1] \quad \frac{\mathrm{d} \log i_0}{\mathrm{d}(1/T)} = -\frac{\Delta H^{0\#}}{2.3R}$$

where $\Delta H^{0\#}$ is the activation energy and R is the gas constant. The Arrhenius plots for all three single-crystal surfaces, Fig. 6, yield the same activation energy of $\Delta H^{0\#} \approx$ 42 kJ/mol. Interestingly, while the variation in catalytic activity is strongly dependent on the three low-index faces, essentially the same activation energies are obtained at the reversible potential for the ORR on the Pt(*hkl*). The value of $\approx \Delta H^{0\#}$ 42 kJ/mol,

© 1997 NRC Canada

Can. J. Chem. Downloaded from www.nrcresearchpress.com by 91.121.58.235 on 09/08/12
For personal use only.

Fig. 6. Arrhenius plots of the exchange current densities at the equilibrium potential for oxygen reduction on Pt(*hkl*) electrodes.



obtained in this work, is smaller than the value of ≈ 57 kJ/mol, previously reported by Appleby for the ORR on "oxide"-free platinum in 85 wt.% orthophosphoric acid (19). Recently, Damjanovic and Sepa reported a value for the activation energy at 0.8 V (vs. the RHE) of ≈25 kJ/mol (23), which is much lower than the activation energy found in this work. Considering that the activation energy is a function of potential (18), and that our value has been extrapolated to the reversible potential for the ORR (1.23 V), it is not surprising that our value is different from the one reported at 0.8 V (23). Damjanovic and Sepa proposed that the Gibbs energy of activation (in our case $\Delta H_E^{\#}$) of an electrochemical reaction, including the ORR, could be experimentally determined at any potential from the intersection of the Tafel lines obtained at different temperatures (23, 24). They found that the Tafel lines intersect at the so-called critical potential, E_{cr}, at which $\Delta H_{E_{cr}}^{\#} = 0$. For the first electron transfer step as rate determining step (rds), $\Delta H_E^{\#}$ at any other potential is given by:

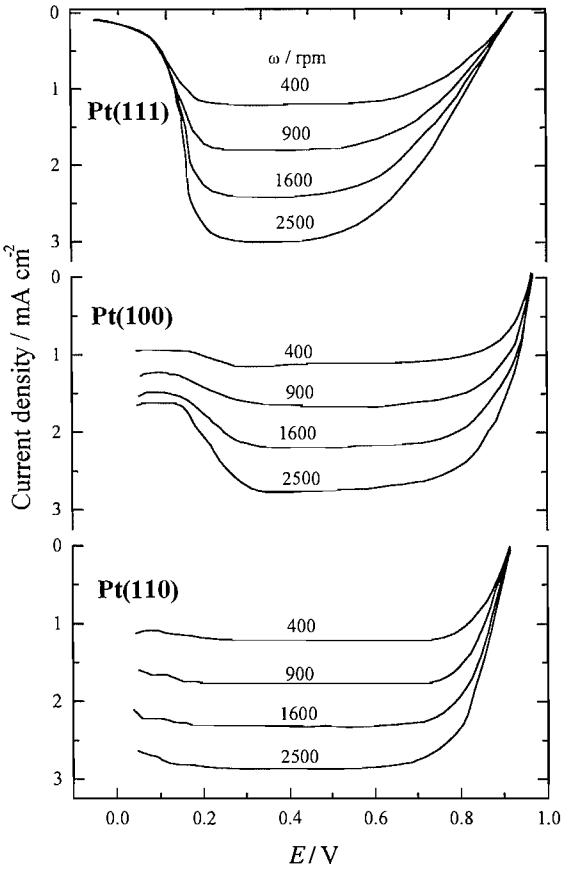
[2] $$\Delta H_E^{\#} = \beta F(E - E_{cr})$$

According to Damjanovic and Sepa (23), for the ORR on polycrystalline Pt at pH ≈1, E_{cr} = 0.3 V vs. RHE. Using this value for E_{cr}, the extrapolated value of their activation energy of 25 kJ/mol at 0.8 V is ≈44 kJ/mol at the theoretical equilibrium potential, in excellent agreement with our experimentally determined value of 42 kJ/mol.

3.4 Peroxide reduction on Pt(*hkl*)

To fully elucidate the structural effects of Pt(*hkl*) on O_2 kinetics in 0.05 mol/L H_2SO_4, the kinetics of H_2O_2 reduction was studied on platinum single crystals in a solution free of oxygen. To simulate the chemical environment during O_2 reduction, we added peroxide to the supporting solutions to a concentration approximating the level of peroxide produced during the oxygen reduction, i.e., the maximum level would be

Fig. 7. Polarization curves for reduction of 1.2×10^{-3} mol/L H_2O_2 on Pt(*hkl*) in 0.05 mol/L H_2SO_4 at 298 K. Sweep rate, 50 mV/s.



equal to the solubility of oxygen in the solutions or ca. 10^{-3} mol/L. Figure 7 shows the family of polarization curves for the reduction of H_2O_2 on the three platinum low-index surfaces. It is important to note that the half-wave potentials for H_2O_2 reduction curves lay well anodic (≈50–100 mV) from the half-wave potentials for O_2 reduction. Thus, if H_2O_2 is formed as an intermediate on the electrode during the ORR, then it should be immediately reduced (electrochemically) to water, since the potential of oxygen reduction is negative of the region of H_2O_2 stability on the platinum single-crystal surfaces. This is also consistent with the ring currents observed during the ORR, which show no measurable amount of peroxide detected above 0.3 V. Below 0.3 V, on the Pt(100) and especially on the Pt(111) surface, the peroxide reduction current drops significantly, an observation reflected in the ring currents during the ORR in Fig. 2. It should also be noted that on Pt(110) a very small decrease in the currents associated with the reduction of peroxide was observed in the hydrogen adsorption region, consistent with a small amount of peroxide formed in the same potential region during the ORR, Fig. 2.

3.5 Reaction pathway for the ORR in sulfuric acid

In this section, the reaction pathway for the ORR on Pt(*hkl*), rather than the reaction mechanism, will be discussed because the $RRD_{Pt(hkl)}E$ technique alone is not capable of detecting all possible reaction intermediates in a complex process such as the ORR. From the many reaction pathways that have been

© 1997 NRC Canada

Can. J. Chem. Downloaded from www.nrcresearchpress.com by 91.121.58.235 on 09/08/12
For personal use only.

proposed in the past (25–27), we will discuss our results in the context of the series pathway, i.e., via an $(O_2H)_{ad}$ intermediate, as proposed by Damjanovic et al. (27). We will not attempt to resolve all of the uncertainties that still persist over the reaction mechanism of the ORR on Pt nor do we claim that our analysis here is definitive. Rather, we attempt to improve the understanding of the reaction pathway by comparing the kinetics of the ORR onto Pt(*hkl*) with the rate of the peroxide reduction under the same experimental conditions. Subsequently, the kinetic parameters, such as Tafel slope, exchange current densities, and activation energies for the ORR on Pt(*hkl*) will be related to the activities and the rds of the ORR on different single-crystal faces.

For the ORR on a polycrystalline platinum electrode there are two views regarding the first reaction step. Damjanovic et al. (28) and Sepa et al. (29) proposed that the first step is electron transfer to the O_2 molecule; this step is rate determining and is either accompanied or followed by a fast proton transfer. On the other hand, Yeager et al. (30) proposed that the first step most likely involves dissociative chemisorption of the O_2 molecules on a platinum surface that occurs simultaneously with the charge transfer. It appears that our results for the ORR on Pt(*hkl*) support the former view, primarily due to two new experimental results that are uniquely related to the enhanced sensitivity of Pt single-crystal electrodes. The first result is that the Tafel slopes, together with the OH_{ad} coverages that can be inferred from the voltammetry curves in Fig.1, are consistent with the first electron transfer to the O_2 molecule as the rds. This is most easily seen for Pt(111) on which a single Tafel slope of $-2 \times 2.3(RT/F)$ mV/dec is observed over the entire potential region; a value of $-2 \times 2.3(RT/F)$ mV/dec is characteristic for the first charge transfer as rds under Langmuirian conditions of adsorption of oxygen-containing species. This is consistent with the voltammetry curve for Pt(111) at 298 K in Fig. 1, which revealed that there is no (apparent) change in coverage of oxygen-containing species on the surface in this potential region. At elevated temperatures (333 K), however, due to a weakening of bisulfate adsorption and simultaneous enhanced adsorption of oxygen-containing species, a second Tafel slope (ca. $-2.3RT/F$) may be inferred from the polarization curves at 333 K in Fig. 3. On the other hand, Pt(100) and Pt(110) have two clearly defined Tafel slopes, as usually observed on a polycrystalline platinum electrode. For Pt(110) and Pt(100) at low overpotentials, the Tafel slope is $\approx -2.3RT/F$ mV/dec, which is also consistent with the first charge transfer step as rds but under Temkin conditions of adsorption of oxygen-containing species (ref. 23, and refs. therein). While the voltammetry curves in Fig. 1 do not provide evidence of Temkin conditions of adsorption, they do show clearly that an irreversible adsorption of OH_{ad} starts at ca. 0.8–0.85 V, and the coverage increases rapidly above 0.85 V. Thus, the transition of the Tafel slopes from $-2 \times 2.3(RT/F)$ to $\approx -2.3RT/F$ mV/dec at ca. 0.85–0.9 V on these surfaces is probably related to the surface coverage by the irreversible adsorption of OH_{ad}, as we previously suggested for an analogous transition that occurs for the ORR on Pt(*hkl*) in alkaline solution (6). It appears, therefore, that at low overpotentials the variations in activity for the ORR between Pt(100) and Pt(110) in sulfuric acid may also arise from highly structure-sensitive irreversible adsorption of OH_{ad} species (7).

A second new result coming from the use of single-crystal electrodes is the data on peroxide reduction in the hydrogen adsorption potential region. In the potential region of hydrogen adsorption, we see direct evidence of the strong inhibition by H_{upd} on oxygen and peroxide reduction on the Pt(111) and Pt(100) surfaces, remarkably so on the Pt(111), but relatively little effect on the Pt(110). We had reported the effects of H_{upd} on the kinetics of both the O_2 and H_2O_2 reduction reactions on Pt(*hkl*) previously, and will not repeat our analysis of these effects in terms of a structural model for H_{upd} and the series reaction pathway (for review see refs. 5–7). For our purposes here, we note only that this model is consistent with the series reaction pathway with the first electron transfer being rate determining.

Finally, we will attempt to resolve the factors that control the kinetics of the ORR, based on the values for the activation energies obtained for the ORR on Pt(*hkl*) in 0.05 mol/L H_2SO_4. Our analysis of Arrhenius plots clearly showed that the *same* activation energy (at the reversible potential) for the ORR, close to 42 kJ/mol, has been found for all three Pt(*hkl*) surfaces. We presented an argument showing that the same reaction mechanism (reaction pathway) is operative on all three single-crystal faces. How then does one account for the very significant differences in kinetic rate, i_o, on the different Pt(*hkl*) surfaces; We had shown previously that this structural sensitivity is most pronounced in solutions in which there is strong adsorption of anions (7), including the sulfuric acid used here. We had also proposed a simple form of Pt site elimination by adsorbed anions (6) and, if the standard free energy of adsorption of molecular O_2 is independent of coverage (Langmuirian conditions), that the rate of O_2 reduction may be expressed as

$$[3] \quad i = nFkC_{O_2}(1 - \theta_{ad})\exp(-\alpha F\eta/RT)$$

where n is the number of the electrons, k is the rate constant, C_{O_2} is the concentration of O_2 in the solution, θ_{ad} is the partial coverage by anion species (e.g., $HSO_{4(ad)}$ and OH_{ad}), i is the observed current, η is applied overpotential, and α is the transfer coefficient. It appears that in this rate equation for the ORR all the variables are independent of surface crystallography, except the surface coverage by bisulfate anions and oxygen-containing species. Therefore, the pre-exponential term $(1 - \theta_{ad})$ will entirely control the kinetics of the ORR on the Pt(*hkl*), as we proposed previously and is now confirmed by these new results for the activation energies for the ORR on Pt(*hkl*) in sulfuric acid solution.

4. Conclusions

Using the rotating ring-disk measurements ($RRD_{Pt(hkl)}E$), the oxygen reduction reaction was studied in sulfuric acid solution over the temperature range 298–333 K. We found that, at the same temperature, the exchange current density increased in the order, $i^0_{111} < i^0_{100} < i^0_{110}$ which gives the order of absolute kinetic activities of Pt(*hkl*): Pt(111) < Pt(100) < Pt(110). We also found that every crystal face has an ideally temperature-dependent Tafel slope for the ORR. For Pt(110) and Pt(100), this slope is $\approx -2.3RT/F$ mV/dec above 0.87 V, with a transition to $-2 \times 2.3RT/F$ mV/dec at higher overpotentials. At 298 K, Pt(111) has a $-2 \times 2.3RT/F$ mV/dec Tafel slope over the entire potential region. At elevated temperatures, however, a

© 1997 NRC Canada

second slope could also be extrapolated from the polarization curves. The activation energy at the reversible potential was determined to be independent of crystallographic orientation of the surface, $\Delta H^{\#}_{hkl} = 42$ kJ/mol. A structure-insensitive activation energy for the ORR implies that the reaction pathway for the ORR is the same on all three single-crystal faces. We concluded that our results are consistent with the "series" reaction pathway, with the first electron transfer step being the rate-determining step (rds). A simple kinetic expression is derived in which all the kinetic parameters are independent of surface structure except the pre-exponential term, $(1 - \theta_{ad})$, where θ_{ad} is the fractional coverage by adsorbed bisulfate and OH_{ad} anions, which are strongly structure sensitive.

Acknowledgment

We are indebted to Hubert Gasteiger for his contribution to all previous measurements and for analysis of the results for the ORR on Pt(*hkl*) at room temperature. This work was supported by the Assistant Secretary for Energy Efficiency and Renewable Energy, Office of Transportation Technologies, of the U.S. Department of Energy under Contract No. DE-AC03-76SF00098.

References

1. N.M. Marković, R.R. Adzić, B.D. Cahan, and E.B. Yeager. J. Electroanal. Chem. **377**, 249 (1994).
2. F. El Kadiri, R. Faure, and R. Durand. J. Electroanal. Chem. **301**, 177 (1991).
3. T. Abe, G.M. Swain, K. Sashikata, and K. Itaya. J. Electroan. Chem. **382**, 73 (1995).
4. H. Kita, Y. Gao, and K. Ohnishi. Chem. Lett. 73 (1994).
5. N.M. Marković, H.A. Gasteiger, and and P.N. Ross. J. Phys. Chem. **99**, 3411 (1995).
6. N.M. Marković, H.A. Gasteiger, and P.N. Ross. J. Phys. Chem. **100**, 6715 (1996).
7. N.M. Marković, H.A. Gasteiger, and P.N. Ross. J. Electrochem. Soc. **144**, 1591 (1997).
8. N.M. Marković, H.A. Gasteiger, S. Sarraf, and P.N. Ross. 189th Electrochem. Soc. Meeting Abstract Book. **96-1**, 1100 (1996).
9. N. Marković, M. Hanson, G. McDougal, and E. Yeager. J. Electroanal. Chem. **241**, 309 (1986).
10. (*a*) I.M. Tidswell, N.M. Marković, and P.N. Ross. Phys. Rev. Lett. **71**, 1601 (1993); (*b*) J. Electroanal. Chem. **376**, 119 (1994).
11. C.A. Lucas, N.M. Marković, and P.N. Ross. Phys. Rev. Lett. **77**, 4922 (1996).
12. N.M. Marković, B.N. Grgur, and P.N. Ross. J. Phys. Chem. **101**, 5405 (1997).
13. N.M. Marković, C.A. Lucas. H.A. Gasteiger, and P.N Ross, Surf. Sci. **365**, 229 (1995).
14. (*a*) K. Al-Jaaf-Golze, D.M. Kolb, and D. Scerson. J. Electroanal. Chem. **200**, 353 (1986); (*b*) F. Wagner and P.N Ross. J. Electroanal. Chem. **250**, 301 (1988); (*c*) N.M. Marković, N.S. Marinković, and R.R. Adzić. J. Electroanal. Chem. **241**, 309 (1988); (*d*) J.M. Orts, R. Gomez, J.M. Feliu, A. Aldaz, and J. Clavilier. Electrochim. Acta, **39**, 1519 (1995).
15. A. Zolfaghari, G. Jerkiewicz, Y. Sung, and A. Wieckowski. Proc. 6th Int. Symp. Electrode Processes. May 1996. *Edited by* A. Wieckowski and K. Itaya. The Electrochemical Society, Pennington, N.J. 1996.
16. S. Morin, H. Dumont, and B.E. Conway. J. Electroanal. Chem. **412,** 39 (1996).
17. F.A. Uribe, M.S. Wilson, T.E. Springer, and S. Gottesfeld. Proc. Workshop Struct. Electrocatal. Oxygen Electrochem. Cleveland, Ohio. October 1991. *Edited by* D. Scherson, D. Tryk, M. Daroux, and X. Xing. Proc. — Electrochem. Soc. **92-11**. 1992.
18. E. Gileadi. *In* Electrode kinetics for chemical engineers and materials scientists. VCH Publisher (UK) Ltd., London. 1993.
19. A.J. Appleby. J. Electrochem. Soc. **117**, 328 (1970); **117**, 641 (1970).
20. M.A. Enayetullah, T.D. DeVibiss, and J.O'M. Bockris. J. Electrochem. Soc. **136**, 3369 (1989).
21. B.R. Scharifker, P. Zelenay, and J.O'M. Bockris. J. Electrochem. Soc. **134**, 2714 (1987).
22. S.J. Clouser, J.C. Huang, and E. Yeager. J. Appl. Electrochem. **23**, 597 (1993).
23. A. Damjanovic and D.B. Sepa. Electrochim. Acta, **35**, 1157 (1990).
24. A. Damjanovic, B.E. Conway, and D.B. Sepa. Ber. Bunsen-ges. Phys. Chem. **93**, 510 (1989).
25. M.R. Tarasevich, A. Sadkowski, and E. Yeager. *In* Comprehensive treatise of electrochemistry. Vol. 7. *Edited by* B.E. Conway, J.O'M. Bockris, E. Yeager, S.U.M. Khan, and R.E. White. Plenum Press, New York. 1983. pp. 301–398.
26. K. Kinoshita. *In* Electrochemical oxygen technology. John Wiley & Sons, Inc., New York. 1992.
27. A. Damjanovic, M.A. Genshaw, and J.O'M Bockris. J. Phys. Chem. **45**, 4057 (1964).
28. A. Damjanovic, V. Brusic, and J.O'M Bockris. J. Phys. Chem. **71**, 2471 (1964).
29. D.B. Sepa, M.V. Vojinovic, Lj.M. Vracar, and A. Damjanovic. Electrochim. Acta, **32**, 129 (1987).
30. E. Yeager, M. Razak, D. Gervasio, A. Razak, and A.D. Tryk. Proc. Workshop Struct. Eff. Electrocatal. Oxygen Electrochem. Cleveland, Ohio. October 1991. *Edited by* D. Scherson, D. Tryk, M. Daroux, and X. Xing. Proc. — Electrochem. Soc. **92-11**. 1992.

Can. J. Chem. Downloaded from www.nrcresearchpress.com by 91.121.58.235 on 09/08/12
For personal use only.

© 1997 NRC Canada

Synthesis of hyperbranched glycodendrimers incorporating α-thiosialosides based on a gallic acid core

Serge J. Meunier, Quigquan Wu, Sho-Nong Wang, and René Roy

Abstract: Hyperbranched glycodendrimers containing sialic acid residues were synthesized in order to further understand the multivalency effect and its role in carbohydrate–protein interactions. Gallic acid **7** as trivalent core and oligoethylene glycol derivatives as hydrophilic spacers were used to scaffold the dendritic backbones. α-Thiosialoside **16** was conjugated onto *N*-chloroacetylated dendritic precursors **13**, **14**, and **26** by nucleophilic substitution to afford trivalent **17**, **18**, and nonavalent **27** sialodendrimers. Complete sugar deprotection furnished water-soluble α-thiosialodendrimers **21**, **22**, and **29**, which were used in protein-binding studies. Turbidimetric analysis confirmed the strong potential of sialodendrimers **29** having nine readily accessible sialic acid residues to bind, cross-link, and precipitate two different lectins. Preliminary results indicated that nonavalent α-sialodendrimer **29** had a greater affinity towards dimeric wheat germ agglutinin (WGA) and the lectin from the slug *Limax flavus* (LFA) than the corresponding trivalent glycodendrimers **21** and **22**.

Key words: carbohydrate, dendrimer, sialic acid, gallic acid, lectin, wheat germ agglutinin, *Limax flavus*.

Résumé : Afin de mieux comprendre l'effet de multivalence et son rôle dans les interactions carbohydrate–protéine, on a synthétisé des glycodendrimères hautement ramifiés contenant des résidus d'acide sialique. On a utilisé l'acide gallique, **7**, comme unité centrale trivalente et des dérivés oligoéthylèneglycol comme intercaleurs hydrophiles pour échafauder les structures de base dendritiques. La conjugaison de l'α-thiosialoside **16** sur les précurseurs dendritiques *N*-chloroacétylés **13**, **14** et **26** par des substitutions nucléophiles conduit aux sialodendrimères trivalents **17** et **18** et nonavalent **27**. Une déprotection complète du sucre conduit aux α-thiosialodendrimères **21**, **22** et **29** qui ont été utilisés dans les études de fixation sur des protéines. Des analyses turbidimétriques ont confirmé que le sialodendrimère **29**, qui incorporent neuf résidus d'acide sialique facilement accessible, possèdent un important potentiel de se lier, de créer des réticulations et de précipiter deux lectines différentes. Les résultats préliminaires indiquent que l'affinité de l'α-sialodendrimère nonavalent **29** pour l'agglutinine dimère du germe de blé (« WGA ») et pour la lectine de la limace *Limax flavus* (« LFA ») est plus grande que celles des glycoden-drimères trivalents correspondants, **21** et **22**.

Mots clés : carbohydrate, dendrimère, acide sialique, acide gallique, lectine, agglutinine du germe de blé, *Limax flavus*.

Introduction

It is now well established that cell surface carbohydrates and sialosides, in particular, are involved as anchoring motifs onto which various pathogenic agents such as viruses (influenza, sendai, and rota-viruses), bacteria (*Helicobacter pilori*, *Escherichia coli*, *Bordetella pertussis*, *Vibrio cholerae*, *Pseudomonas aeruginosa*), and parasites (*Plasmodium falciparum*) adhere and colonize host tissues (1). It has also been demonstrated that bacterial infections (2) and cancer metastasis (3) can be prevented by blocking pathogenic carbohydrate receptors (toxins, lectins, etc.) with high serum carbohydrate concentrations. Additionally, we (4) and others (5)[2] have established that multivalent neoglycoconjugates constitute powerful antiadhesins in a number of generally low affinity carbohydrate–protein binding interactions.

Potent multivalent neoglycoconjugate antiadhesins have been scaffolded onto a wide range of carriers including polymers (6), polyamino acids (7), cyclodextrins (8), calix[4]arenes (9), carbohydrates (10), and dendrimers (11). These last classes of scaffolds proved particularly appealing since the effects of size, shape, and valency can be controlled at will (12, 13). As an extension of our preliminary work on gallic acid (**7**) as seeding trivalent core molecule, we present herein the synthesis of tri- and nona-meric dendrimers bearing α-thiosialosides. The ability of these dendrimers to bind and cross-link sialic acid selective plant (phytohemagglutinins) and animal lectins from wheat germ agglutinin and from the slug *Limax flavus* will be discussed.

Received March 13, 1997.

This paper is dedicated to Professor Brian E. Conway on the occasion of his 70th birthday.

S.J. Meunier, Q. Wu, S.-N. Wang, and R. Roy.[1] Department of Chemistry, University of Ottawa, Ottawa, ON K1N 6N5, Canada.

[1] Author to whom correspondence may be addressed. Telephone: (613) 562-5800, ext. 6055. Fax: (613) 562-5170. E-mail: rroy@science.uottawa.ca

[2] For a review on the "cluster effect" and its implications see ref. 5*a*.

© 1997 NRC Canada

Can. J. Chem. Downloaded from www.nrcresearchpress.com by 91.121.58.235 on 09/08/12
For personal use only.

Can. J. Chem. Downloaded from www.nrcresearchpress.com by 91.121.58.235 on 09/08/12
For personal use only.

Results and discussion

3,4,5-Trihydroxybenzoic acid (gallic acid, **7**) based sialodendrimers were synthesized using commercially available tri- and tetra-ethylene glycol **1** and **2** as spacer arms. The latter were chosen to ensure water solubility of the final product and to counteract the hydrophobic effect of the aromatic backbone. They were also chosen because they are commercially available in different lengths, and they provide sufficient spacing to allow the carbohydrate moieties to be readily accessible by receptor sites. Diols **1** and **2** were ditosylated in 79–81% yields using *p*-toluenesulfonyl chloride (TsCl, triethylamine, Et_2O, reflux). Bistosylated spacers **3** and **4** were then treated with one equivalent of sodium azide (95% EtOH, reflux, 4 h) to afford azidotosylates **5** and **6** in moderate yields (39–44%) (Scheme 1). Under these conditions, a substantial amount of starting material could be recovered (40–50%), together with traces of bisazides and EtOH substitution products, which were minimized when 95% instead of 99% EtOH was used.

The choice of gallic acid as core unit allows dendrimer scaffolding to reach 3^n surface groups at the nth generation. Furthermore, it can be used to generate dendrimers with different valencies than those previously reported (2^n) for sialylated dendrimers (11) in which the seeding molecules L-lysine (12) and 3,3′-iminobis(propylamine) (13) were used. To provide an iterative approach, gallic acid was transformed into an orthogonally protected amino acid derivative (14). Methyl ester **8** was prepared from gallic acid **7** using standard procedure ($SOCl_2$, rt, 2 h, then MeOH, 98%). The white solid ester **8** (mp 199.5–201°C) was then carefully *O*-alkylated with a slight excess of azidotosylate spacers **5** or **6** using K_2CO_3 as base (DMF at 80°C) to afford key dendrimer precursors **9** and **10** in 65 and 68% yields, respectively (Scheme 1). Trisamino esters **11** and **12** were obtained by reduction of azides **9** and **10** (H_2, 10% Pd–C, 93% crude yield for **12**) and used directly in the next step without further purification. An analytical sample of **12** was, however, purified by silica gel chromatography (65% yield). The extent of the reduction was monitored by FTIR spectroscopy, which showed total disappearance of the azido frequency (2106 cm^{-1}). Intermediate amines **11** and **12** were then sequentially transformed into either first generation precursors **13** and **14** or into orthogonally protected amino acid derivatives for further generation buildup. Thus, treatment of **11** or **12** with chloroacetic anhydride ($(ClCH_2CO)_2O$, Et_3N, EtOH) provided tris-*N*-chloroacetylated esters **13** or **14** in 62–65% yields. Completion of the reaction could be readily monitored by a negative ninhydrin reaction and by the appearance of a sharp *N*-chloroacetyl methylene singlet at δ 4.01 ppm ($CDCl_3$) integrating for the expected six proton signals relative to those of the two aromatic protons (δ 7.25 ppm, s) and the three carbomethoxy protons signal at δ 3.85 ppm.

As we previously demonstrated in other glycodendrimer syntheses (11–15), it was found advantageous to attach the carbohydrate residues after the buildup of the dendritic cores. Not only does this strategy permit incorporation of any other carbohydrate haptens at a late stage but it also allows convergent synthesis as well as tethering glycodendrimer building blocks (13*b*). In this last case, tethered glycodendrimers are formed with spherical shapes in all three directions rather than being unidirectional.

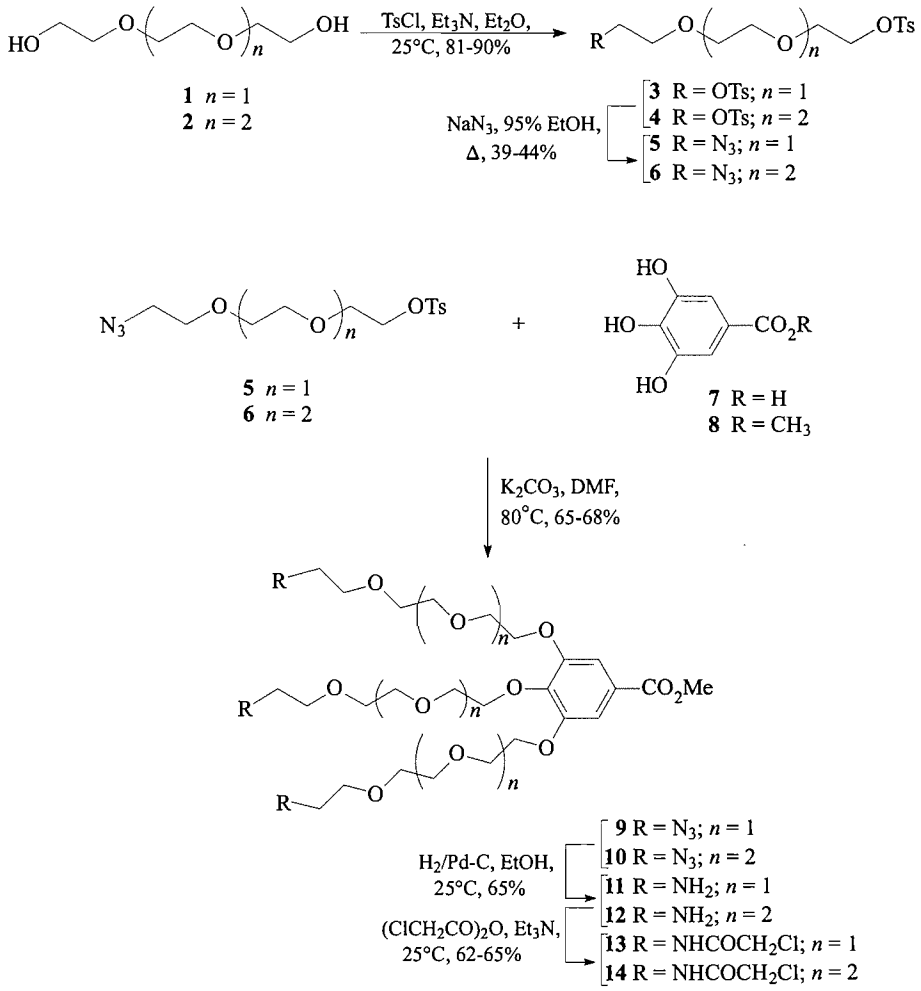
Thus, known α-sialosyl thioacetate **15** (12*a*) was chosen as the nucleophilic carbohydrate moiety to be initially used on the trimeric *N*-chloroacetylated precursors **13** and **14**. Chemoselective hydrolysis of the thioacetate group in **15** was first achieved by mild transesterification conditions (NaOMe, MeOH, −40°C, 15 min), followed by acidic resin treatment at −40°C (16) (Scheme 2). This mild treatment prevented anomeric thiol from both oxidation and anomerization. Thiol derivative **16** was always freshly prepared prior to coupling onto dendrimers. First-generation trivalent α-thiosialosides **17** and **18** were obtained from the coupling of thiol **16** to trimeric *N*-chloroacetylated esters **13** and **14** under a nitrogen atmosphere (CH_3CN, Et_3N, 25°C, 85–95% yields). The extent of thiosialoside incorporation in glycodendrimers **17** and **18** was readily determined by ^1H NMR spectroscopy. The disappearance of the signal due to all three equivalent *N*-chloroacetyl residues at δ 4.01 ppm (6H), along with the integration of well-separated sialic acid associated signals at δ 4.84 ppm (H-4, 3H) and at δ 2.72 ppm (H-3e, 3H) relative to that of the aromatic protons at δ 7.27 ppm (2H), confirmed complete substitution. Peracetylated glycodendrimers **17** and **18** were then treated with NaOMe in MeOH (pH ~9, 25°C) to provide partially deprotected intermediates **19** and **20** in quantitative yields. Their ^1H NMR spectra showed the presence of sialic acid methyl esters and *N*-acetyl residues as well as the disappearance of all *O*-acetyl signals. Methyl ester hydrolysis from both sialosides and gallic acid residues of **19** and **20** was performed simultaneously by treatment with 0.5 M aqueous NaOH in MeOH (1:1, v/v, 25°C , 16 h). This reaction afforded unprotected water-soluble glycodendrimers **21** and **22** in nearly quantitative yields after freeze-drying. Completion of hydrolysis was best monitored using ^{13}C NMR spectroscopy where the methoxy signals at δ ~52–54 ppm were well separated from the remaining carbon signals.

For the preparation of the second generation, readily available amide bond linkages between the subunits were chosen. To this end, orthogonally protected amino acid derivatives were required. Trisamino ester **12**, already obtained from reduction of trisazido ester **10** (see above), was used as an amine partner, while acid precursor **23** was obtained from the same trisazido ester **10** by hydrolysis (Scheme 3). Methyl ester **10** was hydrolyzed under basic conditions (KOH, EtOH, reflux, 2 h) to afford **23** quantitatively. Coupling a slight excess of trisazido acid **23** to trisamino ester **12** using carbodiimide chemistry and hydroxybenzotriazole (EDC, HOBt, EtOH-CH_3CN, 1:1 v/v, DIPEA, 25°C, 3 h) afforded nona-azido ester **24** in 83% yield. After usual work-up and purification by silica gel column chromatography, the ^1H NMR spectrum of **24** showed the expected 1:3 ratio of inner (δ 7.24 ppm, ester) and outer (δ 7.02 ppm, amide) aromatic proton signals. Catalytic hydrogenation (H_2, 10% Pd–C) of azido ester **24** gave nona-amino ester **25**, which was not further purified since it was directly *N*-chloroacetylated as previously shown ($(ClCH_2CO)_2O$, Et_3N), to give **26** in 78% yield . The extent of reduction was ascertained by IR spectroscopy wherein the sensitive azide frequency (2106 cm^{-1}) could be monitored.

Electrophilic nona-*N*-chloroacetylated dendrimer **26** was suitable for nucleophilic substitution with sialic acid thiol **16** (11 equiv.) as described earlier for compounds **17** and **18**. The coupling was done at room temperature overnight (CH_3CN, Et_3N) under nitrogen to provide fully protected nona-sialoside dendrimer **27** in 86% yield as a colorless oil after purification

© 1997 NRC Canada

Scheme 1.



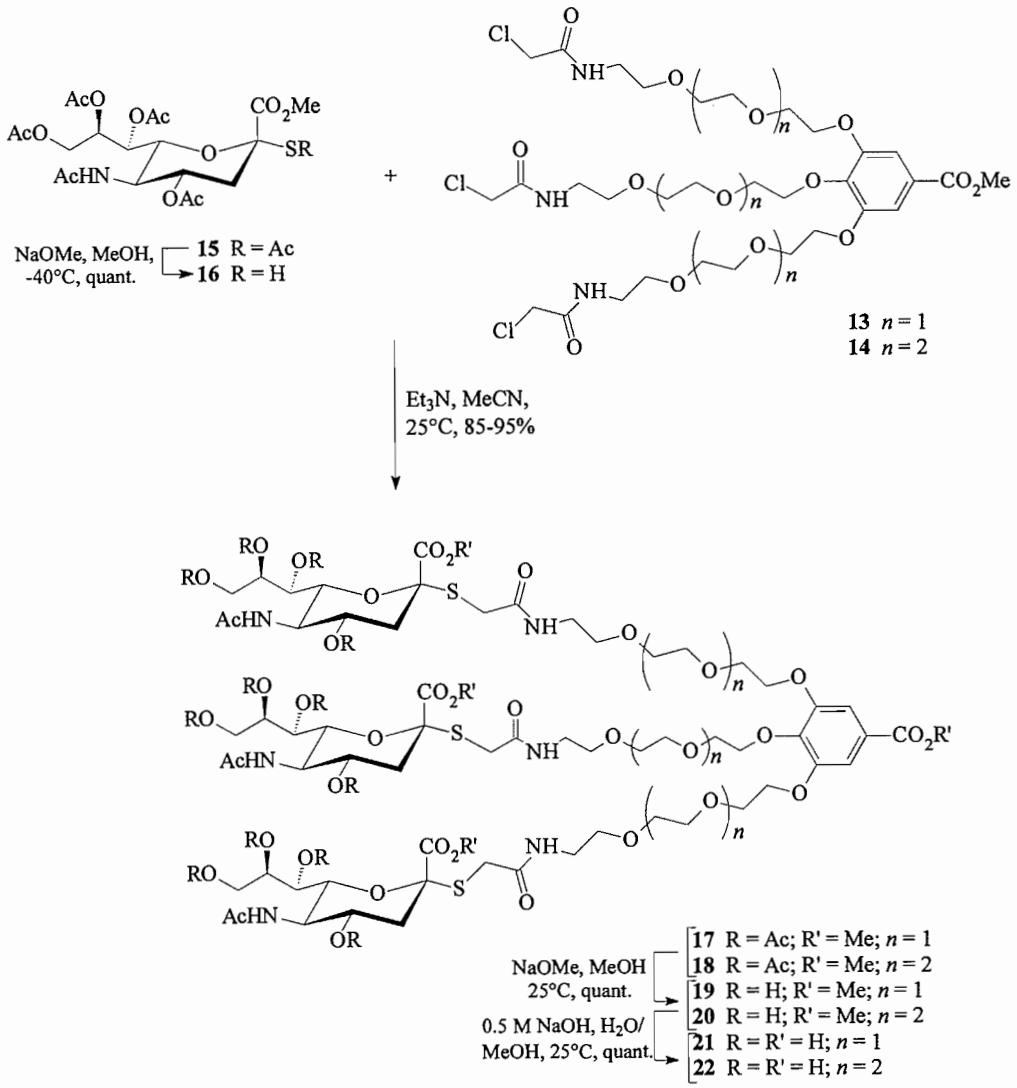
by silica gel column chromatography (Scheme 4). The incorporation level of α-thiosialosides was evaluated as before by using ^{1}H NMR spectroscopy . The aromatic protons of the inner residue (δ 7.25 ppm) integrated for two protons when compared to either H-4 (δ 4.83 ppm) or H-3e (δ 2.71 ppm) of the sialic acid residues, which both integrated for nine protons. De-*O*-acetylation of glycodendrimer **27** was achieved under standard Zemplén conditions (NaOMe, MeOH, pH ~9, 25°C, 45 min) to give compound **28** in quantitative yield. Methyl esters in **28** were hydrolyzed following the procedure described above (aq. NaOH, MeOH), and unprotected nona-α-thiosialylated dendrimer **29** was obtained in quantitative yield.

Preliminary lectin-binding experiments were achieved using microtiter plate turbidimetric analysis (17) wherein solutions of lectin-containing trimeric (**21** or **22**) and nonameric (**29**) sialodendrimers were allowed to form insoluble cross-linked complexes that could be monitored at 490 nm. To this end, two different lectins known to bind α-sialosides were used. Wheat germ agglutinin (WGA) (18) and the lectin from the slug *Limax flavus* (LFA) (19) were used as models. Both lectins are divalent and can therefore form linear one-dimensional (sometimes soluble) or multidimensional cross-linked lattices (20). The results from the time course of turbidimetric analysis are shown in Fig. 1. Interestingly, 9-mer α-thiosialoside **29** showed a clear and rapid cross-linked insoluble complex with both WGA and LFA lectins. This last result with LFA is similar to that previously observed with analogous multivalent α-thiosialosides scaffolded on a 3,3′-iminobis(propylamine) core (13). It differs, however, from both previous studies (13) and the present WGA binding in that the complex seems less stable since there is a steady decrease of cross-linking after the initial 10 min of reaction. The complex does however stabilize after awhile. Additionally, trimeric α-thiosialosides **21** and **22**, only differing by the length of their ethylene glycol spacers, showed no stable insoluble complexes with either lectins. These results can be rationalized by the low valency of the trimers, which fail to form multidimensional cross-linked complexes with the dimeric lectins. This implies that the third arm of the dendrimers does not allow further cross-linking with another lectin molecule. Work is now in progress to determine the intrinsic binding abilities of each sialodendrimer by inhibition assays. This work further stresses the need for a better understanding of carbohydrate-protein interactions of glycodendrimers varying in shape, size, conformation (rigidity), and valency. As antigen presentation is becoming crucial in the design of potent carbohydrate

Can. J. Chem. Downloaded from www.nrcresearchpress.com by 91.121.58.235 on 09/08/12
For personal use only.

© 1997 NRC Canada

Scheme 2.



ligands, which can be used as antiadhesins and as vectors for drug delivery, further work is still needed.

Experimental

General methods

Melting points were determined on a Gallenkamp apparatus and are uncorrected. The ^1H and ^{13}C NMR spectra were recorded on Varian Gemini-200 and Bruker AMX-500 spectrometers. Proton chemical shifts (δ) are given relative to internal chloroform (δ 7.24 ppm) for $CDCl_3$ solutions or to methanol (δ 3.30 ppm) for CD_3OD solutions. Carbon chemical shifts are given relative to deuteriochloroform (δ 77.0 ppm) and to CD_3OD (δ 49.0 ppm). Optical rotations were measured at room temperature (23 ± 1°C) in a 1 dm cell on a Perkin–Elmer 241 polarimeter. Mass spectra were recorded on a VG 7070-E spectrometer (CI, ether) and Kratos Concept IIH (FABMS, thioglycerol). Thin-layer chromatography (TLC) was performed using silica gel 60 F-254 and column chromatography on silica gel 60 (230–400 mesh, E. Merck No. 9385). All solvents and reagents were reagent grade and were used without further purification. Optical densities (O.D.) for the turbidimetric analysis were performed on a Dynatech MR 600 Microplate Reader. The lectins, *Limax flavus* (LFA) and *Triticum vulgaris* (WGA), were obtained from E-Y Laboratories (cat. no. L-5101-1) and Sigma (cat. no. L-9640), respectively.

Synthesis

*1,8-Bis-[(*p*-toluenesulfonyl)oxy]-3,6-dioxaoctane (3)*

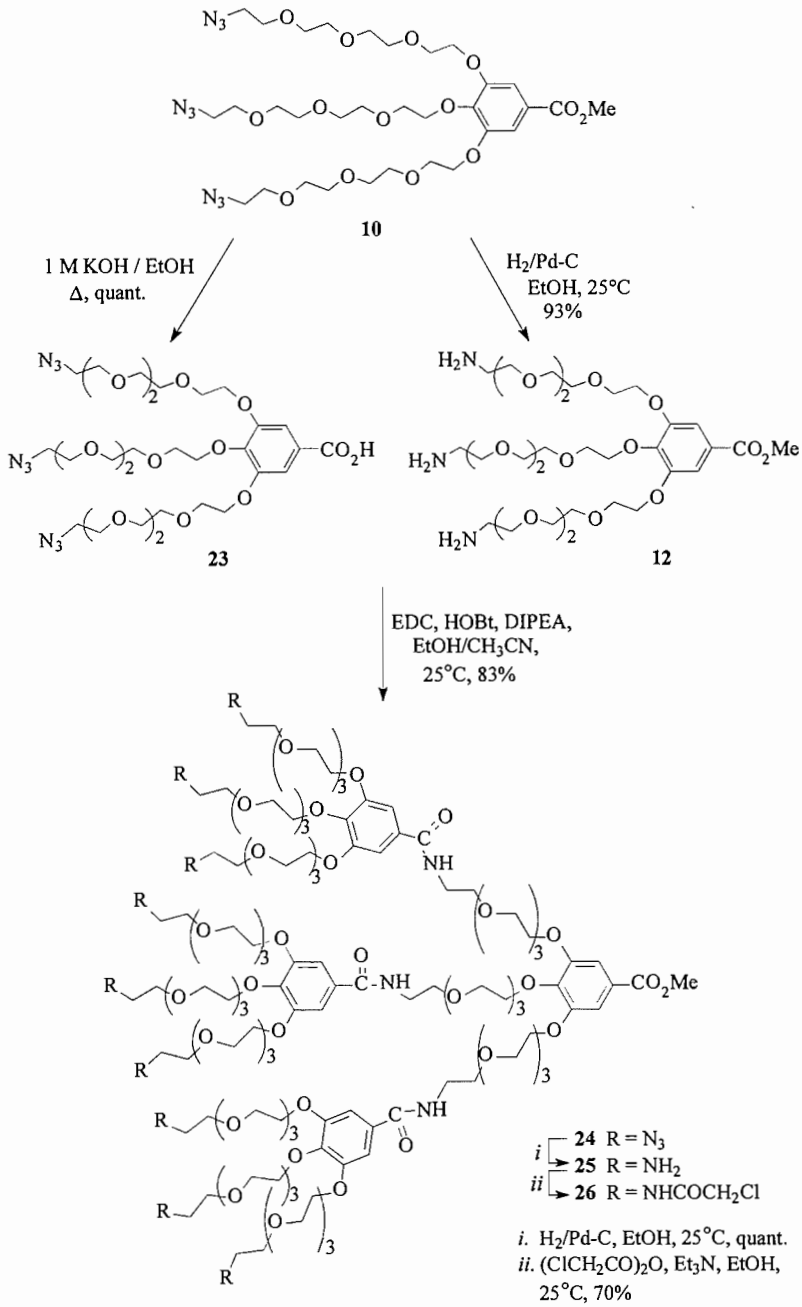
A solution of triethylene glycol (50.0 g, 0.33 mol) in anhydrous diethyl ether (300 mL) was cooled to 0°C under a nitrogen atmosphere. Triethylamine (50 mL) was added followed by *p*-toluenesulfonyl chloride (68.84 g, 0.36 mol) over a 1 h period, and the solution was warmed to room temperature. After stirring for 3 h, the reaction mixture was evaporated in vacuo. The resulting residue was dissolved in CH_2Cl_2 and washed successively with saturated sodium bicarbonate solution (50 mL) and twice with water (50 mL). The organic layer was dried using anhydrous sodium sulfate and concentrated

Can. J. Chem. Downloaded from www.nrcresearchpress.com by 91.121.58.235 on 09/08/12
For personal use only.

© 1997 NRC Canada

Can. J. Chem. Downloaded from www.nrcresearchpress.com by 91.121.58.235 on 09/08/12
For personal use only.

Scheme 3.



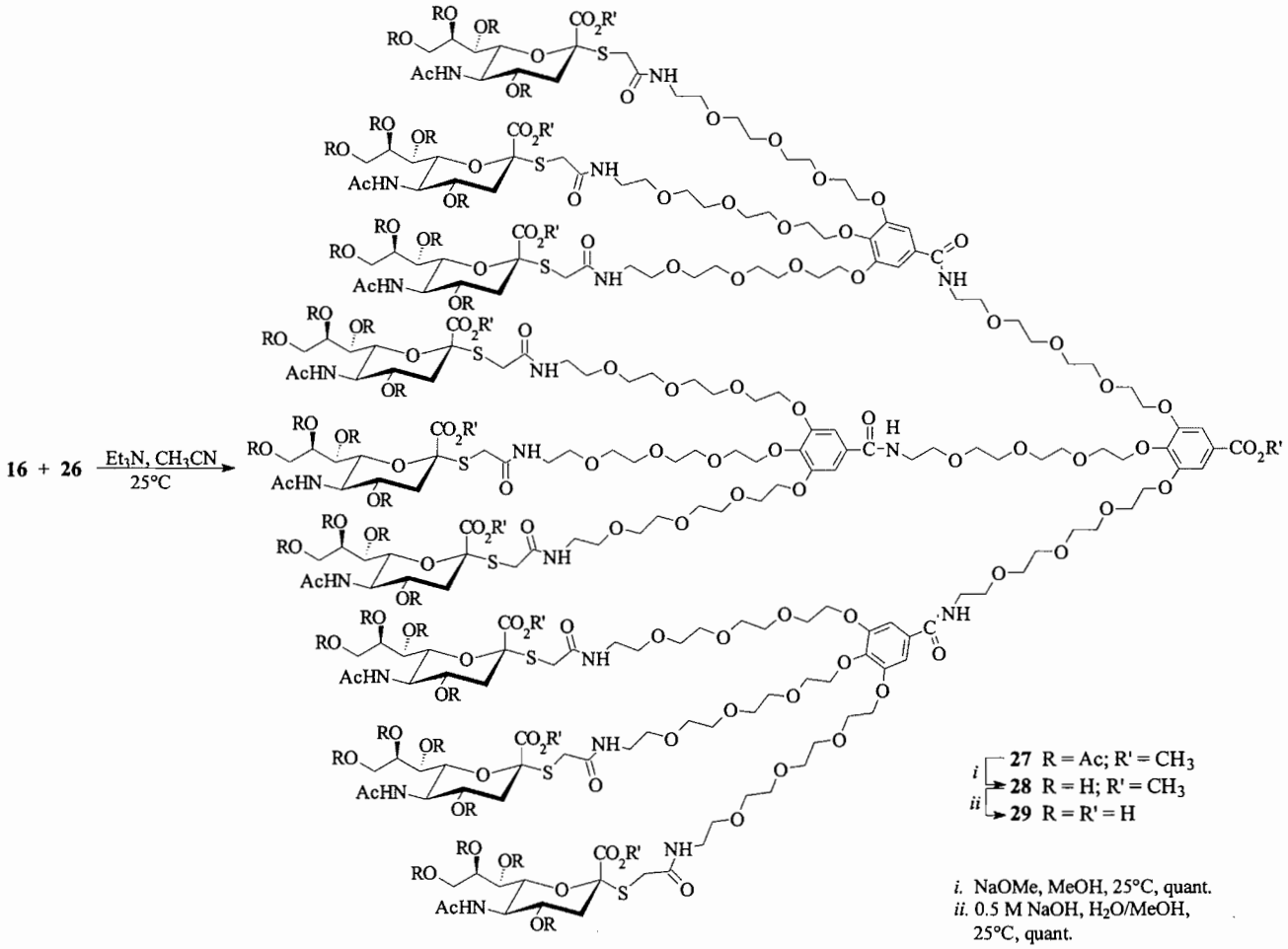
under vacuum to afford 120 g (79%) of **3** as a white solid. After filtration, the remaining crude product was purified by silica gel column chromatography using ethyl acetate/hexanes (1:1, v/v) as eluent to afford 16 g (11%) of **3** (total yield 90%); mp 82–84°C (EtOH); ^{1}H NMR ($CDCl_3$) δ: 7.75 (d, 4H, J 8.3 Hz, H_{ar}), 7.31 (d, 4H, *J* 8.3 Hz, H_{ar}), 4.11 (t, 4H, *J* 4.8 Hz, TsOCH_2), 3.62 (t, 4H, *J* 4.8 Hz, TsOCH$_2CH_2$), 3.49 (s, 4H, OCH_2), 2.41 (s, 6H, CH_3); ^{13}C NMR ($CDCl_3$) δ: 144.8, 132.8, 129.8, 127.9 (C_{ar}), 70.6 (TsOCH_2), 69.2 (CH_2O), 68.6 (CH_2O), 21.6 (CH_3); CIMS: 459 (M+1, 36%), 287 (74).

*1,11-Bis-[(*p*-toluenesulfonyl)oxy]-3,6,9-trioxaundecane (**4**)*
An identical procedure was used to synthesize compound **4** in 81% yield, the difference being that the final product was a colorless oil that was purified by silica gel column chromatography. ^{1}H NMR ($CDCl_3$) δ: 7.76 (d, 4H, *J* 8.2 Hz, H_{ar}), 7.31 (d, 4H, *J* 8.2 Hz, H_{ar}), 4.12 (t, 4H, *J* 4.8 Hz, TsOCH_2), 3.64 (t, 4H, *J* 4.8 Hz, TsOCH$_2CH_2$), 3.53 (s, 8H, OCH_2), 2.41 (s, 6H, CH_3); ^{13}C NMR ($CDCl_3$) δ: 144.6, 132.6, 129.6, 127.7 (C_{ar}), 70.4, 70.2, 69.1, 68.4 (CH_2O), 21.4 (CH_3); CIMS: 503 (M+1, 26%), 331 (46).

*1-Azido-8-[(*p*-toluenesulfonyl)oxy]-3,6-dioxaoctane (**5**)*
To a solution of 500 mg (1.09 mmol) of bistosylate **3** in 95% ethanol (10 mL) was added sodium azide (35.4 mg, 0.545 mmol). The reaction was stirred under reflux for 4 h and monitored by TLC. After cooling the reaction mixture to room temperature and removing the precipitated solid, the filtrate

© 1997 NRC Canada

Scheme 4.



was evaporated under reduced pressure. The oily residue was dissolved in diethyl ether and washed twice with water and brine. The dried organic phase (Na_2SO_4) was concentrated and the crude product purified by silica gel chromatography using a gradient of 1:5 to 1:1 (v/v) ethyl acetate/hexanes as eluent to afford 157.6 mg (44%) of **5** as a colorless oil. FTIR ν_{max} (cm^{-1}): 3015, 2904, 2108, 1738, 1598; ^1H NMR ($CDCl_3$) δ: 7.75 (d, 2H, *J* 8.3 Hz, H_{ar}), 7.32 (d, 2H, *J* 8.3 Hz, H_{ar}), 4.12 (t, 2H, *J* 4.7 Hz, TsOCH_2), 3.68–3.56 (m, 8H, OCH_2), 3.33 (t, 2H, CH_2N_3), 2.41 (s, 3H, CH_3); ^{13}C NMR ($CDCl_3$) δ: 144.6, 132.6, 129.6, 127.6 (C_{ar}), 70.4, 70.2, 69.7, 69.1, 68.4 (CH_2O), 50.3 (CH_2N_3), 21.3 (CH_3); CIMS: 330 (M+1, 3%), 302 (61). Anal. calcd. for $C_{13}H_{19}N_3O_5S$: C 47.40, H 5.81, N 12.76; found: C 47.23, H 6.00, N 12.96.

*1-Azido-11-[(p-toluenesulfonyl)oxy]-3,6,9-trioxaundecane (**6**)*

Compound **6**, prepared under the same conditions described above for **5**, was obtained as an oily residue in 39% yield (15.2 g). FTIR ν_{max} (cm^{-1}): 3015, 2930, 2110, 1727, 1599; ^1H NMR ($CDCl_3$) δ: 7.72 (d, 2H, *J* 8.3 Hz, H_{ar}), 7.27 (d, 2H, *J* 8.3 Hz, H_{ar}), 4.12 (t, 2H, *J* 4.8 Hz, TsOCH_2), 3.63–3.52 (m, 12H, OCH_2), 3.31 (t, 2H, CH_2N_3), 2.39 (s, 3H, CH_3); ^{13}C NMR ($CDCl_3$) δ: 144.7, 132.7, 129.7, 127.8 (C_{ar}), 70.6, 70.5, 70.4, 69.9, 69.2, 68.5 (CH_2O), 50.5 (CH_2N_3), 21.5 (CH_3); CIMS: 374 (M+1, 3%), 346 (67).

*Methyl 3,4,5-trihydroxybenzoate (**8**)*

Gallic acid **7** (3.4 g, 20 mmol) was treated with thionyl chloride (10 mL) at room temperature for 2 h after which time the solvent was removed under vacuum. The oily residue was cooled down using an ice bath followed by addition of methanol (10 mL). The mixture was allowed to react for 30 min and was concentrated in vacuo. The crude residue was recrystallized from ethanol to afford 3.6 g (98%) of a white solid; mp 199.5–201°C (ethanol); ^1H NMR (D_2O) δ: 7.06 (s, 2H, H_{ar}), 3.86 (s, 3H, OCH_3); ^{13}C NMR (DMSO-d_6) δ: 164.9 (C═O), 144.2, 137.0, 117.1, 107.1 (C_{ar}), 50.2 (OCH_3); HREIMS: 184.0372 (calcd. for $C_8H_8O_5$: 184.0367, 15.4%).

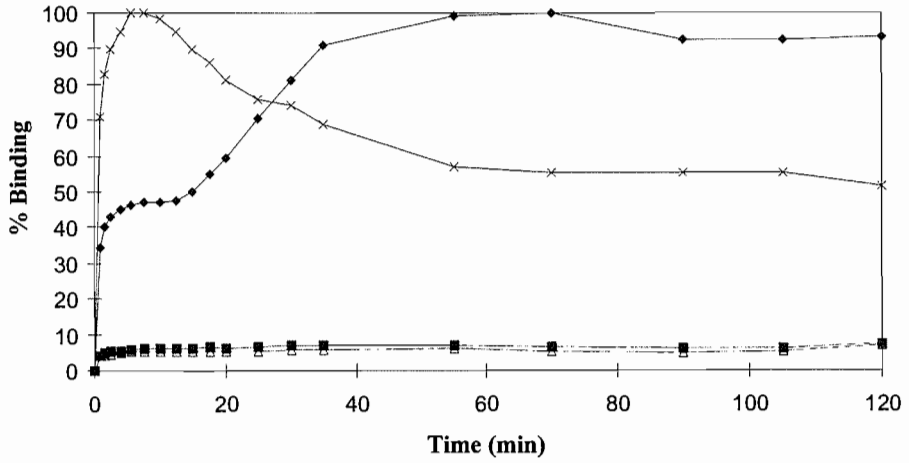
*Methyl 3,4,5-tri-(8-azido-3,6-dioxaoctyloxy)benzoate (**9**)*

To a solution of methyl gallate **8** (184 mg, 1 mmol) in DMF (25 mL) was added potassium carbonate (1.4 g, 10 mmol) and tosylated **5** (1.3 g, 4.0 mmol) dissolved in DMF (5 mL). The mixture was stirred at 80°C for 24 h and allowed to cool to room temperature. The solid was filtered off and the filtrate was evaporated under vacuum, coevaporated with *tert*-butanol, and the remaining residue was partitioned between

© 1997 NRC Canada

Can. J. Chem. Downloaded from www.nrcresearchpress.com by 91.121.58.235 on 09/08/12
For personal use only.

Fig. 1. Time course of turbidimetric analysis of wheat germ agglutinin (WGA) with 9-mer α-thiosialoside **29** (◆), trimers **21** (△) and **22** (■), and *Limax flavus* lectin (LFA) with **29** (X).



CH_2Cl_2 and water. The organic layer was separated and washed further with water, saturated NaCl solution, and dried over sodium sulfate. After removing the solvent, the crude material was purified by silica gel chromatography using a gradient of 1:3 to 2:1 (v/v) ethyl acetate/hexanes to give 426 mg (65%) of **9** as a pure colorless oil. FTIR ν_{max} (cm^{-1}): 3018, 2901, 2107, 1717, 1587; ^1H NMR ($CDCl_3$) δ: 7.27 (s, 2H, H_{ar}), 4.23–4.15 (m, 6H, PhOCH_2), 3.86 (s, 3H, OCH_3), 3.88–3.61 (m, 24H, OCH_2), 3.35 (t, 6H, *J* 5.0 Hz, CH_2N_3); ^{13}C NMR ($CDCl_3$) δ: 166.5 (C═O), 152.2, 142.4, 124.9, 108.9 (C_{ar}), 72.4, 72.3, 70.8, 70.7, 70.5, 70.0, 69.9, 69.6, 68.8 (CH_2O), 52.1 (OCH_3), 50.6 (CH_2N_3); FABMS: 656 (M+1, 11%), 628 (14). Anal. calcd. for $C_{26}H_{41}N_9O_{11}$: C 47.62, H 6.30, N 19.23; found: C 47.69, H 6.22, N 18.97.

*Methyl 3,4,5-tri-(11-azido-3,6,9-trioxaundecyloxy)benzoate (**10**)*

Compound **10** was obtained, the same way as previously shown for **9**, as a colorless oil in 68% yield. FTIR ν_{max} (cm^{-1}): 3009, 2948, 2106, 1717, 1586; ^1H NMR ($CDCl_3$) δ: 7.26 (s, 2H, H_{ar}), 4.22–4.14 (m, 6H, PhOCH_2), 3.85 (s, 3H, OCH_3), 3.87–3.61 (m, 36H, OCH_2), 3.35 (t, 6H, CH_2N_3); ^{13}C NMR ($CDCl_3$) δ: 166.2 (C═O), 152.0, 142.2, 124.6, 108.6 (C_{ar}), 72.1, 70.4, 70.3, 70.3, 69.7, 69.3, 68.5 (CH_2O), 51.8 (OCH_3), 50.3 (CH_2N_3); FABMS: 788 (M+1, 2%), 760 (4). Anal. calcd. for $C_{32}H_{53}N_9O_{14}$: C 48.79, H 6.78, N 16.00; found: C 49.00, H 7.00, N 16.06.

*Methyl 3,4,5-tri-(8-amino-3,6-dioxaoctyloxy)benzoate (**11**)*

To a solution of azide **9** (132 mg, 0.206 mmol) in ethanol (10 mL) was added 50 mg of 10% palladium on carbon. Hydrogen was constantly bubbled through the solution at room temperature and the reaction was monitored by IR (complete disappearance of azide peak). After 3 h, the catalyst was removed by filtration and the filtrate was concentrated under vacuum. The crude product obtained was used in the next step without further purification. FTIR ν_{max} (cm^{-1}): 3450, 3020, 2921, 1716, 1587; FABMS: 579 (M+1, 32%).

*Methyl 3,4,5-tri-(11-amino-3,6,9-trioxaundecyloxy)benzoate (**12**)*

Following the procedure described previously, trisamino **12** was obtained as a yellowish syrup in 93% crude yield. The product was purified by silica gel chromatography using 10% MeOH in CH_2Cl_2 as eluent to give pure **12** in 65% yield. FTIR ν_{max} (cm^{-1}): 3369, 3050, 2897, 1715, 1586; ^1H NMR ($CDCl_3$) δ: 7.25 (s, 2H, H_{ar}), 4.16 (m, 6H, PhOCH_2), 3.85 (s, 3H, OCH_3), 3.84–3.54 (m, 30H, OCH_2), 3.45 (t, 6H, *J* 5.4 Hz, OCH_2), 2.82 (t, 6H, *J* 5.4 Hz, CH_2NH_2), 1.29 (m, 6H, NH_2); ^{13}C NMR ($CDCl_3$) δ: 166.4 (C═O), 152.1, 142.3, 124.8, 108.8 (C_{ar}), 73.3, 72.2, 70.7, 70.5, 70.4, 70.3, 70.1, 69.4, 68.6, (CH_2O), 52.0 (OCH_3), 41.6 (CH_2NH_2); FABMS: 710 (M+1, 45%).

*Methyl 3,4,5-tri-[8-(2-chloroacetamido)-3,6-dioxaoctyloxy]benzoate (**13**)*

To a cooled solution (0°C) of trisamine **11** (119 mg, 0.206 mmol) in ethanol (10 mL) was added triethylamine (0.5 mL) and chloroacetic anhydride (132 mg, 0.772 mmol) in small portions over a 30 min period. The mixture was then stirred at room temperature for 2 h after which time the solvent was evaporated under vacuum. The reaction was monitored by a ninhydrin test. The oily residue was dissolved in H_2O and extracted with CH_2Cl_2. The organic extracts were dried (Na_2SO_4), concentrated under vacuum to give crude **13**, which was purified by silica gel chromatography using 5% methanol in CH_2Cl_2 as eluent to afford 108 mg (65%) of **13** as a colorless oil. FTIR ν_{max} (cm^{-1}): 3316, 3015, 2904, 1715, 1668, 1589; ^1H NMR ($CDCl_3$) δ: 7.25 (s, 2H, H_{ar}), 7.18 (m, 3H, NH), 4.22–4.15 (m, 6H, PhOCH_2), 4.01 (s, 6H, CH_2Cl), 3.85 (s, 3H, OCH_3), 3.85–3.40 (m, 30H, OCH_2 and CH_2NH); ^{13}C NMR ($CDCl_3$) δ: 166.3, 165.9 (C═O), 152.0, 142.0, 124.9, 108.6 (C_{ar}), 72.2, 70.5, 70.4, 70.3, 70.1, 69.4, 69.2, 68.6 (CH_2O), 52.0 (OCH_3), 42.4 (CH_2NH), 39.4 (CH_2Cl); FABMS: 808 (M+1, 14%), 810 (5). Anal. calcd. for $C_{32}H_{50}N_3O_{14}Cl_3$: C 47.62, H 6.24, N 5.21; found: C 47.80, H 6.40, N 5.05.

*Methyl 3,4,5-tri-[11-(2-chloroacetamido)-3,6,9-trioxaundecyloxy]benzoate (**14**)*

Compound **14** was obtained from the amino **12** by the same procedure described above. The pure product was obtained in 62% yield as a colorless syrup. FTIR ν_{max} (cm^{-1}): 3425, 3035, 2904, 1714, 1671, 1588; ^1H NMR ($CDCl_3$) δ: 7.26 (s, 2H, H_{ar}), 7.08–7.04 (m, 3H, NH), 4.18 (t, 2H, *J* 4.9 Hz, PhOCH_2), 4.16

Can. J. Chem. Downloaded from www.nrcresearchpress.com by 91.121.58.235 on 09/08/12
For personal use only.

© 1997 NRC Canada

Can. J. Chem. Downloaded from www.nrcresearchpress.com by 91.121.58.235 on 09/08/12
For personal use only.

(t, 4H, *J* 5.0 Hz, PhOCH_2), 4.00 (s, 6H, CH_2Cl), 3.84 (s, 3H, OCH_3), 3.82 (t, 4H, OCH_2), 3.76 (t, 2H, OCH_2), 3.70–3.66 (m, 6H, OCH_2), 3.64–3.57 (m, 18H, OCH_2), 3.54 (t, 6H, OCH_2), 3.47–3.44 (m, 6H, CH_2NH); ^{13}C NMR ($CDCl_3$) δ: 166.4, 166.0 (C═O), 152.2, 142.2, 125.0, 108.8 (C_{ar}), 72.4, 70.8, 70.6, 70.5, 70.3, 69.6, 69.3, 68.7 (CH_2O), 52.2 (OCH_3), 42.6 (CH_2NH), 39.5 (CH_2Cl); HR-FABMS: 938.3223 (calcd. for $C_{38}H_{63}N_3O_{17}Cl_3$: 938.330, 99%).

Methyl 5-acetamido-4,7,8,9-tetra-O*-acetyl-3,5-dideoxy-2-thio-*D*-glycero-*α*-*D*-galacto-2-nonulo-pyranosidonate (**16**)*

To a solution of thioacetylated sialic acid **15** (12*a*) (63.1 mg, 0.115 mmol) in dry methanol (1.5 mL) cooled to −40°C, was added 1 M sodium methoxide in methanol (109 μL, 0.109 mmol). The reaction, monitored by TLC, took less than 15 min after which time the reaction mixture was treated with H^+ resin (Amberlite IR-120) at −40°C for 15 min. The solution was filtered and evaporated at room temperature under reduced pressure to afford **16**, which was used without further purification. $[\alpha]_D$ +15.6 (*c* 0.99, $CHCl_3$); ^{1}H NMR ($CDCl_3$) δ: 5.33–5.28 (m, 2H, H-7 and H-8), 5.17 (d, 1H, $J_{NH,5}$ 10.5 Hz, NH), 4.91 (ddd, 1H, $J_{4,5}$ 10.3 Hz, $J_{3a,4}$ 11.7, $J_{3e,4}$ 4.8, H-4), 4.49 (dd, 1H, $J_{8,9'}$ 2.1 Hz, $J_{9,9'}$ 12.4, H-9′), 4.10 (dd, 1H, $J_{8,9}$ 5.5 Hz, H-9), 4.06 (m, 1H, H-5), 3.83 (s, 3H, OCH_3), 3.73 (dd, 1H, $J_{6,7}$ 1.9 Hz, $J_{5,6}$ 10.8, H-6), 3.17 (s, 1H, SH), 2.80 (dd, 1H, $J_{3e,3a}$ 12.8 Hz, H-3e), 2.14, 2.13, 2.05, 2.03 (4s, 12H, 4 OAc), 2.04 (dd, 1H, H-3a), 1.88 (s, 3H, NAc); ^{13}C NMR ($CDCl_3$) δ: 170.9, 170.6, 170.4, 170.4, 170.1, 170.0 (C═O), 81.6 (C-2), 75.1 (C-6), 70.1 (C-8), 69.4 (C-4), 67.7 (C-7), 62.2 (C-9), 53.4 (OCH_3), 49.1 (C-5), 38.9 (C-3), 23.1 (NAc), 21.1, 20.8, 20.8 (4 OAc); CIMS: 508 (M+1, 100%), 476 (85).

Methyl 3,4,5-tri-{8-[2-(methyl 5-acetamido-4,7,8,9-tetra-O*-acetyl-3,5-dideoxy-2-thio-*D*-glycero-*α*-*D*-galacto-2-nonulo-pyranosid)-acetamido]-3,6-dioxaoctyloxy}benzoate (**17**)*

To a solution of α-thiosialoside **16** (75.4 mg, 0.149 mmol) in dry acetonitrile (4.5 mL) was added Et_3N (50 μL, 0.358 mmol) and trischloroacetamide precursor **13** (30 mg, 0.037 mmol). The mixture was stirred at room temperature overnight under a nitrogen atmosphere. The solution was concentrated under vacuum, and the crude residue was purified by preparative TLC plate using, first, ethyl acetate, followed by 7% methanol in CH_2Cl_2 as eluent. Pure **17** was extracted using 5% methanol in CH_2Cl_2 and, after evaporation, the residue was dissolved in ethyl acetate and filtered to remove soluble impurities from silica gel. The colorless oil was obtained in 85% (70.7 mg) yield. $[\alpha]_D$ +24.2 (*c* 1.02, $CHCl_3$); ^{1}H NMR ($CDCl_3$) δ: 7.27 (s, 2H, H_{ar}), 6.89 (m, 3H, NH), 5.44 (m, 6H, H-8 and NH), 5.30 (dd, 3H, $J_{6,7}$ 2.0 Hz, $J_{7,8}$ 9.0, H-7), 4.84 (ddd, 3H, $J_{3a,4}$ 11.6 Hz, $J_{3e,4}$ 4.5, H-4), 4.25 (dd, 3H, $J_{8,9'}$ 2.8 Hz, H-9′), 4.21–4.17 (m, 6H, PhOCH_2), 4.06–4.01 (m, 6H, H-5 and H-9), 3.87 (s, 3H, OCH_3), 3.84 (t, 6H, *J* 4.8 Hz, OCH_2), 3.78–3.34 (m, 30H, OCH_2, CH_2N, CH_aS, and H-6), 3.73 (s, 9H, OCH_3), 3.29 (d, 3H, *J* 16.2 Hz, CH_bS), 2.72 (dd, 3H, $J_{3e,3a}$ 12.7 Hz, $J_{3e,4}$ 4.5, H-3e), 2.17, 2.13, 2.03, 2.01 (4s, 36H, 4 OAc), 1.95 (dd, 3H, H-3a), 1.86 (s, 9H, NAc); ^{13}C NMR ($CDCl_3$) δ: 171.1, 170.8, 170.8, 170.7, 170.4, 170.4, 170.1, 168.6, 168.5, 168.4 (C═O), 152.2, 142.2, 125.0 (C_{ar}), 108.9 (C_{ar}-H), 82.1 (C-2), 73.9 (C-6), 72.3, 70.6, 70.5, 70.4, 70.2, 69.6, 69.6, 69.5, 68.7 (OCH_2), 69.4 (C-4), 68.0 (C-8), 67.0 (C-7), 62.3 (C-9), 53.1 (OCH_3), 52.2 (OCH_3), 49.1 (C-5), 39.7 (CH_2N), 37.3 (C-3), 32.4 (CH_2S), 23.1 (NAc), 21.3, 20.8, 20.8, 20.7 (4 OAc); FABMS: 2223 (M+1, 20%). Anal. calcd. for $C_{92}H_{134}N_6O_{50}S_3$: C 49.77, H 6.08, N 3.79; found: C 49.80, H 6.43, N 3.63.

Methyl 3,4,5-tri-{11-[2-(methyl 5-acetamido-4,7,8,9-tetra-O*-acetyl-3,5-dideoxy-2-thio-*D*-glycero-*α*-*D*-galacto-2-nonulo-pyranosid)-acetamido]-3,6,9-trioxaundecyloxy}-benzoate (**18**)*

The sialylated glycodendrimer **18** was obtained in 95% (71.4 mg) yield as a colorless oil in the same way as described for glycodendrimer **17**. $[\alpha]_D$ +22.4 (*c* 1.01, $CHCl_3$); ^{1}H NMR ($CDCl_3$) δ: 7.27 (s, 2H, H_{ar}), 6.83 (m, 3H, NH), 5.41 (ddd, 3H, $J_{8,9'}$ 2.7 Hz, H-8), 5.34 (d, 3H, $J_{NH,5}$ 10.0 Hz, NH), 5.29 (dd, 3H, $J_{6,7}$ 2.1 Hz, $J_{7,8}$ 9.2, H-7), 4.84 (ddd, 3H, $J_{4,5}$ 10.4 Hz, $J_{3a,4}$ 11.6, $J_{3e,4}$ 4.6, H-4), 4.24 (dd, 3H, $J_{8,9'}$ 2.7 Hz, $J_{9,9'}$ 12.4, H-9′), 4.20–4.16 (m, 6H, PhOCH_2), 4.06–4.02 (m, 3H, H-5), 4.03 (dd, 3H, $J_{8,9}$ 5.8 Hz, H-9), 3.87 (s, 3H, OCH_3), 3.83 (t, 4H, *J* 4.9 Hz, OCH_2), 3.79–3.75 (m, 2H, OCH_2), 3.76 (dd, 3H, $J_{5,6}$ 10.7 Hz, H-6), 3.73 (s, 9H, OCH_3), 3.70–3.66 (m, 6H, OCH_2), 3.64–3.60 (m, 18H, OCH_2), 3.54 (d, 3H, *J* 16.0 Hz, CH_aS), 3.58–3.32 (m, 12H, CH_2CH_2N and CH_2CH_2N), 3.28 (d, 3H, *J* 16.0 Hz, CH_bS), 2.72 (dd, 3H, $J_{3e,3a}$ 12.7 Hz, $J_{3e,4}$ 4.6, H-3e), 2.16, 2.12, 2.02, 2.00 (4s, 36H, 4 OAc), 1.95 (dd, 3H, H-3a), 1.85 (s, 9H, NAc); ^{13}C NMR ($CDCl_3$) δ: 171.0, 170.7, 170.6, 170.6, 170.2, 170.0, 168.5, 168.2 (C═O), 152.2, 142.3, 124.9 (C_{ar}), 109.0 (C_{ar}-H), 82.1 (C-2), 73.9 (C-6), 72.3, 72.3, 70.7, 70.5, 70.5, 70.4, 70.2, 69.6, 69.5, 69.4, 69.4, 68.7 (C-4 and OCH_2), 67.9 (C-8), 67.0 (C-7), 62.3 (C-9), 53.1 (OCH_3), 52.2 (OCH_3), 49.1 (C-5), 39.6 (CH_2N), 37.3 (C-3), 32.4 (CH_2S), 23.1 (NAc), 21.3, 20.8, 20.8, 20.7 (4 OAc); FABMS: 2353 (M+1, 26%), 1879 (6), 1405 (2). Anal. calcd. for $C_{98}H_{146}N_6O_{53}S_3$: C 50.04, H 6.26, N 3.57; found: C 49.66, H 6.54, N 3.46.

*Methyl 3,4,5-tri-{8-[2-(methyl 5-acetamido-3,5-dideoxy-2-thio-*D*-glycero-*α*-*D*-galacto-2-nonulo-pyranosid)-acetamido]-3,6-dioxaoctyloxy}benzoate (**19**)*

The dendritic α-thiosialoside **17** (45 mg, 0.020 mmol) was dissolved in dry methanol (3 mL) and a 1 M solution NaOMe–MeOH (pH ~9) was added. The solution was stirred at room temperature for 45 min and then treated with H^+ resin (Amberlite IR-120). The filtrate was evaporated near dryness under reduced pressure and freeze-dried to afford a white powder in quantitative yield. $[\alpha]_D$ +16.3 (*c* 0.49, CH_3OH); ^{1}H NMR (CD_3OD) δ: 7.30 (s, 2H, H_{ar}), 4.24–4.14 (m, 6H, PhOCH_2), 3.94–3.34 (m, 69H, OCH_3, OCH_2, OCH_3, H-4, H-5, H-6, H-7, H-8, H-9, H-9′, CH_2S, and CH_2N), 2.70 (dd, 3H, H-3e), 1.94 (s, 9H, NAc), 1.74 (dd, 3H, H-3a); ^{13}C NMR (CD_3OD) δ: 175.0, 171.5, 171.2, 168.1 (C═O), 153.7, 143.7, 126.3 (C_{ar}), 109.9 (C_{ar}-H), 83.6 (C-2), 77.2 (C-6), 73.6, 71.8, 71.4, 70.8, 70.4, 70.1 (OCH_2), 72.1 (C-8), 70.1 (C-4), 68.8 (C-7), 64.8 (C-9), 53.8 (C-5), 53.6 (OCH_3), 52.8 (OCH_3), 41.8 (C-3), 40.8 (CH_2N), 33.5 (CH_2S), 22.7 (NAc).

*Methyl 3,4,5-tri-{11-[2-(methyl 5-acetamido-3,5-dideoxy-2-thio-*D*-glycero-*α*-*D*-galacto-2-nonulo-pyranosid)-acetamido]-3,6,9-trioxaundecyloxy}benzoate (**20**)*

Zemplén conditions as described above were applied to compound **18** to afford de-O-acetylated glycodendrimer **20** as a white foam (freeze-dried) in quantitative yield. $[\alpha]_D$ +14.4 (*c* 0.52, CH_3OH); ^{1}H NMR (CD_3OD) δ: 7.34 (s, 2H, H_{ar}),

© 1997 NRC Canada

Can. J. Chem. Downloaded from www.nrcresearchpress.com by 91.121.58.235 on 09/08/12
For personal use only.

4.25–4.11 (m, 6H, PhOCH_2), 3.88–3.85 (m, 9H, OCH_3, and PhOCH_2CH_2), 3.81–3.46 (m, 57H, OCH_2, H-4, H-5, H-7, H-8, H-9, H-9′, and OCH_3), 3.50–3.45 (m, 9H, H-6 and CH_2S), 3.40–3.35 (m, 6H, CH_2N), 2.76 (dd, 3H, $J_{3e,3a}$ 12.8 Hz, $J_{3e,4}$ 4.5, H-3e), 1.98 (s, 9H, NAc), 1.80 (dd, 3H, H-3a); ^{13}C NMR (CD_3OD) δ: 174.9, 171.4, 171.0, 168.0 (C═O), 153.6, 143.5, 126.2 (C_{ar}), 109.9 (C_{ar}-H), 83.5 (C-2), 77.1 (C-6), 73.5, 71.6, 71.5, 71.5, 71.2, 70.7, 70.2, 70.0 (OCH_2), 72.0 (C-8), 70.1 (C-4), 68.7 (C-7), 64.7 (C-9), 53.8 (C-5), 53.6 (OCH_3), 52.7 (OCH_3), 41.7 (C-3), 40.7 (CH_2N), 33.4 (CH_2S), 22.6 (NAc).

*3,4,5-Tri-{8-[2-(5-acetamido-3,5-dideoxy-2-thio-D-glycero-α-D-galacto-2-nonulo-pyranosid)-acetamido]-3,6-dioxaoctyloxy}benzoic acid (**21**)*

A solution of α-thiosialoside methyl ester **19** (33 mg, 0.019 mmol), dissolved in a mixture of methanol (2 mL) and 0.5 M NaOH (2 mL), was stirred at room temperature overnight. After treatment with H^+ resin, the filtrate was first evaporated to remove most of the methanol and then freeze-dried. The pure product was obtained in nearly quantitative yield as a yellowish oil. $[\alpha]_D$ +3.4 (*c* 0.5, CH_3OH); ^1H NMR (CD_3OD) δ: 7.36 (s, 2H, H_{ar}), 4.24–4.20 (m, 6H, PhOCH_2), 3.88–3.43 (m, 51H, OCH_2, H-4, H-5, H-6, H-7, H-8, H-9, H-9′, and CH_2S), 3.42–3.35 (m, 6H, CH_2N), 2.78 (dd, 3H, $J_{3e,3a}$ 12.2 Hz, $J_{3e,4}$ 4.3, H-3e), 1.99 (s, 9H, NAc), 1.81 (dd, 3H, H-3a); ^{13}C NMR (CD_3OD) δ: 175.2, 172.5, 171.2, 169.3 (C═O), 153.6, 143.7, 127.0 (C_{ar}), 110.1 (C_{ar}-H), 83.5 (C-2), 77.2 (C-6), 73.6, 71.8, 71.5, 71.3, 70.8, 70.1 (OCH_2), 72.5 (C-8), 70.3 (C-4), 69.0 (C-7), 64.5 (C-9), 53.6 (C-5), 42.0 (C-3), 40.8 (CH_2N), 33.7 (CH_2S), 22.7 (NAc).

*3,4,5-Tri-{11-[2-(5-acetamido-3,5-dideoxy-2-thio-D-glycero-α-D-galacto-2-nonulo-pyranosid)-acetamido]-3,6,9-trioxaundecyloxy}benzoic acid (**22**)*

The methyl esters hydrolysis of **20** was performed in the same manner as above to give a colorless oil after freeze-drying in quantitative yield. $[\alpha]_D$ +5.5 (*c* 0.56, CH_3OH); ^1H NMR (CD_3OD) δ: 7.35 (s, 2H, H_{ar}), 4.25–4.20 (m, 6H, PhOCH_2), 3.90–3.40 (m, 63H, OCH_2, H-4, H-5, H-6, H-7, H-8, H-9, H-9′, and CH_2S), 3.40–3.35 (m, 6H, CH_2N), 2.78 (dd, 3H, $J_{3e,3a}$ 12.6 Hz, $J_{3e,4}$ 4.3, H-3e), 1.99 (s, 9H, NAc), 1.82 (dd, 3H, H-3a); ^{13}C NMR (CD_3OD) δ: 175.1, 172.4, 171.1, 169.2 (C═O), 153.5, 143.5, 126.8 (C_{ar}), 110.1 (C_{ar}-H), 83.5 (C-2), 77.1 (C-6), 73.5, 71.6, 71.5, 71.4, 71.1, 70.7, 70.2, 69.9 (OCH_2), 72.4 (C-8), 70.0 (C-4), 68.9 (C-7), 64.5 (C-9), 53.5 (C-5), 41.8 (C-3), 40.6 (CH_2N), 33.6 (CH_2S), 22.6 (NAc).

*3,4,5-Tri-(11-azido-3,6,9-trioxaundecyloxy)benzoic acid (**23**)*

To a solution of methyl ester precursor **10** (170 mg, 0.215 mmol) in 95% EtOH (6 mL) was added 1 M KOH (400 μL). The reaction mixture was stirred and refluxed for 2 h after which time TLC showed complete hydrolysis of the ester. The solution was cooled to room temperature and neutralized with H^+ resin. The filtrate was concentrated under vacuum to afford 167 mg (quantitative yield) of pure acid **23** as a colorless residue. FTIR ν_{max} (cm^{-1}): 3009, 2903, 2109, 1690, 1587; ^1H NMR ($CDCl_3$) δ: 7.26 (s, 2H, H_{ar}), 4.15–4.10 (m, 6H, PhOCH_2), 3.83–3.78 (m, 6H, OCH_2), 3.66–3.57 (m, 30H, OCH_2), 3.31 (t, 6H, CH_2N_3); ^{13}C NMR ($CDCl_3$) δ: 169.7 (C═O), 152.0, 142.6, 124.4, 109.1 (C_{ar}), 72.2, 70.6, 70.4, 70.4, 69.8, 69.4, 68.6 (CH_2O), 50.4 (CH_2N_3); FABMS: 774 (M+1, 5 %), 746 (17).

*Methyl 3,4,5-tri-{11-[3,4,5-tri-(11-azido-3,6,9-trioxaundecyloxy)-benzamido]-3,6,9-trioxaundecyloxy}benzoate (**24**)*

To a solution of acid **23** (197 mg, 0.254 mmol) in a mixture of EtOH/CH_3CN (20 mL, 1:1 v/v) were added 1-hydroxybenzotriazole hydrate (HOBt, 52 mg, 0.381 mmol), trisamino precursor **12** (50 mg, 0.070 mmol), and diisopropylethylamine (DIPEA, Hünig's base, 89 μL). The mixture was stirred for 5 min under a nitrogen atmosphere after which 73 mg (0.381 mmol) of 1-(3-dimethylaminopropyl)-3-ethylcarbodiimide hydrochloride (EDC) was added. The suspension was stirred for 3 h at room temperature, the solvent was evaporated under vacuum, and the residue dissolved in $CHCl_3$. The organic layer was washed with saturated NH_4Cl, water, and brine, and dried over Na_2SO_4. The crude product was concentrated and purified by silica gel chromatography using 5% MeOH in CH_2Cl_2 as eluent to afford 174 mg (83%) of **24** as a colorless oil. FTIR ν_{max} (cm^{-1}): 3430, 3025, 2899, 2108, 1713, 1653, 1585; ^1H NMR ($CDCl_3$) δ: *7.24 (s, 2H, H_{ar}), 7.02 (s, 6H, $H_{ar'}$)*, 6.78–6.71 (m, 3H, NH), 4.15–4.10 (m, 24H, Ph′OCH_2 and PhOCH_2), 3.82 (s, 3H, OCH_3), 3.80-3.56 (m, 150H, OCH_2), 3.31 (m, 18H, CH_2N_3); ^{13}C NMR ($CDCl_3$) δ: 166.9, 166.5 (C═O), 152.5, 152.2, 142.5, 141.5, 129.7, 125.0 (C_{ar} and C'_{ar}), 109.1, 107.2 (C_{ar}-H and C'_{ar}-H), 72.4, 70.8, 70.7, 70.7, 70.6, 70.6, 70.5, 70.5, 70.2, 70.0, 69.8, 69.7, 68.6, 69.1, 68.8 (CH_2O and CH_2O'), 52.1 (OCH_3), 50.7 (CH_2N_3'), 39.9 (CH_2N).

*Methyl 3,4,5-tri-{11-[3,4,5-tri-(11-amino-3,6,9-trioxaundecyloxy)-benzamido]-3,6,9-trioxaundecyloxy}benzoate (**25**)*

Reduction of the nona-azide **24** was performed by the same method used to synthesize amino precursors **11** and **12**. Compound **25** was obtained by evaporation of the solvent and used without further purification for the next step. FTIR ν_{max} (cm^{-1}): 3358, 3243, 3042, 2896, 1716, 1647, 1582.

*Methyl 3,4,5-tri-{11-[3,4,5-tri-(11-(2-chloroacetamido)-3,6,9-trioxaundecyloxy)-benzamido]-3,6,9-trioxaundecyloxy}benzoate (**26**)*

The chloroacetylation was performed in the same manner as for compounds **13** and **14**. The oily residue was purified by preparative TLC plate to afford 70% yield of pure **26**. FTIR ν_{max} (cm^{-1}): 3344, 3035, 2903, 1717, 1670, 1558; ^1H NMR ($CDCl_3$) δ: 7.24 (s, 2H, H_{ar}), 7.08–6.95 (m, 18H, $H_{ar'}$, NH, and NH′), 4.30–4.13 (m, 24H, Ph′OCH_2 and PhOCH_2), 4.01, 4.01 (2s, 18H, CH_2Cl), 3.84 (s, 3H, OCH_3), 3.82-3.53 (m, 150H, OCH_2, OCH_2', and CH_2N), 3.47-3.43 (m, 18H, CH_2N'); ^{13}C NMR ($CDCl_3$) δ: 167.0, 166.5, 166.2 (C═O), 152.4, 152.2, 142.4, 141.2, 129.8, 125.1 (C_{ar} and C'_{ar}), 109.0, 107.2 (C_{ar}-H and C'_{ar}-H), 72.4, 70.7, 70.7, 70.6, 70.6, 70.5, 70.5, 70.5, 70.3, 70.2, 69.9, 69.7, 69.6, 69.4, 69.0, 68.8 (CH_2O and CH_2O'), 52.2 (OCH_3), 42.6 (CH_2N'), 39.9 (CH_2N), 39.6 (CH_2Cl).

*Methyl 3,4,5-tri-{11-[3,4,5-tri-O-[(methyl 5-acetamido-4,7,8,9-tetra-O-acetyl-3,5-dideoxy-2-thio-D-glycero-α-D-galacto-2-nonulo-pyranosid)-acetamido]-benzamido]-3,6,9-trioxaundecyl oxy}benzoate (**27**)*

Conjugation between α-thiosialoside **16** and chloroacetylated

© 1997 NRC Canada

Can. J. Chem. Downloaded from www.nrcresearchpress.com by 91.121.58.235 on 09/08/12
For personal use only.

monodendron **26** was performed under the same conditions described above for compounds **17** and **18**. The colorless oil obtained after silica gel chromatography was shown to be pure product **27** in 86% yield. $[\alpha]_D$ +19.0 (*c* 1.02, $CHCl_3$); ^1H NMR ($CDCl_3$) δ: 7.25 (s, 2H, H_{ar}), 7.07–7.03 (m, 9H, H'_{ar}, and NH), 6.89–6.83 (m, 9H, N′H), 5.66–5.55 (m, 9H, NH), 5.41 (m, 9H, H-8), 5.28 (dd, 9H, $J_{7,8}$ 9.0 Hz, H-7), 4.83 (ddd, 9H, $J_{3a,4}$ 11.4 Hz, $J_{3e,4}$ 4.6, H-4), 4.23 (dd, 9H, $J_{8,9'}$ 2.5 Hz, $J_{9,9'}$ 12.4, H-9′), 4.20–4.15 (m, 24H, PhOCH_2' and PhOCH_2), 4.06–4.00 (m, 18H, H-5 and H-9), 3.85 (s, 3H, OCH_3), 3.84–3.79 (m, 18H, OCH_2), 3.77–3.31 (m, 159H, OCH_2, OCH_2', CH_2N, CH_2N', and H-6), 3.71 (s, 27H, OCH_3), 3.54 (d, 9H, *J* 16.1 Hz, CH_aS), 3.27 (d, 9H, *J* 16.1 Hz, CH_bS), 2.71 (dd, 9H, $J_{3e,3a}$ 12.6 Hz, $J_{3e,4}$ 4.4, H-3e), 2.15, 2.11, 2.01, 1.99 (4s, 108H, 4 OAc), 1.93 (dd, 9H, H-3a), 1.85 (s, 27H, NAc); ^{13}C NMR ($CDCl_3$) δ: 171.1, 170.7, 170.3, 170.1, 168.6, 168.4, 167.0, 166.5, 166.2 (C═O), 152.4, 152.2, 142.4,, 141.4, 129.7, 125.0 (C_{ar} and C'_{ar}), 109.1, 107.4 (C_{ar}-H and C'_{ar}), 82.2 (C-2), 73.9 (C-6), 72.4, 70.7, 70.6, 70.5, 70.3, 69.7, 69.1 (CH_2O and CH_2O'), 69.5 (C-4), 68.0 (C-8), 67.0 (C-7), 62.4 (C-9), 53.2 (OCH_3), 52.3 (OCH_3), 49.2 (C-5), 39.7 (CH_2N'), 39.7 (CH_2N), 37.4 (C-3), 32.5 (CH_2S), 23.1 (NAc), 21.3, 20.8, 20.8, 20.8 (OAc).

Methyl 3,4,5-tri-{11-[3,4,5-tri-O-*[(methyl 5-acetamido-3,5-dideoxy-2-thio-*D*-glycero-*α*-*D*-galacto-2-nonulo-pyranosid)-acetamido]-benzamido]-3,6,9-trioxaundecyloxy}benzoate (**28**)*

De-O-acetylation of **27** was done by using the Zemplén conditions described earlier for compounds **19** and **20**. After neutralization with H^+ resin, the solution was concentrated, dissolved in H_2O, and freeze-dried to give a yellowish half-powder, half-syrup compound in 98% yield. $[\alpha]_D$ +12.9 (c 1.05, CH_3OH); ^1H NMR (CD_3OD) δ: 7.28 (s, 2H, H_{ar}), 7.18 (s, 6H, H'_{ar}), 4.25–4.15 (m, 24H, PhOCH_2' and PhOCH_2), 3.87 (s, 3H, OCH_3), 3.86–3.32 (m, 276H, OCH_2, OCH_2', CH_2N, CH_2N', CH_2S, OCH_3, H-4, H-5, H-6, H-7, H-8, H-9′, and H-9), 2.76 (dd, 9H, H-3e), 2.01 (s, 27H, NAc), 1.80 (dd, 9H, H-3a); ^{13}C NMR (CD_3OD) δ: 175.3, 171.5, 171.2, 169.4 (C═O), 153.8, 153.7, 143.1, 142.2, 130.6, 126.3 (C_{ar} and C'_{ar}), 109.9, 107.9 (C_{ar}-H and C'_{ar}), 83.7 (C-2), 77.1 (C-6), 72.1 (C-8), 73.7, 71.8, 71.7, 71.6, 71.3, 71.2, 70.8, 70.6, 70.3, 70.1 (CH_2O and CH_2O'), 70.2 (C-4), 68.8 (C-7), 64.8 (C-9), 53.9 (C-5), 53.8 (OCH_3), 53.0 (OCH_3), 41.8 (C-3), 41.2 (CH_2N), 40.9 (CH_2N'), 33.6 (CH_2S), 22.7 (NAc).

3,4,5-Tri-{11-[3,4,5-tri-O-*[(5-acetamido-3,5-dideoxy-2-thio-*D*-glycero-*α*-*D*-galacto-2-nonulo-pyranosid)-acetamido]-benzamido]-3,6,9-trioxaundecyloxy}benzoate (**29**)*

The hydrolysis of the methyl esters on compound **28** was accomplished by treatment with NaOH as described earlier for the sialosylated glycodendrimers **21** and **22**. The yellowish residue was obtained after freeze-drying in nearly quantitative yield. $[\alpha]_D$ +5.2 (*c* 0.5, CH_3OH); ^1H NMR (CD_3OD) δ: 7.30 (s, 2H, H_{ar}), 7.18 (s, 6H, H'_{ar}), 4.25–4.12 (m, 24H, PhOCH_2' and PhOCH_2), 3.94–3.33 (m, 249H, OCH_2, OCH_2', CH_2N, CH_2N', CH_2S, H-4, H-5, H-6, H-7, H-8, H-9′, and H-9), 2.78 (dd, 9H, $J_{3e,4}$ 4.4 Hz, H-3e), 2.01 (s, 27H, NAc), 1.82 (dd, 9H, H-3a); ^{13}C NMR (CD_3OD) δ: 175.3, 172.4, 171.2, 169.5 (C═O), 153.7, 153.6, 143.7, 142.2, 130.6, 126.9 (C_{ar} and C'_{ar}), 110.3, 107.9 (C_{ar}-H and C'_{ar}), 83.6 (C-2), 77.2 (C-6), 72.5 (C-8), 73.7, 71.8, 71.7, 71.6, 71.5, 71.3, 70.8, 70.6, 70.3, 70.0 (CH_2O and CH_2O'), 70.1 (C-4), 69.0 (C-7), 64.6 (C-9), 53.7 (C-5), 42.0 (C-3), 41.2 (CH_2N), 40.8 (CH_2N'), 33.8 (CH_2S), 22.7 (NAc).

Turbidimetric analysis

Turbidimetric experiments were performed in Linbro (Titertek) microtitration plates where 50 μL of stock lectin solutions prepared from WGA (4 mg/mL PBS) were mixed with 12.5, 11.2, and 10.6 μL of glycodendrimer solutions **29**, **22**, and **21**, respectively (0.5 mg/mL PBS). Also, 25 μL of *L. flavus* lectin solution (2 mg/mL PBS) was mixed with 6.25 μL of 9-mer **29** (0.5 mg/mL PBS). The turbidity of the solutions was monitored by reading the optical density at 490 nm for 2 h.

Acknowledgements

The financial support of the Natural Sciences and Engineering Research Council of Canada (NSERC) is gratefully acknowledged. S.J.M. is also thankful to NSERC and Le Fonds pour la formation de chercheurs et l'aide à la recherche (FCAR) for postgraduate scholarships. We thank Dr. Clem Kazakoff for recording mass spectra and Dr. Glenn Facey and Mr. Raj Capoor for recording NMR spectra. A generous gift of sialic acid from Dr. M. Kawase of NGK Insulators, Ltd. (Handa, Japan) is particularly acknowledged.

References

1. K.A. Karlsson. Curr. Opin. Struct. Biol. **5**, 622 (1995).
2. N. Sharon. FEBS Lett. **217**, 145 (1987).
3. J. Beuth, H.L. Ko, G. Pulverer, G. Uhlenbruck, and H. Pichlmaier. Glycoconjugate J. **12**, 1 (1995).
4. (*a*) R. Roy. Curr. Opin. Struct. Biol. **6**, 692 (1996); (*b*) R. Roy. Topics Curr. Chem. **187**, 241 (1997); (*c*) R. Roy. *In* Modern methods in carbohydrate synthesis. *Edited by* S.H. Khan and R. O'Neil. Harwood Academic Publishers, Amsterdam, The Netherlands. 1996. pp. 378–402; (*d*) R. Roy. *In* Carbohydrates: targets for drug design. *Edited by* Z.J. Witczak. Marcel Dekker, New York. 1997. pp. 84–136; D. Zanini and R. Roy. *In* Carbohydrate mimics: concepts and methods. *Edited by* Y. Chapleur. Verlag Chemie, Weinheim, Germany. 1997. In press.
5. (*a*) Y.C. Lee and R.T. Lee. Acc. Chem. Res. **28**, 321 (1995), and ref. cited therein; (*b*) R.T. Lee and Y.C. Lee. Glycoconjugate J. **4**, 317 (1987); (*c*) A. Kichler and F. Schuber. Glycoconjugate J. **12**, 275 (1995); (*d*) G. D. Glick and J.R. Knowles. J. Am. Chem. Soc. **113**, 4701 (1991); (*e*) G.D. Glick, P.L. Toogood, D.C. Wiley, J.J. Skehel, and J.R. Knowles. J. Biol. Chem. **266**, 23660 (1991); (*f*) C. Unverzagt, S. Kelm, and J.C. Paulson. Carbohydr. Res. **251**, 285 (1994); (*g*) G. Kretzschmar, U. Sprengard, H. Kunz, E. Bartnik, W. Schmidt, A. Toepfer, B. Hörsch, M. Krause, and D. Seiffge. Tetrahedron, **51**, 13015 (1995).
6. (*a*) R. Roy. Trends Glycosci. Glycotechnol. **8**, 79 (1996); (b) R. Roy. *In* Carbohydrate chemistry. *Edited by* G.J. Boons. Chapman & Hall, U.K. 1997. In press.
7. (*a*) R. Duncan and J. Kopecek. Adv. Polym. Sci. **57**, 51 (1984); (*b*) M. Monsigny, A.-C. Roche, P. Midoux, and R. Mayer. Adv. Drug Delivery Rev. **14**, 1 (1994).
8. (*a*) L. de Robertis, C. Lancelon-Pin, H. Driguez, F. Attioui, R. Bonaly, and A. Marsura. Bioorg. Med. Chem. Lett. **4**, 1127 (1994); (*b*) V. Lainé, A. Coste-Sarguet, A. Gadelle, J. Defaye, B. Perly, and F. Djedaïni-Pilard. J. Chem. Soc. Perkin Trans. 2, 1479 (1995).
9. (*a*) S.J. Meunier and R. Roy. Tetrahedron Lett. **37**, 5469 (1996); (*b*) A. Marra, M.-C. Scherrmann, A. Dondoni, A. Casnati, P. Minari, and R. Ungaro. Angew. Chem. Int. Ed. Engl. **33**, 2479

© 1997 NRC Canada

(1994); (c) A. Marra, A. Dondoni, and F. Sansone. J. Org. Chem. **61**, 5111 (1996).
10. S.A. DeFrees, W. Kosch, W. Way, J.C. Paulson, S. Sabesan, R.L. Halcomb, D.-H. Huang, Y. Ichikawa, and C.-H. Wong. J. Am. Chem. Soc. **117**, 66 (1995).
11. R. Roy. Polym. News, **21**, 226 (1996).
12. (*a*) R. Roy, D. Zanini, S. J. Meunier, and A. Romanowska. ACS Symp. Ser. **560**, 104 (1994); (*b*) R. Roy, D. Zanini, S. J. Meunier, and A. Romanowska. J. Chem. Soc. Chem. Commun. 1869 (1993); (*c*) D. Zanini, W.K.C. Park, and R. Roy. Tetrahedron Lett. **36**, 7383 (1995).
13. (*a*) D. Zanini and R. Roy. J. Org. Chem. **61**, 7348 (1996); (b) J. Am. Chem. Soc. **119**, 2088 (1997).
14. R. Roy, W.K.C. Park, Q. Wu, and S.-N. Wang. Tetrahedron Lett. **36**, 4377 (1995).
15. (*a*) D. Pagé, D. Zanini, and R. Roy. Bioorg. Med. Chem. **4**, 1949 (1996); (*b*) K. Aoi, K. Itoh, and M. Okada. Macromolecules, **28**, 5391 (1995); (*c*) T. Toyokuni and A.K. Singhal. Chem. Soc. Rev. 231 (1995); (*d*) T.K. Lindhorst and C. Kieburg. Angew. Chem. Int. Ed. Engl. **35**, 1953 (1996); (*e*) D. Pagé, S. Aravind, and R. Roy. Chem. Commun. 1913 (1996).
16. W.K.C. Park, S.J. Meunier, D. Zanini, and R. Roy. Carbohydr. Lett. **1**, 179 (1995).
17. J.M. Singer, J. Hengevels, S.C. Edberg, J.W.T. Lichtenbelt, and P.H. Wiersema. Immunol. Commun. **6**, 517 (1977).
18. B.P. Peters, S. Ebisu, I.J. Goldstein, and M. Flashner. Biochemistry, **24**, 5505 (1979).
19. R. N. Knibbs, S. E. Osborne, G. D. Glick, and I. J. Goldstein. J. Biol. Chem. **268**, 18524 (1993).
20. C.F. Brewer. Chemtracts: Biochem. Mol. Biol. **6**, 165 (1996).

Can. J. Chem. Downloaded from www.nrcresearchpress.com by 91.121.58.235 on 09/08/12
For personal use only.

© 1997 NRC Canada

Morphological, chemical, and electrochemical properties of Ti/(TiO_2 + IrO_2) electrodes

L.A. da Silva, V.A. Alves, M.A.P. da Silva, S. Trasatti, and J.F.C. Boodts

Abstract: Electrodes of general composition $Ir_xTi_{(1-x)}O_2$ with $0.2 \leq x \leq 1.0$ were prepared on a Ti support by calcination of the chlorides at 450°C. Ex situ and in situ characterization included the use of techniques such as scanning electron microscope (SEM), energy dispersive X-ray analysis (EDX), cyclic voltammetry (CV), and electrochemical impedance spectroscopy (EIS). EDX showed a surface enrichment with Ti. The voltammetric charge was found to go through a maximum at 60% IrO_2. O_2 evolution was studied in 1.0 mol dm^{-3} $HClO_4$ by determining Tafel slopes and impedance parameters. Tafel slopes were found to vary between 40 and 60 mV depending on the overpotential range and the oxide composition. Solution and film resistance, film and double layer capacitance, and charge transfer resistance were determined as a function of potential and oxide composition. A reaction mechanism has been proposed. Separation of geometric and electronic effects has been attempted.

Key words: oxygen evolution, oxide electrode, electrocatalysis, electrochemical impedance spectroscopy, iridium dioxide.

Résumé : Procédant par calcination des chlorures à 450°C, on a préparé des électrodes de composition générale $Ir_xTi_{(1-x)}O_2$, avec $0,2 \leq x \leq 1,0$, sur un support de Ti. Les caractérisations ex situ et in situ ont fait appel à des techniques telles que le microscope à balayage électronique, l'analyse de rayons X à dispersion d'énergie (XDE), la voltammétrie cyclique (VC) et la spectroscopie d'impédance électrochimique (SIE). La XDE montre que la surface est enrichie en Ti. On a trouvé que la charge voltammétrique passe par un maximum à 60% d'IrO_2. On a étudié l'évolution du O_2 dans du $HClO_4$ à 1,0 mol/dm^3 en déterminant les pentes de Tafel et les paramètres d'impédance. On a trouvé que les pentes de Tafel varient entre 40 et 60 mV suivant la surtension et la composition de l'oxyde. On a déterminé la résistance en solution et du film, la capacitance du film et de la double couche ainsi que la résistance au transfert de charge en fonction du potentiel et de la composition de l'oxyde. On propose un mécanisme réactionnel. On a essayé de séparer les effets géométriques et électroniques.

Mots clés : évolution de l'oxygène, électrode en oxyde métallique, électrocatalyse, spectroscopie d'impédance électrochimique, dioxyde d'iridium.

[Traduit par la rédaction]

Can. J. Chem. Downloaded from www.nrcresearchpress.com by 91.121.58.235 on 09/08/12
For personal use only.

Introduction

IrO_2 possesses metallic conductivity, catalytic activity, and chemical stability, especially in acids; for this reason it has found application as an anode and cathode material. Its activity for oxygen evolution is lower than that of RuO_2 (1), whereas as a cathode it evolves hydrogen at lower overpotentials than RuO_2 (2). As an anode material it is more stable than RuO_2 and, mixed with the latter, lowers its dissolution rate (3). In turn, IrO_2 is further stabilized either by TiO_2 (4) or Ta_2O_5 (5).

Despite the interest for their potential use as anodes in oxygen evolution, IrO_2 + TiO_2 oxide electrodes have not been investigated exhaustively (6-9). In particular, investigations of the activity-structure correlation are scanty (10, 11) and mainly focused on stability, while mechanistic studies of oxygen evolution are almost nonexistent (12).

Electrochemical impedance has recently received much attention as a technique capable of providing complementary information with respect to more classical methods. However, its application to the study of oxide electrodes is still progressing slowly. In a previous paper (13) we reported on a study of oxygen evolution on an electrode with the specific composition $Ir_{0.3}Ti_{0.7}O_2$. The aim of the present work has been to investigate the relationship between structure and electrocatalytic activity in the case of IrO_2 + TiO_2 mixtures over the whole composition range, using oxygen evolution as a model electrocatalytic reaction. In turn, these data can contribute to a broader understanding of the electrocatalysis of mixed oxides during the course of the oxygen evolution reaction. Surface and electrochemical properties have been studied by both ex situ (SEM, EDX) and in situ (impedance, cyclic voltammetry, quasi-stationary polarization) spectroscopic and electrochemical techniques.

Received February 28, 1997.

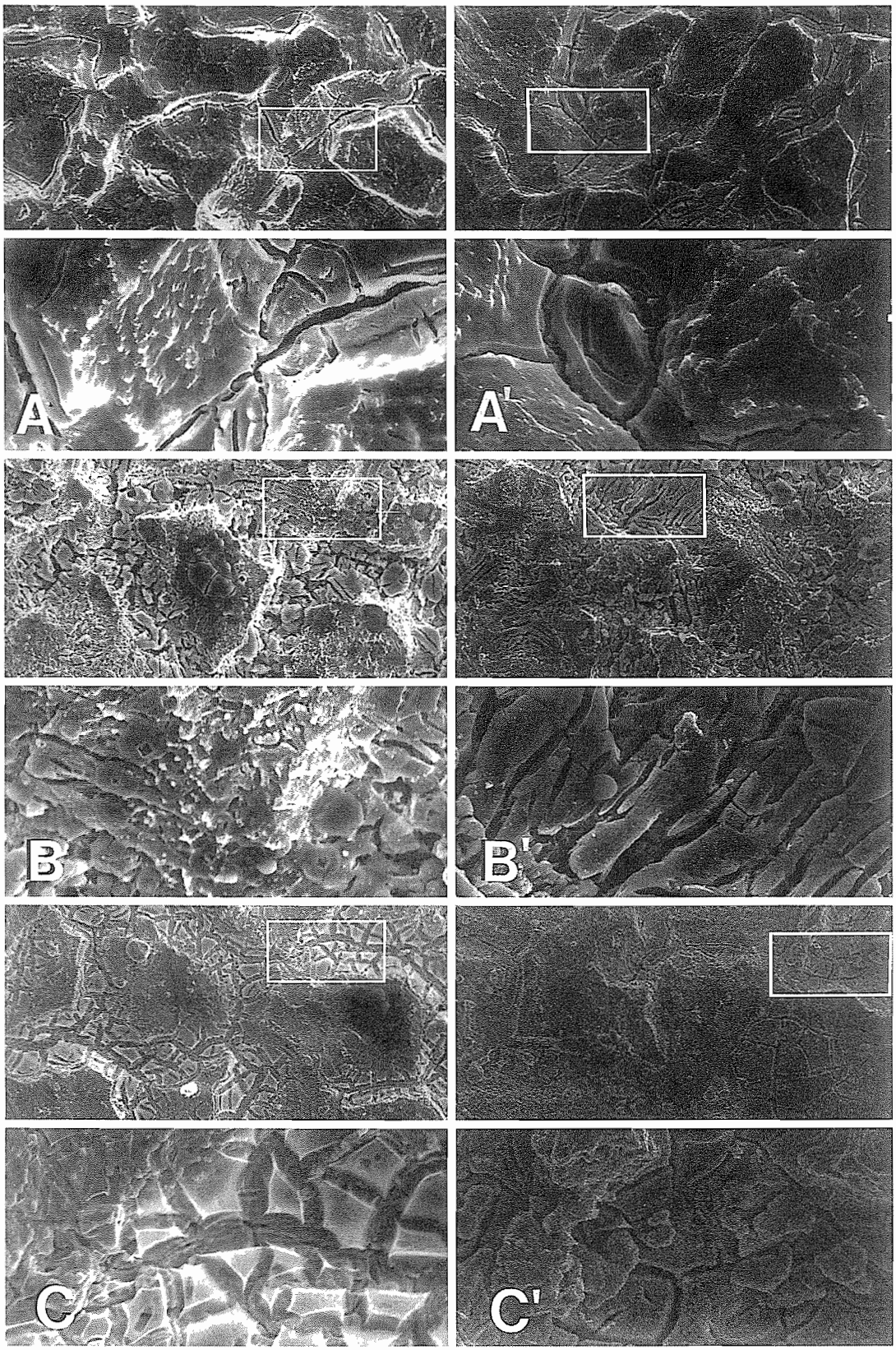
This paper is dedicated to Professor Brian E. Conway on the occasion of his 70th birthday and in recognition of his outstanding contributions to electrochemistry.

L.A. da Silva and V.A. Alves. Instituto de Quìmica de São Carlos, Universidad de São Paulo, São Carlos, Brazil.
M.A.P. da Silva. Instituto de Fisica de São Carlos, Universidade de São Paulo, Carlos, Brazil.
S. Trasatti.[1] Department of Physical Chemistry and Electrochemistry, University of Milan, Via Venezian 21, 20133 Milan, Italy.
J.F.C. Boodts. Departamento de Quìmica, Universidade de São Paulo, Riberão Preto, SP, Brazil.

[1] Author to whom correspondence may be addressed. Telephone: +39.2.26603223. Fax: +39.2.26603224. E-mail: trasatti@icil64.cilea.it

© 1997 NRC Canada

Fig. 1. SEM micrographs of $Ir_xTi_{(1-x)}O_2$ layers calcined at 450°C. (*A*)–(*C*): As prepared; (*A′*)–(*C′*): after the study on O_2 evolution. (*A*), (*A′*): $x = 0.2$; (*B*), (*B′*): $x = 0.6$; (*C*), (*C′*): $x = 1.0$. The lower parts of the micrographs are enlargements (×4) of the area enclosed in the rectangle in the upper part.



Can. J. Chem. Downloaded from www.nrcresearchpress.com by 91.121.58.235 on 09/08/12
For personal use only.

© 1997 NRC Canada

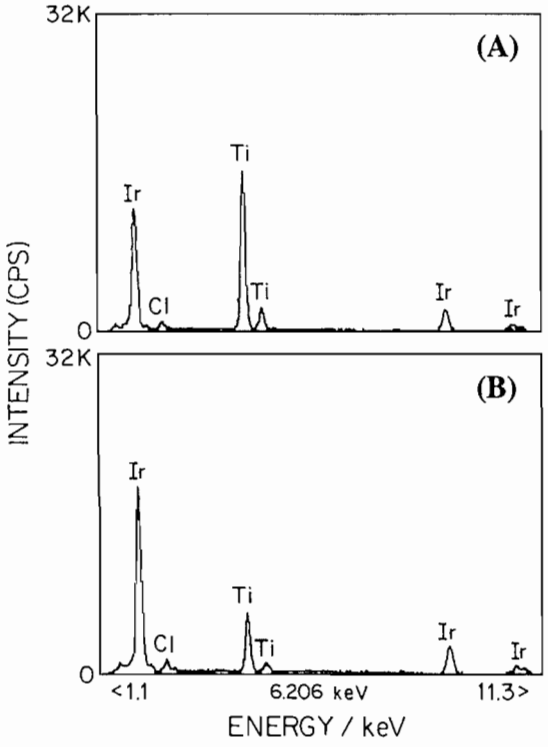
Can. J. Chem. Downloaded from www.nrcresearchpress.com by 91.121.58.235 on 09/08/12
For personal use only.

Table 1. Ir/Ti ratio of the EDX signal as a function of the composition of the IrO_2+TiO_2 system.

Composition (mol% Ir)	Ir/Ti ratio			
	Nominal ratio	Total	Dark area	Bright area
20	0.25	0.19	0.13–0.16	0.32
40	0.67	0.45	0.43–0.47	0.92
60	1.50	0.80	0.76	3.02–3.17
80	4.00	1.50	1.50	2.40–3.00
100[a]	—	4.80	3.30[b]	24.00
	—	(3.3)[c]	(3.9)	(4.80)

[a]A small Ti signal is observed.
[b]Inside a crack.
[c]Intensity of the Ir signal.

Fig. 2. EDX spectra of a $Ir_{0.6}Ti_{0.4}O_2$ layer. (*A*) Taken in dark areas; (*B*) taken in bright areas.



Experimental

Mixed oxides of general composition $Ir_xTi_{(1-x)}O_2$ ($0.2 \leq x \leq 1.0$) were deposited on a Ti support by the thermal decomposition at 450°C of appropriate mixtures of the chlorides dissolved in 1:1 (v/v) concentrated HCl + water solutions to avoid hydrolysis. Details have been provided in a previous paper (14). The oxide loading was such as to correspond to a nominal thickness of 2 μm. Mixtures at IrO_2 content lower than 20 mol% were not used since the properties are then dominated by TiO_2.

SEM micrographs and EDX spectra were obtained with a Zeiss DSM 960 scanning electron microscope equipped with a Link Analytical model QX 2000 microanalyser. The electron energy used was 20 keV.

The electrochemical surface properties were investigated by cyclic voltammetry at 20 mV s^{-1} in the potential range 0.4–1.4 V vs. RHE in 1 mol dm^{-3} $HClO_4$ aqueous solutions. Polarization (E vs. log j) curves were recorded under quasi-stationary conditions (0.056 mV s^{-1}) following a conventional methodology (14). The electrode potential was measured, and is reported (unless otherwise stated), against a hydrogen electrode in the same solution (RHE).

Electrochemical impedance spectra were taken in two distinct potential regions: *(a)* 0.4–1.4 V vs. RHE, where no stationary electrode reaction takes place, and *(b)* 1.4–1.6 V vs. RHE where oxygen is liberated. At fixed potentials, frequencies were scanned in the range 5 mHz – 100 kHz. The multi-sine method was used in the low-frequency range (5 mHz – 10 Hz), while the single-sine method was used in the high-frequency range (10 Hz – 100 kHz). The ac signal was generated by a PARC model 5210 lock-in amplifier.

Electrochemical measurements were carried out using a PARC model 273A potentiostat controlled by a model 55SX PS2 IBM microcomputer. All instruments were connected to a common ground, while the electrochemical cell was placed in a Faraday cage.

Results and discussion

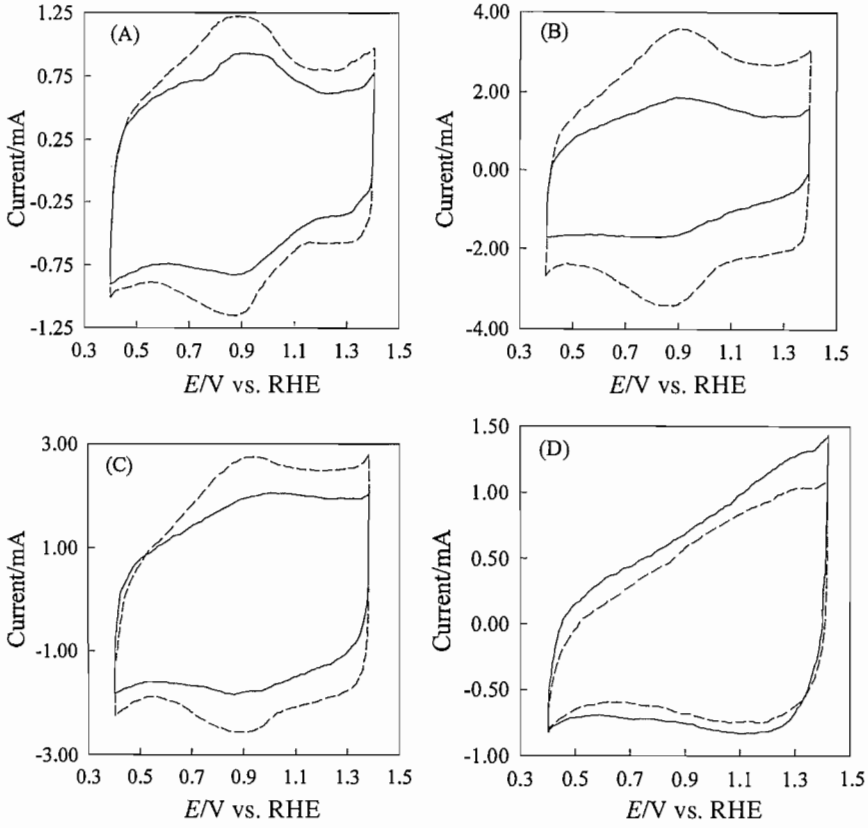
Morphology and chemical composition

Figure 1 shows some representative SEM micrographs. As-prepared layers with IrO_2 contents of 20, 60, and 100 mol% are shown in Figs. 1*A*–1*C*, respectively. IrO_2 + TiO_2 mixtures consist of a large number of small crystallites separated by micro-cracks imparting a very rough texture to the oxide layer. The density of the small crystallites appears to be a function of the oxide composition going through a maximum at 40–60 mol% IrO_2.

A distinct picture is observed with as-prepared pure IrO_2 (Fig. 1*C*, upper part). The oxide layer contains large islands, formed by smaller crystallites, separated by much larger cracks than for the oxide mixtures. This morphology has been described as "cracked mud" structure (15). The magnified view of Fig. 1*C* (lower part) shows that the cracked-mud structure is superimposed on a more homogenous oxide layer. Comparison of the micrograph for the bare Ti support with those for the oxide layers reveals that the edges of the large oxide islands roughly follow the contours of the Ti crystallites.

© 1997 NRC Canada

Fig. 3. Cyclic voltammograms at 20 mV s^{-1} in 1.0 mol dm^{-3} $HClO_4$ of $Ir_xTi_{(1-x)}O_2$ electrodes. (*A*) $x = 0.2$; (*B*) $x = 0.4$; (*C*) $x = 0.6$. (*D*) $x = 1.0$. Curves were recorded (——) with fresh electrodes and (-----) after the study on O_2 evolution.



Micrographs were again taken at the end of the study after intense oxygen evolution. The maximum current experienced by the electrodes during polarization curves was about 50 mA cm^{-2}. Some representative micrographs are shown in Figs. 1*A*′–1*C*′ for the same oxide compositions as for fresh electrodes. No appreciable modifications are visible for binary oxides. However, in the case of pure IrO_2, the heavily cracked outer part of the oxide layer is removed with exposure of the underlying, more compact part. This is indicative of mechanical erosion of the outer layer in the absence of TiO_2, which acts as a stabiliser.

EDX analysis was carried out on the samples subjected to oxygen evolution. Experimental conditions were set to minimize the penetration of the radiation (~0.6 μm, one third of the nominal thickness of the layer). Spectra were recorded both at low SEM magnification to obtain an analysis of the average composition, and at high magnification for local analysis of selected regions of the oxide layers. Special attention was given to the analysis of bright and dark areas of the SEM micrographs.

Typical EDX spectra are shown in Fig. 2. The Ir/Ti peak intensity ratios are summarized in Table 1 as a function of oxide composition. In the bright areas the much higher Ir/Ti ratio indicates enrichment with IrO_2 (with respect to the total average composition). Such segregation seems to be a specific feature of IrO_2 since it has already been observed by us in other multi component systems such as $IrO_2 + TiO_2 + PtO_x$ (16) and $IrO_2 + TiO_2 + CeO_2$ (17). Similar behaviour has been observed by Rolewicz et al. (18) with the $IrO_2 + Ta_2O_5$ system.

It is interesting that, even for pure IrO_2, regions can be found with different Ir signal intensity, thus suggesting a possible variation of IrO_2 density in different places. Moreover, a Ti signal was also unexpectedly observed also in the EDX spectra of pure IrO_2. This can be explained in terms of the preparative methodology, if the strongly acidic solvent of the precursors can attack the Ti support and thus bring some Ti species into the precursor solution.

Comparison of the average Ir/Ti ratio with the nominal one reveals that the former is systematically lower. This can be understood as a consequence of IrO_2 segregation to some specific regions, producing an average surface enrichment with TiO_2. This is in the end the origin of the higher chemical and electrochemical stability of $IrO_2 + TiO_2$ mixtures with respect to pure IrO_2. Surface enrichment with the valve metal oxide has also been observed in the case of $RuO_2 + TiO_2$ (19), $RuO_2 + ZrO_2$ (20), and $IrO_2 + Ta_2O_5$ (21). This is presumably a consequence of the higher affinity of the valve metal for oxygen in the atmosphere of the calcination room.

As-prepared electrodes contain some Cl species; this is not unexpected in view of the nature of the precursors (15). However, at the end of this study, i.e., after intense oxygen evolution, the Cl signal was no longer present. Cl species probably trapped in the layer are apparently pushed away during oxygen evolution.

Voltammetric curves

Figure 3 shows typical voltammetric curves at different oxide compositions for fresh electrodes as well as after intense oxy-

Can. J. Chem. Downloaded from www.nrcresearchpress.com by 91.121.58.235 on 09/08/12
For personal use only.

© 1997 NRC Canada

Can. J. Chem. Downloaded from www.nrcresearchpress.com by 91.121.58.235 on 09/08/12
For personal use only.

Fig. 4. Voltammetric charge, q^*, as a function of $IrO_2 + TiO_2$ oxide composition. (■) Fresh electrodes; (▲) after the O_2 evolution study.

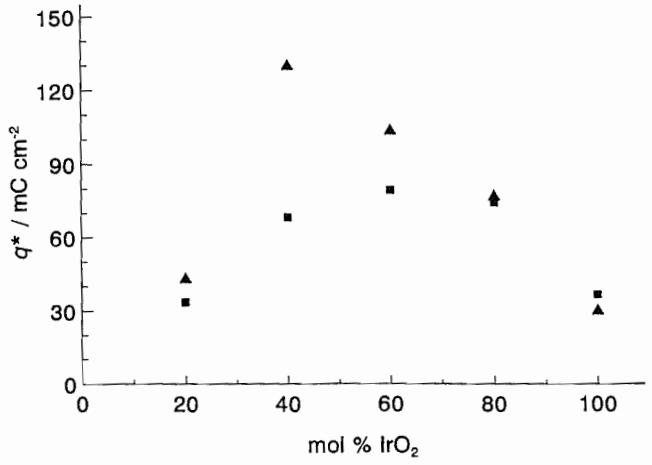


Table 2. Tafel slopes, as a function of composition and overpotential, obtained after correction of the data for ohmic drop. Supporting electrolyte: 1.0 mol dm^{-3} $HClO_4$.

	Tafel slope, *b* (mV)	
Mol% IrO_2	Low overpotential	High overpotential
20	37	59
40	36	56
60	42	53
80	51	58
100	58	58

gen evolution. All curves are rather featureless although a distinct broad peak is evident at the lower IrO_2 content. This peak can be attributed to a surface redox transition related to Ir sites (22). The peak potential is seen to move from <0.9 V at 20% IrO_2 to ca. 1.1 V at 80% IrO_2 (not shown in Fig. 3). No distinct peak is present in the curve for pure IrO_2 although a shoulder is apparent just prior to O_2 evolution. The shift of the redox peak can be understood (23) in terms of the electronic interaction between IrO_2 and TiO_2, the latter drawing the potential to less positive values, this being the main origin of IrO_2 stabilization.

Oxygen evolution produces two effects: *(a)* a variation in the size of the curves, and *(b)* a variation in the shape of the curve. In particular, the size increases at IrO_2 contents <80%, while it decreases for pure IrO_2. Also, at the IrO_2 contents showing a developed redox peak, oxygen evolution produces a better resolution of the peak itself. A higher current and a better resolved peak can be understood in terms of surface enrichment with IrO_2 as a consequence of a possible disruption of the TiO_2-rich surface layer. In other words, regions characterized by a higher IrO_2 concentration are exposed. In the case of pure IrO_2, the decrease in curve size can be explained with the SEM observation of a collapse of the surface islands, replaced by more compact regions. Thus, SEM and CV results converge to provide the same structural picture.

Fig. 5. Typical Tafel plot for O_2 evolution on a $Ir_{0.6}Ti_{0.4}O_2$ electrode in 1.0 mol dm^{-3} $HClO_4$. (■) Forward scan; (□) backward scan; (×) backward scan with *IR* correction; (-----) theoretical Tafel lines.

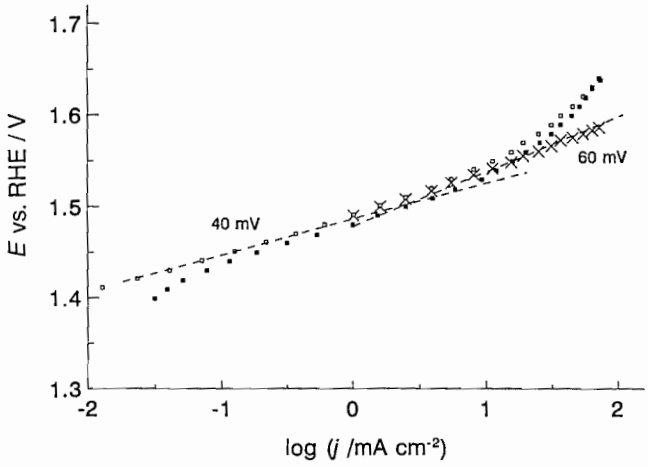
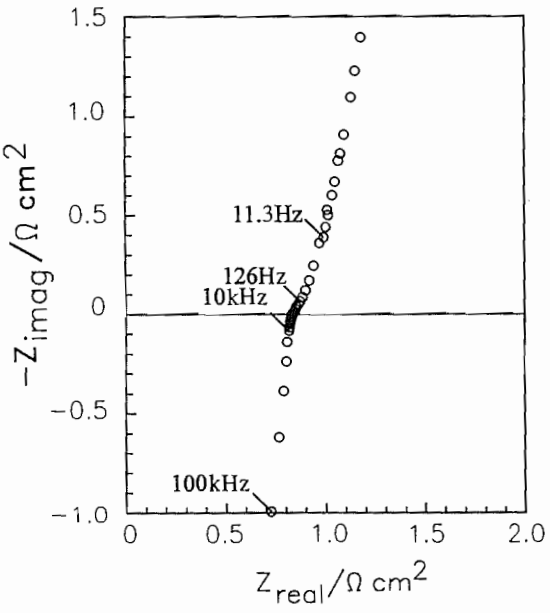


Fig. 6. Complex plane plot of the impedance of a $Ir_{0.6}Ti_{0.4}O_2$ electrode in 1 mol dm^{-3} $HClO_4$. E = 1.0 V vs. RHE.



Voltammetric charge

The voltammetric charge was obtained by integration of the voltammetric curves, and is plotted as a function of oxide composition in Fig. 4. The only processes occurring in the 0.4–1.4 V potential range are the surface redox transitions of Ir species and double-layer charging at the oxide-solution interface. Since the latter is as a rule small compared to the former, q^* measures the number of surface active sites. This is different from the concept of surface area that also includes Ti-containing sites, but it can be defined as proportional to the *electrochemically active* surface area (24).

Figure 4 shows that for fresh electrodes q^* goes through a maximum at about 60 mol% IrO_2. Considering that q^* is due only to Ir sites, one should expect a steady increase of charge with IrO_2 content. The non-monotonic behaviour indicates the presence of two contrasting effects: *(i)* an increase in IrO_2 sur-

© 1997 NRC Canada

Can. J. Chem. Downloaded from www.nrcresearchpress.com by 91.121.58.235 on 09/08/12
For personal use only.

Fig. 7. Bode plots of the impedance of $Ir_xTi_{(1-x)}O_2$ electrodes in 1 mol dm^{-3} $HClO_4$. E = 1.5 V vs. RHE. (*A*) x = 0.2; (*B*) x = 0.6; (*C*) x = 1.0. (○, □) Experimental data; (+) simulated data.

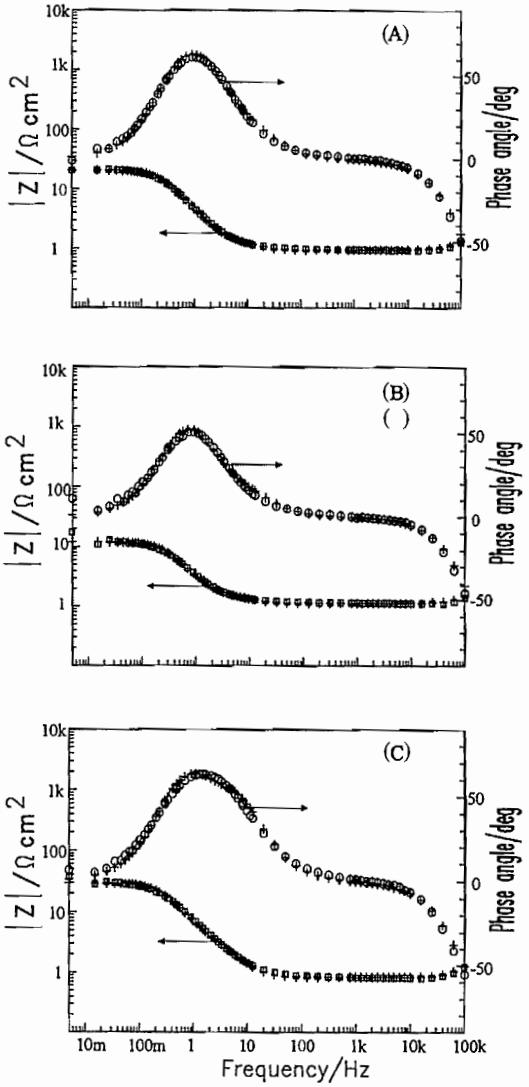
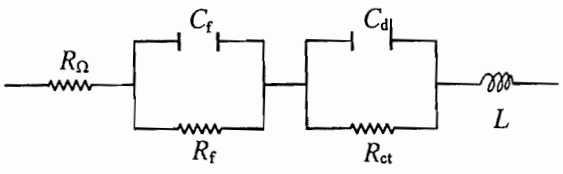


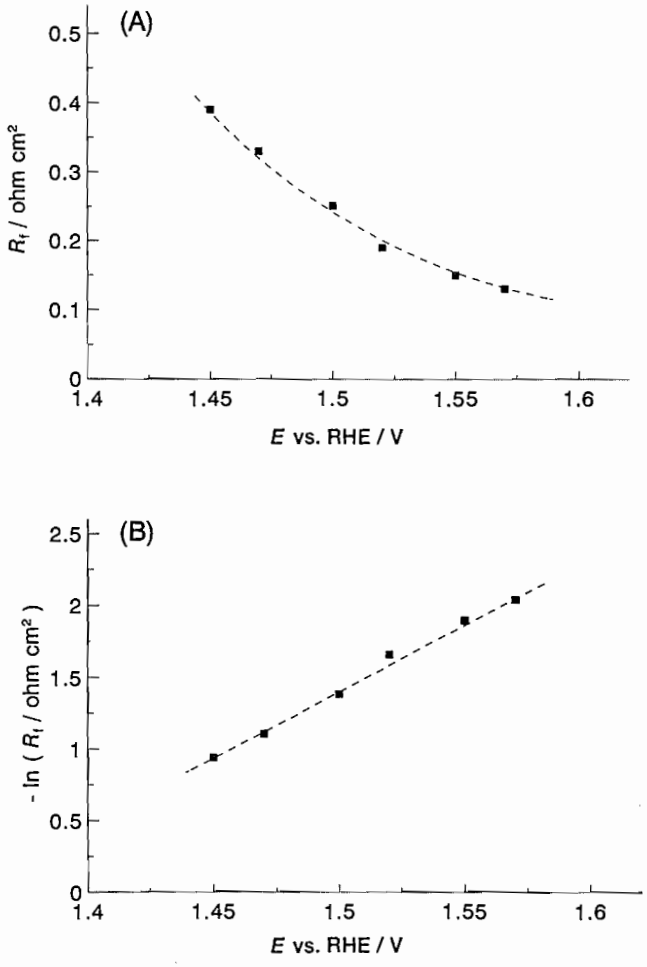
Fig. 8. Scheme of the equivalent circuit used to fit the experimental impedance data. For the meaning of the symbols, see text.



face concentration and *(ii)* a decrease in surface porosity joined with an increase in crystallite size. These two effects are clearly identifiable in the data of Table 1 (EDX data) and of Fig. 1 (SEM micrographs).

Oxygen evolution produces a large increase in q^* in the composition range 20–60% IrO_2. No change is visible at 80% IrO_2, while q^* decreases for pure IrO_2. An explanation has already been offered in the previous section. The variation of q^* is especially dramatic at 40% IrO_2.

Fig. 9. (*A*) Film resistance, R_f, and (*B*) ln R_f as a function of the electrode potential for a $Ir_{0.6}Ti_{0.4}O_2$ electrode.



Tafel lines

Figure 5 shows a typical polarization curve. Only a small hysteresis is visible between up and down runs. The kinetic analysis was carried out using the backward set of data.

For all compositions the deviation from linearity observed at high overpotentials was analysed with the method proposed by Shub et al. (25, 26). The deviations were found to be due to both uncompensated ohmic drop and change in Tafel slope. The only exception is pure IrO_2, for which a single Tafel line was found over the whole current range explored. The uncompensated resistance turned out to be in the range 0.5–0.8 ohm, which suggests it may be due to the solution between the tip of the Luggin capillary and the electrode surface.

Tafel slopes as a function of oxide composition are summarized in Table 2. It is interesting that the average Tafel slope is 40 mV at low current densities and 60 mV at higher overpotentials. However, as the composition approaches pure IrO_2 the Tafel line reduces to just one of nominally 60 mV. Although the difference between the two Tafel slopes is small, it seems real since it has been confirmed by impedance measurements. Tafel slopes close to 60 mV have already been reported for pure IrO_2 in acid solution (1, 27). However, this value is typical of freshly prepared layers; actually, aged electrodes have been found (28) to evolve oxygen with a Tafel

© 1997 NRC Canada

e 3. Electrochemical parameters obtained by fitting the experimental data to an $R_\Omega(R_fC_f)(R_{ct}C_{dl})L$ equivalent circuit. Potentials ized in the OER region. Supporting electrolyte: 1.0 mol dm^{-3} $HClO_4$.

ol% IrO_2	E (V)	R_Ω (Ω cm^2)	R_f (Ω cm^2)	C_f (mF cm^{-2})	C_{dl} (mF cm^{-2})	R_{ct} (Ω cm^2)	j (mA cm^{-2})	b^a (mV)
	1.45	0.95	0.37	73.7	35.2	282.1	0.06	39
	1.47	0.96	0.33	72.9	35.7	84.9	0.20	39
20	1.50	0.95	0.23	57.3	36.4	19.4	1.24	55
	1.52	0.95	0.23	46.8	35.6	9.0	2.55	53
	1.55	0.91	0.14	21.4	33.9	3.2	7.60	56
	1.57	0.91	0.12	19.1	35.1	1.9	16.00	70
	1.45	0.99	0.39	92.6	54.6	198.6	0.09	41
	1.47	1.00	0.35	91.8	55.7	60.6	0.28	39
40	1.50	0.99	0.29	86.4	57.5	12.6	2.03	59
	1.52	0.98	0.21	64.9	56.2	5.1	4.50	53
	1.55	0.95	0.14	47.8	54.7	2.0	12.50	58
	1.57	0.95	0.12	38.7	53.7	1.2	25.00	69
	1.45	0.85	0.39	77.5	56.6	109.6	0.13	33
	1.47	0.86	0.33	73.4	56.3	44.6	0.37	38
60	1.50	1.14	0.25	54.7	57.3	10.1	2.03	47
	1.52	1.09	0.19	54.8	56.7	5.0	4.45	51
	1.55	1.08	0.15	33.0	52.3	2.0	15.5	71
	1.57	1.30	0.13	23.0	52.0	1.1	36.00	—
	1.45	0.78	0.70	71.2	48.7	117.3	0.10	27
	1.47	0.75	0.55	67.8	46.6	54.8	0.25	32
80	1.50	0.76	0.70	42.8	43.3	16.6	1.05	40
	1.52	0.74	0.43	23.6	42.3	9.2	2.80	59
	1.55	0.99	0.17	16.3	38.0	2.1	8.65	42
	1.57	0.85	0.14	18.4	35.9	1.4	19.00	61
	1.45	0.83	2.17	45.0	29.6	238.3	0.05	27
	1.47	0.83	1.64	43.1	27.6	105.5	0.10	24
100	1.50	0.83	0.76	39.2	23.4	26.1	0.35	21
	1.52	0.81	0.42	36.1	20.7	10.9	0.80	20
	1.55	0.82	0.23	27.5	16.9	3.8	2.80	25
	1.57	0.82	0.22	19.8	16.4	2.3	6.25	33

[a]Calculated from $b = 2.303\, jR_{ct}$ (24, 25), eq. [2] in the text.

slope close to 40 mV. The possible presence of two Tafel lines was already previously noted with 30% IrO_2 + 70% TiO_2 electrodes (13). The 80% IrO_2 sample shows an intermediate behaviour, a possibility clearly demonstrated with RuO_2 + IrO_2 electrodes (1).

In a qualitative way, it can be stated that a single-type mechanism can be invoked to explain the dependence of the Tafel slope on oxide composition. The details of the mechanism have been given elsewhere (29). The two Tafel slopes are related to two competing steps, an electrochemical and a chemical one. The chemical step becomes progressively slower as the content of IrO_2 increases. For instance:

[1*a*] $S + H_2O \rightarrow S\text{-}OH^* + H^+ + e$

[1*b*] $S\text{-}OH^* \rightarrow S\text{-}OH$

[1*c*] $S\text{-}OH \rightarrow S\text{-}O + H^+ + e$

[1*d*] $S\text{-}O + S\text{-}O \rightarrow 2S + O_2$

At high IrO_2 contents and at high overpotentials step [1*b*] is rate determining. This step corresponds to a rearrangement of the surface intermediate. At low overpotentials and low IrO_2 contents step [1*c*] becomes rate determining. This may be related to a different surface–intermediate interactions strength which makes step [1*b*] faster. This implies that electronic interactions between IrO_2 and TiO_2 modify the nature of the bond between the surface and the intermediate species. Such an interaction requires that IrO_2 and TiO_2 are intimately mixed, i.e., they form a solid solution. Our experimental approach can only provide an indirect piece of evidence for that.

Impedance spectroscopy

Impedance measurements were carried out both in the "double layer" region, i.e., at potentials before oxygen evolution, and in the O_2 liberation region, i.e., at $E > 1.45$ V.

The impedance spectrum, plotted in the complex plane, for a $Ir_{0.6}Ti_{0.4}O_2$ electrode at 1.0 V is shown in Fig. 6. The features are practically independent of oxide composition. In the low-

Can. J. Chem. Downloaded from www.nrcresearchpress.com by 91.121.58.235 on 09/08/12
For personal use only.

© 1997 NRC Canada

Table 4. Normalized parameters measuring the electrocatalytic behaviour of the IrO_2+TiO_2 system as a function of composition at several potentials.[a]

Mol % IrO_2	E (V)	R_{ct}/C_{dl} (Ω cm^4 mF^{-1})	$(j/C_{dl})/100$ (mA mF^{-1})	$(j/q^*)/100$ (mA mC^{-1})
	1.47	2.380	1.120	1.200
	1.50	0.533	3.407	3.706
20	1.52	0.253	7.163	7.621
	1.55	0.0944	22.419	22.714
	1.57	0.0541	45.584	47.818
	1.47	1.089	1.020	0.830
	1.50	0.219	3.530	2.981
40	1.52	0.0907	8.007	6.609
	1.55	0.0366	22.852	18.358
	1.57	0.0223	46.555	36.716
	1.47	0.793	1.300	0.930
	1.50	0.176	3.543	2.562
60	1.52	0.0882	7.848	5.617
	1.55	0.0382	29.637	19.566
	1.57	0.0212	69.231	45.443
	1.47	1.176	1.080	0.680
	1.50	0.383	2.425	1.415
80	1.52	0.217	6.619	3.773
	1.55	0.0553	22.763	11.655
	1.57	0.0390	52.925	25.600
	1.47	3.817	0.750	0.570
	1.50	1.115	1.496	0.957
100	1.52	0.527	3.860	2.187
	1.55	0.225	16.570	7.654
	1.57	0.140	38.110	17.086

[a]Supporting electrolyte: 1.0 mol dm^{-3} $HClO_4$. Current, allowing for ohmic drops, taken from Tafel experiments.

frequency range a straight line is obtained with an inclination close to 90°C, which is indicative of the capacitive nature of the processes occurring in the 0.4–1.4 V region. At higher frequencies a distorted semicircle is observed, attributable to the presence of less accessible surface regions (walls of microcracks) (30).

Figure 7 shows a few Bode plots ($\log f$ vs. $\log|Z|$, and $\log f$ vs. ϕ) for different oxide compositions recorded at potentials inside the oxygen evolution region. When plotted in the complex plane mode ($|Z'|$ vs. $|Z''|$), a small dispersion of the data is observed at $f \rightarrow 0$, the more appreciable the more positive the electrode potential. This can be attributed to the perturbation introduced by strong gas (O_2) evolution and by the rough nature of the oxide surface. The same feature has been observed by other authors (31, 32).

Figure 8 shows a scheme of the equivalent circuit used to fit the experimental data. R_Ω is the solution ohmic resistance, C_f and R_f capacitance and ohmic resistance of the oxide layer, respectively, C_{dl} the double layer capacitance, and R_{ct} the charge transfer resistance. L is a small inductance (ca. 1 μH) observed in the high-frequency range and which has been related to the equipment (33, 34). Symbols and notations in Fig. 8 are after Boukamp (35). Several equivalent circuits were tested, the one in Fig. 8 giving an excellent fit as evident in Fig. 7. The values of the parameters as obtained from the fitting procedure have been summarized in Table 3.

The impedance analysis allows separation between R_Ω and R_f, which kinetic data do not permit. Table 3 confirms that R_f is small at all compositions, which implies that the conduction in the film is good and the TiO_2 film at the support – film interface is very thin. However, at the higher IrO_2 contents R_f tends to increase a little, which may be related to the morphology of the layers showing larger and deeper cracks. Under similar circumstances a thicker TiO_2 film can grow during calcination.

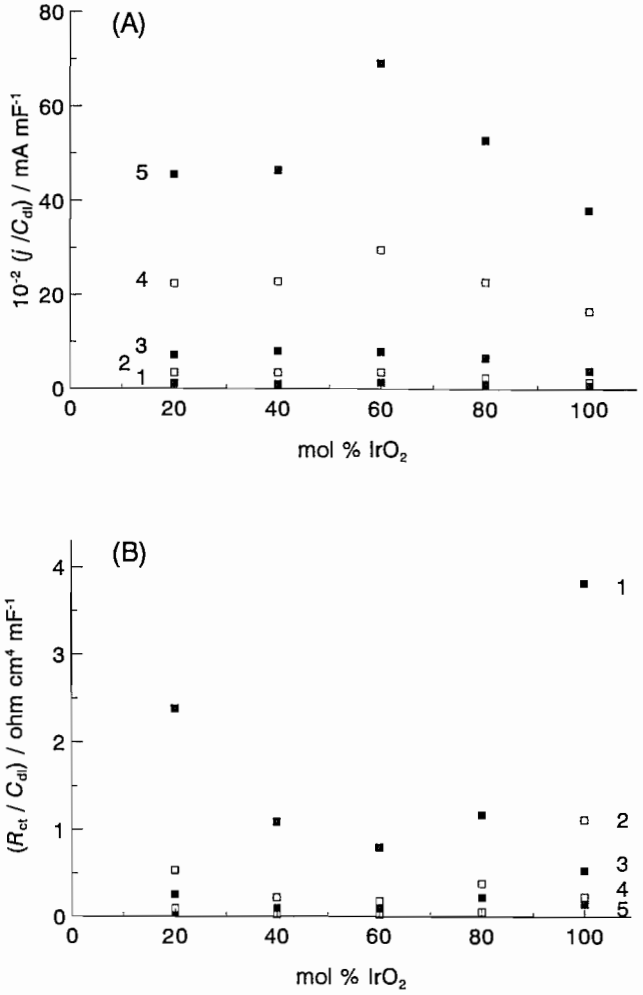
It is noted that for all compositions R_f is potential dependent. If plotted against E, a nonlinear dependence is observed (Fig. 9*A*), contrary to the expected linear behaviour for metallic-type conduction. However, a plot of $\ln R_f$ vs. E results in a straight line (Fig. 9*B*) as predicted by semi-conducting properties (36). This result indicates that the fully metallic nature of IrO_2 is lost in these films, although the conductivity is high. This agrees with previous specific investigations of the conduction behaviour of oxide layers (24). It is, however, possible that the potential dependence of R_f is dominated by the electrical properties of the TiO_2 film formed at the support – active layer interface, even though this film is thin. Compositionally,

Can. J. Chem. Downloaded from www.nrcresearchpress.com by 91.121.58.235 on 09/08/12
For personal use only.

© 1997 NRC Canada

Can. J. Chem. Downloaded from www.nrcresearchpress.com by 91.121.58.235 on 09/08/12
For personal use only.

Fig. 10. (*A*) Current density and (*B*) charge transfer resistance for O_2 evolution, normalized to unit double layer capacitance, as a function of IrO_2 content at different electrode potentials: (1) 1.47, (2) 1.50, (3) 1.52, (4) 1.55, and (5) 1.57 V vs. RHE. 1.0 mol dm^{-3} $HClO_4$.



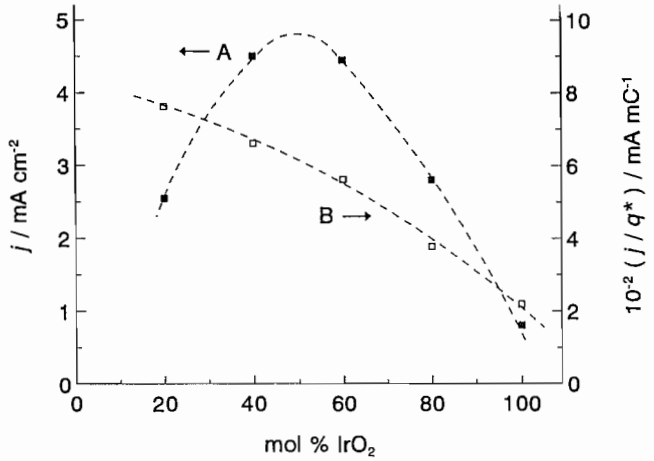
the TiO_2 interlayer could in fact be a substoichiometric oxide with semiconducting properties.

Table 3 shows that R_Ω is independent of both potential and composition, which is reasonable. Values are between 0.8 and 1.1 ohm cm^2, in agreement both with impedance data in the "double layer" region and with the data obtained by applying the method of Shub et al. (25, 26) (see above).

The film capacitance, C_f (Table 3), turns out independent of oxide composition but dependent on electrode potential. As an exception, pure IrO_2 shows C_f values approximately one half of those for the other compositions. The potential dependence of C_f can be understood in terms of a potential-dependent TiO_2 interlayer that plays the role of a dielectric between two conducting plates, the Ti support and the oxide overlayer. The lower C_f values of pure IrO_2 are to be related to the particular surface morphology that allows TiO_2 to grow more than at other compositions. For the same reason R_f of pure IrO_2 is higher.

The double layer capacitance is seen to be independent of potential for IrO_2 contents 20–60%. At higher IrO_2 contents a potential dependence is evident. For its nature C_{dl} is directly related to q^*, going through a maximum at 40–60% IrO_2. The potential dependence of C_{dl} for 80–100% IrO_2 is to be related to the effect of O_2 evolution on the layer morphology (see above). The high absolute values of C_{dl} (of the order of mF) confirm the very high surface areas of these electrodes.

Fig. 11. (*A*) Apparent current density for O_2 evolution and (*B*) current density normalized to unit surface charge, as a function of IrO_2 + TiO_2 oxide composition at 1.52 V vs. RHE. 1.0 mol dm^{-3} $HClO_4$.



The charge transfer resistance, R_{ct}, depends on both potential and composition. The potential dependence is expected from the electrochemical nature of the heterogeneous charge transfer reaction rate. The composition dependence shows a minimum (i.e., a maximum in activity) for 60% IrO_2. This parallels the composition dependence of the current at constant potential as derived from the Tafel lines, which goes through a maximum at the same oxide composition. From a practical point of view, such a composition can be regarded as the most active overall. However, from a fundamental point of view both R_{ct} and j are inadequate to evaluate the true electrocatalytic properties since both are extensive quantities, i.e., they depend on both electronic and geometric (surface area) factors.

Separation of catalytic from geometric effects can be achieved by normalizing the activity to unit, electrochemically active, surface area (24). This can be accomplished by using C_{dl} as a representative parameter of surface area effects. Results are summarized in Table 4, which also includes j/q^* for comparison.

Figures 10*A* and 10*B* show plots of (j/C_{dl}) and (R_{ct}/C_{dl}) as a function of composition. Scrutiny of the plots reveals that the normalized activity does not change appreciably with composition, although a somewhat higher activity is apparent for the electrode with 60% IrO_2. However, if real, the gain is small.

Figure 11 shows the apparent activity (j) as a function of composition at the potential of 1.52 V (the potential value may include some ohmic drop). Clearly, j goes through a maximum at 60% IrO_2. If j is normalized to unit surface charge (nominally, j/q^* measures the reaction rate per Ir site), Fig. 11 shows that the "true" catalytic activity decreases steadily as the IrO_2 content increases.

© 1997 NRC Canada

If the effects in Fig. 11 are real, the trend is for an increase in activity of Ir sites as the IrO_2 content decreases. This is in line with the observed lower Tafel slope at lower IrO_2 contents. It can be explained in terms of synergetic effects between the two oxide components. On the whole, surface area effects appear to be more appreciable than electronic effects, although the latter should not be ruled out.

Armstrong et al. (37, 38) have shown that R_{ct} is related to the Tafel slope, b, by the relationship:

$$[2] \quad b = 2.303\, j\, R_{ct}$$

where j is the steady-state current at the given potential. With the j values from the Tafel line measurements and the R_{ct} values from the impedance data, the calculated b are reported in Table 3, last column. For compositions 20–60% IrO_2, the Tafel values resulting from eq. [2] are in accord with those derived from polarization curves (Table 2). For compositions 80–100% IrO_2 the outcome is not as good, giving Tafel slopes that are too low. This can be attributed to the instability of the systems and their delicate and complex morphology. At the same time this outcome has an impact on the reliability of the separation of geometric from electronic factors. This suggests that the decrease in "true" catalytic activity as the IrO_2 content increases should be considered with caution, although the normalization based on q^* seems more reliable than that in terms of C_{dl}.

Conclusions

1. The average surface composition of TiO_2 + IrO_2 mixed oxides shows enrichment with TiO_2 although there is local segregation of IrO_2 in cracks.
2. The electrochemically active surface area, as measured by the voltammetric charge, goes through a maximum at about 60% IrO_2. This non-monotonic behaviour results from an increase in surface concentration of Ir and a decrease in particle size with Ir content.
3. The evolution of O_2 produces a large increase in voltammetric charge at 20–60% IrO_2, while it decreases for pure IrO_2. The latter is due to mechanical erosion, the former is probably caused by the exposure of new areas where IrO_2 is segregated.
4. O_2 evolution takes place with low Tafel slopes ranging from 40 to 60 mV. The higher Tafel slopes tend to predominate as the IrO_2 content increases. A change in mechanism or, more probably, in the rate-determining step of a single mechanism, is presumably related to the surface concentration of Ir sites.
5. Impedance has shown that the oxide layer does not possess fully metallic properties as would be expected for IrO_2. This can be related to the effect of TiO_2 as well as the small size of the particles for the mixed oxides.
6. Separation of electronic from geometric effects shows that the "true" electrocatalytic activity per "Ir" site probably decreases with the increase in IrO_2 content. This is in line with the conclusions based on the values of the Tafel slopes.

Acknowledgements

J.F.C. Boodts wishes to acknowledge the financial support received from the Conselho Nacional de Desenvolvimento Cientifico e Tecnológico (CNPq) and Fundação de Amparo a Pesquisa do Estado de São Paulo (FAPESP) Foundations (Brazil). Fruitful discussions with Dr. Munir S. Skaf are also acknowledged. S.T. is grateful to Consiglio Nazionale delle Ricerche (C.N.R.) and Ministero per l'Università e per la Ricerca Scientifica e Tecnologica (M.U.R.S.T.) (Italy) for the support of this work.

References

1. C. Angelinetta, S. Trasatti, Lj.D. Atanasoska, Z.S. Minevski, and R.T. Atanasoski. Mater. Chem. Phys. **22**, 231 (1989).
2. I.M. Kodintsev and S. Trasatti. Electrochim. Acta, **39**, 1803 (1994).
3. R. Kötz and S. Stucki. Electrochim. Acta, **31**, 1311 (1986).
4. V.V. Gorodetskii, V.A. Neburchilov, and M.M. Pecherskii. Russ. J. Electrochem. (Transl. Elektrokhimiya), **30**, 916 (1994).
5. G. N. Martelli, R. Ornelas, and G. Faita. Electrochim. Acta, **39**, 1551 (1994).
6. T.V. Varlamova, I.D. Belova, R.R. Shifrina, B.Sh. Galyamov, Yu.E. Roginskaya, and Yu.N. Venevtsev. Zh.Fiz. Khim. **64**, 385 (1990).
7. S. Daolio, B. Facchin, C. Pagura, A. De Battisti, and G. Battaglin. Surf. Interface Anal. **16**, 457 (1990).
8. A. De Battisti, A. Barbieri, A. Giatti, G. Battaglin, S. Daolio, and A.B. Boscoletto. J. Mater. Chem. **1**, 191 (1991).
9. J. Kristóf, J. Liszi, P. Szabó, A. Barbieri, and A. De Battisti. J. Appl. Electrochem. **23**, 615 (1993).
10. Y. Kamegaya, K. Sasaki, M. Oguri, T. Asaki, H. Kobayashi, and T. Mitamura. Electrochim. Acta, **40**, 889 (1995).
11. Ch. Comninellis and G.P. Vercesi. J. Appl. Electrochem. **21**, 335 (1991).
12. Y. Matsumoto, T. Tazawa, and E. Sato. J. Electrochem. Soc. **133**, 2257 (1986).
13. L.A. da Silva, V.A. Alves, M.A.P. da Silva, S. Trasatti, and J.F.C. Boodts. Electrochim. Acta, **42**, 271 (1997).
14. V.A. Alves, L.A. Da Silva, J.C.F. Boodts, and S. Trasatti. Electrochim. Acta, **39**, 1585 (1994).
15. S. Trasatti and G. Lodi. *In* Electrodes of conductive metallic oxides. Part A. *Edited by* S. Trasatti. Elsevier, Amsterdam. 1980. pp. 301–358.
16. L.A. da Silva, V.A. Alves, S. Trasatti, and J.F.C. Boodts, J. Electroanal. Chem. **427**, 97 (1997).
17. V.A. Alves, L.A. da Silva, J.F.C. Boodts, and S. Trasatti. In preparation.
18. J. Rolewicz, Ch. Comninellis, E. Plattner, and J. Hinden. Electrochim. Acta, **33**, 573 (1988).
19. A. De Battisti, G. Lodi, M. Cappadonia, G. Battaglin, and R. Kötz. J. Electrochem. Soc. **136**, 2596 (1989).
20. O.R. Cámara and S. Trasatti. Electrochim. Acta, **41**, 419 (1996).
21. Yu.E. Roginskaya, O.V. Morozova, E.N. Loubnin, A.V. Popov, Yu.I. Ulitina, V.V. Zhurov, S.A. Ivanon, and S. Trasatti. J. Chem. Soc. Faraday Trans. **89**, 1707 (1993).
22. S. Ardizzone, A. Carugati, and S. Trasatti. J. Electroanal. Chem. **126**, 287 (1981).
23. Yu.E. Roginskaya and O.V. Morozova. Electrochim. Acta, **40**, 817 (1995).
24. S. Trasatti. Electrochim. Acta, **36**, 225 (1991).
25. D.M. Shub and M.F. Reznik. Elektrokhimiya, **21**, 855 (1985).
26. D.M. Shub, M.F. Reznik and V.V. Shalagina. Elektrokhimiya, **21**, 937 (1985).
27. C. Iwakura, H. Tada, and H. Tamura. Denki Kagaku, **45**, 202 (1977).
28. H. Chen and S. Trasatti. J. Indian Chem. Soc. **70**, 323 (1993).
29. S. Trasatti. *In* Electrochemical hydrogen technologies. *Edited by* H. Wendt. Elsevier, Amsterdam. 1990. pp. 104–135.

Can. J. Chem. Downloaded from www.nrcresearchpress.com by 91.121.58.235 on 09/08/12
For personal use only.

© 1997 NRC Canada

30. I.R. Burrows, D.A. Denton, and J.A. Harrison. Electrochim. Acta, **23**, 493 (1978).
31. D.T. Shieh and B.J. Hwang. Electrochim. Acta, **38**, 2239 (1993).
32. D.A. Denton, J.A. Harrison, and R.I. Knowles. Electrochim. Acta, **26**, 1197 (1981).
33. B. Savova-Stoynov and Z.B. Stoynov. J. Appl. Electrochem. **17**, 1150 (1987).
34. B.D. Cahan, M.L. Daroux, and E.B. Yeager. J. Electrochem. Soc. **136**, 1585 (1989).
35. B.A. Boukamp. Equivalent circuits. Twente University, Enschede, The Netherlands. 1989.
36. N.W. Ashcroft and N.D. Mermin. Solid state physics. Sauders College, Philadelphia, Pa. 1976. p. 600.
37. R.D. Armstrong, K. Edmondson, and R.E. Firman. J. Electroanal. Chem. **40**, 19 (1972).
38. R.D. Armstrong and M. Henderson. J. Electroanal. Chem. **40**, 121 (1972).

Can. J. Chem. Downloaded from www.nrcresearchpress.com by 91.121.58.235 on 09/08/12
For personal use only.

© 1997 NRC Canada

Zirconium alkyl and borohydride complexes stabilized by a sterically demanding anionic organic amide. The crystal structures of $ZrMeL_3$ (2) and $Zr(BH_4)L_3$ (3) (L = $(3,5\text{-}Me_2Ph)N(Ad)$; Ad = adamantyl)

Aparna Kasani, Sandro Gambarotta, and Corinne Bensimon

Abstract: The lithium amide $[3,5\text{-}Me_2PhN(Ad)]Li\cdot Et_2O$ (**L**) reacts with $ZrCl_4(THF)_2$ to give $ZrClL_3$. Reactions of $ZrClL_3$ with MeLi and $NaBH_4$ produce the corresponding $ZrMeL_3$ (**2**) and $Zr(BH_4)L_3$ (**3**), respectively. The molecular structures of **2** and **3** were determined by X-ray crystallography. Crystal data are as follows. **2**: $C_{55}H_{75}N_3Zr$, FW 869.45, orthorhombic, *Pcab*; a = 19.2436(3) Å, b = 45.9342(4) Å, c = 21.2935(3) Å, V = 18822.2(4) Å^3, Z = 8; **3**: $C_{54}H_{76}BN_3Zr$, FW 869.25, orthorhombic; *Pbc*21, a = 11.5399(3) Å, b = 19.4091(4) Å, c = 20.4471(5) Å, V = 4579.72(19) Å^3, Z = 4.

Key words: zirconium, amide, alkyl, borohydride, structure.

Résumé : L'amide lithié $[3,5\text{-}Me_2PhN(Ad)]Li\cdot Et_2O$ (**L**) réagit avec le $ZrCl_4(THF)_2$ pour donner du $ZrClL_3$. Les réactions du $ZrClL_3$ avec le MeLi et le $NaBH_4$ conduisent respectivement au $ZrMeL_3$ (**2**) et $Zr(BH_4)L_3$ (**3**). On a déterminé les structures moléculaires des composés **2** et **3** par diffraction des rayons X. Les données crystallographiques sont les suivantes : **2** : $C_{55}H_{75}N_3Zr$; PF : 869,45; orthorhombique; *Pcab*; a = 19,2436(3), b = 45,9342(4) et c = 21,2935(3) Å, V = 18822,2(4) Å^3; Z = 8; **3** : $C_{54}H_{76}BN_3Zr$; PF : 869,25; orthorhombique; *Pbc*21; a = 11,5399(3), b = 19,4091(4) et c = 20,4471(5) Å; V = 4579,72(19) Å^3; Z = 4.

Mots clés : zirconium, amide, alkyle, borohydrure, structure.

[Traduit par la rédaction]

Introduction

Among early transition metals, zirconium is certainly the element that has received very special attention as demonstrated by the massive organometallic chemistry that has been developed for this metal. The extensive literature available describes an impressive variety of transformations (1), from metal-promoted organic synthesis (2), to Ziegler–Natta catalysis (3), olefin isomerization (4), insertion reactions (5), C—N bond activation (6), C_1 chemistry (7), etc. Another unique characteristic of zirconium, which is also common to the other group IV metals, is that the majority part of its chemistry was developed with the help of cyclopentadienyl and related ligand systems. Therefore, attempts to explore the reactivity of these metals with alternative ligands is the next and most obvious development in this field. This is certainly the key to understanding the strong revival of interest, which can be observed in the recent literature, for chemistry with non-Cp ligands of these metals and of zirconium in particular. The employment of sterically demanding alkoxides and aryloxides has already proved to be a useful strategy for a number of transformations (8). What remains relatively unexplored for zirconium is the chemistry of the lower oxidation states. The extreme reactivity of low-valent zirconium and the limited resistance of the traditional ligand systems to strong reducing agents (9) is probably the cause of this lacuna in the literature.

Nitrogen donor based ligands (formamidinate, amides, porphyrinogens, etc.) have been shown to be rather versatile in the chemistry of low-valent early transition metals (10), allowing the stabilization of the low oxidation states (11) and displaying a reduced possibility of being involved in the reactivity of the metal center. In addition, what makes these ligands particularly interesting is the possibility of easily adjusting the electronic features and steric hindrance around the transition metal via a virtually unlimited choice of organic substituents attached to the nitrogen donor atom. In the chemistry of zirconium, Fryzuk et al. have demonstrated that the employment of bulky chelating amide–phosphine ligand systems enables the stabilization of rare Zr(III) derivatives (12) and the coordination of highly reduced dinitrogen (13). More recently, anionic organic amides with a particularly large steric hindrance have been employed for a number of

Received April 2, 1997.

This paper is dedicated to Professor Brian E. Conway in recognition of his outstanding contributions to electrochemistry and to Canadian chemistry.

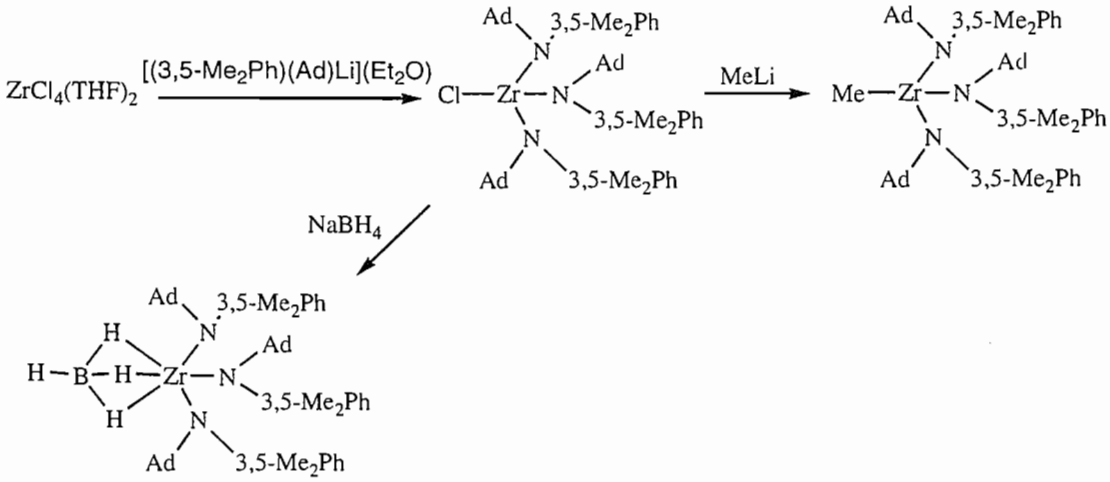
A. Kasani, S. Gambarotta,[1] and C. Bensimon. Department of Chemistry, University of Ottawa, Ottawa, ON K1N 6N5, Canada.

[1] Author to whom correspondence may be addressed. Telephone: (613) 562-5199. Fax: (613) 562-5170. E-mail: sgambaro@oreo.uottawa.ca

© 1997 NRC Canada

Can. J. Chem. Downloaded from www.nrcresearchpress.com by 91.121.58.235 on 09/08/12
For personal use only.

Scheme 1.



remarkable reactions that include dinitrogen cleavage (14), formation of stable and reactive nitrides (15), and assemblage of heterodimetallic structures (16).

The remarkable robustness of these ligands has prompted us to attempt its employment for preparing zirconium complexes that may work as substrates for further reduction towards lower oxidation states or for the trapping of reactive functions (hydride, alkyl, etc.). The large-scale preparation in our lab of the sterically demanding [3,5-Me_2PhN(Ad)] anion (17) has enabled the preparation and characterization of a number of transition metal complexes in the medium oxidation state and the trapping of rare functions. Herein we describe the result of our attempts to use this ligand in zirconium chemistry.

Results and discussion

The reaction between [3,5-Me_2PhN(Ad)]Li·Et_2O and [$ZrCl_4(THF)_2$] in diethyl ether at room temperature resulted in the formation of a pale yellow solution from which [ZrCl{3,5-Me_2PhN(Ad)}$_3$] (**1**) was isolated in moderate yield as a white crystalline solid (Scheme 1).

The product of the reaction was remarkably insensitive to the stoichiometric ratio between the two reagents since similar reactions with different ratios invariably yielded the same compound. The formula of compound **1** was based on chlorine and combustion analyses. The ^{1}H and ^{13}C NMR spectra indicate the presence of a rather symmetric ligand environment in the compound. Two different methylene resonances are observed in equal ratio for the adamantyl group, while a single resonance is observed for the two methyl groups attached to the aryl rings. Two lines present in the aromatic region in a 2:1 ratio are assigned to the *ortho* and *meta* protons of the aryl rings.

Reaction of **1** with methyllithium in ether resulted in the precipitation of lithium chloride and formation of the corresponding zirconium methyl derivative, [ZrMe{3,5-Me_2PhN(Ad)}$_3$] (**2**) (Scheme 1). Compound **2** was isolated in moderate yield from hexane as colorless and very air-sensitive crystals. The infrared spectra of compounds **1** and **2** were nearly identical, thus suggesting that the two complexes may be isostructural. The ^{1}H NMR spectrum of **2** displays amide ligand resonances similar to those observed for **1** with slightly different chemical shifts. The Me group resonance was clearly visible as a sharp new singlet at −0.01 ppm. Similar considerations apply to the ^{13}C NMR spectrum, which shows only one set of ligand resonances, slightly shifted with respect to those of complex **1**, and one additional resonance at 37.4 ppm. DEPT experiments assigned this resonance to the methyl group. The assignment was further supported by HQMC experiments, which showed correlation of the ^{1}H resonance at −0.01 ppm with the ^{13}C NMR resonance of 37.4 ppm. Complex **2** is thermally stable and chemically inert. It does not react with molecular H_2 and carbon monoxide at room temperature and atmospheric pressure, and it is stable for 24 h in refluxing benzene.

The structure of compound **2** (Fig. 1) was elucidated by a single-crystal X-ray diffraction analysis. The coordination geometry around zirconium is distorted tetrahedral and is defined by three nitrogen atoms of the three amide ligands and one methyl group. The bond distances (Zr1—N1 = 2.083(3) Å, Zr1—N2 = 2.072(4) Å, Zr1—N3 = 2.089(4) Å) and angles (N1-Zr1-N2 = 111.52(14)°, N1-Zr1-N3 = 109.57(13)°, N2-Zr1-N3 = 114.82(14)°), as well as the Zr—C bond distance (Zr1—C1 = 2.258 (5) Å) are in the expected range. The amide nitrogen atoms possess the characteristic trigonal planar geometry (sums of the angles around the nitrogen atoms are close to 360°), which indicates the presence of a Zr—N multiple bond character. Relevant bond distances and angles are given in Table 1.

The surprising and unexpected chemical inertness of complex **1** suggested that this particular ligand system may be versatile for the preparation of stable and terminal Zr-H functions. However, since the hydrogenolysis of **2** was not a viable method, we have explored other possible synthetic pathways such as chlorine replacement of **1** with hydridic reagents. Unfortunately, reactions of **1** with NaH, $NaHBEt_3$, Bu_3SnH, and $LiAlH_4$ proved to be unsuccessful since they led only to highly soluble and intractable materials or no reaction. In addition, the ^{1}H NMR spectra were rather complicated and possibly indicative of the presence of a mixture of products. Conversely, the reaction of **1** with an excess of $NaBH_4$ in THF resulted in the precipitation of NaCl and formation of the corresponding tetrahydroborate compound, [Zr(BH_4){3,5-Me_2PhN(Ad)}$_3$] (**3**), in good yield. The infrared spectrum

© 1997 NRC Canada

Can. J. Chem. Downloaded from www.nrcresearchpress.com by 91.121.58.235 on 09/08/12
For personal use only.

Can. J. Chem. Downloaded from www.nrcresearchpress.com by 91.121.58.235 on 09/08/12
For personal use only.

Fig. 1. ORTEP plot of **2**. Thermal ellipsoids are drawn at the 50% probability level.

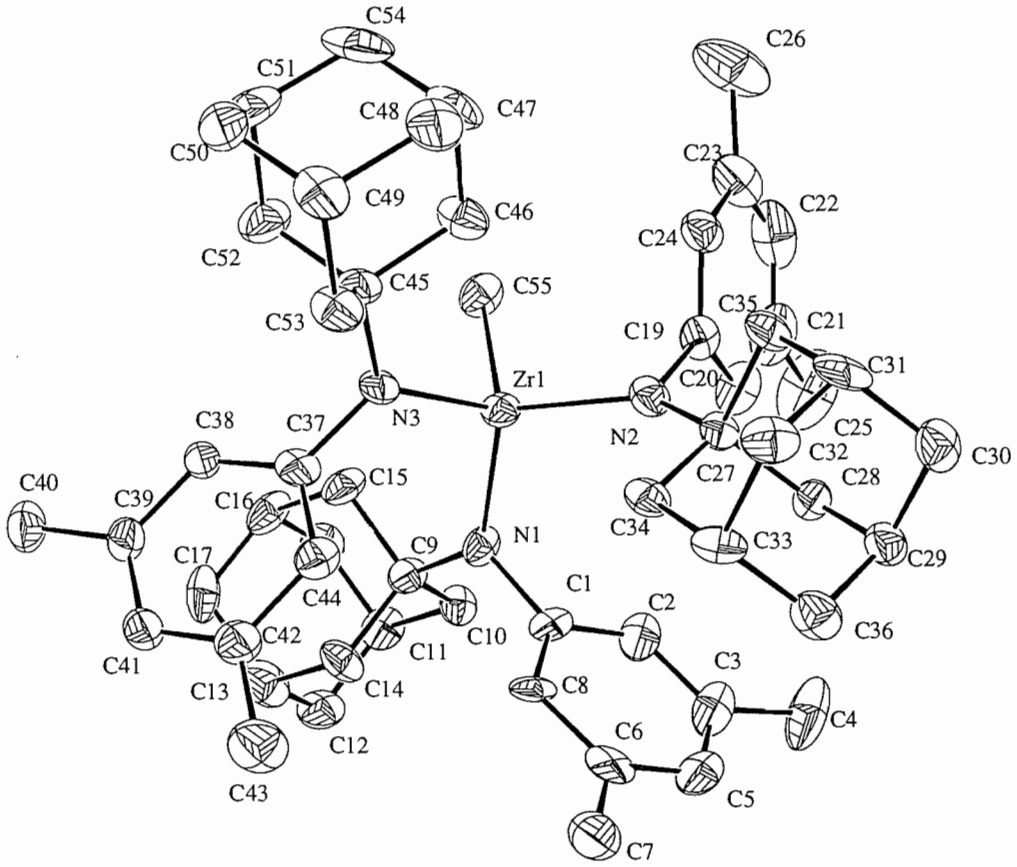


Table 1. Selected bond distances (Å) and angles (deg).

2	3
Zr1—N1 = 2.083(3)	Zr1—N1 = 2.071(3)
Zr1—N2 = 2.072(4)	Zr1—N2 = 2.066(3)
Zr1—N3 = 2.089(4)	Zr1—N3 = 2.072(3)
Zr1—C55 = 2.258(5)	Zr1—B1 = 2.400(4)
N1—C1 = 1.442(6)	Zr1—H = 2.16(4)
N1—C9 = 1.497(6)	Zr1—H = 2.21(4)
N1-Zr1-C55 = 105.26(15)	Zr1—H = 2.23(4)
N2-Zr1-C55 = 108.24(16)	N1-Zr1-N2 = 107.33(11)
N2-Zr1-N3 = 114.82(14)	N1-Zr1-B1 = 110.71(13)
N3-Zr1-N1 = 109.57(13)	B1-Zr1-N3 = 109.88(13)
C1-N1-C9 = 114.9(3)	N3-Zr1-N2 = 106.97(11)
Zr1-N1-C9 = 131.2(3)	C1-N1-C9 = 112.0(3)
Zr1-N1-C1 = 113.2(3)	C9-N1-Zr1 = 128.02(23)
N3-Zr1-C55 = 106.87(16)	N1-Zr1-N3 = 108.05(11)
N1-Zr1-N2 = 111.52(14)	Zr1-N1-C1 = 119.87(23)
	N2-Zr1-N3 = 106.97(11)

showed the characteristic absorptions of $[BH_4]^-$ as an intense sharp line at 2500 cm^{-1} (terminal B-H stretching) and broad doublet at 2172 cm^{-1} (B-H stretching). This pattern usually diagnoses a tridentate bonding mode for the $[BH_4]$ group. The ^1H NMR showed the resonance corresponding to tetrahydroborate as a broad singlet at 1.91 ppm, which nicely correlates with the ^{11}B resonance at −15.6 ppm in HQMC experiments. Attempts to transform complex **3** into terminal hydride by abstracting the BH_3 group with Me_3P or TMEDA were unsuccessful.

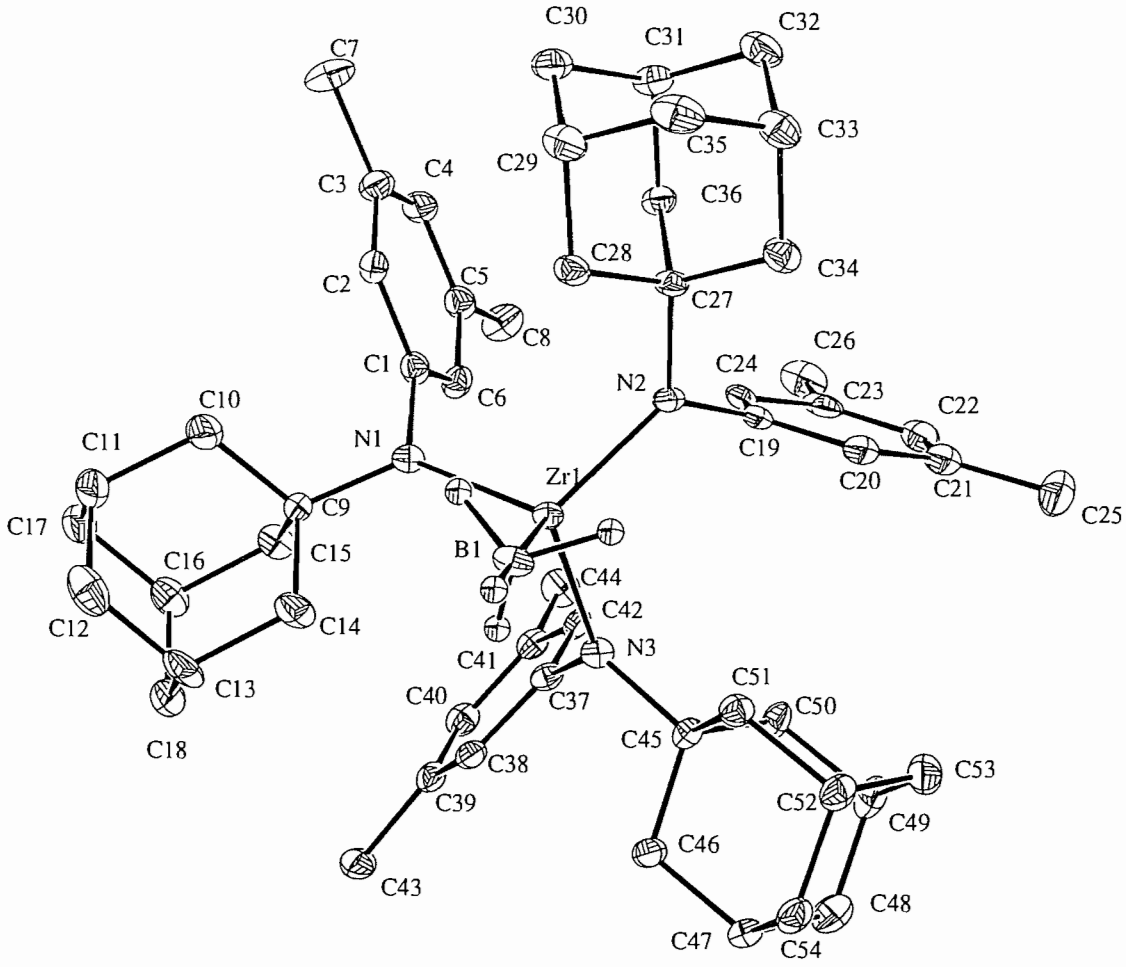
The structure of compound **3** was confirmed by an X-ray crystal structure (Fig. 2). The zirconium metal is coordinated to three amide ligands and one borohydride group. Similar to the case of complex **2**, the geometry around the metal center is distorted tetrahedral and is defined by the three nitrogen atoms (N1-Zr1-N2 = 107.3(1)°, N1-Zr1-N3 = 108.0(1)°, N2-Zr1-N3 = 107.0(1)°) of the three amide groups and one boron atom (N1-Zr1-B1 = 110.7(1)°, N2-Zr1-B1 = 113.7(1)°, N3-Zr1-B1 = 109.9(1)°). The Zr···B nonbonding distance (Zr1-B1 = 2.400(4) Å) is rather short, possibly indicating the presence of an η^3-bonding mode of the BH_4 group. The positions of the tetrahydroborate hydrogen atoms were yielded by difference Fourier maps, thus confirming the tridentate mode (Zr1—H55 = 2.16(4) Å, Zr1—H57 = 2.21(4) Å, Zr1—H58 = 2.23(4) Å). The relatively short Zr—N bond distances (Zr1—N1 = 2.071(3) Å, Zr1—N2 = 2.066(3) Å, Zr1—N3 = 2.072(3) Å) compare well with those of **2** and of other Zr–amide complexes present in the literature, and are consistent with the existence of a Zr—N multiple bond character.

In conclusion, with this work it was possible to prepare and characterize new zirconium alkyl and borohydride complexes supported by bulky amide ligands. These species were found to be remarkably stable and unreactive. At this stage, it is

© 1997 NRC Canada

Can. J. Chem. Downloaded from www.nrcresearchpress.com by 91.121.58.235 on 09/08/12
For personal use only.

Fig. 2. ORTEP plot of **3**. Thermal ellipsoids are drawn at the 50% probability level.



tempting to attribute the surprising stability of these functions to either: (*i*) steric protection, which makes the reactive function inaccessible by incapsulating the metal; or (*ii*) the π-donating ability of the amide ligands that increases the covalency of the M—C and M—H bonds.

Experimental section

All the operations were performed under an inert atmosphere of a nitrogen-filled dry box or by using standard Schlenk techniques. $[ZrCl_4(THF)_2]$ (18) and $[3,5\text{-}Me_2PhN(Ad)]Li\cdot Et_2O$ (Ad = adamantyl) (17) were prepared according to reported procedures. Methyllithium and sodium borohydride (Aldrich) were used as received. Solvents were dried with the appropriate drying agents and distilled prior to use. Infrared spectra were recorded on a Mattson 9000 FTIR instrument from Nujol mulls prepared in a drybox. Elemental analyses were carried out with a Perkin Elmer 2400 CHN analyzer. NMR spectra were recorded with a Bruker AMX 500 MHz spectrometer.

Preparation of $[ZrCl\{3,5\text{-}Me_2PhN(Ad)\}_3]$ (1)

A suspension of $[ZrCl_4(THF)_2]$ (3.35 g, 8.88 mmol) in diethyl ether (150 mL) was stirred with $[3,5\text{-}Me_2PhN(Ad)]Li\cdot Et_2O$ (8.94 g, 26.65 mmol) at room temperature. After stirring for 24 h, the mixture was filtered to eliminate LiCl. After concentrating the filtrate to about 50 mL, colorless crystals of **1** were obtained upon allowing the solution to stand at –30°C for 8 h (5.20 g, 5.84 mmol, 66%). IR (Nujol mull, NaCl, cm^{-1}) *v*: 1599 s, 1585 s, 1356 m, 1343 w, 1303 s, 1290 s, 1188 w, 1151 s, 1106 w, 1088 w, 1067 s, 1029 s, 990 m, 977 w, 950 m, 924 s, 891 w, 851 m, 817 w, 787 w, 763 w, 710 s, 694 s, 682 m, 617 m. ^1H NMR (C_6D_6, 20°C, 500 MHz) δ: 6.82 (s, 2H, Ar), 6.80 (s, 1H, Ar), 2.30 (s, 6H, Me, Ar), 2.03 (bs, 6H, CH_2, Ad), 2.03 (bs, 3H, CH, Ad), 1.56 (q, 6H, CH_2, Ad). ^{13}C NMR (C_6D_6, 20°C, 125.7 MHz) δ: 144.5 (quaternary aryl), 137.4 (quaternary aryl), 130.7 (C-H aryl), 60.1 (quaternary Ad), 43.1 (CH_2, Ad), 36.8 (CH_2, Ad), 30.5 (CH, Ad), 21.7 (CH_3, aryl). Anal. calcd. for $C_{54}H_{72}ClN_3Zr$: C 72.89, H 8.16, N 4.72; found: C 73.52, H 8.00, N 4.85.

Preparation of $[ZrMe\{3,5\text{-}Me_2PhN(Ad)\}_3]$ (2)

A solution of methyllithium (0.80 mL, 1.4 M) in ether was added to a solution of **1** (1.0 g, 1.12 mmol) in the same solvent (80 mL). After stirring the mixture for 8 h at room temperature, the solvent was removed in vacuo. The residue was extracted with hexane (100 mL) and filtered to eliminate LiCl. Upon concentration to about 20 mL and cooling to −30°C for 24 h, colorless crystals of **2** were obtained (0.40 g, 0.46 mmol, 41%). IR (Nujol mull, NaCl, cm^{-1}) *v*: 1592 s, 1304 m, 1290 m, 1261 s, 1152 s, 1074 s, 1027 s, 950 m, 924 s, 848 w, 803 s, 710

© 1997 NRC Canada

Can. J. Chem. Downloaded from www.nrcresearchpress.com by 91.121.58.235 on 09/08/12
For personal use only.

Table 2. Crystal data and structure analysis results.[a]

	2	3
Empirical formula	$C_{55}H_{75}N_3Zr$	$C_{54}H_{76}BN_3Zr$
Formula weight	869.45	869.25
Space group	*Pcab*	*Pbc*21
a (Å)	19.2436(3)	11.5399(3)
b (Å)	45.9342(4)	19.4091(4)
c (Å)	21.2935(3)	20.4471(5)
V (Å^3)	18822.2(4)	4579.72(19)
Z	8	4
Radiation (Å)	0.70930	0.70930
T (°C)	−153	−153
D_{calcd} (g cm^{-3})	1.226	0.819
μ_{calcd} (mm^{-1})	0.27	0.25
R_w	0.077, 0.072	0.038, 0.040

[a] $R = \Sigma||F_o| - |F_c||/\Sigma|F_o|$; $R_w = [(\Sigma(|F_o| - |F_c|)^2/\Sigma w F_o^2)]^{1/2}$.

m, 692 s. ^{1}H NMR (C_6D_6, 20°C, 500 MHz) δ: 7.01 (s, 6H, 2,6-CH, Ar), 6.82 (s, 3H, 4-CH, Ar), 2.34 (s, 18H, CH_3, Ar), 2.06 (s, 9H, CH, Ad), 2.00 (s, 18H, CH_2, Ad), 1.60 (s, 18H, CH_2, Ad), −0.01 (s, 3H, Zr-CH_3). ^{13}C NMR (C_6D_6, 20°C, 125.7 MHz) δ: 142.8 (quaternary aryl), 137.5 (quaternary aryl), 132.0 (C-H aryl), 59.1 (quaternary Ad), 43.9 (CH_2, Ad), 37.4 (Zr-CH_3), 37.1 (CH_2, Ad), 30.5 (CH, Ad), 21.6 (CH_3, Ar).

Preparation of [Zr(BH$_4$){3,5-Me$_2$PhN(Ad)}$_3$] (3)

A solution of **1** (1.62 g, 1.82 mmol) in THF (100 mL) was treated with $NaBH_4$ (0.138 g, 3.64 mmol). After stirring at room temperature for 3 days, the solvent was removed in vacuo and the residue was extracted with diethyl ether (100 mL). After filtration to eliminate NaCl and unreacted $NaBH_4$, the solution was concentrated to 40 mL and allowed to stand at room temperature for 24 h, upon which colorless crystalline **3** was obtained (1.20 g, 1.38 mmol, 76%). IR (Nujol, mull, NaCl, cm^{-1}) *ν*: 2500 s, 2234 bw, 2180 bm, 2154 bw, 1598 s, 1583 s, 1356 s, 1344 w, 1304 s, 1286 s, 1261 m, 1185 m, 1148 s, 1103 m, 1061 s, 1026 s, 975 m, 951 s, 924 s, 888 m, 855 m, 817 m, 801 m, 709 s, 691 s. ^{1}H NMR (C_6D_6, 20°C, 200 MHz) δ: 6.80 (s, 3H, 4-Ar), 6.55 (s, 6H, 2,6-Ar), 2.30 (s, 18H, Me, Ar), 2.05 (s, 9H, CH, Ad), 1.90 (s, 18H, CH_2, Ad), 1.52 (q, 18H, CH_2, Ad). ^{13}C NMR (C_6D_6, 20°C, 125.7 MHz) δ: 146.4 (quaternary aryl), 136.7 (quaternary aryl), 131.1 (C-H aryl), 127.3 (C-H aryl), 60.4 (quaternary Ad), 43.2 (CH_2, Ad), 36.8 (CH_2, Ad), 30.5 (CH, Ad), 21.8 (CH_3, Ar). ^{11}B{^{1}H} NMR (C_6D_6, 20°C, 160.5 MHz) δ: −15.6. Anal. calcd. for $C_{54}H_{76}BN_3Zr$: C 74.62, H 8.81, N 4.83; found: C 75.24, H 9.05, N 4.88.

X-ray crystallography

Data were collected at −158°C using the ω–2θ scan technique to the maximum 2θ value of 50.0° for suitable air-sensitive crystals mounted on glass fibers of the goniometer of a CCD Siemens X-ray diffractometer. Cell constants and orientation matrices were obtained from the least-squares refinement of carefully centered high-angle reflections. Redundant reflections were averaged. The intensities of three representative reflections were measured after every 150 reflections to monitor crystal and instrument stability. Data were corrected for Lorentz and polarization effects and for absorption. The structures were solved by direct methods. The positions of most of the non-hydrogen atoms were refined anisotropically. Hydrogen atom positions were introduced at their idealized positions. The final cycles of full-matrix least-squares refinement were based on the number of observed reflections with $I > 2.5\sigma(I)$. Neutral atomic scattering factors were taken from Cromer and Waber (19)[2]. Anomalous dispersion effects were included in F_c. All calculations were performed using an NRCVAX package on a silicone Graphics station. Complex **2** contains two crystallographically independent and chemically equivalent molecules in the lattice. Details on crystal data and structure solution have been given in Table 2. Selected bond distances and bond angles are given in Table 1. Listings of atomic coordinates and thermal parameters have been given as supplementary information.[3]

Acknowledgments

This work was supported by the Natural Sciences and Engineering Council of Canada (NSERC). We gratefully acknowledge the generosity of Prof. A. Carty for making available to us a CCD Siemens X-ray diffractometer.

References

1. M.F. Lappert. *In* Comprehensive organometallic chemistry II. Vol. 4. *Edited by* E.W. Abel, F.G.A. Stone, and G. Wilkinson. Pergamon Press, Oxford. 1995.
2. S.G. Davies. *In* Organotransition metal chemistry: applications to organic synthesis. Pergamon, Oxford. 1982.
3. (*a*) P.C. Mohring and N.J. Coville. J. Organomet. Chem. **479**, 1 (1994); (*b*) R.F. Jordan. Adv. Organomet. Chem. **32**, 325 (1991); (*c*) J.D. Scollard and D.H. McConville. J. Am. Chem. Soc. **118**, 10008 (1996); (*d*) H.H. Brintzinger, D. Fisher, R. Mulhaupt, B. Rieger, and R.M. Waymouth. Angew. Chem. Int. Ed. Engl. **34**, 1143 (1995); (*e*) A.A. Anderson, H.G. Cordes, J. Herwig, W. Kamisky, A. Merck, R. Mottweiler, J. Pein, H. Sinn, and H.J. Vollmer. Angew. Chem. Int. Ed. Engl. **15**, 630 (1976); (*f*) P. Cossee. J. Catal. **3**, 80 (1964).
4. J. Schwartz and G.A. Labinger. Angew. Chem. Int. Ed. Engl. **15**, 333 (1976).

[2] The discrepancy indices were calculated from the expressions $R(F_o) = \Sigma|F_o - F_c|/\Sigma F_o$ and $R_w(F_o) = \Sigma(w_i)^{1/2}|F_o - F_c|/\Sigma(w_i)^{1/2}F_o$; the standard deviation of an observation of unit weight σ_1 is equal to $[(\Sigma w_i|F_o - F_c|^2)/(n - p)]^{1/2}$, where *n* is the number of observations and *p* is the number of parameters varied during the last refinement cycle.

[3] Supplementary material available includes tables of atomic coordinates, crystal data, bond distances and angles, torsion angles, and temperature factors for both **2** and **3**. Copies of material on deposit may be purchased from: The Depository of Unpublished Data, Document Delivery, CISTI, National Research Council Canada, Ottawa, Canada K1A 0S2. Tables of atomic coordinates and of bond lengths and angles have also been deposited with the Cambridge Crystallographic Data Centre, and can be obtained on request from The Director, Cambridge Crystallographic Data Centre, University Chemical Laboratory, 12 Union Road, Cambridge, CB2 1EZ, U.K.

© 1997 NRC Canada

5. (*a*) J.E. Nelson, J.E. Bercaw, and J.A. Labinger. Organometallics, **8**, 2484 (1989); (*b*) G. Fochi, C. Floriani, A. Chiesi-Villa, and C. Guastini. J. Chem. Soc. Dalton Trans. 445 (1986); (*c*) S. Gambarotta, S. Strologo, C. Floriani, A. Chiesi-Villa, and C. Guastini. Inorg. Chem. **24**, 654 (1985); (*d*) S. Gambarotta, C. Floriani, A. Chiesi-Villa, and C. Guastini. Inorg. Chem. **22**, 2029 (1983).
6. J.R. Agadorn and J. Arnold. Organometallics, **131**, 4670 (1994).
7. (*a*) S. Gambarotta, C. Floriani, A. Chiesi-Villa, and C. Guastini. J. Am. Chem. Soc. **105**, 1690 (1983); (*b*) S. Gambarotta, S. Strologo, C. Floriani, A. Chiesi-Villa, and C. Guastini. J. Am. Chem. Soc. **107**, 6278 (1985).
8. (*a*) G.J. Balaich, J.E. Hill, S.A. Waratuke, P.E. Fanwick, and I.P. Rothwell. Organometallics, **14**, 656 (1995); (*b*) G.J. Balaich, P.E. Fanwick, and I.P. Rothwell. Organometallics, **13**, 4117 (1994); (*c*) A. Van der Linden, C.J. Schaverin, N. Meijboom, C. Ganter, and A.G. Orpen. J. Am. Chem. Soc. **117**, 3008 (1995).
9. Y. Wielstra, S. Gambarotta, and M.Y. Chiang. Recl. Trav. Chim. Pays-Bas, **108**, 1 (1989).
10. (*a*) M. Moore, K. Feghali, and S. Gambarotta. Inorg. Chem. **36**, 2191 (1997); (*b*) J. Song and S. Gambarotta. Chem.—Eur. J. **2**, 1258 (1996); (*c*) M. Moore, S. Gambarotta, G. Yap, L.M. Liable-Sands, and A. Rheingold. J. Chem. Soc. Chem. Commun. In press; (*d*) J. Jubb, L. Scoles, H. Jenkins, and S. Gambarotta. Chem.—Eur. J. **2**, 767 (1996); (*e*) R. Minhas, L. Scoles, S. Wang, and S. Gambarotta. Organometalliscs, **15**, 1113 (1996); (*f*) L. Scoles, R. Minhas, R. Duchateau, J. Jubb, and S. Gambarotta. Organometallics, **13**, 4978 (1994).
11. (*a*) S. Hao, K. Feghali, and S. Gambarotta. Inorg. Chem. **36**, 1745 (1997); (*b*) P. Berno, S. Hao, R. Minhas, and S. Gambarotta. J. Am. Chem. Soc. **116**, 7417 (1994); (*c*) P. Berno and S. Gambarotta. Organometallics, **13**, 2569 (1994); (*d*) J. Jubb and S. Gambarotta. J. Am. Chem. Soc. **115**, 10410 (1993).
12. M.D. Fryzuk and M. Mylvaganam. J. Am. Chem. Soc. **115**, 360 (1993).
13. M.D. Fryzuk, T.S. Haddad, and S.J. Rettig. J. Am. Chem. Soc. **112**, 8185 (1990).
14. C.E. Laplaza and C.C. Cummins. Science, **268**, 861 (1995).
15. (*a*) J. Peters, P.W. Wanandi, A.L. Odom, W.M. Davis, and C.C. Cummins. J. Am. Chem. Soc. **118**, 3515 (1996); (*b*) A.L. Odom and C.C. Cummins. Organometallics, **15**, 898 (1996); (*c*) C.E. Laplaza, A.R. Johnson, and C.C. Cummins. J. Am. Chem. Soc. **118**, 709 (1996).
16. P.W. Wanandi, W.M. Davis, and C.C. Cummins. J. Am. Chem. Soc. **117**, 2110 (1995).
17. K.B. Ruppa, S. Gambarotta, A.L. Rheingold, and G. Yap. Inorg. Chem. **36**, 1194 (1997).
18. L.E. Manzer. Inorg. Synth. **21**, 136 (1982).
19. D.T. Cromer and J.T. Waber. International tables for X-ray crystallography. The Kynoch Press, Birmingham, England. 1974.

Can. J. Chem. Downloaded from www.nrcresearchpress.com by 91.121.58.235 on 09/08/12
For personal use only.

© 1997 NRC Canada

Temperature dependence of activity coefficients and Gibbs energies of transfer of LiBr in acetonitrile, dimethyl sulfoxide, and *N,N*-dimethylacetamide from EMF measurements

J. Barthel, R. Neueder, and A. Schröder

Can. J. Chem. Downloaded from www.nrcresearchpress.com by 91.121.58.235 on 09/08/12
For personal use only.

Abstract: Electromotive force (EMF) measurements based on the redox reaction

$$Li_xHg(l) + TlBr(s) \rightleftharpoons LiBr(solv, c_{LiBr}) + Tl_xHg(l)$$

are reported for solutions of LiBr at concentrations $0.005 < c_{LiBr}/(\text{mol dm}^{-3}) < 0.1$ in acetonitrile (AN), dimethyl sulfoxide (DMSO), and *N,N*-dimethylacetamide (DMA) in the temperature range $278.15 < T/\text{K} < 308.15$. Gibbs energies of transfer and activity coefficients are estimated. The association constants of LiBr in AN, DMSO, and DMA from EMF measurements and the enthalpy of transfer AN → DMSO are compared to those from other methods of determination.

Key words: temperature-dependent EMF measurements, aprotic solvents, LiBr, TlBr(s) | $Tl_xHg(l)$ electrode, activity coefficients, transfer quantities.

Résumé : On rapporte les résultats de mesures de force électromotrice (FÉM) basées sur la réaction rédox

$$Li_xHg(l) + TlBr(s) \rightleftharpoons LiBr(solv, c_{LiBr}) + Tl_xHg(l)$$

pour des solutions de LiBr à des concentrations de $0{,}005 < c_{LiBr}/(\text{mol dm}^{-3}) < 0{,}1$ dans l'acétonitrile (AN), le diméthylsulfoxyde (DMSO) et le *N,N*-diméthylacétamide (DMA), à des températures allant de 278,15 à 308,15 K. On a évalué les énergies de Gibbs de transfert et les coefficients d'activité. On compare les constantes d'association du LiBr dans AN, DMSO et DMA et l'enthalpie de transfert AN → DMSO obtenues par la méthode des mesures de FÉM avec les valeurs correspondantes tirées d'autres méthodes de détermination.

Mots clés : mesures de FÉM en fonction de la température, solvants aprotiques, LiBr, électrode TlBr(s) | $Tl_xHg(l)$, coefficients d'activité, quantités de transfert.

[Traduit par la rédaction]

1. Introduction

The measurement of the electromotive force (EMF) of a galvanic cell requires reversible electrodes. Reversibility depends on the electrode materials and on the solvent of the electrolyte solution. Various reversible electrode systems are known for aqueous electrolyte solutions. For nonaqueous solutions the choice is rather small, especially for solutions in aprotic solvents, despite increasing technological interest. In this paper the galvanic cell without liquid junction

$$Pt \mid Li_xHg(l) \mid LiBr(solv, c_{LiBr}) \mid TlBr(s) \mid Tl_xHg(l) \mid Pt$$

is used for the determination of activity coefficients of lithium bromide at temperatures $278.15 < T/\text{K} < 308.15$ in the dipolar aprotic solvents acetonitrile (AN), dimethyl sulfoxide (DMSO), and *N,N*-dimethylacetamide (DMA), and for the estimation of Gibbs energies and enthalpies of transfer from AN to DMSO and DMA.

1.1 Chemical potentials and equilibria in the solution

The chemical potentials of an electrolyte solution made up by a symmetrical electrolyte E in a solvent S at Temperature T and pressure p are given by the relationships

$$[1a] \qquad \mu_S(p, T) = \mu_S^*(p, T) + RT \ln a_S$$

Received February 14, 1997.

This paper is dedicated to Professor Brian E. Conway on the occasion of his 70th birthday.

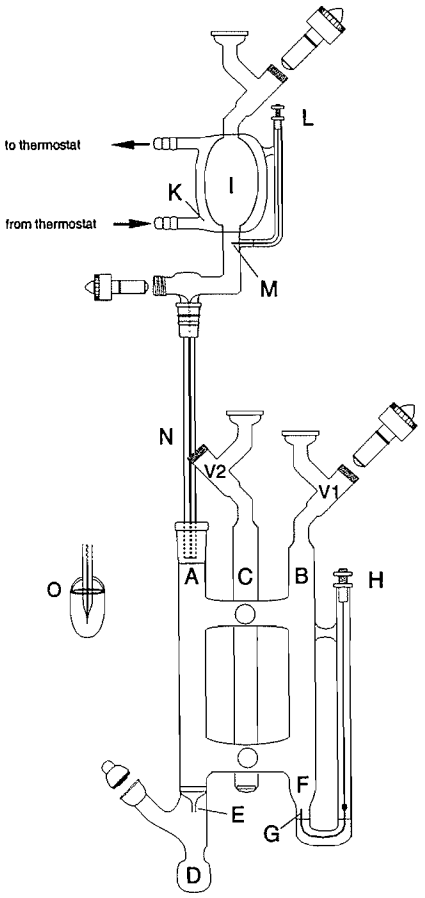
J. Barthel,[1] R. Neueder, and A. Schröder. Institute of Physical and Theoretical Chemistry, University of Regensburg, Universitätsstrasse 31, D-93040 Regensburg, Germany.

[1] Author to whom correspondence may be addressed. Telephone: (941) 943-4044. Fax: (941) 943-4532. E-mail: Josef.Barthel@chemie.uni-regensburg.de

© 1997 NRC Canada

Can. J. Chem. Downloaded from www.nrcresearchpress.com by 91.121.58.235 on 09/08/12
For personal use only.

Fig. 1. Measuring cell. A: electrode compartment, B: reference electrode compartment, C: solution compartment, D: amalgam collecting vessel, E: capillary, F: position of reference electrode, G: platinum wire, H: connection to voltmeter, I: amalgam reservoir, K: water jacket (thermostated), L: connection to voltmeter, M: platinum wire, N: capillary, O: tip of the capillary (modified for measurements in DMSO and DMA), V1, V2: valves.



$$[1b,c] \quad \lim_{x_S \to 1} \mu_S = \mu_S^*; \qquad \lim_{x_S \to 1} f_S = 1$$

$$[2a] \quad \mu_E(p, T) = \mu_E^{\infty(c)}(p, T) + 2\,RT \ln c_E y_\pm$$

$$[2b,c] \quad \lim_{x_S \to 1} [\mu_E - 2\,RT \ln c_E] = \mu_E^{\infty(c)}; \qquad \lim_{x_S \to 1} y_\pm = 1$$

The reference potential of the solvent is the pure solvent (superscript $*$), that of the electrolyte is the infinitely dilute solution (superscript ∞). The activity coefficients of solvent and solute take into account the respective concentration scales (f: mole fraction scale; x; $y_\pm$: molarity scale, c), a_S is the activity of the solvent, $a_S = x_S f_S$.

The formation of neutral ion pairs X in the solution

$$[3] \quad C^+ + A^- \rightleftharpoons X$$

may be taken into account in the chemical potential with the help of the potentials of "free" cations, "free" anions, and ion pairs X (superscript ′) resulting from the analytical concentrations c_E of the electrolyte and the degree of dissociation α of the ion pair X

$$[4a] \quad \mu_E(p, T) = \alpha\mu'_+(p, T) + \alpha\mu'_-(p, T) + (1 - \alpha)\mu'_X(p, T)$$

and underlying the equilibrium condition

$$[4b] \quad \mu'_X(p, T) - \mu'_+(p, T) - \mu'_-(p, T) = 0$$

The combination of eqs. [4a] and [4b] yields the chemical potential of the associating electrolyte

$$[5a] \quad \mu_E(p, T) = \mu_E^{\infty(c)}(p, T) + 2\,RT \ln c_E y_\pm$$

where the overall activity coefficient

$$[5b] \quad y_\pm = \alpha y'_\pm$$

depends on the activity coefficient of the "free" ions $y'_\pm$ and the degree of dissociation α. Equation [4b] yields the association constant K_A

$$[6] \quad K_A^{(c)} = \frac{(1 - \alpha)\, y'_X}{\alpha^2 c_E\, y'^2_\pm}$$

related to the Gibbs energy ΔG_A^∞ of ion-pair formation according to eq. [3]

$$[7] \quad \Delta G_A^\infty = -RT \ln K_A$$

1.2 Electromotive force

The galvanic cell without liquid junction (superscript is phase index)

$$Pt^{(1)}|Li_xHg(l)^{(2)}|LiBr(solv, c_{LiBr})^{(3)}|TlBr(s)^{(4)}|Tl_xHg(l)^{(5)}|Pt^{(1)}$$

involves the chemical reaction

$$[8] \quad Li_xHg(l)^{(2)} + TlBr(s)^{(4)} \rightleftharpoons LiBr(solv, c_{LiBr})^{(3)} + Tl_xHg(l)^{(5)}$$

where $Li_xHg(l)$ is the lithium amalgam electrode and $TlBr(s)\,|\,Tl_xHg(l)$ is the thallium bromide – thallium amalgam reference electrode. The electrolyte solution is a lithium bromide solution at concentration c_{LiBr} in the specified solvent.

The EMF of the galvanic cell without liquid junction shown above is given by the Nernst equation

$$[9] \quad E = E^0 - \frac{RT}{F} \ln a_{LiBr} - \frac{RT}{F} \ln \frac{a_{Tl_xHg}}{a_{Li_xHg}}$$

When, in a series of measurements, the metal concentration of the two amalgams Tl_xHg and Li_xHg is kept constant, eq. [9] may be written

$$[10] \quad E = E'^0 - \frac{2RT}{F} \ln (c_{LiBr} y_\pm)$$

© 1997 NRC Canada

Table 1. EMF data of galvanic cells without liquid junction.[a]

Cell: $Li_xHg(l)$ | LiBr(AN, c_{LiBr}) | TlBr(s) | $Tl_xHg(l)$

278.15 K		288.15 K		293.15 K		298.15 K		308.15 K	
c_{LiBr}	E	c_{LiBr}	E	c_{LiBr}	E	c_{LiBr}	E	c_{LiBr}	E
0.00533	1.2439	0.00526	1.2396	0.00523	1.2395	0.00519	1.2357	0.00511	1.2316
0.00592	1.2449	0.00585	1.2387	0.00581	1.2352	0.00576	1.2337	0.00568	1.2282
0.00871	1.2277	0.00859	1.2231	0.00853	1.2207	0.00847	1.2189	0.00835	1.2147
0.02287	1.1962	0.02257	1.1910	0.02241	1.1878	0.02226	1.1859	0.02194	1.1799
0.03424	1.1827	0.03379	1.1766	0.03356	1.1736	0.03332	1.1708	0.03284	1.1647
0.05371	1.1716	0.05301	1.1651	0.05264	1.1623	0.05227	1.1585	0.05152	1.1537

Cell: $Li_xHg(l)$ | LiBr(DMSO, c_{LiBr}) | TlBr(s) | $Tl_xHg(l)$

293.15 K		298.15 K		303.15 K		308.15 K	
c_{LiBr}	E	c_{LiBr}	E	c_{LiBr}	E	c_{LiBr}	E
0.01151	1.7254	0.01145	1.7251	0.01140	1.7246	0.01135	1.7239
0.01262	1.7211	0.01257	1.7204	0.01251	1.7202	0.01245	1.7195
0.02404	1.6911	0.02393	1.6900	0.02382	1.6895	0.02371	1.6886
0.03525	1.6737	0.03509	1.6724	0.03494	1.6718	0.03478	1.6705
0.05343	1.6558	0.05318	1.6541	0.05294	1.6527	0.05270	1.6514
0.05617	1.6535	0.05592	1.6514	0.08606	1.6296	0.05541	1.6489
		0.08645	1.6317			0.08567	1.6278

Cell: $Li_xHg(l)$ | LiBr(DMA, c_{LiBr}) | TlBr(s) | $Tl_xHg(l)$

288.15 K		298.15 K		308.15 K	
c_{LiBr}	E	c_{LiBr}	E	c_{LiBr}	E
0.03611	1.5427	0.02378	1.5519	0.02354	1.5430
0.05861	1.5213	0.03575	1.5345	0.03540	1.5275
0.07539	1.5088	0.05803	1.5135	0.06028	1.5033
0.09562	1.4980	0.07464	1.5032	0.07390	1.4953
		0.09467	1.4925	0.09373	1.4850

[a]Dimensions of c_{LiBr}: mol dm^{-3}; E: V.

with a reference potential E'^0 depending on the constant activities of the amalgams

$$[11] \qquad E'^0 = E^0 - \frac{RT}{F} \ln \frac{a_{Tl_xHg}}{a_{Li_xHg}}$$

2. Experimental

2.1 Purification of solvents and solutes

Acetonitrile (Baker, analyzed HPLC reagent) was first passed through an Al_2O_3 column (acid Al_2O_3, Woelm, Eschwege) under purified nitrogen, then boiled (48 h) over calcium hydride (1) and distilled. The final distillation over a packed column reduced the water content to less than 30 ppm and the specific conductivity to less than 3×10^{-8} S cm^{-1}.

Dimethyl sulfoxide (Fluka, purum) was dried with molecular sieve (4 Å) and then flushed with pure nitrogen (5–6 days) to remove volatile impurities. After addition of calcium hydride it was refluxed for 2 days and then distilled under reduced pressure (~2 mbar). The water content of the product was less than 50 ppm and the specific conductivity was less than 10^{-8} S cm^{-1}.

N,N-Dimethylacetamide (Aldrich, HPLC-pure) was treated with molecular sieve (4 Å) for some days to reduce the water content to less than 35 ppm.

Lithium bromide (Merck, suprapur) was predried at 80°C under reduced pressure (<10^{-2} mbar) in the presence of P_2O_5. The temperature was then slowly increased and kept at 150°C for several days.

Thallium bromide was obtained from an aqueous solution of thallium(I) sulfate (Aldrich, 99%, gold label) by precipitation with sodium bromide (Merck, suprapur). After filtration the thallium bromide was dried under reduced pressure (<10^{-2} mbar). The preparation and storage took place under exclusion of light.

© 1997 NRC Canada

Can. J. Chem. Downloaded from www.nrcresearchpress.com by 91.121.58.235 on 09/08/12
For personal use only.

Can. J. Chem. Downloaded from www.nrcresearchpress.com by 91.121.58.235 on 09/08/12
For personal use only.

Fig. 2. Chemical model of electrolyte solution. Ion j in an arbitrary position r with regard to ion i; special positions (contact, separation by one or two orientated solvent molecules) are sketched; a, R, distance parameters; W_{ij}, mean force potentials.

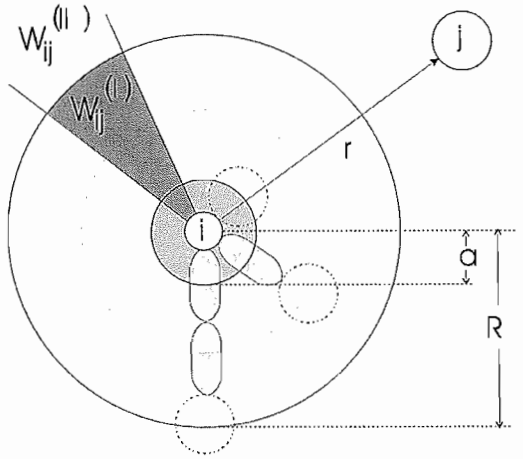
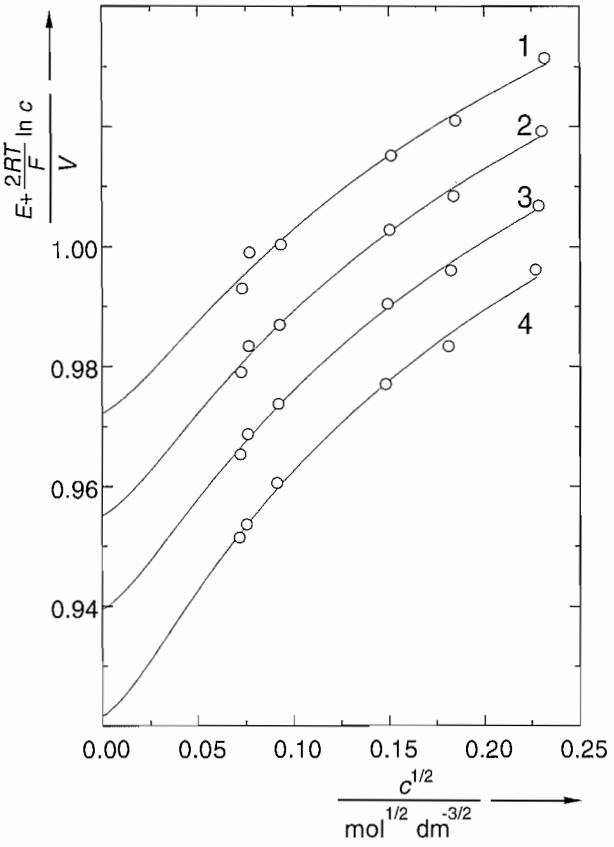


Fig. 3. EMF data of LiBr in AN FROM 278.15 K to 308.15 K. **1**: 278.15 K, **2**: 288.15 K, **3**: 298.15 K, **4**: 308.15 K (explanation in text).



The mercury used for the preparation of the amalgams was repeatedly purified in purification towers (height ~1 m, diameter 2 cm), filled with dilute nitric acid, water, and acetone. At the top of each tower a stream of mercury from a reservoir was directed to the walls, which have small indentations to produce tiny mercury droplets that are forced to pass the purification tower in a zigzag path from the top to the bottom where the mercury was collected. With the help of these towers the mercury was purified several times. Finally the mercury was distilled three times at a pressure below 0.1 mbar.

2.2 Preparation of the amalgams

The lithium amalgam was prepared in a glove box by dissolving a weighed quantity of lithium metal (Chemetall, purity >99.95%) in a known quantity of mercury under pure argon (oxygen, nitrogen, and water content <1 ppm), followed by storage for 6 weeks in special containers from which the amalgam was drawn off for use by a valve at the bottom.

Thallium (Alfa, 99.998% pure) was cleaned of its black oxide layer by rinsing it with argon-saturated dilute sulfuric acid. After carefully rinsing with argon-saturated distilled water the thallium was dried under reduced pressure and stored in a glove box under argon protection. The same method used for the lithium amalgam was applied to the preparation of thallium amalgam (2).

2.3 EMF measurements

The measuring cell, which is made up of two parts, is shown in Fig. 1. The lower part filled with the electrolyte solution is situated in a thermostat with a precision of 10^{-2} K and a reproducibility of 10^{-3} K. The upper part containing the amalgam is kept at equal temperature with the help of a water jacket (K). The electrodes are linked via the connections (L) and (H) to a preamplifier (Knick, 72 W) of input resistance $>5 \times 10^{12}$ Ω. The amplified potential is measured with the help of a digital voltmeter (Data Precision, type 2540A).

EMF measurements carried out using lithium amalgam electrodes require strong protection against oxygen, nitrogen, and water. The capillary (N) of the dropping electrode is introduced (at ground glass joint A) into the measuring cell. The second arm (B) contains the reference electrode and the third arm (C) permits the introduction of the solution and of argon. An amalgam collecting vessel (D) linked to the electrode chamber via a capillary (E) separates the amalgam dripped off the dropping electrode from the solution in the measuring cell, thus avoiding its pollution and chemical reaction with the solvent.

The electrolyte solution is prepared in a separate solution flask and saturated with TlBr to decrease the time for the reference electrode to equilibrate. At the beginning of the measurement the cell is evacuated and flushed several times with argon. The following procedures are all executed under the protection of pure argon.

After a small amount of TlBr is introduced into the cell through valve V1 four drops of thallium amalgam are placed in the reference electrode position (F) with an amalgam level higher than the top of the platinum wire (G). The surface of the amalgam is completely coated by the TlBr crystals previously introduced into the cell. The electrolyte solution is then transferred from the solution flask under slight overpressure through valve V2. The dropping electrode is filled with lithium amalgam (I), which is in contact with the preamplifier via the platinum wire (M). The whole measuring assembly is thermostated for at least 1 h. After reaching thermal equilibrium the amalgam outlet is activated. To increase the stability of the

© 1997 NRC Canada

Can. J. Chem. Downloaded from www.nrcresearchpress.com by 91.121.58.235 on 09/08/12
For personal use only.

Table 2. Reference potentials E'^0 and association constants from EMF measurements of solutions of LiBr in aprotic solvents at various temperatures.[a]

	T	c	E'^0	K_A	$\sigma \times 10^3$
LiBr–acetonitrile					
	278.15	0.005–0.05	0.9722	121.7	2.0
	288.15	0.005–0.05	0.9551	146.9	1.3
	293.15	0.005–0.05	0.9479	147.3	1.0
	298.15	0.005–0.05	0.9394	160.4	1.1
	308.15	0.005–0.05	0.9216	198.4	1.3
LiBr–DMSO					
	293.15	0.01–0.06	1.4889	1.9	0.3
	298.15	0.01–0.09	1.4844	1.6	0.3
	303.15	0.01–0.09	1.4802	1.4	0.3
	308.15	0.01–0.09	1.4752	1.9	0.4
LiBr–DMA					
	288.15	0.04–0.10	1.3619	0.0	0.6
	298.15	0.02–0.09	1.3415	6.2	0.4
	308.15	0.02–0.09	1.3231	10.8	1.0

[a]Dimensions of T: K; c; mol dm^{-3}; E'^0, σ: V; K_A: dm^3 mol^{-1}.

Table 3. Comparison of the association constants of LiBr solutions at 25°C from various experimental methods.[a]

	This paper		Literature		
Solvent	K_A	Conc. range	K_A	Conc. range	Method
AN	160	0.005–0.05	168	0.03–0.15	Vapor pressure (5)
			191	$(0.6–8.0) \times 10^{-3}$	Conductivity (6)
			148	0.1–0.66	Microwave spectroscopy (7)
DMSO	1.5	0.01–0.09	1.4	0.02–0.15	EMF (8)
			6.9	$(0.4–2.5) \times 10^{-3}$	Conductivity (9)

[a]Dimensions of K_A:dm^3 mol^{-1}; conc. range: mol dm^{-3}.

cell voltage in acetonitrile solutions, the diameter of the capillary of the electrode is reduced to produce a thin jet of mercury instead of drops. In contrast, for the measurements in DMSO and DMA solutions, a little beaker (O) is attached at the end of the capillary to produce large drops with a rate of one drop per second. With these variations, a constant cell potential within ±0.1 mV is attained after 2 min. After about 10 min the temperature of the thermostat is changed to the next point of the program. Measurements are carried out in a cycle 25–15–5–35–25°C. The two potentials at the beginning and end of each cycle at 25°C differ by less than 0.3 mV.

3. Results

Table 1 summarizes the results of the EMF measurements in acetonitrile, DMSO, and DMA at different temperatures. The mole fraction of thallium in the thallium amalgam was 0.00595; the mole fraction of lithium in the lithium amalgam was 0.00382 in AN and 0.00401 in DMSO and in DMA.

4. Discussion

4.1 Chemical model

Appropriate equations for the properties of electrolyte solutions in the concentration range studied are obtained with the help of the chemical model (CM) of electrolyte solutions (3, 4), subdividing the space around an ion into three regions (cf. Fig. 2): (*i*) $r \leq a$, a being the minimum distance of two oppositely charged ions, which is assumed to be the sum of the effective cation and anion radii, $a = a_+ + a_-$; (*ii*) $a \leq r \leq R$, within which a paired state of oppositely charged ions, the ion pair, suppresses long-range interactions with other ions in the solution. In dilute solutions the occupancy of this region by ions of equal sign can usually be neglected; (*iii*) $r \geq R$, the region of long-range ion–ion Coulomb interaction.

The chemical model is a Hamiltonian model on the McMillan–Mayer level. Its distance parameters a (minimum distance of two ions) and R (upper limit of the structured region around an ion) are fixed by chemical evidence:

© 1997 NRC Canada

Table 4. Experimental and calculated activity coefficients of LiBr.[a]

AN				DMSO				DMA			
c	$y_{\pm}^{exp}$	$y_{\pm}^{calc}$	α	c	$y_{\pm}^{exp}$	$y_{\pm}^{calc}$	α	c	$y_{\pm}^{exp}$	$y_{\pm}^{calc}$	α
T = 278.15 K				T = 293.15 K				T = 288.15 K			
0.00533	0.648	0.622	0.749	0.01151	0.805	0.808	0.986	0.03611	0.726	0.725	1.000
0.00592	0.572	0.607	0.735	0.01262	0.800	0.802	0.984	0.05861	0.689	0.697	1.000
0.00871	0.556	0.549	0.681	0.02404	0.760	0.755	0.974	0.07539	0.689	0.683	1.000
0.02287	0.409	0.407	0.539	0.03525	0.732	0.725	0.964	0.09562	0.675	0.671	1.000
0.03424	0.362	0.353	0.481	0.05343	0.688	0.690	0.951				
0.05371	0.291	0.298	0.420	0.05617	0.685	0.686	0.949				
T = 288.15 K				T = 298.15 K				T = 298.15 K			
0.00526	0.618	0.601	0.721	0.01145	0.807	0.811	0.988	0.02378	0.701	0.696	0.929
0.00585	0.566	0.585	0.707	0.01257	0.805	0.805	0.987	0.03575	0.654	0.657	0.905
0.00859	0.528	0.526	0.651	0.02393	0.764	0.760	0.978	0.05803	0.606	0.607	0.868
0.02257	0.383	0.385	0.508	0.03509	0.734	0.731	0.971	0.07464	0.576	0.580	0.845
0.03379	0.342	0.333	0.451	0.05318	0.692	0.697	0.960	0.09467	0.559	0.554	0.821
0.05301	0.275	0.280	0.392	0.05592	0.693	0.693	0.958				
				0.08645	0.658	0.657	0.942				
T = 293.15 K				T = 303.15 K				T = 308.15 K			
0.00523	0.596	0.601	0.722	0.01140	0.816	0.813	0.989	0.02354	0.676	0.663	0.888
0.00581	0.584	0.585	0.707	0.01251	0.809	0.807	0.988	0.03540	0.602	0.618	0.854
0.00853	0.530	0.526	0.652	0.02382	0.764	0.762	0.980	0.06028	0.557	0.555	0.799
0.02241	0.387	0.386	0.509	0.03494	0.731	0.733	0.973	0.07390	0.529	0.531	0.775
0.03356	0.342	0.333	0.452	0.05294	0.695	0.701	0.963	0.09373	0.506	0.502	0.745
0.05264	0.273	0.280	0.393	0.08606	0.666	0.661	0.947				
T = 298.15 K				T = 308.15 K							
0.00519	0.603	0.591	0.710	0.01135	0.815	0.811	0.986				
0.00576	0.565	0.575	0.695	0.01245	0.807	0.805	0.985				
0.00847	0.513	0.516	0.639	0.02371	0.758	0.758	0.974				
0.02226	0.371	0.376	0.496	0.03478	0.727	0.728	0.965				
0.03332	0.332	0.324	0.439	0.05270	0.688	0.694	0.951				
0.05227	0.269	0.272	0.381	0.05541	0.685	0.690	0.950				
				0.08567	0.660	0.652	0.930				
T = 308.15 K											
0.00511	0.571	0.565	0.677								
0.00568	0.548	0.548	0.661								
0.00835	0.480	0.489	0.604								
0.02194	0.352	0.352	0.462								
0.03284	0.313	0.302	0.407								
0.05152	0.246	0.252	0.351								

[a]Dimension of c : mol dm^{-3}.

Can. J. Chem. Downloaded from www.nrcresearchpress.com by 91.121.58.235 on 09/08/12
For personal use only.

© 1997 NRC Canada

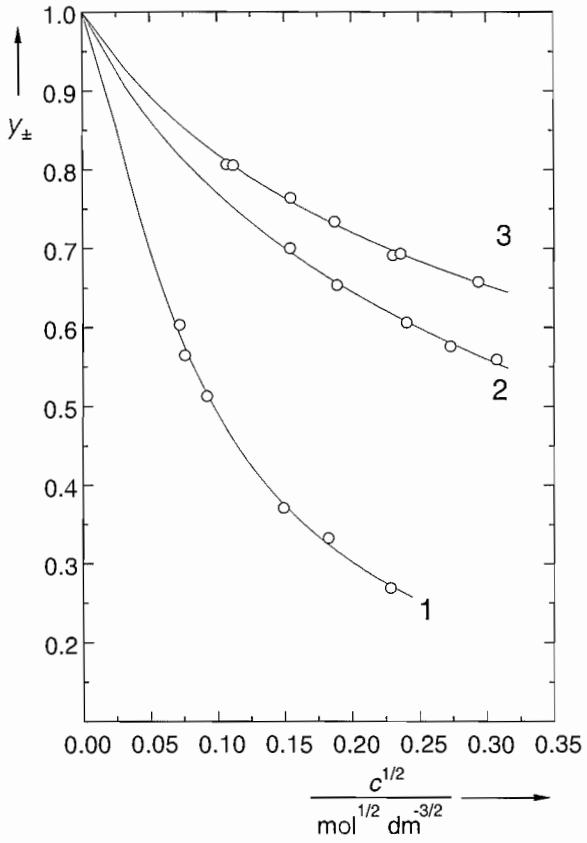
Table 5. Gibbs energy of transfer of LiBr from AN to DMSO and DMA.[a]

T	E'° AN	E'°_{corr} AN	E'° DMSO	E'° DMA	$\Delta_t G^{\infty}$ AN → DMSO	$\Delta_t G^{\infty}$ AN → DMA
288.15	0.9551	0.9564		1.3619		−39.13
293.15	0.9479	0.9492	1.4889		−52.08	
298.15	0.9394	0.9408	1.4844	1.3415	−52.45	−38.66
308.15	0.9216	0.9230	1.4752	1.3231	−53.29	−38.61

[a]Dimensions of T: K; E'°: V; $\Delta_t G^{\infty}$: kJ mol^{-1}.

Can. J. Chem. Downloaded from www.nrcresearchpress.com by 91.121.58.235 on 09/08/12
For personal use only.

Fig. 4. Mean molar activity coefficients of LiBr at 298.15 K. **1**: AN, **2**: DMA, **3**: DMSO (Lines calculated according to the chemical model (Fig. 2) using the association constants from Table 2).



The lower distance a is fixed as a hard-core radius by the center-to-center distance of the ions.

The upper distance R is obtained for 1.1 electrolytes in aprotic solvents of moderate relative permittivity by adding the length of an orientated solvent molecule to the distance of closest approach; $R = a + s$.

The ion-pair concept is introduced into the chemical model when setting the cutoff distance parameter R of the short-range forces equal to the upper limit of association, yielding the integral (3)

$$[12] \quad \int_a^R r^2 \exp\left(-\frac{W_{+-}}{kT}\right) dr = \exp\left[-\frac{2\kappa q}{(1+\kappa R)}\right] \int_a^R r^2 \times \exp\left(\frac{2q}{r} - \frac{W^*_{+-}}{kT}\right) dr$$

where W^*_{+-} is the non-Coulombic part of the potential of mean force W_{+-}. Equation [12] is linked to the ion-pair association constant K_A (dimension: dm^3 mol^{-1}) and the mean activity coefficient $y'_{\pm}$ of the free ions by the relationship

$$[13a] \quad \frac{1-\alpha}{\alpha^2 c y'^2_{\pm}} = K_A^{(c)} = 4000\pi N_A \int_a^R r^2 \exp\left(\frac{2q}{r} - \frac{W^*_{+-}}{kT}\right) dr$$

$$[13b,c] \quad y'_{\pm} = \exp\left(-\frac{\kappa q}{1+\kappa R}\right); \qquad q = \frac{|z_+ z_-| e_0^2}{8\pi\varepsilon_0 \varepsilon kT}$$

The ion pair is represented by an uncharged particle in a spherical box of radius R, meaning that an ion pair is formed if two oppositely charged ions approach to within a distance smaller than R.

4.2 Data analysis

The basis of the data analysis according to eq. [10] for EMF measurements of solutes that exhibit ion-pair formation are the mean molar activity coefficient of the "free ions" (eq. [13*b*]) and the association constant K_A (eq. [13*a*]), which permit the calculation of the degree of ion-pair dissociation needed for the introduction of eq. [5*b*] into eq. [10]. The Debye parameter κ depends on the concentration αc of the free ions.

$$[14] \quad \kappa^2 = \frac{16\pi N_A e_0^2}{8\pi\varepsilon_0 \varepsilon kT} \alpha c_{LiBr}$$

Equation [10] is transformed to fit the EMF data of associated electrolytes

$$[15] \quad E = E'^0 - \frac{2RT}{F} \ln(\alpha c_{LiBr} y'_{\pm})$$

Equation [15] is used to determine the reference potential E'^0 (which is not a standard potential because it contains the activity of the amalgams, eq. [11]) and the association constant K_A as the adjustable parameters. Figure 3 shows EMF data for

© 1997 NRC Canada

Can. J. Chem. Downloaded from www.nrcresearchpress.com by 91.121.58.235 on 09/08/12
For personal use only.

LiBr in acetonitrile at different temperatures as an example. The points are the measured values of $E + (2RT/F) \ln c$ and the lines represent the function $E'^0 - (2RT/F) \ln(\alpha y'_{\pm})$, adapted to the experimental data with the help of the chemical model. This procedure yields the parameters E'^0 and K_A given in Table 2, which also shows the results for LiBr–DMSO and LiBr–DMA solutions.

4.3 Association constants and activity coefficients

Lithium bromide shows a strong tendency to form ion pairs in AN, whereas in DMSO and in DMA this tendency is weak. In AN and DMA the association constant increases with temperature, but in DMSO no significant temperature dependence could be detected. Association constants in AN and DMSO also exist from different experiments and may be compared to the EMF results. Taking into account the different concentration ranges of the experiments, Table 3 shows fair agreement between the association constants obtained by various experimental methods.

The activity coefficients $y_{\pm}$ of LiBr in AN, DMSO, and DMA are available from the E'^0 values of Table 2 and the experimental electrical potentials E with the help of eq. [10]. These experimental values at 25°C are shown in Fig. 4 together with chemical model calculations using the association constants of Table 2.

The much stronger decrease of the activity coefficient of LiBr in AN in comparison with DMSO and DMA is the consequence of the association constant of LiBr being the highest in this series of solvents. In DMSO LiBr is almost completely dissociated. The experimentally determined activity coefficients are given in Table 4 together with the values from CM calculations and of the degree of dissociation.

4.4 Transfer energies

The Gibbs energy of transfer of LiBr at infinite dilution from solvent S_1 to solvent S_2, $\Delta_T G^{\infty}_{LiBr}$, is obtained from the standard electrode potentials

$$[16] \quad \Delta_T G^{\infty}_{LiBr} = -F(E^0_{S_2} - E^0_{S_1}) = -F(E'^0_{S_2} - E'^0_{S_1}) - RT \ln \left[\left(\frac{a_{Tl_xHg}}{a_{Li_xHg}} \right)_{S_2} \left(\frac{a_{Li_xHg}}{a_{Tl_xHg}} \right)_{S_1} \right]$$

At equal amalgam concentrations in each measurement the Gibbs energy of transfer is equal to the difference of the reference potentials $-F(E'^0_{S_2} - E'^0_{S_2})$. Because of the measurements in AN with a slightly different lithium concentration of the lithium amalgam electrode, the electrode potentials were corrected with the help of the activity coefficient data of Mussini et al. (10) according to their equation

$$\log f_{Li} = Q \times x_{Li}, \qquad Q = 18.48 - 3.00 \times 10^{-2}\, T$$

to calculate the activity coefficient of lithium in mercury in the temperature range $283 \leq T/K \leq 313$. The reference potential of acetonitrile ($x_{Li} = x_1 = 0.00382$) solutions corrected to the concentration of DMSO and DMA ($x_{Li} = x_2 = 0.00401$) is then

$$[17] \quad E'^0(x_2) = E'^0(x_1) + \frac{RT}{F} \ln \frac{x_2}{x_1} + \frac{RT}{F} Q \ln 10 (x_2 - x_1)$$

These corrected reference potentials are used to obtain the Gibbs energies of transfer from AN to DMSO or DMA, respectively, see Table 5.

The temperature dependence of the reference potentials yields the entropy of transfer, $\Delta_T S^{\infty}$, and the enthalpy of transfer, $\Delta_T H^{\infty}$, according to

$$[18] \quad \Delta_T S^{\infty} = F \left[\left(\frac{\partial E'^0}{\partial T} \right)_{S_2} - \left(\frac{\partial E'^0}{\partial T} \right)_{S_1} \right]$$

$$[19] \quad \Delta_T H^{\infty} = -F(E'^0_{S_2} - E'^0_{S_1}) + TF \left[\left(\frac{\partial E'^0}{\partial T} \right)_{S_2} - \left(\frac{\partial E'^0}{\partial T} \right)_{S_1} \right]$$

Heat of solution data determined by calorimetric methods in different solvents are another source for enthalpy of transfer data. The enthalpies of solution of LiBr in AN (11), $\Delta_{sol} H^{\infty}_{LiBr}$ (AN) = −38.84 kJ mol^{-1} (transformed to the molarity from the molarity scale), $\Delta_{sol} H^{\infty(m)}_{LiBr}$ (AN) = −39.91 kJ mol^{-1}), and in DMSO (12), $\Delta_{sol} H^{\infty}_{LiBr}$ (DMSO) = −71.5 kJ mol^{-1}, yield a value of −32.7 kJ mol^{-1}, for the enthalpy of transfer from AN to DMSO in agreement with $\Delta_T H^{\infty}_{LiBr}$ = −30.1 kJ mol^{-1} obtained from the temperature dependence of the EMF data. Enthalpies of solution for LiBr–DMA from calorimetric measurements are not known.

References

1. J. Barthel, R. Neueder, M. Poxleitner, J. Seitz-Beywl, and L. Werblan. J. Electroanal. Chem. **344**, 249 (1993).
2. M. Salomon. J. Phys. Chem. **73**, 3299 (1969).
3. J. Barthel. Ber. Bunsen-Ges. Phys. Chem. **83**, 252 (1979).
4. J. Barthel. Pure Appl. Chem. **51**, 2093 (1979).
5. W. Kunz, J. Barthel, L. Klein, T. Cartailler, P. Turq, and B. Reindl. J. Solution Chem. **20**, 875 (1991).
6. H. Roch. Dissertation, Regensburg (1991).
7. M. Kleebauer. Dissertation, Regensburg (1990).
8. M. Salomon. J. Electrochem. Soc. **116**, 1392 (1969).
9. G. Pistoia, A.M. Polcaro, and S. Schiavo. Ric. Sci. **37**, 227 (1967).
10. T. Mussini, P. Longhi, and S. Rondini. Pure Appl. Chem. **57**, 169 (1985).
11. R.F. Rodewald, K. Mahendran, J.L. Bear, and R. Fuchs. J. Am. Chem. Soc. **90**, 6698 (1968).
12. Y.S. Choi and C.M. Criss. J. Chem. Eng. Data, **22**, 297 (1977).

© 1997 NRC Canada

Theory of electrochemical impedance of surface reactions: second-harmonic and large-amplitude response

David A. Harrington

Can. J. Chem. Downloaded from www.nrcresearchpress.com by 91.121.58.235 on 09/08/12
For personal use only.

Abstract: The theory for the electrochemical impedance of surface reactions involving a single adsorbed species is presented. A new methodology is used, in which many harmonics are considered, and the differential equations are reduced to algebraic matrix equations. The amplitude of the ac potential perturbation is not assumed to be small, and nonlinear effects are taken into account. The amplitude dependence of the impedance and the second-harmonic response are investigated. The quasi-reversible electrosorption reaction and the hydrogen evolution reaction are considered in detail, assuming that the adsorbed species obeys the Langmuir isotherm.

Key words: electrochemistry, impedance, adsorption, hydrogen evolution reaction, second harmonic.

Résumé : On présente la théorie relative à l'impédance électrochimique des réactions de surface impliquant une seule espèce adsorbée. On a utilisé une nouvelle méthodologie, dans laquelle on considère plusieurs harmoniques, et les équations différentielles sont réduites à des équations de matrices algébriques. On considère que l'amplitude de la perturbation du potentiel ac n'est pas faible, et on tient compte des effets non linéaires. On a étudié l'influence de l'amplitude sur l'impédance ainsi que la réponse de la seconde harmonique. On a approfondi l'étude de la réaction quasi réversible d'électrosorption et la réaction de dégagement d'hydrogène en faisant l'hypothèse que les espèces adsorbées obéissent à l'isotherme de Langmuir.

Mots clés : électrochimie, impédance, adsorption, réaction de dégagement d'hydrogène, seconde harmonique.

[Traduit par la rédaction]

1. Introduction

In typical electrochemical impedance spectroscopy (EIS), a small ac potential perturbation is applied to the cell, and the ac current response is measured. A small perturbation is chosen so the inherently nonlinear electrochemical system can be approximated by a linear system. In this approximation, the measured impedance is independent of the amplitude of the perturbation and there is no second-harmonic response. Typically, a potential amplitude of $5/n$ mV RMS is assumed to be sufficiently small for linear behaviour, where n is the number of electrons transferred (1). In this work, the amplitude dependence of the impedance and the second-harmonic response are investigated for surface reactions. A new methodology is used that simplifies the differential equations to a system of algebraic equations.

Second and higher harmonics are of interest because they arise from the nonlinear behaviour of the system. This arises mainly from the electrochemical reaction, since double-layer charging effects are only weakly nonlinear and the solution conductivity is linear. Therefore the reaction can be studied free from interference by these other processes. A second potential advantage is that measurement of several harmonics may facilitate extraction of rate parameters at a single dc potential. Measurement of the amplitude dependence of the impedance offers similar advantages, aside from determining the amplitude below which small-signal analysis is valid. Often the number of independent parameters that can be extracted from a normal EIS experiment is less than the number of rate constants in the mechanism. If the second-harmonic response contains the rate constants in new combinations, it may allow more of the rate constants to be determined.

The theory for the second-harmonic response is well developed in the field of ac voltammetry, where the focus is on analytical applications and diffusion of products and reactants is significant (1, 2). Here the focus is on cases where mass transport is fast and diffusion does not influence the rate. These cases are particularly important in industrial electrochemical processes. Frequently, adsorbed species play a significant role, for example, in the hydrogen or chlorine evolution reactions. The case of a simple quasi-reversible electron transfer without adsorption will be considered first as an introduction to the methodology, though the results are equivalent to known results in the literature (3, 4). Single-step adsorption with the Langmuir isotherm follows. Then the hydrogen evolution reaction (HER) is discussed. The special case of the Volmer–Heyrovsky (V–H) mechanism under nonlinear conditions has been the subject of a recent controversy in the literature (5–7). The emphasis here is on the capabilities of the method, and not on an exhaustive investigation of the reactions discussed. The method presented here is easily extended

Received March 7, 1997.

This paper is dedicated to Professor Brian Conway on the occasion of his 70th birthday.

David A. Harrington.[1] Chemistry Department, University of Victoria, P.O. Box 3065, Victoria, BC V8W 3V6, Canada.

[1] Telephone: (250) 721-7166. Fax: (250) 721-7147. E-mail: dharr@uvic.ca

© 1997 NRC Canada

Can. J. Chem. Downloaded from www.nrcresearchpress.com by 91.121.58.235 on 09/08/12
For personal use only.

to other mechanisms with a single adsorbed species, and with a little more difficulty to mechanisms with more than one adsorbed species.

2. Theory

In all cases, mass transport is considered rapid, so that the surface concentration of soluble species is effectively constant and may be subsumed into the rate constants. The potential (or overpotential) is assumed to be the controlled variable, and it consists of dc and ac components:

$$[1] \quad \eta = \eta_{dc} + \Delta E \sin(\omega t)$$

The sine form is chosen here rather than the cosine form because a lock-in amplifier defines zero phase as the position of a zero crossing for a positive-going signal. Higher-harmonic phases are also assumed to be measured relative to sine waves, e.g., $\sin(2\omega t)$ for the second harmonic. After the ac signal has been switched on, there is a transient period that is not considered here. The current density is measured after the system settles. It consists of a dc part and various harmonics:

$$[2] \quad j = j(0) + j(\omega) + j(2\omega) + \ldots = j(0) + j_{1r}\sin(\omega t) + j_{1r}\cos(\omega t) + j_{2r}\sin(2\omega t) + j_{2i}\cos(2\omega t) + \ldots$$

The second and higher harmonics arise because of the nonlinear nature of the electrochemical reaction. That is, the slope of the current–potential characteristic is not constant. The impedance is defined in a way consistent with the way it is measured, for example, by a lock-in amplifier (though other instruments use the same phase conventions). The fundamental frequency part of the response is extracted by the instrument from among the other harmonics:

$$[3] \quad j_{1r}\sin(\omega t) + j_{1i}\cos(\omega t) = \Delta j_1 \cos(\varphi_1)\sin(\omega t) + \Delta j_1 \sin(\varphi_1)\cos(\omega t) = \Delta j_1 \sin(\omega t + \varphi_1)$$

It may be associated with the complex number

$$[4] \quad j_{1r} + j_{1i} i = \Delta j_1 \cos(\varphi_1) + \Delta j_1 \sin(\varphi_1) i = \Delta j_1 \exp(i\varphi_1)$$

The admittance is defined as the complex number for the current divided by the complex number for the potential (which is purely real since its phase has been chosen to be zero):

$$[5] \quad Y = (j_{1r} + j_{1i} i)/\Delta E = \Delta j_1 \exp(i\varphi_1)/\Delta E$$

As defined here, the admittance may depend on ΔE if the current response is not proportional to ΔE. This occurs for larger amplitude perturbations. The effect of the solution resistance and double-layer capacitance may be subtracted in the usual way to leave the faradaic part of the admittance or impedance. Quantities from here on will refer only to the faradaic part.

2.1 Simple electron-transfer reaction

The simplest case is an electron-transfer reaction, in which diffusion of products and reactants is fast compared to the reaction rate. Initially, we consider the irreversible case where only the forward reaction is significant, e.g.,

$$[6] \quad A(aq) \rightarrow A^+(aq) + e^-$$

Then the Tafel relationship links current and potential:

$$[7] \quad j = j_0 \exp(\alpha F \eta / RT)$$

For the conditions of the ac experiment

$$[8] \quad j = j_{dc} \exp(b \sin(\omega t))$$

where

$$[9] \quad j_{dc} = j_0 \exp(\alpha F \eta_{dc} / RT)$$

$$[10] \quad b = \alpha F \Delta E / RT$$

The quantity b should be thought of as a dimensionless potential amplitude. Now the task is simply to find the various harmonics of j, (i.e., $j(0), j(\omega), j(2\omega)$ in eq. [2]). In other words, the current should be expressed as a Fourier series. The Fourier series expansion $\exp(b\sin(\omega t))$ is known (8), though it has not been used much in electrochemistry (ref. 3 and the corrosion literature discussed in ref. 9 being exceptions). The coefficients are the modified Bessel functions:

$$[11] \quad j/j_{dc} = \exp(b\sin(\omega t)) = I_0(b) + 2I_1(b)\sin(\omega t) - 2I_2(b)\cos(2\omega t) - 2I_3(b)\sin(3\omega t) + 2I_4(b)\cos(4\omega t) + \ldots$$

$$= I_0(b) + 2\sum_{k=0}^{\infty} (-1)^k I_{2k+1}(b)\sin((2k+1)\omega t)$$

$$+ 2\sum_{k=1}^{\infty} (-1)^k I_{2k}(b)\cos(2k\omega t)$$

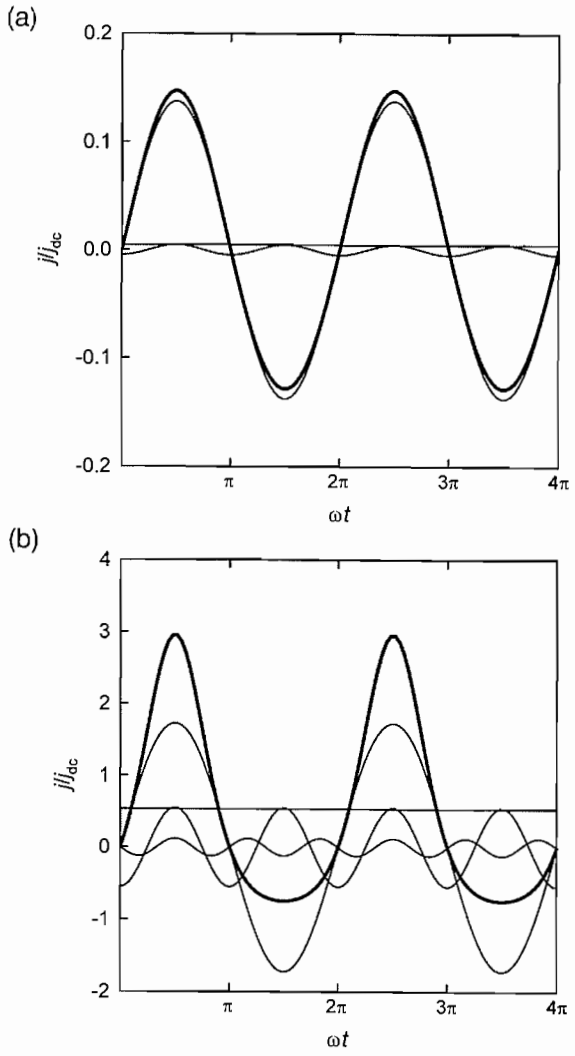
The Bessel functions are just steeply increasing functions of b. Their most important property in this context is that, for small b, they act like powers of b: $I_n(b) \sim (\frac{1}{2}b)^n/n!$. The difference between the actual current and the dc current, expressed as a fraction of the dc current, is plotted in Fig. 1 for two values of b. Taking $\alpha = \frac{1}{2}$ and a typical small-amplitude potential perturbation of 5 mV RMS gives $b = 0.14$. For this case (Fig. 1*a*), the total current response is well approximated by the first harmonic. The second harmonic can be neglected and there is not much change in the dc component (horizontal line is close to zero in the figure). But for a 50 mV RMS potential (Fig. 1*b*), the second harmonic now makes a significant contribution, and significant distortion of the current from the sinusoidal form occurs.

The dc part of the current response in the presence of the ac perturbation, $j(0)$, is different from the dc current without the perturbation, j_{dc} (the horizontal line in Fig. 1*b* is no longer at zero). This is the phenomenon of faradaic rectification (10), and it becomes more marked as the potential amplitude increases. Potentially, this relationship could be used to deter-

© 1997 NRC Canada

Can. J. Chem. Downloaded from www.nrcresearchpress.com by 91.121.58.235 on 09/08/12
For personal use only.

Fig. 1. Fourier components of current for a simple irreversible charge-transfer reaction. Bold line is total current, thinner lines are the first few Fourier components. (*a*) 5 mV RMS potential excitation; (*b*) 50 mV RMS potential excitation.



mine α, but the use of an ac measurement is simpler and avoids base-line errors (see below).

The lack of significant second-harmonic response in Fig. 1*a* suggests that the perturbation is sufficiently small for linear-systems theory to apply. Then the faradaic admittance is the slope of the current–potential curve, and the charge-transfer resistance is defined as the reciprocal of this:

$$[12] \quad Y_f = dj/dE = \alpha F j_{dc}/RT = 1/R_{ct}$$

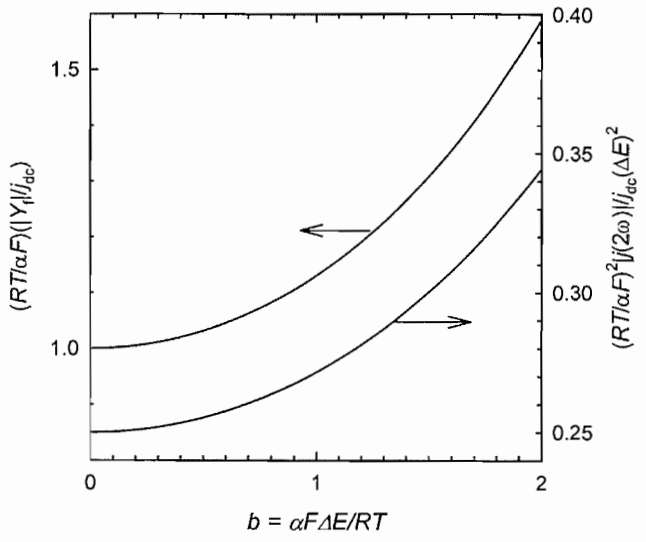
or

$$(RT/\alpha F)(Y_f/j_{dc}) = 1$$

The large-signal analysis above also has the first harmonic in phase with the potential (resistive behaviour):

$$[13] \quad j(\omega) = 2j_{dc}I_1(b)\sin(\omega t)$$

Fig. 2. Amplitude dependence of the fundamental and second-harmonic currents for a simple irreversible charge-transfer reaction.



so that the faradaic admittance is

$$[14] \quad Y_f = 2j_{dc}I_1(b)/\Delta E$$

or

$$(RT/\alpha F)(Y_f/j_{dc}) = 2I_1(b)/b$$

Now for small b, $2I_1(b)/b$ tends to one, so the admittance tends to the small-signal admittance above. But for higher amplitudes, the result departs from the small-signal limit as shown in Fig. 2. For example, the error is about 0.2% for a 5 mV signal, but rises to 26% for a 50 mV signal. Potentially, measurement of the amplitude of the first harmonic and j_{dc}, together with the known ΔE, allows solution of α. However, dc currents are difficult to measure accurately. A better method involves measurement of the current amplitude for a range of ΔE's, and nonlinear fitting to eq. [14]. A slightly less rigorous method involves determination of the current response at a given potential amplitude and at twice the potential amplitude. The quantity $|j(\omega,2\Delta E)|/|j(\omega,\Delta E)|$ is calculated and the equation

$$|j(\omega,2\Delta E)|/|j(\omega,\Delta E)| = I_1(2b)/I_1(b)$$

is solved numerically for b. (Alternatively b can be read off from a working curve of $I_1(2b)/I_1(b)$ vs. b). The transfer coefficient is then obtained from eq. [10]. For accurate results, both measurements should be in the nonlinear regime, say at 30 and 60 mV RMS potential amplitudes. This method measures a ratio, and so calibration issues across different types of measurements do not arise.

The second-harmonic response could be used in a similar fashion to extract α, either from a ratio of second-harmonic responses at different potential amplitudes or from a ratio of second- to first-harmonic responses at a single potential amplitude. Its dependence on b (Fig. 2) is qualitatively similar

© 1997 NRC Canada

Can. J. Chem. Downloaded from www.nrcresearchpress.com by 91.121.58.235 on 09/08/12
For personal use only.

to that of the fundamental frequency response. The second-harmonic has some advantages, in that it arises solely from the electrochemical reaction and not from linear elements in the system, such as the double-layer capacitance or the solution resistance.

If the back-reaction is considered significant, the current–potential characteristic is the Butler–Volmer equation, and a similar procedure to the above leads to the form:

$$[15]\quad j = j_a\exp(b_a\sin(\omega t)) - j_c\exp(-b_c\sin(\omega t))$$

where

$$[16]\quad b_a = \alpha_a F\Delta E/RT$$
$$b_c = \alpha_c F\Delta E/RT$$

and j_a and j_c are the anodic and cathodic partial currents in the absence of an ac perturbation. As before, the exponentials can be expanded in terms of Bessel functions. The Fourier expansion of $\exp(-b\ \sin(\omega t))$ is similar to that of $\exp(b\ \sin(\omega t))$ except that every second term has opposite sign, because $I_n(-b) = I_n(b)$ for n even and $I_n(-b) = -I_n(b)$ for n odd. By collecting terms the expressions for an arbitrary harmonic can be obtained. For small η, the behaviour is linear and uninteresting. Further from equilibrium, either the anodic or cathodic terms dominate, and the irreversible results above apply. A more detailed discussion of this case for the fundamental frequency response is given in ref. 4, although the method of solution of the problem is different.

2.2 Electrosorption reaction

The electrosorption reaction, with Langmuir isotherm, will now be considered:

$$[17]\quad M + A(aq) \rightarrow MA(ads) + e^-$$

The coverage of MA(ads) will be denoted θ, and the coverage of the uncovered surface sites M is $(1 - \theta)$. The surface concentration of sites on the clean surface is Γ_m (mol m^{-2}). The standard state for the adsorbed species will be taken as $\theta = ½$, and for simplicity the symmetry factors will be also be taken as ½. The general quasi-reversible case then has the rate law:

$$[18]\quad \Gamma_m d\theta/dt = k^0[(1 - \theta)\exp(½F(E - E^0)/RT) - \theta\exp(-½F(E - E^0)/RT)]$$

After solution of the above equation, the current is obtained from

$$[19]\quad j = F\Gamma_m d\theta/dt$$

To solve the rate law, the ac and dc parts of the potential may be separated as before:

$$[20]\quad d\theta/dt = k_a(1-\theta)\exp(b\sin(\omega t)) - k_c\theta\exp(-b\sin(\omega t))$$

where

$$k_a = k^0\exp(½F(E_{dc} - E^0)/RT)/\Gamma_m$$
$$k_c = k^0\exp(-½F(E_{dc} - E^0)/RT)/\Gamma_m$$

The new feature here is the coverage, θ, which will vary periodically and may contain higher harmonics:

$$[22]\quad \theta = \theta_0 + \theta_{1r}\sin(\omega t) + \theta_{1i}\cos(\omega t) + \theta_{2r}\sin(2\omega t) + \theta_{2i}\cos(2\omega t) + \ldots$$

Differentiation gives a series form for the left-hand side of the rate law:

$$[23]\quad d\theta/dt = -\omega\theta_{1i}\sin(\omega t) + \omega\theta_{1r}\cos(\omega t) - \omega\theta_{2i}\sin(2\omega t) + \omega\theta_{2r}\cos(2\omega t) - \ldots$$

Already eqs. [19] and [23] together show that the current response has no dc component and there is no faradaic rectification effect. Before coefficients of the various harmonics can be collected, the harmonic expansion of the product $\theta\exp(\pm b\ \sin(\omega t))$ is required. The expansion for each factor is known, and the terms of the product may be obtained from trigonometric relationships such as $\sin(n\omega t)\cos(m\omega t) = ½\sin((n - m)\omega t) + ½\sin((n + m)\omega t)$. This process is tedious, but may be facilitated by the use of a symbolic algebra program. (MAPLE's combine function gives the result immediately.) Then coefficients of each harmonic on the left-hand side of eq. [18] may be equated to the right-hand-side coefficients to give an infinite set of algebraic equations. For example, for $\cos(\omega t)$:

$$[24]\quad \omega\theta_{1r} = (k_a + k_c)(-I_0(b) + I_2(b))\theta_{1i} + (k_a - k_c)(-I_1(b) + I_3(b))\theta_{2r}\,(k_a + k_c)(I_2(b) - I_4(b))\theta_{3i} + \ldots$$

By writing the Fourier series for θ and reducing the differential equation to a set of algebraic equations, the boundary condition has been implicitly assumed to be $\theta(t_2) = \theta(t_1)$ for $t_2 = t_1 + 2\pi/\omega$. The equations are to be solved for θ_0, θ_{nr}, θ_{ni}, n = 1,2,3..., and may be simplified by defining rate constant combinations $k_+ = k_a + k_c$ and $k_- = k_a - k_c$. In matrix form, they are

$$[25]\quad \begin{bmatrix} k_+I_0 & k_-I_1 & 0 & 0 & -k_+I_2 & \ldots \\ 0 & \omega & k_+(I_0 - I_2) & k_-(I_1 - I_3) & 0 & \ldots \\ 2k_-I_1 & k_+(I_0 + I_2) & -\omega & 0 & -k_-(I_1 + I_3) & \ldots \\ -2k_+I_2 & -k_-(I_1 + I_3) & 0 & 2\omega & k_+(I_0 + I_4) & \ldots \\ 0 & 0 & k_-(I_1 - I_3) & k_+(I_0 - I_4) & -2\omega & \ldots \\ \vdots & \vdots & \vdots & \vdots & \vdots & \ddots \end{bmatrix} \begin{bmatrix} \theta_0 \\ \theta_{1r} \\ \theta_{1i} \\ \theta_{2i} \\ \theta_{2i} \\ \vdots \end{bmatrix} = \begin{bmatrix} k_eI_0 \\ 0 \\ 2k_oI_1 \\ -2k_eI_2 \\ 0 \\ \vdots \end{bmatrix}$$

© 1997 NRC Canada

Can. J. Chem. Downloaded from www.nrcresearchpress.com by 91.121.58.235 on 09/08/12
For personal use only.

(The second row originates from eq. [24].) On the right-hand side $k_e = k_o = k_a = \frac{1}{2}(k_+ + k_-)$. k_e is associated with even-order Bessel functions and k_0 is associated with odd-order Bessel functions. (Although in this case k_e and k_o are the same, they will be different for the HER discussed later.) In the matrix, the k_+ rate constants multiply even-order Bessel functions and the k_- multiply odd-order functions. If the rows are indexed by n = 0,1c,1s,2c,2s,3c,3s,... (c and s for cos and sin), and the columns are indexed by 0,1r,1i,2r,2i,3r,3i,... then the combination of Bessel functions in the n,mth entry is made up from Bessel functions of order $n + m$ and $|n - m|$. The rule for the signs of these and the pattern of zero entries can be written down,[2] but in practice generation of the entries by a symbolic algebra program is more convenient.

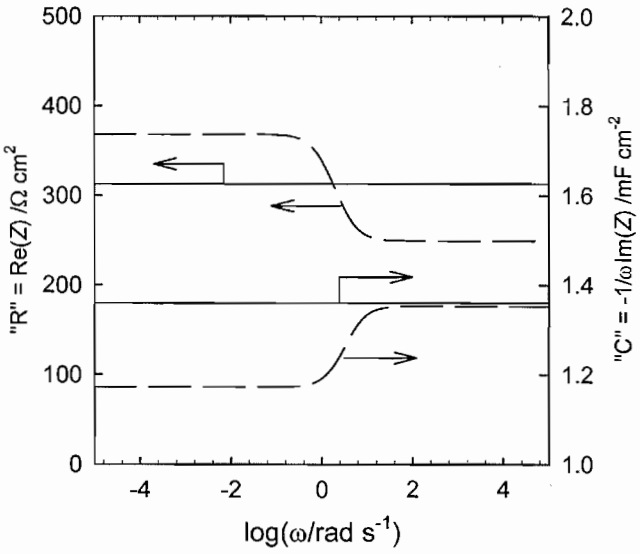
It is interesting to note that the equations have a very simple solution for $k_c = 0$, the case of irreversible production of the adsorbate. Then the solution is $\theta = \theta_0 = 1$. That is, if the surface is fully covered, it remains so in the presence of the ac perturbation. For this irreversible case, it is also clear that there can be no other solutions, because the coverage must always increase and therefore cannot be periodic.

At this point, the solution of linear equations is straightforward, using either symbolic or numerical methods. The matrix is truncated to a finite size and the first few harmonics are calculated. The accuracy of the solutions may be checked by increasing the matrix size and recalculating the answers. All the plots in this paper are obtained for 11×11 matrices, which give better than six-figure accuracy. However, even for 5×5 matrices, the solutions typically have 0.1% accuracy.

The solutions are the ac components of θ. These are converted to $d\theta/dt$ via eq. [23] and thence to current by eq. [19]. The admittance $(j_{1r} + j_{1i}i)/\Delta E$ can be converted to an impedance and the real and imaginary parts of this found. The expected small-signal equivalent circuit is a series RC combination (11), so the real and imaginary parts of the impedance should be R and $-1/\omega C$ for some frequency-independent R and C. This expectation is borne out for small amplitudes, but at higher amplitudes, $R = \mathrm{Re}(Z)$ and $C = -1/\omega\mathrm{Im}(Z)$ show some frequency dependence (Fig. 3). Over a limited frequency range these parameters appear constant, but with values that are not equal to the small-signal limit. In the high-frequency limit, the matrix equation can be solved exactly for R (see Appendix), which then shows a very simple dependence on amplitude.

At the special potential E^0, $k_- = 0$ and the even harmonics of both θ and j are zero. This is true for any amplitude perturbation and for any frequency. At other potentials, the second-harmonic spectrum yields circles in the complex admittance plane (Fig. 4*a*). The potential dependence of the second-harmonic admittance has a characteristic shape not unlike that observed in second-harmonic ac voltammetry of soluble species (Fig. 4*b*). The second-harmonic signal for the reversible, small-signal case has been calculated and measured by Lelievre et al. (12) for a reaction with adsorbed reactant and product.

Fig. 3. Frequency-dependence of the apparent series resistance and capacitance for the Langmuir adsorption reaction. $\Gamma_m = 2 \times 10^{-9}$ mol cm^{-2}, $k^0 = 2 \times 10^{-9}$ mol cm^{-2} s^{-1}, $\beta = \frac{1}{2}$, $E_{dc} = E^0 + 30$ mV. Solid lines, potential amplitude 1 mV RMS; broken lines, potential amplitude 50 mV RMS.



2.3 The hydrogen evolution reaction

$$\begin{aligned} &\mathrm{M(site)} + \mathrm{H^+} + \mathrm{e^-} \underset{k_{-1}}{\overset{k_1}{\rightleftharpoons}} \mathrm{MH(a)} \\ [26]\quad &\mathrm{MH(a)} + \mathrm{H^+} + \mathrm{e^-} \underset{k_{-2}}{\overset{k_{-1}}{\rightleftharpoons}} \mathrm{M(site)} + \mathrm{H_2} \\ &2\mathrm{MH(a)} \underset{k_{-3}}{\overset{k_3}{\rightleftharpoons}} 2\mathrm{M(site)} + \mathrm{H_2} \end{aligned}$$

The HER, eqs. [26], is an important case of a mechanism with a single adsorbed intermediate. Mass transport is assumed to be fast for H^+ and H_2 and the Langmuir isotherm is assumed for the adsorbed species, so that the net rates of the individual steps are given by

$$\begin{aligned} v_1 &= k_1(1 - \theta) - k_{-1}\theta \\ [27]\quad v_2 &= k_2\theta - k_{-2}(1 - \theta) \\ v_3 &= k_3\theta^2 - k_{-3}(1 - \theta)^2 \end{aligned}$$

The rate constants for steps 1 and 2 have exponential potential dependence in the usual way ($\beta_1 = \beta_2 = \frac{1}{2}$ will be assumed).

[2] The nc,mr entry is 0 for m and n even or m and n odd, $-s_{n+m}I_{|n-m|} + s_{n+m}I_{n+m}$ for m even and n odd, $s_{n+m}I_{|n-m|} + s_{n+m}I_{n+m}$ for m odd and n even, where s_i is the sign associated with the ith order Bessel function in the expansion of $\exp(b\sin(\omega t))$, i.e., $s_i = (-1)^{\mathrm{floor}((i \bmod 4)/2)}$. The nc,mi entry is 0 for m even and n odd or for m odd and n even, $s_{n+m}I_{|n-m|} + s_{n+m}I_{n+m}$ for m and n even, $-s_{n+m}I_{|n-m|} + s_{n+m}I_{n+m}$ for m and n odd. The ns,mr entry is 0 for m even and n odd or for m odd and n even, $s_{n+m}I_{|n-m|} - s_{n+m}I_{n+m}$ for m and n even, $-s_{n+m}I_{|n-m|} - s_{n+m}I_{n+m}$ for m and n odd. The ns,mi entry is 0 for m and n even or m and n odd, $s_{n+m}I_{|n-m|} + s_{n+m}I_{n+m}$ for m even and n odd, $-s_{n+m}I_{|n-m|} + s_{n+m}I_{n+m}$ for m odd and n even. The $n = 0$ row follows the same rule as an nc row. For the $m = 0$ column or for the right-hand side, the $n = 0$ entry is I_0, the nc entries are 0 for n odd, $2s_nI_n$ for n even, and the ns entries are 0 for n even, $2s_nI_n$ for n odd.

© 1997 NRC Canada

Can. J. Chem. Downloaded from www.nrcresearchpress.com by 91.121.58.235 on 09/08/12
For personal use only.

Fig. 4. Second-harmonic response for the Langmuir adsorption reaction. (*a*) Complex-plane plot of second-harmonic admittance. Potential amplitude 5 mV RMS; other parameters as for Fig. 3. Selected values of ω marked on the plot. (*b*) Potential dependence of second-harmonic admittance. Potential amplitude 5 mV RMS, $\omega = 6$ rad s^{-1}, other parameters as in Fig. 3.

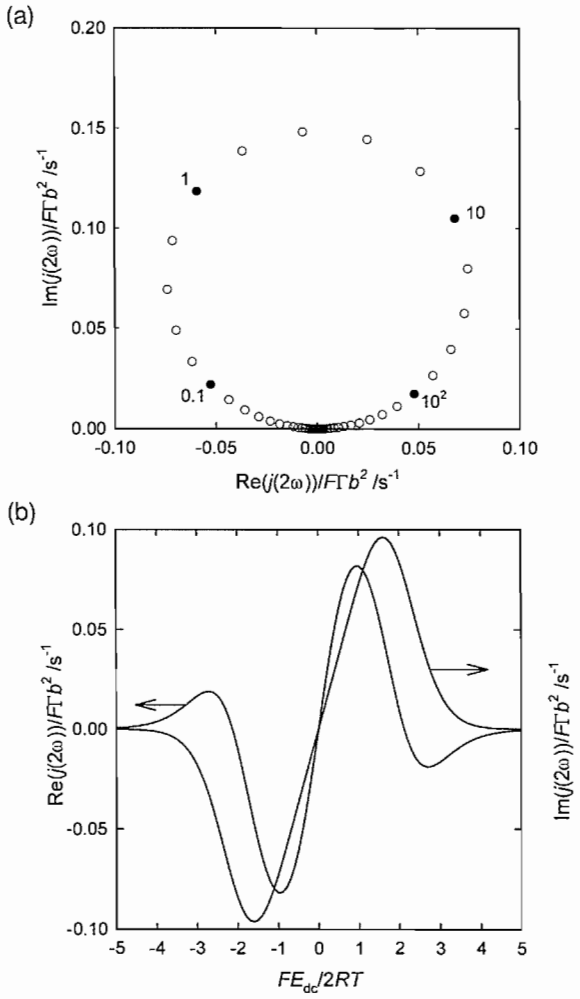
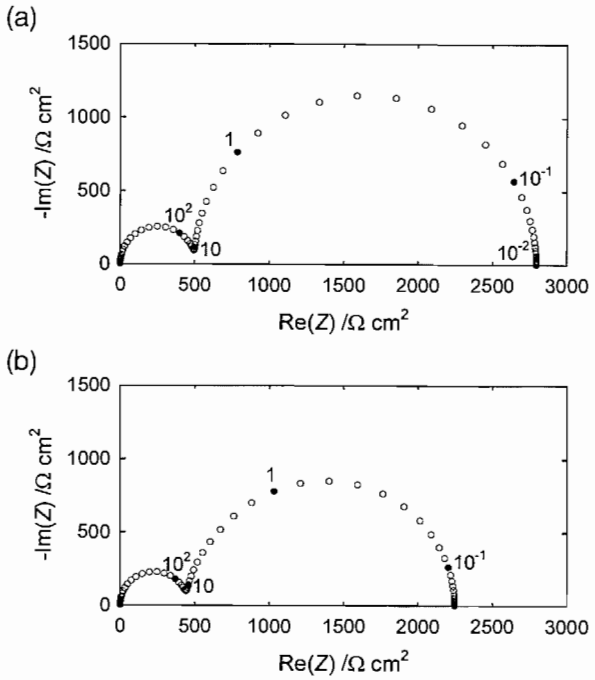


Fig. 5. Impedance of the hydrogen evolution reaction. Rate constants as for Fig. 3, ref. 5, i.e., $k_1/\Gamma_m = k_{-1}/\Gamma_m = 1$ s^{-1}; $k_2/\Gamma_m = k_{-2}/\Gamma_m = 5 \times 10^{-2}$ s^{-1}; $k_3 = k_{-3} = 0$; $\Gamma_m = 1 \times 10^{-9}$ mol cm^{-2}; $\beta_1 = 0.2$; $\beta_2 = 0.6$; $C_{dl} = 1 \times 10^{-5}$ F cm^{-2}. Selected values of ω marked on the plots. (*a*) Potential amplitude $\Delta E = 1$ mV; (*b*) potential amplitude $\Delta E = 70$ mV.



The differential equation to be solved is

[28] $\Gamma_m d\theta/dt = v_1 - v_2 - 2v_3$

The case where $v_3 = 0$ (Volmer–Heyrovsky mechanism) will be considered first. Then the mechanism may be solved in the same way as previously, because eq. [28] is still linear in θ. The rate constants k_+ and k_- in the matrix in eq. [25] are replaced by $(k_1 + k_{-1} + k_2 + k_{-2})/\Gamma_m$ and $(-k_1 + k_{-1} - k_2 + k_{-2})/\Gamma_m$, where these rate constants are now the values at the dc potential. The right-hand side of the matrix equation now has $k_e = (k_1 + k_{-2})/\Gamma_m$ associated with the even-order Bessel functions and $k_o = (k_{-2} - k_1)/\Gamma_m$ associated with odd-order Bessel functions. The four combinations of rate constants appearing in the matrix equation, $k_1 + k_{-1} + k_2 + k_{-2}$, $-k_1 + k_{-1} - k_2 + k_{-2}$, $k_1 + k_{-2}$, and $k_{-2} - k_1$, are linearly independent. Therefore it is at least possible that all four rate constants may be extracted from the data. This possibility will be investigated further in the discussion section.

The case of v_3 non-zero is more complicated because the rate equation is no longer linear in θ. It is still possible to expand the right-hand side of eq. [28] as a Fourier series. The terms in θ^2 are products of two identical Fourier series and can be expanded in a similar way to the other products of two Fourier series, for example, the product $\theta \exp(b \sin(\omega t))$ discussed above. The differential equation can then be converted to a system of algebraic equations, by equating coefficients of the various $\cos(n\omega t)$ and $\sin(n\omega t)$ on the left-hand and right-hand sides. The equations are no longer linear because they contain products like $\theta_{2i}\theta_{3i}$, and they cannot be solved by matrix methods. However, numerical solution of sets of nonlinear equations is possible. Although convergence to a solution is no longer guaranteed, a good strategy is to restrict the search space to between −1 and 1 for each component of θ.

Once the components of θ are found, by matrix or nonlinear methods, they are substituted into the following equation to find the current:

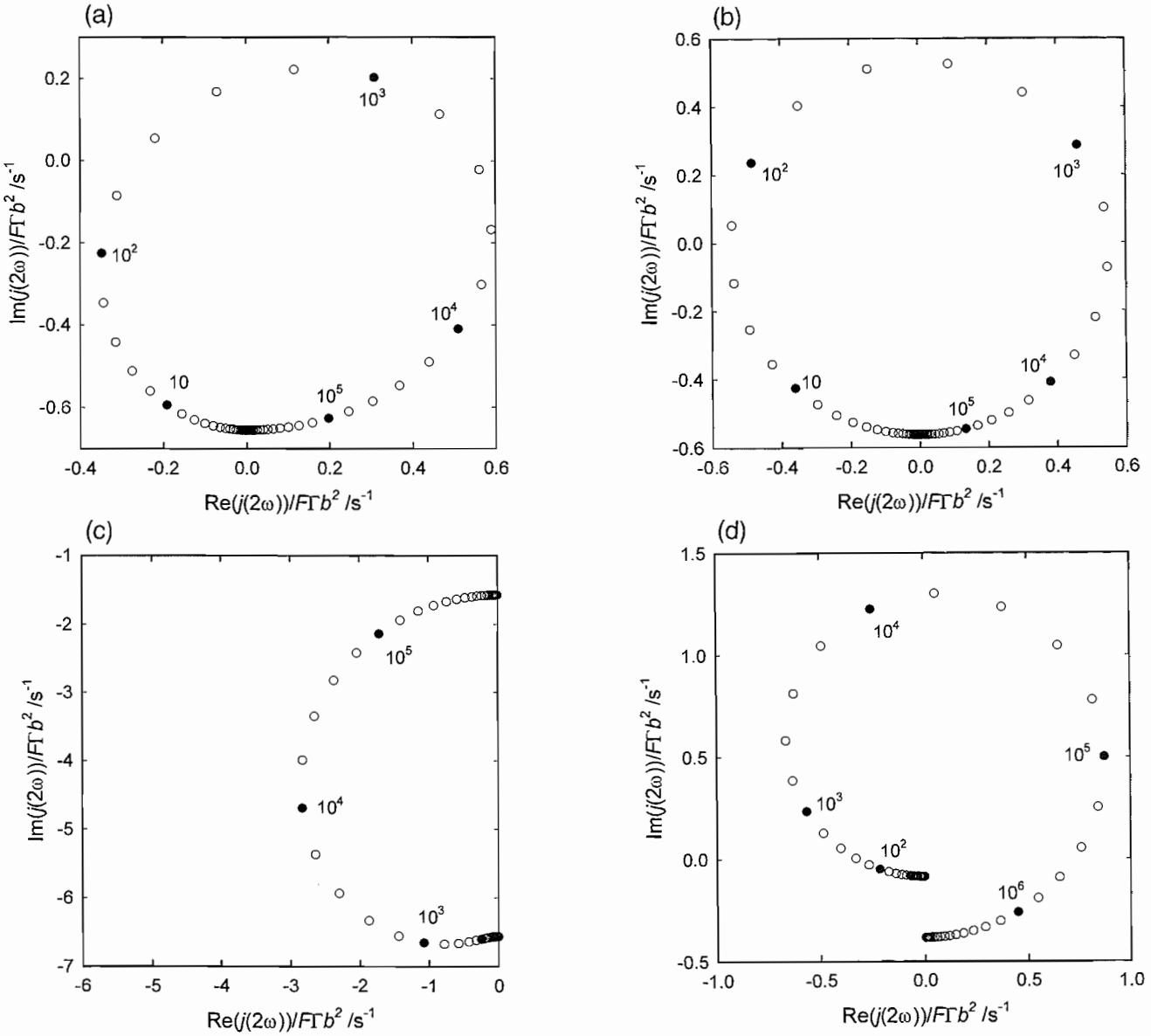
[29] $j = -Fv_1 - Fv_2$

Expanding this into a Fourier series yields the desired complex numbers for each of the current harmonics. The admittance is found as before.

The complex-plane impedance plots show the familiar

© 1997 NRC Canada

Fig. 6. Second-harmonic response for the hydrogen evolution reaction. Complex-plane plots of second-harmonic admittance, with selected values of ω marked. All rate constants are at $\eta_{dc} = -30$ mV. (*a*) Fast first step with slower second step. 50 mV RMS potential amplitude. $k_1/\Gamma_m = 5.6\ s^{-1}$; $k_{-1}/\Gamma_m = 18\ s^{-1}$; $k_2/\Gamma_m = 0.56\ s^{-1}$; $k_{-2}/\Gamma_m = 1.8\ s^{-1}$. $k_3 = k_{-3} = 0$; $\beta_1 = \beta_2 = ½$. (*b*) As for (*a*) but 5 mV RMS potential amplitude. (*c*) Slow first step, fast second step. 5 mV RMS potential amplitude. $k_1/\Gamma_m = 0.56\ s^{-1}$; $k_{-1}/\Gamma_m = 18\ s^{-1}$; $k_2/\Gamma_m = 56\ s^{-1}$; $k_{-2}/\Gamma_m = 18\ s^{-1}$; $k_3 = k_{-3} = 0$; $\beta_1 = \beta_2 = ½$. (*d*) Comparable first and second step rates. 5 mV RMS potential amplitude. $k_1/\Gamma_m = 2.8\ s^{-1}$; $k_{-1}/\Gamma_m = 180\ s^{-1}$; $k_2/\Gamma_m = 5.6\ s^{-1}$; $k_{-2}/\Gamma_m = 0.90\ s^{-1}$. $k_3 = k_{-3} = 0$; $\beta_1 = \beta_2 = ½$.



shapes associated with this mechanism, with the impedances decreasing with increased amplitude (e.g., Fig. 5). The second-harmonic admittance shows two semicircular arcs in the complex plane (Fig. 6).

3. Discussion

The most significant advantage of the present formulation over most others in the literature is the use of the Bessel function expansion for $\exp(b\ \sin(\omega t))$. The use of this expansion has been little used by others (but see refs. 3 and 9). Other treatments typically use Taylor series expansions of the exponential function. Terms involving powers such as $\sin^5(\omega t)$ must then be expanded into their harmonic components, $\sin^5(\omega t) = (1/16)\sin(5\omega t) - (5/16)\sin(3\omega t) + (5/8)\sin(\omega t)$. In general, odd powers lead to all odd harmonics and even powers to all even harmonics. Thus to get accurate evaluation of a given harmonic requires evaluation of a large number of terms

© 1997 NRC Canada

Can. J. Chem. Downloaded from www.nrcresearchpress.com by 91.121.58.235 on 09/08/12
For personal use only.

Can. J. Chem. Downloaded from www.nrcresearchpress.com by 91.121.58.235 on 09/08/12
For personal use only.

in the Taylor series, and this evaluation is complicated by the difficulty of expanding the powers of trigonometric functions into a sum of harmonics.

An alternative approach, as used here, is to write directly the Fourier series for $\exp(b \sin(\omega t))$. In this way, one avoids the difficulty that different terms contribute to a given harmonic. An additional advantage is that the assumption that the perturbation is small is not needed, and the amplitude dependence of the (nonlinear) impedance can be calculated. In the cases with one adsorbed species, an infinite-size matrix must be approximated by a finite-size matrix in order to get a numerical result. However, this approximation is of a different nature than taking a reduced number of terms in a Taylor series, because here the equations are cut off after a specified actual harmonic, which already contains contributions from arbitrarily high-order Taylor-series terms. A relatively small matrix is sufficient to give accuracy far higher than the typical experimental error.

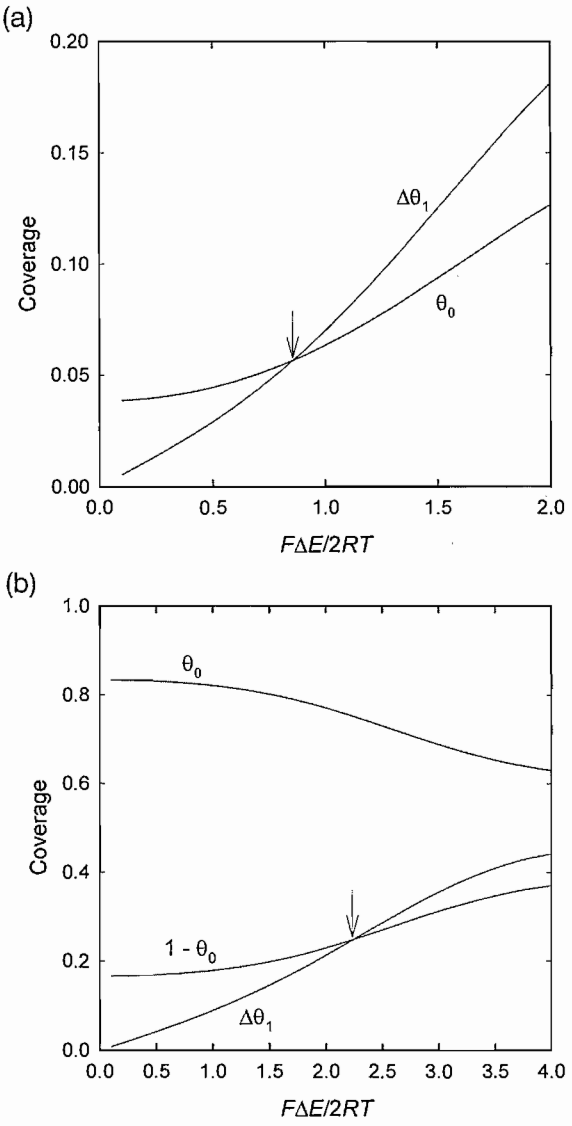
There is some possibility of getting an exact analytical solution to the infinite-size matrix equation, though I have not yet succeeded in this task. For some special cases the infinite-size matrix equation can be solved analytically without reducing its order. For example, in the high-frequency limit for the simple adsorption reaction, the (nonlinear) charge-transfer resistance may be obtained exactly (see Appendix). Its reciprocal has the same simple amplitude dependence as for the admittance of the simple irreversible reaction, eq. [8]. Other special cases may also be tractable. In any case, generation of the matrix equation and numerical solution to any required accuracy is easy using a symbolic algebra program. A MAPLE worksheet for this purpose can be obtained from the author or may be found at http://surface.chem.uvic.ca.

An advantage of high-amplitude impedance measurements or second-harmonic measurements is that they promise to yield kinetic parameters not available from small-amplitude fundamental-frequency impedance measurements. This is especially important for mechanisms in which not all the rate constants may be unambiguously extracted from EIS and steady-state data. The issue of identifiability and distinguishability of mechanisms has been addressed by Berthier et al. (13–15). The last two papers discuss the particular case of the V–H mechanism of the HER, where it was first noted by Lasia and Rami (16) that the replacements $k_1 \leftrightarrow k_2$, $k_{-1} \leftrightarrow k_{-2}$, $\beta_1 \leftrightarrow \beta_2$ do not change the steady-state current–potential curves or the EIS spectra. The present theory also gives the same results for the second-harmonic response under exchange of these rate parameters. Apparently, the equations for the second-harmonic response combine the rate constants in a similar way to conventional EIS.

To investigate this further, recall that the matrix equation contains the four rate constant combinations $k_+ = (k_1 + k_{-1} + k_2 + k_2)/\Gamma_m$, $k_- = (-k_1 + k_{-1} - k_2 + k_{-2})/\Gamma_m$, $k_e = (k_1 + k_{-2})/\Gamma_m$, and $k_o = (k_{-2} - k_1)/\Gamma_m$. The combinations k_e and k_+ originate from the rate law eq. [28] which is $k_e - k_+\theta$. When the Bessel function expansions for $\exp(b \sin(\omega t))$ and $\exp(-b \sin(\omega t))$ are collected, their odd-order terms have opposite signs, and are associated with different combinations k_o and k_-. These are k_e and k_+ with the signs of the cathodic rate constants changed. In the conventional theory the building blocks of the impedance are the partial derivatives $(\partial(v_1 - v_2)/\partial E)_\theta$, $(\partial(-v_1 - v_2)/\partial E)_\theta$, $(\partial(v_1 - v_2)/\partial\theta)_E$, and $(\partial(-v_1 - v_2)/\partial\theta)_E$. The partial derivatives with respect to E contain the steady-state coverage. Because this is found by setting the rate law equal to zero, the same two parameters k_e and k_+ are involved. In the act of taking the partial derivatives with respect to E, the cathodic rate constants change sign, leading again to k_o and k_-. The two theories are quite similar in the way that they combine the rate constants. It is therefore not too surprising that the same rate constant ambiguity that exists for conventional EIS is not resolved by second-harmonic measurements.

The nonlinear impedance of a two-step reaction with an adsorbed intermediate (cf. the V–H mechanism) was first discussed by Gabrielli et al. (17), using a Taylor series approach.

Fig. 7. Amplitude dependence of components of θ in the HER. θ_0 is the dc component of θ, $\Delta\theta_1$ is the amplitude of the fundamental component of θ. Points at which the equations become invalid are marked by an arrow. (*a*) $\omega = 0.001$ rad s^{-1}; $k_1/\Gamma_m = 0.018$ s^{-1}; $k_{-1}/\Gamma_m = 0.056$ s^{-1}; $k_2/\Gamma_m = 1.8$ s^{-1}; $k_{-2}/\Gamma_m = 0.056$ s^{-1}. $k_3 = k_{-3} = 0$; $\beta_1 = \beta_2 = ½$. (*b*) $\omega = 100$ rad s^{-1}; $k_1/\Gamma_m = 36$ s^{-1}; $k_{-1}/\Gamma_m = 6.6$ s^{-1}; $k_2/\Gamma_m = 1.8$ s^{-1}; $k_{-2}/\Gamma_m = 1.1$ s^{-1}. $k_3 = k_{-3} = 0$; $\beta_1 = \beta_2 = ½$.



© 1997 NRC Canada

Can. J. Chem. Downloaded from www.nrcresearchpress.com by 91.121.58.235 on 09/08/12
For personal use only.

More recently, Darowicki (7, 6) and Diard et al. (5) have disagreed over the correct formulation of this problem. Both use Taylor series approaches, and the divergence of opinion seems to arise because of different simplification procedures used. The present method uses a quite different approach, and is able to reproduce the results of Diard et al. (Fig. 5, cf. Fig 3 of ref. 5).

An assumption that is implicit in the physical problem, but not in the mathematical formulation, is that θ must lie between zero and one. This requirement provides an upper limit for ΔE, beyond which the equations must be considered approximate at best. The amplitudes of the components of θ will increase with ΔE. If $\Delta\theta_1$ exceeds θ_0, then θ will be "clipped" at zero for part of its cycle (neglecting the smaller influence of higher harmonics). Clipping also occurs if $\Delta\theta_1 + \theta_0$ exceeds one. Figure 7 shows two cases of the V–H mechanism where there is a maximum ΔE for valid measurements according to this criterion. The factors that enhance the amplitude of the θ oscillations are large rate constants, low frequencies, and steady-state θ near zero or one. Accordingly, it is not easy to make a general statement about which ΔE values are safe.

The method described here opens up the use of second or higher harmonic spectroscopies for surface reactions, though the lack of exact analytical results is a hindrance. At least for the V–H mechanism, with $\beta_1 = \beta_2 = 1/2$, the use of the second-harmonic does not assist in more efficient extraction of rate parameters. The best argument in favour of these measurements is that they are insensitive to the double-layer charging currents, and so a higher precision is possible. Higher precision for second-harmonic measurements has been noted experimentally by Lelievre et al. (12) for a redox reaction in an adsorbed layer.

The method can be used for many cases. Cases where the rate law (expression for $d\theta/dt$) is linear in θ give linear equations and hence can be dealt with by matrix methods. Important examples dealt with in this paper are the simple adsorption reaction and the V–H version of the HER, in the special case of the Langmuir isotherm. Cases that are polynomial in θ, of degree higher than one, cannot be formulated in matrix form, but the equations can be solved numerically. Cases where the rate law is more complex but where a Fourier series is available for the functional form of θ should be soluble numerically, for example, the Frumkin isotherm. The case of more than one adsorbed intermediate is no more difficult than the single-adsorbate case. There are now two or more expressions of the form $d\theta_i/dt$ but these can be reduced to algebraic equations in the same way – the matrix is just larger, with i sets of unknowns, where i is the number of adsorbed species.

4. Conclusions

The method presented here may be used to calculate all the harmonics of the current response to a sinusoidal potential perturbation of arbitrary magnitude. Thus the nonlinear impedance or the second-harmonic impedance is readily calculated. The method is simplest for cases where the rate law is linear in θ, for example, the simple Langmuir adsorption reaction or the V–H mechanism of the HER assuming the Langmuir isotherm. Then matrix methods lead to easy numerical solution, or an exact analytical solution for some simple cases. Other mechanisms can be calculated by similar methods, but only numerical solutions are possible.

5. Acknowledgements

I thank the Natural Sciences and Engineering Research Council of Canada and the University of Victoria for financial support. I thank Dr Andrzej Lasia for making me aware of the rate constant ambiguity of the V–H mechanism and of the existence of refs. 5 and 6.

References

1. D.E. Smith. *In* Electroanalytical chemistry. Vol. 1. *Edited by* A.J. Bard. Marcel Dekker, New York. 1966. pp. 1–155.
2. D.D. Macdonald. Transient techniques in electrochemistry. Plenum, New York. 1977. pp. 229–272.
3. S.G. Canagaratna. J. Electroanal. Chem. **108**, 371 (1980).
4. J.-P. Diard, B. Le Gorrec, and C. Montella. Electrochim. Acta, **39**, 539 (1994).
5. J.-P. Diard, B. Le Gorrec, and C. Montella. Electrochim. Acta, **42**, 1053 (1997).
6. K. Darowicki. Electrochim. Acta, **42**, 1073 (1997).
7. K. Darowicki. Electrochim. Acta, **40**, 767 (1995).
8. M. Abramowitz and I.A. Stegun. Handbook of mathematical functions. Dover, New York. 1965. eq. 9.6.35.
9. N. Bonanos, B.C.H. Steele, E.P. Butler, W.B. Johnson, W.L. Worrell, D.D. Macdonald, and M.C.H. McKubre. *In* Impedance spectroscopy. *Edited by* J.R. Macdonald. Wiley, New York. 1987. p. 270.
10. H.P. Agarwal. *In* Electroanalytical chemistry. Vol. 7. *Edited by* A.J. Bard. Marcel Dekker, New York. 1974. pp. 161–271.
11. P. Dolin and B. Erschler. Acta Physicochimica URSS, **13**, 747 (1940).
12. D. Lelievre, D. Saur, and E. Laviron. J. Electroanal. Chem. **117**, 17 (1981).
13. F. Berthier, J.-P. Diard, P. Landaud, and C. Montella. J. Electroanal. Chem. **362**, 13 (1993).
14. F. Berthier, J.-P. Diard, C. Montella, L. Pronzato, and E. Walter. J. Chim. Phys. **90**, 2069 (1993).
15. F. Berthier, J.-P. Diard, L. Pronzato, and E. Walter. Automatika, **32**, 973 (1996).
16. A. Lasia and A. Rami. J. Electroanal. Chem. **294**, 123 (1990).
17. C. Gabrielli, M. Keddam, and H. Takenouti. *In* Electrochemical methods in corrosion research. Vol. 8 of Materials Science Forum. *Edited by* M. Duprat, Trans Tech Publications, Switzerland. 1986. p. 417.

Appendix

For the high-frequency limit ($\omega \gg k$) in the simple adsorption reaction with $\beta = ½$, it is possible to get an exact result for the charge-transfer resistance at arbitrary amplitude. Cramer's rule is first used to solve the matrix equation [25] for θ_{1i}:

© 1997 NRC Canada

$$[30]\quad \theta_{1i} = \frac{\begin{vmatrix} k_+I_0 & k_-I_1 & k_eI_0 & 0 & -k_+I_2 & \cdots \\ 0 & \omega & 0 & k_-(I_1 - I_3) & 0 & \cdots \\ 2k_-I_1 & k_+(I_0 + I_2) & 2k_oI_1 & 0 & -k_-(I_1 + I_3) & \cdots \\ -2k_+I_2 & -k_-(I_1 + I_3) & -2k_eI_2 & 2\omega & k_+(I_0 + I_4) & \cdots \\ 0 & 0 & 0 & k_+(I_0 - I_4) & 2\omega & \cdots \\ \vdots & \vdots & \vdots & \vdots & \vdots & \ddots \end{vmatrix}}{\begin{vmatrix} k_+I_0 & k_-I_1 & 0 & 0 & -k_+I_2 & \cdots \\ 0 & \omega & k_+(I_0 - I_2) & k_-(I_1 - I_3) & 0 & \cdots \\ 2k_-I_1 & k_+(I_0 + I_2) & -\omega & 0 & -k_-(I_1 + I_3) & \cdots \\ -2k_+I_2 & -k_-(I_1 + I_3) & 0 & 2\omega & k_+(I_0 + I_4) & \cdots \\ 0 & 0 & k_-(I_1 - I_3) & k_+(I_0 - I_4) & -2\omega & \cdots \\ \vdots & \vdots & \vdots & \vdots & \vdots & \ddots \end{vmatrix}}$$

In the large ω limit, the terms with the highest power of ω will dominate. In the bottom determinant, the term with the highest power of ω is formed from the elements in the leading diagonal, i.e., $k_+I_0\omega(-\omega)(2\omega)(-2\omega)\ldots$. In the top determinant, there are two terms associated with $(\omega)(2\omega)(-2\omega)\ldots$. One has the product of the 1,1 entry with the 3,3 entry and the other has the product of the 3,1 entry with the 1,3 entry. Taking the ratio of the top and bottom determinants and cancelling powers of ω gives:

$$\theta_{1i} = \frac{2(k_+I_0k_oI_1 + k_-I_1k_eI_0)}{k_+I_0\omega}$$

A similar argument shows that $\theta_{1r} = 0$, and therefore the imaginary part of the first-harmonic of the current, $\omega F\Gamma_m\theta_{1r}$, is zero. The real part is $-\omega F\Gamma_m\theta_{1i}$ and may be divided by ΔE to give the admittance, or $1/R$. After some simplification, the final result is

$$R(\omega \to \infty) = \frac{RTb(\exp(\tfrac{1}{2}F(E_{dc}-E^0)/RT) + \exp(-\tfrac{1}{2}F(E_{dc}-E^0)/RT))}{2F^2k_oI_1(b)\exp(F(E_{dc}-E^0)/RT} = R_{ct}b/2I_1(b)$$

where R_{ct} is the small-signal charge-transfer resistance.

Can. J. Chem. Downloaded from www.nrcresearchpress.com by 91.121.58.235 on 09/08/12
For personal use only.

© 1997 NRC Canada

Ion–polymer interactions in polypyrrole films

Xiaoming Ren and Peter G. Pickup

Abstract: Formal potentials from cyclic voltammetry and ionic conductivities from impedance measurements are used to probe anion–polymer interactions in electrochemically deposited films of polypyrrole. Hard anions (F^-, Cl^-, ClO_4^-) stabilize the oxidized form of the polymer more than soft anions (I^-, SCN^-). Anions of weak acids (F^- and CN^-) interact with the polymer particularly strongly and exhibit anomalously low mobilities. Hydrogen bonding with the N-H groups of oxidized polypyrrole is proposed.

Key words: conducting polymer, polypyrrole, impedance, ion transport, electrolyte effects, ion exchange.

Résumé : On a utilisé les potentiels formels de la voltampérométrie cyclique et les conductivités ioniques obtenues par des mesures d'impédance pour étudier les interactions anion–polymère dans des films de polypyrrole déposés d'une façon électrochimique. Les anions durs (F^-, Cl^-, ClO_4^-) stabilisent plus la forme oxydée du polymère que les anions mous (I^-, SCN^-). Les anions des acides faibles (F^- et CN^-) interagissent d'une façon particulièrement forte avec le polymère et ils présentent des mobilités anormalement faibles. On suggère l'existence de liaison hydrogène avec les groupes N-H de la forme oxydée du polypyrrole.

Mots clés : polymère conducteur, polypyrrole, impédance, transport ionique, effets d'électrolyte, échange d'ion.

[Traduit par la rédaction]

Can. J. Chem. Downloaded from www.nrcresearchpress.com by 91.121.58.235 on 09/08/12
For personal use only.

Introduction

Ion transport in conducting polymer films has attracted considerable attention since electrochemical studies of these materials began in 1979 (1). The performance of conducting polymers in many applications is strongly influenced by their ion transport properties (2, 3). Furthermore, studies of ion transport can provide valuable information about film structure (4), and chemical interactions within the film (5, 6).

The influence of the anion on the electrochemistry of conducting polymers has been extensively investigated. Many studies (7–13) have involved preparation of the polymer in the presence of different doping anions. In these cases, differences in ion-transport characteristics are mainly due to different film morphologies formed during polymerization.

To probe anion–polymer interactions, films should be grown in the same medium, with subsequent anion exchange. Anion exchange in conducting polymers has been well documented (12, 14–17), although quantitative thermodynamic (18) and kinetic data (15, 16) are limited. There is also a paucity of information on the effects of anion exchange on the electrochemical and transport properties of conducting polymers (19o).

Received February 20, 1997.

This paper is dedicated to Professor Brian E. Conway on the occasion of his 70th birthday.

X. Ren[1] and P.G. Pickup.[2] Department of Chemistry, Memorial University of Newfoundland, St. John's, NF A1B 3X7, Canada.

[1] Present address: Electronics Research Group, Los Alamos National Laboratory, Los Alamos, NM 87545, U.S.A.

[2] Author to whom correspondence may be addressed. Telephone: (709) 737-8657. Fax: (709) 737-3702. E-mail: ppickup@morgan.ucs.mun.ca

Our investigations of ion transport in polypyrrole (4, 5, 20–22) have revealed some surprising dependencies of the ion transport rate on the nature of the mobile ion and the solvent. Perchlorate transport was found to be exceedingly slow when the polymer was immersed in dry acetonitrile, but became faster when a small percentage of water was added (5). In water, the mobility of ClO_4^- in perchlorate-doped polypyrrole was found to be much lower than that of Na^+ in polystyrenesulphonate-doped polypyrrole. We have attributed the low mobility of ClO_4^- in polypyrrole to ion pairing with oxidized sites in the polymer (5), but hydrogen bonding with pyrrole N-H groups (6) may also be important. Schiavon et al. (6) ascribed the lower mobility of anions in unsubstituted polypyrrole, relative to *N*-substituted polypyrroles, to hydrogen bonding. This effect was found to be particularly strong with the hydroxide ion and leads to a substantial negative shift in the polymer's formal potential (19, 23).

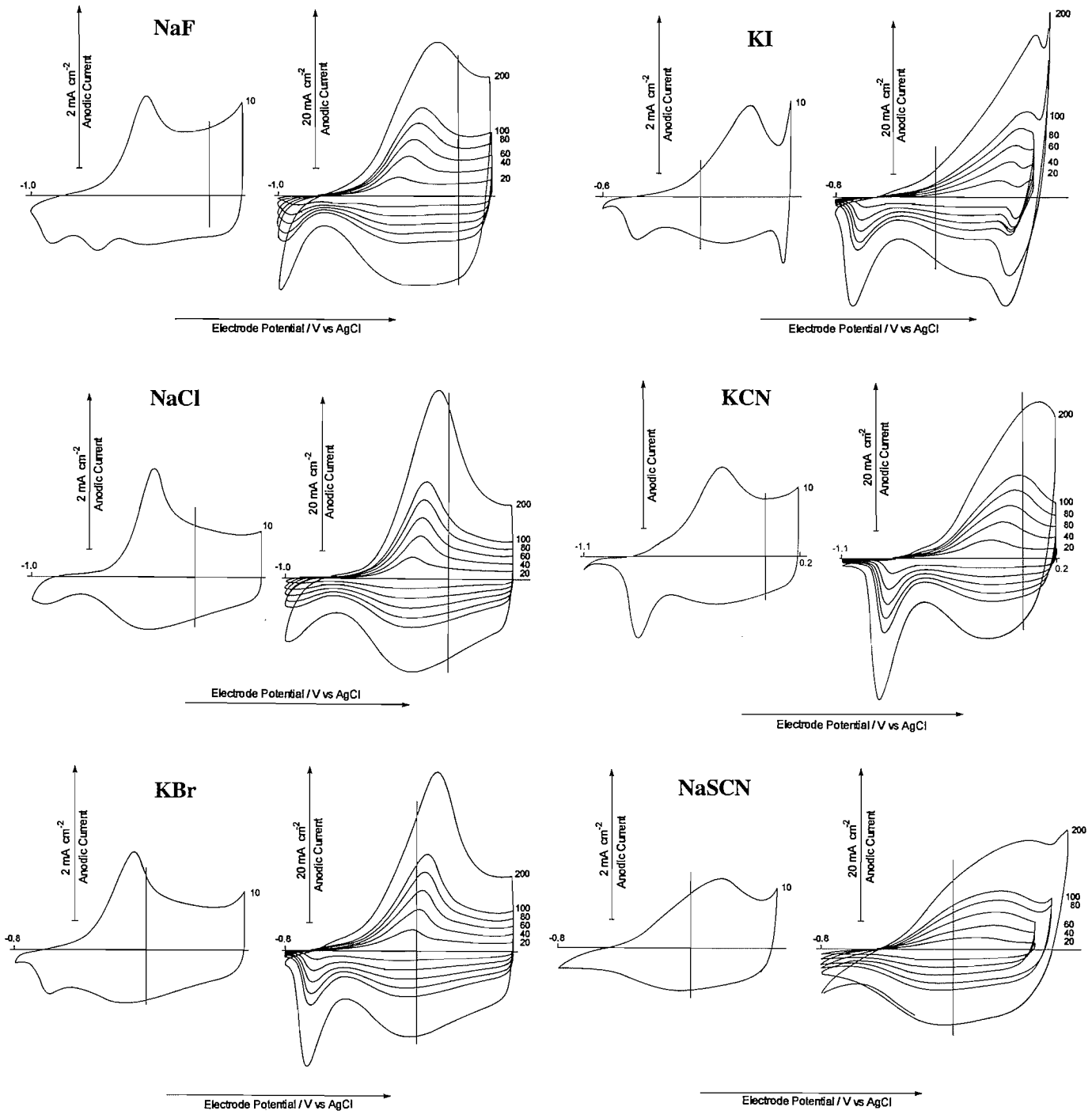
To properly document the influence of the nature of the anion on its mobility in polypyrrole, and to provide further insight into the interactions between anions and the polymer, we report here a comparative study of the electrochemistry and ionic conductivity of polypyrrole in the presence of seven different anions. Evidence for hydrogen bonding between certain anions and oxidized polypyrrole is presented.

Experimental

Experimental procedures and equipment have been described in detail elsewhere (22). Polypyrrole films were prepared electrochemically on Pt disc electrodes (0.0052 cm^2), at constant current (0.80 mA cm^{-2}) from 0.5 M pyrrole in 0.5 M $NaClO_4$(aq), and were nominally 2 μm thick. All voltammetric and impedance measurements were carried out in monomer-free 0.2 M aqueous electrolyte solutions. Before recording voltammograms or impedance data, the potential of each polymer-coated electrode was cycled (at 60 mV s^{-1}) four

© 1997 NRC Canada

Fig. 1. Cyclic voltammograms for Pt electrodes coated with a 2 μm polypyrrole film in 0.20 M aqueous solutions. Scan rates are indicated in mV s^{-1}.



Can. J. Chem. Downloaded from www.nrcresearchpress.com by 91.121.58.235 on 09/08/12
For personal use only.

times between the limits of the voltammograms shown in Fig. 1. Impedance data were collected in the order of decreasing potential.

Results

Cyclic voltammetry

Cyclic voltammograms of polypyrrole-coated electrodes in 0.2 M aqueous solutions of NaF, NaCl, KBr, KI, KCN, and NaSCN are shown in Fig. 1. Voltammograms of a similar film in $NaClO_4$(aq) have been published and discussed previously (22). They are very similar to those in KBr(aq) shown in Fig. 1.

The voltammograms shown in Fig. 1 are all similar, although there are some quite significant differences in peak positions and peak separations. Approximate formal potentials for the main redox process (Table 1) were determined from the slowest voltammograms by taking the average of the

© 1997 NRC Canada

Can. J. Chem. Downloaded from www.nrcresearchpress.com by 91.121.58.235 on 09/08/12
For personal use only.

Table 1. Formal potentials, ionic conductivities, and anion characteristics for polypyrrole in various aqueous electrolyte solutions (all 0.2 M).

Electrolyte	Formal potential (V vs. Ag/AgCl)	Ionic conductivity[a] (μS cm^{-1})	$\Delta H_{hydration}$(anion)[b] (kJ mol^{-1})	Anion radius[b] (nm)
NaCl	−0.27	60	79.5	0.181
KBr	−0.11	43	107.9	0.196
$NaClO_4$	−0.28	25	171.5	0.236
KI	+0.22	9.7	152.7	0.220
NaF	−0.35	7.7	−57.4	0.133
NaSCN	+0.05	5.6	120.5	0.195
KCN	−0.28	3.2	78.5	0.182

[a]At a doping charge of 45 mC cm^{-2}.
[b]Reference 27.

Fig. 2. Plots of ionic conductivity (from impedance spectroscopy) as a function of potential for polypyrrole films in 0.2 M aqueous solutions.

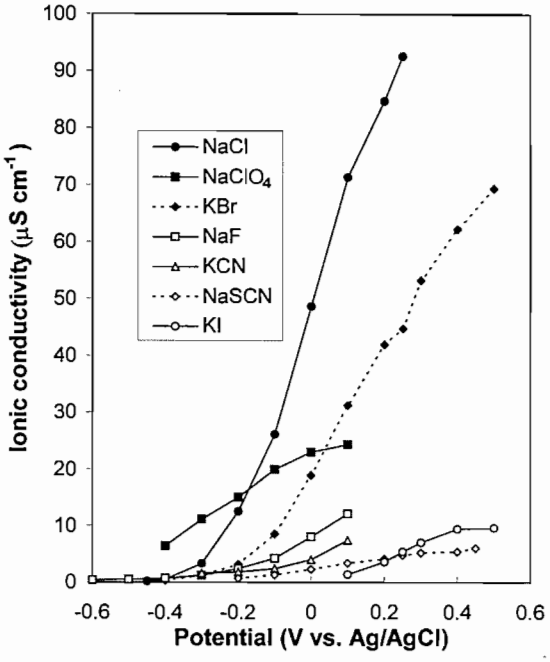
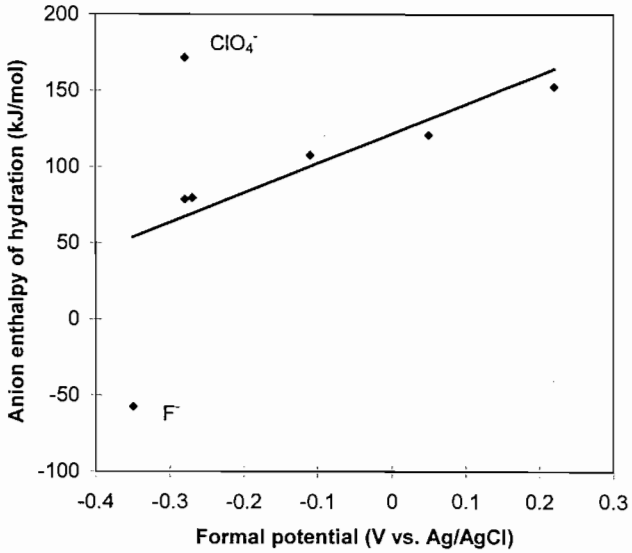


Fig. 3. Formal potentials of polypyrrole in various aqueous solutions vs. the enthalpy of hydration of the anion (data from Table 1).



anodic peak potential and the potential of the corresponding broad cathodic peak. Most of the voltammograms exhibit an additional reduction peak at lower potentials, although the size and location of this peak are quite variable. We believe that it is due to transient cation insertion (22). In KI(aq), peaks for the I_3^-/I^- couple are seen at ca. +0.7 V.

Ionic conductivity

Ionic conductivities of polypyrrole films in 0.2 M aqueous solutions of NaF, NaCl, KBr, KI, $NaClO_4$, KCN, and NaSCN were obtained as a function of potential by impedance spectroscopy as previously described (22). The results are shown in Fig. 2. In all cases, ionic conductivity increases with increasing potential, indicating that it is dominated by anion transport (22). To accurately reflect differences in anion mobilities, conductivities should be compared at the same degree of oxidation of the polymer (doping level). This is done in Table 1, where ionic conductivities at a doping level of 45 mC cm^{-2} (the maximum doping level in the I^- solution before the onset of I^- oxidation) are reported.

Discussion

The data in Table 1 do not follow any obvious trends, and so their explanation will require consideration of a number of factors. First we will consider the thermodynamic information reflected by the formal potentials.

Oxidation of the polymer (eq. [1]) requires uptake of anions from the solution.

$$[1] \quad (\text{-py-})_n^+X^- + e^- \rightleftharpoons (\text{-py-})_n + X^-(\text{solution})$$

where n is the average number of pyrrole rings over which each positive charge is spread. As the potential of the film is increased, n decreases from ∞ to ca. 3 (24).

Weak ion–solvent interactions and strong ion-oxidized polymer interactions will favour oxidation of the polymer and decrease the formal potential. Hence, the formal potentials reflect the ion-exchange selectivity of the polymer. The free

© 1997 NRC Canada

Table 2. Free energies for ion-exchange: $(\text{-py-})_n^+X^- + Y^-(\text{solution}) \rightleftharpoons (\text{-py-})_n^+Y^- + X^-(\text{solution})$.

		ΔG_{ex} (kJ/mol)	
X^-	Y^-	This work	Ref. 18
Cl^-	ClO_4^-	−1	44.7
Cl^-	Br^-	15	1.25
Cl^-	I^-	47	−8.28

energy change (ΔG_{ex}) for the exchange of two ions X^- and Y^- (eq. [2]),

[2] $(\text{-py-})_n^+X^- + Y^-(\text{solution}) \rightleftharpoons (\text{-py-})_n^+Y^- + X^-(\text{solution})$

is given by

[3] $\Delta G_{ex} = F(E_Y^{o'} - E_X^{o'})$

where $E_X^{o'}$ and $E_Y^{o'}$ are the formal potentials in X^- and Y^- solutions, respectively, and F is Faraday's constant. ΔG_{ex} values obtained by using eq. [3] are compared with literature values from experiments involving solid-state cells (18) in Table 2. The lack of even qualitative agreement is difficult to explain, although it should be noted that the literature values are for films prepared in acetonitrile.

From the data in Table 1, the anion preference of polypyrrole is $F^- > CN^- \sim ClO_4^- > Cl^- > Br^- > SCN^- > I^-$, which is virtually opposite to that of conventional anion–exchange polymers (25), and suggests that there is some specific interaction of the anion with the oxidized polymer.

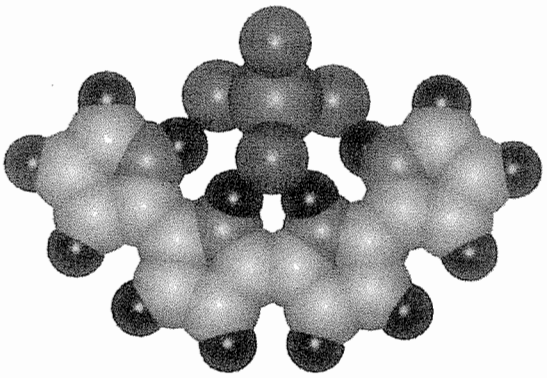
With the exception of perchlorate, enthalpies of hydration for the anions used here (Table 1) become less positive in the order in which they stabilize oxidized polypyrrole. The differences in formal potentials observed in the various solutions cannot, therefore, be due to differences in ion–solvent interactions, which would produce the opposite trend. The anions with the least favourable (most positive) enthalpy of hydration would be preferentially incorporated into the oxidized polymer, stabilizing it most. The differences in formal potentials must therefore be primarily due to differences in the interactions between the anions and the oxidized polymer.

The low formal potentials observed in the F^-, Cl^-, and ClO_4^- solutions indicate that the oxidized polymer interacts most strongly with hard anions (26). This suggests that the oxidized polypyrrole acts as a hard acid, and therefore the positive charge is concentrated at the N-H groups.

Amongst the soft anions, CN^- produces an anomalously low formal potential. Since CN^- is significantly more basic than the other soft anions used here, this suggests that hydrogen bonding with the pyrrole N-H group is important. To test this hypothesis we have plotted the polypyrrole formal potentials against the hydration energies of the anions (Fig. 3). $\Delta H_{hydration}$ is heavily influenced by hydrogen bonding and therefore provides an approximate scale of the strength of hydrogen bonding. The correlation in Fig. 3 is surprisingly good, and provides further evidence for hydrogen bonding.

Turning now to the ion conductivity (mobility) data, the least mobile ions are those of weak acids (CN^-, F^- and SCN^-). Their movement is presumably hindered by hydrogen bonding with the pyrrole N-H groups. For the other ions, size appears to be the main factor in determining the mobility within the polymer, although the mobility of ClO_4^- appears to be anomalously high.

Fig. 4. Molecular model of a $\text{pyrrole}_4^+ClO_4^-$ ion pair.



The perchlorate ion appears to be anomalous, both in terms of its mobility and its effect on the polymer's formal potential. As mentioned in the introduction, it also has a surprisingly low mobility in polypyrrole bathed in acetonitrile. These anomalies could be explained by a strong ion-pairing interaction between ClO_4^- and oxidized polypyrrole. Molecular models (Fig. 4) suggest that the perchlorate ion has an appropriate size and shape to form a strong interaction with a polypyrrole chain, despite its low propensity to hydrogen bond. The nonspecific (directional) nature of this interaction may explain the unexpectedly high mobility of ClO_4^- in polypyrrole bathed in water (i.e., the ClO_4^- ion could roll along the polypyrrole chain with a low activation energy). In acetonitrile, lack of solvation of the polymer may result in local solid phase formation, causing immobilization of the ClO_4^- counterions.

Conclusions

The formal potential and ion mobility data reported here provide evidence for hydrogen bonding between certain anions (F^-, CN^-, and SCN^-) and oxidized polypyrrole. These interactions have a profound influence on the mobility of the anion, leading to differences in mobility of over an order of magnitude between, for example, Cl^- and CN^-.

Acknowledgment

This work was supported by the Natural Sciences and Engineering Research Council of Canada and Memorial University.

References

1. G. Inzelt. *In* Electroanalytical chemistry. Vol. 18. *Edited by* A.J. Bard. Marcel Dekker, New York. 1994. p. 89.
2. R.H. Baughman. Makromol. Chem. Macromol. Symp. **51**, 193 (1991).
3. S. Roth and W. Graupner. Synth. Met. **57**, 3623 (1993).
4. X. Ren and P.G. Pickup. J. Electroanal. Chem. **396**, 359 (1995).
5. G.L. Duffitt and P.G. Pickup. J. Chem. Soc. Faraday Trans. **88**, 1417 (1992).
6. G. Schiavon, G. Zotti, N. Comisso, A. Berlin, and G. Pagani. J. Phys. Chem. **98**, 4861 (1994).

© 1997 NRC Canada

Can. J. Chem. Downloaded from www.nrcresearchpress.com by 91.121.58.235 on 09/08/12
For personal use only.

7. C. Visy, J. Lukkari, and J. Kankare. J. Electroanal. Chem. **319**, 85 (1991).
8. M.S. Kiani and G.R. Mitchell. Synth. Met. **48**, 203 (1992).
9. H. Ge, S.A. Ashraf, K.J. Gilmore, C.O. Too, and G.G. Wallace. J. Electroanal. Chem. **340**, 41 (1992).
10. M. Salmon, A.F. Diaz, A.J. Logan, M. Krounbi, and J. Bargon. Mol. Cryst. Liq. Cryst. **83**, 265 (1982).
11. S. Kuwabata, K. Okamoto, and H. Yoneyama. J. Chem. Soc. Faraday Trans. 1, **84**, 2317 (1988).
12. T. Osaka, K. Naoi, and S. Ogano. J. Electrochem. Soc. **135**, 1071 (1988).
13. D.J. Walton, C.E. Hall, and A. Chyla. Analyst (Cambridge U.K.), **117**, 1305 (1992).
14. L.S. Curtin, G.C. Komplin, and W.J. Pietro. J. Phys. Chem. **92**, 12 (1988).
15. J.B. Schlenoff and J.C.W. Chien. J. Am. Chem. Soc. **109**, 6269 (1987).
16. E.W. Tsai, T. Pajkossy, K. Rajeshwar, and J.R. Reynolds. J. Phys. Chem. **92**, 3560 (1988).
17. V.M. Schmidt and J. Heitbaum. Electrochim. Acta, **38**, 349 (1993).
18. L.S. Curtin, M. McEllistrem, and W.J. Pietro. J. Phys. Chem. **93**, 1637 (1989).
19. G. Zotti, G. Schiavon, and N. Comisso. Synth. Met. **40**, 309 (1991).
20. C.D. Paulse and P.G. Pickup. J. Phys. Chem. **92**, 7002 (1988).
21. H. Mao, J. Ochmanska, C.D. Paulse, and P.G. Pickup. Faraday Discuss. Chem. Soc. **88**, 165 (1989).
22. X. Ren and P.G. Pickup. J. Phys. Chem. **97**, 5356 (1993).
23. G. Zotti, G. Schiavon, S. Zecchin, and G. Daprano. Synth. Met. **80**, 35 (1996).
24. J. Heinze. *In* Topics in current chemistry. Vol. 152. Springer-Verlag, Berlin. 1990 p. 1.
25. C.E. Harland. Ion exchange: theory and practice. 2nd ed. Royal Society of Chemistry, Cambridge, U.K. 1994.
26. R.G. Pearson. J. Am. Chem. Soc. **85**, 3533 (1963).
27. G.A. Krestov. Thermodynamics of solvation. Ellis Horwood, Chichester, U.K., 1991.

Can. J. Chem. Downloaded from www.nrcresearchpress.com by 91.121.58.235 on 09/08/12
For personal use only.

© 1997 NRC Canada

Theory of potential relaxation after interrupting a steady-state current

Keith B. Oldham and Jan C. Myland

Abstract: This article predicts the chronopotentiometric response when a steady-state reductive voltammetric current is interrupted. Although the ohmic polarization disappears instantaneously, the presence of the double-layer capacitance prevents the cessation of faradaic current. The electrode potential adopts a value that reflects three processes — the continuing arrival of electroactive ions, the incomplete reduction of these ions, and the discharging of the capacitor — all of which proceed at a diminishing rate. A nonlinear differential equation is derived to incorporate these three processes and its dimensionless equivalent is solved as a power series. The form of the solution is shown to depend on whether or not the interrupted current was close to the limiting current of the reduction. Methods of analyzing the experimental chronopotentiogram are discussed.

Key words: current interrupt, potential relaxation, chronopotentiometry.

Résumé : Dans cet article on prédit la réponse chronopotentiométrique lorsqu'on interrompt un courant voltampérométrique réducteur à l'état stationnaire. Même si la polarisation ohmique disparaît instantanément, le présence de la capacitance de double couche empêche la cessation du courant faradique. Le potentiel d'électrode adopte une valeur qui est le reflet de trois processus — la continuation de l'arrivée d'ions électroactifs, la réduction incomplète de ces ions et la décharge de la capacitance — qui continuent tous à une vitesse qui s'amenuise. On a dérivé une équation différentielle non linéaire pour incorporer ces trois processus et on a résolu son équivalent sans dimension sous la forme d'une série de puissance. On a démontré que la forme de la solution varie suivant que le courant interrompu était près, ou non, du courant limite de la réduction. On discute des méthodes d'analyse du chronopotentiogramme expérimental.

Mots clés : courant interrompu, relaxation du potentiel, chronopotentiométrie.

[Traduit par la rédaction]

Introduction

The interruption of a faradaic current is a well-established method of studying electrode processes (1–7). Of the three varieties (concentration, activation, and ohmic) of polarization (8), the last two are often considered to disappear instantaneously when the current is interrupted, so that potentials measured immediately after interruption can provide direct access to the extent of concentration polarization, permitting investigation of conditions at the electrode surface. Because ohmic polarization (*IR* drop) can thereby by quantified and nullified, current interruption is particularly useful when the electrolyte solution has high resistivity, or when the material from which the electrode is fabricated is an imperfect conductor of electricity. Rather than relying on a single data point, the first after interruption, it is better to suitably extrapolate a set of measured potentials back to the instant of interruption. In this article, we shall first review the simple theory that applies when nonfaradaic processes can be ignored and then address the much more difficult case in which the discharging of the double layer contributes significantly to changing potential immediately after interruption.

For our present purpose, it is simpler to treat the case in which the electrode reaction generates a species that is at a constant, rather than at a variable, activity and therefore we choose to develop a model based on the *n*-electron reduction

$$[1] \qquad M^{n+}(\text{soln}) + ne^- \rightleftharpoons M(\text{l or s})$$

as the electrode process. However, the canonical case of the reaction

$$[2] \qquad O^{z+}(\text{soln}) + ne^- \rightleftharpoons R^{(z-n)+}(\text{soln})$$

in which both electroactive species are solutes in the solution, may be treated similarly, though the relationships are more elaborate because of the need to take account of two concentrations varying simultaneously. In the interest of further simplification, our attention will be directed solely to cases in which reaction [1] is reversible, so that activation polarization is absent.

The current-interruption procedure is most informative when the current being interrupted is unchanging, for then the behaviour after current cessation is not confounded by changes that were in process before the interruption. Here we shall be exclusively concerned with a current I_{ss} (which to accord with IUPAC's convention is negative) that was in a

Received March 10, 1997.

This article is dedicated to Professor Brian E. Conway on the occasion of his 70th birthday, in recognition of his distinguished and far-ranging contributions to the field of electrochemistry and to chemistry in Canada.

K.B. Oldham[1] **and J.C. Myland.** Department of Chemistry, Trent University, Peterborough, ON K9J 7B8, Canada.

[1] Author to whom correspondence may be addressed. Telephone: (705) 748-1336; Fax: (705) 748-1625; E-mail: KOldham@TrentU.CA

© 1997 NRC Canada

Can. J. Chem. Downloaded from www.nrcresearchpress.com by 91.121.58.235 on 09/08/12
For personal use only.

steady state prior to interruption. This generally implies that the concentration c_{ss} of the electroreactant in the vicinity of the electrode is linearly related

$$[3] \qquad c_{ss} = c_{ss}^{s} + gx$$

to the distance x measured from and normal to the electrode surface. Please note our use of the superscript "s" to denote conditions at the electrode surface, and of the subscript "ss" to indicate the steady state existing prior to interruption. Conditions in the steady state provide the initial conditions of the transient phase that is entered following current interruption. The g term in eq. [3] is the gradient $(dc/dx)^{s}$ of the electroreactant's concentration at the electrode surface and in its vicinity, which is related via Fick's first and Faraday's laws

$$[4] \qquad I_{ss} = -nFAD\left(\frac{dc}{dx}\right)_{ss}^{s} = -nFADg$$

to the steady-state current. Here D denotes the diffusivity (diffusion coefficient) of the electroreductant M^{n+}, A is the electrode area, and F is Faraday's constant. In the case of spherical or hemispherical diffusion (as when steady states are established at microelectrodes), a linear concentration gradient does not accompany a steady state and therefore the findings of this article require modification to address such geometries.

Negligible nonfaradaic interference

Prior to the interruption, the electrode potential displays a steady potential E_{ss}, which can be expressed as

$$[5] \qquad E_{ss} = E^{o\prime} + \frac{RT}{nF}\ln\left\{\frac{c_{ss}^{s}}{c^{o}}\right\} + \eta_{ohm}$$

Here η_{ohm} is the overvoltage attributable to ohmic polarization; it is negative for the reduction under consideration. $E^{o\prime}$ represents the conditional (or formal) potential and c^{o} denotes the standard of chemical concentration, 1000 mol m^{-3}.

At time $t = 0$, the reduction current of reaction [1] is interrupted. The flux of ions across the electrode immediately ceases

$$[6] \qquad \left(\frac{dc}{dx}\right)^{s} = 0$$

However, the concentration gradient elsewhere will continue to drive M^{n+} ions towards the electrode, thereby steadily increasing the concentration c^{s} of ions there. From its constant value E_{ss} prior to $t = 0$, the electrode potential will now change in accordance with the Nernst equation

$$[7] \qquad E = E^{o\prime} + \frac{RT}{nF}\ln\left\{\frac{c^{s}}{c^{o}}\right\}$$

Note that, in the absence of nonfaradaic interference, the Nernst equation could be used after the current interruption, even if reaction [1] were not reversible, because activation polarization, like ohmic polarization, requires a continuing current for its maintenance. However, it is specifically the *faradaic* current that supports activation polarization, whereas the *total* current generates ohmic polarization.

Equation [6] provides one boundary condition for the solution of Fick's second law

$$[8] \qquad D\frac{\partial^2 c}{\partial x^2} = \frac{\partial c}{\partial t}$$

the other boundary condition being

$$[9] \qquad \frac{\partial c}{\partial x} \to g \text{ as } x \to \infty$$

This last expression implies that the linear concentration profile extends indefinitely, which cannot be realized in practice, of course. For short times after interruption, however, which is the prime interest here, limit [9] can be regarded as valid. An initial condition also needs to be supplied to supplement Fick's second law. Equation [3] provides this and it becomes incorporated on Laplace transformation of eq. [8] into

$$[10] \qquad D\frac{d^2\bar{c}}{dx^2} = s\bar{c} - c_{ss}^{s} - gx$$

This is a linear ordinary differential equation and its general solution has the form

$$[11] \qquad \bar{c} = \frac{c_{ss}^{s} + gx}{s} + P(s)\exp\left\{-x\sqrt{\frac{s}{D}}\right\} + Q(s)\exp\left\{x\sqrt{\frac{s}{D}}\right\}$$

where $P(s)$ and $Q(s)$ are presently unknown coefficients that may be functions of the dummy Laplace variable s. In the present case, application of boundary condition [9] shows that $Q(s)$ must be zero. The $P(s)$ term may easily be found but, to establish conformity with the method to be followed in the next section, a solution route will be followed that bypasses the explicit evaluation of $P(s)$. We differentiate eq. [11] with respect to x and then eliminate the $P(s)$ term between this expression for the Laplace transform of the surface concentration of the M^{n+} ion and its derivative. The result may be written

$$[12] \qquad \frac{d\bar{c}}{dx} = \frac{g}{s} - \sqrt{\frac{s}{D}}\left[\bar{c} - \frac{c_{ss}^{s} + gx}{s}\right]$$

Our interest is restricted to the electrode surface, $x = 0$, where

$$[13] \qquad \left(\frac{d\bar{c}}{dx}\right)^{s} = \frac{g}{s} - \sqrt{\frac{s}{D}}\left[\bar{c}^{s} - \frac{c_{ss}^{s}}{s}\right]$$

Because of the presence of the $\sqrt{s}$ multiplier, this transformed equation easily inverts to an expression involving the semiderivative with respect to time of the surface concentration excursion:

$$[14] \qquad \left(\frac{\partial c}{\partial x}\right)^{s} = g - \frac{1}{\sqrt{D}}\frac{d^{1/2}(c^{s} - c_{ss}^{s})}{dt^{1/2}}$$

At this point, use is made of condition [6] to nullify the left-hand member of this equation. After rearrangement, semiintegration then leads easily to

$$[15] \qquad c^{s} = c_{ss}^{s} + 2g\sqrt{\frac{Dt}{\pi}}$$

© 1997 NRC Canada

Can. J. Chem. Downloaded from www.nrcresearchpress.com by 91.121.58.235 on 09/08/12
For personal use only.

Can. J. Chem. Downloaded from www.nrcresearchpress.com by 91.121.58.235 on 09/08/12
For personal use only.

so that, via eqs. [7] and [5], the potential relaxation is found to be described by

$$[16] \qquad E = E_{ss} - \eta_{ohm} + \frac{RT}{nF} \ln\left\{1 + \frac{2g}{c^s_{ss}}\sqrt{\frac{Dt}{\pi}}\right\}$$

c^s_{ss} and η_{ohm} may be found from this chronopotentiometric relation. Alternative routes, not involving the fractional calculus, could have generated eq. [15] more easily; however, our chosen derivation provides a better introduction to the case that now follows.

Effect of nonfaradaic interference

Whereas it is true that the *total* current drops immediately to zero on interruption, this is not true of the individual faradaic and nonfaradaic currents of which the total is composed, except when the latter is negligibly important. Because the individual currents sum to zero after interruption, the expression

$$[17] \qquad nADF\left(\frac{\partial c}{\partial x}\right)^s = -I_{far} = I_{nonfar} = C\frac{dE}{dt} = \frac{CRT}{nFc^s}\frac{dc^s}{dt}$$

holds. The first member in this chain of equalities is analogous to eq. [4], while the last arises from differentiation of eq. [7]. The capacitance C of the electrode has here been assumed potential independent.

As in the previous section, eq. [3] provides the initial condition for the solution of Fick's second law [8], with eq. [9] being one of the boundary conditions. Equation [17], however, now replaces eq. [6] as the boundary condition at the electrode surface. The method of solution remains unchanged from that of the preceding section as far as eq. [14]. At that point eq. [17] may be combined with eq. [14], to give

$$[18] \qquad c^s\frac{d^{1/2}(c^s - c^s_{ss})}{dt^{1/2}} = \sqrt{D}gc^s - \frac{CRT}{n^2F^2A\sqrt{D}}\frac{dc^s}{dt}$$

This is a fractional ordinary differential equation linking the variables c^s and t. It is nonlinear because of the c^s multiplier in the left-hand term. Such equations are rarely soluble in terms of established functions.

To convert eq. [18] into dimensionless form, let us define

$$[19] \qquad \tau = \frac{n^2F^2ADg}{CRT}t = \frac{-nFI_{ss}}{CRT}t$$

and

$$[20] \qquad \varsigma = \frac{nF\sqrt{A}}{\sqrt{CRTg}}c^s = \sqrt{\frac{-n^3F^3D}{CRTI_{ss}}}Ac^s$$

It is also convenient to adopt a as a symbol for the dimensionless equivalent of the preexisting steady-state surface concentration

$$[21] \qquad a = \varsigma_{ss} = \frac{nF\sqrt{A}}{\sqrt{CRTg}}c^s_{ss} = \sqrt{\frac{-n^3F^3D}{CRTI_{ss}}}Ac^s_{ss}$$

These definitions convert the differential equation into

$$[22] \qquad \frac{d\varsigma}{d\tau} = \varsigma - \varsigma\frac{d^{1/2}(\varsigma - a)}{d\tau^{1/2}}$$

an expression that links the ς and τ variables in terms of a single parameter, a. It will now be demonstrated that there exists a power-series solution to eq. [22].

To proceed, let it be assumed that a solution to eq. [22] exists such that

$$[23] \qquad \frac{d\varsigma}{d\tau} = \sum_{j=2}^{\infty} b_j\tau^{(j-2)/2}$$

where the b_j coefficients depend, in a presently unknown fashion, on the a parameter. Then

$$[24] \qquad \varsigma = a + 2\sum_{j=2}^{\infty}\frac{b_j}{j}\tau^{j/2}$$

where the a term, the initial value of ς, appeared as a constant of integration, and

$$[25] \qquad \frac{d^{1/2}(\varsigma - \varsigma_{ss})}{d\tau^{1/2}} = 2\sum_{j=2}^{\infty}\frac{b_j}{j}\frac{\Gamma(\frac{1}{2}j+1)}{\Gamma(\frac{1}{2}j+1/2)}\tau^{(j-1)/2} = \sum_{j=2}^{\infty} b_j\frac{\Gamma(\frac{1}{2}j)}{\Gamma(\frac{1}{2}j+1/2)}\tau^{(j-1)/2}$$

This latter expression arises) either by semiintegration of eq. [23] or by semidifferentiation of eq. [24]. We are free to define $b_1 = -\Gamma(1)/\Gamma(1/2)$ because this term does not occur in eqs. [23]–[25]; then

$$[26] \qquad 1 - \frac{d^{1/2}(\varsigma - \varsigma_{ss})}{d\tau^{1/2}} = 1 - \sum_{k=2}^{\infty} b_k\frac{\Gamma(\frac{1}{2}k)}{\Gamma(\frac{1}{2}k+1/2)}\tau^{(k-1)/2} = -\sum_{k=2}^{\infty} b_{k-1}\frac{\Gamma(\frac{1}{2}k-1/2)}{\Gamma(\frac{1}{2}k)}\tau^{(k-2)/2}$$

Next, we multiply eqs. [24] and [26]

$$[27] \qquad \varsigma\left[1 - \frac{d^{1/2}(\varsigma - \varsigma_{ss})}{d\tau^{1/2}}\right] = -a\sum_{k=2}^{\infty} b_{k-1}\frac{\Gamma(\frac{1}{2}k-1/2)}{\Gamma(\frac{1}{2}k)} \times\tau^{(k-2)/2} - 2\sum_{k=2}^{\infty}\sum_{i=2}^{\infty}\frac{b_{k-1}b_i}{i}\frac{\Gamma(\frac{1}{2}k-1/2)}{\Gamma(\frac{1}{2}k)}\tau^{(k+i-2)/2}$$

It is now convenient to use the summation index j to replace k in the first, and $k+i$ in the second, right-hand terms of eq. [27]. We also make use of the permutation

$$[28] \qquad \sum_{k=2}^{\infty}\sum_{j-k=2}^{\infty} = \sum_{j=4}^{\infty}\sum_{k=2}^{j-2}$$

to simplify the second right-hand term. This leaves us in a position to substitute eqs. [23] and [27] into the differential eq. [22]. Thereby

$$[29] \qquad \sum_{j=2}^{\infty} b_j\tau^{(j-2)/2} = -a\sum_{j=2}^{\infty} b_{j-1}\frac{\Gamma(\frac{1}{2}j-1/2)}{\Gamma(\frac{1}{2}j)}\tau^{(j-2)/2} - 2\sum_{j=4}^{\infty}\sum_{k=2}^{j-2}\frac{b_{j-k}b_{k-1}}{j-k}\frac{\Gamma(\frac{1}{2}k-1/2)}{\Gamma(\frac{1}{2}k)}\tau^{(j-2)/2}$$

© 1997 NRC Canada

Can. J. Chem. Downloaded from www.nrcresearchpress.com by 91.121.58.235 on 09/08/12
For personal use only.

Table 1. Expressions for early coefficients in summation [23]. Note that b_1 does not appear in the series.

j	b_j
1	$\frac{-1}{\sqrt{\pi}}$
2	a
3	$\frac{-2a^2}{\sqrt{\pi}}$
4	$a^3 + a$
5	$\frac{-4a^4}{3\sqrt{\pi}} - \frac{14a^2}{3\sqrt{\pi}}$
6	$\frac{a^5}{2} + \left(\frac{13}{4} + \frac{8}{3\pi}\right)a^3 + \frac{a}{2}$
7	$\frac{-8a^6}{15\sqrt{\pi}} - \left(\frac{128}{45\pi^{3/2}} + \frac{23}{3\sqrt{\pi}}\right)a^4 - \left(\frac{71}{15\sqrt{\pi}}\right)a^2$
8	$\frac{a^7}{6} + \left(\frac{57}{16} + \frac{56}{15\pi}\right)a^5 + \left(\frac{71}{16} + \frac{32}{5\pi}\right)a^3 + \frac{a}{6}$

Notice that the same power of τ now occurs in each of the three terms and that the first (or only) summation is invariably over j-values. It follows that we can equate each of the coefficients of $\tau^{(j-2)/2}$. For the cases $j = 2$ and $j = 3$, there is no contribution from the final term in eq. [29], so that

$$[30] \qquad b_j = -ab_{j-1}\frac{\Gamma(\frac{1}{2}j - 1/2)}{\Gamma(\frac{1}{2}j)} \qquad \text{for } j = 2, 3$$

whereas for all larger j values both right-hand terms contribute

$$[31] \qquad b_j = -ab_{j-1}\frac{\Gamma(\frac{1}{2}j - 1/2)}{\Gamma(\frac{1}{2}j)} - 2\sum_{k=2}^{j-2}\frac{b_{j-k}b_{k-1}}{j-k} \times \frac{\Gamma(\frac{1}{2}k - 1/2)}{\Gamma(\frac{1}{2}k)} \qquad \text{for } j = 4, 5, 6, \ldots$$

Formulas [30] and [31] constitute recursion formulas permitting all the b coefficients to be successively evaluated. Table 1 lists early members, from which an emerging pattern is evident. Writing out the first few terms of the expression for ς, one has

$$[32] \qquad \varsigma = a\left[1 + \tau - \frac{4a\tau^{3/2}}{3\sqrt{\pi}} + \frac{(a^2+1)\tau^2}{2} - \frac{4a(2a^2+7)\tau^{5/2}}{15\sqrt{\pi}} + \cdots\right]$$

Note the absence of a term in $\sqrt{\tau}$. The infinite series of which these are the first few terms effectively constitutes the complete solution to the problem that is being addressed. All that is now required to determine the chronopotentiogram is a return to experimental variables and substitution of c^s into the Nernst equation.

Equation [24] has been shown to be a dimensionless solution to the problem, when the b coefficients are evaluated via recursion relationships [30] and [31] with $b_1 = -\Gamma(1)/\Gamma(1/2) = -1/\sqrt{\tau}$. In experimental variables the solution is the complicated expression

$$[33] \qquad c^s = c^s_{ss}\left[1 - \frac{nFI_{ss}t}{CRT} + \frac{4n^3F^3AI_{ss}c^s_{ss}}{3C^2R^2T^2}\sqrt{\frac{Dt^3}{\pi}} + \frac{n^2F^2I_{ss}[CRTI_{ss} - n^3F^3DA^2(c^s_{ss})^2]t^2}{2C^3R^3T^3} - O(t^{5/2})\right]$$

This gives the concentration at the electrode surface as a function of time in terms of the pertinent experimental parameters. The time evolution of the potential follows from inserting this expression into the Nernstian relationship

$$[34] \qquad E = E_{ss} + \frac{RT}{nF}\ln\left\{\frac{c^s}{c^s_{ss}}\right\} - \eta_{ohm}$$

Magnitude of the a parameter

Table 1 clearly shows that most of the coefficients consist of several terms and that the dominant term among these several depends critically on the magnitude of a. We need to get some idea of typical experimental values of this parameter. Before substituting numerical values into definition [21], it is useful to utilize the concept (ref. 8, pp. 202, 284) of the transport coefficient (or mass transfer constant) m. This links the steady-state current to the difference between the bulk and surface concentrations. In our case

$$[35] \qquad c^b - c^s_{ss} = \frac{-I_{ss}}{nFAm}$$

As the limiting current I_L is approached, the surface concentration of the electroreactant tends toward zero, so that

$$[36] \qquad c^b = \frac{-I_L}{nFAm}$$

Combination of these two equations enables the concentration at the electrode surface to be expressed

$$[37] \qquad c^s_{ss} = c^b\frac{I_L - I_{ss}}{I_L}$$

in terms of more easily measurable quantities. Substitution into definition [21] leads to

$$[38] \qquad a = Ac^b\sqrt{\frac{-n^3F^3D}{CRTI_L}}\frac{I_{ss} - I_L}{\sqrt{I_LI_{ss}}}$$

when the negative sign of I_L and I_{ss} is recognized.

We adopt the following typical voltammetric magnitudes: $c^b = 1$ mol m^{-3}, $n = 2$, $D = 1 \times 10^{-9}$ m^2 s^{-1}, $C/A = 0.3$ F m^{-2}, $T = 300$ K, and $I_L/A = -10$ A m^{-2}. Then, on substitution into eq. [38], we discover

$$[39] \qquad a \approx 30\frac{I_{ss} - I_L}{\sqrt{I_LI_{ss}}}$$

Thus, with these particular values, if the steady-state cur-

© 1997 NRC Canada

Can. J. Chem. Downloaded from www.nrcresearchpress.com by 91.121.58.235 on 09/08/12
For personal use only.

rent exceeds $0.97I_L$ in magnitude, a will be less than unity and, conversely, $a > 1$ if I_{ss} is less than 97% of the limiting current. Both of these alternatives are encountered experimentally, so the possibilities that $a > 1$ and $a < 1$ must both be considered. It is not unreasonable, in the light of these calculations, to assert that a steady-state current on the limiting plateau corresponds to $a \ll 1$, whereas a steady-state experiment not in the limiting region encounters the parameter value $a \gg 1$.

Limiting solutions

In the $a \gg 1$ case, only those components of b_j with the highest power of a will be important. These are the first mentioned terms in Table 1, for example, the $a^5/2$ component of b_6. These terms are, in fact

$$[40] \qquad b_j = \frac{(-a)^j}{a\Gamma(\frac{1}{2}j)} \quad \text{when } a \gg 1$$

so that we learn from eq. [24] that

$$[41] \qquad \varsigma = a + \frac{2}{a}\sum_{j=2}^{\infty}\frac{(-a\sqrt{\tau})^j}{j\Gamma(\frac{1}{2}j)} = a + \frac{1}{a}\sum_{j=2}^{\infty}\frac{(-a\sqrt{\tau})^j}{\Gamma(1+\frac{1}{2}j)}$$

Now the sum from $j = 0$ to ∞ of $(-z)^j/\Gamma(1 + 1/2j)$ is $\exp\{z^2\}\text{erfc}\{z\}$ (10) and therefore

$$[42] \qquad \varsigma = a + \frac{1}{a}\left[2a\sqrt{\frac{\tau}{\pi}} - 1 + \exp\{a^2\tau\}\text{erfc}\{a\sqrt{\tau}\}\right]$$

This is the result, in dimensionless coordinates, when the parameter a is large, i.e., when the current being interrupted is not close to its limiting value.

If not only a, but also $a\sqrt{\tau}$, is large, then we may use an asymptotic expansion of the error function complement (10) to simplify eq. [42] to

$$[43] \qquad \varsigma = a + 2\sqrt{\frac{\tau}{\pi}} - \frac{1}{a} + \frac{1}{a^2\sqrt{\pi\tau}} - \cdots$$

The first two right-hand terms are the dominant ones and it is comforting to find that these two exactly reproduce the right-hand side of eq. [15] when a return is made to dimensional variables. The first right-hand term in eq. [43] represents the surface concentration prior to interruption. The second right-hand term corresponds to the increasing surface concentration of electroreacant arriving by diffusing down the concentration profile. Terms in eq. [43] beyond the first two represent the minor retardation in the buildup of M^{n+} concentration at the electrode caused by the small faradaic burden imposed by the need to discharge the double layer.

Equation [43] is predicated on both a and $a\sqrt{\tau}$ being large. But what magnitude is $a\sqrt{\tau}$ likely to have? Referring to definitions [19] and [21], we find

$$[44] \qquad a\sqrt{\tau} = \frac{n^2F^2Ac^s_{ss}}{CRT}\sqrt{Dt} = \frac{n^2F^2Ac^b}{CRTI_L}(I_L - I_{ss})\sqrt{Dt}$$

and using the previously cited typical voltammetric magnitudes, along with $I_{ss} = I_L/2$, one calculates that $a\sqrt{\tau} \approx (800s^{1/2})\sqrt{t}$. Thus, on this basis, $a\sqrt{\tau}$ exceeds unity soon after 1 μs, so the step from [42] to [43] is valid at most experimentally accessible times. For future use, we shall also estimate the magnitude of $\sqrt{\tau}/a$. We find

$$[45] \qquad \frac{\sqrt{\tau}}{a} = \frac{-I_{ss}}{nFAc^s_{ss}}\sqrt{\frac{t}{D}} = \frac{I_{ss}I_L}{(I_{ss}-I_L)nFAc^b}\sqrt{\frac{t}{D}}$$

$$= (0.7\,s^{-1/2})\sqrt{t}$$

when we use previous values plus the assumption that $I_L/A = 4\text{ A m}^{-2}$.

Next, we consider the $a \ll 1$ case. Then we can ignore all components of the b_j coefficients that involve powers of a larger then unity. A glance at Table 1 shows that this excludes all components when j is odd and that for even j the retained component gives

$$[46] \qquad b_j = \frac{a}{(\frac{1}{2}j-1)!} \quad \text{when } a \ll 1 \text{ and } j = 2,4,6,\ldots$$

It then follows from eq. [24] that

$$[47] \qquad \varsigma = a + 2a\sum_{j=2,4,\ldots}^{\infty}\frac{\tau^{j/2}}{j(\frac{1}{2}j-1)!} = a\exp\{\tau\}$$

a very simple result! Reverting to physical coordinates, we find

$$[48] \qquad \frac{c^s}{c^s_{ss}} = \exp\left\{\frac{-nFI_{ss}t}{CRT}\right\}$$

which shows that the surface concentration rises (recall that I_{ss} is negative) exponentially with time in this limiting case of our model. The Nernst relationship [34] then reveals a linear change in potential with time.

$$[49] \qquad E = E_{ss} - \frac{I_{ss}t}{C} - \eta_{ohm}$$

Result [49] is easily understandable. The small-a case that we are treating corresponds to a steady-state current on the limiting plateau, so that the potential may shift positively after interruption without diminishing the faradaic current significantly. This means that the nonfaradiac current discharging the double-layer capacitor also remains constant. The effect of passing a constant positive current through a negatively charged capacitor is to cause a steady positive shift in potential, at a rate proportional to the current but inversely proportional to the capacitance, which is just what eq. [49] states.

The fact that for both extreme values of a our general result, embedded in eqs. [24], [30], and [31], reduces to limiting forms that can be rationalized, gives confidence that the general result is also correct.

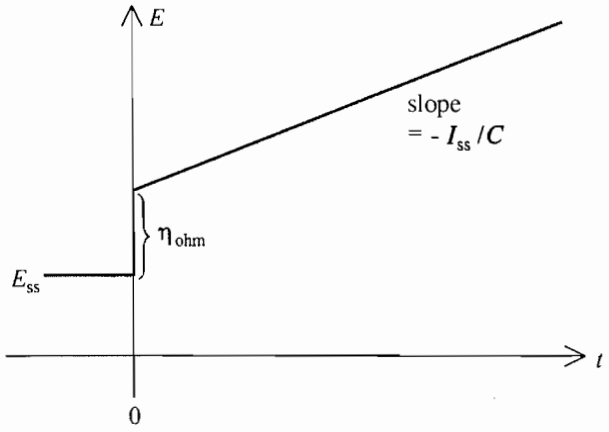
Short-time behaviour

The purpose of interrupting the steady-state current is to measure the ohmic polarization and to learn whatever else is accessible in the way of information about the electrode. This information must be gained from the behaviour of the potential relaxation in the rather short period of time during which the assumption of a linear concentration profile of unlimited

© 1997 NRC Canada

Can. J. Chem. Downloaded from www.nrcresearchpress.com by 91.121.58.235 on 09/08/12
For personal use only.

Fig. 1. Predicted chronopotentiogram from interruption of a steady-state current of magnitude close to the limiting current.



extent remains credible. In this section we briefly describe how information might be extracted from the chronopotentiogram. Of course, an exact method might be based on the full equation, but this would involve repeated or recursive computation in an attempt to match the experimental curve to the theoretical model.

If the steady-state current I_{ss} is close to the limiting current, so that a is small, the problem is simple because eq. [49] applies. If the potential is plotted versus time, before and after interruption, a graph resembling Fig. 1 should be created, from which the ohmic polarization η_{ohm} and the double-layer capacitance C are easily calculable.

The problem may be considerably more difficult when it is eq. [43] that applies. One approach is to ignore all but the first two right-hand terms and reorganize the equation into the form

$$[50] \qquad \frac{c^s}{c^s_{ss}} = \frac{\varsigma}{a} = 1 + \frac{2}{a}\sqrt{\frac{\tau}{\pi}}$$

Then, with the help of eqs. [5] and [7]

$$[51] \qquad E = E_{ss} - \eta_{ohm} + \frac{RT}{nF} \ln\left\{1 + \frac{2}{a}\sqrt{\frac{\tau}{\pi}}\right\}$$

In light of the magnitude calculated in eq. [45] it may, or may not, be legitimate to regard $(2/a)\sqrt{\tau/\pi}$ as small in comparison with unity. If it is, then

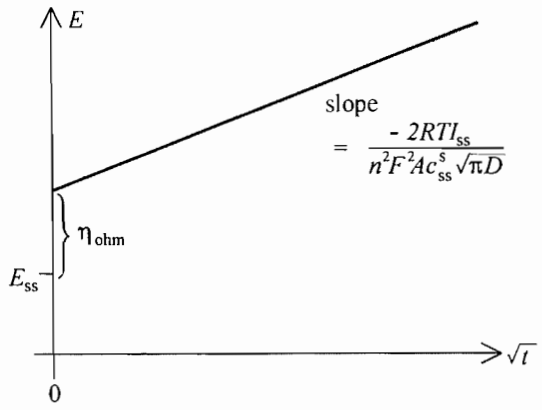
$$[52] \qquad E = E_{ss} - \eta_{ohm} + \frac{2RT}{nFa}\sqrt{\frac{\tau}{\pi}}$$

$$= E_{ss} - \eta_{ohm} - \frac{2RTI_{ss}}{n^2F^2Ac^s_{ss}}\sqrt{\frac{t}{\pi D}}$$

and a graph of the potential E versus the square-root of time will have the characteristics shown in Fig. 2. If not, a less attractive method is needed to analyze eq. [51]. One such relies on pairs of (E,t) data. From these one calculates

$$[53] \qquad c^s_{ss} = \frac{2I_{ss}}{nFA\sqrt{\pi D}} \frac{\varepsilon\sqrt{t_1} - \sqrt{t_2}}{\varepsilon - 1}$$

Fig. 2. Method of analyzing potential-versus-time data for certain cases (see text) of interruption of currents not close to the limiting current.



and

$$[54] \qquad \eta_{ohm} = E_{ss} - E_1 + \frac{RT}{nF} \ln\left\{\frac{\sqrt{t_2} - \sqrt{t_1}}{\sqrt{t_2} - \varepsilon\sqrt{t_1}}\right\}$$

where

$$[55] \qquad \varepsilon = \exp\left\{\frac{nF}{RT}(E_2 - E_1)\right\}$$

Summary

The interruption of a steady-state reductive current at a reversible electrode leads to a sudden positive jump in potential followed by a more gradual potential relaxation. We have derived a series solution describing the course of the relaxation and have investigated some of its limiting cases.

Acknowledgements

The financial support of the Natural Sciences and Engineering Research Council of Canada is acknowledged with gratitude.

References

1. L. Bai, L. Gao, and B.E. Conway. J. Chem. Soc. Faraday Trans. **89**, 235 (1993).
2. B.E. Conway and L. Bai. J. Chem. Soc. Faraday Trans. **81**, 1941 (1985).
3. P. Gu, L. Bai, L. Gau, R. Brousseau, and B.E. Conway. Electrochim. Acta, **37**, 2145 (1992).
4. L.J. Bai. J. Electronanal. Chem. **355**, 37 (1993).
5. C.G. Lee, H. Nakano, T. Nishina, I. Uchida, Y. Izaki, and S. Kuroe. Denki Kagaku, **64**, 486 (1996).
6. M.P. Vinod and K. Vijayamohanan. J. Appl. Electrochem. **24**, 44 (1994).
7. C.Y. Yuh and J.R. Selman. J. Electrochem. Soc. **138**, 3649 (1991).
8. K.B. Oldham and J.C. Myland. Fundamentals of electrochemical science. Academic Press, San Diego. 1994. Chap. 6.
9. K.B. Oldham and J. Spanier. The fractional calculus. Academic Press, New York. 1974. p. 119.
10. J. Spanier and K.B. Oldham. An atlas of functions. Hemisphere, New York, and Springer-Verlag, Berlin. 1987. Sect. 41:6.

© 1997 NRC Canada

The influence of a non-micelle-forming surfactant on the electrocatalytic hydrogenation of carvone and limonene in aqueous medium at Raney nickel electrodes[1]

Valérie Beraud, Jean Lessard, and Marc Thomalla

Abstract: The electrocatalytic hydrogenation (ECH) of carvone (**1**) and limonene (**8**) at a Raney nickel cathode was studied in aqueous solutions containing a non-micelle-forming surfactant (didodecyldimethylammonium bromide, DDAB). The efficiency of ECH of these substrates was markedly increased compared to that observed previously with micelle-forming surfactants, and this for very low DDAB concentrations, as a consequence of the strong adsorption of DDAB on the electrode. For the ECH of **8** in basic medium (pH 10), the major part of organic compounds (60–95%) was shown to be adsorbed on the electrode surface as an organic layer stabilized by an interfacial film of DDAB.

Key words: electrocatalytic hydrogenation, limonene, carvone, surfactant, emulsions, Raney nickel cathodes.

Résumé : L'hydrogénation électrocatalytique (HEC) de la carvone (**1**) et du limonène (**8**) sur cathode de nickel de Raney a été étudiée en solutions aqueuses contenant un surfactant non micellisable (bromure de didodécyldiméthylammonium, DDAB). L'efficacité de l'HEC de ces composés augmente fortement par rapport à celle observée antérieurement en présence de surfactants micellisables et ceci pour de très faibles concentrations en DDAB. Ceci résulte de la forte adsorption de ce type de surfactant sur l'électrode. Dans le cas du limonène en milieu alcalin (pH 10), la majeure partie (60–95%) des composés organiques se retrouve adsorbée sur l'électrode sous forme d'une couche organique stabilisée par un film interfacial de DDAB.

Mots clés : hydrogénation électrocatalytique, limonène, carvone, surfactant, émulsions, cathodes de nickel de Raney.

Can. J. Chem. Downloaded from www.nrcresearchpress.com by 91.121.58.235 on 09/08/12
For personal use only.

Introduction

Electrocatalytic hydrogenation (ECH) at Raney nickel electrodes constitutes a useful method of carrying out the hydrogenation of a variety of unsaturated organic compounds under mild conditions (1). Previous studies have shown that surfactants (especially cationic ones) strongly enhance the extent and the efficiency of the electrocatalytic hydrogenation of unsaturated organic compounds emulsified in an aqueous electrolyte. The conversion rate, the chemical and current yields, and the percentage of fully hydrogenated products were higher in aqueous electrolytes containing a surfactant (emulsified or micellar solutions) than in homogeneous hydroorganic solutions (2).

Received May 16, 1997.

This paper is dedicated to Professor Brian E Conway on the occasion of his 70th birthday.

V. Beraud and M. Thomalla.[2] Laboratoire de chimie organique 3 UMR 56 22, Université Claude Bernard — Lyon I, 43, Bd du 11 Novembre 1918, 69622 Villeurbanne Cedex, France.
J. Lessard.[2] Centre de recherche en électrochimie et électrocatalyse, Département de chimie, Université de Sherbrooke, QC J1K 2R1, Canada.

[1] Part XI in the series Electrocatalytic hydrogenation of organic compounds. For part X and IX, see refs. 1 and 2.

[2] Authors to whom correspondence may be addressed. For J. Lessard, telephone: (819) 821-7091. Fax: (819) 821-8107. For M. Thomalla, telephone: 04-72-431333. Fax: 04-72-431323.

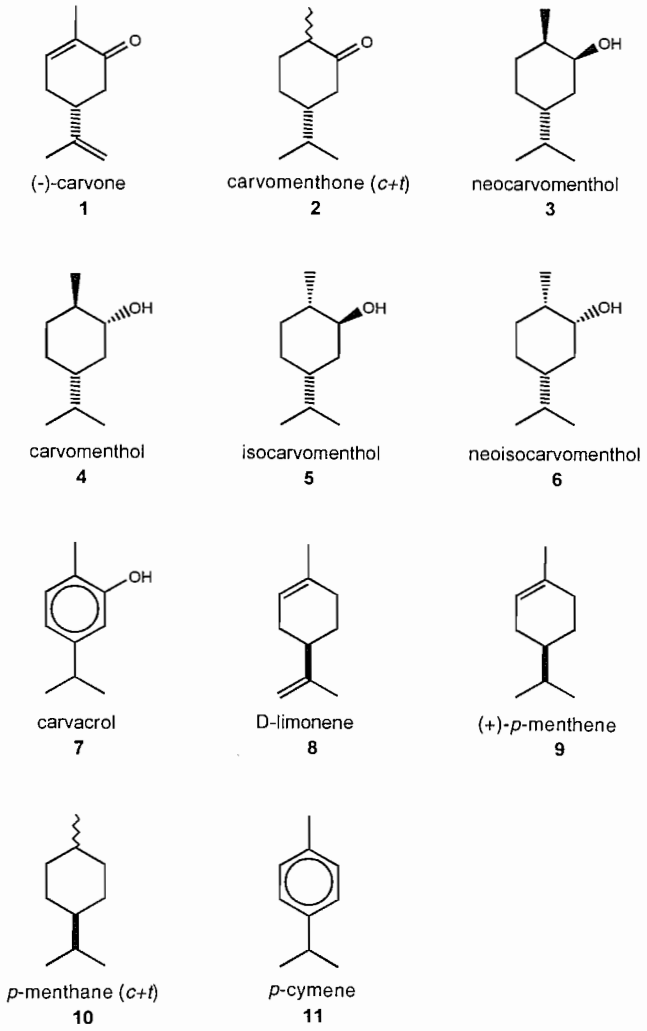
Surfactants can influence the ECH in two ways: (*i*) by increasing the substrate solubility in the whole bulk; (*ii*) by the formation of an adsorbed hydrophobic surfactant layer on the cathode. In the first, the increase of substrate solubility results from its association with the micelles. This occurs only for surfactant concentrations higher than the critical micellar concentration (CMC). In the second, incorporation of the substrate in a hydrophobic layer enhances its adsorption on the cathode and this is operative over the whole range of surfactant concentrations used, including concentrations lower than the CMC. An increase of the local substrate concentration on the catalyst seems to be the main effect of surfactant on the ECH of organic compounds, as shown by the ECH of carvone in emulsions (2). The largest extent and highest efficiency of hydrogenation of carvone were obtained with cetyltrimethylammonium bromide (CTAB) at concentrations lower than the CMC (2). Under those conditions, micelles are not formed and the effect observed on ECH can result only from the presence of a hydrophobic layer on the cathode (2). However, when the surfactant concentration increases, the efficiency of the ECH depends on the solubilization equilibrium between the hydrophobic surfactant layer and the micellar pseudophase. This led to a decrease of the efficiency of the ECH of limonene and carvone at higher surfactant concentrations (2).

In this work, the ECH of carvone (**1**), D-limonene (**8**), and *p*-menthene (**9**) (Fig. 1) was measured in the presence of didodecyldimethylammonium bromide (DDAB). This surfactant, poorly soluble in water (10^{-4} M), does not form micelles, but is strongly adsorbed at the interface, leading to multilayers

© 1997 NRC Canada

Can. J. Chem. Downloaded from www.nrcresearchpress.com by 91.121.58.235 on 09/08/12
For personal use only.

Fig. 1. Structure of substrates and reaction products.



when its concentration increases (3, 4). This property was previously used by Rusling and co-workers (5–7) to enhance the local concentrations of both reactants and mediator on the surface of electrodes for reductive dehalogenation. Thus, in the presence of DDAB, it was possible to study the influence of surfactant adsorption on the ECH of an organic compound in the absence of any micellar effect.

Experimental

Reagents

Some commercially available compounds were used as received: D-limonene (98%) from Eastman Kodak, (+)-*p*-menthene (99%) from Fluka, didodecyldimethylammonium bromide (DDAB) (98%) from Aldrich. Water and (−)-carvone (98%) obtained from Jansen Chimica were distilled before use. Buffers were prepared as described in the *Handbook of chemistry and physics* (8).

Electrolyses

The electrochemical apparatus, the cell, the preparation of Raney Ni electrodes, and the electrolysis procedure have been described previously (1, 2, 9). The electrolysis conditions and the catholyte composition (volume of 100 mL) are indicated in the footnotes of the tables. The anolyte consisted of a 0.1 M H_2SO_4 aqueous solution.

Products

The work-up procedure was the same as that reported in ref. 9. However, taking representative aliquots was not possible in emulsions and therefore the entries in Table 4 correspond to different electrolyses. Yields and product distributions were determined by vapour phase chromatography (VPC), as described in ref. 2, on capillary polar columns (DB-Wax 30 m or DB-5 DE 15 m) using a Varian 3300 or a Hewlett Packard 3390 A chromatograph equipped with a flame ionization detector and nonane (99%, Aldrich) as internal standard. The compounds adsorbed on the cathode were recovered by dipping the electrode in dry ether immediately after the electrolysis and keeping it in the solvent overnight. The cathode was then carefully rinsed several times with dry ether.

Results and discussion

ECH of carvone (1)

In emulsions with DDAB 7.7×10^{-5} M, at pH 2 and 10, after a charge of 6 F mol^{-1}, all the carvone was consumed and a mixture of carvomenthone (**2**), saturated alcohols (**3–6**) and carvacrol (**7**) was obtained (Table 1, entries 1 and 2). In acidic solution (entry 1), the yield of products and the current efficiency were close to those previously obtained with CTAB at similar concentrations (8.2×10^{-5} M)[3] (see entry 3). Lower yields of alcohol and lower current efficiencies were observed at pH 10 (entry 2) as a consequence of the formation of higher amounts of carvacrol. At pH 2, carvacrol can result from acid-catalyzed isomerization of carvone and (or) from enolization and isomerization of the exocyclic double bond through sequential dehydrogenation–hydrogenation. At pH 10, the isomerization of carvone to carvacrol should occur only through a sequential dehydrogenation–hydrogenation process. The latter is faster under alkaline conditions (10, 11*a*), which can explain the higher yield of carvacrol observed at pH 10.

At pH 2, the current efficiency, which is a measure of the competition between substrate hydrogenation (reactions [2]–[4]) and hydrogen evolution (reactions [5]), was higher when a surfactant was present (86–87% with DDAB or CTAB, see entries 1 and 3, respectively) than in the absence of surfactant (77%, entry 4) and was the same with either surfactant.

[1] $H_3O^+ (H_2O) + e^- \Leftrightarrow Hads + H_2O (OH^-)$

[2] $Y = Z \Leftrightarrow Y = Zads$

[3] $Y = Zads + 2Hads \Leftrightarrow YH = ZHads$

[4] $YH - Zhads \Leftrightarrow YH - ZH$

[5] $2Hads \Leftrightarrow H_2$ (Tafel step) and (or) $Hads + H_3O^+ (H_20) + e^- \Leftrightarrow H_2 + H_2O (OH^-)$ (Heyrovsky step)

The extent of hydrogenation as measured by the alcohols-

[3] This concentration is much lower than the CMC and there is no micelles in solution.

© 1997 NRC Canada

Table 1. ECH of carvone (**1**) at Raney Ni cathodes in emulsified solutions.[a]

Entry	Surfactant[b]	pH	Recovered **1** (%)	Yield of products (%)[c] Ketone **2**	Alcohols **3–6**	Carvacrol **7**	(**3** + **4** + **5** + **6**)/**2**	Current efficiency (%)	Material balance (%)
1	DDAB	2	0	1	86	10	86	87	97
2	DDAB	10	0	1.5	68	24	45	67	94
3[d]	CTAB	2	0	4	84	5	21	86	93
4[d]	None	2	8	25[e]	61	1.2	2.5	77	95

[a]Constant potential electrolyses (−0.60 ± 0,05 V vs. SCE in entries 1,3,4; −0,85 ± 0,05 V in entry 2) at 30°C; Q = 6 F mol^{-1}; carvone 15.9 mM in aqueous buffer, NaCl 0.1 M, with or without surfactant.
[b]Cetyltrimethylammonium bromide (CTAB) 8.2 × 10^{-5} M; didodecyldimethylammonium bromide (DDAB) 7.7 × 10^{-5} M.
[c]Determined by VPC and based on the initial amount of **1**.
[d]From ref. 2.
[e]22% of carvomenthone (**2**) and 3% of dihydrocarvone and carvotanacetone.

Table 2. Distribution of the satured alcohols obtained by ECH of carvone (**1**) in emulsified solutions.[a]

Entry	Surfactant[b]	pH	Relative percentage of alcohols[c] **3**	**4**	**5**	**6**	(**3** + **4**)/(**5** + **6**)
1	DDAB	2	41	17	17	25	1.4
2	DDAB	10	36	26	14	24	1.6
3[d]	CTAB	2	40	18	17	25	1.4
4[d]	None	2	36	16	15	33	1.1

[a], [b] and [d]See, respectively, footnotes *a*, *b*, and *d* of Table 1.
[c]Determined by VPC.

to-ketone ratio ((**3** + **4** + **5** + **6**) / **2**) was much higher in the presence (ratio of 21–86, entries 1–3) than in the absence of a surfactant (ratio of 2.5, entry 4).Therefore surfactant adsorption strongly enhances the extent of hydrogenation and, in agreement with the stronger adsorption of DDAB with respect to CTAB (3, 4), higher extents of hydrogenation were observed with DDAB (alcohols/ketones ratio of 86 at pH 2 and 45 at pH 10, entries 1 and 2) than with CTAB (ratio of 21 at pH 2, entry 3).

Concerning the stereochemistry of the ECH of carvone (**1**), the presence of DDAB had no significant influence, as was observed with CTAB (2). Indeed, within experimental error, the relative proportions of the isomeric alcohols (**3–6**) were nearly the same in the presence (Table 2, entries 1–3) and in the absence (entry 4) of surfactant, as seen also in the ratio of isomers with the methyl and isopropyl groups *trans* (alcohols **3** and **4**) to the ratio of isomers with the two substituents *cis* (alcohols **5** and **6**).

ECH of *D*-limonene (8) and *p*-menthene (9)

In the ECH of carvone (**1**) in emulsions, small amounts of a surfactant do significantly improve the efficiency and, in particular, the extent of hydrogenation as seen above. However, due to the easy hydrogenation of carvone and except for the extent of hydrogenation, which was larger with DDAB, the improvement was about the same with the two surfactants (DDAB and CTAB).

To see if DDAB is really more effective than CTAB, a study of the ECH of a substrate more difficult to hydrogenate than carvone, namely limonene (**8**), was carried out in emulsions with and without a surfactant. The results are summarized in Tables 3–5 and Figs. 2 and 3.

In the presence of various concentrations of DDAB, at pH 10, the ECH of limonene gave a mixture of *p*-menthene (**9**), *p*-menthane (**10**) (*cis* + *trans*), *p*-cymene (**11**) resulting from isomerization–dehydrogenation of limonene, and two unidentified products (**X**). The latter have the same mass as *p*-menthene (**9**) and thus could result from its isomerization.

Five main points can be drawn from the results:

1. As previously shown (and discussed) (2), the ECH of limonene (**8**) emulsified in an aqueous buffer without a surfactant did not occur at all, owing to the poor solubility of this substrate. However, a very low concentration of DDAB (6.5 × 10^{-5} M, i.e., 30 mg dm^{-3}) allowed the hydrogenation reaction to occur (Table 3,entry 1). At this concentration, DDAB is entirely soluble and the association between the surfactant and the substrate can be neglected because the number of substrate molecules is 300 times as large as that of surfactant molecules. Thus the occurrence of hydrogenation results only from the surfactant adsorption on the cathode and the association of limonene with this hydrophobic layer and not from an increase of the solubility of limonene in the bulk solution.
2. Concerning the stereochemistry of the ECH of limonene (**8**), the *trans* isomer of *p*-menthane (**10**) is slightly predomi-

© 1997 NRC Canada

Can. J. Chem. Downloaded from www.nrcresearchpress.com by 91.121.58.235 on 09/08/12
For personal use only.

Table 3. ECH of limonene (**8**) at Raney Ni cathodes in emulsions:[a] influence of surfactant concentration [S].

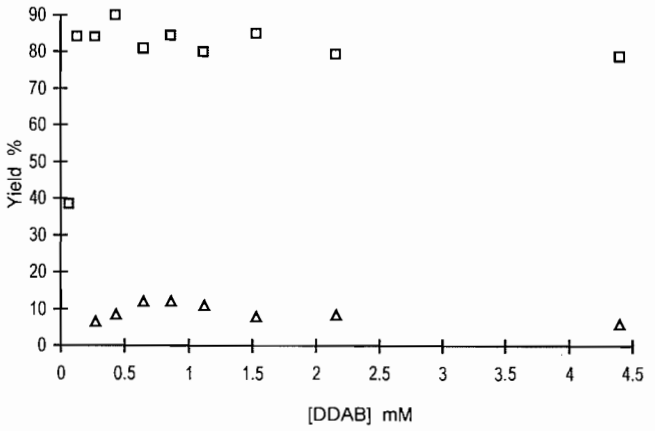
Entry	[S][b] mM	[**8**][c]/[S]	Recovered **8** (%)	Yield (%)[d] **9**	**10** (*c*/*t*)	**11**	**X**[e]	Current efficiency (%)	Material balance (%)
1	6.5×10^{-2}	304	50	11.5	27 (0.9)	—	—	22	88
2	0.13	137	15	36	48 (0.8)	—	—	52	99
3	0.26	69	13	5	69 (0.75)	0.5	0.5	57	92
4	0.27	66	6.5	9	75 (0.75)	5	1.5	70	97
5	0.43	41	6	16	74 (0.8)	5.5	3	65	95
6	0.65	27	7	1	80 (0.8)	7	0.5	64	96
7	0.86	21	5	0.5	80 (0.8)	7	0.5	64	92
8	1.12	16	5	2	78 (0.85)	9	2	63	96
9	1.53	12	3	9	76 (0.9)	6	2	65	96
10	2.16	8	7.5	5.5	74 (0.85)	7	1.5	61	95
11	4.4	4	3	7	72. (0.8)	4	2	60	88
12[f]	1.5	13	80	4	15 (0.6)	—	—	13	94

[a]Constant-potential (−0.9 ± 0.1 V vs. SCE, entries 1–4 and 12) or constant-current (J = 1.25 mA cm^{-2}, entries 5–11) electrolyses at 30°C; Q = 5 F mol^{-1}; aqueous buffer pH 10; NaCl 0.1 M.
[b]DDAB in entries 1–11; CTAB in entry 12.
[c][**8**] = 1.97×10^{-2} M (entries 1 and 12), 1.78×10^{-2} M (entries 2–11).
[d]Determined by VPC and based on the initial amount of **8**.
[e]Two unidentified products (see text).
[f]From ref. 2.

nant. Over the whole range of DDAB concentrations used, the *cis*/*trans* ratio is constant (0.83 ± 0.07) (Table 3). This behavior is different from that observed in the cationic micellar solutions (CTAB or CTACl) in which the *cis*/*trans* ratio varied (0.59–0.85) with the surfactant concentration (2).

3. DDAB adsorption favors the hydrogenation process (reactions [2]–[4]) over hydrogen evolution (reactions [5]) as shown by the following observations. (*i*) In the whole range of DDAB concentrations (Table 3, entries 1–11), except for the three lowest ones (entries 1–3), the current efficiency is constant (60–70%) within experimental error and is higher than the efficiencies observed in homogeneous hydroorganic solutions or in micellar systems, namely, 18–48% (2). As the DDAB concentration increases from 6.5×10^{-5} to 2.7×10^{-4} M (entries 1–4), the overall chemical yield of *p*-menthene (**9**) and *p*-menthane (**10**) reaches a high value (84%) that remains nearly constant (82 ± 8%) upon increasing the concentration further (entries 4–11, see also Fig. 2). With CTAB, the maximum overall yield of hydrogenated products (90 ± 10%)[4] was obtained at much higher surfactant concentrations (90–200 times higher, namely, 2.5×10^{-2} and 5.5×10^{-2} M) than with DDAB (2.7×10^{-4} M). Thus, in regard to the competition between hydrogen evolution and limonene (**8**) hydrogenation (i.e., the ECH efficiency), DDAB is much more efficient than CTAB. This is also clearly evident by comparing the ECH of limonene in emulsions containing similar concentrations of DDAB and CTAB (1.5×10^{-3} M), other things being equal (entries 9 and 12). Indeed, the current efficiency (13%), product yield (19%), and percentage of limonene consumed (20%) were much lower with CTAB (entry 12) than with DDAB (respectively 65%, 93%, and 97%) (entry 9). (*ii*) The extent of hydrogenation, which is measured by the molar fraction of *p*-menthane (**10**) relative to the total amount of hydrogenated products (**9** + **10** + **X**), also depends on the competition between hydrogenation and hydrogen evolution and thus is a measure of the efficiency of ECH. This molar fraction is highest for DDAB concentrations varying between 6.5×10^{-4} and 10.8×10^{-4} M (Fig. 3) and is close to 1 (0.97–0.99). With CTAB, the highest value of this molar fraction is 0.8, but was obtained only at the lowest surfactant concentration (1.5×10^{-3} M), which gave the worst ECH efficiency (current efficiency of 11 ± 1%, overall yield of products of 17 ± 3% with only 38 ± 2% of limonene consumed) (2). (*iii*) Thus, the efficiency and the extent of the ECH of limonene is much higher in DDAB emulsions than in CTAB micelles. With DDAB this

Fig. 2. Variation of the yield of products (□: **9** + **10**; Δ: **11** + **X**) with the DDAB concentration during the ECH of limonene (**8**). Electrolysis conditions: see footnote *a* of Table 3.



[4] The yield is slightly higher than that obtained with DDAB owing to the formation of *p*-cymene (**11**) in the presence of DDAB. *p*-Cymene was not hydrogenated under the experimental conditions used.

Can. J. Chem. Downloaded from www.nrcresearchpress.com by 91.121.58.235 on 09/08/12
For personal use only.

© 1997 NRC Canada

Can. J. Chem. Downloaded from www.nrcresearchpress.com by 91.121.58.235 on 09/08/12
For personal use only.

Fig. 3. Variation of the molar fraction of *p*-menthane (**10**) relative to the total amount of hydrogenated products (**9** + **10** + **X**) with the DDAB concentration. Electrolysis conditions: see footnote *a* of Table 3.

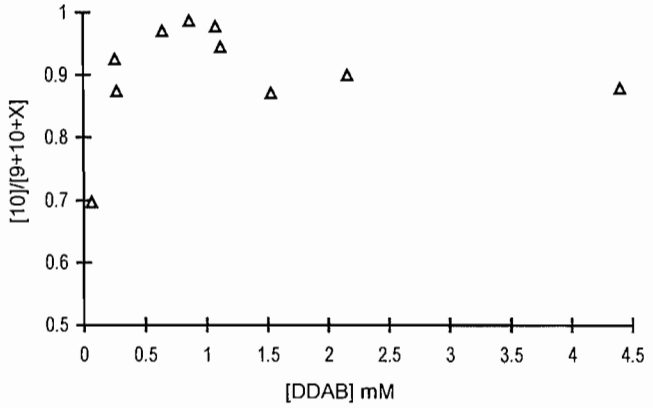


Table 4. Variation of the relative percentage of limonene (**8**) and products with the charge during the ECH of **8** in emulsions.[a]

Entry	Q (F mol^{-1})	Relative percentage of[b] **8**	**9**	**10** (*c*/*t*)	**11**	**X**[c]
1	1	37	46	7	4	6
2	2	20	30	40	6	4
3	5	7	9	77	5	2

[a]Constant-potential electrolyses (–0.97 ± 0.03 V vs. SCE) at 30°C; aqueous buffer pH 10; 2.7×10^{-4} M DDAB; [**8**] = 1.78×10^{-2} M; 0.1 M NaCl.
[b]Determined by VPC (material balance 97–100%).
[c]See footnote *e* of Table 3.

can result only from the adsorption of the surfactant on the cathode owing to the absence of micelles and the low concentrations of DDAB used.

4. The extent of hydrogenation also depends on the DDAB concentration. Indeed the molar fraction of *p*-menthane varies between 0.7 and 0.9 when the surfactant concentration is increased from 6.5×10^{-5} to 4×10^{-3} M with a maximum of 0.99 at a DDAB concentration of 8.6×10^{-4} M (Fig. 3). As previously discussed for the cationic micellar systems (2), this variation can be interpreted as a competition between the hydrogenation of limonene (**8**) to *p*-menthene (**9**) and the hydrogenation of **9** to *p*-menthane (**10**). This competition depends on two parameters. Firstly, in agreement with literature results (11*b*, 12, 13), the hydrogenation of the trisubstituted endocyclic carbon–carbon double bond is more difficult than that of the exocyclic disubstituted one. Indeed, the ECH of **8** follows the sequence **8** ⇒ **9** ⇒**10** as shown by the variation of product distribution during the electrolysis (Table 4). After 1 F mol^{-1}, very little *p*-menthane (**10**) is formed (7%) and the major product is *p*-menthene (**9**) (46%) (entry 1). After 2 F mol^{-1}, *p*-menthane becomes the major product (40%) (entry 2). Secondly, the relative rates of ECH of **8** and **9** depend on the relative amounts of **8** and **9** adsorbed on the catalyst, which is discussed below.

5. The high catalytic efficiency of the Raney nickel cathode in the presence of DDAB is also confirmed by a comparison of the ECH of *p*-menthene (**9**) in cationic micellar solutions (CTAB) and in emulsions with DDAB for surfactant concentrations leading to the highest ECH efficiency with limonene (**8**). In emulsions with a small amount of DDAB (8.6×10^{-4} M) (Table 5, entries 1 and 2), the hydrogenation of **9** to *p*-menthane (**10**), in high yields (69–81%) and with good current efficiencies (65–69%), required only a slight excess of electricity (2–2.5 F mol^{-1}), the theoretical amount being 2 F mol^{-1}, whereas in cationic micelles (5.5×10^{-2} M CTAB, entry 3), a large excess of electricity (7 F mol^{-1}) was required to convert only 60% of *p*-menthene (**9**), resulting in a very low current efficiency (18%). According to previous studies (2), this cannot be attributed to a pH effect.

Fig. 4. Distribution of products (limonene (**8**) and reaction products (**9** + **10** + **11** + **X**)) between the electrode surface and the solution during the ECH of **8** in emulsions for different DDAB concentrations: X, after 1 F mol^{-1}; ◇, after 5 F mol^{-1}. Electrolysis conditions: see footnote *a* of Table 6.

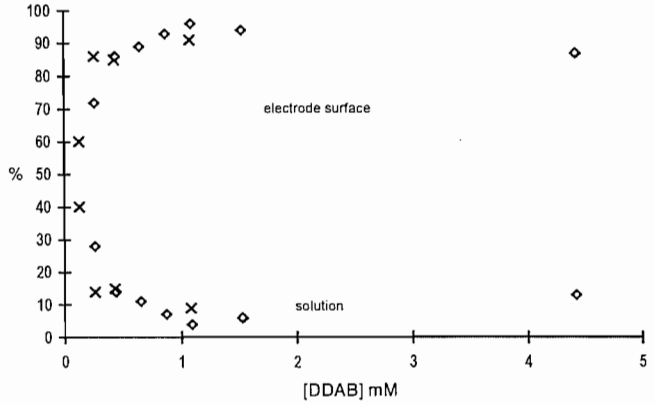
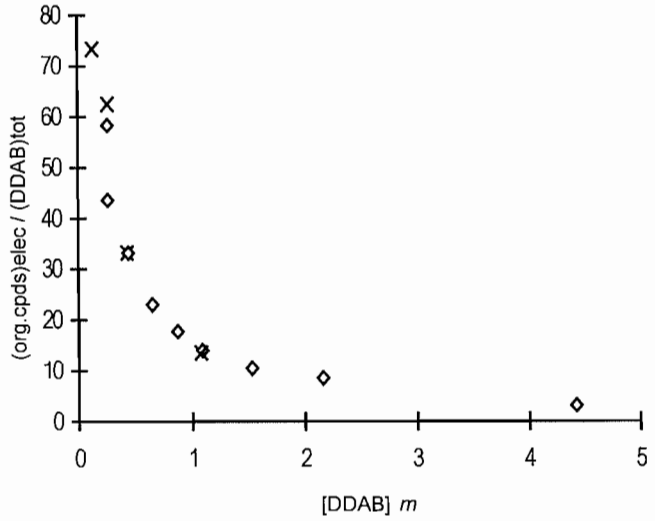


Fig. 5. Variation of the ratio of the number of moles of organic compounds adsorbed on the electrode [$(org.cpds)_{elec}$] to the total number of moles of DDAB [$(DDAB)_{tot}$] vs. the DDAB concentration during the ECH of **8**. Electrolysis conditions: see footnote *a* of Table 6 (X: 1 F mol^{-1},◇ : 5 F mol^{-1}).



© 1997 NRC Canada

Table 5. ECH of *p*-menthene (**9**) at Raney Ni cathodes in emulsions and in cationic micellar solutions.[a]

Entry	Solution[b]	pH	Q (F mol^{-1})	Recovered **9** (%)	Yield (%)[c] **10**	Yield (%)[c] **X**[d]	Current efficiency (%)	Material balance (%)
1	Emulsifed	10	2	23	69	8	69	100
2	Emulsifed	10	2.5	7	81	9	65	97
3[e]	Micellar	2	7	39	61	—	18	100

[a]Constant-current electrolyses (J = 4 mA cm^{-2}) at 30°C.
[b]Emulsified: aqueous buffer, 8.6 × 10^{-4} M DDAB, 0.1 M NaCl; [**9**] = 1.8 × 10^{-2} M; micellar: aqueous buffer, 5.5 × 10^{-2} M CTAB, 0.2 M NaCl; [**9**] = 3 × 10^{-2} M.
[c]Determined by VPC and based on the initial amount of **9**.
[d]See footnote *e* of Table 3.
[e]From ref. 2.

Table 6. Relative amount of **8**, **9**, **10**, **11**, and **X** adsorbed on the cathode, and distribution of **8**, **9**, and **10** between the electrode and the solution during the ECH of **8** in emulsions after 1 F mol^{-1} (entries 1–4) and after 5 F mol^{-1} (entries 5–9).[a]

Entry[b]	[DDAB] mM	Relative amount on the cathode[c] **8**	**9**	**10**	**11**	**X**	Repartition electrode/solution[d] **8**	**9**	**10**
1	0.13	45	32	18	2	3	0.8	9	—
2	0.26	29	51	8	5	7	2	20	—
3	0.43	19	57	8	8	8	1.1	81	—
4	1.08	16	59	6	10	9	1.8	85	—
5	0.26	—	—	95	4	1	—	—	11
6	0.43	—	—	91	8	1	—	—	19
7	1.08	—	—	83	15	2	—	—	68
8	1.53	—	9	82	7	2	—	7	33
9	4.42	—	8	85	4	3	—	3	11

[a]Constant current electrolyses (J = 1.25 mA cm^{-2}) at 30°C; aqueous buffer pH 10; 0.1 M NaCl; [**8**] = 1.78 × 10^{-2} M. The amounts of compounds on the cathode and in solution are determined by VPC (material balance 90–100%).
[b]Entries 1–4 = 1 F mol^{-1}; entries 5–9 = 5 F mol^{-1}.
[c]Relative percentages.
[d]Ratio between the number of molecules adsorbed on the cathode and the number of molecules in the bulk solution.

Study of adsorption phenomena

The adsorption phenomena have been studied, during the ECH of limonene (**8**), by measuring both the amount of limonene and hydrogenation products (**9** + **10** + **11** + **X**) adsorbed on the electrode and the amount of all these compounds present in the bulk solution (see Experimental). The measurements were made after a charge corresponding to 25% (1 F mol^{-1}) of the theoretical amount of electricity and at the end of electrolysis (5 F mol^{-1}). The concentration of limonene was kept constant at 1.78 × 10^{-2} M and the concentration of DDAB was varied from 1.3 × 10^{-4} to 4.4 × 10^{-3} M.

As seen in Fig. 4, for all surfactant concentrations and irrespective of the charge passed, the major part of the organic compounds (substrate and products) is in the surfactant layer on the cathode. This part increases with the DDAB concentration (the amount in solution decreasing accordingly) and reaches a plateau at a DDAB concentration close to 8.5 × 10^{-4} M. After a charge corresponding to 1 F mol^{-1}, limonene (**8**) and *p*-menthene (**9**) represent the major part (75–80%) of the adsorbed compounds (see Table 6, entries 1–4). The DDAB concentration (from 0.13 to 1.08 mM) has little influence on the distribution of limonene (**8**) between the surfactant layer on the electrode surface and the bulk solution, as shown by the small variation of the ratio of the amount of **8** in the surfactant layer adsorbed on the cathode to the amount of **8** in the bulk solution: 0.8 to 2 (entries 1–4). On the other hand, this ratio for *p*-menthene (**9**) increases significantly with the surfactant concentration, from 9 to 85 (entries 1–4). This indicates a preferential absorption of **9** in the surfactant layer on the electrode, which favors its hydrogenation and, hence, leads to the increase of the molar fraction of *p*-menthane (**10**) upon increasing the concentration of DDAB, as already mentioned (see point 4 above). At the end of the electrolysis (after 5 F mol^{-1}), the adsorbed surfactant layer contains mainly *p*-menthane (**10**) (82–95%, see Table 6, entries 5–9), the proportion of which decreases from 95 to 83% upon increasing the concentration of DDAB from 0.26 to 1.08 M and remains constant (83–85%) with further increase of the surfactant concentration to 4.42 M.

It is noteworthy, as shown in Fig. 5, that the amount of organic compounds adsorbed on the cathode is much larger than the total amount of DDAB for all surfactant concentra-

© 1997 NRC Canada

Can. J. Chem. Downloaded from www.nrcresearchpress.com by 91.121.58.235 on 09/08/12
For personal use only.

tions studied. This strongly suggests that there is, on the cathode, an organic layer stabilized by an interfacial film of DDAB. Such a structure corresponds to a microemulsion.

Conclusion

In emulsified solutions, the presence of a non-micelle-forming surfactant at very low concentrations strongly increases the adsorption of organic compounds (formation of a microemulsion on the cathode). As a consequence, the hydrogenation reaction (eq. [3]) is favored over hydrogen evolution (eqs. [5]) and the efficiency and the extent of ECH of an unsaturated organic compound is markedly increased.

Acknowledgments

We gratefully acknowledge financial support from the Ministère des Relations Internationales du Québec and the Ministère des Affaires Étrangères de France (coopération franco-québécoise), the Fonds pour la Formation des chercheurs et l'Aide à la Recherche (FCAR) du Québec, the Natural Sciences and Engineering Research Council of Canada, the Centre National de la Recherche Scientifique (CNRS) de France, and the Ministère de l'Enseignement Supérieur et de la Recherche de France.

References

1. J.M. Chapuzet, A. Lasia, and J. Lessard. *In* Frontiers of electrochemistry. *Edited by* J. Lipkowski. VCH Publishers, Inc., Pennington, N.J. In press.
2. P. Chambrion, L. Roger, J. Lessard, V. Beraud, J. Mailhot, and M. Thomalla. Can. J. Chem. **73**, 804 (1995).
3. M.O. Iwunze and J.-F. Rusling. J. Electroanal Chem. **266**, 197 (1989).
4. K. Fontell, A. Ceglie, B. Lindman, and B. Ninham. Acta Chem. Scand. **A40**, 247 (1986).
5. J.-F. Rusling. Acc. Chem. Res. **24**, 75 (1991).
6. N. Hu and J.-F. Rusling. Anal. Chem. **63**, 2163 (1991).
7. J.-F. Rusling, N. Hu, H. Zhang, D.J. Howe, C.-I. Miaw, and E.C. Couture. *In* Electrochemistry in colloids and dispersions. *Edited by* R.A. Mackay and J. Texter. VCH, New York. 1992. pp. 303–318.
8. R.C. Weast (*Editor*). Handbook of chemistry and physics. 64th ed. CRC Press, Boca Raton, Fla. 1984. D-150.
9. D. Robin, M. Comtois, A. Martel, R. Lemieux, A Kam Cheong, G. Belot, and J. Lessard. Can. J. Chem. **68**, 1218 (1990).
10. N. Campbell. *In* Rodd's chemistry of carbon compounds. Vol. III A. *Edited by* S. Coffey. Elsevier, London. 1971. pp. 137–142, and refs. cited.
11. R.L. Augustine. Catalytic hydrogenation. Marcel Dekker, Inc., New York. 1965. (*a*) p. 46; (*b*) p. 58.
12. A.F. Thomas and Y. Bessière. Nat. Prod. Rep. **6**, 291 (1989), and refs cited.
13. F. Zymalkowski. Katalytische Hydrierungen im Organisch-Chemischen Laboratorium. Ferdinand Enke Verlag, Stuttgart. 1965. p. 76.

Can. J. Chem. Downloaded from www.nrcresearchpress.com by 91.121.58.235 on 09/08/12
For personal use only.

© 1997 NRC Canada

Electrochemical characterization in nonaqueous electrolyte of polyaniline electrochemically prepared from aqueous media[1]

Béatrice Garcia, Florence Fusalba, and Daniel Bélanger

Abstract: Polyaniline film electrodes were characterized in nonaqueous electrolyte following their electrochemical preparation in aqueous media. More specifically, polyaniline films were deposited galvanostatically at the surface of platinum or gold electrodes by anodic electrochemical polymerization from a 0.5 M aniline – 1 M HCl aqueous solution. The polyaniline film electrode was then dried and its electrochemical behavior was evaluated in nonaqueous electrolyte ($LiClO_4$–acetonitrile). Stable cyclic voltammograms were recorded between −0.1 and 1 V in the nonaqueous media, which represents a much wider range than in aqueous acidic media. In the latter case the positive potential limit must be restricted to about 0.7 V in order to avoid oxidative degradation of the polymer. Electrochemical impedance spectroscopy was used to determine the charge capacity of the polyaniline film electrode as a function of film thickness and electrode potential. A linear relationship was observed between the low-frequency capacitance of the polyaniline electrode and the amount of deposited polymer (e.g., charge used to grow the polymer). This indicates that even for the thickest film (deposited charge of 10 C/cm^2) most of the polyaniline is electrochemically accessible at the low frequency of 5 mHz. The thinnest polyaniline film electrode (deposited charge of 0.2 C/cm^2) was also characterized by the electrochemical quartz crystal microbalance technique and it was found that ionic transport is dominated by the movement of anions.

Key words: conducting polymer, polyaniline, nonaqueous electrolyte, capacitance, electrochemical impedance spectroscopy, cyclic voltammetry, electrochemical quartz crystal microbalance.

Résumé : Des électrodes à film de polyaniline préparées d'une façon électrochimique en milieu aqueux ont été caractérisées dans un électrolyte non aqueux. Plus spécifiquement, on a déposé d'une façon galvanostatique des films de polyaniline à la surface d'électrodes de platine ou d'or en procédant à une polymérisation électrochimique anodique à partir d'une solution aqueuse d'aniline 0,5 M contenant du HCl à 1 M. On a alors séché l'électrode à film de polyaniline et on a évalué le comportement électrochimique dans un électrolyte non aqueux ($LiClO_4$–acétonitrile). On a enregistré des voltammogrames cycliques stables entre −0,1 et 1 V dans le milieu non aqueux; ceci correspond à une plage beaucoup plus étendue qu'en milieu acide. Dans le dernier cas, la limite positive du potentiel devrait être fixée à environ 0,7 V si l'on veut éviter la dégradation oxydante du polymère. On a utilisé la spectroscopie d'impédance électrochimique pour déterminer la capacité de charge de l'électrode à film de polyaniline en fonction de l'épaisseur du film et du potentiel de l'électrode. À basse fréquence, on a observé une relation linéaire entre la capacitance de l'électrode à polyaniline et la quantité de polymère déposé (par exemple, la charge utilisée pour faire croître le polymère). Ceci indique que, même pour le film le plus épais (déposé à une charge de 10 C/cm^2), presque toute la polyaniline est électrochimiquement disponible à des fréquences aussi basses que 5 mHz. On a aussi caractérisé l'électrode à film de polyaniline la plus mince (déposée à une charge de 0,2 C/cm^2) par la technique de la microbalance électrochimique à cristal de quartz et on a trouvé que le transport ionique est dominé par le mouvement des anions.

Mots clés : polymère conducteur, polyaniline, électrolyte non aqueux, capacitance, spectroscopie à impédance électrochimique, voltammétrie cyclique, microbalance électrochimique à cristal de quartz.

[Traduit par la rédaction]

Received March 12, 1997.

This paper is dedicated to Professor Brian E. Conway on the occasion of his 70th birthday.

B. Garcia, F. Fusalba, and D. Bélanger.[2] Département de chimie, Université du Québec à Montréal, Case Postale 8888, succursale Centre-Ville, Montréal, QC H3C 3P8, Canada.

[1] This paper (Abstract no. 612) was presented at the 190th Meeting of the Electrochemical Society in San Antonio, Texas, October 6–11, 1996.

[2] Author to whom correspondence may be addressed: Telephone: (514) 987-3000, ext. 3909. Fax: (514) 987-4054. E-mail: belanger.daniel@uqam.ca

© 1997 NRC Canada

Can. J. Chem. Downloaded from www.nrcresearchpress.com by 91.121.58.235 on 09/08/12
For personal use only.

Can. J. Chem. Downloaded from www.nrcresearchpress.com by 91.121.58.235 on 09/08/12
For personal use only.

Introduction

Conducting polymers such as polypyrrole, polyaniline, and polythiophene have been recently proposed as active electrode material for electrochemical supercapacitors (1–3) because of their high charge density (which can be stored in the volume of the polymer layer), fast charge/discharge kinetics, and their low cost. Gottesfeld and co-workers at Los Alamos were the first to recognize that conducting polymers could be used as active material in electrochemical supercapacitors and have proposed a classification for such supercapacitors, which are of three types, designated I, II, and III (1). Type I supercapacitors are based on p-dopable materials such as polyaniline, polypyrrole, or polythiophene as both active anode and cathode and typically yield low cell voltage that is limited by the range of potential over which the polymer is electroactive. Type II is an unsymmetrical supercapacitor in which two p-dopable polymers are characterized by the difference in the potential range over which they can be p-doped (for example polypyrrole with polythiophene). Type III is a high cell voltage supercapacitor by virtue of the difference in potential between n- and p-doping of a polymer that is used for both electrodes.

Polyaniline was previously tested as active material in a Type I symmetrical electrochemical supercapacitor consisting of two polyaniline electrodes and an acid electrolyte (4). Although the charge/discharge behavior and the long-term stability of such a supercapacitor are quite good, its major drawback lies in its low cell voltage. Polyaniline is usually prepared by chemical or electrochemical polymerization in highly concentrated acidic media (5, 6). It is well known that polyaniline degrades under anodic polarization more positive than about 0.8 V vs. SCE (5). However, this limit can be extended to higher potential value if the potential cycling is carried out in nonaqueous media (7–14) and thus could lead to a higher cell voltage for the supercapacitor.

In this paper, we have investigated the effect of film thickness on the electrochemical behavior of polyaniline electrodes, prepared in acidic media, by cyclic voltammetry, electrochemical impedance spectroscopy, and the electrochemical quartz crystal microbalance technique in a nonaqueous electrolyte. Our results indicate that the low-frequency capacitance of the polyaniline film increases linearly with the charge used to grow the film from 0.2 to 10 C/cm^2 and that the ionic transport is dominated by the movement of anions. The loss of charge observed when the polyaniline film was transfered from the aqueous to the nonaqueous medium is due to the fact that the polyaniline film is more compact (less swollen) than in aqueous media.

Experimental

Chemicals

All products were used as received except for aniline, which was freshly distilled before use. Acetonitrile was distilled over CaH_2 prior to use.

Procedure and equipment

The working electrode was a platinum disk (diam. = 1 mm) sealed into a glass tube or epoxy. The platinum disk electrode was polished with a diamond polishing compound to the 1 μm level and then to the 0.05 μm level with aqueous alumina slurry (Techmet, Canada). Platinum gauze and an Ag/AgCl (3 M NaCl) electrode were used as counter and reference electrodes, respectively. All potentials were reported versus the Ag/AgCl reference electrode. Electrochemical measurements were carried out in a one-compartment cell using the three-electrode configuration.

Polyaniline films were prepared galvanostatically from aqueous media (0.5 M aniline + 1 M HCl – H_2O) at a current density of 5 mA/cm^2 (4). Films with deposited charge of 0.2, 1, and 10 C/cm^2 were grown. The as-grown polyaniline electrodes were rinsed with water and a slight jet of acetone. Following that, the electrodes were dried under vacuum at 100°C for 2 days. The electrodes were subsequently tested in a non-aqueous solution consisting of 0.1 M $LiClO_4$ – acetonitrile, except for the electrochemical quartz crystal microbalance experiments for which 0.5 M $LiClO_4$ – acetonitrile was used.

Cyclic voltammetry was performed using either a potentiostat/galvanostat model M273 (EG&G Princeton Applied Research) or an electrochemical interface SI1287 (Solartron Instruments) interfaced with a PC, and the electrochemical set-ups were controlled with the model M270 (EG&G) and DC Corrware (Scribner Associates, version 1.2) software, respectively. Electrochemical impedance experiments were done with an electrochemical interface SI1287 and a frequency response analyser SI1255 (Solartron Instruments) controlled by the Zplot software (Scribner Associates, version 1.2). The impedance measurements were performed at various electrode potentials in the frequency range 65 kHz – 0.05 Hz (except for the 10 C/cm^2 thick film for which the low-frequency limit was 0.005 Hz) using an amplitude of 10 mV for the sine wave.

The electrochemical quartz crystal microbalance (EQCM) system consists of the model EQCN-500 electrochemical quartz crystal nanobalance (Elchema, Potsdam, N.Y.) and a model RDE-4 bipotentiostat (Pine Instruments Inc., Grove City, Pa. and a Kipp and Zonen BD91 *x-y-y′* recorder. A gold-coated 10 MHz AT-cut quartz crystal (International Crystal Mfg. Co. Inc., Oklahoma City, Okla.) was used as working electrode. It was sealed to a 20 ml glass cell by Tub&Tile Silicone Sealant (Canadian Tire Corp., Toronto, Ont.). The geometric area of this working electrode was about 0.25 cm^2. The gold electrode was initially treated to clean its surface by potential cycling between 0 and 1.5 V in 0.1 M aqueous $HClO_4$. The surface area of the electrode was determined by measuring the charge involved in the reduction of gold oxide (generated at 1.2 V vs. SCE) by assuming that a charge of 400 μC/cm^2 and 2 electrons are required per gold atom (15). The microbalance was calibrated by electrodeposition of silver from a 1 mM $AgNO_3$ – 0.2 M H_2SO_4 aqueous solution at 0 V vs. SCE and had an absolute sensitivity of 1.1 ng/Hz.

Results and discussion

Cyclic voltammetry

Figure 1 shows the typical cyclic voltammogram in 1 M HCl – H_2O at a scan rate of 100 mV/s for a polyaniline film electrode grown from acidic media for a charge of 0.2 C/cm^2. The cyclic voltammogram is characterized by a first oxidation wave at about 0.2 V, corresponding to the interconversion between the fully reduced and semiquinone forms, and a second main wave

© 1997 NRC Canada

Can. J. Chem. Downloaded from www.nrcresearchpress.com by 91.121.58.235 on 09/08/12
For personal use only.

Fig. 1. Cyclic voltammetry of a polyaniline (0.2 C/cm^2) electrode in 1 M HCl – H_2O at a scan rate of 100 mV/s.

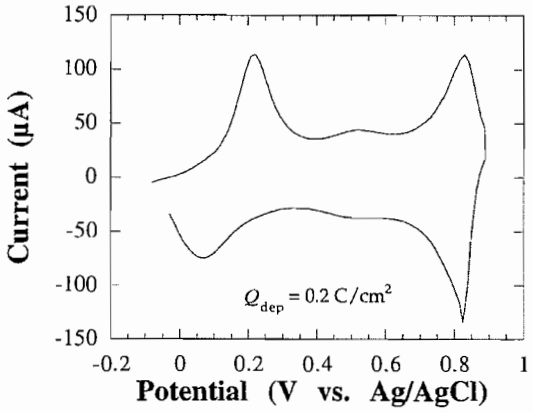
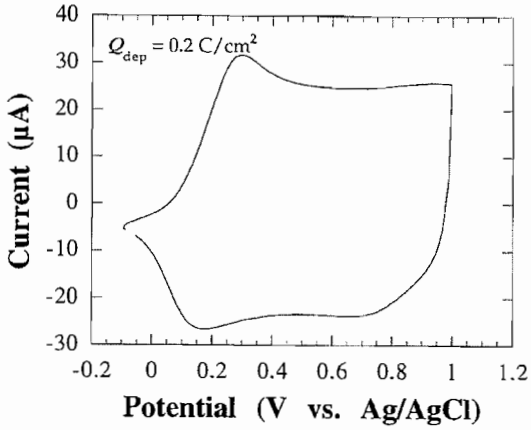


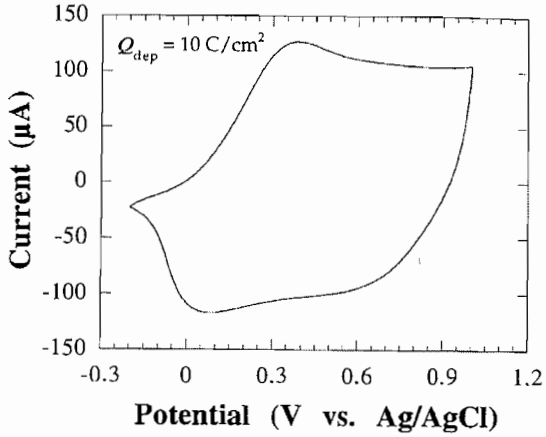
Fig. 2. Cyclic voltammetry of a polyaniline (0.2 C/cm^2) electrode in 0.1 M $LiClO_4$ – acetonitrile at a scan rate of 100 mV/s.



at ca. 0.8 V, related to the interconversion between the semiquinone and fully oxidized forms of polyaniline (6). A small wave attributed either to redox reactions of polyaniline degradation products or to phenazine rings originating in polyaniline from its polymerization is also observed at 0.6 V (5).

Following this initial characterization in acidic media the polyaniline electrodes were dried under vacuum at 100°C for 2 days and soaked in the acetonitrile solution. The cyclic voltammogram of such polyaniline electrodes in 0.1 M $LiClO_4$ – acetonitrile is illustrated in Figs. 2 and 3 for films grown with charge of 0.2 and 10 C/cm^2, respectively. The cyclic voltammogram illustrated in Fig. 2 for the thinnest film (0.2 C/cm^2) shows an oxidation wave at 0.3 V and a fairly high and constant current value is maintained up to 1 V. Contrary to earlier reports (8, 14), a well-developed wave is not observed at the most positive potential. This particular aspect will be discussed further below. An increase of the potential peak separation between the anodic and cathodic peaks (ΔE_p = 340 mV) is clearly observed when the amount of deposited polyaniline is increased to 10 C/cm^2 (Fig. 3) even if a lower scan rate of 10 mV/s was used for the latter. A decrease of peak separation to 160 mV is noticed at a lower scan rate of 2 mV/s. The larger peak separation for the thicker film can be related to the effect

Fig. 3. Cyclic voltammetry of a polyaniline (10 C/cm^2) electrode in 0.1 M $LiClO_4$ – acetonitrile at a scan rate of 10 mV/s.



of the uncompensated resistance. On the other hand, the impedance data demonstrate clearly that the larger peak separation cannot be related to kinetic limitations (vide infra). Nonetheless, an increase of the current is noticeable, as would be expected for higher loading of polymer. The stability of the film subjected to prolonged potential scanning is good even though the positive limit was extended to 1 V. It is important to mention that such a high positive potential value cannot be achieved when a polyaniline electrode is cycled in acidic media, due to oxidative degradation of the polymer (5).

The electrochemical behavior of polyaniline in acidic media has been studied in great detail. However, the number of studies of polyaniline in nonaqueous media is quite scarce. This stems from the ease of polyaniline formation in acidic media. Two main approaches have been used to prepare polyaniline films to be used in nonaqueous media. The first one involves electrochemical preparation in aqueous acidic media, followed by a sequence of steps that are performed to remove the water present in the polymer film electrode after electropolymerization (7–9, 14). The second approach consists of electrochemical polymerization directly from nonaqueous media with or without addition of protons (10–13). The shape and the range of electroactivity of the polymer in the cyclic voltammograms reported in these studies (7–14) differ substantially. For example, the cyclic voltammetry data of Figs. 2 and 3 are in agreement with those reported by Yonezawa et al. (12*b*) and Fiordiponti and Pistoia (7) in 1 M $LiBF_4$ – propylene carbonate (PC) and 1 M $LiClO_4$ – PC-DME (dimethoxyethane), respectively. On the other hand, our cyclic voltammetry data differ from those reported by Daifuku et al. (14) and Desilvestro et al. (8), which were characterized by two pairs of redox waves. The reasons for the discrepancies between the cyclic voltammograms are unclear but they may simply reflect the fact that various growth conditions and treatment (drying procedures) are used before the electrochemical characterization of polyaniline in nonaqueous media. Thus, the variation in cyclic voltammetry behavior cannot be solely attributed to the fact that the resulting polyaniline film electrodes are cycled in different electrolytic solutions.

A comparison of the charge that can be electrochemically addressed during cyclic voltammetry, Q_{cv}, for a polyaniline electrode in aqueous acidic (see Fig. 1) and organic (Fig. 2)

© 1997 NRC Canada

Can. J. Chem. Downloaded from www.nrcresearchpress.com by 91.121.58.235 on 09/08/12
For personal use only.

Fig. 4. Impedance plot for a polyaniline (0.2 C/cm^2) electrode at various potentials in 0.1 M $LiClO_4$ – acetonitrile. Frequency range = 10 kHz–50 mHz. Inset: High-frequency data of the impedance plot.

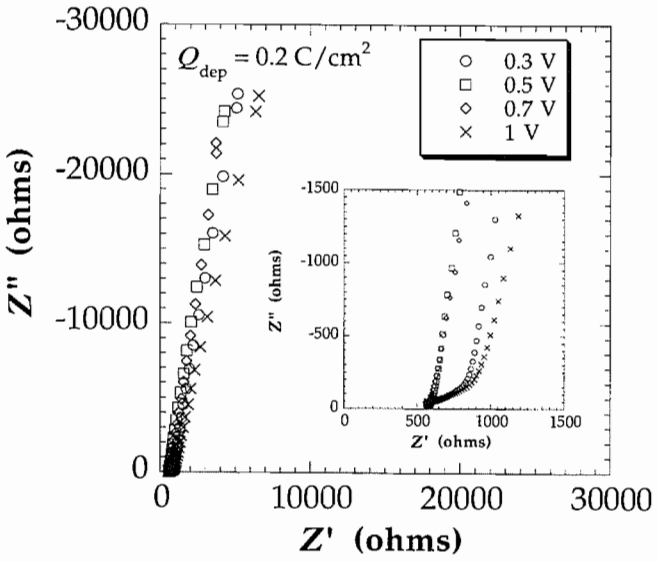
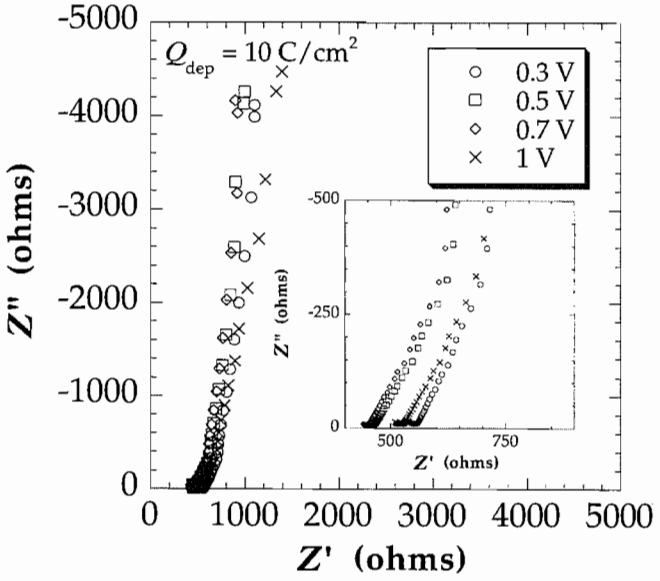


Fig. 5. Impedance plot for a polyaniline (10 C/cm^2) electrode at various potentials in 0.1 M $LiClO_4$ – acetonitrile. Frequency range = 10 kHz–5 mHz. Inset: High-frequency data of the impedance plot.



electrolytes indicates that the charge decreases in the nonaqueous electrolyte. For example, integration of the cyclic voltammograms of Figs. 1 and 2 yields Q_{cv} values of 0.06 and 0.032 C/cm^2 for the aqueous and nonaqueous electrolytes, respectively. Typically, a loss of charge ranging from 25 to 50% is found when polyaniline films, subjected to the drying procedure described in the experimental section, are transferred from aqueous to nonaqueous electrolyte. The decrease in the voltammetric charge contrasts with the results reported by Desilvestro et al., who found that the charge in nonaqueous media amounts to 189% of the value determined from aqueous solutions (8). The decrease of the charge can be ascribed to the fact that the polymer is much less solvated and is swollen to a lower extent in nonaqueous media, which translates to a lower voltammetric charge. To confirm that degradation of the polymer does not occur during the heat treatment, a cyclic voltammogram was recorded in the acidic solution, instead of the nonaqueous electrolyte, after heat treatment. In this case, a slight loss of charge (5–10%) was typically observed, thus confirming that the heat treatment cannot explain the larger decrease (25–50%) of the voltammetric charge. In addition, the voltammetric charge, initially found in acidic media, was restored after heat treatment and cycling in nonaqueous media when the polyaniline electrode was tested again in the acidic electrolyte.

Electrochemical impedance spectroscopy

Electrochemical impedance spectroscopy was used to characterize the polyaniline film electrode in nonaqueous media. Impedance spectra (Z'' vs. Z') measured at various potentials are shown in Figs. 4 and 5 for polyaniline film electrodes grown with a charge of 0.2 and 10 C/cm^2, respectively. For both film thicknesses, the low-frequency data of the impedance plot for the oxidized polyaniline (Nyquist plot) form a straight line that corresponds to capacitive behavior. It should be noted that a 90° line is not observed, as expected for purely capacitive behavior. This is typical behavior for conducting polymer electrodes and is probably due to nonuniform film thickness (16, 17). The inset of Fig. 4 also shows that the real axis intercept at high frequency is independent of potential (between 0. 3 and 1 V). The intercept coincides with the value obtained with a bare Pt electrode (not shown) and represents the uncompensated resistance of the solution. Since the electronic conductivity of oxidized polyaniline is very high (18), the impedance data suggest that the ionic resistance of the polymer increases when the polyaniline electrode is set at either 0.3 or 1 V (19). The Nyquist plot for the thicker film (10 C/cm^2) in the oxidized state (electrode potential between 0.3 and 1 V) does not show a semicircle at higher frequency that could be related to a charge transfer resistance (with an additional double-layer capacitance) at the electrode–polymer interface. On the other hand, a semicircle is observed on the Nyquist plot (not shown) when the electrode potential has been set before the onset of electroactivity of polyaniline; e.g., at a potential of 0.1 or −0.1 V. These impedance plots are in agreement with those previously reported for polyaniline in mixtures of nonaqueous solvents (7). The inset of Fig. 5 shows that the impedance plot shifts to higher real impedance values for electrode potentials of 0.3 and 1 V, indicating that the electronic resistance of the polyaniline layer is higher at these potentials (19). This supports the hypothesis that the increase of the potential peak separation when the film thickness is increased (from a 0.2 to a 10 C/cm^2 film) is due to the resistance of the polyaniline film.

A plot of the imaginary impedance vs. the reciprocal of the frequency (Z'' vs. $1/f$) is linear (Fig. 6) and the slope of this plot yields the low-frequency capacitance, C_{LF}, of the polyaniline electrode ($C_{LF} = (2\ \pi\ \text{slope})^{-1}$) (19, 20). The low-frequency capacitance values are collected in Table 1 for various deposited charges and electrode potentials. The low-frequency capacitance increases as the potential is made more positive than 0.1 V and reaches a nearly constant value between 0.3

© 1997 NRC Canada

Can. J. Chem. Downloaded from www.nrcresearchpress.com by 91.121.58.235 on 09/08/12
For personal use only.

Fig. 6. Plot of the imaginary impedance vs. $1/f$ from the data of Fig. 4 at a potential of 0.7 V. Frequency range corresponding to the $1/f$ data = 650–52 mHz.

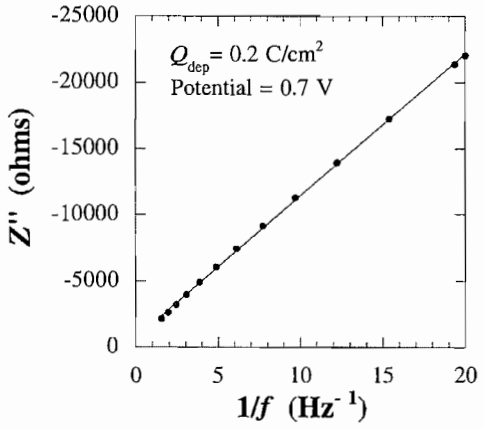


Fig. 7. Cyclic voltammogram and mass–potential plot for a polyaniline-coated gold electrode in 0.5 M $LiClO_4$ – acetonitrile at a scan rate of 10 mV/s. The deposited charge was 0.2 C/cm².

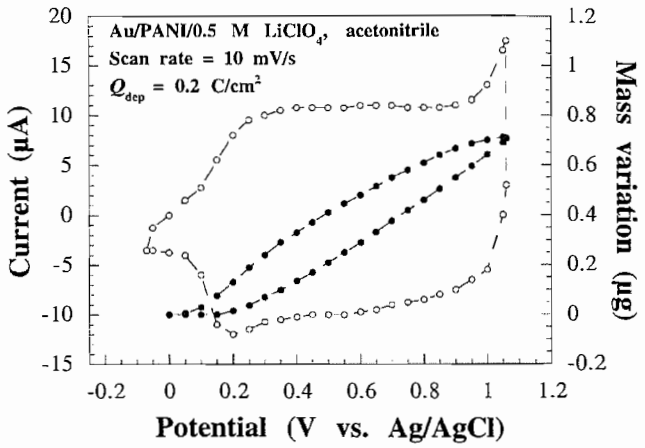


Table 1. Variation of the low-frequency capacitance, C_{LF}, of the polyaniline electrode in 0.1 M $LiClO_4$ – acetonitrile as a function of electrode potential and film thickness (deposited charge, Q_{dep}).

		C_{LF} (F/cm²)		
Potential, V	Q_{dep} (C/cm²):	0.2	1	10
0.1		0.015	0.11	0.75
0.3		0.017	0.10	1.01
0.5		0.018	0.11	0.97
0.7		0.018	0.11	1.0
1.0		0.016	0.10	0.94

and 0.7 V. Further increase of the potential to 1 V leads to a small decrease of the polymer capacitance. A substantial decrease of the low-frequency capacitance is found when the potential is made either more positive than 1 V or more negative than 0.1 V. A similar trend is seen for the three film thicknesses investigated in this study. Typically, the variation of the low-frequency capacitance (from electrochemical impedance) follows the shape of the cyclic voltammogram. The capacitance can be also calculated from the cyclic voltammetry data (capacitance = current/scan rate) (19, 20). As previously reported (20, 21), the capacitance values evaluated from the cyclic voltammetry data are consistently larger than those obtained from electrochemical impedance measurements. For example, a capacitance of 0.032 F/cm² at 0.3 V for the thinnest film (see Fig. 2) should be compared with the value of 0.017 F/cm² (see Table 1). A similar difference is obtained for the other film thicknesses investigated here. The discrepancy between capacitance values evaluated by both techniques has been attributed to conformation changes of the conducting polymer (20).

Table 1 also shows that the low-frequency capacitance scans linearly with the deposited charge for every potential for which low-frequency capacitance values are reported. The latter corresponds to the amount of polyaniline effectively deposited. This can be taken as an indication that the bulk of the polyaniline layer is electrochemically addressed in these experimental conditions. This behavior contrasts with that reported for poly-(3-methylpyrrole-4-carboxylic acid) for which lower capacitance values were calculated for the thinner films (17). The lower capacitance was related to a higher proportion of overoxidized sites in the thinner film. On the other hand, a similar linear relationship between C_{LF} and film thickness has also been reported for chloride-doped polypyrrole electrode (22). The C_{LF} values of Table 1 are in good agreement with those reported previously for polyaniline in acidic media (4). Moreover, they also compare favourably with that reported for a 52 μm thick polyaniline film electrode in 1 M $LiClO_4$ – PC-DME (7). For the latter authors, a value of 0.25 F/cm² can be computed from their data at 0.75 V (C_{LF} = 0.032 F/mg) for a 52 μm thick polyaniline film by taking a density of 1.2 g/cm³. This 52 μm thick film corresponds, in our case, to a deposited charge of ca. 4 C/cm² if we assume that a deposited charge of 20 C/cm² yields a 250 μm thick film (4). Thus, a low-frequency capacitance of 0.4 F/cm² (vs. 0.25 F/cm²) is expected in our case for a 52 μm thick film.

Electrochemical quartz crystal microbalance

The electrochemical quartz microbalance technique allows for the determination of the ionic species (and solvent) involved in the redox switching of electroactive polymer. Figure 7 shows the cyclic voltammogram and the mass–potential curve for a polyaniline film (deposited charge = 0.2 C/cm²) electrode in 0.5 M $LiClO_4$ – acetonitrile at a scan rate of 10 mV/s. The mass of the polyaniline film increases when the potential is scanned linearly from −0.1 to 1 V and decreases upon reduction of the polymer. This information suggests that anion transport is dominant in this system, the anions being inserted (mass increase) during oxidation and expelled (mass decrease) during reduction. Further analysis of the cyclic voltammetry and mass–potential data was carried out by plotting the variation of mass as a function of charge involved in the redox process (by integration of the cyclic voltammogram) to obtain the average molar mass of the chemical species involved. A value of 70 g/mol was computed and can be explained by the insertion of one perchlorate anion (100 g/mol), which is accompanied by the loss of 1.6 molecules of water (29 g). Our results

© 1997 NRC Canada

are in agreement with an in situ gravimetry study of polyaniline in nonaqueous electrolytes that also showed that the main-charge compensating process is the reversible insertion of anions (8, 14).

Concluding remarks

The results presented here indicate that polyaniline could be eventually used in a nonaqueous electrolyte-based electrochemical supercapacitor. The linear increase in the low-frequency capacitance with film thickness is attractive since high polymer loading is required to increase the energy density of a practical supercapacitor. A decrease in the capacitance of polyaniline is observed upon transfer of a film grown in aqueous media to nonaqueous electrolyte and is related to the fact that the polymer is more compact (less swollen). The development of a preparation procedure to obtain polyaniline film electrode with capacitance as high as in aqueous acidic media is currently under investigation in our laboratory.

Acknowledgments

This work was supported by grants from the Natural Sciences and Engineering Research Council of Canada (NSERC), through a Research Grant and two Equipment Grants (EQCM and electrochemical impedance set-up) and by the Université du Québec à Montréal.

References

1. A. Rudge, J. Davey, I. Raistrick, S. Gottesfeld, and J.P. Ferraris. J. Power Sources, **47**, 89 (1994).
2. C. Arbizzani, M. Mastragostino, L. Meneghello, and R. Paraventi. Adv. Mater. (Weinheim, Ger.), **8**, 331 (1996).
3. K. Naoi, M. Asada, Y. Hayashi, and Y. Inoue. Proc. Electrochem. Soc. **93-23**, 86 (1993).
4. D. Bélanger, J. Davey, F. Uribe, and S. Gottesfeld. In preparation.
5. A.A. Pud. Synth. Met. **66**, 1 (1994).
6. Y. Wei, G.-W. Jang, C.-C. Chan, K.F. Hsueh, R. Hariharan, S.A. Patel, and C.K. Whitecar. J. Phys. Chem. **94**, 7716 (1990).
7. P. Fiordiponti and G. Pistoia. Electrochim. Acta, **34**, 215 (1989).
8. J. Desilvestro, W. Scheifele, and O. Haas. J. Electrochem. Soc. **139**, 2727 (1992).
9. K. Kanamura, Y. Kawai, S. Yonezawa, and Z.-i. Takehara. J. Electrochem. Soc. **142**, 2894 (1995).
10. (*a*) T. Osaka, T. Nakajima, K. Shiota, and T. Momma. J. Electrochem. Soc. **138**, 2853 (1991); (*b*) K. Naoi, Y. Nagatomi, and N. Oyama. Denki Kagaku, **60**, 1091 (1992).
11. K. Yamada, K. Teshima, N. Kobayashi, and R. Hirohashi. J. Electroanal. Chem. **394**, 71 (1995).
12. (*a*) S. Yonezawa, K. Kanamura, and Z.-i. Takehara. J. Electrochem. Soc. **142**, 3309 (1995); (*b*) J. Electrochem. Soc. **140**, 629 (1993).
13. N. Pekmez and A. Yildiz. J. Electroanal. Chem. **386**, 121 (1995).
14. H. Daifuku, T. Kawagoe, N. Yamamoto, T. Ohsaka, and N. Oyama. J. Electroanal. Chem. **274**, 313 (1989).
15. S.B. Brummer and A.C. Makrides. J. Electrochem. Soc. **111**, 1122 (1964).
16. I. Rubinstein, J. Rishpon, and S. Gottesfeld. J. Electrochem. Soc. **133**, 729 (1986).
17. X. Ren and P.G. Pickup. J. Electrochem. Soc. **139**, 2097 (1992).
18. E.W. Paul, A.J. Ricco, and M.S. Wrighton. J. Phys. Chem. **89**, 1441 (1985).
19. X. Ren and P.G. Pickup. J. Phys. Chem. **97**, 5356 (1993).
20. X. Ren and P.G. Pickup. J. Electroanal. Chem. **372**, 289 (1994).
21. G. Sandi and P. Vanysek. Synth. Met. **64**, 1 (1994).
22. M.E.G. Lyons. Electroactive polymer electrochemistry. Part 1. Fundamentals. Plenum Press, New York. 1993. p. 311.

Can. J. Chem. Downloaded from www.nrcresearchpress.com by 91.121.58.235 on 09/08/12
For personal use only.

© 1997 NRC Canada

Functionalization and elaboration of ring A taxoid building blocks

Michael W. Tjepkema, Timothy Wong, Peter D. Wilson, and Alex G. Fallis

Abstract: The elaboration of the ring A aldehydes **1**, **7**, and **11** into more highly functionalized intermediates for taxoid synthesis is described. An improved route to the triene **4** and the adduct **28b** is reported. Additional condensations of selected aldehydes (**1**, **7**) with the organolithium reagents derived from the substituted halodienes **8** and **14** afforded the allylic alcohols **10** and **15** with a diastereoselectivity of ~5:1. Further manipulation of these products by the installation of an α-keto-acetylenic dienophile provided a taxoid precursor with the C_2, C_9, C_{10}, C_{13}, and C_{20} oxygens installed in the case of **23** (from **7**), and the less functionalized systems **27** and **27a** (from **1**).

Key words: taxoid, paclitaxel, Diels–Alder, cyclohexene, dienes.

Résumé : On décrit la transformation du cycle A des aldéhydes **1**, **7** et **11** en intermédiaires beaucoup plus fonctionnalisés utiles dans la synthèse de taxoïdes. On a mis au point une voie améliorée pour atteindre le triène **4** et l'adduit **28b**. Des condensations additionnelles d'aldéhydes choisis (**1**, **7**) avec des réactifs organolithiens dérivés des halodiènes substitués **8** et **14** ont fourni les alcools allyliques **10** et **15** avec une diastéréosélectivité d'environ 5 : 1. Des manipulations ultérieures de ces produits par le biais de l'installation d'un diénophile α-cétoacétylénique ont conduit à un précurseur de taxoïde portant les oxygènes en C2, C9, C10, C13 et C20 (**23** obtenu à partir du produit **7**) et d'autres systèmes moins fonctionnalisés (**27** et **27a** à partir du produit **1**).

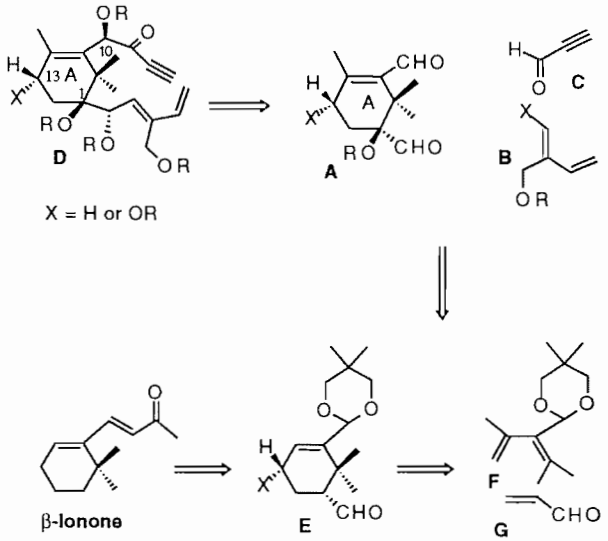
Mots clés : taxoïde, paclitaxel, Diels–Alder, cyclohexène, diènes.

[Traduit par la rédaction]

Introduction

In the preceding paper in this series (1), we described the synthesis of various cyclohexene ring A building blocks as part of a general strategy for the construction of the taxane nucleus. We have been developing an approach that proceeds in the left to right direction (ring A to ABC) (2). For this pathway, it was anticipated that ring A cyclohexene building blocks could be used as anchors to facilitate an intramolecular Diels–Alder reaction for the construction of the B and C rings simultaneously. This is briefly illustrated in Scheme 1 in which the ring A components **A** (previously synthesized), **E** or **F**, plus **G**, may be combined with suitable diene **B** and dienophile **C** units to generate a Diels–Alder precursor **D** for construction of the taxoid nucleus. We have previously developed direct routes to the required diene unit **B** as both the (*E*) and (*Z*) isomers (3). These compounds contain a hydroxymethyl substituent as a control group for the eventual introduction of the oxetane. An acetylenic ketone was selected as the dienophile to minimize the possible stereochemical complications in the transition state and provide a double bond (C_7—C_8) in the C ring as a handle for the eventual introduction of the C_7 hydroxyl and the C_8 methyl groups.

Scheme 1. Retrosynthetic Diels–Alder strategy.



Results and discussion

Initially, in order to demonstrate the synthetic utility of the strategy outlined and establish its convergent nature, a much

Received February 26, 1997.

This paper is dedicated to Professor Brian E. Conway on the occasion of his 70th birthday. Presented with respect and gratitude for his contributions to chemical education and electrochemistry.

M.W. Tjepkema, T. Wong, P.D. Wilson, and A.G. Fallis.[1] Ottawa–Carleton Chemistry Institute, Department of Chemistry, University of Ottawa, 10 Marie Curie, Ottawa, ON K1N 6N5, Canada.

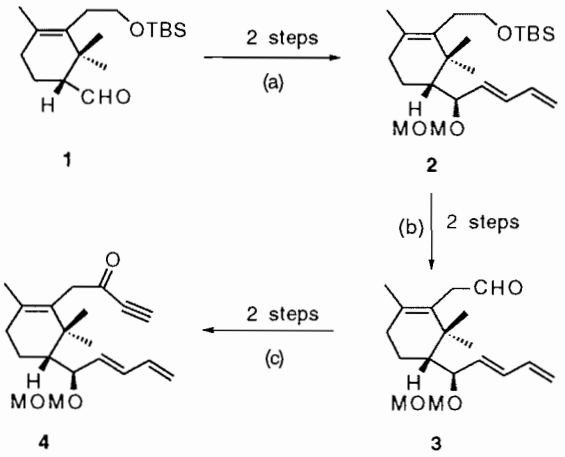
[1] Author to whom correspondence may be addressed. Telephone: (613) 562-5732. Fax: (613) 562-5170. E-mail: afallis@science.uottawa.ca

© 1997 NRC Canada

Can. J. Chem. Downloaded from www.nrcresearchpress.com by 91.121.58.235 on 09/08/12
For personal use only.

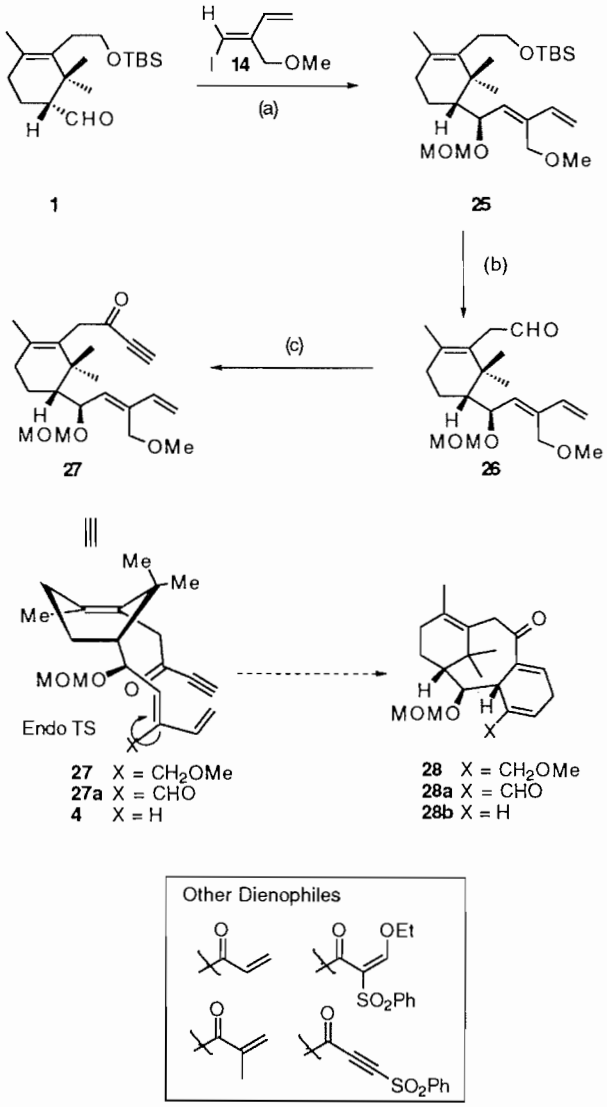
Can. J. Chem. Downloaded from www.nrcresearchpress.com by 91.121.58.235 on 09/08/12
For personal use only.

Scheme 2. Improved synthesis of Diels–Alder precursor **4**.



Reaction conditions: (*a*) **5**, *n*-BuLi, THF, −78°C; **1**, THF, −78°C, 98%; i-Pr_2NEt, MOMCl, CH_2Cl_2, 21°C, 93%; (*b*) *n*-Bu_4NF, THF, 21°C, 92%; $COCl_2$, CH_2Cl_2, DMSO, −78°C, Et_3N, 71%; (*c*) HCCMgCl, THF, 0°C, 90%; Dess–Martin periodinane, CH_2Cl_2, 48°C, 89%.

Scheme 3. Synthesis of Diels–Alder diene **27** (*Z*-series).



Reaction conditions: (*a*) **8**, THF, *s*-BuLi, −78°C; **7**, THF, −78°C, 81%; MOMCl. i-Pr_2NEt, 21°C 66%; (*b*) aq. HCl/ THF, 3:1, 21°C, 99%; (*c*) *n*-BuLi, 1,3-dithiane, THF, −20°C, 49%; (*d*) TBSOTf, collidine, CH_2Cl_2, 21°C; NBS, collidine, aq. CH_3CN, 22%; (*e*) TBSCN, KCN, 18-crown-6, CH_2Cl_2, 21°C, 67%; (*f*) DIBALH, CH_2Cl_2, −78°C, 85%; (*g*) THF, HCCMgCl, 0°C, 40%; Dess–Martin periodinance, CH_2Cl_2, 48°C, 80%.

more direct route to our model Diels–Alder precursor, the diene-ynone **4** (Scheme 2), was developed. This sequence afforded the diene **4** in nine steps commencing with 2-bromo-1,1,3-trimethyl-1,3-pentadiene (4) to provide the aldehyde **1**, as described in the preceding paper (1). Thus the synthesis of the model adduct **28b** (Scheme 3) was accomplished in a total of 10 steps, compared to the 18 steps required in our initial studies (2).

The key aspects of this route are outlined briefly in Scheme 2 and involved the condensation of aldehyde **1** (Table 1) with the organolithium reagent derived from exchange of tri-*n*-butylstannyl-1,3-butadiene (**5**) with *n*-butyllithium to afford the secondary alcohol **6** with a high level of stereoselectivity (15:1). The major diastereomer **6** was treated with chloromethyl methyl ether (MOMCl) and diisopropylethylamine to afford the diether **2**. Removal of the silyl protecting group with fluoride ion released the primary alcohol (96%), which was oxidized under Swern conditions to afford the aldehyde **3**, which was identical to the compound prepared earlier. The subsequent steps to the adduct were also shortened as ethynylmagnesium chloride could be used directly in place of the trimethylsilylethynyllithium previously used.

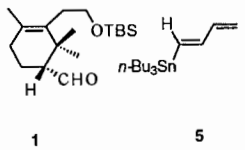
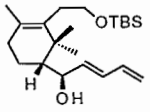
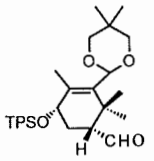
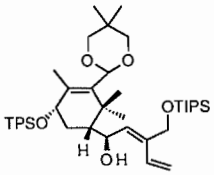
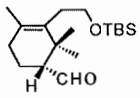
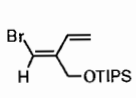
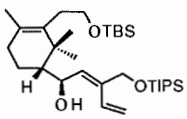
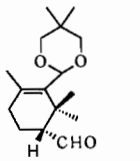
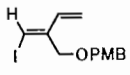
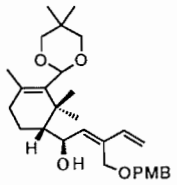
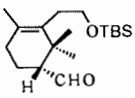
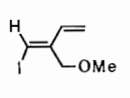
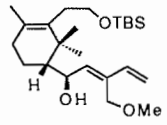
The extension of this chemistry required the introduction of more oxygen functionality and a hydroxymethyl diene substituent for the eventual introduction of the oxetane. The required dienes possess a relatively simple substitution pattern but were not available in a stereo- and regio-controlled manner. Thus various (*E*)- and (*Z*)-1-halo-2-(alkoxymethyloxy)-1,3-butadienes (diene unit **B**) were synthesized from vinylmagnesium chloride addition to trimethylsilylpropargyl alcohol or, alternatively, these were prepared by palladium-mediated addition and coupling of the appropriate alkene unit followed by halodesilylation (3). Table 1 summarizes the results of these additional studies with various aldehydes **1**, **7**, and **11**. The appropriate halodiene **8**, **12**, or **14** was exchanged with *sec*- or *tert*-butyllithium in THF at −78°C to afford the condensation products **9**, **10**, **13**, and **15** in yields of 81–99% with a diastereoselectivity of ~5:1. This stereochemical result is a consequence of preferential attack opposite to the *gem* dimethyl group in which the carbonyl group is also oriented away from these substituents, as illustrated in **16** (Fig. 1) and consistent with our earlier observations (2). As above, the major diastereomers were converted to their methoxymethyl ethers. This set the stage for the attachment of the dienophile unit and the incorporation of additional oxygen. Scheme 4 outlines the sequence developed for the *E*-diene commencing with aldehyde-acetal **7**.

Hydrolysis of the neopentylidene acetal present in **18** was effected smoothly with aqueous hydrochloric acid in THF to

© 1997 NRC Canada

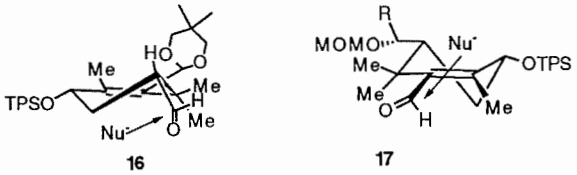
Can. J. Chem. Downloaded from www.nrcresearchpress.com by 91.121.58.235 on 09/08/12
For personal use only.

Table 1. Diene additions to ring A aldehydes.

Aldehyde	Diene	Product[a]
 1	5	 6, 98%, 15:1
 7	 8	 9, 81%, 5:1
 1	 8	 10, 99%, 6:1
 11	 12	 13, 85%, 6:1
 1	 14	 15, 82%, 5:1

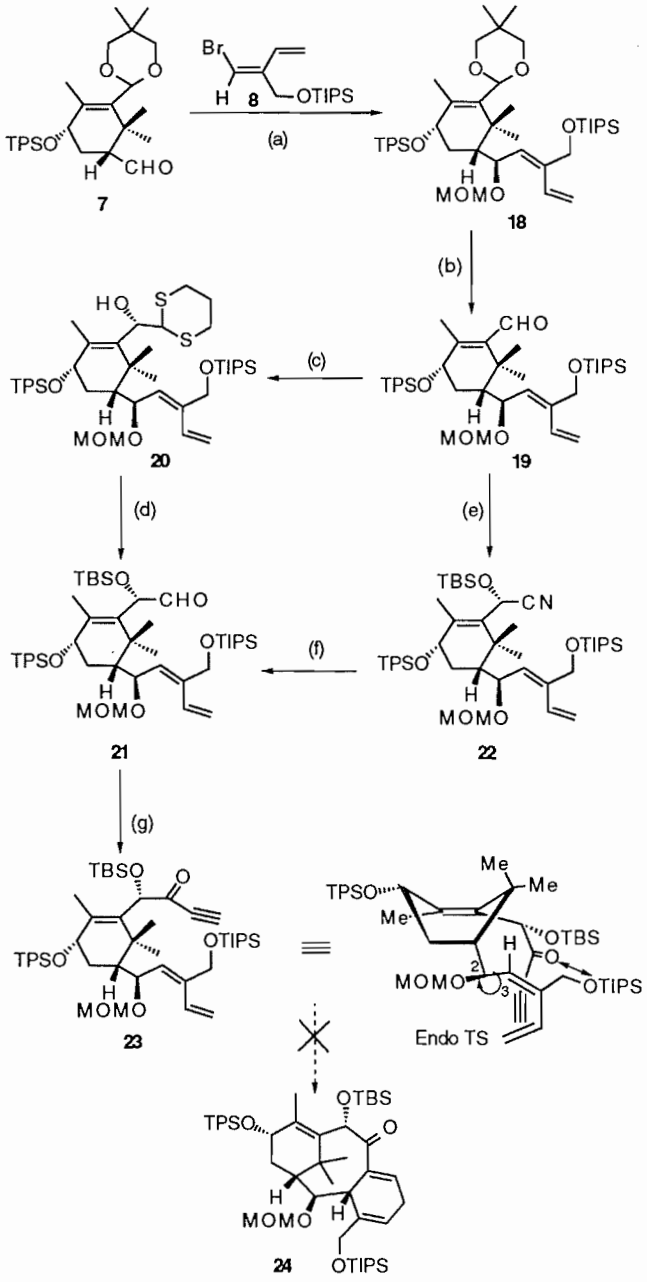
[a]Ratios determined by ^1H and (or) ^{13}C NMR spectroscopy.

Fig. 1. Preferential direction of nucleophilic attack.



provide the aldehyde **19** in quantitative yield. To preserve this oxygen functionality and introduce the new carbonyl group required for C_9 (paclitaxel numbering), aldehyde **19** was condensed with 1,3-dithianyllithium at −20°C. This reaction afforded 24% of the starting aldehyde, accompanied by 49% of the single alcohol diastereomer **20**. This stereochemical result arose from the preferred approach of the nucleophile from the top of the molecule with the carbonyl group oriented downward in order to minimize the interaction with the adjacent methyl groups as illustrated in **17** (Fig. 1). Consequently, the new secondary alcohol has the opposite configuration to the C_9 acetate in paclitaxel (Taxol®). The alcohol **20** was protected by treatment with collidine and *tert*-butyldimethylsilyl

Scheme 4. Synthesis of Diels–Alder diene **25** (*E*-series).

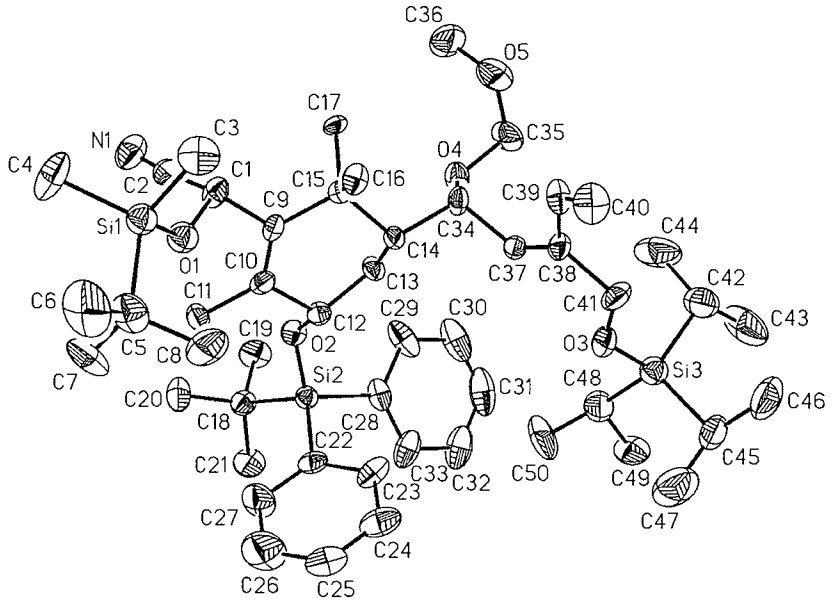


Reaction conditions: (*a*) **14**, *t*-BuLi, THF, −78°C; **1**, THF, −78–0°C, 82%; i-Pr_2NEt, MOMCl, CH_2Cl_2, 0°C, 86%; (*b*) *n*-Bu_4NF, THF, 21°C, 96%; Dess–Martin periodinane, CH_2Cl_2, 48°C, 82%; (*c*) HCCMgCl, THF, 0°C, 67%; Dess–Martin periodinane, CH_2Cl_2, 48°C, 98%.

trifluoromethanesulfonate (TBSTf) and reacted directly with NBS in aqueous acetonitrile–acetone to afford the aldehyde **21**, but in a disappointing yield of only 22%. In view of this low yield a better alternative was examined. This involved the addition of *tert*-butyldimethylsilyl cyanide, in the presence of potassium cyanide, and 18-crown-6 to the aldehyde. This procedure provided the major diastereomer **22** in 67% yield accompanied by its epimer (11%). This implies that, with a small nucleophile, some control over the addition may be possible and lead to a higher yield of the natural stereoisomer. The

© 1997 NRC Canada

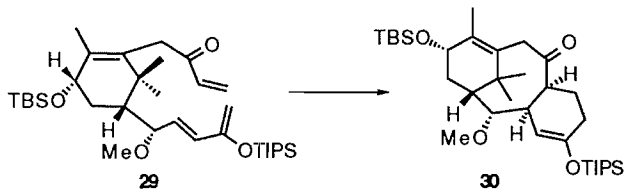
Fig. 2. A view of 1-(2*S**)-*tert*-butyldimethylsilyloxyacetonitrile)-(3*S**)-*tert*-butyldiphenylsilyloxy-(5*R**,1*R**)-methoxymethyloxy-3-triisopropylsilyloxymethyl-2(*E*)-4-pentadienyl-2,6,6-trimethylcyclohexene (**22**).



X-ray structure of **22** (Fig. 2) confirmed the stereochemical relationships of the various centres. Reduction of the nitrile **22** with diisobutylaluminum hydride directly afforded the aldehyde **21** in 85% yield. Ethynylmagnesium chloride was condensed with the aldehyde **21** in THF at 0°C to provide a ~2:1 diastereomeric mixture of acetylenic alcohols. Direct oxidation of the combined epimers with Dess–Martin periodinane afforded the acetylenic ketone **23** in 80% yield.

The final stage of this sequence was expected to provide the tricyclic nucleus **24**. The illustrated transition state suggested, as did computer modeling, that an *endo* cycloaddition should be preferred. This conformation would afford the adduct **24** with the C_2 and C_3 hydrogens *trans*. Rotation about the C_2—C_3 single bond (arrow) would provide the opposite stereochemistry but the potential overlap between the diene and dienophile is less favourable. Unfortunately, despite heating a toluene solution of **23** containing 10 mol% of hydroquinone in a sealed tube in a microwave oven at ~300°C for 8 h until all the starting material was consumed, none of the anticipated adduct **24** (<5%) could be detected. This undesirable result implies that one or more of the nonbonded interactions present in the precursor is sufficient to impede cyclization. Initially we suspected that the 1,3 interaction between the C_{13} ether and the axial bond connecting the diene side chain was the culprit. However, this is not the case, since after completion of these investigations, Winkler et al. (5) reported the successful cyclization of a closely related example, **29** to **30** (Scheme 5), with an *endo* C_{13} ether substituent. Danishefsky and co-workers (6) discovered that an epimeric ether at C_{10} (as contained in **23**) inhibited the Diels–Alder cyclization of ring A in a steroid-based model. This does not seem to be the problem in our case. The geometric difference between the (*E*) and (*Z*) dienes also does not appear to be critical. However, the only way to ascertain the factors responsible for the failure of the Diels–Alder cyclization with certainty was to examine the (*Z*) series and less substituted systems.

Scheme 5. Diels–Alder cycloaddition (ref. 5).



Progress on several fronts, while our work was in progress, has demonstrated that fewer oxygens are required in the precursors to the tricyclic skeleton than previously suspected. For example, the C_{13} oxygen may be introduced by allylic oxidation at a late stage of the synthesis (7), and the C_1 oxygen may be inserted by enolization of an appropriate C_2 ketone (8). It is difficult to introduce a C_{10} oxygen from a C_9 ketone (9); however, the reverse transformation has been accomplished (10). Thus, in an effort to understand the reason(s) for the failure of the cycloaddition, and with the expectation that less oxygenated Diels–Alder precursors would also suffice for the projected total synthesis, simpler systems were synthesized.

To assemble these compounds rapidly, the alcohol **15** from the condensation of aldehyde **1** and **14** (Table 1) was protected as its methyloxymethyl ether to give **25** (Scheme 3). Removal of the *tert*-butyldimethylsilyl ether with fluoride afforded the primary alcohol, which was oxidized directly with Dess–Martin periodinane to the aldehyde **26** (82%). Condensation of this aldehyde with ethynylmagnesium chloride provided a diastereomeric mixture of alcohols (~2:1) that was oxidized with Dess–Martin periodinane to afford the acetylenic ketone **27** (98%). Thermolysis of **27** failed to afford significant quantities of **28**. In a parallel manner, several other Diels–Alder precursors possessing different dienophiles, including activated olefins, were synthesized (box, Scheme 3). Unfortunately none of these new compounds cyclized either.

Can. J. Chem. Downloaded from www.nrcresearchpress.com by 91.121.58.235 on 09/08/12
For personal use only.

© 1997 NRC Canada

Can. J. Chem. Downloaded from www.nrcresearchpress.com by 91.121.58.235 on 09/08/12
For personal use only.

Which nonbonded interaction inhibits the desired cyclization? The key experiment (not the first example studied!) was the attempted cyclization of **27**. This compound differs from our initial, successful model system **4** only by the inclusion of the methoxymethyl ether diene substituent in place of hydrogen (X = CH_2OMe vs. X = H). This leads to the inescapable conclusion that the nonbonded interactions with the diene substituent and another portion of the molecule are sufficient to inhibit cyclization. Here also, the preferred transition state looks quite attractive. The cyclohexene is distorted into a boat-like conformation. This allows for reasonable alignment between the acetylenic ketone and the diene unit. However, the substituent (X = CH_2OMe), due to its rapid free rotation, must inhibit the close approach of the dienophile, despite the fact that in several orientations there does not seem to be excess interference. Even the sterically less demanding aldehyde **27a** (X = CHO) did not cyclize to **28a**, in spite of the fact that carbonyl groups in the 2-position of dienes usually render them particularly reactive (11). The recent Winkler results (5) have provided additional evidence. The diene substituent is the problem. The nonbonded interaction between the diene hydroxymethyl ether substituent and the carbonyl of the dienophile will not allow the required alignment (arrows **23** and **27**) of these two groups into the required orientation for the transition state under the experimental conditions examined. The fact that the diene in **29** (Scheme 5) is both more reactive and lacks this substituent supports this conclusion.

In conclusion, these studies have established the utility of various ring A building blocks and their selective condensation with diverse dienes. This has permitted the synthesis of more complex systems including those with additional oxygen substituents. Despite the fact that only some of the desired synthetic objectives were realized from these investigations, the factors that inhibit the desired intramolecular Diels–Alder cycloaddition have been delineated. Recently it has been reported that a C_4 methoxy substituent has an adverse influence in an aromatic taxane (12).

A beneficial consequence of these difficulties is the revision of our approach to the challenging tricyclo[9.3.1.$0^{3,8}$]pentadecene nucleus. This new synthetic strategy for taxoids capitalizes on the knowledge gained to date using some of the same building blocks prepared above. In addition, a key feature is the use of a chiral tether control group to both impart asymmetry and facilitate the attainment of the requisite transition state for a different intramolecular Diels–Alder cycloaddition. These features allow the inclusion of a hydroxymethyl diene substituent as a handle for the introduction of the oxetane as originally planned (13).

Experimental section

For general methods see ref. 8.

X-ray analysis was conducted on a Rigaku diffractometer with Mo Kα radiation at −130°C using the ω–2θ scan technique to a maximum 2θ value of 44.9. Cell constants and an orientation matrix for data collection were obtained from least-squares refinement using the setting angles of 25 reflections in the range $40 < 2\theta < 45$, corresponding to an orthorombic cell for compound **22** ($C_{50}H_{81}NO_5Si_3$) with dimensions a = 15.127, b = 19.174, c = 18.622 Å. For Z = 4 and FW = 861.83, the calculated density is 1.058 g/cm^3. Based on the systematic absences, the space group was $P2_1c$. The data (6726 reflections) were collected for Lorentz and polarization effects (14). The structure was solved by direct methods with all atoms refined, except hydrogen. The hydrogen atoms were calculated by assuming a distance of 1.07 Å. The final cycle of full matrix least-squares refinement was based on 4549 observed reflections ($I > 2.5\ \sigma(I)$) and 533 variable parameters using weights based on counting statistics. The maximum–minimum peaks on the final differences Fourier map were 0.31 and −0.38 e/Å^3, respectively. All calculations were performed using the NRCVAX crystallographic software package (15). Supplementary material containing experimental details, bond lengths and angles, and torsion angles has been deposited.[2]

(1*R**)-(2-*tert*-Butyldimethylsilyloxyethyl)-(5*R**)-hydroxy-(2*E*)-4-pentadienyl-2,6,6-trimethylcyclohexene

n-Butyllithium (1.50 mL, 2.5 M in hexanes, 3.75 mmol) was added dropwise to a stirred solution of 1(*E*)-(tri-*n*-butylstannyl)-1,3-butadiene **5** (1.31 g, 3.82 mmol) in THF (40 mL) at −78°C over a period of ~1 min. The resultant mixture was stirred at −78°C for 10 min, and then a solution of the aldehyde **1** (952 mg, 2.77 mmol) in THF (6 mL) was added over a period of ~30 s. After a further 30 min, water (40 mL) was added and the reaction mixture was allowed to warm to ambient temperature. The phases were separated and the aqueous phase was extracted further with ether (3 × 40 mL). The combined organic extracts were washed with brine (50 mL), dried, and concentrated. Chromatography (6:1, hexanes/ether) afforded the major alcohol (930 mg, 92%) and the corresponding minor diastereomeric alcohol (64.5 mg, 6%) as colourless oils. Major diastereomer: ^{1}H NMR (200 MHz, $CDCl_3$) δ: 0.03 (s, 6H), 0.88 (s, 9H), 1.05 (s, 6H), 1.20–1.60 (m, 4H), 1.62 (s, 3H), 1.95 (m, 2H), 2.30 (m, 2H), 3.53 (t, J = 8 Hz, 2H), 4.52 (m, 1H), 5.00–5.25 (m, 2H), 5.74 (dd, J = 16, 5 Hz, 1H), 6.15–6.45 (m, 2H).

(1*R**)-(2-*tert*-Butyldimethylsilyloxyethyl)-(5*R**)-methoxymethyloxy-(2*E*)-4-pentadienyl-2,6,6-trimethylcyclohexene (2)

N,N-Diisopropylethyl amine (4.0 mL, 23 mmol) and chloromethyl methyl ether (1.0 mL, 13 mmol) were added sequentially to a stirred solution of the above alcohol (826 mg, 2.27 mmol) in dichloromethane (10 mL) at 0°C. The resultant mixture was stirred at ambient temperature for 24 h and then a saturated aqueous solution of sodium bicarbonate (40 mL) was added. The phases were separated and the aqueous phase was extracted further with dichloromethane (3 × 30 mL). The combined organic extracts were washed with brine (40 mL), dried, and concentrated. Chromatography (20:1, hexanes/ether)

[2] Copies of the supplementary material can be purchased from: The Depository of Unpublished Data, Document Delivery, CISTI, National Research Council Canada, Ottawa, Canada K1A 0S2. With the exception of torsion angles, these data have also been deposited with the Cambridge Crystallographic Data Centre, and can be obtained on request from The Director, Cambridge Crystallographic Data Centre, University Chemical Laboratory, 12 Union Road, Cambridge, CB2 1EZ, U.K.

© 1997 NRC Canada

Can. J. Chem. Downloaded from www.nrcresearchpress.com by 91.121.58.235 on 09/08/12
For personal use only.

afforded the ether **2** (863 mg, 93%) as a colourless oil. ^{1}H NMR (200 MHz, $CDCl_3$) δ: 0.04 (s, 6H), 0.90 (s, 9H), 0.98 (s, 3H), 1.04 (s, 3H), 1.20–1.70 (m, 3H), 1.60 (s, 3H), 1.90 (m, 2H), 2.28 (m, 2H), 3.35 (s, 3H), 3.52 (t, J = 8 Hz, 2H), 4.26 (dd, J = 8, 1.5 Hz, 1H), 4.47 (d, J = 7 Hz, 1H), 4.64 (d, J = 7 Hz, 1H), 5.02–5.24 (m, 2H), 5.65 (dd, J = 15, 8 Hz, 1H), 6.05–6.42 (m, 2H).

(1*R)-(Acetaldehyde)-(5*R**)-methoxymethyloxy-(2*E*)-4-pentadienyl-2,6,6-trimethylcyclohexene (3)**

Tetra-*n*-butylammonium fluoride (10.0 mL, 1.0 M in THF, 10 mmol) was added dropwise to the neat silyl ether **2** (863 mg, 2.11 mmol) at ambient temperature. The resultant mixture was stirred for 1 h and then a saturated aqueous solution of sodium bicarbonate (20 mL) and ether (20 mL) were added. The phases were separated and the aqueous phase was extracted further with ether (3 × 15 mL). The combined organic extracts were washed with brine (25 mL), dried, and concentrated. Chromatography (3:5, hexanes/ether) afforded the corresponding alcohol (569 mg, 92%) as a colourless oil. Oxalyl chloride (0.43 mL, 4.5 mmol) was added dropwise to a stirred solution of dimethyl sulfoxide (0.30 mL, 4.5 mmol) in dichloromethane (20 mL) at −78°C over a period of ~30 s. The resultant mixture was stirred for 15 min and then a solution of the above alcohol (569 mg, 1.93 mmol) in dichloromethane (9 mL) was added dropwise over ~2 min. The reaction mixture was stirred for 1 h and triethylamine (1.25 mL, 8.97 mmol) was added over ~1 min. The reaction mixture was then allowed to warm to 0°C over a period of 1.25 h. Water (15 mL) was added, the phases were separated, and the aqueous phase was extracted further with dichloromethane (3 × 15 mL). The combined organic extracts were then washed with a saturated aqueous solution of ammonium chloride (30 mL), then with brine (30 mL), dried, and concentrated. Chromatography (7:1, hexanes/ether) afforded the aldehyde **3** (401 mg, 71%) as a colourless oil. The spectral data were in accord to that reported previously (2).

(5*R)(1*R**)-Methoxymethyloxy-(2*E*)-4-pentadienyl-1-(2-oxo-3-butynyl)-2,6,6-trimethylcyclohexene (4)**

Ethynylmagnesium chloride (8.0 mL, 0.5 M in THF, 4.0 mmol) was added to a stirred solution of the aldehyde **3** (401 mg, 1.37 mmol) in THF (15 mL) at 0°C. The resultant mixture was stirred at 0°C for 30 min and then a saturated aqueous solution of ammonium chloride (14 mL) was added. The phases were separated and the aqueous phase was extracted further with ether (3 × 10 mL). The combined organic extracts were washed with brine (20 mL), dried, and concentrated. Chromatography (2:1, hexanes/ether) afforded the diastereomeric acetylenic alcohols (393 mg, 90%) as colorless oils. Dess–Martin periodinane (2.0 g, 4.8 mmol) was added to a stirred solution of above acetylenic alcohols (393 mg, 1.23 mmol) in dichloromethane (20 mL). The resultant mixture was heated at reflux for 45 min and then allowed to cool to ambient temperature. The reaction mixture was poured into a mixture of a saturated aqueous solution of sodium bicarbonate (25 mL), an aqueous solution of sodium thiosulfate (1.0 M, 25 mL), and water (25 mL). The phases were separated and the aqueous phase was extracted further with dichloromethane (3 × 25 mL). The combined organic extracts were washed with water (50 mL), then with brine (50 mL), dried, and concentrated. Chromatography (5:1, hexanes/ether) afforded the ketone **4** (346 mg, 89%) as a colourless oil. The spectral data were in accord to that reported previously (2).

(3*S)-*tert*-Butyldiphenylsilyloxy-(5*R**)(1*R**)-hydroxy-3-triisopropylsilyloxymethyl-(2*E*)-4-pentadienyl-2,6,6-trimethylcyclohexene-1-carboxaldehyde neopentylidene acetal (9)**

A solution of the dienyl bromide **8** (577 mg, 1.81 mmol) in THF (3 mL) was added to a stirred solution of *sec*-butyllithium (3.2 mL, 1.21 M in hexanes, 3.9 mmol) in THF (10 mL) over a period of 2 min at −78°C. After 20 min a solution of the aldehyde **7** (664 mg, 1.27 mmol) in THF (3.5 mL) was added over a period of 1 min. The reaction mixture was stirred at −78°C for a further 10 min and then allowed to warm to ambient temperature over 30 min. Water (30 mL) was added, the phases separated, and the aqueous phase was extracted further with ether (3 × 30 mL). The combined organic extracts were dried and concentrated. Chromatography (3:1, petroleum ether/ether) afforded, as a ~5:1 mixture of diastereomers, the corresponding secondary alcohols (782 mg, 81%) as colourless oils. Major isomer **9**: IR ($CHCl_3$): 3607, 3017, 1466, 1427, 1216, 1065 cm^{-1}; ^{1}H NMR (200 MHz, $CDCl_3$) δ: 0.72, (s, 3H), 0.99–1.08 (m, 36H), 1.25–1.30 (m, 1H), 1.26 (s, 3H), 1.61–1.69 (m, 1H), 1.95–2.01 (m, 1H), 2.04 (s, 3H), 3.43–3.75 (m, 4H), 4.13 (dd, J = 10.2, 5.0 Hz, 1H), 4.30 (s, 2H), 4.72 (m, 1H), 4.78 (s, 1H), 5.05 (d, J = 11.3 Hz, 1H), 5.15 (d, J = 17.5 Hz, 1H), 5.50 (d, J = 10.0 Hz, 1H), 6.70 (dd, J = 17.5, 11.3 Hz, 1H), 7.31–7.40 (m, 6H), 7.67–7.72 (m, 4H); ^{13}C NMR (50 MHz, $CDCl_3$) δ: 11.9, 14.1, 16.9, 18.0, 19.5, 21.0, 22.2, 22.4, 24.1, 26.3, 27.2, 30.1, 38.0, 48.8, 60.4, 63.5, 65.8, 73.8, 77.2, 78.5, 78.6, 102.1, 115.2, 127.3, 127.4, 129.5, 130.4, 130.8, 133.9, 134.6, 135.0, 136.1, 136.2, 138.6; HRMS (EI) calcd. for $C_{46}H_{70}O_4Si_2$ ($M^+ - H_2O$): 742.4718; found: 742.4764.

1-(2-*tert*-Butyldimethylsilyloxyethyl)-(5*R)(1*R**)-hydroxy-3-triisopropylsilyloxymethyl-(2*E*)-4-pentadienyl-2,6,6-trimethylcyclohexene (10)**

A solution of the dienyl bromide **8** (918 mg, 2.87 mmol) in THF (4 mL) was added to a stirred solution of *sec*-butyllithium (5.0 mL, 1.21 M in cyclohexane, 6.03 mmol) in THF (25 mL) over a period of 2.5 min at −78°C. After 20 min a solution of the aldehyde **1** (377 mg, 1.48 mmol) in THF (4 mL) was added. The reaction mixture was stirred at −78°C for a further 10 min and then allowed to warm to ambient temperature over 30 min. Water (10 mL) was added, the phases separated, and the aqueous phase was extracted further with ether (2 × 10 mL). The combined organic extracts were dried and concentrated. Chromatography (9:1, hexanes/ether) afforded, as a ~6:1 mixture of diastereomers, the corresponding secondary alcohols (656 mg 99%) as colourless oils. Major isomer **10**: ^{1}H NMR (200 MHz, $CDCl_3$) δ: 0.05 (s, 6H), 0.88 (s, 9H), 0.90–1.70 (m, 31H), 1.62 (s, 3H), 1.95 (m, 2H). 2.28 (m, 2H), 3.53 (t, J = 9 Hz, 2H), 4.38 (s, 2H), 4.85–5.27 (m, 3H), 5.89 (m, 1H), 6.48–6.67 (m, 1H); HRMS (EI) calcd. for $C_{32}H_{60}O_2Si_2$ ($M^+ - H_2O$): 532.4135; found: 532.4158. *N*,*N*-Diisopropylethyl amine (7.0 mL, 40 mmol) and chloromethyl methyl ether (1.5 mL, 20 mmol) were added sequentially to a stirred solution of the above alcohols (1.19 g, 2.17 mmol) in dichloromethane (10 mL) at 0°C. The resultant mixture was stirred at ambient temperature for 41 h, and then

© 1997 NRC Canada

Can. J. Chem. Downloaded from www.nrcresearchpress.com by 91.121.58.235 on 09/08/12
For personal use only.

water (10 mL) and ether (10 mL) were added. The phases were separated and the aqueous phase was extracted further with ether (3 × 5 mL). The combined organic extracts were washed with brine (15 mL), dried, and concentrated. Chromatography (25:1, hexanes/ether) afforded, as a single diastereomer, the corresponding methyloxymethyl ether (939 mg, 73%) as a colourless oil. ^{1}H NMR (200 MHz, $CDCl_3$) δ: 0.04 (s, 6H), 0.77–2.80 (m, 30H), 0.88 (s, 9H), 1.60 (s, 3H), 1.90 (m, 2H), 2.28 (m, 2H), 3.34 (s, 3H), 3.50 (m, 2H), 4.36–4.80 (m, 5H), 5.05–5.24 (m, 2H), 5.88 (m, 1H), 6.67 (m, 1H).

(5*R)(1*R**)-Hydroxy-3-*para*-methoxybenzyloxymethyl-(2*E*)-4-pentadienyl-2,6,6-trimethylcyclohexene-1-carboxaldehyde neopentylidene acetal (13)**

A solution of the dienyl iodide **12** (537 mg, 1.66 mmol) in THF (3 mL) was added to a stirred solution of *sec*-butyllithium (2.70 mL, 1.21 M in cyclohexane, 3.51 mmol) in THF (10 mL) over a period of 1 min at −78°C. After 4 min a solution of the aldehyde **11** (299 mg, 1.12 mmol) in dry THF (3 mL) was added over a period of 15 s. The reaction mixture was stirred at −78°C for a further 20 min and then at ambient temperature for 5 min. Water (10 mL) was next added, the phases were separated, and the aqueous phase was extracted further with ether (3 × 10 mL). The combined organic extracts were washed with brine (20 mL), dried, and concentrated. Chromatography (1:1, hexanes/ether) afforded, as a ~6:1 mixture of diastereomers, the corresponding secondary alcohols (437 mg, 85%) as a colourless oil. Mayor isomer **13**. IR (neat) 3458, 2909, 1611, 1586, 1514, 1247, 1089 cm^{-1}; ^{1}H NMR (200 MHz, $CDCl_3$) δ: 0.73 (s, 3H), 1.03 (s, 3H), 1.04 (s, 3H), 1.20–2.10 (m, 6H), 1.26 (s, 3H), 1.90 (s, 3H), 3.42–3.53 (m, 2H), 3.66–3.75 (m, 2H), 3.79 (s, 3H), 4.06–4.25 (m, 2H), 4.37–4.52 (m, 2H), 4.70 (m, 1H), 4.82 (s, 1H), 5.07 (d, J = 11 Hz, 1H), 5.28 (d, J = 18 Hz, 1H), 5.83 (d, J = 8 Hz, 1H), 6.30 (dd, J = 18, 11 Hz, 1H), 6.86 (d, J = 9 Hz, 2H), 7.25 (d, J = 9 Hz, 2H); HRMS (EI) calcd. for $C_{29}H_{42}O_5$: 470.3034; found: 470.3033.

1-(2-*tert*-Butyldimethylsilyloxyethyl)-(5*R)(1*R**)-hydroxy-3-methoxymethyl-(2*Z*)-4-pentadienyl-2,6,6-trimethylcyclohexene (15)**

A solution of *tert*-butyllithium (12.4 mL, 1.58 M in pentane, 19.6 mmol) was added to a stirred solution of the dienyl iodide **14** (2.09 g, 9.33 mmol) in THF (80 mL) over a period of 3 min at −78°C. The resultant mixture was stirred at −78°C for 3 min, at 0°C for 20 min, and was then recooled to −78°C. A solution of the aldehyde **1** (2.05 g, 6.60 mmol) in dry THF (14 mL) was then added over a period of 30 s. The reaction mixture was stirred at −78°C for 15 min and then at 0°C for a further 15 min. Water (50 mL) was added, the phases were separated, and the aqueous phase was extracted with ether (3 × 50 mL). The combined organic extracts were washed with brine (100 mL), dried, and concentrated. Chromatography (7:3, hexanes/ether) afforded, as a ~5:1 mixture of diastereomers, the corresponding secondary alcohols (2.22 g, 82%) as colourless oils. Major isomer **15**. IR ($CHCl_3$): 3443, 2911, 1083 cm^{-1}; ^{1}H NMR (200 MHz, $CDCl_3$) δ: 0.05 (s, 6 H), 0.88 (s, 9H), 1.05 (s, 3H), 1.06 (s, 3H), 1.17–1.70 (m, 3H), 1.62 (s, 3H), 1.97 (m, 2H), 2.24 (t, J = 7 Hz, 2H), 3.33 (s, 3H), 3.56 (t, J = 7 Hz, 2H), 4.15 (s, 2H), 4.80 (m, 1H), 5.16 (d, J = 11 Hz, 1H), 5.32 (d, J = 17.5 Hz, 1H), 5.85 (d, J = 8.5 Hz, 1H), 6.29 (dd, J = 17.5, 11 Hz, 1H); ^{13}C NMR (75 MHz, $CDCl_3$) δ: −5.5, 18.3, 18.5, 20.3, 22.9, 26.0, 27.5, 32.5, 32.6, 38.4, 50.8, 58.2, 62.9, 66.6, 67.2, 113.7, 129.5, 133.5, 134.5, 138.6, 139.3; HRMS (EI) calcd. for $C_{24}H_{42}O_2Si$ ($M^+ - H_2O$): 390.2956; found: 390.2973.

(3*S)-*tert*-Butyldiphenylsilyloxy-(5*R**)(1*R**)-methoxymethyloxy-3-triisopropylsilyloxymethyl-(2*E*)-4-pentadienyl-2,6,6-trimethylcyclohexene-1-carboxaldehyde neopentylidene acetal (18)**

N, N-Diisopropylethyl amine (1.25 mL, 7.19 mmol) and chloromethyl methyl ether (460 μL, 6.06 mmol) were added sequentially to a stirred solution of the diastereomeric alcohols **9** (497 mg, 0.654 mmol) in dichloromethane (3 mL) at ambient temperature (21°C). The resultant mixture was stirred for 14 h and then a saturated aqueous solution of sodium bicarbonate (10 mL) and ether (100 mL) were added. The organic phase was separated, washed with a saturated aqueous solution of sodium bicarbonate (5 mL), then with brine (2 × 10 mL), dried, and concentrated. Chromatography (100% hexanes to 20% ether in hexanes) afforded, as a single diastereomer, the ether **18** (354 mg, 66%) as a colourless oil. IR ($CHCl_3$): 2915, 1465, 1427, 1216, 1067 cm^{-1}; ^{1}H NMR (500 MHz, $CDCl_3$) δ: 0.72 (s, 3H), 0.99–1.08 (m, 36H), 1.25–1.30 (m, 1H), 1.26 (s, 3H), 1.60–1.68 (m, 1H), 1.95–2.01 (m, 1H), 2.05 (s, 3H), 3.15 (s, 3H), 3.42–3.74 (m, 4H), 4.12 (dd, J = 10.3, 5.1 Hz, 1H), 4.26 (d, J = 6.7 Hz, 1H), 4.31 (s, 2H), 4.46 (d, J = 6.7 Hz, 1H), 4.50 (dd, J = 9.8, 4.0 Hz, 1H), 4.77 (s, 1H), 5.06 (d, J = 11.4 Hz, 1H), 5.15 (d, 17.7 Hz, 1H), 5.49 (d, J = 9.8 Hz, 1H), 6.58 (dd, J = 17.7 Hz, 11.4 Hz, 1H), 7.31–7.40 (m, 6H), 7.67–7.72 (m, 4H); ^{13}C NMR (125 MHz, $CDCl_3$) δ: 12.0, 16.8, 17.9, 18.0, 19.5, 21.8, 22.2, 24.1, 26.7, 27.2, 30.0, 30.2, 38.1, 48.5, 56.0, 63.2, 69.8, 74.0, 78.5, 78.6, 93.5, 102.3, 114.7, 127.2, 127.5, 128.2, 129.3, 129.4, 130.9, 133.9, 134.8, 136.2, 136.3, 136.7, 139.1.

(3*S)-*tert*-Butyldiphenylsilyloxy-1-carboxaldehyde-(5*R**)(1*R**)-methoxymethyloxy-3-triisopropylsilyloxymethyl-(2*E*)-4-pentadienyl-2,6,6-trimethylcyclohexene (19)**

Hydrochloric acid (4%, 300 μL) was added to a stirred solution of the acetal **18** (30.0 mg, 0.037 mmol) in THF (1 mL) at ambient temperature. The resultant mixture was stirred for 3 h and then a saturated aqueous solution of sodium bicarbonate (2 mL) was added. On removal of the THF, in vacuo, the resultant aqueous residue was extracted with ether (100 mL). The organic extract was washed with water (5 × 10 mL), a saturated aqueous solution of sodium bicarbonate (5 mL), and then with brine (2 × 10 mL), dried, and concentrated to afford the aldehyde **19** (27 mg, 99%) as a colourless oil. IR (neat): 2913, 2758, 1677, 1464, 1076 cm^{-1}; ^{1}H NMR (200 MHz, $CDCl_3$) δ: 1.01–1.08 (m, 30H), 1.19 (s, 3H), 1.22 (s, 3H), 1.67–1.74 (m, 1H), 2.04–2.12 (m, 1H), 2.07 (s, 3H), 3.17 (s, 3H), 4.20 (apparent t, 1H), 4.27 (d, J = 6.7 Hz, 1H), 4.33 (s, 2H), 4.49 (d, J = 6.7 Hz, 1H), 4.57 (dd, J = 9.8, 3.7 Hz, 1H), 5.09 (d, J = 11.3 Hz, 1H), 5.17 (d, J = 18.1 Hz, 1H), 5.52 (d, J = 9.8 Hz, 1H), 6.60 (dd, J = 18.1, 11.3 Hz, 1H), 7.32–7.44 (m, 6H), 7.67–7.75 (m, 4H), 10.06 (s, 1H); ^{13}C NMR (75 MHz, $CDCl_3$) δ: 11.9, 15.0, 17.9, 19.5, 21.1, 26.7, 27.0, 27.1, 29.3, 37.5, 48.3, 56.0, 62.9, 68.9, 74.3, 93.4, 114.8, 127.4, 127.5, 127.6, 129.6, 129.7, 130.6, 133.4, 134.1, 136.0, 136.8, 141.2, 155.6, 193.9.

© 1997 NRC Canada

Can. J. Chem. Downloaded from www.nrcresearchpress.com by 91.121.58.235 on 09/08/12
For personal use only.

(3*S)-*tert*-Butyldiphenylsilyloxy-1-(2*S**)-hydroxyacetaldehyde propylidene dithioacetal)-(5*R**)(1*R**)-methoxymethyloxy-3-triisopropylsilyloxymethyl-(2*E*)-4-pentadienyl-2,6,6-trimethylcyclohexene (20)**

n-Butyllithium (180 μL, 2.5 M in hexanes, 0.45 mmol) was added to a stirred solution of 1,3-dithiane (54 mg, 0.45 mmol) in THF (3.5 mL) at −20°C. The resultant mixture was stirred for 1 h and then cooled to −78°C. A solution of the aldehyde **19** (154 mg, 0.214 mmol) in THF (1 mL) was then added. After 1 h the reaction mixture was warmed to −20°C and a saturated aqueous solution of sodium bicarbonate (10 mL) was added. On removal of the THF, in vacuo, the resultant aqueous residue was extracted with ether (100 mL). The ether extract was then washed with a saturated aqueous solution of sodium bicarbonate (10 mL), then with brine (10 mL), dried, and concentrated. Chromatography (100% hexanes to 20% ether in hexanes) afforded the starting aldehyde **19** (37 mg, 24%) and the alcohol **20** (88 mg, 49%) as colourless oils. IR ($CHCl_3$): 3451, 2947, 2865, 1593, 1464, 1379, 1216, 1107 cm^{-1}; ^1H NMR (500 MHz, $CDCl_3$) δ: 0.86 (s, 3H), 1.00–1.03 (m, 30H), 1.05 (s, 3H), 1.10–1.30 (m, 1H), 1.48–1.63 (m, 1H), 1.82 (s, 3H), 1.91–2.09 (m, 3H), 2.74–2.79 (m, 2H), 2.87–2.91 (m, 2H), 3.13 (s, 3H), 4.16 (dd, *J* = 10.3, 5.7 Hz, 1H), 4.22 (d, *J* = 10.2 Hz, 1H), 4.23 (d, *J* = 6.7 Hz, 1H), 4.32 (s, 2H), 4.48 (d, *J* = 6.7 Hz, 1H), 4.49 (dd, *J* = 10.0, 4.0 Hz, 1H), 4.52 (d, *J* = 10.2 Hz, 1H), 5.07 (d, *J* = 11.4 Hz, 1H), 5.15 (d, *J* = 17.9 Hz, 1H), 5.53 (d, *J* = 10.0 Hz, 1H), 6.58 (dd, *J* = 17.9, 11.4 Hz, 1H), 7.29–7.40 (m, 6H), 7.68–7.73 (m, 4H); ^{13}C NMR (125 MHz, $CDCl_3$) δ: 12.0, 17.7, 18.0, 19.7, 22.4, 22.6, 25.4, 27.1, 27.2, 28.3, 29.4, 29.7, 29.9, 39.5, 48.5, 51.6, 56.0, 63.1, 69.8, 71.1, 74.9, 93.4, 114.7, 127.3, 127.5, 128.1, 129.3, 129.4, 130.9, 134.4, 134.9, 136.0, 136.1, 136.7, 138.1, 138.6.

1-(2*S)-*tert*-Butyldimethylsilyloxyacetonitrile)-(3*S**)-*tert*-butyldiphenylsilyloxy-(5*R**)(1*R**)-methoxymethyloxy-3-triisopropylsilyloxymethyl-(2*E*)-4-pentadienyl-2,6,6-trimethylcyclohexene (22)**

Potassium cyanide (27.0 mg, 0.42 mmol), 18-crown-6 (30.0 mg, 0.12 mmol), and *tert*-butyldimethylsilyl cyanide (87.0 mg, 0.62 mmol) were added sequentially to a stirred solution of the aldehyde **19** (212 mg, 0.295 mmol) in dichloromethane (2 mL) at ambient temperature. The resultant mixture was stirred for 7 h and then ether (100 mL) and a saturated aqueous solution of sodium bicarbonate (5 mL) were added. The organic phase was separated, washed with a saturated aqueous solution of sodium bicarbonate (5 mL), then with brine (2 × 10 mL), dried, and concentrated to afford the product as a 6:1 mixture of diastereomers. Chromatography (100% hexanes to 5% ether in hexanes) afforded the major diastereomer **22** (170 mg, 67%) as a crystalline solid and the corresponding minor diastereomer (28 mg, 11%) as a colourless oil. Major diastereomer **22**: mp 132–134.5°C; IR ($CHCl_3$): 3019, 2947, 2863, 1467, 1216, 1109 cm^{-1}; ^1H NMR (200 MHz, $CDCl_3$) δ: 0.13 (s, 3H), 0.26 (s, 3H), 0.88 (s, 9H), 0.82–1.06 (m, 36H), 1.30–1.38 (m, 1H), 1.58–1.64 (m, 1H), 1.92–2.05 (m, 1H), 1.98 (s, 3H), 3.12 (s, 3H), 4.11 (dd, *J* = 9.7, 5.4 Hz, 1H), 4.25 (d, *J* = 6.7 Hz, 1H), 4.32 (s, 2H), 4.45 (d, *J* = 6.7 Hz, 1H), 4.47 (dd, *J* = 10.0, 4.2 Hz, 1H), 4.95 (s, 1H), 5.09 (d, *J* = 11.6 Hz, 1H), 5.17 (d, *J* = 18.3 Hz, 1H), 5.49 (d, *J* = 10.0 Hz, 1H), 6.56 (dd, *J* = 18.3, 11.6 Hz, 1H), 7.32–7.43 (m, 6H), 7.67–7.76 (m, 4H); ^{13}C NMR (75 MHz, $CDCl_3$) δ: −5.2, −5.1, 11.9, 16.5, 18.0, 19.5, 22.3, 25.4, 25.5, 26.3, 27.1, 29.8, 38.9, 48.1, 56.0, 58.9, 63.0, 69.4, 73.6, 93.3, 115.0, 120.0, 127.3, 127.5, 127.9, 129.4, 129.5, 130.6, 133.9, 134.7, 135.7, 135.9, 136.0, 136.1, 136.9, 141.0.

1-(2*S)-*tert*-Butyldimethylsilyloxyacetaldehyde)-(3*S**)-*tert*-butyldiphenylsilyloxy-(5*R**)(1*R**)-methoxymethyloxy-3-triisopropylsilyloxymethyl-(2*E*)-4-pentadienyl-2,6,6-trimethylcyclohexene (21)**

*From **20***: Collidine (100 μL, 0.75 mmol) and *tert*-butyldimethylsilyltrifluoromethanesulfonate (100 μL, 0.44 mmol) were added sequentially to a stirred solution of the alcohol **20** (77.0 mg, 0.092 mmol) in dichloromethane (2 mL) at 0°C. The resultant mixture was stirred at 0°C for 10 h and then a saturated aqueous solution of sodium bicarbonate (5 mL) and ether (100 mL) were added. The organic phase was washed with a saturated aqueous solution of sodium bicarbonate (5 mL), then with brine (2 × 5 mL), dried, and concentrated. Chromatography (100% hexanes to 5% ether in hexanes) afforded the corresponding silyl ether (38 mg, 43%) as a colourless oil. ^1H NMR (500 MHz, $CDCl_3$) δ: 0.11 (s, 3H), 0.21 (s, 3H), 0.81–1.04 (m, 39H), 1.25–1.30 (m, 1H), 1.33 (s, 3H), 1.41 (s, 3H), 1.60–1.68 (m, 1H), 1.62 (s, 3H), 1.91–2.09 (m, 3H), 2.74–2.91 (m, 4H), 3.28 (s, 3H), 4.16–4.22 (m, 2H), 4.30 (s, 2H), 4.32–4.50 (m, 5H), 4.81 (d, *J* = 8.0 Hz, 1H), 5.02 (d, *J* = 11.4 Hz, 1H), 5.12 (d, *J* = 17.0 Hz, 1H), 5.57 (d, 10.0 Hz, 1H), 6.53–6.61 (m, 1H), 7.29–7.40 (m, 6H), 7.68–7.73 (m, 4H). Collidine (60 μL, 0.45 mmol) and *N*-bromosuccinimide (60 mg, 0.33 mmol) were added sequentially to a stirred solution of the above silyl ether (35 mg, 0.037 mmol) in aqueous acetonitrile (80%, 1.5 mL) and acetone (2.5 mL) at 0°C. The resultant mixture was stirred for 5 min and then a saturated aqueous solution of sodium bicarbonate (5 mL), an aqueous solution of sodium thiosulfate (20%, 5 mL), and ether (100 mL) were added. The organic phase was separated, washed with a saturated aqueous solution of sodium bicarbonate (5 mL), then with brine (10 mL), dried, and concentrated. Chromatography (5% ether in hexanes) afforded the aldehyde **21** (7 mg, 22%) as a colourless oil. IR (neat): 2912, 2720, 1737, 1592, 1465, 1080 cm^{-1}; ^1H NMR (200 MHz, $CDCl_3$) δ: 0.02 (s, 3H), 0.13 (s, 3H), 0.82–1.04 (m, 45H), 1.31–1.39 (m, 1H), 1.65–1.70 (m, 1H), 1.69 (s, 3H), 1.98–2.08 (m, 1H), 3.15 (s, 3H), 4.15 (dd, *J* = 9.9, 6.6 Hz, 1H), 4.27 (d, *J* = 6.6 Hz, 1H), 4.33 (s, 3H), 4.48 (d, *J* = 6.6 Hz, 1H), 4.52 (dd, *J* = 10.4, 4.4 Hz, 1H), 4.60 (s, 1H), 5.09 (d, *J* = 11.6 Hz, 1H), 5.18 (d, *J* = 18.3 Hz, 1H), 5.53 (d, *J* = 10.4 Hz, 1H), 6.59 (dd, *J* = 18.3, 11.6 Hz, 1H), 7.35–7.42 (m, 6H), 7.66–7.73 (m, 4H), 9.57 (s, 1H); ^{13}C NMR (75 MHz, $CDCl_3$) δ: −4.7, −4.3, 11.9, 16.5, 18.0, 18.3, 19.5, 22.3, 25.7, 25.9, 27.0, 27.1, 29.9, 38.8, 48.4, 56.0, 63.1, 69.7, 73.8, 77.4, 93.4, 114.8, 127.3, 127.5, 128.2, 129.3, 129.5, 130.7, 134.1, 134.8, 136.0, 136.4, 136.7, 201.2.

*From **22***: Diisobutylaluminum hydride (70 μL, 1 M in toluene, 0.07 mmol) was added to a stirred solution of the nitrile **22** (40 mg, 0.047 mmol) in dichloromethane (2 mL) at −78°C. The resultant mixture was stirred for 30 min and then allowed to warm to ambient temperature. A saturated aqueous solution of ammonium chloride (5 mL) was added and the resultant mixture was stirred for a further 3 h. The aqueous phase was then extracted with ether (100 mL) and the extract was washed

© 1997 NRC Canada

Can. J. Chem. Downloaded from www.nrcresearchpress.com by 91.121.58.235 on 09/08/12
For personal use only.

with a saturated aqueous solution of ammonium chloride (5 mL), then with brine (10 mL), dried, and concentrated to afford the aldehyde **21** (34 mg, 85%) as a colourless oil. The spectral data for this material were in accord to that recorded above. Anal. calcd. for $C_{50}H_{82}O_6Si$: C 69.79, H 9.49; found: C 69.96, H 9.23.

1-(1*S)-*tert*-Butyldimethylsilyloxy-2-oxo-3-butynyl)-(3*S**)-*tert*-butyldiphenylsilyloxy-(5*R**)(1*R**)-methoxymethyloxy-3-triisopropylsilyloxymethyl-(2*E*)-4-pentadienyl-2,6,6-trimethylcyclohexene (23)**

Ethynylmagnesium chloride (850 μL, 0.5 M in THF, 0.42 mmol) was added to a stirred solution of the aldehyde **21** (170 mg, 0.197 mmol) in THF (10 mL) at 0°C. The resultant mixture was stirred for 30 min and then a saturated aqueous solution of ammonium chloride (10 mL) was added. On removal of the THF, in vacuo, the resultant aqueous residue was extracted with ether (100 mL). The ether extract was washed with a saturated aqueous solution of ammonium chloride (5 mL), a saturated aqueous solution of sodium bicarbonate (5 mL), and then with brine (2 × 5 mL), dried, and concentrated to afford a ~2:1 mixture of corresponding diastereomeric acetylenic alcohols. Chromatography (100% hexanes to 20% ether in hexanes) afforded the minor diastereomer (31 mg, 15%), followed by the major diastereomer (51 mg, 25%), both as colourless oils. Major diastereomer: IR (neat): 3309, 2944, 2862, 1593, 1465, 1105, 1039 cm^{-1}; ^1H NMR (200 MHz, $CDCl_3$) δ: 0.02 (s, 3H), 0.16 (s, 3H), 0.84 (s, 9H), 0.97 (s, 3H), 1.01–1.07 (m, 33H), 1.25–1.30 (m, 1H), 1.50–1.62 (m, 1H), 1.96 (s, 3H), 2.01–2.10 (m, 1H), 2.43 (d, 1H, J = 2.0 Hz), 3.14 (s, 3H), 4.12 (dd, J = 10.0, 5.7 Hz, 1H), 4.24 (d, J = 6.8 Hz, 1H), 4.33 (s, 2H), 4.38 (d, J = 8.2 Hz, 1H), 4.46 (d, J = 6.8 Hz, 1H), 4.46–4.54 (m, 2H), 5.10 (d, J = 11.7 Hz, 1H), 5.18 (d, J = 18.4 Hz, 1H), 5.49 (d, J = 11.2 Hz, 1H), 6.59 (dd, J = 18.4, 11.7 Hz, 1H), 7.34–7.43 (m, 6H), 7.66–7.76 (m, 4H); ^{13}C NMR (75 MHz, $CDCl_3$) δ: −4.2, −3.8, 11.9, 16.7, 18.0, 18.4, 19.5, 22.3, 25.9, 26.2, 27.2, 27.9, 30.0, 39.4, 48.3, 56.0, 63.1, 66.0, 69.5, 73.3, 74.6, 74.8, 85.0, 93.3, 114.9, 127.3, 127.5, 128.0, 129.4, 129.5, 130.7, 134.0, 134.7, 136.0, 136.8, 138.6, 139.3. Dess–Martin periodinane (597 mg, 1.40 mmol) was added to a stirred solution of the above acetylenic alcohols (80 mg, 0.09 mmol) in dichloromethane (6 mL). The resultant mixture was heated at reflux for 16 h and then cooled to ambient temperature. A saturated aqueous solution of sodium bicarbonate (25 mL), sodium thiosulfate (1.0 g), and ether (100 mL) were then added and the resultant mixture stirred for 30 min. The organic phase was separated and washed with a saturated aqueous solution of sodium bicarbonate (5 mL), then with brine (2 × 5 mL), dried, and concentrated. Chromatography (100% hexanes to 10% ether in hexanes) afforded the ketone **23** (64 mg, 80%) as a colourless oil. IR ($CHCl_3$): 3299, 3020, 2948, 2862, 1690, 1467, 1216 cm^{-1}; ^1H NMR (500 MHz, $CDCl_3$) δ: 0.02 (br s, 3H), 0.15 (s, 3H), 0.89 (s, 9H), 1.01–1.07 (m, 45H), 1.30–1.35 (m, 1H), 1.58–1.64 (m, 1H), 1.62 (br s, 3H), 1.99–2.04 (m, 1H), 3.17 (s, 3H), 3.23 (d, 1H, J = 2.4 Hz), 4.15–4.18 (m, 1H), 4.27 (d, J = 6.7 Hz, 1H), 4.32 (s, 2H), 4.47 (d, J = 6.7 Hz, 1H), 4.55 (m, 1H), 4.58 (br s, 1H), 5.08 (d, J = 11.3 Hz, 1H), 5.17 (d, J = 17.7 Hz, 1H), 5.53 (d, J = 9.8 Hz, 1H), 6.57 (dd, J = 17.7, 11.3 Hz, 1H), 7.30–7.42 (m, 6H), 7.67–7.71 (m, 4H); ^{13}C NMR (125 MHz, $CDCl_3$) δ: −4.6, −4.0, 12.0, 14.1, 15.3, 18.0, 18.5, 19.6, 22.3, 25.9, 26.0, 27.1, 29.8, 31.6, 39.1, 56.0, 63.1, 65.8, 69.6, 73.9, 80.6, 81.1, 93.5, 114.8, 127.3, 127.5, 127.6, 128.2, 129.3, 129.5, 130.8, 134.3, 134.9, 136.0, 136.1, 136.8, 165.8, (CO, δ: 188.3 recorded at 230 K). Anal. calcd. for $C_{52}H_{82}O_6Si_3$: C 70.38, H 9.31; found: C 70.51, H 9.34.

1-(2-*tert*-Butyldimethylsilyloxyethyl)-(5*R)-(3-methoxymethyl-(1*R**)-methoxymethyloxy-(2*Z*)-4-pentadienyl-2,6,6-trimethylcyclohexene (25)**

N,*N*-Diisopropylethyl amine (15 mL, 86 mmol) and chloromethylmethyl ether (3.0 mL, 40 mmol) were added sequentially to a stirred solution of the alcohol **15** (2.22 g, 5.43 mmol) in dichloromethane (20 mL) at 0°C. The resultant mixture was stirred at 0°C for 10 min and then at ambient temperature for 20 h. A saturated aqueous solution of sodium bicarbonate (80 mL) was added, the phases were separated, and the aqueous phase was extracted further with dichloromethane (3 × 50 mL). The combined organic extracts were washed with a saturated aqueous solution of sodium bicarbonate (100 mL), then with brine (100 mL), dried, and concentrated. Chromatography (9:1, hexanes/ether) afforded the silyl ether **25** (2.12 g, 86%) as a colourless oil. IR ($CHCl_3$): 2912, 1092 cm^{-1}; ^1H NMR (200 MHz, $CDCl_3$) δ: 0.05 (s, 6 H), 0.88 (s, 9H), 1.00 (s, 3H), 1.07 (s, 3H), 1.14–1.40 (m, 3H), 1.60 (s, 3H), 1.90 (m, 2H), 2.28 (m, 2H), 3.31 (s, 3H), 3.34 (s, 3H), 3.50 (t, J = 7 Hz, 2H), 4.12 (dd, J = 2, 11 Hz, 2H), 4.55 (dd, J = 2, 11 Hz, 2H), 4.72 (m, 1H), 5.20 (d, J = 11 Hz, 1H), 5.35 (d, J = 17.5 Hz, 1H), 5.73 (d, J = 9 Hz, 1H), 6.26 (dd, J = 17.5, 11 Hz, 1H); ^{13}C NMR (75 MHz, $CDCl_3$) δ: −5.16, 18.3, 19.3, 20.3, 22.4, 26.0, 27.0, 32.7, 32.9, 38.6, 51.0, 56.2, 58.1, 63.0, 66.5, 71.1, 94.4, 114.1, 129.1, 133.6, 135.4, 136.6, 138.4; HRMS (EI) calcd. for $C_{26}H_{48}O_4Si$: 452.3324; found: 452.3344.

1-Acetaldehyde-(5*R)-(3-methoxymethyl-(1*R**)-methoxymethyloxy-(2*Z*)-4-pentadienyl-2,6,6-trimethylcyclohexene (26)**

A solution of *n*-tetrabutylammonium fluoride (25 mL, 1.0 M in THF, 25 mmol) was added to the neat silyl ether **25** (2.12 g, 4.68 mmol) at ambient temperature. The resultant mixture was stirred for 2 h and then a saturated aqueous solution of sodium bicarbonate (25 mL) was added. The phases were separated and the aqueous phase was extracted further with ether (3 × 20 mL). The combined organic extracts were washed with brine (40 mL), dried, and concentrated. Chromatography (3:4, hexanes/ether) afforded the corresponding alcohol (1.51 g, 96%) as a colourless oil. IR ($CHCl_3$): 3374, 2910, 1095 cm^{-1}; ^1H NMR (200 MHz, $CDCl_3$) δ: 0.97 (s, 3H), 1.03 (s, 3H), 1.10–1.30 (m, 3H), 1.58 (s, 3H), 1.85 (m, 2H), 2.23 (m, 2H), 3.22 (s, 3H), 3.25 (s, 3H), 3.50 (t, J = 7 Hz, 2H), 4.05 (dd, J = 2, 11 Hz, 2H), 4.42 (dd, J = 2, 11 Hz, 2H), 4.62 (m, 1H), 5.00 (d, J = 11 Hz, 1H), 5.29 (d, J = 17.5 Hz, 1H), 5.68 (d, J = 9 Hz, 1H), 6.21 (dd, J = 17.5, 11 Hz, 1H); ^{13}C NMR (75 MHz, $CDCl_3$) δ: 19.3, 20.3, 22.5, 27.1, 32.3, 32.8, 38.6, 50.9, 56.3, 58.1, 62.5, 66.5, 71.1, 94.4, 114.1, 129.5, 133.1, 135.4, 136.6, 138.3. Dess–Martin periodinane (2.70 g, 6.55 mmol) was added to a stirred solution of the above alcohol (679 mg, 2.01 mmol) in dichloromethane (20 mL) at ambient temperature. The resultant mixture was heated at reflux for 1 h and then cooled to ambient temperature. A saturated aqueous solution of sodium bicarbonate (12 mL), aqueous sodium thiosulfate solution (1.0 M, 15 mL), and water (10 mL) were then added.

© 1997 NRC Canada

Can. J. Chem. Downloaded from www.nrcresearchpress.com by 91.121.58.235 on 09/08/12
For personal use only.

The phases were separated and the aqueous phase was extracted further with dichloromethane (2 × 15 mL). The combined organic extracts were washed with brine (30 mL), dried, and concentrated. Chromatography (2:1, hexanes/ether) afforded the aldehyde **26** (591 mg, 87%) as a colourless oil. IR ($CHCl_3$): 2905, 1072 cm^{-1}; ^1H NMR (200 MHz, $CDCl_3$) δ: 0.99 (s, 3H), 1.02 (s, 3H), 1.4–1.8 (m, 3H), 1.54 (s, 3H), 2.04 (m, 2H), 3.07 (d, J = 2 Hz, 2H), 3.30 (s, 3H), 3.33 (s, 3H), 4.13 (dd, J = 2, 11 Hz, 2H), 4.52 (dd, J = 2, 11 Hz, 2H), 4.71 (m, 1H), 5.12 (d, J = 11 Hz, 1H), 5.39 (d, J = 17.5 Hz, 1H), 5.77 (d, J = 9 Hz, 1H), 6.29 (dd, J = 17.5, 11 Hz, 1H), 9.73 (t, J = 2 Hz, 1H); ^{13}C NMR (75 MHz, $CDCl_3$) δ: 19.2, 20.2, 21.9, 26.7, 33.0, 38.5, 43.7, 43.8, 51.0, 56.2, 58.1, 66.4, 71.0, 94.4, 114.1, 129.0, 132.5, 135.7, 136.2, 138.2, 201.2.

(5*R)-(3-Methoxymethyl-(1*R**)-methoxymethyloxy-(2*Z*)-4-pentadienyl-1-(2-oxo-3-butynyl)-2,6,6-trimethylcyclohexene (27)**

A solution of ethynylmagnesium chloride (10 mL, 0.5 M in THF, 5.0 mmol) was added to a stirred solution of the aldehyde **26** (630 mg, 1.87 mmol) in THF (20 mL) at 0°C. The resultant mixture was stirred for 1.5 h and then water (40 mL) was added. The phases were separated and the aqueous phase was extracted further with ether (3 × 40 mL). The combined organic extracts were washed with brine (50 mL), dried, and concentrated. Chromatography (1:1, hexanes/ether) afforded the corresponding acetylenic alcohols (454 mg, 67%) as colourless oils. Dess–Martin periodinane (2.20 g, 5.33 mmol) was added to a stirred solution of the above acetylenic alcohols (454 mg, 1.25 mmol) in dichloromethane (20 mL) at ambient temperature, and the resultant mixture was then heated at reflux for 1.5 h. The reaction mixture was then cooled to ambient temperature and poured into a mixture of a saturated aqueous solution of sodium bicarbonate (15 mL), an aqueous sodium thiosulfate solution (1.0 M, 15 mL), and water (30 mL). The aqueous phase was then extracted with dichloromethane (3 × 15 mL) and the combined organic extracts were washed with brine (30 mL), dried, and concentrated. Chromatography (2:1, hexanes/ether) afforded the ketone **27** (441 mg, 98%) as a colourless oil. IR ($CHCl_3$): 2920, 2090, 1680, 1095 cm^{-1}; ^1H NMR (200 MHz, $CDCl_3$) δ: 0.99 (s, 3H), 1.01 (s, 3H), 1.40–1.60 (m, 3H), 1.56 (s, 3H), 1.71 (m, 2H), 2.04 (m, 2H), 3.15 (s, 1H), 3.34 (s, 3H), 3.41 (s, 3H), 4.12 (dd, J = 2, 11 Hz, 2H), 4.48 (dd, J = 2, 11 Hz, 2H), 4.70 (m, 1H), 5.08 (d, J = 11 Hz, 1H), 5.36 (d, J = 17.5 Hz, 1H), 5.73 (d, J = 9 Hz, 1H), 6.29 (dd, J = 17.5, 11 Hz, 1H); ^{13}C NMR (75 MHz, $CDCl_3$) δ: 19.2, 20.8, 22.3, 26.6, 32.9, 38.4, 45.2, 50.5, 56.3, 58.1, 66.5, 71.1, 78.3, 81.7, 94.5, 114.1, 129.7, 132.8, 135.7, 136.3, 138.3, 186.0: Anal. calcd. for $C_{22}H_{32}O_4$: C 73.30, H 8.95; found: C 73.42, H 8.86.

Acknowledgment

We are grateful to the Natural Sciences and Engineering Research Council of Canada, Rhône-Poulenc Rorer, the Canadian Breast Cancer Research Initiative of the National Cancer Institute of Canada, and the Saunders–Matthey Foundation for Breast Cancer Research for financial support of this research and to Corrine Bensimon for the X-ray analysis.

References

1. M.W. Tjepkema, P.D. Wilson, H. Audrain, and A.G. Fallis. Can. J. Chem. **75**, 1215 (1997).
2. (*a*) Y.-F. Lu and A.G. Fallis. Tetrahedron Lett. **34**, 3367 (1993); (*b*) Can. J. Chem. **73**, 2239 (1995).
3. (*a*) T. Wong, M.A. Romero, and A.G. Fallis. J. Org. Chem. **59**, 5527 (1994); (*b*) T. Wong, M.W. Tjepkema, H. Audrain, P.D. Wilson, and A.G. Fallis. Tetrahedron Lett. **37**, 755 (1996).
4. (*a*) P.S. Skell and A.Y. Garner. J. Am. Chem. Soc. **78**, 5430 (1956); (*b*) W. von E. Doering and W.A. Henderson, Jr. J. Am. Chem. Soc. **80**, 5274 (1958).
5. J.D. Winkler, S.K. Bhattacharya, and R.A. Batey. Tetrahedron Lett. **37**, 8069 (1996).
6. I.J. Kim, T.K. Park, and S.J. Danishefsky. Tetrahedron Lett. **36**, 1015 (1995).
7. (*a*) K.C. Nicolaou, Z. Yang, J.J. Liu, H. Ueno, P.G. Nantermet, R.K. Guy, C.F. Claiborne, J. Renaud, E.A. Couladouros, K. Paulvannan, and E.A. Sorensen. Nature (London) **367**, 630 (1994); (*b*) K.C. Nicolaou, P.G. Nantermet, H. Ueno, R.K. Guy, E.A. Couladouros, and E.J. Sorensen. J. Am. Chem. Soc. **117**, 624 (1995); (*c*) K.C. Nicolaou, J.-J. Liu, Z. Yang, H. Ueno, E.J. Sorensen, C.F. Claiborne, R.K. Guy, C.K. Hwang, M. Nakada, and P.G. Nantermet. J. Am. Chem. Soc. **117**, 634 (1995); (*d*) K.C. Nicolaou, Z. Yang, J.J. Liu, P.G. Nantermet, C.F. Claiborne, J. Renaud, R.K. Guy, and K. Shibayama. J. Am. Chem. Soc. **117**, 645 (1995); (*e*) K.C. Nicolaou, H. Ueno, J.J. Liu, P.G. Nantermet, Z. Yang, J. Renaud, K. Paulvannan, and R. Chadha. J. Am. Chem. Soc. **117**, 653 (1995).
8. (*a*) K.J. Shea and S.T. Sakata. Tetrahedron Lett. **33**, 4261 (1992); (*b*) S.L. Gawltney II, S.T. Sakata, and K.J. Shea. J. Org. Chem. **61**, 7438 (1996).
9. J.D. Winkler, C.-S. Lee, L. Rubo, C.L. Muller, P.J. Squattrito. J. Org. Chem. **54**, 4491 (1989).
10. (*a*) J.J. Masters, J.T. Link, L.B. Snyder, W.B. Young, and S.J. Danishefsky. Angew. Chem. Int. Ed. Engl. **34**, 1723 (1995); (*b*) S.J. Danishefsky, J.J. Masters, W.B. Young, J.T. Link, L.B. Snyder, T.V. Magee, D.K. Jung, R.C.A. Isaacs, W.G. Bornmann, C.A. Alaimo, C.A. Coburn, and M.J. Di Grandi. J. Am. Chem. Soc. **118**, 2843 (1996).
11. (*a*) C. Spino and J. Crawford. Can. J. Chem. **71**, 1094 (1993); (*b*) C. Spino, J. Crawford, and J. Bishop. J. Org. Chem. **60**, 844 (1995).
12. P.A. Wender, T.E. Glass, N.E. Krauss, M. Mühlebach, B. Peschke, and D.B. Rawlins. J. Org. Chem. **61**, 7662 (1996).
13. A.G. Fallis. Pure Appl. Chem. **69**, 495 (1997).
14. D.F. Grant and E.J. Gabe. J. Appl. Crystallogr. **11**, (1978).
15. E.J. Gabe, F.L. Lee, and Y. Lepage. J. Appl. Crystallogr. **22**, 384 (1989).

© 1997 NRC Canada

The chemical history of a current

Keith J. Laidler

Abstract: The electric current was born two centuries ago, and its precise nature is still being elucidated. Various lines of investigation have been pursued. The discovery of electrolysis in 1800 was followed in 1834 by Faraday's laws, and led to the realization that there is a fundamental particle of electricity. In the 1840s, Joule's studies on batteries and electric motors led him to the formulation of the principle of conservation of energy. Clerk Maxwell's theory of electromagnetic radiation owed much to measurements of the speed of an electric current in a good conductor. The existence of ions in solution was not accepted until late in the century, and has led to a much deeper understanding in the whole field of electrochemistry. The electrode processes that occur in a galvanic cell and in electrolysis usually control the rate with which the current flows, and the mechanisms of such processes have presented a great challenge to research workers. Brian Conway has made important contributions to the understanding of electrode processes, and to related electrochemical problems, over a period of more than 40 years.

Key words: electric current, electrochemistry, electrode processes.

Résumé : La découverte de l'électricité remonte à deux siècles et sa nature précise est encore à découvrir. Plusieurs voies d'études ont été poursuivies. La découverte de l'électrolyse en 1800 suivie en 1834 par les lois de Faraday, a permis de réaliser qu'il existe une particule fondamentale d'électricité. Dans les années 1840, les études de Joule sur les batteries et les moteurs électriques l'ont conduit à formuler le principe de la conservation de l'énergie. La théorie de Clerk Maxwell sur la radiation électromagnétique est surtout due à la mesure de la vitesse d'un courant électrique dans un bon conducteur. L'existence des ions en solution n'a été acceptée que très tard dans le courant du siècle, et a conduit à une connaissance plus approfondie de l'électrochimie en général. La réaction à l'électrode qui se produit dans une cellule galvanique et dans l'électrolyse contrôle habituellement la vitesse à laquelle le courant circule, et le mécanisme de ces réactions a constitué un grand défi pour les chercheurs. Brian Conway, sur une période de 40 ans, a apporté une contribution importante à la compréhension des réactions à l'électrode, ainsi qu'aux problèmes électrochimiques qui y sont reliés.

Mots clés : courant, électrique, électrochimie, réactions à l'électrode.

[Traduit par la rédaction]

Introduction

The electric current was born in 1800 and continues to be investigated after nearly 200 years. When an electric current is generated by a galvanic cell, or when an electrolysis occurs, several different processes have to be taken into consideration. One is the flow through the conducting wires; another is the movement of ions in the chemical solutions. Of particular importance are the processes that take place at the electrodes. Almost always the rate with which the current flows is determined by these electrode processes. The story of the experimental and theoretical studies made over so many years is a complex one, and the present account can cover only some of the most fundamental aspects.

The exact date of birth of the electric current is debatable, but 2 March 1800 is a reasonable suggestion. It was on that day that the Italian physicist Alessandro Volta (1745–1827), of the University of Padua, sent his famous letter to Sir Joseph Banks (1743–1820), the President of the Royal Society, of which Volta was a Fellow. In this letter Volta described the pile, now known by his name, consisting of a series of discs of two different metals, such as silver and zinc, separated by paper moistened with brine. He found that electricity was produced, and his great achievement was to realize that it was caused by the contact between the metals and solutions present in his pile. Later in the year Volta's paper appeared in the *Philosophical Transactions* (1).

It is true that nine years previously Galvani had produced electricity by inserting metals into frogs' legs. He had, however, misinterpreted the effect as due to some particular property of living systems, and he used the expression "animal electricity." Volta's work showed this idea to be incorrect. His important contribution was to isolate the physical phenomenon of electricity from its connection with living systems. He recognized that in Galvani's experiments the function of the frog's leg was to provide the salt solution, and to act as a detector of electricity. It took about four more decades for it to become clear that chemical energy released in a reaction is the source of the electrical energy produced in a Voltaic pile.

For some time after Volta's announcement there was confusion about just what he had discovered. Much work had previously been done on static electricity, and the new phenomenon obviously had some connection with static electricity, but just what was the relationship? It gradually became clear that Volta had discovered how to create a flow of elec-

Received March 25, 1997.

This article is dedicated to Professor Brian E. Conway on the occasion of his 70th birthday.

K.J. Laidler.[1] Department of Chemistry, University of Ottawa, Ottawa, ON K1N 6N5, Canada.

[1] Telephone: (613) 749–3316. Fax: (613) 562–5170.

© 1997 NRC Canada

Can. J. Chem. Downloaded from www.nrcresearchpress.com by 91.121.58.235 on 09/08/12
For personal use only.

Can. J. Chem. Downloaded from www.nrcresearchpress.com by 91.121.58.235 on 09/08/12
For personal use only.

tricity, but many questions remained. Just what happens when a current flows along a wire? How fast does it flow? What happens at the metals that are introduced into a solution in order to generate electricity? In the case of an electrolysis, there was a question of how electricity flows through a solution, and of how fast it flows. What happens at the electric poles (which Faraday preferred to call electrodes) that are introduced into a solution in order to bring about electrolysis?

The discovery of electrolysis

The news of Volta's discovery spread rapidly by word of mouth, and there was much excitement among scientific investigators. As a result, even before Volta's letter appeared in print, another paper (2) was published, which described experiments making use of the information presented by Volta, and using piles of the same kind. This paper showed that the electricity generated in the piles was capable of bringing about the decomposition of water into hydrogen and oxygen gases. The author of this paper was William Nicholson (1753–1815), and the experiments had been done in collaboration with his friend Anthony Carlisle (1768–1840). Nicholson was a competent amateur scientist, and Carlisle was a fashionable London surgeon. On learning of Volta's work the two men constructed Voltaic piles of their own, and introduced the wires coming from the piles into weakly acid solutions. When they used either platinum or gold wires they found that hydrogen gas was evolved at one wire and oxygen gas at the other. Nicholson was the founder and editor of the *Journal of Natural Philosophy, Chemistry and the Arts*, usually known as *Nicholson's Journal*, and, as a result, was able to publish his results in July 1800 (before Volta's own paper was published). Much later, in 1834, Michael Faraday first used the word *electrolysis* to describe this kind of molecular splitting.

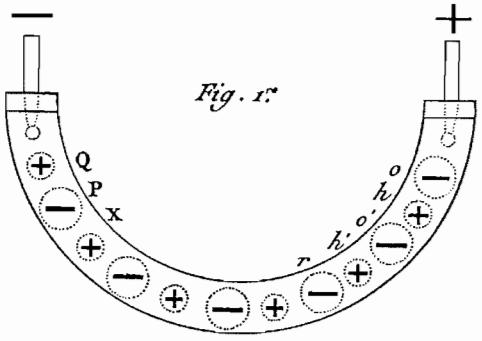
Nicholson and Carlisle's discovery that electricity can split water into hydrogen and oxygen created as great a stir as any scientific discovery ever made. The surprise was not so much at the *fact* that the gases were produced, but with *where* they were produced. It seemed to most investigators that, if the gases were produced at all, they should be produced *together*. If water is split into hydrogen and oxygen, why do they not appear in one place? Does one of the gases burrow through the solution from one wire to the other?

There was much confusion about this for a number of years, and the Institut de France even set up a committee to consider the problem. Its members came to no firm conclusion, but suggested various possibilities, one of which was that there actually was some unknown mechanism by which gases and other materials could travel invisibly through a solution. In 1806 such a mechanism was suggested (3) by a young German, Theodor Christian Johann Diedrich von Grotthuss (1785–1822; Fig. 1). While still a student in Italy he postulated that "galvanic action" polarizes water to such a degree that the elements can pass through the solution in opposite directions, always remaining bound to a partner until released at the poles. The diagram he used to explain his mechanism is shown in Fig. 2. It seems remarkable today that von Grotthuss should have represented a molecule of water as if it were completely dissociated into charged species (many people at the time thought that water was HO, so that he may have been thinking of H^+ and O^-). In fact, von Grotthuss did not believe that ions

Fig. 1. An engraving of Theodor Christian Johann Diedrich von Grotthuss (1784–1822). Besides suggesting a theory of electrolysis in 1805, he discovered in 1809 that for photochemical action the light must be absorbed. This was rediscovered by J.W. Draper in 1841, and is now often called the Grotthuss–Draper law. Von Grotthuss inherited a disease that caused him great suffering, and, as a result, he committed suicide at the age of 37. (Photograph courtesy of Mrs. Brian Conway.)



Fig. 2. The diagram given by von Grotthuss to explain his theory of electrolysis. He did not believe that ions exist in solution, but that they are produced transiently by the electrical action, and jump from one molecule to another.



were really present in solution; he thought that the ions were always bound to one another, but that one charged species could jump from one molecule to another. He envisioned something like what happens in a square dance in which each person passes along a chain of people, continually taking the hands of those moving in the opposite direction. We now know that von Grotthuss's mechanism does not apply in gen-

© 1997 NRC Canada

eral, the current instead being carried by ions that can move without always being attached to a partner. However, a mechanism similar to that of von Grotthuss is believed to apply to the movement of a hydrogen or hydroxide ion through a solution. In the case of a hydrogen ion, a proton is transferred from H_3O^+ along a stream of water molecules, and such a mechanism is today called a *Grotthuss mechanism.* More is said later of this type of mechanism.

Electric batteries

Volta's work, and that of Nicholson and Carlisle, stimulated much further work on the production of electric currents. It was soon realized that Voltaic piles were awkward to use, and that it was more convenient to immerse rods or plates of two different metals in a bath containing a suitable solution. Such a device was, and is, often called a *battery*, although strictly speaking it should be called a cell; the word battery should be reserved for several cells connected together. Many different combinations of metals were used, and there was much rivalry among investigators. Some, notably John George Children (1777–1852), delighted in making batteries of enormous size, by means of which they produced spectacular sparks and brought about the melting of metals. Some of this work had little scientific value.

Batteries of a more modest size were used at the Royal Institution by Sir Humphry Davy (1778–1829) to isolate a number of chemical elements. On 6 October 1807 he electrolyzed fused potash and obtained the element potassium, and later he isolated sodium, calcium, strontium, barium, and magnesium (4).[2] On the basis of work of this kind, Davy advanced the hypothesis that electrical attractions are responsible for the formation of chemical compounds. In this he was quite right, although the situation is much more complicated than he thought.

In 1808 Davy brought together two carbon rods, which were connected to the poles of a battery, and produced a brilliant arc (5). This can be said to be the first lamp powered by electricity, but it was not for another half century that arc lamps could be used for public lighting.

Later, several useful electric cells were devised by John Frederick Daniell (1790–1845), who was professor of chemistry at King's College, London. One of Daniell's cells (6), constructed in 1836, consisted of an outer vessel containing copper sulphate solution, inside which was an ox-gullet bag containing a rod of amalgamated zinc in dilute sulphuric acid. It produced about 1.1 V. In a later modification the ox gullet was replaced by a porous pot that contained the acid and the zinc electrode (7). In 1839 he put together a battery of 70 of his cells and produced a brilliant electric arc, which caused some skin blistering and some eye injury to himself and others (8).

William Robert Grove (1811–1896) also devised some useful electric cells. In 1838, when a professor at the London Institution, he devised a cell consisting of zinc in sulphuric acid and platinum in nitric acid, the two liquids being separated by porous material (9). This cell produced 1.8–2.0 V (greater than that given by Daniell's cells). A little later he described what he called a *gas voltaic battery*, consisting of platinum electrodes immersed in acid solution, with hydrogen bubbled over one electrode and oxygen over the other (10).[3] The source of the voltage is the energy released by the combination of the two gases. Later Grove used other combinations of gases, such as hydrogen and chlorine, and oxygen and carbon monoxide. Cells of this type are today called *fuel cells,* and they are still the subject of much research to make them more effective for commercial use.

The electrical euphoria

The invention of batteries for the generation of current electricity led in the early 19th century to what has been called an electrical euphoria. After electric motors had been invented in the early 1830s the idea became prevalent that one could run a motor by a battery, and gain an unlimited amount of energy (although the actual word energy was rarely used at that time). One of the enthusiastic proponents of this point of view was Moritz Hermann von Jacobi (1801–1874), whose work was done first at Dorpat, which was then in Russia (it is now called Tartu and is in Estonia), and then in St. Petersburg. In 1834 von Jacobi constructed an electric motor, and he carried out interesting experiments with it (11). Three years later he published a paper (12) that created something of a sensation. He argued that if certain imperfections of the electric motor, such as friction and what is now called back-emf, could be eliminated, a motor would go on accelerating indefinitely, producing enormous amounts of power — all at no cost! These arguments seemed compelling at the time, and many electric motors were built in order to take advantage of what seemed a utopian opportunity.

It was James Prescott Joule (1818–1899), an amateur scientist living in Manchester, who first pricked the bubble, showing that one could not get something for nothing by using a battery to operate a motor. He began his investigations at the age of 19, and at first he too was carried away by the electrical euphoria. In 1840 he made careful experiments on the mechanical effect that could be obtained from a motor, and related it to the amounts of metal used up in the battery operating the motor (13). He was disappointed to find that the consumption of a given amount of zinc in a battery of the Daniell type led to the production of only about one-fifth of the mechanical work that would be produced by the same weight of coal in a steam engine. Since zinc was much more expensive than coal, it followed that an electric motor would be far from being a competitor to a steam engine for the primary production of energy. For Joule, the electrical euphoria was over.

Joule then decided to study the heating effect of an electric current. Using simple equipment, but working with great care, he established that a current passing through a wire of resistance r generates heat in proportion to r, and in proportion to i^2, the square of the current passing; this is his well-known i^2r law (14). He also concluded that the heat produced is equal to the energy released by the chemical action occurring in the battery. Although this conclusion had later to be modified (to

[2] This was Davy's Bakerian Lecture, delivered on 20 November 1806.

[3] Reference 10 gives only a brief preliminary account of the gas battery; further details are in papers that appeared in 1842, 1843, and 1845.

Can. J. Chem. Downloaded from www.nrcresearchpress.com by 91.121.58.235 on 09/08/12
For personal use only.

© 1997 NRC Canada

take into account entropy changes as well as energy changes), it was important in confirming that, contrary to von Jacobi's prediction, energy could not be created from nothing. With regard to the applications of electricity to practical use, Joule wrote that "electricity is a grand agent for carrying, arranging and converting chemical heat." This was indeed a shrewd prophesy.

In 1843 Joule carried out an investigation that is remarkable for its ingenuity. He enclosed the revolving part ("armature") of an electric generator (sometimes later called a "dynamo") in a vessel containing water, and determined the heat generated when he rotated the armature for a fixed period of time (15). He also measured the heat produced by the current that was generated. In this way he established the equivalence between the heat produced as a result of rotating the armature, and the mechanical work required for the rotation.

As is well known, Joule carried out a great many other investigations that led firmly to the law of conservation of energy, also known as the first law of thermodynamics. Modern textbooks tend to stress the investigations Joule made in which he generated heat in liquids by the use of large paddles. It is important to recognize, however, that it was his work on batteries and electric motors that first set him on the right track.

Joule also made progress towards establishing the general thermodynamic relationships involved in electrical batteries. He was not, however, completely successful, since the concept of entropy had not yet been introduced, and he necessarily neglected its role. Correct treatments of the thermodynamics of electric cells were first worked out by Hermann von Helmholtz (1821–1894) and further developed by Walther Nernst (1864–1941).

Electromagnetism

Twenty years after the discoveries of current electricity and of electrolysis there was another discovery that had momentous consequences. This was Oersted's discovery of electromagnetism,[4] which showed for the first time that there was an important relationship between electricity and magnetism. Early in 1820 Hans Christian Oersted (1777–1851), professor of physics at the University of Copenhagen, brought a compass needle near to a wire connected to the poles of a battery and found that the needle tended to turn. When the direction of the current was reversed, the needle turned in the opposite direction.

There are three unusual features of this discovery. In the first place, it was made in front of a class of students. Oersted and his assistant had set up the experiment but had no time to try it out before the students arrived. Oersted first decided to defer the experiment until later, but during the lecture he began to feel confident that it would work, and performed it successfully. The second remarkable feature is that, since the deflection of the needle had been small, Oersted was so little impressed by the result that he performed no further experiments on the subject for 3 months.

The third remarkable feature was that the compass needle turned in an unexpected direction; the poles of the magnet were not attracted or repelled by the current, but moved in a direction at right angles to the expected direction. At the time, in the scientific tradition established in particular by Newton, theories were formulated in terms of so-called central forces acting in straight lines between points; these forces were believed to follow Coulomb's law, the force being inversely proportional to the square of the distance between the points. The fact that the magnetized needle was subjected to a deflecting force (i.e., it moved in a sideways direction) was therefore particularly surprising. It suggested a force not acting in a straight line but circularly, which most scientists thought to be impossible. However, within a short time many investigators had confirmed the experimental result obtained by Oersted. In particular, the distinguished scientific statesman François Arago (1786–1853), at first sceptical, himself repeated Oersted's experiment, and called attention to the discovery at a meeting of the Académie des Sciences in Paris on 4 September 1820.

The French physicist André Marie Ampère (1775–1836) was in the audience at that meeting, and heard Arago announce Oersted's discovery. He had not worked previously on electricity, but within a week had made careful quantitative experiments and formulated a mathematical treatment. As early as 18 and 25 September 1820 he gave verbal reports to the Académie, confirming Oersted's results and presenting some significant additional experimental results he had obtained himself (17).[5] He also explained a hypothesis he had formulated on the relationship between electricity and magnetism. His work during the next few years gave strong support to the conclusions he had reached so quickly. The *Mémoire* (18) published on the subject by Ampère in 1823 is still regarded as a masterpiece; Clerk Maxwell later described it as "perfect in form and unassailable in accuracy" (19). It is appropriate that the unit of electric current is called the ampere; it is one of the base units in the Système Internationale d'Unités (SI).

Ampère's detailed mathematical treatment of the interactions was based on the assumption that current-carrying elements of the wires interacted with one another according to the inverse square law. By adding up (by integration) the effects of all the elements, he arrived at expressions that were consistent with the experimental results. His treatment was very impressive, and Clerk Maxwell in his *Treatise on Electricity and Magnetism* (19) referred to Ampère as the "Newton of electricity." There is something of an irony about this, because Maxwell's own work caused the later development of the theory of electromagnetism to follow a completely different path. Ampère nevertheless deserves great credit for his experimental and theoretical work, since it played a significant part in the later developments of the subject.

To explain the effect of an electric current on a magnet, Ampère supposed that magnetism arises from electricity moving in circular orbits round the axis of the magnet; that is, the planes of the orbits are at right angles to the magnetic axis. He coined the word *solenoid* to refer to a current moving in a

[4] H.C. Oersted wrote a four-page note in Latin, and sent it on 21 July 1820 to a number of scientific journals in different countries; announcements of the discovery then appeared in various languages; for example, see ref. 16.

[5] This paper was received on 4 December 1820, and there were a number of papers later on the same theme.

Can. J. Chem. Downloaded from www.nrcresearchpress.com by 91.121.58.235 on 09/08/12
For personal use only.

© 1997 NRC Canada

Can. J. Chem. Downloaded from www.nrcresearchpress.com by 91.121.58.235 on 09/08/12
For personal use only.

Fig. 3. A daguerreotype of Michael Faraday (1791–1865), taken by Antoine Claudet (1797–1867) in the early or mid 1840s.



small circuit and creating a magnet. He carried out experiments with solenoids in which wires were wound around glass tubes, and confirmed that when a current passed, a magnetic effect was obtained. He then developed an elegant mathematical treatment of the interactions between electric currents and the circular currents around the magnets, and was able to explain Oersted's results in terms of central forces.

Ampère's work was at once recognised by most investigators as an achievement of great significance, but a few objections were raised. It was pointed out that there was no experimental evidence for a flow of electricity round magnets, and no suggestion as to how it could arise. Volta had found that a current results when two dissimilar metals are present, but not if only one metal is present. Ampère later modified his theory to relate to the molecules in the magnets, suggesting that perpetual electric currents moved in orbits around them (we know today, of course, that electrons do move in orbits about the nuclei of atoms).

Faraday's scepticism

Michael Faraday (1791–1867; Fig. 3) was particularly unhappy with what Ampère had done. He knew little mathematics, and was ill-versed in physical theories: he simply could not understand the treatment. He was quite content to think of a circular force arising from a current flowing in a wire. Hardly anyone brought up on the physics of the time could accept such an idea, and yet it was the origin of Faraday's important concept of the electromagnetic field, which was to be the core of the later, more advanced, ideas of Faraday himself and of Clerk Maxwell.

In late 1820, prodded by his friend Richard Phillips, an editor of the *Philosophical Magazine*, Faraday somewhat reluctantly began to investigate electromagnetism. His reluctance was partly because he was employed at the Royal Institution as a chemist, and not as a physicist, and all his previous work had been in chemistry (he was later, in 1832, appointed professor of *chemistry* at the Institution). At the time, however, the distinctions between the sciences were fainter than today, and no one at the Institution seems to have objected to the fact that Faraday's subsequent work was more in physics than in chemistry.

Faraday at once repeated Oersted's experiments, and noticed that when a small magnetic needle was moved round a wire carrying a current, one of the poles turned in a circle. He then speculated that a single magnetic pole, if it could exist, would move continuously around a wire as long as the current flowed. This led him to perform an experiment of great simplicity, and also of great importance. In 1821 he attached a magnet upright to the bottom of a deep basin, and then filled the basin with mercury so that only the pole of the magnet was above the surface. A wire free to move was attached above the bowl and dipped into the mercury. When Faraday passed a current through the wire and the magnet, the wire continuously rotated around the magnet (20). In an adaptation of the experiment he caused the magnet to rotate around the wire. He also succeeded in rotating a wire by use of the magnetism of the earth. The great practical significance of these simple demonstrations is that electrical energy was being converted into mechanical energy for the first time. Faraday had anticipated the electric motor by about 10 years.

The experiment also had a great theoretical significance, at first appreciated only by Faraday, but later by the world of science. Faraday's conclusion was that there were circular *lines of force* round the current-carrying wire, and he accepted this as a simple experimental fact. Almost everyone else at first ridiculed this suggestion, and concluded that the force could not be simple, but must be explained in some way in terms of central forces, as had been done successfully by Ampère. For the next 10 years Faraday worked only sporadically on electricity, but quietly maintained his unconventional ideas about electromagnetism.

In 1831 Michael Faraday made one of his most famous discoveries, *electromagnetic induction*. From time to time he had experimented with the idea in his mind that a wire bearing a current might induce a current in a nearby wire. Until 29 August 1831, however, he always failed to find any effect. On that day he wound one side of a soft-iron ring with insulated wire, and arranged a secondary winding, connected to a galvanometer, around the other side. At first he thought that the experiment was again a failure. He noticed, however, that when he *turned off* the electric current in the primary coil, believing the experiment to have failed, the galvanometer revealed a sudden short flow in the secondary circuit. Closer investigation showed that a *continuous* current in the primary circuit had no effect; it was only when the current was started or stopped that there was an effect on the galvanometer (21).

Soon after his discovery of electromagnetic induction in 1831, Faraday demonstrated that if he pushed a magnet into a coil of wire, a transient current was produced (22). A current was generated in the opposite direction when the magnet was withdrawn. No current passed when the magnet was station-

© 1997 NRC Canada

Can. J. Chem. Downloaded from www.nrcresearchpress.com by 91.121.58.235 on 09/08/12
For personal use only.

ary; to generate a current the magnet must be moved in relation to the coil. The important point is that electromagnetic induction only occurs if there is a *change* in an electric current or if a magnet is *moved*.

Faraday's laws of electrolysis

Soon after Faraday carried out these experiments, which supported his unconventional ideas about the nature of an electric current, he began to devote much attention to the electrolysis of water. In 1833 he showed (23) that electrolysis can be brought about by electricities produced in a variety of ways, such as from electrostatic generators, voltaic cells, and even electric fish. In particular, he charged two metal spheres with static electricity and brought them close to one another in the neighbourhood of a solution; the passage of the discharge through the solution brought about electrolysis, even though no wires had been introduced into it. An extremely powerful electrostatic field, however, would not in itself bring about electrolysis (which it would be expected to do if central forces were involved); a current or an electric discharge must pass through the solution.

Besides being important to Faraday's investigations of electrolysis, these results for the first time clarified the relationship between static and current electricity, a matter that had never been properly understood. They are essentially the same, but exist under different circumstances. With static electricity the quantities of electricity are usually small, but enormous potential differences may exist. With current electricity, the potential differences are usually smaller, but the quantities are larger.

Experiments done by Faraday in 1834 (24) finally convinced him that if electrolysis is brought about by inserting wires into a solution, and then a current is passed, the effect cannot be explained in terms of action at a distance. He performed one experiment in which two solutions were separated from one another by a 70 ft string soaked in brine. Gases were evolved at the two wires, and Faraday thought it impossible that the inverse square law could explain an effect extending over such a distance. He also showed that the effects of electrolysis do not follow straight lines, which they would do if there were action at a distance. Also, Faraday argued, if a substance were attracted to a wire by the inverse square law, would it not remain bound to the wire rather than being released from it?

Faraday's conclusion that action at a distance does not apply led him to dislike the word *pole* that had come to be used in connection with electrolysis, since he felt that it implied a centre of force. In its place, at the suggestion of his friend and personal physician Whitlock Nicholl (1786–1838), he introduced the word *electrode*, from the Greek ελεκτρων (electron) and όδος (hodos), meaning "way." Nicholl also suggested the word *electrolysis*, from λυσις (lysis), meaning "splitting," and also the word *electrolyte*, to mean something that undergoes electrolysis.

For other help with words, in 1834 Faraday approached William Whewell of Trinity College, Cambridge, who had shown much interest in Faraday's research. The details of the discussions with Whewell are of great interest, but since they have been presented in detail (25, 26) they will be given here only in outline. In 1834 Faraday asked Whewell for words that would refer to the regions of solution present at the surfaces of the positive and negative electrodes. Whewell suggested the words *anode* and *cathode*, and for species present in solution he suggested *anion, cation*, and *ion*; Faraday made good use of the words cation and anion, but regarded them as always transient species. He commented to Whewell that he thought he would find little use for the word ion. Now that it is known (which Faraday did not know) that ions do exist in solution, the word has found a wide use.

As Faraday proceeded with his investigations into electrolysis he came to view the process as follows. He considered that the electrical effect is transmitted from molecule to molecule, and that the affinities of the components of water, or of a dissolved salt, are weakened, so that each component would be able to leave its partner and jump to another close by.

In 1834 Faraday suggested, on the basis of these ideas, two fundamental laws of electrolysis (27). It is often thought that he discovered these two laws empirically, but this is not the case; they were deduced by him on the basis of his ideas about how electricity interacts with a solution. He later confirmed them by experiment. If electrolysis had proceeded by action at a distance, as had been thought previously, the amount of material deposited or evolved would have depended on the electric potential and on the size of the vessel used. According to Faraday's ideas, however, the amount would depend only on the product of the current and the time, i.e., on the *quantity* of electricity that passes through the solution, and Faraday confirmed that this is the case; this was his *first law of electrolysis*. And since, in Faraday's view, the electricity was concerned with weakening the affinities between the constituents of matter, the amount should depend on the equivalent weight of the substance evolved or deposited. This is his *second law of electrolysis*. Faraday never expressed the second law in quite this form, but his experiments showed this law to be obeyed.

It is somewhat ironic that Faraday should have deduced his laws of electrolysis on the basis of ideas that we now know to be not entirely correct. The effect of the current is not to *bring about* dissociation, as Faraday thought; instead, the ions are *already present* and the electric field brings about their movement towards the electrodes, where they are neutralized. The relationship between the quantity of electricity and the amount of material deposited or evolved arises not because the electricity is concerned with dissociation, but because it is concerned with the neutralization of ions that are already present. This, however, did not matter as far as Faraday's conclusion was concerned.

Faraday's laws of electrolysis were of great theoretical significance, since they suggested that electricity itself is not continuous, and that fundamental particles of electricity are in some way associated with atoms. In one of his later papers on electrolysis (28) Faraday wrote:

> ...if we adopt the atomic theory or phraseology, then the atoms of bodies which are equivalent to each other in their ordinary chemical action, have equal quantities of electricity naturally associated with them.

However, Faraday was always rather reticent in referring to atoms, preferring the idea that electricity is a fluid. It was left to others, notably von Helmholtz and Johnstone Stoney, to develop the idea of a fundamental unit of electricity.

© 1997 NRC Canada

Can. J. Chem. Downloaded from www.nrcresearchpress.com by 91.121.58.235 on 09/08/12
For personal use only.

Electrolytic dissociation

It was not until later in the 19th century that much thought was given to the existence of independent ions in solution. Although Faraday had used the words cation and anion since 1834, he thought that they only existed in close association with ions of opposite sign. When he spoke of the movement of cations and anions through a solution, he was thinking of them as formed only transiently when the current flowed. His assumption was that, for example, sodium chloride molecules are present intact in solution, and he explained electrolysis in terms of the dissociation of salt molecules by the action of the electric current. It is true that von Grotthuss, in 1808, had given a diagram showing independent ions (Fig. 2), and that similar diagrams had been presented by Daniell and Miller (29) and by Hittorf (30). But these diagrams had been thought to be purely schematic, intended to help the understanding of what occurs during the passage of electricity through a conducting solution.

The first modification to this point of view was put forward in 1857 by Rudolph Julius Emmanuel Clausius (1822–1888), who was then at the Polytechnicum in Zürich. Clausius (31) found that Ohm's law was accurately obeyed in measurements of conductivities of solutions; i.e., the current is proportional to the electromotive force. This result presented difficulties for the idea that the electric current has to perform the work of splitting molecules into ions. He suggested that a small number of ions are always present as a result of collisions between solvent and solute molecules, some of the collisions being sufficiently energetic to cause dissociation into ions. The movement of these ions would provide the transport of charge when a current was passed.[6]

In 1853 Johann Wilhelm Hittorf (1824–1914) began work on conductivity at the Royal Academy of Münster. At first he followed Faraday's ideas as to the nature of the process, but after the appearance of Clausius's 1857 paper he accepted the idea that a small number of free ions are always present. He made measurements of the concentration changes in the neighbourhood of the two electrodes when the current is passed, and measured the relative speeds with which ions moved through solutions (32).

Further significant experimental advances were made in the 1860s and 1870s by Friedrich Wilhelm Georg Kohlrausch (1840–1910). In Göttingen, Zürich, and Würzburg he carried out extensive studies, using novel techniques, on the conductivities of electrolytes (33). He too was impressed by the fact that Ohm's law was accurately obeyed, and, like Clausius, he assumed that free ions were always present in small amounts.

In 1874 Kohlrausch and Otto Natalis August Grotrian (1847–1921) found evidence for the law of independent migration of ions (34). They were also able to deduce the speeds with which various ions move under a unit potential gradient. Other important measurements of ionic speeds were also made by Oliver Joseph Lodge (1851–1940), who followed the ions as they moved through a gel coloured by an indicator sensitive to acid. This so-called moving-boundary method was also used by William Cecil Dampier Whetham (later known as Sir William Dampier, 1867–1952), who studied the movement of neutral ions by observing their motion in coloured salts or by the formation of precipitates.

A great advance, the theory of electrolytic dissociation, was made by Svante August Arrhenius (1859–1927) in 1889. The details are so well known[7] that only brief comments need be made here. According to Arrhenius, there exists an equilibrium in solution between undissociated molecules AB and the ions A^+ and B^-:

$$AB \rightleftharpoons A^+ + B^-$$

This proposal was significantly different from the previous idea that only trace amounts of ions are present at all times. Arrhenius proposed that the ions are always present, sometimes in substantial amounts, in equilibrium with the undissociated molecules, and that the effect of an applied voltage is not to produce them but to cause them to move through the solution.

This theory was quickly accepted by many prominent scientists, including van't Hoff, Ostwald, and Nernst. There was also much opposition to the theory. A particularly vigorous critic was Henry Edward Armstrong (1848–1937), a distinguished organic chemist who also did a considerable amount of work in electrochemistry. He was particularly outspoken on the subject of the Arrhenius theory and even lampooned the idea of ionic dissociation in two ironic fairy tales, *A Dream of Fair Hydrone* and *The Thirst of Salt Water*.

The essence of the criticisms of electrolytic dissociation was that the theory assumed that the solvent was playing only a passive role; in Armstrong's words, "the solvent was merely a dance floor for ions," as far as the theory was concerned. Armstrong, incidentally, was quite beside himself when Laurence Bragg (35, 36) insisted that in solid sodium chloride no molecules of NaCl are present, but only the ions Na^+ and Cl^-. Armstrong published a Letter in *Nature* (37)[8] ridiculing the idea (which of course was perfectly correct).

There was indeed some substance to the criticisms, in that the Arrhenius theory did seem to imply that dissociation into ions was a result merely of the high dielectric constant of a solvent such as water, and that chemical interactions were unimportant. The remedy, however, was not to overturn the theory, but to modify it.

An important advance (38) was made in 1894 by Walter Nernst (1864–1941) and Paul Karl Ludwig Drude (1863–1906), who treated the binding of ions to water molecules, a process they referred to as *electrostriction*. This idea answered the criticisms that the role of the solvent was being ignored, and led to a wider acceptance of Arrhenius's ideas. During the early years of his career Nernst made many outstanding contributions to electrochemistry, particularly to the thermody-

[6] The idea that ions exist free in solution is sometimes referred to as the Williamson–Clausius hypothesis, but this expression does not seem justified. In papers in 1851 and 1852 the British chemist Alexander William Williamson (1824–1904) suggested the dissociation of substances, but not into charged species, and his proposal was in no way related to the conductances of solutions.

[7] See ref. 26, pp. 209–218.

[8] This letter refers to a statement by Bragg in ref. 35; the work had been done 14 years previously, but Armstrong had not realized its significance!

© 1997 NRC Canada

Can. J. Chem. Downloaded from www.nrcresearchpress.com by 91.121.58.235 on 09/08/12
For personal use only.

namics of electrochemical cells, and to the theory of the behaviour of ions at interfaces.

In spite of developments such as these, the opposition to the theory of electrolytic dissociation lasted in some quarters even until the 1930s. As late as that, for example, Louis Kahlenberg (1870–1941) was still giving, at the University of Wisconsin, a course on electrochemistry that took no account of the existence of ions in solution. Some confusion arose from the fact that strong electrolytes are completely dissociated, and that their conductivity behaviour has to be interpreted in terms of the interactions betweeen ions (the Debye–Hückel theory). Arrhenius himself, to the day of his death, never accepted that this is the case.

The speed of an electric current

The question of the speed with which an electric current travels along a metal wire turned out to be a matter of special significance. The realization that this speed is the same as the speed of light was a determining factor in leading Clerk Maxwell to his theory of electromagnetic radiation.

The speed of a current can be obtained indirectly by comparing electrical results expressed in the two different sets of units, electrostatic and electromagnetic. The electrostatic units are particularly appropriate to static electricity, and relate the force of attraction and repulsion between two charged bodies to the quantities of electricity that they hold. The electromagnetic units, on the other hand, relate force to electric current. The quantity of electricity residing on a wire at a given time depends on the speed with which the current travels along the wire. It can be shown that the ratio of the value of an electrical quantity expressed in electromagnetic units to that expressed in electrostatic units is the speed with which the current travels.

Several investigations made in the midde of the 19th century showed the speed of light to be about 3×10^8 m s^{-1}. In 1856–1857 the German physicists Wilhelm Edouard Weber (1804–1891) and Rudolph Herrmann Arndt Kohlrausch[9] (1809–1858) made a careful measurement of an electric charge, first in one set of units and then in the other (39, 40). When they divided one value by the other they obtained a velocity that was very similar to the speed of light. Similar investigations (41) were carried out at about the same time by Gustav Robert Kirchhoff (1824–1887). Both sets of investigators concluded that a current travels along perfectly conducting material with the speed of light.

A little later Clerk Maxwell carried out similar experimental investigations, and obtained the same result (42). He also used an alternative procedure, comparing the electrical quantity now called the *permittivity* of a vacuum, ε_0, with the magnetic quantity now called the *permeability* of a vacuum, η_0. Maxwell's mathematical treatment of Faraday's lines of force led to the conclusion that the speed v of an advancing electromagnetic field was given by

$$[1] \quad v = (\eta_0 \varepsilon_0)^{-1/2}$$

The two quantities had been measured by a number of people, and this expression also led to the result that v was the speed of light. These investigations of Clerk Maxwell were of great significance, since they led him to his great contribution, the theory of electromagnetic radiation.

A significant aspect of these investigations was that they led to a decision between the two alternative theories of electricity that were held at the time. One theory was that there were two electrical fluids, positive and negative, which moved in opposite directions when a current flowed. Use of the method of comparison of units led to the conclusion that if there were two fluids they would each flow with half the speed of light. The evidence thus supports the theory (which Benjamin Franklin, among others, had advocated a century earlier) that only one type of electricity flows along a wire when a current passes.

The fundamental particle of electricity

Faraday's laws of electrolysis, and other investigations, pointed to the fact that there is a fundamental particle of electricity that plays an essential role. A specific idea about such a particle of electricity was advanced (43) in 1874[10] by George Johnstone Stoney (1826–1911), an Irish physicist who did much of his scientific work in London. He based his conclusion on the value of the Faraday constant, which relates the amount of substance deposited in an electrolysis to the amount of electricity passed through the system. His reasoning led to the conclusion that if the charge on this particle is the same as that on a hydrogen ion (although of opposite sign), its mass must be about 1/2000 that of the hydrogen atom.

In 1891 Johnstone Stoney even went so far as to suggest that the negative particles move in orbits within the atoms (44). He tried to develop this idea into detailed explanations of the spectra of atoms and molecules, but since essential theories (particularly the quantum theory) were still to come, these were inevitably in disagreement with experiment. For this reason his idea did not receive much attention, although we now know that it was essentially correct. Stoney suggested that the unit of negative electricity should be called an *electron*.

The actual discovery of the electron can be said to have occurred in 1897, when Joseph John Thomson (1856–1940), Cavendish professor at Cambridge, announced his conclusion that the negative particles present in a cathode-ray discharge have a mass about 2000 times smaller than that of a hydrogen atom. These were obviously the electrons that Johnstone Stoney had predicted.

By the end of the 19th century the conclusion had therefore been reached that electrons play the important role in electricity. With static electricity, a body that has a positive charge has a deficit of electrons; one that is negative has an excess of electrons. The transfer of a charge is a movement of electrons.

In current electricity, the current is carried through solids by a flow of electrons. During recent years there have been great advances in the understanding of the structures of solids. It is known that in metals at the absolute zero the electrons fill a number of quantized energy levels up to a particular level

[9] R.H.A. Kohlrausch was the father of Friedrich Wilhelm Georg Kohlrausch (1840–1910), who is well known to electrochemists for his accurate measurements of the conductivities of solutions (refs. 33, 34).

[10] Stoney had presented his ideas at the 1874 meeting of the British Association, but they were not published until 1881.

© 1997 NRC Canada

known as the *Fermi level*. At higher temperatures electrons pass into higher levels and they are then in what is called the *conduction band*. The electrons can easily pass along this conduction band. Other solids are poor conductors, and some are superconductors at lower temperatures. Detailed treatments are to be found in books on the theory of the solid state, and are beyond the scope of the present article.

In an electrolytic cell, the electrons are not the carriers of the current; instead it is carried through the cell by the ions. The electrons are involved in the neutralization of ions at the electrodes.

When electrolysis occurs, the flow of the electrons through the metal wires and the movement of the ions in the solution, are not the only factors to be considered. There is also the important matter of the electrode processes. If, for example, hydrogen gas is being evolved at an electrode, there is a question of exactly how the hydrogen ions in the solution are discharged, and how they become hydrogen molecules. The hydrogen ions must first pass through a layer (the "double layer") at the electrode surface, and this layer has different properties from the bulk of the solution. When the hydrogen ions reach the surface there may be an electron transfer from the Fermi level at the surface to the ion, with the formation of a hydrogen atom. Two hydrogen atoms can then recombine to form a hydrogen molecule. Several processes take place, and the rate with which the current flows depends on the rates of these processes. One of these processes may be slower than the others, and therefore controls the rate of deposition. Usually these electrode processes are slower than the movement of the ions through the solution, and therefore control the rate with which the current passes.

The mechanisms of surface processes are complicated, and are still being actively investigated. Only a very brief summary can be given here.

The kinetics of electrode processes

It was not until the early years of the 19th century that the time was ripe for study of the electrode processes occurring during an electrolysis, or during the operation of an electrochemical cell. The first significant work along these lines was done by Julius Tafel (1862–1918; Fig. 4) at the University of Würzburg. Tafel was primarily an organic chemist; he had been an assistant to Emil Fischer and was active in the field of preparative electro-organic chemistry, which was a popular field in the late 19th century.

In the early 1900s Tafel investigated the electrolysis of solutions in which hydrogen gas is evolved at the negative electrode. By that time it had been realized that in order for electrolysis to proceed at an appreciable rate, the voltage applied must be greater than a certain equilibrium or reversible voltage; the additional voltage is called the *overvoltage*. The overvoltage η is thus defined as

$$[2] \quad \eta = V - V_{rev}$$

where V is the potential at which electrolysis is actually proceeding, and V_{rev} is the reversible potential under the same conditions.

At the equilibrium or reversible voltage the rate of deposition of ions on an electrode is equal to the rate of reionization of the deposited substance; the net rate of deposition is therefore zero. When the additional voltage (the overvoltage) is applied, the rate of deposition is increased, and the rate of the reverse reaction is decreased; there is then net deposition. The greater the overvoltage, the greater the current. One of Tafel's important contributions (45) was to obtain an empirical expression for the relationship between the overvoltage η and the current density i (the current per unit area of electrode):

$$[3] \quad \eta = a + b \ln i$$

This equation, fundamental to the study of the kinetics of electrode processes, has come to be called the *Tafel equation*.

The overvoltage varies considerably with the nature of the electrodes. Electrodes consisting of "platinized platinum," which is platinum electrodeposited with a layer of platinum black, have a fairly low overvoltage for the evolution of hydrogen and oxygen gases in the electrolysis of water. For electrolysis to occur, the voltage that has to be applied to an aqueous solution of an acid or a base when platinized platinum electrodes are used is about 1.7 V. With zinc, on the other hand, the overvoltage is higher, and a potential of about 2.4 V has to be applied in order to have an appreciable evolution of gases.

It took a number of years for the significance of the Tafel equation to be understood in terms of theories of overvoltage. In 1930 Erdey-Gruz and Max Volmer (1885–1965) gave kinetic equations for the rates of the electrode processes occurring in forward and reverse directions (46): when the cell is operating reversibly these rates are equal, but when a current flows the rate in one direction is not exactly balanced by the rate in the other, and there is then an overvoltage. Erdey-Gruz and Volmer based their treatment on the fact that,

Fig. 4. Julius Tafel (1862–1918). (Photograph courtesy of the Institüt für Organische Chemie der Universität Würzburg.)



Can. J. Chem. Downloaded from www.nrcresearchpress.com by 91.121.58.235 on 09/08/12
For personal use only.

© 1997 NRC Canada

Can. J. Chem. Downloaded from www.nrcresearchpress.com by 91.121.58.235 on 09/08/12
For personal use only.

according to the Arrhenius equation for reaction rates, the rate of a reaction is related exponentially to the height E of the energy barrier for the reaction (the activation energy). They also recognized that when there is an overvoltage η, the contribution of the electrical energy to the energy change in the overall reaction is ηF, where F is the Faraday constant. However, only a fraction of this enters into the activation energy for the forward reaction. If the fraction is α, the energy of activation for the forward reaction is therefore lowered by $\alpha\eta F$. For the reverse reaction the fraction $1 - \alpha$ of the electrical energy causes the activation energy to increase by $(1 - \alpha)\eta F$. The current that passes is proportional to the net rate of reaction, and the resulting rate equation is therefore of the form

$$[4] \quad i = i_0(e^{\alpha\eta F/RT} - e^{-(1-\alpha)\eta F})$$

The overvoltage has thus increased the rate of the forward reaction and decreased that of the reverse reaction. When the overvoltage is zero the two exponential terms are zero, and no current flows. When the overvoltage is large the second exponential approaches zero, so that the equation becomes

$$[5] \quad i = i_0 e^{\alpha\eta F/RT}$$

which can be written as

$$[6] \quad \eta = -\frac{RT}{\alpha F}\ln i_0 + \frac{RT}{\alpha F}\ln i$$

This is of the same form as the empirical Tafel equation [3], so that the empirical b in that equation is given by $RT/\alpha F$.

In the early 1930s Ronald Wilfred Gurney (1898–1953), then at the University of Manchester, published an important theoretical treatment of the electrolytic evolution of hydrogen gas from an acidified solution (47, 48). In 1932 Ralph Howard Fowler (1889–1944), with whom Gurney had worked at Cambridge, gave a similar theoretical discussion (49). These treatments dealt with the transfer of a proton from H_3O^+ in solution to the surface of the metal electrode, taking into account hydration effects but not considering the possible adsorption of hydrogen atoms at the surface. Account was taken of the distribution of energy of the electrons in the metal (in modern terms, of the Fermi levels) and of the energy levels in the H_3O^+ ion. An important feature of Gurney's treatment is that he suggested, for the first time for any process, that there might be quantum-mechanical tunnelling through the energy barrier. His idea was that the rate is controlled by the transfer of electrons and that these might not have to surmount the barrier but could tunnel through it, a possibility not permitted in classical mechanics.

The Gurney–Fowler treatment of electrode processes was extended in various ways. In 1934 Bawn and Ogden, at the University of Manchester, presented a quantum-mechanical treatment of the transfer of a *proton* (rather than an electron, as in Gurney's treatment) at the surface of an electrode (50). An important feature of their work was that they postulated that the transfer of a proton can also occur by quantum-mechanical tunnelling. However, as will be seen in more detail later, careful studies by Brian Conway and others have not yet revealed any positive evidence for quantum-mechanical tunnelling in any electrode process.

In 1936 John Alfred Valentine Butler (1899–1977), then at the University College of Swansea, gave a treatment in which he took account, in addition, of adsorption (e.g., of hydrogen atoms) at the surface of the electrode (51, 52). When adsorption was neglected, as in Gurney's treatment, the predicted activation energies for the discharge of a proton were much higher than the experimental values and were independent of the nature of the surface. Better agreement was found when adsorption was taken into account, and Butler was able to explain the substantial differences in activation energy for nickel and mercury surfaces.

In 1939, an interpretation of electrode processes was given by Eyring, Glasstone, and Laidler on the basis of potential-energy surfaces and transition-state theory (53, 54). The resulting equation is of the form

$$[7] \quad i = A\exp(-\Delta^{\ddagger}G^0/RT)\exp(\alpha\eta F/RT)$$

where $\Delta^{\ddagger}G^0$ is the Gibbs energy of activation. The constant A can be expressed in terms of fundamental constants, and also involves the concentration of species involved in the reaction that controls the rate and therefore the current.

The significance of the fraction α that appears in these equations has been much discussed, and is a little complicated. It depends on the rate-controlling process, and the form of the potential-energy surface for that process. If the rate-controlling step is proton transfer and the energy barrier is a symmetrical one, the value of α (which can be obtained experimentally from the Tafel factor b, which is $RT/\alpha F$) will be 0.5. Conway and Salomon (55), and others, have pointed out that the constancy of the α values in electrochemical reactions provides excellent examples of the Brønsted relationships (linear free-energy relationships) that apply to many chemical reactions.

If, on the other hand, the slow step in the process of hydrogen evolution is the combination of hydrogen atoms at the surface, it can be shown that the Tafel b is $RT/2F$, so that α is equal to 2. This has sometimes been observed experimentally.

The Gibbs energy of activation can be expressed in terms of the entropy of activation $\Delta^{\ddagger}S^0$ and the enthalpy of activation $\Delta^{\ddagger}H^0$, and eq. [7] becomes

$$[8] \quad i = A\exp(\Delta^{\ddagger}S^0/R)\exp(-\Delta^{\ddagger}H^0/RT)\exp(\alpha\eta F/RT)$$

Much work has been concerned with the nature of the rate-controlling step when hydrogen gas is evolved at an electrode. Work by the Russian electrochemist Alexander Naimovitch Frumkin (1895–1976) showed that under certain circumstances the overvoltage passes through a minimum when the pH of the solution is varied (56). This suggests that in acid solution the slow step is the transfer of a proton from the solution to the surface, where it is neutralized. In alkaline solution, however, the hydrated protons are present only at low concentrations, and the slow step is then the transfer of a proton from a water molecule. As already mentioned, the slow step is sometimes the combination of hydrogen atoms.

Ionic solvation and double layers

The processes that occur at electrode surfaces during electrolysis or the operation of an electrochemical cell are greatly

© 1997 NRC Canada

Can. J. Chem. Downloaded from www.nrcresearchpress.com by 91.121.58.235 on 09/08/12
For personal use only.

influenced by two factors: the solvation of the ions involved, and the structure of the thin layer that is present at the electrode, and which differs in properties from the bulk solution.

Mention has been made of the work of Drude and Nernst (38) on the solvation of ions, which they called electrostriction. An interesting advance was made in 1920 by the German physicist Max Born (1882–1970), who gave a very simple and useful interpretation of solvation (57). He considered an ion to be a conducting sphere of radius r, carrying a charge ze, where e is the charge on a proton and z is a whole number (for Na^+, for example, $z = +1$; for the sulphate ion SO_4^- $z = -2$). He considered the solvent to be a continuous medium having a dielectric constant of ε. He then derived an expression for the work required to charge a sphere of radius r in a continuum of dielectric constant ε, and found it to be

$$[9] \qquad w = \Delta G = \frac{z^2e^2}{4\pi\varepsilon_0\varepsilon r}$$

where ε_0 is the permittivity of a vacuum. This work is the increase ΔG in Gibbs energy of the ion as it is charged. This expression can easily be extended to give the Gibbs energy of hydration of an ion, i.e., the Gibbs energy change when the ion is transferred from the gas phase to a liquid. Since entropy is the negative of the partial derivative of the Gibbs energy with respect to the temperature, eq. [9] also leads to an expression for the entropy of hydration.

In spite of the simplicity of Born's model, it leads to surprisingly satisfactory results. The Gibbs-energy changes during the hydration of ions do vary more or less linearly with the values of z^2/r for most ions. The expression that eq. [9] leads to for the entropy of hydration of ions is also in reasonably good agreement with experiment.

An obvious weakness of the Born procedure is that it assumed that the effective dielectric constant of the solvent close to an ion is the same as it is in the bulk liquid. Water, for example, has a dielectric constant of about 78, and this high value is due to the extent with which the water molecules can orient with respect to an electric field. At high field strengths, however, the molecules have become fully oriented, and then respond much less to the field. Solvent molecules that are close to an ion are in fact in a very intense field (especially if the ion is small), and become aligned in the field. Since they cannot be oriented further, the effective dielectric constant of the solvent near to an ion is greatly reduced. As a result, the effective dielectric constant of water in the near neighbourhood of a small ion is close to 2, which is characteristic of nonpolar molecules.

In 1957 Laidler and Pegis (58) gave a theoretical treatment of the solvation of simple ions in which they took account of the variation of the dielectric constant with the electric field strength. They found that their treatment gave a significantly better interpretation of the Gibbs energies and entropies of ions than was given by the simple Born equation [9]. In considering chemical reactions beween ions, and processes occurring at electrodes, it is obviously of great importance not to neglect these field effects (59), since in the region in which reaction occurs the ions are close together; the effective dielectric constant is therefore less (in the case of aqueous solutions, about 40 times less) than in the bulk solution.

An alternative procedure, due mainly to H.S. Frank and his co-workers (60, 61), is to take into account the molecular nature of the solvent instead of treating it as a continuous dielectric. The idea is that next to an ion in aqueous solution there is a layer of water molecules that are held fairly tightly, forming a *hydration shell*. Outside this layer there is a *disorder zone*, where the water molecules are arranged in a less orderly fashion than in the bulk solution. This zone arises because of the competition between the electrical forces produced by the ion and the hydrogen-bonding forces resulting from the surrounding water molecules. Quantitative calculations of ionic properties based on this idea (62, 63) have been carried out, with fairly satisfactory results.

Another important matter relating to electrode processes is the nature of the layer of solution next to an electrode, since it is in that layer that the electrode processes occur. It was suggested in 1879 by Helmholtz (64) that any surface can be regarded as bearing a positive or a negative charge, and that in the solution a layer of ions of opposite charge will be attracted to the surface and held to it. This fixed double layer is now often referred to as the *Helmholtz double layer*.

This idea was modified in 1910 (65) by the French physicist Georges Gouy (1854–1926) and in 1913 (66) by the British chemist David Leonard Chapman (1869–1959). They pointed out that the Helmholtz theory is deficient in neglecting the Boltzmann distribution of the ions. They suggested that on the solution side of the interface there is not a simple layer of ions but an ionic distribution that extends some distance from the surface; in other words, there is a *diffuse double layer*. The idea behind the Gouy–Chapman theory is very similar to that in the later Debye–Hückel theory of the ionic atmosphere surrounding an ion. Indeed, Chapman's mathematical treatment in 1913 of the distribution of ions at a surface is essentially a two-dimensional version of the Debye–Hückel theory, which appeared 10 years later.

The Gouy–Chapman theory did not prove entirely satisfactory, and in 1924 a further modification was made (67) by the German physicist Otto Stern (1888–1969). Stern combined the fixed double-layer model of Helmholtz with the diffuse double-layer model of Gouy and Chapman; there is a fixed layer at the surface and also a diffuse layer. To explain certain results, however, it has been found necessary to develop even more elaborate models. For example, Nevill Francis Mott (1905–1994) and J. Watts-Tobin gave in 1961 an important treatment of the double layer in which they took into account charge-dependent orientation of solvent molecules (68).

Brian Conway's electrochemistry

During recent years a number of schools of electrochemistry have made important advances in the understanding of electrode processes, which are the most complex of the processes occurring when an electric current passes through a solution. Among the most prominent workers in the field may be mentioned A.N. Frumkin (see, for example, ref. 56); John O'M. Bockris, at the Imperial College of Technology (University of London), the University of Pennsylvania, and Texas A & M University; Roger Parsons, at the University of Southampton; Allen Bard, at the University of Texas at Austin; and the late Heinz Gerischer, at the Fritz–Haber Institüt in Berlin. The present account focusses on Conway's work, and must of necessity overlook much important work done by others.

© 1997 NRC Canada

Can. J. Chem. Downloaded from www.nrcresearchpress.com by 91.121.58.235 on 09/08/12
For personal use only.

Conway has made important contributions to a range of electrochemical problems. Most of his work falls into one of two complementary areas. One of these is concerned with the behaviour of individual ions in solution, in particular their solvation. The other deals with the detailed mechanisms of electrode processes of various kinds. He has linked these two areas together by his parallel investigations of the adsorption of ions in the electric double layer. This adsorption is influenced by the solvation of the ions, and by their electronic interaction with the metal of the electrode.

In the 1960s Conway carried out several investigations of ionic solvation, in collaboration with J.E. Desnoyers, R.E. Verrell, and L. Laliberté (69, 70). They made theoretical calculations of the electrostriction of ions, taking into account dielectric saturation in the hydration co-sphere that exists in the immediate neighbourhood of the ions. They also made experimental studies of ionic volumes and compressibilities. Their conclusion was that the effect of electrostriction is to bring about changes in the effective volume of the solvent shell around the ion. In some of the work, parallel measurements were made in H_2O and D_2O, and the results interpreted in terms of "structure-making" and "structure-breaking" effects. Studies with quaternary ammonium salts, having cations of the R_4N^+ type, gave information about what are known as *hydrophobic interactions*.

A related contribution by Conway et al. (71) was to treat, for the first time, the hydration of polyelectrolytes. Their work was based on their measurements of partial molar volumes of polyelectrolytes, and also involved a theoretical treatment of the interaction between polycations and polyanions with the solvent, account being taken of dielectric saturation.

It was mentioned earlier that suggestions have been made that quantum-mechanical tunnelling may be involved when hydrogen is evolved at an electrode. For certain ordinary chemical reactions, tunnelling of hydrogen atoms and protons has been confirmed (72, 73). A good way of detecting quantum-mechanical tunnelling is to carry out experiments down to low temperatures. At a sufficiently low temperature a chemical reaction involving an energy barrier will effectively cease, but tunnelling, having a low temperature coefficient, will continue to occur. The result is that an Arrhenius plot (of the logarithm of the rate against the reciprocal of the absolute temperature), instead of being linear, will show curvature, the rates at the lower temperatures being abnormally high. Another test for tunnelling is to replace hydrogen by deuterium, which because of its greater mass is much less likely to tunnel; the H/D isotopic ratios will therefore be abnormal.

In 1956 an important theoretical analysis of tunnelling in an electrolytic process was carried out by Conway, Bockris, and Linton (74). They considered a Grotthuss-type mechanism in which a proton is transferred from an H_3O^+ ion to a water molecule, a process that had earlier been discussed in a classical paper by Bernal and Fowler (75). With a particular type of barrier, called an Eckart barrier, they concluded that, for the actual transfer of the proton, the tunnelling mechanism should occur with a higher rate than the process in which the proton passes over the barrier. In a related investigation Conway (76) concluded that if there is appreciable participation of electron tunnelling, the Tafel relationship [3] will be different from that with classical proton transfer.

A complication arises from the fact that after a proton is transferred there has to be a rotation of a neighboring water molecule, in order for the proton to be transferred to that water molecule. The theoretical treatment led to the conclusion that the rate is in fact limited by the rate of this rotation and not by the proton transfer itself. It follows that the H/D isotope ratio of rates is also determined by the rotation rates of the water molecules rather than by the rates of proton or deuteron transfer. The expected isotope ratio for the rates of rotation of H_2O and D_2O molecules is $\sqrt{2}$.

In an attempt to detect tunnelling in an electrochemical process, Conway and Salomon (77, 78) carried out detailed experiments, using mercury electrodes, over the temperature range from 333 K down to 180 K. Curved Arrhenius plots were not obtained, so that there was no evidence for tunnelling. Also, at the low temperatures, there were no observed deviations from Tafel behaviour, which Conway (76) had predicted for proton transfer by tunnelling. Conway and Salomon (77, 78) also investigated the H/D isotopic ratios, and again could find no evidence for tunnelling. Studies of the same kind by other workers has also failed to find evidence for tunnelling.

A series of investigations by Conway (79–82) have shown that the constant α that appears in equations such as [6] is a function of temperature. It was seen (eq. [6]) that the Tafel slope b (in eq. [3]) is, according to transition-state theory, equal to $RT/\alpha F$. Experiments carried out over a range of temperature showed instead that for some systems the Tafel slope b was practically *independent* of temperature, which means that α *increases* with increasing temperature. Conway and his co-workers showed in these investigations that the temperature dependence of α was given by equations of the form

$$[10] \quad \alpha = \alpha_H + T\alpha_S$$

Insertion of this expression into eq. [8] gives an expression in which α_H enters into the enthalpy of activation, and α_S enters into the entropy of activation (because of the cancellation of the temperatures). This result was interpreted in terms of the influence of the electric field on the solvation of the transition state, associated with potential-dependent solvent dipole orientation in the double layer.

Conway's more recent work has been concerned with what may be called *electrochemical surface science* (83–85). He has dealt, for example, with the influence of different anions on the early sub-monolayer stages of oxide film formation on transition metals such as platinum. Even at very low concentrations (Cl^- and Br^- at 10^{-7} M) anions were found to interfere with surface oxide formation. They also influence the place-exchange reconstruction that occurs during the conversion of monolayer arrays of OH and O into growing three-dimensional films. His later research extended this type of study to single-crystal surfaces of platinum and gold, and led to improved interpretations of the kinetic behaviour.

Acknowledgements

I have presumed that Michael Faraday would have had no objection to my taking inspiration, in my title, from his delightful book *The Chemical History of a Candle*. My many discussions with Brian Conway, over the last 41 years, have always been of great help to me, and I am grateful. His assis-

© 1997 NRC Canada

tance with the preparation of the latter part of this article, and his comments on the whole article, are much appreciated.

References

1. A. Volta. Philos. Trans. R. Soc. London, **92**, 403 (1800).
2. J. Nicholson. Nicholson's Journal, **4**, 179 (1800).
3. C.J.D. von Grotthuss. Mémoire sur la décomposition de l'eau et des corps, qu'elle tient en dissolution, à l'aide de l'électricité galvanique. Rome. 1805. Milan, 1806; Ann. Chim. (Paris), **58**, 54 (1806) (English version in Philos. Mag. **25**, 330 (1806)).
4. H. Davy. Philos. Trans. R. Soc. London, **98**, 1 (1808).
5. H. Davy. Philos. Trans. R. Soc. London, **98**, 333 (1808).
6. J.F. Daniell. Philos. Trans. R. Soc. London, **126**, 107 (1836); **126**, 125 (1836).
7. J.F. Daniell. Philos. Trans. R. Soc. London, **127**, 141 (1837).
8. J.F. Daniell. Philos. Trans. R. Soc. London, **129**, 89 (1839).
9. W.R. Grove. Philos. Mag. [3], **20**, 294 (1839).
10. W.R. Grove. Philos. Mag. [3], **14**, 127 (1839).
11. M.H. von Jacobi. L'Institut; Journal des Académies et Sociétés Scientifiques de la France et de l'Étranger, Paris, **2**, 394 (1834) (German versions in (Poggendorff's) Ann. Phys. Chem. [2], **31**, 367 (1834); [2], **36**, 366 (1835)).
12. M.H. von Jacobi. Bull. Acad. Imp. Sci. St.-Pétersbourg, **2**, 17 (1837); **2**, 37 (1837).
13. J.P. Joule. Proc. R. Soc. Edinburgh, **4**, 280 (1840).
14. J.P. Joule. Philos. Mag. [3], **19**, 260 (1841).
15. J.P. Joule. Philos. Mag. [3], **23**, 204 (1843); **23**, 263 (1843).
16. H.C. Oersted. Ann. Philos. **16**, 273 (1820); Journal de physique, de chimie d'histoire naturelle et des arts (Rozier's Journal), **91**, 72 (1820).
17. A.M. Ampère. Journal de physique, de chimie d'histoire naturelle et des arts (Rozier's Journal), **91**, 226, (1820).
18. A.M. Ampère. Mémoires de la Classe des Sciènces mathématiques et physiques de l'Institut, Paris, **6**, 175, 1823 (submitted 1820).
19. J. Clerk Maxwell. *In* A treatise on electricity and magnetism. *Edited by* W.D. Niven. 2 vols. Oxford University Press, U.K. 1873.
20. M. Faraday. The quarterly journal of science, literature, and the arts, **12**, 74 (1821); **12**, 186 (1821); **12**, 283 (1821).
21. M. Faraday. Philos. Trans. R. Soc. London, **122**, 125 (1832).
22. M. Faraday. Philos. Trans. R. Soc. London, **122**, 163 (1832).
23. M. Faraday. Philos. Trans. R. Soc. London, **123**, 23 (1833).
24. M. Faraday. Philos. Trans. R. Soc. London, **124**, 55 (1834); **124**, 77 (1834); **124**, 427 (1834).
25. S. Ross. Royal Society (Great Britain) Notes & records of the Royal Society of London, **16**, 187 (1961).
26. K.J. Laidler. The world of physical chemistry. Oxford University Press, U.K. 1993; paperback edition, 1995.
27. M. Faraday. Philos. Trans. R. Soc. London, **124**, 77 (1834).
28. M. Faraday. Philos. Mag. [3], **24**, 136 (1844).
29. J.F. Daniell and W.A. Miller. Philos. Trans. R. Soc. London, **134**, 1 (1844); Philos. Mag. [3], **25**, 175 (1844).
30. J.W. Hittorf. (Poggendorff's) Ann. Phys. Chem. [2], **89**, 177 (1853).
31. R. Clausius.(Poggendorff's) Ann. Phys. Chem. **101**, 338 (1857).
32. J.W. Hittorf. (Poggendorff's) Ann. Phys. Chem. [2] **98**, 1 (1856); **103**, 1 (1858); **106**, 337 (1859); **106**, 513 (1859).
33. F. Kohlrausch and W.A. Nippoldt. (Poggendorff's) Ann. Phys. Chem. [2], **138**, 28 (1869); **138**, 370 (1869) (English summary in Philos. Mag. [4], **40**, 227 (1870)).
34. F. Kohlrausch and O. Grotrian. Nachr. Ges. Wiss. Göttingen. 405 (1874); (Poggendorff's) Ann. Phys. Chem. [2], **154**, 1 (1875); **154**, 215 (1875) (English version in Philos. Mag. [4], **49**, 417 (1875)).
35. W.L. Bragg. Proc. R. Soc. London Ser. A, **89**, 246 (1913).
36. W.L. Bragg. Nature (London), **120**, 414 (1927).
37. H.E. Armstrong. Nature (London), **120**, 478 (1927).
38. P. Drude and W. Nernst. Z. Phys. Chem. **15**, 79 (1894).
39. W.E. Weber and R.H.A. Kohlrausch. (Poggendorff's) Ann. Phys. Chem. [2], **99**, 10 (1856).
40. W.E. Weber and R.H.A. Kohlrausch. Abt. Math. Phys. Leipzig, **3**, 219 (1857); (Poggendorff's) Ann. Phys. Chem. **49**, 115 (1857).
41. G. Kirchhoff. (Poggendorff's) Ann. Phys. Chem. [2], **100**, 193 (1857); **100**, 251 (1857) (English translation in Philos. Mag. [4], **13**, 393 (1857)).
42. J. Clerk Maxwell. British Association Reports, **32**, 130 (1863).
43. G. Johnstone Stoney. Philos. Mag. [5], **11**, 381 (1881).
44. G. Johnstone Stoney. Trans. R. Soc. Dublin, **4**, 563 (1891).
45. J. Tafel. Z. Phys. Chem. **50**, 641 (1905).
46. T. Erdey-Gruz and M. Volmer. Z. Phys. Chem. **150**, 203 (1930); T. Erdey-Gruz and H. Wick. Z. Phys. Chem. **162**, 53 (1932); **162**, 63 (1932).
47. R.W. Gurney. Proc. R. Soc. London Ser. A, **134**, 137 (1931).
48. R.W. Gurney. Proc. R. Soc. London Ser. A, **136**, 378 (1932).
49. R.H. Fowler. Trans. Faraday Soc. **28**, 368 (1932).
50. C.E.H. Bawn and G. Ogden. Trans. Faraday Soc. **30**, 432 (1934).
51. J.A.V. Butler. Trans. Faraday Soc. **28**, 379 (1932).
52. J.A.V. Butler. Proc. R. Soc. London Ser. A, **157**, 423 (1936).
53. H. Eyring, S. Glasstone, and K.J. Laidler. J. Chem. Phys. **7**, 1053 (1939).
54. S. Glasstone, K.J. Laidler, and H. Eyring. The theory of rate processes. McGraw–Hill, New York. 1941. Ch. 10.
55. B.E. Conway and M. Salomon. J. Chem. Educ. 44, 554 (1967).
56. A.N. Frumkin. Z. Phys. Chem. **160**, 116 (1932).
57. M. Born. Z. Phys. **1**, 45 (1920).
58. K.J. Laidler and C. Pegis. Proc. R. Soc. London Ser. A, **240**, 80 (1957).
59. K.J. Laidler. Can. J. Chem. **37**, 138 (1959).
60. H.S. Frank and M.H. Evans. J. Chem. Phys. **13**, 507 (1945).
61. H.S. Frank and W.V. Wen. Discuss. Faraday Soc. **24**, 133 (1957).
62. J.S. Muirhead-Gould and K.J. Laidler. Trans. Faraday Soc. **63**, 944 (1967).
63. J.S. Muirhead-Gould and K.J. Laidler. *In* Chemical physics of ionic solutions. *Edited by* B.E. Conway and R.G. Barradas. Wiley, New York. 1967. p. 75.
64. H. Helmholtz. (Wiedemann's) Ann. Phys. Chem. **7**, 337 (1879).
65. G. Gouy. Colloq. Phys. **9**, 457 (1910).
66. D.L. Chapman. Philos. Mag. [6], **25**, 475 (1913).
67. O. Stern. Z. Elektrochem. Angew. Phys. Chem. **30**, 508 (1924).
68. R.J. Watts-Tobin. Philos. Mag. [8], **6**, 133 (1961); N.F. Mott and R.J. Watts-Tobin. Electrochim. Acta, **4**, 79 (1961).
69. J.E. Desnoyers, R.E. Verrall, and B.E. Conway. J. Chem. Phys. **43**, 243 (1965).
70. B.E. Conway, R.E. Verrall, and J.E. Desnoyers. Trans. R. Soc. London, Faraday Soc. **62**, 2738 (1966).
71. B.E. Conway, J.E. Desnoyers, and A.C. Smith. Philos. Trans. R. Soc. London Ser. A, **256**, 389 (1964).
72. E.F. Caldin. Fast reactions in solution. Blackwell, Oxford. 1964. pp. 272–275.
73. R.P. Bell. The tunnel effect in chemistry. Chapman and Hall, London. 1980.
74. J.D. Bernal and R.H. Fowler. J. Chem. Phys. **1**, 515 (1933).
75. B.E. Conway, J.O'M. Bockris, and H. Linton, J. Chem. Phys. **24**, 834 (1956).
76. B.E. Conway. Can. J. Chem. **37**, 178 (1959).
77. B.E. Conway and M. Salomon. J. Chem. Phys. **41**, 3169 (1964).
78. B.E. Conway and M. Salomon. Discuss. Faraday Soc. **39**, 223 (1965).

Can. J. Chem. Downloaded from www.nrcresearchpress.com by 91.121.58.235 on 09/08/12
For personal use only.

© 1997 NRC Canada

79. B.E. Conway, D.J. MacKinnon, and B.V. Tilak. Trans. R. Soc. London, Faraday Soc. **66**, 1203 (1970).
80. B.E. Conway and D.J. MacKinnon. J. Electroanal. Chem. **199**, 249 (1986).
81. B.E. Conway, D.F. Tessier, and D. Wilkinson. J. Electroanal. Chem. 204, 111 (1986).
82. B.E. Conway. *In* Modern aspects of electrochemistry. Vol. 16. *Edited by* B.E. Conway and J.O'M. Bockris. Plenum, New York. 1986. Chap. 2.
83. H.A. Kozlowska, B.E. Conway, and W. Sharp. J. Electroanal. Chem. **43**, 9 (1973).
84. B.E. Conway and H.A. Kozlowska. Acc. Chem. Res. **14**, 49 (1981).
85. H.A. Kozlowska, B.E. Conway, and A. Hamelin. Electrochim. Acta, **31**, 1051 (1986).

Can. J. Chem. Downloaded from www.nrcresearchpress.com by 91.121.58.235 on 09/08/12
For personal use only.

© 1997 NRC Canada

Application of electrochemical methods in the development of models for fuel dissolution and container corrosion under nuclear waste disposal conditions

D.W. Shoesmith, W.H. Hocking, B.M. Ikeda, F. King, J.J. Noël, and S. Sunder

Can. J. Chem. Downloaded from www.nrcresearchpress.com by 91.121.58.235 on 09/08/12
For personal use only.

Abstract: The permanent disposal of nuclear fuel wastes requires the development of models that can assess the performance of a disposal vault over long periods of time. Models to assess the long-term stability of the nuclear fuel (UO_2) and the corrosion performance of the waste container (either copper or titanium) have been based on electrochemical principles. Here we review the chemical/electrochemical performance of fuel and the two candidate container materials, and describe some of the electrochemical studies undertaken either to develop the mechanistic understanding upon which these models are based or to measure the values of parameters required to evaluate long-term performance. These include the following: the anodic dissolution of UO_2; the reduction of O_2 on various specimens of UO_2; the crevice corrosion of various titanium alloys; the impedance characteristics of passive films on Ti alloys; the anodic dissolution of copper in chloride solutions; the reduction of O_2 on copper; the effect of various transport barriers on the corrosion of copper; and the prediction of the corrosion potential of copper in aerated chloride solutions.

Key words: uranium dioxide, copper, titanium, nuclear waste, oxygen.

Résumé : Pour effectuer la décharge permanente des déchets nucléaires, il est important de disposer de modèles qui permettent d'évaluer la performance sur de longues périodes des voûtes d'enfouissement. Des modèles permettant d'évaluer la stabilité à long terme de combustible nucléaire (UO_2) ainsi que la performance vis-à-vis de la corrosion de contenants de déchets (cuivre out titane) ont été développés en se basant sur des principes électrochimiques. Dans ce travail, on passe en revue la performance chimique/électrochimique du combustible et des deux matériaux pouvant servir de contenant et on décrit un certain nombre d'études électrochimiques effectuées soit pour développer une compréhension mécanistique des modèles utilisés comme base ou pour mesurer les valeurs de paramètres nécessaires pour évaluer la performance à long terme. Celles-ci incluent : la dissolution anodique du UO_2; la réduction du O_2 sur divers spécimens de UO_2; la corrosion des crevasses de divers alliages du titane; les caractéristiques d'impédance de films passifs sur des alliages de Ti; la dissolution anodique dans des solutions de chlorure; la réduction du O_2 sur le cuivre; l'effet de diveres barrières au transport sur la corrosion du cuivre; et la prédicton du potentiel de corrosion du cuivre dans des solutions de chlorure aérées.

Mots clés : dioxyde d'uranium, cuivre, titane, déchets nucléaires, oxygène.

[Traduit par la rédaction]

1. Introduction

The Canadian nuclear fuel waste disposal concept involves the permanent burial of fuel wastes at depths of 500–1000 m in plutonic rock in the Canadian Shield. The waste would be sealed in corrosion-resistant containers, and a clay-based buffer material placed between the containers and the rock. If this concept is to be justified, then models must be developed to demonstrate that the rate of release of radionuclides will be slow compared to their radioactive decay. A problem with such models is the lack of any opportunity to refine them on the basis of observational experience or failure analysis. This means the models must be based on sound mechanistic understanding and substantial databases.

In this review we are interested in the chemical performance of two barriers within this engineered vault: the corrosion/dissolution of the fuel wasteform, and the corrosion of the metallic container encapsulating the waste. Models to predict how these processes will evolve with time in a waste vault have recently been developed (1–4) and incorporated into assessments of waste vault performance (5, 6). These models are based on electrochemical principles since both fuel dissolution and container degradation are corrosion processes requiring that the oxidative dissolution of the fuel or container material be coupled to the reduction of available oxidants within the waste vault. Since the unperturbed environment is

Received April 7, 1997.

This paper is dedicated to Professor Brian E. Conway in recognition of his outstanding contributions to Canadian electrochemistry.

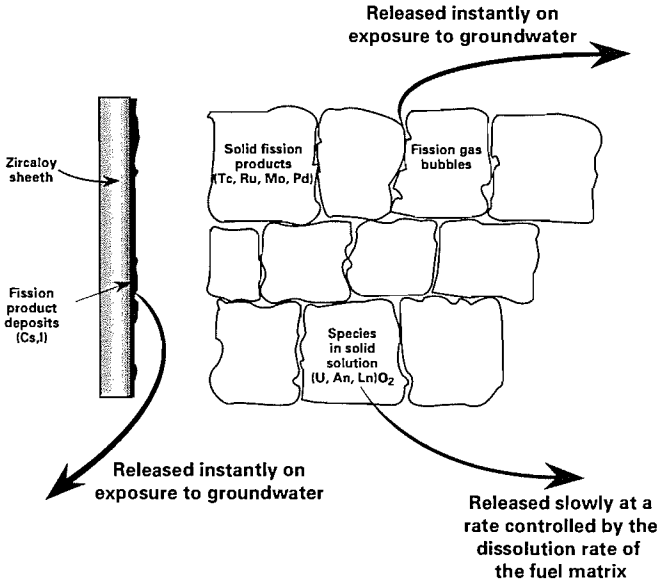
D.W. Shoesmith,[1] W.H. Hocking, B.M. Ikeda, F. King, J.J. Noël, and S. Sunder. Atomic Energy of Canada Ltd. (AECL), Whiteshell Laboratories, Pinawa, MB R0E 1L0, Canada.

[1] Author to whom correspondence may be addressed. Telephone: (204) 753-2311. Fax: (204) 753-2455. E-mail: shoesmithd@aecl.ca

© 1997 NRC Canada

Can. J. Chem. Downloaded from www.nrcresearchpress.com by 91.121.58.235 on 09/08/12
For personal use only.

Fig. 1. Schematic showing the distribution of radionuclides in used fuel. Radionuclides located at the fuel–Zircaloy cladding gap and at grain boundaries within the fuel are assumed to be released instantly.



reducing, the oxidants available will be those trapped within the waste vault on sealing (effectively O_2) and, for passive metals, H_2O and those produced by the radiolytic decomposition of the water expected to eventually saturate the vault.

Many electrochemical methods have been used either to develop the mechanistic understanding upon which these models are based or to measure the values of parameters required to evaluate long-term performance. In this paper, we will describe the basic electrochemistry/chemistry of fuel dissolution and container corrosion and describe some of the electrochemical studies undertaken.

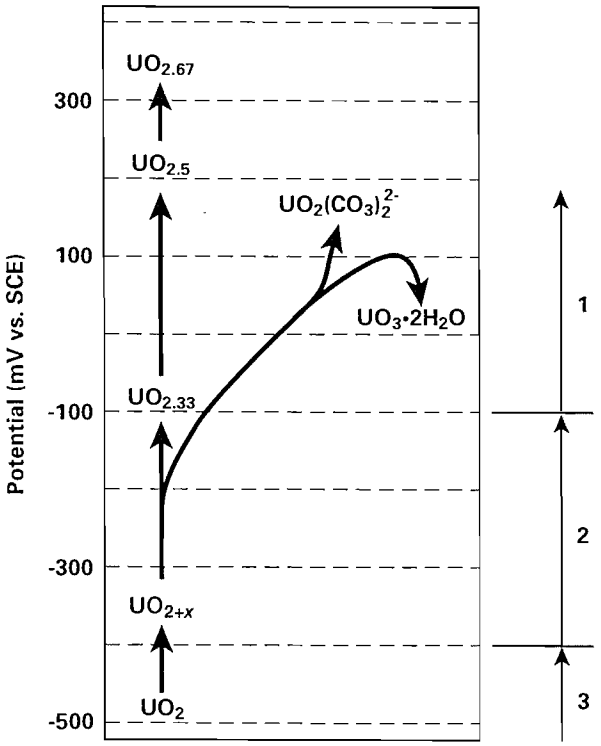
2. Corrosion/dissolution of nuclear fuel (UO_2)

Nuclear fuel is basically uranium dioxide (UO_2) fabricated by sintering pressed compacts of very fine grained powder at ~1700°C under a reducing atmosphere. These sintered ceramics typically have 92–99% of the theoretical density with grain sizes of 2–15 μm. The as-fabricated fuel is a slightly hyperstoichiometric oxide, UO_{2+x} where $x \leq 0.001$. The presence of excess oxygen, as interstitial oxide ions (O_I^{2-}), requires further ionization of a small fraction of the U^{IV} ions, to the U^V and (or) U^{VI} valence state, which creates holes in the narrow occupied U 5*f* sub-band that can migrate by a small polaron-hopping process with a low activation energy (7–9).

On burning in a nuclear reactor, many fission products and actinides with widely varying solubilities in the host matrix are created. The radionuclide release model used in safety assessments includes three main release mechanisms (Fig. 1). Since the great majority of radionuclides (90–99%) are contained within the grains of the fuel pellets, they will be released at a rate governed by the dissolution rate of the UO_2 matrix.

The solubility of uranium increases by many orders of magnitude when conditions become more oxidizing, and it is necessary to treat fuel dissolution as a corrosion process and to attempt the prediction of rates based on electrochemical principles. Many studies have demonstrated the electrochemical nature of UO_2 dissolution (10).

Fig. 2. Chemistry/electrochemistry of UO_2 oxidation and dissolution as a function of corrosion potential or electrochemically applied potential.



2.1 Electrochemistry/chemistry of UO_2 oxidation/dissolution

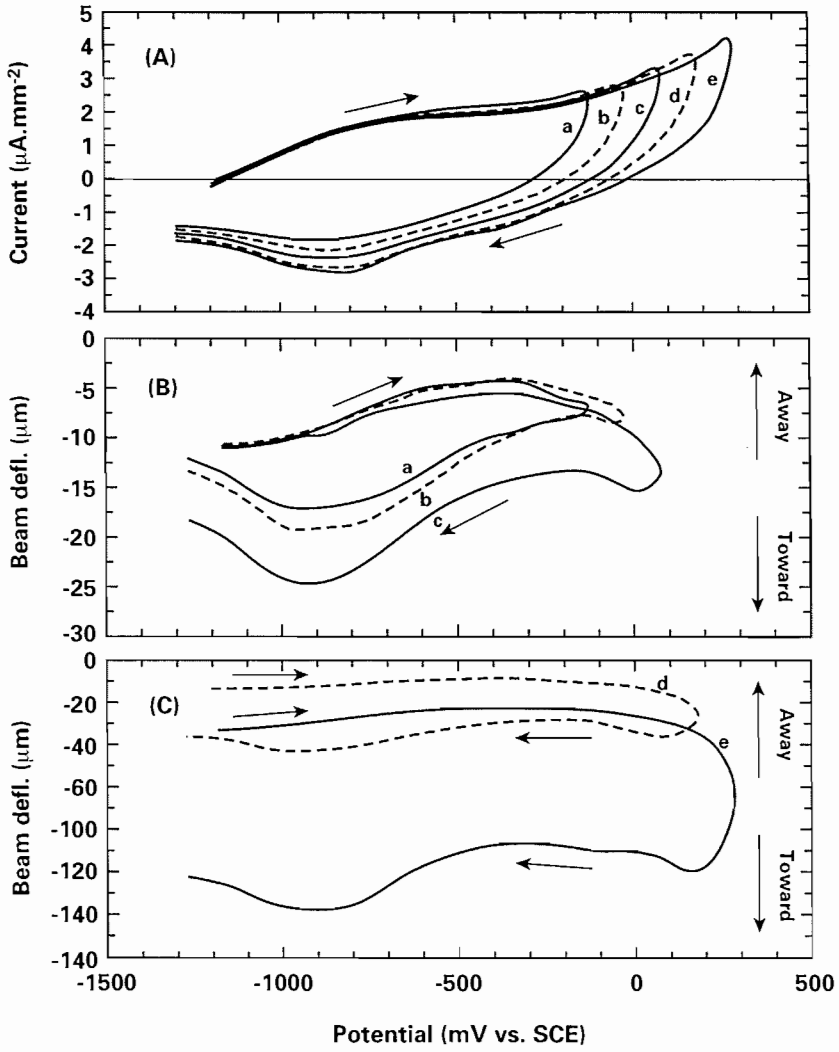
Figure 2 shows the expected composition of a UO_2 surface as a function of either the corrosion potential achieved or the electrochemical potential applied. The compositions indicated have been established by a combination of electrochemical, corrosion, and X-ray photoelectron spectroscopic (XPS) techniques (11–14). The behaviour can be divided into three regions.

For $E \lesssim -400$ mV (vs. SCE), region 3 (Fig. 2), no oxidative dissolution can be detected, even by techniques as sensitive as photothermal deflection spectroscopy (PDS) (15). The observation of positive current flow under voltammetric conditions clearly indicates some degree of oxidation, although this appears to be either confined to submonolayer levels or concentrated at more readily oxidizable sites such as defects and grain boundaries (10).

For potentials -400 mV $\leq E \leq -100$ mV (vs. SCE), region 2 (Fig. 2), the composition of the surface (UO_{2+x}) and the extent of oxide formation are directly determined by potential (16). The loss of *p*-type photocurrent, observed at $E < E_{fb}$ (where E_{fb} is the flatband potential (~ −1.2 V (vs. SCE)), after voltammetric excursions into this potential region shows that dissolution is accompanied by the at least partially irreversible oxidation of UO_2 (10, 17). XPS analyses show that a surface

© 1997 NRC Canada

Fig. 3. Electrochemical/photo-deflection spectroscopy experiment in 0.5 mol L^{-1} Na_2SO_4 (pH = 10.5) for five voltammetric scans (20 mV s^{-1}) to progressively more positive potential limits. (*A*) current response; (*B*) beam deflection for the first three scans; (*C*) beam deflection for the last two scans. The deflection of the probe beam is proportional to the dissolved uranium concentration, and deflection of the probe beam towards the electrode surface is an indication that dissolution is occurring. (Reprinted from J. Electroanal. Chem. Vol. 372, J.D. Rudnicki et al., "Photothermal deflection spectroscopy investigations of uranium dioxide oxidation", 63–74 (1994) with kind permission from Elsevier Science S.A., P.O. Box 564, 1001 Lausanne, Switzerland.)



composition of $UO_{2.33}$ is achieved by $E \sim -100$ mV (vs. SCE) (18) and that its subsequent reduction on a negative-going voltammetric scan yields a surface of composition $\sim UO_{2.1}$. A combination of PDS and electrochemistry shows that an increase in anodic current for $E \gtrsim -300$ mV (vs. SCE) is partially attributable to dissolution (Fig. 3) (15). That dissolution is enhanced by excursions to more positive potentials is clearly indicated by the larger beam deflection shown in Fig. 3C. The PDS technique is based on the deflection of a probe laser as it passes adjacent to an electrode surface, and the degree to which the beam is deflected is directly proportional to the gradient of the solution refractive index. The release of chemical species from the electrode (i.e., dissolution) can then be detected by a deflection of the probe beam towards the electrode due to the local increase in refractive index of the electrolyte.

By comparing the electrochemical/PDS behaviour of a sintered UO_2 pellet and a UO_2 single crystal it has been shown that the oxidative dissolution process is dependent on surface structure.[2] For a single crystal, in which grain boundaries are absent, insignificant dissolution was observed (for $E \lesssim -100$ mV (vs. SCE)). By contrast, as shown in Fig. 3 and discussed elsewhere (15), anodic dissolution from the surface of a sintered pellet containing many grain boundaries is observed at potentials as low as -300 mV (vs. SCE).

When $E \geq -100$ mV, region 1 (Fig. 2), oxidation beyond $UO_{2.33}$ is observed and dissolution becomes extensive as the potential increases. For $E \gtrsim 200$ mV (vs. SCE) the $UO_{2.33}$ surface may oxidize to $UO_{2.67}$. While XPS results suggest this is possible at room temperature under electrochemical conditions (13, 14), its occurrence at high temperatures ($\geq$150°C) is

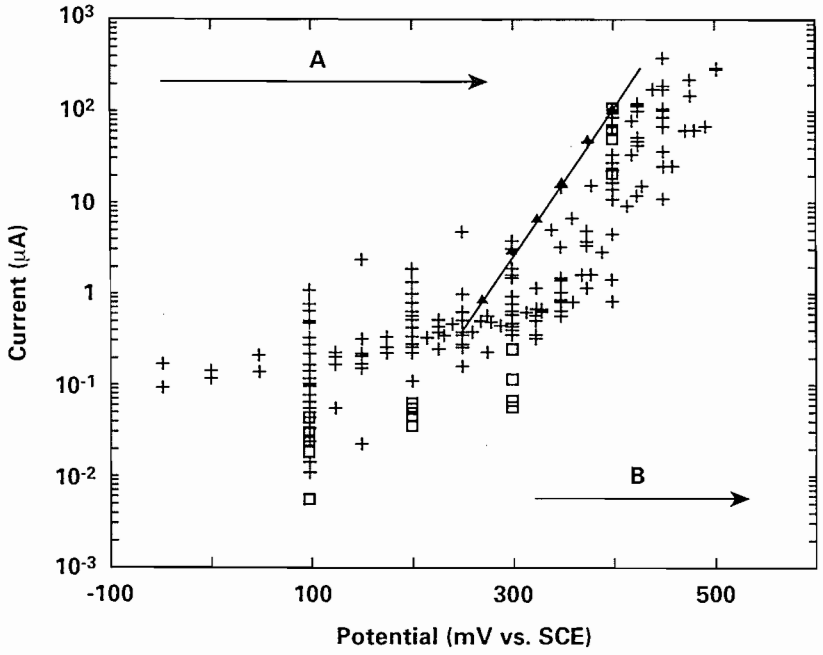
[2] J.D. Rudnicki and R. Russo. Private communication.

© 1997 NRC Canada

Can. J. Chem. Downloaded from www.nrcresearchpress.com by 91.121.58.235 on 09/08/12
For personal use only.

Can. J. Chem. Downloaded from www.nrcresearchpress.com by 91.121.58.235 on 09/08/12
For personal use only.

Fig. 4. Electrochemically determined dissolution currents as a function of applied potential recorded on a number of different unirradiated UO_2 specimens in 0.1 mol L^{-1} Na_2SO_4 (pH = 9.5). In region A, currents are non-steady-state; in region B, currents are steady-state values. The line connects the data points used in a recent assessment of fuel performance (6) (from ref. 23).



well documented under hydrothermal (19) and radiolytic oxidizing conditions (20). Simultaneously, dissolution as UO_2^{2+} occurs and, for solutions in which uranyl species have a low solubility, secondary phases (such as $UO_3{\cdot}2H_2O$) precipitate on the electrode surface

[1] $UO_2^{2+} + 3H_2O \rightarrow (UO_3{\cdot}2H_2O)_S + 2H^+$

where $(\ )_S$ denotes a solid phase or species. In the presence of uranyl-complexing anions (e.g., CO_3^{2-}) dissolution is enhanced

[2] $UO_2^{2+} + 2CO_3^{2-} \rightarrow UO_2(CO_3)_2^{2-}$

and secondary phase formation avoided (10, 21).

For redox conditions sufficiently oxidizing to drive the corrosion potential (E_{CORR}) to values $\gtrsim -100$ mV (vs. SCE), UO_2 dissolution is clearly a corrosion process requiring the coupling of oxide dissolution and oxidant reduction. We recently published an electrochemical procedure to determine the rates of UO_2 dissolution based on a Tafel extrapolation of anodic dissolution currents as a function of applied potential to values of E_{CORR} measured in environments with controlled redox potential (22). This procedure yields rates of fuel dissolution (as corrosion currents, I_{CORR}) as a function of oxidant concentration, and has been incorporated into a model to assess fuel behaviour under waste vault conditions (6). A natural extension of this procedure is the development of a mixed potential model to describe and predict UO_2 fuel behaviour. For the application of such a model to be justified, a good understanding of both the anodic dissolution of UO_2 and the cathodic reduction of oxidants on UO_2 is required.

2.2 Anodic dissolution of UO_2

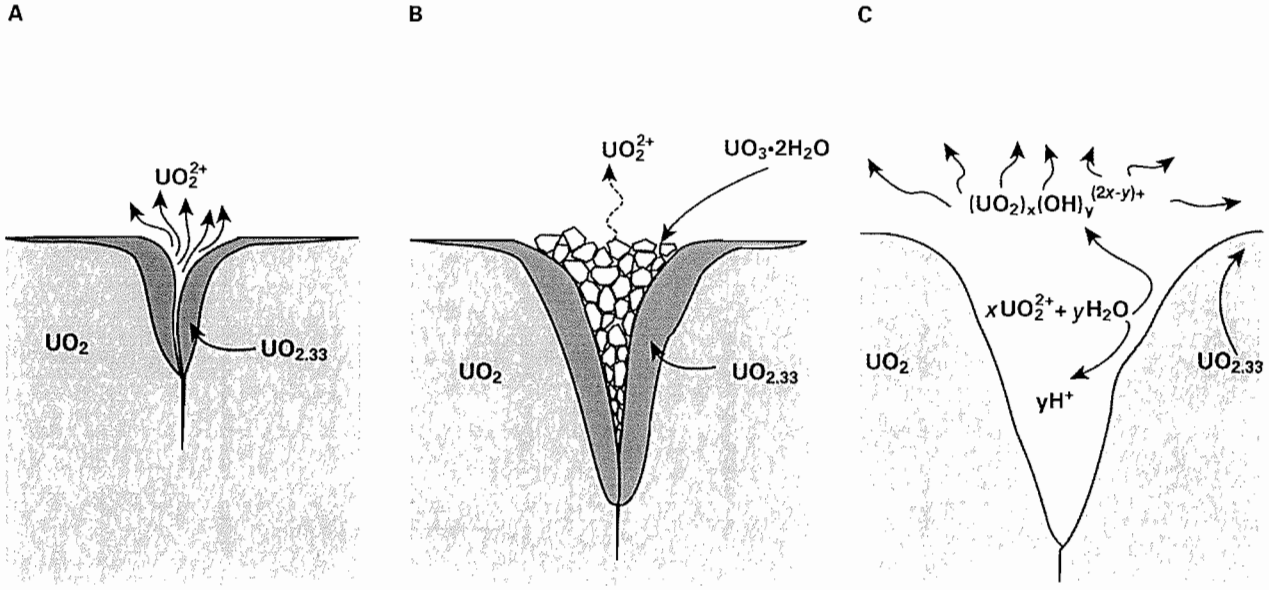
Figure 4 shows electrochemically determined dissolution currents as a function of applied potential recorded on a number of different UO_2 specimens (in the form of rotating disc electrodes (RDE)) in 0.1 mol L^{-1} $NaClO_4$ (pH ~ 9.5), a solution representative of the noncomplexing groundwaters anticipated in the Canadian Shield (23). Two distinct regions of behaviour (A and B) are observed.

For $E \leq 300$ mV (region A) the currents are non-steady-state, progressively decreasing as the accumulation of secondary phases ($UO_3{\cdot}2H_2O$) blocks dissolution of the UO_2 surface. For $E \gtrsim 300$ mV (region B), steady-state dissolution currents are obtained. The wide distribution of points at 100 mV reflects the various lengths of time for which the potential was held before recording the current. The open squares show currents recorded after 24 h of oxidation.

In region A the currents fall by more than two orders of magnitude over a 24-h period and even after 24 h, by which time currents $\leq$5 nA were obtained, no steady state was achieved. Voltammetric reduction of the anodically oxidized surface clearly indicates that the dissolution product accumulates by deposition on the electrode surface, the amount of electrochemical charge recovered by reduction of these deposits being equal to that consumed in their formation. That this should occur on the surface of a rotating disc electrode is evidence that deposition is occurring at occluded sites, such as within grain boundaries. An attempt to represent this situation schematically is shown in Figs. 5*A* and 5*B*. That dissolution should preferentially occur at grain boundaries is not unexpected for UO_2. The conductivity of UO_2 increases markedly with the degree of non-stoichiometry (7, 9) and the reductive sintering process used to fabricate the

© 1997 NRC Canada

Fig. 5. Schematic illustrating the oxidation and dissolution of UO_2 localized at grain boundaries. (*A*) Dissolution at short times in potential region A (Fig. 4); (*B*) dissolution at long times (1.5 h) in potential region A (Fig. 4); (*C*) steady-state dissolution in potential region B (Fig. 4).



pellets is likely to leave some degree of non-stoichiometry in the grain boundaries.

For $E \geq 300$ mV, region B (Fig. 4), a logarithmic dependence of the dissolution current on applied potential is obtained, and the steady-state nature of the currents makes a Tafel extrapolation to determine corrosion currents at measured values of E_{CORR} acceptable. The scatter in data points at a given potential in region B is approximately one order of magnitude and can be attributed to a combination of variability in UO_2 reactivity between specimens and the unavoidable irreproducibility of a dissolution process largely confined to small areas at grain boundaries. The line drawn through the triangular points in Fig. 4 is that extrapolated to determine the corrosion rates in performance assessment calculations (6). These data points are from a previous, less rigorous, attempt to determine dissolution currents as a function of applied potential (23).

At high potentials in region B anodic dissolution of $UO_{2.33}$,

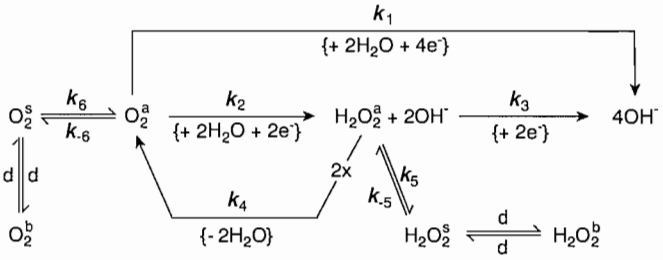
[3] $(UO_{2.33})_S + 0.33H_2O \rightarrow UO_2^{2+} + 0.66OH^- + 1.34e^-$

is sufficiently rapid that extensive hydrolysis to produce local acidity at the occluded dissolution site can occur; i.e.,

[4] $xUO_2^{2+} + yH_2O \rightarrow (UO_2)_x(OH)_y^{(2x-y)+} + yH^+$

For pH $\leq$ 5.5, a $UO_{2.33}$ layer does not form as a dissolution intermediate (24), and an increase in the solubility of $UO_3{\cdot}2H_2O$ (25) prevents its local precipitation, leaving the dissolution site unblocked, Fig. 5*C*. That only a very thin surface film was present on the UO_2 surface after anodic oxidation in region B (Fig. 4) is confirmed by the absence of a major reduction peak in a subsequent voltammetric scan to negative potentials. The Tafel slope measured in region B is 58 $\pm$ 5 mV, suggesting rate control by a single two-electron transfer. This is unlikely, and it is possible that local acidification is non-uniform, and the slope is some average value between the 40 mV in acidic solutions and the 70–80 mV in neutral solutions observed by Nicol and Needes (26).

Fig. 6. General reaction scheme for O_2 reduction. Superscripts b, s, and a denote species in bulk solution, near the electrode surface and adsorbed on the electrode, respectively; d denotes diffusion.



2.3 Oxygen reduction on UO_2

While study of the anodic dissolution may produce a relationship between dissolution current and applied potential that can be used to predict corrosion (dissolution) rates under natural corrosion conditions, the destruction of the UO_2 surface disguises many subtleties of its electrochemical reactivity. Not only is a knowledge of the kinetics of O_2 reduction necessary for the development of a complete mixed potential model (to describe the corrosion behaviour of fuel), the reduction is an electron transfer reaction that can also probe many features of the surface reactivity of UO_2.

Two major pathways exist for O_2 reduction (Fig. 6): the direct pathway (characterized by the overall four-electron reduction to OH^-) and the series pathway (which proceeds via a peroxide intermediate). In the absence of detectable peroxide formation it is difficult to distinguish between these two routes. On UO_2, Tafel slopes ($dE/d \log i$) larger (in magnitude) than -120 mV, coupled with reaction orders of $\sim$1, indicate

Can. J. Chem. Downloaded from www.nrcresearchpress.com by 91.121.58.235 on 09/08/12
For personal use only.

© 1997 NRC Canada

Fig. 7. Schematic showing the mechanism of O_2 reduction at donor–acceptor sites on the surface of UO_2.

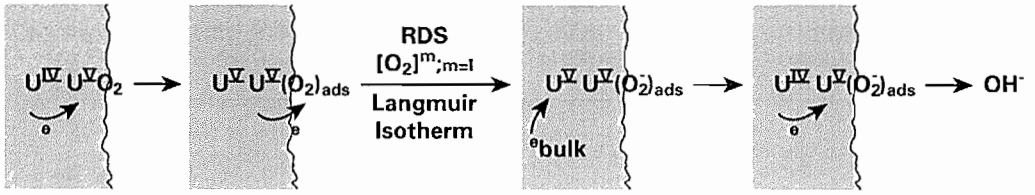
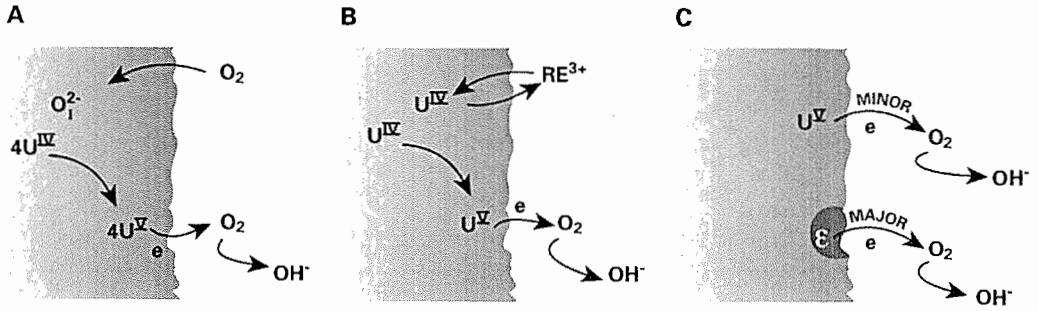


Fig. 8. Schematic showing the effects of various fuel treatments and properties on O_2 reduction on a UO_2 surface. (*A*) Effect of corrosion in aerated solution on the number density of surface donor–acceptor sites (shown as U^V); (*B*) effect of rare earth doping on number density of donor–acceptor surface sites; (*C*) effect of noble metal particles (ε phase).



that the first electron transfer is rate determining and occurs before O—O bond cleavage. This is more consistent with a series mechanism, with the absence of detectable peroxide suggesting $k_3 \gg k_5$, than with a direct mechanism involving early O—O bond rupture.

Recently, we showed that the cathodic reduction of O_2 on nearly stoichiometric *p*-type UO_2 in dilute alkaline solution (0.1 mol L^{-1} $NaClO_4$, pH ~9.5) proceeds by an overall four-electron series route involving single electron and proton transfer steps (27, 28). Electron transfer appears to occur exclusively at surface sites where adjacent uranium cations are present in different valence states, U^{VI} or U^V above U^V or U^{IV}. This is an adaptation of the theory of donor–acceptor reduction sites developed by Presnov and Trunov (29, 30) to explain O_2 reduction on transition metal oxides with *p*-type semiconductivity, and is illustrated schematically for UO_2 in Fig. 7. A first-order dependence on $[O_2]$ and a Tafel slope >-120 mV (generally around -180 to -200 mV) are consistent with adsorption under Langmuir conditions and control of the rate by the first electron transfer step. Surface oxidation by corrosion in aerated solutions significantly increases the cathodic current for O_2 reduction, consistent with an increase in the number density of donor–acceptor sites, Fig. 8*A*. By contrast, high concentrations of carbonate, which preferentially coordinates U^{VI} and U^V but not U^{IV} (25, 28), cause a decrease in O_2 reduction current by an order of magnitude and lead to the release of copious amounts of peroxide to solution (27).

In the absence of peroxide release to solution, and for weak absorption of O_2 at donor–acceptor sites, the current for O_2 reduction (I_k), corrected for any contribution from diffusion, is given by

$$[5] \quad I_k = 4FAN_S^D(N_S^U)^{-1}\, kK[O_2] \exp\left\{-\frac{\alpha F\eta}{RT}\right\}$$

where F is Faraday's constant, A is the surface area of the electrode, k is the rate constant (s^{-1}) for the rate-determining electron transfer, K is the equilibrium constant for adsorption of O_2 at donor–acceptor sites, and $N_S^D(N_S^U)^{-1}$ is the ratio of the number density of donor–acceptor sites (N_S^D) to the number density of uranium atoms in the electrode surface. This ratio changes with potential since N_S^D is potential dependent.

While the general features of the reduction reaction remain unchanged, the kinetic details vary depending on the distribution of donor–acceptor sites. This was clearly indicated by experiments on a UO_2 specimen exhibiting *n*-type photocurrent characteristics (31). A near square-root dependence on $[O_2]$ suggested coupling of the adsorption and first electron transfer steps under Temkin isotherm conditions,

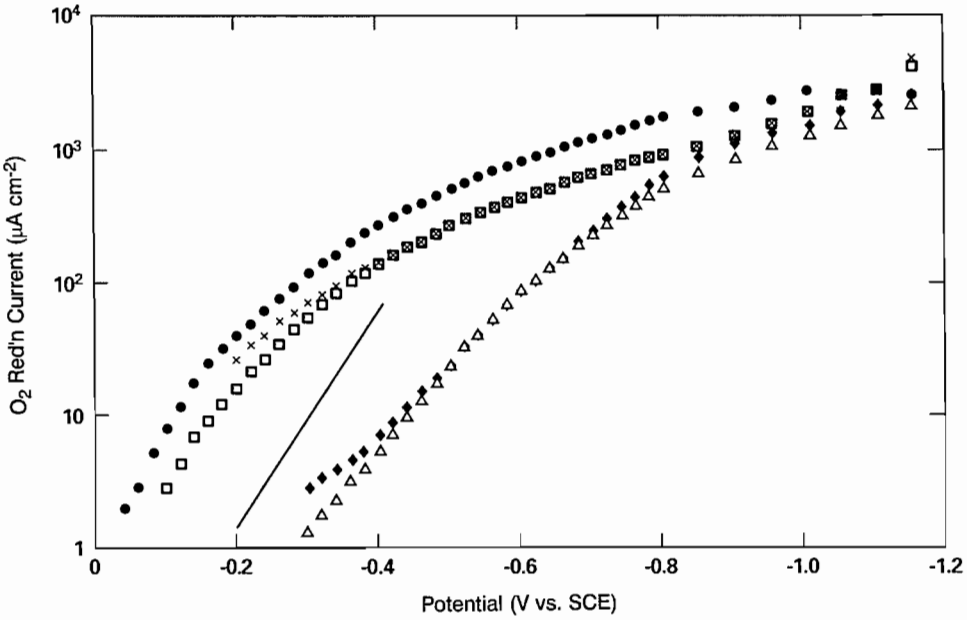
$$[6] \quad \{U^V\} + O_2 \xrightarrow{k_1'} \{U^V\}\,(O_2)_{ads} \xrightarrow[e^-]{k_2'} \{U^{VI}\}\,(O_2^-)_{ads}$$

This was attributed to a severely localized distribution of donor–acceptor sites due to pronounced heterogeneity in the degree of non-stoichiometry. *n*-Type characteristics suggest the presence of a significant degree of non-stoichiometry, an observation apparently inconsistent with X-ray diffraction results that show the UO_2 composition is effectively close to stoichiometry. This suggests that the non-stoichiometric material responsible for the *n*-type behaviour is either highly localized, possibly in grain boundaries, or randomly distributed at levels undetectable by X-rays. In view of the reductive sintering process used to produce UO_2 pellets from oxidized powders, the former appears the more likely explanation. The kinetic limiting current was calculated to be

Can. J. Chem. Downloaded from www.nrcresearchpress.com by 91.121.58.235 on 09/08/12
For personal use only.

© 1997 NRC Canada

Fig. 9. Tafel plots for O_2 reduction on a number of UO_2 rotating disc electrodes (16.7 Hz) recorded in 0.1 mol L^{-1} $NaClO_4$ (pH ~ 9.5) containing 2.5×10^{-4} mol L^{-1} dissolved oxygen: (•) SIMFUEL with 6 at.% burnup (SF1); (□) SIMFUEL with 3 at.% burnup (SF2); (Δ) SIMFUEL (3 at.% burnup) containing only species soluble in UO_2 (SS1); (×) SIMFUEL (3 at.% burnup) containing only noble metal segregants (SS2); (◆) neodymium-doped UO_2 (1 at.% Nd) (ND1). The line indicates a slope of 120 mV.



$$[7] \quad I_k = 4FAk'N_S^D(N_S^U)^{-1}[O_2]^{1/2} \exp\left\{-\frac{\alpha F\eta}{2RT}\right\}$$

where k' is an effective rate constant related to the fraction of donor–acceptor sites occupied by adsorbed O_2 molecules (θ_S),

$$[8] \quad k' = [\theta_S(1-\theta_S)k_2'k_1']^{1/2}$$

and k_2', k_1' are the rate constants in reaction [6] (31).

Equation [7] not only yields the observed square-root dependence on $[O_2]$ but also predicts large Tafel slopes of −240 mV (for α = 0.5). Observed Tafel slopes were usually between −240 and −310 mV.

While much can be learned from the study of these UO_2 specimens, neither is truly representative of used nuclear fuel, which will contain a multiplicity of fission products and actinides. Recently, we have studied O_2 reduction on simulated nuclear fuel (SIMFUEL). SIMFUEL contains 11 stable elements in proportions appropriate to replicate the chemical effects caused by reactor irradiation to various degrees of burnup. The principal microstructure of SIMFUEL (32) is virtually identical to that of ceramic UO_2, but secondary metallic (Mo, Ru, Rh, Pd) and perovskite ((Ba, Sr)ZrO_3) phases are present as submicron particles on grain boundaries, and the additives Y, Ce, Nd, La, and Zr are present dissolved in the UO_2 grains.

Figure 9 shows plots of O_2 reduction current in 0.1 mol L^{-1} $NaClO_4$ (pH ~ 9.5) for a neodymium-doped UO_2 (1 at.% Nd) (ND1), two SIMFUEL electrodes: SF1 (6 at.% burnup); SF2 (3 at.% burnup), a SIMFUEL electrode with a nominal 3 at.% burnup containing only the species soluble in UO_2 (SS1), and a SIMFUEL with 3 at.% nominal burnup containing only the noble metal segregants (SS2) (33). The noble metal segregants, present in SF1, SF2, and SS2, are predominantly a hexagonal close-packed alloy, known as the ε-phase, with an average composition in at.% of Ru(47)Mo(28)Pd(22)Rh(3) (32). These particles are a few hundred nanometres in diameter and are distributed along grain boundaries in the fuel.

As on a standard CANDU fuel specimen (*p*-type UO_2), the overall O_2 reduction reaction is a four-electron process with a close to first-order dependence on $[O_2]$ (33). For electrodes containing only rare earth dopants (SS1, ND1) the currents are typical of those measured on slightly hyperstoichiometric, but otherwise undoped, *p*-type UO_2. As for *p*-type UO_2, the Tafel slopes are >−120 mV, Fig. 9. Electrodes containing noble metal segregants (SF1, SF2, SS2) exhibit currents that are enhanced by up to two orders of magnitude, especially at lower overpotentials when Tafel slopes approaching −90 mV are observed, Fig. 9.

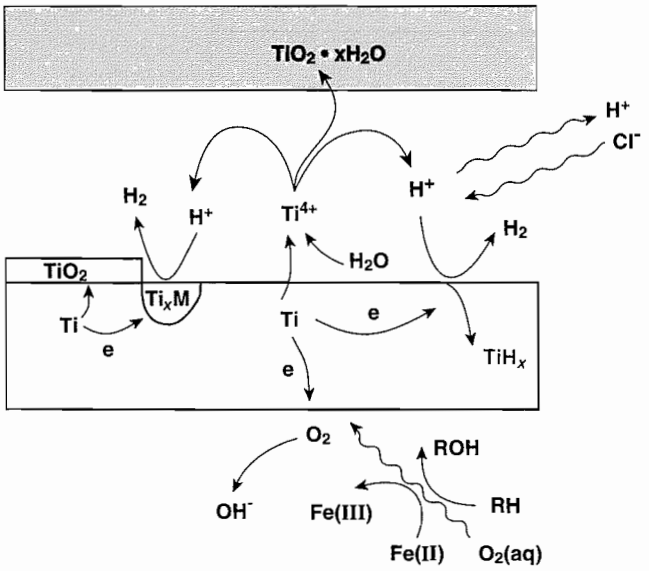
The introduction of lower valence rare earth elements into the uraninite structure will increase both the electrical conductivity and the number of available donor–acceptor sites by creating additional holes in the U 5*f* sub-band (Fig. 8*B*). However, despite the excellent electrical conductivity of ND1 and SS1 there is no significant enhancement in the kinetics of O_2 reduction. Conversely, the poorly conducting SS2 electrode, without rare earth dopants to produce an increased number density of donor–acceptor sites, shows marked electrocatalysis, especially at lower overpotentials, comparable with that found for the SIMFUEL electrodes, SF1 and SF2. Clearly, the high reactivity of the SIMFUEL electrodes must arise predominantly from the noble-metal particles rather than from rare-earth doping of the UO_2 lattice (Fig. 8*C*). The observation of a Tafel slope <−120 mV at low overpotentials is also consistent with reduction at noble metal particles: Tafel plots for O_2 reduction on Pd, Rh, and Ru generally exhibit two

© 1997 NRC Canada

Can. J. Chem. Downloaded from www.nrcresearchpress.com by 91.121.58.235 on 09/08/12
For personal use only.

Can. J. Chem. Downloaded from www.nrcresearchpress.com by 91.121.58.235 on 09/08/12
For personal use only.

Fig. 10. Chemical and electrochemical processes involved in the crevice corrosion of titanium under waste disposal vault conditions. The crevice exists under the $TiO_2 \cdot xH_2O$ deposit, which is itself a product of the crevice corrosion process. The initial crevice would require the presence of a crevice former above this deposit (not shown).



distinct regions, with slopes of −60 mV at low current densities and −120 to −180 mV at high current densities (34–36).

In the oxidation/dissolution of used nuclear fuel the noble metal particles will act as preferential cathodes for the oxidant reduction processes driving fuel dissolution. A valid mixed-potential model for the corrosion of used nuclear fuel under waste disposal conditions will need to accommodate these processes.

3. Corrosion of nuclear waste containers

Conditions within a nuclear waste vault are expected to evolve from initially warm and oxidizing (<100°C, aerated groundwater) to eventually cool and nonoxidizing, as the heat-generating radioactive processes decay and oxidants are consumed by reaction with oxidizable minerals in the vault buffer/backfill materials or by the container corrosion process. Two materials have been chosen as candidates for the construction of the container: dilute α-titanium alloys and copper. For both of these materials it is expected that most corrosion damage will be sustained during the early, warm oxidizing period of the lifetime of the vault (37). If long-term containment is to be achieved, then this damage, expressed as a depth of penetration of the available corrosion allowance, must be minimized.

To assess the effect of container performance on the release of radionuclides, models have been developed to predict lifetimes of containers and how these lifetimes will be affected by materials selection, evolution in vault conditions, and various vault engineering scenarios. These approaches and predictions have been reviewed (1, 2, 38). Much of the mechanistic information upon which these models and lifetime predictions are based has been developed electrochemically. Here, we review the chemistry/electrochemistry of corrosion processes and discuss some of the ways in which electrochemical procedures have been utilized.

3.1 Crevice corrosion of titanium alloys

For titanium alloys, crevice corrosion and hydrogen-induced cracking (HIC) are the corrosion processes most likely to cause container failure (1). While crevice corrosion under waste vault conditions is not expected (1, 39) it remains the corrosion mechanism most likely to lead to significant wall penetration while the vault is warm and oxidizing. Our present understanding of the chemical/electrochemical processes important in the crevice corrosion of titanium alloys is illustrated schematically in Fig. 10.

Once initiation of a crevice has occurred, O_2 reduction on surfaces external to the crevice will lead to the development of acidity due to the hydrolysis of dissolved metal cations at active sites within the crevice. In this manner, an oxygen concentration cell is established in which neutral oxidizing conditions exist outside, and acidic nonoxidizing conditions inside, the creviced area. The reduction of protons within the crevice not only causes further metal dissolution, but also leads to hydrogen absorption and the formation of precipitated metal hydrides within the metal, eventually rendering the material susceptible to HIC. If crevice corrosion proceeds unchecked for extended periods of time, then container failure by either crevice corrosion or HIC would be a danger.

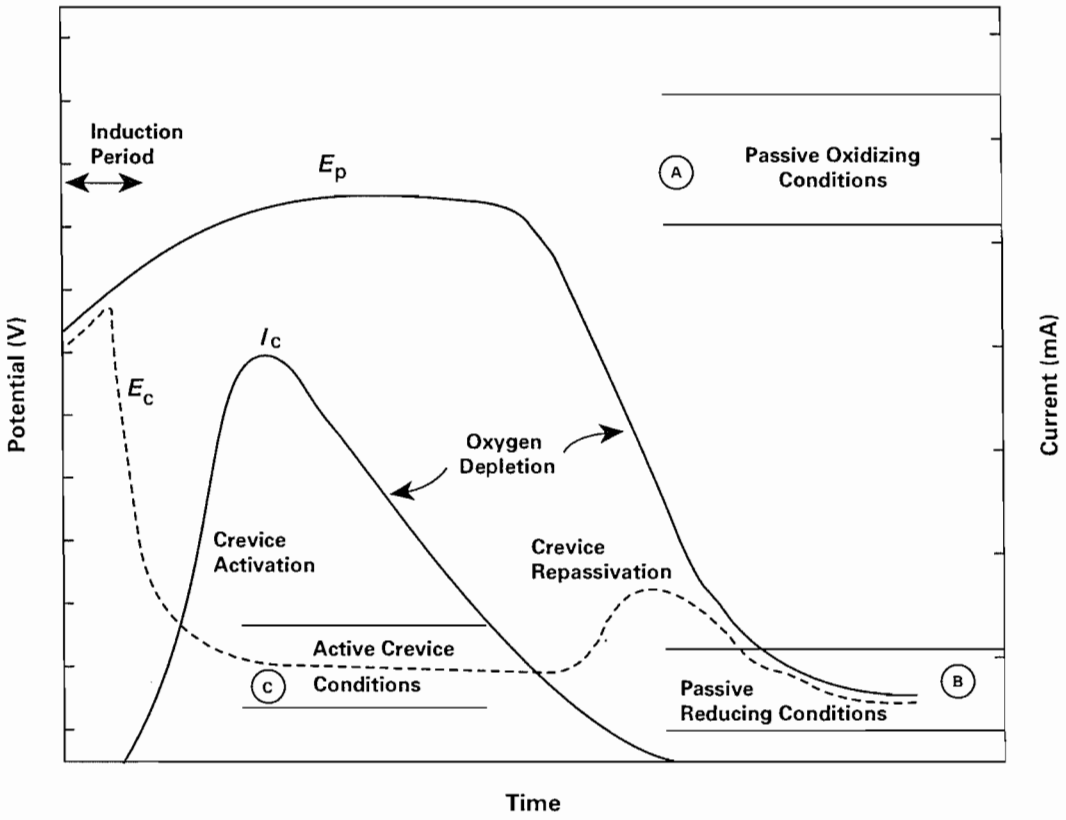
Two limitations on the extent of crevice corrosion appear possible. For susceptible alloys, crevice propagation can continue until all available O_2 within the vault is consumed, and the extent of damage will be limited by the consumption of O_2 by reaction with Fe^{II} and (or) organic material (RH) (Fig. 10). For impure Grade-2 titanium (Ti-2), or materials containing alloying elements to decrease crevice corrosion susceptibility (Ni and Mo in Ti-12; Pd in Ti-16), proton reduction on the surfaces of intermetallics (Ti_xM in Fig. 10) could induce repassivation (40).

To study the propagation of crevice corrosion we have employed a galvanic coupling technique in which an artificially creviced working electrode is coupled to a large Ti counter electrode through a zero-resistance ammeter (41). This arrangement simulates the conditions that could lead to crevice corrosion in a waste vault when metal dissolution within a relatively small occluded area on a container wall is supported by O_2 reduction on a much larger area of the wall, i.e., the potentially dangerous situation of a small anode coupled to a large surrounding cathode. The experiment is performed inside a sealed pressure vessel, an arrangement that limits the amount of available oxygen as expected in a sealed waste vault.

Figure 11 shows the general form of the coupled current (I_C), creviced electrode potential (E_C), and the non-creviced electrode potential (E_P), for an experiment on an alloy of titanium susceptible to crevice corrosion. After a short induction period, I_C rises and E_C falls as the crevice activates, and I_C falls once the available O_2 is consumed. O_2 depletion is also accompanied by a fall in E_P. As I_C approaches zero, a loop in E_C is generally taken to be an indication that repassivation is underway. The value of I_C is the rate of crevice propagation supported by the reduction of O_2 on passive surfaces external to the crevice. It underestimates the true rate since no current flows in the external measuring circuit due to propagation driven by proton reduction within the crevice, which is a short-circuit reaction (Fig. 10). However, our experiments suggest that, for extensive propagation, the ratio of externally

© 1997 NRC Canada

Fig. 11. The general form of the coupled current (I_C), crevice potential (E_C), and the planar potential (E_P) measured using the galvanic coupling technique: (*A*) range of corrosion potentials (E_P) measured for passive corrosion under oxidizing conditions; (*B*) range of corrosion potentials (E_P) measured for passive corrosion under nonoxidizing conditions; (*C*) range of crevice potentials (E_C) measured on an active crevice.



to internally supported crevice propagation is approximately constant. Once this ratio is established from weight-change measurements, which measure the total extent of crevice propagation, the real propagation rate can be obtained by multiplying I_C by an attenuation factor (42).

The influences of many parameters, including chloride concentration (43, 44), groundwater composition (1), temperature (45, 46), O_2 concentration (1, 42), γ irradiation (1), welding (1), and material composition (40, 47), on crevice corrosion have been studied by this method, Here, as an example, we will confine our discussion to the effects of material composition.

3.2 Influence of impurities and alloying additives on the crevice corrosion of titanium

Figure 12 shows values of I_C and E_C measured on two specimens of Ti-2, and on Ti-12 and Ti-16 in 0.27 mol L^{-1} NaCl at 150°C (Ti-2 and Ti-12) or 100°C (Ti-16). It is clear that the rate ($\propto I_C$) and the extent (Q_C = area under the I_C-t curve) of crevice propagation decrease by many orders of magnitude from Ti-2 to Ti-12 and Ti-16. The distinctly different behaviours observed for the two Ti-2 materials reflect the diverse properties of materials that differ in the amount and distribution of impurities, particularly Fe (40, 47). Very large values of I_C are accompanied by negative values of E_C and are indicative of fully activated, rapidly propagating crevices. Small currents accompanied by less negative potentials are observed when propagation is limited, and are indicative of partially activated crevices (i.e., with limited active area) capable of repassivation even in the presence of substantial concentrations of O_2.

The two Ti-2 specimens differ in their Fe content (~0.02 and >0.1 wt.%) and grain size (30–40 μm and ~15 μm, respectively) (47). Crevice propagation is clearly suppressed in the high Fe material, and repassivation, indicated by a fall in I_C to zero accompanied by a positive shift in E_C (Fig. 12*B*), occurs before all the O_2 is consumed. The critical feature in suppressing propagation appears to be the presence of small amounts of Ni with Fe in intermetallic particles. These particles appear to possess a lower overvoltage for proton reduction than the adjacent α-Ti grains and act as local cathodes driving the latter to repassivate (40).

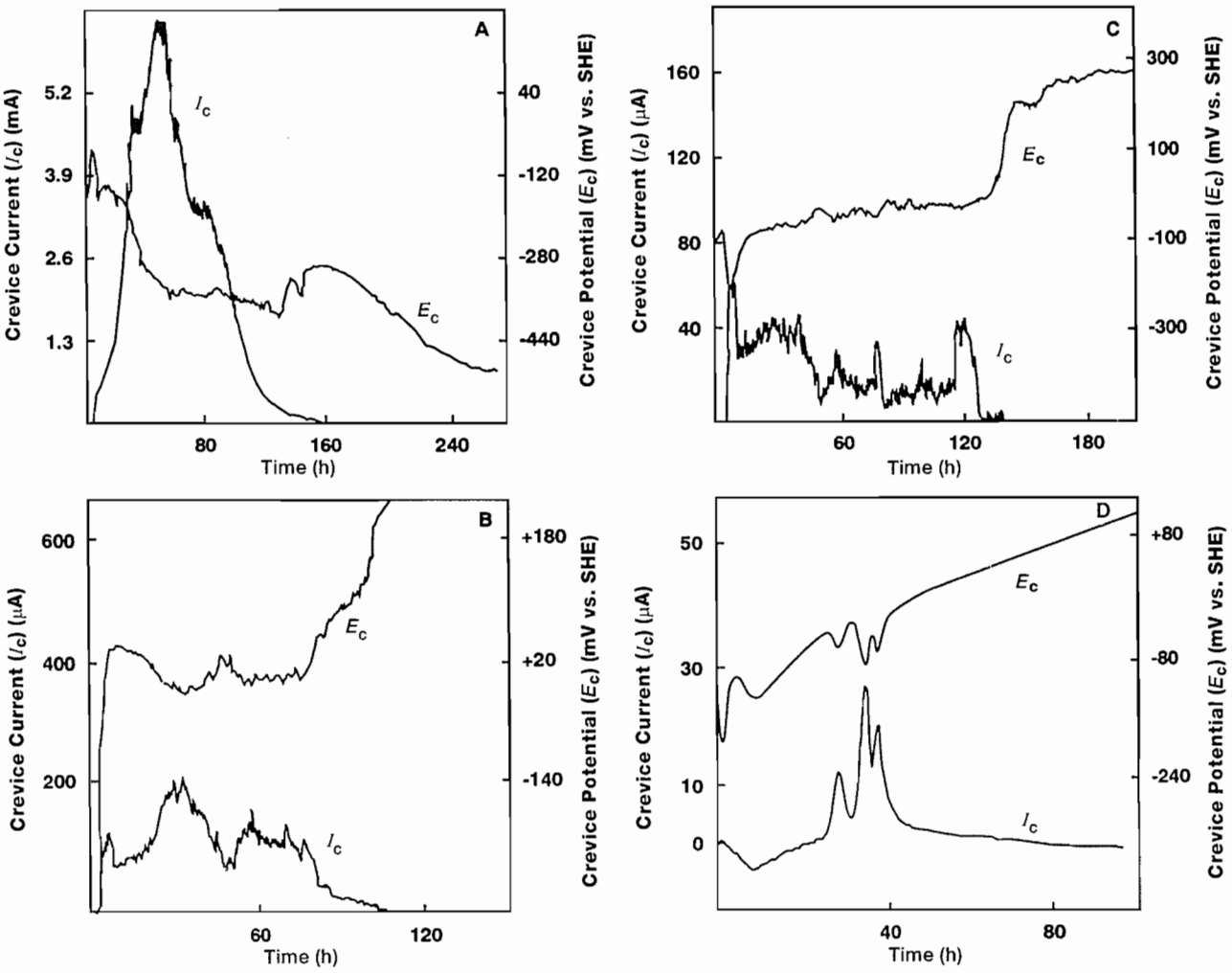
For Ti-12 (0.8 wt.% Ni, 0.3 wt.% Mo) the extent of propagation before repassivation is minor. Two possible explanations have been proposed: (*i*) repassivation is driven by catalysis of the proton reduction reaction on intermetallic Ti_2Ni particles within the creviced area of the surface (Fig. 9) (48); (*ii*) dissolution of the intermetallic particles leads to nickel ion enrichment of the corrosive crevice solution, and redeposition of metallic nickel on adjacent titanium surfaces then produces catalytic sites for proton reduction (49). Similar mechanisms have been claimed for Ti-16 (0.05 wt.% Pd) (50) on which crevice propagation is insignificant. Pd enrichment at the surface of corroding specimens may also be a factor (51,

Can. J. Chem. Downloaded from www.nrcresearchpress.com by 91.121.58.235 on 09/08/12
For personal use only.

© 1997 NRC Canada

Can. J. Chem. Downloaded from www.nrcresearchpress.com by 91.121.58.235 on 09/08/12
For personal use only.

Fig. 12. Coupled currents (I_C) and crevice potentials (E_C) measured in 0.27 mol L^{-1} NaCl on artificially formed crevices of various Ti alloys. (*A*) Ti-2 (Fe-0.024 wt.%) at 150°C; (*B*) Ti-2 (Fe-0.13 wt.%) at 150°C; (*C*) Ti-12 at 150°C; (*D*) Ti-16 at 100°C.



52). This ability of Ti-12 and Ti-16 to repassivate under oxidizing conditions renders these two materials much less dependent than Ti-2 on the evolution of the waste vault environment from warm and oxidizing to cool and nonoxidizing.

3.3 Impedance characteristics of passive films on titanium alloys

Providing that the extent of crevice corrosion can be limited, or better still, its initiation avoided, then the corrosion of titanium waste containers would proceed extremely slowly under passive conditions and long container lifetimes (>10^5 years) would be expected (3). If predictions of such long lifetimes are to be assured, then the properties of the passive films, upon which such good performance depends, must be thoroughly understood. With this aim in mind, we have studied the properties of the oxide films formed on pure Ti, Ti-2, Ti-12, and Ti-16 under open-circuit corrosion conditions in deaerated 0.27 mol L^{-1} NaCl as a function of temperature using electrochemical impedance spectroscopy (53).

Figure 13 shows Bode plots of the frequency response of these materials at 80°C. For all the materials the total impedance (|Z|) depends on frequency in a manner suggesting that the behaviour is dominated by the capacitative response of the film (i.e., $|Z| \propto \log f$). This is confirmed by the value of the phase angle (θ) at intermediate frequencies, which is >80° out of phase. That the phase angle is <90° out of phase indicates this capacitative behaviour is less than ideal. For low frequencies (<1 Hz) differences in both |Z| and θ are observed between the different alloys.

The impedance data can be accurately fitted by the equivalent circuit shown in Fig. 14. The non-ideal capacitative response of the oxide film, which suggests a non-homogeneous distribution in film capacitance, is represented by a constant phase element (CPE). The film is considered to be breached by defects that may be either grain boundaries in the oxide, physical defects introduced by compressive stresses, or incomplete film formation at the sites of surface intermetallics known to be distributed throughout all these materials (except for pure Ti). These defects are represented in the equivalent circuit by an interfacial impedance, Z_I, which could be specified as a parallel combination of an interfacial polarization resistance (R_P) and an interfacial capacitance (C_I), in series with a pore, or defect, resistance, R_{PORE}. The resistance, R_S, is the electrolyte resistance, which is negligible in this case.

© 1997 NRC Canada

Fig. 13. Bode plots for various Ti alloys recorded after 24 h on open circuit in 0.27 mol L^{-1} NaCl at 80°C: (—·—·) pure Ti; (—) Ti-2; (– – –) Ti-12; (----) Ti-16.

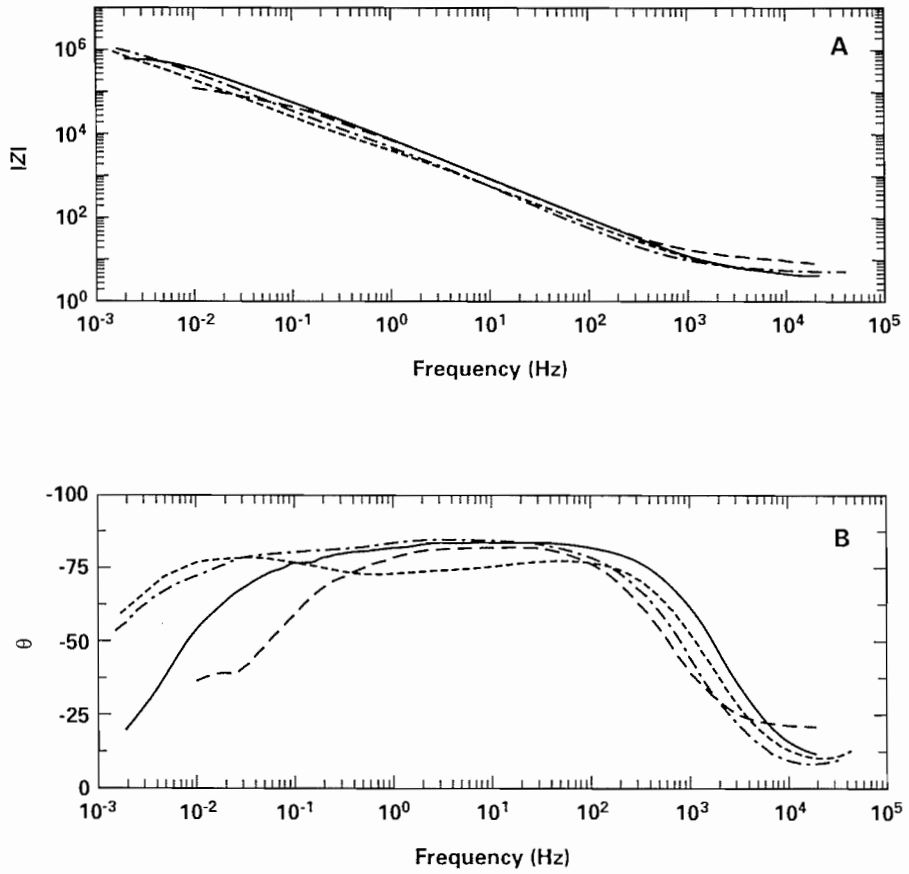
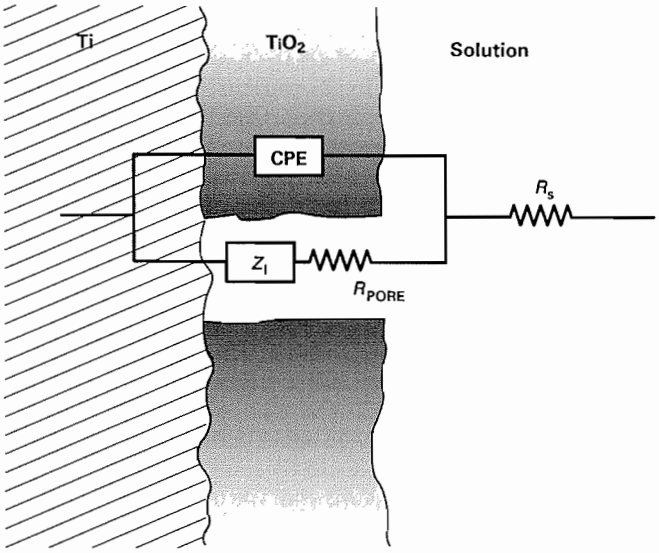


Fig. 14. Equivalent circuit used to analyze electrochemical impedance spectroscopy data for passive Ti alloys.



Within this circuit, R_P will be inversely related to the corrosion rate of the material if it is assumed that charge transfer, either electrochemically or as film dissolution, does not occur across the intact oxide–solution interface.

A comprehensive discussion of the impedance behaviour as a function of temperature is beyond the scope of this paper and will be published elsewhere (53). At lower temperatures, all four materials are covered by a passive film with a very high impedance and hence the capability of providing excellent corrosion protection. However, at 80°C the impedance spectra show clear differences at low frequencies (Fig. 13). For pure Ti and Ti-16, a generally capacitative response is maintained even at $f \lesssim 10^{-2}$ Hz, i.e., the phase angle, θ, remains numerically large and the impedance Z continues to increase. By contrast, for Ti-2 and Ti-12 the impedance begins to level off at the lowest frequencies (Fig. 13*A*), and to become more resistive in character (Fig. 13*B*).

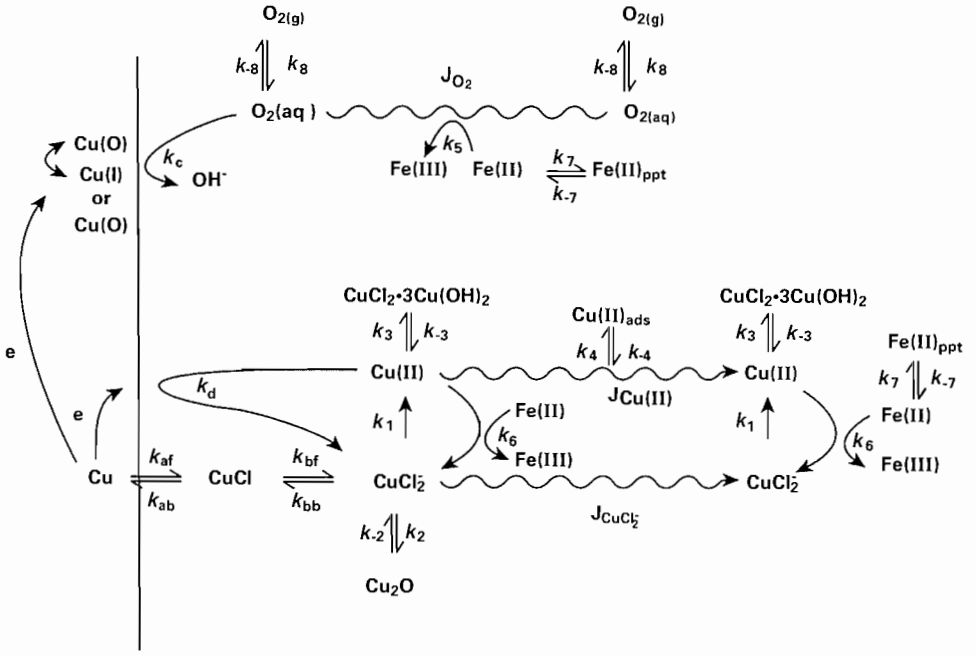
It has been shown by various electrochemical and analytical methods (ellipsometry, Raman, XPS) that, for $T \gtrsim 70$°C, film breakdown/recrystallization followed by film thickening occurs (54–57). These experiments were performed on commercially pure Ti (i.e., Ti-2). Under creviced conditions on Ti-2 this process leads to the development of acidity, oxide dissolution, and, in chloride solutions, the initiation of localized corrosion (58). The generation of acidity in this manner is a clear indication of the occurrence of metal dissolution/metal cation hydrolysis. Under non-creviced conditions this process cannot develop the local low pH (<1 at 70°C) required for the initiation of localized corrosion (59).

For both Ti and Ti-2 a simple parallel combination of the constant phase element, CPE, and R_{PORE} gave the best fit for

© 1997 NRC Canada

Can. J. Chem. Downloaded from www.nrcresearchpress.com by 91.121.58.235 on 09/08/12
For personal use only.

Fig. 15. Proposed mechanism for the corrosion of copper nuclear fuel waste containers.



the data, although the value of R_{PORE} for Ti-2 (~0.6 Mohm cm^2) is significantly lower than that for Ti (~2 Mohm cm^{-2}). This is consistent with a loss in film resistance for Ti-2 due to the film breakdown – recrystallization – film thickening process that would introduce a high density of grain boundaries, thereby providing short diffusion paths for the ions involved in film growth. The much higher value of R_{PORE} suggests this process does not occur on Ti. The specimen of Ti-2 used contained sufficient Fe as an impurity (0.105 wt.%) for the separation of Ti_xFe intermetallics (60). It would appear that the presence of these intermetallics facilitates the film breakdown – recrystallization process.

For Ti-12, the number density of intermetallics (Ti_2Ni) would be much higher than in Ti-2. The data for Ti-12 cannot be accurately fitted to a circuit with only one time constant (as for Ti and Ti-2) and the equivalent circuit involving film defects (Z_I, R_{PORE}, Fig. 14) is required. The value of R_{PORE} (~0.1 Mohm cm^2) is substantially lower than that for Ti-2, consistent with a much higher density of defect sites within which an interfacial impedance (Z_I) is now detectable in the impedance spectrum.

For Ti-16 there is clear evidence for two time constants in the impedance spectrum despite the fact that the film maintains its essentially capacitative nature to very low impedances. Apparently, the intermetallic particles known to exist in this alloy (61) do not lead to the introduction of low-resistance defects into the film. However, the value of R_{PORE} for Ti-16 is approximately an order of magnitude lower than that calculated for Ti-12. The value of R_P, associated with Z_I (the interfacial impedance within the defect/pore), is >2 Mohm cm^{-2} compared to a value for Ti-12 of ~0.1 Mohm cm^2. This combination of relatively low-resistance pores R_{PORE} with a high interfacial polarization resistance (R_P) suggests the presence of a large number of exposed noble particles on a generally passive surface.

These results indicate that the order of stability of the different alloys of titanium is different for general passive corrosion than it is for crevice corrosion. For crevice corrosion the extent of damage decreased in the order

$$\text{Ti} > \text{Ti-2} > \text{Ti-12} \gg \text{Ti-16}$$

For general passive corrosion, the susceptibility to corrosion decreases in the order

$$\text{Ti-12} > \text{Ti-2} > \text{Ti-16} \sim \text{Ti}$$

Some caution should be exercised in accepting the order for general passive corrosion, which could change if determined at a higher temperature than the 80°C used in the present work.

3.4 General corrosion of copper

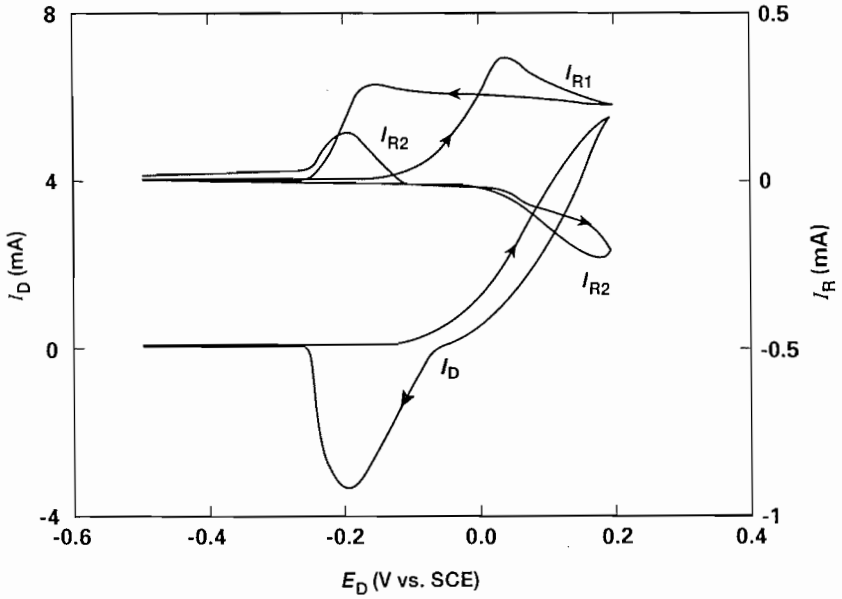
Figure 15 shows the mechanism of the uniform corrosion of Cu containers in Cl^--rich groundwaters. A number of interfacial and homogeneous redox reactions are involved, including the anodic dissolution of Cu as $CuCl_2^-$ (k_{af}, k_{ab}, k_{bf}, k_{bb}) supported by the interfacial reduction of dissolved O_2 (k_c), the oxidation of $CuCl_2^-$ by O_2 (k_1), the consumption of O_2 by reaction with dissolved Fe^{II} (k_5), and the reduction of Cu^{II} by Fe^{II} (k_6). The corrosion rate of the container will also be significantly affected by the adsorption properties of the compacted buffer materials surrounding the container and the precipitation of solids, either locally at the container surface or throughout the surrounding media. Finally, the transport fluxes (J_{O_2}, $J_{Cu^{II}}$, $J_{CuCl_2^-}$) will be restricted since the effective diffusion coefficients of species in water-saturated compacted buffer material will be ~10^2 lower than in bulk solution due to the constrictive and tortuous nature of the pore structure.

Here we describe the two interfacial processes and the measurement and prediction of the corrosion potential (E_{CORR})

© 1997 NRC Canada

Can. J. Chem. Downloaded from www.nrcresearchpress.com by 91.121.58.235 on 09/08/12
For personal use only.

Fig. 16. Rotating split-ring disc electrode study of the dissolution of copper in deaerated 0.1 mol L^{-1} NaCl/0.1 mol L^{-1} Na_2SO_4. I_{R1} is the ring current for the oxidation of Cu^I (E_{R1} = +0.4 V vs. SCE), I_{R2} is the ring current for the reduction of Cu^{II} to Cu^I (E_{R2} = −0.1 V vs. SCE), and the disc potential was scanned between −0.5/+0.2/−0.5 V vs. SCE at a scan rate of 10 mV s^{-1}. Collection efficiency for each half-ring 0.2, disc surface area 0.33 cm^2, rotation rate 14.3 Hz.



and corrosion rate (i_{CORR}). Since transport rates are extremely important in determining Cu container corrosion, particular attention has been paid to E_{CORR} measurements under restricted mass transport conditions. The results of these studies have been used to develop a detailed finite-difference model to predict E_{CORR} and i_{CORR} for Cu containers in a waste vault.

3.5 Anodic dissolution of Cu in chloride solutions

The anodic dissolution of Cu in acidic and neutral Cl^- solutions has been extensively studied (ref 62, and refs. therein). As first proposed by Deslouis et al. (62), the mechanism can best be described by the reactions

[9] $Cu + Cl^- \leftrightarrow CuCl_{ads} + e^-$

[10] $CuCl_{ads} + Cl^- \leftrightarrow CuCl_2^-(s)$

[11] $CuCl_2^-(s) \xrightarrow{RDS} CuCl_2^-(b)$

where the diffusion of $CuCl_2^-$ from the surface of the electrode (s) to the bulk of solution (b) is rate determining (reaction [11]). Various mechanisms for the preceding interfacial reactions ([9] and [10]) are best distinguished by considering the E and [Cl^-] dependence of the intercepts and slopes of Koutecky–Levich (K–L) plots, in which the inverse of the observed current from RDE measurements is plotted against the inverse of the square root of the rotation frequency. Extrapolation of these plots to infinite rotation frequency permits the mathematical separation of the transport and interfacial components of the observed current. Our own work has confirmed this mechanism and has shown the conditions under which reaction [10] can be considered to be at equilibrium (62, 63). In addition, we have determined values for k_{bb} and the parameter ($k_{af}k_{bf}/k_{ab}$) used in our mixed-potential model.

Pore water in compacted buffer is expected to contain a significant [SO_4^{2-}] from the dissolution of gypsum ($CaSO_4 \cdot 2H_2O$) impurities. Unlike Cl^-, SO_4^{2-} does not stabilize Cu^I species, and generally Cu^{II} corrosion products are observed (64). To determine the speciation of Cu in mixed Cl^-/SO_4^{2-} solutions we have used a Au–Cu RSRDE (rotating split ring disc electrode) (Fig. 16). One half-ring is used to detect Cu^I dissolution from the Cu disc ($Cu^+ \rightarrow Cu^{2+} + e$; E = +0.4 V (vs. SCE)) while the other half-ring is used to detect Cu^{II} dissolved from the Cu disc ($Cu^{2+} + e \rightarrow Cu^+$; E = −0.1 V (vs. SCE)). In chloride solutions (0.1 mol L^{-1}, not shown in Fig. 16), Cu dissolves as Cu^I for $E \lesssim 0.1$ V (vs. SCE), as indicated by the absence of a ring current for Cu^{II} reduction. Virtually identical behaviour is observed when 0.1 mol L^{-1} Na_2SO_4 is added (Fig. 16). Thus, Cl^- dominates the speciation of dissolved Cu, at least up to 0.0 V (vs. SCE) and reactions [9]–[11] represent Cu dissolution even in sulphate-containing pore waters.

Invariably, Cu exposed to natural environments is covered by a thin layer of Cu_2O. Except in alkaline solutions (65), the mechanism of Cu_2O formation has not been extensively examined in Cl^- solutions. There are two possible mechanisms,

(*i*) the hydrolysis of $CuCl_{ads}$:

[12] $2CuCl_{ads} + H_2O \leftrightarrow (Cu_2O)_S + 2H^+ + 2Cl^-$

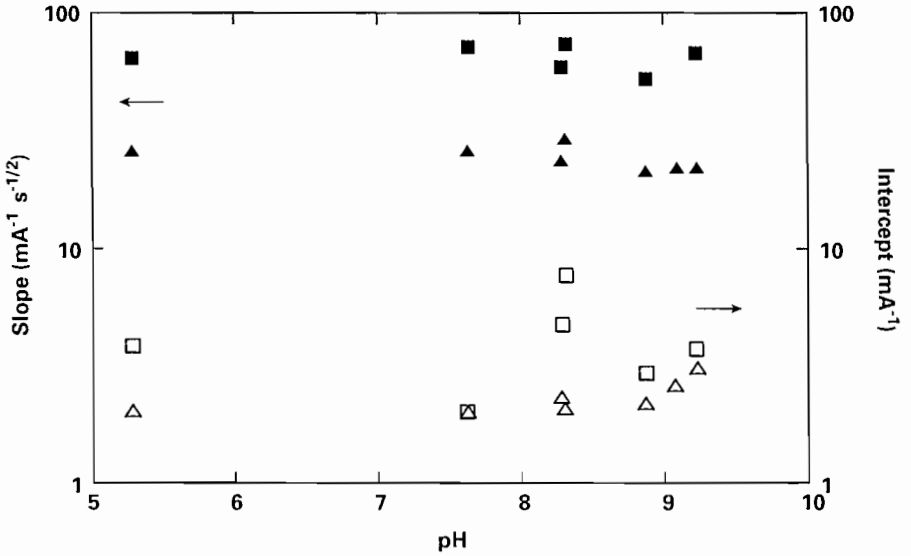
and (*ii*) the hydrolysis of dissolved $CuCl_2^-$:

[13] $2CuCl_2^- + H_2O \leftrightarrow (Cu_2O)_S + 2H^+ + 4Cl^-$

Can. J. Chem. Downloaded from www.nrcresearchpress.com by 91.121.58.235 on 09/08/12
For personal use only.

© 1997 NRC Canada

Fig. 17. pH dependence of Koutecky–Levich (K–L) slopes and intercepts for a copper RDE in 0.1 mol L^{-1} NaCl. ■, slope at a disc potential (E_D) of −0.125 V vs. SCE; □, intercept at E_D = −0.125 V vs. SCE; ▲, slope at E_D = −0.100 V vs. SCE; Δ, intercept at E_D = −0.100 V vs. SCE.



Can. J. Chem. Downloaded from www.nrcresearchpress.com by 91.121.58.235 on 09/08/12
For personal use only.

These hydrolysis reactions may proceed via CuOH intermediate species, either $Cu(OH)_{ads}$ in the case of eq. [12] or a dissolved complex in the case of eq. [13]. Both of these mechanisms account for the experimental observation that the amount of Cu_2O formed increases with (*i*) increasing pH, (*ii*) decreasing [Cl^-], and (*iii*) decreasing rate of mass transport. The plausibility of reactions [12] and [13] can be determined from the *E*, [Cl^-], and pH dependence of K–L slopes and intercepts shown in Fig. 17 as a function of pH in 0.1 mol L^{-1} NaCl. Both slopes and intercepts are pH independent up to pH = 9.2, above which Cu_2O formation (identified by cathodic stripping voltammetry) passivates the electrode. An identical critical pH is obtained in 1.0 mol L^{-1} NaCl. If Cu_2O formation were in competition with dissolution as $CuCl_2^-$ (reaction sequence [9]–[11] then [13]), then the critical pH might be expected to increase with [Cl^-]. While the exact mechanism remains to be demonstrated, this favours the reaction sequence [9]–[11] followed by reaction [12].

3.6 Cathodic reduction of oxygen on copper

A generalized mechanism for the reduction of O_2 is given in Fig. 6 and indicates that two products, OH^- and (or) H_2O_2, may be released from the disc of an RRDE (rotating ring disc electrode). We have used a Au ring to detect peroxide released as an intermediate in O_2 reduction and a Bi ring to detect the four-electron end product, OH^- (66). The Bi surface oxidizes in air to produce a pH-sensitive Bi_2O_3 ring electrode.

Figure 18 shows steady-state currents for the reduction of O_2 on Cu in 1.0 mol L^{-1} NaCl for three [O_2]. At negative potentials a well-defined limiting current and no ring current for HO_2^- oxidation are obtained, consistent with an overall four-electron reduction of O_2 to OH^-. For aerated solutions and solutions equilibrated with low O_2 partial pressures, a single wave and no detectable ring current are obtained. For atmospheres of ≥50 vol.% O_2/N_2 a cathodic peak and measurable peroxide formation are observed in the joint kinetic/transport potential region. This suggests that a catalytic surface is formed in this potential range. The [O_2] at which the cathodic peak is observed varies with pH (67), a peak being observed in aerated solution at pH =10, but not in neutral NaCl. Also, the peak observed in oxygenated neutral solution (Fig. 18) disappears when the solution is buffered at pH 7.

Significant pH changes are detected at a Bi ring electrode in neutral 1.0 mol L^{-1} $NaClO_4$ solution (Fig. 19). The hysteresis observed in the disc current on a potentiodynamic scan is also obtained in the pH measurement that follows the disc current. In the transport-limited region for O_2 reduction, the interfacial pH reaches a maximum value of ~10.5.

Kinetic parameters were determined from steady-state measurements in 1.0 mol L^{-1} NaCl. Reaction orders with respect to [O_2] varied from ~1 for $E \lesssim -0.5$ V (vs. SCE) to >1 at more positive potentials, corresponding to the cathodic peak at higher [O_2]. Transport-corrected Tafel slopes increased with [O_2], from −135 mV for 2 vol.% O_2/N_2 to −160 to −180 mV for ≥ 21 vol.% O_2/N_2. These values are consistent with control of the overall process by the first electron transfer.

To explain the observation of the cathodic peak, it is conjectured that O_2 reduction occurs on two different surface sites: (*i*) "bare" Cu sites (type A), present on cathodically reduced Cu at negative potentials and at low [O_2]; (*ii*) catalytic sites (type B) formed at more positive potentials and at higher [O_2]. Then, the kinetic current (I_k) is given by (67),

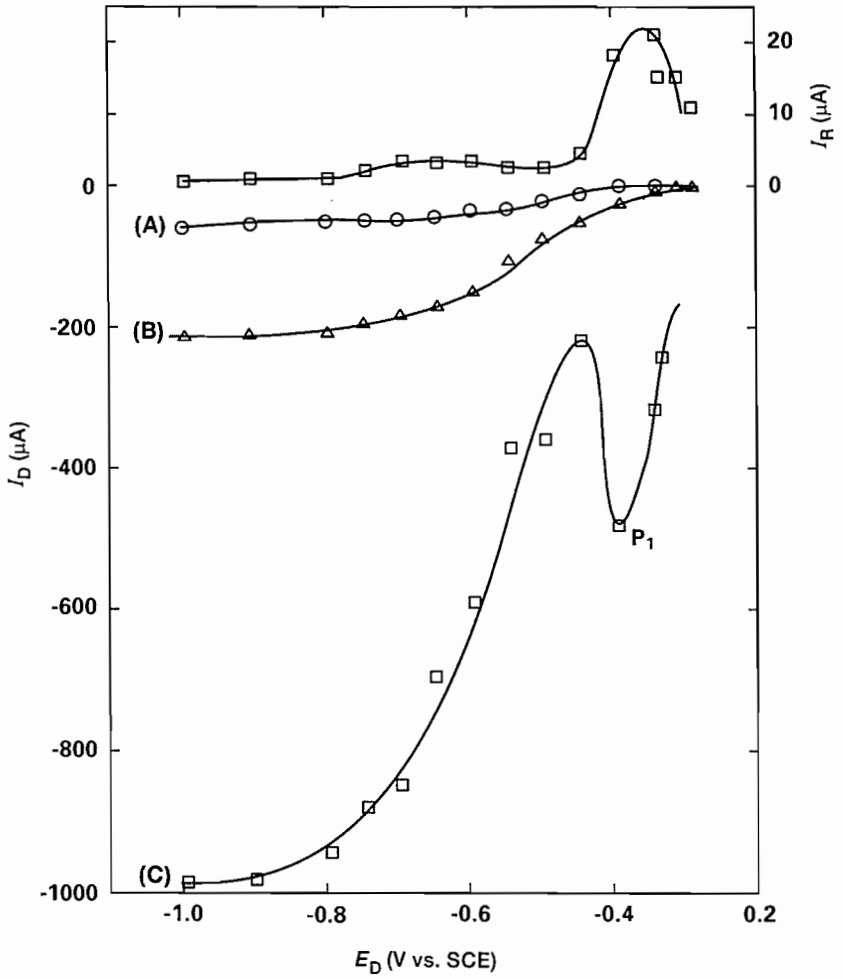
$$[14] \quad -I_k = nFA[O_2](\theta_A k^\circ_{CA} + \theta_B k^\circ_{CB}) \exp\left\{-\frac{\alpha F(E-E_C^\circ)}{RT}\right\}$$

where *n* is the overall number of electrons, *A* is the surface area, k°_{CA} and k°_{CB} are standard rate constants for sites A and B ($k^\circ_{CB} \gg k^\circ_{CA}$), θ_A and θ_B are the fractional surface coverages, and E°_C is the standard potential for O_2 reduction on both sites, assumed here to occur via the same mechanism. It is further assumed that the reaction is first order with respect to [O_2].

Because θ_B is a function of *E* and, through the interfacial pH, a function of [O_2], eq. [14] can be used to explain the observed variations in Tafel slope and reaction order. At negative potentials and (or) low [O_2], $\theta_B \rightarrow 0$ and a reaction order

© 1997 NRC Canada

Fig. 18. Steady-state oxygen reduction currents on copper in 1 mol L^{-1} NaCl in atmospheres of (*A*) 5 vol.% O_2/N_2 (○), (*B*) air (Δ), and (*C*) 100% O_2 (□), and the corresponding ring current for the oxidation of peroxide for 100% O_2. Disc surface area 0.33 cm^2, collection efficiency 0.4, rotation rate 14.3 Hz. (Reprinted from J. Electroanal. Chem.Vol. 385, F. King et al., "Oxygen reduction on copper in neutral NaCl solution", 44–55 (1995) with kind permission from Elsevier Science S.A., P.O. Box 564, 1001 Lausanne, Switzerland.)



of 1 with a Tafel slope of −120 mV (α = 0.5) are predicted. At more positive potentials and (or) higher $[O_2]$ (i.e., higher interfacial pH), $\theta_B k^\circ_{CB} \gg \theta_A k^\circ_{CA}$. The current increases as a consequence of the formation of catalytic type-B sites. At more positive potentials the current decreases, both because of the decrease in the overpotential for the reduction of O_2 and because the activity of the surface decreases as it becomes covered by Cu^I (see below). By considering the potential dependence of θ_B, it can be shown that reaction orders between 1 and 2 are possible with Tafel slopes of $2.3RT/(\beta\text{-}2\alpha)F$, where β is the potential dependence of the formation of catalytic sites of type B (67)).

Evidence from cyclic voltammetry suggests the catalytic site may be composed of $Cu(OH)_{ads}$ or submonolayer Cu_2O. Voltammetry in deaerated solutions shows that the onset of the cathodic reduction peak coincides with the initial stages of Cu_2O formation, and Elsner et al. (68) suggest that $Cu(OH)_{ads}$ may be a precursor of Cu_2O. The presence of Cu^I on Cu^0 may provide the donor–acceptor sites thought to catalyse O_2 reduction on UO_2 and transition metal oxides (see Section 2.3 above). O_2 reduction at these sites (type B) also leads to the release of peroxide, which is not observed for O_2 reduction on "bare" Cu (type A sites).

3.7 Measurement and prediction of E_{CORR} in O_2-containing chloride solutions

Because the rate of mass transport of reactants and products to and from the container surface will be restricted by the compacted clay, we have made E_{CORR} measurements under different mass transport conditions. Under steady-state conditions, the relative permeability of the diffusion layer can be characterized by a steady-state mass transfer coefficient k_M, equal to D/δ, where D is the effective diffusion coefficient and δ the diffusion layer thickness. Two attempts were made to restrict mass transport: (*i*) by placing a porous nylon membrane over the electrode (MCE) ($k_M = 10^{-4}$ cm s^{-1}); (*ii*) by placing a clay layer (0.1 or 1.0 cm thick) over the electrode (CCE) ($k_M = 10^{-6}$–10^{-7} cm s^{-1}) (Fig. 20). Internal reference electrodes built into some of these electrodes (MCE, CCE) allowed us to correct for the small (<20 mV) membrane potential (69). By comparison, in bulk solution $k_M = 10^{-2}$ cm s^{-1}.

E_{CORR} measurements with an RDE in bulk solution as a

© 1997 NRC Canada

Can. J. Chem. Downloaded from www.nrcresearchpress.com by 91.121.58.235 on 09/08/12
For personal use only.

Fig. 19. Oxygen reduction on a Cu disc electrode in oxygenated unbuffered 0.1 mol L^{-1} $NaClO_4$ and the corresponding variation of the interfacial pH determined with a Bi_2O_3 ring electrode. Disc surface area 0.33 cm^2, rotation rate 14.3 Hz, potential scan rate 10 mV s^{-1}.

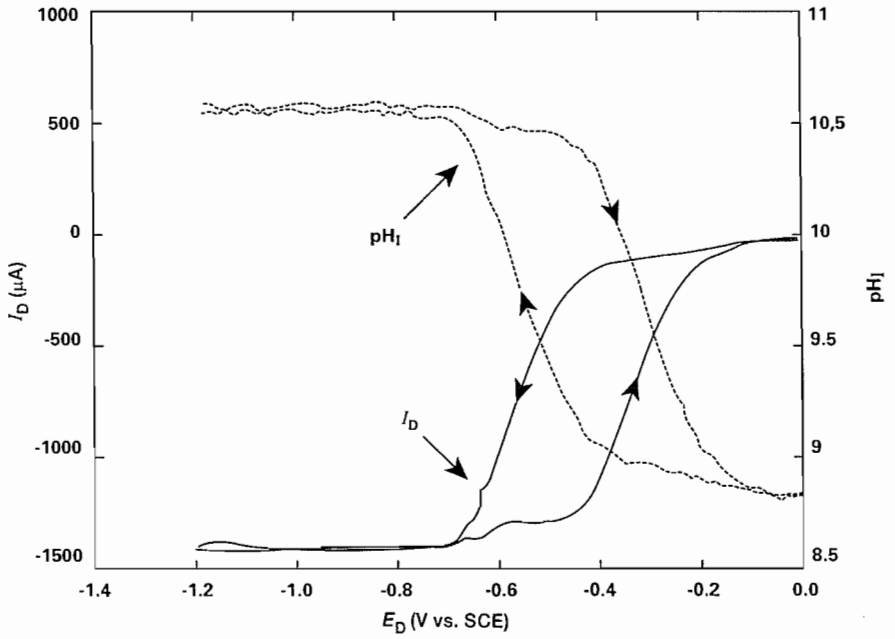


Table 1. Dependence of steady-state E_{CORR} of a copper rotating disc electrode in 1.0 mol L^{-1} NaCl solution on rotation rate and bulk oxygen concentration.

(a) Experimental measurements.

$[O_2]_\infty$ (mol L^{-1})	E_{CORR} at f = 2 Hz[a] (V (vs. SCE))	$\frac{dE_{CORR}}{d \log f}$ (V)	$\frac{dE_{CORR}}{d \log[O_2]_\infty}$ (V)
2.0×10^{-4} (air)	−0.306 ± 0.008	-0.019_8	0.049
1.9×10^{-5} (2% O_2/N_2)	−0.356 ± 0.011	-0.015_4	0.056
1.9×10^{-6} (0.2% O_2/N_2)	−0.413 ± 0.011	-0.014_7	0.032
7×10^{-7} (deaerated est.)	−0.426 ± 0.014	-0.011_1	

(b) Theoretical predictions.

$[O_2]_\infty$ (mol L^{-1})	E_{CORR} at f = 2 Hz (V (vs. SCE))	$\frac{[O_2]_0}{[O_2]_\infty}$	$\frac{dE_{CORR}}{d \log f}$ (V)	$\frac{dE_{CORR}}{d \log[O_2]_\infty}$ (V)
2×10^{-4}	−0.294	0.963	−0.016	0.040
1.9×10^{-5}	−0.335	0.921	−0.015	0.041
1.9×10^{-6}	−0.376	0.839	−0.015	0.042
7×10^{-7}	−0.393	0.789	−0.014	

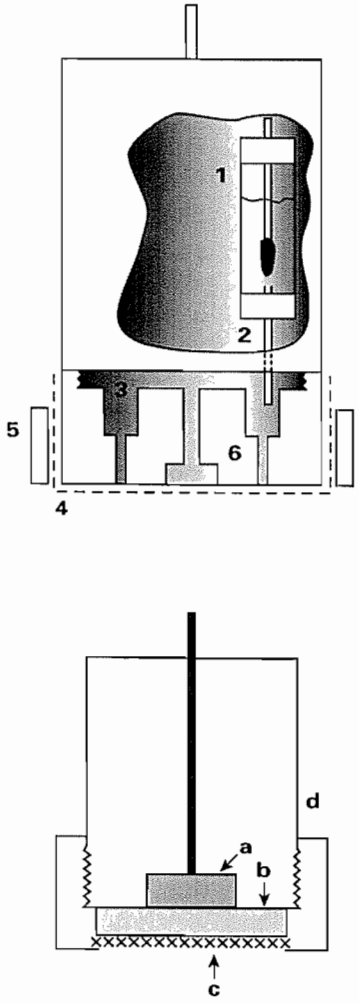
[a]Variability in E_{CORR} is given as ± one standard deviation for between 20 and 27 experiments under each set of conditions.

Can. J. Chem. Downloaded from www.nrcresearchpress.com by 91.121.58.235 on 09/08/12
For personal use only.

© 1997 NRC Canada

Can. J. Chem. Downloaded from www.nrcresearchpress.com by 91.121.58.235 on 09/08/12
For personal use only.

Fig. 20. Schematics of electrodes with reduced rates of mass transport to and from the surface. Top: Schematic of the membrane-covered electrode (MCE). (1) Internal Ag/AgCl/0.1 mol L^{-1} KCl reference electrode, (2) reference electrode wick, (3) solution-filled annular channel, (4) porous nylon membrane, (5) membrane retaining ring, (6) Cu disc electrode. Bottom: Schematic of the clay-covered electrode (CCE). (*a*) Cu disc, (*b*) layer of compacted clay, (*c*) Pt gauze frit, (*d*) Plexiglass electrode mount.



function of rotation rate frequency (f) and $[O_2]$ (69) demonstrated that in aerated solutions the transport of $CuCl_2^-$ away from the electrode was rate determining (i.e., reaction [11]) for the anodic reaction (Table 1). The cathodic reaction (O_2 reduction) is activation controlled, but becomes increasingly transport controlled as $[O_2]$ decreases (i.e., $dE_{CORR}/d \log f$ becomes less negative). Full transport control is never established even in nominally deaerated solutions (69).

Measurements with the MCE and CCE are consistent with transport control of both the anodic and cathodic reactions, as might be expected for electrodes with rates of mass transport 2–5 orders of magnitude lower than in bulk solution. E_{CORR} values measured with the MCE varied with neither the mean pore size of the membrane, nor f (69). Using the CCE, E_{CORR} was measured as a function of $[O_2]$ (Fig. 21). As expected, E_{CORR} decreases with $[O_2]$, but the time to establish steady state between each change in $[O_2]$ was ~50 h for the 0.1-cm-thick electrode (not shown) and 500–1000 h for the thicker clay layer (Fig. 21). E_{CORR} was relatively insensitive to the clay-layer thickness, but decreased by 40–60 mV per decade decrease in $[O_2]$ (69).

From the mechanisms of the anodic and cathodic reactions we have constructed mixed potential models (MPM) to predict E_{CORR} and i_{CORR}. These models allow us to interpret our experimental E_{CORR} measurements, and to predict container lifetimes and assess the probability of localized corrosion under waste disposal conditions. For the second of these two purposes, the interfacial processes are coupled to the mass transport, adsorption/desorption, precipitation/dissolution, and redox processes included in the full reaction mechanism (Fig. 15).

In our MPM, the anodic reaction is described by reactions [9] and [10] and the cathodic reaction by the overall mechanism

[15] $O_2 + 2H_2O + 4e^- \rightarrow 4OH^-$

The use of these simplified mechanisms is relatively unimportant in our MPM since mass transport processes determine the rates of anodic and cathodic reactions.

Table 1 gives the predicted values of E_{CORR} for comparison with the RDE measurements. The predicted values differ from experimental data by 30–40 mV at worst, and show the same trend of decreasing rotation–rate dependence with decreasing $[O_2]$. The MPM can also be used to predict the interfacial $[O_2]$ ($[O_2]_0$). The predicted $[O_2]_0/[O_2]_\infty$ ratio (Table 1) confirms the conclusion that the cathodic reaction becomes increasingly transport limited with decreasing $[O_2]$, but never completely ($[O_2]_0/[O_2]_\infty = 0$), even in deaerated solution.

The predicted steady-state E_{CORR} values for the CCE are marked on Fig. 21. Again, agreement between theory and experiment is within 30 mV, but in this case $[O_2]_0/[O_2]_\infty < 0.01$, suggesting essentially complete transport control of the cathodic reaction. The figure also compares the measured E_{CORR} as a function of time to that predicted using our full MPM model incorporating the processes detailed in Fig. 15 (70). The maximum difference between measured and experimental values is ~20 mV. Furthermore, the MPM accounts reasonably well for the period required for reestablishment of the steady state between each change in $[O_2]_\infty$.

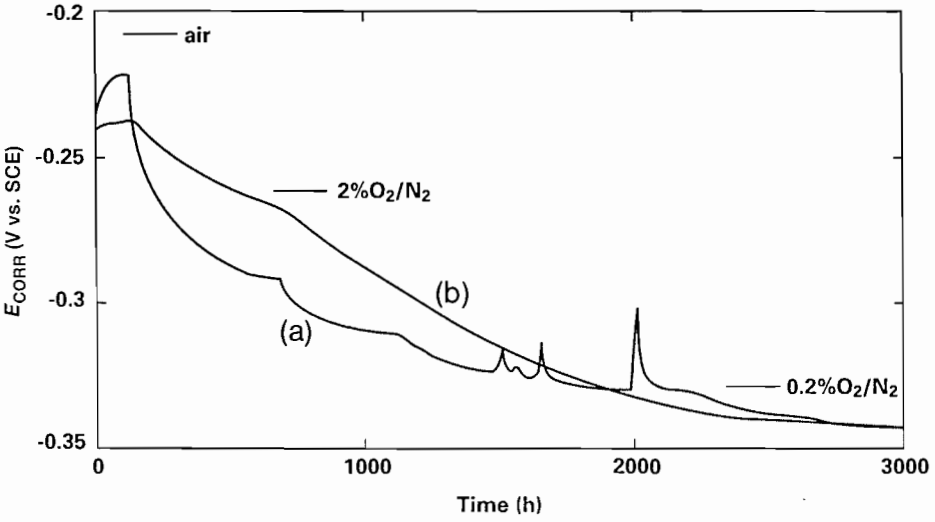
These agreements between measurement and prediction give us confidence that such modelling procedures can be justifiably applied to the prediction of waste container lifetimes.

4. Summary

A number of different electrochemical studies relevant to the disposal of nuclear waste have been described. These include studies of fuel dissolution and the localized and general corrosion of the potential waste container materials Cu and Ti. These studies have provided the mechanistic basis for the development of models to predict fuel and container behaviour as well as providing the values of parameters used in evaluating and applying these models. While the application of electrochemical methods to nuclear waste disposal problems has been described, it is clear that electrochemical processes are central to the description and prediction of a wide range of environmental issues involving redox processes.

© 1997 NRC Canada

Fig. 21. Comparison of measured and predicted corrosion potentials for a clay-covered copper electrode (CCE) in 1.0 mol L^{-1} NaCl with a clay-layer thickness of 1.0 cm. (*a*) Measured E_{CORR} (69), (*b*) predicted E_{CORR} (70). The horizontal lines represent the predicted steady-state values for the respective O_2/N_2 mixtures (69). For the experimental measurements, the initial air atmosphere was changed to atmospheres of 2 vol.% O_2/N_2 and 0.2 vol.% O_2/N_2 at times of 110 and 675 h, respectively. The spikes in the experimental curve resulted from accidental additions of aerated solution or loss of the gas overpurge.



Can. J. Chem. Downloaded from www.nrcresearchpress.com by 91.121.58.235 on 09/08/12
For personal use only.

Acknowledgement

This work was jointly funded by Ontario Hydro and AECL under the auspices of the CANDU Owners Group (COG).

References

1. D.W. Shoesmith, B.M. Ikeda, M.G. Bailey, M.J. Quinn, and D.M. LeNeveu. Atomic Energy of Canada Limited Report, AECL-10973, COG-94-558 (1995).
2. F. King. Atomic Energy of Canada Limited Report, AECL-11552, COG-95-105 (1996).
3. D.W. Shoesmith, F. King, and B.M. Ikeda. Atomic Energy of Canada Limited Report, AECL-10972, COG-94-534 (1995).
4. D.W. Shoesmith and S. Sunder. J. Nucl. Mater. **190**, 20 (1992).
5. L.H. Johnson, D.M. LeNeveu, D.W. Shoesmith, D.W. Oscarson, M.N. Gray, R.J. Lemire, and N.C. Garisto. Atomic Energy of Canada Limited Report, AECL-10714, COG-93-4 (1994).
6. L.H. Johnson, D.M. LeNeveu, F. King, D.W. Shoesmith, M. Kolar, D.W. Oscarson, S. Sunder, C. Onofrei, and J.L. Crosthwaite. Atomic Energy of Canada Limited Report, AECL-11494-2, COG-95-552-2 (1996).
7. S. Aronson, J.E. Rulli, and B.E. Schaner. J. Chem. Phys. **35**, 1382 (1961).
8. G.J. Hyland and J. Ralph. High Temp. – High Pressures, **15**, 179 (1983).
9. P.W. Winter. J. Nucl. Mater. **161**, 38 (1989).
10. D.W. Shoesmith, S. Sunder, and W.H. Hocking. *In* Electrochemistry of novel materials. *Edited by* J. Lipkowski and P.N. Ross. VCH Publishers, New York. 1994. p. 297.
11. S. Sunder and D.W. Shoesmith. Atomic Energy of Canada Limited Report, AECL-10395 (1991).
12. D.W. Shoesmith and S. Sunder. Atomic Energy of Canada Limited Report, AECL-10488 (1991).
13. S. Sunder, D.W. Shoesmith, M.G. Bailey, F.W. Stanchell, and N.S. McIntyre. J. Electroanal. Chem. **130**, 163 (1981).
14. N.S. McIntyre, S. Sunder, D.W. Shoesmith, and F.W. Stanchell. J. Vac. Sci. Technol. **18**, 714 (1981).
15. J.D. Rudnicki, R. Russo, and D.W. Shoesmith. J. Electroanal. Chem. **372**, 63 (1994).
16. D.W. Shoesmith, S. Sunder, M.G. Bailey, and G.J. Wallace. Corros. Sci. **29**, 1115 (1989).
17. W.H. Hocking, D.W. Shoesmith, and J.S. Betteridge. J. Nucl. Mater. **190**, 36 (1992).
18. S. Sunder, D.W. Shoesmith, N.H. Miller, and G.J. Wallace. Mater. Res. Soc. Symp. Proc. **257**, 345 (1992).
19. P. Taylor, D.D. Wood, and A.M. Duclos. J. Nucl. Mater. **189**, 116 (1992).
20. S. Sunder and N.H. Miller. Atomic Energy of Canada Limited Report, AECL-11351 (1995).
21. D.W. Shoesmith, S. Sunder, M.G. Bailey, G.J. Wallace, and F.W. Stanchell. Appl. Surf. Sci. **20**, 39 (1984).
22. S. Sunder, D.W. Shoesmith, M. Kolar, and D.M. LeNeveu. J. Nucl. Mater. Submitted.
23. S. Sunder, L.K. Strandlund, and D.W. Shoesmith. Atomic Energy of Canada Limited Report, AECL-11440, COG-95-461 (1996).
24. S. Sunder, D.W. Shoesmith, R.J. Lemire, M.G. Bailey, and G.J. Wallace. Corros. Sci. **32**, 373 (1991).
25. I. Grenthe, J. Fuger, R.J.M. Konings, R.J. Lemire, A.B. Muller, C. Nguyen-Trung, and H. Wanner. Chemical thermodynamics of uranium. Vol. 1. *Edited by* H. Wanner and I. Forest. North Holland, Amsterdam. 1992.
26. M.J. Nicol and C.R.S. Needes. Electrochim. Acta, **20**, 585 (1975).
27. W.H. Hocking, J.S. Betteridge, and D.W. Shoesmith. Atomic Energy of Canada Limited Report, AECL-10402 (1991).
28. W.H. Hocking, J.S. Betteridge, and D.W. Shoesmith. J. Electroanal. Chem. **379**, 339 (1994).
29. V.A. Presnov and A.M. Trunov. Elektrokhimiya, **11**, 71 (1975).
30. A.M. Trunov and V.A. Presnov. Electrokhimiya, **11**, 77 (1975); **11**, 290 (1975).
31. D.W. Shoesmith, J.S. Betteridge, and W.H. Hocking. J. Electroanal. Chem. **406**, 69 (1996).
32. P.G. Lucuta, R.A. Verrall, Hj. Matzke, and B.J. Palmer. J. Nucl. Mater. **178**, 48 (1991).

© 1997 NRC Canada

33. J.S. Betteridge, N.A.M. Scott, D.W. Shoesmith, L.A. Bahen, W.H. Hocking, and P.G. Lucuta. Atomic Energy of Canada Limited Report, AECL-11647, COG-96-331-I (1997).
34. N.A. Anastasijevic, Z.M. Dimitrijevic, and R.R. Adzic. J. Electroanal. Chem. **199**, 351 (1986).
35. Lj.M. Vracar, D.B. Sepa, and A. Damjanovic. J. Electrochem. Soc. **133**, 1835 (1986).
36. Lj.M. Vracar, D.B. Sepa, and A. Damjanovic. J. Electrochem. Soc. **134**, 1695 (1987).
37. D.W. Shoesmith, B.M. Ikeda, and F. King. *In* Modelling aqueous corrosion. *Edited by* K.R. Trethewey and P.R. Roberge. Kluwer Academic Publishers, London. 1994. p. 201.
38. D.W. Shoesmith, B.M. Ikeda, F. King, and S. Sunder. *In* Life predictions of structures subjected to environmental degradation. NACE International, Houston, Tex. 1996. p. 101.
39. D.W. Shoesmith, B.M. Ikeda, M.J. Quinn, and M. Kolar. Atomic Energy of Canada Limited Report, AECL-11255, COG-95-18 (1995).
40. B.M. Ikeda, R.C. Styles, M.G. Bailey, and D.W. Shoesmith. *In* Compatibility of biomedical implants. *Edited by* P. Kovacs and N.S. Istephanous. Proc. Electrochem. Soc. **94-15**, 368 (1994).
41. B.M. Ikeda, M.G. Bailey, C.F. Clarke, and D.W. Shoesmith. Atomic Energy of Canada Limited Report, AECL-9508 (1989).
42. B.M. Ikeda, M.G. Bailey, M.J. Quinn, and D.W. Shoesmith. *In* Applications of accelerated corrosion tests to service life predictions of materials. *Edited by* G. Cragnolino and N. Sridhar. ASTM STP 1194, 126 (1994).
43. M.G. Bailey, B.M. Ikeda, M.J. Quinn, and D.W. Shoesmith. Atomic Energy of Canada Limited Report, AECL-10971, COG-95-279 (1996).
44. B.M. Ikeda, M.G. Bailey, M.J. Quinn, and D.W. Shoesmith. *In* Critical factors in localized corrosion. *Edited by* G. Frankel and R.C. Newman. Proc. Electrochem. Soc. **92-9**, 431 (1992).
45. D.W. Shoesmith, B.M. Ikeda, D. Hardie, M.G. Bailey, and C.F. Clarke. *In* Focus '91. American Nuclear Society, LaGrange, Ill. 1992. p. 193.
46. B.M. Ikeda, M.G. Bailey, M.J. Quinn, and D.W. Shoesmith. *In* Proc. Int. Corrosion Congress, 11th, Florence, Italy. **5**, 5.371 (1990).
47. B.M. Ikeda, M.G. Bailey, C.D. Cann, and D.W. Shoesmith. *In* Advances in localized corrosion. *Edited by* H.S. Isaacs, U. Bertocci, J. Kruger, and S. Smialowska. NACE International, Houston, Tex. 1990. p. 439.
48. R.S. Glass. Electrochim. Acta, **28**, 1507 (1983).
49. A.J. Sedriks, J.A.S. Green, and D.L. Novak. Corrosion, **28**, 137 (1972).
50. R.W. Schutz and M. Xiao. *In* Proc. Int. Corrosion Congress 12th, Houston, Tex. NACE Int. Symp. 1213 (1993).
51. R.D. Armstrong, R.E. Firman, and H.R. Thirsk. Corros. Sci. **13**, 409 (1973).
52. S. Kitayama, Y. Shida, and M. Oshiyama. Sumitomo Search, **41**, 23 (1990).
53. J.J. Noël. To be published.
54. T. Shibata and Y.-C. Zhu. Corrosion Sci. **37**, 253 (1995).
55. T. Shibata and Y.-C. Zhu. Corrosion Sci. **36**, 1735 (1994).
56. J. Yahalom and J. Zahavi. Electrochim. Acta, **15**, 1429 (1970).
57. C.K. Dyer and J.S.L. Leach. J. Electrochem. Soc. **125**, 1032 (1978).
58. J.J. Noël, B.M. Ikeda, N.H. Miller, D.W. Shoesmith, S. Sunder, and Z. Tun. Symp. Surface Oxide Films. *Edited by* J.A. Bardwell. Proc. Electrochem. Soc. **96-18**, 246 (1996).
59. D.W. Shoesmith and B.M. Ikeda. Atomic Energy of Canada Limited Report, AECL-11709, COG-96-557-I (1997).
60. T. Watanabe, M. Kondo, H. Naito, and K. Sakai. Nippon Steel Technical Report, **39**, **40**, 29 (1989).
61. R.W. Schutz. Paper No. 244, Corrosion 95, NACE International, Houston, Tex. (1995).
62. C. Deslouis, B. Tribollet, G. Mengoli, and M.M. Musiani. J. Appl. Electrochem. **18**, 374 (1988).
63. F. King, C.D. Litke, and Y. Tang. In preparation.
64. F. King, Y. Tang, M.J. Quinn, and C.D. Litke. Paper No. 424, Corrosion 95, NACE International, Houston, Tex. 1995.
65. H.-H. Strehblow and B. Titze. Electrochim. Acta, **25**, 839 (1980).
66. F. King, C.D. Litke, and Y. Tang. J. Electroanal. Chem. **384**, 105 (1995).
67. F. King, M.J. Quinn, and C.D. Litke. J. Electroanal. Chem. **385**, 45 (1995).
68. C.I. Elsner, R.C. Salvarezza, and A.J. Arvia. Electrochim. Acta, **33**, 1735 (1988).
69. F. King, C.D. Litke, M.J. Quinn, and D.M. LeNeveu. Corros. Sci. **37**, 833 (1995).
70. F. King and M. Kolar. Proc. Int. Conf. Deep Geological Disposal of Radioactive Waste, Canadian Nuclear Society, Toronto, Ont. 1996. pp. 5-39–5-50.

Can. J. Chem. Downloaded from www.nrcresearchpress.com by 91.121.58.235 on 09/08/12
For personal use only.

© 1997 NRC Canada

Tafel behaviour and competitive adsorption of amino acids and peptides with surface oxide formation at the Pt electrode

R. Julia Petrie, Stephanie M. MacDonald, Katherine L. Fuller, and Sharon G. Roscoe

Can. J. Chem. Downloaded from www.nrcresearchpress.com by 91.121.58.235 on 09/08/12
For personal use only.

Abstract: The electrochemical oxidation reactions and competitive adsorption behaviour of glycine, the peptides glycyl-glycine and glycyl-glycyl-glycine, α- and β-alanine, and α-, β-, and γ-aminobutyric acid have been investigated by cyclic voltammetry at a platinum electrode in a pH 7.0 phosphate buffer solution at ambient temperature. Strong adsorption of all species at anodic potentials in neutral solution was accompanied by an efficient ability to block both the initial stages of OH monolayer deposition as well as the second stage involving an irreversible process of continued deposition of OH or O species. Glycine and the peptides blocked the initially and more reversibly deposited OH species in preference to those formed at higher potentials. Surface concentrations determined with the lower anodic end potentials (0.50 V) gave information on the orientation of the adsorbed molecules. Steady-state polarization measurements gave Tafel slopes in the range of 253-498 mV, considerably higher than that normally seen for oxygen evolution from a phosphate buffer solution. These results suggest that, in the pH 7.0 buffer, the negatively charged carboxylate group preferentially adsorbs under these anodic potentials in a mechanism similar to the Kolbe reaction, with the decarboxylation step being rate determining.

Key words: electrochemical oxidation, glycine, alanine, aminobutyric acid, peptides, platinum oxide.

Résumé : Opérant à la température ambiante, dans une solution tampon de phosphate à pH 7,0 et faisant appel à la voltampérométrie cyclique à une électrode de platine, on a étudié les réactions d'oxydation électrochimiques et le comportement compétitif d'adsorption de la glycine, des peptides glycyl-glycine et glycyl-glycyl-glycine, des α- et β-alanines et des acides α-, β- et γ-aminobutyriques. La forte adsorption de toutes les espèces à des potentiels anodiques en solution neutre est accompagnée d'une habilité efficace à bloquer tant les étapes initiales des dépôts de monocouches de OH que la deuxième étape impliquant le processus irréversible de dépôt continue des espèces OH ou O. La glycine et les peptides bloquent les espèces OH qui se forment initialement et qui sont déposées d'une façon plus réversible de préférence à celles qui se forment à des potentiels plus élevés. Les concentrations à la surface qui ont été déterminées aux potentiels anodiques les plus bas (0,50 V) fournissent de l'information sur l'orientation des molécules adsorbées. Des mesures de polarisation à l'état stationnaire permettent d'obtenir les pentes de Tafel à des valeurs allant de 253 à 498 mV, des valeurs beaucoup plus élevées que celles généralement observées pour l'évolution de l'oxygène à partir d'une solution tampon de phosphate. Ces résultats suggèrent que, à ces potentiels anodiques, à un pH de tampon égal à 7,0, il y a adsorption préférentielle des groupes carboxylates chargés négativement; le mécanisme est semblable à celui de la réaction de Kolbe et la décarboxylation est alors l'étape cinétiquement déterminante.

Mots clés : oxydation électrochimique, glycine, alanine, acide aminobutyrique, peptides, oxyde de platine.

[Traduit par la rédaction]

1. Introduction

Anodic reactions in aqueous solutions at the Pt electrode are characterized by the electrocatalytic surface oxide film that develops on the metal surface. This oxide film is known to be electrocatalytic for such reactions as O_2 (1, 2), Cl_2 (3–8), and N_2 (from N_3^-) (9–13) evolution and for the oxidation of acetate ions that produce ethane by the Kolbe mechanism (14). Therefore it is of interest to compare the adsorption and oxidation behaviour of amino acids with that of acetic acid and to examine the role of the surface oxide film at platinum in the electrochemical (EC) oxidation mechanism. In addition, since amino acids form the building blocks of proteins, the oxidation and adsorption behaviour of amino acids at an electrode surface is relevant to the interfacial behaviour of proteins and, hence, to the immense industrial and medical problems associated with the fouling of surfaces by proteins (15–19). These studies are also relevant to the development of biosensors such as those used for EC detection in HPLC and other LC systems on noble metal electrodes such as platinum and gold (20–23),

Received March 17, 1997.

This paper is dedicated to Professor Brian E. Conway in recognition of his distinguished contributions to the field of electrochemistry and to chemistry in Canada.

R.J. Petrie, S.M. MacDonald, K.L. Fuller, and S.G. Roscoe.[1]
Chemistry Department, Acadia University, Wolfville, NS B0P 1X0, Canada.

[1] Author to whom correspondence may be addressed. Telephone: (902) 585-1156. Fax: (902) 585-1074. E-mail: sharon.roscoe@acadiau.ca

© 1997 NRC Canada

Can. J. Chem. Downloaded from www.nrcresearchpress.com by 91.121.58.235 on 09/08/12
For personal use only.

active Langmuir–Blodgett films of enzyme on platinum (24), enzymes immobilized between platinum electrode surfaces and membranes (25–30), enzyme entrapment in polymers on platinum (31), and also phospholipid bilayers (32–34) and bilayer conducting polymers (35) formed on platinum electrode surfaces that may be used for the incorporation of enzymes (36–38).

A number of studies have been made to obtain information on the mechanisms of the oxidation of amino acids at platinum. The anodic oxidation of simple amino acids such as glycine (39), α- and β-alanine (40), and α-, β-, and γ-aminobutyric acid (41) at pH 1 and 13 at a platinum electrode have been found to result in the formation of the next lower aldehyde in the homologous series. These studies were undertaken to investigate the role of the amino group in the oxidation process. Kinetic analysis showed the reactions to proceed in a manner similar to the Kolbe mechanism with adsorption through the carboxylate group accompanied by electron transfer, followed by decarboxylation as the rate-determining step. However, rather than dimerization of the adsorbed radicals as in the Kolbe mechanism (14), the adsorbed radicals were further oxidized to the next lower aldehyde in the homologous series accompanied by the transfer of a second electron. In the electro-oxidation of glycine, product analysis showed the intermediate species to be hydrolyzed to formaldehyde and ammonia. However, with the larger amino acids, product analysis was complicated by further reactions of the newly formed aldehydes, particularly by condensation reactions with the amino acids in the bulk solution (40, 41). HPLC analysis of the products of electrolysis of the dipeptide tyrosyl-glycine (Tyr-Gly) at potentials of 1.8–2.2 E_{SCE} indicated that although minimal cleavage of the peptide bond occurred, cleavage of the dipeptide was not the predominant pathway in the anodic oxidation process (42). In the case of tryptophyl-glycine (Trp-Gly), polymerization at the metal surface may have predominated as a film formed on the surface of the electrode after electrolyzing the solution for long periods of time at these high anodic potentials.

Investigations with other techniques have also indicated the important role of the carboxyl functional group in the surface adsorption behaviour of related molecules. In recent investigations of the interaction of acetic acid with platinum electrodes using infrared spectroscopy, Krauskopf and Wieckowski (43) have shown that both carboxylate oxygens were oriented toward the metal surface. Corrigan et al. (44) found maximum adsorption of acetic acid at a platinum electrode at 0.5 V (E_{SCE}) by both infrared analysis and radiotracer techniques. Horanyi (45) carried out a systematic radiotracer study of the behaviour of amino acids at a platinum electrode in order to investigate the role of the carboxyl functional group in the adsorption of aliphatic acids. The adsorption behaviour of acetic acid and glycine was reported to be similar in acidic medium. Strong chemisorption of both species occurred in alkaline medium. No adsorption was found at potentials less than 0 V, but adsorption increased steadily with anodic potentials and maximized at 0.4–0.5 V (E_{SCE}). A rapid exchange of adsorbed labeled glycine with nonlabeled species suggested that the protonated $^{+}H_3N\text{-}CH_3$ group does not influence the adsorption behaviour of glycine. To obtain further evidence concerning the role of the -COOH group in the adsorption of amino acids, the adsorption of labeled $CH_3\text{-}NH_2$ and $NH_2\text{-}CH_2\text{-}CH_2\text{-}NH_2$ was studied. No adsorption of these compounds was observed in the potential range in which the adsorption of glycine and γ-aminobutyric acid occurred. Masui et al. (46) found that the oxidation of several N-methyl amino acids at a glassy carbon plate electrode and pH 10 proceeded by decarboxylation and produced the corresponding aldehyde and methylamine as the major electrolysis products. A two electron oxidation mechanism was proposed for this degradation.

In the present studies, the adsorption behaviour of glycine, the peptides glycyl-glycine (Gly-Gly) and glycyl-glycyl-glycine (Gly-Gly-Gly), α- and β-alanine, and α-, β-, and γ-aminobutyric acid were investigated by cyclic voltammetry at a platinum electrode in a pH 7.0 phosphate buffer solution at ambient temperature. Steady-state polarization measurements provide information regarding the kinetics and mechanisms of the electrochemical oxidation processes. Therefore comparisons of the adsorption and oxidation reaction properties may be made (*i*) between the α-amino acids with the amino group positioned on the carbon containing the carboxylate group, i.e., glycine, α-alanine, and α-aminobutyric acid; (*ii*) between those with the amino group on the terminal chain carbon relative to the carbon with the attached carboxylate group, i.e., glycine, β-alanine, and γ-aminobutyric acid; and (*iii*) between similar α-amino acids in the absence and presence of peptide bonds, i.e., glycine, Gly-Gly, Gly-Gly-Gly. These results are also compared to those obtained previously in this laboratory for glycine (39), α- and β-alanine (40), and α-, β-, and γ-aminobutyric acid (41) at pH 1 and 13 in order to explore the response to changes in pH.

2. Experimental

Reagents and solutions

Individual solutions of glycine (>99% purity, gold label reagent), the peptides Gly-Gly and Gly-Gly-Gly, α- and β-alanine, and α-, β-, and γ-aminobutyric acid (all of the highest possible quality, Sigma Chemical Company) were prepared in 0.05 mol L^{-1} phosphate buffer (pH 7.0) using anhydrous monobasic potassium phosphate (KH_2PO_4) (Sigma Chemical Company, cell culture tested) and sodium hydroxide (prepared from standardized BDH Chemical Company concentrate). Conductivity water (Nanopure, resistivity = 18.3 megohm cm) was used in the preparation of all aqueous solutions.

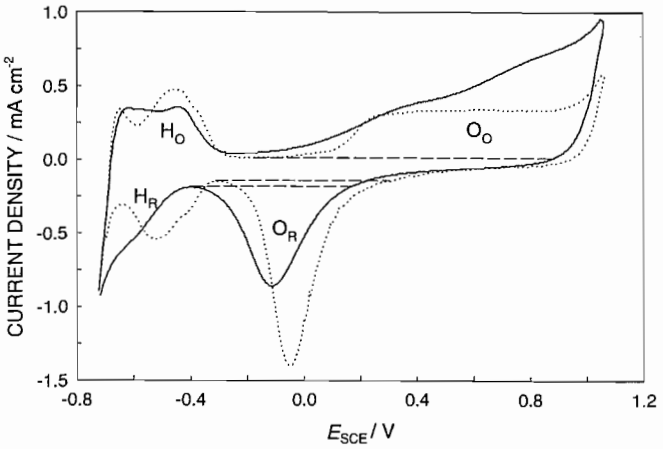
Electrochemical cell and electrodes

Three-compartment all-glass electrochemical cells were constructed with two glass-sleeved stopcocks as two of the separate compartments. The working and counter electrode compartments were purged continuously with nitrogen gas (Linde, commercial purity 99.7%) that was deoxygenated by passage through a copper furnace at 573 K. This also provided a well-mixed bulk solution. Electrodes of high-purity platinum wire or mesh (99.99%, Johnson, Matthey and Mallory) were degreased by refluxing in acetone, sealed in soft glass, electrochemically cleaned by potential cycling in 0.5 mol L^{-1} sulfuric acid (Aristar grade purity, BDH Chemicals Limited), and stored in 98% sulfuric acid. The real surface area of the platinum electrode was obtained from the charge under the hydrogen underpotential deposition (upd) peaks (47). Saturated calomel reference electrodes were constructed by a

© 1997 NRC Canada

Can. J. Chem. Downloaded from www.nrcresearchpress.com by 91.121.58.235 on 09/08/12
For personal use only.

Fig. 1. Cyclic voltammogram at a Pt electrode (E_{SCE}) (sweep rate 500 mV s^{-1}) of the phosphate buffer, pH 7.0 (dotted line) and 0.092 mol L^{-1} Gly-Gly-Gly in the phosphate buffer (solid line). O_o indicate the anodic oxidation regions and O_r the oxide reduction regions, which are integrated to obtain Q_{O_o}, Q_{O_r}, $Q_{O_o}{}^A$, and $Q_{O_r}{}^A$. H_o and H_r are the hydrogen oxidation and reduction regions, respectively.



standard procedure (48). Their potentials were checked frequently against a standard hydrogen electrode and compared with the literature value (49). The saturated calomel electrodes were found to be reproducible to within ±1 mV.

Methods

Cyclic voltammograms were obtained using a Hokuto Denko potentiostat (model HD-301) and a Hokuto Denko function generator (model HD-111) and were recorded on an Allen Datagraph, Inc. X-Y recorder–plotter (model 720M). The sweep rate used throughout was 500 mV s^{-1}.

The surface charge density, Q_{ADS}, resulting from the deposition of the amino acid (or peptide) on the electrode following additions of specific aliquots of analyte, was determined from the difference between the integrated areas of anodic oxidation, O_o, and oxide reduction, O_r, in the presence of the adsorbing species (Fig. 1). The small surface charge density that resulted from the phosphate buffer in the absence of amino acid was subtracted from that measured for the amino acid and the remainder was attributed to the amino acid adsorption, as follows:

$$[1] \quad Q_{ADS} = (Q_{O_o}{}^A - Q_{O_r}{}^A) - (Q_{O_o} - Q_{O_r})$$

where Q_{O_o} is the anodic oxidation charge density in phosphate buffer, Q_{O_r} is the oxide reduction charge density in phosphate buffer, $Q_{O_o}{}^A$ is the anodic oxidation charge density in the presence of the amino acid (or peptide) species and $Q_{O_r}{}^A$ is the oxide reduction charge density in the presence of the adsorbing species. Cyclic voltammograms were recorded after each aliquot of amino acid was added to the buffer solution in the electrochemical cell and steady-state conditions had been attained, giving identical, reproducible cyclic voltammograms with continued potential sweeps. The reproducibility of determining areas of different cyclic voltammogram tracings from different experiments for phosphate buffer at anodic end potential 0.5 V was within ±3%. The standard deviation of the surface charge densities, Q_{ADS}, of the plateau values for amino acid surface adsorption were found to be ±5%.

From the surface charge densities, the surface concentration of amino acid, Γ_A, in molecules nm^{-2}, was calculated using:

$$[2] \quad \Gamma_A = Q_{ADS} N_A / nF$$

where N_A is Avogadro's number, $n = 2$ is the number of electrons transferred, and F is the Faraday constant.

The % decrease in the oxide reduction area as a result of the competitive behaviour of the amino acids was calculated using the following relationship:

$$[3] \quad \% \text{ oxide blocked} = 100\,(Q_{O_r} - Q_{O_r}{}^A)/Q_{O_r}$$

where Q_{O_r} and $Q_{O_r}{}^A$ are the surface charge densities measured for the oxide reduction peak in the phosphate buffer in the absence and presence of amino acid, respectively.

Steady-state polarization measurements were made using a computer-controlled EG&G Princeton Applied Research (model 273) potentiostat to vary the potential of the working electrode. Before each run, the working electrode was conditioned at −600 mV to reduce the electrode surface. Tafel slopes were obtained from the plot of potential versus log of the current density (amp cm^{-2}) with corrections made to correct for "uncompensated solution resistance" obtained from the ac impedance measurements using a Solatron HF frequency response analyzer (model 1255). The solution resistance was determined from the x-intercept in the Nyquist plot of the imaginary versus real components of impedance.

3. Results and discussion

3.1 Cyclic voltammetric measurements

The formation of surface oxide films on Pt has been the subject of many investigations (50–60) and it is well known that there are three qualitatively different stages in surface oxide formation distinguishable by electrochemical (52) and optical methods (59–61). The first stage consists of a submonolayer of underpotential deposited (upd) OH species which behave reversibly in electrochemical measurements (52, 59, 60). A second irreversible process involves continued deposition of OH or O species associated with the initial stages of a place inversion of Pt and O in the oxide film (1–3, 14, 50–52, 59, 60, 62). The third is an oxide-thickening process resulting from high-field oxide film growth (1, 2, 59, 60). The first and second stages of oxide film growth are the regions of interest in the cyclic voltammetric measurements. The anodic end potential was initially varied to determine the potential at which the charge due to a monolayer of adsorbed OH species in the phosphate buffer solution was equivalent to the total H charge in the cathodic upd region. This potential was found to be 0.50 V, which includes 30% of the total oxide formed up to the anodic end potential 1.1 V (similar to that observed in alkaline solution (52)) and represents the first stage of oxide formation. Data, to be discussed later, were evaluated at this potential as well as the whole anodic upd region to the higher end potential of 1.1 V, which includes both the first and second stages of oxide film formation.

To characterize the behaviour of the amino acids and related compounds, it was first necessary to determine the

© 1997 NRC Canada

Can. J. Chem. Downloaded from www.nrcresearchpress.com by 91.121.58.235 on 09/08/12
For personal use only.

Fig. 2. Surface charge density at the Pt electrode for the anodic end potential 1.1 V as a function of bulk concentration of: ●, glycine; ○, Gly-Gly; Δ, Gly-Gly-Gly.

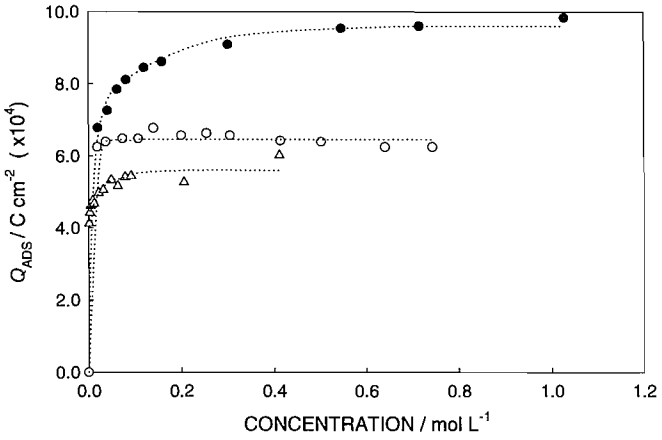
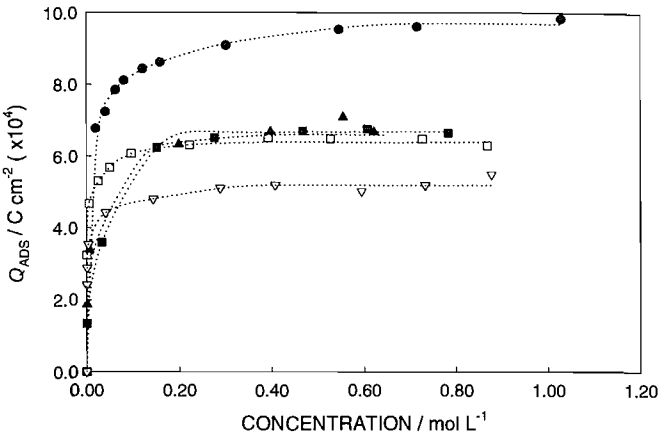


Fig. 3. Surface charge density at the Pt electrode for the anodic end potential 1.1 V as a function of bulk concentration of: ●, glycine; ■, α-alanine; □, β-alanine; ▲, α-aminobutyric acid; ▽, γ-aminobutyric acid.



cyclic voltammogram for phosphate buffer, pH 7.0 (Fig. 1). Cyclic voltammograms were then recorded for additions of each aliquot of amino acid to the electrochemical cell containing the phosphate buffer. As an example, Fig. 1 also shows the tracing of 0.092 mol L^{-1} Gly-Gly-Gly in the phosphate buffer. Strong adsorption of all the species studied in neutral solution was evident by a significant increase in the area of the anodic oxidation region (O_o) and the decrease in the area of the oxide reduction region (O_r) due to blocking the deposition of the surface oxide by the adsorbing species. The surface charge density was determined from the corresponding cyclic voltammogram with anodic end potentials 0.5 and 1.1 V for each addition of amino acid as described earlier.

The relationships between surface charge density, Q_{ADS}, determined using eq. [1], and concentration of amino acid in the bulk solution are shown in Figs. 2 and 3 for the end potential 1.1 V, for concentrations up to about 1 mol L^{-1}. The plateau values obtained for glycine and its peptides (Fig. 2) show a very nice trend, with surface charge density values for glycine > Gly-Gly > Gly-Gly-Gly that reflect the ability of the molecules to pack efficiently on the electrode surface; i.e., glycine with the smallest structure showing the greatest packing density and charge due to oxidation. Fig. 3 shows the similarity between the surface charge densities of the two molecules, α-alanine and β-alanine, in the plateau region that reflects the similar sizes in their structures. However, β-alanine adsorbs more readily than α-alanine at the lower concentrations. The plateau values of surface charge densities for the alanines (~650 μC cm^{-2}) are very similar to the value obtained for Gly-Gly. This again reflects the similarity in structural sizes of the three compounds. If we now compare the results in Fig. 3 for the α-amino acids (glycine, α-alanine, and α-aminobutyric acid), glycine again shows the highest surface charge density, with α-alanine and α-aminobutyric acid giving lower, but very comparable results. Also in Fig. 3, a comparison with the effect of the amino group placed on the terminal carbon in the chain shows glycine still with the highest surface charge density at about 960 μC cm^{-2}, β-alanine with ~630 μC cm^{-2}, and γ-aminobutyric acid with the lowest value of ~500 μC cm^{-2}.

The competitive nature between the adsorption of amino acids and the two stages of oxide film formation may be evaluated from the % decrease in the oxide reduction area in the presence of increasing concentrations of amino acids. The blocking of the first stage in the formation of the oxide layer, i.e., monolayer OH deposition, has been determined from results for % oxide blocked obtained with anodic end potential 0.5 V. The efficiency of the amino acid to block both the first and second stages, i.e., continued deposition of OH or O species associated with the electrochemically irreversible initial stages of place exchange of Pt–O in the oxide film, has been examined by the blocking efficiency over the whole anodic upd region to 1.1 V.

An examination of the blocking efficiency of glycine and the peptides of the first stage of oxide film formation (Fig. 4*a*) shows a large blocking effect by glycine that curves and tends to level off at about 80% of the oxide blocked. An even greater effect results from the tripeptide, Gly-Gly-Gly, as the curve representing the blocking increases to 90%. However, the blocking efficiency of glycine and the peptides becomes somewhat diminished over the large upd region representing both the first and second stages of oxide film formation. Figure 4*b* instead shows a long linear relationship of % oxide blocked versus logarithm of the concentration of amino acid in the bulk solution for glycine, Gly-Gly, and Gly-Gly-Gly. At the higher concentrations the tripeptide was more efficient in blocking oxide deposition than the smaller dipeptide, Gly-Gly, and amino acid, glycine. However, glycine and the peptides block the initially and more reversibly deposited OH species in preference to those formed at higher potentials. The linear logarithmic regions of Fig. 4*b* arise mainly from a continuing blocking of surface oxide.

Unlike the behaviour by glycine, a linear behaviour is observed for the % oxide blocked by α-alanine in the first stage of monolayer surface oxide growth (Fig. 5*a*), which continues past the upper limiting values for glycine. However, the efficiency is significantly less than that of glycine in the concentration range 10^{-5}–10^{-3} mol L^{-1}. At the higher concentrations, β-alanine also showed a linear behaviour but with a blocking efficiency similar to that of glycine. A comparison of

© 1997 NRC Canada

Can. J. Chem. Downloaded from www.nrcresearchpress.com by 91.121.58.235 on 09/08/12
For personal use only.

Fig. 4. The % oxide formation blocked by the amino acid at the Pt electrode as a function of logarithm of concentration for: ●, glycine; ○, Gly-Gly; △ , Gly-Gly-Gly. (*a*) Anodic end potential 0.5 V; (*b*) anodic end potential 1.1 V.

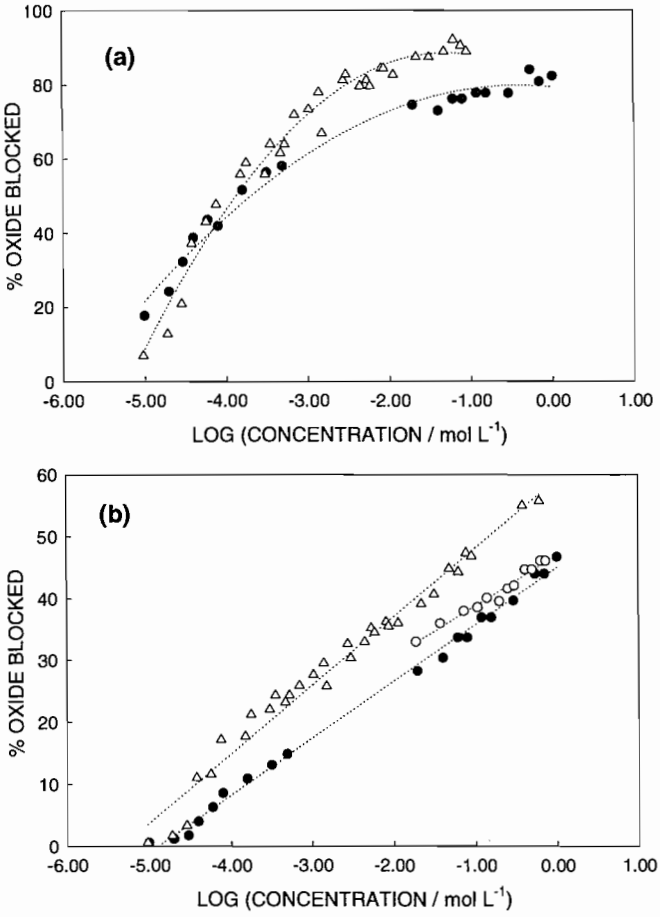
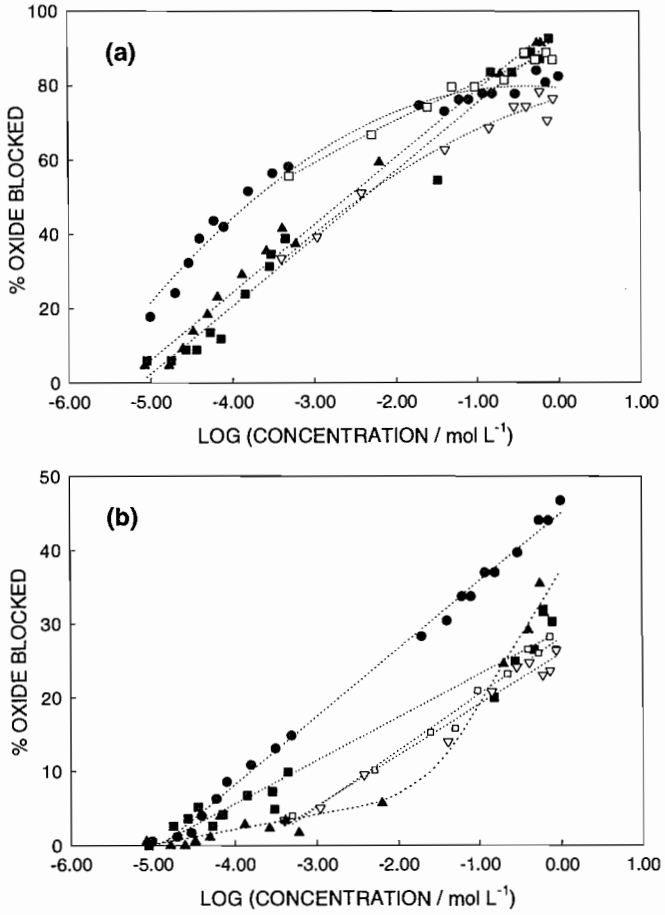


Fig. 5. The % oxide formation blocked by the amino acid at the Pt electrode as a function of logarithm of concentration for: ●, glycine; ■, α-alanine; □, β-alanine; ▲, α-aminobutyric acid; ▽, γ-aminobutyric acid. (*a*) Anodic end potential 0.5 V; (*b*) anodic end potential 1.1 V.



glycine and α- and β-alanine over the whole upd region (Fig. 5*b*) showed glycine to be significantly more efficient at blocking oxide deposition than α- and β-alanine at the higher concentrations, although the efficiency was similar at low concentrations for glycine and α-alanine.

A comparison of the three α-amino acids for monolayer surface coverage (Fig. 5*a*) displayed a long linear behaviour with almost identical slopes for α-alanine and α-aminobutyric acid, but with the larger α-aminobutyric acid having a slightly greater efficiency for blocking. Glycine was much more effective in the lower concentrations. When we consider the whole upd region to 1.1 V, the three α-amino acids at low concentrations showed a consistent increasing blocking efficiency trend with decreasing hydrocarbon chain length (Fig. 5*b*). However, at higher concentrations, the efficiency of α-aminobutyric acid increased significantly in a nonlinear manner to give values at the higher concentrations similar to that of α-alanine.

When the amino group is positioned on the terminal carbon, a curved effect can be seen with γ-aminobutyric acid that causes the blocking efficiency in the first stage of oxide formation to fall off at the higher concentrations in a manner similar to that observed for glycine but with less efficiency (Fig. 5*a*). However, at lower concentrations the blocking efficiency is very similar to that of α-aminobutyric acid. The behaviour of β-alanine is linear over the same concentration range as that of γ-aminobutyric acid. In contrast, the results for blocking efficiency over the whole upd region (Fig. 5*b*) show a linear behaviour with significantly less efficiency in blocking oxide deposition by β-alanine and γ-aminobutyric acid than glycine.

These results indicate that the most effective amino acids for blocking the initial stage of oxide deposition, particularly at low concentrations, were glycine and the peptides. Since Cl^- is also known to selectively block this initially deposited OH monolayer at Pt in 0.1 mol L^{-1} H_2SO_4 and 0.1 mol L^{-1} $HClO_4$ (62), it was of interest to examine the blocking efficiency of Cl^- in phosphate buffer in the presence of $H_2PO_4^-$ ions. The onset of blocking surface oxide by Cl^- occurred at a concentration of about 3×10^{-6} mol L^{-1} Cl^- in the presence of HSO_4^- or ClO_4^- (62). In contrast, as shown in Fig. 6, additions of Cl^- to concentrations as high as 3×10^{-2} mol L^{-1} Cl^- were required before the onset of oxide blocking occurred in the presence of $H_2PO_4^-$ ions. This was a factor of 10^4 increase in concentration required of Cl^- in the presence of $H_2PO_4^-$ ions compared with that required in the presence of HSO_4^- or ClO_4^-. As the concentration of Cl^- increased to 0.9 mol L^{-1}, the blocking efficiency abruptly increased to 92%. To

© 1997 NRC Canada

Can. J. Chem. Downloaded from www.nrcresearchpress.com by 91.121.58.235 on 09/08/12
For personal use only.

Fig. 6. The % oxide formation blocked at the Pt electrode by chloride as a function of logarithm of concentration of Cl^- in the presence of: △, phosphate buffer, pH 7.0; ●, 1.0 mol L^{-1} glycine solution in phosphate buffer, pH 7.0.

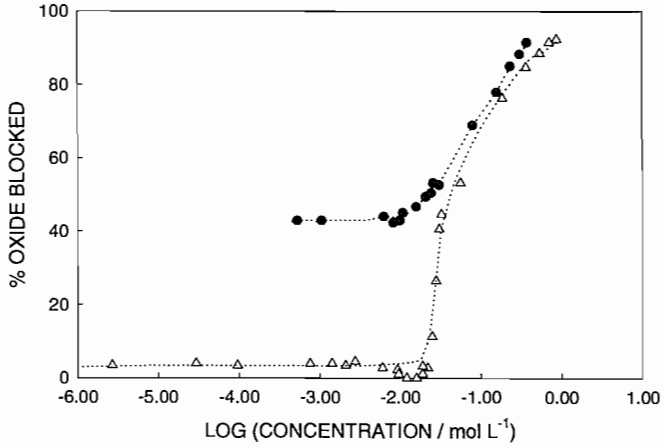


Fig. 7. Surface charge density at the Pt electrode from: ●, additions of glycine to the phosphate buffer; △, followed by additions of HCl.

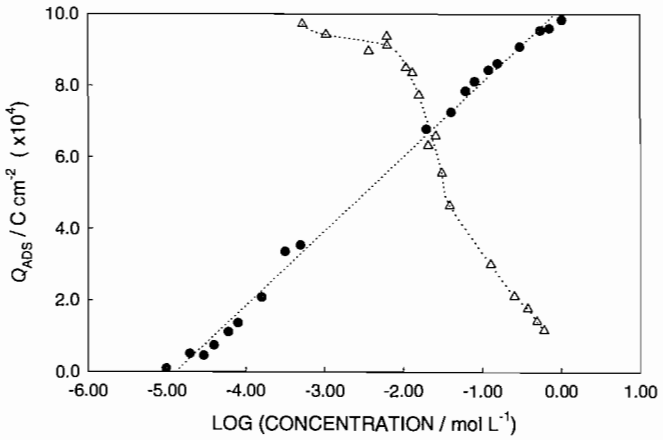


Fig. 8. Tafel behaviour of oxygen evolution from a phosphate buffer pH 7.0, and of glycine, Gly-Gly, and Gly-Gly-Gly in phosphate buffer pH 7.0.

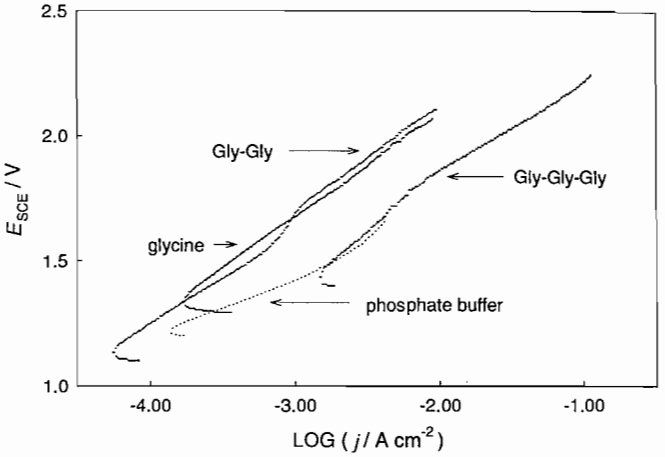
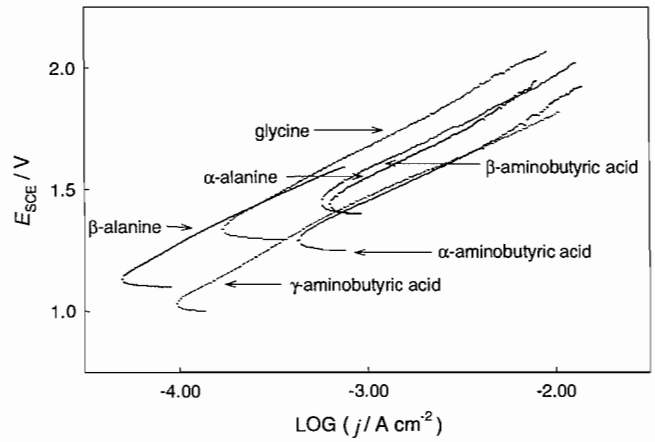


Fig. 9. Tafel behaviour of glycine, α- and β-alanine, and α-, β-, and γ-aminobutyric acid in phosphate buffer pH 7.0.



examine the competitive % oxide blocking behaviour between Cl^- and glycine, experiments were made in which Cl^- concentrations were incrementally increased in a solution containing 0.9 mol L^{-1} glycine in the phosphate buffer, which had already blocked 50% of the formation of oxide. Again, no change in the % oxide blocked was observed until a concentration of 3×10^{-2} mol L^{-1} Cl^- was attained in the bulk solution. At that point, an abrupt increase in the % oxide blocked was again observed and the oxide blocking continued to an efficiency of 85%, similar to that obtained in the absence of glycine. Fig. 7 shows the surface charge density for increments of glycine followed by the additions of Cl^-. Again no substantial change was observed in the surface charge density until the concentration of Cl^- reached 3×10^{-2} mol L^{-1} and at that point there was a steady decrease with increasing Cl^- that indicates that Cl^- was efficient in blocking glycine as well.

Comparisons of the trends in the ratio $Q_{O_o}{}^A/Q_{O_r}{}^A$ for the anodic oxidation region (Table 1) of these compounds with those previously studied can be used to examine the adsorption properties over a range of pH values. A higher value of the ratio corresponds to a greater adsorption by the organic compounds. The most distinct trend shows the decreasing ratio of $Q_{O_o}{}^A/Q_{O_r}{}^A$ for each amino acid with decreasing pH. This is consistent with the adsorption of the carboxylate anion being more strongly attracted to and adsorbed at the anodic electrode. There is also a decreasing trend in $Q_{O_o}{}^A/Q_{O_r}{}^A$ with increasing hydrocarbon chain length. In addition, as the amino group is positioned farther along the hydrocarbon chain from the carboxylate group, there is generally a decrease in $Q_{O_o}{}^A/Q_{O_r}{}^A$.

3.2 Steady-state polarization measurements

Tafel plots from the steady-state potential measurements in the faradaic region at potentials significantly more positive than those used in the cyclic voltammetric measurements are shown in Fig. 8 for solutions of glycine, Gly-Gly, and Gly-Gly-Gly, and in Fig. 9 for glycine, α- and β-alanine, and α-, β-, and γ-aminobutyric acid. Oxygen evolution from phosphate buffer pH 7.0 in the absence of amino acid is shown in Fig. 8. The experimentally obtained Tafel slopes at pH 7.0 for

© 1997 NRC Canada

Can. J. Chem. Downloaded from www.nrcresearchpress.com by 91.121.58.235 on 09/08/12
For personal use only.

Table 1. Surface charge density values from cyclic voltammograms.

Compound pH	Potential range (E_{SCE}/V)	$Q_{O_o}{}^A$ (μC cm^{-2})	$Q_{O_r}{}^A$ (μC cm^{-2})	$Q_{O_o}{}^A/Q_{O_r}{}^A$
Glycine (0.45 mol L^{-1})				
13.0 (NaOH)	−0.854–0.816	2136	223	9.6 (39)
7.0 (KH_2PO_4)	−0.650–1.100	974	313	3.1
1.0 (H_2SO_4)	−0.317–1.220	1315	451	2.9 (39)
Gly-Gly (0.77 mol L^{-1})				
7.0 (KH_2PO_4)	−0.650–1.100	1038	314	3.3
Gly-Gly-Gly (0.092 mol L^{-1})				
7.0 (KH_2PO_4)	−0.650–1.100	942	241	3.9
α-Alanine (0.45 mol L^{-1})				
13.0 (NaOH)	−0.962–0.454	1582	315	5.0 (40)
7.0 (KH_2PO_4)	−0.650–1.100	1150	374	3.1
1.0 (H_2SO_4)	−0.322–1.220	1055	448	2.4 (40)
β-Alanine (0.45 mol L^{-1})				
13.0 (NaOH)	−0.926–0.800	1323	162	8.2 (40)
7.0 (KH_2PO_4)	−0.650–1.100	1091	364	3.0
1.0 (H_2SO_4)	−0.316–1.217	1184	455	2.6 (40)
α-Aminobutyric acid (0.45 mol L^{-1})				
13.0 (NaOH)	−1.050–0.800	1111	225	4.9 (41)
7.0 (KH_2PO_4)	−0.700–1.100	1103	355	3.1
1.0 (H_2SO_4)	−0.292–1.475	775	381	2.0 (41)
β-Aminobutyric acid (0.45 mol L^{-1})				
13.0 (NaOH)	−1.100–0.845	1205	242	5.0 (41)
7.0 (KH_2PO_4)	−0.650–1.100	1024	364	2.8
1.0 (H_2SO_4)	−0.314–1.530	972	430	2.3 (41)
γ-Aminobutyric acid (0.45 mol L^{-1})				
13.0 (NaOH)	−0.900–0.850	1072	265	4.1 (41)
7.0 (KH_2PO_4)	−0.800–1.100	1170	437	2.7
1.0 (H_2SO_4)	−0.290–1.430	543	432	1.3 (41)

the stirred solutions are presented in Table 2 along with those previously obtained at pH 1.0 and 13.0. The Tafel slopes for the amino acids and dipeptides at pH 7.0 ranged from 253 to 498 mV, considerably higher than the Tafel slope of 208 mV for oxygen evolution from a phosphate buffer solution. This Tafel slope for oxygen evolution is also significantly higher than the value of 120 mV normally observed in H_2SO_4 and NaOH solutions (63). This may result from strong adsorption by phosphate anions at these potentials that thereby inhibit the oxygen evolution reaction. In acidic conditions the slopes for the amino acids ranged from 223 to 250 mV, while in alkaline solutions above the inflection point the values ranged from 153 to 212 mV, with the exception of glycine, which gave a much higher slope of 363 mV. Thus the highest slopes in the presence of amino acids occurred at pH 7.0 in the phosphate buffer. The oxidation reactions of the amino acids may therefore also be inhibited by the adsorption of phosphate anions.

Quantitative product analysis from controlled electrolysis of glycine at 1.8 V and pH 13 has been reported previously (39). Based on the measured charge passed through the cell during the reaction, the yield of formaldehyde was 85–90% and the yield of ammonia was 83%, indicating that the oxygen evolution reaction was suppressed in the presence of the amino acid. If it is assumed that the amino acid oxidation reactions at pH 7.0, with similar concentrations of carboxylate anion, proceed in a similar manner with the suppression of the oxygen evolution reaction, and since previous results have suggested that the carboxylate group adsorbs at the anodic electrode surface (14, 39–41, 43–45, 64), a comparison may be made of the experimental Tafel slopes with theoretical values for the rate-determining step of the mechanism in a manner similar to that observed for the Kolbe reaction by the method described by Conway and Dzieciuch (64). Considering the mechanism as shown for the electrochemical oxidation of glycine, with the initial two steps similar to the Kolbe reaction (14)

Step I $^+H_3N\text{-}CH_2\text{–}COO^- \rightarrow {}^+H_3N\text{-}CH_2\text{–}COO(M) + e^-$

Step II $^+H_3N\text{-}CH_2\text{–}COO(M) \rightarrow {}^+H_3N\text{-}CH_2(M) + CO_2$

Step III $^+H_3N\text{-}CH_2(M) + H_2O \rightarrow NH_4^+ + CH_2O + H^+ + e^-$

and with Step I as rate determining, then

$$[4] \quad i_1 = zFk_1(1 - \theta_{G\cdot})C_{G^+}\exp -[(\Delta G_1^{\ddagger} - \beta VF + \beta r_1\theta)/RT]$$

where G· refers to the radical species on the electrode surface, G^+ refers to the free amino acid or dipeptide in the bulk solution, θ designates the fractional surface coverage, β is the symmetry factor (usually 0.5), and r corrects for variation of

© 1997 NRC Canada

Can. J. Chem. Downloaded from www.nrcresearchpress.com by 91.121.58.235 on 09/08/12
For personal use only.

Table 2. Tafel parameters of amino acids and peptides.

Compound and pH	Potential range (E_{SCE}/V)	Tafel Slope b (mV)
Phosphate buffer (I = 0.33 mol L^{-1})		
7.0 (KH_2PO_4)	1.25–1.40	208
Glycine (0.45 mol L^{-1})		
13.0 (NaOH)	0.90–1.10	239 (39)
13.0 (NaOH)	1.48–1.70	363 (39)
7.0 (KH_2PO_4)	1.50–2.08	414
1.0 (H_2SO_4)	1.28–1.68	237 (39)
Gly-Gly (0.77 mol L^{-1})		
7.0 (KH_2PO_4)	1.20–1.50	358
7.0 (KH_2PO_4)	1.75–2.10	420
Gly-Gly-Gly (0.092 mol L^{-1})		
7.0 (KH_2PO_4)	1.50–1.80	379
7.0 (KH_2PO_4)	1.80–2.20	498
α-Alanine (0.45 mol L^{-1})		
13.0 (NaOH)	0.91–1.06	183 (40)
13.0 (NaOH)	1.30–1.50	192 (40)
7.0 (KH_2PO_4)	1.50–1.70	376
1.0 (H_2SO_4)	1.15–1.50	223 (40)
β-Alanine (0.45 mol L^{-1})		
13.0 (NaOH)	0.80–1.06	555 (40)
13.0 (NaOH)	1.15–1.30	193 (40)
7.0 (KH_2PO_4)	1.20–1.60	365
1.0 (H_2SO_4)	1.30–1.80	234 (40)
α-Aminobutyric acid (0.45 mol L^{-1})		
13.0 (NaOH)	0.71–0.90	320 (41)
13.0 (NaOH)	1.30–1.50	198 (41)
7.0 (KH_2PO_4)	1.40–1.60	352
1.0 (H_2SO_4)	1.50–1.90	250 (41)
β-Aminobutyric acid (0.45 mol L^{-1})		
13.0 (NaOH)	0.73–0.95	310 (41)
13.0 (NaOH)	1.30–1.60	212 (41)
7.0 (KH_2PO_4)	1.50–2.00	386
1.0 (H_2SO_4)	1.50–2.00	250 (41)
γ-Aminobutyric acid (0.45 mol L^{-1})		
13.0 (NaOH)	0.80–1.10	350 (41)
13.0 (NaOH)	1.20–1.40	153 (41)
7.0 (KH_2PO_4)	1.15–1.40	448
7.0 (KH_2PO_4)	1.40–1.80	340
1.0 (H_2SO_4)	1.20–1.40	183 (41)
1.0 (H_2SO_4)	1.40–2.00	250 (41)

the heat of adsorption with coverage. By differentiating the above equation, the Tafel slope is

$$[5] \quad dV/d \log i_1 = 2.3(2RT/F)$$

If the assumption is made that the rate-determining step is the decarboxylation of the adsorbed radical, then the electrochemical equation is:

$$[6] \quad i_2 = zFk_2 (1 - \theta_{G1.}) (\theta_{G.}) \times \exp -[(\Delta G_2^{\ddagger} - \beta r_1\theta + (1 - \beta)r_2\theta)/RT]$$

where G· refers to the adsorbed radical from Step I and G_1· refers to the adsorbed radical formed following decarboxylation. By making the further presumption that Step I is in quasi-equilibrium and that β = 0.5, then the above equation becomes:

$$[7] \quad i_2 = zFk_2 (1 - \theta_{G1.}) (\theta_{G.}) \times \exp -[(\Delta G_2^{\ddagger} + (VF/2r_1)(r_2 - r_1))/RT]$$

After simplifying and differentiating, the Tafel slope becomes:

$$[8] \quad dV/d \log i_2 = 2.3(2RT/F)(r_1/(r_1 - r_2))$$

If Step III, the formation of the next lower aldehyde in the homologous series accompanied by transfer of a second

© 1997 NRC Canada

Table 3. Theoretical Tafel slopes.

Rate-determining step	Theoretical Tafel slope	Calculated Tafel slope (mV)	r_2/r_1
Step I	$2.3(2RT/F)$	120	—
Step II	$2.3(2RT/F)(r_1/(r_1 - r_2))$	180	0.33
		240	0.50
		360	0.66
Step III	$2.3(2RT/F)(r_1/(r_1 + r_2))$	90	0.33
		80	0.50
		72	0.66

Can. J. Chem. Downloaded from www.nrcresearchpress.com by 91.121.58.235 on 09/08/12
For personal use only.

electron, is postulated to be the rate-determining step in the mechanism, then the electrochemical equation is modified to:

[9] $$i_3 = zFk_3\,\theta_{G1}.\,\exp -[(\Delta G_3^{\ddagger} - \beta VF - \beta r_2\theta)/RT]$$

Subsequent rearrangement and differentiation shows the predicted Tafel slope to be

[10] $$dV/d\log i_3 = 2.3(2RT/F)(r_1/(r_1 + r_2))$$

By varying the numerical values of r_1 and r_2 for each of the equations, the predicted Tafel ranges may be calculated, and are shown in Table 3.

The range of values obtained experimentally (Table 2) compare favourably with those shown in Table 3 for Step II, the decarboxylation of the terminal carboxyl group, as the rate-determining step. This is consistent with results obtained previously with glycine (39), α- and β-alanine (40), and α-, β-, and γ-aminobutyric acid (41). Thus the Tafel slopes obtained in phosphate buffer may be attributed to a suppression of the oxygen evolution reaction by the kinetically favoured oxidation of the amino acid or peptide similar to that observed in the Kolbe mechanism (14).

3.3 Surface charge density calculations

By monitoring the surface charge density at an anodic end potential of 0.5 V, information can be obtained on the surface concentration of the adsorbed species in comparison with monolayer surface coverage of OH species, thereby gaining information about structural orientation of the organic molecules at the surface. A series of plots of surface charge density versus concentration for the same concentration ranges were made for each amino acid. Table 4 presents a summary of the surface charge density plateau values of these molecules for the 0.5 V anodic end potentials and the corresponding calculated surface concentrations (Γ_A) from eq. [2], which represent approximate maximum values for surface concentrations up to this anodic potential. This method was used as an approximation for surface concentrations because of the difficulty in determining the pzc (potential of zero charge) for the platinum electrode, and therefore the absolute charge density (65).

The thermodynamic analysis of the charge data is based on the electrocapillary equation:

[11] $$-d\gamma = Q dE + \Gamma_A d\mu_A$$

Table 4. Surface charge densities and surface concentrations for 0.5 V anodic end potentials.

Compound	Q_{ADS} (μC cm^{-2})	$\Gamma_A \times 10^{10}$ (mol cm^{-2})	Γ_A (molecules nm^{-2})
Glycine	60	3.1	1.9
Gly-Gly	128	6.7	4.0
Gly-Gly-Gly	88	4.5	2.7
α-Alanine	105	5.5	3.3
β-Alanine	105	5.5	3.3
α-Aminobutyric acid	189	9.8	6.0
γ-Aminobutyric acid	141	7.3	4.4

where γ is the interfacial tension, Q is the charge density, E is the electrode potential, Γ_A is the Gibbs excess of adsorbed amino acid (approximately equal to the surface concentration), and μ_A is the chemical potential of the amino acid. Since the interfacial tension is a function of the surface charge density, Gibbs excess, and chemical potential of all the species in solution, we will first review the method used in the integration of the cyclic voltammograms and subsequent calculations. Since $Q_T = f(\Gamma_{O_o}, \Gamma_P, \Gamma_A)$, the Gibbs excess may be described by Γ_{O_o} for adsorption of OH^-, Γ_P for adsorption of phosphate anions ($H_2PO_4^-$ + HPO_4^{2-} + PO_4^{3-}), and Γ_A for adsorption of amino acid anions + neutral species. The experiments were carried out at constant ionic strength and constant concentrations of all species in the bulk solution. Therefore if we consider only the contribution due to the surface charge density and recall eq. [1] used to evaluate the cyclic voltammograms,

$$Q_{ADS} = (Q_{O_o}{}^{A} - Q_{O_r}{}^{A}) - (Q_{O_o} - Q_{O_r})$$

then the contribution due to anodic charges may be described as follows:

[12] $$Q_T = Q_{O_o} + Q_A + Q_P$$

where Q_T represents the total charge resulting from the adsorption of oxide (Q_{O_o}), amino acid (Q_A), and phosphate anions (Q_P). Since the anodic oxide charge (Q_{O_o}) due to OH^- adsorption is equal to the oxide reduction charge (Q_{O_r}) in the absence of other adsorbing species, and if we represent the

© 1997 NRC Canada

Can. J. Chem. Downloaded from www.nrcresearchpress.com by 91.121.58.235 on 09/08/12
For personal use only.

charge resulting from the electrolyte solution in the absence of amino acid (Q_E) as:

[13] $$Q_E = Q_{O_o} + Q_P$$

then:

[14] $$Q_{ADS} = Q_T - Q_E = Q_A$$

Differentiation of eq. [11] gives the charge number:

[15] $$\gamma' = \frac{1}{F}\left(\frac{\partial Q}{\partial \Gamma_A}\right)_E = \frac{1}{F}\left(\frac{\partial \mu_A}{\partial E}\right)_\Gamma$$

where γ' is the electrosorption valency or the number of electrons transferred to the interface per one adsorbed amino acid molecule. The integral of the voltammetric current is equal to :

[16] $$\Delta Q = \int i dt = \frac{1}{\nu}\int i dE = Q_{ADS}$$

Since $i = \nu C$ with ν being the sweep rate and C being the differential capacity, the charge may also be given as:

[17] $$\Delta Q = \int C dE$$

In the case of specific adsorption, the capacity C may be represented as a sum of two terms; the so-called infinite frequency capacity and a pseudocapacity. This can be derived in the following way. In the presence of specific adsorption, the charge Q is a function of two variables, the potential E and the amount of adsorbed amino acid Γ_A, i.e.; $Q = f(E, \Gamma_A)$. The total differential of charge is therefore given by:

[18] $$dQ = \left(\frac{\partial Q}{\partial E}\right)_\Gamma dE + \left(\frac{\partial Q}{\partial \Gamma_A}\right)_E d\Gamma_A$$

Differentiation of eq. [18] gives the desired expression for the differential capacity:

[19] $$C = \left(\frac{dQ}{dE}\right) = \left(\frac{\partial Q}{\partial E}\right)_\Gamma + \left(\frac{\partial Q}{\partial \Gamma_A}\right)_E \frac{d\Gamma_A}{dE}$$

where the term $(\partial Q/\partial E)_\Gamma = C_\Gamma$ is called the infinite frequency capacity (or the true capacity) and the second term on the right-hand side of eq. [19] is called the pseudocapacity. The term $(\partial Q/\partial \Gamma_A)_E = \gamma' F$ where γ' is the electrosorption valency. Substitution of C in eq. [17] by the right-hand side of eq. [19] gives the following expression for ΔQ:

[20] $$\Delta Q = \int C dE = \int \left(\frac{\partial Q}{\partial E}\right)_\Gamma dE + \int \left(\frac{\partial Q}{\partial \Gamma_A}\right)_E d\Gamma_A$$

If the integration starts at a potential at which $\Gamma = 0$, and if it is assumed that the electrosorption valency or charge number is independent of the electrode potential and coverage, then eq. [17] may be written as:

[21] $$\Delta Q = \int \left(\frac{\partial Q}{\partial E}\right)_\Gamma dE + \gamma' F \Gamma_A$$

Equation [21] shows that the charge measured by integration of the cyclic voltammogram is not equal to $\gamma' F \Gamma_A$, but also contains a term that is due to charging of the infinite frequency capacity. However, in the present studies, the integration was begun as the charge increased above that of the double-layer region for the anodic area and below the double layer for the oxide reduction area, and because these areas are subtracted, the term for charging the infinite frequency capacity is eliminated. Therefore rearranging eq. [21] for surface concentration gives:

[22] $$\Gamma_A = \Delta Q/\gamma' F = Q_{ADS}/nF$$

where n (or γ', the electrosorption valency of amino acid) was used as 2 in these calculations based on the results of quantitative coulometric product analysis (39). From the Tafel measurements, initial adsorption is assumed to be quasi-reversible (Step I) with decarboxylation (Step II) as the rate-determining step. In situ FTIR measurements of glycine have shown that adsorption occurs through the carboxylate groups at the Pt(111) surface (66). The production of CO_2 from the asymmetric stretching frequency at 2344 cm^{-1} coincided with the potential for maximum adsorption at this surface. Therefore the use of $n = 2$ as the charge number appears to be appropriate, particularly for a comparative study of the adsorption behaviour of a series of amino acids.

It is interesting to compare the calculated approximate maximum values for surface concentrations (Table 4) with those estimated from molecular dimensions. The area of a glycine molecule lying on its side may be estimated as an upper limit from the sum of the bond lengths (67) N—H (0.1001 nm), C—N (0.1467 nm), C—C (0.1526 nm), C—O (0.1355 nm), and O—H (0.0966 nm), which gives 0.6324 nm. If half this value is taken as the radius of a circle occupied by the molecule, then the calculated area is 0.31 nm^2 $molecule^{-1}$ or 3.2 molecules nm^{-2}. Therefore it appears that glycine is likely in a horizontal position at these small anodic potentials with both the ammonium ion and carboxylate group positioned on the electrode surface. It is interesting to compare the similarity of the surface concentration for glycine with that for the calculated value of 2.9 molecules nm^{-2} taken from the experimental results reported for the surface concentration for acetic acid adsorption at the Pt electrode from a solution of 10^{-3} mol L^{-1} acetic acid in 0.1 mol L^{-1} $HClO_4$ (44). When the area is calculated for Gly-Gly in a similar manner, only 0.8 molecules nm^{-2} would be allowed for the dipeptide to be oriented on its side. Since a much higher surface concentration is observed, this suggests that a more vertical arrangement occurs with adsorption through the carboxylate group. An estimate of the area of a circle described by the rotation of this functional group using geometrical calculations from C═O (0.1205 nm), C—O (0.1355 nm), O—H (0.966 nm), and an O═C—O angle of 123° (67) gave approximately 13 molecules nm^{-2}. Thus, the remaining molecules appear to be in a tilted position, rather than in a horizontal position on the surface.

© 1997 NRC Canada

Can. J. Chem. Downloaded from www.nrcresearchpress.com by 91.121.58.235 on 09/08/12
For personal use only.

4. Summary

Electrochemical oxidation of the amino acids and peptides at a platinum electrode has shown that there is strong adsorption of all species at anodic potentials in neutral solution, accompanied by an efficient ability to block both the initial stages of OH monolayer deposition as well as the second stage involving an irreversible process of continued deposition of OH or O species associated with the initial stages of a place inversion of Pt and O in the oxide film. Glycine and the peptides, however, blocked the initially and more reversibly deposited OH species in preference to those formed at higher potentials. The surface charge densities of the amino acids and peptides were measured at the anodic end potential of 0.50 V, which corresponds to the first stage resulting in monolayer OH coverage. This was the same potential at which maximum adsorption of acetic acid at a platinum electrode was observed in infrared and radiotracer studies (44) and where maximum adsorption of amino acids occurred in Horanyi's radiotracer studies (45). The present results at pH 7.0 indicate that adsorption occurred through the negatively charged carboxylate groups, similar to results observed previously (39–41). The infrared experiments of Krauskopf and Wieckowski (43) with acetic acid at a platinum electrode support these results, as they determined that both carboxylate oxygens were oriented toward the metal surface. Results of the present study also indicated that, at the lower anodic end potentials (0.50 V), the glycine may be arranged predominately in a horizontal position on the electrode surface, but the larger amino acids and peptides appear to be in a modified vertical configuration with adsorption through the carboxylate groups.

Steady-state polarization measurements gave Tafel slopes in the range of 253–498 mV, considerably higher than that normally seen for oxygen evolution from a phosphate buffer solution. These results suggest that, in the pH 7.0 buffer, the negatively charged carboxylate group preferentially adsorbs under these anodic potentials in a mechanism similar to the Kolbe reaction, with the decarboxylation step being rate determining. Previous results have shown that at potentials greater than 1.8 V, less than 10% of the yield of oxidation products from the dipeptides Tyr-Gly and Trp-Gly could be attributed to the cleavage of the peptide bond (42). Therefore, this type of reaction was not expected to contribute to any extent to the oxidation mechanisms at the lower potentials used in the present study.

Acknowledgments

Grateful acknowledgment is made to the Natural Sciences and Engineering Research Council of Canada for support of this research. The authors would like to thank Professor Jacek Lipkowski for helpful discussions on the thermodynamics in this manuscript.

References

1. A. Damjanovic. *In* Modern aspects of electrochemistry. Vol. 5. *Edited by* J.O'M. Bockris and B.E. Conway. Plenum, New York. 1969. pp. 369–483.
2. A. Damjanovic, L.S.R. Yeh, and J.F. Wolf. J. Electrochem. Soc. **127,** 784 (1980); **127**, 1951 (1980).
3. A. Damjanovic, L.S.R. Yeh, and J.F. Wolf. J. Electrochem. Soc. **122,** 471 (1975).
4. E.L. Littauer and L.L. Shrier. Electrochim. Acta, **11**, 527 (1966).
5. B.E. Conway and D.M. Novak. J. Chem. Soc. Faraday Trans. 1, **75**, 2454 (1979).
6. B.E. Conway and D.M. Novak. J. Electroanal. Chem. **99**, 133 (1979).
7. B.E. Conway and J. Mozota. J. Chem. Soc. Faraday Trans. 1, **78**, 1717 (1982).
8. S.G. Roscoe and B.E. Conway. J. Electroanal. Chem. **224,** 163 (1987).
9. H.P. Stout. Trans. Faraday Soc. **41**, 64 (1945).
10. L. Krishtalik and G.E. Titova. Elektrokhimiya, **4**, 285 (1968).
11. S.G. Roscoe and B.E. Conway. J. Chem. Soc. Chem. Commun. 900 (1988).
12. S.G. Roscoe and B.E. Conway. J. Electroanal. Chem. **249**, 217 (1988).
13. A. Dalmia, S. Wasmus, R.F. Savinell, and C.C. Liu. J. Electrochem. Soc. **143**, 556 (1996).
14. A.K. Vijh and B.E. Conway. Chem. Rev. **67**, 623 (1967).
15. S.G. Roscoe. *In* Modern aspects of electrochemistry. Vol. 29. *Edited by* J.O'M. Bockris, B.E. Conway, and R.E. White. Plenum, New York. 1996. pp. 319–399.
16. S.G. Roscoe, K.L. Fuller, and G. Robitaille. J. Colloid Interface Sci. **160**, 243 (1993).
17. S.G. Roscoe and K.L. Fuller. J. Colloid Interface Sci. **152,** 429 (1992).
18. K.L. Hanrahan, S.M. MacDonald, and S.G. Roscoe. Electrochim. Acta, **41**, 2469 (1996).
19. S.M. MacDonald and S.G. Roscoe. J. Colloid Interface Sci. **184**, 449 (1996).
20. D.C. Johnson, S.G Weber, A.M. Bond, R.M. Wightman, R.E. Shoup, and I.S. Krull. Anal. Chim. Acta, **180**, 187 (1986).
21. L.E. Welch, W.R. LaCourse, D.A. Mead, Jr., D.C. Johnson, and T. Hu. Anal. Chem. **61**, 555 (1989).
22. D.C. Johnson and W.R. LaCourse. Anal. Chem. **62**, 589 (1990).
23. H. Gunasingham, K.P. Ang, and C.C. Ngo. Anal. Chem. **57**, 505 (1985).
24. S. Sun, P-H. Ho-Si, and J.D. Harrison. Langmuir, **7**, 727 (1991).
25. C.E Hall and E.A.H. Hall. Anal. Chim. Acta, **310**, 199 (1995).
26. E.A.H. Hall, J.J. Gooding, and C.E Hall. Mikrochim. Acta, **121**, 119 (1995).
27. O. Adeyoju, E.I. Iwuoha, and M.R. Smyth. Electroanalysis, **7**, 924 (1995).
28. W. Schuhmann. Biosens. Bioelectron. **10**, 181 (1995).
29. H. Durliat, C. Causserand, and M. Comtat. Anal. Chim. Acta, **231**, 309 (1990).
30. J.S. Redinha, A.M. Oliveira Brett, J.L.C. Pereira, M. Alves da Silva, and M.H. Gil. Bioelectrochem. Bioenerg. **22**, 379 (1988).
31. L. Coche-Guerente, S. Cosnier, C. Innocent, P. Mailley, J.-C. Moutet, R.M. Morelis, B. Leca, and P.R. Coulet. Electroanalysis, **5**, 647 (1993).
32. H.T. Tien and S. Salamon. Bioelectrochem. Bioenerg. **22**, 211 (1989).
33. T. Hianik, J. Dlugopolsky, V.I. Passechnik, D.F. Sargent, and S.A. Ivanov. Colloids Surf. A: **106**, 109 (1996).
34. K.M.R. Kallury, V. Ghaemmaghami, U.J. Krull, and M. Thompson. Anal. Chim. Acta, **225**, 369 (1989).
35. Z. Gao, J. Bobacka, and A. Ivaska. J. Electroanal. Chem. **364**, 127 (1994).
36. J.J. Ramsden, G.I. Bachmanova, and A.I. Archakov. Biosens. Bioelectron. **11**, 523 (1996).
37. E. Sackman. Science, **271**, 43 (1996).
38. F. Sommer, S. Alexandre, N. Dubreuil, D. Lair, T. Due, and J.M. Valleton. Langmuir, **13**, 791 (1997).
39. D.G. Marangoni, R.S. Smith, and S.G. Roscoe. Can. J. Chem. **67**, 921 (1989).

© 1997 NRC Canada

40. D.G. Marangoni, I.G.N. Wylie, and S.G. Roscoe. Bioelectrochem. Bioenerg. **25**, 269 (1991).
41. I.G.N. Wylie and S.G. Roscoe. Bioelectrochem. Bioenerg. **28**, 367 (1992).
42. S.M. MacDonald and S.G. Roscoe. Electrochim. Acta, **41**, 2469 (1996).
43. E.K. Krauskopf and A. Wieckowski. *In* Adsorption of molecules at metal electrodes. Vol. 1. *Edited by* J. Lipkowski and P.N. Ross. VCH Publishers, Inc., New York. 1992. pp. 119–169.
44. D.S. Corrigan, E.K. Krauskopf, L.M. Rice, A. Wieckowski, and M.J. Weaver. J. Phys. Chem. **92**, 1596 (1988).
45. G. Horanyi. Electrochim. Acta, **35**, 919 (1990).
46. M. Masui, Y. Kamada, T. Iizuka, and S. Ozaki. Chem. Pharm. Bull. **32**, 4740 (1984).
47. H. Angerstein-Kozlowska. *In* Comprehensive treatise of electrochemistry. Vol. 9. *Edited by* E. Yeager, J.O'M. Bockris, B.E. Conway, and S. Sarangapani. Plenum Press, New York. 1984. pp. 15–59.
48. J.H. Kennedy. Analytical chemistry. Harcourt Brace Jovanovich, San Diego. 1984. p. 481.
49. G.J. Shugar and J.A. Dean. The chemist's ready reference handbook. McGraw–Hill, New York. 1990. p. 179.
50. A.K.N. Reddy, M.A. Genshaw, and J.O'M. Bockris. J. Chem. Phys. **48**, 671 (1968).
51. D. Gilroy and B.E. Conway. Can. J. Chem. **46**, 875 (1968).
52. H.A. Kozlowska, B.E. Conway, and W.B.A. Sharp. J. Electroanal. Chem. **43**, 9 (1973).
53. Y.B. Vassiliev, V.S. Bagotsky, and V.A. Gromyko. J. Electroanal. Chem. **178**, 247 (1984).
54. A.J. Appleby. J. Electrochem. Soc. **120**, 1205 (1973).
55. S. Shibata. Bull. Chem. Soc. Jpn. **36**, 526 (1963); **40**, 696 (1967).
56. S. Shibata and M.P. Sumino. Electrochim. Acta, **16**, 1089 (1971); **17**, 395 (1972); **17**, 2215 (1972).
57. S. Shibata. Electrochim. Acta, **22**, 175 (1977).
58. J.W. Schultze and K.J. Vetter. J. Electroanal. Chem. **34**, 131 (1972); **34**, 141 (1972).
59. J.L. Ord and F.C. Ho. J. Electrochem. Soc. **118**, 46 (1971).
60. R. Parsons and W. Visscher. J. Electroanal. Chem. **36**, 329 (1972).
61. S. Gottesfeld and B.E. Conway. J. Chem. Soc. Faraday Trans. 1, **69**, 1090 (1973).
62. D.M. Novak and B.E. Conway. J. Chem. Soc. Faraday Trans. 1, **77**, 2341 (1981).
63. M. Tarasevich, A. Sadkowski, and E. Yeager. *In* Comprehensive treatise of electrochemistry. Vol. 7. *Edited by* B.E. Conway, J.O'M Bockris, E. Yeager, S.U.M. Khan, and R.E. White. Plenum Press, New York. 1983. pp. 301–397.
64. B.E. Conway and M. Dzieciuch. Can. J. Chem. **43**, 38 (1963).
65. W. Savich, S-G. Sun, J. Lipkowski, and A. Wieckowski. J. Electroanal. Chem. **388**, 233 (1995).
66. F. Huerta, E. Morallon, F. Cases, A. Rodes, J.L. Vazquez, and A. Aldaz. J. Electroanal. Chem. **421**, 179 (1997).
67. C-H. Hu, M. Shen, and H.F. Schaefer III. J. Am. Chem. Soc. **115**, 2923 (1993).

Can. J. Chem. Downloaded from www.nrcresearchpress.com by 91.121.58.235 on 09/08/12
For personal use only.

© 1997 NRC Canada

$Cu_xCo_{3-x}O_4$/$LaPO_4$-bonded Ni electrodes for oxygen evolution in alkaline solution: preparation, physicochemical properties, and electrochemical behavior

Khalid Fatih and Benoît Marsan

Can. J. Chem. Downloaded from www.nrcresearchpress.com by 91.121.58.235 on 09/08/12
For personal use only.

Abstract: Copper-cobalt oxide, prepared by thermal decomposition of nitrate precursors on a highly porous lanthanum phosphate-bonded nickel support, was investigated as an anode material for alkaline water electrolysis. Physicochemical characterization shows that this nonstoichiometric oxide possesses a spinel structure ($Cu_{0.9}Co_{2.1}O_4$) and that it is also highly porous. FTIR spectroscopy indicates that the oxide is not decomposed in 5 M KOH at room temperature. The highest electrocatalytic activity for the oxygen evolution reaction is obtained when the electrode is prepared at 300°C from a solution containing 0.5 M $Cu(NO_3)_2{\cdot}2.5H_2O$ and 1.0 M $Co(NO_3)_2{\cdot}6H_2O$, with a catalyst loading of 52 mg cm^{-2}. The activity is reduced when an excess of either Co or Cu is present in the spinel oxide film beyond the stoichiometric ratio of the precursors, probably due to some phase change. Cyclic voltammetry indicates that a quasi-reversible Co^{IV}/Co^{III} surface redox transition occurs prior to the onset of oxygen evolution; this process is diffusion controlled at low OH^- concentration and at high scan rate when $[OH^-] \geq 1$ M. In the negative potential domain, a Cu^{II}/Cu^{I} surface redox transition is observed.

Key words: copper-cobalt oxide, oxygen evolution, highly porous electrode, cyclic voltammetry.

Résumé : L'oxyde de cuivre et de cobalt, préparé par décomposition thermique des nitrates précurseurs sur un substrat très poreux constitué de nickel finement divisé lié par un polymère de phosphate de lanthane, a été étudié comme matériau d'anode pour le procédé d'électrolyse de l'eau en milieu alcalin. Les analyses physico-chimiques montrent que cet oxyde non stoéchiométrique possède une structure spinelle ($Cu_{0.9}Co_{2.1}O_4$) et qu'il est également très poreux. La spectroscopie infrarouge indique que l'oxyde n'est pas décomposé lorsqu'il est immergé dans une solution de KOH 5 M à la température ambiante. L'activité électrocatalytique pour le dégagement de l'oxygène est la plus élevée lorsque l'électrode est préparée à 300°C à partir d'une solution contenant du $Cu(NO_3)_2{\cdot}2{,}5H_2O$ 0,5 M et du $Co(NO_3)_2{\cdot}6H_2O$ 1,0 M, à un recouvrement d'oxyde de 52 mg cm^{-2}. L'activité est diminuée lorsqu'un excès de cobalt ou de cuivre est présent dans le film d'oxyde au-delà du rapport stoéchiométrique des nitrates précurseurs, probablement en raison d'un changement de phase partiel. Les études de voltammétrie cyclique indiquent qu'une transition rédox de surface Co^{IV}/Co^{III} quasi-réversible se produit avant le dégagement de l'oxygène; ce processus est contrôlé par la diffusion des ions OH^- à faible concentration et à concentration plus élevée ($[OH^-] \geq 1$ M) lorsque la vitesse du balayage de potentiel est grande. Dans le domaine des potentiels négatifs, une transition rédox de surface Cu^{II}/Cu^{I} est observée.

Mots clés : oxyde de cuivre et de cobalt, dégagement de l'oxygène, électrode très poreuse, voltammétrie cyclique.

Introduction

The oxygen evolution reaction (OER) is highly irreversible with a significant activation overpotential in aqueous solution. Selection of an electrode material is based on several parameters, including excellent electrocatalytic properties, high active surface area as for heterogeneous catalysts, long-term chemical, electrochemical, and mechanical stabilities, and low cost. Cobaltite spinel oxides (MCo_2O_4 with M = Co, Ni, Mn, Cu) have shown interesting electrocatalytic activities for the OER in alkaline solutions (1–6); among these materials, $NiCo_2O_4$ and Co_3O_4 were the most studied. Different preparation techniques have been used such as thermal decomposition (2, 4), sol–gel synthesis (7), cryochemical synthesis (6), and coprecipitation (5); sometimes an effect of the nature of the substrate (Pt, Ni, Ti) was noticed (2, 3).

Recently, we reported that the nonstoichiometric oxide $Cu_xCo_{3-x}O_4$, prepared by thermal decomposition of nitrate precursors on a sandblasted nickel support, shows fairly low overvoltages for the OER in 1 M KOH at 25°C (280 mV at 10 mA cm^{-2} and 320 mV at 100 mA cm^{-2}) (2). Based on the same

Received March 24, 1997.

This paper is dedicated to Professor Brian E. Conway on the occasion of his 70th birthday.

K. Fatih and B. Marsan.[1] Département de chimie, Université du Québec à Montréal, C.P. 8888, Succ. Centre-Ville, Montréal, QC H3C 3P8, Canada.

[1] Author to whom correspondence may be addressed. Telephone: (514) 987-3000, ext. 7980. Fax: (514) 987-4054. E-mail: marsan.benoit@uqam.ca

© 1997 NRC Canada

Can. J. Chem. Downloaded from www.nrcresearchpress.com by 91.121.58.235 on 09/08/12
For personal use only.

electrochemically active surface area, the $Cu_xCo_{3-x}O_4$/Ni electrode demonstrated a better activity than the most active perovskite, $LaNiO_3$, and a much greater activity than Co_3O_4 and $NiCo_2O_4$ (8). Lee et al. (9) investigated the effect of intercalation of Cu^{2+} and Zn^{2+} on the electrochemical properties of Co_3O_4; the intercalation, respectively, enhances (Cu^{2+}) and depresses (Zn^{2+}) the electrocatalytic activity of the cobaltite spinel oxide for the OER. It has been demonstrated that $Cu_xCo_{3-x}O_4$ is a *p*-type semiconductor with a metallized surface in the potential region of oxygen evolution (10). Its resistivity (0.047 Ω cm) is situated between the values reported for $NiCo_2O_4$ and Co_3O_4, prepared by the same method.

Electrochemical studies suggested that the experimentally observed currents are strongly correlated to the roughness factor of the oxide film (2). Recent works by Dumont et al. (11) into developing new anode and cathode materials for water electrolysis have been directed toward the use of a new process of cementation of metallic nickel powder to produce highly porous electrodes; the nickel particles were bonded by $LaPO_4$, leading to three-dimensional electrodes. The present work deals with the use of lanthanum phosphate-bonded nickel (LPBN) as support for $Cu_xCo_{3-x}O_4$; we recall that our previous papers were related to the use of a much smoother Ni substrate (2, 10). The new optimum conditions (concentration of the nitrate precursors, Cu:Co atomic ratio, decomposition temperature, and catalyst loading) for thermal decomposition of the nitrate precursors on this highly porous support were established, based on the electrode activity for the OER in 1 M KOH at 25°C. Furthermore, the electrochemical behavior of the oxide deposited on a Pt wire was studied in detail in order to understand the nature, reversibility, and mechanism of the surface redox transition occurring prior to the onset of oxygen evolution. Also, the redox transition observed in the negative potential region was investigated.

Experimental

Preparation of copper-cobalt oxide electrodes

$Cu_xCo_{3-x}O_4$ electrodes were prepared by thermal decomposition of nitrate precursors (2, 4, 12) deposited on a highly porous substrate consisting of lanthanum phosphate ($LaPO_4$ 10% w/w)-bonded spiky filamentary particles of nickel (LPBN) (11), supplied by the Université de Sherbrooke. In this procedure, $Co(NO_3)_2{\cdot}6H_2O$ and $Cu(NO_3)_2{\cdot}2.5H_2O$ (Fisher Scientific, ACS) were dissolved in the solvent mixture isopropanol:nanopure water (4:1), with the appropriate atomic ratio (Cu:Co) and concentration. The solution was deposited uniformly with a micropipet onto a 1 cm^2 LPBN pellet, which had been previously degreased in dichloromethane (Anachemia, ACS) and thoroughly washed with nanopure water. The solvent was then evaporated at 110°C, and the nitrate coating was heated for 15 min in a triple-zone quartz furnace (Lindberg 59744) under air atmosphere at an appropriate temperature. The procedure was repeated several times until the desired catalyst loading was achieved, and the electrodes were thereafter annealed over 1 h under the same conditions. To reach the highest electrocatalytic activity for the OER, the following preparation variables were optimized. Concentration of the nitrate precursors, with a constant atomic ratio Cu:Co = 1:2, was varied from 0.2 M to 1.4 M $Co(NO_3)_2{\cdot}6H_2O$. The Cu:Co atomic ratio was changed (1:5, 1:2, and 1:1) using the optimized total nitrate concentration. The electrodes were heated at temperatures ranging from 250 to 400°C and the catalyst loading was varied from 0 to 83 mg cm^{-2}.

Bulk and surface characterization of the oxide

X-ray diffraction patterns of the oxide electrodes were obtained using a Siemens model D5000 instrument with Co-K_α radiation (λ = 1.789 Å); the scan rate was 1° min^{-1}. Oxide powder was analyzed by FTIR spectroscopy (Perkin–Elmer, model 1600) to evaluate its chemical stability in alkaline medium. FTIR spectra were obtained between 800 and 400 cm^{-1} using KBr pellets (Aldrich, 99+%) containing the oxide (1% w/w). The powder was prepared as follows. An aqueous solution of copper and cobalt nitrates (Cu:Co = 1:2) was evaporated to dryness and the residue was dried (110°C), ground, and annealed in air for 1 h at 300°C. The oxide was then finely ground and annealed for an extra 5 h. Analysis was made on fresh oxide and on oxide that had been dipped for 7 days in aqueous 5 M KOH (A&C, Baker analyzed) solution without stirring. Surface morphology of the electrodes was examined with a scanning electron microscope (Hitachi, model S-2300) and the surface composition was assessed through semiquantitative EDAX analysis.

Electrochemical studies

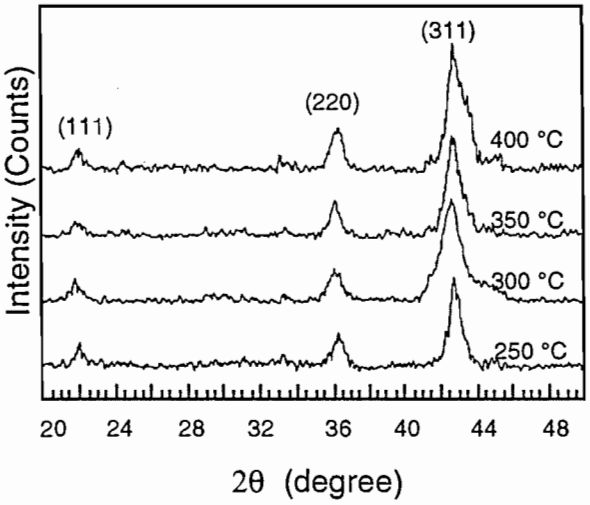
Electrochemical behavior of $Cu_xCo_{3-x}O_4$ electrodes was studied using cyclic voltammetry; a potentiostat (Pine Instruments AFRDE4) coupled with an X-Y recorder (Kipp & Zonen BD 90) was used. For this experiment, $Cu_xCo_{3-x}O_4$ was prepared (optimum deposition conditions) on a Pt (Johnson Matthey, 99.9%) wire substrate (0.14 cm^2) sealed in a glass tube, instead of LPBN. This is because the highly porous surface of $Cu_xCo_{3-x}O_4$/LPBN masks the real electrochemical behavior of the oxide film. Cyclic voltammetry measurements were carried out at room temperature in a cylindrical Pyrex glass cell. Potentials of the working electrode are measured against a Ag/AgCl reference electrode (0.21 V vs. NHE) and reported with respect to a Hg/HgO/1 M KOH electrode (0.110 V vs. NHE at 25°C); the auxiliary electrode consisted of a Pt foil (Alfa, 99.9%) (11 cm^2). The electrolyte was prepared from KOH (Mallinckrodt, ACS) and nanopure water. To study the influence of pH on the mean peak potential of the redox transition, the ionic strength of the electrolyte was corrected using KNO_3 (Mallinckrodt, A.R.). Cyclic voltammetry was also used to determine the electrochemical surface area of the LPBN substrate through double-layer charging curves in deaerated 1 M KOH solution at 25°C (2). The potential was scanned (20–100 mV s^{-1}) between −0.20 and −0.05 V vs. Hg/HgO.

To determine the electrocatalytic activity of the $Cu_xCo_{3-x}O_4$/LPBN electrodes for the OER, steady-state galvanostatic measurements were carried out at 25°C using a three-compartment Teflon cell, which has been described previously (10). In this case, ohmic drops were minimized by using a Luggin capillary approaching the front of the electrode; IR-corrected potentials are reported against a Hg/HgO/1 M KOH reference electrode. A 7 cm^2 Pt disc (Alfa, 99.9%), 3 cm away from the anode, was used as the auxiliary electrode. A potentiostat (PAR, model 273) controlled by a microcomputer (Packard Bell, Pack-Mate III) working with software developed at the Université de Sherbrooke was used. The polarization time varied with the current (e.g., 600 s at 2 μA and 60 s at 700 mA).

© 1997 NRC Canada

Can. J. Chem. Downloaded from www.nrcresearchpress.com by 91.121.58.235 on 09/08/12
For personal use only.

Fig. 1. X-ray diffractograms of $Cu_xCo_{3-x}O_4$ prepared at various temperatures as a thin film on a LPBN support. $Cu(NO_3)_2 \cdot 2.5H_2O$ = 0.5 M; $Co(NO_3)_2 \cdot 6H_2O$ = 1.0 M; catalyst loading: 52 mg cm^{-2}.



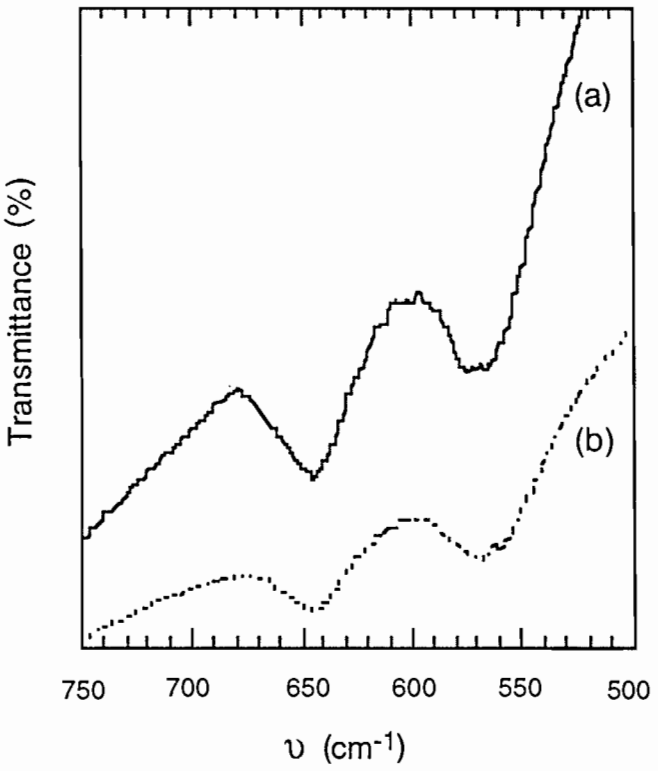
Results and discussion

Physicochemical characterization of the oxide phase

Figure 1 shows X-ray diffraction patterns of $Cu_xCo_{3-x}O_4$/LPBN electrodes prepared under the optimum conditions (see below) at temperatures ranging from 250 to 400°C. Diffractograms are limited to Bragg angles lying between $2\theta = 20°$ and 50° because of the high intensity of the diffraction lines of the nickel substrate in comparison to those of the oxide phase in the region 50°–90°. Relative intensities of the diffraction lines of the spinel (face-centered cubic structure) oxide are in good agreement with ASTM data for $CuCo_2O_4$ (13). We observe that the intensity of the peaks increases when the temperature of nitrate decomposition is raised; this indicates a better crystallization of the oxide film at high temperature. The lattice parameter a_0 was estimated at each temperature from the *d*-spacings of the planes (311) and (220), in a similar way to that used in a previous work (2). The values show a discontinuous variation from 8.13 to 8.10 Å with increasing temperature. These values are higher than the one calculated from the *d*-spacings given in the ASTM table for the same planes of $CuCo_2O_4$: 8.06 Å (13). Petrov et al. (14) obtained almost the same values of a_0, up to 8.13 Å, for copper-cobalt oxide prepared by thermal decomposition. Since diffraction lines of $CuCo_2O_4$ and Co_3O_4 are very close, it is difficult to exclude the possibility of the presence of a Co_3O_4 phase. However, there are no diffraction lines characteristic of monoclinic copper oxide (CuO), so we can conclude that the diffractograms almost correspond to the spinel $CuCo_2O_4$ at each temperature. According to EDAX analysis, copper-cobalt oxide presents a nonstoichiometric phase ($Cu_{0.9}Co_{2.1}O_4$), which is in agreement with the oxide formed on a smooth nickel substrate (2). However, we have to consider that backscattered electrons influence EDAX measurements in the case of a porous electrode.

Figure 2(*a*) shows the FTIR spectrum of as-prepared oxide powder. We observe two broad bands around 570 and 645 cm^{-1}, which may be assigned, respectively, to the octahedrically and tetrahedrically coordinated cations in the spinel crystal lattice (15). Figure 2(*b*) shows the FTIR spectrum of the oxide powder, which had been dipped for 7 days in 5 M KOH solution at room temperature. We can see the same absorption bands with a decrease of their intensities. We observe that the weight of the oxide has been weakly reduced after its contact with the solution; this may be due to a partial dissolution of the oxide in highly concentrated KOH solutions. However, it seems that there is no decomposition of the mixed oxide $Cu_xCo_{3-x}O_4$ to simple oxides, as reported by Cherkashin et al. (16) for Co_3O_4. These authors noticed the appearance of a new absorption band at 450 cm^{-1}, attributed to the partial decomposition of Co_3O_4 to CoO and Co_2O_3, after contact with a 12 M KOH solution.

Fig. 2. FTIR spectra of the $Cu_xCo_{3-x}O_4$ powder prepared at 300°C: (*a*) as prepared oxide powder; (*b*) oxide powder dipped for 7 days in 5 M KOH solution at 25°C.



Characterization of the highly porous LPBN substrate

The highly porous LPBN substrate has been mainly studied as a cathode and anode material for alkaline water electrolysis (11). SEM micrograph (Fig. 3) reveals the Ni particles that ensure the highly porous surface of the substrate. The electrochemical surface area of this support was determined from double-layer charging curves using cyclic voltammetry. Figure 4 depicts the cyclic voltammograms recorded in deaerated 1 M KOH solution (25°C), at various scan rates ($\partial E/\partial t$), in the small capacitive region (−0.20 to −0.05 V vs. Hg/HgO). When there is no adsorption pseudo-capacitance, the double-layer capacitance (C_{dl}) is calculated from the slope of the linear curve i_{cap} vs. ($\partial E/\partial t$) (2):

$$[1] \quad C_{dl} = \frac{d_{icap}}{d(\partial E/\partial t)}$$

© 1997 NRC Canada

Can. J. Chem. Downloaded from www.nrcresearchpress.com by 91.121.58.235 on 09/08/12
For personal use only.

Fig. 3. SEM micrograph of the LPBN support.

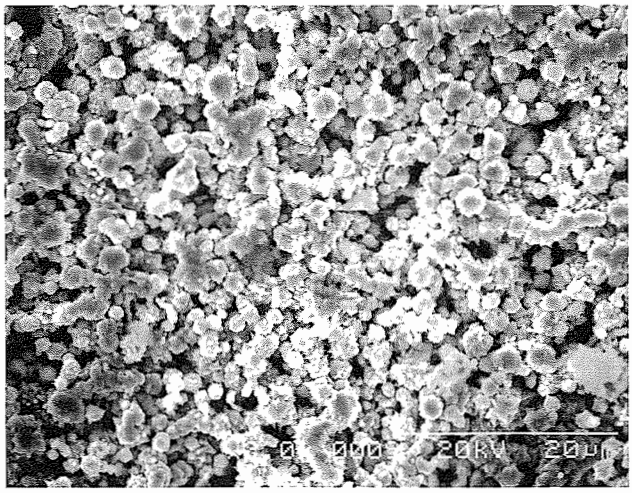
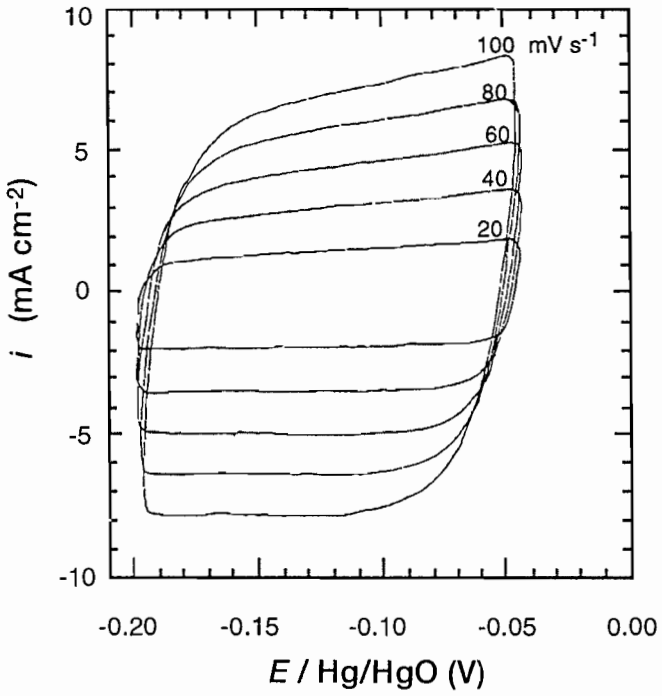


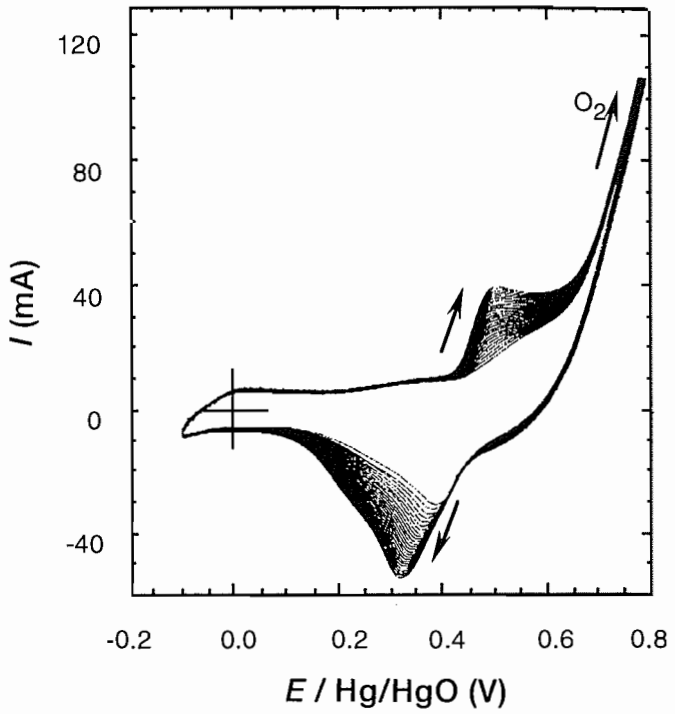
Fig. 4. Cyclic voltammograms of the LPBN support recorded at various scan rates in the capacitive region. Electrolyte: deaerated 1 M KOH solution at 25°C.



where i_{cap} is the capacitive current density measured at −0.125 V vs. Hg/HgO. The high roughness factor (4050), determined by assuming a double-layer capacitance of 20 μF cm^{-2} for a smooth metallic surface (17), indicates that the LPBN substrate is highly porous.

Figure 5 shows the voltammetric curve (several cycles) recorded in 1 M KOH solution (25°C) between −0.10 and 0.80 V vs. Hg/HgO, i.e., between a potential near the open-circuit potential and a potential in the oxygen evolution region. There is a single anodic peak and the corresponding cathodic peak. This voltammetric curve shows the characteristic behavior of a Ni electrode; the peaks are associated with the $NiOOH/Ni(OH)_2$ redox couple:

Fig. 5. Cyclic voltammograms of the LPBN support in 1 M KOH (25°C) at 20 mV s^{-1}.



[2] $Ni(OH)_2 + OH^- \rightleftharpoons Ni(OOH) + H_2O + e^-$

Electrocatalytic activities for the OER

Influence of the nitrate concentrations

Concentration of the nitrate precursors in the solvent mixture has a direct effect on $Cu_xCo_{3-x}O_4$/LPBN electrocatalytic activity for the OER. Figure 6 shows SEM micrographs (after anodic polarization, the SEM being out of order before) of electrodes prepared at 300°C from different concentrations of copper and cobalt nitrates, with constant metal atomic ratio (Cu:Co = 1:2) and oxide loading (~41 mg cm^{-2}). We observe that the electrode is more porous when the copper nitrate concentration is 0.5 M (Fig. 6(*c*)). Table 1 gives the electrode potential values at a current density of 250 mA cm^{-2} (geometric surface area), as determined from steady-state galvanostatic polarization measurements. As expected, the lower potential was obtained for the more porous electrode. It is interesting to note that we reported an optimum copper nitrate concentration of 0.3 M when the spinel oxide is formed on a smooth titanium substrate (2).

The morphology of copper-cobalt oxide films is mainly determined by the volume of gases (NO_2, O_2) that evolve during decomposition of the nitrate precursors. At low concentration, the number of coating layers is increased in order to obtain the same catalyst loading. This leads to the formation of smoother oxide films (Fig. 6(*a*)). When concentration of the precursors is increased above the optimum value, a compact film with large cracks and a poor mechanical stability is obtained (Fig. 6(*d*)).

© 1997 NRC Canada

Can. J. Chem. Downloaded from www.nrcresearchpress.com by 91.121.58.235 on 09/08/12
For personal use only.

Fig. 6. SEM micrographs of $Cu_xCo_{3-x}O_4$/LPBN electrodes (after anodic polarization) prepared at 300°C from different concentrations of nitrate precursors: [Cu]/[Co] = (*a*) 0.1 M/0.2 M; (*b*) 0.3 M/0.6 M; (c) 0.5 M/1.0 M; (d) 0.7 M/1.4 M. Catalyst loading: 41 mg cm^{-2}.

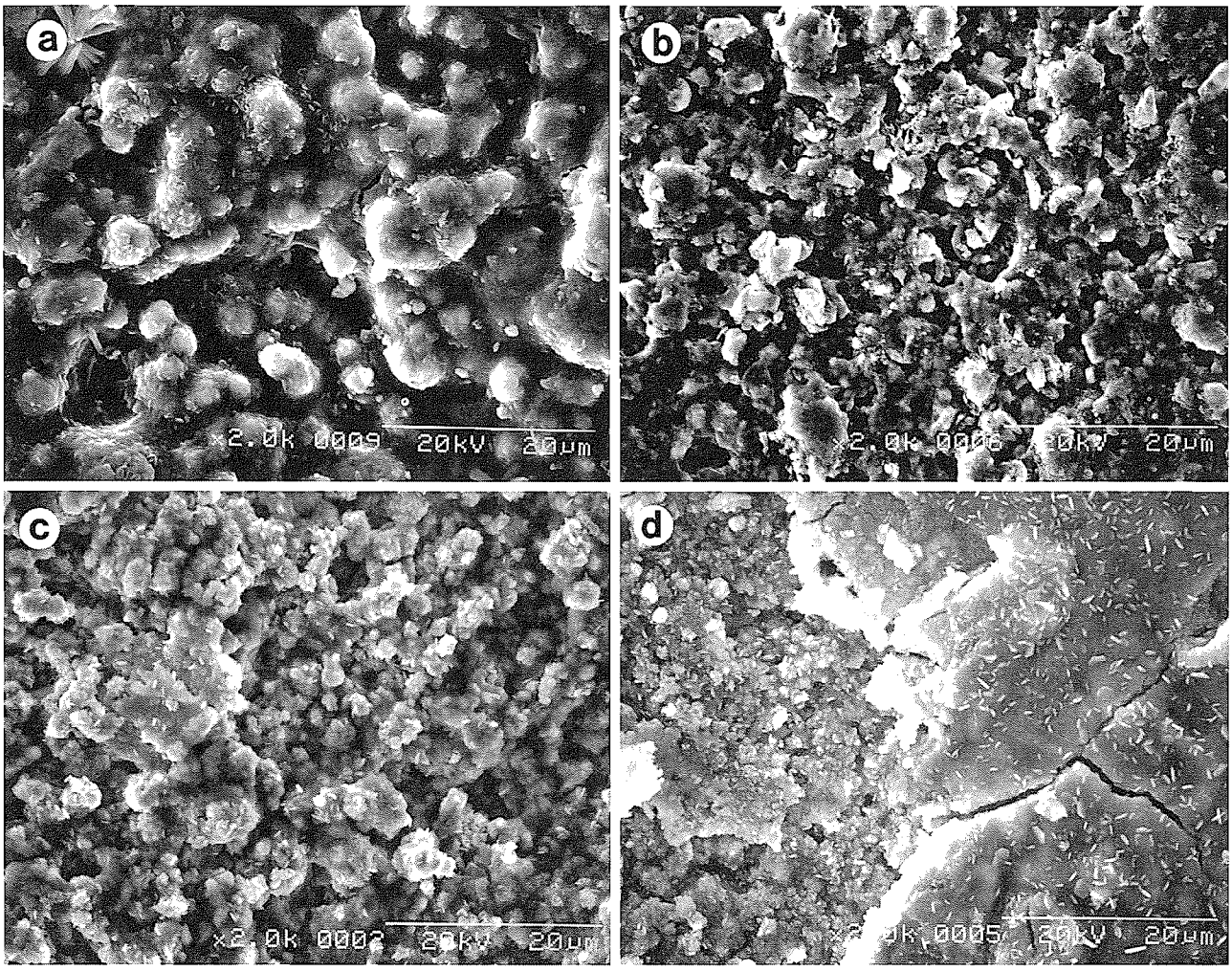


Table 1. Influence of the concentration of nitrate precursors on $Cu_xCo_{3-x}O_4$/LPBN electrode potential in 1 M KOH (25°C); electrodes prepared at 300°C.

$[Cu(NO_3)_2{\cdot}2.5H_2O]$: $[Co(NO_3)_2{\cdot}6H_2O]$ (M)	*E* vs. Hg/HgO (at 250 mA cm^{-2})[a] (mV)	Catalyst loading (mg cm^{-2})
0.1:0.2	780	41.3
0.3:0.6	760	40.8
0.5:1.0	735	41.6
0.7:1.4	765	40.0

[a]Geometric surface area.

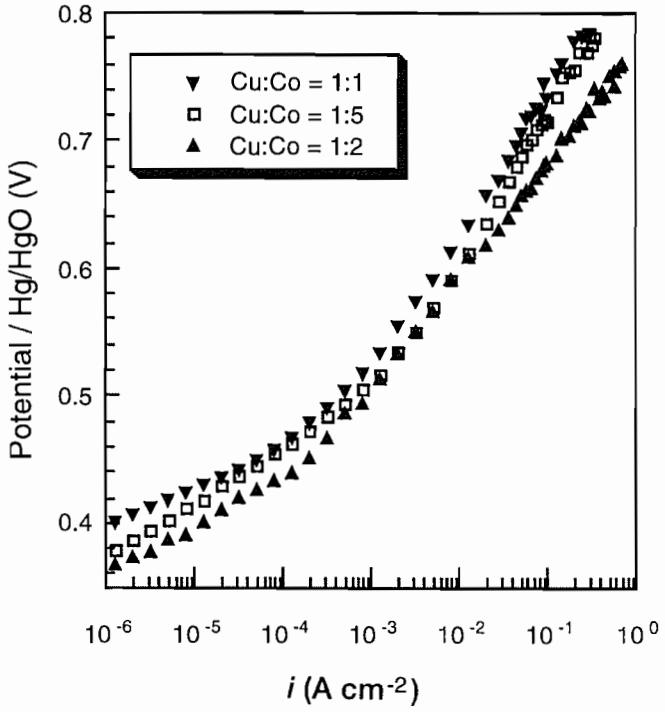
Influence of the Cu:Co atomic ratio

$Cu_xCo_{3-x}O_4$/LPBN electrodes were prepared with the following Cu:Co atomic ratios: 1:5, 1:2, and 1:1. Total concentration of the nitrates was kept at 1.5 M, and the electrodes were prepared at 300°C with a catalyst loading of 50 mg cm^{-2}. Figure 7 shows IR-corrected galvanostatic polarization curves obtained in 1 M KOH solution at 25°C: two Tafel regions are observed. Table 2 gives Tafel slopes (*b*) and exchange current densities (i_0) for the different electrodes at low and high overpotentials. At low overpotential, the Tafel slope is nearly constant (~40 mV dec^{-1}) whereas the exchange current density is lower for the electrode with the highest copper content: i_0[1:2] > i_0[1:5] >> i_0[1:1]. At high overpotential, the electrode prepared from a stoichiometric Cu:Co nitrate ratio (1:2) shows the lowest Tafel slope (~90 mV dec^{-1} instead of ~110 mV dec^{-1}), which gives rise to a better electrocatalytic activity for the OER. Therefore, the activity is reduced when an excess of either Co or Cu is present in the oxide film beyond the stoichiometric ratio of the precursors. This can be explained by the fact that some phase change might occur in these particular cases. Indeed, an excess of cobalt may favor the formation of the spinel Co_3O_4, which is less active than $CuCo_2O_4$; on the other hand, an excess of copper may lead to the formation of a highly resistive monoclinic CuO phase. Similar results were reported for $Ni_xCo_{3-x}O_4$ by Jasem and Tseung (18), and Gennero De Chialvo and Chialvo (15), which indicate higher activity for $NiCo_2O_4$.

© 1997 NRC Canada

Can. J. Chem. Downloaded from www.nrcresearchpress.com by 91.121.58.235 on 09/08/12
For personal use only.

Fig. 7. IR-corrected galvanostatic polarization curves obtained at $Cu_xCo_{3-x}O_4$/LPBN electrodes prepared at 300°C (50 mg cm^{-2}) from various Cu:Co precursors ratios. Electrolyte: 1 M KOH solution (25°C).



Influence of the decomposition temperature

On a smooth Ni substrate, temperature of nitrate decomposition affects the crystalline properties and surface morphology of the oxide coating (8); these parameters have an effect on the electrode activity for the OER. $Cu_xCo_{3-x}O_4$/LPBN electrodes were prepared between 250 and 400°C. This interval was chosen considering the stability of the spinel phase between 300 and 400°C, and also the specific surface area of the substrate, which decreases above 400°C by reduction of the fractal character of the nickel particles (11). Figure 8 illustrates SEM micrographs of electrodes prepared at 300, 350, and 400°C from solutions containing the optimum concentration of the nitrate precursors; the catalyst loading is 52 mg cm^{-2}. Electrodes prepared at 300 and 350°C present a highly porous surface, similar to the surface of the LPBN substrate (Fig. 3). At 400°C (Fig. 8(*c*)), the surface is less porous due to the packing of the oxide particles. These results are in good agreement with those obtained by other authors for $NiCo_2O_4$ (5) and Co_3O_4 (19), and by us for $Cu_xCo_{3-x}O_4$ (2), prepared at high temperature on a smooth metallic support.

Figure 9 shows the variation of the electrode potential, in 1 M KOH solution at 25°C, with the decomposition temperature at three anodic current densities. The thermal treatment seems to have little effect on the electrode activity in the temperature range studied, except at low current density where the overpotential is higher for the electrodes prepared at 350 and 400°C. If the activity for the OER is strongly dependent upon the $Cu_xCo_{3-x}O_4$/LPBN electrochemical surface area, we must conclude that this area is mainly controlled by the morphology of the highly porous substrate.

Table 2. Comparison of the kinetic parameters for the OER on $Cu_xCo_{3-x}O_4$/LPBN, for various atomic ratios in 1M KOH (25°C); [Cu] + [Co] = 1.5 M. Electrodes prepared at 300°C with a catalyst loading of 50 mg cm^{-2}.

	Tafel slope, b (mV dec^{-1})		Exchange current density, $i_0{}^a$ (A cm^{-2})	
Cu:Co	Low η^b	High η	Low η	High η
1:5	43	112	2.0×10^{-8}	1.9×10^{-5}
1:2	40	88	3.3×10^{-8}	4.7×10^{-6}
1:1	36	109	3.2×10^{-9}	1.9×10^{-5}

[a]Geometric surface area.
[b]Overpotential.

Influence of the catalyst loading

The variation in electrode activity for the OER with the catalyst loading can give an answer to the degree of covering of the oxide layer. Figure 10 shows that the lowest overpotential is observed at several current densities when the oxide loading is 52 mg cm^{-2}. The significant decrease in overpotential with increasing catalyst loading until 52 mg cm^{-2} indicates an enhancement of the electrocatalytic activity by adding more layers of $Cu_xCo_{3-x}O_4$. At this value the substrate is likely completely covered and the roughness of the electrode is still controlled by the morphology of the substrate. Above 52 mg cm^{-2}, the overpotential is increased, taking into account the semiconducting nature of $Cu_xCo_{3-x}O_4$, which raises the ohmic drop inside the spinel oxide.

Electrochemical behavior prior to oxygen evolution

Figure 11 displays typical voltammograms recorded in deaerated 1 M KOH solution (25°C) at a $Cu_xCo_{3-x}O_4$/Pt electrode prepared under the optimum conditions; however, the oxide loading was much lower than 52 mg cm^{-2} and corresponded to a single dipping of the Pt wire in the nitrate solution. The curve obtained between 0.10 and 0.65 V vs. Hg/HgO exhibits a single anodic peak A_1 at 0.55 V, prior to the onset of oxygen evolution, and a corresponding cathodic peak C_1 at 0.54 V. The voltammograms were almost the same regardless of the variation in the catalyst loading that possibly occurred during preparation of the electrodes. To establish the relationship between the oxidation and reduction peaks, the positive potential limit was varied (Fig. 11, broken curves). It can be seen that C_1 appears only once A_1 is obtained; furthermore, the cathodic peak current increases slightly when the potential limit becomes more positive; thus C_1 is associated with A_1. For comparison, voltammograms recorded at the bare Pt wire, at the same scan rate (20 mV s^{-1}), show currents higher than 0.1 mA when the electrode potential is more positive than 0.85 V.

A number of spinel oxides have shown similar electrochemical behavior, sometimes at different potentials. Table 3 summarizes the values of the mean peak potential ($E_p = [E_{pa} + E_{pc}]/2$) or the anodic peak potential (E_{pa}) for some of the most studied systems; in each case, the proposed redox transition reaction is also given. The peaks A_1 and C_1 obtained in this work are most likely associated to the CoO_2/CoOOH redox couple formed at the surface of $Cu_xCo_{3-x}O_4$ prior to the OER:

© 1997 NRC Canada

Can. J. Chem. Downloaded from www.nrcresearchpress.com by 91.121.58.235 on 09/08/12
For personal use only.

Fig. 8. SEM micrographs of $Cu_xCo_{3-x}O_4$/LPBN electrodes prepared at various temperatures: (*a*) 300°C; (*b*) 350°C; (*c*) 400°C. $Cu(NO_3)_2 \cdot 2.5H_2O$ = 0.5 M; $Co(NO_3)_2 \cdot 6H_2O$ = 1.0 M; catalyst loading: 52 mg cm^{-2}.

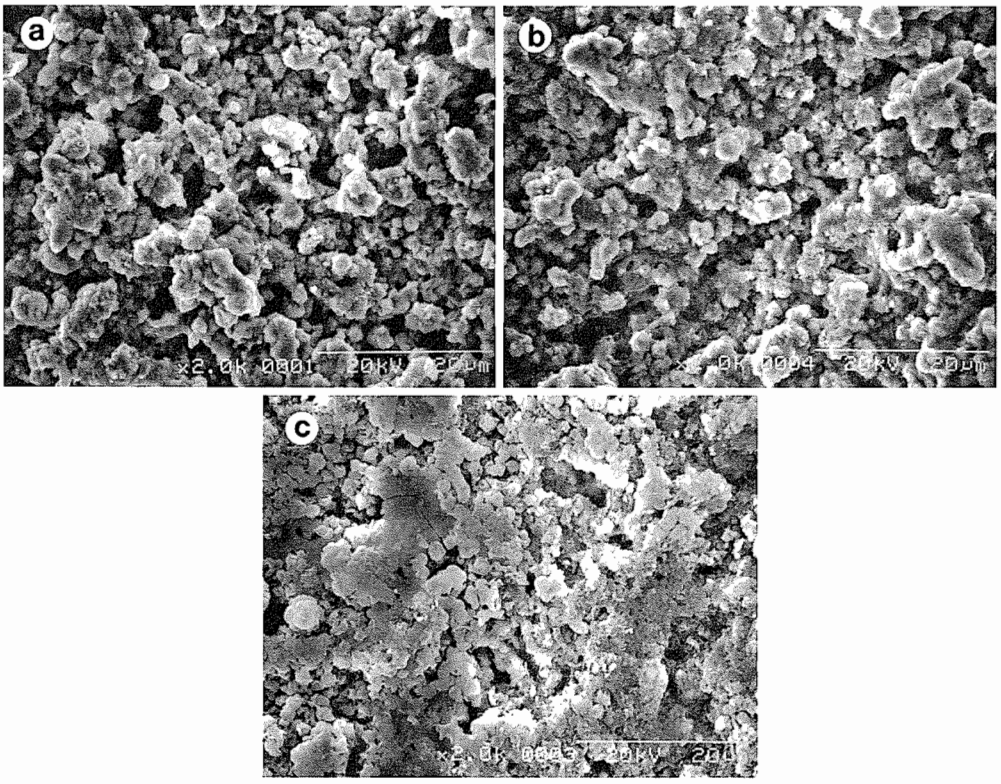


Table 3. Potentials E_p or E_{pa} obtained for several of the most studied spinel oxides in 1 M KOH (NaOH) at 25°C.

Oxide electrode	Preparation	E_p/Hg/HgO (mV)	Reference
Co_3O_4/Ti	S.P.[a]	525[c]	20
Co_3O_4/RuO_2/Ti	T.D.[b]	490[c] (E_{pa})	12
$NiCo_2O_4$/Ti	S.P.	420[d]	20
Co_3O_4/CdO/glass	S.P.	515[c]	21
$NiCo_2O_4$/CdO/glass	S.P.	400[d]	21
La_2CuO_4	T.D.	600[e]	22
$Cu_xCo_{3-x}O_4$/Ni	T.D.	536[c] (E_{pa})	2

[a]Spray pyrolysis.
[b]Thermal decomposition.
[c]Equation [3].
[d]Equation [2].
[e]Equilibrium reaction involving hydrated species and copper oxyhydroxide that may include Cu^{II} and Cu^{III} species.

[3] $CoOOH + OH^- \rightleftharpoons CoO_2 + H_2O + e^-$

This is in agreement with our work presenting the electrochemical behavior of thin colloidal films of $Co(OH)_2$ and $Cu(OH)_2$ deposited on Pt wires (10). According to Pourbaix diagram (23), reaction [3] should occur at 0.54 V vs. Hg/HgO at pH = 14, which is very close to E_{pa} found in this work. Pourbaix diagram also shows that the reaction

[4] $Co_2O_3 + 2OH^- \rightleftharpoons 2CoO_2 + H_2O + 2e^-$

is thermodynamically possible in the same potential range: reactions [3] and [4] involve the same redox species Co^{III} and Co^{IV}. Hamdani et al. (21) have concluded that a CoOOH layer is spontaneously produced when Co_3O_4 is in contact with an alkaline electrolyte. This indicates that reaction [3] is the most probable. However, it should be noted that the assignment of redox peaks is speculative and that other measurements should be performed to verify their validity.

Tarasevich et al. (24) have assigned the peak A_1 to the electrochemical adsorption of OH^- ions at the surface of a Co_3O_4 film according to

[5] $2OH^- \rightleftharpoons H_2O_2^- + e^-$

Their suggestion came after observing a shift of 140 mV pH^{-1} of the anodic peak potential. Therefore, the influence of pH on the electrochemical behavior of $Cu_xCo_{3-x}O_4$/Pt has been studied by varying the KOH concentration from 0.5 to 2.0 M. For each concentration, the scan rate ranged from 20 to 700 mV s^{-1}. Figure 12 presents stabilized voltammograms recorded in 2 M KOH, between 20 and 200 mV s^{-1}. It can be seen that E_{pa} and E_{pc} move only slightly, respectively, to more positive and negative values with increasing the scan rate. This indicates that the Co^{IV}/Co^{III} transition is quasi-reversible. The dependence of pH on the mean peak potential is displayed in Fig. 13 at several scan rates; $\partial E_p/\partial pH$ is 60 mV pH^{-1} and this value does not change with the scan rate. These results confirm that reaction [5] does not take place on $Cu_xCo_{3-x}O_4$.

© 1997 NRC Canada

Can. J. Chem. Downloaded from www.nrcresearchpress.com by 91.121.58.235 on 09/08/12
For personal use only.

Fig. 9. $Cu_xCo_{3-x}O_4$/LPBN electrode potential as a function of the nitrate decomposition temperature at various current densities. Catalyst loading: 52 mg cm^{-2}; electrolyte: 1 M KOH solution (25°C).

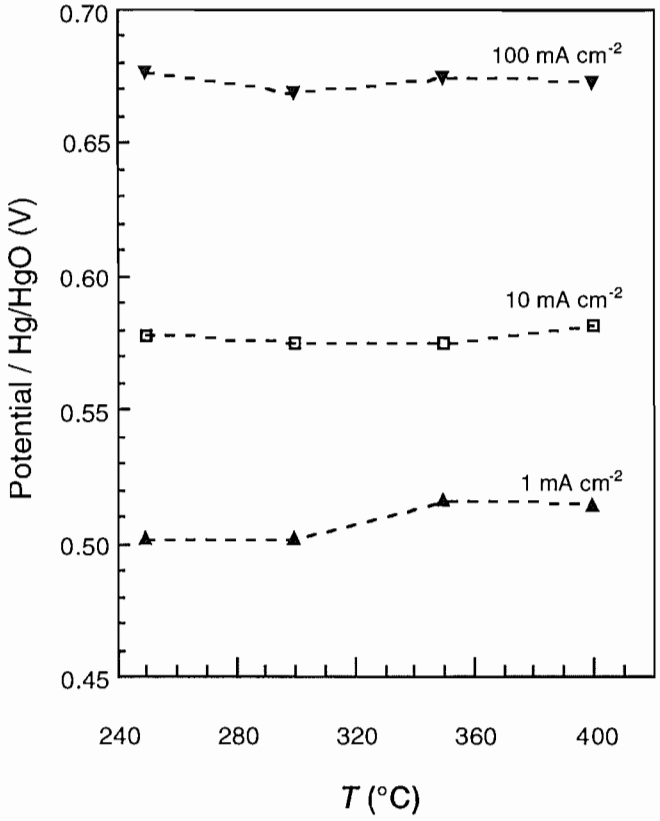


Fig. 10. $Cu_xCo_{3-x}O_4$/LPBN anodic overpotential as a function of the catalyst loading at various current densities. Electrodes prepared at 300°C; electrolyte: 1 M KOH solution (25°C).

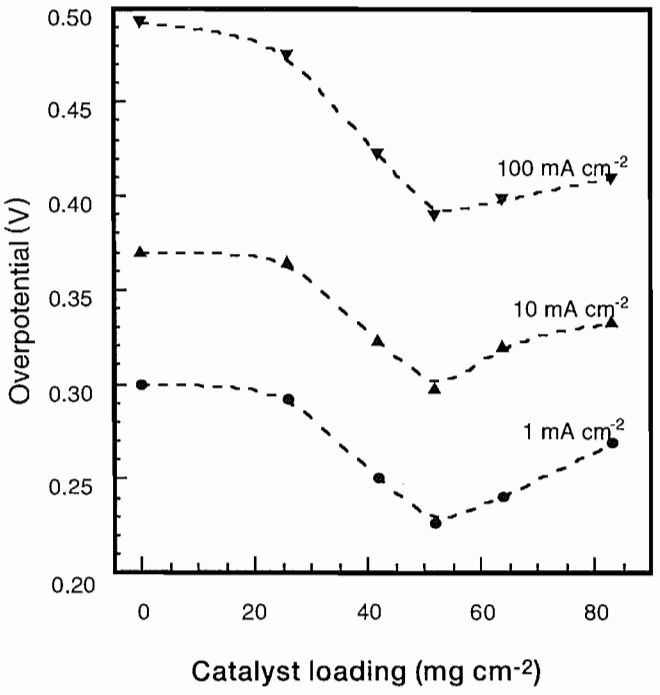


Fig. 11. Cyclic voltammograms of a $Cu_xCo_{3-x}O_4$/Pt electrode obtained by varying the positive potential limit in 1 M KOH solution (25°C). Scan rate: 20 mV s^{-1}.

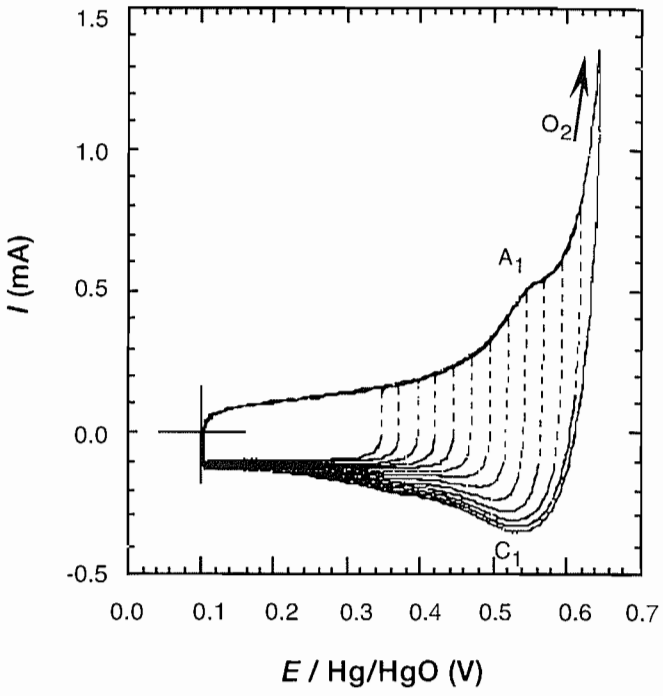
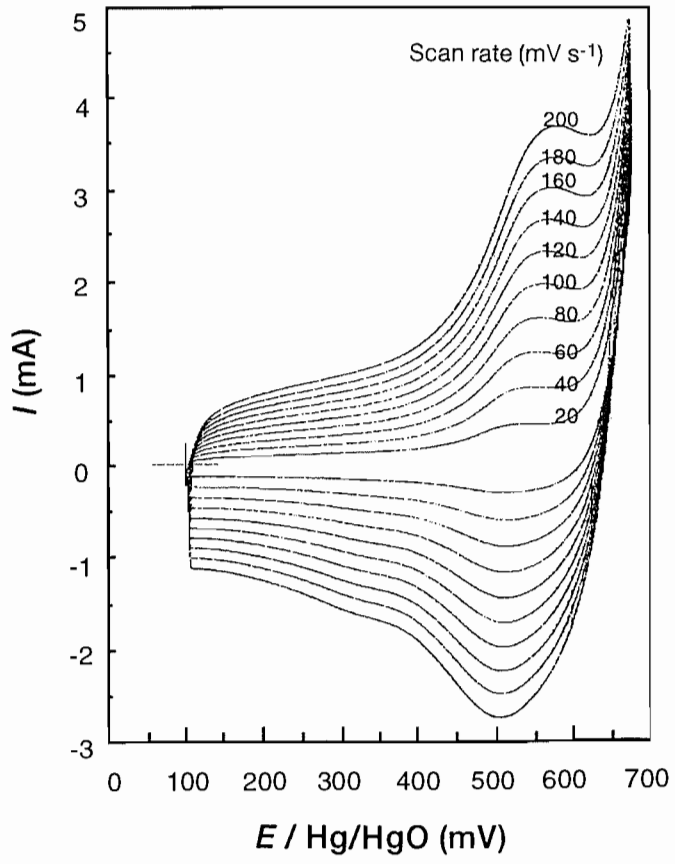


Fig. 12. Cyclic voltammograms of a $Cu_xCo_{3-x}O_4$/Pt electrode obtained at several scan rates in 2 M KOH solution (22°C).



© 1997 NRC Canada

Can. J. Chem. Downloaded from www.nrcresearchpress.com by 91.121.58.235 on 09/08/12
For personal use only.

Fig. 13. Dependence of pH on the mean peak potential of the process observed in Fig. 12 for various scan rates.

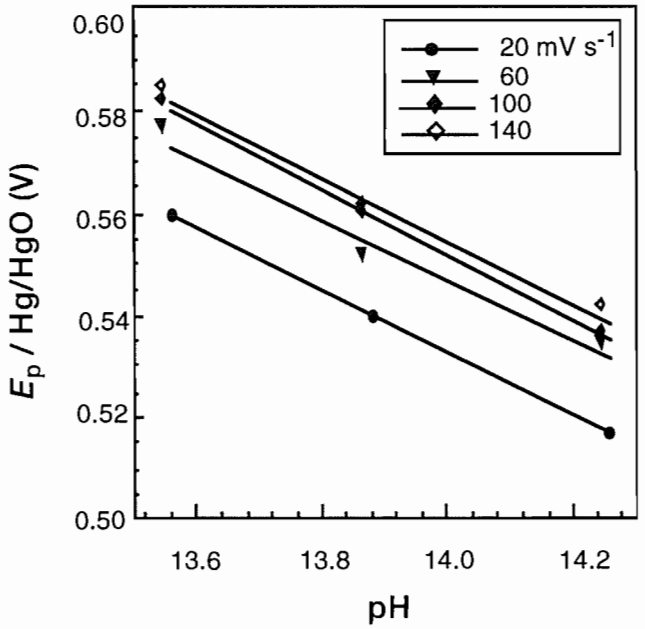
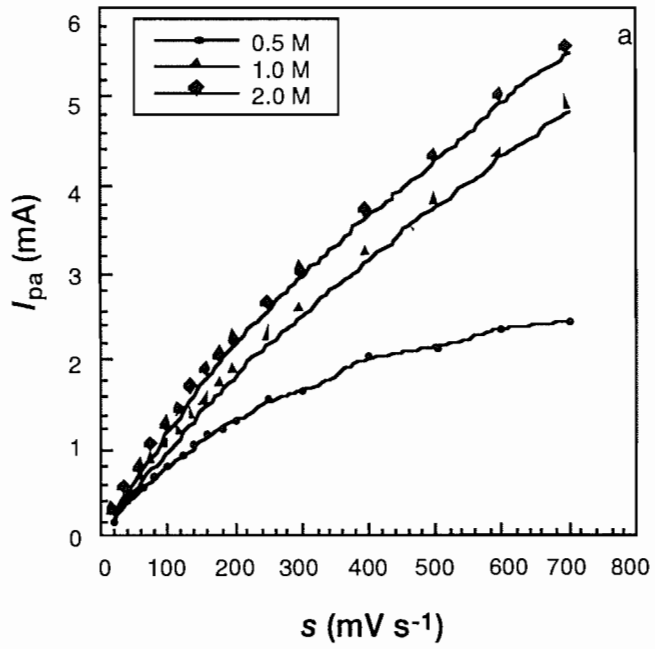


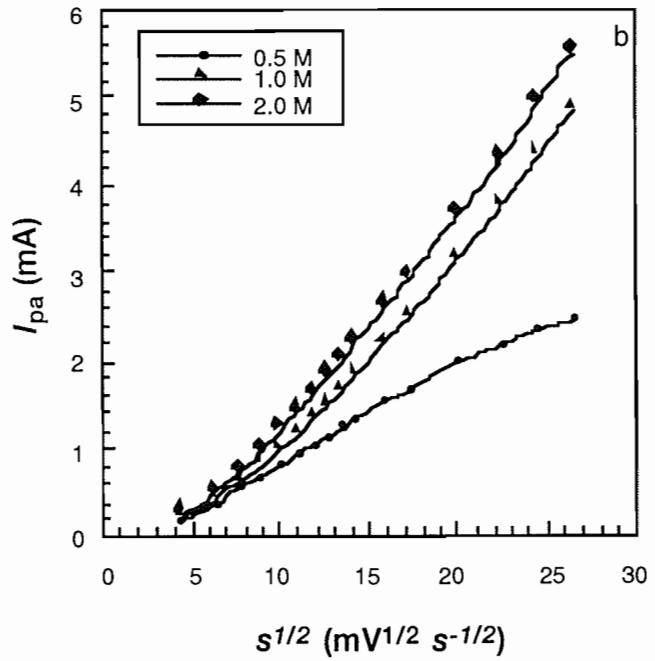
Figure 14(*a*) depicts the dependence of the anodic peak current (I_{pa}) on the scan rate at three KOH concentrations. It was not possible to accurately determine the same dependence for the cathodic peak current, due to its width and consequent difficulties in determination of the baseline. Figure 14(*b*) shows the corresponding variation of I_{pa} with the square root of the scan rate ($s^{1/2}$). We clearly notice that I_{pa} increases linearly with $s^{1/2}$ in 0.5 M KOH at all scan rates, and in 1 M and 2 M KOH at the higher scan rates. This suggests that the surface redox transition process is diffusion controlled at low OH^- concentration and at high scan rate when $[OH^-] \geq 1$ M. The shift of 60 mV pH^{-1} of the mean peak potential, determined in this work, corresponds to a 1:1 ratio of hydroxide ions to electrons. This situation suggests that one electron is removed from the oxide film during the oxidation process (reaction [3]), while one OH^- is injected into the film.

Figure 15 shows cyclic voltammograms obtained in 1 M KOH (22°C) by varying the negative potential limit between 0 and −0.37 V vs. Hg/HgO. These voltammograms demonstrate the presence of a significant cathodic current around −0.35 V leading to the appearance of a new anodic peak (A_2) at −0.1 V, while the peaks A_1 and C_1 remain almost unchanged. Our previous work (10) has shown that the electrochemical behavior of $Co(OH)_2$/Pt exhibits two redox transition processes assigned to the couples Co^{III}/Co^{II} and Co^{IV}/Co^{III}, the former being absent on $Cu_xCo_{3-x}O_4$/Pt presented in this work. On the other hand, $Cu(OH)_2$/Pt indicated the presence of one redox transition corresponding to Cu^{II}/Cu^{I} with $E_p = -0.270$ V vs. Hg/HgO at 100 mV s^{-1}. By comparison with the behavior of $Cu_xCo_{3-x}O_4$/Pt in the negative potential region (Fig. 15), one can associate the cathodic current with the reduction of surface Cu^{II} species. Cu^{I} species thus produced are oxidized at A_2 according to:

[6] $Cu_2O + H_2O + 2OH^- \rightleftharpoons 2\,Cu(OH)_2 + 2\,e^-$

Fig. 14. Dependence of the anodic peak current obtained in various KOH solutions on: (*a*) the scan rate; (*b*) the square root of the scan rate.



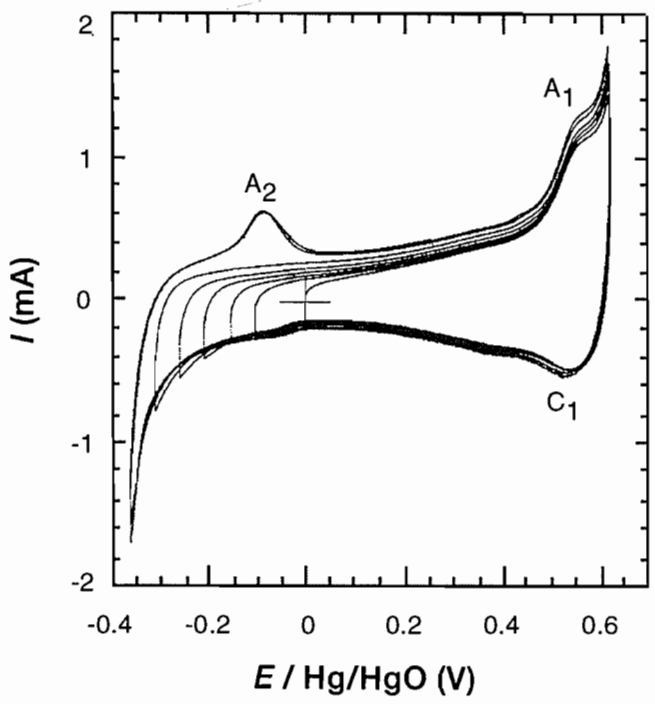


From the above results, we can assume that the surface of $Cu_xCo_{3-x}O_4$ in contact with the alkaline electrolyte is mostly composed of Co^{III} and Cu^{II} species. XPS measurements have shown that the surface of a freshly prepared $Cu_xCo_{3-x}O_4$/Ni electrode is mainly composed of octahedral Co^{III} and Cu^{II} species when the oxide is prepared at 300°C (10).

© 1997 NRC Canada

Can. J. Chem. Downloaded from www.nrcresearchpress.com by 91.121.58.235 on 09/08/12
For personal use only.

Fig. 15. Cyclic voltammograms of a $Cu_xCo_{3-x}O_4$/Pt electrode obtained by varying the negative potential limit in 1 M KOH solution (22°C). Scan rate: 20 mV s^{-1}.



Conclusion

In this work, the spinel oxide $Cu_xCo_{3-x}O_4$ was prepared by thermal decomposition of nitrate precursors on a highly porous lanthanum phosphate-bonded nickel support (LPBN) with a roughness factor of ~4050. The highest electrocatalytic activity for the OER is obtained when the electrode is prepared at 300°C from a solution containing 0.5 M $Cu(NO_3)_2 \cdot 2.5\ H_2O$ and 1.0 M $Co(NO_3)_2 \cdot 6\ H_2O$, with a catalyst loading of 52 mg cm^{-2}. The activity is reduced when an excess of either Co or Cu is present in the spinel oxide film beyond the stoichiometric ratio of the precursors, probably due to some phase change. The nitrate decomposition temperature seems to have little effect on the electrocatalytic activity; the $Cu_xCo_{3-x}O_4$/LPBN electrochemical surface area is likely controlled by the morphology of the highly porous support. Below the optimum catalyst loading, the support is not completely covered, which decreases the electrode activity; above this value, the semiconducting properties of $Cu_xCo_{3-x}O_4$ increase the electrode resistivity, which also decreases the activity. Kinetics and mechanistic studies have been carried out at the optimum electrode using steady-state galvanostatic measurements and impedance spectroscopy. The results will be presented in a forthcoming publication.

This work indicates that the quasi-reversible Co^{IV}/Co^{III} surface redox transition, which likely takes place prior to the onset of oxygen evolution, is diffusion controlled at low OH^- concentration and at high scan rate when $[OH^-] \geq 1$ M. The results suggest that one electron is removed from the oxide film during the oxidation process while one OH^- is injected into the film. In the negative potential domain, a Cu^{II}/Cu^{I} surface redox transition was observed. Thus, the surface of $Cu_xCo_{3-x}O_4$ in the alkaline solution is mainly composed of Co^{III} and Cu^{II} species, which are most likely the active sites and (or) the precursors of the active sites for the OER.

Acknowledgments

The authors are grateful to the Natural Sciences and Engineering Research Council of Canada (NSERC) for financial support. We also acknowledge the assistance of Mr. M. Preda (Département des sciences de la terre, Université du Québec à Montréal (UQAM)) for recording the X-ray diffraction patterns, Mr. R. Mineau (Département des sciences de la terre, UQAM) for the SEM and EDAX analyses, and Dr. H. Ménard (Département de chimie, Université de Sherbrooke) for supplying the nickel supports and for useful discussions. K. Fatih wishes to thank La Fondation de l'UQAM for a graduate scholarship.

References

1. M.R. Tarasevich and B.N. Efremov. *In* Electrodes of conductive metallic oxides. Part A. *Edited by* S. Trasatti. Elsevier, Amsterdam. 1980. pp. 221–260.
2. B. Marsan, N. Fradette, and G. Beaudoin. J. Electrochem. Soc. **139**, 1889 (1992).
3. A.C.C. Tseung and S. Jasem. Electrochim. Acta. **22**, 31 (1977).
4. G. Singh, M.H. Miles, and S. Srinivasan. *In* Electrocatalysis on non-metallic surfaces. NBS Special Publ. No. 455. *Edited by* A.D. Franklin. U.S. Government Printing Office, Washington. 1976. pp. 289–296.
5. J. Haenen, W. Visscher, and E. Barendrecht. J. Appl. Electrochem. **15**, 29 (1985).
6. A.C.C. Tseung, S. Jasem, and M.N. Mahmood. *In* Hydrogen energy systems. Vol I. *Edited by* T.N. Verziroglu and W. Seifritz. Pergamon Press, Oxford. 1978. pp. 215–226.
7. M. El Baydi. Ph.D. thesis, Université Louis Pasteur, Strasbourg. 1993.
8. N. Fradette. M.Sc. thesis, Université du Québec à Montréal, Montréal. 1992.
9. Y.-S. Lee, C.-C. Hu, and T.-C. Wen. J. Electrochem. Soc. **143**, 1218 (1996).
10. N. Fradette and B. Marsan. J. Electrochem. Soc. Submitted.
11. H. Dumont, P. Los, L. Brossard, A. Lasia, and H. Ménard. J. Electrochem. Soc. **139**, 2143 (1992).
12. P. Boggio, A. Carugati, and S. Trasatti. J. Appl. Electrochem. **17**, 828 (1987).
13. W.F. McClune. Powder diffraction file of inorganic phases. International Center for Diffraction Data, Swarthmore, Pa. 1984.
14. K. Petrov, K. Krezhov, and P. Konstantinov. J. Phys. Chem. Solids, **50**, 577 (1989).
15. M.R. Gennero De Chialvo and A.C. Chialvo. Electrochim. Acta, **38**, 2247 (1993).
16. A.E. Cherkashin, F.I. Vilisov, G.L. Semin, and L.G. Matvienko. Fiz. Tverd. Tela, **11**, 189 (1969).
17. S. Trasatti and O.A. Petrii. Pure Appl. Chem. **63**, 711 (1991).
18. S. Jasem and A.C.C. Tseung. J. Electrochem. Soc. **126**, 1353 (1979).
19. C. Iwakura, A. Honji, and H. Tamura. Electrochim. Acta, **26**, 1319 (1981).
20. R.N. Singh, J.F. Koeing, G. Poillerat, and P. Chartier. J. Electrochem. Soc. **137**, 1408 (1990).

© 1997 NRC Canada

21. M. Hamdani, J.F. Koeing, and P. Chartier. J. Appl. Electrochem. **18**, 568 (1988).
22. J.-C. Grenier, A. Wattiaux, N. La Gueyte, J.-C. Park, E. Marquestaut, J. Etourneau, and M. Pouchard. Physica A, **173**, 139 (1991).
23. M. Pourbaix. *In* Atlas d'équilibres électrochimiques. Gauthier-Villars, Paris. 1963.
24. M.R. Tarasevich, G.I. Zakharin, A.M. Khutornoi, F.V. Makordei, and V.I. Nikitin. Zh. Prikl. Khim. (S.-Peterburg), **51**, 731 (1976).

Can. J. Chem. Downloaded from www.nrcresearchpress.com by 91.121.58.235 on 09/08/12
For personal use only.

© 1997 NRC Canada

Comparison of the thermodynamic and transport properties of lithium bis(trifluoromethylsulfonyl)imide (LiTFSI) with $LiClO_4$ and Bu_4NBr in water at 25°C

Gérald Perron, Dany Brouillette, and Jacques E. Desnoyers

Can. J. Chem. Downloaded from www.nrcresearchpress.com by 91.121.58.235 on 09/08/12
For personal use only.

Abstract: Lithium bis(trifluoromethylsulfonyl)imide (LiTFSI) is a promising electrolyte for lithium batteries. While it presents many interesting features in aprotic solvents (high solubility and conductivity, electrochemical stability, etc.), little is known about its properties in water. The solid–liquid phase diagram, surface tension, volume, heat capacity, and conductivity were therefore measured at 25°C and compared with the same properties of typical hydrophilic ($LiClO_4$) and hydrophobic (Bu_4NBr) electrolytes. To help in the comparison, some of the literature data for $LiClO_4$ and Bu_4NBr were extended. The standard Λ_0, V_2^0, and $C_{P,2}^0$ are respectively 71.12 S cm^2 mol^{-1}, 139.7 cm^3 mol^{-1}, and 543 J K^{-1} mol^{-1} at 25°C. LiTFSI is quite soluble, and shows surface activity and a small tendency for self-association in water. The aggregation number estimated from a mass-action model is of the order of 4.

Key words: lithium bis(trifluoromethylsulfonyl)imide, lithium perchlorate, tetrabutylammonium bromide, volume, heat capacity, phase diagram, thermal analysis, surface tension, conductance.

Résumé : Le bis(trifluorométhylsulfonyl)imide de lithium (LiTFSI) est un électrolyte prometteur pour les batteries au lithium. Même s'il présente plusieurs caractéristiques intéressantes dans les solvants aprotiques (solubilité et conductivités élevées, stabilité électrochimique, etc.), ses propriétés en milieu aqueux sont peu connues. Opérant à 25°C, on a donc mesuré les propriétés suivantes : diagramme de phase solide–liquide, tension superficielle, volume, capacité calorifique et conductivité; on a comparé ces propriétés avec celles d'électrolytes hydrophile ($LiClO_4$) et hydrophobe (Bu_4NBr) typiques. Afin de faire une meilleure comparaison, certaines données relatives au $LiClO_4$ et au Bu_4NBr ont été ramenées aux conditions désirées. À 25°C, les valeurs standards de Λ_0, V_2^0 et $C_{P,2}^0$ sont respectivement égales à 71,12 S cm^2 mol^{-1}, 139,7 cm^3 mol^{-1} et 543 J K^{-1} mol^{-1}. Le LiTFSI est assez soluble; il présente une certaine activité superficielle et une faible tendance à s'autoassocier dans l'eau. En se basant sur un modèle d'action de masse, on a évalué que le nombre d'agrégation est d'environ 4.

Mots clés : bis(trifluorométhylsulfonyl)imide de lithium, perchlorate de lithium, bromure de tétrabutylammonium, volume, capacité calorifique, diagramme de phase, analyse thermique, tension superficielle, conductivité.

[Traduit par la rédaction]

Introduction

The conducting medium of high-energy lithium batteries requires a lithium salt that is electrochemically stable, chemically inert to the electrodes (passivation film), highly soluble in aprotic solvents, and that has a high conductivity under the operating conditions. The most commonly used lithium salts for liquid lithium batteries are $LiClO_4$, $LiAsF_6$, and $LiBF_4$. Lithium bis(trifluoromethylsulfonyl)imide (LiTFSI), or $Li(CF_3SO_2)_2N$, has been shown to be one of the most effective electrolytes for electrolyte–polymer lithium batteries (1), and recent work (2) shows that it also has most of the required qualities for a promising electrolyte for liquid lithium batteries. Relatively little is known about the properties of this electrolyte in solution (3–7). It has good conductivity, it is stable electrochemically and thermally, and is quite soluble in many solvents. The anionic crystal radius has been estimated by Ue (8), and this anionic radius appears to be consistent with Stokes law in propylene carbonate. On the other hand, there are many peculiarities with this electrolyte in solvents of low dielectric constants such as 1,2-dimethoxyethane (DME) (2). It has a very high association constant, but its specific conductivity at high concentration is still large. It forms a stable 3:1 solvate, which seems to persist in the solution state. The apparent molar heat capacity has an anomalous concentration dependence.

It is not easy to understand solute–solute interactions in aprotic solvents in general, since most of the thermodynamic studies have been limited to the standard infinite dilution stan-

Received March 20, 1997.

This paper is dedicated to Professor Brian E. Conway, the former research director of J.E.D., on the occasion of his 70th birthday.

G. Perron,[1] D. Brouillette, and J.E. Desnoyers. Institut National de la Recherche Scientifique — Énergie et Matériaux, 1650 boulevard Lionel Boulet, Varennes, QB J3X 1S2, Canada.

[1] Author to whom correspondence may be addressed. Telephone: (514) 929 8251. Fax: (514) 929 8102. E-mail: perron@inrs-ener.uquebec.ca

© 1997 NRC Canada

Can. J. Chem. Downloaded from www.nrcresearchpress.com by 91.121.58.235 on 09/08/12
For personal use only.

dard state. On the other hand, aqueous electrolyte solutions have been well investigated over a wide concentration range. We therefore felt that it would be useful to compare some of the thermodynamic properties (phase diagram, surface tension, apparent molar volume, and heat capacity) and conductivity of LiTFSI in water over a wide concentration range with well-characterized hydrophilic and hydrophobic electrolytes such as $LiClO_4$ and tetrabutylammonium bromide, Bu_4NBr. Such comparisons should help in understanding any peculiarities in the properties of LiTFSI that may be related to its molecular structure. In the course of this comparative study, we realised that some of the data for $LiClO_4$ and Bu_4NBr at high concentration were lacking. The literature data were therefore extended by new measurements.

Experimental

$LiClO_4$ and Bu_4NBr were both obtained from Omega. $LiClO_4$ was dried under vacuum at 150°C. Bu_4NBr was recrystallized from acetone and dried under vacuum at 70°C. LiTFSI, produced by 3M, was supplied free of charge by Hydro-Quebec. This salt is quite soluble in many solvents and attempts to purify large quantities of salt by recrystallization, as suggested by Dominey et al. (7),[2] were not successful. It often fails to recrystallize at low temperatures and forms a glass. It was therefore assumed pure.

Although LiTFSI is quite hygroscopic, water or acetonitrile can be removed fairly readily during the drying process. It was dried under vacuum at 150°C for 10 h and kept under an argon atmosphere in a Gallenkamp dry box, where the atmospheric humidity was maintained at less than 2%, or in a model HE-493 argon dry box (from Vacuum Atmospheres Company) equipped with a Dri-Train. This latter dry box, lent by Hydro-Quebec, contains less than 0.01% relative humidity. The salt was weighed in the dry box and the solutions prepared with deionized distilled water (Barnstead Nanopure II). The weights of the salt were corrected for the presence of argon in the bottles. The aqueous solutions prepared with the present lot of LiTFSI had a pH of 8.0. Since it was observed that the aqueous solutions were reacting slowly with stainless steel at concentrations above 0.5 mol kg^{-1}, flow cells made of platinum–rhodium alloy were used for this study in the flow densimeter and microcalorimeter.

The phase diagrams were obtained from thermal analysis using the Heat Leak Modulus (HLM) technique (9) since this technique is well adapted for hygroscopic and volatile liquids at low temperatures. The solution in a small tube containing a platinum resistor was rapidly frozen and the temperature was followed as the sample was warmed.

The surface tensions (γ) were measured with a Fisher Tensiomat, model 20, having a precision of ± 1 dyne cm^{-1}. The purpose of these measurements was mostly to see the trends in γ with concentration since it was observed that the aqueous solutions had a tendency to foam when shaken. For these studies, small quantities of salt were added successively to the solvent to obtain different concentrations, even though such a procedure is less accurate than the preparation of individual solutions.

The volumetric heat capacities were measured with a Picker flow microcalorimeter (SODEV model CP-C) (10). Essentially, two liquids at the same initial temperature and flowing at the same rate in twin cells were heated. The difference in the applied power ΔW necessary to maintain the final temperature of the laboratory cell identical to that of the reference cell is proportional to the difference in the heat capacity per unit volume, $\Delta\sigma$, of the two liquids. If there is no heat loss (11),

$$[1] \quad \frac{\Delta W}{W_0} = \frac{\Delta\sigma}{\sigma_0}$$

where W_0 is the basic power applied to the cells and σ_0 is the heat capacity per unit volume of the reference liquid. The difference in specific heat capacity, in J K^{-1} g^{-1}, can be calculated from

$$[2] \quad c_P = (1 + \Delta\sigma/\sigma_0)c_{P,0}d_0/d$$

where d and d_0 are the densities of the solution and of the solvent in g cm^{-3} and $c_{P,0}$ is the heat capacity of the reference water in J K^{-1} g^{-1} (12). The differences in heat capacities can be obtained to $\pm 0.5\%$ under the best conditions.

The density is related to the resonance frequency of the U-shaped vibrating capillary tube adapted to the flow regime by Picker et al. (13). The difference in density between the solution and a reference solvent is given by

$$[3] \quad d - d_0 = k(\tau^2 - \tau_0^2)$$

where k is the calibration constant obtained using pure water (12), dry nitrogen (12), and a vacuum as references. The calibration constant obtained for various organic liquids against a vacuum or nitrogen is slightly different from the one for water and a vacuum or nitrogen in the commercial version of the instrument. The densities of nonaqueous solvents should therefore be measured and calibrated against an organic reference solvent. Densities can be measured to $\pm 3 \times 10^{-6}$ g cm^{-3} under the most favourable conditions.

The ionic conductivities were measured with a bridge similar to the Beckman model RC-15 commercial bridge. The platinized platinum cells had constants of 1 or 0.1 cm^{-1} depending on the concentrations of the solutions. Resistance measurements were made at 1 and 3 kHz and extrapolated to 0 kHz. The precision is 0.05%.

Results and discussion

Thermal analysis and solid–liquid phase diagram

Some examples of thermograms for the system LiTFSI–H_2O are shown in Fig. 1 and the derived solid–liquid phase diagram is given in Fig. 2. The original data are available as Supplementary Material.[3]

The information obtained from the HLM thermal analysis is similar to that from a DSC. The temperatures associated with various transitions are given as maxima, minima, or inflection

[2] Also L.A. Dominey. Private communication.

[3] A complete set of data may be purchased from: The Depository of Unpublished Data, Document Delivery, CISTI, National Research Council Canada, Ottawa, Canada K1A 0S2.

© 1997 NRC Canada

Can. J. Chem. Downloaded from www.nrcresearchpress.com by 91.121.58.235 on 09/08/12
For personal use only.

Fig. 1. Examples of thermograms of the system LiTFSI–H_2O for different mole fractions x. The inset is an expanded scale for different rates of cooling. One or two peaks will appear in this region for different conditions of slow cooling (see text).

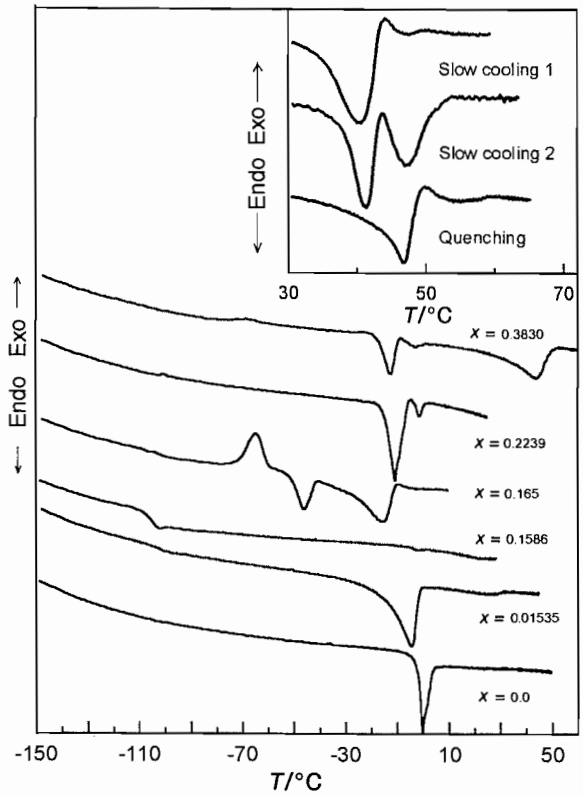
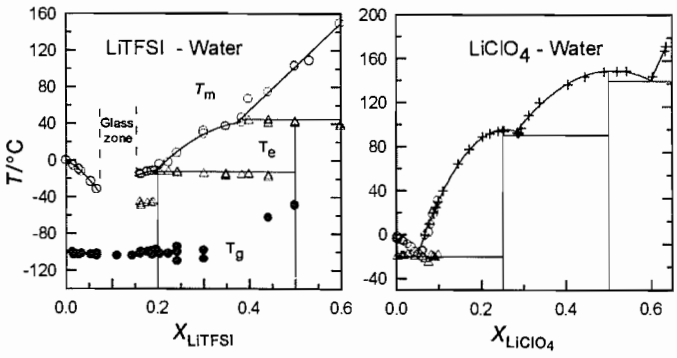


Fig. 2. Solid–liquid phase diagram of the system LiTFSI–H_2O: ○, melting points; Δ, eutectic points; ● glass transition temperatures; +, melting point data from ref. 20.



points and the enthalpy associated with the phenomena are derived from the area under the curves. The change in the base line at the melting point, as illustrated, for example, with pure H_2O, reflects the difference in heat capacity between the solid and the liquid phases. This difference decreases rapidly as the concentration of LiTFSI increases. Measurements were made up to mole fractions of LiTFSI of 0.6. Pure LiTFSI has a melting point of 234°C and a heat of fusion of 13.2 kJ mol^{-1} (14).

All the thermograms below 0.08 mole fraction show only melting points and glass transition temperatures, T_g. Only a small peak corresponding to T_g is observed if the quenching process is slow. For rapid quenching, the T_g is followed by a crystallization peak, T_c. T_g is constant up to approximately 0.3 mole fraction. Between mole fractions of 0.08 and 0.16, only a T_g is seen, corresponding to an amorphous zone in the phase diagram. Such zones, which are also present with other electrolytes such as LiBr in water, have been studied in detail by Angel et al. (15, 16). Similar phenomena are also observed in metallurgy (17). We have observed that, for some mixtures, the presence of an amorphous zone corresponds to the convergence of the melting point (T_m) with T_c (5).

Above 0.16 mole fraction, eutectic temperatures, T_e, in addition to melting points (T_m), are observed. At 0.38 mole fraction, the thermogram depends on the quenching and rate of heating. Depending on the experimental conditions, T_m is either split into a double peak or only one of these peaks is observed, as shown in the upper corner of Fig. 2. Such splitting of peaks, which depends on the kinetics of crystallization, has been observed in the literature (18) and could be a case of polymorphism (19). This phenomenon was not investigated further.

The phase diagram of LiTFSI indicates the presence of unstable solvates, which show incongruent melting, at 0.2 and 0.5 mole fractions with well-defined T_e.

The phase diagrams of $LiClO_4$ and H_2O obtained from the present thermal analysis technique are compared with the literature values (20) in Fig. 2. The thermograms do not depend on the rate of cooling in this case. The excellent agreement with the literature confirms that the HLM method is well adapted to the study of phase diagrams of aqueous solutions. $LiClO_4$ forms two stable hydrates and has a well-defined eutectic in water.

Surface tension

The surface tensions of LiTFSI are given elsewhere[3] and are compared with Bu_4NBr in Fig. 3. Some values of γ of Bu_4NBr were also measured to complement the literature data (22, 23). The γ of Bu_4NBr were also measured by Arnett et al. (21) but these values are systematically lower by about 5 dynes cm^{-1} and were not included in Fig. 3. The excellent agreement of the present measurements with the two sets of literature data is a good indication of the reliability of the present technique.

Contrary to inorganic electrolytes, which increase the γ of the aqueous solutions, LiTFSI decreases γ and reaches a minimum value in the same concentration range as Bu_4NBr, i.e., ~1–1.5 mol kg^{-1}, but the value of γ at saturation is 35 dyne cm^{-1} compared with 45 dyne cm^{-1} for Bu_4NBr. Liquid fluorocarbons generally have lower γ than liquid hydrocarbons. Such lowering and levelling off of γ with concentration is usually associated with micellization. These results therefore indicate that LiTFSI, like Bu_4NBr, is surface active and shows some tendency for self-association above 1 mol kg^{-1}.

Apparent molar quantities

The volumes and heat capacities of electrolyte solutions are usually expressed as apparent molar quantities $Y_{2,\phi}$. The apparent molar volume of component 2 is calculated from

$$[4] \quad V_{2,\varphi} = \frac{M_2}{d} - \frac{1000(d - d_0)}{m_2 d d_0}$$

© 1997 NRC Canada

Can. J. Chem. Downloaded from www.nrcresearchpress.com by 91.121.58.235 on 09/08/12
For personal use only.

Fig. 3. Surface tension of LiTFSI and Bu_4NBr in water at 25°C on a logarithmic and linear scale of the molality.

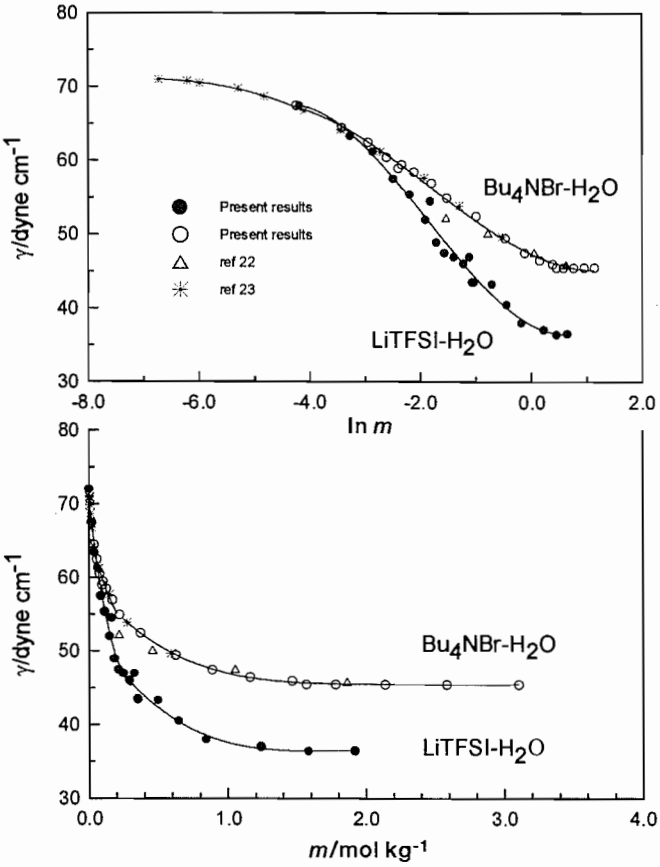


Fig. 4. Excess apparent molar volume of LiTFSI, $LiClO_4$, and Bu_4NBr in water at 25°C. Data for Bu_4NBr from Wen and Saito (26). Low-concentration data for $LiClO_4$ (○) are compared to those compiled by Lobo (24) (Δ, □). The full line in the case of LiTFSI is from mass-action model.

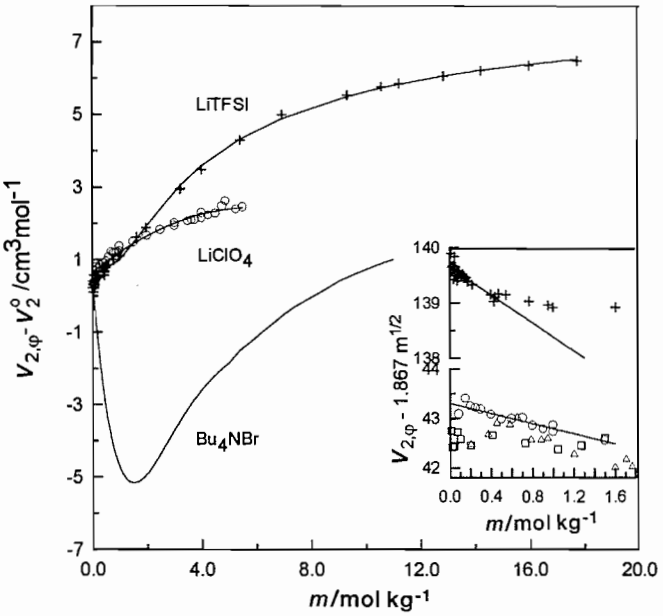
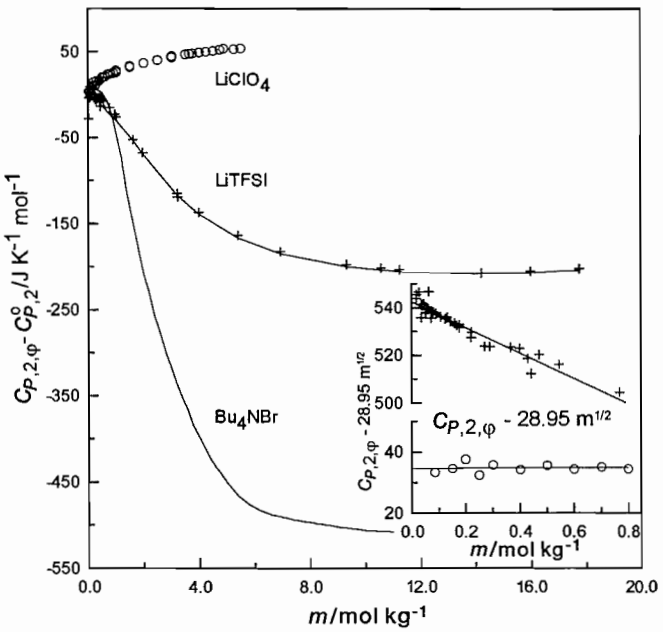


Fig. 5. Excess apparent heat capacity of LiTFSI, $LiClO_4$, and Bu_4NBr in water at 25°C. Data for Bu_4NBr from Perron et al. (27) and de Visser et al. (28). Full line in the case of LiTFSI is from mass-action model.



where M_2 is the molar mass and m_2 the molality of component 2, and the apparent molar heat capacity is calculated from

$$[5] \quad C_{P,2,\varphi} = M_2 c_P + \frac{1000(c_P - c_{P,0})}{m_2}$$

The difference in densities $(d - d_0)$, the relative changes in heat capacities per unit volume $(\Delta\sigma/\sigma_0)$, and the derived $V_{2,\varphi}$ and $C_{P,2,\varphi}$ are given elsewhere.[3] The low-concentration data were analysed with the Redlich–Meyer equation,

$$[6] \quad Y_{2,\varphi} = Y_2^0 + y_{DH} m^{1/2} + B_Y m$$

where Y_2^0 is the standard partial molar quantity, y_{DH} is the Debye–Hückel limiting slope, taken as 1.867 $cm^3\ kg^{1/2}\ mol^{-3/2}$ and 28.95 $J\ kg^{1/2}\ K^{-1}\ mol^{-3/2}$, respectively, for volumes and heat capacities at 25°C, and B_Y are empirical constants. The volume data reported by Lobo (24) on $LiClO_4$ disagree with the present data at low concentration (Fig. 4). This is not unexpected since the volumes were calculated from densities at four decimal places only. The parameters of eq. [6] are given in Table 1. The absolute value of V_2^0 ($TFSI^-$), based on the scale V_2^0 (H^+) = −5.4 $cm^3\ mol^{-1}$ (25) is 150.9 $cm^3\ mol^{-1}$, and the conventional $C_{P,2}^0$ ($TFSI^-$), based on $C_{P,2}^0$ (H^+) = 0, is 481 $J\ K^{-1}\ mol^{-1}$. Since data for LiTFSI were obtained at rather high concentrations in water and in other solvents, it is possible to estimate the intrinsic volume and heat capacity Y_2^*, or the molar property of the hypothetical liquid solute at 25°C, from a plot of the apparent quantity against $1/m$ (2). Since this function must be independent of the solvent, the best values

© 1997 NRC Canada

Can. J. Chem. Downloaded from www.nrcresearchpress.com by 91.121.58.235 on 09/08/12
For personal use only.

Table 1. Thermodynamic properties of LiTFSI, $LiClO_4$, and Bu_4NBr in water at 25°C.

Solute	Properties	Y_2^0	B_Y	m_{max}	Y_2^*
LiTFSI	V_2/cm^3 mol^{-1}	139.67 ± 0.05	−1.33	0.44	148 ± 2
	$C_{P,2}$/J K^{-1} mol^{-1}	542.6 ± 0.5	−53.9	0.8	300 ± 20
$LiClO_4$	V_2/cm^3 mol^{-1}	43.33 ± 0.05	−0.59	1.0	45 ± 5
	$C_{P,2}$/J K^{-1} mol^{-1}	34.7 ± 0.5	−0.2	1.0	125 ± 25
Bu_4NBr	V_2/cm^3 mol^{-1}	300.4			305 ± 5
	$C_{P,2}$/J K^{-1} mol^{-1}	1208			670 ± 25

Table 2. Least-squares analysis of the thermodynamic data of LiTFSI at high concentration using a mass-action model.

Property	Y_2^0	B_Y	N	m_I	Y_2^M	B_Y^M	RELAX
$V_{2,\varphi}$ /cm^3 mol^{-1}	(139.67)[a]	−1.07	(4)	(1.5)	149.6	−0.01	
$C_{P,2,\varphi}$ /J K^{-1} mol^{-1}	(542.6)	−55.8	(4)	(1.5)	241.7	4.58	94.1

[a]Values in parentheses were fixed.

Table 3. Conductance parameters of LiTFSI using the Fuoss–Hsia/Fernandez–Prini equation, modified to include the Chen and echo terms.[a]

	Λ_0	J	$J(3/2)$	K_A	r	m_{max}
Present data	71.12 ± 0.20	260.7	−1588.1	0	9.65	0.0147
Salomon (3)	70.56 ± 0.06	207.9	−994.1	0	9.65	0.0141

[a]Conductance units in S cm^2 mol^{-1}.

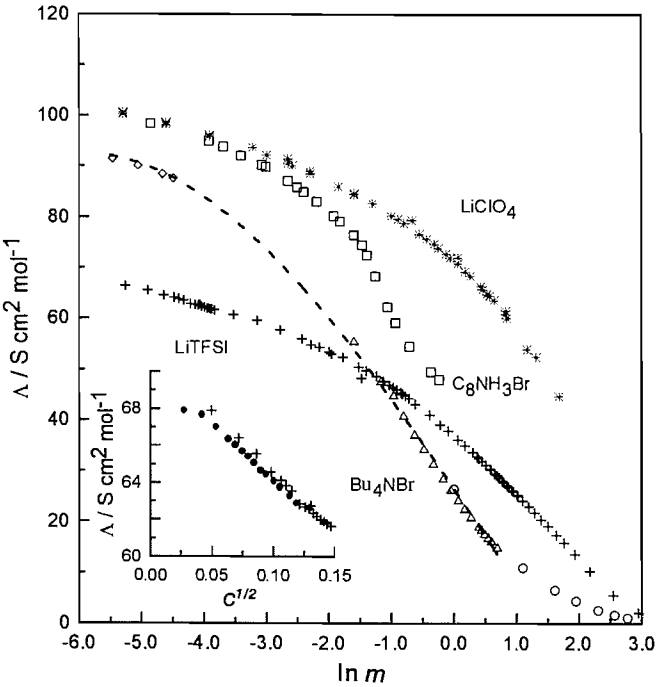


Fig. 6. Equivalent conductivity of LiTFSI, Bu_4NBr, $LiClO_4$, and $OctNH_3Br$ in water at 25°C. Data for LiTFSI (●) from Salomon (3), $LiClO_4$(∗) from Haase and Duecker (40), Bu_4NBr (Δ) from Quentin and Justice (36) and (○) from Wirth and Lesordo (38), and $OctNH_3Br$ from Desnoyers et al. (41).

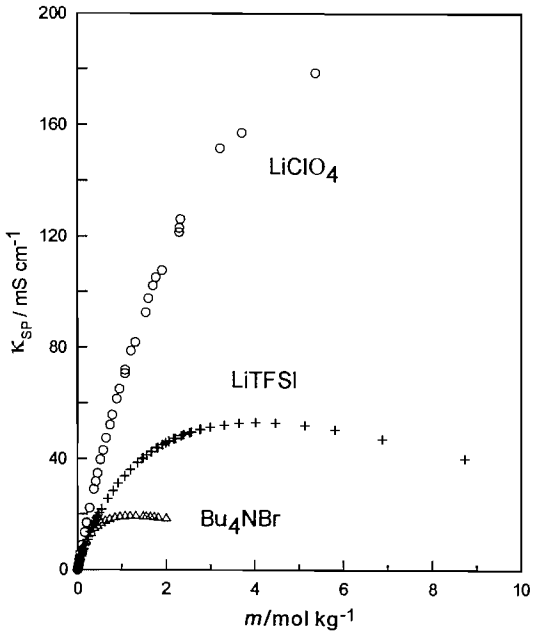
for V_2^* and $C_{P,2}^*$ are, respectively, 148 ± 2 cm^3 mol^{-1} and 300 ± 20 J K^{-1} mol^{-1}. The corresponding values for $LiClO_4$ and Bu_4NBr are given in Table 1.

To facilitate the comparison between different electrolytes, $Y_{2,\varphi} - Y_2^0$ are plotted in Figs. 4 and 5. The decrease in $V_{2,\varphi} - V_2^0$ of Bu_4NBr below 1.5 mol kg^{-1} arises because the term $B_V m$ is much more negative than $\nu_{DH} m^{1/2}$ of eq. [6]. A large negative value for B_V is usually associated with hydrophobic pair interactions (29). This term is also negative for the other electrolytes in Fig. 4 but the overall trend is governed by the Debye–Hückel contribution. There are many examples of hydrophobic electrolytes that show an overall increase in volume at low concentration, for example, many surfactants such as sodium alkanoates (30), amine hydrobromides (31) and perfluoroalkanoates (32). The trends in $V_{2,\varphi} - V_2^0$ at higher molalities are more informative. At about 1–1.5 mol kg^{-1}, $V_{2,\varphi} - V_2^0$ of LiTFSI shows a further increase as in the case of Bu_4NBr, while $V_{2,\varphi} - V_2^0$ of $LiClO_4$ simply levels off. The decrease in $C_{P,2,\varphi} - C_{P,2}^0$ of LiTFSI in Fig. 5 is also qualitatively similar to that of Bu_4NBr although the magnitude is smaller. No such changes are observed with $LiClO_4$ or alkali halides. The increase in $V_{2,\varphi} - V_2^0$ and decrease in $C_{P,2,\varphi} - C_{P,2}^0$ beyond a certain concentration is usually taken as evidence of self-association of the hydrophobic ions. The changes occur at approximately the same concentration as the break in γ in Fig. 3. Treatment of the data with a mass-action model (33, 34) would suggest that the aggregation number of LiTFSI would be of the order of 4. Such a model fits the volumes and heat capacities

© 1997 NRC Canada

Can. J. Chem. Downloaded from www.nrcresearchpress.com by 91.121.58.235 on 09/08/12
For personal use only.

Fig. 7. Specific conductivity of LiTFSI, Bu_4NBr, and $LiClO_4$ in water at 25°C. Data sources are the same as for Fig. 6.



remarkably well, as seen from Figs. 4 and 5, with a minimum number of parameters. These new parameters, given in Table 2, have the following meaning: N is the aggregation number, m_I is the molality at the inflexion point of the fraction of monomers (equivalent to a critical micellar concentration or CMC), Y_2^M is the molar property of the solute in the micellar state, B_Y^M is an interaction parameter for the micelles, and RELAX is the relaxational contribution to heat capacity which takes into account the shift in CMC with temperature. In the data analysis, Y_2^0 was fixed to the value given in Table 1 in all cases. To get a good convergence of the least-squares analyses, at least one more parameter had to be fixed. After a few trials, N and m_I were fixed at reasonable mean values for volumes and heat capacities and the other parameters were determined by the least-squares fit. The mass-action model is a good fitting equation for LiTFSI; the parameters B_Y in Tables 2 and 3 are comparable, and the quantity $Y_2^M + B_Y^M(m - m_I)$ is tending to the parameter Y_2^* in Table 2. With such small aggregation numbers and large values of m_I, the aggregates can probably not be associated with real micelles but more with the kind of time-averaged clusters that are observed in alcohol–water mixtures (35).

Ionic conductivity

The equivalent conductances, Λ, of LiTFSI are given elsewhere.[3] Some data were also obtained for Bu_4NBr at intermediate concentrations to partially fill the gap in the available data in the literature (24, 36–38). The low concentration data ($m < 0.01$) were analyzed with the Fuoss–Hsia/Fernandez–Prini equation, modified to include the Chen and echo terms using the programs developped by Justice (39). The parameters are given in Table 3. The value of Λ_0 of LiTFSI was found to be 71.12 S cm^2 mol^{-1} at 25°C, which is in good agreement with the value obtained by Salomon (3), 70.89 S cm^2 mol^{-1}, once his data are analyzed with the same equation, considering the precision of our conductance bridge and the relative purity of different samples of this electrolyte. The values of Λ_0 of LiTFSI in various solvents were discussed in detail by Salomon (3) and by Ue (8). Our interest is more in the high-concentration behaviour.

The large decrease in conductivity at low concentrations resulting from the long-range Coulombic force hides most of the additional attractive interactions due to self-association. To see if the results can show any evidence of self-association, Λ values were plotted against $\ln(m)$ in Fig. 6 and compared with those of Bu_4NBr, $LiClO_4$, and of a typical short-chain surfactant. Bu_4NBr shows some evidence of self-association, when the trends in Λ are compared with those of octylammonium bromide, $OctNH_3Br$ (41). On the other hand, the concentration dependence of LiTFSI seems to be closer to that of $LiClO_4$. The only explanation we can offer to explain why the conductance of LiTFSI does not show the expected trends of a surface-active solute, considering the observed trends of the thermodynamic properties, is that different properties are reflecting different effects. The changes in volumes and heat capacities during micellization are essentially due to a loss of hydrophobic hydration while the corresponding changes in conductance are due to a change in the number of free ions and to changes in the size of the moving particles. With systems undergoing changes above 1.5 mol kg^{-1} involving only three or four molecules, the effects may be too small to be detected in conductances.

The specific conductivities, κ_{sp}, are plotted as a function of m in Fig. 7. κ_{sp} reaches the maximum value of 53 mS cm^{-1} at 4.3 mol kg^{-1}, which can be compared with the maximum value of 19.9 mS cm^{-1} for Bu_4NBr at 1.2 mol kg^{-1} and a value tending to 200 mS cm^{-1} for $LiClO_4$. The decrease in κ_{sp} following the order $LiClO_4$ > LiTFSI > Bu_4NBr probably reflects the increasing size of the pairs of ions.

Conclusion

LiTFSI is highly soluble and shows some surface activity in water. Above 1 mol kg^{-1}, the surface tension, volume, and heat capacity data all show some evidence of self-association. Using a mass-action model, the aggregation number would be of the order of 4. The behaviour of LiTFSI in water is therefore similar to weakly hydrophobic electrolytes such as Pr_4NBr. The surface activity character of LiTFSI is not reflected in conductances. The anomalous thermodynamic properties and equivalent conductivities of LiTFSI observed in DME (2) are not present in water. This suggests that LiTFSI has most of the expected properties of a weakly surface-active electrolyte in water, and the anomalous trends in solvents of low dielectric constant are due to specific interactions and not to the chemical structure of this large anion.

Acknowledgement

The authors are grateful to the Natural Sciences and Engineering Research Council of Canada for financial assistance and to Yves Choquette of Hydro-Quebec for supplying a sample of LiTFSI for these studies.

© 1997 NRC Canada

References

1. M. Armand, J.Y. Sanchez, M. Gauthier, and Y. Choquette. *In* Electrochemistry of novel materials. *Edited by* J. Lipkowski and P.N. Ross. VCH Publishers, New York. 1994. p. 65.
2. D. Brouillette, G. Perron, M. Pesant, and J.E. Desnoyers. J. Solution Chem. Submitted.
3. M. Salomon. J. Solution Chem. **22**, 715 (1993).
4. A. Webber. J. Electrochem. Soc. **138**, 2586 (1991).
5. G. Perron, D. Brouillette, M. Pesant, and J.E. Desnoyers. Proc. Electrochem. Soc. **95–2**, 147 (1995).
6. C.L. Matthias, P.M. Shah, M.L. Kronenberg. Proc. Electrochem. Soc. **95–2**, 141 (1995).
7. L.A. Dominey, V.R. Koch, and T. Blakley. Electrochim. Acta, **37**, 1551 (1992).
8. M. Ue. Denki Kagaku, **62**, 620 (1994); J. Electrochem. Soc. **143**, L270 (1996).
9. F. Quirion, D. Lambert, and G. Perron. Can. J. Chem. **70**, 2745 (1992).
10. P. Picker, P.-A. Leduc, P. Philip, and J.E. Desnoyers. J. Chem. Thermodyn. **3**, 631 (1971).
11. J.E. Desnoyers, C. De Visser, G. Perron, and P. Picker. J. Solution Chem. **5**, 605 (1976).
12. R.C. Weast (*Editor*). Handbook of chemistry and physics. 70th ed. CRC Press, Boca Raton, Fla. 1990.
13. P. Picker, E. Tremblay, and C. Jolicoeur. J. Solution Chem. **3**, 377 (1974).
14. C. Labrèche, L. Lévesque, and J. Prud'homme. Macromolecules, **29**, 7795 (1996).
15. C.A. Angel and E.J. Sare. J. Chem. Phys. **52**, 1058 (1970).
16. C.A. Angel and R.D. Bressel. J. Phys. Chem. **76**, 3244 (1972).
17. A.D. Pelton. *In* Physical metallurgy. *Edited by* R.W. Cahn and P. Haasen. North-Holland Physics Publ., The Netherlands. 1983. Part 1, Chap. 7.
18. H. Senapati, R.K. Kadiyala, and C.A. Angel. J. Phys. Chem. **95**, 7050 (1991).
19. B. Perrenot and G. Widmann. Thermochim. Acta, **234**, 31 (1994).
20. A. Seidell. Solubilities of inorganic and metal organic compounds. Vol. 1. 3rd ed. D. Van Nostrand, New York. 1940. p. 920.
21. E.M. Arnett, M. Ho, and L.L. Schaleger. J. Am. Chem. Soc. **92**, 7039 (1970).
22. K. Tamaki. Bull. Chem. Soc. Jpn. **40**, 38 (1967).
23. S.K. Kang and M.S. Jhon J. Polym. Sci. Part A: Polym. Chem. **31**, 1243 (1993).
24. V.M.M. Lobo. Electrolyte solutions: literature data on thermodynamic and transport properties. Vol. 1. 1981; Vol. 2, 1984; Coimbra, Portugal.
25. R. Zana and E. Yeager. J. Phys. Chem. **70**, 954 (1966); **71**, 521 (1967).
26. W.Y. Wen and S. Saito. J. Phys. Chem. **68**, 2639 (1964).
27. G. Perron, N. Desrosiers, and J.E. Desnoyers. Can. J. Chem. **54**, 2163 (1976).
28. C. de Visser, G. Perron, and J.E. Desnoyers. J. Am. Chem. Soc. **99**, 5894 (1977).
29. J.E. Desnoyers and C. Jolicoeur. *In* Comprehensive treatise of electrochemistry. *Edited by* B.E. Conway, J.O'M. Bockris, and E. Yeager. Plenum Press, New York. 1983. Chap. 1.
30. R. DeLisi, G. Perron, and J.E. Desnoyers. Can. J. Chem. **58**, 959 (1980).
31. J.E. Desnoyers and M. Arel. Can. J. Chem. **45**, 359 (1967).
32. G. Perron and J.E. Desnoyers. J. Chem. Eng. Data, **42**, 172 (1997).
33. J.E. Desnoyers, G. Caron, R. DeLisi, D. Roberts, A. Roux, and G. Perron. J. Phys. Chem. **87**, 1397 (1983).
34. J.E. Desnoyers and G. Perron. Langmuir, **12**, 4044 (1996).
35. F. Franks and J.E. Desnoyers. *In* Water science reviews 1. *Edited by* F. Franks. Cambridge University Press, London. 1985. pp. 171–232.
36. M. Quentin and M.-C. Justice. C. R. Acad. Sci. Paris, **261**, 1287 (1965).
37. A. LeSurdo and H.E. Wirth. J. Phys. Chem. **83**, 879 (1979).
38. H.E. Wirth and A. LeSurdo. J. Phys. Chem. **76**, 1333 (1972).
39. J.-C. Justice. *In* Comprehensive treatise of electrochemistry. Vol. 5. *Edited* by B.E. Conway, J.O'M. Bockris, and E. Yeager. Plenum Press, New York. 1983. Chap. 3.
40. R. Haase and K.H. Duecker. Z. Phys. Chem. NF, **46**, 140 (1965).
41. J.E. Desnoyers, M. Arel, and P.-A. Leduc. Can. J. Chem. **47**, 547 (1969).

Can. J. Chem. Downloaded from www.nrcresearchpress.com by 91.121.58.235 on 09/08/12
For personal use only.

© 1997 NRC Canada

Influence of adsorption of organic compounds and surface heterogeneity on the hydrogen evolution reaction

Andrzej Lasia

Can. J. Chem. Downloaded from www.nrcresearchpress.com by 91.121.58.235 on 09/08/12
For personal use only.

Abstract: The hydrogen evolution reaction on rough or porous surfaces often leads to low Tafel slopes that cannot be explained in terms of the Volmer–Heyrovsky–Tafel mechanism. In addition, adsorption of organic compounds and ions causes an increase in the Tafel slopes. To explain such behavior, a concept of distribution of adsorption energies on heterogeneous surfaces, leading to a distributed kinetics, was studied. Simulations of the dependence of the current and the surface coverage by adsorbed hydrogen on overpotential are presented for different values of the kinetic parameters in the absence and presence of the adsorbed foreign substances. These results were compared with those obtained using the Frumkin/Temkin adsorption isotherm. It was found that for some kinetic parameters and a flat distribution of adsorption energies, low Tafel slopes, similar to those observed experimentally, are obtained.

Key words: hydrogen evolution, adsorption, heterogeneous surfaces, distributed kinetics, Frumkin/Temkin isotherm.

Résumé : La réaction de dégagement d'hydrogène sur des surfaces poreuses ou rugueuses conduit souvent à de faibles pentes de Tafel que l'on ne peut expliquer en fonction du mécanisme de Volmer–Heyrovsky–Tafel. De plus, l'adsorption de composés organiques et d'ions provoque une augmentation des pentes de Tafel. Dans le but d'expliquer un tel comportement, on a étudié un concept de distribution des énergies d'adsorption sur des surfaces hétérogènes conduisant à une cinétique répartie. On présente des simulations relatives à l'influence d'une surtension sur le courant et sur la surface couverte par l'hydrogène adsorbé, pour différentes valeurs des paramètres cinétiques, en l'absence et en présence de substances étrangères adsorbées. On a comparé ces résultats à celles obtenues dans les conditions de l'isotherme de Frumkin/Temkin. On a trouvé que l'on obtient, pour quelques paramètres cinétiques et pour une distribution en palier des énergies d'adsorption, de faibles pentes de Tafel semblables à celles observées expérimentalement.

Mots clés : dégagement d'hydrogène, adsorption, surfaces hétérogènes, cinétique répartie, isotherme de Frumkin/Temkin.

[Traduit par la rédaction]

Introduction

The real electrode surfaces used in electrocatalysis are usually very rough or porous and heterogeneous. However, in electrochemistry, a homogenous approach is usually used and it is assumed that there is only one set of reaction rates describing the kinetics of the system. In the heterogeneous systems the adsorption energy and the rate constants depend on the nature of the site. The main sources of heterogeneity are (1): (*i*) different types of crystal planes, steps, edges, etc. exposed for adsorption, (*ii*) irregularities in crystallographic surface structure, (*iii*) impurities strongly bound to the surface, and (*iv*) the different chemical nature of the surface centers. Such concepts are well known in adsorption studies (1–9). They were applied to electrosorption by Nikitas and Papqutsis (10, 11). The concept of distributed kinetics as a distribution of rate constants was adopted for electrochemistry by Albery et al. (12, 13), used by Rowe et al. (14) and, recently, by Chialvo and Chialvo (15, 16).

Rough and porous electrodes are usually used in the hydrogen evolution reaction (HER). On Ni–Zn Raney electrodes, after leaching out the zinc in alkaline solutions, the observed Tafel plots vary between 50 and 90 mV dec^{-1}, depending on the deposited layer thickness and composition (17–21). Such slopes cannot be explained in terms of the classical Volmer–Heyrovsky–Tafel mechanism. The porous electrode model predicts even doubling of the Tafel slopes. Rausch and Wendt (17, 18) tried to explain such behavior by hydrogen pressure buildup in pores, using an approximate model; however, recently Lasia (22), using correct treatment, showed that such low slopes predicted due to the hydrogen pressure buildup cannot be observed experimentally in the linear Tafel range. It was also suggested (21) that hydrogen absorption in the topmost surface layers may be responsible for low Tafel slopes.

In our earlier papers (20, 21) it was found that adsorption of organic compounds (pyridine, thiourea) or ions (CN^-) causes an increase of the observed Tafel slopes. The influence of adsorption of organic compounds on the HER was

Received March 10, 1997.

This paper is dedicated to Professor Brian E. Conway on the occasion of his 70th birthday.

A. Lasia.[1] Département de chimie, Université de Sherbrooke, Sherbrooke, QC J1K 2R1, Canada.

[1] Telephone: (819) 821-7097. Fax: (819) 821-8017. E-mail: alasia@courrier.usherb.ca

© 1997 NRC Canada

Can. J. Chem. Downloaded from www.nrcresearchpress.com by 91.121.58.235 on 09/08/12
For personal use only.

discussed by Conway and Jerkiewicz (23) and Jerkiewicz et al. (24, 25). They carried out simulations of the surface coverage by adsorbed hydrogen, Θ_H, assuming homogeneous surface conditions. It was suggested earlier (20) that the distribution of adsorption energies may play an important role in the kinetics of the hydrogen evolution on heterogeneous surfaces. In the present paper the model of the distribution of adsorption energies, leading to distributed kinetics, is applied to the HER, and the influence of the adsorption of other species on this reaction is studied. These results are compared with those obtained assuming unique rate constants and with adsorption under Frumkin/Temkin isotherms. The HER kinetics was expressed in terms of the rate constants, in contrast with the earlier approach (15, 16) using the exchange current densities and the surface coverage at the equilibrium potential.

Hydrogen adsorption in the absence of organic compounds

The hydrogen evolution reaction may proceed through three reaction paths:

[1] $H_2O + e \rightleftharpoons OH^- + MH$ Volmer

[2] $MH + H_2O + e \rightleftharpoons H_2 + OH^-$ Heyrovsky

[3] $MH + MH \rightleftharpoons H2$ Tafel

where MH denotes hydrogen adsorbed on the electrode surface. For reasons of simplicity only the Volmer–Heyrovsky reaction mechanism will be considered below. The rate constants of these reactions depend on the standard hydrogen adsorption Gibbs energy (26), ΔG^0_H, which can be represented as $G^0_H = (\Delta G^0_H - \Delta G^0_{H,r}) + \Delta G^0_{H,r} = \Delta\Delta G^0_H + \Delta G^0_{H,r}$ where $\Delta G^0_{H,r}$ is the hydrogen adsorption Gibbs energy at a reference state. Then, the reaction rates, assuming the Langmuir isotherm for hydrogen adsorption, may be written as:

$$[4]\quad v_1 = k_1^0 \, e^{-\beta_1(\Delta\Delta G^0_H/RT)} e^{-\alpha_1 f\eta}(1 - \Theta_H) - k_{-1}^0 \, e^{(1-\beta_1)(\Delta\Delta G^0_H/RT)} e^{(1-\alpha_1)f\eta}\Theta_H$$

$$[5]\quad v_2 = k_2^0 \, e^{(1-\beta_2)(\Delta\Delta G^0_H/RT)} e^{-\alpha_2 f\eta}\Theta_H - k_{-2}^0 \, e^{-\beta_2(\Delta\Delta G^0_H/RT)} e^{(1-\alpha_2)f\eta}(1-\Theta_H)$$

where k_i^0 are the standard rate constants, including term $\Delta G^0_{H,r}$; α_i and β_i are the symmetry coefficients for the electrochemical and adsorption processes, respectively; η is the overpotential; Θ_H is the surface coverage by adsorbed hydrogen; and $f = F/RT$. The adsorption energy enters into the rate constants: $k_i = k_i^0 \, e^{-\beta_i(\Delta\Delta G^0_H/RT)}$ for $i = 1, -2$, and $k_i = k_i^0 \, e^{(1-\beta_i)(\Delta\Delta G^0_H/RT)}$ for $i = -1, 2$. Taking into account that, in the steady state, rates of the Volmer and Heyrovsky reactions are identical, the following equation is obtained:

$$[6]\quad v = v_1 + v_2 = \vec{k}_1 (1 - \Theta_H) - \overleftarrow{k}_{-1}\Theta_H + \vec{k}_2\Theta_H + \overleftarrow{k}_{-2}(1 - \Theta_H) = 2v_1 = 2v_2$$

where $\vec{k}_i$ and $\overleftarrow{k}_i$ are the potential-dependent rate constants, $\vec{k}_i = k_i^0 \exp(-\alpha_i f\eta)$ for $i = 1,2$ and $\overleftarrow{k}_i = k_i^0 \exp[(1 - \alpha_i)f\eta)$ for $i = -1, -2$, and the total observed current equals $i = Fv$. Equation [6] allows for the determination of the surface coverage by adsorbed hydrogen:

$$[7]\quad \Theta_H = \frac{\vec{k}_1 + \overleftarrow{k}_{-2}}{\vec{k}_1 + \overleftarrow{k}_{-1} + \vec{k}_2 + \overleftarrow{k}_{-2}}$$

or

$$[8]\quad \frac{\Theta_H}{1 - \Theta_H} = \frac{\vec{k}_1 + \overleftarrow{k}_{-2}}{\overleftarrow{k}_{-1} + \vec{k}_2} = \overline{K}_H$$

where $\overline{K}_H$ is the potential-dependent equilibrium constant of hydrogen adsorption. It also allows for the elimination of one out of four rate constants, because:

$$[9]\quad \frac{k_1 k_2}{k_{-1} k_{-2}} = 1$$

It can be noticed that $\Theta_H = k_{-2}/(k_{-1} + k_{-2})$ at very positive overpotentials, $\Theta_H = k_1/(k_1 + k_{-1}) = k_{-2}/(k_2 + k_{-2})$ at the equilibrium potential, and $\Theta_H = k_1/(k_1 + k_2)$ at very negative overpotentials. These relations may be used when the solution is saturated with hydrogen and its diffusion may be neglected. However, because of a very small hydrogen solubility in aqueous solutions, the anodic limit predicted above is not reached and the surface coverage reaches zero at positive potentials. Langmuir (27) assumed that the heterogeneous surface is composed of a number of patches, which are independent of each other and behave as separate. However, adsorption on each patch follows the Langmuir isotherm. Later, this concept was extended to random distribution of adsorption heterogeneities. To describe this behavior a distribution of adsorption energies is introduced. It is assumed that the surface can be divided into a number of macroscopic sites possessing the surface area dS and at each site the Langmuir isotherm is valid; however, each site may be characterized by a different adsorption energy (1–3, 15, 16, 27). Such a model is usually used in the adsorption studies.

In such cases the macroscopically observed surface coverage, Θ_H, and total reaction rate, V, are obtained by integration over all sites:

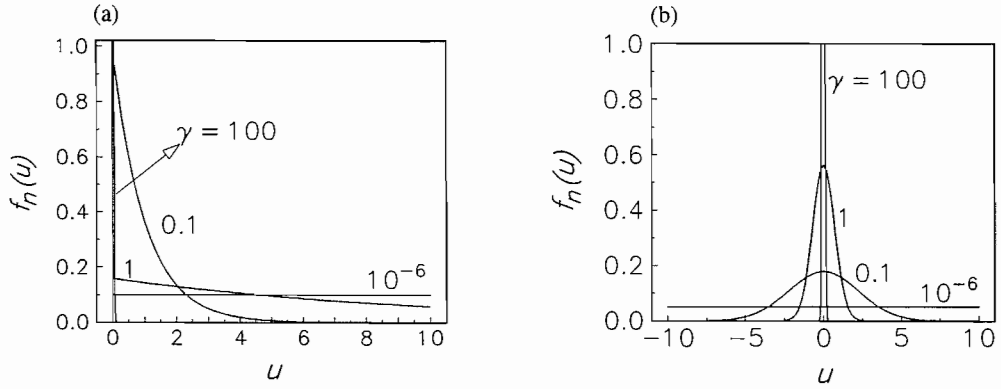
$$[10]\quad \Theta_H = \frac{\int_{u_1}^{u_2} \theta_H(\eta, u) f(u) du}{\int_{u_1}^{u_2} f(u) du} = \int_{u_1}^{u_2} \theta_H(\eta, u) f_n(u) du \qquad \text{where} \quad u = \Delta\Delta G^0_H/RT$$

$$[11]\quad V = \frac{\int_{u_1}^{u_2} v(\eta, u) f(u) du}{\int_{u_1}^{u_2} f(u) du} = \int_{u_1}^{u_2} v(\eta, u) f_n(u) du$$

© 1997 NRC Canada

Can. J. Chem. Downloaded from www.nrcresearchpress.com by 91.121.58.235 on 09/08/12
For personal use only.

Fig. 1. Distribution functions $f(u)$ as a function of $u = \Delta\Delta G^0_H/RT$ for different values of parameter γ: (*a*) exponential, (*b*) Gaussian.



where $f(u)$ is the distribution function and $f_n(u)$ is the normalized distribution function:

$$[12] \quad f_n(u) = \frac{f(u)}{\int_{u_1}^{u_2} f(u)\mathrm{d}u}$$

and the integration runs between the lowest, u_1, and the highest, u_2, adsorption energies in the system. The distribution function is directly related to the fraction of the surface area, dS, characterized by the adsorption energy between u and $u + du$: d$S = f_n(u)\,du$. By integration, a fraction of the surface area characterized by a given range of adsorption energies may be obtained. Popular choices of distribution functions in catalysis are Gaussian and exponential (1, 2), eq. [13], or skewed,

$$[13] \quad f(u) = \mathrm{e}^{-\gamma u^2} \qquad \text{or} \qquad f(u) = \mathrm{e}^{-\gamma u}$$

where γ is the distribution parameter. Gaussian distribution means that there is a normal distribution of adsorption energies around one value, $\Delta\Delta G^0_H = 0$, and the exponential distribution means that the number of sites decreases exponentially with the increase of the adsorption energy, that is, there are many sites characterized by low and fewer characterized by high adsorption energy. Parameter γ is related to the surface heterogeneity (2). A few examples of the normalized distribution functions are shown in Fig. 1. When $\gamma \to \infty$ there is no dispersion and only one adsorption energy exists (surface is homogeneous), and $\gamma = 0$ means that there is "flat" distribution and each center contributes equally to the total adsorption energy. In experimental studies of adsorption, more complex distribution functions, e.g., composed of a few Gaussian peaks, were found. To simulate such cases more experimental information on the distribution function should be known. Because of the exponential dependence of the rate constants on the adsorption energy, the rate constants of the Volmer and Heyrovsky reactions are distributed and the logarithm of the rate constants is distributed according to the function $f(u)$. Equations [4] and [5] show that as the adsorption energy increases, i.e., $\Delta\Delta G^0_H$ becomes more negative, the hydrogen adsorption rates, k_1 and k_{-2}, increase and the desorption rates, k_{-1} and k_2, decrease.

In the above discussion the Langmuir isotherm was assumed; however, hydrogen adsorption may also proceed according to other isotherms, for example, the Frumkin/Temkin isotherms (28–30). The Frumkin/Temkin isotherm assumes that the adsorption energy depends on the surface coverage:

$$[14] \quad \Delta G^0_H = \Delta G^0_{H,0} + r\Theta$$

Such behavior may be due to interactions between adsorbed species or to the surface heterogeneity. Equation [14] leads to the following kinetic equations:

$$[15] \quad v_1 = k_1^0\,\mathrm{e}^{-\beta_1 g\Theta_H}\mathrm{e}^{-\alpha_1 f\eta}(1 - \Theta_H) - k_{-1}^0\,\mathrm{e}^{(1-\beta_1)g\Theta_H}\,\mathrm{e}^{(1-\alpha_1)f\eta}\Theta_H$$

$$[16] \quad v_2 = k_2^0\,\mathrm{e}^{(1-\beta_2)g\Theta_H}\mathrm{e}^{-\alpha_2 f\eta}\Theta_H - k_{-2}^0\,\mathrm{e}^{-\beta_2 g\Theta_H}\mathrm{e}^{(1-\alpha_2)f\eta}(1 - \Theta_H)$$

where $g = r/RT$, and to the adsorption isotherm:

$$[17] \quad \frac{\Theta_H}{1-\Theta_H}\mathrm{e}^{g\Theta_H} = \frac{\vec{k}_1 + \overleftarrow{k}_{-2}}{\overleftarrow{k}_{-1} + \vec{k}_2} = \overline{K}_H$$

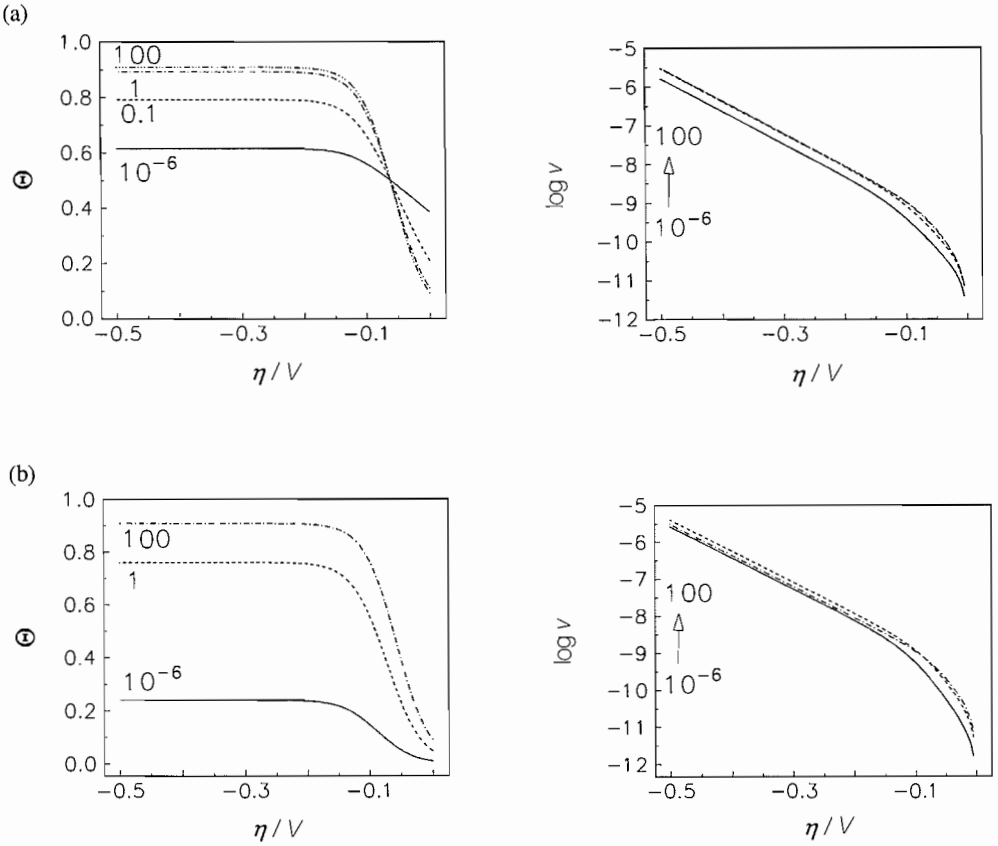
Because these equations also describe heterogeneous surfaces, the results obtained will be compared with those obtained using distributed kinetics.

Gaussian and exponential distributions

The values of the total surface coverage, Θ_H, and the total reaction rate, V, were simulated for different values of the kinetic parameters. Rate constants chosen were similar to those used in the earlier simulations (31, 32). The distribution parameter γ has a strong influence on the total surface coverage, Θ_H, but a much smaller influence on the total reaction rate (i.e., current). The results of the simulations are presented in Fig. 2. Although Θ_H is very sensitive to the parameter γ, it has a very small influence on the observed currents. In addition, for the lowest values of parameter γ, change in the Tafel slope at low overpotentials is observed; however, at more negative overpotentials, where the surface coverage is constant, the classical Tafel slope is $RT\ln(10)/0.5F$ = 118 mV dec^{-1} (at 25°C). Similar results were obtained for the exponential distri-

© 1997 NRC Canada

Fig. 2. Influence of parameter γ on the surface coverages and the global rate of the HER for (*a*) Gaussian and (*b*) exponential distribution of adsorption energies; parameters used: $k_1^0 = 10^{-9}$, $k_{-1}^0 = 10^{-8}$, $k_2^0 = 10^{-10}$ mol cm^{-2} s^{-1}, $\alpha_i = \beta_i = 0.5$, $u = \Delta\Delta G_H^0/RT = \pm 10$, $\gamma = 10^{-6}$, 0.1, 1, 100.



bution of adsorption energies; these results are also presented in Fig. 2. Because the changes in the Tafel slope were observed for flat distribution of adsorption energies (low γ), further calculations were mainly carried out for low values of γ ($\gamma = 10^{-6}$).

The influence of the energy range used, $\pm\Delta\Delta G_H^0$, on Θ_H and V is shown in Fig. 3. An increase in $\Delta\Delta G_H^0$ causes a decrease in the values of the surface coverage, Θ_H, and an almost parallel decrease of the Tafel curves. These curves are obtained by integration of currents for different values of the parameter u. A change in the adsorption energies affects the currents and the surface coverages. Examples of Tafel curves for various adsorption energies (in the absence of the adsorption energy distribution, i.e., for homogeneous surfaces) are presented in Fig. 4. For $\Delta\Delta G_H^0$ equal to -10, $\Theta_H \ll 1$; for $\Delta\Delta G_H^0 = 10$, $\Theta_H \to 1$; and for $\Delta\Delta G_H^0 = 0$, Θ_H increases with overpotential from 0.09 to 0.91.

When the ratio of the rate constants k_1/k_2 increases, the overpotential range, where low Tafel slopes are observed, also increases, Fig. 5. The Tafel slopes obtained at low overpotentials are equal to 52–60 mV dec^{-1}. They are larger than the slopes observed at low overpotentials for the unique rate constants and, for a small ratio of k_1/k_{-1}, $RT \ln 10/1.5F = \sim 40$ mV dec^{-1}. The above analysis shows that low Tafel slopes may be obtained for distributed kinetics. It should be kept in mind that for very low values of γ there is no difference between the Gaussian and exponential distribution; the difference lies only in the initial k_i values and the energy range used for integration.

Frumkin adsorption isotherm

Similar simulations were carried out for the Frumkin adsorption isotherm. The parameter g (>0) has a very strong influence on the surface coverage by adsorbed hydrogen but relatively small influence on the Tafel curves, Fig. 6. Similarly, an increase in the ratio of k_1/k_2 extends the low slope range, Fig. 7, in a way similar to the results in Fig. 5. The Tafel slope is ~56 mV dec^{-1} at low overpotentials and 118 mV dec^{-1} at high overpotentials. These results are similar to those found for a flat distribution of adsorption energies under local Langmuir isotherms. Comparison of the dependence of Θ_H on overpotential for the flat distribution of adsorption energies under the Langmuir adsorption isotherm, Fig. 5, and for the Frumkin isotherm, Fig. 7, shows that at low overpotentials the surface coverage changes linearly with overpotential. This effect indicates that, under such conditions, Θ_H is described by the Temkin isotherm, i.e., it depends linearly on the free energy of adsorption (28, 33). It was shown (33) that the Temkin isotherm leads to a flat distribution function of adsorption energies ($\gamma \sim 0$) in a limited adsorption energy range, preceded and followed by a sharp decrease in $f(u)$. However, the Temkin adsorption isotherm is valid only for the surface coverages around 0.5 (~0.2 to ~0.8).

Can. J. Chem. Downloaded from www.nrcresearchpress.com by 91.121.58.235 on 09/08/12
For personal use only.

© 1997 NRC Canada

Fig. 3. (*a*) Influence of $\pm\Delta\Delta G_H^0/RT$ for Gaussian distribution and (*b*) of $\Delta\Delta G_H^0/RT$ for exponential distribution of adsorption energies; $\gamma = 10^{-6}$, other parameters as in Fig. 2.

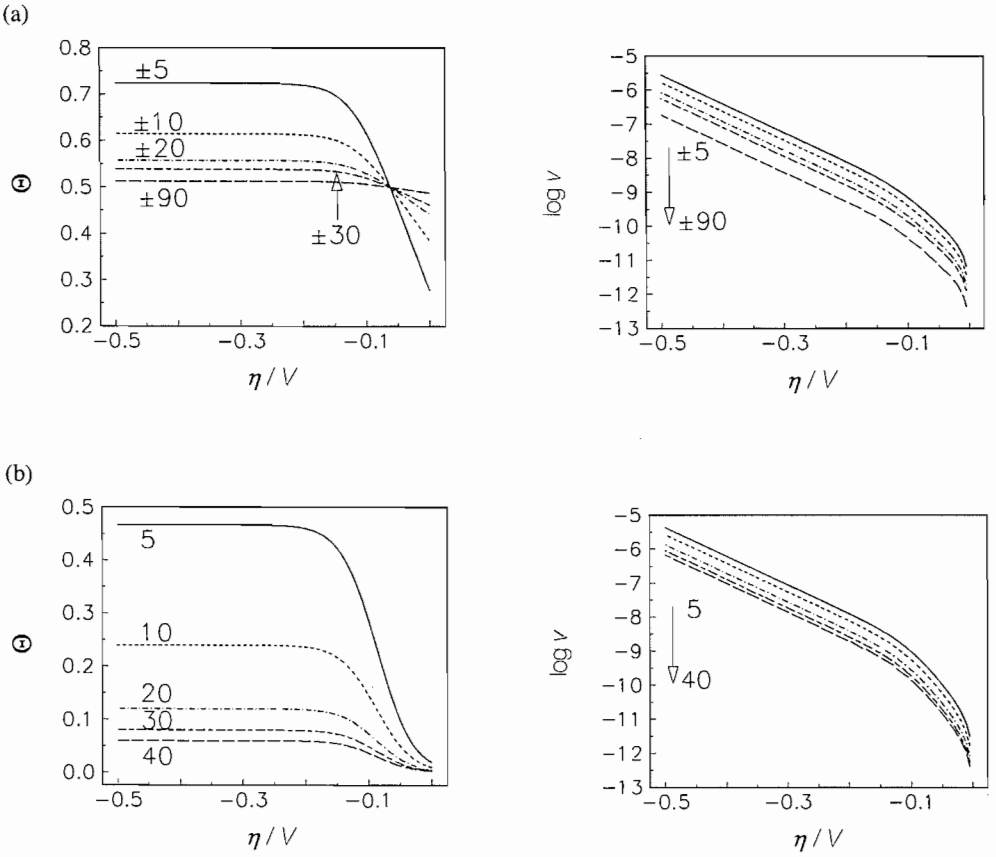
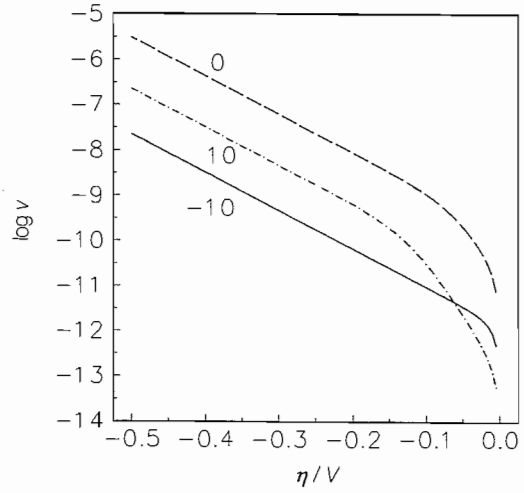


Fig. 4. Individual currents for different values of the adsorption energy; rate constants as in Fig. 2; the rate constants are, for $\Delta\Delta G_H^0/RT = -10$: $k_1 = 1.48 \times 10^{-7}$, $k_{-1} = 6.74 \times 10^{-11}$, $k_2 = 6.74 \times 10^{-13}$, for $\Delta\Delta G_H^0/RT = 0$ they are equal to k_i^0, for $\Delta\Delta G_H^0/RT = 10$: $k_1 = 6.74 \times 10^{-12}$, $k^{-1} = 1.48 \times 10^{-6}$, $k_2 = 1.48 \times 10^{-8}$ mol cm^{-2} s^{-1}.



Adsorption of organic compounds

If an organic compound, R, is present in the solution there is a competition between hydrogen and R for a free space. The kinetic equation for the hydrogen evolution displays a decrease of the free surface from $1 - \theta_H$ to $1 - \theta_H - \theta_R$:

[18] $$v_1 = k_1 e^{-\alpha_1 f\eta}(1 - \theta_H - \theta_R) - k_{-1} e^{(1-\alpha_1)f\eta}\theta_H$$

[19] $$v_2 = k_2 e^{-\alpha_2 f\eta}\theta_H - k_{-2} e^{(1-\alpha_2)f\eta}(1 - \theta_H - \theta_R)$$

and produces the following isotherm:

[20] $$\frac{\theta_H}{1 - \theta_H - \theta_R} = \frac{\vec{k}_1 + \overleftarrow{k}_{-2}}{\overleftarrow{k}_{-1} + \vec{k}_2} = \overline{K}_H$$

It indicates that the chemical potential of adsorbed hydrogen remains unchanged (24). Two different cases of the adsorption of organic compounds were considered: (*i*) competitive equilibrium adsorption of H and R, in which both species are always at equilibrium and a change in the adsorption of one component causes a change in the adsorption of the other:

[21] $$\frac{\theta_R}{1 - \theta_H - \theta_R} = K_R C_R$$

and (*ii*) slow, i.e., irreversible, adsorption of an organic compound, in which R is first adsorbed (in the absence of adsorbed hydrogen) according to its adsorption isotherm and then its surface coverage remains unchanged during the experiment:

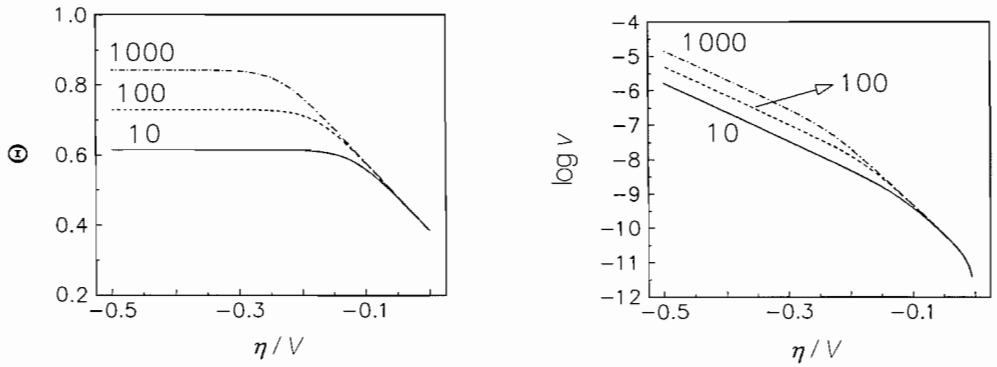
[22] $$\frac{\theta_R}{1 - \theta_R} = K_R C_R$$

Can. J. Chem. Downloaded from www.nrcresearchpress.com by 91.121.58.235 on 09/08/12
For personal use only.

© 1997 NRC Canada

Fig. 5. Dependence of the surface coverage by adsorbed hydrogen and current on overpotential for (*a*) Gaussian and (*b*) exponential distribution of adsorption energies; the ratio of k_1/k_2 is indicated in the graph, $\gamma = 10^{-6}$, $\Delta\Delta G^0_H/RT = \pm 10$, $\alpha_i = \beta_i = 0.5$, $k_1/k_{-1} = 0.1$, $k_2 = 10^{-10}$ mol cm^{-2} s^{-1}.

(a)



(b)

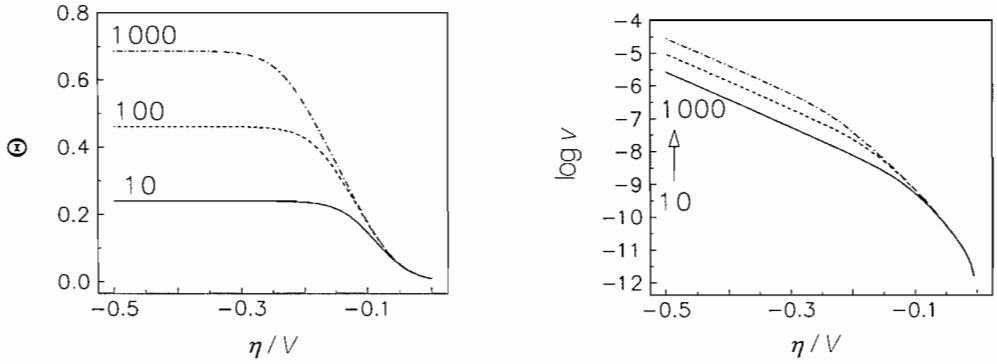
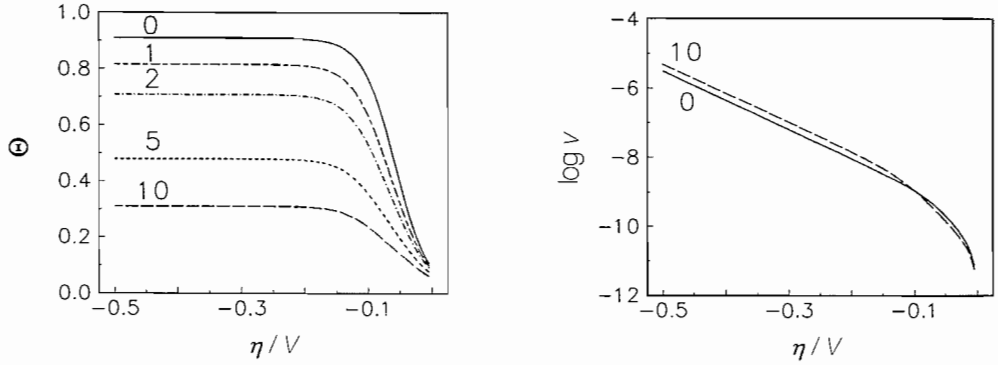


Fig. 6. Dependence of the parameter *g*, indicated in the graphs, on the surface coverage and the total rate of the HER; rate constants and transfer coefficients as in Fig. 2.



In the following simulations it was assumed that the centers, which have the highest hydrogen adsorption energy, also have the highest adsorption energy of organic molecules. This implies that the equilibrium constant K_R depends on the adsorption energy according to: $K_R = K^0_R \exp(-\Delta\Delta G^0_H/RT)$. The simulations were carried out for the Gaussian distribution of adsorption energies with flat distribution function, $\gamma = 10^{-6}$. Assuming $\Delta\Delta G^0_H/RT = \pm 10$, the equilibrium constant changes from 2.20×10^4 K^0_R to 4.54×10^{-5} K^0_R. Figure 8 presents the dependence of the surface coverage by adsorbed hydrogen and by organic molecules as functions of the overpotential. For reversible adsorption, an increase in the hydrogen adsorption at more negative potentials causes desorption of the organic compound. In the case of irreversible adsorption, Θ_R is constant and the adsorption of hydrogen changes with overpotential but remains low to satisfy eq. [20]. The current is only slightly lower at more negative potentials, at which the total reaction rate is given by:

$$[23] \quad v = 2k_1 e^{-\alpha_1 f\eta}(1 - \Theta_H - \Theta_R)$$

Can. J. Chem. Downloaded from www.nrcresearchpress.com by 91.121.58.235 on 09/08/12
For personal use only.

© 1997 NRC Canada

Fig. 7. Influence of the ratio k_1/k_2 on the surface coverage and total rate of the HER under the Frumkin isotherm; $g = 10$; other kinetic parameters as in Fig. 5.

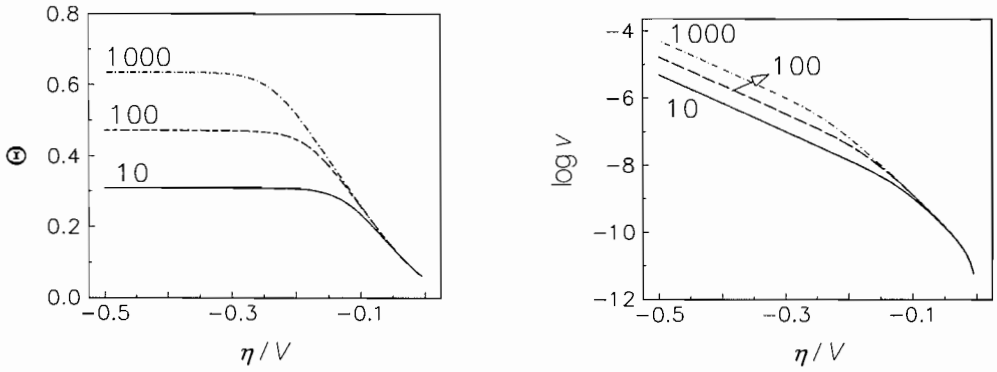
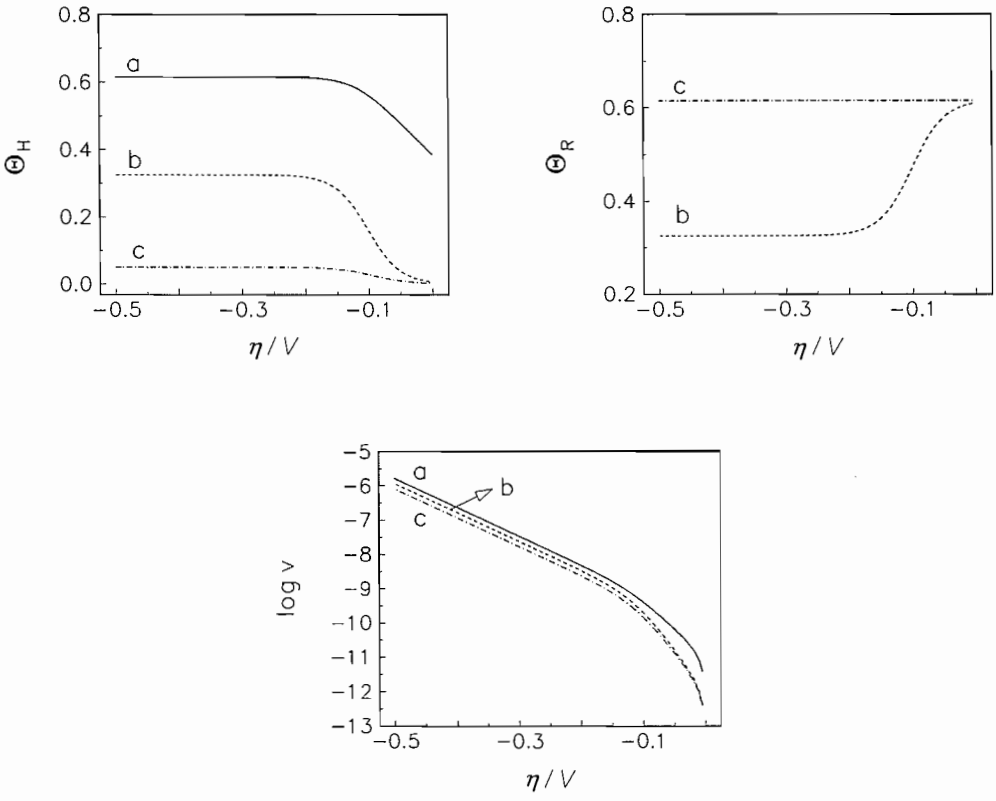


Fig. 8. Dependence of surface coverages and total current on overpotential for Gaussian distribution of adsorption energies: (*a*) in the absence of the adsorption of organic compound; (*b*) assuming reversible adsorption of H and R; (*c*) assuming irreversible adsorption of R; $K^0_R C_R = 10$, $k_1 = 10^{-9}$, $k_{-1} = 10^{-8}$, $k_2 = 10^{-10}$ mol cm^{-2} s^{-1}, $\Delta\Delta G^0_H/RT = \pm 10$, $\gamma = 10^{-6}$, $\alpha = \beta = 0.5$.



therefore the whole effect arises from changing $(1 - \Theta_H)$ to $(1 - \Theta_H - \Theta_R)$. It should be stressed that for some individual adsorption energies this effect is important, but for the flat dispersion of adsorption energies it is quite small. In fact, for the rate constants shown in Fig. 8 this parameter equals 0.385 in the absence of R, 0.350 for reversible, and 0.335 for irreversible adsorption of R. Similar curves for $k_1/k_2 = 1000$ and stronger adsorption of the organic compound, $K^0_R C_R = 100$, are presented in Fig. 9. It should be noticed that the Tafel slope at low overpotentials changes from 60 mV dec^{-1} in the absence of organic compound to 43 mV dec^{-1} in its presence, for the kinetic parameters given in Fig. 9. Because of the dispersion of the adsorption energies, the effect of adsorption of the organic compound on the observed current is smaller. For comparison, Tafel curves obtained in the absence of energy dispersion (in the presence and absence of R) are also included in Fig. 9.

Similar studies were carried out using the Frumkin isotherm. In this case an irreversible adsorption of the organic compound was assumed, that is, adsorbed organic molecules decreased only the available surface area, without affecting other parameters. Examples of the Tafel curves in the absence

Can. J. Chem. Downloaded from www.nrcresearchpress.com by 91.121.58.235 on 09/08/12
For personal use only.

© 1997 NRC Canada

Fig. 9. Dependence of surface coverages and total current on overpotential for Gaussian distribution of adsorption energies: (*a*) in the absence of the adsorption of organic compound; (*b*) assuming reversible adsorption of H and R; (*c*) assuming irreversible adsorption of R; (*d*) assuming nondistributed rate constants in the absence of R; (*e*) assuming nondistributed rate constants in the presence of irreversible adsorption of R; $K^0_R C_R = 100$, $k_1 = 10^{-7}$, $k_{-1} = 10^{-6}$, $k_2 = 10^{-10}$ mol cm^{-2} s^{-1}; other parameters as in Fig. 8.

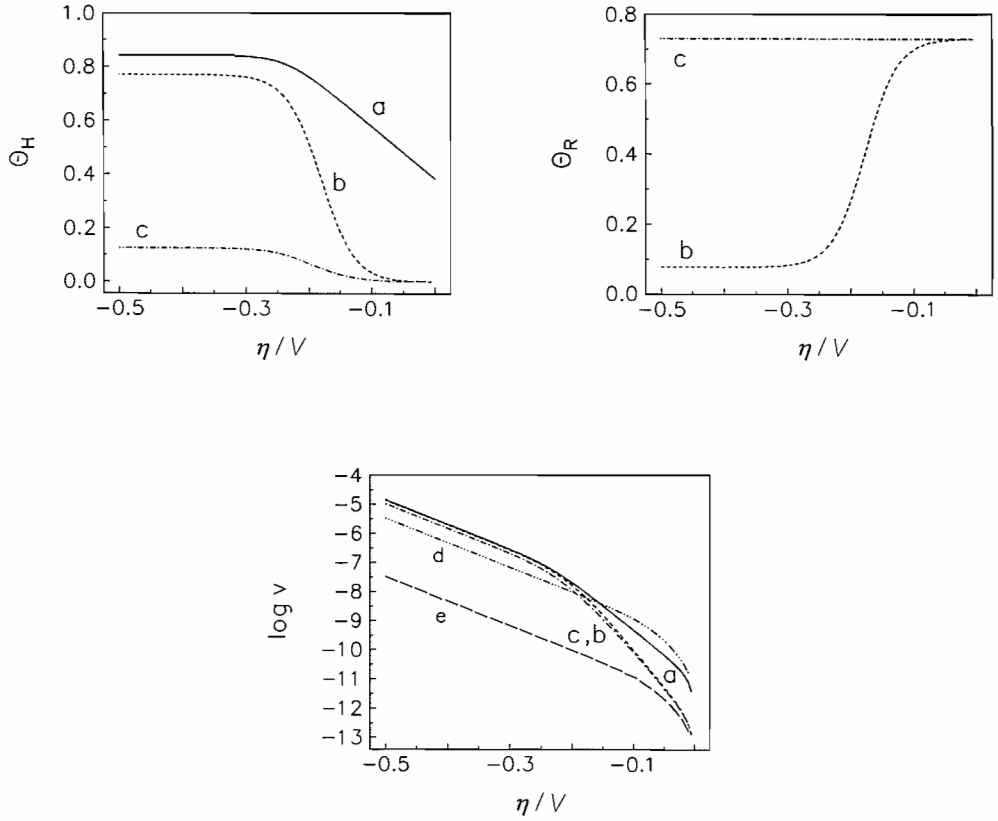
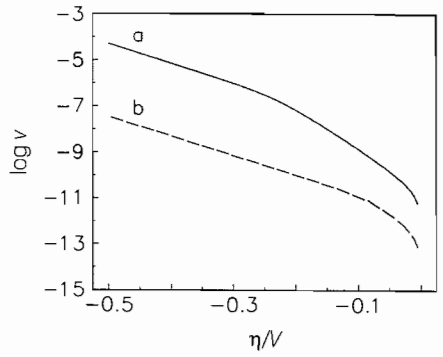


Fig. 10. Tafel curves for the HER using the Frumkin isotherm: (*a*) without organic compound; (*b*) in the presence of organic compound. Parameters used: $k_1 = 10^{-7}$, $k_{-1} = 10^{-6}$, $k_2 = 10^{-10}$ mol cm^{-2} s^{-1}, $K^0_R C_R = 100$, $g = 10$.



and in the presence of organic compounds are shown in Fig. 10. In the presence of the adsorption of the organic compound only one Tafel slope of 118 mV dec^{-1} is observed over the whole potential range. In this case of strong adsorption of the poison, the surface coverage by adsorbed hydrogen decreases significantly and the exponential term $\exp(g\Theta_H)$ in eq. [17] is negligible. Therefore the observed behavior is similar to the Langmuir isotherm.

It should be added that similar results were obtained for more realistic values of the γ parameter (e.g., $\gamma = 0.1$), but with further increase of γ the potential range, where low Tafel slopes were observed, decreased. Some more complex interactions are also possible, including repulsion forces between adsorbed H and R and (or) R and R, changes in the adsorption energy of H induced by adsorption of R, changes of symmetry coefficients α_i and β_i, etc. They also affect the observed Tafel slopes.

Discussion

Heterogeneity of the surface leads to the distribution of the adsorption energies. A model, including distribution of adsorption energies, leading to the distributed kinetics was applied to the hydrogen adsorption during the HER. Surface heterogeneity strongly affects the surface coverage by adsorbed hydrogen; however, this parameter cannot be directly measured (34, 35). Its effect on the observed currents depends on the values of the rate constants of the Volmer and Heyrovsky reactions. First, our simulations were carried out assuming the Langmuir adsorption isotherm. When the ratio $k_1/k_2 \leq 10$, only a small change in the slope is observed at low overpotentials. At higher overpotentials, for all cases studied, i.e., different kinetic and energy distribution parameters and different adsorption isotherms, the Tafel slope always equals that theoretically predicted for the Volmer–Heyrovsky mech-

© 1997 NRC Canada

Can. J. Chem. Downloaded from www.nrcresearchpress.com by 91.121.58.235 on 09/08/12
For personal use only.

anism without distribution, that is, $RT \ln 10 / 0.5F = 118$ mV dec^{-1} (at 25°C). Lower slopes of 42–60 mV dec^{-1} are observed only when the surface coverage changes with overpotential, that is, at low overpotentials. At low overpotentials, for low values of parameter γ, the adsorption of hydrogen is linear with overpotential, which is equivalent to the Temkin isotherm (28).

When the ratio k_1/k_2 increases, the potential range where low Tafel slopes are observed increases, especially for low values of the distribution parameter γ. Such slopes were observed experimentally for the HER on Ni–Zn electrodes in alkaline solutions. However, for the same kinetic parameters and $\gamma \rightarrow \infty$ (i.e., without adsorption-free energy distribution) only one Tafel slope of 118 mV dec^{-1} is observed.

Similar effects were found for the Frumkin adsorption isotherm with positive values of the parameter g; with an increase in the ratio of k_1/k_2, the potential range in which low Tafel slopes (~56 mV dec^{-1}) are observed increased.

In the case of the distributed kinetics, adsorption of organic compounds has a large effect on the surface coverage by adsorbed hydrogen but a much smaller effect on the observed currents, even for relatively strong adsorption (large $K_R C_R$). Because of the distribution of adsorption energies, values of the adsorption equilibrium constant vary from very small to very large, and the portion of the surface to which the very large values apply is limited. In addition, at negative overpotentials, the current depends on k_1 and a free surface unoccupied by H and R, eq. [23]. For large ratios of k_1/k_2 the surface coverage by adsorbed hydrogen is large ($\Theta_H \rightarrow 1$) and the free surface $1 - \Theta_H - \Theta_R$ does not change significantly with $K_R C_R$. It should be mentioned that in the presence of adsorption of foreign compounds the Tafel slope changes from ~60 to ~43 mV dec^{-1}.

In the case of the Frumkin adsorption isotherm, adsorption of R causes a change in the Tafel slope and only one slope of 118 mV dec^{-1} was observed. This behavior is related to a strong decrease of the surface coverage by adsorbed hydrogen and, consequently, change of the isotherm from Frumkin to Langmuir (at low coverages they are identical). Moreover, the observed HER current is reduced. Such behavior was earlier observed experimentally (20, 21).

The above simulations were carried out for a simple case of the Gaussian or exponential distributions of adsorption energies and $\alpha_i = \beta_i = 0.5$. For real electrodes the distribution function may vary from that theoretically assumed. In fact, in the case of physical adsorption, more complex distribution functions have been found experimentally (8, 9). Nevertheless, the distributed energy model predicts current–overpotential curves similar to those found experimentally and explains the influence of the adsorption of foreign substances on these curves.

Acknowledgment

The financial support of the Natural Sciences and Engineering Research Council of Canada (NSERC) is gratefully acknowledged.

References

1. M. Jaroniec and R. Madey. Physical adsorption on heterogeneous solids. Elsevier, Amsterdam. 1988.
2. W. Rudzinski and D.H. Everett. Adsorption of gases on heterogeneous surfaces. Academic Press, London. 1992.
3. S. Ross and J.P. Olivier. On physical adsorption. Interscience, New York. 1964.
4. A.W. Adamson and I. Ling. *In* Solid surfaces and the gas–solid interface. Trans. Symp. Honoring S. Brunauer. Division of Colloid and Surface Chemistry. 139th Meeting of the American Chemical Society, St. Louis, Mo. March 1961. Adv. Chem. Ser. **33**, 51 (1961).
5. C.F. Cerofloni. Thin Solid Films, **23**, 129 (1974).
6. W.A. House. J. Colloid Interface Sci. **67**, 166 (1978).
7. K.F. Scott. J. Chem. Soc. Faraday Trans. 1, **76**, 2065 (1980).
8. B. Hunger, M. Heuchel, S. Matysik, K. Beck, and W.D. Einicke. Thermochim. Acta, **269/270**, 599 (1995).
9. M. Heuchel, M. Jaroneic, R.K. Gilpin, P. Bräuer, aned M. v. Szombathely. Langmuir, **9**, 2537 (1993).
10. P. Nikitas. Electrochim. Acta, **33**, 647 (1988).
11. P. Nikitas and A. Papqutsis. Electrochim. Acta, **33**, 683 (1988).
12. W.J. Albery, P.N. Bartlett, C.P. Wilde, and J.R. Darwent. J. Am. Chem. Soc. **107**, 1854 (1985).
13. W.J. Albery, M.G. Boutelle, P.J. Colby, and A.R. Hillman. J. Electroanal. Chem. **133**, 135 (1982).
14. G.K. Rowe, M.T. Carter, J.N. Richardson, and R.W. Murray. Langmuir, **11**, 1797 (1995).
15. M.R. Gennero de Chialvo and A.C. Chialvo. J. Electroanal. Chem. **372**, 209 (1994).
16. M.R. Gennero de Chialvo and A.C. Chialvo. J. Electroanal. Chem. **388**, 215 (1995).
17. S. Rausch and H. Wendt. J. Appl. Electrochem. **22**, 1025 (1992).
18. S. Rausch and H. Wendt. J. Electrochem. Soc. **143**, 2852 (1996).
19. L. Chen and A. Lasia. J. Electrochem. Soc. **138**, 3321 (1991).
20. L. Chen and A. Lasia. J. Electrochem. Soc. **139**, 1058 (1992).
21. A.C.D. Angelo and A. Lasia. J. Electrochem. Soc. **142**, 3313 (1995).
22. A. Lasia. J. Electroanal. Chem. **428**, 155 (1997).
23. B.E. Conway and G. Jerkiewicz. J. Electroanal. Chem. **357**, 47 (1993).
24. G. Jerkiewicz, J.J. Borodzinski, W. Chrzanowski, and B.E. Conway. Proc. Electrochem. Mater. Sci. Cathodic Hydrogen Absorpt. Adsorpt. *In* Proc. – Electrochem. Soc. **94-32**, 44 (1994).
25. G. Jerkiewicz, J.J. Borodzinski, W. Chrzanowski, and B.E. Conway. J. Electrochem. Soc. **142**, 3755 (1995).
26. R. Parsons. Trans. Faraday Soc. **54**, 1053 (1958).
27. I. Langmuir. J. Am. Chem. Soc. **40**, 1361 (1918).
28. E. Gileadi and B.E. Conway. Mod. Aspects Electrochem. **3**, 347 (1964).
29. A. Saraby-Reintjes. J. Chem. Soc. Faraday Trans. 1, **83**, 271 (1987).
30. J. Divisek. J. Electroanal. Chem. **214**, 615 (1986).
31. D.A. Harrington and B.E. Conway. J. Electroanal. Chem. **221**, 1 (1987).
32. A. Lasia and A. Rami. J. Electroanal. Chem. **294**, 123 (1990).
33. J. O'M. Bockris and S.U.M. Khan. Surface electrochemistry. Plenum Press, New York. 1993. p. 200.
34. A. Lasia. Curr. Top. Electrochem. **2**, 239 (1993).
35. A. Lasia. Pol. J. Chem. **69**, 639 (1995).

Can. J. Chem. Downloaded from www.nrcresearchpress.com by 91.121.58.235 on 09/08/12
For personal use only.

© 1997 NRC Canada

The role of crystal imperfections in electrochemical phase formation and growth

G. Staikov and W.J. Lorenz

Abstract: The role of different crystal imperfections and surface inhomogeneities in the processes of electrochemical phase formation and crystal growth is discussed on the basis of experimental results obtained by electrodeposition of metals on native and foreign single crystal substrates in selected model systems. The major role of screw dislocations in the electrochemical growth of real crystals is demonstrated in the case of silver electrodeposition on silver single crystal faces prepared by the so-called capillary technique. Experimental results show that the electrochemical spiral growth of silver crystal faces with low dislocation density can be used for a preparation of surfaces with a defined and uniform density of monatomic steps. Combined electrochemical and in situ scanning probe microscopy (SPM) studies of underpotential deposition (UPD) of metals on foreign single crystal substrates show that surface inhomogeneities induce a stepwise formation of different low-dimensional (0D, 1D, and 2D) metal phases. The thermodynamic, kinetic, and structural aspects of the stepwise formation of Me phases of different dimensionality in the UPD range are discussed on an atomic level using results of electrochemical and in situ SPM measurements in various systems.

Key words: electrocrystallization, screw dislocations, spiral growth, surface inhomogeneities, underpotential deposition, low-dimensional phases, scanning tunneling microscopy.

Résumé : Se basant sur les résultats expérimentaux obtenus par électrodéposition de métaux sur des substrats constitués de cristal unique naissant et étranger, on discute du rôle des différentes imperfections du cristal et de l'inhomogénéité des surfaces lors de la formation et de la croissance des cristaux. On a mis en évidence le rôle prépondérant des dislocations hélicoïdales dans la croissance électrochimique de vrais cristaux dans le cas de l'électrodéposition de l'argent sur les faces d'un cristal unique d'argent préparé par la technique dite capillaire. Les résultats expérimentaux montrent que l'on peut faire appel à la croissance électrochimique en spirale des faces du cristal d'argent avec de faibles densités de dislocations pour la préparation des surfaces avec une densité définie et uniforme d'étapes monoatomiques. Des études combinées de microscopie de sonde à balayage «SPM» in situ et électrochimique du dépôt de métaux à faibles potentiels «UPD» sur des substrats de cristaux uniques étrangers ont permis de montrer que les inhomogénéités superficielles induisent une formation par étapes de différentes phases métalliques de faible dimension (0D, 1D et 2D). En se basant sur les résultats électrochimiques et des mesures in situ de «SPM» dans divers systèmes, on discute à un niveau atomique des aspects thermodynamiques, cinétiques et structuraux de la formation par étapes de phases Me de dimensions différentes dans le domaine du dépôt à de faibles potentiels.

Mots clés : électrocristallisation, dislocations hélicoïdales, croissance en spirale, inhomogénéités superficielles, dépôt à de faibles potentiels, phases de faibles dimensions, microscopie à balayage de l'effet tunnel.

[Traduit par la rédaction]

Introduction

Real crystals are always imperfect in some respect and exhibit various structural imperfections of different dimensionality:

0D or point imperfections (atomic disorder, chemical impurities, etc.),

1D or line imperfections (edge and screw dislocations, etc.),

2D or planar imperfections (grain or subgrain boundaries, stacking faults, etc.),

3D or volume imperfections (crystal domains with different chemical and (or) physical properties).

The crystal surface, which can also be considered as a 2D crystal imperfection, plays an important role in the processes of phase formation and crystal growth. The structure and homogeneity of a crystalline surface depend strongly on the structure and perfection of the corresponding bulk crystal and on the surface treatment used. Generally the following surface inhomogeneities can be distinguished:

0D inhomogeneities (kinks, adatoms, vacancies, chemical impurities, emergence points of edge and screw dislocations, etc.),

1D inhomogeneities (monatomic steps, intersection lines of grain or subgrain boundaries, and stacking faults, etc.),

2D inhomogeneities (reconstructed surface domains, 2D islands and pits, surface domains or terraces with different chemical and (or) physical properties).

Received March 18, 1997.

This paper is dedicated to Professor Brian E. Conway on the occasion of his 70th birthday.

G. Staikov and W.J. Lorenz.[1] Institute of Physical Chemistry and Electrochemistry, University of Karlsruhe, Kaiserstr. 12, D-76131 Karlsruhe, Germany.

[1] Author to whom correspondence may be addressed. Telephone: 0049-721-6083303. Fax: 0049-721-6082917. E-mail: wolfgang.lorenz@chemie.uni-karlsruhe.de

© 1997 NRC Canada

Can. J. Chem. Downloaded from www.nrcresearchpress.com by 91.121.58.235 on 09/08/12
For personal use only.

Can. J. Chem. Downloaded from www.nrcresearchpress.com by 91.121.58.235 on 09/08/12
For personal use only.

Fig. 1. In situ STM image of an electrochemically polished Au(111) surface in the system Au(111)/5×10^{-3} M $AgClO_4$ + 5×10^{-1} M $HClO_4$ at T = 298 K and ΔE = 200 mV.

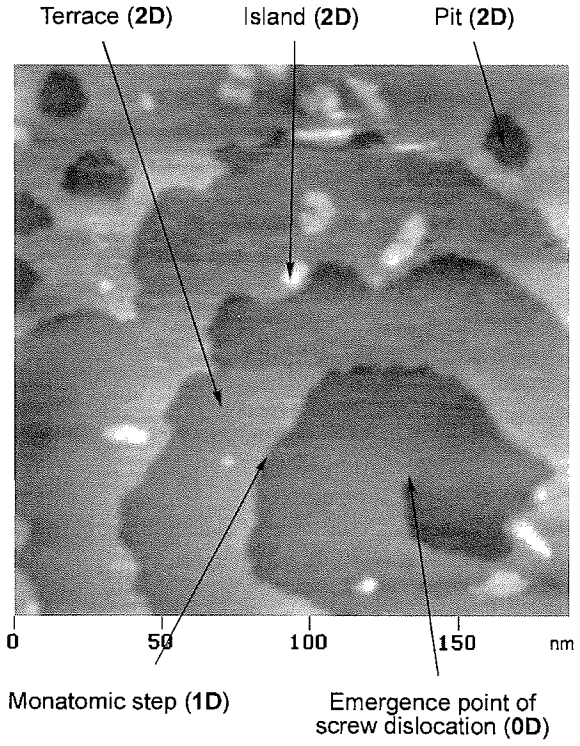


Fig. 2. In situ STM image with lateral atomic resolution of an atomically flat Ag(111) terrace in the system Ag(111)/10^{-2} M $HClO_4$ at T = 298 K and E_H = 350 mV.

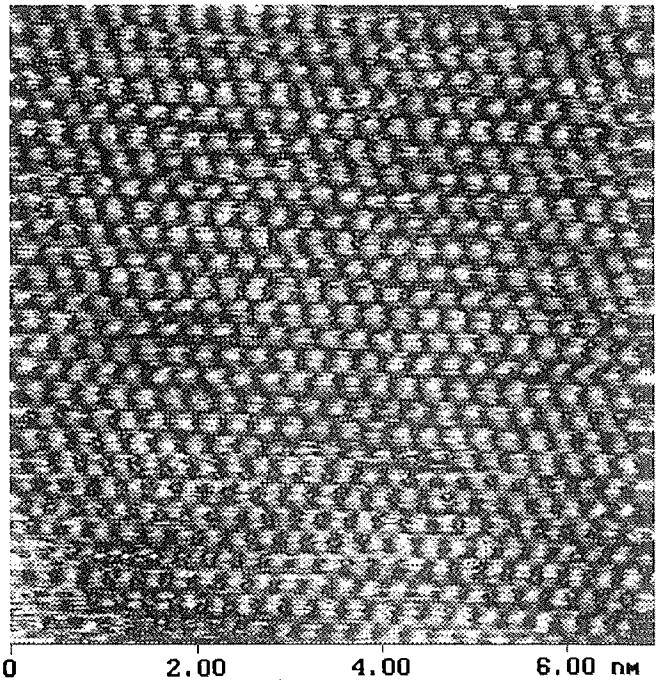
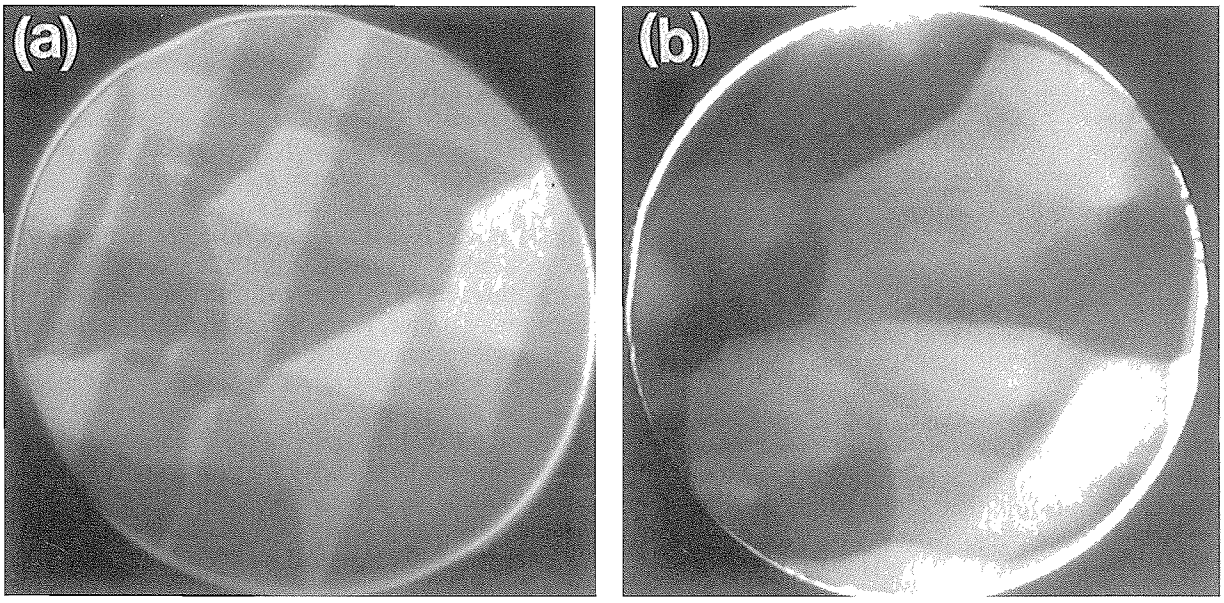


Fig. 3. Morphology of electrochemically growing Ag(100) crystal faces in the systems: (*a*) Ag(100)/6M $AgNO_3$ (aq) at T = 318 K; (*b*) Ag(100)/$AgNO_3$ (melt) at T = 573 K. Face area $A = 2 \times 10^{-3}$ cm^2.

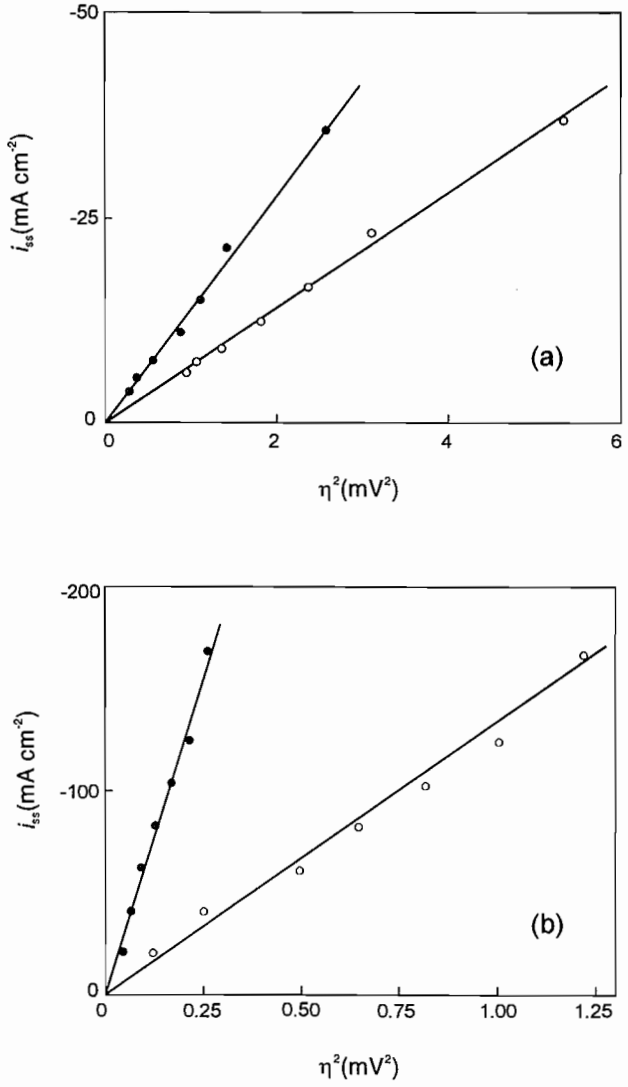


The heterogeneity of a real crystal surface can be well characterized on a nanometer scale by in situ scanning probe microscopy (SPM) techniques such as scanning tunneling microscopy (STM) and atomic force microscopy (AFM). Emergence points of screw dislocations, monatomic steps separated by atomically flat terraces, 2D islands and pits, etc. can be directly observed under defined electrochemical conditions as illustrated in Fig. 1. In addition, in situ SPM imaging with lateral atomic resolution provides important information about the local atomic structure of crystalline surfaces (Fig. 2).

© 1997 NRC Canada

Can. J. Chem. Downloaded from www.nrcresearchpress.com by 91.121.58.235 on 09/08/12
For personal use only.

Fig. 4. Steady state current density – overpotential dependencies obtained by a spiral growth of Ag(111) and Ag(100) crystal faces in the systems: (*a*) Ag(*hkl*)/6M $AgNO_3$ (aq) at $T = 318$ K; (*b*) Ag(*hkl*)/$AgNO_3$ (melt) at $T = 573$ K. (*hkl*) = (111) (●); (100) (○).



The introduction of SPM techniques in electrochemistry opened a new window not only for the characterization of solid surfaces but also for studies of electrochemical phase formation on an atomic level.

The aim of this paper is to discuss the role of crystal imperfections and surface inhomogeneities in the processes of electrochemical phase formation and crystal growth on the basis of experimental results obtained by electrodeposition of metals on native and foreign single crystal substrates.

Formation of three-dimensional Me phases on native substrates induced by surface inhomogeneities

The growth of a crystal from an ambient phase takes place at supersaturation by incorporation of crystal building units in kink site positions. At undersaturation the 3D bulk crystal phase becomes unstable and dissolves.

In the case of electrochemical growth and dissolution of a metal crystal (1), i.e. electrochemical deposition and dissolution of a metal (Me) on native substrate (S = Me), the stability limit of the 3D Me bulk crystal phase is given by the Nernst equilibrium potential, $E_{3D\,Me}$:

$$[1] \quad E_{3D\,Me} = E^0_{3D\,Me} + \frac{RT}{zF} \ln\left(\frac{a_{Me^{z+}}}{a_{3D\,Me}}\right)$$

where $E^0_{3D\,Me}$ denotes the standard potential of the bulk Me phase, $a_{Me^{z+}}$ is the activity of Me^{z+} ions in the electrolyte phase, $a_{3D\,Me}$ and represents the activity of the 3D Me bulk phase, which is related to the activity of a Me atom in a kink site position. For a pure 3D Me bulk phase, $a_{3D\,Me}$ is equal to unity .

Assuming that charge transfer, diffusion, and chemical reactions of Me^{z+} are fast processes (i.e., do not determine the rate of crystal growth and dissolution), the supersaturation ($\Delta\mu > 0$) and undersaturation ($\Delta\mu < 0$) with respect to the 3D Me bulk crystal can be defined by the difference between the actual electrode potential, E, and the equilibrium potential, $E_{3D\,Me}$:

$$[2] \quad \Delta\mu^{def} = -zF(E - E_{3D\,Me}) = -zF\eta$$

where $\eta = E - E_{3D\,Me} < 0$ and $\eta = E - E_{3D\,Me} > 0$ represent the cathodic and anodic overpotential, respectively.

Crystal imperfections and surface inhomogeneities influence significantly the kinetics and mechanism of crystal growth and dissolution. As shown by Frank (2), screw dislocations are the most important crystal defects playing a major role in the growth of real crystal faces. Due to the helicoidal structure of this 1D crystal imperfection, a step originates from the point where the screw dislocation line intersects the crystal face. This step is constrained to terminate at the dislocation emergence point and winds up into a spiral during the growth process. The spiral step can never disappear and the crystal face grows perpetually, even at relatively low supersaturations, without the need of a 2D nucleation.

Screw dislocations are also active in crystal dissolution (cf. Fig. 1). For a given dislocation, however, the sense of the dissolution spiral is opposite to that of the corresponding growth spiral. Spirals are polygonized if the propagation rate of the steps is anisotropic. Formation of absolutely polygonized spirals, however, can only be expected at very low temperature. At room temperature spiral steps are usually curved on a nanometer scale (cf. Fig. 1). The height of spiral steps is related to the Burgers vector of the screw dislocation. In metal crystals the modulus of the Burgers vector usually does not exceed atomic dimensions, so that single screw dislocations produce monatomic steps (cf. Fig. 1).

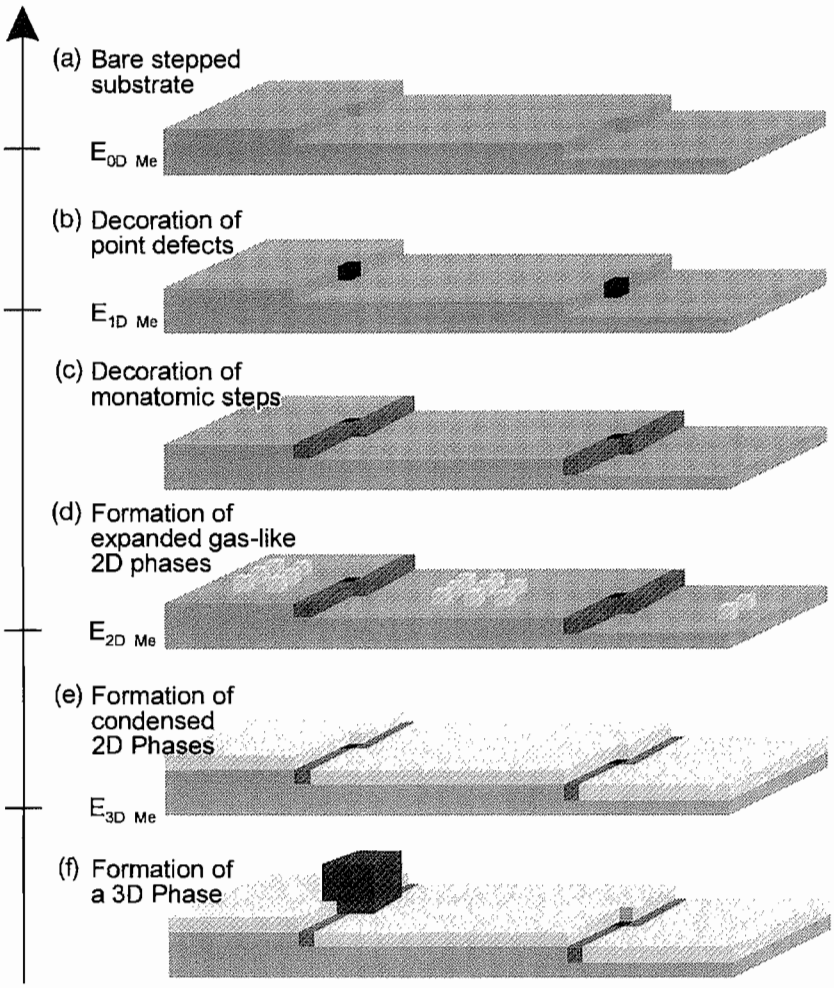
According to the theory of spiral growth (1, 3–5), the steady state distance, d_S, between monatomic spiral steps generated by a single screw dislocation is given by

$$[3] \quad d_S(\eta) = 19\rho_{crit}(\eta) = \frac{19\varepsilon}{q_{mon}|\eta|}$$

where $\rho_{crit}(\eta)$ is the radius of the circle inscribed into the geometrical form of the 2D nucleus, ε is the specific edge energy

© 1997 NRC Canada

Fig. 5. Stepwise formation of Me phases of different dimensionally in the UPD and OPD ranges and the corresponding stability ranges indicated by E_{iD}.



of monatomic steps, q_{mon} is the charge density for deposition of a monolayer, and η is the overpotential.

Real crystal faces are usually intersected by more than one screw dislocation. If these dislocations are separated by a distance much larger than the size of the 2D nucleus, they operate independently of each other and d_S is given by eq. [3]. The problem becomes more complex if the emergence points of screw dislocations are located at distances comparable to the size of the 2D nucleus (1, 3).

Two screw dislocations of opposite sign produce at equilibrium only one step, which connects both emergence points of the dislocations. If the distance between emergence points is smaller than the size of the 2D nucleus, the step is not active and cannot grow at the given overpotential. If this distance, however, is larger than the size of the 2D nucleus, the screw dislocation pair produces loops of steps.

A group of n screw dislocations of the same sign that are closer than the size of the 2D nucleus generate n non-intersecting spirals. The resultant activity of such a screw dislocation group is approximately n times that of a single screw dislocation.

Circular or polygonized spirals or loops of steps with a monatomic height, h_{mon}, appear macroscopically as low cones or pyramids with a slope $\tan(\alpha) = (h_{mon}/d_S)$. The corresponding steady state current density, $i_{ss}(\eta)$, is given by (1)

$$[4] \quad i_{ss}(\eta) = - q_{mon}\, \nu(\eta)\, d_S^{-1}(\eta)$$

where $\nu(\eta)$ is the step propagation rate and $d_S^{-1}(\eta) = L_S(\eta)$ represents the step density.

For low cathodic overpotentials and a crystal face intersected by well-separated single screw dislocations from eqs. [3] and [4] follows

$$[5] \quad i_{ss}(\eta) = - \frac{q_{mon}^2\, \kappa_\nu}{19\varepsilon}\, \eta^2$$

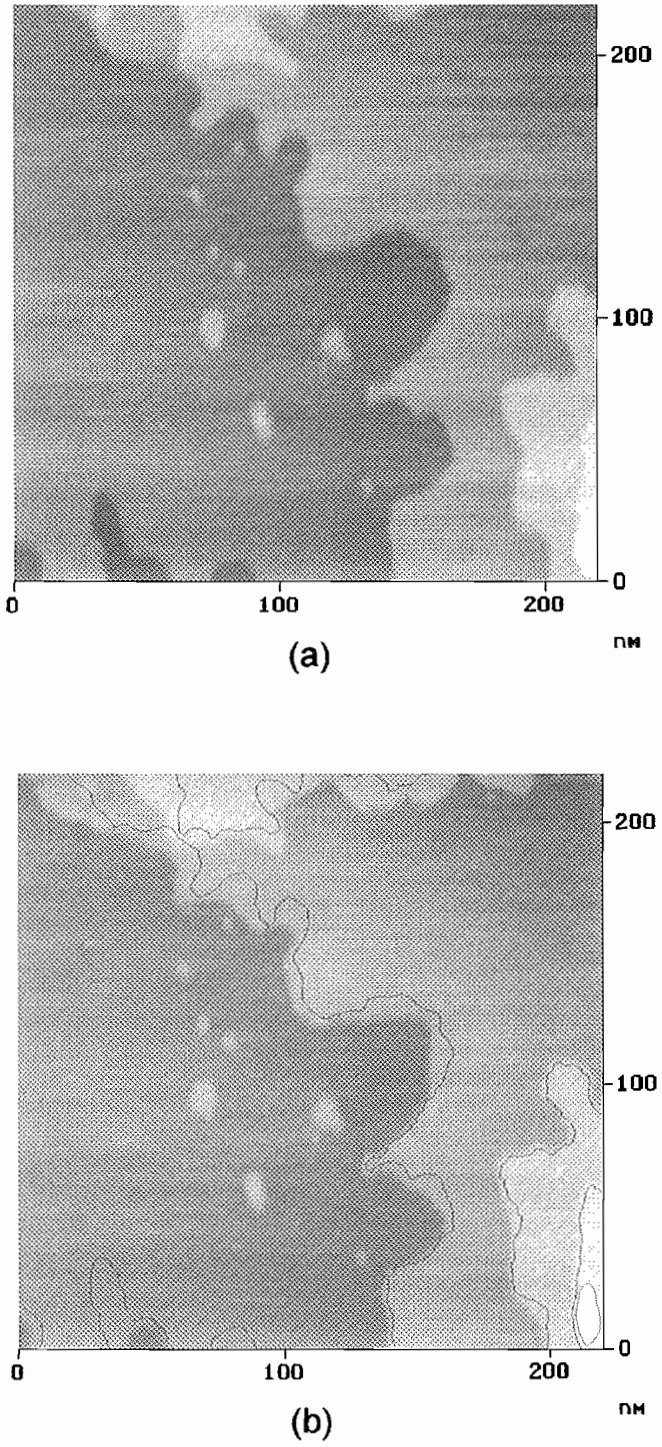
where $\kappa_\nu = \nu(\eta)/|\eta|$ represents the propagation rate constant of monatomic steps, which is related to the exchange current density (1).

Well-defined and relatively simple conditions for an experimental investigation of the spiral growth mechanism offer silver single crystal faces prepared by the so-called capillary technique (1, 6–13). Such crystal faces have an extremely low crystal imperfection density and are usually intersected by only a few screw dislocations. Using this capillary technique,

© 1997 NRC Canada

Can. J. Chem. Downloaded from www.nrcresearchpress.com by 91.121.58.235 on 09/08/12
For personal use only.

Fig. 6. In situ STM images showing a decoration of monatomic steps in the system Ag(100)/5 × 10^{-3} M $Pb(ClO_4)_2$ + 10^{-2} M $HClO_4$ at T = 298 K. (*a*) Stepped bare Ag(100) substrate at ΔE = 300 mV; (*b*) decorated monatomic steps at ΔE = 300 mV (lines indicate the location of step edges in (*a*).



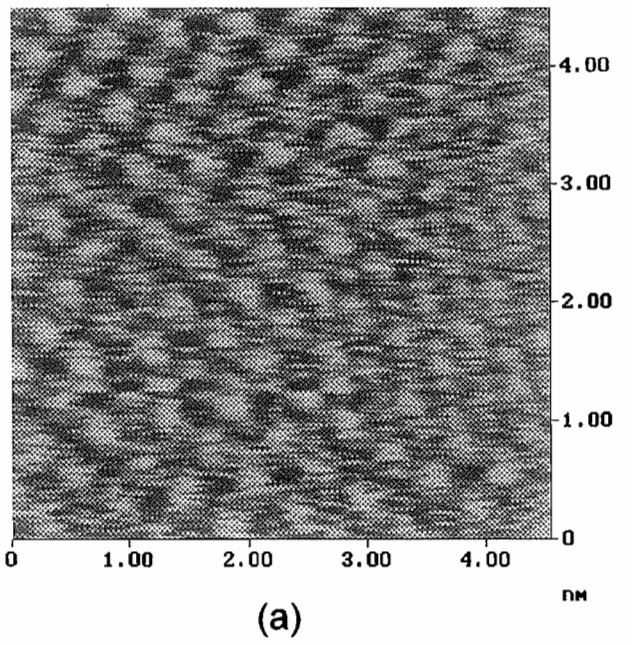
Can. J. Chem. Downloaded from www.nrcresearchpress.com by 91.121.58.235 on 09/08/12
For personal use only.

both the morphology and kinetics of electrochemical growth of Ag(100) and Ag(111) faces have been studied in a 6 M $AgNO_3$ aqueous solution at T =318 K and in a $AgNO_3$ melt at T = 573 K (1, 9–11). As an example, Fig. 3 shows growing pyramids and cones with a uniform slope as observed by the electrochemical spiral growth of Ag(100) faces in 6 M $AgNO_3$ aqueous solution and $AgNO_3$ melt, respectively. Due to the elevated temperature in the second case (Fig. 3*b*) the propagation rate of monatomic steps becomes isotropic and leads to formation of low cones. Parabolic $i_{ss} - \eta^2$ dependencies have been found experimentally in both systems in good agreement with eq. [5] (Fig. 4). From experimental results the values of

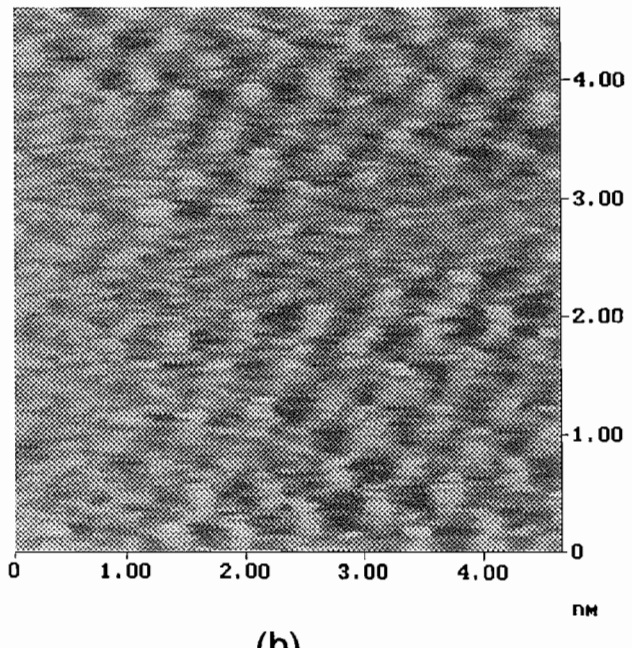
© 1997 NRC Canada

Can. J. Chem. Downloaded from www.nrcresearchpress.com by 91.121.58.235 on 09/08/12
For personal use only.

Fig. 7. In situ STM images of 2D Ag(100)–c(2 × 2) Pb and Au(100)–c(2 × 2) Pb domains in the systems: (*a*) Ag(100)/5 × 10^{-3} M $Pb(ClO_4)_2$ + 10^{-2} M $HClO_4$ at T = 298 K and ΔE = 175 mV; (*b*) Au(100)/5 × 10^{-3} M $Pb(ClO_4)_2$ + 10^{-2} M $HClO_4$ at T = 298 K and ΔE = 550 mV.



(a)



(b)

the specific edge energy ε and (or) the density of monatomic steps $L_S(\eta)$ can be determined (1, 9–11). In this way stepped silver crystal faces with a regular step spacing and an exactly known step density can be prepared by electrochemical growth at constant overpotential η. Such crystal faces can successfully be used as substrates in various studies related to the influence of surface inhomogeneities on different electrochemical processes (1, 14–18).

Formation of low-dimensional Me phases on foreign substrates induced by surface inhomogeneities

The first step of electrodeposition of a metal (Me) on a foreign substrate (S ≠ Me) is the formation of isolated Me adatoms (Me_{ads}). If the binding energy of Me_{ads} on a more noble foreign substrate is higher than that on the native substrate, a phase formation process starts even at undersaturations with respect to the 3D Me bulk phase. This phenomenon is known as underpotential deposition (UPD) of metals (1). The undersaturation range is denoted by convention as underpotential range $\Delta E = E - E_{3D\,Me} > 0$.

Metal UPD processes can be strongly influenced by cosorption or competitive adsorption of electrolyte constituents such as anions. Such sorption processes accompanying Me UPD can be quantitatively characterized by the electrosorption valency defined by $\gamma = F^{-1}(\partial q/\partial\Gamma)_E = F^{-1}(\partial\mu/\partial E)_\Gamma$, where q and Γ denote the charge density and the Me surface coverage, respectively, and μ represents the chemical potential of Me^{z+} in the electrolyte. The elctrosorption valency can be directly measured, for example, by different thin-layer techniques as described in detail elsewhere (1).

However, for all Me UPD systems discussed in this paper, the electrosorption valency was found to be $\gamma = z$ by Twin-Electrode Thin-Layer (TTL) measurements. Consequently, cosorption and competitive adsorption phenomena of anions can be excluded for the systems under test (1).

Electrochemical and in situ SPM studies of UPD of metals on real single crystal substrates show that different substrate surface inhomogeneities play an important role in this process, leading to formation of different Me phases with lower dimensionality (1, 19–21).

Generally, surface inhomogeneities are characterized by significant differences of the adatom binding energy and can induce formation of low-dimensional (0D, 1D, and 2D) Me phases with different energetics and structure in well-separated underpotential ranges. The condition for such stepwise phase formation process can be expressed by

$$[6]\quad \Psi_{Me_{ads}-S_{0D}} \gg \Psi_{Me_{ads}-S_{1D}} \gg \Psi_{Me_{ads}-S_{2D}} \gg \Psi_{Me_{ads}-Me}$$

where $\Psi_{Me_{ads}-S_{iD}}$ (i = 0, 1, 2) denotes the binding energy of a Me_{ads} on an iD surface inhomogeneity of the foreign substrate S and $\Psi_{Me_{ads}-Me}$ represents the binding energy of a Me adatom on native substrate.

The stability ranges of iD Me phases can be described by Nernst-type equations:

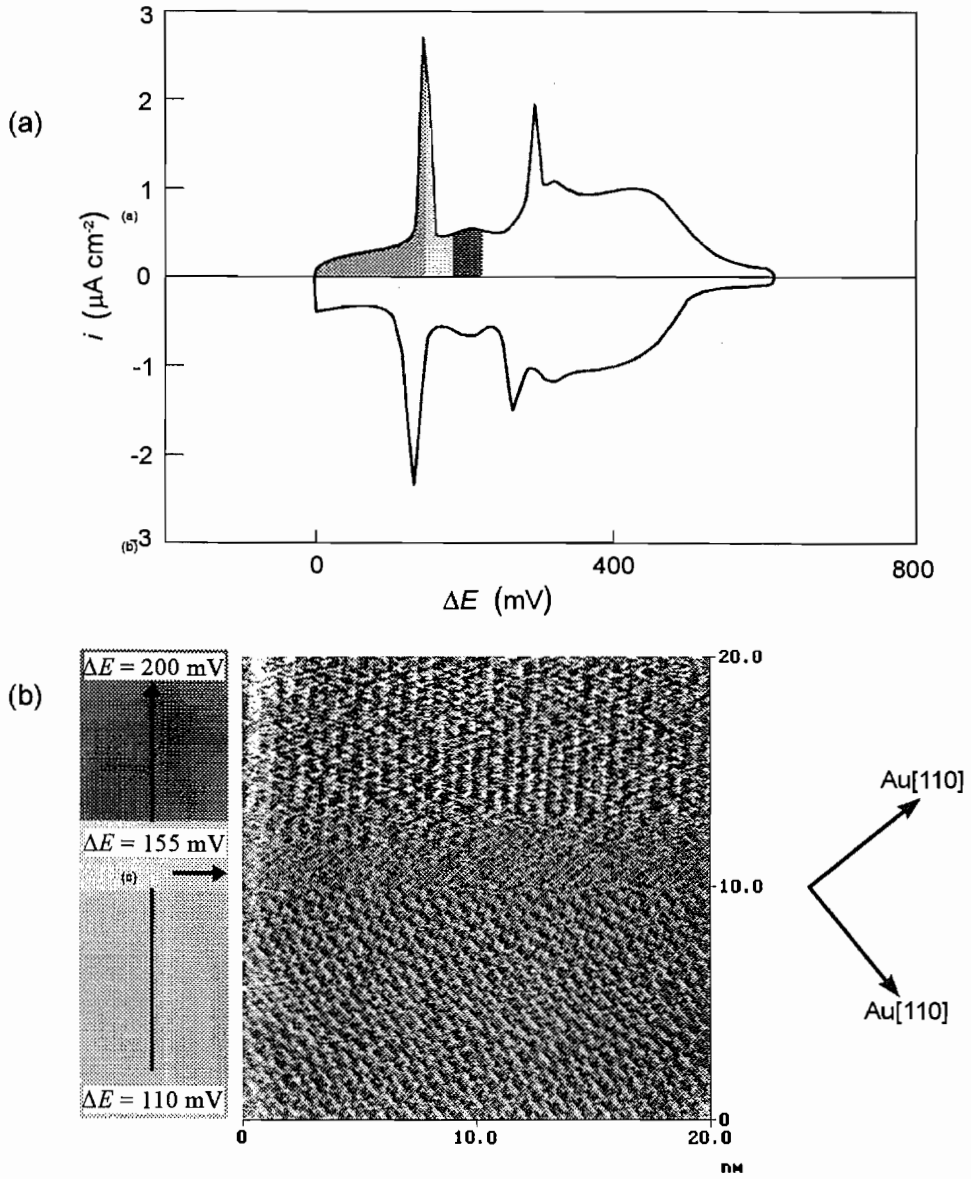
$$[7]\quad E_{i\mathrm{D\,Me}} = E^0_{i\mathrm{D\,Me}} + \frac{RT}{zF}\ln\left(\frac{a_{Me^{z+}}}{a_{i\mathrm{D\,Me}}}\right) \qquad \text{with } i = 0,1,2$$

where $a_{i\mathrm{D\,Me}}$ is a constant for condensed iD Me phases and $E_{i\mathrm{D\,Me}}$ represents the corresponding equilibrium potential. The supersaturation and the undersaturation with respect to a condensed iD Me phase are defined by:

$$[8]\quad \Delta\mu^{\mathrm{def}} = -zF(E - E_{i\mathrm{D\,Me}})$$

© 1997 NRC Canada

Fig. 8. First-order phase transformation in the system Au(100)/5 × 10^{-3} M $Pb(ClO_4)_2$ + 10^{-2} M $HClO_4$ at T = 298 K. (*a*) Cyclic voltammogram at a scan rate 10 mV s^{-1}; (*b*) in situ STM image during an anodic potential sweep from ΔE = 110 mV to ΔE = 200 mV. A condensed 2D hcp Pb phase showing an Au(100)–c(6 × 2) Pb moiré superstructure is imaged at ΔE < 155 mV in the lower part of this image. At ΔE > 170 mV the upper part of the STM image shows an expanded 2D Pb phase with an Au(100)–2c($3\sqrt{2} \times \sqrt{2}$) Pb R 45° superstructure. In the intermediate part of this STM image, the Au(100) substrate appears, indicating a very mobile Pb UPD adlayer.



For expanded *i*D Me phases formed by a continuous adsorption process (without first-order phase transition), $a_{i\mathrm{D\ Me}}$ becomes a function of $E_{i\mathrm{D\ Me}}$ at constant $\mu_{Me^{z+}}$, and eq. [7] represents the corresponding adsorption isotherm.

The stepwise formation of low-dimensional Me phases on a stepped substrate in the UPD range is shown schematically in Fig. 5.

0D Me phase formation can start at extremely high underpotentials by a decoration of 0D surface inhomogeneities. For instance single Me adatoms or small Me clusters deposited on kink sites of the foreign substrate can be considered as 0D Me phases (cf. Fig. 5*b*).

The decoration of monatomic steps represents an 1D Me phase formation (cf. Fig. 5*c*). Such a preferential decoration of monatomic steps at relatively high underpotentials was directly observed by in situ SPM in various Me UPD systems (1, 19–24). The width of this step decoration extends up to several nanometers, indicating a high activity of the step edge. Figure 6 shows an example for step decoration in the system Ag(100)/Pb^{2+} (24).

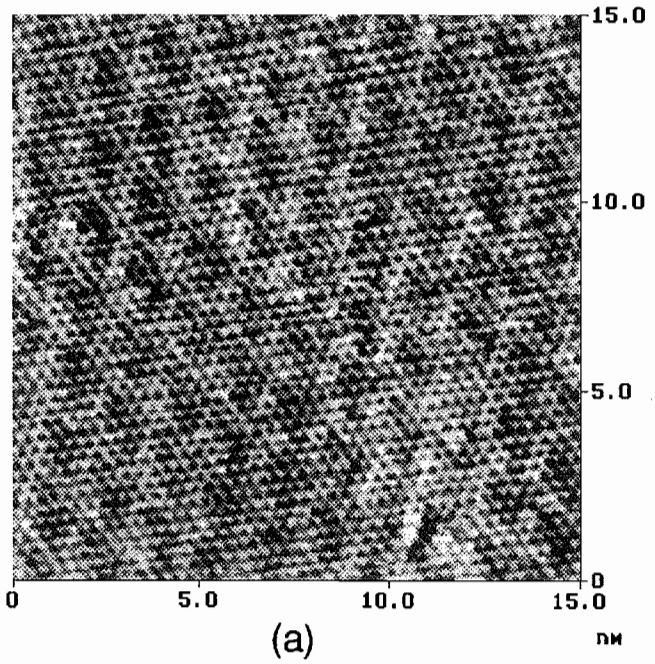
The processes of decoration of kinks and steps are followed by formation of different 2D Me phases on 2D surface inhomogeneities (1). At medium underpotentials, expanded commensurate 2D Me adlayers can be formed by localized

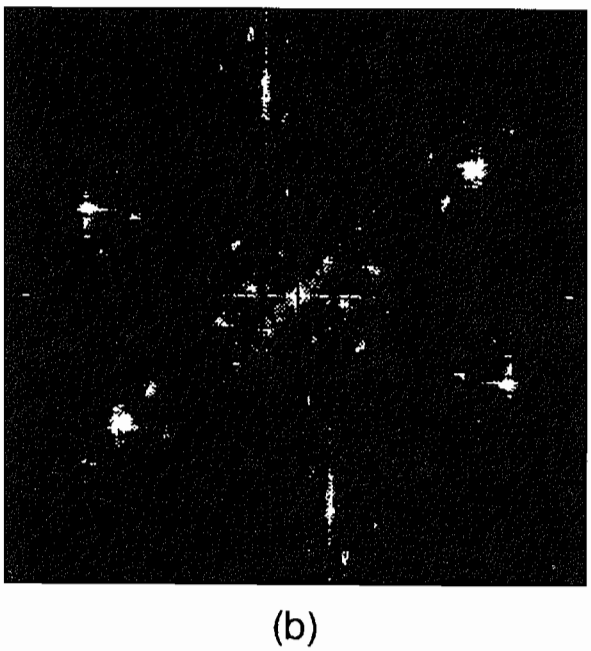
© 1997 NRC Canada

Can. J. Chem. Downloaded from www.nrcresearchpress.com by 91.121.58.235 on 09/08/12
For personal use only.

Can. J. Chem. Downloaded from www.nrcresearchpress.com by 91.121.58.235 on 09/08/12
For personal use only.

Fig. 9. Compressed 2D hcp Pb UPD overlayer showing a superstructure with moiré pattern in the system Au(111)/5 × 10^{-3} M $Pb(ClO_4)_2$ + 10^{-2} M $HClO_4$ at T = 298 K and ΔE = 50 mV. (*a*) In situ STM image; (*b*) 2D Fourier transform of (*a*).

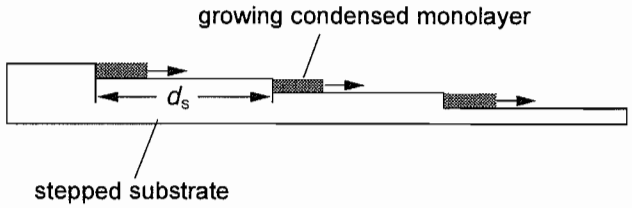




adsorption on atomically flat terraces (cf. Fig. 5*d*). Typical examples of Ag(100) − c(2 × 2)Pb and Au(100) − c(2 × 2)Pb superlattice structures are shown in Fig. 7 (1, 24).

At lower undersaturation, expanded 2D Me phases usually transform into condensed Me monolayers via a first order phase transition (cf. Fig. 5*e*). Such a phase transition is demonstrated in Fig. 8 for Pb UPD on Au(100) (1, 24). A stable

Fig. 10. Schematic representation of a growing condensed monolayer on a foreign substrate exhibiting parallel steps with a constant step spacing d_S.



condensed 2D hcp Pb phase showing an Au(100) − c(6 × 2) Pb moiré superstructure and an expanded 2D Pb phase with an Au(100)–2c($3\sqrt{2} \times \sqrt{2}$) Pb R 45° superstructure are observed at low and medium underpotentials, respectively. The phase transition occurs within a narrow underpotential range of about 15 mV at the applied anodic potential scan rate of $|dE/dt|$ = 10 mV s^{-1}.

Condensed Me UPD overlayers are either commensurate, higher order commensurate, or incommensurate depending on the crystallographic Me–S misfit (1). As an example, the moiré structure of a close-packed Pb UPD overlayer on Au(111) at low underpotentials is shown in Fig. 9 (1, 19). Due to the significant crystallographic Pb–Au misfit the overlayer is incommensurate, isotropically compressed, and rotated with respect to the Au(111) substrate. Analysis of the corresponding 2D Fourier transform (Fig. 9*b*) indicates a modulation of Pb–Pb interatomic distances, in good agreement with the static distortion waves (SDW) model proposed by Novaco and McTague (1, 25–27).

The formation of condensed 2D phases in the UPD range involves 2D nucleation and growth phenomena. It is well known that surface inhomogeneities of the foreign substrate such as monatomic steps significantly influence the thermodynamics and kinetics of 2D nucleation (1, 28). Sites at monatomic steps are energetically more favorable for 2D nucleation than sites at atomically flat terraces. Thus, at relatively low supersaturations the nucleation of the condensed 2D Me phase takes place, practically, only on monatomic steps. As shown above, monatomic steps of the substrate are usually modified by a 1D Me phase that acts as precursor for the formation of the condensed 2D Me phase.

The heterogeneity of the substrate surface influences not only the nucleation act, but also the 2D growth of the condensed monolayer. Thus the theoretical treatment of 2D nucleation and growth kinetics on real crystal substrates is complicated due to the presence of different edge effects related to surface inhomogeneities. A relatively simple situation is obtained in the case of formation of a condensed monolayer on a foreign substrate exhibiting, as surface inhomogeneities, only parallel monatomic steps with a constant step spacing d_S (Fig. 10), Assuming that the phase formation process starts only at monatomic steps and that the steps are instantaneously (at t = 0) covered by the condensed 2D phase, the current density connected with the spreading of the condensed monolayer can be described by (1, 19, 21)

$$[9] \quad -i(t) = \begin{cases} q_{cd}\, d_S^{-1}\, v = q_{cd}\, L_S\, v & \text{for } 0 \le t < d_S\, v^{-1} \\ 0 & \text{for } t = d_S\, v^{-1} \end{cases}$$

© 1997 NRC Canada

Fig. 11. Schematic representation of current transients for lateral growth of a condensed monolayer starting at monatomic steps. (*a*) foreign substrate exhibiting parallel steps with a regular step spacing; (*b*) foreign substrate exhibiting parallel steps with an irregular step spacing (arbitrary step distribution).

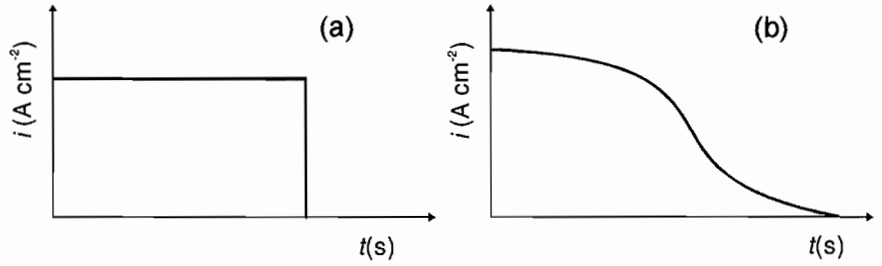
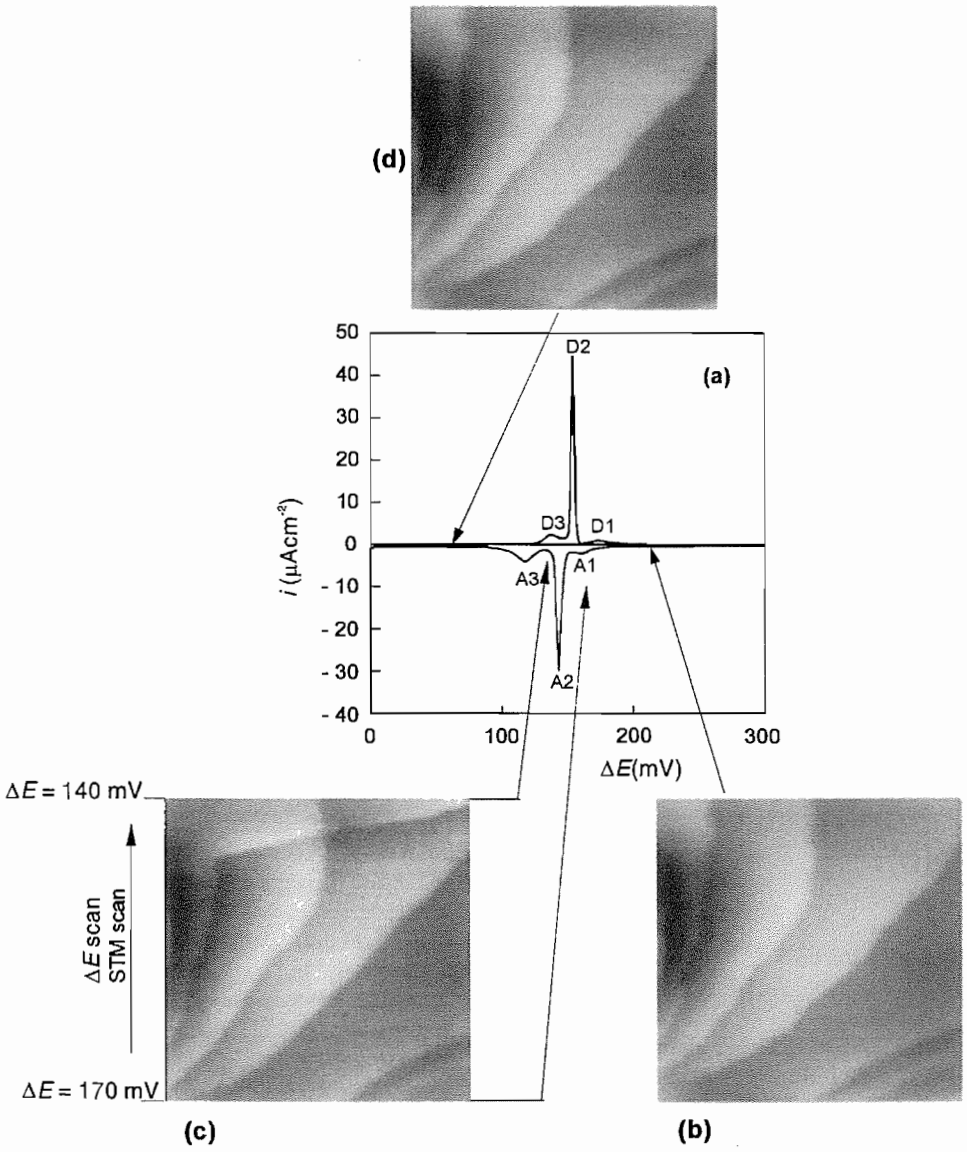


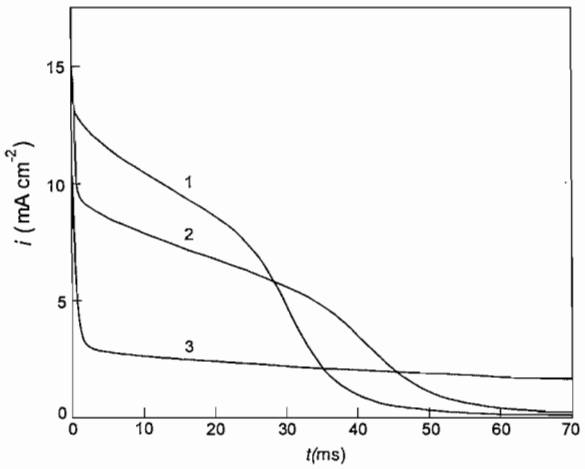
Fig. 12. UPD of Pb on a stepped Ag(111) substrate in the system Ag(111)/5 × 10^{-3} M $Pb(ClO_4)_2$ + 10^{-2} M $HClO_4$ at T = 298 K. (*a*) Cyclic voltammogram at a scan rate 1 mV s^{-1}; (*b*) in situ STM image of the bare substrate; (*c*) in situ STM image during the cathodic potential sweep in the range of peak A_2; (*d*) in situ STM image of the substrate covered by the condensed Pb monolayer. STM scan size: 70 nm × 70 nm.



Can. J. Chem. Downloaded from www.nrcresearchpress.com by 91.121.58.235 on 09/08/12
For personal use only.

© 1997 NRC Canada

Fig. 13. Current transients for the formation of a condensed Pb monolayer on a stepped Ag(111) substrate in the system Ag(111)/5 × 10^{-3} M $Pb(ClO_4)_2$ + 5 × 10^{-1} M $NaClO_4$ + 5 × 10^{-3} M $HClO_4$ at T = 298 K. Potential pulses from ΔE_i = 300 mV to ΔE_f = 20 mV (1); 50 mV(2); 110 mV(3).



where q_{cd} and v represent the charge density and the propagation rate of the condensed monolayer, respectively. The corresponding current transient is shown in Fig. 11*a*.

Surfaces of real crystals, however, are usually characterized by atomically flat terraces, 2D islands and pits, as well as by a nonuniform distribution of monatomic steps that can be rough and frizzy, leading to a "fractal dimensionality" of *i*D with $1 \leq i \leq 2$ (1, 29, 30). These inhomogeneities can strongly influence the shape of the corresponding current transients (Fig. 11*b*). Thus analysis of experimental current transients requires exact information about the local mechanism of monolayer formation and the substrate surface morphology on an atomic level.

Direct evidence for formation of a condensed monolayer starting exclusively at monatomic steps was obtained recently by combined electrochemical and in situ STM studies of Pb UPD on Ag(100) and Ag(111) substrates (1, 23, 24). The process of monolayer formation occurs at monatomic steps that are modified by an 1D Pb phase (cf. Fig. 8) formed at undersaturations with respect to the condensed 2D phase. Figure 12 shows the change of the surface morphology during the formation of the condensed 2D Pb phase on a Ag(111) substrate. The appearance of a growth front starting at monatomic steps is clearly seen in the in situ STM image (Fig. 12*c*) corresponding to peak A_2 of the cyclic voltammogram (Fig. 12*a*). The shape of experimental current transients (Fig. 13) is in good agreement with the model discussed above (cf. Fig. 11*b*).

Conclusions

The influence of crystal imperfections and surface inhomogeneities on the processes of electrochemical phase formation and crystal growth is demonstrated in various studies of electrodeposition of metals on native and foreign single crystal substrates.

Screw dislocations play the most important role in electrodeposition of metals on native substrate. A quantitative investigation of the spiral growth mechanism, however, is possible only on single crystal faces with a relatively low screw dislocation density. Experiments on such crystal faces prepared by the so-called capillary technique conform to Frank's spiral growth theory. Surfaces with uniform and well-defined step density can be prepared by electrochemical growth of crystal faces with low screw dislocation density.

A significant progress in understanding the role of surface inhomogeneities in the initial stages of electrochemical metal phase formation on foreign solid substrates is achieved by introducing in situ SPM techniques. Combined electrochemical and in situ SPM studies of the UPD of metals show that surface inhomogeneities induce a formation of low-dimensional (0D, 1D, and 2D) metal phases in different underpotential ranges.

Further development of theories and experiments on an atomic level is necessary for a better understanding of the role of crystal imperfections in the electrochemical formation of phases of different dimensionality.

Acknowledgments

Financial support for this work given by the Deutsche Forschungsgemeinschaft (DFG), contracts No. Lo 184/21/1-8 and Lo 184/29/1,2, Arbeitsgemeinschaft Industrieller Forschungsvereinigungen (AIF), contracts No. 9521, 10029, and 2046, and the Bundeswirtschaftsministerium is gratefully acknowledged. The authors thank E. Budevski, V. Bostanov, and W. Obretenov (Bulgarian Academy of Sciences, Sofia, Bulgaria), C. Mayer, D. Salinas, and S. Garcia (Universidad Nacional del Sur, Bahia Blanca, Argentina), and U. Schmidt, S. Vinzelberg, and R. Pötzschke (University of Karlsruhe) for successful scientific cooperation.

References

1. E. Budevski, G. Staikov, and W.J. Lorenz. Electrochemical phase formation and growth – an introduction in the initial stages of metal deposition. VCH, Weinheim.1996.
2. F.C. Frank. Discuss. Faraday Soc. **5**, 48 (1949); **5**, 67 (1949).
3. W.K. Burton, N. Cabrera, and F.C. Frank. Philos. Trans. R. Soc. London, Ser. A: **243**, 299 (1951).
4. N. Cabrera and M. Levine. Philos. Mag. **1**, 450 (1956).
5. E. Budevski, G. Staikov, and V. Bostanov. J. Cryst. Growth, **29**, 316 (1975).
6. E. Budevski and V. Bostanov. Electrochim. Acta, **9**, 477 (1964).
7. E. Budevski, V. Bostanov, T. Vitanov, Z. Stoynov, A. Kotzeva, and R. Kaischew. Electrochim. Acta, **11**, 1697 (1966).
8. V. Bostanov, A. Kotzeva, and E. Budevski. Bull. Inst. Phys. Chem. (Bulg. Acad. Sci.) **6**, 33 (1967).
9. V. Bostanov, R. Roussinova, and E. Budevski. Commun. Dept. Chem. (Bulg. Acad. Sci.) **2**, 885 (1969).
10. V. Bostanov, G. Staikov, E. Budevski, and R. Kaischew. Commun. Dept. Chem. (Bulg. Acad. Sci.) **4**, 311 (1971).
11. G. Staikov, W. Obretenov, V. Bostanov, E. Budevski, and H. Bort. Electrochim. Acta, **25**, 1619 (1980).
12. E. Budevski, V. Bostanov, and G. Staikov. Annu. Rev. Mater. Sci. **10**, 85 (1980).
13. E. Budevski. *In* Comprehensive treatise of electrochemistry. Vol. 7. *Edited by* B.E. Conway, J.O'M. Bockris, E. Yeager, S.U.M. Khan, and R.E. White. Plenum Press, New York. 1983. p. 399.

© 1997 NRC Canada

Can. J. Chem. Downloaded from www.nrcresearchpress.com by 91.121.58.235 on 09/08/12
For personal use only.

14. T. Vitanov and A. Popov. SAEST Trans. **5**, 10 (1975).
15. A. Hamelin,T. Vitanov, E. Sevastyanov, and A. Popov. J. Electroanal. Chem. **145**, 225 (1983).
16. T. Vitanov, E. Sevastyanov, Z. Stoynov, and E. Budevski. Elektrokhimiya, **5**, 238 (1969).
17. G. Staikov, K. Jüttner, W.J. Lorenz, and E. Budevski. Electrochim. Acta, **23**, 319 (1978).
18. T. Vitanov, A. Popov, G. Staikov, E. Budevski, W.J. Lorenz, and E. Schmidt. Electrochim. Acta, **31**, 981 (1986).
19. W.J. Lorenz and G. Staikov. Proc. Int. Symp. Electrode processes, 6th, Los Angeles. May 1996. Vol. **96-8**. *Edited by* A. Wieckowski and K. Itaya. The Electrochemical Society, Pennington, N.J. 1996. p. 189.
20. W.J. Lorenz and G. Staikov. Proc. Symp. Electrochemically Deposited Thin Films, 3rd, San Antonio. 1996. Vol. **96-19**. *Edited by* M. Paunovic and D.A. Scherson. The Electrochemical Society, Pennington N.J. 1997. p. 171.
21. G. Staikov and W.J. Lorenz. Proc. Symp. Electrochemically Deposited Thin Films, 3rd, San Antonio. 1996. Vol. **96-19**. *Edited by* M. Paunovic and D.A. Scherson. The Electrochemical Society, Pennington N.J. 1997. p. 3.
22. D. Carnal, P.I. Oden, U. Müller, E. Schmidt, and H. Siegenthaler. Electrochim. Acta, **40**, 1223 (1995).
23. E. Ammann. Master Thesis, University of Bern. 1995.
24. U. Schmidt, S. Vinzelberg, and G. Staikov. Surf. Sci. **348**, 261 (1996).
25. A.D. Novaco and J.P. McTague. Phys. Rev. Lett. **38**, 1286 (1977).
26. J.P. McTague and A.D. Novaco. Phys. Rev. B: Condens. Matter, **19**, 5299 (1979).
27. G. Staikov. *In* Proceedings of NATO Advanced Study Institute on nanoscale probes of the solid/liquid interface, Sophia Antipolis, July 1993. *Edited by* H. Siegenthaler and A. Gewirth. Kluwer Acad. Publ., Dordrecht. 1995. p. 193.
28. R. Kaischew. Commun. Bulg. Acad. Sci. (Phys. Ser.), **1**, 100 (1950).
29. R.Q. Hwang, J. Schröder, C. Günther, and R.J. Behm. Phys. Rev. Lett. **67**, 3279 (1991).
30. R.J. Hamers, U.K. Kohler, and J.E. Demuth. Ultramicroscopy, **31**, 10 (1989).

Can. J. Chem. Downloaded from www.nrcresearchpress.com by 91.121.58.235 on 09/08/12
For personal use only.

© 1997 NRC Canada

Impact of electrode geometry, depth of immersion, and size on impedance measurements

Petr Vanýsek

Can. J. Chem. Downloaded from www.nrcresearchpress.com by 91.121.58.235 on 09/08/12
For personal use only.

Abstract: Although the platinum electrode is used regularly in the practice of electroanalytical chemistry, there are some caveats that should be considered in experimental design and data interpretation when ac impedance measurements are made. A wire electrode was immersed only partially with the purpose of decreasing its effective area. Impedance was used to study the effect of partial immersion. In the case of an NaOH solution, a good impedance fit was found if a transmission line was added to the equivalent circuit. Transmission line behavior corresponds to the transversal conductivity in the wet, though not immersed, surface. Impedance was further compared for a wire electrode, as well as for short wire electrodes with metal spheres attached to their end. The shorter, predominantly spherical, electrode minimizes impedance artifacts at higher frequencies, thus serving as a better electrode for impedance studies. The change in impedance after depositing platinum black was used to estimate the effective surface area increase.

Key words: electrochemical impedance spectroscopy, platinum, electrode shape, partial immersion, platinum black, sodium hydroxide.

Résumé : Même si l'électrode de platine est régulièrement utilisée dans la pratique de la chimie électroanalytique, il est nécessaire de considéré certaines de ses limites dans la mise au point des expériences et dans l'interprétation des données découlant de mesures d'impédance à ca. On n'a immergé que partiellement une électrode à fil afin de diminuer sa surface effective. On a utilisé l'impédance pour étudier l'effet de l'immersion partielle. Dans le cas d'une solution de NaOH, on a obtenu une bonne corrélation d'impédance à la condition d'ajouter une ligne de transmission au circuit équivalent. Le comportement de la ligne de transmission correspond à une conductivité transversale d'une surface mouillée, mais non immergée. On a aussi comparé l'impédance d'une électrode à fil ainsi que celles d'électrodes à fil court auxquelles on a fixé des sphères métalliques à leur extrémité. L'électrode plus courte, qui est essentiellement sphérique, minimise les artefacts de l'impédance à des fréquences plus élevées et elle est donc une meilleure électrode pour les études d'impédance. On a utilisé le changement d'impédance après dépôt de noir de platine pour évaluer l'augmentation de la surface effective.

Mots clés : spectroscopie électrochimique d'impédance, platine, forme de l'électrode, immersion partielle, noir de platine, hydroxyde de sodium.

[Traduit par la rédaction]

Introduction

Platinum is the most typically encountered metal in electrodes used in research laboratories. It is routinely regarded as an inert metal, which does not itself enter into a chemical or an electrochemical reaction. It is used as a stable gauze electrode in electrogravimetry for bulk electrodeposition and, in various forms, sizes, and shapes, it is used as the working electrode both in electroanalytical and electrokinetic applications. In addition, it is often discussed as the oxidation–reduction electrode, or the electrode of the zeroth kind, a piece of metal immersed in a solution of two oxidation states of certain species. The metal merely mediates the transfer of electrons between the two species. Platinum as the working electrode is used by a wide range of individuals with various degrees of experience in order to obtain impedance in a solution. Impedance can be probed for such tasks as measurements of the double-layer capacitance, adsorption, surface area, or reaction kinetics.

In many of these studies, impedance is used as one of the techniques to probe the kinetics or mechanism of the reaction or surface state. However, there has been some indication in the literature that the shape of the electrode, or the arrangement of all the electrodes, can influence the quality of the measurement. In particular, capacitance obtained from ac data is often used for the area measurement of Pt as well as of other electrodes. Therefore, the goal of this experiment is to examine the impact of the shape of the electrode, as well as depth of immersion into solution, on the obtained impedance data.

Received April 24, 1997.

This paper is presented in honour of Professor Brian Evans Conway's outstanding contributions to electrochemistry on the occasion of his 70th birthday.

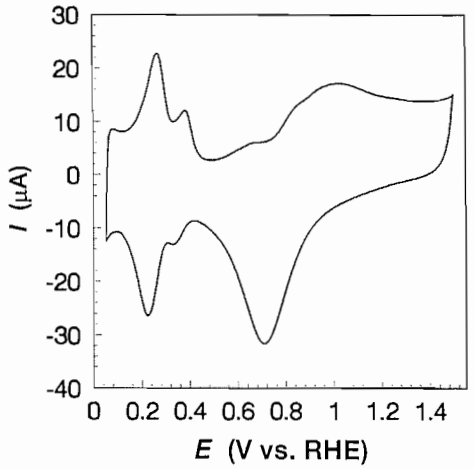
P. Vanýsek.[1] Northern Illinois University, Department of Chemistry and Biochemistry, DeKalb, IL 60115-2862, U.S.A.

[1] Telephone: (815) 753-6876. Fax: (815) 753-4802. E-mail: pvanysek@niu.edu

© 1997 NRC Canada

Can. J. Chem. Downloaded from www.nrcresearchpress.com by 91.121.58.235 on 09/08/12
For personal use only.

Fig. 1. Voltammogram of polycrystalline platinum in 1 mol/L NaOH. Scan rate 100 mV/s. Electrode area 11 mm^2.



General cyclic voltammetry response

Figure 1 is an example of a voltammogram of platinum in 1.0 mol/L NaOH. One can obtain this result with standard chemicals, without special purification. The positive scan from 0.6 V shows a current increase that is due to the formation of platinum oxide. The additional current increase toward the upper end of the scan (1.5 V vs. RHE) corresponds to oxygen evolution (oxidation of water) and a further continuation of the scan in the positive direction would result in an increase of the recorded current. The prominent peak observed on the negative scan (at about 0.76 V vs. RHE) is due to the reduction of the surface oxide. The "butterfly" peaks, as they are named for their shape, at 0.3 V and below, correspond to surface adsorption of a monolayer of hydrogen atoms (negative current) and their subsequent desorption (positive current). The scan is reversed slightly before 0.0 V vs. RHE, as scanning any further would result in the massive evolution of hydrogen gas; there is already a hint of this evolution in the voltammogram.

The region between 0.35 and 0.75 V vs. RHE corresponds primarily to the charging of the double layer. Impedance was measured at 0.6 V vs. RHE where little or no faradaic process takes place, and the impedance response is due to the electrode capacitance.

Electrochemical impedance

Impedance as a method for characterization of the electrical parameters of a material has been embraced by electrochemists for quite some time. The method is, at least in principle, suitable for resolving the resistive, capacitive, and inductive components of a system under study. The available instrumentation is adequate for such a task. Interpretation, however, is sometimes problematic because, often, individual factors contributing to the impedance cannot be resolved, or the impedance data lend themselves to a number of interpretations. Platinum metal in a solution can be investigated by impedance on several fronts. At the potentials of electrochemical inactivity, the metal surface behaves as a capacitive double layer, and its capacitance can be directly measured. During hydrogen adsorption, the adsorptive layer also appears to the impedance probe as capacitance, although much higher than the double-layer capacitance. This result can, again, be interpreted as capacitance and is often labeled as pseudocapacitance. On the positive side of the polarization potential, where metal oxides are formed, the impedance signature can reveal the presence of an additional layer at the surface.

A number of impedance studies in electrochemistry on Pt have been reported by Conway (1–11). The work was mostly concerned with interpretation of faradaic reactions, adsorption, supercapacitors (devices with especially high pseudocapacitive values), and even work in nonaqueous solvents. Using impedance also allows one to probe the roughness or porosity of metal surfaces (5, 6). Although true inductance in electrochemistry (source of current) is not seen, behavior appearing as inductance is; it is labeled as pseudoinductance (8). A comprehensive book on impedance, emphasizing solid materials, has been edited by Macdonald (12).

Impedance measurements are based on determining the dynamic ac resistance of a system as a function of the ac frequency. The parameter obtained consists of two values, the ratio of the potential and current (i.e., the "resistance"), and the phase shift between the potential and the current. The measurement of impedance at a number of frequencies (electrochemical impedance spectroscopy) can provide kinetic parameters as well as an insight into the structural properties of the electrode–solution interface. Resistive components of the impedance are often associated with a charge transfer process or a faradaic current, whereas capacitive response has to do with separation of charge and dielectric behavior. A double layer is an example of a structure that has electrical capacitance; in impedance study it is seen as a capacitor. In the case of Pt in NaOH solution, the double-layer capacitance can be seen.

Ideally, a capacitor will have its impedance Z as a function of frequency ω expressed as

$$[1] \quad Z(\omega) = R - 1/(j\omega C)$$

where C is the capacitance, j is the imaginary unit $j = \sqrt{-1}$, ω the angular frequency ($\omega = 2\pi f$, where f is frequency in Hz), and R is a resistance of the system in series with C, usually originating from the solution resistance. However, in practice, the electrochemical equivalents of capacitors and resistors are not point, localized, components. They tend to be spread or distributed over a distance. The impedance of such distributed parameters usually needs to be written in a more complex form as (13, 14)

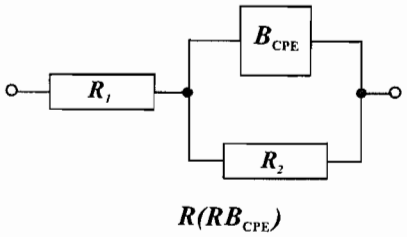
$$[2] \quad Z(\omega) = R - 1/B_{CPE}(j\omega)^n$$

where the fraction $1/B_{CPE}(j\omega)^n$ is known as the constant phase element (CPE), a value with two parameters. The parameter B_{CPE} is the magnitude of the constant phase element and is often called just the constant phase element.[2] The power fac-

[2] Symbol B is used in electricity and magnetism for susceptance. Here it is used for the value of the constant phase element, B_{CPE}. Though not strictly susceptance, the CPE is in close relationship to it. The B symbol is less misleading than Q, which is used for the CPE value in the EQUIVCRT program, but is otherwise used routinely as a symbol for charge.

© 1997 NRC Canada

Fig. 2. Diagram of the simple equivalent circuit coded as $R(RB_{CPE})$ used in the text. R: resistance (R_1, solution resistance; R_2, charge transfer resistance), B_{CPE}: constant phase element (CPE).



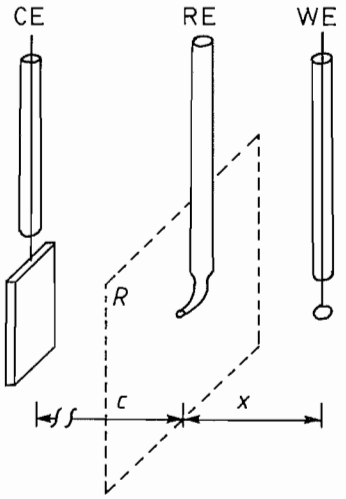
tor, n, can attain values between 0 and 1. For $n \rightarrow 1$, eq. [2] becomes eq. [1], with $B_{CPE} = C$. It has been shown that the parameter n becomes smaller for rougher surfaces (13, 15). In some work, the $n < 1$ was interpreted in terms of fractal analysis (13, 15–17). In much of practical work, when n is not too far from unity, the B_{CPE} is simply reported as capacitance, C. However, the use of CPE in modeling can account for non-idealities, without their quantitative description (18). The value of $n = 0.5$ has special meaning. Experimentally, it corresponds to resistance caused by diffusion control. This special case of CPE is called the Warburg impedance.

In many cases, a simple model, expressed as $R(RB_{CPE})$ and shown in Fig. 2, was used to evaluate impedance at potentials without electron transfer. The first R in the notation is R_1, a series resistance usually associated with the resistance of solution. The notation of the two elements in parentheses implies that they are in parallel. B_{CPE} is the value of the constant phase element and R is a resistance, R_2, which corresponds to a charge transfer (reaction) resistance.

Experimental

Both the voltammetric and the impedance work were carried out in a standard glass electrochemical cell with two compartments, separating the reference electrode part from the rest of the system by a ground-glass stopcock and a Haber–Luggin capillary terminating in the vicinity of the working electrode. Hydrogen gas (compressed gas, Airco), at a rate of about 10 mL/min, was allowed in the compartment of the reference reversible hydrogen electrode (RHE), which was filled with 1.0 mol/L NaOH. Nitrogen (compressed gas, Airco) gas was bubbled through the working electrode compartment prior to the measurements to displace the solution oxygen. In some experiments a fourth electrode, in the form of a platinum wire connected through a 0.47 μF or 2.4 μF capacitor to the reference electrode, was used to compensate for high-frequency distortion. However, in most measurements, this connection was deliberately omitted to observe the natural behavior of the system. From our experience, the size, shape, or even the placement of this fourth electrode in the cell has very little effect on the overall impedance response, as long as such electrode is present in the working solution compartment. The physical layout of the electrode placement in the cell is shown in Fig. 3. The distance between the working and counter electrode (i.e., $c + x$) was 20 mm. The cell was open to the atmosphere; therefore, the gas pressure was close to

Fig. 3. Physical cell layout of the electrode placement. CE: Pt foil counter electrode, RE: Luggin capillary of the reference electrode, WE: working electrode. R: isopotential plane between the working and the counter electrode where the solution impedance (along distance x) is measured. c: the distance between plane R and CE, electrically compensated by the potentiostat.



that of atmospheric pressure. The solutions were prepared from distilled water redistilled from glass. Sodium hydroxide was of analytical purity (Fisher). Wire, mesh, and foil metal for the polycrystalline Pt electrodes, which were used as the working, counter, and fourth compensating electrodes, was obtained from Aldrich. The sizes and the shapes of the electrodes, when relevant for the actual experiment, are described in the appropriate results subsection. The electrodes were cleaned electrochemically before experiment by 16 voltammetric sweeps between −0.05 V and 1.8 V vs. RHE, the reversible hydrogen electrode, at 0.1 V/s. The cleanliness of the electrode was ascertained by a voltammogram between 1.5 and 0.05 V at 0.1 V/s. The work was done at laboratory temperature, ~24°C. If a platinum black surface on an electrode was desired, it was prepared by a 10 min electrolysis at 30 mA/cm^2, reversing polarity every 30 s, from a solution of 3.5% chloroplatinic acid and 0.005% lead acetate.

The voltammetric experiments were carried out using the EG&G 273A potentiostat, controlled by M270 software. Impedance was measured with the Solartron 1250/1286 analyzer/potentiostat, controlled by Z-Plot software (Scribner Associates). The frequency range was between 65 kHz and 0.1 Hz, with 12 points per decade. The amplitude of the ac signal was 10 mV (rms). The impedance data were evaluated with the help of the nonlinear least-squares-fit software utility, EQUIVCRT, written by B. Boukamp (University of Twente). Because the potentiostat was engaged in the impedance measurement, the impedance of the system is that of the path between the working electrode, towards the counter electrode but ending in the plane where the reference electrode is placed. Therefore, barring an instrument artifact, the counter electrode and, for that matter, the nature of the reference electrode should not be contributing factors towards the measured impedance (cf. ref. 19).

© 1997 NRC Canada

Can. J. Chem. Downloaded from www.nrcresearchpress.com by 91.121.58.235 on 09/08/12
For personal use only.

Can. J. Chem. Downloaded from www.nrcresearchpress.com by 91.121.58.235 on 09/08/12
For personal use only.

Results and discussion

A. The shape of the working electrode

(i) Solution resistance and the shape of an electrode

The original paper by Nicholson and Shain (20) describing cyclic voltammetry also introduced the component of spherical correction (21), then needed for the widely used mercury dropping electrode. The implication of the correction was that in spherical or hemispherical diffusion, as opposed to semi-linear diffusion, the currents are higher and, at infinite time, the limiting current has a nonzero value. This follows from the geometry, in which radially increasing volume around the electrode supplies an ever-increasing pool of electroactive species. This notion is applicable to contemporary ultramicroelectrodes as well, with the additional importance of diminished solution resistance.

The resistance between an electrode and a plane in which a reference electrode is placed can be calculated by various mathematical methods, in principle identical to those used in heat conduction (22). The usual approach to solving a heat conduction problem is to draw upon previously solved equations for a particular "shape factor" and substitute appropriate dimensions. This approach should be applicable to the problems of conductivities in solutions involving shapes of electrodes as well. For example a wire electrode placed a certain distance away from a flat counter electrode is electrically equivalent to a horizontal isothermal cylinder buried in a semi-infinite medium, while a spherical electrode has its equivalent in an isothermal sphere. The electrodes are well conductive, thus isopotential, and heat flux and charge flux are phenomenologically the same. Drawing on previously solved cases in ref. 22, the resistance of the solution was evaluated as a function of the distance from the working electrode to a plane away from the electrode at a distance x, where the reference electrode is placed. The counter electrode is assumed to be placed still further, past the plane of the reference electrode. The counter electrode is assumed to be planar, with infinite area, compared to the working electrode.

For a large foil electrode, the solution resistance is simply proportional to the working–reference electrode distance x and inversely proportional to the solution conductivity κ:

$$[3] \quad R = (1/\kappa)x$$

For a wire electrode of diameter d and length l parallel to the counter electrode, the resistance relationship, based on the similarity with an isothermal cylinder and assuming that its length $l >> d$ and also that its distance from the reference electrode plane is greater than $3d/2$, is written as:

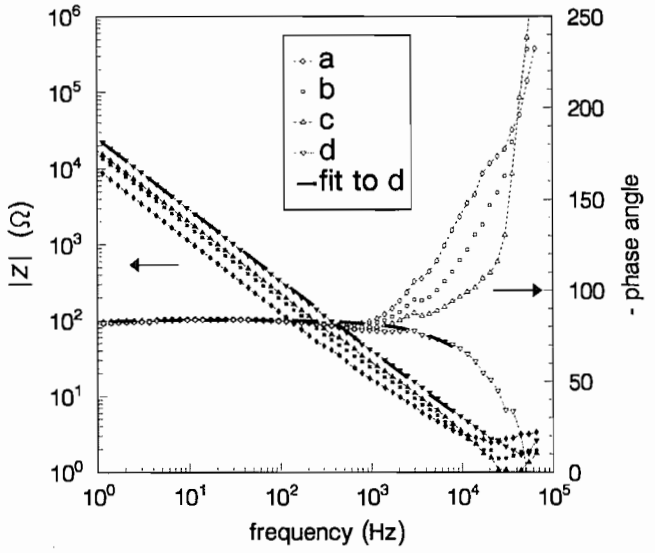
$$[4] \quad R = (1/\kappa)(\ln(4x/d))/(2\pi l)$$

and for a spherical electrode with diameter d, where it is assumed that the distance from the reference electrode plane is greater than $d/2$, the relationship is

$$[5] \quad R = (1/\kappa)(1 - (d/4x))/(2\pi d)$$

From relationships [3]–[5] it follows that for a planar large electrode the solution resistance always changes with electrode distance. For a wire electrode, the change with position, at larger distances, is less pronounced, due to the logarithmic function in eq. [4]. For a spherical electrode, the changes of resistance with distance diminish sharply and, eventually, become independent of further electrode movement. This effect on the solution resistance parameter R_1 in an experiment with wire-sphere electrodes is described in the following section.

Fig. 4. The Bode impedance plot for a platinum wire electrode with a sphere attached to its end. Solid symbols, |Z|; hollow symbols, the phase angle. The plots are shown for (*a* - ◇) a wire electrode only (19.2 mm^2 area); and for the three consecutively larger spheres and therefore shorter wires, with decreasing surface area: (*b* - □) 11.7 mm^2; (*c* - △) 9.4 mm^2; and (*d* - ▽) 6.16 mm^2. The bold broken line is the best-fit curve for electrode (*d*) (cf. Table 1). Only one fit overlay is shown to maintain clarity.



(ii) Spherical electrode

In past experience with various shapes of electrodes, the most ideal impedance results, i.e., the best fit to the expected equivalent circuit (cf. Fig. 2) and a constant phase element (CPE) having its value n close to 1 (cf. eq. [2]), corresponding to a pure capacitance, were those obtained with a mercury hanging drop electrode. For other shapes of electrodes, n differed more or less from 1. Our thesis was that the shape, and perhaps the size, of the electrode, relative to the size of the cell, was an important factor. To further investigate the effect of the electrode shape and its size, a piece of 20-mm-long platinum wire sealed in a soft glass was used. The first set of measurements was done with this electrode. The geometry of this electrode was modified for subsequent experiments. The tip of the platinum wire was carefully heated in a pointed glass-blowing flame until it melted and gathered in a sphere; thus, a small spherical electrode was created, still connected to a length of exposed platinum wire. Following an impedance measurement, the electrode was again reheated, and more metal was gathered in a sphere. Each such step shortened the connecting wire and increased the diameter of the sphere. The geometric area of such an electrode was calculated for a cylinder and sphere whose sizes were obtained using a caliper and a micrometer. Three such melting steps were performed.

Figure 4 compares the Bode plot impedance response of the

© 1997 NRC Canada

Table 1. Impedance response of Pt electrode in NaOH with gradually increasing ball size/decreasing surface area. Impedance fit model $R(RB_{CPE})$.

Apparent area (mm^2)	Corresponding curve in Fig. 4	R_1 (Ω)	R_2 (Ω)	B_{CPE} (μF)	n	Calculated capacitance ($\mu F/cm^2$)
19.2	*a*	4.2	79 000	18.8	0.947	93
11.7	*b*	5.3	85 000	11.1	0.956	94
9.39	*c*	6.1	110 000	10.0	0.947	106
6.16	*d*	8.4	150 000	6.9	0.945	111

four Pt shape/size electrodes. It should be noted that for the first three experiments with a longer wire (smaller sphere) electrode, the response at the higher frequencies is nonstandard, i.e., the phase angle goes beyond 90°. This is an artifact caused by the reference electrode impedance, the geometry of the working electrode, and the relative placement of the working and the reference electrode in the cell. The result appears to mean that the current precedes the applied potential by more than 90°, which a capacitor cannot attain. However, a time lag in the reference electrode channel may increase this apparent delay past 90°. The smallest electrode with a minimum amount of wire and essentially a spherical surface does not display this behavior.

Table 1 summarizes the impedance results for the electrode shape experiment. The apparent area of the electrode was calculated from its physical dimensions. A simple circuit $R(RB_{CPE})$ (cf. Fig. 2) was used for the evaluation. For the three cases in which the phase angle exceeds 90°, the high-frequency data were excluded from the fit, because it was not possible to fit such behavior with a realistic impedance component. Therefore, there were more usable impedance points for the smallest electrode, which resulted in the smallest value of the fitting error. Figure 4 shows the overlay for the smallest electrode (broken line). The overlays for the full frequency range show that the $R(RB_{CPE})$ model is too simple to account for the total behavior. The equivalent circuit fit was adequate for frequencies from approximately 4 to 400 Hz. The retained high-frequency data for the smallest electrode have a good fit at the highest values, but deviate around 1 kHz, a likely experimental artifact. All four fits deviate somewhat at the low frequencies. The parameter evaluated as the solution resistance, R_1 (Table 1), decreases with increasing electrode area, but not linearly. When the R_1 is normalized by multiplying by the electrode area, then the smallest electrode has the smallest resistance. This deserves special mention, because solution resistance, a path between the working and the reference electrode, should be constant, i.e., the normalization mentioned should not be necessary. Alternatively, the resistance could possibly increase with diminishing cross section of the solution at the working electrode, assuming the major contribution of the solution resistance is near the surface of the reference electrode. In such case the normalization would render the solution resistance constant. However, the decrease following the electrode size seems to be unique to the modification of the size and shape of the electrode. As the derivation and eqs. [4] and [5] in part (*i*) show, solution resistance of a sphere should be smaller than that of a wire, which was observed.

To calculate the Pt capacitance, the assumption was made that the CPE can be regarded directly as capacitance (with n about 0.95). From such calculated values, divided by the geometrical area, the average apparent electrode capacitance is about 100 $\mu F/cm^2$. Using the literature data for double-layer capacitance, 28 $\mu F/cm^2$ (21), the roughness of the electrode would be about 3.6. This is still in agreement with commonly accepted data. Impedance interpretation in which B_{CPE} is equated to C, although n is less than 1, tends to overestimate the capacitance compared to the typical double-layer capacitance values in the literature (23); thus, the actual roughness of our electrodes might be closer to 1.7–2, as reported by others (23, 24). However, from the tabulated results, it can be seen that the evaluated capacitance per unit area shows a steady increase with decrease of the electrode size. From this it would appear that a smaller, spherical platinum electrode will tend to overestimate the capacitance in the impedance measurement. It is interesting to see that the n value does not approach closer to unity upon transition from a wire to a sphere. Within experimental error it is independent of the electrode shape. This refutes our thesis that a sphere is a better shape for an electrode used to measure capacitance.

The value R_2 is associated with leakage current, a charge transfer resistance parallel to the double-layer capacitance. The value in Table 1 is inversely proportional to the surface area. This qualitative trend, consistent with the expected behavior, is usually all one can get from R_2 values, because their uncertainty is typically large.

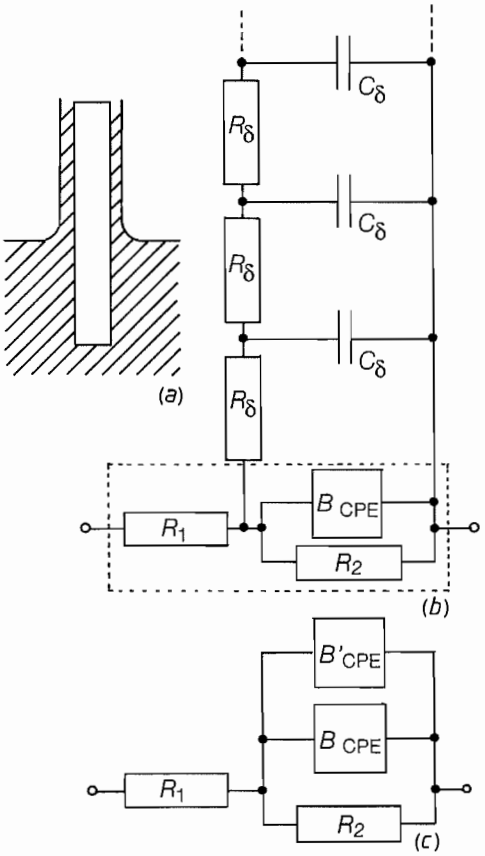
The advantage of a small spherical electrode may be that its impedance response at higher frequencies is more free of artifacts. Some workers in impedance use another electrode in addition to the three conventional electrodes (working, reference, counter) used with the usual potentiostats (25, 26). This additional electrode, usually platinum wire, is capacitively coupled to the reference electrode input of the potentiostat. Such an arrangement compensates for experimental artifacts brought about by relatively high resistance of a typical reference electrode and, in particular, its Luggin capillary. The error introduced by the uncompensated reference electrode, without the fourth electrode, also appears to be a function of the shape of the working electrode and its overall size. Whereas the three larger electrodes reveal major artifact at the higher frequencies in absence of the fourth electrode, the smallest electrode does not suffer in such a pronounced way. In fact, curve fitting reveals that the data deduced from the measurements with and without the fourth electrode yield essentially the same results, suggesting that the ideal geometry for the working electrode used for impedance measurement, without the need for the fourth electrode, may be a sphere.

Can. J. Chem. Downloaded from www.nrcresearchpress.com by 91.121.58.235 on 09/08/12
For personal use only.

© 1997 NRC Canada

Can. J. Chem. Downloaded from www.nrcresearchpress.com by 91.121.58.235 on 09/08/12
For personal use only.

Fig. 5. Illustration used in discussing impedance of a partially immersed electrode: (*a*) diagram of the partially immersed electrode, assuming a thin layer of an electrolyte spreading over the entire surface; (*b*) equivalent circuit of such a partially immersed electrode. Outlined segment is the equivalent circuit of the electrode surrounded by bulk electrolyte; (*c*) conversion of the infinite branch in Fig. 5*b* into a second constant phase element (B'_{CPE}).



B. Partial immersion of a wire electrode

A wire electrode used in electrochemical work is often ≥1 cm long. Thus, it is possible to immerse it only partially. This can happen by accident, if the electrode is not fully inserted, not enough solution is used, or if the cell is tilted. But partial immersion also can be used on purpose, for example, to grow films of different thickness along the wire length. The location of the growth may be regulated by the depth of immersion. Partial immersion results in a smaller active surface area. However, partial immersion does not lead to a proportional decrease in response. Solutions that have a tendency to creep along surfaces will form a thin, conductive layer on the part of the wire electrode above the solution, thus distorting the results. This can happen, in particular, if the electrode was first fully immersed and then partially emersed. The emersed surface would be expected to have some degree of electrochemical activity. In the model used in this paper it is assumed that the emersed wet surface retains at least some level of double-layer capacitance.

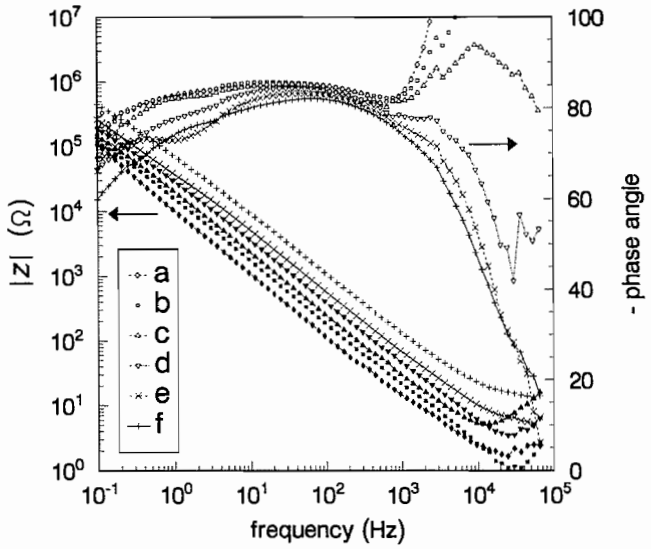
The effect of partial immersion can best be seen by the analysis of the impedance data. Figure 5*a* depicts the situation that can be expected to arise for a wire electrode that has been totally immersed, then partially emersed, and is still wet. A corresponding equivalent circuit is shown next to it (Fig. 5*b*). Its lower part, outlined by a dotted box, $R(RB_{CPE})$ is the impedance response of a wire electrode fully immersed. As determined in the previous section (A), the experimental data more appropriately require B_{CPE} with n about 0.95 instead of a pure capacitor. The upper part, with an infinite ladder arrangement of resistors and capacitors, is the assumed impedance of the wet electrode surface, with the series resistors on the side of the ladder being the incremental resistance of the wet surface, R_δ, and C_δ representing the corresponding incremental capacitances. If a long wire is assumed, then this resistance/capacitance ladder can be considered infinite. The total impedance Z_x of such an infinite motif has a finite value and can be obtained through straightforward formalism. Since the motif is infinite, the removal of one segment (series resistor R_δ and parallel capacitor C_δ) will not change the impedance of the remaining infinite structure Z_x. By adding back the impedance of the capacitor ($Z_c = -j/\omega C_\delta$) and the impedance of the resistor (R_δ), a new impedance may be written as:

$$[6] \quad Z_x = (R_\delta Z_c + R_\delta Z_x + Z_c Z_x)/(Z_c + Z_x)$$

Solving for Z_x leads to a quadratic equation that yields a rather long expression for the real and imaginary components of Z_x. However, the impedance of Z_x is also equal to the constant phase element from eq. [2], with n in this case equal to 1/2. The value of B_{CPE} is $(C_\delta/R_\delta)^{0.5}$.

The impedance data obtained for the partially immersed electrode (Fig. 6 curves *c*,*d*,*e*,*f*) show that there is a need for more than one capacitor (or CPE) in the equivalent circuit intended for evaluation of the behavior. From the model in Fig. 5, a possible equivalent circuit could be that of Fig. 5*c*,

Fig. 6. The Bode impedance plot for a platinum wire electrode (12.5 mm^2) fully immersed and partially immersed in 1.0 mol/L NaOH, measured at 600 mV vs. RHE. Solid symbols, |Z|; hollow symbols, the phase angle. Estimated amount of immersion: (*a* – ◇) 100%; (*b* – □) 67%; (*c* – △) 50%; (*d* – ▽) 25%; (*e* – ×) 20%; and (*f* – +) 10%. Evaluated data are in Table 2.



© 1997 NRC Canada

Table 2. Partially immersed electrode. Impedance response evaluated using two different equivalent circuits. Electrode area 12.5 mm^2.

Percent immersed	Corresponding curve in Fig. 6	Model $R(RB_{CPE})$ R_1 (Ω)	R_2 (Ω)	B_{CPE} (μF)	n	Model $R(RCB_{CPE})$ R_1 (Ω)	R_2 (Ω)	C (μF)	R_2C (s)	B_{CPE} (μF)	n
100	a	5.2	39 700	17	0.967	No convergence					
67	b	5.7	67 200	10.4	0.971						
50	c	5.7	81 500	8.1	0.963	2.0	380 000	5.3	2.0	4.4	0.780
25	d	9.4	89 700	5.4	0.955	2.2	623 000	3.2	2.0	4.0	0.860
20	e	12.5	88 900	3.9	0.944	5.7	1 300 000	1.5	1.9	3.9	0.814
10	f	22.7	171 000	2.3	0.929	13.5	2 000 000	0.60	1.2	2.4	0.871

i.e., R(RCB_{CPE}), or, since even a fully immersed electrode is not a perfect capacitor (cf. Sect. C), the circuit could be $R(RB_{CPE}B'_{CPE})$. The data fitting, however, revealed that the nonlinear optimization pins the n of one of the CPEs at 1, thus effectively turning the $R(RB_{CPE}B'_{CPE})$ circuit into $R(RCB_{CPE})$. Therefore, circuit $R(RCB_{CPE})$ was used in further evaluation.

A need to use a more complicated circuit than the simple $R(RB_{CPE})$ also follows from the impedance data. Table 2 shows the results for full immersion and four partial immersions of Pt wire electrodes. Whereas it is possible to fit the middle frequency range of data of all partial immersions to the $R(RB_{CPE})$ circuit, it is difficult to reconcile this with the calculated value of the charge transfer resistance R_2. While the immersion decreases ×10 (from 100% to 10%), R_2 increases only about ×4.3, indicating another contribution to system conductivity. The B_{CPE} of the CPE, on the other hand, when normalized for surface area, is constant, without apparent trend. The n value of the CPE decreases with the amount of electrode withdrawn from the solution, indicating that the thin wet film is increasingly contributing to the overall impedance with its distributed parameters.

It is important to realize that, with the additional C in $R(RCB_{CPE})$ vs. the original $R(RB_{CPE})$, R_2 and C can be resolved in a very satisfactory manner. With the area of immersion changing, the capacitance should be directly proportional to the area immersed, whereas the resistance should be inversely proportional. Thus, the product R_2C (cf. Table 2), for a particular electrode but for different extent of immersion, should be a constant value, which is, within the experimental error of the data fit, the actual case. It should be noted here that the percent immersion indicated is approximate, because the capillary elevation made the exact immersion measurement uncertain. Therefore, it should come as no surprise that, although R_2 and C change with the immersion as expected, the data spread is quite large. The B_{CPE} value in the $R(RCB_{CPE})$ fit of the right-hand side of Table 2 should be constant if the behavior was as expected from eq. [6] and the model of Fig. 5*b*. Such behavior is fulfilled for the first three data points, with the fit value for the 10% immersion deviating from the rest. The thin layer modeled by a single constant phase element is a simplification. In actuality, the n of the CPE is higher than the calculated 0.5. However, the approach to impedance evaluation of partially immersed electrodes via CPE appears to be a valid one.

C. Platinized electrodes

The usual approach to preparing a platinum electrode of large surface area is to deposit a platinum black layer on its surface. This procedure (27) roughens the surface, thus increasing the effective surface area. In this work, impedance was used to measure the increase in surface area of the platinized electrode. The impedance fit for the bright and platinized electrodes was done using equivalent circuit $R(RB_{CPE})$.

The solution resistance values, R_1, for both the bright platinum electrode and the same electrode subsequently plated with platinum black, were identical. This indicates that the value obtained from such measurement, and the subsequent evaluation, is a function of the electrode placement relative to the reference electrode. Since the geometrical area, the shape, and the placement for both electrodes are identical, the same R_1 is obtained. The platinum black surface had a lower n value of the CPE, 0.93, than a comparable electrode of bright wire, with n = 0.95–0.96. This lower value is consistent with the knowledge that the exponent n corresponds to surface roughness. The approximate surface area increase upon the deposition of platinum black can be estimated by ratioing the B values of the constant phase elements, tacitly assuming that they correspond to capacitance. In the present work, it is estimated that the surface increase resulting from the Pt black deposition was about ×40.

Conclusions

The probing of the impedance of a platinum electrode is often performed either singly, as the only assessment of the metal surface state, or as an experiment used in support of other techniques. In this paper, the contribution of electrode shape to the impedance data was investigated in a simple 1 mol/L NaOH solution at potential of 600 mV vs. RHE. A difference in impedance response was found for a straight wire electrode (20 mm long) and a shorter wire electrode with a sphere on its end (ultimately a sphere on a 1.6-mm-long wire). The sphere electrode tends to overestimate the electrode capacitance but, at the same time, provides response with the least amount of high-frequency artifacts, possibly eliminating the need to use a secondary reference electrode for high-frequency compensation. The impedance response of an electrode only partially immersed, but with the non-immersed part wet with solution, corresponds to an apparent decrease of the electrode surface, but it introduces an additional impedance component, the con-

Can. J. Chem. Downloaded from www.nrcresearchpress.com by 91.121.58.235 on 09/08/12
For personal use only.

© 1997 NRC Canada

stant phase element, derived from a transmission line. A platinum surface, coated with platinum black in order to increase its effective surface area, can be assessed by impedance probe. The constant phase element, corresponding to the surface capacitance of the electrode immersed in solution, can be used to measure the apparent increase in the surface area.

References

1. G. Tremiliosi-Filho, G. Jerkiewicz, and B.E. Conway. Langmuir, **8**, 658 (1992).
2. L. Bai, D.A. Harrington, and B.E. Conway. Electrochim. Acta, **32**, 1713 (1987).
3. D.A. Harrington and B.E. Conway. Electrochim. Acta, **32**, 1703 (1987).
4. B.E. Conway and S.Y. Quian. Electrochim. Acta, **34**, 1785 (1989).
5. L. Bai, L. Gao, and B.E. Conway. J. Chem. Soc. Faraday Trans. **89**, 235 (1993).
6. L. Bai, L. Gao, and B.E. Conway. J. Chem. Soc. Faraday Trans. **89**, 243 (1993).
7. L. Bai and B.E. Conway. J. Electrochem. Soc. **138**, 2897 (1991).
8. L. Bai and B.E. Conway. Electrochim. Acta, **38**, 1803 (1993).
9. B.E. Conway and S. Gottesfeld. J. Chem. Soc. Faraday Trans. I **69**, 1090 (1973).
10. B.E. Conway. *In* Transition from "supercapacitor" to "battery" behavior in electrochemical energy storage. Proc. 34th Int. Power Sources Symp. June 25–28, 1990. Cherry Hill, N.J. pp. 319–327.
11. S. Morin, H. Dumont, and B.E. Conway. J. Electroanal. Chem. **412**, 39 (1996).
12. J.R. Macdonald (*Editor*). Impedance spectroscopy. Wiley, New York. 1987.
13. M. Leibig and T. Halsey. Electrochim. Acta, **38**, 1985 (1993).
14. E. Gileadi. *In* Electrode kinetics for chemists, chemical engineers and material scientists. VCH, New York. 1993.
15. R.D. Armstrong and R.A. Burnham. J. Electroanal. Chem. **72**, 257 (1978).
16. M. Leibig and T.C. Halsey. J. Electroanal. Chem. **358**, 77 (1993).
17. J. Hubrecht, M. Embrechts, and W. Bogaerts. Electrochim. Acta, **38**, 1867 (1993).
18. A.J. Zhang, V.I. Birss, and P. Vanýsek. J. Electroanal. Chem. **378**, 63 (1994).
19. D.D. Macdonald. Transient techniques in electrochemistry. Plenum Press, New York. 1977. p. 233.
20. R.S. Nicholson and I. Shain. Anal. Chem. **36**, 706 (1964).
21. A.J. Bard and L.R. Faulkner. *In* Electrochemical methods. Fundamentals and applications. John Wiley, New York. 1980. p. 218.
22. F.P. Incropera and D.P. De Witt. *In* Fundamentals of heat and mass transfer. 2nd ed. John Wiley, New York. 1985. p. 140; *In* Introduction to heat transfer. 3rd ed. John Wiley, New York. 1996. p. 170.
23. T. Biegler and R.W. Woods. J. Electroanal. Chem. **29**, 269 (1971).
24. I. Bakos and G. Horanyi. J. Electroanal. Chem. **332**, 147 (1992).
25. F. Mansfeld, S. Lin, Y.C. Chen, and H. Shih. J. Electrochem. Soc. **135**, 906 (1988).
26. C.A. Gervasi and J.R. Vilche. Electrochim. Acta, **37**, 1389 (1992).
27. D.T. Sawyer and J.L. Roberts. *In* Experimental electrochemistry for chemists. Wiley, New York. 1974. p. 37.

Can. J. Chem. Downloaded from www.nrcresearchpress.com by 91.121.58.235 on 09/08/12
For personal use only.

© 1997 NRC Canada

SERS studies of monoprotonated pyrazine (pyrazinium) cations adsorbed onto positively charged silver electrodes

A.G. Brolo and D.E. Irish

Abstract: The surface-enhanced Raman scattering (SERS) spectra of monoprotonated pyrazine cations adsorbed on silver electrodes have been measured. The molecular orientation of the pyrazinium cation is dependent on the electrode potential. At potentials more positive than −170 mV the monoprotonated pyrazine is adsorbed end-on. However, the spectral features suggest a flat orientation as the potential becomes more negative than −300 mV. Monoprotonated pyrazine cations with both orientations can coexist at potentials between these limits. The adsorption of the positive ion to a positively charged electrode is mediated by specifically adsorbed bromide ions.

Key words: SERS; monoprotonated pyrazine cation, silver electrode, pyrazinium.

Résumé : On a mesuré les spectres de diffusion Raman rehaussés par la surface «SERS» de cations de pyrazine monoprotonée adsorbée sur des électrodes d'argent. L'orientation moléculaire du cation pyrazinium dépend du potentiel de l'électrode. À des potentiels plus positifs que −170 mV, la pyrazine monoprotonée est adsorbée par son extrémité. Toutefois, les caractéristiques spectrales suggèrent que l'orientation est plate lorsque le potentiel devient plus négatif que −300 mV. Des cations de pyrazine monoprotonée ayant les deux orientations peuvent coexister à des potentiels entre ces limites. L'adsorption de l'ion positif sur une électrode chargée positivement se fait avec l'aide d'ions bromures adsorbés d'une façon spécifique.

Mots clés : diffusion Raman rehaussés par la surface «SERS», cation pyrazine monoprotoné, électrode d'argent, pyrazinium.

[Traduit par la rédaction]

Can. J. Chem. Downloaded from www.nrcresearchpress.com by 91.121.58.235 on 09/08/12
For personal use only.

Introduction

Pyrazine is a centrosymmetric molecule that belongs to the D_{2h} point group. Protonation of one nitrogen will suppress the centre of inversion and reduce the symmetry to C_{2v}. This symmetry lowering will "activate" all the pyrazine vibrational modes in the Raman spectrum. However, pyrazine is a very weak base, and its low pK values (pK_{a1} = 0.65 and pK_{a2} = −5.8) (1) make protonation possible only in very acidic media.

A Raman spectral study of pyrazine and its protonated forms in aqueous solution has been performed in our laboratory (2). By observation of the shifts of the bands from the positions measured for neutral solutions, it has been possible to identify the unique characteristic bands of unprotonated pyrazine and its two protonated forms. The majority of the vibrational bands of the monoprotonated pyrazine (pzH^+) were identified and assigned (2). The diprotonated pyrazine cation spectrum was only observed from very concentrated H_2SO_4 and $HClO_4$ solutions, and the presence of strong bands from these acids masked some of its bands (2). The positions of these masked bands have been predicted theoretically (3). The ab initio calculations for pyrazine and its two protonated forms provided useful confirmation of the assignments of the observed bands within 10% accuracy.

The identification and assignment of the vibrational bands from pyrazine and monoprotonated pyrazinium cation (pzH^+) in solution proved to be useful in the interpretation of the Raman spectrum of pyrazine adsorbed onto metallic surfaces (4). The positions of the vibrational bands in the surface-enhanced Raman scattering (SERS) spectrum of pyrazine adsorbed on a polycrystalline silver electrode are more similar to those of aqueous pyrazine than those of its monoprotonated derivative. However, several "forbidden" pyrazine modes were activated by the electrode surface (4). The presence of Raman forbidden bands in the SERS spectrum of pyrazine can be explained either by the "chemical" (charge transfer (CT)) or by the "electromagnetic" enhancement mechanisms (5). The intensities of all bands in the SERS spectrum of pyrazine are potential dependent, and their maxima depend on the electrolyte and on the activation procedure (4). The spectrum is mainly dominated by the ring stretch (number 8a) mode at ca. 1590 cm^{-1}. The ring breathing (number 1) mode at ca. 1019 cm^{-1} is the second most intense band, followed by the other A_g modes at 630 and 1235 cm^{-1}. Vibrational bands at ca. 360, 432, 700, 1225, and 1520 cm^{-1} were also observed.

Received February 20, 1997.

This paper is dedicated to Professor Brian Conway on the occasion of his 70th birthday.

A.G. Brolo and D.E. Irish.[1] Guelph–Waterloo Centre for Graduate Work in Chemistry, Department of Chemistry, University of Waterloo, Waterloo, ON N2L 3G1, Canada.

[1] Author to whom correspondence may be addressed. Telephone: (519) 888-4567, ext. 2500. Fax: (519) 746-0435. E-mail: dirish@sciborg.uwaterloo.ca

© 1997 NRC Canada

Can. J. Chem. Downloaded from www.nrcresearchpress.com by 91.121.58.235 on 09/08/12
For personal use only.

New features have been observed in the SERS spectrum of pyrazine adsorbed on a silver electrode immersed in a 1.0 M KBr solution when the applied potential is more negative than −900 mV (6). These new bands were assigned to the main reduction product of pyrazine, the 1,4-dihydropyrazinium cation (7, 8). The 1,4-dihydropyrazinium cation, formed at negative potentials, can be adsorbed on the electrode surface even at potentials more positive than the pzc for silver in that medium. In this case, the reduced pyrazine cation binds to the halide layer (6). The halide, which is adsorbed on the positively charged metal surface, acts like a bridge. The same phenomenon has been observed for the adsorption of other cations like pyridinium (9) and tetramethylammonium (10). Hence, the presence of the 1,4-dihydropyrazinium cation on the silver electrode at positive potentials suggests that the monoprotonated pyrazine can also be adsorbed on a positively charged silver electrode by a similar mechanism. We have thus explored the adsorption of pzH^+ on a polycrystalline silver electrode in acidic media. This work complements the preliminary results that we presented elsewhere (11).

Experimental section

Reagents

The following chemicals were used without further purification: pyrazine 99+%, from Aldrich; KBr AnalR grade, from BDH; and concentrated $HClO_4$, from Baker. All solutions were prepared with Milli-Q-water.

Electrochemistry

The three-electrode spectroelectrochemical cell has been described elsewhere (12). A potentiostat PAR model 273 was used to control the potential applied to the working electrode. The counter electrode was a 0.3 mm platinum wire (99.9%). A saturated calomel electrode (SCE) was used as reference. The working electrode was made from 99.9% polycrystalline silver rod. A silver disk of ca. 2 mm radius was mounted in a Teflon holder. The working electrode was first polished with emery paper and then with progressively finer grades of alumina powder down to 0.3 μm. The electrode was rinsed with an abundant amount of Milli-Q-water, sonicated, rinsed again, and transferred to the spectroelectrochemical cell. The solution was degassed with Ar for 0.5 h prior to the experiment, and a gentle stream of Ar was kept on during the data acquisition.

Activation procedure

The process of roughening the metal surface electrochemically, in order to create the necessary SERS active sites, is called the activation procedure. In this work we activated the electrode electrochemically by a sequence of Oxidation–Reduction Cycles (ORCs). ORCs were performed on the silver electrode from an aqueous solution containing 1.0 M KBr and 1.0 M $HClO_4$ by sweeping from −800 to −50 mV at 5 mV/s. The potentiostat was turned off, and pyrazine was added to the system. This sequence prevents decomposition, which might occur during the ORC; trapped decomposition products have been observed when the analyte was present during the ORC (6). The pyrazine concentration used in all experiments was 0.1 M. After pyrazine was introduced into the system, the potentiostat was switched on again, the ORC cycle was resumed, and the SERS spectrum of pyrazinium adsorbed on silver was recorded at the desired potential values.

Raman spectra

Raman spectra were measured with a Dilor OMARS 89 spectrometer equipped with an optical multichannel analyzer (OMA). The intensified diode array (512 diodes) detector was thermoelectrically cooled to ca. −10°C. The spectrometer was interfaced to an IBM computer. The data were transferred to an IBM 486 computer on which baseline correction, band-fitting, and plotting programs were available. The spectra were excited by using a 514.5 nm (100 mW at the head) line from a Coherent Innova 70 argon ion laser chopped at a 1 s cycle. The chopping is a feature of the Dilor OMARS 89 spectrometer to improve signal-to-noise; it has the added advantage of diminishing photodegradation.

Results and discussion

Figure 1 shows the spectrum obtained for pyrazine adsorbed from a 1.0 M KBr + 1.0 M $HClO_4$ + 0.1 M pyrazine solution onto the SERS activated silver surface at the open circuit potential (OCP) for several spectral regions. The band positions and assignments are presented in Table 1. Table 1 also shows the band positions of the pyrazine SERS spectrum obtained from a neutral solution (4) and the pyrazine and monoprotonated pyrazine bands from aqueous solution (2). A comparison between the spectrum presented in Fig. 1 and the SERS spectrum of pyrazine adsorbed from a nonacidic solution shows striking differences in the peak positions and intensities. It has been proposed that the adsorption of neutral pyrazine onto a metallic surface would remove the molecular centre of symmetry (13). Consequently, the molecular symmetry should be reduced from D_{2h} to C_{2v} due to the adsorption. In this case, it can be expected that the spectrum of adsorbed neutral pyrazine (under C_{2v} symmetry) should have some similarities with the spectrum of the monoprotonated pyrazine cation (also C_{2v}) in solution. However, as observed in Table 1, the vibrational wave numbers found for pyrazine adsorbed onto a silver electrode from acidic solution more closely match the wave numbers of the monoprotonated pyrazine cation in solution, and the peak positions in the SERS spectrum of pyrazine adsorbed from neutral solution are more similar to those from the pyrazine spectrum of the aqueous solution. This is an indication that symmetry reduction, due to formation of a metal – organic molecule complex, is not a necessary consequence of adsorption, and that the interaction of pyrazine with the metal is not strong enough to induce a symmetry change.

The SERS spectra at potentials more positive than ca. −100 mV were time dependent. The SERS signal decreased with time, and the rate of decrease became faster as the potential became more positive. A simple explanation is that a silver bromide film is formed during the silver oxidation step, and this film quenches the SERS effect, which is a near-surface phenomenon. The time dependence of the SERS signals made the study of medium intensity and weak bands very difficult at these potentials. Hence, we focused our work in the 1000, 1200, and 1600 cm^{-1} regions where the strongest bands were found.

© 1997 NRC Canada

Can. J. Chem. Downloaded from www.nrcresearchpress.com by 91.121.58.235 on 09/08/12
For personal use only.

Fig. 1. SERS spectrum of pyrazinium on a silver electrode adsorbed from a 1.0 M KBr + 1.0 M $HClO_4$ + 0.1 M pyrazine solution at the open circuit potential (OCP). The asterisks (*) mark the bands that are not present in the SERS spectrum of pz adsorbed from neutral solution (see text). The plus sign (+) marks the ClO_4^- symmetrical stretch mode.

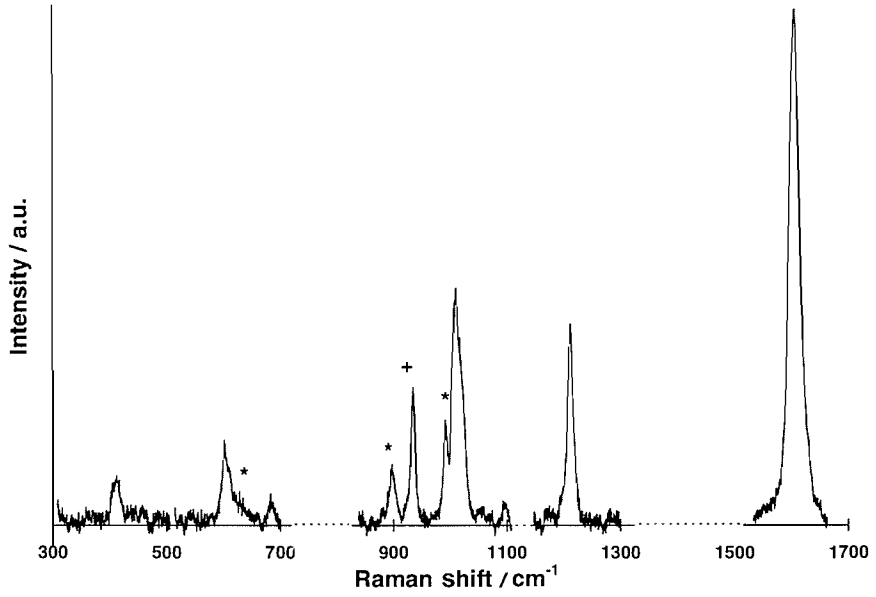


Table 1. Vibrational frequencies (in cm^{-1}) and assignments for pyrazine (pz) in solution; monoprotonated pyrazine (pzH^+) in solution; pyrazine adsorbed from acidic solution onto silver electrodes; pyrazine adsorbed from nonacidic solutions onto silver electrodes.

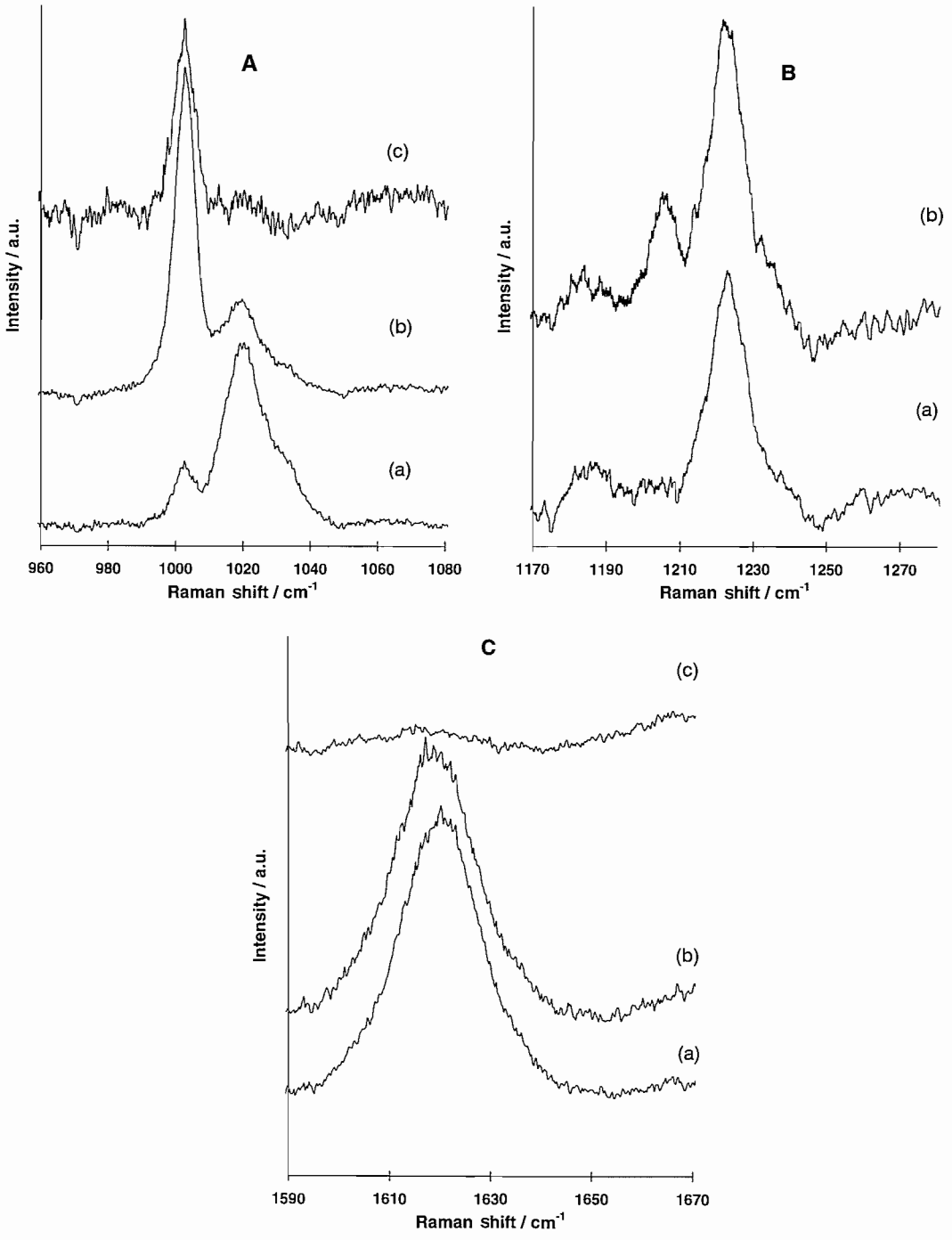
Adsorption from a 1.0 M KBr + 1.0 M $HClO_4$ + 0.1 M pz solution			pzH^+ in solution (0.1 M pz + 2.7 M HCl) (from ref. 2)	Adsorption from a 1.0 M KBr + 0.1 M pz solution, E = −700 mV (from ref. 4)	Pyrazine in solution (0.1 M pz) (from ref. 2)	Vibrational assignments.[a] D_{2h}/C_{2v}
OCP	E ≈ −100 mV[b]	E ≈ −300 mV[c]				
411 (w)			417 (vvw)	432 (w)		B_{2u}/B_2 (16*b*)
602 (m)			606 (w)			A_g/A_1 (6*a*)
611 (sh)				630 (m)	620 (w)	
710 (w)			688 (m)	697 (w)	702 (m)	B_{2g}/B_1 (6*b*)
898 (m)		898 (m)	898 (vw)		922 (w)	B_{1g}/A_2 (10*a*)
934 (s)	934 (s)	934 (s)				ClO_4^-
1002 (s)		1002 (s)				A_g/A_1 (1)
1018 (s)	1018 (s)		1020 (vs)	1019 (vs)	1020 (vs)	
1031 (sh)	1031 (sh)		1031 (s)			B_{1u}/A_1 (12)
1090 (w)			1112 (w)			B_{1u}/A_1 (18*a*)
1222 (s)	1222 (s)	1200 (m)	1223 (m)	1225 (m)	1218 (m)	A_g/A_1 (9*a*)
				1235 (m)	1238 (sh)	A_g/A_1 (11 + 16*b*)
1616 (vs)	1616 (vs)		1618 (m)	1590 (vs)	1593 (m)	A_g/A_1 (8*a*)
1635 (sh)					1618 (vw)	A_g/A_1 (1 + 6*a*)

[a]The symmetry species are presented for both D_{2h} (for pyrazine) and C_{2v} (for monoprotonated pyrazine) point groups (D_{2h}/C_{2v}). A correlation table was used (see ref. 2).
[b]Perpendicular-adsorbed pzH^+.
[c]Flat-adsorbed pzH^+.
v = very; s = strong; m = medium; w = weak; sh = shoulder.

Figures 2, *A–C*, show the SERS spectra of pyrazine adsorbed from acidic solution on a silver electrode at several potentials. The point of zero charge for silver in bromide medium is expected to be more negative than −900 mV (14) and, thus, the surface charge is positive. As the potential is swept to values more positive than −170 mV, the band intensity at 1002 cm^{-1} decreases, and one can just notice two bands near 1020 cm^{-1} at potentials close to the onset of the silver oxidation (around −100 mV). These two bands coalesce into a broad envelope that can be resolved using a band-fitting computer program. The experimental trace in this region and its band-fitted components are presented in Fig. 3. From the

© 1997 NRC Canada

Fig. 2. SERS spectrum of pyrazinium on a silver electrode adsorbed from a 1.0 M KBr + 1.0 M $HClO_4$ + 0.1 M pyrazine solution at several potentials. For (*A*): (*a*) −160 mV; (*b*) −250 mV; (*c*) −340 mV. For (*B*): (*a*) −170 mV; (*b*) −235 mV. For (*C*): (*a*) −170 mV; (*b*) −250 mV; (*c*) −310 mV.



band-fitting analysis one can locate the positions of these two bands at ca. 1018 and at ca. 1031 cm^{-1}, respectively. Just one band is observed at 1222 (Fig. 2*B*) and 1616 cm^{-1} (Fig. 2*C*) at potentials more positive than −170 mV.

As the potential was swept to less positive values, the SERS intensity of pzH^+ was recovered following the silver ion reduction around ca. −200 mV. In this case, the 1002 cm^{-1} band was present and it was more intense than the envelope at ca. 1020 cm^{-1}. The 1002 cm^{-1} band is the only one left in the spectrum in the 1000 cm^{-1} region at potentials more negative than ca. −280 mV (Fig. 2*A*). Two bands showed up in the 1200 cm^{-1} region after the silver ion reduction (Fig. 2*B*), one band at 1222 cm^{-1} and another at ca. 1200 cm^{-1}. The 1616 cm^{-1} intensity decreased as the potential became negative (Fig. 2*C*), and its position remained unchanged. This band vanished completely near −300 mV.

The results presented above are consistent with an adsorption of pyrazinium cation with different orientations at

© 1997 NRC Canada

Can. J. Chem. Downloaded from www.nrcresearchpress.com by 91.121.58.235 on 09/08/12
For personal use only.

Can. J. Chem. Downloaded from www.nrcresearchpress.com by 91.121.58.235 on 09/08/12
For personal use only.

Fig. 3. Observed SERS spectrum of pyrazinium on a silver electrode and its band-fitted components. PzH^+ adsorbed from a 1.0 M KBr + 1.0 M HClO4 + 0.1 M pyrazine solution. $E = -170$ mV.

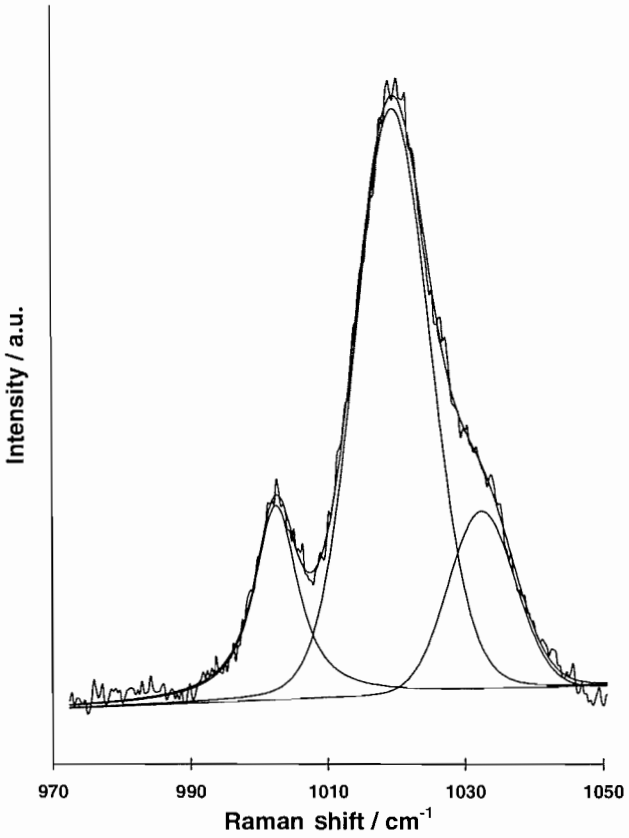
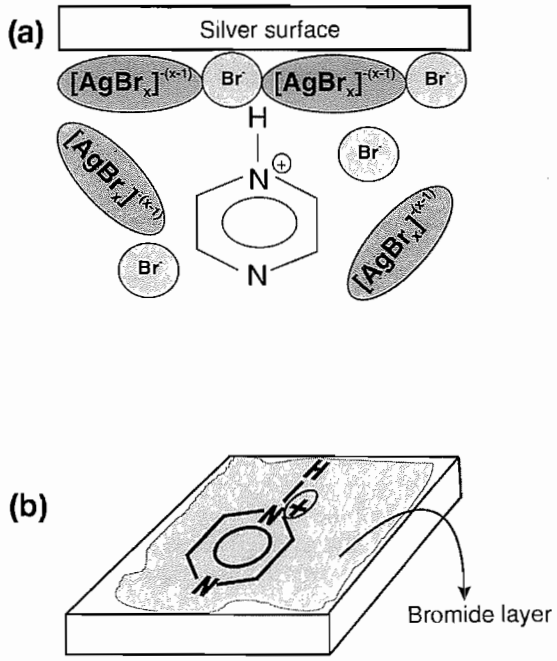


Fig. 4. (*a*) PzH^+ adsorbed end-on is the predominant species at potentials more positive than −170 mV. The cation may interact with either the halide or the soluble silver oxidation products, which are adsorbed at the positively charged electrode. (*b*) The positive charge can be delocalized throughout the entire pyrazine ring due to the protonation of pz, which enables pzH^+ to be adsorbed flat through the halide layer. Flat-adsorbed pzH^+ is the predominant species at potentials more negative than −300 mV.



different potentials. One adsorption orientation is predominant during the silver oxidation ($E > -170$ mV), and the other dominates at potentials more negative than −300 mV. These two different orientations of adsorbed monoprotonated pyrazine can coexist on the metallic surfaces at intermediate potentials. Actually, the pyrazinium ion spectrum at OCP presented in Fig. 1 is an example of this. The two different orientations proposed for the monoprotonated pyrazine cation are illustrated in Fig. 4.

The surface selection rules for SERS predict that the vibration modes with polarizability changes perpendicular to the electrode surface will be more enhanced than the parallel ones (5). Pyrazine adsorbed from neutral solution is thought to bind to the metallic surface by means of one of its nitrogen atoms (4). This end-on adsorption mode is confirmed by a SERS spectrum dominated mainly by the 630, 1019, 1225, and 1590 cm^{-1} bands; for end-on adsorption these bands have components perpendicular to the surface.

The most predominant band in the pzH^+ spectrum at potentials more positive than −170 mV is the ring stretch mode 8*a* at 1616 cm^{-1} (Fig. 2*C*). This band is, at least, 3 times more intense than the ring breathing mode at ca. 1000 cm^{-1}. The 8*a* mode is more intense than the ring breathing mode in the SERS spectra of the perpendicular-adsorbed pyrazine (4). Even considering that a CT contribution may be relevant for the large intensity of the band at 1616 cm^{-1} (15), the intensity ratio between this mode and the ring breathing mode (at ca. 1000 cm^{-1}), observed in Fig. 2, suggests that pyrazinium is adsorbed end-on at those potentials where the silver oxidation occurs. The presence of the 1031 cm^{-1} δ ring mode (number 12) also supports an end-on adsorption. This mode is forbidden in the normal Raman spectrum of pyrazine, but becomes active (with very weak intensity) in the SERS spectrum of pyrazine (4). It also appears with fair intensity in the SERS spectrum of end-on adsorbed pyridine (7). On the other hand, this mode is completely absent in the flat-adsorbed benzene SERS spectrum (16).

Another point to be addressed is how a positive monoprotonated pyrazine can adsorb on a positively charged electrode (the pzc for silver in this bromide medium is expected to be more negative than −900 mV (14)). It is well known in the literature that positive species can use a halide layer as bridge to adsorb onto a positively charged surface (6, 9, 10). During the silver oxidation, a AgBr film is expected to form. It is possible that film dissolution can occur in a highly concentrated halide medium, by formation of $(AgBr_x)^{-(x-1)}$ anions. We can conclude that the pyrazinium cation is bound to either a halide or to the $(AgBr_x)^{-(x-1)}$ and these anions are adsorbed to the positively charged electrode (see Fig. 4*a*). A low wave number band at 150 cm^{-1}, attributed to adsorbed Br^-, decreases in intensity as the electrode is made more negative; concomitantly the band of pzH^+ decreases in intensity. These observa-

© 1997 NRC Canada

tions are consistent with the potential-dependent Br^- surface coverage determined electrochemically (14).

Different features in the pzH^+ spectrum were observed when the potential sweep was continued in the negative direction and the reduction of the silver oxidation products occurred. The Ag^+ ions reduced to Ag, forming the SERS-active sites, and the spectral lines became more intense. The intensity of the SERS bands decreased again, starting at ca. −300 mV. The main features of this pyrazinium spectrum in the 1000 cm^{-1} region are the decrease in the intensities of the envelope that contains the 1018 and 1031 cm^{-1} bands and the appearance of a very strong band at 1002 cm^{-1} (Fig. 2*A*). In the 1200 cm^{-1} region (Fig. 2*B*) one can also notice the decrease in the 1222 cm^{-1} band and the appearance of a 1200 cm^{-1} band. New bands are not formed in the 1600 cm^{-1} region (Fig. 2*C*). The 1616 cm^{-1} band intensity just decreases as the potential becomes negative and vanishes completely at −330 mV.

The spectral observations at potential values more negative than −200 mV suggest that the pyrazinium cation is either tilted or flat-adsorbed on the metallic surface. The bands at 1002 cm^{-1} and at 1200 cm^{-1} can be assigned to the ring modes, numbers 1 and 9*a*, respectively. The shifts of flat-adsorbed pyrazine ring modes to lower wave numbers have been observed by Moskovits et al. (17). Similar changes were also observed in the benzene SERS spectrum (16). When aromatic molecules interact with the surface by π-electrons of the ring they adsorb flat. This interaction is expected to shift the ring stretch frequencies downward. The flat-adsorbed benzene SERS spectrum is also completely dominated by the ring breathing mode (number 1) (16). For instance, this mode is several times more intense than the ring stretch mode number 8*a*, which dominates the spectrum of the end-on adsorbed pyrazine. In Fig. 2, at a potential of ca. −300 mV, the 8*a* mode is hardly observed, but the ring breathing mode is still intense. Another interesting band is at 898 cm^{-1}, marked with an asterisk (*) in Fig. 1. This band is assigned to the γ ring mode number 10*a* (out-of-plane), and it is completely absent in the SERS spectrum of pyrazine (4). However, this band is fairly intense in the benzene spectrum (16) and, following the SERS selection rules, it is expected to be active only for a flat-adsorbed molecule. Similarly, the presence of the 1002 cm^{-1} band (also marked with an asterisk (*) in Fig. 1) is consistent with the flat orientation.

In the potential range where the monoprotonated pyrazine is adsorbed flat, the silver oxidation products, AgBr or $(AgBr_2)^-$, have largely been reduced to metallic silver. This process increases the specific halide surface concentration very significantly. Hence, the flat-adsorbed pyrazinium cation may be bound to the halide layer, which is adsorbed to the positively charged silver surface, as shown in Fig. 4*b*.

Conclusions

The SERS spectrum of monoprotonated pyrazine was measured. The pyrazinium cation can adsorb onto the electrode surface by two different orientations. The end-on adsorbed monoprotonated pyrazine is predominant at potentials more positive than −170 mV. The flat-adsorbed pyrazinium cation is thought to be the only specie on the surface at potentials more negative than −300 mV. The positively charged pyrazinium cation must use either the halide or the $(AgBr_x)^{-(x-1)}$ complex as a bridge to adsorb to a positive electrode surface.

Acknowledgment

This research was supported by grants from the Natural Sciences and Engineering Research Council of Canada.

References

1. A.S.-C. Chia and R.F. Trimble, Jr. J. Phys. Chem. **65**, 863 (1961).
2. A.G. Brolo and D.E. Irish. Z. Naturforsch. A: Phys. Sci. **50**, 274 (1995).
3. A.G. Brolo. Ph.D. thesis, University of Waterloo, Waterloo, Ontario. In preparation.
4. A.G. Brolo and D.E. Irish. J. Electroanal. Chem. **414**, 183 (1996).
5. J.A. Creighton. *In* Advances in spectroscopy. Vol. 16. Spectroscopy of Surfaces. *Edited by* R.H. Clark and R.E. Hester. Wiley, New York. 1988. p. 37.
6. A.G. Brolo and D.E. Irish. J. Chem. Soc. Faraday Trans. **93**, 419 (1997).
7. L.N. Klatt and R.L. Rouseff. J. Am. Chem. Soc. **94**, 7295 (1972).
8. J. Swartz and F.C. Anson. J. Electroanal. Chem. **114**, 117 (1984).
9. D.J. Rogers, S.D. Luck, D.E. Irish, D.A. Guzonas, and G.F. Atkinson. J. Electroanal. Chem. **167**, 237 (1984).
10. Z. Deng and D.E. Irish. Langmuir, **10**, 586 (1994).
11. A.G. Brolo and D.E. Irish. *In* Solid–liquid electrochemical interfaces. *Edited by* G. Jerkiewicz, M.P. Soriaga, K. Uosaki, and A. Wieckowski. ACS Symposium Series No. 656. ACS Books, Washington, D.C. 1997. Chap. 22. p. 310.
12. A.G. Brolo, B.D. Smith, and D.E. Irish. J. Mol. Struct. **405**, 29 (1997).
13. G.R. Erdheim, R.L. Birke, and J.R. Lombardi. Chem. Phys. Lett. **69**, 495 (1980).
14. G. Vallete and R. Parsons. J. Electroanal. Chem. **229**, 87 (1987).
15. J.F. Arenas, M.S. Woolley, J.C. Otero, and J.I. Marcos. J. Phys. Chem. **100**, 3199 (1996).
16. M. Moskovits and D.P. DiLella. Chem. Phys. **73**, 6068 (1980).
17. M. Moskovits, D.P. Dilella, and K.J. Maynard. Langmuir, **4**, 67 (1988).

Can. J. Chem. Downloaded from www.nrcresearchpress.com by 91.121.58.235 on 09/08/12
For personal use only.

© 1997 NRC Canada

The mean spherical approximation and medium effects in the kinetics of solution reactions involving ions

W. Ronald Fawcett, Alex C. Tikanen, and Douglas J. Henderson

Can. J. Chem. Downloaded from www.nrcresearchpress.com by 91.121.58.235 on 09/08/12
For personal use only.

Abstract: The mean spherical approximation has been applied to describe medium effects in the kinetics of reactions between ions in water. When the ionic strength of the medium is altered by the addition of an inert electrolyte, the rate of reaction can be accurately predicted with the inert electrolyte concentration up to 1 M. The theoretical rate constant at the limit of infinite dilution k_{r0} has been estimated for five earlier kinetics studies for which data are available in the literature.

Key words: kinetic medium effects, mean spherical approximation, activity coefficients.

Résumé : On a appliqué l'approximation sphérique moyenne pour décrire les effets de milieu sur les cinétiques de réactions entre des ions dans l'eau. Lorsqu'on modifie la force ionique du milieu par l'addition d'un électrolyte inerte, on peut prédire correctement la vitesse de la réaction avec l'électrolyte inerte à des concentrations allant jusqu'à 1 M. Pour les cinq études cinétiques antérieures pour lesquelles des données sont disponibles dans la littérature, on a évalué la constante de vitesse théorique à la limite de la dilution infinie, k_{r0}.

Mots clés : effets cinétiques du milieu, approximation sphérique moyenne, coefficients d'activité.

[Traduit par la rédaction]

Introduction

Interest in medium effects in the kinetics of reactions involving ions dates from the work of Brönsted (1, 2) and Brönsted and Livingston (3). Somewhat later, these effects were described within the context of transition state theory (4). This led to the conclusion that the logarithm of the reaction rate constant should be linear in the square root of the ionic strength of the solution when the latter is very dilute. Furthermore, the slope of this relationship should be proportional to the product of the charges on the reacting ions. Data illustrating this medium effect can be found in most textbooks dealing with chemical reaction kinetics. The effect in very dilute solutions is easily accounted for on the basis of Debye–Hückel theory in its simple or extended version (5). However, it is clear that the details of the behavior of these systems at higher ionic strengths cannot be dealt with on the basis of the Debye–Hückel model. For example, Kautz and Robinson (6) showed that the rate constant for hydrolysis of sucrose by hydrochloric acid increases markedly with the addition of alkali or alkaline earth chlorides to the system, and that the extent of the increase depends on the nature of the cation. According to the simple theory, the rate of this reaction, which involves an uncharged reactant, should be independent of ionic strength.

In recent work (7, 8), two of us have shown that the nonideality of simple electrolyte solutions can be described up to quite high concentrations on the basis of the mean spherical approximation (MSA). The conclusion from these studies is that the finite size of all solute species, charged or uncharged, must be considered in a complete description of the system. This effect, which is modeled on the basis of the statistical mechanical description of a hard sphere fluid, leads to the well-known increase in the mean ionic activity coefficient at higher concentrations. A second factor that should be considered is the decrease in the dielectric permittivity of the solution with addition of electrolyte. This leads to an increase in the strength of ion–ion interactions with increase in ionic strength.

Examination of the data presented earlier in the literature led us to conclude that it would be worthwhile to reconsider the medium effect for this class of solution reactions within the context of recent work on the MSA. Details of this investigation are given in the present paper.

The MSA utilizing the actual solvent permittivity

The details of the MSA applied to a system involving an ionic reaction are now summarized. It is assumed that the various ions in solution have different sizes so that the unrestricted version of the MSA is applied as described by Blum and coworkers (9–12). The bimolecular reaction involved is

Received March 13, 1997.

This paper is dedicated to Professor Brian E. Conway on the occasion of his 70th birthday.

W.R. Fawcett[1] **and A.C. Tikanen.** Department of Chemistry, University of California, Davis, CA 95616, U.S.A.
D.J. Henderson. Department of Chemistry and Biochemistry, Brigham Young University, Provo, UT 84602, U.S.A.

[1] Author to whom correspondence may be addressed. Telephone: (530) 752-1105. Fax: (530) 752-8995. E-mail: fawcett@indigo.ucdavis.edu

© 1997 NRC Canada

Can. J. Chem. Downloaded from www.nrcresearchpress.com by 91.121.58.235 on 09/08/12
For personal use only.

[1] $A + B \rightleftharpoons X^*$

where A and B are ionic reactants (including the case where the charge on A or B is zero), and X^* is the activated complex whose charge is equal to the sum of that on A and B. The reaction occurs in the presence of an inert 1-1 electrolyte MY. As a result, the solution contains five species, each of which may have a different size. Therefore, activity coefficients for each of these five species should be estimated.

The quantity of fundamental interest in deriving an expression for the single ion activity coefficient is the excess Helmholtz energy ΔA^{EX}. This is made up of two contributions, ΔA^{ES}, the electrostatic part due to the ionic atmosphere, and ΔA^{HS}, the hard sphere part due to the finite size of the solute species. Thus, one writes

[2] $$\Delta A^{EX} = \Delta A^{ES} + \Delta A^{HS}$$

The first contribution becomes more negative as concentration increases, expressing the fact that the ionic atmosphere becomes more effective in screening ion–ion interactions. The second becomes more positive with increasing concentration, expressing the fact that an increasing amount of work must be done to introduce a new solute species into the solution.

The electrostatic contribution can be written as follows

[3] $$\Delta A^{ES} = \Delta U^{ES} + \frac{kT\Gamma^3}{3\pi}$$

where ΔU^{ES} is the excess internal energy due to ion–ion interactions, Γ is the MSA screening parameter defined below, and k is the Boltzmann constant. The general electrolyte solution contains at least two different ions, each of which has a number density ρ_i, a valence z_i, and an effective diameter σ_i. The excess internal energy of any ion i is then

[4] $$\Delta U_i^{ES} = -\frac{e_0^2 \rho_i z_i N_i}{4\pi\varepsilon_0\varepsilon_s}$$

where

[5] $$N_i = \frac{\Gamma z_i + \zeta\sigma_i}{1 + \Gamma\sigma_i}$$

[6] $$\zeta = \frac{\pi}{2\Omega\Delta}\sum_k \frac{\rho_k\sigma_k z_k}{1 + \Gamma\sigma_k}$$

[7] $$\Omega = 1 + \frac{\pi}{2\Delta}\sum_k \frac{\rho_k\sigma_k^3}{1 + \Gamma\sigma_k}$$

[8] $$\Delta = 1 - \frac{\pi}{6}\sum_k \rho_k\sigma_k^3$$

and

[9] $$\Gamma^2 = \frac{\beta e_0^2}{4\varepsilon_0\varepsilon_S}\sum_i \rho_i[(z_i - \zeta\sigma_i^2)/(1 + \Gamma\sigma_i)]^2$$

In these expressions e_0 is the fundamental electronic charge; ε_S, the relative permittivity of the solvent; ε_0, the permittivity of free space; and $\beta = 1/kT$. The screening parameter Γ must be determined by an iterative technique. A convenient starting point in this regard is the value of Γ in the limit that the size of the ions goes to zero. This result gives

[10] $$\Gamma|_{\sigma_i=0} = \frac{\kappa}{2} = \frac{1}{2}\left(\frac{\beta e_0^2}{\varepsilon_0\varepsilon_S}\sum_i \rho_i z_i^2\right)^{1/2}$$

where κ is the Debye–Hückel screening parameter.

Once the screening parameter Γ has been determined, the values of ΔU_i^{ES} and ζ are found by solving eqs. [4]–[8]. The total electrostatic contribution to the excess internal energy is obtained by adding up the contributions from individual ions

[11] $$\Delta U^{ES} = \sum_i \Delta U_i^{ES}$$

The electrostatic contribution to the single ion activity coefficient is determined by differentiating the excess Helmholtz energy due to electrostatic effects with respect to the corresponding ionic number density:

[12] $$\ln y_i^{ES} = \left(\frac{\partial\beta\Delta A^{ES}}{\partial\rho_i}\right)_\Gamma$$

The result obtained by Simonin et al. (12) is

[13] $$\ln y_i^{ES} = \frac{-\beta e_0^2}{4\pi\varepsilon_0\varepsilon_s}\left[\frac{\Gamma z_i^2}{1 + \Gamma\sigma_i} + \zeta\sigma_i\left(\frac{2z_i - \zeta\sigma_i^2}{1 + \Gamma\sigma_i} + \frac{\zeta\sigma_i^2}{3}\right)\right] - \frac{\beta\Delta U^{ES}}{4\pi\varepsilon_0\varepsilon_s}\frac{\partial\varepsilon_s}{\partial\rho_i}$$

The value of $\partial\varepsilon_S/\partial\rho_i$ is unknown for the reactants and the activated complex. However, in the kinetic studies examined here, the concentration of the reactants was always low except in the case of the sucrose study (6). As a result, the only species affecting the solution permittivity are the ions from the inert electrolyte. This means that $\ln y_i^{ES}$ may be estimated for the reactants and activated complex, assuming that $\partial\varepsilon_S/\partial\rho_i$ for each of these species is zero. The value of $\partial\varepsilon_S/\partial\rho_i$ would be required if one wished to estimate individual activity coefficients for the ions of the inert electrolyte, but that is not the object of the present study. Finally, the value of the experimentally observed permittivity ε_S, which involves knowing how this quantity varies with inert electrolyte concentration, was used in calculations based on eq. [13].

The permittivity data for the aqueous inert salt solutions were obtained from the recent compilation of Barthel et al. (13). This compilation provides detailed information about the frequency dependence of the permittivity at each concentration. To avoid the effects of possible ion pairing at low frequencies, and of any high-frequency relaxations, the in-phase component ε_{in} of the permittivity was plotted against the out-of-phase component ε_{out} in order to determine the static

© 1997 NRC Canada

Can. J. Chem. Downloaded from www.nrcresearchpress.com by 91.121.58.235 on 09/08/12
For personal use only.

Table 1. Values of the constants δ_s and b_s, which describe the concentration dependence of ε_s in eq. [15], along with the maximum concentration for which permittivity data are available $c_{max}(\varepsilon_s)$.

Electrolyte	δ_s (L mol^{-1})	b_s (L$^{3/2}$ mol$^{-3/2}$)	$c_{max}(\varepsilon_s)$ (M)
KCl	14.7	3.0	4.0
NaCl	16.2	3.1	4.0
KNO_3	14.4	4.5	4.0
$NaNO_3$	16.9	4.3	4.0

permittivity of the solvent ε_S. According to the Debye model, the relationship between these quantities is

$$[14] \quad \varepsilon_{in} = \varepsilon_S - \omega\tau\varepsilon_{out}$$

where ω is the angular frequency, and τ, the Debye relaxation time. Excellent linear plots were obtained for most of the frequency range above 8 GHz for the electrolytes considered here.

The concentration dependence of ε_S was analyzed on the basis of the relationship

$$[15] \quad \varepsilon_s = \varepsilon_{s0} - \delta_s c_e + b_s c_e^{3/2}$$

where ε_{S0} is the permittivity of the *pure* solvent (for H_2O, 78.45 at 25°C), c_e, the electrolyte concentration in M, δ_S, the dielectric decrement for the given electrolyte, and b_S, a parameter describing the nonlinear part of this dependence. Values of δ_S and b_S, determined by a least-squares fit of eq. [15] to the ε_S data, are summarized in Table 1 for the inert electrolytes included in this study.

Finally, the unrestricted hard sphere contribution may be calculated by differentiating the expression for the Helmholtz energy of a mixture of hard spheres (14, 15). The hard sphere contribution to $\ln y_i$ for the case that there are two or more particles of differing size, regardless of their charge, is evaluated as follows:

$$[16] \quad \ln y_i^{HS} = \left(\gamma_i - 1 - \frac{2\eta_i}{\eta} y_3\right) \ln X + \frac{\eta}{X^2}\left[3(1-\alpha_i) + \gamma_i + \frac{3\eta}{2}(\alpha_i - \beta_i - \gamma_i - 1)\right] + \frac{\eta_i}{X^3}\left\{\eta\left[5y_3 - \frac{9}{2}y_1 - 2 + \eta\left(\frac{3}{2}y_1 - 3y_2 - 4y_3 + 1\right)\right] - 2y_3 + 4\right\}$$

where

$$\eta_i = \frac{\pi}{6}\rho\sigma_i^3, \qquad \eta = \sum_i \kappa_i\eta_i, \qquad \kappa_i = \frac{\rho_i}{\rho}, \qquad \rho = \sum_i \rho_i$$

and

$$[17] \quad X = 1 - \eta$$

The other quantities introduced in eq. [16] are as follows

$$[18] \quad y_1 = \sum_{i>j} \Delta_{ij} \frac{\sigma_i + \sigma_j}{(\sigma_i\sigma_j)^{1/2}}$$

$$[19] \quad y_2 = \sum_{i>j} \Delta_{ij} \sum_k \kappa_k \frac{\eta_k}{\eta} \frac{(\sigma_i\sigma_j)^{1/2}}{\sigma_k}$$

$$[20] \quad y_3 = \left[\sum_i \kappa_i \left(\frac{\eta_i}{\eta}\right)^{2/3}\right]^3$$

$$[21] \quad \Delta_{ij} = \kappa_i\kappa_j \frac{(\eta_i\eta_j)^{1/2}}{\eta} \frac{(\sigma_i - \sigma_j)^2}{\sigma_i\sigma_j}$$

$$[22] \quad \alpha_i = \frac{1}{\eta}\sum_k \kappa_k \frac{(\sigma_i + \sigma_k)(\sigma_i - \sigma_k)^2(\eta_i\eta_k)^{1/2}}{(\sigma_i\sigma_k)^{3/2}}$$

$$[23] \quad \beta_i = \sum_{i>j} \Delta_{ij} \frac{\eta_i}{\eta} \frac{(\sigma_i\sigma_j)^{1/2}}{\sigma_i} + \sum_j \kappa_j \frac{(\eta_i\eta_j)^{1/2}}{\eta} \frac{(\sigma_i - \sigma_j)^2}{\sigma_i\sigma_j} \times \sum_k \kappa_k \frac{\eta_k}{\eta} \frac{(\sigma_i\sigma_j)^{1/2}}{\sigma_k}$$

and

$$[24] \quad \gamma_i = 3\left(\frac{\eta_i}{\eta} y_3\right)^{2/3}$$

The present model assumes that the size of the reactants are equal, so eqs. [16]–[24] are solved for only four, instead of five, species in solution, that is, the reactants, the activated complex, the cation of the inert salt, and the anion of the inert salt. By adding the logarithms of the electrostatic and the hard sphere contributions, one obtains the activity coefficient on the molar scale y_i:

$$[25] \quad \ln y_i = \ln y_i^{ES} + \ln y_i^{HS}$$

The medium effect in solution reactions involving ions

The description of the medium effect for a reaction in solution is based on transition state theory (4), and involves estimation of the concentration of the activated complex X^* formed in a pseudoequilibrium with the reactants A and B (eq. [1]). The equilibrium constant for this process is K^* given by

$$[26] \quad K^* = \frac{a_{X^*}}{a_A a_B}$$

where a_i is the activity of component i. Since all of these species can be charged, the activity coefficients are not unity, and are expected to vary significantly with ionic strength. The rate of reaction υ_r is given by

$$[27] \quad \upsilon_r = \nu^* c_{X^*} = \frac{\nu^* K^* a_A a_B}{y_{X^*}} = \frac{y_A y_B}{y_{X^*}} \nu^* K^* c_A c_B$$

where ν^* is the frequency of decomposition of the activated complex into products; c_i, the molar concentrations of the species A, B, and X^*; and y_i, the corresponding activity coefficients on the molarity scale. The rate constant k_r for reaction [1] is

© 1997 NRC Canada

Table 2. The reactants in the systems considered here, their charges z_A and z_B, along with values obtained for the diameters σ_+ and σ_- for the ions of the inert electrolyte on the basis of an earlier study (8).

Reactants A, B	Ref.	z_A, z_B	Inert salt	σ_+ (pm)	σ_- (pm)
$BrCH_2COO^{1-}$, $S_2O_3^{2-}$	17	−1, −2	$NaNO_3$	454	266
Nitrourethane anion, OH^{1-}	16	−1, −1	KCl	528	434
Sucrose, H_3O^{1+}	6	0, +1	KCl	528	434
$CoBr(NH_3)_5^{2+}$, OH^{1-}	17	+2, −1	NaBr	454	450
$CoBr(NH_3)_5^{2+}$, Hg^{2+}	3	+2, +2	KNO_3	528	266

Can. J. Chem. Downloaded from www.nrcresearchpress.com by 91.121.58.235 on 09/08/12
For personal use only.

$$[28] \quad k_r = \frac{\upsilon_r}{c_A c_B} = \frac{y_A y_B}{y_{X^*}} k_{r0}$$

where

$$[29] \quad k_r = \nu^* K^*$$

The rate constant k_{r0} is that measured in the absence of medium effects and, in general, cannot be determined experimentally. This follows from the fact that the solution always has a finite ionic strength even in the absence of an inert electrolyte.

In the Debye–Hückel description of this effect, each activity coefficient is given by its value in the concentration region where the limiting law applies, that is

$$[30] \quad \ln y_i = -Az_i^2 I^{1/2}$$

where I is the ionic strength and A, the Debye–Hückel constant. Substituting this expression for y_i in eq. [28], one obtains, after some simple algebra,

$$[31] \quad \ln (k_r/k_{r0}) = +2Az_A z_B I^{1/2}$$

This result involves the assumption that the charge on the activated complex is $z_A + z_B$. It has often been presented in textbooks, but is limited in validity to the concentration range over which the limiting Debye–Hückel law is valid. When data are available at these low concentrations, eq. [31] is quite useful, because it allows one to confirm the nature of ions involved in the rate-determining step by plotting ln k_r against $I^{1/2}$. The value of the product $z_A z_B$ can then be extracted from the slope of such a plot.

In the present study, attention is focused on eq. [28], and the question of whether medium effects can be understood beyond the range of applicability of the limiting Debye–Hückel law. Thus, it is always assumed that z_A and z_B are known from the analysis of data at lower ionic strengths. Details of our analysis and the results are presented in the following sections.

Data analysis

A basic requirement in the literature search for rate constant data demonstrating the "kinetic salt effect" was that the reactants be kept at the same concentrations while the ionic strength was increased only by the addition of an inert 1-1 electrolyte. This requirement follows from the fact that the activity coefficients of the reactants do not depend on their concentration in a simple way. Moreover, the purpose of this study is to show that the theoretically determined activity coefficients for the reactants and activated complex can be directly related to the reaction rate. In all cases, the MSA effective ion sizes for the inert salt were obtained in earlier work (8) and are given in Table 2. To keep the analysis simple, the sizes of the reacting ions A and B were assumed to be the same. Although this is not always a reasonable assumption, it reduces the number of assumed parameters by one. However, this assumption is expected to have an effect on the best value of the size of the activated complex σ_{X^*}, which is also required to carry out the analysis. The best value of σ_{X^*} was found by requiring that a plot of $\log_{10} k_r$ against $\log_{10}(y_A y_B/y_{X^*})$ be linear with a slope of unity. The maximum ionic strength considered was 1 M. Although data for most systems studied involve lower ionic strengths, data for the inversion of sucrose (6) have been reported to ionic strengths as high as 3 M. A proper analysis of data at high ionic strengths should consider the effects of ion pairing, which are not negligible under these conditions (8).

Two other features of the analysis need to be mentioned. Since the reactants A and B are usually ions, their presence in solution adds other ions to the system. For example, if A and B are cations, they come into solution with anions. These anions were assumed to be the same as the anion of the inert electrolyte, and its concentration was adjusted in the appropriate way. Thus, all calculations were performed with a strictly electroneutral system, and the estimation of the ionic strength and the screening parameter Γ were made considering all ions in the system.

In all cases except two, the kinetic data were obtained in studies made at 25°C, that is, at the same temperature at which the dielectric permittivity data are available. However, in the case of the $CoBr(NH_3)_5^{2+}$–OH^{1-} and $CoBr(NH_3)_5^{2+}$–Hg^{2+} systems, the kinetic data were obtained at 15°C. For these systems, the value of ε_{S0} was taken to be 82.44, as reported for pure water at 15°C in the literature (13), and the values of δ_S and b_S for the inert salt were assumed to have the same values obtained at 25°C (see Table 1). No dielectric decrement data are available for NaBr, which was used as the inert electrolyte for the $CoBr(NH_3)_5^{2+}$–OH^{1-} study. The permittivity parameters were assumed to be the same as those for the NaCl system as reported in Table 1. On the basis of our previous work this is a reasonable assumption.

For each system, the linear regression line obtained by a plot of $\log_{10} k_r$ against $\log_{10}(y_A y_B/y_{X^*})$ was extrapolated to

© 1997 NRC Canada

Can. J. Chem. Downloaded from www.nrcresearchpress.com by 91.121.58.235 on 09/08/12
For personal use only.

Table 3. Values for the diameter of the reactants σ_A and σ_B ($\sigma_A = \sigma_B$) and the activated complex σ_{X^*}, which produce a slope of unity for the plot of $\log_{10}k$ against the MSA estimate of $\log_{10}(y_A y_B/y_{X^*})$, along with the logarithm of the rate constant in the limit of infinite dilution $\log_{10}k_{r0}$, and the linear least-squares correlation coefficient r.

Reactants A, B	$\sigma_{A,B}$ (pm)	σ_{X^*} (pm)	$\log_{10}k_{r0}$	r
$BrCH_2COO^{1-}$, $S_2O_3^{2-}$	400	687	−0.551	0.998
Nitrourethane anion, OH^{1-}	800	1074	−0.844	0.992
Sucrose, H_3O^{1+}	800	1057	−0.525	0.994
$CoBr(NH_3)_5^{2+}$, OH^{1-}	700	1065	2.04	0.999
$CoBr(NH_3)_5^{2+}$, Hg^{2+}	700	674	1.84	0.996

zero, and the value of the rate constant in the limit of infinite dilution k_{r0} was estimated. This value was then used in eq. [31] to obtain a plot of $\log_{10}(k/k_{r0})$ against the square root of the ionic strength. The initial slope of this plot estimated by the limiting Debye–Hückel law for ionic strengths below 0.01 M is also shown in Figs. 1–5. The results for each system, along with the correlation coefficient for the MSA are reported in Table 3.

Discussion

Kinetic data were examined for five systems, corresponding to values of $z_A z_B$ equal to 4, 2, 1, 0, and −2. The nature of the reactants, the inert electrolyte, and the values of the size parameters for this electrolyte obtained in earlier work are summarized in Table 2.

The results of our analysis are summarized in Table 3 and in Figs. 1–5. First of all, it should be noted that excellent fits to the data were obtained in all cases. This allows one to extrapolate the plots of $\log_{10}k_r$ against $\log_{10}(y_A y_B/y_{X^*})$ to obtain values of the rate constant at infinite dilution k_{r0}. It should be noted that values of k_{r0} reported in the early literature often corresponded to the rate constant measured at finite ionic strength in the absence of an inert electrolyte. In our analysis, the concentration of *all* ions was considered in calculating the ionic strength so that k_{r0} is a hypothetical rate constant not measurable in the laboratory, but it is a proper point of reference.

Results for the bromoacetate–thiosulphate reaction for which $z_A z_B$ is equal to 2 are shown in Fig. 1. As can be seen, the MSA estimates of the ratio $y_A y_B/y_{X^*}$ successfully describe the kinetic data for ionic strengths up to 1 M. The values of the assumed diameters for the reactants and activated complex, namely 400 and 600 pm, respectively, are quite reasonable. The traditional plot of $\log_{10}(k_r/k_{r0})$ against $I^{1/2}$ demonstrates the severe departure of the kinetic data from limiting Debye–Hückel behavior over most of the experimental range that data have been reported. This analysis underscores the necessity of considering the size of all ions in the electrolyte solution in order to make realistic estimates of ionic activity coefficients.

Results for the nitrourethane–hydroxyl system for which $z_A z_B$ is equal to 1 are shown in Fig. 2. Much larger values of the hard sphere diameter were required to get an acceptable fit in the MSA analysis. In the traditional Debye–Hückel plot all of

Fig. 1. Kinetic data for the $BrCH_2COO^{1-}$–$S_2O_3^{2-}$ system. The top graph shows the plot of $\log_{10}k$ against $\log_{10}(y_A y_B/y_{X^*})$, along with the linear regression line with a slope of unity. The bottom graph shows the plot of $\log_{10}(k_r/k_{r0})$ against the square root of the ionic strength $I^{1/2}$. The dotted line shows the prediction of the medium effect on the basis of the unrestricted MSA, and the solid line shows the prediction on the basis of the limiting Debye–Hückel law (eq. [31]).

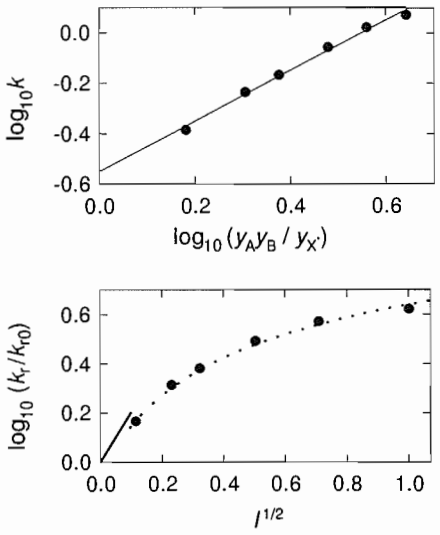
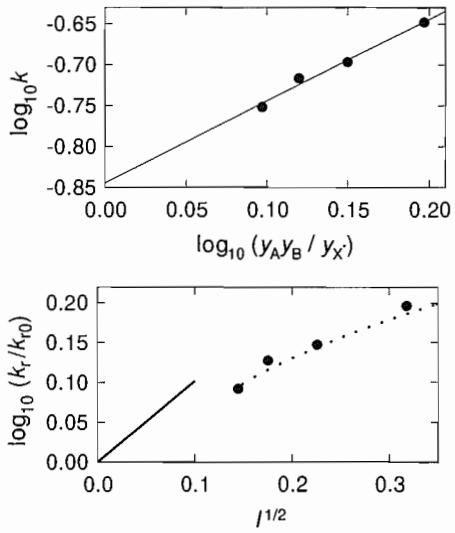


Fig. 2. Kinetic data for the nitrourethane anion–OH^{1-} system. The top graph shows the plot of $\log_{10}k$ against $\log_{10}(y_A y_B/y_{X^*})$, along with the linear regression line with a slope of unity. The bottom graph shows the plot of $\log_{10}(k_r/k_{r0})$ against the square root of the ionic strength $I^{1/2}$. The dotted line shows the prediction of the medium effect on the basis of the unrestricted MSA, and the solid line shows the prediction on the basis of the limiting Debye–Hückel law (eq. [31]).



the data points fall below the limiting Debye–Hückel behavior. This is not unexpected because the data were obtained at ionic strengths greater than 0.01. The hard sphere approximation is probably weakest for this system because of the charge

© 1997 NRC Canada

Can. J. Chem. Downloaded from www.nrcresearchpress.com by 91.121.58.235 on 09/08/12
For personal use only.

Fig. 3. Kinetic data for the sucrose–H_3O^{1+} system. The top graph shows the plot of $\log_{10}k$ against $\log_{10}(y_A y_B/y_{X^*})$, along with the linear regression line with a slope of unity. The bottom graph shows the plot of $\log_{10}(k_r/k_{r0})$ against the square root of the ionic strength $I^{1/2}$. The dotted line shows the prediction of the medium effect on the basis of the unrestricted MSA, and the solid line shows the prediction on the basis of the limiting Debye–Hückel law (eq. [31]).

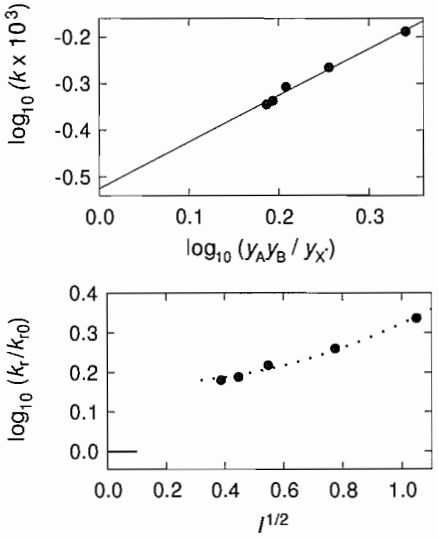
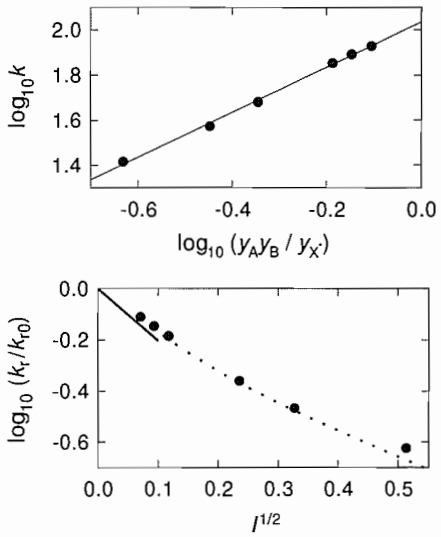


Fig. 4. Kinetic data for the $CoBr(NH_3)_5^{2+}$–OH^{1-} system. The top graph shows the plot of $\log_{10}k$ against $\log_{10}(y_A y_B/y_{X^*})$, along with the linear regression line with a slope of unity. The bottom graph shows the plot of $\log_{10}(k_r/k_{r0})$ against the square root of the ionic strength $I^{1/2}$. The dotted line shows the prediction of the medium effect on the basis of the unrestricted MSA, and the solid line shows the prediction on the basis of the limiting Debye–Hückel law (eq. [31]).

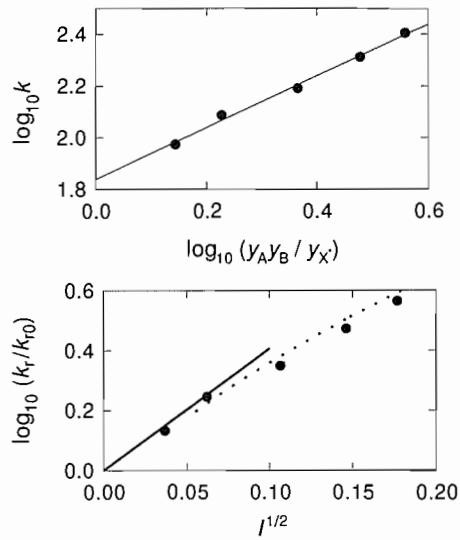


distribution on the nitrourethane–hydroxyl activated complex. It is probable that the negative charge on the nitrourethane anion is several atoms away from the site of attack of the hydroxyl ions, so that this complex behaves more like a species with a charge of -1 with respect to ionic atmosphere effects. This would explain the fact that deviations from the Debye–Hückel line are lower than one might anticipate.

Results for the inversion of sucrose in the presence of KCl are shown in Fig. 3. In this case, the reactants sucrose and hydronium ion were held at fixed concentrations of 0.5843 M and 0.1 M, respectively. The large hard sphere contribution from the reactant sucrose correctly holds the ratio $y_A y_B/y_{X^*}$ above unity even in the limit of zero ionic strength. The application of the MSA in this case allows one to estimate the rate constant k_{r0} in the limit of infinite dilution of the uncharged reactant sucrose, a very useful result. Since the product of $z_A z_B$ is zero, the rate constant for this reaction should be independent of ionic strength on the basis of Debye–Hückel theory. The increase in k_r, seen experimentally, is clearly due to the hard sphere effect only, that is, the finite size of the solute species in the electrolyte solution. An excellent description of this effect is obtained on the basis of the MSA, assuming rather large diameters for the reactants and activated complex. The assumption that σ_A is equal to σ_B is clearly incorrect here because the effective size of the hydronium ion should be much smaller than that of a sucrose molecule. However, making the calculation more carefully would involve adding at least one more adjustable parameter. Since our purpose is only to demonstrate the effectiveness of the MSA in a qualitative way, the present results are quite satisfying.

Results for the bromopentaamino Co(III) – hydroxyl ion system for which $z_A z_B$ is equal to -2 are shown in Fig. 4. This is the only system considered here in which the charges on the

Fig. 5. Kinetic data for the $CoBr(NH_3)_5^{2+}$–Hg^{2+} system. The top graph shows the plot of $\log_{10}k$ against $\log_{10}(y_A y_B/y_{X^*})$, along with the linear regression line with a slope of unity. The bottom graph shows the plot of $\log_{10}(k_r/k_{r0})$ against the square root of the ionic strength $I^{1/2}$. The dotted line shows the prediction of the medium effect on the basis of the unrestricted MSA, and the solid line shows the prediction on the basis of the limiting Debye–Hückel law (eq. [31]).



reacting ions are opposite one another. The fit is again very successful with reasonable values being obtained for σ_A, σ_B, and σ_{X^*}.

The last system considered involved ions with high charges

© 1997 NRC Canada

and a value of $z_A z_B$ equal to 4 (Fig. 5). Although ion pairing is expected to play a role in medium effects for this system, a very good fit was obtained to the kinetic data, with reasonable values for the size parameters.

The present study is especially valuable in the estimation of the work terms in homogeneous electron transfer reactions. In Marcus' detailed description of the theory of electron transfer (18), w_r was defined as the work done to bring the reactants from points very far from one another to contact. This work is equivalent to the factor $RT \ln(y_A y_B / y_{X^*})$ discussed in this paper. In most estimates of w_r (19, 20), the extended Debye–Hückel theory has been used. However, this model is limited to ionic strengths of 0.1 M, whereas experimental studies are often carried out at higher ionic strengths. This is especially true of studies of self-exchange reactions such as the Fe^{3+}/Fe^{2+} system, which often involve highly charged reactants. The MSA is clearly superior to the extended Debye–Hückel model because it considers the sizes of all the solute particles in the system. Its application to existing data would help considerably in obtaining better estimates of the Gibbs activation energy for electron transfer in the limit of infinite dilution.

In summary, the present study has shown conclusively that the MSA provides a very reasonable extension of the Debye–Hückel theory. It can be applied to describe the thermodynamic properties of 1-1 electrolytes for ionic strengths up to 1 M, provided it is used in its unrestricted version in which different sizes are assumed for each ionic species in solution. The main feature of this model, which enabled the present successful treatment of medium effects for ionic reactions in solution, is the consideration of the finite size of all solute species in the system, not just a central ion as in the Debye–Hückel model. Further improvement in the description of these systems would require the addition of ion pairing to the model. This has been done for simple electrolyte solutions (8) but does not seem worthwhile in the analysis of kinetic data, at least, considering the fact that so few studies are available.

Can. J. Chem. Downloaded from www.nrcresearchpress.com by 91.121.58.235 on 09/08/12
For personal use only.

Acknowledgment

W.R.F. acknowledges support from the Office of Naval Research, Washington, D.C., and D.J.H., from the Petroleum Research Foundation (grant number 31573-AC9).

References

1. J.N. Brönsted. Z. Phys. Chem. **102**, 169 (1922).
2. J.N. Brönsted. Z. Phys. Chem. **115**, 337 (1925).
3. J.N. Brönsted and R. Livingston. J. Am. Chem. Soc. **49**, 435 (1927).
4. S. Glasstone, K.J. Laidler, and H. Eyring. The theory of rate processes. 1st ed. McGraw–Hill, New York. 1941.
5. R.A. Robinson and R.H. Stokes. Electrolyte solutions. 2nd ed. Butterworths Scientific Publications, London. 1959.
6. C.F. Kautz and A.L. Robinson. J. Am. Chem. Soc. **50**, 1022 (1928).
7. W.R. Fawcett and A.C. Tikanen. J. Phys. Chem. **100**, 4251 (1996).
8. A.C. Tikanen and W.R. Fawcett. J. Electroanal. Chem. In press.
9. L. Blum. Mol. Phys. **30**, 1529 (1975).
10. L. Blum and J.S. Hoye. J. Phys. Chem. **81**, 1311 (1977).
11. C. Sanchez-Castro and L. Blum. J. Phys. Chem. **93**, 7478 (1989).
12. J.-P. Simonin, L. Blum, and P. Turq. J. Phys. Chem. **100**, 7704 (1996).
13. J. Barthel, R. Buchner, and M. Münsterer. DECHEMA Chemistry Data Series. Vol. XII. Part 2. DECHEMA, Frankfurt a. M. 1995.
14. W. Ebeling and K. Scherwinski. Z. Phys. Chem. (Leipzig), **264**, 1 (1983).
15. A.A. Humffray. J. Phys. Chem. **87**, 5521 (1983).
16. J.N. Brönsted and A. Delbanco. Z. Anorg. Chem. **144**, 248 (1925).
17. A.R. Olsen and T.R. Simonson. J. Chem. Phys. **17**, 1167 (1949).
18. R.A. Marcus. J. Chem. Phys. **43**, 679 (1965).
19. B. Perlmutter-Hayman. Prog. React. Kinet. **6**, 239 (1971).
20. N. Sutin. *In* Progress in inorganic chemistry. Vol. 30. *Edited by* S.J. Lippard. John Wiley & Sons, New York. 1983. p. 441.

© 1997 NRC Canada

Comprehensive studies of formation and reduction of surface oxides at rhodium electrodes at 298 K

Francis Villiard and Gregory Jerkiewicz

Can. J. Chem. Downloaded from www.nrcresearchpress.com by 91.121.58.235 on 09/08/12
For personal use only.

Abstract: Surface oxides on Rh were formed by anodic polarization at various potentials, E_p, from 0.70 to 1.40 V, RHE, for polarization times, t_p, up to 10^4 at 298 K; their thickness expressed as a charge density, q_{OX}, was evaluated from cyclic voltammetry, CV, profiles. The oxide growth proceeds in two steps whereas its reduction occurs in one. Upon extension of E_p and (or) t_p to higher values, q_{OX} increases. Under the above experimental conditions, q_{OX} varied from 110 ± 5 to 985 ± 10 μC cm^{-2}; after conversion, these charge densities correspond to 0.5 monolayer, ML, of RhOH and 1.56 ML of $Rh(OH)_3$, respectively. Augmentation of E_p and t_p results in thermodynamically more stable oxides. Plots of q_{OX} versus log t_p are linear over the whole range of q_{OX} whereas plots of $1/q_{OX}$ versus log t_p are linear only when q_{OX} >210 μC cm^{-2}. Thus, the oxide growth is either logarithmic in time over the whole region of q_{OX} or it is logarithmic when q_{OX} <210 μC cm^{-2} and inverse-logarithmic when q_{OX} >210 μC cm^{-2}. It was observed that the oxide growth continues when the positive-going scan is stopped in the oxide-formation potential region. Similarly, the oxide reduction proceeds when the negative-going scan is stopped in the oxide-reduction potential range. Finally, the authors present the first-ever studies of the Rh oxide reduction. The results indicate that the reduction takes place at $E \leq 0.70$ V, RHE. The oxide reduction kinetics are not understood but, in general, the lower the reduction potential and the longer the reduction time, the greater the amount of the reduced oxide.

Key words: rhodium oxides, oxide films, growth kinetics, reduction kinetics.

Résumé : La polarisation anodique à des potentiels, E_p, allant de 0,70 à 1,40 V, RHE, pour des temps de polarisation, t_p, allant jusqu'à 10^4 s à 298 K, conduit à la formation d'oxydes de surface sur le Rh; on a évalué leur épaisseur en fonction de la densité de charge, q_{OX}, à partir de leurs profils de voltampérométrie cyclique, VC. La croissance de l'oxyde se fait en deux étapes alors que la réduction n'en implique qu'une. Si l'on augmente les valeurs de E_p et (ou) de t_p, la valeur de q_{OX} augmente. Dans les conditions expérimentales décrites plus haut, q_{OX} varie de 110 ± 5 à 985 ± 10 μC cm^{-2}; après conversion, ces densités de charge correspondent respectivement à 0,5 d'une monocouche, MC, de RhOH et à 1,56 MC de $Rh(OH)_3$. Des augmentations de E_p et de t_p conduisent à des oxydes thermodynamiquement plus stables. Les courbes de q_{OX} en fonction de log t_p sont linéaires sur l'ensemble de q_{OX} alors que celles de $1/q_{OX}$ en fonction du log t_p ne sont linéaires que lorsque q_{OX} >210 μC cm^{-2}. Ainsi, la croissance de l'oxyde est soit logarithmique avec le temps sur l'ensemble de q_{OX} soit elle est logarithmique quand q_{OX} <210 μC cm^{-2} et logarithmique inverse quand q_{OX} >210 μC cm^{-2}. On a observé que la croissance de l'oxyde se poursuit lorsqu'on arrête le balayage positif dans la région de potentiel conduisant à la formation d'oxyde. De la même manière, la réduction de l'oxyde se poursuit lorsqu'on arrête le balayage négatif dans la région de potentiel conduisant à la réduction de l'oxyde. Enfin, les auteurs présentent les toutes premières études sur la réduction de l'oxyde de Rh. Les résultats indiquent que la réduction se produit à $E \leq$ 0,70 V, RHE. On ne comprend pas la cinétique de la réduction de l'oxyde, mais, en général, la quantité d'oxyde réduit augmente avec une diminution du potentiel de réduction et une augmentation du temps de réduction.

Mots clés : oxydes de rhodium, oxydes en film, cinétique de la croissance, cinétique de la réduction.

[Traduit par la rédaction]

Introduction

Surface oxides on metals can be formed by application of gas phase and electrochemical techniques (1–7). The oxide development under gas phase conditions requires the presence of an oxidizing atmosphere containing molecular oxygen. During oxidation, the O_2 molecule approaching the metal surface undergoes dissociation and the oxygen atoms become chemisorbed, O_{chem}. Subsequently, the transfer of two electrons to O_{chem} takes place, resulting in creation of O^{2-}. The formation of O^{2-} is accompanied by formation of the metal cation, M^{Z+}, or M^{2+} in the case of a divalent metal, at the metal–oxide interface (Fig. 1). In the case of electroformation of surface oxides, the process requires the presence of an oxidizing electrolyte and an external current source. In acidic solutions, for instance, the water molecule discharge results in formation of adsorbed OH species, and subsequent electron transfer with simultaneous H departure from OH_{ads} groups leads to formation of O^{2-} (Fig. 1); the process is

Received April 14, 1997.

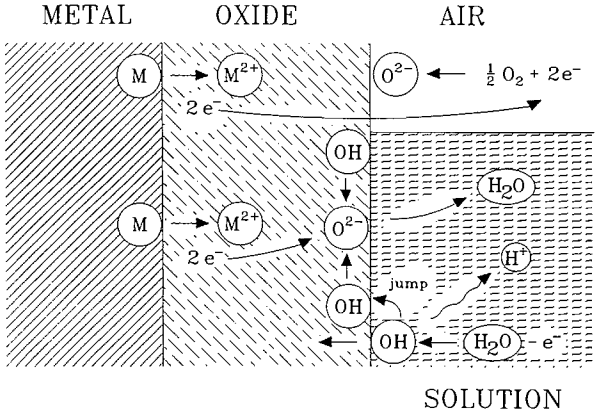
This paper is dedicated to Professor Brian E. Conway on the occasion of his 70th birthday.

F. Villiard and G. Jerkiewicz.[1] Département de chimie, Université de Sherbrooke, Sherbrooke, QC J1K 2R1, Canada.

[1] Author to whom correspondence may be addressed. Telephone: (819) 821-7085. Fax: (819) 821-8017. E-mail: gregory.jerkiewicz@courrier.usherb.ca

© 1997 NRC Canada

Fig. 1. Visual representation of surface-oxide development under gas-phase and electrochemical conditions. Under gas-phase conditions, the O_2 undergoes dissociation and the process leads to development of O_{chem}; simultaneous formation of the metallic cation, M^{2+}, and the electron transfer through the oxide film result in creation of a surface metal–oxide structure that comprises M^{2+} and O^{2-}. Under electrochemical conditions, the adsorbed O_{chem} or OH_{chem} results from discharge of the O-containing species of electrolyte (here the H_2O molecule); accompanying creation of M^{2+} and the electron transfer through the oxide leads to development of a surface oxide or surface hydroxide.



followed by creation of M^{Z+} cations at the inner metal–oxide interface; the transport of electrons, O^{2-}, and M^{Z+}, is assisted by the externally applied electric field. The extent of surface oxidation accomplished by utilization of electrochemical means is related to nature of the metal and the polarization conditions as well as to the electrolyte composition and pH. Metal oxidation does not necessarily involve development of an oxide film since, for instance, a surface sulfide can be grown in a nonaqueous solvent containing S^{2-} or HS^-, or in a molten sulfide (1–3). It has been discussed elsewhere that a stable surface oxide affects the kinetics and mechanism of various faradaic and redox anodic processes (8–14). In particular, the surface valence band structure of an oxidized metal differs from that of the native metal, giving rise to (*i*) distinguishable adsorption properties of the reaction intermediates and products and (*ii*) creation of a barrier to charge transfer. In the case of anodic oxidation of adsorbed inorganic/organic species, the potential region in which the process takes place can overlap that of the oxide formation, thus the overall current corresponds to both electrode processes occurring concurrently. Presence of the surface oxide can alter the kinetics, mechanism, and the pathways of the process, resulting in reduced or enhanced electrochemical activity as well as in new reaction products.

Growth of the surface oxide on noble-metal electrodes can be conveniently studied by application of electrochemical techniques such as cyclic voltammetry, CV, and linear-sweep voltammetry, LSV, because the oxide can be completely reduced within one CV cycle or LSV sweep, respectively (11, 12, 15–26). This approach allows one to (*i*) evaluate the overall oxide-reduction charge density, q_{OX}, with the precision of some 2–3% of a monolayer; (*ii*) identify different oxidation states of the metal cation in the oxide; and (*iii*) distinguish various energetic states of the oxide that can arise from different surface structures or different degrees of hydration. However, this procedure cannot be applied to scrutinize the thickness of oxides on certain transition metals such as Ni, Ti, Zr, Hf, etc., because the passive films are not reducible by utilization of electrochemical techniques.

X-ray photoelectron spectroscopy, XPS, Auger electron spectroscopy, AES, core-level electron energy loss spectroscopy, CEELS, and ellipsommetry experiments (27–32) are of importance to the electrochemical surface science of oxides because they provide means of elucidating the oxidation state of the metal cation within the oxide, identifying the presence of other surface species, and evaluating thickness of the oxide. Coupling of UHV-based surface-science techniques with electrochemical procedures results in detailed characterization of the electrified solid–liquid interface and in assessment of the relation between the mechanism and kinetics of the electrode process under scrutiny as well as the chemical and electronic structure of the surface of the electrode without contaminating it by transfer via air.

Rhodium, being a noble metal, forms surface oxides upon anodic polarization even in the region of water stability, thus below the thermodynamic reversible potential of the oxygen evolution reaction, E°_{OER} = 1.23 V, SHE (4–6, 8–26). In aqueous 0.50 M H_2SO_4 solution, the oxide growth on Rh commences at 0.55 V versus the reversible hydrogen electrode, RHE, and a complete monolayer, ML, of $Rh(OH)_3$ is formed upon reaching the potential of 1.40 V, RHE, as revealed by CV and XPS measurements (27). Short potentiostatic polarization at potentials between 3.00 and 4.00 V, RHE, or prolonged polarization at potentials above 2.00 V, RHE, leads to formation of oxides comprising two species, namely, $Rh(OH)_3$ and RhO(OH) (12, 27). Elsewhere (13), it was shown that the $Rh(OH)_3$ layer grows to a limiting thickness of 3 ML and that it is sandwiched between Rh and the outer film consisting of RhO(OH). In the case of Rh oxides formed in 0.50 M aqueous H_2SO_4 by anodic polarization at potentials from 0.80 to 2.40 V, RHE, and for times up to 10^4 s, it was observed that these conditions resulted in development of thin films and that once a monolayer of RhOH had been formed, the oxide growth followed inverse-logarithmic kinetics with the process being limited by the rate of escape of the Rh^{3+} cation from the metal into the oxide (12). Subsequently, the kinetics of the oxygen evolution reaction, OER, on preoxidized Rh electrodes were evaluated and a relation between the oxide thickness and the kinetic parameters of the OER was established (13).

In this paper, the authors demonstrate a comprehensive study of the formation and reduction of Rh monolayer oxides in 0.50 M aqueous H_2SO_4 solution at 298 K. The present results are an extension to the previous work (12–14) and they show detailed investigation of the development of Rh oxides upon polarization at $0.70 \leq E_p \leq 1.40$ V, RHE, with an interval, ΔE, of 0.05 V for $t_p \leq 10^4$ s; these data have not been presented before. The paper also presents first-ever data on the reduction behavior of Rh surface oxides under potential-controlled conditions, namely, at $0.70 \geq E_r \geq 0.25$ V, RHE, with ΔE of 0.05 V and for $t_r \leq 10^4$ s.

Can. J. Chem. Downloaded from www.nrcresearchpress.com by 91.121.58.235 on 09/08/12
For personal use only.

© 1997 NRC Canada

Can. J. Chem. Downloaded from www.nrcresearchpress.com by 91.121.58.235 on 09/08/12
For personal use only.

Experimental

Electrode preparation and oxide charge density examination.

The Rh electrode was a wire (99.99% in purity); the preparation methodology and pretreatment of the electrode are described elsewhere (12–14). The shape of the CV profiles recorded in 0.50 M aqueous H_2SO_4 indicated that both the electrode and the electrolyte were free of impurities (33, 34). Elsewhere (12–14), it was discussed that growth of oxides did not affect the surface of the electrode, which sustained its characteristics as revealed from the CV profile features in the 0.05–0.30 V, RHE, potential range. The real surface area of the Rh electrode was determined by accepting the charge of 210 $\mu C\ cm^{-2}$ as that necessary to form a monolayer of H_{UPD} (4, 12, 13), allowing for the double-layer charging; it was found to be 0.26 ± 0.01 cm^2. No dissolution of the anodically formed oxides was observed during the course of research. This conclusion is based on the observation that the q_{OX} versus log t_p or the $1/q_{OX}$ versus relations do not deviate from linearity (11).

It is essential to elaborate on the possible presence of molecular oxygen in the electrolyte upon electrode polarization at potentials above E°_{OER} = 1.23 V, SHE. Indeed, the latter is the thermodynamic reversible potential of the OER but, due to a significant overpotential of the OER, no molecular oxygen is present in the electrolyte and the oxide-reduction profiles are not obscured; this aspect is discussed in refs. 11–13.

Because the potential region corresponding to oxide reduction overlaps that of hydrogen and anion adsorption, it is necessary to explain how the oxide charge density was examined. The procedure applied is as follows. A CV profile between 0.05 and 0.55 V, RHE, thus prior to the oxide growth, was applied and the charge density of the double-layer charging, as well as the hydrogen and anion adsorption, was determined. This charge density was subsequently subtracted from the total charge density as determined from the oxide-reduction CV profile (11–13).

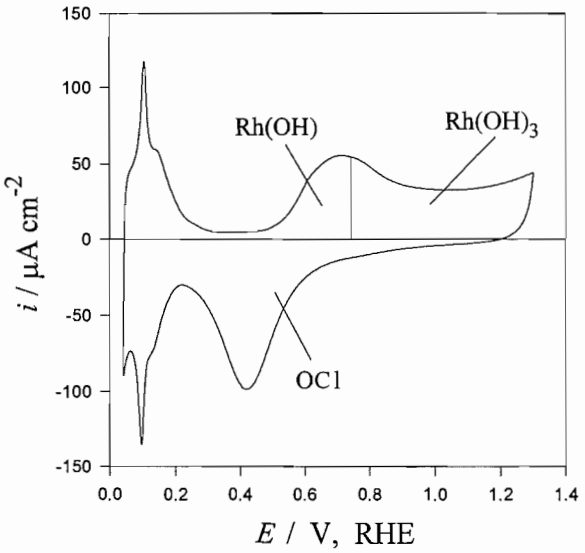
Solution and electrochemical cell

A high-purity 0.50 M solution was prepared from BDH Aristar grade and Nanopure water. Oxygen was removed from the solution by passing high-purity nitrogen through and over the cell solution at all times. The cleanliness of the solution was verified by recording CV profiles, which were found in agreement with those in the literature (1, 12–14, 21, 22). The electrochemical cell employed was a standard, all-glass, three-compartment cell with sleeved stopcocks. The glassware was precleaned according to well-established procedure (33, 34). During the experiments, H_2 gas that had been precleaned and presaturated with water vapor was bubbled through the reference electrode, RE, compartment in which a Pt/Pt black electrode was immersed.

Temperature control

The electrochemical cell was immersed in a Haake W13 water bath, and the temperature was maintained at 298 ± 0.5 K by means of a Haake D1 thermostat; the water level in the bath was kept above the electrolyte in the cell. The temperatures in the water bath and in the electrochemical cell were controlled by means of thermometers and a 80 TK Fluke K-type thermocouple; the readings were in agreement to within ±0.5 K.

Fig. 2. CV profile for Rh in 0.50 M aq. H_2SO_4. The oxide growth proceeds in two steps and involves formation of Rh(OH) followed by its transition to $Rh(OH)_3$. The oxide reduction takes place in one step, peak OC1. Sweep rate s = 50 mV s^{-1}, T = 298 K.



Instrumentation

The instrumentation included: (*a*) an EG&G model 273 potentiostat–galvanostat, (*b*) an 80486 computer, and (*c*) EG&G M270 electrochemical software. All potentials quoted in the paper were measured with respect to the RHE immersed in the same electrolyte and kept at the same temperature. Upon anodic polarization the potential was held constant to within 1 mV and was monitored on a Fluke 45 digital multimeter.

Results and discussion

Oxide development and chemical identity of the surface oxide species

To present a meaningful discussion of the growth of Rh oxides formed under well-defined potentiostatic conditions, it is essential to consider the surface processes involved in their development and on their surface-chemical composition. Peuckert (27) studied the surface-chemical composition of Rh oxides by means of X-ray photoelectron spectroscopy, XPS, and established that their formation proceeds in two steps: the first step involves electrodeposition of OH and the process occurs in the 0.55–0.75 V, RHE, potential range (eq. [1]); the second step leads to creation of $Rh(OH)_3$ (eq. [2]). The two potential regions with the respective surface-oxide species are shown in Fig. 2. It is worthwhile emphasizing that while the oxide growth proceeds in two steps, the oxide reduction is a one-step process (the OC1 peak in Fig. 2 and eq. [3]).

Formation

[1] $Rh + H_2O \rightarrow RhOH + H^+ + e$, 0.55–0.75 V

[2] $RhOH + 2\ H_2O \rightarrow Rh(OH)_3 + 2\ H^+ + 2\ e$, 0.75–1.40 V

© 1997 NRC Canada

Reduction

[3] $Rh(OH)_3 + 3\ H^+ + 3\ e \rightarrow Rh + 3\ H_2O$

The mechanism of the surface-oxide development on Rh is not yet well understood. For instance, at the present state of knowledge, it is unclear if $Rh(OH)_2$ acts as an intermediate in the $Rh(OH)_3$ formation (eqs. [4*a*] and [4*b*]) or whether $Rh(OH)_3$ is formed in a single step involving discharge of two water molecules (eq. [5]).

[4*a*] $RhOH + H_2O \rightarrow Rh(OH)_2 + H^+ + e$

[4*b*] $Rh(OH)_2 + H_2O \rightarrow Rh(OH)_3 + H^+ + e$

[5] $RhOH + 2\ H_2O \rightarrow Rh(OH)_3 + 2\ H^+ + 2\ e$

An answer to this question can be provided only by combined electrochemistry–XPS–CEELS measurements or X-ray scattering experiments. Another aspect of the very initial development of RhOH that requires investigation is the possibility of place exchange between the Rh surface atoms and the electroadsorbed OH groups, leading to a new surface structure (10, 19, 35, 36). Because the formation of surface oxides on noble metals reveals many similarities, it is reasonable to assume that, as in the case of Pt, the electroadsorption of OH groups on Rh is accompanied by place exchange between the Rh surface atoms and OH_{ads}. Evidence for place exchange in Pt oxidation is based on theoretical treatment of the oxide growth mechanism and X-ray scattering data (35–37). However, AC voltammetry results of Harrington and co-workers (38) on Pt oxidation do not support the place-exchange mechanism and indicate the electro-oxidation of Pt is a two-electron process. Moreover, they propose a different growth model in which the metal cation being immersed in the "electron sea" is pulled to the surface by the electroadsorbed OH groups. The authors also discuss the surface diffusion of Pt^{2+} cations and present a quantitative interpretation of their data. Numerical simulations of the formation of Pt surface oxides agree well with the experimentally observed CV profile. Clearly, despite some 25 years of research on the topic (37), the electro-oxidation of noble metals is still not well understood and calls for more research by means of state-of-the-art surface-science techniques.

Anodic polarization of Rh at E_p between 0.70 and 1.40 V, RHE, with an interval of 0.05 V, for t_p up to 10 000 s at 298 K leads to growth of thin oxide films (Figs. 3 and 4). The oxide-formation CV profiles reveal one peak and a wide wave overlapping each other in the 0.55–1.40 V, RHE, range. The CV oxide-reduction profiles show only one feature, designated the OC1 peak (12–14). The reduction charge density of OC1 increases and the peak shifts towards less positive potentials upon extension of E_p or t_p to higher values. In Fig. 3, the authors show CV oxide-reduction profiles for polarization for t_p = 1000 s at potentials from 0.70 to 1.40 V, RHE. The diagrams demonstrate that upon increase of E_p (for t_p = const.) the oxide-reduction charge density increases and the reduction peak shifts towards less positive values, in this particular case from 0.55 to 0.29 V, RHE. In Fig. 4, the authors demonstrate CV oxide-reduction profiles for polarization at E_p = 1.40 V, RHE, for $t_p = 10^0, 10^1, 10^2, 10^3$, and 10^4 s. The diagrams show that upon increase of t_p (for E_p = const.) the oxide-reduction

Fig. 3. Series of CV profiles for Rh in 0.50 M aq. H_2SO_4 solution taken at the sweep rate s = 50 mV s^{-1}, T = 298 K. The profiles demonstrate examples of the effect of increase of the polarization potential, E_p, from 0.70 to 1.40 V, RHE, on the oxide charge density and the reduction peak potential for t_p = 1000 s. The CV reduction profiles reveal only one state, OC1, which shifts towards less positive potentials.

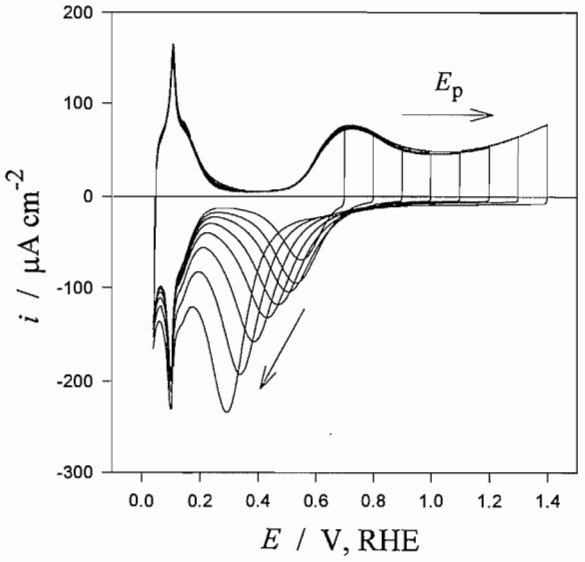
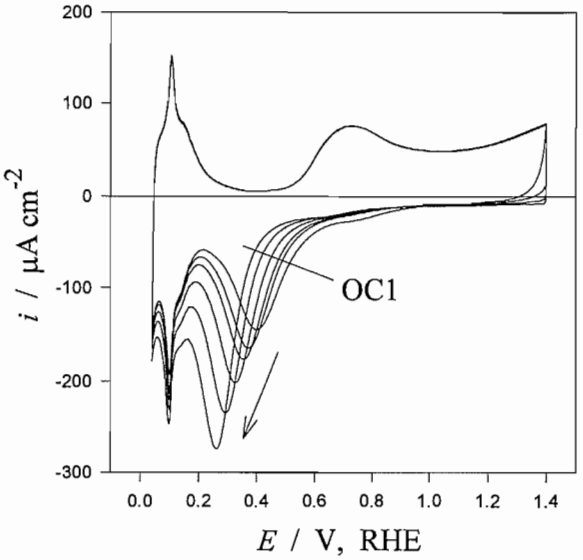


Fig. 4. Series of CV profiles for Rh in 0.5 M aq. H_2SO_4 solution taken at the sweep rate s = 50 mV s^{-1}, T = 298 K. The profiles demonstrate examples of the effect of increase of the polarization time, $t_p = 10^0, 10^1, 10^2, 10^3$, and 10^4 s, on the oxide charge density and the reduction peak potential for E_p = 1.40 V, RHE. The CV reduction profiles reveal only one state, OC1, which shifts towards less positive potentials.



charge density expands and the reduction peak moves towards less positive values, in the case presented above, from 0.40 to 0.26 V, RHE. Similar behavior is observed for values of E_p and t_p other than those referred to in Figs. 3 and 4. For all the E_p or t_p values studied in the course of this research, it was

Can. J. Chem. Downloaded from www.nrcresearchpress.com by 91.121.58.235 on 09/08/12
For personal use only.

© 1997 NRC Canada

Can. J. Chem. Downloaded from www.nrcresearchpress.com by 91.121.58.235 on 09/08/12
For personal use only.

observed that an increase of E_p or t_p always led to enhanced oxide-reduction charge densities, thus to thicker oxide films that reveal the same surface-chemical composition (12–14, 27). The authors base their viewpoint on the observation that the same oxide state is distinguishable in the CV reduction profiles, namely OC1, and the XPS data show that it corresponds to a surface film. Elsewhere (14), it was discussed that extension of E_p and t_p towards higher values had a dual impact on the oxide films: (*i*) thickness increased upon augmentation of E_p and t_p; and (*ii*) thermodynamics of the oxide reduction were changed upon augmentation of E_p and t_p because a lower potential was required to reduce the same chemically equivalent but thicker oxide film when E_p or t_p was increased. Observation (*ii*) leads to the conclusion that thicker oxides are thermodynamically more stable than thin ones. The impact of temperature variation on the thermodynamics of oxide formation is discussed in ref. 14.

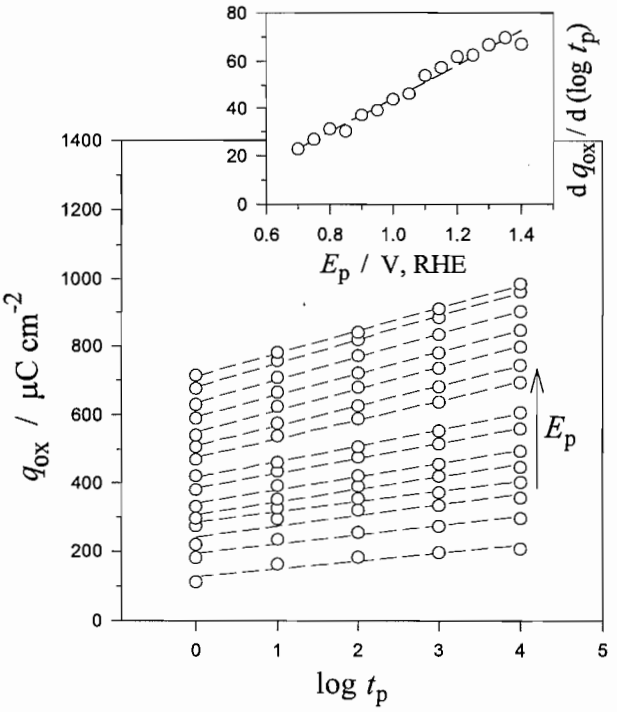
Oxide growth kinetics and mechanism

A study of oxide growth kinetics over a wide range of E_p and t_p, followed by theoretical treatment of the results by fitting them into existing oxide-formation theories, leads to assessment of important kinetic parameters of the process as a function of E_p and t_p as well as to examination of the applicable growth mechanism with emphasis on the rate-determining step. Application of CV to scrutiny of the oxide states and subsequent integration of the CV profiles collected in the course of the research allowed the authors to evaluate q_{OX} as a function of E_p and t_p. CV is a very suitable technique in a study of oxide films because it leads to evaluation of the oxide thickness, here expressed as the charge density of the oxide, with great precision (10–19, 23–26, 32, 35). In the case of the development of very thin oxide films (of submonolayer and monolayer thickness) on noble metals, it is well known that the growth often proceeds by logarithmic or inverse-logarithmic kinetics. In the first case, the rate-determining step is the transition from a submonolayer or monolayer of O_{chem} or OH_{chem} residing on the surface of the metal substrate, through place exchange or another surface process, to a new surface structure (1–3, 10, 34, 35, 38). In the case of inverse-logarithmic growth, the escape of the metal cation from metal into the oxide at the inner metal–oxide interface can be the rate-determining step. At present, it is unclear whether another surface process could be responsible for these kinetics and further research is needed to provide an unambiguous answer.

The authors plotted q_{OX} and $1/q_{OX}$ versus log t_p for various E_p in order to examine which growth kinetics are applicable to the system under investigation (Figs. 5 and 6). Under the experimental condition reported above, q_{OX} has values from 110 ± 5 to 985 ± 10 μC cm^{-2}, which correspond to 0.5 ML of Rh(OH) and 1.56 ML of $Rh(OH)_3$, respectively. Clearly, the Rh oxide films are very thin and of submonolayer and monolayer nature. It ought to be added that anodic polarization of Pt under similar E_p and t_p conditions results in thicker oxides than those formed on Rh, thus the electroformation of Rh oxides proceeds more slowly than that of Pt (11, 24–26).

The data shown in Fig. 5 indicate that the q_{OX} versus log t_p relations are linear for the whole range of E_p, thus indicating that the growth kinetics might be logarithmic in polarization (growth) time. The slope of the q_{OX} versus log t_p plots increases when E_p is raised towards higher polarization

Fig. 5. Rh oxide growth plots expressed as the charge density, q_{OX}, versus log of the polarization time, log t_p, at $T = 298$ K for various polarization potentials, E_p; the arrow indicates the increase of E_p from 0.70 to 1.40 V, RHE. The data demonstrate linear relations between q_{OX} and log t_p for the whole range of q_{OX}. The inset shows the $dq_{OX}/d(\log t_p)$ versus E_p plot, which expresses the growth rate as a function of E_p. The data show that the oxide growth rate becomes accelerated when E_p is increased.



potentials. The authors examined the relation between the growth rate and the polarization potential and expressed it as a $dq_{OX}/d(\log t_p)$ versus E_p plot (see the inset in Fig. 5); the results show that the oxide growth rate becomes accelerated when the polarization potential is increased. The $1/q_{OX}$ versus log t_p relations (Fig. 6) are also linear for $q_{OX} > 210$ μC cm^{-2} whereas the $1/q_{OX}$ versus log t_p plots reveal deviations from linearity for $q_{OX} < 210$ μC cm^{-2}. Thus on the basis of the data presented in Figs. 5 and 6, it may be concluded that the Rh electro-oxidation follows either logarithmic kinetics over the whole range of E_p and t_p or that it follows inverse-logarithmic kinetics once the oxide thickness has reached the charge density of 210 μC cm^{-2}, in other words, once the oxide has grown to the extent of 1 ML of Rh(OH). These results clearly illustrate that the distinction between logarithmic and inverse-logarithmic kinetics is difficult to make on the basis of linearity of q_{OX} versus log t_p or versus $1/q_{OX}$ versus log t_p plots. To identify which kinetics are applicable to the system under investigation, it is necessary to evaluate the relation between the actual oxide thickness, X, and the X_o and X_1 parameters as defined below (12–14):

$$[6] \quad X_o = \sqrt{\frac{\kappa kT}{8\,\pi n q^2}}, \qquad X_1 = \frac{qaV}{kT}$$

where κ is the relative permittivity of the film, n the number of

© 1997 NRC Canada

Can. J. Chem. Downloaded from www.nrcresearchpress.com by 91.121.58.235 on 09/08/12
For personal use only.

Fig. 6. Rh oxide growth plots expressed as reciprocals of the charge density, $1/q_{OX}$, versus log of the polarization time, log t_p, at $T = 298$ K, for various polarization potentials, E_p; the arrow indicates the increase of E_p from 0.70 to 1.40 V, RHE. The data demonstrate that the $1/q_{OX}$ versus log t_p relations are linear when $q_{OX} > 210$ μC cm^{-2}.

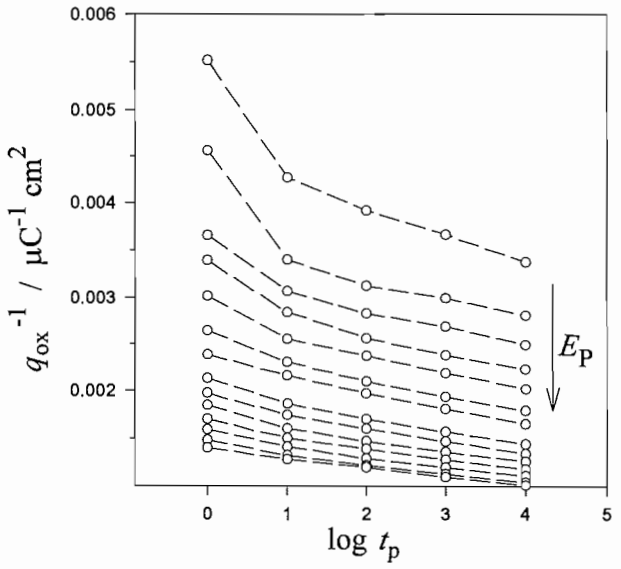
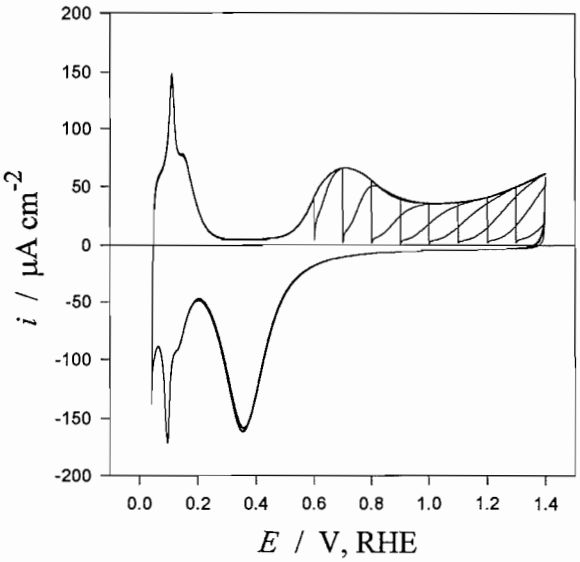


Fig. 7. Series of CV profiles for Rh in 0.5 M aq. H_2SO_4 solution taken at the sweep rate $s = 50$ mV s^{-1}, $T = 298$ K. The profiles demonstrate the effect of holding E at various values from 0.70 to 1.35 V, RHE, for 30 s. The results indicate that regardless of E, the amount of the oxide formed is the same as indicated in the CV oxide-reduction profiles.



metal ions per unit volume (cm^3), q the metal cation charge, V the potential across the oxide, a the distance between metal cations in the film (or between the metal atom and the metal cation at the inner metal–oxide interface, designated a'), k is Boltzmann's constant, and T the temperature. These parameters represent particular (critical) oxide thicknesses that determine the oxide growth kinetics. If the experimentally observed oxide thickness, X, is below or above X_1 (or X_o), then a specific oxide growth mechanism may become applicable. In ref. 14, the authors showed that in the case of very thin Rh oxide films $X < X_o$ and that $X < X_1$, thus the growth kinetics are typical of thin films. At present, it is almost impossible to discriminate between either of the kinetics. If the oxide growth proceeds by logarithmic kinetics, then the O-containing species create a surface dipole moment that induces the place-exchange mechanism, thus the O-containing species (here water molecules) and the metal surface atoms, M, undergo place exchange, which results in development of a new 2D surface structure. The oxide growth through place exchange might give rise to the logarithmic kinetics (10, 35). While the change of the surface dipole moment is significant during electrosorption of the first ML of OH groups, it seems sensible to conclude that this variation would be less pronounced upon commencement of the place exchange, which results in creation of a structure with OH and M occupying adjacent sites. Moreover, the deposition of the second, third, etc., ML of OH would result in a much smaller change of the surface dipole moment than the adsorption of the first ML of OH. Therefore logarithmic kinetics may be applied to the growth of the first oxide ML, giving rise to logarithmic kinetics but unlikely to the development of the subsequent MLs. If the growth of the following MLs does not occur through logarithmic kinetics, then another mechanism and kinetics should govern the process. At present there is only one other mechanism that can explain the experimentally observable inverse-logarithmic kinetics, and it implies that the escape of the metal cation from the metal into the oxide is the rate-determining step. This kinetic approach was applied by the current authors who based their calculations on the Mott–Cabrera formalism (14) and determined that the electric field across the oxide film is of the order of 10^9 V m^{-1} (details of the calculations are provided in refs. 12 and 14). In conclusion, it is difficult to evaluate the kinetics that can unambiguously explain the observable logarithmic or inverse-logarithmic growth, and more research on well-defined surfaces using modern surface-science techniques is needed to provide an indisputable explanation of the growth mechanism.

Impact of potential holding on oxide growth

In a separate set of experiments, the authors investigate the effect of holding the potential at E from 0.70 to 1.35 V, RHE, for 30 or 60 s while forming the oxide in a single CV transient (Fig. 7). The data demonstrate that when the potential was held at a constant value, the current density did not fall to zero, indicating that the oxide growth continued while the transient was stopped. The subsequent oxide-reduction CV profiles show that the amount of oxide formed was unaffected regardless of the holding potential. The same behavior was noted when the positive-going scan was stopped for 60 s. To the knowledge of the authors, this behavior has never been reported for Rh electrodes and the results represent a new contribution, which will lead to subsequent detailed assessment of the oxide growth kinetics and mechanism on Rh electrodes.

Influence of restricted range potential cycling on oxide growth and stability.

In a separate series of experiments the authors studied the influence of cycling the electrode some 50 times over a restricted potential range in order to evaluate possible changes

© 1997 NRC Canada

Can. J. Chem. Downloaded from www.nrcresearchpress.com by 91.121.58.235 on 09/08/12
For personal use only.

Fig. 8. Series of CV profiles for Rh in 0.5 M aq. H_2SO_4 solution taken at the sweep rate s = 50 mV s^{-1}, T = 298 K. The profiles demonstrate the effect of cycling the electrode 50 times over a restricted potential range. The upper potential limit, E_U, is 1.40 V and the lower one, E_L, is above the OC1 peak potential (see the reference curve referring to cycling between 0.05 and 1.40 V); here E_L = 0.40, 0.44, 0.48, and 0.52 V, RHE, respectively. Upon cycling to E_L, which is greater than the peak potential in the reference CV profile (0.38 V), q_{OX} is unaffected but the peak potential shifts towards more positive values and the peak current density decreases.

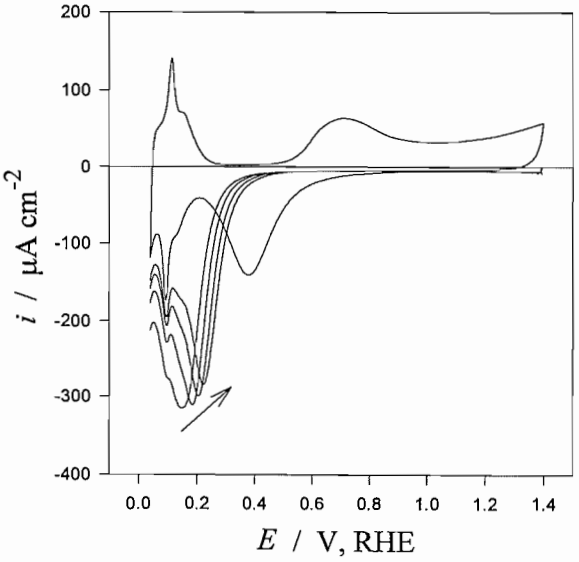
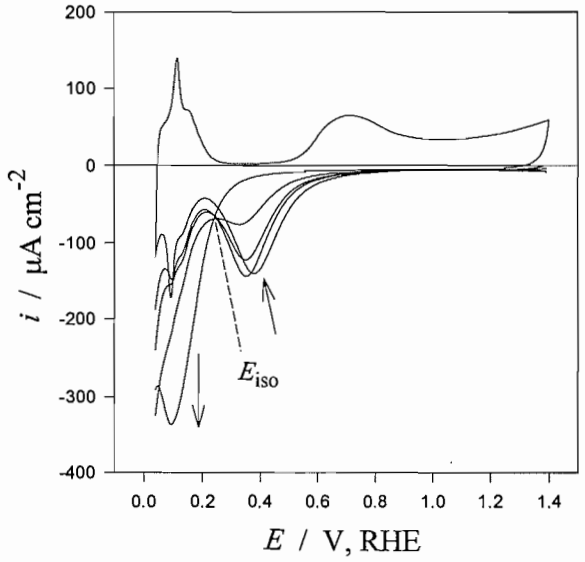


Fig. 9. Series of CV profiles for Rh in 0.5 M aq. solution taken at the sweep rate s = 50 mV s^{-1}, T = 298 K. The profiles demonstrate the effect of cycling the electrode 50 times over a restricted potential range. The upper potential limit, E_U, is 1.40 V and the lower one, E_L, is below the OC1 peak potential (see the reference curve referring to cycling between 0.05 and 1.40 V); here E_L = 0.36, 0.32, 0.28, and 0.24 V, RHE, respectively. Upon cycling to an upper limit, which is lower than the peak potential in the reference CV profile (0.38 V), q_{OX} is unaffected but the peak potential drastically shifts towards less positive values and the peak current density increases. E_{iso} refers to an isopotential point.



of the oxide thickness and its reduction potential (39). The potential ranges were selected with respect to the OC1 peak potential representative of the Rh oxide reduction within a single sweep. Because the oxide-reduction peak potential is at 0.38 V, RHE, (Fig. 2) the upper potential limit, E_U, of the restricted cycling was at 1.40 V while the lower one, E_L, was selected either above (E_L = 0.40, 0.44, 0.48, and 0.52 V, RHE) or below the peak potential (E_L = 0.36, 0.32, 0.28, and 0.24 V, RHE); the results of these experiments are shown in Figs. 8 and 9. The data shown in Fig. 8 indicate that upon increase of E_L from 0.40 to 0.52 V, RHE, the oxide-reduction peak shifts towards more positive values while the oxide-reduction charge density, determined by integrating the CV profiles, stays the same and close to 230 ± 5 μC cm^{-2}. The results demonstrate that upon decrease of E_L from 0.36 to 0.24 V, RHE, (Fig. 9) the oxide-reduction profile undergoes dramatic qualitative changes because it shifts towards less positive potentials and the peak current increases (the deconvolution of the peak becomes troublesome because it overlaps the UPD H peak). Interestingly, the charge density under the oxide peak remains almost constant and close to 215 ± 10 μC cm^{-2} (determination of q_{OX} is more complex because of the overlap of the oxide-reduction and the UPD H potential regions; in the charge-density determination, one has to account for the charge density of the UPD H and the double-layer charging as assessed on the basis of a standard CV profile between 0.05 and 1.40 V without arresting the scan or restricting its cycling range; see refs. 12 and 13). The displacement of the peak potential towards lower values may be assigned to changes in the stability of the oxide — it becomes thermodynamically more stable, because lower potentials are required to reduce the same oxide although its charge density is not altered. In the case of cycling to E_L >0.38 V, RHE, q_{OX} is greater than in the case of cycling to E_L <0.38 V, RHE, simply because the lower potential limit is too low and the oxide film is not completely reduced, and multiple cycling over the potential range increases its charge density.

Oxide reduction and its kinetics

Reduction of the electrochemically formed Rh oxides has never been a subject of research and it became an integral part of the project. The authors studied the process by application of the following procedure. An oxide of well-established and reproducible charge density (thickness) was formed by polarizing the electrode at E_P = 1.40 V, RHE, for t_p = 10^4 s. The charge density of such an oxide was 945 μC cm^{-2}, corresponding to 1.5 ML of $Rh(OH)_2$. This oxide was subsequently reduced at various potentials, E_r (see below), according to the following procedure: (*i*) a negative-going sweep that started at 1.40 V, RHE, was stopped at E_r, which was adjusted between 0.70 and 0.25 V with an interval of 0.05 V; (*ii*) the reduction time, t_r, was t_r = 10^0, 10^1, 10^2, 10^3, and 10^4 s; (*iii*) after the oxide reduction, the negative-going sweep was continued down to 0.05 V, RHE, and it led to complete reduction of the surface oxide as revealed from the subsequent CV profile. We emphasize that the CV profile that follows the reduction at E_r allows determination of the amount of the unreduced oxide that stayed on the surface; subtraction of this charge density

© 1997 NRC Canada

Can. J. Chem. Downloaded from www.nrcresearchpress.com by 91.121.58.235 on 09/08/12
For personal use only.

Fig. 10. Series of CV profiles for Rh in 0.5 M aq. H_2SO_4 solution taken at the sweep rate s = 50 mV s^{-1}, T = 298 K. The profiles demonstrate samples of the effect of reduction at E_r = 0.60 V for t_r = 10^0, 10^1, 10^2, 10^3, and 10^4 s. Increase of t_r leads to enhancement of the amount of the reduced oxide.

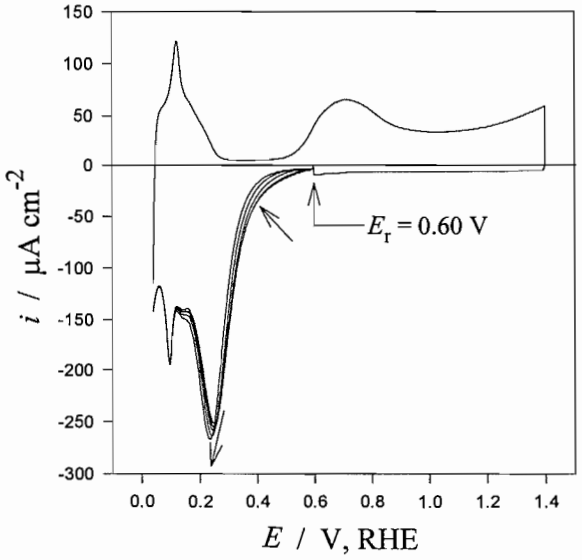
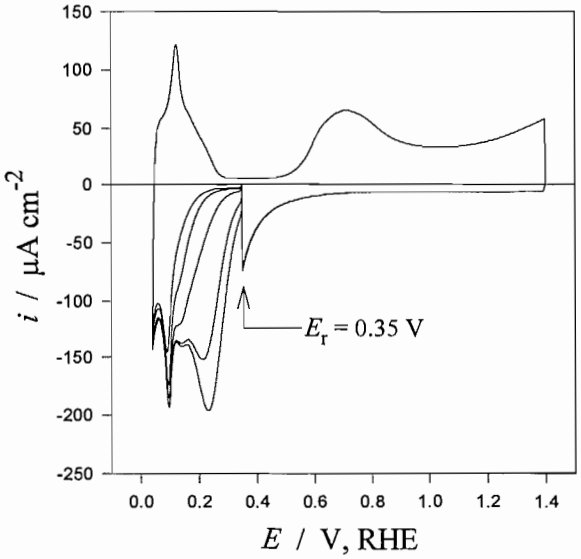


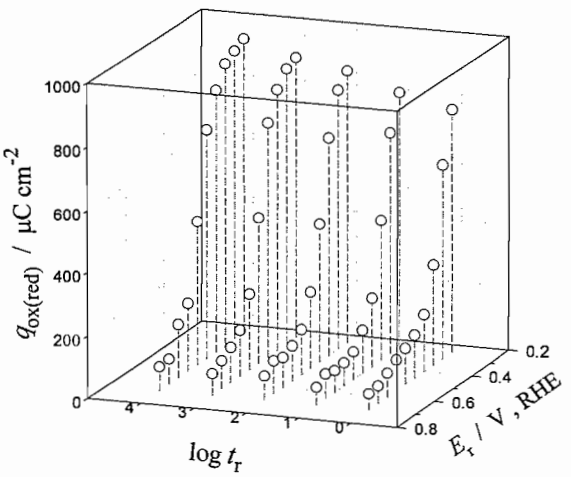
Fig. 11. Series of CV profiles for Rh in 0.5 M aq. H_2SO_4 solution taken at the sweep rate s = 50 mV s^{-1}, T = 298 K. The profiles demonstrate samples of the effect of reduction at E_r = 0.35 V for t_r = 10^0, 10^1, 10^2, 10^3, and 10^4 s. Increase of t_r leads to enhancement of the amount of the reduced oxide.



from 945 μC cm^{-2} allows determination of the amount of the reduced oxide. Two representative sets of CV oxide-reduction profiles are shown in Figs. 10 and 11. The data presented in Fig. 10 refer to E_r = 0.60 V, RHE, and the arrows reveal changes in the CV profiles that result from the reduction. The behavior at E_r = 0.60 V, RHE, may be summarized as follows: (*i*) upon stopping the negative-going sweep, the current density does not fall to zero but has a small value that indicates that the oxide reduction continues; (*ii*) extension of t_r from 10^0 to 10^4 s results in minute reduction of the oxide because its charge density decreases by only some 5%; (*iii*) changes in the shape of the CV profiles represented by arrows show that the oxide film undergoes some qualitative transition during the reduction because its half-width changes and the peak current density increases. At the present time, the authors are unable to relate these changes to structural parameters of the oxide, and XPS and X-ray scattering experiments are required to further explain these data. The behavior at E_r = 0.35 V, RHE, (Fig. 11) is simpler and the profiles show that upon extension of the reduction time from to s, the quantity of the oxide reduced, $q_{OX(red)}$, significantly increases.

In evaluation of the reduction behavior, the Rh oxide was always formed under the same E_p and t_p conditions and it resulted in an oxide of the same charge density, namely, 945 μC cm^{-2}. Integration of the CV oxide-reduction profiles for between 0.70 and 0.25 V, RHE, with an interval of 0.05 V (see Figs. 10 and 11) allowed the authors to assess the amount of the unreduced oxide, and its comparison with 945 μC cm^{-2} led to accurate determination of the amount of the Rh surface oxide reduced, $q_{OX(red)}$. This procedure was used for all the reduction potentials and the reduction times applied in the course of research, permitting evaluation of $q_{OX(red)}$ as a function of E_r and t_r. The results are shown in Fig. 12 as a 3-dimensional $q_{OX(red)}$ versus (E_r, log t_r) plot. The authors

Fig. 12. Rh oxide reduction plots expressed as the reduction charge density, $q_{OX(red)}$, versus the reduction potential, E_r, and log of the reduction time, log t_r, at T = 298 K; E_r is between 0.70 and 1.40 V, RHE, and t_r = 10^0, 10^1, 10^2, 10^3, and 10^4 s. The data demonstrate nonlinear relations between $q_{OX(red)}$ and log t_r

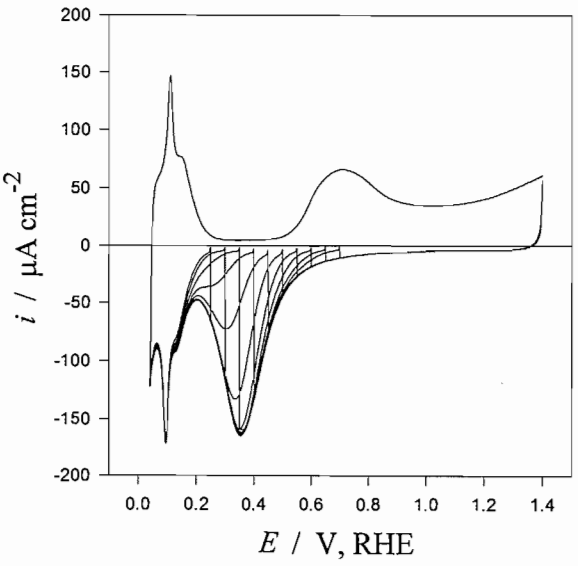


selected a logarithmic scale for the oxide-reduction time in order to compare this behavior with the growth behaviour albeit at present there is no reason to believe that the reduction should be logarithmic in time. The data (Fig. 12) indicate that the relations between $q_{OX(red)}$ and log t_r (for E_r = const.) are nonlinear; similarly, the $q_{OX(red)}$ versus E_r plots (for log t_r = const.) are also nonlinear. An analysis of the $q_{OX(red)}$ versus (E_r, log t_r) relations leads to the conclusion that the lower the reduction potential and can longer the reduction time, the

© 1997 NRC Canada

Can. J. Chem. Downloaded from www.nrcresearchpress.com by 91.121.58.235 on 09/08/12
For personal use only.

Fig. 13. Series of CV profiles for Rh in 0.5 M aq. H_2SO_4 solution taken at the sweep rate s = 50 mV s^{-1}, T = 298 K. The profiles demonstrate the effect of holding E at various values from 0.70 to 0.25 V, RHE, for 30 s. The results indicate that the oxide reduction continues when the scan is stopped. The lower the potential, the greater the amount of the reduced oxide.



greater the amount of the reduced oxide. Since there exists no theory of oxide reduction, the authors are unable to apply any theoretical methodology to explain the experimental data and can only present a qualitative discussion of the results. The interesting results presented in this section point to the necessity of conducting further experimental and theoretical research on reduction of oxide films on noble metals.

Impact of potential holding on oxide reduction

In a manner similar to the study of the impact of potential holding on the oxide formation, the authors examined the effect of holding the potential at E values varying from 0.70 to 0.25 V, RHE, with an interval of 0.05 V, for 30 or 60 s while reducing the oxide in a single CV transient (Fig. 13). The data reveal that when the potential was held at constant value, the current density did not fall to zero, indicating that the oxide reduction continued when the transient was stopped. Continuation of the reduction transient down to 0.05 V, RHE, and its comparison with the reference CV profile (see Fig. 2) indicates that some of the oxide was reduced while the scan was stopped. Integration of the CV profiles allowed determination of the charge density that was unreduced during the potential arrest as well as the charge density of the oxide that was reduced during the arrest. An analysis of the data showed that the lower the holding potential, the greater the amount of oxide that was reduced. The same behavior was noticed when the positive-going scan was stopped for 60 s but the reduction was more pronounced since a longer reduction period led to enhanced reduction. This observation is of significance in understanding the oxide-reduction mechanism and the kinetics.

Conclusions

1. Anodic polarization of Rh at E_p between 0.70 and 1.40 V, RHE, for $t_p = 10^0$, 10^1, 10^2, 10^3, and 10^4 s at 298 K results in thin oxides that reveal only one state in the CV reduction profiles, with q_{OX} values from 110 to 985 μC cm^{-2}, thus between 0.5 ML of Rh(OH) and 1.56 ML of $Rh(OH)_3$. Oxide development occurs in two steps whereas its reduction occurs in one.
2. Enhancement of E_p (for t_p = const.) or increase of t_p (for E_p = const.) leads to thicker oxides but of the same physical nature. Upon increase of E_p and (or) t_p the reduction peak shifts towards less positive potentials, indicating that thicker oxides are thermodynamically more stable.
3. Plots of q_{OX} versus log t_p are linear over the whole range of q_{OX} whereas plots of $1/q_{OX}$ versus log t_p are linear only when q_{OX} >210 μC cm^{-2}, that is, when the thickness is greater than 1 ML of RhOH. Therefore, the growth is either logarithmic in time over the whole region of q_{OX}, or it is logarithmic when q_{OX} <210 μC cm^{-2} and inverse-logarithmic when q_{OX} >210 μC cm^{-2}.
4. Oxide growth continues when the positive-going scan is stopped in the oxide-formation potential region. Similarly, oxide reduction proceeds when the negative-going scan is stopped in the oxide-reduction potential range.
5. Oxide reduction takes place at $E \leq 0.70$ V, RHE. The oxide reduction kinetics are not understood but, in general, the lower the reduction potential and the longer the reduction time, the greater the amount of the reduced oxide.

Acknowledgments

Acknowledgment is made to the Natural Sciences and Engineering Research Council (NSERC) of Canada and le Fonds pour la formation de chercheurs et l'aide à la recherche (FCAR) du Québec for support of this research.

References

1. N. Cabrera and N.F. Mott. Rep. Prog. Phys. **12**, 163 (1948–1949); N.F. Mott. J. Chim. Phys. Phys.-Chim. Biol. **44**, 172 (1949).
2. O. Kubaschewski and B.E. Hopkins. Oxidation of metals and alloys. Butterworths, London. 1962.
3. K. Hauffe. Oxidation of metals. Plenum Press, New York. 1965.
4. R. Woods. *In* Electroanalytical chemistry. Vol. 9. *Edited by* A.J. Bard. Marcel Dekker, New York. 1977. pp. 27–90.
5. L.D. Burke. *In* Electrodes of conductive metallic oxides. Part A. *Edited by* S. Trasatti. Elsevier, New York. 1980. pp. 141–181.
6. L.D. Burke. *In* Modern aspects of electrochemistry. No. 18. *Edited by* J.O'M. Bockris and B.E. Conway. Plenum Press, New York. 1986. pp. 169–248.
7. S. Trasatti. *In* The electrochemistry of novel materials. *Edited by* J. Lipkowski and P.N. Ross. VCH Publishers, New York. 1994. Chap. 5.
8. A. Damjanovic, A. Dey, and J.O'M. Bockris. J. Electrochem. Soc. **113**, 739 (1966).
9. A. Damjanovic and V.I. Birss. J. Electrochem. Soc. **130**, 1688 (1983); **133**, 1621 (1986); **134**, 113 (1987).
10. K.J. Vetter and J.W. Schultze. J. Electroanal. Chem. **34**, 131 (1972); **34**, 141 (1972).
11. G. Tremiliosi-Filho, G. Jerkiewicz, and B.E. Conway. Langmuir, **8**, 658 (1992).
12. G. Jerkiewicz and J.J. Borodzinski. Langmuir **9**, 2202 (1993).
13. G. Jerkiewicz and J.J. Borodzinski. J. Chem. Soc. Faraday Trans. **90**, 3669 (1994).
14. F. Villiard and G. Jerkiewicz. *In* Solid–liquid electrochemical interfaces. *Edited by* G. Jerkiewicz, M.P. Soriaga, K. Uosaki, and A. Wieckowski. ACS Symposium. Series Vol. 656. ACS, Washington, D.C. 1997. Chap. 23.

© 1997 NRC Canada

15. S. Shibata. Bull. Chem. Soc. Jpn. **38**, 1330 (1965); J. Electroanal. Chem. **89**, 37 (1978); S. Shibata and M. Sumino. Electrochim. Acta, **20**, 739 (1975).
16. S.D. James. J. Electrochem. Soc. **116**, 1681 (1969).
17. J. Balej and O. Spalek. Collect. Czech. Chem. Commun. **37**, 499 (1972).
18. D.A.J. Rand and R. Woods. J. Electroanal. Chem. **35**, 209 (1972).
19. H. Angerstein-Kozlowska, B.E. Conway, and W.B.A. Sharp. J. Electroanal. Chem. **43**, 9 (1973).
20. S. Gottesfeld. J. Electrochem. Soc. **127**, 272 (1980).
21. Z. Cataldi, N.R. De Tacconi, and A.J. Arvia. J. Electroanal. Chem. **122**, 367 (1981).
22. C. Pallotta, N.R. De Tacconi, and A.J. Arvia. Electrochim. Acta, **26**, 261 (1981); see also Z. Cataldi, R.O. Lezna, M.C. Giordano, and A.J. Arvia. J. Electroanal. Chem. **261**, 61 (1988).
23. H. Angerstein-Kozlowska, B.E. Conway, A. Hamelin, and L. Stoicoviciu. Electrochim. Acta **31**, 1051 (1986); H. Angerstein-Kozlowska, B.E. Conway, K. Tellefsen, and B. Barnett. Electrochim. Acta, **34**, 1045 (1989).
24. B.E. Conway, G. Tremiliosi-Filho, and G. Jerkiewicz. J. Electroanal. Chem. **297**, 435 (1991).
25. G. Jerkiewicz, G. Tremiliosi-Filho, and B.E. Conway. J. Electroanal. Chem. **334**, 359 (1992).
26. B.E. Conway and G. Jerkiewicz. J. Electroanal. Chem. **339**, 123 (1992).
27. M. Peuckert. Surf. Sci. **141**, 500 (1984).
28. K.S. Kim, N. Winograd, and R.E. Davis. J. Am. Chem. Soc. **93**, 6296 (1971).
29. G.C. Allen, P.M. Tacker, A. Capon, and R. Parsons. J. Electroanal. Chem. **50**, 335 (1974); J.S. Hammond and N. Winograd. J. Electroanal. Chem. **78**, 55 (1977).
30. G. Jerkiewicz, H. Strzelecki, and A. Wieckowski. Langmuir, **12**, 1005 (1996).
31. Y.-E. Sung, W. Chrzanowski, A. Zolfaghari, G. Jerkiewicz, and A. Wieckowski. J. Am. Chem. Soc. **119**, 194 (1997).
32. G. Tremiliosi-Filho, L.-H. Dall'Antonia, and G. Jerkiewicz, J. Electroanal. Chem. **422**, 149 (1997).
33. B.E. Conway, W.B.A. Sharp, H. Angerstein-Kozlowska, and E.E. Criddle. Anal. Chem. **45**, 1331 (1973).
34. H. Angerstein-Kozlowska. *In* Comprehensive treatise of electrochemistry. Vol. 9. *Edited by* E. Yeager, J.O'M. Bockris, B. E. Conway, and S. Sarangapani. Plenum Press, New York. 1984. pp. 15–59.
35. B.E. Conway, B. Barnett, H. Angerstein-Kozlowska, and B.V. Tilak. J. Chem. Phys. **93**, 8361 (1990).
36. H. You, D.J. Zurawski, Z. Nagy, and R.M. Yonco. J. Chem. Phys. **100**, 4699 (1994).
37. B.E. Conway. Prog. Surf. Sci. **49**, 331 (1995).
38. M.E. van der Geest, N.J. Dangerfield, and D.A. Harrington. J. Electroanal. Chem. **420**, 89 (1997); D.A. Harrington. J. Electroanal. Chem. **420**, 101 (1997).
39. S.G. Roscoe and B.E. Conway. J. Electroanal. Chem. **224**, 163 (1987).

Can. J. Chem. Downloaded from www.nrcresearchpress.com by 91.121.58.235 on 09/08/12
For personal use only.

© 1997 NRC Canada

A new electrocatalyst consisting of a molecularly homogeneous platinum–aerogel nanocomposite

Siyu Ye, Ashok K. Vijh, Zheng-Yu Wang, and Lê H. Dao

Abstract: Aerogels offer interesting opportunities for (electro)catalysis due to their high porosity and specific surface area. A new electrocatalytic material consisting of a molecularly homogeneous platinum–aerogel nanocomposite was prepared. The mixed components represent, at the microscopic level, very homogeneous combinations originating from chemical interactions at the molecular scale in the liquid phase that can be viewed as "frozen in" in the solid state via supercritical drying. Transmission electron microscopy (TEM) images of this material clearly show that nanometer-size platinum particles are homogeneously distributed and are a part of the molecular architecture of the composite. An X-ray photoelectronic spectroscopy (XPS) study indicates that there exists a special interaction between platinum and the support within a polyacrylonitrile–Pt (PAN-Pt) electrocatalyst. This material is a promising electrocatalyst for oxygen reduction, and its electrocatalytic activity arises from the nanodispersed platinum particles present in the nanocomposite.

Key words: electrocatalyst, aerogel, nanocomposite, oxygen reduction, metal–support interaction.

Résumé : Les aérogels présentent des possibilités intéressantes d'(électro)catalyse résultant des valeurs élevées de leur porosité et de la superficie de leur spécifique. On a préparé un nouveau matériel électrocatalytique formé d'un nanocomposite moléculairement homogène de platine–aérogel. Les composants mélangés représentent, au niveau microscopique, des combinaisons très homogènes ayant leur origine dans les interactions chimiques, à l'échelle moléculaire, dans la phase liquide qui peuvent être considérées «fixées» dans l'état solide par le biais d'un séchage supercritique. Les images dérivées de la microscopie électronique de transmission («TEM») de ce matériel montrent clairement que les particules de platine d'une grosseur de l'ordre du nanomètre sont distribuées d'une façon homogène et qu'elles font partie de l'architecture moléculaire du composite. Une étude par spectroscopie photoélectronique des rayons X («XPS») indique qu'il existe une interaction spéciale entre le platine et le support dans un électrocatalyseur de polyacrylonitrile–Pt (PAN-Pt). Ce matériel est un catalyseur prometteur pour la réduction de l'oxygène et son activité électrocatalytique découle des particules nanodispersées de platine dans le nanocomposite.

Mots clés : électrocatalyseur, aérogel, nanocomposite, réduction de l'oxygène, interaction métal–support.

[Traduit par la rédaction]

Introduction

Aerogels possess unique morphological and chemical properties, originating from their wet-chemical preparation by the solution–sol–gel (SSG) method or phase-separation techniques and the subsequent solvent removal via supercritical drying (SCD) (1). Aerogels have been extensively investigated with regard to their preparation (2–5), characterization (6, 7), and applications such as optical, thermal, acoustic, and electronic (8), capacitive deionization (9), biosensor (10), and electroanalysis (11). Due to the "structure-preserving" ability of SCD, aerogels are solids of high porosity and specific surface area. These aerogels thus offer interesting opportunities for (electro)catalysis (12–14). The motivation to combine the SSG or phase-separation techniques with the method of SCD for the preparation of aerogel catalysts or supports resides mainly in the highly controllable SSG or phase-separation preparation route with the structure-preserving ability of SCD, embracing features such as molecular-scale mixing of the constituents; homogeneity of SSG or phase-separation products with pronounced isotropy of chemical, physical, and morphological properties; and use of various wet-chemical tools for tailoring the preparation. Thus, by exploiting these properties, catalysts with unique structural and chemical properties can be prepared that are not easily accessible by means of other preparation techniques.

Received March 13, 1997.

This paper is dedicated to Professor Brian E. Conway on the occasion of his 70th birthday in recognition of his distinguished and far-ranging contributions to the field of electrochemistry and to chemistry in Canada.

Siyu Ye and Ashok K. Vijh.[1] Institut de recherche d'Hydro-Québec (IREQ), 1800 Boul. Lionel-Boulet, Varennes, QC J3X 1S1, Canada.
Zheng-Yu Wang and Lê H. Dao. Laboratoire de recherche sur les matériaux avancés, INRS – Energie et matériaux, Institut national de la recherche scientifique, 1650 Boul. Lionel-Boulet, C.P. 1020, Varennes, QC J3X 1S2, Canada.

[1] Author to whom correspondence may be addressed. Telephone: (514) 652–8234. Fax: (514) 652–8424. E-mail: ashok@ireq.ca

© 1997 NRC Canada

Can. J. Chem. Downloaded from www.nrcresearchpress.com by 91.121.58.235 on 09/08/12
For personal use only.

Can. J. Chem. Downloaded from www.nrcresearchpress.com by 91.121.58.235 on 09/08/12
For personal use only.

We have previously reported a method for the preparation of an electrocatalyst based on carbonized polyacrylonitrile (PAN) aerogels in which we achieved a homogeneous distribution of nanoparticles of platinum in the carbonized PAN matrix by dipping a carbonized PAN in H_2PtCl_6 solution (15–19). Here we report on a new method in which a homogeneous platinum–aerogel composite is obtained, in which platinum nanoparticles are uniformly incorporated as part of the molecular architecture of the composite, in distinction from the mere uniform physical distribution of platinum particles. This was achieved by adding the metal precursor prior to the gelation stage. Using this approach, the metal is incorporated directly into the support framework structure, at the molecular level. The mixed aerogels or their parent gels thus represent, at the microscopic level, very homogeneous combinations originating from the chemical interactions at the molecular scale in the liquid that can be viewed as "frozen in" in the solid state. Aerogels are, in this respect, sort of a three-dimensional dry picture of the sol–gel product, with all their catalytic potentialities intact and available for revelation (1, 13, 14). It is surmised that the uniform three-dimensional distribution of the metal component throughout the PAN matrix with large surface area thus achieved may help to prevent sintering and coking of the active metal phase and improve its mechanical stability.

In this paper, we describe the preparation and characterization (conducted by combining microscopic methods, XPS, and electrochemical approaches) of the new material (hereafter denoted as PAN-Pt). PAN-Pt was used as an electrocatalyst for the oxygen reduction, and compared with the behavior of the bulk platinum electrode as well as with the PAN-based material prepared by the previously described method (15–19, hereafter denoted as PAN/Pt).

Hence, PAN/Pt denotes the material prepared by dipping a carbonized PAN in H_2PtCl_6 solution, and PAN-Pt signifies the catalyst in which a homogeneous solution of PAN and K_2PtCl_6 was the starting material.

Experimental

Preparation

The carbonized PAN aerogel incorporated with platinum, PAN-Pt, was prepared as follows: a platinum salt (e.g., K_2PtCl_6) or an organometallic compound (e.g., platinum acetylacetonate) was mixed with PAN (5 wt.%) in *N*,*N*-dimethylformamide (DMF)/water (v/v:84/16). This mixture became a clear solution as the temperature was increased. At about 120°C, the solution was degassed and then poured into a mold. Upon cooling the solution, a polymer gel containing platinum compounds was obtained by thermally induced phase-separation. After reducing the platinum salt with 1 wt.% $NaBH_4$ aqueous or alcoholic solution, or by bubbling hydrogen into the aqueous or alcoholic solution containing the gel, the remaining solvent in the polymer gel was exchanged with acetone or ethanol, and the latter solvent was removed by CO_2 supercritical extraction. The dry platinum containing PAN aerogel was pretreated in a forced-air convection oven at 210°C, followed by pyrolysis at 900°C under an argon atmosphere.

The preparation of PAN/Pt has been described in detail in the literature (15–19).

Electrode materials and chemicals

The electrode structure can be fabricated by grinding the powder (by mortar and pestle) of the PAN/Pt or PAN-Pt foam. The ground powder was dispersed in a solution of the carrier polymer to yield a slurry. Here, Nafion (5 wt.% solution in alcohols) was used as the carrier polymer. A small amount of the slurry (typically 10 μL) was spread on a previously cleaned (20) glassy carbon disk electrode (diam. 4.0 mm, EG&G), and the solvent allowed to evaporate from its surface.

In a typical experiment on PAN-Pt, 3.5 mg of PAN-Pt powder (5 wt.% of platinum) was added to 1167 μL solution of Nafion (5 wt.% solution in a mixture of lower aliphatic alcohols and 10% water, from Aldrich, diluted with ethanol with v/v: 2/1). The suspension was placed in an ultrasonic bath for 15 min; 10 μL of this slurry was spread onto a glossy carbon disk electrode (diam. 5 mm). The platinum loading (i.e., the total amount in the aerogel), using the geometric area of the substrate electrode, was thus calculated to be 7.6 μg cm^{-2}.

In a typical experiment on PAN/Pt, 6.6 mg of PAN-Pt powder (4.95 w/o of platinum) was added to 2000 μL solution of Nafion (5 wt.% solution in a mixture of lower aliphatic alcohols and 10% water, from Aldrich). The suspension was placed in an ultrasonic bath for 15 min; 10 μL of this slurry was spread onto a glassy carbon disk electrode (diam. 3 mm). The platinum loading (i.e., the total amount in the aerogel), using the geometric area of the substrate electrode, was thus calculated to be 23 μg cm^{-2}.

All chemicals were of analytical grade purity and were used without further purification. Solutions were prepared using doubly-distilled water. All experiments were performed at room temperature.

Instrumentation

The electrochemical experiments were performed by using a PAR model 273 potentiostat–galvanostat coupled with a model 616 rotating disk electrode. A conventional H-type glass cell with a platinum foil or wire spiral counter-electrode was used for all electrochemical experiments. An Ag/AgCl/4 M NaCl electrode was used as the reference electrode; all potentials in this paper are referred to the normal hydrogen electrode (NHE). The geometric surface area of the electrode was used to calculate the current density, and the sign of a cathodic current was defined as positive. A platinum disk electrode (diam. 4.0 mm, EG&G) was used for comparison in this study, and was polished according to the procedure described in ref. 8. High-purity N_2 or O_2 was bubbled through the 0.5 M H_2SO_4 aqueous solution for more than 30 min before each electrochemical experiment and during the experiment.

Transmission electron microscopy (TEM) was performed on a Hitachi H9000 operating at 300 kV and equipped with a Link EDX detector. The platinum particle size was evaluated using a Tracor Northern TN-8500 image analyzer.

The XPS studies were performed using a Fisons Instruments Escalab 220i-XL surface microanalysis system with an Al $K\alpha$ X-ray source (1486.6 eV). The spectrometer was calibrated by assuming the binding energy (BE) of the Ag $3d_{2/5}$ line to be at 368.25 eV. The C 1*s* peak of carbon at 284.6 eV was used as an internal reference. The sample powders were mounted onto a standard sample holder by using double-sided adhesive tape. Survey scan photoelectron spectra in the range of 0–1100 eV were recorded at a pass energy of 100 eV

© 1997 NRC Canada

Fig. 1. TEM image of PAN-Pt at a magnification of 45 K.



Can. J. Chem. Downloaded from www.nrcresearchpress.com by 91.121.58.235 on 09/08/12
For personal use only.

with a step size of 1 eV and a dwell time of 0.1 s step^{-1}. Narrow-scan photoelectron spectra (50 eV pass energy, 0.1 eV step^{-1}, and 0.1 s step^{-1} dwell time) were obtained for the C 1*s*, N 1*s*, O 1*s*, Pt 4*f*, Pt 4*d*, and Pt 4*p* regions. The pressure in the analysis chamber during the scans was approximately 10^{-7} Pa or less. All core-level spectra were deconvoluted by using the ECLIPSE program, version 1.7T, from Fisons/VG.

Results and discussion

Microscopic characterization

A TEM image of the PAN-Pt is shown in Fig. 1, from which a homogeneous distribution of dark spots with relatively uniform size distribution (except for a very few large-sized spots in some special positions) can be observed. From the EDX data of these spots, we can unambiguously assign them to platinum. PAN-Pt presents, in this magnification, TEM features similar to those of PAN/Pt (15, 17–19). By using high-resolution TEM (Fig. 2), however, one can see dramatically different features between these two materials. For PAN/Pt (Fig. 2*A*), the platinum particles seen at lower magnification are actually aggregates of smaller particles. By contrast, in PAN-Pt (Fig. 2*B*), the finer platinum particles are well separated, indicating a much higher homogeneity of the platinum particle distribution in the PAN-Pt material than in the PAN/Pt.

The distribution of particle size in PAN-Pt catalyst, as mea-

© 1997 NRC Canada

Can. J. Chem. Downloaded from www.nrcresearchpress.com by 91.121.58.235 on 09/08/12
For personal use only.

Fig. 2. High-resolution TEM images of PAN/Pt (*A*) and PAN-Pt (*B*) at a magnification of 900 K.

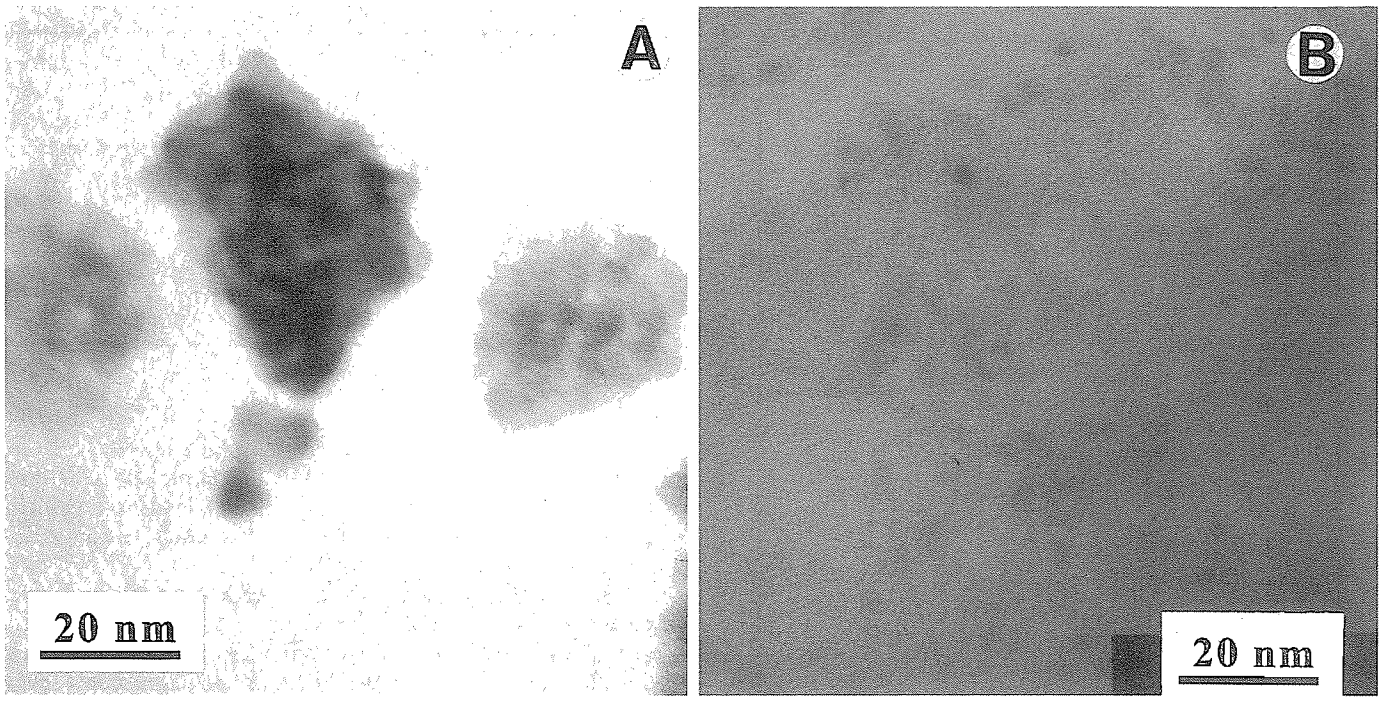


Fig. 3. Particle-size distribution measured from high-resolution TEM image of PAN-Pt. The percentage frequency denotes the percentage of total particles of a given diameter.

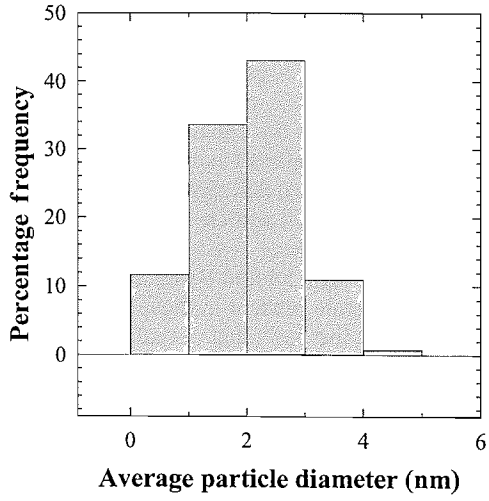
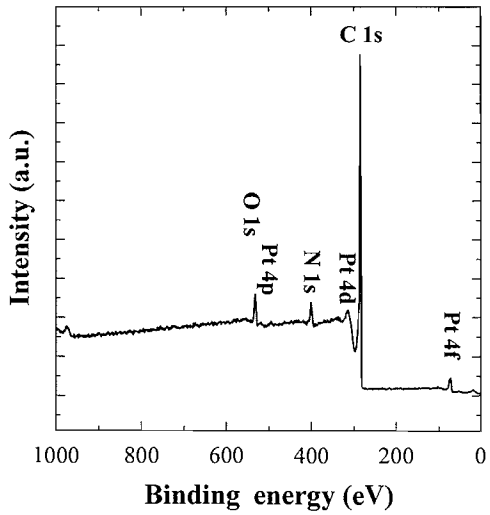


Fig. 4. XPS survey scan spectrum for PAN-Pt.



sured from high-resolution TEM images, is shown in Fig. 3, which is obtained by measuring the area of a sufficiently large number of particles (>100) to ensure good statistics. It can be seen in Fig. 3 that most platinum particles have diameters smaller than 5 nm, 59% of the platinum particles have diameters of 2–3 nm, and 46% of them range from 1 to 2 nm. The surface mean particle size $\bar{d}$ can be estimated (21) to be 2.7 nm according to the equation:

$$[1] \quad \bar{d} = \frac{\Sigma f_i d_i^3}{\Sigma f_i d_i^2}$$

where f_i is the frequency of occurrence of the particles of diameter d_i in the sample, from the particle size distribution shown in Fig. 3. The surface mean particle size of the platinum particles in PAN-Pt is much smaller than that of the platinum particles in PAN/Pt (17 nm, ref. 18), which suggests that a much better dispersion has been achieved in PAN-Pt.

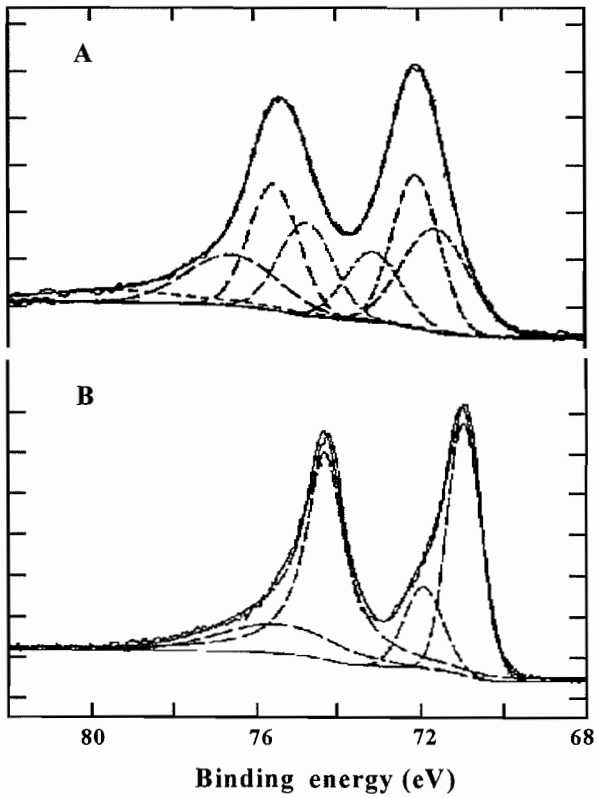
XPS study

Figure 4 shows the survey scan spectrum for PAN-Pt, which consists of the C 1*s* peak at 284.6 eV, the N 1*s* peak at 400.9 eV, the O 1*s* peak at 532.5 eV, Pt 4*f* peaks at 73.1 and 75.5 eV, Pt 4*d* peaks at 315.9 and 331.3 eV, and the Pt 4*p* peak at 520.7 eV. It is evident from the survey scan spectra for PAN-Pt that platinum has been incorporated into the PAN matrix, as indicated by the appearance of these Pt peaks.

© 1997 NRC Canada

Can. J. Chem. Downloaded from www.nrcresearchpress.com by 91.121.58.235 on 09/08/12
For personal use only.

Fig. 5. Pt 4*f* narrow scan spectra and line-shape analysis for (*A*) PAN-Pt and (*B*) PAN/Pt. The solid line is the experimental data, and the broken lines are the fits to the data (see the text).



The narrow scan XPS spectrum of the Pt 4*f* core level for PAN-Pt is shown in Fig. 5*A* along with that of PAN/Pt (Fig. 5*B*). It has been reported that the Pt 4*f* spectrum of PAN/Pt did not show any shifts in comparison with the literature values for Pt^0 (18). In contrast, the maxima of the Pt 4*f* peaks of PAN-Pt shift 1.2 eV to higher energy. Obviously, such a high value cannot be due to the measurement error. For platinum on a zeolite support, a significant chemical shift (~+0.7 eV) of peak maximum for the Pt $4f_{7/2}$ was detected (21), and was considered to be due to the formation of charge-transfer complexes between platinum and the Lewis-acid sites of zeolite. For Pt/C catalysts, the peak maximum for the Pt $4f_{7/2}$ has been observed to shift to higher values by 0–1.8 eV, depending on the content of the surface functional groups of the support. This was interpreted as being due to the presence of a platinum–support electronic effect (22). For PAN/Pt, no chemical shift of Pt 4*f* signals was detected, which was tentatively interpreted as follows. (*i*) Only a small fraction of the total charge of platinum particles participates in the charge-transfer process from platinum to support. (*ii*) The specific metal–support interaction is mainly through the electron transfer from platinum to pyridine-type nitrogen, and the lone-pair electrons of the nitrogen atoms in PAN are localized within the large aromatic rings, which results in a lower electron density of these nitrogen atoms. (*iii*) The complicated structure of the polymer might result in the charge transfer from platinum to polymer being less than that to the surface functional groups of inorganic supports, or even non-unidirectional in some location of the polymer matrix. In addition, the platinum particles are larger and are aggregated in PAN/Pt, in comparison with those in PAN-Pt, as seen in Figs. 2 and 3, which leads to less interaction with the support and thus may explain the apparent differences between PAN/Pt and PAN-Pt.

Table 1. Deconvolution parameters for the Pt 4*f* narrow scan XPS spectra of PAN/Pt and PAN-Pt.

Material	Binding energy (eV) / FWHM[a] (eV) $4f_{7/2}$	Binding energy (eV) / FWHM[a] (eV) $4f_{5/2}$	Relative peak area (%)
PAN/Pt	70.9 / 1.0	74.3 / 1.1	74.5
	71.9 / 1.1	75.5 / 3.4	25.4
PAN-Pt	71.4 / 1.5	75.1 / 1.6	26.1
	72.0 / 1.4	75.5 / 1.7	41.9
	73.1 / 2.2	76.7 / 3.3	32

[a]FWHM is the full width at half maximum.

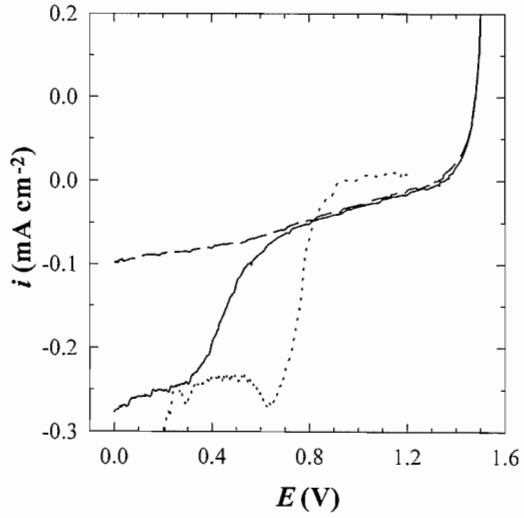
For PAN-Pt, the chemical interactions on the molecular scale are established in the liquid phase, which then gets "frozen in" in the solid state through the special aerogel preparation procedures. This should lead to, at the microscopic level, very homogeneous three-dimensional structures, not only in morphology but also in the chemical interactions between metal and support. In this case, all platinum particles, in principle, participate in this interaction, which is different from that for PAN/Pt, where only a small fraction of the total charge of platinum particles participate in the charge-transfer process from platinum to support. The large shift of the Pt 4*f* peaks in PAN-Pt may indicate a stronger metal–support interaction than in PAN/Pt. The specific metal–support interaction is considered to be beneficial to the enhancement of catalytic properties (21), and for the improved stability of the electrocatalyst (23). It can thus be surmised that the stability of PAN-Pt is better than that of PAN/Pt; this point is under experimental investigation at the present time.

It is obvious from Figs. 5*A* and *B* that there is more than one platinum oxidation state present in these spectra. The spectra are deconvoluted on the basis that not all of the Pt sites are in the metallic state. They contain some or all of the Pt^0, Pt^{II}, and Pt^{IV} components, and each has two corresponding peaks in the envelope spectrum. Based on the previous work reported in the literature (24, 25), and considering the effect of metal–support interaction, these deconvoluted peaks can be assigned; the results are presented in Table 1 along with other deconvolution parameters. It can seen from Fig. 5 and Table 1 that there are only two Pt components present in PAN/Pt (Pt^0 and Pt^{II}), while three components (Pt^0, Pt^{II}, and Pt^{IV}) are present in PAN-Pt. Based on the relative peak area, the percentage of Pt^0 in PAN/Pt is 74.5%, which is similar to that in 20% Pt/Vulcan XC-72 (Electrochem, Inc., Woburn, Mass.) where 77.8% Pt^0 was obtained (25). In PAN-Pt, only 26.1% was in the Pt^0 state, which suggests that a large fraction of platinum is in the oxidized states and may indicate the difficulty of reducing the platinum encapsulated inside the PAN micropores. As H_2PtCl_6 and K_2PtCl_6 were used as precursors to prepare these two materials, Cl might have been present in these two materials, with platinum residing as chloride. However, no Cl sig-

© 1997 NRC Canada

Can. J. Chem. Downloaded from www.nrcresearchpress.com by 91.121.58.235 on 09/08/12
For personal use only.

Fig. 6. Linear sweep voltammograms of the PAN-Pt in 0.5 M H_2SO_4 solution saturated with oxygen (———) and nitrogen (– – –). Cyclic voltammogram of a smooth Pt bulk electrode in 0.5 M H_2SO_4 solution saturated with oxygen (·····) is also shown for comparison. Scan rate: 5 mV s^{-1}. Rotating rate: 0 rpm.



nal was detected in these two samples. It can be concluded, therefore, that at least most of the Pt^{II} and Pt^{IV} sites are not present as chloride. They may be present as oxides or hydroxides, as those assigned in Pt/C (25). The presence of oxygen species in PAN-Pt is verified by the survey scan spectrum (Fig. 4), and is probably due to the special preparation procedures (see Experimental), i.e., the PAN aerogel containing dry platinum was pretreated in a forced-air convection oven at 210°C.

Electrocatalysis for the oxygen reduction

The electrocatalytic properties of PAN-Pt have been tested for the reduction of oxygen. Cyclic voltammograms of the PAN-Pt electrode in 0.5 M H_2SO_4 saturated with O_2 and N_2 are shown in Fig. 6. For comparison, the cyclic voltammogram of a smooth platinum bulk electrode in 0.5 M H_2SO_4 saturated with O_2 is also shown in Fig. 6. The platinum loading of the PAN-Pt electrode material is 7.6 μg cm^{-2}. An enhancement of the cathodic current in the oxygen-reduction region at the PAN/Pt electrode in the O_2-saturated solution, in comparison with that in N_2-saturated solution, indicates the electrocatalytic activity of the PAN/Pt for the reduction of oxygen. At the PAN/Pt electrode, the values of the cathodic current at higher overpotential range are comparable to those at the smooth platinum bulk electrode in 0.5 M H_2SO_4 saturated with O_2.

Figure 7 compares the current–potential curves of the PAN-Pt electrode (with a platinum loading of 7.6 μg cm^{-2}) and PAN/Pt electrode (with a platinum loading of 23 μg cm^{-2}) in 0.5 M H_2SO_4 saturated with O_2. Appreciable values of the cathodic current in the oxygen-reduction region have been observed at both electrodes. In comparison with the features of the current–potential curve for PAN/Pt, the cathodic current of the PAN-Pt is smaller (in mA cm^{-2}). It should be noted, however, that the platinum loading of these two electrodes is different (see above). If the current scale is changed to A g^{-1} Pt, the cathodic current of PAN-Pt, as also shown in Fig. 7, would be larger than that of PAN/Pt at more negative potentials, indicating a better mass electrocatalytic activity of the PAN-Pt material. This better mass electrocatalytic activity obviously originates from the higher homogeneity of the platinum particle distribution and the lesser degree of aggregation of the small particles in the PAN-Pt than in the PAN/Pt.

Fig. 7. Current–potential curves of PAN-Pt (– – –) and PAN/Pt (———) in 0.5 M H_2SO_4 solution saturated with oxygen. Scan rate: 5 mV s^{-1}. Rotating rate: 0 rpm.

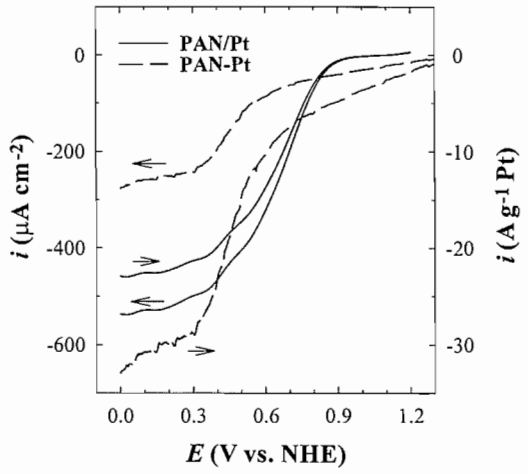
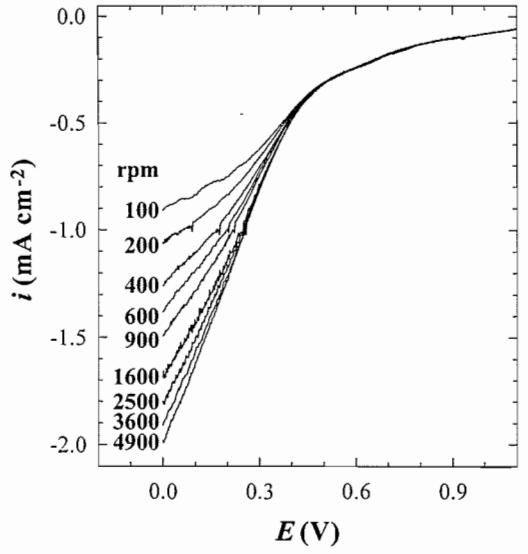


Fig. 8. Current–potential curves of PAN-Pt in 0.5 M H_2SO_4 solution saturated with oxygen at different rotating rates as shown in figure. Scan rate: 20 mV s^{-1}.



Since the oxygen-reduction current depends strongly on hydrodynamic conditions, a rotating disk electrode was used to study the kinetics of oxygen reduction at the PAN-Pt electrode. Figure 8 presents the current–potential curves at different rotation rates (ω in revolutions per minute, rpm) obtained by scanning the potential from 1.2 to 0.0 V at 20 mV s^{-1} in 0.5 M H_2SO_4 saturated with O_2. The platinum loading of this electrode material is 7.6 μg cm^{-2}. An ω-independent non-zero current value appeared at 1.0–0.6 V. Mass transport contributions became significant at lower potentials, i.e., at higher values of the oxygen-reduction overpotentials. The curves do not

© 1997 NRC Canada

level off as expected at large overpotentials of O_2 reduction. In general, the diffusion-limiting current density is not well defined; we plan to examine the possible cause for this behavior in our future work.

Concluding remarks

A new electrocatalytic material consisting of a molecularly homogeneous platinum–aerogel nanocomposite has been prepared. TEM images of this material clearly show that nanometer-size platinum particles are homogeneously distributed, and form part of a molecular architecture of the composite. Compared with the PAN/Pt previously studied (16–19), it is (*i*) the highly homogeneous distribution of the nanometer-size platinum particles within the PAN-Pt nanocomposite, and (*ii*) the suitable interparticle distance that make PAN-Pt possess highly electrocatalytic activity. If the mean distance between these particles is too small, a depletion of the reactant (dissolved oxygen) concentration due to slow mass transfer occurs around each particle, and this process seems to be the rate-determining step in this type of system. A suitable mean distance between these particles could thus lead to enhancement of the mass transfer process. This PAN-Pt system seems to act as a "collection of nanoelectrodes" with ideal spacing between the platinum particles. XPS study indicates that there exists a special interaction between the platinum and the support within a PAN-Pt electrocatalyst, which is stronger than that in the PAN/Pt material. The long time stability of the PAN/Pt electrocatalyst should be, in principle, improved by this special interaction, which has indeed been indicated by our preliminary experimental results, and is a subject of our continuing study. This material is a promising electrocatalyst for oxygen reduction, and its electrocatalytic activity is due to the nanodispersed platinum particles present in the nanocomposite.

The PAN-Pt material can be considered to be a molecularly mixed inorganic–organic polymer nanocomposite. At the microscopic level, the mixed components represent very homogeneous combinations originating from chemical interactions at the molecular scale in the liquid phase that can be viewed as "frozen in" in the solid state via supercritical drying. Thus, by using aerogel preparation methods, control of the morphological properties is well advanced by comparison with conventional preparation techniques such as impregnation, ion exchange, and so on. The synthesis of such composites is believed to open promising new possibilities for the (electro)catalytic application of aerogels as catalysts or catalyst supports with novel structural and chemical properties (14). However, in such molecularly mixed preparation routes, it must be remembered that at least part of the precious metal component is submerged within the body of the matrix (26), thus no longer being accessible for (electro)catalytic surface processes. Also, it was found from the analysis of XPS data that a large fraction of platinum is in oxide or hydroxide states. It is known that platinum oxides are electrochemically inactive for oxygen reduction, which is believed to be one of the main reasons that PAN-Pt is not such a good electrocatalyst for oxygen reduction as would be expected by taking into account its molecularly homogeneous nanocomposite structure. In addition, one can see from Fig. 6 that it takes a higher overpotential to generate the same current density on PAN-Pt as on a platinum bulk electrode, the reason being still unclear. Further studies are being carried out in order to achieve a more efficient use of this electrocatalyst, by converting the higher oxide states of platinum to the metallic state.

Acknowledgements

This work was supported by the Institut de Recherche d'Hydro-Québec (IREQ) and the Natural Sciences and Engineering Research Council of Canada (NSERC). Thanks are due to Dr. Guy Bélanger of IREQ for his interest in this work. We thank Dr. R. Schulz and Mr. A. Joly of IREQ, and Mr. G. Veilleux of the Institut National de la Recherche Scientifique (INRS) for their invaluable help in the TEM and XPS measurements.

References

1. C.J. Brinker and G.W. Scherer. Sol–gel Science — The physics and chemistry of sol–gel processing. Academic Press, San Diego. 1990.
2. J.D. LeMay, R.W. Hopper, L.W. Hrubesh, and R.W. Pekala. MRS Bull. 19 (1990).
3. J.H. Albert and A.P. Sylwester. CHEMTECH. **21**, 290 (1991).
4. L. Sawtschenko, K. Jobst, M. Schwarzenberg, and G. Paasch. Synth. Met. **47**, 287 (1992).
5. G.M. Pajonk, E. Elaloui, P. Achard, B. Chevalier, J.-L. Chevalier, and M. Durant. J. Non-Cryst. Solids, **186**, 1 (1995).
6. X. Lu, O. Nilsson, J. Fricke, and R.W. Pekala. J. Appl. Phys. **73**, 581 (1993).
7. D.W. Schefer, R. Pekala, and G. Beaucage. J. Non-Cryst. Solids, **186**, 159 (1995).
8. L.W. Hrubesh and J.F. Poco. J. Non-Cryst. Solids, **186**, 46 (1995).
9. J.C. Farmer, D.V. Fix, G.V. Mack, R.W. Pekala, and J.F. Poco. J. Electrochem. Soc. **143**, 159 (1996).
10. J. Wang, P.V.A. Pamidi, C.L. Renschler, and C. White. J. Electroanal. Chem. **404**, 137 (1996).
11. J. Wang, A. Brennsteiner, and A.P. Sylwester. Anal. Chem. **62**, 1102 (1990).
12. G.M. Pajonk. Appl. Catal. **72**, 217 (1991).
13. E.I. Ko. CHEMTECH, 31 (1993).
14. M. Schneider and A. Baiker. Catal. Rev. Sci. Eng. **37**, 515 (1995).
15. S. Ye, A. K. Vijh, and L. H. Dao. *In* New materials for fuel cell systems I, Proceedings of the First International Symposium on New Materials for Fuel Cell Systems, Montreal, Quebec, Canada, July 9–13, 1995. *Edited by* O. Savadogo, P.R. Roberge, and T.N. Veziroglu. Les Éditions de l'École Polytechnique de Montreal, Montreal. 1995. p. 532.
16. S. Ye, A.K. Vijh, and L.H. Dao. J. Electrochem. Soc. **143**, L7 (1996).
17. S. Ye, A.K. Vijh, and L.H. Dao. J. Electroanal. Chem. **415**, 115 (1996).
18. S. Ye, A.K. Vijh, and L.H. Dao. J. Electrochem. Soc. **144**, 90 (1997).
19. S. Ye, A.K. Vijh, and L.H. Dao. J. Electrochem. Soc. **144**, 1734 (1997).
20. S. Ye, S. Besner, L.H. Dao, and A.K. Vijh. J. Electroanal. Chem. **381**, 71 (1995).
21. J.C. Vedrine, M. Dufaux, C. Naccache, and B. Imelik. J. Chem. Soc. Faraday Trans. 1. **74**, 440 (1978).
22. P.L. Antonucci, V. Alderucci, N. Giordano, D.L. Cocke, and H. Kim. J. Appl. Electrochem. **24**, 58 (1994).

Can. J. Chem. Downloaded from www.nrcresearchpress.com by 91.121.58.235 on 09/08/12
For personal use only.

© 1997 NRC Canada

23. A. Biloul, F. Coowar, O. Contamin, G. Scarbeck, M. Savy, D. van den Ham, J. Riga, and J. Verbist. J. Electroanal. Chem. **289**, 189 (1990).
24. C.D. Wagner, W.M. Riggs, L.E. Davis, J.F. Moulder, and G.E. Muilenberg (*Editors*). *In* Handbook of X-ray photoelectron spectroscopy. Perkin–Elmer Co., Eden Prairie, Minn. 1979. p. 152.
25. A.S. Arico, P. Creti, H. Kim, R. Mantegna, N. Giordano, and V. Antonucci. J. Electrochem. Soc. **143**, 3950 (1996).
26. T. López, M. Villa, and R. Gómez. J. Phys. Chem. **95**, 1690 (1991).

Can. J. Chem. Downloaded from www.nrcresearchpress.com by 91.121.58.235 on 09/08/12
For personal use only.

© 1997 NRC Canada

Response of the EQCM to specific adsorption on gold electrodes: adsorption of pyridine and benzene

Galit Zilberman, Vladimir Tsionsky, and Eliezer Gileadi

Can. J. Chem. Downloaded from www.nrcresearchpress.com by 91.121.58.235 on 09/08/12
For personal use only.

Abstract: The electrochemical quartz crystal microbalance (EQCM) is used to study adsorption of pyridine and benzene on gold. The most important result observed is that *the frequency increases when the organic molecule is adsorbed*, namely, the total mass of the species rigidly adsorbed is reduced as a result of adsorption. This is consistent with the accepted idea that electrosorption is a replacement reaction, in which a number of water molecules are replaced from the interface for each organic molecule adsorbed. However, this is the first time, to the best of our knowledge, that it has been observed experimentally. If the number of water molecules desorbed to make place for one molecule of pyridine is larger than 4.4, a decrease in mass should be observed. When independent data on the dependence of surface coverage on potential is available, this number can be estimated. In the case of pyridine, the EQCM data best fit the adsorption results if each molecule is assumed to replace 10–12 water molecules. In the case of benzene a similar calculation could not be performed since there are no adsorption data collected under comparable experimental conditions. Nevertheless, a positive shift of frequency is observed, indicating that this number must be >4.4.

Key words: electrochemical quartz crystal microbalance, electrical double layer, gold, pyridine, benzene.

Résumé : On a utilisé une microbalance électrochimique à cristal de quartz («EQCM») pour étudier l'adsorption de la pyridine et du benzène sur l'or. Le résultat le plus important à être observé est que *la fréquence augmente lors de l'adsorption de la molécule organique*, à savoir que l'adsorption provoque une réduction de la masse totale de l'espèce adsorbée d'une façon rigide. Cette observation est en accord avec l'idée généralement acceptée à l'effet que l'électrosorption est une réaction de substitution dans laquelle un certain nombre de molécules d'eau sont remplacées de l'interface par les molécules organiques adsorbées. Toutefois, à notre connaissance, c'est la première fois que ce phénomène est observé expérimentalement. Si le nombre de molécules désorbées pour faire de la place pour une molécule de pyridine est supérieur à 4,4, on devrait observer une diminution de la masse. Quand on dispose de données indépendantes relatives à la relation entre la couverture de la surface et le potentiel, il est possible d'évaluer ce nombre. Dans le case de la pyridine, les données de «EQCM» s'ajustent bien aux résultats d'adsorption si l'on fait l'hypothèse que chaque molécule remplace de 10 à 12 molécules d'eau. Dans le cas du benzène, il n'a pas été possible de faire un calcul semblable parce qu'aucune donnée d'adsorption, obtenue dans des conditions expérimentales semblables, n'est disponible. On observe toutefois un déplacement positif de fréquence; ceci indique que ce nombre doit être >4,4.

Mots clés : microbalance électrochimique à cristal de quartz, double couche électrique, or, pyridine, benzène.

[Traduit par la rédaction]

Introduction

We have pointed out in several previous publications (1–4) that the responses of the quartz crystal microbalance (QCM) and its electrochemical version, the EQCM, reflect a variety of phenomena taking place at the interface between the surface of the vibrating crystal and the medium in which it is immersed. In particular it was shown (4) that electrostatic interactions between the charge on the metal surface and the ionic species in solution, which lead to significant changes in the concentration of the ions in the diffuse double layer, can lead to substantial changes in the frequency of the quartz crystal resonator. These changes in frequency are commensurate with the mass effect associated with the adsorption of one or two monolayers of typical adsorbates of interest in the study of the metal–solution interface. It was concluded that these changes in frequency are caused by the combined effects of the change in concentration and the resulting change in viscosity in the layer of liquid very close to the surface.

In the present work we embarked on a study of the use of the EQCM for the determination of specific adsorption, using the electrosorption of pyridine and benzene from aqueous solutions on a gold electrode as an example. The electrosorption of pyridine on gold has been studied in detail by different techniques (electrochemical, radiotracer, and Raman spectroscopy), and the results were recently reviewed by Lipkowski

Received June 12, 1997.

This paper is dedicated to Professor Brian E. Conway on the occasion of his 70th birthday.

G. Zilberman, V. Tsionsky,[1] and E. Gileadi. School of Chemistry, Raymond and Beverly Sackler, Faculty of Exact Sciences, Tel-Aviv University, Ramat-Aviv, Tel-Aviv 69978, Israel.

[1] Author to whom correspondence may be addressed. Fax: 972-3-6409293. E-mail: tsionsky@ccsg.tau.ac.il

© 1997 NRC Canada

Can. J. Chem. Downloaded from www.nrcresearchpress.com by 91.121.58.235 on 09/08/12
For personal use only.

et al. (5). In a previous publication (1), we reported on our studies of the adsorption of the same two compounds from the gas phase on gold, with the use of the QCM.

Experimental

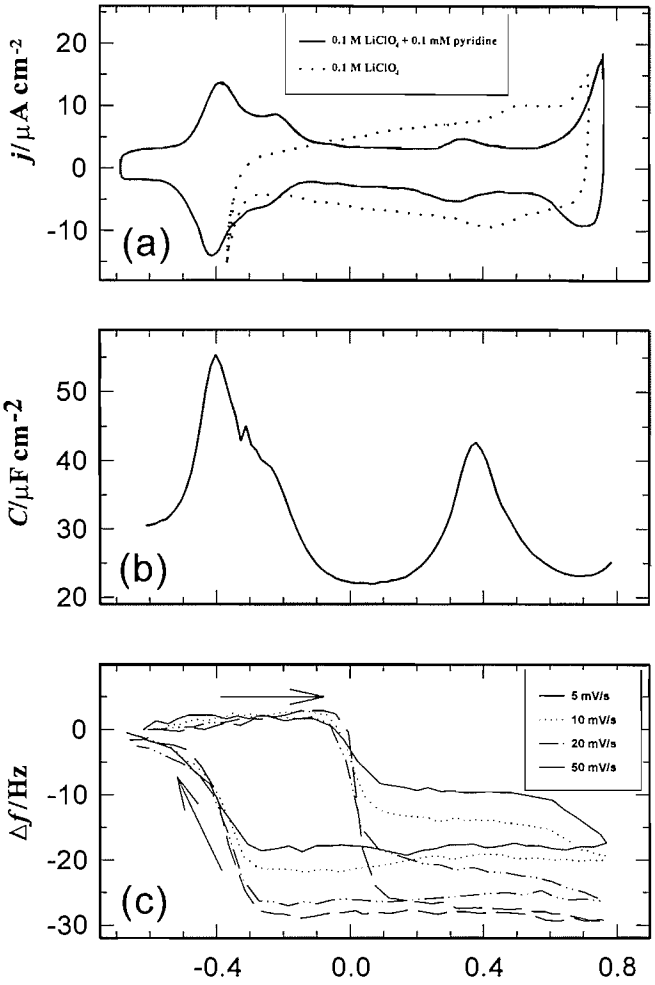
The quartz crystals employed in this work (diam. 14 mm) were of the "AT-cut" type, coated on both sides with vacuum-sputtered gold. The fundamental frequency of the crystal was f_0 = 6 MHz. A Leybold Inficon model XTC/2 or model IC/4 thin-film deposition controller, employing the "modelock" method for controlling and measuring the frequency, was used. Details of the measuring technique and the instrumentation employed were given in a recent publication (4). As in ref. 4, different compartments of the glass cell were separated by wetted glass stopcocks. Removal of oxygen traces from the solution by pure helium flow and preparing solutions with different concentrations of pyridine or benzene were performed in a separate cell compartment. This was used as a stock compartment to refill the working-electrode compartment. The latter was tubular and closed at the bottom by the disk of the quartz resonator. At the top of this tube, at a distance of 10 cm from the working electrode, an auxiliary platinum disc electrode was placed. This was used for ac measurement only and was connected through a capacitor, with the main counter platinum electrode placed in a separate compartment. This avoided polarization by the dc current and decreased the possibility of contamination of solution in the working-electrode compartment. At the same time, most of the ac current was passed through the solution, thus improving the uniformity of ac current distribution on the working electrode. A Solartron 1250 frequency-response analyzer was used to measure the double-layer capacitance as a function of potential. The potential was swept at a rate of 5 mV/s and modulated at a frequency of 25 Hz with a sine wave of 5 mV amplitude.

The gold surface sputtered on the quartz crystal was used as the working electrode. It was degreased and cleaned by standard procedures, as described earlier (4). To enhance reproducibility of the surface, the electrode was cycled overnight in the supporting electrolyte (0.1 M $LiClO_4$), between −0.40 V vs. NHE (the onset of hydrogen evolution) and 1.50 V vs. NHE. Only after this procedure, and replacement of the solution in the working-electrode compartment with a new portion of solution, did the current–potential (j–E) curve become symmetrical in current over the potential region of interest (Fig. 1*a*, broken line). The cell construction permitted maintenance of the experimental conditions for many hours without any sign of contamination of solution or electrode. All the measurements were performed at 25 ± 0.5°C with unstirred solutions.

Preliminary results

The cyclic voltammogram and the dependence of capacitance on voltage obtained for solutions containing pyridine are shown in Figs. 1*a* and *b*, respectively. There is good correspondence between the j–E and the C–E plots. These results coincide with the results published by Lipkowski and coworkers (6). This is very important for us, because we used the data on charge density and surface excess obtained in ref. 6 to process the data on the EQCM response. The dependence of charge on potential, obtained in the supporting electrolyte in

Fig. 1. (*a*) Cyclic voltammetry, 50 mV/s; (*b*) double-layer capacitance; and (*c*) EQCM response. Gold electrode in 0.1 M $LiClO_4$ + 0.1 mM pyridine. Arrows show the potential scan directions.



the absence of pyridine, agrees well with literature data (7) if we assume a roughness factor of approximately 1.5, which is reasonable in view of the roughness of the gold surfaces we have been using, as discussed earlier (2).

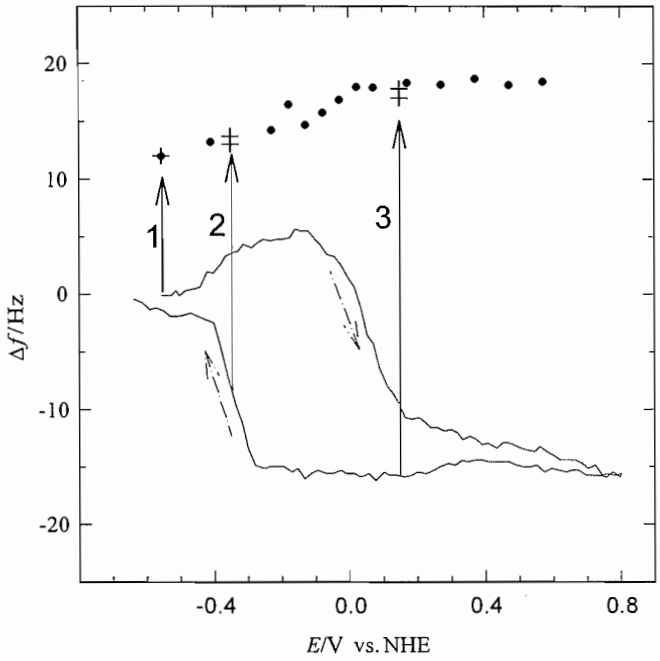
In preliminary experiments with dilute solutions of pyridine (0.1 mM) it was observed that the response of the EQCM during cycling over a given potential region is strongly dependent on the sweep rate and the direction of the sweep, as shown in Fig. 1*c*.[2] The hysteresis decreases with increasing pyridine concentration. It should be noted that the curves shown in Fig. 1*c* were reproducible only after the first 5–10 cycles. The initial Δf–E curves appear at higher frequencies. There are two possible reasons for this behavior. One of them is transport limitation. It is known (5, 6) that in the case of pyridine, measurements of the double-layer capacitance during cycling over a given range of potentials do not yield the true size and shape of the capacitance dependence on potential

[2] The value of Δf was arbitrarily taken as zero at a potential of −0.6 V, where adsorption of pyridine does not occur.

© 1997 NRC Canada

Can. J. Chem. Downloaded from www.nrcresearchpress.com by 91.121.58.235 on 09/08/12
For personal use only.

Fig. 2. Comparison between the data obtained in the 0.1 M $LiClO_4$ + 1 mM pyridine solution by potential-sweep (solid line) and potential-step (points) techniques. Dashed arrows show the direction of the sweep (50 mV/s). For other details see text.



and, as a result, misrepresent the data on surface excess. Transport limitations give rise to the diffusion layer, the viscosity of which may differ from that of the bulk solution. The EQCM response is very sensitive to changes of viscosity at the interface. The influence of diffusion kinetics on the EQCM response has been shown (8). Kinetic limitations of the adsorption–desorption process, which do not allow equilibrium adsorption of pyridine during cycling, are probably an additional cause of the hysteresis observed.

To avoid this complication, we employed a potential-step rather than potential-sweep technique. The gold electrode was held for a few minutes at an initial potential E_i (−0.6 vs. NHE), where adsorption of pyridine does not take place. The potential was then stepped to a desired value E_1, maintained there for a few minutes to ensure that steady state had been reached, then stepped back to the initial value E_i to ensure that the state of the surface had not changed, as determined by the fact that the frequency resumed its original value. This procedure was repeated for a series of potentials, E_2, E_3, E_4, etc. The frequency was monitored throughout this procedure, and the dependence of frequency on potential was determined from the steady state values observed at each potential. This steady state was usually reached within 10–30 s of changing the potential and was stable to within ±0.5 Hz. The difference between the frequency at E_i and E_n is used below as a function of potential.

Correlation between the data obtained by potential-step and potential-sweep techniques is shown in Fig. 2. The solid line corresponds to the Δf–E curve for the 50 mV/s scan. If the sweep is stopped at negative potential, where there is no adsorption of pyridine, Δf increases by more than 10 Hz in about 3 min. These changes are shown by the vertical arrow 1. In practice, it is impossible to compare the absolute values of fundamental frequency of the quartz resonator obtained in different independent experiments. Therefore, as seen in Fig. 2 we took the limiting steady state value of the frequency (a cross at the end of arrow 1) as background for the data obtained by the potential-step technique (points). In this manner one can see the difference between the two sets of data. If the sweep is stopped at any arbitrary potential (arrows 2 and 3) the frequency begins to increase and its limiting values (crosses) coincide with the dependence obtained by the potential-step method. These limiting values are independent of the sweep direction. Thus the data on the EQCM response obtained during the potential-sweep do not reflect equilibrium adsorption and do not represent an intrinsic hysteresis in the adsorption behavior of pyridine from aqueous solutions.

Contrary to experiments with pyridine, the EQCM responses obtained with benzene from potential-step experiments and from cyclic voltammetry practically coincide. This may be due to different energies of adsorption–desorption of the two substances, different kinetics of this process, and partially to the higher diffusion coefficient of benzene (1.02×10^5 cm^2/s) compared to that of pyridine (0.58×10^{-5} cm^2/s) (9). All the data on pyridine adsorption presented in Figs. 3 and 4, and discussed below, were obtained by the potential-step technique.

Results and discussion

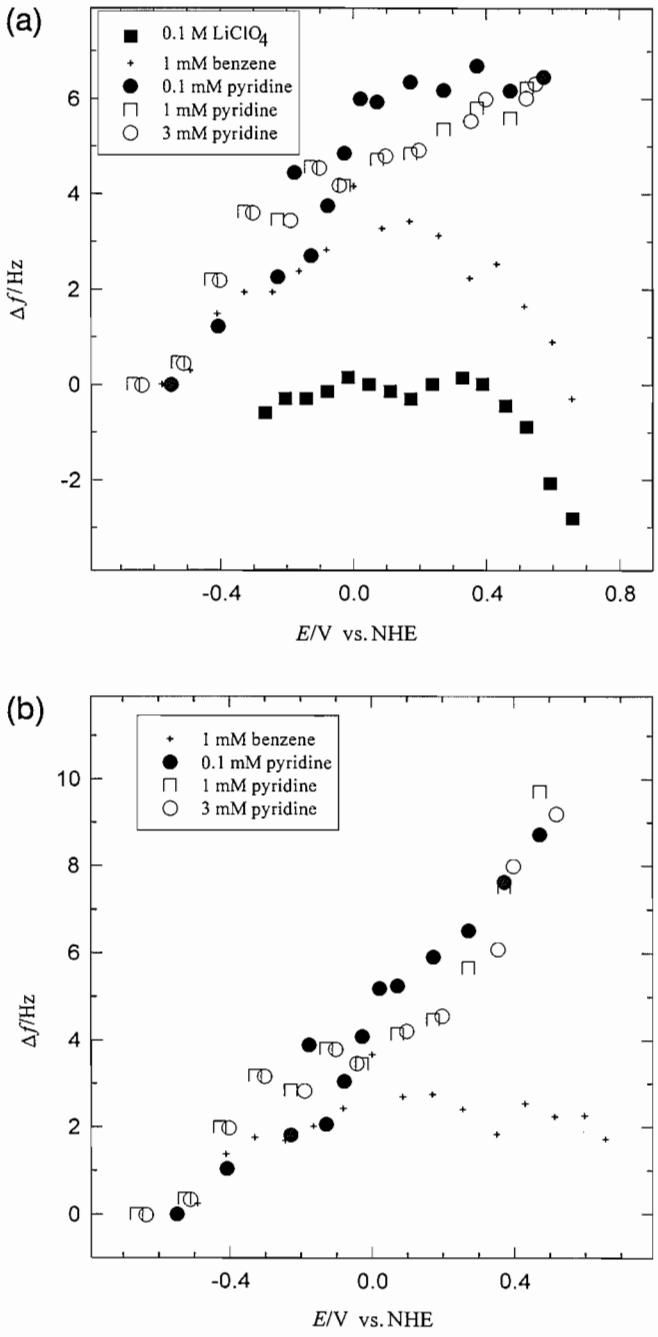
The frequency of the EQCM depends in a complex manner on the detailed structure of the interface between the metal coating on the quartz crystal and the solution (4). The concentrations of pyridine and of benzene used in the present series of experiments are sufficiently low, so that the bulk viscosity and density of the solution may be considered to be independent of the presence of the organic adsorbate. Moreover, when switching from the initial potential to a chosen value, the frequency changes in a relatively short time, i.e., on the time scale of seconds, and upon switching back to the initial potential the frequency resumes its original value, ruling out the possibility of major changes in the surface roughness. We are therefore left to interpret the change in frequency in terms of the changes in the diffuse double layer, alluded to above (3, 4), and, of course, the change in mass resulting from electrosorption.

The properties of the diffuse double layer depend directly on the surface charge density of the metal and not on the potential. Thus, in order to correct for this effect quantitatively, we first need to convert the dependence of frequency on potential $\Delta f(E)$ to its dependence on charge density, $\Delta f(q)$. In Fig. 3*a*, the potential regions, where the EQCM response was measured in the presence and absence of pyridine, do not coincide because hydrogen evolution in the supporting electrolyte starts at a more positive potential than in the presence of pyridine (cf. Fig. 1*a*). However, because of peculiarities of the shape of charge–potential dependence and a shift of the PZC on gold to more negative potentials in pyridine-containing solutions (6), the range of charge densities practically coincide. In this new coordinate ($\Delta f(q)$) we shift all the curves along the frequency axis, so that at the initial potential, where no adsorption occurs, the value of Δf coincides with its value on the Δf vs. q plot for the supporting electrolyte. We then fol-

© 1997 NRC Canada

Can. J. Chem. Downloaded from www.nrcresearchpress.com by 91.121.58.235 on 09/08/12
For personal use only.

Fig. 3. Response of the EQCM on gold in 0.1 M $LiClO_4$, in the presence of pyridine or benzene at the concentrations marked in the figure. (*a*) The measured shift in frequency as a function of potential; (*b*) the same as (*a*) corrected for the effect of the diffuse double layer (see text).



low the curve to all other potentials, subtracting the value of $\Delta f(q)$, caused by changes in the diffuse double layer in the supporting electrolyte, from the value obtained in the presence of pyridine or benzene. This is done on the tacit assumption that the structure of the diffuse double layer, as far as changes in the surface excess of the different ions is concerned, is independent of the presence of the organic adsorbate, *as long as the comparison is made at the same charge density*. The dependence of charge density on potential is, of course, influenced by electrosorption, so a similar correction would not have been justified had we used the dependence of frequency on potential. We use the dependence of charge on potential obtained for pyridine in the literature (6) from potential-step experiments, i.e., by the same techniques used to obtain the EQCM response. The dependence of charge on potential for the case of benzene is obtained by numerical integration of the capacitance as a function of potential. Such a corrected plot is shown in Fig. 3*b* for one concentration of benzene and two concentrations of pyridine. Comparison between Figs. 3*a* and *b* shows the overwhelming importance of taking the potential dependence of frequency, resulting from the effects of ions in the diffuse double layer, into account when interpreting of EQCM data in the submonolayer region (3, 4). The change in frequency caused by specific adsorption in the present case is similar in magnitude to that caused by the change in potential in systems where specific adsorption is known to be absent. Ignoring this effect, which has been discussed in some detail earlier (4), could therefore lead to totally erroneous conclusions regarding specific adsorption.

Having corrected for the effect of the diffuse double layer, and considering that all other conditions (viscosity, density, surface roughness) are constant in the course of the experiment, the only cause for a change in frequency is the mass effect of the adsorbed species. We can hence employ the Sauerbrey equation (10):

$$[1] \quad \Delta f = -C_m \Delta m$$

The constant C_m, which represents the sensitivity of the EQCM, is 0.082 Hz ng^{-1} cm^2 in our experimental setup.

It should first be noted that the change of frequency caused by adsorption is positive, *implying a decrease rather than an increase in mass.* This is not unexpected, considering that electrosorption is a replacement process in which the adsorbate replaces a certain number of water molecules from the surface (11, 12). Thus, depending on the number of water molecules displaced for each organic molecule adsorbed, the total mass could increase, decrease, or remain essentially constant. The change of mass resulting from electrosorption can be expressed in the form

$$[2] \quad \Delta m = \Gamma_{ads}(M_{ads} - vM_W)$$

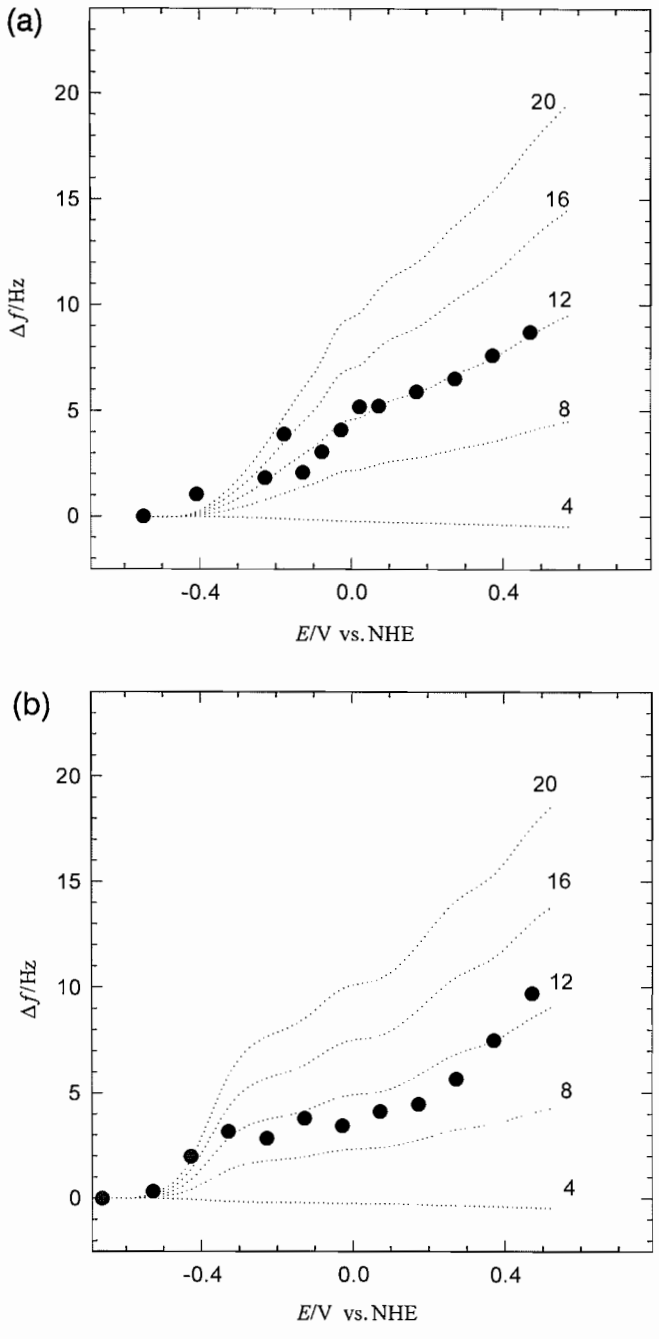
where M_{ads} and M_W are the molecular weights of the adsorbate and water, respectively, Γ_{ads} is the surface excess of the adsorbate, and v is the number of water molecules replaced by each adsorbed organic molecule. It is obvious from the above that for values of v equal to 4–5, there would hardly be any change in frequency upon adsorption of benzene or pyridine. The increase of frequency observed in our experiments (cf. Fig. 3*b*) indicates that the number of water molecules replaced from the surface is higher.

In the case of the adsorption of pyridine on gold electrodes, the dependence of Γ_{ads} and of the charge density on potential has been determined in great detail (6). This allowed us to calculate the expected values of the change in frequency as a function of potential, assuming different values of the size parameter v. The results of such calculations, for values of v

© 1997 NRC Canada

Can. J. Chem. Downloaded from www.nrcresearchpress.com by 91.121.58.235 on 09/08/12
For personal use only.

Fig. 4. Comparison between the calculated shift of frequency of the EQCM upon adsorption of pyridine, assuming different values of the size parameter v (dashed lines) and the experimental results, corrected for the effect of the diffuse double layer. (*a*) 0.1 mM; (*b*) 1 mM pyridine.



ranging from 4 to 20, are shown in Figs. 4*a* and *b* for 0.1 mM and 1.0 mM solutions of pyridine, respectively. It can be seen that the experimental points best fit the curve calculated for a value of v = 10–12. A specific physical interpretation of these values can be given only in the framework of a simplified model of the interface, consisting of the metal surface, a film of water molecules adsorbed on this surface, followed by "bulk" water. The film is assumed to be rigidly attached to the metal (as in chemisorption) and to vibrate with the crystal. The hydrodynamic velocity profile leads from the plane of this rigid film outwards. Thus, adsorption of pyridine gives rise to substitution of a number of water molecules (v) from the rigidly adsorbed film. The real situation at the interface is undoubtedly more complicated, and the structure of water changes gradually with distance from the metal surface, until bulk properties are reached at a distance of a few layers from the surface. Thus, the value of v estimated in the above manner should be regarded as an effective value, reflecting the total effect of an adsorbed species on the structure of the water in the interface.

At potentials more positive than −0.05, the effective value of v, calculated from the EQCM response (points), has the same shape as that obtained from surface excess (lines). This indicates that the effective number of water molecules replaced is unchanged, and reorientation of adsorbed pyridine molecules is not likely to have taken place in this region. At more negative potentials the response of the EQCM is too small for sufficiently precise determination of v. The PZC values are equal to 0.01 and −0.06 V vs. NHE for 0.1 mM and 1 mM pyridine, respectively (6). Thus, at positive charge densities, there is no change of configuration of the pyridine molecule at the interface. It has been reported in the literature (6) that, in the same region, pyridine is adsorbed on gold in a perpendicular configuration.

Figures 4*a* and *b* present only low concentrations of pyridine. For higher concentrations of pyridine and for benzene we could not perform this type of calculation, because accurate data for the dependence of Γ_{ads} and of the charge density on potential are not available. In the case of benzene, a direct comparison between the available radiotracer data on gold (13) and the present EQCM measurements cannot be made because of the great difference in the experimental conditions. This makes the interpretation of the dependence of frequency on potential difficult for benzene. We do observe, however, that the change in frequency is positive, as in the case of pyridine (cf. Fig. 3*b*), indicating that the number of water molecules replaced from the surface for each molecule of benzene adsorbed is larger than 4, and probably not less than 6. We note here the difference between our earlier measurements in the gas phase (1) and the present measurements from solution. In the former, pyridine is adsorbed in a perpendicular configuration occupying a smaller area on the surface, and hence a monolayer contains more molecules, leading to a larger shift of frequency *in the negative direction*. Here, the perpendicular configuration of the pyridine molecule disturbs the structure of water further away from the metal surface, thus leading to *a larger positive shift in frequency*, which is indicative of a larger apparent number of water molecules replaced by each molecule of pyridine adsorbed.

Conclusions

The concept of electrosorption as a replacement reaction has long been established and the energetics of the process is commonly discussed in terms of the difference between the energy of adsorption of the organic molecule and the energy of desorption of the number of water molecules v (14). The present study is the first, to the best of our knowledge, in which direct

© 1997 NRC Canada

evidence for this displacement process is presented, in that the frequency of the EQCM is found to *increase* upon adsorption of organic molecules, showing that the total mass loading the crystal has effectively decreased. This is a very important central finding in our work, the importance of which transcends the detailed discussion of the configuration of different molecules adsorbed on the surface.

If independent adsorption data are available, one can fit the EQCM data to curves, calculated by assuming different numbers of water molecules replaced for each organic molecule adsorbed, and determine the effective size parameter of the molecule.

It is shown that meaningful adsorption data can only be obtained if the change of frequency, resulting from changes in concentration and viscosity inside the diffuse double layer, is taken into account, as discussed in our earlier publications (3, 4).

The frequency of the quartz crystal resonator is sensitive to a host of physical phenomena occurring at the interface, and should not be interpreted only in terms of a change in mass (1–4). This calls for tight control of these parameters, if meaningful data concerning adsorption are to be extracted. In electrochemical systems it is best to use the EQCM in conjunction with other methods, such as measurement of the double-layer capacitance, the charge density, and the surface excess, to obtain a clear picture of the interface, and the configuration of different molecular species in it.

Acknowledgments

Financial support for this work by the Israel Science Foundation of the Israel Academy of Science and Humanities is gratefully acknowledged. The authors wish to thank Dr. L. Daikhin of this department for useful discussions. We also thank M. Brand and B. Agam for their diligent and skillful technical assistance.

References

1. V. Tsionsky and E. Gileadi. Langmuir, **10**, 2830 (1994).
2. V. Tsionsky, L. Daikhin, M. Urbakh, and E. Gileadi. Langmuir, **11**, 674 (1995).
3. V. Tsionsky, L. Daikhin, and E. Gileadi. J. Electrochem. Soc. **142**, L-233 (1995).
4. V. Tsionsky, L. Daikhin and E. Gileadi. J. Electrochem. Soc. **143**, 2240 (1996).
5. J. Lipkowski, L. Stolberg, S. Morin, D.E. Irish, P. Zelenay, M. Gamboa, and A. Wieckowski. J. Electroanal. Chem. **355**, 147 (1993).
6. L. Stolberg, J. Richer, J. Lipkowski, and D.E. Irish. J. Electroanal. Chem. **207**, 213 (1986).
7. J. Clavilier and C. Nguen VanHuong. J. Electroanal. Chem. **80**, 101 (1977).
8. W.-W. Lee , H.S. White, and M.D. Ward. Anal. Chem. **65**, 3232 (1993).
9. D.R. Lide (*Editor*). CRC handbook of chemistry and physics. CRC Press, Boca Raton, Fla. 1996. p. 6-220.
10. G. Sauerbrey. Z. Phys. **155**, 206 (1959).
11. J.O'M. Bockris, M.A.V. Devanathan, and K. Muller. Proc. R. Soc. London Ser. A, **274**, 55 (1963).
12. E. Gileadi. *In* Electrosorption. *Edited by* E. Gileadi. Plenum Press, New York. 1967. Chap. 1. pp. 1–18.
13. H. Dahams and M. Green. J. Electrochem. Soc. **110**, 1075 (1963).
14. W. Heiland, E. Gileadi, and J. O'M. Bockris. J. Phys. Chem. **70**, 1207 (1966).

Can. J. Chem. Downloaded from www.nrcresearchpress.com by 91.121.58.235 on 09/08/12
For personal use only.

© 1997 NRC Canada

Réorganisation de la double couche électrique suivant la désorption réductive d'une monocouche auto-assemblée d'alcanethiols sur l'or<111>

Dong Fang Yang et Mario Morin

Résumé : Nous avons utilisé la spectroscopie vibrationnelle pour suivre la réorganisation de la double couche électrique suite à la réduction d'une monocouche auto-assemblée de nonanethiols chimisorbés sur une électrode monocristalline d'or<111>. L'absence de changements vibrationnels importants dans la région de la double couche démontre que la monocouche de nonanethiols est stable sur plus de 800 mV. Lorsque le potentiel de l'électrode est plus négatif que le potentiel de réduction de la monocouche de nonanethiols, des changements sont observés dans le spectre vibrationnel des molécules d'eau. L'interaction entre les molécules d'eau et la surface d'or change selon le potentiel appliqué à l'électrode. Pour un potentiel correspondant au début de la réduction de la monocouche de thiols, les résultats spectroscopiques suggèrent que les molécules d'eau interagissent faiblement avec la surface d'or<111>. Lorsque le potentiel de l'électrode devient suffisamment négatif pour produire de l'hydrogène gazeux, le mode de déformation de l'eau se déplace vers une plus basse énergie. Ce dernier résultat indique une plus forte interaction entre les molécules d'eau et l'électrode d'or. De plus, des mesures vibrationelles résolues dans le temps suggèrent la formation d'agrégats de molécules d'eau immédiatement après la désorption réductive des thiols et avant la production d'une quantité détectable d'hydrogène.

Mots clés : électrochimie, double couche électrique, spectroscopie vibrationnelle, thiols.

[Traduit par la rédaction]

Abstract: We report a vibrational study of the reorganization of the electrical double layer following the reduction of a self-assembled nonanethiol monolayer on a Au <111> electrode. The absence of changes in the vibrational spectra taken in the potential range covering the double layer shows that the nonanethiol monolayer is stable over 800 mV. Important changes in the vibrational spectra of the water molecules are observed when the applied potential is more negative than the reduction potential of the thiol monolayer. The interaction between the water molecules and the gold electrode is modified by the electrode potential. For a potential corresponding to the onset of the reduction of the nonanethiol monolayer the spectroscopic results suggest that the water molecules interact weakly with the gold surface. However, when the potential is sufficiently negative to cause the evolution of hydrogen, the deformation mode of the water molecules moves to a lower energy, indicating a stronger interaction between the water molecule and the gold surface. Time-resolved vibrational measurements suggest that water clusters are formed immediately after the reductive desorption of the thiols and before a significant amount of molecular hydrogen is produced.

Key words: electrochemistry, electrical double layer, vibrational spectroscopy, thiols.

Introduction

Les monocouches auto-assemblées de thiols chimisorbés sur des électrodes métalliques sont utilisées comme systèmes électrochimiques modèle car elles sont compactes et bien ordonnées (1–8). Ces monocouches permettent l'étude de l'interface entre des composés organiques et une solution électrolyte aqueuse car il est possible de varier l'affinité des composés organiques pour le solvant à l'aide de la fonction du groupe terminal du thiol. Plusieurs études théoriques ont d'ailleurs porté sur la structure de la double couche à l'interface organique en présence des groupes fonctionnels chargés (9–11). Dans le cas de monocouches d'alcanethiols, l'interaction entre absorbats et la solution électrolyte est faible et une capacité de la double couche faible est mesurée (1). Cependant, lorsque la monocouche d'alcanethiols est oxydée ou réduite, la formation d'une double couche à la surface de l'électrode donne lieu à une augmentation du courant capacitif (12). Le contraste important entre la surface hydrophobe formée par les alcanethiols chimisorbés et la surface de l'électrode d'or<111> obtenue après la réduction des

Reçu le 15 mai 1997.

Cet article est dédié au Professeur Brian Conway à l'occasion de son 70ième anniversaire.

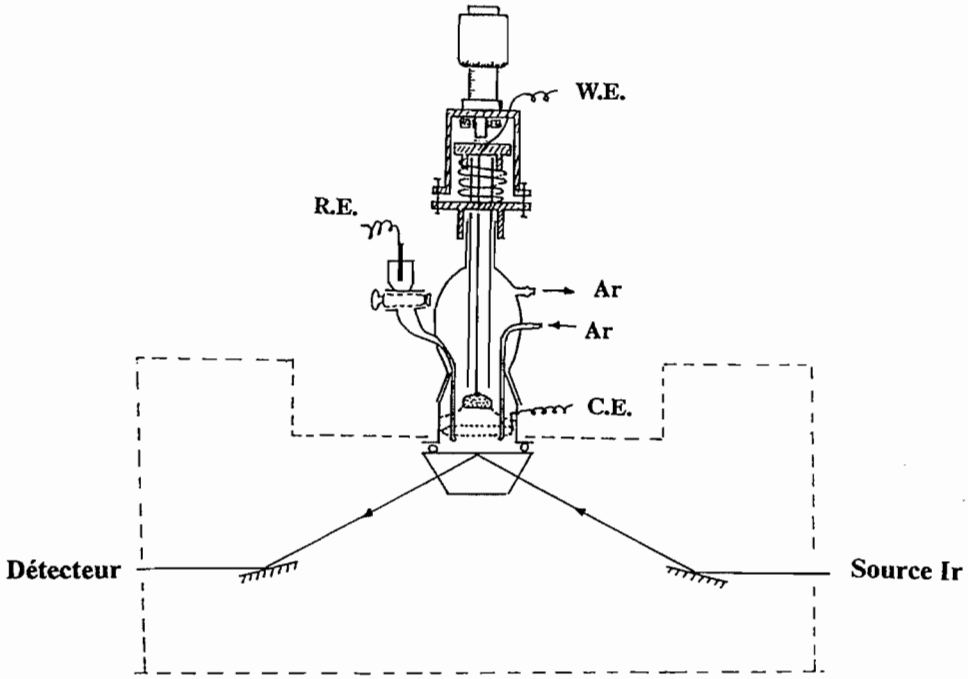
D.F. Yang et M. Morin.[1] Département de chimie, Université d'Ottawa, 10 Marie Curie, Ottawa, ON K1N 6N5, Canada.

[1] Auteur à qui adresser toute correspondance. Téléphone : (613) 562-5800, ext. 6037. Fax : (613) 562-5170. courrier électronique : mgmorin@science.uottawa.ca

© 1997 NRC Canada

Can. J. Chem. Downloaded from www.nrcresearchpress.com by 91.121.58.235 on 09/08/12
For personal use only.

Fig. 1. Schéma de la cellule spectro-électrochimique. C. E.: contre-électrode de platine; R. E.: électrode de référence (calomel saturé); W. E.: électrode de travail (or<111>). Le prisme de Dove est coupé à 60° et fait de CaF_2. Le détecteur infrarouge est de type MCT (mercure–cadmium–tellurium). Le spectromètre est purgé avec de l'azote.



alcanethiols cause des variations importantes de l'orientation des molécules d'eau à l'interface suivant la réduction des alcanethiols. Ces changements d'orientation pourraient être mesurés par spectroscopie vibrationnelle et utilisés pour suivre la formation de la double couche suivant la réduction des thiols. Une telle étude serait difficile avec des électrodes d'or polycristallines car le courant d'évolution d'hydrogène est superposé à celui de la réduction de thiols (13–16). Cependant, nous avons démontré dans une série d'études récentes que l'utilisation d'électrodes monocristallines d'or<111> permet la formation de monocouches ayant très peu de défauts et dont la réduction est séparée du courant d'évolution de l'hydrogène (12, 17). Dans la présente étude les changements du spectre vibrationnel des molécules d'eau observés suite à la désorption réductive d'une monocouche de thiols chimisorbés sur l'or<111> seront présentés. Ces résultats démontrent que l'interaction des molécules d'eau avec la surface de l'électrode d'or<111> varie selon le potentiel.

Expérimental

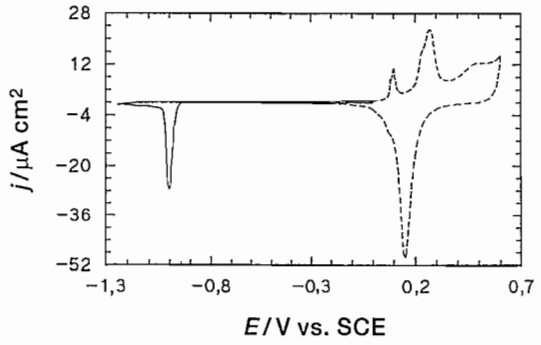
La préparation du monocristal d'or<111> a été décrite précédemment (12). La solution d'hydroxyde de potassium (Aldrich, semiconductor grade) de 0,1 M a été faite à partir d'eau distillée traitée avec un système Milli-Q (Millipore). L'eau deutérée utilisée pour les mesures isotopiques avait une pureté de 99,9% (Cambridge Isotopes). Les potentiels cités dans ce travail sont relatifs à celui d'une électrode de calomel saturée (SCE). La monocouche de nonanethiol est obtenue en déposant une électrode d'or dans une solution 1 mM de nonanethiol dans l'éthanol pour une durée de 1 h. Ce protocole de déposition donne une monocouche complète et bien ordonnée (12). Un schéma de la cellule spectro-électrochimique est présenté dans la Fig. 1. Elle est faite de verre. Au fond de la cellule, il y a un prisme de Dove de 60° en CaF_2 qui sert de fenêtre infrarouge. L'électrode de référence est à l'extérieur de la cellule et est reliée à la cellule principale par un capillaire de Luggin, afin de minimiser les contaminations dues aux chlorures. La contre-électrode est un anneau de platine qui entoure le monocristal d'or. Le monocristal est poussé sur la fenêtre infrarouge à l'aide d'un micromètre afin de former une couche mince d'électrolyte. Il est également possible en remontant l'électrode de former un ménisque pour effectuer des mesures électrochimiques exclusivement sur la surface <111> (12). Le spectromètre FTIR (Nicolet Magna 550) est équipé d'un détecteur MCT (mercure–cadmium–tellurium) refroidi avec de l'azote liquide. Le faisceau infrarouge est polarisé à l'aide d'un réseau de fils métalliques déposés sur un substrat de ZnSe. Le faisceau entre dans la fenêtre de CaF_2 avec une incidence normale afin de minimiser les pertes d'intensité par réflexion. Il est ensuite réfléchit par la surface de l'électrode monocristalline. L'angle d'incidence du faisceau par rapport à la normale à la surface d'or<111> est environ 70°. Le faisceau réfléchi est dirigé vers le détecteur MCT à l'aide d'un miroir. Ce design simple permet une transmission de la radiation infrarouge de l'ordre de 70–90%. La technique spectroscopique utilisée pour l'acquisition des spectres est connue sous l'acronyme SNIFTIRS (18). Elle consiste à mesurer un spectre à un potentiel de référence et un spectre à un autre potentiel. Le spectre de référence est celui d'une électrode recouverte de nonanethiols à un potentiel de −0,5 V. Par la suite, la différence entre ces spectres est calculée et elle est normalisée par le spectre de référence. Ceci donne un

© 1997 NRC Canada

Can. J. Chem. Downloaded from www.nrcresearchpress.com by 91.121.58.235 on 09/08/12
For personal use only.

Can. J. Chem. Downloaded from www.nrcresearchpress.com by 91.121.58.235 on 09/08/12
For personal use only.

Fig. 2. Voltampérogramme cyclique d'une électrode d'or<111> recouverte d'une monocouche de nonanethiols dans une solution de 0,1 M KOH. Le balayage débute à −0,5 V vers les potentiels négatifs. La vitesse de balayage est de 20 mV/s.



spectre de réflectance différentielle dans lequel les bandes négatives correspondent à une augmentation de l'intensité des modes vibrationnels et les bandes positives correspondent à une di-minution de l'intensité des modes vibrationnels par rapport au spectre de référence. Les spectres présentés correspondent à une moyenne de 64 spectres dont la résolution est de 2 cm^{-1}. Le temps d'acquisition de 64 spectres est d'environ 30 s. La radiation infrarouge est polarisée dans le plan d'incidence (c.-à-d., p-polarisée) afin de maximiser le champ électrique perpendiculaire à la surface (19).

La Fig. 2 illustre le voltamogramme de la réduction d'une monocouche de nonanethiols dans une solution de 0,1 M KOH. Ce voltamogramme a été discuté antérieurement (12). Nous n'en ferons qu'une brève description afin de donner les caractéristiques principales du processus de réduction de la monocouche de nonanethiols. On note que la monocouche est réduite à un potentiel de −1,04 V (pour une vitesse de balayage de 20 mV/s) et que le pic de réduction est symétrique. Lors du balayage vers des potentiels plus positifs, suivant la réduction de la monocouche de thiols, on observe la formation de l'oxyde de surface correspondant à celle d'une surface d'or<111> propre. Nous avons démontré lors d'études précédentes (20) que la réduction des thiols suit un mécanisme dit de «création de trous et croissance». Ce mécanisme consiste en la création de trous de forme circulaire causée par la désorption réductive de thiols. Par la suite, la désorption réductive des thiols ne se produit qu'à la périphérie de ces trous qui prennent ainsi de l'expansion. Lorsqu'un thiol est réduit et quitte la surface, il y a formation d'une double couche électrique à l'interface électrolyte–or<111>. Un courant dit capacitif est associé à la formation de cette double couche électrique. Ce courant capacitif est causé le fait qu'il est possible d'accumuler une charge plus importante à la surface d'un électrode métallique qu'à la surface d'une électrode métallique recouverte d'une monocouche d'alcanethiols.

Résultats

Les spectres SNIFTIRS de la Fig. 3 couvrent la région de 1300 à 3600 cm^{-1} pour différents sauts de potentiel à des valeurs finales allant de −0,1 V à −1,2 V. On observe, pour des sauts de potentiel entre −0,10 V et −0,90 V, qu'il n'y a pas de changements dans la région des modes d'étirements CH entre 2800 et 3000 cm^{-1}. Seule une légère variation d'intensité dans la région entre 3200 et 3600 cm^{-1} correspondant aux modes d'étirements de l'eau est observée. La monocouche de nonanethiols chimisorbés sur une surface monocristalline d'or<111> ne subit donc pas de modifications importantes de l'orientation des molécules d'eau et aucun changement de l'orientation des thiols entre −0,10 V et −0,90 V. Ces résultats sont en accord avec les résultats voltampérométriques (12) et chronoampérométriques (20) qui démontrent que seul le chargement de la double couche se produit dans ce domaine de potentiel.

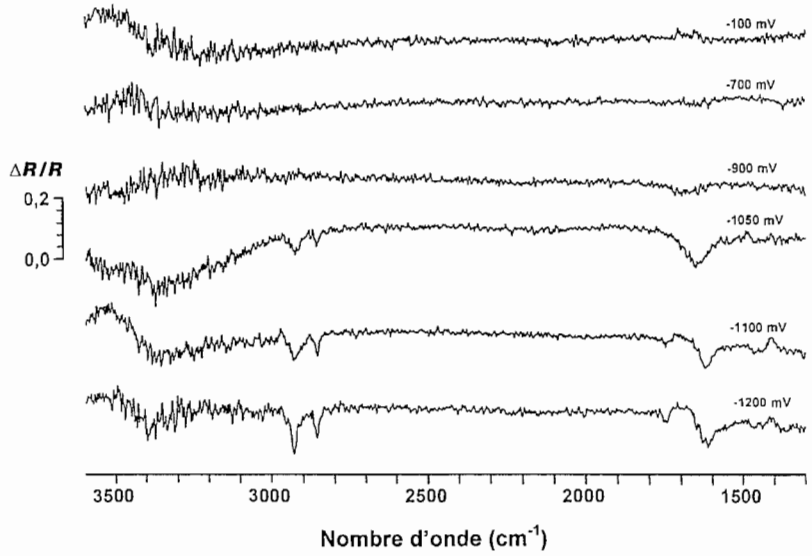
Lorsque le potentiel final est de −1,05 V ou plus négatif des changements importants sont observés dans le spectre vibrationel. On remarque dans ce domaine de potentiel des bandes négatives entre 2800 et 3000 cm^{-1} qui indiquent une augmentation de l'intensité des modes d'étirements CH des nonanethiols. Ces changements ont été discutés précédemment comme étant reliés à la formation de micelles de nonanethiolates (21). Un mode de faible intensité est observé à 1750 cm^{-1}. L'origine de ce mode est incertaine, mais il semble relié aux molécules de thiols (21). On voit également une augmentation de l'intensité (c.-à-d. des bandes négatives) de modes entre 1550 et 1700 cm^{-1} et entre 3000 et 3600 cm^{-1}. Ces modes correspondent respectivement au mode de déformation et aux modes d'étirement symétrique et asymétrique des molécules d'eau et ils sont le sujet de la présente étude.

Plusieurs observations indiquent que les spectres SNIFTIRS dans la Fig. 3 représentent principalement les molécules d'eau à la surface. En effet, lors d'une étude précédente, on a démontré que les bandes vibrationelles de l'eau dans le spectre p-polarisé diffèrent de celles observées dans un spectre s-polarisé (polarisation perpendiculaire au plan d'incidence) (21). Elles sont plus intenses et situées dans certains cas à des nombres d'onde différents. En conséquence, ceci indique, d'après les règles de sélection interfaciales en spectroscopie infrarouge (19), que les molécules d'eau observées dans les spectres p-polarisés sont surtout celles qui sont à l'interface. L'intensité similaire des modes vibrationels de l'eau et des modes d'étirements CH suggère qu'un nombre restreint de molécules d'eau (c.-à-d. une ou quelques monocouches) contribuent à ce spectre. Finalement, la bande négative correspondant au mode de déformation de l'eau n'est pas bipolaire. C'est à dire qu'elle consiste en une augmentation régulière de l'intensité et non à une variation complexe de l'intensité en fonction du nombre d'onde (18). Cette observation peut s'expliquer par un changement important dans l'intensité et (ou) du nombre d'onde de ce mode vibrationnel des molécules d'eau à l'interface qui masquerait des changements moins importants du spectre vibrationel des molécules d'eau dans la solution.

Le mode de déformation de l'eau se déplace de façon soudaine entre −1,05 V et −1,10 V. Il est à 1670 cm^{-1} pour un potentiel final de −1,05 V et il est à 1620 cm^{-1} pour un potentiel final plus négatif que −1,10 V. La bande de ce mode devient plus étroite (~70 cm^{-1}) pour le potentiel de −1,10 V. L'intensité relative du mode de déformation et des modes d'étirement varie également en fonction du potentiel. Pour un potentiel final de −1,05 V, le mode de déformation est environ deux fois moins intense que les modes d'étirement. Ceci a été observé lors d'études spectro-électrochimiques précédentes (22). Cependant, pour un potentiel final de −1,20

© 1997 NRC Canada

Fig. 3. Spectres SNIFTIRS d'une électrode d'or<111> recouverte d'une monocouche de nonanethiols. Les spectres sont exprimés en terme de réflectance différentielle (%). Le potentiel de référence est de −0,50 V et le potentiel final est indiqué sur la figure. Les spectres représentent les 30 premières secondes après le saut de potentiel.



V, on remarque que le mode de déformation est aussi intense que les modes d'étirement. Ces différences spectrales entre les potentiels de −1,05 V et −1,20 V suggèrent que l'interaction des molécules avec l'électrode d'or<111> est influencée par le potentiel.

L'évolution temporelle des spectres vibrationels pour un potentiel final de −1,05 V illustrés sur la Fig. 4 montre une augmentation graduelle des bandes négatives dues aux modes vibrationels de l'eau. Le mode de déformation à 1670 cm^{-1} ne subit pas de déplacement durant les 115 premières secondes. Les modes d'étirements consistent en une large bande négative centrée à 3400 cm^{-1} qui est environ deux à trois fois plus intense que la bande du mode de déformation. Ceci suggère une accumulation des molécules d'eau à la surface de l'électrode. Les variations d'intensité des modes d'étirements et de déformation pour un potentiel final de −1,20 V sont beaucoup plus importantes qu'à −1,05 V comme ceci est illustré dans la Fig. 5. Le spectre correpondant aux 30 premières secondes après le saut de potentiel montre une augmentation de l'intensité du mode de déformation situé à 1620 cm^{-1} par rapport à l'état de référence à −0,50 V. Entre 45 et 75 s, la bande positive indique une diminution de l'intensité du mode de déformation qui se déplace à 1660 cm^{-1}. La bande correspondant aux modes d'étirement de l'eau subit des changements similaires. Durant les 30 premières secondes il y a une légère augmentation de l'intensité de ces modes situés à environ 3350 cm^{-1}. Par la suite, l'intensité de ces modes diminue (bande positive) et se déplace vers 3450 cm^{-1}. Après 250 s, les modes vibrationels de l'eau dominent le spectre vibrationel avec des augmentations de réflectivité supérieurs à 1%. Cette importante diminution de l'intensité des modes vibrationels reliés aux molécules d'eau ne peut s'expliquer par un changement des moments de transition vibrationnel d'une monocouche de molécules d'eau. Il doit y avoir une diminution du nombre de molécules d'eau dans la mince couche d'électrolyte entre le monocristal et la fenêtre de CaF_2. Cette diminution s'explique par la décomposition de molécules d'eau lors de l'évolution d'hydrogène qui se produit à un potentiel de −1,20 V (12, 23). Les différentes évolutions temporelles des spectres vibrationels décrites dans ce paragraphe confirment que l'interaction des molécules d'eau avec la surface d'or<111> lorsque le potentiel est moins négatif que −1,05 V est différente de celle à des potentiel plus négatif que −1,05 V.

Nous avons effectué des mesures avec de l'eau deutérée, comme solvant, pour mieux comprendre l'interaction des molécules d'eau avec la surface d'or<111> à un potentiel final de −1,20 V. Les résultats de cette étude sont présentés dans la Fig. 6. On voit une augmentation de l'intensité des modes d'étirements de l'eau deutérée entre 2200 et 2800 cm^{-1} et du mode de déformation à 1220 cm^{-1}. Le rapport des nombres d'onde des modes de déformation de l'eau et de l'eau deutérée est 1,33. Ce rapport isotopique est proche de celui prévu pour une molécule d'eau dans un puits d'énergie potentielle de forme harmonique (24). L'évolution temporelle du spectre vibrationel obtenu lorsque l'eau deutérée est utilisée comme solvant est similaire à celle observée avec de l'eau. On observe lors des 100 premières secondes des bandes négatives qui indiquent une augmentation de l'intensité des modes vibrationels de l'eau deutérée relativement au spectre de référence. Ceci est suivi d'une diminution importante (supérieure à 1%) de l'intensité de ces modes après 250 s. Sur le spectre correspondant aux 30 premières secondes après le saut de potentiel, on voit dans la région des modes d'étirement, deux bandes négatives centrées à 2700 cm^{-1} et 2500 cm^{-1}. La bande à 2500 cm^{-1} est attribuée aux modes d'étirement symétrique et asymétrique de molécules d'eau deutérées ayant des liaisons hydrogènes avec d'autres molécules d'eau (22, 24). La bande à 2700 cm^{-1} est attribuée à des molécules d'eau deutérée ayant au maximum une liaison hydrogène (22, 24). Durant les 100 premières secondes, l'intensité du mode à 2700 cm^{-1} varie peu tandis que celle du

Can. J. Chem. Downloaded from www.nrcresearchpress.com by 91.121.58.235 on 09/08/12
For personal use only.

© 1997 NRC Canada

Fig. 4. Évolution temporelle d'un spectre SNIFTIRS d'une électrode d'or<111> recouverte d'une monocouche de nonanethiols pour un saut de potentiel de −0,50 V à −1,05 V. Le spectre est exprimé en terme de réflectance différentielle (%) : (*a*) de 0 à 30 s; (*b*) de 45 à 75 s; (*c*) de 85 à 115 s.

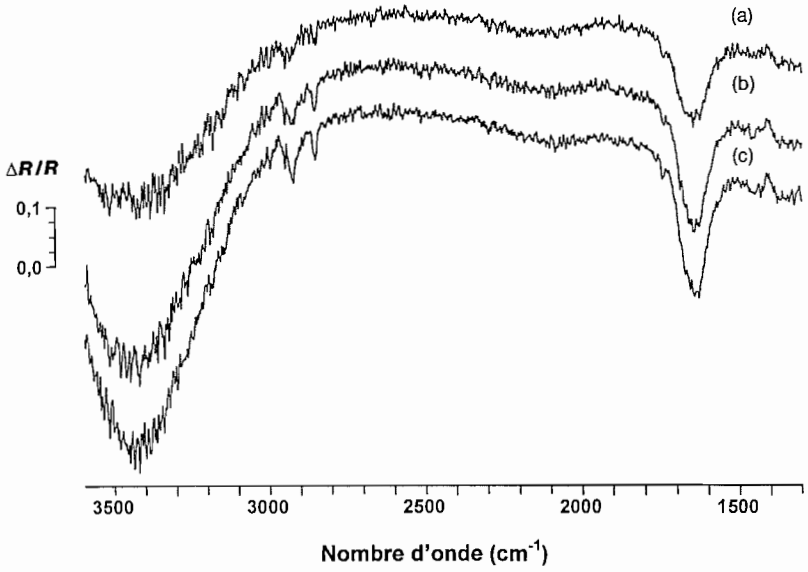
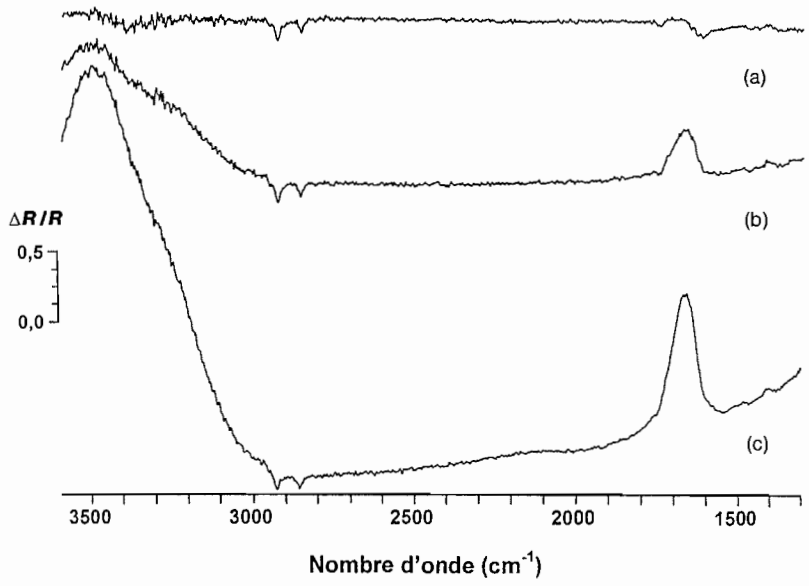


Fig. 5. Évolution temporelle d'un spectre SNIFTIRS d'une électrode d'or<111> recouverte d'une monocouche de nonanethiols pour un saut de potentiel de −0,50 V à −1,20 V. Le spectre est exprimé en terme de réflectance différentielle (%) : (*a*) de 0 à 30 s; (*b*) de 45 à 75 s; (*c*) de 85 à 115 s.



mode à 2500 cm^{-1} augmente fortement. Ce résultat indique une augmentation des liaisons hydrogène entre les molécules d'eau à l'interface électrolyte–or<111>.

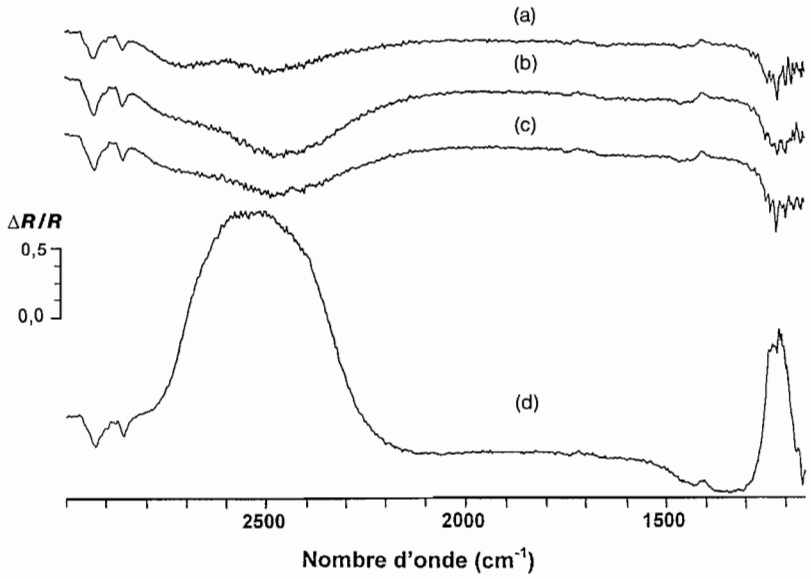
Discussion

Les mesures vibrationnelles in situ démontrent que le potentiel électrique appliqué à l'électrode a un effet peu important sur l'orientation des molécules d'eau à l'interface nonanethiols–or<111> et des nonanethiols chimisorbés entre −0,1 V et −0,8 V. Comme mentionnés ci-dessus, ces résultats sont compatibles avec les mesures électrochimiques que l'on a obtenues précédemment et qui indiquaient une capacité constante dans ce domaine de potentiel (12, 20). On peut conclure de ces différentes observations qu'il est possible de former une monocouche de nonanethiols ayant très peu de défauts et qui bloque efficacement la surface de l'électrode métallique

© 1997 NRC Canada

Can. J. Chem. Downloaded from www.nrcresearchpress.com by 91.121.58.235 on 09/08/12
For personal use only.

Fig. 6. Évolution temporelle d'un spectre SNIFTIRS d'une électrode d'or<111> recouverte d'une monocouche de nonanethiols pour un saut de potentiel de −0,50 V à −1,20 V dans une solution 0,1 M KOH dans le D_2O. Le spectre est exprimé en terme de réflectance différentielle (%) : (*a*) de 0 à 30 s; (*b*) de 45 à 75 s; (*c*) de 85 à 115 s; (*d*) de 250 à 275 s.



lorsqu'un substrat monocristallin est utilisé. Ces résultats suggèrent également que l'observation de changements électrochimiques importants dans la région de la double couche d'une électrode d'or polycristalline recouverte d'alcanethiols est reliée à la qualité du substrat (1). Il est raisonnable de croire que pour un substrat d'or polycristallin, il y aura une plus forte proportion de défauts dans la monocouche et que celle-ci aura une plus grande perméabilité ionique.

Deux types de molécules d'eau peuvent être identifiés à partir des spectres vibrationels. Le premier type est observé à des potentiels finaux allant de −0,95 V jusqu'à environ −1,05 V. L'autre type de molécule d'eau est observé à des potentiels plus négatifs. Pour le premier type de molécules d'eau, l'augmentation de l'intensité des modes d'étirement et de déformation par rapport à ceux de l'état de référence indique que les molécules d'eau adoptent une orientation dans laquelle les moments de transition de ces modes sont, en moyenne, orientés plus perpendiculairement à la surface d'or<111>. L'intensité du mode de déformation est environ 1/3 de celle des modes d'étirement. Ce rapport est similaire à ce qui est observé pour la glace (22) et dans des études vibrationnelles in situ d'électrodes de platine dans la région d'adsorption d'hydrogène (25, 26). On remarque également que les nombres d'onde de ces modes sont similaires à ce qui est observé dans le cas du platine. Les molécules d'eau interagissent donc faiblement avec la surface d'or<111> puisque leur spectre est similaire à celui de molécules d'eau à l'état solide. Cette interaction se fait probablement via un des doublets libres de l'oxygène puisque l'énergie du mode de déformation de l'eau est identique à celle mesurée en solution.

La variation temporelle des spectres vibrationnels entre −0,95 V et −1,05 V indique que l'augmentation de l'intensité des modes vibrationels de l'eau est corrélée avec l'augmentation de l'intensité des modes d'étirements CH causée par la lente désorption réductive de la monocouche de nonanethiols. Les nombres d'onde et l'intensité relative des modes de déformation et d'étirements des molécules d'eau varient peu en fonction du temps. Ces résultats suggèrent que les molécules d'eau forment une double couche à la surface de l'électrode d'or<111> au fur et à mesure que les thiolates désorbent de la surface.

Le deuxième type de molécules d'eau est observé à des potentiels plus négatifs que −1,10 V. Le spectre vibrationnel correspondant aux 30 premières secondes dans ce domaine de potentiel indique des différences importantes avec celui du premier type de molécule d'eau. Le mode de déformation est à un plus bas nombre d'onde (1620 cm^{-1}) que celui du premier type de molécules d'eau et les intensités des modes de déformation et d'étirement sont similaires (voir la Fig. 5). Les bandes négatives dans le spectre de réflectance différentielle indiquent que l'orientation des molécules d'eau à la surface d'or<111> est telle que les moments de transition de ces modes sont en moyenne plus perpendiculaires à la surface que ce qui est observé à l'interface nonanethiols–or<111> au potentiel de référence. Le déplacement du mode de déformation vers une plus basse énergie indique une plus grande interaction des molécules d'eau avec la surface métallique et suggère un affaiblissement de la liaison OH (22, 24). Cette interaction modifie également l'intensité relative des modes d'étirement et de déformation par rapport au premier type de molécules d'eau. Le mode de déformation devient aussi intense que les modes d'étirement. Ces observations soutiennent notre suggestion d'une interaction plus directe des liaisons OH avec la surface d'or<111>. En nous basant sur ces résultats, nous suggérons qu'à un potentiel de −1,20 V, la molécule d'eau interagit, en moyenne, avec la surface métallique via ses hydrogènes.

Le spectre vibrationnel des modes d'étirement de molécules d'eau deutérées fournit d'autres évidences que les molécules d'eau aux potentiels plus négatifs que −1,10 V interagissent différemment avec la surface d'or<111>. La présence de deux

© 1997 NRC Canada

Can. J. Chem. Downloaded from www.nrcresearchpress.com by 91.121.58.235 on 09/08/12
For personal use only.

bandes négatives dans la région des modes d'étirement de l'eau durant les 30 premières secondes après un saut de potentiel à −1,20 V, surtout celle qui est à 2700 cm^{-1}, suggère la formation d'agrégats de molécules d'eau. Les molécules d'eau à la périphérie des agrégats n'auraient pas tous leurs hydrogènes formant des liaisons hydrogènes et donneraient lieu au mode à 2700 cm^{-1} (24). Ce résultat quoiqu'inattendu peut s'expliquer par des mesures réalisées lors d'études précédentes démontrant que les alcanethiols les moins solubles demeurent physisorbés à la surface après leur réduction pour une période allant de quelques secondes pour le nonanethiol (12) à plusieurs heures pour l'hexadecanethiol (17). Il est donc possible que la formation d'agrégats de molécules d'eau soit due à l'insertion de molécules d'eau entre la surface d'or<111> et les thiolates immédiatement après la réduction des thiols et avant que les thiolates ne soient dissous dans la solution alcaline. La diminution continue de l'intensité des modes vibrationnels de l'eau ne peut s'expliquer que par la consommation de molécules d'eau dans le processus d'évolution de l'hydrogène en milieu alcalin (23). Nous interprétons donc la séquence des spectres vibrationnels pour un potentiel final de −1,20 V comme une indication que les molécules d'eau observées lors des 30 premières secondes sont des intermédiaires dans la production d'hydrogène sur l'or<111>. Nous n'avons pas observé de modes vibrationnels Au–H qui seraient situés entre 1700 et 1900 cm^{-1}. Cependant, dans le cas de l'or, il n'y a pas d'hydrogène chimisorbé avant l'application d'un surpotentiel. De plus, des études d'impédance ac ont suggéré que la concentration d'hydrogène adsorbé est inférieure à 1% à l'état de pseudo-équilibre pour l'évolution d'hydrogène à des surpotentiels assez importants (27, 28).

Sommaire

Des mesures vibrationnelles in situ résolues en temps ont permis de suivre la réorganisation des molécules d'eau à l'interface entre −0,1 V et −1,20 V. Dans la région de la double couche, la monocouche de nonanethiol est très stable car très peu de changements spectroscopiques sont observés. Pour des potentiels finaux correspondants à la réduction de la monocouche de nonanethiols, des changements importants dus à la formation d'une double couche à l'interface solution électrolyte–or<111> sont observés. Le spectre vibrationnel des molécules d'eau à l'interface change de façon soudaine entre −1,05 V et −1,10 V. À des potentiels inférieurs à −1,05 V les molécules d'eau interagissent faiblement avec la surface métallique probablement via les doublets libres de l'oxygène. Pour des potentiels plus négatifs que −1,10 V les molécules d'eau interagissent plus fortement avec l'électrode via leurs hydrogènes. Finalement, les résultats spectroscopiques suggèrent la formation d'agrégats de molécules d'eau à un potentiel de −1,20 V dans les 30 secondes suivant la réduction de la monocouche de nonanethiols.

Remerciements

Nous remercions le Conseil de la Recherche en Sciences Naturelles et en Génie du Canada pour une subvention de recherche de projet concerté.

Bibliographie

1. H.O. Finklea. *Dans* Electroanalytical chemistry. Vol. 15. *Édité par* A.J. Bard et I. Rubenstein. Marcel Dekker, New-York. 1996. pp. 109–335.
2. C.E.D. Chidsey. Science, **251**, 919 (1991).
3. S.E. Creager et K.G. Olsen. Anal. Chim. Acta, **307**, 277 (1995).
4. M. Becka et C.J. Miller. J. Phys. Chem. **96**, 2675 (1991).
5. H. Demoz et D.J. Harrison. Langmuir, **9**, 1046 (1993).
6. G.E. Poirier et M.J. Tarlov. Langmuir, **10**, 2853 (1994).
7. N. Camillone III, T.Y.B. Leung, P. Schwartz, P. Eisenberg et G. Scoles. Langmuir, **12**, 2737 (1996).
8. L.H. Dubois, B.R. Zegarski et R.G. Nuzzo. J. Electron Spectrosc. Relat. Phenom. **54/55**, 1143 (1990).
9. C.P. Smith et H.S. White. Anal. Chem. **64**, 2398 (1992).
10. R. Andreu et W.R. Fawcett. J. Phys. Chem. **98**, 12753 (1994).
11. W.R. Fawcett, M. Fedurco et Z. Kovacova. Langmuir, **10**, 2403 (1994).
12. D.F. Yang, C.P. Wilde et M. Morin. Langmuir, **12**, 6570 (1996).
13. C.A. Widrig, C. Chung et M.D. Porter. J. Electroanal. Chem. **310**, 335 (1991).
14. D.E. Weisshaar, M.M. Walczak et M.D. Porter. Langmuir, **7**, 2687 (1991).
15. K.A. Bunding-Lee, R. Mowry, S. McLennan et H.O. Finklea. J. Electroanal. Chem. **246**, 217 (1988).
16. T.W. Schneider et D.A. Buttry. J. Am. Chem. Soc. **115**, 12391 (1993).
17. D.-F. Yang, C.P. Wilde et M. Morin. Langmuir, **13**, 243 (1997).
18. K. Ashley et S. Pons. Chem. Rev. **88**, 673 (1988)
19. R.G. Greenler. J. Chem. Phys. **44**, 310 (1966).
20. D.F. Yang et M. Morin. J. Electroanal. Chem. **429**, 1 (1997)
21. D.-F. Yang, H. Al-Maznai et M. Morin. J. Phys. Chem. B, **101**, 1158 (1997).
22. P.A. Thiel et T.E. Madey. Surf. Sci. Rep. **7**, 211 (1987).
23. J.O'M. Bockris et S.U.M. Khan. Surface electrochemistry. Plenum, New-York. 1993.
24. H. Ibach et S. Lehwald. Surf. Sci. **91**, 187 (1980).
25. A. Bewick et J.W. Russel. J. Electroanal. Chem. **132**, 329 (1982).
26. M.A. Habib et J.O'M. Bockris. Langmuir, **2**, 388 (1986).
27. B.E. Conway et L. Bai. Electrochim. Acta, **31**, 1013 (1986).
28. A. Hamelin et M.J. Weaver. J. Electroanal. Chem. **223**, 171 (1987).

Can. J. Chem. Downloaded from www.nrcresearchpress.com by 91.121.58.235 on 09/08/12
For personal use only.

© 1997 NRC Canada

Hydrous Ir oxide films: the mechanism of the anodic prepeak reaction

V.I. Birss, C. Bock, and H. Elzanowska

Abstract: The origin and significance of the anodic prepeak (peak A_0), seen in cyclic voltammetric studies of hydrous Ir oxide films in acidic solution just prior to the large Ir(III)/(IV) redox peaks (A_1/C_1), has been examined in this work. By also studying only very thin films, a corresponding cathodic feature (peak C_0) has also been identified. The pH dependence of the A_0/C_0 peaks, assumed to also depict the Ir(III)/(IV) process, has been examined in sulfuric acid solutions, indicating that a ca. −80 mV shift per pH unit applies to this reaction. By also taking into consideration the measured in situ mass changes as the potential is scanned through the A_0/C_0 peaks, it is shown that these peaks are associated with a greater involvement of anions and more extensive water exchange than is the reaction in the main A_1/C_1 peaks. Other results also indicate that the film sites that react in the A_0/C_0 peaks are located deep within the oxide film, likely near the Ir – oxide film interface.

Key words: Ir oxide, hydrous oxide films, cyclic voltammetry, quartz crystal microbalance (QCMB), prepeak, pH dependence, electrochemistry.

Résumé : On a examiné l'origine et la signification du prépic anodique (pic A_0) observé dans les études de voltampérométrie cyclique de fils d'oxyde d'Ir hydreux, en solution acide, juste avant les importants pics redox Ir(III)/(IV) ((A_1/C_1). En n'étudiant que des films extrêmement minces, on a pu identifier aussi une caractéristique cathodique correspondante (pik C_0). La dépendance des pics A_0/C_0 sur le pH, qui décrirait aussi le processus Ir(III)/(IV), a fait l'objet d'un examen en solutions d'acide sulfurique; ces études suggèrent que, pour cette réaction, il faut appliquer un déplacement d'environ −80 mV par unité de pH. Si l'on tient aussi compte des changements de masse in situ mesurés lors du balayage du potentiel à travers les pics A_0/C_0, il est démontré que ces pics sont associés à une implication plus importante des anions et à un échange d'eau plus important que dans la réaction dans les pics A_1/C_1 principaux. D'autres résultats indiquent aussi que les sites de film qui réagissent dans les pics A_0/C_0 sont situés en profondeur de l'oxyde de film, probablement près de l'interface Ir – film d'oxyde.

Mots clés : oxyde d'Ir, films d'oxyde hydreux, voltampérométrie cyclique, microbalance à cristal de quartz (MBCQ), prépic, dépendance sur le pH, électrochimie.

[Traduit par la rédaction]

Introduction

There is a significant amount of interest in the electrochemical properties of hydrous Ir oxide films, primarily due to their very promising and wide-ranging applications as electrochromic materials, in supercapacitive devices, as battery electrodes, as interneural stimulating electrodes, etc. The particular advantage of Ir oxide films is their very rapid (reversible) redox kinetics, even when very thick films of this material are being used, as well as their long-term stability.

In some of our previous work (1–4) with electrochemically formed, hydrous Ir oxide films, carried out in a range of aqueous solutions, one of the points of focus has been the problems associated with the aging/unaging of the electrochemical response of the oxide film, as seen most readily in cyclic voltammetry (CV) experiments. Reversible aging is characterized by a notable positive shift of the main anodic peak (peak A_1, representing the oxidation of Ir(III) to Ir(IV) within the oxide film) and is also associated with a diminishment in the kinetics of this reaction. In our prior work (1, 2), it was suggested that reversible aging, which is induced primarily by time spent at sufficiently negative potentials, may be connected with the reaction that occurs in the prepeak, A_0, seen in most solutions at the foot of the principal A_1 peak in CV experiments. This was partly justified on the basis of the observation that time spent at negative potentials also has a marked effect on the A_0 peak by shifting it positively so that it merges together with peak A_1, especially for relatively thick films. Also, Mozota and Conway (5, 6) have shown that the kinetics of the A_0 process are very slow and have suggested that the reaction involves a slow rearrangement of atoms. Therefore, it is reasonable to expect that the kinetically slow A_0 reaction, which is the first step in the conversion of the film from its Ir(III) to Ir(IV) state, may have a significant impact on the overall Ir oxide redox kinetics.

There is little agreement in the literature concerning the

Received April 23, 1997.

This paper is dedicated to Professor Brian E. Conway on the occasion of his 70th birthday.

V.I. Birss,[1] C. Bock, and H. Elzanowska.[2] Department of Chemistry, University of Calgary, Calgary, AB T2N 1N4, Canada.

[1] Author to whom correspondence may be addressed. Telephone: (403) 220-6432. Fax: (403) 289-9488. E-mail: birss@acs.ucalgary.ca

[2] Permanent address: University of Warsaw, Department of Chemistry, Warsaw, Poland.

© 1997 NRC Canada

Can. J. Chem. Downloaded from www.nrcresearchpress.com by 91.121.58.235 on 09/08/12
For personal use only.

Can. J. Chem. Downloaded from www.nrcresearchpress.com by 91.121.58.235 on 09/08/12
For personal use only.

nature of the process occurring in peak A_0. It has been suggested by some that it reflects the oxidation of Ir sites in a particular region of the film, likely to be near the metal–oxide interface, or at Ir sites that are partially complexed to solution anions (5–8). Peak A_0 is readily seen for films formed in sulfuric acid solutions, but its presence and characteristics depend strongly on the oxide growth conditions employed in solutions such as phosphoric acid (3) and the peak has sometimes been reported to be absent altogether in this solution (5–9). Therefore, it is feasible that peak A_0 reflects the oxidation of a region of the film having a different microstructure, degree of hydration, etc., or possibly that it represents a reaction of different stoichiometry from that in the principal redox peaks, A_1/C_1. Another interpretation of prepeaks of this kind is that they are artifactual, in that they arise as the consequence of the large change in conductivity of these films as they are oxidized (10). However, it has subsequently been pointed out (1, 2) that this explanation for the Ir oxide prepeak would be inconsistent with its absence during the oxidation of Ir oxide in alkaline solutions, where the transition from nonconducting Ir(III) to conducting Ir(IV) oxide also takes place.

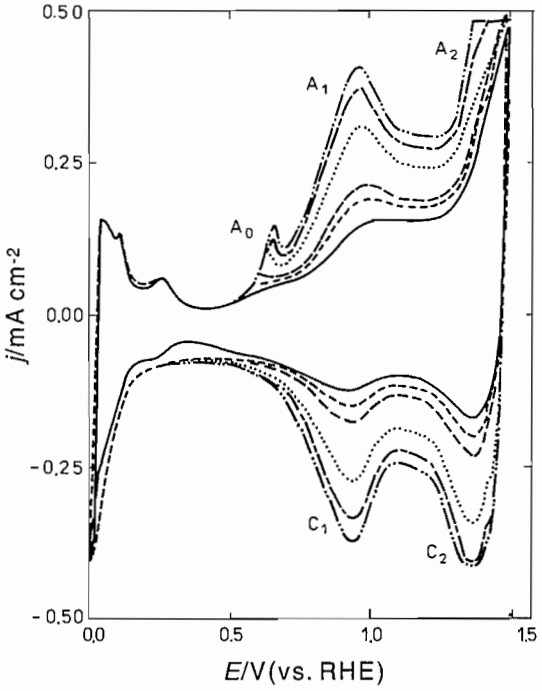
In the present work, the electrochemical properties of the process occurring in peak A_0 have been examined more closely, with the goal being to better understand the origin and significance of the peak. As part of this, the pH dependence of the A_0 peak, as well as the mass changes associated with it, as determined using the in situ quartz crystal microbalance (QCMB) technique, have been examined in sulfuric acid solutions. Based on these results, a mechanism for the reaction in the A_0/C_0 peaks is suggested.

Experimental

The experimental details concerning the growth of Ir oxide films (carried out by cycling at either 0.1 or 1 V/s, or by using 1 s pulses, usually between a lower potential limit, E_-, of −0.05 or 0.0 V vs. RHE and an upper potential limit, E_+, of 1.55 V vs. RHE) in the appropriate solution and the transfer of the electrode between various solutions have been described previously (1–4, 11). Briefly, the working electrode (WE) in the electrochemical experiments consisted of an Ir wire (99.9% purity, 0.5 mm diam., ca. 0.1 cm^2 geometric area) embedded in soft glass tubing. For the WE used in the mass measurements, standard 5 MHz AT-cut quartz crystals (2.5 cm diam.) were obtained from Valpey–Fisher and were sputter-coated in the usual keyhole pattern, first with 25–35 nm of Ti and then with 100–150 nm of Ir. Electrical contact was made on each side of the crystal to Pt wires using conducting epoxy. Frequency (mass) data were collected using a Philips (model 6654C) frequency counter, connected to a standard oscillator (12). Ir wire electrodes were cleaned by heating in a fuel-rich flame, while Ir-coated quartz crystals were used as sputtered. A Pt gauze counter electrode, and either the reversible hydrogen (RHE) or a saturated calomel (SCE) electrode, were employed as the reference electrodes. All potentials are given versus the RHE in this paper.

All experiments were carried out at room temperature, with oxygen removal from solution achieved by vigorous bubbling with argon or nitrogen gas. All reagents were Fisher Certified or ACS grade and were used as received.

Fig. 1. CV response during Ir oxide growth at 100 mV/s with continuous cycling between 0 and 1.5 V in 0.5 M H_2SO_4 (maximum CEF = 12). The response is shown for cycle number 1, 4, 7, 15, 21, and 24.



Results and discussion

(a) General cyclic voltammetric behavior

Figure 1 shows a typical set of CVs, obtained in 0.5 M sulfuric acid at 100 mV/s, as a series of Ir oxide films of increasing thickness were formed via the continuous potential cycling method. It is notable that the principal redox peaks, A_1/C_1, remain reversible and centered at a constant potential as the film thickens. For these relatively thin films, the potentials of peaks A_1 and C_1 are independent of the normally achievable sweep rates, and the peak currents are linearly proportional to sweep rate, up to ca. 1 V/s. Thicker films become diffusion controlled, even at sweep rates lower than 0.1 V/s. A general form of the reaction, which can be suggested to represent the A_1/C_1 process in acidic solutions and is consistent with the >60 mV/pH dependence of the A_1/C_1 peaks (7, 8, 11–13), is as follows,

[1] $$\text{Ir(IV)oxide}\cdot n\text{H}_2\text{O} + \text{e}^- + x\text{H}_3\text{O}^+ + y\text{A}^- <===> \text{Ir(III)oxide}\cdot m\text{H}_2\text{O}(\text{H}_3\text{O}^+)_x(\text{A}^-)_y + (n-m)\text{H}_2\text{O}$$

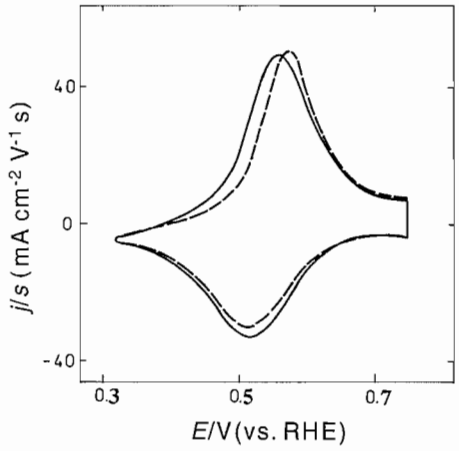
where A^- represents the electrolyte anion and the x, y, m, and n coefficients depend on the particular experimental conditions employed. Peaks A_2/C_2 in Fig. 1 reflect the Ir(IV)/Ir(V or VI) redox process.

In contrast, peak A_0, which also increases in magnitude as the film thickens, is seen in Fig. 1 to move positively as more Ir oxide film is formed. Also, unlike the A_1/C_1 reaction, a complementary cathodic peak to A_0 is not seen when the high E_+ value of Fig. 1 is employed. The oxide film in the last cycle shown in Fig. 1 has a charge enhancement factor (CEF) of ca. 12, where the CEF is considered to be an estimate of the

© 1997 NRC Canada

Can. J. Chem. Downloaded from www.nrcresearchpress.com by 91.121.58.235 on 09/08/12
For personal use only.

Fig. 2. Normalized CV response (j/s) of Ir oxide film (CEF = 35, grown in 0.5 M H_2SO_4) in 1.0 M NaOH at s = 2 (—) and 100 (---) mV/s.



number of monolayers of hydrous film present (5, 6, 14, 15). CEFs of up to 500 or more can be readily achieved with Ir oxide films. Therefore, the film formed in Fig. 1 is still very thin and should not be susceptible to film aging effects, which would be seen, in part, by the merging together of the A_0 and A_1 peaks (1, 2).

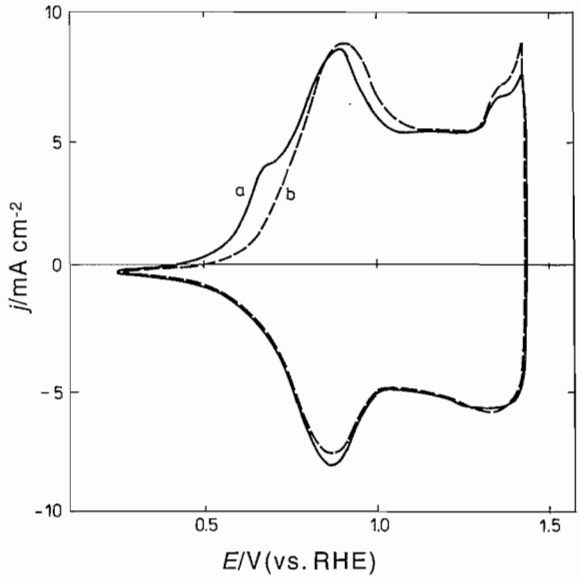
A positive shift of the A_0 peak with increasing film thickness, similar to that shown in Fig. 1, has also been reported for oxides grown in 1 M perchloric acid (5, 6, 13, 16), 1 M nitric acid (1–4), and in 0.5 M Na_2CO_3 (5, 6) solutions. The A_0 peak is seen only if particular growth conditions (pulsing times) are employed in phosphoric acid solutions (1, 3), and other previously published work has suggested that the peak is absent entirely in this growth medium (5, 6, 9, 16). Based on the proposed involvement of solution anions in reaction [1], peak A_0 has sometimes been linked to the presence of anions in the oxide film, particularly as the A_0 peak represents the first step in film oxidation (5, 6). It is interesting to note that when Ir oxide films, grown in 0.5 M H_2SO_4, are transferred to a highly alkaline solution, e.g., 1 M NaOH (Fig. 2), the CV shows no evidence of the A_0 peak, even when thin films and very slow sweep rates are employed. Reaction [2] shows that, in base, hydroxide ions and solution cations are involved in the reaction (no anions are available other than OH^-) and that, in the reduced state, the film has a negligible ion content, compared to the oxidized form of the film (11, 12).

$$[2]\quad \text{Ir(IV)oxide}\cdot n\text{H}_2\text{O}(\text{OH}^-)_x(\text{M}^+)_y + e^- + m\text{H}_2\text{O} <===> \text{Ir(III)oxide}\cdot(n+m)\text{H}_2\text{O} + x\text{OH}^- + y\text{M}^+$$

It is expected that when Ir oxide films are transferred from typical growth media such as sulfuric or nitric acid solutions into alkaline solutions, protons and anions incorporated in the film would be replaced by hydroxide and alkali metal ions in the first few cycles of potential cycles. Indeed, it is possible to see a trace of the A_0 peak in the first one or two cycles in base, especially in 0.1 M KOH solutions (11, 12), but the peak then disappears with longer cycling times.

The results shown above lend support to the notion that the presence of anions in the oxide film, particularly in the reduced state, may be related to the appearance of the A_0 peak.

Fig. 3. CV response of Ir oxide electrode (CEF = 200) at 100 mV/s in 0.5 M H_2SO_4 before (curve a) and after (curve b) potential holding at E_- = 0.20 V for 75 min.



It should also be noted that reactions [1] and [2] show that water may be expelled during Ir oxide reduction in acidic solutions, but injected in alkaline media, and hence these differences in the water content of the reduced form of the film may also be significant in terms of whether or not the A_0 peak appears.

The existence of a prepeak prior to the main oxidation peak has been reported for some polymer films (10) for which, like Ir oxide, the conductivity is very much lowered as the film becomes fully reduced. It has been suggested that film oxidation is initially delayed until a small fraction of the film has been oxidized. The sudden increase in film conductivity then results in a prepeak in a CV experiment. According to this model, the prepeak would not be related to the oxidation of any specific region or component of the film. When modelled mathematically, it is seen (10) that a positive shift and an increase of the prepeak with increasing sweep rate is predicted, but that the prepeak must be crossed before the reaction in the main peak can commence. That is, the film conductivity must be substantially increased before the bulk of the film can react, and the merging together of the prepeak and the main peak would not be predicted by this model. In the case of Ir oxide films, experiments carried out at somewhat higher sweep rates result in the merging together of the A_0 and A_1 peaks (1–3). Figure 3 shows an example of this, where the potential has been first continuously cycled (curve a), revealing peak A_0 as distinct from peak A_1, whereas complete film reduction by maintaining the potential at 0.2 V for a period of time results in the (reversible) merging together of peaks A_0 and A_1 in the next set of potential cycles. This is not consistent with the explanation given (10) for the prepeak. Also, this model does not predict that the prepeak would be present in one solution (acidic) and would disappear in another (basic) when the identical film is transferred back and forth between the solutions and the same conductivity changes occur. Rather, this strongly suggests that the A_0/C_0 peaks are associ-

© 1997 NRC Canada

Table 1. Dependence of potentials (vs. RHE) of peaks A_0 and A_1 on sweep rate and on sulfuric acid concentration.

Sweep rate (mV/s)	0.5 M H_2SO_4		0.1 M H_2SO_4		0.5 M vs. 0.1 M	
	A_0 (mV)	A_1 (mV)	A_0 (mV)	A_1 (mV)	A_0 (mV)	A_1 (mV)
20	645	970	625	960	20	10
50	680	970	660	965	20	5
100	705	975	690	965	15	10
200	735	975	715	960	20	15

Can. J. Chem. Downloaded from www.nrcresearchpress.com by 91.121.58.235 on 09/08/12
For personal use only.

ated with the particular nature of the involvement of ions and (or) solvent in this reaction in acidic solutions.

(*b*) pH dependence of the A_0/C_0 reaction

It has previously been reported that the principal Ir(III)/(IV) redox process, which occurs in peaks A_1/C_1, exhibits a super-Nernstian pH response over the bulk of the pH range (7, 8 ,11–13). An example of this can be seen by comparing Figs. 1 and 2, where the potential of the main peaks, which is independent of the sweep rate in both solutions under these conditions, is >300 mV more negative (vs. RHE) in the 1 M NaOH solution than in the 0.5 M sulfuric acid medium, leading to an overall pH dependence of ca. −80 mV/pH unit. This is similar to what has previously been reported, when many different pH's were examined (11, 12). It is also consistent with the formulation of reactions [1] and [2], in which the ratio of the pH-determining ion to the number of electrons passed is greater than 1, in both acidic and alkaline conditions, such that the pH dependence must be greater than −59 mV. A recent more careful study (3) of the pH dependence of the hydrous Ir oxide redox potential over a narrow range of acidic pH's in various acidic solutions has shown values between ca. −65 and −70 mV/pH unit. The value in sulfuric acid, in particular, is −68 mV/pH unit, which is consistent with the following reaction stoichiometry for the A_1/C_1 peaks in solutions between 0.1 to 0.75 M sulfuric acid:

$$[3]\quad \text{Ir(IV)oxide}\cdot n\text{H}_2\text{O} + \text{e}^- + 1.15\ \text{H}_3\text{O}^+ + 0.15\ \text{HSO}_4^- <===> \text{Ir(III)oxide}\cdot m\text{H}_2\text{O}(\text{H}_3\text{O}^+)_{1.15}(\text{HSO}_4^-)_{0.15} + (n-m)\text{H}_2\text{O}$$

In the present work, the pH dependence of the peak A_0 potential was compared in two solutions, 0.5 and 0.1 M sulfuric acid, in order to determine whether the stoichiometry of reaction [3] also applies to the reaction in peak A_0. The Ir oxide films in this study were formed in the 0.5 M acid solution by cycling at 200 mV/s between 0 and 1.5 V vs. RHE. Only very thin oxide films were formed (CEF ca. 14) in order to ensure that peaks A_0 and A_1 would remain separated, even at higher sweep-rates. The sweep-rate dependence of peak A_0 was then established in the growth solution, after which the film was transferred to a 5× diluted acid solution in which the A_0 peak was examined once again for the sweep-rate dependence of its potential. It is notable that the shape and width of peak A_0 was the same in these two solutions.

As the pH of these two acidic solutions is not known with certainty, the pH dependence of peak A_0 was established by tracking its potential relative to the A_1/C_1 peak potentials in the two solutions. As stated earlier, the pH dependence of the A_1/C_1 process is now known to be −68 mV/pH unit in sulfuric acid solutions, based on careful measurements of the variation in the peak potential with solution pH and corroborated by the determination of the HSO_4^- content of the oxidized vs. reduced form of the film by ion chromatographic methods (3).

Table 1 lists the potentials of the A_0 and A_1 peaks, at four different sweep-rates, in the two sulfuric acid solutions after equilibration of the films by multicycling between 0.05 and 1.4 V for a period of time. It can be seen that the A_1 peak potential is independent of sweep-rate in each solution, and there is a small negative shift by 5–15 mV (this range depicts the error in identifying peak potentials from the CVs recorded on an X/Y recorder) in the 0.1 vs. 0.5 M sulfuric acid solution, consistent with that reported previously (3). It is also seen from the data in Table 1 that the A_0 peak potential is shifted more negatively in the 0.1 M solution vs. than in the 0.5 M sulfuric acid solution, than is peak A_1, by an average of ca. 20 mV, i.e., by 5–15 mV more than the shift of the A_1/C_1 peaks. Based on the −68 mV pH dependence of the main redox peaks, this translates to a ca. −73 to −83 mV pH dependence for the A_0/C_0 process, which in turn indicates a greater anionic involvement in the reaction in peak A_0 than in peak A_1 (compare reaction [4] with reaction [3]). The following stoichiometry is suggested for the prepeak reaction, assuming a −80 mV per pH dependence.

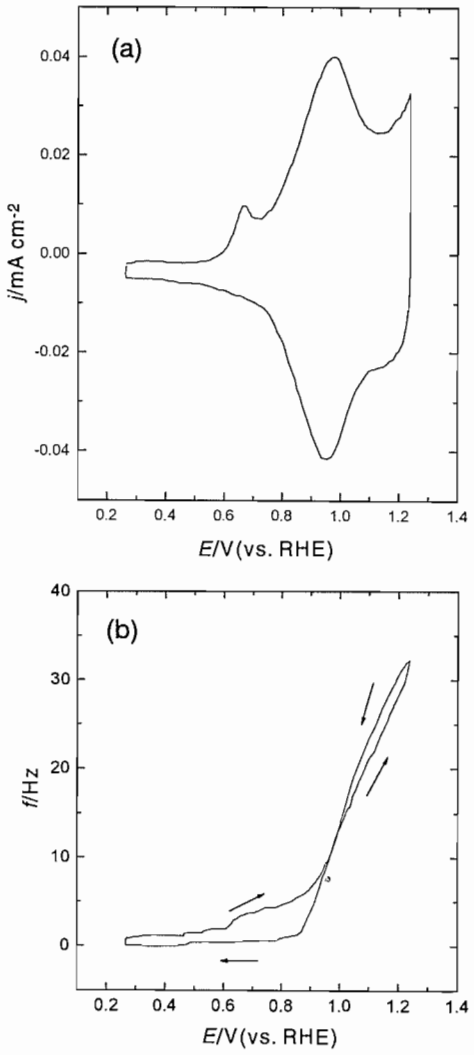
$$[4]\quad \text{Ir(IV)oxide}\cdot n\text{H}_2\text{O} + \text{e}^- + 1.35\ \text{H}_3\text{O}^+ + 0.35\ \text{HSO}_4^- <===> \text{Ir(III)oxide}\cdot m\text{H}_2\text{O}(\text{H}_3\text{O}^+)_{1.35}(\text{HSO}_4^-)_{0.35} + (n-m)\text{H}_2\text{O}$$

It is also notable (although not shown in Table 1) that when the oxide film was transferred between solutions, the initial potential scans were carried out only over the range of the A_0/C_0 peaks, i.e., between 0.05 and 0.7 or 0.8 V. Under these conditions, the A_0/C_0 peak potentials were more similar to those of the prior test solution than indicated in Table 1, and it was only after the completion of several full potential cycles, up to 1.4 V or more, that the steady-state potentials of Table 1 were obtained. This was not the case for the potential of the A_1/C_1 peaks, which immediately reflected the new solution conditions and did not change further with time, potential limits, or sweep rate. These results suggest that, unless the ionic

© 1997 NRC Canada

Can. J. Chem. Downloaded from www.nrcresearchpress.com by 91.121.58.235 on 09/08/12
For personal use only.

Fig. 4. CV at 10 mV/s (*a*) and associated frequency response (*b*) of Ir oxide film (CEF = 10) on Ir sputter-coated quartz crystal in 0.5 M H_2SO_4.



content from the prior solution is fully expelled from the oxide film by scanning to sufficiently positive potentials, the local conditions of the Ir oxide sites that react in the A_0/C_0 peaks remain similar to those of the prior test solution. This, in turn, suggests that the A_0/C_0 sites are located deep within the film, probably in the region of the metal–oxide interface.

(*c*) Mass change associated with the A_0/C_0 reaction

To attempt to corroborate the pH dependence data for the A_0 peak (reaction [4]) and to complete the reaction stoichiometry, the film mass change was measured as the potential was scanned very slowly through the potential range of peak A_0. Figure 4 shows a typical CV and the corresponding frequency change in a full cycle of potential for a very thin Ir oxide film (CEF = 10), conditions under which the A_0 and A_1 peaks are again well separated. A mass loss during film oxidation, and corresponding mass gain during reduction, is seen to be consistent with the predictions of reactions [1], [3], and [4] in acidic solutions. It is notable that the mass gain observed during Ir oxide reduction is essentially complete at potentials just negative of peak C_1; neither peak C_0 nor any additional mass gain associated with this process are seen. This suggests that the A_0 sites reduce in peak C_1 under the conditions of this experiment. When the frequency change over peak A_0 is converted to a mass change, using a crystal constant of -57 Hz μg^{-1} cm^2 from the Sauerbrey equation (17), and the charge density in peak A_0 is also taken into consideration, a mass change of ca. 11 grams per mole of electrons passed is obtained in this particular case. Several other experiments have shown that this ratio varied between 10 and 12, considering both experimental error and the fact that slightly thicker films result in some shift of the A_0 charge into the foot of the A_1 peak, making charge measurement more difficult.

Considering the stoichiometry of reaction [4], this overall net mass change would predict that $n - m$ is 2.7, i.e., that 2.7 moles of water are gained by the film per mole of electrons passed (i.e., per mole of Ir sites reacted) during the A_0 reaction, and vice versa, during its reduction. In comparison, the mass-to-charge ratio for the A_1/C_1 reaction is ca. 6–7 grams per mole of electrons, which suggests that only ca. 1.5 moles of water are injected into the oxide per mole of Ir sites reacted, based on the stoichiometry of reaction [3]. This interpretation of the data would indicate that the A_0/C_0 sites are characterized by a proportionally greater water exchange per mole of Ir sites reacted, as well as a higher anionic to protonic ratio, as compared to the case in the main A_1/C_1 peaks (cf. reactions [3] and [4]).

It should be pointed out that the mass-to-charge ratio of 10–12 grams per mole of electrons observed experimentally for the A_0 process could also be explained on the basis of only protonic and water exchange. Based on reaction [5], $(n - m)$ would then be much smaller, ca. 0.4, such that 0.4 moles of water would be injected into the film for each mole of electrons and hydronium ions expelled during film oxidation in peak A_0, and vice versa, during film reduction.

$$[5]\quad \text{Ir(IV)oxide}\cdot n\text{H}_2\text{O} + \text{e}^- + \text{H}_3\text{O}^+ <===> \text{Ir(III)oxide}\cdot m\text{H}_2\text{O}(\text{H}_3\text{O}^+) + (n - m)\text{H}_2\text{O}$$

However, a pH dependence of ca. -59 mV would then be observed, which is not the case here; therefore, reaction [5] can be ruled out.

A final possibility is that the greater negative shift of the A_0 peak vs. the A_1 peak with increasing pH (Table 1) originates, not from a higher ratio of anionic to protonic charge compensation than in the main A_1/C_1 peaks, but rather from the large changes in water content and hence complex activity changes deep within the Ir oxide film. In this case, if the stoichiometry of the principal redox peaks (reaction [3]) is also assumed to hold for the A_0/C_0 reaction, then the mass-to-charge ratio of ca. 10–12 would yield an $n - m$ value of 1.3, whereas for the A_1/C_1 process, $n - m$ would remain equal to 1.5. This would suggest that more water exchange is occurring in the main redox peaks vs. in the A_0/C_0 peaks and that large changes in water content in the A_0/C_0 reaction are not responsible for anomalous activity effects, which would then be expected to be more predominant in the A_1/C_1 redox reaction.

Overall, it is clear that the mass-to-charge ratio obtained for the A_0 peak as compared to that in the main A_1/C_1 redox peaks is significantly larger, 10–12 vs. 6–7 grams per mole of elec-

© 1997 NRC Canada

Can. J. Chem. Downloaded from www.nrcresearchpress.com by 91.121.58.235 on 09/08/12
For personal use only.

trons. This most likely represents both a greater involvement of anions in the A_0 reaction and a greater degree of water exchange during this process.

(*d*) Suggested mechanism of the A_0/C_0 reaction

In their examination of the kinetics of the A_0 process, Mozota and Conway (5, 6) showed that at slow sweep-rates the A_0 peak current depends linearly on sweep-rate, while the peak potential depends on the log of sweep-rate. They suggested that the A_0 reaction involves a slow surface adsorption process, limited by the slow rearrangement of sites. However, even at the slowest sweep-rates employed, the A_0 peak potential continued to move negatively, and hence the reaction rate constant could not be determined using sweep methods. Films of reasonable thickness were examined in their work and, under these conditions, a complementary cathodic process, C_0, could not be distinguished. It was assumed, therefore, that the C_0 peak was located negative of the potential for the hydrogen evolution reaction. Taking into account the pronounced positive shift of the A_0 peak potential with sweep-rate and the presumed very negative shift of C_0, substantial kinetic limitations of the A_0/C_0 process were suggested (5, 6).

In the present paper, the CV behavior of the A_0/C_0 process was examined more closely using very thin Ir oxide films. The CVs presented in Fig. 5*a* show that a cathodic counterpart, C_0, of the A_0 peak can be seen for this very thin film (CEF = 12), as long as the upper potential limit is restricted to the range of the A_0 peak. After first examining the anodic peak, it is seen that the peak current is linearly dependent on the sweep-rate, as reported by Mozota and Conway (5, 6), and that the peak potential shifts anodically with increasing sweep-rate, both characteristics of a kinetically irreversible surface reaction. However, as long as the same E_+ value is used (Fig. 5*b*), the C_0 peak potential remains constant with increasing sweep-rate, instead of the more typical opposing shifts of the potential of the anodic and cathodic peaks expected for a slow surface process. The apparent positive shift of peak C_0 with increasing sweep-rate in Fig. 5*a* arises from the need to increase E_+, hence including some of peak A_1 in the scan, in order to cross peak A_0.

Based on the QCMB and pH dependence results described in sections (b) and (c) above, the following mechanism could apply to the A_0/C_0 reaction. It is assumed that the reduced film sites that react in the prepeak are more hydrated and contain more solution anions as charge-compensating species than do the oxidized form. After examining the oxidation reaction, the first step is expected to be a slow electron transfer reaction, as suggested earlier (5, 6), consistent with the notable anodic shift of the A_0 peak with increasing sweep-rate.

[6] $\mathrm{Ir(III)oxide{\cdot}}m\mathrm{H_2O(H_3O^+)_{1.35}(HSO_4^-)_{0.35}} \overset{\text{slow}}{\Longrightarrow} \mathrm{Ir(IV)oxide{\cdot}}m\mathrm{H_2O} + e^- + 1.35\ \mathrm{H_3O^+} + 0.35\ \mathrm{HSO_4^-}$

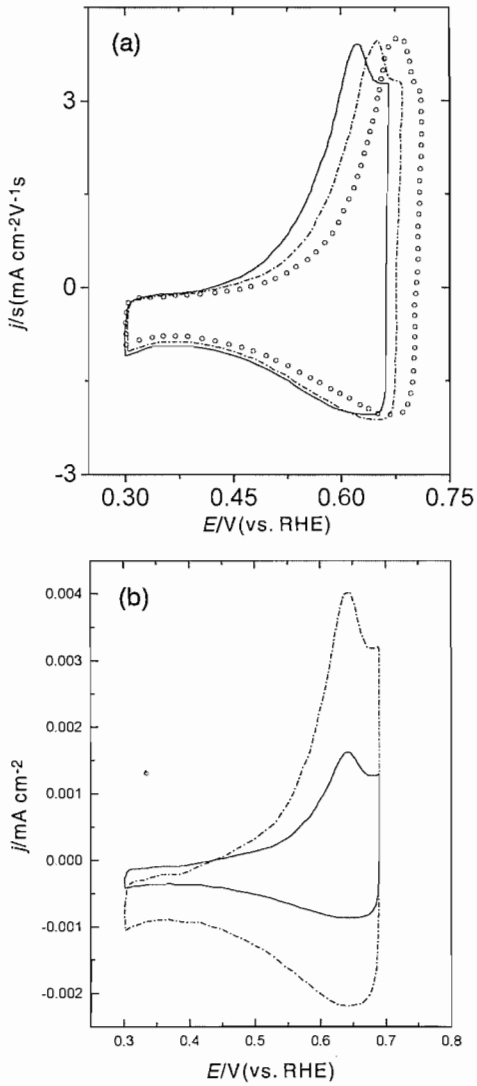
This is then followed by a rapid film hydration process:

[7] $\mathrm{Ir(IV)oxide{\cdot}}m\mathrm{H_2O} + 2.7\ \mathrm{H_2O} \overset{\text{fast}}{\Longleftrightarrow} \mathrm{Ir(IV)oxide{\cdot}}(m + 2.7)\mathrm{H_2O}$

It can be argued that this hydration process changes the formal potential of these sites, such that the cathodic reaction can occur at more positive potentials (Fig. 5). Reactions [8] and [9] are suggested for the C_0 process, based also on the electrochemical results. Reaction [8] is a rapid electron-transfer reaction, consistent with the independence of its peak potential on sweep-rate at constant E_+ (Fig. 5*b*). The slow dehydration process (reaction [9]) is consistent with the fact that holding the potential negative of the A_0/C_0 peaks constant for a long period of time causes a minor increase and a small positive shift of the A_0 peak (although not affecting its kinetics).

[8] $\mathrm{Ir(IV)oxide{\cdot}}(m + 2.7)\mathrm{H_2O} + e^- + 1.35\ \mathrm{H_3O^+} + 0.35\ \mathrm{HSO_4^-} \overset{\text{fast}}{\Longleftrightarrow} \mathrm{Ir(III)oxide{\cdot}}(m + 2.7)\mathrm{H_2O(H_3O^+)_{1.35}(HSO_4^-)_{0.35}}$

Fig. 5. (*a*) Normalized CV responses (*j*/*s*) over restricted potential range of peaks A_0/C_0 at 5 (—), 20 (-·-·-) and 50 (○○○) mV/s in 0.5 M H_2SO_4 (CEF = 12). Note that E_+ was increased with increasing sweep-rate in order to cross the A_0 peak. (*b*) CV at 10 (—) and 20 (-·-·-) mV/s of peaks A_0/C_0 using constant E_+ and E_- values.



© 1997 NRC Canada

This is followed by a relatively slow dehydration process:

$$[9]\quad \text{Ir(III)oxide}\cdot(m + 2.7)H_2O(H_3O^+)_{1.35}(HSO_4^-)_{0.35} \overset{\text{slow}}{===>} \text{Ir(III)oxide}\cdot mH_2O(H_3O^+)_{1.35}(HSO_4^-)_{0.35} + 2.7\ H_2O$$

The different shapes of the A_0 and C_0 peaks, seen in Fig. 5, can perhaps therefore be explained by the fact that the state of hydration of the reacting sites is different in the two forms, introducing different lateral interactions between redox sites in the two cases (18). Alternatively, it has previously been shown (13) that the Ir oxide A_1/C_1 peaks are broader in solutions of lower ionic strength. Therefore, it is possible that the narrower A_0 peak reflects the higher ionic and lower water content of the reduced state, versus the broader cathodic C_0 peak, reflecting reduction of sites from which ions have been lost and a significant amount of water has been gained.

A final issue to address is the possible reason for the development of energetically different sites in these electrochemically grown Ir oxide films, i.e., those that react in peaks A_0/C_0 and those that oxidize and reduce in the principle redox peaks A_1/C_1. It is possible that this relates back to the fact that, in order to form these films, the lower potential limit in each growth cycle is usually made more negative than 0 V, at which point hydrogen evolution commences. This reaction, which involves the consumption of water as well as the generation of locally alkaline conditions, occurs at the film–metal interface, as the oxide film is in its reduced, nonconductive state at these potentials. This may lead to the partial dehydration, as well as other possible structural–compositional alterations, of the oxide film in the region of this interface. Consistent with this, it has been found (3) that the potential of peak A_0 depends somewhat on the length of time spent at the negative potential limit in each cycle during the growth of Ir oxide films using potential pulsing techniques.

Acknowledgements

The authors gratefully acknowledge the financial support of this work by the Natural Sciences and Engineering Research Council of Canada.

References

1. H. Elzanowska and V.I. Birss. J. Appl. Electrochem. **23**, 646 (1993).
2. H. Elzanowska, J. Segal, and V.I. Birss. Extended Abstract, Electrochem. Soc. Spring Meeting, Los Angeles, Calif. 1989.
3. C. Bock. Ph.D. thesis, University of Calgary, Calgary, Alta. 1997.
4. C. Bock and V.I. Birss. Extended Abstracts, Electrochem. Soc. Fall Meeting, San Antonio, Tex. October, 1996.
5. B.E. Conway and J. Mozota. Electrochim. Acta, **28**, 9 (1983).
6. J. Mozota and B.E. Conway. Electrochim. Acta, **28**, 1 (1983).
7. L.D. Burke and D.P. Whelan. J. Electroanal. Chem. **162**, 121 (1984).
8. L.D. Burke and R.A. Scannell. J. Electroanal. Chem. **175**, 119 (1984).
9. J.O. Zerbino and A.J. Arvia. J. Electrochem. Soc. **126**, 93 (1979).
10. S. Gottesfeld, A. Redondo, I. Rubenstein, and S.W. Feldberg. J. Electroanal. Chem. **265**, 15 (1989).
11. P.G. Pickup and V.I. Birss. J. Electroanal. Chem. **240**, 126 (1988).
12. V.I. Birss, H. Elzanowska, and S. Gottesfeld. J. Electroanal. Chem. **318**, 327 (1991).
13. M.F. Yuen, I. Lauks, and W.C. Dautremont-Smith. Solid State Ionics. **11**, 19 (1983).
14. P.G. Pickup and V.I. Birss. J. Electroanal. Chem. **135**, 171 (1988); 185 (1988).
15. V.I. Birss, R. Meyers, H. Angerstein-Kozlowska, and B.E. Conway. J. Electroanal. Chem. **131**, 1502 (1984).
16. S.H. Glarum and J.H. Marshall. J. Electrochem. Soc. **127**, 1467 (1980).
17. D.A. Buttry and M.D. Ward. Chem. Rev. (Washington, D.C., **92**, 1355 (1992).
18. H.A. Kozlowska and B.E. Conway. J. Electroanal. Chem. **95**, 1 (1979).

Can. J. Chem. Downloaded from www.nrcresearchpress.com by 91.121.58.235 on 09/08/12
For personal use only.

© 1997 NRC Canada

Electrochemical and Raman spectroscopic studies of pyrazine adsorption at the Au(210) electrode surface

Anna Iannelli, Alexandre G. Brolo, Donald E. Irish, and Jacek Lipkowski

Can. J. Chem. Downloaded from www.nrcresearchpress.com by 91.121.58.235 on 09/08/12
For personal use only.

Abstract: Chronocoulometry and Raman spectroscopy have been applied to study pyrazine adsorption at the Au(210) electrode surface. The adsorption isotherms, Gibbs energies of adsorption, and the electrosorption valency for pyrazine adsorption at the Au(210) electrode surface have been determined. Surface-enhanced Raman Scattering (SERS) spectra of pyrazine adsorbed on an "unroughened" Au(210) electrode surface have been obtained for the first time. The thermodynamic data and the SERS spectra indicate that pyrazine adsorbs on the Au(210) electrode via the nitrogen lone pair (N-bonded configuration) over the whole range of electrode potentials investigated. Consequently, the pyrazine molecule assumes only the vertical orientation at this surface of gold. The adsorption of pyrazine at the Au(210) and Au(111) surfaces is compared and the influence of the surface crystallography on the adsorption of this molecule at gold electrodes is discussed.

Key words: adsorption at Au(210), pyrazine, SERS, chronocoulometry.

Résumé : On a utilisé la chronocoulométrie et la spectroscopie Raman pour étudier l'adsorption de la pyrazine sur la surface (210) d'une électrode d'or. On a déterminé les isothermes d'adsorption, les énergies de Gibbs pour l'adsorption ainsi que la valence d'électrosorption pour l'adsorption de la pyrazine sur la surface (210) d'une électrode d'or. On a déterminé pour la première fois les spectres de diffusion Raman rehaussés par la surface («SERS») de la pyrazine adsorbée sur une surface (210) «polie» d'une électrode d'or. Les données thermodynamiques et les spectres «SERS» indiquent que, à tous les potentiels d'électrode étudiés, la pyrazine s'adsorbe sur la sruface (210) de l'électrode d'or par le biais de la paire d'électrons libres de l'azote (configuration liées par l'azote). En conséquence, la molécule de pyrazine ne prend que l'orientation verticale par rapport à la surface de l'or. On a comparé l'adsorption de la pyrazine sur les surfaces (210) et (111) de l'or et on discute de l'influence de la cristallographie de la surface sur l'adsorption de cette molécule sur les électrodes d'or.

Mots clés : adsorption sur la surface (210) de l'or, pyrazine, «SERS», chronocoulométrie.

[Traduit par la rédaction]

Introduction

The adsorption onto an electrode of an organic molecule from solution is a complex process that involves direct interaction of the adsorbed molecule with the metal electrode surface, displacement of solvent molecules that were previously adsorbed, interaction with the solvent molecules constituting the solution phase, and lateral interactions between the adsorbate molecules and their modified cospheres (1). Brian Conway et al. (2–4) have shown that the pyrazine molecule, which has a zero net dipole moment in the gas phase, is an ideal probe for the study of the displacement of field-oriented water dipoles from the electrode surface. These papers stimulated our interest in the study of the adsorption of pyrazine at gold electrodes. We have already performed extensive research of pyridine adsorption at group IB metals electrodes (5–19). The size of pyrazine is almost the same as that of pyridine but, in contrast to pyrazine, the pyridine molecule has an appreciable dipole moment. In addition, the presence of the second nitrogen heteroatom in the *para* position of the aromatic ring should significantly affect the interaction of the adsorbed molecule with the aqueous subphase and, consequently, the lateral interactions between the adsorbed molecules (20). Therefore, a comparison of pyrazine and pyridine adsorption at gold electrodes may give insight into the role of the different forces involved in molecular adsorption at metal electrodes.

We have already described the adsorption of pyrazine at the Au(111) (21) and the Au(poly) (22) surfaces. Most recently, the pyrazine monolayer on the Au(111) electrode emersed from an electrolyte solution and transferred to a UHV chamber was investigated by X-ray photoelectron spectroscopy

Received April 8, 1997.

This paper is dedicated to Brian E. Conway on the occasion of his 70th birthday and in recognition of his contributions to electrochemistry.

A. Iannelli and J. Lipowski.[1] Guelph–Waterloo Centre for Graduate Work in Chemistry, Department of Chemistry and Biochemistry, University of Guelph, Guelph, ON N1G 2W1, Canada.

A.G. Brolo and D.E. Irish. Guelph–Waterloo Centre for Graduate Work in Chemistry, Department of Chemistry, University of Waterloo, Waterloo, ON N2L 3G1, Canada.

[1] Author to whom correspondence may be addressed. Telephone: (519) 824-4120, ext. 8543. Fax: (519) 766-1499. E-mail: lipkowski@chembio.uoguelph.ca

© 1997 NRC Canada

Can. J. Chem. Downloaded from www.nrcresearchpress.com by 91.121.58.235 on 09/08/12
For personal use only.

(XPS) by Hamm et al. (23). The objective of this paper is to describe the adsorption of pyrazine at the Au(210) surface. We have selected this plane because it has the most open structure. Structurally, it constitutes the opposite extreme to the Au(111) surface, which has the highest packing density. Chronocoulometry has been employed to measure the charge density at the electrode surface. The energetics of pyrazine adsorption have been determined from a thermodynamic analysis of the charge density data. Surface-enhanced Raman scattering, SERS, of pyrazine molecules adsorbed onto the "unroughened" Au(210) surface has been measured. In this way we have determined the character of pyrazine adsorption at this electrode. The adsorption of pyrazine at the Au(210) surface is compared with that at the Au(111) surface and the influence of surface crystallography on adsorption of this molecule at gold electrodes has been assessed. Preliminary results of the chronocoulometric measurements were included in a recent review (5) and preliminary results of SERS studies have been described in a recent letter (24).

Experimental

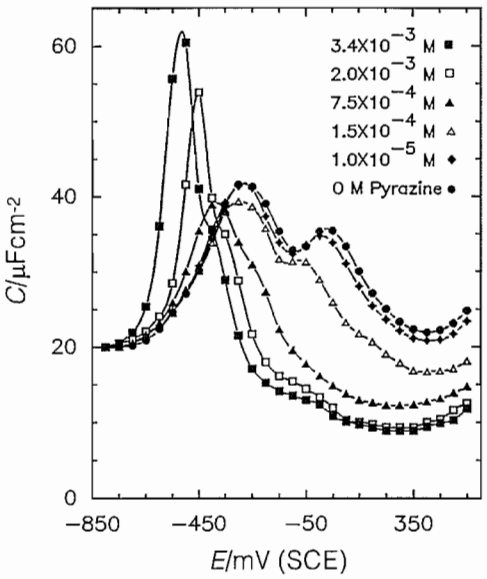
The experimental procedures and instrumentation have been described in previous communications (21, 22, 25). All solutions were prepared from Milli-Q water (Waters) with a resistivity higher than 17 MΩ cm. The supporting electrolyte was 0.1 M $KClO_4$, which was purified by calcination at 300°C and recrystallization. Pyrazine (Aldrich, Gold Label 99+%) was utilized without further purification. A three-electrode cell was used in the measurements. The reference electrode was an external saturated calomel electrode (SCE). The counter-electrode was a coil of gold wire. The Au(210) crystal was grown, oriented, and cut in our laboratory. The electrode was cleaned by flame annealing and quenching with ultrapure water before each experiment (26). Contact between the gold surface and the solution was made using the hanging electrolyte method (27). The temperature was 20 ± 2°C.

The experiments were performed using a PAR model 173 potentiostat, a homemade voltage generator, and an IBM computer equipped with an IS-16 analog–digital interface (RC Electronics, California) for digital data acquisition at a 1 MHz analog–digital conversion frequency with a resolution of 1 mV.

The "unroughened" gold electrode for the SERS experiments was prepared using the technique developed in our previous work (11). A clean gold electrode was placed in the SERS cell containing 0.1 M $KClO_4$ and the desired concentration of the adsorbate. The electrode was submitted to continuous cleaning cycles between the limits −0.8 V and +1.1 V at 20 mV s^{-1}. This cycling persisted until a cyclic voltammogram reproduced itself from one cycle to the next and displayed the features of a clean electrode. After the SERS experiment, the electrode was rinsed with copious amounts of Milli-Q water, and flame annealed. The electrode was then transferred to a clean electrochemical cell containing 0.1M $KClO_4$ solution. Cyclic voltammograms were obtained in the region −0.8 to +1.1 V at 20 mV s^{-1}. The voltammograms presented features uniquely characteristic of a Au(210) surface (16). This surface characterization was carried out to confirm that the electrode surface was preserved during the SERS experiment.

A Renishaw system 1000 Raman microscope equipped with a 385 × 578 pixel Peltier-cooled Wright Instruments charge coupled device (CCD) was used in the SERS experiments. A macro point accessory, with 40 mm focal length, was used to redirect the laser light to the electrode surface in the spectro-electrochemical cell, described elsewhere (28). The spectrometer was interfaced to a PC computer containing programs for data acquisition, baseline correction, smoothing, and bandfitting. A potentiostat PAR model 273 was used in the electrochemical SERS experiments. A 35 mW Melles Griot He-Ne laser provided excitation at 632.8 nm. The laser power was ca. 6 mW at the sample; the diameter of the focal spot was ca. 5 μm.

Fig. 1. Differential capacity curves for the Au(210) electrode recorded in 0.1 M $KClO_4$ solutions of varying pyrazine concentrations as indicated in the figure. The curves were recorded for the potential sweep in the positive direction. The capacitance was determined using a 5 mV rms sine wave modulated at 25 Hz and a 5 mV s^{-1} voltage sweep rate. A series RC equivalent circuit was assumed in the calculations.



Results and discussion

Cyclic voltammetry and differential capacity

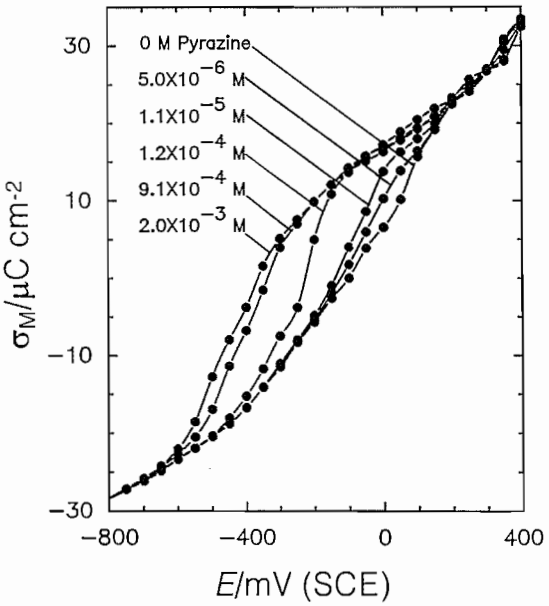
The cyclic voltammograms (CVs) and the differential capacity curves were recorded in order to determine the potential range in which pyrazine adsorption occurred. The shape of the CV recorded for the supporting electrolyte gave the characteristic "fingerprint " of the Au(210) surface (16, 29). Cyclic voltammetry also indicated that the Au(210) surface behaves as an ideally polarizable electrode in the potential range between −0.85 and +0.6 V/SCE.

The differential capacity of the electrode was measured using an ac signal of 25 Hz and 5 mV rms superimposed onto a 5 mV s^{-1} voltage ramp. Figure 1 shows the differential capacity curves for supporting electrolyte without and with a few selected concentrations of pyrazine. We note that at the potential −0.85 V/SCE the capacity is independent of the pyrazine concentration and equal to the capacity of the pure supporting electrolyte. This feature indicates that pyrazine is totally desorbed from the electrode surface at this potential.

© 1997 NRC Canada

Can. J. Chem. Downloaded from www.nrcresearchpress.com by 91.121.58.235 on 09/08/12
For personal use only.

Fig. 2. The absolute charge density of the Au(210) electrode plotted versus the electrode potential in 0.1 M $KClO_4$ solutions of varying pyrazine concentrations as indicated in the figure.



The capacity curves recorded in the presence of pyrazine display a characteristic adsorption/desorption peak followed by a broad minimum. These features show the potential range within which pyrazine molecules are adsorbed at the electrode surface.

The differential capacity curve for the pure supporting electrolyte displays a characteristic minimum at $E = -100$ mV/SCE. The minimum was much more pronounced when the differential capacity was recorded in a dilute (0.005 M $KClO_4$) solution, indicating that this is the diffuse-layer minimum. The potential of the minimum corresponds, therefore, to the potential-of-zero-charge (pzc) of the Au(210) electrode. The pzc value is consistent with the data reported in the literature (16, 29). Finally, we would like to emphasize that the differential capacity curves recorded in the presence of pyrazine displayed a frequency dispersion and thus can not be considered as corresponding to the equilibrium between the electrode surface and the bulk of the solution. Therefore, we used the differential capacities exclusively to characterize the pyrazine adsorption qualitatively.

The charge densities

The chronocoulometric technique (6, 25) was employed to determine the charge density on the metal side of the interface σ_M. The electrode was held at a potential at which pyrazine adsorption occurred for a sufficiently long period of time for the equilibrium between the electrode surface and the bulk of the solution to be established. For pyrazine concentrations lower than 10^{-4} M, the solution was stirred in order to enhance mass transport to the surface. The potential was then stepped to $E = -0.85$ V/SCE, where the pyrazine molecules were desorbed from the electrode surface and the difference between the charge densities at the two potentials was measured. Next, the value of the pzc was used to calculate the absolute charge densities using the procedure described in our earlier papers (6, 25).

Fig. 3. (*a*) Surface pressure at a constant potential plotted versus *E*, and (*b*) surface pressure at a constant charge plotted versus σ_M for 0.1 M $KClO_4$ solutions of the following pyrazine concentrations: (a) 5.0×10^{-6} M; (b) 1.1×10^{-5} M; (c) 5.6×10^{-5} M; (d) 1.2×10^{-4} M; (e) 4.1×10^{-4} M; (f) 9.1×10^{-4} M; (g) 2.0×10^{-3} M.

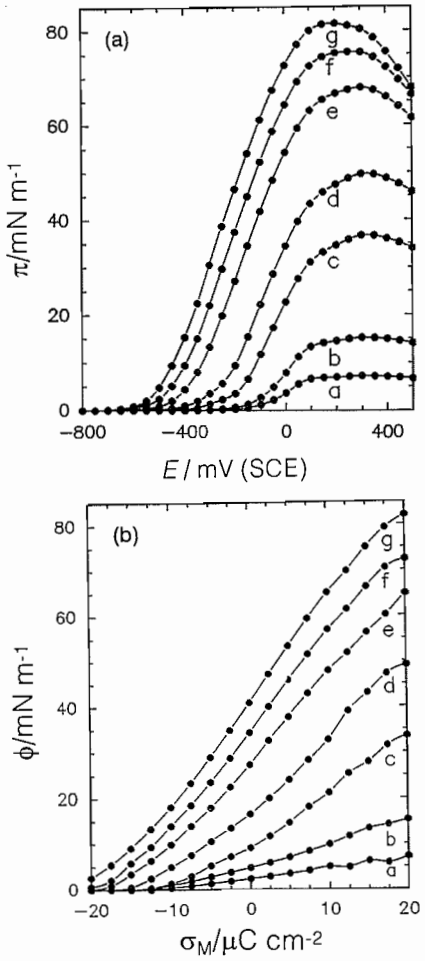


Figure 2 shows the charge density curves determined for the pure supporting electrolyte and for a few selected concentrations of pyrazine. Adsorption of pyrazine is responsible for the appearance of a characteristic step on the charge–potential curves. At positive potentials the curves acquired in the presence of pyrazine intersect the curve for the pure supporting electrolyte solution. The intersection point corresponds to the charge and potential of the maximum adsorption of the pyrazine molecule. The potential of maximum adsorption shifts from about 350 to about 200 mV/SCE with increasing bulk concentration of pyrazine molecules. The potentials of maximum adsorption corresponding to the intersection points on the charge–potential curves correlate well with the potentials of the minimum on the differential capacity curves in Fig. 1.

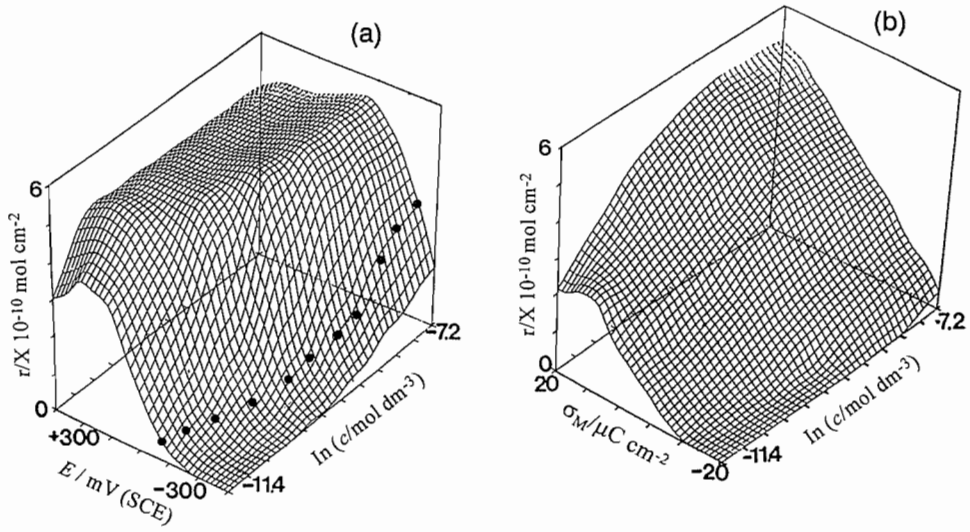
Surface pressure

The surface pressure at constant potential, defined as $\pi = \gamma_{c=0} - \gamma_c$, where $\gamma_{c=0}$ and γ_c correspond to the specific surface energies in the absence and presence of pyrazine, are calculated by integration of the charge density curves (6, 26). Figure 3*a* shows the surface pressure versus potential plots for

© 1997 NRC Canada

Can. J. Chem. Downloaded from www.nrcresearchpress.com by 91.121.58.235 on 09/08/12
For personal use only.

Fig. 4. Three-dimensional graphs representing the isotherms for the adsorption of pyrazine onto a Au(210) surface calculated for (*a*) potential and (*b*) charge used as the independent electrical variable.



seven bulk concentrations of pyrazine. The surface pressure curves display a characteristic bell shape, typical for adsorption of an organic molecule at a metal electrode. In addition, the surface pressure at constant charge, defined as $\phi = \xi_{c=0} - \xi_c$, where $\xi = \gamma + \sigma_M E$ is the Parsons function, can be calculated for charge used as an independent electrical variable. The surface pressures at a constant charge are plotted versus σ_M in Fig. 3*b*. These data show that pyrazine adsorption at the Au(210) surface takes place predominantly at a positively charged surface. The surface pressures data were used to calculate the Gibbs excess of adsorbed pyrazine.

Adsorption isotherms

The relative Gibbs excess, Γ, of pyrazine was calculated by differentiation of the plots of π or ϕ versus the logarithm of the bulk pyrazine concentration. The calculated Gibbs excesses are plotted in three-dimensional coordinates in Figs. 4*a* and 4*b*. The potential or charge axes and the axis of the logarithm of the bulk pyrazine concentration are in the horizontal plane of the figure and the Gibbs excess is plotted on the vertical axis. Figure 4*a* shows one well-defined plateau corresponding to the limiting surface concentration, $\Gamma_{max} = 5.6 \times 10^{-10}$ mol cm^{-2}, of adsorbed pyrazine molecules. A cross section of the three-dimensional graph in the Γ–E plane gives the dependence of the surface concentration of pyrazine on potential at a constant bulk concentration of this molecule. Likewise, a cross section of the 3-D graph in the Γ – ln c plane gives the dependence of the surface concentration of pyrazine on the logarithm of its bulk concentration at a constant electrode potential. All these Γ–E and Γ – ln c curves have a sigmoidal shape with only one inflection point. These properties of the isotherm suggest that pyrazine molecules assume only one orientation when adsorbed at the Au(210) surface. The limiting surface concentration corresponds to an effective molecular area of about 0.25 nm^2. This value is consistent with a vertical orientation of the adsorbed pyrazine (5, 6). The black dots in Fig. 4*a* show the position of the pzc for different concentrations of pyrazine. Apparently, the pzc is located at the rising section of the isotherm and pyrazine molecules are predominantly adsorbed at the positively charged surface. This result shows that adsorption of pyrazine displays a remarkable asymmetry with respect to the charge at the electrode surface.

The character of pyrazine adsorption at the Au(210) surface is therefore distinctly different than at the Au(111) surface. The results of our chronocoulometric experiments (21) and recent XPS studies by Hamm et al. (23) demonstrated that at the Au(111) electrode, the adsorption of pyrazine has a two-state character. The molecule assumes a flat, π-bonded orientation at the negatively charged surface and a vertical N-bonded coordination at positive charge densities. The influence of the surface crystallography of gold on the adsorption of this aromatic heterocycle is dramatic.

Gibbs energy of adsorption

The Gibbs energy of adsorption was determined from the surface pressure data. In the limit of zero coverage, all isotherms simplify to the Henry isotherm and the following relationship holds (6):

$$[1] \quad \pi \text{ (or } \phi) = RT\,\Gamma_{max}\beta c/55.5$$

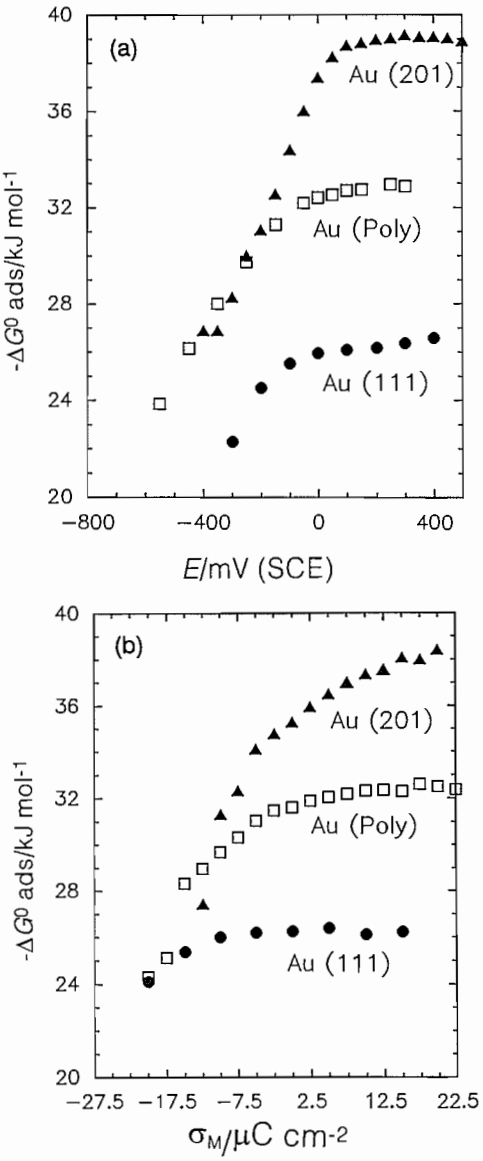
where β is the adsorption equilibrium constant, which is related to the Gibbs energy of adsorption through the equation $\Delta G^\circ = -RT \ln \beta$. The equilibrium constants were calculated from the initial slopes of the surface pressure versus the bulk concentration plots, and the Gibbs energies of adsorption, determined in this way, are plotted in Figs. 5*a* and 5*b* against the potential and charge, respectively. The standard state corresponds to unit mole fraction of the organic species in the bulk of the solution and to monolayer coverage by the noninteracting adsorbates.

For comparison, the Gibbs energies of adsorption determined for pyrazine adsorption at a Au(111) and a polycrystalline Au electrode surface, taken from our previous papers (21, 22), are also included in Figs. 5*a* and 5*b*. The impact of the crystallographic orientation on the energetics of pyrazine

© 1997 NRC Canada

Can. J. Chem. Downloaded from www.nrcresearchpress.com by 91.121.58.235 on 09/08/12
For personal use only.

Fig. 5. Gibbs energy of pyrazine adsorption at the Au(210), Au(111), and Au(poly) surfaces plotted versus (*a*) electrode potential and (*b*) charge density at the metal surface.



adsorption is significant. These data corroborate the above-discussed differences between the character of pyrazine coordination to the Au(210) and Au(111) surfaces of gold and show that the differences have not only a qualitative but also a quantitative character. It is also interesting to note that the Gibbs energies of adsorption at the polycrystalline Au electrode are intermediate between the energies for Au(111) and Au(210) surfaces. We note also that the minimum values of the Gibbs energies of pyrazine adsorption on all gold electrodes are significantly smaller than the minimum value of ΔG°_{ads} at mercury, reported by Conway et al. to be -21 kJ mol^{-1} (2–4). Apparently, pyrazine is physisorbed at Hg while the adsorption at gold electrodes has a character of weak chemisorption that involves mixing of the electronic states of the adsorbed molecule with the electronic states of the metal (21).

Fig. 6. Curves of the charge density at the Au(210) surface versus surface excess of pyrazine for different values of the electrode potential as indicated in the figure. The straight lines were drawn through the points corresponding to low values of the surface excess.

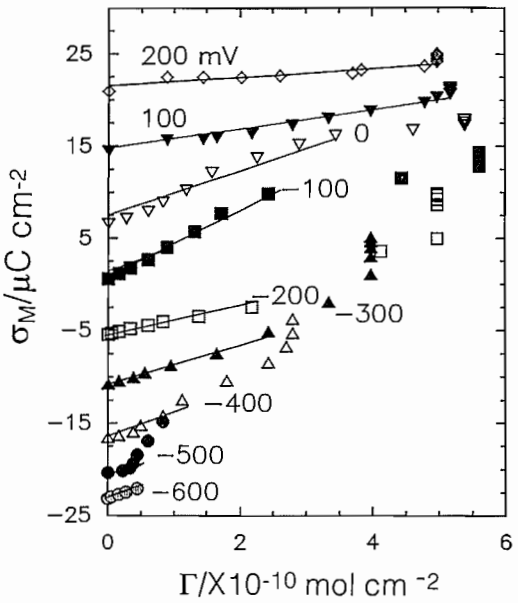
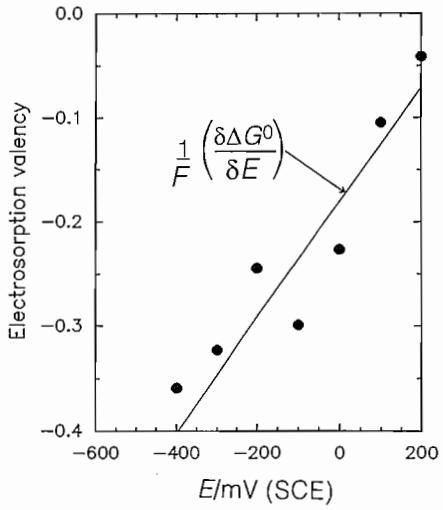


Fig. 7. Dependence of the electrosorption valency on the electrode potential. The dots correspond to the data that were obtained from the slopes of the plots in Fig. 6. The straight line corresponds to the first derivative of a second-order polynomial used to fit the Gibbs energy data given in Fig. 5*a*.



The first derivative of the ΔG°_{ads} versus E plot is equal to the electrosorption valency γ'. The electrosorption valency can be determined independently from the slope of the charge density versus surface concentration plots:

$$[2] \quad \gamma' = (\partial \Delta G^{\circ}_{ads}/\partial E)_{\Gamma} = -(\partial \sigma_M/\partial \Gamma)_E$$

In addition, the first derivative of the Gibbs energy of adsorp-

© 1997 NRC Canada

Fig. 8. Plots of the electrode potential as a function of the surface excess of pyrazine for different values of the charge density at the Au(210) surface. The values of σ_M are given in the figure. The straight lines were drawn through the points corresponding to low values of the surface excess.

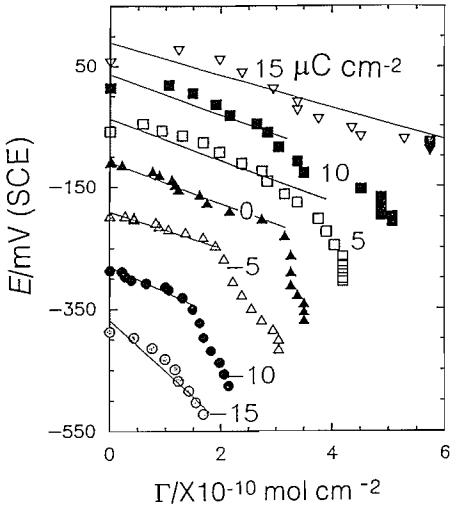
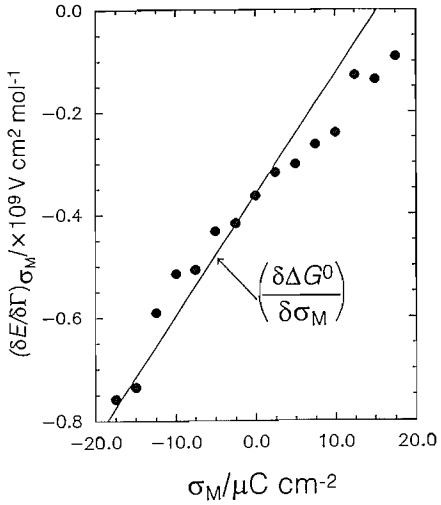


Fig. 9. Dependence of $\partial E/\partial\Gamma$ on the charge density, for pyrazine adsorption at the Au(210) surface. The black points were calculated from the initial slopes of the plots in Fig. 8. The solid line corresponds to the first derivative of a second-order polynomial used to fit the Gibbs energy data in Fig. 5*b*.



tion with respect to charge is equal to the derivative of the electrode potential with respect to the Gibbs excess taken at a constant charge:

$$[3] \quad (\partial\Delta G^{\circ}_{ads}/\partial\sigma_M)_\Gamma = (\partial E/\partial\Gamma)\sigma_M$$

Equations [2] and [3] may be used to check that no major errors have been introduced in the data processing.

Figure 6 shows a series of σ_M versus Γ plots at selected electrode potentials. The initial sections of these plots display good linearity. The data corresponding to higher values of Γ deviate from these linear relationships. However, only the initial slopes of these plots need to be measured, since the Gibbs energies were determined by linear extrapolation of the surface pressures to zero coverage and are considered as zero coverage data. The electrosorption valencies determined from the initial slopes of the charge versus surface concentration curves are plotted as black points in Fig. 7. In addition, the Gibbs energy versus potential curve was fitted by a polynomial and differentiated. The solid line in Fig. 7 is the derivative of the Gibbs energy curve. The agreement between the two sets of data is quite good and it indicates that no major errors were made in the numerical data processing. The electrosorption valency displays a linear dependence on the electrode potential, which points to a quadratic dependence of the Gibbs energy on E. For a one-state adsorption of an organic molecule, the energy of adsorption is expected to be a quadratic function of the electrode potential (20, 30).

Figure 8 shows the dependence of the electrode potential on the surface concentration of pyrazine at selected values of the charge density at the metal. The E versus Γ plots are nonlinear; however, as in the case of electrosorption valency, only the initial slopes of these curves need to be compared to the derivative of the Gibbs energy with respect to charge. The initial slopes of the E versus Γ curves are plotted as points against the charge in Fig. 9. The solid line in Fig. 9 is the derivative of the Gibbs energy with respect to charge. With the exception of a few points corresponding to small values of $(\partial E/\partial\Gamma)\sigma_M$ the agreement between the two sets of data is very good.

In Fig. 8, the E versus Γ curve for zero charge contains useful information about the orientation of adsorbed molecules. For an uncharged electrode, a change of the potential with coverage is caused by the displacement of surface dipoles of water by the dipoles of the adsorbed molecule. This change is described by the Helmholtz formula:

$$[4] \quad \Delta E_{pzc} = (\mu/\varepsilon)\Gamma$$

where ε is the permittivity and $\mu = \mu^{org} - n\mu^{w}$ is the effective dipole moment, where μ^{org} and μ^{w} are the components of the dipole moment of the organic molecule and water in the direction normal to the surface and n is the number of water molecules displaced by one adsorbed organic molecule.

The E versus Γ curve for zero charge is nonlinear, which indicates that the magnitude of the effective dipole moment changes with coverage. Due to the nonlinear character of this dependence it is difficult to determine the shift of pzc due to displacement of water molecules by a monolayer of close-packed pyrazine molecules; that is, for Γ_{max}. However, we may estimate that this shift may be as large as −0.5 V. Independent studies have shown that the interaction of water molecules with the Au(111) surface is weak (31, 32). Consequently, at the pzc the preferential orientation of water is weak and the magnitude of μ^{w} is small. The relatively large shift of the pzc indicates therefore that μ^{org} must be quite large and the negative sign of the shift indicates that, in the organic molecule, the negative pole of the dipole is turned towards the metal and the positive pole towards the solution. The isolated pyrazine molecule has a zero dipole moment. However, at the electrode surface the adsorbed pyrazine molecule can acquire a dipole moment, induced by asymmetric interactions with the solvent and the metal phase. In the case of the vertical orientation, the lone pair of electrons from one nitrogen atom can mix with the electronic states of the metal, while the lone pair

Can. J. Chem. Downloaded from www.nrcresearchpress.com by 91.121.58.235 on 09/08/12
For personal use only.

© 1997 NRC Canada

Fig. 10. SERS spectra of pyrazine adsorbed on a Au(210) electrode. The applied potentials are indicated in the figure. Concentrations are 0.1 M $KClO_4$ and 1 mM pyrazine.

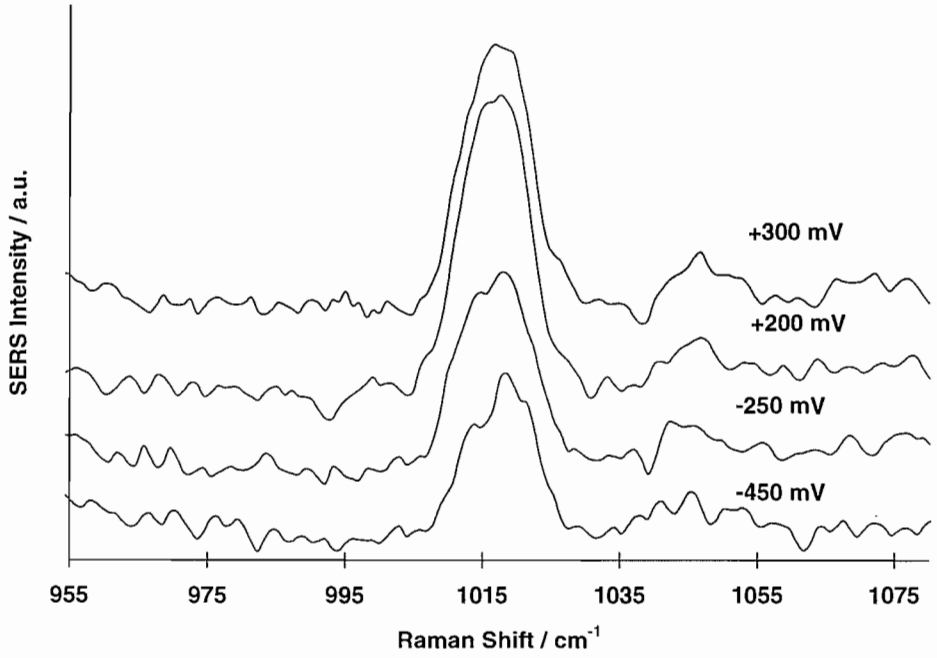
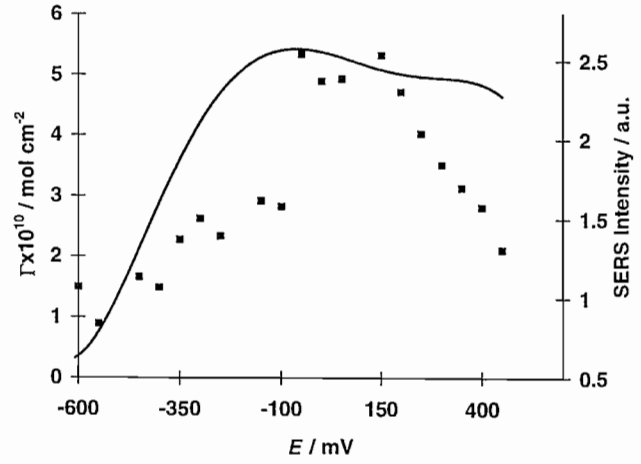


Fig. 11. Dependence of surface coverage (line) and the normalized SERS intensities (squares) on the applied potential for pyrazine adsorbed on a Au(210) electrode. Concentrations are 0.1 M $KClO_4$ and 1 mM pyrazine.



from the second nitrogen atom can form hydrogen bonds with the water molecules. Therefore the dipole moment for the vertical orientation may be significant. The observed shift of the pzc is consistent with the vertical N-bonded orientation of pyrazine molecules at the Au(210) electrode surface.

SERS spectra of pyrazine at the Au(210) surface

Further information about the orientation of pyrazine molecules adsorbed at the Au(210) surface may be obtained from SERS experiments. Until recently, measurements of the SERS for adsorbed molecules were performed at electrode surfaces which had been roughened or activated by oxidation–reduction cycles (ORCs). These roughening procedures affected the crystallographic structure of the surface and the surface crystallography of the roughened electrode was always poorly defined. Recently, due to the advent of a new generation of high-sensitivity Raman spectrometers equipped with CCD detectors, the signal-to-noise ratio for Raman spectra has been significantly improved. Consequently, both the enhanced and unenhanced Raman spectra from molecules adsorbed at "smooth" surfaces of polycrystalline (33) and single crystal electrodes (34) have been reported. In this work we have taken advantage of the possibilities brought by the new instruments to record SERS spectra for pyrazine adsorbed at an "unroughened" gold electrode.

Figure 10 shows the SERS spectra of pyrazine adsorbed on Au(210) at several potentials. The peak at 1019 cm^{-1} corresponds to the ring breathing vibration. The weak peak at ca. 1030 cm^{-1} is due to the ring stretching mode. This mode is forbidden in the normal Raman spectrum of pyrazine in solution. We have recently shown (35) that this mode becomes active for adsorbed pyrazine due to a field gradient enhancement mechanism. Raman spectra of aqueous pyrazine solutions (36) show the ring breathing mode at 1015 cm^{-1}. This band for adsorbed pyrazine on Au(210) is at 1019 cm^{-1}; its frequency is, therefore, higher than for pyrazine in solution. This difference can provide qualitative information about the orientation of the adsorbed pyrazine molecule. For instance, a flat adsorbed pyrazine would interact with the electrode surface through π-electrons of the aromatic ring. This interaction is expected to decrease the frequency of the ring breathing mode when compared to the spectrum of the free molecule in the liquid state. The data presented in Fig. 10 show that the ring breathing mode of adsorbed pyrazine is shifted to higher frequences. This strongly suggests that pyrazine is adsorbed on the Au(210) electrode in an end-on configuration. Moreover,

Can. J. Chem. Downloaded from www.nrcresearchpress.com by 91.121.58.235 on 09/08/12
For personal use only.

© 1997 NRC Canada

Can. J. Chem. Downloaded from www.nrcresearchpress.com by 91.121.58.235 on 09/08/12
For personal use only.

Fig. 10 shows that the Raman peak position of pyrazine adsorbed on Au(210) is independent of the electrode potential. This indicates that the pyrazine orientation does not change with the applied potential, consistent with the electrochemical data.

Figure 11 shows the relationship between the surface coverage for pyrazine adsorbed on Au(210) and the SERS intensities (normalized using the perchlorate stretch mode from the solution). The increase of surface coverage correlates with the increase of SERS intensities for low surface coverage values. However, as the surface coverage increases and reaches a saturation value, the SERS intensities reach a maximum around ca. +100 mV and then decline (24). The difference in the dependence of these quantities (surface coverage and SERS intensity) on the potential has been observed before for the adsorption of pyridine on polycrystalline gold electrodes (11). The lack of relationship between surface coverage and SERS intensities for a heavily packed surface is due to electromagnetic effects. The interaction between dipoles of molecules adsorbed on a highly covered surface can depolarize the local electromagnetic field, causing a decrease in the SERS intensities (11).

Summary and conclusions

The major features of pyrazine adsorption at the Au(210) surface are as follows. The adsorption takes place predominantly at the positively charged surface and hence displays a remarkable asymmetry with respect to the sign of the electrode charge density. The charge and potential of maximum adsorption are large (σ_M varies between 26 and 20 $\mu C\ cm^{-2}$ and $E_{max} - E_{pzc}$ varies between +400 and +300 mV). The absolute values of the Gibbs energy of adsorption are large and their sign is negative (ΔG°_{ads} at E_{max} is equal to -39 kJ mol^{-1}). The Gibbs energy of adsorption displays a quadratic dependence on the electrode potential. The adsorption isotherms have only one inflection point and their plateau corresponds to the limiting surface concentration expected for a close-packed monolayer of vertically adsorbed molecules. These features suggest that the pyrazine molecule is chemisorbed at the Au(210) surface with one of the two nitrogen atoms directed towards the metal, at all potentials and charge densities. The SERS experiments demonstrated that the chemisorption must involve a mixing of the nonbonding orbital of the nitrogen atom with the electronic states of the metal. This behaviour is in contrast to the two-state character of pyrazine adsorption at the Au(111) electrode surface, where a flat, π-bonded, surface coordination was observed at the negatively charged surface and the vertical N-bonded coordination at positive charge densities. Apparently, the character of pyrazine adsorption onto gold depends strongly on the surface crystallography.

The present result shows also that pyrazine adsorption at gold and mercury is significantly different. Conway and coworkers (2–4) demonstrated that pyrazine assumes only one orientation, i.e., flat, at the mercury surface over the whole range of electrode charge densities and bulk pyrazine concentrations. The adsorption of pyrazine at the Au(210) surface constitutes, therefore, the opposite case where only the vertical orientation is observed. These extreme behaviours of pyrazine at the two metals show that different forces are involved in pyrazine adsorption at mercury and at gold. The interaction of a pyrazine molecule with Hg is weak and hence, as was shown by Conway et al., the character of its adsorption at mercury is influenced by the interaction of the adsorbed molecules with the solvent and by the strength of the metal–solvent interaction. The interaction between the pyrazine molecule and the Au(210) surface is stronger and the character of adsorption is determined by the metal–adsorbate interaction.

This point is further reinforced by the remarkable similarities between the adsorption of pyrazine and pyridine at gold electrodes (5, 6). The two molecules display the same two-state adsorption at the Au(111) electrode surface and the one state, N-bonded, adsorption at the Au(210) surface. Very similar differences between the magnitude of the Gibbs energies of adsorption at the Au(111) and Au(210) surfaces are observed for the two molecules. The main differences between surface properties of pyrazine and pyridine at gold electrodes are displayed in the slope of the adsorption isotherms at the Au(210) surface and the sharpness of the phase transition at the Au(111) surface. For pyridine adsorption at the Au(210) surface, the adsorption isotherms display extremely steep changes of the surface concentration from a value close to zero to the limiting surface concentration. These features are characteristic of a phase transition from a gaseous to a condensed state of the monolayer (37, 38). For pyrazine, the adsorption isotherms are less steep and display a continuous change of the surface concentration from zero coverage to the limiting, saturation value. Likewise, at the Au(111) surface, reorientation from the flat to the vertical geometry, observed around the pzc, is rapid for pyridine and gradual for pyrazine.

These differences show that a small change in the structure of the azabenzene molecule has quite an impact on the character of the lateral interactions between adsorbed molecules. Specifically, for monolayers of vertically oriented molecules at the Au(210) surface, the differences may be explained in terms of the different character of the adsorbate–solvent interaction (21). In the vertical orientation the pyridine molecule is coordinated to the metal surface through the nitrogen atom and its aromatic ring is directed toward the solution. The interaction of the surface molecule with the solvent must have a strongly hydrophobic character. In contrast, the second nitrogen atom of the pyrazine molecule can participate in hydrogen bonding to the solvent molecule. Therefore, it is not surprising that a miscibility gap occurs in a two-dimensional mixture of water and N-bonded pyridine, while surface pyrazine and water form a continuous series of solutions. Once again, the similarity between the surface behaviour of pyrazine and pyridine at gold electrodes is in remarkable contrast to the difference between the adsorption of these two molecules at mercury (1–4). These behaviours indicate that the surface properties of azabenzenes at electrodes of group IB metals are determined by the strength of the metal–adsorbate interaction.

Acknowledgments

This work was supported by grants from the Natural Sciences and Engineering Research Council of Canada.

References

1. B.E. Conway, J.G. Mathieson, and H.P. Dahr. J. Phys. Chem. **78**, 1226 (1974).
2. B.E. Conway and H.P. Dahr. Croat. Chem. Acta, **45**, 109 (1973).

© 1997 NRC Canada

Can. J. Chem. Downloaded from www.nrcresearchpress.com by 91.121.58.235 on 09/08/12
For personal use only.

3. B.E. Conway, H.P. Dhar, and S. Gottesfeld. J. Colloid Interface Sci. **43**, 303 (1973).
4. B.E. Conway and H. Angerstei-Kozlowska. Electrochim. Acta, **19**, 455 (1974).
5. J. Lipkowski and L. Stolberg. *In* Adsorption of molecules at metal electrodes. *Edited by* J. Lipkowski and P.N. Ross. VCH, New York. 1992. p. 171.
6. J. Lipkowski, L. Stolberg, D.-F. Yang, B. Pettinger, S. Mirwald, F. Henglein, and D.M. Kolb. Electrochim. Acta, **39**, 1045 (1994).
7. F. Henglein, J. Lipkowski, and D.M. Kolb. J. Electroanal. Chem. **303**, 245 (1991).
8. B. Pettinger, J. Lipkowski, S. Mirwald, and A. Friedrich. J. Electroanal. Chem. **329**, 289 (1992).
9. J. Lipkowski, L. Stolberg, S. Morin, D.E. Irish, P. Zelenay, M. Gamboa, and A. Wieckowski. J. Electroanal. Chem. **355**, 147 (1993).
10. L. Stolberg, J. Richer, J. Lipkowski, and D.E. Irish. J. Electroanal. Chem. **207**, 213 (1986).
11. L. Stolberg, J. Lipkowski, and D.E. Irish. J. Electroanal. Chem. **300**, 563 (1991).
12. L. Stolberg, J. Lipkowski, and D.E. Irish. J. Electroanal. Chem. **238**, 333 (1987).
13. L. Stolberg, J. Lipkowski, and D.E. Irish. J. Electroanal. Chem. **296**, 171 (1990).
14. L. Stolberg, J. Lipkowski, and D.E. Irish. J. Electroanal. Chem. **322**, 357 (1992).
15. L. Stolberg, J. Lipkowski, and D.E. Irish. J. Electroanal. Chem. **307**, 241 (1991).
16. D.-F. Yang, L. Stolberg, J. Lipkowski, and D.E. Irish. J. Electroanal. Chem. **329**, 259 (1992).
17. A. Hamelin, S. Morin, J. Richer, and J. Lipkowski. J. Electroanal. Chem. **272**, 241 (1989).
18. A. Hamelin, S. Morin, J. Richer, and J. Lipkowski. J. Electroanal. Chem. **285**, 249 (1990).
19. A. Hamelin, S. Morin, J. Richer, and J. Lipkowski. J. Electroanal. Chem. **304**, 195 (1991).
20. R. Guidelli. *In* Adsorption of molecules at metal electrodes. *Edited by* J. Lipkowski and P.N. Ross. VCH, New York. 1992. p. 1.
21. A. Iannelli, J. Merza, and J. Lipkowski. J. Electroanal. Chem. **376**, 49 (1994).
22. A. Iannelli, J. Richer, and J. Lipkowski. Langmuir, **5**, 466 (1989).
23. U.W. Hamm, V. Lazarescu, and D.M. Kolb. J. Chem. Soc. Faraday Trans. **92**, 3785 (1996).
24. A.G. Brolo, D.E. Irish, and J. Lipkowski. J. Phys. Chem. **101**, 3906 (1997).
25. J. Richer and J. Lipkowski. J. Electrochem. Soc. **133**, 121 (1986).
26. J. Clavilier. J. Electroanal. Chem. **107**, 211 (1980).
27. D. Dickermann, J.W. Schultze, and F.D. Koppitz. Electrochim. Acta, **21**, 967 (1976).
28. A.G. Brolo, B.D. Smith, and D.E. Irish. J. Mol. Struct. **405**, 29 (1997).
29. A. Hamelin, L. Stoicoviciu, and F. Silva. J. Electroanal. Chem. **229**, 107 (1987).
30. S. Trasatti. J. Electroanal. Chem. **53**, 335 (1974).
31. J. Lipkowski, C. Nguyen Van Hong, C. Hinnen, R. Parsons, and J. Cevalet. J. Electroanal. Chem. **143**, 375 (1983).
32. P. Thiel and T. Madey. Surf. Sci. Rep. **7**, 211 (1987).
33. N. Matsuda, T. Sawaguchi, M. Osawa, and I. Uchida. Chem. Lett. 145 (1995).
34. T. Sueoka, J. Inukai, and M. Ito. J. Electron Spectrosc. Relat. Phenom. **64/65**, 363 (1993).
35. A.G. Brolo and D.E. Irish. J. Electroanal. Chem. **414**, 183 (1996).
36. A.G. Brolo and D.E. Irish. Z. Naturforsch. A: Phys. Sci. **50**, 274 (1995).
37. R. de Levie. Chem. Rev. **88**, 599 (1988).
38. C. Buess-Herman. *In* Adsorption of molecules at metal electrodes. *Edited by* J. Lipkowski and P.N. Ross. VCH, New York. 1992. p. 77.

© 1997 NRC Canada

Anodic oxidation of Au(111)

Marie Anne Schneeweiss, Dieter M. Kolb, DeZhong Liu, and Daniel Mandler

Abstract: The initial stages of the anodic oxidation of Au(111) were investigated by means of cyclic voltammetry as well as in situ scanning tunneling microscopy (STM). The results suggest that the place exchange process, which initiates the oxide formation, starts at step edges. The oxide phase was imaged in situ by scanning tunneling and atomic force microscopy (AFM). The topographic information acquired by the two techniques is compared.

Key words: gold, gold oxide, corrosion, scanning tunneling microscopy (STM), atomic force microscopy (AFM).

Résumé : Faisant appel à la voltampérométrie cyclique ainsi qu'à la microscopie à balayage de l'effet tunnel «STM» in situ, on a étudié les étapes initiales de l'oxydation anodique de Au(111). Les résultats suggèrent que le processus d'échange de place qui initie la formation de l'oxyde débute aux arêtes. Faisant appel à la microscopie à balayage de l'effet tunnel et à la microscopie de la force atomique «AFM», on a obtenu une image in situ de la phase oxyde. On a comparé les informations topographiques obtenues par les deux méthodes.

Mots clés : or, oxyde d'or, corrosion, microscopie à balayage de l'effet tunnel «STM», microscopie de la force atomique «AFM».

[Traduit par la rédaction]

1. Introduction

The use of metal in industrial processes or daily life often entails the problem of oxidation and corrosion. The first step towards protection of metal surfaces from corrosion is obviously a full mechanistic understanding of the processes involved in metal oxidation and corrosion.

As many of the metals concerned are reactive and, at ambient conditions, tend to be covered with a thin oxide layer, it is desirable to perform studies of the initial stages of oxidation and corrosion on structurally well-defined surfaces of an inert noble metal, for which the oxidation reaction can be controlled by the electrode potential, thus serving as a model system. Au and Pt have long since been used for this purpose.

Electrochemical oxide formation on gold single-crystal electrodes has been investigated in great detail by Conway and co-workers (1, 2). The mechanism that they proposed is generally accepted and will be summarized briefly as follows. A recent review article by Conway gives an excellent overview on oxide formation on noble metals, exemplified by the cases of Au and Pt (3).

In general, the anodic oxidation reaction comprises a number of steps, the first of which is the deposition of OH on the surface, the second one a restructuring process that involves a turnover of the MOH[2] dipoles in the surface, accompanied by the transfer of the second electron to form the oxide. In the absence of any specific adsorption on the surface during oxidation, a continuous deposition of OH should be expected, the repulsive interactions between the parallel-oriented MOH dipoles then causing the turnover process (restructuring). The presence of an adsorbate, however, can change the reaction path. An anion like sulfate, which adsorbs strongly at potentials less positive than the oxidation potential, affects the extent of OH deposition on the precovered surface. In such a case the adsorption of anions from the electrolyte constitutes the very first step in the oxidation reaction, as it has a profound influence on the following steps. The role of anion adsorption as a competitive effect in the initial stages of OH electrosorption was demonstrated by Angerstein–Kozlowska et al. (2) by creating conditions referred to as "anions on" and "anions off." In the latter case the electrosorption of OH and O could be resolved in the cyclic voltammogram (2). As the fourth and final step the formation of bulk oxide should be added to this list. This is generally proposed to proceed by a high-field-type mechanism as described by Mott and Cabrera (4, 5).

Detailed studies performed by Conway and co-workers (ref. 1, and literature cited therein) resulted in the following three-step model for the oxide formation on Au(111) in H_2SO_4: (*i*) sulfate (or, more likely, hydrogen sulfate) adsorption up to a complete $(\sqrt{3}\times\sqrt{7})$ adlayer precedes (*ii*) the electrosorption of OH or O, which are incorporated in the ordered sulfate adlattice. During the latter process, which takes place in the potential range of the peaks labeled OA1/2, OA3 (see Fig. 2), a repulsive interaction between the AuOH dipoles builds up and causes (*iii*) a turnover process, resulting in a two atom thick oxide layer. The turnover process takes place simultaneously with anion desorption and replacement (i.e., replacement–turnover process, RTO) in the potential range of the OA4 peak. For the discussion of the cyclic voltammograms,

Received May 22, 1997.

This paper is dedicated to Professor Brian E. Conway on the occasion of his 70th birthday.

M.A. Schneeweiss and D.M. Kolb.[1] Department of Electrochemistry, University of Ulm, D-89069 Ulm, Germany. **D.-Z. Liu and D. Mandler.** Department of Inorganic and Analytical Chemistry, The Hebrew University of Jerusalem, Jerusalem 91904, Israel.

[1] Author to whom correspondence may be addressed. Telephone: ++49-731-502-5400. Fax: ++49-731-502-5409. E-mail: dieter.kolb@chemie.uni-ulm.de

[2] MOH in this case describes the chemisorbed state of OH on the M surface (1).

© 1997 NRC Canada

Can. J. Chem. Downloaded from www.nrcresearchpress.com by 91.121.58.235 on 09/08/12
For personal use only.

Can. J. Chem. Downloaded from www.nrcresearchpress.com by 91.121.58.235 on 09/08/12
For personal use only.

however, we choose the expressions "first oxidation peak" and "second oxidation peak" instead of "OA1–3" and "OA4" as a means of simplification.

It has been known for quite some time, from conventional electrochemical studies (1, 6, 7), that an oxidation–reduction cycle (ORC) causes roughening of the electrode surface. Trevor et al. (8) were the first to employ in situ scanning tunneling microscopy (STM) to image a Au(111) surface in dilute $HClO_4$ prior to and after an ORC. They found that the formation of a complete monolayer of oxide was necessary in order to observe monoatomic deep pits on flat terraces after reduction, and they attributed the pit formation to a place exchange process during oxidation. Honbo et al. (9) were able to show that pit formation takes place during reduction rather than during oxidation. The same conclusions for Ag(111) were made earlier on the basis of reflectance measurements (10).

Meanwhile, several STM studies (11–16) and one AFM study (17) on this subject were performed. Our group (15, 16) has shown that the morphology of the gold surface after ORCs depends on whether the reduction was achieved by a cathodic potential sweep (resulting in pits only) or a potential step (leading to the formation of islands as well as pits).

For a long time it was not clear whether electrochemical surface oxidation would generate a crystalline oxide that would grow according to the laws of crystal growth. All STM results, though, have shown so far that the gold oxide layer is never anything else but rough and amorphous (9, 11–13). Reproducibly, we have found that the oxide layer as imaged by STM is rough, consisting of small hillocks 0.1–0.25 nm in height (16). Reports on crystalline gold oxide in the literature are rare and limited exclusively to the use of hydrothermal synthesis, which yields stable ruby red crystals of Au_2O_3 (18, 19).

The quantitative evaluation of data acquired by STM, in spite of its great power in monitoring processes on electrode surfaces on the nanometer scale, can nevertheless be problematic when the surface under investigation is an oxide rather than a metal. Topographic information (derived from imaging constant local density of states) cannot be taken at face value. Thus it was also desirable to image the oxide layer by AFM in order to compare and cross-check information from these two techniques. In addition, the use of AFM allows the imaging of thicker oxide layers. In this work, we compare the results for the oxide layer on Au(111) obtained by STM and AFM.

Furthermore, recent voltammetric studies with stepped Au(111) surfaces performed in the course of this investigation suggest a possible modification of the currently employed mechanistic model concerning the assignment of the various current peaks to the initial stages of oxide formation. We will discuss preliminary results about the dependence of the first oxidation peak on the defect density of the Au(111) surface.

2. Experimental

The STM measurements were performed with a Topometrix TMX 2010, using W tips electrochemically etched from a 0.25 mm diameter wire in 2 M NaOH and Pt–Ir tips (Pt to Ir ratio 80:20) etched in 3.4 M NaCN. To minimize faradaic currents at the tip–electrolyte interface, all tips were coated with Apiezon wax (20, 21). Tip and sample potentials were controlled independently of each other by means of a bipotentiostat.

The AFM measurements were performed with a Nanoscope II in the Department of Inorganic and Analytical Chemistry of the Hebrew University of Jerusalem, Israel. Commercial Si_3N_4 tips were used.

The electrolyte solutions were prepared from H_2SO_4 (Merck, suprapure), $CuSO_4$ (Fluka, puriss. p.), and Milli-Q water. For the STM measurements, a copper wire served as a convenient, low-noise reference electrode. For this purpose, $CuSO_4$ was added to the solution in all STM experiments. In the case of the AFM measurements homemade Hg/Hg_2SO_4 microelectrodes (0.41 V vs. SCE) were used as a reference electrode. In all cases, electrode potentials are quoted versus SCE.

The gold samples used for STM and AFM experiments consisted of 200 nm thick films evaporated onto a special glass (AF 45, Berliner Glas KG) on top of a 2 nm Cr layer for better adhesion. The samples were annealed in a hydrogen flame for 2 min at yellow heat to yield large, atomically flat (111) terraces (22).

All STM data were recorded in the constant current mode, AFM data in the constant force mode. All images are displayed either as top views with different shades of grey, representing different heights (dark areas indicating low parts, and light areas high parts of the surface), or as three-dimensional plots based on shaded top views.

The cyclic voltammograms were obtained with standard electrochemical equipment and a conventional electrochemical cell with separated compartments for reference and counter electrode. Here, the Au(111) electrodes were single-crystal discs (MaTecK, Jülich), each with a diameter of about 4 mm and a gold wire attached to the back for better handling. Two of them were oriented and mechanically polished to better than 1°, but two were 3° and 6° off the [111] direction to yield stepped surfaces with an average terrace width of 6 and 3 nm, respectively. Prior to each experiment the gold crystals were annealed for 2 min in a Bunsen-burner flame and brought into contact with the electrolyte under potential control by the so-called dipping technique. In a previous STM study it was shown that flame annealing did not endanger the step structure by facetting, but produced regularly stepped surfaces with flat terraces of the expected width (23, 24).

3. Results and discussion

3.1. Cyclic voltammetry

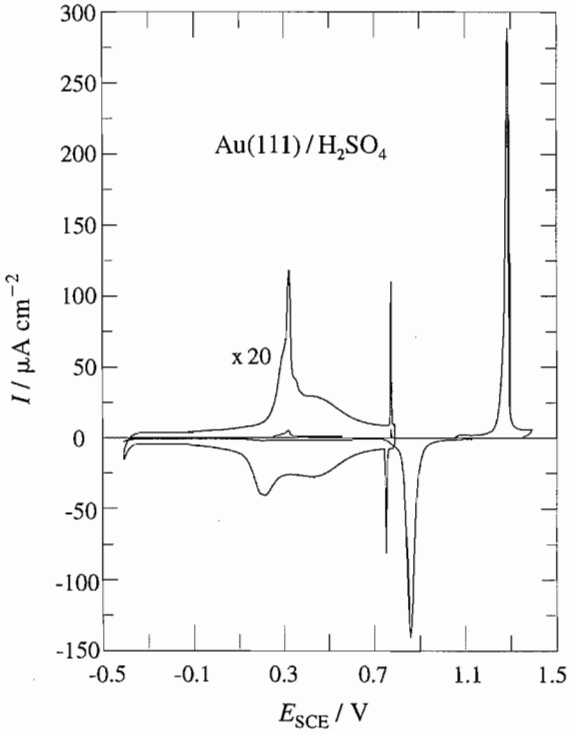
Although the cyclic voltammograms for Au(111) in sulfuric acid solution are well known (1), our recent measurements with the stepped electrodes revealed some new aspects, which will be discussed here briefly.

Figure 1 shows a cyclic voltammogram for a freshly annealed Au(111) (<1°) single-crystal electrode in 0.1 M H_2SO_4 at 10 mV/s. The double-layer region (shown in Fig. 1 on an enlarged scale) displays these well-known characteristics: the sharp peak at about 0.3 V, associated with lifting of the reconstruction, and the sharp spike at 0.73 V, caused by a phase transition within the sulfate adlayer between random adsorption and an ordered structure (25). The current density of the sulfate spike has been shown to be a good indicator for the quality of a (111) surface, as it decreases with increasing defect (step) density of the surface (24). The double-layer diagram thus indicated that the crystal was extremely well prepared. Ex situ STM measurements showed that this crystal

© 1997 NRC Canada

Can. J. Chem. Downloaded from www.nrcresearchpress.com by 91.121.58.235 on 09/08/12
For personal use only.

Fig. 1. Cyclic voltammogram for Au(111) in 0.1 M H_2SO_4 at 10 mV/s. The scale for the current density in the double-layer region is enhanced to show details of anion adsorption.



exhibited terraces up to 1 μm in width. Compared to *I–E* curves from the literature, the first oxidation peak (at ca. 1.1 V vs. SCE), which corresponds to the so-called OA1/2 peak, is very small for such a surface. The maximum current density of the second peak (at ca. 1.28 V vs. SCE, corresponding to OA4), on the other hand, is extremely high. Cycling the potential again (see Fig. 2(*b*)) caused the first peak to increase slightly, whereas the height of the second peak decreased markedly. Similar effects have been reported by Hamelin (26) and were attributed to a change of surface topography with the first ORC.

It is by now a well-known fact that the first ORC causes roughening of a virgin Au(111) surface by way of creating monoatomic deep pits. Thus it seems likely that the changes observed in the second cycle are due to changes in the surface topography caused by the preceding ORC, i.e., the increase in surface defects. This would indicate that the process related to the first peak is confined to defects, as the peak height depends on the defect density. This hypothesis is supported by preliminary results from experiments with stepped single-crystal electrodes. These crystals present the possibility of working with surfaces exhibiting a quantitatively assessable number of defects.

Figure 2 shows a compilation of ORCs for different Au(111) electrodes in 0.1 M H_2SO_4 (at 10 mV/s from −0.4 V vs. SCE to 1.4 V and back), illustrating our findings. Curve (*a*) refers to the first ORC on a freshly annealed, well-prepared electrode; this is the same curve as the one shown in Fig. 1. Curve (*b*) shows the second cycle on the very same electrode. Curve (*c*) is the first cycle of a different (111) crystal that, according to the manufacturer, also has a tilt of less than 1° from the [111] direction, but is obviously not as perfect as the former crystal. This voltammogram compares very well with the curves known from the literature and was used in ref. 16. The reduction peak in this curve is slightly smaller than in the others, as the potential was only scanned up to 1.3 V. Curves (*d*) and (*e*) show ORCs performed with the stepped electrodes, their surfaces tilted by 3° and 6° from the (111) plane, respectively.

The trend clearly shows an increase of the first peak with increasing defect (step) density on the surface. At the same time, the second peak decreases markedly in height. Within a certain margin of error, the total charge passed under both peaks on the anodic scan seems to be of the same order of magnitude in all five cases (570–630 μC/cm^2).

The first peak (OA1/2) is usually associated with OH^- deposition on the sulfate-covered surface. We reported in an earlier STM study that cycling the potential to an anodic limit within this peak causes no defects on the atomically flat terraces (16). We called the process associated with this peak reversible, in the sense that it leaves the surface intact after reduction. This observation seemed to agree with the established mechanism described above. The pronounced defect dependence of the first peak, however, appears to be at variance with the suggestion that peak OA1/2 represents OH^- adsorption and incorporation in the sulfate adlayer, which would be mainly at flat terraces.

We offer what at this point seems to be a reasonable explanation: turnover processes at step edges, which might be energetically favoured and hence occur at less positive potentials than those taking place on terraces, may be responsible for the majority of the charge passing under the first peak. This assumption does not necessarily disagree with the reversibility stated before, as the reduction of turned-over material on step edges would not affect the terraces. A more detailed study also taking into account the presence of islands, which are formed by lifting of the reconstruction (15), is in progress and is hoped to shed more light on the defect dependence of the onset of oxidation.

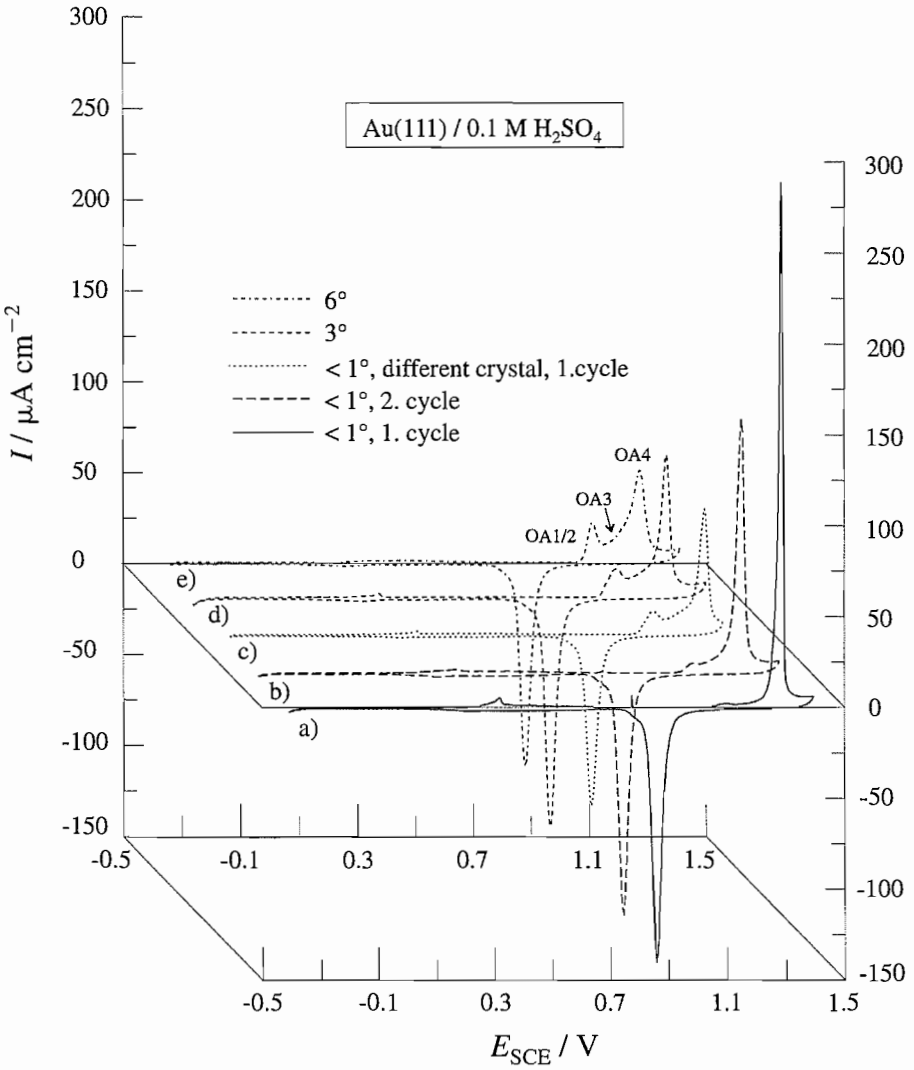
4. STM and AFM measurements

For slow anodic potential sweeps it is possible to show with in situ STM that oxidation (formation of a rough, turned-over phase) indeed begins preferably (although not exclusively) at step edges. Figure 3 shows a Au(111) surface during such an anodic sweep (0.5 mV/s) to 1.15 V. At 1.15 V, the step edges are densely decorated with a rough crust of 0.1–0.3 nm height, which is completely absent at 1.04 V, i.e., before entering the potential region of the first peak. Since, at even lower sweep rates, the turnover process can be observed to begin on terraces as well as on the step edges, it may be concluded that the onset of the turnover process at flat terraces is to a large extent governed by kinetics.

It is generally agreed that the main step in the oxidation process is the so-called turnover process, which is reflected in the STM image by roughening of the surface. The complete transformation of atomically flat terraces into a rough oxide-covered surface is illustrated in Fig. 4. Figures 4(*a*) and (*b*) are three-dimensional in situ STM images (125 nm × 125 nm) acquired at 0.8 V and 1.3 V, respectively, before and after the

© 1997 NRC Canada

Fig. 2. Cyclic voltammograms for different Au(111) electrodes in 0.1 M H_2SO_4. (*a*) and (*b*) First and second cycles for a well-prepared Au(111) electrode. (*c*) A different Au(111) electrode. (*d*) Stepped Au(111) single crystal with its surface tilted 3° from the (111) plane. (*e*) Stepped Au(111) single crystal tilted 6° from the (111) plane. Increasing defect density leads to an enhancement of the first oxidation peak and diminution of the second.



corresponding potential step. The topography of the rough, amorphous oxide layer has been characterized by several groups (11, 13, 16, 17) with AFM as well as STM, and will be discussed in some detail below.

Even at a potential just beyond the oxidation peak OA4, oxidation is assumed to continue, and thus thickening of the oxide film is expected. On the time scale accessible with STM, however, no increase in the surface roughness was found. In our experiment, the surface remained unchanged even after about 35 min at 1.3 V. At significantly longer times in the oxidation range, imaging of the surface with STM becomes increasingly difficult. (Experiments with AFM, however, showed that in the course of 16 h no marked change in the surface topography takes place and only a slight increase in roughness is found.) Figure 4(*c*) finally shows the effect of the surface-oxide reduction by a potential step down to 0.5 V. After reduction the surface exhibits the well-known characteristics, namely, monoatomic deep holes and monoatomic high islands.

In a previous study, we reported that the oxide-covered surface consists mainly of small hillocks about 0.1–0.25 nm in height and about 2–4 nm in width (16). Such dimensions correlate well with results of other authors (11, 13). In the meantime, however, we have been able to image the oxide layer with much better resolution, by STM as well as AFM, the latter resulting in a distinctly different appearance of the oxide-covered surface.

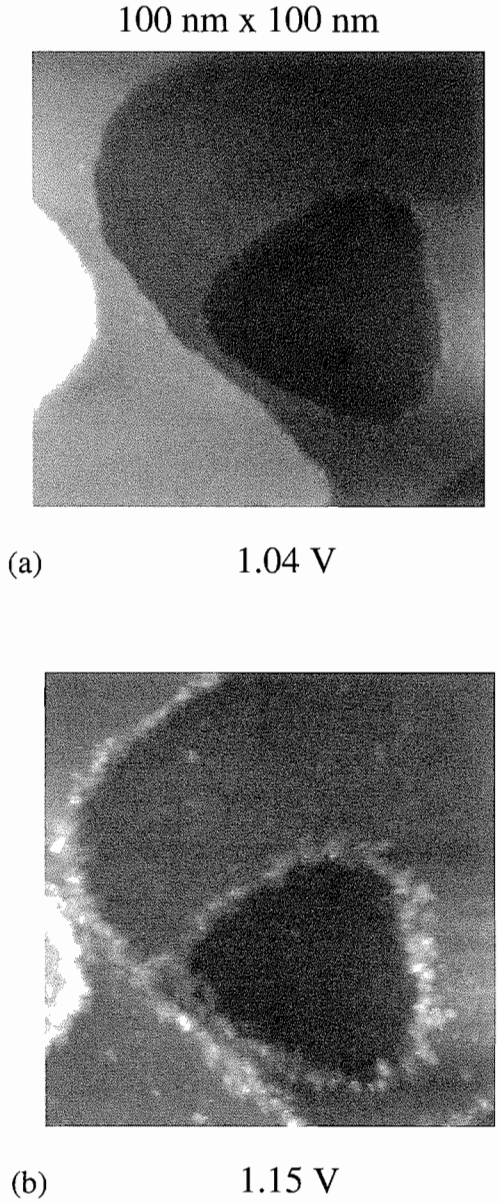
Figure 5 compares three images of the oxide layer under different instrumental conditions. Figure 5(*a*) represents an STM image obtained with a poorly resolving tip, while Fig. 5(*b*) shows higher resolution; Fig. 5(*c*) shows an AFM image. All three images were acquired on different samples but under similar conditions, namely at 1.3 V, which is just beyond the

© 1997 NRC Canada

Can. J. Chem. Downloaded from www.nrcresearchpress.com by 91.121.58.235 on 09/08/12
For personal use only.

Can. J. Chem. Downloaded from www.nrcresearchpress.com by 91.121.58.235 on 09/08/12
For personal use only.

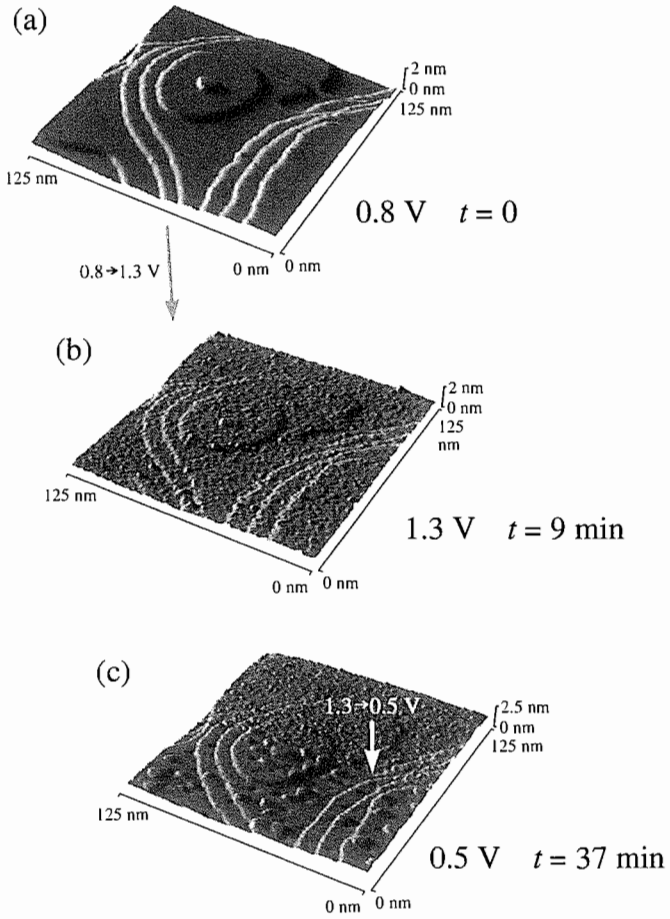
Fig. 3. STM images showing the onset of oxidation at the steps of a Au(111) electrode during a potential sweep to 1.15 V. Sweep rate: 0.5 mV/s. (*a*) At 1.04 V vs. SCE, the terraces are smooth, and the step edges sharp and distinct. (*b*) At about 1.15 V: the step edges are decorated with a crust of turned-over material. I_T: 2 nA. E_{tip}: 0 mV.



second peak. Images (*a*) and (*c*) were recorded after about 10 min of oxidation, image (*b*) immediately after reaching the oxidation potential. Because we have never found any indication that the structure of the oxide at this potential changes with time, it seems justified to regard the experimental conditions as equivalent. The images in Fig. 5 are accompanied by typical cross sections all drawn to the same scale. Figure 5(*a*) shows the oxide layer as a disordered arrangement of small clusters of oxide. A three-dimensional rendering of such an image would yield the familiar picture of hillocks 2–4 nm wide. In the cross section such a hill is marked with a circle.

At first sight the STM image in Fig. 5(*b*) presents the same

Fig. 4. STM images (125 nm × 125 nm) showing the oxidation of Au(111) in 0.1 M H_2SO_4 ($+10^{-3}$ M $CuSO_4$) and subsequent reduction by potential step: (*a*) before oxidation and (*b*) after a potential step to 1.3 V and 9 min at this potential. (*c*) After 35 min at 1.3 V, the surface topography did not change. Reduction was achieved by a potential step to 0.5 V (see arrow) and resulted in the appearance of monoatomic deep (high) pits (islands). I_T: 2 nA. U_T: −300 mV.

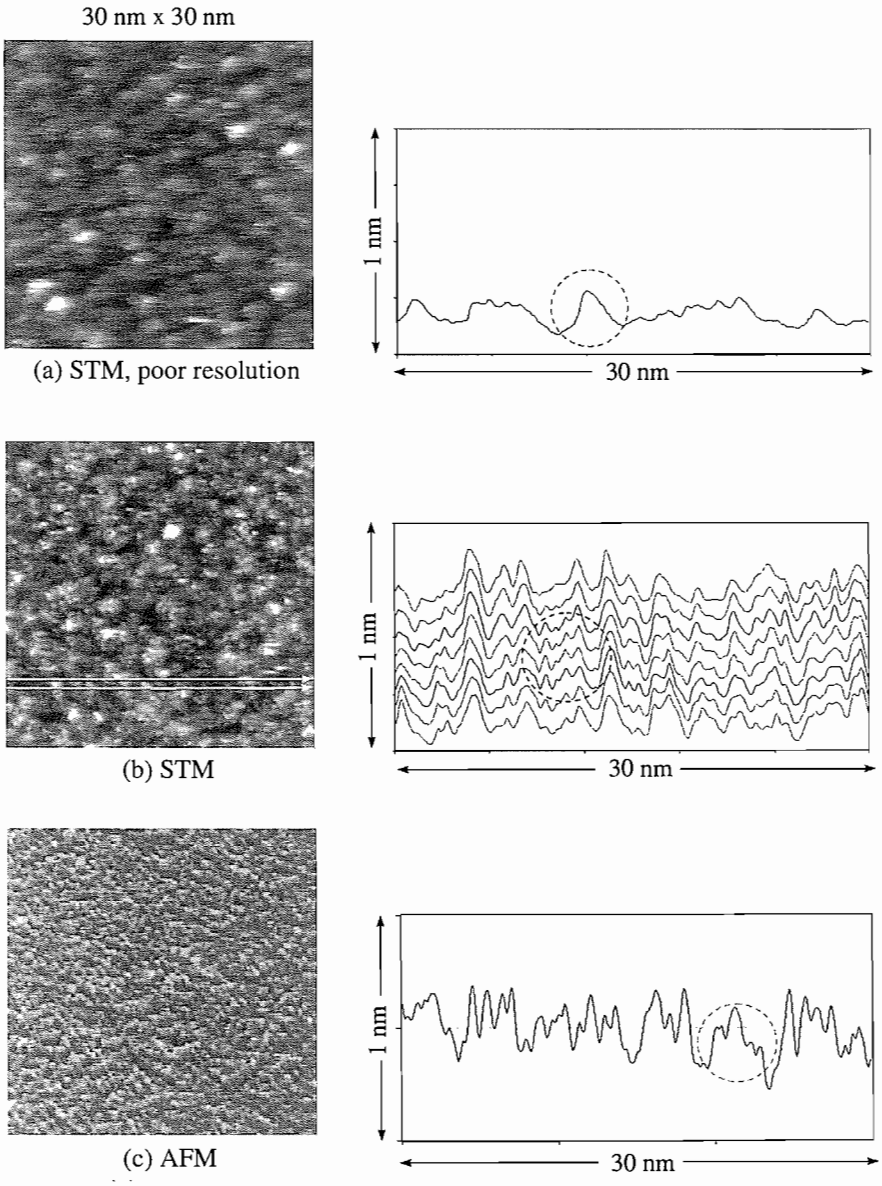


structure. On close examination, however, the hillocks are found to be aggregates of smaller structures, which can be resolved in the cross sections as well as in a three-dimensional display (see Fig. 6(*a*)). Here, the circle marks such an aggregation of small structures, which, in a less well-resolved image, would simply be shown as one hillock. Arrows in the STM image mark the uppermost and lowest of those scan lines, which are shown as cross sections. This sequence of scan lines is depicted to demonstrate the continuity of the small structures in real space, which serves to distinguish them from noise.

Finally, Fig. 5(*c*) shows an AFM image of the same structure. Here, the fine structure is even better resolved, and only the cross section reveals a certain bunching of the spiky structures in groups. In a similar AFM study of gold oxidation Manne et al. (17) also found aperiodic atomic-scale features in the oxidation regime, associating these with Au–OH moieties, but not commenting on height or width.

© 1997 NRC Canada

Fig. 5. Images (30 nm × 30 nm) of the oxide layer on Au(111) in 0.1 M H_2SO_4 ($+10^{-3}$ M $CuSO_4$) at 1.3 V. Also shown are cross sections that are typical for the image, all drawn to the same scale to allow a direct comparison. (*a*) Poorly resolved STM image showing the familiar surface structure consisting of small round hillocks. I_T: 2 nA. U_T: −300 mV. (*b*) A high-resolution STM image showing fine structure within the hillocks. I_T: 2 nA. U_T: −300 mV. (*c*) AFM image, where again the fine structure is well resolved.



Can. J. Chem. Downloaded from www.nrcresearchpress.com by 91.121.58.235 on 09/08/12
For personal use only.

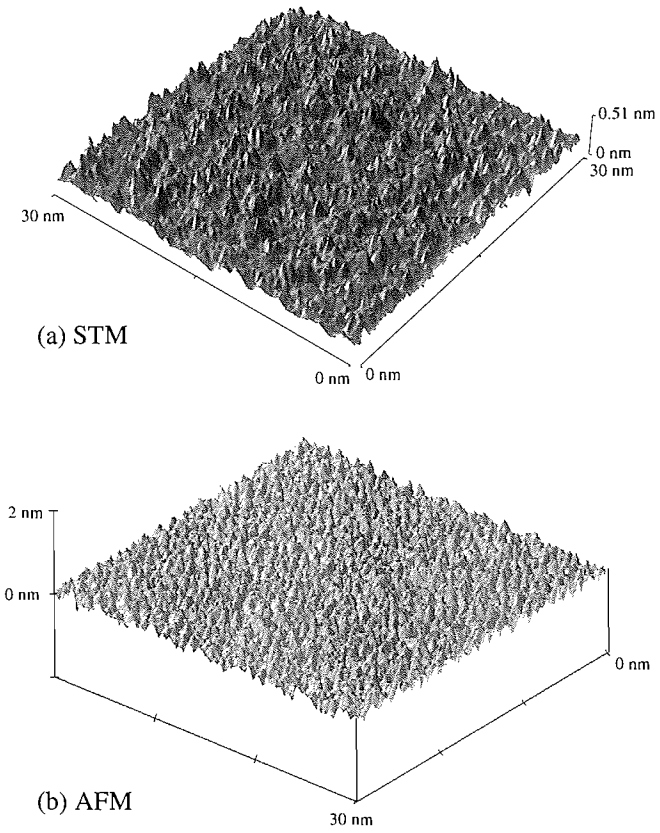
For a better comparison, in Fig. 6 the topographical three-dimensional plots of a high-resolution STM image (*a*) and an AFM image (*b*) are set against each other (because of the two different image-analysis softwares used, the two *z* scales could not be drawn to match each other exactly). Although the small clusters are of similar width (1–2 nm), the corrugation is larger in the AFM image (about 0.3 nm). It thus appears that the STM image of the oxide-covered surface is obscured by electronic effects, which are responsible for differences between the two images, particularly for smearing out the topographical fine structure.

5. Conclusions

We were able to show that the height of the first oxidation peak (OA1/2) in the well-known cyclic voltammogram for Au(111) in sulfuric acid solution depends strongly on the defect density of the surface. Curves obtained with an extremely well-oriented, freshly prepared crystal showed a sharp, and unusually high, second current peak (OA4) for the main oxidation process, whereas the smaller first peak at more negative potentials was almost nonexistent. After roughening of this electrode by an ORC, the height of the first peak

© 1997 NRC Canada

Fig. 6. (*a*) Three-dimensional plot (30 nm × 30 nm) of the STM data shown in Fig. 5(*b*). The small spiky features within the hillocks are clearly visible. (*b*) Three-dimensional plot (30 nm × 30 nm) of the AFM data shown in Fig. 5(*c*).



increased whereas the second peak decreased. Experiments with stepped single-crystal electrodes confirmed that this effect is due to an increased defect density on the surface. STM images obtained in the potential range of the first peak support the assumption that at least a large part of the charge passing under the first peak is caused by turnover processes at step edges. The second, very pronounced, current peak is assigned to turnover processes at terraces in accordance with existing theories.

The topography of the completely oxidized surface was imaged by STM and AFM, with superior lateral resolution. We have shown that the broad hillocks reported in previous STM studies consist of small clusters, which can be even better imaged by AFM. The results of both scanning probe techniques show that the Au(111) surface at 1.3 V is covered by these small disordered entities, which are about 0.1–0.3 nm in height and 1–2 nm in width. From a comparison of STM and AFM images we are led to conclude that the former are obscured by electronic effects. A more systematic comparison of images from STM and AFM might lead to interesting insights into the imaging mechanism of STM for oxide surfaces.

Can. J. Chem. Downloaded from www.nrcresearchpress.com by 91.121.58.235 on 09/08/12
For personal use only.

Acknowledgements

This work was supported by the Volkswagen Foundation through grant no. I/68 222-223. We thank Dipl.-Phys. Harald Hagenström and Dipl.-Chem. Ludwig Kibler for performing the cyclic voltammograms with the gold single crystals.

References

1. H. Angerstein-Kozlowska, B.E. Conway, A. Hamelin, and L. Stoicoviciu. Electrochim. Acta, **31**, 1051 (1986); J. Electroanal. Chem. **228**, 429 (1987).
2. H. Angerstein-Kozlowska, B.E. Conway, K. Tellefsen, and B. Barnett. Electrochim. Acta, **34**, 1045 (1989).
3. B.E. Conway. Prog. Surf. Sci. **49**, 331 (1995).
4. N.F. Mott. Trans. Faraday Soc. **35**, 1175 (1939); **36**, 472 (1940); **43**, 429 (1949).
5. N. Cabrera and N.F. Mott. Rep. Prog. Phys. **12**, 163 (1949).
6. S. Bruckenstein and M. Shay. J. Electroanal. Chem. **188**, 131 (1985).
7. R. Schumacher, G. Borges, and K.K. Kanazawa. Surf. Sci. **163**, L621 (1985).
8. D.J. Trevor, C.E.D. Chidsey, and D.N. Loiacano. Phys. Rev. Lett. **62**, 929 (1989).
9. H. Honbo, S. Sugawara, and K. Itaya. Anal. Chem. **62**, 2424 (1990).
10. D.M. Kolb. *In* Spectroelectrochemistry: theory and practice. *Edited by* R.J. Gale. Plenum, New York. 1988. p. 152.
11. R.J. Nichols, O.M. Magnussen, J. Hotlos, T. Twomey, R.J. Behm, and D.M. Kolb. J. Electroanal. Chem. **290**, 21 (1990).
12. C.M. Vitus and A.J. Davenport. J. Electrochem. Soc. **141**, 1291 (1994).
13. X. Gao and M.J. Weaver. J. Electroanal. Chem. **367**, 259 (1994).
14. K.J. Hanson and M.P. Green. Mater. Res. Soc. Symp. Proc. **237**, 323 (1992).
15. D.M. Kolb, A.S. Dakkouri, and N. Batina. *In* Nanoscale probes of the solid–liquid interface. NATO-ASI, Vol. E288. *Edited by* A.A. Gewirth and H. Siegenthaler. Kluwer, Dordrecht. 1995. p. 263.
16. M.A. Schneeweiss and D.M. Kolb. Solid State Ionics, **94**, 171 (1997).
17. S. Manne, J. Massie, V.B. Elings, P.K. Hansma, and A.A. Gewirth. J. Vac. Sci. Technol. B, **9**, 950 (1991).
18. P.G. Jones, H. Rumpel, E. Schwarzmann, G.M. Sheldrick, and H. Paulus. Acta. Crystallogr. Sect. B: Struct. Crystallogr. Cryst. Chem. **35**, 1435 (1979).
19. E. Schwarzmann, J. Mohn, and H. Rumpel. Z. Naturforsch. B: Anorg. Chem. Org. Chem. **31**, 135 (1976).
20. J. Wiechers, T. Twomey, D.M. Kolb, and R.J. Behm. J. Electroanal. Chem. **248**, 451 (1988).
21. L.A. Nagakara, T. Mundat, and S.M. Lindsay. Rev. Sci. Instrum. **60**, 3128 (1989).
22. T. Will. Ph.D. thesis, University of Ulm, Germany. 1994.
23. M.H. Hölzle, V. Zwing, and D.M. Kolb. Electrochim. Acta, **40**, 1237 (1995).
24. M.H. Hölzle. Ph.D. thesis, University of Ulm, Germany. 1995.
25. O.M. Magnussen, J. Hageböck, J. Hotlos, and R.J. Behm. Faraday Discuss. **94**, 329 (1992).
26. A. Hamelin. J. Electroanal. Chem. **407**, 1 (1996).

© 1997 NRC Canada

A practical approach to modeling the electrical double layer in the presence of specific adsorption of ions

Bruno Pettinger and Karl Doblhofer

Abstract: Model calculations are presented that yield in a straightforward manner the quantitative dependence of the specific adsorption of ions at electrode surfaces on the applied electrode potential (electrode charge). Furthermore, the double-layer capacitance and the potential at the outer Helmholtz plane (ϕ_2) are obtained. The derivation is based on Devanathan's three-capacitor model for the interfacial electric-potential distribution. A convenient correction function for the ϕ_1 potential accounting for the discreteness-of-charge effect is derived, largely on the basis of recent work by Conway et al. The results are shown to be in very good agreement with published work by Lawrence and Parsons on the double layer between Br^- electrolyte and the mercury electrode.

Key words: electrochemistry, specific adsorption, electric double layer, discreteness-of-charge effect.

Résumé : On présente des calculs modèles qui conduisent d'une manière directe à la relation qui existe entre l'adsorption spécifique d'ions sur des surfaces d'électrode et le potentiel d'électrode (charge de l'électrode) appliqué. De plus, on peut déduire la capacitance de la double couche et le potentiel au niveau du plan extérieur de Helmholtz (ϕ_2). Cette dérivation est basée sur le modèle de trois capacitances de Devanathan pour la distribution interfaciale du potentiel électrique. On a aussi dérivé une correction pour le ϕ_1 potentiel appropriée pour l'effet de discrétion de la charge; elle est basée principalement sur des travaux récents de Conway et al. On montre que les résultats sont en bon accord avec ceux publiés par Lawrence et Parsons sur la double couche entre l'électrolyte Br^- et l'électrode de mercure.

Mots clés : électrochimie, adsorption spécifique, double couche électrique, effet de discrétion de la charge.

1. Introduction

In modelling the electric double layer at the electrode–electrolyte interface, the discreteness of ionic charges (DC) constitutes a complicating feature. The DC effect has an important consequence: the potential that operates on ions in the electric double layer is different from its classical expression. The latter is derived for a double layer model where charges are distributed homogeneously in the inner Helmholtz plane (IHP) at x_1 for specifically adsorbed ions or in the diffuse layer for nonspecifically adsorbed ions. However, it is the potential difference, $\phi^{DC}(x_1) - \phi(s)$, between the IHP and the bulk solutions (and not the classical expression, $\phi(x_1) - \phi(s)$), that controls the adsorption process.

In a recent series of publications Marshall and Conway (1) proposed a new way of dealing with the problem of discreteness of ionic charge at the interface. Based on Conway's approach (1), along with classical double layer concepts (2–12), we have developed a straightforward way of simulating the parameters characterizing the electric double layer in the absence and presence of specific adsorption. In this paper we present our simulation procedure.

One might suppose that simulating the electric double layer is a subject that had been dealt with exhaustively about 30 years ago. Indeed, the basic concepts were developed at that time (13–26, see also refs. cited in ref. 27), and a number of experimental findings were related to theory via model calculations. See, for example, Grahame's comparison of experimental and theoretical work (21) or subsequent papers of Parry and Parsons (28), of D'Alkaine et al. (29), or of de Levie (30). However, to our knowledge there does not exist a convenient approach that would yield, for instance, the complete relationships between double layer capacitance and potential/charge, or the potential at the OHP as a function of the different double layer parameters in the presence of specific adsorption.

In presenting the model, the classical Gouy–Chapman–Stern theory and Devanathans's three-capacitor model of the interface are first briefly reviewed (13, 14). Second, a correction for the ϕ_1 potential, which accounts for the discreteness-of-charge effect, is introduced. Finally, model calculations are conducted. The results are compared with experimental data on the specific adsorption of Br^- ions on Hg electrodes (31).

Received March 10, 1997.

This paper is dedicated to Professor Brian E. Conway on the occasion of his 70th birthday.

B. Pettinger and K. Doblhofer.[1] Fritz-Haber-Institut der Max-Planck-Gesellschaft, Faradayweg 4-6, D-14195 Berlin (Dahlem), Germany.

[1] Author to whom correspondence may be addressed. Telephone: +049-30-8413-3100. Fax: +049-30-8413-3101. E-mail: doblhofer@fhi-berlin.mpg.de

2. The model

2.1 Ion adsorption at the interface

(*a*) *Nonspecific adsorption*

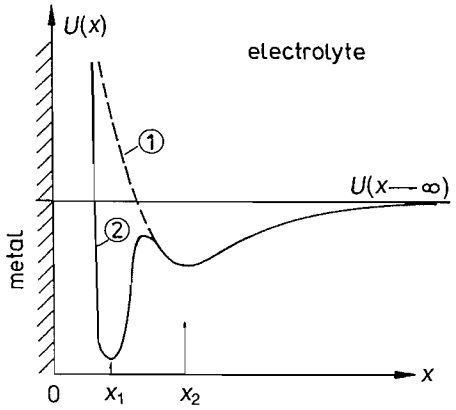
This is caused exclusively by electrostatic attraction between the ions and the excess charge of the metal electrode, q_M.

© 1997 NRC Canada

Can. J. Chem. Downloaded from www.nrcresearchpress.com by 91.121.58.235 on 09/08/12
For personal use only.

Can. J. Chem. Downloaded from www.nrcresearchpress.com by 91.121.58.235 on 09/08/12
For personal use only.

Fig. 1. Illustration of the dependence of the free energy of ionic species (U) on the distance from the electrode surface (x). The situation (1) represents nonspecific adsorption, with x_2 (the equilibrium distance of the ions from the surface) defining the "outer Helmholtz plane," OHP. (2) Specific adsorption: x_1 defines the location of the "inner Helmholtz plane," IHP.



The ions are considered completely solvated, forming the diffuse ("Gouy") layer. The centers of the charge carriers can approach the electrode only to a minimum distance x_2, defining the position of the "outer Helmholtz plane" (OHP). The electric charge of the nonspecifically adsorbed ions will be designated as q_G.

(b) Specific adsorption

The surface excess may be enhanced by specific ("chemical") bonds formed between the adsorbed ions and the electrode surface. If such specific interactions are effective, the surface excess and the corresponding ionic excess charge q_1 are larger than in the case of nonspecific adsorption at the same value of q_M. Thus, q_M will be overcompensated, and additional adsorption of ions of the same sign as q_M is required to provide interfacial electroneutrality. It is assumed that only one ionic species is specifically adsorbed, i.e., the charge overcompensation is neutralized by q_G. The condition of interfacial electroneutrality may thus be formulated:

$$[1] \quad q_M = -(q_1 + q_G)$$

In Fig. 1, the case of specific adsorption at the interface is illustrated schematically by a potential distribution exhibiting a pronounced minimum at x_1, which denotes the distance between the electrode surface and the center of specifically adsorbed ions (which lose, at least partly, their solvation shell).

2.2 The adsorption isotherm

For convenience and clarity, but also because of the practical relevance, the emphasis in the presentation will be on the specific adsorption of anions. The situation may be characterized by the reversible reaction

$$[2] \quad X^- \rightleftharpoons X_1^-$$

where X^- is an anionic species in solution, and the subscript 1 indicates the specifically adsorbed state. At some point below, explicit reference will be made to the corresponding cations. Where this is not done, the extension to specific adsorption of cations is considered to be straightforward. Note that the potential of the electrolyte, ϕ_S, is taken as the reference value for the potential scale, i.e., $\phi_S \equiv 0$. The partial molar free energy of transferring an ion from the bulk electrolyte to the IHP is ΔG^0_{ad} at $\phi_1 = 0$.

Any partial electron transfer (32–36) between the electrode and the adsorbate is taken into account only via an appropriate choice of x_1; the ions are assumed to be present in a fully charged state at the IHP. This assumption appears justified in most cases, see, for example, Chap. 9.5 of ref. 36, and ref. 37, or the recent work of Philpott and co-workers on the adsorption of Br^- on Ag electrodes (38, 39). In some cases (e.g., the specific adsorption of OH^-) it is generally accepted that the ionic species itself is weakly specifically adsorbed ($\Delta G^0_{ad}(OH^-) \approx 0$) while the product of surface oxidation, (OH_{ad}), binds strongly to some metal substrates: $OH^- \rightleftharpoons OH_{ad} + e^-$, see for instance Gerischer (40).

Since the adsorbed ions "i" are considered fully charged, their surface density at the IHP, Γ_i^1, can be represented by the charge density at the IHP, q_1, where $q_1 = z_i F \Gamma_i^1$; z_i defines the sign and number of the ionic unit charges. Thus, a Langmuir isotherm can be used in the following form:

$$[3] \quad \frac{q_1}{q_1^0 - q_1} = \frac{c}{c^0} \exp\left(-\frac{\Delta G^0_{ad} + zF\phi_1}{RT}\right)$$

where q_1^0 is the surface charge corresponding to full coverage; c is the bulk concentration of the adsorbing ions in the electrolyte, c^0 is the reference concentration, $c^0 = 1$ mol cm^{-3}. Note that at relatively low coverages $q_1 \ll q_1^0$, and disregarding activity coefficients, the above isotherm corresponds straightforwardly to the condition of equal electrochemical potentials of the ions "i" in the bulk electrolyte and at the IHP.

The Langmuir isotherm alone, which implies that ΔG^0_{ad} is independent of Γ_i^1, is a poor approximation for describing the adsorption equilibrium (41, 42). It is necessary to make an appropriate correction see the discussion of the "discreteness-of-charge" effect below.

2.3 The three-capacitor model of the interface

In Fig. 2 the distribution of the excess charge density, q, and of the electric potential, ϕ, across the interface between a polarized metal electrode (M) and an electrolyte solution (S) are shown schematically. Again, specific adsorption of anions is assumed.

From Gauss' law one can derive (6, 13) eqs. [4] and [5], relating the potential drop between the metal and the IHP, $\Delta\phi_{01}$, and the potential drop between the IHP and the OHP, $\Delta\phi_{12}$, with the excess charge density on the metal electrode, q_M, and in the Gouy layer, q_G, respectively.

$$[4] \quad \phi_M - \phi_1 = \Delta\phi_{01} = \frac{x_1}{\varepsilon_{01}\varepsilon^0} q_M = \frac{q_M}{C_1}$$

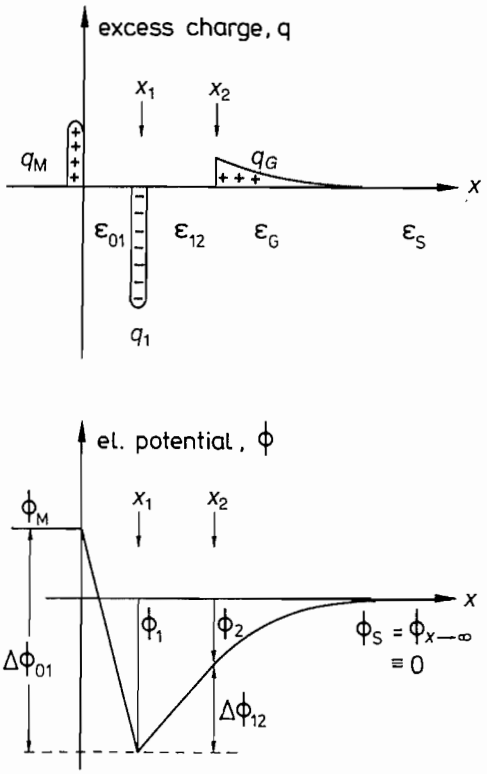
$$[5] \quad \phi_1 - \phi_2 = \Delta\phi_{12} = -\frac{(x_2 - x_1)}{\varepsilon_{12}\varepsilon^0} q_G = -\frac{q_G}{C_{12}}$$

The capacitances C_1 and C_{12} are defined by eqs. [4] and [5]. According to the classical concepts of diffuse-double-layer

© 1997 NRC Canada

Can. J. Chem. Downloaded from www.nrcresearchpress.com by 91.121.58.235 on 09/08/12
For personal use only.

Fig. 2. Summary of the parameters used in the discussion of the interface between the polarized metal electrode (subscript M) and an electrolyte (subscript S). x_1 and x_2 mark the positions of the inner and outer Helmholtz planes, q_G is the charge of the diffuse part of the double layer ("Gouy layer"), and ε are the dielectric constants.



theory, the potential at the OHP, ϕ_2, and the diffuse-layer capacitance, C_G, are defined for a z–z type electrolyte by (12):

$$[6] \quad \phi_2 - \phi_S = \phi_2 = \frac{2RT}{zF} \sinh^{-1}\left(-\frac{q_G}{(8\varepsilon_G\varepsilon^0 RTc)^{1/2}}\right)$$

$$[7] \quad C_G = -\frac{dq_G}{d\phi_2} = zF\sqrt{\frac{2\varepsilon_G\varepsilon^0 c}{RT}} \cosh\left(\frac{zF\phi_2}{2RT}\right)$$

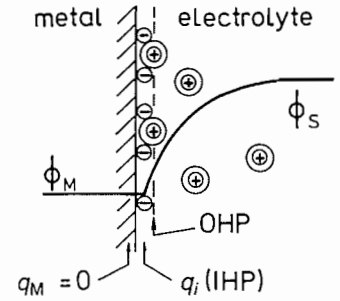
where c is the bulk concentration of this electrolyte, ε_G the relative dielectric constant of the electrolyte in the region of the diffuse layer (it is usually assumed to equal the bulk value), and ε^0 is the permittivity of free space. It is important to realize that the above equations are derived under the assumption of homogeneous charge distribution, i.e., "smeared out" charges.

From Fig. 2 it follows that the total interfacial potential drop is the sum of the three potential differences defined above:

$$[8] \quad E_z = \phi_M = \Delta\phi_{01} + \Delta\phi_{12} + \phi_2$$

where E_z is the rational potential, i.e., the electrode potential relative to the potential of zero charge observed in absence of specific adsorption. For convenience, the E_z potential scale will be used throughout the following discussions.

Fig. 3. Illustration of the potential distribution across the electrochemical interface at $q_M = 0$, in the presence of specifically adsorbed anions, disregarding the DC effect. According to this picture, the specifically adsorbed ions are at the same potential as the metal, $\phi_1 = \phi_M$.



2.4 The discreteness-of-charge (DC) effect

(*a*) *The necessity for considering the DC effect*

To emphasize the need for considering the discreteness-of-charge effect, we make use of the special interfacial situation prevailing at the potential of the electrocapillary maximum (E^{ecm}) in the presence of specific adsorption of ions. In Fig. 3, the interfacial potential distribution based on the three-capacitor model (disregarding the DC effect) is represented for anion adsorption. Since $q_M = 0$ at E^{ecm}, the potential drop between the electrode surface and the IHP should be zero (eq. [4]). Furthermore, the charge of the anions adsorbed at the IHP is compensated exactly by the charge q_G of counterions in the "Gouy" layer, i.e., for $q_M^{ecm} = 0$ the condition $q_1^{ecm} = -q_G^{ecm}$ is valid. Thus, at E_z^{ecm} the shift of E^{ecm} observed experimentally in going from absence to presence of specific adsorption equals ϕ_1, the electrical potential at the IHP:

DC effect disregarded:

$$[9] \quad \phi_1^{ecm} = E_z^{ecm}$$

Since values of E_z^{ecm} and q_1^{ecm} are well known for mercury electrodes (12), the standard free energy of adsorption (ΔG_{ad}^0) can be derived for such systems from the Langmuir isotherm considered, eq. [3]:

DC effect disregarded:

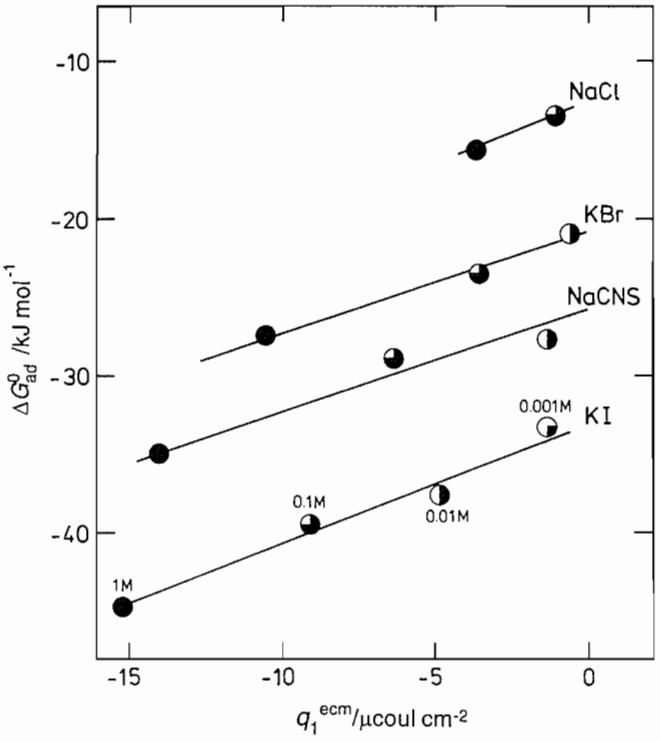
$$[10] \quad \Delta G_{ad}^0 = -zFE_z^{ecm} - RT \ln\left(\frac{q_1^{ecm}}{c(q_1^{max} - q_1^{ecm})}\right)$$

In Fig. 4, ΔG_{ad}^0 values are represented that were obtained with eq. [10] from the experimental data summarized by Grahame on p. 451 of ref. 12. Clearly, a variation of ΔG_{ad}^0 is found, suggesting increasing bond strength at increasing coverage with all the anions considered. This is an unsatisfactory result (41), demonstrating the limitations of the simple model. Similar conclusions, which point to the necessity for considering the DC effect, are reached on the basis of Esin and Markov's analysis of the experimental E_z^{ecm} values (43) see, for example, Parson's review (5) or Grahame's work on the DC effect (22), and the references given therein.

© 1997 NRC Canada

Can. J. Chem. Downloaded from www.nrcresearchpress.com by 91.121.58.235 on 09/08/12
For personal use only.

Fig. 4. Summary of ΔG^0_{ad} values obtained from the data of Grahame (12) with eq. [10], i.e., disregarding the discreteness-of-charge effect.



(*b*) *Deriving a correction for the DC effect*

An excess of electronic countercharge will accumulate in the metal surface near adsorbed ions because of the discreteness of the adsorbed-ion charge. The overall (average) condition $q_M = 0$ at E^{ecm} is fulfilled because of the effect of ions in the OHP on the charge distribution in the metal. Thus, the picture in Fig. 3 has to be modified (5) in a manner illustrated by Fig. (5). It follows that even when $q_M = 0$ there exists a significant potential drop between the metal and the specifically adsorbed ions that reduces the electrostatic repulsion experienced by the adsorbing ion approaching the interface from the electrolyte.

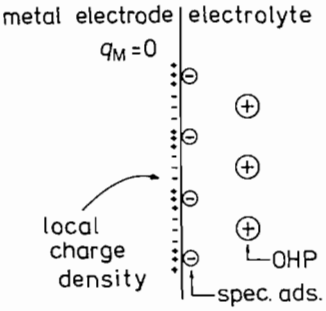
To approach this problem, we derive a DC-corrected value of the potential at the IHP in the Langmuir isotherm. This is done by adding a correction term, $\Delta\phi_{corr}$, to ϕ_1 in the isotherm equation. The following derivation of the DC correction is closely related to the one proposed recently by Marshall and Conway (1).

First, eq. [4] is reformulated to separate the effects of q_1 and q_G on $\Delta\phi_{01}$ (using eq. [1]: $q_M = -(q_1 + q_G)$):

$$[11] \quad \Delta\phi_{01} = -\frac{x_1}{\varepsilon_{01}\varepsilon^0}\, q_1 - \frac{x_1}{\varepsilon_{01}\varepsilon^0}\, q_G$$

The DC effect is assumed to operate only on the first term. The metal surface and the OHP are considered to form a parallel-plate capacitor (5), which can be approximated by a homogeneous charge distribution. For convenience we name the first term $\Delta\phi^{nG}_{01}$. It corresponds to the potential drop between metal and the IHP under the condition that the specifically adsorbed charge is completely compensated by

Fig. 5. The interfacial situation of Fig. 3, considering the discreteness-of-charge effect. A specifically adsorbed anion experiences a less negative potential ϕ_1 than would be predicted by the classical picture, Fig. 3.



q_M ("no Gouy", $q_G = 0$):

$$[12] \quad \Delta\phi^{nG}_{01} = -\frac{x_1}{\varepsilon_{01}\varepsilon^0}\, q_1 = -\frac{q_1}{C_1}$$

As shown in the Appendix, $\Delta\phi^{nG}_{01}$ can be straightforwardly corrected for the DC effect of specifically adsorbed ions. A correction factor f_{corr} is derived (eq. [24], Appendix) that leads to $\Delta\phi_{corr}$, the potential difference between the $\Delta\phi^{nG}_{01}$ value obtained for the homogeneous charge distribution (according to eqs. [4] or [12]) and the DC-corrected value of $\Delta\phi^{nG}_{01}$:

$$[13] \quad \Delta\phi_{corr} = f_{corr} \times \Delta\phi^{nG}_{01}$$

where the $\Delta\phi^{nG}_{01}$ is not DC corrected. The value of f_{corr} varies between zero and one:

$$\lim_{q_1 \to 0} f_{corr} = 1, \qquad \lim_{q_1 \to \infty} f_{corr} = 0$$

It was found convenient to use analytical functions $f_{fit\text{-}corr}$ for describing the $f_{corr}(q_1)$ relation.

$$[14] \quad f_{corr} \approx f_{fit\text{-}corr} = \{[a q_1^{1/3}]^n + [c^m + (b q_1^{1/13})^m]^{n/m}\}^{-1/n}$$

where the parameters a, b, and c, used to draw the curves $f_{fit\text{-}corr}$, vary slightly with ε_1, as follows. For $\varepsilon_1 = 10$: $a = 0.318$; $b = 1.26$; $c = 1.01$. For $\varepsilon_1 = 7$: $a = 0.322$; $b = 1.32$; $c = 1.01$. For $\varepsilon_1 = 5$: $a = 0.318$; $b = 1.37$; $c = 1.01$. The fit function $f_{fit\text{-}corr}$ is easily applicable. Since it is sufficiently precise, it has been used to obtain the data discussed in the following.

3. Modelling the electrical double layer

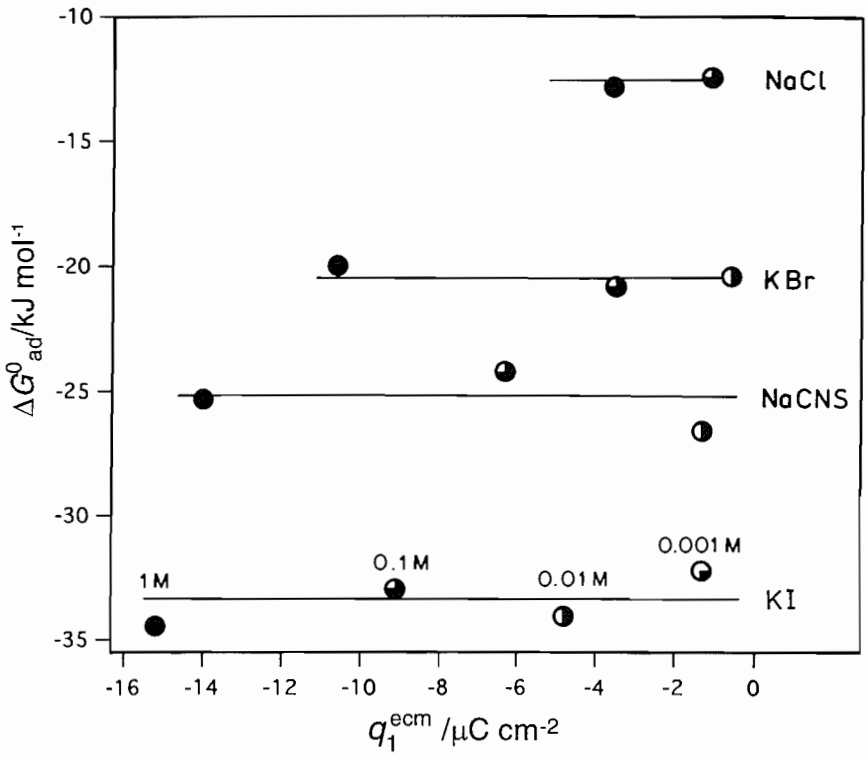
3.1 General considerations

In the calculations, the values of ϕ_1 and $\Delta\phi^{nG}_{01}$ are first determined classically, i.e., disregarding the DC effect. Then, the $\Delta\phi_{corr}$ term, describing the potential shift due to the DC correction, is added to the ϕ_1 term in the isotherm equation [15]. This $\Delta\phi_{corr}$ term is additionally weighted by a factor f_{DC}, where $0 < f_{DC} < 1$. Thus, the isotherm takes the form:

$$[15] \quad \frac{q_1}{q_1^0 - q_1} = c \exp\left(-\frac{\Delta G^0_{ad} + zF(\phi_1 + f_{DC}\Delta\phi_{corr})}{RT}\right)$$

© 1997 NRC Canada

Fig. 6. Summary of ΔG^0_{ad} values derived from Grahame's data (12), as for Fig. 4, but under consideration of the discreteness-of-charge effect (eq. [15]). Values of $q_1^0 = 120\ \mu C\ cm^{-2}$, $\varepsilon_1 = 5$, $x_1 = 0.1$ nm, $x_2 = 0.2$ nm, $f_{dce} = 0.5$, and the DC-correction fit function from eq. [14] are used.



Using $f_{DC} = 0$ means that a DC correction is not applied. In this case one obtains results corresponding to the straightforward three-capacitor model, similar to those derived by Devanathan (13). Significant qualitative discrepancies are observed between such results and the experimental findings (see below).

Using the full DC correction ($f_{DC} = 1$) will usually overcompensate the DC effect. This is understandable, considering the simplifications made in the derivations (in particular, disregarding the DC effect of the counterions in the OHP, see Fig. 5). We find that values of $f_{DC} \approx 0.5$ lead to results that agree with experiment.

It should be noted that the correction for the DC effect is derived for one value of the dielectric constant: $\varepsilon_1 = \varepsilon_{01} = \varepsilon_{12}$. However, the correction is valid also when $\varepsilon_{01} \neq \varepsilon_{12}$, as long as $(\varepsilon_{01} + \varepsilon_{12})/2 = \varepsilon_1$. The agreement with experimental values tends to be better when a value of $\varepsilon_{01} < \varepsilon_{12}$ is used for the model calculations (see below).

3.2 Procedure for the model calculations

To minimize the chances of an error in the numerical calculations, each author developed independently a suitable computer program, (*a*) by programming directly in the Macintosh Graphing and Data Analysis System "IGOR Pro" (Wave Metrics), and (*b*) in FORTRAN.

In the numerical procedure, first, an array of q_M values is defined by the range (typically −20.0 to +100.0 μC cm^{-2}), and the intervals (0.25 or 0.5 μC cm^{-2}). Each q_M value is subjected to the following numerical routine:

(*a*) $\Delta\phi_{01}$ is determined via eq. [4].

(*b*) With a chosen value of ϕ_2 the values of q_G, $\Delta\phi_{12}$, and ϕ_1 are obtained.

(*c*) With the value of q_1 from the previous calculation $\Delta\phi_{corr}$ is determined.

With eq. [15] a new value of q_1 is found. The sum $q_1 + q_G$ is compared with $-q_M$; ϕ_2 is varied until the electroneutrality condition is fulfilled. The routine is repeated once, starting at (*b*) with the new values of ϕ_2 and q_1.

(*d*) The electrode potential E_z is evaluated (eq. [8]).

(*e*) The differential capacitance, C_{dl}, is found by dividing the differences between the actual and previous values of q_M and E_z.

3.3 Comparing simulation with experiment

(*a*) *The DC-corrected values of* ΔG^0_{ad}

In Fig. 6, the same experimental data as in Fig. 4 are analyzed on the basis of eq. [15], i.e., the correction for the DC effect, with $f_{DC} = 0.5$, is applied. As in all the following analyses, a value of $q_1^0 = 120\mu C\ cm^{-2}$ is used; see, for example, refs. 44 and 45. Clearly, as they should, the values of ΔG^0_{ad} obtained in this way are largely independent of the surface coverage (q_1^{ecm}). The value obtained for bromide adsorption, $\Delta G^0_{ad} = -20.4$ kJ mol^{-1}, will be used in the following model calculations.

(*b*) *Modelling adsorption isotherms and related quantities*

With the concepts discussed above, adsorption isotherms, $q_1(E_z, q_M)$, along with the corresponding values of ϕ_2 and C_{dl} are derived. The parameters $q_1^0 = 120\ \mu C\ cm^{-2}$, $x_1 = 0.1$ nm,

© 1997 NRC Canada

Can. J. Chem. Downloaded from www.nrcresearchpress.com by 91.121.58.235 on 09/08/12
For personal use only.

Can. J. Chem. Downloaded from www.nrcresearchpress.com by 91.121.58.235 on 09/08/12
For personal use only.

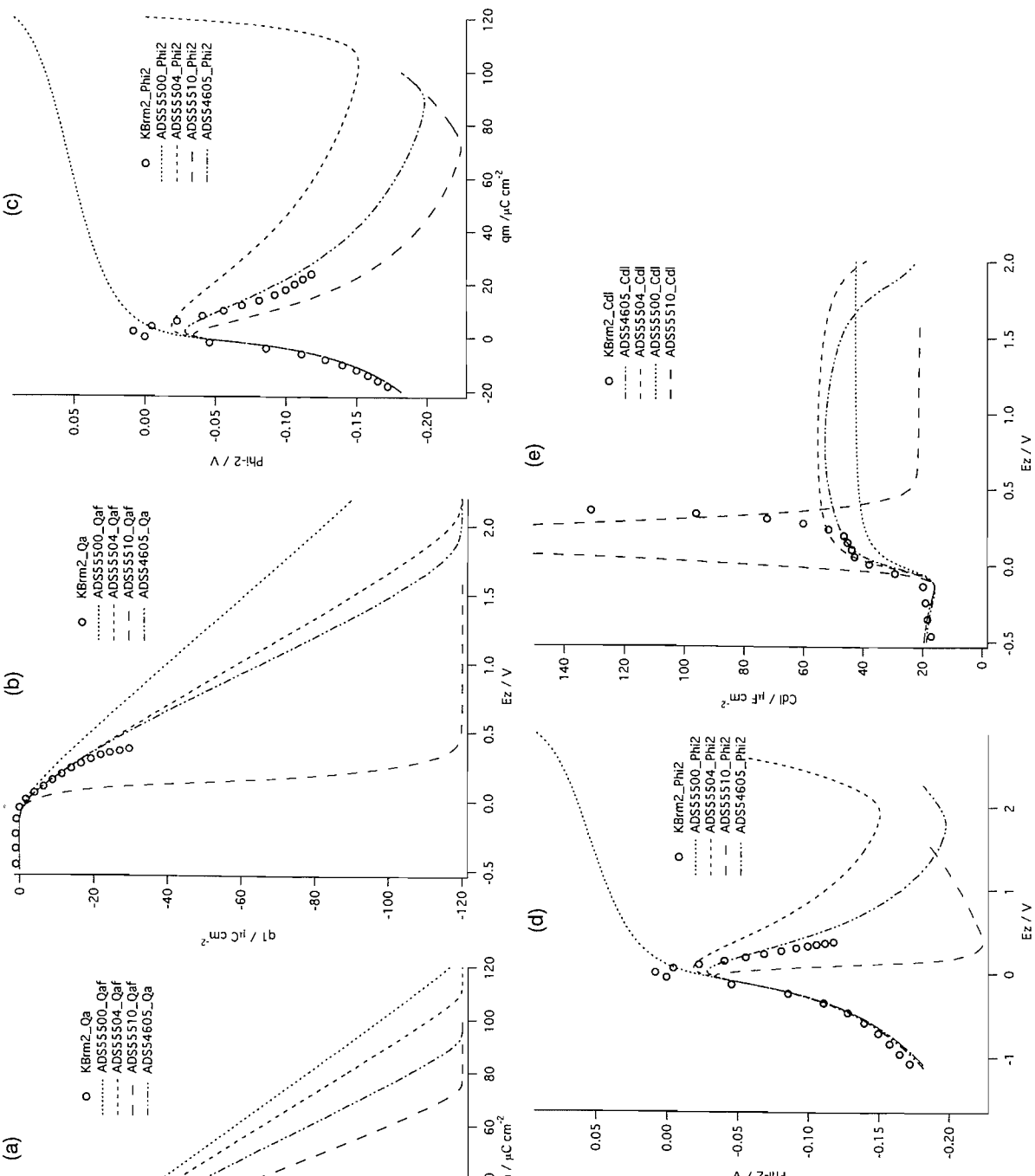


Fig. 7. (*a*)–(*e*) Results of model calculations corresponding to the electrical double layer between 0.01 M KBr and mercury electrodes. "ql" (= q_1) is the amount of anions adsorbed at the IHP, "qm" (= q_M) is the surface charge on the metal electrode; "Ez" (= E_z) is the electrode potential relative to the ecm in absence of specific adsorption; "Phi-2" (= ϕ_2) is the electric potential at the OHP. The experimental results of Lawrence and Parsons for 0.01 M Br^- (31) are included as circles ("KBrm2"). For the calculations the following parameters were used: $q_1^0 = 120$ μC cm^{-2}, $x_1 = 0.1$ nm, $x_2 = 0.2$ nm, and the DC-correction fit function for $\varepsilon_1 = 5$. The values of ε_{01}, ε_{12}, and of f_{DC} are given as the numbers following "ADS5" in the inset, e.g., ADS54605 means $\varepsilon_{01} = 4$, $\varepsilon_{12} = 6$, and $f_{DC} = 0.5$.

© 1997 NRC Canada

$x_2 = 0.2$ nm, the DC-correction fit function from the Appendix for $\varepsilon_1 = 5$, and an appropriate value of f_{dce} are used. The electrolyte concentration is chosen to be $c = 1 \times 10^{-5}$ mol cm^{-3}, so that the results may be compared with the experimental results of Lawrence and Parsons for 0.01 M Br^- (31), which are included in all the following diagrams, Figs. 7 (*a*)–(*e*), as circles.

4. Conclusions

From the comparison between the experimental double-layer parameters and those obtained by the simulation method outlined above, one may derive the following conclusions:

1. The state of the electrochemical interface Br^-/Hg is generally very well described by the model, in particular with $\varepsilon_{01} = 4$, $\varepsilon_{12} = 6$, see Figs. 7 (*a*)–(*e*).
2. The results obtained disregarding the discreteness-of-charge effect deviate significantly from the experimental findings, indicating the importance of the DC correction. Note in particular the significant qualitative deviations in the ϕ_2 results, Figs. 7 (*c*) and (*d*).
3. Preliminary studies on other systems have shown that the model presented above is appropriate for modelling a number of adsorption processes, e.g., I^- on Hg and Au electrodes.

References

1. S.L. Marshall and B.E. Conway. J. Electroanal. Chem. **337**, 1 (1992); **337**, 19 (1992); **337**, 45 (1992); **337**, 67 (1992).
2. H.L. von Helmholtz. Wied. Ann. **7**, 337 (1879).
3. G. Guy. Ann. Phys. **7**, 129 (1917).
4. O. Stern. Z. Elektrochem. **30**, 508 (1924).
5. R. Parsons. *In* Advances in electrochemistry and electrochemical engineering. Vol. 1. *Edited by* P. Delahay. Interscience Publishers, New York. 1961. pp. 1–64.
6. D.M. Mohilner. *In* Electroanalytical chemistry. *Edited by* A.J. Bard. M. Dekker, New York. 1966. pp. 241–409.
7. P. Delahay. Double layer and electrode kinetics. Interscience Publishers, New York. 1965.
8. J.O'M. Bockris. *In* Comprehensive treatise of electrochemistry. Vol. 1: The double layer. *Edited by* B.E. Conway and E. Yeager. Plenum Press, New York. 1980.
9. D.M. Kolb and D.A. Scherson. Proc. IX Int. Vacuum Congress and V Int. Conf. Solid Surfaces, Madrid 1983. pp. 158–178.
10. A. Hamelin. *In* Modern aspects of electrochemistry. Vol. 16. *Edited by* B.E. Conway, R.E. White, and J.O'M. Bockris. Plenum Press, New York. 1985. pp. 1–101.
11. M.A. Vorotyntsev. *In* Modern aspects of electrochemistry. Vol. 17. *Edited by* J.O'M. Bockris, B.E. Conway, and R.E. White. Plenum Press, New York. 1986. pp. 131–222.
12. D.C. Grahame. Chem. Rev. **41**, 441 (1947).
13. (*a*) M.A.V. Devanathan. Trans. Faraday Soc. **50**, 373 (1954); (*b*) M.A.V. Devanathan and B.V.K.S.R.A. Tilak. Chem. Rev. **65**, 635 (1965).
14. R. Payne. J. Electroanal. Chem. **41**, 277 (1973).
15. S. Lamperski. J. Electroanal. Chem. **379**, 445 (1994).
16. P.A. Rikvold, J. Zhang, Y.E. Sung, and A. Wieckowski. Electrochim. Acta, **41**, 2175 (1996).
17. Z. Samec and K. Doblhofer. J. Electroanal. Chem. **367**, 141 (1994).
18. A. Hamelin. Port. Electrochim. Acta, 77 (1987).
19. A. Frumkin. Z. Elektrochem. **59**, 807 (1955).
20. O.A. Esin and V.M. Shikov. Russian J. Phys. Chem. **17**, 236 (1943); B.V. Ershler. Russ. J. Phys. Chem. **20**, 679 (1946).
21. D.C. Grahame. J. Am. Chem. Soc. **80**, 4201 (1958).
22. D.C. Grahame. Z. Elektrochem. **62**, 264 (1958).
23. S. Levine, J. Mingins, and G.M. Bell. J. Electroanal. Chem. **13**, 280 (1967).
24. M.A. Habib and J.O'M. Bockris. *In* Modern aspects of electrochemistry. Vol. 16. *Edited by* B.E. Conway, R.E. White, and J.O'M. Bockris. Plenum Press, New York. 1985. pp. 189–203.
25. C.A. Barlow and J.R. Macdonald. J. Chem. Phys. **40**, 1535 (1964); **43**, 2575 (1965); J.R. Macdonald and C.A. Barlow. J. Electrochem. Soc. **113**, 978 (1966).
26. S. Levine, G.M. Bell, and D. Calvert. Can. J. Chem. **40**, 518 (1962).
27. B.E. Conway. Electrochim. Acta, **40**, 1501 (1995).
28. J.M. Parry and R. Parsons. Trans. Faraday Soc. **59**, 241 (1963).
29. C.V. D'Alkaine, E.R. Gonzalez, and R. Parsons. J. Electroanal. Chem. **32**, 57 (1971).
30. R. de Levie. J. Electrochem. Soc. **118**, C185 (1971).
31. J. Lawrence and R. Parsons. J. Electroanal. Chem. **16**, 193 (1968).
32. R. Parsons. Chem. Rev. **90**, 813 (1990).
33. W. Lorenz and G. Salié. Z. Phys. Chem. **218**, 259 (1961); Z. Physik. Chem. N.F. **29**, 390 (1961); **29**, 408 (1961).
34. J.W. Schultze and F.D. Koppitz. Electrochim. Acta, **21**, 327 (1976).
35. W.J. Plieth and K.J. Vetter. Z. Phys. Chem. N.F. **61**, 282 (1968).
36. M.A. Habib and J.O'M. Bockris. *In* Modern aspects of electrochemistry. Vol. 16. *Edited by* B.E. Conway, R.E. White, and J.O'M. Bockris. Plenum Press, New York. 1985. pp. 180–186.
37. R. Parsons. *In* Advances in electrochemistry and electrochemical engineering. Vol. 7. *Edited by* P. Delahay. Interscience Publishers, New York. 1970. pp. 177–219.
38. G. Pacchioni, P.S. Bagus, and M.R. Philpott. Z. Phys. D: At. Mol. Clusters, **12**, 543 (1989).
39. G. Pacchioni, P.S. Bagus, and M.R. Philpott. J. Chem. Phys. **90**, 4293 (1989).
40. H. Gerischer. *In* Electrocatalysis on non-metallic surfaces. NBS Spec. Publ. (US), 455, U.S. Department of Commerce. 1976. pp. 1–19.
41. R. Parsons. Trans. Faraday Soc. **51**, 1518 (1955); **55**, 999 (1959).
42. J.E.B. Randles. J. Electroanal. Chem. **41**, 272 (1973).
43. O.A. Esin and B.F. Markov. Acta Physicochim. URSS, **10**, 353 (1939).
44. D.M. Kolb, D.L. Rath, R. Wille, and W.N. Hansen. Ber. Bunsen-Ges. Phys. Chem. **87**, 1108 (1983).
45. W. Paik, M.A. Genshaw, and J.O'M. Bockris. J. Phys. Chem. **74**, 4266 (1970).

A. Appendix: The discreteness of charge effect

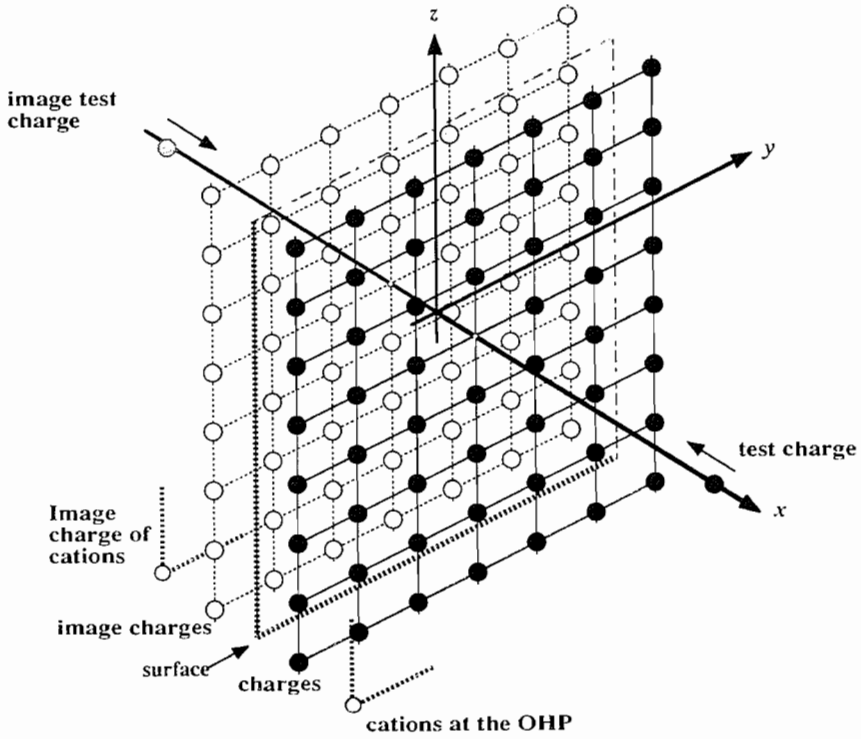
A.1 The concept

Very often, only homogeneous charge (HC) distributions are assumed when modeling the electric double layer (2–8). This simplification leads to a straightforward one-dimensional solution of the Poisson–Boltzman equation (PBE), but neglects the discrete nature of charges. The correct model would be a solution of the PBE or, better, a corresponding quantum mechanical formalism in three dimensions based on the correct charge distribution in space and time. This is, however, beyond the capability of today's theory and computers.

© 1997 NRC Canada

Can. J. Chem. Downloaded from www.nrcresearchpress.com by 91.121.58.235 on 09/08/12
For personal use only.

Fig. A1. Diagram of the an ionic array and its image array at the metal surface. The central ion and its image are removed. Both arrays and the image test charge constitute the local potential for the test charge.



A reasonable approximation is to consider point-like charges (and point-like dipoles) and to organize them at the interface in form of a lattice(s) (1, 25, 26). Usually, the next step of simplification is to consider only the specifically adsorbed ions and their images as discrete charges, but to treat the charges in the diffuse double layer and the excess charges on the metal side within the framework of homogeneous charge distribution. A number of approaches of that type, associated with the name of discreteness of charge (DC), have been employed during the last decades (1, 25, 26). Classically calculating the potential distribution across the interface one finds two different situations: at large distances from the surface both the hc and dc models yield the same result, but for locations close to the surface they differ (these differences in the potential distribution are illustrated in Fig. A4.

What is known in the literature as the discreteness of charge effect is just this difference of the potentials for the 1-D solution and the 3-D solution of the PBE, usually taken at the location of the anion. It is important, because the adsorption of anions is controlled by this 3-D potential difference existing between the locations $x_S = x_\infty$ and x_1.[2] $\Delta\phi_{1S}^{DC} = \phi^{DC}(\infty, 0, 0) - \phi^{DC}(x_1, 0, 0) \neq \Delta\phi_{1S}$. In this context, see also eqs. [5] and [6].

The precise calculation of the 3D-potential is rather difficult, not from the theoretical aspect but due to the fact that the sums involved are slowly convergent. This point and possible conceptional and mathematical solutions to this specific topic have been addressed in several papers (1, 25, 26).

Since we are interested in arriving at easy practical expressions, we will not focus on the details of how to convert slowly convergent sums into fast convergent ones. Instead we will present approximate, but sufficiently precise, expressions to describe the dc effect. On this basis we model specific adsorption (main section of this paper), of course in the framework of a rather classical concept. Our objective is to show that such a concept is fairly sufficient to reproduce experimental data, such as the ϕ_2 potential.

Let us consider a metal surface (perfect conductor) in contact with a dielectricum (electrolyte) and adapt the Gouy–Chapman–Stern model for the double layer: (*i*) an inner Helmholtz plane (IHP) at x_1 where the specific adsorbed anions are located, (*ii*) the outer Helmholtz plane (OHP) at x_2, and (*iii*) the diffuse layer or Gouy layer. The dielectric functions are denoted as $\varepsilon_{01}, \varepsilon_{12}, \varepsilon_G (= \varepsilon_S)$, respectively. Cationic or anionic charges are accumulated in the diffuse layer, depending on the actual Gouy potential, ϕ_G. A regular array of anionic charges is positioned at the plane z_1, with the origin of the coordinate system located in the plane of the metal surface. At the metal surface the corresponding countercharges are accumulated for electric neutrality.

The discreteness of charge is taken into account only for the charges at the IHP and their image charges. The array of anionic charges may be of hexagonal or quadratic nature or of any other regular type; the structural differences affect "only" the way the summation over the lattice has to be performed and, thus, the quantity of the computed numbers but not the general results.

[2] Note that in this appendix we use x as the direction vertical to the electrode surface and y, z as Cartesian coordinates located in the surface plane (see Fig. A1).

© 1997 NRC Canada

Can. J. Chem. Downloaded from www.nrcresearchpress.com by 91.121.58.235 on 09/08/12
For personal use only.

Can. J. Chem. Downloaded from www.nrcresearchpress.com by 91.121.58.235 on 09/08/12
For personal use only.

The central ion is located at the point $(x_1, 0, 0)$; therefore, the coordinates of the charges (anions) are given as $(x_1, y_k = kd, z_m = md)$, with $m, k = -\infty \cdots + \infty$. Similarly, we assume an array of image charges at $(-x_1, y_k = kd, z_m = md)$. m, k are integer numbers and d is the spacing of the lattice (this holds for a quadratic array; the modification for a hexagonal array is straightforward; see Fig. A1). Since we are seeking the potential felt by the central ion, we have to remove the central ion and its image charge from both arrays. Therefore, the summation runs over $m, k = -\infty \cdots + \infty$, with $k \neq 0$! The potential, $\Delta\phi$, at the point (x, y, z) provided by all n ions located at (x_1, y_k, z_m) and their images is given as:

$$[16] \quad \Delta\phi(x,y,z) = \frac{2e}{\varepsilon\varepsilon^0} \sum_{\substack{m=0 \\ k=1}}^{+\infty} \frac{1}{2} \left\{ \frac{1}{\sqrt{(x-x_1)^2 + (y-y_k)^2 + (z-z_m)^2}} - \frac{1}{\sqrt{(x+x_1)^2 + (y-y_k)^2 + (z-z_m)^2}} \right\}$$

with $y = z = 0$ and, substituting $\xi = x/d, \xi_1 = x_1/d$, one can replace the double sum by a function $S_0(\xi, \xi_1)$:

$$[17] \quad \Delta\phi = \frac{2e}{\varepsilon\varepsilon^0} S_0(\xi, \xi_1)$$

Note that lattice sums of this type are essentially an electrochemical equivalent of Madelung constants known in the field of calculations of lattice energies of ionic crystals (1).

The infinite sums over an ionic lattice alone are necessarily divergent, but the summation over ion array and image–ion array is slowly convergent. Marshall and Conway have shown how to transform these difference series into a fast converging sum (1). We show here the result and include the modifications to account for the two structures ($r = 3$, $l = 1$ and $r = 4$, $l = 0$ hold for the hexagonal or quadratic lattice, respectively):

$$[18] \quad S_0(\xi, \xi_1) = 2 \ln \left\{ \frac{|\sinh[2\pi(\xi + \xi_1)/\sqrt{r}]|}{|\sinh[2\pi(\xi - \xi_1)/\sqrt{r}]|} \left| \frac{\xi - \xi_1}{\xi + \xi_1} \right| \right\} + 8 \sum_{k=1}^{\infty} \sum_{n=1}^{\infty} (-1)^{lkn} \left\{ K_0 \left[2n\pi a_- \left(\sqrt{\frac{r}{4}}\, k \right) \right] - K_0 \left[2n\pi a_+ \left(\sqrt{\frac{r}{4}}\, k \right) \right] \right\}$$
$$+ 2 \int_0^{\infty} J_1(u) \ln \left[\frac{1 - \exp(-uA_1)}{1 - \exp(uB_1)} \right] du$$

where $K_0[w]$ is the modified Bessel function of zero order, $J_1(u)$ is the Bessel function of first order, and $A_1 = (x - x_1)/d$ and $B_1 = (x + x_1)/d$.

Next, for a four-layer interface (metal–IHP–OHP – diffuse layer), we have to consider that imaging of charges is occurring at all phase boundaries (1). Due to the mutual imaging of ionic and image charges there are further infinite series of images. If one locates the anions on the phase boundary IHP–OHP one can treat the IHP and OHP layers as a single layer with an average dielectric function of $\varepsilon_1 = \frac{1}{2}(\varepsilon_{01} + \varepsilon_{12})$. One has then to consider only two series of image charges for the phase boundaries (01) and (12) (see Fig. A2). To illustrate this, the potential vs. x for a single charge at $(x_1, 0, 0)$ including the infinite series of imaging is given:

$$[19] \quad \phi_{\mathrm{I}} = \frac{q}{\varepsilon_1 r} + \frac{q_{\mathrm{M}}}{\varepsilon_1 r_{\mathrm{M}}} + \left(\frac{q_1}{\varepsilon_1 r_1} + \frac{q_{1,\mathrm{M}}}{\varepsilon_1 r_{1,\mathrm{M}}} \right) + \ldots = \frac{q}{\varepsilon_1} \left(\frac{1}{x - a} - \frac{1}{x + a} + \ldots \right)$$

$$[20] \quad \phi_{\mathrm{II}} = \frac{q_2}{\varepsilon_2 r} + \frac{q_{2,\mathrm{M}}}{\varepsilon_2 r_{2,\mathrm{M}}} = \frac{2q}{\varepsilon_1 + \varepsilon_2} \left(\frac{1}{r} - \frac{1}{(r + 2a)} \pm \ldots \right)$$

The adaption of the above equation for an array of charges is obtained by substituting:

$$[21] \quad \left[\frac{1}{X(x) - a} - \frac{1}{X(x) + a} \right] \rightarrow dS_0 \left(\frac{X(x)}{d}, \xi_1 \right)$$

where $\xi_1 = z_1/d = z_1 * \sqrt{q_1/(100e)}$ and $a = z_1$. For further details on single and multiple imaging see ref. 1.

A.2 The DC correction

For a comparison of the two concepts, the homogeneous and the discrete charge distributions in the IHP, we have to calculate for both cases the potential distribution across the interface, $\phi^{\mathrm{DC}}(x)$ and $\phi(x)$. There are three contributions to this potential that are provided by the charges on the metal, the anions at IHP, and the ions in the diffused layer. Since we restrict the DC effect to the anion layer alone, only its contribution differs for the two cases, whereas all other contributions to the potential at any x remain unaffected and are additive (for a given/fixed interfacial charge distribution). Thus, we have

$$[22] \quad \phi(x) = \begin{cases} \phi_{\mathrm{a}}^{\mathrm{HC}}(x) + \phi_{\mathrm{M}}(x) + \phi_{\mathrm{G}}(x) & \text{hc model} \\ \phi_{\mathrm{a}}^{\mathrm{DC}}(x) + \phi_{\mathrm{M}}(x) + \phi_{\mathrm{G}}(x) & \text{dc model} \end{cases}$$

Note that

$$[23] \quad E_z = \phi^{\mathrm{DC}}(0) - \phi^{\mathrm{DC}}(\infty) = \phi(0) - \phi(\infty)$$

© 1997 NRC Canada

Can. J. Chem. Downloaded from www.nrcresearchpress.com by 91.121.58.235 on 09/08/12
For personal use only.

Fig. A2. Multiple imaging of the anion array. Note that for the actual calculation $a = \frac{1}{2}b$.

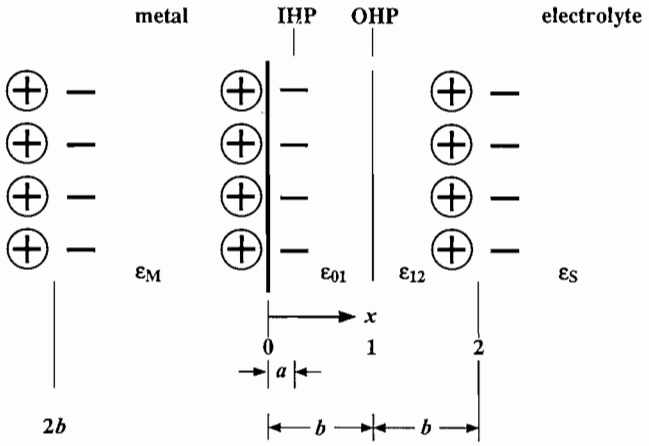


Fig. A3. Correction factor f_{corr} vs. charge density q_1 for three ε_1 values (ε_1 = 10, 7, and 5). Broken lines indicate the corresponding $f_{fit\text{-}corr}$ curves. ε_S = 78; z_1 = 1 Å, x_2 = 2 Å. For fit-equation and parameters see text.

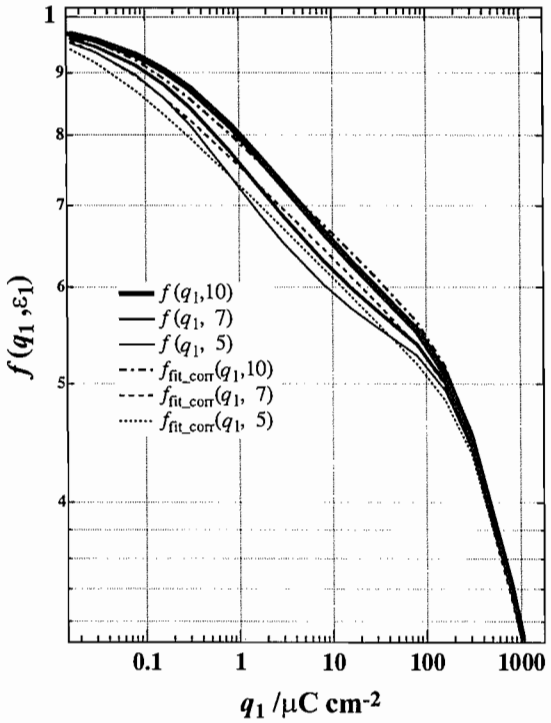
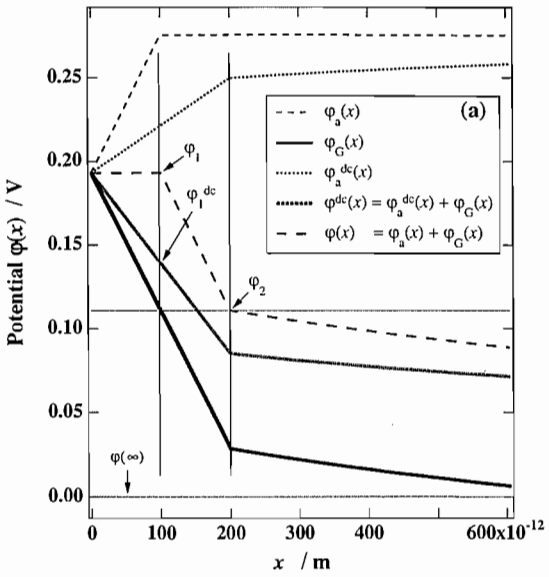
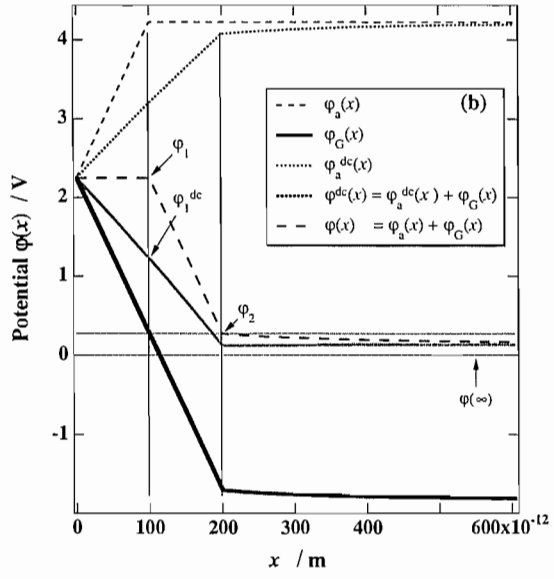


Fig. A4. Comparison of HC and DC potential distribution across the metal–electrolyte interface for the pzc case. Panel (*a*): charge density: 5 μC. Panel (*b*): charge density: 120 μC. The vertical lines indicate the x_1 and x_2 locations.





Since $\phi_a^{DC}(x, \xi_1, \varepsilon)$ depends via ξ_1 on q_1, it is convenient to plot the ratio of $f_{corr} = (\phi_a^{DC}/\phi_a) - 1$ vs. the anion charge density q_1. By multiplying this correction factor by ϕ_a we obtain the shift of the potential at x_1 from the classical to the DC value. Thus,

$$\Delta\phi_a^{(DC-(HC))}(x_1) = \phi_a^{DC}(x_1) - \phi_a^{HC}(x_1) = \left(\frac{\phi_a^{DC}(x_1)}{\phi_a^{HC}(x_1)} - 1\right)\phi_a^{HC}(x_1) = f_{corr}\phi_a^{HC}(x_1)$$

[24]

$$\phi_a^{DC}(x_1) = \phi_a^{HC}(x_1) + \Delta\phi_a^{(DC-(HC))}(x_1)$$

The dependence of f_{corr} on q_1 is shown in Fig. A3 in a semilogarithmic plot covering five decades of q_1. At low charge densities, f_{corr} is close to one. With increasing charge density the factor decreases. There are two regions of relatively linear behavior. Curves of this type can be easily approximated by fit-curves, which are given in Fig. A3 as broken curves. The analytical formula for the fit-curve is given in the main part of the paper (eq. [14]).

© 1997 NRC Canada

A.3 Potential distribution across the metal–electrolyte interface

For a given charge distribution, the comparison of HC and DC reveals a significant difference of the local potential across the interface. In contrast, the (external) potential, E_x remains unaffected. Figure A4 illustrates this behaviour for the case of potential of zero charge (pzc) and two distinct charge densities. Note the rather linear variation of the potential within $0 < x < x_2$. Since for the case of pzc the countercharges are located within the diffuse double layer, the total interfacial potential has to include the potential drop in the diffuse layer. Its relative contribution is, under pzc condition, larger the lower the ion concentration at IHP.

In addition, note that the HC case shows a zero potential gradient between the IHP and the metal surface, much in contrast to the DC case where a noticeable gradient is possible. This underlines the necessity of including the DC for an adequate determination of the adsorption isotherm and other related quantities of the electric double layer.

Can. J. Chem. Downloaded from www.nrcresearchpress.com by 91.121.58.235 on 09/08/12
For personal use only.

© 1997 NRC Canada

In situ X-ray absorption fine structure and optical reflectance studies of electrodeposited nickel hydrous oxide films in alkaline electrolytes

Yining Hu, In Tae Bae, Yibo Mo, Mark R. Antonio, and Daniel A. Scherson

Can. J. Chem. Downloaded from www.nrcresearchpress.com by 91.121.58.235 on 09/08/12
For personal use only.

Abstract: X-ray absorption fine structure (XAFS) and optical reflectance spectroscopy (RS) have been used to examine in situ electronic and structural aspects of nickel hydrous oxide, α-$Ni(OH)_2$(hyd), electrodes supported on gold in alkaline electrolytes as a function of their state of charge. The extended X-ray absorption fine structure (EXAFS) of α-$Ni(OH)_2$(hyd) electrodes in the uncharged (UC, or discharged) and overcharged (OC, or *fully* charged) states yielded, in each case, a single set of two distinct nearest-neighbor shells, with distances, $d(Ni—O)_1 = 2.05 \pm 0.02$ Å and $d(Ni—Ni)_1 = 3.11 \pm 0.02$ Å for UC, and $d(Ni—O)_1 = 1.87 \pm 0.02$ Å and $d(Ni—Ni)_1 = 2.83 \pm 0.02$ Å for OC. The in situ EXAFS of films allowed to self-discharge following overcharge could be fit with contributions from both sets of shells, suggesting that only two types of nickel sites are sufficient to account for the redox chemistry of this material. These data, in addition to information derived both from quantitative X-ray absorption near-edge structure (XANES) and optical RS in the visible range, indicate that the excess anodic charge, i.e., beyond the one-electron oxidation of Ni^{2+} sites, observed during the first oxidation of freshly prepared α-$Ni(OH)_2$(hyd) electrodes may not be related to oxidation state changes involving nickel sites in the lattice, and, therefore, do not support the existence of nickel sites with a formal oxidation state higher than three for charged or overcharged electrodes in this media.

Key words: nickel oxide, reflectance spectroscopy, EXAFS, in situ measurements.

Résumé : On a fait appel à la spectroscopie d'absorption des rayons X («XAFS») et à la spectroscopie optique par réflexion (diffuse) («RS») pour étudier in situ, en fonction de leur état de charge, les aspects électroniques et structuraux d'électrodes formées d'oxyde de nickel hydraté, α-$Ni(OH)_2$(hyd), supporté sur de l'or, en présence d'électrolytes alcalins. La technique de la spectroscopie d'absorption des rayons X loin du seuil («EXAFS») d'électrodes de α-$Ni(OH)_2$(hyd) dans les états sans charge («UC») ou déchargé) et surchargé («OC») ou *complètement* chargé) ont permis, dans chaque cas, d'obtenir un seul ensemble de deux couches distinctes voisines les plus près, avec des distances de : $d(Ni—O)_1 = 2{,}05 \pm 0{,}02$ Å et $d(Ni—Ni)_1 = 3{,}11 \pm 0{,}02$ Å pour UC et $d(Ni—O)_1 = 1{,}87 \pm 0{,}02$ Å et $d(Ni—Ni)_1 = 2{,}83 \pm 0{,}02$ Å pour OC. Les spectres d'absorption des rayons X loin du seuil («EXAFS») in situ de films que l'on a laissé s'autodécharger après les avoir surchargés peuvent être ajustés aux contributions des deux ensembles de couches; ceci suggère que deux types de sites de nickel sont suffisants pour expliquer la chimie redox de ce produit. Ces données, prises en relation avec les informations obtenues à partir de la technique quantitative de spectroscopie de seuil d'absorption des rayons X («XANES») et de la spectroscopie optique par réflexion (diffuse) («RS»), indiquent que la charge anodique en excès, c'est-à-dire au-delà des sites de Ni^{2+} d'oxydation à un électron observés au cours de la première oxydation d'électrodes de α-$Ni(OH)_2$(hyd) fraîchement préparées, ne peut pas être reliée à des changements dans l'état d'oxydation impliquant des sites de nickel du réseau et que, en conséquence, elle n'apporte pas de support à l'existence, dans ce milieu, de sites de nickel dans un état d'oxydation formel supérieur à trois pour les électrodes chargées ou surchargées.

Mots clés : oxyde de nickel, spectroscopie optique par réflexion (diffuse) («RS»), spectroscopie d'absorption des rayons X loin du seuil («EXAFS»), mesures in situ.

[Traduit par la rédaction]

Received March 24, 1997.

This paper is dedicated to Professor Brian E. Conway on the occasion of his 70th birthday.

Y. Hu, I.T. Bae, Y. Mo, and D.A. Scherson.[1] Ernest B. Yeager Center for Electrochemical Sciences and the Department of Chemistry, Case Western Reserve University, Cleveland, OH 44106-7078, U.S.A.
M.R. Antonio. Argonne National Laboratory, Chemistry Division, Argonne, IL 60439, U.S.A.

[1] Author to whom correspondence may be addressed. Telephone: (216) 368-5186. Fax: (216) 368-3006. E-mail: dxs16@po.cwru.edu

Introduction

Considerable insight into the physicochemical properties of nickel hydrous oxide electrodes for rechargeable batteries and fuel cells (1) has been gained from UV–vis reflectance spectroscopy (RS) (2), substrate-enhanced Raman scattering (3), X-ray absorption fine structure (XAFS) (4), atomic force microscopy (5), and microgravimetric (6) measurements performed in situ. At least two, possibly related, issues still remain to be elucidated: the origin of the excess anodic charge observed during the first cycle of electrodeposited α-$Ni(OH)_2$(hyd) films (7), and the actual oxidation state of the nickel sites as a function of the state of charge of the electrode (8).

© 1997 NRC Canada

Can. J. Chem. Downloaded from www.nrcresearchpress.com by 91.121.58.235 on 09/08/12
For personal use only.

This paper presents in situ XAFS data for α-$Ni(OH)_2$ films electrodeposited onto a Au-coated polymeric film substrate (Melinex) acquired with a newly designed cell that enables detection of fluorescent X-rays through the back of the electrode. This arrangement, introduced originally by Kerkar et al. (9), and used extensively by Isaacs, Davenport, and coworkers in their studies of metal oxides (10), made it possible to record in situ Ni K-edge XAFS of nickel hydrous oxide films at potentials positive to that ascribed to their nominal full oxidation, without problems associated with oxygen evolution. Within the resolution of the EXAFS measurements, the results obtained were consistent with the presence of a single type of site for films in each of the fully reduced and the fully oxidized states. Evidence that the excess charge may be largely unrelated to changes in the oxidation state of the nickel sites in the lattice was obtained from quantitative in situ X-ray absorption near-edge structure (XANES) and complementary in situ optical reflectance spectra of electroprecipitated α-$Ni(OH)_2$(hyd) films on Au(111) recorded during the first and subsequent cycles.

Experimental

A. Film deposition

The electroprecipitation of α-$Ni(OH)_2$ films on Au(poly)/Melinex (XAFS) or Au(111)/quartz (RS) (11), was performed potentiostatically at −0.75 V vs. SCE from a 0.05 M $Ni(NO_3)_2$ aqueous solution, following the procedure described by Corrigan (12) in the same cells where the in situ spectroscopic measurements were carried out. The average current during deposition was in the range −1.0 to −1.4 mA/cm^2 for periods of 1–4 min for XAFS and 10–30 s for RS experiments. Subsequently, the SCE reference electrode (RE) was removed (and later replaced with a $Hg/HgO,OH^-$ RE), the nitrate solution discarded, and the cells then rinsed thoroughly with deionized water and filled with 1.0 M KOH. The amount of Ni per unit cross-sectional area of film can be estimated from the faradaic efficiency for the α-$Ni(OH)_2$(hyd) electrodeposition process (6*c*), determined in this and other laboratories (13), i.e., $2e^-$ per Ni site in the α-$Ni(OH)_2$(hyd) film. For the in situ XAFS measurements, the calculated value corresponds to ca. $(3.7–13.5) \times 10^{-7}$ mol/cm^2, that is, to less than 1/20 of one absorption length at the Ni K-edge (8333 eV). Under these conditions, all fluorescence spectra reported in this work are expected to be free of artifacts derived from self-absorption effects.

B. In situ spectroscopic measurements: cell design, data acquisition, and data analysis

In situ measurements were performed in 1.0 M KOH using either a $Hg/HgO,OH^-$ (XAFS) or a SCE (RS) reference electrode placed beside the working electrode, away from the path of the X-ray or optical beams.

a. X-ray absorption fine structure

The main body of the electrochemical cell designed for in situ Ni K-edge XAFS measurements in the fluorescence mode through the back of the electrode is a block of Kel-F machined in the form shown in Fig. 1. The working electrode is a piece of Au-coated Melinex (2.2 cm × 1.2 cm × 0.02 cm thick) (14), with the three edges immersed in the solution covered by Kapton tape (50 μm thick), exposing an area of ca. 1.0 cm^2 to the electrolyte. The edge masking was found to stabilize the gold film against delamination during the rather long times (>6 h) required for the acquisition of a series of spectra. The electrode was affixed onto a much larger piece of Kapton tape, which was, in turn, attached to the cell to form a cavity that was filled first with the electrodeposition solution and, after forming and rinsing the film, with 1 M KOH. The thickness of the Au layer on Melinex, ca. 0.05 μm, is much thinner than one absorption length of Au at the Ni K-edge (ca. 2.7 μm). External connection to the working electrode was made using a clamp attached to the protruding end of the bare Au-coated film. The counter electrode was a ca. 1.3 cm × 1.3 cm Pt foil facing the working electrode at a distance of 1.2 cm.

Spectra were acquired at the Stanford Synchrotron Radiation Laboratory (SSRL, line 4-1) and at the National Synchrotron Light Source (NSLS, line X-23A2) with beam currents in the range of 40 to 100 mA at 3 GeV (SSRL) and of 100 to 180 mA at 2.6 GeV (NSLS). The beam was monochromatized with a set of Si(111) crystals (SSRL) or a servo-feedback stabilized Si(311) (NSLS) crystal. The fluorescence radiation was collected with a Lytle-type (SSRL) or a PIN diode detector (NSLS) (see Fig. 1). The Ni K-edge energy, defined as the first maximum in the derivative curve, i.e., 8333 eV, was calibrated using a Ni foil. The X-ray energy was scanned in the range −150 to −50 eV, and −50 to 50 eV (X-ray absorption near-edge structure, XANES) with respect to the Ni K-edge energy, in increments of 2 and 0.4 eV, respectively. In the extended X-ray absorption fine structure (EXAFS) region, i.e., 8383–9300 eV, the step size was 0.05 $Å^{-1}$.

Based on the results of more than five independent measurements over a period of 2 years, no significant differences could be found between data obtained at the two synchrotron facilities. For many of the experiments, in situ XAFS was recorded for the film in the reduced state before cycling; or in the uncharged state, after polarization at 0.6 V vs. $Hg/HgO,OH^-$ for a few minutes; or in the nominally oxidized state, following subsequent reduction; or the fully discharged state, after polarization at 0.6 V for an extended period of time, i.e., 1 h or more; or in the overcharged state; and, finally, after disconnecting the potentiostat while the electrode was overcharged, or the self-discharged state. Except for the self-discharged state, the potential was scanned at 1 or 2 mV/s until the desired value was achieved.

The features in the pre-edge region were resolved by subtracting from the normalized spectra an arctan fit to the tail of the main edge, excluding data in the energy range in which the peaks occurred (15).

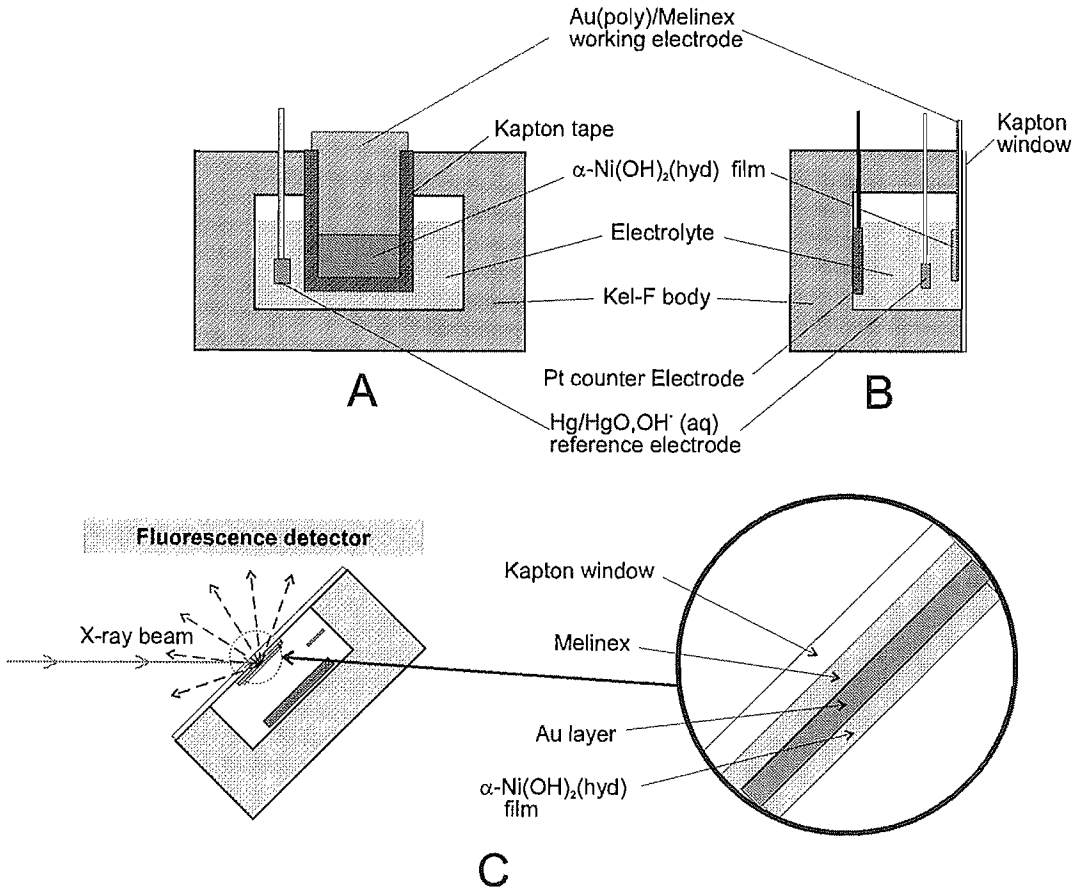
The analysis of the EXAFS data was performed using EXAFPAK, a set of routines developed by I. Pickering and G. George at SSRL (16). Theoretical phase and amplitude functions calculated from FEFF 5.05 (17) were used for fitting the reduced EXAFS functions. Fourier transforms (FT) of the k^3-multiplied reduced EXAFS function ($k^3\chi(k)$) were obtained over the range 3.0-13.5 $Å^{-1}$ (Δk = 10.5 $Å^{-1}$). The first two prominent shells in the resulting FTs were back-Fourier transformed collectively using a window of 0.6–3.6 Å (Δr = 3.0 Å).

b. Reflectance spectroscopy

The cell used for the optical experiments was the same as that described earlier for simultaneous electrochemical, spectroscopic, and microgravimetric measurements involving the

© 1997 NRC Canada

Fig. 1. Schematic diagram of the electrochemical cell for in situ fluorescence XAFS measurements through the back of the electrode (*A*, front view; *B*, side view; *C*, top view).



adsorption of bromide ions on Au(111) (11). As indicated therein, the highly oriented Au(111) layer was formed by sputtering, in sequence, a layer of Ni (5 nm) and then a layer of Au (520 nm) on the surface of an optically polished quartz crystal wafer for quartz crystal microgravimetric (QCM) measurements. The specimens were subsequently removed from the chamber and then flame-annealed with a hydrogen torch.

The spectrum of the nickel hydrous film in the nominally fully oxidized state was acquired with a Harrick rapid scan spectrophotometer and found to be in agreement with that published much earlier by Lamy and co-workers (2). The reflectivity was monitored at constant wavelength, λ = 540 nm, while cycling the electrode linearly between 0.0 and 0.45 V vs. SCE. Each run always started with a freshly deposited α-$Ni(OH)_2$(hyd) film, to enable comparisons with coulometric data reported by Corrigan and Knight (7) for similar films.

Results and discussion

The cyclic voltammogram of α-$Ni(OH)_2$/Au(poly) on Melinex in 1 M KOH (not shown in this work), displayed characteristic features associated with the oxidation and reduction of the nickel hydrous film (see, for example, panel (*a*), Fig. 9) with essentially no overlap between the trailing edge of the oxidation peak and the onset of oxygen evolution.

Figure 2 shows in situ XANES obtained for a single α-$Ni(OH)_2$(hyd) film in the uncharged (UC, solid line), nominally charged (OX, broken line), overcharged (OC, dotted line), after full discharge (FD, not shown), and self-discharged (SD, dot–dash line) states following overcharge. Also shown in this figure is the pre-edge region in expanded form for clarity.

Plots of $k^3\chi(k)$ vs. k, for the film in the UC and OC states, and their corresponding non-phase corrected Fourier transforms are given in Figs. 3 (UC, curve *a*; OC, curve *b*) and 4 (UC, dotted line; OC, solid line), respectively. As clearly seen there, the $k^3\chi(k)$ EXAFS (Fig. 3) and the corresponding FT data (Fig. 4) for the film in the OC state displayed much larger amplitudes than those in the UC (or FD) states. The results of the statistical analysis of the entire series of in situ XAFS spectra run are compiled in Tables 1 and 2. The best two-shell (Ni—O and Ni—Ni) fits to the Fourier-filtered $k^3\chi(k)$ EXAFS for the UC and OC films are shown in Fig. 5. The subsections to follow address separately the pre-edge and edge regions, as well as the results of the EXAFS analysis.

A. XANES

a. Pre-edge region

The XANES pre-edge features associated with transitions between the 1*s* and *p*-hybridized *d*-states after background subtraction (see Fig. 6), yielded for all states of charge

© 1997 NRC Canada

Can. J. Chem. Downloaded from www.nrcresearchpress.com by 91.121.58.235 on 09/08/12
For personal use only.

Can. J. Chem. Downloaded from www.nrcresearchpress.com by 91.121.58.235 on 09/08/12
For personal use only.

Fig. 2. in situ normalized Ni K-edge XANES for a single α-$Ni(OH)_2$(hyd) film recorded in the fluorescence mode through the back of the electrode in 1 M KOH at room temperature, recorded in the sequence: freshly prepared (UC, solid line), nominally charged (OX, broken line), overcharged (OC, dotted line), after full discharge (FD, not shown), and self-discharged states following overcharge (SD, dot–dash). The region below the main absorption edge has been expanded for clarity.

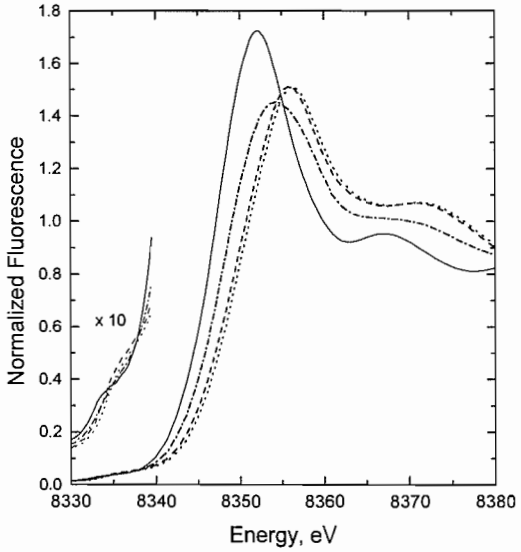
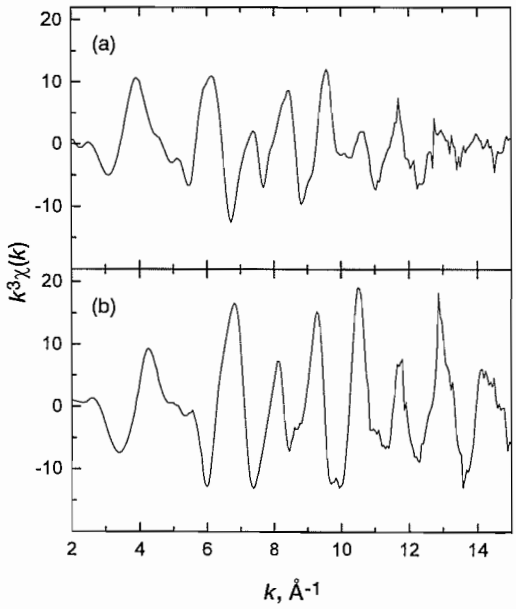
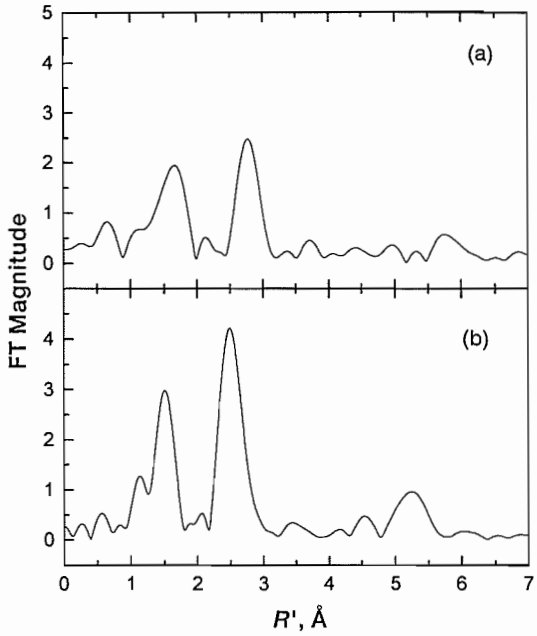


Fig. 3. In situ $k^3\chi(k)$ vs. k EXAFS data for the films in the (*a*) UC and (*b*) OC states of Fig. 2.



well-defined, asymmetric peaks with maxima at energies (E_{peak}) in the range 8333.9–8335.9 eV (see Table 1). The magnitude of the peak separation, ΔE_{peak} = 2.1 (SSRL) or 1.6 (NSLS) eV, for the films in the UC and OC states (see Table 1 and Fig. 6) is up to twice as high as values reported by other

Fig. 4. Non-phase-corrected Fourier transform of the reduced EXAFS data in Fig. 3 for the (*a*) UC and (*b*) OC states.



authors for nickel hydrous oxide electrodes in the charged and discharged states (see Table 3, and ref. 4); however, it is well within the range of ΔE_{peak} values found ex situ for other oxides of transition metals of the first row per unit change in state of charge, e.g., ΔE_{peak} = 1.6 and 2.7 eV for Mn (18) and Fe (19), respectively. Particularly noteworthy is the shift in E_{peak} toward smaller values, found for the film in the SD state, to values intermediate between OC (or OX) states and FD states. This effect is consistent with the spontaneous reduction of the film, due, most probably, to a reaction with water. In addition, the kinetics for full oxidation (or overcharge) and full reduction were found to be relatively slow, despite the fact that the films are thin. This is evidenced by the time (more than 1 h) required for the edge to achieve its lowest (full reduction) or highest values (full oxidation or overcharge) following a change in oxidation state, i.e., polarization at 0.6 V for OX and OC, and 0.0 (or −0.15) V for UC (or FD). This is illustrated in Fig. 7 for a film that was first oxidized (curve *b*: long dashed line), starting from the UC state (*a*: solid line), and then overcharged (*c*: solid thick line). The in situ XANES in dot–dash lines (curve *d*) was acquired immediately after the potential had reached −0.15 V and that in short broken lines (curve *e*) an hour later under the same conditions, showing a clear shift toward lower energies.

Furthermore, as shown in Fig. 8, no significant differences could be discerned between the unnormalized in situ XANES of a freshly prepared film after the first (curve *b*: dashed line) and second oxidation without overcharge (curve *d*: thick solid line), even though the charge under the oxidation peak (not shown in this work) decreased by 9% in the second compared to the first linear scan in the positive direction. This observation suggests that the excess charge may not be related to nickel sites in the film (see below). Curves *a* (solid line) and *c* (dot–dashed line) in this figure are the corresponding

© 1997 NRC Canada

Can. J. Chem. Downloaded from www.nrcresearchpress.com by 91.121.58.235 on 09/08/12
For personal use only.

Table 1. Pre-edge energy (E_{peak}, eV), main absorption edge energy (E_{edge}, eV), and energy shifts (ΔE) for electroprecipitated α-$Ni(OH)_2$(hyd) films in 1 M KOH in various states of charge, obtained from in situ fluorescence Ni K-edge XANES, and for $Ni(OH)_2$ crystalline recorded ex situ.

α-$Ni(OH)_2$ (hyd) film in situ (SSRL)	E_{peak} (eV) (peak maximum)[a]	ΔE_{peak}[b] (eV)	E_{peak} (eV) (inflection point)[c]	ΔE_{peak}[b] (eV)	E_{edge} (eV) (half-height)[d]	ΔE_{edge}[b] (eV)	E_{edge} (eV) (inflection point)[e]	ΔE_{edge}[b] (eV)
Uncharged (UC)	8333.8	0.0	8332.6	0.0	8344.4	0.0	8347.3	0.0
	(8333.7)[f]	(0.0)	(8332.9)	(0.0)	(8344.0)	(0.0)	(8347.4)	(0.0)
Nominally charged (OX)	8335.7	1.9	8333.8	1.2	8347.0	2.6	8349.8	2.5
Fully discharged (FD)	8333.8	0.0	8332.5	−0.1	8344.2	−0.2	8347.2	−0.1
Overcharged (OC)	8335.9	2.1	8334.4	1.8	8347.4	3.0	8350.2	2.9
	(8335.3)	(1.6)	(8334.3)	(1.4)	(8347.0)	(3.0)	(8350.5)	(3.1)
Self-discharged (SD)	8335.1	1.3	8333.5	0.9	8345.8	1.4	8348.0	0.7
$Ni(OH)_2$ (crystalline) ex situ	8333.5		8332.1		8344.1		8347.1	

[a] E_{peak} defined as the energy of the peak maximum.
[b] Energy shifts are given with respect to the values obtained for freshly prepared α-$Ni(OH)_2$ (hyd) film in situ, i.e., UC state.
[c] E_{peak} defined as the energy of the inflection point of the leading edge of the pre-edge peak.
[d] E_{edge} defined as the energy at half-height the normalized fluorescence.
[e] E_{edge} defined as the energy of inflection point of the main absorption edge.
[f] Values in parentheses were obtained from virtually identical measurements performed at NSLS.

Table 2. Structural parameters for α-$Ni(OH)_2$(hyd) films recorded in situ and for $Ni(OH)_2$ (crystalline) acquired ex situ extracted from the reduced EXAFS functions.

α-$Ni(OH)_2$(hyd)	Shell	N[a]	r, Å	σ^2, Å^2	ΔE_0,[b] eV	F
In situ						
(SSRL)						
Uncharged (UC)	(Ni—O)$_1$	5.6(4)[c]	2.05[d]	0.004(1)	−2.0(6)	20
	(Ni—Ni)$_1$	6.8(7)	3.11[d]	0.007(1)		
Charged (OX)	(Ni—O)$_1$	5.7(5)	1.87[d]	0.003(1)	−2.7(9)	52
	(Ni—Ni)$_1$	5.3(5)	2.83[d]	0.003(1)		
Discharged (DC)	(Ni—O)$_1$	6.2(6)	2.05(1)	0.005(1)	−2(1)	268
	(Ni—Ni)$_1$	6.6(9)	3.11(1)	0.007(1)		
Overcharged (OC)	(Ni—O)$_1$	6.0(7)	1.87(1)	0.003(1)	−3(1)	79
	(Ni—Ni)$_1$	5.3(6)	2.83[d]	0.003(1)		
Self-discharged (SD)	(Ni—O)$_1$	2.8(4)	1.85(1)	0.003(1)	−3(2)	36
	(Ni—O)$_2$	3.2	2.02(1)	0.003[e]		
	(Ni—Ni)$_1$	4(1)	2.84(1)	0.006(2)		
	(Ni—Ni)$_2$	2.4	3.09(1)	0.004(1)		
(NSLS)						
Uncharged (UC)	(Ni—O)$_1$	7.2(6)	2.04(1)	0.006(1)	−0.8(9)	33
	(Ni—NI)$_1$	6.3(8)	3.11(1)	0.006(1)		
Overcharged (OC)	(Ni—O)$_1$	5.3(5)	1.87[d]	0.002(1)	−4.1(9)	51
	(Ni—Ni)$_1$	5.0(5)	2.82[d]	0.002[f]		
Ex situ						
$Ni(OH)_2$ (crystalline)	(Ni—O)$_1$	6	2.05(1)	0.004(1)	−2(2)	35
	(Ni—Ni)$_1$	6	3.13(1)	0.006(1)		

[a] The scale factor, 0.777, was obtained by fitting the ex situ EXAFS function of $Ni(OH)_2$(cryst) fixing N for both Ni—O and Ni—Ni shells to 6.0.
[b] A single ΔE_0 value was used for all shells[15b].
[c] The numbers in parentheses are three times the standard deviation.
[d] $3\sigma < 0.005$.
[e] σ^2 for this shell was set the same as that for (Ni—O)$_1$.
[f] $3\sigma < 0.0005$.

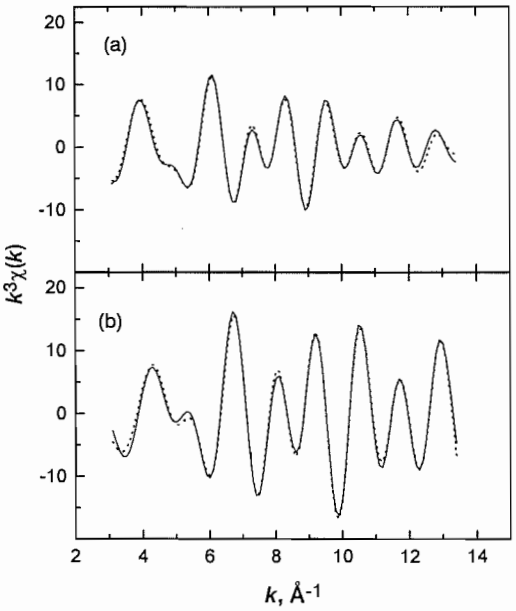
© 1997 NRC Canada

Table 3. Pre-edge peak (E_{peak}) and main absorption edge (E_{edge}) energies, energy shifts (ΔE, eV), bond distances (d), and coordination numbers (N) for nickel hydroxide films in the uncharged (or discharged) and charged states in alkaline electrolytes reported in the literature (4).

Nickel hydroxide electrode in situ	E_{peak} (eV)	E_{peak} (eV)	E_{edge} (eV) (half-height)	ΔE_{edge} (eV)	E_{edge} (eV) (inflection point)	ΔE_{edge} (eV)	d(Å)		N
Uncharged or discharged	8332	0.0	8343.0	0.0	8342.9–8346.0	0.0	Ni—O	2.04–2.08	3.8–7.1
							Ni—Ni	3.07–3.16	2.9–8.5
							Ni—O	1.94–2.12	0–2.2
Charged	8333	1.0	8345.3	2.3	8345.0–8346.9	0.9–2.5	Ni—O	1.86–1.89	1.7–9.2
							Ni—Ni	3.00–3.19	0–1.9
							Ni—Ni	2.79–2.88	4.2–7.9

Can. J. Chem. Downloaded from www.nrcresearchpress.com by 91.121.58.235 on 09/08/12
For personal use only.

Fig. 5. Fourier-filtered EXAFS for the films in the UC and OC states (solid lines in *a* and *b*, respectively) as obtained by back-transforming the FT data of Fig. 3 between 0.6 and 3.6 Å. The broken lines are the best two-shell (Ni—O and Ni—Ni) fits to the filtered data.

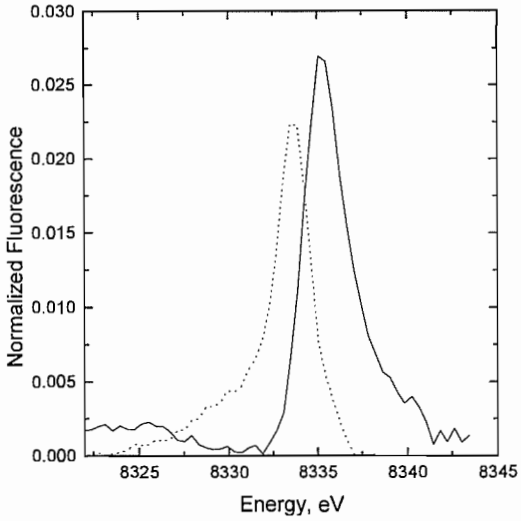


unnormalized in situ XANES recorded for the film after preparation and after reduction following the first oxidation, respectively.

b. Edge region

The edge shift between films in the UC and OC states, as measured by the difference (Δ) in the magnitude of the energy at half the normalized fluorescence (E_{edge}, see Table 1), was 3.0 eV. This value is larger than that observed for the film in the OX state and indeed larger than any other reported previously for nickel hydrous oxides in the oxidized state (see Table 3). The same trend is also found for the edge position defined by the inflection point of the absorption edge (see Table 1). The

Fig. 6. Background-subtracted pre-edge features for an α-$Ni(OH)_2$(hyd) film in the UC (dotted line) and OC (solid line) states recorded in situ.



results obtained for the film in the five states of charge strongly suggest that E_{edge} is a monotonic, albeit not necessarily linear, function of the extent of oxidation. As was the case with ΔE_{peak}, E_{edge} are displaced toward lower energy upon self-discharge to yield values intermediate between OC and FD, supporting the view that the films reduce by a spontaneous reaction with the solvent.

B. EXAFS

A statistical analysis of the Fourier-filtered $k^3\chi(k)$ EXAFS for the films in the UC and OC states (shown as solid lines in Figs. 5*a* and 5*b*, respectively) produced the best fits shown in broken lines in Fig. 5. The bond distances, d, coordination numbers, N, and other relevant parameters, have been collected in Table 2. As shown therein, the first $(Ni—O)_1$ and second $(Ni—Ni)_1$ nearest-neighbor shell distances yielded, for films in the UC state, the values $d(Ni—O)_1 = 2.05 \pm 0.02$ Å and

© 1997 NRC Canada

Can. J. Chem. Downloaded from www.nrcresearchpress.com by 91.121.58.235 on 09/08/12
For personal use only.

Fig. 7. In situ XANES for an α-Ni(OH)$_2$(hyd) film that was first oxidized (curve *b*, long dashed line), starting from the UC state (curve *a*, solid line), and then overcharged (curve *c*, thick solid line). The in situ XANES in dot–dashed lines (curve *d*) was acquired immediately after the potential had reached −0.15 V, whereas that in short dashed lines (curve *e*) was recorded an hour later under the same conditions.

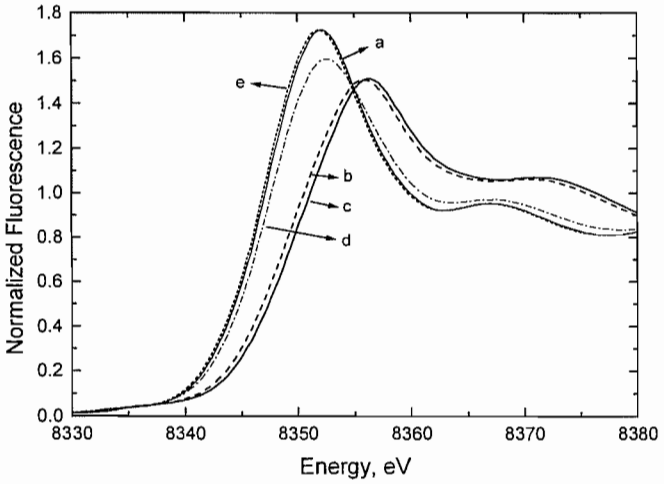
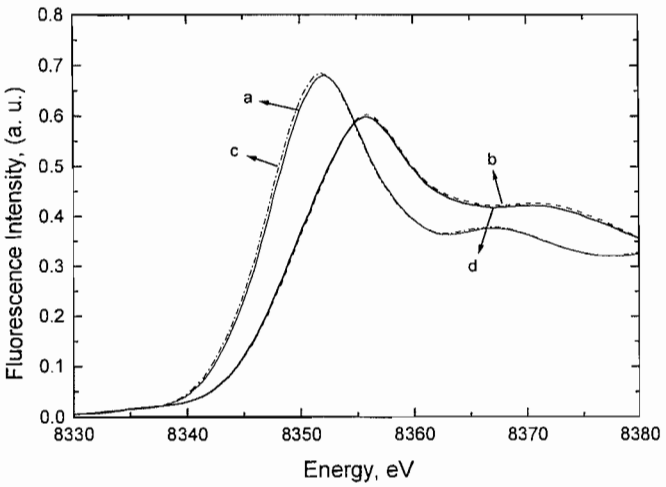


Fig. 8. Unnormalized in situ Ni K-edge XANES of a freshly prepared film (curve *a*: thin solid line), after the first oxidation (curve *b*: dashed line), following subsequent reduction (curve *c*: dash–dotted line), and after a second oxidation (curve *d*: thick solid line). The film was not overcharged.



d(Ni—Ni)$_1$ = 3.11 ± 0.02 Å, which are substantially longer than those in the OC state, i.e., d(Ni—O)$_1$ = 1.87 ± 0.02 Å and d(Ni—Ni)$_1$ = 2.83 ± 0.02 Å. These distances are in excellent agreement with those obtained earlier in this laboratory using different measurement conditions (4*f*), and are well within the range reported elsewhere for uncharged (or discharged) and charged nickel hydrous electrodes (Table 3). Also in accordance with other work (4) are the corresponding values of N that, due to uncertainties in the magnitudes of the scale factors, exhibit much higher variability. The contraction of both Ni—O and Ni—Ni interatomic distances from the UC to the OC state may be responsible for the development of wide cracks upon oxidation of nickel hydrous oxide films supported on Au electrodes observed in this laboratory by in situ atomic force microscopy in the same electrolyte (5*d*).

The most significant aspect of the present study is that no evidence for the presence of a second set of shells could be obtained for films in the OC state by attempting to fit the in situ EXAFS with four (as opposed to two) shells. This observation affords rather strong evidence that, to the level of uncertainty of these measurements, there exists only one type of site for each — the fully reduced and fully oxidized species in these films. This finding is at variance with the results for nickel hydrous oxide electrodes in the oxidized state reported by other workers (see Table 3), who have found an additional Ni—O shell with d(Ni—O)$_2$ = 1.94 — 2.12 Å and, occasionally, a second Ni—Ni shell, with d(Ni—Ni)$_2$ = 3.00 — 3.19 Å. Three explanations have been offered (4*b*) to account for these extra feature(s): an incomplete oxidation of the film, a distortion of the octahedral symmetry, and the formation of a highly oxidized form of nickel, denoted as Ni^{4+}. The first of these possibilities appears strongly favored since, as shown in this work, films in the OC state yield, upon self-discharge, shells with the same bond distances as those found for the film in the UC or FD state, and the level of distortion of the octahedral symmetry around the nickel site, as judged by the intensity of the pre-edge peaks is low (< 3%) for both the UC and OC states.

C. On the question of the oxidation state of nickel in Ni hydrous oxide films

Attempts have been made to correlate the position of the absorption edge jump and the effective atomic charge of transition metal ions (20). As noted by Bianconi (21), however, there exists no linear relationship between these two parameters, since (*i*) the absorption edge jump is determined by the threshold of dipole-allowed transitions, and, hence, on the mixing of *d* and *sp* orbitals of the unoccupied states, and (*ii*) the energy of multiple scattering resonances depends markedly on the interatomic distance, giving rise to a much larger energy shift compared to that of the core exciton (pre-edge peak).

A good illustration of this lack of correlation was obtained for Mn oxides by Schultze et al. (18), who concluded that a simple measure of the edge energy is unsatisfactory for determining the oxidation states of unknown oxides.

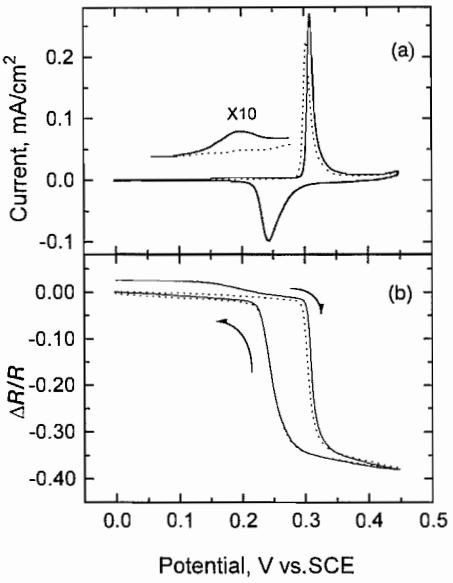
In contrast, excellent correspondence has been found between the maximum energy of the pre-edge peak (E_{peak}) and the oxidation state, by Schultze et al. (18) for Mn oxides and by Bajt et al. (19) for Fe oxides. However, for oxides of transition metals of the first row, ΔE_{peak}, the difference in E_{peak}, per unit oxidation state, spans a wide range of values; hence, it becomes impossible, based solely on the magnitude of ΔE_{peak}, to establish the oxidation state of nickel in the overcharged films. This assignment is further complicated in this case by the lack of well-characterized, genuine inorganic Ni^{3+} and Ni^{4+} oxide species that could serve as standards for comparison.

Much of the controversy surrounding the oxidation state in these charged or overcharged materials may be traced to the work of Corrigan and Knight (7), who noted that the charge obtained during the initial oxidation of electrodeposited

© 1997 NRC Canada

Can. J. Chem. Downloaded from www.nrcresearchpress.com by 91.121.58.235 on 09/08/12
For personal use only.

Fig. 9. First (solid line) and second (broken line) cyclic voltammograms (panel (*a*)) and normalized reflectivity data $\Delta R/R$ vs. E, where $\Delta R/R = [R(E) - R(E_{ref})]/R(E_{ref})$ and E_{ref} is the potential just before the onset of film oxidation (ca. 0.3 V in the first cycle) (panel (*b*)), recorded simultaneously for an α-$Ni(OH)_2$(hyd) film, ca. 15 nm thick, in 1 M KOH (see text for details). Scan rate = 2 mV/s.



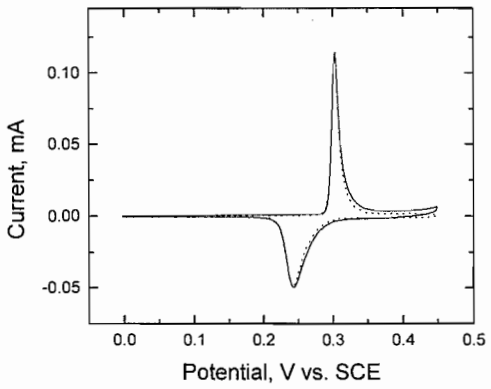
α-$Ni(OH)_2$(hyd) on Au(poly) was larger, ca. 1.5 e^- per nickel site, than that expected for the full one-electron oxidation of the film. Rather good agreement with a single one-electron process was obtained, however, after the first oxidation–reduction cycle, leading these authors to suggest that the redox process involves the oxidation (and reduction) of Ni(2.5) (and Ni(3.5)). Some insight into the origin of this effect was gained from in situ reflectance spectroscopy (RS) measurements to be described in the next section.

D. Reflectance spectroscopy

Figure 9 displays the first two cyclic voltammetry curves (panel (*a*) for an α-$Ni(OH)_2$(hyd) film (ca. 15 nm thick) in 1 M KOH, deposited via the method described in the experimental section for a Au(111) electrode. The optical data recorded at a constant wavelength (λ = 540 nm) during these scans are shown in the form of $\Delta R/R$ vs. E plots (see panel (*b*) in this figure), where $\Delta R/R = [R(E) - R(E_{ref})]/R(E_{ref})$ and E_{ref} is the potential just before the onset of film oxidation, ca. 0.3 V. As indicated therein, the optical signal during the first scan in the positive direction remained constant up to a potential of 0.15 V vs. SCE and decreased linearly thereafter down to the onset of the prominent oxidation peak, ca. 0.3 V vs. SCE. The optical behavior in the range 0.0–0.3 V is characteristic of gold in aqueous electrolytes. In particular, the potential at which the reflectivity curve undergoes a change in slope (ca. 0.15 V in this case) corresponds to the onset of gold oxide formation (see expanded section of the voltammogram in panel (*a*), Fig. 9) (cf. ref. 11). As the film was gradually oxidized, the reflectivity was found to decrease markedly, down to the trailing edge of the oxidation peak (ca. 0.35 V vs. SCE), and much more slowly thereafter.

The change in reflectivity associated with the film oxidation

Fig. 10. Cyclic voltammogram (solid line) and derivative of the normalized reflectivity (dotted line) based on the data shown in Fig. 9.



was found to be virtually reversible, within 1%, as judged by a comparison between values of $\Delta R/R$ observed just before the onset of oxidation and following full reduction.[2] In addition, virtually identical $\Delta R/R$ vs. E curves were observed during the second and subsequent 10 cycles. If it is assumed that the changes in the optical signal are proportional to the extent of oxidation of the film, the number of oxidized nickel sites generated during the very first scan appear to be essentially the same as those produced in the second and subsequent scans. On this basis, the additional charge observed during the first oxidation does not seem to be associated with nickel sites in the lattice, but with some other phenomenon (see below).

Particularly revealing is a comparison between the cyclic voltammogram and curves obtained by taking the derivative of the optical signal. Figure 10 shows both these plots, where the optical scale has been adjusted to match the current observed during the scan in the negative direction. As indicated, the charge, for which no account can be made by the optics, becomes especially evident for potentials positive to the oxidation peak.

Several possible sources could contribute to this excess charge, including the presence of partially reduced forms of nitrate within the film (such as nitrite), produced during the electrodeposition of the films, which could undergo oxidation to form nitrate during the first oxidation scan; the oxidation of hydroxyl ions to generate precursor species in the evolution of dioxygen (22); and structural changes, i.e., crevice formation, in the film induced by the first oxidation as has been observed in this laboratory by in situ AFM measurements using the basal plane of highly oriented pyrolytic graphite as the film substrate (5).

Summary

The in situ XAFS results presented in this work have shown that α-$Ni(OH)_2$(hyd) films in the uncharged (or discharged) and overcharged states are characterized by distinct sets of Ni—O and Ni—Ni shells. In particular, the EXAFS of over-

[2] As evidenced by both the cyclic voltammogram and optical reflectivity data, the Au surface appears to remain in the oxidized state even after the nickel hydrous oxide layer is reduced.

© 1997 NRC Canada

charged films provided no evidence for contributions due to shells at distances longer than those attributed to oxidized nickel sites in those films.

Within experimental uncertainty, the in situ XAFS and RS spectral data for nickel hydrous oxides films in the oxidized state were found to be virtually identical after the first and subsequent oxidations, despite the decrease in the charge under the anodic peak following the first oxidation. These results indicate that the excess charge observed during the very first oxidation may not be related to changes in the redox state of nickel sites in the lattice, but rather to other processes, and, thereby, are consistent with Ni^{3+} being the most oxidized species in charged nickel hydrous oxide films in alkaline solutions.

Acknowledgements

This work was supported by the Department of Energy, Office of Basic Energy Sciences. M.R.A. is supported by the U.S. DoE, Basic Energy Sciences – Chemical Sciences, under contract No. W-31-109-ENG-38. The research was carried out at the National Sychrotron Light Source, Brookhaven National Laboratory, which is supported by the US Department of Energy, Division of Materials Sciences and Division of Chemical Sciences, and at the Stanford Synchrotron Radiation Laboratory, which is operated by the Department of Energy, Office of Basic Energy Sciences.

References

1. D. Linden. *In* Handbook of batteries. McGraw-Hill, New York. 1995.
2. F. Hahn, D. Floner, B. Beden, and C. Lamy. Electrochim. Acta, **32**, 1631 (1987).
3. (*a*) B.A. Lopez de Mishima, T. Ohtsuka, and N. Sato. Electrochim. Acta, **38**, 341 (1993); (*b*) J. Desilvestro, D.A. Corrigan, and M.J.J. Weaver, Phys. Chem. **90**, 6408 (1986).
4. (*a*) J. McBreen, W.E. O'Grady, G. Tourillon, E. Dartyge, A. Fontaine, and K.I. Pandya. J. Phys. Chem. **93**, 6308 (1989); (*b*) K.I Pandya, R.W. Hoffman, J. McBreen, and W.E. O'Grady. J. Electrochem. Soc. **137**, 383 (1990); (*c*) K.I. Pandya, W.E. O'Grady, D.A. Corrigan, J. McBreen, and R.W.J. Hoffman. J. Phys. Chem. **94**, 21 (1990); (*d*) T.W. Capehart, D.A. Corrigan, R.S. Conell, K.I. Pandya, and R.W. Hoffman. Appl. Phys. Lett. **58**, 865 (1991); (*e*) D. Guay, G. Tourillon, E. Dartyge, A. Fontaine, J. McBreen, K.I. Pandya, and W.E. O'Grady. J. Electroanal. Chem. **305**, 83 (1991); (*f*) S. Kim, D.A. Tryk, M.E. Antonio, R. Carr, and D. Scherson. J. Phys. Chem. **98**, 10269 (1994); (*g*) W.E. O'Grady, K.I. Pandya, K.E. Swider, and D.A. Corrigan. J. Electrochem. Soc. **143**, 1613 (1996).
5. (*a*) R.R. Chen, Y. Mo, and D.A. Scherson. Langmuir, **11**, 3933 (1994); (*b*) P. Haring and R.J. Kotz. Electroanal. Chem. **395**, 243 (1995); (*c*) A. Kowal, R. Niewiara, B. Peronczyk, and J. Haber. Langmuir, **12**, 2332 (1996). (*d*) Y. Hu and D.A. Scherson. J. Phys. Chem. **101**, 5370 (1997).
6. (*a*) I. Cordoba-Torresi, C. Gabrielli, A. Hugot-Le Goff, and R.J. Torresi. J. Electrochem. Soc. **138**, 1548 (1991); (*b*) G.T. Cheek and W.E. O'Grady. Extended Abstracts Electrochemical Society Meeting, Abstract no. 259, p. 374, Fall 1990; (*c*) Y. Mo, E. Hwang, and D.A. Scherson. J. Electrochem. Soc. **143**, 37 (1996).
7. D.A. Corrigan and S.L. Knight. J. Electrochem. Soc. **136**, 613 (1989).
8. J. McBreen. *In* Modern aspects of electrochemistry. Vol. 23. *Edited by* B.E. Conway, R. White, and J.O'.M. Bockris. Plenum Press, New York. 1991, p. 29.
9. M. Kerkar, J. Robinson, and A.J. Forty. Faraday Discuss. Chem. Soc. **89**, 31 (1990).
10. A.J. Davenport, H.S. Isaacs, G.S. Frankel, A.G. Schrott, and M.A.J. Russak. J. Electrochem. Soc. **138**, 337 (1991).
11. Y. Mo, E. Hwang, and D.A. Scherson. Anal. Chem. **67**, 2415 (1995).
12. D.A. Corrigan. J. Electrochem. Soc. **134**, 377 (1987).
13. J. Desilvestro, D.A. Corrigan, and M.J.J. Weaver. J. Electrochem Soc. **135**, 885 (1988).
14. K. Kordesch and R.W. Hoffman. Thin Solid Films, **107**, 365 (1983).
15. A. Manceau, A.I. Gorshkov, and V.A. Drits. Am. Mineral. **77**, 1133 (1992).
16. (*a*) I.J. Pickering and G.N. George. Inorg. Chem. **34**, 3142 (1995); (*b*) P.A. O'Day, J.J.J. Rehr, S.I. Zabinsky, and G.E. Brown, Jr. J. Am. Chem. Soc. **116**, 2938 (1994).
17. (*a*) J.J. Rehr, J. Mustre de Leon, S.I. Zabinsky, and R.C. Albers. J. Am. Chem. Soc. **113**, 5135 (1991); (*b*) J. Mustre de Leon, J.J. Rehr, S.I. Zabinsky, and R.C. Albers. Phys. Rev. B: Condens. Matter, **44**, 4146 (1991).
18. D.G. Schulze, S.R. Sutton, and S. Bajt. Soil Sci. Soc. Am. J. **59**, 1540 (1995).
19. A. Bajt, S.R. Sutton, and J.S. Delaney. Geochim. Cosmochim. Acta, **58**, 5209 (1994).
20. (*a*) S.P. Cramer. *In* X-ray absorption: principles, applications, techniques of EXAFS, SEXAFS and XANES. *Edited by* D.C. Koningsberger and R. Prins. Wiley, New York. 1988 p. 257; (*b*) A.N. Mansour and C.A. Melendres. Physica B: (Amsterdam), **208 & 209**, 583 (1995).
21. A. Bianconi. *In* X-ray absorption: principles, applications, techniques of EXAFS, SEXAFS and XANES. *Edited by* D.C. Koningsberger and R. Prins. Wiley, New York. 1988 p. 573.
22. R.E. Carbonio, V.A. Macagno, and A.J. Arvia. J. Electroanal. Chem. **177**, 217 (1984).

Can. J. Chem. Downloaded from www.nrcresearchpress.com by 91.121.58.235 on 09/08/12
For personal use only.

© 1997 NRC Canada

Electrochemical and ^{1}H NMR studies of proton behavior of ImCl and LiCl solution in acetonitrile

Ping He and Keith E. Johnson

Can. J. Chem. Downloaded from www.nrcresearchpress.com by 91.121.58.235 on 09/08/12
For personal use only.

Abstract: The role of the proton in extending the electrochemical window and promoting the stripping efficiency of alkali metals has been studied in acetonitrile solution. The platinum hydride surface generated in the hydrogen evolution was considered responsible for the potential shift of 1-ethyl-3-methyl-1*H*-imidazolium (Im^+) reduction in the absence of lithium. In lithium chloride solution, the lithium layer deposited on the electrode may be the main cause for the stretch of the solvent electrochemical window because of the high overpotential of Im^+ reduction on that surface. The proton may affect the properties of the passive layer on newly deposited alkali metal surfaces and then improve the performance of the alkali metal anodes.

Key words: 1-ethyl-3-methyl-1*H*-imidazolium chloride, protons, acetonitrile, lithium reduction.

Résumé : Opérant en solution dans l'acétonitrile, on a étudié le rôle du proton pour provoquer une extension de la fenêtre électrochimique et pour promouvoir l'efficacité d'arrachement des électrons des métaux alcalins. On considère qu'une surface d'hydrure de platine générée dans l'évolution d'hydrogène est responsable du déplacement de potentiel lors de la réduction de l'ion 1-éthyl-3-méthyl-1*H*-imidazolium (Im^+) en l'absence de lithium. En solution de chlorure de lithium, la couche de lithium déposée sur l'électrode pourrait être la cause principale de l'extension de la fenêtre électrochimique du solvant à cause du surpotentiel élevé de la réduction du Im^+ sur cette surface. Le proton peut affecter les propriétés de la couche passive sur les nouvelles surfaces du métal alcalin déposé et il peut alors augmenter la performance des anodes de métal alcalin.

Mots clés : chlorure de 1-éthyl-3-méthyl-1*H*-imidazolium, protons, acétonitrile, réduction du lithium.

[Traduit par la rédaction]

Introduction

In studies of chloroaluminate room temperature melts as electrolytes in high-energy batteries, the lower depositing and stripping efficiency of the alkali metals is one of the major hindrances (1). It has been reported (2) that in neutral ImCl–$AlCl_3$ (Im ≡ 1-ethyl-3-methyl-1*H*-imidazolium) melt, Li^+ can be plated and stripped on tungsten and aluminum electrodes, although the plated lithium is not stripped quantitatively. This may be because in neutral LiCl-buffered ImCl–$AlCl_3$ melt[2] the reduction potential of lithium is close to that of Im^+ on the electrodes and the organic reduction product of the melt reacts with the newly deposited lithium to form a passive layer that damps the stripping of the metal (3, 4). The reduction of Na^+ and K^+ in neutral ImCl–$AlCl_3$ melts cannot be observed, since the reduction potentials of Na^+ and K^+ are overlapped or beyond the negative limit of the melts.

Riechel and Wilkes (3) have recently found that proton, added to NaCl-buffered neutral melts, can shift the reduction of ImCl to a more negative potential and thus stretch the electrochemical window of the melt. Proton addition also led to an improvement in the reversibility of lithium deposition–stripping behavior. They suggested that these phenomena may be related to the reaction product of proton and Im^+. However, no spectroscopic evidence showed that Im^+ reacted with the proton except for solid neutron diffraction data that demonstrated that HCl_2^- could hydrogen bond to the ring hydrogen on Im^+ (5). The results of Carlin and co-workers (1) showed that by adding HCl_2^- to MCl (M = Li^+, Na^+)-buffered ImCl–$AlCl_3$ neutral melts, the negative limit of the electrochemical window changed from −2.2 to −2.4 V vs. Al(III)/Al (in 0.6:0.4 ImCl–$AlCl_3$) and nearly reversible plating and stripping behavior for both lithium and sodium could be obtained, although the reduction potential of Li^+ shifted to a more negative potential as well. Using triethanolamine hydrogen chloride (TEOA·HCl) as a stable proton source, Piersma et al. (4) observed similar phenomena to those of Riechel and Wilkes (3). They considered that the stretch of the electrochemical window was related to the alkali metal plated surfaces. The reason that the proton leads to the potential shift and promotes the reversibility of metals is still not clear.

We have undertaken studies employing a nonaqueous solvent as medium, to better understand the role of the proton in

Received March 10, 1997.

This paper is dedicated to Professor Brian E. Conway on the occasion of his 70th birthday and in recognition of his contributions to electrochemistry.

P. He and K.E. Johnson.[1] Department of Chemistry, The University of Regina, Regina, SK S4S 0A2, Canada.

[1] Author to whom correspondence may be addressed. Fax: (306) 585–4894; E-mail: johnsonke@meena.cc.uregina.ca

[2] A buffered neutral melt is an approximately stoichiometric tetrachloroaluminate melt to which a slightly soluble alkali chloride is added to reduce Cl^- and $Al_2Cl_7^-$ concentrations to a minimum, i.e., to provide Lewis neutrality.

© 1997 NRC Canada

Can. J. Chem. Downloaded from www.nrcresearchpress.com by 91.121.58.235 on 09/08/12
For personal use only.

the electrochemical behavior of alkali and Im^+. In some nonaqueous solutions, the dielectric constant is sufficiently high to allow the dissolved salt to dissociate, although the interaction between ions and solvent is not as strong as that in water; to some extent we could say that the ion is more "naked" than in aqueous solution. Thus, the behavior of ions in a nonaqueous solvent is close to that in an ionic liquid (an assemblage of "naked" ions) rather than in aqueous solution, except for the ionic strength. A number of experimental results have confirmed (6, 7) that the spectroscopic and electrochemical characteristics of ions dissolved in room temperature chloroaluminate molten salts are similar to those in nonaqueous rather than in aqueous solutions. This indicates that the behavior of the ions in nonaqueous solutions could be analogous, to some extent, to that in ionic liquids. Moreover, using a solvent medium allows us to separate the effects of those ions that compose the ionic liquid. For buffered neutral melts, the dominant ions are $AlCl_4^-$ and Im^+, with the alkali cation and proton, in the form of HCl_2^- and (or) $H_2Cl_3^-$ etc., dispersed in the melt. It is reported (3, 8) that component ions of the melt are involved in blocking the newly deposited alkali metal surface and proton could help to get rid of the passive surface. In a nonaqueous solution the effects of the component ions can be easily separated. In this study acetonitrile was chosen as the solvent for it has a wide electrochemical window, and a medium dielectric constant, so that some alkali chloride salts can dissolve and dissociate in it sufficiently. Previous studies have shown (9) that under certain conditions, as when HCl is added to an acetonitrile solution containing chloride, the proton can exist as a form of dichloride anion, HCl_2^-, the same species of proton as in the melts. Fortunately, all the ions existing in the melt are stable in acetonitrile, except that they are surrounded by the solvent molecules. Therefore, taking acetonitrile solution as a simulated system to study the behavior of the proton is feasible.

Experimental

Reagents

ImCl was made from 1-methylimidazole and chloroethane (Aldrich) using the method reported by Wilkes et al. (10). 1-Ethyl-3-methyl-1*H*-imidazolium hydrogen dichloride ($ImHCl_2$) was made by passing HCl(g) over the weighed solid ImCl (8). Anhydrous LiCl, NaCl, and the other inorganic chemicals were dried overnight under vacuum at ca. 120°C. Acetonitrile was obtained from Fisher Scientific, and distilled from calcium hydride suspension. Tetraethylammonium chloride (TEAC) was recrystallized twice before it was used. HCl gas was generated by dropping hydrochloric acid into concentrated sulfuric acid. All the chemicals used in the experiment were reagent grade.

In the preparation of electrolyte, because the solubilities (11) of LiCl and NaCl are low (LiCl: 2.6×10^{-2} M, NaCl: 3×10^{-5} M) and dissolution requires a long time (1 day), we usually first allowed the solution to become saturated by alkali chloride, and then added the weighed ImCl to the filtered solution. $ImHCl_2$ was readily soluble. Starting HCl:ImCl ratios were determined by weight change.

Instrumentation

All the experimental work connected with the hygroscopic chemicals was carried out in a LabConco glove box under a dry nitrogen atmosphere. Electrochemical measurements were performed by using a BAS 100A electrochemical analyzer. Three-electrode electrochemical cells were used with various working electrodes: platinum (BAS, MF-2013), glassy carbon (BAS, MF-2012), and tungsten (custom fabrication, diam. 1 mm). A platinum foil auxiliary electrode was used. A screw-type platinum wire was placed in another chamber containing 0.003 M ferrocene in acetonitrile solution to act as a pseudo-reference electrode, which contacted the studied electrolyte via a fine frit. Some experimental results were obtained on platinum (diam. 30 μm) and tungsten (diam. 20 μm) microelectrodes, leading to waves rather than peaks. In these measurements the BAS PA-1 preamplifier was employed. ^1H NMR spectra were acquired with a Bruker AC 200 MHz spectrometer; DMSO-d_6 was used as an exterior reference. UV–VIS spectroscopic experiments were performed on a Hewlett–Packard model 8452A diode array spectrophotometer.

Results and discussion

The states of proton in acetonitrile

The states of proton in a series of aprotic solvents have been studied by NMR spectroscopy in the work of Fujiwara and Martin (9). When HCl was added to tetraalkylammonium chloride solutions they found that HCl associates with chloride anions:

$$[1] \quad HCl(g) + Cl^-(l) = HCl_2^-(l)$$

and protonates the solvent.

The suggested association constant in acetonitrile is ca. 600. Thus, if the chloride is in excess, the dihalide anion HCl_2^- will form quantitatively. In the case where HCl is in excess, $[Cl^-] < [HCl]$, Fujiwara and Martin (9) obtained a broader and weaker ^1H NMR signal that was shifted downfield with increase in the ratio of HCl to the chloride salt. This phenomenon was presumed to be a consequence of slow H^+ exchange between the dihalide ion or $Cl(HCl)_n^-$ and the protonated solvent. In this case there were at least two kinds of protons, HCl_2^- and protonated solvent.

In our experiments, it is difficult to determine exactly the relative quantity of HCl and chlorides (LiCl and (or) ImCl); however, HCl can be added as $ImHCl_2$, since HCl_2^- could transform to HCl(g) or other proton forms in the transfer process. In some cases we had to add proton by bubbling HCl through the electrolyte. Figure 1 gives the voltammetric curves on a Pt electrode in 0.01 M ImCl acetonitrile solution. Curve 1 was obtained for the solution with a ratio of HCl:ImCl = 1.7 (HCl in excess). Two proton reduction current waves can be observed with potentials at −0.3 and −0.7 V, respectively. With removal of HCl by passing nitrogen through the electrolyte, the current wave at −0.3 V decayed steeply, while the current at −0.7 V declined quite slowly. We have compared curve 4 with the voltammetric curve obtained from the solution with a feed ratio of HCl:ImCl = 0.5 (HCl in deficit). The two curves have the same features: no detectable current at −0.3 V but a reduction current at −0.7 V. This means that the quantity of HCl in the solutions represented by curves 4 and 5 was less than that of ImCl.

The electrochemical behavior of the proton on glassy carbon and tungsten electrodes in the same electrolytes as in

© 1997 NRC Canada

Can. J. Chem. Downloaded from www.nrcresearchpress.com by 91.121.58.235 on 09/08/12
For personal use only.

Fig. 1. Voltammetric curves of HCl added to 0.01 M ImCl acetonitrile solutions with a platinum electrode. Sweep rate: 100 mV/s. Curve 1, initial solution with HCl:ImCl = 1.7; from curve 2 to curve 5, the quantity of HCl was decreased gradually by passing N_2 through the solution to remove the HCl.

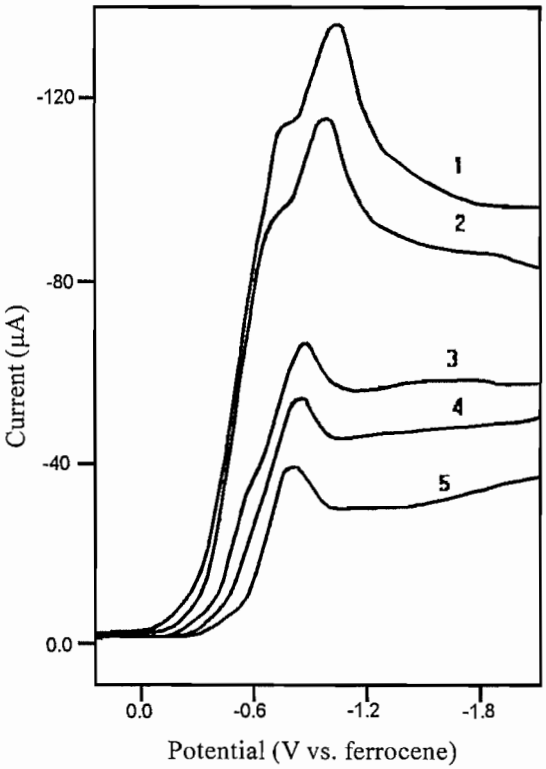


Fig. 2. Voltammetric curves of HCl added to 0.01 M ImCl acetonitrile solutions with a glassy carbon electrode. Sweep rate: 100 mV/s. From curve 1 to curve 3, the quantity of HCl decreased gradually; curve 4 without HCl.

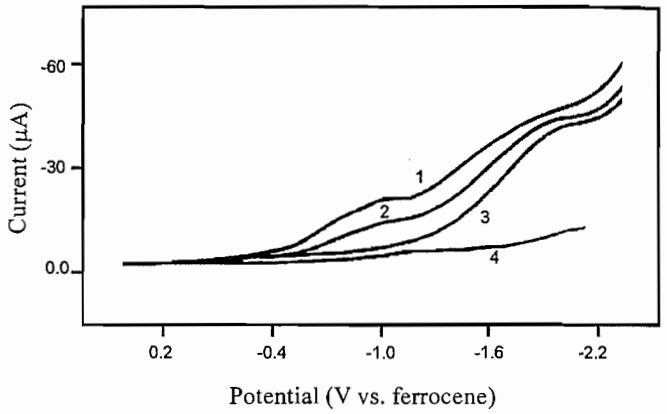
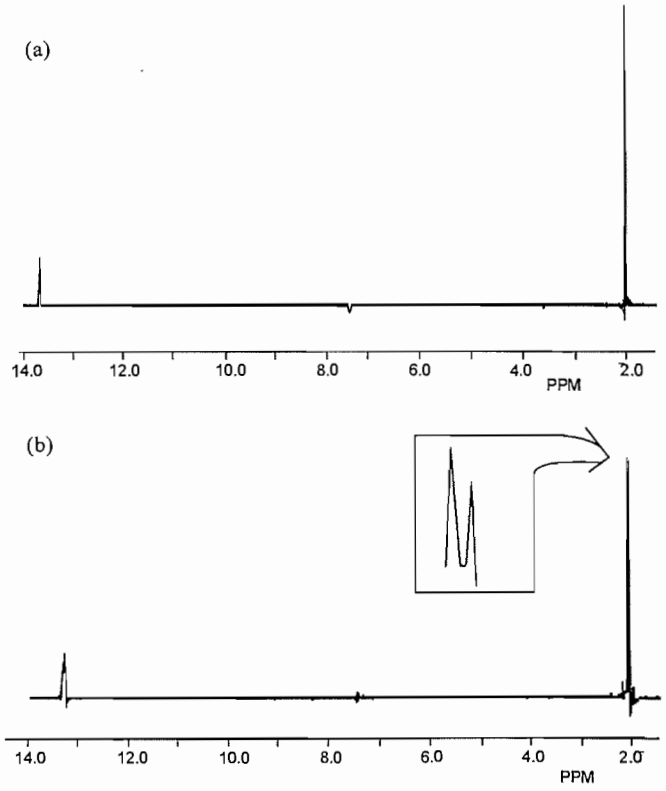


Fig. 3. H NMR spectra of 0.01 M ImCl solutions (*a*) without HCl and (*b*) with HCl (HCl:ImCl = 1.7) added. Inset: amplified graph as given by the arrow.



the above experiment was measured. Similar phenomena can be observed. The two current waves on tungsten and glassy carbon electrodes are different from those on the platinum electrode. On tungsten the potentials are −0.9 and −1.4 V, while on the glassy carbon electrode they are −1.0 and −2.0 V, respectively, which are separated from each other more than those on platinum (Fig. 2). Substituting the chloride, ImCl, with tetraethylammonium chloride did not change the above results.

The mass-transfer characteristics of the proton reduction on platinum and tungsten electrodes show that there are at least two protonic species in the acetonitrile solution in the case of HCl in excess. According to Fujiwara's analysis, when the concentration of HCl is lower than that of chloride, HCl_2^- should be the dominant proton form. Therefore, the second cathodic current wave on electrodes corresponds to the reduction of HCl_2^-. The current at −0.3 V on platinum may result from some other proton forms. In the following experiments, for the sake of keeping the proton form in acetonitrile the same as that in the melt, proton forms other than HCl_2^- are not necessary, so one can bubble enough HCl through the solution, followed by nitrogen to get rid of the excess. The quantity of HCl can be roughly controlled by monitoring the current on the potential–current curve.

The ^1H NMR spectra of the electrolytes with HCl in excess and deficit were measured, and are shown in Fig. 3. As the signal of HCl_2^- is far away from that of the solvent proton, we did not use deuterated solvent in the measurement. There was a downfield resonance signal observed in both cases which had been ascribed in the literature to the hydrogen-bonded proton of the HCl_2^- ion (9). When HCl is in excess (HCl:ImCl = 1.7) the downfield signal is broader than the signal obtained when the solution chloride is in excess, and the location of the

© 1997 NRC Canada

Can. J. Chem. Downloaded from www.nrcresearchpress.com by 91.121.58.235 on 09/08/12
For personal use only.

Fig. 4. Voltammetric curves obtained with a platinum microelectrode of a 1-ethyl-3-methyl-1*H*-imidazolium solution (0.01 M) in acetonitrile (1) with and (2) without HCl. Sweep rate: 100 mV/s.

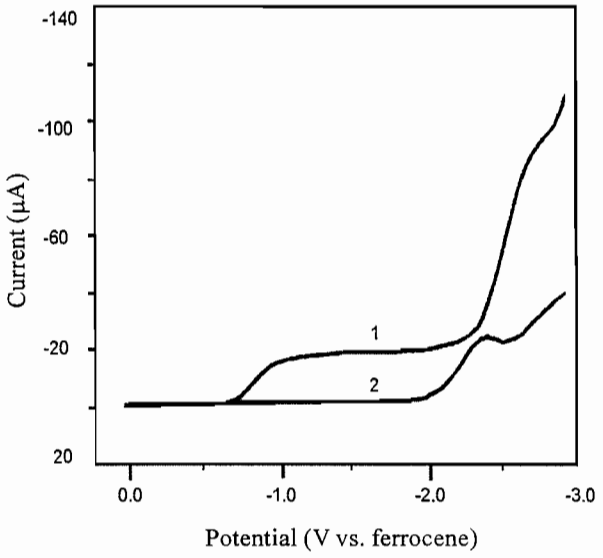
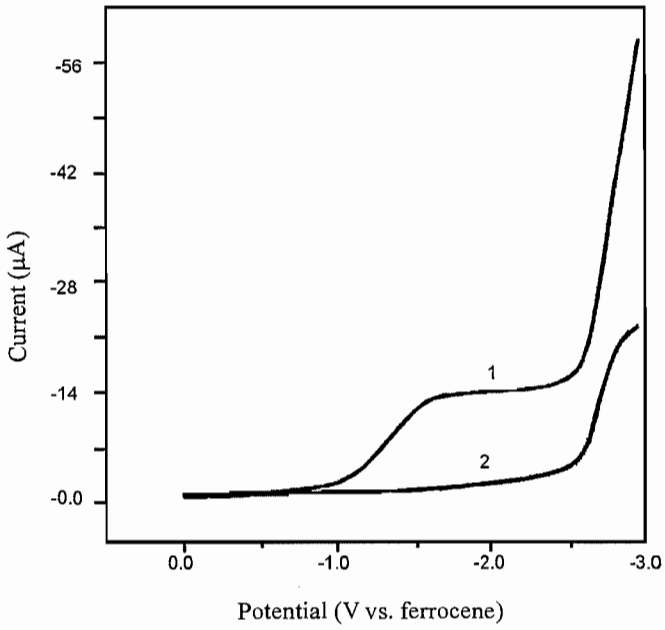


Fig. 5. Voltammetric curves obtained with a tungsten microelectrode of a 1-ethyl-3-methyl-1*H*-imidazolium solution (0.01 M) in acetonitrile (1) with and (2) without HCl. Sweep rate: 100 mV/s.



former is slightly downfield (δ = 13.7) from the latter (δ = 13.2). These results are consistent with those given by Fujiwara. The upfield signal was caused by the solvent protons, and its appearance is sensitive to the quantity of HCl. In the case of chloride in excess it is a simple signal, in a solution of HCl:ImCl = 1.7 (HCl in excess) it is a doublet signal, while increasing the quantity of HCl by passing HCl gas into the solution gave rise to a complex spectrum. The reaction between acetonitrile and HCl has been studied for decades (12). The products are quite complex and are dependent on the reaction conditions. They include nitrilium, iminium, dimerized iminium, or some other polymerized salts. In the solution of HCl:ImCl = 1.7, nitrilium salt is the most probable protonated solvent species, because only the proton on the nitrilium nitrogen atom may generate the doublet splitting signal of the methyl group proton on the solvent molecules. The proton exchange between HCl_2^- and nitrilium leads to the broadening and shift of the downfield signal.

The effect of proton on the reduction of Im^+ cation

In acetonitrile the reduction of Im^+ is at −2.0 V vs. ferrocene on platinum electrodes, within the electrochemical window of the solvent. The voltammetric curves of 0.01 M ImCl acetonitrile solution on platinum and tungsten electrodes with and without HCl are shown in Figs. 4 and 5, respectively. The current at −0.7 V in curve 1 is due to the reduction of HCl_2^-. On platinum electrodes, the onset of reduction of Im^+ has been moved from −2.0 to −2.2 V by adding HCl to the electrolyte. No effect of the proton on the reduction potential of Im^+ on tungsten electrodes could be observed, although the reaction occurred at a more negative potential. The situation on glassy carbon is the same as on tungsten electrodes.

The above phenomena are very similar to those taking place in melts. Campbell and Johnson (13) have reported that adding HCl to a basic melt ($AlCl_3$:ImCl = 0.495:0.505) shifted the reduction of Im^+ ca. 200 mV to a more negative potential as long as the partial pressure of HCl was higher than 0.2 atm (1 atm = 101.3 kPa). On tungsten and glassy carbon electrodes the potential shift could not be distinguished in the melt.

We consider that the effect of the proton on the potential shift of Im^+ reduction on a platinum electrode is related to the adsorption of proton on the platinum surface. It is well known that platinum is a good catalytic electrode for hydrogen evolution and the catalytic mechanism has been extensively reported in the literature. The results of previous studies (14) have confirmed that in the process of hydrogen evolution a number of equivalent monolayers of overpotential-deposited (OPD) H species in the near-surface region of the platinum interface will form a hydride phase. The electrode behavior is closely associated with the formation of this hydride layer. In solutions of low proton concentration the hydride layer would be depressed by impurities or reduced on the electrode. This means that in the process of hydrogen evolution the platinum hydride surface has been generated under conditions of sufficient acidity. Since the reduction potential of Im^+ is located in the potential range of the hydrogen evolution, the reaction in the electrolyte with HCl was conducted on a platinum hydride surface rather than on platinum itself. Therefore, it is reasonable that the reduction of Im^+ on two different electrode surfaces should have different overpotentials. This conclusion can also explain why the potential shift occurred under the condition of high HCl concentration in Campbell's experiment. Presumably Piersma failed to observe the shift phenomenon on platinum electrodes because of the low proton content. Protons adsorb only weakly on glassy carbon and tungsten electrode surfaces. At very negative potentials, pro-

© 1997 NRC Canada

Can. J. Chem. Downloaded from www.nrcresearchpress.com by 91.121.58.235 on 09/08/12
For personal use only.

Fig. 6. Cyclic voltammetric curves for a platinum microelectrode in LiCl saturated 0.01 M ImCl acetonitrile solution (1) with HCl and (2) without HCl. Sweep rate: 100 mV/s.

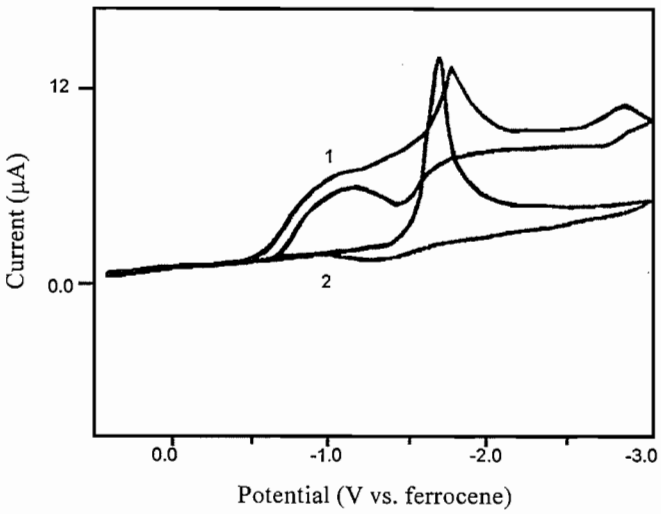
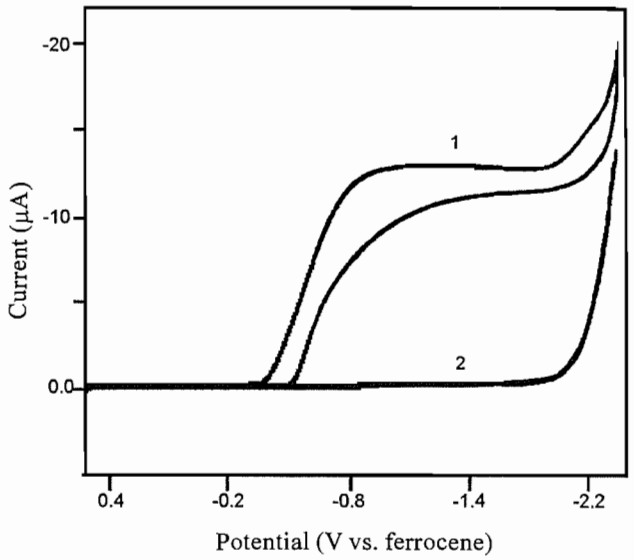


Fig. 7. Cyclic voltammetric curves for a platinum microelectrode in NaCl saturated 0.01 M ImCl acetonitrile solution (1) with HCl and (2) without HCl. Sweep rate: 100 mV/s.



ton reduction is merely a competitive reaction to the Im^+ reduction. The electrode surface does not change and no potential shift of Im^+ reduction could be observed.

The stripping efficiency of alkali metals in acetonitrile

The lithium ion can be reduced on Pt and W electrodes ahead of the reduction of Im^+ in the electrolytes with and without HCl. Figure 6 shows the deposition and stripping behavior on Pt electrodes; it is apparent that the deposition current in the HCl-containing electrolyte is lower than that without HCl. This may be caused by the competing reaction of proton reduction on the same electrode. Adding HCl to the electrolyte caused the Li^+ reduction potential to shift slightly in the negative direction, possibly caused by the adsorption of H on the platinum. By integrating the plating and stripping peaks on the cyclic voltammograms, the stripping efficiency on platinum electrodes in electrolytes with and without HCl is estimated to be 60 and 10%, respectively. The data indicate that HCl considerably improved the reversibility of the Li^+/Li couple.

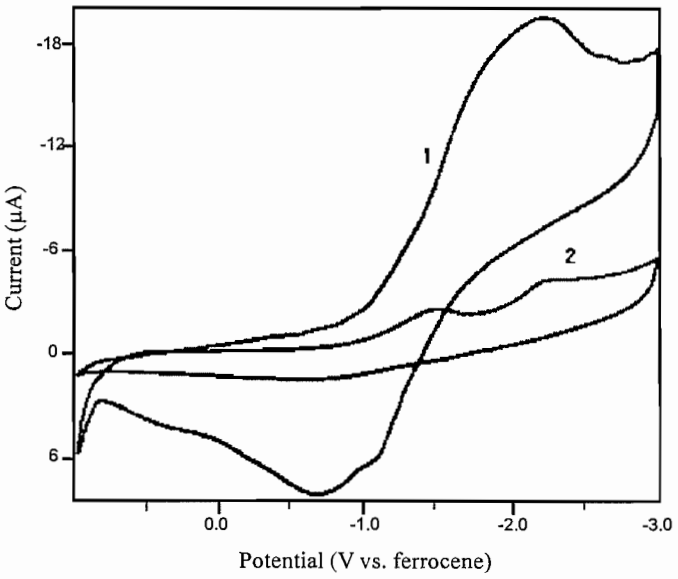
After the deposition of lithium, the reduction of Im^+ shifts to more negative potentials, beyond the potential range of the BAS instrument, no matter whether the electrolyte contains HCl or not. The higher overpotential of Im^+ reduction on a lithium surface than on a platinum electrode may account for this. On glassy carbon electrodes lithium cannot deposit from the acetonitrile in this experiment, and we cannot observe the stretching of the solvent electrochemical window. Similar results were observed in Piersma's experiments in the melts (4). In their staircase cyclic voltammetry measurement, even with the negative limit set to −2.8 V (vs. Al(III)/Al), no obvious solvent decomposition current was recorded. They concluded that the lithium or sodium layer plated on the platinum or tungsten electrode is responsible for the stretching of the electrochemical windows.

As the Im^+ cation may react with newly deposited lithium metal (15) to form an Im-Li layer on the lithium surface, it is easy to think that the product may block the electrode surface, and the passive surface layer may barricade the stripping of the lithium layer. Some authors (16) have observed the in situ formation of a passive layer on the lithium surface by using an optical microscope. In this connection, an analogous experiment was performed in the electrolyte without Im^+ cation. The result showed that the low stripping efficiency of the deposited lithium layer can also be distinctly increased by adding proton. Nevertheless, we cannot exclude the formation of an Im^+-participating passive layer in the melt or in the acetonitrile solution. It has been suggested (17, 18) that in nonaqueous solutions the alkali metals are always covered by a surface layer that is instantly formed by the reaction of the metal with the electrolyte. This layer, which acts as an interphase between the metal and the solution, has the properties of a solid electrolyte. The electrochemical behavior of the alkali electrodes will be governed by the properties of this layer. Water contamination or other proton agents will lead to its breakdown or change the properties of the passive film. In this study, although the surface film on the lithium in acetonitrile may be different from that in the melts, we consider that adding proton to the electrolytes could improve the surface layer's properties, i.e., increase the permeability of lithium cation or the transportation ability for other ions and the electron, and thus improve the performance of the alkali electrodes.

Figure 7 gives the cyclic voltammetric curves of sodium chloride solutions on a platinum electrode. In the electrolyte without HCl, no sodium deposition current could be observed. After adding HCl, the deposition and dissolution current appeared. As the solubility of sodium chloride in acetonitrile is low, the deposition current peak is small. In the melt without proton the sodium current can also not be distinguished on the cyclic voltammetric curves (3), due to the potential overlap of the sodium reduction with Im^+ reduction. Their SEM/EDS results verified the passivation of the sodium layer by the organic compound. This experiment shows that the proton in

© 1997 NRC Canada

Fig. 8. Cyclic voltammetric curves on tungsten electrode in LiCl saturated 0.01 M ImCl acetonitrile solution (1) with HCl and (2) without HCl. Sweep rate: 100 mV/s.



acetonitrile solution may play a similar role to that in the melt. We consider that the improvement of sodium redox behavior in proton-containing solutions can be attributed to the improvement of the surface layer on sodium.

On tungsten electrodes, proton brought about a great change in the lithium redox behavior (see Fig. 8). The stripping effect was noticeabley enhanced. On the cathodic branch, the hydrogen reduction current overlapped with the lithium reduction current, so it is impossible to calculate the stripping efficiency from the voltammograms. As we know, tungsten is a good electrochromic material, widely used in photo-electrochemistry: lithium can be electrochemically embedded in the tungsten electrode under certain conditions. Studies (19, 20) have shown that the proton can help lithium insertion into the tungsten interface. The above processes may take place in our situation although the surface layer is different. More research is clearly required to fully explain the phenomena in these systems.

Summary

The effect of proton in shifting the Im^+ reduction potential and promoting the reversibility of the redox behavior of alkali ions has been studied. It is found that the above phenomena not only take place in room temperature molten salts but also in nonaqueous solutions.

In this study at least two kinds of proton species have been identified in chloride acetonitrile solutions by an electrochemical method. HCl_2^-, which is the species existing in the melt, can be controlled as the only proton form in acetonitrile solution. It is suggested that the potential shift of Im^+ reduction on platinum electrodes is related to the formation of a platinum hydride phase during the hydrogen evolution. In alkali chloride solutions the stretch of the solvent electrochemical window is due to the high overpotential of Im^+ reduction on the alkali metal surface that is deposited before the solvent decomposition. The instantly established solid electrolyte film on a newly deposited alkali metal surface controls the performance of the alkali electrode. Adding proton to the system improves the properties of the film and then promotes the reversibility of the alkali redox couples.

Acknowledgment

Financial support from the Natural Sciences and Engineering Research Council of Canada and the University of Regina is gratefully acknowledged.

References

1. C. Scordilis-Kelley, J. Fuller, R.T. Carlin, and J.S. Wilkes. J. Electrochem. Soc. **139**, 694 (1992).
2. M. Lipsztajn and R.A. Osteryoung. Inorg. Chem. **24**, 716 (1985).
3. T.L. Riechel and J.S. Wilkes. J. Electrochem. Soc. **139**, 977 (1992).
4. B.J. Piersma, D.M. Ryan, E.R. Schumacher, and T.L. Riechel. J. Electrochem. Soc. **143**, 908 (1996).
5. S. Takahashi, M.-L. Saboungi, K. Suzuya, and N. Koura. *In* Molten salts, Ninth International Symposium. *Edited by* C.L. Hussey, D.S. Newman, G. Mamantov, and Y. Ito. The Electrochemistry Society, Inc. 1994. p. 69.
6. R. Moy and F.-P. Emmenegger. Electrochim. Acta, **37**, 1061 (1992).
7. R.A. Osteryoung. NTIS Report, No. Ad-A279, 396 (1994).
8. D.R. Chang, A.M. Elias, R.T. Carlin, and J.S. Wilkes. *In* Molten salts, Ninth International Symposium. *Edited by* C.L. Hussey, D.S. Newman, G. Mamantov, and Y. Ito. The Electrochemistry Society, Inc. 1994. p. 132.
9. F.Y. Fujiwara and J.S. Martin. J. Chem. Phys. **56**, 4091 (1972).
10. J.S. Wilkes, L.A. Levinsky, R.A. Wilson, and C.L. Hussey. Inorg. Chem. **21**, 1263 (1982).
11. J.F. Coetzee. Prog. Phys. Org. Chem. **4**, 45 (1967).
12. S. Yanagida and M. Okahara. Synthesis, 189 (1973).
13. J.L.E. Campbell and K.E. Johnson. J. Am. Chem. Soc. **117**, 7791 (1995).
14. L. Bai. J. Electroanal. Chem. **355**, 21 (1993), and refs. therein.
15. M.R. Grimmett. *In* Comprehensive heterocyclic chemistry. Vol. 5. Part 4A. *Edited by* A.R. Katritsky and C.W. Rees. Pergamon Press, New York. 1984. p. 415.
16. Scordilis-Kelley and R.T. Carlin. J. Electrochem. Soc. **141**, 873 (1994); J. Fuller, R.T. Carlin, and R.A. Osteryoung. J. Electrochem. Soc. **143**, L145 (1996).
17. E. Peled. J. Electrochem. Soc. **126**, 2047 (1979).
18. M. Odziemkowski and D.E. Irish. J. Electrochem. Soc. **140**, 1546 (1993).
19. R.A. Batchelor, M.S. Burdis, and J.R. Siddle. J. Electrochem. Soc. **143**, 1050 (1996).
20. P.K. Shen, K.Y. Chen, and A.C.C. Tseung. J. Electrochem. Soc. **141**, 1758 (1994).

Can. J. Chem. Downloaded from www.nrcresearchpress.com by 91.121.58.235 on 09/08/12
For personal use only.

© 1997 NRC Canada

Voltammetric determination of surface active compounds at Au and Pt ultramicroelectrodes in flowing solutions

Andrzej S. Baranski and Parviz Norouzi

Can. J. Chem. Downloaded from www.nrcresearchpress.com by 91.121.58.235 on 09/08/12
For personal use only.

Abstract: A new detection method was developed that takes advantage of changes in cyclic voltammograms (recorded with either a platinum or a gold ultramicroelectrode) caused by the adsorption, of inorganic and organic molecules. These changes may include reduction or oxidation of the adsorbate, inhibition of oxygen adsorption, inhibition of hydrogen adsorption, and also changes in the charging current. The detection is carried out in a stripping mode after the accumulation of analyte on the electrode surface for 50–1000 ms. Typical scan rates are between 10 and 1000 V/s. Removal of oxygen from the solutions studied is not required. Electrochemical conditioning of the working electrode is sufficient to insure a stable response for a period of several hours. For strongly adsorbing molecules the linear dynamic range extends over two orders of magnitude from about 10^{-7} M to 10^{-5} M with the relative standard deviation for replicate determinations lower than 5%. The smallest discernable signal is associated with about 0.1% surface coverage, which corresponds to the adsorption of about 10^{-18} mol of analyte on a ultramicroelectrode 5 μm in radius.

Key words: adsorption, cyclic voltammetry, ultramicroelectrode, flow injection.

Résumé : On a mis au point une nouvelle méthode de détection qui tire profit des changements dans les voltampérogrammes cycliques (enregistrés avec une ultramicroélectrode de platine ou d'or) qui sont causés par l'adsorption de molécules organiques ou inorganiques. Ces changements peuvent comporter la réduction ou l'oxydation de l'adsorbat, l'inhibition de l'adsorption de l'oxygène, l'inhibition de l'adsorption d'hydrogène ainsi que des changements dans le courant de charge. On effectue la détection dans le mode de redissolution après avoir effectué une accumulation de l'analyte sur la surface de l'électrode pendant 50 à 1000 ms. Les vitesses typiques de balayage se situent entre 10 et 1000 V/s. Il n'est pas nécessaire d'enlever l'oxygène des solutions étudiées. Le conditionnement électrochimique de l'électrode de travail est suffisant pour assurer une réponse stable pendant une période de plusieurs heures. Pour les molécules fortement adsorbées, l'amplitude de la réponse dynamique linéaire est de plus de deux ordres de grandeur allant d'environ 10^{-7} M à 10^{-5} M; la déviation relative standard pour la reproduction des déterminations est inférieure à 5%. Le plus faible signal détectable est associé à une couverture d'environ 1% de la surface; ceci correspond à une adsorption d'environ 10^{-18} mol d'analyte sur une ultramicroélectrode de 5 μm de rayon.

Mots clés : adsorption, voltampérométrie cyclique, ultramicroélectrode, injection à écoulement.

[Traduit par la rédaction]

Introduction

Electrochemical techniques provide the means for relatively simple, inexpensive, and very sensitive detection in flowing solutions, including Liquid Chromatography (LC), Capillary Electrophoresis (CE), and Flow-Injection Analysis (FIA). By far the most popular technique is simple amperometric detection at a fixed potential, which offers excellent detection limits (1–3). The most serious limitation of this detection method is associated with the stability of the working electrode. In general, amperometric detection is not appropriate for kinetically controlled electrode processes or electrode processes involving the electrodeposition of insoluble products. In many such cases, however, pulse amperometric detection has been successfully applied. The best illustration of this approach is pulse amperometric detection of carbohydrates (4). Carbohydrates can be oxidized in basic solutions on a Pt or Au electrode but the process is catalyzed by intermediate forms of oxide formation on the noble metals (AuOH or PtOH) (5). To maintain high catalytic activity of the detector the electrode potential has to be continuously cycled between positive and negative values. The detection strategy involves application of three potential steps per each cycle. First, a potential suitable for electrocatalytic oxidation of the carbohydrate is applied for 100–400 ms and the current is sampled for a short time at the end of this potential. Then the electrode is oxidatively cleaned by a positive step lasting 50–200 ms, and cathodically reactivated for 100–400 ms. A similar method was used in the detection of amino acids (6) and metal ions (7).

Alternatively, a potential scanning technique such as cyclic voltammetry or square-wave voltammetry could be used. This allows the maintenance of a clean and active electrode surface, and also the monitoring of the electrode response as a function

Received June 12, 1997.

This paper is dedicated to Professor Brian E. Conway on the occasion of his 70th birthday.

A.S. Baranski[1] and P. Norouzi. Department of Chemistry, University of Saskatchewan, 110 Science Place, Saskatoon, SK S7N 5C9, Canada.

[1] Author to whom correspondence may be addressed. Fax: (306) 966-4730. E-mail: baranski@sask.usask.ca

© 1997 NRC Canada

Can. J. Chem. Downloaded from www.nrcresearchpress.com by 91.121.58.235 on 09/08/12
For personal use only.

of potential. The option of recording current–potential curves is very important because it may improve the selectivity of some determinations, and it allows quick tracking of any change in the detector performance, often providing information sufficient to draw conclusions about the possible causes of observed changes. Such an option is also extremely useful in research on the development and optimization of electrochemical detectors because it provides detailed information about electrode processes under exactly the same conditions as used in a given analytical procedure. However, in order to use potentiodynamic techniques for detection in flowing solutions the scan rate must be sufficiently high so that a single sweep is several times shorter than the time needed for the analyte zone to pass through the detector. This means that in LC and FIA the scan rate should be higher than about 1 V/s and in CE higher than about 10 V/s. Fulfilling this condition may have an adverse effect on the detection limit under some conditions (8). It is well known that an increase in the sweep rate causes a deterioration of the signal-to-background ratio for redox processes involving soluble reactants, because background current is directly proportional to the sweep rate but the signal (controlled by the rate of diffusion) increases with the square root of the sweep rate. This argument, however, is not applicable to electrochemical detection carried out in a stripping mode after accumulation of the analyte on the electrode surface by means of electrodeposition or adsorption (9). If ultramicroelectrodes are employed, a meaningful accumulation can be obtained in a 100-ms time period, which then can be followed by a stripping scan carried out at, for example, a 100 V/s sweep rate.

Following these lines, a new detection method was developed that takes advantage of all changes in cyclic voltammograms (recorded with either a platinum or gold ultramicroelectrode) caused by the adsorption of inorganic and organic molecules. These changes may include reduction or oxidation of adsorbate, inhibition of oxygen adsorption, inhibition of hydrogen adsorption, and also changes in the charging current. The inspiration for this work came from papers published by Conway and co-workers (e.g., refs. 10–12), which show that surface processes on Pt and Au electrodes can be monitored with exceptional precision by cyclic voltammetry. In particular, it has been demonstrated that the cyclic voltammetric method is sensitive enough to detect very small changes, down to 0.25%, in OH coverage on a polycrystalline gold electrode (10). A simple calculation shows that in the case of a disk ultramicroelectrode (5 μm in radius) such coverage corresponds to about 2×10^{-18} mol, or 4×10^4 molecules.

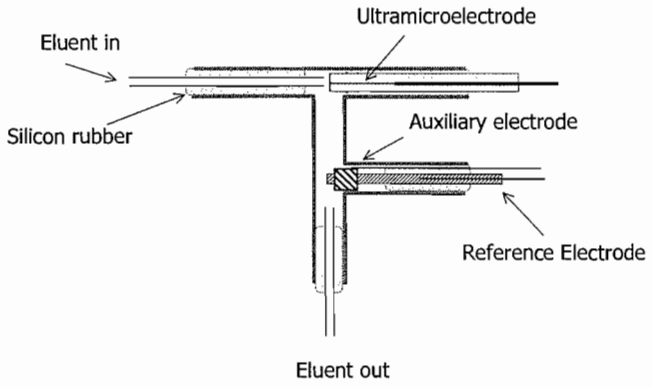
This paper describes only initial testing of the method under flow-injection conditions, but the method is nonselective (with the exception of heavy metal analysis); therefore it can be effectively used only in conjunction with a separation technique. Currently, this detection method is tested under capillary electrophoresis conditions.

Experimental

Reagents

All solutions were prepared in double-distilled deionized water (Corning Mega-Pure System, MP-6A and D-2) using analytical grade reagents. Reagents employed in preparation of the stock eluent solution for flow-injection analysis (H_3PO_4, NaOH, $Na_4BO_7 \cdot 10H_2O$, and $NaHCO_3$) were obtained from BDH Chemicals. In all experiments all solutions were used without removal of dissolved oxygen.

Fig. 1. Electrochemical cell used in flow-injection experiments.



Flow-injection setup

The equipment for flow-injection analysis included a 10 roller peristaltic pump (Microperpex) and a four-way injection valve (Supelco Rheodyne model 5020) with a 50 μL sample loop. Solutions were introduced into the sample loop by means of a plastic syringe. The electrochemical cell used in flow–injection analysis is shown in Fig. 1. In all experiments described in this paper the flow rate of eluent solution was 2.0 mL/min. The dispersion coefficient for an injection volume of 50 μL was approximately equal to 1.85.

Electrodes

Gold and platinum ultramicroelectrodes (radius 5.0 and 12.5 μm, respectively) served as the working electrodes. Electrodes of that size are usually employed in end-column electrochemical detection in capillary electrophoresis (7). The electrodes were prepared by sealing metal microwires (Goodfellow Metals Ltd., U.K.) into a soft glass capillary. The capillary was then cut perpendicular to its length to expose the wire. Electrical contacts were made using silver epoxy (Johnson Matthey Ltd., U.K.). Before each experiment the electrode surface was polished for 1 min using extra-fine carborundum paper and then for 10 min with 0.3 μm alumina. The electrode was washed with water prior to being placed in the cell. The true surface area of the working electrodes was estimated from the charge required for the oxidation of adsorbed hydrogen on the Pt electrode and from the charge due to the reduction of adsorbed oxygen on the gold electrode (15). This method yielded $(9.4 \pm 0.8)) \times 10^{-6}$ and $(1.6 \pm 0.2) \times 10^{-6}$ cm^2 for the Pt and Au electrode, respectively.

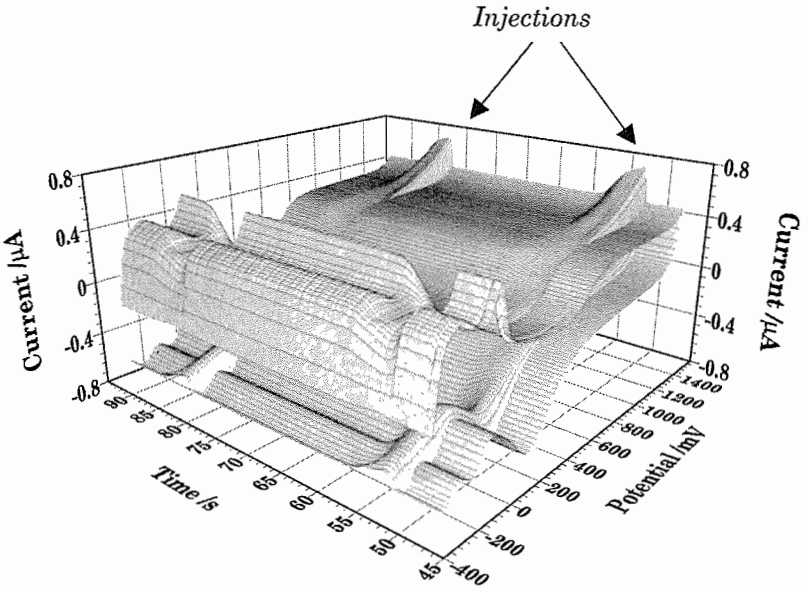
In all measurements an Ag(s)|AgCl(s)|1 M KCl(aq) reference electrode was used. The auxiliary electrode was made of a Pt wire, 0.5 mm in diameter.

Data acquisition and processing

All electrochemical experiments were done using a setup comprising a PC 486, 66-MHz microcomputer equipped with a data acquisition board (PCL-818PG, PC-Labcard Co.) and a custom-made potentiostat. The diagram of the potentiostat and details of the computer interfacing are described else-

© 1997 NRC Canada

Fig. 2. Cyclic voltammograms at a 12.5 μm Pt ultramicroelectrode recorded during a flow-injection experiment. The eluent was 0.05 M H_3PO_4, the flow rate was 2.0 mL/min, and the sweep rate was 100 V/s. Each scan was preceded by a 200 ms preconcentration period at −0.4 V. The injected solution (50 μL) contained 1 mM aniline in 0.05 M H_3PO_4.



where (13). All data acquisition and data processing programs were developed in this laboratory using Microsoft Visual C++, version 4.0, and Visual Basic, version 4.0. Electrochemical experiments used in this work involved continuous monitoring of the electrode response under cyclic voltammetric conditions. The cycle was started by holding the electrode at the arbitrary selected potential (called here the rest potential) for a fixed time period (called the delay time). Then the electrode potential was scanned from the initial to the vertex potential and back to the initial. Immediately after scanning, the rest potential was applied and the cycle was repeated. The current passing through the electrode was sampled only during the scanning of potential. It should be noted that in this method all processes studied involve adsorption of analytes, hence both charging and faradaic currents potentially carry useful analytical information. For this reason it was important to sample current at a frequency at least two times higher than the current transducer bandwidth, so that according to the Nyquist sampling theorem (14) complete information about current passing through the electrode could be obtained. To fulfill this requirement the sampling frequency was always between 40 and 70 kHz. In addition, a second-order low-pass filter with a 20 kHz cutoff frequency was placed between the current output of the potentiostat and the data acquisition board. The highest sampling rate used in this work was intentionally lower than the 100 kHz limit specified by the manufacturer of the data acquisition board because it was noted that a significant increase in the noise level occurs for sampling rates greater than about 75 kHz. Typically the scan rates in cyclic voltammetric experiments were between 10 and 1000 V/s. The delay time was usually between 0.05 and 3 s. During that time the collected data were processed and displayed graphically on the computer screen. The number of data points collected during each scan was user-selectable, but in this work it was always set to 256 points. Consequently, at lower sweep rates each data point represented an average of two or more analog-to-digital conversions. Part of the computer code used for the acquisition of data was written in assembly language and placed in a dynamic link library (this library is available on request from the corresponding author). The data processing involved background subtraction and the integration of the current between two user-selectable potential limits; details of these procedures will be described later. Results of the data acquisition were stored in the computer memory as matrices with 256 columns (typically) and up to 4096 rows.

Results and discussion

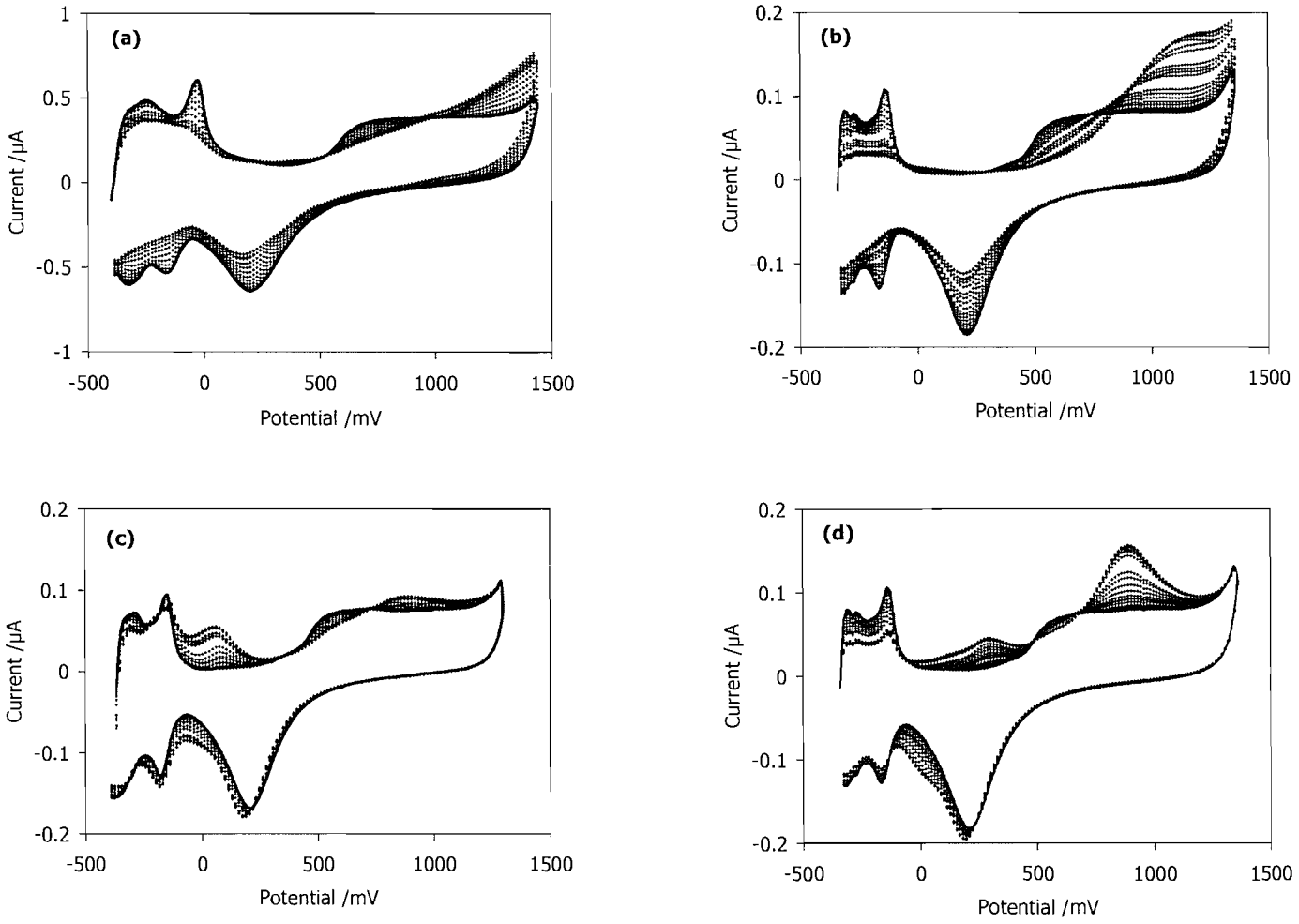
Analytical method

Figure 2 shows a sequence of cyclic volumetric (CV) curves recorded during the flow injection of 50 μL of 1×10^{-3} M aniline in 0.05 M H_3PO_4 into the eluent solution containing 0.05 M H_3PO_4. The working electrode was a Pt disk ultramicroelectrode. The potential axis on this graph represents potential applied to the working electrode during each scan. The time axis represents the time passing between the beginning of the flow injection experiment and the beginning of a particular scan (i.e., it represents a quantity proportional to the scan number). In the absence of aniline the shape of the CV curves is typical for a polycrystalline Pt electrode in acidic media. At negative potentials the electrode is covered with chemisorbed hydrogen. The charge needed to produce a monolayer of hydrogen on polycrystalline Pt is 2.20 C/m^2 (15). At positive potentials water decomposition takes place, leading to the formation of a two-dimensional phase of platinum oxide. The process is initiated by the electrosorption of the hydroxyl ion, which at more positive potentials undergoes deprotonation and structural rearrangements (16). When the electrode–solution interface is exposed to the analyte both the process of hydrogen adsorption and the process of platinum

© 1997 NRC Canada

Can. J. Chem. Downloaded from www.nrcresearchpress.com by 91.121.58.235 on 09/08/12
For personal use only.

Fig. 3. Overlapping cyclic voltammograms recorded during flow-injection experiments at a platinum electrode 12.5 μm in radius: (*a*) 1 mM aniline; (*b*) 0.1 mM NaSCN; (*c*) 0.1 mM Na_2MoO_4; (*d*) 0.1 mM $NaAsO_2$. The eluant was 0.05 M H_3PO_4; delay time: 0.2 s; rest potential: −0.35 V; scan rate: (*a*) 100 V/s, (*b*), (*c*), and (*d*) 20 V/s. Solid curves represent overlapping cyclic voltammograms recorded in the absence of analyte before and after the injection. The dotted lines illustrate changes caused by injection of the analyte.



oxide formation are strongly inhibited. In addition, at sufficiently positive potentials, the oxidation of adsorbed molecules is often observed (17). As a result profound changes in the shape of cyclic voltammograms take place, as is shown in Fig. 2. These changes are even more obvious when all CV curves are superimposed on one another (Fig. 3*a*). In this figure a solid line represents the electrode response to the supporting electrolyte alone (it actually consists of four CV curves recorded before the injection and four curves recorded after the analyte was flushed out by eluent, superimposed on each other). The dotted lines represent the electrode response in the presence of the analyte. The most notable changes in the current are observed in the hydrogen adsorption region or in the oxide formation region, and those changes may be either negative or positive depending on the electrode potential. Information about the concentration of aniline in solution can be obtained from the value of the current monitored at a fixed potential (e.g., 1100 mV). This is the simplest method but it provides a relatively poor signal-to-noise (S/N) ratio. Better precision can be obtained by integrating the change in the electrode response over a certain potential range (e.g., from E_1 to E_2) and expressing the result in terms of electrical charge. In reality, CV curves are recorded numerically by sampling current in equal time intervals. Consequently, the integration must be replaced by a summation carried out between two points (*a* and *b*) that correspond to potentials E_1 and E_2.

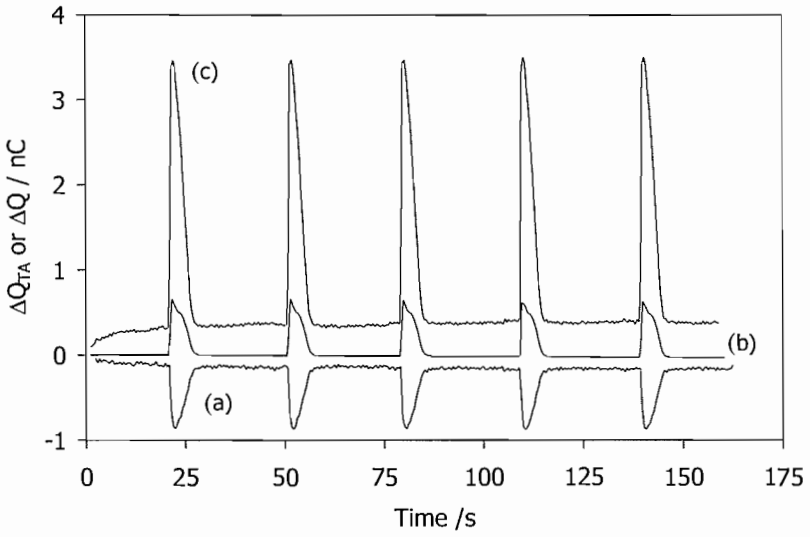
$$[1] \quad \Delta Q(k\tau) = \frac{\Delta E}{\nu}\left(\sum_{j=a}^{j=b} I(k,j) - \sum_{j=a}^{j=b} I(k_r,j)\right)$$

In this equation k is the scan number, τ is the time period between subsequent scans, ν is the scan rate, ΔE is the potential difference between two subsequent points on the CV curves, $I(k,E)$ represents the CV curve recorded during the kth scan, and $I(k_r,E)$ is the reference CV curve. The reference CV curve is obtained by averaging a few CV curves recorded at the beginning of the experiment (i.e., before injection of the analyte). Typically the averaging included the 5th to 11th curves. The integration can be carried out in the forward scan ($a = |E_i - E_1|/\Delta E$ and $b = |E_i - E_2|/\Delta E$, where E_i is the initial potential) or in the reverse scan ($a = (|E_i - E_v| + |E_v - E_1|)/\Delta E$ and $b = (|E_i - E_v| + |E_v - E_2|)/\Delta E$, where E_v is the vertex potential).

Can. J. Chem. Downloaded from www.nrcresearchpress.com by 91.121.58.235 on 09/08/12
For personal use only.

© 1997 NRC Canada

Fig. 4. Response of a Au ultramicroelectrode to five consecutive injections of 1 mM aniline. All experimental conditions as in Fig. 2. Curves (*a*) and (*b*) represent the ΔQ function calculated according to eq. [1] for the integration limits −0.4 to 0.1 V and 0.9–1.25 V, respectively. Curve (*c*) represents the ΔQ_{TA} function calculated according to eq. [2].



If the main contribution to the baseline noise is from the "white" noise generated by the potentiostat, the integration procedure usually provides a 3- to 4-fold improvement in the S/N ratio compared to the simple monitoring of the current at a fixed potential. However, in the case of severe environmental noise (e.g., power line noise) the improvement may be much greater.

All CV curves collected during the entire experiment (typically 200–4000 curves) were always stored in computer memory and could be saved onto a hard drive for future analysis, if desired. This means that, for the same flow-injection experiment, the electrode response can be obtained using different reference CV curves and (or) different integration limits. The choice of the reference curve has little or no effect on the results, as long as the curve is acquired in the absence of analyte; however, the electrode response expressed in terms of ΔQ strongly depends on the selection of the integration limits.

For example, in the case of aniline, the integration carried out in the forward scan between −400 and 100 mV (hydrogen adsorption region) produces negative peaks (Fig. 4, curve *a*). If the integration is done in the oxide formation region, between 900 and 1250 mV, the peaks on the ΔQ vs. time curve are positive (Fig. 4, curve *b*). However, integration between 500 and 1280 mV produces no peaks, because negative changes in the current between 500 and 950 mV are cancelled by positive changes occurring between 950 and 1280 mV. Hence, a proper selection of the integration region requires careful examination of changes in CV curves caused by a given analyte.

Alternatively, a total absolute difference function (ΔQ_{TA}) can be calculated in the following way:

$$[2] \quad \Delta Q_{TA}(k\tau) = \frac{\Delta E}{\nu} \sum_{j=1}^{N} |I(k, j) - I(k_r, j)|$$

where N is the number of data points collected during each scan and all other symbols have the same meaning as in eq. [1].

A plot of the total absolute difference parameter for the injection of aniline is shown in Fig. 4 (curve *c*). As expected, the magnitude of the peaks is larger than for ΔQ vs. time plots. Despite this, the signal-to-noise ratio is a few times lower than for curve *b*. The deterioration in the S/N ratio occurs partially because some regions of the CV curve (e.g., 0–500 mV in the forward scan and 1000–600 mV in the reverse scan) do not contribute significantly to the analytical signal, but (since they are included in ΔQ_{TA} calculations) they contribute to the baseline noise. Moreover, on the platinum electrode the level of baseline noise in the hydrogen region is a few times larger than in the "double layer" or oxygen region; this interesting finding will be discussed at the end of the paper.

The detector response can be reliably expressed in terms of the total absolute difference only if the baseline drift is small (say, less than 1% during the entire experiment). Such a situation is commonly encountered in flow-injection experiments. However, in CE or HPLC detection the baseline drift is sometimes significant, and in such cases the magnitude of the ΔQ_{TA} peaks is strongly affected by the choice of the reference CV curve. It should be stressed that both the baseline drift and the choice of reference CV curve have practically no effect on the detector response peaks expressed in terms of ΔQ based on eq. [1].

The detection method described is nearly universal for organic compounds since nearly all organic compounds adsorb on noble metal electrodes. In addition, many inorganic compounds, particularly anions, can also be detected. The shape of CV curves is strongly affected by the nature of the electrode material and the nature of the adsorbates. We will begin the discussion of the results by describing the role of these two primary factors.

Pt electrode

It is interesting that changes in the CV curve caused by adsorption of different species on Pt are quite similar. For example, the changes caused by injection of 1×10^{-3} M aniline and 1×10^{-4} M NaSCN are shown in Figs. 3*a* and 3*b*, respectively. In

© 1997 NRC Canada

Can. J. Chem. Downloaded from www.nrcresearchpress.com by 91.121.58.235 on 09/08/12
For personal use only.

Can. J. Chem. Downloaded from www.nrcresearchpress.com by 91.121.58.235 on 09/08/12
For personal use only.

Table 1. Values of ΔQ_{TA} per electrode surface area due to injection of 1×10^{-4} M analyte solutions in 0.05 M H_3PO_4.

	Pt electrode		Au electrode	
Analyte	Normalized response ($\mu C/cm^2$)	Reproducibility (%)	Normalized response ($\mu C/cm^2$)	Reproducibility (%)
NaI	1852	2.7	1056	1.5
NaSCN	1351	3.0	683	1.4
$NaIO_3$	1258	3.5	642	1.3
Thiourea	973	4.0	627	1.7
1,3-Dinitrobenzene	962	3.0	242	2.0
$NaAsO_2$	834	2.6	177	1.6
NaBr	741	2.5	702	1.8
Bipyridyl	727	2.0	214	1.7
Sodium mercaptoacetate	713	3.5	386	1.2
Na_2MoO_4	617	4.0	217	2.0
H_2SeO_3			215	2.3
Aniline	607	2.5	161	2.7
Pyridine	571	3.0	172	2.5
NaCl	562	2.3		
Benzoic acid	412	3.0	63	4.9
Buthylnitrile	317	3.5	30	4.1
$KMnO_4$	252	5.5	214	2.6
$Cd(NO_3)_2$	231	4.5	46	2.5
EDTA	128	3.2	152	2.4
$NaBrO_3$	83	7.0	16	12
Glycine	72	5.5	62	3.1
Ethanediol	36	23	24	8.4
N,*N*-Dimethylformamide	16	13	5	20
$LiAsF_6$	8	15	25	5.1
Methanesulfonic acid	2	29	8	14
KNO_3			7	18

the group of 26 compounds studied in this work only MoO_4^{2-}, AsO_2^-, and Cd^{2+} produced a significantly different pattern. A set of CV curves recorded during injection of 1×10^{-4} M Na_2MoO_4 and 1×10^{-4} M $NaAsO_2$ are shown in Fig. 3*c* and Fig. 3*d*, respectively.

To establish what type of compounds could be detected at the Pt electrode a series of experiments involving replicate injections of 1×10^{-4} M solutions of various analytes in 0.05 M H_3PO_4 was performed. In all cases the preconcentration time was 0.1 s, the scan rate was 20 V/s, and the injection loop was 50 μL. The rest potential was in all cases equal to −0.4 V. The normalized electrode response and reproducibility of results are listed in Table 1. The normalized response represents ΔQ_{TA} divided by the true surface area of the electrode. The reproducibility is expressed as the relative standard deviation of four replicate injections.

The results indicate that the Pt electrode is well suited for detection of aromatic compounds, thio-componds, heavy metals, and a number of inorganic anions; however, it exhibits very low sensitivity towards methanesulfonic acid, $LiAsF_6$, ethanediol, and *N*,*N*-dimethylformamide. The relative standard deviation of the results is typically 2–4% except for these compounds, which produce a very weak response.

Au electrode

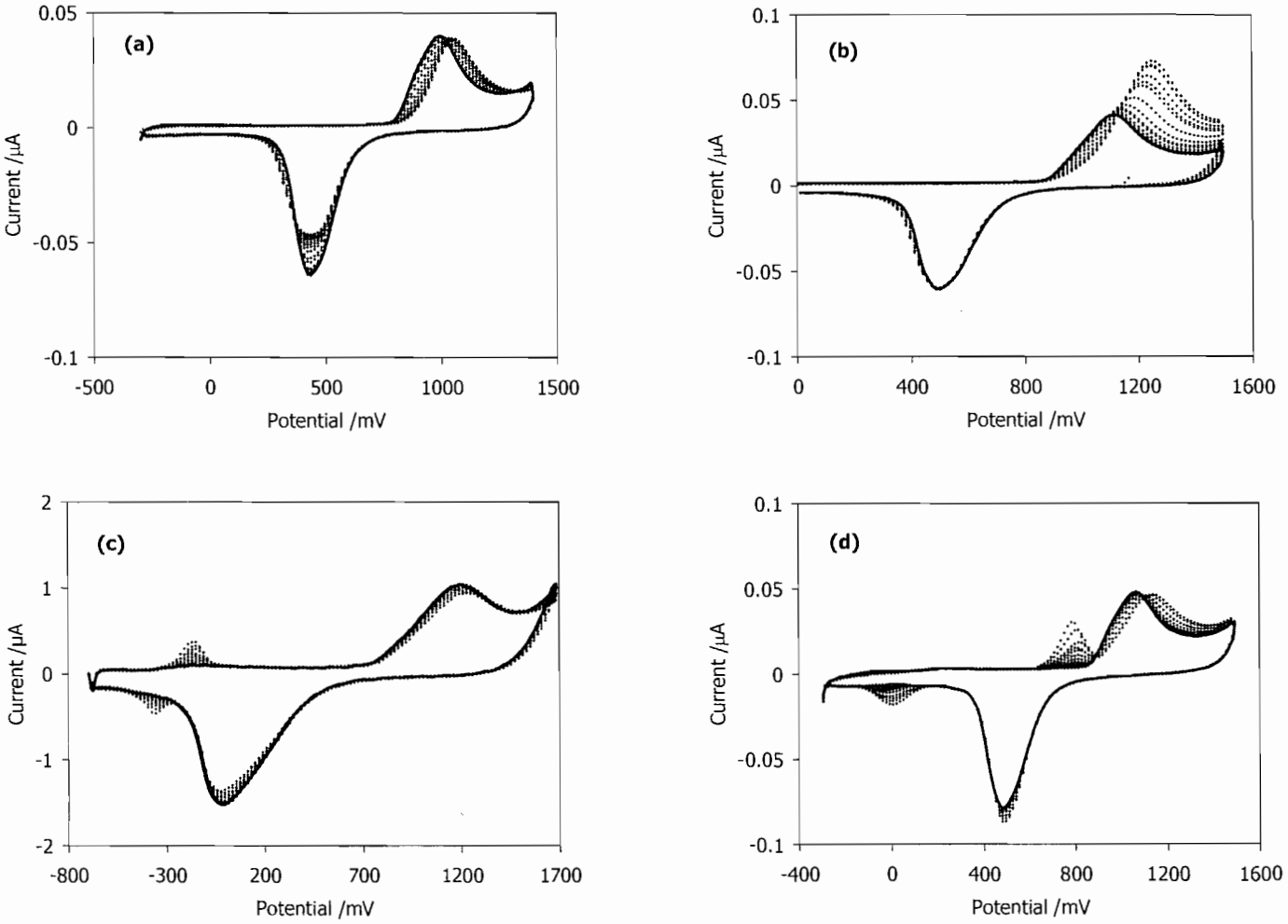
The characteristic feature of cyclic voltammograms at a gold electrode is a set of peaks associated with the formation and dissolution of a surface oxide layer at about 1.0 and 0.45 V, respectively. Most organic compounds and some inorganic anions cause a shift of the oxide formation peak towards a more positive potential, as can be seen in the case of 1×10^{-3} M pyridine (Fig. 5*a*).

For many organic compounds some increase of current, presumably due to their catalytic oxidation, can be noted at the most positive potentials; however, these kinetic currents are usually not very strongly pronounced in high sweep rate experiments. Exceptional in this regard are thio-compounds as well as some inorganic anions (e.g., IO_3^-, I^-, Br^-, SCN^-) that produce a well-defined oxidation current at potentials more positive than the gold oxide formation peak. This behavior is exemplified by a set of CV curves recorded during the injection of 1×10^{-4} M thiocyanate (Fig. 5*b*).

Since there is no significant adsorption of hydrogen on gold, Au electrodes have a relatively wide polarizibility range and, because of that, they are more suitable than Pt electrodes for the determination of metal ions. Cyclic voltammograms recorded during the injection of 1×10^{-5} M $Pb(NO_3)_2$ are

© 1997 NRC Canada

Fig. 5. Overlapping cyclic voltammograms recorded during flow-injection experiments at a 5 μm (radius) gold electrode: (*a*) 1 mM pyridine; (*b*) 0.1 mM NaSCN; (*c*) 0.02 mM $Pb(NO_3)_2$; (*d*) 0.1 mM H_2SeO_3. Eluant: 0.05 M H_3PO_4; delay time: 0.2 s; rest potential: (*a*) and (*b*) 0 V, (*c*) −0.7 V, (*d*) −0.3 V; scan rate: (*a*), (*b*), and (*d*) 20 V/s, (*c*) 670 V/s. Solid curves represent overlapping cyclic voltammograms recorded in the absence of analyte before and after the injection. The dotted lines illustrate changes caused by injection of the analyte.



shown in Fig. 5*c*. In this case the scan rate was 665 V/s and a preconcentration of Pb at the microelectrode was carried out for 0.4 s at −700 mV before each potential scan. An injection of Pb^{2+} ions under these conditions causes the appearance of a well-defined stripping peak at −150 mV and a corresponding reduction peak at −350 mV, as well as some inhibition of the oxide formation process. Similar behavior was observed for Cd^{2+}, Tl^{+}, Cu^{2+}, AsO_2^{-}, and SeO_3^{2-}. A set of CV curves recorded for that last ion is shown in Fig. 5*d*.

The normalized response of the gold electrode due to injection of various compounds is shown in Table 1. All experimental parameters were the same as in the Pt electrode study, except for the electrode radius, which was 5 μm. Despite significant differences in the electrochemical behavior of gold and platinum electrodes, the normalized responses of either electrode towards different compounds usually follow the same order. In most cases the sensitivity of the Pt electrode was higher than the Au electrode sensitivity due to a contribution from the hydrogen adsorption region; however, the reproducibility of results obtained with the gold electrode was somewhat better.

It should be stressed that the data in Table 1 allow only identification of compounds that can be detected by this method; the higher normalized response to an injection of 1×10^{-4} M analyte does not necessarily indicate a lower detection limit. For example, the normalized response of the Au electrode to a 1×10^{-4} M glycine solution is slightly higher than to an injection of $Cd(NO_3)_2$ at the same concentration; however, as it will be shown later, the detection limit for Cd^{2+} ($\sim 3 \times 10^{-8}$ M) is about 20 times smaller than the detection limit for glycine.

In general, the electrode response can be affected by the thermodynamic and kinetic parameters of adsorption, the rate of mass transport, and the electrochemical behavior of the adsorbed species. The free energy and the rate of adsorption depend on the electrode potential, the electrode material, and, to some extent, on the choice of the supporting electrolyte. The mass transport rate is strongly affected by the radius of the ultramicroelectrode, the solution flow rate, and the delay time between subsequent scans. Finally, the electrochemical behavior of adsorbates is affected by the choice of initial and vertex potential, the scan rate, the supporting electrolyte, and

© 1997 NRC Canada

Can. J. Chem. Downloaded from www.nrcresearchpress.com by 91.121.58.235 on 09/08/12
For personal use only.

Fig. 6. The effect of scan rate on the response of a Au electrode (5 μm in radius) to injections of 2×10^{-5} M Cd^{2+}, 2×10^{-5} M pyridine, and 4×10^{-5} M Br^- in 0.05 M H_3PO_4. The delay time was 400 ms and the rest potential was 0.2 V for both pyridine and Br^- and −0.5 V for Cd. The electrode response was expressed as ΔQ_{TA} (left-side scale) in the case of pyridine and Br^- and as the stripping peak charge (right-side scale) in the case of Cd.

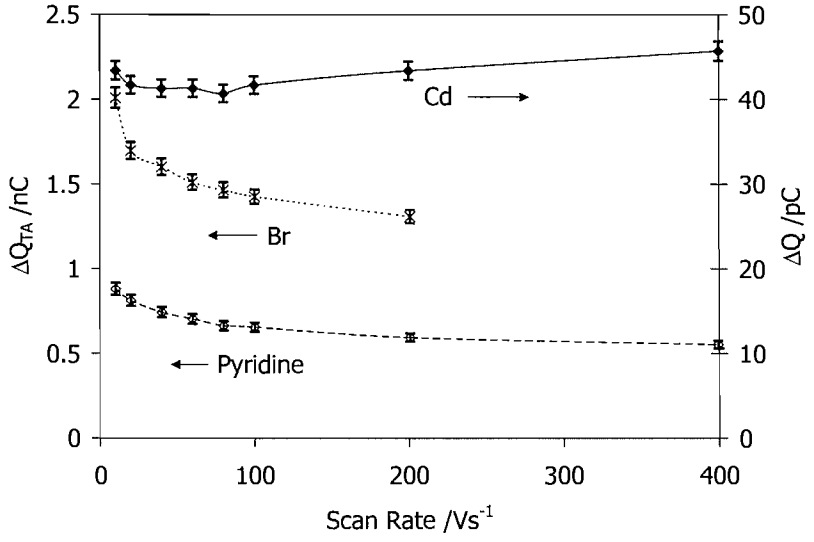
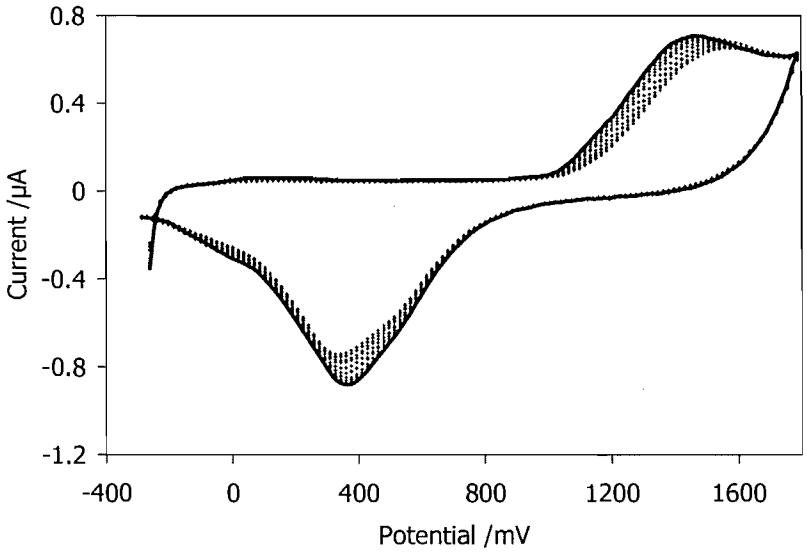


Fig. 7. Overlapping cyclic voltamograms for flow injection of 2×10^{-5} M pyridine in 0.05 M H_3PO_4 at a 5-μm Au electrode. The flow rate was 2.0 mL/min, and the sweep rate was 400 V/s. Each scan was preceded by a 200 ms preconcentration period at −0.5 V.



the electrode material. More detailed studies of the effect of experimental conditions on the electrode response were done for only a few compounds, mainly pyridine, Br^- and Cd^{2+}.

Effect of sweep rate

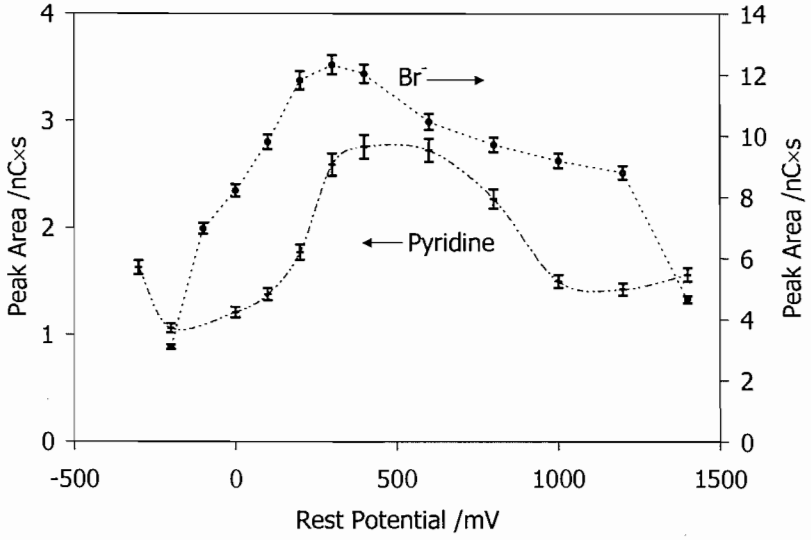
The use of this detection method in conjunction with fast separation techniques such as capillary electrophoresis requires the employment of high scan rates. From this point of view it is important to examine how the sensitivity of the method is affected by the scan rate. The results obtained for Cd^{2+} on the Au electrode show that the height of the flow-injection peak is constant within experimental error for scan rates between 10 and 400 V/s (see Fig. 6). This is not surprising since in this case the main contribution to the signal arises from the electrical charge needed to remove cadmium from the electrode. This charge depends on preconcentration conditions but should be independent of the scan rate.

In the cases of Br^- and pyridine the signal (expressed in terms of ΔQ_{TA}) decreases somewhat with scan rate (see Fig. 6). In this case the analytical signal originates mainly from changes in the oxide-formation and oxide-reduction peaks. Due to slow electrode kinetics and ohmic drops these peaks are flattened at very high scan rates (see Fig. 7), their charge decreases, and, consequently, changes caused by adsorption of analytes become smaller. Despite this, for all analytes studied (Cd^{2+}, Br^-, and pyridine) the signal-to-noise ratio was the

Can. J. Chem. Downloaded from www.nrcresearchpress.com by 91.121.58.235 on 09/08/12
For personal use only.

© 1997 NRC Canada

Fig. 8. The effect of rest potential on the response of a Au electrode (5 μm in radius) to injections of 2×10^{-5} M pyridine or 4×10^{-5} Br^- in 0.05 M H_3PO_4. The delay time was 400 ms and the scan rate was 20 and 30 V/s for pyridine and Br^-, respectively.



highest for scan rates between 200 and 700 V/s. The most dramatic improvement was observed for Cd, where the change in the scan rate from 10 to 700 V/s caused an increase in the S/N ratio from 26 to 410. It should be noted that currents measured in these experiments are essentially proportional to the scan rate and higher currents are obviously less affected by external interference coming from the power line, the computer monitor, or the separation current in capillary electrophoresis experiments.

The response of the Pt electrode is affected by the scan rate in a similar way to that described above; however, on this electrode the oxide-formation and oxide-reduction processes are slower than on gold and, consequently, the optimum scan rate is about 100 V/s.

Effect of the preconcentration potential

In Fig. 8 is shown the effect of the rest potential on the Au electrode response to injection of a solution of 2×10^{-5} M pyridine and 4×10^{-5} M Br^- in 0.05 M H_3PO_4. The optimum potential for preconcentration of these analytes is similar, about 0.4 V and 0.5 V for pyridine and Br^-, respectively. The relation observed for Br^- can be easily explained: at negative potentials the efficiency of preconcentration drops because adsorption of anions on the negatively charged electrode becomes thermodynamically unfavorable. Some drop of response at positive potentials is likely due to the competitive adsorption of hydroxyl ions. At even more positive potentials an irreversible oxidation of Br^- (presumably to BrO_3^-) takes place and at this point the electrode response declines rapidly (it should be noted that the Au electrode shows only residual response to BrO_3^- ions). The curve obtained for pyridine most likely reflects the dependence of the free energy of adsorption on potential. Extensive studies in this area were done by Lipkowski and Stolberg (18); however, direct comparison of results is difficult because of differences in the supporting electrolyte. The effect of the rest potential on the response at the Pt electrode for pyridine and bromide is similar to that observed at the Au electrode, but the optimum rest potential is about 200 mV more negative.

The effect of the rest potential on preconcentration of other compounds listed in Table 1 was also studied. For most anions and all neutral organic compounds on both Pt and Au electrodes the optimum preconcentration potentials were within ±150 mV of those reported for pyridine. This means that efficient preconcentration of different compounds can be carried out at the same rest potential, which is essential for the wide application of the method in CE or HPLC detection. However, as data in Fig. 9 indicate, the sensitive detection of metal ions (such as Cd^{2+}, Cu^{2+}, and Pb^{2+}) requires a different setting of the rest potential.

It is very interesting that these metal ions can be preconcentrated on the Au electrode at either negative or positive potentials. This is clearly evident from experiments with a normal ($E_{vertex} > E_{initial}$) or reversed scan direction but, to observe this effect, high scan rates must be employed so that the scanning step is short in comparison with the preconcentration period. It is well known that lead can be preconcentrated on the anode as PbO_2, but anodic preconcentration of Cd^{2+} and Cu^{2+} was rather unexpected. It is possible that at sufficiently positive potentials hydroxyl groups at the gold-solution interface undergo dissociation and some metal ions may become covalently attached to the surface via oxygen as Au-O-Me. The anodic preconcentration of Cd and Cu is not very efficient, perhaps because the adsorption equilibrium constants are relatively small; however, in the case of Pb the accumulation can be carried out equally well at negative or positive potentials.

Similar experiments were also done for Cd^{2+} on a Pt electrode but the anodic preconcentration of Cd^{2+} was not observed in this case.

Effect of the delay time

Preconcentration of analytes on the electrode takes place during the delay period (assuming that an appropriate rest poten-

Can. J. Chem. Downloaded from www.nrcresearchpress.com by 91.121.58.235 on 09/08/12
For personal use only.

© 1997 NRC Canada

Fig. 9. The effect of rest potential on the response of a Au electrode (5 μm in radius) to injections of 2×10^{-5} M Pb^{2+}, Cd^{2+}, or Cu^{2+} in 0.05 M H_3PO_4. The delay time was 400 ms and the scan rate was 750 V/s for Cd and 665 V/s for Pb and Cu. The potential was scanned between −0.6 and 1.7 V. The initial scanning direction was towards negative potentials in graph (*a*), and towards positive potentials in graph (*b*).

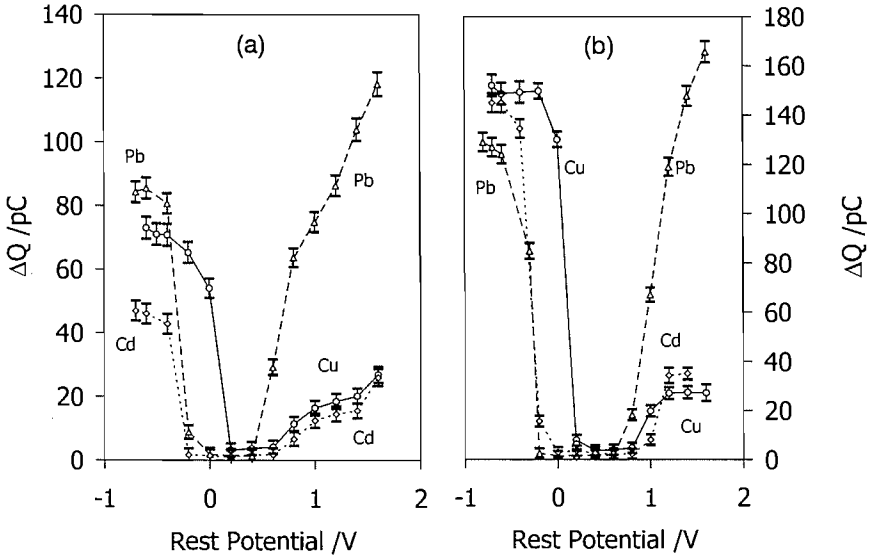
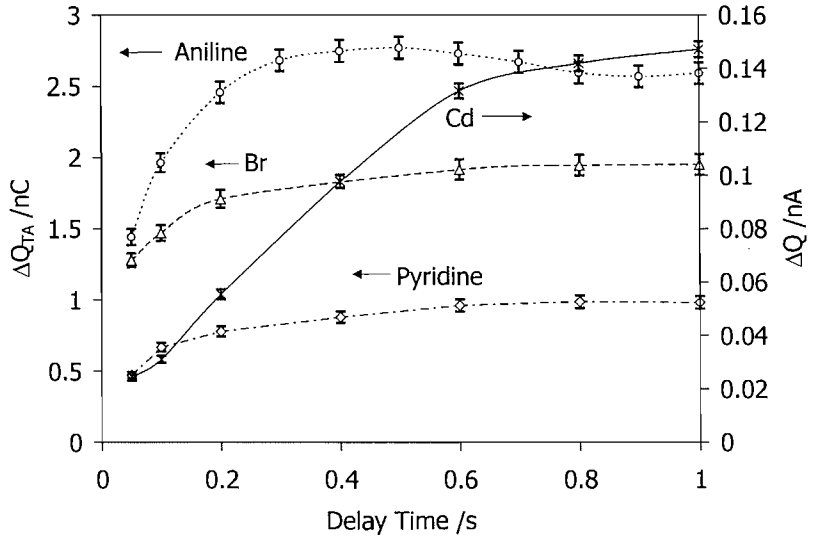


Fig. 10. The effect of delay time on the electrode response to injections of 3×10^{-5} M aniline, 2×10^{-5} M Cd^{2+}, 2×10^{-5} M pyridine, or 4×10^{-5} M Br^- in 0.05 M H_3PO_4. The following scan rates were used: aniline 100 V/s, Cd^{2+} 750 V/s, pyridine 20 V/s, Br^- 30 V/s. Measurements for aniline were done with a 12.5-μm Pt electrode, and all others were done with a 5-μm Au electrode. The rest potential was 0.2 V for pyridine and Br^-, −0.1 V for aniline, and −0.5 V for Cd^{2+}. The electrode response was expressed as ΔQ_{TA} (left-side scale) in the case of aniline, pyridine, and Br^-, and as the stripping peak charge (right-side scale) in the case of Cd^{2+}.



tial has been selected) and during scanning, when the electrode potential passes through the region of spontaneous adsorption. This last contribution, however, is very small at high scan rates (for example, results in Fig. 9 indicate that it is less than 3%). Studies of the functional relation between the electrode response and the delay time may provide some information about the kinetics of the adsorption process; here, however, only a brief discussion of this topic will be provided. In Fig. 10 the electrode response (expressed in terms of the stripping peak charge for Cd^{2+} and in terms of ΔQ_{TA} for pyridine, aniline, and Br^-) is shown as a function of the delay time. In the case of Cd^{2+}, pyridine, and Br^- the data were obtained at a Au ultramicroelectrode in 0.05 M H_3PO_4 solution. Concentration of the analyte was 2×10^{-5} M for both Cd and pyridine and 4×10^{-5} M for Br^-. Aniline at a concentration of 3×10^{-5} M in 0.05 M H_3PO_4 was studied on a Pt ultramicroelectrode. An examination of the CV curves indicates that the underpotential deposition (UPD) of Cd on gold is electrochemically reversible, consequently the accumulation of Cd on the electrode must be controlled by the mass transport. Results pre-

Can. J. Chem. Downloaded from www.nrcresearchpress.com by 91.121.58.235 on 09/08/12
For personal use only.

© 1997 NRC Canada

sented in Fig. 10 show that the electrode surface becomes saturated with cadmium within a 1-s time window. The limiting surface concentration calculated from the limiting charge was $(9.7 \pm 1.5) \times 10^{-10}$ mol/cm^2. Based on the initial slope of the ΔQ vs. time curve, the flux of the analyte was estimated as $(1.4 \pm 0.2) \times 10^{-9}$ mol s^{-1} cm^{-2}. In quiescent solutions the flux of a depolarizer at a disk ultramicroelectrode under steady-state conditions can be expressed as (19):

$$[3] \quad v = \frac{4DC_0}{\pi r}$$

where D is the diffusion coefficient, C_0 is the bulk concentration of electroactive species, and r is the electrode radius.

The steady-state mass transport is reached for times longer than $\tau_{ss} \approx r^2/D$ (19). By taking a likely value of the diffusion coefficient $D = 1 \times 10^{-5}$ cm^2/s and $C_0 = 2 \times 10^{-8}$ mol/cm^3, $v = 5.1 \times 10^{-10}$ mol s^{-1} cm^{-2} and $\tau_{ss} = 25$ ms can be obtained. The difference between observed and calculated fluxes can be explained by taking into account a convectional mass transport caused by the flow of solution (the linear velocity of solution near the electrode in this experiment was about 8.7 cm/s). This large contribution from convectional mass transport was confirmed by brief experiments involving amperometric detection of a 1 mM $Ru(NH_3)_6^{3+}$ solution in 0.05 M H_3PO_4 with a gold electrode. In this case the steady-state limiting current in the flowing (2.0 mL/min) electrolyte was about 1.9 times larger than that observed at the same electrode in a quiescent solution of the same composition. Because of this large contribution from convection the rate of mass transport to a 12.5 μm Pt electrode is not expected to be significantly different from that observed at the Au electrode.

Curves obtained for Br^-, pyridine, and aniline are similar to the one obtained for Cd, but in general the plateau is reached more quickly and the difference in the electrode response for the delay times 0.05 s and 1.0 s is much smaller than for Cd. These differences can be partially explained by the smaller limiting surface concentration for the organic adsorbates, more extensive preconcentration during the potential scan, and larger bulk concentration in the case of Br^- and aniline. However, the major cause of the observed differences may be due to slow cleaning of the electrode surface. It is very likely that large organic molecules adsorbed during the delay period are not completely oxidized during a single high-speed scan. Consequently, for some molecules the average residence time on the electrode surface may extend over a few cycles and, if this is the case, a smaller number of surface sites is available for adsorption during the delay period. Slow oxidation is clearly evident from analysis of CV curves obtained for pyridine with both Au and Pt electrodes (the total charge consumed in the oxygen adsorption region drops when the adsorbate is injected). For aniline on Pt and bromide on Au and Pt the total charge consumed in the oxygen adsorption region increases after the injection, but this does not exclude the possibility of incomplete oxidation. Besides, the oxidation processes likely go through several stages, and intermediates as well as products may reside on the interface for some time.

It should be stressed, however, that all substances studied in this work are eventually completely removed from the electrode. In all cases studied the cleaning of the electrode was complete after 20 or fewer scanning cycles. This conclusion can be derived from the fact that the electrode response always returns to normal within a few seconds after the supporting electrolyte flushes out the analytes.

It is difficult to conclude at this stage whether the rate of adsorption for aniline on Pt or pyridine on gold is controlled by mass transport or by interfacial kinetics, but there is no doubt that rates of adsorption for these substances are large. In all experiments the electrode was exposed to adsorbates for only a few seconds. Therefore in all cases when a high sensitivity of detection was obtained, the rate of adsorption had to be very high. This is in sharp contrast with results published by Bockris and Jeng (20), who reported that for many organic compounds (including aniline) several minutes of exposure to 10^{-4} M solution are needed in order to obtain a significant surface coverage on platinum. Wieckowski (21) pointed out that kinetic measurements reported by Bockris and Jeng (20) may be seriously skewed by slow mass transport through micropores in the platinum-black electrode employed in these measurements. It should also be emphasized that continuous scanning of the electrode potential between the hydrogen-adsorption and oxide-formation regions carried out several times per second may produce a very reactive interface, and this could explain high rates of adsorption observed in this work. Despite this, in some cases (e.g., ethanediol on Pt) slow adsorption kinetics may be the limiting factor in obtaining good sensitivity in detection.

Stability of response

Both electrodes tested provide a stable response for several hours without any mechanical or chemical treatment. The longest test (48 h) involved replicate measurements of the response for 1×10^{-5} M pyridine on a gold electrode in continuously flowing 0.05 M H_3PO_4 with the sweep rate of 20 V/s, the rest potential equal to 0.4 V, and the delay time equal to 0.1 s. The relative standard deviation of the results was 4.6% and there was no definite drift in the electrode sensitivity. A Pt electrode was tested during a 16-h period for the determination of 2×10^{-6} M Br^- in 0.05 M H_3PO_4 solution and gave similar results. In this experiment the sweep rate was 20 V/s, the rest potential was 0.2 V, and the delay time was 0.2 s.

Calibration curves and the detection limits

From an analytical point of view, the relation between concentration of analyte and the electrode response, called the calibration curve, is the most important. It is expected that for most substances the electrode response is proportional to electrode coverage. This is obviously the case when ΔQ due to oxidation of adsorbates is monitored. This assumption may be less obvious, but not unlikely, when inhibition of oxide formation or hydrogen adsorption by adsorbates is considered. For example, it has been shown that a decrease of charge in the oxide-formation region on platinum caused by adsorption of Cl^- is proportional to the surface coverage (ref. 17, p. 139). Consequently, if the electrode coverage is controlled by the rate of mass transport, a linear calibration curve is expected, up to the point when full electrode coverage is reached during the preconcentration period. When thermodynamics of adsorption or kinetics of the interfacial step control the electrode coverage, a linear calibration curve can be expected only for very small (perhaps <5%) coverages. Under typical experimental conditions used in this work and for strongly adsorb-

Can. J. Chem. Downloaded from www.nrcresearchpress.com by 91.121.58.235 on 09/08/12
For personal use only.

© 1997 NRC Canada

Fig. 11. Calibration curve obtained for Br^- on a 5-μm Au electrode in 0.05 M H_3PO_4. Circles represent the average peak area under the ΔQ vs. time curve measured for three to five injections. The ΔQ function was obtained by integrating CV curves between 1.1 and 1.4 V in the forward scan. The scan rate was 20 V/s and the delay time was 0.1 s.

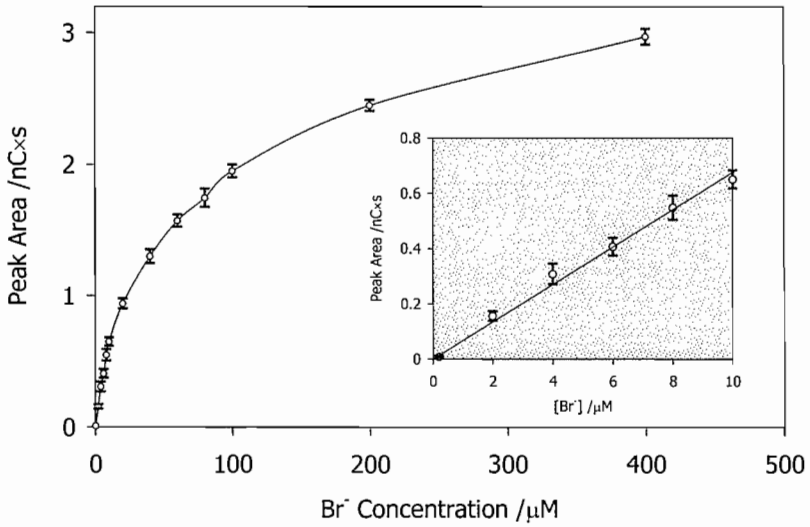


Table 2. Detection limits at Au and Pt electrodes in 0.05 M H_3PO_4.

Analyte	Electrode	Scan rate (V/s)	Rest potential (V)	Integration limits (V)	Detection limit (mol/L)
$Cd(NO_3)_2$	Au	750	–0.7	–0.4–0.0	3×10^{-8}
Glycine	Au	580	0.4	0.7–1.3	6×10^{-7}
$NaAsO_2$	Pt	100	–0.4	0.7–1.4	1×10^{-8}
NaBr	Au	580	0.4	0.7–1.3	3×10^{-8}
NaCl	Pt	100	0.2	0.5–1.0	2×10^{-8}
Pyridine	Au	580	0.4	0.7–1.3	4×10^{-8}
Pyridine	Pt	100	0.2	0.5–1.0	3×10^{-8}

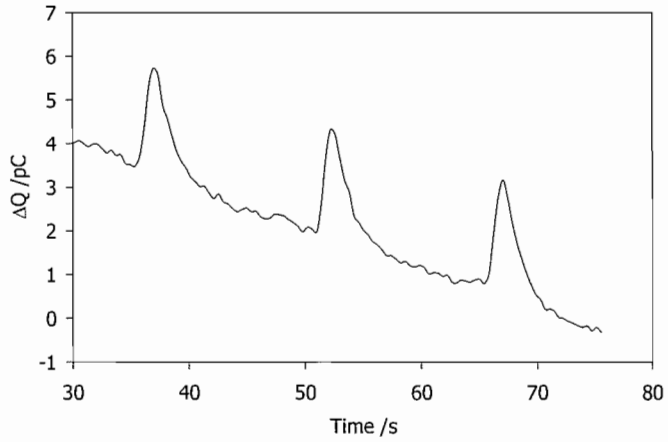
ing substances (such as pyridine, Br^-, or Cd^{2+} on gold) the linear portion of the calibration curve extends from about 10^{-7} M to about 10^{-5} M. A typical calibration curve obtained for the detection of Br^- on a Au ultramicroelectrode in 0.05 M H_3PO_4 is shown in Fig. 11. It should be noted that electrode response can be expressed in various ways as peak heights or peak areas. In addition, the magnitude of the flow-injection peaks depends on choice of the data processing methods (see eqs. [1] and [2], and Fig. 4). Results shown in Fig. 11 represent the average peak area under the ΔQ vs. time curve measured for three to five consecutive injections of a standard solution; the ΔQ function was obtained by integrating CV curves between 1.1 and 1.4 V in the forward scan. The scan rate was 20 V/s and the delay time was 0.1 s.

Measurements carried out for small analyte concentrations allow the detection limit C_{DL} to be estimated:

$$[4] \quad C_{DL} = \frac{3s_b}{m}$$

where s_b is the standard deviation of the baseline around the flow-injection peak and m is the sensitivity of the method

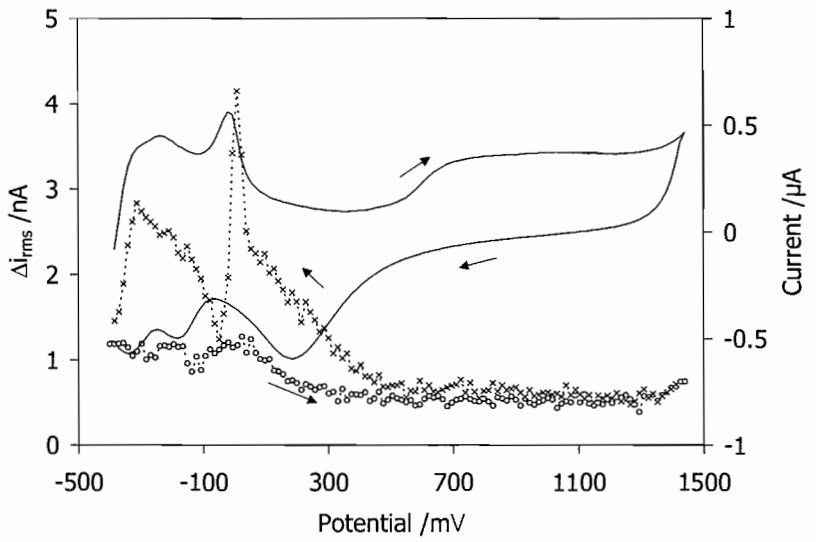
Fig. 12. Response of a 5-μm Au electrode to three consecutive injections of 2×10^{-7} M $Cd(NO_3)_2$ in 0.05 M H_3PO_4. The scan rate was 750 V/s, the rest potential was −0.5 V, and the delay time was 0.4 s. The electrode response is expressed in terms of the stripping peak charge.



Can. J. Chem. Downloaded from www.nrcresearchpress.com by 91.121.58.235 on 09/08/12
For personal use only.

© 1997 NRC Canada

Fig. 13. Potential dependence of the root-mean-square current noise (–×–×– forward scan, –○–○– reverse scan) and the current–potential relation (solid line) for a 12.5-μm Pt electrode in 0.05 M H_3PO_4. The scan rate was 100 V/s, the rest potential was −0.4 V, and the delay time was 0.2 s.



(a change in the peak height divided by the change in concentration) near the detection limit.

The detection limits obtained for several substances at Au and Pt electrodes are given in Table 2. To insure the best signal-to-noise ratio the measurements were carried out at high scan rates. In all cases the delay time was 0.4 s, but the rest potential and integration limits in the calculation of the $\Delta Q(t)$ function were optimized to obtain the maximum S/N ratio. Details of experimental conditions are given in Table 2. For all analytes, except Cd^{2+}, the potential scanning range was from −0.7 to 1.7 V on gold and −0.4 to 1.5 V on platinum.

In the case of cadmium the vertex potential was +0.7 V; this means that the potential scan was reversed before reaching the oxide formation peak. It should be noted that the stripping peak for cadmium occurs in a relatively narrow potential range and is superimposed on a relatively small background current. Because of that, it was possible to obtain a good detection limit despite a relatively small signal. The actual trace of the $\Delta Q(t)$ curve for the flow injection of 2×10^{-7} M $Cd(NO_3)_2$ is shown in Fig. 12. Despite some baseline drift, the response for consecutive injections is quite reproducible; the relative standard deviation for six replicates was 6.6 and 9.0%, based on peak height and peak area measurements, respectively. Peaks of this magnitude can easily be used in quantitative analysis although they represent only 2.5 pC of electrical charge generated by the oxidation of 1.3×10^{-17} mol of Cd. The electrode coverage in this case does not exceed 0.7%. At the detection limit the typical electrode coverage is about 0.1% and the quantity of substance adsorbed at a 5-μm electrode is about 1 attomol, hence the method is suitable for analysis of very small samples. In this regard the method offers very significant improvement over existing electroanalytical methods.

Data in Table 2 also indicate that this method can compete with well-established methods when the ability to detect small concentrations is compared. The detection limit for Cl^- on Pt is a few times lower than the limit reported for the pulse amperometric detection method (22). Our detection limit for AsO_2^- is comparable with the detection limit obtained for the same analyte using dc amperometric detection with a much larger working electrode (23). The same authors also determined the detection limit for AsO_2^- at a Pt electrode, 12.5 μm in radius, and reported a value 5 times higher value than ours. This comparison is significant, because amperometric detection is considered to be the most sensitive electrochemical detection method in flowing solutions (2). It should also be stressed that amperometric detection is applicable only to substances that can be easily oxidized or reduced, whereas the method described in this work can be used for the detection of any surface-active substance.

The detection limit can be further decreased by increasing the preconcentration time in cases where the adsorption process is limited by mass transport or surface kinetics; however, in some applications (e.g., CE or HPLC detection) this may lead to a deterioration of the zone resolution.

An improvement in the detection limit can also be achieved by lowering the baseline noise. The noise level in such measurements depends to a large extent on the quality of the electronic equipment. In this case a relatively inexpensive 12-bit data acquisition board was used, together with an in-house-built potentiostat. Certainly there is room for improvement; for example, the potentiostat could be redesigned to allow grounding of the auxiliary electrode (hence grounding of the electrolyte solution). Hopefully this would provide better shielding from environmental noise. Also, increasing the resolution of the analog-to-digital converter from 12- to 16-bit should be very beneficial.

Interestingly, however, the level of the background noise is also determined by the properties of the electrode. For example, in the case of the Pt ultramicroelectrode the level of noise was much higher in the hydrogen region than in the oxygen adsorption region. In Fig. 13 the $\Delta i_{rms}(E)$ function represents the standard deviation of current measured at a given potential

© 1997 NRC Canada

Can. J. Chem. Downloaded from www.nrcresearchpress.com by 91.121.58.235 on 09/08/12
For personal use only.

for 64 consecutive CV curves. Analyses of current fluctuations in the hydrogen region done both in the time domain and after the Fourier transformation did not reveal an obvious trend or pattern. At this stage it is difficult to explain the details of this phenomenon; however, it may be related to the fact that the hydrogen-adsorption process is very fast and the current strongly depends on potential (sharp peaks). Consequently, a small fluctuation in the electrode potential may cause a relatively large fluctuation in the current. The noise level for the Au electrode was independent of potential and comparable to that observed for the Pt electrode in the oxygen-adsorption region.

All experiments described up to now in this paper were done using dilute H_3PO_4 solutions as eluents; however, other supporting electrolytes were also briefly tested. The experiments involved detection of Br^-, pyridine, and glycine with a Au electrode. Acidic solutions containing weakly adsorbing anions such as HNO_3 or $HClO_4$ gave results similar to those described in this paper. In NaH_2PO_4/Na_2HPO_4 buffer or in dilute KOH solutions the sensitivity of the method drops by one or two orders of magnitude. In a borax solution (pH = 9.2) or in a carbonate buffer (pH $\approx$ 10) many organic compounds can be detected with sensitivity only 2 to 3 times worse than in acidic solutions. However, a Au electrode appears less stable in basic solutions than in acidic solutions. For example, during detection of glycine, a 10% decrease in sensitivity was observed over a period of 25 h in a continuously flowing 0.05 M $Na_2B_4O_7$ solution.

Acknowledgment

The financial support of the Natural Sciences and Engineering Research Council of Canada (NSERC), through a research grant, is gratefully acknowledged.

References

1. P.T. Kissinger. *In* Laboratory techniques in electroanalytical chemistry. *Edited by* P.T. Kissinger and W.R. Heineman. Dekker, New York. 1984. p. 611.
2. D.C. Johnson, S.G. Weber, A.M. Bond, R.M. Wightman, R.E. Shoup, and I.S. Krull. Anal. Chim. Acta, **180**, 187 (1986).
3. S.F.Y. Li. Capillary electrophoresis: principles, practice and applications. Elsevier, Amsterdam. 1992.
4. D.C. Johnson and W.R. LaCourse. Anal. Chem. **62**, 589A (1990).
5. L.D. Burke and K.J. O'Dwyer. Electrochim. Acta, **34**, 1659 (1989).
6. L.E. Welch, W.R. LaCourse, D.A. Mead, Jr., D.C. Johnson, and T. Hu. Anal. Chem. **61**, 555 (1989).
7. J. Wen and R.M. Cassidy. Anal. Chem. **68**, 1047 (1996).
8. P.T. Kissinger. J. Liq. Chromatogr. **4**, 321 (1981).
9. H. Gunasingham, K.P. Ang, and C.C. Ngo. Anal. Chem. **57**, 505 (1985).
10. D.M. Novak, B.V. Tilak, and B.E. Conway. In Modern aspects of electrochemistry. Vol. 14. *Edited by* J.O'M. Bockris, B.E. Conway, and R.E. White. Plenum Press, New York. 1982. p. 250.
11. H. Angerstein-Kozlowska, J. Klinger, and B.E. Conway. J. Electroanal. Chem. **75**, 45 (1977).
12. H. Angerstein-Kozlowska, B.E. Conway, K. Tellefsen, and B. Barnett. Electrochim. Acta, **34**, 1045 (1989).
13. A.S. Baranski and A. Szulborska. J. Electroanal. Chem. **373**, 157 (1994).
14. M. Bellanger. Digital processing of signals. Wiley, Chichester. 1984. p. 14.
15. B.E. Conway, H. Angerstein-Kozlowska, F.C. Ho, J. Klinger, B. MacDugall, and S. Gottesfeld. Faraday Discuss. Chem. Soc. **56**, 199 (1973).
16. H. Angerstein-Kozlowska, B.E. Conway, and W.B.A. Sharp. J. Electroanal. Chem. **43**, 9 (1973).
17. S. Gilman. *In* Electroanalytical chemistry. *Edited by* A.J. Bard. Dekker, New York. 1967. p. 161.
18. J. Lipkowski and L. Stolberg. *In* Adsorption of molecules at metal electrodes. *Edited by* J. Lipkowski and P.N. Ross. VCH, New York. 1992. p. 202.
19. R.M. Wightman and D.O. Wipf. *In* Electroanalytical chemistry. Vol. 5. *Edited by* A.J. Bard. Dekker, New York. 1988.
20. J. O'M. Bockris and K.T. Jeng. J. Electroanal. Chem. **330**, 637 (1992).
21. A. Wieckowski. J. Electroanal. Chem. **352**, 313 (1993).
22. D.S. Austin, J.A. Polta, T.Z. Polta, A.P.-C. Tang, T.D. Cabelka, and D.C. Johnson. J. Electroanal. Chem. **168**, 227 (1984).
23. R.S. Stojanovic, A.M. Bond, and E.C.V. Butler. Anal. Chem. **62**, 2692 (1990).

Can. J. Chem. Downloaded from www.nrcresearchpress.com by 91.121.58.235 on 09/08/12
For personal use only.

© 1997 NRC Canada

The partial discharge of electrosorbates and its influence in electrocatalysis

J.W. Schultze and D. Rolle

Abstract: The integral charge flow during electrosorption processes can be described by the electrosorption valency, γ. This dimensionless thermodynamic parameter consists of contributions from the penetration of the substance into the double layer, g, and the partial charge transfer, λ. g varies between 1 for discharged substances and very small values, g_{min}, for electrostatic adsorption without transfer. The charge transfer coefficient, λ, can be estimated empirically using Pauling's concept of electronegativity, χ, but the quantitative correlation is different for anions and cations due to the different type of bonding. The γ value of special electrosorbates depends on the nature of the solvent and ligands. Theoretical model calculations justify the influence of χ and solvation. The partial discharge of ions causes a decreasing electrostatic influence in electrocatalysis. Examples are given for ion (ITR) and electron transfer reactions (ETR).

Key words: electrosorption valency, partial charge transfer, bond formation, solvation, double layer.

Résumé : Il est possible de décrire l'écoulement intégral de la charge accompagnant les processus d'électrosorption par la valence d'électrosorption γ. Ce paramètre thermodynamique sans dimension est formé de contributions provenant de la pénétration de la substance dans la double couche, g, et du transfert partiel de charge, λ. Les valeurs de g varient entre l'unité, pour les substances déchargées, et des valeurs très faibles, g_{min}, pour une adsorption électrostatique sans transfert. Il est possible de faire une évaluation empirique du coefficient de transfert de charge, λ, en utilisant le concept d'électronégativité de Pauling, χ; toutefois, la corrélation quantitative est différente pour les anions et les cations à cause des différences dans les types de liaison. La valeur de γ pour des électrosorbats spéciaux dépend de la nature du solvant et des coordinats. Des calculs sur un modèle théorique justifient l'influence de χ et de la solvatation. La décharge partielle des ions provoque une diminution de l'influence électrostatique dans l'électrocatalyse. On donne des exemples pour des réactions de transfert d'ion (RTI) et de transfert d'électron (RTE).

Mots clés : valence d'électrosorption, transfert partiel de charge, formation de liaison, solvatation, double couche.

[Traduit par la rédaction]

1. Introduction

Since the classical paper of Helmholtz (1), the structure of the metal–electrolyte interface has been the subject of many investigations. Important contributions have been made by Brian Conway, in particular, with many papers on electrosorption processes and electrocatalysis (2–6).

In spite of careful investigations, the relation between molecular electrosorption models and macroscopically determined parameters is open to discussion. Taking into account the partial charge transfer coefficient λ, an electrosorption reaction can formally be written as

$$[1] \quad \nu M - OH_2 + S^z aq \rightleftharpoons M_\nu - S^{z+\lambda} + \lambda e^- + \nu H_2O$$

Received May 22, 1997.

This paper is dedicated to Professor Brian E. Conway on the occasion of his 70th birthday.

J.W. Schultze[1] **and D. Rolle.** Arbeitsgemeinshaft Electrochemischer Forschungsinstitutionen e.V. - Institut an der Heinrich-Heine-Universität Duesseldorf, D 40225 Duesseldorf, Germany.

[1] Author to whom correspondence may be addressed. Telephone: 49-211-81-14750. Fax: 49-211-81-12803.

Electrochemical experiments, on the other hand, yield the macroscopic parameters, i.e., metal charge q_m, and the surface excess Γ of the specifically adsorbed substance S^z and the (mostly nonspecifically) cosorbed counterions X to maintain the condition of electroneutrality

$$[2] \quad -q_m = z_s F \Gamma_s + z_x F \Gamma_x$$

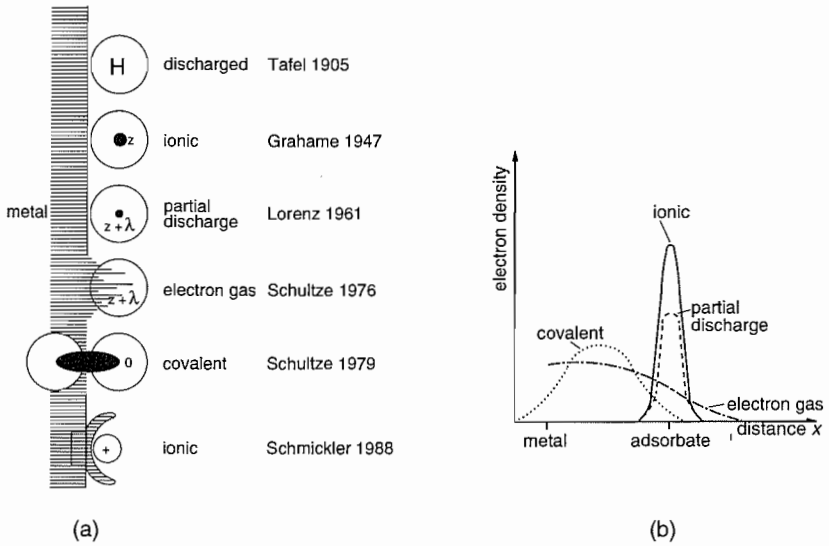
Therefore, the role of partial charge transfer is controversial, since it cannot directly be determined in electrochemical experiments, but it is involved in the metal charge q_m (7). While λ was neglected in the fundamental papers of Grahame (8), it was overemphasized in the papers by Lorenz and Salié (9, 10).

In extension of a recent analysis, the possibilities and limitations of charge transfer and the accompanying charge distribution will be analysed in dependence on the molecular parameters of the systems. In general, the analysis will be valid for all substances such as small or large ions, and neutral molecules. To show the most important contributions, however, we confine the following discussion to mononuclear ions. Due to its practical relevance, the impact of the charge transfer on the rate of ion (ITR) and electron transfer reactions (ETR) will be discussed. New results on the electrosorption valency of organic molecules are given elsewhere (11).

© 1997 NRC Canada

Can. J. Chem. Downloaded from www.nrcresearchpress.com by 91.121.58.235 on 09/08/12
For personal use only.

Fig. 1. (*a*) Schematic representation of the electron density in electrosorbates according to various authors; (*b*) density along the distance normal to the surface.



2. The physical model of the charge distribution

Physical models of charge distribution and the energetics of the system have been developed for some limiting cases. Figure 1*a* shows the charge distribution according to the concepts of various authors. While Tafel assumed complete discharge for hydrogen on platinum without specification of bond formation (12), Grahame (8) used ionic charges in his double layer models. On the other hand, he assumed that electrosorption is enhanced by the formation of covalent bonds, in contradiction to his electrostatic models. The model of Lorenz (10) of partially discharged ions is reasonable, but also neglects both bond formation and charge accumulation between the metal atoms of the surface and the electrosorbate. For underpotential deposition (UPD) layers, we have introduced the model of the adsorbed ion penetrating into the electron gas (13), while for metal–halide systems, the role of the covalent bond has been emphasized (14, 15). In this case, the electrons are enriched along the metal–anion axis. Since the orbitals of the metal atom are involved, even a demetallization may be discussed, but at least the electron gas within the surface will be modulated. Schmickler, on the other hand, postulated the formation of a dipole image for the limiting case of electrostatic adsorption (16), for example, an accumulation of negative charge around a positive ion. The corresponding electron densities normal to the surface are described in Fig. 1*b*. All the models shown in Fig. 1 refer to limiting cases, while in real systems intermediate electron distributions may be observed.

The electronic interaction in complexes $M–S^{z+\lambda}$ and the charge transfer have a great impact on energetic models as is shown in Fig. 2. The energies of the ion, the electrons, or of the total interface may be discussed as a function of weak or strong interaction. The traditional model considers the potential energy of the ion in the outer and inner layer, respectively (Fig. 2*a*). The model by Plieth and Vetter (17) considers separately the electron states of the metal and adsorbate, respectively, which corresponds to a weak interaction. The broadening of the energetic states of the adsorbate was explained by interaction with the solvent. A fast electronic exchange between the states in the metal and the electrosorbate was assumed. The Anderson–Newns model for gas phase adsorption (18) is similar, but here the broadening of the adsorbed state is due to the strong interaction with the solid. It was later applied by Kornyshev and Schmickler (19) for electrosorption.

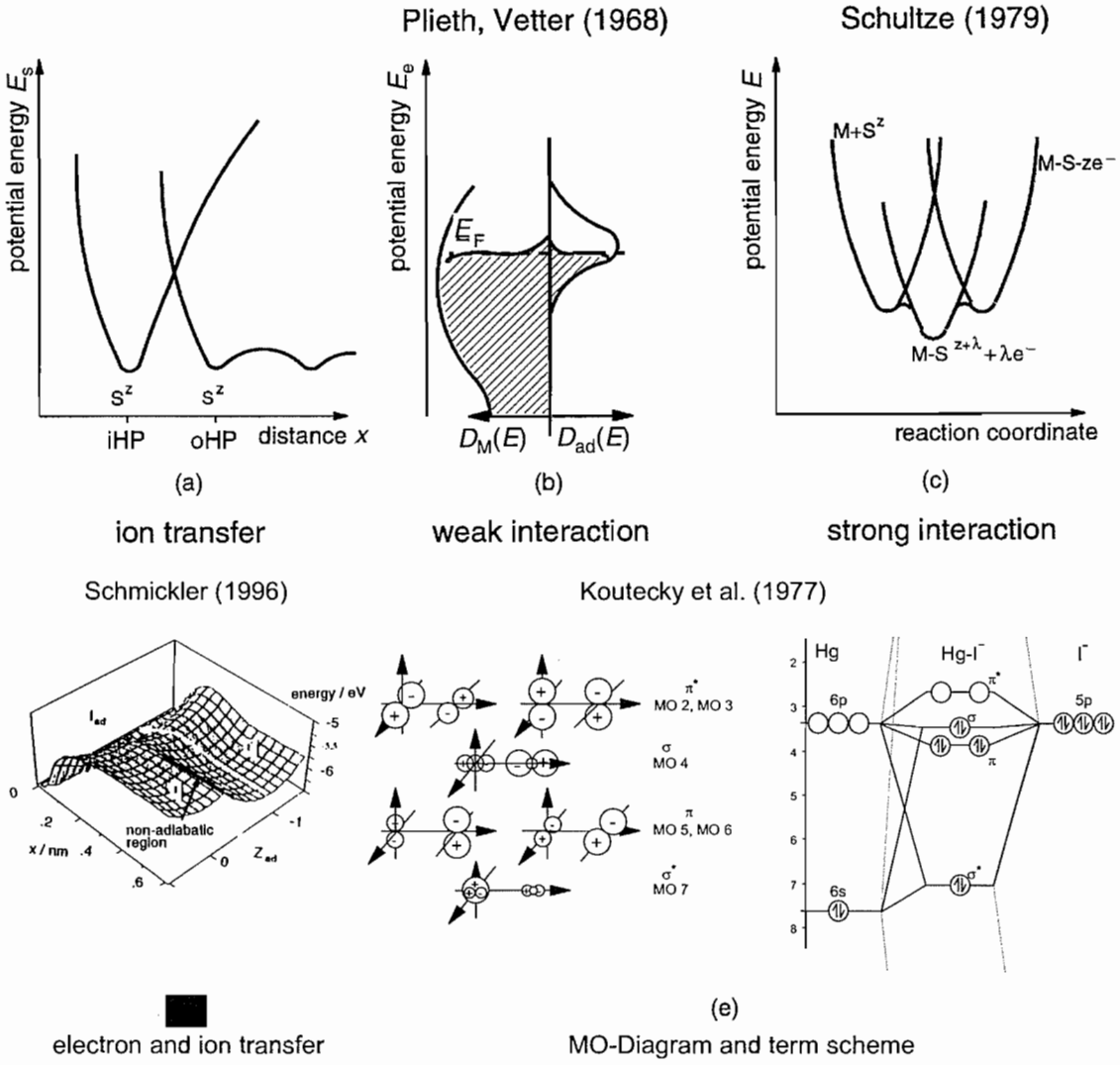
For strong interaction, on the other hand, the total energy of the interface has to be considered instead of that of single electron states. Following a suggestion by R.A. Marcus, the potential energy surfaces of the whole system have to be taken into acccount (14). In addition to the energy surfaces of reactants and products, that of the adsorbate has to be included (Fig. 2*c*). In the case of strong electrosorption, this causes the formation of a new minimum. This diagram plotted along the reaction coordinate is the one-dimensional part of a three-dimensional model used by Schmickler for the general treatment of ion and electron transfer reactions in the double layer (Fig. 2*d*) (20). For the example of Pt/I^-, the potential energy minimum of the adsorbed state is clearly pronounced at a small distance of about 0.1 nm just in front of the electrode and at a partial charge of about -0.5.

In all of these models the chemical interaction between the atoms is not taken into account directly. Therefore, the models are more or less useful for cationic adsorbates interacting with the electron gas of the metal. For covalent systems, however, the atomic orbitals and the formation of molecular orbitals must be considered. EHMO calculations yield MO diagrams and term schemes of the MO levels (15). The most important parts of the full diagrams are shown for Hg/Br^- and Hg/I^-, respectively, in Fig. 2*e*. It can be seen that the most important orbitals are the π-orbitals MO 5,6 formed by the *p*-orbitals of Hg and the halide. Contributions from the other orbitals are smaller (15). The quantitative results of these calculations were not reliable, but the calculations did show the localization of the binding electrons along the Hg—X axis. These pictures may be appropriate for the case of halide adsorption with strong covalent bonds, while they may be less useful for UPD systems.

Can. J. Chem. Downloaded from www.nrcresearchpress.com by 91.121.58.235 on 09/08/12
For personal use only.

© 1997 NRC Canada

Fig. 2. Energetic description of electrosorption reactions. (*a*) Classical ion transfer ($\lambda = 0$). (*b*) Model of Plieth and Vetter for the energy of electronic states E_e at the interface for a solvated adsorbate with weak interaction (17). (*c*) Potential energy E of the systems $M + S^z$, $M - S - ze^-$, and $M - S^{z+\lambda} + \lambda e^-$ versus the generalized reaction coordinate according to Marcus theory (14). (*d*) Schmickler's generalized description of ion and electron transfer reactions for the case of a partially discharged iodide ion on platinum (20). $I^- \rightarrow I_{ad}$ (ITR), $I^- \rightarrow I + e^-$ at 0.5 nm (nonadiabatic ETR). E = relative energy consisting of various contributions. (*e*) MO diagram for $Hg–Br^-$ and term scheme for $Hg–I^-$ from EHMO calculations. Most important MOs are shown; for full diagrams see ref. 15.



3. The electrosorption valency γ

The determination of the charge distribution in electrosorbates is more difficult than for bulk materials. X-ray diffraction (21) and scanning probe microscopy (SXM) methods (22, 23) have a high sensitivity to structures and symmetries, but the electronic structure of the interface remains unknown. Spectroscopic investigations show surface vibrations and symmetries, but not the electronic distribution. The electrical conductivity of ultrathin metal films usually decreases with electrosorption. New results for halide ions adsorbed on epitactically grown Ag(100) films indicate a qualitative connection with the discharge of the ions (24) at which the electron waves are scattered. A quantitative relation, however, has not yet been obtained.

Many electrochemical data of electrosorbates reflect the charge transfer: e.g., the shift of the potential of zero charge (25). From eq. [1] it may be assumed that the charge flow of an electrosorption reaction yields the charge transfer coefficient λ directly. This is, however, not true, since capacitive effects are combined with the change of the interface structure. A straightforward analysis of electrosorption reactions is possible using the Gibbs equation for systems with excess supporting electrolyte. Corresponding to the Nernst equation and Faraday's law, the electrosorption valency γ was defined by the partial derivatives given in eq. [3] (26):

$$[3] \quad -(\delta q_m/\delta \Gamma_S)_U = (\delta \mu_S/\delta U)_{\Gamma_S} = \gamma F$$

with q_m = metal charge, Γ_S = surface concentration of S, μ_S = chemical potential, and U = electrode potential. This thermodynamic analysis can be applied to all electrosorbates, i.e., ions as well as neutral molecules, for all charge transfer coef-

© 1997 NRC Canada

Can. J. Chem. Downloaded from www.nrcresearchpress.com by 91.121.58.235 on 09/08/12
For personal use only.

Can. J. Chem. Downloaded from www.nrcresearchpress.com by 91.121.58.235 on 09/08/12
For personal use only.

Table 1. Electrosorption valencies (γ) for various systems in aqueous solutions.

M	S^z	γ	Reference
Anions			
Au(111)	Cl^-	–0.8	38
Au(111)	Br^-	–0.78	39, 40
Au	Br^-	–0.39	41
Au	I^-	–1.01	41
Au	S^{2-}	–2.0	42
Au	SO_4^{2-}	–1.0	43
Ag(110)	Cl^-	–0.53	38, 44
Ag(100)	Br^-	–0.68	40
Ag(111)	S^{2-}	–1.4	22
Pt	Br^-	–0.9	6
Cations			
Au	Cu^{2+}	1.84	45
		1.40	46
Au	Cd^{2+}	1.6–2.0	46
Au	Bi^{3+}	2.2	45
		2.4	47
		2.7	46
Au	Tl^+	0.61	45
Au	Hg_2^{2+}	0.94	45, 48
Au	Pb^{2+}	2.0	46
Pt(111)	Zn^{2+}	2.0	49
Cosorption			
Au(111)	Cu^{2+}, Br^-	1.6–1.8	50
Pt	Cu^{2+}, ClO_4^-	2.0	51
Pt	Cu^{2+}, SO_4^{2-}	1.75	51
		1.4–2.0	52

ficients $0 < -\lambda/z < 1$ (26, 27). But the analysis has to be extended for dilute electrolytes due to the increasing influence of the diffuse double layer (5) or in the case of specific interaction with other ions or molecules X (28).

In contrast to Faraday reactions at electrodes, γ is a fractional value, in general between 0 and z. Moreover, it can change with Γ and with U. This is especially observed with ordered structures on single crystal planes where the cosorption changes stepwise. Therefore, it is useful to take the thermodynamic value γ_N as reference value. This refers to small coverages at the potential of zero charge, i.e., the electrocapillary maximum. This procedure eliminates capacitive terms and the sorbate–sorbate interaction.

Experimental methods for the determination of γ have been described and compared in refs. 13 and 26. A critical comparison showed that experimental reproducibility of different methods and papers is typically better than 0.1. Data were collected for inorganic systems in water and nonaqueous solvents (13) as well as for organic molecules (29–31). Recent measurements, often on well-defined single crystal planes, are evaluated in Table 1. Most of these values are based on a complete thermodynamic analysis of chronocoulometric data as a function of U and μ_S. A final analysis of q/Γ or μ/U diagrams gives electrosorption valencies showing a reasonable agreement.

For comparison with vacuum measurements, an effective "surface dipole" m can be obtained from γ and the Helmholtz capacity C_H using eq. [4] (32, 33):

$$[4] \quad m = (ze_0/4\pi C_H)(1 - \gamma/z)$$

but there is no additional information on the structure of the interface, since this dipole refers to contributions from the electrosorbate as well as cosorbed counterions (see eq. [2]).

4. Correlation between γ and microscopic parameters

To correlate γ with the microscopic parameters λ and g, the structure of the double layer and the shape of the electric potential at the interface must be discussed. For well-defined systems with a strong surface bond, the position of the electrosorbate can be determined exactly by X-ray diffraction methods (21), or by STM (22, 23). The positions of the fast-moving water molecules or counterions, however, are rather difficult to detect. Therefore, the picture given in Fig. 3 remains speculative. Following the fundamental ideas of Grahame, an inner Helmholtz layer iHp is assumed for the position of the electrosorbate, while the nonspecifically adsorbed and solvated ions stay in the outer Helmholtz plane oHp. In Fig. 3*a*, a cation is electrostatically adsorbed, corresponding to the concept of Grahame ($\lambda = 0$). From electrostatic calculations (neglecting the charge transfer), Grahame obtained a value equivalent to γ, which was called the "thickness ratio" r:

$$[5] \quad |\gamma| = r = (x_2 - x_1)/x_2$$

with x_2 = double layer thickness $\approx$ diameter of the solvent molecule, and x_1 = radius of the specifically adsorbed ion. The thickness ratio is, however, in conflict with experimental results as was shown in refs. 13 and 26. This will also be shown in Sect. 5. Due to the increase in the permittivity of the solvent with increasing distance from the surface and other nonlinear effects, a more flexible definition of a geometric factor g according to eq. [6] was proposed (7, 26)

$$[6] \quad g = (\Phi_{ad} - \Phi_e)/(\Phi_m - \Phi_e)$$

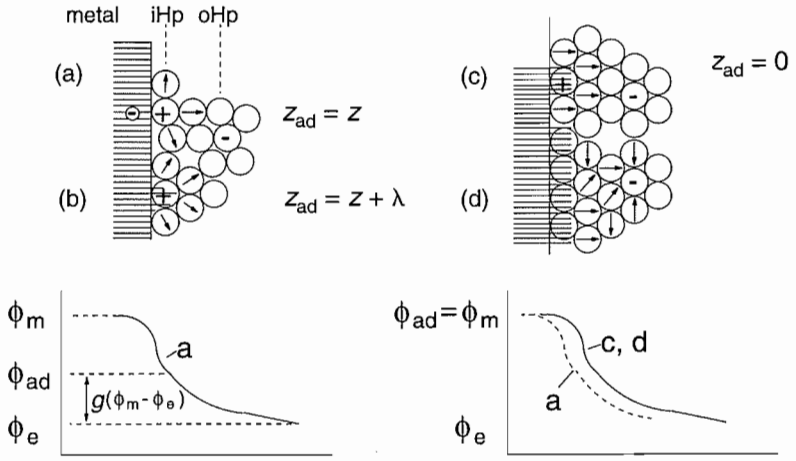
with the Galvani potentials Φ of the metal m, adsorbate ad, and electrolyte e. Note that eq. [6] again is an approximation for excess supporting electrolytes. The value of g can be estimated from experimental data of ionic electrosorbates (see Sect. 5 and ref. 13). Further parts of Fig. 3 show partially ($-\lambda/z < 1$, Fig. 3*b*) or completely ($-\lambda/z = 1$, Fig. 3*c*, 3*d*) discharged ions. In the case of complete discharge, e.g., with UPD layers, the whole double layer shifts towards the electrolyte side (13). This means that the geometric factor for such systems becomes almost 1. Hence, g cannot be considered as constant, but has to be considered as varying with the discharge of the electrosorbate (13).

From an electrostatic model, the relation between the model parameters g (eq. [6]), λ (eq. [1]), and the dipole terms κ with γ_N was derived (7):

$$[7] \quad \gamma_N = gz - \lambda(1 - g) + \kappa_S - \nu\kappa_w$$

© 1997 NRC Canada

Fig. 3. Potential drop at the interface and schematic double layer model with nonadsorbed ions in the outer Helmholtz plane (oHp), adsorbed water molecules and adsorbed ions in the inner layer (iHp). Effects of the diffuse layer are neglected (supporting electrolyte); g is defined by eq. [6]. Cation adsorbed electrostatically (*a*), partially discharged (*b*), and completely discharged (*c*) and (*d*).



Since the charge and sign of the ions differ, it is useful to analyse normalized values γ_N/z in the theoretical treatments. Dipole terms κ_i are important for neutral molecules (27, 29), but they can be neglected for ionic systems. In the following, we refer to the approximation, eq. [8]:

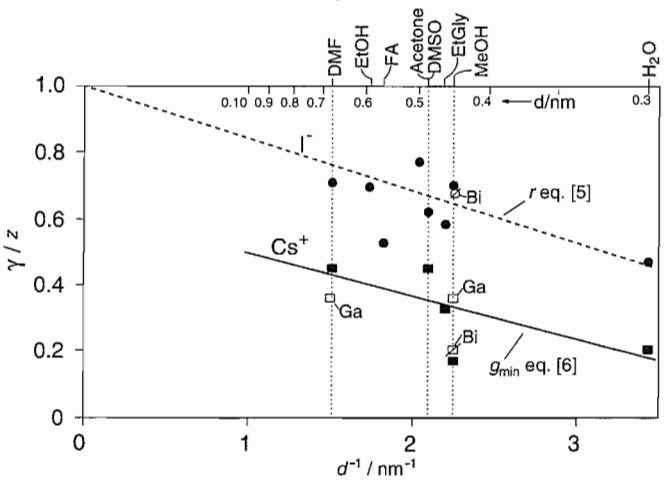
[8] $\gamma_N/z = g - (\lambda/z)(1 - g)$

5. Experimental estimation of *g*

As eq. [8] still includes two unknown parameters g and λ, it is impossible to determine these values by thermodynamic experiments only. However, the models of Figs. 1 and 3 can be tested by comparison of data for various systems with known geometric parameters. A plot of normalized electrosorption valencies versus the radius $r_S = x_1$ of the electrosorbate has shown that γ increases with r_S instead of showing the decrease predicted by eq. [5]. The result for water was supported by similar data for methanol and DMF (13). Only data for very electropositive or electronegative electrosorbates can be used to estimate g, which is much smaller than the value predicted by eq. [5]. Moreover, in the electrostatic model of Grahame, x_2 should be given by the thickness of the solvent molecule. Thus, a plot of "$\gamma_N = r$" (eq. [5]) versus the diameter of the solvent molecule should be on the broken line shown in Fig. 4. Experimental data of the normalized electrosorption valency γ/z are plotted versus the reciprocal diameter d of various solvents. The values for Cs^+ ions are definitely below the broken line, indicating that the solvent diameter plays a much less significant role than would be expected from eq. [5]. The flexible eq. [6], however, can be applied and experimental values of g_{min} can be obtained from minimum γ_N values (13, 26). From Fig. 4, minimum geometric factors of about 0.2 for water and methanol and 0.4 for DMF can be estimated. In the original treatments (34, 35), values for the so-called thickness ratio (in fact, the electrosorption valency) of iodide ions were discussed that seemed to verify the idea of the thickness ratio, as is also shown in Fig. 4. However, this apparent agreement was an artefact, since λ is definitely positive for iodide on mercury.

The distribution of the electric potential changes strongly if

Fig. 4. The normalized electrosorption valency ratio γ/z as a function of the reciprocal diameter of the solvent. Values are taken from ref. 13. Full symbols refer to Hg, other data for Ga and Bi are marked. The thickness ratio corresponding to eq. [5] is indicated by dotted lines. The values for Cs^+ can be taken as a geometric factor according to eq. [6]. Values for I^- cannot be taken for g, since they contain contributions from discharge.



the ions are completely discharged, for example, in the case of UPD layers. In that case the whole double layer shifts to the electrolyte as shown in Fig. 3*c* and 3*d*.

6. Experimental estimate of the partial charge transfer coefficient λ

Using Pauling's concept for the covalent character of a bond (36, 37), eq. [9] was successfully applied by Koppitz and Schultze (13):

[9] $-\lambda/z = \exp[-a(\Delta\chi)^2]$

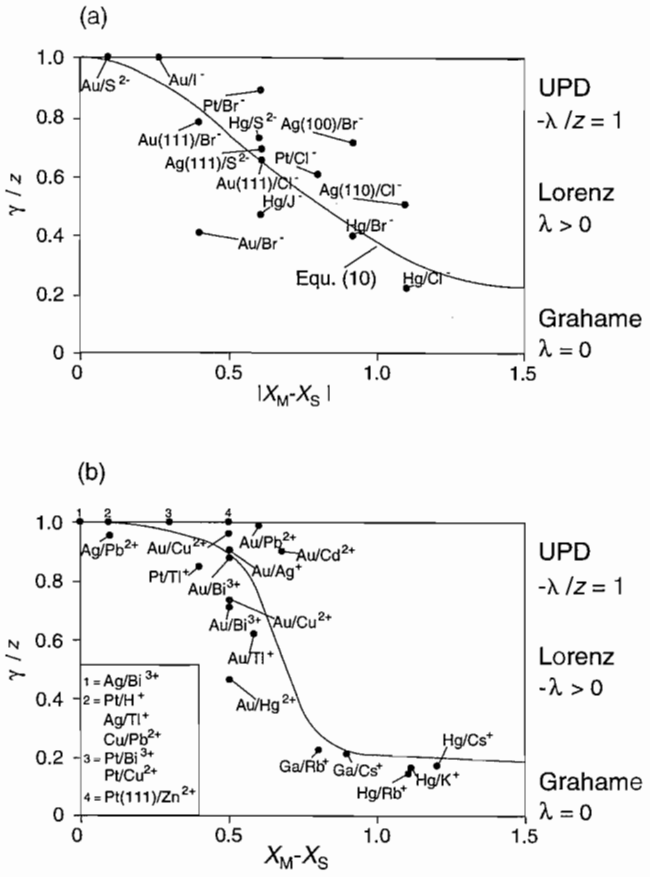
$\Delta\chi$ is the difference of the electronegativities between the

Can. J. Chem. Downloaded from www.nrcresearchpress.com by 91.121.58.235 on 09/08/12
For personal use only.

© 1997 NRC Canada

Can. J. Chem. Downloaded from www.nrcresearchpress.com by 91.121.58.235 on 09/08/12
For personal use only.

Fig. 5. Normalized electrosorption valency versus the absolute difference of electronegativity, data taken from ref. 13 and, in addition, from Table 1 (Au–Cu^{2+} and Au–Bi^{3+}). (*a*) Anions in water. (*b*) Cations in water. The full line in (*a*) gives the charge transfer according to eq. [10]; in (*b*) it is an empirical description.



metal electrode and the adsorbate. Originally, the normalized value γ/z was plotted versus the absolute difference of electronegativity for all ions. The advantage was the simultaneous treatment of anions and cations. This should be questioned, considering the different models for anion and cation bonding shown in Fig. 1. Moreover, new data for the adsorption systems summarized in Table 1 show that a separate treatment is necessary. Finally, some older data for the silver–halide systems (53) referred to the formation of layers, possibly involving place exchange reactions. These data could not be confirmed in new measurements at low coverage and had to be discarded. The corresponding new plots for anions and cations in water are shown in Fig. 5*a* and *b*.

The general tendency of both diagrams is the same as in ref. 13: At small electronegativity differences, γ/z approaches 1, i.e., the charge transfer dominates. With increasing difference, γ/z decreases and approaches a minimum value that can be attributed to the geometric factor of the electrostatic electrosorbates, g_{min}. The difference between the two diagrams lies in the almost stepwise transition for cations at about $|\Delta\chi| = 0.5$, while γ/z for anionic systems changes continuously following eq. [9]. This seems to be connected with the different bonding models discussed in Fig. 1. The bonding of cations may be described by a delocalized electron gas model that favours an autocatalytically increasing discharge of the ions: with increasing bonding, Φ_{ad} approaches Φ_m, thus causing $g \rightarrow 1$. The result for cations resembles the traditional, separate treatment of UPD systems and electrostatic systems such as those with alkali ions. It should be emphasized that an increasing interaction with ligands smoothes the step, since the γ/z values decrease, indicating an increasing ionicity of the metal–metal bond, as will be discussed in the next section.

In contrast to cations, the bonding electrons of anionic electrosorbates will not be included in the electron gas of the metal, and the geometric factor probably remains constant. Figure 2*e* may illustrate the different character of the bond. In such a case, the Pauling model valid for the field free vacuum seems to be more appropriate than for cations. Combining eqs. [8] and [9], we get:

$$[10a] \quad \gamma/z = g_{min} + (1 - g_{min}) \exp(-a(\Delta\chi)^2)$$

In Fig. 5*a*, values of $a = 1.5$ and $g_{min} = 0.2$ give the best fit:

$$[10b] \quad \gamma/z = 0.2 + 0.8 \exp(-1.5(\Delta\chi)^2)$$

The value, $a = 1.5$, of course, exceeds that of the vacuum, $a = 0.25$, which will be explained in Sect. 7. We have estimated the charge transfer data for the much studied system of Hg – halide ions. Using the assumptions $\gamma_{Cl} = g_{min}$, the point charge model, neglection of dipole terms, and no specific interaction with counterions, we obtained the lower values $\lambda = 0$ (Cl^-), 0.2 (Br^-), and 0.3 (I^-).

7. The influence of solvent and ligands

Increasing solvation or complexation of the electrosorbate stabilizes the ionic charge. Therefore, it causes a weakening of the surface bond (54). The prediction can be tested by investigating the electrosorption data for various solvents. With increasing solvation, the constant *a* of the Pauling eq. [9] should increase. It was shown, using DMF as an example, that the values for anions and cations could only be simulated with different values of *a*. The increase in *a*, from 0.25 for vacuum to 3 for water and methanol and to 6 for cations in DMF, parallels the solvation strength. Model calculations (19, 55, 56) discussed in Sect. 8 also show this strong influence of the solvation.

Ligands have a similar, strong influence. First determinations of the electrosorption valency for the Cu^{2+}–sulfate system from thermodynamic and kinetic measurements (51, 52) yielded surprisingly low values between 1.4 and 2, which indicates a cosorption of the anion. In this case, the electrosorption valency has to be written

$$[11] \quad \gamma_{mix} = \gamma_{Cu} + \gamma_{SO_4}(\delta\Gamma_{SO_4}/\delta\Gamma_{Cu})_U$$

X-ray diffraction measurements in the system Au (111)/Cu^{2+}, SO_4^{2-} proved the coadsorption at low coverages. From the structural data (21), the coupling factor

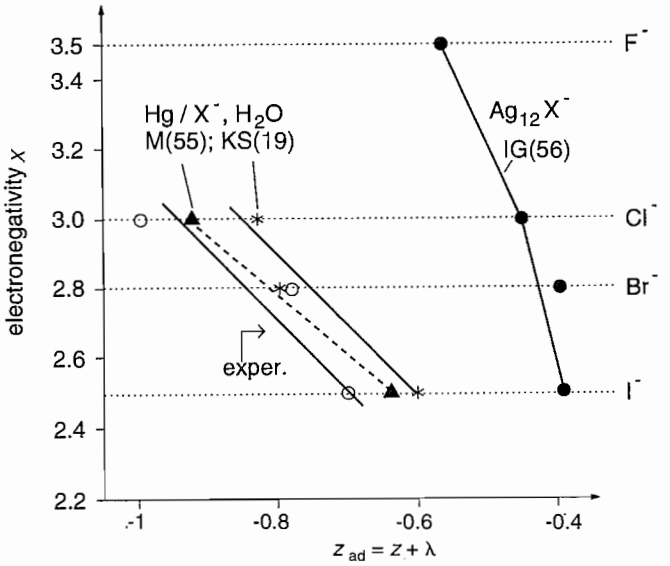
$$[12] \quad \rho = (\delta\Gamma_{SO_4}/\delta\Gamma_{Cu})_U = 0.33$$

can be derived. A careful coulometric analysis was carried out

© 1997 NRC Canada

Can. J. Chem. Downloaded from www.nrcresearchpress.com by 91.121.58.235 on 09/08/12
For personal use only.

Fig. 6. z_{ad} as a function of electronegativity χ. Comparison of z_{ad} values estimated from γ and theoretical calculations. Values from Kornyshev and Schmickler for 1/3 hydration (19), from Mishra et al. for 1/3 hydration for I^- and 2/3 for Cl^- (55), and from Ignaczak and Gomes for small clusters without solvation (56). The open circles represent experimental data.

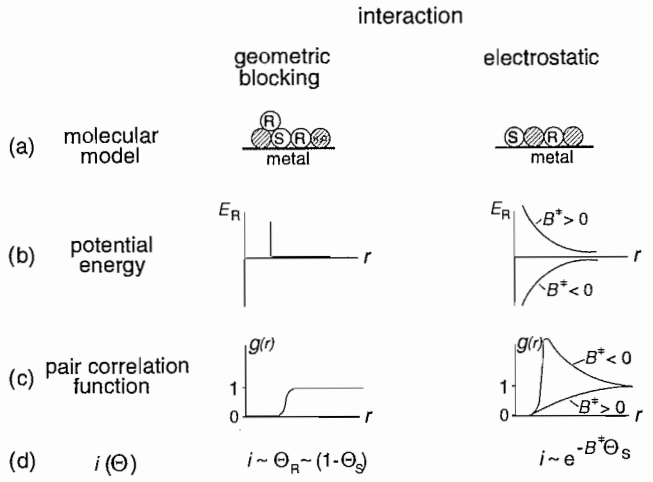


by Lipkowski et al. (50, 57, 58) for Au (111)/Cu^{2+}, X with X = Br^-, Cl^-, SO_4^{2-}. For SO_4^{2-} a coupling factor of 0.5, and for Br^- $\rho = 0.25$, was found for low coverages, but it must be noted that γ and ρ change with Γ_{Cu} and the electrode potential (50). Calculations by Mishra based on the Anderson–Newns model yield a partial discharge of the copper, approaching +0.4 for a monolayer (59). For these systems, a final interpretation of the charge distribution is still open to discussion.

8. Comparison with theoretical calculations

Figure 6 shows a comparison of the above-mentioned evaluations based on thermodynamic experiments as well as on theoretical calculations. Such experiments and calculations were carried out preferentially for the halide ions on mercury, where reliable experimental data are available, and where a continuously decreasing electronegativity or electron affinity promises interesting results. First, calculations were carried out with the Extended Hückel Method (15). The results were only of qualitative interest, since the limitation to a Hg–X^- complex with a single metal atom without water was too restricted. Therefore, the charge transfer was overestimated. Later calculations were carried out using the Anderson–Newns model for clusters with increasing hydration (19). Many-body effects were taken into account in ref. 55. New calculations with the density-functional method were carried out without solvent molecules. Here again, the charge transfer is overemphasized (56), since the hydration of the ion is neglected. As Fig. 6 shows, the quantitative data obtained with various parameters and methods differ due to arbitrary assumptions, but all agree in indicating a decreasing charge transfer with increasing solvation and with increasing electron affinity of the halide. Thus,

Fig. 7. Schematic representation of molecular arrangement, potential energy, pair correlation functions, and rate equations for electrostatic catalysis and geometric blocking. S = electrosorbate, R = reactant.



the agreement with our empirical estimates is reasonable. Calculations based on molecular dynamics and density-functional theory are not yet available for electrosorbates (60).

9. The role of partial discharge in electrocatalysis

The rate of ion transfer reactions, ITR, can either be enhanced or inhibited by catalytically active electrosorbates. In general, the influence of a substance S on the reaction rate of a reactant R can be due to electrostatic or chemical interaction or to geometric blocking (61, 62). Here we will consider the electrostatic influence, the geometric blocking taken only as reference. Models, potential energies, and pair correlation functions are schematically shown in Fig. 7. While the electrostatic forces decrease with $1/r$, the geometric blocking is only observed for $r < r_S$. Therefore, the positive or negative electrostatic influence is reflected in the potential energy curves and in the pair correlation function as well, at much larger distances. The potential energy curves for the electrostatic influence differ only by sign, but the pair correlation function for catalysis can change much more than that for electrostatic inhibition. As was shown by Parsons (63, 61), the electrostatic influence yields a relation

$$[13a] \quad \log i_\Gamma / i_{\Gamma=0} = -2B^\ddagger \cdot \Gamma$$

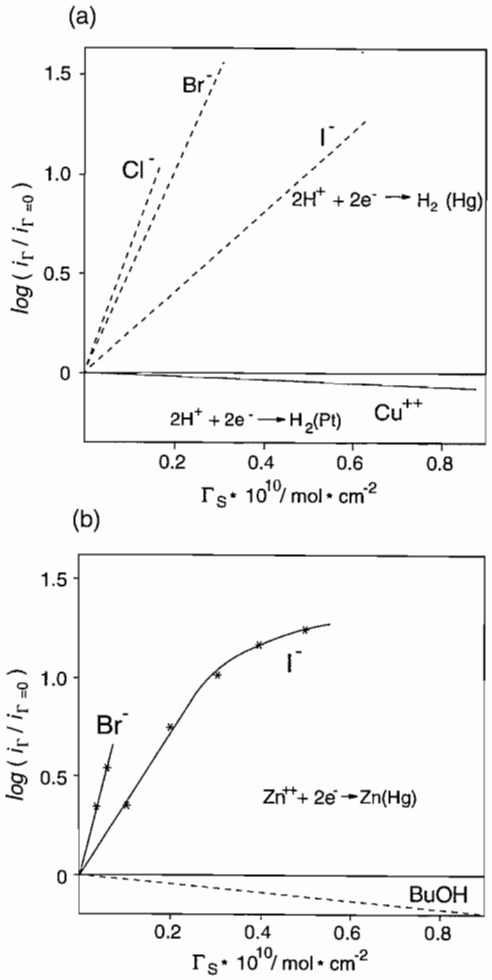
$$[13b] \quad B^\ddagger \sim z_{ad} z_R$$

with a constant $B^\ddagger$ depending on the activity of the transition complex, i.e., on the charges z_{ad} and z_R, respectively. Figure 8 shows the corresponding plots of the normalized current densities of hydrogen evolution on mercury (63) and zinc deposition on mercury (64, 61). Both reactions are accelerated by adsorbed halide ions, since $B^\ddagger < 0$. Straight lines are observed at low coverages as predicted by eq. [13]. The important observation is that for both reactions the slope decreases with

© 1997 NRC Canada

Can. J. Chem. Downloaded from www.nrcresearchpress.com by 91.121.58.235 on 09/08/12
For personal use only.

Fig. 8. Normalized current density ($i_\Gamma/i_{\Gamma=0}$) of various reactions as a function of the surface concentration Γ. (*a*) Cathodic hydrogen evolution on mercury with electrosorbed halide ions (63) and on platinum with electrosorbed Cu (65). (*b*) Cathodic deposition of Zn on mercury with electrosorbed halide ions (64) and butanol (66).

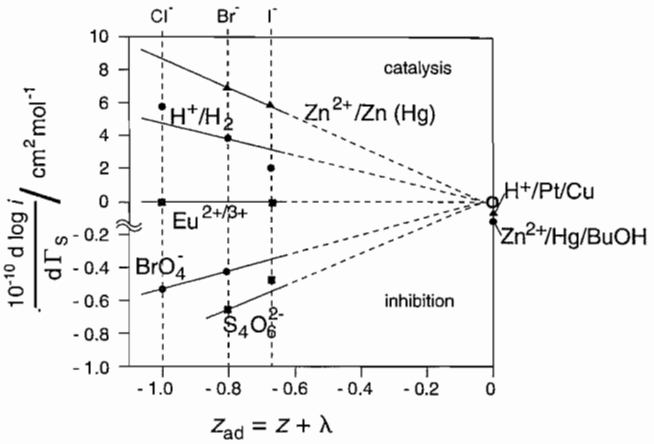


decreasing charge of the adsorbed ion in the sequence $Cl^- > Br^- > I^-$. For comparison, data for an only geometrically blocking adsorbate are plotted, as well. Cu on Pt, for example, slightly hinders the hydrogen evolution due to geometric blocking (65) with an almost negligible electrostatic effect. For the zinc deposition, data for completely discharged ionic electrosorbates were not available. Hence, the data for butanol (66) with a small geometric effect are plotted for comparison.

Taking the results of the estimate for the charge z_{ad} into account, the results can easily be explained using eq. [13]. The slope d log i/dΓ should be proportional to z_{ad} and z_R. In Fig. 9 the slope of the straight lines of Fig. 8 is plotted vs. the charge z_{ad}. The lines expected from eq. [13] are laid through the fixed point 0 at $z_{ad} = 0$. Considering the geometric blocking, the fixed point would be at about -0.1. The agreement with the experimental points confirms the general idea and the tendency. The proportionality to z_R, $B_{Zn^{2+}} \approx 2B_{H^+}$, is roughly fulfilled, as well.

For inner-sphere electron transfer reactions, ETR, the same behaviour is expected, while for outer sphere ETR the electrostatic influence should vanish. Figure 9 shows relevant data for the reduction of BrO_4^- and $S_4O_6^{2-}$ according to ref. 61. In that case, the adsorbed halide ions reduce the reaction rate, since $B^{\pm}$ is positive. The proportionality of the experimental slope to the real charge of the adsorbed halide ion is qualitatively confirmed. The quantitative influence is much smaller than in the case of catalysis, since the exclusion of the volume near the halide ion is not so important as the catalysis in the same volume. This can be derived from the pair correlation functions shown in Fig. 7. The influence of adsorbed halide ions on the outer-sphere ETR is almost negligible. Hence, the charge z_{ad} is without influence (67).

Fig. 9. Slope of the lines in Fig. 8 for $\Gamma \rightarrow 0$ as a function of the partial charge z_{ad} of the adsorbed halide ions. Upper part: electrocatalysis; lower part: inhibition (extended scale). On the right ordinate, the fixed points for $z_{ad} = 0$ and geometric blocking are shown.



10. Conclusions

The problem of charge distribution in electrosorbates can be qualitatively approached. Experimental values of γ/z are known for many systems, with a typical reliability of ± 0.1. The estimate of λ is a bit speculative, but comparison with various chemical and molecular parameters shows that in spite of these assumptions the results may have an accuracy of ± 0.1–± 0.2. It is shown that the discharge of ions increases with decreasing difference of electronegativities. For the real influence, the type of bonding plays an important role. Due to the metallic bonding, UPD systems are separated from electrostatic systems, and partial discharge plays a role only in the case of complexing ligands. Anions are covalently bound with a charge transfer continuously increasing with decreasing electronegativity. Theoretical calculations are in reasonable agreement, but may be improved by consideration of the specific metal–sorbate interaction.

The catalytic influence of electrosorbed halide ions can be explained by an electrostatic effect taking the partial discharge into account.

Acknowledgement

The support of this work by the Fonds der Chemischen Industrie is gratefully acknowledged. Helpful discussions with A.

© 1997 NRC Canada

Otto, W. Schmickler, and Th. Wandlowski are gratefully acknowledged.

References

1. H. Helmholtz. Ann. Phys. Chem. **7**, 337 (1879).
2. B.E. Conway. Theory and principles of electrode processes. The Ronald Press Company, New York. 1965.
3. B.E. Conway. J. Electrochem. Soc. **124**, 410C (1977).
4. B.E. Conway, H. Angerstein-Kozlowska, and W.B.A. Sharp. Z. Phys. Chem. NF, **98**, 61 (1975).
5. B.E. Conway and S. Marshall. Electrochim. Acta, **28**, 1003 (1983).
6. B.E. Conway, Y. Phillips, and S.Y. Quian. J. Chem. Soc. Faraday Trans. **91**, 283 (1995).
7. K.J. Vetter and J.W. Schultze. Ber. Bunsenges. Phys. Chem. **76**, 920 (1972); **76**, 927 (1972).
8. D.C. Grahame. Chem. Rev. **41**, 441 (1947).
9. W. Lorenz and G. Salié. Z. Phys. Chem. **218**, 259 (1961).
10. W. Lorenz and G. Salié. Z. Phys. Chem. NF, **29**, 390 (1961); **29**, 408 (1961).
11. J.W. Schultze and D. Rolle. Proc. Grahame Symp. 1997. Montreal. In press.
12. J. Tafel. Z. Phys. Chem. **50**, 641 (1905).
13. J.W. Schultze and F.D. Koppitz. Electrochim. Acta, **21**, 327 (1976); **21**, 337 (1976).
14. J.W. Schultze. III Int. Symp. Electrode Processes, Boston. 1979. p. 167.
15. D. Döhnert, J. Koutecky, and J.W. Schultze. J. Electroanal. Chem. **82**, 81 (1977).
16. W. Schmickler. J. Electroanal. Chem. **249**, 25 (1988).
17. W.J. Plieth and K.J. Vetter. Z. Phys. Chem. NF, **61**, 282 (1968).
18. D.M. Newns. Phys. Rev. **178**, 1123 (1969).
19. A.A. Kornyshev and W. Schmickler. J. Electroanal. Chem. **185**, 253 (1985).
20. W. Schmickler. Grundlagen der Elektrochemie. Vieweg, Braunschweig, Wiesbaden. 1996.
21. M.F. Toney, J.N. Howard, J. Richer, G.L. Borges, J.G. Gordon, O.R. Melroy, D. Yee, and L.B. Sorensen. Phys. Rev. Lett. **75**, 4472 (1995).
22. G.D. Aloisi, M. Cavallini, M. Innocenti, M.L. Foresti, G. Pezzatini, and R. Guidelli. 191st Meet. Electrochem. Soc., Montreal. 1997.
23. E. Budevski, G. Staikov, and W.J. Lorenz. Electrochemical phase formation and growth. VCH, Weinheim. 1996.
24. A. Otto, D. Schumacher, and H. Winkes. To be published; H. Winkes. Diss. Heinrich-Heine-Universität, Düsseldorf (1996).
25. B.E. Conway. Electrochim. Acta, **40**, 1501 (1995).
26. J.W. Schultze and K.J. Vetter. J. Electroanal. Chem. **44**, 63 (1973).
27. D. Rolle and J.W. Schultze. Electrochim. Acta, **31**, 991 (1986).
28. J.W. Schultze and K.J. Vetter. Electrochim. Acta, **19**, 913 (1974).
29. F.D. Koppitz, J.W. Schultze, and D. Rolle. J. Electroanal. Chem. **170**, 5 (1984).
30. D. Rolle and J.W. Schultze. J. Electroanal. Chem. **229**, 141 (1987).
31. C. Fontanesi and L. Benedetti. Electrochim. Acta, **42**, 1373 (1997).
32. K. Bange, B. Straehler, J.K. Sass, and R. Parsons. J. Electroanal. Chem. **229**, 87 (1987).
33. W. Schmickler. Ber. Bunsen-Ges. Phys. Chem. **92**, 1203 (1988).
34. D.C. Grahame. J. Am. Chem. Soc. **80**, 4201 (1958).
35. D.C. Grahame and R. Parsons. J. Am. Chem. Soc. **83**, 1291 (1961).
36. L. Pauling. J. Am. Chem. Soc. **54**, 3570 (1932).
37. L. Pauling. The nature of the chemical bond. 3rd ed. Cornell Univ. Press, Ithaca, N.Y. 1960.
38. Zh. Shi and J. Lipkowski. J. Electroanal. Chem. **403**, 225 (1996).
39. C.N. van Huong, C. Hinnen, and A. Rousseau. J. Electroanal. Chem. **151**, 149 (1983).
40. Th. Wandlowski, J.X. Wang, and B.M. Ocko. 191st Meet. Electrochem. Soc., Montreal. 1997.
41. M.R. Deakin, T.T. Li, and O.R. Melroy. J. Electroanal. Chem. **243**, 343 (1988).
42. D. Wierse, M.M. Lohrengel, and J.W. Schultze. J. Electroanal. Chem. **92**, 121 (1978).
43. Zh. Shi, J. Lipkowski, S. Mirwald, and B. Pettinger. J. Electroanal. Chem. **396**, 115 (1995).
44. G. Valette and R. Parsons. J. Electroanal. Chem. **204**, 291 (1986).
45. G. Salié and K. Bartels. Electrochim. Acta, **39**, 1057 (1994).
46. M.R. Deakin and O.R. Melroy. J. Electroanal. Chem. **239**, 321 (1988).
47. J.W. Schultze and D. Dickertmann. Faraday Discuss. Chem. Soc. **12**, 36 (1978).
48. J. Li and H.D. Abruna. J. Phys. Chem. **B**, **101**, 2907 (1997).
49. S. Taguchi and A. Aramata. J. Electroanal. Chem. **396**, 131 (1995).
50. Z. Shi and J. Lipkowski. J. Phys. Chem. **99**, 4170 (1995).
51. G. Horanyi. J. Electroanal. Chem. **55**, 45 (1974).
52. J.W. Schultze. Ber. Bunsenges. Phys. Chem. **74**, 705 (1970).
53. E. Schmidt and S. Stucki. Ber. Bunsenges. Phys. Chem. **77**, 913 (1973).
54. S.L. Marshall and B.E. Conway. J. Electroanal. Chem. **337**, 19 (1992).
55. A.K. Mishra, D.F. Milner, M.J. Weaver, and S.K. Rangarajan. J. Electroanal. Chem. **271**, 351 (1989).
56. A. Ignaczak and J.A.N.F. Gomes. J. Electroanal. Chem. **420**, 71 (1997).
57. Z. Shi, S. Wu, and J. Lipkowski. Electrochim. Acta, **40**, 9 (1995).
58. Z. Shi and J. Lipkowski. J. Electroanal. Chem. **365**, 303 (1994).
59. A.K. Mishra. Private communication, paper submitted for publication.
60. D.L. Price and J.W. Halley. J. Chem. Phys. **102**, 6603 (1995).
61. J.W. Schultze and M.A. Habib. J. Appl. Electrochem. **9**, 255 (1979).
62. J.W. Schultze. DECHEMA-Monogr. **102**, 273 (1986).
63. R. Parsons. J. Electroanal. Chem. **21**, 35 (1969).
64. M. Sluyters-Rehbach, J.S.C.M. Brenkel, and J.H. Sluyters. J. Electroanal. Chem. **19**, 85 (1968).
65. N. Furuya and S. Motoo. J. Electroanal. Chem. **72**, 165 (1976).
66. J. Lipkowski and Z. Galus. J. Electroanal. Chem. **61**, 11 (1975).
67. M.J. Weaver and F.C. Anson. J. Electroanal. Chem. **65**, 737 (1975).

Can. J. Chem. Downloaded from www.nrcresearchpress.com by 91.121.58.235 on 09/08/12
For personal use only.

© 1997 NRC Canada

Preparation and characterization of oxide film electrodes

A. De Battisti, G. Lodi, L. Nanni, G. Battaglin, and A. Benedetti

Abstract: In this paper are presented data on the preparation and characterization of different oxide electrodes. RuO_2–TiO_2, IrO_2–TiO_2, and SnO_2–Sb_2O_5 mixed-oxide films have been taken as model systems. For the first, the traditional preparation method based on the pyrolysis of precursor salt deposits was adopted. For the SnO_2-based films, the spray pyrolysis preparation has been used. The characterization of RuO_2–TiO_2 films confirms the existence of a solid solution between the two component oxides over a wide composition range. Rutherford backscattering spectrometry confirms the occurrence of segregation of titanium oxide species in the outermost part of the films. Nuclear reaction analysis indicates that large amounts of carbon and hydrogen impurities are trapped in the oxide films. SnO_2-based films were found to be less porous and chemically more simple. The differences between the two systems have been discussed in terms of the preparation method and the differences in chemical properties of the precursors.

Key words: oxide film electrodes, mixed-oxide films, Rutherford backscattering spectrometry, nuclear reaction analysis.

Résumé : Dans ce travail, on présente des données sur la préparation d'électrodes de divers oxydes. On a utilisé les films d'oxydes mixtes suivants comme modèles : RuO_2–TiO_2, IrO_2–TiO_2 et SnO_2–Sb_2O_5. Pour le premier, on a adopté la méthode de préparation traditionnelle qui repose sur la pyrolyse de dépôts de sels précurseurs. Pour les films incorporant du SnO_2, on a fait appel à une préparation par pyrolyse de vapeurs. La caractérisation des films de RuO_2–TiO_2 confirme que, pour une large plage de composition, il existe une solution solide entre les deux oxydes les composant. La spectroscopie de rétrodiffusion de Rutherford confirme l'existence d'une ségrégation des espèces de l'oxyde de titane dans la partie extérieure des films. Une analyse par réaction nucléaire indique que de grandes quantités de carbone et d'oxygène sont piégées dans les oxydes de films sous la forme d'impuretés. On a trouvé que les films incorporant du SnO_2 sont les moins poreux et chimiquement plus simples. On discute des différences entre les deux systèmes en fonction de la méthode de préparation et des différences dans les propriétés chimiques des précurseurs.

Mots clés : électrodes des films d'oxydes, films d'oxydes mixtes, spectroscopie de rétrodiffusion de Rutherford, analyse par réaction nucléaire.

[Traduit par la rédaction]

1. Introduction

Thermally prepared oxide electrodes based on different metal components have quite important industrial applications. The wide choice of possible compositions of the active film allows the modification of catalytic properties of these electrodes in a significant range. The well-known dimensionally stable anodes (DSA®), mixtures of group VIII noble-metal oxides stabilized with other components such as TiO_2, Ta_2O_5, and ZrO_2, are certainly the most important and have been well studied (1–3). Materials based essentially on IrO_2–TiO_2 mixtures perform well in chloralkali cells (e.g., ref. 3), while materials based on IrO_2–Ta_2O_5 exhibit better performance under oxygen evolution conditions (4). The high selectivity and efficiency of IrO_2 electrodes in some oxidative organic electrosyntheses seem to open further perspectives of application (5, 6).

Drastic modification of catalytic properties is caused when the group VIII noble-metal oxide is substituted by tin dioxide (7–9). In this case the occurrence of oxygen evolution at very high overpotentials allows efficient oxidative destruction of organic pollutants, and good efficiency in the electrochemical ozone generation.

The difference in chemical properties of the oxide metal ions plays a dominant role, affecting the stability of hydroxyl radicals, intermediates in all electrooxidative processes (e.g., ref. 6, and literature therein). Other factors, such as their microstructure and surface texture, related to the preparation method, also strongly affect the behaviour of oxide electrodes. A study of electrochemistry at these electrodes must therefore treat the electrode preparation and characterization in detail. When, as in the case of materials based on group VIII noble-metal oxides and SnO_2, not only the chemical properties, but also the preparation methods are substantially different, this aspect of the research may be particularly important.

In the present work, an attempt is made to show the role played by the preparation method on the properties of model

Received May 14, 1997.

A. De Battisti,[1] G. Lodi, and L. Nanni. Dipartimento di Chimica dell'Università, via L. Borsari, 46, I-44100 Ferrara, Italy.
G. Battaglin and A. Benedetti. Unità INFM, Dipartimento di Chimica Fisica dell'Università Calle Larga S. Marta 2137, I-30123 Venezia, Italy.

[1] Author to whom correspondence may be addressed. Telephone: +39-532-294-124. Fax: +39-532-240-709. E-mail: dba@dns.unife.it

© 1997 NRC Canada

Can. J. Chem. Downloaded from www.nrcresearchpress.com by 91.121.58.235 on 09/08/12
For personal use only.

Can. J. Chem. Downloaded from www.nrcresearchpress.com by 91.121.58.235 on 09/08/12
For personal use only.

oxide electrocatalysts. The traditional methods based on pyrolytic oxidation of precursor deposits (ink methods) and pyrolytic oxidation of aerosols (spray pyrolysis) will be considered in this study. Data relative to RuO_2-and IrO_2-based electrocatalysts prepared by "ink" procedures (an example of pyrolytic oxidation of precursor deposits), will be dealt with. Some comparison with data on SnO_2–Sb_2O_5 electrocatalysts prepared by spray pyrolysis and pyrolytic oxidation of precursor deposits has been attempted. The microstructural study was carried out by wide-angle X-ray scattering (WAXS). Considering that a correct interpretation of the microstructural data requires an extended compositional study, Rutherford Backscattering Spectrometry (RBS) and Nuclear Reaction Analysis (NRA) have been used for oxide films prepared by deposit pyrolytic oxidation methods, for which, as shown later, the composition may be quite complex.

2. Experimental

RuO_2–TiO_2 electrodes were prepared by pyrolysis of Ti-supported deposits consisting of mixtures of ruthenium(III) hydrated chloride and titanium diisopropoxide bis-2,4-pentanedionate reactants, in molar rations corresponding to those of the two metal components in the product mixed-oxide film. Deposits were prepared by painting the Ti substrates with isopropanol solutions of the two precursors in the required ratios. After solvent evaporation, such deposits were pyrolyzed in dry oxygen at 400°C for 20 min and the procedure repeated until an oxide film thickness of about 0.7–0.8 μm was reached. Titanium substrates were mirror-finished by mechanical polishing, then cleaned by quick chemical etching with hot 20% oxalic acid, rinsed with water and acetone, and dried. The Ti substrates were 1 cm × 1 cm plates (thickness 0.3 mm), with stem. Groups of different sample compositions were prepared, with noble-metal concentrations ranging between 20 and 100 mol%,

Details on the spray pyrolysis preparation of SnO_2–Sb_2O_5 films have been given elsewhere (8, 9). $SnCl_4 \cdot 5HO_2O$ (Aldrich) and $SbCl_3$ (Fluka) were used as precursors and the solvent was an ethanol – hydrochloric acid mixture. The oxide thickness was 4 μm in most of the cases, and the preparation temperature was 550°C.

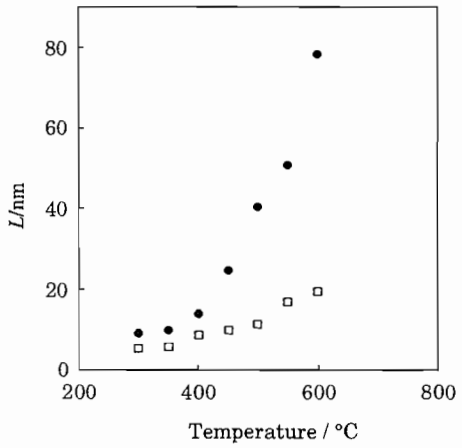
The preparation of SnO_2–Sb_2O_5 films (6 mol% Sb) by pyrolytic oxidation of precursor deposits, the traditional "brushing" or "ink" method, was also carried out for the sake of direct comparison of film properties. In this case the precursors $SnCl_2$ and $Sb_4O_5Cl_2$ (Carlo Erba) were used, dissolved in a mixed water–ethanol solvent.

Depth profiles of Ru, Ti, and O were determined by RBS. A $^4He^+$ ion beam with an energy of 2.2 MeV was used. Scattered particles were detected at an angle $\theta = 160°$, with respect to the direction of the incident beam. A surface-barrier silicon detector was used. The depth resolution in the near-surface region was generally 15–20 nm. The depth profiles were obtained by a procedure based on fitting of experimental spectra (10).[2] The operational depth profiles were adjusted until a satisfactory fit of the synthesized spectrum to the experimental one was obtained. Estimated uncertainties in Ru and Ti concentrations were 1–2%, reaching larger values for oxygen, due to the smaller elastic cross section and the superimposition of the signal from oxygen in the film with those from the elements in the substrate. Carbon total amount was measured by NRA. Use was made of the $^{12}C(d,p)^{13}C$ nuclear reaction. The energy of the deuteron beam was 620 keV and the detection angle was 150°. A 12 μm thick Mylar foil was placed in front of the detector to stop elastically scattered deuterons.

X-ray diffractometric studies were carried out with a Siemens D-500 instrument. Ni-filtered CuK_α radiation was used. The goniometer rate was 2° min^{-1}. The apparent size of the solid solution crystallites was determined by the Scherrer formula, under the assumption that the line broadening is due to microcrystallinity only.

[2] Also, A. Carnera. University of Padova, Italy, unpublished results, 1979.

Fig. 1. Average crystallite size for RuO_2 (●) and IrO_2 (□) rutile phases in films prepared at different temperatures, by pyrolytic oxidation of precursor deposits.



3. Results and discussion

3.1. Microstructural study of RuO_2–TiO_2 and IrO_2–TiO_2 films

Making use of the Scherrer formula, the average crystallite size, L, of RuO_2 and IrO_2 rutile phases prepared at different pyrolysis temperatures between 300 and 600°C were measured and results are shown in Fig. 1. As expected L increases with increasing pyrolysis temperature in both cases. The effect is, however, quite small for the IrO_2 phase. Since the same preparation procedure was applied for the two series of samples, the reasons for this significant difference must be sought in the different reactivity of the two hydrated chloride precursors. Thermoanalytical investigations (11–13) have shown that, in fact, the reactivity of Ir(III) hydrated chloride films is lower at intermediate stages of the pyrolytic process, probably due to the formation of stable oxychlorides. These results have been interpreted by assuming the passivation of parts of the precursor deposits, due to partial oxidation of the most external part, with further occurrence of the pyrolysis under "anaerobic" conditions. The reactivity of Ru(III) hydrated chloride and its oxidation intermediates is apparently sufficiently high to minimize these effects (14). Resistivity data reported in ref. 12 for IrO_2 films of different thickness support the idea that the deposit pyrolysis procedure enhances the effects of differences of reactivity of the type described above.

© 1997 NRC Canada

Can. J. Chem. Downloaded from www.nrcresearchpress.com by 91.121.58.235 on 09/08/12
For personal use only.

Fig. 2. Interplanar lattice spacing d_{110}, for the RuO_2–TiO_2 solid solution in mixed-oxide films.

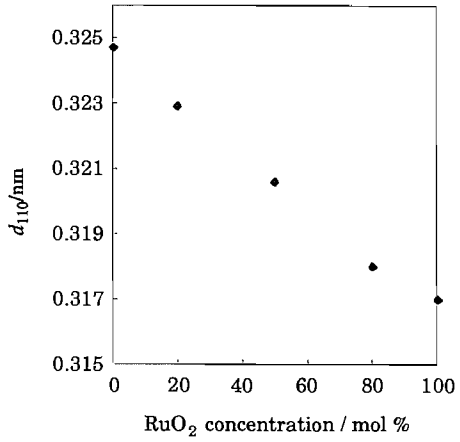
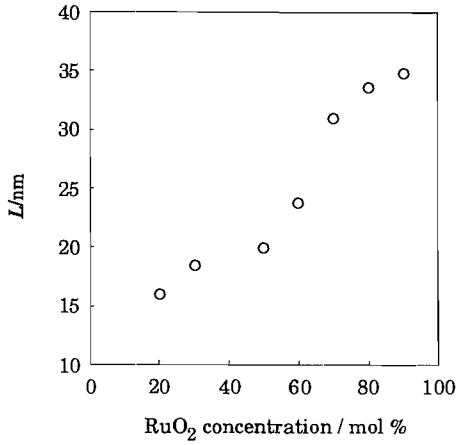


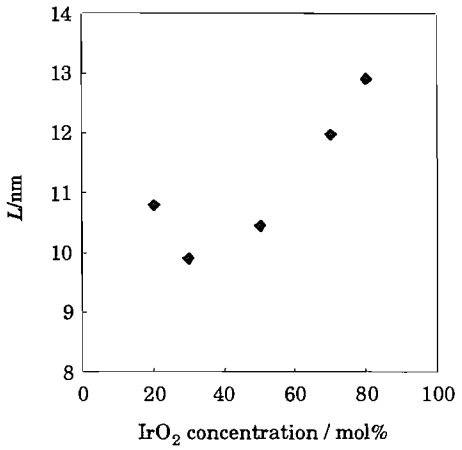
Fig. 3. Average crystallite size of the RuO_2–TiO_2 solid solution as a function of the nominal bulk composition of the electrode film.



As proved in other studies (15, 16), the presence of ruthenium oxide induces the formation of RuO_2–TiO_2 solid solutions with rutile structure. The same holds for the IrO_2–TiO_2 quasi-binary system (17). It has been shown elsewhere (10) that, for RuO_2–TiO_2 samples containing 20–30 mol% of noble-metal oxide, the solid solution is formed independent of the nature of the ruthenium precursor salt (acetylacetonate, nitrosyl nitrate, chloride). It was also shown that the cell parameters of a solid solution follow the Vegard law with excellent approximation. This feature is confirmed also for the samples studied in this work (Fig. 2). In spite of the different reactivity of the precursors, the interplanar distances of the crystalline structure of the two solid solutions change regularly with the noble-metal/titanium ratio.

A microstructural characterization of RuO_2–TiO_2 and IrO_2–TiO_2 films was also carried out, using the same method. The influence of film composition on the average crystallite size for two series of samples prepared at 400°C is shown in Figs. 3 and 4, respectively. For both series the decrease of the noble-metal oxide causes a decrease of the solid solution crystallite size. The trend to develop larger crystallite sizes for the RuO_2-based samples is confirmed at any noble-metal concentration. The increase of reactivity caused by the addition of the titanium precursor (13, 14) is not sufficient to cancel this feature. In other mixed-oxide films like RuO_2–Ta_2O_5 (18) and IrO_2–ZrO_2 (19), for which formation of solid solutions, if any, is limited, different trends are observed. In the first case a decrease of the RuO_2 crystallite size with decreasing noble-metal concentration has been found. In the latter case, however, the crystallite size is small, compared with data reported in the present paper (minima around 10 nm). The immobilizing role of Ta(V) species should be probably taken into account in this case. For the IrO_2–ZrO_2 films the crystallite size of the IrO_2-rich phase is unaffected by the bulk film composition. In this case experimental results suggest that small amounts of ZrO_2 are dissolved in the IrO_2 (rutile) phase. The ZrO_2-rich phase, however, changes from a crystalline morphology at low IrO_2 contents, to amorphous at intermediate to high IrO_2 contents. This transformation is likely to involve mutually compensating effects on the formation of the conjugated IrO_2-rich phase.

Fig. 4. Average crystallite size of the IrO_2–TiO_2 solid solution as a function of the nominal bulk composition of the electrode film.



Synthesis by the spray pyrolysis method leads to quite different microstructural properties (20). In the case of the SnO_2–Sb_2O_5 mixed-oxide films, crystallite size is much larger, of the order of about 1 μm, at a synthesis temperature of 550°C. Further, the average crystallite size decreases linearly with increasing temperature of synthesis. On the contrary, in SnO_2–Sb_2O_5 films prepared by thermal decomposition of precursor deposits in this work, the crystallite size is again of the order of 10–20 nm, and crystallinity of the films increases with the pyrolysis temperature.

3.2. Film composition

3.2.1. RBS results for group VIII noble-metal oxides

As previously mentioned, the ruthenium, titanium, and oxygen stoichiometry of the RuO_2–TiO_2 films has been studied by RBS. The ruthenium and titanium stoichiometries in two series (A, B) of mixed-oxide films are shown in Table 1. The oxygen stoichiometry was 2 in all the investigated samples. Depth profiling, also determined by RBS, indicates the occurrence of an enrichment with titanium oxide species in the most

© 1997 NRC Canada

Table 1. Ru and (Ru + Ti) total metal load "up to the interface" (measured by RBS) in two different groups of samples (A and B).

	Sample A		Sample B	
Mol% RuO_2 (nominal)	Ru: at $cm^{-2} \times 10^{17}$	Ru + Ti: at $cm^{-2} \times 10^{17}$	Ru: at $cm^{-2} \times 10^{17}$	Ru + Ti: at $cm^{-2} \times 10^{17}$
20	1.1	5.0	1.0	4.3
30	2.6	8.0	1.3	5.0
50	3.2	5.5	3.5	6.0
70	5.6	8.0	3.9	5.9
80	7.8	9.2	6.0	7.2
100	—	—	—	—

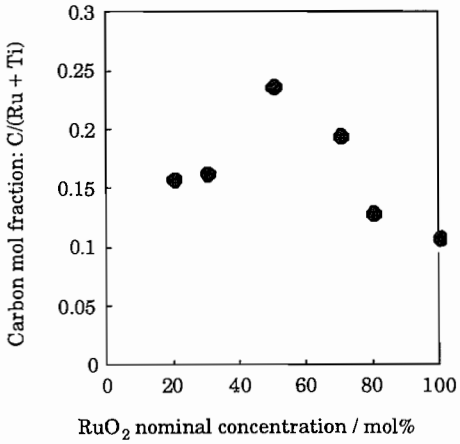
external part of the mixed-oxide films. The compositional features of several films with effective ruthenium concentrations between 22 and 30 mol% also showed the occurrence of "encapsulation" by titanium oxide species (10). In ref. 10 it was also shown that this phenomenon already appears at pyrolysis temperatures as low as 200°C and that it is not affected by the nature of the ruthenium precursor salt, even when a complexing anion like acetylacetonate is bound to ruthenium ions. In addition, the substitution of ruthenium with iridium does not change the shape of the concentration depth profiles (17). Utilization of stabilizing components other than TiO_2 may induce, on the contrary, some changes (19).

3.2.2. NRA results for RuO_2–TiO_2 and IrO_2–TiO_2 films

NRA measurements, also reported in ref. 10, have shown that carbon- and (or) hydrogen-containing impurities may be present in thermally prepared oxide films in amounts that are quite comparable with those of the main components (metal ions, oxygen). These impurities are due to incomplete oxidative conversion of organic components in the precursor mixture (solvent, organic anions) and incomplete elimination of water of hydration. This interpretation has been confirmed by thermoanalytical data (13, 14) and thermoanalytical and resistivity data on IrO_2 films (12). In ref. 11, the anomalous formation of iridium metal in the oxidative pyrolysis of iridium(III) hydrated chloride films has been explained by passivation of the outermost part of the reacting particles, and consequent hindrance of oxygen uptake from the oven atmosphere. Blocking of the thermal decomposition process of iridium(III) hydrated chloride and anomalous behaviour of the electrical resistivity of thermal IrO_2 films upon annealing has also been explained along the same lines (12). Accumulation of impurities is likely to occur around the film regions where oxide crystallites are formed. The previously mentioned areas of sparse crystallinity, for which evidence has been given in ref. 10, may therefore coincide with the "passivation" areas, encapsulating the crystallite clusters, mentioned in refs. 11 and 12, and could be the reason for the low density of the oxide films.

In the present work, NRA measurements were also carried out for the RuO_2–TiO_2 films containing 20, 30, 50, 70, 80, and 100 mol% of RuO_2, making use of the $^{12}C(d,p)^{13}C$ nuclear reaction. As expected on the basis of literature data (10, 14), large amounts of carbon were detected. Interestingly, the differences in the preparation method adopted in ref. 10 (a classical sol–gel method) with respect to that adopted in the present work (an "ink" method) were not sufficient to distinguish significant changes in the amount of residual carbon. The latter is, otherwise, affected by the amount of noble-metal salt present in the precursor films. In Fig. 5, the dependence of the C/(Ru+Ti) atom ratio on noble-metal content is shown. It can be observed that lower residual carbon contents are found at high or low noble-metal concentrations. This feature results from the combination of two factors. One is, of course, the content of organics in the precursor mixture, which increases with increasing titanium precursor salt concentration. The other is the reactivity of the precursor mixture towards the cracking and successive combustion of the organic species in the mixture. TGA–GC–MS results described in ref. 14 have demonstrated that the reactivity of the ruthenium(III) hydrated chloride+titanium(IV) diisopropoxide bis-pentane-2,4-dionate precursor mixture towards the cracking and combustion of organics is larger at noble-metal concentrations as low as 10 mol%. NRA measurements repeated after different electrochemical treatments have shown that no significant change in the carbon content is caused during electrochemical perfor-

Fig. 5. Dependence of the carbon content, expressed as the ratio between carbon atoms per square centimeter and total number of metal atoms per square centimeter (RBS), on the nominal RuO_2 concentration, in RuO_2–TiO_2 mixed oxide.



Can. J. Chem. Downloaded from www.nrcresearchpress.com by 91.121.58.235 on 09/08/12
For personal use only.

© 1997 NRC Canada

Can. J. Chem. Downloaded from www.nrcresearchpress.com by 91.121.58.235 on 09/08/12
For personal use only.

Table 2. Amount of residual C, as C/Ru molar ratio, in RuO_2–TiO_2 of different noble-metal concentration.

RuO_2 bulk conc. (mol%)	C/Ru molar ratio (%)
20	33 ± 9
30	35 ± 10
50	23 ± 6
70	18 ± 4
80	12 ± 3
100	11 ± 3

Table 3. Anodic peak charge, $(q_p)_A$, roughness factor (from CV data), number of electroactive sites, n_S, per square centimeter (effective surface area), for RuO_2–TiO_2 electrodes.

c_{Ru} (mol%)	$(q_p)_A$ (mC cm^{-2})	Roughness factor	n_S(× 10^{13})
20	1.0	115	5.5
30	1.4	175	5.1
50	1.1	172	4.1
70	0.8	141	3.6
80	0.4	97	3.0

mance. The dependence of the C/Ru atom ratio on noble-metal content is shown in Table 2. The increase in the number of carbon atoms per ruthenium atom can be taken as indirect evidence of a larger degree of dispersion of the active (or noble-metal containing) phase in the electrode material, at low noble-metal concentrations. NRA measurements repeated after cyclic voltammetry experiments in the polarization range −0.25–1.25 V (vs. SCE) have shown that no significant change in the carbon content takes place, even after repeated cycling. This excludes the possibility that the presence of carbon in the films is due to surface contamination phenomena. It is also interesting to observe that, even when no titanium organometallic compound is present, in the case of the 100% RuO_2 films, quite significant amounts of residual carbon are present. This indicates that the use of isopropanol as the solvent of the precursor mixture is sufficient to cause the phenomenon of C incorporation. Substitution of crystal water molecules around Ru(III) ions by isopropanol molecules or their decomposition products is likely to take place during the first stages of the thermolytic process. As shown in ref. 10, the amount of hydrogen impurities in this type of oxide films is comparable with that of carbon. Although the methods based on pyrolytic oxidation of precursor deposits allow attainment of an average MO_2 stoichiometry (M = Ru(IV), Ti(IV)) for the oxide phase(s), large amounts of C and H impurities are trapped in the film texture, due to the hindrance of oxygen uptake and of the release of cracking products of organics in the precursor film. The final result is a highly dispersed oxide phase, in a porous matrix.

3.3. Electrochemical characterization

3.3.1. RuO_2–TiO_2 film electrodes

Voltammetric charge can serve as a powerful tool for the study of the electrochemical or catalytic properties of oxide electrodes (21). Typical voltammograms exhibit the peak generally assigned to the Ru(IV)/Ru(III) redox couple (21). Following the procedure in ref. 22, faradaic peak charges and currents were estimated (after establishing a base line for the peaks). The total voltammetric charges and peak charges were found to be independent of the potential scan rate. The peak charges are significantly lower than those encountered in the case of IrO_2-based materials. This indicates that in RuO_2–TiO_2 mixtures a lower degree of dispersion of the active and conducting phase is achieved and is in good agreement with the previously discussed microstructural data. Both total charge and peak charge depend on the electrode film composition, exhibiting maxima around 30 mol% RuO_2. Attempts to account for the experimental results should be based on the degree of dispersion of the active phase in the electrode materials. As discussed in the literature (e.g., refs. 10–14, and literature cited therein) and further proved in the present work, when precursor deposits are pyrolyzed, the mechanism of formation of the phases is quite complicated and affects microstructural features quite strongly. When precursor salt mixtures are taken into account, the situation is further complicated by the formation of metastable solid solutions, such as in the RuO_2–TiO_2 and IrO_2–TiO_2 systems.

The roughness factor of the electrode films can be estimated from the cyclic voltammetry data. If a reasonable value is assumed for the capacity per effective unit surface area, roughness factors can be evaluated from the capacitive component of the cyclic voltammograms (21, 22). The results for RuO_2–TiO_2 film electrodes with noble-metal concentrations between 20 and 80 mol% are shown in Table 3. Larger values are found for the samples containing 30 mol% of RuO_2; minimum values are typical of samples containing 80 mol% of RuO_2. The high values attained indicate a considerable degree of porosity. More generally, the low to intermediate ruthenium concentration range is characterized by larger porosity. From peak charges (anodic, cathodic) the number of electroactive (Ru) sites, n_S, can be calculated. Results are also reported in Table 3, referred to the geometric electrode area (anodic charge densities $(q_p)_A$) and to the estimated effective area (number of electroactive sites, n_S). Interestingly, the first are themselves quite large, compared with the expected values, which should range between 10^{14} and 7×10^{14} (19, 22). Only after normalizing to the effective surface area are these figures approached, also considering the lower ruthenium concentration at the surface of the films, due to the combined effects of nominal composition and surface segregation of Ti species. At the same time the dependence of the n_S on the film composition is damped. This may be better understood if we consider that, due to segregation phenomena, the surface composition does not depend on the bulk composition. On the basis of the above results, we can therefore conclude that maxima of voltammetric charge of the type shown in Table 3 are essentially due to larger surface roughness of the oxide film. The latter, in turn, may find a tentative explanation in the high decomposition rate of the precursors at lower concentrations of the ruthenium precursor salt (14).

With reference to the above considerations about the signif-

© 1997 NRC Canada

Can. J. Chem. Downloaded from www.nrcresearchpress.com by 91.121.58.235 on 09/08/12
For personal use only.

Fig. 6. Dependence of the ratio m_S between n_S and the total amount of metal atoms Ru+Ti in the film, as measured by RBS.

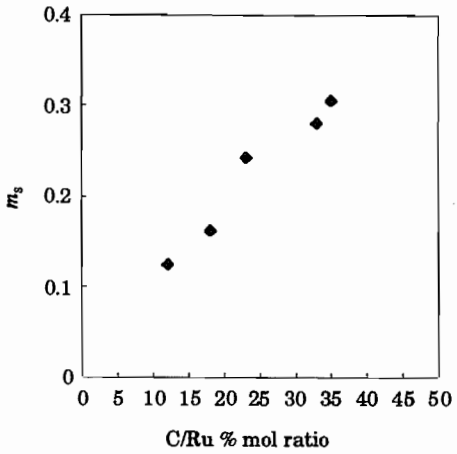
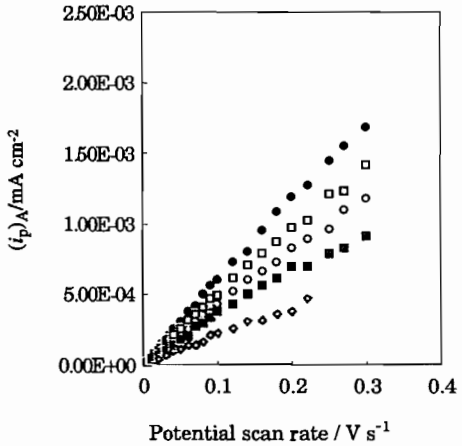


Fig. 7. Anodic peak current density ($(j_p)_A$ as a function of potential scan rate s: □, 20; ●, 30; ○, 50; ■, 70; ◇, 80 mol% Ru.



icance of residual carbon content, the correlation between the latter and the voltammetric charge of oxide electrodes has been studied. To compensate for the effect of relatively small differences in mixed-oxide loading on the voltammetric charge, the voltammetric peak charges (anodic) were divided by the total number of atoms of metal species (Ru + Ti) in the films, as determined by RBS. For homogeneity of units, peak charges were expressed as numbers of electroactive sites. The carbon content has been expressed in terms of C/Ru atom ratio, and results are shown in Fig. 6. As expected on the basis of previous considerations, larger mole fractions of electroactive sites are found in samples with larger C/Ru atom ratios. Thermoanalytical results indicate that larger amounts of organics in the reacting films enhance the reactivity towards the formation of the final oxide products, which is related to an increase of nucleation sites. According to the above consideration on the accumulation of impurities in the intergranular regions, growth of crystallites of the oxide phases should then be hindered by large amounts of carbon. Both factors should favour a better dispersion of the oxide solid solution. These properties of noble-metal based oxide electrodes are typically due to the character of volume reactions of the pyrolytic processes taking place in the precursor films.

The relatively large porosity of the RuO_2–TiO_2 films has suggested an extension of the study to the changes in voltammetric peak current densities ($(i_p)_A$, anodic, $(i_p)_C$, cathodic) with the potential sweep rate, S. Figure 7 shows that for all electrode materials the voltammetric peak current is linear in S, as expected for electrodes whose surface has been modified by insertion of electroactive sites. According to this result, mass transport does not seem to play a significant role in controlling the rate of oxidation state changes occurring in RuO_2–TiO_2 films. For IrO_2–TiO_2 and IrO_2–ZrO_2 film electrodes, exhibiting larger roughness factors, the i_p/S plots are more complicated, and peak current densities become linear in S^x, with $0.6 < x < 0.8$ (19). In these cases the surface texture is probably more microporous and diffusion of counterions taking part in the charging process is hindered.

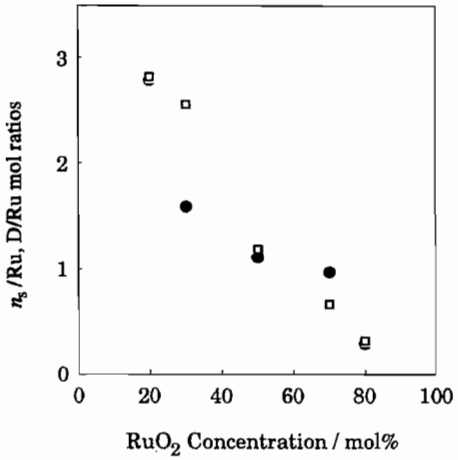
As shown in previous work on IrO_2–TiO_2 films (22), polarization experiments carried out in D_2SO_4 solutions in D_2O can supply information on the surface texture of oxide electrodes, complementary to cyclic voltammetry data. In the present work, the electrochemical behaviour of RuO_2–TiO_2 films was studied in 1 N D_2SO_4 in D_2O by following the procedure outlined in ref. 22. Analogous experiments could be carried out, in principle, tracing hydrogen by the $^1H(^{15}N, \alpha\gamma)^{12}C$ nuclear reaction, or by ERD. However, as shown by the previous ERD measurements, the amount of hydrogen present is quite high, and essentially bound to the hydrocarbon species, or to other products of incomplete oxidative decomposition of organics taking part in the precursor reactions. This high background of essentially non-exchangeable hydrogen would make more difficult the interpretation of the data of counterion exchange under polarization. The electrodes to be analyzed by NRA were conditioned in the test solution by repeated cycling between −0.25 and 1.25 V (vs. SCE). A first measurement was then carried out after polarization for 30 min at −0.20 V. Other NRA measurements were repeated after polarization at 1.20 V, again for 30 min. After the polarization at 1.20 V a decrease in the amount of deuterium in all the electrodes was observed. This is in agreement with the double injection–ejection mechanism of charging proposed for noble-metal oxides. The cyclic voltammetry data obtained in 1 N D_2SO_4 – D_2O were similar to those obtained in 1 M aqueous $HClO_4$. Comparison between the number of electroactive sites (from anodic peak charges) per ruthenium ion and the number of exchanged deuterium (difference between the amount taken up at −0.20 V and the residual at 1.20 V), are shown in Fig. 8, as a function of the nominal bulk concentration of ruthenium. For both quantities a decrease with increasing noble-metal concentration is observed. With the exception of the result for the sample containing 30 mol% RuO_2, the correspondence between amount of exchangeable deuterium and number of electroactive sites is also satisfactory.

4. Conclusions

Compositional studies of electrode films based on RuO_2–TiO_2 mixtures, prepared by pyrolytic oxidation of $RuCl_3 \cdot 3H_2O$–Ti

© 1997 NRC Canada

Fig. 8. Comparison between the peak charge and number of exchangeable deuterium ions normalized to the ruthenium content, for RuO_2–TiO_2 electrodes of different composition: □, electroactive site fraction; ●, D/Ru mol fraction.



diisopropoxide bis-2,4-pentanedionate deposits show that these materials contain large amounts of carbon and hydrogen impurities. This evidence supports the idea that crystallites of the RuO_2–TiO_2 solid solution are separated by large amorphous areas where these chemical impurities have accumulated. The porosity of these areas is responsible for the relatively high charge-storage capacity of the mixed-oxide electrodes found by cyclic voltammetry. The results presented here are in good agreement with thermoanalytical – mass spectrometric investigations reported in other papers (11–14).

SnO_2–Sb_2O_5 film electrodes, which are generally more conveniently prepared by spray pyrolysis, exhibit a much more compact microstructural texture and less open surface texture. Smaller amounts of impurities, such as carbon and hydrogen, are incorporated in the films during their growth. This is because the pyrolytic oxidation takes place in spray pyrolysis processes as a surface reaction, which favours a more complete reaction of the precursors. Preparation based on a sol–gel method leads to smaller average crystallite size (10–20 nm). RuO_2–TiO_2 films studied in the present work are prepared by pyrolytic oxidation of precursor deposits. This essentially involves volume reactions and hindered oxygen uptake during precursor oxidation, which necessarily results in incomplete combustion of organics and more porous structures. The complexity of the volume reactions occurring during the deposit oxidation is also the main reason for the poor reproducibility of the properties of electrodes prepared by this method.

References

1. S. Trasatti and G. Lodi. *In* Electrodes of conductive metallic oxides, Part B. *Edited by* S. Trasatti. Elsevier, Amsterdam. 1981. pp. 301–358.
2. S. Trasatti and G. Lodi. *In* Electrodes of conductive metallic oxides. *Edited by* S. Trasatti. Elsevier, Amsterdam. 1981. pp. 521–626.
3. D.M. Novak, B.V. Tilak, and B.E. Conway. *In* Modern aspects of electrochemistry. Vol. 14. *Edited by* B.E. Conway and J.O'M. Bockris. Plenum Press, New York. 1982. pp. 195–317.
4. J. Rolewicaz, Ch. Comninellis, E. Plattner, and J. Hinden. Electrochim. Acta, **33**, 573 (1988).
5. Ch. Comninellis. Electrochim. Acta, **39**, 1857 (1994).
6. Ch. Comninellis and A. De Battisti. J. Chim. Phys. In press.
7. R. Kötz, S. Stucki, and B. Carcer. J. Appl. Electrochem. **21**, 14 (1991).
8. B. Correa-Lozano. EPFL Thése No. 1297, Lausanne, Switzerland. (1994).
9. B. Correa-Lozano, Ch. Comninellis, and A. De Battisti. J. Appl. Electrochem. **26**, 83 (1996).
10. M. Guglielmi, P. Colombo, V. Rigato, G. Battaglin, A. Boscolo, and A. De Battisti. J. Electrochem. Soc. **139**, 1655 (1993).
11. G. Lodi, A. De Battisti, A. Benedetti, G. Fagherazzi, and J. Kristóf. J. Electroanal. Chem. **256**, 441 (1988).
12. G. Lodi, A. De Battisti, G. Bordin, C. De Asmundis, and A. Benedetti. J. Electroanal. Chem. **277**, 139 (1990).
13. J. Kristóf, J. Liszi, P. Szabó, A. Barbieri, and A. De Battisti. J. Appl. Electrochem. **23**, 615 (1993).
14. J. Kristóf, J. Liszi, A. De Battisti, A. Barbieri, and P. Szabó. Mater. Chem. Phys. **37**, 23 (1994).
15. W.A. Gerrard and B.C.H. Steele. J. Appl. Electrochem. **8**, 417 (1978).
16. Yu, E. Roginskaya, B.Sh. Galyamov, I.D. Belova, R.R. Shifrina, V.B. Kozhevnikov, and V.I. Bystrov. Elektrokhimiya, **18**, 1327 (1982).
17. A. De Battisti, A. Barbieri, A. Giatti, G. Battaglin, S. Daolio, and A. Boscolo. J. Mater. Chem. **1**, 191 (1991).
18. A. De Battisti, R. Brina, G. Gavelli, A. Benedetti, and G. Fagherazzi. J. Electroanal. Chem. **200**, 83 (1986).
19. A. Benedetti, P. Riello, G. Battaglin, A. De Battisti, and A. Barbieri. J. Electroanal. Chem. **376**, 195 (1994).
20. B. Correa-Lozano, Ch. Comninellis, and A. De Battisti. J. Electrochem. Soc. **143**, 203 (1996).
21. S. Trasatti and G. Lodi. *In* Electrodes of conductive metallic oxides. Part A. *Edited by* S. Trasatti. Elsevier, Amsterdam. 1980. pp. 522–626.
22. G. Battaglin, A. De Battisti, A. Barbieri, A. Giatti, and A. Marchi. Surf. Sci. **251/252**, 73 (1991).

Can. J. Chem. Downloaded from www.nrcresearchpress.com by 91.121.58.235 on 09/08/12
For personal use only.

© 1997 NRC Canada

Interlamellar amino functionalization of kaolinite

James J. Tunney and Christian Detellier

Abstract: The interlamellar surface of kaolinite has been modified with molecules possessing amino functionalities. Either the dimethyl sulfoxide intercalate of kaolinite (Kao/DMSO) or the *N*-methylformamide intercalate of kaolinite (Kao/NMF) were used as starting materials. One of the products, an ethanolamine functionalized kaolinite (Kao–EOA) was resistant to thermal decomposition in both air and N_2 atmospheres up to temperatures greater than 150°C. Based on results from thermal analysis, IR analysis, ^{13}C CP/MAS NMR spectroscopy, and elemental analysis, a structural model is proposed in which every third interlayer surface hydroxyl group on the aluminol (Al-OH) surface of kaolinite is either replaced with an interlayer Al-$OCH_2CH_2NH_2$ group or is strongly H-bonded to an aminoalcohol molecule. A mixture of both types of linkages could coexist. The amino groups that point away from this surface are each keyed into the -$(SiO-)_6$ macro-rings of the adjacent silicate surface, resulting in an amino-functionalized ordered two-dimensional organo-mineral assembly.

Key words: kaolinite, halloysite, organo-mineral nanocomposites, clay functionalization, supramolecular assemblies.

Résumé : On a modifié la surface interlamellaire de la kaolinite avec des molécules portant des fonctions amino. Comme produits de départ, on a utilisé de la kaolinite intercalée de diméthylsulfoxyde (Kao/DMSO) ou de *N*-méthylformamide (Kao/NMF). Sur l'un des produits, une kaolinite fonctionnalisée à l'éthanolamine (Kao–EAO) est résistante à la décomposition thermique, jusqu'à des températures supérieures à 150°C, dans des atmosphères tant d'air que de N_2. En se basant sur les résultats d'analyses thermiques, d'analyses élémentaires, de spectroscopies IR et RMN ^{13}C avec polarisation croisée/rotation à l'angle magique, «CP/MAS», on propose un modèle structural selon lequel un sur trois groupes hydroxyles de la surface de l'intercouche de l'aluminol (Al-OH) de la kaolinite sont soit remplacés par une intercouche de groupes Al-$OCH_2CH_2NH_2$ soit fortement liés, par liaisons hydrogènes, à une molécule d'aminoalcool. Il est possible que les deux types de liaisons coexistent. Les groupes amino qui sont orientés vers l'extérieur de cette surface sont insérés dans les macrocycles de -$(SiO-)_6$ de la surface adjacente de silicate qui conduit à un arrangement organominéral aminofonctionnalisé ordonné d'une façon bidimensionnelle.

Mots clés : kaolinite, halloysite, nanocomposites organominéraux, fonctionnalisation de l'argile, arrangement supramoléculaires.

[Traduit par la rédaction]

Introduction

It has previously been shown that it is possible to rigidly fix small alcohol moieties onto the interlamellar aluminate surface of kaolinite ($Al_2Si_2O_5(OH)_4$), through the grafting reaction of the alcohol group to the Al-O-H surface of the kaolinite (1–3). These interesting materials are organo-mineral nanocomposites with organic units covalently attached to the inorganic substrate in an ordered stacking of organo-mineral layers. The non-centrosymmetric kaolinite layers may act as a rigid inorganic supramolecular organizing medium, since the dipole moment that exists across the interlayer space of kaolinite (4–6) may act to orient molecules in a preferred orientation (1–3, 7–16). It would thus be of interest to expand the interlayer grafting chemistry of kaolinite to include other systems than the previously reported alcohol/diol organo-kaolinite system (1–3). It has been demonstrated that despite the slow kinetics of many kaolinite intercalation reactions (8), it is nonetheless possible to intercalate large molecules, such as polyethylene glycol of average molecular weight 3400, into the interlayers of kaolinite by first preswelling with either DMSO or NMF (17). This suggests that kaolinite could be used as a non-centrosymmetric inorganic organizing medium. One may thus envisage rationally assembling sophisticated non-centrosymmetric organo-mineral materials based on rigid inorganic asymmetric kaolinite layers.

With the diol-based organo-kaolinites, the interlayer cohesive forces for these new materials prevented easy layer swelling (1, 2). This was presumably due to the strong hydrogen bonding between the pendant hydroxyl groups of the diols and the silicate surface of the kaolinite layers. As a result, even though the alcohol functionality of the diol unit offers an

Received May 16, 1997.

This paper is dedicated to Professor Brian E. Conway on the occasion of his 70th birthday.

J.J. Tunney[1] **and C. Detellier.**[2] Ottawa–Carleton Chemistry Institute, Department of Chemistry, University of Ottawa, Ottawa, ON K1N 6N5, Canada.

[1] Present address: Institute for Chemical Process and Environmental Technology, National Research Council of Canada, Ottawa, ON K1A 0R6. Telephone: (613) 990-2102. Fax: (613) 991-2383. E-mail: Jim.Tunney@nrc.ca

[2] Author to whom correspondence may be addressed. Telephone: (613) 562-5707. Fax: (613) 562-5170. E-mail: dete@science.uottawa.ca

© 1997 NRC Canada

Can. J. Chem. Downloaded from www.nrcresearchpress.com by 91.121.58.235 on 09/08/12
For personal use only.

Can. J. Chem. Downloaded from www.nrcresearchpress.com by 91.121.58.235 on 09/08/12
For personal use only.

attractive site for further interlayer modification reactions, it is inaccessible to reactant molecules. Other types of organo-kaolinites, preferably with weaker interlayer cohesion and consequently greater swelling properties, are required if one wishes to use them as the first step in the development of more sophisticated structures. Part of the appeal in attaching molecules with pendant amine groups in the interlayer space of kaolinite lies with the possibility of using the free amine group to attach larger molecules to the interlayer surface kaolinite. Amines could, for example, provide an ideal site for the attachment of a carbonyl-functionalized moiety.

Organo-kaolinites with organic guests possessing amino groups have previously been reported. Kaolinite-hydrazine (Kao/Hz) (8, 18–21) is rapidly formed by exposing untreated kaolinite to hydrazine vapours or to a hydrazine solution. Despite its ease of formation, Kao/Hz is much less stable than either Kao/DMSO or Kao/NMF, decomposing in ambient conditions within less than an hour. This ease of formation and inherent instability allows Kao/Hz to be used to advantage as an intermediate in the preparation of other organo-kaolinites via the displacement method (21–23). In related work, Inoue et al. (24) prepared a series of aminoalcohol-based organoboehmite materials in which they proposed that the organic units were attached to the boehmite via Al-O-$(CH_2)_n NH_2$ bonds.

Experimental

Materials

All chemicals used were of reagent grade quality and were not further purified unless otherwise specified. KGa-1, well-crystallized kaolinite, was obtained from the Source Clay Repository of the Clay Mineral Society (Department of Geology, University of Missouri, Columbia, Mo.). Halloysite (coded as Halloysite no. 13 from Eureka, Utah), a polytype of kaolinite, was obtained from Ward's Natural Science Establishment Inc. (Rochester, N.Y.) in the form of hard rocklike chunks. This had to first be ground up to the consistency of a coarse powder before proceeding with the purification procedure. For both kaolinite and halloysite, purification by standard sedimentation procedures to remove the >2 μm size fraction was required (25–27). Even after purification, in the case of kaolinite small amounts of anatase (TiO_2) impurities could be detected by XRD as a sharp weak reflection at d = 3.52 Å, corresponding to the (101) reflection of anatase. The purified clays were then characterized by XRD, FTIR, and TGA/DSC, and were found to be consistent with literature data for purified natural kaolinite and halloysite (28, 29).

Characterization

XRD powder patterns were measured on a Philips PW 3710 automated diffractometer using Cu Kα radiation (wavelength = 1.5416 Å). All measurements were taken using a generator voltage of 45 kV and a generator current of 40 mA. A step size of 0.04° 2Θ was used with a dwell time of 0.5 seconds per step. The sample was spun during pattern acquisition, and an automatic divergent slit and a 0.1 mm receiving slit were used without employing any mask. Samples were mounted on a circular glass disk by first dispersing 20–30 mg of sample with 1 mL of methanol, sonicating for 10 s, and allowing the suspension to dry on the glass disk. Some samples were mounted dry by first smearing a small quantity of vaseline to the glass disk and then placing the powder directly on this. The intercalation ratio (I.R.), which is an indication of the extent of modification, was calculated from the relative intensities of the (001) reflections of the modified organo-kaolinite phase and the unexpanded kaolinite phase (8). The c-spacing or basal spacing is calculated based on the indexed (00*l*) reflections (8). Reflections due to the presence of residual unreacted kaolinite are identified with the symbol K. All *d*-values are given in Ångstrom units (Å), with the relative intensities given in parentheses on a scale where 100 is the intensity of the most intense reflection. The assigned indexing of the reflection is also given in parentheses.

Infrared spectra were obtained on a Bomem Michelson MB 100 FTIR spectrometer using 30–50 averaged scans at 4 cm^{-1} resolution. The samples were prepared as KBr pellets (0.25–0.50% by weight in KBr). X-ray fluorescence (XRF) measurements to measure the Si/Al ratio were performed on a Philips PW 2400 fluorimeter equipped with a Philips PW 2510 sample holder, with the scans referenced to a mixture of SiO_2 and Al_2O_3. Ceramic yields were determined by measuring the residual mass (as a percentage of the starting mass) of the product after calcination at 1100°C for 3 h in air atmosphere. Thermal analyses (TGA and DSC) runs were performed on a Polymer Labs 1500H instrument under either flowing nitrogen or air (20–90 cm^3/min) and a heating rate of 20°C/min. Approximately 10 mg of sample was used for each run using alumina sample and reference pans.

^{13}C cross polarization/magic angle spinning (CP/MAS) spectra (50.33 MHz) were performed on a Bruker ASX-200 instrument with a magic angle spinning rate of 3–4 kHz. The ^{13}C CP/MAS spectra were referenced to hexamethylbenzene at 16.9 ppm. Solution state NMR (^1H and ^{13}C) were performed on either a Varian XL-300 or a Bruker AMX-500, and both ^1H and ^{13}C chemical shifts are reported relative to TMS in $CDCl_3$.

Starting materials

The preparations of both Kao/DMSO and Kao/NMF and starting materials have been described elsewhere and are based on standard literature procedures (1, 2, 8). Briefly, this involves allowing 20 g of the unexpanded purified kaolinite to remain in contact with DMSO or NMF in an enclosed jar for at least 2 months at room temperature, followed by washing with 1,4-dioxane to remove excess DMSO or NMF, and air drying. After this time, both Kao/DMSO and Kao/NMF are found by XRD to be formed with an intercalation ratio (I.R.) exceeding 90%. XRD patterns, IR spectra, and TGA were all consistent with literature data (8). The DMSO intercalate of halloysite (Hal/DMSO) was formed in an identical manner. In this case, no residual unexpanded halloysite was observed by XRD (8).

Reactions with amines

Kao/DMSO + ethanolamine (Rxn 1)

The reaction of Kao/DMSO with ethanolamine was repeated a number of times and in all cases nearly identical materials resulted. The following is a typical example: 1.0 g of Kao/DMSO (I.R. = 0.97) was refluxed with 50 mL of freshly distilled ethanolamine (EOA) for 22 h under N_2 atmosphere. This was then filtered and washed with 1,4-dioxane to remove excess EOA. Air drying at 40°C for 2 h yielded 0.76 g of an

© 1997 NRC Canada

Can. J. Chem. Downloaded from www.nrcresearchpress.com by 91.121.58.235 on 09/08/12
For personal use only.

off-white powder. XRD: 10.64 (100, d_{001}); 7.14 (1.5, d_{001}K); 5.34 (0.1, d_{002}); 4.46 (1.4); 4.34 (2.3); 4.28 (2.1); 4.20 (2.0); 4.15 (1.4); 3.72 (1.2); 3.56 (16.5, d_{003}); 3.32 (0.5); 3.19 (1.2); 3.14 (0.9); 2.84 (0.1); 2.67 (0.7, d_{004}); 2.13 (1.2, d_{005}); 1.78 (0.2, d_{006}); 1.487 (0.3, d_{060}). $d = 10.67 \pm 0.03$ Å, I.R. = 0.985. FTIR (cm^{-1}), ν(O-H): 3693 (s), 3628 (s), 3558 (m), 3486 (s) ν(NH): 3354 (m), 3311 (m); ν(C-H): 3074 (w, br), 2964 (vw), 2946 (w), 2935 (vw), 2889 (w); δ(HOH): 1663 (w); δ(C-H, N-H): 1613 (w), 1525 (w), 1476 (w), 1353 (w), 1197 (w); Si-O vibrations: 1125 (s), 1092 (s), 1045 (vs), 1016 (vs); δ(AlOH): 974 (m), 908 (s); other bands: 2792 (vw), 2691 (w), 2612 (w), 1385 (w, impurity), 874 (w), 796 (w), 740 (w), 683 (m), 604 (w, sh), 552 (s), 471 (s), 433 (s). ^{13}C CP/MAS NMR (Bruker CXP-180, spinning speed = 6 kHz, 45.27 MHz, δ(ppm)): 42 ($-CH_2NH_2$), 60 ($-CH_2O-$); no dipolar dephasing signal detected after 40 μs dephasing time for either resonance. Elemental analysis: %C 8.06, %N 4.12; %H 2.72, ceramic yield 72.5%. Calculated for $Al_2Si_2O_5(OH)_{4.0}(HOCH_2CH_2NH_2)_{1.0}$: %C 7.52, %N 4.39, %H 3.45, ceramic yield 69.6%. Calculated for $Al_2Si_2O_5(OH)_{3.0}(OCH_2CH_2NH_2)_{1.0}$: %C 7.97, %N 4.65, %H 2.99, ceramic yield 73.8%.

*Kao/NMF + ethanolamine (Rxn **2**)*
Kao/NMF (2.0 g) (I.R. = 0.91) was refluxed with 60 mL of ethanolamine (freshly distilled) for 23 h under N_2 atmosphere. This was then filtered and washed with 1,4-dioxane to remove excess ethanolamine. Air drying yielded 20 g of an off-white powder. The FTIR and XRD patterns proved to be nearly identical to product (**1**). XRD (vaseline mounted, vacuum dried at 40°C for 3 h): 10.36 (100, d_{001}); 7.02 (3.7, d_{001}K); 4.41 (7.5); 4.31 (9.8); 4.25 (11); 4.15 (9.1); 4.00 (5.6); 3.69 (5.9); 3.53 (23, d_{003}); $d = 10.5 \pm 0.2$ Å; I.R. = 0.96.

*Kaolinite + ethanolamine (Rxn **3**)*
Kaolinite (1.0 g) was refluxed with 50 mL of ethanolamine in a round-bottom flask fitted with a reflux condenser for 17 h under N_2 atmosphere. After filtering and washing the reaction mixture with methanol, the product was air dried, yielding 0.9 g of a light grey product. The FTIR pattern of this product was indicative of the well-crystallized kaolinite starting material.

*Hal/DMSO + ethanolamine (Rxn **4**)*
Hal/DMSO (10 g) was refluxed with 40 mL of ethanolamine (freshly distilled) for 20 h under N_2 atmosphere. This was then filtered and washed with ethanol to remove excess ethanolamine. Air drying yielded 0.70 g of an off-white powder. XRD: 10.61 (100, d_{001}); 3.55 (13, d_{003}). $d = 10.6 \pm 0.1$ Å; I.R. = 1.0. FTIR (cm^{-1}), ν(O-H): 3695 (s), 3630 (s), 3558 (s), 3491 (s); ν(NH): 3356 (m), 3313 (m); ν(C-H): 3076 (w, br), 2948 (w), 2889 (w); ν(C=O): 1614 (m); δ(C-H, N-H): 1478 (vw), 1355 (vw); Si-O vibrations: 1125 (s), 1035 (vs); δ(AlOH): 908 (s); other bands: 2620 (w), 744 (w), 680 (m), 551 (s), 468 (s), 434 (s).

*Kao/DMSO + ethylene diamine (Rxn **5**)*
Kao/DMSO (1.2 g) (I.R. = 0.97) was refluxed with 60 mL reagent grade ethylene diamine (Aldrich, BP 118°C) in a round-bottom flask fitted with a reflux condenser for 18 h under N_2 atmosphere. After filtering and washing the reaction mixture with 1,4-dioxane, the product was air dried, yielding 0.8 g of a light grey product. The FTIR pattern of this product was indicative of partially collapsed Kao/DMSO.

Table 1. Summary of the organo-kaolinite products formed from the treatment of amines with kaolinite.

Starting material	Reactant	Rxn code[a]	Basal spacing[b] (Å)	I.R.[c]
Kao/DMSO	Ethanolamine	**1**	10.7	0.98
Kao/NMF	Ethanolamine	**2**	10.5	0.96
Kaolinite	Ethanolamine	**3**	NR	
Hal/DMSO	Ethanolamine	**4**	10.6	1.0
Kao/DMSO	Ethylene diamine	**5**	NR	
Kao/DMSO	3-Amino-1-propanol	**6**	11.1	0.58
Kao/DMSO	DL-1-Amino-2-propanol	**7**	NR	
Kao/DMSO	Nitroaniline	**8**	NR	

[a]See experimental section for details.
[b]This refers to the basal spacing of the principal modified product phase. NR, no reaction.
[c]Intercalation ratio.

*Kao/DMSO + 3-amino-1-propanol (Rxn **6**)*
Kao/DMSO (1.0 g) (I.R. = 0.97) was refluxed with 50 mL of 3-amino-1-propanol (Aldrich, $NH_2(CH_2)_3OH$, bp 187–188°C) for 19 h under N_2 atmosphere. Work-up consisted of cooling, filtering, and washing with methanol; 0.82 g of an off-white powder was recovered after air drying for 1 h. XRD and FTIR patterns were indicative of a partially modified product. XRD: 11.07 (90, d_{001}), 7.10 (66, d_{001}K). I.R. = 0.58. FTIR (cm^{-1}), ν(O-H): 3698 (s), 3652 (m), 3622 (s), 3626 (w, br); ν(NH): 3364 (vw); ν(C-H): 2941 (w), 2878 (w); δ(C-H, N-H): 1574 (w), 1482 (w), 1322 (vw); Si-O vibrations: 1110 (s, sh), 1085 (s), 1046 (vs), 1032 (vs), 1013 (vs); δ(Al-OH): 914 (s); other bands: 791 (w), 752 (w), 685 (m), 539 (s), 472 (s), 431 (s).

*Kao/DMSO + DL-1-amino-2-propanol (Rxn **7**)*
Kao/DMSO (1.0 g) (I.R. = 0.97) was refluxed with 50 mL of DL-1-amino-1-propanol (Aldrich, $NH_2CH_2CH_2OHCH_3$, bp 160°C) for 19 h under N_2 atmosphere. Work-up consisted of cooling, filtering, and washing with methanol; 0.72 g of an off-white powder was recovered after air drying for 1 h. FTIR indicated that no modification had occurred, and the Kao/DMSO starting material had reverted to a collapsed kaolinite.

*Kao/DMSO + nitroaniline (Rxn **8**)*
A preliminary attempt to intercalate nitroaniline into the interlayer space of kaolinite was made by reacting 1.0 g of Kao/DMSO in 10 g of melted nitroaniline (mp 149°C) at 175°C for 40 h under N_2 atmosphere. During the course of reaction, the mixture slowly turned black. Work-up consisted of repeated washings with methanol to remove as much of the excess organic material as possible. FTIR and XRD patterns were both consistent with a collapsed kaolinite structure.

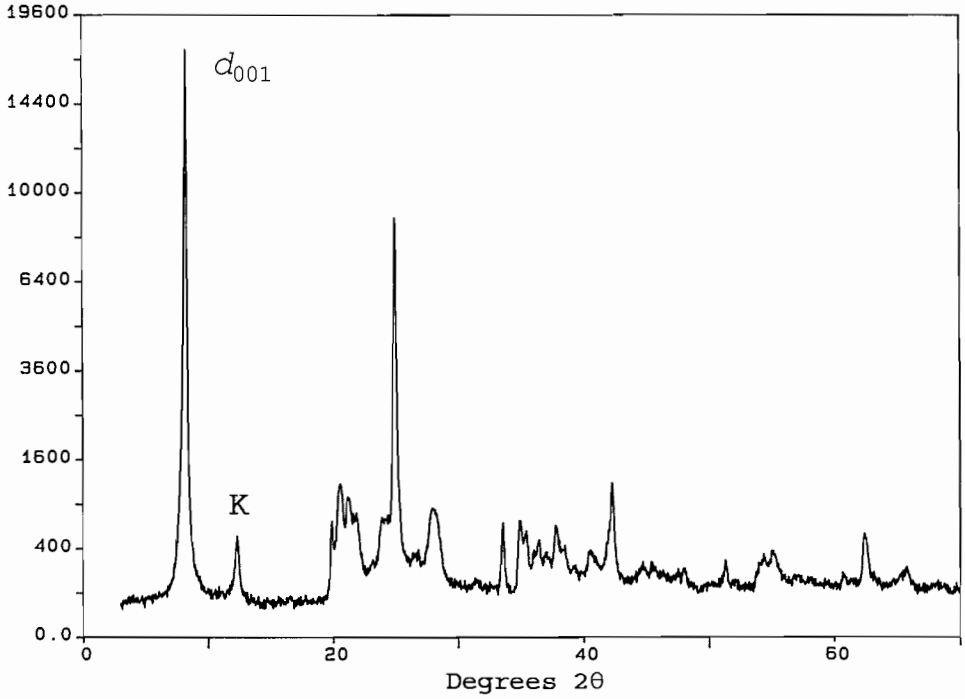
Results and discussion

Preparation

A series of amines were reacted with Kao/DMSO and Kao/NMF (Table 1). These included the aminoalcohols ethanol-

© 1997 NRC Canada

Fig. 1. XRD pattern (2°–70° 2Θ) for Kao–EOA. K indicates (001) reflection from residual kaolinite.



amine (EOA) and 3-amino-1-propanol (3,1-AP), which formed new organo-kaolinite intercalates. The reactions involving ethylene diamine (**5**), DL-1-amino-2-propanol (**7**), and nitroaniline (**8**) were unsuccessful and yielded only collapsed unmodified kaolinite and Kao/DMSO starting material. For Kao–3,1-AP (**6**), the modified phase had a basal spacing of 11.1 Å, and the intercalation ratio (I.R.) was only 0.58. IR results for this material definitely show that the Kao/DMSO starting material has been altered, and one observes bands attributable to the 3-amino-1-propanol guest species. For example, faint ν(NH) bands were detected at 3426 (vw) and 3364 (vw) cm^{-1}, ν(CH) bands at 2941 (w) and 2878 (w) cm^{-1}, and deformation bands at 1574 (w), 1482 (w), and 1322 cm^{-1}. The fact that 3-amino-1-propanol formed an intercalate with kaolinite, whereas DL-1-amino-2-propanol did not, may plausibly be due to the higher reaction temperature for Kao–3,1-AP formation (187°C vs. 160°C), which permitted a more rapid diffusion of 3-amino-1-propanol into the interlayers of kaolinite before structural collapse could occur. Alternately, the presence of an end methyl group in 1-amino-2-propanol may have also made interlayer diffusion more difficult and contributed to a weaker host–guest interaction.

In view of the fact that ethylene diamine may intercalate into halloysite to form an 11.7 Å intercalation complex (30, 31), it is surprising that an organo-kaolinite product was not formed via the displacement of DMSO. Reaction with *para*-nitroaniline was also unsuccessful, presumably due to the hydrophobic nature of *para*-nitroaniline and the weaker basicity of *para*-nitroaniline compared to primary amines.

Clearly, the greatest success was achieved using ethanolamine as the reactant, and this product (Kao–EOA) will be examined in some detail. It was possible to form nearly identical Kao–EOA products from both Kao/DMSO and Kao/NMF starting materials but not from unexpanded kaolinite. This indicates that the intercalating agent (DMSO or NMF) that was used to provide access to the interlamellar space of kaolinite plays a passive role and is not directly involved in the actual chemical reaction between ethanolamine and the interlamellar surface of kaolinite. DMSO and NMF are required only to provide access to the clay interlayers.

The Kao–EOA product exhibited a remarkable crystallinity as exhibited by the strong reflections of the XRD pattern (Fig. 1). The main product had a basal spacing of 10.67 Å. This product was found to be stable with respect to vacuum drying over phosphorus pentoxide for 24 h at 25°C, but was unstable when washed with water overnight, reverting slowly to the parent kaolinite 7.2 Å phase.

It was also possible to form the halloysite analogue of Kao–EOA (Hal–EOA), by reacting Hal/DMSO with ethanolamine (**4**). These materials exhibited similar basal spacings and IR patterns. Hal–EOA was much less crystalline than Kao–EOA, as evidenced by the very broad diffraction peaks. This was presumably due to the turbostratic nature of halloysite and Hal–EOA compared to kaolinite and Kao–EOA. No residual unexpanded parent mineral could be detected for the Hal–EOA, indicating that 100% modification was achieved. This was not the case for Kao–EOA, where a reflection at 7.2 Å representing 1.5% relative intensity indicates the presence of a small amount of residual unexpanded kaolinite.

To our knowledge, an ethanolamine derivative (intercalate or otherwise) of kaolinite has not been previously reported in the literature. Ethanolamine has, however, been reported intercalated in halloysite (31), forming a material with a basal spacing of 10.7 Å, which is similar to what is reported here (**4**). This corresponded to a layer expansion of 3.5 Å, which is less than the 4.0 Å minimum clearance space that was calculated

© 1997 NRC Canada

Can. J. Chem. Downloaded from www.nrcresearchpress.com by 91.121.58.235 on 09/08/12
For personal use only.

Can. J. Chem. Downloaded from www.nrcresearchpress.com by 91.121.58.235 on 09/08/12
For personal use only.

Fig. 2. IR spectra (3800–2400 cm^{-1}) of Kao–EOA.

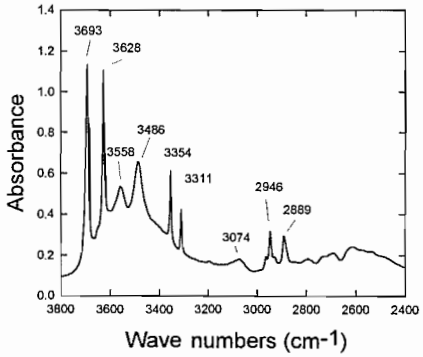
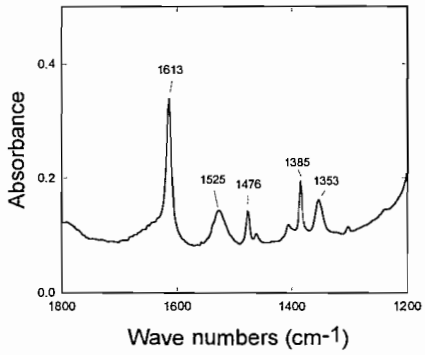


Fig. 3. IR spectra (1800–1200 cm^{-1}) of Kao–EOA.



for ethanolamine. This is in accord with many other intercalates that show a smaller than expected basal spacing due to some keying in of the guest (1–3, 8).

IR analysis

The IR patterns of Hal–EOA and Kao–EOA showed strong evidence of modification of the respective host minerals. In particular, the O-H stretching region was greatly perturbed and additional N-H stretching bands could be seen due to the ethanolamine units (Fig. 2). The ν(OH) bands of kaolinite normally found at 3695, 3670, 3652, and 3620 cm^{-1} have been replaced by bands at 3693, 3628, 3558, and 3486 cm^{-1} for Kao–EOA. These last two bands represent significant red shifts, indicating the effects of increased hydrogen bonding between the kaolinite host and ethanolamine guest.

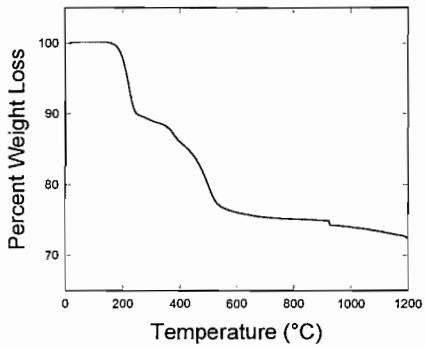
The inner hydroxyl kaolinite peak at 3620 cm^{-1} peak has been blue shifted to 3628 cm^{-1}. A similar blue shift phenomenon for an evacuated (0.01 Torr; 1 Torr = 133.3 Pa) hydrazine intercalated kaolinite was previously attributed to keying of the -NH_2 moiety of hydrazine into the siloxane ditrigonal cavity of kaolinite (20). A partial collapse of the hydrazine intercalate from 10.4 to 9.6 Å was associated with this phenomenon. This 8 cm^{-1} shift of the inner hydroxyl ν(OH) band, therefore, provides some evidence for the keying in of the -NH_2 group of ethanolamine into the (Si-O-)$_6$ macro-ring of kaolinite. In addition to the O-H stretching region, further evidence for ethanolamine modification includes the presence of two sharp N-H stretching bands at 3354 and 3311 cm^{-1}. C-H stretching bands were observed at 2946 and 2889 cm^{-1} (Fig. 2).

In the deformation region (Fig. 3), an NH bending band at 1613 cm^{-1}, a δ(CH) band at 1476 cm^{-1}, and a C-N stretching band at 1353 cm^{-1} could all be observed. The kaolinite host material also showed signs of perturbation in the lattice vibrations region. The very strong in-plane Si-O-Si stretching vibrations of kaolinite at 1010 and 1033 cm^{-1} (26) are shifted to higher frequencies in Kao–EOA to 1016 and 1045 cm^{-1}. The δ(Al-OH) band of the inner hydroxyl of kaolinite is shifted from 915 to 908 cm^{-1}, and the δ(Al-OH) band of the inner surface kaolinite hydroxyls at 938 cm^{-1} is replaced by a band at 974 cm^{-1}. All this indicates strong host–guest interactions between kaolinite and the ethanolamine moiety.

^{13}C NMR analysis

The solid state ^{13}C CP/MAS NMR spectrum (45.3 MHz) of Kao–EOA showed two broad resonances, one at 43 ppm and the other at 60.5 ppm corresponding, respectively, to the ^{13}C-NH_2 carbon and the ^{13}C-O- carbon of the ethanolamine unit. This was consistent with the insertion of the ethanolamine units in the interlayers of kaolinite. A dipolar dephasing experiment (32) (40 μs interrupted decoupling) led to the complete disappearance of both signals, indicating the existence of a rigidly bound ethanolamine unit, plausibly grafted to the aluminate interlamellar surface via $\equiv$Al-O-CH_2CH_2-NH_2 linkages. Alternatively, the ethanolamine molecule may be intercalated, but held rigidly in place by the inorganic host.

Fig. 4. TGA (20–1200°C) for Kao–EOA. Flowing nitrogen (40 cc/min); the heating rate was 20°C/min.



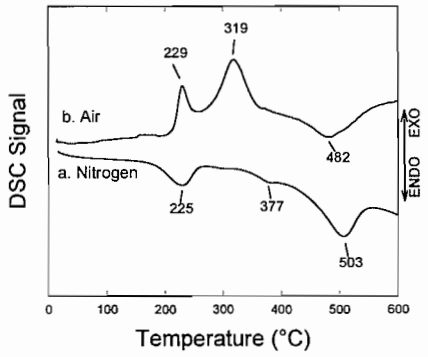
Thermal analysis

Thermal analysis of Kao–EOA shows that decomposition does not occur until about 150°C, and then there appears to be a three-step decomposition ending at 600°C (Fig. 4). The total calcination weight loss after heating to 1100°C in air for 3 h is 27.5%. Hal–EOA differs from Kao–EOA in that there is a preliminary decomposition step (7.6% weight loss) beginning almost immediately upon heating.

The thermal decomposition in nitrogen between 150 and 600°C is characterized by endothermic peaks at 225, 377, and 503°C (Fig. 5*a*). The peaks at 225 and 377°C are assigned to the endothermic pyrolysis of the interlayer organic material, and the peak at 503°C is assigned to the dehydroxylation of the kaolinite host. In air atmosphere (Fig. 5*b*), one observes an endothermic peak at 482°C assigned to the dehydroxylation of the kaolinite host material. However, instead of two endothermic events corresponding to the decomposition of interlayer organic material, two exotherms with peaks at 229 and 319°C

© 1997 NRC Canada

Fig. 5. DTA for Kao–EOA under flowing nitrogen (40 cc/min), and flowing air (40 cc/min). The heating rate was 20°C/min.



are observed. They are assigned to the exothermic combustion of the interlayer organic material. When the TGA/DSC run was done in air atmosphere, the product after heating to 1100°C was white, indicating that complete combustion of the interlayer organic material had occurred.

Based on elemental analysis of Kao–EOA (**1**), one can assign the formula $Al_2Si_2O_5(OH)_{3.0}(OCH_2CH_2NH_2)_{1.0}$. Here one assumes that grafting has occurred via the condensation reaction of the alcohol group of the ethanolamine with the interlamellar Al-O-H groups of kaolinite. This is consistent with the model for the aminoalcohol-derivatized organoboehmites of Inoue et al. (24) and with the methoxy-functionalized kaolinite (3). There is one ethanolamine unit per $Al_2Si_2O_5(OH)_4$ structural unit of kaolinite, allowing each amino group to key into one $(Si\text{-}O\text{-})_6$ macro-ring of the silicate surface of the adjacent layer. Alternately, if one were to consider an ethanolamine unit that is intercalated into the interlamellar surface of kaolinite without grafting, one could assign a chemical formula of $Al_2Si_2O_5(OH)_4(CH_2OHCH_2NH_2)_{1.0}$. The discrepancy between the calculated (3.45%) and found (2.72%) values for the%H of this last assignment suggests that the chemical formula based on the grafting of ethanolamine units ($Al_2Si_2O_5(OH)_{3.0}(OCH_2CH_2NH_2)_{1.0}$) may be a better representation of the structure.

Conclusions

The well-ordered organo-kaolinite material, Kao–EOA, was prepared from the reaction of ethanolamine with both Kao/DMSO and Kao/NMF. A model in agreement with the characterization data can be suggested: an organo-kaolinite material where ethanolamine units are attached to the aluminate interlamellar surface of kaolinite via $\equiv Al\text{-}O\text{-}CH_2CH_2NH_2$ covalent linkages, with the pendant NH_2 group keyed into the $(SiO\text{-})_6$ macro-ring of the adjacent silicate surface. This model accounts for both the rigidity of the ethanolamine units observed from ^{13}C DD/MAS NMR results, and the relative thermal stability of Kao–EOA. Elemental analysis and IR are also consistent with this structure, representing a supramolecular assembly of dipolar organo-mineral layers, stacked upon each other in an ordered non-centrosymmetric manner. However, on the basis of the basal spacing (10.7 Å) and of the lesser thermal and hydrolytic stability than the corresponding methoxy (3) and ethylene glycol derivatives (2), one can not unambigously disprove a structure when EOA units would be rigidly intercalated with EOA units keyed into the silicate macro-rings and the aluminol sheets. The prepared material could be a mixture of both types of compounds, intercalated and grafted EOA–kaolinite. A similar mixture could be obtained under certain experimental conditions in the case of the two previously reported ethylene glycol – kaolinite derivatives (1, 2).

Regarding Hal–EOA, the short-range structure of this intercalate appears to be similar to Kao–EOA. The long-range ordering, as evidenced from XRD, indicates that Hal–EOA is arranged in a turbostratic manner whereas Kao–EOA appears to have some three-dimensional ordering. This could be expected on the basis that the parent materials show this same difference in long-range ordering (8, 29).

References

1. J.J. Tunney and C. Detellier. Chem. Mater. **5**, 747 (1993).
2. J.J. Tunney and C. Detellier. Clays Clay Miner. **42**, 552 (1994).
3. J.J. Tunney and C. Detellier. J. Mater. Chem. **6**, 1679 (1996).
4. R.F. Giese. Clays Clay Miner. **26**, 51 (1978).
5. R.F. Giese. Bull. Mineral. **105**, 417 (1982).
6. M. Cruz, H. Jacobs, and J.J. Fripiat. Proc. Int. Clay Conf. 35 (1973).
7. J.A. Raussell-Colom and J.M. Serratosa. *In* Chemistry of clays and clay Minerals. *Edited by* A.C.D. Newman. Mineralogical Society, London. 1987. p. 371.
8. B.K.G. Theng. *In* The chemistry of clay-organo reactions. Adam Hilger, London. 1974. p. 239.
9. S. Hayashi. J. Phys. Chem. **99**, 7120 (1995).
10. M.J. Duer, J. Rocha, and J. Klinowski. J. Am. Chem. Soc. **114**, 6867 (1992).
11. J.G. Thompson and C. Cuff. Clays Clay Miner. **33**, 490 (1985).
12. J.G. Thompson. Clays Clay Miner. **33**, 173 (1985).
13. M. Raupach, P.F. Barron, and J.G. Thompson. Clays Clay Miner. **35**, 208 (1987).
14. S. Olejnik, L.A.G. Aylmore, A.M. Posner, and J.P. Quirk. J. Phys. Chem. **72**, 241 (1968).
15. S. Olejnik, A.M. Posner, and J.P. Quirk. Clay Miner. **8**, 421 (1970).
16. C.T. Johnston, G. Sposito, D.F. Bocian, and R.R. Birge. J. Phys. Chem. **88**, 5959 (1984).
17. J.J. Tunney and C. Detellier. Chem. Mater. **8**, 927 (1996).
18. R.L. Ledoux and J.L. White. J. Colloid. Interface Sci. **21**, 137 (1966).
19. J. Barrios, A. Plançon, M.I. Cruz, and C. Tchoubar. Clays Clay Miner. **25**, 422 (1977).
20. C.T. Johnston and D.A. Stone. Clays Clay Miner. **38**, 121 (1990).
21. A. Weiss, W. Thielepape, G. Göring, W. Ritter, and H. Schäfer. Proc. Int. Clay Conf. 287 (1963).
22. P. Sidheswaran, S.V. Ram Mohan, P. Ganguli, and A.N. Bhat. Indian J. Chem. Sect. A: Inorg. Phys. Theor. Anal. **26A**, 994 (1987).
23. P. Sidheswaran, A.N. Bhat, and P. Ganguli. Clays Clay Miner. **38**, 29 (1990).
24. M. Inoue, H. Tanino, and Y. Kondo. Clays Clay Miner. **39**, 151 (1991).
25. M.L. Jackson, L.D. Whittig, and R.P. Pennington. Soil Sci. Soc. Am. Proc. **14**, 77 (1949).
26. C.B. Tanner and M.L. Jackson. Soil Sci. Soc. Am. Proc. **12**, 60 (1947).

Can. J. Chem. Downloaded from www.nrcresearchpress.com by 91.121.58.235 on 09/08/12
For personal use only.

© 1997 NRC Canada

27. R.K. Schofield and H.R. Samson. Discuss. Faraday Soc. **18**, 135 (1954).
28. H. van Olphen and J.J. Fripiat. Data handbook for clay minerals and other non-metallic minerals. Pergamon Press, Oxford. 1979.
29. S.W. Bailey. *In* Crystal structures of clay minerals and their X-ray identification. *Edited by* G.W. Brindley and G. Brown. Mineralogical Society, London. 1984. p. 1.
30. D.M.C. MacEwan. J. Chem. Soc. Faraday Trans. **44**, 349 (1948).
31. R.M. Carr and H.W.A. Chih. Clay Miner. **9**, 153 (1971).
32. L.B. Alemany, D.M. Grant, T.D. Alger, and R.J. Pugmire. J. Am. Chem. Soc. **105**, 6697 (1983).

Can. J. Chem. Downloaded from www.nrcresearchpress.com by 91.121.58.235 on 09/08/12
For personal use only.

© 1997 NRC Canada

Capacitive and kinetic characteristics of Ru–Ti oxide electrodes: influence of variation in the Ru content

B.V. Tilak, C.-P. Chen, V.I. Birss, and J. Wang

Can. J. Chem. Downloaded from www.nrcresearchpress.com by 91.121.58.235 on 09/08/12
For personal use only.

Abstract: A systematic investigation has been carried out of thermally formed Ru–Ti oxide electrodes of varying Ru content, correlating their voltammetric and impedance characteristics in NaCl solutions with the kinetics of the chlorine evolution reaction. The Tafel slope increases markedly with lower Ru content (< ca. 25 at.%), indicative either of the contribution of increasing oxide resistance or of a change in mechanism. The exchange current density is linearly proportional to the Ru content down to <10 at.% Ru, below which the film appears to respond more like a highly resistive film material. The film resistance and capacitance, determined by equivalent circuit fitting in the absence of dissolved chlorine, were used to calculate the expected impedance response of the oxide film, based on a model of an activation-controlled surface redox reaction occurring in a porous matrix. The calculated results show the dominant signature of the matrix resistance at low Ru loadings, in both the phase angle impedance data and in the Tafel plots, in agreement with the experimental observations.

Key words: Ru oxide, Ru–Ti oxide, chlorine evolution, kinetics, capacitance, equivalent circuit, impedance, Tafel data.

Résumé : On a effectué une étude systématique d'électrodes de l'oxyde de Ru–Ti, formées thermiquement, contenant diverses quantités de Ru; on a établi une corrélation entre leurs caractéristiques voltampérométriques et d'impédance dans des solutions de NaCl avec la cinétique de la réaction d'évolution du chlore. La pente de Tafel augmente d'une façon importante aux faibles concentrations de Ru (inférieures à environ 25 at.%); ceci suggère une augmentation de contribution de la résistance de l'oxyde ou un changement de mécanisme. La densité du courant d'échange est linéairement proportionnelle à la concentration du Ru jusqu'à des valeurs inférieures à 10 at.% de Ru; en dessous de ces valeurs, le film semble répondre plus comme un film ayant au grande résistivité. On a utilisé la résistance et la capacitance du film, déterminées par un ajustement de circuit équivalent en l'absence de chlore dissous, pour calculer la réponse attendue de l'impédance de l'oxyde de film; à cette fin, on a fait appel à un modèle de réaction redox de surface contrôlée par l'activation et se produisant dans une matrice poreuse. Les résultats calculés montrent que la signature dominante de la résistance de la matrice à de faibles doses de Ru est en accord avec les données expérimentales, tant pour les données d'impédance que pour les courbes de Tafel.

Mots clés : oxyde de ruthénium, oxyde de Ru–Ti, évolution de chlore, cinétique, capacitance, circuit équivalent, impédance, données de Tafel.

[Traduit par la rédaction]

1.0 Introduction

Understanding the electrochemical properties of thermally formed Ru–Ti oxide electrodes, commonly used as anodes in the chlor-alkali industry, is very important in order to forecast, and to enable the optimization of, their overall performance during chlorine evolution in industrial operations. Extensive prior investigations have been directed towards understanding Ru–Ti oxide electrode characteristics and to establishing the relationship between their structural and electrical properties and their Ru content. Several comprehensive and critical analyses of these prior results have been presented previously (1–3).

The effect of the temperature employed during the formation of Ru–Ti oxides on their structure has been examined (4–6), and it was reported that the oxide obtained at 400°C is a metastable solid solution, while a crystalline mixture is obtained at 700–800°C. Spasskaya et al. (7) concluded that the change of the roughness factor (200 to 800) that occurs with composition has little effect on the oxide surface properties. It was also reported by various groups (5–9) that the resistance of Ru–Ti oxide films increases sharply with decreasing Ru content for films containing less than ca. 25 at.% Ru (7, 8).

Doblhofer et al. (10) studied the effect of sweep rate on the charge passed in cyclic voltammetry (CV) experiments by thermally formed Ru–Ti oxide electrodes, allowing the diffusion coefficients to be estimated. A study of the effect of the Ru composition on the CV charge of the Ru–Ti oxide electrodes (6, 11–13) showed that it could be used to measure their

Received June 10, 1997.

This paper is dedicated to Dr. Brian E. Conway, in honour of his many scientific contributions and on the occasion of his 70th birthday.

B.V. Tilak and C.-P. Chen. Occidental Chemical Corporation, Technology Centre, Grand Island, NY 14072, U.S.A.
V.I. Birss[1] **and J. Wang.** Department of Chemistry, University of Calgary, Calgary, AB T2N 1N4, Canada.

[1] Author to whom correspondence may be addressed. Telephone: (403) 220-6432. Fax: (403) 289-9488. E-mail: birss@acs.ucalgary.ca

© 1997 NRC Canada

Can. J. Chem. Downloaded from www.nrcresearchpress.com by 91.121.58.235 on 09/08/12
For personal use only.

true surface area. Shieh and Hwang (14) studied the electrochemical behavior of Ru–Ti oxide electrodes doped with small amounts of Sn and found the relationship between the CV charge and the double layer capacity (obtained from ac impedance experiments) to be linear and also that the capacity could yield the electrochemically active surface area. Investigations of the influence of temperature on the CV response (13, 15, 16) revealed the Arrhenius relation to be obeyed, yielding an activation enthalpy of ca. 4–5 kJ/mol.

Vallet et al. (17, 18) studied the properties of ion-implanted Ru– and Ir–Ti electrodes and found the electrochemical activity of Ru-implanted electrodes to be 2 to 3 times higher than that of the Ir-implanted ones, while the corrosion rate of the latter was only ca. 1% of the former. They also reported that the mechanism of electrical conductance of these oxides changes from semiconducting to metallic when a surface Ru concentration of 2.6×10^{21} atoms cm^{-3} is exceeded, corresponding to about 25 at.% Ru in the Ru–Ti oxide film.

Most of the investigations performed in the past with thermally formed Ru–Ti oxide electrodes have focussed on the kinetics of the chlorine evolution reaction on these oxide surfaces. However, no systematic studies have to date been reported relating the electrochemical and impedance properties of these metal oxide electrodes, under conditions when only the oxide film is redox-active, to the kinetic characteristics of these materials in the faradaic domain of the chlorine evolution reaction. In the present paper, attempts have been made to explain the changes in the chlorine evolution Tafel data, in terms of the combined effect of changing film resistivity and of the density of active Ru sites, with the change in the Ru content of the films. This study was also considered relevant in terms of attempting to further the understanding of the origin of the problematic loss of kinetic activity, seen with some Ru–Ti oxide anodes, in practice.

2.0 Experimental

The working electrode substrate consisted of 99.99% Ti wire of 2 mm diameter, purchased from Johnson Matthey, Inc. The cross-sectional end (0.0314 cm^2) of each fresh titanium wire electrode was first polished with 600 grit emery paper, and then dipped in hot oxalic acid (1.25 mol/L) + 2.2 mol/L hydrochloric acid to remove the air-formed oxide film from the surface. It was then rinsed with acetone, dried, rinsed with methylene chloride, dried again, and then rinsed with triply distilled water.

Ruthenium(III) chloride (18.2 g, Johnson Matthey & Mallory Ltd.), titanium(VI) butoxide (45 ml, Aldrich Chemical Co. Inc.), and 4.4 mol/L hydrochloric acid (6 mL) were mixed together to make the coating solution.[2] The Ti wire electrodes were then painted with a thin layer of this solution and allowed to air-dry. A single coat under normal conditions yielded a coating thickness, estimated by its weight gain, to be ca. 2 μm. In other experiments, a thinner film of 0.6–0.7 μm thickness was deposited in two coats from a 5 × diluted Ru–Ti coating solution. These coatings were then converted to the oxide by heating at a rate of 5°C/min to 100°C, and then remaining at 100°C for 15 min to remove the solvent. The temperature was then increased at 10°C/min to 440°C in air and maintained at 440°C for 30 min to decompose the Ru–Ti compounds into the corresponding oxides. Afterwards, the side of each oxide-coated Ti wire was insulated with Teflon tape, leaving only the cross-sectional end to serve as the working electrode (WE) in the NaCl test solution.

All experiments were carried out in 5 mol/L NaCl (EM Science) made up with triply distilled water. The pH of the NaCl solution was adjusted both before and during electrolysis to ca. 4 by the addition of either 0.5 or 2 mol/L HCl at regular intervals. All electrolysis experiments were carried out without additional stirring of the solution or removal of the dissolved oxygen, in a one-compartment cell at both room temperature (20–22°C) and at 90°C. IR compensation was employed for the Tafel analysis of the chlorine evolution data in all of the experiments.

The counter electrode (CE) was a 40 at.% Ru oxide coating on a Ti substrate, of more than 100 times the apparent surface area of the WE. It was positioned inside a Teflon tube to minimize the amount of hydrogen gas that passed into the solution in the main compartment. An Ag/AgCl electrode was employed as the reference electrode (RE) at high temperatures, while an SCE generally served as the RE at room temperature. All potentials are given versus the SCE in this paper.

An EG&G PAR 273 potentiostat/galvanostat was used in all electrolysis and CV experiments, with the data plotted on an HP 7044B X-Y recorder. A Solartron 1255 HF frequency response analyzer, coupled with a Solartron 1286 electrochemical interface, was employed for the ac impedance measurements, using frequencies from 0.1 to 65 kHz and a 10 mV rms amplitude (effective) applied at the open circuit potential (OCP). As the SCE reference electrode introduces a time delay to the potentiostat, seen as a phase shift at high frequencies due to its resistance and capacitance characteristics, an additional Pt wire electrode was placed in the cell and was connected via a 6.8 μF capacitor to the RE lead (19–21). Data acquisition was carried out using Z-Plot software (Scribner Associates) and its evaluation was achieved using a nonlinear least-squares fit program (Equivalent Circuit, Version 3.97, written by B. Boukamp, University of Twente).

3.0 Results and discussion

3.1 Cyclic voltammetric (CV) behavior of Ru–Ti oxide films

As part of the early steps in the characterization of the films, CV data were collected in fresh 5 mol/L NaCl solutions prior to the electrolysis experiments. It is known (1, 2, 22–24) that the CV response of these electrodes reflects the reversible conversion of the Ru sites at the film surface from Ru(II) at the negative end of the scan to Ru(IV) at more positive potentials. The CV behavior at 100 mV/s for oxide electrodes of varying Ru content is shown in Fig. 1 at 20–22°C (solid lines) and at 90°C (dotted lines) in 5 mol/L NaCl, between 0.5 and 1.0 V vs. SCE. It can be seen from Fig. 1 that the magnitude of the CV currents decreases with decreasing Ru content, particularly for the less than 15 at.% Ru oxide films. Also, the effect of temperature on the response is negligible down to 10 at.% Ru, below which increased temperature yields significantly higher currents, especially for the 5 at.% Ru oxide.

Figure 2 (open symbols) shows a plot of the reciprocal of

[2] B.V. Tilak. Private communication.

© 1997 NRC Canada

Fig. 1. Cyclic voltammograms of Ru–Ti oxide electrodes (2 μm thick) with varying Ru content in 5 mol/L NaCl (pH ca. 4) at 100 mV/s at room temperature (solid lines) and at 90°C (dotted lines).

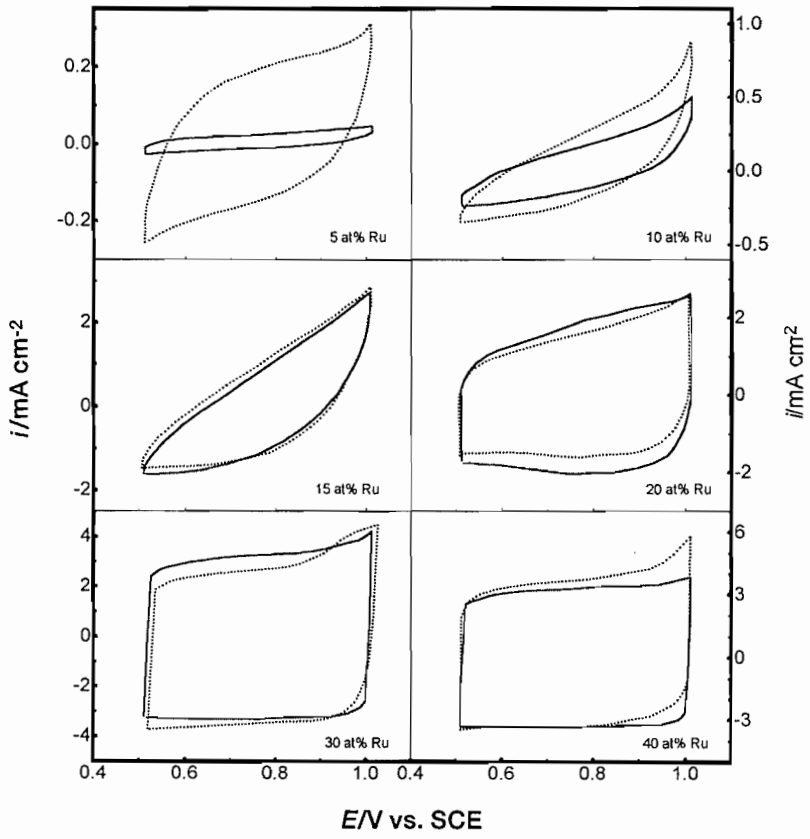
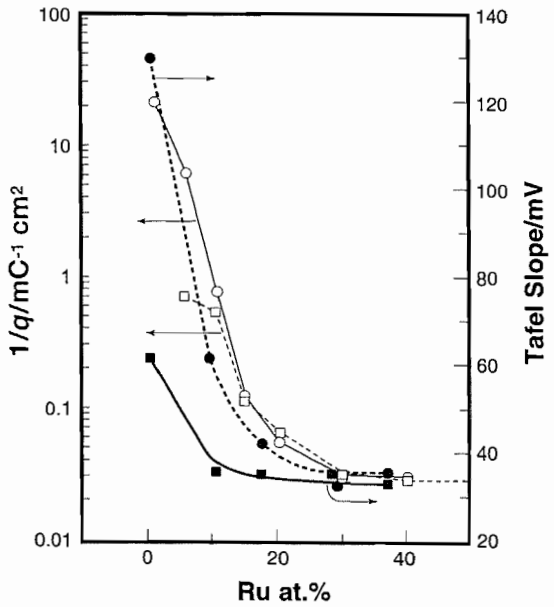


Fig. 2. Relationship of reciprocal CV charge densities (room temperature, open circles; 90°C, open squares) and of the Tafel slope obtained during chlorine evolution (room temperature, closed circles; 90°C, closed squares) on the Ru content for 2 μm thick Ru–Ti oxide films in 5 mol/L NaCl (pH ca. 4).



the logarithm of the integrated charge density (passed in a single anodic scan) as a function of the Ru content of the film. The inverse log of the charge density decreases linearly up to ca. 25 at.% Ru, and then takes on a close to steady-state value at higher Ru compositions. Clearly, the addition of Ru to the Ti oxide film not only results in a proportional increase in the density of surface-active Ru sites, but also leads to other changes in film properties.

Figure 3(*a*) shows the room temperature CV response for a pure, thermally formed Ti oxide film, demonstrating the very low capacitance of this semiconducting material. Figure 3 (*b* and *c*) displays the CV responses for pure Ru oxide films at room temperature and at 90°C, respectively. The higher charges and the more capacitive appearance of the CV response in Figs. 3*b* and 3*c* for pure Ru oxide films appears very similar to the CV data for mixed Ru–Ti oxide films of more than 20 at.% Ru, shown in Fig. 1. Clearly, the CV response for Ti oxide (Fig. 3*a*) is more similar to those of the 5 and 10 at.% Ru films in Fig. 1, suggesting that the more marked effect of temperature in Fig. 1 for these oxides reflects an increase in conductivity.

The effect of film thickness on the CV response of 40 at.% Ru oxide films is shown in Fig. 4. The currents and charge densities are seen to be approximately proportional to the estimated film thicknesses of 0.6 and 2 μm. If the Ru–Ti oxide CV response is proportional to the available surface area, as was reported earlier for thermally formed films (12, 25, 26), then these results suggest that these films are homogeneously

© 1997 NRC Canada

Can. J. Chem. Downloaded from www.nrcresearchpress.com by 91.121.58.235 on 09/08/12
For personal use only.

Can. J. Chem. Downloaded from www.nrcresearchpress.com by 91.121.58.235 on 09/08/12
For personal use only.

Fig. 3. Cyclic voltammograms in 5 mol/L NaCl (pH ca. 4): (*a*) thermally formed TiO_2, formed on Ti at 440°C for 30 min, room temperature; (*b*) anodically formed RuO_2 on Ru (2 V for 5 min); room temperature; (*c*) same as (*b*), but at 90°C.

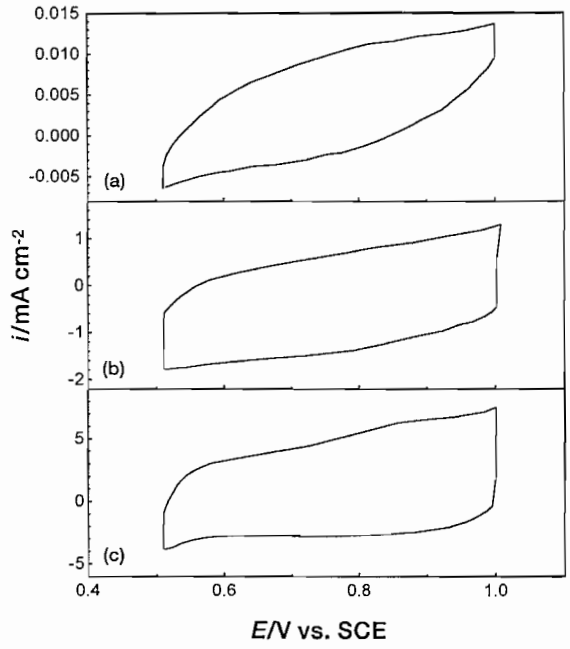
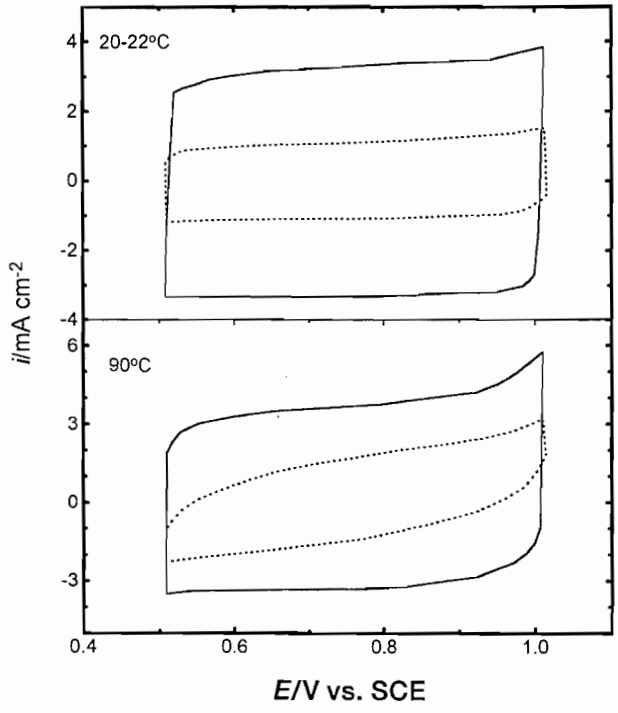
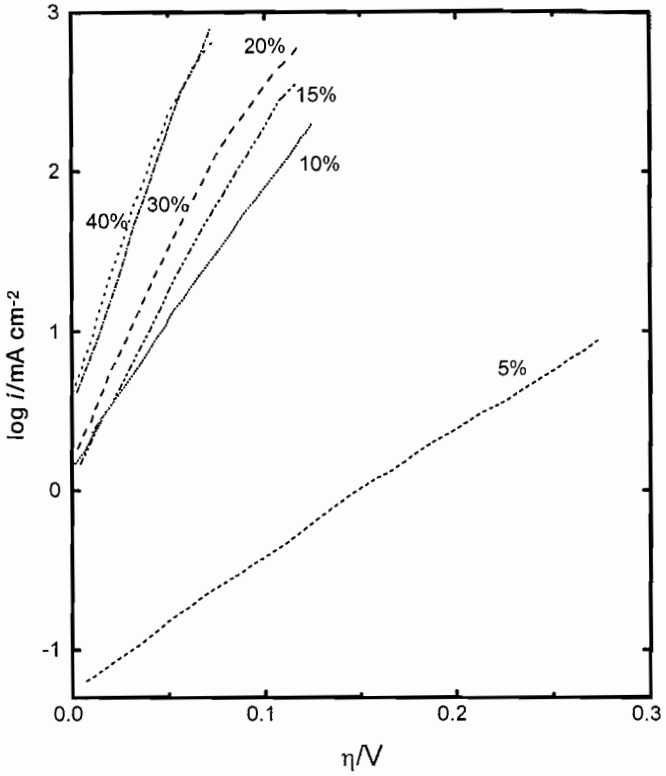


Fig. 4. Cyclic voltammograms of Ru(40 at.%) – Ti oxide electrodes at room temperature and 90°C in 5 mol/L NaCl (pH 3–5) at 100 mV/s: 2 μm thick coatings (solid lines); 0.6 μm coatings (dotted lines).



porous materials and that all of the Ru surface sites are accessible for reaction under these experimental conditions. The research of Burke and O'Neil (13) also concluded that the CV charge is a measure of the true surface area of the oxide film,

Fig. 5. Polarization behavior of Ru–Ti oxide electrodes with varying at.% Ru in 5 mol/L NaCl (pH ca. 4) at room temperature.



and that it is proportional to the Ru content of the film (from 10 to 100 at.% Ru).

3.2 Effect of Ru content of the oxide films on chlorine evolution Tafel plots

The *i/E* relationship of the chlorine evolution reaction was established after electrolysis had been carried out for a relatively long period of time, such that the solution could be considered to have equilibrated in terms of dissolved chlorine and hypochlorite, at both temperatures studied. In these experiments, the potential was scanned at 1 mV/s from the OCP (1.05 V) to a maximum current of ca. 800 mA cm^2 (potentiostat oscillations occurred during IR compensation at currents higher than this) and then back to the OCP. Figure 5 shows a typical set of Tafel data for the chlorine evolution reaction at freshly formed, 2 μm thick, Ru–Ti oxide films of varying Ru contents at room temperature. Both the Tafel slope and the exchange current density of the reaction are clearly affected by the oxide composition, with the most notable difference being observed for the 5 at.% Ru film. These results are in agreement with those reported earlier (8, 16) for thermally formed Ru–Ti oxide films.

The effect of the Ru content on the Tafel slopes is shown more clearly in Fig. 2 (closed symbols). It is seen that, at room temperature, the Tafel slope increases for oxide films containing less than 25 at.% Ru, while, at 90°C, an effect on the slope is seen only when the Ru content is less than 10 at.%. At high Ru contents, the Tafel slope is in the range of 30–40 mV, while, at low contents, a higher ca. 120 mV slope is seen, in agreement with prior literature reports (8, 16).

Figure 6 shows the exchange current density for the chlo-

© 1997 NRC Canada

Can. J. Chem. Downloaded from www.nrcresearchpress.com by 91.121.58.235 on 09/08/12
For personal use only.

Fig. 6. Effect of at.% Ru in Ru–Ti oxide films of 2 μm thickness on exchange current density of chlorine evolution reaction in 5 mol/L NaCl (pH ca. 4) at room temperature (circles) and at 90°C (squares).

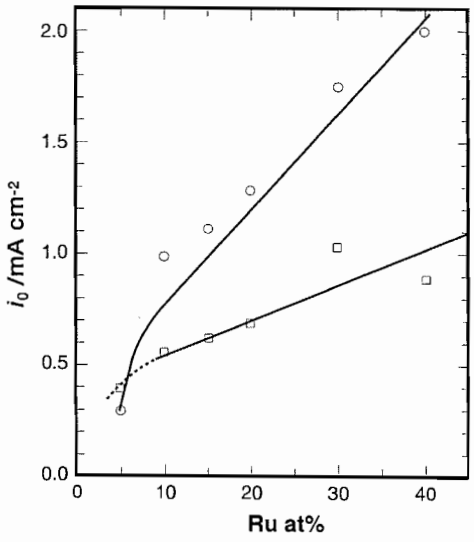
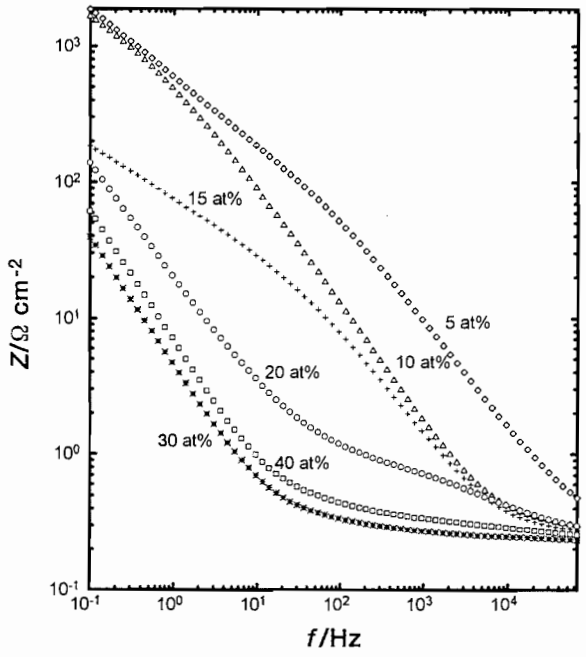


Fig. 7. Frequency dependence of total impedance of Ru–Ti oxide electrodes with different Ru contents in 5 mol/L NaCl (chlorine-free) at room temperature at the OCP.



rine evolution reaction as a function of oxide composition. At both temperatures, the relationship between the exchange current density and the Ru content of the oxide film is linear down to ca. 10 at.% Ru. For the 5 at.% Ru films, the exchange currents are clearly very much reduced. Figure 6 also shows that the exchange current densities at 90°C are lower than the corresponding values at room temperature. This presumably reflects a difference in the nature of the adsorbed surface species participating in the rate-determining step at these two temperatures.

It is widely accepted that the Tafel slope for the chlorine evolution reaction should be ca. 40 mV (1, 2), indicative of a slow desorption step. The 30 mV slope seen in Fig. 2 for high Ru contents may indicate the slow diffusion of the product away from the electrode surface, such that it becomes super-

Fig. 8. Frequency dependence of phase angle of Ru–Ti oxide electrodes with different Ru contents in 5 mol/L NaCl (chlorine-free) at room temperature at the OCP.

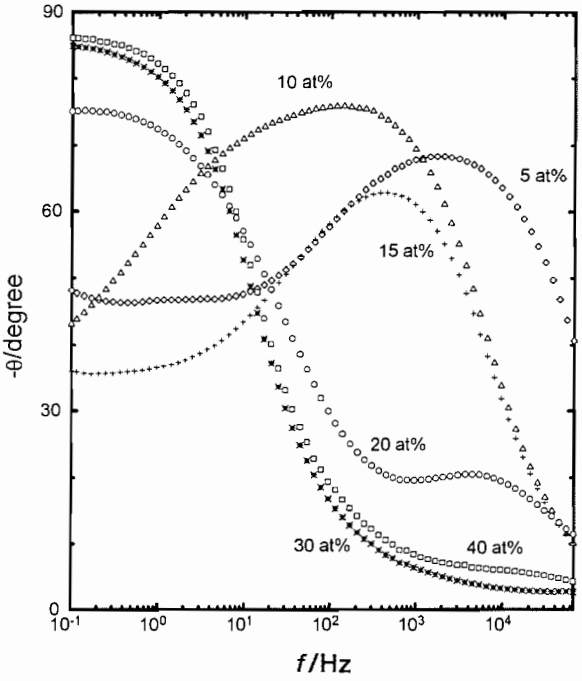
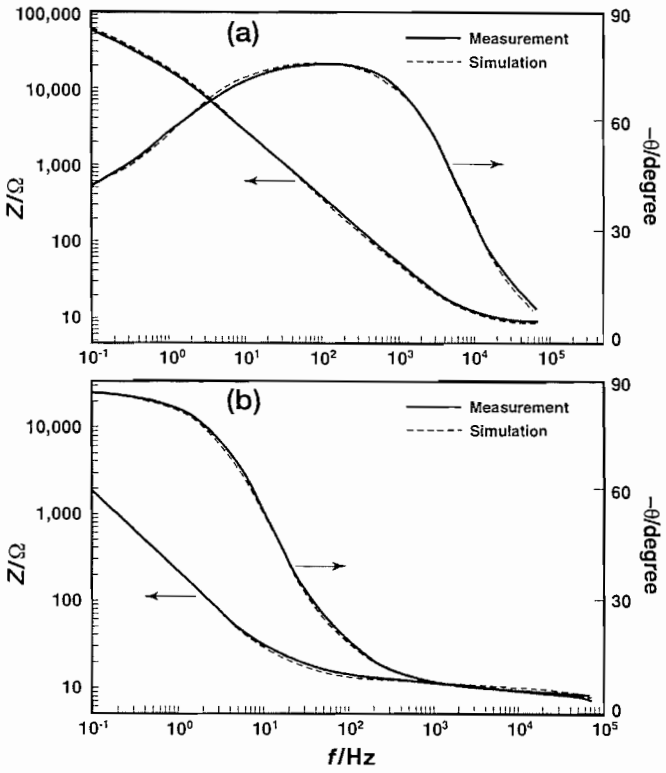


Fig. 9. Comparison of experimental impedance (Z) and phase angle (θ) data with values calculated using the best-fit equivalent circuit parameters in Table 1. (*a*) 10 at.% Ru; (*b*) 40 at.% Ru.



© 1997 NRC Canada

Can. J. Chem. Downloaded from www.nrcresearchpress.com by 91.121.58.235 on 09/08/12
For personal use only.

saturated with adsorbed chlorine, or that a rapid discharge reaction is followed by a slow recombination step (2). To explain the increasing Tafel slope with decreasing Ru content, several possibilities can be considered. First, as the Ru site density decreases with lower Ru content, the probability of interaction of a chloride ion with an adsorbed chlorine atom intermediate (expected to yield a 40 mV Tafel slope) is likely to decrease, and therefore the mechanism may change to one in which the discharge reaction is slow (120 mV Tafel slope). The Tafel slopes of between 40 and 120 mV at intermediate Ru contents might then reflect the fact that both of these mechanisms are occurring simultaneously on the surface for films of between 10 and 25 at.% Ru. A second option to explain the data of Fig. 2 is that, at high Ru surface site densities (>25 at.% Ru), the surface coverage of adsorbed chlorine atoms is close to zero, which would yield the expected Tafel slope of ca. 40 mV for this reaction. However, at lower Ru contents, as the reaction rate decreases, it is possible that the surface coverage by adsorbed chlorine atoms increases to unity, which would be consistent with a 120 mV slope. A still more likely possibility is that the experimental Tafel slope reflects not only the mechanism of the chlorine evolution reaction, but also the resistance of the oxide film substrate (27, 28). This would then suggest that the trends in the Tafel slope should be paralleled by similar trends in the oxide resistance. This will be discussed below, based on the impedance results shown.

The exchange current density would be expected to vary linearly with the Ru surface site density, which should be proportional to the Ru content of the film, consistent with what is seen in Fig. 6 down to 10 at.% Ru. The lower value for the 5 at.% film suggests that either some of the Ru sites are no longer accessible or that the oxide surface does not reflect the bulk oxide composition and is behaving anomalously, i.e., more like a poorly conducting Ti oxide film.

3.3 Effect of oxide film Ru content on the ac impedance response

All of the ac impedance data were collected at room temperature in a 5 mol/L NaCl solution. Solution stirring and deaeration were found not to affect the ac response and therefore no attempts were made to remove oxygen or agitate the solution. Most previous ac impedance studies of this system have been carried out in chlorine-saturated solutions near the chlorine–chloride equilibrium potential (29–32), i.e., at ca. 1.05 V vs. SCE. As the emphasis in the present study has been on examining the oxide film properties in the absence of the chlorine evolution reaction, the ac impedance data were gathered primarily at the OCP of the mixed oxide electrodes in solutions containing no dissolved chlorine, i.e., near 0.4 V vs. SCE.

Figures 7 and 8 show the total impedance and phase angle Bode representations for oxide films ranging between 5 and 40 at.% Ru at the oxide OCP in chlorine-free solutions. It is seen that the 20–40 at.% Ru oxides are generally quite similar in their response, and that the biggest change occurs at 15 at.% Ru and lower. This pattern is consistent with the CV data of Fig. 1 and the Tafel slope data in Fig. 2, showing the impact of the oxide properties on the chlorine evolution reaction. The impedance at low frequencies indicates that the resistance of the oxide film is particularly high for the 5–10 at.% Ru films, with the 15 and 20% films exhibiting intermediate resistances, in agreement with prior published results (7). At high frequencies, a resistance value of ca. 6 Ω, corresponding to the solution resistance, is seen in all cases.

The phase angle data in Fig. 8 is particularly interesting in terms of revealing the changing electrical properties of these films with Ru content. Again, the transition in properties is most notable at 15–20 at.% Ru. With decreasing Ru content, it is seen that a second time constant appears at high frequencies, with its phase angle maximum increasing in magnitude and moving to lower frequencies from 20 to 10 at.% Ru in the coating. Interestingly, for the 5 at.% Ru containing Ru–Ti oxide film, the phase angle maximum decreases somewhat, and moves back to higher frequencies, perhaps indicating that the 5% Ru film is significantly different from the others and behaves more like a conventional capacitive oxide material, with the large fraction of TiO_2 likely serving as its ohmic component.

The analogous set of experiments were carried out with these oxide films in a chlorine-saturated solution at 1.05 V. The phase angle data, in particular, displayed several important trends (not shown in a figure) in common with those at the oxide OCP in Fig. 8, namely, that, with decreasing Ru content, a new high-frequency time constant develops, with its phase angle maximum increasing and moving to lower frequencies. The data for the 5 at.% Ru containing Ru–Ti oxide film was again anomalous, in that its high-frequency time constant has moved to higher frequencies.

3.4 Interpretation of impedance data for mixed Ru–Ti oxides

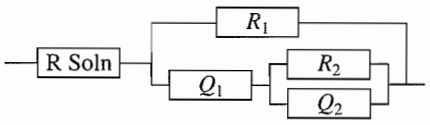
Two approaches were taken in this work to understand and interpret the impedance data, shown in Figures 7 and 8. The first involved identifying the best-fit equivalent circuit (EQC), based on Boukamp's EQUIVCIRC software, in order to establish the values of the circuit elements. The intention of this work was to then correlate their values with the Tafel and CV data as a function of oxide film composition. The usual guidelines for the selection of the best-fit EQC were followed, i.e., that a minimum number of circuit elements be employed; that, as far as possible, the same circuit is used for all film compositions; and that the χ^2 error, as well as the errors associated with each element, is suitably low (33). Many equivalent circuits were examined, but only that shown in Table 1 obeyed these criteria. Also, this circuit fit well to the impedance data obtained at both the OCP in chlorine-free solutions and at 1.05 V in chlorine-saturated media.

Figure 9 depicts the overlay of the experimental (at the OCP in chlorine-free solutions) and the calulated Bode data, using the EQC shown in Table 1, for the 10 and 40 at.% Ru oxide films, respectively, and shows a high quality of fit over the entire frequency range. The fit for the 5 at.% Ru oxide film was somewhat less satisfactory, again indicating that the properties of this film are quite different from those of the other films, consistent with the apparently anomalous positive shift of the second high-frequency time constant (Fig. 8).

Table 1 gives the values of the circuit elements for the six oxide films at the OCP, based on this EQC. It should be noted that the solution resistance, R_{soln}, was ca. 6 Ω in all of this work, in agreement with the expected electrolyte resistance between the oxide electrode surface and the SCE. R_1, the parallel resistance, lies between ca. 10^3 and 10^4 Ω cm^{-2} in all cases. R_1 is likely to represent the dc leakage current arising

© 1997 NRC Canada

Table 1. Best-fit "equivalent circuit" data.



% Ru	R_1 (Ω cm^{-2})	R_2 (Ω cm^{-2})	Q_1 (mF cm^{-2})	n_1	Q_2 (mF cm^{-2})	n_2
5	4 500	120	0.53	0.70	0.16	0.80
10	3 000	300	0.66	0.87	0.66	0.85
15	300	30	4.50	0.70	1.20	0.79
20	—	0.9	11.66	0.83	18.23	0.50
30	24 000	1.2	26.66	0.95	—	—
40	4 500	0.3	41.66	0.97	—	—

from faradaic reactions involving trace impurities in solution (e.g., the reduction of trace oxygen), which occurs at the OCP (32). As R_1 does not appear to depend on the oxide film properties, its impact on the observations is ignored in the present discussion.

Q_1 and Q_2 represent constant phase elements (CPEs), with n_1 and n_2 reflecting how similar these elements are to a pure capacitor, for which $n = 1$. Notably, both Q_1 and Q_2 increase with the Ru content in the film, with Q_1 likely reflecting the oxide pseudocapacitance and, hence, the number of active Ru sites at the oxide–solution interface. In fact, a rough comparison between these Q_1 values (without converting them to capacitance values through their n values) and the oxide capacitance, estimated from the CV responses in Fig. 1 (current divided by sweep rate), yield very similar pseudocapacitances, confirming this suggestion. The fact that the n_1 values are so close to unity for the 30 and 40 at.% Ru oxide films indicates the formation of nearly perfectly capacitive films, whereas the decreasing n_1 values with decreasing Ru content show the development of nonideality in the capacitive characteristics, probably due to decreasing matrix conductivity (34).

The R_2 values also show an interesting trend with increasing Ru content of the film, decreasing from ca. 10^2 to ca. 0.5 Ω cm^{-2}, consistent with the expected change in film conductivity. The Q_2 value also increases with increasing Ru content. For the 30 and 40 at.% Ru films, the best-fit Q_2 values were unreasonably high, up to 1 F cm^{-2} (larger than any possible capacitance in the system). However, as their n values were very low, less than 0.2, this indicates that the second CPE is not a valid part of the EQC, and that Q_2 should be replaced by a resistor (33).

Overall, it should be stated that, while the data could be best accounted for by the equivalent circuit shown in Table 1, the circuit itself cannot be said to have any absolute physical meaning. However, it is interesting that, even when the data were fit (although with higher error) to several other equivalent circuits containing the same or almost the same number of elements, the Q and R values were very similar to the R_2 and Q_1 values in Table 1. This strongly suggests that these values do, in fact, accurately reflect the electrical characteristics of these oxide films and were therefore used in the treatment below.

The second approach used in the present work to understand and interpret the impedance response of these Ru–Ti oxide films follows an earlier mechanistic description (35) employed to explain the response of Ru oxide based capacitors to small signal ac perturbations. Attempts were made here to verify this mechanistic approach by comparing the calculated impedance data (specifically the phase angle Bode plots) with those obtained experimentally. The equivalent circuit for a simple one-electron, activation-controlled surface redox process occurring on a planar Ru–Ti oxide surface at the OCP (reaction [1]),

[1] $Ru^{4+} + e^- <==> Ru^{3+}$

was shown (33) to be represented by the circuit in Fig. 10*a*. The double layer capacitance (C_d) is located in parallel with the charge transfer resistance (R_t) and the film pseudocapacitance (C_ϕ), which are in series with each other.

The impedance of the same reaction [1], but occurring in a porous matrix structure, was shown (35) to be represented by the following relationship:

$$[2] \quad Z(p) = \frac{1}{\sigma' S}\left(\frac{\coth(ml)}{m}\right)$$

where

$$[3] \quad \sigma' = \frac{\sigma A}{S}$$

and

$$[4] \quad m = \sqrt{\frac{1}{\sigma'}\left(pC_d + \frac{pC_\phi}{(pC_\phi R + 1)}\right)}$$

$Z(p)$ refers to the generalized impedance, p to the Laplace transform variable in the Heaviside notation, σ to the specific conductance of the solution phase (Ω^{-1} cm^{-1}), A to the cross-sectional area (cm^2), l to the pore length, R to the sum of the charge transfer and film matrix resistance, and S to the surface

Can. J. Chem. Downloaded from www.nrcresearchpress.com by 91.121.58.235 on 09/08/12
For personal use only.

© 1997 NRC Canada

Can. J. Chem. Downloaded from www.nrcresearchpress.com by 91.121.58.235 on 09/08/12
For personal use only.

Fig. 10. Theoretical equivalent circuit for an activation-controlled surface redox reaction reaction [1]) occurring (*a*) at a planar surface; (*b*) at a porous electrode.

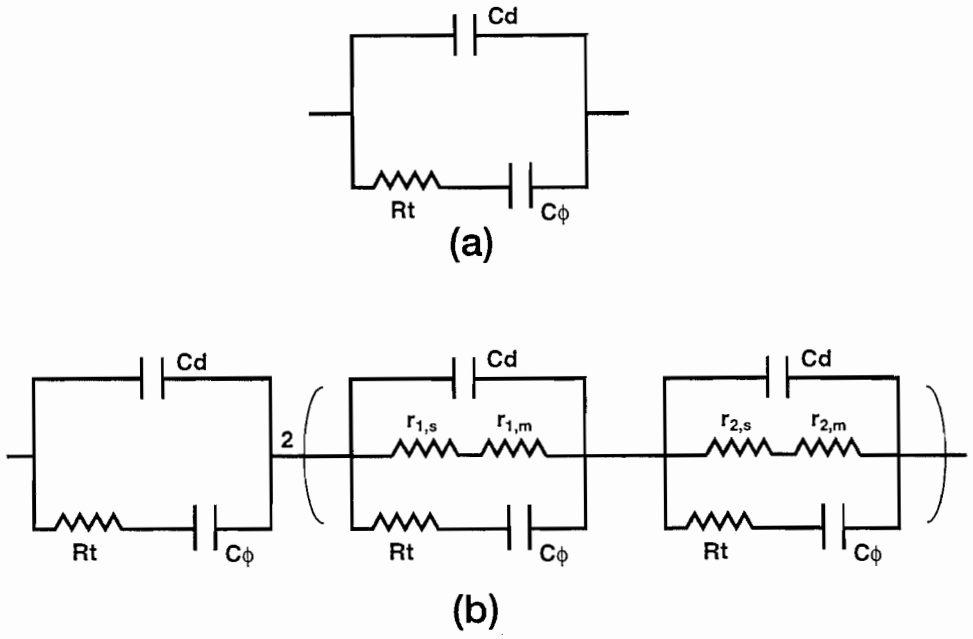
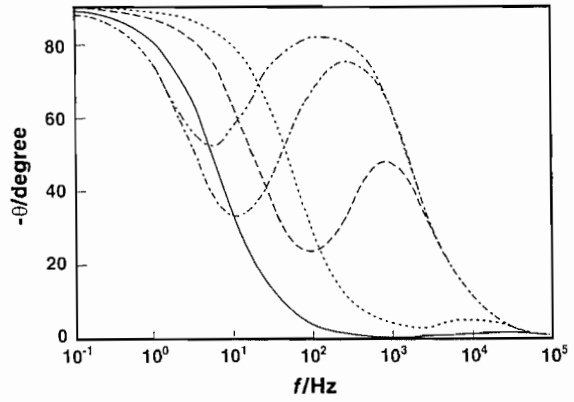


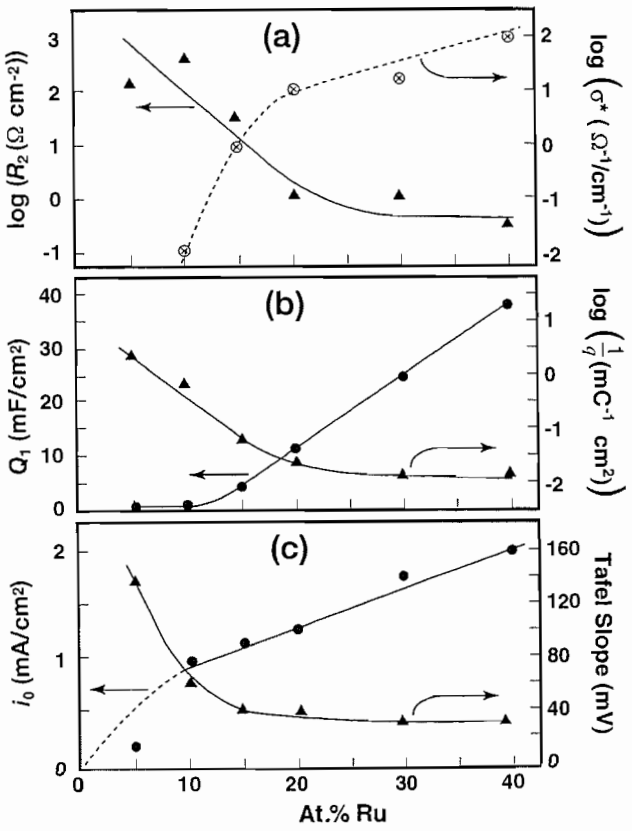
Fig. 11. Phase angle vs. frequency plots, calculated using eq. [2]. C_ϕ = 30 mF, R = 0.3 Ω (————). C_ϕ = 3 mF; R = 1 Ω (.....). C_ϕ = 1.5 mF; R = 30 Ω (– – – – – –). C_ϕ = 1 mF; R = 300 Ω (-·-·-·-·-·-). C_ϕ = 0.3 mF; R = 1300 Ω (-·-·-·-·-·-·-).



area of the porous matrix per unit film thickness. The capacitances and resistances are both defined per unit surface area; the solution resistance in the pores of the film is accounted for in the calculation of σ.

The equivalent circuit derived from eq. [2] is shown in Fig. 10*b*. The outer surface of the oxide film is represented by the same circuit as shown in Fig. 10*a* for a planar electrode, while charge transport in the pores of the film matrix yields the transmission line component, with only two units (of a possible n units) of the transmission line shown in parentheses in Fig. 10*b*. The resistance of the oxide matrix, r_m, has been added in the present treatment, and appears (36) in series with the pore solution resistance, r_s, in Fig. 10*b*. The separation of R_t, r_m, and r_s is difficult, if not impossible, as these elements are lumped together with the capacitors (37), constituting the overall system resistance.

Fig. 12. Variations of electrochemical characteristics of Ru–Ti oxide films as a function of at.% Ru. (*a*) R_2 and log σ. (*b*) Q_1 (Table 1) and log (1/*q*) (Fig. 2). (*c*) i_0 and Tafel slope (from Figs. 2 and 6) at room temperature.



© 1997 NRC Canada

Can. J. Chem. Downloaded from www.nrcresearchpress.com by 91.121.58.235 on 09/08/12
For personal use only.

Phase angle calculations were performed by inserting the R_t (same as R_2 in Table 1), and C_ϕ (same as Q_1 in Table 1) values, obtained at the OCP (in chlorine-free solutions) from the best-fit EQC method, into eq. [2]. R_s was taken to be 5 Ω and C_d was set at 100 μF cm^{-2}, which appears reasonable, based on the discussion presented in ref. 1. The calculated results shown in Fig. 11 reveal the essential features of the experimental phase angle Bode plots in Fig. 8. It is seen that, as the sum of the charge transfer resistance and the oxide matrix resistance increases, a peak develops in the high-frequency region of the Bode plot, moving to lower frequencies as the at.% Ru in the coating decreases. The peculiar experimental result for the 5 at.% Ru films in Fig. 8 could not be obtained by this calculation, perhaps as a result of the very high resistivity of this film and the likely existence of a TiO_2 dielectric capacitance in this case.

It is notable that this mechanistic derivation of the impedance, based on the assumption of the activation-controlled reaction of surface Ru sites occurring throughout a porous matrix, and employing the R and C values obtained from the EQC fitting procedure, leads to a very similar phase angle response as seen experimentally (except for the 5 at.% film). This lends support to the validity of the heuristic EQC approach, the suggested mechanism of the reaction, as well as the porous character of these films. This also confirms the data in Table 1, showing the development of matrix resistivity and a loss in pseudocapacitance with decreasing Ru content of the film. The most significant increase in the resistivity occurs below about 20 at.% Ru, in agreement with the conductivity data published in the literature (4, 7, 9, 34).

Figure 12 correlates the kinetic results obtained here for the chlorine evolution reaction and the impedance data at the oxide OCP, obtained from EQC fitting. It is interesting to note that, while the exchange current density for the chlorine evolution reaction shows a linear dependence on the Ru content (Fig. 12*c*) for films of more than 5 at.% Ru, this behavior is not revealed in either the Tafel slope variations (Fig. 12*c*) or in the Q_1 and R_2 parameters deduced from the EQC in Table 1 (Figs. 12*a* and 12*b*). This is to be anticipated, as the magnitude of Tafel slope and the impedance of the system are both a function of the mechanism of the reactions involved at the OCP or during the course of the chlorine evolution reaction, the mechanism being controlled not only by the number of active Ru sites in the film, but also dictated by the matrix resistivity. It should also be noted that the variations in R_2, Q_1, and $1/q$ change significantly in the range of 10–20 at.% Ru, similar to the change in the Ru–Ti oxide conductivity (σ'), determined independently (4, 7, 9, 34).

The results presented in this investigation show clearly that the signature of the developing matrix resistance with decreasing Ru content of the oxide film is revealed more dominantly in the phase angle Bode plots than in either the Tafel slopes or the overall impedance plots, although the latter parameters are also affected by the coating resistance. It will be shown in a forthcoming communication that, in practice, the performance characteristics of electrodes that have become electrochemically inactive after long times of electrolysis closely resemble those of freshly formed oxides of low Ru content. This implies that anode deactivation results from the selective loss of Ru from the oxide film with time of chlorine evolution and hence a markedly increased increase in resistance, as well as a loss in active surface sites.

Acknowledgements

Grateful acknowledgement is made to the Natural Sciences and Engineering Research Council of Canada for partial support of this work, and to Dr. Petr Vaný́sek, Northern Illinois University, for helpful discussions.

References

1. S. Trasatti. *In* The electrochemistry of novel materials. *Edited by* J. Lipkowski and P.N. Ross. VCH Publishers, New York. 1994. Chap. 5, p. 207.
2. B.E. Conway and B.V. Tilak. Adv. Catal. **38**, 1 (1992).
3. S. Trasatti. Electrochim. Acta, **32**, 369 (1987).
4. W.A. Gerrard and B.C.H. Steele. J. Appl. Electrochem. **8**, 417 (1978).
5. F. Hine, M. Yasuda, and T. Yoshida. J. Electrochem. Soc. **124**, 500 (1977).
6. L.D. Burke, O.J. Murphy, and J.F. O'Neill. J. Electroanal. Chem. **81**, 391 (1977).
7. E.K. Spasskaya, Y.B. Makarychev, A.A. Yakovleva, and L.M. Yakimenko. Soviet Electrochem. **13**, 327 (1977).
8. M.D. Spasojevic, N.V. Krstajic, and M.M. Jaksic. J. Res. Inst. Catal. Hokkaido Univ. **31**, 77 (1983).
9. P.H. Duvigneaud and A. Coussement. J. Solid State Chem. **52**, 22 (1984).
10. K. Doblhofer, M. Metikos, Z. Ogumi, and H. Gerischer. Ber. Bunsen-Ges. Phys. Chem. **82**, 1046 (1978).
11. L.D. Burke and O.J. Murphy. J. Electroanal. Chem. **96**, 19 (1979).
12. L.D. Burke and O.J. Murphy. J. Electroanal. Chem. **112**, 39 (1980).
13. L.D. Burke and J.F. O'Neil. J. Electroanal. Chem. **101**, 431 (1979).
14. D.T. Shieh and B.J. Hwang. Electrochim. Acta, **38**, 2239 (1993).
15. E.W. Tsai and K. Rajeshwar. Electrochim. Acta, **36**, 27 (1991).
16. A.T. Kuhn and C.J. Mortimer. J. Electrochem. Soc. **120**, 231 (1973).
17. C.E. Vallet, D.E. Heatherly, and C.W. White. J. Electrochem. Soc. **137**, 579 (1990).
18. C.E. Vallet. J. Electrochem. Soc. **138**, 1234 (1991).
19. C.A. Gervasi and J.R. Vilche. Electrochim. Acta, **37**, 1389 (1992).
20. S.G. Real, J.R. Vilche, and A.J. Arvia. J. Electroanal. Chem. **341**, 181 (1992).
21. E.B. Castro, S.G. Real, R.H. Milocco, and J.R. Vilche. Electrochim. Acta, **36**, 117 (1991).
22. S. Trasatti and G. Buzzanca. J. Electroanal. Chem. **29**, App 1 (1971).
23. V.I. Birss, R. Meyers, H. Angerstein-Kozlowska, and B.E. Conway. J. Electrochem. Soc. **131**, 1502 (1984).
24. S. Ardizzone, G. Fregonara, and S. Trasatti. Electrochim. Acta, **35**, 263 (1990).
25. D. Mitchell, D.A.J. Rand, and R. Woods. J. Electroanal. Chem. **89**, 11 (1978).
26. L.D. Burke and E.J.M. O'Sullivan. J. Electroanal. Chem. **117**, 155 (1989).
27. S.K. Rangarajan, M.J. Dignam, and B.E. Conway. Can. J. Chem. **45**, 422 (1967).
28. B.V. Tilak, S. Venkatesh, and S.K. Rangarajan. J. Electrochem. Soc. **136**, 1977 (1989).
29. I.R. Burrows, D.A. Denton, and J.A. Harrison. Electrochim. Acta, **23**, 493 (1978).
30. D.A. Denton, J.A. Harrison, and R.I. Knowles. Electrochim. Acta, **24**, 521 (1979).

© 1997 NRC Canada

31. D.A. Denton, J.A. Harrison, and R.I. Knowles. Electrochim. Acta, **25**, 1147 (1980).
32. J.A. Harrison, D.L. Caldwell, and R.E. White. Electrochim. Acta, **29**, 203 (1984).
33. A.J. Zhang, V.I. Birss, and P. Vanýsek. J. Electroanal. Chem. **378**, 63 (1994).
34. C.E. Vallet. J. Electrochem. Soc. **138**, 1234 (1991).
35. B.V. Tilak, C.-P. Chen, and S.K. Rangarajan. J. Electroanal. Chem. **324**, 405 1992; **356**, 319 (1993).
36. B. Pillay and J. Newman. J. Electrochem. Soc. **143**, 1806 (1996).
37. S.K. Rangarajan. J. Electroanal. Chem. **22**, 89 (1969); **41**, 459 (1973).

Can. J. Chem. Downloaded from www.nrcresearchpress.com by 91.121.58.235 on 09/08/12
For personal use only.

© 1997 NRC Canada

A non-enzymatic synthesis of (*S*)-(−)-rosmarinic acid and a study of a biomimetic route to (+)-rabdosiin

David E. Bogucki and James L. Charlton

Abstract: The synthesis of (*S*)-(−)-rosmarinic acid (**30**) in 9% overall yield is described. The synthesis was achieved by a convergent route in which 3-(3′,4′-dihydroxyphenyl)-(*S*)-lactic acid (**23**) and caffeic acid (**25**), both appropriately protected, were coupled to produce a pentaallyl precursor **29**, which was then deprotected to give (*S*)-(−)-rosmarinic acid (**30**). A triallyl derivative **35** was similarly prepared and converted to (+)-rabdosiin (**41**) and its (1*R*,2*S*) isomer (**42**) via a biomimetic oxidative free radical coupling–cyclization followed by deallylation. The coupling–cyclization gave a ratio of rabdosiin diastereomers unlike that found in nature. A preliminary study showed that methyl (*R*)-mandelyl sinapate (**15**) could be dimerized diastereoselectively to give a 1,2-*trans* thomasidioate diester (**16**).

Key words: rabdosiin, rosmarinic acid, lignan, oxidative coupling.

Résumé : On décrit la synthèse de l'acide (*S*)-(−)-rosmarinique (**30**) avec un rendement global de 9%. On a réalisé la synthèse par le biais d'une route convergente dans laquelle on procède au couplage des acides 3-(3′,4′-dihydroxyphényl)-(*S*)-lactique (**23**) et caféique (**25**) adéquatement protégés pour conduire à un précurseur pentaallylique (**29**) qui, par déprotection, fournit l'acide (*S*)-(−)-rosmarinique (**30**). Procédant de la même manière, on a aussi préparé un dérivé triallylique (**35**) qui a été transformé en (+)-rabdosiin, (**41**) et en son isomère 1*R*,2*S* (**42**) par le biais d'une cyclisation biomimétique par couplage radicalaire oxydant, suivie d'une déallylation. La cyclisation par couplage conduit à un mélange de diastéréomères de la rabdosiine différent de celui observé dans la nature. Une étude préliminaire a permis de montrer que le (*R*)-mandélyl sinapate de méthyle (**15**) peut être soumis à une dimérisation diastéréosélective qui conduit au diester **16** de l'acide 1,2-*trans*-thomasidioïque.

Mots clés : rabdosiine, acide rosmarinique, lignane, couplage oxydant.

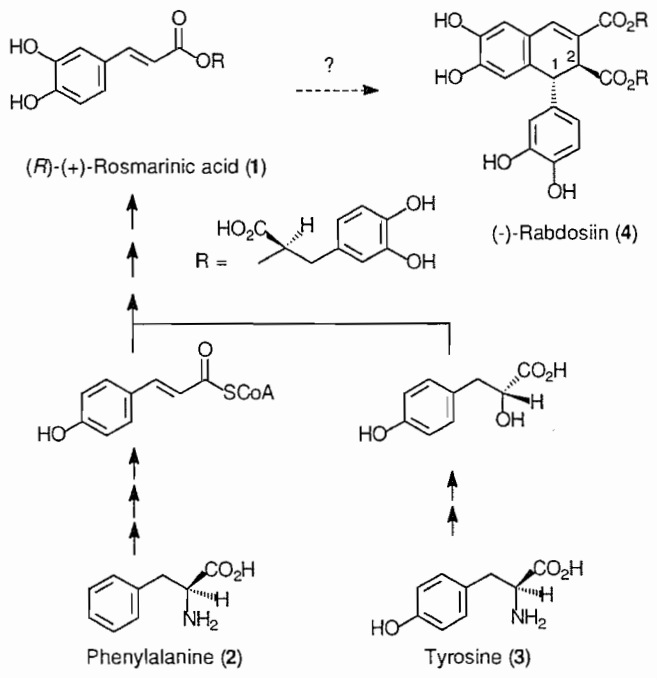
[Traduit par la rédaction]

Introduction

(*R*)-(+)-Rosmarinic acid (**1**) (Scheme 1) is a caffeic acid dimer whose structure was first elucidated by Scarpati and Oriente (1) almost 40 years ago. It has been the subject of many studies due to its anti-inflammatory properties and its association with phytotherapies (2–10). It is a major constituent of the Chinese medicinal herb Danshen, which has been used for the treatment of heart disease (11). Its other biological activities include antioxidative (8, 12–15), antihistamine (16), antibacterial (2, 17, 18), antiviral (19), and antihormonal (20) effects. Rosmarinic acid was originally isolated from extracts of *Rosmarinus officinalis* (1), but it can be found throughout the plant kingdom in such families as Lamiaceae, Boraginaceae, and Apiaceae (13).

The biosynthetic pathway for rosmarinic acid production has been determined from investigations of *Coleus blumei* and *Anchusa officinalis* plant cell suspension cultures (21–25, 26).

Scheme 1.



Received May 5, 1997.

D.E. Bogucki and J.L. Charlton.[1] Department of Chemistry, University of Manitoba, Winnipeg, MB R3T 2N2, Canada.

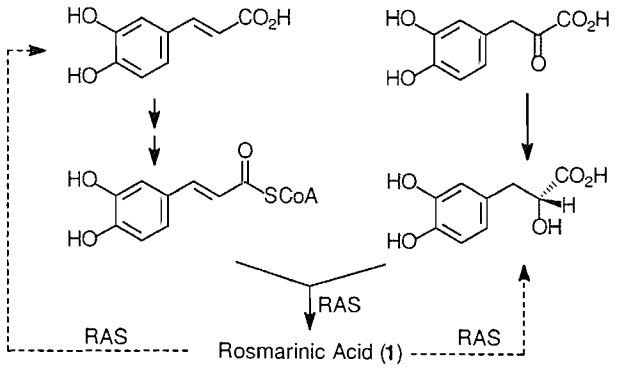
[1] Author to whom correspondence may be addressed. Telephone: (204) 474-9267. Fax: (204) 474-7608. E-mail: charltn@cc.umanitoba.ca

© 1997 NRC Canada

Can. J. Chem. Downloaded from www.nrcresearchpress.com by 91.121.58.235 on 09/08/12
For personal use only.

Can. J. Chem. Downloaded from www.nrcresearchpress.com by 91.121.58.235 on 09/08/12
For personal use only.

Scheme 2.



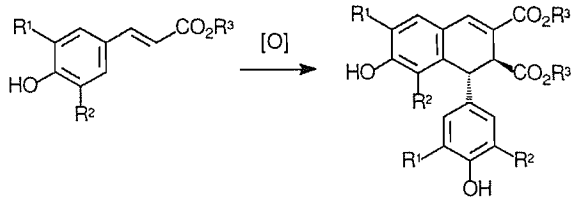
RAS = rosmarinic acid synthase

(*S*)-Phenylalanine (**2**) and (*S*)-tyrosine (**3**) (Scheme 1) were first established as precursors to (*R*)-rosmarinic acid in 1970 by introducing radioactively labeled amino acids to plants of *Mentha* (27). With the subsequent discovery that cell cultures of *Coleus blumei* (21, 22) and *Anchusa officinalis* (23) generated large amounts of rosmarinic acid, these cell cultures became the focus of research. In 1977, the *Coleus blumei* cell cultures were used to confirm the biosynthetic precursors **2** and **3** and to determine that phenylalanine ammonia-lyase was one of the enzymes involved in the biosynthesis (21). The other enzymes of the biosynthetic pathway were unknown until 10 years later when tyrosine aminotransferase activity was implicated (24, 25). Determination of the remaining enzymes soon followed.[2] This led to a chemo-enzymatic synthesis of (*R*)-rosmarinic acid (**1**) (9) (see Scheme 2) and the proposal of a total biosynthetic pathway (26) (see Scheme 1). However, no non-enzymatic route to this compound has been published, and no one has investigated the possibility that it may be involved in the biosynthesis of (−)-rabdosiin (**4**).

(−)-Rabdosiin (**4**) (Scheme 1), a caffeic acid tetramer, was first isolated in 1988 by Agata et al. (28, 29) from the stems of *Rabdosia japonica* (Labiatae) and it has since been isolated from *Arnebia euchroma* (Boraginaceae), also known as *Macrotomia euchroma* (30, 31). It is a constituent of a household medicine (enmeiso) that has been used in Japan for treating gastrointestinal disorders (28). It is a constituent in anti-inflammatory, antipyretic, and antibacterial medicines that have been used in China (31). A recent study showed that (−)-rabdosiin, its (1*S*,2*R*) diastereomer, and particularly the monopotassium and monosodium salts thereof, have potent anti-HIV activity (31). Like some other aryltetralin lignan analogs, (−)-rabdosiin was also found to be a strong inhibitor of DNA topoisomerase I and II (32). Considering that rabdosiin is formally a dimer of rosmarinic acid, it seems possible that it is biosynthesized by the diastereoselective oxidative coupling of two molecules of (*R*)-(+)-rosmarinic acid (Scheme 1).

Although no one has investigated the possibility that the aryltetralin lignan rabdosiin can be formed by oxidative coupling and cyclization of rosmarinic acid, oxidative coupling studies have been carried out on other hydroxycinnamic acid

Scheme 3.



5 R^1 = OH, R^2 = H, R^3 = CH_3 **6** R^1 = OH, R^2 = H, R^3 = CH_3
7 R^1 = OH, R^2, R^3 = H **8** R^1 = OH, R^2, R^3 = H
9 R^1, R^2 = OCH_3, R^3 = CH_3 **10** R^1, R^2 = OCH_3, R^3 = CH_3

esters similar to rosmarinic acid. For instance, methyl caffeate (**5**) is converted to aryltetralin **6** on oxidation with ferric chloride (29) and even caffeic acid (**7**) itself forms the corresponding diacid **8** on treatment with oxygen in aqueous base (Scheme 3) (33). Methyl sinapate (**9**) also yields dimethyl thomasidioate (**10**) on oxidation with ferric chloride (34), or with horseradish peroxidase and hydrogen peroxide (Scheme 3) (35). Based on these precedents, it seemed at least possible that rabdosiin could be prepared from rosmarinic acid by oxidative coupling–cyclization.

Natural rabdosiin has been isolated in both a (−)-(1*R*,2*S*), **4**, and a (+)-(1*S*,2*R*) form although the 3-(3′,4′-dihydroxyphenyl)lactyl ester groups are *R* in both compounds. Rabdosiin is probably synthesized in the plant by an enzyme-catalyzed process that produces one of the two forms of rabdosiin preferentially. While a non-biosynthetic formation of rabdosiin from rosmarinic acid might not proceed with the same stereoselectivity, there was at least the possibility that the chiral lactyl groups could influence the oxidation–cyclization such that rabdosiin would be produced diastereoselectively.

As a prelude to the preparation of rabdosiin, we sought a practical route to both the (*R*) and (*S*) enantiomers of rosmarinic acid. In this paper, we report the first non-enzymatic preparation of the (*S*) enantiomer of rosmarinic acid (**30**) from (*S*)-tyrosine (**19**) and caffeic acid (**25**). The procedure should be equally valid for the preparation of (*R*)-rosmarinic acid from (*R*)-tyrosine.

Before attempting to oxidatively couple and cyclize rosmarinic acid to rabdosiin, a model study was performed. Sinapic acid, esterified by the chiral and bulky methyl (*R*)-mandelyl group, was chosen for the model study. This compound has an ester portion that is similar to that found in rosmarinic acid, and an acid residue that is known to readily cyclize to the desired aryltetralin on oxidative coupling. The model study was undertaken primarily to determine the effect of the bulkier ester group on cyclization (methyl sinapate was already known to cyclize readily) and to look for asymmetric induction.

Finally, attempts were made to oxidatively couple and cyclize (−)-rosmarinic acid itself to rabdosiin. While unsuccessful, the conversion of a protected form of (−)-rosmarinic acid (**35**) was accomplished. Interestingly, both (+)-rabdosiin (1*S*,2*R*) and (−)-rabdosiin (1*R*,2*S*) were formed with the (−) isomer being predominant.

Results and discussion

In preparation for the model oxidative coupling reaction (see above) the (methyl (*R*)-mandelyl) ester of sinapic acid, **15**,

[2] Petersen et al. (ref. 26) have cited the relevant literature regarding the enzymes involved in rosmarinic acid biosynthesis.

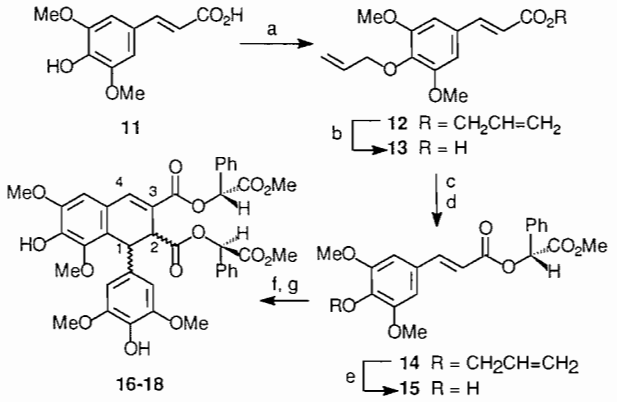
© 1997 NRC Canada

Can. J. Chem. Downloaded from www.nrcresearchpress.com by 91.121.58.235 on 09/08/12
For personal use only.

Table 1. Solvent and temperature effects on the oxidative coupling of mandelyl sinapate.

Reaction conditions			Product ratio from ^{1}H NMR		
Solvent	Temperature	Time	Major 1,2-*trans* isomer	Minor 1,2-*trans* isomer	Starting material
THF–H_2O	25°C	20 h	1.6	1.2	1.0
AcOH-H_2O	25°C	10 min	1.9	1.0	1.6
i-PrOH–H_2O	25°C	1 h	5.6	3.5	1.0
CH_3CN–H_2O	25°C	30 min	7.3	3.8	1.0
Acetone–H_2O	25°C	30 min	12.1	6.0	1.0
Acetone–H_2O	2°C	20 h	7.9	4.8	1.0

Scheme 4.



a: K_2CO_3, $CH_2=CHCH_2Br$; b: KOH, MeOH-H_2O; c: $SOCl_2$; d: methyl (*R*)-mandelate; e: $(Ph_3P)_3RhCl$; f: $FeCl_3$; g: *p*-TsOH

was prepared by the coupling of methyl (*R*)-mandelate with 4-*O*-allylsinapic acid (**13**) (Scheme 4). Direct coupling to sinapic acid was not possible due to interference from the phenolic hydroxyl group. Sinapic acid (**11**) was treated with allyl bromide in the presence of anhydrous base to give allyl 4-*O*-allylsinapate (**12**) (36). The allyl ester group was removed by hydrolysis to give 4-*O*-allylsinapic acid (**13**) in 98% crude yield from **11**. Acid **13** was transformed to the acid chloride with thionyl chloride and subsequently reacted with methyl (*R*)-mandelate to produce ester **14** in 79% yield. The deprotected sinapate ester **15** was obtained in 98% yield by the deallylation of **14** with tris(triphenylphosphine)rhodium(I) chloride (37, 38).

The mandelyl sinapate ester **15** was oxidized and cyclized using a method similar to that used by Wallis (34) for methyl sinapate (**9**). Treatment of **15** with ferric chloride in acetone–water (2:1) followed by dehydration gave a crude product that appeared by ^{1}H NMR to be a mixture of two isomers of the desired lignan in a 2:1 ratio. Very little starting material remained. The time for complete reaction was similar to that for methyl sinapate (34), suggesting that the bulky mandelyl group had not significantly hindered the reaction. The crude product was chromatographed on a preparative HPLC reverse-phase column using 53:47 MeOH–H_2O as the eluant. Three aryltetralin lignans were isolated in a 8.1:4.0:1.0 ratio. The ^{1}H NMR spectra of the two major compounds showed that each had an H-2 doublet with a coupling constant of 1.2 Hz ($J_{1,2}$). Based on these coupling constants, these dimers, **16** and **17**, were assigned the 1,2-*trans* stereochemistry (Scheme 4). The coupling constant of 8.8 Hz ($J_{1,2}$) exhibited by the minor isomer (**18**) indicated it had the 1,2-*cis* geometry. The absolute configurations at C-1 and C-2 for compounds **16–18** were not determined.

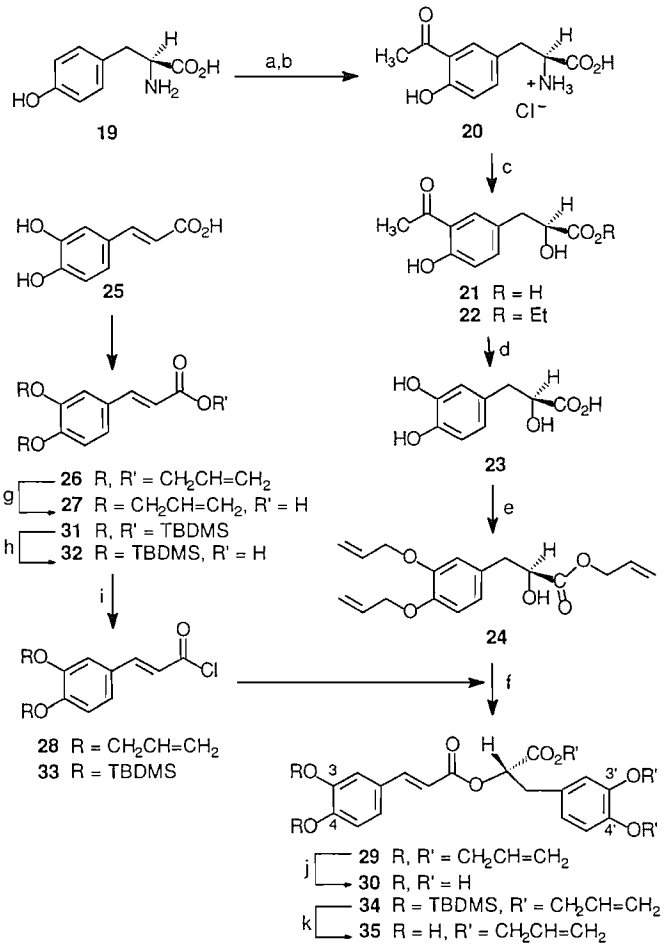
The 53% yield of the major diastereomer was impressive but attempts were made to try to improve the diastereoselectivity by changing the reaction medium. The results of the study are displayed in Table 1. The general procedure for the study was to add 2.2 equiv. of ferric chloride in water to ester **15** in organic solvent (2:1 organic solvent – H_2O) at room temperature, dehydrate the product with a catalytic amount of acid, and analyze the product mixture by ^{1}H NMR spectroscopy. Aqueous acetone solvent gave the best diastereoselectivity for the major 1,2-*trans* isomer relative to the minor *trans* isomer and resulted in the least unreacted starting material. Most of the solvents used resulted in similar diastereoselectivity except for THF, in which the reaction was very slow and unselective. Performing the reaction at a lower temperature also resulted in decreased diastereoselectivity. The successful oxidative cyclization of the model compound led us to believe that rosmarinic acid could be dimerized to rabdosiin in a similar manner.

In considering the retrosynthesis of rosmarinic acid, the disconnection of the caffeic acid ester bond was an obvious first step. This disconnection gave 3-(3′,4′-dihydroxyphenyl)lactic acid (**23**) and caffeic acid (**25**) (Scheme 5) as synthetic intermediates. A synthetic route with these compounds as intermediates was pursued since it provided an efficient convergent synthesis not unlike the one that occurs in nature (Scheme 1). The problem of establishing the chiral center was overcome at the beginning of the synthesis by making use of enantiomerically pure (*S*)-tyrosine (**19**) as the starting material for the synthesis of 3-(3′,4′-dihydroxyphenyl)-(*S*)-lactic acid (**23**).

The complete synthesis of (*S*)-rosmarinic acid is depicted in Scheme 5. (*S*)-Tyrosine (**19**) was acylated using a Friedel–Crafts reaction, as described by Boger and Yohannes (39), providing the hydrogen chloride salt of acetyl-(*S*)-tyrosine (**20**). Amino acid **20** was transformed into hydroxy acid **23** by using the two-step procedure described by Wunsch and Zott (40). Diazotization of **20** followed by in situ hydrolysis led to

© 1997 NRC Canada

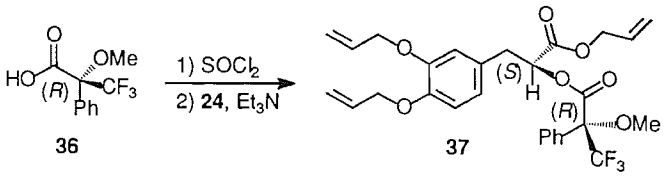
Scheme 5.



a: AcCl, $AlCl_3$; b: HCl; c: $NaNO_2$, H_2O; d: H_2O_2, NaOH, H_2O; e: K_2CO_3, CH_2 = $CHCH_2Br$; f: Et_3N; g: KOH, MeOH-H_2O; h: K_2CO_3, MeOH-H_2O; i: $SOCl_2$; j: $(Ph_3P)_3RhCl$; k: *n*-Bu_4NF

α-hydroxy acid **21** (81% yield) with retention of configuration. The enantiomeric purity of **21** was tentatively verified by converting it to the known ester **22**. The specific rotation, measured at the sodium D line was comparable to that which could be extrapolated from literature values measured at two other wavelengths (see experimental) (40). Aryllactic acid **21** was then subjected to Baeyer–Villiger oxidation. The resulting base-sensitive phenolic acetate was not isolated but was directly hydrolyzed to **23** (61% yield) in the alkaline environment. The moderate yield could be attributed to the loss of the highly polar polyhydroxy acid during chromatographic purification (it should be noted that the (*R*) form of 3-(3′,4′-dihydroxyphenyl)lactic acid (**23**), also known as danshensu, has a wide range of pharmacological activities and is found in traditional Chinese medicine (41, 42)). The phenolic and carboxylic hydroxyl groups of **23** were protected by allyl groups by treating it with allyl bromide (36) and potassium carbonate to give **24**. Only the α-hydroxyl group, needed in the subsequent coupling reaction, was left unprotected. The moderate yield of **24** (42%) was unexpected since TLC and ^1H NMR analysis of

Scheme 6.



the crude product was indicative of a complete reaction. It appeared that some product was lost during chromatography. The overall yield of **24** from tyrosine was improved from 15% to 30% by not chromatographing intermediates **21** and **23**.

Caffeic acid (**25**) was allylated to provide ester **26** in good yield (86%). Hydrolysis of **26** gave the diallyl ether of caffeic acid (**27**) in 83% yield. The coupling of **24** and **27** was accomplished by preparing the acid chloride of **27** (**28**) and reacting it with alcohol **24** in the presence of triethylamine. Fully allylated rosmarinic acid (**29**) was obtained in 65% yield. The overall yield of **29**, like that of alcohol **24**, was increased from 9% to 29% by omitting all of the intermediate chromatographic steps. **29** was deprotected by isomerizing and hydrolyzing the allyl groups in one step using Wilkinson's catalyst (37, 38) in an aqueous medium. Chromatographically pure (*S*)-rosmarinic acid (**30**) was obtained from **29** in 29% yield and in 3% overall yield (9% overall yield when chromatography was not performed prior to the isolation of **29**). However, the crude rosmarinic acid, isolated in the final step by base extraction, would probably be sufficiently pure for most purposes, and the loss of material that occurred during chromatography on silica gel could be avoided.

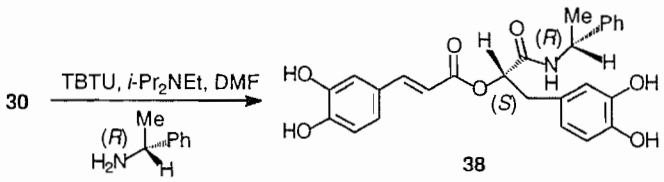
Although all of the spectral data were consistent with the structure of rosmarinic acid, it was disturbing to observe that the magnitude of the specific rotation of our sample ($[\alpha]_D^{25}$ = −86, *c* 0.53, 95% EtOH) was noticeably different than that reported for the natural product ($[\alpha]_D^{25}$ = +145, *c* 1.4, 95% EtOH) (1), indicative of only 59% ee for the synthetic material. To verify the enantiomeric purity of the synthetic rosmarinic acid, various stages of the synthesis were investigated for possible isomerization. Derivatization of the (*S*)-tyrosine starting material and analysis by GC on a chiral column revealed that it was greater than 99% enantiomerically pure. As mentioned above, the enantiomeric purity of **21** was confirmed from the optical rotation of **22**. To verify the optical purity of alcohol **24**, it was reacted with (*R*)-Mosher's acid chloride (43, 44) (Scheme 6), prepared from Mosher's acid (**36**) (43, 44), to give diester **37**. Only a single diastereomer could be detected in the crude ^1H and ^{19}F NMR spectra, indicating that **24** had an enantiomeric purity of at least 84% (this value was calculated from the integrated ratio of the ^{19}F NMR singlet to the largest of the remaining ^{19}F NMR signals). Attempts to isomerize **37** with strong base failed, giving back recovered starting material.[3] The fact that crude **37** could not be isomerized indicated that it was also unlikely that **23** could have been isomerized during allylation.

[3] Crude diester **37** in THF was treated with a 1.0 M solution of lithium bis(trimethylsilyl)amide in hexanes (5 equiv.) under nitrogen at −55°C, stirred for 10 min, and worked up with 10% HCl.

Can. J. Chem. Downloaded from www.nrcresearchpress.com by 91.121.58.235 on 09/08/12
For personal use only.

© 1997 NRC Canada

Scheme 7.



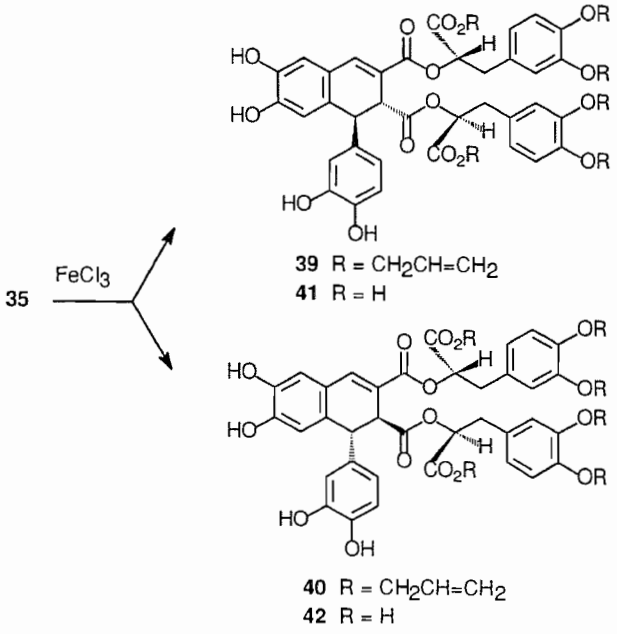
Finally, the enantiomeric purity of rosmarinic acid was tested. Although diastereomeric salts, prepared from rosmarinic acid and racemic α-methylbenzylamine, could not be distinguished by ^{1}H NMR,[4] the corresponding diastereomeric amides were easily distinguishable. Thus, **30** was converted to amide **38** (Scheme 7) with (*R*)-α-methylbenzylamine and TBTU (*O*-benzotriazol-1-yl-*N*,*N*,*N*′,*N*′-tetramethyluronium tetrafluoroborate) (45). The ^{1}H NMR spectra of crude amide **38** in both deuterated acetone and deuterated DMSO exhibited only very minor peaks that could possibly be attributed to the (*R*,*R*) diastereomer. This indicated that the synthetic rosmarinic acid was at least 90% *S*. The discrepancy between the specific rotation of the synthetic material and the rotation reported for the natural material remains unexplained.

Efforts to cyclize (*S*)-rosmarinic acid with ferric chloride failed, as no aryltetralin lignans could be observed in the ^{1}H NMR spectrum of the crude product. It was believed that the poor reactivity of **30** was due to the coordination of the extraneous phenolic substituents on C-3′ and C-4′ with the oxidant. To overcome this problem, (*S*)-rosmarinic acid was prepared with only the two phenolic groups on C-3 and C-4 unprotected as shown in Scheme 5. Caffeic acid (**25**) was fully silylated to **31** with TBDMS triflate (46) and hydrolyzed to acid **32** in 76% yield. The coupling of **32** with **24** via an acid chloride intermediate (**33**) resulted in the formation of ester **34** in 97% yield, and removal of the silyl protecting groups with fluoride ion (47) gave a 51% yield of triallyl (*S*)-rosmarinic acid (**35**).

Protected rosmarinic acid **35** was treated with ferric chloride on a small scale, and the ^{1}H NMR spectrum of the crude product showed the presence of aryltetralins along with significant starting material. The crude product was chromatographed on a preparative HPLC reverse-phase column using 72:28 MeOH – 0.06% $TFA_{(aq)}$ as the eluant, and two aryltetralin lignans were isolated. According to HPLC analysis, the lignans were produced in a 1.0:1.6 ratio. A comparison of the ^{1}H NMR spectra of both lignans with those reported (28, 30, 31) for (−) rabdosiin and its (1*S*,2*R*) isomer led to the conclusion that these compounds were the allylated enantiomers of these natural lignans. The minor diastereomer was tentatively assigned structure **39** (see Scheme 8) based on the higher chemical shift of its H-1 signal (ca. 4.54 ppm) relative to that of the major diastereomer (4.31 ppm). Consequently, the major diastereomer was assigned structure **40**. The low yield of the reaction may have been the result of steric hindrance from the allyl groups. Methyl caffeate (**5**), a less sterically hindered analog, can be cyclized in higher yield under similar conditions (29). **39** and **40** were deprotected using tributyltin

[4] The diastereomeric salt of **30** was prepared by adding racemic α-methylbenzylamine (1.2 equiv.) in acetone to (*S*)-rosmarinic acid in acetone.

Scheme 8.



hydride and bis(triphenylphosphine)palladium dichloride under acidic conditions (48–51) to give (+)-rabdosiin (**41**) and its (1*R*,2*S*) isomer (**42**), respectively (see Scheme 8). The identities of the crude products were confirmed from the direction of their optical rotations and their ^{1}H NMR data as compared with those of their enantiomers in the literature (28, 30, 31).

The observation that the (1*R*,2*S*) isomer was produced selectively over (+)-rabdosiin was unexpected. Extraction of their enantiomers from natural sources has always led to greater yields of the (1*R*,2*S*) isomer, (−)-rabdosiin (30, 31). This implies that the production of the natural isomers may be diastereoselectively controlled, not only by the chiral aryllactyl groups, but by the oxidizing system as well. It could also mean that the natural isomers are not formed by the oxidative coupling of two rosmarinic acid molecules. Although less likely, perhaps the basic aryltetralin structure is first established by the non-asymmetric dimerization of caffeic acid (**25**), and the aryllactyl moieties are subsequently added selectively to the (1*R*,2*S*) enantiomer.

Conclusion

(*S*)-Rosmarinic acid was synthesized in 9% overall yield, and the synthetic route that has been described has advantages over the previously reported enzymatic procedure. In the enzymatic process, rosmarinic acid synthase (RAS) not only catalyses the formation of rosmarinic acid but also catalyses its hydrolysis (Scheme 2) (9), thereby diminishing its yield. Furthermore, the non-enzymatic synthesis is applicable to both the (*R*) and (*S*) forms of rosmarinic acid.

(Methyl (*R*)-mandelyl) sinapate, synthesized in 76% overall yield, was dimerized to give three thomasidioate diester isomers with the major diastereomer being obtained in a 53% yield. This reaction has shown that a bulky chiral ester group does not hinder the efficient dimerization of a sinapate ester and that it induces diastereoselectivity. Other chiral ester groups are currently being investigated for their ability to

Can. J. Chem. Downloaded from www.nrcresearchpress.com by 91.121.58.235 on 09/08/12
For personal use only.

© 1997 NRC Canada

induce stereoselectivity in similar reactions. This type of reaction, especially if the diastereomeric excess could be improved, would be very useful for asymmetrically synthesizing lignans such as thomasidioic acid since the chiral groups can be removed following the cyclization. The mechanism of the free radical coupling process is also being investigated.

Triallylated (*S*)-rosmarinic acid was synthesized (15% overall yield) and oxidatively coupled to give two isomeric intermediates that were subsequently deallylated resulting in the formation of (+)-rabdosiin and its (1*R*,2*S*) diastereomer. The low yield of the cyclization products has shown that this is not an efficient synthetic route for obtaining these caffeic ester tetramers. However, the fact that the observed ratio of the cyclization adducts is not consistent with that of (−)-rabdosiin and the (1*S*,2*R*) isomer found in nature suggests that further studies are required in order to better understand how these lignans are biosynthesized and what factors control the predominant formation of one isomer over the other.

Experimental

General methods

The general experimental procedures and instrumentation have been described in a previous publication (52).

Allyl ether allyl ester of sinapic acid, 12

Sinapic acid (**11**) (706 mg, 3.15 mmol) was refluxed in allyl bromide (7 mL, 81 mmol) and acetone (13 mL) in the presence of anhydrous K_2CO_3 (1.76 g, 12.7 mmol) under a drying tube ($CaCl_2$) for 22 h using a 50 mL round-bottom flask. The solution was allowed to cool to room temperature, and CH_2Cl_2 (15 mL) was added and washed with H_2O (20 mL). After extracting the aqueous layer four times with CH_2Cl_2 (10 mL), the combined organic layers were dried ($MgSO_4$) and evaporated to give an orange liquid (960 mg, 100%). A portion of the crude product was chromatographed on silica gel (25% EtOAc – hexanes) to afford an analytically pure sample of a colourless liquid: IR (CH_2Cl_2): 1708 (CO) cm^{-1}; ^1H NMR ($CDCl_3$) δ: 3.87 (s, 6H, CH_3), 4.56 (dt, 2H, J = 6.1, 1.2, CH_2), 4.71 (dt, 2H, J = 5.7, 1.4, CH_2), 5.17–5.41 (m, 4H, CH_2), 5.93–6.06 (ddt, 1H, J = 17.1, 10.4, 5.7, CH), 6.02–6.15 (ddt, 1H, J = 17.2, 10.3, 6.1, CH), 6.37 (d, 1H, J = 15.8, CH), 6.75 (s, 2H, aromatic), 7.62 (d, 1H, J = 15.9, CH); ^{13}C NMR ($CDCl_3$) δ: 56.2 (2 × CH_3), 65.2 (CH_2), 74.2 (CH_2), 105.3 (2 × CH), 117.0 (CH), 118.0 (CH_2), 118.2 (CH_2), 129.8 (C), 132.3 (CH), 134.1 (CH), 138.8 (C), 145.0 (CH), 153.6 (2 × C), 166.5 (C); mass spectrum *m/z* (relative intensity): 304 (M^+, 13), 263 (100), 247 (6), 177 (13); HRMS calcd. for $C_{17}H_{20}O_5$: 304.1310; found: 304.1274.

Allyl ether of sinapic acid, 13

Diallyl sinapate **12** (832 mg, 2.73 mmol) was stirred in 9:1 MeOH–H_2O (20 mL) with KOH (1.82 g, 32.4 mmol) at room temperature for 3 h using a 50 mL round-bottom flask. Some of the MeOH was evaporated using a rotary evaporator. H_2O (10 mL) was added and washed with EtOAc (30 mL), and the organic layer was extracted with saturated $NaHCO_{3(aq)}$ (3 × 10 mL) followed by H_2O (10 mL). The combined aqueous layers were washed once with EtOAc (10 mL), acidified with 10% $HCl_{(aq)}$, then extracted with CH_2Cl_2 (4 × 20 mL). The combined CH_2Cl_2 extracts were dried ($MgSO_4$) and evaporated to give beige crystals (708 mg, 98%). Some of the crude product was recrystallized from 10% EtOAc – hexanes to afford an analytically pure sample of colourless crystals: mp 99–100°C; IR (CH_2Cl_2): 1690 (CO) cm^{-1}; ^1H NMR ($CDCl_3$) δ: 3.89 (s, 6H, CH_3), 4.57 (dt, 2H, J = 6.1, 1.2, CH_2), 5.20 (m, 1H, CH_2), 5.32 (m, 1H, CH_2), 6.03–6.16 (ddt, 1H, J = 17.1, 10.3, 6.1, CH), 6.35 (d, 1H, J = 15.9, CH), 6.77 (s, 2H, aromatic), 7.70 (d, 1H, J = 15.9, CH); ^{13}C NMR ($CDCl_3$) δ: 56.2 (2 × CH_3), 74.2 (CH_2), 105.6 (2 × CH), 116.3 (CH), 118.1 (CH_2), 129.5 (C), 134.1 (CH), 139.2 (C), 147.1 (CH), 153.6 (2 × C), 172.2 (C); mass spectrum *m/z* (relative intensity): 264 (M^+, 14), 223 (100), 163 (17), 149 (36), 119 (19), 81 (44), 69 (90); HRMS calcd. for $C_{14}H_{16}O_5$: 264.0998; found: 264.0984.

Allyl ether (methyl (*R*)-mandelyl) ester of sinapic acid, 14

Monoallyl sinapic acid, **13**, (201 mg, 0.761 mmol) in a 25 mL round-bottom flask was refluxed with $SOCl_2$ (0.16 mL, 2.2 mmol) in CCl_4 (7 mL) under a drying tube ($CaCl_2$) for 19.5 h. After the flask was allowed to cool to room temperature, the solvent was evaporated using a rotary evaporator, and CCl_4 (4 mL) was added and evaporated twice to remove traces of $SOCl_2$. The crude acid chloride was refluxed with methyl (*R*)-mandelate (255 mg, 1.53 mmol) in CCl_4 (2.5 mL) in a 10 mL round-bottom flask under a drying tube ($CaCl_2$) for 23 h. The solution was slightly cooled, the solvent was evaporated, and the crude yellow solid was chromatographed on silica gel (10% EtOAc – toluene) to give colourless crystals (249 mg, 79%): mp 83–84°C (hexanes); $[\alpha]_D^{25}$ −67 (*c* 0.51, $CHCl_3$); IR (CH_2Cl_2): 1757 (CO), 1717 (CO) cm^{-1}; ^1H NMR ($CDCl_3$) δ: 3.75 (s, 3H, CH_3), 3.87 (s, 6H, CH_3), 4.56 (dt, 2H, J = 6.1, 1.2, CH_2), 5.19 (m, 1H, CH_2), 5.31 (m, 1H, CH_2), 6.02–6.15 (ddt, 1H, J = 17.2, 10.3, 6.1, CH), 6.09 (s, 1H, CH), 6.48 (d, 1H, J = 15.9, CH), 6.76 (s, 2H, aromatic), 7.41 (m, 3H, aromatic), 7.53 (m, 2H, aromatic), 7.69 (d, 1H, J = 15.9, CH); ^{13}C NMR ($CDCl_3$) δ: 52.7 (CH_3), 56.2 (2 × CH_3), 74.2 (CH_2), 74.4 (CH), 105.4 (2 × CH), 116.1 (CH), 118.0 (CH_2), 127.7 (2 × CH), 128.8 (2 × CH), 129.3 (CH), 129.6 (C), 134.0 (C), 134.1 (CH), 139.0 (C), 146.3 (CH), 153.6 (2 × C), 166.0 (C), 169.3 (C); mass spectrum *m/z* (relative intensity): 412 (M^+, 4), 371 (12), 237 (33), 149 (100), 121 (25), 117 (77), 71 (47), 57 (97); HRMS calcd. for $C_{23}H_{24}O_7$: 412.1522; found: 412.1526.

(Methyl (*R*)-mandelyl) sinapate 15

Monoallyl (methyl mandelyl) sinapate, **14**, (170 mg, 0.412 mmol), tris(triphenylphosphine)rhodium(I) chloride (26 mg, 0.028 mmol), and DABCO (24 mg, 0.21 mmol) were placed in a 10 mL round-bottom flask and refluxed in a 7:3:1 mixture of ethanol–benzene–H_2O (5 mL) for 4 h. The solution was allowed to cool to room temperature, acidified with 10% $HCl_{(aq)}$ (2 mL), diluted with H_2O (5 mL), and extracted with CH_2Cl_2 (4 × 5 mL). The combined organic layers were dried ($MgSO_4$), evaporated, and the resulting yellow residue was chromatographed on silica gel (55% EtOAc – hexanes) to yield a colourless amorphous solid (150 mg, 98%): $[\alpha]_D^{25}$ −63 (*c* 1.2, $CHCl_3$); IR (CH_2Cl_2): 3523 (OH), 1752 (CO), 1714 (CO) cm^{-1}; ^1H NMR ($CDCl_3$) δ: 3.75 (s, 3H, CH_3), 3.92 (s, 6H, CH_3), 5.78 (s, 1H, OH), 6.09 (s, 1H, CH), 6.43 (d, 1H, J = 15.9, CH), 6.79 (s, 2H, aromatic), 7.42 (m, 3H, aromatic), 7.54 (m, 2H, aromatic), 7.69 (d, 1H, J = 15.8, CH); ^{13}C NMR ($CDCl_3$) δ: 52.6 (CH_3), 56.4 (2 × CH_3), 74.4 (CH), 105.3 (2 × CH), 114.6 (CH), 125.7 (C), 127.7 (2 × CH), 128.8 (2 × CH),

Can. J. Chem. Downloaded from www.nrcresearchpress.com by 91.121.58.235 on 09/08/12
For personal use only.

© 1997 NRC Canada

Can. J. Chem. Downloaded from www.nrcresearchpress.com by 91.121.58.235 on 09/08/12
For personal use only.

129.2 (CH), 134.0 (C), 137.4 (C), 146.5 (CH), 147.2 (2 × C), 166.2 (C), 169.4 (C); mass spectrum *m/z* (relative intensity): 372 (M^+, 46), 223 (27), 207 (100), 180 (25), 149 (11), 121 (15), 105 (17), 91 (22) 77 (20); HRMS calcd. for $C_{20}H_{20}O_7$: 372.1209; found: 372.1193.

Lignans 16, 17, and 18 from the oxidative cyclization of (methyl (*R*)-mandelyl) sinapate

A solution of sinapate **15** (24 mg, 0.064 mmol) in acetone (0.6 mL) was stirred at rt (room temperature) while a solution of $FeCl_3$ (24 mg, 0.15 mmol) in H_2O (0.4 mL) was added dropwise over 3 min. After 25 min, the brown solution was diluted with EtOAc (4 mL) and H_2O (4 mL), acidified with 10% $HCl_{(aq)}$ (1 mL), and stirred for 1 min. The aqueous layer was separated and extracted with CH_2Cl_2 (3 × 3 mL). The combined organic layers were dried ($MgSO_4$), filtered, stirred with Amberlite® IRC-718 ion-exchange resin for 5 min, filtered, and evaporated to give a brown amorphous solid. The crude residue was refluxed in benzene (1.3 mL) with *p*-TsOH·H_2O (2 mg, 0.01 mmol) for 40 min. The solution was diluted with CH_2Cl_2 (4 mL), washed with H_2O (5 mL), and the aqueous phase was extracted with CH_2Cl_2 (3 × 3 mL). The combined organic phases were dried ($MgSO_4$) and evaporated to give a brown amorphous solid (24 mg). The ^1H NMR spectrum ($CDCl_3$) of the crude product indicated the presence of the 1,2-*trans* diastereomers **16** and **17** in a ratio of 2:1, respectively (from ratio of H-4 singlets at 7.79 ppm, and 7.81, ppm respectively). A portion of the crude product (7.8 mg) was chromatographed on a preparative HPLC reverse-phase column (5 μm CSC-S ODS2 (25 × 0.46 cm)) using 53:47 MeOH–H_2O to give the 1,2-*trans* diastereomers **16** (4.1 mg, 53%) and **17** (1.8 mg, 23%) and the 1,2-*cis* diastereomer **18** (0.6 mg, 8%) as colourless amorphous solids. The HPLC chromatogram (Varian 9050 UV–VIS detector, λ = 254 nm) indicated the presence of **16**, **17**, and **18** in a ratio of 8.1:4.0:1.0, respectively.

1,2-trans *Lignan* ***16***

$[\alpha]_D^{25}$ −160 (*c* 0.10, $CHCl_3$); IR (CH_2Cl_2): 3525 (OH), 1754, 1715 (CO) cm^{-1}; ^1H NMR ($CDCl_3$) δ: 3.62 (s, 3H, CH_3), 3.67 (s, 3H, CH_3), 3.72 (s, 3H, CH_3), 3.78 (s, 6H, CH_3), 3.92 (s, 3H, CH_3), 4.26 (d, 1H, *J* = 1.2, H-2), 5.10 (s, 1H, H-1), 5.35 (s, 1H, OH), 5.77 (s, 1H, OH), 5.86 (s, 1H, CH), 6.01 (s, 1H, CH), 6.41 (s, 2H, aromatic), 6.71 (s, 1H, aromatic), 7.26–7.45 (m, 10H, aromatic), 7.79 (s, 1H, H-4); ^{13}C NMR ($CDCl_3$) δ: 39.2 (CH), 45.8 (CH), 52.5 (2 × CH_3), 56.3 (3 × CH_3), 60.6 (CH_3), 74.6 (CH), 74.9 (CH), 104.3 (2 × CH), 107.7 (CH), 121.5 (C), 122.7 (C), 124.5 (C), 127.3 (2 × CH), 127.6 (2 × CH), 128.6 (2 × CH), 128.7 (2 × CH), 129.0 (CH), 129.1 (CH), 133.7 (3 × C), 134.0 (C), 139.3 (CH), 141.3 (C), 145.0 (C), 146.6 (C), 146.8 (2 × C), 165.6 (C), 168.8 (C), 169.1 (C), 171.0 (C); mass spectrum *m/z* (relative intensity): 742 (M^+, 10), 548 (31), 457 (8), 426 (16), 400 (36), 383 (30), 356 (11), 274 (12), 231 (11), 149 (84), 121 (41), 107 (99), 91 (100), 79 (45), 69 (33), 57 (58); HRMS calcd. for $C_{40}H_{38}O_{14}$: 742.2262; found: 742.2251.

1,2-trans *Lignan* ***17***

^1H NMR ($CDCl_3$) δ: 3.56 (s, 3H, CH_3), 3.64 (s, 3H, CH_3), 3.65 (s, 3H, CH_3), 3.73 (s, 6H, CH_3), 3.94 (s, 3H, CH_3), 4.25 (d, 1H, *J* = 1.2, H-2), 5.01 (s, 1H, H-1), 5.33 (s, 1H, OH), 5.77 (s, 1H, OH), 5.83 (s, 1H, CH), 6.00 (s, 1H, CH), 6.35 (s, 2H, aromatic), 6.75 (s, 1H, aromatic), 7.26–7.45 (m, 10H, aromatic), 7.81 (s, 1H, H-4).

1,2-cis *Lignan* ***18***

^1H NMR ($CDCl_3$) δ: 3.46 (s, 3H, CH_3), 3.57 (s, 6H, CH_3), 3.64 (s, 3H, CH_3), 3.73 (s, 3H, CH_3), 3.92 (s, 3H, CH_3), 4.29 (dd, 1H, *J* = 8.8, 2.7, H-2), 4.85 (d, 1H, *J* = 8.8, H-1), 5.11 (s, 1H, OH), 5.49 (s, 1H, OH), 5.68 (s, 1H, CH), 6.18 (s, 1H, CH), 6.30 (s, 2H, aromatic), 6.68 (s, 1H, aromatic), 7.03–7.55 (m, 10H, aromatic), 7.60 (d, 1H, *J* = 2.7, H-4).

3-(3′-Acetyl-4′-hydroxyphenyl)-(*S*)-alanine hydrochloride 20

Compound **20** was prepared using the method of Boger and Yohannes (39) from (*S*)-tyrosine (**19**) (14.5 g, 80.0 mmol), anhydrous $AlCl_3$ (42.4 g, 318 mmol), and acetyl chloride (7.8 mL, 110 mmol). The crude product was recrystallized from 5 M $HCl_{(aq)}$ to give beige crystals (14.6 g, 70%): IR (KBr): 3418 (OH), 1747 (CO) cm^{-1}; ^1H NMR (D_2O) δ: 2.67 (s, 3H, CH_3), 3.22 (dd, 1H, *J* = 14.7, 7.3, CH_2), 3.32 (dd, 1H, *J* = 14.7, 5.8, CH_2), 4.27 (dd, 1H, *J* = 7.3, 5.9, CH), 7.00 (d, 1H, *J* = 8.6, aromatic), 7.49 (dd, 1H, *J* = 8.6, 2.2, aromatic), 7.82 (d, 1H, *J* = 2.2, aromatic); ^{13}C NMR (D_2O) δ: 27.5 (CH_3), 36.0 (CH_2), 55.6 (CH), 119.5 (CH), 121.0 (C), 126.6 (C), 133.6 (CH), 138.9 (CH), 161.0 (C), 173.0 (C), 208.2 (C); mass spectrum *m/z* (relative intensity): 223 ($[M - HCl]^+$, 2), 177 (13), 149 (100), 131 (44), 107 (13), 77 (20). The ^1H NMR spectrum was similar to that previously reported (39).

3-(3′-Acetyl-4′-hydroxyphenyl)-(*S*)-lactic acid 21

Compound **21** was prepared using the method of Wunsch and Zott (40) from acetyl-(*S*)-tyrosine hydrochloride **20** (3.00 g, 11.6 mmol) and $NaNO_2$ (1.20 g, 17.4 mmol). The product was chromatographed on silica gel (200:32:5:1 $CHCl_3$–MeOH–AcOH–H_2O) to afford a yellow amorphous solid (2.10 g, 81%): $[\alpha]_D^{25}$ −12 (*c* 0.64, MeOH); IR ($CHCl_3$): 3674 (OH), 1729 (CO) cm^{-1}; ^1H NMR ($CDCl_3$) δ: 2.62 (s, 3H, CH_3), 2.97 (dd, 1H, *J* = 14.3, 6.8, CH_2), 3.16 (dd, 1H, *J* = 14.3, 4.1, CH_2), 4.50 (dd, 1H, *J* = 6.8, 4.2, CH), 6.92 (d, 1H, *J* = 8.5, aromatic), 7.37 (dd, 1H, *J* = 8.5, 2.1, aromatic), 7.63 (d, 1H, *J* = 2.0, aromatic), 12.16 (s, 1H, OH); ^{13}C NMR ($CDCl_3$) δ: 26.6 (CH_3), 39.1 (CH_2), 70.8 (CH), 118.5 (CH), 119.5 (C), 126.3 (C), 131.6 (CH), 137.7 (CH), 161.4 (C), 177.4 (C), 204.4 (C); mass spectrum *m/z* (relative intensity): 224 (M^+, 3), 206 (1), 191 (2), 178 (3), 149 (100), 131 (47), 117 (42), 77 (13), 43 (34); HRMS calcd. for $C_{11}H_{12}O_5$: 224.0685; found: 224.0699.

3-(3′-Acetyl-4′-hydroxyphenyl)-(*S*)-lactic acid ethyl ester 22

Ethyl ester **22** was prepared using the method of Wunsch and Zott (40) from acetyl-(*S*)-tyrosine hydrochloride **20** (200 mg, 0.77 mmol), by repeating the above procedure and refluxing the crude aryllactic acid, **21**, with EtOH (4 mL) and H_2SO_4 (0.02 mL, 0.4 mmol). The crude ester was chromatographed on silica gel (40:8:1 hexanes–EtOAc–AcOH) to afford colourless crystals (95 mg, 49%): mp 96–98°C ($CHCl_3$) (lit. (40) mp 97–98°C); $[\alpha]_D^{25}$ −30 (*c* 2.7, $CHCl_3$) (lit. (40) $[\alpha]_{546}$ −38.8, $[\alpha]_{578}$ −34.2 (*c* 2.39, $CHCl_3$)); IR (CH_2Cl_2): 3537 (OH), 1733 (CO) cm^{-1}; ^1H NMR ($CDCl_3$) δ: 1.30 (t, 3H, *J* = 7.2, CH_3), 2.62 (s, 3H, CH_3), 2.93 (dd, 1H, *J* = 14.2, 6.6, CH_2), 3.10 (dd, 1H, *J* = 14.2, 4.3, CH_2), 4.24 (q, 2H, *J* = 7.1, CH_2), 4.41 (dd, 1H, *J* = 6.5, 4.3, CH), 6.91 (d, 1H, *J* = 8.5, aromatic), 7.34 (dd, 1H, *J* = 8.5, 2.2, aromatic), 7.61 (d, 1H, *J* = 2.1, aromatic),

© 1997 NRC Canada

Can. J. Chem. Downloaded from www.nrcresearchpress.com by 91.121.58.235 on 09/08/12
For personal use only.

12.15 (s, 1H, OH); ^{13}C NMR ($CDCl_3$) δ: 14.3 (CH_3), 26.6 (CH_3), 39.3 (CH_2), 61.9 (CH_2), 71.0 (CH), 118.3 (CH), 119.4 (C), 126.8 (C), 131.5 (CH), 137.7 (CH), 161.3 (C), 174.0 (C), 204.3 (C); mass spectrum *m/z* (relative intensity): 252 (M^+, 6), 234 (5), 179 (8), 149 (100), 131 (36), 77 (12), 55 (10); HRMS calcd. for $C_{13}H_{16}O_5$: 252.0997; found: 252.0988. The ^{1}H NMR spectrum was similar to that previously reported (40).

3-(3′,4′-Dihydroxyphenyl)-(*S*)-lactic acid 23

Compound **23** was prepared using the method of Wunsch and Zott (40) from aryllactic acid, **21** (2.04 g, 9.10 mmol), NaOH (1.27 g, 31.8 mmol), and 30% H_2O_2 (1.56 g, 13.8 mmol H_2O_2). The yellow crude product was chromatographed on silica gel (200:50:5:1 $CHCl_3$–MeOH–AcOH–H_2O) to give a yellow amorphous solid (1.10 g, 61%): $[\alpha]_D^{25}$ −10 (*c* 0.50, MeOH); IR (neat): 3651 (OH), 1726 (CO) cm^{-1}; ^{1}H NMR (acetone-d_6) δ: 2.78 (dd, 1H, *J* = 14.0, 7.5, CH_2), 2.97 (dd, 1H, *J* = 13.9, 4.3, CH_2), 4.32 (dd, 1H, *J* = 7.5, 4.3, CH), 6.60 (dd, 1H, *J* = 8.0, 2.0, aromatic), 6.71 (d, 1H, *J* = 8.0, aromatic), 6.78 (d, 1H, *J* = 2.0, aromatic); ^{13}C NMR (acetone-d_6) δ: 40.6 (CH_2), 72.2 (CH), 115.7 (CH), 117.5 (CH), 121.7 (CH), 130.0 (C), 144.4 (C), 145.4 (C), 175.3 (C); mass spectrum *m/z* (relative intensity): 198 (M^+, 4), 152 (9), 136 (5), 123 (100), 77 (16), 44 (35); HRMS calcd. for $C_9H_{10}O_5$: 198.0529; found: 198.0508.

Diallyl ether allyl ester of 3-(3′,4′-dihydroxyphenyl)-(*S*)-lactic acid, 24

3-(3′,4′-dihydroxyphenyl)lactic acid (**23**) (940 mg, 4.7 mmol) was dissolved in acetone (14 mL) in a 50 mL round-bottom flask and stirred at room temperature while allyl bromide (7 mL, 80 mmol) and anhydrous potassium carbonate (1.97 g, 14.3 mmol) were added. The mixture was refluxed under a drying tube ($CaCl_2$) in a silicone oil bath (70°C) for 22 h and then cooled to room temperature. The insoluble salts were filtered, washed with CH_2Cl_2, and the combined filtrate and CH_2Cl_2 portions were evaporated. The residue was dissolved in CH_2Cl_2 (10 mL), washed with water (10 mL), and the aqueous layer was extracted three times with CH_2Cl_2 (5 mL). The combined organic layers were dried ($MgSO_4$), evaporated, and the crude product (1.28 g) was chromatographed on silica gel (20% EtOAc – hexanes) to give colourless fibers (640 mg, 42%): mp 72–73°C; $[\alpha]_D^{25}$ −29 (*c* 0.73, $CHCl_3$); IR (CH_2Cl_2): 3545 (OH), 1738 (CO) cm^{-1}; ^{1}H NMR ($CDCl_3$) δ: 2.91 (dd, 1H, *J* = 14.1, 6.5, CH_2), 3.06 (dd, 1H, *J* = 14.0, 4.4, CH_2), 4.44 (dd, 1H, *J* = 6.5, 4.5, CH), 4.58 (d, 4H, *J* = 5.2, CH_2), 4.65 (dt, 2H, *J* = 5.8, 1.3, CH_2), 5.23–5.44 (m, 6H, CH_2), 5.84–5.97 (ddt, 1H, *J* = 17.1, 10.4, 5.9, CH), 6.01–6.14 (m, 2H, CH), 6.73 (dd, 1H, *J* = 8.1, 2.0, aromatic), 6.78 (d, 1H, *J* = 1.9, aromatic), 6.82 (d, 1H, *J* = 8.2, aromatic); ^{13}C NMR ($CDCl_3$) δ: 40.0 (CH_2), 66.2 (CH_2), 70.0 (2 × CH_2), 71.3 (CH), 114.2 (CH), 115.7 (CH), 117.4 (CH_2), 117.5 (CH_2), 119.2 (CH_2), 122.1 (CH), 129.1 (C), 131.4 (CH), 133.4 (CH), 133.6 (CH), 147.6 (C), 148.4 (C), 173.7 (C); mass spectrum *m/z* (relative intensity): 318 (M^+, 40), 259 (29), 229 (24), 203 (100), 161 (32), 123 (38), 81 (62); HRMS calcd. for $C_{18}H_{22}O_5$: 318.1467; found: 318.1445.

(*R*)-Mosher's acid ester of alcohol 24, 37

(*R*)-α-Methoxy-α-(trifluoromethyl)phenylacetic acid (Mosher's acid, **36**) (19 mg, 0.081 mmol) was refluxed in $SOCl_2$ (0.56 mL, 7.7 mmol) and CCl_4 (0.5 mL) in a 10 mL conical flask under a drying tube ($CaCl_2$) for 4 h. The solution was cooled slightly, evaporated, and CCl_4 was added and evaporated once to remove traces of $SOCl_2$. A solution of freshly distilled Et_3N (37 μL, 0.27 mmol), DMAP (2 mg, 0.02 mmol), and alcohol **24** (7.0 mg, 0.02 mmol) in CCl_4 (0.4 mL) was added to the stirred crude acid chloride at rt to immediately give a colourless precipitate. The mixture was stirred under a drying tube ($CaCl_2$) for 1 h, diluted with CH_2Cl_2 (6 mL), and washed successively with 10% $HCl_{(aq)}$ (2 × 3 mL), saturated $NaHCO_{3(aq)}$ (2 × 3 mL), and H_2O (3 mL). The organic layer was dried ($MgSO_4$) and evaporated to give a yellow oil (11.8 mg, 100%): ^{1}H NMR ($CDCl_3$) δ: 3.04 (dd, 1H, *J* = 14.5, 10.0, CH_2), 3.25 (dd, 1H, *J* = 14.5, 3.6, CH_2), 3.36 (d, 3H, *J* = 1.1, CH_3), 4.48 (dt, 2H, *J* = 5.3, 1.5, CH_2), 4.57 (m, 3H, CH, CH_2), 4.65 (dt, 2H, *J* = 5.9, 1.2, CH_2), 5.22–5.43 (m, 6H, CH_2), 5.80–5.93 (ddt, 1H, *J* = 17.2, 10.4, 5.9, CH), 5.96–6.13 (m, 2H, CH), 6.74 (m, 2H, aromatic), 6.81 (d, 1H, *J* = 8.0, aromatic), 7.32 (m, 5H, aromatic). The ^{1}H NMR spectrum ($CDCl_3$) showed no alcohol present, and only one diastereomer could be detected. The ^{19}F NMR spectrum ($CDCl_3$) displayed one major signal (−75.00 ppm) and four very minor signals, and the ratio of the major signal to the largest minor signal (−75.11 ppm) was 92:8 from integration.

Diallyl ether allyl ester of caffeic acid, 26

Caffeic acid (**25**) (1.50 g, 8.33 mmol) was dissolved in acetone (22 mL) in a 100 mL round-bottom flask and stirred at room temperature while allyl bromide (11 mL, 130 mmol) and anhydrous potassium carbonate (5.18 g, 37.5 mmol) were added. The mixture was refluxed under a drying tube ($CaCl_2$) in a silicone oil bath for 19 h and then cooled to room temperature. The insoluble salts were filtered, washed with CH_2Cl_2, and the combined filtrate and CH_2Cl_2 portions were evaporated. The residue was dissolved in CH_2Cl_2 (15 mL), washed with water (10 mL), and the aqueous layer was extracted three times with CH_2Cl_2 (3 mL). The combined organic layers were dried ($MgSO_4$), evaporated, and the crude product (2.50 g) was chromatographed on silica gel (20% EtOAc – hexanes) to give colourless crystals (2.15 g, 86%): mp 50–51°C; IR (CH_2Cl_2): 1711 (CO) cm^{-1}; ^{1}H NMR ($CDCl_3$) δ: 4.64 (m, 4H, CH_2), 4.70 (dt, 2H, *J* = 5.7, 1.4, CH_2), 5.25–5.47 (m, 6H, CH_2), 5.93–6.15 (m, 3H, CH), 6.30 (d, 1H, *J* = 15.9, CH), 6.87 (d, 1H, *J* = 8.9, aromatic), 7.08 (dd, 1H, *J* = 8.8, 2.0, aromatic), 7.08 (d, 1H, *J* = 2.0, aromatic), 7.63 (d, 1H, *J* = 15.9, CH); ^{13}C NMR ($CDCl_3$) δ: 65.1 (CH_2), 69.7 (CH_2), 70.0 (CH_2), 112.7 (CH), 113.4 (CH), 115.6 (CH), 117.9 (2 × CH_2), 118.1 (CH_2), 122.7 (CH), 127.5 (C), 132.4 (CH), 132.9 (CH), 133.1 (CH), 144.9 (CH), 148.5 (C), 150.7 (C), 166.8 (C); mass spectrum *m/z* (relative intensity): 300 (M^+, 100), 259 (73), 243 (33), 229 (63), 173 (32), 145 (41), 133 (74), 117 (34), 105 (34), 77 (54); HRMS calcd. for $C_{18}H_{20}O_4$: 300.1362; found: 300.1342.

Diallyl ether of caffeic acid, 27

Triallyl caffeate **26** (2.14 g, 7.13 mmol) and KOH (4.00 g, 71.3 mmol) were stirred in 9:1 MeOH–H_2O (48 mL) in a 100 mL round-bottom flask at room temperature for 4 h. The volume of MeOH was reduced to approximately half of the original volume by evaporation using a rotary evaporator, and the remaining mixture was acidified with 10% $HCl_{(aq)}$ (30 mL) followed by concentrated HCl (5 mL). The solution was satu-

© 1997 NRC Canada

Can. J. Chem. Downloaded from www.nrcresearchpress.com by 91.121.58.235 on 09/08/12
For personal use only.

rated with NaCl and extracted with EtOAc (10 mL) five times. The combined organic layers were dried ($MgSO_4$), evaporated, and the crude product (1.85 g) was recrystallized twice with 10% MeOH – $CHCl_3$ to give colourless crystals (1.54 g, 83%): mp 157–159°C; IR (CH_2Cl_2): 1686 (CO) cm^{-1}; ^1H NMR (acetone-d_6) δ: 4.65 (dt, 2H, J = 5.1, 1.6, CH_2), 4.68 (dt, 2H, J = 5.2, 1.6, CH_2), 5.26 (m, 2H, CH_2), 5.47 (m, 2H, CH_2), 6.04–6.18 (m, 2H, CH), 6.39 (d, 1H, J = 15.9, CH), 7.02 (d, 1H, J = 8.3, aromatic), 7.20 (dd, 1H, J = 8.3, 2.0, aromatic), 7.34 (d, 1H, J = 2.0, aromatic), 7.60 (d, 1H, J = 15.9, CH); ^{13}C NMR (acetone-d_6) δ: 70.0 (CH_2), 70.2 (CH_2), 113.5 (CH), 114.4 (CH), 116.8 (CH), 117.3 (CH_2), 117.4 (CH_2), 123.5 (CH), 128.5 (C), 134.4 (CH), 134.6 (CH), 145.4 (CH), 149.6 (C), 151.5 (C), 167.9 (C); mass spectrum *m/z* (relative intensity): 260 (M^+, 100), 219 (72), 189 (53), 179 (26), 145 (28), 133 (25), 117 (32), 105 (21), 91 (21), 77 (47); HRMS calcd. for $C_{15}H_{16}O_4$: 260.1048; found: 260.1044.

Tetraallyl ether allyl ester of (*S*)-rosmarinic acid, 29

Diallyl caffeic acid **27** (1.05 g, 4.03 mmol) and thionyl chloride (0.90 mL, 12 mmol) were refluxed in CCl_4 (15 mL) in a 25 mL round-bottom-flask under a drying tube ($CaCl_2$) for 17.5 h. After slight cooling, the solvent was evaporated using a rotary evaporator, and CCl_4 was added and evaporated once to remove traces of $SOCl_2$. Alcohol **24** (585 mg, 1.84 mmol) in CH_2Cl_2 (6 mL) was added to the crude acid chloride, **28**, to give a homogeneous solution that was stirred at room temperature while freshly distilled, dry triethylamine (2.25 mL, 16.1 mmol) was added. The solution was stirred under a drying tube ($CaCl_2$) for 3.5 h and then evaporated. The residue was dissolved in CH_2Cl_2 (10 mL), and the solution was extracted successively with 10% $HCl_{(aq)}$ (2 × 5 mL), H_2O (5 mL), saturated $NaHCO_{3(aq)}$ (2 × 5 mL), and H_2O (5 mL). The aqueous layers, except for the acidic layers, were combined and extracted twice with CH_2Cl_2 (1 mL). The combined organic layers were dried ($MgSO_4$), evaporated, and the crude product was chromatographed on silica gel (20% EtOAc – hexanes) to give a colourless oil (673 mg, 65%): $[\alpha]_D^{25}$ −42 (*c* 1.08, $CHCl_3$); IR (CH_2Cl_2): 1753 (CO), 1715 (CO) cm^{-1}; ^1H NMR ($CDCl_3$) δ: 3.11 (dd, 1H, J = 14.3, 7.9, CH_2), 3.18 (dd, 1H, J = 14.4, 5.2, CH_2), 4.56–4.66 (m, 10H, CH_2), 5.21–5.46 (m, 11H, CH, CH_2) 5.80–5.93 (ddt, 1H, J = 17.1, 10.5, 5.7, CH), 5.99–6.14 (m, 4H, CH), 6.29 (d, 1H, J = 15.9, CH), 6.82 (m, 4H, aromatic), 7.07 (m, 2H, aromatic), 7.61 (d, 1H, J = 15.9, CH); ^{13}C NMR ($CDCl_3$) δ: 37.1 (CH_2), 65.9 (CH_2), 69.7 (CH_2), 70.0 (3 × CH_2), 73.0 (CH), 112.7 (CH), 113.4 (CH), 114.2 (CH), 114.7 (CH), 115.6 (CH), 117.5 (2 × CH_2), 117.9 (CH_2), 118.0 (CH_2), 118.7 (CH_2), 122.0 (CH), 123.0 (CH), 127.3 (C), 128.8 (C), 131.5 (CH), 132.8 (CH), 133.0 (CH), 133.4 (CH), 133.5 (CH), 145.9 (CH), 147.6 (C), 148.4 (C), 148.6 (C), 150.9 (C), 166.3 (C), 169.5 (C); mass spectrum *m/z* (relative intensity): 560 (M^+, 2), 300 (100), 259 (37), 243 (27), 229 (23), 201 (11), 173 (14), 161 (10), 145 (15), 133 (24), 117 (12), 105 (10), 81 (21); HRMS calcd. for $C_{33}H_{36}O_8$: 560.2410; found: 560.2412.

(*S*)-(−)-Rosmarinic acid 30

Pentaallyl (*S*)-rosmarinate 29 (645 mg, 1.15 mmol) in 7:3:1 ethanol–benzene–H_2O (22 mL) in a 50 mL round-bottom flask was refluxed in the presence of tris(triphenylphosphine)rhodium(I) chloride (700 mg, 0.757 mmol) under a drying tube ($CaCl_2$) for 43 h. After slight cooling, most of the solvent was evaporated, and EtOAc (40 mL) was added. The mixture was extracted sequentially with H_2O (2 × 10 mL), saturated $NaHCO_{3(aq)}$ (3 × 10 mL), H_2O (10 mL), saturated $NaHCO_{3(aq)}$ (3 × 10 mL), and H_2O (10 mL). The combined aqueous layers were washed once with CH_2Cl_2 (10 mL), filtered, and acidified with concentrated HCl to approximately pH 1–2. The mixture was filtered, saturated with NaCl, and extracted 10 times with EtOAc (20 mL). The combined EtOAc layers were dried ($MgSO_4$), evaporated, and the crude product (247 mg) was chromatographed on silica gel (200:40:5:1 $CHCl_3$–MeOH–AcOH–H_2O) to give a light yellow amorphous solid (121 mg, 29%). A colourless amorphous solid was obtained from lyophilization of the product in H_2O: $[\alpha]_D^{25}$ −86 (*c* 0.54, 95% EtOH); IR (neat): 3316 (OH), 1729 (CO), 1690 (C) cm^{-1}; ^1H NMR (acetone-d_6) δ: 3.03 (dd, 1H, J = 14.3, 8.4, CH_2), 3.13 (dd, 1H, J = 14.3, 4.4, CH_2), 5.22 (dd, 1H, J = 8.4, 4.4, CH), 6.29 (d ,1H, J = 15.9, CH), 6.67 (dd, 1H, J = 8.1, 2.0, aromatic), 6.75 (d, 1H, J = 8.0, aromatic), 6.86 (m, 2H, aromatic), 7.05 (dd, 1H, J = 8.2, 2.0, aromatic), 7.16 (d, 1H, J = 2.1, aromatic), 7.56 (d, 1H, J = 15.9, CH); ^{13}C NMR (acetone-d_6) δ: 37.4 (CH_2), 73.6 (CH), 114.9 (CH), 115.2 (CH), 115.9 (CH), 116.3 (CH), 117.2 (CH), 121.6 (CH), 122.6 (CH), 127.4 (C), 129.1 (C), 144.7 (C), 145.6 (C), 146.2 (C), 146.4 (CH), 148.8 (C), 166.7 (C), 171.0 (C); mass spectrum (FAB^+) *m/z* (relative intensity): 361 ($[M + H]^+$, 13), 180 (63), 163 (100), 123 (17).

(*S*)- and (*R*)-α-Methylbenzyl amide of (*S*)-rosmarinic acid, (*SS*) and (*SR*)-38

(*S*)-Rosmarinic acid (**30**) (7.5 mg, 0.021 mmol) in DMF (0.2 mL) in a 5 mL round-bottom flask was stirred at rt under N_2 atmosphere while (i–Pr)$_2$NEt (3.3 mg, 0.026 mmol) in DMF (0.2 mL) was added. The solution was cooled in an ice bath for 7 min, treated with *O*-benzotriazol-1-yl-*N*,*N*,*N*′,*N*′-tetramethyluronium tetrafluroborate (TBTU, 7.5 mg, 0.023 mmol), stirred for 5 min to allow the TBTU to dissolve, stirred at rt for 10 min, cooled in an ice bath for 7 min, and treated dropwise with a solution of racemic α-methylbenzylamine (3.4 mg, 0.028 mmol) in DMF (0.2 mL). The solution was stirred for 1.5 h, slowly allowed to warm to rt, stirred for 24 h, diluted with EtOAc (7 mL), and washed with saturated $NaHCO_{3(aq)}$ (3 × 2 mL) followed by 10% $HCl_{(aq)}$ (2 mL). The combined aqueous phases were extracted with EtOAc (3 mL). The combined organic phases were dried ($MgSO_4$) and evaporated to give a yellow amorphous solid (7.9 mg, 82%). The ^1H NMR spectrum (acetone-d_6) showed the presence of the (*S*,*S*) diastereomer and the (*S*,*R*) diastereomer in a ratio of 1.3:1.0, respectively. The best separation of diastereomeric signals was observed for an aromatic doublet at 6.71 ppm (J = 8.0, (*S*,*R*) isomer) and an aromatic doublet at 6.72 ppm (J = 8.0, (*S*,*S*) isomer).

(*R*)-α-Methylbenzyl amide of (*S*)-rosmarinic acid, (*RS*)-38

The synthesis was performed in a similar manner as for the (*S*)/(*R*)-α-methylbenzyl amide of (*S*)-rosmarinic acid (see above procedure) using (*S*)-rosmarinic acid (**30**) (7.3 mg, 0.020 mmol), (i–Pr)$_2$NEt (2.6 mg, 0.020 mmol), *O*-benzotriazol-1-yl-*N*,*N*,*N*′,*N*′-tetramethyluronium tetrafluroborate (TBTU 6.9 mg, 0.021 mmol), (*R*)-α-methylbenzylamine (3.3 mg, 0.027 mmol), and the same volumes of DMF. The crude product was obtained as a light yellow amorphous solid (7.0 mg, 74%). The ^1H NMR spectrum (acetone-d_6) showed a large

© 1997 NRC Canada

Can. J. Chem. Downloaded from www.nrcresearchpress.com by 91.121.58.235 on 09/08/12
For personal use only.

doublet at 6.71 ppm and only minor peaks that could possibly be attributed to the (*R*,*R*) diastereomer. A ratio of 9:1 was obtained from integration of the (*S*,*R*) isomer doublet at 6.71 ppm and the signal that could possibly be attributed to the (*R*,*R*) isomer doublet at 6.72 ppm.

Bis(*tert*-butyldimethylsilyl) ether of caffeic acid, 32

TBDMS triflate was freshly prepared (46) by adding triflic acid (14 mL, 160 mmol) to TBDMSCl (24 g, 160 mmol) in a 100 mL round-bottom flask at room temperature and stirring the mixture in a silicone oil bath (65°C) for 12 h. The solution was distilled at reduced pressure (ca. 2.5 Torr (1 Torr = 133.3 Pa). A minor amount of TBDMSCl was collected first at ca. 60°C, followed by TBDMS triflate, a colourless liquid, at ca. 83°C (33.4 g, 79%).

Caffeic acid (**25**) (4.00 g, 22.2 mmol) was stirred as a suspension in CH_2Cl_2 (100 mL) in a 250 mL round-bottom flask at room temperature while TBDMS triflate (23 mL, 100 mmol) was added, followed by freshly distilled, anhydrous Et_3N (20.5 mL, 147 mmol). The Et_3N had to be added carefully due to the vigorous effervescence of gas. The mixture immediately became a homogeneous, dark brown solution that was stirred under N_2 atmosphere for 17 h. The solution was washed successively with 10% $HCl_{(aq)}$ (2 × 20 mL) and H_2O (20 mL), and the organic layer was dried ($MgSO_4$) and evaporated to give crude trisilyl caffeate **31** as a mixture of a brown oil and light brown solid (11.5 g, 99%): ^{1}H NMR ($CDCl_3$) δ: 0.21 (s, 6H, CH_3), 0.22 (s, 6H, CH_3), 0.33 (s, 6H, CH_3), 0.98 (s, 9H, CH_3), 0.99 (s, 9H, CH_3), 1.00 (s, 9H, CH_3), 6.20 (d 1H, *J* = 15.8, CH), 6.82 (d, 1H, *J* = 8.7, aromatic), 7.00 (m, 2H, aromatic), 7.50 (d, 1H, *J* = 15.8, CH).

Crude trisilyl caffeate **31** was dissolved in 1:1 MeOH–H_2O (220 mL) in a 500 mL round-bottom flask and stirred at room temperature while H_2O (20 mL) was slowly added over 5 min followed by $K_2CO_3 \cdot 1.5H_2O$ (3.63 g, 22.0 mmol). The mixture was stirred for 3 h, filtered, and the filtrate was evaporated to ca. 50% of the original volume using a rotary evaporator. EtOAc (150 mL) and H_2O (20 mL) were added to the solution, which was then cooled in an ice bath, acidified with concentrated HCl, and saturated with NaCl at rt. The aqueous phase was removed and extracted four times with EtOAc (20 mL). The combined organic phases were dried ($MgSO_4$), evaporated, and the grey crystalline solid obtained was chromatographed on silica gel (5:1 $CHCl_3$–MeOH) to give a colourless crystalline solid (6.90 g, 76% from **25**): mp 152–155°C; IR (CH_2Cl_2): 1686 (CO) cm^{-1}; ^{1}H NMR ($CDCl_3$) δ: 0.22 (s, 6H, CH_3), 0.23 (s, 6H, CH_3), 0.99 (s, 9H, CH_3), 1.00 (s, 9H, CH_3), 6.25 (d, 1H, *J* = 15.8, CH), 6.84 (d, 1H, *J* = 8.8, aromatic), 7.05 (m, 2H, aromatic), 7.67 (d, 1H, *J* = 15.9, CH); ^{13}C NMR ($CDCl_3$) δ: −4.1 (2 × CH_3), −4.0 (2 × CH_3), 18.5 (2 × C), 25.9 (6 × CH_3), 114.7 (CH), 120.6 (CH), 121.1 (CH), 122.6 (CH), 127.6 (C), 147.0 (CH), 147.2 (C), 149.9 (C), 172.1 (C); mass spectrum *m*/*z* (relative intensity): 408 (M^+, 1), 351 (6), 335 (6), 219 (55), 149 (14), 73 (100), 57 (11); HRMS calcd. for $C_{21}H_{36}O_4Si_2$: 408.2152; found: 408.2169.

Bis(*tert*-butyldimethylsilyl) ether diallyl ether allyl ester of (*S*)-rosmarinic acid, 34

Disilyl caffeic acid **32** (4.31 g, 10.5 mmol) was refluxed with $SOCl_2$ (2.4 mL, 33 mmol) in CCl_4 (40 mL) in a 100 mL round-bottom flask under a drying tube ($CaCl_2$) for 4.75 h. The solution was cooled to room temperature, the solvent was evaporated, and CCl_4 (10 mL) was added and evaporated once to remove traces of $SOCl_2$. Triallyl alcohol **24** (2.13 g, 6.69 mmol) in CH_2Cl_2 (20 mL) was added to the crude acid chloride **33**, and the resulting homogeneous solution was stirred at rt while freshly distilled, anhydrous Et_3N (5.9 mL, 42 mmol) was added. The solution was stirred under a drying tube ($CaCl_2$) for 4 h, and most of the solvent was evaporated. EtOAc (50 mL) was added and washed successively with 10% $HCl_{(aq)}$ (2 × 11 mL) and H_2O (11 mL). The combined aqueous layers were extracted with CH_2Cl_2 (2 × 10 mL). The combined organic layers were dried ($MgSO_4$), evaporated, and the crude yellow oil was chromatographed on silica gel (20% EtOAc – hexanes) to afford a light yellow oil (4.61 g, 97%): $[\alpha]_D^{25}$ −34 (*c* 0.50, $CHCl_3$); IR (CH_2Cl_2): 1751 (CO), 1719 (CO) cm^{-1}; ^{1}H NMR ($CDCl_3$) δ: 0.21 (s, 6H, CH_3), 0.22 (s, 6H, CH_3), 0.98 (s, 9H, CH_3), 0.99 (s, 9H, CH_3), 3.11 (dd, 1H, *J* = 14.3, 7.9, CH_2), 3.18 (dd, 1H, *J* = 14.3, 5.2, CH_2), 4.57 (br d, 4H, *J* = 5.2, CH_2), 4.63 (dt, 2H, *J* = 5.7, 1.3, CH_2), 5.21–5.43 (m, 7H, CH, CH_2), 5.80–5.93 (ddt, 1H, *J* = 17.1, 10.5, 5.7, CH), 5.99–6.12 (m, 2H, CH), 6.25 (d, 1H, *J* = 16.0, CH), 6.81 (m, 4H, aromatic), 7.00 (m, 2H, aromatic), 7.59 (d, 1H, *J* = 15.9, CH); ^{13}C NMR ($CDCl_3$) δ: −4.1 (2 × CH_3), −4.0 (2 × CH_3), 18.4 (C), 18.5 (C), 25.9 (6 × CH_3), 37.1 (CH_2), 65.9 (CH_2), 70.0 (2 × CH_2), 73.0 (CH), 114.2 (CH), 114.5 (CH), 115.5 (CH), 117.5 (2 × CH_2), 118.7 (CH_2), 120.5 (CH), 121.1 (CH), 121.9 (CH), 122.5 (CH), 127.8 (C), 128.9 (C), 131.5 (CH), 133.3 (CH), 133.5 (CH), 146.0 (CH), 147.2 (C), 147.6 (C), 148.4 (C), 149.7 (C), 166.4 (C), 169.6 (C); mass spectrum *m*/*z* (relative intensity): 708 (M^+, 1), 465 (3), 408 (3), 391 (11), 351 (19), 335 (15), 300 (6), 261 (8), 236 (5), 219 (100), 191 (10), 115 (17), 73 (100), 59 (17); HRMS calcd. for $C_{39}H_{56}O_8Si_2$: 708.3514; found: 708.3460.

Diallyl ether allyl ester of (*S*)-rosmarinic acid, 35

Disilyl triallyl (*S*)-rosmarinate **34** (4.23 g, 5.97 mmol) in THF (30 mL) in a 100 mL round-bottom flask was stirred at room temperature under N_2 atmosphere while tetra-*n*-butylammonium fluoride (1.0 M in THF, 12 mL, 12 mmol) was added over ca. 1 min. The resultant dark brown solution was stirred for 15 min, acidified with 10% $HCl_{(aq)}$ (10 mL), diluted with H_2O (10 mL), and extracted with EtOAc (1 × 35 mL, then 3 × 10 mL). The combined organic phases were dried ($MgSO_4$), evaporated, and the crude yellow oil was chromatographed on silica gel (25:25:1 EtOAc–hexanes–AcOH) to produce a colourless crystalline solid (1.47 g, 51%): mp 116–118°C (EtOAc); $[\alpha]_D^{25}$ −51 (*c* 0.51, $CHCl_3$); IR (CH_2Cl_2): 3542 (OH), 3369 (OH), 1741 (CO), 1717 (CO) cm^{-1}; ^{1}H NMR ($CDCl_3$) δ: 3.12 (dd, 1H, *J* = 14.3, 7.7, CH_2), 3.18 (dd, 1H, *J* = 14.2, 5.1, CH_2), 4.57 (br d, 4H, *J* = 5.3, CH_2), 4.65 (dt, 2H, *J* = 5.7, 1.2, CH_2), 5.21–5.42 (m, 7H, CH, CH_2), 5.80–5.93 (ddt, 1H, *J* = 17.1, 10.5, 5.7, CH), 5.98–6.11 (m, 3H, CH, OH), 6.17 (s, 1H, OH), 6.20 (d, 1H, *J* = 16.0, CH), 6.80 (m, 4H, aromatic), 6.91 (dd, 1H, *J* = 8.2, 1.9, aromatic), 6.99 (d, 1H, *J* = 1.9, aromatic), 7.51 (d, 1H, *J* = 15.9, CH); ^{13}C NMR ($CDCl_3$) δ: 37.1 (CH_2), 66.1 (CH_2), 70.0 (CH_2), 70.1 (CH_2), 73.0 (CH), 114.2 (2 × CH), 114.4 (CH), 115.4 (CH), 115.7 (CH), 117.7 (2 × CH_2), 119.0 (CH_2), 122.1 (CH), 122.5 (CH), 127.2 (C), 128.7 (C), 131.2 (CH), 133.2 (CH), 133.4 (CH), 143.9 (C), 146.2 (CH), 146.6 (C), 147.6 (C), 148.3 (C), 166.6 (C), 170.1 (C); mass spectrum *m*/*z* (relative intensity): 480 (M^+, 2), 318

© 1997 NRC Canada

Can. J. Chem. Downloaded from www.nrcresearchpress.com by 91.121.58.235 on 09/08/12
For personal use only.

(14), 300 (53), 259 (32), 229 (18), 219 (10), 203 (50), 191 (6), 175 (14), 163 (100), 145 (20), 135 (28), 117 (22), 105 (15), 89 (23), 77 (23), 55 (20); HRMS calcd. for $C_{27}H_{28}O_8$: 480.1784; found: 480.1752.

(+)-Rabdosiin 41, and its (1*R*, 2*S*) isomer 42

A slow stream of oxygen was passed through a stirred solution of triallyl rosmarinate **35** (26 mg, 0.054 mmol) in acetone (2.4 mL) at rt while a solution of $FeCl_3$ (19.3 mg, 0.119 mmol) in H_2O (1.2 mL) was added dropwise over 2 min. The dark green reaction mixture, protected from light, was stirred for 23 h, diluted with H_2O (5 mL), and extracted with EtOAc (3 × 3 mL). The combined organic layers were dried ($MgSO_4$) and evaporated to give a brown amorphous solid (30 mg). The ^{1}H NMR spectrum (acetone-d_6) showed that a significant amount of starting material was present and that diastereomers **40** and **39** were present in a ratio of 1.6:1.0 from integration of their H-2 doublets at 3.97 and 3.94 ppm, respectively. The reaction was repeated, due to the low yield of products, in the same manner as for above using **35** (21 mg, 0.044 mmol), $FeCl_3$ (16 mg, 0.099 mmol), and the same volumes of solvents. The crude products from both reactions were combined and chromatographed on a preparative HPLC reverse-phase column using 72:28 MeOH – 0.06% $TFA_{(aq)}$ to give 1,2-*trans* diastereomers **40** (3.0 mg, 6.4%) and **39** (2.6 mg, 5.5%) as colourless amorphous solids. The HPLC chromatogram indicated the presence of **40** and **39** in a ratio of 1.6:1.0, respectively.

*Tetraallyl ether diallyl ester (1R,2S)-diastereomer of (+)-rabdosiin, **40***

^{1}H NMR (acetone-d_6) δ: 3.01 (m, 4H, CH_2), 3.97 (d, 1H, J = 2.1, H-2), 4.31 (d, 1H, J = 1.9, H-1), 4.45–4.58 (m, 12H, CH_2), 5.06 (dd, 1H, J = 8.0, 4.8, CH), 5.11–5.25 (m, 9H, CH, CH_2), 5.38–5.46 (m, 4H, CH_2), 5.68–5.86 (m, 2H, CH), 6.01–6.14 (m, 4H, CH), 6.39 (dd, 1H, J = 8.1, 2.1, aromatic), 6.44 (d, 1H, J = 2.1, aromatic), 6.53 (s, 1H, aromatic), 6.67 (d, 1H, J = 8.1, aromatic), 6.76 (m, 2H, aromatic), 6.90 (m, 5H, aromatic), 7.66 (s, 1H, H-4).

*Tetraallyl ether diallyl ester of (+)-rabdosiin, **39***

^{1}H NMR (acetone-d_6) δ: 3.07 (m, 4H, CH_2), 3.94 (d, 1H, J = 1.6, H-2), 4.54 (m, 13H, H-1, CH_2), 5.09–5.29 (m, 10H, CH, CH_2), 5.38–5.46 (m, 4H, CH_2), 5.74–5.90 (m, 2H, CH), 6.01–6.13 (m, 4H, CH), 6.40 (m, 2H, aromatic), 6.62–6.97 (m, 9H, aromatic), 7.65 (s, 1H, H-4).

To a stirred mixture of the hexaallyl (1*R*,2*S*)-isomer of (+)-rabdosiin **40** (3.0 mg, 0.0031 mmol), bis(triphenylphosphine)palladium dichloride (0.9 mg, 0.001 mmol), and acetic acid (0.0036 mL, 0.063 mmol) in acetone (0.3 mL) at rt was added tributyltin hydride (0.0051 mL, 0.019 mmol) every 10 min for a total of five additions (0.0255 mL, 0.095 mmol) over 40 min. The mixture was stirred for 10 min, diluted with EtOAc (5 mL), saturated $NaHCO_{3(aq)}$ (1 mL), and H_2O (2 mL), and stirred for 1 min. The organic phase was separated and extracted twice with saturated $NaHCO_{3(aq)}$ (0.5 mL) and H_2O (2 mL). The aqueous phase was filtered, washed once with EtOAc (1 mL), carefully acidified to pH 1–2 using concentrated HCl, and evaporated. The resulting residue was washed with acetone, and the solvent was filtered and evaporated to give the (1*R*,2*S*) diastereomer of (+)-rabdosiin (**42**) as a yellow amorphous solid (2.1 mg, 95%).

(+)-Rabdosiin (**41**) was prepared in the same manner as for **42** using hexaallyl (+)-rabdosiin **39** (2.6 mg, 0.0027 mmol), bis(triphenylphosphine)palladium dichloride (0.8 mg, 0.001 mmol), acetic acid (0.0030 mL, 0.052 mmol), tributyltin hydride (5 × 0.0050 mL, 0.019 mmol; 0.0250 mL, 0.093 mmol total), and the same volume of acetone. The crude product was obtained as a light yellow amorphous solid (1.9 mg, 100%).

*(1R,2S)-Diastereomer of (+)-rabdosiin, **42***

^{1}H NMR (acetone-d_6) δ: 3.01 (m, 4H, CH_2), 3.96 (d, 1H, J = 2.0, H-2), 4.22 (d, 1H, J = 2.0, H-1), 5.01 (dd, 1H, J = 8.6, 4.6, CH), 5.12 (t, 1H, J = 6.2, CH), 6.35–6.90 (m, 11H, aromatic), 7.62 (s, 1H, H-4). Plane polarized light was rotated in a counterclockwise direction (negative optical rotation).

*(+)-Rabdosiin **41***

^{1}H NMR (acetone-d_6) δ: 3.05 (m, 4H, CH_2), 3.94 (d, 1H, J = 1.3, H-2), 4.57 (br s, 1H, H-1), 5.06 (t, 1H, J = 6.2, CH), 5.09 (dd, 1H, J = 7.1, 5.4, CH), 6.39–6.93 (m, 11H, aromatic), 7.63 (s, 1H, H-4). Plane polarized light was rotated in a clockwise direction (positive optical rotation).

Acknowledgements

We are grateful to the Natural Sciences and Engineering Research Council of Canada for financial support of this project.

References

1. M.L. Scarpati and G. Oriente. Ric. Sci. **28**, 2329 (1958).
2. M. Kuhnt, A. Pröbstle, H. Rimpler, R. Bauer, and M. Heinrich. Planta Med. **61**, 227 (1995).
3. P.W. Peake, B.A. Pussell, P. Martyn, V. Timmermans, and J.A. Charlesworth. Int. J. Immunopharmacol. **13**, 853 (1991).
4. W. Englberger, U. Hadding, E. Etschenberg, E. Graf, S. Leyck, J. Winkelmann, and M.J. Parnham. Int. J. Immunopharmacol. **10**, 729 (1988).
5. Y. Kimura, H. Okuda, T. Okuda, T. Hatano, and S. Arichi. J. Nat. Prod. **50**, 392 (1987).
6. M. Rampart, J.R. Beetens, H. Bult, A.G. Herman, M.J. Parnham, and J. Winkelmann. Biochem. Pharmacol. **35**, 1397 (1986).
7. H. Bult, A.G. Herman, and M. Rampart. Br. J. Pharmacol. **84**, 317 (1985).
8. L. Gracza, H. Koch, and E. Löffler. Arch. Pharm. **318**, 1090 (1985).
9. K. Pabsch, M. Petersen, N.N. Rao, A.W. Alfermann, and C. Wandrey. Recl. Trav. Chim. Pays-Bas, **110**, 199 (1991).
10. J.K.S. Nuytinck, R.J.A. Goris, E.S. Kalter, and P.H.M. Schillings. Agents Actions, **17**, 373 (1985).
11. H. Kohda, O. Takeda, S. Tanaka, K. Yamasaki, A. Yamashita, T. Kurokawa, and S. Ishibashi. Chem. Pharm. Bull. **37**, 1287 (1989).
12. J.L. Lamaison, C. Petitjean-Freytet, and A. Carnat. Pharm. Acta Helv. **66**, 185 (1991).
13. J.L. Lamaison, C. Petitjean-Freytet, and A. Carnat. Ann. Pharm. Fr. **48**, 103 (1990).
14. K.P.M. van Kessel, E.S. Kalter, and J. Verhoef. Agents Actions, **17**, 375 (1985).
15. G.T. Liu, T.M. Zhang, B.E. Wang, and Y.W. Wang. Biochem. Pharmacol. **43**, 147 (1992).
16. L.R. Simpol, H. Otsuka, K. Ohtani, R. Kasai, and K. Yamasaki. Phytochemistry, **36**, 91 (1994).

© 1997 NRC Canada

17. N.Z. Alimkhodzhaeva and R.L. Khazanovich. Chem. Abstr. **82**, 167491r (1975).
18. T.E. Van Dyke, L. Braswell, and S. Offenbacher. Agents Actions, **19**, 376 (1986).
19. Z. Dimitrova, B. Dimov, N. Manolova, S. Pancheva, D. Ilieva, and S. Shishkov. Acta Microbiol. Bulg. **29**, 65 (1993).
20. M. Auf'mkolk, J. Kohrle, H. Gumbinger, H. Winterhoff, and R.D. Hesch. Horm. Metab. Res. **16**, 188 (1984).
21. A. Razzaque and B.E. Ellis. Planta, **137**, 287 (1977).
22. M.H. Zenk, H. El-Shagi, and B. Ulbrich. Naturwissenschaften, **64**, 585 (1977).
23. W. De-Eknamkul and B.E. Ellis. Planta Med. **50**, 346 (1984).
24. W. De-Eknamkul and B.E. Ellis. Phytochemistry, **26**, 1941 (1987).
25. W. De-Eknamkul and B.E. Ellis. Arch. Biochem. Biophys. **257**, 430 (1987).
26. M. Petersen, E. Häusler, B. Karwatzki, and J. Meinhard. Planta, **189**, 10 (1993).
27. B.E. Ellis and G.H.N. Towers. Biochem. J. **118**, 291 (1970).
28. I. Agata, T. Hatano, S. Nishibe, and T. Okuda. Chem. Pharm. Bull. **36**, 3223 (1988).
29. I. Agata, T. Hatano, S. Nishibe, and T. Okuda. Phytochemistry, **28**, 2447–2450 (1989).
30. M. Nishizawa, M. Tsuda, and K. Hayashi. Phytochemistry, **29**, 2645 (1990).
31. Y. Kashiwada, M. Nishizawa, T. Yamagishi, T. Tanaka, G. Nonaka, L.M. Cosentino, J.V. Snider, and K. Lee. J. Nat. Prod. **58**, 392 (1995).
32. Y. Kashiwada, K.F. Bastow, and K. Lee. Bioorg. Med. Chem. Lett. **5**, 905 (1995).
33. J.J.L. Cilliers and V.L. Singleton. J. Agric. Food Chem. **39**, 1298 (1991).
34. A.F.A. Wallis. Aust. J. Chem. **26**, 1571 (1973).
35. H. Setälä, A. Pajunen, I. Kipeläinen, and G. Brunow. J. Chem. Soc. Perkin Trans. 1, 1163 (1994).
36. J.L. Charlton, V.A. Sayeed, K. Koh, W.F. Lau, H.K. Lai, and A.R. Bell. J. Agric. Food Chem. **38**, 1719 (1990).
37. J.A. Osborn, F.H. Jardine, J.F. Young, and G. Wilkinson. J. Chem. Soc. A: 1711 (1966).
38. R. Gigg. J. Chem. Soc. Perkin Trans. 1, 738 (1980).
39. D.L. Boger and D. Yohannes. J. Org. Chem. **52**, 5283 (1987).
40. B. Wünsch and M. Zott. Liebigs Ann. Chem. 39 (1992).
41. N.N. Rao and H.J. Roth. Arch. Pharm. **321**, 179 (1988).
42. J. Wang, H. He, Y. Zhu, D. Shi, Y. Li, and Y. Zhang. Chem. Abstr. **115**, 120154t (1991).
43. J.A. Dale, D.L. Dull, and H.S. Mosher. J. Org. Chem. **34**, 2543 (1969).
44. D.E. Ward and C.K. Rhee. Tetrahedron Lett. **32**, 7165 (1991).
45. V. Dourtoglou, B. Gross, V. Lambropoulou, and C. Zioudrou. Synthesis, 572 (1984).
46. E.J. Corey, H. Cho, C. Rücker, and D.H. Hua. Tetrahedron Lett. **22**, 3455 (1981).
47. M. Lalonde and T.H. Chan. Synthesis, 817 (1985).
48. F. Guibe and Y. Saint M'Leux. Tetrahedron Lett. **22**, 3591 (1981).
49. E. Keinan and P.A. Gleize. Tetrahedron Lett. **23**, 477 (1982).
50. P. Four and F. Guibe. Tetrahedron Lett. **23**, 1825 (1982).
51. F. Guibe, O. Dangles, and G. Balavoine. Tetrahedron Lett. **27**, 2365 (1986).
52. J.L. Charlton, G.L. Plourde, K. Koh, and A.S. Secco. Can. J. Chem. **68**, 2022 (1990).

Can. J. Chem. Downloaded from www.nrcresearchpress.com by 91.121.58.235 on 09/08/12
For personal use only.

© 1997 NRC Canada

Products from photochemical reactions and electrochemical oxidation of methylenecyclopropane[1]

H.J.P. de Lijser, T. Stanley Cameron, and Donald R. Arnold

Abstract: The reactivity of methylenecyclopropane (MCP, **1**) and its radical cation ($\mathbf{1}^{+\bullet}$) have been studied in the presence and absence of a nucleophile (methanol). Photochemical reactions of **1** in the presence of an electron-acceptor (1,4-dicyanobenzene, **6**) and a codonor (biphenyl, **7**) in acetonitrile (with and without methanol present) or chloroform lead to cycloadditions (*ortho*, *meta*, and *para*; products **12–17**) rather than products from photoinduced electron transfer (PET). Based on the measured (cyclic voltammetry, CV) oxidation potential, using the Weller equation, electron transfer (ET) was predicted to occur. It was shown that the measured oxidation potential of **1** represents the adiabatic ionization potential. For PET processes the value for the vertical ionization potential must be used. Electrochemical (EC) generation of $\mathbf{1}^{+\bullet}$ without a nucleophile present results in the formation of one major product: *tert*-butyl acetamide (**25**). A series of rearrangements leading to the *tert*-butyl cation is proposed. Addition of a nucleophile (methanol) to the mixture leads to the formation of 3-methoxy-2-(methoxymethyl)-1-propene (**26**). This product may arise from trapping of the initially formed ring-opened (trimethylenemethane) radical cation ($\mathbf{1a}^{+\bullet}$), which undergoes a second oxidation and nucleophilic addition (ECE).

Key words: methylenecyclopropane, radical cation, photochemistry, electrochemistry, photocycloaddition.

Résumé : On a étudié la réactivité du méthylènecyclopropane (MCP, **1**) et de son cation radical ($\mathbf{1}^{+\bullet}$) en présence et en l'absence d'un nucléophile (méthanol). Les réactions photochimiques du produit **1** en présence d'un accepteur d'électron (1,4-dicyanobenzène, **6**) et d'un codonneur (biphényle, **7**) dans l'acétonitrile (en présence et en l'absence de méthanol) ou dans le chloroforme conduit à des cycloadditions (*ortho*, *méta* et *para*; produits **12–17**) plutôt qu'aux produits résultant d'un transfert photoinduit d'électron (TPE). Sur la base du potentiel d'oxydation mesuré (voltampérométrie cyclique, VC) en faisant appel à l'équation de Weller, il est prédit qu'il se produira un transfert d'électron (TE). On a montré que le potentiel mesuré d'oxydation du produit **1** correspond au potentiel d'ionisation adiabatique. Pour le processus de TPE, on doit faire appel à la valeur du potentiel vertical d'ionisation. La génération électrochimique (EC) du cation radical $\mathbf{1}^{+\bullet}$ en l'absence d'un nucléophile conduit à la formation d'un produit principal: *tert*-butylacétamide (**25**). On propose une série de réarrangements conduisant à la formation du cation *tert*-butyle. L'addition d'un nucléophile (méthanol) au mélange conduit à la formation du 3-méthoxy-2-(méthoxyméthyl)prop-1-ène (**26**). Ce produit pourrait se former par le piégeage du cation radical ($\mathbf{1a}^{+\bullet}$) (triméthylèneméthane) à cycle ouvert qui se forme initialement et qui peut subir une deuxième oxydation suivie d'une addition nucléophile («ECE»).

Mots clés : méthylènecyclopropane, cation radical, photochimie, électrochimie, photocycloaddition.

[Traduit par la rédaction]

Introduction

Radical cations are reactive species that readily undergo interconversions and rearrangements. Many examples of these types of reactions are known (3). In an earlier paper we reported on the relative energies and the possible interconversions and rearrangements of the five related C_4H_6 and C_8H_{12} species shown in Fig. 1 (1*a*).

According to our ab initio calculations (1*a*), methylenecyclopropane radical cation ($\mathbf{1}^{+\bullet}$)[3] has the highest energy of these five species. From Scheme 1, it is clear that reaction of this radical cation with its neutral precursor is highly exothermic. Because of the large exothermicity of this reaction it is hard to make predictions concerning the ultimate outcome of the reaction, i.e., the type of product(s) that will be formed.

The dimerization of $\mathbf{1}^{+\bullet}$ with **1** in the gas phase, as calculated by ab initio methods (1*a*), leads to the formation of only one type of dimer (Scheme 2). However, carrying out these reactions in the liquid phase could have a dramatic effect on product formation.

Received June 20, 1997.

H.J.P. de Lijser, T.S. Cameron, and D.R. Arnold.[2] Department of Chemistry, Dalhousie University, Halifax, NS B3H 4J3, Canada.

[1] Part 3 of the series Interconversion and Rearrangement of Radical Cations. Parts 1 and 2 are listed in ref. 1. This is also Part 43 of the series Radical Ions in Photochemistry; see ref. 2 for recent parts of this series.

[2] Author to whom correspondence may be addressed. Telephone: (902) 494-3714. Fax: (902) 494-1310. E-mail: arnold@chem1.chem.dal.ca

[3] It must be noted that ring opening of $\mathbf{1}^{+\bullet}$ to give $\mathbf{1a}^{+\bullet}$ will proceed rapidly. It is most likely that in these reactions the reactive species is $\mathbf{1a}^{+\bullet}$, not $\mathbf{1}^{+\bullet}$.

© 1997 NRC Canada

Can. J. Chem. Downloaded from www.nrcresearchpress.com by 91.121.58.235 on 09/08/12
For personal use only.

Scheme 1.

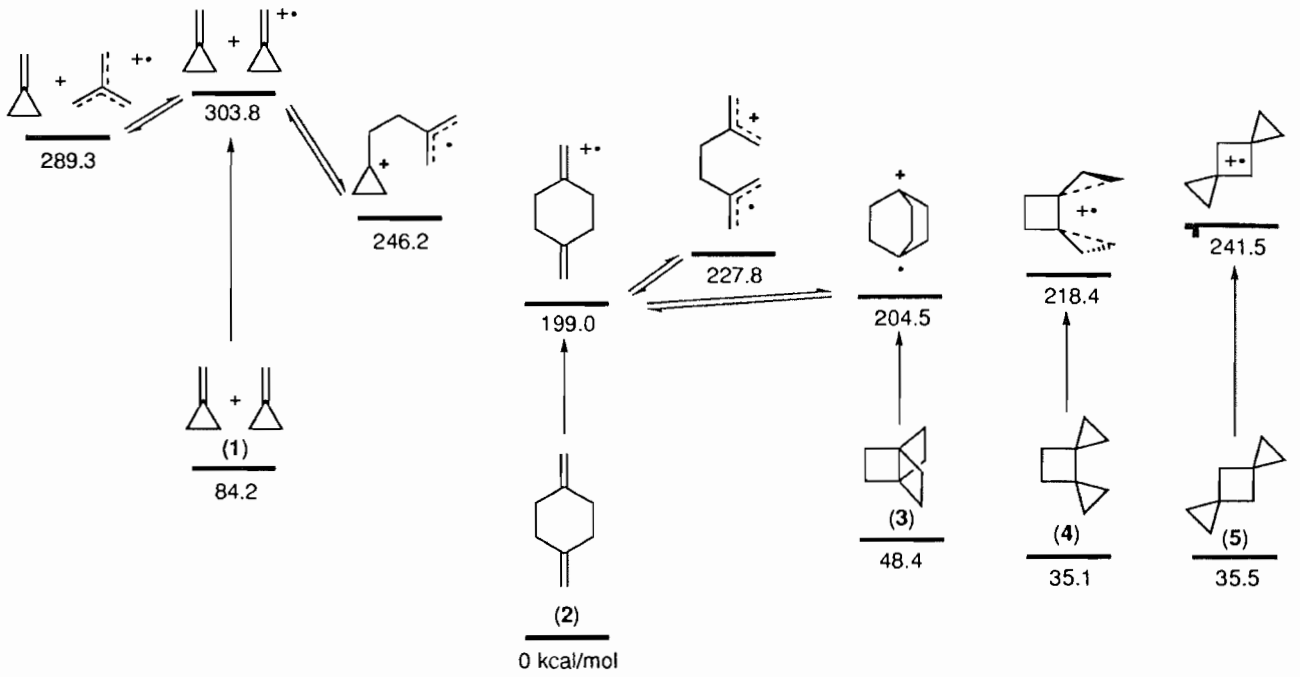
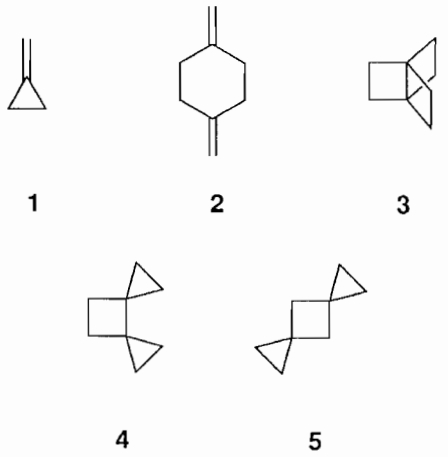


Fig. 1. Compounds of interest for the study on the interconversion and rearrangement of radical cations (see ref. 1 for earlier studies).

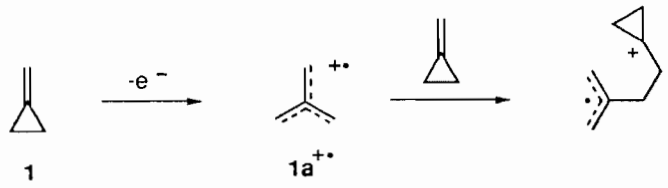


The dimerization of **1** to yield **4** and **5** has been reported (4). These reactions, however, do not involve the radical cations.

In the preceding part of this series (*1b*), product formation from the radical cation of 1,4-bis(methylene)cyclohexane (**2**) was discussed. This isomer is the most stable species of the compounds **1**–**5** and it is likely that some of the products arising from the reaction of $\mathbf{1}^{+\cdot}$ with **1** will resemble those from the reaction of $\mathbf{2}^{+\cdot}$.

Little experimental work has been done on the radical cations of methylenecyclopropane (MCP) and trimethylenemethane (TMM) (5–9) The parent molecules have never been studied, except for a recent ESR study (9). The ESR spectrum of $\mathbf{1}^{+\cdot}$ shows that even at temperatures as low as 4 K all the hydrogens in the radical cation are equivalent. This can only be explained by a ring-opened species, i.e., TMM radical

Scheme 2.



cation ($\mathbf{1a}^{+\cdot}$). This is consistent with the ab initio calculations (*1a*).

Other studies have involved substituted methylenecyclopropanes. Painter and Blackstock (5) recently generated a TMM radical cation using diazene (**8**) with tetracyanoethylene (TCNE) as the electron acceptor. Addition products were formed in this reaction (Scheme 3). The authors claimed that only product **11** was formed by a radical cation mechanism; products **9** and **10** resulted from reaction of a biradical. Evidence for this conclusion was the absence of an appreciable solvent effect on the formation of **9** and **10** and the fact that **9** and **10** were also formed in a thermal (dark) reaction.

The thermal reaction of 2-phenyl-1-methylenecyclopropane and 2,2-diphenyl-1-methylenecyclopropane with TCNE also results in the formation of cycloaddition products (6). The mechanism for this reaction is believed to involve a concerted pathway. Diradical intermediates or dipolar (zwitterionic) intermediates were ruled out on the basis of the observation of a lack of a solvent effect and the fact that the reaction was not quenched by radical scavengers.

Earlier, Roth and co-workers studied the radical cation of 2,2-dianisyl-1-methylenecyclopropane (7). The radical cation was generated by photoinduced electron transfer using chloranil (triplet) as the electron acceptor. The products from this reaction were 1:1 (MCP–chloranil) addition products. CIDNP studies (7) indicated the presence of two different types of

Can. J. Chem. Downloaded from www.nrcresearchpress.com by 91.121.58.235 on 09/08/12
For personal use only.

© 1997 NRC Canada

Can. J. Chem. Downloaded from www.nrcresearchpress.com by 91.121.58.235 on 09/08/12
For personal use only.

Scheme 3.

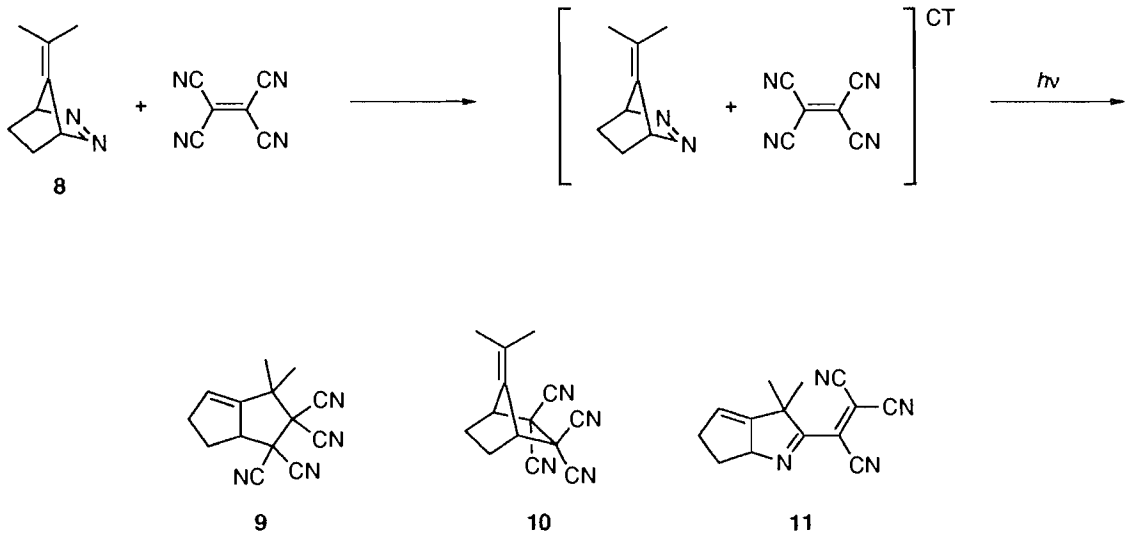
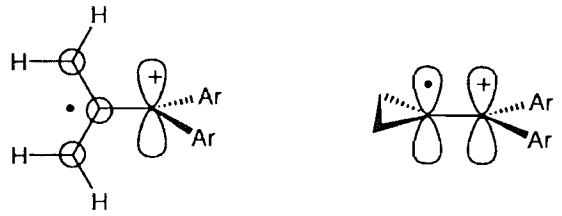


Fig. 2. Intermediates detected in the photoreaction of 2,2-dianisyl-1-methylenecyclopropane with chloranil using CIDNP (7).



radical cations: (*a*) a ring-opened species in which the spin is delocalized in an allyl moiety and the charge is localized on the diarylmethylene group, and (*b*) a ring-closed species in which the spin is localized on the tertiary cyclopropane carbon and the charge is localized on the diarylmethylene group (Fig. 2).

It is clear that the reactivity of the radical cation of methylenecyclopropane ($\mathbf{1}^{+\cdot}$) and that of the trimethylenemethane radical cation ($\mathbf{1a}^{+\cdot}$) are interesting and that there is some controversy regarding reaction pathways. Obviously, the structure and reactivity of these substituted species will be different from that of the unsubstituted compound, and it is perhaps surprising that the reactions of the parent molecules (radical cations) have not been studied.

In this paper, the results of the reactions of methylenecyclopropane (**1**) studied by photochemical and electrochemical methods in the presence and in the absence of nucleophiles are presented and possible mechanisms for product formation are discussed.

Results and discussion

Photochemistry of methylenecyclopropane (1)

It has been shown that radical cations undergo rapid nucleophilic addition (1, 2, 10). This is useful because the product distribution will enable us to assess spin and charge distributions in the radical cations. However, a main goal of this research is to determine whether the radical cation of methylenecyclopropane (MCP, **1**) undergoes dimerization and, if so, what is the structure(s) of the dimeric product(s). Addition of a nucleophile to the reaction mixture might compete with the dimerization as was observed before (1*b*). Dimerization is also more likely to occur when the concentration of MCP is greater. To favour dimerization, an attempt was made to generate the radical cation of MCP by photoinduced electron transfer using 1,4-dicyanobenzene (DCB, **6**) as the electron acceptor, biphenyl (**7**) as the codonor,[4] with the alkene present in excess (MCP:DCB = 5:1), and in the absence of a nucleophile.

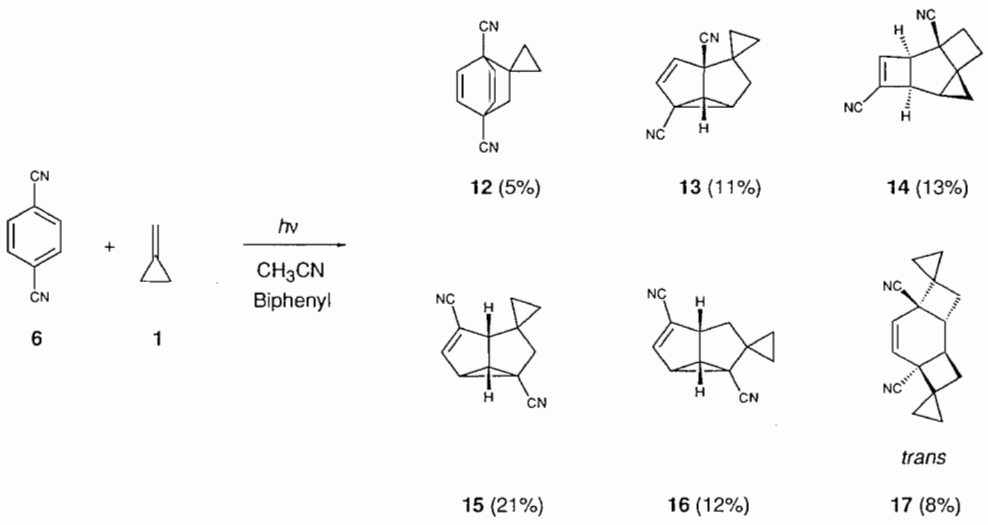
Irradiation of a 0.5 M solution of MCP (**1**) in acetonitrile using DCB (**6**, 0.1 M) as the electron acceptor and biphenyl (**7**, 0.1 M) as the codonor leads to the formation of photocycloaddition (*ortho*, *meta*, and *para*) products (Reaction [1]). Identification of the products was initially made largely on the basis of the ^{1}H and ^{13}C nmr and mass spectra; X-ray crystallography confirmed the proposed structures.[5] Progress of the reaction was followed by gc/ms and gc/fid. The product ratios did not change over the duration of the irradiation. The final product ratios are **12**:**13**:**14**:**15**:**16**:**17** = 1.0:1.8:1.8:2.9:1.7:1.1. Formation of this type of cycloaddition product in the photo-

[4] The use of biphenyl (**7**) as a codonor in photoinduced electron transfer (PET) processes to increase the yield of the free radical ion pairs by reducing back electron transfer has been discussed (1*b*,2).

[5] Data for **12–16** may be purchased from: The Depository of Unpublished Data, Document Delivery, CISTI, National Research Council Canada, Ottawa, Canada K1A 0R6. Details of data collection, structural analysis and refinement, and tables of interatomic distances and bond angles have also been deposited with the Cambridge Crystallographic Data Centre, University Chemical Laboratory, 12 Union Road, Cambridge, CB2 1EZ, U.K.

© 1997 NRC Canada

Reaction [1]



reactions of 1,4-dicyanobenzene is quite uncommon. The only previously reported example is that resulting from the irradiation of a mixture of **6** and 1,5-hexadiene (2*a*).

Another interesting example is the formation of cycloaddition products in the photochemical reaction of 1,4-dicyanonaphthalene with 2,3-dimethyl-2-butene (11). However, in this reaction, the initial intermediates are believed to be the radical ions. Also, in this reaction there are several rearrangements taking place (deprotonation–reprotonation) that are inconsistent with a simple cycloaddition reaction.

Photocycloaddition reactions generally do not occur with exocyclic double bonds. One reported example of such a reaction is that of methylenecyclobutane with benzene (12).

Three of the major products (**13**, **15**, and **16**) in the photoreaction of MCP and **6** in acetonitrile are the result of a *meta* photocycloaddition. The mechanism for the formation of *meta* photocycloaddition products has been studied extensively (13). From the observed *meta* addition products in the photoreaction of **1** with **6**, and the relative yields of the products, it can be concluded that there is a preference for 1,3-addition; in fact, all three *meta* adducts isolated from this mixture are products of initial 1,3-bond formation. This is in accord with studies on other disubstituted arenes carrying electron-acceptor substituents (13, 14). Addition of the alkene moiety to the 1 and 3 positions of the arene allows for charge stabilization of the intermediate. The favoured additions for **1** with **6** (^1S state) are shown in Scheme 4. Clearly, the formation of **15** and **16** proceeds through the same intermediate, the difference being the orientation of the MCP moiety.

Mattay (15) established guidelines for predicting the type of reaction that will take place upon irradiation of a mixture containing an arene and an alkene. The guidelines are based on the reduction potential of the arene and the oxidation potential of the alkene. The energetics can be calculated using the Weller equation (eq. [1]) (16).

$$[1] \quad \Delta G_{et} = F[E_{ox}(D) - E_{red}(A) - e/\varepsilon\alpha] - E_{0,0}(A)$$

It was shown that electron transfer and substitution take place when ΔG is less than 0.0 eV. *ortho* Cycloadditions take place when ΔG is between 0.0 and +1.5 eV, and *meta* cycloadditions occur when ΔG is larger than +1.5 eV. It must be noted that these boundaries are not sharp; several exceptions are known. *para* Photocycloadditions are rarely observed and it was shown by Scharf et al. (17) that this mode of reaction occurs from a secondary photochemical event.

In the photoreaction of **1** with **6** one *para* cycloaddition product was observed. A possible mechanism is combination of the radical cation and the radical anion pair to yield the observed cycloaddition product. This mechanism is unlikely since calculations (1*a*, 18) and ESR experiments (9) have shown that the MCP radical cation ($\mathbf{1}^{+\bullet}$) undergoes a rapid ring opening to give the TMM radical cation ($\mathbf{1a}^{+\bullet}$).

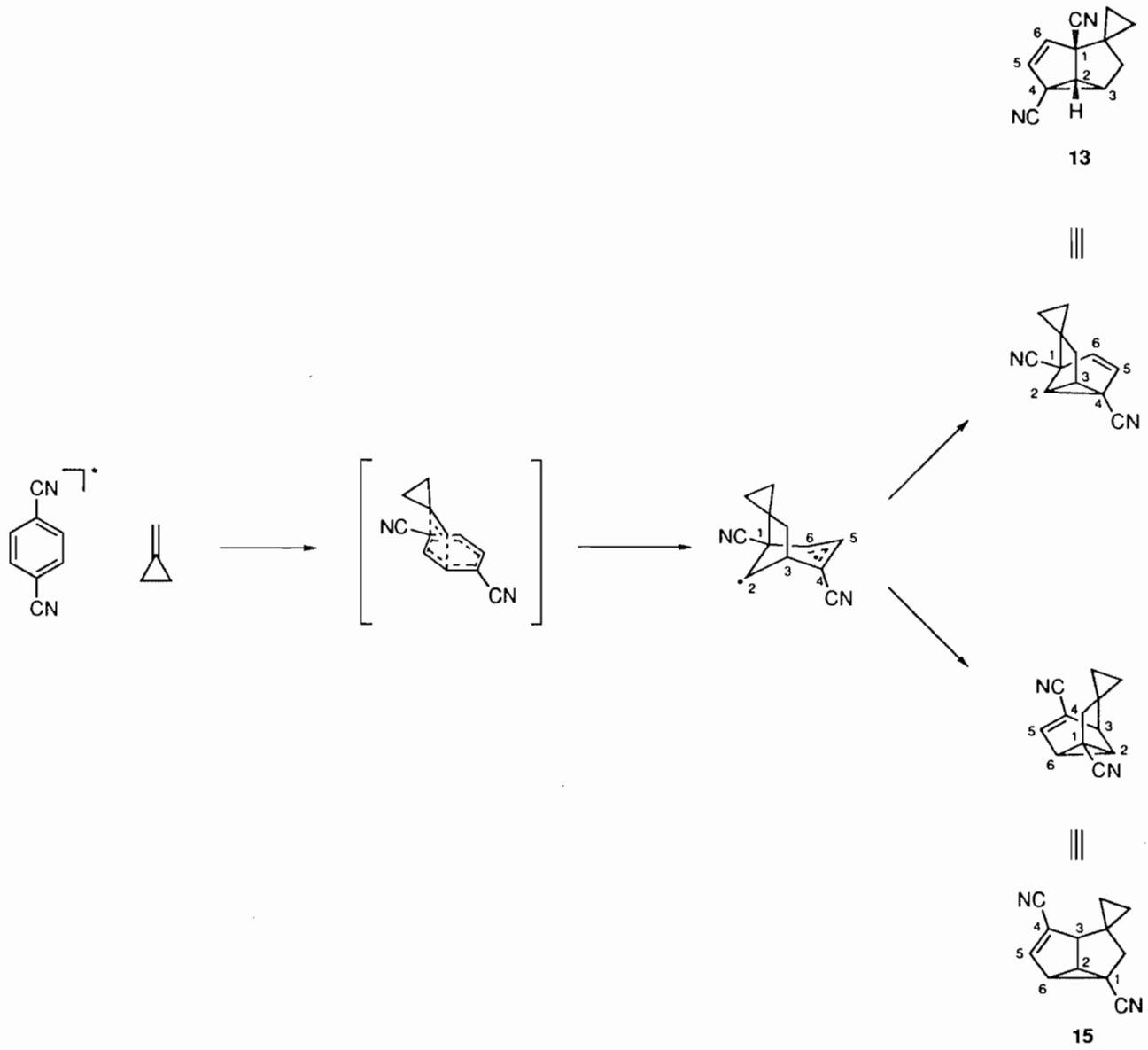
An interesting observation is the formation of the 2:1 (alkene:arene) adduct (**17**). Mattay and co-workers claim to have observed this type of adduct in the photoreaction of *m*-bis(trifluoromethyl)benzene with cyclopentene (14*a*). However, the product identification was based on mass spectra only; no attempt to isolate these 2:1 adducts was undertaken in this case, and their structural assignment remains tentative. Gilbert and co-workers claimed the formation of 2:1 adducts in the photoreaction of benzene and cyclopropene. Again, no pure compounds were isolated but several possible structures were proposed, based on the assumption that the products are the result of a 1:1 addition of the cyclopropene dimer to benzene (14*b*).

A single *ortho* photocycloaddition reaction of MCP to **6** can be used to explain the formation of product **14** (Scheme 5; pathway I). *ortho* Addition of MCP to **6** leads to the intermediate bicyclooctadiene **18**, which can undergo a ring opening to give the cyclooctatriene **19**. There is precedence in the literature for these types of (secondary) reactions (2*a*, 19). Formation of the final product (**14**) can be accounted for by a modified cyclopropyl–π-methane rearrangement (20). This reaction, discovered by Zimmerman and co-workers, pro-

© 1997 NRC Canada

Can. J. Chem. Downloaded from www.nrcresearchpress.com by 91.121.58.235 on 09/08/12
For personal use only.

Scheme 4.



ceeds by a mechanism (Scheme 6) that parallels that of the well-known di-π-methane rearrangement (21). The cyclopropyl–π-methane rearrangement of **19**, however, would lead to compound **22** (Scheme 5, pathway II), which was not observed.[6] Instead, the 1,5-diradical intermediate (**20**) undergoes a ring closure to give the observed product (**14**).

It is not clear why the observed product (**14**) is preferred over the product expected from the cyclopropyl π-methane rearrangement (**22**). One possible explanation is that intermediate **21** is disfavoured due to the presence of two primary radical centres. Furthermore, the presence of two cyano groups could have a significant effect on the stability of the radical centres in **20**, favouring pathway I rather than pathway II (Scheme 5).

The measured (CV) oxidation potential of **1** is 2.41 V.[7] Using the Weller equation (eq. [1]), this leads to a value of −5 kcal mol^{-1} for ΔG_{et}. Electron transfer is therefore expected to

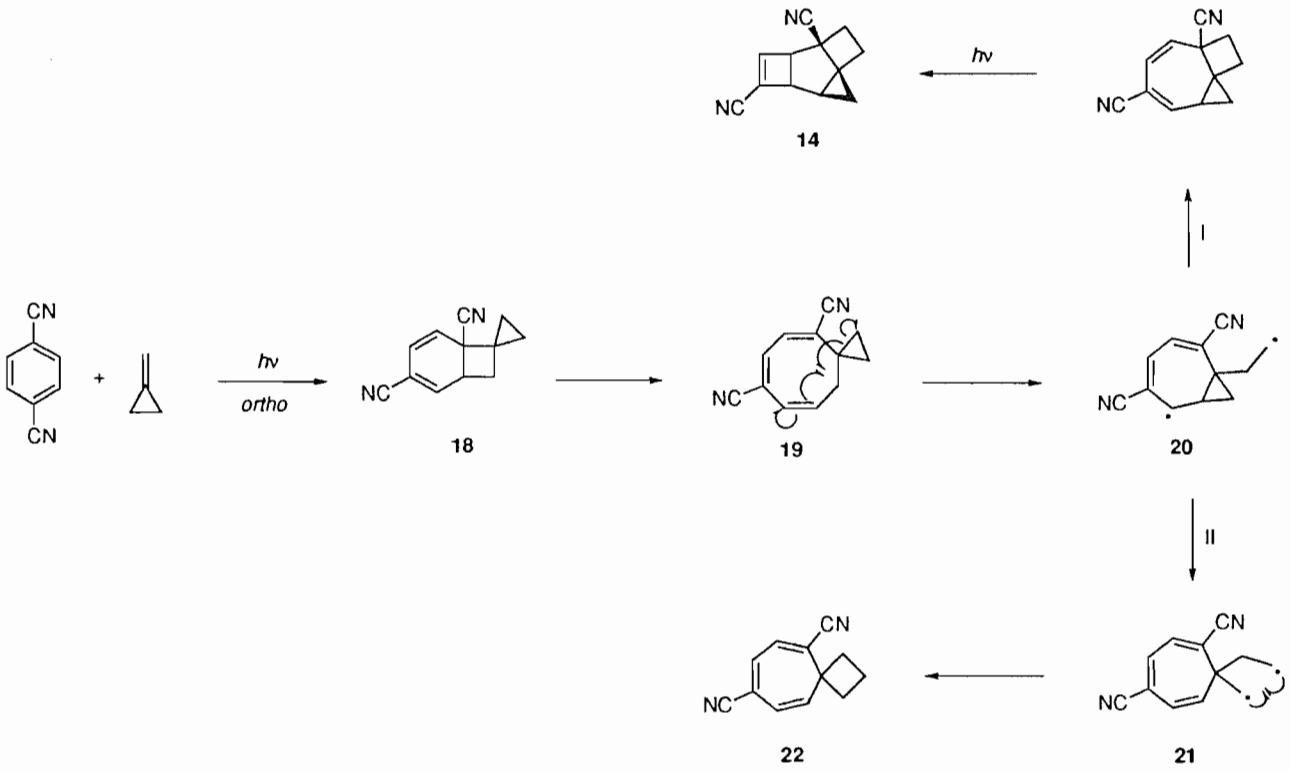
[6] It must be noted that the six isolated products are the major products of the photoreaction of MCP with **6**. Analysis of the final product mixture indicated the presence of at least six additional products with mass spectra very similar to those of the isolated products. However, since all of these additional products are only minor products, it can be concluded that the normal cyclopropyl–π-methane rearrangement is not an important pathway in this reaction.

[7] It must be noted that the oxidation potentials of the alkenes are irreversible, i.e., the number has no thermodynamic significance. However, it has been well established that in many cases reliable values for the E_{ox} can be obtained from the measured peak potentials (36).

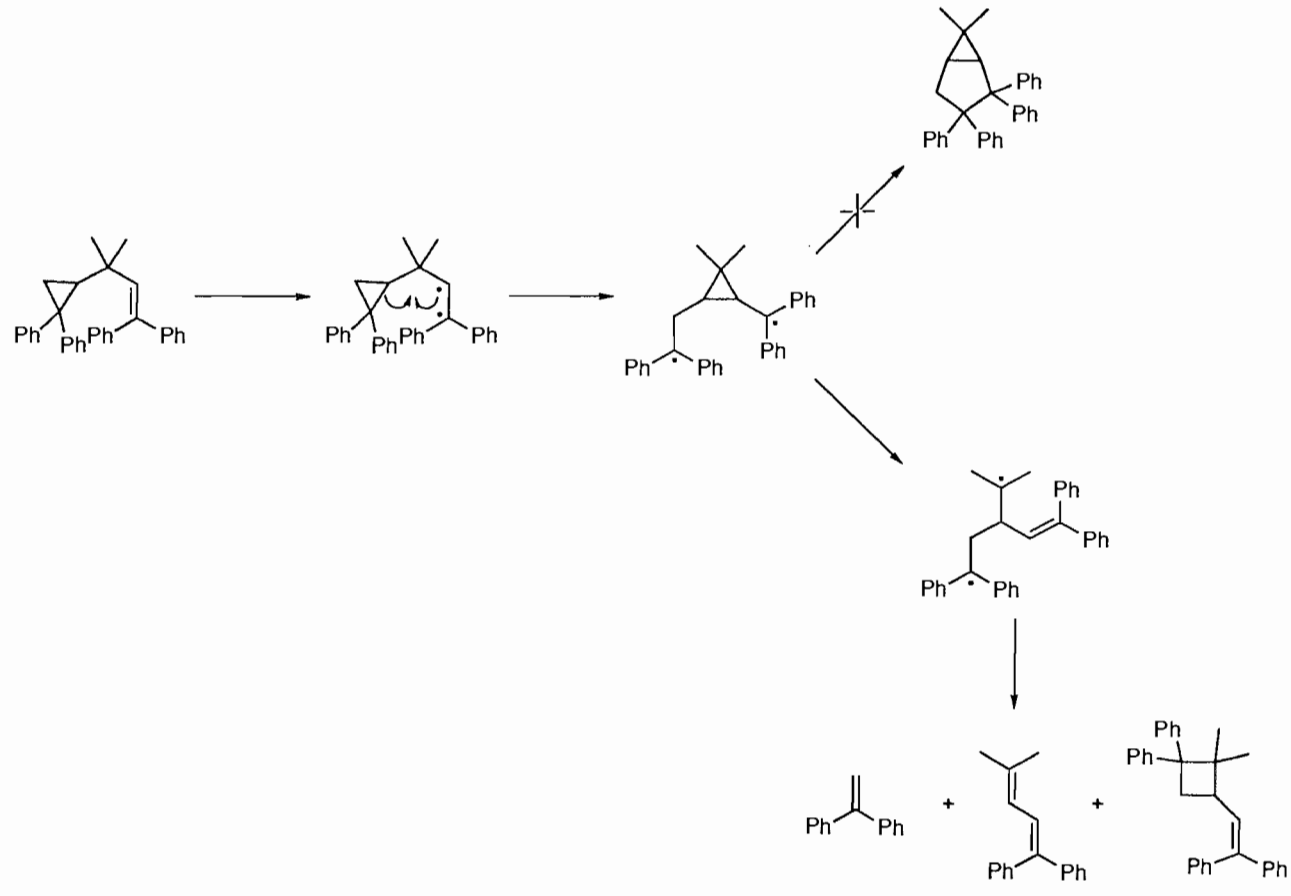
Can. J. Chem. Downloaded from www.nrcresearchpress.com by 91.121.58.235 on 09/08/12
For personal use only.

© 1997 NRC Canada

Scheme 5.



Scheme 6.



Can. J. Chem. Downloaded from www.nrcresearchpress.com by 91.121.58.235 on 09/08/12
For personal use only.

© 1997 NRC Canada

Table 1. Comparison of the calculated and experimentally determined oxidation potentials and ionization potentials of several alkenes.

Compound	IP_v[a] (eV)	IP_v[b] (eV)	IP_a[c] (eV)	$E_{ox,v}$[d] (V)	$E_{ox,v}$[e] (V)	$E_{ox,v}$[f] (V)	E_{ox}[g] (V)
Methylenecyclopropane (**1**)	9.6	9.8[h]	8.89[h]	2.88	3.04	2.29	2.41[i]
2-Methylpropene (**23**)	9.24	9.39[j]	8.81[j]	2.58	2.71	2.23	2.99[k]
1,4-Bis(methylene)cyclohexane (**2**)	9.0	9.2[h]	8.51[h]	2.38	2.55	1.98	2.49[l]
2-Methyl-2-butene	8.68	8.93[j]	8.27[j]	2.12	2.33	1.78	2.03[m]
2-Methyl-1,3-butadiene	8.85	8.67[j]	8.45[j]	2.26	2.11	1.93	2.25[n]
4-Methyl-1,3-pentadiene	8.28	8.23[j]	7.90[j]	1.79	1.75	1.47	1.51[j]
2,4-Dimethyl-1,3-pentadiene	8.49	8.62[j]	7.58[j]	1.96	2.07	1.21	1.53[j]

[a]Experimental (vertical) ionization potential (ref. 25).
[b]Calculated (vertical) ionization potential (taken from the eigenvalue of the HOMO).
[c]Calculated adiabatic ionization potential (taken as the difference between the calculated total energy of the minimized neutral molecule and the minimized radical cation).
[d]Calculated oxidation potential (eq. [2]) using the experimental (vertical) ionization potential.
[e]Calculated oxidation potential (eq. [2]) using the calculated (vertical) ionization potential.
[f]Calculated oxidation potential (eq. [2]) using the calculated (adiabatic) ionization potential.
[g]Measured (CV) oxidation potential (vs. sce).
[h]Reference 1*a*.
[i]This work.
[j]Reference 2*e*.
[k]Reference 23.
[l]Reference 1*b*.
[m]Reference 2*c*.
[n]Reference 2*b*.

take place at the diffusion-controlled rate. However, the product mixture clearly indicates that ET does not occur; formation of the radical cation of **1** is expected to lead to the ring-opened trimethylenemethane radical cation (see above) (1*a*, 18). This was shown to be true by a recent ESR study on the MCP radical cation (9). None of the isolated products of the reaction of **1** with **6** show any indication of a ring-opened MCP unit, another good indication that electron transfer does not take place.

Lowering the MCP concentration to 0.1 M does not lead to different results, except for the fact that the reaction becomes less efficient. The efficiency of the reaction is also reduced upon increasing the biphenyl (**7**) concentration. However, no other products are formed as a result of a higher biphenyl or a lower MCP concentration.

It is well known that cycloadditions occur more rapidly in nonpolar solvents since polar solvents favour electron transfer. When the photoreaction of **1** with **6** is carried out in a nonpolar solvent ($CHCl_3$, ε = 4.8) rather than a polar solvent (CH_3CN, ε = 35.7) the same products are observed. The relative product ratios **12**:**13**:**14**:**15**:**16**:**17** are now 1.0:1.8:1.2:2.8:1.4:0.3. With the exception of products **14** and **17** these ratios are close to those observed for the reaction in acetonitrile, providing strong evidence that in both cases the same mechanism is operative.

Analysis of the product mixture shows that in all cases the cyclopropyl moiety remained closed. The rearrangement leading to product **14** does cleave the cyclopropyl unit but the initially formed *ortho* adduct must have the cyclopropyl (ring-closed) group (Scheme 5). This indicates that the mechanism does not proceed through a diradical, radical ionic, or zwitterionic intermediate, because these intermediates are expected to give mainly products resulting from addition of the ring-opened species to the arene.

To be able to understand the observation that no electron transfer takes place, even though the measured (CV) oxidation potential is low enough for the rate of electron transfer to be diffusion controlled, the ionization potential (IP, gas phase) of MCP was taken into account. It has been established that there is a good correlation between the oxidation potential (OP, solution) and the ionization potential (IP, gas phase) of a compound. Neikam et al. (22) measured the oxidation potentials and the ionization potentials of a large number of arenes and alkenes and determined the correlation, eq. [2].[8] (There are several correlations available; for others see refs. 23 and 24.)

$$[2] \quad E_{ox} = (0.827 \times IP - 5.40)\ V$$

Using this correlation and the experimentally determined IP (vertical) (25), the E_{ox} of **1** was calculated to be 2.88 V (sce). Using the Weller equation (eq. [1]) the calculated ΔG for the reaction with **6** is now +5.8 kcal mol^{-1} (+0.25 eV). Based on these numbers it is clear that electron transfer is unlikely and that the major reaction pathway will be cycloaddition. Other alkenes were also considered in this study; the results are shown in Table 1.

Ab initio molecular orbital calculations (MP2/6–31G*//HF/6–31G*) were used to calculate the ionization potentials of the alkenes listed in Table 1. Both the adiabatic and the vertical ionization potentials were considered. The experimental (vertical) ionization potentials were found in the literature (25).

Plots of the experimental (CV) oxidation potential against the vertical ionization potential (calculated) (Fig. 3; r^2 = 0.774) and against the adiabatic ionization potential (calculated) (Fig. 4; r^2 = 0.903) show that the correlation between the adiabatic IP and the experimental E_{ox} is better. Note that

[8] This correlation gives the oxidation potential vs. Ag/Ag^+. To convert this oxidation potential to the value relative to sce, 0.34 V has to be added.

© 1997 NRC Canada

Can. J. Chem. Downloaded from www.nrcresearchpress.com by 91.121.58.235 on 09/08/12
For personal use only.

Fig. 3. Correlation between the vertical ionization potentials (calculated) and the experimentally determined oxidation potentials (□) of the alkenes listed in Table 1. The line represents the expected oxidation potential based on the vertical ionization potential (calculated) using eq. [2].

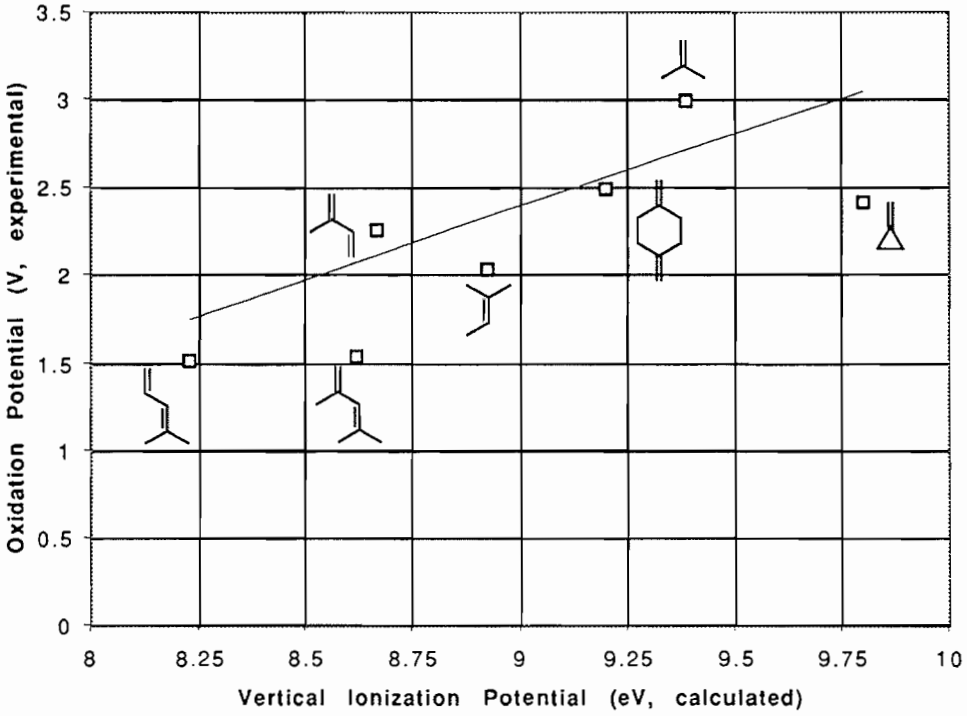
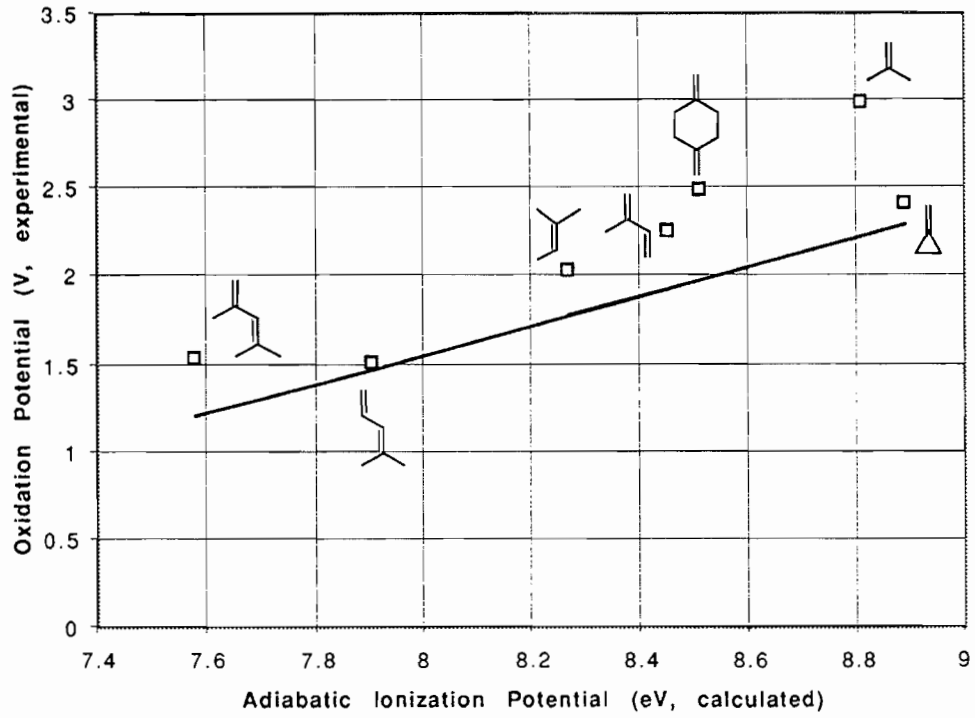


Fig. 4. Correlation between the adiabatic ionization potentials (calculated) and the experimentally determined oxidation potentials (□) of the alkenes listed in Table 1. The line represents the expected oxidation potential based on the adiabatic ionization potential (calculated) using eq. [2].



the line does not represent the best fit of the measured points; it represents the expected oxidation potential based on the ionization potential (calculated) using eq. [2].

It can be seen from Fig. 3 that there are two IP points (MCP and 2,4-dimethyl-1,3-pentadiene) that deviate markedly from the expected oxidation potential based on the vertical IP (calculated). Ignoring these two points significantly improves the correlation ($r^2 = 0.925$). The oxidation potentials of these two

© 1997 NRC Canada

Can. J. Chem. Downloaded from www.nrcresearchpress.com by 91.121.58.235 on 09/08/12
For personal use only.

Can. J. Chem. Downloaded from www.nrcresearchpress.com by 91.121.58.235 on 09/08/12
For personal use only.

compounds show a much better correlation with the adiabatic IP (calculated) (Fig. 4).

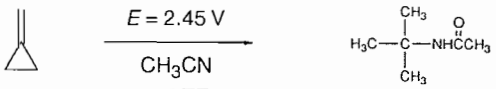
It must be concluded that for MCP in the electrochemical experiments the measured OP reflects the adiabatic IP rather than the vertical IP. In the photochemical experiments it is the vertical IP that determines the reactivity. This variation could result from an interaction (formation of a complex) between the alkene and the Pt electrode. MCP is a highly strained molecule and interaction with the electrode might lead to a relief of strain by a partial ring opening. This type of reaction has precedence; there are many examples of metal-catalyzed ring-opening reactions of methylenecyclopropanes (26, 27). A commonly observed reaction is metal atom insertion. The metals frequently used for this type of reaction are Ni and Pd; however, there are also examples of Pt-catalyzed reactions.

The other major exception listed in Table 1 is 2,4-dimethyl-1,3-pentadiene. This molecule has an E_{ox} of 1.53 V, a value close to that of 4-methyl-1,3-pentadiene (1.51 V). The major difference between these two neutral molecules is that the latter is planar, (s-*trans*) conjugated whereas the former is not. The calculated dihedral angle between the double bonds of 2,4-dimethyl-1,3-pentadiene is ca. 50°, i.e., significantly twisted from the s-*cis* conformation. It was shown by ab initio MO calculations that the global minimum of the radical cation of 2,4-dimethyl-1,3-pentadiene is planar (2*e*). All four methyl groups stabilize the radical cation. However, the initially formed radical cation (vertical ionization) will have a twisted geometry (s-*cis*) and must overcome the barrier to become planar (adiabatic). Based on this data one would expect a higher OP for 2,4-dimethyl-1,3-pentadiene than for 4-methyl-1,3-pentadiene. However, the measured values are essentially the same. Interaction of the twisted diene with the electrode surface might reduce the twist of the dihedral angle, resulting in a lower oxidation potential (adiabatic) than expected on the basis of the measured (vertical) ionization potential. However, in the photoinduced electron transfer reactions of this diene, there will be no assistance for the neutral molecule to become planar and therefore the electron transfer will reflect the vertical rather than the adiabatic IP. This is also evident from a comparison of the results of the PET reactions of these two molecules (4-methyl-1,3-pentadiene and 2,4-dimethyl-1,3-pentadiene) (2*e*). The efficiency of the reaction of the twisted diene is significantly lower than that of the planar diene. For the twisted diene to reach the same amount of conversion as the planar diene it has to be irradiated almost twice as long as the planar diene even though the measured oxidation potentials are virtually the same (2*e*). This once again supports the conclusion that, in photochemical reactions, electron transfer is dependent on the vertical ionization potential rather than the adiabatic IP.

Photochemistry of methylenecyclopropane (1) in the presence of a nucleophile

Irradiation of a mixture of methylenecyclopropane (**1**, 0.1 M), biphenyl (**7**, 0.1 M), and 1,4-dicyanobenzene (**6**, 0.1 M) in acetonitrile–methanol (3:1) leads to the formation of essentially the same products as the irradiation without methanol. The reaction was followed by gc/ms and gc/fid; identification of the products was based on their retention times and mass spectra. A careful analysis of the chromatograms and the mass spectra revealed the presence of a few additional minor products. The mass spectra of these compounds were very similar to those of the cycloaddition products with the exception that the molecular ion was at *m/z* 184 rather than *m/z* 182. These compounds are most likely the reduced cycloaddition products. These minor products were not isolated from the mixture.

Reaction [2]



23

The observed ratios of the cycloaddition products are different from those obtained in the experiments using acetonitrile or chloroform as the solvent. With methanol present the ratios are **12**:**13**:**14**:**15**:**16**:**17** = 1.0:1.8:0.1:1.4:0.6:1.7. The most significant difference is the almost complete absence of product **14** in this product mixture. The mechanism for the formation of this compound (a "modified" cyclopropyl–π-methane rearrangement) was discussed earlier (Scheme 5). The mechanism for the cyclopropyl–π-methane rearrangement shows that the fate of the reaction is determined by the pathway of the diradical intermediate (e.g., **20**). Opening of the cyclopropyl group followed by ring closure to give a cyclobutane moiety is the normal course of the reaction (Schemes 5 and 6). However, in a similar reaction, Zimmerman and Carpenter discovered that the diradical intermediate reacted to give a very small amount of the cyclobutane product when the reaction was carried out in pentane but none when the solvent was *tert*-butanol (20*b*). It is possible that the diradical (**20**) in the reaction of MCP with **6** is trapped by the solvent (methanol), leading ultimately to a reduced species.

The results of this reaction once again clearly indicate that, upon irradiation of a mixture of **6** and **1**, no electron transfer takes place. Under these conditions (i.e., the use of **6** as the electron acceptor) the energetic requirements for ET are not met. Formation of an exciplex between the first singlet excited state of **6** and MCP followed by cycloaddition is the preferred reaction pathway.

Electrochemical oxidation of methylenecyclopropane (1) in the absence of a nucleophile

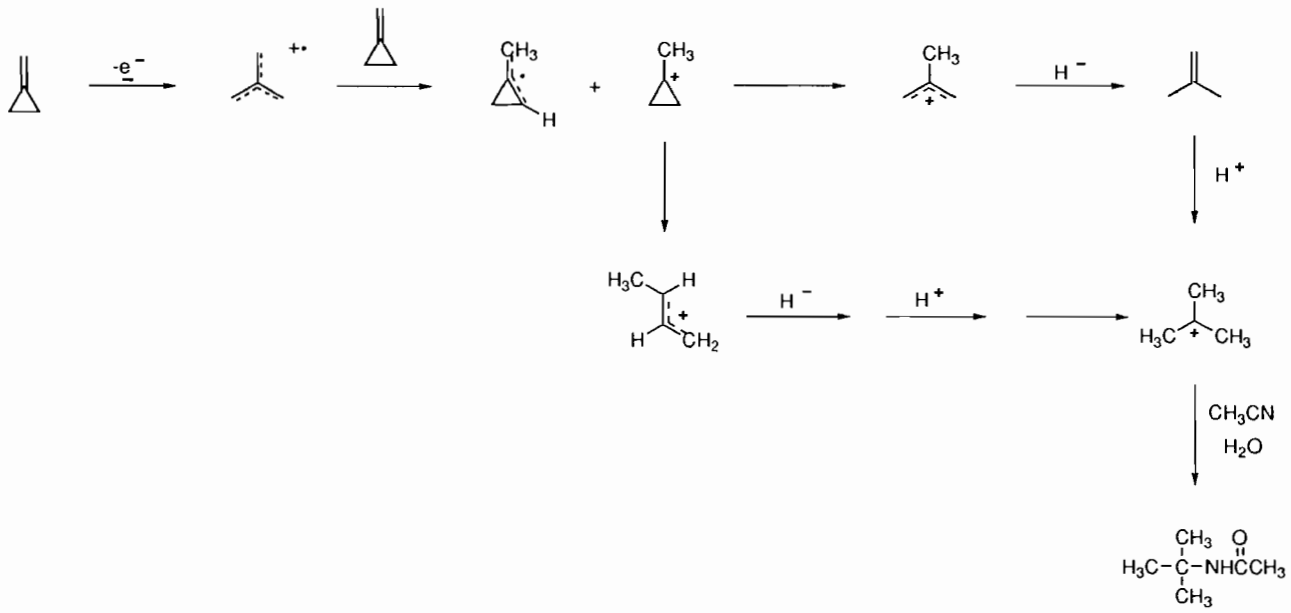
Attempts to generate the MCP radical cation by photoinduced electron transfer using 1,4-dicyanobenzene (**6**) as the electron acceptor (see above) were not successful due to the high vertical IP of MCP. However, it was shown that the measured (CV) E_{ox} was only 2.41 V, close to the value expected based on the calculated adiabatic IP. Anodic oxidation of MCP at a low (<2.5 V) potential should therefore lead to the formation of the radical cation. Its reactivity can then be studied in the presence and absence of nucleophiles.

Anodic oxidation of MCP at a potential difference of 2.45 V in acetonitrile (no methanol) using TEAP as the electrolyte results in the formation of one major product: *tert*-butylacetamide (**23**) (Reaction [2]).

This product (*tert*-butylacetamide, **23**) can be rationalized by the formation of the (relatively) stable *tert*-butyl cation, which then goes on to react with acetonitrile to give the

© 1997 NRC Canada

Scheme 7.



23

observed product (after hydrolysis). A possible mechanism for the formation of the *tert*-butyl cation is shown in Scheme 7.

An important intermediate is the 2-methylallyl cation, a result of a proton transfer from $\mathbf{1a}^{+\bullet}$ to **1** followed by ring opening. It was shown in the previous part of this series that, under non-nucleophilic conditions, anodic oxidation of alkenes can lead to deprotonation (1*b*). Even in the presence of methanol, a good nucleophile, one of the major products in the anodic oxidation of 1,4-bis(methylene)cyclohexane (**2**) was the result of a protonation of the methylene group as the initial step. The proton source is the highly acidic alkene radical cation. Furthermore, a recent ESR study on $\mathbf{1}^{+\bullet}$ showed that this species exists as the ring-opened TMM radical cation, $\mathbf{1a}^{+\bullet}$ (9). However, upon warming the matrix from 77 to 120 K, the radical cation lost a proton and supposedly underwent a ring closure to give the allylic 2-methylenecyclopropyl radical (Scheme 7, step 2).[9]

Protonation of MCP (i.e., MCP acting as the base) leads to the methylcyclopropylium ion, which can undergo a ring opening to give the 2-methylallyl cation or the 1-methylallyl cation. Hydride transfer from a suitable donor (e.g., MCP) followed by protonation (and a rearrangement in the case of the 1-methylallyl cation pathway) leads to the *tert*-butyl cation. The pathway leading to isobutylene as an intermediate seems the most likely one because this involves fewer rearrangements. It has also been shown that *tert*-butylacetamide can be prepared from isobutylene and acetonitrile using an acid catalyst (28). The formation of the *tert*-butyl cation through rearrangements has additional precedence. Anodic oxidation of bromoalkanes leads to the formation of their corresponding acetamido compounds (29). For example, *tert*-butylacetamide was observed as a product in the reactions of 2-bromobutane and 1-bromo-2-methylpropane (29*b*). The anodic oxidation of 1-bromopentane leads to the formation of *N*-1-pentylacetamide, *N*-2-pentylacetamide, and *N*-3-pentylacetamide in equal amounts, indicating that the initially formed carbocation undergoes multiple rearrangements (29*a*).

The precursor to the methylcyclopropylium ion (1-bromo-1-methylcyclopropane) has not been studied by electrochemistry. However, a gas phase study (MS) on the radical cation revealed that loss of a bromine atom leads to the 1-methylcyclopropylium ion, which then undergoes a ring opening to the 1-methylallyl cation rather than the 2-methylallyl cation (30). The results were in agreement with MNDO calculations on these species. In solution, formation of the 2-methylallyl cation seems more likely (see above). As mentioned above, formation of the *tert*-butyl cation from MCP may involve one or more rearrangements. Both experimental (31) and theoretical (32) results on the $C_4H_7^+$ species have indicated that there is evidence for an equilibrium involving the nonclassical bicyclobutonium ion and the bisected cyclopropylcarbinyl cation. Rearrangements to other $C_4H_7^+$ species do not require much energy and are also expected to happen rapidly. For a four-carbon cationic species, the *tert*-butyl cation is the lowest energy structure that can be formed. The driving force for reaction towards this species will be large, even though this may involve several rearrangements, including hydride transfers.

Electrochemical oxidation of methylenecyclopropane (1) in the presence of a nucleophile

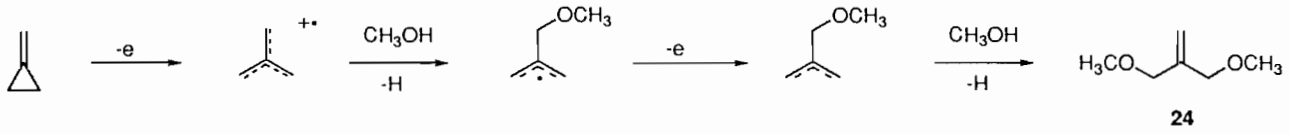
To see whether any of the possible radical cation or cation intermediates could be trapped, the anodic oxidation of MCP was carried out in the presence of a nucleophile (methanol). Under these conditions, one major product was formed: 3-methoxy-2-(methoxymethyl)-1-propene (**24**) (Reaction [3]).

[9] The authors did not propose a mechanism for this reaction and it must be noted that, in principle, the radical cation $\mathbf{1a}^{+\bullet}$ could abstract a hydrogen atom from a neutral molecule (MCP, **1**) to yield the allylic radical and the allylic cation. Either way, this reaction involves two species: the neutral (**1**) and the radical cation ($\mathbf{1a}^{+\bullet}$).

Can. J. Chem. Downloaded from www.nrcresearchpress.com by 91.121.58.235 on 09/08/12
For personal use only.

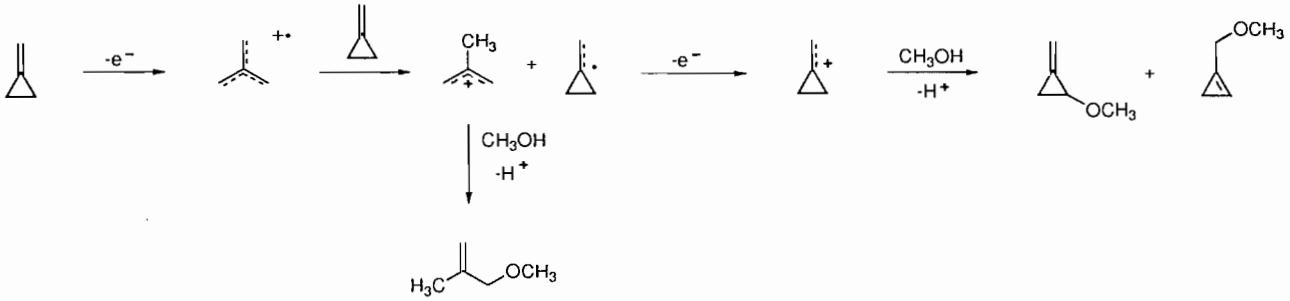
© 1997 NRC Canada

Scheme 8.

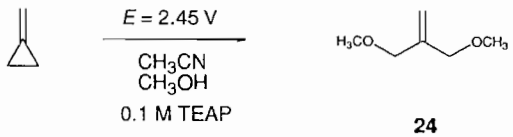


24

Scheme 9.



Reaction [3]



24

Based on the results of the anodic oxidation of **2** under similar conditions (1*b*) this is an expected product. Formation of the (ring-opened; TMM) radical cation (**1a**$^{+\bullet}$) followed by nucleophilic addition and loss of a proton from the distonic radical cation leads to the allylic radical. A second oxidation followed by a second nucleophilic addition and deprotonation yields the final product (Scheme 8). This sequence parallels that of the formation of several products found in the anodic oxidation of 1,4-bis(methylene)cyclohexane (**2**) (1*b*).

It must be noted that it is possible that some of the primary products of this reaction may be too volatile to be observed with conventional gc/fid and gc/ms. For example, it was shown before that anodic oxidation of alkenes in the presence of a nucleophile can lead to allylic substituted products (1*b*, 33) Even though the formation of these types of products from MCP would most likely require a ring-closed species (**1**$^{+\bullet}$, an unlikely intermediate), their presence cannot be ruled out. Furthermore, it was also suggested that the ring-closed radical species that was observed by ESR (9), upon warming of the matrix in which the TMM radical cation had been generated, resulted from a hydrogen atom abstraction by the TMM radical cation from a neutral MCP molecule (see footnote 9). Oxidation of this species and nucleophilic addition would also give the allylic substitution products (Scheme 9).

The previous section described the anodic oxidation of MCP in the absence of methanol; under those conditions the formation of the *tert*-butyl cation is favoured. Formation of this species in the presence of methanol is highly unlikely since it involves multiple rearrangements and the reactive intermediates would be trapped before the final intermediate (*tert*-butyl cation) is formed. However, the possible formation of the product resulting from this intermediate (*tert*-butyl methyl ether) cannot be ignored. Analysis of the expected product (*tert*-butyl methyl ether) by gc/fid showed that the retention time is short and its presence in the reaction mixture cannot be ruled out.

Conclusions

The photochemical reactions of methylenecyclopropane (MCP, **1**) in the presence of an electron acceptor (1,4-dicyanobenzene, **6**) were studied under a number of conditions. Using the measured (CV) oxidation potential (E_{ox}) of MCP, electron transfer (ET) was predicted to occur at the diffusion-controlled rate. However, no products resulting from ET were detected; only photocycloaddition products were formed under these conditions. The mechanism is believed to be addition of MCP to the ^1S state of **6**. Only products with ring-closed MCP moieties were formed, indicating that radical ions, diradicals or ionic species are not involved. Additional evidence for this conclusion is based upon the fact that product formation was shown to be virtually independent of solvent (MeCN, MeOH, $CHCl_3$) and codonor (biphenyl, **7**) concentration. On the basis of these results it is hypothesized that for PET reactions, formation of the radical ion pair is dictated by the vertical IP. In many cases the measured E_{ox} reflects the vertical IP; however, for certain molecules (e.g., MCP) the difference between the vertical and the adiabatic IP is large. In these cases the initially generated (vertical) radical cation is expected to relax to the adiabatic energy level. For these types of molecules the measured E_{ox} reflects the adiabatic IP rather than the vertical IP. This can be explained in terms of an interaction between the alkene and the Pt electrode that will result in a partial release of strain.

Generation of the radical cation of MCP by anodic oxidation at a potential close to the measured (CV) E_{ox} in the absence of a good nucleophile leads to several rearrangements, resulting in the ultimate formation of the most stable

Can. J. Chem. Downloaded from www.nrcresearchpress.com by 91.121.58.235 on 09/08/12
For personal use only.

© 1997 NRC Canada

C_4-cation: the *tert*-butyl cation. This species is then trapped by the solvent (acetonitrile) to give the observed product *tert*-butyl-acetamide. In the presence of methanol this intermediate is believed not to be formed; however, it cannot be completely ruled out. Under these conditions the major product is 3-methoxy-2-(methoxymethyl)-1-propene, a result of nucleophilic addition to the ring-opened radical cation followed by a second oxidation and nucleophilic addition. This reactivity was also observed in the anodic oxidation of 1,4-bis(methylene)cyclohexane (**2**) in the presence of methanol (*1b*).

Experimental

General information

The ^1H and ^{13}C nmr spectra were obtained on a Bruker AC250 spectrometer. Frequencies are relative to tetramethylsilane. Infrared spectra were recorded on a Nicolet 205 spectrometer and are reported in wave numbers (cm^{-1}). Exact mass determinations were obtained using a CEC 21–110B spectrometer. Melting points were determined using a Cybron Corporation Thermolyne apparatus with a digital thermocouple and are corrected. Product yields were determined using a Hewlett–Packard (HP) 5890 gas chromatograph with a DB-1701 fused silica WCOT column (30 m × 0.25 mm, 0.25 μm film thickness) and a calibrated flame ionization detector (gc/fid). An HP 3392A integrator was interfaced with the gc/fid to obtain peak areas. An HP 5890 gas chromatograph with a 5% phenyl methyl silicone fused silica WCOT column (25 m × 0.20 mm, 0.33 μm film thickness) interfaced with an HP 5970 mass selective detector (gc/ms) was also used for product analyses. Mass spectra are reported as *m/z* (relative intensity). Separation of product mixtures was generally carried out using preparative medium-pressure liquid chromatography (mplc), followed by dry column flash chromatography (dcfc) (34). The mplc consists of a 2.5 cm × 1 m column packed with thin-layer chromatography (tlc) grade silica gel (Rose Scientific Ltd., Silica Gel G/UV-254 with gypsum binder, cat. no. 81632) at a pressure of 18 psi using helium (1 psi = 6.9 kPa). Connected to the mplc was a uv spectrophotometer – fraction collector that collects ca. 20 mL fractions. For dcfc the column was packed with thin-layer chromatography grade silica gel (Rose Scientific Ltd., Silica Gel G/UV-254 with gypsum binder, cat. no. 81632). Fraction sizes were ca. 10 mL.

Materials

Anhydrous acetonitrile (Aldrich) and anhydrous methanol (Aldrich) were stored over molecular sieves (3 Å) upon arrival and used without further purification. 1,4-Dicyanobenzene (**6**) (Aldrich) was purified by treatment with Norite in methylene chloride, followed by recrystallization from 95% ethanol. Biphenyl (**7**) (Eastman Kodak) was recrystallized from methanol. Tetraethylammonium perchlorate (TEAP) (Fisher) was recrystallized three times from water and then dried in a vacuum oven for 15 h, 70°C, 0.25 Torr (1 Torr = 133.3 Pa). Methylenecyclopropane (**1**) was prepared as described below. *tert*-Butyl methyl ether, sodium amide, di-*n*-butyl ether, methallyl chloride (2-chloromethyl-1-propene), and potassium *tert*-butoxide (1.0 M solution in *tert*-butanol) were all received from Aldrich and used without further purification.

Irradiations

Irradiations were generally carried out on solutions of acetonitrile (with or without methanol as the nucleophile) with 1,4-dicyanobenzene (**6**), the alkene, and with or without a codonor (biphenyl, **7**). Solutions were irradiated in either 2 cm i.d. Pyrex tubes or 5 mm Pyrex nmr tubes. The samples were irradiated at 10°C using a CGE 1 kW medium-pressure mercury vapour lamp contained in a water-cooled quartz immersion well.

Cyclic voltammetric measurements

Cyclic voltammetry at a sweep rate of 100 mV/s was used to obtain the oxidation potential of the alkene. The apparatus has been described (35). The working electrode was a platinum sphere (1 mm diameter) and the counter electrode was a platinum wire. The reference electrode was a saturated calomel electrode (sce), which was connected to the solution (TEAP 0.1 M, acetonitrile) through a Luggin capillary. The alkene concentration was ca. 0.005 M. Since the anodic wave was irreversible, the half-wave potential was taken as 0.028 V before the anodic peak potential (36).

Controlled potential electrolyses

Controlled potential electrolyses of **1** were performed with a double-wall two-electrode cell (total volume 200 mL) containing the working electrode and the reference electrode (sce). The counter electrode compartment, containing the counter electrode, was fitted into the cell; the two compartments were connected by means of fine glass frit. Both the working electrode and counter electrode were platinum mesh (6.5 cm^2). The reference electrode was the standard calomel electrode (sce). The cell was kept at a temperature of 10 (±0.5)°C.

The electrochemical measurements were obtained with a Princeton Applied Research (PAR) 173 potentiostat in combination with a PAR 175 universal programmer and a PAR 179 digital coulometer.

Synthesis of methylenecyclopropane (1)

Methylenecyclopropane (**1**) was synthesized according to literature procedures (37) with some minor modifications. A 250 mL 3-neck round-bottom flask equipped with a pressure equalizing dropping funnel (with a nitrogen inlet) and a condenser was charged with 20 g sodium amide and 50 mL di-*n*-butyl ether. This mixture was refluxed under nitrogen for ca. 15 min after which 40 mL of methallyl chloride was added dropwise over a period of 40 min. The volatile products were removed from the flask by a small nitrogen flow through a trap containing 50 mL 5 N H_2SO_4 followed by an empty trap (kept at room temperature), and were then condensed in a trap cooled by an acetone – Dry Ice mixture. Analysis of this mixture by ^1H and ^{13}C nmr indicated the presence of both methylenecyclopropane and methylcyclopropene in a ratio of about 1:4. The mixture was transferred to a flask containing 50 mL dimethyl sulfoxide after which 10 mL of a 1.0 M solution of potassium *tert*-butoxide in *tert*-butanol was added. The mixture was stirred for 1 h at room temperature and then for 2 h at reflux temperature. During this reflux period the volatiles were carried over through an empty trap (room temperature) to a cold trap (cooled by an acetone – Dry Ice mixture) with a small nitrogen flow. Afterwards, the trap contained ca. 10 mL

© 1997 NRC Canada

Can. J. Chem. Downloaded from www.nrcresearchpress.com by 91.121.58.235 on 09/08/12
For personal use only.

Can. J. Chem. Downloaded from www.nrcresearchpress.com by 91.121.58.235 on 09/08/12
For personal use only.

of product (≈50% yield). Analysis of the contents of the trap by ^{1}H and ^{13}C nmr indicated the presence of pure methylenecyclopropane (**1**) (37).

Irradiation of a mixture of methylenecyclopropane (1), 1,4-dicyanobenzene (6), and biphenyl (7) in acetonitrile

A solution containing 6 g (1.1×10^{-1} mol) methylenecyclopropane (**1**), 3.1 g (2.4×10^{-2} mol) 1,4-dicyanobenzene (**6**), and 3.7 g (2.4×10^{-2} mol) biphenyl (**7**) dissolved in 240 mL anhydrous acetonitrile was irradiated for 20 days. After this period the solvent and the volatile products were removed by rotary evaporation. The residue was chromatographed on silica gel (mplc) using a hexanes–ether gradient. Further purification of the products was achieved by dcfc. Identification of the products was based on the ^{1}H and ^{13}C nmr spectra and the X-ray diffraction spectra. The yields of the reaction were determined by calibrated gc/fid. All yields are based on the amount of 1,4-dicyanobenzene (**6**) that was consumed in the reaction.

*2,5-Dicyanobicyclo[2.2.2]octa-3,7-diene spiro cyclopropane (**12**)*

Recrystallized from cyclohexane; mp 100–101°C; ir (KBr) ν: 3087 (s), 3074 (m), 3001 (m), 2978 (m), 2944 (m), 2879 (m), 2856 (w), 2255 (s), 1650 (w), 1603 (w), 1583 (w), 1463 (m), 1455 (m), 1426 (m), 1356 (s), 1324 (w), 1266 (m), 1236 (w), 1173 (m), 1160 (m), 1110 (w), 1056 (m), 1041 (m), 1023 (m), 1012 (m), 971 (m), 961 (m), 949 (m), 882 (m), 867 (m), 716 (s), 691 (s), 657 (w); ^{1}H nmr ($CDCl_3$) δ: 6.66–6.49 (m, 7.93 Hz, 12.82 Hz, 4H), 1.92 (s, 2H), 0.96 (m, 5.49 Hz, 6.10 Hz, 2H), 0.56 (t, 6.10 Hz, 2H); ^{13}C nmr ($CDCl_3$) δ: 133.82 (d), 133.40 (d), 120.70 (s), 118.53 (s), 45.57 (s), 42.75 (t), 38.68 (s), 24.77 (s), 10.15 (t); ms *m/z*: 182 ($M^{+\cdot}$, 4%), 181 (19), 167 (12), 154 (19), 140 (19), 128 (30), 115 (10), 101 (13), 89 (5), 75 (17), 64 (16), 54 (100); Exact Mass of ion $C_{12}H_{10}N_2$: 182.0844; measured: 182.0843.

*2,5-Dicyanotricyclo[3.3.0.^{2,6}0^{5,7}]oct-3-ene spiro cyclopropane (**13**)*

Recrystallized from cyclohexane; mp 90–91°C; ir (KBr) ν: 3095 (m), 3073 (m), 3006 (m), 2957 (m), 2943 (m), 2236 (s), 1695 (w), 1602 (w), 1452 (m), 1421 (s), 1360 (w), 1330 (w), 1317 (m), 1294 (w), 1075 (m), 1064 (m), 1031 (s), 1021 (s), 1002 (m), 989 (w), 969 (m), 948 (m), 931 (s), 919 (w), 896 (m), 871 (s), 846 (s), 811 (s), 782 (s), 764 (s), 710 (s); ^{1}H nmr ($CDCl_3$) δ: 5.81 (d, 5.47 Hz, 1H), 5.60 (d, 5.47 Hz, 1H), 3.56 (d, 7.3 Hz, 1H), 2.66 (dt (unresolved), 1.2 Hz, 6.7 Hz, 6.1 Hz, 1H), 2.05 (d, 14.0 Hz, 1H), 1.78 (dd, 6.7 Hz, 14.6 Hz, 1H), 1.15–1.03 (m, 1H), 0.72–0.49 (m, 3H); ^{13}C nmr ($CDCl_3$) δ: 132.75 (d), 125.67 (d), 118.33 (s), 116.54 (s), 55.23 (s), 47.28 (d), 37.56 (d), 36.59 (s), 31.62 (t), 27.90 (s), 13.07 (t), 4.90 (t); ms *m/z* 182 ($M^{+\cdot}$, 19%), 181 (70), 167 (38), 155 (56), 154 (100), 140 (67), 127 (37), 116 (41), 103 (25), 89 (17), 76 (29), 67 (55), 54 (40), 51 (50); Exact Mass of ion $C_{12}H_{10}N_2$: 182.0844; measured: 182.0835.

*1,4-Dicyanotetracyclo[2.0.^{3,10}0.^{4,7}2.0.^{7,9}1]decene (**14**)*

Recrystallized from cyclohexane; mp 123–124°C; ir (KBr) ν: 3080 (w), 3063 (m), 3000 (m), 2976 (m), 2945 (m), 2869 (w), 2860 (w), 2227 (s), 2217 (s), 1601 (w), 1584 (w), 1448 (m), 1430 (m), 1286 (w), 1263 (w), 1248 (m), 1230 (w), 1196 (w), 1254 (w), 1135 (w), 1059 (m), 1043 (m), 1029 (m), 1006 (w), 966 (m), 955 (m), 909 (w), 873 (m), 865 (m), 848 (m), 838 (m), 652 (m), 641 (w); ^{1}H nmr ($CDCl_3$) δ: 6.83 (s, 1H), 4.23 (4 line multiplet: 3.05 Hz, 3.66 Hz, 4.27 Hz, 1H), 3.66 (dd, 1.22 Hz, 3.66 Hz, 1H), 2.75 (dd, 1.83 Hz, 10.38 Hz, 1H), 2.60–2.35 (m, 2H), 2.00–1.88 (m, 1H), 1.50–1.41 (m, 1H), 1.23–1.13 (m, 2H); ^{13}C nmr ($CDCl_3$) δ: 152.18 (d), 122.11 (s), 121.14 (s), 112.90 (s), 62.34 (d), 55.53 (d), 52.27 (s), 43.08 (s), 30.88 (t), 25.51 (t), 20.73 (d), 18.06 (t); ms *m/z*: 182 ($M^{+\cdot}$, 5%), 181 (37), 167 (26), 154 (100), 140 (88), 127 (59), 116 (53), 103 (44), 89 (19), 77 (38), 63 (37), 54 (18), 51 (57); Exact Mass of ion $C_{12}H_{10}N_2$: 182.0844; measured: 182.0849.

*3,7-Dicyanotricyclo[3.3.0.^{2,6}0^{5,7}]oct-3-ene spiro cyclopropane (**15**)*

Recrystallized from cyclohexane; mp 106–107°C; ir (KBr) ν: 3084 (w), 3058 (w), 3004 (w), 2968 (w), 2937 (m), 2235 (s), 2216 (s), 1596 (m), 1443 (w), 1425 (m), 1305 (w), 1277 (w), 1247 (w), 1146 (w), 1059 (m), 1031 (m), 1019 (w), 998 (m), 950 (m), 903 (m), 882 (m), 854 (m), 788 (w), 629 (m); ^{1}H nmr ($CDCl_3$) δ: 6.53 (d, 3.05 Hz, 1H), 3.39 (t, 6.10 Hz, 1H), 2.82 (dd, 1.83 Hz, 5.48 Hz, 1H), 2.69 (dd, 2.44 Hz, 6.73 Hz, 1H), 2.26 (d, 14.05 Hz, 1H), 1.83 (dd, 1.23 Hz, 14.03 Hz, 1H), 0.93–0.54 (m, 4H); ^{13}C nmr ($CDCl_3$) δ: 140.73 (d), 119.11 (s), 115.18 (s), 58.65 (d), 44.86 (d), 40.35 (d), 35.36 (s), 34.98 (t), 24.37 (s), 14.21 (t), 5.75 (t); ms *m/z*: 182 ($M^{+\cdot}$, 29%), 181 (100), 167 (25), 155 (66), 154 (92), 140 (81), 127 (46), 116 (74), 103 (21), 89 (23), 77 (31), 63 (43), 54 (21), 51 (46); Exact Mass of ion $C_{12}H_{10}N_2$: 182.0844; measured: 182.0855.

*4,6-Dicyanotricyclo[3.3.0.^{3,7}0^{6,8}]oct-4-ene spiro cyclopropane (**16**)*

Recrystallized from cyclohexane; mp 106–108°C; ir (KBr) ν: 3080 (m), 3054 (w), 2998 (w), 2985 (w), 2971 (w), 2954 (w), 2939 (w), 2870 (w), 2230 (s), 2217 (s), 1601 (m), 1505 (w), 1455 (m), 1430 (m), 1313 (w), 1293 (w), 1277 (w), 1261 (w), 1212 (w), 1153 (m), 1063 (m), 1029 (s), 1006 (m), 987 (w), 966 (s), 949 (w), 923 (w), 909 (m), 876 (s), 847 (s), 838 (s), 784 (w), 699 (w), 607 (w); ^{1}H nmr ($CDCl_3$) δ: 6.60 (3.05 Hz, 1H), 3.51 (6-line multiplet, 5.49 Hz, 6.11 Hz, 4.88 Hz, 11.60 Hz, 12.20 Hz, 1H + 1H), 2.84 (dd, 4.27 Hz, 12.20 Hz, 1H), 2.69 (dd, 2.44 Hz, 6.10 Hz, 1H), 1.53 (d, 12.20 Hz, 1H), 1.15–1.03 (m, 1H), 0.97–0.84 (m, 1H), 0.67–0.45 (m, 2H); ^{13}C nmr ($CDCl_3$) δ: 143.43 (d), 120.84 (s), 118.77 (s), 114.86 (s), 52.13 (d), 50.45 (t), 46.60 (d), 42.60 (d), 31.71 (s), 22.28 (s), 15.15 (t), 7.92 (t); ms *m/z*: 182 ($M^{+\cdot}$, 11%), 181 (28), 167 (27), 155 (15), 154 (23), 140 (16), 128 (14), 116 (21), 103 (12), 89 (2), 76 (12), 63 (10), 54 (100), 51 (17); Exact Mass of ion $C_{12}H_{10}N_2$: 182.0844; measured: 182.0850.

*Dispiro[2.4.2.4]-11,14-dicyanotricyclo[2.2.2.0.^{5,14}0^{6,11}]tetradec-12-ene (**17**)*

Recrystallized twice from cyclohexane and once from 95% ethanol; mp 176–177°C; ir (KBr) ν: 3078 (w), 3001 (m), 2988 (w), 2967 (s), 2935 (m), 2925 (s), 2858 (m), 2237 (m), 2224 (m), 1446 (m), 1425 (m), 1244 (m), 1211 (w), 1177 (w), 1131 (w), 1118 (w), 1064 (w), 1060 (w), 1051 (w), 1033 (m), 1026 (m), 991 (w), 913 (m), 904 (w), 885 (m), 873 (m), 807 (m), 761 (s); ^{1}H nmr ($CDCl_3$) δ: 5.84 (s, 2H), 3.15 (m, 8.55 Hz, 9.15 Hz, 2H), 2.26 (m, 10.98 Hz, 9.77 Hz, 2H), 2.04 (m, 1.84 Hz, 9.15 Hz, 2H), 1.14–1.01 (m, 2H), 0.85–0.73 (m, 2H), 0.73–0.61 (m, 2H), 0.50–0.38 (m, 2H); ^{13}C nmr ($CDCl_3$) δ:

© 1997 NRC Canada

Can. J. Chem. Downloaded from www.nrcresearchpress.com by 91.121.58.235 on 09/08/12
For personal use only.

124.43 (d), 119.85 (s), 35.94 (d), 35.77 (s), 30.62 (t), 26.23 (s), 12.02 (t), 6.78 (t); ms *m/z*: 236 ($M^{+\cdot}$, 1%), 235 (7), 221 (4), 207 (27), 194 (8), 179 (21), 167 (7), 154 (21), 140 (10), 129 (11), 116 (20), 104 (13), 91 (10), 77 (15), 63 (11), 54 (100), 51 (21); Exact Mass of ion $C_{16}H_{16}N_2$: 236.1313; measured: 236.1290.

Irradiation of methylenecyclopropane (1) and 1,4-dicyanobenzene (6) in acetonitrile

A 0.1 M solution (40 mL) of MCP (**1**) in acetonitrile containing 0.5 g (3.9×10^{-3} mol) 1,4-dicyanobenzene (**6**) and 0.6 g (3.9×10^{-3} mol) biphenyl (**7**) was irradiated through Pyrex with the 1 kW lamp for 30 days. The reaction was followed by gc/fid and gc/ms. Analysis of the product mixture indicated the presence of the same products as in the reaction with a larger MCP concentration; however, the reaction was less efficient than before.

Influence of the biphenyl (7) concentration on the product formation in the irradiation of methylenecyclopropane (1) and 1,4-dicyanobenzene (6) in acetonitrile

Solutions (2 mL) containing 0.1 M (50 μL) MCP (**1**) and 0.1 M (25 mg) 1,4-dicyanobenzene (**6**), as well as 0.1 M (30 mg), 0.25 M (78 mg), and 0.5 M (154 mg) biphenyl (**7**) were irradiated through Pyrex with the 1 kW lamp for 40 h. The reactions were followed by gc/fid and gc/ms. Analysis of the product mixtures indicated that the same products were formed in each reaction. Increasing the biphenyl concentration decreases the efficiency of the reaction. No other products were formed.

Irradiation of methylenecyclopropane (1) and 1,4-dicyanobenzene (6) in chloroform

A solution of 0.7 g (1.3×10^{-2} mol) methylenecyclopropane (**1**) and 1.55 g (1.2×10^{-2} mol) 1,4-dicyanobenzene (**6**) in 200 mL chloroform was irradiated for 5 days through Pyrex with the 1 kW lamp. The reaction was followed by gc/ms and gc/fid. Analysis of the product mixture by gc/fid and gc/ms indicated the formation of the same products that were observed in the experiment with acetonitrile as the solvent.

Irradiation of a mixture of methylenecyclopropane (1) and 1,4-dicyanobenzene (6) in acetonitrile–methanol (3:1)

A solution of 0.2 g (3.7×10^{-3} mol) methylenecyclopropane (**1**), 0.5 g (3.9×10^{-3} mol) 1,4-dicyanobenzene (**6**), and 0.6 g (3.9×10^{-3} mol) biphenyl (**7**) in 40 mL acetonitrile–methanol (3:1 by volume) solution was irradiated through Pyrex with the 1 kW lamp for 40 days. The reaction was followed by gc/fid and gc/ms. Product identification was based on retention time (two different columns) and mass spectra. Several other products were tentatively identified as the reduced 1:1 cycloadducts; identification is based on their mass spectra.

Electrolysis of a solution of methylenecyclopropane (1) in acetonitrile

A solution of 4.6 g (2.0×10^{-2} mol) tetraethylammonium perchlorate (TEAP) in 200 mL acetonitrile was deaerated for 30 min by nitrogen ebullition. After this period 6.5 mL (9.6×10^{-2} mol) methylenecyclopropane (**1**) was added to the solution and a potential difference of 2.45 V was applied to the cell. The reaction was stopped after 1080 coulombs had been consumed (ca. 10% conversion; calculated on basis of a one-electron oxidation).[10] The solvent was evaporated and the residue was washed with benzene to remove the residual TEAP. Evaporation of the benzene left the crude product, which was identified as *N-tert*-butylacetamide (**23**, 25%) based on its ^{1}H nmr, ^{13}C nmr (38*a*,*b*), and mass spectra (38*b*).

N-tert-Butylacetamide (23): ^{1}H nmr ($CDCl_3$) δ: 7.36 (s, 1H), 1.94 (s, 3H), 1.35 (s, 9H); ^{13}C nmr ($CDCl_3$) δ: 170.11 (s), 51.36 (s), 28.63 (q), 24.22 (q); ms *m/z*: 115 ($M^{+\cdot}$, 7%), 100 (10), 64 (5), 60 (21), 59 (17), 58 (100), 56 (7).

Electrolysis of a solution of methylenecyclopropane (1) in acetonitrile–methanol (3:1)

A solution of 4.6 g TEAP (2.0×10^{-2} mol) in 200 mL acetonitrile–methanol (3:1) was purged with nitrogen for 45 min. A potential difference of 2.45 V was applied to the cell for 2 h for background correction. After this period the coulometer was reset and 6.5 mL MCP (5.2 g, 9.6×10^{-2} mol) was added to the solution and the potential difference (2.45 V) was applied to the cell again. The reaction was allowed to continue until 2085 C had been consumed (ca. 11% conversion; calculated on basis of a two-electron oxidation) (see footnote 10). Analysis of the product mixture by gc/ms revealed the presence of one major product (**24**) and several minor products. Identification of product **24** (3-methoxy-2-(methoxymethyl)-1-propene) is based on its mass spectrum.

3-Methoxy-2-(methoxymethyl)-1-propene (24): ms *m/z*: 116 ($M^{+\cdot}$, 0.1%), 115 (1), 101 (2), 85 (18), 84 (47), 75 (18), 71 (100), 69 (12), 58 (9), 56 (16), 55 (55), 53 (13).

Acknowledgement

This work was supported by grants from the Natural Sciences and Engineering Research Council of Canada. We thank Dr. D.L. Hooper the Atlantic Region Magnetic Resonance Centre at Dalhousie University for help in the preparation of the manuscript. Exact Mass determinations were carried out by Dr. J.-H. Kim (Dalhousie Chemistry Mass Spectrometry Lab). H.J.P.dL. is grateful for a scholarship from the Izaak Walton Killam Memorial foundation.

References

1. (*a*) H.J.P. de Lijser and D.R. Arnold. J. Phys. Chem. **100**, 3996 (1996); (*b*) J. Chem. Soc. Perkin Trans. 2, 1369 (1997).
2. (*a*) D.R. Arnold, K.A. McManus, and X. Du. Can. J. Chem. **72**, 415 (1994); (*b*) K.A. McManus and D.R. Arnold. Can. J. Chem. **72**, 2291 (1994); (*c*) Can. J. Chem. **73**, 2158 (1995); (*d*) D.R.

[10] Calculation of the conversion of MCP was done using the formula (1*b*): $a = (Q^*M)/(n^*F)$. In this equation, n is the number of electrons involved in the oxidation process per molecule substrate, Q is the total amount of coulombs consumed, M is the molecular weight of the substrate, a is the amount of substrate that has been converted (in grams), and F is Faraday's constant. Based on our previous experiments (ref. 1*b*) the electrooxidation in the presence of a nucleophile is known to be a two-electron process, whereas the electrooxidation in acetonitrile is a one-electron process. Using these assumptions, and the values of Q, the conversion of MCP can be calculated.

© 1997 NRC Canada

Can. J. Chem. Downloaded from www.nrcresearchpress.com by 91.121.58.235 on 09/08/12
For personal use only.

Arnold, D.A. Connor, K.A. McManus, P.K. Bakshi, and T.S. Cameron. Can. J. Chem. **74**, 602 (1996); (*e*) D.R. Arnold, M.S.W. Chan, and K.A. McManus. Can. J. Chem. **74**, 2143 (1996); (*f*) A.L. Perrott, H.J.P. de Lijser, and D.R. Arnold. Can. J. Chem. **75**, 384 (1997); (*g*) D.R. Arnold, K.A. McManus, and M.S.W. Chan. Can. J. Chem. **75**, 1055 (1997).

3. (*a*) D.R. Arnold and S.A. Mines. Can. J. Chem. **65**, 2312 (1987); (*b*) Can. J. Chem. **67**, 689 (1989); (*c*) J.P. Dinnocenzo and D.A. Conlon. J. Am. Chem. Soc. **110**, 2324 (1988); (*d*) Tetrahedron, **36**, 7415 (1995); (*e*) G.-F. Chen and F. Williams. J. Am. Chem. Soc. **113**, 7792 (1991); (*f*) D. Vollmer, D.L. Rempel, M.L. Gross, and F. Williams. J. Am. Chem. Soc. **117**, 1669 (1995); (*g*) A. Lund and M. Shiotani (*Editors*). Radical ionic systems. Kluwer Academic Publishers, Dordrecht. 1991.
4. (*a*) P. Binger. Angew. Chem. Int. Ed. Engl. **11**, 309 (1972); **11**, 433 (1972); (*b*) W.R., Dolbier, Jr., D. Lomas, T. Garza, C. Harmon, and P. Tarrant. Tetrahedron, **28**, 3185 (1972); (*c*) M.J. Doyle, J. McMeeking, and P. Binger. J. Chem. Soc. Chem. Commun. 376 (1976); (*d*) P. Binger, M.J. Doyle, and R. Benn. Chem. Ber. **116**, 1 (1983); (*e*) P. Binger, A. Brinkmann, and P. Wedemann. Chem. Ber. **116**, 2920 (1983).
5. S.L. Painter and S.C. Blackstock. J. Am. Chem. Soc. **117**, 1441 (1995).
6. R. Noyori, N. Hayashi, and M. Katô. J. Am. Chem. Soc. **93**, 4948 (1971).
7. T. Miyashi, Y. Takahashi, T. Mukai, H.D. Roth, and M.L.M. Schilling. J. Am. Chem. Soc. **107**, 1079 (1985).
8. (*a*) Y. Takahashi, T. Miyashi, and T. Mukai. J. Am. Chem. Soc. **105**, 6511 (1985); (*b*) T. Miyashi, M. Kamata, and T. Mukai. J. Am. Chem. Soc. **108**, 2755 (1986); (*c*) J. Am. Chem. Soc. **109**, 2780 (1987); (*d*) T. Miyashi, Y. Takahashi, M. Kamata, K. Yokogowa, H. Ohaku, and T. Mukai. Stud. Org. Chem. (Amsterdam), **31**, 363 (1987).
9. K. Komaguchi, M. Shiotani, and A. Lund. Chem. Phys. Lett. **265**, 217 (1997).
10. (*a*) L.J. Johnston and N.P. Schepp. Adv. Electron Transfer Chem. **5**, 41 (1996); (*b*) N.P. Schepp and L.J. Johnston. J. Am. Chem. Soc. **116**, 6895 (1994); (*c*) J. Am. Chem. Soc. **118**, 2872 (1996); (*d*) L.J. Johnston and N.P. Schepp. Pure Appl. Chem. **67**, 71 (1995).
11. D.R. Arnold, P.C. Wong, A.J. Maroulis, and T.S. Cameron. Pure Appl. Chem. **52**, 2609 (1980).
12. R. Srinivasan. Tetrahedron Lett. **32**, 2725 (1974).
13. (*a*) J. Cornelisse. Chem. Rev. **93**, 615 (1993); (*b*) F. Müller and J. Mattay. Chem. Rev. **93**, 99 (1993); (*c*) P.A. Wender, L. Siggel, and J.M. Nuss. Org. Photochem. **10**, 357 (1989).
14. (*a*) G. Weber, J. Runsink, and J. Mattay. J. Chem. Soc. Perkin Trans. 1, 2333 (1987); (*b*) D. Bryce-Smith, B. Foulger, J. Forrester, A. Gilbert, B.H. Orger, and H.M. Tyrrell. J. Chem. Soc. Perkin Trans. 1, 55 (1980).
15. (*a*) J. Mattay. Tetrahedron, **41**, 2293 (1985); (*b*) Tetrahedron, **41**, 2405 (1985); (*c*) J. Photochem. **37**, 167 (1987).
16. D. Rehm and A. Weller. Isr. J. Chem. **8**, 259 (1970).
17. (*a*) H.-D. Scharf and J. Mattay. Tetrahedron Lett., 401 (1977); (*b*) J. Mattay, H. Leismann, and H.-D. Scharf. Chem. Ber. **112**, 577 (1979).
18. P. Du and W.T. Borden. J. Am. Chem. Soc. **109**, 5330 (1987).
19. (*a*) P.J. Wagner and K. Nahm. J. Am. Chem. Soc. **109**, 6528 (1987); (*b*) K.B. Cosstick, M.G.B. Drew, and A. Gilbert. J. Chem. Soc., Perkin Trans. 1, 1867 (1987).
20. (*a*) H.E. Zimmerman and C.J. Samuel. J. Am. Chem. Soc. **97**, 4025 (1975); (*b*) H.E. Zimmerman and C.W. Carpenter. J. Org. Chem. **53**, 3298 (1988); (*c*) S.M. Nevill and J.A. Pincock. Can. J. Chem. **75**, 232 (1997); (*d*) S.M. Nevill, A.L. Pincock, and J.A. Pincock. J. Org. Chem. **62**, 2680 (1997).
21. H.E. Zimmerman and G.L. Grunewald. J. Am. Chem. Soc. **88**, 448 (1966).
22. W.C. Neikam, G.R. Dimeler, and M.M. Desmond. J. Electrochem. Soc. **111**, 1190 (1964).
23. L.L. Miller, G.D. Nordblum, and E.A. Mayeda. J. Org. Chem. **37**, 916 (1972).
24. (*a*) L. Eberson. Adv. Phys. Org. Chem. **18**, 79 (1982); (*b*) Electron transfer reactions in organic chemistry. Springer-Verlag, Berlin. 1987.
25. G. Bieri, F. Burger, E. Heilbronner, and J.P. Maier. Helv. Chim. Acta, **60**, 2213 (1977).
26. P. Binger and H.M. Büch. Top. Curr. Chem. **135**, 77, (1987), and cited references.
27. M. Lautens, Y. Ren, and H.M. Delanghe. J. Am. Chem. Soc. **116**, 8821 (1994).
28. D.Z. Samedova, K.Ya. Alieva, S.S. Avanesova, F.K. Ismailov, Z.A. Ekhtibarova, and T.N. Shakhtakhtinskii. Dokl. Akad. Nauk Az. SSR, **32**, 42 (1976); Chem. Abstr. **87**, 52718f (1977).
29. (*a*) J.Y. Becker and M. Münster. Tetrahedron Lett. 455 (1977); (*b*) J.Y. Becker and D. Zemach. J. Chem. Soc. Perkin Trans. 2, 336 (1981).
30. R.D. Bowen, J. Chandrasekhar, G. Frenking, P. v. R. Schleyer, H. Schwartz, C. Wesdemiotis, and D.H. Williams. Chem. Ber. **113**, 1084 (1980).
31. J.S. Staral, I. Yavari, J.D. Roberts, G.K.S. Prakash, D.J. Donovan, and G.A. Olah. J. Am. Chem. Soc. **100**, 8016 (1978).
32. H. Kollmar and H.O. Smith. Tetrahedron Lett., 3133 (1970).
33. (*a*) T. Shono and A. Ikeda. J. Am. Chem. Soc. **94**, 7892 (1972); (*b*) T. Shono, A. Ikeda, J. Hayashi, and S. Hakozaki. J. Am. Chem. Soc. **97**, 4261 (1975).
34. L.M. Harwood. Aldrichimica Acta, **18**, 25 (1985).
35. D.R. Arnold and D.D.M. Wayner. Can. J. Chem. **64**, 100 (1986).
36. (*a*) R.S. Nicholson and I. Shain. Anal. Chem. **36**, 706 (1964); (*b*) Anal. Chem. **37**, 178 (1965).
37. (*a*) I.S. Krull and D.R. Arnold. Org. Prep. Proced. **1**, 283 (1969); (*b*) J.R. Salaun, J. Champion, and J.M. Conia. Org. Synth. **57**, 36 (1977); (*c*) R. Köster, S. Arora, and P. Binger. Angew. Chem. **8**, 205 (1969); (*d*) R. Köster, S. Arora, and P. Binger. Synthesis, 322 (1971); (*e*) Liebigs Ann. Chem. 1219 (1973).
38. (*a*) J. Llinarés, J. Elguero, R. Faure, and E.-J. Vincent. Org. Magn. Reson. **14**, 20 (1980); (*b*) N. Kalayanam and S. Sivaram. Org. Mass Spectrom. **22**, 43 (1987).

© 1997 NRC Canada

Photochemical nucleophile–olefin combination, aromatic substitution (photo-NOCAS) reaction, Part 15. Investigations involving fluoride anion as the nucleophile and the effect of fluorine substitution on the relative stability of the reaction intermediates[1]

Mary S.W. Chan and Donald R. Arnold

Abstract: The scope of the photochemical nucleophile–olefin combination, aromatic substitution (photo-NOCAS) reaction has been extended to include fluoride anion as the nucleophile. The 4-cyanophenyl substituted fluoroalkanes were obtained in moderate yields with 2,3-dimethyl-2-butene and 2-methyl-2-butene reacting as the olefin. The yields were lower with 2-methylpropene, and no photo-NOCAS products were detected when conjugated dienes were used as the olefin. The selectivity of the fluoride anion towards alkenes can be explained in terms of the Hard–Soft-Acid–Base (HSAB) principle. The regiochemistry of this reaction can be described as predominantly following the *anti*-Markovnikov mode of addition. The fluoride anion adds preferentially to the less alkyl-substituted end of an unsymmetrical alkene radical cation to produce the more heavily substituted β-fluoroalkyl radical. Ab initio molecular orbital calculations (MP2/6-31G*//HF/6-31G*) were used to determine the relative stability of the β-fluoroalkyl radical intermediates. The more heavily substituted β-fluoroalkyl radical is NOT the more stable. The addition step is kinetically, rather than thermodynamically, controlled.

Key words: photochemistry, radical ions, electron transfer, alkyl fluorides, nucleophilic addition.

Résumé : On a élargi le domaine d'application de la réaction photochimique de combinaison nucléophile–oléfine avec substitution aromatique («photo-NOCAS») de façon à inclure l'anion fluorure comme nucléophile. Utilisant le 2,3-diméthylbut-2-ène et le 2-méthylbut-2-ène comme oléfine pour la réaction, on a obtenu des rendements modérés de fluoroalcanes substitués par le 4-cyanophényle. Les rendements ont été inférieurs avec le 2-méthylpropène et on n'a observé aucun produit «photo-NOCAS» lorsqu'on a utilisé des diènes comme oléfines. On peut expliquer la sélectivité de l'anion fluorure pour les alcènes en termes du concept des acides et des bases dures et molles. On peut décrire la régiochimie de cette réaction à l'aide du mode d'addition *anti*-Markovnikov. L'anion s'additionne d'une façon préférentielle à l'extrémité la moins substituée par des groupes alkyles du cation radical d'un alcène non symétrique; ceci conduit à la formation préférentielle du radical β-fluoroalkyle le plus substitué. On a fait appel à des calculs d'orbitales moléculaires ab initio (MP2/6-31G*//HF/6-31G*) pour déterminer les stabilités relatives des radicaux β-fluoroalkyles intermédiaires. Le radical β-fluoroalkyle le plus substitué n'est PAS le plus stable. L'étape d'addition est contrôlée d'une façon cinétique plutôt que d'une façon thermodynamique.

Mots clés : photochimie, ions radicaux, transfert d'électron, fluorures d'alkyles, addition nucléophile.

[Traduit par la rédaction]

Introduction

Organofluorine compounds can be found in a variety of industrial applications. Some of these include lubricants, coatings, propellants, pharmaceuticals, blood substitutes, liquid crystals, and textile chemicals (1). One of the more important applications is isosteric replacement, the replacement of a hydrogen atom, hydroxyl group, or another halogen by a fluorine atom. The similarity in size of the fluorine and the hydrogen atom results in negligible steric effects, yet the significant difference in electronegativity produces pronounced effects on the electronic distribution within the molecule. These characteristics make isosteric replacement an ideal structural modification for altering the chemical and biological activities of organic compounds. For this reason, the selective formation of a carbon–fluorine bond has been, and continues to be, the focus of intensive research (2). In this paper, we report a highly selective, one-step synthesis for fluoroalkanes starting from simple alkenes. The fluoro-substituted compounds were obtained from the photochemical nucleophile–olefin combi-

Received August 6, 1997.

M.S.W. Chan and D.R. Arnold.[2] Department of Chemistry, Dalhousie University, Halifax, NS B3H 4J3, Canada.

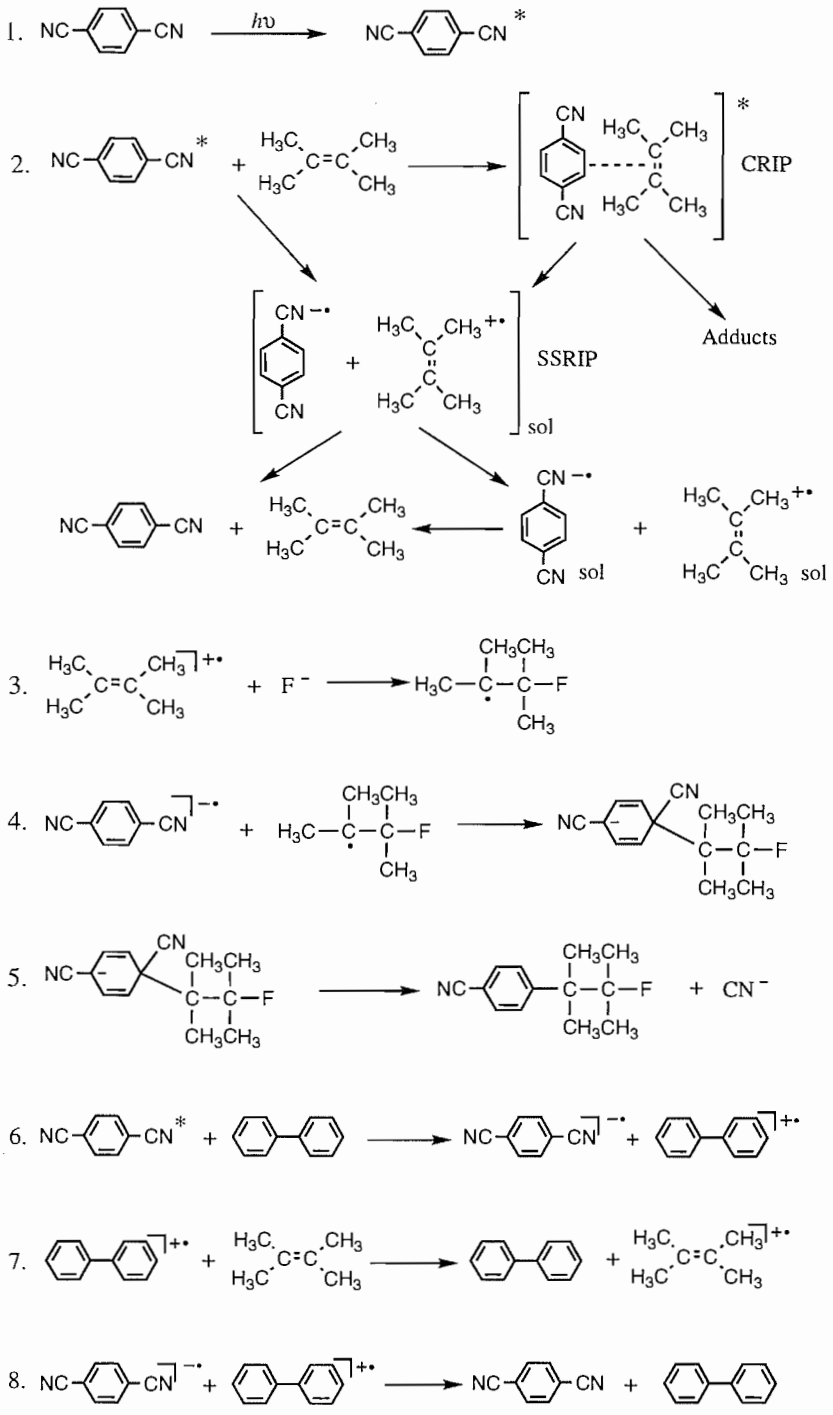
[1] This is also Part 45 of the series Radical Ions in Photochemistry. See ref. 3 for preceding parts of these series.

[2] Author to whom correspondence may be addressed. Telephone: (902) 494-3714. Fax: (902) 494-1310. E-mail: arnold@chem1.chem.dal.ca

© 1997 NRC Canada

Can. J. Chem. Downloaded from www.nrcresearchpress.com by 91.121.58.235 on 09/08/12
For personal use only.

Scheme 1. Mechanism for the photo-NOCAS reaction.



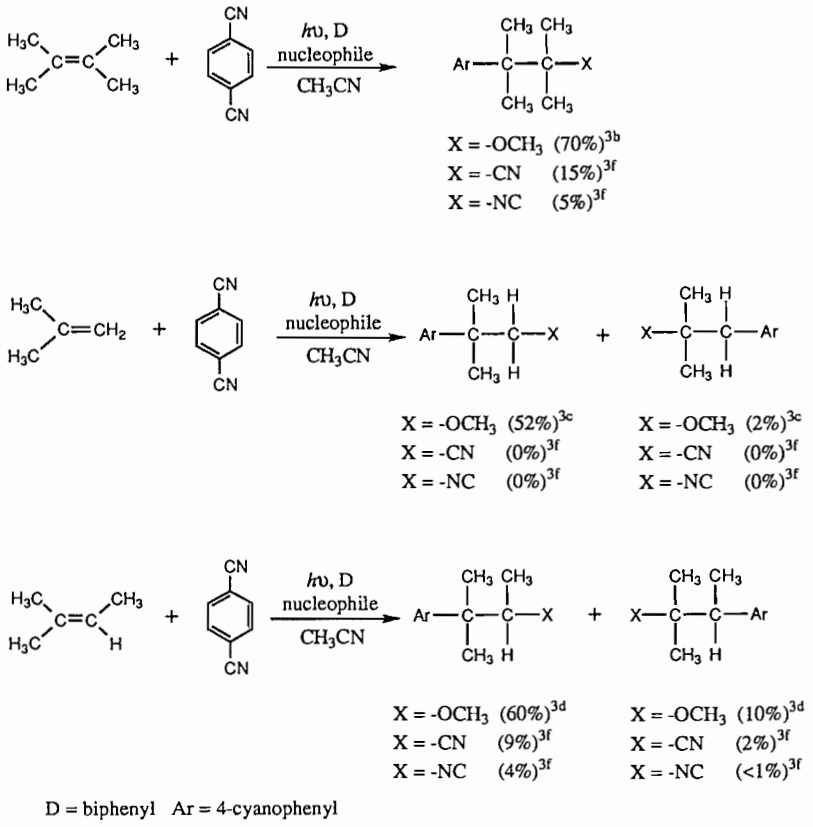
nation, aromatic substitution (photo-NOCAS) reaction with fluoride anion serving as the nucleophile.

The mechanism of the photo-NOCAS reaction had been analyzed and documented (3). The proposed mechanism for the reaction, using 2,3-dimethyl-2-butene as the olefin, is shown in Scheme 1. The scope and limitations of this reaction with regard to the olefin in combination with alcoholic nucleophiles have been extensively investigated; only recently has this study been extended to other nucleophiles (3*f*). Figure 1 summarizes the results of the reaction involving simple alkenes when methanol or cyanide anion serves as the nucleophile. The regiochemistry in all cases can be considered as predominately *anti*-Markovnikov, where the nucleophile adds to the less substituted carbon of the double bond. The reasons for this preference have also been rationalized (3*e*, *f*). In the case of methanol serving as the nucleophile, distonic radical cations that can equilibrate via a bridged structure are initially formed. The regiochemistry is thermodynamically controlled and the product distribution is dependent on the stability of the β-alkoxyalkyl radical intermediates (Scheme 1, step 3). When

© 1997 NRC Canada

Can. J. Chem. Downloaded from www.nrcresearchpress.com by 91.121.58.235 on 09/08/12
For personal use only.

Fig. 1. Isolated yields of photo-NOCAS products.



cyanide anion reacts as the nucleophile, the β-cyano or β-isocyano alkyl radicals cannot bridge, the regiochemistry is kinetically controlled, and steric factors dominate. Similar experimental and theoretical investigation of the photo-NOCAS reaction with fluoride anion serving as the nucleophile will be described. The olefins chosen for this study were 2,3-dimethyl-2-butene (**1**), 2-methylpropene (**2**), and 2-methyl-2-butene (**3**).

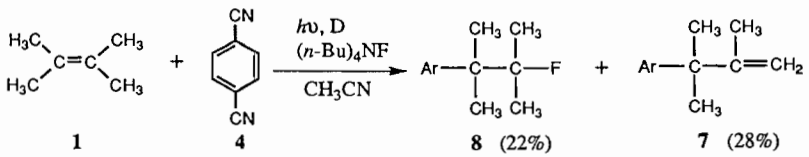
Results

Irradiation of an acetonitrile solution of 1,4-dicyanobenzene (**4**), biphenyl (**5**), tetrabutylammonium fluoride (**6**), and 2,3-dimethyl-2-butene (**1**) resulted in one major 1:1 (alkene:1,4-dicyanobenzene) adduct and one photo-NOCAS product (Reaction [1]). The 1:1 adduct, 3-(4-cyanophenyl)-2,3-dimethyl-1-butene (**7**), was obtained in 28% yield. The yield of the photo-NOCAS product, 3-(4-cyanophenyl)-2-fluoro-2,3-dimethylbutane (**8**), was 22%. The addition of the codonor, biphenyl, increased the efficiency of the reaction, but had no affect on the relative amounts of these reaction products.

The photo-NOCAS reaction of 2,3-dimethyl-2-butene (**1**) was also attempted using potassium fluoride as the fluoride ion source. These irradiations were identical to the ones involving **6** with the exception that an equal molar amount of KF and 18-crown-6 was added instead. The use of KF as a source of fluoride ion did not affect the identity of the products, but significantly more 1:1 (alkene: 1,4-dicyanobenzene) adducts were observed. For this reason, tetrabutylammonium fluoride (**6**) was used in the subsequent large-scale reactions to improve the yield of the photo-NOCAS products.

A similar irradiation of an acetonitrile solution of **4**, **5**, **6**, and 2-methylpropene (**2**) resulted in a 1:1 (alkene:1,4-dicyanobenzene) adduct and two photo-NOCAS products (Reaction [2]). The 1:1 adduct, 3-(4-cyanophenyl)-2-methylpropene (**9**), was obtained in 8% yield. The *anti*-Markovnikov photo-NOCAS product, 2-(4-cyanophenyl)-1-fluoro-2-methylpropane (**10**), was isolated in 5% yield. A trace amount of the Markovnikov isomer, 1-(4-cyanophenyl)-2-fluoro-2-methylpropane, was identified (gc/ms, ^{1}H and ^{13}C nmr) but it was not isolated. Integration of a gc/ms chromatograph obtained from single ion monitoring for the molecular ion

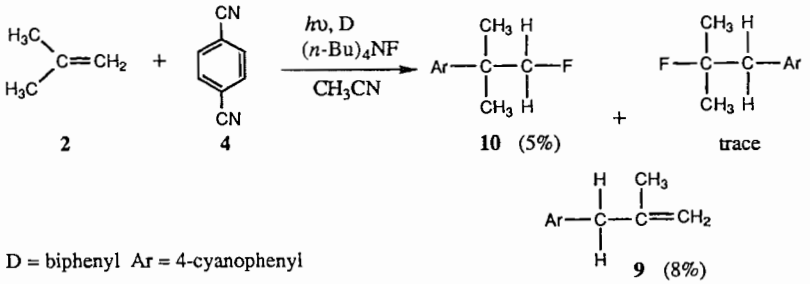
Reaction [1]



Can. J. Chem. Downloaded from www.nrcresearchpress.com by 91.121.58.235 on 09/08/12
For personal use only.

© 1997 NRC Canada

Reaction [2]



Reaction [3]

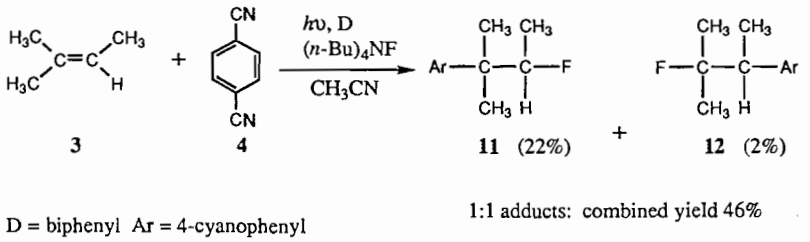


Table 1. Calculated enthalpy change for reaction 2b as a function of theoretical model.

Theoretical model	2-Fluoro-2-methylpropane (au)	1-Fluoro-2-methylpropane (au)	ΔH (kJ/mol)
HF/6-31G*//HF/6-31G*	−256.159 00	−256.148 10	28.62
MP2/6-31G*//HF/6-31G*	−256.855 96	−256.842 52	35.29
MP2/6-31G*//MP2/6-31G*	−256.857 00	−256.843 76	34.76
MP2/6-311+G*//MP2/6-31G*	−256.988 41	−256.975 13	34.87

gave a ratio of 95: 5 (*anti*-Markovnikov:Markovnikov) for the two photo-NOCAS products. This ratio remained constant as a function of irradiation time. Again, the addition of the codonor, biphenyl, increased the efficiency of the reaction, but did not have any affect on the product ratios.

The stability of the radical intermediates resulting from the reaction of the 2-methylpropene radical cation with fluoride anion was estimated by ab initio molecular orbital calculations. The relevant isodesmic reactions, along with enthalpy changes calculated from MP2/6-31G*//HF/6-31G* energies, are shown in Fig. 2. The isodesmic reaction 2a is a direct comparison of the two β-fluoroalkyl radical intermediates resulting from the Markovnikov (**2a**·) and *anti*-Markovnikov (**2b**·) modes of addition. Reactions 2b and 2c separate the effect of alkyl substitution on the fluoro and radical moiety, respectively. The sum of these two reactions shows the combined effect of the two factors on the overall stability of the β-fluoroalkyl radicals (reaction 2d). The isodesmic reaction 2e is an alternative way of separating these two effects. β-Fluoroalkyl radicals do not show a tendency to bridge (4), and the results of the calculations were consistent with this. Geometry optimization starting from a symetrically bridged radical converged to the more stable open radical (**2a**·).

The calculated thermodynamic stability of fluoro-substituted compounds has not been extensively investigated, and the question of an appropriate theoretical model to evaluate the enthalpy changes of these isodesmic reactions should be addressed. Therefore, the influence of the theoretical model on the ΔH of reaction 2b was examined and the results are summarized in Table 1.

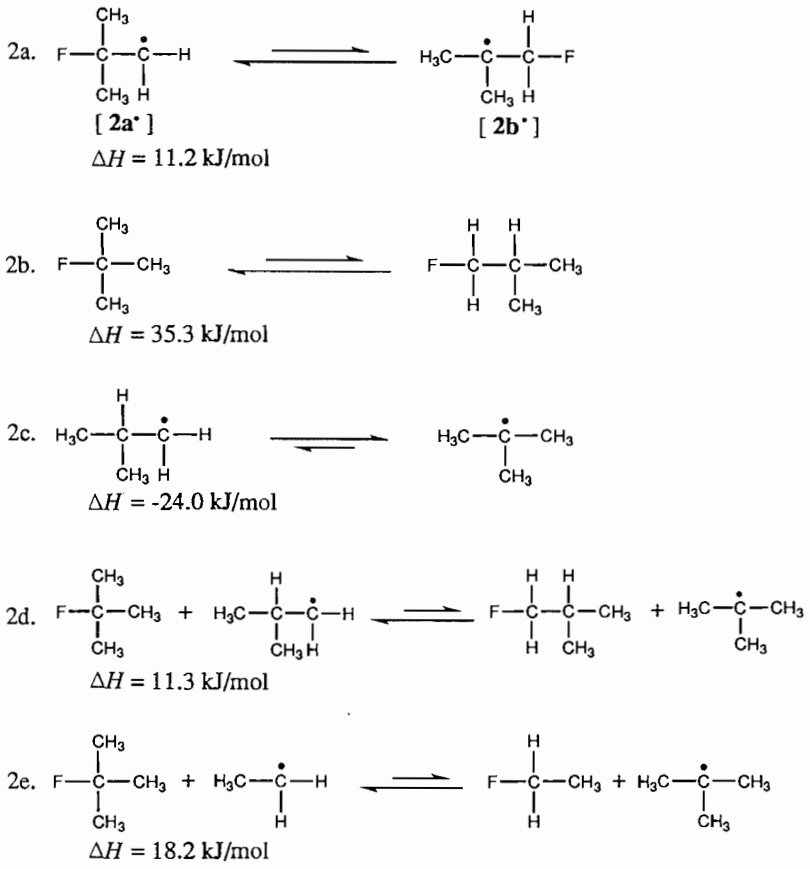
Irradiation of an acetonitrile solution of **4**, **5**, **6**, and 2-methyl-2-butene (**3**) resulted in four 1:1 (alkene:1,4-dicyanobenzene) adducts and two photo-NOCAS products (Reaction [3]). The combined yield of the four 1:1 adducts was 46%. The *anti*-Markovnikov photo-NOCAS product, 3-(4-cyanophenyl)-2-fluoro-3-methylbutane (**11**), was isolated in 22% yield; whereas the Markovnikov product, 3-(4-cyanophenyl)-2-fluoro-2-methylbutane (**12**), was obtained in only 2% yield. The ratio of *anti*-Markovnikov to Markovnikov prod-

[3] The total energies, selected geometrical parameters, charge and spin distributions of all species in this figure are available as supplementary material, and can be purchased from: The Depository of Unpublished Data, Document Delivery, CISTI, National Research Council Canada, Ottawa, Canada K1A 0S2.

Can. J. Chem. Downloaded from www.nrcresearchpress.com by 91.121.58.235 on 09/08/12
For personal use only.

© 1997 NRC Canada

Fig. 2. Isodesmic reactions for 2-methylpropene reaction intermediates.[3]



ucts was found to be 89:11 by integration of a gc/ms chromatograph obtained by single ion monitoring for the molecular ion. This ratio is independent of irradiation time. The addition of a codonor, biphenyl, increased the efficiency of the reaction but had no effect on the product ratios.

The stability of the radical intermediates for this reaction was also evaluated by ab initio molecular orbital calculations. Figure 3 shows the relevant isodesmic reactions and their enthalpy changes. The analysis for this alkene is identical to that described above for the 2-methylpropene reaction. Again, there was no evidence for bridging of the β-fluoroalkyl radical intermediate for this alkene.

The feasibility of the photo-NOCAS reaction with fluoride anion serving as the nucleophile and conjugated dienes serving as the olefin was also investigated. The dienes chosen for this study were 1,3-butadiene, 2-methyl-1,3-butadiene, 4-methyl-1,3-pentadiene, 2,4-dimethyl-1,3-pentadiene, and 2,5-dimethyl-2,4-hexadiene. Irradiation of an acetonitrile solution of 1,4-dicyanobenzene (**4**), biphenyl (**5**), diene, and tetrabutylammonium fluoride (**6**) did not result in any photo-NOCAS products. The mass spectrum obtained from the gc/ms chromatographs of these reaction mixtures suggested that 1:1 (diene:1,4-dicyanobenzene) adducts and dimers of the dienes were the major products.

Discussion

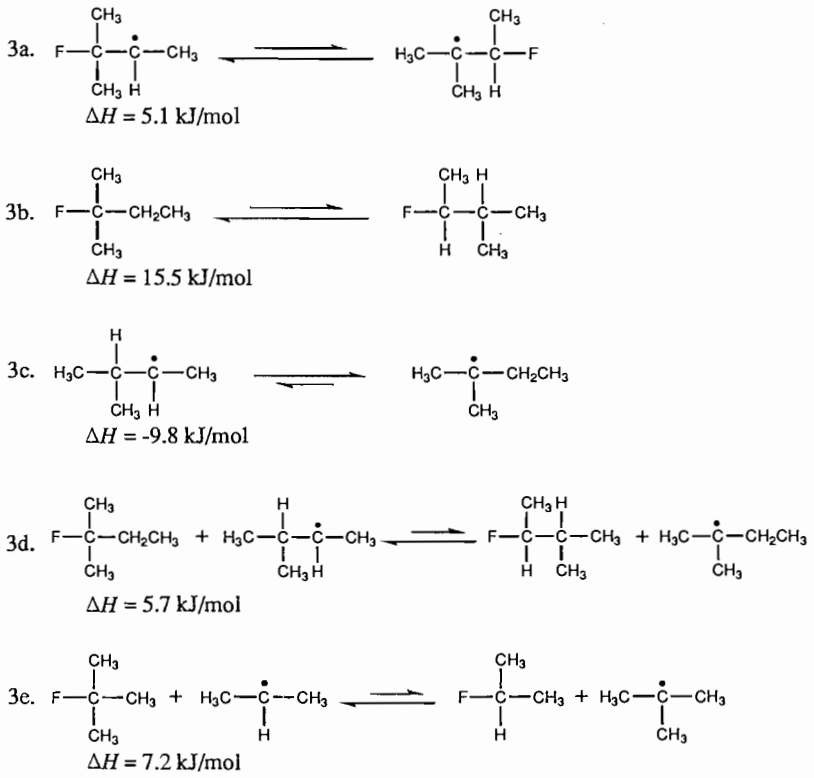
The results of this study illustrate that the photo-NOCAS reaction with fluoride anion serving as the nucleophile is feasible. The photo-NOCAS products incorporating fluoride anion were obtained in reasonable yields with little attempt to optimize the reaction conditions. The fluoride anion has been shown to react as a nucleophile (n_{CH_3I} = 2.7) (5) and as a base (pK_a of HF = 3.2) (6). Therefore, it is not surprising that deprotonation of the alkene radical cation, where the fluoride anion behaves as a base rather than a nucleophile, is a major competing reaction. In fact, the 1:1 adducts resulting from the coupling of the allylic radical and the radical anion of 1,4-dicyanobenzene (Scheme 1, step 10) were the major product(s) in all of the reactions studied. This type of adduct is commonly observed when irradiations are carried out in the absence of a nucleophile (3*a*,*b*). Even though radical cations are known to be highly acidic species (7), there is direct evidence that the fluoride anion enhances the deprotonation step. The radical cation of 2-methylpropene does not deprotonate easily; the resultant allylic radical is primary on both ambident ends (Scheme 1, step 9). The 1:1 adduct (**9**) resulting from the deprotonation of the radical cation followed by coupling with the radical anion of the 1,4-dicyanobenzene is only observed in trace amounts in the absence of added base (8). The fluoride anion reacting as a base is also the major competing pathway in the preparation of alkyl fluorides by normal (S_N1, S_N2) nucleophilic substitution (5*b*, 9).

The addition of fluoride anion to the radical cation of unsymmetrical alkenes shows high regioselectivity. The regiochemistry can be described as predominately following the *anti*-Markovnikov mode of addition, where the nucleo-

Can. J. Chem. Downloaded from www.nrcresearchpress.com by 91.121.58.235 on 09/08/12
For personal use only.

© 1997 NRC Canada

Fig. 3. Isodesmic reactions for 2-methyl-2-butene reaction intermediates.[3]



phile (fluoride) adds preferentially to the less substituted olefinic carbon to produce the more heavily alkyl-substituted radical. At this point, one may be tempted to conclude that the regioselectivity is governed by the relative stability of the β-fluoroalkyl radical intermediates. However, the theoretical calculations show that this is not the case. For both unsymmetrical alkenes studied, the radical resulting from the Markovnikov addition of fluoride is the more stable of the two alternative β-fluoroalkyl radicals (isodesmic reactions 2a and 3a). Nucleophilic addition to the alkene radical cation is highly exothermic, this results in an early transition state, and the product distribution is determined before the relative stability of the alternative intermediate radicals becomes important. These experimental and theoretical results indicate that the fluoride anion behaves like the cyanide anion: the addition is kinetically controlled, steric and polar factors dominate.

Contrary to expected trends, the ab initio molecular orbital calculations indicate that the primary radical (**2a**·) is 11 kJ/mol more stable than the tertiary radical (**2b**·) (isodesmic reaction 2a). The validity of the level of theory employed for these calculations is a question that should be addressed. The MP2/6-31G*//HF/6-31G* theoretical model was shown to be sufficient for estimating the relative stability of ethers (3*e*) and alkyl radicals (the ΔH of reaction 2c is −15.9 kJ/mol calculated from experimentally determined heats of formation (10)). However, there is little information with regard to fluoro-substituted compounds. Calculations on fluorinated aromatic compounds suggest that electron correlation and diffuse functions were not important for evaluating the enthalpy change of isodesmic reactions (11). The isodesmic reaction 2b compares the relative stability of a primary and a tertiary fluoro-substituted alkane. The enthalpy change of this reaction was calculated at various theoretical levels, and the results are reported in Table 1. Including electron correlation (MP2) in the form of single-point energy calculations produces notable differences in the ΔH value. However, including electron correlation in the optimization procedure and further increasing the basis set to 6-311+G* in the single-point calculations did not change the ΔH value significantly. These results suggest that the MP2/6-31G*//HF/6-31G* level of theory is sufficient for estimating the relative stability of fluoro-substituted compounds using isodesmic reactions.

The relative stabilities of the β-fluoroalkyl radicals were further investigated by calculating the enthalpy change of isodesmic reactions 2b–2e and 3b–3e. Reaction 2b indicates that a tertiary substituted fluoroalkane is 35 kJ/mol more stable than a primary substituted fluoroalkane, whereas a tertiary alkyl radical is more stable than a primary alkyl radical by only 24 kJ/mol (reaction 2c). Obviously the effect of the fluoro substitutent dominates when the two effects are combined (reaction 2d). The isodesmic reaction 2e is an alternative method of separating these two effects. The general agreement between reactions 2a, 2d, and 2e is reassuring. In the case of 2-methyl-2-butene, the comparison is now between a secondary β-fluoroalkyl radical and a tertiary β-fluoroalkyl radical. Still, the effect of the fluoro substitutent dominates: the secondary radical is more stable than the tertiary radical by 5 kJ/mol (isodesmic reaction 3a). The energy difference between a secondary and a tertiary alkyl radical is 10 kJ/mol (reaction 3c), and that between a secondary and tertiary substituted fluoro-

Can. J. Chem. Downloaded from www.nrcresearchpress.com by 91.121.58.235 on 09/08/12
For personal use only.

© 1997 NRC Canada

alkane is 16 kJ/mol (reaction 3b). The sum of these two reactions (reaction 3d) agrees well with the relative stability of the two β-fluoroalkyl radicals (reaction 3a). The tendency for fluoro substituents to cause abnormal behavior as compared to their hydrocarbon analogs has been well documented and this effect has been used to advantage in organic synthesis and mechanistic studies (12).

The attempted photo-NOCAS reaction with fluoride anion reacting as the nucleophile did not result in the desired products when conjugate dienes were employed as the olefin. This behavior is related to that observed when cyanide anion was used as the nucleophile. The nitrogen atom of the ambident cyanide anion reacts as a nucleophile to produce isonitrile products only with alkenes. No trace of the isonitrile products were found when conjugate dienes were used. This selectivity was explained in terms of the hard–soft-acid–base (HSAB) principle. The fluoride anion falls into the hard category (13). Relatively speaking, the radical cations of alkenes can be considered as harder than those of conjugated dienes. Therefore, the hard fluoride anion nucleophile prefers to react with hard alkene radical cations. The photo-NOCAS reaction incorporating fluoride as the nucleophile is then limited to hard electrophiles.

Conclusions

The fluoride anion can serve as an effective nucleophile in the photo-NOCAS reaction. The 4-cyanophenyl substituted fluoroalkanes were obtained in reasonable yields with monoalkenes. The reaction is not effective with conjugated dienes. This reactivity can be explained in terms of the HSAB principle; the hard fluoride anion prefers to react with the relatively harder alkene radical cation.

The reaction is regioselective, with the fluoride anion adding preferentially to the less substituted end of an unsymmetrical alkene. The product ratios are not a reflection of the relative stability of the alternative β-fluoroalkyl radical intermediates; the addition is kinetically controlled, and the product ratio is determined before the relative stability of the resulting radicals becomes important; steric and polar effects dominate.

The degree of alkyl substitution on the carbon atom bearing the fluorine substituent produces substantial differences in stability. This can be attributed to the highly electronegative nature of the fluorine atom. In fact, the effect of alkyl substitution on a fluoroalkane is larger than on a carbon radical center. Consequently the more heavily substituted β-fluoroalkyl radical in not the more stable of the two possible intermediates for the unsymmetrical alkenes studied.

Computational details

The GAUSSIAN 94 package of programs (14) was employed for all ab initio molecular orbital calculations. The geometries of the open-shell systems were fully optimized at the unrestricted Hartree–Fock level with the 6-31G* basis set.[4] Single-point energies were calculated to second order in Møller–Plesset perturbation theory (MP2) (16) using the 6-31G* basis set at the HF/6-31G* optimized geometries, and were corrected for spin contamination where appropriate. Unless otherwise noted, all of the structures were optimized using the Berny optimization procedure (17) without symmetry constraints and were confirmed, by harmonic frequency analyses, to be minima on their respective potential energy surfaces. The charge and spin density distributions were obtained from Mulliken population analysis (18).

Experimental

General information

Progress of the reactions was monitored by using a Hewlett–Packard (HP) 5890 gas chromatograph with a BD-1701 fused silica WCOT column (20 m × 0.25 mm, 0.4 μm film thickness) and a flame ionization detector (gc/fid). An HP 3392A integrator is interfaced with the gc/fid to obtain peak areas. An HP 5890 gas chromatograph with a 5% phenyl methyl silicone fused silica WCOT column (25 m × 0.20 mm, 0.33 μm film thickness) interfaced with an HP 5970 mass selective detector (gc/ms) was also used for product analysis. Exact Mass determinations were obtained using a CEC 21-110 mass spectrometer. The mass spectra are reported as *m/z* (relative intensity). The ^{1}H and ^{13}C nmr spectra were obtained from a Bruker 250 or 400 MSL spectrometer. Spectra were recorded in parts per million and frequencies are relative to tetramethylsilane. Infrared spectra (ir) were recorded on a Nicolet 205 spectrometer and are reported in wave numbers (cm^{-1}). Separation of the reaction mixtures was carried out using a combination of the following chromatographic methods: preparative, centrifugally accelerated, radial, thin-layer chromatography (chromatotron),[5] using 1, 2, or 4 mm plates prepared with thin-layer chromatography (tlc) grade silica gel (with binder and fluorescent indicator, Merck 7749); dry column flash chromatography (dcfc) (19) packed with tlc grade silica gel (with binder, Rose Scientific Ltd. 81632); preparative thin-layer chromatography using precoated silica gel plates (2 mm thickness, Merck 5717).

Materials

Acetonitrile was distilled twice, first from sodium hydride and then from phosphorus pentoxide. It was then passed through a column of basic alumina, refluxed over calcium hydride for 24 h (under a nitrogen atmosphere), fractionally distilled, and stored over 3Å molecular sieves. 1,4-Dicyanobenzene (Aldrich) was purified by treatment with activated carbon in methylene chloride, followed by recrystallization from 95% ethanol. Biphenyl was recrystallized three times from methanol before use. Tetrabutylammonium fluoride (Aldrich) was dried at 55°C under vacuum for 24 h just prior to use. 2-Methylpropene (Matheson), 2,3-dimethyl-2-butene (Aldrich), and 2-methyl-2-butene (Aldrich) were used as received.

Irradiations

Irradiations were carried out on acetonitrile solutions of 1,4-dicyanobenzene (**4**), the alkene, tetrabutylammonium fluoride (**6**), and biphenyl (**5**) (serving as a codonor). These solutions were irradiated in either 2 cm inner diameter Pyrex tubes or

[4] For an in-depth discussion of theoretical methods and basis sets see ref. 15.

[5] Purchased from Harrison Research, Palo Alto, Calif.

© 1997 NRC Canada

Can. J. Chem. Downloaded from www.nrcresearchpress.com by 91.121.58.235 on 09/08/12
For personal use only.

Can. J. Chem. Downloaded from www.nrcresearchpress.com by 91.121.58.235 on 09/08/12
For personal use only.

5 mm Pyrex nmr tubes, which were degassed by either nitrogen or alkene ebullition. The samples were irradiated at 10°C using a CGE 1 kW medium-pressure mercury vapor lamp contained in a water-cooled quartz immersion well. The yields of the reaction products were calculated based on the amount of 1,4-dicyanobenzene consumed.

Reaction of 2,3-dimethyl-2-butene with 1,4-dicyanobenzene and tetrabutylammonium fluoride

A solution of 1,4-dicyanobenzene (**4**) (1.0401 g, 0.0081 mol), biphenyl (**5**) (1.2151 g, 0.0079 mol), and tetrabutylammonium fluoride (**6**) (3.7161 g, 0.014 mol) in acetonitrile (160 mL) was degassed by nitrogen ebullition. 2,3-Dimethyl-2-butene (**1**) (2.0 mL, 0.017 mol) was added to the reaction mixture, and the solution was irradiated for 24.0 h. Removal of the solvent yielded the crude photolysate. Initial separation of the irradiation mixture was achieved by dcfc using an ether–hexanes gradient. Further purification of the products 3-(4-cyanophenyl)-2,3-dimethyl-1-butene (**7**) and 3-(4-cyanophenyl)-2-fluoro-2,3-dimethylbutane (**8**) was carried out by repeated chromatography (chromatotron) using 100% hexanes as the eluant. Final separation of the 1:1 (alkene:1,4-dicyanobenzene) adduct from the fluoride adduct was achieved by preparative tlc using a 2.5% ether – hexanes gradient (developed twice).

3-(4-Cyanophenyl)-2,3-dimethyl-1-butene (7)

The yield of **7** was 28%. The ^{1}H nmr spectrum agrees well with previously reported results (3*a*): ^{1}H nmr (250.13 MHz, $CDCl_3$) δ_{TMS}: 1.43 (s, 6H, H's of methyl groups adjacent to aryl-substituted carbon), 1.50 (s, 3H, H's of vinylic methyl group), 4.94 (d, 1H, $^2J_{H\text{-}H}$ = 1.2 Hz, vinylic hydrogen), 5.01 (d, 1H, $^2J_{H\text{-}H}$ = 1.2 Hz, vinylic hydrogen), 7.41 (d, 2H, $^3J_{H\text{-}H}$ = 8.5 Hz, H's adjacent to alkyl-substituted aryl carbon), 7.58 (d, 2H, $^3J_{H\text{-}H}$ = 8.5 Hz, H's adjacent to cyano-substituted aryl carbon); ^{13}C nmr (62.90 MHz, $CDCl_3$) δ: 20.09 (q, vinylic methyl group), 28.08 (q, methyl groups adjacent to aryl-substituted carbon), 44.42 (s, aryl-substituted carbon), 109.61 (s, quaternary aryl carbon, cyano substituted), 110.78 (t, terminal olefinic carbon), 119.13 (s, CN), 126.98 (d, aromatic CH adjacent to alkyl-substituted aryl carbon), 132.02 (d, aromatic CH adjacent to cyano-substituted aryl carbon), 151.08 (s, quaternary aryl carbon, alkyl substituted), 154.15 (s, alkyl-substituted olefinic carbon).

3-(4-Cyanophenyl)-2-fluoro-2,3-dimethylbutane (8)

The yield of **8** was 22%: infrared (Nicolet 205) ν: 2989(s), 2229(s), 1608(m), 1506(m), 1474(m), 1377(s), 1098(m), 844(s); ^{1}H nmr (250.13 MHz, $CDCl_3$) δ_{TMS}: 1.22 (d, 6H, $^3J_{H\text{-}F}$ = 22.0 Hz, H's of methyl groups adjacent to fluoro-substituted carbon), 1.42 (s, 6H, H's of methyl groups adjacent to aryl-substituted carbon), 7.55 (d, 2H, $^3J_{H\text{-}H}$ = 9.1 Hz, H's adjacent to alkyl-substituted aryl carbon), 7.60 (d, 2H, $^3J_{H\text{-}H}$ = 9.1 Hz, H's adjacent to cyano-substituted aryl carbon); ^{13}C nmr (62.90 MHz, $CDCl_3$) δ: 23.59 (q, d, $^2J_{C\text{-}F}$ = 24.8 Hz, methyl groups adjacent to fluoro-substituted carbon), 24.14 (q, d, $^3J_{C\text{-}F}$ = 5.7 Hz, methyl groups adjacent to aryl-substituted carbon), 45.12 (s, d, $^2J_{C\text{-}F}$ = 20.0 Hz, aryl-substituted carbon), 98.74 (s, d, $^1J_{C\text{-}F}$ = 175.5 Hz, fluoro-substituted carbon), 109.99 (s, quaternary aryl carbon, cyano substituted), 119.04 (s, CN), 128.80 (d, aromatic CH adjacent to alkyl-substituted aryl carbon), 131.31 (d, aromatic CH adjacent to cyano-substituted aryl carbon), 151.61 (s, quaternary aryl carbon, alkyl substituted); ms *m/z*: 40(25), 61(7), 116(30), 130 (20), 144(100), 145(95), 205(1). Exact Mass calcd. for $C_{13}H_{16}FN$: 205.1267; found: 205.1262.

Reaction of 2-methylpropene with 1,4-dicyanobenzene and tetrabutylammonium fluoride

2-Methylpropene (**1**) was bubbled into a solution of 1,4-dicyanobenzene (**4**) (1.5572 g, 0.012 mol), biphenyl (**5**) (1.9684 g, 0.013 mol), and tetrabutylammonium fluoride (**6**) (3.8249 g, 0.015 mol) in acetonitrile (240 mL). This reaction mixture was irradiated for 50.5 h. The solvent was then removed to afford the crude photolysate. Initial separation of the reaction mixture was achieved by dcfc using a solvent gradient of hexanes and ether. 1,4-Dicyanobenzene (**4**) (0.9318 g, 0.0073 mol) was recovered in this manner (40% conversion). Subsequent purification of the products 3-(4-cyanophenyl)-2-methylpropene (**9**) and 2-(4-cyanophenyl)-1-fluoro-2-methylpropane (**10**) was carried out by repeated chromatography (chromatotron) with 100% hexanes and 0.25% ether – hexanes as eluants, respectively.

A trace amount of 1-(4-cyanophenyl)-2-fluoro-2-methylpropane was also detected. Evidence for this compound consisted of a doublet at 2.95 ppm ($^3J_{H\text{-}F}$ = 21.7 Hz) in the ^{1}H nmr spectrum, indicative of the aryl-substituted methylene group, and, a doublet at 26.69 ppm ($^2J_{C\text{-}F}$ = 24.8 Hz) in the ^{13}C nmr spectrum, indicative of methyl groups adjacent to a fluoro-substituted carbon. Integration of a gc/ms chromatograph obtained from single-ion monitoring mode for the molecular ion (*m/z* = 177) gave a ratio of 95:5 (*anti*-Markovnikov: Markovnikov) for the two photo-NOCAS products.

3-(4-Cyanophenyl)-2-methylpropene (9)

The yield of **9** was 8%: ^{1}H nmr (250.13 MHz, $CDCl_3$) δ_{TMS}: 1.66 (s, 3H, CH_3), 3.36 (s, 2H, methylene group), 4.72 (s, 1H, vinylic hydrogen), 4.86 (s, 1H, vinylic hydrogen), 7.29 (d, 2H, $^3J_{H\text{-}H}$ = 8.5 Hz, H's adjacent to alkyl-substituted aryl carbon), 7.58 (d, 2H, $^3J_{H\text{-}H}$ = 8.5 Hz, H's adjacent to cyano-substituted aryl carbon); ^{13}C nmr (62.90 MHz, $CDCl_3$) δ: 22.06 (q, CH_3), 44.64 (t, aryl-substituted methylene carbon), 110.07 (s, quaternary aryl carbon, cyano substituted), 113.23 (t, terminal olefinic carbon), 119.09 (s, CN), 129.71 (d, aromatic CH adjacent to alkyl-substituted aryl carbon), 132.16 (d, aromatic CH adjacent to cyano-substituted aryl carbon), 143.56 (s), 145.44 (s). These spectral data agree well with previously reported results (20).

2-(4-Cyanophenyl)-1-fluoro-2-methylpropane (10)

The yield of **10** was 5%: infrared (Nicolet 205) ν: 2974(s), 2898(m), 2229(s), 1608(m), 1507(m), 1473(m), 1370(m), 1020(s), 839(s); ^{1}H nmr (250.13 MHz, $CDCl_3$) δ_{TMS}: 1.37 (d, 6H, $^4J_{H\text{-}F}$ = 1.8 Hz, H's of methyl groups), 4.38 (d, 2H, $^2J_{H\text{-}F}$ = 47.6 Hz, H's of fluoro-substituted methylene group), 7.49 (d, 2H, $^3J_{H\text{-}H}$ = 8.5 Hz, H's adjacent to alkyl-substituted aryl carbon), 7.63 (d, 2H, $^3J_{H\text{-}H}$ = 8.5 Hz, H's adjacent to cyano-substituted aryl carbon); ^{13}C nmr (62.90 MHz, $CDCl_3$) δ: 24.61 (q, d, $^3J_{C\text{-}F}$ = 5.8 Hz, methyl groups), 39.81 (s, d, $^2J_{C\text{-}F}$ = 18.1 Hz, aryl-substituted carbon), 90.65 (t, d, $^1J_{C\text{-}F}$ = 178.0 Hz, fluoro-substituted carbon), 110.35 (s, quaternary aryl carbon, cyano substituted), 118.86 (s, CN), 127.02 (d, aromatic CH adjacent to alkyl-substituted aryl carbon), 132.12 (d, aromatic

© 1997 NRC Canada

Can. J. Chem. Downloaded from www.nrcresearchpress.com by 91.121.58.235 on 09/08/12
For personal use only.

CH adjacent to cyano-substituted aryl carbon), 151.13 (s, d, $^3J_{C\text{-}F}$ = 2.9 Hz, quaternary aryl carbon, alkyl substituted); ms *m/z*: 38(13), 40(12), 116(48), 144(100), 145(17), 177(32). Exact Mass calcd. for $C_{11}H_{12}FN$: 177.0954; found: 177.0955.

Reaction of 2-methyl-2-butene with 1,4-dicyanobenzene and tetrabutylammonium fluoride

A solution of 1,4-dicyanobenzene (**4**) (1.6289 g, 0.013 mol), biphenyl (**5**) (1.8685 g, 0.012 mol), and tetrabutylammonium fluoride (**6**) (6.1549 g, 0.024 mol) in acetonitrile (240 mL) was degassed by nitrogen ebullition. 2-Methyl-2-butene (**3**) (3.0 mL, 0.028 mol) was added to the reaction mixture, and the solution was irradiated for 24.0 h. Removal of the solvent yielded the crude photolysate. Initial separation of the irradiation mixture was achieved by dcfc using an ether–hexanes gradient. 1,4-Dicyanobenzene (**4**) (0.4193 g, 0.0033 mol) was recovered in this manner (74% conversion). Four 1:1 adducts (combined yield of 46%) were also separated from the reaction mixture by dcfc. The identity of these products was deduced by the mass of the molecular ion (*m/z* = 171) and the fragmentation pattern in the mass spectrum. Subsequent purification of the fluoride adducts was carried out by repeated chromatography (chromatotron) using 100% hexanes as the eluant. Final separation of the two isomers was attempted by preparative tlc using a 1.0% ether – hexanes gradient (developed 12 times). Integration of a gc/ms chromatograph obtained from single-ion monitoring mode for the molecular ion (*m/z* = 191) gave a ratio of 89:11 (*anti*-Markovnikov: Markovnikov) for the two photo-NOCAS products.

*3-(4-Cyanophenyl)-2-fluoro-3-methylbutane (**11**)*

The yield of **11** was 22%: infrared (Nicolet 205) ν: 2985(s), 2924(m), 2229(s), 1608(m), 1507(m), 1453(m), 1382(m), 1067(s), 841(s); ^{1}H nmr (250.13 MHz, $CDCl_3$) δ_{TMS}: 1.10 (d, d, 3H, $^3J_{H\text{-}H}$ = 6.1 Hz, $^3J_{H\text{-}F}$ = 24.4 Hz, H's of methyl group adjacent to fluoro-substituted carbon), 1.38 (s, 6H, H's of methyl groups adjacent to aryl-substituted carbon), 4.66 (q, d, 1H, $^3J_{H\text{-}H}$ = 6.1 Hz, $^2J_{H\text{-}F}$ = 47.0 Hz, methine proton), 7.50 (d, 2H, $^3J_{H\text{-}H}$ = 8.5 Hz, H's adjacent to alkyl-substituted aryl carbon), 7.61 (d, 2H, $^3J_{H\text{-}H}$ = 8.5 Hz, H's adjacent to cyano-substituted aryl carbon); ^{13}C nmr (100.61 MHz, $CDCl_3$) δ: 16.23 (q, d, $^2J_{C\text{-}F}$ = 24.2 Hz, methyl groups adjacent to fluoro-substituted carbon), 24.07 (q, d, $^3J_{C\text{-}F}$ = 5.3 Hz, methyl group adjacent to aryl-substituted carbon), 24.25 (q, d, $^3J_{C\text{-}F}$ = 4.7 Hz, methyl group adjacent to aryl-substituted carbon), 42.83 (s, d, $^2J_{C\text{-}F}$ = 18.7 Hz, aryl-substituted carbon), 96.36 (s, d, $^1J_{C\text{-}F}$ = 176.5 Hz, fluoro-substituted carbon), 110.48 (s, quaternary aryl carbon, cyano substituted), 119.10 (s, CN), 127.89 (d, aromatic CH adjacent to alkyl-substituted aryl carbon), 132.10 (d, aromatic CH adjacent to cyano-substituted aryl carbon), 151.32 (s, quaternary aryl carbon, alkyl substituted); ms *m/z*: 47(2), 104(8), 116(35), 144(100), 145(10), 191(8). Exact Mass calcd. for $C_{12}H_{14}FN$: 191.1110; found: 191.1105.

*3-(4-Cyanophenyl)-2-fluoro-2-methylbutane (**12**)*

The yield of **12** was 2%. Spectral information obtained from a 7:3 (**12**:**11**) mixture: ^{1}H nmr (250.13 MHz, $CDCl_3$) δ_{TMS}: 1.26 (d, 6H, $^3J_{H\text{-}F}$ = 22.0 Hz, H's of methyl groups adjacent to fluoro-substituted carbon), 1.34 (d, 3H, $^3J_{H\text{-}H}$ = 7.3 Hz, H's of methyl group adjacent to aryl-substituted carbon), 2.96 (q, d, 1H, $^3J_{H\text{-}H}$ = 7.3 Hz, $^3J_{H\text{-}F}$ = 19.5 Hz, methine proton), 7.35 (d, 2H, $^3J_{H\text{-}H}$ = 8.3 Hz, H's adjacent to alkyl-substituted aryl carbon), 7.59 (d, 2H, $^3J_{H\text{-}H}$ = 8.3 Hz, H's adjacent to cyano-substituted aryl carbon); ^{13}C nmr (62.90 MHz, $CDCl_3$) δ: 15.57 (q, d, $^3J_{C\text{-}F}$ = 5.7 Hz, methyl group adjacent to aryl-substituted carbon), 24.90 (q, d, $^2J_{C\text{-}F}$ = 24.7 Hz, methyl group adjacent to fluoro-substituted carbon), 25.76 (q, d, $^2J_{C\text{-}F}$ = 24.8 Hz, methyl group adjacent to fluoro-substituted carbon), 49.08 (s, d, $^2J_{C\text{-}F}$ = 21.7 Hz, aryl-substituted carbon), 96.51 (s, d, $^1J_{C\text{-}F}$ = 172.1 Hz, fluoro-substituted carbon), 110.49 (s, quaternary aryl carbon, cyano substituted), 118.97 (s, CN), 129.67 (d, aromatic CH adjacent to alkyl-substituted aryl carbon), 131.85 (d, aromatic CH adjacent to cyano-substituted aryl carbon), 148.44 (s, quaternary aryl carbon, alkyl substituted); ms *m/z*: 61(90), 77(20), 103(27), 116(21), 129(19), 130(100), 156(34), 191(5).

Acknowledgments

This work was supported financially by the Natural Sciences and Engineering Research Council of Canada. We thank Drs. D.L. Hooper and M.D. Lumsden at the Atlantic Regional Magnetic Resonance Center at Dalhousie University for the high-field nmr spectra, Dr. R.J. Boyd for computer time, and Dr. J.-H. Kim for the Exact Mass measurements. M.S.W.C. is grateful for scholarships from the Natural Sciences and Engineering Research Council of Canada, the Izaak Walton Killam Memorial Foundation, and the Walter C. Sumner Foundation.

References

1. E.R. Banks, D.W.A. Sharp, and J.C. Tatlow (*Editors*). Fluorine: the first hundred years. Elsevier Sequoia, New York. 1986.
2. (*a*) O.A. Mascaretti. Aldrichimica Acta, **26**, 47 (1993); (*b*) J.A. Wilkinson. Chem. Rev. **92**, 505 (1992).
3. (*a*) D.R. Arnold, P.C. Wong, A.J. Maroulis, and T.S. Cameron. Pure Appl. Chem. **52**, 2609 (1980); (*b*) R.M. Borg, D.R. Arnold, and T.S. Cameron. Can. J. Chem. **62**, 1785 (1984); (*c*) D.R. Arnold and M.S. Snow. Can. J. Chem. **66**, 3012 (1988); (*d*) K.A. McManus and D.R. Arnold. Can. J. Chem. **73**, 2158 (1995); (*e*) D.R. Arnold, M.S.W. Chan, and K.A. McManus. Can. J. Chem. **74**, 2143 (1996); (*f*) D.R. Arnold, K.A. McManus, and M.S.W. Chan. Can. J. Chem. **75**, 1055 (1997).
4. (*a*) J.K. Kochi. Free radicals. Vol. II. John Wiley & Sons, Toronto. 1973, Chap. 26; (*b*) D.J. Edge and J.K. Kochi. J. Am. Chem. Soc. **94**, 6485 (1972); (*c*) Tetrahedron Lett. 2427 (1972).
5. (*a*) C.M. Sharts and W.A. Sheppard. Org. React. **21**, 125 (1974); (*b*) D.P. Cox, J. Terpinski, and W. Lawrynowicz. J. Org. Chem. **49**, 3216 (1984).
6. J.H. Clark. Chem. Rev. **80**, 429 (1980).
7. A.M.deP. Nicholas and D.R. Arnold. Can. J. Chem. **60**, 2165 (1982).
8. H.J.P. de Lijser and D.R. Arnold. J. Org. Chem. Submitted.
9. (*a*) J.M. Gerdes, R.N. Keil, A.T. Shulgin, and C.A. Mathis. J. Fluorine Chem. **78**, 121 (1996); (*b*) J.-I. Hayami, N. Ono, and A. Kaji. Tetrahedron Lett. 2727 (1970).
10. D.R. Lide (*Editor*). C.R.C. Handbook of chemistry and physics. 76th ed. (1995–1996). CRC Press, Inc., New York. 1995.
11. A. Skancke. *In* Fluorine-containing molecules: structure, reactivity, synthesis, and applications. *Edited by* J.F. Liebman, A. Greenberg, and W.R. Dolbier. VCH Publishers, Inc., New York. 1988. Chap. 3.
12. (*a*) W.R. Dolbier and H. Koroniak. *In* Fluorine-containing molecules: structure, reactivity, synthesis, and applications. *Edited by* J.F. Liebman, A. Greenberg, and W.R. Dolbier. VCH Publishers, Inc. New York. 1988. Chap. 4; (*b*) J.T. Welch and S.

© 1997 NRC Canada

Eswarakrishnan. *In* Fluorine-containing molecules: structure, reactivity, synthesis, and applications. *Edited by* J.F. Liebman, A. Greenberg, and W.R. Dolbier. VCH Publishers, Inc. New York. 1988. Chap. 7.
13. T.-L. Ho. Hard and soft acids and bases principle in organic chemistry. Academic Press, New York. 1977. Chap. 2.
14. M.J. Frisch, G.W. Trucks, H.B. Schlegel, P.M.W. Gill, B.G. Johnson, M.A. Robb, J.R. Cheeseman, T. Keith, G.A. Petersson, J.A. Montgomery, K. Raghavachari, M.A. Al-Laham, V.G. Zakrzewski, J.V. Ortiz, J.B. Foresman, J. Cioslowski, B.B. Stefanov, A. Nanayakkara, M. Challacombe, C.Y. Peng, P.Y. Ayala, W. Chen, M.W. Wong, J.L. Andres, E.S. Replogle, R. Gomperts, R.L. Martin, D.J. Fox, J.S. Binkley, D.J. Defrees, J. Baker, J.P. Stewart, M. Head-Gordon, C. Gonzalez, and J.A. Pople. GAUSSIAN 94, Revision B.2. Gaussian, Inc., Pittsburgh, Pa. 1995.
15. (*a*) W.J. Hehre, L. Radom, P.v.R. Schleyer, and J.A. Pople. *Ab initio* molecular orbital theory. Wiley–Interscience, New York. 1987; (*b*) P.C. Hariharan and J.A. Pople. Theor. Chim. Acta. **28**, 213 (1973).
16. C. Møller and M.S. Plesset. Phys. Rev. **46**, 618 (1934).
17. (*a*) H.B. Schlegel. J. Chem. Phys. **77**, 3676 (1982); (*b*) J. Comput. Chem. **3**, 214 (1982).
18. (*a*) R.S. Mulliken. J. Chem. Phys. **23**, 1833 (1955); (*b*) J. Chem. Phys. **23**, 1841 (1955).
19. L.H. Harwood. Aldrichimica Acta, **18**, 25 (1985).
20. K. Nakanishi, K. Mizuno, and Y. Otsuji. Bull. Chem. Soc. Jpn. **66**, 2371 (1993).

Can. J. Chem. Downloaded from www.nrcresearchpress.com by 91.121.58.235 on 09/08/12
For personal use only.

© 1997 NRC Canada

Generation and spectroscopic and kinetic characterization of methoxy-substituted phenoxyl radicals in solution and on paper[1]

D. Shukla, N.P. Schepp, N. Mathivanan, and L.J. Johnston

Can. J. Chem. Downloaded from www.nrcresearchpress.com by 91.121.58.235 on 09/08/12
For personal use only.

Abstract: A number of methoxy-substituted phenoxyl radicals have been generated and characterized by laser flash photolysis techniques in solution and on paper. The radicals have been produced by three routes in solution: hydrogen abstraction from phenols by *tert*-butoxyl radical, photolysis of α-aryloxyacetophenones, and direct excitation of phenols. Most of the phenoxyl radicals studied have a characteristic absorption near 400 nm; the *ortho*-substituted radicals have an additional broad absorption in the visible in non-hydroxylic solvents (e.g., 650 nm for 2-methoxyphenoxyl radical). The relative intensities of the 400 nm and the long-wavelength bands vary with substitution pattern and solvent, with the long wavelength band being much weaker in hydroxylic solvents. Direct excitation of phenols provides an alternate source of phenoxyl radicals in some cases. However, for 4-methoxyphenol there are overlapping absorptions due to triplet phenol and phenol radical cation, both of which absorb in the 400–460 nm region. The 4-methoxyphenol radical cation is formed in a biphotonic process and decays by deprotonation to give the phenoxyl radical. The 4-methoxyphenoxyl radical can also be generated on paper from either the ketone or phenol precursor and decays with complex kinetics that depend on the precursor loading and laser intensity. There is no evidence for the formation of significant amounts of long-lived ketone or phenol triplets on paper. The decay kinetics for the phenoxyl radical are modified by the addition of the radical scavenger dithioerythritol. The results indicate both static and dynamic components to the radical scavenging process. The generation of phenoxyl radicals on paper in the presence and absence of scavengers provides the basis for the development of a new method for screening potential photoyellowing inhibitors and understanding their mode of action.

Key words: phenoxyl radicals, paper photoyellowing, laser flash photolysis, triplets, radical cations.

Résumé : On a généré un certain nombre de radicaux phénoxyles substitués par des groupes méthoxyles et on les a caractérisés par les techniques de la photolyse laser éclair en solution et sur papier. On a produit les radicaux par trois méthodes en solution: utilisation du radical *tert*-butyloxyle pour l'enlèvement d'hydrogène à partir de phénols, la photolyse d'α-aryloxyacétophénones et l'excitation directe de phénols. La plupart des radicaux phénoxyles étudiés présentent une bande d'absorption caractéristique vers 400 nm; les radicaux substitués en *ortho* présentent en plus une large bande d'absorption dans le visible dans les solvants non hydroxyliques (environ 650 nm pour le radical 2-méthoxyphénoxyle). Les intensités relatives des bandes à 400 nm et à longueur d'onde plus élevée varient avec le patron de substitution et avec le solvant; la bande à longueur d'onde plus élevée est la plus faible dans les solvants hydroxyliques. Dans certains cas, l'excitation directe des phénols est une voie alternative d'obtention de radicaux phénoxyles. Toutefois, pour le 4-méthoxyphénol, il y a superposition de bandes dues au phénol triplet et au cation radical phénol qui absorbent tous les deux dans la région de 400 à 460 nm. Le cation radical 4-méthoxyphénol se forme par un processus biphotonique et il se décompose par déprotonation pour donner le radical phénoxyle. Le radical 4-méthoxyphénoxyle peut aussi être obtenu sur papier à partir soit de la cétone ou du phénol approprié et il se décompose avec une cinétique complexe qui dépend de la concentration du précurseur et de l'intensité du laser. Sur le papier, on n'a obtenu aucune indication pouvant suggérer qu'il y a formation de quantités appréciables d'états triplets de longue vie de cétone ou de phénol. La cinétique de la décomposition du radical phénoxyle est modifiée par l'addition du piège à radical dithioérythritol. La génération de radicaux phénoxyles sur papier, en présence ou en l'absence de pièges à radicaux, fournit une base pour le développement d'une nouvelle méthode d'évaluer les inhibiteurs potentiels de jaunissement photochimique et de comprendre leur mode d'action.

Mots clés : radicaux phénoxyles, jaunissement photochimique du papier, photolyse laser éclair, triplets, cations radicaux.

[Traduit par la rédaction]

Received June 5, 1997.

D. Shukla, N.P. Schepp, N. Mathivanan, and L.J. Johnston.[2] Steacie Institute for Molecular Sciences, National Research Council Canada, Ottawa, ON K1A 0R6, Canada.

[1] Issued as NRCC 40834.

[2] Author to whom correspondence may be addressed. Telephone: (613) 990-0973. Fax: (613) 991-4278. E-mail: ljj@ned1.sims.nrc.ca

© 1997 NRC Canada

Can. J. Chem. Downloaded from www.nrcresearchpress.com by 91.121.58.235 on 09/08/12
For personal use only.

The light-induced yellowing of lignin-rich mechanical and high-yield pulps has recently attracted considerable mechanistic interest (1, 2). It is now well established that phenoxyl radicals are key intermediates in the photooxidation of lignin and that their oxidation leads to quinones and other decomposition products that are responsible for the yellow color. Lignin-derived phenoxyl radicals are generated by several different routes, including β-cleavage reactions of substituted α-aryloxyacetophenones, hydrogen abstraction reactions of phenols, and cleavage of ketyl radicals derived from the photoreduction of aromatic ketones or hydrogen abstraction from arylglycerol β-arylethers (1, 3–7). Reactions of other chromophores such as stilbenes and phenylcoumarones may also play a role, particularly for pulps that have been chemically treated to remove free phenols and aromatic ketones (8–10).

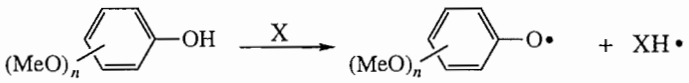
Much of the mechanistic evidence in support of these reaction pathways comes from detailed studies using model compounds in solution since the direct detection of reactive intermediates in pulp or the isolation of products from irradiated pulp samples is relatively difficult. Although such model studies provide much useful background information, it is becoming increasingly obvious that extrapolating from the behavior in homogeneous solution to that in a heterogeneous environment such as that provided by pulp is not straightforward. In some cases the irradiation of model compounds on solid supports, including paper, has been used to obtain mechanistic information as to the manner in which a heterogeneous environment may modify the outcome of a photochemical reaction. For example, earlier work indicates that the triplet states of α-guaiacoxylacetoveratrone are relatively unreactive on a variety of solid supports, including cellulose and the crystalline ketone, despite their efficient β-cleavage in hydroxylic solvents (4, 11, 12). Relatively long-lived transients assigned to triplet aryl ketones have also been observed on thermomechanical wood pulps (13).

There are several reports that indicate that phenoxyl radicals have relatively long lifetimes in paper and pulp samples. For example, phenoxyl radicals with lifetimes of hours or days have been detected in solid matrices by esr (14). The 2,4,6-trimethylphenoxyl radical has been generated by hydrogen abstraction by triplet benzophenone on cellulose and observed directly by diffuse reflectance flash photolysis (15). The recognized importance of phenoxyl radicals in the photoreversion of lignin-rich pulps has prompted us to examine a number of potential phenoxyl precursors on paper using diffuse reflectance laser flash photolyis. The latter technique has now been applied to the study of a variety of reactive intermediates in opaque solids (16). We report herein our initial results on the generation of methoxy-substituted phenoxyl radicals from phenol and ketone precursors in solution and on paper, and their spectroscopic and kinetic characterization. This work provides the necessary background for studies of the reactivity of lignin-derived phenoxyl radicals with potential free-radical scavengers and for examining the mode of action of compounds that are effective in inhibiting the photoreversion process. It also raises interesting questions concerning the involvement of phenol triplet excited states and radical cations in photoyellowing.

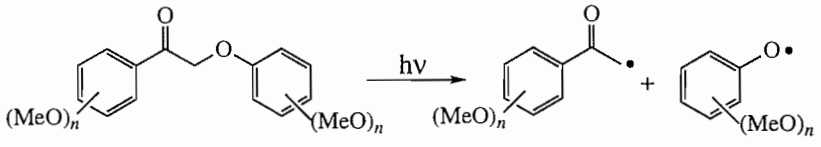
Results and discussion

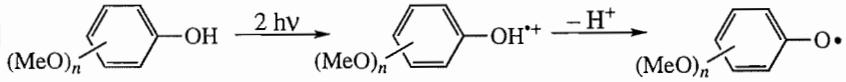
Generation of phenoxyl radicals in solution

There are a number of efficient photochemical sources of phenoxyl radicals for transient absorption measurements in solution. These include hydrogen abstraction from the appropriately-substituted phenol using triplet ketones or *tert*-butoxyl radicals (eq. [1]), β-cleavage reactions of α-aryloxyacetophenones (eq. [2]), and direct excitation of phenols (17–22). The latter reaction has been suggested to occur via biphotonic ionization of phenol followed by deprotonation of the resulting radical cation (eq. [3]) in alcohols and *n*-butyl chloride, although direct homolysis of the O—H bond may play a role in nonpolar solvents (17, 22–25). A number of substituted phenoxyl radicals have been generated using each of these routes in order to evaluate the effects of substitution pattern and solvent on the spectroscopic properties of these radicals and to identify the radicals and methods for their generation that are most suitable for spectroscopic and kinetic studies on paper.

[1] 

X = ^{3}Ketone, ^{t}BuO•

[2] 

[3] 

© 1997 NRC Canada

Can. J. Chem. Downloaded from www.nrcresearchpress.com by 91.121.58.235 on 09/08/12
For personal use only.

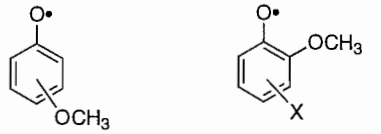
Table 1. Spectroscopic data for substituted phenoxyl radicals generated by hydrogen abstraction from the corresponding phenols using *tert*-butoxyl radical.

Phenoxyl radical	Solvent	Spectrum (nm)	I_S/I_L[a]
1 (2-OCH_3)	Benzene	390, 660	1.8
	Isooctane	390, 640	1.2
	Freon-113	390, 650	1.5
	Acetonitrile	390, 660	1.7
	tert-Butanol	390, 660	3.3
	Methanol	390, 660	3.7
2 (3-OCH_3)	Benzene	435, >700[b]	
3 (4-OCH_3)	Benzene	410	
4 (2-OCH_3-4-CH_3)	Benzene	390, 625	2.8
	Methanol	390, 650	~4
5 (2,6-$(OCH_3)_2$)	Benzene	<350, 700	
	Methanol	400, ~700[b]	
6 (2,6-$(OCH_3)_2$-4-CH_2OH)	Acetonitrile	360, 700[b]	
7 (2,6-$(^tBu)_2$-4-CH_3)	Benzene	400, 610	3.4
	Methanol	400, 620	3.2
8 (2,6-$(^tBu)_2$-4-OCH_3)	Benzene	400, 550	~8

[a] I_S/I_L refers to the ratio of the intensities of the absorption bands in the 400 nm and 650 nm regions and is based on measurements at the respective λ_{max} values for each radical.
[b] Broad and weak.

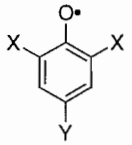
(a) Hydrogen abstraction from phenols

Various mono-substituted phenoxyl radicals have been generated by hydrogen abstraction from the corresponding phenols using *tert*-butoxyl radical in 2:1 di-*tert*-butyl peroxide/benzene (18). The rate constants for the hydrogen abstraction reaction for most of the phenols that have been studied are in the 10^8–10^9 M^{-1} s^{-1} range. The same method has been used to generate a number of substituted phenoxyl radicals (**1**–**8**) with one or more methoxy groups in both polar and nonpolar solvents. The data are summarized in Table 1 and representative spectra for the 2-methoxyphenoxyl radical in Freon-113 and methanol are shown in Fig. 1. In agreement with literature results for various phenoxyl radicals, radicals **1**–**8** have a moderately strong absorption band in the 400 nm region that is characteristic of nonaryl-substituted phenoxyl radicals. As noted previously (20), the spectrum for the 2,6-dimethoxyphenoxyl radical (**5**) is somewhat different in that the usual 400 nm band is blue-shifted and does not show a well-defined maximum. The data in Table 1 demonstrate that most of the 2- and 2,6-substituted phenoxyl radicals have a second broad absorption band at longer wavelengths (~650 nm for **1**, Fig. 1). The parent phenoxyl radical also shows a broad weak visible absorption that has recently been simulated using ab initio quantum chemical methods and shown to correspond to a $\pi\pi^*$ transition (20). This long-wavelength band is of comparable intensity to the 400 nm absorption for a variety of *ortho*-substituted phenoxy radicals, but is much weaker in the 3-methoxyphenoxyl radical and nondetectable in the 4-methoxy analog (17, 20). Note that the reported spectra for radicals **1**–**8** are in good agreement with the available literature data for the 400 nm transition of phenoxyl radicals, although in most cases the weaker visible absorption has not been characterized in detail (18, 22).



1 2-OCH_3
2 3-OCH_3
3 4-OCH_3

4 X = 4-CH_3
5 X = 6-OCH_3



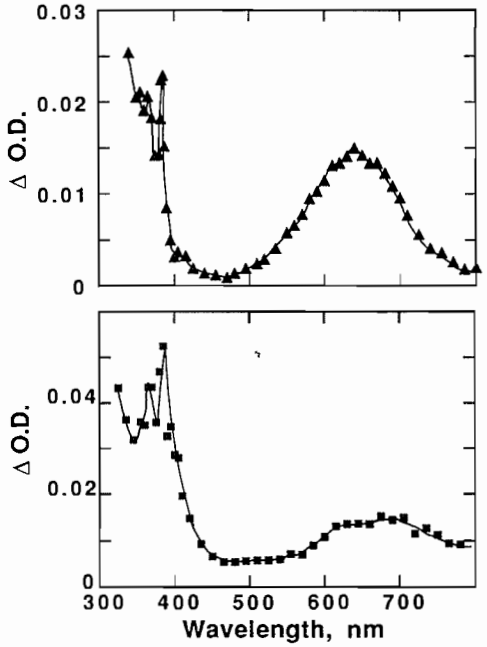
6 X = OCH_3; Y = CH_2OH
7 X = ^tBu; Y = CH_3
8 X = ^tBu; Y = OCH_3

The visible absorption band observed for most of the radicals in Table 1 is potentially useful for monitoring phenoxyl radicals on paper or pulp since it should permit the detection of the radical in a region free of absorptions due to other potential intermediates such as aryl ketone triplets. However, preliminary experiments indicated that the long-wavelength absorption was much weaker on a variety of solid supports. Accordingly phenoxyl **1** was generated in a number of solvents and the data are reported in Table 1. Note that in all cases the

© 1997 NRC Canada

Can. J. Chem. Downloaded from www.nrcresearchpress.com by 91.121.58.235 on 09/08/12
For personal use only.

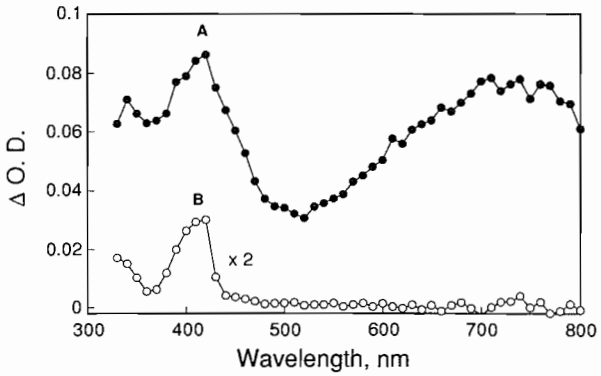
Fig. 1. Transient absorption spectra for the 2-methoxyphenoxyl radical in Freon-113 (*top*) and methanol (*bottom*). The radicals were generated by hydrogen abstraction from 2-methoxyphenol by *tert*-butoxyl radicals produced by 308 nm excitation of 4% di-*tert*-butyl peroxide.



experiments were carried out with sufficiently high concentrations of phenol to minimize decay of the initial *tert*-butoxyl radical by α-cleavage or hydrogen abstraction from the solvent (e.g., methanol, isooctane). The data show that the relative ratio of the 390 nm and long-wavelength absorptions varies substantially with solvent. For example, the ratio of short- to long-wavelength bands for **1** increases from 1.2 in isooctane to 3.7 in methanol. This change appears to be related mainly to the presence of hydroxyl groups since *tert*-butanol and methanol have similar ratios for the two bands, whereas the spectrum in acetonitrile is similar to those in less polar solvents such as benzene and Freon-113. Reasonably strong visible absorptions in the 600–650 nm region are also observed for radicals **4**, **5**, and **7** in benzene. The ratio of the intensities of the short- and long-wavelength bands decreases substantially for **4** and **5** in methanol; by contrast, the spectrum of phenoxyl **7** is virtually identical in both benzene and methanol. Phenoxyls **6** and **8** have quite weak visible absorptions bands with apparent λ_{max} values of ≥700 and 550 nm, respectively, and their spectra have been measured in only a single solvent.

It is clear from the above results that the relative intensity, position, and broadness of the long-wavelength transition in substituted phenoxyl radicals depend on the substituent, its position of attachment to the aromatic ring, and the solvent. Based on the data in Table 1, it appears that the hydrogen-bonding ability of the solvent is more important than its polarity. In general, *ortho* substitution seems to be a necessary but not a sufficient prerequisite for a strong visible absorption. In any event the solvent effects indicate that this band is unlikely to be of general utility for characterization of methoxy-substituted phenoxyl radicals on a hydroxylic support such as cellulose or paper.

Fig. 2. Transient absorption spectra measured after 308 nm excitation of 4-methoxyphenol in nitrogen-(*A*; 0.2 μs) and oxygen-(*B*, ×2, 0.2 μs) purged 1:1 ethanol/water (v/v).



(b) Direct excitation of phenols

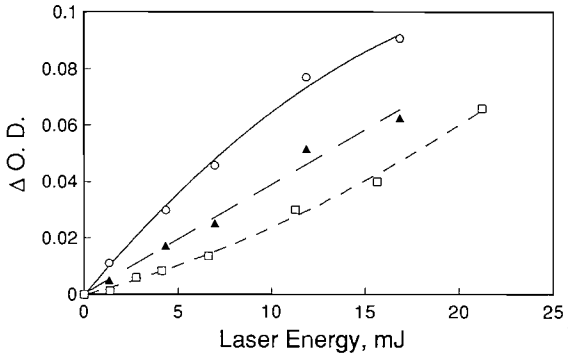
Although a number of time-resolved studies have used the direct excitation of phenols as a source of phenoxyl radicals, the literature results also indicate that this route may lead to competing absorptions due to triplet phenol, phenol radical cation, and solvated electron, depending on the reaction conditions (22, 24–27). For example, laser excitation of several phenols in aqueous solution has been reported to generate triplet–triplet absorptions at wavelengths between 250 and 450 nm and with lifetimes on the order of several microseconds, in addition to phenoxyl radicals (25); matrix studies indicate a λ_{max} value of 440 nm for triplet 4-methoxyphenol (26). A number of early studies using conventional flash photolysis indicate that phenoxyl radical formation is biphotonic and occurs via the triplet manifold (24, 27). Although the solvated electron had been observed in several cases, the initial radical cation precursor to the phenoxyl radical has only recently been characterized in solution using both pulse radiolysis and laser photolysis methods in *n*-butyl chloride (22). These results and previous studies in matrices demonstrate that a variety of methoxy-substituted phenol radical cations have absorptions in the 400–500 nm region that overlap with phenoxyl radical signals. We have carried out a number of experiments using the direct excitation of 4-methoxy-, 2-methoxy-, and 2,6-dimethoxyphenol as a source of phenoxyl radicals in order to investigate the mechanism for their formation under various conditions and to determine whether this method is suitable for kinetic studies on paper.

The transient spectrum obtained following 308 nm laser excitation of 4-methoxyphenol in nitrogen-purged 1:1 aqueous ethanol is shown in Fig. 2*A*. At early times there is a broad absorption at long-wavelength (>600 nm) that decays with a rate constant of 1.5×10^6 s^{-1} and is completely removed by purging the sample with oxygen, consistent with its assignment to the solvated electron (28). Figure 2*A* also shows a strong absorption with λ_{max} at 410 nm and a shoulder at 440 nm. The shoulder at 440 nm decays more rapidly than the 410 nm signal ($k_{obs} \sim 10^6$ s^{-1}), clearly demonstrating that two species contribute to the signal in the 400–450 nm region at early times. At long times (10 μs) or in oxygen-saturated solutions only the 410 nm transient remains (Fig. 2*B*); this species has an additional absorption band at ~330 nm and is clearly the 4-methoxyphenoxyl radical (**3**), based on the known spec-

© 1997 NRC Canada

Can. J. Chem. Downloaded from www.nrcresearchpress.com by 91.121.58.235 on 09/08/12
For personal use only.

Fig. 3. Plots of signal intensity as a function of incident laser energy for 308 nm excitation of 4-methoxyphenol in 1:1 ethanol/water: (○) 410 nm, nitrogen purged; (▲) 410 nm, oxygen purged; (□) 650 nm, nitrogen purged.

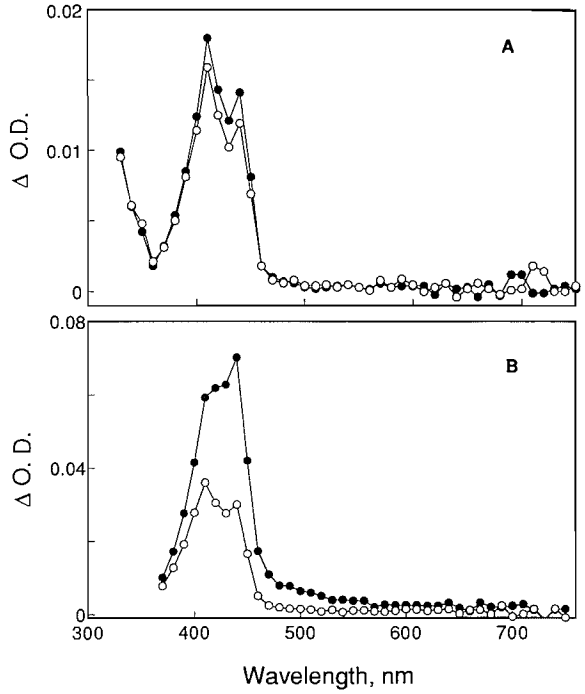


trum for this radical (Table 1) and its insensitivity to oxygen (20). Note that the relative intensities for the early and late spectra or for nitrogen vs. oxygen saturation indicate that the 440 nm transient also absorbs at 410 nm. This species can be quenched by the addition of 1,3-cyclohexadiene. These data indicate that the longer-wavelength transient is the triplet phenol, in agreement with its reported spectrum in a matrix (26). There is no evidence for the phenol radical cation, presumably due to rapid deprotonation in protic solvents.

The yield of the various transients generated by excitation of 4-methoxyphenol in aqueous ethanol was examined as a function of the laser intensity (Fig. 3). The yield of the solvated electron (measured at 650 nm) showed pronounced positive curvature; plots of signal intensity vs. the square of the laser intensity were reasonably linear (R = 0.995), indicating that the formation of the solvated electron is a two-photon process. By contrast, plots of the signal intensities at both 410 and 450 nm vs. the laser intensity showed negative curvature. Since the signals at these wavelengths are the sums of contributions from both the triplet and phenoxyl radical **3**, the experiment was repeated for an oxygenated sample. In this case the signal intensity at 410 nm was substantially lower and the plot showed much less curvature. These results suggest that most of the curvature is due to the triplet absorption. However, if all of the phenoxyl radical was produced by deprotonation of the radical cation formed by photoionization, then a similar intensity dependence would be expected for the phenoxyl radical signal (at 410 nm in the presence of triplet quencher) and the solvated electron. The two are clearly different, which suggests that there is a second pathway for phenoxyl radical formation, presumably direct homolysis of the first or an upper excited singlet state.

The transient phenomena observed upon excitation of 4-methoxyphenol in methanol were qualitatively similar to those described above in aqueous ethanol. In acetonitrile, both phenoxyl radical and triplet were also observed, with the latter reacting with both oxygen and 1,3-cyclohexadiene. A plot of the observed rate constant for decay of the 440 nm transient as a function of diene concentration gives a rate constant of 3.6×10^9 $M^{-1}s^{-1}$. In the presence of 1,3-cyclohexadiene (0.5–3 mM) the transient decays at various wavelengths from 400 to

Fig. 4. Transient absorption spectra measured (*A*) 0.3 (●) and 0.7 (○) μs after 308 nm excitation of 4-methoxyphenol in oxygen-purged acetonitrile and (*B*) 0.2 (●) and 0.6 (○) μs after 355 nm excitation of a solution of 5.6×10^{-3} M 1,4-dicyanonaphthalene, 0.3 M biphenyl, and 0.008 M 4-methoxyphenol in oxygen-purged acetonitrile.



460 nm clearly show two components: a rapid decay that increases with diene concentration and a much slower one assigned to the phenoxyl radical, with the relative contributions of the two varying with wavelength. Note that in acetonitrile the solvated electron exists as a dimer radical anion that does not absorb appreciably below 750 nm and is not detectable under our experimental conditions (28).

The transient spectrum measured for an oxygenated solution of 4-methoxyphenol in dry acetonitrile (Fig. 4*A*) was somewhat different from that obtained in aqueous ethanol. In addition to the radical signal at 410 nm, there was clearly still a residual unquenched signal at 440 nm that decayed with a rate constant of $\sim 8 \times 10^5$ s^{-1}. This is not triplet 4-methoxyphenol, but is consistent with spectra of radical cations of related phenols in *n*-butyl chloride (22). The 440 nm signal was efficiently quenched by water ($k_q \sim 8 \times 10^7$ M^{-1} s^{-1}). The 4-methoxyphenol radical cation was generated by photosensitized electron transfer in acetonitrile, as outlined below in order to confirm that its spectrum and lifetime were in agreement with the residual 440 nm signal observed upon excitation of an oxygenated solution of the phenol.

Excitation (355 nm) of 5.6×10^{-3} M 1,4-dicyanonaphthalene in the presence of 0.3 M biphenyl in acetonitrile leads to rapid electron transfer quenching of the singlet sensitizer with concomitant formation of biphenyl radical cation, λ_{max} at 680 and 380 nm. The radical anion can be completely removed by purging the sample with oxygen. The biphenyl radical cation reacts with 4-methoxyphenol with a rate constant of 1.6×10^{10} M^{-1} s^{-1} and yields a transient spectrum with λ_{max} at 440 nm

© 1997 NRC Canada

Can. J. Chem. Downloaded from www.nrcresearchpress.com by 91.121.58.235 on 09/08/12
For personal use only.

and a shoulder at 410 nm (Fig. 4*B*). The 440 nm band decays with a rate constant of 1.6×10^5 s^{-1}, leaving a spectrum that can clearly be assigned to phenoxyl radical **3**. The early spectrum shown in Fig. 4*B* may contain a small contribution from the phenoxyl radical; however, it is clear that most of the signal is attributable to the 4-methoxyphenol radical cation generated by quenching of biphenyl radical cation. The 4-methoxyphenol radical cation has substantial absorption between 400 and 450 nm and is similar to the reported matrix spectrum of the 1,4-dimethoxybenzene radical cation (29); generation of this species using 1,4-dicyanonaphthalene–biphenyl in acetonitrile gave a spectrum with λ_{max} values of 430 and 460 nm. Measurement of the decay of the 4-methoxyphenol radical cation at 440 nm as a function of water concentration gave a quenching rate constant of 6.0×10^7 M^{-1} s^{-1}, in good agreement with the rate constant measured for water quenching of the transient produced by direct excitation of 4-methoxyphenol in acetonitrile–diene. It is likely that the measured lifetime of the radical cation in acetonitrile reflects deprotonation by traces of water, even in "dry" acetonitrile.

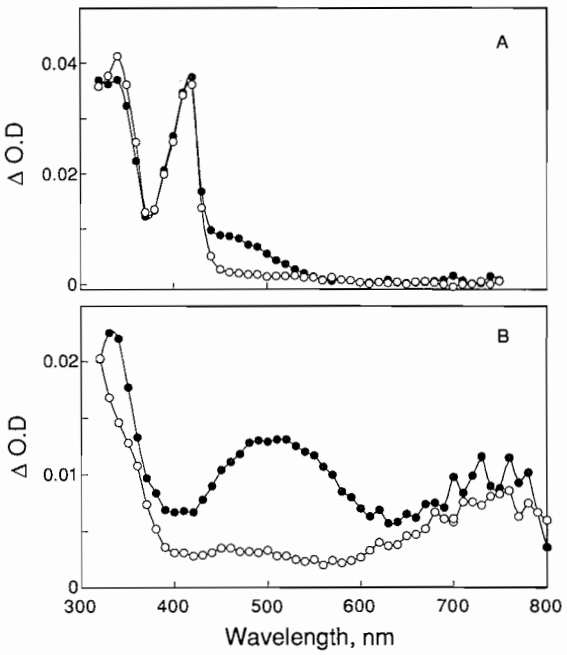
The results noted above indicate that direct excitation of 4-methoxyphenol generates triplet, radical cation, and phenoxyl radical. In solution, the triplet and radical cation can be easily eliminated by addition of triplet quenchers (oxygen or diene) and water or alcohols, respectively. Photoionization occurs via a biphotonic process, in agreement with previous work (22, 24, 27). The measured singlet lifetimes for 4-methoxyphenol are 2.1 and 1.8 ns in acetonitrile and methanol; this suggests that either the singlet or triplet excited state of the phenol is a potential candidate for absorption of a second photon during the ~6 ns laser pulse employed in our experiments. The variation in the yields of phenoxyl radical and solvated electron with laser intensity in ethanol indicates that the phenoxyl radical is produced by both photoionization–deprotonation and direct homolysis, at least in this solvent.

Direct excitation of carefully purified samples of 2,6-dimethoxyphenol (266 nm) in either acetonitrile or aqueous ethanol does not lead to any significant absorptions between 700 and 320 nm. This phenol is difficult to work with since it rapidly forms impurities that absorb at slightly longer wavelength than the phenol and generate a transient with absorption at 400 nm. Direct excitation (266 nm) of 2-methoxyphenol gives at best only very weak signals due to phenoxyl radical. Both the low radical yields and the rapid formation of products that interfere with transient experiments are substantial limitations to the use of these two *ortho*-substituted phenols as phenoxyl sources on paper.

(c) β-*Cleavage of* α-*aryloxyacetophenones*

Excitation of a variety of α-aryloxyacetophenones has been shown to lead to rapid excited state cleavage (< 1 ns) to generate aryloxyl and phenacyl radicals (12, 21, 30–32). The singlet excited state of the ketone has been identified as the radical precursor for a number of α-aryloxyacetophenones and α-aryloxy-4-methoxyacetophenones (21, 31, 32), although both singlet and triplet excited states lead to cleavage for α-aryloxy-3,4-dimethoxyacetophenones (12, 33). Figure 5*A* shows the transient absorption spectrum produced by 308 nm laser excitation of α-(4-methoxyphenoxy)acetophenone in nitrogen-purged acetonitrile. In addition to the phenoxyl radical there is a weak absorption between 400 and 500 nm that is removed by oxygen purging (Fig. 5*A*), consistent with its assignment to the phenacyl radical (34). There is no indication for a long-lived triplet ketone, as expected from the previous estimate of 166 ps for the lifetime of this intermediate (30). A similar experiment for α-(2,6-dimethoxyphenoxy)-4-methoxyacetophenone in acetonitrile is shown in Fig. 5*B*. The visible absorptions due to the 2,6-dimethoxyphenoxyl and 4-methoxyphenacyl radicals are clearly observed at >700 and 500 nm, respectively. There is additional absorption below 400 nm that contains contributions from both radicals as demonstrated by the spectrum measured in the presence of sufficient oxygen to remove the phenacyl radical signal.

Fig. 5. Transient absorption spectra measured after 308 nm laser excitation of α-(4-methoxyphenoxy)acetophenone (*A*, 1.5×10^{-3} M) and α-(2,6-dimethoxyphenoxy)-4-methoxyacetophenone (*B*, 1.0×10^{-3} M) in nitrogen-(●) and oxygen-(○) purged acetonitrile.



Generation of phenoxyl radicals on paper

The direct excitation of either phenols or α-aryloxyacetophenones is the most suitable method for generation of phenoxyl radicals for kinetic studies on solid supports. This choice is dictated primarily by the fact that these precursors provide rapid unimolecular routes to the required phenoxyl radicals whereas the hydrogen abstraction route involves a bimolecular reaction between phenol and an excited ketone or a photochemically generated free radical. This results in slower generation of the required radical, which is expected to be more of a problem in solids than in homogeneous solution. The phenol and ketone precursors are also better models for the lignin-derived chemistry that occurs on paper. Radical **3** was selected as an appropriate model for initial experiments on paper since it can be generated from both the ketone and phenol precursor using 308 nm excitation. The use of 308 nm excitation for paper samples is desirable since our ultimate goal is to develop routes for generating phenoxyl radicals on paper and studying their decay kinetics in the presence of

© 1997 NRC Canada

Fig. 6. Transient spectra obtained by 308 nm laser excitation of 2% 4-methoxyphenol (*A*) and 4% α-(4-methoxyphenoxy)acetophenone (*B*) on paper. Spectra were measured ~0.5 μs after laser excitation in each case.

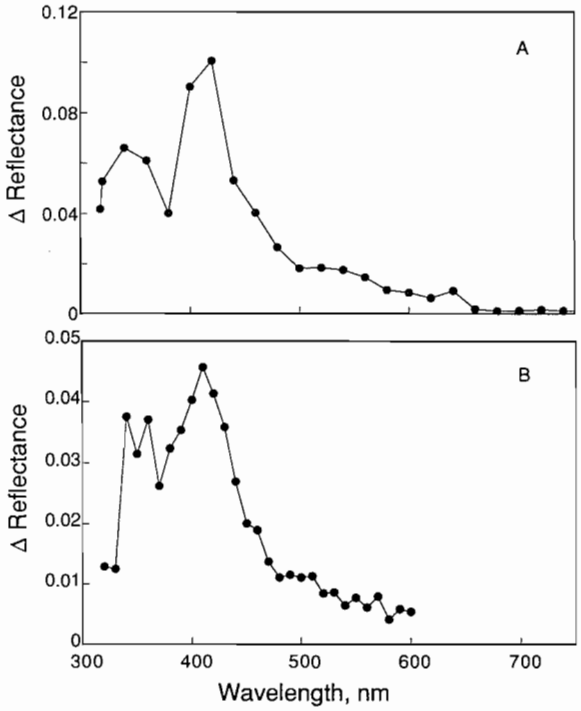
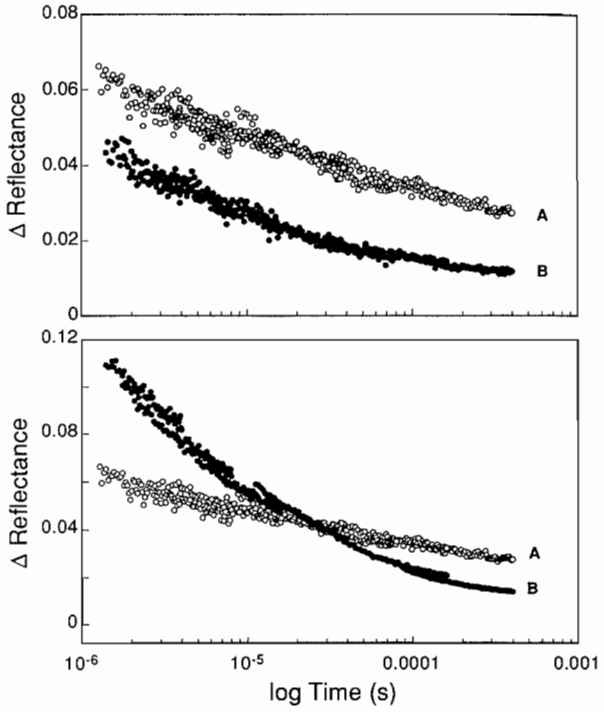


Fig. 7. *Top*: Decay of the 410 nm transient generated by 308 nm excitation of 4-methoxyphenol (*A*, 2%) and α-(4-methoxyphenoxy)acetophenone (*B*, 2%) on paper. *Bottom*: Decay of the 410 nm transient generated by 308 nm excitation of 2% (*A*) and 4% (*B*) 4-methoxyphenol on paper.



potential free radical scavengers, many of which absorb below 300 nm. The ability to generate the phenoxyl radical from two different precursors is also an advantage for initial experiments on paper.

The spectrum obtained by 308 nm excitation of an aerated sample of 4-methoxyphenol on paper is shown in Fig. 6*A*. The observed transient shows λ_{max} at 410 nm, in good agreement with the solution spectra for radical **3**. A similar transient is obtained upon excitation of α-(4-methoxyphenoxy)acetophenone on paper (Fig. 6*B*) under air. Although the transient spectra observed from the two precursors are similar and are in good agreement with the solution spectrum for **3**, it is important to demonstrate whether phenol or ketone triplets are formed in significant yield on paper. Note that the efficient reaction of the 4-methoxyphenol radical cation with water and the relatively high water content of paper (typically 5–10%) make it unlikely that the radical cation will have a significant lifetime on paper. Initial experiments to eliminate contributions due to triplet excited states focused on the use oxygen as a selective quencher of triplet excited states but not phenoxyl radicals. Transient absorption spectra obtained by excitation of both 4-methoxyphenol and α-(4-methoxyphenoxy)acetophenone were not significantly different for oxygen vs. nitrogen equilibrated samples, nor were there significant changes in intensity. Similar results were also observed for triplet benzophenone on paper, indicating that it is not possible to substantially modify the oxygen concentration in paper, at least using our experimental procedure (see Experimental). This is consistent with previous reports of the lack of oxygen effect on triplet excited states of arylketones in cellulose (11, 35, 36).

Experiments were therefore carried out using 1,3,5,5-tetramethylcyclohexadiene as a triplet quencher. Preliminary experiments used acetophenone triplet as a model in order to identify appropriate conditions for measuring triplet quenching on paper. The only transient observed upon 308 nm excitation of a sample of acetophenone on paper (4% w/w) is the triplet ketone with λ_{max} at ~380 nm. Addition of 6% (w/w) diene resulted in an approximately 60% decrease in the initial signal intensity, but no change in either the transient spectrum or decay kinetics (after normalization). This demonstrates that a static quenching mechanism is operative. Similar experiments using both the phenol and ketone precursors for radical **3** in the presence of 7% diene on paper showed little change in either the overall signal intensity at 410 nm (±15%, within the reproducibility of the experiment) or in the spectrum of the transient. This indicates that the transient spectra in Fig. 6 do not include significant contributions from triplet excited states of the phenol and ketone precursors.

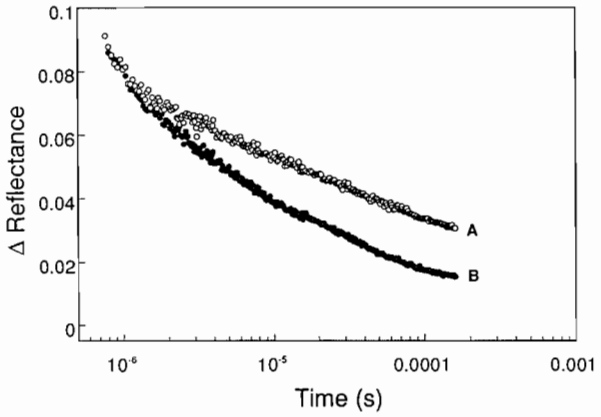
The decay of phenoxyl radical **3** on paper occurs slowly and follows complex kinetics that cannot be fit to simple kinetic expressions. Examples of composite kinetic traces (see Experimental) measured at 410 nm under air for the ketone and phenol precursors are shown in Fig. 7. For the phenol precursor approximately half the signal has decayed on the longest time scale measured whereas approximately one third of the signal remains for the ketone precursor. The decay kinetics also vary with the precursor loading level as shown in Fig. 7. A twofold

© 1997 NRC Canada

Can. J. Chem. Downloaded from www.nrcresearchpress.com by 91.121.58.235 on 09/08/12
For personal use only.

Can. J. Chem. Downloaded from www.nrcresearchpress.com by 91.121.58.235 on 09/08/12
For personal use only.

Fig. 8. Normalized decay traces for the 410 nm transient generated by 308 nm excitation of 3% 4-methoxyphenol on paper alone (*A*) and with 7% added dithioerythritol (*B*). The initial signal intensity for trace *B* is 0.75 times that of trace *A*.



increase in the amount of phenol increases the initial signal intensity by ~70% and results in much more rapid disappearance of the radical. Similarly, decreasing the laser intensity results in a decreased signal intensity and less rapid decay of the radical. These results are consistent with some contribution from radical–radical coupling to the decay kinetics, at least at the radical concentrations produced at higher laser intensity or higher precursor loading.

The kinetics for the decay of phenoxyl radical **3** were also examined in the presence of dithioerythritol, which has been shown to inhibit photoyellowing of lignin-containing paper and has been suggested to function as a phenoxyl radical scavenger (14, 37). Since the signal intensity and decay kinetics for **3** vary substantially with the precursor used, as well as the loading level and the laser intensity, it is essential to compare results for samples with and without the scavenger measured under identical conditions on the same day. Such a comparison for **3** generated from the phenol precursor in the presence and absence of dithioerythritol (7% w/w) is shown in Fig. 8. The decay traces have been normalized to more clearly show the difference in kinetics; the initial signal intensity in the presence of dithioerythritol is approximately 25% lower than that measured in the absence of scavenger. This indicates that some static quenching occurs, presumably as a result of the generation of a phenoxyl radical in the vicinity of a thiol quencher. The normalized decay traces shown in Fig. 8 demonstrate that **3** decays somewhat more rapidly in the presence of the thiol scavenger, with less long-lived residual signal remaining on the longest time scale measured. This is consistent with a dynamic component in the quenching process that must result from diffusional mobility of either the radical or the thiol on the time scale of the experiment. Note that the diene experiments described above suggest that the quenching observed with the thiol scavenger is not simply related to the added loading of the scavenger causing displacement of the phenoxyl precursor to sites for which the decay kinetics are more rapid.

Conclusions

The solution spectra for a number of methoxy-substituted phenoxyl radicals that provide models for lignin-derived radicals have been measured. The results show that most of the *ortho*-substituted phenoxyls have moderately strong visible absorptions in addition to the characteristic sharp absorption at ~400 nm. However, the relative intensities of the long-wavelength bands vary substantially with substitution pattern and solvent; the decreased intensity in hydroxylic solvents means that this absorption is not generally useful for experiments in a hydroxylic matrix such as paper. The generation of phenoxyl radicals via direct photolysis of 4-methoxyphenol has been investigated in some detail in solution. The results demonstrate that triplet phenol, phenol radical cation, and phenoxyl radical are all produced upon 308 nm excitation of this phenol, with all three intermediates having lifetimes in the microsecond region and absorptions in the 400–460 nm range. Photoionization is biphotonic and the phenol radical cation decays via deprotonation to generate phenoxyl radical, although it appears that some phenoxyl radical may also be formed via direct homolysis, at least in aqueous ethanol. The results suggest that both phenol triplets and radical cations should be considered as potential intermediates in the photochemistry of lignin-derived phenols. For example, although there is no evidence for direct phenoxyl radical formation from the triplet excited state, this species has a sufficiently long lifetime to undergo electron transfer reactions that can generate phenoxyl radical via deprotonation of the initial phenol radical cation.

Both α-(4-methoxyphenoxy)acetophenone and 4-methoxyphenol have been used as precursors for 4-methoxyphenoxyl radical on paper. The above results demonstrate that this radical can be readily generated in sufficient concentrations for its direct detection using transient techniques on paper. The transient spectra are comparable to solution results for the same radical and quenching experiments indicate that triplet states of the ketone or phenol precursor do not contribute significantly to the transient phenomena on paper. The 4-methoxyphenoxyl radical is long-lived and follows complex decay kinetics as observed for other radicals on solid supports such as zeolites and cellulose (15, 38–40). More importantly, the decay of the radical can be monitored reproducibly in the presence and absence of potential scavengers such as thiols. This provides the necessary background for studies of phenoxyl radicals in the presence of potential radical scavengers and should allow the development of a routine method for screening photoyellowing inhibitors. Correlation of the results obtained by diffuse reflectance flash photolysis and steady state irradiation will also allow important mechanistic conclusions as to the mode of action of inhibitors. In this context it is obviously of interest to extend our studies to 2-methoxy-substituted radicals that more closely resemble the lignin-derived radicals and to paper samples made from high-yield pulps. Such experiments are in progress.

Experimental

Materials

The paper used in these experiments was Whatman no. 2 filter paper. Biphenyl, dithioerythritol, 1,4-dimethoxybenzene, and all phenols were obtained from Aldrich. The phenols were purified by sublimation followed by recrystallization (twice) from hexanes or by distillation before use. Di-*tert*-butyl peroxide was purified by passage through a small alumina column before use. α-(4-Methoxyphenoxy)acetophenone was

© 1997 NRC Canada

synthesized by reaction of α-bromoacetophenone with 4-methoxyphenol in acetone in the presence of potassium carbonate according to a literature procedure (41). Similarly, reaction of 2,6-dimethoxyphenol with α-bromo-4-methoxyacetophenone in acetone in the presence of potassium carbonate afforded α-(2,6-dimethoxyphenoxy)-4-methoxyacetophenone, which was purified by recrystallization from ethanol. 1,4-Dicyanonaphthalene was synthesized according to a literature procedure (42, 43) and purified by chromatography (neutral alumina, CH_2Cl_2) followed by recrystallization from toluene. 1,3-Cyclohexadiene (Aldrich) and 1,3,5,5-tetramethylcyclohexadiene (Wiley Organics) were distilled before use. Ethanol and methanol were used as received. Acetonitrile was distilled over calcium hydride in an inert atmosphere.

Sample preparation on paper

A methanol or THF (ca. 2.0 mL) solution of phenol–α-aryloxyacetophenone (5–10 mg) was applied to a pre-weighed Whatman no. 2 filter paper (7×7 cm^2). The paper was placed on a petri dish and sample (phenol or phenoxyacetophenone) solution was applied to it with the aid of a syringe or pipette. The paper was allowed to dry and then turned over and sample solution applied to the other side in a similar manner. The paper was dried in air overnight in the dark and weighed again (the amount of substrate on the paper was determined by the difference in weight of the sample before and after loading). There was no evidence for degradation of the phenol over this time period. A similar method was used to prepare paper samples containing both substrate and scavenger, viz., dithioerythritol (DTE). In general, paper samples were made the day before the laser experiments were carried out.

Laser flash photolysis

The laser flash photolysis setup for both transmission and diffuse reflectance measurements has been described in detail (40). For these experiments either a Lumonics EX530 excimer laser (XeCl, 308 nm; ≤40 mJ/pulse; ~8 ns pulses) or a Lumonics HY750 Nd:YAG laser (266 nm, ≤60 mJ/pulse; 355nm, ≤50 mJ/pulse; ~10 ns pulses) was used for sample excitation. All solution experiments were done using a 7×7 mm^2 quartz flow cell attached to a sample reservoir to minimize problems related to sample depletion and buildup of products. Samples were purged with either nitrogen or oxygen before and during the experiments. For the diffuse reflectance experiments in air, the paper samples were folded and placed directly in the sample holder; the paper was moved during the experiments to provide a fresh sample surface for each laser shot. For experiments under O_2 and N_2, thin strips (~ 2×6 mm^2) of the paper samples were placed in 3×7 mm^2 quartz cuvettes. The quartz cuvettes, with paper sample inside, were placed in a round-bottomed flask and evacuated under an atmosphere of N_2 or O_2. The cuvettes were taken out of the flask, sealed with a rubber septum, and then purged with N_2 or O_2 for 15–20 min before use. The diffuse reflectance data are reported as ΔReflectance = $(J_0 - J_t)/J_0$, where J_0 is the initial reflected light before the laser pulse and J_t is the reflected light at time t after the laser excitation. The composite decay traces shown in Figs. 7 and 8 were produced by measuring decay traces on a number of different time scales and then combining these into a single plot. It was necessary to normalize some of the traces in the region where they overlap in time, but these corrections were relatively small (<15%). The first reliable data point could only be recorded ~500 ns after the laser pulse, due to the presence of a relatively strong luminescence (at the monitoring wavelength of 400–410 nm at short delays) for which complete correction is difficult.

Acknowledgements

This work was supported by the Mechanical Wood Pulps Network of Centres of Excellence.

References

1. C. Heitner and J.C. Scaiano (*Editors*). Photochemistry of lignocellulosic materials. ACS Symp. Ser. **531** (1993).
2. G.J. Leary. J. Pulp Paper Sci. **20**, J154 (1994).
3. J.A. Schmidt and C. Heitner. J. Wood Chem. Technol. **13**, 309 (1993).
4. J.C. Scaiano, A.B. Berinstain, M.K. Whittlesey, P.R.L. Malenfant, and C. Bensimon. Chem. Mater. **5**, 700 (1993).
5. Y. Huang, D. Page, D.D.M. Wayner, and P. Mulder. Can. J. Chem. **73**, 2079 (1995).
6. L.R.C. Barclay, G.R. Cromwell, and J.W. Hilborn. Can. J. Chem. **72**, 35 (1994).
7. D.S. Argyropoulos and Y. Sun. Photochem. Photobiol. **64**, 510 (1996).
8. C. Noutary, P.F. de Violet, J. Vercauteren, and A. Castellan. Res. Chem. Intermed. **21**, 247 (1995).
9. D.F. Wong, G. Leary, and G. Arct. Res. Chem. Intermed. **21**, 329 (1995).
10. W.J. Leigh, T.J. Lewis, V. Lin, and J.A. Postigo. Can. J. Chem. **74**, 263 (1996).
11. L. Hurrell, L.J. Johnston, N. Mathivanan, and D. Vong. Can. J. Chem. **71**, 1340 (1993).
12. J.A. Schmidt, A.B. Berinstain, F. de Rege, C. Heitner, L.J. Johnston, and J.C. Scaiano. Can. J. Chem. **69**, 104 (1991).
13. J.A. Schmidt, C. Heitner, G.P. Kelly, P.A. Leicester, and F. Wilkinson. J. Photochem. Photobiol. **57**, 111 (1991).
14. J.K.S. Wan and M.C. Depew. Res. Chem. Intermed. **22**, 241 (1996).
15. P.P. Levin, L.F.V. Ferreira, and S.M.B. Costa. Chem. Phys. Lett. **173**, 277 (1990).
16. F. Wilkinson and G. Kelly. *In* Handbook of photochemistry. Vol. 1. *Edited by* J. C. Scaiano. CRC Press Inc., Boca Raton, Fla. 1989. Chap. 12.
17. E.J. Land, G. Porter, and E. Strachan. Trans. Faraday Soc. 1885 (1961).
18. P.K. Das, M.V. Encinas, S. Steenken, and J.C. Scaiano. J. Am. Chem. Soc. **103**, 4162 (1981).
19. P.K. Das, M.V. Encinas, and J.C. Scaiano. J. Am. Chem. Soc. **103**, 4154 (1981).
20. L.J. Johnston, N. Mathivanan, F. Negri, and W. Siebrand. Can. J. Chem. **71**, 1655 (1993).
21. J.C. Scaiano, J.K. Whittlesey, A.B. Berinstain, P.R.L. Malenfant, and R.H. Schuler. Chem. Mater. **6**, 836 (1994).
22. O. Brede, H. Orthner, V. Zubarev, and R. Hermann. J. Phys. Chem. **100**, 7097 (1996).
23. G. Dobson and L.I. Grossweiner. Trans. Faraday Soc. **61**, 708 (1965).
24. J. Feitelson and E. Hayon. J. Phys. Chem. **77**, 10 (1975).
25. D.V. Bent and E. Hayon. J. Am. Chem. Soc. **97**, 2599 (1975).
26. H. Yamada, N. Nakashima, and H. Tsubomura. J. Phys. Chem. **74**, 2897 (1970).
27. J. Feitelson, E. Hayon, and A. Treinin. J. Am. Chem. Soc. **95**, 1025 (1973).

© 1997 NRC Canada

Can. J. Chem. Downloaded from www.nrcresearchpress.com by 91.121.58.235 on 09/08/12
For personal use only.

28. Y. Hirata and N. Mataga. Prog. React. Kinet. **18**, 273 (1993).
29. T. Shida. Electronic absorption spectra of radical ions. Elsevier, Amsterdam. 1988.
30. J.C. Netto-Ferreira, I.G.J. Avellar, and J.C. Scaiano. J. Org. Chem. **55**, 89 (1990).
31. W.U. Palm and H. Dreeskamp. J. Photochem. Photobiol. A: **52**, 439 (1990).
32. W.U. Palm, H. Dreeskamp, H. Bouas-Laurent, and A. Castellan. Ber. Bunsen-Ges Phys. Chem. **96**, 50 (1992).
33. J.K.S. Wan, M.Y. Tse, and M.C. Depew. Res. Chem. Intermed. **17**, 59 (1992).
34. S.V. Jovanovic, J. Renaud, A.B. Berinstain, and J.C. Scaiano. Can. J. Chem. **73**, 223 (1995).
35. J. Murtagh and J.K. Thomas. Chem. Phys. Lett. **148**, 445 (1988).
36. F. Wilkinson, P.A. Leicester, L.F.V. Ferreira, and V.M.M.R. Freire. Photochem. Photobiol. **54**, 599 (1991).
37. L.R.C. Barclay, K.A. Dakin, and J.A.Y. Khor. Res. Chem. Intermed. **21**, 467 (1995).
38. G. Kelly, C.J. Willsher, F. Wilkinson, J.C. Netto-Ferreira, A. Olea, D. Weir, L.J. Johnston, and J.C. Scaiano. Can. J. Chem. **68**, 812 (1990).
39. L.J. Johnston, J.C. Scaiano, J.-L. Shi, W. Siebrand, and F. Zerbetto. J. Phys. Chem. **95**, 10018 (1991).
40. S. Kazanis, A. Azarani, and L.J. Johnston. J. Phys. Chem. **95**, 4430 (1991).
41. E. Adler, B.O. Lindgren, and U. Saeden. Sven. Papperstidn. **55**, 245 (1952).
42. R.W. Bayer and E.J. O'Reilley, Jr. J. Org. Chem. **23**, 311 (1958).
43. M.S. Newman. Org. Synth. Coll. Vol. **3**, 631 (1995).

Can. J. Chem. Downloaded from www.nrcresearchpress.com by 91.121.58.235 on 09/08/12
For personal use only.

© 1997 NRC Canada

Synthesis of *C*-aryl-*N*-(2-hydroxyphenylmethyl)-nitrones and their reaction with diphenylborinic or carboxylic acid derivatives. Crystal and molecular structures of a free nitrone ligand and its diphenyl–boron chelate[1]

Wolfgang Kliegel, Jörg Metge, Steven J. Rettig, and James Trotter

Abstract: The syntheses of a number of aromatic aldonitrones of *N*-(2-hydroxyphenylmethyl)hydroxylamine and their subsequent reactions with diphenylborinic or carboxylic acid derivatives are reported. Crystals of 8-(4-dimethylaminophenylmethylene)-6,6-diphenyl-5,7-dioxa-8-azonia-6-borata-5*H*-6,7,8,9-tetrahydrobenzocycloheptene, **2***b*, are triclinic, $a = 10.6802(8)$, $b = 11.1809(4)$, $c = 10.1520(3)$ Å, $\alpha = 105.847(3)°$, $\beta = 92.567(4)°$, $\gamma = 84.610(5)°$, $Z = 2$, space group $P\bar{1}$, and those of *C*-(4-dimethylaminophenyl)-*N*-(2-hydroxyphenylmethyl)nitrone, **6***e*, are monoclinic, $a = 12.2319(8)$, $b = 7.071(1)$, $c = 17.2005(9)$ Å, $\beta = 107.520(4)°$, $Z = 4$, space group $P2_1/a$. The structures were solved by direct methods and refined by full-matrix least-squares procedures to $R = 0.035$ and 0.032 ($R_w = 0.036$ and 0.032) for 3379 and 1800 reflections with $I \geq 3\sigma(I)$, respectively. Compound **2***b* is representative of a new type of heterocyclic *B*,*N*-betaine. The solid state structure of **6***e* (the precursor to **2***b*) shows that only small topological changes, but significant changes in the electron distribution, occur upon the formation of the diphenylboron chelate.

Key words: aromatic aldonitrones, organoboron compounds, crystal structures.

Résumé : On a réalisé la synthèse d'un certain nombre d'aldonitrones aromatiques de la *N*-(2-hydroxyphénylméthyl)-hydroxylamine dont on a examiné les réactions subséquents avec des dérivés des acides diphénylborinique ou carboxylique. Les cristaux du 8-(4-diméthylaminophénylméthylène)-6,6-diphényl-5,7-dioxa-8-azonia-6-borata-5*H*-6,7,8,9-tétrahydrobenzocycloheptène, **2***b*, sont tricliniques, groupe d'espace $P\bar{1}$, avec $a = 10{,}6802(8)$, $b = 11{,}1809(4)$ et $c = 10{,}1520(3)$ Å, $\alpha = 105{,}847(3)°$, $\beta = 92{,}567(4)°$ et $\gamma = 84{,}610(5)°$, et $Z = 2$ alors que ceux de la *C*-(4-diméthylaminophényl)-*N*-(2-hydroxyphénylméthyl)nitrone, **6***e*, sont monocliniques, groupe d'espace $P2_1/a$, avec $a = 12{,}2319(8)$, $b = 7{,}071(1)$ et $c = 17{,}2005(9)$ Å, $\beta = 107{,}520(4)°$ et $Z = 4$. On a résolu les structures par des méthodes directes et on les a affinées par la méthode des moindres carrés jusqu'à des valeurs respectives de $R = 0{,}035$ et 0,032 ($R_w = 0{,}036$ et 0,032) pour 3379 et 1800 réflexions avec $I \geq 3\sigma(I)$. Le composé **2***b* représente un nouveau type de composé de *B*,*N*-bétaïne hétérocyclique. La structure du composé **6***e* (précurseur du composé **2***b*) à l'état solide indique que, lors de la formation du chélate diphénylbore, il n'y a que de faibles changements topologiques, toutefois significatifs, qui se produisent dans la distribution électronique.

Mots clés : aldonitrones aromatiques, composés organobore, structures cristallines.

[Traduit par la rédaction]

Introduction

Nitrones of salicylaldehyde react as bidentate ligands with various chelate-forming boron compounds to give heterocyclic *B*,*N*-betaines such as **1** (1) (Scheme 1). An X-ray crystallographic analysis of the diphenylboron derivative of the *N*-methylnitrone (**1**, R = Me) established the seven-membered chelate ring structure with an endocyclic nitrone C=N double bond (2). In the course of this continuing investigation we were interested in the related seven-membered boron chelates **2**, utilizing a similar type of bidentate *N*-oxide–phenolate ligand, differing by having the nitrone C=N bond located outside of the chelate ring ("exocyclic" or "semicyclic" (3)).

An analogous boron chelate ring **3** containing an alcoholate instead of a phenolate ligand moiety had been postulated previously for the crystalline diphenylboron derivatives of *C*-aryl-*N*-(3-hydroxypropyl)nitrones (4). The stability of these type **3** chelates, however, turned out to depend on the *C*-aryl residue, which influences the basicity of the nitrone *N*-oxide function. Thus the derivative of 4-(dimethylamino)benzaldehyde (**3**, Ar = 4-$Me_2NC_6H_4$) proved to be by far the most

Received June 27, 1997.

W. Kliegel and J. Metge. Institut für Pharmazeutische Chemie der Technischen Universität Braunschweig, Beethovenstrasse 55, 38106 Braunschweig, Germany.
S.J. Rettig and J. Trotter.[2] Department of Chemistry, University of British Columbia, 2036 Main Mall, Vancouver, BC V6T 1Z1, Canada.

[1] Structural studies of organoboron compounds LXVI. Previous paper in this series: ref. 34.

[2] Author to whom correspondence may be addressed. Telephone: (604) 822-4865. Fax: (604) 822-2847. E-mail: jtrt@xray4.chem.ubc.ca

© 1997 NRC Canada

Can. J. Chem. Downloaded from www.nrcresearchpress.com by 91.121.58.235 on 09/08/12
For personal use only.

Can. J. Chem. Downloaded from www.nrcresearchpress.com by 91.121.58.235 on 09/08/12
For personal use only.

stable of all isolated type **3** chelates, whereas the 4-nitrobenzaldehyde derivative (**3**, Ar = 4-$NO_2C_6H_4$) could not be obtained at all (4). To provide information on the chelate-forming properties of *N*-(2-hydroxyphenylmethyl)nitrones, a series of aromatic aldonitrones was synthesized. The synthesis of these aromatic aldonitrones proceeded from salicylaldoxime **4** via the intermediate hydroxylamine **5** (which could not be isolated) to the nitrones **6**. These aromatic aldonitrones **6** were reacted with diphenylborinic acid anhydride to achieve the synthesis of the diphenylboron chelates **2**. In addition, a possible ring–chain isomerism or a rearrangement of the ligand (**6** ⇌ **7**) was examined by acylation experiments using an example compound (**6***e*). The same example ligand **6***e* and its diphenylboron chelate **2***b* were subjected to single crystal X-ray crystallographic analysis to provide unambiguous proof of the respective molecular structures and elucidation of possible changes in the molecular geometry concomitant with chelate formation.

Experimental

General procedures

All preparations and reactions were carried out under normal conditions, without protective gas atmosphere. Commercial solvents were used as supplied. Oxybis(diphenylborane) was prepared according to literature methods, from sodium tetraphenylborate (5) or from 2-(diphenylboryloxy)ethylamine (6). Melting points, measured on a Linström SPA-1 apparatus, are uncorrected. Elemental analyses: (C, H, N, O) Carlo Erba Elemental Analyzer 1106; (B) oxidative disintegration (Schöninger) and potentiometric titration. Infrared spectra: Phillips PU 9800 FT-IR spectrometer, V 3.00, and Mattson Genesis Series FTIR Rev. I (ATI Unicam); ^{1}H nmr: Varian EM 390; ^{11}B nmr: Bruker AC 200. Mass spectra: Finnigan MAT 8430.

8-(4-Methoxyphenylmethylene)-6,6-diphenyl-5,7-dioxa-8-azonia-6-borata-5*H*-6,7,8,9-tetrahydrobenzocycloheptene,[3] 2*a*

6*b* (0.26 g, 1.0 mmol) and oxybis(diphenylborane) (0.17 g, 0.5 mmol) are dissolved in 20 mL of absolute ethanol and refluxed for 10 min. The solvent is distilled off to dryness. Yield: 0.41 g (97%) of slightly discolored white crystals; mp 170–173°C. Infrared (KBr, cm^{-1}): 1650 (C═N), 1599 (C═C); ^{1}H nmr (90 MHz, $CDCl_3$–TMS), δ (ppm): 3.80 (s, OCH_3), 4.93 (s, NCH_2), 6.85 and 8.09 (d and d, J = 9 Hz, AA′BB′ system, OC_6H_4), 6.9–8.0 (m, 14 aromatic H and CH═N); ^{11}B nmr (64 MHz, $CDCl_3$–Et_2OBF_3), δ (ppm): 8.7 ($W_{1/2}$ = 342 Hz), 30.6 ($W_{1/2}$ = 342 Hz), and 46.3 ($W_{1/2}$ = 257 Hz); ratio of peak areas 1:1:1. Anal. calcd. for $C_{27}H_{24}BNO_3$: C 76.97, H 5.74, B 2.57, N 3.32; found: C 76.88, H 5.76, B 2.68, N 3.20. The product gives a blue-colored solution upon the addition of diphenylcarbazone in ethanol, indicating the presence of the chelated diphenylborenium (Ph_2B^+) ion (7).

8-(4-Dimethylaminophenylmethylene)-6,6-diphenyl-5,7-dioxa-8-azonia-6-borata-5*H*-6,7,8,9-tetrahydrobenzocycloheptene,[4] 2*b*

6*e* (0.27 g, 1.0 mmol) and oxybis(diphenylborane) (0.17 g, 0.5 mmol) are dissolved in 20 mL of absolute ethanol and refluxed for 10 min. Upon cooling to room temperature crystallization commences. Yield: 0.42 g (97%) of yellow crystals; mp 205°C (from ethanol). Infrared (KBr, cm^{-1}): 1640 (C═N), 1593 (C═C); ^{1}H nmr (90 MHz, $CDCl_3$–TMS), δ (ppm): 3.10 (s, $(CH_3)_2N$), 5.06 (s, $N(O)CH_2$), 6.75 and 8.21 (d and d, J = 9 Hz, AA′BB′ system, NC_6H_4), 6.9–8.0 (m, 14 aromatic H and CH═N); ^{1}H nmr (90 MHz, DMSO-d_6–TMS), δ (ppm): 3.05 (s, $(CH_3)_2N$), 5.05 (s, $N(O)CH_2$), 6.79 and 8.13 (d and d, J = 9 Hz, AA′BB′ system, NC_6H_4), 6.6–8.0 (m, 14 aromatic H), 8.36 (s, CH═N); ^{11}B nmr (64 MHz, $CDCl_3$–Et_2OBF_3), δ (ppm): 8.5 ($W_{1/2} \approx$ 300 Hz) and 46.5 ($W_{1/2}$ = 260 Hz); ratio of peak areas 1:2. Anal. calcd. for $C_{28}H_{27}BN_2O_2$: C 77.43, H 6.27, B 2.49, N 6.45; found: C 77.43, H 6.24, B 2.45, N 6.48. **2***b* gives a blue-colored solution upon addition of diphenylcarbazone as described for **2***a*. Crystals suitable for X-ray analysis were obtained by slow crystallization from absolute ethanol.

8-(4-Diethylaminophenylmethylene)-6,6-diphenyl-5,7-dioxa-8-azonia-6-borata-5H-6,7,8,9-tetrahydrobenzocycloheptene, 2*c*

6*f* (0.30 g, 1.0 mmol) and oxybis(diphenylborane) (0.17 g, 0.5 mmol) are dissolved in 20 mL of absolute ethanol and refluxed for 10 min. Crystallization starts upon cooling. Yield: 0.26 g (56%) of yellowish crystals; mp 183°C (from ethanol). Infrared (KBr, cm^{-1}): 1642 (C═N), 1593 (C═C); ^{1}H nmr (90 MHz, $CDCl_3$ – TMS), δ (ppm): 1.16 (t, J = 8 Hz, 2 CH_3), 3.35 (q, J = 8 Hz, 2 NCH_2), 4.83 (s, $N(O)CH_2$), 6.55 and 7.95 (d and d, J = 9 Hz, AA′BB′ system, NC_6H_4), 6.7–7.8 (m, 14 aromatic H and CH═N); ^{11}B nmr (64 MHz, $CDCl_3$–Et_2OBF_3), δ (ppm): 8.8 ($W_{1/2}$ = 550 Hz) and 46.6 ($W_{1/2}$ = 430 Hz); ratio of peak areas 5:1. Mass spectrum (EI, 150°C), *m/z* (%): 385 (74) [$M^+ - C_6H_5$], 369 (43) [$M^+ - C_6H_5 - O$], 298 (44) [**6***f*$^+$], 282 (21) [**6***f*$^+ - O$], 192 (59), 177 (100), 161 (42), 133 (32), 105 (26), 78 (38), 77 (32). Anal. calcd. for $C_{30}H_{31}BN_2O_2$: C 77.93, H 6.76, B 2.34, N 6.06; found: C 77.93, H 6.90, B 2.35, N 6.09. **2***c* gives a blue-colored solution upon addition of diphenylcarbazone as described for **2***a*.

Synthesis of *C*-aryl-*N*-(2-hydroxyphenylmethyl)nitrones, 6 (general procedure)

Salicylaldoxime, **4** (13.7 g, 100 mmol) is dissolved in 50 mL of methanol. After the addition of sodium cyanotrihydroborate[5] (4.2 g, 67 mmol), 50 mL of 2 N HCl solution is added dropwise under stirring, the mixture being kept at a constant pH of 3 using a pH-stat automatic titrator. The consumption is finished after about 40 min and the solution is brought to pH 6.5 with 2 N NaOH solution. A third of this solution (~40 mL), containing the hydroxylamine **5**, is mixed with 30 mmol

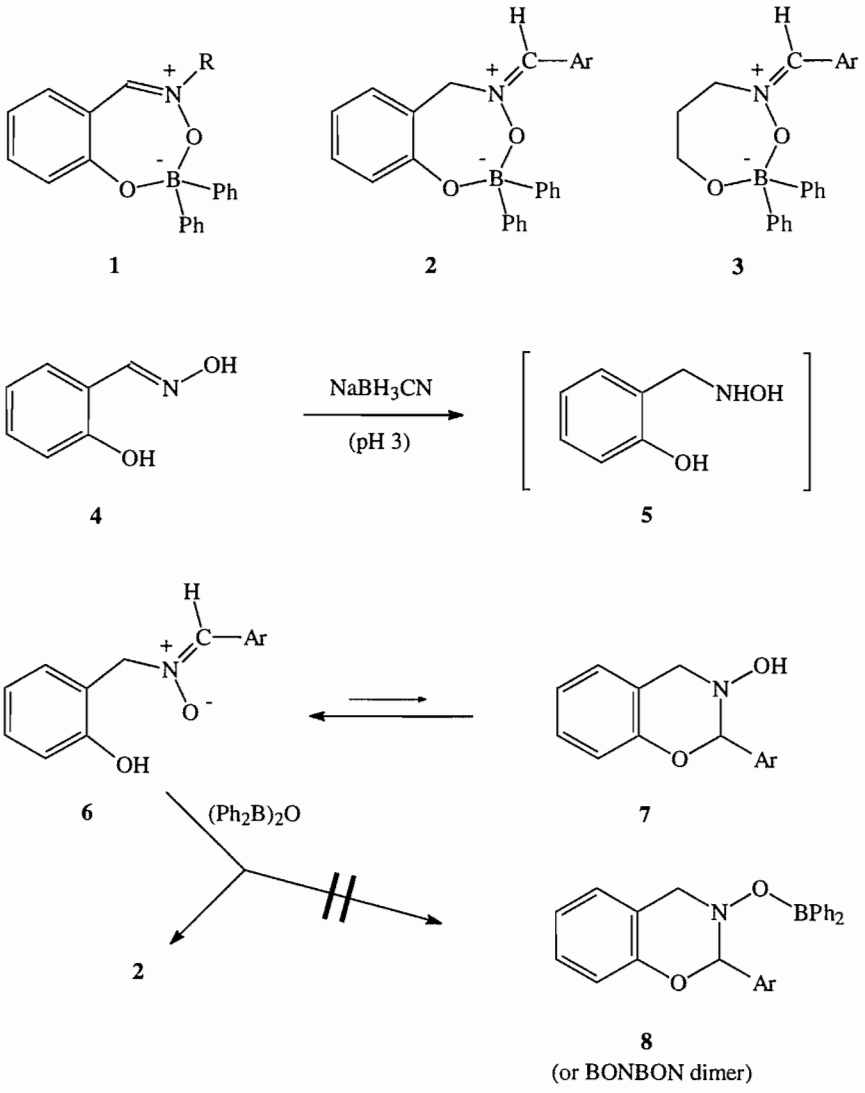
[3] Alternative nomenclature: *N*-(4-methoxyphenylmethylene)-*N*-[(2-diphenylboryloxyphenyl)methyl]amine *N*-oxide (O→B complex).

[4] Alternative nomenclature: *N*-(4-dimethylaminophenylmethylene)-*N*-[(2-diphenylboryloxyphenyl)methyl]amine *N*-oxide (O→B complex).

[5] Sodium cyanoborohydride ($NaBH_3CN$).

© 1997 NRC Canada

Scheme 1.



1 2 3 4 5 6 7 2 8

(or BONBON dimer)

	Ar
2*a*	4-$MeOC_6H_4$
2*b*	4-$Me_2NC_6H_4$
2*c*	4-$Et_2NC_6H_4$

	Ar
6*a*	C_6H_5
6*b*	4-$MeOC_6H_4$
6*c*	4-$O_2NC_6H_4$
6*d*	4-ClC_6H_4
6*e*	4-$Me_2NC_6H_4$
6*f*	4-$Et_2NC_6H_4$
6*g*	2,4,6-$Me_3C_6H_2$
6*h*	1-naphthyl

of an aromatic aldehyde and is refluxed for 30 min.[6] Upon cooling, the nitrone **6** precipitates and is recrystallized from ethanol.

[6] The remaining two thirds of the solution are reacted similarly with aromatic aldehydes to give the nitrones **6**.

C-*Phenyl*-N-*(2-hydroxyphenylmethyl)nitrone,* **6***a*
From benzaldehyde (3.18 g, 30 mmol). Yield: 5.46 g (80%) of colorless crystals; mp 174°C. Infrared (KBr, cm^{-1}): 3000–1700 ("curtain", O-H), 1609 (C═N), 1595 (C═C); ^1H nmr (90 MHz, $CDCl_3$–TMS), δ (ppm): 5.07 (s, NCH_2), 6.8–7.5 (m, 7 aromatic H), 7.50 (s, CH═N), 8.1–8.3 (m, 2 aromatic H), 11.35 (s, broad, exchangeable, OH). Anal. calcd. for

Can. J. Chem. Downloaded from www.nrcresearchpress.com by 91.121.58.235 on 09/08/12
For personal use only.

© 1997 NRC Canada

Can. J. Chem. Downloaded from www.nrcresearchpress.com by 91.121.58.235 on 09/08/12
For personal use only.

Table 1. Crystallographic data.[a]

Compound	**2***b*	**6***e*
Formula	$C_{28}H_{27}BN_2O_2$	$C_{16}H_{18}N_2O_2$
FW	434.34	270.33
Crystal system	Triclinic	Monoclinic
Space group	$P\bar{1}$ (No. 2)	$P2_1/a$ (No. 14)
a, Å	10.6802(8)	12.2319(8)
b, Å	11.1809(4)	7.071(1)
c, Å	10.1520(3)	17.2005(9)
α, °	105.847(3)	90
β, °	92.567(4)	107.520(4)
γ, °	84.610(5)	90
V, Å^3	1160.8(1)	1418.8(2)
Z	2	4
ρ_{calc}, g/cm^3	1.242	1.265
F(000)	460	576
μ(Cu K_α), cm^{-1}	5.74	6.42
Crystal size, mm	0.12 × 0.30 × 0.35	0.08 × 0.25 × 0.40
Transmission factors	0.90–1.00	0.88–1.00
Scan type	ω–2θ	ω–2θ
Scan range, deg in ω	1.31 + 0.20 tan θ	1.31 + 0.20 tan θ
Scan speed, deg/min	32 (up to 9 scans)	32 (up to 9 scans)
Data collected	+*h*, ±*k*, ±*l*	+*h*, +*k*, ±*l*
$2\theta_{max}$, deg	155	155
Crystal decay, %	Negligible	Negligible
Total reflections	5015	3266
Total unique reflections	4754	3116
R_{merge}	0.023	0.011
Reflections with $I \geq 3\sigma(I)$	3379	1800
No. of variables	383	254
R	0.035	0.032
R_w	0.036	0.032
gof	2.37	2.08
Max Δ/σ (final cycle)	0.0007	0.0003
Residual density e/Å^3	–0.10 to 0.12	–0.08 to 0.13

[a]Temperature 294 K, Rigaku AFC6S diffractometer, Cu K_α radiation (λ = 1.54178 Å), graphite monochromator, takeoff angle 6.0°, aperture 6.0 × 6.0 mm at a distance of 285 mm from the crystal, stationary background counts at each end of the scan (scan/background time ratio 2:1), $\sigma^2(F^2) = [S^2(C + 4B)]/Lp^2$ (*S* = scan rate, *C* = scan count, *B* = normalized background count), function minimized $\Sigma w(|F_o| - |F_c|)^2$ where $w = 4F_o^2/\sigma^2(F_o^2)$, $R = \Sigma||F_o| - |F_c||/\Sigma|F_o|$, $R_w = (\Sigma w(|F_o| - |F_c|)^2/\Sigma w|F_o|^2)^{1/2}$, and gof = $[\Sigma w(|F_o| - |F_c|)^2/(m - n)]^{1/2}$. Values given for *R*, R_w, and gof are based on those reflections with $I \geq 3\sigma(I)$.

$C_{14}H_{13}NO_2$: C 74.00, H 5.77, N 6.16; found: C 73.94, H 5.78, N 6.09.

C-*(4-Methoxyphenyl)*-N-*(2-hydroxyphenylmethyl)nitrone,* **6**b
From 4-methoxybenzaldehyde (4.08 g, 30 mmol). Yield: 6.20 g (80%) of colorless crystals; mp 166°C. Infrared (KBr, cm^{-1}): 3100–1700 ("curtain", O-H), 1603 (C═N, C═C); ^{1}H nmr (90 MHz, $CDCl_3$–TMS), δ (ppm): 3.80 (s, OCH_3), 5.02 (s, NCH_2), 6.86 and 8.13 (d and d, *J* = 9 Hz, AA′BB′ system, OC_6H_4), 6.66–7.36 (m, 4 aromatic H), 7.43 (s, CH═N), 11.75 (s, exchangeable, OH). Anal. calcd. for $C_{15}H_{15}NO_3$: C 70.02, H 5.88, N 5.44; found: C 69.90, H 5.87, N 5.37.

C-*(4-Nitrophenyl)*-N-*(2-hydroxyphenylmethyl)nitrone,* **6**c
From 4-nitrobenzaldehyde (4.53 g, 30 mmol). Yield: 6.42 g (79%) of yellow crystals; mp 174°C. Infrared (KBr, cm^{-1}): 3200–1700 ("curtain", O-H), 1598 and 1579 (C═N, C═C); ^{1}H nmr (90 MHz, $CDCl_3$ – TMS), δ (ppm): 5.15 (s, NCH_2), 6.76–7.43 (m, 4 aromatic H), 7.66 (s, CH═N), 8.20 and 8.35 (d and d, *J* = 9 Hz, AA′BB′ system, $O_2NC_6H_4$), 10.43 (s, exchangeable, OH). Anal. calcd. for $C_{14}H_{12}N_2O_4$: C 61.76, H 4.44, N 10.29; found: C 61.21, H 4.47, N 9.99.

C-*(4-Chlorophenyl)*-N-*(2-hydroxyphenylmethyl)nitrone,* **6**d
From 4-chlorobenzaldehyde (4.22 g, 30 mmol). Yield: 5.78 g (74%) of colorless needles; mp 174°C. Infrared (KBr, cm^{-1}): 3000–1700 ("curtain", O-H), 1588 (C═N, C═C); ^{1}H nmr (90 MHz, $CDCl_3$–TMS), δ (ppm): 5.10 (s, NCH_2), 6.73–7.56 (m, 4 aromatic H), 7.38 and 8.20 (d and d, *J* = 9 Hz, AA′BB′ sys-

© 1997 NRC Canada

Can. J. Chem. Downloaded from www.nrcresearchpress.com by 91.121.58.235 on 09/08/12
For personal use only.

tem, ClC_6H_4), 7.52 (s, CH═N), 11.13 (s, exchangeable, OH). Anal. calcd. for $C_{14}H_{12}ClNO_2$: C 64.25, H 4.62, Cl 13.55, N 5.35; found: C 64.25, H 4.60, Cl 13.19, N 5.23.

C-*(4-Dimethylaminophenyl)*-N-*(2-hydroxyphenylmethyl)-nitrone,* ***6e***

From 4-dimethylaminobenzaldehyde (4.48 g, 30 mmol). Yield: 7.20 g (89%) of pale yellow crystals; mp 200°C. Infrared (KBr, cm^{-1}): 3000–1700 ("curtain", O-H), 1618 (C═N), 1589 (C═C); ^1H nmr (90 MHz, $CDCl_3$–TMS), δ (ppm): 3.07 (s, $(CH_3)_2N$), 5.04 (s, $N(O)CH_2$), 6.96 and 8.13 (d and d, J = 9 Hz, AA′BB′ system, NC_6H_4), 6.80–7.33 (m, 4 aromatic H), 7.36 (s, CH═N), 12.25 (s, exchangeable, OH). Anal. calcd. for $C_{16}H_{18}N_2O_2$: C 71.09, H 6.71, N 10.36; found: C 71.07, H 6.77, N 10.37. Crystals suitable for X-ray analysis were obtained by very slow cooling of a saturated solution of ***6e*** in ethyl acetate, mp 201°C.

C-*(4-Diethylaminophenyl)*-N-*(2-hydroxyphenylmethyl)-nitrone,* ***6f***

From 4-diethylaminobenzaldehyde (5.32 g, 30 mmol). Yield: 5.43 g (61%) of pale yellow crystals; mp 176°C. Infrared (KBr, cm^{-1}): 3100–1700 ("curtain", O-H), 1597 and shoulder at 1610 (C═N, C═C); ^1H nmr (90 MHz, $CDCl_3$–TMS), δ (ppm): 1.18 (t, J = 8 Hz, 2 CH_3), 3.38 (q, J = 8 Hz, 2 NCH_2), 5.02 (s, $N(O)CH_2$), 6.63 and 8.08 (d and d, J = 9 Hz, AA′BB′ system, NC_6H_4), 6.50–7.30 (m, 4 aromatic H), 7.33 (s, CH═N), 12.36 (s, exchangeable, OH). Anal. calcd. for $C_{18}H_{22}N_2O_2$: C 72.45, H 7.43, N 9.39; found: C 72.52, H 7.39, N 9.39.

C-*(2,4,6-Trimethylphenyl)*-N-*(2-hydroxyphenylmethyl)-nitrone,* ***6g***

From 2,4,6-trimethylbenzaldehyde (4.45 g, 30 mmol). Yield: 4.96 g (61%) of a colorless powder; mp 166°C. Infrared (KBr, cm^{-1}): 3200–1900 ("curtain", O-H), 1592 and shoulder at 1600 (C═N, C═C); ^1H nmr (90 MHz, $CDCl_3$–TMS), δ (ppm): 2.16 (s, 2 *o*-CH_3), 2.26 (s, *p*-CH_3), 5.08 (s, NCH_2), 6.70–7.40 (m, 6 aromatic H), 7.75 (s, CH═N), 11.30 (s, exchangeable, OH). Anal. calcd. for $C_{17}H_{19}NO_2$: C 75.81, H 7.11, N 5.20; found: C 75.96, H 7.12, N 5.20.

C-*(1-Naphthyl)*-N-*(2-hydroxyphenylmethyl)nitrone,* ***6h***

From 1-naphthylbenzaldehyde (4.69 g, 30 mmol). Yield: 6.34 g (76%) of colorless crystals; mp 164°C. Infrared (KBr, cm^{-1}): 3100–1800 ("curtain", O-H), 1604 (C═N), 1590 (C═C); ^1H nmr (90 MHz, $CDCl_3$–TMS), δ (ppm): 5.23 (s, NCH_2), 6.73–8.10 (m, 10 aromatic H), 8.30 (s, CH═N), 9.35 (d, J = 7.5 Hz, 1 aromatic H), 11.30 (s, exchangeable, OH). Anal. calcd. for $C_{18}H_{15}NO_2$: C 77.96, H 5.45, N 5.05; found: C 77.89, H 5.26, N 4.74.

3-Acetyloxy-2-(4-dimethylaminophenyl)-3,4-dihydro-2*H*-1,3-benzoxazine, 9*a* (Scheme 2)

A solution of acetylchloride (0.08 g, 1.0 mmol) in 5 mL of benzene is slowly added to a solution of ***6e*** (0.27 g, 1.0 mmol) and triethylamine (0.10 g, 1.0 mmol) in 20 mL of dry benzene. After 2 h of stirring at 50°C the precipitated triethylammonium chloride is filtered off, and the solution is evaporated in vacuo. The remaining oil is brought to crystallization with petroleum ether and (or) diethyl ether. Yield: 0.20 g (64%) of a slightly discolored white powder; mp 129°C (from benzene). Infrared (KBr, cm^{-1}): 1749 (C═O), 1612 (C═C); ^1H nmr (90 MHz, $CDCl_3$–TMS), δ (ppm): 1.93 (s, CH_3CO), 2.96 (s, $(CH_3)_2N$), 4.33 (s, broad, $N(O)CH_2$), 6.02 (s, O-CH-N), 6.72 and 7.46 (d and d, J = 7 Hz, AA′BB′ system, NC_6H_4), 6.9–7.4 (m, 4 aromatic H). Anal. calcd. for $C_{18}H_{20}N_2O_3$: C 69.21, H 6.45, N 8.97; found: C 68.90, H 6.56, N 8.84.

3-Benzoyloxy-2-(4-dimethylaminophenyl)-3,4-dihydro-2*H*-1,3-benzoxazine, 9*b*

6e (0.27 g, 1.0 mmol), triethylamine (0.10 g, 1.0 mmol), and benzoylchloride (0.14 g, 1.0 mmol) are reacted as described for ***9a***. Yield: 0.25 g (67%) of a colorless white powder; mp 129°C (from benzene – petroleum ether). Infrared (KBr, cm^{-1}): 1748 (C═O), 1615 (C═C); ^1H nmr (90 MHz, $CDCl_3$–TMS), δ (ppm): 2.90 (s, $(CH_3)_2N$), 4.50 (m, $N(O)CH_2$), 6.16 (s, O-CH-N), 6.68 and 7.88 (d and d, J = 8 Hz, AA′BB′ system, NC_6H_4), 6.8–7.6 (m, 9 aromatic H). Anal. calcd. for $C_{23}H_{22}N_2O_3$: C 73.78, H 5.92, N 7.48; found: C 74.06, H 6.10, N 7.27.

***C*-(4-Dimethylaminophenyl)-*N*-[2-(phenylcarbamoyloxy)-phenylmethyl]nitrone, 10**

6e (0.27 g, 1.0 mmol) in 30 mL of dry benzene is mixed with phenylisocyanate (0.12 g, 1.0 mmol) and refluxed for 6 h. The solvent is distilled off and the residue recrystallized from benzene – petroleum ether. Yield: 0.17 g (44%) of pale yellow crystals; mp 131°C. Infrared (KBr, cm^{-1}): 3409 (N-H), 1755 and 1741 (C═O), 1618 and 1590 (C═N, C═C); ^1H nmr (90 MHz, $CDCl_3$–TMS), δ (ppm): 3.04 (s, $(CH_3)_2N$), 5.03 (s, $N(O)CH_2$), 6.68 and 8.12 (d and d, J = 9 Hz, AA′BB′ system, NC_6H_4), 6.7–7.4 (m, 9 aromatic H), 7.35 (s, CH═N), ~11 (very broad, exchangeable, NH). Anal. calcd. for $C_{23}H_{23}N_3O_3$: C 70.93, H 5.95, N 10.79; found: C 70.72, H 5.99, N 10.75.

X-ray crystallographic analyses of 2*b* and 6*e*

Crystallographic data appear in Table 1. The final unit-cell parameters were obtained by least squares on the setting angles for 25 reflections with 2θ = 86.6°–93.5° for ***2b*** and 88.2°–95.9° for ***6e***. The intensities of three standard reflections, measured every 200 reflections throughout the data collections, showed only small random fluctuations for both compounds. The data were processed,[7] and corrected for Lorentz and polarization effects and for absorption (based on azimuthal scans).

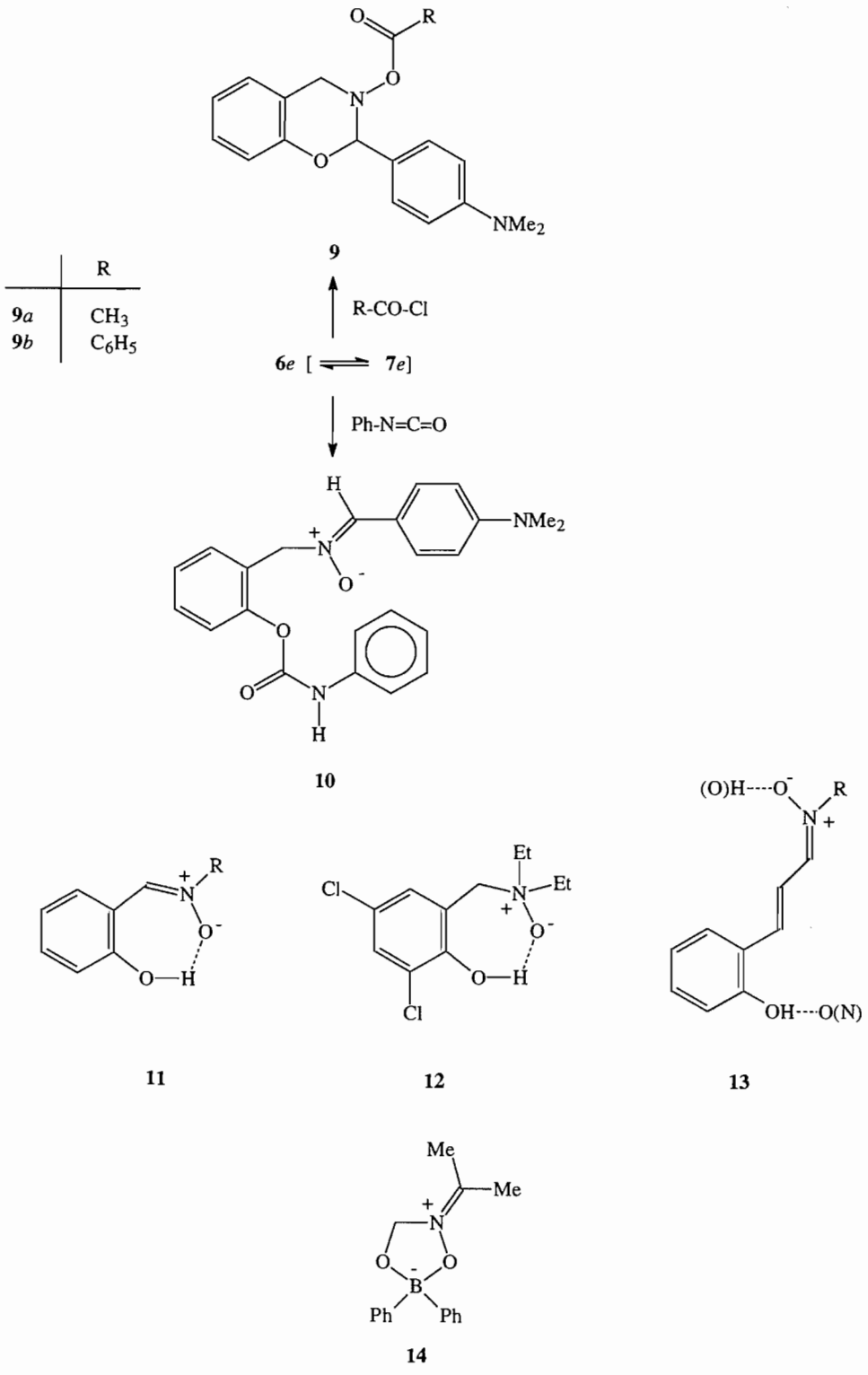
The structures were solved by direct methods, the coordinates of the non-hydrogen atoms being determined from *E*-maps or from subsequent difference Fourier syntheses. All non-hydrogen atoms were refined with anisotropic thermal parameters. For ***2b*** a difference map indicated that the NMe_2 hydrogen atoms (associated with C(27) and C(28)) were 3:2 twofold disordered with respect to rotation about

[7] *teXsan*: Crystal structure analysis package. Unix version 1.7. Molecular Structure Corporation. The Woodlands, Tex., U.S.A. 1995.

© 1997 NRC Canada

Can. J. Chem. Downloaded from www.nrcresearchpress.com by 91.121.58.235 on 09/08/12
For personal use only.

Scheme 2.



the N—C bonds. These disordered hydrogen atoms were fixed in calculated positions with C—H = 0.98 Å and B_H = 1.2 $B_{\text{bonded atom}}$ and all remaining hydrogen atoms of **2***b* and all those of **6***e* were refined with isotropic thermal parameters. Corrections for secondary extinction were applied (Zachariasen type, isotropic, Gaussian), the final values of the extinction coefficients being $7.8(2) \times 10^{-6}$ for **2***b* and $7.73(11) \times 10^{-6}$ for **6***e*. Neutral atom scattering factors for all atoms and anomalous dispersion corrections for the non-hydrogen atoms were taken from the *International tables for X-ray crystallography* (8). Final atomic coordinates and equivalent isotropic thermal parameters, bond lengths, bond

© 1997 NRC Canada

Can. J. Chem. Downloaded from www.nrcresearchpress.com by 91.121.58.235 on 09/08/12
For personal use only.

Table 2. Final atomic coordinates (fractional) and B_{eq} (Å^2).[a]

Atom	*x*	*y*	*z*	B_{eq}
		2*b*		
O(1)	0.25618(9)	0.18444(8)	0.47205(10)	3.44(2)
O(2)	0.2527(1)	0.05590(10)	0.2275(1)	4.41(3)
N(1)	0.3157(1)	0.0955(1)	0.5285(1)	3.34(3)
N(2)	0.3279(1)	0.5637(1)	1.0859(1)	4.43(3)
C(1)	0.3158(2)	–0.0357(1)	0.4446(2)	3.95(4)
C(2)	0.1918(1)	–0.0593(1)	0.3732(2)	3.65(3)
C(3)	0.1647(2)	–0.0087(1)	0.2637(2)	3.94(3)
C(4)	0.0523(2)	–0-0303(2)	0.1904(2)	5.26(5)
C(5)	–0.0309(2)	–0.1022(2)	0.2285(2)	5.90(5)
C(6)	–0.0049(2)	–0.1517(2)	0.3369(2)	5.43(5)
C(7)	0.1063(2)	–0.1299(1)	0.4103(2)	4.48(4)
C(8)	0.3524(1)	0.1250(1)	0.6557(2)	3.44(3)
C(9)	0.3475(1)	0.2419(1)	0.7561(2)	3.37(3)
C(10)	0.2905(2)	0.3561(1)	0.7420(2)	3.80(3)
C(11)	0.2858(2)	0.4610(1)	0.8487(2)	4.04(4)
C(12)	0.3365(1)	0.4604(1)	0.9794(2)	3.61(3)
C(13)	0.3957(2)	0.3460(2)	0.9936(2)	4.11(4)
C(14)	0.3996(2)	0.2418(2)	0.8860(2)	4.00(4)
C(15)	0.1924(1)	0.2904(1)	0.2910(2)	3.77(4)
C(16)	0.1589(2)	0.4028(2)	0.3861(2)	4.91(4)
C(17)	0.0859(2)	0.5001(2)	0.3521(2)	5.77(5)
C(18)	0.0445(2)	0.4864(2)	0.2197(3)	6.11(6)
C(19)	0.0749(2)	0.3769(2)	0.1229(3)	6.30(6)
C(20)	0.1472(2)	0.2806(2)	0.1580(2)	5.18(5)
C(21)	0.4309(1)	0.1925(1)	0.3049(2)	3.77(3)
C(22)	0.4999(2)	0.1192(2)	0.1935(2)	4.47(4)
C(23)	0.6246(2)	0.1355(2)	0.1756(2)	5.68(5)
C(24)	0.6844(2)	0.2267(2)	0.2701(3)	6.22(6)
C(25)	0.6198(2)	0.3014(2)	0.3804(3)	5.99(6)
C(26)	0.4949(2)	0.2841(2)	0.3974(2)	4.85(4)
C(27)	0.2654(2)	0.6803(2)	1.0723(2)	5.98(5)
C(28)	0.3744(2)	0.5619(2)	1.2219(2)	5.44(5)
B(1)	0.2839(2)	0.1774(2)	0.3215(2)	3.59(4)
		6*e*		
O(1)	0.37986(9)	0.1588(2)	0.28554(8)	5.29(3)
O(2)	0.4404(1)	0.3113(2)	0.17254(9)	6.46(4)
N(1)	0.2665(1)	0.1598(2)	0.25789(8)	4.08(3)
N(2)	0.2872(1)	0.1491(2)	0.64420(8)	4.55(4)
C(1)	0.2183(2)	0.1708(3)	0.1674(1)	4.60(5)
C(2)	0.2375(1)	0.3613(3)	0.13453(9)	3.94(4)
C(3)	0.3467(1)	0.4187(3)	0.13657(10)	4.64(4)
C(4)	0.3610(2)	0.5893(4)	0.1002(1)	5.91(6)
C(5)	0.2675(2)	0.6995(4)	0.0631(1)	6.30(7)
C(6)	0.1598(2)	0.6461(4)	0.0617(1)	6.13(6)
C(7)	0.1448(2)	0.4763(3)	0.0975(1)	4.95(5)
C(8)	0.2001(1)	0.1543(2)	0.3037(1)	4.02(4)
C(9)	0.2309(1)	0.1491(2)	0.39115(10)	3.73(4)
C(10)	0.3423(1)	0.1462(3)	0.4454(1)	4.02(4)
C(11)	0.3602(1)	0.1443(3)	0.5280(1)	4.07(4)
C(12)	0.2689(1)	0.1468(2)	0.5616(1)	3.80(4)
C(13)	0.1575(1)	0.1469(3)	0.5071(1)	4.27(4)
C(14)	0.1401(1)	0.1484(3)	0.4246(1)	4.17(4)
C(15)	0.4016(2)	0.1581(4)	0.7000(1)	5.86(6)
C(16)	0.1921(2)	0.1616(4)	0.6775(1)	5.24(5)

[a] $B_{eq} = (8/3)\pi^2\Sigma\Sigma(U_{ij}a_i{*}a_j{*}(\mathbf{a}_i.\mathbf{a}_j))$.

© 1997 NRC Canada

Can. J. Chem. Downloaded from www.nrcresearchpress.com by 91.121.58.235 on 09/08/12
For personal use only.

Table 3. Bond lengths (Å) with estimated standard deviations in parentheses.

Bond	Length	Bond	Length
		2b	
O(1)—N(1)	1.371(1)	O(1)—B(1)	1.549(2)
O(2)—C(3)	1.357(2)	O(2)—B(1)	1.488(2)
N(1)—C(1)	1.482(2)	N(1)—C(8)	1.294(2)
N(2)—C(12)	1.349(2)	N(2)—C(27)	1.445(2)
N(2)—C(28)	1.451(2)	C(1)—C(2)	1.492(2)
C(2)—C(3)	1.387(2)	C(2)—C(7)	1.388(2)
C(3)—C(4)	1.389(2)	C(4)—C(5)	1.385(3)
C(5)—C(6)	1.368(3)	C(6)—C(7)	1.379(3)
C(8)—C(9)	1.419(2)	C(9)—C(10)	1.402(2)
C(9)—C(14)	1.408(2)	C(10)—C(11)	1.361(2)
C(11)—C(12)	1.412(2)	C(12)—C(13)	1.413(2)
C(13)—C(14)	1.361(2)	C(15)—C(16)	1.387(2)
C(15)—C(20)	1.392(2)	C(15)—B(1)	1.613(2)
C(16)—C(17)	1.390(2)	C(17)—C(18)	1.369(3)
C(18)—C(19)	1.366(3)	C(19)—C(20)	1.383(3)
C(21)—C(22)	1.396(2)	C(21)—C(26)	1.394(2)
C(21)—B(1)	1.616(2)	C(22)—C(23)	1.387(3)
C(23)—C(24)	1.378(3)	C(24)—C(25)	1.371(3)
C(25)—C(26)	1.391(3)		
		6e	
O(1)—N(1)	1.324(2)	O(2)—C(3)	1.359(2)
N(1)—C(1)	1.491(2)	N(1)—C(8)	1.291(2)
N(2)—C(12)	1.370(2)	N(2)—C(15)	1.440(2)
N(2)—C(16)	1.446(2)	C(1)—C(2)	1.507(3)
C(2)—C(3)	1.385(2)	C(2)—C(7)	1.385(2)
C(3)—C(4)	1.394(3)	C(4)—C(5)	1.372(3)
C(5)—C(6)	1.363(3)	C(6)—C(7)	1.387(3)
C(8)—C(9)	1.437(2)	C(9)—C(10)	1.400(2)
C(9)—C(14)	1.396(2)	C(10)—C(11)	1.371(2)
C(11)—C(12)	1.404(2)	C(12)—C(13)	1.403(2)
C(13)—C(14)	1.370(2)		

angles, and intra-annular torsion angles appear in Tables 2–5, respectively. Hydrogen atom parameters, anisotropic thermal parameters, and torsion angles, intermolecular contacts, and least-squares planes are included as supplementary material.[8]

Results and discussion

Synthesis and structure of the nitrones 6

N-(2-Hydroxyphenylmethyl)hydroxylamines **5** were generated by the reduction of salicylaldoximes **4** with $NaBH_3CN$ at pH 3 (9) for the synthesis of the nitrones **6**. The hitherto unknown hydroxylamine **5** appears to be a very unstable compound and could not be isolated, neither as a free base nor as a hydrochloride salt. It was possible, however, to trap compound **5** in situ as its nitrone derivatives **6** by the addition of an aromatic aldehyde to the reaction mixture of the salicylaldoxime reduction. The condensation products **6** crystallized in good yields.

Since it has been reported that *N*-(2-hydroxyalkyl)nitrones (10), *N*-(3-hydroxyalkyl)nitrones (11), and also *N*-(2-hydroxynaphthylmethyl)nitrones (12) can isomerize to cyclotautomeric *N*-hydroxy-oxazolidine or *N*-hydroxy-perhydro-1,3-oxazine derivatives, an isomerism between the open-chain nitrone form **6** and the cyclic form **7** had to be considered. It is known from the literature (4, 10–13) that nitrones derived from aromatic aldehydes are very stable in their open-chain nitrone form, and that no trace of the ring form is detectable by spectroscopic means in inert solvents. Only aliphatic aldo- or ketonitrones display evidence of both forms in their nmr spectra.

The nitrone structure cannot be deduced unequivocally from the infrared spectra of **6** (KBr pellets) because the

[8] Copies of material on deposit may be purchased from: The Depository of Unpublished Data, Document Delivery, CISTI, National Research Council Canada, Ottawa, Canada K1A 0S2. Tables of hydrogen atom coordinates and bond lengths and angles involving hydrogen atoms have also been deposited with the Cambridge Crystallographic Data Centre and can be obtained on request from The Director, Cambridge Crystallographic Data Centre, University Chemical Laboratory, 12 Union Road, Cambridge CB2 1EZ, UK.

© 1997 NRC Canada

Table 4. Bond angles (deg) with estimated standard deviations in parentheses.

Bonds	Angle(deg)	Bonds	Angle(deg)
	2*b*		
N(1)-O(1)-B(1)	118.3(1)	C(3)-O(2)-B(1)	119.7(1)
O(1)-N(1)-C(1)	116.5(1)	O(1)-N(1)-C(8)	120.3(1)
C(1)-N(1)-C(8)	122.4(1)	C(12)-N(2)-C(27)	121.7(1)
C(12)-N(2)-C(28)	121.8(1)	C(27)-N(2)-C(28)	116.4(1)
N(1)-C(1)-C(2)	110.8(1)	C(1)-C(2)-C(3)	116.8(1)
C(1)-C(2)-C(7)	123.0(2)	C(3)-C(2)-C(7)	120.2(2)
O(2)-C(3)-C(2)	118.4(1)	O(2)-C(3)-C(4)	122.0(2)
C(2)-C(3)-C(4)	119.6(2)	C(3)-C(4)-C(5)	119.2(2)
C(4)-C(5)-C(6)	121.4(2)	C(5)-C(6)-C(7)	119.6(2)
C(2)-C(7)-C(6)	120.1(2)	N(1)-C(8)-C(9)	131.0(1)
C(8)-C(9)-C(10)	126.9(1)	C(8)-C(9)-C(14)	116.5(1)
C(10)-C(9)-C(14)	116.5(1)	C(9)-C(10)-C(11)	121.5(2)
C(10)-C(11)-C(12)	121.8(1)	N(2)-C(12)-C(11)	121.6(1)
N(2)-C(12)-C(13)	121.5(1)	C(11)-C(12)-C(13)	116.8(1)
C(12)-C(13)-C(14)	120.6(2)	C(9)-C(14)-C(13)	122.7(1)
C(16)-C(15)-C(20)	115.4(2)	C(16)-C(15)-B(1)	125.3(1)
C(20)-C(15)-B(1)	119.2(2)	C(15)-C(16)-C(17)	122.8(2)
C(16)-C(17)-C(18)	119.6(2)	C(17)-C(18)-C(19)	119.5(2)
C(18)-C(19)-C(20)	120.4(2)	C(15)-C(20)-C(19)	122.3(2)
C(22)-C(21)-C(26)	115.9(2)	C(22)-C(21)-B(1)	122.1(2)
C(26)-C(21)-B(1)	121.9(2)	C(21)-C(22)-C(23)	122.3(2)
C(22)-C(23)-C(24)	119.8(2)	C(23)-C(24)-C(25)	119.7(2)
C(24)-C(25)-C(26)	120.0(2)	C(21)-C(26)-C(25)	122.3(2)
O(1)-B(1)-O(2)	111.2(1)	O(1)-B(1)-C(15)	103.5(1)
O(1)-B(1)-C(21)	110.6(1)	O(2)-B(1)-C(15)	110.5(1)
O(2)-B(1)-C(21)	108.2(1)	C(15)-B(1)-C(21)	112.8(1)
	6*e*		
O(1)-N(1)-C(1)	114.7(1)	O(1)-N(1)-C(8)	124.3(1)
C(1)-N(1)-C(8)	121.0(1)	C(12)-N(2)-C(15)	120.9(2)
C(12)-N(2)-C(16)	120.8(2)	C(15)-N(2)-C(16)	118.0(2)
N(1)-C(1)-C(2)	112.4(1)	C(1)-C(2)-C(3)	120.7(2)
C(1)-C(2)-C(7)	119.9(2)	C(3)-C(2)-C(7)	119.3(2)
O(2)-C(3)-C(2)	121.5(2)	O(2)-C(3)-C(4)	119.0(2)
C(2)-C(3)-C(4)	119.5(2)	C(3)-C(4)-C(5)	120.0(2)
C(4)-C(5)-C(6)	121.1(2)	C(5)-C(6)-C(7)	119.2(2)
C(2)-C(7)-C(6)	120.8(2)	N(1)-C(8)-C(9)	128.7(2)
C(8)-C(9)-C(10)	126.4(1)	C(8)-C(9)-C(14)	116.2(1)
C(10)-C(9)-C(14)	117.4(2)	C(9)-C(10)-C(11)	120.7(2)
C(10)-C(11)-C(12)	121.9(2)	N(2)-C(12)-C(11)	121.7(2)
N(2)-C(12)-C(13)	121.1(1)	C(11)-C(12)-C(13)	117.2(2)
C(12)-C(13)-C(14)	120.6(2)	C(9)-C(14)-C(13)	122.2(2)

Table 5. Intra-annular torsion angles (deg) for **2*b*** with standard deviations in parentheses.

Atoms	Value (deg)	Atoms	Value (deg)
O(1)-N(1)-C(1)-C(2)	–40.0(2)	C(3)-O(2)-B(1)-O(1)	25.7(2)
N(1)-C(1)-C(2)-C(3)	73.2(2)	O(2)-B(1)-O(1)-N(1)	58.3(2)
C(1)-C(2)-C(3)-O(2)	1.3(2)	B(1)-O(1)-N(1)-C(1)	–46.6(2)
C(2)-C(3)-O(2)-B(1)	–67.7(2)		

Can. J. Chem. Downloaded from www.nrcresearchpress.com by 91.121.58.235 on 09/08/12
For personal use only.

© 1997 NRC Canada

Fig. 1. Stereoview of **6*e***; 33% probability thermal ellipsoids are shown for the non-hydrogen atoms. Unfilled bonds and fine lines represent hydrogen bonds and C—H···O interactions, respectively.

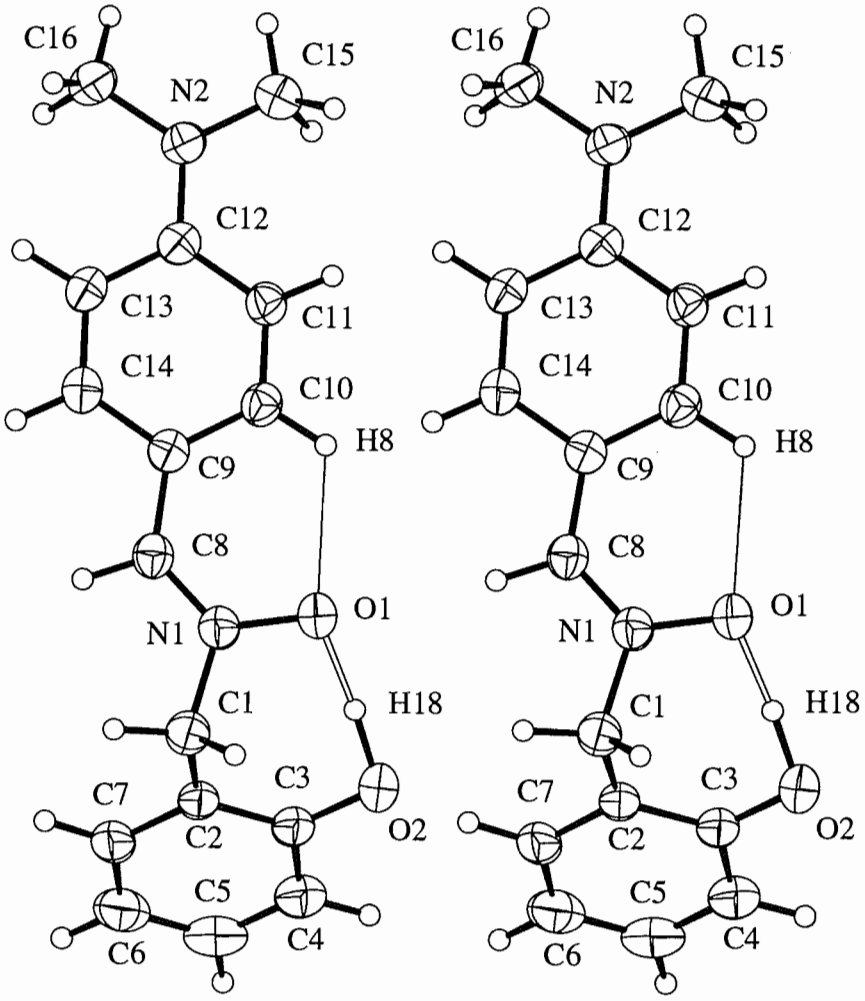


Table 6. Comparison of selected ^{1}H nmr data of 4-substituted benzaldehyde nitrones **6** and pK_a values of the corresponding *N*-methylnitrones (15).

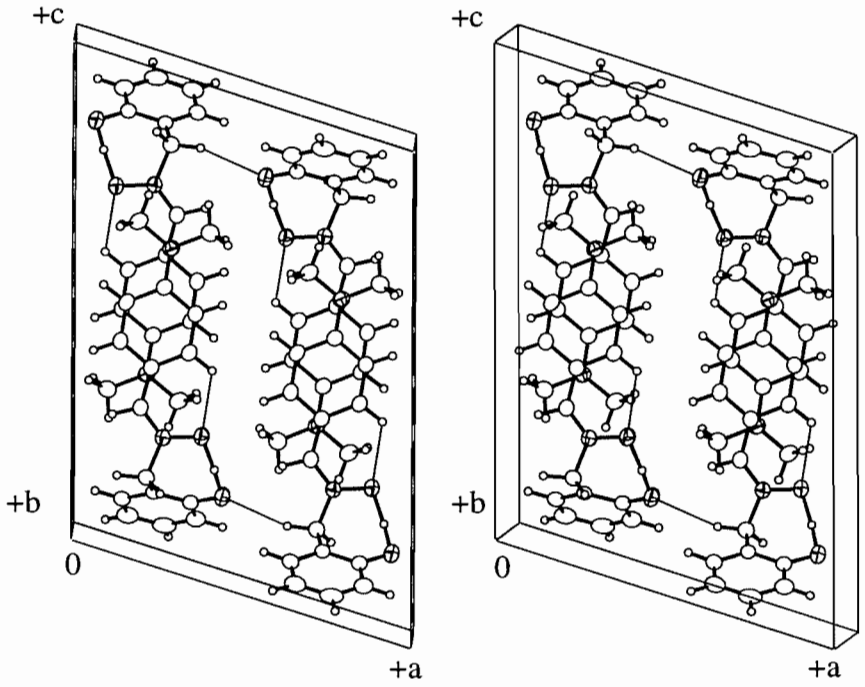
Ar	$\delta_{CH=N}$ (ppm)	δ_{OH} (ppm)	p*K*a values for Ar-CH=N(O)Me (15)
4-$NO_2C_6H_4$ (**6*c***)	7.66	10.43	6.10
4-ClC_6H_4 (**6*d***)	7.52	11.13	7.67
C_6H_5 (**6*a***)	7.50	11.35	8.26
4-$MeOC_6H_4$ (**6*b***)	7.43	11.75	9.43
4-$Me_2NC_6H_4$ (**6*e***)	7.36	12.25	11.94
4-$Et_2NC_6H_4$ (**6*f***)	7.33	12.36	—

expected C=N stretching vibrations near 1600 cm^{-1} coincide with the ν_{16} C=C ring stretching of the aromatic ring systems in these molecules, and the distinction is further complicated by resonance interactions between the nitrone and the conjugated aryl group. Very broad "curtain" type O-H association bands between 3100 and 1700 cm^{-1}, however, are consistent with the nitrone form **6** having an intramolecular hydrogen bond involving the "chelated" phenolic proton like those known for salicylaldonitrones **11** (1, 14) (Scheme 2). The nitrone form is clearly demonstrated in the ^{1}H nmr spectra of **6** by signals for the CH=N methine proton at ~7.5 ppm, similar to those observed for other *C*-arylnitrones (1, 4, 10*a*, 12, 14*b*, 15). Signals for the O-CH-N methine protons of the cyclic form **7**, typically around 5–6 ppm, were not detected. In accor-

Can. J. Chem. Downloaded from www.nrcresearchpress.com by 91.121.58.235 on 09/08/12
For personal use only.

© 1997 NRC Canada

Fig. 2. Stereoview of the packing arrangement of **6*e***; 33% probability thermal ellipsoids are shown for the non-hydrogen atoms. Unfilled bonds and fine lines represent hydrogen bonds and C—H···O interactions, respectively.



Can. J. Chem. Downloaded from www.nrcresearchpress.com by 91.121.58.235 on 09/08/12
For personal use only.

dance with the predominant or exclusive open-chain nitrone form **6** in solution, the "chelated" phenolic proton gives rise in each case to a downfield signal at ~11.4 ppm, characteristic for intramolecular hydrogen bonds of this type (1, 12*a*, 12*c*, 14*a*, 16). Comparison of the ^{1}H nmr spectra of the 4-substituted benzaldonitrones **6** (see Table 6) shows that the increasing downfield shift of the OH signal reflects the strengthening of the hydrogen bond due to the increasing basicity of the azomethine *N*-oxide group, going from the 4-nitro- to the 4-diethylaminophenyl derivative. For comparison, Table 6 also lists the pK_a values reported for the *N*-methylnitrones having the corresponding 4-substituents at the *C*-aryl residue (17). There is also an increasing, though less distinct, balancing upfield shift of the signals assigned to the CH═N methine protons in the same sequence of nitrones **6** (Table 6), indicating the gain in shielding by the electron-donating substituents in the 4-position.

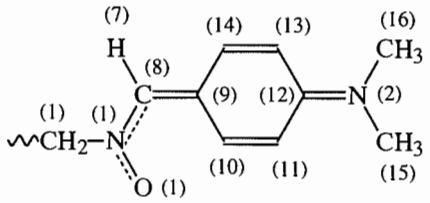
The X-ray analysis of **6*e*** establishes the nitrone structure of the type **6** compounds, at least in the crystalline state, and shows the intramolecular hydrogen bond between the phenolate and *N*-oxide oxygen atoms, already suggested by the ^{1}H nmr and infrared spectra (Fig. 1). In the crystal of **6*e*** this O(2)—H(18)···O(1) hydrogen bond (O—H = 1.13(3) Å, O···H = 1.40(3) Å, O···O = 2.521(3) Å, O—H···O = 174(2)°) represents a strong hydrogen bond (18) within a seven-membered "proton chelate" having metrical parameters similar to those of two other phenolic *N*-oxides with intramolecular H-bridges: the *N-tert*-butylsalicylaldonitrone **11** (R = CMe_3) (19) and the 2-(diethylaminomethyl)-4,6-dichlorophenol *N*-oxide **12** (20) with H···O (O···O) distances of 1.53 Å (2.47 Å) and 1.22/1.31 Å (2.407/2.425 Å), respectively. The nearly linear O—H...O angle in **6*e*** may contribute to the bonding energy and lies in between the corresponding values of 170.6° in **11** (19) and 175/177° in **12** (20). The nearly linear intramolecular O—H...O angles in **6*e***, **11**, and **12** are comparable to those reported for *inter*molecular O—H···O(N) hydrogen bonds in various vinyl salicylaldonitrones like **13** (21) that cannot form intramolecular H-bridges and crystallize in "head-to-tail" chains via O–H...O hydrogen bonds (O···H = 1.44–1.96 Å, O···O = 2.567–2.662 Å, O—H···O = 135°–180°). Furthermore, the (*Z*) arrangement at the nitrone double bond allows the formation of an intramolecular C—H···O hydrogen bond (C(10)—H(8)...O(1): C—H = 1.00(1) Å, O···H = 2.30(1) Å, C···O = 2.922(2) Å, C—H...O = 119(1)°). The geometry of this intramolecular C—H···O interaction is clearly consistent with the presence of a hydrogen bond (22) which may play a role in determining the solid state molecular conformation.

The crystal packing of **6*e*** (Fig. 2) is dominated by three intermolecular C—H···O contacts that meet the requirements of hydrogen bonding (22): C(1)—H(2) and C(8)—H(7) both interact with the same phenolic oxygen atom O(2) to link *a*-glide related "helical enantiomers" into linear chains, and one of the *N*-methyl groups forms the C(15)—H(14)...O hydrogen bond to a neighboring nitrone oxygen atom cross-linking the chains along *b*. The geometry of these interactions is as follows: C(1)—H(2)...O(2)($-1/2 + x$, $1/2 - y$, z), C(8)—H(7)···O(2)($-1/2 + x$, $1/2 - y$, z), C(15)—H(14)···O(1)($1 - x$, $-y$, $1 - z$); C—H = 1.03(2), 1.00(2), 1.01(2) Å; H···O = 2.47(2), 2.48(2), 2.47(2) Å; C···O = 3.429(2), 3.306(2), 3.439(2) Å; and C—H···O = 153(1)°, 165(1)°, 160(2)°; respectively.

The C═N bond length (1.291(2) Å) does not differ significantly from the values found for other nitrones (19, 21, 23, 24) whereas the N—O bond (1.324(2) Å) is slightly longer, prob-

© 1997 NRC Canada

Fig. 3. Mesomeric electron distribution in the 4-dimethylaminophenylmethylidene resonance system.



ably because of the involvement of the nitrone oxygen atom in the very strong intramolecular hydrogen bond. As a consequence of the interaction of the nitrone group and the 4-dimethylaminophenyl π-system, an approximate coplanarity is seen in this part of the molecule. The relatively short bond lengths for N(2)—C(12) (1.370(2) Å), C(10)—C(11) (1.371(2) Å), C(13)—C(14) (1.370(2) Å), and C(8)—C(9) (1.437(2) Å) are indicative of a significant contribution from the 4-dimethylaminomethylidene resonance form having double bonds at these locations (Fig. 3). The phenolic ring system of C(2)—C(7) plus O(2) is twisted out of the mean plane of the remainder of the molecule by about 60°.

Synthesis and structure of the boron chelates 2

To examine the chelate-forming properties of the nitrones **6** by replacement of the "chelated" phenolic proton with a diphenylborenium ion (Ph_2B^+), the compounds **6** were reacted with diphenylborinic acid anhydride, $(Ph_2B)_2O$, in ethanol. Only the 4-dialkylaminophenyl derivatives **6***e* and **6***f* gave crystalline diphenylboron chelates (**2***b* and **2***c*) stable enough for recrystallization. The 4-methoxyphenyl derivative **2***a* could be obtained only as a crude crystalline product that decomposes easily by solvolysis. In all the other cases the respective bidentate ligand **6** was recovered unchanged, even from water-free aprotic media like benzene with continuous removal of reaction water by azeotropic distillation (Dean–Stark trap).

Thus details of the formation of the seven-membered boron chelates **2** resembles the results reported for the synthesis of type **3** chelates (4). Both ring systems show that the ring enlargement of stable six-membered boron chelates derived from aromatic aldonitrones (10*a*) to seven-membered chelates is disadvantageous with respect to the stability of these compounds if the nitrone N=C bond appears as a substitutive (exocyclic) double bond. In the case of the salicylaldonitrone boron chelates **1**, however, with the N=C nitrone double bond being part of the chelate ring (endocyclic), the chelate stability is adequate for various derivatives that could be recrystallized without difficulties despite the enlarged ring system (1, 2). As for the boron chelates **3**, the electron-donating 4-dialkylamino substituent of the *C*-aryl residue of the chelates **2***b* and **2***c* increases the basicity at the nitrone oxygen enough to enable the formation of a chelate sufficiently stable for recrystallization or for analyses of solutions. A similar, though weaker, effect is achieved by the 4-methoxy substituent in the chelate **2***a*.

The solvolytic sensitivity of **2** becomes obvious in the ^{11}B nmr spectra where, in addition to signals for tetracoordinate (sp^3) boron at δ (Et_2OBF_3) = 8.5–8.8 ppm, second signals appear at 46.3–46.6 ppm indicating the presence of a trivalent (sp^2) boron atom of a Ph_2B-O-R moiety (25) that might result from ring opening at the weaker O—B bond to the nitrone oxygen ligand in solution. The solvolysis observed in the $CDCl_3$ solutions of the ^{11}B nmr experiments is a partial solvolysis, the mechanism of which is not yet clear. Other solvents like DMSO-d_6 are even less suitable because of water content. While we are not sure just what Ph_2B-O-R moiety (possibly the ring-opened compound **2** or free diphenylborinic acid) gives rise to the signal at 46.6 ppm, this species should be a trivalent Ph_2B-O-R moiety. The additional peak at 30.6 ppm in the spectrum of **2***a* points to more extensive decomposition of the diphenylborinic acid component that may result from dephenylation by moisture (H_2O traces, or even HCl traces in the $CDCl_3$) or from oxidation by atmospheric oxygen in the solvent, resulting in a $Ph_2B(OR)_2$ phenylboronic acid derivative (25). Experiments with special precautions to exclude water or oxygen in the nmr experiments have not been performed.

The ^1H nmr spectra of **2** do not display any signals at 5–6 ppm indicative of an N-CH-O methine signal that could be assigned to the diphenylborinate **8** (or its BONBON dimer[9]) deriving from a possible cyclotautomer **7**. The CH=N methine signal indicating the nitrone form **2** appears hidden behind the multiplets arising from the aromatic proton signals in each case.

The infrared spectra of **2** show a distinct shift, about 30 cm^{-1}, of the nitrone C=N stretching band to higher frequencies compared to the respective free ligands **6**, indicating the increased iminium salt character of the nitrone moiety in the boron chelates **2**. Similar tendencies have also been observed in the formation of boron chelates from other nitrone ligands (1, 4, 10).

No molecular ion peak was observed in the mass spectrum of **2***c* (investigated as an example). As noted earlier for the seven-membered boron chelates **3** (4), only a dephenylated fragment ($M^+ - 77$) could be detected. This is typical for diphenylboron chelates and points to a preferred transition of the zwitterionic compound **2***c* to the stable $(2c - C_6H_5)^+$ ion.

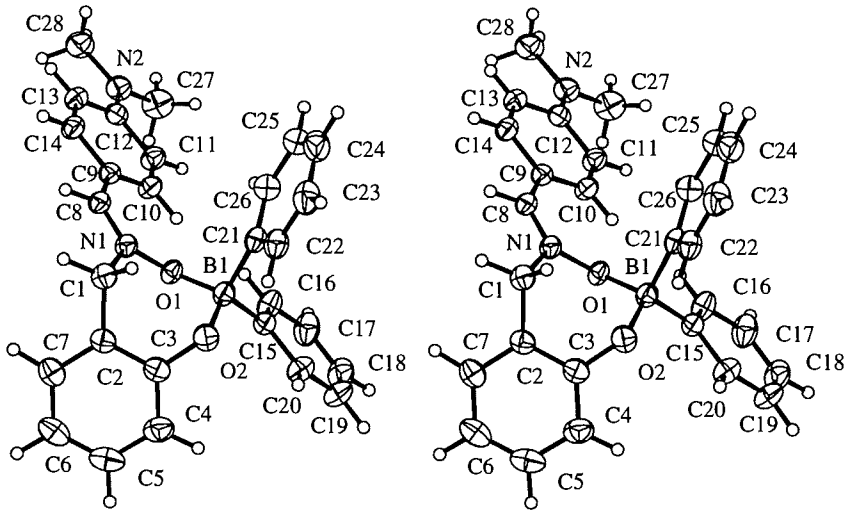
An X-ray analysis of **2***b*, derived from the free ligand **6***e* (see above), establishes the seven-membered boron chelate structure **2** (Fig. 4), which represents a new type of heterocyclic *B,N*-betaine (27). The proton of the intramolecular O—H···O moiety in **6***e* is replaced by the diphenylborenium cation, leading to some changes in the geometry of **2***b*. Besides the C(10)—H(8)...O(1) intramolecular contact, which is maintained in the chelate **2***b* without any significant changes, three additional intramolecular C—H···O interactions (all involving the phenolate oxygen atom O(2)) are noted: (C(10)—H(8)···O(1), C(1)—H(1)···O(2), C(20)—H(16)···O(2), C(22)—H(17)···O(2); C—H = 0.96(2), 0.99(2), 1.02(2), 0.96(2) Å; H···O = 2.32(2), 2.43(2), 2.50(2), 2.46(2) Å; C···O = 2.915(2), 2.708(2), 2.906(2), 2.857(2); Å; C—H···O = 119(1)°, 95(1)°, 103(1)°, 103(1)°, respectively). The relatively acute C—H···O angles for the three interactions involving O(2) suggest that these weak interactions probably have little influence on the molecular conformation (22). As noted above for **6***b*, the *C*-arylnitrone moiety is

[9] For more information about BONBON dimers of borinates from hydroxylamine derivatives see ref. 26 and papers cited therein.

© 1997 NRC Canada

Can. J. Chem. Downloaded from www.nrcresearchpress.com by 91.121.58.235 on 09/08/12
For personal use only.

Fig. 4. Stereoview of **2***b*; 33% probability thermal ellipsoids are shown for the non-hydrogen atoms.



roughly coplanar. The *C*-arylnitrone mean plane makes a dihedral angle of about 67° with that of phenolate system C(2)—C(7) plus O(2), indicating a somewhat larger rotation in **2***b* than in the free ligand **6***e*. The centrosymmetric structure of **2***b*, like that of **6***e*, contains pairs of "helical enantiomers." Molecules of **2***b* are separated by normal van der Waals distances, the shortest intermolecular distance between non-hydrogen atoms being N(2)···C(13) = 3.407(2) Å.

The insertion of the Lewis acid diphenylboron group in place of the phenolic hydrogen of **6***e* enhances the iminium salt character of the nitrone moiety in **2***b*. Within the 4-dimethylaminophenylmethylidene moiety (Fig. 3) of **2***b*, the double bond character of the N(2)—C(12), C(10)—C(11), C(13)—C(14), and C(8)—C(9) bonds is even more pronounced than in **6***e* (for **2***b*: 1.349(2), 1.361(2), 1.361(2), and 1.419(2) Å, respectively; for **6***e*: 1.370(2), 1.371(2), 1.370(2), and 1.437(2) Å). The N—O bond of the nitrone group in **6***e* (1.324(2) Å), already longer than those for nitrone groups not involved in hydrogen bonding, is further lengthened by about 0.05 Å in the boron chelate **2***b* (1.371(1) Å). This represents a decrease in the π-bond order of the nitrone N—O bond from 0.35 in the free ligand **6***e* to 0.22 in the chelate **2***b*, estimated from plots of bond distance vs. HMO–π-bond order (28*b*). The C=N$^+$ nitrone double bond, however, remains practically unchanged (1.291(2) Å in **6***e* and 1.294(2) Å in **2***b*) with an estimated (28*a*) HMO–π-bond order of 0.82 in both the ligand and the chelate, and is comparable to the C=N$^+$ bond in **1** (R = Me) (1.291(4) Å) (2). It is somewhat surprising that the chelate formation, i.e., the incorporation of the Lewis acid boron nucleus, has a more profound effect on the more distant 4-dimethylaminophenyl resonance system than on the conjugated nitrone C=N$^+$ group.

As in **1** (R = Me) (2) and other boron chelates obtained from bidentate ligands having *N*-oxide and alcoholate or phenolate oxygen donor atoms (23, 29), the (N)O—B bond in **2***b* is longer (1.549(2) Å) than the (C)O—B bond (1.488(2) Å). The sum of the bond lengths about the boron atom in **2***b* (6.266 Å) is about the same as in the other type of seven-membered diphenylboron chelate **1** (R = Me) (6.276 Å) (2), consistent with the observation that for a given chelate ring size this sum is essentially constant (30). The mean (phenyl)C—B bond length in **2***b* (1.615(2) Å) is similar to corresponding values observed for **1** (R = Me) (2) and other Ph_2BO_2 chelates (29*a*–*d*, 29*g*, 30–32). The mean C—B/mean O—B bond length ratio for **2***b* (1.063) indicates a slightly increased binding strength of the bidentate ligand with respect to the diphenylboron moiety compared to the other type of seven-membered chelate **1** (R = Me) (2), which has an average C—B/O—B ratio of 1.054. Similar values calculated from the bond lengths observed for various six-membered "Ph_2BO_2" chelates provide a good estimate of overall chelate binding strength (31).

The chelate ring geometry of **2***b* (with an exocyclic N=C double bond) generally allows somewhat smaller intracyclic angles at the ring member atoms than does the geometry of **1** (2) with an endocyclic N=C double bond. In **1** nearly all of the chelate ring angles are widened: the sum of the intracyclic bond angles is 858.4° compared to 811.7° in **2***b*. If the differing alkylidene substituents are not considered, the new boron chelates **2** may be formally regarded as ring-enlarged "phenylogues" (by *o*-phenyl insertion) of the five-membered diphenylboron chelate **14**, which has been fully characterized by X-ray crystallographic analysis (29*g*). Comparing the dimensions of the chelate rings in **2***b* and **14**: similar bond distances are found at the "Ph_2BO_2" moiety and wider ring angles are found at all ring member atoms of **2***b*, in particular the N-O-B angle that changes from 104.7(2)° in **14** to 118.3(1)° in **2***b*.

Acylation of the nitrones 6

Since the attack of the Lewis acid diphenylborinic acid at the nitrone groups leads preferentially to the boron chelates **2** rather than to an *O*-borylated cyclotautomerization product **8**, acylation was attempted with an acyl halide and an isocyanate. Thus the reaction of **6***e* with acetyl chloride (R = Me) and benzoyl chloride (R = Ph) resulted in the crystalline benzoxazine derivatives **9**, whereas the reaction with phenyl isocyanate gave the phenylcarbamoylated phenol **10** with an intact nitrone function. The *N*-acyloxy derivatives **9***a,b* display ester carbonyl C=O stretching bands in the infrared spectra at

Can. J. Chem. Downloaded from www.nrcresearchpress.com by 91.121.58.235 on 09/08/12
For personal use only.

© 1997 NRC Canada

about 1750 cm^{-1} and have the typical O-CH-N acetalic methine proton signal near $\delta = 6.1$ ppm in the ^1H nmr spectra. Comparable acylations of the ring tautomers of *N*-(2-hydroxyalkyl)nitrones (10), *N*-(3-hydroxyalkyl)nitrones (4), and *N*-(2-hydroxynaphthylmethyl)nitrones (12*b*, 12*c*, 33) have been reported. Compound **10** is not only characterized by urethane C=O and nitrone C=N stretching bands in the infrared spectrum, but also by the typical $CH{=}N^+$ methine proton signal at 7.35 ppm in the ^1H nmr spectrum. The latter excludes not only a 1,3-benzoxazine derivative like **9**, but also an isoxazolidine derivative as a result of the possible 1,3-dipolar cycloaddition of phenylisocyanate to the nitrone group. It should be noted that the ester or urethane C=O stretch is not a good means for discrimination and it serves only for the characterization of both compounds. It is also *not* the 7.35 ppm signal in the ^1H nmr (buried under the multiplet of aromatic protons) that discriminates, but rather the *absence* of the acetalic O-CH-N methine signal around 6 ppm that suggests the open-chain nitrone form of **10**. X-ray analysis would certainly establish these structures, but it has not yet been possible to obtain suitable crystals of **9** and **10**.

Acknowledgments

We thank the Natural Sciences and Engineering Research Council of Canada and the Fonds der Chemischen Industrie, Frankfurt am Main, for financial support. We are grateful to the Chemische Institute der Technischen Universität Braunschweig for the ^{11}B nmr and mass spectra.

References

1. W. Kliegel and D. Nanninga. J. Organomet. Chem. **243**, 373 (1983).
2. W. Kliegel, U. Lauterbach, S.J. Rettig, and J. Trotter. Can. J. Chem. **65**, 1457 (1987).
3. (*a*) G. Zinner. Chem.-Ztg. **109**, 436 (1985); (*b*) H. Hopf and G. Maas. Angew. Chem. **104**, 953 (1992); see footnote for "exocyclic" double bonds, p. 954.
4. W. Kliegel and L. Preu. Liebigs Ann. Chem. 1937 (1983).
5. R. Neu. Chem. Ber. **87**, 802 (1954).
6. G.N. Chremos, H. Weidmann, and H.K. Zimmerman. J. Org. Chem. **26**, 1683 (1961).
7. (*a*) R. Neu. Z. Anal. Chem. **176**, 334 (1960); (*b*) B. Friese and F. Umland. Anal. Chim. Acta, **96**, 303 (1978).
8. (*a*) International tables for X-ray crystallography. Vol. IV. Kynoch Press, Birmingham, U.K. (present distributor Kluwer Academic Publishers, Boston, Mass.). 1974. pp. 99–102; (*b*) International tables for crystallography. Vol. C. Kluwer Academic Publishers. Boston, Mass. 1992. pp. 200–206.
9. (*a*) R.F. Borch, M.D. Bernstein, and H.D. Durst. J. Am. Chem. Soc. **93**, 2897 (1971); (*b*) J. Beyersdorf. Dissertation, Braunschweig. 1990.
10. (*a*) W. Kliegel and H. Becker. Chem. Ber. **110**, 2067 (1977); (*b*) Chem. Ber. **110**, 2090 (1977); (*c*) W. Kliegel, B. Enders, and H. Becker. Liebigs Ann. Chem. 1712 (1982); (*d*) Chem. Ber. **116**, 27 (1983).
11. W. Kliegel and L. Preu. Chem.-Ztg. **108**, 283 (1984).
12. (*a*) H. Möhrle, M. Lappenberg, and D. Wendisch. Monatsh. Chem. **108**, 273 (1977); (*b*) H. Möhrle and M. Lappenberg. Arch. Pharm. (Weinheim), **311**, 897 (1978); (*c*) H. Möhrle and K. Tröster. Arch. Pharm. (Weinheim), **314**, 836 (1981).
13. U. Paulsen and B. Lindeke. Acta Pharm. Suec. **15**, 264 (1978).
14. (*a*) N. Harada, Y. Mori, and I. Tanaka. Mol. Photochem. **2**, 153 (1970); (*b*) V.I. Minkin, E.A. Medyantseva, I.M. Andreeva, and G.V. Gorshkova. Zh. Org. Khim. **9**, 148 (1973); J. Org. Chem. USSR, **9**, 148 (1973).
15. N. Arumugam, P. Manisankar, S. Sivasubramanian, and D.A. Wilson. Magn. Reson. Chem. **22**, 592 (1984).
16. N. Arumugam, P. Manisankar, S. Sivasubramanian, and D.A. Wilson. Magn. Reson. Chem. **23**, 246 (1985).
17. V.A. Bren′, E.A. Medyantseva, I.M. Andreeva, and V.I. Minkin. Zh. Org. Khim. **9**, 767 (1973); J. Org. Chem. USSR, **9**, 790 (1973).
18. (*a*) J. Emsley. Q. Rev. Chem. Soc. **9**, 91 (1980); (*b*) Structure Bonding, **57**, 147 (1984); (*c*) F. Hibbert and J. Emsley. Adv. Phys. Org. Chem. **26**, 255 (1980); (*d*) G.A. Jeffrey and W. Saenger. Hydrogen bonding in biological structures. Springer, Berlin. 1991; (*e*) J. Bernstein, M.C. Etter, and L. Leiserowitz. *In* Structure correlation. Vol. 2. *Edited by* H.B. Bürgi and J.D. Dunitz. VCH, Weinheim. 1994. p. 431.
19. D. Christensen, K.A. Jørgensen, and R.G. Hazell. J. Chem. Soc. Perkin Trans. 1, 2391 (1990).
20. A. Koll, M. Rospenk, L. Sobczyk, and T. Glowiak. Can. J. Chem. **64**, 1850 (1986).
21. A.N. Utenyshev and S.M. Aldoshin. Zh. Strukt. Khim. **37**, 349 (1996); J. Struct. Chem. **37**, 305 (1996).
22. G.R. Desiraju. Acc. Chem. Res. **29**, 441 (1996).
23. W. Kliegel, L. Preu, S.J. Rettig, and J. Trotter. Can. J. Chem. **63**, 509 (1985), and refs. cited therein.
24. (*a*) L. Greci and P. Sgarabotto. J. Chem. Soc. Perkin Trans. 2, 1281 (1984); (*b*) C.P. Falshaw, N.A. Hashi, and G.A. Taylor. J. Chem. Soc. Perkin Trans. 1, 1837 (1985); (*c*) P.J. Carroll, G.B. Mullen, and V.S. Georgiev. Acta Crystallogr. Sect. C: Cryst. Struct. Commun. **C45**, 821 (1989); (*d*) R.G. Pritchard, R.E. Banks, R.A. DuBoisson, and A.E. Tipping. Acta Crystallogr. Sect. C: Cryst. Struct. Commun. **C47**, 230 (1991); (*e*) L. Cardellini, P. Carloni, E. Damiani, L. Greci, P. Stipa, C. Rizzoli, and P. Sgarabotto. J. Chem. Soc. Perkin Trans. 2, 1589 (1994); (*f*) P.K. Olszewski and K. Stadnicka. Acta. Crystallogr. Sect. C: Cryst. Struct. Commun. **C51**, 98 (1995).
25. (*a*) H. Nöth and B. Wrackmeyer. Nuclear magnetic resonance spectroscopy of boron compounds. Springer, Berlin. 1978; (*b*) R. Köster (*Editor*) Houben-Weyl: Organobor-Verbindungen III. Vol. XIII/3c. Thieme, Stuttgart. 1984.
26. W. Kliegel, D. Nanninga, U. Riebe, S.J. Rettig, and J. Trotter. Can. J. Chem. **72**, 1735 (1994).
27. W. Kliegel. Organomet. Chem. Rev. A, **8**, 153 (1972).
28. (*a*) G. Häfelinger. Chem. Ber. **103**, 2902 (1970); (*b*) Chem. Ber. **103**, 3370 (1970).
29. (*a*) S.J. Rettig, J. Trotter, and W. Kliegel. Can. J. Chem. **52**, 2531 (1974): (*b*) W. Kliegel, H.W. Motzkus, S.J. Rettig, and J. Trotter. Can. J. Chem. **62**, 838 (1984); (*c*) W. Kliegel, M. Tajerbashi, S.J. Rettig, and J. Trotter. Can. J. Chem. **66**, 2621 (1988); (*d*) E. Ebeling, W. Kliegel, S.J. Rettig, and J. Trotter. Can. J. Chem. **67**, 933 (1989); (*e*) W. Kliegel, U. Schumacher, S.J. Rettig, and J. Trotter. Can. J. Chem. **69**, 681 (1991); (*f*) E. Ahlenstiel, W. Kliegel, S.J. Rettig, and J. Trotter. Can. J. Chem. **71**, 263 (1993); (*g*) W. Kliegel, U. Riebe, S.J. Rettig, and J. Trotter. Can. J. Chem. **73**, 835 (1995).
30. C. Orvig, S.J. Rettig, and J. Trotter. Can. J. Chem. **65**, 590 (1987).
31. W.R. Cullen, S.J. Rettig, J. Trotter, and E.B. Wickenheiser. Can. J. Chem. **66**, 2007 (1988).
32. C. Orvig, S.J. Rettig, J. Trotter, and Z. Zhang. Can. J. Chem. **68**, 1803 (1990).
33. J.M.J. Tronchet, M. Koufaki, G. Zosimo-Landolfo, and G. Bernardinelli. J. Chem. Res. (S), 293 (1992); (M), 2501 (1992).
34. W. Kliegel, J. Metge, S.J. Rettig, and J. Trotter. Can. J. Chem. **75**, 1203 (1997).

Can. J. Chem. Downloaded from www.nrcresearchpress.com by 91.121.58.235 on 09/08/12
For personal use only.

© 1997 NRC Canada

X^+ transfer from the halonium ions of adamantylideneadamantane to acceptor olefins. The possibility of chiral induction in the transfer process

Alexei A. Neverov, Theresa L. Muise, and R.S. Brown

Can. J. Chem. Downloaded from www.nrcresearchpress.com by 91.121.58.235 on 09/08/12
For personal use only.

Abstract: The bromonium ion of adamantylideneadamantane (Ad═Ad-Br^+) has been used to induce the bromocyclization of a 4-pentenyl glycoside (**10**) and a 5-hexenyl glycoside (**11**) in dichloroethane. The kinetics of these processes have been studied at 25°C in the presence of varying [Ad═Ad] and, in the case of the transfer to **10**, in the presence of pentanol. The second-order rate constants for bromocyclization of these two alkenes are $(1.04 \pm 0.06) \times 10^{-1}$ M^{-1} s^{-1} and $(5.34 \pm 0.2) \times 10^{-2}$ M^{-1} s^{-1}, respectively, and in no case does added Ad═Ad or pentanol alter the reaction rate. The kinetic behavior is interpreted in terms of cyclization occurring directly from a 1:1 complex of Ad═Ad-Br^+ and **10** or **11**. The chiral induction for the bromocyclization of **10** promoted by AdAd-Br^+ was measured at 20% e.e., the (−)-(*S*)-tetrahydrofurfuryl bromide being the dominant stereoisomer. Ad═Ad molecules substituted at one of the homoallylic carbons by an axial methyl group (**12**), or by two methyl groups (axial and equatorial), were synthesized and the ^1H NMR spectra of their bromonium ions is given. These materials are not stable for prolonged times at room temperature. A limited kinetic study of the reaction of **12**-Br^+ and 4-pentenol indicated that the Br^+ transfer is 500 times faster than the comparable transfer from Ad═Ad-Br^+ to 4-pentenol. The possibility of using these materials to induce chiral bromocyclization is discussed.

Key words: bromonium ion, halonium, transfer, chiral, adamantylideneadamantane.

Résumé : On a utilisé l'ion bromonium de l'adamantylidèneadamantane (Ad═Ad-Br^+) pour induire la bromocyclisation des glucosides de pent-4-énule (**10**) et d'hex-5-énule (**11**) dans le dichlorométhane. On a étudié la cinétique de ces processus à 25°C, en présence de concentrations variables de Ad═Ad et, dans le cas du transfert vers le composé **10**, en présence de pentanol. Les constantes de vitesse du deuxième ordre pour la bromocyclisation de ces deux alcènes sont respectivement de $(1{,}04 \pm 0{,}06) \times 10^{-1}$ M^{-1} s^{-1} et $(5{,}34 \pm 0{,}2) \times 10^{-1}$ M^{-1} s^{-1} et il n'y a aucun cas où l'addition de Ad═Ad ou de pentanol provoque des changements dans la constante de vitesse. On interprète ce comportement cinétique en fonction d'une cyclisation qui se produirait directement à partir d'un complexe 1 : 1 de Ad═Ad-Br^+ et des composés **10** ou **11**. On a déterminé que l'induction chirale pour la bromocyclisation du composé **10** sous l'influence de Ad═Ad-Br^+ est égale à 20% d'e.e., alors que le bromure de (−)-(*S*)-tétrahydrofurfuryle est le stéréoisomère prédominant. On a synthétisé des molécules d'Ad═Ad substituées à l'un des carbones homoallyliques soit par un groupe méthyle axial (**12**) ou par deux groupes méthyles (axial et équatorial) et l'on rapporte les spectres RMN du ^1H de leurs ions bromonium. À la température ambiante, ces produits ne sont pas stables pour des périodes prolongées. Une étude cinétique limitée de la réaction du composé **12**-Br^+ avec le pent-4-énol indique que le transfert de Br^+ est 500 fois plus rapide que le transfert comparable du Ad═Ad-Br^+ vers le pent-4-énol. On discute des possibilités d'utiliser ces composés pour induire des bromocyclisations chirales.

Mots clés : ion bromonium, halonium, transfert, chiral, adamantylidèneadamantane.

[Traduit par la rédaction]

Recent work from these laboratories (1–3) has shown that the bromonium and iodonium ions of adamantylideneadamantane (Ad═Ad) rapidly transfer X^+ to acceptor olefins such as cyclohexene, and those capable of undergoing halocyclizations, see Scheme 1. A detailed analysis (1, 2) of the process for Br^+ transfer to 1,ω-alkenols and alkenoic acids indicated that: (*i*) the reaction usually exhibits some common species rate suppression by added Ad═Ad and an acceleration by added bases and alcohols such as pentanol; and (*ii*) formation of the cyclized product (**3**) occurs from the nascent bromonium ion **2** or in some cases from a 1:1 complex of Ad═Ad-Br^+ and **1**. The fact that the nascent bromonium ion **2** and the cyclized product both contain a potentially asymmetric center (marked with an asterisk in Scheme 1) suggests that it might be possible to use a suitably constructed Ad═Ad bromonium ion to induce chirality in the cyclized product. If so, this would be an important synthetic contribution since there are relatively few cases of asymmetric induction accompanying Br_2/Br^+ electrophilic additions to olefins **1** (4–10).

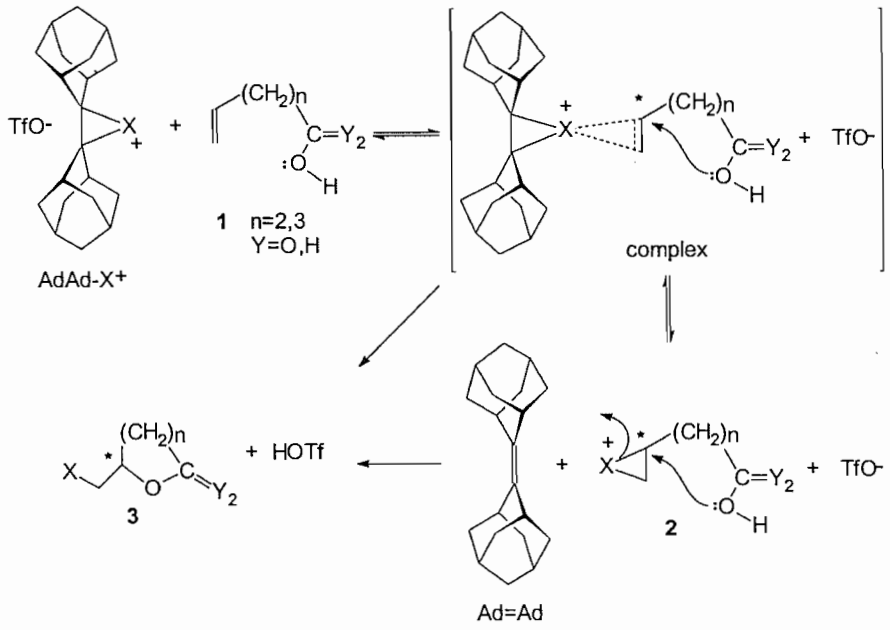
Received May 30, 1997.

A.A. Neverov, T.L. Muise,[1] and R.S. Brown.[2] Department of Chemistry, Queen's University, Kingston, ON K7L 3N6, Canada.

[1] Summer Undergraduate Research Assistant, 1996.
[2] Author to whom correspondence may be addressed: Telephone (613) 545-2624. Fax: (613) 545-6669. E-mail: rsbrown@chem.queensu.ca

© 1997 NRC Canada

Scheme 1.

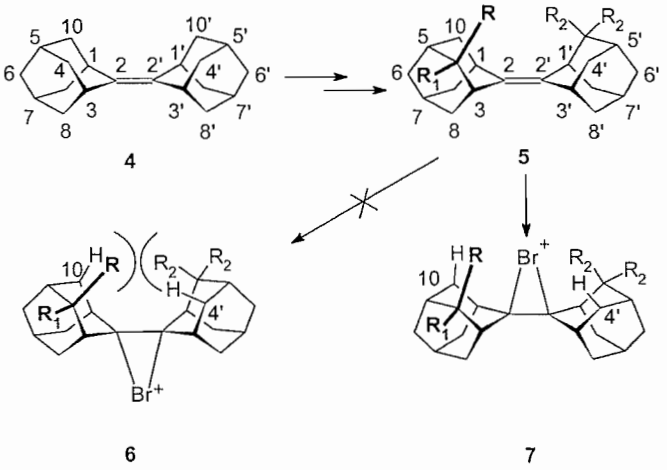


Induction of chirality in the Br^+ transfer process requires a chiral Ad═Ad-bromonium ion, a chiral acceptor olefin, or both. Conceivably the Ad═Ad could be made chiral by appropriate functionalization of any carbon not lying on the plane that includes carbons 8, 6, 7, 2, 2′, 6′, 7′, and 8′. The most appropriate functionalization places a nonreactive alkyl group in the axial positions of any of the eight homoallylic carbons since these are closest to the Π-face of the double bond. In the ideal case the homoallylic carbons could be substituted pairwise in order to preserve a C_2 symmetry in the olefin as in **5** (R_2 = R, R_1, Scheme 2). An axial homoallylic substituent also prohibits bromination at the distal Π-face since the so-formed ion (**6**) would experience severe interactions between the R group(s) and the $C_{4'}$, C_{10} hydrogens. Therefore, bromonium ion formation can only occur on the Π-face of the double bond proximal to the axial homoallylic groups as in **7**.[3]

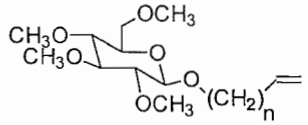
An alternative way to promote chiral induction requires that the alkene contain an asymmetric center either permanently or temporarily installed as a chiral auxiliary. Rodebaugh and Fraser-Reid (11*a*, *b*) have studied the NBS-induced cyclizations of the *n*-pentenyl and *n*-hexenyl benzyl-protected glycosides **8** and **9**, and noted that a 20% enantiomeric excess is produced in the tetrahydrofurfuryl bromide product of the cyclization of **8** (11*b*), Scheme 3. Given the fact that Br^+ transfer from Ad═Ad-Br^+ to **8** or **9** could occur through diastereomeric complexes between the bulky partners, it seemed likely that enhanced induction of chirality could occur if Ad═Ad-Br^+ were used as the transfer agent.

As an initial undertaking for this research the permethylated

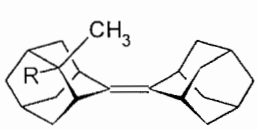
Scheme 2.



glycosides **10** and **11** were synthesized and the kinetics of their reaction with Ad═Ad-Br^+ and -I^+ were studied to determine the mechanism for X^+ transfer. Also, the enantiomeric excess induced in the product of the reaction of **10** and Ad═Ad-Br^+ was determined. Finally, we have synthesized racemic methylated alkenes **12** and **13** and their corresponding bromonium ions to assess the likelihood of producing useful chiral Br^+ transfer agents from such substituted adamantylideneadamantanes. Herein we report the results of this study.



10, n=3
11, n=4



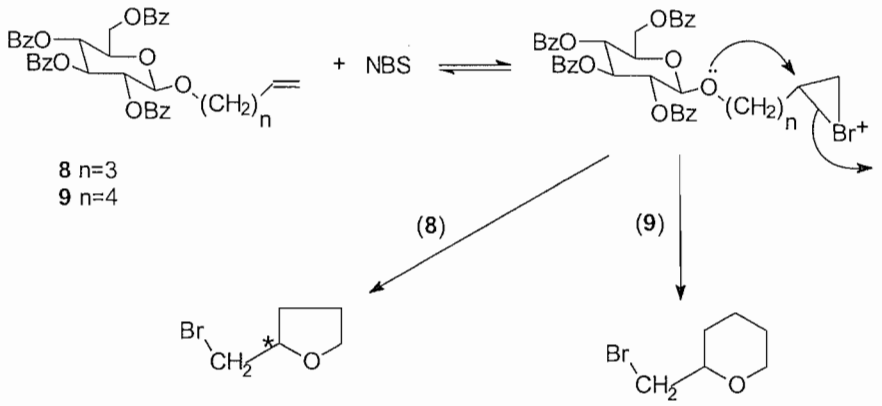
12, R=H
13, R=CH_3

[3] MMX calculations using PC Model (Serena Software, Box 3076, Bloomington, IN 47402-3076, U.S.A.) with CF-Br^+ force constants and parameters set to produce the known structure of the Ad═Ad-Br^+ (3) indicate that it is energetically favorable to brominate proximal and not distal to the C_4 axial substituents.

Can. J. Chem. Downloaded from www.nrcresearchpress.com by 91.121.58.235 on 09/08/12
For personal use only.

© 1997 NRC Canada

Scheme 3.



Experimental

(a) Materials and methods

Dichloromethane was purified as described (12). 1,2-Dichloroethane was distilled over P_2O_5. Adamantylideneadamantane (Ad=Ad) and the corresponding bromonium and iodonium triflates were prepared as previously described (1, 3, 13). ^1H NMR and ^{13}C NMR data were obtained using Bruker WH-200 and Bruker AM-400 instruments. Kinetic measurements were done using an OLIS modified Cary 17 UV–VIS spectrophotometer or an Applied Photophysics SX-17MV stopped-flow reaction analyzer.

(b) Synthesis

*4, 4-Dimethyl-2-tricyclo[3.3.1.1^{3,7}]decylidene tricyclo-[3.3.1.1^{3,7}]decane (**13**)*

Approximately 12 mmol of dimethyltitanium(IV) dichloride were prepared by mixing 12 mL of a 1 M solution of $TiCl_4$ in CH_2Cl_2 and 6 mL of a 2 M solution of dimethylzinc in toluene in 10 mL of dry CH_2Cl_2 under argon at −78°C. The mixture was kept for 30 min at −30°C and then treated with 10 mL of a solution containing 1.3 g of 2-oxo-4-tricyclo[3.3.1.1^{3,7}]-decylidene tricyclo[3.3.1.1^{3,7}]decane (13) in dry CH_2Cl_2 at −78°C. The reaction mixture was allowed to warm to room temperature and then immediately quenched by pouring onto ice. The product was extracted with 100 mL of CH_2Cl_2, which was then washed with an equal amount of water, saturated K_2CO_3, and dried over Na_2SO_4. Recrystallization from 15 mL of methanol yielded 0.9 g (67%) of a white solid, mp 71–72°C. IR (cm^{-1}, $CHCl_3$ cast): 2905, 2845, 1447; ^1H NMR (CD_2Cl_2) δ: 2.93 (s, 1H), 2.90 (s, 1H), 2.84 (s, 1H), 2.39 (s, 1H), 2.14 (d, 2H, J = 12 Hz), 1.98 (d, 1H, J = 12 Hz), 1.9–1.6 (m, 17H), 1.48 (d, 1H, J = 12 Hz), 1.39 (s, 1H), 1.08 (s, 3H), 0.92 (s, 3H); ^{13}C NMR (see Table 7); MS (*m/z*) calcd for $C_{22}H_{32}$: 296.2504; found: 296.2500.

*Bromonium ion of **12***

To a Teflon reaction vessel equipped with a stirring bar and charged with a small excess of Br_2 under Ar, was slowly added 21.8 mg of **12** (0.078 mmol) (kindly supplied by Prof. A. J. Bennet, Simon Fraser University) dissolved in 1 mL of dry CH_2Cl_2. The precipitate was separated by centrifugation and, after the addition of 20 μL (0.084 mmol) of methyl trifluoromethylsulfonate in 2 mL of dry CH_2Cl_2, was redissolved using sonication for 30 min at room temperature. The solvent and volatile by-products were removed by a stream of Ar and the product was recrystallized from CH_2Cl_2–hexane.

*Bromonium ion of **13***

To 22.4 mg of **13** (0.077 mmol) dissolved in 1 mL of dry CH_2Cl_2 cooled by Dry Ice was slowly added a small excess of Br_2 (24.5 mg) in 0.65 mL of CH_2Cl_2 under Ar. The orange precipitate formed was then separated from the liquid phase and redissolved in 2 mL of CH_2Cl_2 solution containing 67.9 mg (0.077 mmol) of the sodium salt of tetra(3,5-di(trifluoromethyl)phenyl)borate. While the system was kept at Dry Ice temperature the bulk of the solvent was removed by a stream of Ar and the product was precipitated by the addition of dry hexane.

*4-Pentenyl-2,3,4,6-tetra-*O*-methyl-β-D-glucopyranoside **10***

A 20 mL solution of anhydrous methanol containing 1.3 g (3.12 mmol) of 4-pentenyl-2,3,4,6-tetra-*O*-acetyl-β-D-glucopyranoside (11) and 100 mg of K_2CO_3 was stirred for 5 h. The reaction was filtered through a Celite pad and the solvent was removed, leaving a crude product that was added to a suspension of 0.72 g of NaH (30 mmol) in 50 mL of dry dimethylformamide. The reaction mixture was cooled in an ice bath and 2 mL of methyl iodide were added dropwise. The system was allowed to warm to room temperature overnight, after which the product was extracted with 100 mL of ether. The ether layer was washed with 100 mL each of water, saturated $NaHCO_3$ (twice), and saturated KCl (twice), dried over $MgSO_4$, and then concentrated by rotary evaporation. The residue was flash chromatographed (95:5 to 85:15 petroleum spirit:EtOAc) to give 0.54 g (62%) of the liquid product. ^1H NMR (200 MHz, $CDCl_3$) δ: 5.80 (m, 1H), 5.00 (m, 2H), 4.20 (d, J = 7.4 Hz, 1H), 3.92 (m, 1H), 3.61 (s, 3H), 3.60–3.20 (m, 4H), 3.57 (s, 3H), 3.51 (s, 3H), 3.38 (s, 3H), 3.10 (m, 2H), 2.98 (m, 1H), 2.12 (m, 2H), 1.70 (m, 2H): MS *m/z*: 304.(M^+), 303 ($M^+ - 1$).

*5-Hexenyl-2,3,4,6-tetra-*O*-methyl-β-D-glucopyranoside (**11**)*

This was prepared in the same manner as above from 5-hexenyl-2,3,4,6-tetra-*O*-acetyl-β-D-glucopyranoside: yield, 55%. ^1H NMR (200 MHz, $CDCl_3$) δ: 5.78 (m, 1H), 4.95 (m, 2H), 4.20 (d, J = 7.6 Hz, 1H), 3.90 (m, 1H), 3.61 (s, 3H), 3.60–3.20 (m, 4H), 3.56 (s, 3H), 3.51 (s, 3H), 3.38 (s, 3H), 3.10 (m, 2H), 2.95 (m, 1H), 2.05 (m, 2H), 1.70–1.4 (m, 4H).

© 1997 NRC Canada

Can. J. Chem. Downloaded from www.nrcresearchpress.com by 91.121.58.235 on 09/08/12
For personal use only.

Can. J. Chem. Downloaded from www.nrcresearchpress.com by 91.121.58.235 on 09/08/12
For personal use only.

(c) Product analysis for the reaction of 4-pentenyl-2,3,4,6-tetra-*O*-methyl-β-D-glucopyranoside (10) with Ad═Ad-Br$^+$

To a solution of 29.4 mg of **10** (0.1 mmol) in 1 mL of dry CH_2Cl_2 was added 58 mg of Ad═Ad-Br$^+$ (0.11 mmol, prepared according to the procedure given in refs. (1 and 3) and the system was kept at room temperature overnight. The solvent was removed and tetrahydrofurfuryl bromide was dissolved in CH_3CN. The product was further purified by using preparative GC (30% SE-30 Chrom AW 3/8 in × 3 ft, 150°C, 30 mL/min). The enantiomeric excess at C_2 in the tetrahydrofurfuryl bromide was determined by ^{1}H NMR using the chiral shift reagent tris[3-heptafluoropropylhydroxymethylene-(+)-camphorato] europium(III), (Eu(hfp)$_3$). The sample was dissolved in 0.7 mL of $CDCl_3$ containing 9.5 mg of Eu(hfp)$_3$ and the ratio between the different stereoisomers determined by comparison of the integrated intensities of the signals at δ 9.5 and 9.1 corresponding to the C-H protons at C_2. Absolute configuration was determined on the basis of comparison of the optical rotation of the sample solution in $CHCl_3$ with the reported assignment (11*c*).

(d) Kinetics

The kinetics of the reactions of the bromonium and iodonium ions of Ad═Ad with olefins **10** and **11** were monitored by observing the rate of disappearance of the halonium ions in purified 1,2-dichloroethane (DCE) at 25°C under pseudo-first-order conditions of excess olefin. A limited number of kinetic runs were conducted with the bromonium ion of **12**. In the case of **12**-Br$^+$/OTf$^-$, 3.5×10^{-4} M solutions were used and the reactions were followed at 260 nm (ε_{260} = 6330 M^{-1} cm^{-1}). The observed rate constants were determined by initial rate methods, monitoring the ΔAbs for the initial 5–10% of the reaction. The pseudo-first-order rate constants, k_{obs}, were evaluated as $k_{obs} = (\Delta Abs)/(\Delta t[\mathbf{1}\text{-}X^+]\varepsilon)$, where X = Br or I, Δt = the initial time span, and ε the extinction coefficient at 260 nm given above. The second-order rate constants for the reaction, k_2, were determined from plots of k_{obs} vs. [olefin] using four to six different concentrations of olefin from 0 to 10^{-2} M.

Results and discussion

(a) Kinetics of X$^+$ transfer to pentenyl and hexenyl glucopyranosides 10 and 11

Rodebaugh and Fraser–Reid (11) have studied the transfer of Br$^+$ from NBS to the tetrabenzyl analogues of **10** and **11** for production of the cyclized tetrahydrofurfuryl and pyranyl bromides (Scheme 3). They observed, for competitive reactions containing excess and equal amounts of both alkenes, that the product ratio changes when the initial concentrations of **10** and **11** were equally reduced. Thus, there must be communication between the bromonium ions formed from each of the *n*-pentenyl and the *n*-hexenyl glycosides and the two parent olefins. When studied alone, the cyclization of the *n*-pentenyl glycoside was shown to give a 20% enantiomeric excess in the tetrahydrofurfuryl bromide product, which indicates that there is some chiral induction attributable to the remote glycoside. This reaction is an ideal candidate for kinetics studies using Ad═Ad-Br$^+$ as the Br$^+$ source since the bromonium ion has a strong chromophore with which to monitor the reaction progress. Furthermore, at some point, the transfer requires that the bulky Ad═Ad and alkene must share the Br$^+$ in a transition state or complex as in Scheme 1, so the resulting steric interactions could further discriminate between the diastereomeric transition states and lead to enhanced chiral induction.

Table 1. Pseudo-first-order rate constants for the reaction of Ad═Ad-Br$^+$/OTf$^-$ with 4-pentenyl-2,3,4,6-tetra-*O*-methyl-β-D-glucopyranoside (**10**), $C_2H_4Cl_2$, T = 25°C.[a]

10^3[**10**], M	10^3[Ad═Ad], M	10^4 k_{obs}, s^{-1}[b]
0	0	0.25
0.5	0	1.0
1.0	0	1.5
1.0	0.5	1.6
1.0	1.0	1.5
1.0	1.5	1.5
1.5	0	1.9
2.0	0	2.1
2.0	0	2.8
2.5	0	2.9
3.0	0	3.3
3.0	0	3.6

[a][Ad═Ad-Br$^+$] = 3.5×10^{-4} M.
[b]From initial rates, errors in k_{obs} do not exceed 10%.

Table 2. Pseudo-first-order rate constants for the reaction of Ad═Ad-I$^+$/OTf$^-$ with 4-pentenyl-2,3,4,6-tetra-*O*-methyl-β-D-glucopyranoside (**10**), $C_2H_4Cl_2$, T = 25°C.[a]

10^4 [**10**], M	10^3 [Ad═Ad], M	10^3 k_{obs}, s^{-1}[b]
5.0	0	5.6
2.5	0	2.95
1.25	0	1.64

[a][Ad═Ad-I$^+$] = 8.0×10^{-5} M.
[b]From initial rates, errors in k_{obs} do not exceed 10%.

In our study the permethylated derivatives **10** and **11** were used for the reaction instead of the perbenzylated ones in order to avoid interference form the highly absorbing phenyls in conducting the UV–VIS kinetic studies. Given in Tables 1 and 2 are the pseudo-first-order rate constants (k_{obs}) for the reaction of the Ad═Ad-Br$^+$ and -I$^+$ with excess **10** in the presence and absence of added [Ad═Ad]. In Tables 3 and 4 are the analogous data for the reaction of these ions with excess **11**. The second-order rate constants were determined from a plot of k_{obs} vs. [**10**] or [**11**]: for bromine transfer the values are $(1.04 \pm 0.06) \times 10^{-1}$ M^{-1} s^{-1} and $(5.34 \pm 0.2) \times 10^{-2}$ M^{-1} s^{-1} with olefins **10** and **11**, respectively, while the corresponding values for the iodonium ion are roughly 100 times faster at (10.6 ± 0.1) and (5.3 ± 0.2) M^{-1}s^{-1}. These are the same general trends noted for X$^+$ transfer from Ad═Ad-X$^+$ to 4-pentenol and 5-hexenol (1, 2) where the respective rate constants for Br$^+$ cyclization are 3.4 and 0.35 M^{-1} s^{-1}, and the I$^+$ cyclizations are 70- and 28-fold faster.

Of note is the fact that added Ad═Ad does not lead to a reduction in the rate of any reaction of **10** or **11** nor, from the data in Table 5, does 1-pentanol accelerate the process.

© 1997 NRC Canada

Scheme 4.

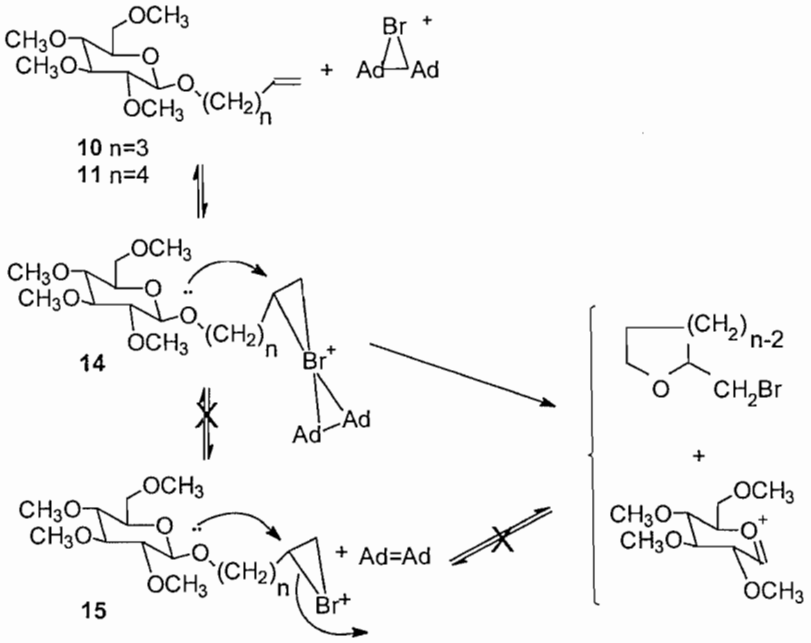


Table 3. Pseudo-first-order rate constants for the reaction of Ad═Ad-Br$^+$/OTf$^-$ with 5-hexenyl-2,3,4,6-tetra-*O*-methyl-β-D-glucopyranoside, (**11**), $C_2H_4Cl_2$, T = 25°C.[a]

10^3[**11**], M	10^4[Ad═Ad], M	10^4 k_{obs}, s^{-1}[b]
0	0	0.18
2.5	0	1.6
2.5	0	1.6
5.0	0	3.3
5.0	5.0	3.3
5.0	10.0	3.5
7.5	0	4.1
10.0	0	5.6

[a][Ad═Ad-Br$^+$] = 3.5×10^{-4} M.
[b]From initial rates, errors in k_{obs} do not exceed 10%.

Table 4. Pseudo-first-order rate constants for the reaction of Ad═Ad-I$^+$/OTf$^-$ with 5-hexenyl-2,3,4,6-tetra-*O*-methyl-β-D-glucopyranoside (**11**), $C_2H_4Cl_2$, T = 25°C.[a]

10^3 [**11**], M	10^4 [Ad═Ad], M	10^2 k_{obs}, s^{-1}[a]
2.5	0	1.3
5.0	0	2.55
7.5	0	3.95

[a][Ad═Ad-I$^+$] = 8.0×10^{-5} M.
[b]From initial rates, errors in k_{obs} do not exceed 10%.

This stands in contrast with the situation for Ad═Ad-Br$^+$-induced cyclization of 1-pentenol (1, 2) and rules out the process given in Scheme 4 where a free bromonium ion (**15**) is produced during the course of the reaction with **10** or **11**. The most favored explanation is a process where the cyclization occurs directly and irreversibly from the Ad═Ad-X$^+$ complex (**14**) of the olefins.

Table 5. Pseudo-first-order rate constants for the reaction of Ad═Ad-Br+/OTf$^-$ with 4-pentenyl-2,3,4,6-tetra-*O*-methyl-β-D-glucopyranoside (**10**) in the presence of pentanol-1, $C_2H_4Cl_2$, T = 25°C.[a]

10^3 [**10**], M	10^3 [Pentanol-1], M	10^4 k_{obs}, s^{-1}[b]
0.5	.0	1.02
0.5	4.0	0.91
0.5	10.0	0.92
0.5	20.0	1.04

[a][Ad═Ad-Br$^+$] = 3.5×10^{-4} M.
[b]From initial rates, errors in k_{obs} do not exceed 10%.

Since the kinetic study indicates that the cyclization occurs within the complex, we expected to see enhanced chirality in the tetrahydrofurfuryl bromide produced from the glucopyranoside auxiliary **10**. This expectation was predicated on the fact that approach of the Ad═Ad-Br$^+$ to the olefin can occur from either of two faces, and the cyclization must occur by a *trans* displacement of the β-anomeric oxygen on the remote C-Br$^+$. This brings the sterically demanding complexed Ad═Ad-Br$^+$-olefinic portion into close proximity with the chiral glucopyranoside. To test this, equimolar Ad═Ad-Br$^+$ and **10** were allowed to react overnight and the tetrahydrofurfuryl bromide products were separated and purified. ^{1}H NMR analysis of the CH methine protons at δ 9.5 and 9.1 ppm using a chiral shift reagent indicated a 20% enantiomeric excess in the product. On the basis of the sign of the net optical rotation of the product (11*a*), the predominant stereoisomer was (−)-(*S*)-tetrahydrofurfuryl bromide. These results are similar to those reported by Rodebaugh and Fraser–Reid for the cyclization of the perbenzyl analogue of **10** (11*a*), which indicates

© 1997 NRC Canada

Can. J. Chem. Downloaded from www.nrcresearchpress.com by 91.121.58.235 on 09/08/12
For personal use only.

Can. J. Chem. Downloaded from www.nrcresearchpress.com by 91.121.58.235 on 09/08/12
For personal use only.

Table 6. ^{13}C NMR chemical shifts observed for **12** and **12**-Br^+/TfO^-.

Carbon no.[a]	Chemical shift for **12**[b] (ppm)	Chemical shift for **12**-Br^+/TfO^-[c] (ppm)
1		38.72
2	130.26	160.51
3	38.3	42.46
4		43.37
5		31.0
6		43.93
7		26.16
8		40.16
9		40.72
10		46.65
1′		34.78
2′	136.35	142.77
3′		36.30
4′		34.44
5′		25.97
6′		35.96
7′		26.13
8′		41.35
9′		39.80
10′		37.07
CH_3	19.51	18.98

[a]See Scheme 1 for numbering assignments.
[b]At 25°C in $CDCl_3$.
[c]At −50°C in CD_2Cl_2.

Table 7. ^{13}C NMR chemical shifts observed for **13** and **13**-$Br^+/B(Ph(CF_3)_2)_4^-$.

Carbon no.[a]	Chemical shift for **13**[b] (ppm)	Chemical shift for **13**-$Br^+/B(Ph(CF_3)_2)_4^-$[c] (ppm)
1	31.79	40.74
2	132.07	168.31
3	42.30	47.53
4	36.7	40.10
5	38.46	34.83
6	33.65	30.87
7	29.05	26.0
8	35.13	41.16
9	41.56	n.d.
10	35.31	35.69
1′	32.68	34.62
2′	135.20	139.59
3′	32.45	36.96
CH_3 (ax)	28.91	27.86
CH_3 (eq)	27.14	27.02

[a]See Scheme 2 for numbering assignments.
[b]At 25°C in CD_2Cl_2.
[c]At −50°C in CD_2Cl_2.

that the use of the bulky Ad═Ad-Br^+ moiety confers no advantage over NBS in promoting chiral cyclization of these alkenes.

(b) Axially methylated derivatives 12 and 13

Olefin **12** was generously provided by Prof. A. J. Bennet (13) while **13** was prepared by treatment of the corresponding ketone (14) with dimethyltitanium dichloride (15). The corresponding bromonium ions were made by simple treatment of **12** with Br_2 and methyl triflate as was the case for the parent Ad═Ad (3), and treatment of **13** with Br_2 and the sodium salt of tetra (3,5-di(trifluoromethyl)phenyl)borate. We had anticipated that the interaction of the axial CH_3 group and the proximal Br would lead to considerable distortion of the three-membered ring, but unfortunately this could not be confirmed directly since crystals of the bromonium ions of sufficient quality for X-ray diffraction analysis could not be obtained.

The olefins and their bromonium ions were subjected to extensive ^1H and ^{13}C NMR studies using COSY, NOE, and long- and short-range NMR experiments. Given in Tables 6 and 7 are the ^{13}C NMR data for **12**, **12**-Br^+/ OTF^- and **13**, **13**-Br^+/ $B(Ph(CF_3)_2)_4^-$. By comparison with the olefinic carbons of adamantylideneadamantane at δ 133.66 ppm (3), the C_2 and $C_{2'}$ olefinic carbons of **12** and **13** appear at δ 130.26, 136.35 and 132.07, 135.20 ppm, respectively. Bromination of the parent Ad═Ad to give the symmetrical bromonium ion produces a downfield shift in both carbons of 22.58 ppm to δ 156.24 (3): in the case of **12**-Br^+ C_2 and $C_{2'}$ appear at δ 160.51 and 142.77 while for **13**-Br^+ these carbons are at δ 168.31 and 139.59 ppm, respectively. The more pronounced downfield shift of C_2 (30 and 36 ppm) than that of $C_{2'}$ (6.4 and 4.4 ppm) upon bromonium ion formation from **12** and **13** indicates a high degree of asymmetry in these ions as would be expected if the axial methyl group and Br are sterically buttressed. This buttressing is the source of some instability and although the ions are indefinitely stable at −50°C, they decompose readily at room temperature to unknown materials.

Despite the instability of **12**-Br^+ at room temperature, a few kinetics experiments were conducted to determine its efficacy in promoting the cyclization of 4-pentenol in dichloroethane at 25°C. At 260 nm **12**-Br^+/ OTF^- has an extinction coefficient (6330 ± 50 M^{-1} cm^{-1}) that is roughly 2-fold greater than that of Ad═Ad-Br^+ (3200 M^{-1} s^{-1}) (1, 2). From the slopes of plots of the pseudo-first-order rate constants for loss of **12**-Br^+ as a function of excess 4-pentenol, a second-order rate constant of about 2000 ± 300 M^{-1} s^{-1} is obtained. This value is 500–600 times greater than the value obtained for Ad═Ad-Br^+ (1, 2), which probably results from a destabilized ground state for the distorted bromonium ion in **12**-Br^+.

Conclusions

In the above research we have attempted to design Br^+ transfer agents based on the adamantylideneadamantane skeleton to induce chirality in the cyclization of alkenes. The kinetics results indicate that cyclization of the 4-pentenyl permethylated glycoside, **10**, must occur through a complex of the olefin and Ad═Ad-Br^+. Disappointingly, there is no additional enantiomeric excess in the tetrahydrofurfuryl bromide product over what is observed using NBS and the perbenzylated analogue of **10** (11). An attempt to build chirality into the Ad═Ad system using axial methylation of one of the homoallylic car-

© 1997 NRC Canada

bons was undertaken and the racemic derivatives **12** and **13** were synthesized for preliminary studies. Unfortunately, the bromonium ions of these materials are not stable when held at room temperature for prolonged periods. The results of this research indicate that it is unlikely that the Ad=Ad system will prove of utility in inducing chiral Br^+ transfer to olefins. Alternative ways of effecting this important process are currently under investigation in these laboratories.

Acknowledgement

The authors gratefully acknowledge the financial support of the Natural Sciences and Engineering Research Council of Canada and Queen's University. In addition, they are grateful to Prof. A.J. Bennet (Simon Fraser University) for a generous gift of olefin **12**.

References

1. A.A. Neverov and R.S. Brown. J. Org. Chem. **61**, 962 (1996).
2. A.A. Neverov and R.S. Brown. Can. J. Chem. **72**, 2540 (1994).
3. R.S. Brown, R.W. Nagorski, A.J. Bennet, R.E.D. McClung, G.H.M. Aarts, M. Klobukowski, R. McDonald, and B.D. Santarsiero. J. Am. Chem. Soc. **116**, 2448 (1994).
4. (*a*) K. Penzien and G.M. Schmidt. Angew. Chem. Int. Ed. Engl. **8**, 608 (1969); (*b*) Y. Tanaka, H. Sakuraba, and H. Nakanishi. J. Chem. Soc. Chem. Commun. 947 (1983).
5. (*a*) G. Belluci, G. Berti, and R. Bianchini. Gazz. Chim. Ital. **116**, 77 (1987); (*b*) G. Bellucci, G. Berti, F. Marioni, and A Marzilli. Tetrahedron, **26**, 4627 (1970); (*c*) L. Duhamel, G. Ple′, P. Angibaud, and J.R. Desmurs. Synth. Commun. **23**, 2423 (1993).
6. (*a*) C. Giordano, L. Coppi, and A. Restelli. J. Org. Chem. **55**, 5400 (1990); (*b*) G. Castaldi and C. Giordano. Synthesis, 1039 (1987); (*c*) G. Castaldi, S. Cavicchioli, C. Giordano, and F. Uggeri. Angew. Chem. Int. Ed. Engl. **25**, 259 (1986).
7. P. Angibaud, J.L. Chaumette, J.R. Desmurs, L. Duhamel, G. Ple′, J.Y. Valnot, and P. Duhamel. Tetrahedron: Asymmetry, **6**, 1919 (1995).
8. (*a*) W. Oppolzer, R. Pedrosa, and R. Moretti. Tetrahedron Lett. **27**, 831 (1986); (*b*) W. Oppolzer and P. Dudfield. Tetrahedron Lett. **26**, 5037 (1985); (*c*) W. Oppolzer. Pure Appl. Chem. **62**, 1241 (1990).
9. (*a*) D.A. Evans, T.C. Britton, J.A. Ellman, and R.L. Dorow. J. Am. Chem. Soc. **112**, 4011 (1990); (*b*) D.A. Evans and J.A. Ellman. Tetrahedron Lett. **28**, 1123 (1987).
10. S.-S. Jew, J.-W. Kim, B.-S. Jeong, and Y.-S. Cho. *In* Advances in organobromine chemistry, II. Industrial chemistry library. Vol. 7. *Edited by* J.R. Desmurs, B. Gerard, and M.J. Goldstein. Elsevier, Amsterdam. 1995 pp. 171–173.
11. (*a*) R. Rodebaugh and B. Fraser-Reid. Tetrahedron, **52**, 7663 (1996); (*b*) R. Rodebaugh and B. Fraser-Reid. J. Am. Chem. Soc. **116**, 3155 (1994); (*c*) H. Merz, K. Stockhaus, and H. Wick. J. Med. Chem. **18**, 996 (1975).
12. D.D. Perrin, W.L.F. Armagero, and D.R. Perrin. *In* Purification of laboratory chemicals. 2nd ed. Pergamon Press, Oxford. 204 1980. p. 204.
13. X. Huang, R.J. Batchelor, F.W.B. Einstein, and A.J. Bennet. J. Org. Chem. **59**, 7108 (1994).
14. E.W. Meijer, R.M. Kellogg, and H. Wynberg. J. Org. Chem. **47**, 2005 (1982).
15. M.T. Reets, J. Westerman, and R. Steinbach. Angew. Chem. Int. Ed. Engl. **19**, 900 (1980).

Can. J. Chem. Downloaded from www.nrcresearchpress.com by 91.121.58.235 on 09/08/12
For personal use only.

© 1997 NRC Canada

Conformational behavior and electronic structure of silylketenes studied with quantum chemical calculations and photoelectron spectroscopy

Heidi M. Muchall, Nick H. Werstiuk, Jiangong Ma, Thomas T. Tidwell, and Kuangsen Sung

Can. J. Chem. Downloaded from www.nrcresearchpress.com by 91.121.58.235 on 09/08/12
For personal use only.

Abstract: The He(I) photoelectron spectra of silylketenes $(Me_3Si)_2C{=}C{=}O$ (**1**), $Me_5Si_2CH{=}C{=}O$ (**2**), $Me_2Si(CH{=}C{=}O)_2$ (**3**), $MeSi(CH{=}C{=}O)_3$ (**4**), $(SiMe_2CH{=}C{=}O)_2$ (**5**), and $(CH_2SiMe_2CH{=}C{=}O)_2$ (**6**) have been recorded and their structures and orbital energies have been calculated by ab initio methods. Orbital energies for disilanes **2** and **5** are strongly dependent on a Si-Si-C-C torsional angle due to σ–π orbital interaction. Comparisons between experimental and simulated spectra show that **2** and **5** prefer conformations in which the Si—Si bond and ketene group(s) are approximately orthogonal (113° and 111°, respectively). Silylalkenes $Me_5Si_2CH{=}CH_2$ (**7**) and $(SiMe_2CH{=}CH_2)_2$ (**8**), which have been included in the computational study, show the same behavior as their corresponding silylketenes. Silylbis- and trisketenes **3–6** do not exhibit π–π interaction of any significance. For Si—Si containing compounds, the best agreement between experimental and computed data was obtained when Becke3LYP/6-31G*//HF/3-21G* was employed.

Key words: conformational behavior, electronic structure, photoelectron spectroscopy, quantum chemical calculations, silylketenes.

Résumé : On a déterminé les spectres photoélectroniques He(I) des silylcétènes $(Me_3Si)_2C{=}C{=}O$ (**1**), $Me_5Si_2CH{=}C{=}O$ (**2**), $Me_2Si(CH{=}C{=}O)_2$ (**3**), $MeSi(CH{=}C{=}O)_3$ (**4**), $(SiMe_2CH{=}C{=}O)_2$ (**5**) et $(CH_2SiMe_2CH{=}C{=}O)_2$ (**6**) et on a calculé leurs structures et leurs énergies orbitalaires par des méthodes ab initio. Les énergies orbitalaires des disilanes **2** et **5** dépendent fortement d'un angle de torsion Si-Si-C-C dû à une interaction σ–π. Des comparaisons entre les spectres expérimentaux et simulés montrent que les composés **2** et **5** adoptent préférentiellement des conformations dans lesquelles la liaison Si—Si et le(s) groupe(s) cétène(s) sont approximativement orthogonaux (113° et 111° respectivement). Les silylalcènes $Me_5Si_2CH{=}CH_2$ (**7**) et $(SiMe_2CH{=}CH_2)_2$ (**8**) dont on a aussi calculé les énergies présentent le même comportement que celui des silylcétènes correspondants. Les silylbis- et triscétènes **3–6** ne présentent pas d'interactions π–π significatives. Pour les composés comportant une liaison Si—Si, l'utilisation de la méthode Becke3LYP/6-31G*//HF/3-21G* conduit au meilleur accord entre les données expérimentales et calculées.

Mots clés : comportement conformationnel, structure électronique, spectroscopie photoélectronique, calculs quantiques de chimie, silylcétènes.

[Traduit par la rédaction]

Introduction

Studies on ketenes have shown a remarkable stabilizing effect of silyl substituents on the ketene group, giving persistent mono- and bisketenes (1). In a previous study (2), the availability of a number of conformationally flexible silylketenes had prompted us to employ photoelectron (PE) spectroscopy, *the* technique giving information about bonding in organic molecules. PE spectroscopy has been of continued use for conformational analyses where orbital energies depend on torsional angles (3) and has proved especially suited for systems with neighboring electron lone pairs or π electrons. Besides the expected π–π interaction in the bisketenes studied, ab initio calculations suggested an interesting σ–π interaction in *t*-$BuMe_2SiCH{=}C{=}O$ involving an energetically high-lying orbital of the *tert*-butylsilyl bond (2). Using Koopmans' theorem (4) to correlate HF ab initio orbital energies and experimental ionization potentials, we interpreted and accurately simulated the experimental PE spectra, thereby confirming the applicability of the combination of ab initio calculations and PE spectroscopy to the study of the conformational behavior of silylketenes. PE spectra of disilanes (5) and ketenes (6) are well known, yet there are no spectra reported of compounds combining disilane and ketene moieties, compounds of potential interest with respect to σ–π orbital interactions. Further-

Received June 20, 1997.

H.M. Muchall,[1] N.H. Werstiuk,[1] and J. Ma. Department of Chemistry, McMaster University, Hamilton, ON L8S 4M1, Canada.
T.T. Tidwell and K. Sung. Department of Chemistry, University of Toronto, Toronto, ON M5S 3H6, Canada.

[1] Authors to whom correspondence may be addressed. Telephone: (905) 525-9140. Fax: (905) 522-2509. E-mail: muchall@mcmaster.ca, werstiuk@mcmaster.ca

© 1997 NRC Canada

Can. J. Chem. Downloaded from www.nrcresearchpress.com by 91.121.58.235 on 09/08/12
For personal use only.

more, while we presented PE spectra of some silylketenes and silylbisketenes (2), there are no reports of such studies of compounds having more than one ketene group connected to a silicon atom, which are sources of possible remote π–π orbital interactions.

The preparation of such compounds has been reported recently (7, 8), and in this paper we report the conformational behavior of silylketenes **1–6** using ab initio calculations and PE spectroscopy. Where necessary for the interpretation of the experimental spectra, Becke3LYP (9) of density functional theory (DFT) has been employed alongside HF (10) theory.[2] Computational studies for silylalkenes **7** and **8** are included for comparison. The ionization potentials of these species have been presented (12) but representations of their PE spectra have not been reported. The interpretation of the spectra for **7** and **8** (12) does not agree with our conclusions on similar systems (2), and so we have studied **7** and **8** in more detail computationally.

$(Me_3Si)_2C{=}C{=}O$ **1**

$Me_5Si_2CH{=}C{=}O$ **2**

$Me_2Si(CH{=}C{=}O)_2$ **3**

$MeSi(CH{=}C{=}O)_3$ **4**

$(SiMe_2CH{=}C{=}O)_2$ **5**

$(CH_2SiMe_2CH{=}C{=}O)_2$ **6**

$Me_5Si_2CH{=}CH_2$ **7**

$(SiMe_2CH{=}CH_2)_2$ **8**

Experimental

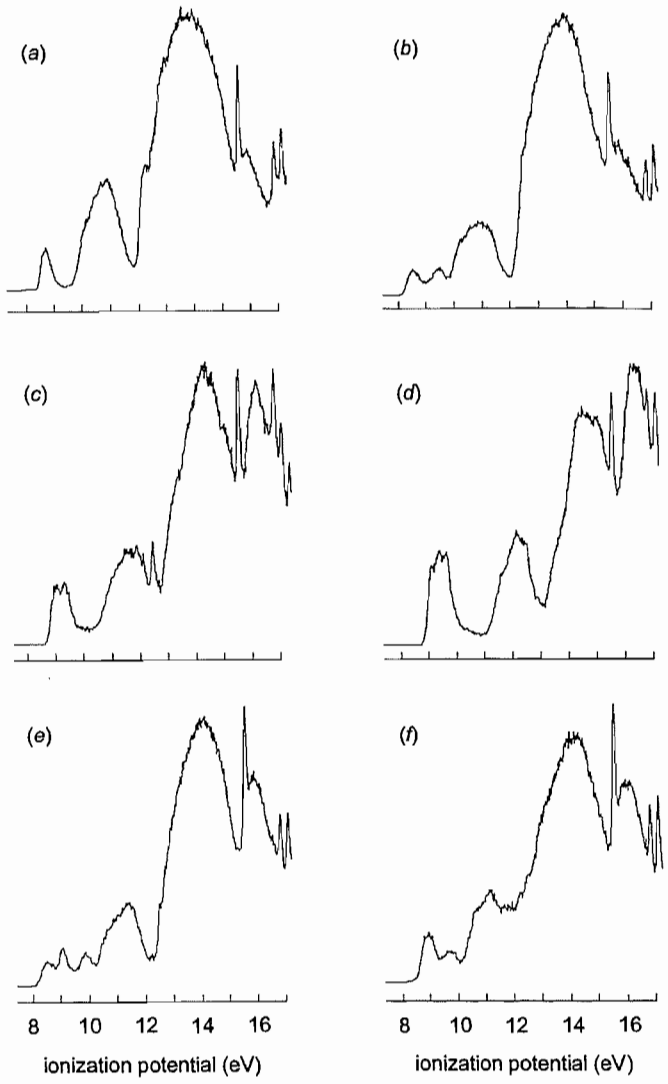
Ab initio HF (10) and Becke3LYP (9) calculations were carried out on IBM RS/6000 model 39H, 350, and 530 computers with GAUSSIAN 94 (13).[3] Semiempirical PM3 (14) calculations were performed with the MOPAC (15) program package (version 6.00) on an IBM RS/6000 model 320H computer. Except for those dihedral angles fixed in torsional analyses and indicated in the text, all geometry parameters were optimized. Synthetic spectra were calculated from the MO results with a Fortran program PESPEC (16). Graphical representations of the computationally determined eigenvectors (PM3//HF/3-21G*; these were checked against HF/3-21G*//HF/3-21G* as well as Becke3LYP/6-31G*//HF/3-21G* eigenvectors and were found to compare well) were plotted from HyperChem 4.[4]

[2] A rationale for the successful application of the Koopmans' theory-like interpretation of the orbital energies obtained at the DFT level of theory in a PE spectroscopic study of a series of carbenes has recently been provided by Arduengo et al. (11). It is clear that applying a uniform shift based on the difference in calculated HOMO energy and the experimental first vertical IP to the DFT orbital energies nicely reproduces the PE spectra of compounds presented here, which are vastly different from the carbenes studied by Arduengo.

[3] Total energies are uncorrected; for a discussion of the inclusion of zero-point vibrational energies in these studies, see Werstiuk et al. (2).

[4] Hypercube, Inc., Waterloo, Ont. 1994.

Fig. 1. UV photoelectron spectra of silylketenes (*a*) **1**, (*b*) **2**, (*c*) **3**, (*d*) **4**, (*e*) **5**, and (*f*) **6**.



He(I) PE spectra were measured with a locally built instrument (17) by signal averaging 40–50 scans, with nitrogen (15.6 eV) as the calibrant. Linearity of the scale was ensured through calibrations with methyl iodide (9.54 and 10.16 eV) and O_2 (12.30 eV) performed prior to the experiments.

Silylketenes **1–6** were synthesized as reported (7, 8).

Calculations and photoelectron spectra

Bis(trimethylsilyl)ketene (1)

Except for the rotation of the two trimethylsilyl groups, there is no conformational flexibility in this simple silylketene. According to HF/3-21G*, the preferred conformation **1a** has C_2 symmetry, one methyl group of each Me_3Si moiety being twisted out of the *syn*-periplanar (*sp*) arrangement with the ketene group by 17.7° to avoid eclipsing. Fixing these torsional angles at 0° (*sp* conformation **1b**) leads to an increase in total energy of 2.90 kJ mol^{-1}, whereas keeping them at 180° (*anti*-periplanar conformation **1c**) causes a destabilization of 18.49 kJ mol^{-1}. Neither **1b** nor **1c** are minima on the potential energy surface with HF/3-21G*.

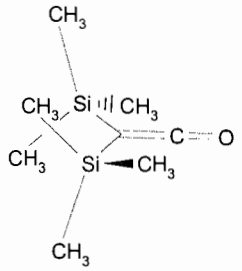
© 1997 NRC Canada

Can. J. Chem. Downloaded from www.nrcresearchpress.com by 91.121.58.235 on 09/08/12
For personal use only.

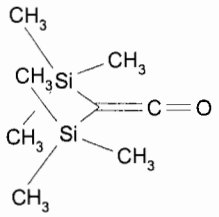
Table 1. Selected experimental vertical ionization potentials IP (eV) and calculated orbital energies ε (eV) of silylketenes **1–6** and silylalkenes **7** and **8**.

		$-\varepsilon^a$		
	IP	HF/3-21G*//HF/3-21G*	PM3//HF/3-21G*	B3LYP/6-31G*//HF/3-21G*
1	8.75	9.24	8.52	6.18
	10.2	11.23	9.93	7.81
2[b]	8.52	8.92	8.36	6.00
	9.51	10.42	9.69	7.20
	10.2	11.53	10.44	7.96
3	9.10	9.56	8.90	6.47
	9.38	9.81	9.10	6.64
	10.9	12.34	11.06	8.69
4	9.12	9.73	8.97	6.64
	9.42	9.96	9.14	6.80
	9.61	9.96	9.14	6.80
	11.6	13.08	11.56	9.35
5	8.52	8.75	8.17	5.93
	9.10	9.82	9.21	6.64
	9.88	10.95	10.08	7.64
	10.5	11.84	10.59	8.25
6	8.9	9.26	8.74	6.20
	8.9	9.60	8.99	6.46
	9.73	10.90	9.95	7.53
	10.6	11.90	10.59	8.31
7	8.56[c]	9.11	8.67	6.32
	10.0[c]	10.55	10.15	7.43
8[d]	8.63[c]	8.90	8.59	6.22
	10.0[c]	10.25	10.11	7.29

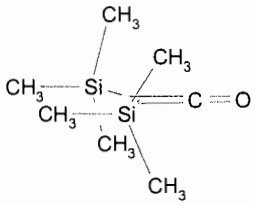
[a]Given for the most stable conformer according to HF/3-21G*.
[b]Orbital energies are given for conformer **2a**.
[c]Reference 12.
[d]Orbital energies are given for conformer **8b**.



1a



1b



1c

The HOMO of **1**, which is mainly π_{CCO} with only minor contributions from Si—CH_3 bonds, is followed by a group of five orbitals (HOMO-1 to HOMO-5; 11.23, 11.73, 11.84, 12.07, and 12.12 eV), all of which have σ Si—C character. Upon rotation of one trimethylsilyl group, there is essentially no dependence of the orbital energies on the torsional angle.

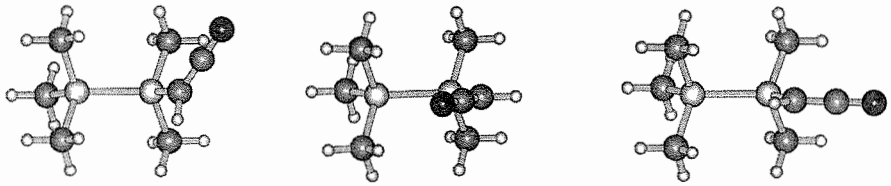
The PE spectrum of ketene **1**, which resembles that of $Me_3SiCH{=}C{=}O$ (**2**), exhibits two separate bands in the low-energy region (Fig. 1(*a*)). The first band (8.75 eV) belongs to just one ionization, the second, centered at 10.7 eV, to five. Another band at 12.29 eV is resolved in front of the σ region. Compared to the first ionization of $Me_3SiCH{=}C{=}O$ (8.95 eV) (**2**), that of **1** is shifted to a slightly lower IP, showing the destabilization of the π_{CCO}-HOMO due to further $SiMe_3$ substitution. The relative positions of the bands correspond well to the computed relative orbital energies for **1** (Table 1); in particular, the HOMO energy taken from a PM3 single-point calculation on the HF/3-21G* optimized geometry of 8.52 eV is very close to the experimental value of 8.75 eV for the first ionization.

© 1997 NRC Canada

Can. J. Chem. Downloaded from www.nrcresearchpress.com by 91.121.58.235 on 09/08/12
For personal use only.

Table 2. Calculated total (hartrees) and relative (kJ mol^{-1}) energies of conformers of silylketenes **2–6** and silylalkenes **7** and **8**.

	HF/3-21G*//HF/3-21G*		Becke3LYP/6-31G*//HF/3-21G*	
	Total energy	Relative energy	Total energy	Relative energy
2a	−922.371 105	0.73	−930.634 892	0.00
2b	−922.371 385	0.00	−930.634 682	0.55
2c	−922.369 523	4.88	−930.632 989	4.99
3a	−666.976 824	0.00	−673.387 789	1.53
3b	−666.976 810	0.04	−673.388 374	0.00
3c	−666.975 340	3.89	−673.387 614	1.99
4a	−777.897 465	0.00	−785.486 598	0.00
4b	−777.896 452	2.66	−785.486 226	0.98
4c	−777.895 114	6.17	−785.485 459	2.99
5a	−1033.290 507	0.00	−1042.733 900	0.00
5b	−1033.290 475	0.08	−1042.733 897	0.01
5c	−1033.286 794	9.74	−1042.729 943	10.38
5d	−1033.290 172	0.88	−1042.733 053	2.22
6a	−1110.951 768	0.00	−1121.368 596	0.00
6b	−1110.951 752	0.04	−1121.368 400	0.51
6c	−1110.951 559	0.55	−1121.368 461	0.35
7a	−849.081 419	0.00	−856.610 379	0.00
7b	−849.080 692	1.91	−856.609 137	3.26
8a	−886.711 307	0.00	−894.685 432	0.76
8b	−886.711 296	0.03	−894.685 723	0.00



2a **2b** **2c**

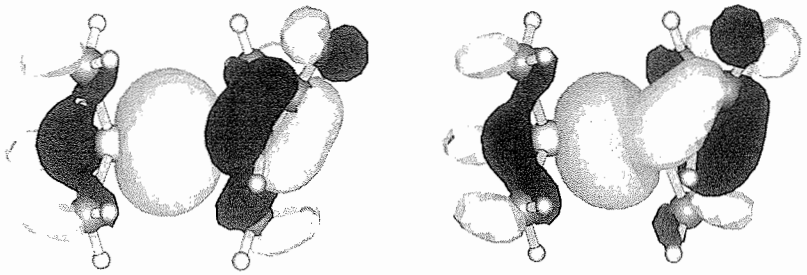
(Trimethylsilyldimethylsilyl)ketene (2)

The most stable conformation of the related (*tert*-butyldimethylsilyl)ketene was found to be one in which one methyl group is oriented *sp* to the ketene group, the Bu^t-Si-C-C dihedral angle being 115.4° (2). We studied three conformations, **2a–2c**, of disilylketene **2**. While HF/3-21G* calculations predict the 0° conformer (Si-Si-C-C torsional angle) **2b** to be lowest in energy, both HF/6–31G*//HF/3-21G* and Becke3LYP/6–31G*//HF/3-21G* calculate **2a** to be more stable than **2b**, the 180° conformer **2c** showing the highest energy (Table 2). For *t*-$BuMe_2SiCH{=}C{=}O$ the conformation analogous to **2a** was also found to be most stable (2). In **2a**, the Si—Si bond length is 234.7 pm and the Si-Si-C-C dihedral angle is 112.6°. The semiempirical PM3 method stretches the Si—Si bond considerably (to 246.0 pm in the optimized **2a**), which allows the ketene group to adopt a smaller torsional angle of 92.5°.

The geometries of **2** and (*tert*-butyldimethylsilyl)ketene are comparable but there is a distinct difference in their electronic structures. In the *tert*-butyl carbon analog of **2**, orbital energies do not seem to be a function of the Bu^t-Si-C-C torsional angle (2). For **2a**, HOMO and HOMO-1 are the antisymmetrical and symmetrical combinations of π_{CCO} with σ-type contribution of electron density on the Si—Si bond. HOMO-1 is followed by a group of four orbitals (HOMO-2 to HOMO-5, σ Si—C type, values not given) that are energetically close together. In disilane **2**, the HOMO/HOMO-1 splitting is strongly dependent on the Si-Si-C-C torsional angle, regardless of the level of theory applied. HOMO (σ_{SiSi}) and HOMO-1 (π_{CCO}) show no mixing and are quite similar in energy in the 0° conformer **2b**, Δε of these two orbitals being 0.33 (PM3), 0.27 (HF/3-21G*), and 0.42 eV (Becke3LYP/6–31G*//HF/3-21G*). This difference grows as the torsional angle is increased and the orbitals are allowed to mix. The greatest Δε of 1.73 (PM3), 1.63 (HF/3-21G*), and 1.28 eV (Becke3LYP/6–31G*//HF/3-21G*), due to maximal σ–π interaction, is found at 90°, decreasing again to about the 0° value on going to 180°. An explanation for the preference of a dihedral near 90° (**2a** is the global minimum) in spite of this destabilizing interaction is given by the very low lying LUMO of σ^*_{SiSi} character: the σ*–π interaction is stabilizing.

The potential for this twisting about the Si—CCO bond was obtained by fixing the Si-Si-C-C dihedral at 0°, 45°, 90°, 135°, and 180° and relaxing the rest of the molecule. Fitted curves as calculated by PESPEC (16) on HF/3-21G* and Becke3LYP/6–

© 1997 NRC Canada

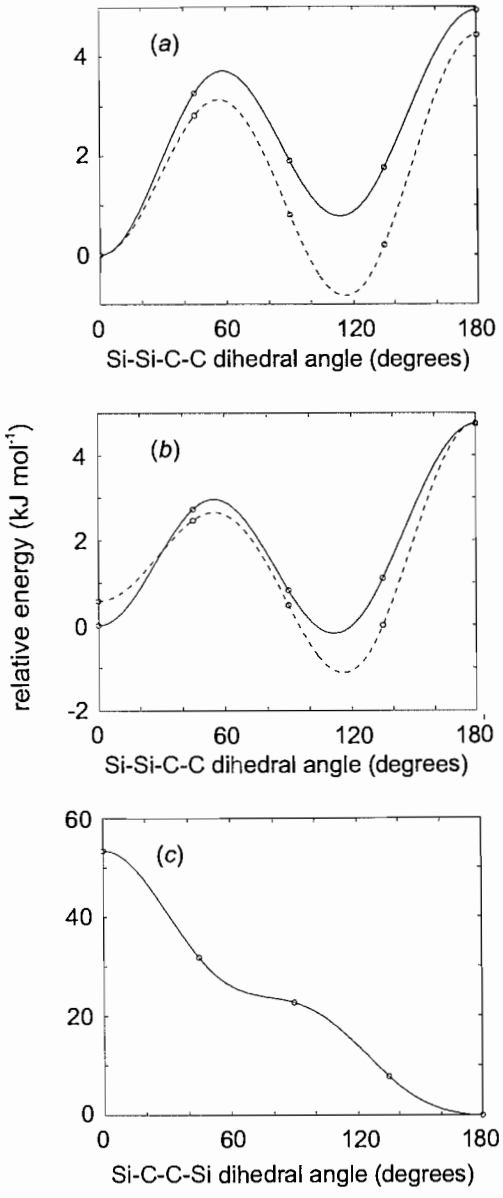


Can. J. Chem. Downloaded from www.nrcresearchpress.com by 91.121.58.235 on 09/08/12
For personal use only.

31G*//HF/3-21G* relative energies are shown in Fig. 2(*a*). The change in orbital energies of the four highest occupied molecular orbitals upon increase of the Si-Si-C-C torsional angle is given in Fig. 3(*a*) (Becke3LYP/6-31G*//HF/3-21G* values). The progression of HOMO and HOMO-1 clearly shows the pronounced σ–π interaction in disilane **2** that was previously proposed on the basis of UV data for **2** (8).

In the PE spectrum of disilylketene **2** depicted in Fig. 1(*b*), the first (8.52 eV) and second (9.51 eV) ionization each give rise to a separate band; the third band (centered at 10.9 eV) is formed by four ionizations. The overall appearance of the spectrum is similar to that of (*tert*-butyldimethylsilyl)ketene (2), yet the first IP of **2** is found at a lower value than that of the corresponding *tert*-butyl carbon analog (8.79 eV), which indicates a greatly destabilized HOMO. This and the experimentally determined gap of 1 eV between the first two ionizations of **2** shows the extent of interaction between σ_{SiSi} and π_{CCO} in **2**, which was predicted by the calculations (Fig. 3(*a*)). While both HF/3-21G*//HF/3-21G* and HF/6-31G*//HF/3-21G* overestimate the σ–π interaction, leading to an exaggerated splitting of the first two orbitals, there is excellent agreement between the relative ionization energies and the relative calculated orbital energies of **2** when Becke3LYP is employed. Electron correlation, therefore, cannot be neglected when describing the electronic structure of this disilane. The simulated PE spectrum obtained with PESPEC and based on the calculated potential (Fig. 2(*a*)) is given in Fig. 4(*a*). Twelve eigenvalues (HOMO to HOMO-11) were used to synthesize the partial spectrum of **2**, convoluted with a Gaussian lineshape with a full width at half height (FWHH) of 0.4 and the temperature set at 300 K. The simulated spectrum correctly reproduces the low-energy part of the experimental spectrum of **2**, suggesting that disilylketene **2** prefers a conformation in which the Si—Si bond and ketene group are close to orthogonal for maximum orbital interaction. While Becke3LYP values are excellent in terms of relative orbital energies, they differ by several eV from the experimental values.[2] As for **1**, the energy of the first ionization can be predicted well using PM3//HF/3-21G*.

Fig. 2. Torsional potential calculated with PESPEC (HF/3-21G*, solid line; Becke3LYP/6–31G*//HF/3-21G*, broken line): twisting about (*a*) the Si—CCO bond of **2**, (*b*) one Si—CCO bond of **5**, and (*c*) the CH_2—CH_2 bond of **6**.

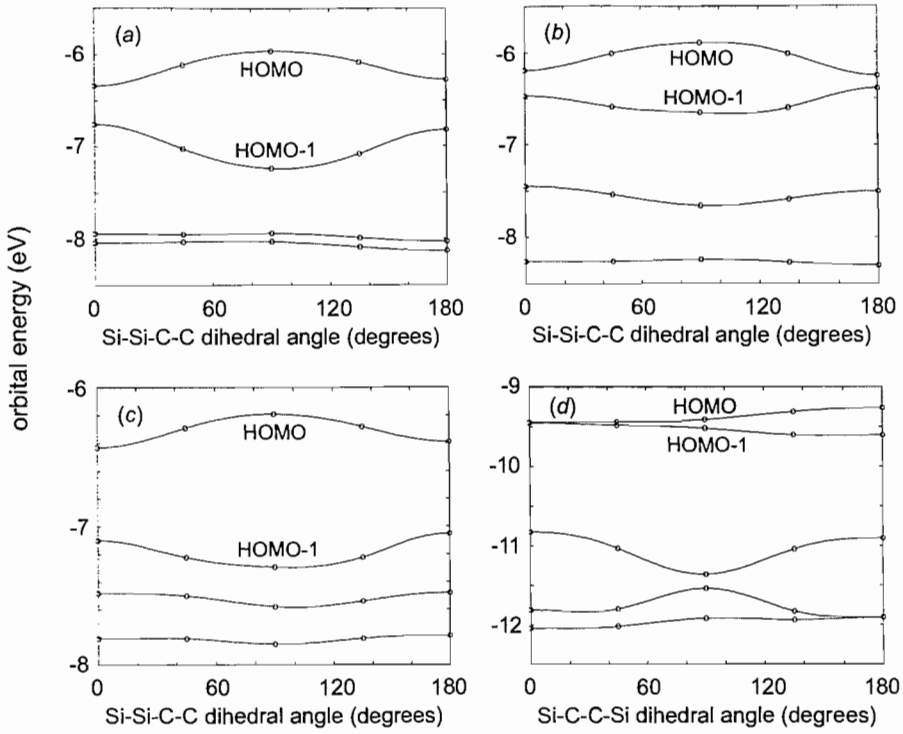


(Trimethylsilyldimethylsilyl)ethene (7)

A comparison of (*tert*-butyldimethylsilyl)ketene and (*tert*-butyldimethylsilyl)ethene revealed similar conformational behavior and orbital interactions, with more σ–π interaction for the alkene as judged by the angular dependence of the HOMO/HOMO-1 gap (2). Khvostenko et al. (12) reported an absence of σ–π conjugation for (trimethylsilyldimethylsilyl)ethene (**7**) based on the first IP in the PE spectra of the

© 1997 NRC Canada

Fig. 3. Angular dependences of the MO energies of HOMO to HOMO-3 of (*a*) **2**, (*b*) **5**, and (*c*) **8** (Becke3LYP/6-31G*//HF/3-21G*), as well as (*d*) HOMO to HOMO-4 of **6** (HF/3-21G*).



series **7** (8.56 eV), 1,2–divinyl-1,1,2,2–tetramethyldisilane (**8**) (8.63 eV), and hexamethyldisilane (8.69 eV), which they claimed to be constant. As this was quite unexpected, we calculated the potential for the rotation of the ethylene moiety in alkene **7**. Two conformations, **7a** and **7b**, correspond to **2a** and **2b**, respectively. The Si—Si bond length (235.0 pm) and Si-Si-C-C dihedral angle (109.4°) in the optimized **7a** (HF/3-21G*) compare to those in **2a**, as do the orbitals (LUMO of **7a** is a low-lying σ^*_{SiSi}, HOMO the antibonding combination of σ_{SiSi} with $\pi_{C=C}$). Likewise, the Becke3LYP/6-31G*//HF/3-21G* fitted potential for the rotation in **7** resembles that found for **2**, except for the energy difference of 3.26 kJ mol^{-1} between **7a** and the 0° conformation **7b** being larger than for the respective conformations of **2** (0.73 kJ mol^{-1}). This is due to the greater steric interaction experienced by the vinyl hydrogen atom, which points inwards in **7**, compared to that for the ketene group in **2** and can be seen in the different Si-C-C angles (122.7° **2a**/125.2° **7a**, 121.2° **2b**/125.9° **7b**), as for the *tert*-butyl analogs (2). Yet in contrast to these *tert*-butyl compounds, the σ–π interaction seems to be greater in ketene **2** (the HOMO/HOMO-1 gap increasing from 0.42 to 1.28 eV) than in alkene **7** (from 0.50 to 1.18 eV, Becke3LYP/6-31G*// HF/3-21G*, plot not shown). The torsional dependence of HOMO and HOMO-1 resulting from the relative orientations of the Si—Si bond and the C—C double bond in alkene **7** is clearly in contrast to the absence of σ–π conjugation published by Khvostenko et al. (12). The simulated PE spectrum for **7** (Becke3LYP/6-31G*//HF/3-21G*, 12 eigenvalues, FWHH 0.4, temperature 300 K), which unfortunately cannot be compared to the experimental spectrum, is shown in Fig. 4(*b*). Yet it was stated (12) that the second and the third band in the spectrum of **7** are poorly resolved and this is correctly reproduced by the calculations as can be seen in the synthesized spectrum. Thus we can conclude that alkene **7** exhibits the same conformational properties as ketene **2**.

Dimethylsilylbisketene (3)

Five conformations of bisketene **3** were studied at the ab initio level. Conformer **3a**, shaped like a partial propeller (where one "blade" is represented by a methyl group) with one ketene group *sp* to the other Si—CCO bond and one ketene group *sp* to one Si—CH_3 bond (the torsional angles being 12.6° and 5.2°, respectively), and conformer **3b**, another propeller, with C_2 symmetry and ketene groups each *sp* to one Si—CH_3 bond (OC-C-Si-CH_3 dihedrals are 4.2°) and *anti* with respect to each other, are essentially equal in energy at HF/3-21G*. The related *syn* conformer **3c** with ketene groups *sp* to the same Si—CH_3 bond (OC-C-Si-CH_3 dihedrals are 8.4°) is 3.9 kJ mol^{-1} higher in energy (Table 2). While HF/6-31G*//HF/3-21G* total energies of the three conformers (not given) follow the same ordering, Becke3LYP/6-31G*//HF/3-21G* reverses the energetic order of **3a** and **3b**. Two in-plane conformations (U and W shaped), which are still higher in energy at the semiempirical level (PM3), are not stationary points according to ab initio calculations.

Orbital energies for the three low-energy conformations **3a–3c** are very similar, according to all computational methods applied. HOMO and HOMO-1 (symmetrical and antisymmetrical combinations of π_{CCO}'s) are close in energy, followed by a group of three orbitals (HOMO-2 to HOMO-4, values not given) that are mainly σ Si—C type. To obtain the potential energy surface and determine the extent of orbital

© 1997 NRC Canada

Can. J. Chem. Downloaded from www.nrcresearchpress.com by 91.121.58.235 on 09/08/12
For personal use only.

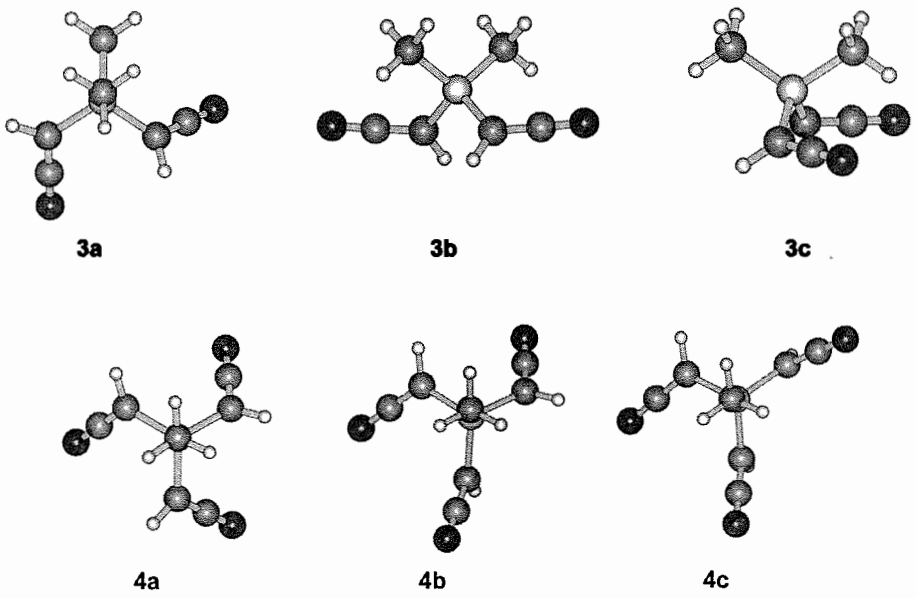
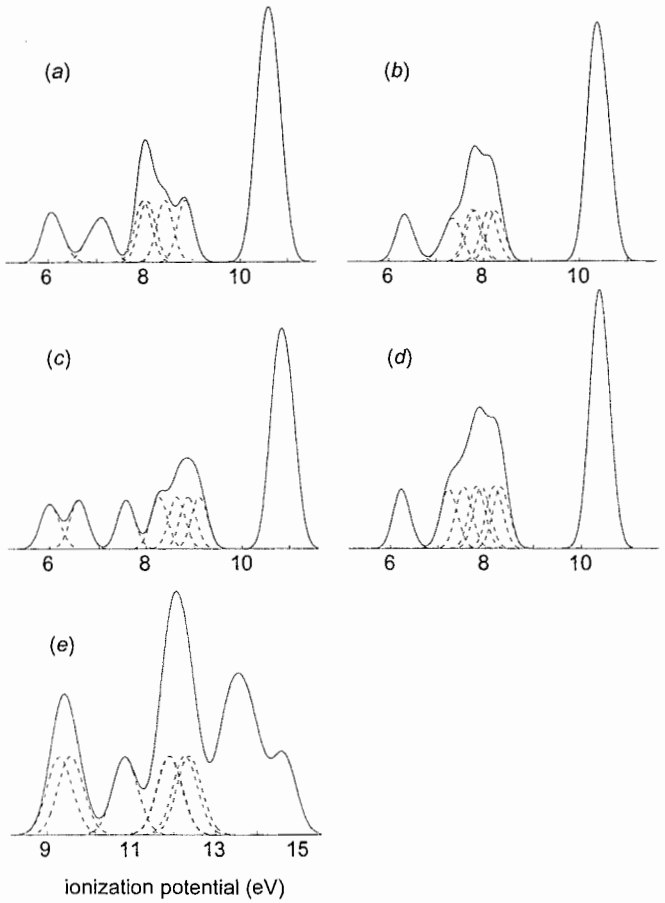


Fig. 4. Synthetic partial UV photoelectron spectrum calculated with PESPEC of (*a*) **2**, (*b*) **7**, (*c*) **5**, (*d*) **8**, and (*e*) **6**.



energy dependence on changes in the orientation of the two ketene groups, one dihedral (of the ketene group *sp* to the Si—CH_3 bond) was restrained at its original value and the other varied (plots not shown). As suggested by the similar energies of HOMO and HOMO-1 of **3a**–**3c**, the orbital energies are almost independent of the torsional angle. This fact, as well as the near degeneracy of HOMO and HOMO-1, shows that there is little π–π interaction between the two ketene moieties in bisketene **3**.

Like **1**, the PE spectrum of bisketene **3** (Fig. 1(*c*)) closely resembles that of $Me_3SiCH{=}C{=}O$ (2). For **3**, the first band is made up of two ionizations (9.10 and 9.38 eV) and the second, centered at 11.7 eV, corresponds to three (the sharp peak at 12.51 eV is due to traces of water). The stabilization of the HOMO (and therefore greater value for the first IP), upon substitution of one methyl group in $Me_3SiCH{=}C{=}O$ by a second ketene moiety, and the very small splitting of the first two ionizations arising from the absence of significant π–π interaction are accurately predicted by the calculations (Table 1).

Methylsilyltrisketene (4)

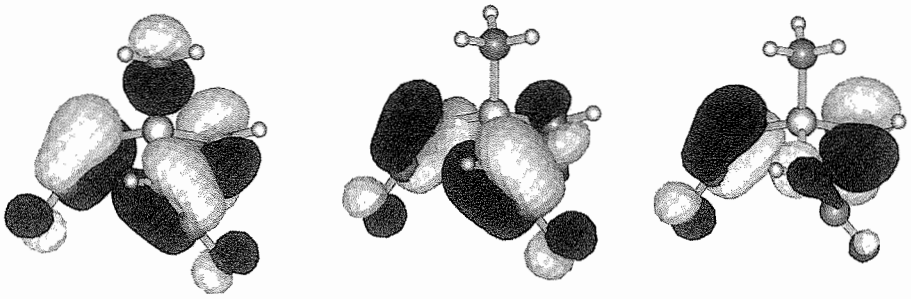
The most stable conformation of trisketene **4** is the symmetrical propeller **4a**, as found with all computational methods (Table 2). All ketene groups in **4a** are oriented *sp* to a Si—CCO bond; the respective torsional angles OC-C-Si-CCO are 10°. Two further low-energy conformations **4b** and **4c** can be derived from the propeller **4a** by twisting one or two ketene groups, respectively, into an arrangement *sp* to the Si—CH_3 bond.

Molecular orbitals HOMO to HOMO-5 for **4a**–**4c** come in two groups of three centered around 9.8 and 13.2 eV as calculated by HF/3-21G*. The first group is made up of three combinations of three π_{CCO}'s, one symmetrical and two antisymmetrical. The energy difference $\Delta\varepsilon$ between the first (HOMO) and last (HOMO-2) orbital in this group is 0.23 (**4a**), 0.53 (**4b**), and 0.67 eV (**4c**). In **4a**, HOMO-1 and HOMO-2 are degenerate because of the symmetry of the conformer; as the orbitals split in **4b** and **4c**, $\Delta\varepsilon$ becomes bigger. Orbitals in the second group (HOMO-3 to HOMO-5) are three combinations of σ Si—C type and show a similar behavior to those of the first group with respect to $\Delta\varepsilon$.

For the determination of the potential energy surface (plot not shown), two ketene dihedrals in **4a** were kept at their original values while the remaining one was twisted. Again, as in

© 1997 NRC Canada

Can. J. Chem. Downloaded from www.nrcresearchpress.com by 91.121.58.235 on 09/08/12
For personal use only.



4a-HOMO **4a**-HOMO-1 **4a**-HOMO-2

the case of dimethylsilylbisketene (**3**), the orbital energy dependence on the torsional angle is small, further confirming the lack of significant π–π interaction between the ketene groups in these molecules.

The PE spectrum of trisketene **4**, which on going from $Me_3SiCH{=}C{=}O$ has two methyl groups replaced by ketene groups, shown in Fig. 1(*d*) resembles that of bisketene **3**. For **4**, there are two bands of similar intensity in the low-energy region, one around 9.4 eV for which three maxima can be given, the other at about 12.2 eV. Each is composed of three ionizations. Again, this spectrum displays the computationally predicted small splitting of the first three IPs coherent with a small π–π interaction between the ketene groups (Table 1). The fact that we are able to assign three maxima in the first band suggests that **4** to a certain degree exists in unsymmetrical conformations that do not permit HOMO-1 and HOMO-2 to be degenerate.

1,2–Bis(ketenyl)-1,1,2,2-tetramethyldisilane (5)

Three conformations of disilylbisketene **5** with the OCC-Si-Si-CCO dihedral at 180° were studied and, except for the semiempirical PM3 method, all calculations predict **5a** to be lowest in energy (Table 2). Ketene groups in the C_2 symmetrical **5a** are oriented *sp* to Si—CH_3 bonds (C-Si-C-C dihedral is 9°) and *syn* towards each other. The corresponding *anti* conformer **5b**, which is the global minimum with PM3, is only slightly destabilized. Conformer **5c** with Si-Si-C-C dihedral angles at 180° is higher in energy. The Si—Si bond length (234.2 pm) and Si-Si-C-C torsional angles (111.0°) of **5a** obtained with HF/3-21G* resemble those of **2a**, the other disilane studied. Again, PM3 lengthens the Si—Si bond to 246.7 pm, which allows the ketene groups to approach the optimal right angle. The fourth conformation studied with ab initio methods, **5d**, differs from the other three in that the OCC-Si-Si-CCO dihedral is at 65.3°. Conformer **5d** is lower in energy than **5c** (Table 2).

As was the case for disilylketene **2**, there is a pronounced difference in orbital energies for conformers **5a** and **5c** that is once more indicative of a σ–π interaction. For **5a** with the Si—Si bond and ketene groups near orthogonal (ab initio calculations), HOMO to HOMO-2 are more or less equally spaced orbitals followed by a group of four (mainly σ Si—C character). HOMO and HOMO-2 show a symmetrical combination of π_{CCO}'s with σ contribution of electron density on the Si—Si bond ($\pi^+_{CCO}/\sigma_{SiSi}$); HOMO-1 is the antibonding combination of π_{CCO}'s (π^-_{CCO}). As for disilylketene **2**, the LUMO is a low-lying σ^*_{SiSi}. In the "stretched" **5c**, HOMO and HOMO-1 (π^-_{CCO} and π^+_{CCO}, respectively) are almost degenerate, and HOMO-2 is the unperturbed σ_{SiSi}.

Conformers **5a**–**5d** suggest that there are three bonds in this disilane that should be included in a conformational study, one Si—Si and two Si—CCO bonds. To study this problem computationally, rotations about the Si—Si bond and one Si—CCO bond were examined separately. Neither total energy nor orbital energies depend on the OCC-Si-Si-CCO torsional angle (no plots shown) but the rotation of one ketene moiety has an effect on the orbital energies. For the calculation of the respective potential, one Si-Si-C-C dihedral was fixed at its optimized value[5] and the other rotated through 0°, 45°, 90°, 135°, and 180°. The fitted potentials for HF/3-21G* and Becke3LYP/6-31G*//HF/3-21G* relative energies are shown in Figure 2(*b*). Figure 3(*b*) gives the Becke3LYP/6–31G*//HF/3-21G* eigenvalues for the four highest occupied molecular orbitals as a function of the torsional angle. To judge the extent of the effect of σ–π mixing on the orbital energies is not simple because of multiple interactions; UV spectra seem to indicate that it is smaller in bisketene **5** than it is in monoketene **2** (8).

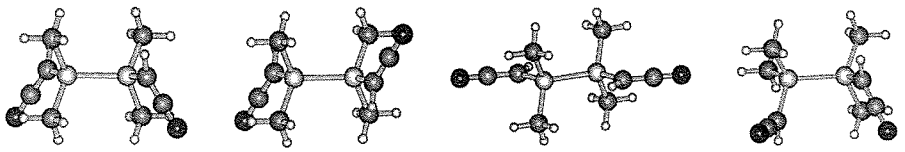
As is the case for bisketene **3** and trisketene **4**, there is only a small π–π interaction in **5**. A simple "uncoupling" of π^+_{CCO} and σ_{SiSi}, which form HOMO and HOMO-2, gives a π^+_{CCO} that is in the energetic neighborhood of π^-_{CCO}. This is confirmed by isodesmic considerations on the unsubstituted bis(ketenyl)disilane (H_2Si-$CH{=}C{=}O)_2$ (7).

The PE spectrum of disilylbisketene **5** (Fig. 1(*e*)) shows three bands (8.52, 9.10, and 9.88 eV) of comparable intensity belonging to one ionization each, followed by a broad band centered at 11.2 eV that is composed of four ionizations. The first band in the spectrum of **5** is found at the same low value as that for **2**, again indicating an interaction between σ_{SiSi} and π_{CCO}. As for **2**, the best simulated spectrum was obtained using the Becke3LYP/6-31G*//HF/3-21G* calculated surface and eigenvalues, which again shows the importance of including electron correlation in calculations of the electronic structure of disilanes. The synthesized partial PE spectrum based

[5] The assumption that keeping the second dihedral at its optimized value would lead to correct results was drawn from the PM3 surface obtained for the rotation of *both* ketene groups of disilylbisketene **5**. This hypersurface obtained from 25 points (0°, 45°, 90°, 135°, and 180°) suggests that conformations lying on the lowest energy path have one Si-Si-C-C dihedral angle at 90°. This is near the optimized PM3 value for this dihedral in **5a**.

© 1997 NRC Canada

Can. J. Chem. Downloaded from www.nrcresearchpress.com by 91.121.58.235 on 09/08/12
For personal use only.



5a 5b 5c 5d

on the 13 highest occupied molecular orbitals from PESPEC with a Gaussian convolution of 0.4 and a temperature of 300 K displayed in Fig. 2(*c*) is an excellent match of the experimental low-energy region in the spectrum of **5**. Like disilylketene **2**, disilylbisketene **5** prefers conformations in which its ketene moieties are arranged approximately orthogonal to the Si—Si bond to allow for maximum orbital interaction.

1,2-Divinyl-1,1,2,2-tetramethyldisilane (8)

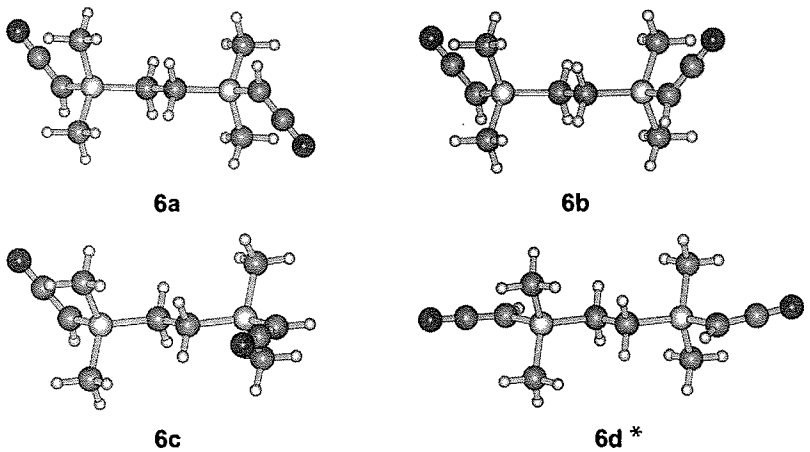
We also performed a conformational analysis for disilane **8**, which according to Khvostenko et al. (12) does not exhibit σ–π interaction. Two low-energy conformers **8a** (ethylene groups *syn*) and **8b** (ethylene groups *anti*) correspond to **5a** and **5b**, respectively. With HF/3-21G*, **8b** is less stable than **8a** by 0.03 kJ mol^{-1} (the HF/6-31G*//HF/3-21G* value is 0.22 kJ mol^{-1}), their geometries are similar to those found for disilane **5**: the Si-Si-C-C dihedral in **8a** is 110°, the C-Si-C-C dihedral is at 11°. Becke3LYP/6-31G*//HF/3-21G* predicts **8b** to be more stable by 0.76 kJ mol^{-1}. The fitted potential (Becke3LYP/6-31G*//HF/3-21G*, plot not shown) for the torsion about one Si—CC bond (with the other one kept at approx. 110°) resembles that for **5** except for energy differences in **8** being more pronounced: ΔE between the two minima in the plot for **5** is 1.5 (Fig. 6), for **8** it is 4.5 kJ mol^{-1}. This can be explained as was done for alkene **7**. The dependence of the orbital energies on the Si-Si-C-C dihedral in **8** can be seen in Fig. 3(*c*). Just as for disilylbisketene **5**, the HOMO of **8** ($\pi^{+}_{CC}/\sigma_{SiSi}$) is destabilized by about 0.2 eV on increasing the torsional angle from 0° to 90° while HOMO-1 and HOMO-2 are stabilized in both cases to about the same extent. This suggests that there are similar σ–π interactions in disilanes **5** (ketene substituents) and **8** (alkene substituents). The simulated PE spectrum of **8** (Becke3LYP/6-31G*//HF/3-21G*, 12 eigenvalues, FWHH 0.4, temperature 300 K) is shown in Fig. 4(*d*). Again, the experimental PE spectrum for **8** was not published but the stated poor resolution of the second and third bands (12) can be seen in the simulation.

1,2-Bis(ketenyldimethylsilyl)ethane (6)

According to HF/3-21G*, conformation **6a** with ketene groups *anti* and *sp* to the Si—CH_3 bonds (H_3C-Si-C-CO dihedral at 2.1°) is the global minimum. The related *syn* conformation **6b** is essentially equal in energy while **6c**, with one ketene group *sp* to a Si—CH_2 bond, is slightly destabilized by 0.55 kJ mol^{-1} (Table 2). This energetic order is confirmed by HF/6-31G*//HF/3-21G* calculations whereas Becke3LYP/6-31G*//HF/3-21G* reverses the sequence of **6b** and **6c**, but all energy differences stay small. Conformation **6d**, which has both ketene groups *anti*-periplanar (*ap*) to the Si—CH_2 bonds, is the most stable conformation as determined by PM3, but is not a stationary point on the potential energy surface with HF/3-21G*.

HF/3-21G* HOMO to HOMO-6 orbital energies of **6a** come as groups of two (9.26 and 9.60 eV), one (10.90 eV), and four (11.90, 11.91, 12.28, and 12.37 eV), with the groups well separated. HOMO (π^{+}_{CCO}) and HOMO-1 (π^{-}_{CCO}) only show a small splitting. HOMO-2 has an in-phase electron contribution on the Si—CH_2 bonds and HOMO-3 is the antibonding combination of π_{CH_2}'s ($\pi^{-}_{CH_2}$) on the central C—C bond with electron density on the Si—CH_3 bonds. Orbital energies for **6a** and **6b** do not differ; for **6c** the HOMO/HOMO-1 splitting is smaller and the HOMO-2 is slightly raised.

Conformationally, bisketene **6** is the most complex of all the molecules studied. There are five important bonds here and the orbitals of **6** suggest that three of them, one CH_2—CH_2 and two Si—CCO bonds, could be of interest for an investiga-



6a 6b 6c 6d *

* Representation of the PM3 geometry.

Can. J. Chem. Downloaded from www.nrcresearchpress.com by 91.121.58.235 on 09/08/12
For personal use only.

© 1997 NRC Canada

Can. J. Chem. Downloaded from www.nrcresearchpress.com by 91.121.58.235 on 09/08/12
For personal use only.

tion of orbital energy dependences. Again, the torsions about these bonds were examined separately. For the rotation about the central CH_2—CH_2 bond, the other four dihedral angles of the backbone of **6a** were kept at their optimized values and the Si-C-C-Si torsional angle was twisted through 0°, 45°, 90°, 135°, and 180°. Figure 2(*c*) shows the potential obtained from the calculated relative energies. Since **6** is a bisketene with an ethylene spacer, its potential is that of a 1,2-disubstituted ethane. The strong destabilization of the 60° conformation, which is obvious from Fig. 2(*c*), can be interpreted by the large direct interaction between the methyl groups of the two silicon substituents. From this potential, **6** is expected to be exclusively in a 180° conformation; the often-found 60° conformation of 1,2-disubstituted ethanes in the gas phase will not be occupied to a great extent.

Orbital energies of HOMO to HOMO-4 as a function of the central torsional angle are displayed in Fig. 3(*d*). The change of the Si-C-C-Si dihedral does not influence HOMO and HOMO-1 (π_{CCO}'s) significantly, which again is an indication of no π–π interaction of any importance. HOMO-2 is lowest in energy at 90° and highest at 0° and 180° while HOMO-3 energies exhibit the opposite behavior. These two orbitals are almost degenerate in the 90° conformation, the point of avoided crossing, as can be seen in Fig. 3(*d*). They split to a maximum of about 1 eV as the dihedral is changed and, as a result of this, HOMO-2 moves up in energy and into the gap formed by HOMO/HOMO-1 and HOMO-3/HOMO-4 groupings.

In addition, the rotation about just one Si—CCO bond was examined, as in the case of disilane **5**. The remaining four dihedral angles of the backbone of **6a** were fixed at their optimized values. The potential obtained for twisting the CH_2–Si-C-C torsional angle resembles that for **5** but the energy differences for **6** are smaller. This is reflected in the orbital energy dependence, which shows smaller changes but otherwise is the same as for **5** (plots not shown).

In the PE spectrum of bisketene **6** shown in Fig. 1(*f*), three bands are resolved from the main groups of the σ bands, belonging to two (8.9 eV), one (9.73 eV), and four (centered at 11.0 eV) ionizations. Even though the first band, which comprises ionizations from the two π orbitals (π^+_{CCO} and π^-_{CCO}), shows individual maxima, they cannot be ascribed to discrete bands: a deconvolution would lead to a very small splitting. As for silylketenes **3**, **4**, and **5** bearing more than one ketene group, the π–π interaction in **6** is almost nonexistent. The value of 8.9 eV for the first IP is close to that of (*tert*-butyldimethylsilyl)ketene (8.79 eV) (2), which indicates a similar destabilization of the ketene π orbital due to alkyl substitution, and no further interaction. The most prominent feature in the spectrum, in spite of its size, is the band at 9.73 eV. It is situated in an energy gap of about 1.5 eV made up by the larger bands. From Fig. 3(*d*) it is clear that HOMO-2 is destabilized enough for this only when the substituents on the ethane moiety are arranged *ap* (Si-C-C-Si torsional angle at 180°, the 0° conformation is a maximum, see Fig. 2(*c*)). There is remarkable agreement between the simulated partial spectrum for this torsion (HF/3-21G*, 11 eigenvalues, FWHH 0.7, temperature 300 K) as displayed in Fig. 4(*e*) and the experimental PE spectrum of **6**. Unlike the cases of disilanes **2** and **5**, using DFT values for **6** gives a similar simulation with no further improvement, which clearly shows that it is important to consider electron correlation for silylketenes containing a Si—Si bond, while it can be neglected for silylketenes without a Si—Si bond. For the latter, it is sufficient to employ HF/3-21G*// HF/3-21G*. There is no change in the synthesized spectrum when the torsion of one ketene group is considered, emphasizing the lack of importance of this motion on the electronic structure of **6**.

Conclusion

The PE spectra presented for silylketenes **1**–**6** have been interpreted on the basis of the conformational flexibility of the molecules. Calculated energy differences between conformers are small and all are significantly populated. For disilanes **2** and **5**, whose orbital energies are a function of a Si-Si-C-C torsional angle, this seriously affects the PE spectra. Because of a strong σ–π interaction, the preferred conformation for **2** and **5** is one in which the Si—Si bond and ketene group are approximately orthogonal. The same is true for the corresponding silylalkenes **7** and **8**, contrary to what has been reported (12). In contrast to the strong σ–π interaction, there is no π–π interaction of any significance in bis- and trisketenes **3**–**6**. While HF calculations describe the electronic structure of silylketenes **1**, **3**, **4**, and **6** well, this level of theory is not sufficient for disilanes **2** and **5**. For these Si—Si containing compounds, Becke3LYP must be employed for accurate representations of the experimental PE spectra.

Acknowledgment

Financial support by the Natural Sciences and Engineering Research Council of Canada is gratefully acknowledged.

References

1. D. Zhao, A.D. Allen, and T.T. Tidwell. J. Am. Chem. Soc. **115**, 10097 (1993); L. Gong, M.A. McAllister, and T.T. Tidwell. J. Am. Chem. Soc. **113**, 6021 (1991); M.A. McAllister and T.T. Tidwell. J. Org. Chem. **59**, 4506 (1994).
2. N.H. Werstiuk, J. Ma, M.A. McAllister, T.T. Tidwell, and D. Zhao. J. Chem. Soc. Faraday Trans. **90**, 3383 (1994).
3. R.S. Brown and F.S. Jørgensen. *In* Electron spectroscopy: theory, techniques and applications. Vol. 5. *Edited by* C.R. Brundle and A.D. Baker. Academic Press, London. 1984; M. Klessinger and P. Rademacher. Angew. Chem. **91**, 885 (1979); Angew. Chem. Int. Ed. Engl. **18**, 826 (1979).
4. T. Koopmans. Physica, **1**, 104 (1933).
5. H. Bock and W. Ensslin. Angew. Chem. **83**, 435 (1971); Angew. Chem. Int. Ed. Engl. **10**, 404 (1971); H. Bock, W. Ensslin, F. Fehér, and R. Freund. J. Am. Chem. Soc. **98**, 668 (1976).
6. C. Baker and D.W. Turner. Chem. Commun. 480 (1969); H. Bock, T. Hirabayashi, and S. Mohmand. Chem. Ber. **114**, 2595 (1981); D. Colbourne and N.P.C. Westwood. J. Chem. Soc. Perkin Trans. 2, 2049 (1985); R. Sammynaiken and N.P.C. Westwood. J. Chem. Soc. Perkin Trans. 2, 1987 (1989).
7. K. Sung and T.T. Tidwell. J. Am. Chem. Soc. **118**, 2768 (1996).
8. K. Sung and T.T. Tidwell. Organometallics, **16**, 78 (1997).
9. A.D. Becke. J. Chem. Phys. **98**, 5648 (1993); C. Lee, W. Yang, and R.G. Parr. Phys. Rev. B: Condens. Matter, **37**, 785 (1988).
10. W.J. Hehre, L. Radom, P.v.R. Schleyer, and J.A. Pople. Ab initio molecular orbital theory. John Wiley & Sons, New York. 1986.

© 1997 NRC Canada

11. A.J. Arduengo III, H. Bock, H. Chen, M. Denk, D.A. Dixon, J.C. Green, W.A. Herrmann, N.L. Jones, M. Wagner, and R. West. J. Am. Chem. Soc. **116**, 6641 (1994).
12. V.I. Khvostenko, B.G. Zykov, V.P. Yuriev, V.F. Mironov, G.I. Kovel'zon, A.A. Panasenko, V.D. Sheludyakov, and I.A. Gailyunas. J. Organomet. Chem. **218**, 155 (1981).
13. M.J. Frisch, G.W. Trucks, H.B. Schlegel, P.M.W. Gill, B.G. Johnson, M.A. Robb, J.R. Cheeseman, T. Keith, G.A. Petersson, J.A. Montgomery, K. Raghavachari, M.A. Al-Laham, V.G. Zakrzewski, J.V. Ortiz, J.B. Foresman, C.Y. Peng, P.Y. Ayala, W. Chen, M.W. Wong, J.L. Andres, E.S. Replogle, R. Gomperts, R.L. Martin, D.J. Fox, J.S. Binkley, D.J. Defrees, J. Baker, J.P. Stewart, M. Head-Gordon, C. Gonzalez, and J.A. Pople. Gaussian 94, Revision B.3. Gaussian, Inc., Pittsburgh, Pa. 1995.
14. J.J.P. Stewart. J. Comput. Chem. **10**, 209 (1989).
15. J.J.P. Stewart. QCPE, 455 (1983).
16. N.H. Werstiuk, G. Timmins, J. Ma, and T.A. Wildman. Can. J. Chem. **70**, 1971 (1992).
17. N.H. Werstiuk, D.N. Butler, and E. Shahid. Can. J. Chem. **65**, 760 (1986).

Can. J. Chem. Downloaded from www.nrcresearchpress.com by 91.121.58.235 on 09/08/12
For personal use only.

© 1997 NRC Canada

Electrocatalytic hydrogenation of phenol on various electrode materials

Anna Martel, Behzad Mahdavi, Jean Lessard, Louis Brossard, and Hugues Ménard

Can. J. Chem. Downloaded from www.nrcresearchpress.com by 91.121.58.235 on 09/08/12
For personal use only.

Abstract: The electrocatalytic hydrogenation (ECH) of phenol was investigated at room temperature under galvanostatic control in aqueous sulfuric acid solutions on platinized platinum (Pt/Pt) electrodes and on composite Rh/Ni and Ru/Ni electrodes consisting of rhodium or ruthenium chemically deposited on nickel particles dispersed in a lanthanum polyphosphate matrix. The order of electrocatalytic activity at a current density (based on the geometric area) of 1 mA/cm^2 was found to be Ru/Ni > Pt/Pt > Rh/Ni. The efficiency decreased with increased current density. For the Ru/Ni electrodes, the efficiency increased with the percentage of Ru (2.3 to 5%). On Ru 5%/Ni electrodes and at a current density of 5 mA/cm^2, cyclohexanol was obtained with a high selectivity of 91% and a current efficiency of 23% after 94% conversion. In neutral aqueous boric acid containing sodium chloride as supporting electrolyte, the Rh/Ni and Ru/Ni electrodes showed very low activity. The influence of the supporting electrolyte, periodic current control, and temperature was studied in the neutral medium with composite Raney nickel (RaNi) electrodes consisting of Raney nickel particles dispersed in a nickel matrix. At 60°C and a current density of 10 mA/cm^2, the selectivity of cyclohexanol formation was 100% with a 11% current efficiency after 92% conversion with sodium chloride as supporting electrolyte.

Key words: electrocatalytic hydrogenation, phenol, ruthenium on nickel cathodes, rhodium on nickel cathodes, Raney nickel cathodes.

Résumé : L'hydrogénation électrocatalytique (HEC) du phénol a été étudiée à la température ambiante en solution aqueuse d'acide sulfurique sur des électrodes de platine platinisé (Pt/Pt) et sur des électrodes composites de Rh/Ni et Ru/Ni, consistant en rhodium ou ruthénium métallique déposé chimiquement sur des particules de nickel dispersées dans une matrice de polyphosphate de lanthane. On a trouvé une activité décroissante dans l'ordre Ru/Ni, Pt/Pt et Rh/Ni à une densité de courant de 1 mA/cm^2 (basée sur la surface géométrique) et une diminution de l'activité des électrodes avec l'augmentation de la densité de courant. Avec les électrodes de Ru/Ni, une augmentation de l'efficacité de l'HEC a été observée avec le pourcentage de Ru de 2.3 à 5%. Sur les électrodes de Ru 5%/Ni, on a obtenu le cyclohexanol avec une très bonne sélectivité de 91% et une efficacité de courant de 23% après 94% de conversion. En solution neutre d'acide borique contenant du chlorure de sodium comme électrolyte support, les électrodes Ru/Ni et Rh/Ni se sont avérées pratiquement inactives. L'influence de l'électrolyte support, d'un courant pulsé et de la température a été étudiée en solution neutre avec des électrodes de RaNi faites de particules de nickel de Raney dispersées dans une matrice de nickel. Le phénol a été électrohydrogéné en cyclohexanol avec une sélectivité de 100% et une efficacité de courant de 11% après 92% de conversion, en effectuant l'électrolyse à 60°C et à une densité de courant de 10 mA/cm^2 en présence de chlorure de sodium comme électrolyte support.

Mots clés : hydrogénation électrocatalytique, phénol, cathodes de ruthénium sur nickel, cathodes de rhodium sur nickel, cathodes de nickel de Raney.

[Traduit par la rédaction]

Introduction

The electrocatalytic hydrogenation (ECH) of organic compounds constitutes a mild and efficient method for hydrogenating a variety of organic substrates (for a recent review, see ref. 1). The mechanism is described by reactions [1]–[4] where M represents the metallic surface. Chemisorbed hydrogen, (H)M, generated in situ by electroreduction of water (or the hydronium ion) (reaction [1]), reacts with the adsorbed organic substrate, (Y = Z)M, (reactions [2]–[4]). Hydrogenation (reaction [3]) competes with hydrogen desorption (reactions [5] and (or) [6]) (2, 3). The efficiency of ECH depends on the relative rates of these two processes, which are influenced by a number of factors such as the substrate and its concentration (2, 4), the electrode material and surface (5, 6), the reaction medium (organic cosolvent (2), pH (2, 4), buffer (2, 4), supporting electrolyte (2), surfactants (7)), the temperature (2), the current density (2, 4, 8) and current pulsation (8).

[1] $2H_2O\ (H_3O^+) + 2e^- + M \rightarrow 2(H)M + OH^-\ (H_2O)$

[2] $Y = Z + M \rightarrow (\ Y = Z)M$

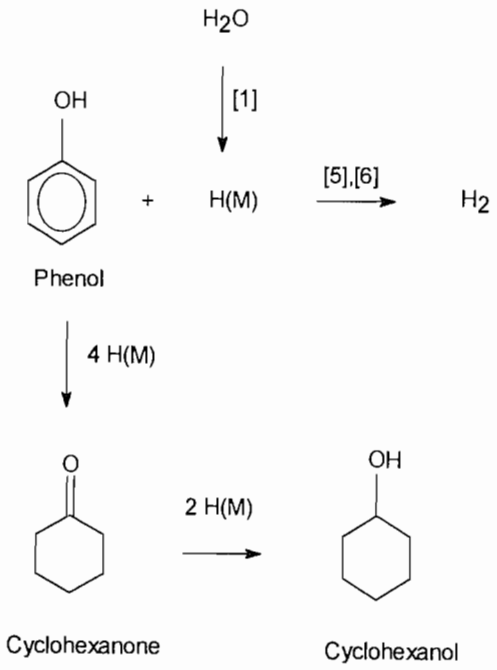
Received April 14, 1997.

A. Martel, B. Mahdavi, J. Lessard,[1] and H. Ménard.[1]
Département de Chimie, Université de Sherbrooke, Sherbrooke, QC J1K 2R1, Canada.
L. Brossard Institut de Recherche d'Hydro-Québec, 1800 Montée Sainte-Julie, Varennes, QC J3X 1S1, Canada.

[1] Authors to whom correspondence may be addressed. Telephone: (819) 821–7084 or 7091. Fax: (819) 821–8017.

© 1997 NRC Canada

Scheme 1.



[3] $(Y = Z)M + 2(H)M \rightarrow (YH - ZH)M$

[4] $(YH - ZH)M \rightarrow YH - ZH + M$

[5] $(H)M + H_2O + e^- \rightarrow H_2 + M + OH^-$

[6] $(H)M + (H)M \rightarrow H_2 + M$

This paper reports the results of a study on the effect of current density, current pulsation, pH (acidic and neutral), and electrode material on the efficiency of the ECH of phenol to cyclohexanol in aqueous solutions. Scheme 1 shows the conversion of phenol to cyclohexanol via cyclohexanone as intermediate. The electrode materials investigated in acidic medium were: platinized platinum (Pt/Pt), rhodium on nickel (Rh/Ni) (9), ruthenium on nickel (Ru/Ni) (10), and ruthenium on stainless steel (Ru/Inox). The electrodes consisted of rhodium or ruthenium metal chemically deposited on nickel or stainless steel particles dispersed in a lanthanum polyphosphate matrix (lanthanum phosphate-bonded electrodes) (9, 10). In neutral medium, the electrodes studied were made of Rh/Ni, Ru/Ni, or RaNi particles dispersed in a nickel matrix (2). The ECH of phenol to cyclohexanol has been reported before in aqueous acid solutions on platinum (11–14), Pd/C (12), and Rh/C (12) electrodes. Cyclohexanol is an important industrial product as a starting material for preparing adipic acid used in the production of nylon 6 and nylon 6–6 (15).

Experimental

Electrolysis

Electrolysis was carried out at room temperature with an Electrosynthesis (ESC) 410 potentiostat coupled to an ESC 640 digital coulometer and an ESC 2830 digital multimeter or with an EG&G Princeton Applied Research (PAR) 173 potentiostat coupled to a PAR 179 digital coulometer. For the pulse current electrolysis, the PAR 173 potentiostat coupled to a PAR 175 universal programmer was used. A two-compartment glass H-cell with a jacketed cathodic compartment (volume of each compartment 25 mL) with a Nafion-324 (E.I. du Pont de Nemours & Co.) membrane (1.8 cm^2) was used. For the electrolysis at 60°C, it was connected to a Haake D8 constant-temperature circulating bath filled with water – ethylene glycol. The counter electrode was a glassy carbon plate (~12 cm^2) or a platinum grid cylinder (4 cm long and 6 cm in diameter). The neutral electrolyte consisted of a solution of boric acid (0.5 M) (ACS from BDH) and sodium chloride (0.005 to 0.05 M) (ACS from Anachemia) in distilled water. To ensure a high concentration of protons, the concentration of boric acid in the anolyte was sometimes increased to saturation. The pH was measured at the beginning (pH = 4) and at the end (pH = 6) of the electrolysis with a pHydrion Vivid 6–8 (Micro Essential Laboratory) or a Spezialindikator pH 2.5–4.5 (Merck) paper indicator. The acid electrolyte consisted of a solution of sulfuric acid (0.1 M) (ACS from Fisher Scientific) in distilled water. The anodic and cathodic compartments were filled with one of the above solutions. Phenol (ACS from BDH) was dissolved in the cathodic compartment (20 mg, 8.5×10^{-3} M solution), the anode and cathode were immersed, and the catholyte stirred with a magnetic bar and stirrer. The progress of the electrolysis was followed by gas–liquid chromatography (glc) on a Hewlett Packard (HP) 5790a chromatograph equipped with a FID detector and an HP integrator using a 30 m long DB-5 fused silica capillary column heated at 78°C. Aliquots (0.5 mL) from the catholyte were added to a saturated NaCl solution (1 mL), acidified (pH ≈ 1) with concentrated HCl, and extracted with ether. The products were identified by comparing their retention time with that of an authentic sample. The mass balance (92–100%) was determined by the internal standard method.

Electrodes

The Raney nickel (RaNi) electrodes were prepared as already described (2) by codeposition on a stainless steel grid (1.6 cm × 2.2 cm) of nickel and of particles of Raney alloy suspended in a nickel-plating bath, followed by leaching the aluminum in 30% aqueous NaOH at 70°C for 7 h. The composite rhodium–nickel (Rh/Ni) (9) and ruthenium–nickel (Ru/Ni) (10) electrodes consisted of metal/Ni particles (98% by weight) dispersed in a lanthanum polyphosphate matrix (2% by weight). They were prepared as previously described: chemical deposition of Rh or Ru from $RhCl_3$ or $RuCl_3$ on Ni (Rh 3.5%/Ni; Ru 2.3, 3.5, and 4.4%/Ni); thorough mixing of Rh/Ni or Ru/Ni powder and an homogeneous mixture of $La(H_2PO_4)_3$ and $La(OH)_3$; pressing of the resulting mixture under vacuum at room temperature at 1000 lbs/in^2 (1 lb/in^2 = 7.03×10^2 kg/m^2) in a stainless steel cylindrical mould (diameter: 1.33 cm); polymerization by heating the pellet at 300°C for 3–4 h under a flow of argon. The pellet was coated on one side and along the edge with Epoxyfix resin (Struers) after a Ni foil had been introduced (to ensure electrical contact) to obtain a 1.33 cm^2 geometric area. The Ru 4.4%/Inox electrode was prepared in the same way with stainless steel particles 316-L (100 mesh, Consolidated Astronautics) and 90% Ru/Inox in 10% lantha-

Can. J. Chem. Downloaded from www.nrcresearchpress.com by 91.121.58.235 on 09/08/12
For personal use only.

© 1997 NRC Canada

Table 1. ECH of phenol (8.5×10^{-3} M) in a 0.1 M H_2SO_4 aqueous solution on Pt/Pt, Rh/Ni, and Ru/Ni electrodes at $J = 1$ mA/cm^2[a] and at room temperature.

Entry	Cathode[b]	F/mol	Unreacted phenol[c] (%)	Yield of products[c]		Current efficiency (%)
				Cyclohexanone (%)	Cyclohexanol (%)	
1	Pt/Pt	2	77	23	1	44
2		4	58	41	1	43
3		12	—	38	62	42
4	Rh 3.5%/Ni	2	61	29	10	~87[d]
5		6	39	38	23	~46[d]
6		14	—	51	49	~36[d]
7	Ru 3.5%/Ni	2	32	7	60	—[e]
8		12	—	—	100	—[e]

[a]Based on the geometric area.
[b]See the experimental section.
[c]Determined by glc (mass balance = 92–100%).
[d]Some dissolution of nickel was observed, so the true current efficiencies are probably lower.
[e]Could not be determined due to dissolution of nickel (see text).

Can. J. Chem. Downloaded from www.nrcresearchpress.com by 91.121.58.235 on 09/08/12
For personal use only.

num polyphosphate. The composite electrodes were activated by cathodic polarization curves obtained by decreasing the applied current galvanostatically from 250 to 0.01 mA/cm^2 after applying a current density of 250 mA/cm^2 for 30 min and repeating the cycle until superimposable Tafel curves were obtained. The platinized platinum electrodes (16) were prepared by electrodeposition of platinum from a 2% platinic chloride solution in hydrochloric acid (2 N) for 10–20 min at 10–20 mA/cm^2 on a platinum plate (1.2 cm × 1.1 cm). This electrode was activated by cathodic and anodic polarization (5 cycles of 15 s in each direction) in sulfuric acid (0.01 M) at 0.5 mA/cm^2 just before electrolysis.

Results and discussion

Electrolysis in an acid medium

Previous studies on the ECH of phenol (11–14) were carried out in aqueous sulfuric (0.05 to 0.2 M) and aqueous perchloric (1 M) acid solutions at different current densities (0.02–12.7 mA/cm^2 based on the geometric area) and different phenol concentrations (0.001–0.2 M).The latter two factors influence the competition between hydrogenation (reactions [2]–[4]) and hydrogen desorption (reactions [5] and (or) [6]) and, hence, the efficiency (current efficiency and conversion rate) of ECH: higher current densities usually favor hydrogen evolution over ECH (2, 4, 8, 13) and higher substrate concentrations favor ECH over hydrogen evolution (4, 13). Thus, it is not possible to make a strict comparison between the various results presented in the literature. Our studies in an acidic medium were carried out in aqueous sulfuric acid (0.1 M) with a 8.5 mM phenol concentration. The results are summarized in Tables 1 and 2.

Table 1 reports the results of a comparison of Pt/Pt, Rh/Ni, and Ru/Ni electrodes at a relatively low current density ($J = 1$ mA/cm^2). Both cyclohexanone and cyclohexanol were identified as products, cyclohexanone being formed first and then hydrogenated to cyclohexanol (Scheme 1), as already reported by Miller and Christensen (12) and Amouzegar and Savadogo (14). As the charge increased (theoretical charge = 6 F/mol), more cyclohexanol was formed and the current efficiency decreased due to a decrease in substrate concentration that causes a decrease of the rate of hydrogenation (reaction [3]). It was not possible to determine the current efficiency for the ECH on Ru 3.5%/Ni electrodes (entries 7 and 8) because of electrons provided by the dissolution of nickel during the electrolysis as evidenced by the green coloration of the catholyte. An open-circuit experiment under the same conditions confirmed that the dissolution of nickel did lead to the formation of chemisorbed hydrogen, (H)M, and then to the hydrogenation of phenol: after a period of time corresponding to the end of the electrolysis of entries 7 and 8, 95% of phenol had been converted to 3% cyclohexanone and 92% cyclohexanol. This experiment shows that the Ru/Ni electrode is very active for the hydrogenation of phenol in dilute aqueous sulfuric acid. The Pt/Pt and Rh/Ni electrodes are less active. After 12–14 F/mol, the yield of cyclohexanol was slightly higher with the Pt/Pt electrode (62%, 12 F/mol, entry 3) than with the Rh/Ni electrode (49%, 14 F/mol, entry 6), which suggests that the former electrode is more active. On a Pt/Pt electrode, Miller and Christensen (12) reported the following results in 0.2 M H_2SO_4, after a charge corresponding to 6 F/mol, at a current density of 1.45 mA/cm^2 and a phenol concentration of 0.2 M: 50% conversion, 7% cyclohexanone, 17% cyclohexanol, 22% current efficiency.

Since ruthenium was shown to be an active metal in such composite catalysts in aqueous sulfuric acid, we investigated the Ru/Ni electrodes further, looking at how their activity was affected by current density, the percentage of ruthenium on nickel, and the replacement of nickel with stainless steel. The results are recorded in Table 2 and those of entries 1–10 show that, as reported in the literature with other electrode materials (2, 4, 8, 13), an increase of current density (from 3 to 15 mA/cm^2) led to a decrease in ECH efficiency due to an increase in the rate of hydrogen desorption as already mentioned. There was no dissolution of nickel at current densities of 3 mA/cm^2 and greater so the current efficiencies of entries 1–16 repre-

© 1997 NRC Canada

Table 2. ECH of phenol (8.5×10^{-3} M) in a 0.1 M H_2SO_4 solution on ruthenium electrodes at room temperature: effect of %Ru, metal support, and current density.

Entry	Cathode	J^a (mA/cm^2)	F/mol	Unreacted phenol^b (%)	Yield of products^b		Current efficiency (%)
					Cyclohexanone (%)	Cyclohexanol (%)	
1	Ru 2.3%/Ni	3	2	94	2	4	15
2			6	75	5	20	23
3			13	50	6	45	23
4			24	23	7	70	20
5	Ru 2.3%/Ni	10	2	98	1	1	4
6			4	97	1	2	4
7			42	48	8	44	7
8	Ru 2.3%/Ni	15	2	98	1	2	6
9			6	92	2	6	7
10			13	82	5	14	8
11	Ru 4.4%/Ni	10	3	89	1	10	22
12			6	75	3	22	23
13			12	60	4	37	20
14	Ru 5%/Ni	5	3	69	4	27	66
15			6	41	6	52	56
16			25	6	3	91	23
17	Ru 4.4%/Inox^c	1	2	96	2	3	11
18			6	92	3	6	7
19			12	88	5	7	5

[a]Based on the geometric area.
[b]Determined by glc.
[c]Ruthenium deposited on stainless steel particles (see the experimental section).

Can. J. Chem. Downloaded from www.nrcresearchpress.com by 91.121.58.235 on 09/08/12
For personal use only.

sent true current efficiencies. An increase in the percentage of ruthenium did lead to an increase in efficiency as shown by a comparison of entries 5 and 6 (Ru 2.3%/Ni, J = 10 mA/cm^2) with entries 11 and 12 (Ru 4.4%/Ni, J = 10 mA/cm^2) and a comparison of entries 1 and 2 (Ru 2.3%/Ni, J = 3 mA/cm^2) with entries 14 and 15 (Ru 5%/Ni, J = 5 mA/cm^2): the conversion rate, yield of cyclohexanol and current efficiency are higher in entries 11 and 12 as well as in entries 14 and 15 (despite the fact that the current density was larger in the electrolysis of entries 14 and 15 than in that of entries 1 and 2). As revealed by a comparison of entries 7 and 8 of Table 1 with entries 17–19 of Table 2, replacing nickel with stainless steel led to a notable decrease in electrode activity. This shows that the metal supporting ruthenium does have an influence on the competition (relative rates) between hydrogenation (reaction [3]) and hydrogen desorption (reactions [5] and (or) [6]). This is not surprising since the supporting metal is not completely covered with ruthenium at percentages of ruthenium lower than 10%, as previously shown by X-ray (EDX) mapping (10).

The Ru 5%/Ni electrode appears the most interesting for the ECH of phenol in an aqueous acidic medium with a 94% conversion rate, a 91% yield of cyclohexanol, and a 23% current efficiency at a current density of 5 mA/cm^2 after a charge corresponding to 25 F/mol (Table 2, entry 16). After 6 F/mol (entry 15), the conversion rate was 59%, the yield of cyclohexanol 52%, and the current efficiency 56%. These results can be compared with those of Amouzegar and Savadogo (14) in 0.05 M H_2SO_4 on a Pt/C/Teflon electrode: 100% conversion, 5% cyclohexanone, 95% cyclohexanol, and 85% current efficiency at 6 F/mol. However, they used a much lower current density (0.02 mA/cm^2) and larger phenol concentration (0.05 M), both of which strongly favor the ECH process over hydrogen evolution as pointed out above. On the other hand, the results of entry 12 (Ru 4.4%/Ni electrode, J = 10 mA/cm^2, 6 F/mol, 25% conversion, 3% cyclohexanone, 22% cyclohexanol, 23% current efficiency), could be compared to those obtained by Miller and Christensen (12) for their most active electrode (Rh/C) (J = 11 mA/cm^2, 6 F/mol, 100% conversion, 15% cyclohexanone, 74% cyclohexanol, 84% current efficiency), bearing in mind, however, that they used a much larger concentration of phenol (0.2 M), which again markedly favors the ECH process over hydrogen evolution.

Electrolysis in a neutral medium

For the ECH of phenanthrene in ethylene glycol – water solutions, we reported earlier that the presence of boric acid at concentrations between 0.1 to 0.5 M was beneficial in favoring hydrogenation over hydrogen desorption and thus improving the efficiency of the ECH process (2). It also served as a buffer to maintain the pH between 3.5 and 6.5 during electrolysis (14 F/mol) since hydoxide ions are produced (see eq. [1]) (2). We thus investigated the ECH of phenol on the various electrodes used in the above section as well as on Raney nickel (RaNi) electrodes in an aqueous solution of boric acid (0.5 M) containing sodium chloride (0.05 M) as supporting electrolyte. The pH varied from 4 to 6 during the electrolysis. The

© 1997 NRC Canada

Table 3. ECH of phenol (8.5×10^{-3} M) at room temperature in an aqueous solution containing H_3BO_3 (0.5 M) and NaCl (0.05 M) on Pt/Pt, Rh/Ni, Ru/Ni, and RaNi electrodes.[a]

Entry	Cathode	J^b (mA/cm^2)	F/mol	Unreacted phenol[c] (%)	Yield of products[c]		Current efficiency (%)
					Cyclohexanone (%)	Cyclohexanol (%)	
1	Pt/Pt	1	12	41	36	23	23
2		10	12	91	9	—	3
3		30	12	97	2	1	1
4	Rh 3.5%/Ni	1	13	100	—	—	0
5		10	13	100	—	—	0
6		30	10	100	—	—	0
7	Ru 3.5%/Ni	1	6	98	2	—	1
8			12	96	4	—	1
9		10	6	100	—	—	0
10			12	>99	<1	<1	<1
11		30	6	99	<1	6	6
12			11	89	<1	11	6
13	Ru 2.3%/Ni	30	6	98	<1	2	2
14			15	95	1	4	2
15	Ru 4.4%/Ni	30	6	90	1	8	10
16			16	79	2	19	8
17	RaNi 56%	1	6	100	—	—	0
18			27	83	—	17	4
19	RaNi 58%	10	6	95	—	5	5
20			27	59	—	41	9
21			56	25	—	75	8
22	RaNi 60%	30	6	96	—	4	4
23			12	91	—	9	5
24			21	82	—	18	5

[a]pH before starting the electrolysis: 4.5; pH after the electrolysis: 6.4–8.0.
[b]Based on the geometric area.
[c]Determined by glc (mass balance = 98–100%).

results of the studies carried out at room temperature are recorded in Table 3. It is clear from the current efficiencies and the yield of cyclohexanol that the ECH of phenol on Pt/Pt, Rh/Ni, and Ru/Ni electrodes under those conditions was much less efficient than in aqueous sulfuric acid: compare entry 1 of Table 3 with entry 3 of Table 1 for the Pt/Pt electrodes; no hydrogenation occurred on the Rh/Ni electrodes (entries 4–6) and little hydrogenation occurred on the Ru/Ni electrodes (entries 7–18), which were the most active electrodes in the aqueous acid medium. The RaNi electrodes (entries 17–24) appear somewhat more active than the Ru/Ni electrodes. Thus, under these neutral electrolysis conditions, desorption of chemisorbed hydrogen (reactions [5] and (or) [6]) was much faster than hydrogenation of phenol (reaction [3]). Increasing the current density caused a decrease in ECH efficiency in the case of the Pt/Pt electrodes (entries 1–3) as usually observed (see previous section), had little effect on the low efficiencies of ECH on RaNi electrodes (entries 17–24), but caused a small increase in ECH efficiency on the Ru/Ni electrodes (entries 7–18). However, the reproducibility of these experiments was not assessed since the current efficiencies were very low. The charge had also little effect on the low current efficiency (compare entries 19–21), so it was possible to reach 75% conversion with the quantitative formation of cyclohexanol at a charge corresponding to 56 F/mol (see entry 21). It is noteworthy that no cyclohexanone was detected during the electrolysis on RaNi electrodes, which strongly suggests that its hydrogenation is much faster on these electrodes than that of phenol under the conditions used.

We had previously reported for the ECH of phenanthrene in ethylene glycol — water on RaNi electrodes that replacing sodium chloride as supporting electrolyte by sodium sulfate caused some decrease in efficiency (2) and that pulsating the current (8) and increasing the temperature (2) improved efficiency. We looked at the influence of these factors on the efficiency of the ECH of phenol in a neutral medium. The results of Table 4 show that the ECH of phenol was similarly less efficient when using sodium sulfate as supporting electrolyte (entries 3–5) and that the efficiency was also significantly improved when carrying out the electrolysis at 60°C instead of at room temperature (entries 9–11: 92% conversion, quantitative formation of cyclohexanol, 11% current efficiency in entry 11). However, the ECH of phenol was significantly less efficient when pulsating the current (entries 6–8), contrary to the ECH of phenanthrene. We have no satisfactory explanation for this difference in behavior.

Can. J. Chem. Downloaded from www.nrcresearchpress.com by 91.121.58.235 on 09/08/12
For personal use only.

© 1997 NRC Canada

Table 4. ECH of phenol (8.5×10^{-3} M) in an aqueous H_3BO_3 (0.5 M) solution on RaNi: effect of supporting electrolyte, periodic current control, or temperature.

Entry	Supporting electrolyte	T (°C)	Current density[a] (mA/cm^2)	F/mol	Unreacted phenol[b] (%)	Yield of cyclohexanol[b] (%)	Current efficiency (%)
1[c]	NaCl 0.05 M	R.T.	10	6	95	5	5
2[c]				56	25	75	8
3	Na_2SO_4 0.5 M	R.T.	10	6	98	2	2
4				12	95	5	2
5				57	68	32	3
6	NaCl 0.05 M	R.T.	10	6	99	1	1
7			Periodic current	12	96	4	2
8			control[d]	41	86	14	2
9	NaCl 0.05 M	60	10	6	79	20	20
10				12	60	40	19
11				51	8	92	11

[a]Based on the geometric area.
[b]Determined by glc (mass balance = 98–100%).
[c]Taken from Table 3 (entries 19 and 21).
[d]T_1 = 100 ms at 0.05 mA/cm^2; T_2 = 200 ms at 10 mA/cm^2.

Conclusions

We have shown that composite electrocatalysts consisting of a small amount of rhodium or ruthenium metal chemically deposited on nickel particles (2–4% Rh or Ru/Ni) dispersed in a polyphosphate matrix were active for the ECH of phenol *in aqueous sulfuric acid*. Ruthenium supported on stainless steel was much less active, which shows that nickel has an influence on electrocatalytic activity. At a relatively low current efficiency of 1 mA/cm^2, dissolution of nickel generating active chemisorbed hydrogen occurred but no dissolution was observed at J = 3–15 mA/cm^2. The order of activity of the electrodes was Ru/Ni > Pt/Pt > Rh/Ni. The best results were obtained with a Ru 5%/Ni electrode, which gave, at a current density of 5 mA/cm^2, a conversion rate of 94%, a 91% yield of cyclohexanol, and a current efficiency of 23%. A meaningful comparison with literature data on other electrocatalysts could not be made because of the widely different electrolysis conditions used which have an influence on the competition between the reaction of phenol with chemisorbed hydrogen and desorption of chemisorbed hydrogen and thus the efficiency of ECH. *In aqueous boric acid (neutral medium)*, the Rh/Ni and Ru/Ni electrodes were found to be practically inactive, whereas a composite Raney nickel electrocatalyst consisting of Raney nickel particles dispersed in a nickel matrix did quantitatively electrohydrogenate phenol to cyclohexanol (no cyclohexanone detected) at 60°C although with low current efficiencies (≈17%).

Acknowledgements

Financial support from the Natural Sciences and Engineering Council of Canada, the Fonds pour la formation de chercheurs et l'aide à la recherche (FCAR) du Québec, and the Institut de recherche d'Hydro-Québec is gratefully acknowledged.

References

1. J.M. Chapuzet, A. Lasia, and J. Lessard. *In* Frontiers of electrochemistry: Electrocatalysis. 5th ed. *Edited by* J. Lipkowski. VCH Publishers, Inc., New York. 1997. In press.
2. D. Robin, M. Comtois, A. Martel, R. Lemieux, A. Kam Cheong, G. Belot, and J. Lessard. Can. J. Chem. **68**, 1218 (1990).
3. T. Osa, T. Matsue, A. Yokozawa, and T. Yamada. Denki Kagaku, **54**, 484 (1986).
4. B. Mahdavi, P. Chambrion, J. Binette, E. Martel, and J. Lessard. Can. J. Chem. **73**, 846 (1995).
5. J.M. Chapuzet, B. Mahdavi, and J. Lessard. J. Chim. Phys. **93**, 1252 (1996).
6. B. Mahdavi, P. Los, M.J. Lessard, and J. Lessard. Can. J. Chem. **72**, 2268 (1994).
7. P. Chambrion, L. Roger, J. Lessard, V. Béraud, J. Mailhot, and M. Thomalla. Can. J. Chem. **73**, 804 (1995).
8. B. Mahdavi, J.M. Chapuzet, and J. Lessard. Electrochim. Acta, **38**, 1377 (1993).
9. H. Dumont, P. Los, L. Brossard, A. Lasia, and H. Ménard. J. Electrochem. Soc. **139**, 2143 (1992).
10. H. Dumont, P. Los, A. Lasia, L. Brossard, and H. Ménard. J. Appl. Electrochem. **23**, 684 (1993).
11. R.A. Misra and B.L. Sharma. Electrochim. Acta, **24**, 727 (1978).
12. L.L. Miller and L. Christensen. J. Org. Chem. **43**, 2059 (1978).
13. K. Sasaki, A. Kunai, J. Harada, and S. Nakabori. Electrochim. Acta, **28**, 671 (1983).
14. K. Amouzegar and O. Savadogo. Electrochim. Acta, **39**, 557 (1994).
15. J. Haggin. Chem. Eng. News, **2**, 22 (1994).
16. G.J. Hills. J. Chem. Soc. 305 (1961).

Can. J. Chem. Downloaded from www.nrcresearchpress.com by 91.121.58.235 on 09/08/12
For personal use only.

© 1997 NRC Canada

Electrokinetic study of the adsorption of ethyl violet and crystal violet by montmorillonite clay particles[1]

Laurier L. Schramm, Shmuel Yariv, Dipak K. Ghosh, and Loren G. Hepler

Abstract: Electrophoretic mobilities of mixtures of a montmorillonite clay (in different exchangeable metal cation forms) and increasing amounts of two cationic dyes (ethyl violet and crystal violet) were measured. Electrophoretic mobilities were found to vary between -60×10^{-5} and $+40 \times 10^{-5}$ cm^2 s^{-1} V^{-1}. For both the dyes, the degree of saturation at which the isoelectric point (IEP) occurs, decreases with increasing valency of the metal cations. An effort was made to connect the IEP, maximum flocculation, and dye adsorption parameters. An important adsorption parameter is the transition saturation (TS), the saturation beyond which adsorption by organophilic attractions occurs in addition to adsorption by electrical and (or) π-interactions. It was found that maximum flocculation occurs before the IEP for all the exchangeable cations tested, but the IEP is reached at similar saturations to the TS for most of the cations. These results have been interpreted in terms of different types of adsorption phenomena and particle associations.

Key words: clay, adsorption, dye, ion exchange, electrokinetic charge.

Résumé : On a mesuré les mobilités électrophorétiques de mélanges d'une argile montmorillonite (dans diverses formes de cations métalliques échangeables) et de quantités croissantes de deux colorants cationiques (violet d'éthyle et cristal violet). On a trouvé que les mobilités électrophorétiques varient entre -60×10^{-5} et $+40 \times 10^{-5}$ cm^2 s^{-1} V^{-1}. Pour chacun des colorants, le degré de saturation auquel se produit le point isoélectrique (PIE) diminue avec une augmentation de la valence des cations métalliques. On a aussi fait un effort pour relier le PIE, le maximum de floculation et les paramètres d'adsorption des colorants. Un paramètre d'adsorption important est la saturation de transition (ST), la saturation au-delà de laquelle il se produit une adsorption organophile en plus de l'adsorption par des interactions électriques et (ou) π. On a observé que, pour tous les cations échangeables évalués, le maximum de floculation se produit avant le PIE; toutefois pour la plupart des cations, on atteint le PIE à des saturations semblables à la ST. On peut interpréter ces résultats en fonction des divers types de phénomènes d'adsorption et d'associations de particules.

Mots clés : argile, adsorption, colorant, échange d'ions, charge électrocinétique.

[Traduit par la rédaction]

Introduction

The adsorption of aromatic cationic dyes by clay minerals was investigated because of its importance in nature and in various technologies in which aromatic compounds or dyes are involved, and also because of the fact that these staining reactions are used as tests for the identification of various clay minerals (1–3). These adsorption reactions may serve as models for the interactions between aromatic compounds and clay minerals in soils and sediments (3, 4). The adsorption of cationic dyes by clays normally takes place through cation exchange, where the positively charged dye species replace the exchangeable metal cations (2–4), but other mechanisms are possible.

Several aromatic dyes show metachromic properties. In metachromasy the visible spectrum of a very dilute aqueous dye solution shows one absorption band in the visible range, due to the $\pi \rightarrow \pi^*$ transition, called band α, whereas that of the more concentrated solution shows an additional band, called band β, at a shorter wavelength. At still higher concentrations of metachromic dyes band α disappears. Band β is considered to represent a blue shift of band α owing to π interactions in which the aromatic dye is involved. In aqueous solutions band α represents monomeric species whereas band β represents dimeric species. An additional blue-shifted band, band γ, may appear in very concentrated aqueous solutions, which represents trimers, tetramers, etc.

Previous studies of the interaction between several metachromic dyes and montmorillonite (5–8) showed that adsorption from very dilute dye solutions was accompanied by metachro-

Received June 9, 1997.

L.L. Schramm.[2] Department of Chemistry, University of Calgary, and Petroleum Recovery Institute, Calgary, AB T2L 2A6, Canada.
S. Yariv. Department of Inorganic and Analytical Chemistry, The Hebrew University of Jerusalem, 91 904, Israel.
D.K. Ghosh and L.G. Hepler. Department of Chemistry, University of Alberta, Edmonton, AB T6G 2G2, Canada.

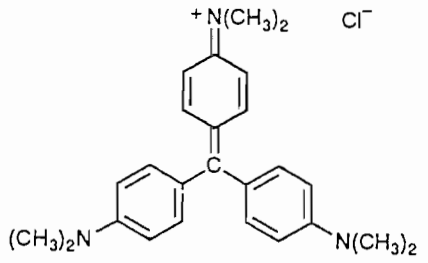
[1] Dedicated to the memory of Professor Loren G. Hepler, 1928–1996.

[2] Corresponding author. Telephone: (403) 282-1211. Fax: (403) 289-1988. E-mail: schramm@pri.ab.ca.

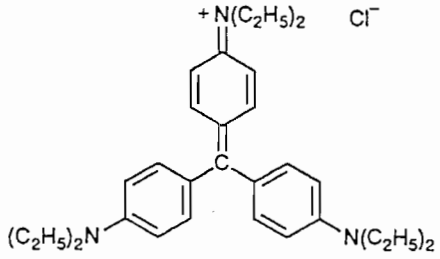
© 1997 NRC Canada

Can. J. Chem. Downloaded from www.nrcresearchpress.com by 91.121.58.235 on 09/08/12
For personal use only.

Fig. 1. Illustration of dye structures for I: crystal violet (N-{4-[bis(4-dimethylaminophenyl)methylene]cyclohexa-2,5-dienylidene}dimethylaminium chloride) and II: ethyl violet (N-{4-[bis(4-diethylaminophenyl)methylene]cyclohexa-2,5-dienylidene}dimethylaminium chloride). Adapted from ref. 9.



I



II

masy. In these cases, the appearance of a metachromatic, or blue-shifted band resulted from π-interactions between the aromatic rings of the organic dyes and the oxygen planes of the aluminosilicate platelets, and from the adsorption of aggregated dye cations, probably into the interparticle space of flocs. These investigations also suggested that visible-light spectroscopy might be a useful tool for the study of flocculation–peptization processes in clay–dye systems, because the molar absorbance of both bands α and β (of the adsorbed dye) decreased as a result of the flocculation of the adsorbing phase, but returned to its initial values if the adsorbing phase was peptized. When the clay–dye complexes are intensely coloured the flocculation and peptization processes are easily observed by the naked eye.

In a study of the adsorption of two metachromic cationic dyes (see Fig. 1) crystal violet (CV; **I**; *N*-{4-[bis(4-dimethylaminophenyl)methylene]cyclohexa-2,5–dienylidene}dimethylaminium chloride) and ethyl violet (EV; **II**; *N*-{4-[bis(4-diethylaminophenyl)methylene]cyclohexa-2,5-dinylidene}dimethylaminium chloride) by Na-montmorillonite four types of adsorption interactions were identified from the visible spectra of the clay–dye aqueous suspensions (10, 11). Types A_1 and B_1 (previously named A and B) were identified with the help of band α. This band is located at 590 and 595 nm in the spectra of very dilute aqueous solutions of CV and EV, respectively. In the clay–dye suspensions this band is located at the same wavelength in the spectrum of type A_1 and is shifted to higher wavelengths (red shift) in the spectrum of type B_1 clay–dye complexes. From the location of the band maximum it was assumed that type A_1 represents monomeric cationic species located in an environment in which polarity is very similar to that of the aqueous phase, and therefore should be outside the "interlayer space," on the external surfaces of the tactoids or platelets. Type B_1 represents monomeric cationic species located inside the interlayer space, an environment in which polarity is different from that of the aqueous phase. The red shift is more significant in the spectra of adsorbed CV than in those of adsorbed EV. Band β is located below 590 nm. Type B_2 (previously named C) was identified with the help of band β. It represents monomeric cationic species that are located in the interlayer space, with the aromatic ring parallel to the clay layers and bound to the oxygen planes by π-interactions. Type D, which represents polymeric species trapped in the interparticle space of a floc, was identified with the help of band γ. This type of interaction is negligible for this system and will not be further discussed here. In a study of the adsorption of CV by Laponite (a synthetic hectorite) it was shown that at the stage when the smectite flocculates, dimers of CV are obtained in the interparticle space of the flocs (type C) giving rise to band β. In the spectrum of type C, band β is located at a lower wavelength compared to the spectrum of type B_2 (12). In the presence of excess dye dimeric cations are adsorbed and are located on the external surfaces of peptized particles (type A_2). Band β of this association is located between that of type B_2 and that of type C. Figure 2 illustrates the different types of association.

Electrokinetic measurements, either expressed simply as electrophoretic mobilities or through the zeta potentials, have been applied to many clay dispersions (13–18). Clays saturated with metallic cations typically have negative electrophoretic mobilities due to the negative surface charge of the clay platelets (arising from isomorphic lattice substitution). The charge is compensated for by the presence of the metallic cations in the electrical double layer. If the metallic cations are exchanged by specifically adsorbing cations, the charge on the kinetic unit (particle plus adsorbed layer out to the shear plane) may change from negative, through the isoelectric point (IEP), to positive. Delgado et al. (17) studied in detail the effects of clay–electrolyte interactions on the zeta potential and interpreted these interactions by considering the structural characteristics of the clay particles and their electrical double layers. Black et al. (15) also observed the reversal in the sign of electrophoretic mobilities during adsorption of the polycation *N*-substituted piperidinium chloride polymer on kaolinite.

Being large organic cations, CV and EV are water-structure breakers and their adsorption by montmorillonite should be, to some extent, specific. Consequently, this should have an effect on the electrokinetic potential of the clay particles. The present investigation was undertaken to study the electrophoretic mobility changes that result from the adsorption of the dyes. We shall make comparisons between the measured electrokinetic and spectroscopic results in terms of the various types of bondings and the flocculation process of the clay–dye suspensions.

Experimental

Materials

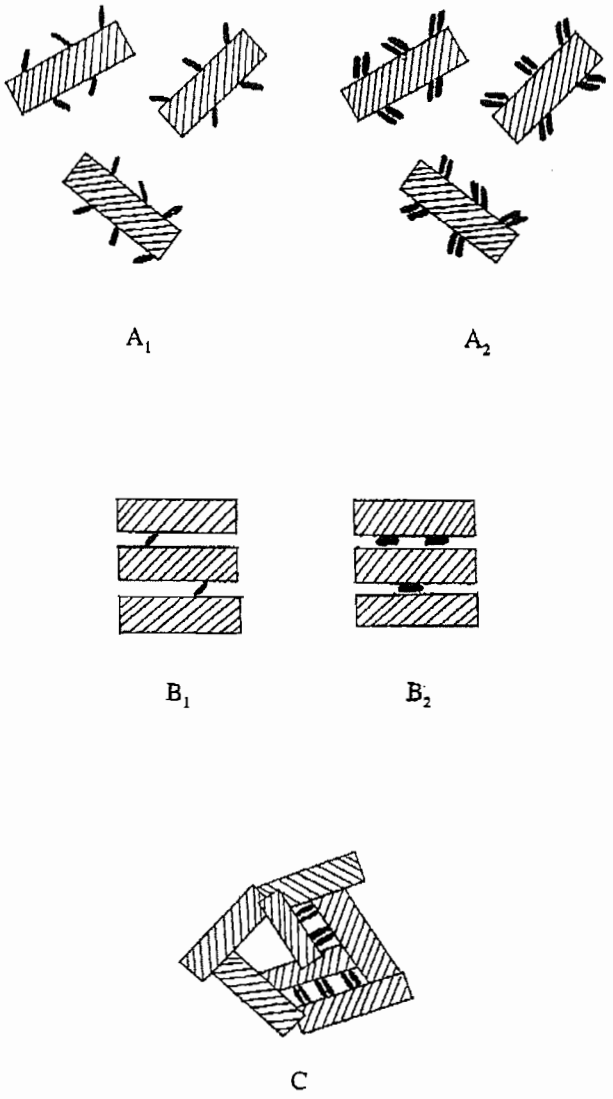
The organic dyes (BDH) were used as supplied as the chlorides. Their concentrations in the powder were determined by C, N, and Cl microanalysis. Montmorillonite (Upton Wyo-

© 1997 NRC Canada

Can. J. Chem. Downloaded from www.nrcresearchpress.com by 91.121.58.235 on 09/08/12
For personal use only.

Can. J. Chem. Downloaded from www.nrcresearchpress.com by 91.121.58.235 on 09/08/12
For personal use only.

Fig. 2. Illustration of the different types of dye–clay associations. Adapted from S. Yariv. (Manuscript in preparation.)



ming montmorillonite, A.P.I. 25, Wards Natural Science Est., Rochester, N.Y.) was gently ground to about −80 mesh. The elemental analysis and related data for this montmorillonite are given in ref. 19. Homoionic montmorillonites were prepared by equilibrating 10 g of natural clay with 1 L of 0.02 M chloride solution of the corresponding cation (20, 21). The excess salt was washed out after 3 days, by centrifugation at 7000 G. The resulting stable suspensions were kept as stock suspensions.

For ethyl violet (EV), five homoionic montmorillonites (Li, K, Mg, Ba, and Al), and for crystal violet (CV), three homoionic montmorillonites (Li, Mg, and Al) were used for electrophoretic measurements. For each cation, the degree of saturation varied from 5 to 130 mmol dye per 100 g clay.

Spectrophotometric measurements

For spectrophotometric measurements suspensions containing a constant amount of dye (4.0×10^{-6} M) and increasing amounts of clay (in the concentration range ($2–400 \times 10^{-4}$ mass%) were used. Spectra were recorded at room temperature using a Cary 219 double-beam spectrophotometer, in the 700–400 nm range. Each suspension was subjected to ultrasound for 7 min immediately after its preparation. Each spectrum was recorded within 3 h after preparation of the suspension.

Flocculation and peptization

Since the clay–dye complexes are intensely coloured the flocculation and peptization processes were readily observed by the naked eye in the present study. Flocculated particles were separated by sedimentation and (or) centrifugation and the supernatants were examined for residual nonflocculated (peptized) clay (12). The amount of residual peptized clay decreased with decreasing absorbance of bands α and β. When the absorbance reached the minimum, the supernatant was colourless because the total amount of clay was flocculated. The light absorption spectrum of peptized suspensions was not affected by the ultrasound treatment, whereas the absorbance of flocculated suspensions was increased as a result of mechanical peptization due to the ultrasound treatment (6).

Electrokinetic measurements

Bulk clay suspensions of 0.05 wt.% of different homoionic montmorillonites and dye solutions EV and CV (10^{-4} M) were used as stock solutions to prepare the clay–dye mixtures. To each 2 mL of clay suspensions, increasing amounts of dye solutions were added and the total volume of the suspensions was made up to 15 mL by adding distilled water. In this way dye/clay mixing ratios (in mmol dye/100 g clay) from 5 to 133 were obtained. For all of these the total clay concentration was constant at 0.0667 g/L. The suspensions were well dispersed and electrokinetic measurements were carried out within 24 h of preparing the clay–dye suspensions.

Particle electrophoretic mobilities were measured with a Rank Brothers, microelectrophoresis apparatus Mark II (Rank Brothers, Cambridge, England) fitted with a rotating prism and video viewing system. A rectangular cell was employed, fitted with hydrogen-charged palladium electrodes. Particle mobilities were determined at 25.0 ± 0.5°C, using a horizontal viewing plane through the centre of the cell, at one of the stationary levels. A direct voltage over distance mode was utilized and particle motions were matched with the opposite scanning motion of a calibrated microprocessor-controlled rotating prism (Rank Brothers Mark II). The apparatus, techniques, and precautions have been discussed elsewhere (18, 22). The cell was used and stored in a constantly water-wet condition; detergent-washing procedures proved to be satisfactory.

For the systems used in this work, the relation between zeta potential, ζ, and electrophoretic mobility, μ_E, is sufficiently well described by the Helmholtz–Smoluchowski equation:

$$[1] \quad \mu_E = \zeta\epsilon/\eta$$

where ϵ and η are the dielectric constant and viscosity of the medium, respectively. The zeta potential can be taken to provide a reasonable approximation of the potential at the Stern layer boundary, hence as an indication of the extent of specific adsorption of dye onto the oxygen plane.

© 1997 NRC Canada

Can. J. Chem. Downloaded from www.nrcresearchpress.com by 91.121.58.235 on 09/08/12
For personal use only.

Fig. 3. The effect of degree of Li-montmorillonite clay saturation by ethyl violet dye on (*a*) the wavelength of the absorption maxima of bands α (●) and β (○), (*b*) the maximum absorbance values corresponding to bands α (●) and β (○), and (*c*) the clay particle electrophoretic mobilities (in units of 10^{-5} cm^2 s^{-1} V^{-1}).

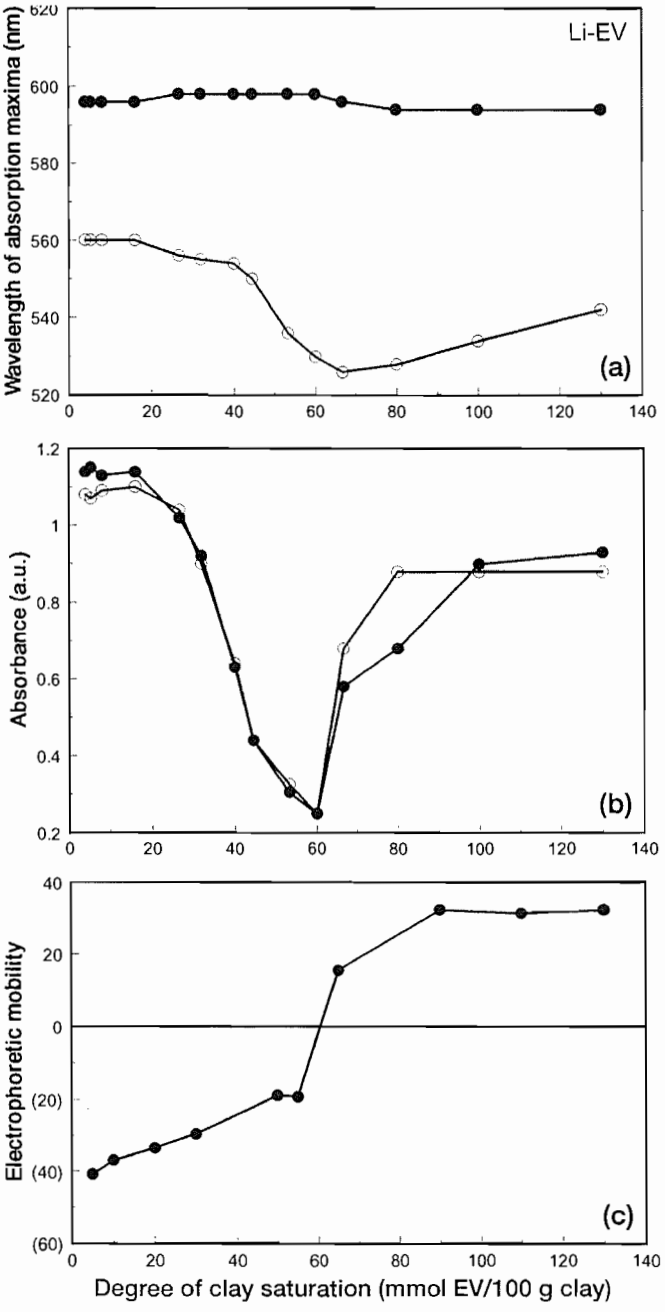
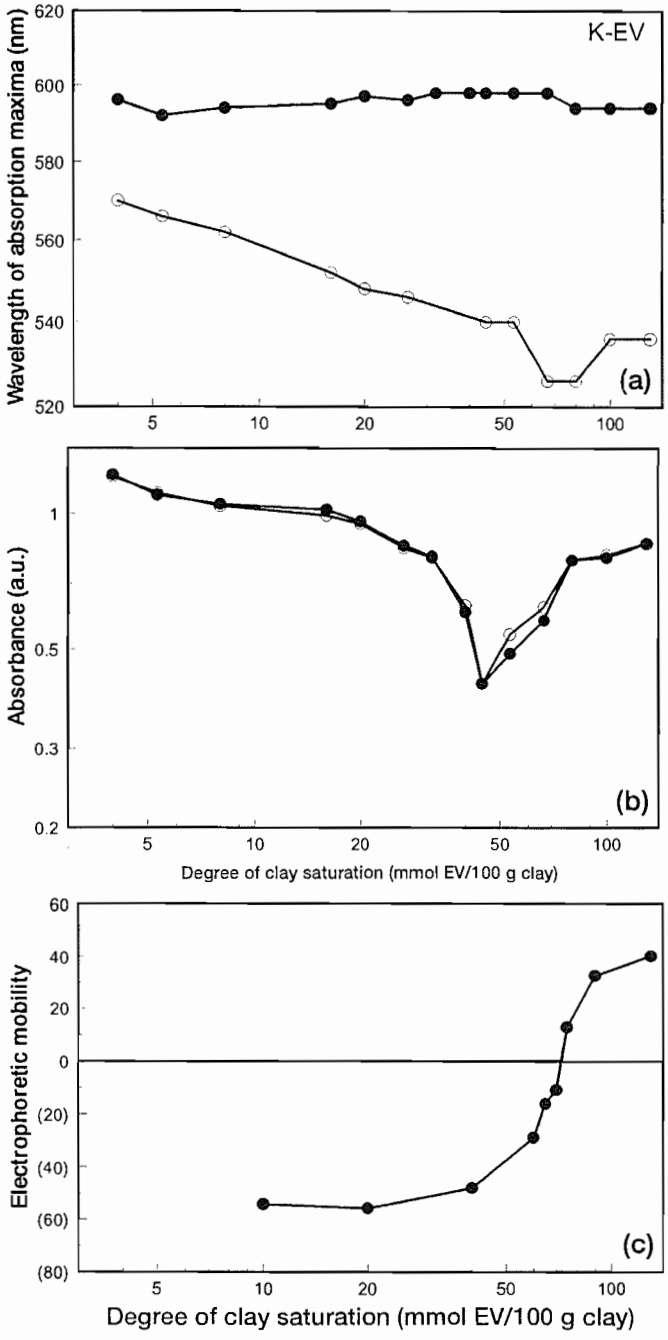


Fig. 4. The effect of degree of K-montmorillonite clay saturation by ethyl violet dye on (*a*) the wavelength of the absorption maxima of bands α (●) and β (○), (*b*) the maximum absorbance values corresponding to bands α (●) and β (○), and (c) the clay particle electrophoretic mobilities (in units of 10^{-5} cm^2 s^{-1} V^{-1}).



Results and discussion

Three kinds of results are shown in Figs. 3–10. In accordance with previous spectrophotometric investigations of dye–clay interactions (10, 11) the minimum degree of saturation for which the spectrophotometric measurements did not exhibit type B_1 but did exhibit type A_1 adsorption interactions was defined as the "transition saturation" (TS). Figures 3–10 show: (*a*) the wavelengths of the absorption maxima of bands α and β. The locations of these bands depend on the degree of saturation. Below the TS band α shows a red shift, more significant in the spectra of CV than in those of EV. The red shift also depends on the acid strength of the exchangeable inorganic cation and increases with its charge. The wavelength maximum of band β is first relatively high (type B_2), then shifts to lower wavelengths (type C), and later to higher wave-

© 1997 NRC Canada

Can. J. Chem. Downloaded from www.nrcresearchpress.com by 91.121.58.235 on 09/08/12
For personal use only.

Fig. 5. The effect of degree of Mg-montmorillonite clay saturation by ethyl violet dye on (*a*) the wavelength of the absorption maxima of bands α (●) and β (○), (*b*) the maximum absorbance values corresponding to bands α (●) and β (○), and (c) the clay particle electrophoretic mobilities (in units of 10^{-5} cm^2 s^{-1} V^{-1}).

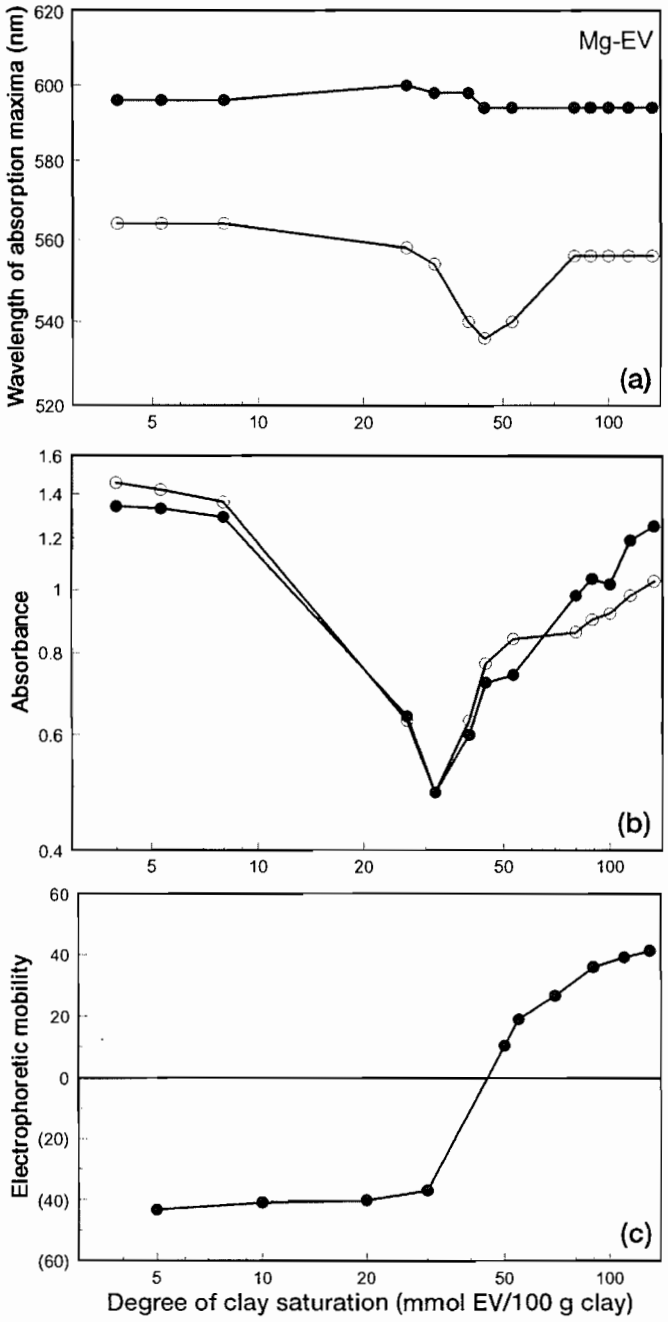
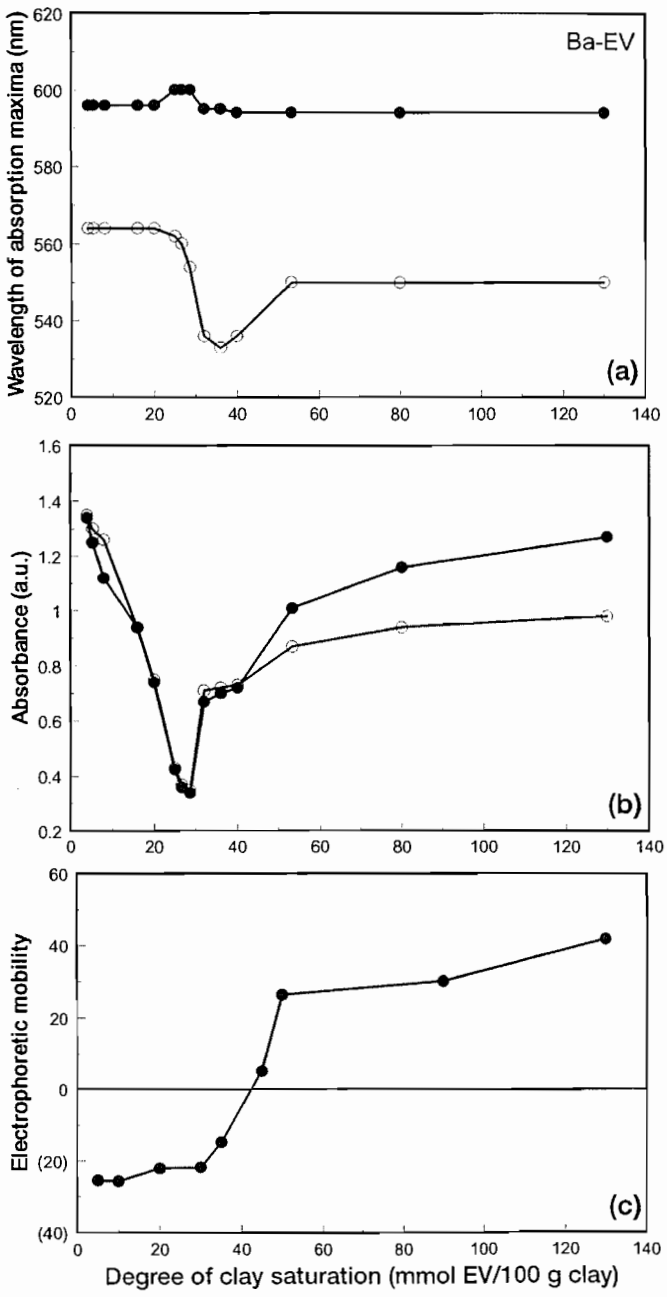


Fig. 6. The effect of degree of Ba-montmorillonite clay saturation by ethyl violet dye on (*a*) the wavelength of the absorption maxima of bands α (●) and β (○), (*b*) the maximum absorbance values corresponding to bands α (●) and β (○), and (*c*) the clay particle electrophoretic mobilities (in units of 10^{-5} cm^2 s^{-1} V^{-1}).



lengths (type A_2). As the clay/dye ratio increases, the absorbance values for bands α and β are first constant, or decrease very slightly, then considerably decrease with clay flocculation, and later increase with peptization;

(*b*) the absorbance values corresponding to bands α and β;

(*c*) the clay particle electrophoretic mobilities, which ranged in continuous fashion from negative values at low degrees of saturation (as large as -56×10^{-5} cm^2 s^{-1} V^{-1}) to positive values at high degrees of saturation (as large as $+42 \times 10^{-5}$ cm^2 s^{-1} V^{-1}). It can be seen that the electrophoretic mobility curves are asymptotic with mobilities remaining almost constant at both low and high dye/clay ratios. In the following discussion the clay–dye system will be treated from the point of view of a titration in which the degree of saturation increases, and three regions of behaviour will be distinguished.

© 1997 NRC Canada

Can. J. Chem. Downloaded from www.nrcresearchpress.com by 91.121.58.235 on 09/08/12
For personal use only.

Fig. 7. The effect of degree of Al-montmorillonite clay saturation by ethyl violet dye on (*a*) the wavelength of the absorption maxima of bands α (●) and β (○), (*b*) the maximum absorbance values corresponding to bands α (●) and β (○), and (*c*) the clay particle electrophoretic mobilities (in units of 10^{-5} cm^2 s^{-1} V^{-1}).

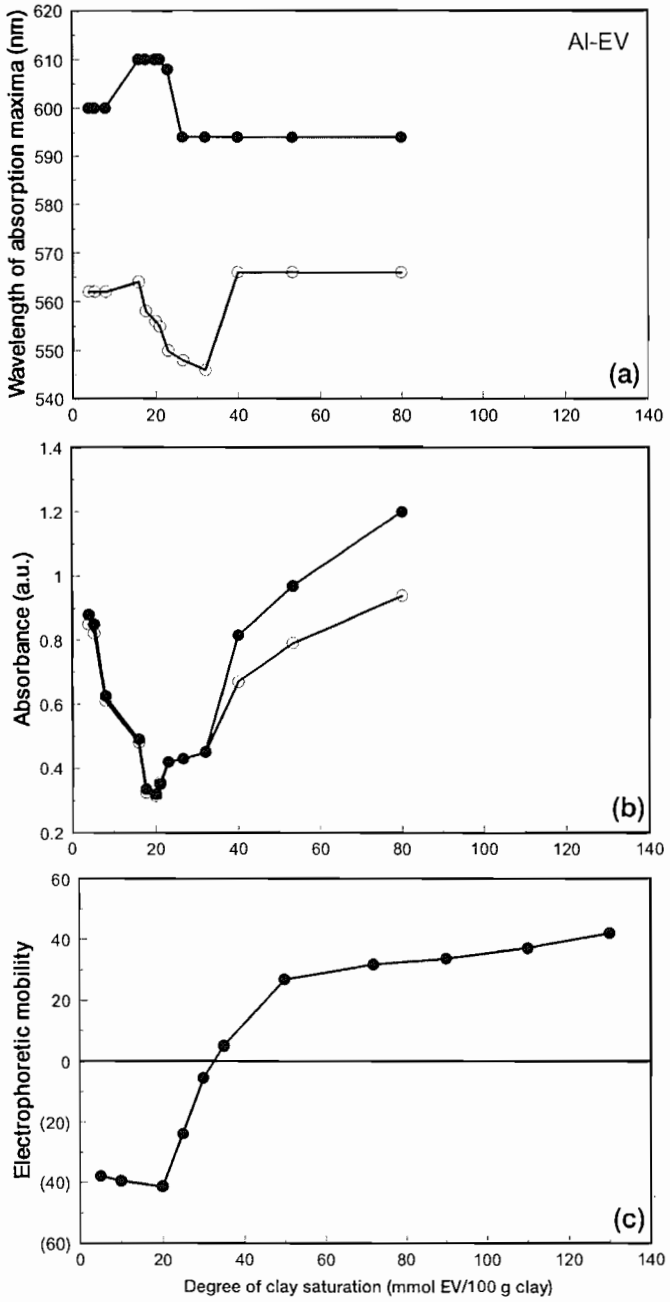
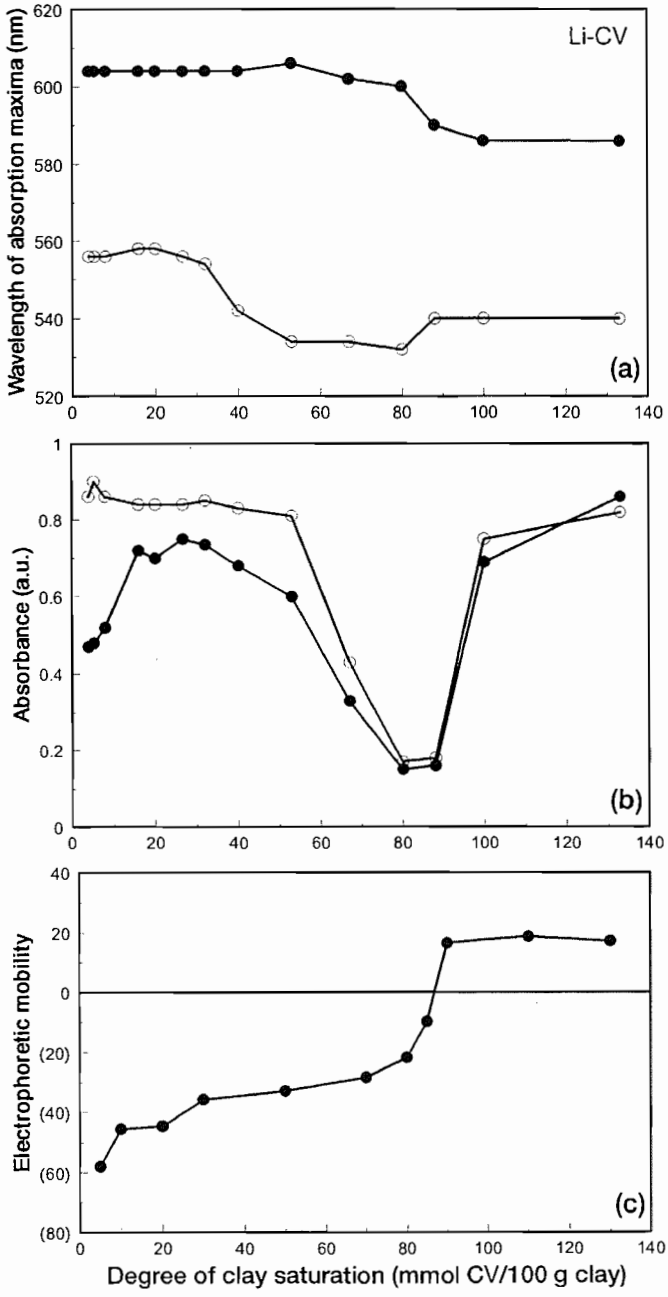


Fig. 8. The effect of degree of Li-montmorillonite clay saturation by crystal violet dye on (*a*) the wavelength of the absorption maxima of bands α (●) and β (○), (*b*) the maximum absorbance values corresponding to bands α (●) and β (○), and (*c*) the clay particle electrophoretic mobilities (in units of 10^{-5} cm^2 s^{-1} V^{-1}).



First, a hypothesis may be advanced for the most likely kinds of adsorption of the dyes and their effects on the mobility curves. When monovalent metallic cations exchange polyvalent cations, they are first adsorbed onto the outer tactoid surfaces, and later into the interlayer spaces, causing breakup of the original tactoids into smaller sizes (23–27). In the case of CV and EV the dyes, although monovalent, are organic cations. They will tend to adsorb first where the clay is most hydrophobic and offers the greatest chance for π-bonding, namely, on the oxygen plane (type B_2). It is likely that a certain degree of cation exchange saturation will be required (type B_1 bonding) before the organic cations can orient themselves to permit π-bonding (type B_2). Such adsorption should not lead to a large change in the electrophoretic mobility of the montmorillonite, because there will be little if any change in the net charge on the tactoid whose size remains relatively constant. The titrations began with 4 mmol dye per 100 g clay; by this degree of saturation band β was clearly observed.

© 1997 NRC Canada

Can. J. Chem. Downloaded from www.nrcresearchpress.com by 91.121.58.235 on 09/08/12
For personal use only.

Fig. 9. The effect of degree of Mg-montmorillonite clay saturation by crystal violet dye on (*a*) the wavelength of the absorption maxima of bands α (●) and β (○), (*b*) the maximum absorbance values corresponding to bands α (●) and β (○), and (*c*) the clay particle electrophoretic mobilities (in units of 10^{-5} cm^2 s^{-1} V^{-1}).

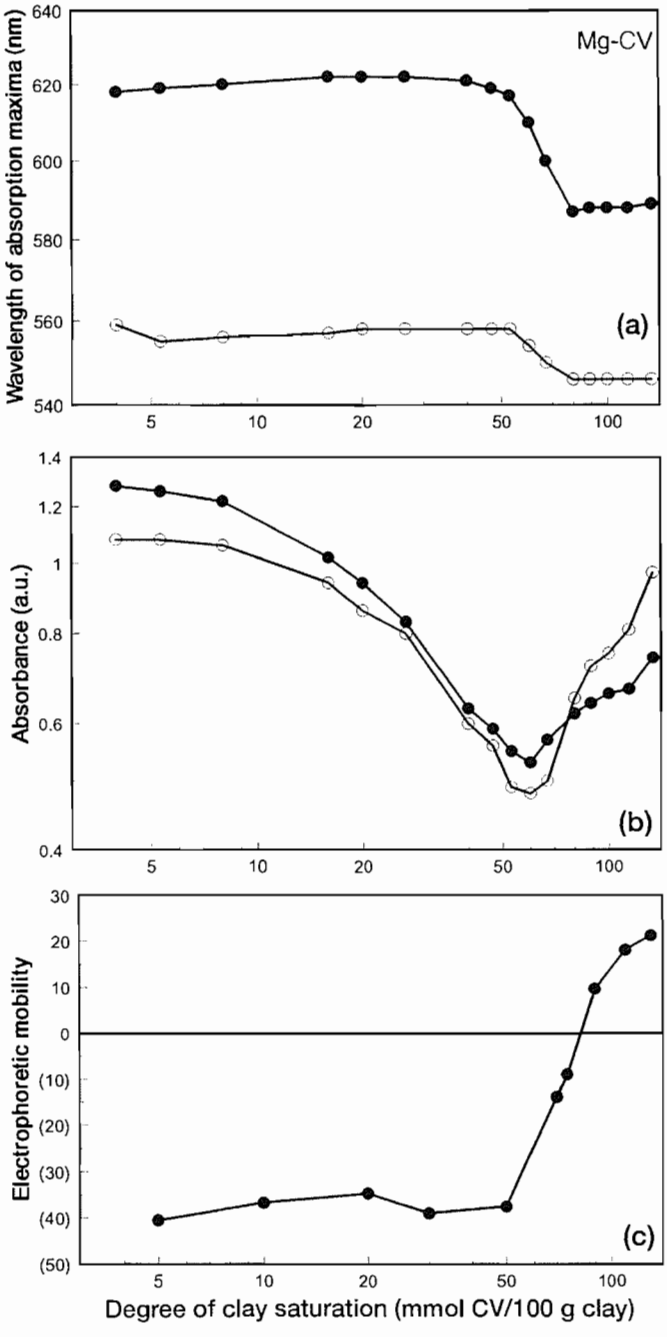
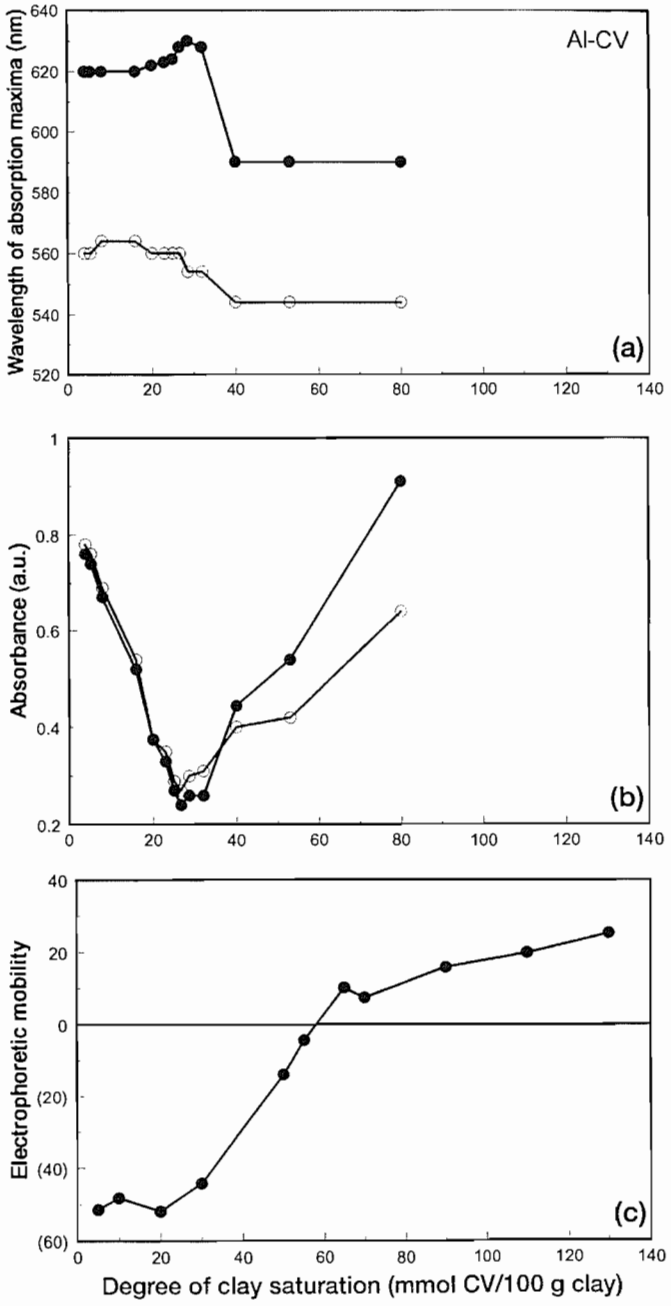


Fig. 10. The effect of degree of Al-montmorillonite clay saturation by crystal violet dye on (*a*) the wavelength of the absorption maxima of bands α (●) and β (○), (*b*) the maximum absorbance values corresponding to bands α (●) and β (○), and (*c*) the clay particle electrophoretic mobilities (in units of 10^{-5} cm^2 s^{-1} V^{-1}).



At a certain degree of saturation, which depends on the exchangeable metal cation, the clay particle electrokinetic potential will be reduced to near zero (near zero electrophoretic mobility) causing flocculation. At this point CV or EV dimeric cations can be located in the interparticle space as well (12). The fact that dimeric CV and EV are present in the interparticle space is envisaged from the location of band β. The wavelength curves, Figs. 3–10*a*, which describe the maximum of band β as a function of the degree of saturation, show shorter wavelengths, which represent associations of type C.

Once the external tactoid surfaces have been filled, then additional bonding could take place by organophilic interactions. Type A_1 and A_2 bonding on the saturated external surfaces would cause the clay particle electrokinetic potential to become increasingly positive (increasing positive electrophoretic mobility), causing peptization. At this stage the maximum of band α is located at the same wavelength as in the dilute aqueous solution.

© 1997 NRC Canada

Table 1. Electrokinetic and spectrophotometric properties of homoionic montmorillonite as a function of degree of saturation with cationic dye.

Original counterion	Dye cation	Saturation for IEP (mequiv./100 g)	Transition saturation (mequiv./100 g)	Maximum flocculation saturation (mequiv./100 g)	Original tactoid size, n (mequiv./100 g)	Minimum Γ (mequiv./100 g)
Li	EV	61	70	60	1.0	90
K	EV	73	73	45	1.5	60
Mg	EV	45	45	32	5.5	16
Ba	EV	42	36	29	6.3	14
Al	EV	32	32	20	6.4	14
Li	CV	87	80	84	1.0	90
Mg	CV	80	80	60	5.5	16
Al	CV	60	40	27	6.4	14

Can. J. Chem. Downloaded from www.nrcresearchpress.com by 91.121.58.235 on 09/08/12
For personal use only.

Region 1

Although the adsorption of the dye by the clay will take place principally by cation exchange reaction, we showed in a previous calorimetric study of the adsorption of CV by different monoionic montmorillonites (20) that the initial exchangeable metallic cations have a great influence on the products of adsorption due to the fact that the initial tactoid is preserved during the first stages of the titration. Again in the present work, the first region exhibits a constant absorbance, indicating that at this stage the adsorption of the dye did not change the size of the original tactoids. Bonding of types B_1 (monomers in the interlayer space) and B_2 (monomers π-bonded to the oxygen planes) is formed from the very beginning of the titration of the homoionic montmorillonite with either CV or EV (10, 11). It is for this reason that in the first region of the mobility curves the initial size of the tactoid is preserved for both dyes. Li-montmorillonite has very small tactoids (1–2 layers) and some of the type B_2 adsorption takes place on the external surface. Thus the negative surface charge decreases only very slightly. Al-montmorillonite has the largest tactoid size and a very small specific surface area. Adsorption via cation exchange takes place into the interlayer space and the charge of the tactoid is not changed.

Region 2

The second region in the mobility curves is the jump to the isoelectric point. This jump is obtained during the flocculation of the clay. This region exhibits a decrease in absorbance, indicating that at this stage the adsorption of the dye resulted in the flocculation of the system (the flocculation of the clay became most efficient at the stage in which the absorbance curve showed its minimum). The degree of saturation with minimum absorbance was considered as the degree of saturation with maximum flocculation. Selected values are given in Table 1.

This region also begins, together with the second region in the wavelength curves of band β, when this band shifts to shorter wavelengths. The IEP is reached at different degrees of saturation for different homoionic montmorillonites (Table 1). The dye/clay ratios at which the mobility becomes zero (IEP) decreased with increasing valency of the exchangeable metallic cations. The exchange capacity of the Wyoming bentonite is about 90 mequiv. per 100 g clay (28–31). The IEP is almost always reached at lower degrees of saturation, which means that only part of the exchangeable metallic cations are replaced by either CV or EV.

Several studies (32–34) have noted that with low molecular weight polycations and cationic surfactants, maximum aggregation typically occurs at a zeta potential of about zero. However, other studies (35–37) have shown that for high molecular weight polycations, optimum dosage (i.e., the concentration at which maximum aggregation occurs) can be less than that needed to lower the zeta potential to zero when interparticle bridging occurs concurrently with charge reduction (36, 37).

During the study of the adsorption of methylene blue by various homoionic montmorillonites, Bodenheimer and Heller (38) concluded that this dye coats the montmorillonite tactoid. Brindley and Thompson (39) showed that this coating prevented the completion of the cation exchange reaction and that this prevention increased with increasing size of the tactoid, owing to the slow diffusion of the cations through the big tactoid. Similar observations on the effect of the metallic cations and the coating of CV or EV on the extent of the cation exchange are obtained in the present study. As coating by the organic cations (type A) causes the external negative charge of the particles to approach zero, the system begins to flocculate. During the flocculation process in Region 2 inorganic and organic cations may become trapped in the flocs to some extent, causing even more rapid charge decrease. The IEP is obtained at the stage where the external charge on the floc is near zero and does not require complete cation exchange.

Most montmorillonites flocculate before their charge reaches zero, in agreement with the results in Table 1. Only Li-montmorillonite was required to reach the IEP saturation to reach maximum flocculation. The highest degrees of saturation for IEP are observed with the monovalent cations, which initially had the smallest tactoids. The lowest degrees are observed with Al-montmorillonite, which initially had the biggest tactoids (Table 1).

In general, the flocs formed in advance of the IEP are likely of the "book-house" type, and due to edge–face particle interactions. At the transition saturation the particle charges are near zero and the flocs may change their structure. A change

© 1997 NRC Canada

Fig. 11. Degree of saturation to reach the isoelectric point as a function of the degree of saturation to reach the transition saturation. The points correspond to montmorillonites in the presence of ethyl violet (●) and crystal violet (○).

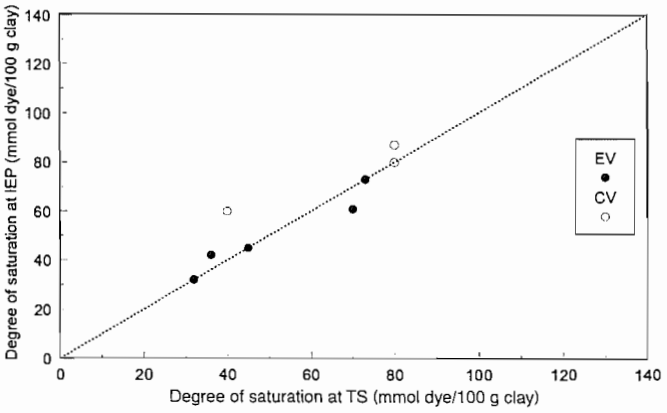
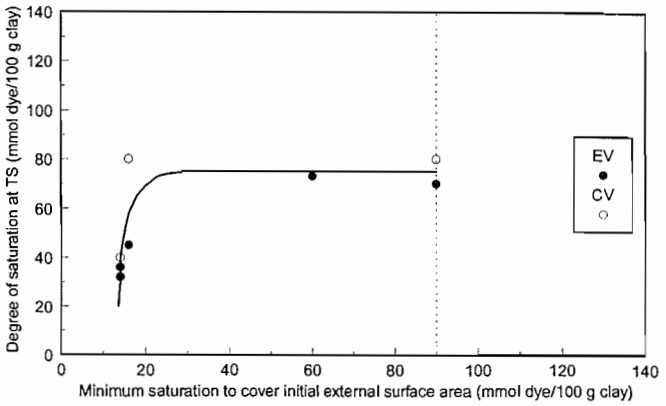


Fig. 12. Degree of saturation to reach the transition saturation as a function of the degree of saturation to cover the initial external tactoid surface area. The points correspond to montmorillonites in the presence of ethyl violet (●) and crystal violet (○). The vertical, broken line represents the total surface charge density of the clay.



from book-house to "card-house" structure would be consistent with the shift of band α in the wavelength curves to lower wavelengths, which characterizes the disappearance of type B_1.

The IEP is reached for CV always at a higher degree of saturation than for EV. This difference between the two dyes is due to size and bonding strength effects. EV is larger and is more hydrophobic and the coating of the clay tactoids by this dye is more efficient. Thus smaller dye concentrations are necessary to reach the IEP.

Region 3

After the IEP the mobility curves show increasingly positive particle surface charges. This is the third region of the titration curve and exhibits increasing absorbance values corresponding to the repeptization of the clay and the exposure of additional surfaces. Bondings of type A are the principal adsorption products that are formed at this stage of the titration. In previous work we have concluded that this adsorption results from "organophilic attraction" forces between the organo-clay complex and the cationic dye, after the latter had been in excess in the aqueous phase. We also concluded that these bondings are formed outside the interlayer space (10, 11). Thus, the type A cations are attached to the external surfaces of peptized platelets or small tactoids, contributing positive charge to the mobile particles. At well past the IEP there eventually is little surface area available for further adsorption and only small increases in electrokinetic potential result.

Transition saturation and the isoelectric point

Some TS values that were determined in our spectrophotometric study are shown in Table 1. With most montmorillonites at this stage, band β reaches its shortest wavelength (dimers in the interparticle space). A comparison of the degree of saturation for TS to that for IEP is shown in Fig. 11. It can be seen that there is reasonably good agreement. The type B_1 bonding disappears by the IEP. It seems that, once the external surfaces of the tactoids become positive as a result of coating, this stage defines the TS. This stage will be reached before all ion exchange is complete. We can calculate the minimum degree of saturation required to reach TS as follows. Before the tactoid size changes, the external surface must be covered with dye. The amount of dye required depends on the original tactoid size. If Γ° is the total surface charge density of the clay (mequiv./100 g clay), then the effective charge density (exposed charge density) of the tactoids (Γ) is given by

$$[2] \quad \Gamma = \Gamma^\circ/n^\circ$$

where n° is the original tactoid thickness in number of plates per tactoid. Γ° is 90 mequiv./100 g (the CEC). The average tactoid sizes can be estimated from the measurements of Banin and Lahav (21) and applying the tactoid volume correction of Schramm and Kwak (26). The values obtained this way yield a good estimate of tactoid sizes, as would be obtained from independent experimental methods such as light scattering, viscosity, and anion exclusion (26, 27). The values are shown in Table 1. The relation between TS and Γ is shown in Fig. 12. It can be seen that the TS values increase strongly with Γ at first and then reach a plateau.

From Fig. 12 the values of Γ that equal TS can be found. These are about 70 mequiv./100 g for EV and 80 mequiv./100 g for CV. These should be the final external surface areas for the dye montmorillonite tactoids and correspond to tactoid sizes of 1.3 for EV and 1.1 for CV. A consistent interpretation of these results would involve dye adsorption to an extent that creates the tactoid size favoured by each cation (as happens for metal cation exchange). At this point all the external surfaces are covered; this is TS. With more dye addition to the system dye cations can adsorb at the tactoid surfaces by types A_1 and A_2 bonding. The previous results (10, 11) show that indeed both occur after TS.

Conclusions

In this work we have investigated the electrokinetic properties of a number of initially homoionic (metal cation) montmorillonites in the presence of the cationic dyes, crystal violet and ethyl violet. The electrophoretic mobility changes taking place with increasing amounts of dye in the systems were

© 1997 NRC Canada

Can. J. Chem. Downloaded from www.nrcresearchpress.com by 91.121.58.235 on 09/08/12
For personal use only.

explained in terms of different types of dye adsorption as identified by spectrophotometric measurements. Dye adsorption apparently occurs initially by ion exchange, followed by some more specific adsorption due to π and H interactions with the clay particle surface.

The spectroscopic and electrophoretic mobility curves can be divided into three regions. In the first region the clay is relatively well peptized and the initial size of the tactoid, which is determined by the metal cation, is preserved during the adsorption of both dyes. Most dye is adsorbed into the interlayer space of the tactoids but some of the B_2 adsorption takes place on the external oxygen planes of the tactoids. Thus the surface negative charge decreases very slightly. In the second region the clay is in a flocculated state and dimeric cations are mostly adsorbed into the interparticle spaces of the flocs (type C) with some cations adsorbed on the external surfaces. When the process of adsorption and particle rearrangements is complete, the transition saturation and isoelectric point are reached. In the third region, beyond the IEP, the clay is peptized and new, smaller, tactoids are obtained which gain a positive charge from types A_1 and A_2 adsorption of CV or EV cations. The size of these tactoids is determined by the adsorbed dye.

Acknowledgements

S.Y. is grateful to the Alexander Silberman Hebrew University Foundation for Applied Science for financial support. We are grateful to the Petroleum Recovery Institute, Syncrude Canada Ltd., the Natural Sciences and Engineering Research Council of Canada, and the Alberta Oil Sands Technology and Research Authority for their support of the collaborations involved in this research.

References

1. R.E. Grim. Clay mineralogy. McGraw–Hill Book Co., New York. 1968.
2. B.K.G. Theng. The chemistry of clay-organic reactions. Wiley, New York. 1974.
3. S. Yariv. Int. J. Trop. Agric. **6**, 1 (1988).
4. S. Yariv and H. Cross. Geochemistry of colloid systems. Springer-Verlag, Berlin. 1979.
5. S. Yariv and D. Lurie. Isr. J. Chem. **9**, 537 (1971).
6. Z. Grauer, G.L. Grauer, D. Avnir, and S. Yariv. J. Chem. Soc. Faraday Trans. 1, **83**, 1685 (1987).
7. R. Cohen and S. Yariv. J. Chem. Soc. Faraday Trans. I. **80**, 1705 (1984).
8. D. Garfinkel-Shweky and S. Yariv. J. Colloid Interface Sci. **188**, 168 (1997).
9. S. Yariv, D.K. Ghosh, and L.G. Hepler. J. Chem. Soc. Faraday Trans. 1, **87**, 1201 (1991).
10. S. Yariv, M. Müller-Vonmoos, G. Kahr, and A. Rub. Thermochim. Acta, **148**, 457 (1989).
11. C. Dobrogowska, L.G. Hepler, D.K. Ghosh, and S. Yariv. J. Therm. Anal. **37**, 1347 (1991).
12. S. Yariv, A. Nasser, and P. Bar-On. J. Chem. Soc. Faraday Trans. 1, **86**, 1593 (1990).
13. H. van Olphen. An introduction to clay colloid chemistry. 2nd ed. Wiley–Interscience, New York. 1977.
14. R.J. Hunter and A.E. Alexander. J. Colloid Sci. **18**, 833 (1963).
15. A.P. Black, F.B. Birkner, and J. Morgan. J. Colloid Sci. **21**, 626 (1966).
16. N.S. Srinivasan and L.G. Hepler. J. Can. Pet. Technol. **21**, 25 (1982).
17. A. Delgado, F. Gonzalez-Gabalero, and J.M. Brugue. J. Colloid Interface Sci. **113**, 203 (1985).
18. L.L. Schramm and R.G. Smith. Colloids Surfaces, **14**, 67 (1985).
19. H. van Olphen and J.J. Fripiat (*Editors*). Data handbook for clay materials and other non-metallic minerals. Pergamon Press, Oxford. 1979.
20. L.G. Hepler, S. Yariv, and C. Dobrogowska. Thermochim. Acta, **121**, 373 (1987).
21. A. Banin and N. Lahav. Isr. J. Chem. **6**, 235 (1968).
22. L.L. Schramm, K. Mannhardt, and J.J. Novosad. Colloids Surf. **55**, 309 (1991).
23. I. Shainberg and H. Otoh. Isr. J. Chem. **6**, 251 (1968).
24. I. Shomer and U. Mingelgrin. Clays Clay Miner. **26**, 135 (1978).
25. J.E. Dufey, A. Banin, H.G. Laudelout, and Y. Chen. Soil Sci. Soc. Am. J. **40**, 310 (1976).
26. L.L. Schramm and J.C.T. Kwak. Clays Clay Miner. **30**, 40 (1982).
27. L.L. Schramm and J.C.T. Kwak. Colloids Surf. **3**, 43 (1982).
28. D. Lurie and S. Yariv. Isr. J. Chem. **6**, 203 (1968).
29. P. Bar-On and I. Shainberg. Soil Sci. **109**, 241 (1970).
30. J. Kamil and I. Shainberg. Soil Sci. **106**, 193 (1968).
31. I. Shainberg, P.F. Low, and U. Kafkafi. Soil Sci. Soc. Am. Proc. **38**, 751 (1974).
32. R.H. Ottewill and A.C. Rastogi. Trans. Faraday Soc. **56**, 866 (1960).
33. J.C.Kane, V.K. La Mer, and H.B. Lindford. J. Phys. Chem. **68**, 2273 (1964).
34. J.K. Dixon, V.K. LaMer, C.L.S. Messinger, and H.B. Lindford. J. Colloid Interface Sci. **23**, 465 (1967).
35. B. Vincent. Adv. Colloid Interface Sci. **4**, 193 (1974).
36. W. Heller. Pure Appl. Chem. **12**, 149 (1966).
37. J. Gregory. Trans. Faraday Soc. **65**, 2260 (1969).
38. W. Bodenheimer and L. Heller. Isr. J. Chem. **6**, 307 (1968).
39. G.W. Brindley and T.D. Thompson. Isr. J. Chem. **8**, 409 (1970).

Can. J. Chem. Downloaded from www.nrcresearchpress.com by 91.121.58.235 on 09/08/12
For personal use only.

© 1997 NRC Canada

Oxidative addition and isomerization reactions. The synthesis of *cis*- and *trans*-$ArSF_4Cl$ and *cis*- and *trans*-$PhTeF_4Cl$

Xiaobo Ou, Guy M. Bernard, and Alexander F. Janzen

Abstract: The stereoselective synthesis and isomerization of *cis*- and *trans*-$ArSF_4Cl$ is described, where Ar = Ph, *p*-MeC_6H_4, and *p*-$O_2NC_6H_4$. Also briefly described is the synthesis of $ArSF_5$, *cis*- and *trans*-$PhTeF_4Cl$, and $PhTeF_5$. The oxidative halogenating reagent is a mixture of XeF_2 and Cl^-, and suitable starting compounds are ArSSAr, $ArSF_3$, and PhTeTePh. Products were characterized by ^{19}F, ^{13}C, and ^{125}Te NMR spectroscopy, and by the $^{37}Cl/^{35}Cl$ and $^{34}S/^{32}S$ isotope effects on the ^{19}F NMR chemical shifts. A mechanism of oxidative halogenation is proposed to account for the stereoselective synthesis of *cis*- and *trans*-$ArSF_4Cl$. Ab initio calculations of optimized geometries of anionic and radical intermediates, i.e., $PhSF_3X^-$ and $PhSF_3X^{\cdot}$ (X = F, Cl), were carried out with the aid of the GAUSSIAN 92 program.

Key words: synthesis of *cis*- and *trans*-$ArSF_4Cl$, *cis*- and *trans*-$PhTeF_4Cl$, $ArSF_5$, and $PhTeF_5$, mechanism of oxidative fluorination and oxidative chlorination, $^{37}Cl/^{35}Cl$ and $^{34}S/^{32}S$ isotope effects on ^{19}F NMR spectra.

Résumé : On décrit la synthèse stéréosélective et l'isomérisation des *cis*- et *trans*-$ArSF_4Cl$ dans lesquels Ar = Ph, *p*-MeC_6H_4 et *p*-$O_2NC_6H_4$. On décrit aussi brièvement la synthèse des $ArSF_5$, *cis*- et *trans*-$PhTeF_4Cl$ et $PhTeF_5$. Le réactif provoquant une halogénation oxydante est un mélange de XeF_2 et de Cl^- pour lesquels les ArSSAr, $ArSF_3$ et PhTeTePh sont des produits de départ appropriés. On a caractérisé les produits par la spectroscopie RMN du ^{19}F, du ^{13}C et du ^{125}Te ainsi que par les effets isotopiques $^{37}Cl/^{35}Cl$ et $^{34}S/^{32}S$ sur les déplacements chimiques dans la RMN du ^{19}F. On propose un mécanisme pour l'halogénation oxydante qui tient compte de la synthèse stéréosélective des *cis*- et *trans*-$ArSF_4Cl$. Faisant appel au programme GAUSSIAN 92, on a effectué des calculs ab initio sur les géométries optimisées des intermédiaires anioniques et radicalaires, soit $PhSF_3X^-$ et $PhSF_3X^{\cdot}$ (X = F, Cl).

Mots clés : synthèse des *cis*- et *trans*-$ArSF_4Cl$, *cis*- et *trans*-$PhTeF_4Cl$, $ArSF_5$, and $PhTeF_5$, méchanisme de la fluoration oxydante et de la chloration oxydante, effets isotopiques $^{37}Cl/^{35}Cl$ et $^{34}S/^{32}S$ sur les spectres RMN du ^{19}F.

[Traduit par la rédaction]

Can. J. Chem. Downloaded from www.nrcresearchpress.com by 91.121.58.235 on 09/08/12
For personal use only.

Introduction

cis and *trans* isomers of six-coordinate S, Se, and Te fluorides are known (1–3), and the preparation of chlorofluoro derivatives, RSF_4Cl, can be carried out with oxidizing agents such as ClF (4), or with oxidizing agents in the presence of fluoride ion, e.g., Cl_2 and CsF (5).

We have shown that oxidation with XeF_2 can be carried out in the presence of a catalytic amount of Cl^-, e.g., oxidative fluorination of Ph_2TeF_2 to Ph_2TeF_4 (6) and of Ph_2SO to $Ph_2S(O)F_2$ (7), but it is generally difficult to predict the stereochemical outcome of oxidation reactions because of the complexity brought about by competition among oxidative fluorination, isomerization, and ligand-exchange processes. If, for example, a Lewis acid such as SbF_5 or PF_5 is added to S(VI) or Te(VI) fluorides, then isomerization can occur (6, 8, 9), presumably via cationic and fluorine-bridged intermediates, but the H_2O–HF–glass system may also, inadvertently, introduce Lewis acids such as BF_3 or SiF_4 into a reaction mixture (10). All attempts were made in this study to avoid the introduction of Lewis acids; furthermore, traces of moisture are eliminated by in situ reaction with sulfur(IV) fluorides and, consequently, pathways involving cationic intermediates are unlikely. If that is indeed the case, then the stereochemical outcome of the reactions discussed below may provide information about anionic and radical intermediates that participate in the oxidation of sulfur(IV) compounds.

Received August 28, 1997.

X. Ou, G.M. Bernard, and A.F. Janzen.[1] Department of Chemistry, University of Manitoba, Winnipeg, MB R3T 2N2, Canada.

[1] Author to whom correspondence may be addressed. Telephone: (204) 474-9731. Fax: (204) 474-7608. E-mail: ajanzen@cc.umanitoba.ca

Results and discussion

cis- and trans-$ArSF_4Cl$

The preparation of *cis*- and *trans*-$ArSF_4Cl$ was carried out in a polytetrafluoroethene (ptfe) bottle by using ~0.06 mmol of either ArSSAr or $ArSF_3$ as starting compound, and XeF_2 and Et_4NCl as oxidizing and halogenating reagents, in CD_2Cl_2 or CD_3CN solution at room temperature, according to eqs. [1] and [2].

$$[1]\quad ArSSAr + 2\,Cl^- + 5\,XeF_2 \xrightarrow{CD_2Cl_2 \text{ or } CD_3CN} 2\ cis\text{- and } trans\text{-}ArSF_4Cl + 2\,F^- + 5\,Xe$$

© 1997 NRC Canada

Can. J. Chem. Downloaded from www.nrcresearchpress.com by 91.121.58.235 on 09/08/12
For personal use only.

[2] $ArSF_3 + Cl^- + XeF_2 \xrightarrow{CD_2Cl_2}$ *cis*- and *trans*-$ArSF_4Cl + F^-$ + Xe, Ar = Ph, *p*-MeC_6H_4, and *p*-$O_2NC_6H_4$

Attempts were made to optimize the yield of *cis*- and *trans*-$ArSF_4Cl$, and experimental results are summarized in Table 1. The molar ratio of reactants was systematically varied, two solvents were used, CD_2Cl_2 or CD_3CN, and substituents *p*-Me and *p*-NO_2 were introduced into the benzene ring.

All products were characterized by ^{19}F and ^{13}C NMR spectroscopy (Tables 2 and 3), and the presence of a chlorine substituent in $ArSF_4Cl$ was confirmed by chlorine isotope shift measurements (Table 4). The ^{19}F NMR spectrum of *cis*-$ArSF_4Cl$ has an A_2BC spin pattern, of which the two equivalent F^A fluorines can be assigned uniquely; however, for the assignment of F^B versus F^C, the method of Dean and Evans (11) was used (Table 2).



cis-$ArSF_4Cl$ *trans*-$ArSF_4Cl$ $ArSF_5$

The experimental results of Table 1 confirm that either *cis* or *trans* isomers can be prepared in high yield, depending on the reaction conditions. *trans*-$ArSF_4Cl$ is the predominant isomer in entries 8–11, 14–16 of Table 1. The highest yield of *trans*-$ArSF_4Cl$ is 89% (entry 11), and five reactions give yields greater than 80% (entries 8–11, 16). Each of these reactions was carried out with a stoichiometric excess of XeF_2 and, in each case, excess XeF_2 was identified at the completion of the reaction, as noted in the last column of Table 1.

The highest yield of *cis*-$ArSF_4Cl$ is 83% (entry 1), and there are five reactions in which the *cis* isomer is formed in greater than 70% yield (entries 1–3, 5, 12). In none of these cases was excess XeF_2 observed at the completion of the reaction. It thus appears that the synthesis of *trans*-$ArSF_4Cl$ is favoured by an excess of XeF_2.

Although the reactions of Table 1 were generally completed within 3–20 min, as judged by the cessation of xenon gas evolution, the ^{19}F NMR spectra, on which the yields are based, were recorded after 24 h. On standing for 1 week, or longer, the yield of *cis* isomer slowly increased at the expense of the *trans* isomer (entries 3–6). In view of the time delay in recording the NMR spectra, and because there is a slow *trans*-to-*cis* isomerization in solution, we cannot attach significance to small differences in yield.

The slow isomerization of *trans*-$ArSF_4Cl$ to *cis*-$ArSF_4Cl$ in solution is clearly evident after 1 week, or longer (entries 3–6), and is enhanced by Et_4NCl. The effect of Cl^- on isomerization was confirmed by adding Et_4NCl to a sample containing a 2:1 ratio of *trans*:*cis* isomers and an excess of XeF_2. After 16 h, the sharp single ^{19}F NMR peak of *trans*-$PhSF_4Cl$ was replaced by a broad peak of reduced intensity but at nearly the same chemical shift, suggesting the onset of a ligand-exchange process in *trans*-$ArSF_4Cl$. The A_2BC peaks of *cis*-$PhSF_4Cl$ remained sharp and at the same chemical shift. Integration of all ^{19}F NMR spectra showed that the original *trans*:*cis* ratio of 2:1 changed to 1:2 after 16 h, 1:4 after 48 h, and 1:8 after 5 days. After 1 week nearly all *trans*-$PhSF_4Cl$ had isomerized to *cis*-$PhSF_4Cl$.

Generally, ArSSAr was the starting compound of choice, because of its ease of preparation and commercial availability. However, $ArSF_3$ can also be used (entries 3, 7, 9), and we assume that $ArSF_3$ is formed *in situ* in all reactions of ArSSAr in Table 1. In those reactions of ArSSAr that were carried out with a stoichiometric deficiency of XeF_2, unreacted $ArSF_3$ can be identified at the completion of the reaction, thus confirming the presence of $ArSF_3$ in these reactions (entries 4, 6, 7).

A small amount of $ArSF_5$ is produced in most reactions, but generally less than ~3% (entries 3, 5, 9–11, 13–16). The yield of $ArSF_5$ can be increased by decreasing the amount of Et_4NCl. For example, at a lower ratio of Cl^-, i.e., $PhSF_3$:Et_4NCl:XeF_2 = 1:0.3:1, the yield of $ArSF_5$ is increased to 20% (entry 7).

In most reactions, but not all, a small amount of $ArSOF_3$ was identified by ^{19}F and ^{13}C NMR, as noted in the last column of Table 1. Trace amounts of water in the reaction mixture produce $ArSOF_3$, and this hydrolysis product serves as an indicator of our experimental technique. Careful purification of reactants and solvents avoids completely the appearance of $ArSOF_3$, whereas the deliberate introduction of water to a reaction mixture containing some $ArSOF_3$ leads immediately to the appearance of $ArSO_2F$. On the other hand, *cis*- and *trans*-$PhSF_4Cl$ appear to be stable towards water for at least several days.

Also listed in the last column of Table 1 are the products CD_2F_2, CD_2FCl, and CD_2FCN, identified by ^{19}F and ^{13}C NMR. It has previously been noted that solvents react with XeF_2 and with anhydrous fluoride ion (12). An exchange-broadened ^{19}F NMR peak at about −153 ppm is seen in all samples and is assigned to a mixture of FHF^-, FDF^-, HF and DF.

Proposed mechanism of oxidative halogenation

The experimental results of Table 1 are explained by the mechanism of Scheme 1. The *N*-X-*L* notation (13) is used to specify the valence electron count and coordination number of sulfur-containing compounds and intermediates as 10-S-4, 12-S-5, 11-S-5, and 12-S-6. It may be noted that fluorinated analogues of these sulfur species have been identified experimentally, i.e., SF_4, SF_5^- (14), $SF_5^\bullet$ (15), and SF_6, respectively. Cations with 10-S-5 sulfur are also known, e.g. RSF_4^+ (16), but cationic intermediates are not considered in Scheme 1 because of the absence of strong Lewis acids in all reaction mixtures.

Some of the proposals in Scheme 1 have been discussed previously, including the reaction of XeF_2 and Cl^- to give $Cl^\bullet$ and F^- in eq. [3] (7), the *trans* arrangement of aryl substituents and nonbonding electrons in eqs. [4] and [5] (6), anion-to-radical oxidation in eq. [4] (17), and cleavage of oxidizing agents such as XeF_2 and Cl_2 via bridged $[S\text{--}F\text{--}Xe]^\bullet$ and $[S\text{--}Cl\text{--}Cl]^\bullet$ intermediates in eqs. [6] and [7] (7).

It is postulated in eq. [4] that addition of F^- to $ArSF_3$, followed by anion-to-radical oxidation, gives the radical $ArSF_4^\bullet$. Further addition of $Cl^\bullet$ then leads to *trans*-$ArSF_4Cl$. The experimental finding that excess XeF_2 favours the synthesis of *trans*-$ArSF_4Cl$ (Table 1) is consistent with eqs. [3] and [4], since excess XeF_2 favours the synthesis of F^- and $Cl^\bullet$ (eq. [3]) and the latter species are required for the synthesis of *trans*-$ArSF_4Cl$ (eq. [4]).

It is also postulated in eq. [4] that interaction of radical

© 1997 NRC Canada

Can. J. Chem. Downloaded from www.nrcresearchpress.com by 91.121.58.235 on 09/08/12
For personal use only.

Table 1. Experimental conditions for the synthesis of *cis*- and *trans*-$ArSF_4Cl$ and $ArSF_5$ at 25°C in CD_2Cl_2 or CD_3CN solvent.[a]

Entry	Molar ratio of reactants	Reaction time	$ArSF_4Cl$ *cis*	$ArSF_4Cl$ *trans*	$ArSF_5$	Other products identified
Stoichiometric ratio, or less, of XeF_2; solvent CD_2Cl_2						
1	$(p\text{-}O_2NC_6H_4)_2S_2$:$Et_4NCl$:$XeF_2$/1:2:6	24 h	83%	11%	Nil	$ArSOF_3$, CD_2F_2, CD_2FCl, DF_2^-/DF
2	Ph_2S_2:Et_4NCl:XeF_2/1:4:5	24 h	75%	14%	Nil	$PhSOF_3$, CD_2F_2, CD_2FCl,DF_2^-/DF
3	$PhSF_3$:Et_4NCl:XeF_2/1:1:1	24 h	54%	37%	3%	$PhSOF_3$, CD_2F_2, CD_2FCl, DF_2^-/DF
		1 week	79%	12%		
4	Ph_2S_2:Et_4NCl:XeF_2/1:2:4	24 h	39%	19%	Nil	$PhSF_3$, $PhSOF_3$, CD_2F_2, CD_2FCl, DF_2^-/DF
		1 week	44%	6%		
5	Ph_2S_2:Et_4NCl:XeF_2/1:2:6	24 h	38%	53%	<1%	$PhSOF_3$, CD_2F_2, CD_2FCl, DF_2^-/DF
		1 week	72%	11%		
6	$(p\text{-}MeC_6H_4)_2S_2$:Et_4NCl:XeF_2/1:2:5	24 h	38%	35%	Nil	$ArSF_3$, $ArSOF_3$, CD_2F_2, CD_2FCl, DF_2^-/DF
		1 week	46%	13%		
7	$PhSF_3$:Et_4NCl:XeF_2/1:0.3:1	24 h	<1%	34%	20%	XeF_2, $PhSF_3$, $PhSOF_3$, CD_2F_2, CD_2FCl, DF_2^-/DF
		1 month	<1%	46%		
Excess XeF_2, solvent CD_2Cl_2						
8	$(p\text{-}O_2NC_6H_4)_2S_2$:$Et_4NCl$:$XeF_2$/1:2:8	24 h	14%	80%	Nil	XeF_2, $ArSOF_3$, CD_2F_2, CD_2FCl, DF_2^-/DF
9	$PhSF_3$:Et_4NCl:XeF_2/1:1:2	24 h	<1%	84%	<1%	XeF_2, $PhSOF_3$, CD_2F_2, CD_2FCl, DF_2^-/DF
10	$(p\text{-}MeC_6H_4)_2S_2$:Et_4NCl:XeF_2/1:2:8	24 h	Nil	83%	2%	XeF_2, $ArSOF_3$, CD_2F_2, CD_2FCl, DF_2^-/DF
11	Ph_2S_2:Et_4NCl:XeF_2/1:2:8	24 h	1%	89%	2%	XeF_2, $PhSOF_3$, CD_2F_2, CD_2FCl, DF_2^-/DF
Solvent CD_3CN						
12	Ph_2S_2:Et_4NCl:XeF_2/1:3:5	24 h	77%	7%	Nil	$PhSOF_3$, CD_2FCN, DF_2^-/DF
13	Ph_2S_2:Et_4NCl:XeF_2/1:2:5	24 h	55%	25%	<1%	XeF_2, $PhSOF_3$, CD_2FCN, DF_2^-/DF
14	Ph_2S_2:Et_4NCl:XeF_2/1:2:6	24 h	27%	60%	<1%	XeF_2, $PhSOF_3$, CD_2FCN, DF_2^-/DF
15	Ph_2S_2:Et_4NCl:XeF_2/1:2:7	24 h	12%	75%	<1%	XeF_2, $PhSOF_3$, CD_2FCN, DF_2^-/DF
16	Ph_2S_2:Et_4NCl:XeF_2/1:2:8	24 h	4%	84%	<1%	XeF_2, $PhSOF_3$, CD_2FCN, DF_2^-/DF

[a]Reactions were complete within 3-20 min, but ^{19}F NMR spectra were recorded after ~24 h. Yields are based on integration of ^{19}F NMR signals of all sulfur fluoride compounds.

Table 2. ^{19}F NMR data of *cis*- and *trans*-$ArSF_4Cl$, $ArSF_5$, and *cis*- and *trans*-$PhTeF_4Cl$ in CD_2Cl_2.

Compound	Spin system	^{19}F chemical shifts, ppm[a,b] δF^A	δF^B	δF^C	F–F coupling constants, Hz $J(F^AF^B)$	$J(F^BF^C)$	$J(F^AF^C)$
cis-$PhSF_4Cl$	A_2BC	99.6 (130.4)	164.3 (152.6)	65.8 (68.8)	164.2	81.4	149.1
cis-*p*-$MeC_6H_4SF_4Cl$	A_2BC	100.2 (131.0)	165.4 (153.5)	66.5 (69.4)	165.5	81.2	149.8
cis-*p*-$O_2NC_6H_4SF_4Cl$	A_2BC	100.6 (130.5)	159.5 (148.8)	66.7 (68.9)	163.3	84.9	153.6
trans-$PhSF_4Cl$	A_4	136.8 (130.4)					
trans-*p*-$MeC_6H_4SF_4Cl$	A_4	139.1 (131.0)					
trans-*p*-$O_2NC_6H_4SF_4Cl$	A_4	135.1 (130.5)					
$PhSF_5$	A_4B	62.1	84.3				
p-$MeC_6H_4SF_5$	A_4B	62.7	85.2				
p-$O_2NC_6H_4SF_5$	A_4B	62.2	80.8				
cis-$PhTeF_4Cl$[c]	A_2BC	–46.5	–33.7[d]	–24.1[d]	120.1[d]	150.9	120.7[d]
trans-$PhTeF_4Cl$[e]	A_4	–39.4					

[a]For assignment of F^A, F^B, and F^C fluorines in *cis*-$ArSF_4Cl$, see text.
[b]Chemical shifts in parentheses calculated by the method of Dean and Evans (11).
[c]δTe = 46.8 ppm; $J(TeF^A)$ = 2994 Hz; $J(TeF^B)$ = 3024 Hz; $J(TeF^C)$ = 3020 Hz.
[d]Assignment of F^B versus F^C is arbitrary.
[e]δTe = 23.1 ppm; $J(TeF^A)$ = 3281 Hz.

© 1997 NRC Canada

Can. J. Chem. Downloaded from www.nrcresearchpress.com by 91.121.58.235 on 09/08/12
For personal use only.

Table 3. ^{13}C NMR data (ppm) of *cis*- and *trans*-$ArSF_4Cl$ in CD_2Cl_2[a]

Compound	δC1	δC2	δC3	δC4	δCH_3
cis-$PhSF_4Cl$	168.5 (m)	126.0 (m)	129.1	134.3	—
cis-p-$MeC_6H_4SF_4Cl$	167.4 (m)	124.4 (m)	129.1	142.6	20.8
cis-p-$O_2NC_6H_4SF_4Cl$	170.3 (m)	125.9 (m)	124.4	148.9	—
trans-$PhSF_4Cl$	155.4 (q, 17.5 Hz)	125.9 (q, 4.7 Hz)	129.1	132.1	—
trans-p-$MeC_6H_4SF_4Cl$	153.3 (q, 17.7 Hz)	125.8 (q, 4.7 Hz)	129.2	143.0	21.1
trans-p-$O_2NC_6H_4SF_4Cl$	159.2 (q, 20.1 Hz)	127.9 (q, 4.8 Hz)	124.3	149.4	—

[a]m = multiplet, q = quintet.

Table 4. ^{19}F NMR chemical shifts (ppm) of *trans*-$ArSF_4Cl$, and chlorine $^{37}Cl/^{35}Cl$ and sulfur $^{34}S/^{32}S$ isotope effects.[a,b]

Compound	$\delta^{19}F$	$^2\Delta F(^{37}Cl/^{35}Cl)$	$^1\Delta F(^{34}S/^{32}S)$	$^3J(F, H_o)$
trans-$PhSF_4Cl$	136.85(2)	−2.09(6) Hz[c]	−16.7(2) Hz[c]	Decoupled
		−7.4(2) ppb	−59.1(7) ppb	
trans-p-$MeC_6H_4SF_4Cl$	139.13(3)	−1.96(9) Hz[c]		Decoupled
		−6.9(3) ppb	Not resolved	
trans-p-$O_2NC_6H_4SF_4Cl$	135.21(1)	−2.04(3) Hz[c]	−16.7(1) Hz[c]	0.89(2) Hz
		−7.2(1) ppb	−59.1(4) ppb	

[a]Numbers in parentheses are the uncertainty in the last digit.

[b]A negative sign implies increased shielding as a result of substitution with the heavier isotope, i.e., $^2\Delta^{19}F(^{37}Cl/^{35}Cl) = \delta^{19}F(^{37}Cl) - \delta^{19}F(^{35}Cl)$.

[c]At 282.4 MHz.

$ArSF_4^{\bullet}$ with an $F^{\bullet}$ donor leads to $ArSF_5$. A competition thus exists for radical $ArSF_4^{\bullet}$, and the yield of $ArSF_5$ should increase as the concentration of $Cl^{\bullet}$ donors decreases, which is consistent with our experimental results (Table 1, entry 7). However, the overall synthesis of $ArSF_5$ still requires a catalytic amount of Cl^- because of the role of Cl^- in the production of F^-, $ArSF_4^-$, and $ArSF_4^{\bullet}$, according to eqs. [3] and [4].

Fluoride-catalyzed oxidation of sulfur(IV) compounds in eq. [4] thus follows the sequence: 10-S-4 → 12-S-5 → 11-S-5 → 12–S-6. If the same sequence is adopted by the F^--catalyzed oxidation of SF_4, then the following pathway is predicted: $SF_4 \rightarrow SF_5^- \rightarrow SF_5^{\bullet} \rightarrow SF_6$. In the absence of F^- (and SF_5^-), the mechanism of oxidation is presumably simplified to $SF_4 \rightarrow SF_5^{\bullet} \rightarrow SF_6$, and the latter sequence of 10-S-4 → 11-S-5 → 12-S-6 is proposed in eq. [5] for the stereospecific synthesis of *cis*-$ArSF_4Cl$.

It is postulated in eqs. [6] and [7] that oxidizing agents such as XeF_2 and Cl_2 interact with radicals $ArSF_4^{\bullet}$ and $ArSF_3Cl^{\bullet}$, with bond cleavage occurring via bridged [S--F--Xe]$^{\bullet}$ and [S--Cl--Cl]$^{\bullet}$ intermediates. Bridged bonds are expected to be very weak, and the role of F^- in the formation of these weak bonds provides an explanation for the catalytic role of F^- in oxidative addition reactions. In the absence of F^-, the oxidizing agents XeF_2 or Cl_2 would have to function as sources of free radicals, and that would require the cleavage of bonds in the oxidizing agents themselves, perhaps under more drastic conditions of heat, or photochemically. Indeed, free-radical reactions with oxidizing agents such as $FO_2SO\text{-}OSO_2F$ or $F_5SO\text{-}OSF_5$ generally require elevated temperatures (18).

Scheme 1 is necessarily vague in several respects. Oxidation of ArSSAr is not discussed, instead we assume that $ArSF_3$ is a common sulfur(IV) intermediate in all reactions. Our experimental results do not allow us to identify the electron acceptor that converts $ArSF_4^-$ to $ArSF_4^{\bullet}$, eq. [4]. However, anion-to-radical oxidations are known for related fluorinated species, e.g., $PhSiF_5^{2-}$ to $PhSiF_5^{-\bullet}$, and numerous one-electron acceptors can be used for this oxidation, including halogen compounds, tetracyanoethylene, metal ions, etc. (19). It is also not possible to identify with certainty the halogen donors in Scheme 1. While Cl_2, $Cl^{\bullet}$, XeF_2, and $XeF^{\bullet}$ are sources of halogen atoms, it is likely that $ArSF_4^{\bullet}$, $ArSF_3Cl^{\bullet}$, and other intermediates can also function as halogen donors. An evaluation of the relative importance of various halogen donors is not possible, and specific halogen donors are not identified in eqs. [4] and [5]. We do not attempt to explain why Cl^- and excess XeF_2 favour the slow isomerization of *trans*-$ArSF_4Cl$ to *cis*-$ArSF_4Cl$, although it may be noted that Michalak and Martin (8) reported previously that the stereochemical outcome of oxidative fluorination depends on the ratio of oxidizing agent, with $\frac{2}{3}$ mol of BrF_3 favouring the synthesis of *trans*-$F_2S[OC(CF_3)_2C_6H_4]_2$, whereas more than $\frac{2}{3}$ mol of BrF_3 favours the *cis* isomer.

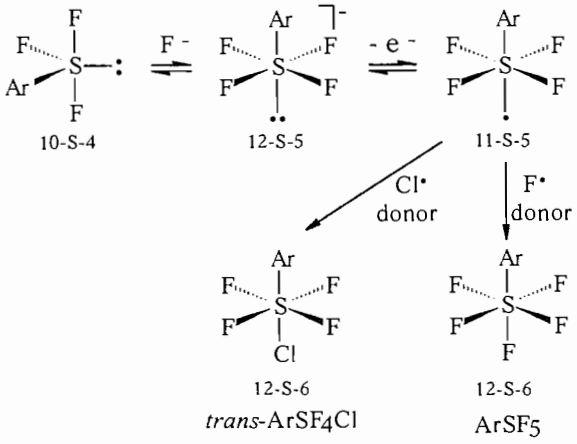
Ab initio calculations

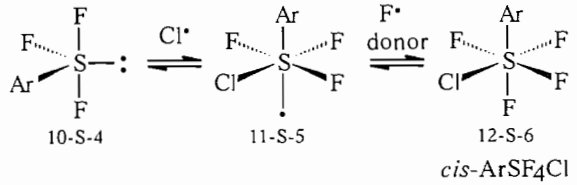
The mechanism of Scheme 1 assumes that only F^- forms an anionic intermediate $ArSF_4^-$, but not Cl^-, whereas both fluoro and chloro radical intermediates are postulated, i.e., $ArSF_4^{\bullet}$ and $ArSF_3Cl^{\bullet}$. A difference between the catalytic role of

© 1997 NRC Canada

Scheme 1. Proposed mechanism of formation of *cis*- and *trans*-$ArSF_4Cl$ and $ArSF_5$.

[3] $XeF_2 + 2\,Cl^- \longrightarrow 2\,Cl^{\bullet}\,(\rightleftharpoons Cl_2) + 2\,F^- + Xe$

[4] 

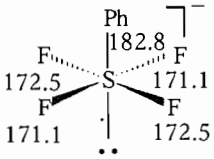
[5] 

[6] $ArSF_3X^{\bullet} \underset{11\text{-}S\text{-}5}{\overset{XeF_2}{\rightleftharpoons}} ArSF_3X\text{--}F\text{--}XeF^{\bullet} \overset{-\,XeF^{\bullet}}{\rightleftharpoons} \underset{12\text{-}S\text{-}6}{ArSF_4X}$ X = F, Cl

[7] $ArSF_4^{\bullet} \underset{11\text{-}S\text{-}5}{\overset{Cl_2}{\rightleftharpoons}} ArSF_4\text{--}Cl\text{--}Cl^{\bullet} \overset{-\,Cl^{\bullet}}{\rightleftharpoons} \underset{12\text{-}S\text{-}6}{ArSF_4Cl}$

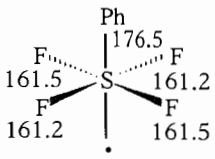
F^- and Cl^- was discussed previously and attributed, based on ab initio calculations of optimized geometries, to the reduced stability and lower concentration of chloro anions in solution (7). Experimental support for this view is based on ion–molecule reactions, which show that SF_4 readily abstracts a fluoride ion to produce SF_5^-, but SF_4Cl^- is formed much more slowly, and SF_4Br^- is not observed (20). Calculations based on density functional theory show a relatively long S—Cl bond in SF_4Cl^-, 223–241 pm, but a shorter S—Cl bond in radical $SF_4Cl^{\bullet}$, 207–219 pm (21). Calculations also reveal a shorter S—F bond length in radical $SF_5^{\bullet}$, 156.2 pm, than in anion SF_5^-, 163.3 pm (22).

Ab initio calculations were carried out for species **1–4**. Of these, **1**, **2**, **4** are postulated intermediates in Scheme 1, but not chloro anion **3**. The calculated (3-21G*) structure of chloro anion **3** shows a very long S--Cl bond of 313.8 pm, which approaches the sum of the van der Waals radii of 350–370 pm (23), implying that $PhSF_3Cl^-$ is probably unimportant in oxidation reactions because of its short lifetime and low concentration. On the other hand, fluoro anion **1** shows four approximately equal S—F bonds in the range 171.1–172.5 pm.



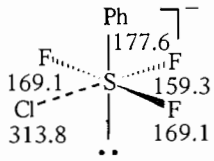
∠CSF = 84.5-87.8°

1 (3-21G*)



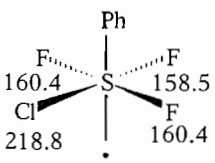
∠CSF = 94.3-94.4°

2 (3-21G*)



∠CSF = 88.8, 89.5, 100.5°
∠CSCl = 84.9°

3 (3-21G*)



∠CSF = 91.9, 91.9, 95.7°
∠CSCl = 99.7°

4 (STO-3G*)

All S—F bonds in fluoro radical **2**, 161.2–161.5 pm, are shorter than those of anion **1**, in fact, the bonds in **2** approach those of SF_4, 154–165 pm (24), and SF_6, 156.22 pm (25). The S—Cl bond in radical **4** is significantly shorter and stronger than in anion **3**, and the S—Cl bond length in **4**, 218.8 pm, is only 6.9% longer than in SF_5Cl, 204.7 pm (26). These calculations thus support the mechanism of Scheme 1, which postulates that fluoro anion $ArSF_4^-$ and fluoro and chloro radicals $PhSF_4^{\bullet}$ and $PhSF_3Cl^{\bullet}$, but not chloro anion $ArSF_3Cl^-$, are intermediates in the oxidation of S(IV) to S(VI) compounds.

It is assumed in Scheme 1 that a *trans* arrangement is adopted by aryl substituents and nonbonded electrons. This assumption is in agreement with ab initio calculations (3-21G*), which show that the energy of **1** is 29.3 kJ/mol lower than that of an isomer of **1** in which fluorine is placed *trans* to a nonbonded electron pair. A similar geometry has been assumed for related anions $CF_3SF_4^-$ and $(CF_3)_2CFSF_4^-$ (27).

cis- and *trans*-$PhTeF_4Cl$, $PhTeF_3Cl_2$, and $PhTeF_5$

The method described above for the synthesis of *cis*- and *trans*-$ArSF_4Cl$ was briefly extended to analogous tellurium compounds. Oxidative halogenation of PhTeTePh was carried out on a ~0.06–0.12 mmol scale in a ptfe bottle in CD_3CN solution, using slightly less XeF_2 than required by the stoichiometry of eq. [8].

[8] $PhTeTePh + 2\,Cl^- + 5\,XeF_2 \xrightarrow[25\ ^{\circ}C]{CD_3CN} 2$ *cis*- and *trans*-$PhTeF_4Cl + 2\,F^- + Xe$

Reaction [8] proceeds rapidly to give a mixture of *cis*- and *trans*-$PhTeF_4Cl$, as confirmed by the ^{19}F and ^{125}Te NMR spectra (Table 2). The ^{19}F NMR spectrum shows an additional peak with an AB_2 spin pattern that we attribute to $PhTeF_3Cl_2$. If an excess of XeF_2 is used in reaction [8], then the dominant product is $PhTeF_5$, a known compound (2).

Experimental

NMR spectra were recorded on a Bruker AM300 spectrometer at 282.4 (^{19}F), 75.47 (^{13}C), and 94.76 (^{125}Te) MHz, with the

© 1997 NRC Canada

Can. J. Chem. Downloaded from www.nrcresearchpress.com by 91.121.58.235 on 09/08/12
For personal use only.

Can. J. Chem. Downloaded from www.nrcresearchpress.com by 91.121.58.235 on 09/08/12
For personal use only.

use of internal C_6F_6 (−162.9 ppm with respect to $CFCl_3$), internal CD_2Cl_2 (53.8 ppm with respect to TMS), internal CD_3CN (1.3 ppm with respect to TMS), and external Ph_2Te (692.3 ppm with respect to Me_2Te) as references. NMR tubes contained ptfe inserts, and samples were prepared in a glove box under a N_2 atmosphere. Yields quoted in Table 1 were measured by ^{19}F NMR integration at several time intervals.

The structures of *cis*-$ArSF_4Cl$, *trans*-$ArSF_4Cl$, and $ArSF_5$ are confirmed by the A_2BC, A_4, and A_4B spin patterns of the ^{19}F NMR spectra, respectively, and by the characteristic ^{13}C NMR spectra of the aromatic substituents. The two equivalent F^A fluorines in *cis*-$ArSF_4Cl$ can be assigned uniquely, but for the assignment of F^B versus F^C the method of Dean and Evans (11) was used. Empirical constants C and T in the linear function $\Delta\delta^{19}F = pC + qT$, where p and q, are respectively, the number of substituents *cis* and *trans* to the fluorine atom, were derived from literature values of the chemical shifts of SF_5Cl (28), and of $ArSF_5$ from this work, relative to SF_6, 57.0 ppm (29). In this way, the following values for C and T were obtained: C = 68.3, T = 6.7 for Cl; C = 5.1, T = 27.3 for Ph; C = 5.7, T = 28.2 for *p*-MeC_6H_4; C = 5.2, T = 23.8 for *p*-$O_2NC_6H_4$. The calculated values of the chemical shifts are given in parentheses in Table 2, and it can be seen that the agreement is good for δF^C, and acceptable for δF^B, thus providing a reasonable basis for the assignment of F^B versus F^C. Agreement with experimental values for δF^A is much poorer, but the assignment of F^A is not in doubt.

The high-resolution ^{19}F NMR spectrum of *trans*-$ArSF_4{}^{35}Cl$ contains an additional peak of approximately one-third intensity that is assigned to *trans*-$ArSF_4{}^{37}Cl$. The chlorine $^{37}Cl/^{35}Cl$ isotope effect on the ^{19}F chemical shift in *trans*-$ArSF_4Cl$ is −6.9 to −7.4 ppb, or −1.96 to −2.09 Hz at 282.4 MHz, a negative sign implying increased shielding for the heavier isotopomer. Although $^{37}Cl/^{35}Cl$ isotope shifts in *cis*-$ArSF_4Cl$ are visible, the isotope peaks were difficult to resolve because of the more complex A_2BC spin pattern. Sulfur $^{34}S/^{32}S$ isotope shifts in *trans*-$ArSF_4Cl$ were also measured (Table 4).

The following compounds were identified by NMR on the basis of literature values: $PhSF_3$ (30), $PhSF_5$ (31), $PhSOF_3$ (32), $PhSO_2F$ (32), and $PhTeF_5$ (2). XeF_2 (Air Products), deuterated solvents (Aldrich), Ph_2S_2 (Aldrich), $(p\text{-}O_2NC_6H_4)_2S_2$ (Aldrich), and Ph_2Te_2 (Aldrich) were used without further purification. $(p\text{-}MeC_6H_4)_2S_2$ was prepared from *p*-MeC_6H_4SH according to the literature method (33). Et_4NCl (Eastman) was recrystallized from dry CH_3CN and stored in a desiccator over P_2O_5.

Ab initio molecular orbital calculations were carried out with the GAUSSIAN 92 program (34).

Preparation of *trans*-$PhSF_4Cl$

Method A

In a typical reaction, solid XeF_2 (30 mg, 0.18 mmol) was added to a mixture of Ph_2S_2 (12.8 mg, 0.059 mmol) in CD_2Cl_2 at 25°C in a ptfe bottle. A small amount of Et_4NCl (2 mg, 0.01 mmol) was added and $PhSF_3$ was formed in almost quantitative yield within 20 min, as determined by ^{19}F NMR examination. To this solution more Et_4NCl (19.5 mg, 0.12 mmol) and XeF_2 (30 mg, 0.18 mmol) were added, and a rapid reaction occurred with vigorous evolution of xenon gas. The colour of the solution changed to deep yellow, but the solution became colourless again after gas evolution ceased. The ^{19}F NMR spectrum of the solution showed that *trans*-$PhSF_4Cl$ was the dominant product; experimental details and yields of products are summarized in Table 1.

Method B

trans-$PhSF_4Cl$ could be made more conveniently in one stage, directly from Ph_2S_2 but without identifying $PhSF_3$. Typically, solid XeF_2 (80 mg, 0.47 mmol) was added to a mixture of Ph_2S_2 (12.8 mg, 0.059 mmol) and Et_4NCl (19.5 mg, 0.12 mmol) in CD_3CN at 25°C in a ptfe bottle. A rapid reaction occurred, with vigorous evolution of xenon gas. The colour of the solution changed to deep yellow, and back to colourless after gas evolution ceased. The reaction was complete within 3 min, and *trans*-$PhSF_4Cl$ was formed in high yield (reactions are summarized in Table 1).

Preparation of *cis*-$PhSF_4Cl$

Method A or method B, as described above, could be used for the synthesis of *cis*-$ArSF_4Cl$, but the amount of XeF_2 was reduced. In a typical reaction, solid XeF_2 (60 mg, 0.35 mmol) was added to Ph_2S_2 (12.8 mg, 0.059 mmol) and Et_4NCl (19.5 mg, 0.12 mmol) in CD_3CN at 25°C in a ptfe bottle. The reaction proceeded as described above and *cis*-$PhSF_4Cl$ was formed in high yield (reaction conditions are summarized in Table 1).

Numerous reactions were carried out in order to optimize the preparation of *cis*-$ArSF_4Cl$ and *trans*-$ArSF_4Cl$, as summarized in Table 1. The ^{19}F and ^{13}C NMR data are given in Tables 2 and 3, and $^{37}Cl/^{35}Cl$ and $^{34}S/^{32}S$ isotope effects on the ^{19}F NMR chemical shifts of *trans*-$ArSF_4Cl$ are given in Table 4.

Reaction of Ph_2S_2 or $PhSF_3$ with XeF_2, but without Cl^-

In typical reactions, solid XeF_2 (50 mg, 0.30 mmol) was added to a solution of Ph_2S_2 (12.8 mg, 0.059 mmol), or to $PhSF_3$ (0.12 mmol), in CD_2Cl_2 or CD_3CN at 25°C in a ptfe bottle. No sulfur(VI) product was found after 1 week, as judged by ^{19}F NMR.

Isomerization of *trans*- to *cis*-$ArSF_4Cl$

Solid XeF_2 (20 mg, 0.12 mmol) and Et_4NCl (15 mg, 0.09 mmol) were added to a solution of *cis*-$PhSF_4Cl$ (20 mg, 0.09 mmol) in CD_2Cl_2. A rapid reaction occurred between XeF_2 and Et_4NCl, with vigorous evolution of xenon gas, but no *cis*-$ArSF_4Cl$ was converted into *trans*-$ArSF_4Cl$.

Solid XeF_2 (5 mg, 0.03 mmol) and Et_4NCl (20 mg, 0.12 mmol) were added to a solution of *trans*-$PhSF_4Cl$ (20 mg, 0.09 mmol) in CD_2Cl_2. The colour of the solution changed from colourless to faint yellow, and *trans*-$PhSF_4Cl$ was gradually converted to *cis*-$PhSF_4Cl$ over a period of several weeks. Some reduction of *cis*-$ArSF_4Cl$ to $ArSF_3$ was observed in solution after 1 month.

Reaction of BF_3 with *cis*- and *trans*-$ArSF_4Cl$

Excess BF_3 was bubbled into a mixture of *cis*- and *trans*-$ArSF_4Cl$ in CD_2Cl_2 at 25°C. All $ArSF_4Cl$ gradually disappeared and the product $PhSF_5$ was identified by ^{19}F NMR.

Preparation of *cis*- and *trans*-$PhTeF_4Cl$

Ph_2Te_2 (24 mg, 0.059 mmol) was partially dissolved in

© 1997 NRC Canada

CD_3CN (0.3 mL) in a ptfe bottle. Solid XeF_2 (20 mg, 0.12 mmol) was added slowly, and Ph_2Te_2 dissolved gradually as xenon gas evolved, but the reddish-orange colour remained. Et_4NCl (19.5 mg, 0.12 mmol) was added to this mixture, and more XeF_2 (20 mg, 0.12 mmol) was added. Gas evolution ceased within 5 min and the colour of the solution became fainter. The presence of both *cis*- and *trans*-$PhTeF_4Cl$ was confirmed by ^{19}F and ^{125}Te NMR (Table 2).

Acknowledgements

We thank the University of Manitoba for a graduate fellowship award (to X.O.). Dr. R.G. Syvret (Air Products, Allentown, Pa.) is thanked for a sample of XeF_2.

References

1. (*a*) J.M. Shreeve. *In* Sulfur in organic and inorganic chemistry. Vol. 4. *Edited by* A. Senning. Marcel Dekker, New York. 1982. Chap. 4; (*b*) D.B. Denny, D.Z. Denny, and Y.F. Hsu. J. Am. Chem. Soc. **95**, 8191 (1973); (*c*) C. Lau and J. Passmore. J. Fluorine Chem. **7**, 261 (1976); (*d*) C. Lau, J. Passmore, E.K. Richardson, T.K. Whidden, and P.S. White. Can. J. Chem. **63**, 2273 (1985); (*e*) H. Baba, K. Kodaira, S. Nagase, and T. Abe. Bull. Chem. Soc. Jpn. **50**, 2809 (1977); (*f*) G. Klein and D. Naumann, J. Fluorine Chem. **30**, 259 (1985); (*g*) H.M. Marsden and J.M. Shreeve. Inorg. Chem. **25**, 4021 (1986).
2. K. Alam and A.F. Janzen. J. Fluorine Chem. **27**, 467 (1985).
3. (*a*) A.F. Janzen and M. Jang. Can. J. Chem. **67**, 71 (1989); (*b*) A.F. Janzen. Coord. Chem. Rev. **130**, 355 (1994).
4. T. Abe and J.M. Shreeve. J. Fluorine Chem. **3**, 187 (1973/74).
5. J.J. Darragh and D.W.A. Sharp. J. Chem. Soc. Chem. Commun. 864 (1969).
6. M. Jang and A.F. Janzen. J. Fluorine Chem. **52**, 45 (1991).
7. X. Ou and A.F. Janzen. Can. J. Chem. **74**, 2002 (1996).
8. R.S. Michalak and J.C. Martin. J. Am. Chem. Soc. **104**, 1683 (1982).
9. (*a*) A.S. Secco, K. Alam, B.J. Blackburn, and A.F. Janzen. Inorg. Chem. **25**, 2125 (1986); (*b*) A.F. Janzen, K. Alam, M. Jang, B.J. Blackburn, and A.S. Secco. Can. J. Chem. **66**, 1308 (1988).
10. T.Q. Nguyen, F. Qu, X. Huang, and A.F. Janzen. Can. J. Chem. **70**, 2089 (1992).
11. P.A.W. Dean and D.F. Evans. J. Chem. Soc. A, 1154 (1968).
12. (*a*) J.A. Gibson and A.F. Janzen. Can. J. Chem. **49**, 2168 (1971); (*b*) K.O. Christe and W.W. Wilson. J. Fluorine Chem. **47**, 117 (1990); (*c*) W.W. Dukat, J.H. Holloway, E.G. Hope, P.J. Townson, and R.L. Powell. J. Fluorine Chem. **62**, 293 (1993).
13. C.W. Perkins, J.C. Martin, A.J. Arduengo, W. Lau, A. Alegria, and J.K. Kochi. J. Am. Chem. Soc. **102**, 7753 (1980).
14. J. Bittner, J. Fuchs, and K. Seppelt. Z. Anorg. Allg. Chem. **557**, 182 (1988).
15. (*a*) J.R. Morton and K.F. Preston. Chem. Phys. Lett. **18**, 98 (1973); (*b*) J. Gawlowski and J.A. Herman. Can. J. Chem. **52**, 3631 (1974); (*c*) R.A. De Marco and J.M. Shreeve. Adv. Inorg. Chem. Radiochem. **16**, 109 (1974); (*d*) J.R. Morton and K.F. Preston. J. Chem. Phys. **58**, 2657 (1973); (*e*) W.B. Gara, B.P. Roberts, C.M. Kirk, B.C. Gilbert, and R.O.C. Norman. J. Magn. Reson. **27**, 509 (1977).
16. T. Meier and R. Mews. Angew. Chem. Int. Ed. Engl. **24**, 344 (1985).
17. X. Ou and A.F. Janzen. Inorg. Chem. **36**, 392 (1997).
18. (*a*) C.I. Merrill and G.H. Cady. J. Am. Chem. Soc. **85**, 909 (1963); (*b*) F.B. Dudley and G.H. Cady. J. Am. Chem. Soc. **85**, 3375 (1963).
19. K. Tamao, J. Yoshida, H. Yamamoto, T. Kakui, H. Matsumoto, M. Takahashi, A. Kurita, M. Murata, and M. Kumada. Organometallics, **1**, 355 (1982).
20. L.M. Babcock and G.E. Streit. J. Chem. Phys. **75**, 3864 (1981).
21. G.L. Gutsev and T. Ziegler. Inorg. Chem. **31**, 1909 (1992).
22. T. Ziegler and G.L. Gutsev. J. Chem. Phys. **96**, 7623 (1992).
23. J.E. Huheey, E.A. Keiter, and R.L. Keiter. Inorganic chemistry, principles of structure and reactivity. 4th ed. Harper Collins, New York. 1993. p. 292.
24. (*a*) F.A. Cotton and G. Wilkinson. Advanced inorganic chemistry. 5th ed., John Wiley and Sons, New York. 1988. p. 509; (*b*) W.M. Tolles and W.D. Gwinn. J. Chem. Phys. **36**, 1119 (1962); (*c*) K. Kimura and S.H. Bauer. J. Chem. Phys. **39**, 3172 (1963).
25. B.R. Miller and M. Fink. J. Chem. Phys. **75**, 5326 (1981).
26. C.J. Marsden and L.S. Bartell. Inorg. Chem. **15**, 3004 (1976).
27. (*a*) R. Minkwitz and A. Werner. J. Fluorine Chem. **37**, 397 (1987); (*b*) W. Heilemann, R. Mews, S. Pohl, and W. Saak. Chem. Ber. **122**, 427 (1989).
28. C.I. Merrill, S.M. Williamson, G.H. Cady, and D.F. Eggers. Inorg. Chem. **1**, 215 (1962).
29. M.G. Marlow, R.R. Dean, and J. Lee. Trans. Faraday Soc. **65**, 321 (1969).
30. R.W. Braun, A.H. Cowley, M.C. Cushner, and R.J. Lagow. Inorg. Chem. **17**, 1679 (1978).
31. D.R. Eaton and W.A. Sheppard. J. Am. Chem. Soc. **85**, 1310 (1963).
32. I. Ruppert. Chem. Ber. **113**, 1047 (1980).
33. J. Drabowicz and M. Mikolajczyk. Synthesis, 32 (1980).
34. M.J. Frisch, G.W. Trucks, M. Head-Gordon, P.M.W. Gill, M.W. Wong, J.B. Foresman, B.G. Johnson, H.B. Schlegel, M.A. Robb, E.S. Replogle, R. Gomperts, J.L. Andres, K. Raghavachari, J.S. Binkley, C. Gonzalez, R.L. Martin, D.J. Fox, D.J. Defrees, J. Baker, J.J.P. Stewart, and J.A. Pople. Gaussian 92, Revision C. Gaussian, Inc., Pittsburgh, Pa. 1992.

Can. J. Chem. Downloaded from www.nrcresearchpress.com by 91.121.58.235 on 09/08/12
For personal use only.

© 1997 NRC Canada

Courbes de solubilité de sels congruents présentant une branche croissante dans la représentation de Jänecke

Néji Bourguiba, Tahar Jouini et Mohamed Jemal

Résumé : La représentation de Jänecke de la coupe quasi-ternaire K_2SO_4–KH_2PO_4–H_2O du système quaternaire réciproque H^+, K^+, PO_4^{3-}, SO_4^{2-}, H_2O à 75°C et du ternaire limite K_3PO_4–H_3PO_4–H_2O a révélé des courbes de solubilité présentant une allure croissante inhabituelle pour des sels congruents KH_2PO_4 et K_2HPO_4. Ce comportement est a priori surprenant si l'on admet que la teneur en eau joue le même rôle que la température dans un système polytherme. Afin de lever cette «anomalie», l'influence du mode de représentation sur l'allure de la courbe de solubilité a été examinée et un traitement thermodynamique de ce phénomène a été proposé.

Mots clés : courbe de solubilité, représentation de Jänecke, allure anormale, traitement thermodynamique, phosphates de potassium.

Abstract: The solubility curves at 75°C, represented in Jänecke's mode, of the quasi-ternary section K_2SO_4–KH_2PO_4–H_2O and the limiting ternary system K_3PO_4–H_3PO_4–H_2O of the reciprocal quaternary system H^+, K^+, PO_4^{3-}, SO_4^{2-}, H_2O reveal an unusual increasing shape for the congruent salts KH_2PO_4 and K_2HPO_4. This shape is surprising when one considers the similarities that exist between the role of water content and that of temperature in polytherm systems. The effect of the representation mode on the shape of the solubility curves has been studied in order to explain this unusual behaviour. A thermodynamic treatment of this phenomenon is also proposed.

Key words: solubility curve, Jänecke's mode, abnormal shape, thermodynamic treatment, potassium phosphates.

Can. J. Chem. Downloaded from www.nrcresearchpress.com by 91.121.58.235 on 09/08/12
For personal use only.

Introduction

Dans des travaux antérieurs effectués par deux d'entre nous (N.B. et T.J.) sur le système quaternaire réciproque H_3PO_4–K_2SO_4–H_2SO_4–K_3PO_4–H_2O à 75°C, la représentation de Jänecke de la coupe quasi-ternaire K_2SO_4–KH_2PO_4–H_2O (1) et du système ternaire limite K_3PO_4–H_3PO_4–H_2O (2) a révélé des courbes de solubilité présentant une allure croissante inhabituelle pour les sels congruents KH_2PO_4 et K_2HPO_4.

Ce résultat a été, en un premier temps, signalé par un referee comme étant une erreur. En effet, ce comportement paraît a priori anormal dans la mesure où l'on considère communément que la variable intensive «teneur en eau» joue le même rôle que la température dans un système polytherme. Dans ces conditions un composé à solubilité congruente devrait correspondre à un maximum de la courbe de solubilité. Nous l'avons, en réponse au referee, en partie justifié dans le cas de KH_2PO_4 (1). Ce travail est consacré à une étude plus générale de cette question.

Une recherche bibliographique nous a permis de relever deux exemples utilisant également la représentation de Jänecke, où les courbes de solubilité des sels congruents $Na_2Cu(SO_4)_2 \cdot 2H_2O$ (3) et $K_2HPO_4 \cdot 3H_2O$ (4) manifestent le même phénomène.

L'influence du mode de représentation sur l'allure de la courbe de solubilité est examinée et un traitement thermodynamique de ce phénomène est proposé.

Reçu le 20 mai 1997.

N. Bourguiba, T. Jouini[1] et M. Jemal. Département de chimie, Faculté des sciences de Tunis, Campus Universitaire, 1060 Tunis, Tunisie.

1. Auteur à qui adresser toute correspondence. Téléphone : 872 600 poste 220. Fax : 216 1 885 008. E-mail : sonia.zghal@cck.rnrt.tn

I. Influence du mode de représentation sur l'allure de la courbe de solubilité

I.1. Coupe quasi-ternaire K_2SO_4–KH_2PO_4–H_2O à 75°C

Dans cette section (Fig. 1*a*) on observe en particulier que la courbe de solubilité de KH_2PO_4 (Z en fonction du complément de X soit ($U = 100 - X$)) est croissante du point **c** vers **b**.

Les coordonnées de Jänecke définies précédemment (1, 2) s'écrivent dans le cas de liquides dont les points représentatifs appartiennent à la courbe **cb** comme suit : $X = 3 \times 10^2\ n{PO_4}^{3-} / N$; $Z = 10^2\ n{H_2O}/N$ avec $N = n{H^+} + n{K^+} = 2\ n{SO_4}^{2-} + 3\ n{PO_4}^{3-}$.

La concentration en ions H^+ est négligeable. Celle des ions PO_4^{3-} l'est aussi à cette valeur du pH (≃5). De ce fait, les espèces ioniques prépondérantes sont K^+ et $H_2PO_4^-$ (5) provenant de la dissolution de KH_2PO_4 :

$$KH_2PO_4(\text{solide}) \leftrightarrows (K^+)_{aq} + (H_2PO_4^-)_{aq}$$

En définissant pour cette isoplèthe de nouvelles coordonnées faisant intervenir les espèces présentes réellement en quantités non négligeables, on obtient : $X' = 10^2\ n{H_2PO_4}^-/N'$; $Z' = 10^2\ n{H_2O}/N'$ avec $N' = n{K^+} = 2\ n{SO_4}^{2-} + n{H_2PO_4}^-$.

© 1997 NRC Canada

Can. J. Chem. Downloaded from www.nrcresearchpress.com by 91.121.58.235 on 09/08/12
For personal use only.

Fig. 1. (*A*) Coupe quasi-ternaire K_2SO_4–KH_2PO_4–H_2O à 75°C (coordonnées de Jänecke). ○—○—○— Courbe (*Z*, *X*) (d'après réf. 1); ■—■—■— courbe (*Z*′, *X*′). (*B*) Coupe quasi-ternaire K_2SO_4–KH_2PO_4–H_2O à 75°C (composition pondérale).

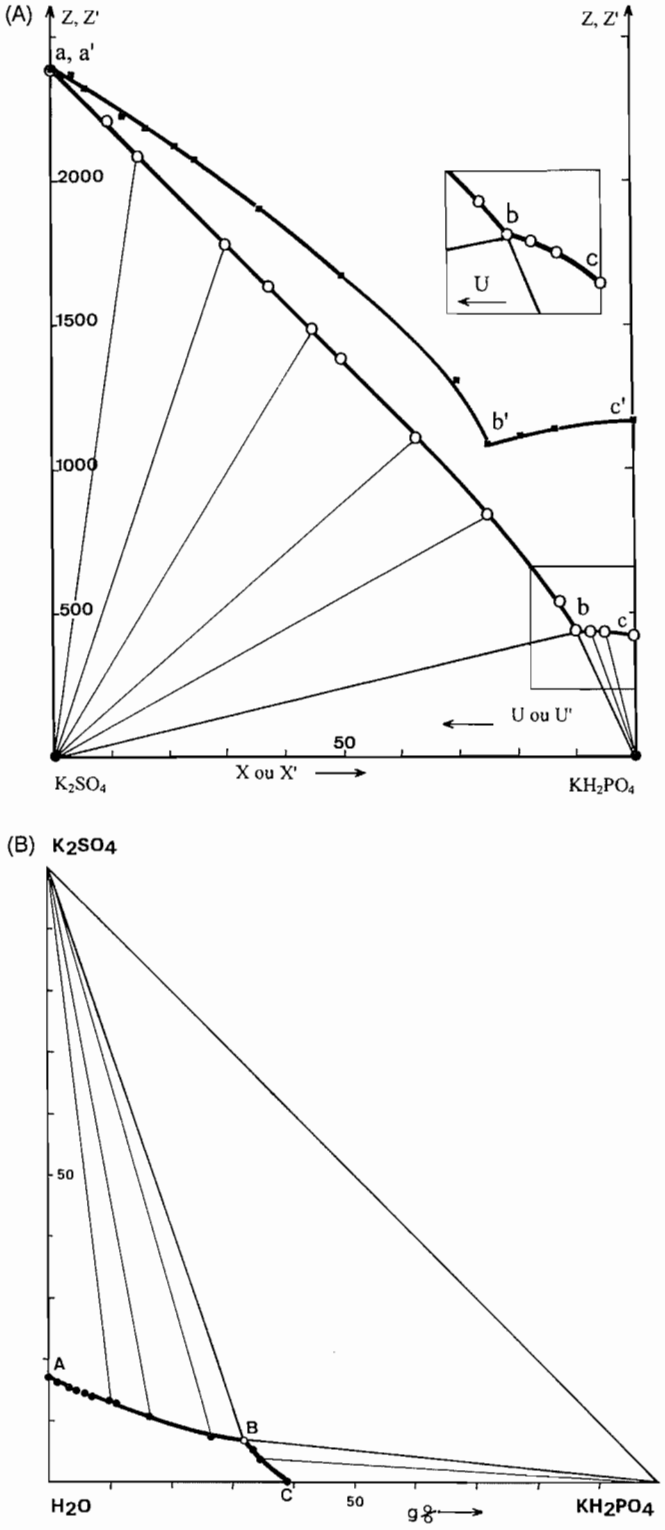
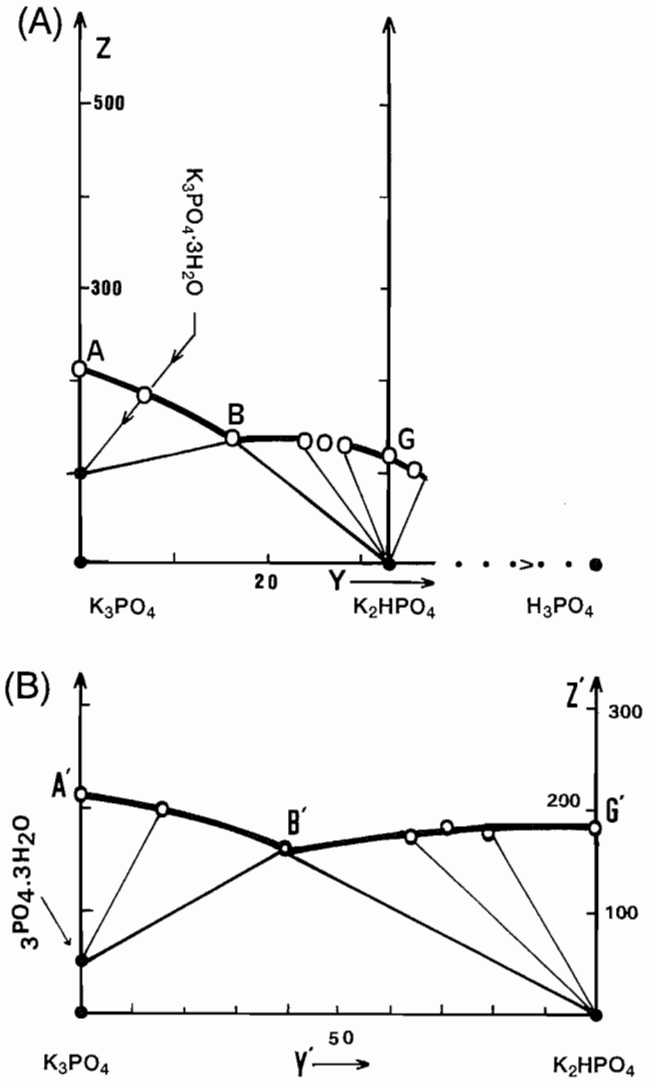


Fig. 2. (*A*) Système ternaire limite K_3PO_4–H_3PO_4–H_2O à 75°C. Courbe (*Z*, *Y*) (d'après réf. 2). (*B*) Système ternaire limite K_3PO_4–H_3PO_4–H_2O à 75°C. Courbe (*Z*′, *Y*′).



Un calcul utilisant ces dernières définitions a été effectué. Les résultats présentés à la figure 1*a* révèlent cette fois que la courbe *Z*′ en fonction de *U*′(= 100 − *X*′) est décroissante du point **c**′ vers **b**′, comme attendu. Cependant pour une raison d'homogénéité de représentation nous devons garder les mêmes définitions de *X* et *Z* dans tout le quaternaire.

Notons également que la représentation classique en triangle rectangle utilisant les coordonnées pondérales conduit à un diagramme où la courbe de solubilité de KH_2PO_4 présente une allure normale (Fig. 1*b*).

Ainsi l'allure croissante de la courbe (**cb**) de solubilité de KH_2PO_4 représentée dans le mode de Jänecke (Fig. 1*a*) est due à la définition du nombre d'équivalents ioniques *N* et donc de la cote *Z*.

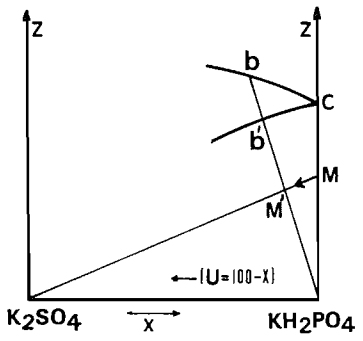
I.2. Système ternaire limite K_3PO_4–H_3PO_4–H_2O à 75°C

Dans la région basique de ce ternaire (Fig. 2*a*) on constate que le composé à solubilité congruente K_2HPO_4 ne correspond pas

© 1997 NRC Canada

Can. J. Chem. Downloaded from www.nrcresearchpress.com by 91.121.58.235 on 09/08/12
For personal use only.

Fig. 3.



à un maximum de la courbe de solubilité, la portion de cette dernière (**GB**) étant croissante du point **G** vers **B**.

Nous rappelons que les coordonnées de Jänecke s'écrivent dans le cas de solutions dont les points représentatifs appartiennent à la portion de courbe **GB** : $Y = 10^2\ n\mathrm{H}^+/N$; $Z = 10^2\ n\mathrm{H_2O}/N$ avec $N = n\mathrm{H}^+ + n\mathrm{K}^+ = 3\ n\mathrm{PO_4}^{3-}$.

Comme ces solutions sont basiques (pH $\geq$ 8,75), la concentration des ions H^+ est négligeable. Les entités prédominantes dans ce domaine de pH sont en fait K^+, PO_4^{3-} et HPO_4^{2-} (5). Dans ces conditions, il convient de définir pour le sous-système ternaire K_3PO_4–K_2HPO_4–H_2O, de nouvelles coordonnées faisant intervenir les entités mises en évidence ci-dessus : $Y' = 2 \times 10^2\ n\mathrm{HPO_4}^{2-}/N'$; $Z' = 10^2\ n\mathrm{H_2O}/N'$ avec $N' = n\mathrm{K}^+ = 3\ n\mathrm{PO_4}^{3-} + 2n\mathrm{HPO_4}^{2-}$.

Un calcul utilisant ces nouvelles définitions a été effectué. Les résultats représentés la figure 2*b* montrent, dans ce cas aussi, que la courbe Z' en fonction de U' (= 100 − Y') est décroissante du point **G'** vers **B'** (Fig. 2*b*). Signalons également que K_2HPO_4 est un extremum du diagramme K_3PO_4–H_3PO_4–H_2O tracé en utilisant les coordonnées pondérales (2). La portion de courbe (**GB**) y est bien décroissante du point **G** vers **B**. Ainsi on confirme que l'allure croissante de la courbe (**GB**) de solubilité de K_2HPO_4 représentée dans le mode de Jänecke (Fig. 2*a*) est bien due à la définition de la cote *Z*.

II. Traitement thermodynamique

II.1. Courbe de solubilité de KH_2PO_4

En se situant à l'extrémité droite du diagramme, l'allure d'un liquidus est déterminée, dans le cadre de la représentation de Jänecke, par le signe de la dérivée de la cote *Z* par rapport à *U*, complément de *X* ($U = 100 - X$). On peut établir l'expression de cette dérivée dans le cas de solutions idéales et réelles.

II.1.1. Cas de solutions idéales

Partant d'un mélange M où coexistent KH_2PO_4(sd) et la solution saturée représentée par le point **c** (Fig. 3), l'addition de *n* moles de K_2SO_4 à un litre de cette solution provoque le déplacement du point représentatif de ce mélange de M à M' et le point représentatif de la solution résultante de **c** vers **b**, ou vers **b'**.

L'équation de dissociation de KH_2PO_4 s'écrit :

$$\mathrm{KH_2PO_4(solide)} \leftrightarrows (\mathrm{K}^+)_{aq} + (\mathrm{H_2PO_4}^-)_{aq}$$

En présence de K_2SO_4, la concentration des différentes entités ioniques à l'équilibre sera : $[K^+] = 2n + S$ et $[H_2PO_4^-] = S$ où *S* est la solubilité de KH_2PO_4.

La condition d'équilibre se traduit par l'expression du produit de solubilité P_S de ce sel :

$$[1] \quad P_S = [\mathrm{K}^+][\mathrm{H_2PO_4}^-] = (S + 2n)S$$

Les coordonnées de Jänecke définies avec $N = n\mathrm{H}^+ + n\mathrm{K}^+ = 2n\mathrm{SO_4}^{2-} + 3\ n\mathrm{PO_4}^{3-}$ s'écrivent pour la solution saturée :

$$[2] \quad X = 3 \times 10^2\ S/(3S + 2n)$$

$$[3] \quad Z = 10^2\ n\mathrm{H_2O}/(3S + 2n)$$

L'allure de la courbe de solubilité (**cb**) dépendra du signe de dZ/dU avec $U = 100 - X = 200n/(3S + 2n)$.

En posant :

$$[4] \quad dZ/dU = (dZ/dn)(dn/dU)$$

La dérivée de *Z* par rapport à *n* donne :

$$[5] \quad dZ/dn = -10^2\ n\mathrm{H_2O}\ (2 + 3\ dS/dn)/(3S + 2n)^2$$

À température constante le produit de solubilité P_S est constant. Sa différentielle est donc nulle $d(P_S) = 2S\ dS + 2n\ dS + 2S\ dn = 0$, d'où $dS/dn = -S/(S + n)$.

En remplaçant dS/dn par son expression, la relation [5] devient :

$$[6] \quad dZ/dn = -10^2\ n\mathrm{H_2O}(2n - S)/(3S + 2n)^2(S + n)$$

La dérivation de *U* par rapport à *n* donne :

$$[7] \quad dU/dn = 200(3S^2 + 6nS)/(3S + 2n)^2(S + n)$$

En remplaçant, dans la relation [4], dZ/dn et dU/dn par leur expression, on obtient :

$$[8] \quad dZ/dU = -(nZ/U)(2n - S)/(3S^2 + 6nS)$$
$$= -(nZ/U)(2n\text{-}S)/3S(S + 2n)$$

Sachant que $P_S = S\ (S + 2n)$, l'expression [8] peut s'écrire encore :

$$[9] \quad dZ/dU = -\ (nZ/3UP_S)(2n - S)$$

Comme KH_2PO_4 est suffisamment soluble (S = 2,9 moles dans 1000 g de solution saturée (2)), lors de l'addition des premières quantités de K_2SO_4, on a $2n < S$ et l'expression [9] est positive. Ainsi dans l'hypothèse d'un comportement idéal des solutions considérées, on prévoit une courbe de solubilité croissante de **c** vers **b**, dans la représentation de Jänecke.

II.1.2. Cas de solutions réelles

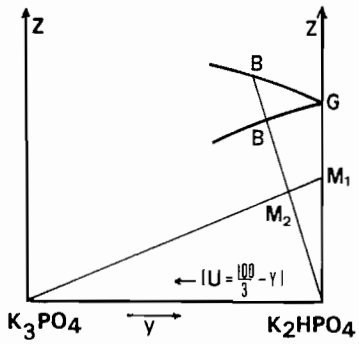
Les calculs relatifs à ces solutions doivent faire intervenir les activités $a_i = \gamma(i)[i]$.

La même démarche suivie pour l'établissement de l'expression de dZ/dU dans le cas de solutions idéales nous conduit, dans ce cas, à l'expression suivante :

$$[10] \quad dZ/dU = -(nZ\gamma_{\pm}^2/3UPs)(2n - S)$$
$$+ (nZ/U\gamma_{\pm}^2)\ (d\gamma_{\pm}/dn)$$

© 1997 NRC Canada

Fig. 4.



L'allure de la courbe de solubilité dépendra du signe de $(d\gamma_{\pm}/dn)$ et de l'importance relative de chacun des termes de la relation [10] par rapport à l'autre. Le terme $(d\gamma_{\pm}/dn)$ varie dans le même sens que $(d\gamma_{\pm}/dI)$, I étant la force ionique du milieu. Or le signe de $(d\gamma_{\pm}/dI)$ dépend de la force ionique I de la solution (6, 7). Il en résulte que l'allure de la courbe de solubilité ne peut être prévue à l'avance. Elle sera croissante où décroissante selon le signe de l'expression [10]. Ainsi dans le cas considéré (courbe **cb** Fig. 1*a*), l'allure croissante du point **c** vers **b** n'est pas contradictoire avec la théorie.

On peut constater qu'en maintenant le coefficient d'activité moyen égal à l'unité, l'expression [10] se ramène à celle précédemment établie pour les solutions idéales.

II.2. Courbe de solubilité de K_2HPO_4

Comme précédemment, l'allure de la courbe de solubilité (**GB**) représentée dans le mode de Jänecke, dépend du signe de la dérivée de la cote Z par rapport à la variable U ($U = (100/3) - Y$).

II.2.1. Cas de solutions idéales

Partant d'un mélange biphasé M_1 où K_2HPO_4 solide est en équilibre avec la solution saturée **G** (Fig. 4), l'addition de n moles de K_3PO_4 à un litre de cette solution provoque le déplacement du point représentatif de ce mélange de M_1 en M_2 et le point représentatif de la solution de **G** vers **B**, ou vers **B′**.

En supposant que K_2HPO_4 est complètement dissocié dans la phase liquide, l'équation de dissociation en présence de K_3PO_4 ajouté s'écrit :

$$K_2HPO_4(\text{solide}) \leftrightarrows 2\,(K^+)_{aq} + (HPO_4^{2-})_{aq}$$

La concentration des différentes entités ioniques à l'équilibre sera : $[K^+] = (3n + 2S)$ et $[HPO_4^{2-}] = S$ où S est la solubilité de K_2HPO_4.

La condition d'équilibre se traduit par :

$$[1'] \quad P_S = [K^+]_{eq}^2[HPO_4^{2-}]_{eq} = (3n + 2S)^2S$$

Les coordonnées de Jänecke définies avec $N = nH^+ + nK^+ = 3nPO_4^{3-}$ s'écrivent pour la solution saturée : $Y = 10^2\, nH^+/N = 10^2\, S/3(S + n)$; $Z = 10^2\, nH_2O/3(S + n)$. La variable U, complément de Y est : $U = (100/3) - Y = 100\, n/3(S + n)$.

La dérivation de Z par rapport à n donne :

$$[2'] \quad dZ/dn = -10^2\, nH_2O(1 + dS/dn)/3(S + n)^2$$

La différentielle de l'expression [1′] permet de tirer :

$$[3'] \quad dS/dn = -2S/(2S + n)$$

On peut aisément établir les expressions :

$$[4'] \quad dU/dn = US(2S + 3n)/n(S + n)(2S + n)$$

et

$$[5'] \quad dZ/dU = -n^2Z/SU(2S + 3\,n)$$

L'expression [5′] peut s'écrire :

$$dZ/dU = -n^2Z(2S + 3n)/UP_S$$

Cette expression montre que la dérivée de Z par rapport à U est toujours négative. Il en résulte que l'hypothèse d'un comportement idéal des solutions ne permet pas d'expliquer l'allure croissante de la courbe (**GB**) de solubilité de K_2HPO_4, représentée dans le mode de Jänecke (Fig. 4). Ce désaccord ne peut s'expliquer que par l'écart des solutions considérées par rapport à l'idéalité. K_2HPO_4 étant très soluble, sa solubilité dans l'eau pure à 75°C est de 72,74 g de sel pour 100 g de solution saturée (2).

II.2.2. Cas de solutions réelles

Dans ce cas, l'expression de dZ/dU devient :

$$dZ/dU = -n^2Z\gamma_{\pm}^3(2S + 3n)/UPs + n^2Z\gamma_{\pm}^2S(2S + 3n)/UP_S\,(d\gamma_{\pm}/dn)$$

Comme précédemment, l'allure de la courbe de solubilité dépendra du signe de $(d\gamma_{\pm}/dn)$ et de l'importance relative de chacun des termes par rapport à l'autre. Ainsi, l'allure croissante de Z en fonction de U n'est pas en désaccord avec la théorie.

III. Conclusion

Les équilibres de dissolution de KH_2PO_4 et de K_2HPO_4 dans les solutions aqueuses :

$$KH_2PO_4(\text{solide}) \leftrightarrows (K^+)_{aq} + (H_2PO_4^-)_{aq}$$

et

$$K_2HPO_4(\text{solide}) \leftrightarrows 2\,(K^+)_{aq} + (HPO_4^{2-})_{aq}$$

doivent, par augmentation de la concentration des ions K^+ et conformement à la loi d'action de masse, se déplacer vers la formation du sel congruent correspondant. Il en résulte que la solubilité de ces sels doit décroître. En revanche les courbes de solubilité correspondantes, tracées en utilisant le mode de représentation de Jänecke, peuvent manifester une allure croissante.

Bibliographie

1. N. Bourguiba et T. Jouini. Can. J. Chem. **72**, 2212 (1994).
2. N. Bourguiba et T. Jouini. Can. J. Chem. **70**, 2197 (1992).

© 1997 NRC Canada

Can. J. Chem. Downloaded from www.nrcresearchpress.com by 91.121.58.235 on 09/08/12
For personal use only.

3. F. Carrilo et J. Said. Douzièmes journées d'études des equilibres entre phases, Bordeaux. Mars 1986. pp. 15–19.
4. R. Lazrak, M. Nadifiyine, B. Tanouti, A. Mokhlisse, J. Guion, R. Tenu, J. Berthet et J.J. Counioux. J. Solid State Chem. **119**, 68 (1995).
5. D.G. Peters, J.M. Hayes et G.M. Hiefje. Chemical separations and measurements. Theory and practice of analytical chemistry. Saunders Golden Sunburst Series, Philadelphia. 1974. pp. 111–112.
6. G.N. Lewis et M. Randall. Thermodynamics. 2e éd. révisé par K.S. Pitzer et L. Brewer. McGraw-Hill, New York. 1961. p. 343.
7. N.A. Gokcen. Thermodynamique. Vol. 3. (Traduction de l'ouvrage Thermodynamics. Copyright 1975 par N.A. Gokcen. ISBN 0-918910-01-3). Publié par le C.I.R.P. (Centre interdépartemental de recherche et de perfectionnement), Paris. 1978. p. 346.

Can. J. Chem. Downloaded from www.nrcresearchpress.com by 91.121.58.235 on 09/08/12
For personal use only.

© 1997 NRC Canada

Excess molar volumes and viscosities of binary mixtures of propylene carbonate with (C_5–C_8) *n*-alkanols at 298.15 K

Mohamed M. El-Banna

Can. J. Chem. Downloaded from www.nrcresearchpress.com by 91.121.58.235 on 09/08/12
For personal use only.

Abstract: Excess molar volumes (V^E) and changes in viscosity ($\Delta\eta$) have been determined for binary liquid mixtures of propylene carbonate (PC) with (C_5–C_8) *n*-alkanols at 298.15 K and atmospheric pressure, over the whole composition range. The positive V^E corresponding to negative $\Delta\eta$, for all the mixtures studied, suggests the presence of specific interactions, namely, involving the intermolecular hydrogen bonds. The results are correlated by means of a Redlich–Kister type equation. The fitting of viscosities to the parameter (N_{12}) of Nissan–Grunberg or to the (H_{12}) parameter of Hind et al. provides models for the dynamic viscosities; the two-parameter (ν_{12} and ν_{12}) McAllister equation and the three parameters (*a*, *b*, and *c*) Heric–Brewer provide models for the kinematic viscosities, allowing us to gain greater knowledge of the interactions between unlike molecules. However, this analysis suggests that the McAllister model fits the data better than the others.

Key words: excess volumes, propylene carbonate, *n*-alkanols, liquid mixtures, hydrogen bonding.

Résumé : Opérant à 298,15 K, à la pression atmosphérique et sur l'ensemble des compositions, on a mesuré les volumes molaires en excès (V^E) et les changements de viscosité ($\Delta\eta$) de mélanges binaires liquides de carbonate de prophylène (CP) avec des *n*-alcanols (C_5–C_8). Pour tous les mélanges étudiés, une valeur positive de V^E correspond à une valeur négative de $\Delta\eta$; cette observation suggère la présence d'interactions spécifiques, à savoir des liaisons hydrogènes intermoléculaires. On a établi une corrélation des résultats à l'aide d'une équation du type Redlich–Kister. L'ajustement des viscosités au paramètre (N_{12}) de Nissan–Grunberg ou au paramètre (H_{12}) de Hind et al. fournit un modèle pour les viscosités dynamiques; par ailleurs, l'équation à deux paramètres (ν_{12} et ν_{12}) de McAllister ainsi que l'équation à trois paramètres (a, b et c) de Heric–Brewer fournit un modèle cinématique des viscosités qui permet d'obtenir une meilleure compréhension entre les molécules qui ne sont pas semblables. Toutefois, cette analyse suggère que le modèle de McAllister conduit à un meilleur ajustement que les autres.

Mots clés : volumes en excès, carbonate de propylène, alcanols, mélanges liquides, liaison hydrogène.

[Traduit par la rédaction]

Introduction

Previous papers (1–4) explained that *n*-alkanols in the pure state are self-associated, forming both open and cyclic aggregates; the probability of the latter increases from smaller alkanols, but in nonpolar solvents is independent of the chain length. Both (4-methyl-1,3-dioxolan-2-one) propylene carbonate (PC) and *n*-alkanols find a wide range of applications as solvents and solubilizing agents in organic synthesis and electrochemical studies (5–7).

In the present study, the excess molar volume (V^E) and the deviation of the viscosity ($\Delta\eta$) of binary mixtures of propylene carbonate + (C_5–C_8) *n*-alkanols have been determined over the entire composition range at 298.15 K and atmospheric pressure. The alkanols considered are 1-pentanol, 1-hexanol, 1-heptanol, and 1-octanol. Mixtures containing the alkanols 1-nonanol and 1-decanol could not be studied because of the partial miscibility of propylene carbonate in these solvents. From these properties, attempts have been made to explain the behaviour of the liquid mixtures. We applied the Nissan–Grunberg (8) and Hind et al. (9) models to dynamic viscosities, and the McAllister (10) and Heric–Brewer (11) models to kinematic viscosities to gain greater knowledge of the specific interaction parameters.

Received May 21, 1997.

M.M. El-Banna.[1] Department of Chemistry, Faculty of Education, El-Shatby, 21526, Alexandria University, Egypt.

[1] Fax: 203-5421 526.

Experimental

The pure liquids were obtained from Aldrich (purity >99.5 mol%). All chemicals were used without further purification, other than storing over molecular sieve to remove any possible traces of moisture.

Density (ρ) measurements of the pure components and binary mixtures, over the complete composition range, were carried out using a Kyoto electronic vibrating tube densimeter (model DA 110) with a temperature sensor keeping the temperature within ±0.005 K. The apparatus was calibrated several times with the well-known density values of deionized doubly-distilled and degassed water, benzene, and dry air at atmospheric pressure.

The mixtures were prepared by syringe, inserting a weighed amount (Mettler A 160 range balance ±0.01 mg) of the pure liquids into stoppered bottles to prevent preferential evaporation. The experimental technique has previously been

© 1997 NRC Canada

Can. J. Chem. Downloaded from www.nrcresearchpress.com by 91.121.58.235 on 09/08/12
For personal use only.

Table 1. Comparison of measured densities (g cm^{-3}) and viscosities (mPa s) of the pure constituents with literature values at 298.15 K.

	ρ/g cm^{-3}		η/mPa s	
Substance	Expt.	Lit. (ref.)	Expt.	Lit. (ref.)
Propylene carbonate	1.199 53	1.199 57 (5)	2.474	2.471 (15)
		1.199 50 (14)		2.480 (16)
		1.199 30 (16)		
1-Pentanol	0.810 81	0.810 84 (6)	3.316	3.318 (6)
		0.810 80 (17)		3.347 (17)
		0.810 30 (18)		3.310 (19)
1-Hexanol	0.815 28	0.815 25 (6)	4.593	4.595 (6)
		0.815 30 (17)		4.920 (17)
		0.815 16 (20)		4.950 (7,21)
1-Heptanol	0.818 85	0.818 87 (6)	4.860	4.836 (6)
		0.818 69 (7,20)		4.970 (7)
		0.818 70 (22)		
		0.818 71 (23)		
1-Octanol	0.822 20	0.822 14 (6)	6.135	6.130 (6)
		0.822 09 (21)		6.125 (17)

described (12). The precision of the densities was ±0.001% g cm^{-3} and of the mole fraction ±0.005 mol%.

Viscosity (η) measurements of both pure components and their mixtures were determined by using an Ubbelohde level viscometer that was calibrated with doubly distilled water and benzene as described previously (13). The accuracy was estimated to be ±0.05%. The density and viscosity values and those from the literature for all the pure compounds are listed in Table 1.

Results and discussion

The experimental data of the densities and viscosities for the (x) PC + (1−x) n-alkanol mixtures at 298.15 K are reported in Table 2. The density values were used to calculate the V^E values from the following equation:

$$[1] \quad V^E / \text{cm}^3\text{mol}^{-1} = x_1 M_1 (\rho_m^{-1} - \rho_1^{-1}) + x_2(\rho_m^{-1} - \rho_2^{-1})$$

where x_i, ρ_i, and M_i are the mole fraction, density, and relative mole mass of the pure components, respectively, with i = 1 for the PC and i = 2 for the n-alkanols, and ρ_m is the mixture at given composition.

The deviations of the viscosity ($\Delta\eta$) were calculated from:

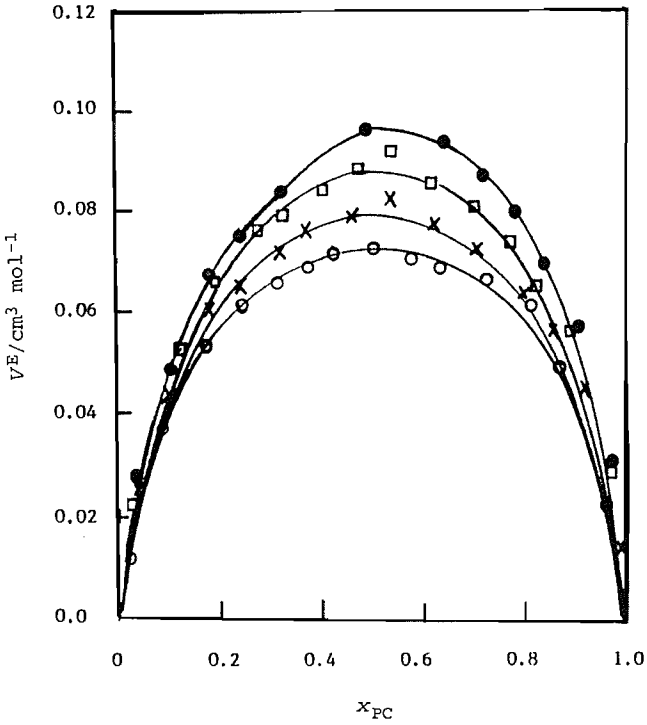
$$[2] \quad \Delta\eta = \eta_m - x_1\eta_1 - x_2\eta_2$$

where η_m, η_1, and η_2 are the viscosities of the mixtures and the pure components, respectively. The V^E and $\Delta\eta$ values are presented in Table 2. Each set of results was fitted with the Redlich–Kister equation (24):

$$[3] \quad X^E - x(1-x)\sum_{j=0}^{n} A_j(2x-1)^j$$

where E^X is V^E or $\Delta\eta$, and A_j are the parameters obtained by a least-squares fitting procedure. In each case the optimum number of coefficients are ascertained from an examination of the variation of the standard error of estimate (σ) with n,

Fig. 1. Excess molar volumes, V^E, of mixtures vs. x_{pc} (○, 1-pentanol; ×, 1-hexanol; □, 1-heptanol; ●, 1-octanol) at 298.15 K.



$$[4] \quad \sigma(F) = [\Sigma\,(X^E_{obs} - X^E_{cal})^2 / (n_{obs} - n)\,]^{0.5}$$

where n_{obs} is the number of measurements. The values of A_j and the standard error estimates associated with the use of eq. [4] are given in Table 3.

In all the mixtures studied the values of V^E are positive over the whole range of composition (Fig. 1). A regular pattern of behaviour for each of the four sets of the binary system is

© 1997 NRC Canada

Can. J. Chem. Downloaded from www.nrcresearchpress.com by 91.121.58.235 on 09/08/12
For personal use only.

Table 2. Experimental density (ρ), absolute viscosity (η), excess molar volume (V^E), and viscosity deviation (Δη) for the binary mixtures of (x) PC + (1–x) (C_5–C_8) n-alkanols at 298.15 K.

x	ρ/g cm^{-3}	Δη/mPa s	V^E/cm^3 mol^{-1}	Δη/mPa s
		(x) PC + (1 – x) 1-pentanol		
0.0218	0.817 39	3.297	0.011	0.0835
0.0861	0.837 22	3.235	0.037	0.0515
0.1654	0.862 58	3.161	0.053	–0.0825
0.2433	0.888 45	3.094	0.061	–0.1495
0.3101	0.911 40	3.029	0.066	–0.2145
0.3740	0.934 04	2.973	0.069	–0.2705
0.4207	0.951 01	2.933	0.072	–0.3105
0.5003	0.980 88	2.865	0.073	–0.3785
0.5691	1.007 67	2.808	0.070	–0.4355
0.6326	1.033 21	2.756	0.069	–0.4875
0.7214	1.070 34	2.685	0.067	–0.5585
0.8072	1.107 90	2.618	0.061	–0.6255
0.8655	1.134 52	2.574	0.049	–0.6695
0.9573	1.178 28	2.505	0.022	–0.7385
		(x) PC + (1 – x) 1-hexanol		
0.0254	0.821 83	4.523	0.020	–0.1209
0.0901	0.839 19	4.346	0.044	–0.0561
0.1722	0.862 40	4.130	0.061	–0.2721
0.2303	0.879 68	3.984	0.065	–0.4181
0.3087	0.904 12	3.796	0.072	–0.6061
0.3846	0.929 13	3.621	0.076	–0.7811
0.4521	0.952 57	3.473	0.079	–0.9291
0.5332	0.982 35	3.303	0.083	–1.0991
0.6124	1.013 39	3.145	0.078	–1.2571
0.7005	1.050 29	2.978	0.073	–1.4241
0.7883	1.089 90	2.821	0.064	–1.5811
0.8455	1.117 36	2.722	0.057	–1.6801
0.9112	1.150 71	2.614	0.046	–1.7881
0.9770	1.186 48	2.509	0.013	–1.8931
		(x) PC + (1 – x) 1-heptanol		
0.0321	0.826 13	4.755	0.024	0.1818
0.1202	0.847 35	4.481	0.053	–0.0922
0.1934	0.866 27	4.281	0.066	–0.3082
0.2735	0.888 95	4.035	0.077	–0.5382
0.3226	0.902 85	3.909	0.079	–0.6642
0.4002	0.927 00	3.709	0.084	–0.8642
0.4717	0.950 88	3.534	0.089	–1.0392
0.5334	0.972 89	3.390	0.092	–1.1832
0.6111	1.002 74	3.217	0.086	–1.3562
0.6990	1.039 61	3.031	0.081	–1.5422
0.7602	1.067 52	2.909	0.074	–1.6642
0.8226	1.098 09	2.789	0.066	–1.7842
0.8925	1.135 17	2.662	0.056	–1.9112
0.9674	1.178 89	2.529	0.029	–2.0442
		(x) PC + (1 – x) 1-octanol		
0.0305	0.828 34	5.992	0.025	0.2198
0.0991	0.842 99	5.607	0.049	–0.1652
0.1708	0.859 40	5.253	0.068	–0.5192
0.2441	0.877 53	4.915	0.075	–0.8572
0.3107	0.895 22	4.627	0.084	–1.1452
0.4055	0.922 75	4.245	0.092	–1.5272

© 1997 NRC Canada

Table 2 (*concluded*).

x	ρ/g cm^{-3}	$\Delta\eta$/mPa s	V^E/cm^3 mol^{-1}	$\Delta\eta$/mPa s
0.4882	0.949 32	3.938	0.097	−1.8342
0.5632	0.975 72	3.679	0.110	−2.0932
0.6277	1.000 72	3.469	0.094	−2.3032
0.7091	1.035 32	3.222	0.088	−2.5502
0.7824	1.069 98	3.015	0.081	−2.7572
0.8415	1.070 10	2.857	0.070	−2.9152
0.9046	1.100 94	2.698	0.058	−3.0742
0.9710	1.179 22	2.540	0.033	−3.2322

Table 3. Coefficients A_j of eq. [3] and the standard error $\sigma(F)$ of the binary mixtures.

Function	A_o	A_1	A_2	A_3	$\sigma(F)$
		(x) PC + (1 − x) 1-pentanol			
V^E	0.2826	−0.0117	0.2501	−0.0036	0.0016
$\Delta\eta$	−1.3620	0.4941	−3.3012	0.7323	0.0115
		(x) PC + (1 − x) 1-hexanol			
V^E	0.3112	−0.0219	0.2775	0.0476	0.0038
$\Delta\eta$	−3.6230	0.8843	−9.4489	0.9436	0.0422
		(x) PC + (1 − x) 1-heptanol			
V^E	0.3446	−0.0054	0.2813	−0.0458	0.0050
$\Delta\eta$	−3.9192	1.1081	−9.5426	1.1023	0.0381
		(x) PC + (1 − x) 1-octanol			
V^E	0.3906	−0.0616	0.1790	0.1571	0.0082
$\Delta\eta$	−6.7160	1.0555	−11.7185	1.3719	0.0640

observed, starting from 1-pentanol to 1-octanol with the maximum V^E value, 0.097 cm^3 mol^{-1} at x = 0.5, and the standard error changes from ±0.0016 to ±0.0082. The equimolar excess volume, V^E (x = 0.5), increases with increasing length of the hydrocarbon chain of the alkanol (from methanol to 1-butanol) (5); in our work, the values of V^E (x = 0.5) show a slight increase in the sequence: 1-octanol>1-heptanol> 1-hexanol>1-pentanol (Fig. 2).

Molar excess volumes of liquid mixtures reflect the result of different contributions arising from the structural changes undergone by the pure cosolvents. It is expected that positive contributions arise from the breakup interactions between the molecules, namely, the rupture of the hydrogen-bonded chains of the alcohols and the loosening of the dipole interactions between propylene carbonate molecules (25, 26), given that PC is a poor proton acceptor and alkanols are relativity poor proton donors (27, 28). Therefore, steric effects and proton-accepting abilities increase as the alkanol chain length increases (29), with a net increase in the positive contributions to V^E. Figure 2 supports such an assumption.

From Fig. 3, the observed negative $\Delta\eta$ values, decrease from 1-pentanol to 1-octanol. The absence of any minima in the intermediate composition gives an indication of the possibility of intermolecular hydrogen bonds between PC and the alcohols. The deviations are negatively defined by the ideal behaviour and additivity of viscosities of the two components (5). Figure 4 shows the plot of $\Delta\eta$ vs. n, the alcohol chain length, at x = 0.5; such $\Delta\eta$ values are negative and their absolute values increase with increasing chain length of the alkanols (7).

Different equations exist in the literature that can calculate viscosity coefficients from the models for the dynamic viscosities, namely:
Nissan–Grunberg (8)

$$[5] \quad \ln \eta_m = x_1 \ln \eta_2 + x_2 \ln \eta_2 + x_1 x_2 N_{12}$$

Hind et al. (9)

$$[6] \quad \eta_m = x_1^2 \eta_1 + x_2^2 \eta_2 + 2 x_1 x_2 H_{12}$$

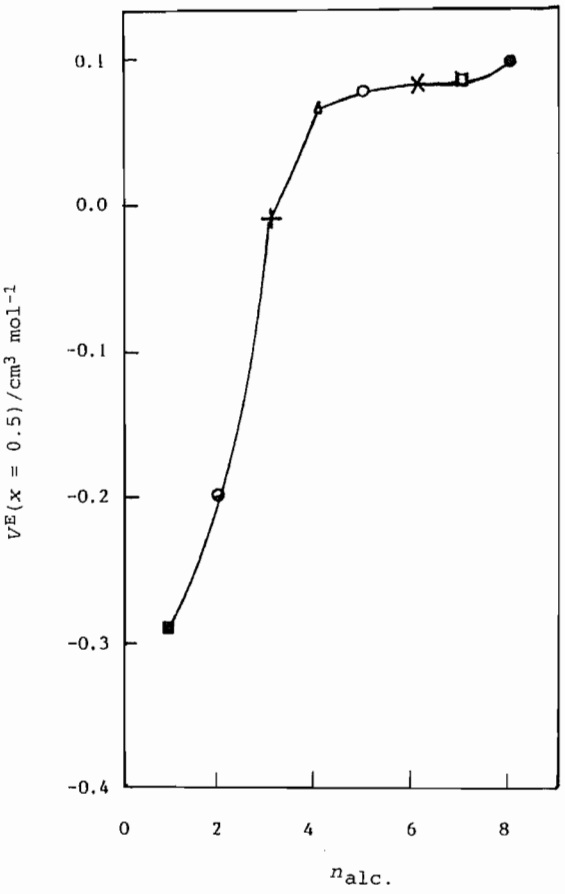
where N_{12} and H_{12} values are the new interaction parameters (viscosity coefficients) and reflect the nonideality of the system. These parameters have usually been regarded as an approximate measure of the strength of the interaction between the components. The N_{12} and H_{12} values are found to be positive for all mixtures and are similar in magnitude; they are summarized in Table 4 together with the percent error. Also, these can be interpreted in a similar way to the V^E values (Fig. 5).

Can. J. Chem. Downloaded from www.nrcresearchpress.com by 91.121.58.235 on 09/08/12
For personal use only.

© 1997 NRC Canada

Can. J. Chem. Downloaded from www.nrcresearchpress.com by 91.121.58.235 on 09/08/12
For personal use only.

Fig. 2. $V^E(x = 0.5)$ vs. n (number of carbon atoms in alkanols molecules) at 298.15 K. (■, methanol; ◒, ethanol; +, 1-propanol; Δ, 1-butanol; from ref. 5); this work, ○, 1-pentanol; ×, 1-hexanol; □, 1-heptanol; ●, 1-octanol.



The McAllister correlation for viscosities of liquid mixtures was fitted to the kinematic viscosities, which consider that interaction occurs between three bodies:

$$\ln \nu = x_1^3 \ln \nu_1 + x_2^3 \ln \nu_2 + x_1^3 \ln M_1 + x_2^3 \ln M_2 - \ln(x_1 M_1 + x_2 M_2) + 3x_1^3 x_2 \ln(2M_1 + M_2/3) + 3x_1 x_2^3 \ln(M_1 + 2M_2/3) + 3x_1^3 x_2 \ln \nu_{12} + 3x_1 x_2^2 \ln \nu_{21} \quad [7]$$

where ν_1, ν_2,and ν refer to the kinematic viscosities (η/ρ) of the pure components 1, 2, and the mixture, respectively. The interaction parameters were determined by a non-linear least-squares analysis. The values of ν_{12} and ν_{21} are presented in Table 4, along with their percent error. In a simplified model the parameter ν_{12} would represent the 1-1-2 or 1-2-1 interactions, whereas ν_{21} accounts for the 1-2-2 or 2-1-2 type of interaction. From an examination of the values of ν_{12} and ν_{21}, it is obvious that the values are of the same order of magnitude but they do differ slightly from each other. The ν_{21} values were always greater than ν_{12} (Fig. 5), the difference increasing with the alcohol chain length.

Heric and Brewer (11) suggested the equation:

Fig. 3. $\Delta\eta$ vs. x_{pc} at 298.15 K for the binary systems (○, 1-pentanol; ×, 1-hexanol; □, 1-heptanol; ●, 1-octanol).

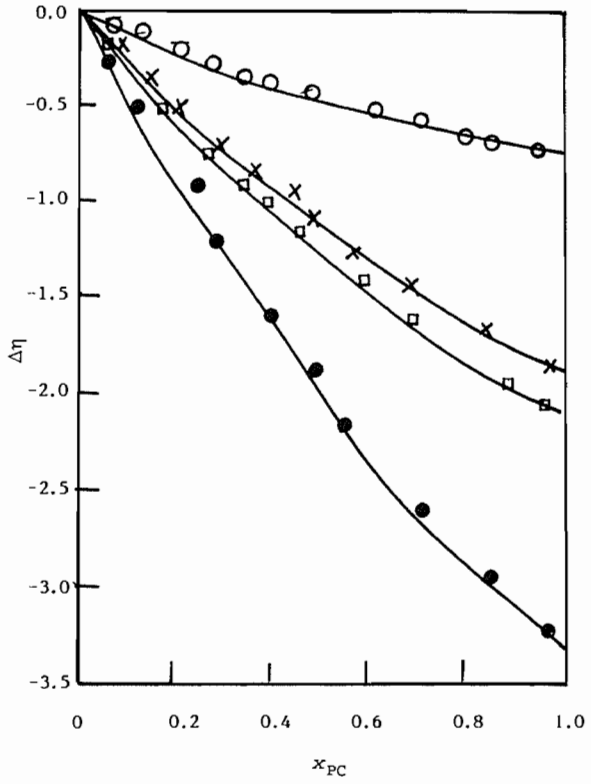
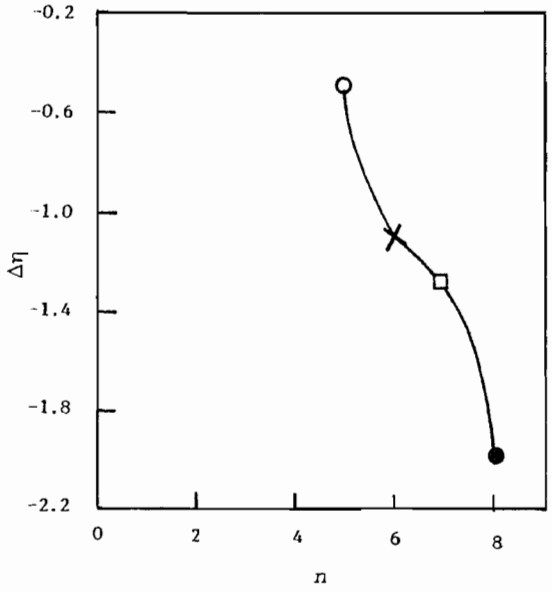


Fig. 4. $\Delta\eta(x = 0.5)$ vs. n (number of carbon atoms in alkanol molecule) at 298.15 K. (○, 1-pentanol; ×, 1-hexanol; □ 1-heptanol; ●, 1-octanol).



$$\nu = x_1\nu_1 + x_2\nu_2 + x_1x_2[a + b(x_1 - x_2) + c(x_1 - x_2)^2] \quad [8]$$

for the kinematic viscosity of binary mixtures. The values of parameters a, b, and c (Table 5) were found to be negative for

© 1997 NRC Canada

Can. J. Chem. Downloaded from www.nrcresearchpress.com by 91.121.58.235 on 09/08/12
For personal use only.

Fig. 5. Variation of parameters (*a*) N_{12}, (*b*) H_{12}, (*c*) v_{12}, and (*d*) v_{21} with *n* (number of carbon atoms in alkanol molecule) at 298.15 K. (○, 1-pentanol; ×, 1-hexanol; □ 1-heptanol; ●, 1-octanol).

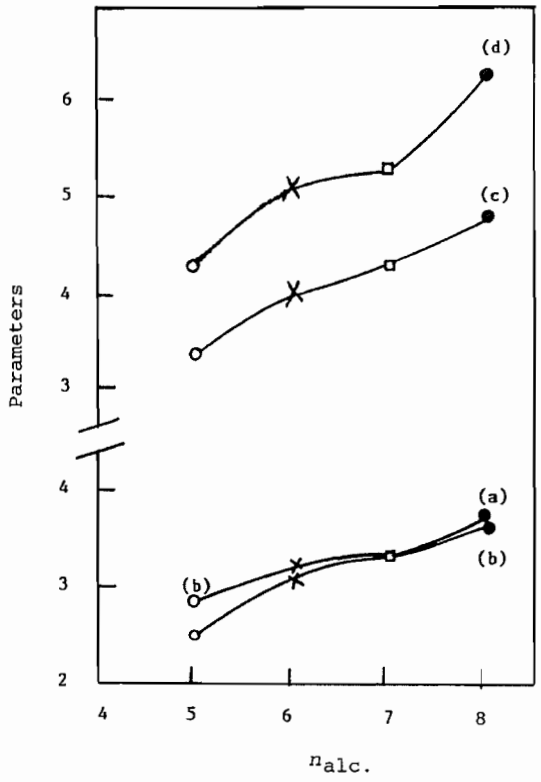


Table 4. Parameters of eqs. [5], [6], and [7] of the (*x*) PC + (1 − *x*) *n*-alkanols at 298.15 K.

N_{12}	H_{12}	v_{12}	v_{21}	% Error
		(*x*) PC + (1 − *x*) 1-pentanol		
2.8344	2.5031	2.3527	3.3213	±0.16
		(*x*) PC + (1 − *x*) 1-hexanol		
3.2278	3.1127	2.9707	4.1251	±0.38
		(*x*) PC + (1 − *x*) 1-heptanol		
3.3058	3.2679	3.3643	4.3191	±0.50
		(*x*) PC + (1 − *x*) 1-octanol		
3.5912	3.7360	3.7822	5.2711	±0.82

Table 5. Parameters of eq. [8] of (*x*) PC + (1 − *x*) *n*-alkanols at 298.15 K.

a	*b*	*c*	% Error
	(*x*) PC + (1 − *x*) 1-pentanol		
−0.6486	−0.1821	0.3943	±0.09
	(*x*) PC + (1 − *x*) 1-hexanol		
−1.0493	−0.1653	−0.0265	±0.11
	(*x*) PC + (1 − *x*) 1-heptanol		
−1.5596	0.2056	−0.0121	±0.32
	(*x*) PC + (1 − *x*) 1-octanol		
−2.8582	−0.0101	0.2335	±0.45

mixed fluids that manifest negative deviation from ideal behaviour. Generally, from different equations for calculating viscosity mixtures, the McAllister model shows the best agreement with experimental data with a smaller deviation, compared with the other relationships.

References

1. A. D'Aprano, D. Donato, and E. Caponetti. J. Solution Chem. **8**, 135 (1979).
2. L. Wilson, R. Bicca de Alencastro, and C. Sandorfy. Can. J. Chem. **63**, 40 (1985).
3. R.K. Dewan, S.K. Mehta, R. Parashar, and K. Bala. J. Chem. Soc. Faraday Trans. **87**, 1561 (1991).
4. M. Iwamashi, Y. Mayashi, N. Mahiya, H. Matsuzawa, and H. Kobayashi. J. Chem. Soc. Faraday Trans. **89**, 707 (1993).
5. R. Francesconi and F. Comilli. J. Chem. Eng. Data, **41**, 1397 (1996).
6. M.M. El-Banna. J. Chem. Eng. Data, **42**, 31 (1997).
7. F.J. Hoyuelos, B. Garcia, R. Alcalde, S. Ibeas, and J.M. Leal. J. Chem. Soc. Faraday Trans. **92**, 219 (1996).
8. A.H. Nissan and L. Grunberg. Nature (London), **164**, 799 (1949).
9. R.K. Hind, E. McLaughlin, and A.R. Ubbelohde. Trans. Faraday Soc. **56**, 328 (1960).
10. P.A. McAllister. AIChE J. **6**, 427 (1960).
11. E.L. Heric and J. Brewer. J. Chem. Eng. Data, **12**, 574 (1967).
12. J. Ortega, M.I. Paz-Andrade, E. Rodriguez-Nunez, and L. Romani. Aust. J. Chem. **38**, 1435 (1985).
13. M. Singh, P.C. Gupta, and R.N. Kesharwani. J. Chem. Eng. Data, **40**, 358 (1995).
14. G. Moumouzias, D.K. Panopoulos, and G. Ritzoulis. J. Chem. Eng. Data, **36**, 20 (1991).
15. P.K. Muhuri, B. Das, and D. Hazra. J. Chem. Eng. Data, **41**, 1473 (1996).
16. M.L. Jansen and H.L. Yeager. J. Phys. Chem. **78**, 1380 (1974).
17. J.A. Riddick, W.B. Bunger, and T.K. Sakato. Techniques of chemistry; organic solvents, physical properties and method of purification. Vol. II. 4th ed. Wiley, New York. 1986.
18. K.J. Kim and C.H. Lee. J. Chem. Eng. Data, **19**, 228 (1994).
19. J.A. Manick. Alcohols. Their chemistry, properties and manufacture. Reinhold Book Corp: New York. 1968. Chap. 3.
20. R. Francesconi and F. Comelli. J. Chem. Eng. Data, **42**, 45 (1997).
21. R.P. Singh, C.P. Sinha, and P. Ghosh. J. Chem. Eng. Data, **35**, 93 (1990).
22. C.H. Yu and F.N. Tasi. J. Chem. Eng. Data, **39**, 441 (1994).
23. J. Ortega and J.D. Garcia. Can. J. Chem. **66**, 1520 (1988).
24. O. Redlich and A.T. Kister. Ind. Eng. Chem. **40**, 341 (1948).
25. N.V. Riggs. Aust. J. Chem. **38**, 1585 (1985).
26. G. Ritzoulis. Can. J. Chem. **67**, 1105 (1989).
27. A.S.N. Murthy and C.N.R. Rao. Appl. Spectrosc. Rev. **2**, 69 (1968).
28. A.M. Hafez and H. Sadek. Acta Chim. Acad. Sci. Hung. **89**, 257 (1976).
29. C. Pikkarainen. Finn. Chem. Lett. **7**, 109, (1980).

© 1997 NRC Canada

Thermodynamic properties of ternary mixtures containing nitrobenzene

V.K. Sharma, Khem Chand Kalra, and A. Katoch

Abstract: Molar excess volumes, V^E_{ijk}, and molar excess enthalpies, H^E_{ijk}, of nitrobenzene (i) + benzene (j) + cyclohexane (k), nitrobenzene (i) + benzene (j) + *n*-hexane (k), and nitrobenzene (i) + benzene (j) + *n*-heptane (k) ternary mixtures have been determined dilatometrically and calorimetrically as a function of composition at 298.15 K. The data have been analyzed in terms of (*i*) the graph-theoretical approach and (*ii*) Flory's Theory. It has been observed that V^E_{ijk} data calculated by graph theoretical as well as Flory's approach compare well with their corresponding experimental values.

Key words: molar excess volumes, molar excess enthalpies, specific interactions, molar volume interaction parameter, molar interaction enthalpy parameter.

Résumé : Opérant à 298,15 K et faisant appel à la dilatométrie et à la calorimétrie, on a déterminé les volumes molaires partiels, V^E_{ijk}, et les enthalpies molaires en excès, H^E_{ijk}, de mélanges ternaires de nitrobenzène (i) + benzène (j) + cyclohexane (k), de nitrobenzène (i) + benzène (j) + *n*-hexane (k) et de nitrobenzène (i) + benzène (j) + *n*-heptane (k) en fonction de la composition. On a analysé les données en termes (*i*) de l'approche théorique des graphes et (*ii*) de la théorie de Flory. On a observé que les données de V^E_{ijk} calculées par l'approche théorique des graphes ainsi que par la théorie de Flory se comparent bien avec les valeurs expérimentales correspondantes.

Mots clés : volumes molaires en excès, enthalpies molaires en excès, interactions spécifiques, paramètre volumique d'interaction molaire, paramètre de l'enthalpie d'interaction molaire.

[Traduit par la rédaction]

Can. J. Chem. Downloaded from www.nrcresearchpress.com by 91.121.58.235 on 09/08/12
For personal use only.

Introduction

In our earlier communication (1) molar excess volumes, V^E_{ij}, and molar excess enthalpies, H^E_{lj}, for nitrobenzene (i) + benzene or + toluene or + xylenes (j) binary mixtures were reported. The observed data were analysed in terms of the graph-theoretical approach as well as Flory's theory. Recent studies have shown that the thermodynamic properties of ternary (i + j + k) mixtures (2–5) can be determined from the properties of the respective (i + j), (j + k), and (i + k) binary mixtures. Thus it would be of interest to see how the graph approach and Flory's theory explain the V^E_{ijk} and H^E_{ijk} of the various ternary mixtures of non-electrolytes if corresponding data for the (i + j), (j + k), and (i + k) binary mixtures are known. Therefore, in the present investigation molar excess volumes, V^E_{ijk}, and molar excess enthalpies, H^E_{ijk}, of nitrobenzene (i) + benzene (j) + cyclohexane or + *n*-hexane or + *n*-heptane (k) of ternary mixtures have been determined.

Experimental

Nitrobenzene (NB), benzene, cyclohexane, *n*-hexane, and *n*-heptane (AR Grade) were purified by standard methods (6). The purities were checked by measuring their densities at 298 ± 0.01 K and these agreed to within $\pm 5 \times 10^{-5}$ g cm^{-3} with their corresponding literature (7–10) values.

Molar excess volumes, V^E_{ijk}, for various ternary mixtures were measured by means of a dilatometer as has been described elsewhere (11). The dilatometer used had three limbs for three components. The temperature of the thermostat was controlled to better than ±0.1° by means of a toluene regulator. The change in liquid level of the dilatometer capillary was measured with a cathetometer that could read up to ±0.001 cm. The uncertainty in our measured V^E value is ±0.5%. The reliability of the dilatometer was checked by measuring V^E values for the benzene (i) + cyclohexane (j) mixture at 298.15 K and these values agreed with their corresponding literature values (12) within the reported accuracy.

Molar excess enthalpies for ternary (i + j + k) mixtures were determined in a flow calorimeter (LKB Broma, Sweden) in exactly the same manner (4, 13) as that described for the (i + j) binary mixtures, except that now the composition of the third liquid was varied by taking pure component in one syringe and running the mixture of known composition (by weight) of i + j or j + k or i + k in the second syringe. Molar excess enthalpies for the i + j + k mixtures were then calculated from the relation:

$$[1] \quad H^E_{ijk} = (Q_{i+j+k} + Q_{j+k})/(n_i + n_j + n_k)$$

where Q_{i+j+k} is the heat evolved, in joules, when pure liquid (i) is allowed to run in one syringe while, in the other, a mixture of (j + k) of known composition is taken. Q_{j+k} is the heat

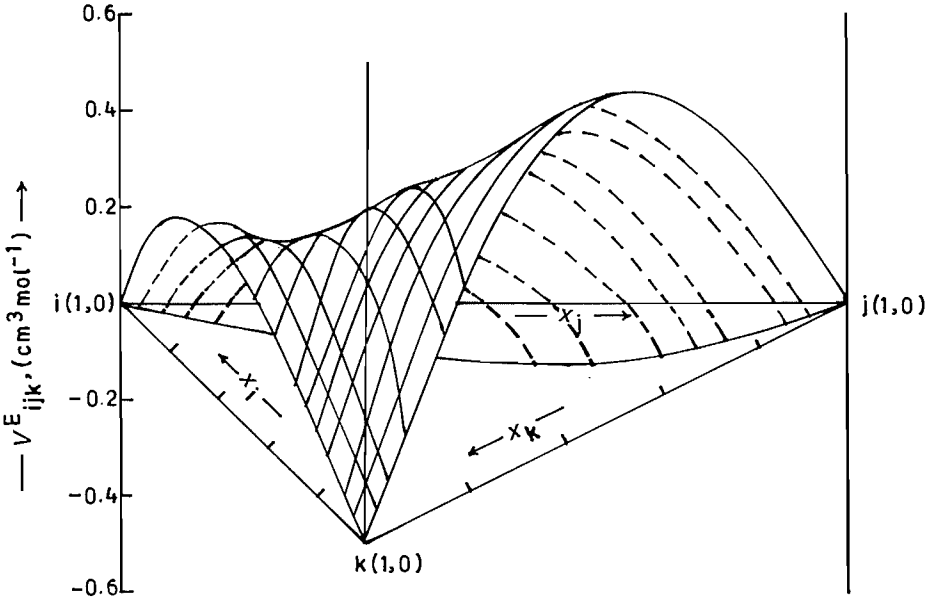
Received December 18, 1996.[1]

V.K. Sharma,[2] K.C. Kalra, and A. Katoch. Department of Chemistry, Maharishi Dayanand University, Rohtak-124001, India.

[1] Revision received September 11, 1997.
[2] Author to whom correspondence may be addressed. Telephone: (01262) 41598.

© 1997 NRC Canada

Fig. 1. Molar excess volumes, V^E_{ijk}, of nitrobenzene (i) + benzene (j) + cyclohexane (k) at 298.15 K.



evolved in the binary system of j + k of known composition. Since

$$[2] \quad Q_{j+k} = H^E_{j+k}\, n_{j+k}$$

where n_{j+k} is the total number of moles of the (j + k) binary system in the ternary mixture at the desired flow rate, eq. [1] takes the form:

$$[3] \quad H^E_{ijk} = (H^E_{j+k}\, n_{j+k} + Q_{i+j+k})/(n_i + n_j + n_k)$$

Further, the number of moles and the mole fraction of the various components in the ternary mixture were calculated from the following relations:

$$[4] \quad n_i = r_{f1}/V_i$$

$$[5] \quad n_j = (x_j r_{f2})/[V^E_{j+k} + (x_j V_j + x_k V_k)]$$

$$[6] \quad n_k = (n_k r_{f2})/(V^E_{j+k} + (x_j V_j + x_k V_k)]$$

where V^E_{j+k} is the excess volume at the known composition of j in a j + k mixture, V_i, etc. are the molar volumes of the i, etc. entities, and x_j and x_k are the mole fractions of j and k in the j + k mixture, respectively. r_{f1} is the flow rate of the liquid running in the syringe no. 1 and r_{f2} is the flow rate of liquid running in syringe no. 2. The reliability of the instrument was checked by measuring H^E_{ij} for the benzene (i) + carbon tetrachloride (j) system at 298.15 K and the experimental values agreed with the corresponding literature values (14) within the reported accuracy. The uncertainty in our H^E values is ±1%.

Results

V^E_{ijk} and H^E_{ijk} data for the various (i + j + k) ternary mixtures as a function of composition at 298.15 K (recorded in Tables 1 and 2 and plotted in Figs. 1–6) were fitted to eq. [7].

$$[7] \quad X^E_{ijk}\,(X = V \text{ or } H) = x_i x_j\left[\sum_{n=0}^{2} X_{ij}(n)(x_i - x_j)^n\right] + x_j x_k\left[\sum_{n=0}^{2} X_{jk}(n)(x_j - x_k)^n\right] + x_k x_i\left[\sum_{n=0}^{2} X_{ki}(n)(x_k - x_i)^n\right] + x_i x_j x_k\left[\sum_{n=0}^{2} X_{ijk}(n)(x_j - x_k)^n x_i^n\right]$$

where x_i and x_j are the mole fractions of the ith and jth components in the (i + j + k) mixture and $X_{ijk}(n)$ ($X = V$ or H; n = 0–2) etc. are the parameters characteristic of the ternary mixture. $X_{ij}(n)$ ($X = V$ or H; n = 0–2) etc. are the parameters characteristic of the (i + j), (j + k), and (k + i) binary mixtures and have been taken from the literature (1, 15–21). The $X_{ijk}(n)$ parameters of eq. [7] were evaluated by fitting X^E_{ijk} data to eq. [8].

$$[8] \quad \left[X^E_{ijk} - \left\{x_i x_j\left[\sum_{n=0}^{2} X_{ij}(n)(x_i - x_j)^n\right] - x_j x_k\left[\sum_{n=0}^{2} X_{jk}(n)(x_j - x_k)^n\right] - x_k x_i\left[\sum_{n=0}^{2} X_{ki}(n)(x_k - x_i)^n\right]\right\}\right] \Big/ x_i x_j x_k = \left[\sum_{n=0}^{2} X_{ijk}(n)(x_j - x_k)^n x_i^n\right]$$

Can. J. Chem. Downloaded from www.nrcresearchpress.com by 91.121.58.235 on 09/08/12
For personal use only.

© 1997 NRC Canada

Can. J. Chem. Downloaded from www.nrcresearchpress.com by 91.121.58.235 on 09/08/12
For personal use only.

Table 1. Comparison of measured V^E_{ijk} values for the various (i + j + k) ternary mixtures at 298.15 K with the corresponding values evaluated from graph and Flory theory; also included are the various $V^{(n)}_{ijk}$ (n = 0–2) parameters along with the standard deviation, $\sigma(V^E_{ijk})$, of X^E_{ijk} ($X = V$ or H), the interaction parameters (χ'_{ij}, χ'_{jk}, ...), and $^3\xi_i$, etc.[a]

		V^E_{ijk} (cm^3 mol^{-1})		
x_i	x_j	Flory	Exptl.	Graph
Nitrobenzene (i) + benzene (j) + cyclohexane (k)				
0.0237	0.5614	1.036	0.611	0.302
0.0476	0.7870	0.550	0.318	0.184
0.0638	0.3817	0.990	0.606	0.383
0.0865	0.6560	0.728	0.433	0.282
0.1156	0.7848	0.256	0.153	0.131
0.1756	0.5488	0.654	0.400	0.330
0.1868	0.1154	0.719	0.427	0.425
0.2311	0.7441	–0.128	–0.059	–0.061
0.3035	0.3235	0.672	0.432	0.427
0.3923	0.5470	–0.068	–0.029	–0.061
0.4008	0.4471	0.198	0.135	0.129
0.4131	0.5641	–0.199	–0.093	–0.168
0.5303	0.2114	0.393	0.256	0.300
0.6634	0.1790	0.185	0.133	0.133
0.7471	0.1267	0.136	0.098	0.099
0.9137	0.0421	0.030	0.024	0.021
$V^{(0)}_{ijk}$ = 0.465; $V^{(1)}_{ijk}$ = –5.025; $V^{(2)}_{ijk}$ = –41.836; $\sigma(V^E_{ijk})$ = 0.001				
$^3\xi_i$ = 1.30; $^3\xi_j$ = 0.667; $^3\xi_k$ = 1.50				
χ'_{ii} = –0.968; χ'_{ij} = –0.229; χ'_{jk} = 1.888				
χ_{ij} = 14.372; χ_{jk} = 58.383; χ_{ik} = 75.094				
θ_j = 0.466; θ_k = 0.523; θ_i = 0.489				
Nitrobenzene (i) + benzene (j) + *n*-hexane (k)				
0.0652	0.8392	0.158	0.048	–0.023
0.1382	0.1933	0.134	–0.208	–0.025
0.1833	0.6653	0.039	–0.070	–0.070
0.2329	0.2526	–0.066	–0.436	–0.055
0.2330	0.4664	0.047	–0.206	–0.076
0.2580	0.0474	–0.482	–0.615	–0.019
0.3073	0.6148	–0.196	–0.163	–0.131
0.3975	0.5628	–0.263	–0.174	–0.173
0.4136	0.5178	–0.273	–0.205	–0.173
0.5146	0.4384	–0.299	–0.195	–0.207
0.5345	0.3870	–0.309	–0.240	–0.200
0.6248	0.3135	–0.310	–0.214	–0.213
0.6892	0.2106	–0.354	–0.287	–0.180
0.7893	0.1057	–0.342	–0.307	–0.119
$V^{(0)}_{ijk}$ = –5.325; $V^{(1)}_{ijk}$ = 34.097; $V^{(2)}_{ijk}$ = –146.764; $\sigma(V^E_{ijk})$ = 0.001				
$^3\xi_i$ = 1.30; $^3\xi_j$ = 0.667; $^3\xi_k$ = 0.957				
χ'_{ii} = –0.671; χ'_{ij} = –0.215; χ'_{jk} = 0.044				
χ_{ij} = 14.372; χ_{jk} = 58.522; χ_{ik} = 53.338				
θ_j = 0.466; θ_k = 0.526; θ_i = 0.560				
Nitrobenzene (i) + benzene (j) + *n*-heptane (k)				
0.0528	0.6122	0.541	0.392	0.068
0.0563	0.7297	0.954	0.278	0.138
0.0804	0.0917	0.033	0.108	0.033
0.1001	0.8343	0.005	0.037	0.392

© 1997 NRC Canada

Can. J. Chem. Downloaded from www.nrcresearchpress.com by 91.121.58.235 on 09/08/12
For personal use only.

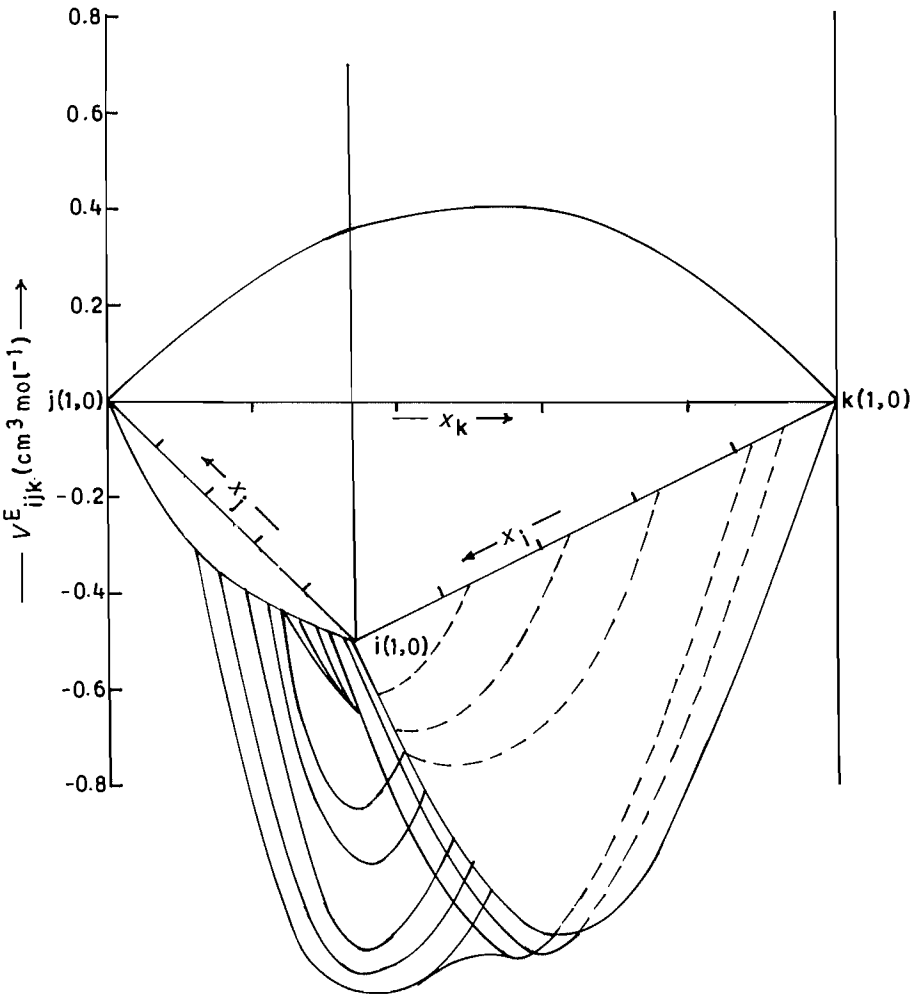
Table 1 (*concluded*).

		V^E_{ijk} (cm^3 mol^{-1})		
x_i	x_j	Flory	Exptl.	Graph
0.1200	0.5926	0.265	0.234	0.251
0.1514	0.1157	−0.124	0.041	0.033
0.1951	0.3017	0.035	0.125	0.126
0.2458	0.4126	−0.063	0.053	0.223
0.3013	0.5477	−0.145	−0.044	0.406
0.3214	0.5654	−0.214	−0.068	0.439
0.3508	0.2519	−0.376	−0.097	−0.031
0.4274	0.2219	−0.378	−0.165	−0.165
0.5054	0.3857	−0.352	−0.134	−0.052
0.5858	0.0462	−0.764	−0.320	−0.321
0.7006	0.1428	−0.465	−0.188	−0.564
0.8712	0.0852	−0.204	−0.071	−0.554

$V^{(0)}_{ijk} = -2.300$; $V^{(1)}_{ijk} = -8.174$; $V^{(2)}_{ijk} = 48.985$; $\sigma(V^E_{ijk}) = 0.001$
$^3\xi_i = 1.30$; $^3\xi_j = 0.667$; $^3\xi_k = 1.10$
$\chi'_{ii} = -7.950$; $\chi'_{ij} = 3.060$; $\chi'_{jk} = -0.833$
$\chi_{ij} = 14.372$; $\chi_{jk} = 43.212$; $\chi_{ik} = 58.852$
$\theta_j = 0.466$; $\theta_k = 0.547$; $\theta_i = 0.580$

[a] $V^{(0)}_{ijk}$ etc., $\sigma(V^E_{ijk})$, and χ'_{ii} etc. are in cm^3 mol^{-1}, χ_{ij}, etc. are in J mol^{-1}.

Fig. 2. Molar excess volumes, V^E_{ijk}, of nitrobenzene (i) + benzene (j) + *n*-hexane (k) at 298.15 K.



© 1997 NRC Canada

Can. J. Chem. Downloaded from www.nrcresearchpress.com by 91.121.58.235 on 09/08/12
For personal use only.

Table 2. Comparison of measured H^{E}_{ijk} values for the various (i + j + k) ternary mixtures at 298.15 K with the corresponding values evaluated from graph and Flory theory; also included are the various $H^{(n)}_{ijk}$ (n = 0–2) parameters along with standard deviation, $\sigma(H^{E}_{ijk})$, of X^{E}_{ijk} (X = V or H), the interaction parameters χ'_{ii} etc.

		H^{E}_{ijk} (J mol^{-1})		
x_i	x_j	Flory	Exptl.	Graph
Nitrobenzene (i) + benzene (j) + c-hexane (k)				
0.0436	0.7662	716.7	657.8	604.0
0.0488	0.1819	824.5	741.8	874.7
0.0920	0.7274	735.2	788.1	769.7
0.1137	0.1695	1014.2	1071.4	1177.0
0.1542	0.6776	745.9	962.4	933.9
0.1704	0.1586	1147.9	1355.1	1402.3
0.2042	0.1522	1217.0	1519.6	1518.2
0.2331	0.6144	749.1	1174.3	1107.1
0.2550	0.1424	1294.7	1734.3	1664.8
0.3131	0.5503	736.5	1325.9	1263.4
0.3392	0.1263	1375.9	1992.4	1833.7
0.3780	0.4983	710.5	1376.9	1377.8
0.4769	0.4190	657.6	1311.8	1520.5
0.5066	0.0943	1358.2	1983.5	1890.8
0.6063	0.0753	1238.5	1683.9	1751.0
0.6458	0.2837	508.9	884.4	1592.9
0.6725	0.0626	1113.4	1407.5	1587.9
0.7549	0.0469	908.7	1033.6	1309.1
$H^{(0)}_{ijk}$ = 13 046.4; $H^{(1)}_{ijk}$ = 2884.9; $H^{(2)}_{ijk}$ = 861 230.7; $\sigma(H^{E}_{ijk})$ = 1.45				
χ'_{ii} = 5428.12; χ'_{ij} = 229.81; χ'_{jk} = 4974.26				
Nitrobenzene (i) + benzene (j) + *n*-hexane (k)				
0.0125	0.2004	797.9	544.3	585.5
0.0457	0.7558	891.8	599.9	523.1
0.1308	0.1649	1024.7	718.6	778.2
0.1607	0.6647	875.2	600.6	619.7
0.1940	0.1529	1130.1	886.2	889.6
0.2420	0.6003	847.2	672.8	674.2
0.2863	0.1354	1230.8	1143.8	1023.5
0.3238	0.5355	803.8	741.9	727.0
0.3757	0.1184	1276.0	1308.1	1111.7
0.3897	0.4834	764.9	767.3	768.2
0.4452	0.1052	1273.9	1352.3	1145.2
0.4892	0.4046	683.5	730.4	820.6
0.5462	0.0861	1208.3	1259.4	1132.1
0.6224	0.3218	461.1	543.7	746.5
0.6435	0.0676	1077.8	1039.1	1043.0
0.6570	0.2716	511.5	504.6	834.4
0.7065	0.0557	956.5	861.4	943.3
0.7831	0.0411	2655.7	629.5	774.4
$H^{(0)}_{ijk}$ = −8510.2; $H^{(1)}_{ijk}$ = −5482.4; $H^{(2)}_{ijk}$ = 740 150.9; $\sigma(H^{E}_{ijk})$ = 1.61				
χ'_{ii} = 3190.02; χ'_{ij} = −470.65; χ'_{jk} = 3797.34				
Nitrobenzene (i) + benzene (j) + *n*-heptane (k)				
0.0232	0.2053	694.8	641.4	861.7
0.0514	0.7851	672.6	650.9	506.2
0.1005	0.7023	812.4	789.0	600.3
0.1420	0.1723	1040.8	1027.9	1072.0
0.1653	0.6614	802.2	806.4	513.9
0.2093	0.1588	1199.4	1218.9	1213.9

© 1997 NRC Canada

Can. J. Chem. Downloaded from www.nrcresearchpress.com by 91.121.58.235 on 09/08/12
For personal use only.

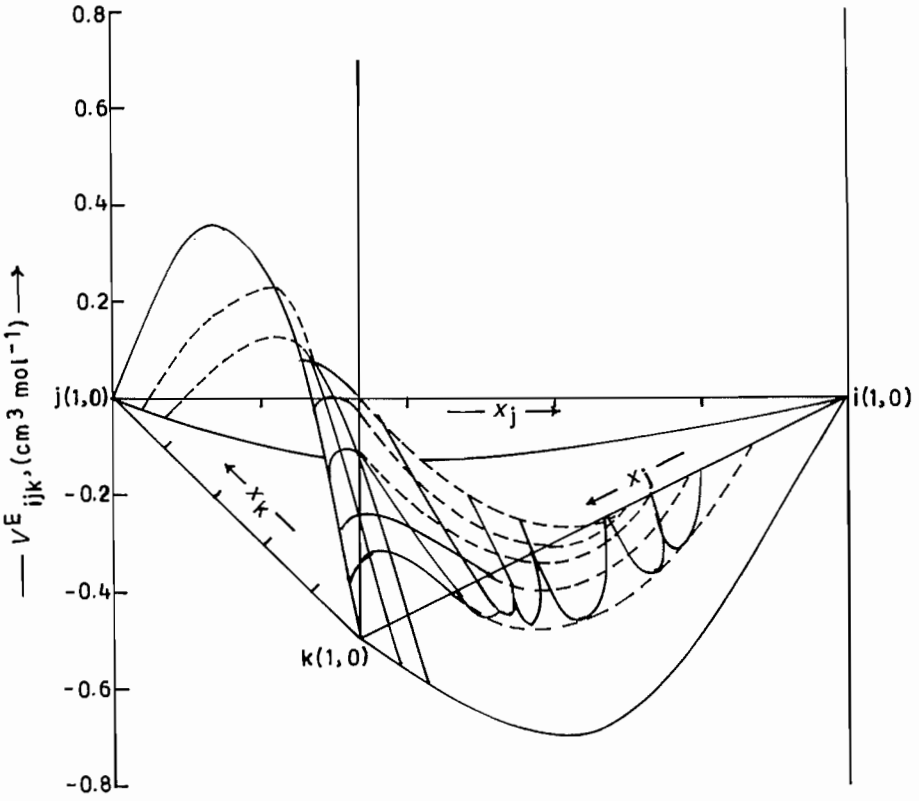
Table 2 (*concluded*).

		H^E_{ijk} (J mol^{-1})		
x_i	x_j	Flory	Exptl.	Graph
0.2482	0.5957	811.1	850.1	463.6
0.2486	0.1509	1275.6	1311.4	1290.8
0.3062	0.1393	1361.2	1416.6	1389.7
0.3312	0.5299	797.8	872.1	446.1
0.3977	0.4772	772.1	860.1	456.9
0.3983	0.1208	1440.1	1500.0	1500.3
0.4688	0.1067	1451.7	1485.1	1535.8
0.4976	0.3981	712.0	792.8	504.1
0.5697	0.0864	1386.8	1354.1	1499.9
0.6646	0.2658	551.6	570.2	593.8
0.6651	0.0672	1240.7	1138.0	1362.7

$H^{(0)}_{ijk}$ = 1756.2; $H^{(1)}_{ijk}$ = −2894.3; $H^{(2)}_{ijk}$ = 270 632.0; $\sigma(H^E_{ijk})$ = 1.26
χ'_{ii} = 4478.77; χ'_{ij} = −2255.91; χ'_{jk} = 5679.23

[a] $H^{(0)}_{ijk}$ etc., $\sigma(H^E_{ijk})$, and χ_{ij} etc. are in J mol^{-1}.

Fig. 3. Molar excess volumes, V^E_{ijk}, of nitrobenzene (i) + benzene (j) + *n*-heptane (k) at 298.15 K.



by the method of least squares and are recorded together with the standard deviation σ (X^E_{ijk}) of X^E_{ijk} defined by

$$[9] \quad \sigma(X^E_{ijk}) = [\Sigma\{X^E_{ijk(expt.)} - X^E_{ijk\ [calcd.\ from\ eq.\ [1]}\}^2/(m-n)]^{0.5}$$

where m is the number of data points and n is the number of adjustable parameters of eq. [7] in Tables 1 and 2.

Discussion

We are unaware of any V^E_{ijk} and H^E_{ijk} values for the mixtures studied with which to compare our results. The observed data for these mixtures were analysed in terms of the graph-theoretical approach.

Conceptual aspect of the graph approach and results

Our earlier studies on the NB (i) + benzene (j) mixture (1)

© 1997 NRC Canada

Fig. 4. Molar excess enthalpies, H^E_{ijk}, of nitrobenzene (i) + benzene (j) + cyclohexane (k) at 298.15 K.

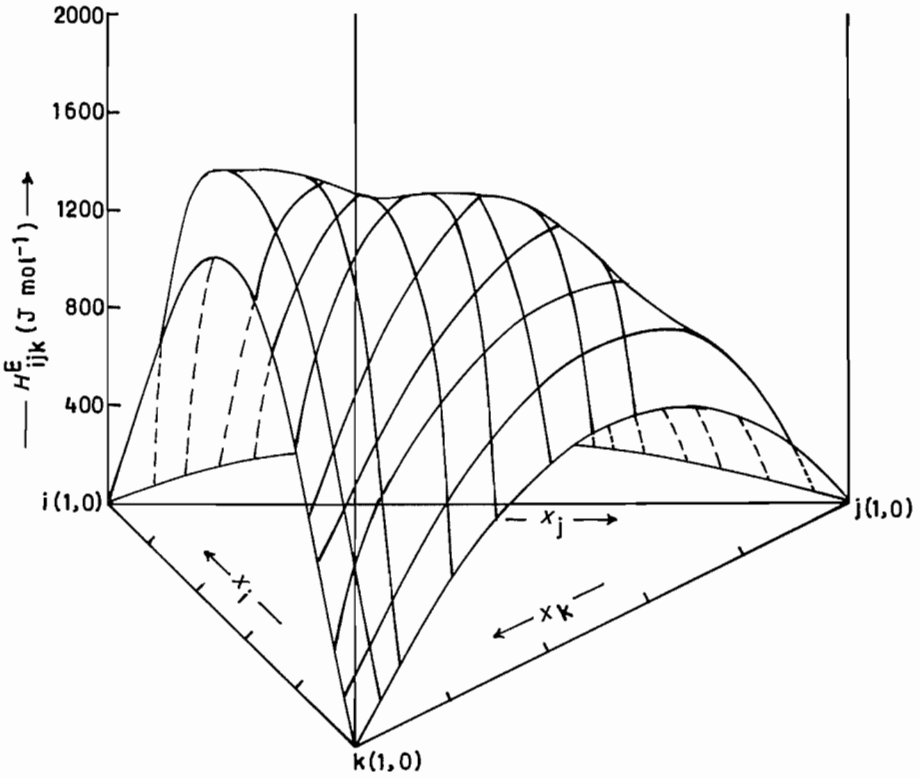
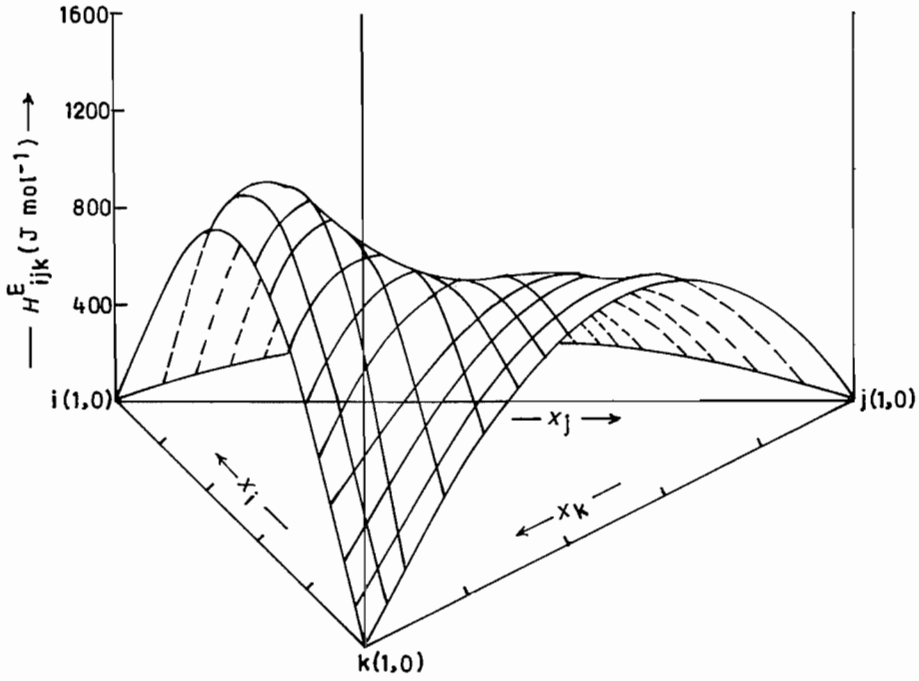


Fig. 5. Molar excess enthalpies, H^E_{ijk}, of nitrobenzene (i) + benzene (j) + *n*-hexane (k) at 298.15 K.



have suggested that (*i*) NB exists as an associated entity in the pure state and (*ii*) the NB (i) + benzene (j) binary mixture formation involves (*a*) the establishment of i_n–j contact between i_n and j; (*b*) the unlike contact formation between i_n and j would then cause depolymerization of i to yield monomers of i; (*c*) monomers of i and j then form an i–j molecular entity. Consequently if χ_{ij}, χ_{ii}, and χ_{12} are the molar volume or enthalpy interaction parameters due to unlike i–j contact formation, j–j and specific interactions, then change in the molar X ($X = V$ or H) property due to processes (*a*), (*b*), and (*c*) would be given (22–24) by

[10] $\Delta X_1 = x_i x_j \chi_{ij} V_j / \Sigma x_i V_i$

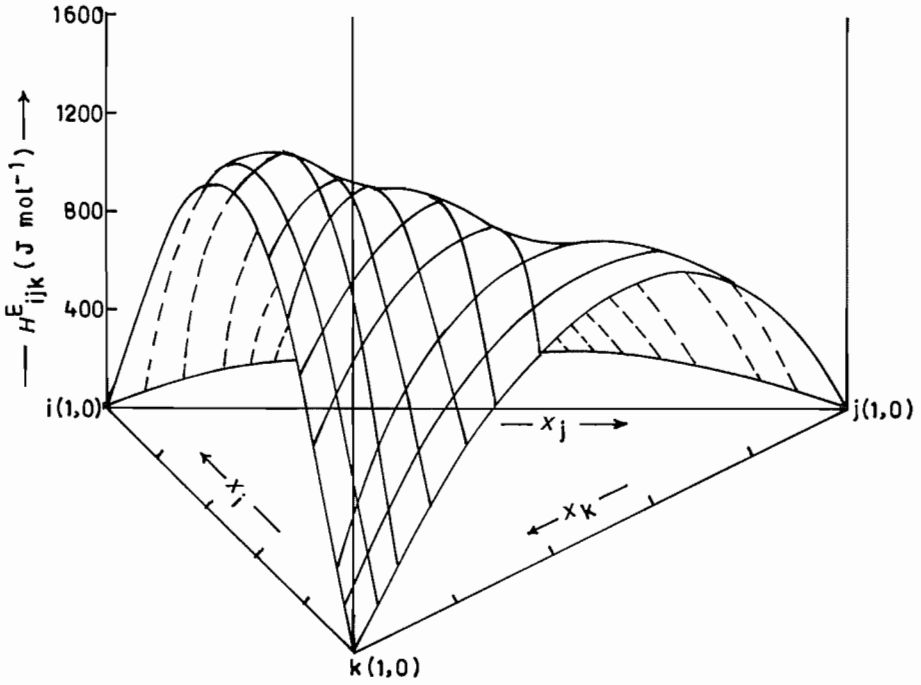
[11] $\Delta X_2 = x_i^2 x_j V_j \chi_{ii} / \Sigma x_i V_i$

Can. J. Chem. Downloaded from www.nrcresearchpress.com by 91.121.58.235 on 09/08/12
For personal use only.

© 1997 NRC Canada

Can. J. Chem. Downloaded from www.nrcresearchpress.com by 91.121.58.235 on 09/08/12
For personal use only.

Fig. 6. Molar excess enthalpies, H^E_{ijk}, of nitrobenzene (i) + benzene (j) + *n*-heptane (k) at 298.15 K.



[12] $\Delta X_3 = x_i x_j^2 V_j \chi_{12}/\Sigma x_i V_i$

The overall changes in molar property X due to processes (a)–(c) were then expressed by

[13] $X^E = \sum_{i=1}^{3} \Delta X_i = [x_i x_j V_j/\Sigma x_i V_i][(1 + x_j)\chi_{ij} + x_i \chi_{jj}]$

However, in the NB (i) + cyclohexane or + *n*-hexane or + *n*-heptane (k) mixture, if i and k are assumed to undergo weak specific interactions, then this binary mixture formation would involve processes (*a*) and (*b*) and the X^E data of these binary mixtures would be expressed by using (21, 25)

[14] $X^E = [x_i x_k V_i/\Sigma x_i V_i][\chi_{ii} + x_i \chi_{12}]$

Equations [13] and [14] contain two parameters and these were evaluated from arbitrary X^E ($X = V$ or H; $x_i = 0.4$ and 0.5 at 298.15 K) data. Since the X^E data of binary systems determined by employing eqs. [13] and [14] compare reasonably well (1, 21) with their corresponding experimental values, it suggests that our basic assumptions in deriving eqs. [13] and [14] are valid.

When an inert hydrocarbon (k) (cyclohexane or *n*-hexane or *n*-heptane) is added to a NB (i) + benzene (j) binary mixture, then this ternary mixture formation involves (*i*) the establishment of (*a*) i_n–j, (*b*) j–k, (*c*) i_n–k unlike contacts between i_n, j, and k components of the mixture; (*ii*) unlike contact formation would then cause depolymerization of i_n to yield monomers of i; and (*iii*) the monomers of i would undergo specific interactions to give an i–j molecular entity. Consequently if χ'_{ij}, χ'_{jk}, and χ'_{ki}, are the molar interaction energies of the i_n–j, j–k, and i_n–k contacts, then change in the molar property due to process (*i*) would be given by

[15] $\Delta X_1 = x_i \chi'_{ij} S_j + x_j \chi'_{jk} S_k + x_k \chi'_{ik} S_i$

where S_i etc. are defined by $S_i = x_i V_i/\Sigma x_i V_i$. Further, if χ'_{ii} and χ'_{12} are the molar interactions of i–i and specific interactions (leading to the formation of i:j entities), then a change in molar property due to processes (*ii*) and (*iii*) can be expressed by

[16] $\Delta X_2 = x_i^2 x_j V_j \chi'_{ii}/\Sigma x_i V_i$

and

[17] $\Delta X_3 = x_i x_j^2 V_j \chi'_{12}/\Sigma x_i V_i$

The overall change in the thermodynamic property due to the processes (*i*)–(*iii*) is given by

[18] $X^E = \sum_{j=1}^{3} \Delta X_i = [x_i x_j V_j/\Sigma x_i V_i][\chi'_{ij} + x_i \chi'_{ii} + x_j \chi'_{12}]$

$+ [x_j x_k V_k/\Sigma x_j V_j]\chi'_{jk} + [x_k x_i V_i/\Sigma x_k V_k]\chi'_{ik}$

Since $V_i/V_j = {}^3\xi_j/{}^3\xi_i$, where ${}^3\xi_i$ etc. are the connectivity parameters of the third degree of pure i, etc. and are defined (24) by

[19] ${}^3\xi_i = \sum_{m<n<o<p} \delta_m{}^v \delta_n{}^v \delta_o{}^v \delta_p{}^v$

where $\delta_m{}^v$, etc. reflect explicitly the valency of the *m*th vertex in the molecular graph of i, in forming bonds, eq. [18] then reduces to

[20] $X^E = [x_i x_j({}^3\xi_i/{}^3\xi_j)/x_i + x_j({}^3\xi_i/{}^3\xi_j)][\chi'_{ij} + x_i \chi'_{jj} + x_j \chi'_{12}]$

$+ [x_j x_k({}^3\xi_j/{}^3\xi_k)/x_j + x_k({}^3\xi_j/{}^3\xi_k)][\chi'_{jk}]$

$+ [x_k x_i({}^3\xi_k/{}^3\xi_i)/x_k + x_i({}^3\xi_k/{}^3\xi_i)][\chi'_{ki}]$

© 1997 NRC Canada

Can. J. Chem. Downloaded from www.nrcresearchpress.com by 91.121.58.235 on 09/08/12
For personal use only.

Further, let it be assumed that $\chi'_{ij} = \chi'_{12}$ and $\chi'_{jk} \approx \chi'_{ik}$; then eq. [20] reduces to

$$[21] \quad X^E = [x_i x_j ({}^3\xi_i/{}^3\xi_j)/x_i + x_j({}^3\xi_i/{}^3\xi_j)][x_i\chi'_{ii} + (1 + x_j)\chi'_{ij}] + [x_j x_k({}^3\xi_j/{}^3\xi_k)/x_j + x_k({}^3\xi_j/{}^3\xi_k) + x_k x_i({}^3\xi_k/{}^3\xi_i)/x_k + x_i({}^3\xi_k/{}^3\xi_i)][\chi'_{jk}]$$

Equation [21] contains three unknown parameters (χ'_{ii}, χ'_{ij}, and χ'_{jk}) that were evaluated from the experimental V^E_{ijk} and H^E_{ijk} of the ternary mixture data at three compositions. Such evaluated parameters along with V^E_{ijk} and H^E_{ijk} for the various mixtures studied are recorded in Tables 1 and 2.

Examination of data in Tables 1 and 2 reveals that V^E_{ijk} and H^E_{ijk} data calculated from the graph approach reproduce well the experimental V^E_{ijk} and H^E_{ijk} data (for $x_i \leq 0.12$, the calculated V^E_{ijk} values are of the right order of magnitude, but the quantitative agreement is not impressive). This lends additional support to the assumption made in deriving eq. [21] and also to the validity of the assumption that $V_j/V_i = {}^3\xi_i/{}^3\xi_j$. The V^E_{ijk} and H^E_{ijk} for these mixtures were then analysed in terms of Flory's theory (26, 27). According to this theory V^E_{ijk} and H^E_{ijk} for a ternary mixture are given by

$$[22] \quad V^E_{ijk} = \overline{V}^E_{cal.}\,(\Sigma\, x_i V_i^*)$$

$$[23] \quad H^E_{ijk} = \Sigma\, x_i P_i^* V_i^* (\overline{V}_i^{-1} - \overline{V}^{-1}_{cal.}) + x_i V_i^* \theta_j \chi_{ij}\, \overline{V}^{-1}_{cal.} + x_j V_j^* \theta_k\, \chi_{jk} \overline{V}^{-1}_{cal.} + x_k V_k \theta_i \chi_{ki} \overline{V}^{-1}_{cal.}$$

$$[24] \quad \overline{V}^E_{cal.} = \overline{V}_0^{7/3}\,[(4/3) - \overline{V}_0^{1/3}]^{-1}(\overline{T} - \overline{T}^0]$$

where all the symbols have the same significance as described elsewhere (25, 26).

Evaluation of V^E_{ijk} and H^E_{ijk} by this theory thus depends upon a knowledge of the reduced temperature $\overline{T}$, and hence on the adjustable parameters θ_j and χ_{ij} of the various binary mixtures. The χ_{ij}, etc. parameters characteristic of (i + j), (j + k), and (k + i) binary mixtures were evaluated by fitting the corresponding $H^E_{exptl.}$ ($x_i = 0.5$) data (1, 15–20) to eq. [24]:

$$[25] \quad H^E_{ij} = x_i P_i^* V_i^* (\overline{V}_i^{-1} - \overline{V}^{-1}_{cal.}) + x_j P_j^* V_j^* (\overline{V}_j^{-1} - \overline{V}^{-1}_{cal.}) + x_i V_i^* \theta_j \chi_{ij}\, \overline{V}^{-1}_{cal.}$$

The parameters of the pure components were determined by using isothermal compressibility (k_T) values reported in the literature (28). These parameters were then utilised to obtain V^E_{ijk} and H^E_{ijk} values at various values of x_i. Such V^E_{ijk} and H^E_{ijk} are recorded in Tables 1 and 2 and are also compared with their corresponding experimental values.

Examination of the data in Tables 1 and 2 has shown that X^E_{ijk} ($X = V$ or H) values calculated from Flory's theory compare reasonably well with the corresponding experimental values. Even in those cases where the agreement between the two values is not good, the predicted X^E_{ijk} values are of the right order of magnitude.

Acknowledgement

The authors are grateful to the Head, Chemistry Department, and authorities of M.D. University, Rohtak, for providing research facilities.

References

1. K.C. Kalra, V.K. Sharma, and A. Katoch. Indian J. Chem. **36A**, 46 (1997).
2. P.P. Singh and V.K. Sharma. Can. J. Chem. **61**, 2321 (1983).
3. P.P. Singh and V.K. Sharma. Z. Phys. Chim. **265**, 915 (1984).
4. P.P. Singh, R. Malik, S. Maken, William E. Acree, Jr., and A. Sheryl. Thermochim. Acta, **162**, 291 (1990).
5. P.P. Singh, S. Maken, and R. Malik. Indian J. Chem. **32A**, 942 (1993).
6. J.A. Riddick and W.B. Bunger. Techniques of organic chemistry by Weissberger. Wiley Interscience, New York. 1970.
7. J. Timmermans. Physico-chemical constants of pure organic compounds. Elsevier Publishing Co., Inc., New York. 1950. p. 276.
8. E. Aicart, G. Tardojos, and M. Pena Diaz. J. Chem. Eng. Data, **25**, 140 (1980).
9. M. Pena Diaz and J. Delego Nunez. J. Chem. Thermodyn. **7**, 201 (1975).
10. A.J. Treszczanowicz, C.J. Halpin, and G.C. Benson. J. Chem. Eng. Data, **27**, 321 (1982).
11. P.P. Singh and S.P. Sharma. J. Chem. Eng. Data, **30**, 477 (1985).
12. G. Scatchard and L.B. Ticknor. J. Am. Chem. Soc. **74**, 3722 (1952).
13. H.P. Dahiya, P.P. Singh, and S. Dagar. Fluid Phase Equilib. **33**, 191 (1987).
14. R.H. Stokes, K.N. Marsh, and R.P. Tomlines. J. Chem. Thermodyn. **1**, 211 (1969).
15. K.N. Marsh. Int. DATA Ser. Sel. Data Mixtures, Ser. A: 5 (1973).
16. K.N. Marsh. Int. DATA Ser. Sel. Data Mixtures, Ser. A: 23 (1973).
17. M.K. Kumaran and G.C. Benson. J. Chem. Thermodyn. **16**, 599 (1984).
18. M.I. Paz-Andrade. Int. DATA Ser. Sel. Data Mixtures, Ser. A: 100 (1973).
19. K.R. Harris and P.J. Dunlop. J. Chem. Thermodyn. **2**, 813 (1970).
20. J.P.E. Grolier. Int. DATA Ser. Sel. Data Mixtures, Ser. A: 223 (3) (1974).
21. K.C. Kalra, V.K. Sharma, and A. Katoch. Indian J. Chem. In press.
22. M.L. Huggins. J. Phys. Chem. **34**, 371 (1970).
23. M.L. Huggins. Polymer, **12**, 389 (1971).
24. P.P. Singh and M. Bhatia. J. Chem. Soc. Faraday Trans. 1, **86**, 3807 (1990).
25. L.B. Kier. *In* Physico-chemical properties of drugs. *Edited by* S.H. Yalkowski, A.A. Sinkula, and S.C. Valvani. Marcel Dekker, New York. 1980. p. 295.
26. P.J. Flory. J. Am. Chem. Soc. **87**, 1833 (1965).
27. P.J. Flory and A. Abe. J. Am. Chem. Soc. **87**, 1838 (1965).
28. R.C. Weast (*Editor*). Handbook of chemistry and physics. 68th ed. CRC Press, Boca Raton, Fla. 1987.

© 1997 NRC Canada

Selective aromatic chlorination of activated arenes with sodium chlorite, (salen)manganese(III) complex, and alumina in dichloromethane

Masao Hirano, Shigetaka Yakabe, Hiroyuki Monobe, and Takashi Morimoto

Can. J. Chem. Downloaded from www.nrcresearchpress.com by 91.121.58.235 on 09/08/12
For personal use only.

Abstract: The reaction of alkyl phenyl ethers with sodium chlorite in dichloromethane in the presence of a (salen)manganese(III) complex and alumina preloaded with a small amount of water afforded monochlorination products with unusually high *para* selectivities under mild conditions. The $NaClO_2$-based biphasic system can also be successfully used for the regioselective monochlorination of substituted anisoles and polymethoxybenzenes.

Key words: aromatic chlorination, alkyl aryl ethers, sodium chlorite, (salen)manganese(III) complex, alumina.

Résumé : La réaction des phénoxyalcanes avec le chlorite de sodium, dans le dichlorométhane et en présence d'un complexe (salen)manganèse(III) et d'alumine à laquelle on a préalablement ajouté une faible quantité d'eau, conduit, dans des conditions douces, à des produits de monochloration avec des sélectivités élevées en faveur des produits *para*. On peut aussi utiliser avec succès le système biphasique basé sur le $NaClO_2$ pour effectuer la monochloration régiosélective d'anisoles et de polyméthoxybenzènes substitués.

Mots clés : chloration aromatique, oxydes d'alkyles et d'aryles, chlorite de sodium, complexe (salen)manganèse(III), alumine.

[Traduit par la rédaction]

Introduction

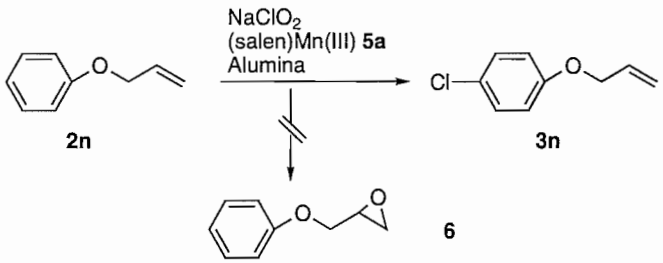
Sodium chlorite **1** has enjoyed an important position in pulp and carbohydrate chemistry (1) because of its mild oxidative property. As an organic synthetic reagent, **1** has been utilized for the selective oxidation of formyl groups to the carboxylic acids in aqueous acidic media (eq. [1]) in the presence of what is generally termed a "chlorine scavenger" such as sulfamic acid (2, 3), resorcinol (2, 4), DMSO (5, 6), hydrogen peroxide (5, 7), or 2-methylbut-2-ene (8) for scavenging HClO and unpleasant ClO_2 (eqs. [1] and [2]). However, there has been no synthetically useful reaction using **1** other than for the aldehyde-to-carboxylic acid oxidations. Indeed, aromatic hydrocarbons or alcohols, upon treatment with **1** in strongly acidic media, undergo competitive chlorination and oxidation, affording only complex mixtures of products (9). In addition, the conventional reactions (1–10) were conducted under aqueous or semiaqueous conditions owing to the negligible solubility of **1** in organic solvents, and therefore its synthetic utility in a water-free medium has so far remained unexplored.

Received May 13, 1997.

Masao Hirano,[1] Shigetaka Yakabe, Hiroyuki Monobe, and Takashi Morimoto. Department of Applied Chemistry, Faculty of Technology, Tokyo University of Agriculture and Technology, Koganei, Tokyo 184, Japan.

[1] Author to whom correspondence may be addressed. Fax: +81-423-88-7033.

Scheme 1.



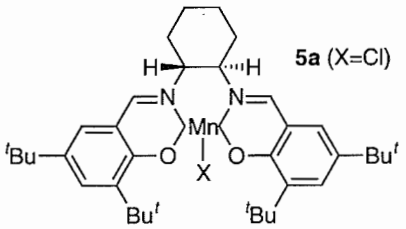
[1] $R\text{-}CHO + ClO_2^- \rightarrow R\text{-}COO^- + HOCl$

[2] $HOCl + 2\ ClO_2^- \rightarrow ClO_2 + Cl^- + OH^-$

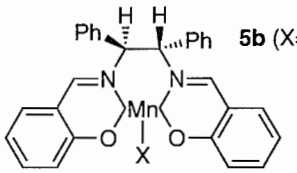
In connection with one of our ongoing projects, we recently needed a simple procedure for the transformation of functionalized alkenes, such as allyl phenyl ether **2n**, into the corresponding epoxide **6** (Scheme 1). Attempted reaction of **2n** with a combination of **1**, chromatographic alumina, and a (salen)manganese(III) complex **5a** (11), a recently developed catalyst for the epoxidation of alkenes (12), in dichloromethane failed to yield the desired product **6**,[2] but resulted in the formation of monochlorinated ether **3n** in good yield (see

[2] Oxidation of sulfides with a reagent combination of sodium chlorite, **5a**, and alumina in dichloromethane under comparable conditions to those employed in the present chlorination led to the formation of chiral sulfoxides, albeit with moderate to low ee's (13).

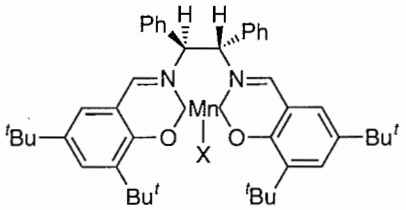
© 1997 NRC Canada



5a (X=Cl)



5b (X=OAc)



5c (X=OAc)

also entry 25 in Table 2). Intrigued by the unexpected and facile incorporation of a chlorine atom into the aromatic moiety, our attention was drawn to the chlorination since this procedure is expected to provide a mild and convenient aromatic chlorination method (for preliminary results, see ref. 14). In this article, we would like to report a new nuclear monochlorination of activated arenes under heterogeneous conditions.[3]

Experimental

Instruments

^{1}H NMR spectra were measured with a JEOL JNM-FX200 or JNM-FX500 spectrometer for solutions in deuteriochloroform using TMS as an internal standard. Analytical GC was carried out on a Shimazdu GC-4BM or GC-14B instrument, equipped with a flame ionization detector through a 2 m × 6 mm diam. glass column packed with 5% PEG-20M on Chromosorb WAW-DMCS and interfaced with a Shimazdu Chromatopac C-R6A integrator, with temperature programming. Mass spectra were determined on a JEOL model SX-102A mass spectrometer, which was coupled with a Hewlett Packard model GC5890 Series II GC apparatus via a heated capillary column. Atomic absorption analyses were carried out on a Hitachi model 170–30 instrument.

Starting materials

Dichloromethane was rigorously dried, distilled, and stored over molecular sieves. Sodium chlorite was purchased from Kanto Chemical Co., Ltd. (Japan). Anisole **2a**, phenetole **2b**, butyl phenyl ether **2e**, allyl phenyl ether **2n**, benzyl phenyl ether **2o**, substituted anisoles **6a–d**, xylenes, mesitylene, and di- and tri-methoxybenzenes **10a–d** and **12a,b**, respectively, are commercial chemicals and the reagents can be used without further purification. Cycloalkyl phenyl ethers, **2l** and **2m**, were prepared by heating a mixture of phenol, potassium hydroxide, and cycloalkyl chlorides in DMSO (16). Other alkyl phenyl ethers **2c**, **2d**, and **2f–k** were synthesized by the reactions of sodium phenoxide with alkyl bromides in ethanol (17). The purities of all substrates were checked by GC prior to use; *p*- and *o*-chloroanisole **3a** and **4a**, respectively, and mesityl chloride **9** were commercially available as reference compounds. *Moist* alumina was prepared by adding deionized water (0.2 g) to oven-dried (500°C, 6 h) chromatographic neutral alumina (ICN BIOMEDICALS: Alumina N, Super I; 1 g) in portions, followed by vigorous shaking of the mixture for a few minutes after every addition until a free-flowing powder was obtained, 1 g of which was immediately used for the chlorination. Optically active (salen)manganese(III) complexes **5a** (11), **5b** (18), and **5c** (18) were synthesized according to standard methods. Commercial inorganic cobalt and manganese salts (vide infra) were finely ground prior to use.

Chlorination procedures

The following procedure for anisole **2a** is representative. A 30 mL, round-bottom, two-necked flask, equipped with a 1.5 cm long Teflon-coated stirrer bar, a 25 cm long condenser, and a glass gas-inlet tubing connected to an argon-filled balloon, was arranged in order to perform the reaction under dry conditions by linking the top of the condenser to a liquid paraffin trap via a flexible silicone rubber tubing. In the flask were placed **2a** (1.5 mmol), freshly prepared *moist* alumina (1 g), the catalyst **5a** (1 mol% with respect to **2a**), and dichloromethane (10 mL) in that order, and the resultant dark mixture was stirred for a few minutes. Sodium chlorite **1** (2.85 mmol; [**1**]/[**2a**] = 1.9) was added in one portion with magnetic stirring and the flask was then deaerated by passing a gentle stream of dry argon through the system. The reaction was carried out by vigorously stirring the heterogeneous mixture; care should be taken in continuing efficient stirring during the reaction to ensure smooth chlorination and to attain reproducible results. After a given time (agitation periods after addition of **1** are indicated in Tables 1–3), the whole mixture was transferred onto a sintered glass funnel, and the insoluble residues were thoroughly washed with portions of dry ether (in toto ca. 100 mL). The combined clear filtrate was condensed on a rotary evaporator under reduced pressure to leave an oil contaminated with a catalyst residue. Chromatography on a silica gel column (Merck Silica Gel 60, hexane – ethyl acetate) afforded a mixture of monochloroanisoles in 97% yield based on starting **2a**.

[3] For recent developments in supported reagent chemistry, see the books listed in ref. 15.

Can. J. Chem. Downloaded from www.nrcresearchpress.com by 91.121.58.235 on 09/08/12
For personal use only.

© 1997 NRC Canada

Can. J. Chem. Downloaded from www.nrcresearchpress.com by 91.121.58.235 on 09/08/12
For personal use only.

The recovery of anisole and the yield of *para*- and *ortho*-chloroanisole **3a** and **4a** were determined by GC using biphenyl as an internal standard. Reuse of **5a** was found to be impractical because of the tedious recovery of the catalyst in such low concentration from a mixture of spent reagents and products, and of some skeleton destruction of **5a** during the chlorination.

The other mono-, di-, and tri-alkoxybenzenes were similarly subjected to the chlorination with a **1–5a** – *moist* alumina system, followed by common work-up and chromatographic separation, to yield the indicated products, which were characterized by NMR and MS spectroscopies.

3b: δ ($CDCl_3$), ^{1}H NMR: 1.40 (t, 3H), 4.95 (q, 2H), 6.70 (d, 2H), 7.15 (d, 2H); *m/e*: 158 (M+2, 32.2% of M^+), 156 (M^+).

3c: δ ($CDCl_3$), ^{1}H NMR: 1.03 (t, 3H), 1.74–1.85 (m, 2H), 3.88 (t, 2H), 6.81 (d, 2H), 7.21 (d, 2H); *m/e*: 172 (M+2, 34.2% of M^+), 170 (M^+).

3d: δ ($CDCl_3$), ^{1}H NMR: 1.31 (d, 6H), 4.89–5.03 (m, 1H), 6.80 (d, 2H), 7.21 (d, 2H); *m/e*: 172 (M+2, 32.2% of M^+), 170 (M^+).

3e: δ ($CDCl_3$), ^{1}H NMR: 0.97 (*t*, 3H), 1.39–1.56 (m, 2H), 1.71–1.83 (m, 2H), 3.92 (t, 2H), 6.81 (d, 2H), 7.21 (d, 2H); *m/e*: 186 (M+2, 34.0% of M^+), 184 (M^+).

3f: δ ($CDCl_3$), ^{1}H NMR: 0.96 (t, 3H), 1.27 (d, 3H), 1.59–1.77 (m, 2H), 4.19–4.28 (m, 1H), 6.81 (d, 2H), 7.21 (d, 2H); *m/e*: 186 (M+2, 33.0% of M^+), 184 (M^+).

3g: δ ($CDCl_3$), ^{1}H NMR: 1.01 (d, 6H), 2.00–2.13 (m, 1H), 3.67 (d, 2H), 6.81 (d, 2H), 7.20 (d, 2H); *m/e*: 186 (M+2, 31.3% of M^+), 184 (M^+).

3h: δ ($CDCl_3$), ^{1}H NMR: 1.33 (s, 9H), 6.92 (d, 2H), 7.22 (d, 2H); *m/e*: 186 (M+2, 29.7% of M^+), 184 (M^+).

3i: δ ($CDCl_3$), ^{1}H NMR: 0.92 (t, 3H), 1.32–1.47 (m, 4H), 1.70–1.84 (m, 2H), 3.90 (t, 2H), 6.80 (d, 2H), 7.21 (d, 2H); *m/e*: 200 (M+2, 33.2% of M^+), 198 (M^+).

3j: δ ($CDCl_3$), ^{1}H NMR: 0.90 (t, 3H), 1.28–1.69 (m, 6H), 1.70–1.83 (m, 2H), 3.91 (t, 2H), 6.81 (d, 2H), 7.21 (d, 2H); *m/e*: 214 (M+2, 32.6% of M^+), 212 (M^+).

3k: δ ($CDCl_3$), ^{1}H NMR: 0.89 (t, 3H), 1.29–1.52 (m, 10H), 1.67–1.85 (m, 2H), 3.90 (t, 2H), 6.81 (d, 2H), 7.20 (d, 2H); *m/e*: 242 (M+2, 33.0% of M^+), 240 (M^+).

3l: δ ($CDCl_3$), ^{1}H NMR: 1.58–1.84 (m, 8H), 4.65–4.77 (m, 1H), 6.79 (d, 2H), 7.20 (d, 2H); *m/e*: 198 (M+2, 32.3% of M^+), 196 (M^+).

3m: δ ($CDCl_3$), ^{1}H NMR: 1.17–2.17 (m, 10H), 4.12–4.24 (m, 1H), 6.81 (d, 2H), 7.21 (d, 2H); *m/e*: 212 (M+2, 33.0% of M^+), 210 (M^+).

3n: δ ($CDCl_3$), ^{1}H NMR: 4.50 (d, 2H), 5.25–5.45 (q, 2H), 5.93–6.12 (m, 1H), 6.83 (d, 2H), 7.21 (d, 2H); ^{13}C NMR: 69.1, 116.0, 117.8, 125.7, 129.3, 132.9, 157.2; *m/e*: 170 (M+2, 34.8% of M^+), 168 (M^+).

3o: δ ($CDCl_3$), ^{1}H NMR: 5.02 (s, 2H), 6.90 (d, 2H), 7.22 (d, 2H), 7.33–7.41 (m, 5H); ^{13}C NMR: 70.3, 116.9, 125.8, 127.4, 128.0, 128.6, 129.3, 136.6, 157.3; *m/e*: 220 (M+2, 33.1% of M^+), 218 (M^+).

7a: δ ($CDCl_3$), ^{1}H NMR: 2.18 (s, 3H), 3.80 (s, 3H), 6.73 (d, 1H), 7.08 (s, 1H), 7.10 (d, 1H); ^{13}C NMR: 16.1, 55.5, 110.9, 124.9, 126.3, 128.5, 130.3, 156.3; *m/e*: 158 (M+2, 31.8% of M^+), 156 (M^+).

7b: δ ($CDCl_3$), ^{1}H NMR: 2.33 (s, 3H), 3.75 (s, 3H), 6.65 (d, 1H), 6.75 (s, 1H), 7.20 (d, 1H); ^{13}C NMR: 20.2, 55.4, 112.5, 116.4, 125.8, 129.5, 136.9, 158.1; *m/e*: 158 (M+2, 32.8% of M^+), 156 (M^+).

7c: δ ($CDCl_3$), ^{1}H NMR: 2.17 (s, 3H), 2.31 (s, 3H), 3.78 (s, 3H), 6.63 (d, 1H), 7.14 (d, 1H); ^{13}C NMR: 12.5, 16.7, 55.7, 108.8, 126.2, 126.3, 126.9, 135.2, 156.1; *m/e*: 172 (M+2, 31.9% of M^+), 170 (M^+).

7d: δ ($CDCl_3$), ^{1}H NMR: 2.24 (s, 6H), 3.68 (s, 3H), 6.98 (s, 2H); ^{13}C NMR: 15.9, 59.7, 128.4, 128.4, 132.5, 155.6; *m/e*: 172 (M+2, 32.2% of M^+), 170 (M^+).

9: δ ($CDCl_3$), ^{1}H NMR: 2.24 (s, 3H), 2.33 (s, 6H), 6.88 (s, 2H); ^{13}C NMR: 20.6, 20.6, 129.2, 131.6, 135.5, 135.8; *m/e*: 156 (M+2, 32.0% of M^+), 154 (M^+).

11a: δ ($CDCl_3$), ^{1}H NMR: 3.86 (s, 3H), 3.88 (s, 3H), 6.75–6.91 (m, 3H); ^{13}C NMR: 56.0, 56.1, 112.0, 112.1,120.3, 125.7, 149.6, 149.6; *m/e*: 174 (M+2, 32.4% of M^+), 172 (M^+).

11b: δ ($CDCl_3$), ^{1}H NMR: 3.78 (s, 3H), 3.86 (*s*, 3H), 6.40 (s, 1H), 6.47 (d, 1H), 7.23 (d, 1H); ^{13}C NMR: 55.5, 56.0, 100.0, 105.2, 114.2, 130.1, 155.7, 159.5; *m/e*: 174 (M+2, 34.6% of M^+), 172 (M^+).

11c: δ ($CDCl_3$), ^{1}H NMR: 3.78 (s, 3H), 3.85 (s, 3H), 6.75 (d, 1H), 6.85 (d, 1H), 6.95 (s, 1H); ^{13}C NMR: 55.9, 56.8, 112.9, 113.3, 116.2, 123.0, 149.4, 153.9; *m/e*: 174 (M+2, 32.9% of M^+), 172 (M^+).

11d: δ ($CDCl_3$), ^{1}H NMR: 2.16 (s, 3H), 3.79 (s, 6H), 6.55 (d, 1H), 7.13 (d, 1H); ^{13}C NMR: 55.8, 60.3, 60.3, 106.8, 119.6, 121.9, 126.8, 154.7, 157.5; *m/e*: 188 (M+2, 31.0% of M^+), 186 (M^+).

13a: δ ($CDCl_3$), ^{1}H NMR: 3.84 (s, 3H), 3.89 (s, 3H), 3.91 (s, 3H), 6.62 (d, 1H), 7.05 (d, 1H); ^{13}C NMR: 56.2, 61.1, 61.1, 107.8, 107.9, 123.9, 143.6,150.0, 152.7; *m/e*: 204 (M+2, 34.1% of M^+), 202 (M^+).

13b: δ ($CDCl_3$), ^{1}H NMR: 3.80 (s, 3H), 3.89 (s, 6H), 6.18 (s, 2H); ^{13}C NMR: 55.6, 56.3, 91.8, 156.7, 159.5; *m/e*: 204 (M+2, 33.3% of M^+), 202 (M^+).

Results and discussion

Chlorination of anisole

The current chlorination can be readily carried out only by efficiently stirring a heterogeneous mixture of an aromatic ether, catalyst **5a**, **1**, chromatographic alumina, and an aprotic solvent. Independent experiments were first made to estimate reaction parameters such as solvents, temperature, and water content of the alumina using anisole **2a** as the test substrate in order to optimize reaction conditions. When **2a** was treated with **1** without metal catalyst in the absence and presence of commercial or oven-dried or water-loaded alumina in dichloromethane, no reaction took place, **2a** being recovered essentially unchanged (**2a** recovery 98% by GC on every run). In the presence of oven-dried alumina or when no alumina was added, no reaction occurred even though catalyst **5a** was added. On the other hand, when **2a** was treated with a $NaClO_2$–**5a** system in the presence of the optimally water-loaded alumina (*moist* alumina; water content 17% by weight) in dichloromethane at ambient temperature it was completely consumed within 30 min, affording a mixture of *p*-chloroanisole **3a** (92.6%) and *o*-chloroanisole **4a** (4.5%) in quasi quantitative yield (Scheme 2, R = Me; total 97%) with high selectivity to the *para* isomer (*para*/*ortho* ratio, 41 after statistical correction), but no *meta*-chloroanisole. Consequently, the catalyst **5a** and *moist* alumina are essential for chlorination to occur under mild conditions.

The choice of solvent was found to be another important

© 1997 NRC Canada

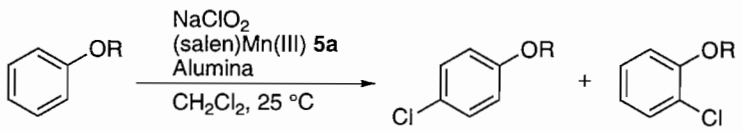
Can. J. Chem. Downloaded from www.nrcresearchpress.com by 91.121.58.235 on 09/08/12
For personal use only.

Table 1. Aromatic chlorination of anisole in various solvents.[a]

Entry no.	Solvent	Distribution (%)[b] PhOMe	*p*-ClC_6H_4OMe	*o*-ClC_6H_4OMe
1[c]	Dichloromethane	0	93	4.5
2	Chloroform	98	0	0
3	Tetrachloromethane	94	0	0
4	1,2-Dichloroethane	99	0	0
5	Acetone	98	0	0
6	Acetonitrile	97	0	0
7	1,4-Dioxane	98	0	0
8	Ethanol	98	0	0
9	Ether	98	0	0
10	Ethyl acetate	99	0	0
11	Hexane	99	0	0
12	Tetrahydrofuran	98	0	0

[a]Reaction conditions: 25°C; 2 h; anisole, 1.5 mmol; $NaClO_2$, 3 mmol; (salen)Mn(III) catalyst **5a**, 0.015 mmol; solvent, 10 mL, *moist* alumina, 1 g.
[b]Determined by GC using biphenyl as an internal standard.
[c]30 min.

Scheme 2.



2 **3** **4**

a R = Me **e** R = *n*-Bu **i** R = *n*-Pentyl **m** R = *c*-Hexyl
b R = Et **f** R = *s*-Bu **j** R = *n*-Hexyl **n** R = Allyl
c R = *n*-Pr **g** R = i-Bu **k** R = *n*-Octyl **o** R = $PhCH_2$
d R = *i*-Pr **h** R = *t*-Bu **l** R = *c*-Pentyl

factor: of common solvents examined, only dichloromethane favored the chlorination whereas no chlorination occurred in the other solvents during extended periords of time (Table 1). In contrast to the remarkable solvent effect, the chlorination exhibited little temperature dependence — control experiments conducted in the range of 0–30°C revealed that there was no significant change in the yield of monochloroanisoles or the *para* selectivity with a change of the temperature. Another comparative study using related (salen)manganese(III) complexes **5a**, **5b**, and **5c** showed that, although there is no significant difference in the activity of the catalysts and the *para* selectivity, the reaction using **5a** gave monochloroanisoles in slightly superior yield to those with use of **5b** and **5c** (97, 91, and 91%, respectively). In addition, **5a** can be synthesized by a simpler method (11) than those used for the preparation of **5b** and **5c** (18). Consequently, the subsequent chlorinations were carried out by using **5a** as the catalyst, in dichloromethane in the presence of *moist* alumina.

Although it is known that some heterogeneous reactions are affected by the presence of water (19, 20), the remarkable sensitivity of the current reaction towards the water content of the alumina and towards the solvent was unexpected and unusual. Sodium chlorite is insoluble in dichloromethane, no reaction occurred in the absence of alumina, and atomic absorption analyses of the reaction solvent showed no detectable amount of manganese species. These observations suggest that the chlorination presumably occurs on the alumina surface and that the solvent – alumina surface interface plays a decisive role in the present reaction. There might be a fine balance between keeping the right amount of water on the alumina surface to help break up the sodium chlorite lattice[4] and moderate solvent polarity to enable the chlorination to take place under mild conditions. It should be noted that no evidence was found for the formation of 2,4-dichlorinated or poly-chlorinated product(s), or for demethylation (22) or rearrangement to phenolic compound in the experiments described above.

Chlorination of aromatic monoethers

Applicability of the $NaClO_2$–**5a** – *moist* alumina system to a series of simple alkyl phenyl ethers **2b–o** was then tested (Scheme 2) and the results are collected in Table 2. Although it is known that some heterogeneous chlorinations have been considerably affected by a slight structual change in the substrates (23), there is apparently no serious dependence of the reactivity of the ethers on the shape and size of the alkyl moiety in the current reactions. For example, comparative studies

[4] A similar explanation has been given for the acceleration of reactions with the use of solid reagents by a small amount of water: see ref. 21.

© 1997 NRC Canada

Scheme 3.

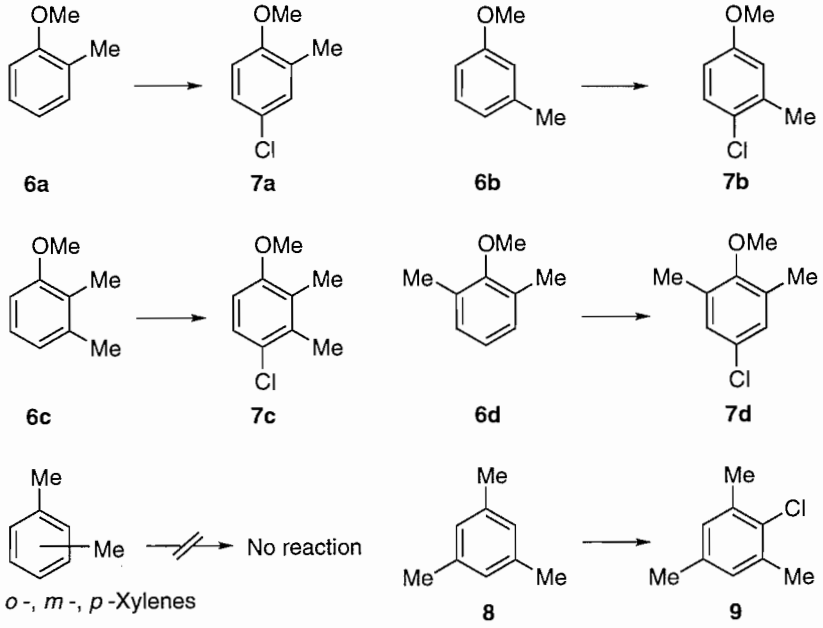


Table 2. Aromatic monochlorination of alkyl pheny ethers **2**.[a]

Entry no.	Ether	$NaClO_2$ (mmol)	Time (min)	Product	Yield (%)[b]
1[c]	**2a**	2.85	30	**3a**+**4a** (95:5)[d]	97
13[c]	**2b**	2.85	30	**3b**	Quant.
14[c]	**2c**	2.7	30	**3c**	96
15	**2d**	2.7	30	**3d**	96
16[c]	**2e**	2.85	30	**3e**	97
17	**2f**	2.85	30	**3f**	96
18	**2g**	2.85	30	**3g**	98
19	**2h**	2.7	30	**3h**	93
20[c]	**2i**	3.0	40	**3i**	94
21[c]	**2j**	2.7	30	**3j**	Quant.
22[c]	**2k**	3.0	30	**3k**	Quant.
23	**2l**	2.7	30	**3l**	93
24	**2m**	3.0	50	**3m**	91
25	**2n**	3.0	45	**3n**	56 (60)[e]
26	**2o**	3.0	60	**3o**	97

[a]Reaction conditions: 25°C; **2**, 1.5 mmol; *moist* alumina, 1 g; (salen)Mn(III) catalyst **5a**, 0.015 mmol (1 mol% with respect to **2**); CH_2Cl_2, 10 mL.
[b]Isolated yield of *para*-chlorinated ether **3** (plus **4a** in the case of **2a**) based on the starting **2**.
[c]Reference 14.
[d]Product ratio, **3a**:**4a**, determined by GC using biphenyl as an internal standard.
[e]GC yield (internal standard: biphenyl); number in parentheses is the yield of **3n** based on consumed **2n**.

Table 3. Selective monochlorination of various activated arenes.[a]

Entry no.	Ether	$NaClO_2$ (mmol)	Time (min)	Product	Yield (%)[b]
27	**6a**	3.3	30	**7a**	83
28	**6b**	2.4	30	**7b**	87
29	**6c**	2.7	50	**7c**	85
30	**6d**	3.9	35	**7d**	92
31	**8**	3.5	70	**9**	81 (85)
32	**10a**	3.0	30	**11a**	89 (93)
33	**10b**	2.4	40	**11b**	82 (86)
34	**10c**	3.6	30	**11c**	84 (92)
35	**10d**	2.2	55	**11d**	94
36	**12a**	2.4	50	**13a**	89
37	**12b**	2.6	40	**13b**	84 (87)

[a]Reaction conditions: 20°C; substrate, 1.5 mmol; *moist* alumina, 1 g; (salen)Mn(III) catalyst **5a**, 0.015 mmol (1 mol% with respect to **2**); CH_2Cl_2, 10 mL.
[b]Based on the starting ether (numbers in parentheses are yields based on consumed substrates).

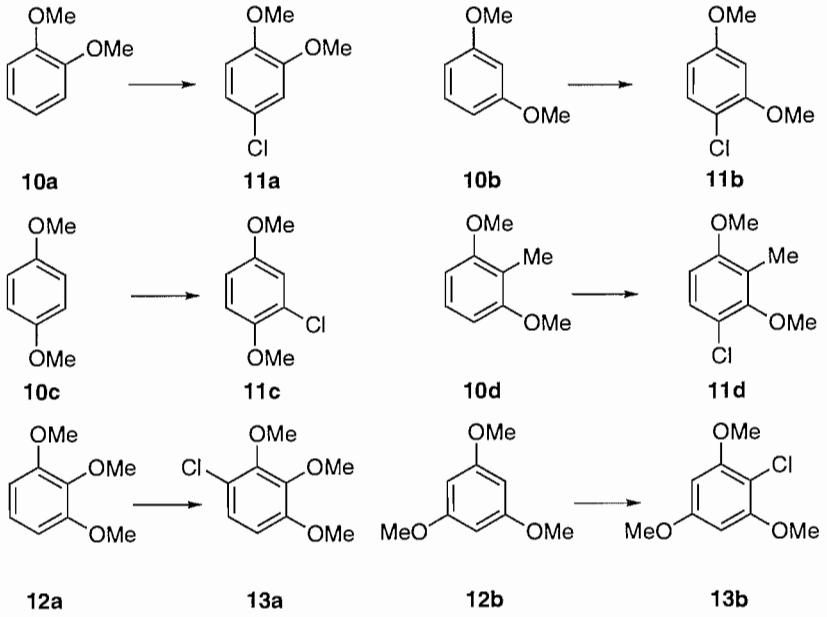
using ethers having C_3- (**2c–d**) and C_4-alkyl groups (**2e–h**) clearly indicated that the reactivity of the ethers is little influenced by steric bulk around the ether linkage. Interestingly, the reactions of **2b–o** led to exclusive *para*-chlorination, giving **3b–o** in excellent to quantitative yields. The side chain of **2n** is assumed to be highly susceptible to chlorination, but it gave **3n** in good yield (60% based on **2n** consumed).

Encouraged by the unusually high *para* selectivity in the chlorination of simple monoether substrates **2a–o**, chlorination of methyl- and dimethyl-substituted anisoles **6a,b** and **6c,d**, respectively, with a **1**–**5a** – *moist* alumina system was also investigated. As shown in Scheme 3, the chlorination occurred selectively at positions *para* to the MeO groups, producing monochlorination products **7a–d** in excellent yields (entries 27–30 in Table 3). In sharp contrast to the facile chlorination of **6a** and **6b**, xylenes resisted chlorination, leading to the recovery of unchanged substrates even after prolonged reactions (120 min; substrate recovery 97–99%). This might suggest that activation by the two methyl groups is not adequate for the nuclei to undergo chlorination, since mesitylene **8** afforded mesityl chloride **9** in fairly good yield (Entry 31).

Can. J. Chem. Downloaded from www.nrcresearchpress.com by 91.121.58.235 on 09/08/12
For personal use only.

© 1997 NRC Canada

Scheme 4.



Can. J. Chem. Downloaded from www.nrcresearchpress.com by 91.121.58.235 on 09/08/12
For personal use only.

Chlorination of di- and tri-methoxybenzenes

The reactions of a series of di- and tri-methoxybenzenes, **10** and **12**, were carried out in order to examine the regiospecificity in the chlorination of the polyether substrates (Scheme 4). Chlorinations of 1,2- and 1,3-dimethoxybenzene **10a** and **10b** occurred at the position *para* to the MeO group, affording **11a** and **11b**, respectively. 1,4-Dimethoxybenzene **10c** has no substitutable hydrogen at the position *para* to each MeO group, but it was readily chlorinated to give **11c** in excellent yield. The usefulness of the present procedure for the monochlorination of triether substrates, **12a** and **12b**, is also apparent.

Aromatic chlorination has been an important reaction in organic chemistry (for reviews, see ref. 24) and many interesting methods have been developed employing molecular chlorine, sulfuryl chloride, hypochlorite and its esters, metal chlorides, N-chloro compounds, etc. as chlorinating agents (24–34). So far as we are aware, both the yield and the selectivity of the chlorination product resulting from solid–solution biphasic systems (23, 28–31) are, in general, superior to those from simple solution-phase counterparts. For example, chlorination of aralkyl ethers (**2a–c**, **2e**, and **2i**) by alumina-supported $CuCl_2$ reagent ([$CuCl_2$]/[**2**], ca. 5 (mole ratio); 100°C, 2–3 h) gives excellent yields and *para* selectivity (30). Our chlorination compared favorably with this procedure in terms of the generally *higher* yield, much *milder* conditions (< 25°C), *shorter* reaction periods, and use of *smaller* amounts of the *cheaper* chlorinating reagent ([$NaClO_2$]/[**2**] $\leq$ 2). In addition, the chlorination of a wide variety of substrates can be performed readily and efficiently, and the regioselectivities are impressive. These advantages, together, may make the new system an attractive alternative to conventional chlorination methodologies.

The current alumina-promoted chlorination formally amounts to a simple chlorine transfer to arenes. This study had a preparative rather than a mechanistic purpose and, in addition, convincing evidence to permit a physicochemical interpretation of the reaction has not been yet provided, since there is uncertainty with regard to the catalysis of **5a** and the active species wherein the chlorite itself and (or) its degradation product(s) might be involved. The following observations and comparisons with related literature data, however, might show interesting aspects of the chlorination.[5] Since chlorine itself is very reactive and small in size, the recent development in selective chlorinations owes its success either to the use of bulky chlorinating agents (27, 32) or shape-selective catalysts such as cyclodextrin (25), zeolites (27, 28), or, as noted above, to the reaction performance under biphasic conditions (23, 27–31), all of which are based on the sterically (or dimensionally) controlled access of chlorinating agents to the reactive, electron-rich position(s) of aromatic nuclei. For the present chlorination, it might be expected that chlorine transfer from a bulky **5a**–chlorine complex to arenes is responsible for the high regioselectivity. However, this should be unlikely, since simple inorganic metal salts, e.g., $CoSO_4$, $Co(NO_3)_2$, $CoCl_2$, $CoBr_2$, $MnSO_4$, $MnCl_2$, $Mn(OAc)_2$, $KMnO_4$, $NaMnO_4$, can be used in place of **5a** for the chlorination of **2a** and there has been no significant change in the **3a/4a** ratios and the yields of chloroanisoles; typically, **3a/4a** = 95:5 and 94:6 with use of $CoSO_4$ and $MnSO_4$, respectively (total yields of **3a** plus **4a** were 94 and 95%, respectively). Thus **5a** is considered to serve as a catalytic activator of **1** or to be involved in the degradation process of **1** en route to the generation of the active chlorine species. In addition, the chlorination of simple aromatic ethers occurred selectively or exclusively at positions *para* to the alkoxy groups (entries 1 and 13–26). It is noteworthy that, in the case of methyl- (entries 27, 28, and 35) and dimethyl-substituted anisoles (entries 29 and 30), positions *para* to the MeO groups are chlorinated, but not those *para* to the Me substituent(s), indicating clearly that chlorine displaces hydrogens attached to the more nucleophilic carbon atoms on the benzene rings (ref. 24*d*, Chap. 2; ref. 24*e*, p. 513; 33, 34). Together, these results undoubtedly support the view that electronic effects are a decisive factor in controlling the

[5] Valuable suggestions from one of the referees regarding the observed regioselectivities are gratefully acknowledged.

© 1997 NRC Canada

regioselectivy of the current chlorination, in which the alumina might contribute not only to facilitating the reaction, but to enhancing the regioselectivity of the product (23*a*, 30). Smooth reactions of **6b**,**c**, **8**, **10b–d**, and **12a**,**b** may account for the lesser influence of steric factors. Finally, even if some interaction between electron-rich ether oxygen (34) and the alumina surface is present, it seems unimportant in determining the reactivity of an ether and the regioselectivity of the chlorination product, since **2h**, for example, was readily chlorinated to afford exclusively **3h** (entry 19).

Conclusion

We have demonstrated here that the $NaClO_2$-based biphasic system serves as an efficient electrophilic chlorine source that is capable of regiospecifically chlorinating the electron-rich position on the benzene ring of a variety of aromatic ethers under mild and neutral conditions.

Can. J. Chem. Downloaded from www.nrcresearchpress.com by 91.121.58.235 on 09/08/12
For personal use only.

Acknowledgements

The authors thank Messrs. Tsuyoshi Kimura and Nobutake Akioka, and Miss Yasuko Tonami, Tokyo University of Agriculture and Technology, for their involvement in carrying out some preliminary experiments. We also thank Dr. Masahiro Natsume and Mrs. Junko Takizawa for their help in GC–MS and NMR measurements, respectively. This work was partially supported by Grant No. 08651001 from the Ministry of Education of Japan.

References

1. T.P. Nevell. Methods Carbohydr. Chem. **3**, 182 (1963).
2. B.O. Lindgren and T. Nilsson. Acta Chem. Scand. **27**, 888 (1973).
3. J.A. Moore and E.M. Partain III. Org. Prep. Proced. Int. **17**, 203 (1985); L. Colombo, C. Gennari, M. Santandrea, E. Narisano, and C. Scolastico. J. Chem. Soc. Perkin Trans. 1, 136 (1980); F. M. Hauser and S. R. Ellenberger. Synthesis, 723 (1987).
4. G.S. Arora, H. Shirahama, and T. Matsumoto. Chem. Ind. (London), 318 (1983).
5. E. Dalcanale and F. Montanari. J. Org. Chem. **51**, 567 (1986).
6. J.P. Bayle, F. Perez, and J. Courtieu. Bull. Soc. Chim. Fr. **127**, 565 (1990).
7. M. Floor, L.P.M. Hofsteede, W.P.T. Groenland, L.A.Th. Verhaar, A.P.G. Kieboom, and H. van Bekkum. Recl. Trav. Chim. Pays-Bas, **108**, 384 (1989).
8. B.S. Bal, W.E. Childers, Jr., and H.W. Pinnick. Tetrahedron, **37**, 2091 (1981); G.A. Kraus and B. Roth. J. Org. Chem. **45**, 4825 (1980); G.A. Kraus and M.J. Taschner. J. Org. Chem. **45**, 1175 (1980); D.S. Matteson and E.C. Beedle. Tetrahedron Lett. **28**, 4499 (1987); L.R. Hills and R.C. Ronald. J. Org. Chem. **50**, 470 (1985).
9. K. Paluch, J. Otto, and R. Starski. Rocz. Chem. **48**, 1453 (1974) (Chem. Abstr. **82**, 111821 (1975)); K. Paluch and J. Jogielski. Zesz. Nauk Politech. Szczecin., Chem., 113 (1972) (Chem. Abstr. **80**, 59772 (1974)); J. Otto and K. Paluch. Rocz. Chem. **47**, 967 (1973) (Chem. Abstr. **79**, 136679 (1973)); Rocz. Chem. **46**, 1551 (1972) (Chem. Abstr. **78**, 57909 (1973)).
10. B.R. Babu and K.K. Balasubramaniam. Org. Prep. Proced. Int. **26**, 123 (1994); E.A. Harrison, Jr., K. C. Rice, and M. E. Rogers. J. Heterocycl. Chem. **14**, 909 (1977).
11. L. Deng and E.N. Jacobsen. J. Org. Chem. **57**, 4320 (1992).
12. K. Srinivasan, P. Michaud, and J.K. Kochi. J. Am. Chem. Soc. **108**, 2309 (1986); E.N. Jacobsen, W. Zhang, A.R. Muci, and J.R. Ecker. J. Am. Chem. Soc. **113**, 7063 (1991); T. Katsuki. J. Mol. Catal. A: Chem. **113**, 87 (1996).
13. M. Hirano, S. Yakabe, J.H. Clark, H. Kudo, and T. Morimoto. Synth. Commun. **26**, 1875 (1996).
14. M. Hirano, S. Yakabe, H. Monobe, J.H. Clark, and T. Morimoto. Synth. Commun. **27**, 3749 (1997).
15. J.H. Clark, A.P. Kybett, and D.J. Macquarrie. Supported reagents. Preparation, analysis, and applications, VCH, New York. 1992; J.H. Clark. Catalysis of organic reactions by supported inorganic reagents. VCH, New York. 1994; K. Smith (*Editor*). Solid supports and catalysts in organic synthesis. Ellis Horwood, Chichester. 1992; P. Laszlo (*Editor*). Preparative chemistry using supported reagents. Academic Press, San Diego. 1987; M. Balogh and P. Laszlo. Organic chemistry using clays. Springer-Verlag, Berlin. 1993; K. Smith, C.V. Fry, and M. Tzimas. *In* Chemistry of waste minimization. *Edited by* J.H. Clark. Chapman and Hall, London. 1995. Chap. 4.
16. M. Siskin, G. Brons, A.R. Katritzky, and R. Murugan. Energy Fuels, **4**, 482 (1990).
17. R.A. Smith. J. Am. Chem. Soc. **55**, 3718 (1933).
18. R. Irie, Y. Noda, Y. Ito, N. Matsumoto, and T. Katsuki. Tetrahedron: Asymmetry, **2**, 481 (1991).
19. T. Nishiguchi and F. Asano. J. Org. Chem. **54**, 1531 (1989); M. Kodomari, H. Satoh, and S. Yoshitomi. Bull. Chem. Soc. Jpn. **61**, 4149 (1988); S. Yasui, M. Fujii, K. Nakamura, and A. Ohno. Bull. Chem. Soc. Jpn. **60**, 963 (1987); M.O. Brimeyer, A. Mehrota, S. Quici, A. Nigam, and S.L. Regen. J. Org. Chem. **45**, 4254 (1980); F.M. Menger and C. Lee. J. Org. Chem. **44**, 3446 (1979); E. Keinan and Y. Mazur. J. Org. Chem. **43**, 1020 (1978); M. Hojo and R. Masuda. Synth. Commun. **5**, 169 (1975); Tetrahedron Lett., 613 (1976); B.B. Jarvis and M.M. Evans. J. Org. Chem. **39**, 643 (1974).
20. M. Onaka, K. Sugita, and Y. Izumi. J. Org. Chem. **54**, 1116 (1989); T. Ando, T. Kawate, J. Yamawaki, and T. Hanafusa. Chem. Lett. 935 (1982).
21. L.A. Carpino and A.C. Sau. J. Chem. Soc. Chem. Commun. 514 (1979); M. Tanaka and M. Koyanagi. Synthesis, 973 (1981).
22. M. Tiecco. Synthesis, 749 (1988).
23. (*a*) M. Kodomari, S. Takahashi, H. Watanabe, and S. Yoshitomi. Nippon Kagaku Kaishi, 1753 (1987) (Chem. Abstr. **109**, 37557 (1988)); (*b*) I. Tanimoto, K. Kushioka, T. Kitagawa, and K. Maruyama. Bull. Chem. Soc. Jpn. **52**, 3586 (1979).
24. (*a*) D.E. Pearson and C.A. Buehler. Synthesis, 455 (1971); (*b*) H. Heavy. *In* Comprehensive organic chemistry. Vol. 1. *Edited by* D.H.R. Barton and W.D. Ollis. Pergamon Press, Oxford. 1979. p. 291; (*c*) E.B. Merkushev. Synthesis, 923 (1988); (*d*) R. Taylor. Electrophilic aromatic substitution. John Wiley & Sons, Chichester. 1990. p. 363; (*e*) J. March. Advanced organic chemistry. Reactions, mechanisms, and structure. 4th ed. John Wiley & Sons, New York. 1992. p. 531.
25. R. Breslow and P. Campbell. J. Am. Chem. Soc. **91**, 3085 (1969); Bioorg. Chem. **1**, 140 (1971); Tetrahedron Lett. 1645 (1976).
26. H.A. Muathen. Tetrahedron Lett. **52**, 8863 (1996); F. Bellesia, F. Ghelfi, U.M. Pagnoni, and A. Pinetti. J. Chem. Res. (S), 284 (1991); G.A. Olah, L. Ohanneslan, and M. Arvanaghi. Synthesis, 868 (1986); I. Tanimoto, K. Kushioka, T. Kitagawa, and K. Maruyama. Bull. Chem. Soc. Jpn. **52**, 3586 (1979); J.G. Lee, H.T. Cha, U.C. Yoon, Y.S. Suh, K.C. Kim, and I.S. Park. Bull. Korean Chem. Soc. **12**, 4 (1991).
27. W.D. Watson. J. Org. Chem. **50**, 2145 (1985); R. Rathore, S.H. Loyd, and J.K. Kochi. J. Am. Chem. Soc. **116**, 8414 (1994).
28. K. Smith and M. Butters. Tetrahedron Lett. **29**, 1319 (1988).
29. K. Smith, M. Butters, and B. Nay. Synthesis, 1157 (1985); L. Delaude and P. Laszlo. J. Org. Chem. **55**, 5260 (1990).

© 1997 NRC Canada

30. M. Kodomari, S. Takahashi, and S. Yoshitomi. Chem. Lett. 1901 (1987).
31. L. Delaude, P. Laszlo, and K. Smith. Acc. Chem. Res. **26**, 607 (1993); L. Delaude and P. Laszlo. Catal. Lett. **5**, 35 (1990); M. Kodomari, H. Satoh, and S. Yoshitomi. J. Org. Chem. **53**, 2093 (1988).
32. J.R. Lindsay Smith, L.C. McKeer, and J.M. Taylor. J. Chem. Soc. Perkin Trans. 2, 1533 (1987); 385 (1988); 1529 (1989); 1537 (1989).
33. G. Castelfranchi and G. Borra. Ann. Chim. (Rome), **43**, 293 (1953).
34. Y. Ogata, M. Kimura, and Y. Kondo. J. Chem. Soc. Perkin Trans. 2, 451 (1984).

Can. J. Chem. Downloaded from www.nrcresearchpress.com by 91.121.58.235 on 09/08/12
For personal use only.

© 1997 NRC Canada

Iodine and iodine supported on polyvinylpyrrolidone as catalysts and reagents for alcoholysis, hydrolysis, and acetolysis of epoxides and thiiranes

Nasser Iranpoor, Bahman Tamami, and Khodabakhsh Niknam

Can. J. Chem. Downloaded from www.nrcresearchpress.com by 91.121.58.235 on 09/08/12
For personal use only.

Abstract: Iodine and iodine supported on polyvinylpyrrolidone (betadine) have been used as catalysts for ring opening of epoxides and as reagent for ring-opening dimerization of thiiranes in alcohols, water, and acetic acid. The reactions occur with high regio-, chemo-, and stereoselectivity. The reaction of *R*-(+)-styrene oxide with I_2 supported on PVP in methanol was found to be very stereospecific and the product was isolated in 93% ee.

Key words: iodine, support, polyvinylpyrrolidone, ring opening, epoxides, thiiranes.

Résumé : On a utilisé de l'iode et de l'iode supporté sur de la polyvinylpyrrolidone (PVP, bétadine) comme catalyseurs pour l'ouverture de cycle d'époxydes et comme réactifs pour l'ouverture de cycle dimérisante de thiiranes dans l'acide acétique, l'eau ou des alcools. Les réactions se produisent avec des régio-, chimio- et stéréosélectivités élevées. On a trouvé que la réaction du *R*-(+)-oxyde de styrène avec de l'iode supporté par de la PVP dans le méthanol est hautement stéréospécifique; le produit isolé présente un ee de 93%.

Mots clés : iode, support, polyvinylpyrrolidone, ouverture de cycle, époxydes, thiiranes.

[Traduit par la rédaction]

Introduction

Various reactions of halogens with organic compounds have been reported in the literature. Among these reactions, the addition reactions of halogens to unsaturated compounds have been extensively studied (1–3). Iodine has also been used in many other organic transformations such as conversion of unsaturated carboxylic acids to iodolactones (4) and addition to alkenes to form diiodo compounds (5), halohydrins (6), and β-alkoxy and acetoxy iodides (7). Very recently some new applications of iodine, such as preparation of phosphate ester via activation of trialkyl phosphites (8), catalysis of some Diels–Alder reactions (9), and the conversion of alcohols to alkyl iodides (10), have also been reported. In this study we report that iodine and iodine supported on polyvinyl pyrrolidone (I_2/PVP, betadine, a commercially available disinfectant) can act as efficient catalysts for ring opening of epoxides and as reagents for ring-opening dimerization of thiiranes in alcohols, water, and acetic acid with high regio-, chemo-, and stereoselectivity under neutral conditions.

Received June 26, 1996.[1]

N. Iranpoor,[2] B. Tamami,[2] and K. Niknam. Chemistry Department, Shiraz University, Shiraz 71454, Iran.

[1] Revision received August 7, 1997.

[2] Authors to whom correspondence may be addressed. Fax: (071) 20027.

Results and discussion

Ring-opening reactions of different epoxides in primary, secondary, and tertiary alcohols were performed in the presence of 0.1–1.5 molar equivalents of iodine. The molar ratio of iodine to the substrate depends on the structure of both epoxide and nucleophile. The corresponding β-alkoxy alcohols were formed in 75–98% yields. NMR and GC analysis showed that the reactions are highly regioselective. The products obtained from cyclic epoxides showed the formation of the *trans* isomer as the sole product of the reaction. The results obtained from alcoholysis of epoxides are shown in Table 1. High chemoselectivity in the reaction of **1d**, which contains a double bond, was observed in methanol. The reaction of **1d** with methanol in the presence of 0.4 molar equivalent of I_2 and at room temperature occurred only on the epoxide ring and the double bond remained unreacted. However, when this reaction was performed in the presence of excess I_2 (1.5 molar equivalent) and under reflux conditions, in addition to the ring opening of epoxide, the double bond reacted with the methanol and iodine (Table 1, entries 10–12).

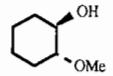
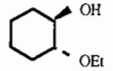
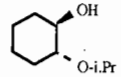
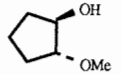
The reactions of these epoxides in water and acetic acid also took place efficiently and in the presence of 0.2–1.3 molar equivalent of I_2. The corresponding β-diols and β-acetoxy alcohols were obtained in high to excellent yields (Table 2). Identification of these compounds was done by comparison with authentic samples, which were prepared according to known procedures (11–24).

As far as we know, there is no report in the literature concerning the selective opening of an epoxide in the presence of other epoxides. We observed that, in the presence of 0.1 molar

© 1997 NRC Canada

Can. J. Chem. Downloaded from www.nrcresearchpress.com by 91.121.58.235 on 09/08/12
For personal use only.

Table 1. Reaction of epoxides with I_2 and I_2/PVP in different alcohols.

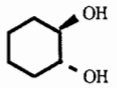
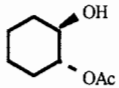
			I_2			I_2/PVP			
Entry	Epoxide	Solvent	Mole ratio of I_2/epoxide	Time (h)/ temp. (°C)	% Yield	Mole ratio of I_2/PVP/epoxide	Time (h)/ temp. (°C)	% Yield[a]	Product[b] (lit)
1	**1a**	MeOH	0.1	1/25	98	0.2	$1\frac{1}{2}$/25	92	$PhCH(OMe)CH_2OH$ (11–13)
2	**1a**	EtOH	0.2	1/25	97	0.2	$1\frac{3}{4}$/25	90	$PhCH(OEt)CH_2OH$ (11–13)
3	**1a**	*n*-PrOH	0.2	$3\frac{1}{4}$/25	98	0.2	$1\frac{3}{4}$/25	91	$PhCH(O\text{-}Pr^i)CH_2OH$ (11–13)
4	**1a**	i-PrOH	0.2	4/25	96	0.2	9/25	90	$PhCH(O\text{-}Pr^i)CH_2OH$ (11–13)
5	**1a**	*t*-BuOH	1	$\frac{1}{3}$/85	60	0.8	1/85	60	$PhCH(O\text{-}Bu^t)CH_2OH$ (11–13)
6	**1b**	MeOH	0.5	$1\frac{1}{2}$/80	98	0.4	10/25	88	$PhOCH_2CH(OH)CH_2OMe$ (11–14)
7	**1b**	EtOH	1	$\frac{3}{4}$/80	96	0.5	6/25	84	$PhOCH_2CH(OH)CH_2OEt$ (11–14)
8	**1b**	i-PrOH	1	$\frac{3}{4}$/80	94	0.6	2/85	90	$PhOCH_2CH(OH)CH_2O\text{-}Pr^i$ (11–13)
9	**1c**	MeOH	1	7/80	75	0.7	$5\frac{1}{2}$/25	86	$ClCH_2CH(OH)CH_2OMe$ (11)
10	**1d**	MeOH	0.4	1/25	94	0.5	5/25	98	$CH_2{=}CHCH_2OCH_2CH(OH)CH_2OMe$ (11–13)
11	**1d**	MeOH	1.5	$\frac{1}{10}$/80	93	1.6	2/80	94	$CH_2\text{-}CHCH_2OCH_2CH(OH)CH_2OMe$ (11–13) | | OMe I
12	**1d**	EtOH	1.5	$\frac{1}{5}$/80	92	—	—	—	$CH_2\text{-}CHCH_2OCH_2CH(OH)CH_2OEt$ (11–13) | | OEt I
13	**1d**	i-PrOH	1.5	$\frac{1}{3}$/90	98	—	—	—	$CH_2CHCH_2OCH_2CH(OH)CH_2O\text{-}Pr^i$ (11, 13) | | OPr^i I
14	**1e**	MeOH	0.1	$\frac{3}{4}$/25	98	0.2	$5\frac{1}{2}$/25	91	 (11, 13, 15)
15	**1e**	EtOH	0.3	$\frac{1}{2}$/25	92	0.3	11/25	88	 (11, 13, 15)
16	**1e**	i-PrOH	0.3	$\frac{3}{4}$/25	96	0.4	2/85	90	 (11, 13, 15)
17	**1f**	MeOH	0.1	$\frac{3}{4}$/25	93	0.2	6/25	88	 (11, 16)

[a]Yield refers to isolated product.
[b]Products were identified by comparison with authentic samples.

© 1997 NRC Canada

Can. J. Chem. Downloaded from www.nrcresearchpress.com by 91.121.58.235 on 09/08/12
For personal use only.

Table 2. Reaction of epoxides with water and acetic acid in the presence of I_2 and I_2/PVP.

			I_2			I_2/PVP			
Entry	Epoxide	Solvent	Mole ratio of I_2/epoxide	Time (h)/ temp. (°C)	% Yield	Mole ratio of I_2/PVP/epoxide	Time (h)/ temp. (°C)	% Yield[a]	Product[b] (lit)
1	**1a**	H_2O–CH_3CN	0.2	6/25	92	0.2	$1\frac{3}{4}$/25	94	$PhCH(OH)CH_2OH$ (17)
2	**1b**	H_2O–CH_3CN	1.2	$1\frac{1}{2}$/80	93	0.5	$4\frac{1}{2}$/25	91	$PhOCH_2CH(OH)CH_2OH$ (18)
3	**1c**	H_2O–CH_3CN	1.2	$1\frac{1}{2}$/80	94	0.7	1/80	87	$ClCH_2CH(OH)CH_2OH$ (18)
4	**1d**	H_2O–CH_3CN	1.5	1/80	74	1.7	1/80	70	CH_2-$CHCH_2OCH_2CH(OH)CH_2OH$ (19) | | OH I
5	**1e**	H_2O–CH_3CN	0.2	4/25	92	0.3	$1\frac{1}{2}$/25	95	 (20)
6	**1a**	HOAc	0.3	2/25	91	0.2	2/25	88	$PhCH(OAC)CH_2OH$ (21)
7	**1b**	HOAc	1.3	7/80	94	0.6	$1\frac{3}{4}$/80	27+diol	$PhOCH_2CH(OH)CH_2OAc$ (22)
8	**1c**	HOAc	1.3	13/80	92	0.7	$5\frac{1}{2}$/80	33+diol	$ClCH_2CH(OH)CH_2OAc$ (23)
9	**1e**	HOAc	0.3	3/25	98	0.4	5/25	90	

[a]Yield refers to isolated product.
[b]Products were compared with known samples.

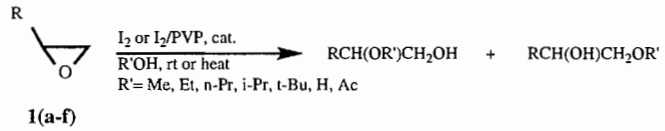
© 1997 NRC Canada

Table 3. Competitive ring opening of epoxides in methanol in the presence of I_2.

Entry	Epoxides mixture	Mole ratio of I_2/epoxide	Time (h)/ (temp) (°)	% Conversion of epoxide[a]
1	**1a** + **1b**	0.1	$\frac{1}{2}$/25	100% of **1a** 0% of **1b**
2	**1a** + **1d**	0.1	$\frac{1}{2}$/25	100% of **1a** 0% of **1d**
3	**1e** + **1c**	0.1	$\frac{3}{4}$/25	100% of **1e** 0% of **1c**
4	**1e** + **1b**	0.1	$\frac{3}{4}$/25	100% of **1e** 0% of **1b**
5	**1e** + **1d**	0.1	$\frac{3}{4}$/25	100% of **1e** 0% of **1d**
6	**1a** + **1e**	0.1	16/25	100% of **1a** 75% of **1e**

[a]GC yield.

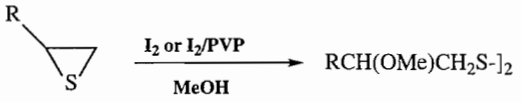
Scheme 1.



1(a-f)

1	R	1	Epoxide
a	Ph-	**e**	
b	$PhOCH_2$-		
c	$ClCH_2$-	**f**	
d	CH_2=$CHCH_2$-		

Scheme 2.



2a, 2b

R or thiirane: **2a** R=Ph, **2b** Cyclohexene sulfide

equivalent of I_2 and in methanol, a competitive ring-opening reaction of styrene oxide in the presence of those epoxides carrying electron-withdrawing substitutents (**1b**, **1c**, **1d**) can be carried out efficiently at room temperature. Very high selectivity was observed in these reactions and styrene oxide reacted quantitatively while the other epoxides remained intact (Table 3). However, the reaction of styrene oxide in the presence of cyclohexene oxide as a disubstituted epoxide in methanol did not show high selectivity under these conditions (Table 3, entry 6).

The ring-opening reaction of epoxides has been studied extensively (23) but, due to the ready polymerization of thiiranes, fundamental information abour their ring-opening reactions is still scarce. Most of the reported data concerning ring-opening reactions of this important class of compounds has been obtained in the presence of higly acidic catalysts such as H_2SO_4, HCl, or BF_3 and at high temperature (25). We studied the possibility of using iodine for ring opening of thiiranes in alcohols and aqueous acetonitrile.

The reactions of thiiranes in alcohols and aqueous acetonitrile were carried out in the presence of an equimolar amount of iodine at room temperature or under reflux (Scheme 2, Table 4). In these reactions, ring opening of thiiranes and dimerization occurred together with the formation of the corresponding disulfides in 66–90% yields.

Iodine, whose handling is not safe due to easy vaporization and ready sublimation at high temperature, has recently found very interesting applications in organic synthesis (8–10) and it is therefore important to overcome the problems of handling and sublimation. We decided to prepare I_2 supported on polyvinylpyrrolidone, to investigate its reactions with epoxides and thiiranes, and to compare the results with those obtained with iodine. Iodine supported on polyvinylpyrrolidone (I_2/PVP) has been reported in the literature and has also been used commercially as a disinfectant (betadine) (25–27) but, as far as we know, there is no report in the literature concerning its uses in organic synthesis. We prepared this reagent according to the literature and studied its reactions with both epoxides and thiiranes. The results obtained from the reaction of epoxides and thiiranes with I_2/PVP are shown in Tables 1, 2, and 4 (entries 5 and 9). Although the reactions with I_2/PVP are somewhat slower than those with iodine, the regio-, chemo-, and stereoselectivities are still very high and the same products were obtained in high yields with the advantage of overcoming the problem of handling of the reagent.

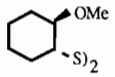
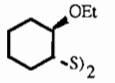
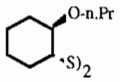
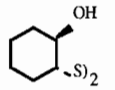
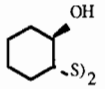
The mechanism of these reactions is not clear, but due to the formation of disulfides from the noncatalytic reaction of thiiranes in the presence of both iodine and I_2/PVP, the occurrence of a one-electron transfer reaction between I_2 and

© 1997 NRC Canada

Can. J. Chem. Downloaded from www.nrcresearchpress.com by 91.121.58.235 on 09/08/12
For personal use only.

Can. J. Chem. Downloaded from www.nrcresearchpress.com by 91.121.58.235 on 09/08/12
For personal use only.

Table 4. Reaction of thiiranes with alcohols and water in the presence of I_2 and I_2/PVP.

Entry	Thiirane	Solvent	Mole ratio of I_2/thiirane	Time (h)/ temp (°C)	% Yield[a]	Product[b] (ref. 24)
1	**4a**	MeOH	1	2/25	86	$PhCH(OMe)CH_2S]_2$
2	**4a**	EtOH	1	24/25	95	$PhCH(OEt)CH_2S]_2$
3	**4a**	EtOH	1	1/80	86	$PhCH(OEt)CH_2S]_2$
4	**4a**	*n*-PrOH	1	2/85	82	$PhCH(OPr^n)CH_2S]_2$
5	**4a**	MeOH	1[c]	17/85	82	$PhCH(OPr^n)CH_2S]_2$
6	**4b**	MeOH	1	$2\frac{3}{4}$/25	78	
7	**4b**	EtOH	1	1/80	73	
8	**4b**	*n*-PrOH	1	$3\frac{1}{3}$/85	66	
9	**4b**	MeOH	1[c]	29/85	74	
10	**4b**	H_2O–CH_3CN	1	5/25	90	$PhCH(OH)CH_2S]_2$
11	**4b**	H_2O–CH_3CN	1	9/25	72	

[a]Yield refers to isolated product.
[b]Products were identified by comparison with authentic samples.
[c]Reaction was performed in the presence of I_2/PVP.

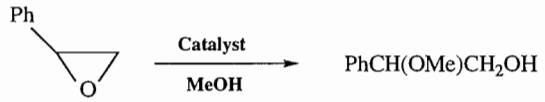
thiiranes with the formation of a radical cation (**I**) is the most probable. Attack of a molecule of alcohol on the radical cation **I** followed by dimerization of the radical obtained (**II**) could be responsible for the formation of disulfides in these reactions. To show the possibility of formation of radical in the reaction, ring opening of styrene sulfide in alcohols was studied in the presence of excess acrylamide. A great decrease in the reaction rate was observed with the formation of some polyacrylamide. Under similar conditions but in the absence of thiirane, no polymerization was observed. The formation of radical cation **I** followed by the generation of radical **II** has also been suggested in the reaction of thiiranes with other one-electron transfer agents such as Ce(IV)-based oxidants and DDQ (24).



I **II**

The possibility of the formation of an alkoxy thiol from thiiranes followed by oxidation–dimerization to the corresponding disulfide is ruled out, since neither I_2 nor I_2/PVP oxidize cyclohexyl, *meta*-thiocresol, or benzyl thiol to their corresponding disulfides under the conditions used for ring opening of thiiranes. In addition, the UV spectrum of I_2 in methanol does not show any change after 24 h. This shows that no oxidation reaction occurs between I_2 and methanol with subsequent formation of proton (13*e*). Therefore, the possibility of an acid catalysis reaction similar to that reported for Ce(IV) is also ruled out (13*e*).

Scheme 3.



The stereospecificity of the ring-opening reaction of optically active styrene oxide was studied with both iodine and different amounts of I_2/polyvinylpyrrolidone, Scheme 3. The results are shown in Table 5.

The highest optical purity was obtained by using 0.1 molar equivalent of I_2/PVP at 0°C. The optical rotation of the product was determined and compared with that reported in the literature (28). When using iodine for alcoholysis of optically

© 1997 NRC Canada

Table 5. Raction of *R*-(+)-styrene oxide[a] with methanol in the presence of I_2 and I_2/PVP.

Catalyst	Mole ratio of catalyst/epoxide	Time (h)/ temp. (°C)	% Yield[b]	%ee[c]
I_2	0.1	1/25	96	34.4
I_2	0.1	2/10	90	53.6
I_2/PVP	0.2	2/25	93	67.3
I_2/PVP	0.1	3/25	94	75
I_2/PVP	0.1	3/0	95	93

[a]Optically active styrene oxide $[\alpha]_D$ +33.0 (neat), product of Aldrich, was used without further purification. The highest value reported in the literature is $[\alpha]_D$ +35.17 (neat) (29).
[b]Yield of isolated product.
[c]Values not corrected for the optical purity of the starting material and determined according to the literature (28).

active styrene oxide at both 0°C and 25°C (Table 5), the optical purity of the product obtained was not high. These results could show the more S_N1 character of the reactions under these conditions. The low optical purity of the product in these cases could not be due to the racemization of the product after its formation, since the optical rotation of the pure product is not lowered in methanol and in the presence of I_2.

In conclusion, I_2 and I_2/PVP can be regarded as neutral catalysts or reagents for efficient ring opening of epoxides and thiiranes, respectively. Due to this neutrality, they may find application for ring opening of those epoxides and thiiranes which contain acid-sensitive functional groups. The results obtained in the competitive ring-opening reaction of certain classes of epoxides with iodine show the mildness of the catalyst. In comparison with I_2, the reactions of I_2/PVP with optically active styrene oxide are more enantioselective. I_2 supported on PVP is also very stable, nonvolatile, and its toxicity is greatly reduced. Availability, ease of procedure, high regio-, chemo-, and stereoselectivties, mild reaction conditions, and high yields of products indicate a new synthetic application for iodine in organic synthesis. In addition, the formation of disulfides from thiiranes demonstrates an interesting possible application for iodine and iodine/PVP as one-electron transfer reagents.

Experimental

Products were characterized by comparison of their physical data, IR, NMR, and mass spectra with those reported in the literature (11–24). All yields refer to isolated products. IR spectra were recorded on a Perkin Elmer IR-157 G and a Perkin Elmer 781 spectrometer. NMR spectra were recorded on a Hitachi R-2413 60 MHz or a Bruker DPX 250 MHz spectrometer. Mass spectra were recorded on a Shimadzu GCMS-QP 1000 EX. Determination of the purity of the substrate and reaction monitoring were accomplished by TLC on silica gel polygram SILG/UV 254 plates or by GLC on a Shimadzu GC-14A instrument.

Procedure for preparation of polyvinylpyrrolidone-supported iodine (I_2/PVP)

Polyvinylpyrrolidone "Fluka, 81420 Mr 40000" (5 g) was added to a solution of iodine (10 g) in diethyl ether (300 mL). The resulting suspension was stirred for 24 h at room temperature. The mixture was filtered and the resulting solid was washed several times with ether to remove the excess of iodine. The brown solid was dried in vacuum. The capacity of the reagent was found, by titration with $Na_2S_2O_3$ solution, to be 1.88 mmol iodine per gram of polymer.

General procedure for the reaction of epoxides with alcohols in the presence of iodine and iodine/PVP

Iodine (1–16 mmol) was added to a solution of epoxide (10 mmol) in the appropriate alcohol (60 mL). The reaction mixture was stirred for the specified time and at the appropriate temperature according to Table 1. The progress of the reaction was monitored by GLC. The solvent was evaporated, ether (50 mL) was added, and the mixture was washed with 10% aqueous solution of $Na_2S_2O_3$ until disappearance of the iodine colour was observed. The aqueous layer was separated and washed with ether (3 × 10 mL) The combined organic solution was dried. Evaporation of the organic solution followed by vacuum distillation or column chromatography on a short column of silica gel afforded the pure product in 60–98% yield.

General procedure for the reaction of epoxides in aqueous acetonitrile with iodine and iodine/PVP

To a solution of epoxide (10 mmol) in an equal mixture of acetonitrile–water (60 mL) was added I_2 or I_2/PVP (2–15 mmol). The reaction mixture was stirred for the specified time at room temperature according to Table 2. The progress of the reaction was monitored by TLC using CCl_4–CH_3OH (10/1) as eluent. Acetonitrile was removed and the aqueous mixture was washed with a 10% aqueous solution of $Na_2S_2O_3$ until disappearance of the iodine colour was observed. The mixture was saturated with sodium chloride and extracted with ether (3 × 40 mL, or by continuous extraction). The combined organic solution was dried and evaporated. Vacuum distillation or column chromatography of the product on a short column of silica gel afforded the pure product in 70–94% yield.

General procedure for the reaction of thiiranes with alcohols and water in the presence of iodine

Iodine (3 mmol) was added to a solution of thiirane (3 mmol) in the appropriate alcohol (30 mL) or in aqueous acetonitrile

© 1997 NRC Canada

Can. J. Chem. Downloaded from www.nrcresearchpress.com by 91.121.58.235 on 09/08/12
For personal use only.

(1:1). The reaction mixture was stirred for the required time and at the appropriate temperature according to Table 4. The progress of the reaction was monitored by GLC. The solvent was evaporated, ether (50 mL) was added, and the mixture was washed with 10% aqueous solution of $Na_2S_2O_3$. The aqueous layer was separated and washed with ether (3×20 mL) The combined organic solution was dried. Evaporation of the organic solution followed by vacuum distillation or column chromatography on a short column of silica gel afforded the pure product in 66–90% yield.

Acknowledgments

We would like to acknowledge the support of this work by Shiraz University Research Council. Helpful discussions with Professor H. Firouzabadi and the assistance of Mr. N. Maleki for running the NMR spectra and Dr. A.A. Jarahpoor for running the mass spectra are also greatly appreciated.

References

1. J.H. Rolston and K. Yates. J. Am. Chem. Soc. **9**, 1469 (1969).
2. G.H. Olah, L.M. Bollinger, and J. Brinich. J. Am. Chem. Soc. **69**, 3581 (1974),
3. (*a*) M.L. Poutsma. J. Am. Chem. Soc. **87**, 2161 (1965); (*b*) R.C. Fabey. J. Am. Chem. Soc. **88**, 4681 (1966); (*c*) **87**, 5172 (1965).
4. M.D. Domle and D.I. Davis. Chem. Soc. Rev. **8**, 171 (1979).
5. (*a*) P.S. Skell and R.R. Pavlis. J. Am. Chem. Soc. **86**, 2956 (1964); (*b*) R.L. Ayres, C.J. Michejda, and E.P. Rack. J. Am. Chem. Soc. **93**, 1389 (1971).
6. R.C. Cambie, W.I. Noall, G.J. Potter, P.S. Rutledge, and P.D. Woodgate. J. Chem. Soc. Perkin Trans. 1, 226 (1977).
7. C. Georgoulis and J.M. Valery. Bull. Soc. Chim. Fr. 2361 (1975).
8. J.K. Stomell and T.S. Widlanski. Tetrahedron Lett. **36**, 1825 (1995).
9. O. Kitagawa, K. Aoki, T. Inoue, and T. Taguchi. Tetrahedron Lett. **36**, 593 (1995).
10. R. Joseph, P.S. Pallan, A. Sudalai, and T. Ravindranathan. Tetrahedron. Lett. **36**, 609 (1995).
11. N. Iranpoor and P. Salehi. Synthesis, 1152 (1994).
12. M. Chini, P. Crotti, C. Cardelli, and F. Macchia. Synlett, 673 (1992).
13. (*a*) N. Iranpoor and I. Mohammadpour Baltork. Tetrahedron Lett. **31**, 735 (1990); (*b*) Synth. Commun. **20**, 2789 (1990); (*c*) N. Iranpoor, I. Mohammadpour Baltork, and F. Shiriny. Tetrahedron, **47**, 986 (1991); (*d*) N. Iranpoor and F. Shiriny. Synth. Commun. **24**, 1959 (1994), (*e*) J.-M. Chapuzet, S. Beauchemin, B. Daoust, and J. Lessard. Tetrahedron, **52**, 4175 (1996).
14. S. Mamedov and F. Gadzehi-Zade. Zh. Obshch. Khim. **34**, 47 (1964) (Chem. Abstr. **59**, 12628g (1963)).
15. N. Sonoda and S. Tsutsumi. Bull. Chem. Soc. Jpn. **38**, 958 (1965).
16. M. Mousseron and R. Granger. C.R. Hebd. Seances Acad. Sci. **205**, 327 (1937).
17. W. Treibs and W. Schroth. Justus Liebigs Ann. Chem. **639**, 204 (1961).
18. S. Winstein and L.L. Ingraham. J. Am. Chem. Soc. **77**, 1738 (1955).
19. Kh. Niknam. M.Sc. thesis, Shiraz University, Shiraz, Iran. 1995.
20. CRC handbook of chemistry and physics. 42nd ed. CRC Press, Boca Raton, Fla. 1961.
21. A. Roebuck and H. Adkins. Org. Synth. Coll. Vol. **III**, 217 (1955).
22. E. Detilleux and J. Jadot. Bull. Soc. R. Sci. Liege, **29**, 208 (1960).
23. (*a*) C. Smith. Synthesis, 629 (1984); (*b*) G.H. Posner and D.Z. Rogers. J. Am. Chem. Soc. **99**, 8208 (1977); **99**, 8214 (1977); (*c*) G.A. Olah, A.P. Fung, and D. Meider. Synthesis, 280 (1981).
24. N. Iranpoor and J. Owji. Synth. Commun. **20**, 1047 (1990); Tetrahedron, **47**, 149 (1991).
25. M. Sander. Chem. Rev. **66**, 297 (1966).
26. R.F. Cournoyer and S. Siggia. J. Polym. Sci. Polym. Chem. Ed. **12**, 603 (1974).
27. The Merck index. 8th ed. Merck and Co., Inc., Rahway, N.J. 1968.
28. C. Moberg, L. Rakos, and L. Toottie. Tetrahedron Lett. **23**, 2191 (1992).
29. C.R. Johnson and C.W. Shroeke. J. Am. Chem. Soc. **95**, 7418 (1973).

Can. J. Chem. Downloaded from www.nrcresearchpress.com by 91.121.58.235 on 09/08/12
For personal use only.

© 1997 NRC Canada